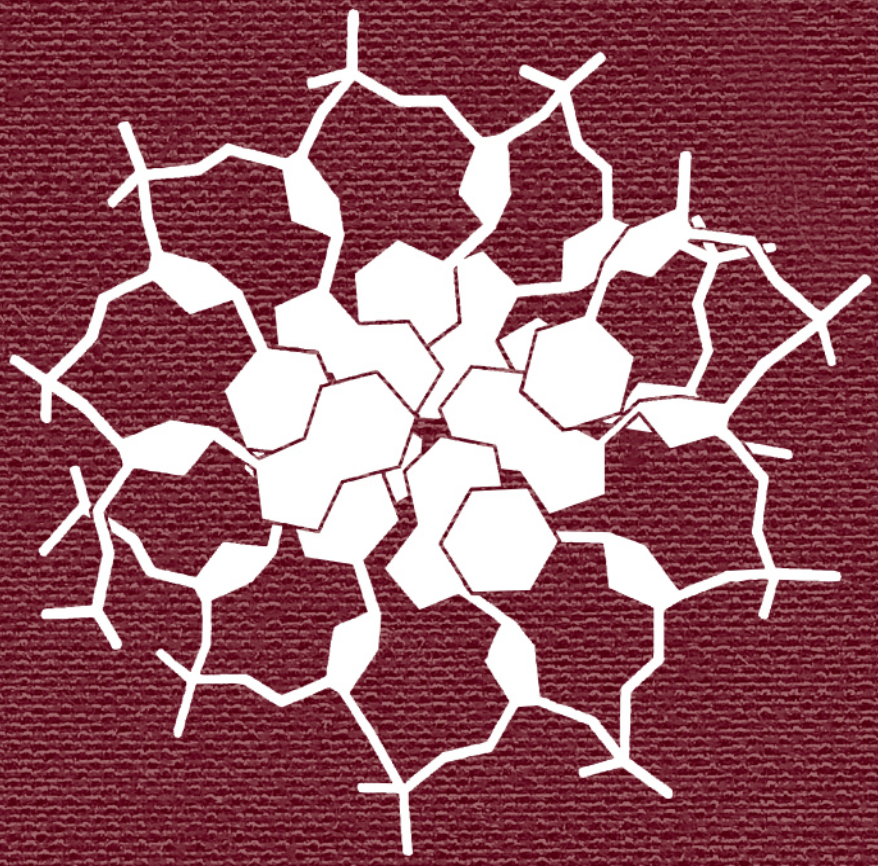
Biochemistry

TENTH EDITION

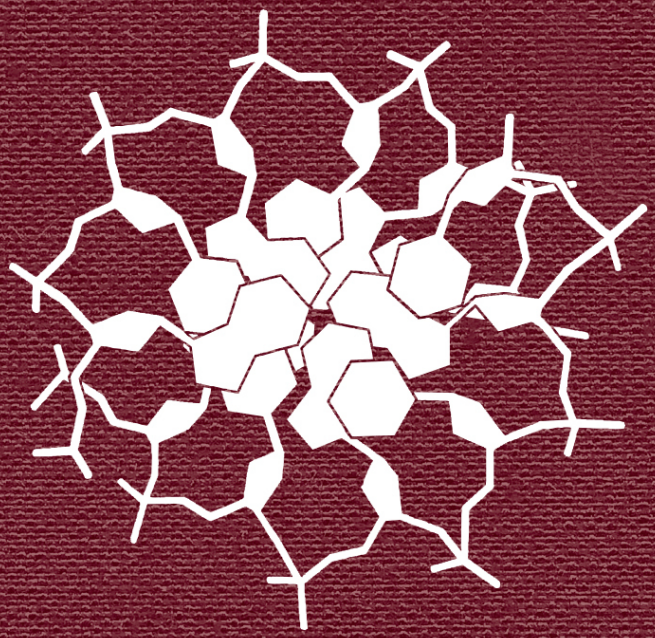


Jeremy M. Berg
Gregory J. Gatto, Jr.
Justin K. Hines
John L. Tymoczko
Lubert Stryer

macmillan learning™

Biochemistry

TENTH EDITION



Jeremy M. Berg
Gregory J. Gatto, Jr.
Justin K. Hines
John L. Tymoczko
Lubert Stryer

macmillan learning™



Accessibility

Macmillan Learning is committed to the goal of providing equal access to all products regardless of an individual's age, ability, or situation and embraces the opportunity to develop services and information technologies that are accessible and usable by all individuals. Accessibility at Macmillan Learning is about extending the power of education to all users. In addition to addressing product compatibility with assistive technologies such as screen reader software, alternative keyboard devices, and voice recognition products, we are working to ensure that the content and platforms we provide are fully accessible.

Our E-books

Macmillan Learning became the first education solutions company to become Global Certified Accessible™, providing "born accessible" digital learning (e-book) options for students with disabilities. Books that are born accessible are developed to ensure that all students, no matter their ability, have the same access to information. This is increasingly important for students and instructors, as more than one out of every ten students who attends college has a disability.

To become Global Certified Accessible, Benetech evaluated Macmillan Learning's workflow for creating accessible books, as well as many samples of content across the disciplines they publish in, and certified conformance to the accessible EPUB creation guidelines, which are based on WCAG 2.0 AA+ standards put in place by the international standards organizations and the publishing community. Using a collaborative process, Benetech evaluated and

provided feedback on more than one hundred accessibility features. The certification applies to all books created using Macmillan Learning's updated process, which includes all e-books with a 2019 copyright and beyond.

Extended Descriptions

In this book, extended descriptions are present for complex images and graphs that may be helpful to understanding content. These extended descriptions can be accessed via a link on this icon:



Alternative Text

When an image provides important pedagogical information, alternative text (which is also known as alt text) is provided for the image. This text is not visible on the page but can be accessed and read with screen reader technology and other assistive technologies. Our alt text is written and reviewed by subject matter experts.

Color Contrast

All of our book designs and illustrations are checked to ensure that they meet contrast requirements for WCAG 2.0 AA. Meeting these standards ensures ease of use for users with low vision and color

blindness, and can create a more supportive learning environment for users with learning disabilities.

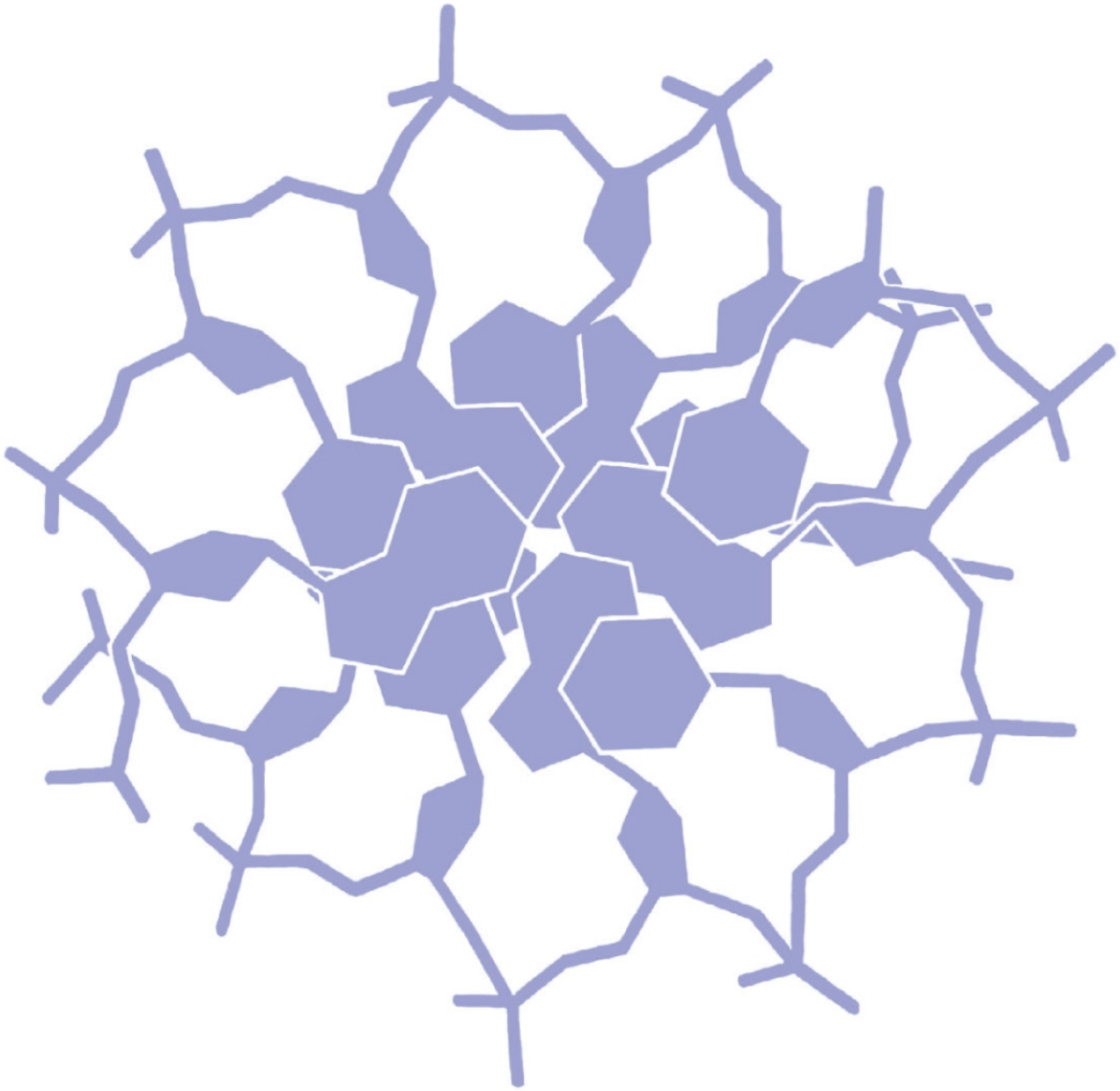
Navigation

E-book navigation is designed to make it easy for users, with or without assistive technology, to discover and learn from content within the textbook. Text reflows when resized so there is no horizontal scrolling on the page, and page numbers are embedded in the book so that students can always find where they are compared to classmates using the print equivalent. Heading structures are clearly marked up so it's easy to see where you are within the book as you work your way through.

Accessibility Help

If you have any questions about the accessibility of this e-book or other Macmillan Learning e-books, please reach out to us at webaccessibility@macmillan.com. For student resources, visit our knowledge base.

Biochemistry



Biochemistry

TENTH EDITION

Jeremy M. Berg
Gregory J. Gatto, Jr.
Justin K. Hines
Jutta Beneken Heller
John L. Tymoczko
Lubert Stryer



Austin • Boston • New York • Plymouth



Senior Vice President, STEM: Daryl Fox
Executive Program Director: Sandy Lindelof
Senior Program Manager: Liz Simmons
Marketing Manager: Maureen Rachford
Director of Development: Barbara Yien
Senior Development Editor: Jennifer Angel
Editorial Project Manager: Jennifer Hart
Director of Content: Heather Southerland
Executive Media Editor: Amy Thorne
Senior Media Editors: Cassandra Korsvik, Kelsey Hughes
Senior Lead Content Developer: Lily Huang
Assistant Editor: Angelica Hernandez
Senior Director of Content Management Enhancement: Tracey Kuehn
Senior Managing Editor: Lisa Kinne
Senior Content Project Manager: Peter Jacoby
Workflow Project Manager: Paul Rohloff
Director of Design, Content Management: Diana Blume
Senior Design Services Manager: Natasha A. S. Wolfe
Senior Cover Design Manager: John Callahan
Text Designer: Maureen McCutcheon
Art Manager: Matthew McAdams
Illustrations: Jeremy Berg with Network Graphics, Gregory J. Gatto, Jr., Adam Steinberg, Lumina Datamatics, Inc.
Senior Director of Digital Production: Keri deManigold
Senior Media Production Manager: Elton Carter
Senior Media Permissions Manager: Christine Buese
Photo Researchers: Richard Fox and Krystyna Borgen, Lumina Datamatics, Inc.
Composition: Lumina Datamatics, Inc.

Library of Congress Control Number: 2022943738

Gregory J. Gatto, Jr., is an employee of GlaxoSmithKline (GSK), which has not supported or funded this work in any way. Any views expressed herein do not necessarily represent the views of GSK.

ISBN-13: 978-1-319-41746-8 (Amazon)

© 2023, 2019, 2015, 2012 by Macmillan Learning
© 1995, 1988, 1981, 1975 by Lubert Stryer

All rights reserved.

1 2 3 4 5 6 28 27 26 25 24 23

Macmillan Learning
120 Broadway
New York, NY 10271
www.macmillanlearning.com



In 1946, William Freeman founded W. H. Freeman and Company and published Linus Pauling's *General Chemistry*, which revolutionized the chemistry curriculum and established the prototype for a Freeman text. W. H. Freeman quickly became a publishing house where leading researchers can make significant contributions to mathematics and science. In

1996, W. H. Freeman joined Macmillan and we have since proudly continued the legacy of providing revolutionary, quality educational tools for teaching and learning in STEM.



To our teachers and our students,

including our late coauthor John Tymoczko,

whose devotion to his students was an inspiration

Brief Contents

1 Biochemistry in Space and Time
2 Protein Composition and Structure
3 Binding and Molecular Recognition
4 Protein Methods
5 Enzymes: Core Concepts and Kinetics
6 Enzyme Catalytic Strategies
7 Enzyme Regulatory Strategies
8 DNA, RNA, and the Flow of Genetic Information
9 Nucleic Acid Methods
10 Exploring Evolution and Bioinformatics
11 Carbohydrates and Glycoproteins
12 Lipids and Biological Membranes
13 Membrane Channels and Pumps
14 Signal-Transduction Pathways
15 Metabolism: Basic Concepts and Themes
16 Glycolysis and Gluconeogenesis
17 Pyruvate Dehydrogenase and the Citric Acid Cycle
18 Oxidative Phosphorylation
19 Phototrophy and the Light Reactions of Photosynthesis
20 The Calvin–Benson Cycle and the Pentose Phosphate Pathway
21 Glycogen Metabolism
22 Fatty Acid and Triacylglycerol Metabolism
23 Protein Turnover and Amino Acid Catabolism
24 Integration of Energy Metabolism
25 Biosynthesis of Amino Acids
26 Nucleotide Biosynthesis
27 Biosynthesis of Membrane Lipids and Steroids
28 DNA Replication, Repair, and Recombination
29 RNA Functions, Biosynthesis, and Processing
30 Protein Biosynthesis

31 Control of Gene Expression
32 Principles of Drug Discovery and Development

Contents

PREFACE
ACKNOWLEDGMENTS
ABOUT THE AUTHORS
CHAPTER 1
Biochemistry in Space and Time
- **1.1 Biochemical Unity Underlies Biological Diversity**
- **1.2 DNA Illustrates the Interplay Between Form and Function**
  - DNA is constructed from four building blocks
  - Two single strands of DNA combine to form a double helix
  - DNA structure explains heredity and the storage of information
- **1.3 Concepts from Chemistry Explain the Properties of Biological Molecules**
  - The formation of the DNA double helix is a key example
  - The double helix can form from its component strands
  - Atoms and molecules undergo random motions that help define the timescales for biochemical interactions
  - Covalent bonds and noncovalent interactions are important for the structure and stability of biological molecules
  - The formation of DNA's double helix is an expression of the rules of chemistry
  - The laws of thermodynamics govern the behavior of biochemical systems
  - By releasing heat, the formation of the double helix obeys the Second Law of Thermodynamics

Double-helix formation can be monitored one molecule at a time
Acid–base reactions are central in many biochemical processes
Acid–base reactions can disrupt the double helix
Buffers regulate pH in organisms and in the laboratory
EXAMPLE Applying the Henderson–Hasselbalch Equation
1.4 DNA Sequencing Is Transforming Biochemistry, Medicine, and Other Fields
Genome sequencing has become remarkably fast and inexpensive
Characterization of genetic variation between individuals is powerful for many applications
The most important function of genomic sequences is to encode proteins
Comparing genomes offers great insights into evolution
1.5 Biochemistry Is an Interconnected Human Endeavor
CHAPTER 2
Protein Composition and Structure
2.1 Several Properties of Protein Structure Are Key to Their Functional Versatility
2.2 Proteins Are Built from a Repertoire of 20 Amino Acids
The diversity of amino acids arises from the different side chains
Biochemists postulate several reasons why this set of amino acids is conserved across all species
2.3 Primary Structure: Amino Acids Are Linked by Peptide Bonds to Form Polypeptide Chains
Proteins have unique amino acid sequences specified by genes
Polypeptide chains are flexible yet conformationally restricted

2.4 Secondary Structure: Polypeptide Chains Can Fold into Regular Structures

The alpha helix is a coiled structure stabilized by intrachain hydrogen bonds
SCIENTIST PROFILE Herman Branson
Beta sheets are stabilized by hydrogen bonding between polypeptide strands
Polypeptide chains can change direction by making reverse turns and loops

2.5 Tertiary Structure: Proteins Can Fold into Globular or Fibrous Structures

Globular proteins form tightly packed structures
Fibrous proteins form extended structures that provide support for cells and tissues

2.6 Quaternary Structure: Polypeptide Chains Can Assemble into Multisubunit Structures

2.7 The Amino Acid Sequence of a Protein Determines Its Three-Dimensional Structure

Amino acids have different propensities for forming α helices, β sheets, and turns
Protein folding is a highly cooperative process
Proteins fold by progressive stabilization of intermediates rather than by random search
Prediction of three-dimensional structure from sequence remains a great challenge

 Protein misfolding and aggregation are associated with some neurological diseases
Posttranslational modifications confer new capabilities to proteins

CHAPTER 3
Binding and Molecular Recognition

3.1 Binding Is a Fundamental Process in Biochemistry

Binding depends on the concentrations of the binding partners
Proteins can selectively bind certain small molecules
Binding is a dynamic process involving association and dissociation

3.2 Myoglobin Binds and Stores Oxygen

More myoglobin binds oxygen as the oxygen partial pressure is increased
A bond is formed between oxygen and iron in heme
The structure of myoglobin prevents the release of reactive oxygen species
Compared with model compounds, myoglobin discriminates between oxygen and carbon monoxide

3.3 Hemoglobin Is an Efficient Oxygen Carrier

Human hemoglobin is an assembly of four myoglobin-like subunits
Hemoglobin binds oxygen cooperatively
Oxygen binding markedly changes the quaternary structure of hemoglobin
Hemoglobin cooperativity can be potentially explained by several models
Structural changes at the heme groups are transmitted to the $\alpha_1\beta_1-\alpha_2\beta_2$ interface
2,3-Bisphosphoglycerate in red blood cells is crucial in determining the oxygen affinity of hemoglobin
Hydrogen ions and carbon dioxide promote the release of oxygen
Mutations in genes encoding hemoglobin subunits can result in disease

3.4 The Immune System Depends on Key Binding Proteins

The innate immune system recognizes molecules characteristic of pathogens

Antibodies bind specific molecules through specific hypervariable loops
Antibodies possess distinct antigen-binding and effector units
Recombination events equip the adaptive immune system with millions of unique antibodies
Major-histocompatibility-complex proteins present peptide antigens on cell surfaces for recognition by T-cell receptors
3.5 Quantitative Terms Can Describe Binding Propensity
Dissociation constants are useful in describing binding reactions quantitatively
SCIENTIST PROFILE Pamela Bjorkman
EXAMPLE Determining the Fraction of Bound Receptors
Specificity can be quantified by comparing dissociation constants
Kinetic parameters can also describe binding processes
CHAPTER 4
Protein Methods
4.1 The Purification of Proteins Is an Essential First Step in Understanding Their Function
The assay: How do we recognize the protein we are looking for?
Proteins must be released from the cell to be purified
Proteins can be purified according to solubility, size, charge, and binding affinity
Proteins can be separated by gel electrophoresis and displayed
A protein purification scheme can be quantitatively evaluated
EXAMPLE Calculating the Effectiveness of Protein Purification
Ultracentrifugation is valuable for separating biomolecules and determining their masses

Recombinant DNA technology can make protein purification easier
4.2 Immunology Provides Important Techniques for Investigating Proteins
Antibodies to specific proteins can be generated
Monoclonal antibodies with virtually any desired specificity can be readily prepared
Proteins can be detected and quantified by using an enzyme-linked immunosorbent assay
Western blotting permits the detection of proteins separated by gel electrophoresis
Co-immunoprecipitation enables the identification of binding partners of a protein
Fluorescent markers make the visualization of proteins in the cell possible
4.3 Mass Spectrometry Is a Powerful Technique for the Identification of Peptides and Proteins
Peptides can be sequenced by mass spectrometry
Proteins can be specifically cleaved into small peptides to facilitate analysis
Genomic and proteomic methods are complementary approaches to deducing protein structure and function
The amino acid sequence of a protein provides valuable information
Individual proteins can be identified by mass spectrometry
The proteome is the functional representation of the genome
4.4 Peptides Can Be Synthesized by Automated Solid-Phase Methods
4.5 Three-Dimensional Protein Structures Can Be Determined Experimentally
X-ray crystallography reveals three-dimensional structure in atomic detail

SCIENTIST PROFILE Rosalind Franklin
Nuclear magnetic resonance spectroscopy can reveal the structures of proteins in solution
Cryo-electron microscopy can be used to determine the structures of large proteins and macromolecular complexes
CHAPTER 5
Enzymes: Core Concepts and Kinetics
5.1 Enzymes Are Powerful and Highly Specific Catalysts
Most enzymes are classified by the types of reactions they catalyze
Many enzymes require cofactors for activity
Enzymes can transform energy from one form into another
5.2 Gibbs Free Energy Is a Useful Thermodynamic Function for Understanding Enzymes
The free-energy change provides information about the spontaneity but not the rate of a reaction
The standard free-energy change of a reaction is related to the equilibrium constant
EXAMPLE Calculating and Comparing $\Delta G^{\circ\prime}$ and ΔG
Enzymes alter only the reaction rate and not the reaction equilibrium
5.3 Enzymes Accelerate Reactions by Facilitating the Formation of the Transition State
The formation of an enzyme–substrate complex is the first step in enzymatic catalysis
The active sites of enzymes have some common features
The binding energy between enzyme and substrate is important for catalysis
Because the transition state collapses randomly, the activation energies determine the accumulation of either product or substrate

5.4 The Michaelis–Menten Model Accounts for the Kinetic Properties of Many Enzymes

- Kinetics is the study of reaction rates
- The steady-state assumption aids a description of enzyme kinetics
- The Michaelis–Menten model explains many observations of enzyme kinetics
- The Michaelis–Menten equation describes the relationship between initial velocity and substrate concentration
- **SCIENTIST PROFILE** Maud Menten
- **EXAMPLE** Applying the Michaelis–Menten Equation
-  Variations in K_M can have physiological consequences
- K_M and V_{max} values can be determined by several means
- K_M and k_{cat} values are important enzyme characteristics
- k_{cat}/K_M is a measure of catalytic efficiency
- Most biochemical reactions include multiple substrates
- Allosteric enzymes often do not obey Michaelis–Menten kinetics
- Temperature affects enzymatic activity

5.5 Enzymes Can Be Studied One Molecule at a Time

- Single-molecule kinetics confirm results obtained from ensemble studies
- Single-molecule studies continue to reveal new information about enzyme molecular dynamics

5.6 Enzymes Can Be Inhibited by Specific Molecules

- The different types of reversible inhibitors are kinetically distinguishable
- Transition-state analogs are potent competitive inhibitors
- Irreversible inhibitors can be used to map the active site

EXAMPLE Determining Inhibitor Type from Data

 Penicillin irreversibly inactivates a key enzyme in bacterial cell-wall synthesis

CHAPTER 6

Enzyme Catalytic Strategies

6.1 Enzymes Use a Core Set of Catalytic Strategies

6.2 Proteases Facilitate a Fundamentally Difficult Reaction

Chymotrypsin possesses a highly reactive serine residue

Chymotrypsin action proceeds in two steps linked by a covalently bound intermediate

Serine is part of a catalytic triad that also includes histidine and aspartate

Catalytic triads are found in other hydrolytic enzymes

Scientists have dissected the catalytic triad using site-directed mutagenesis

Some proteases cleave peptides at other locations besides serine residues

 Protease inhibitors are important drugs

6.3 Carbonic Anhydrases Make a Fast Reaction Faster

Carbonic anhydrase contains a bound zinc ion essential for catalytic activity

Catalysis involves zinc activation of a water molecule

Rapid regeneration of the active form of carbonic anhydrase depends on proton availability

6.4 Restriction Enzymes Catalyze Highly Specific DNA-Cleavage Reactions

Cleavage is by direct displacement of 3′-oxygen from phosphorus by magnesium-activated water

Restriction enzymes require magnesium for catalytic activity

The complete catalytic apparatus is assembled only within complexes of cognate DNA molecules, ensuring specificity
Host-cell DNA is protected by the addition of methyl groups to specific bases
6.5 Molecular Motor Proteins Harness Changes in Enzyme Conformation to Couple ATP Hydrolysis to Mechanical Work
ATP hydrolysis proceeds by the attack of water on the gamma phosphoryl group
Formation of the transition state for ATP hydrolysis is associated with a substantial conformational change
The altered conformation of myosin persists for a substantial period of time
Actin forms filaments along which myosin can move
CHAPTER 7
Enzyme Regulatory Strategies
7.1 Allosteric Regulation Enables Control of Metabolic Pathways
Many allosterically regulated enzymes do not follow Michaelis–Menten kinetics
ATCase consists of separable catalytic and regulatory subunits
Allosteric interactions in ATCase are mediated by large changes in quaternary structure
Allosteric regulators modulate the T-to-R equilibrium
7.2 Isozymes Provide a Means of Regulation Specific to Distinct Tissues and Developmental Stages
7.3 Covalent Modification Is a Means of Regulating Enzyme Activity
Kinases and phosphatases control the extent of protein phosphorylation
Phosphorylation is a highly effective means of regulating the activities of target proteins

Cyclic AMP activates protein kinase A by altering the quaternary structure
Mutations in protein kinase A can cause Cushing's syndrome
The phosphorylation states of the proteome can be measured
7.4 Many Enzymes Are Activated by Specific Proteolytic Cleavage
Chymotrypsinogen is activated by specific cleavage of a single peptide bond
Proteolytic activation of chymotrypsinogen leads to the formation of a substrate-binding site
The generation of trypsin from trypsinogen leads to the activation of other zymogens
Some proteolytic enzymes have specific inhibitors
7.5 Enzymatic Cascades Allow Rapid Responses Such as Blood Clotting
Prothrombin must bind to Ca^{2+} to be converted to thrombin
Fibrinogen is converted by thrombin into a fibrin clot
Vitamin K is required for the formation of γ-carboxyglutamate
The clotting process must be precisely regulated
CHAPTER 8
DNA, RNA, and the Flow of Genetic Information
8.1 A Nucleic Acid Consists of Four Kinds of Bases Linked to a Sugar–Phosphate Backbone
RNA and DNA differ in the sugar component and one of the bases
Nucleotides are the monomeric units of nucleic acids
DNA molecules are very long and have directionality

8.2 A Pair of Nucleic Acid Strands with Complementary Sequences Can Form a Double-Helical Structure
- The double helix is stabilized by hydrogen bonds and van der Waals interactions
- DNA can assume a variety of structural forms
- The major and minor grooves are lined by sequence-specific hydrogen-bonding groups
- Some DNA molecules are circular and supercoiled
- Single-stranded nucleic acids can adopt elaborate structures

8.3 The Double Helix Facilitates the Accurate Transmission of Hereditary Information
- Differences in DNA density established the validity of the semiconservative replication hypothesis
- The double helix can be reversibly melted

8.4 DNA Is Replicated by Polymerases That Take Instructions from Templates
- DNA polymerase catalyzes phosphodiester-bridge formation
- The genes of some viruses are made of RNA

8.5 Gene Expression Is the Transformation of DNA Information into Functional Molecules
- Several kinds of RNA play key roles in gene expression
- All cellular RNA is synthesized by RNA polymerases
- RNA polymerases take instructions from DNA templates
- Transcription begins near promoter sites and ends at terminator sites
- Transfer RNAs are the adaptor molecules in protein synthesis

8.6 Amino Acids Are Encoded by Groups of Three Bases Starting from a Fixed Point
- Major features of the genetic code
- **SCIENTIST PROFILE** Har Gobind Khorana

Messenger RNA contains start and stop signals for protein synthesis
The genetic code is nearly universal
8.7 Most Eukaryotic Genes Are Mosaics of Introns and Exons
RNA processing generates mature RNA
Many exons encode protein domains
CHAPTER 9
Nucleic Acid Methods
9.1 The Exploration of Genes Relies on Key Tools
Restriction enzymes split DNA into specific fragments
Restriction fragments can be separated by gel electrophoresis and visualized
DNA can be sequenced by controlled termination of replication
DNA probes and genes can be synthesized by automated solid-phase methods
Selected DNA sequences can be greatly amplified by the polymerase chain reaction
PCR is a powerful technique in medical diagnostics, forensics, and studies of molecular evolution

The tools for recombinant DNA technology have been used to identify disease-causing mutations
9.2 Recombinant DNA Technology Has Revolutionized All Aspects of Biology
Restriction enzymes and DNA ligase are key tools in forming recombinant DNA molecules
Plasmids and λ phage are choice vectors for DNA cloning in bacteria
Specific genes can be cloned from digests of genomic DNA
Complementary DNA prepared from mRNA can be expressed in host cells

Proteins with new functions can be created through directed changes in DNA
9.3 Complete Genomes Have Been Sequenced and Analyzed
The genomes of organisms ranging from bacteria to multicellular eukaryotes have been sequenced
The sequence of the human genome has been completed
Next-generation sequencing methods enable the rapid determination of a complete genome sequence
Comparative genomics is a powerful research tool
9.4 Eukaryotic Genes Can Be Quantitated and Manipulated with Considerable Precision
Gene-expression levels can be comprehensively examined
New genes inserted into eukaryotic cells can be efficiently expressed
Transgenic animals harbor and express genes introduced into their germ lines
Gene disruption and genome editing provide clues to gene function and opportunities for new therapies
RNA interference enables disruption of gene expression and presents new therapeutic opportunities
SCIENTIST PROFILE Emmanuelle Charpentier and Jennifer Doudna
Foreign DNA can be introduced into plants
CHAPTER 10
Exploring Evolution and Bioinformatics
10.1 Homologs Are Descended from a Common Ancestor and Can Be Detected by Sequence Alignments
Orthologs and paralogs are two different classes of homologous proteins
Statistical analysis of sequence alignments can detect homology

The statistical significance of alignments can be estimated by shuffling
Distant evolutionary relationships can be detected through the use of substitution matrices
Databases can be searched to identify homologous sequences
10.2 Examination of Three-Dimensional Structure Enhances Our Understanding of Evolutionary Relationships
Tertiary structure is more conserved than primary structure
Knowledge of three-dimensional structures can aid in the evaluation of sequence alignments
Repeated motifs can be detected by aligning sequences with themselves
Convergent evolution illustrates common solutions to biochemical challenges
Comparison of RNA sequences can be a source of insight into RNA secondary structures
EXAMPLE Interpreting an RNA Alignment
10.3 Evolutionary Trees Can Be Constructed on the Basis of Sequence Information
Evolutionary trees can be calibrated using fossil record data
Horizontal gene transfer events may explain unexpected branches of the evolutionary tree
SCIENTIST PROFILE Russell Doolittle
10.4 Modern Techniques Make the Experimental Exploration of Evolution Possible
Ancient DNA can sometimes be amplified and sequenced
Molecular evolution can be examined experimentally
CHAPTER 11
Carbohydrates and Glycoproteins

11.1 Monosaccharides Are the Simplest Carbohydrates

There are many monosaccharides but they are structurally similar
Most monosaccharides exist as interchanging cyclic forms
Pyranose and furanose rings can assume different conformations
D-Glucose is an important fuel for most organisms
Glucose is a reducing sugar and reacts nonenzymatically with hemoglobin
Monosaccharides are joined to alcohols and amines through glycosidic linkages by specific enzymes
Phosphorylated sugars are key intermediates in metabolism

11.2 Monosaccharides Are Linked to Form Complex Carbohydrates

Sucrose, lactose, and maltose are common disaccharides
 Maltase inhibitors can help to maintain blood glucose homeostasis
 Human milk oligosaccharides protect newborns from infection
Glycogen and starch are storage polysaccharides of glucose
Cellulose is the main structural polysaccharide of plants
Chitin is the main structural polysaccharide of fungi and arthropods
Chitin can be processed to a molecule with a variety of uses

11.3 Carbohydrates Can Be Linked to Proteins to Form Glycoproteins

Carbohydrates can be linked to proteins through asparagine (*N*-linked) or through serine or threonine (*O*-

linked) residues
 The glycoprotein erythropoietin is a vital hormone
Glycosylation functions in nutrient sensing
Proteoglycans have important structural roles
Proteoglycans are important components of cartilage
Mucins are glycoprotein components of mucus
Protein glycosylation takes place in the lumen of the endoplasmic reticulum and in the Golgi complex
Specific enzymes are responsible for oligosaccharide assembly
Blood groups are based on protein glycosylation patterns
 Errors in glycosylation can result in pathological conditions
Biochemists use several techniques to analyze the oligosaccharide components of glycoproteins
11.4 Lectins Are Specific Carbohydrate-Binding Proteins
Lectins promote interactions between cells and within cells
Lectins are organized into two large classes
Influenza virus binds to sialic acid residues
SCIENTIST PROFILE Carolyn Bertozzi
CHAPTER 12
Lipids and Biological Membranes
12.1 Fatty Acids Are Key Constituents of Lipids
Fatty acid names are based on their parent hydrocarbons
Chain length and degree of unsaturation affect fatty acid properties
12.2 Biological Membranes Are Composed of Three Common Types of Membrane Lipids
Phospholipids are the major class of membrane lipids
Glycolipids include carbohydrate moieties

Cholesterol is a lipid based on a steroid nucleus
SCIENTIST PROFILE Marie M. Daly
Archaeal membranes are built from ether lipids with branched chains
A membrane lipid is an amphipathic molecule containing a hydrophilic and a hydrophobic moiety
12.3 Phospholipids and Glycolipids Readily Form Bimolecular Sheets in Aqueous Media
Lipid vesicles can be formed from phospholipids
Lipid bilayers are highly impermeable to ions and most polar molecules
12.4 Proteins Carry Out Most Membrane Processes
Proteins associate with the lipid bilayer in a variety of ways
Proteins interact with membranes in a variety of ways
Some proteins associate with membranes through covalently attached hydrophobic groups
Transmembrane helices can be accurately predicted from amino acid sequences
12.5 Lipids and Many Membrane Proteins Diffuse Rapidly in the Plane of the Membrane
The fluid mosaic model allows lateral movement but not rotation through the membrane
Membrane fluidity is controlled by fatty acid composition and cholesterol content
Lipid rafts are highly dynamic complexes formed between cholesterol and specific lipids
All biological membranes are asymmetric
12.6 Prokaryotes and Eukaryotes Differ in Their Use of Biological Membranes
Eukaryotic cells contain compartments bounded by internal membranes
Membrane budding and fusion are highly controlled processes

CHAPTER 13
Membrane Channels and Pumps
13.1 The Transport of Molecules Across a Membrane May Be Active or Passive
Many molecules require protein transporters to cross membranes
Free energy stored in concentration gradients can be quantified
EXAMPLE Calculating the Energetic Cost of Ion Transport
13.2 Two Families of Membrane Proteins Use ATP Hydrolysis to Actively Transport Ions and Molecules Across Membranes
P-type ATPases couple phosphorylation and conformational changes to pump calcium ions across membranes
Digoxin specifically inhibits the Na^+-K^+ pump by blocking its dephosphorylation
P-type ATPases are evolutionarily conserved and play a wide range of roles
Multidrug resistance highlights a family of membrane pumps with ATP-binding cassette domains
13.3 Lactose Permease Is an Archetype of Secondary Transporters That Use One Concentration Gradient to Power the Formation of Another
13.4 Specific Channels Can Rapidly Transport Ions Across Membranes
Action potentials are mediated by transient changes in Na^+ and K^+ permeability
Patch-clamp conductance measurements reveal the activities of single channels

The structure of a potassium ion channel is an archetype for many ion-channel structures
SCIENTIST PROFILE Baldomero Olivera
The structure of the potassium ion channel reveals the basis of ion specificity
The structure of the potassium ion channel explains its rapid rate of transport
Voltage gating requires substantial conformational changes in specific ion-channel domains
A channel can be inactivated by occlusion of the pore: the ball-and-chain model
The acetylcholine receptor is an archetype for ligand-gated ion channels
Action potentials integrate the activities of several ion channels working in concert
EXAMPLE Calculating Equilibrium Potentials
Disruption of ion channels by mutations or chemicals can be potentially life-threatening
Hyperpolarization-activated ion channels enable pacemaker activity in the heart
13.5 Gap Junctions Allow Ions and Small Molecules to Flow Between Communicating Cells
13.6 Specific Channels Increase the Permeability of Some Membranes to Water
CHAPTER 14
Signal-Transduction Pathways
14.1 Many Signal-Transduction Pathways Share Common Themes
Signal transduction depends on molecular circuits
14.2 Epinephrine Signaling: Heterotrimeric G Proteins Transmit Signals and Reset Themselves
Ligand binding to 7TM receptors leads to the activation of heterotrimeric G proteins

Activated G proteins transmit signals by binding to other proteins
Cyclic AMP stimulates the phosphorylation of many target proteins by activating protein kinase A
G proteins spontaneously reset themselves through GTP hydrolysis
Some 7TM receptors activate the phosphoinositide cascade
Calcium ion is a widely used second messenger
Calcium ion often activates the regulatory protein calmodulin
Some receptors signal through G proteins that inhibit rather than stimulate adenylate cyclase
G-protein βγ-dimers can also directly participate in signaling
7TM receptors trigger signaling through G proteins in many other cell types
SCIENTIST PROFILE Eva Neer
14.3 Insulin Signaling: Phosphorylation Cascades Are Central to Many Signal-Transduction Processes
The insulin receptor is a protein kinase that is autoinhibited prior to insulin binding
Insulin binding results in the cross-phosphorylation and activation of the insulin receptor
The activated insulin-receptor kinase initiates a kinase cascade
Insulin signaling is terminated by the action of phosphatases
14.4 Epidermal Growth Factor: Receptor Dimerization Can Drive Signaling
The EGF receptor undergoes phosphorylation of its carboxyl-terminal tail
EGF signaling leads to the activation of Ras, a small G protein

Activated Ras initiates a protein kinase cascade
EGF signaling is terminated by protein phosphatases and the intrinsic GTPase activity of Ras

 **14.5 Defects in Signal-Transduction Pathways Can Lead to Cancer and Other Diseases**

Monoclonal antibodies can be used to inhibit signal-transduction pathways activated in tumors
Protein kinase inhibitors can be effective anticancer drugs

14.6 Sensory Systems Are Based on Specialized Signal-Transduction Pathways

A huge family of 7TM receptors detect a wide variety of organic compounds
Vision relies on a specialized 7TM receptor to signal in response to absorbed light
Light absorption induces a specific isomerization of bound 11-*cis*-retinal
Color vision is mediated by three cone receptors that are homologs of rhodopsin
Hearing depends on hair cells that use mechanosensitive ion channels to detect tiny motions
Comparison of different organisms yields insights into sensory system evolution

CHAPTER 15
Metabolism: Basic Concepts and Themes

15.1 Metabolism Is Composed of Many Interconnected Reactions

Metabolism consists of destructive and constructive reactions that typically yield or require energy
A thermodynamically unfavorable reaction can be driven by a favorable reaction

15.2 ATP Is the Universal Currency of Free Energy in Biological Systems

ATP hydrolysis is exergonic
ATP hydrolysis drives metabolism by shifting the equilibrium of coupled reactions
The high phosphoryl potential of ATP results from structural differences between ATP and its hydrolysis products
Phosphoryl-transfer potential is an important form of cellular energy transformation
EXAMPLE Calculating ΔG for a Coupled Reaction Under Real Conditions
15.3 The Oxidation of Carbon Fuels Is an Important Source of Cellular Energy
Compounds with high phosphoryl-transfer potential can couple carbon oxidation to ATP synthesis
Ion gradients across membranes provide an important form of cellular energy that can be coupled to ATP synthesis
Phosphates play a prominent role in biochemical processes
Energy from food is extracted in three stages
15.4 Metabolic Pathways Contain Many Recurring Motifs
Activated carriers exemplify the modular structure and economy of metabolism
Many activated carriers are derived from vitamins
Key reactions are reiterated throughout metabolism
Metabolic processes are regulated in three principal ways
CHAPTER 16
Glycolysis and Gluconeogenesis
16.1 Glycolysis Is an Energy-Conversion Pathway in Most Organisms
Glucose is generated from dietary carbohydrates
A family of transporters enables glucose to enter and leave animal cells

16.2 Glycolysis Can Be Divided into Two Parts

- Stage 1 begins: Hexokinase traps glucose in the cell and begins glycolysis
- Fructose 1,6-bisphosphate is generated from glucose 6-phosphate
- The six-carbon sugar is cleaved into two three-carbon fragments
- Mechanism: Triose phosphate isomerase salvages a three-carbon fragment
- Stage 2 begins: The oxidation of an aldehyde powers the formation of a compound with high phosphoryl-transfer potential
- Mechanism: Phosphorylation is coupled to the oxidation of glyceraldehyde 3-phosphate by a thioester intermediate
- ATP is formed by phosphoryl transfer from 1,3-bisphosphoglycerate
- Additional ATP is generated with the formation of pyruvate
- Two ATP molecules are formed in the conversion of glucose into pyruvate
- NAD^+ is regenerated from the metabolism of pyruvate
- Fermentations provide usable energy in the absence of oxygen
- Fructose is converted into glycolytic intermediates by fructokinase
- Galactose is converted into glucose 6-phosphate
- Galactose can be highly toxic with a defective metabolic pathway
- Many adults worldwide are intolerant of milk because they are deficient in lactase

16.3 The Glycolytic Pathway Is Tightly Controlled

Glycolysis in muscle is regulated to meet the need for ATP
The regulation of glycolysis in the liver illustrates the biochemical versatility of the liver
The enzymes of glycolysis are physically associated with one another
 Aerobic glycolysis is a property of tumor cells and other rapidly growing cells
 Cancer and endurance training affect glycolysis in a similar fashion
16.4 Glucose Can Be Synthesized from Noncarbohydrate Precursors
Gluconeogenesis is not a reversal of glycolysis
The conversion of pyruvate into phosphoenolpyruvate begins with the formation of oxaloacetate
Oxaloacetate is shuttled into the cytoplasm and converted into phosphoenolpyruvate
The conversion of fructose 1,6-bisphosphate into fructose 6-phosphate and orthophosphate is an irreversible step
The generation of free glucose occurs only in some tissues and is an important control point
Six high-transfer-potential phosphoryl groups are spent in synthesizing glucose from pyruvate
16.5 Gluconeogenesis and Glycolysis Are Reciprocally Regulated
Glycolysis and gluconeogenesis are regulated by adenosine nucleotides and other metabolic intermediates
In mammals, glycolysis and gluconeogenesis in the liver are controlled by hormones sensitive to blood-glucose concentration

Substrate cycles amplify metabolic signals and produce heat
Lactate and alanine formed by contracting muscle and peripheral tissues are used by other organs
 Deficiencies in glycolytic or gluconeogenic enzymes are rare genetic disorders
SCIENTIST PROFILE Gerty Cori
Glycolysis and gluconeogenesis are evolutionarily intertwined
CHAPTER 17
Pyruvate Dehydrogenase and the Citric Acid Cycle
17.1 The Citric Acid Cycle Harvests High-Energy Electrons
17.2 The Pyruvate Dehydrogenase Complex Links Glycolysis to the Citric Acid Cycle
Mechanism: The synthesis of acetyl coenzyme A from pyruvate requires three enzymes and five coenzymes
Flexible linkages allow lipoamide to move between different active sites
17.3 The Citric Acid Cycle Oxidizes Two-Carbon Units
Citrate synthase forms citrate from oxaloacetate and the acetyl group from acetyl coenzyme A
Mechanism: The mechanism of citrate synthase prevents undesirable reactions
Citrate is isomerized into isocitrate
Isocitrate is oxidized and decarboxylated to alpha-ketoglutarate
Succinyl coenzyme A is formed by the oxidative decarboxylation of alpha-ketoglutarate
A compound with high phosphoryl-transfer potential is generated from succinyl coenzyme A
Mechanism: Succinyl coenzyme A synthetase transforms types of biochemical energy

Oxaloacetate is regenerated by the oxidation of succinate
SCIENTIST PROFILE Hans Krebs
The citric acid cycle produces high-transfer-potential electrons, ATP, and CO_2
17.4 Entry to the Citric Acid Cycle and Metabolism Through It Are Controlled
The pyruvate dehydrogenase complex is regulated allosterically and by reversible phosphorylation
 Diabetic neuropathy may be due to inhibition of the pyruvate dehydrogenase complex
The citric acid cycle is regulated at several points
17.5 The Citric Acid Cycle Is a Source of Biosynthetic Precursors
The citric acid cycle must be capable of being rapidly replenished
 The disruption of pyruvate metabolism is the cause of beriberi and poisoning by mercury and arsenic
The citric acid cycle likely evolved from preexisting pathways
17.6 The Glyoxylate Cycle Enables Plants and Bacteria to Grow on Acetate
 Blocking the glyoxylate cycle may lead to new treatments for tuberculosis
CHAPTER 18
Oxidative Phosphorylation
18.1 Cellular Respiration Drives ATP Formation by Transferring Electrons to Molecular Oxygen
Eukaryotic oxidative phosphorylation takes place in mitochondria

Mitochondria are the result of an endosymbiotic event
SCIENTIST PROFILE Lynn Margulis
18.2 Oxidative Phosphorylation Depends on Electron Transfer
The electron-transfer potential of an electron is measured as redox potential
EXAMPLE Calculating the Standard Free Energy of a Reaction from Reduction Potentials
Electron flow from NADH to molecular oxygen powers the formation of a proton gradient
18.3 The Respiratory Chain Consists of Four Complexes: Three Proton Pumps and a Physical Link to the Citric Acid Cycle
Iron–sulfur clusters are common components of the electron-transport chain
The high-potential energy electrons of NADH enter the respiratory chain at NADH-Q oxidoreductase
Ubiquinol is the entry point for electrons from $FADH_2$ of flavoproteins
Electrons flow from ubiquinol to cytochrome *c* through Q-cytochrome *c* oxidoreductase
The Q cycle funnels electrons from a two-electron carrier to a one-electron carrier while pumping protons
Cytochrome *c* oxidase catalyzes the reduction of molecular oxygen to water
Most of the electron-transport chain is organized into a larger complex called the respirasome
Toxic derivatives of molecular oxygen such as superoxide radicals are scavenged by protective enzymes
Electrons can be transferred between groups that are not in contact
18.4 A Proton Gradient Powers the Synthesis of ATP

The chemiosmotic hypothesis suggested that ATP formation is powered by a proton gradient
ATP synthase is composed of a proton-conducting unit and a catalytic unit
Proton flow through ATP synthase leads to the release of tightly bound ATP via the binding-change mechanism
Rotational catalysis is the world's smallest molecular motor
Proton flow around the c ring powers ATP synthesis
ATP synthase and G proteins have several common features

18.5 Many Shuttles Allow Movement Across Mitochondrial Membranes

Electrons from cytoplasmic NADH enter mitochondria by shuttles
The entry of ADP into mitochondria is coupled to the exit of ATP by ATP-ADP translocase

18.6 The Regulation of Cellular Respiration Is Governed Primarily by the Need for ATP

The complete oxidation of glucose yields about 30 molecules of ATP
The rate of oxidative phosphorylation is determined by the need for ATP
ATP synthase can be regulated
Regulated uncoupling leads to the generation of heat
Reintroduction of UCP-1 into pigs may be economically valuable
Oxidative phosphorylation can be inhibited at many stages
 New mitochondrial diseases are constantly being discovered
Mitochondria play a key role in apoptosis

18.7 Proton Gradients Generated by Respiratory Chains Drive Many Biochemical Processes

Proton flow through a rotary motor allows bacteria to swim

Power transmission by proton gradients is a central motif of bioenergetics

CHAPTER 19

Phototrophy and the Light Reactions of Photosynthesis

19.1 Phototrophy Converts Light Energy into Chemical Energy

Photosynthesis comprises light reactions and dark reactions

The same biochemical principles govern both respiration and photosynthesis

Two kinds of light reactions take place in the green plants

19.2 In Eukaryotes, Photosynthesis Takes Place in Chloroplasts

The primary events of photosynthesis take place in thylakoid membranes

Chloroplasts arose from an endosymbiotic event

19.3 Light Absorption by Chlorophyll Molecules Induces Electron Transfer

Transferring electrons allows energy to be captured instead of lost as heat

A “special pair” of chlorophylls initiate charge separation

A proton gradient across the membrane is established

Cyclic electron flow reduces the cytochrome of the reaction center

19.4 Two Photosystems Generate a Proton Gradient and Reducing Power in Cyanobacteria and Photosynthetic Eukaryotes

Photosystem II transfers electrons from water to plastoquinone and generates a proton gradient
Photosystem II is comparable to the purple bacterial reaction center
Cytochrome *bf* links photosystem II to photosystem I
Photosystem I uses light energy to generate reduced ferredoxin, a powerful reductant
Ferredoxin–$NADP^+$ reductase converts $NADP^+$ into NADPH
SCIENTIST PROFILE Peter Mitchell and André Jagendorf
19.5 A Proton Gradient across the Thylakoid Membrane Drives ATP Synthesis
The ATP synthase of chloroplasts closely resembles those of mitochondria and prokaryotes
The activity of chloroplast ATP synthase is regulated
Cyclic electron flow through photosystem I leads to the production of ATP instead of NADPH
The absorption of eight photons yields one O_2, two NADPH, and three ATP molecules
19.6 Accessory Pigments Funnel Energy into Reaction Centers
Resonance energy transfer allows energy to move from the site of initial absorbance to the reaction center
Accessory pigments also protect plants from reactive oxygen
Increasing the efficiency of photosynthesis will increase crop yields
The components of photosynthesis are highly organized
Many herbicides inhibit the light reactions of photosynthesis
19.7 The Ability to Convert Light into Chemical Energy Is Ancient

Artificial photosynthetic systems may provide clean, renewable energy
 Photosensitive proteins are transforming other fields
CHAPTER 20
The Calvin–Benson Cycle and the Pentose Phosphate Pathway
20.1 The Calvin–Benson Cycle Synthesizes Hexoses from Carbon Dioxide and Water
Stage 1: Carbon dioxide reacts with ribulose 1,5-bisphosphate to form two molecules of 3-phosphoglycerate
SCIENTIST PROFILE Andrew Benson
Rubisco activity depends on magnesium and carbamate
Rubisco also catalyzes a wasteful oxygenase reaction
Stage 2: Hexose phosphates are made from phosphoglycerate
Stage 3: Ribulose 1,5-bisphosphate is regenerated
18 ATP and 12 NADPH molecules are used to bring six carbon dioxides to the level of a hexose
Starch and sucrose are the major carbohydrate stores in plants
Inspired by the Calvin–Benson cycle, scientists are developing new methods for fixing carbon dioxide
20.2 The Activity of the Calvin–Benson Cycle Depends on Environmental Conditions
Rubisco is activated by light-driven changes in proton and magnesium ion concentrations
Thioredoxin plays a key role in regulating the Calvin–Benson cycle
The C_4 pathway of tropical plants and grasses accelerates photosynthesis by concentrating carbon dioxide

Crassulacean acid metabolism permits growth in arid ecosystems
20.3 The Pentose Phosphate Pathway Generates NADPH and Synthesizes Pentoses
Two molecules of NADPH are generated in the conversion of glucose 6-phosphate into ribulose 5-phosphate
The pentose phosphate pathway and glycolysis are linked by transketolase and transaldolase
Transketolase and transaldolase stabilize carbanionic intermediates by different mechanisms
20.4 The Metabolism of Glucose 6-Phosphate by the Pentose Phosphate Pathway Is Coordinated with Glycolysis
The rate of the oxidative phase of the pentose phosphate pathway is controlled by the level of $NADP^+$
The flow of glucose 6-phosphate depends on the need for NADPH, ribose 5-phosphate, and ATP
The pentose phosphate pathway is required for rapid cell growth
The Calvin–Benson cycle and the pentose phosphate pathway are essentially mirror images of one another
20.5 Glucose 6-Phosphate Dehydrogenase Plays a Key Role in Protection Against Reactive Oxygen Species
 Glucose 6-phosphate dehydrogenase deficiency causes a drug-induced hemolytic anemia
A deficiency of glucose 6-phosphate dehydrogenase can be protective against malaria
CHAPTER 21
Glycogen Metabolism
21.1 Glycogen Metabolism Is the Regulated Release and Storage of Glucose in Multiple Tissues

21.2 Glycogen Breakdown Requires the Interplay of Several Enzymes

- Phosphorylase catalyzes the phosphorolytic cleavage of glycogen to release glucose 1-phosphate
- Mechanism: Pyridoxal phosphate participates in the phosphorolytic cleavage of glycogen
- Debranching enzyme also is needed for the breakdown of glycogen
- Phosphoglucomutase converts glucose 1-phosphate into glucose 6-phosphate
- The liver contains glucose 6-phosphatase, a hydrolytic enzyme absent from muscle

21.3 Phosphorylase Is Regulated by Allosteric Interactions and Controlled by Reversible Phosphorylation

- Liver phosphorylase produces glucose for use by other tissues
- Muscle phosphorylase is regulated by changes in AMP and ATP concentrations
- Biochemical characteristics of muscle fiber types differ
- Phosphorylation promotes the conversion of phosphorylase *b* to phosphorylase *a*
- Phosphorylase kinase is activated by phosphorylation and calcium ions

21.4 Glucagon and Epinephrine Signal the Need for Glycogen Breakdown

- G proteins transmit the signal for the initiation of glycogen breakdown
- Glycogen breakdown must be rapidly turned off when necessary

21.5 Glycogen Synthesis Requires Several Enzymes and Uridine Diphosphate Glucose

- UDP-glucose is an activated form of glucose
- Glycogen synthase catalyzes the transfer of glucose from UDP-glucose to growing chains

A branching enzyme forms α-1,6 linkages
Glycogen synthase is the key regulatory enzyme in glycogen synthesis
Glycogen is an efficient storage form of glucose
21.6 Glycogen Breakdown and Synthesis Are Reciprocally Controlled by Hormones
Protein phosphatase 1 reverses the effects of kinases on glycogen metabolism
Insulin stimulates glycogen synthesis by inactivating glycogen synthase kinase
Glycogen metabolism in the liver regulates the blood-glucose concentration
 Biochemists have uncovered the biochemical basis of multiple glycogen-storage diseases
CHAPTER 22
Fatty Acid and Triacylglycerol Metabolism
22.1 Triacylglycerols Are Highly Concentrated Energy Stores
Dietary lipids are digested by pancreatic lipases
Dietary lipids are transported in chylomicrons
22.2 The Use of Fatty Acids as Fuel Requires Three Stages of Processing
Mobilization: Triacylglycerols are hydrolyzed by hormone-stimulated lipases
Mobilization continues: Free fatty acids and glycerol are released into the blood
Activation: Fatty acids are linked to coenzyme A before they are oxidized
Transport: Carnitine carries long-chain activated fatty acids into the mitochondrial matrix
Breakdown: Acetyl CoA, NADH, and $FADH_2$ are generated in each round of fatty acid oxidation

The complete oxidation of palmitate yields 106 molecules of ATP
22.3 Unsaturated and Odd-Chain Fatty Acids Require Additional Steps for Degradation
An isomerase and a reductase are required for the oxidation of unsaturated fatty acids
Odd-chain fatty acids yield propionyl CoA in the final thiolysis step
Vitamin B_{12} contains a corrin ring and a cobalt atom
Mechanism: Methylmalonyl CoA mutase catalyzes a rearrangement to form succinyl CoA
SCIENTIST PROFILE Dorothy Hodgkin
Fatty acids are also oxidized in peroxisomes
Some fatty acids contribute to the development of pathological conditions
22.4 Ketone Bodies Are a Fuel Source Derived from Fats
Ketone bodies are a major fuel in some tissues
Diabetic ketoacidosis is a dangerous pathological condition caused by excessive ketone body formation
Animals cannot convert fatty acids into glucose
22.5 Fatty Acids Are Synthesized by Fatty Acid Synthase
Fatty acid degradation and synthesis mirror each other in their chemical reactions
Fatty acids are synthesized and degraded by different pathways
The formation of malonyl CoA is the committed step in fatty acid synthesis
Intermediates in fatty acid synthesis are attached to an acyl carrier protein
Fatty acid synthesis consists of a series of condensation, reduction, dehydration, and reduction reactions

Fatty acids are synthesized by a multifunctional enzyme complex in animals
The synthesis of palmitate requires 8 molecules of acetyl CoA, 14 molecules of NADPH, and 7 molecules of ATP
Citrate carries acetyl groups from mitochondria to the cytoplasm for fatty acid synthesis
Several sources supply NADPH for fatty acid synthesis
 Fatty acid metabolism is altered in tumor cells
Triacylglycerols may become an important renewable energy source
22.6 The Elongation and Unsaturation of Fatty Acids Are Accomplished by Accessory Enzyme Systems
Membrane-bound enzymes generate unsaturated fatty acids
Eicosanoid hormones are derived from polyunsaturated fatty acids
22.7 Acetyl CoA Carboxylase Plays a Key Role in Controlling Fatty Acid Metabolism
Acetyl CoA carboxylase is regulated by conditions in the cell
Acetyl CoA carboxylase is controlled by a variety of hormones
AMP-activated protein kinase is a key regulator of metabolism
CHAPTER 23
Protein Turnover and Amino Acid Catabolism
23.1 Proteins Are Degraded to Amino Acids
The digestion of dietary proteins begins in the stomach and is completed in the intestine
Cellular proteins are degraded at different rates
23.2 Protein Turnover Is Tightly Regulated
Ubiquitin tags proteins for destruction
The proteasome digests the ubiquitin-tagged proteins

The ubiquitin pathway and the proteasome have prokaryotic counterparts
Protein degradation can be used to regulate biological function
23.3 The First Step in Amino Acid Degradation Is the Removal of Nitrogen
Alpha-amino groups are converted into ammonium ions by the oxidative deamination of glutamate in the liver
SCIENTIST PROFILE Cecile Pickart
Mechanism: Pyridoxal phosphate forms Schiff-base intermediates in aminotransferases
Aspartate aminotransferase is an archetypal pyridoxal-dependent transaminase
 Blood levels of aminotransferases serve a diagnostic function
Pyridoxal phosphate enzymes catalyze a wide array of reactions
Serine and threonine can be directly deaminated
Peripheral tissues transport nitrogen to the liver
23.4 Ammonium Ions Are Converted into Urea in Most Terrestrial Vertebrates
The urea cycle begins with the formation of carbamoyl phosphate
Carbamoyl phosphate synthetase I is the key regulatory enzyme for urea synthesis
Carbamoyl phosphate reacts with ornithine to begin the urea cycle
The urea cycle is linked to gluconeogenesis
 Inherited defects of the urea cycle cause hyperammonemia and can lead to brain damage
Urea is not the only means of disposing of excess nitrogen

23.5 Carbon Atoms of Degraded Amino Acids Emerge as Major Metabolic Intermediates

Pyruvate is an entry point into metabolism for a number of amino acids
Oxaloacetate is an entry point into metabolism for aspartate and asparagine
Alpha-ketoglutarate is an entry point into metabolism for amino acids with five-carbon chains
Succinyl coenzyme A is a point of entry for several amino acids
Methionine degradation requires the formation of a key methyl donor, *S*-adenosylmethionine
Threonine deaminase initiates the degradation of threonine
The branched-chain amino acids yield acetyl CoA, acetoacetate, or propionyl CoA
Oxygenases are required for the degradation of aromatic amino acids
Protein metabolism helps to power the flight of migratory birds
EXAMPLE Determining Metabolic Products of Amino Acid Degradation

23.6 Inborn Errors of Metabolism Can Disrupt Amino Acid Degradation

Branched-chain ketoaciduria is a serious disorder of branched-chain amino acid degradation
Phenylketonuria is one of the most common metabolic disorders

CHAPTER 24
Integration of Energy Metabolism

24.1 Caloric Homeostasis Is a Means of Regulating Body Weight

The brain plays a key role in caloric homeostasis

Short-term signals from the gastrointestinal tract induce feelings of satiety
Leptin and insulin regulate long-term control over caloric homeostasis
Leptin is one of several hormones secreted by adipose tissue
Leptin resistance may be a contributing factor to obesity
24.2 The Fasted–Fed Cycle Is a Response to Eating and Sleeping Behaviors
The postprandial state follows a meal
The postabsorptive state occurs at the beginning of a fast
The refed state occurs at the end of a long fast
 **24.3 Diabetes Is a Common Metabolic Disease Often Resulting from Obesity**
Insulin initiates a complex signal-transduction pathway in muscle
Metabolic syndrome often precedes type 2 diabetes
Excess fatty acids in muscle modify metabolism
Insulin resistance in muscle facilitates pancreatic failure
Metabolic alterations in type 1 diabetes result from insulin insufficiency and glucagon excess
24.4 Exercise Beneficially Alters the Biochemistry of Cells
Fuel choice during exercise is determined by the intensity and duration of activity
 The perplexing symptoms of McArdle disease result from the distinct ways skeletal muscle produces ATP
Mitochondrial biogenesis is stimulated by muscular activity
Exercise alters muscle and whole-body metabolism

EXAMPLE Measuring the Impact of a Single Athletic Activity on Caloric Homeostasis
24.5 Starvation Induces Protein Wasting and Ketone Body Formation
The first priority during starvation is the maintenance of blood-glucose concentration
Metabolic adaptations in prolonged starvation minimize protein degradation
24.6 Ethanol Alters Energy Metabolism in the Liver
Ethanol metabolism leads to an excess of NADH
Ethanol metabolites cause liver damage
Excess ethanol consumption disrupts vitamin metabolism
 Ethanol and defects in central energy metabolism contribute to the development of cancer
CHAPTER 25
Biosynthesis of Amino Acids
25.1 Nitrogen Fixation: Microorganisms Use ATP and a Powerful Reductant to Reduce Atmospheric Nitrogen to Ammonia
Biological nitrogen fixation is catalyzed by the nitrogenase complex
The iron–molybdenum cofactor of nitrogenase binds and reduces atmospheric nitrogen
Ammonium ion is assimilated into an amino acid through glutamate and glutamine
25.2 Amino Acids Are Made from Intermediates of the Citric Acid Cycle and Other Major Pathways
Human beings can synthesize some amino acids but must obtain others from their diet
Aspartate, alanine, and glutamate are formed by the addition of an amino group to an alpha-ketoacid
SCIENTIST PROFILE Beverly Guirard

A common step determines the chirality of all amino acids
The formation of asparagine from aspartate requires an adenylated intermediate
Glutamate is the precursor of glutamine, proline, and arginine
3-Phosphoglycerate is the precursor of serine, cysteine, and glycine
Tetrahydrofolate carries activated one-carbon units at several oxidation levels
S-Adenosylmethionine is the major donor of methyl groups
Cysteine is synthesized from serine and homocysteine
 High homocysteine levels correlate with vascular disease
Shikimate and chorismate are intermediates in the biosynthesis of aromatic amino acids
Tryptophan synthase illustrates substrate channeling in enzymatic catalysis
25.3 Feedback Inhibition Regulates Amino Acid Biosynthesis
Branched pathways require sophisticated regulation
The sensitivity of glutamine synthetase to allosteric regulation is altered by covalent modification
25.4 Amino Acids Are Precursors of Many Biomolecules
Glutathione, a gamma-glutamyl peptide, serves as a sulfhydryl buffer and an antioxidant
Nitric oxide, a short-lived signal molecule, is formed from arginine
Amino acids are precursors for a number of neurotransmitters
Porphyrins are synthesized from glycine and succinyl coenzyme A

 Porphyrins accumulate in some inherited disorders of porphyrin metabolism
CHAPTER 26
Nucleotide Biosynthesis
26.1 Nucleotides Can Be Synthesized by de Novo or Salvage Pathways
26.2 The Pyrimidine Ring Is Assembled from CO_2, Ammonia, and Aspartate
Bicarbonate and other oxygenated carbon compounds are activated by phosphorylation
The side chain of glutamine can be hydrolyzed to generate ammonia
The pyrimidine ring is completed and coupled to ribose
Nucleotide mono-, di-, and triphosphates are interconvertible
CTP is formed by amination of UTP
Salvage pathways recycle pyrimidine bases
26.3 Purine Bases Can Be Synthesized from Glycine, Aspartate, and Other Components
The purine ring system is assembled on ribose phosphate
The purine ring is assembled by successive steps of activation by phosphorylation followed by displacement
AMP and GMP are formed from IMP
Enzymes of the purine biosynthesis pathway associate with one another
Salvage pathways economize intracellular resource consumption
An alternative to adenine is used by some viruses
26.4 Deoxyribonucleotides Are Synthesized by the Reduction of Ribonucleotides
Ribonucleotide reduction occurs via a radical mechanism

Stable radicals are present in ribonucleotide reductases
SCIENTIST PROFILE JoAnne Stubbe
Thymidylate is formed by the methylation of deoxyuridylate
 Several valuable anticancer drugs block the synthesis of thymidylate
26.5 Key Steps in Nucleotide Biosynthesis Are Regulated by Feedback Inhibition
Pyrimidine biosynthesis is regulated by aspartate transcarbamoylase
The synthesis of purine nucleotides is controlled by feedback inhibition at several sites
The synthesis of deoxyribonucleotides is controlled by the regulation of ribonucleotide reductase
26.6 Disruptions in Nucleotide Metabolism Can Cause Pathological Conditions
 The loss of adenosine deaminase activity results in severe combined immunodeficiency
 Gout is induced by high serum levels of urate
 Lesch–Nyhan syndrome is a dramatic consequence of mutations in a salvage-pathway enzyme
CHAPTER 27
Biosynthesis of Membrane Lipids and Steroids
27.1 Phosphatidate Is a Common Intermediate in the Synthesis of Phospholipids and Triacylglycerols
The synthesis of phospholipids requires an activated intermediate
Some phospholipids are synthesized from an activated alcohol

Phosphatidylcholine is an abundant phospholipid
Base-exchange reactions can generate phospholipids
Sphingolipids are synthesized from ceramide
Tay–Sachs disease results from the disruption of lipid metabolism
Phosphatidic acid phosphatase is a key regulatory enzyme in lipid metabolism
27.2 Cholesterol Is Synthesized from Acetyl Coenzyme A in Three Stages
Stage 1: The synthesis of mevalonate initiates the synthesis of cholesterol
Stage 2: Squalene (C_{30}) is synthesized from six molecules of isopentenyl pyrophosphate (C_5)
Stage 3: Squalene cyclizes to form cholesterol
27.3 The Regulation of Cholesterol Biosynthesis Takes Place at Several Levels
Lipoproteins transport cholesterol and triacylglycerols throughout the organism
Low-density lipoproteins play a central role in cholesterol metabolism
The absence of the LDL receptor leads to hypercholesterolemia and atherosclerosis
Mutations in the LDL receptor prevent LDL release and result in receptor destruction
Cycling of the LDL receptor is regulated
HDL appears to protect against atherosclerosis
The clinical management of cholesterol levels can be understood at the biochemical level

27.4 Important Biochemicals Are Synthesized from Cholesterol and Isoprene

Steroids are hydroxylated by cytochrome P450 monooxygenases that use NADPH and O_2

 Cytochrome P450s are widespread and perform many functions

SCIENTIST PROFILE Namandjé Bumpus

Pregnenolone is a precursor of many other steroids

Vitamin D is derived from cholesterol by the ring-splitting activity of light

Five-carbon units are joined to form a wide variety of biomolecules

Some isoprenoids have industrial applications

CHAPTER 28

DNA Replication, Repair, and Recombination

28.1 DNA Replication Proceeds by the Polymerization of Deoxyribonucleoside Triphosphates Along a Template

DNA polymerases require a template and a primer

DNA polymerases have common structural features

Bound metal ions participate in the polymerase reaction

The specificity of replication is dictated by complementarity of shape between bases

An RNA primer enables DNA synthesis to begin

SCIENTIST PROFILE Tsuneko and Reiji Okazaki

One strand of DNA is made continuously, whereas the other strand is synthesized in fragments

DNA ligase seals breaks in double-stranded DNA

The separation of DNA strands requires specific helicases and ATP hydrolysis

28.2 DNA Unwinding and Supercoiling Are Controlled by Topoisomerases

The linking number, a topological property, determines the degree of supercoiling

Topoisomerases prepare the double helix for unwinding
Type I topoisomerases relax supercoiled structures
Type II topoisomerases introduce negative supercoils through coupling to ATP hydrolysis
28.3 DNA Replication Is Highly Coordinated
DNA replication requires highly processive polymerases
The leading and lagging strands are synthesized in a coordinated fashion
DNA replication in *E. coli* begins at a unique site
DNA replication in eukaryotes is initiated at multiple sites
The eukaryotic cell cycle ensures coordination of DNA replication and cell division
Telomeres are protective structures at the ends of linear chromosomes
Telomeres are replicated by telomerase, a specialized polymerase that carries its own RNA template
28.4 Many Types of DNA Damage Can Be Repaired
Errors can arise in DNA replication
DNA can be damaged by oxidizing agents, alkylating agents, and light
DNA damage can be detected and repaired by a variety of systems
The presence of thymine instead of uracil in DNA permits the repair of deaminated cytosine
 Some genetic diseases are caused by the expansion of repeats of three nucleotides
Many cancers are initiated by the defective repair of DNA
Many potential carcinogens can be detected by their mutagenic action on bacteria
28.5 DNA Recombination Plays Important Roles in Replication, Repair, and Other Processes

RecA can initiate recombination by promoting strand invasion
Some recombination reactions proceed through Holliday-junction intermediates
CHAPTER 29
RNA Functions, Biosynthesis, and Processing
29.1 RNA Molecules Play Different Roles, Primarily in Gene Expression
RNAs play key roles in protein biosynthesis
Some RNAs can guide modifications of themselves or other RNAs
Some viruses have RNA genomes
 Messenger RNA vaccines provide protection against diseases
29.2 RNA Polymerases Catalyze Transcription
RNA synthesis comprises three stages: initiation, elongation, and termination
RNA polymerases catalyze the formation of a phosphodiester bond
RNA chains are formed de novo and grow in the $5'$-to-$3'$ direction
RNA polymerases backtrack and correct errors
RNA polymerase binds to promoter sites on the DNA template in bacteria to initiate transcription
Sigma subunits of RNA polymerase in bacteria recognize promoter sites
The template double helix must be unwound for transcription to take place
Elongation takes place at transcription bubbles that move along the DNA template
Sequences within the newly transcribed RNA signal termination

In bacteria, the rho protein helps to terminate the transcription of some genes
29.3 Transcription Is Highly Regulated
Alternative sigma subunits in bacteria control transcription in response to changes in conditions
Some messenger RNAs directly sense metabolite concentrations
Control of transcription in eukaryotes is highly complex
Eukaryotic DNA is organized into chromatin
Three types of RNA polymerase synthesize RNA in eukaryotic cells
Three common elements can be found in the RNA polymerase II promoter region
Regulatory cis-acting elements are recognized by different mechanisms
The TFIID protein complex initiates the assembly of the active transcription complex in eukaryotes
Enhancer sequences can stimulate transcription at start sites thousands of bases away
29.4 Some RNA Transcription Products Are Processed
Precursors of transfer and ribosomal RNA are cleaved and chemically modified after transcription
RNA polymerase I produces three ribosomal RNAs
RNA polymerase III produces transfer RNAs
The product of RNA polymerase II, the pre-mRNA transcript, acquires a $5'$ cap and a $3'$ poly(A) tail
Sequences at the ends of introns specify splice sites in mRNA precursors
Splicing consists of two sequential transesterification reactions
Small nuclear RNAs in spliceosomes catalyze the splicing of mRNA precursors

 Mutations that affect pre-mRNA splicing cause disease
Most human pre-mRNAs can be spliced in alternative ways to yield different proteins
Transcription and mRNA processing are coupled
Small regulatory RNAs are cleaved from larger precursors
RNA editing can lead to specific changes in mRNA
29.5 The Discovery of Catalytic RNA Revealed a Unique Splicing Mechanism
Some RNAs can promote their own splicing
RNA enzymes can promote many reactions, including RNA polymerization
SCIENTIST PROFILE Thomas Cech
CHAPTER 30
Protein Biosynthesis
30.1 Protein Biosynthesis Requires the Translation of Nucleotide Sequences into Amino Acid Sequences
The biosynthesis of long proteins requires a low error frequency
Transfer RNA (tRNA) molecules have a common design
Some transfer RNA molecules recognize more than one codon because of wobble in base-pairing
30.2 Aminoacyl-tRNA Synthetases Establish the Genetic Code
Amino acids are first activated by adenylation
Aminoacyl-tRNA synthetases have highly discriminating amino acid activation sites
Proofreading by aminoacyl-tRNA synthetases increases the fidelity of protein biosynthesis
Kinetic proofreading increases the fidelity of protein biosynthesis

Synthetases recognize various features of transfer RNA molecules
Aminoacyl-tRNA synthetases are divided into two classes
30.3 The Ribosome Is the Site of Protein Biosynthesis
Ribosomal RNAs (5S, 16S, and 23S rRNA) play central roles in protein biosynthesis
Ribosomes have three transfer RNA-binding sites that bridge the 30S and 50S subunits
The start signal is usually AUG preceded by several bases that pair with 16S rRNA
Bacterial protein biosynthesis is initiated by *N*-formylmethionyl-transfer RNA
N-Formylmethionyl-$tRNA^{fMet}$ is placed in the P site of the ribosome in the formation of the 70S initiation complex
Elongation factors deliver aminoacyl-tRNAs to the ribosome
Peptidyl transferase catalyzes peptide-bond formation
GTP hydrolysis-driven translocation of tRNAs and mRNA follows peptide-bond formation
In bacteria, transcription and translation are coupled in space and time
Protein biosynthesis is terminated by release factors that read stop codons
Eukaryotic protein biosynthesis differs from bacterial protein biosynthesis primarily in translation initiation
Ribosomes selectively control gene expression
Scientists have manipulated protein biosynthesis pathways to incorporate unnatural amino acids in preselected positions
SCIENTIST PROFILE Ada Yonath
30.4 Ribosomes Bound to the Endoplasmic Reticulum Manufacture Secretory and Membrane Proteins

Protein biosynthesis begins on ribosomes that are free in the cytoplasm
Signal sequences mark proteins for translocation across the endoplasmic reticulum membrane
Transport vesicles carry cargo proteins to their final destinations
30.5 A Variety of Antibiotics and Toxins Inhibit Protein Biosynthesis
Some antibiotics inhibit protein biosynthesis
Diphtheria toxin blocks protein biosynthesis in eukaryotes by inhibiting translocation
Some toxins modify 28S ribosomal RNA
CHAPTER 31
Control of Gene Expression
31.1 Bacterial DNA-Binding Proteins Bind to Specific Regulatory Sites
Many DNA-binding proteins match the symmetry in their target DNA sequences
The helix-turn-helix motif is common to many bacterial DNA-binding proteins
31.2 In Bacteria, Genes Are Often Arranged into Clusters Under the Control of a Single Regulatory Sequence
An operon consists of regulatory elements and protein-encoding genes
The *lac* repressor protein can block transcription
Ligand binding can induce structural changes in regulatory proteins
The operon is a common regulatory unit in bacteria
Some DNA-binding proteins stimulate transcription
31.3 Regulatory Circuits Can Result in Switching Between Patterns of Gene Expression
The λ repressor regulates its own expression

A circuit based on the λ repressor and Cro forms a genetic switch
31.4 Regulation of Gene Expression Is More Complex in Eukaryotes
A range of DNA-binding motifs are employed by eukaryotic DNA-binding proteins
Activation domains interact with other proteins
Multiple transcription factors interact with eukaryotic regulatory regions
31.5 The Control of Gene Expression in Eukaryotes Can Require Chromatin Remodeling
Chromatin remodeling and DNA methylation regulate access to DNA-binding sites
Epigenetic modifications influence gene expression
SCIENTIST PROFILE Sarah Stewart
Enhancers stimulate transcription by recruiting activator proteins that alter chromatin structure
Nuclear hormone receptors are transcription factors that cause changes in chromatin structure
Nuclear hormone receptors regulate transcription by recruiting coactivators to the transcription complex
Chromatin structure is modulated through covalent modifications of histone tails
Transcriptional repression can be achieved through histone deacetylation and other modifications
31.6 Gene Expression Can Be Controlled at the Posttranscriptional Level
Attenuation regulates transcription in bacteria through the modulation of nascent RNA secondary structure
Eukaryotes use different mechanisms to control gene expression at the posttranscriptional level
Genes associated with iron metabolism are translationally regulated in animals

Small RNAs are involved in posttranscriptional gene regulation in eukaryotes
CHAPTER 32
Principles of Drug Discovery and Development
32.1 Drug Discovery Begins with Target Identification and Validation
Drug targets must be validated and tractable
Serendipitous observations can drive drug development
32.2 Lead Molecules Can Be Discovered in Many Ways
Natural products are a valuable source of lead molecules
High-throughput screening expands the opportunity for lead identification
Screening libraries can be prepared using combinatorial chemistry
DNA-encoded libraries provide very large compound libraries for lead identification
Phenotypic screening provides an alternative to the target-centered approach
32.3 Compounds Must Meet Stringent Criteria to Be Developed into Drugs
Drugs must be potent and selective
EXAMPLE Determining the IC_{50} for an Inhibitor
Drugs must have suitable properties to reach their targets
Toxicity can limit drug effectiveness
Lead molecules can be optimized on the basis of three-dimensional structural information about their targets
32.4 Biologics Are a Growing Family of Drugs
The majority of biologics are recombinant proteins
Monoclonal antibodies are highly specific and potent recombinant protein biologics
SCIENTIST PROFILE Gertrude Elion
32.5 The Clinical Development of Medicines Proceeds Through Several Phases

Clinical trials are time-consuming and expensive
The evolution of drug resistance can limit the utility of drugs for infectious agents and cancer
CHEMISTRY REVIEW
ANSWERS TO SELF-CHECK QUESTIONS
ANSWERS TO PROBLEMS
INDEX

Preface

Fifty years ago, the first edition of *Biochemistry* hit the market and forever changed the way biochemistry is taught. In the tenth edition, we remain true to the hallmarks of Lubert Stryer's vision while presenting molecular structure and function, metabolism, regulation, and laboratory techniques in new ways that engage students actively in the process of learning biochemistry.

Thematic Threads

It has always been our goal to help students connect biochemistry to their own lives and the world around them. We use an evolutionary perspective to reveal the threads that bind organisms, clinical applications to show physiological relevance, and biotechnological and industrial applications to show how biochemistry is used to improve our lives. Pathways and processes are presented in a physiological context so students can see how biochemistry works in the body when it is at rest and during exercise, during health and disease, and under stress. Many of these examples are tagged with a caduceus symbol. (For a full list of these clinical applications, see p. xxxii.) New for this edition, we have highlighted the importance of time as a variable, linking the time scales associated with fundamental molecular processes, enzymatic reactions, physiological responses, and evolutionary change.

Several chapters provide the foundation for students' understanding of key aspects of biochemistry.

- Chapter 3 illustrates the remarkable abilities of biological molecules to interact specifically with one another, using as

examples the oxygen-binding proteins myoglobin and hemoglobin and key molecules from the immune system.

- Chapters 5 through 7 explain where enzymes derive the catalytic power, specificity, and control they have to drive chemical and energetic transformations.
- Chapter 15 introduces the basic concepts and design of metabolic pathways before students dive into the chapters on specific pathways.
- Chapter 24 integrates the concepts of energy metabolism by focusing on healthy caloric homeostasis and its dysfunctional extremes: obesity and starvation. The chapter also presents the biochemical basis for the many benefits of regular exercise and the pathology of diabetes.

Areas of Focus in the Tenth Edition

In developing the tenth edition of *Biochemistry*, we stayed true to the integrity of Lubert Stryer's original textbook while updating our approach to reflect today's biochemistry instructors and students. Within our main text, you will find our hallmark clear writing and straightforward illustrations, which together make the language of biochemistry accessible for students learning the subject for the first time. We present a logical flow of ideas, clearly written text, and informative figures to help students grasp and retain biochemical concepts and details.

The strengths of the tenth edition textbook are enhanced with videos, interactive figures, and more in our interactive e-book. The e-book is available within our Achieve platform and is downloadable through the VitalSource app, enabling students to read offline. Students can highlight, take notes, search by keyword, and even have the book

read aloud. The Achieve course further builds on the strengths of the tenth edition with interactive assessments, media, and abundant resources for use during class time or during study.

The tenth edition supports three organizing principles:

- Advances in biochemistry rely on diverse teams.
- Visualization is a critical teaching tool in biochemistry.
- Biochemistry requires conceptual understanding, critical thinking, effective problem solving, and practice.

Advances in Biochemistry Rely on Diverse Teams

In the tenth edition, we include short profiles of scientists, some very well-known and some less so, who have contributed to different aspects of biochemistry. In addition to introducing some fascinating people, the purpose of these profiles is to illustrate some of the wide range of training and career paths that different individuals have taken to allow them to make important contributions to biochemistry. Some profiles highlight how different life experiences have contributed to the selection of scientific problems or approaches. ▶

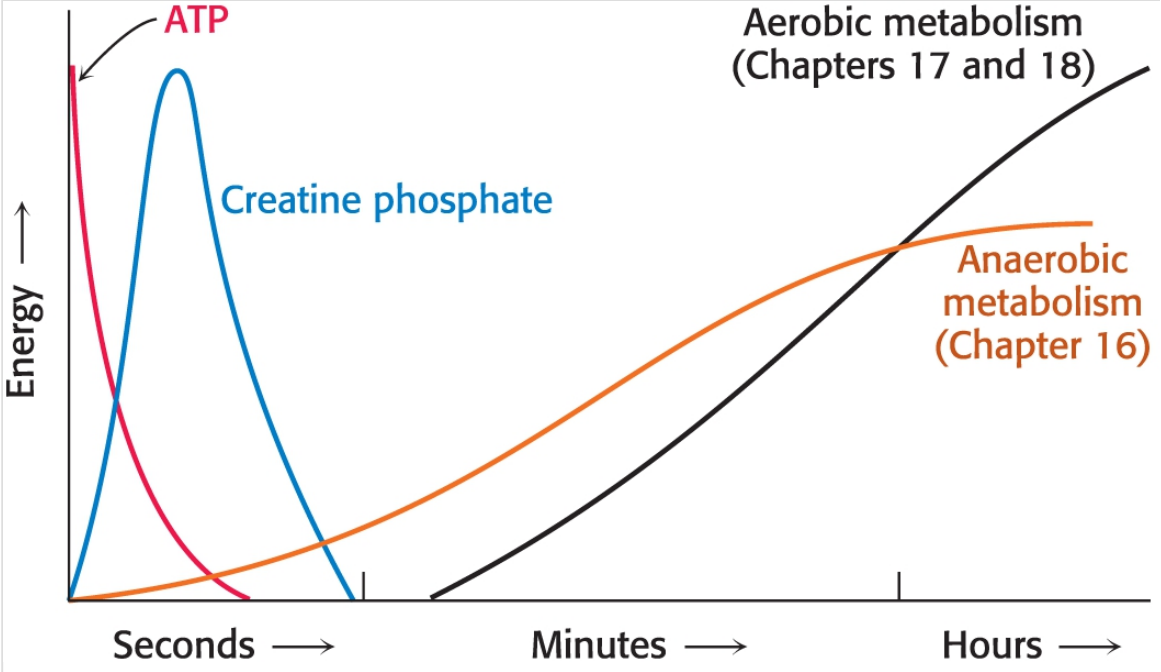


FIGURE 15.6 The sources of ATP change as exercise duration increases, even within the first few seconds. In the initial seconds of exertion, power is generated by existing high-phosphoryl-transfer compounds (ATP and creatine phosphate). Subsequently, the ATP must be regenerated by metabolic pathways.

Through these profiles, students may be able to apply their own experiences to understanding topics in biochemistry and other sciences. A list of all the profiles is on p. xxxiii.

Visualization Is a Critical Teaching Tool in Biochemistry

The ability to visualize concepts and how they are connected helps students gain a deeper conceptual understanding. Two innovations introduced in the first edition of *Biochemistry* were an open, uncluttered layout of text and figures that was easy on the eyes (and brain) and the presentation of one concept per figure. We continue these traditions in the tenth edition, while also presenting an updated art program that

enhances the power of figures to help students learn. Concise figures and ample margins are part of a layout that is well organized and easy to read.

- **One Idea at a Time.** Each figure illustrates a single concept, which helps students zoom in on the main points without the distraction of excess detail. **Figure captions** begin by identifying the concept in the figure.

- **Macromolecular Structures.** Beautifully rendered art depicting structures and structural models were prepared by authors Jeremy Berg and Gregory Gatto, based on the latest x-ray crystallographic, NMR, and cryo-electron microscopy data. For most molecular models, the **PDB number** at the end of the figure gives the student easy access to the file used in generating the structure (https://www.wwpdb.org).



JAMES TENSUAN/The New York Times/Redux

CAROLYN BERTOZZI Chemist Carolyn Bertozzi is a leader in developing the field of glycobiology and communicating its exciting possibilities. Initially planning to go to medical school, her interest in chemistry developed in college, and she went on to complete a PhD focused on synthesizing

In the tenth edition, chapter reading is enhanced with a variety of embedded multimedia tools in Achieve to enliven the narrative, while promoting strong visual understanding of the material. Each of these enhancements are available for stand-alone use in Achieve or within interactive questions and activities:

- **Interactive Figures.** Bring protein structures to life with interactive 3-D models using Jmol. Students can zoom and rotate structures and experiment with different display styles (space-filling, ball-and-stick, ribbon, and backbone) by means of a user-friendly interface. These interactive molecular structures can be launched within the e-book wherever you see the INTERACT callouts. ▼

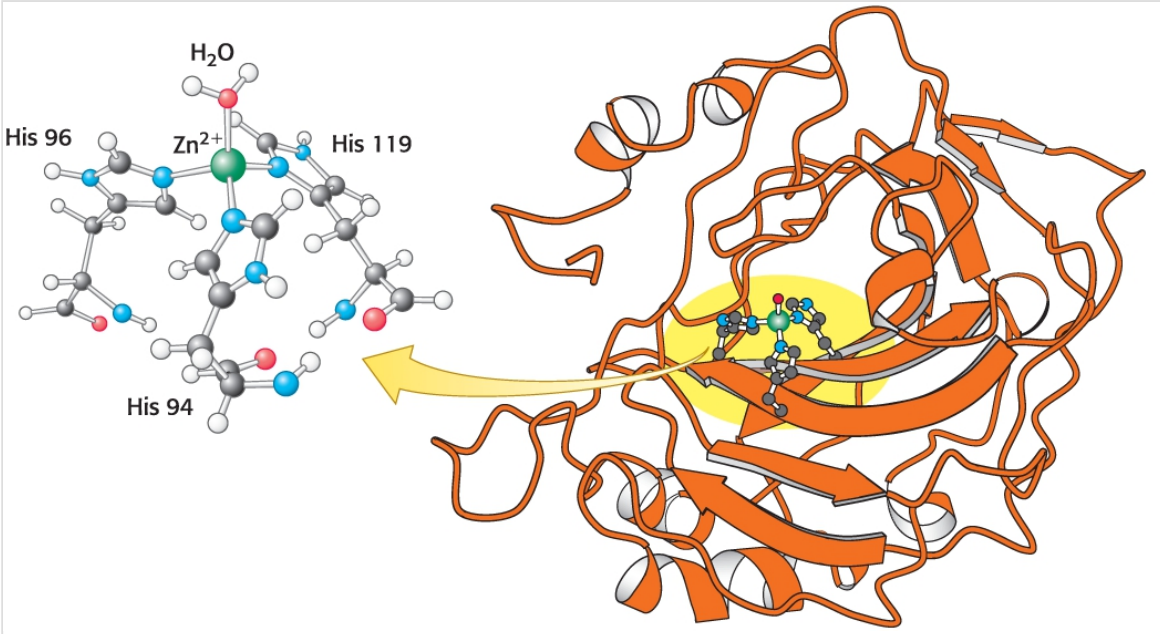


FIGURE 6.18 The active site of human carbonic anhydrase II includes a bound zincion. The active site includes a zinc ion that is bound to the imidazole rings of three histidine residues as well as to a water molecule in a cleft near the center of the enzyme.

[Drawn from 1CA2.pdb.]

INTERACT with this model in Achieve

- **Animated Mechanisms.** Watch the mechanisms of iconic enzymes as short animations.

- **Animated Technique Videos.** Reinforce understanding of laboratory techniques by watching animations that include an overview of protocol and then show what is happening at the

chemical level. Laboratory technique animations can be launched within the e-book wherever you see the VIEW callouts.

- **Interactive Metabolic Map.** EXPLORE callouts highlight metabolic processes that students can study in greater depth in 

. 

With this interactive tool, students can navigate and zoom between overviews and detailed views of the most commonly taught metabolic pathways. Embedded Tours take students through the pathways step by step. Such intimate interaction helps students visualize concepts in isolation as well as understand how concepts are interconnected. Metabolic Map Pathways include glycolysis, gluconeogenesis, the citric acid cycle, oxidative phosphorylation, the pentose phosphate pathway, glycogen metabolism, fatty acid synthesis, the urea cycle, and β oxidation.

Biochemistry Requires Conceptual Understanding, Critical Thinking, Effective Problem Solving, and Practice

Every chapter of *Biochemistry*, Tenth Edition, provides numerous opportunities for students to practice problem-solving skills and apply the concepts described in the text.

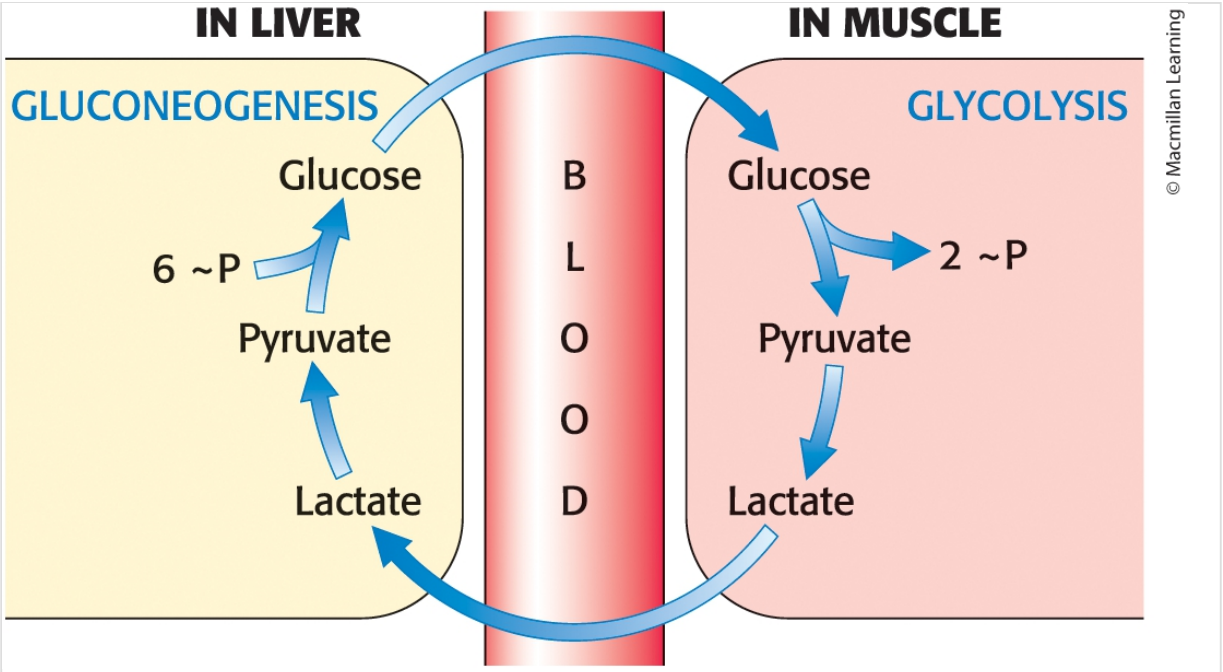


FIGURE 16.36 The Cori cycle allows the liver to better support other tissues, such as skeletal muscle. Lactate formed by active muscle is converted into glucose by the liver. This cycle shifts part of the metabolic burden of active muscle to the liver. The symbol, ~P represents nucleoside triphosphates.

EXPLORE this pathway further in the Metabolic Map in Achieve

- **NEW! Self-Check Questions.** New Self-Check questions provide periodic "speed bumps" in the chapter narrative to allow students to assess their comprehension and practice applying concepts they have just learned.

Self–Check Question

Recall our study of enzymes in previous chapters: Why do isolated F_1 subunits of ATP synthase catalyze ATP hydrolysis?

- **NEW! Examples.** The boxed examples (listed on p. xxxiii) provide point-of-use, worked-through examples of the types of quantitative and reasoning questions students will frequently encounter in biochemistry courses and in laboratory work. ▶

Example

Determining the Fraction of Bound Receptors

Problem:

What fraction of receptors are occupied with ligand at a ligand concentration of 5 μM, given that half of the receptors are occupied with ligand at a total ligand concentration of 20 μM?

Getting Started:

Equation 2 gives the relationship between the fraction of receptors occupied with ligands as a function of the total ligand concentration and the dissociation constant:

$$[RL]/R_{total} = L_{total}/(K_d + L_{total})$$

We are interested in what happens at a total ligand concentration of 5 μM. In order to use equation 2, we need to know the dissociation constant

Solve:

We showed that the half of the receptors are occupied with ligands when the total ligand concentration is equal to the dissociation constant. Since half of the receptors are occupied when the ligand concentration is 20 μM, we know that $K_d = 20\ nM$. Substituting this and $L_{total} = 5\ \mu M$ into equation 2, we find that

$$[RL]/R_{total} = 5\ \mu M/(20\ \mu M + 5\ \mu M) = 0.20$$

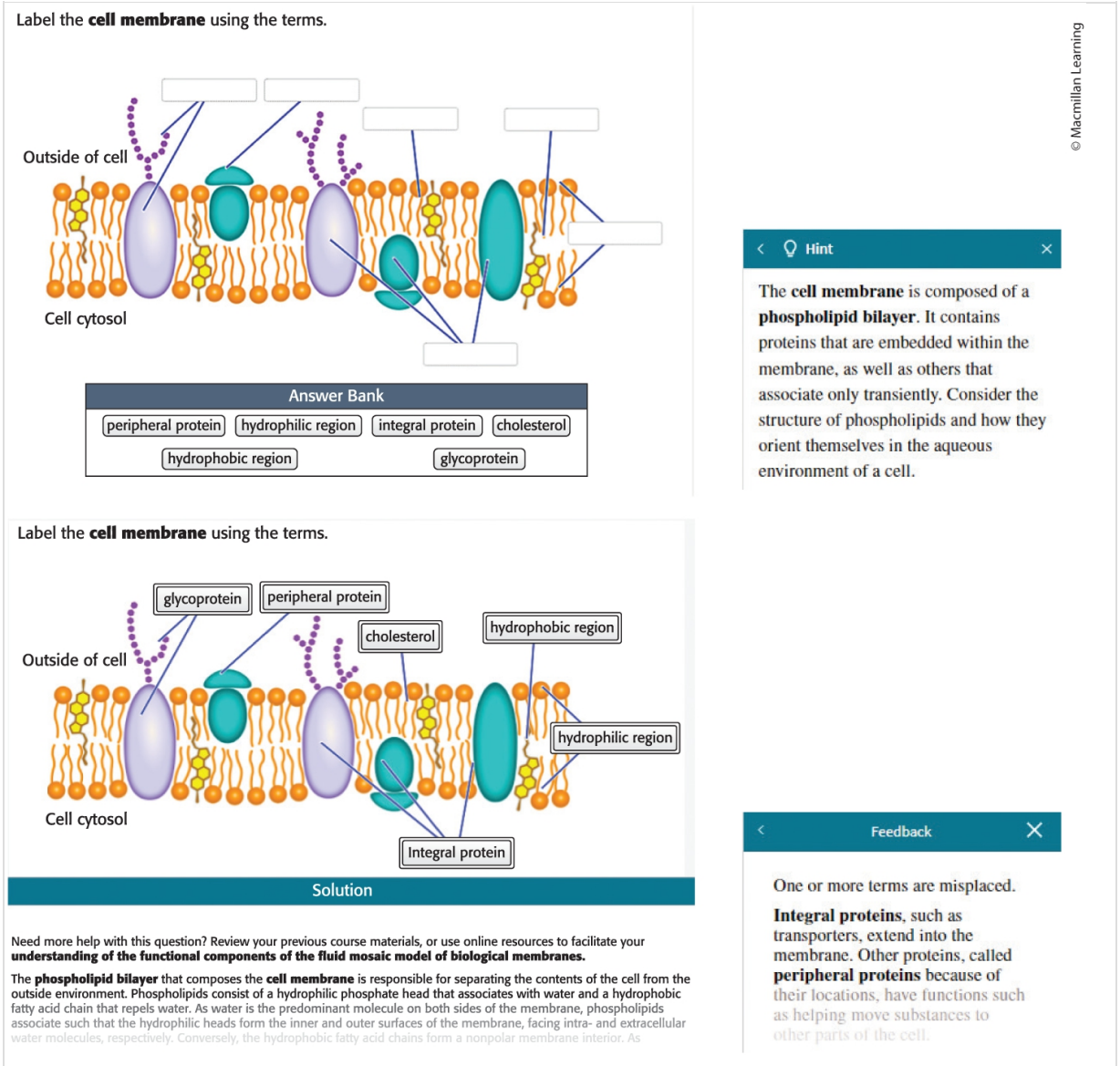
Reflect:

This result makes sense since the total ligand concentration is somewhat less than 20 μM, the ligand concentration at which half (0.50) of the receptors are occupied.

In Achieve, engagement is encouraged with adaptive quizzing, feedback-rich problem-solving practice, case study applications, and more.

- Achieve **Adaptive Quizzing.** This game-like activity motivates reading and provides individualized learning and feedback as students build towards a target score. All questions are tied back to the e-book to encourage students to explore the reading, figures, and interactive resources at hand. Adaptive quizzing includes a student dashboard with their progress and a personalized study plan. ▼

- **NEW! Every end-of-chapter problem from *Biochemistry*, Tenth Edition, is assignable in** Achieve**.** Raise comprehension and problem-solving skills with robust end-of-chapter questions, that are available as pencil-and-paper assignments or as autograded, feedback-rich online homework. The end-of-chapter problems in *Biochemistry*, Tenth Edition, vary in presentation and degree of difficulty; they include higher-level critical thinking questions that ask students to suggest or describe a chemical mechanism, draw conclusions from data taken from real research papers, and connect concepts across chapters.



- In Achieve, each autograded question delivers hints and immediate, individualized feedback so students get guidance targeted to the underlying misconception of each specific wrong answer. Upon completion of each question, students can see fully worked solutions that explain how to reason through and solve the question. ▼

- Achieve **Question Bank.** In addition to end-of-chapter problems, instructors can explore and assign thousands of additional interactive, autograded questions for more problem-solving practice. Questions in the question bank are frequently customizable and algorithmic so students working together see variations of the same problems. Achieve promotes student success through practice and targeted feedback, while saving instructors time and providing meaningful insights with assessment reports.

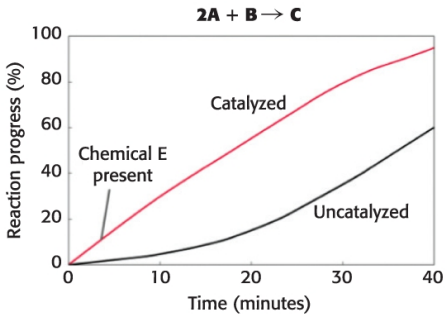
Most chemical reactions occur in a step-wise fashion, requiring more than one **elementary step** (or **elementary reaction**) to form the final products. During a step-wise reaction process, a later elementary step consumes the **intermediate** or intermediates formed by an earlier elementary step. Therefore, like catalysts, reaction intermediates do not appear in the overall schematic of a chemical reaction.

Uncatalyzed reaction

Step 1: $A + B \longrightarrow D$
Step 2: $A + D \longrightarrow C$
Overall: $2A + B \longrightarrow C$

Catalyzed reaction

Step 1: $A + B + E \longrightarrow EAB$
Step 2: $A + EAB \longrightarrow C + E$
Overall: $2A + B \longrightarrow C$



Consider the given series of **elementary reactions** and their **overall reaction**.

reaction 1:	$A + B \longrightarrow AB$
reaction 2:	$AB + C \longrightarrow AC + B$
overall:	$A + C \longrightarrow AC$

© Macmillan Learning

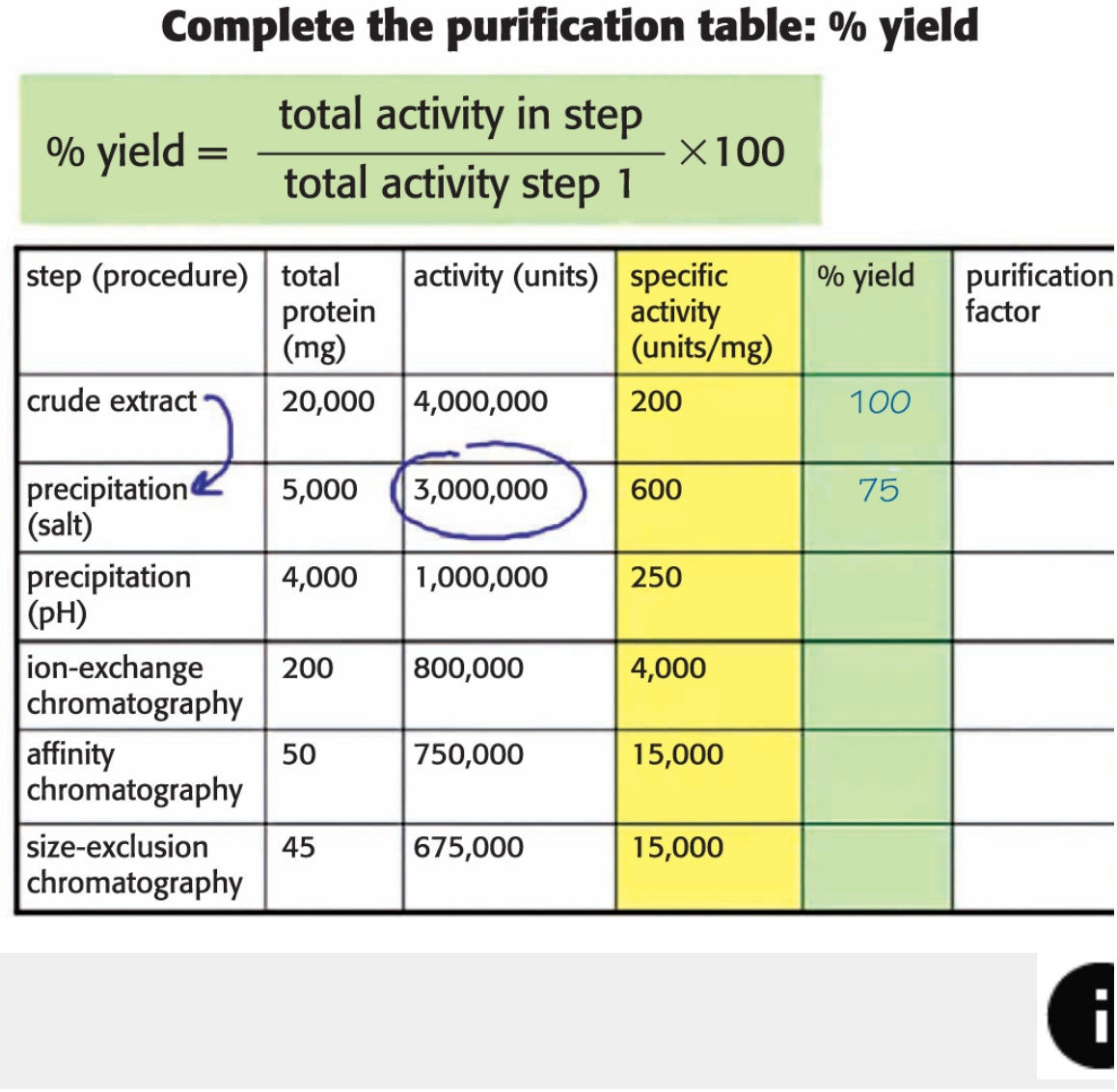
Which species is an **intermediate** in the reaction?

- C
- AC
- B
- A
- AB

Which species is a **catalyst** in the reaction?

- B
- C
- A
- AB
- AC

- Achieve **NEW! Skills You Need Activities.** Each chapter includes a short activity that identifies one to three skills or concepts that students may have learned in prerequisite courses — such as general chemistry, organic chemistry, biology, and math — and will need to apply to the current biochemistry chapter. Developed with guidance from student reviewers, these activities provide short refreshers on the prerequisite content then allow students to assess their mastery of the content and provide helpful feedback and search terms they can apply through their preferred methods of study. ▶



-  **Readiness Activities.** Whereas Skills You Need activities are aligned with one chapter at a time, Readiness Activities are designed to get students ready for the course as a whole. Students can review the math, general chemistry, and organic chemistry skills they will need to use as biochemistry students, and each question provides hints, answer-specific feedback, and solutions.

-  **Problem-Solving Videos.** With diagrams, graphs, and narration, these videos walk students through problems on topics that typically prove difficult — such as data interpretation — helping students understand the right approach to the solution.

-  **Case Studies.** Each case study introduces students to a biochemical mystery and allows them to determine what investigations will solve it. Accompanying assessments ensure that students have fully completed and understood the case study, showing that they have applied their knowledge of the concepts. ▼ ▶

Case Study Topics

Biomolecules

- Observation Over Intuition: Thermodynamics of Protein Folding
- pH Peril: pH and Amino Acid Structure
- Profound Relevance: Hemoglobin Regulation (Bohr Effect)
- **NEW!** Mile High Stadium and Silent Killer: Hemoglobin Dysfunction
- **NEW!** Toxic Alcohols: Enzyme Function
- A Likely Story: Enzyme Inhibition

Signal Transduction/Metabolism

- **NEW!** Failure to Propagate: Signal Transduction
- **NEW!** Sudden Onset: Introduction to Metabolism
- An Unexplained Death: Carbohydrate Metabolism
- A Day at the Beach: Fatty Acid Metabolism
- **NEW!** The Narrow Window: Electron Transport Chain and Oxidative Phosphorylation
- Runner's Experiment: Integration of Energy Metabolism

Mile High Stadium and the Silent Killer
Case Study on Hemoglobin Regulation and Dysfunction
By Justin Hines, Lafayette College



Photo Credit: Zoonar /A. Kravchenko /AGE Fotostock

Act 1 - Trouble at Mile High Stadium

Gino had hemoglobin on the mind. He had been embarrassed earlier when he failed to remember how pH was related to oxygen transport in the human body.

As an undergraduate in his junior year who hoped to go to medical school, Gino's day job shadowing emergency room physician Dr. Rose Smith was otherwise going well. But the routine patient visits were interrupted when he saw a large crowd gathered just outside in the hospital lobby. Most had flowers, but some, strangely, were carrying footballs and wearing jerseys.

"Dr. Smith, what's that all about?" Gino pointed to the noisy crowd.

"Oh that... yes, we have a patient up on three recovering from a sickle cell attack."

"But why so many people?" asked Gino. "And why do some have footballs? Is it a child or something?"

"No, actually he's an NFL star... plays defensive end. Most of those people are just fans. He played a game last night here in Denver at the new Mile High Stadium. The combination of vigorous exercise from sprinting all over a 100-yard field and the fact that the game was here in Denver triggered a sickle cell crisis. He'll probably never play in Denver again."

"He has sickle cell anemia and plays in the NFL??!"

"Actually, he has sickle cell *trait*, meaning he is heterozygous for the sickle cell allele, HbS. Some people with sickle cell trait can be top athletes. But, the right conditions can still bring about a crisis."

Achieve: Your One-Stop-Shop For Instructional Resources

Integrated with the tenth edition are activities, media, and resources to support in-person, virtual, and hybrid teaching. The resources found in the Achieve platform include tools for class preparation, instruction, practice and assessment, and reporting and analytics:

Class Preparation

- **Transition Guide** for navigating the changes between editions
- **Goal-Setting and Reflection Surveys** to help students identify their goals, develop strategies to reach those goals, and realign their study habits throughout the course
- Assignable chapter-by-chapter **Skills You Need** and course-level **Readiness Activities** to refresh students on content from courses frequently taken as prerequisites
- **Interactive e-book** with assignable sections and chapters
- Assignable **LearningCurve Adaptive Quizzing** tasks to ensure reading comprehension

Instruction

- Editable all-in-one **Lecture Slides** that include content, images, iClicker questions, multimedia tools, and activities
- **Standalone Slide Decks** streamlined to just include content, images, and iClicker activities
- **Problem-Solving Activities** and other **In-Class Activities** with **Instructor Activity Guides** and student **Worksheets** that follow a consistent approach for solving biochemistry problems and include recommendations for use in face-to-face, virtual, and hybrid classes
- **Cloud-based iClicker**, an in-class response system with integrated Gradebook
- Presentation-ready media such as the **Interactive Metabolic Map**, **Animated Mechanisms**, **Animated Techniques**, **Problem-Solving**

Videos, **Living Figures**, and **Case Studies** integrated into **Lecture Slides**, **Problem-Solving Activities**, and other **In-Class Activities**; they are also available as stand-alone resources.

Practice and Assessment

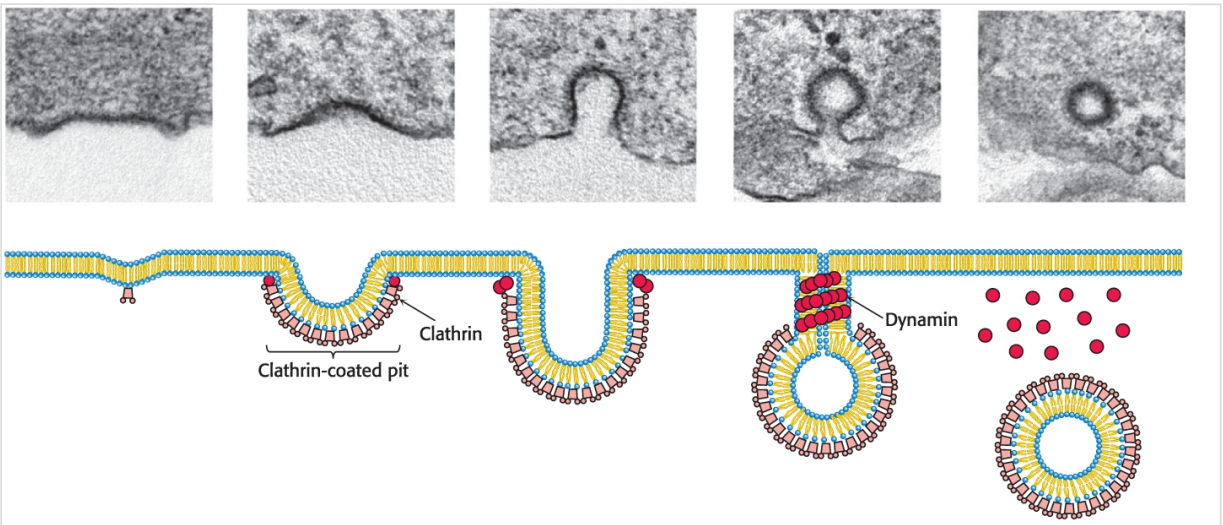
- **Editable, curated, autograded homework assignments** that match the order and question in the text
- **Question Bank** with thousands of additional questions to create an assignment from scratch or add to a curated assignment
- **Abbreviated Solutions** and **Extended Solutions** for all end-of-chapter questions
- **Assignable Case Studies**
- **Test Banks** and accompanying software (located on Macmillan Learning's catalog page) to create tests outside of the Achieve environment

Reporting and Analytics

- **Learning Objectives** aligned with course content and resources
- **Insights** on student performance on top learning objectives and course data, such as time on task and other metrics
- **Detailed reporting** by class, by individual student, and by learning objective
- **Gradebook that syncs with iClicker** for an all-in-one gradebook
- **Integration** with most campus Learning Management Systems

Recent Advances and Discoveries Included in the New Edition

Biochemistry is an exciting and dynamic field of study. In the tenth edition of *Biochemistry*, we have updated examples and explanations to provide the latest and most interesting discoveries in biochemistry, along with material essential for understanding biochemical concepts. Some of these new topics are:



Credit: *Top*: Republished with permission of Company of Biologists, from Membrane remodeling in clathrin-mediated endocytosis. Volker Haucke, Michael M. Kozlov, J Cell Sci (2018) 131 (17): jcs216812. Figure 1. Permission conveyed through Copyright Clearance Center, Inc.; *Bottom*: Schmid SL. Reciprocal regulation of signaling and endocytosis: Implications for the evolving cancer cell. J Cell Biol. 2017 Sep 4;216(9):2623-2632. doi: 10.1083/jcb.201705017. Epub 2017 Jul 3. PMID: 28674108; PMCID: PMC5584184. Copyright © 2017 Schmid. Illustration by Marcel Mettlen. Used with permission.

FIGURE 12.38 Many cells take up molecules by receptor-mediated endocytosis. Receptor binding on the surface of the cell induces the membrane to invaginate, with the assistance of specialized intracellular proteins such as clathrin and dynamin. The process results in the formation of a vesicle within the cell.

Discussion of SARS-CoV-2 and COVID-19 in multiple contexts (Chapter 1–4, 14, 29)
Discussion and illustration of binding phenomena at the single-molecule level (Chapter 1)

Expanded discussion of the interpretation of variations in genome sequences in terms of ancestry and evolutionary timescales (Chapter 1)
New section highlighting different career paths related to biochemistry, and the importance of diverse teams of people for advancing our field of knowledge (Chapter 1)
Updated discussion of protein structure prediction, including the development of AlphaFold (Chapter 2)
New chapter focused on molecular recognition, using the examples of steroid-hormone binding, oxygen transport by hemoglobin, and key proteins from the immune system (Chapter 3)
Expanded discussion of timescale and single-molecule kinetics, including new figures and equations (Chapter 5)
Expanded discussion of molecular motor proteins, particularly myosin (Chapter 6)
Updated discussion of anticoagulant medicines (Chapter 7)
Discussion of the major and minor grooves of double-stranded DNA (Chapter 8)
Expanded discussion of the methods for quantitation of gene expression to include RNA-seq (Chapter 9)
Updated presentation of carbohydrate structures and the role of glycoproteins in biology (Chapter 11)
Expanded discussion of lipid rafts (Chapter 12) ▲
Updated discussion of the ion channels responsible for cardiac pacemaker activity (Chapter 13)
Illustration of signal-transduction processes in the context of the “fight-or-flight” response (Chapter 14)
Discussion of signal-transduction processes involved in sensory systems, including sight, smell, and hearing (Chapter 14)
Updated information regarding the health effects of fructose consumption (Chapter 16)
Discussion of inborn errors of metabolism (Chapter 16)
Discussion of the role of the proton motive force in the flagellar motor (Chapter 18)
New emphasis on phototrophy versus photosynthesis, and autotrophy versus heterotrophy (Chapter 19)

Discussion of optogenetics, including bacteriorhodopsin and its relationship to rhodopsin and channelrhodopsin (Chapter 19)
Updated discussion of the evolution and enzymology of C_4 plants (Chapter 20)
Updated discussion of the UPS system, the role of degrons in regulation, and the alternative functions of ubiquitin (Chapter 23)
Updated discussion of the fasted-fed cycle, diabetes, and obesity (Chapter 24)
Discussion of McArdle glycogen storage disease and its effects on the fuel choices available to muscles (Chapter 24)
Discussion of metabolism and cancer (Chapter 24)
Discussion of some viruses that utilize an alternative nucleobase (Chapter 26)
Discussion of the involvement of 3-metal ions in catalysis by DNA polymerase (Chapter 28)
Added examples of RNA function (Chapter 29)
Discussion of the role of kinetic proofreading in increasing the fidelity of protein synthesis (Chapter 30)
Discussion of the manipulation of protein-synthesis pathways to incorporate unnatural amino acids in preselected positions (Chapter 30)
Discussion of how ribosomes selectively control gene expression (Chapter 30)
Updated and greatly revised discussion on drug discovery to emphasize target identification, validation, and tractability (Chapter 32)
Expanded discussion of the role of high-throughput screening in lead identification during drug discovery (Chapter 32)
Discussion of biologics (Chapter 32)

Clinical Applications

 This icon signals the start of a clinical application in the text.

Additional, briefer clinical correlations appear in the text as appropriate.

Osteogenesis imperfecta
Protein-misfolding diseases
2,3-BPG and fetal hemoglobin
Carbon monoxide poisoning
Sickle-cell anemia
Vaccines, including for SARS-CoV-2
Monoclonal antibodies
Aldehyde dehydrogenase deficiency
Competitive inhibitors as drugs
Action of penicillin
Toxins that modify reactive serine residues
Protease inhibitors as drugs
Protein kinase A mutations and Cushing's syndrome
Deficiency of α_1-antitrypsin and lung disease
Anticoagulant drugs
Identifying disease-causing mutations using recombinant DNA technology
Using RNAi to treat disease
Monitoring changes in glycosylated hemoglobin (A1C levels)
Using maltase inhibitors to control blood glucose
Human milk oligosaccharides and newborn protection
Erythropoietin (EPO)
Mucin overexpression and disease
Blood type O and cholera susceptibility
Errors in glycosylation and I-cell disease
Liposomes for drug delivery
Demyelinating diseases
Action of aspirin and ibuprofen
Gram staining to characterize bacterial infections
Digoxin and congestive heart failure
ATP-binding cassette domains and multidrug resistance
Drug side effects caused by interaction with the K^+ channel hERG

Signal-transduction pathways and cancer
COVID-19 effects on sense of smell
Vitamins

Effects of excessive fructose consumption
Galactosemia
Lactose intolerance
Glucokinase and type 2 diabetes
Aerobic glycolysis and cancer
Activation of transcription factor HIF1 by both cancer and endurance training
Effects of substrate cycles on health and disease
Deficiencies of glycolytic or gluconeogenic enzymes
Pyruvate dehydrogenase complex inhibition and diabetic neuropathy
Beriberi and mercury and arsenic poisoning
Blocking the glyoxylate cycle as potential tuberculosis treatment
Frataxin mutations and Friedreich's ataxia
Reactive oxygen species (ROS) and signal transduction
Mild uncouplers as drugs
Mitochondrial diseases
Photosensitive proteins and optogenetics
Glucose 6-phosphate dehydrogenase deficiency and drug-induced hemolytic anemia
Drugs for type 2 diabetes that target liver phosphorylase
Glycogen-storage diseases
Carnitine deficiency
Zellweger syndrome
Fatty acids and pathological conditions
Ketogenic diets as treatment for epilepsy
Diabetic ketosis
Fatty acid synthase inhibitors as drugs
Effects of aspirin on signaling pathways
Diseases resulting from defects in E3 proteins
Proteasome inhibitors and tuberculosis treatment
Blood levels of aminotransferases as indicators of liver damage
Inherited defects of the urea cycle and hyperammonemia
Phenylketonuria and other disorders of amino acid degradation
Causes of type 1 and type 2 diabetes
McArdle disease
Effects of ethanol on energy metabolism and link to cancer

High homocysteine levels and vascular disease
Inherited disorders of porphyrin metabolism
Herpes drug that targets viral thymidine kinase
Anticancer drugs that block the synthesis of thymidylate
Adenosine deaminase and severe combined immunodeficiency
Gout
Lesch–Nyhan syndrome
Cardiolipin and Parkinson's disease
Disruption of lipid metabolism and Tay–Sachs disease
Hypercholesterolemia and atherosclerosis
Mutations in the LDL receptor
Role of the protease PCSK9 in cardiovascular disease
Clinical management of cholesterol levels
Protective function of the cytochrome P450 system
Aromatase inhibitors in the treatment of breast and ovarian cancer
Rickets and vitamin D
Antibiotics that target DNA gyrase
Using DNA-repair mechanisms to study disease
Huntington's disease
mRNA vaccines
Burkitt lymphoma and B-cell leukemia
Diseases of defective RNA splicing
Diphtheria
Serendipitous discovery of penicillin
HMG-CoA reductase inhibitors
HIV protease inhibitors

Boxed Example Problems

The boxed Examples provide point-of-use, worked-through examples of the types of quantitative and reasoning questions students will frequently encounter in the course.

Applying the Henderson–Hasselbalch Equation

Determining the Fraction of Bound Receptors
Calculating the Effectiveness of Protein Purification
Calculating and Comparing $\Delta G^{\circ\prime}$ and $\Delta G^{\circ\prime}$
Applying the Michaelis–Menten Equation
Determining Inhibitor Type from Data
Interpreting an RNA Alignment
Calculating the Energetic Cost of Ion Transport
Calculating Equilibrium Potentials
Calculating ΔG for a Coupled Reaction Under Real Conditions
Calculating the Standard Free Energy of a Reaction from Reduction Potentials
Determining Metabolic Products of Amino Acid Degradation
Measuring the Impact of a Single Athletic Activity on Caloric Homeostasis
Determining the IC_{50} for an Inhibitor

Scientist Profiles

Scientist profiles throughout the book illustrate some of the wide range of training and career paths that different individuals have taken to allow them to make important contributions to biochemistry.

Herman Branson
Pamela Bjorkman
Rosalind Franklin
Maud Menten
Har Gobind Khorana
Emmanuelle Charpentier and Jennifer Doudna
Russell Doolittle
Carolyn Bertozzi
Marie M. Daly
Baldomero Olivera
Eva Neer

Gerty Cori
Hans Krebs
Lynn Margulis
Peter Mitchell and André Jagendorf
Andrew Benson
Dorothy Hodgkin
Cecile Pickart
Beverly Guirard
JoAnne Stubbe
Namandjé Bumpus
Tsuneko and Reiji Okazaki
Thomas Cech
Ada Yonath
Sarah Stewart
Gertrude Elion

Acknowledgments

With the publication of this tenth edition of *Biochemistry*, we are reminded of the tremendous responsibility in continuing the tradition started by Lubert Stryer in 1975. Throughout our preparation and writing of this edition, we sought to reaffirm our commitment to the guiding principles that make this book special: clear and precise writing, simple and informative illustrations, and the awareness that our work would be consumed by clever and engaged students and their dedicated and meticulous teachers. It is an honor that we do not take lightly. We are grateful to all our colleagues who supported and advised us throughout this process, and to all the pioneering scientists whose discoveries and insights provide us with the subject material that inspires our passion for biochemistry.

It has been a joy to work with the Macmillan Learning team throughout the creative process. While the undertaking was invariably arduous, they continually kept our spirits up and our eyes focused on the ultimate goal by coaxing without nagging, and critiquing while supporting us. We have many people to thank for this experience, some of whom are first timers to *Biochemistry*. We were delighted to work with Senior Program Manager Liz Simmons for the first time. She was unfailing in her enthusiasm and tremendous leadership through an enormously tumultuous time during the pandemic. Senior Development Editor Jennifer Angel provided countless thoughtful suggestions to improve the book in every facet, from the writing to the page layout. Director of Development Debbie Hardin (and Barbara Yien in the final months of the project), provided support and encouragement throughout the project. A special word of thanks to our Senior Media Editor, Cassandra Korsvik,

who provided extraordinary support as we worked to synchronize our print and online assessments. Special thanks also to Assistant Editor Angelica Hernandez, who tirelessly juggled countless tasks in support of our team.

It is almost impossible to put into words the amount of coordination and effort required to shepherd a textbook project from authors' first draft to publication. We have many to thank for directing us through this complex process. Editorial Project Manager Jennifer Hart and Content Project Manager Peter Jacoby managed the flow of the entire project, from draft writing to copyediting to bound book, with amazing efficiency. Diana Blume, Director of Design, Content Management; Natasha Wolfe, Design Services Manager; and Maureen McCutcheon, Designer, produced a design and layout that makes the book uniquely attractive and modern, while still emphasizing its ties to past editions. Permissions Manager Christine Buese and Photo Researchers Richard Fox and Krystyna Borgen found many new photographs in addition to diligently tracking down classics from the published literature. Matthew McAdams, Art Manager, deftly directed the rendering of new illustrations and the conversion of legacy art for a new printing process. Paul Rohloff, Senior Workflow Project Manager, made sure that the significant difficulties of scheduling, composition, and manufacturing were smoothly overcome. Heather Southerland, Amy Thorne, Cassandra Korsvik, Kelsey Hughes, and Lily Huang did a wonderful job in their management of the media program. Maureen Rachford, Marketing Manager for the Physical Sciences, enthusiastically introduced this newest edition of *Biochemistry* to the academic world. We are deeply appreciative of Greg David and his sales staff for their support. Without their able and enthusiastic presentation of our text to the academic community, all of our efforts would be in vain.

Thanks also to our many colleagues at our own institutions as well as throughout the country who patiently answered our questions and

encouraged us on our quest. Finally, we owe a debt of gratitude to our families: our spouses — Wendie Berg, Megan Williams, Catherine Hines, and Mark Heller — and our children. Without their support, comfort, and understanding, this endeavor could never have been undertaken, let alone successfully completed.

We also especially thank those who served as reviewers for this tenth edition. Their thoughtful comments, suggestions, and encouragement have been of immense help to us in maintaining the excellence of the preceding editions. These reviewers are listed below.

Balasubrahmanyam Addepalli
University of Cincinnati, Main Campus

Dolapo Adedeji
Elizabeth City State University

James Ames
University of California, Davis

Mary Anderson
Texas Woman's University

Gerald Audette
York University

Dana Baum
Saint Louis University, Main Campus

Donald Beitz
Iowa State University

Matthew Berezuk
Azusa Pacific University

Mark Berry
Memorial University

Joshua Blose
State University of New York, Brockport

Paul Bond
Shorter University

Michael Borenstein
Temple University

Adam Brummett
University of Iowa

Christopher Calderone
Carleton College

Sara C. Zapico
New Jersey Institute of Technology

Michael Cascio
Duquesne University

Nancy Castro
University of Southern California

Yongli Chen
Hawaii Pacific University, Hawaii Loa

Greg Ciesielski
Auburn University, Montgomery

Jade Clement
Texas Southern University

Robert Congdon
State University of New York, Broome Community College

Douglas Conklin
University of Albany

John Conrad
University of Nebraska, Omaha

Rebecca Corbin
Ashland University

Rikki Corniola
California North State University, College of Health Sciences

Garland Crawford
Mercer University

Tuhin Das
City University of New York, John Jay College of Criminal Justice

Madeleine De Beer
University of Dayton

Tomas Ding
North Carolina Central University

Brittney A. Dinkel
Buena Vista University

Cassidy Dobson
Truman State University

Pasha Ebrahimi
El Camino Community College District

Shawn Ellerbroek
Wartburg College

Steven R. Ellis
University of Louisville

Nuran Ercal
Missouri University of Science and Technology

Stylianos Fakas
Alabama A&M University

Kirsten Fertuck
Northeastern University

Sheree J. Finley
Alabama State University

Barbara S. Frank
Idaho State University

Linnea Freeman
Furman University

Brooke Gardner
University of California, Santa Barbara

Yulia Gerasimova
University of Central Florida

Dipak K. Ghosh
North Carolina A&T State University

Christina Goode
Western University of Health Sciences

Sarah Goomeshi Nobary
Columbia College

Neena Grover
Colorado College

Christopher S. Hamilton
Hillsdale College

Tiffany Hayden
Erskine College And Seminary

James A. Hebda
Austin College

Newton P. Hilliard Jr.
Arkansas Tech University

Cheryl Ingram-Smith
Clemson University

Lori Isom
University of Central Arkansas

Kelly E. Johanson
Xavier University of Louisiana

Brian Kalet
Colorado State University, Fort Collins

Dmitry Kolpashchikov
University of Central Florida

Ivan Korendovych
Syracuse University

Chandrika Kulatilleke
City University of New York, Bernard M Baruch College

Allison C. Lamanna
University of Michigan, Ann Arbor

Yun Li
Delaware Valley University

Jie Li
University of South Carolina, Columbia

Zhengchang Liu
University of New Orleans

Debra Martin
Saint Mary's University of Minnesota

Jonathon Mauser
Winona State University

Karen McPherson
Delaware Valley University

Michael Mendenhall
University of Kentucky

Jonathan M. Meyers
Columbus State University

Geoffrey Mitchell
Wofford College

David Mitchell
Saint John's University

Victoria Del Gaizo Moore
Elon University

Ifedayo Victor Ogungbe
Jackson State University

S. Ryan Oliver
University of Alaska, Fairbanks

Justin P'Pool
Franklin College

Siva S. Panda
Augusta University

Ann Paterson
Williams Baptist College

John D. Patton
Southwest Baptist University

Alfred S. Ponticelli
State University of New York at Buffalo Medical School

Ramin Radfar
Wofford College

Supriyo Ray
Bowie State University

Katarzyna Roberts
Rogers State University

Douglas Root
University of North Texas

Gillian E. A. Rudd
Georgia Gwinnett College

Megan E. Rudock
Wake Forest University

Usha Sankar
Fordham University

Michael Sehorn
Clemson University

Kavita Shah
Purdue University, Main Campus

Juyoung K. Shim
University of Maine, Augusta

Aaron J. Sholders
Colorado State University, Fort Collins

Gabriela M. Smeureanu
City University of New York, Hunter College

Sarah Smith
Bucknell University

Jennifer Sniegowski
Arizona State University, Downtown Phoenix

Amy L. Stockert
Ohio Northern University

Nina V. Stourman
Youngstown State University

Kent Strodtman
Columbia College

Suresh Kumar Thallapuranam
University of Arkansas

Kerstin Tiedemann
Concordia University, Loyola Campus

Peter Tieleman
University of Calgary

Candace Timpte
Georgia Gwinnett College

Yufeng Tong
University of Windsor

Andrew T. Torelli
Ithaca College

Vishwa D. Trivedi
Bethune Cookman University

Robert J. Warburton
Shepherd University

Kathrine Weeks
Centenary College of Louisiana

Rodney Weilbaecher
Southern Illinois University, Carbondale

Cindy L. White
Harding University

Vladimira Wilent
Temple University

Jacek Wower
Auburn University

Adrienne Wright
University of Alberta, Edmonton

Naciem Yousif
University of the District of Columbia

Alexander G. Zestos
American University

Joshua Zhu
Dordt College

About the Authors



Courtesy Jeremy Berg

JEREMY M. BERG received his BS and MS degrees in Chemistry from Stanford University (where he did research with Keith Hodgson and

Lubert Stryer) and his PhD in Chemistry from Harvard with Richard Holm. He then completed a postdoctoral fellowship with Carl Pabo in Biophysics at Johns Hopkins University School of Medicine. He was an Assistant Professor in the Department of Chemistry at Johns Hopkins from 1986 to 1990. He then moved to Johns Hopkins University School of Medicine as Professor and Director of the Department of Biophysics and Biophysical Chemistry, where he remained until 2003. He then became Director of the National Institute of General Medical Sciences at the National Institutes of Health. In 2011, he moved to the University of Pittsburgh, where he is now Professor of Computational and Systems Biology and Pittsburgh Foundation Chair and Director of the Institute for Personalized Medicine. He served as President of the American Society for Biochemistry and Molecular Biology from 2011 to 2013 and as Editor-in-Chief for *Science* magazine and the *Science* family of journals from 2016 to 2019. Dr. Berg has received numerous awards for his research, teaching, and public service. He is an elected member of the National Academy of Medicine and the American Academy of Arts and Sciences. He is coauthor, with Stephen J. Lippard, of the textbook *Principles of Bioinorganic Chemistry*. He greatly enjoys sharing his life with his wife, three grown children, and grandchildren.



Karpagam Aravindhan

GREGORY J. GATTO, JR., received his AB degree in Chemistry from Princeton University, where he worked with Martin F. Semmelhack and was awarded the Everett S. Wallis Prize in Organic Chemistry. In 2003, he received his MD and PhD degrees from the Johns Hopkins University School of Medicine, where he studied the structural biology of peroxisomal targeting signal recognition with Dr. Berg and received the Michael A. Shanoff Young Investigator Research Award. He completed a postdoctoral fellowship in 2006 with Christopher T.

Walsh at Harvard Medical School, where he studied the biosynthesis of the macrolide immunosuppressants. Dr. Gatto is currently a Scientific Director in the Novel Human Genetics Research Unit at GlaxoSmithKline. While he enjoys losing at board games, attempting but not completing crossword puzzles, and watching baseball games at every available opportunity, he treasures most the time he spends with his wife Megan and sons Timothy and Mark.



Clay Wegrzynowicz/Lafayette College Communications Dept

JUSTIN K. HINES is Professor of Chemistry at Lafayette College, where he teaches general chemistry and biochemistry courses and conducts education and NIH-funded laboratory research on protein misfolding with undergraduates. He received both his BS and PhD in Biochemistry from Iowa State University, where he studied the structure and regulation of the enzymes of central metabolism with Richard B. Honzatko and Herbert J. Fromm. He then completed a postdoctoral fellowship with Elizabeth A. Craig in Biochemistry at the University of Wisconsin–Madison. Professor Hines has won numerous awards for teaching and research, including being named a Cottrell Scholar by the Research Corporation for Science Advancement and a Henry-Dreyfus Teacher-Scholar by the Camille and Henry Dreyfus Foundation. He is also the author of the case-studies series for Macmillan's three biochemistry textbooks. He enjoys running, hiking, games of any kind, and spending time with his wife and children. He would like to dedicate his work on this book to his loving mother Kathryn, who passed away in 2021.



Jutta B. Heller

JUTTA BENEKEN HELLER is a Teaching Professor at the University of Washington Tacoma. She primarily teaches upper-division undergraduate courses in the Biomedical Sciences, with a focus on molecular biology. She also acts as a faculty mentor in an NSF-funded program that supports the academic success of undergraduate students with low-income or underrepresented backgrounds. Professor Heller's top priority is the academic and personal success

of her students as she strives to create a welcoming and equitable learning environment for everyone. She received her AB in Molecular Biology from Princeton University in 1995 and her PhD from Johns Hopkins University School of Medicine in 2001. Her PhD thesis work was completed in the lab of Dr. Daniel Leahy, where she determined the crystal structure of the Homer EVH1 domain in complex with a peptide ligand. She completed a postdoctoral fellowship at the University of Chicago and began her teaching career at Loyola University Chicago in 2004. She received the 2010 Edwin T. and Vivijeanne F. Sujack Award for Teaching Excellence at Loyola University. She enjoys exploring mountains, forests, and beaches with her husband Mark and their dog Ziggy.



Hai Ngo

JOHN L. TYMOCZKO was Towsley Professor of Biology Emeritus at Carleton College, where he taught from 1976 until his death in 2019. He taught a variety of courses, including Biochemistry, Biochemistry Laboratory, Oncogenes and the Molecular Biology of Cancer, and Exercise Biochemistry, and cotaught an introductory course, Energy Flow in Biological Systems. Professor Tymoczko received his BA from the University of Chicago in 1970 and his PhD in Biochemistry from the University of Chicago with Shutsung Liao at the Ben May Institute

for Cancer Research. He then had a postdoctoral position with Hewson Swift of the Department of Biology at the University of Chicago. The focus of his research was on steroid receptors, ribonucleoprotein particles, and proteolytic processing enzymes.



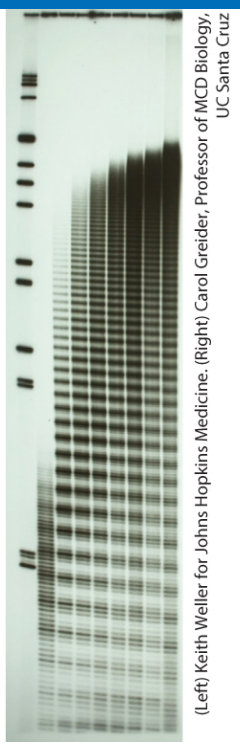
Saul Loeb/AFP/Getty Images

LUBERT STRYER is Winzer Professor of Cell Biology, Emeritus, in the School of Medicine and Professor of Neurobiology, Emeritus, at

Stanford University, where he has been on the faculty since 1976. He received his MD from Harvard Medical School. Professor Stryer has received many awards for his research on the interplay of light and life, including the Eli Lilly Award for Fundamental Research in Biological Chemistry, the Distinguished Inventors Award of the Intellectual Property Owners' Association, and election to the National Academy of Sciences and the American Philosophical Society. He was awarded the National Medal of Science in 2006. The publication of his first edition of *Biochemistry* in 1975 transformed the teaching of biochemistry.

Chapter 1
Biochemistry in Space and Time





(Left) Keith Weller for Johns Hopkins Medicine. (Right) Carol Greider, Professor of MCD Biology, UC Santa Cruz

Nobel Prize winners Peter Agre, MD, and Carol Greider, PhD, celebrated on the occasion of the announcement that Dr. Greider was sharing the Nobel Prize in Medicine or Physiology in 2009. Dr. Agre had won a Nobel in 2003. Dr. Greider was honored for determining a key aspect of how chromosomes are replicated faithfully. Some data from Dr. Greider's laboratory notebook (right) shows regularly spaced signals, indicating that she had found a biochemical process suspected to exist, but not previously discovered. This work not only helped Dr. Greider earn her PhD degree but was also cited when she shared the Nobel Prize.

Outline

1.1 Biochemical Unity Underlies Biological Diversity
1.2 DNA Illustrates the Interplay Between Form and Function

1.3 Concepts from Chemistry Explain the Properties of Biological Molecules
1.4 DNA Sequencing Is Transforming Biochemistry, Medicine, and Other Fields
1.5 Biochemistry Is an Interconnected Human Endeavor

Learning Goals



By the end of this chapter, you should be able to:

1. Provide examples of the unity of biology at the biochemical level.
2. Describe the double-helical structure of DNA including its formation from two component strands in the context of important atomic interactions: covalent bonds, ionic interactions, hydrogen bonds, van der Waals interactions, and the hydrophobic effect.
3. Discuss the first and second laws of thermodynamics and the concepts of entropy and enthalpy.
4. Discuss the importance of single-molecule experiments in terms of understanding reaction rates.
5. Explain the roles of buffers in stabilizing the pH of solutions.
6. Perform calculations using the definitions of pH and pK_a and the Henderson–Hasselbalch equation.
7. Briefly describe some discoveries enabled by advances in DNA sequencing technologies, including the concept of molecular clocks.

Biochemistry is the study of the chemistry of life processes. Scientists have explored the chemistry of life with great intensity for nearly two centuries. Many of the most fundamental mysteries of how living things function at a biochemical level have been solved. However, much remains to be investigated. As is often the case, each discovery raises at least as many new questions as it answers. We are now in an age of unprecedented opportunity for the application of this tremendous body of knowledge of biochemistry to problems in

medicine, agriculture, forensics, environmental sciences, and many other fields.

1.1 Biochemical Unity Underlies Biological Diversity

The biological world is magnificently diverse. Plant and animal species range from nearly microscopic insects to elephants, whales, and giant sequoias. This variability extends further when we descend into the microscopic world. A great diversity of organisms such as protozoa, yeast, and bacteria are found in water, in soil, and both on and within larger organisms. Some organisms can survive and even thrive in seemingly hostile environments such as hot springs, deep-sea vents, and glaciers.

The development of the microscope revealed a key unifying feature that underlies this diversity: large organisms are built up of **cells**, resembling, to some extent, single-celled microscopic organisms. The construction of animals, plants, and microorganisms from cells suggested that these diverse organisms might have more in common than is apparent from their outward appearance. With the development of biochemistry, this notion has been tremendously supported and expanded. At the biochemical level, all organisms have many common features (**Figure 1.1**).

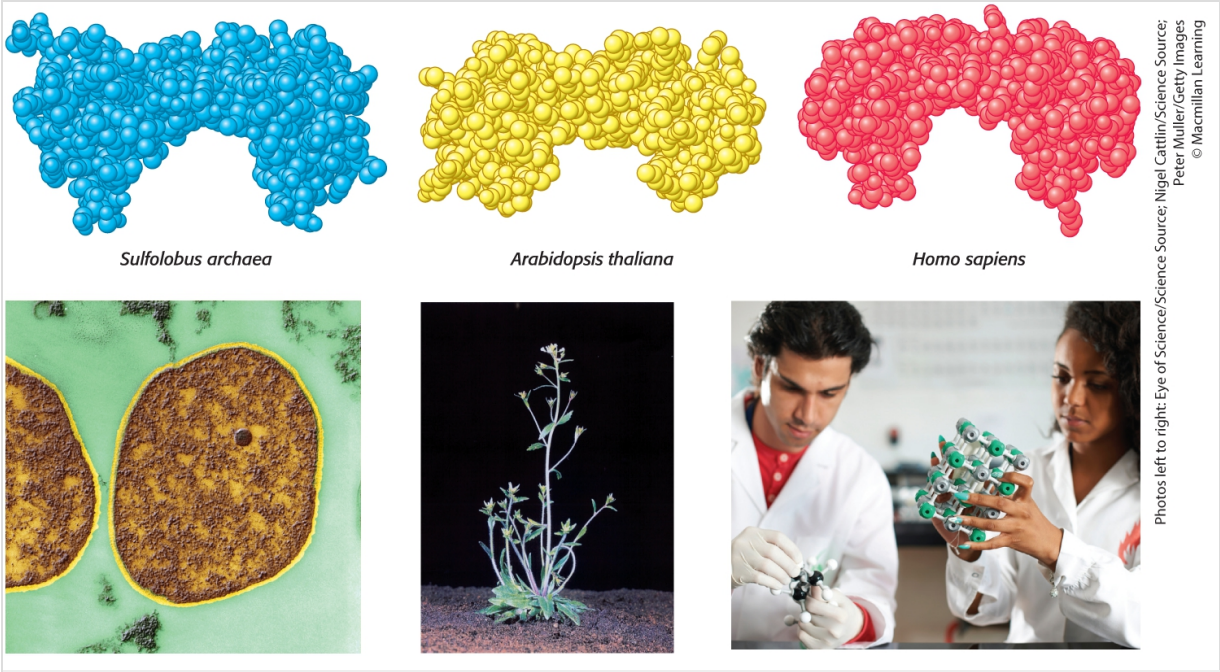
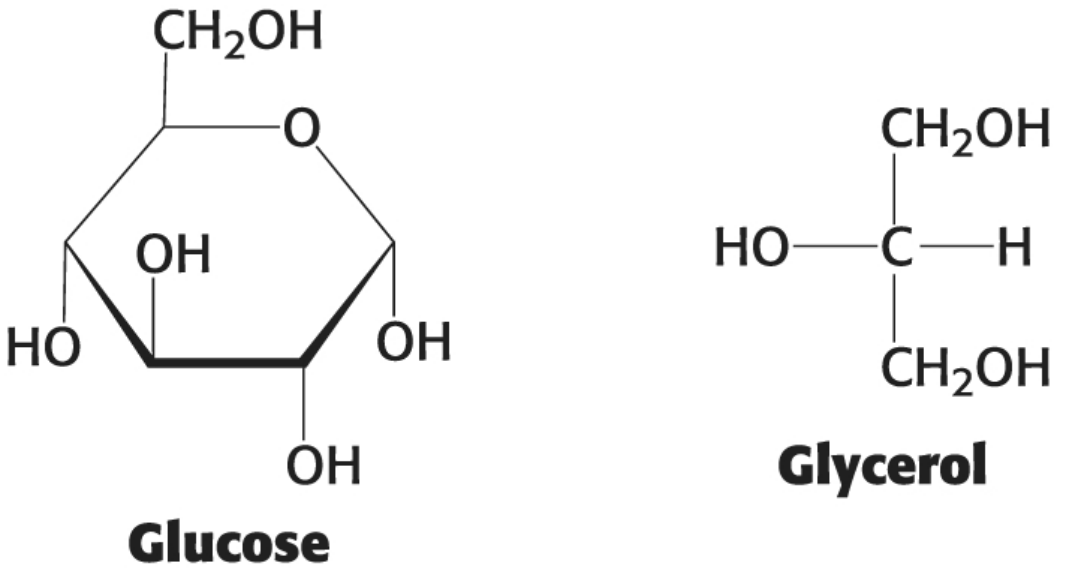


FIGURE 1.1 Despite tremendous biological diversity, there is remarkable similarity in the molecules that make up living organisms. The shape of a key molecule in gene regulation (the TATA-box-binding protein) is similar in three very different organisms that are separated from one another by billions of years of evolution.

Biochemical processes entail the interplay of two different classes of molecules: large molecules such as proteins and nucleic acids, referred to as **biological macromolecules**, and low-molecular-weight molecules such as glucose and glycerol, referred to as **metabolites**, that are chemically transformed in biological processes.



Examples of metabolites

Members of both these classes of molecules are common, with minor variations, to all living things. For example, **deoxyribonucleic acid (DNA)** stores genetic information in all cellular organisms. **Proteins**, macromolecules that are the key participants in most biological processes, are built from the same set of 20 building blocks in all organisms. Furthermore, proteins that play similar roles in different species often have very similar, or sometimes identical, three-dimensional structures (Figure 1.1).

Key metabolic processes also are common to many organisms. For example, the set of chemical transformations that converts glucose and oxygen into carbon dioxide and water is essentially identical in simple bacteria such as *Escherichia coli* (*E. coli*) and human beings. Even processes that appear to be quite distinct often have common features at the biochemical level. Remarkably, the biochemical processes by which plants capture light energy and convert it into

more-useful forms are strikingly similar to steps used in animals to capture energy released from the breakdown of glucose.

These observations overwhelmingly suggest that all living things on Earth have a **common ancestor** and that modern organisms have evolved from this ancestor into their present forms. Geological and biochemical findings support a timeline for this evolutionary path (**Figure 1.2**).

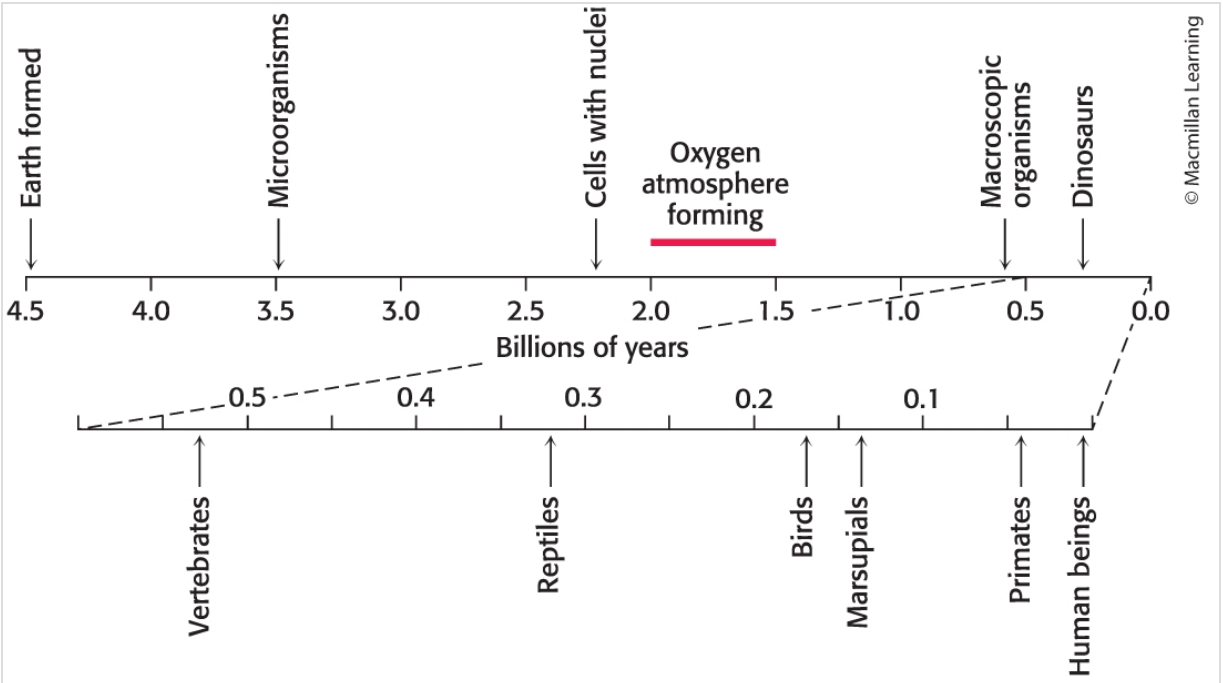


FIGURE 1.2 A possible timeline for biochemical evolution shows that life on Earth began approximately 3.5 billion years ago. Selected key events are indicated, including the relatively recent emergence of human beings. The times of emergence of classes of animals from the fossil record are shown below the main timeline.

On the basis of their biochemical characteristics, the diverse organisms of the modern world can be divided into three

fundamental groups called *domains:* Eukarya, Bacteria, and Archaea.

Domain **Eukarya** (also called **eukaryotes**) comprises all multicellular organisms, including all animals, plants, and human beings, as well as many microscopic unicellular organisms such as yeast. The defining characteristic of eukaryotes is the presence of a well-defined nucleus within each cell.

Unicellular organisms that lack a nucleus are referred to as **prokaryotes**. The prokaryotes were classified as two separate domains in response to Carl Woese's discovery in 1977 that certain unicellular organisms are biochemically quite distinct from previously characterized bacterial species. These organisms, now recognized as having diverged from the domain **Bacteria** early in evolution, make up the domain **Archaea**.

Evolutionary paths from a common ancestor to modern organisms can be deduced on the basis of biochemical information, with one possible such path shown in **Figure 1.3**. Much of this book will explore the chemical reactions and the associated biological macromolecules and metabolites that are found in biological processes common to all organisms. The unity of life at the biochemical level makes this approach possible. At the same time, different species have specific needs, depending on the particular biological niche in which they evolved and live. By comparing and contrasting details of particular biochemical pathways in different species, we can learn how biological challenges have been solved at the biochemical level. In most cases, these challenges are addressed by the adaptation of existing macromolecules to new roles rather than by the evolution of entirely new ones.

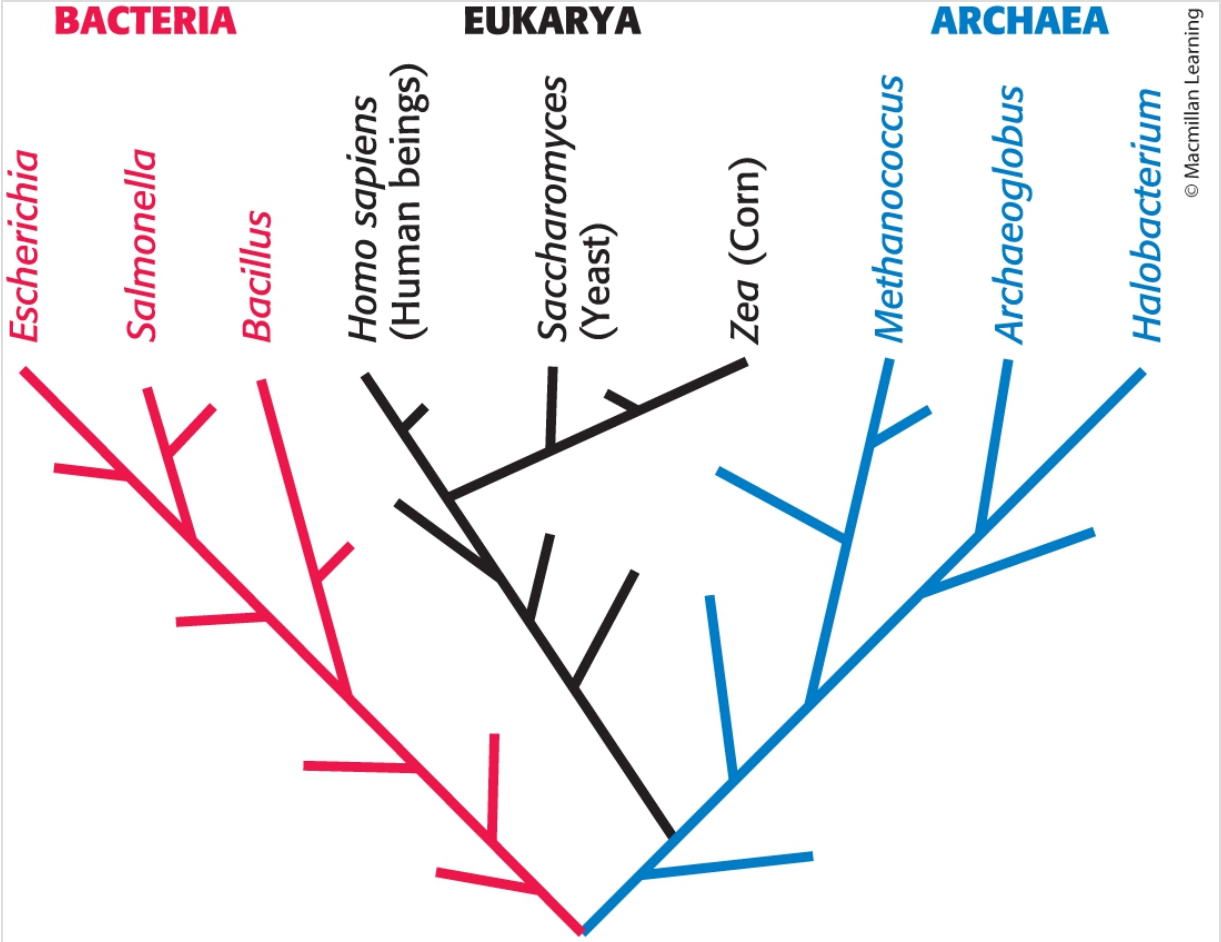


FIGURE 1.3 The relationships of all modern organisms can be displayed on a tree of life with just three major branches. A possible evolutionary path from a common ancestor is represented at the bottom of the tree, with organisms found in the modern world at the top.

Biochemistry has been greatly enriched by our ability to examine the three-dimensional structures of biological macromolecules in exquisite detail. Some of these structures are simple and elegant, whereas others are incredibly complicated. In any case, these structures provide an essential framework for understanding function. We begin our exploration of the interplay between structure and function with the genetic material, DNA.

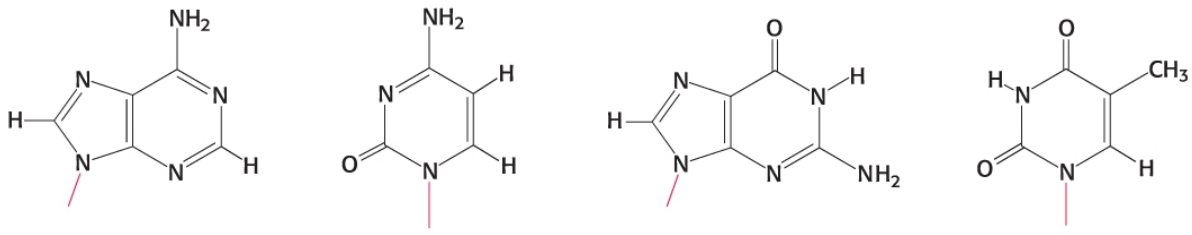
1.2 DNA Illustrates the Interplay Between Form and Function

A fundamental biochemical feature common to all cellular organisms is the use of DNA for the storage of genetic information. The discovery that DNA plays this central role was first made in studies of bacteria in the 1940s. A compelling proposal for the three-dimensional structure of DNA followed in 1953, setting the stage for many of the advances in biochemistry and numerous other fields, extending to the present.

The structure of DNA powerfully illustrates a basic principle common to all biological macromolecules: the intimate relationship between structure and function. The remarkable chemical properties of this substance allow it to function as an efficient and robust vehicle for storing information. We start with an examination of the covalent structure of DNA and its extension into three dimensions.

DNA is constructed from four building blocks

DNA is a linear polymer made up of four different types of monomers. It has a fixed backbone from which protrude variable substituents, referred to as **nitrogenous bases**, or simply, **bases** (**Figure 1.4**). The backbone is built of repeating sugar–phosphate units. The sugars are molecules of deoxyribose from which DNA receives its name. Each sugar is connected to two phosphate groups through different linkages. Moreover, each sugar is oriented in the same way, and so each DNA strand has directionality, with one end distinguishable from the other. This **polarity** is very important for many processes involving DNA. Joined to each deoxyribose is one of four possible nitrogenous bases: adenine (A), cytosine (C), guanine (G), and thymine (T).



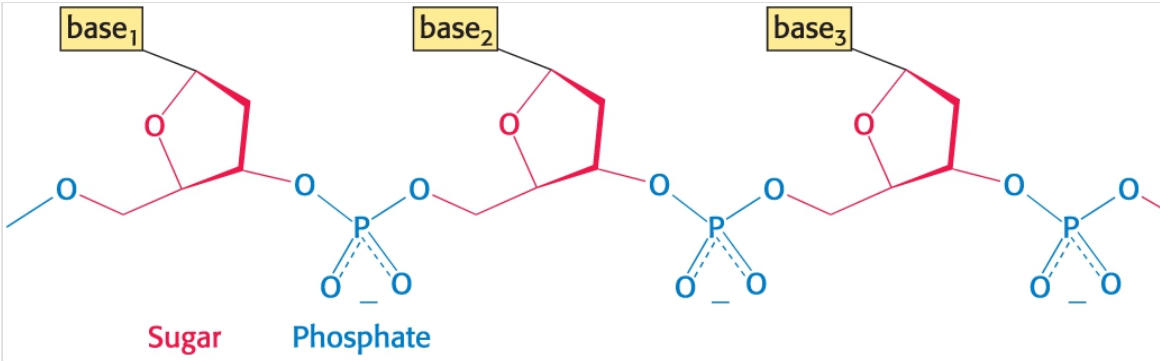


FIGURE 1.4 The covalent structure of DNA is a linear polymer of monomeric units. Each monomer is composed of a sugar (deoxyribose), a phosphate, and a variable nitrogenous base that protrudes from the sugar–phosphate backbone.

These bases are connected to the sugar components in the DNA backbone through the bonds shown in black in Figure 1.4. All four bases are planar but differ significantly in other respects. Thus, each monomer of DNA, called a *nucleotide*, consists of a sugar–phosphate unit and one of four bases attached to the sugar. These bases can be arranged in any order along a strand of DNA.

Two single strands of DNA combine to form a double helix

Most DNA molecules consist of not one but two strands (**Figure 1.5**). In 1953, James Watson and Francis Crick deduced the arrangement of these strands and proposed a three-dimensional structure for DNA molecules based, in part, on experimental data from Rosalind Franklin. This structure is a **double helix** composed of two intertwined strands arranged such that the sugar–phosphate backbone lies on the outside and the bases on the inside. The key to this structure is that the bases form specific **base pairs** held together by noncovalent interactions called *hydrogen bonds* (Section 1.3): adenine pairs with thymine (A–T) and guanine pairs with cytosine (G–C), as shown in **Figure 1.6**. Hydrogen bonds are much weaker than covalent bonds such as the carbon–carbon or carbon–nitrogen bonds that define the structures of the bases themselves. Such weak interactions are crucial to biochemical systems; they are weak enough to be reversibly broken in biochemical processes, yet they are strong enough, particularly when many form simultaneously, to help stabilize specific structures such as the double helix.



FIGURE 1.5 The double helix has two antiparallel strands. This representation of the double-helical structure of DNA proposed by Watson and Crick shows the sugar–phosphate backbones the two chains in red and blue, and the bases in green, purple, orange, and yellow. The two strands are antiparallel, running in opposite directions with respect to the axis of the double helix, as indicated by the arrows.

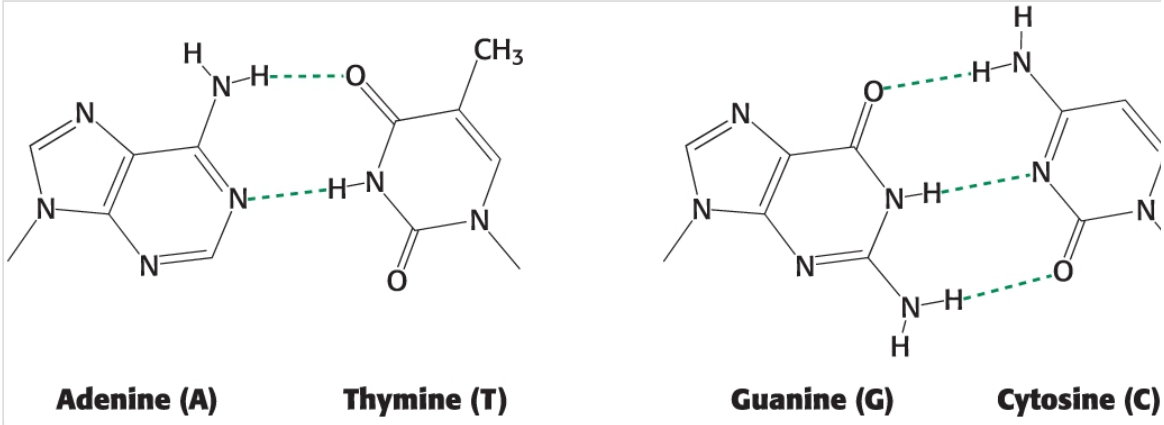


FIGURE 1.6 The nitrogenous bases in DNA form specific Watson–Crick base pairs. Adenine pai with thymine (A–T) and guanine with cytosine (G–C). The dashed green lines represent hydroge bonds.

DNA structure explains heredity and the storage of information

The structure proposed by Watson and Crick has two properties of central importance to the role of DNA as the hereditary material. First, the structure is compatible with any sequence of bases. While the bases are distinct in structure, the base pairs have essentially the same shape and thus fit equally well into the center of the double-helical structure of any sequence. Without any constraints, the sequence of bases along a DNA strand can act as an efficient means of encoding information. Indeed, the sequence of bases along DNA strands is how genetic information is stored. The DNA sequence determines the sequences of

the ribonucleic acid (RNA) and protein molecules that carry out most of the activities within cells.

Second, because of base pairing, the sequence of bases along one strand completely determines the sequence along the other strand. As Watson and Crick so coyly wrote: “It has not escaped our notice that the specific pairing we have postulated immediately suggests a possible copying mechanism for the genetic material.” Thus, if the DNA double helix is separated into two single strands, each strand can act as a template for the generation of its partner strand through specific base-pair formation (Figure 1.7). The three-dimensional structure of DNA beautifully illustrates the close connection between molecular form and function.

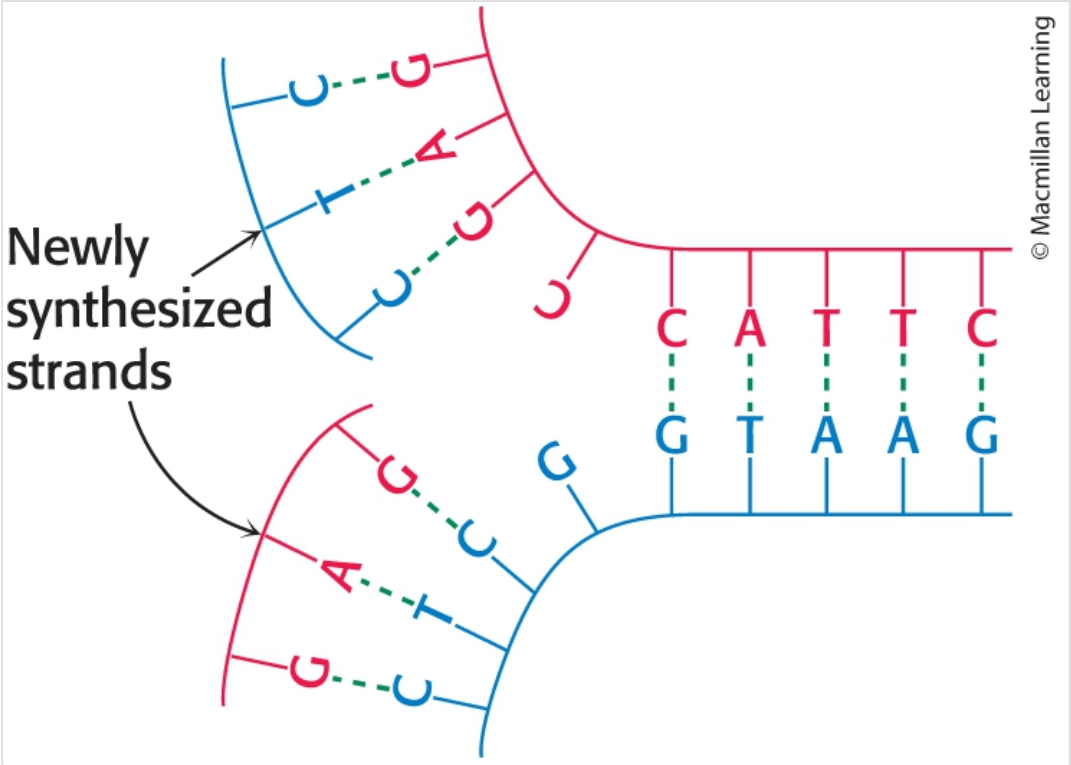


FIGURE 1.7 Once separated, each strand of the DNA double helix can act as a template for the generation of its partner strand.

1.3 Concepts from Chemistry Explain the Properties of Biological Molecules

We have seen how a chemical insight into the hydrogen-bonding capabilities of the bases of DNA led to a deep understanding of a fundamental biological process. To lay the groundwork for the rest of the book, we begin our study of biochemistry by examining selected concepts from chemistry and showing how these concepts apply to biological systems. The concepts include the types of chemical interactions; the structure of water, the solvent in which most biochemical processes take place; the First and Second Laws of Thermodynamics; and the principles of acid–base chemistry.

The formation of the DNA double helix is a key example

We will use these concepts to examine an archetypical biochemical process — the formation of a DNA double helix from its two component strands. The process is but one of many examples that could have been chosen to illustrate these topics. Keep in mind that, although the specific discussion is about DNA and double-helix formation, these concepts are quite general and will apply to many other classes of molecules and processes that will be discussed in the remainder of the book.

The double helix can form from its component strands

The discovery that DNA from natural sources exists in a double-helical form with Watson–Crick base pairs suggested, but did not prove, that such double helices would form spontaneously outside biological systems. Suppose that two short strands of DNA were chemically synthesized to have **complementary sequences** so that they could, in principle, form a double helix with Watson–Crick base pairs. Two such sequences are CGATTAAT and ATTAATCG. In this context, the term *complementary* refers to the fact that the two sequences can form Watson–Crick base pairs when the sequence of one of them is written in the reverse order.

The structures of these molecules in solution can be examined through a variety of techniques. In isolation, each sequence exists almost exclusively as a single-stranded molecule. However, when the two sequences are mixed, a double helix with Watson–Crick base pairs does form (**Figure 1.8**).

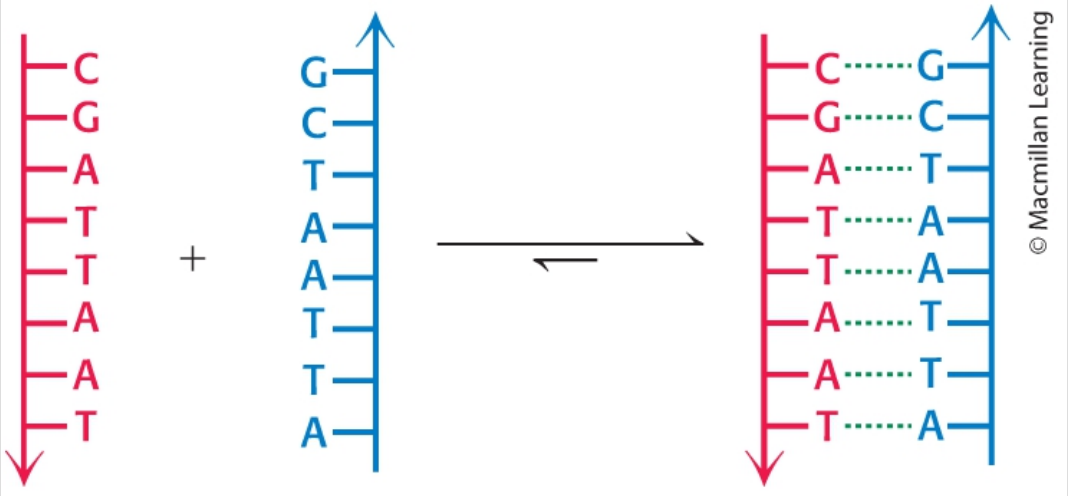


FIGURE 1.8 When two DNA strands with complementary sequences are mixed, they spontaneously assemble to form a double helix.

Self-Check Question



What DNA sequence can form a double helix with $5'-AGGTCCGATA-3'$?

What forces cause the two strands of DNA to bind to each other? To analyze this binding process, we must consider several factors: the types of interactions and bonds in biochemical systems, the thermal motion of molecules, the energetic favorability of the process, and the influence of the solution conditions — in particular, the consequences of acid–base reactions. Remarkably, this process proceeds nearly to completion in less than a millisecond when the single strands are mixed at appropriate concentrations. How does this process occur so rapidly?

Atoms and molecules undergo random motions that help define the timescales for biochemical interactions

The atoms and molecules within and around us are in constant thermal motion: translating, vibrating, rotating, and colliding with one another very rapidly. How fast do these processes occur? One useful estimate to consider is that the gas molecules that make up the air you are breathing now are colliding with one another about 1 billion (10^9)

times per second, meaning the relevant timescale for these interactions is best measured in nanoseconds (10^{-9} s).

On a similar timescale to these gaseous molecular interactions are the biochemical interactions taking place in your cells. The timescale for biochemical interactions and processes are broadly on the order of picoseconds to microseconds (10^{-12}-10^{-6} s), which we shall refer to as the **biochemical timescale**. Consideration of this timescale can be quite illuminating in understanding biochemical phenomena. The rates of molecular interactions can be challenging to comprehend because, relative to them, human beings perceive time very slowly. Indeed, our perceptions are dependent on complex cascades of these very interactions. By carefully considering this timescale from the molecular perspective, we can improve our intuitions about the speed of chemical and biochemical events. For example, imagine a reaction that occurs once per millisecond (10^{-3} s), or 1000 times per second. Is this reaction occurring quickly or slowly? Our intuition about the passage of time might compel us to consider this a very fast reaction; this is, in fact, an imperceptibly short time for a human being. However, consider that molecules colliding one billion times per second will experience 1 million (10^{6}) unproductive collisions in this timeframe, on average, before a single reaction event occurs. From the perspective of a molecule undergoing these interactions, this reaction does not seem to be occurring particularly fast at all, but rather is the result of events that occur only rarely.

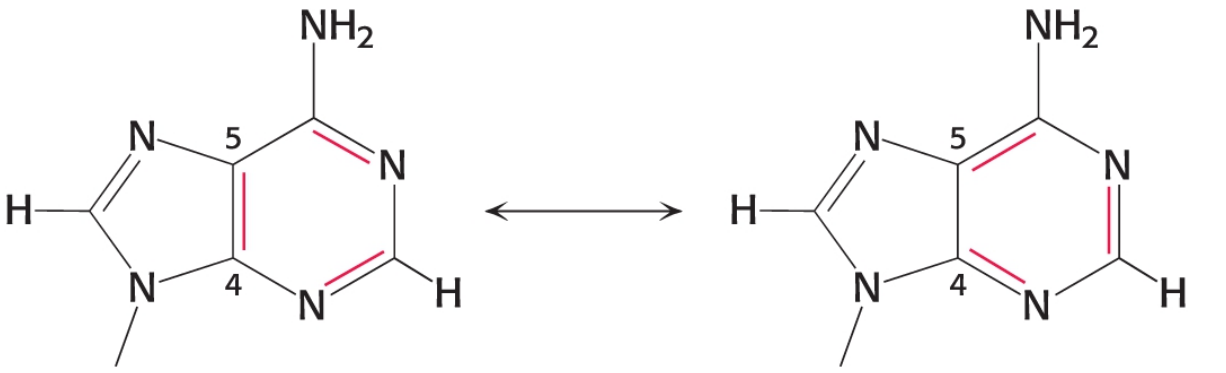
Many aspects of biochemistry depend on promoting specific processes and reactions so that they occur at biologically useful rates, harnessing the underlying rates of molecular interactions. In Chapters 5–7, we will focus explicitly on biochemical reaction rates and their control. In addition, we will visit the topic of biological timescale many times throughout the book as we explore molecular interactions in the context of biological systems.

Covalent bonds and noncovalent interactions are important for the structure and stability of biological molecules

Counteracting the chaos of thermal motion are attractive interactions that stabilize biological molecules. Atoms favorably interact with one another in several ways, including through the covalent bonds that define the structure of molecules, as well as a variety of noncovalent interactions that are of great importance to biochemistry. Among the strongest chemical interactions are **covalent bonds**, such as the bonds that hold the atoms together within DNA's individual bases. A covalent bond is formed by the sharing of a pair of electrons between adjacent atoms. A typical carbon–carbon ($C—C$) covalent bond has a bond length of $1.54\ Å$ — where $1\ Å$ (angstrom) is equivalent to one ten-billionth of a meter, or approximately 1/750,000th the width of a human hair — and a bond energy of $355\ kJ\ mol^{-1}$ ($85\ kcal\ mol^{-1}$). Because covalent bonds are so strong, considerable energy must be expended to break them. Recall that one joule (J) is the amount of energy required to move 1 meter against a force of 1 newton, and a kilojoule (kJ) is 1000 joules.

More than one electron pair can be shared between two atoms to form a multiple covalent bond. For example, three of the bases in Figure 1.6 include carbon–oxygen ($C=O$) double bonds. These bonds are shorter in length and even stronger than $C—C$ single bonds, with energies near $730\ kJ\ mol^{-1}$, or $175 kilocalories (kcal) mol^{-1}$.

For some molecules, more than one pattern of covalent bonding can be written; these alternative patterns are called **resonance structures**.



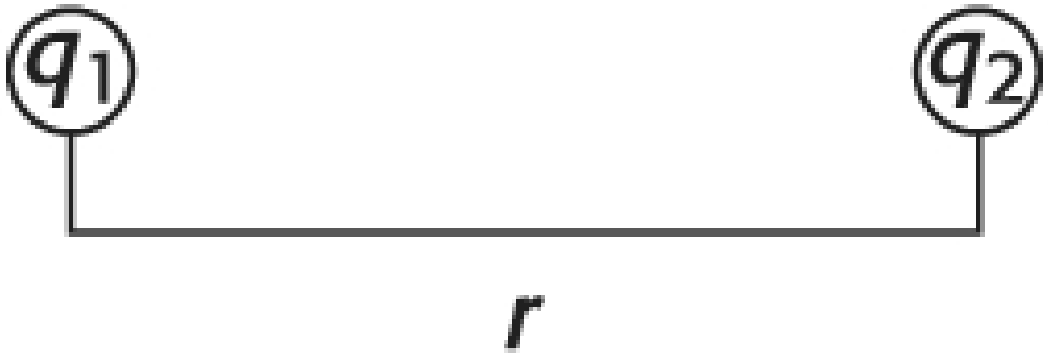
These adenine structures depict alternative arrangements of single and double bonds that are possible within the same structural framework, but the true structure of adenine is a composite of its two resonance structures. The composite structure has properties that are a blend of the two alternative states. For example, the observed length for the bond joining carbon atoms C-4 and C-5 is $1.40\ \text{Å}$, which is in between that expected for a $\text{C}-\text{C}$ single bond ($1.54\ \text{Å}$) and a $\text{C}=\text{C}$ double bond ($1.34\ \text{Å}$). A molecule that can be written as several resonance structures of approximately equal energies generally has greater stability than does a molecule without multiple resonance structures.

Noncovalent interactions are weaker than covalent bonds but are crucial for biochemical processes such as the formation of a double helix. Four fundamental noncovalent interaction types are ionic interactions, hydrogen bonds, van der Waals interactions, and hydrophobic interactions. They differ in geometry, strength, specificity, and physical origin. Furthermore, these interactions are affected in vastly different ways by the presence of water. Let us consider the characteristics of each type:

Ionic interactions

In an **ionic interaction**, a charged group on one molecule can attract an oppositely charged group on the same or another molecule. The energy of an ionic interaction (sometimes called an *electrostatic interaction*) is given by the Coulomb energy:

$$E = kq_1q_2 / Dr$$



where E is the energy, q_1 and q_2 are the charges on the two atoms (in units of the electronic charge), r is the distance between the two atoms (in angstroms), D is the dielectric constant (which decreases the Coulomb energy depending on the intervening solvent or medium), and k is a proportionality constant ($k = 1389$ for energies in units of kJ mol^{-1}, or 332 for energies in kcal mol^{-1}).

The ionic interaction between two ions bearing single opposite charges separated by $3\ \text{Å}$ in water (which has a dielectric constant of 80) has an energy of $5.8\ \text{kJ mol}^{-1}$ $(1.4\ \text{kcal mol}^{-1})$. Note the importance of the dielectric constant of the medium. For the same ions separated by $3\ \text{Å}$

in a solvent such as hexane (which has a dielectric constant of 2), the energy of this interaction is $232\ \text{kJ mol}^{-1}$ ($55\ \text{kcal mol}^{-1}$).

Thus far we have considered interactions between ions, atoms, or molecules that have one or more full electric charges. However, even molecules that have no overall charge can have regions where the electron distribution is uneven, such they are partially negatively or partially positively charged. This leads to **electric dipoles** (or simply **dipoles**) that can interact with ions or with other dipoles (**Figure 1.9**).

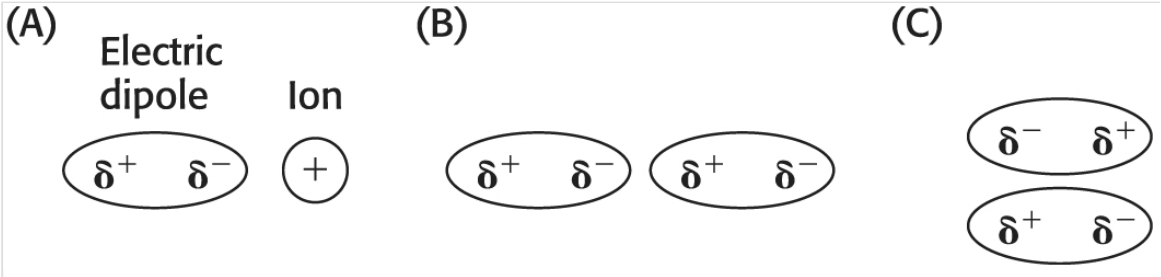


FIGURE 1.9 Electric dipoles can form a variety of noncovalent interactions. (A) An electric dipole can interact with an ion, with the negative end of the dipole pointing toward the positive charged ion. (B) Two dipoles can interact, with the negative end of one pointing toward to the positive end of the other. (C) Two dipoles position themselves so that both the positive and negative ends can favorably interact.

Hydrogen bonds

Hydrogen bonds are a specific type of dipole-dipole interactions that are so important in biochemistry that we single them out for a separate discussion. We already introduced hydrogen bonds in the context of their role in specific base-pair formation in the DNA double helix. In a **hydrogen bond**, an electropositive hydrogen atom is partially shared by two electronegative atoms such as nitrogen or oxygen. The **hydrogen-bond donor** is the group that includes both the atom to which the

hydrogen atom is covalently bonded and the hydrogen atom itself, whereas the **hydrogen-bond acceptor** is the lone pair of electrons that is on the atom less tightly linked to the hydrogen atom (Figure 1.10). The electronegative atom to which the hydrogen atom is covalently bonded pulls electron density away from the hydrogen atom, which thus develops a partial positive charge (δ^+). This hydrogen atom with a partial positive charge can interact with a lone pair of electrons on an atom having a partial negative charge (δ^-) through a dipole-dipole interaction.

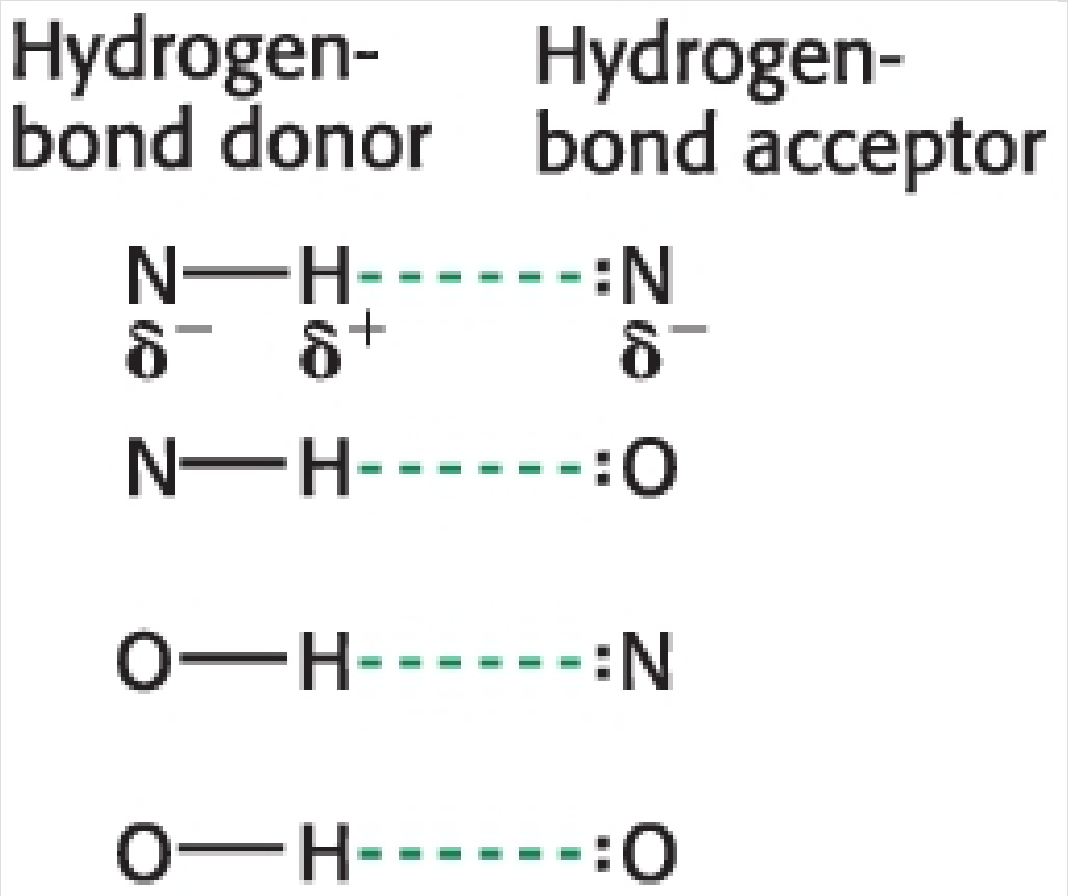
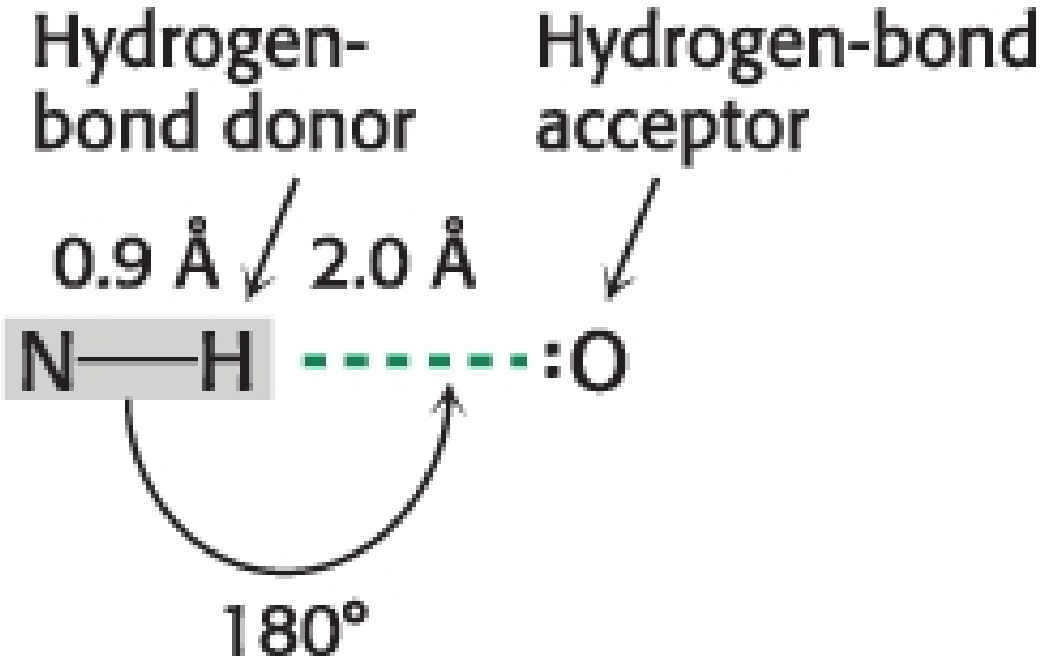


FIGURE 1.10 Hydrogen bonds are weak noncovalent interactions between specific hydrogen atoms and lone pairs of electrons. Hydrogen bonds are depicted as dashed green lines and the positions of the partial charges as δ^+ and δ^-.

Hydrogen bonds are much weaker than covalent bonds. They have energies ranging from 4 to $20\ \text{kJ mol}^{-1}$ (from 1 to $5\ \text{kcal mol}^{-1}$). Accordingly, hydrogen bonds are also somewhat longer than covalent bonds; their bond lengths (measured from the hydrogen atom) range from $1.5\ \text{Å}$ to $2.6\ \text{Å}$. Hence, a distance ranging from $2.4\ \text{Å}$ to $3.5\ \text{Å}$ separates the two nonhydrogen atoms in a hydrogen bond.



Hydrogen bonds tend to be straight, such that the hydrogen-bond donor, the hydrogen atom, and the hydrogen-bond acceptor lie in a line. This tendency toward linearity can be important for orienting interacting molecules with respect to one another. Hydrogen-bonding interactions

are responsible for many of the properties of water that make it such an important solvent, as will be described shortly.

van der Waals interactions

The basis of a **van der Waals interaction** is that the distribution of electronic charge around an atom fluctuates with time. At any instant, the charge distribution is not perfectly symmetric, leading to a dipole. This dipole acts through dipole-dipole interactions to induce a complementary dipole in its neighboring molecules, causing an attraction between the molecules. This attraction increases as the two atoms come closer to each other, until they are separated by what is termed the **van der Waals contact distance** (**Figure 1.11**). At distances shorter than the van der Waals contact distance, very strong repulsive forces become dominant because the outer electron clouds of the two atoms overlap.

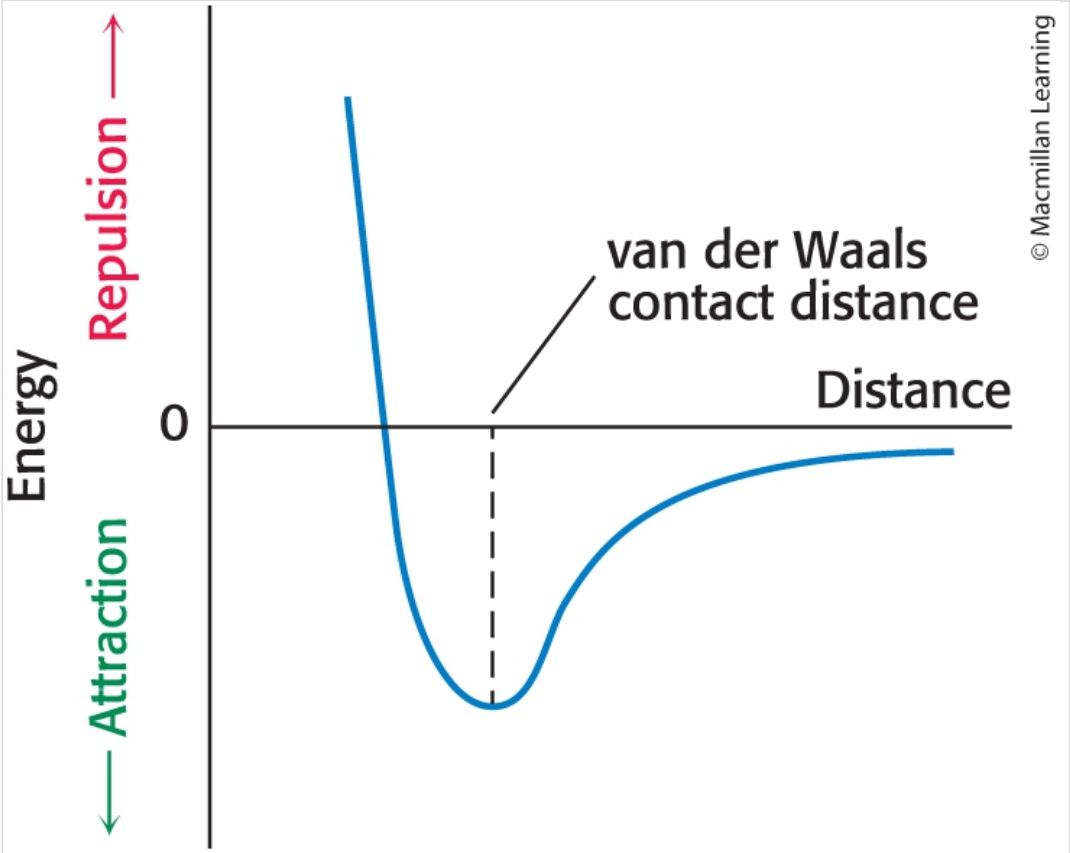


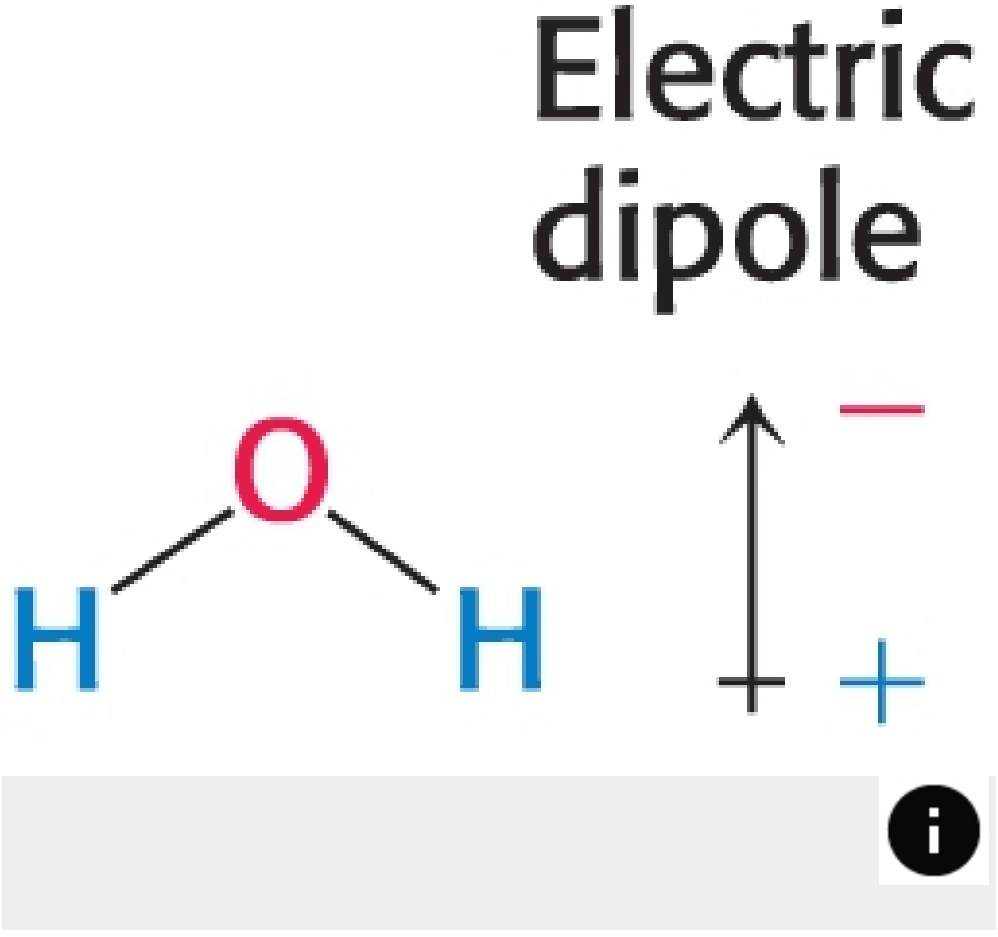
FIGURE 1.11 The energy of a van der Waals interaction varies and is most favorable at the van der Waals contact distance. Owing to electron–electron repulsion, the energy rises rapidly as the distance between the atoms becomes shorter than the contact distance.

Energies associated with van der Waals interactions are quite small; typical interactions contribute from 2 to $4\ \text{kJ mol}^{-1}$ (0.5 to $1\ \text{kcal mol}^{-1}$) per atom pair. When the surfaces of two large molecules come together, however, a large number of atoms are in van der Waals contact; the net effect, summed over many atom pairs, can be substantial.

The hydrophobic effect

Before we define the last noncovalent interaction, it's important to remember that water is the solvent in which most biochemical reactions take place; thus its properties are essential to the formation of macromolecular structures and the progress of chemical reactions. Two properties of water are especially relevant:

- *Water is a polar molecule*. The water molecule is bent, not linear, and so the distribution of charge is asymmetric. The oxygen nucleus draws electrons away from the two hydrogen nuclei, which leaves the region around each hydrogen atom with a net positive charge. The water molecule thus has a permanent electric dipole.



The polar nature of water is responsible for its high dielectric constant of 80. Molecules in aqueous solution interact with water molecules through the formation of hydrogen bonds and through ionic interactions. These interactions make water a versatile solvent, able to readily dissolve many species, especially polar and charged compounds that can participate in these interactions.

- *Water is highly cohesive*. Water molecules interact strongly with one another through hydrogen bonds. These interactions are apparent in the structure of ice (**Figure 1.12**). Networks of hydrogen bonds hold the structure together; similar interactions link molecules in liquid water and account for many of the properties of water. In the liquid state, approximately one in four of the hydrogen bonds present in ice is broken.

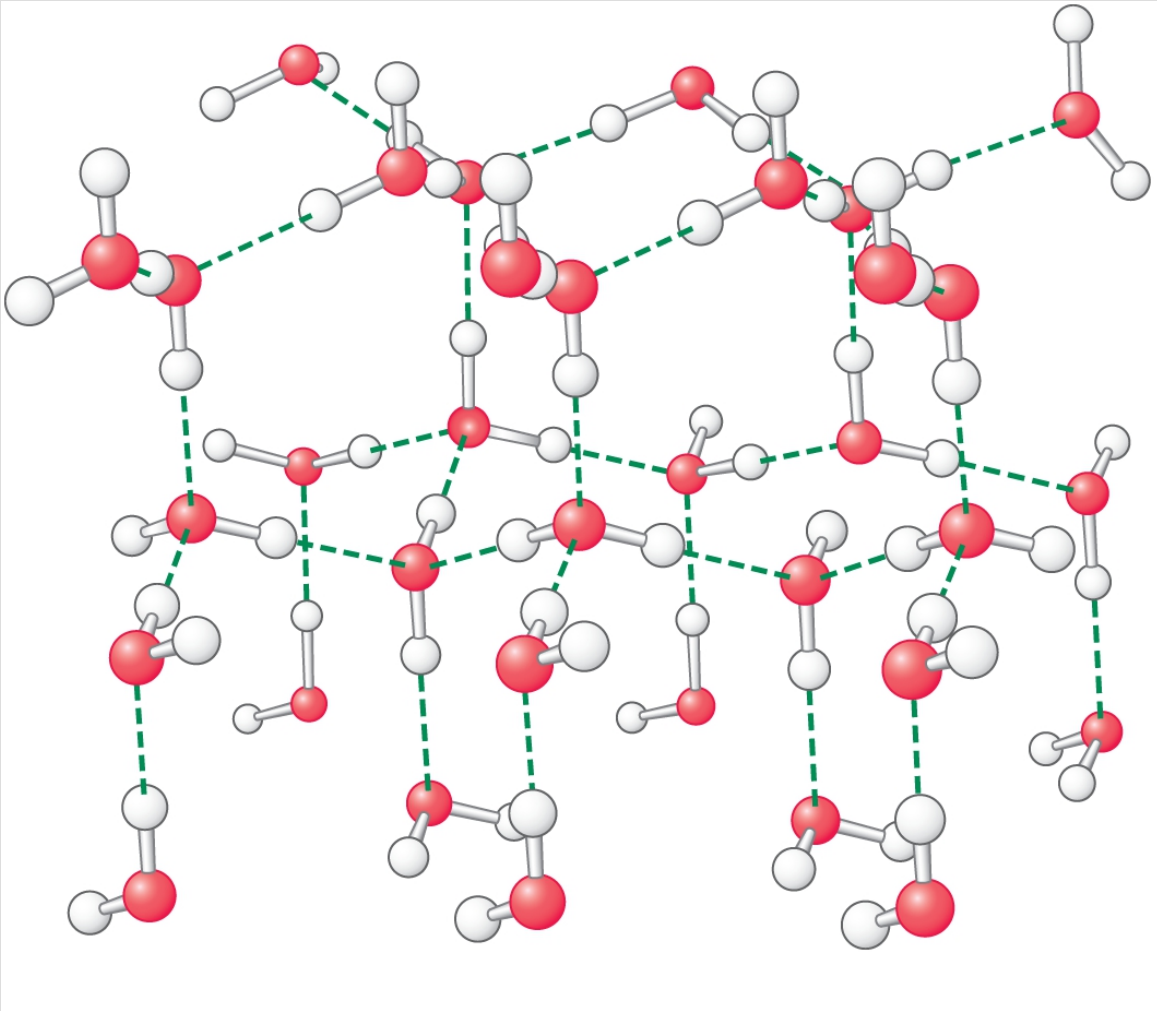


FIGURE 1.12 The structure of ice involves extensive hydrogen bonding. Hydrogen bonds (shown as dashed green lines) are formed between water molecules, producing a highly ordered and open structure.

The **hydrophobic effect** is a manifestation of the properties of water just described: it is the increased tendency for nonpolar molecules to aggregate in water compared with other, less polar and less self-associating, solvents. Some molecules (termed **nonpolar molecules**) lack any dipoles and therefore cannot participate in hydrogen bonding or ionic interactions. Polar water molecules interact much more favorably with each other than they do with nonpolar molecules. In the presence of nonpolar molecules, water molecules form cage-like structures around them, becoming more ordered than water molecules free in solution. However, when two such nonpolar molecules come together, some of the water molecules that had been surrounding them are released from the "cage." The released water molecules interact freely with bulk water (**Figure 1.13**). Why the release of water from such cages is favorable will be considered shortly. The result is that nonpolar molecules show an increased tendency to associate with one another in water. This tendency is called the *hydrophobic effect*; the associated interactions are called *hydrophobic interactions*.

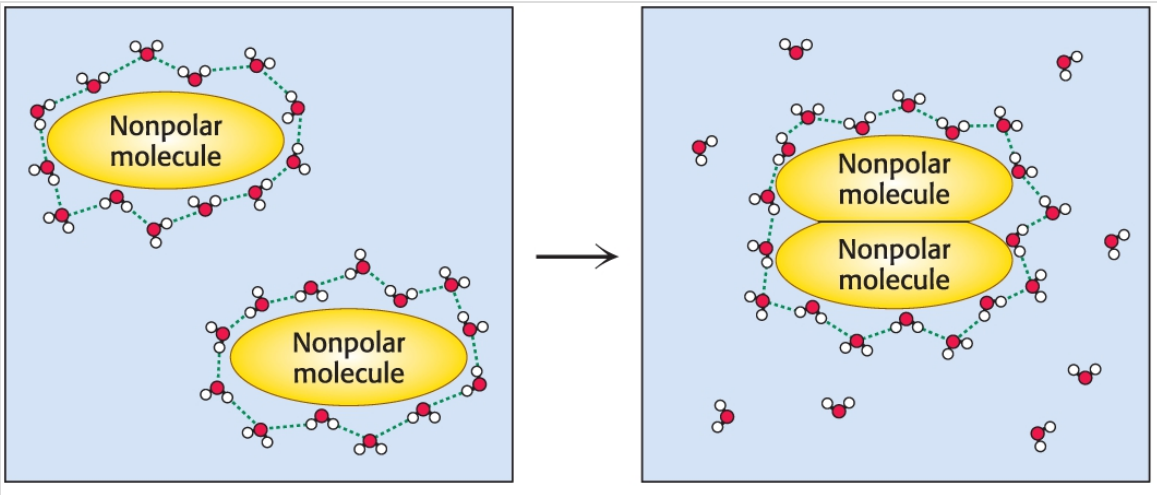


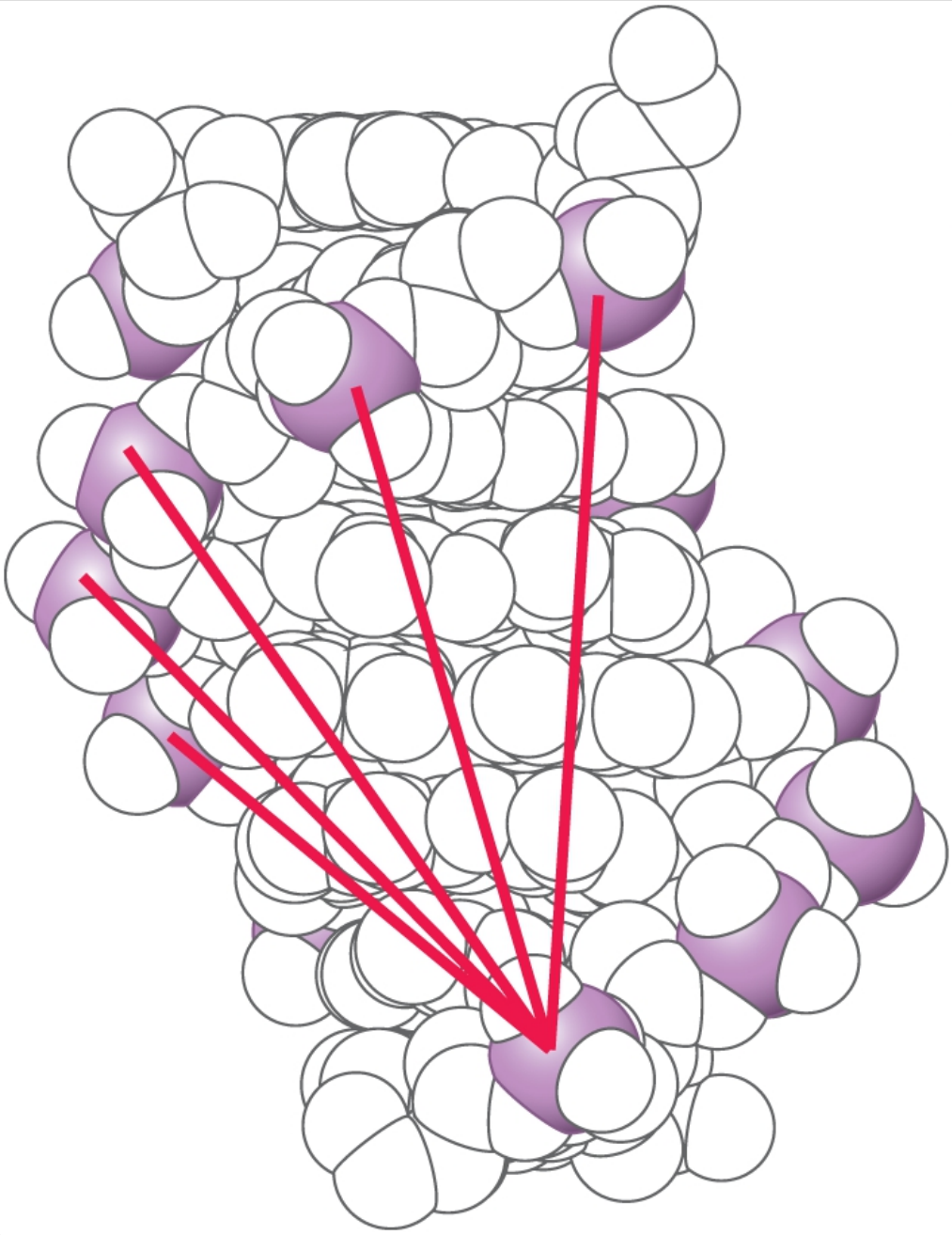
FIGURE 1.13 The hydrophobic effect is due to the behavior of water molecules. The aggregation of nonpolar groups in water leads to the release of water molecules, initially interacting with the nonpolar surface, into bulk water. The release of water molecules into solution makes the aggregation of nonpolar groups favorable.



The formation of DNA's double helix is an expression of the rules of chemistry

Let us now explore how these noncovalent interactions work together to drive the association of two strands of DNA to form a double helix.

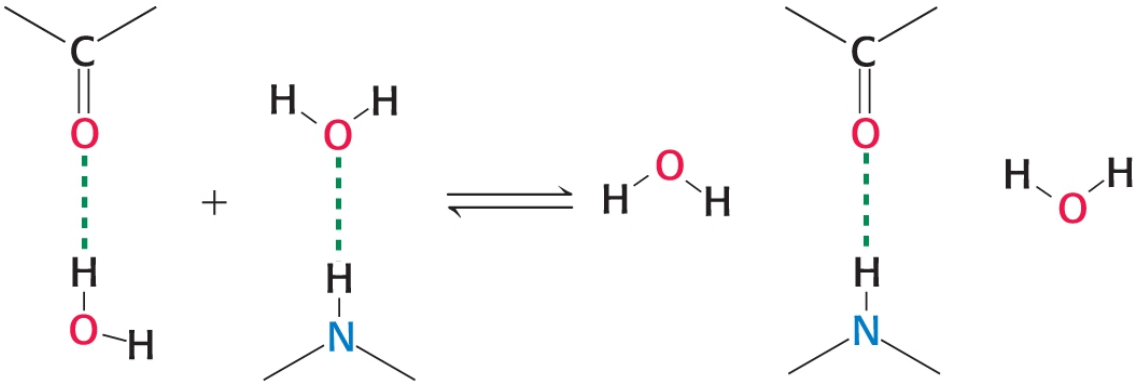
- *The aqueous environment surrounding DNA favors helix formation, overcoming the ionic repulsion between charged phosphate groups.* Each phosphate group in a DNA strand carries a negative charge and thus interacts unfavorably with other phosphate groups over distances. Even though the phosphate groups are far apart in the double helix, with distances greater than $10\ \text{Å}$, many such interactions take place (**Figure 1.14**). Thus, ionic interactions oppose the formation of the double helix. However, the strength of these repulsive ionic interactions is diminished by the high dielectric constant of water and the presence of ionic species such as Na^+ or Mg^{2+} ions in solution. These positively charged species interact with the phosphate groups and partly neutralize their negative charges.



© Macmillan Learning

FIGURE 1.14 Ionic interactions among phosphate groups oppose the formation of the DNA double helix. Each unit within the double helix includes a phosphate group (the phosphorus atom shown in purple) that bears a negative charge. The unfavorable (repulsive) interactions of one phosphate with several others are shown by red lines.

- *Hydrogen bonds help ensure the specificity of base-pairing.* The second type of noncovalent interactions to consider in the formation of the double helix are hydrogen bonds. In single-stranded DNA, the hydrogen-bond donors and acceptors are exposed to solution and can form hydrogen bonds with water molecules. When two single strands come together, these hydrogen bonds with water are broken and new hydrogen bonds between the bases are formed.



Because the number of hydrogen bonds that are broken is the same or greater than the number that are formed, these new hydrogen bonds do not contribute substantially to driving the overall process of double-helix formation. However, they do contribute greatly to the specificity of binding. Suppose two bases that cannot form Watson–Crick base pairs (adenine and cytosine, for example) are brought together. Hydrogen bonds with water must be broken as the bases come into contact, but because the bases are not complementary in structure, not all of the broken bonds can be simultaneously replaced by hydrogen bonds between the bases. Thus, the formation of a double helix between noncomplementary sequences is disfavored.

- *Within a double helix, van der Waals interactions encourage base stacking*. The base pairs are parallel and stacked nearly on top of one another, with a typical separation of $3.4\ \text{Å}$ between the planes of adjacent base pairs and approximately $3.6\ \text{Å}$ between the most closely approaching atoms. This separation distance corresponds nicely to the van der Waals contact distance (Figure 1.15). Bases tend to stack even in single-stranded DNA molecules. However, the base stacking and associated van der Waals interactions are nearly optimal in a double-helical structure.

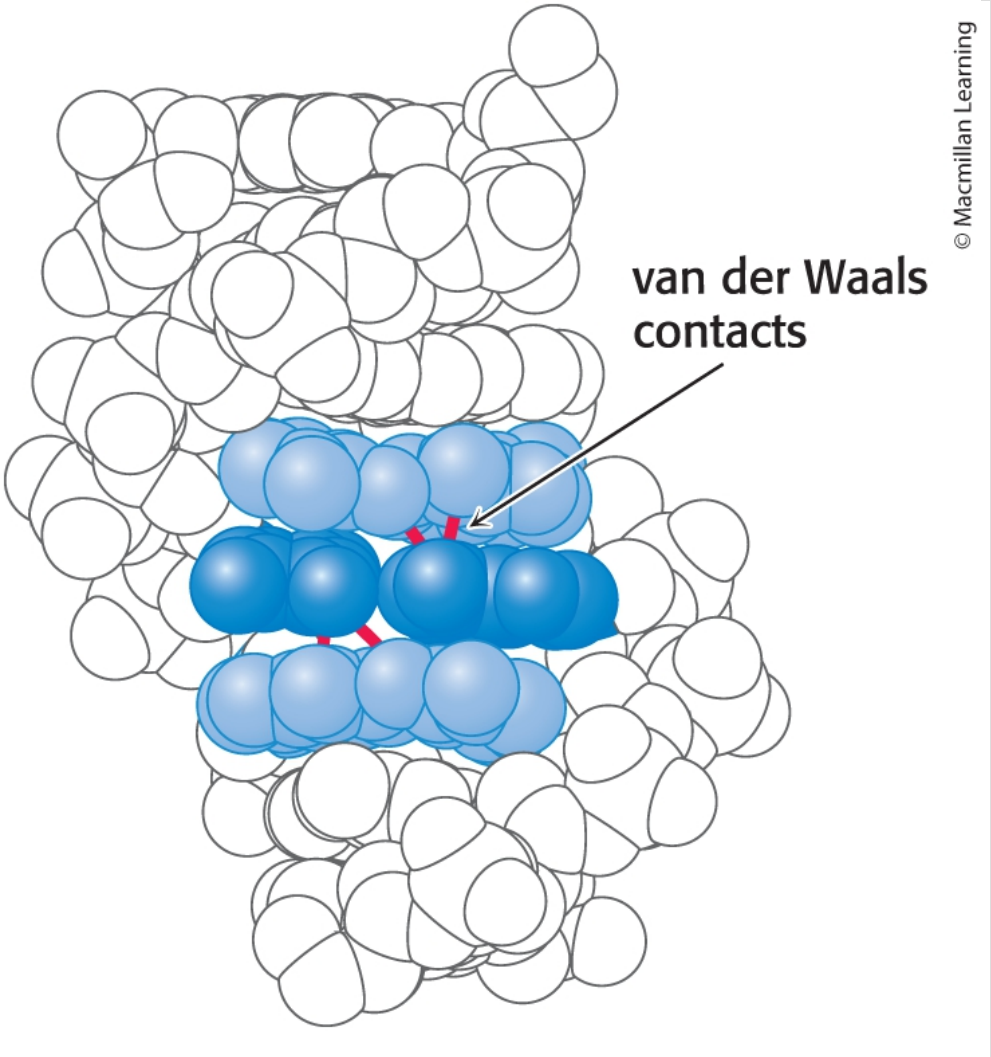


FIGURE 1.15 Optimal base stacking allows many weak, but favorable, van der Waals contacts that drive double-helix formation. In the DNA double

helix, adjacent base pairs are stacked nearly on top of one another, and so many atoms in each base pair are separated by their van der Waals contact distance. The central base pair is shown in dark blue and the two adjacent base pairs in light blue. Several van der Waals contacts are shown in red.



- *The hydrophobic effect also contributes to the favorability of base stacking.* More-complete base stacking moves the nonpolar surfaces of the bases away from water molecules and into contact with each other.

The principles of double-helix formation between two strands of DNA apply to many other biochemical processes. Many weak interactions contribute to the overall energetics of the process, some favorably and some unfavorably. Furthermore, **surface complementarity** is a key feature: when complementary surfaces meet, hydrogen-bond donors align with hydrogen-bond acceptors, and nonpolar surfaces come together to maximize van der Waals interactions and minimize nonpolar surface area exposed to the aqueous environment. The properties of water play a major role in determining the importance of these interactions. Interactions between complementary surfaces play central roles in a great many biochemical processes, and we will encounter them repeatedly throughout the book.

The laws of thermodynamics govern the behavior of biochemical systems

We can look at the formation of the double helix from a different perspective by examining the laws of thermodynamics, general principles that apply to all physical (and biological) processes. The laws distinguish between a system and its surroundings; a *system* refers to the

matter and energy within a defined region of space, and the matter and energy in the rest of the universe is called the *surroundings.*

The laws of thermodynamics are of great importance because they determine the conditions under which specific processes can or cannot take place. We will consider these laws from a general perspective first and then apply the principles that we have developed to the formation of the double helix.

- *The First Law of Thermodynamics states that the total energy of a system and its surroundings is constant.* In other words, the energy content of the universe is constant; energy can be neither created nor destroyed. Energy can take different forms, however. Heat, for example, is one form of energy. Heat is a manifestation of the *kinetic energy* associated with the random motion of molecules. Alternatively, energy can be present as *potential energy* — energy of position that will be released on the occurrence of some process. Consider, for example, a ball held at the top of a tower. In this position the ball has considerable gravitational potential energy because, when it is released, the ball will develop kinetic energy associated with its motion as it falls. Chemical potential energy is related to the plausible ways that atoms might react with one another. For instance, a mixture of gasoline and oxygen has a large potential energy because these molecules can react to form carbon dioxide and water and release energy as heat.

  Energy is always required to break chemical bonds and is released when new bonds form. The First Law requires that any energy released in the formation of chemical bonds must be used to break other bonds, released as heat or light, or stored in some other form.

- *The Second Law of Thermodynamics states that the total entropy of a system plus that of its surroundings always increases.* **Entropy** is a measure of the degree of randomness or disorder in a system. For example, the hydrophobic effect — the release of water from nonpolar surfaces — is favorable because water molecules that are

free in solution are more disordered than they are when they are associated with nonpolar surfaces.

At first glance, the Second Law appears to contradict much common experience, particularly about biological systems. Many biological processes, such as the generation of a leaf from carbon dioxide gas and other nutrients, clearly increase the level of order and hence decrease entropy. Entropy may be decreased locally in the formation of such ordered structures only if the entropy of other parts of the universe is increased by an equal or greater amount. The local decrease in entropy is usually accomplished by a release of heat, which increases the entropy of the surroundings.

We can analyze this process in quantitative terms. First, consider the system. The entropy (*S*) of the system may change in the course of a chemical reaction by an amount ΔS_{system}. If heat flows from the system to its surroundings, then the heat content, often referred to as the **enthalpy** (*H*), of the system will be reduced by an amount ΔH_{system}. To apply the Second Law, we must determine the change in entropy of the surroundings. If heat flows from the system to the surroundings, then the entropy of the surroundings will increase.

The precise change in the entropy of the surroundings depends on the temperature; the change in entropy is greater when heat is added to relatively cold surroundings than when heat is added to surroundings at high temperatures; these surroundings are already in a high degree of disorder. To be even more specific, the change in the entropy of the surroundings will be proportional to the amount of heat transferred from the system and inversely proportional to the temperature (*T*) of the surroundings. In biological systems, *T*, absolute temperature in kelvins (K), is usually assumed to be constant. Thus, a change in the entropy of the surroundings is given by

$$\Delta S_{surroundings} = -\Delta H_{system} / T$$

(1)

The total entropy change is given by the expression

$$\Delta S_{\text{total}} = \Delta S_{\text{system}} + \Delta S_{\text{surroundings}}$$

(2)

Substituting equation 1 into equation 2 yields

$$\Delta S_{\text{total}} = \Delta S_{\text{system}} - \Delta H_{\text{system}} / T$$

(3)

Multiplying by $-T$ gives

$$-T\Delta S_{\text{total}} = \Delta H_{\text{system}} - T\Delta S_{\text{system}}$$

The function $-T\Delta S$ has units of energy and is referred to as **free energy** or **Gibbs free energy**, after Josiah Willard Gibbs, who developed this function in 1878:

$$\Delta G = \Delta H_{\text{system}} - T\Delta S_{\text{system}}$$

The free-energy change, ΔG, will be used throughout this book to describe the energetics of biochemical reactions. The Gibbs free energy can also be considered the energy available to do useful work; it is essentially an accounting tool that keeps track of both the entropy of the system (directly) and the entropy of the surroundings (in the form of heat released from the system).

Recall that the Second Law of Thermodynamics states that, for a process to take place, the entropy of the universe must increase. Examination of equation 3 shows that the total entropy will increase if and only if

$$\Delta S_{\text{system}} > \Delta H_{\text{system}} / T$$

Rearranging gives $T\Delta S_{\text{system}} > \Delta H_{\text{system}}$ or, in other words, entropy will increase if and only if

$$\Delta G = \Delta H_{\text{system}} - T\Delta S_{\text{system}} < 0$$

Thus, the free-energy change must be negative for a process to take place spontaneously. There is negative free-energy change when and only when the overall entropy of the universe is increased.

Self-Check Question



The free energy can be calculated based on the system only. Why don't the surroundings need to be considered separately?

By releasing heat, the formation of the double helix obeys the Second Law of Thermodynamics

Let's see how the principles of thermodynamics apply to the formation of the double helix (**Figure 1.16**). Suppose solutions containing each of the two single strands are mixed. Before the double helix forms, each of the single strands is free to translate (change position) and rotate in solution, whereas each matched pair of strands in the double helix must move together. Additionally, the free single strands exist in more conformations than possible when bound together in a double helix. Thus, the formation of a double helix from two single strands appears to result in a decrease rather than an increase in disorder, and therefore entropy, of the system.

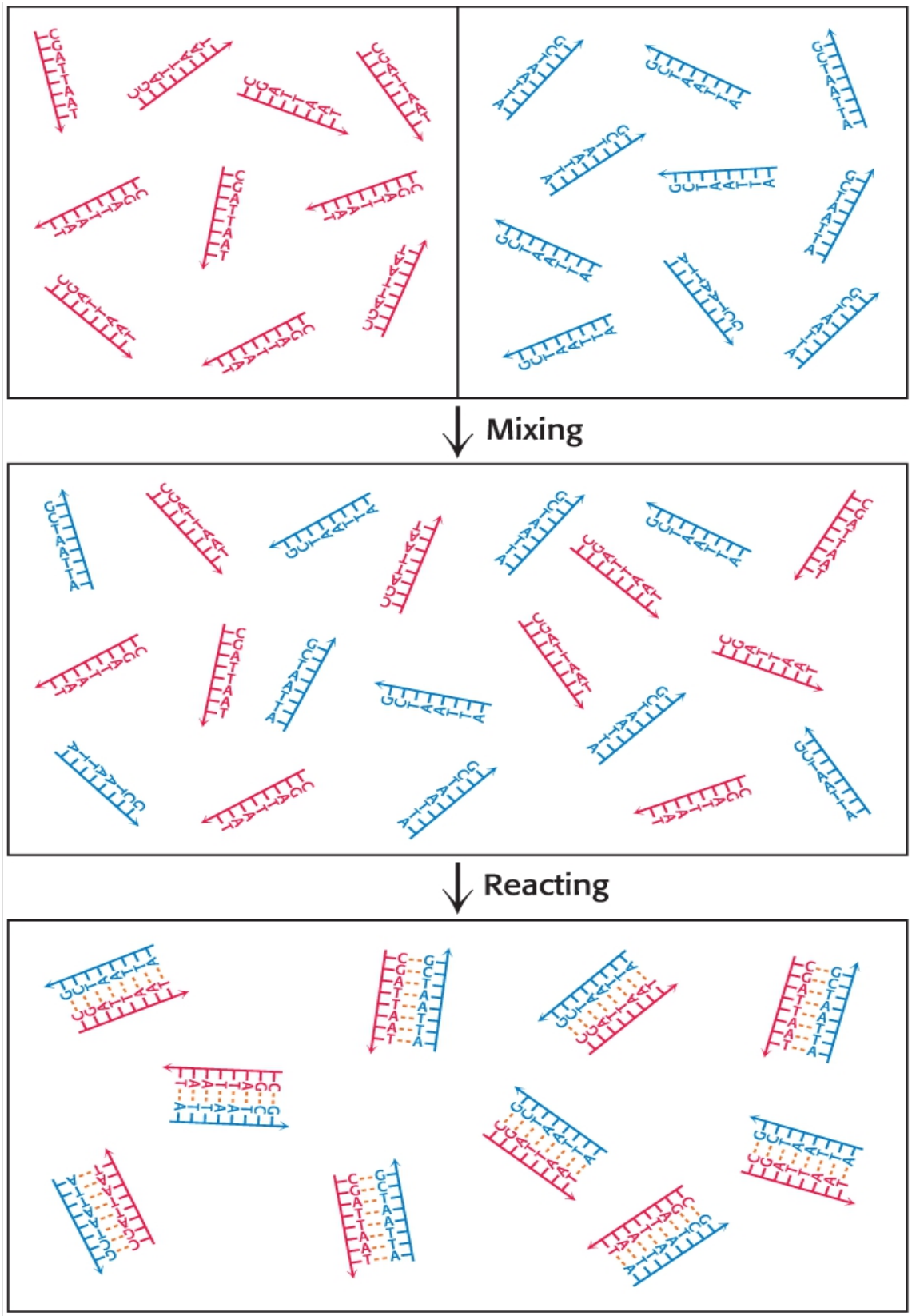

Mixing
Reacting

FIGURE 1.16 Double-helix formation entails a loss of entropy. When solutions containing DNA strands with complementary sequences are mixed, the strands react to form double helices. Th process results in a loss of entropy from the system, indicating that heat must be released to th surroundings to prevent a violation of the Second Law of Thermodynamics.



On the basis of this analysis, we expect that the double helix cannot form without violating the Second Law of Thermodynamics unless heat is released to increase the entropy of the surroundings. Experimentally, we can measure the heat released by allowing the solutions containing the two single strands to come together within a water bath, which here corresponds to the surroundings. We then determine how much heat must be absorbed by the water bath or released from it to maintain it at a constant temperature.

This experiment establishes that a substantial amount of heat is released — namely, approximately $250\ \text{kJ mol}^{-1}$ ($60\ \text{kcal mol}^{-1}$) — consistent with our expectation that significant heat would have to be released to the surroundings for the process not to violate the Second Law. We see in quantitative terms how order within a system can be increased by releasing sufficient heat to the surroundings to ensure that the entropy of the universe increases. We will encounter this general theme throughout this book.

Double-helix formation can be monitored one molecule at a time

One of the most exciting advances in biochemistry in recent years has been the development of methods to monitor some types of biochemical reactions one molecule at a time. To see why this is such an astounding achievement, recall that chemistry typically deals in terms

of fractions of moles, and that a mole contains Avogadro's number (6.0×10^{23}) of molecules, a truly astronomical number. Being able to observe single molecules requires technological improvements to provide adequate signal to noise, as well as clever conceptions of experiments that often utilize other discoveries in biochemistry. We will discuss examples of these so-called *single-molecule methods* in some detail several times in this book. For now, we will examine the results when single molecules are monitored during the formation of double helices from single-stranded DNA molecules.

New methods allow one single-stranded DNA molecule to be exposed very abruptly to a solution containing a normal laboratory concentration, typically on the order of $1\ \mu M\ (10^{-6}\ moles/liter)$ of the complementary single-stranded DNA. Once exposed to the solution, the potential double-helix formation process is allowed to occur for a fixed period of time on the millisecond ($10^{-3}\ s$) timescale. At the completion of this period, the result of the process can be probed, to see if the exposed single-stranded molecule found and bound a partner to form a double helix (**Figure 1.17**).

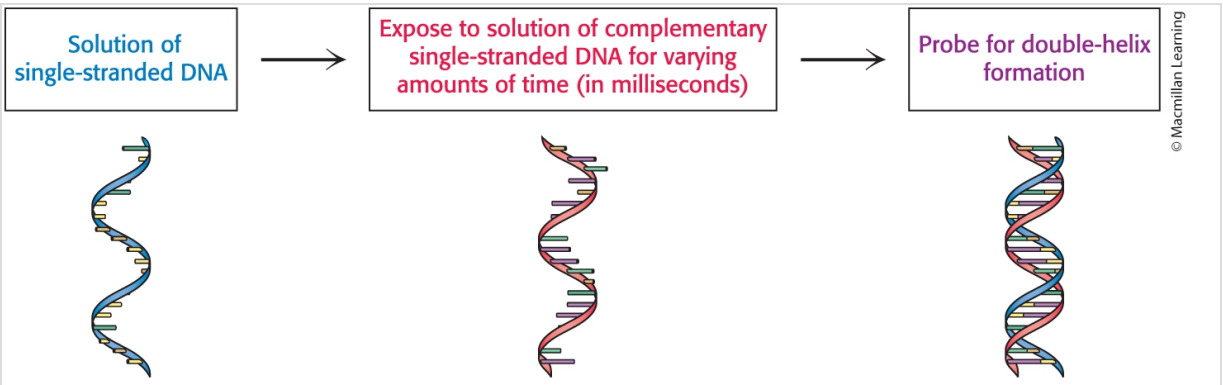


FIGURE 1.17 DNA double-helix formation can be probed at the single-molecule level. After one DNA single strand is exposed to a solution containing the complementary strand for a specific period of time, double-helix formation is probed. This experiment can be repeated many times with different individual DNA single strands.

Suppose that the first time we do the experiment, with an exposure time of 2.0 milliseconds, we observe that the double helix is formed. Perhaps surprisingly, however, when we repeat the identical experiment, no double helix is observed. We push on and repeat the experiment 800 times and observe that sometimes double-helix formation is observed, but usually it is not (Figure 1.18).

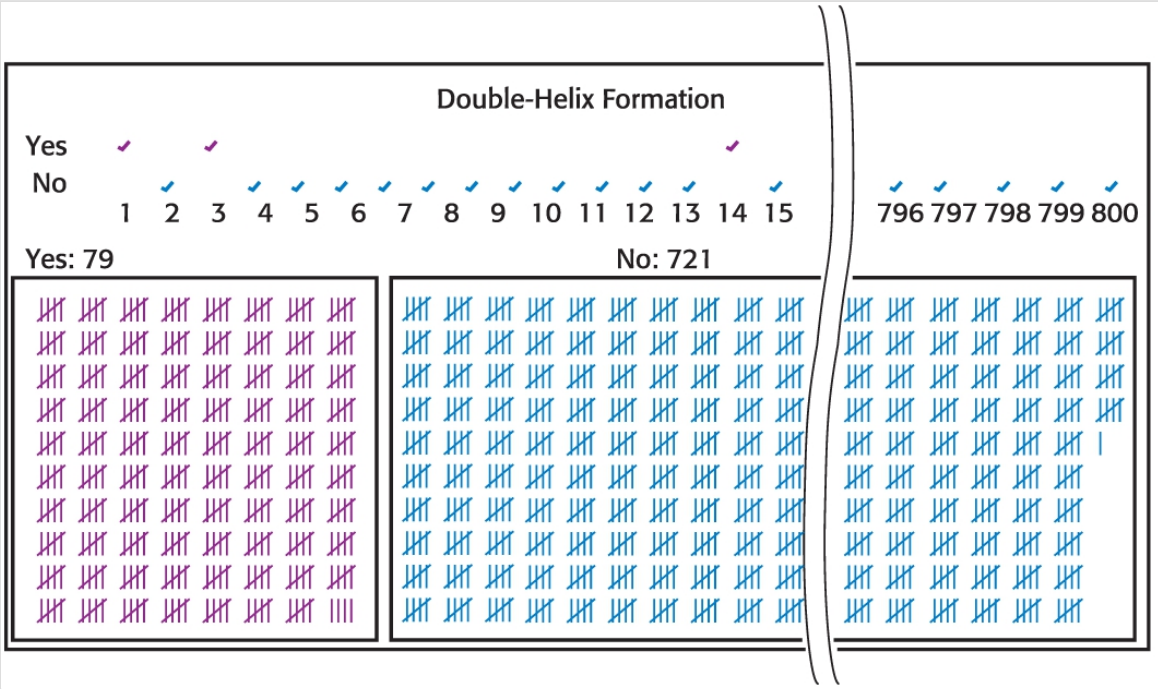


FIGURE 1.18 A tally sheet for repeating a single-molecule experiment shows the combined results of numerous individual trials. DNA double-helix formation was probed 800 times with a exposure time of 2.0 milliseconds, resulting in 79 times when a double helix was detected and 721 times where it was not.

Overall, the double-helix formation was observed in 9.9% (79/800) of the experiments. This value fluctuates somewhat as the number of experiments increases. For example, after 100 experimental runs were completed, 15 (or 15.0%) showed double-helix formation, whereas after 500 runs, 51 instances (or 10.2%) of double-helix formation were seen. A plot of the percentage showing double-helix formation as a function of the number of experimental runs reveals fluctuations prior to reaching a stable value (Figure 1.19).

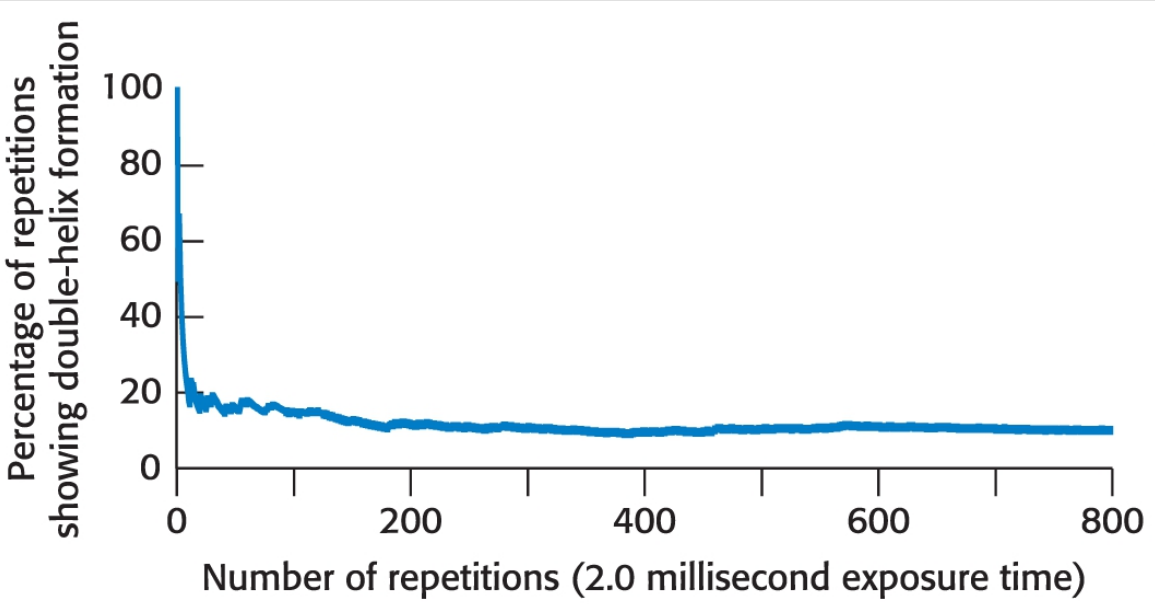


FIGURE 1.19 A plot of the running average of the number of experimental repetitions observing double-helix formation reveals eventual convergence on a stable value. For example, for the point at 500 repetitions, 51 had shown double-helix formation, for a percentag of $51/500 = 10.2\%$.

These results show that, at the single molecule level, the outcome of a particular attempt is not predictable — sometimes the double-helix forms, and sometimes it does not. Such processes are often referred to as **stochastic**. However, when averaged over hundreds of repetitions, the chance of double-helix formation converges to a well-defined

probability. Under most circumstances, we observe processes involving thousands, billions, or billions of billions of molecules, so that the variability at the single-molecule level is not apparent. However, it is best to keep in mind the reality of the variability at the level of single molecules; understanding this stochasticity is key to understanding some biochemical processes.

Acid–base reactions are central in many biochemical processes

Throughout our consideration of the formation of the double helix, we have dealt only with the noncovalent interactions that occur or are disrupted in this process. In addition, many biochemical processes entail the formation and cleavage of covalent bonds. A particularly important class of reactions prominent in biochemistry is **acid–base reactions**, in which hydrogen ions are added to molecules or removed from them. Throughout the book, we will encounter numerous processes in which the addition or removal of hydrogen ions is crucial.

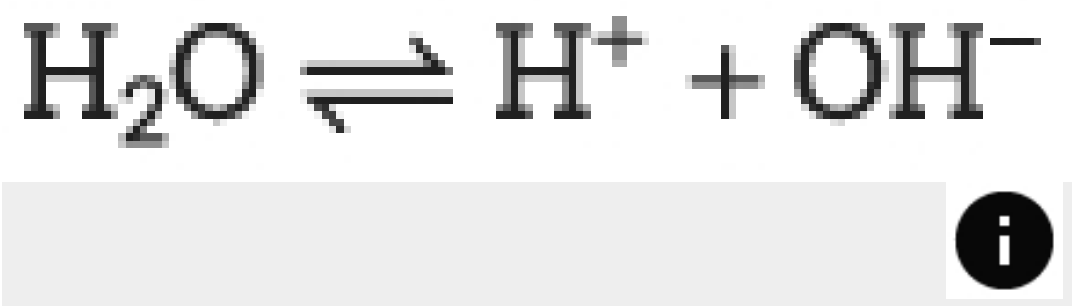
A hydrogen ion, often written as H^+, corresponds to a proton. In fact, hydrogen ions exist in solution bound to water molecules, thus forming what are known as *hydronium ions*, H_3O^+. For simplicity, we will continue to write H^+, but we should keep in mind that H^+ is shorthand for the actual species (H_3O^+) that is present.

The concentration of hydrogen ions in solution is expressed as the pH Specifically, the **pH** of a solution is defined as

$$pH = -\log[H^+]$$

where $[H^+]$ is in units of molarity (M). Thus, pH 7.0 refers to a solution for which $-\log[H^+] = 7.0$, and so $\log[H^+] = -7.0$ and $[H^+] = 10^{\log[H^+]} = 10^{-7.0} = 1.0 \times 10^{-7}$ M.

The pH also indirectly expresses the concentration of hydroxide ions, $[OH^-]$, in solution. To see how, we must realize that water molecules can dissociate to form H^+ and OH^- ions in an equilibrium process:



The equilibrium constant (K) for the dissociation of water is defined as

$$K = [H^+][OH^-]/[H_2O]$$

and has a value of $K = 1.8 \times 10^{-16}$. Note that an equilibrium constant does not formally have units. Nonetheless, the value of the equilibrium constant given assumes that particular units are used for concentration (sometimes referred to as standard states); in this case and in many others, units of molarity (M) are assumed.

The concentration of water, $[H_2O]$, in pure water is 55.5 M, and this concentration is constant under most conditions. Thus, we can define a new constant, K_W:

$$\begin{aligned} K_W &= K[H_2O] = [H^+][OH^-] \\ K[H_2O] &= 1.8 \times 10^{-16} \times 55.5 \\ &= 1.0 \times 10^{-14} \end{aligned}$$

Because $K_W = [H^+][OH^-] = 1.0 \times 10^{-14}$, we can calculate

$$[OH^-] = 10^{-14}/[H^+] \text{ and } [H^+] = 10^{-14}/[OH^+]$$

With these relationships in hand, we can easily calculate the concentration of hydroxide ions in an aqueous solution, given the pH. For example, at $pH = 7.0$, we know that $[H^+] = 10^{-7}\ M$ and so $[OH^-] = 10^{-14}/10^{-7} = 10^{-7}\ M$. In acidic solutions, the concentration of hydrogen ions is higher than 10^{-7} and, hence, the pH is below 7. For example, in $0.1\ M\ HCl$, $[H^+] = 10^{-1}\ M$ and so $pH = 1.0$ and $[OH^-] = 10^{-14}/10^{-1} = 10^{-13}\ M$.

Acid–base reactions can disrupt the double helix

The formation process that we have been considering between two strands of DNA to form a double helix takes place readily at pH 7.0. Suppose that we take the solution containing the double-helical DNA and treat it with a solution of concentrated base (i.e., with a high concentration of OH^-). As the base is added, we monitor the pH and

the fraction of DNA in double-helical form (Figure 1.20). When the first additions of base are made, the pH rises, but the concentration of the double-helical DNA does not change significantly. However, as the pH approaches 9, the DNA double helix begins to dissociate into its component single strands. As the pH continues to rise from 9 to 10, this dissociation becomes essentially complete.

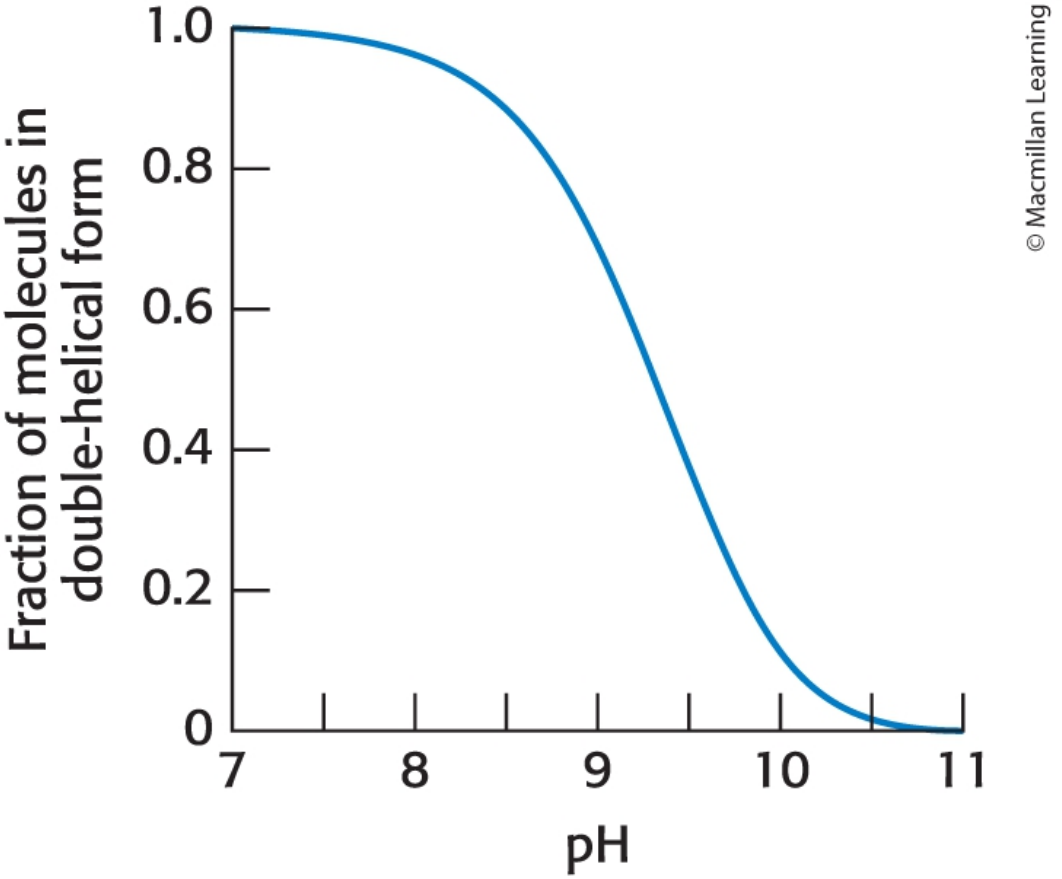
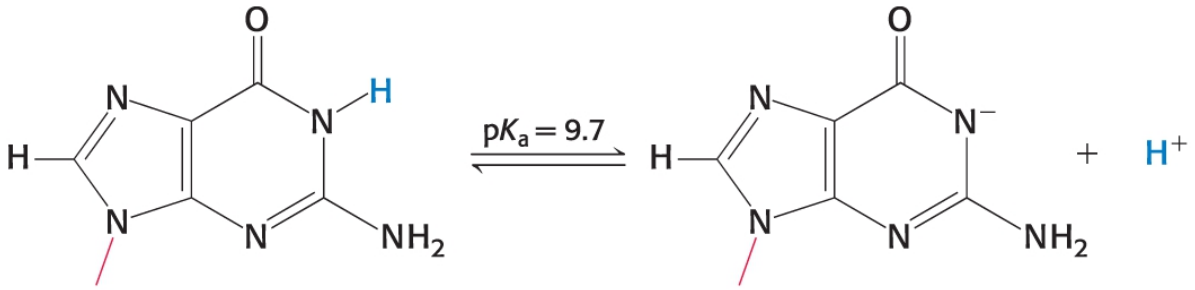


FIGURE 1.20 DNA strands are separated by the addition of a base. The addition of a base to a solution of double-helical DNA initially at pH 7 causes the double helix to separate into single strands. The process is half complete at slightly above pH 9.

Why do the two strands dissociate as pH increases? The hydroxide ions can react with nitrogenous bases in DNA base pairs to remove certain

protons. The most susceptible proton is the one bound to the N-1 nitrogen atom in a guanine base.



Guanine (G)

Proton dissociation for a substance HA (such as that bound to N-1 on guanine) has an equilibrium constant defined by the expression

$$K_a = [H^+][A^-]/[HA]$$

The susceptibility of a proton to removal by reaction with a base is often described by its **pK_a value**:

$$pK_a = -\log(K_a)$$

When the pH is equal to the pK_a, we have $pH = pK_a$

$$pH = pK_a$$

and so

$$-\log[H^+] = -\log([H^+][A^-]/[HA])$$

and

$$[H^+] = [H^+][A^-]/[HA]$$

Dividing by $[H^+]$ reveals that

$$1 = [A^-]/[HA]$$

and so

$$[A^-] = [HA]$$

So, when the pH equals the pK_a, the concentration of the deprotonated form of the group or molecule is equal to the concentration of the protonated form; the deprotonation process is halfway to completion. The pK_a for the proton on N-1 of guanine is typically 9.7. When the pH approaches this value, the proton on N-1 is lost (see Figure 1.20). Replacement of the partial positive change on the proton with a full negative charge substantially destabilizes the DNA double helix.

The DNA double helix is also destabilized by low pH. Below pH 5, some of the hydrogen-bond acceptors that participate in base-pairing become protonated. In their protonated forms, these bases can no longer form

these hydrogen bonds, and the double helix separates. So, acid–base reactions that either remove or donate protons at specific positions on the DNA bases can disrupt the double helix.

Buffers regulate pH in organisms and in the laboratory

These observations about DNA reveal that a significant change in pH can disrupt molecular structure. The same is true for many other biological macromolecules; changes in pH can protonate or deprotonate key groups, potentially disrupting structures and initiating harmful reactions. Thus, biological systems have evolved to mitigate changes in pH.

Solutions that resist changes in pH are called **buffers**. Specifically, when acid is added to an unbuffered aqueous solution, the pH drops in proportion to the amount of acid added. In contrast, when acid is added to a buffered solution, the pH drops more gradually. Buffers also mitigate the pH increase caused by the addition of base and changes in pH caused by dilution.

Compare the result (shown in **Figure 1.21**) of adding a 1 M solution of the strong acid HCl drop by drop to (1) pure water, versus (2) adding it to a solution containing 100 mM of the buffer sodium acetate ($Na^+CH_3COO^-$). The process of gradually adding known amounts of reagent to a solution with which the reagent reacts while monitoring the results is called a **titration**. For pure water, the pH drops from 7 to close to 2 on the addition of the first few drops of acid. However, for the sodium acetate solution, the pH first falls rapidly from its initial value near 10, then changes more gradually until the pH reaches 3.5, and then falls more rapidly again.

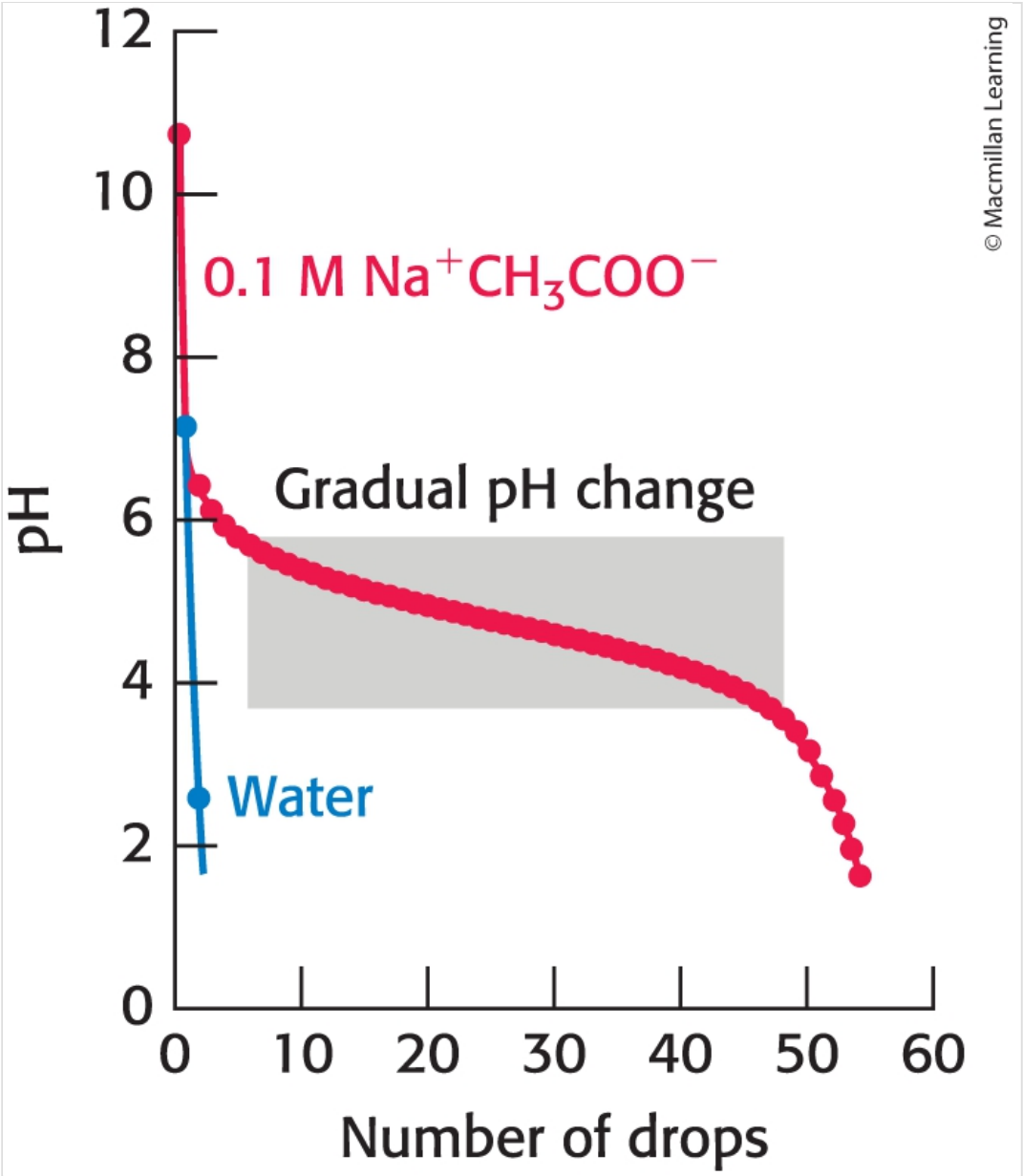


FIGURE 1.21 Buffers resist changes in pH over a narrow pH range. The addition of a strong acid, 1 M HCl, to pure water results in an immediate drop in pH to near 2. In contrast, the addition of the acid to a 0.1 M sodium acetate $(Na^+CH_3COO^-)$ solution results in a much more gradual change in pH until the pH drops below 3.5.

Why does the pH decrease so gradually in the middle of the titration? The answer is that when hydrogen ions are added to this solution, they react with acetate ions to form acetic acid. This reaction consumes some of the added hydrogen ions so that the pH does not drop. Hydrogen ions continue reacting with acetate ions until essentially all the acetate ion is converted into acetic acid. After this point, added protons remain free in solution and the pH begins to fall sharply again.

We can analyze the effect of the buffer in quantitative terms. The equilibrium constant for the deprotonation of an acid is

$$K_a = [H^+][A^-]/[HA]$$

Taking logarithms of both sides yields

$$\log(K_a) = \log([H^+]) + \log([A^-]/[HA])$$

Recalling the definitions of pK_a and pH and rearranging gives

$$pH = pK_a + \log([A^-]/[HA])$$

This expression is referred to as the **Henderson–Hasselbalch equation**.

We can apply the equation to our titration of sodium acetate. The pK_a of acetic acid is 4.75. We can calculate the ratio of the concentration of acetate ion to the concentration of acetic acid as a function of pH by slightly rearranging the Henderson–Hasselbalch equation:

$$[\text{Acetate ion}]/[\text{Acetic acid}] = [A^-]/[HA] = 10^{pH - pK_a}$$

At pH 9, this ratio is $10^{9 - 4.75} = 10^{4.25} = 17{,}800$; very little acetic acid has been formed.

At pH 4.75 (when the pH equals the pK_a), the ratio is $10^{4.75 - 4.75} = 10^0 = 1$.

At pH 3, the ratio is $10^{3 - 4.75} = 10^{-1.25} = 0.02$; almost all the acetate ion has been converted into acetic acid.

We can follow the conversion of acetate ion into acetic acid over the entire titration (**Figure 1.22**). The graph shows that the region of relatively constant pH corresponds precisely to the region in which acetate ion is being protonated to form acetic acid.

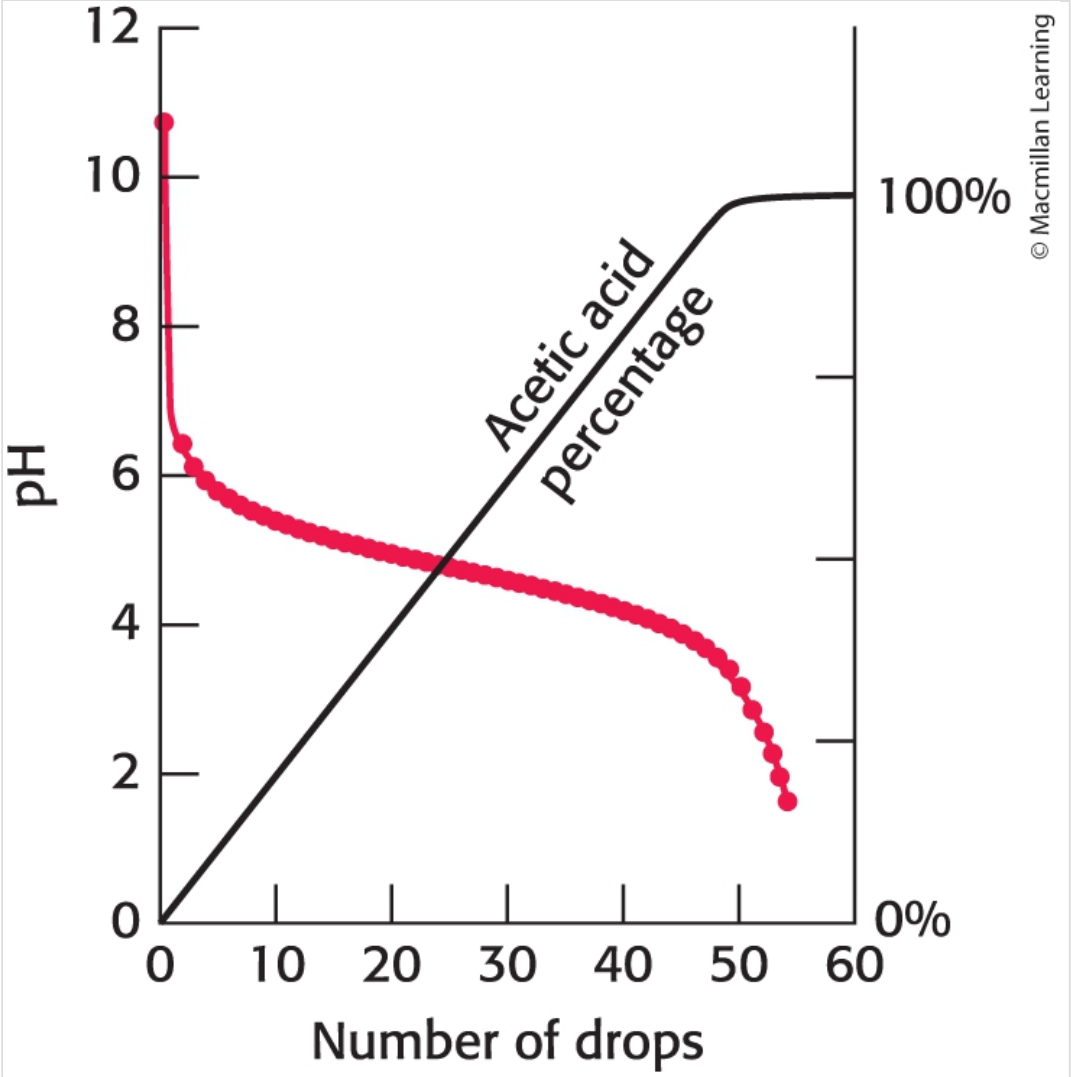
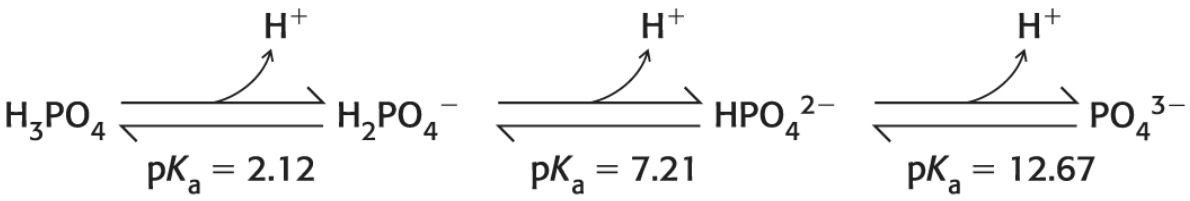


FIGURE 1.22 Added hydrogen ions protonate buffer components rather than remaining free. When acid is added to sodium acetate, the added hydrogen ions are used to convert acetate ion into acetic acid. Because the proton concentration does not increase significantly, the pH remains relatively constant until all the acetate has been converted into acetic acid.

From this discussion, we see that a buffer functions best close to the pK_a value of its acid component. Physiological pH is typically about 7.4.

An important buffer in biological systems is based on phosphoric acid (H_3PO_4). The acid can be deprotonated in three steps to form a phosphate ion.



At about pH 7.4, inorganic phosphate exists primarily as a nearly equal mixture of $H_2PO_4^-$ and HPO_4^{2-}. Thus, phosphate solutions function as effective buffers near $pH 7.4$. The concentration of inorganic phosphate in blood is typically approximately 1 mM, providing a useful buffer against processes that produce either acid or base.

Self-Check Question



Butyric acid ($CH_3CH_2CH_2COOH$) has a pK_a of 4.82. What is the ratio of butyrate ($CH_3CH_2CH_2COO^-$) to butyric acid at pH 6.0?

Example

Applying the Henderson—Hasselbalch Equation

Problem:

You need to prepare 2 liters of 0.100 M acetate buffer, pH 5.00 for acetic acid, sodium acetate, and water. How much acetic acid and sodium acetate do you use?

Getting Started:

The Henderson–Hasselbalch equation relates the pH to the ratio of ionized and unionized buffer components

$$pH = pK_a + \log([A^-]/[HA])$$

where $[A^-]$ is the concentration of acetate ion and [HA] is the concentration of acetic acid. We know that the pK_a of acetic acid is 4.75 and the buffer is supposed to have a pH of 5.00 with a total concentration of acetate-containing species of 0.100 M; that is, $[CH_3COO^-] + [CH_3COOH] = 0.100\ M$.

Solve:

Substituting into the Henderson–Hasselbalch equation, we find that

$$5.00 = 4.75 + \log([CH_3COO^-]/[CH_3COOH])$$

Solving for the ratio of species, we find that

$$\log([CH_3COO^-]/[CH_3COOH]) = 5.00 - 4.75 = 0.25$$

so that $[CH_3COO^-]/[CH_3COOH] = 10^{0.25} = 1.78$.

Thus, $[CH_3COO^-] = 1.78[CH_3COOH]$.

We can then substitute this expression into the expression for the total concentration of acetate-containing species,
$[CH_3COO^-] + [CH_3COOH] = 0.100\ M$

That is, $1.78[CH_3COOH] + [CH_3COOH] = 0.100\ M$

so that $(1.78 + 1.00)[CH_3COOH] = 2.78[CH_3COOH] = 0.100\ M$.

Thus, $[CH_3COOH] = (1/2.78)(0.100\ M) = 0.036\ M$ and
$[CH_3COO^-] = 1.78(0.036\ M) = 0.064\ M$.

We need to make 2 liters of buffer, so we need
$(2\ liters)(0.036\ M) = 0.072$ moles of acetic acid and
$(2\ liters)(0.064\ M) = 0.128$ moles of acetate ion, provided as sodium acetate.

The molecular weights of acetic acid and sodium acetate are
$60.052\ g/mol$ and $82.034\ g/mol$, respectively.

Thus, we need $(0.072\ moles)(60.052\ g/mol) = 4.32\ g$ of acetic acid

and $(0.128\ \text{moles})(82.034\ \text{g/mol}) = 10.50\ \text{g}$ of sodium acetate.

After weighing out these materials, we add water to make a total volume of 2 liters.

Reflect:

You can confirm the result by calculating the pH using the Henderson–Hasselbalch equation with the concentrations of acetic acid and acetate ion that you added.

1.4 DNA Sequencing Is Transforming Biochemistry, Medicine, and Other Fields

The discovery of the structure of DNA suggested the hypothesis that hereditary information is stored as a sequence of nitrogenous bases along long strands of DNA. This remarkable insight provided an entirely new way of thinking about biology. However, for years this hypothesis remained unconfirmed, and many features needed to be elucidated. How is the sequence information read and translated into action? What are the sequences of naturally occurring DNA molecules, and how can such sequences be experimentally determined?

Through advances in biochemistry and related sciences, we now have essentially complete answers to these questions. Indeed, in the past two decades, scientists have determined the complete genome sequences of thousands of different organisms, including simple microorganisms, plants, animals of varying degrees of complexity, and human beings. Comparisons of these genome sequences, with the use of methods discussed in Chapter 10, have provided many insights that have transformed biochemistry. In addition to its experimental and clinical aspects, biochemistry has now become an information science.

Genome sequencing has become remarkably fast and inexpensive

The sequencing of a human genome was a daunting task, because it contains approximately 3 billion (3×10^9) base pairs. We can look at a small section of the human genome to get a sense of its overall complexity. For example, the sequence

ACATTTGCTTCTGACACAACTGTGTTCACTAGCAACCTC
AAACAGACACCATGGTGCATCTGACTCCTGAGGAGAAGT
CTGCCGTTACTGCCCTGTGGGGCAAGGTGAACGTGGA...

is a part of one of the genes that encodes hemoglobin, the oxygen carrier in our blood, discussed in Chapter 3. This gene is found on the end of chromosome 9 of our 24 distinct chromosomes. If we were to include the complete sequence of our entire genome, this chapter would run to more than 500,000 pages. The sequencing of our genome is truly a landmark in human history. This sequence contains a vast amount of information, some of which we can now extract and interpret, but much of which we are only beginning to understand. For example, some human diseases have been linked to particular variations in genomic sequence. Sickle-cell anemia is caused by a single base change of an A (noted in boldface red type in the preceding sequence) to a T. In this course of this book, we will encounter many other examples of diseases that have been linked to specific DNA sequence changes.

Determining the first human genome sequences was a huge challenge. It required the efforts of large teams of geneticists, molecular biologists, biochemists, and computer scientists, as well as billions of dollars, because there was no previous framework for aligning the sequences of various DNA fragments: many methods had to be developed along the way. Fortunately, one human genome sequence can serve as a reference for others: the availability of reference sequences and modern techniques enables much more rapid characterization of partial or complete genomes from other individuals, as we will discuss in Chapter 9.

Methods for sequencing DNA have improved rapidly, resulting in dramatic increases in the sequencing rate and decreases in costs (**Figure 1.23**). The availability of such powerful sequencing technology is transforming many fields, including medicine, dentistry,

microbiology, pharmacology, and ecology, although a great deal remains to be done to improve the interpretation of these large data sets.

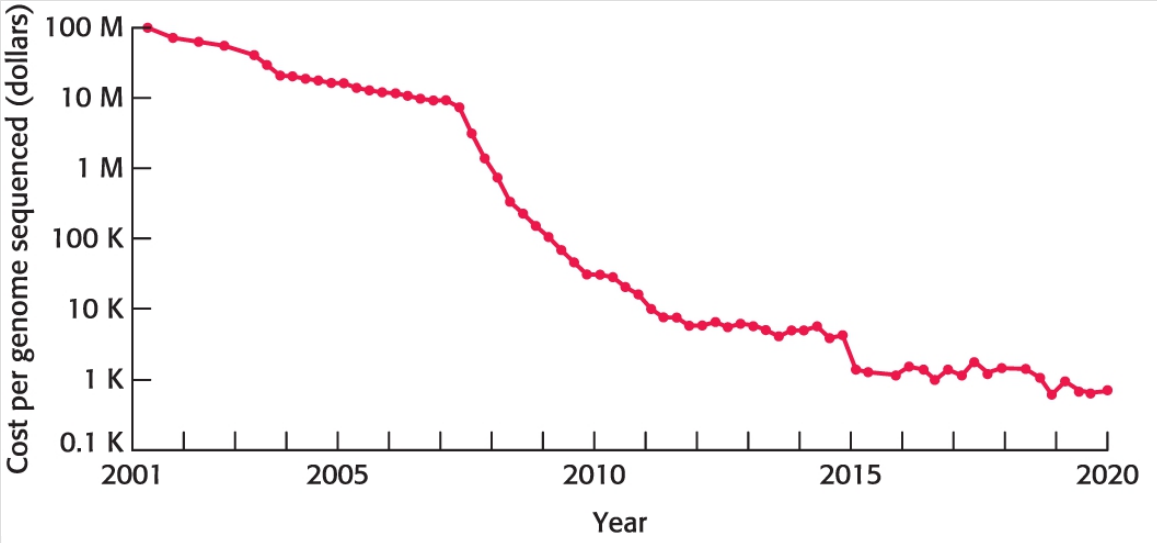


FIGURE 1.23 The cost to sequence a human genome has decreased dramatically over the pas two decades. Through the Human Genome Project, the costs of DNA sequencing dropped steadily due to new methods and are now under $1000 for a complete human genome sequenc

[National Human Genome Research Institute. https://www.genome.gov/about-genomics/fact-sheets/Sequencing-Human-Genome-cost]

Characterization of genetic variation between individuals is powerful for many applications

Each person has a unique sequence of DNA base pairs. How different are we from one another at the genomic level? Examination of the differences in our genomes reveals that, on average, each pair of individuals has a different base in one position per 200 bases; that is,

the difference is approximately 0.5%. This genomic variation between individuals who are not closely related is quite substantial compared with differences in populations. The average difference between two people within one population or ethnic group is greater than the difference between the averages of two different populations or ethnic groups (Figure 1.24).

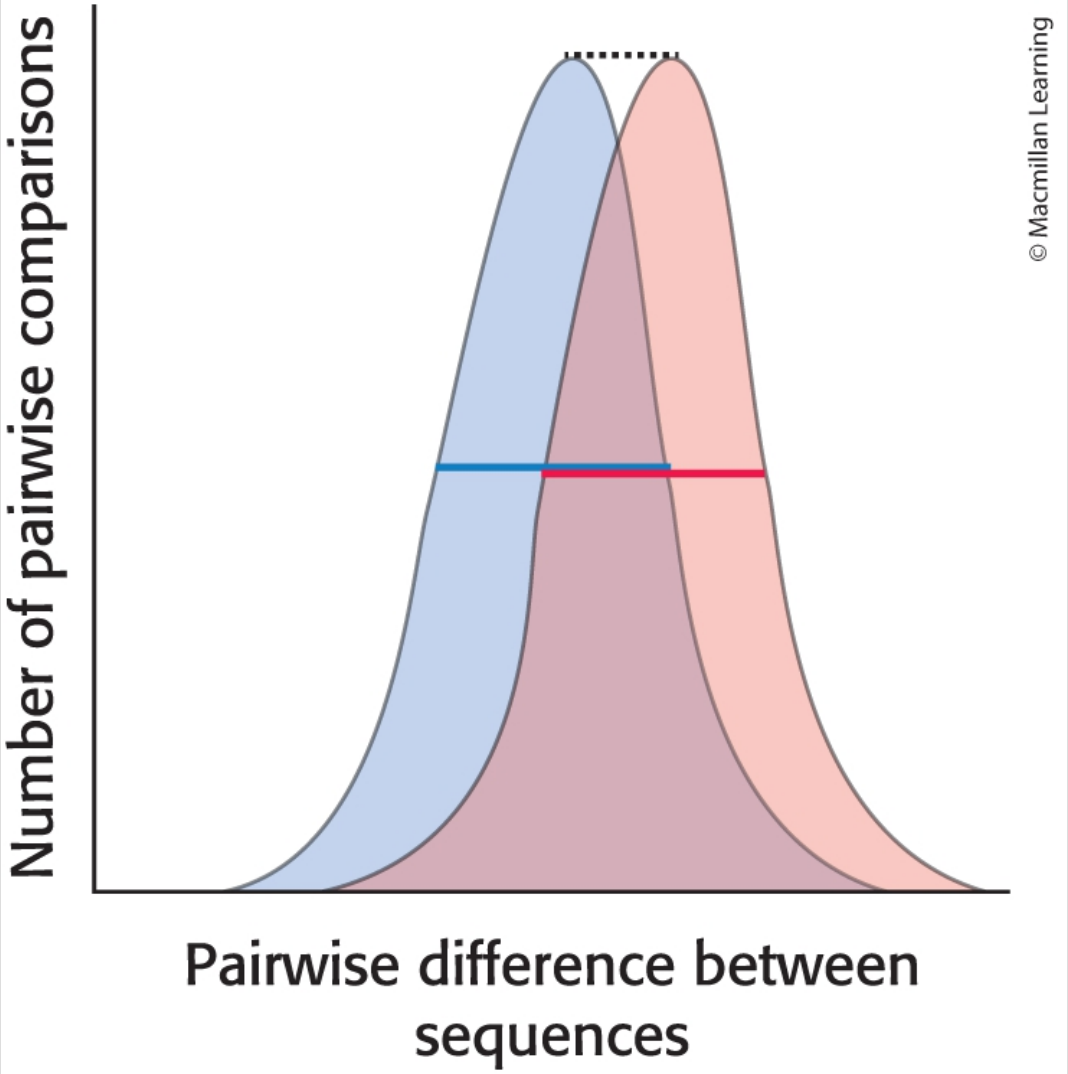


FIGURE 1.24 DNA sequences vary more within populations than they do between populations. The distribution of differences between pairs of individuals within two populations (from Europe and Sub-Saharan Africa) are shown in blue and red, respectively. The widths of these two distributions (shown by the blue and red lines) are larger than the average difference between the two populations (shown by the black dotted line).

[Adapted from Witherspoon *et al.* Genetic differences between and within human populations. *Genetics* **176,** 351–359 (2007).]

- *Providing insights into ancestry.* While average differences in DNA sequence between different human populations are relatively small, DNA analysis can be a powerful tool for providing information about ancestry. In a landmark study, DNA from more than 1300 individuals with known ancestry from different parts of Europe was analyzed. The study looked at more than 200,000 positions spanning the genome that were known to vary across populations and visualized the differences in two dimensions. Breathtakingly, this plot reflected a remarkably accurate map of Europe (**Figure 1.25**)! More recent studies of individuals from 50 ethnolinguistic groups across Africa have revealed greater genomic variation than is seen in European populations and have suggested migrations of groups of people across this continent that have occurred over the course of 2000 years.

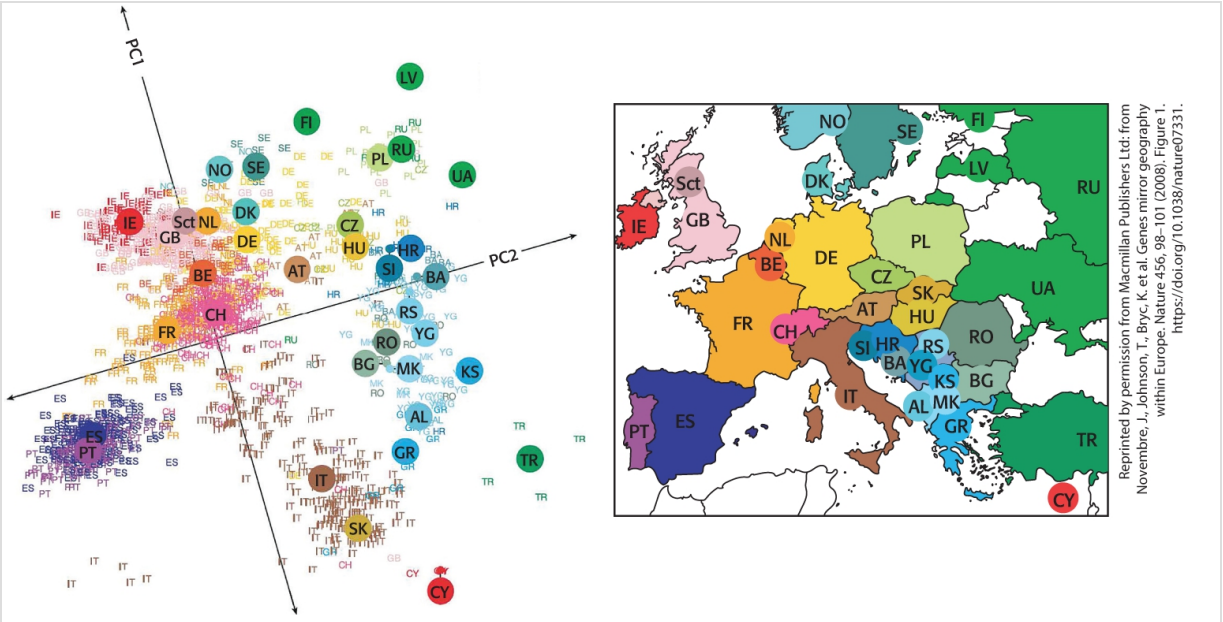


FIGURE 1.25 Genomic information can confirm locations of ancestry. Statistical analysis of the genomes of more than 1300 Europeans reproduced a map of Europe, providing a framework for inferring ancestry from genomic information.



- *Understanding the molecular basis of disease.* Scientists have identified the genetic variations associated with thousands of diseases, such as sickle-cell anemia, for which the cause can be traced to a single gene. For other diseases and traits, such as heart disease, we know that variation in many different genes contributes to disease in significant and often complex ways. Furthermore, in most cases, the presence of a particular variation or set of variations does not inevitably result in the onset of a disease but, instead, leads to a predisposition, or a heightened probability, for the development of the disease.

  The observation that genes alone do not determine disease outcomes is vividly illustrated through twin studies. Monozygotic (or "identical") twins share the same genome, whereas dizygotic (or "fraternal") twins share the same parents and typically develop in the same environment, but are not more genetically similar on average than any two siblings. By examining pairs of twins, scientists can begin to dissect the roles of genes versus environmental and other factors. For diseases like sickle-cell disease, monozygotic twins are always concordant; meaning, if one twin has the disease, so does the other. Most concordance rates, even for monozygotic twins, are well below 50%, indicating that environmental factors and chance are important in determining disease occurrence (**Table 1.1**). These often-modest levels of concordance reveal that environmental effects, and chance, can affect who gets any particular disease, revealing the complexity of biochemistry and biology that will be explored throughout the book.

- *Assessing the identity and role of our microbiome.* Our own genes are not the only ones that can contribute to our health and disease. Our bodies, including our skin, mouth, digestive tract, genitourinary

tract, respiratory tract, and other areas, contain a large number of microorganisms. These complex communities, collectively called the human **microbiome**, have been characterized through powerful methods that allow sequences from these biological samples to be examined without any previous knowledge of the organisms present.

Remarkably, we are outnumbered in our own bodies! Each of us contains more microbial cells than human cells, and these microbial cells collectively include many more genes than do our own genomes. These microbiomes differ between regions of the body, from one person to another, and in the same individual over time (**Figure 1.26**). They appear to play roles in health and in diseases such as obesity and dental caries.

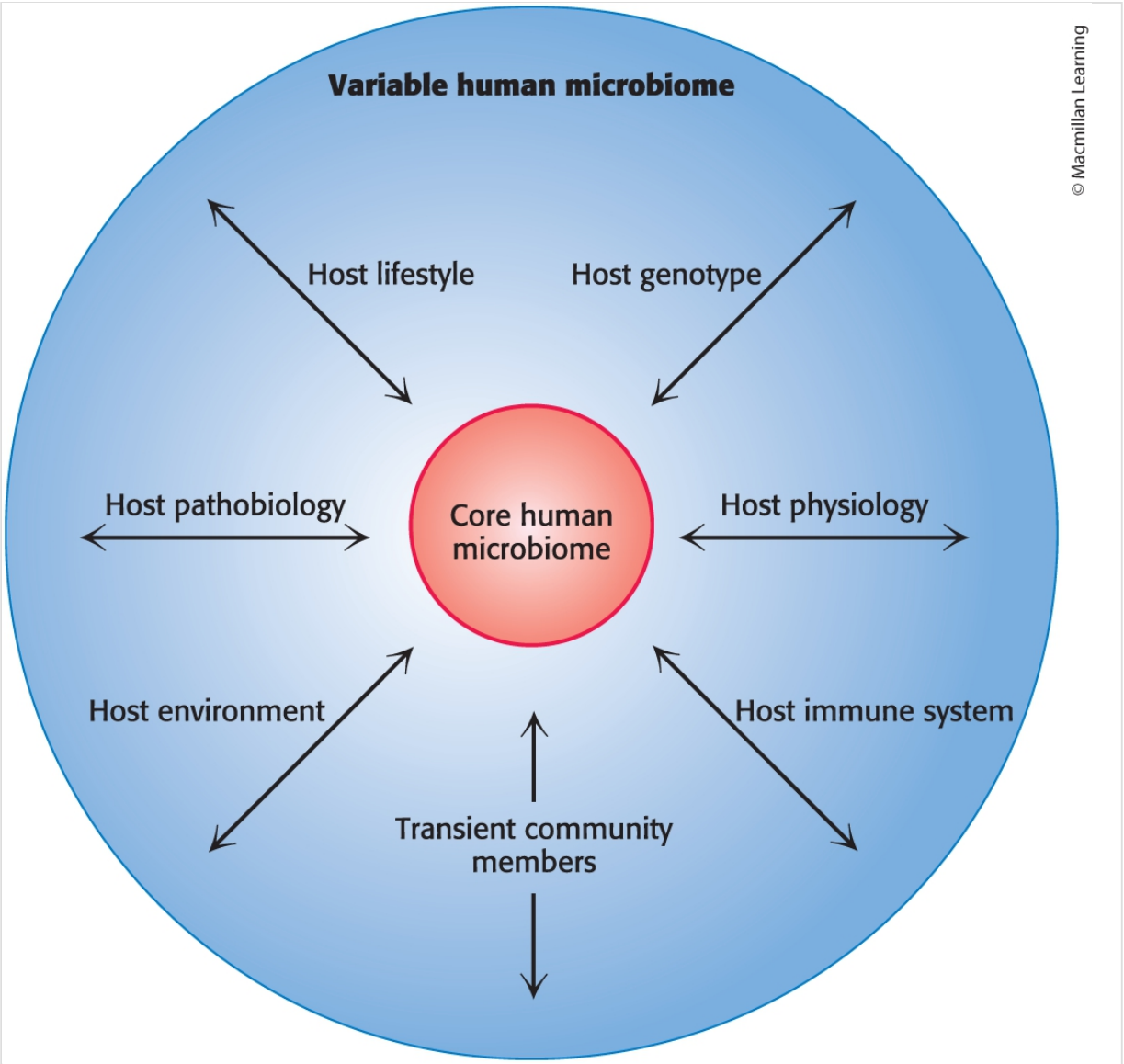


FIGURE 1.26 The human microbiome comprises many different bacterial and fungal species. The species composition varies greatly between individuals and within a given individual depending on a range of biological and environmental factors.

[From Turnbaugh, P., Ley, R., Hamady, M. *et al.* The human microbiome project. *Nature* **449,** 804–810 (2007). https://doi.org/10.1038/nature06244]

TABLE 1.1 Disease concordance rates in twins

	Monozygotic twins (%)	Dizygotic twins (%)
Diabetes (Type 1)	23	5
Diabetes (Type 2)	45	19
Breast cancer (Women)	17	11
Prostate cancer (Men)	33	15
Stroke	18	4
Amyotrophic lateral sclerosis	18	< 3
Alzheimer's disease	67	22

Note: Given one twin who has a disease, the percentage whose twin partner also has the disease is called the *concordance rate.*

The most important function of genomic sequences is to encode proteins

What kinds of information do DNA's base sequences store, and how is it expressed? The most fundamental role of DNA is to encode the sequences of proteins. Like DNA, proteins are linear polymers. However, proteins differ from DNA in two important ways. First, proteins are built from 20 building blocks, called **amino acids**, rather than just 4, as in DNA. The chemical complexity provided by this variety of building blocks enables proteins to perform a wide range of functions. Second, proteins spontaneously fold into elaborate three-dimensional structures, determined almost exclusively by their amino acid sequences (**Figure 1.27**). This enables the transition from a largely one-dimensional world of DNA sequences into a three-dimensional world of intricate, interacting objects with diverse properties that

characterize biochemistry. Proteins and protein folding will be discussed extensively in the next chapter. Interestingly, the human genome includes approximately 21,000 protein-coding genes, much smaller than earlier estimates of up to 100,000 or more.

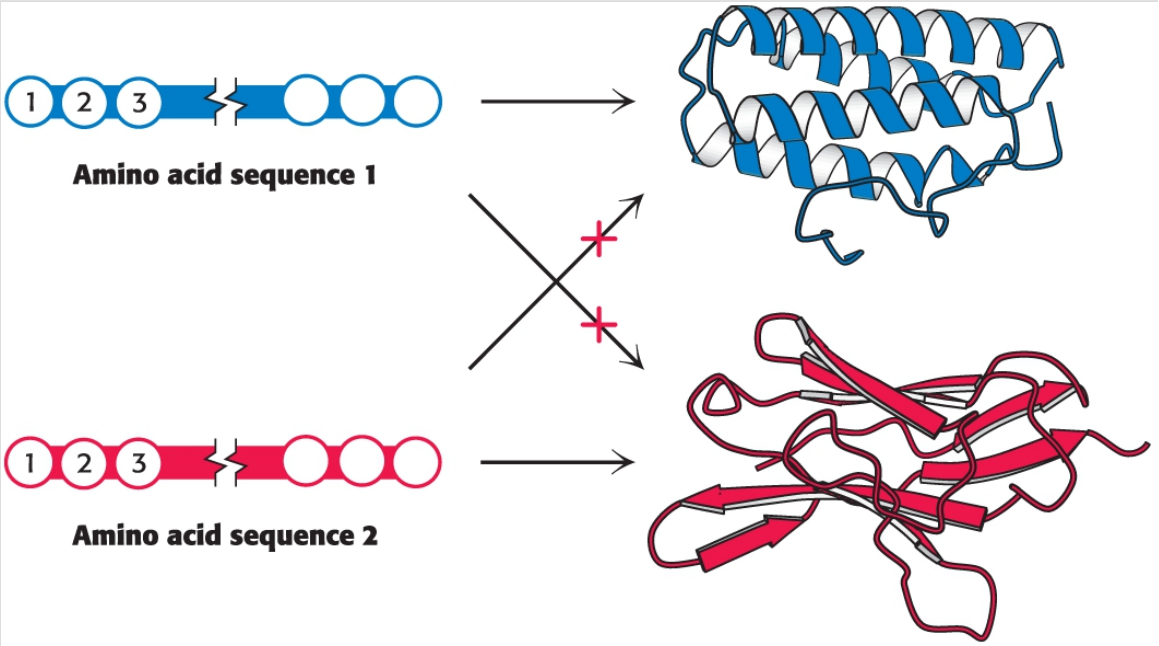


FIGURE 1.27 Protein folding is primarily dictated by the specific sequence of amino acids. Proteins are linear polymers of amino acids that fold into elaborate structures. The sequence of amino acids is the most important factor that determines the three-dimensional structure. Thus, amino acid sequence 1 gives rise only to a protein with the shape depicted in blue, not the shape depicted in red.

Comparing genomes offers great insights into evolution

Studies of comparative genomics, in which one organism's genome is compared with the genomes of other organisms, are confirming the tremendous unity that exists at the level of biochemistry. Comparative

genomics is also revealing key steps in the course of evolution. For example, many genes that are key to the function of the human brain and nervous system have evolutionary and functional relatives, even in the genomes of bacteria. Sequence comparisons can reveal a fascinating connection between biochemistry, evolution, and time.

The major mechanism for evolution involves the accumulation of small changes in DNA sequences. In rare cases, these changes (mutations) help the organism survive and reproduce under a particular set of conditions, leading to selection of organisms that carry these changes. More often, the changes are neutral, providing no advantage but causing no significant harm, and they accumulate because there is no reason or mechanism to remove them. Linus Pauling, a two-time Nobel Prize winner (for Chemistry and Peace) and his colleague followed this logic and suggested that the extent of sequence difference between the same protein from two organisms could be used as a measure of the time that had passed since these organisms had a common ancestor. This is called the **molecular clock hypothesis**.

To give one example of the sorts of conclusions we can reach from applying the molecular clock hypothesis, let us examine the number of sequence differences between one component of human hemoglobin and the same component from other species. The sequences of this hemoglobin subunit from human beings and our closest living relatives, chimpanzees, are identical, while those from human beings and a slightly more distant relative, gorillas, are 99.3% identical. In contrast, the sequences between human beings and chickens are only 70.4% identical. We can plot these differences and those from representatives from the classes of animals from Figure 1.2 versus the times for the emergence of these classes from the fossil record (**Figure 1.28**).

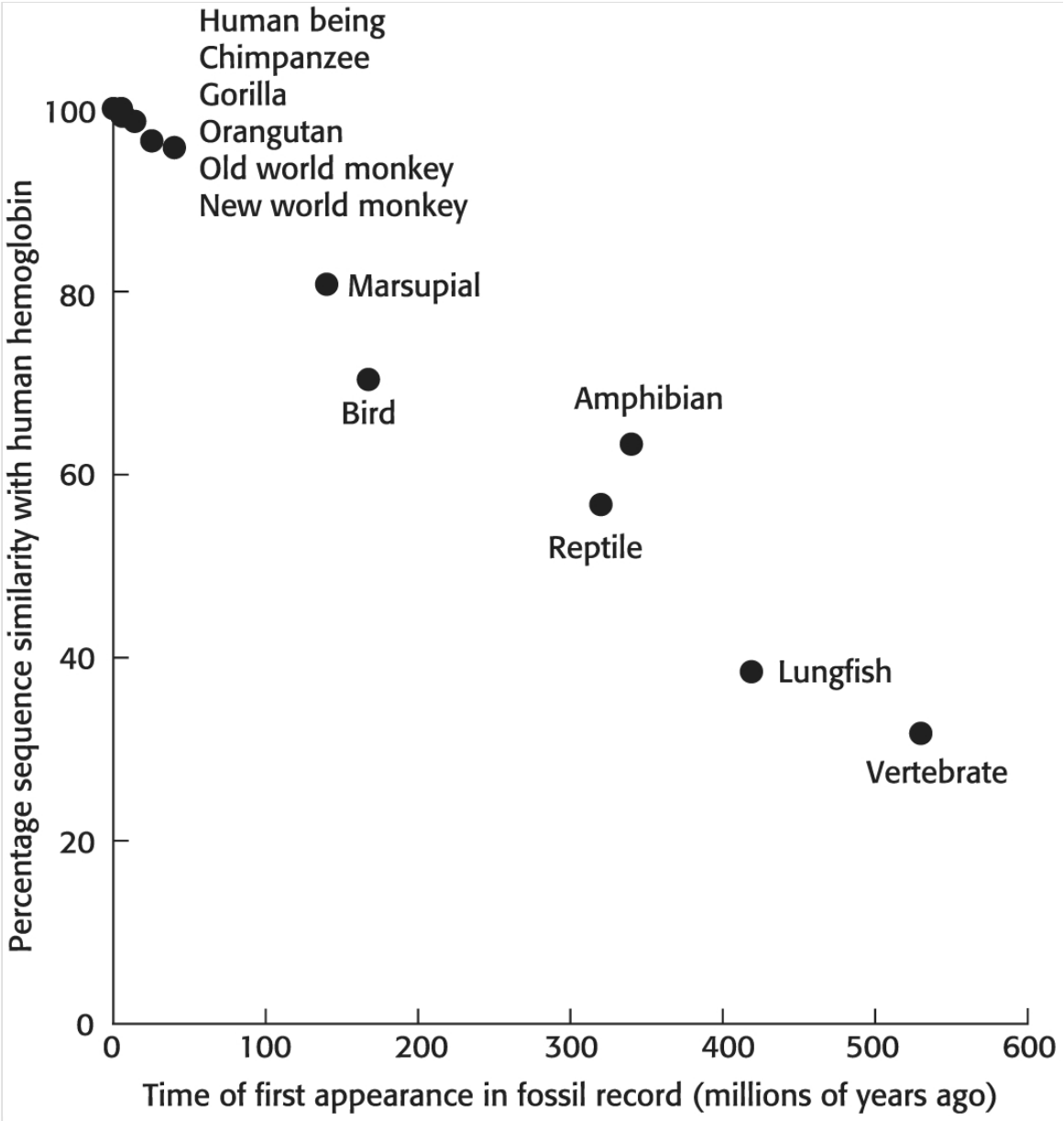


FIGURE 1.28 The similarities between hemoglobin sequences from different species provide evidence for a molecular clock. A comparison of the sequence identity between a component o the protein hemoglobin from human beings and those from representation of modern species from different classes of animals is shown. The nearly linear relationship between the sequence similarity and the time of emergence of the class of animals suggests that sequence similarity o this protein between two species can be used to measure evolutionary time since these species had a common ancestor.

Self-Check Question



The amino acid sequence of hemoglobin from an unknown species is found to be 83.5% identical to that from human beings. Could this be from a primate?

Different molecular clocks are also used for entities such as viruses that evolve very rapidly. In essence, a **virus** comprises a nucleic acid genome (DNA or the related molecule ribonucleic acid, abbreviated RNA) surrounded by a protein coat. Viruses are not alive in that they cannot grow or reproduce on their own, but instead infect specific cells and take advantage of the components of these cells to produce new virus particles by copying their genomes and synthesizing their protein coats and other components encoded by the viral genome. These virus particles then escape from these cells to go on and infect other cells. The sequence of a viral genome changes over time, even slightly every time the virus replicates.

Comparison of viral sequences allows the timing of key evolutionary events to be estimated. For example, both the virus that caused Severe Acute Respiratory Syndrome (SARS) in 2002–2004, termed SARS-CoV, and the virus that causes COVID-19, SARS-CoV-2, diverged over periods of a few years from viruses found in horseshoe bats. Sequence comparison also helps reveal the origins and spread of variant viruses across the human population.

Molecular clocks provide a framework that will be used throughout the book. Specifically, we can infer evolutionary relatedness from sequence comparison, with the simple rule of thumb that nearly identical sequences had a recent common evolutionary ancestor whereas more different versions of the same sequence have had more time to diverge.

1.5 Biochemistry Is an Interconnected Human Endeavor

Biochemical knowledge is generated through the research efforts of human beings, individually and in teams, at many different stages along a variety of career paths, some of which are outlined in **Figure 1.29**. To give some examples of the human journeys involved in establishing this knowledge, we will introduce you to a sampling of interconnected career paths and collegial partnerships.

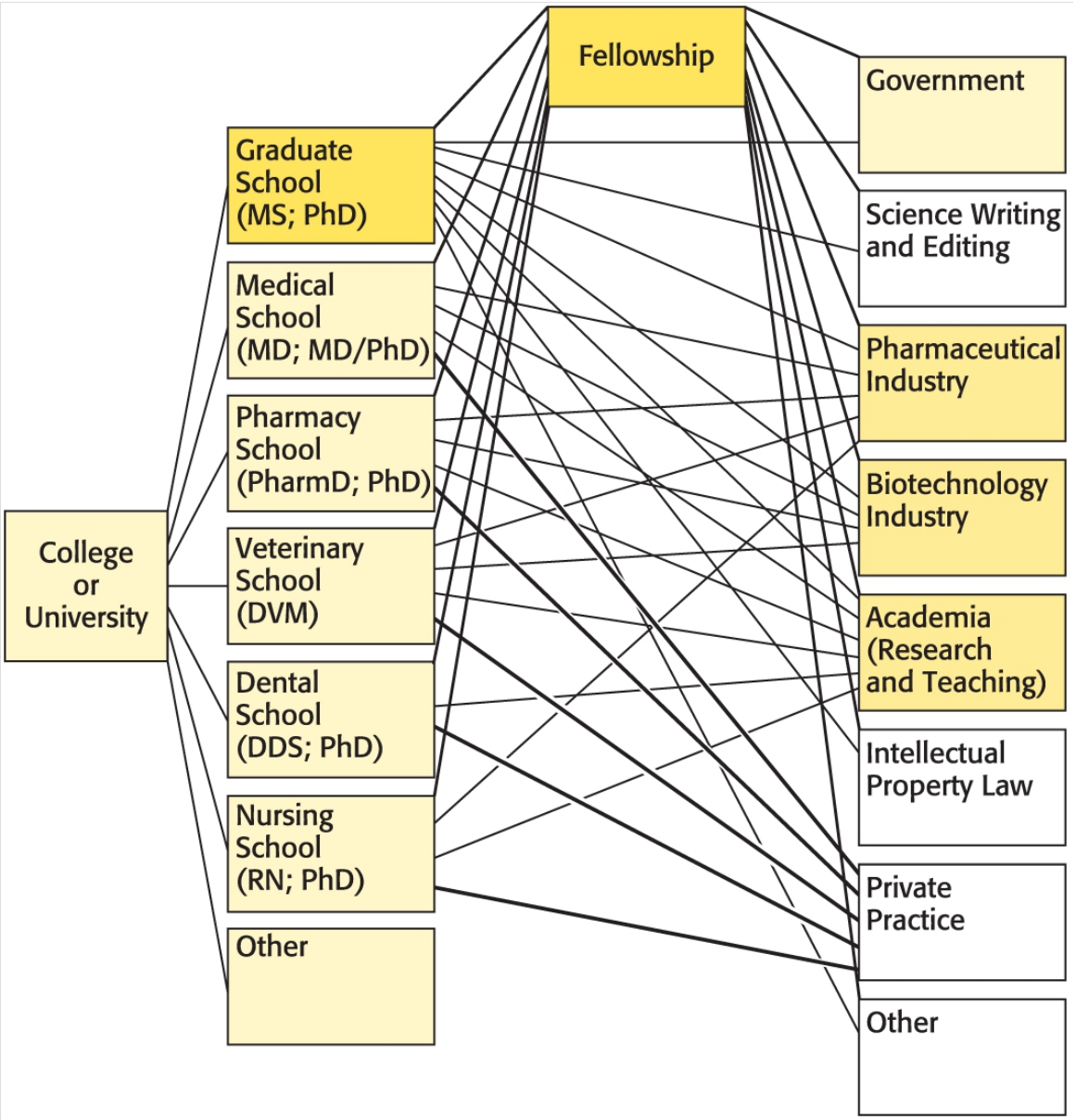


FIGURE 1.29 There are a variety of possible career paths for those involved in biochemical research. The intensity of the yellow shading corresponds to the intensity of the biochemical research activity in different positions and the lines highlight career paths that are commonly pursued.

This chapter opened with a photograph of Carol Greider, PhD, celebrating with Peter Agre, MD, on the occasion of her award of the

Nobel Prize in Medicine or Physiology in 2009 for research she started as a graduate student. Her discoveries, which were initially motivated by curiosity about fundamental biological process, have continued throughout her career, shedding light on both cancer and mechanisms of cellular aging. Her path to success was not always clear or easy, however. Although she was a strong student, she had struggled to get into college and graduate school because of relatively poor performance on standardized tests due to dyslexia.

Dr. Agre, shown with Dr. Greider in the photograph, had been awarded a Nobel Prize six years earlier. He was trained as a hematologist; his research was on Rh factor, a molecule important for blood compatibility for transfusions and in other contexts. In the course of this work, Dr. Agre and his coworkers discovered an abundant but uncharacterized component of red blood cells that turned out to be a long-hypothesized protein that allows red blood cells to take up and release water rapidly. For this discovery, Dr. Agre shared the Nobel in Chemistry, and he found this ironic, since he had temporarily withdrawn from high school because he received a “D” in chemistry.

One of the authors of this book, Jeremy Berg, PhD, was fortunate to have been colleagues with both Dr. Agre and Dr. Greider at Johns Hopkins University. Dr. Berg’s research experience began as an undergraduate in the laboratory of Lubert Stryer, MD. Based on this and other experiences, his interests focused on the roles of metal ions in biological systems. After completing a PhD in chemistry, his research changed directions as a postdoctoral fellow, focusing on the structures of proteins that bind DNA. He was able to combine these interests with the discovery that certain DNA- and RNA-binding proteins contained bound metal ions such as zinc. During his career in academia and in government, Dr. Berg worked with undergraduates, PhD and MD/PhD students, and postdoctoral fellows with a wide range of backgrounds, interests, and future career directions.

Science often involves friendly competitions between research teams working on the same problems. For Dr. Berg, one such team was led by Michael Summers, PhD, who also began in inorganic chemistry and expanded into the structures of biological molecules. Dr. Summers and his coworkers were the first to determine the three-dimensional structure of an RNA-binding protein from Human Immunodeficiency Virus (HIV) that contains zinc and is essential for this virus to incorporate its own genome into its protein coat. Summers is a co-leader of a nationally recognized program directed to providing substantial research experiences for undergraduate students. He and an ever-changing group of undergraduates, along with some PhD students, technicians, and postdoctoral fellows (**Figure 1.30**), have continued this research over many years, elucidating more details about how this protein performs its function and expanding into other areas of HIV research.

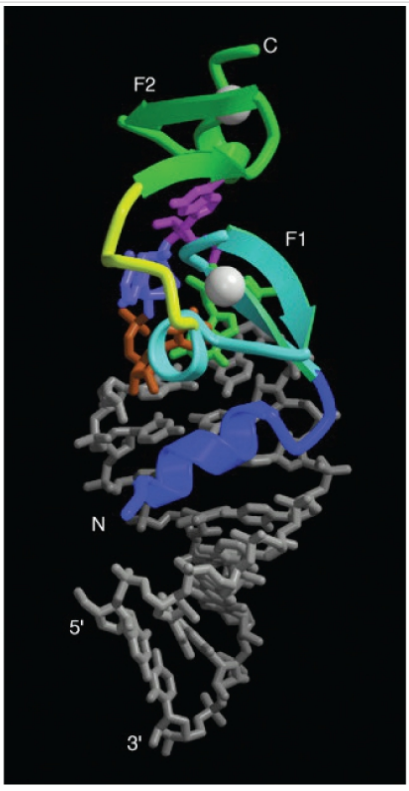


FIGURE 1.30 The research team of Professor Michael Summers at the University of Maryland, Baltimore County, is diverse in many dimensions. His team consists primarily of undergraduat

students, with some graduate students and postdoctoral fellows.

Among those who conducted research with Dr. Summers is Chelsea Pinnix, MD/PhD (Figure 1.31), who worked with Dr. Summers while she was an undergraduate student and contributed to the work that detailed the three-dimensional structure of the zinc-containing HIV protein bound to an RNA target. After graduating, she completed a combined MD/PhD program, earning her PhD in cell and molecular biology. She then completed additional medical training in radiation oncology and now uses her knowledge in all of these fields as a faculty member at an academic medical center.





(left) Courtesy of Dr. Chelsea Pinnix; (right) Republished with permission of American Association for the Advancement of Science, from Roberto N. De Guzman, Zheng Rong Wu, Chelsea C. Stalling, Lucia Pappalardo, Philip N. Borer, Michael F. Summers, "Structure of the HIV-1 Nucleocapsid Protein Bound to the SL3 Ψ-RNA Recognition Element." Science 16 Jan 1998: Vol. 279, Issue 5349, pp. 384–388, DOI: 10.1126/science.279.5349.384, Figure 4a. Permission conveyed through Copyright Clearance Center, Inc.

FIGURE 1.31 Chelsea Pinnix, MD/PhD, helped to determine the three-dimensional structure of an HIV zinc-containing protein bound to RNA.

Our knowledge of biochemistry is constantly expanding through the efforts of many individuals and teams working in universities and research institutes, and also in private industrial and government

laboratories. One of Dr. Berg's former students and coauthor of this book is Gregory Gatto, MD/PhD, who works on developing new drugs at a pharmaceutical company. Coauthor Justin Hines, PhD, began conducting research on protein structure and function as an undergraduate and now teaches and investigates protein misfolding with a research team made up solely of undergraduates. Coauthor Jutta Heller, PhD, studied protein structure in graduate school and now teaches molecular biology to undergraduates. Many students of biochemistry, however, pursue nonacademic careers, applying their biochemical knowledge to other aspects of human endeavor, such as medicine, intellectual property law, communication, and finance.

Biochemistry enriches many aspects of modern society. Throughout this book, we will continue to highlight individuals who have made important contributions to biochemistry while pursuing various career paths. We hope these profiles help you learn about some outstanding scientists and appreciate the varied paths available to students of biochemistry.

Chapter 1 Summary

1.1 Biochemical Unity Underlies Biological Diversity

- Many biochemical processes and pathways are quite similar even in organisms that appear quite different from one another.
- Organisms can be divided into three fundamental groups called domains.
- Eukarya (eukaryotes) includes all multicellular organisms, including all animals, plants, and human beings as well as some unicellular organisms, whereas Bacteria and Archaea represent two distinct groups of microscopic microorganisms (prokaryotes).

1.2 DNA Illustrates the Interplay Between Form and Function

- Each DNA strand consists of a phosphodiester backbone with four nitrogenous bases.
- Most DNA molecules consist of two strands that wind around a common axis to form a double helix with specific base pairs in the center.
- The double-helical structure of DNA can explain the role of DNA in storing hereditary information; the information is stored in the sequence of bases, and each strand can serve as a template for the synthesis of a new copy of the opposite strand.

1.3 Concepts from Chemistry Explain the Properties of Biological Molecules

- The DNA double helix serves as a useful example to illustrate how concepts from chemistry apply to essentially all other molecules in biochemistry.

- Most biochemical interactions take place on timescales from picoseconds to microseconds ($10^{-12}-10^{-6}$ s).
- Covalent bonds are strong bonds formed by the sharing of a pair of electrons between adjacent atoms.
- Noncovalent interactions are generally weaker than covalent bonds and include ionic interactions, hydrogen bonds, van der Waals interactions, and interactions associated with the hydrophobic effect.
- Most biochemical processes take place in water, which has a highly cohesive structure due to water molecules (H_2O) interacting with one another through hydrogen bonds.
- The hydrophobic effect refers to the tendency of nonpolar groups, those that lack the ability to participate in ionic interactions and hydrogen bonds, to come together, minimizing exposure to aqueous solution.
- A variety of methods have been developed to observe single molecules participating in different processes, revealing the underlying randomness of chemical processes.
- The laws of thermodynamics are general principles that apply to all physical and chemical processes: The First Law states that the total energy of a system and its surroundings is constant, and The Second Law states that the total entropy of a system plus that of its surroundings always increases.
- Acid–base reactions, which involve the addition or removal of hydrogen ions from molecules, are generally characterized by the equilibrium constant $K_a = [H^+][A^-]/[HA]$.
- Buffers are solutions that resist changes in pH due to the fact that they contain both a weak acid and the associated base.

1.4 DNA Sequencing Is Transforming Biochemistry, Medicine, and Other Fields

- DNA sequencing has become rapid and inexpensive and is transforming many fields, including biochemistry and medicine.
- On average, the genome sequences of two individual human beings differ by 0.5%; this difference is generally larger than the average difference between populations.
- While variations in genome sequences can be important in contributing to traits such as disease susceptibility, environmental factors and chance are also important.
- A major role of the genome sequence is to encode the amino acid sequences of proteins, the molecules that perform most of the functions within cells.
- Molecular clocks have been developed based on analyzing variations in DNA or protein sequences between different organisms to infer how long ago these organisms shared a common ancestor.

1.5 Biochemistry Is an Interconnected Human Endeavor

- Knowledge of biochemistry advances through the efforts of scientists generally working together in small teams.
- A wide variety of career paths is accessible to individuals who study biochemistry.

Key Terms

cell
biological macromolecule
metabolite
deoxyribonucleic acid (DNA)
protein
common ancestor
Eukarya (eukaryotes)

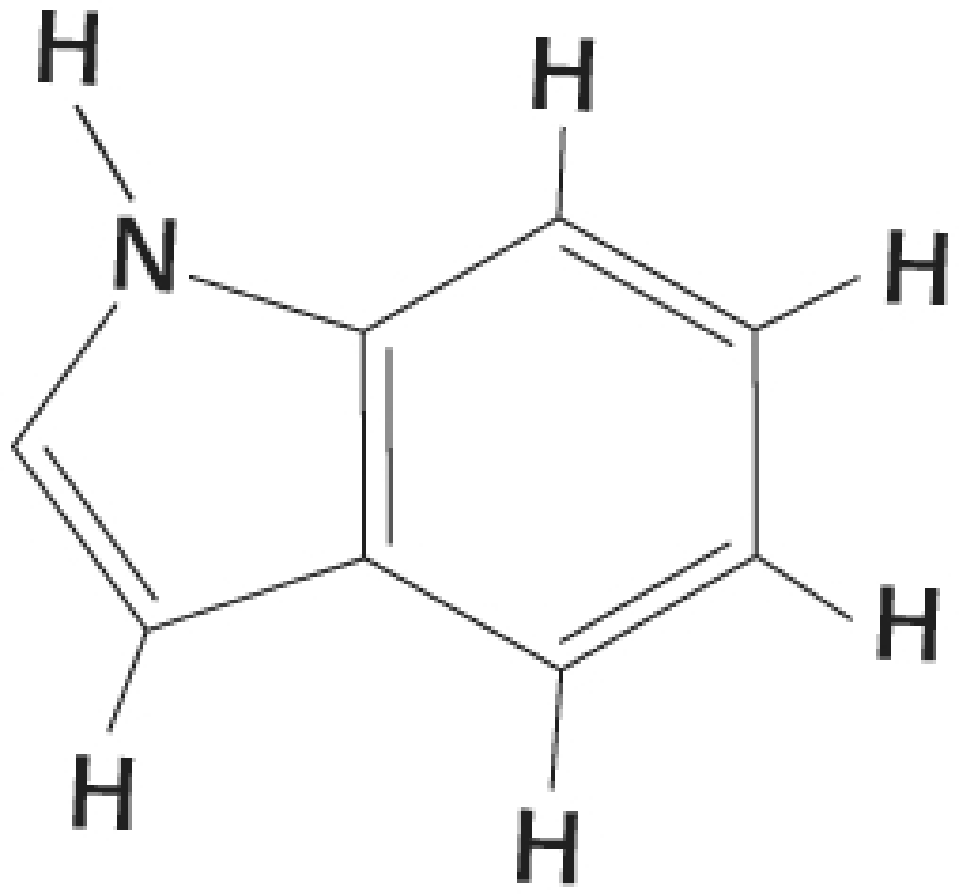
prokaryotes
Bacteria
Archaea
nitrogenous bases (bases)
polarity
double helix
base pair
complementary sequences
biochemical timescale
covalent bond
resonance structure
ionic interaction
electric dipole (dipole)
hydrogen bond
hydrogen-bond donor
hydrogen-bond acceptor
van der Waals interaction
van der Waals contact distance
hydrophobic effect
nonpolar molecule
surface complementarity
entropy
enthalpy
free energy (Gibbs free energy)
stochastic
acid–base reactions
pH
pK_a value
buffer
titration
Henderson–Hasselbalch equation
microbiome
amino acid
molecular clock hypothesis

virus

Problems

1. Identify the hydrogen-bond donors and acceptors in each of the four bases on page 4. 2

2. Draw a stable, uncharged resonance form for the structure shown. Be sure to include lone pairs of electrons. 2



3. What types of noncovalent interactions hold together the following solids? 2

a. Table salt (NaCl), which contains Na^+ and Cl^- ions.
b. Graphite (C), which consists of sheets of covalently bonded carbon atoms.

4. Given the following values for the changes in enthalpy (ΔH) and entropy (ΔS), which of the following processes can take place at 298 K without violating the Second Law of Thermodynamics? 3

a. $\Delta H = -84\ \text{kJ mol}^{-1}\ (-20\ \text{kcal mol}^{-1})$,

$\Delta S = +125\ \text{J mol}^{-1}\ \text{K}^{-1}\ (+30\ \text{cal mol}^{-1}\ \text{K}^{-1})$

b. $\Delta H = -84\ \text{kJ mol}^{-1}\ (-20\ \text{kcal mol}^{-1})$,

$\Delta S = -125\ \text{J mol}^{-1}\ \text{K}^{-1}\ (-30\ \text{cal mol}^{-1}\ \text{K}^{-1})$

c. $\Delta H = +84\ \text{kJ mol}^{-1}\ (+20\ \text{kcal mol}^{-1})$,

$\Delta S = +125\ \text{J mol}^{-1}\ \text{K}^{-1}\ (+30\ \text{cal mol}^{-1}\ \text{K}^{-1})$

d. $\Delta H = +84\ \text{kJ mol}^{-1}\ (+20\ \text{kcal mol}^{-1})$,

$$\Delta S = -125\ \text{J mol}^{-1}\ \text{K}^{-1}\ (-30\ \text{cal mol}^{-1}\ \text{K}^{-1})$$

5. For double-helix formation, ΔG can be measured to be $-54\ \text{kJ mol}^{-1}\ (-13\ \text{kcal mol}^{-1})$ at pH 7.0 in $1\ \text{M NaCl}$ at $25°\text{C}\ (298\ \text{K})$. The heat released indicates an enthalpy change of $-251\ \text{kJ mol}^{-1}\ (-60\ \text{kcal mol}^{-1})$. For this process, calculate the entropy change for the system and the entropy change for the surroundings. 3

6. Calculate the pH of a solution that is 0.153 M HCl. 6

7. Given a density of $1\ \text{g/ml}$ and a molecular weight of $18\ \text{g/mol}$, calculate the concentration of water in water.

8. A solution is prepared by adding $0.01\ \text{M}$ acetic acid $(pK_a = 4.75)$ and $0.01\ \text{M}$ ethylamine to water and adjusting the pH to 7.4. The pK_a of the ethylammonium ion $(CH_3CH_2NH_3^+)$ is 10.70. What is the ratio of acetate to acetic acid? What is the ratio of ethylamine to ethylammonium ion? 6

9. 100 mL of a solution of hydrochloric acid with pH 5.0 is diluted to 1 L. Similarly, $100\ \text{mL}$ of a 0.1 mM buffer solution made from acetic acid and sodium acetate with pH 5.0 is diluted to 1 L. What are the pH values of the two diluted solutions? 5

10. A dye that is an acid and that appears as different colors in its protonated and deprotonated forms can be used as a pH indicator. Suppose that you have a 0.001 M solution of a dye

with a pK_a of 7.2. From the color, the concentration of the protonated form is found to be 0.0002 M. Assume that the remainder of the dye is in the deprotonated form. What is the pH of the solution? 6

11. During exercise when the body lacks an adequate supply of oxygen to support energy production, a compound called pyruvate that is produced from the breakdown of glucose is converted into lactic acid.

The dissociation of lactic acid to lactate is shown in the reaction. Lactic acid has a pK_a of 3.86.

A solution containing a mixture of lactic acid and lactate was found to have a pH of 4.13. Calculate the ratio of the lactate concentration to the lactic acid concentration in this solution. 6

12. Through the use of nuclear magnetic resonance spectroscopy, it is possible to determine the ratio between the protonated and deprotonated forms of buffers. Use the Henderson–Hasselbalch equation for a propanoic acid solution ($CH_3CH_2CO_2H$, $pK_a = 4.87$) to calculate the quotient $[A^-]/[HA]$ at three different pH values:

a. $pH = 4.52$;
b. $pH = 4.87$;
c. $pH = 5.08$.

13. Given that phosphoric acid (H_3PO_4) can give up three protons with different pK_a values, sketch a plot of pH as a function of added drops of sodium hydroxide solution, starting with a solution of phosphoric acid at pH 1.0. 6

14. Your laboratory is out of materials to make phosphate buffer and you are considering using sulfate to make a buffer instead. The pK_a values for the two hydrogens in H_2SO_4 are -10 and 2.

a. Will this approach work for making a buffer effective near pH 7?
b. Around what pH might a sulfate-based buffer be useful? 6

15. You wish to prepare a buffer consisting of acetic acid and sodium acetate with a total acetic acid plus acetate concentration of 250 mM and a pH of 5.0. What concentrations of acetic acid and sodium acetate should you use? Assuming you wish to make 2 liters of this buffer, how many moles of acetic acid and sodium acetate will you need? How many grams of each will you need (molecular weights: acetic acid $60.05\ g\ mol^{-1}$, sodium acetate, $82.03\ g\ mol^{-1}$)? 5

16. Norman Good and his colleagues developed a series of compounds that are useful buffers near neutral pH. Three of these buffers are abbreviated MES $(pK_a = 6.15)$, MOPS $(pK_a = 7.15)$, and HEPPS $(pK_a = 8.00)$.

a. Which of these buffers would be most effective near pH 7.0?
b. Near 6.0? 5

17. Would you expect the double helix in a short segment of DNA to be more stable in 100 sodium phosphate buffer at pH 7.0 or in pure water? Why? 2

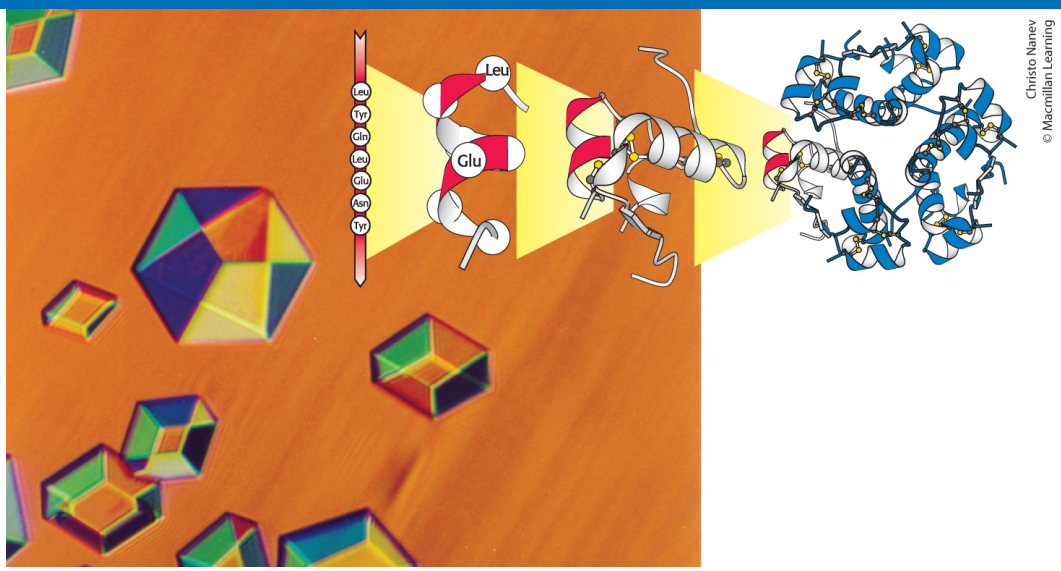
18. Suppose two phosphate groups in DNA (each with a charge of -1) are separated by $12\ \text{Å}$. What is the energy of the ionic interaction between these two phosphates, assuming a dielectric constant of 80? Repeat the calculation, assuming a dielectric constant of 2. 2

19. Describe the noncovalent interactions that are primarily responsible for the fact that oil and water do not mix easily. 2

20. Hemoglobin from the Galapagos tortoise is 64% identical to that from human beings. In contrast, a protein called histone H2B is 98% identical in these two organisms. What level of identity would you expect for histone H2B for gorillas compared with human beings? Would histone H2B be as useful a molecular clock as hemoglobin? 7

21. Assume that 10% of the members of a population will get a particular disease over the course of their lifetime. Genomic studies reveal that 5% of the population have sequences in their genomes such that their probability of getting the disease over the course of their lifetimes is found to be 50%. What is the average lifetime risk of this disease for the remaining 95% of the population without these sequences? 7

Chapter 2
Protein Composition and Structure



Christo Nanev
© Macmillan Learning

A protein is defined by a specific sequence of amino acids, which uniquely determines its folded three-dimensional structure. For example, consider the protein insulin, a hormone that is crucial for maintaining blood sugar at appropriate levels. In this protein's chain of amino acids, the interactions of amino acids close to one another in the sequence produce spiraled chains (helices) that fold further into the precisely defined shape of a single insulin molecule. Complexes of six insulin molecules can be induced in the laboratory to form well-defined crystals (photograph at left), which allows the experimental determination of these structures at atomic-level resolution.

Outline

2.1 Several Properties of Protein Structure Are Key to Their Functional Versatility
2.2 Proteins Are Built from a Repertoire of 20 Amino Acids
2.3 Primary Structure: Amino Acids Are Linked by Peptide Bonds to Form Polypeptide Chains
2.4 Secondary Structure: Polypeptide Chains Can Fold into Regular Structures
2.5 Tertiary Structure: Proteins Can Fold into Globular or Fibrous Structures
2.6 Quaternary Structure: Polypeptide Chains Can Assemble into Multisubunit Structures
2.7 The Amino Acid Sequence of a Protein Determines Its Three-Dimensional Structure

---

Learning Goals



By the end of this chapter, you should be able to:

1. Identify the 20 amino acids and their corresponding three-letter and one-letter abbreviations, and group them according to the chemical properties of their side chains.
2. Distinguish between primary, secondary, tertiary, and quaternary structures.
3. Describe the properties of the principal types of secondary structure, including the α helix, the β sheet, and the reverse turn.
4. Explain how the hydrophobic effect serves as the primary driving force for folding of polypeptide chains into globular proteins.
5. Describe the nucleation-condensation model of protein folding, and explain why it is preferable to a random sampling model.

Proteins are the most versatile macromolecules in living systems and serve crucial functions in essentially all biological processes. They function as catalysts, transport and store other molecules such

as oxygen, provide mechanical support and immune protection, generate movement, transmit nerve impulses, and control growth and differentiation. Indeed, much of this book will focus on understanding what proteins do and how they perform these functions. In order to fully appreciate this functional diversity, we must first understand the essential structural components shared by all proteins. For the biochemist, recognition of this architectural composition is critical and fundamental, akin to learning the alphabet of a new language.

2.1 Several Properties of Protein Structure Are Key to Their Functional Versatility

As we shall see throughout this text, proteins can adopt a breathtakingly wide variety of structures, which, in turn, enables them to participate in a broad range of functions. There are several key features of protein structure that allow for this remarkable diversity:

- *Proteins are linear polymers built of monomer units called amino acids, which are linked end to end*. The sequence of linked amino acids is called the primary structure. Remarkably, proteins spontaneously fold up into three-dimensional structures that are determined by the sequence of amino acids in the protein polymer. Three-dimensional structure formed by hydrogen bonds between amino acids near one another is called secondary structure, whereas tertiary structure is formed by long-range interactions between amino acids. Protein function depends directly on this three-dimensional structure (**Figure 2.1**). Thus, proteins are the embodiment of the transition from the one-dimensional world of sequences to the three-dimensional world of molecules capable of diverse activities. Many proteins also display quaternary structure, in which the functional protein is composed of several distinct polypeptide chains.

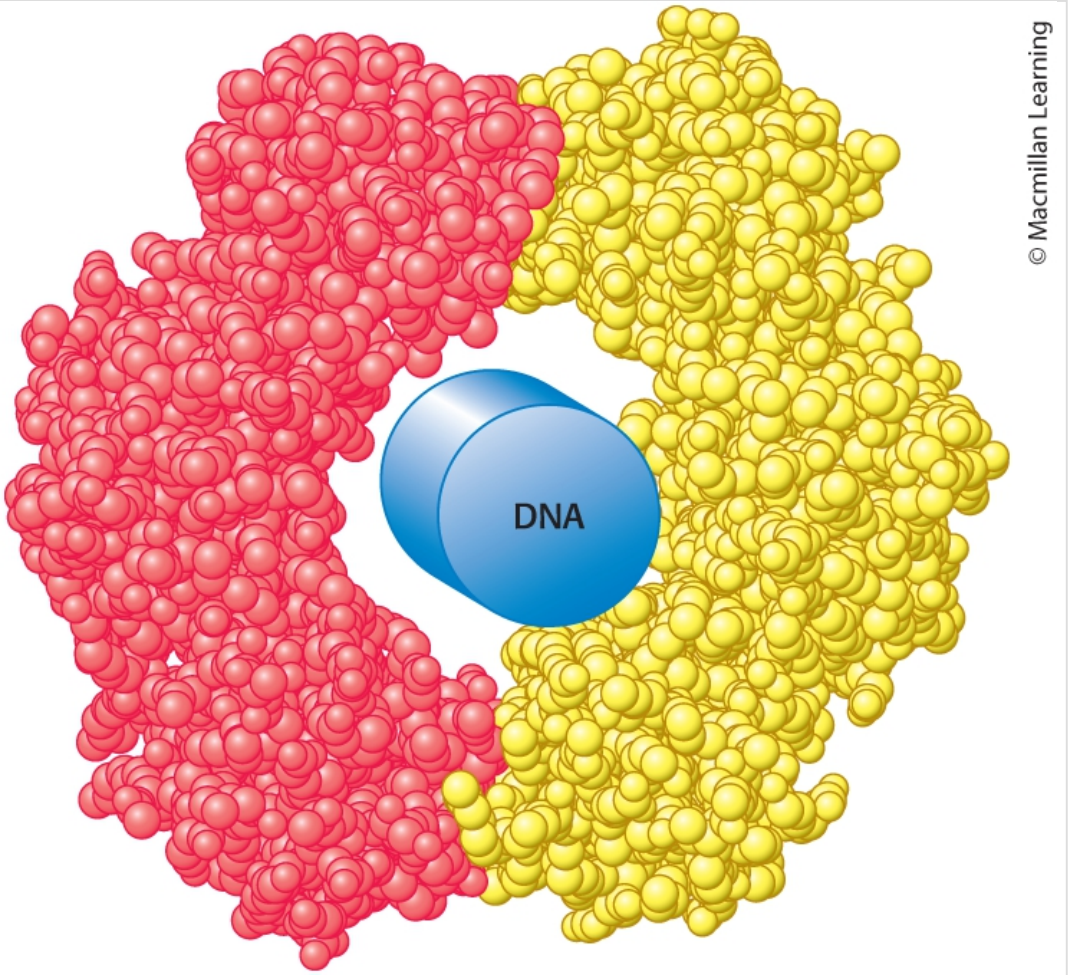


FIGURE 2.1 The structure of a protein determines its function. The protein component of the DNA replication machinery, which consists of two identical subunits (shown in red and yellow), acts as a clamp that allows large segments of DNA (depicted as a cylinder) to be copied without the replication machinery dissociating from the DNA.

[Drawn from 2POL.pdb.]

INTERACT with this model in Achieve

- *Proteins contain a wide range of functional groups*. These functional groups include alcohols, thiols, thioethers, carboxylic acids, carboxamides, and a variety of basic groups, such as amines. Most of these groups are chemically reactive. When combined in various

sequences, this array of functional groups accounts for the broad spectrum of protein function. For instance, their reactive properties are essential to the function of **enzymes** — the proteins that catalyze specific chemical reactions in biological systems (Chapters 5 through 7).

- *Proteins can interact with one another and with other biological macromolecules to form complex assemblies*. The proteins within these assemblies can act synergistically to generate capabilities that individual proteins may lack. Examples of these assemblies include macromolecular machines that replicate DNA, transmit signals within cells, and enable muscle cells to contract (**Figure 2.2**).

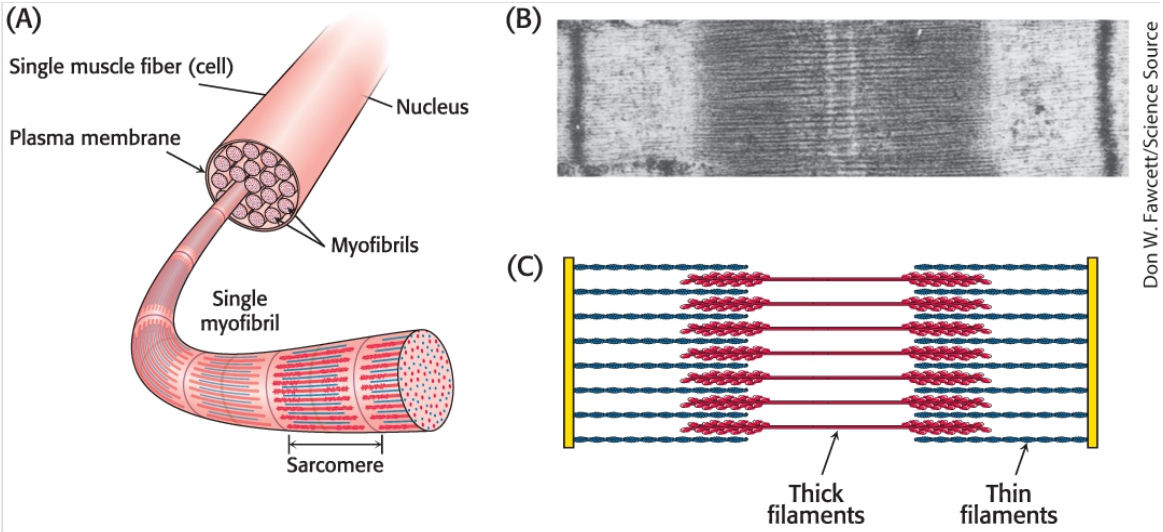


FIGURE 2.2 Some proteins form complex assemblies. (A) A single muscle cell contains multiple myofibrils, each of which is comprised of numerous repeats of a complex protein assembly known as the sarcomere. (B) The banding pattern of a sarcomere is evident by electron microscopy. (C) The banding is caused by the interdigitation of filaments made up of many individual proteins.

- *Some proteins are quite rigid, whereas others display considerable flexibility*. Rigid units can function as structural elements in the cytoskeleton (the internal scaffolding within cells) or in connective

tissue. Proteins with some flexibility may act as hinges, springs, or levers. In addition, conformational changes within proteins enable the regulated assembly of larger protein complexes as well as the transmission of information within and between cells (Figure 2.3).

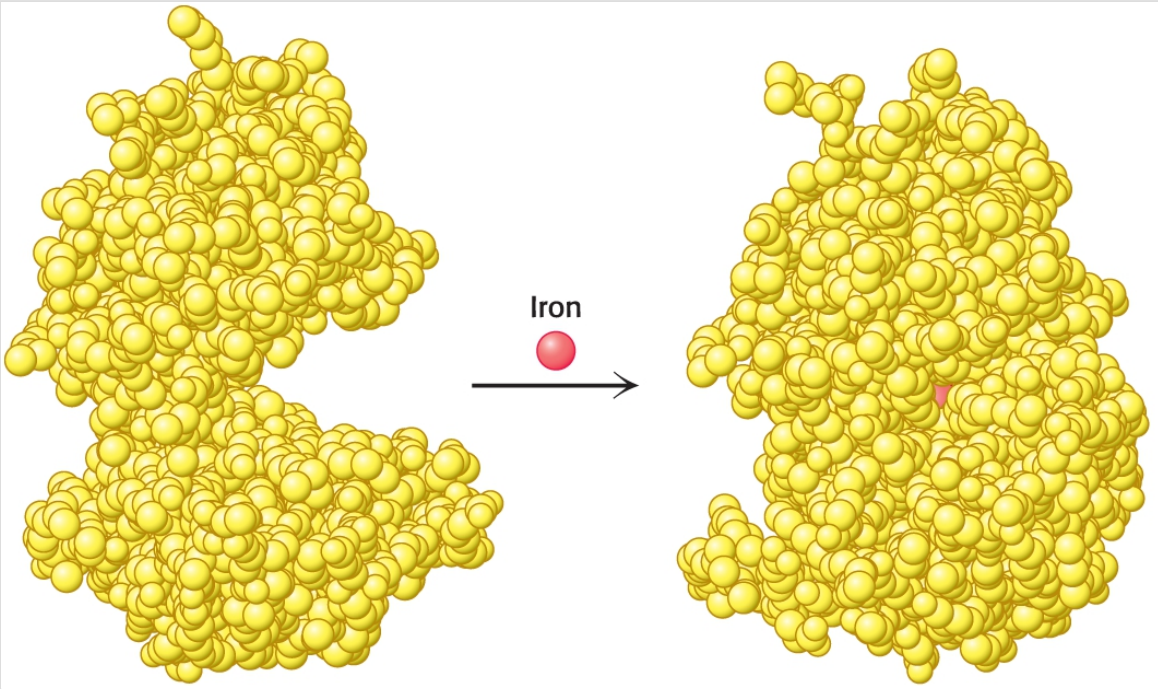


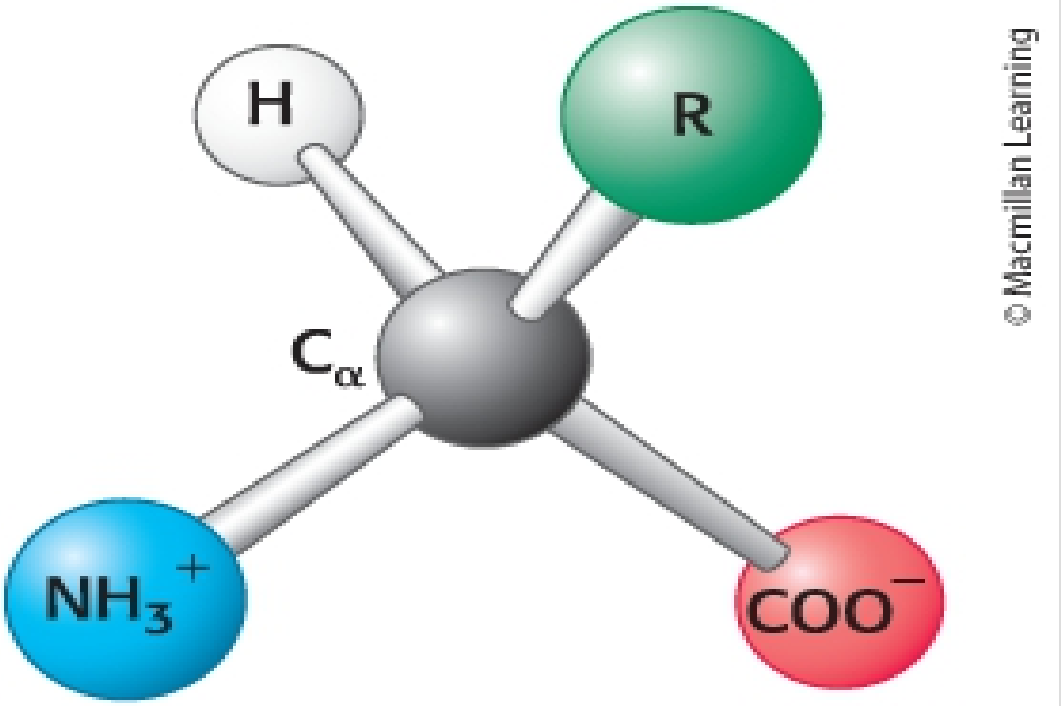
FIGURE 2.3 Conformational changes allow flexibility in protein function. On binding iron, the protein lactoferrin undergoes a substantial change in conformation that allows other molecules to distinguish between the iron-free and the iron-bound forms.

[Drawn from 1LFH.pdb and 1LFG.pdb.]

INTERACT with this model in Achieve

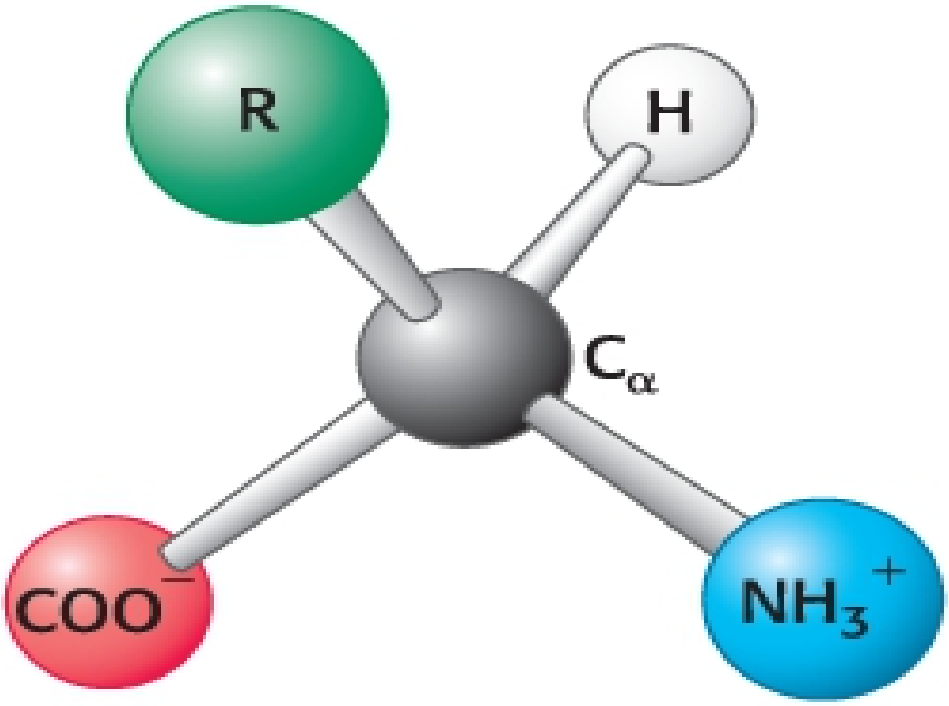
2.2 Proteins Are Built from a Repertoire of 20 Amino Acids

Amino acids are the building blocks of proteins. An α-amino acid consists of a central carbon atom, called the **α carbon**, linked to an amino group, a carboxylic acid group, a hydrogen atom, and a distinctive **R group** (also referred to as the **side chain**). With four different groups connected to the tetrahedral α-carbon atom, α-amino acids are **chiral**: they may exist in one or the other of two mirror-image forms, called the *L isomer* and the *D isomer* (**Figure 2.4**).



© Macmillan Learning

L isomer



D isomer

FIGURE 2.4 The L and D isomers of amino acids are mirror images of each other.
The letter R refers to the side chain. Only the L amino acids are found in proteins.



Only L isomers of amino acids (called *L amino acids*) are constituents of proteins. What is the basis for the preference for L amino acids? The answer has been lost to evolutionary history. It is possible that the preference for L over D amino acids was a consequence of a chance selection. However, there is evidence that L amino acids are slightly more soluble than a racemic mixture of D and L amino acids, which tend to form crystals. This small solubility difference could have been amplified over time so that the L isomer became dominant in solution.

Amino acids in solution at physiological pH (around 7.4) exist predominantly as **dipolar ions** (also called **zwitterions**). In the dipolar form, the amino group is protonated $(-NH_3^+)$ and the carboxyl group is deprotonated $(-COO^-)$. The ionization state of an amino acid varies with pH (**Figure 2.5**). In acid solution (e.g., pH 1), the amino group is protonated $(-NH_3^+)$ and the carboxyl group is not dissociated $(-COOH)$. As the pH is raised, the carboxylic acid is the first group to give up a proton, inasmuch as its pK_a is near 2. (The concept of pK_a was explained in Section 1.3.) The dipolar form persists until the pH approaches 9.5, when the protonated amino group loses a proton.

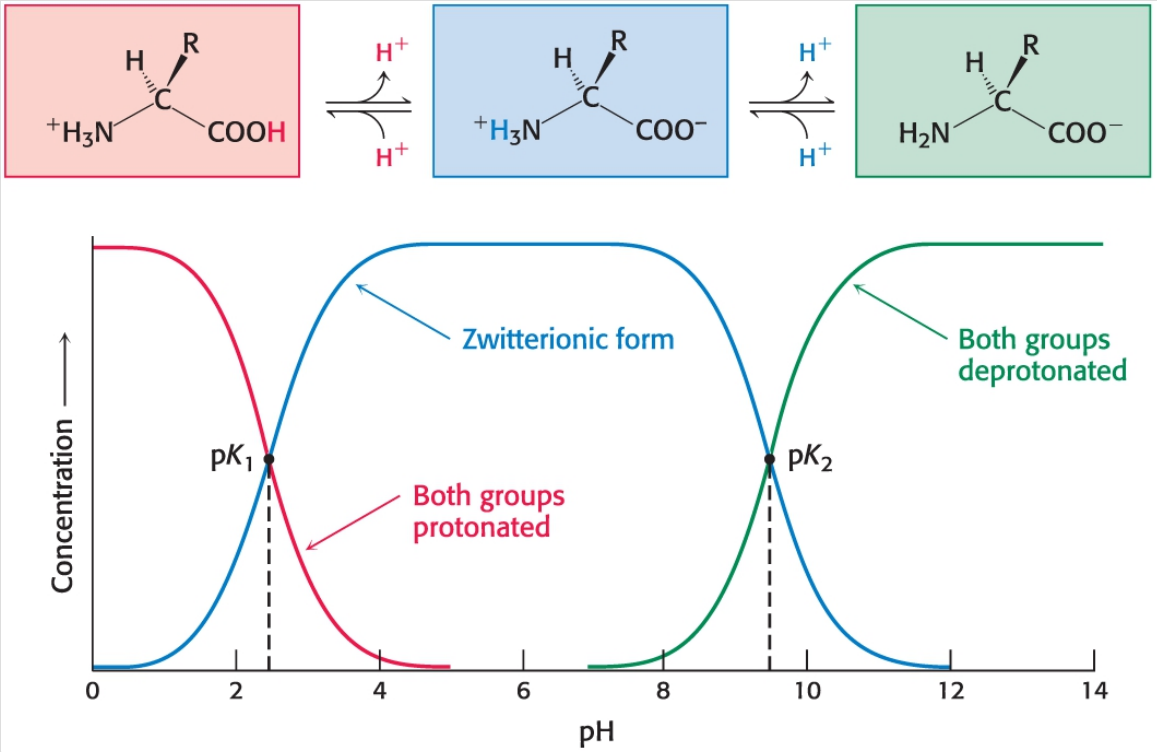


FIGURE 2.5 The ionization state of amino acids is altered by changes in pH. At low pH, near th pK_a for the carboxylic acid, pK_1, the $-COOH$ proton is lost from the fully protonated form. As the pH approaches physiological levels, the zwitterionic form predominates. At high pH near the pK_a for the amino group, pK_2, one of the $-NH_3^+$ protons is lost to form the ful deprotonated species.

The diversity of amino acids arises from the different side chains

Twenty kinds of side chains varying in size, shape, charge, hydrogen-bonding capacity, hydrophobic character, and chemical reactivity are commonly found in proteins. Indeed, all proteins in all species — bacterial, archaeal, and eukaryotic — are constructed from the same set of 20 amino acids with only a few exceptions. This fundamental

alphabet for the construction of proteins is several billion years old. The remarkable range of functions mediated by proteins results from the diversity and versatility of these 20 building blocks. Understanding how this alphabet is used to create the intricate three-dimensional structures that enable proteins to carry out so many biological processes is an exciting area of biochemistry, and one that we will return to in Section 2.7.

Although there are many ways to classify amino acids, we will sort these molecules into four groups, on the basis of the general chemical characteristics of their R groups:

1. Hydrophobic amino acids with nonpolar R groups
2. Polar amino acids with neutral R groups but the charge is not evenly distributed
3. Positively charged amino acids with R groups that have a positive charge at physiological pH
4. Negatively charged amino acids with R groups that have a negative charge at physiological pH

Hydrophobic amino acids

The simplest amino acid is glycine, which has a single hydrogen atom as its side chain. With two hydrogen atoms bonded to the α-carbon atom, glycine is unique in being achiral; that is, its mirror images are superimposable. Alanine, the next simplest amino acid, has a methyl group $(-CH_3)$ as its side chain (**Figure 2.6**).

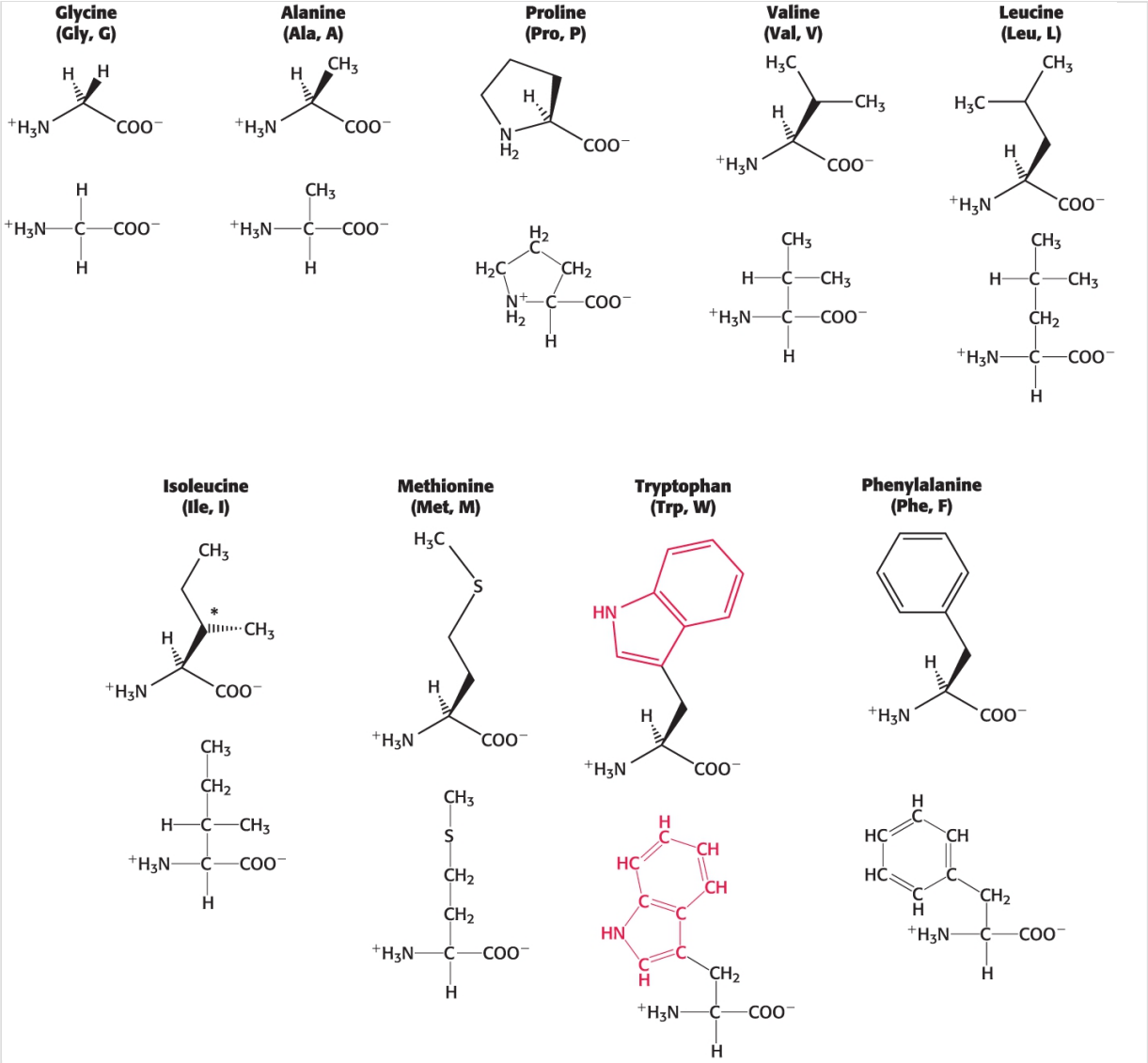


FIGURE 2.6 The hydrophobic amino acids have nonpolar R groups. For each amino acid, a stereochemically realistic formula (top) shows the geometric arrangement of bonds around atoms and a Fischer projection (bottom) shows all bonds as being perpendicular for a simplified representation. The additional chiral center in isoleucine is indicated by an asterisk. The indole group in the tryptophan side chain is shown in red.

Larger hydrocarbon side chains are found in valine, leucine, and isoleucine. Methionine contains a largely aliphatic side chain that includes a thioether (—S—) group. The side chain of isoleucine includes

an additional chiral center; only the isomer shown in Figure 2.6 is found in proteins. These aliphatic side chains are especially hydrophobic; that is, they tend to cluster together rather than contact water. The three-dimensional structures of water-soluble proteins are stabilized by this tendency of hydrophobic groups to come together (the hydrophobic effect, Section 1.3). The different sizes and shapes of these hydrocarbon side chains enable them to pack together to form compact structures with little empty space. Proline also has an aliphatic side chain, but it differs from other members of the set of 20 in that its side chain is bonded to both the nitrogen and the α-carbon atoms, yielding a pyrrolidine ring. Proline markedly influences protein architecture because its cyclic structure makes it more conformationally restricted than the other amino acids.

Two amino acids with relatively simple aromatic side chains are part of the fundamental repertoire. Phenylalanine, as its name indicates, contains a phenyl ring attached in place of one of the hydrogen atoms of alanine. Tryptophan has an indole group joined to a methylene $(-CH_2-)$ group; the indole group comprises two fused rings containing an NH group (Figure 2.6, shown in red). Phenylalanine is purely hydrophobic, whereas tryptophan is less so because of its side chain NH group.

Polar amino acids

Seven amino acids are polar but uncharged at physiological pH. Three amino acids, serine, threonine, and tyrosine, contain hydroxyl groups $(-OH)$ attached to a hydrophobic side chain (**Figure 2.7**). Serine can be thought of as a version of alanine with a hydroxyl group attached. Threonine resembles valine with a hydroxyl group in place of one of valine's methyl groups. Tyrosine is a version of phenylalanine with the hydroxyl group replacing a hydrogen atom on the aromatic ring. The hydroxyl group makes these amino acids much more hydrophilic (water

loving) and reactive than their hydrophobic analogs. Threonine, like isoleucine, contains an additional asymmetric center; again, only one isomer is present in proteins.

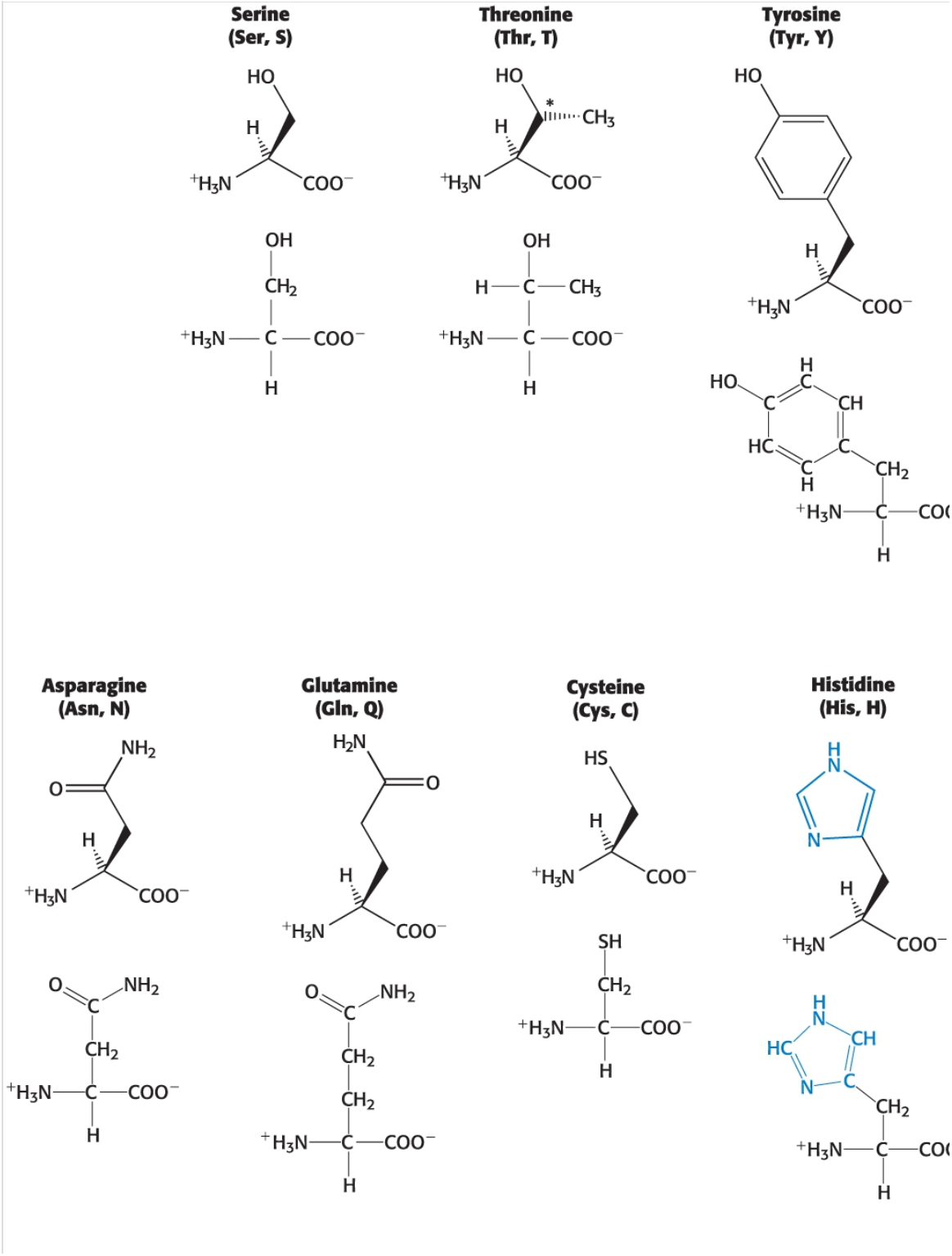


FIGURE 2.7 The polar amino acids have polar but uncharged R groups at physiological pH. Th additional chiral center in threonine is indicated by an asterisk. The carboxamide groups of asparagine and glutamine are shown in red. The imidazole group of histidine is shown in blue.



In addition, the set includes asparagine and glutamine, two amino acids that contain a terminal carboxamide, highlighted in red in Figure 2.7. The side chain of glutamine is one methylene group longer than that of asparagine.

Cysteine is structurally similar to serine but contains a sulfhydryl, or thiol $(-SH)$, group in place of the hydroxyl group. The sulfhydryl group is much more reactive. Pairs of sulfhydryl groups may come together to form disulfide bonds, which are particularly important in stabilizing some proteins, as will be discussed shortly.

Histidine contains an imidazole group, an aromatic ring that is uncharged at pH 7 (Figure 2.7, shown in blue). However, with a pK_a value near 6, the imidazole group can be uncharged or positively charged near neutral pH, depending on its local environment (**Figure 2.8**). Histidine is often found in the active sites of enzymes, where the imidazole ring can bind and release protons in the course of enzymatic reactions.

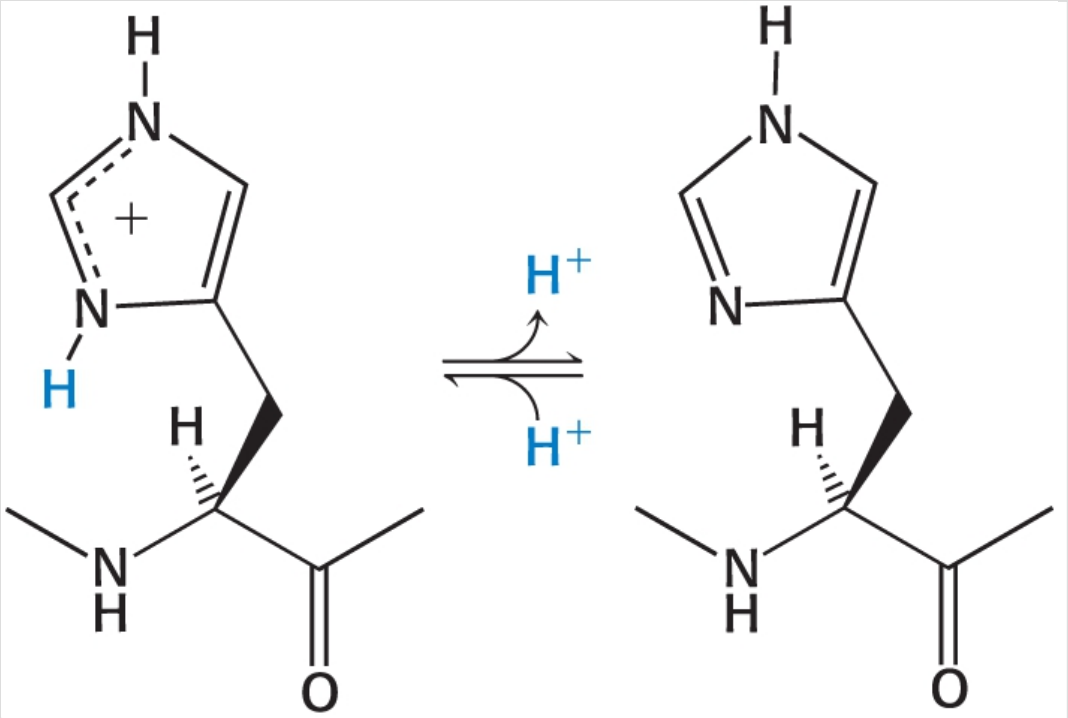
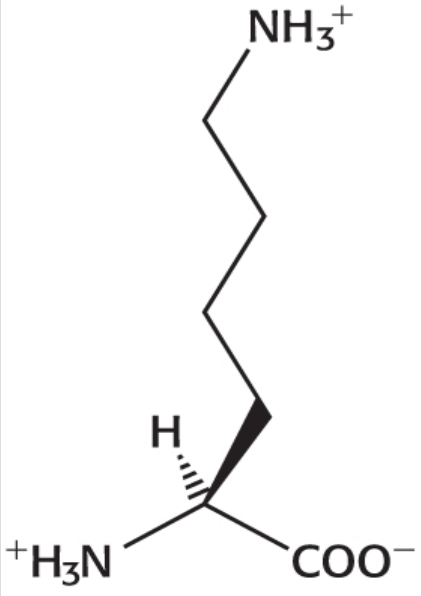


FIGURE 2.8 Histidine can bind or release protons near physiological pH.

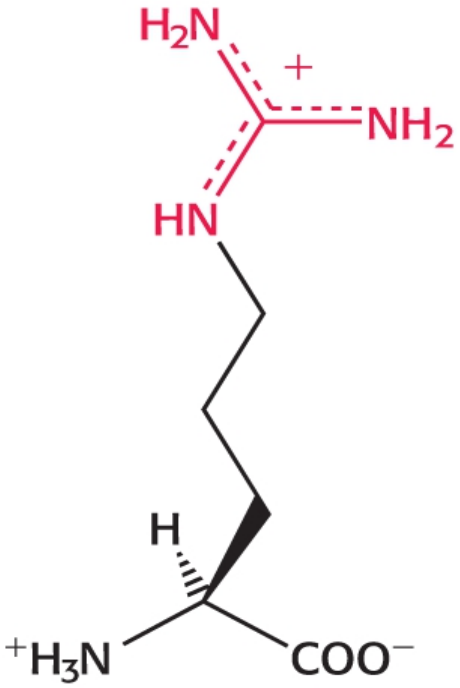
Positively charged amino acids

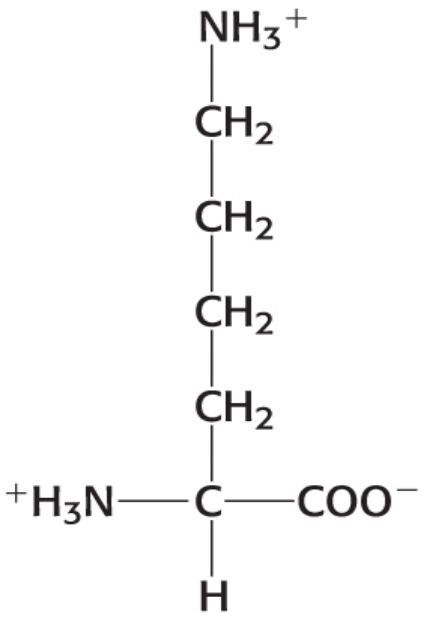
We turn now to amino acids with complete positive charges that render them highly hydrophilic (**Figure 2.9**). Lysine and arginine have long side chains that terminate with groups that are positively charged at neutral pH. Lysine is capped by a primary amino group and arginine by a guanidinium group (Figure 2.9, shown in red).

Lysine
(Lys, K)



Arginine
(Arg, R)





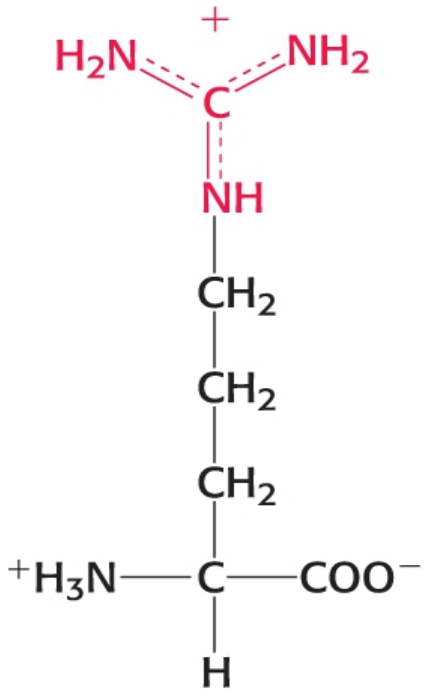


FIGURE 2.9 Two amino acids are positively charged at physiological pH. The guanidinium group in the arginine side chain is shown in red.

Negatively charged amino acids

This set of amino acids contains two with acidic side chains: aspartic acid and glutamic acid (**Figure 2.10**). These amino acids are charged derivatives of asparagine and glutamine (Figure 2.7), with a carboxylic acid in place of a carboxamide. Aspartic acid and glutamic acid are often called *aspartate* and *glutamate* to emphasize that, at physiological pH, their side chains usually lack a proton that is present in the acid form and hence are negatively charged. Nonetheless, these side chains can accept protons in some proteins, often with functionally important consequences.

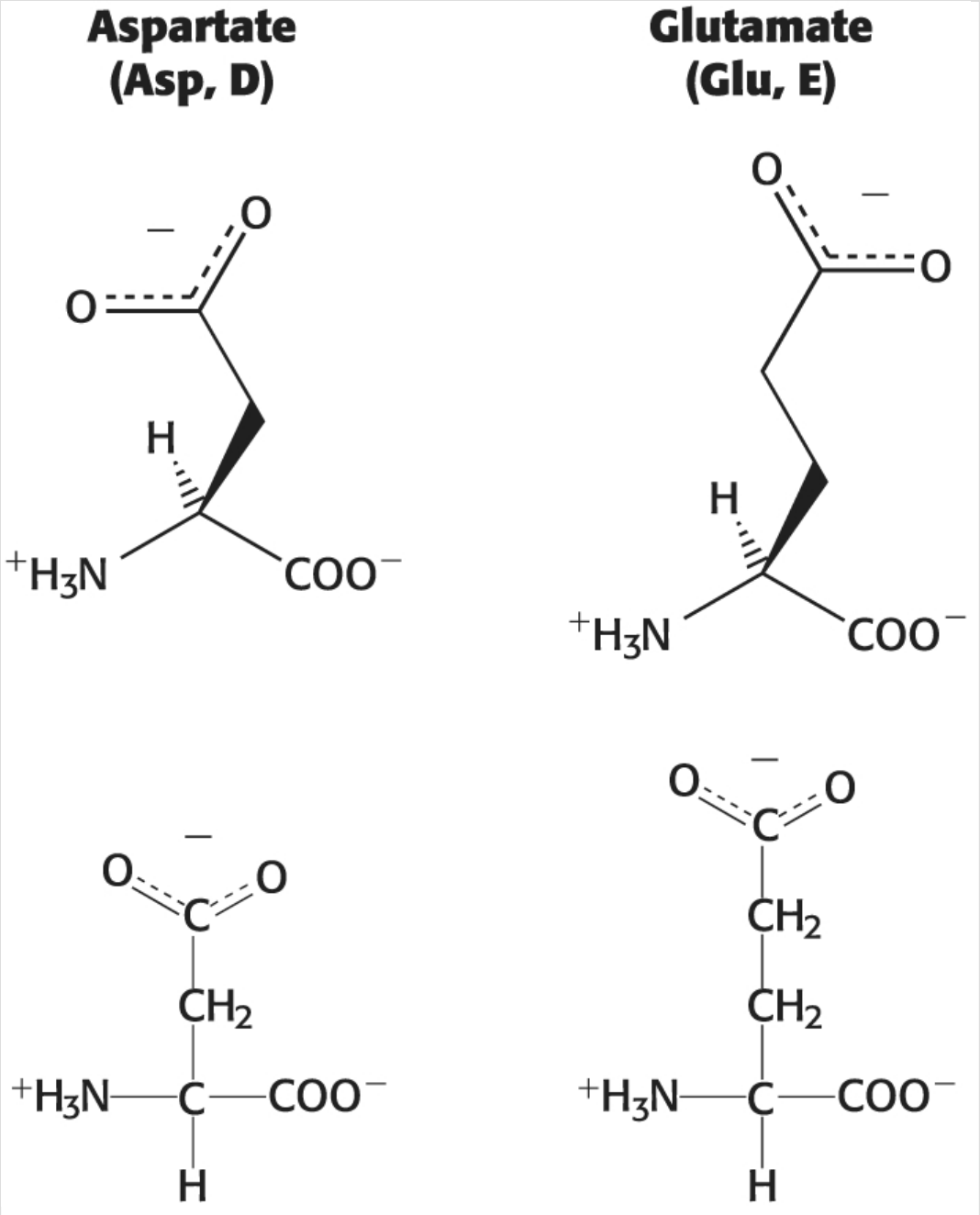
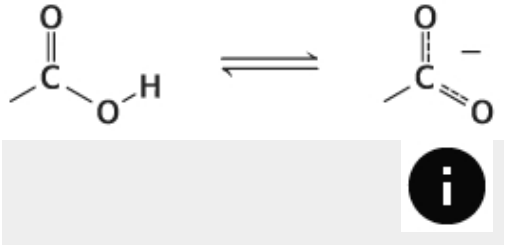
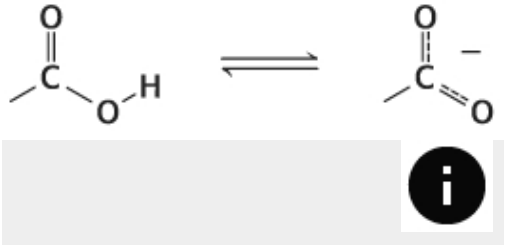


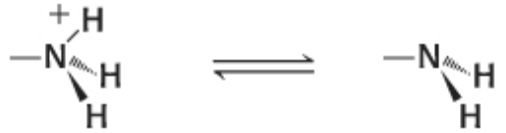
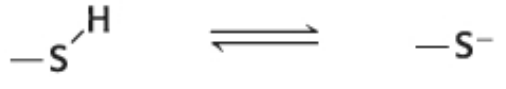
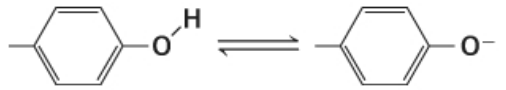
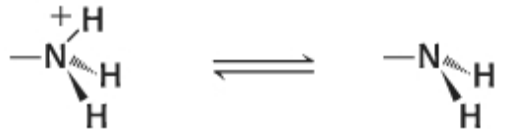
FIGURE 2.10 Two amino acids are negatively charged at physiological pH.

Seven of the 20 amino acids have readily ionizable side chains. These 7 amino acids are able to donate or accept protons to facilitate reactions

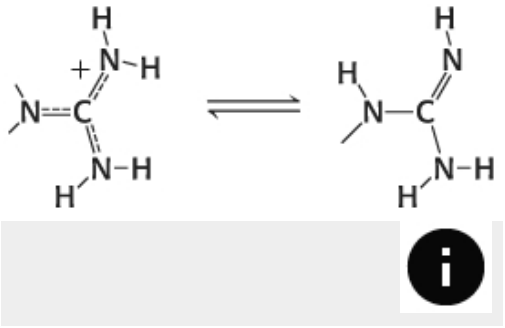
as well as to form ionic bonds. Table 2.1 gives equilibria and typical pK_a values for ionization of the side chains of tyrosine, cysteine, arginine, lysine, histidine, and aspartic and glutamic acids in proteins. Two other groups in proteins — the terminal α-amino group and the terminal α-carboxyl group — can be ionized, and typical pK_a values for these groups also are included in Table 2.1.

TABLE 2.1 Typical pK_a values of ionizable groups in proteins

Group	Acid ⇌ Base	Typical pK_a*
Terminal α-carboxyl group		3.1
Aspartic acid Glutamic acid		4.1
Histidine		6.0

Terminal α-amino group		8.0
Cysteine		8.3
Tyrosine		10.0
Lysine		10.4

Arginine	12.5



*pK_a values depend on temperature, ionic strength, and the microenvironment of the ionizable group

Amino acids are often designated by either a three-letter abbreviation or a one-letter symbol (Table 2.2). The abbreviations for amino acids are the first three letters of their names, except for asparagine (Asn), glutamine (Gln), isoleucine (Ile), and tryptophan (Trp). The symbols for many amino acids are the first letters of their names (e.g., G for glycine and L for leucine); the other symbols have been agreed on by convention. These abbreviations and symbols are an integral part of the vocabulary of biochemists.

TABLE 2.2 Abbreviations for amino acids

Amino acid	Three-letter abbreviation	One-letter abbreviation
Alanine	Ala	A
Arginine	Arg	R
Asparagine	Asn	N
Aspartic acid	Asp	D
Cysteine	Cys	C

Glutamine	Gln	Q
Glutamic acid	Glu	E
Glycine	Gly	G
Histidine	His	H
Isoleucine	Ile	I
Leucine	Leu	L
Lysine	Lys	K
Methionine	Met	M
Phenylalanine	Phe	F
Proline	Pro	P
Serine	Ser	S
Threonine	Thr	T
Tryptophan	Trp	W
Tyrosine	Tyr	Y
Valine	Val	V
Asparagine or aspartic acid	Asx	B
Glutamine or glutamic acid	Glx	Z

Biochemists postulate several reasons why this set of amino acids is conserved across all species

How did this particular set of amino acids become the building blocks of proteins? First, as a set, they are diverse: their structural and chemical properties span a wide range, endowing proteins with the versatility to assume many functional roles. Second, many of these amino acids were probably available from prebiotic reactions; that is, from reactions that took place before the origin of life. Finally, other possible amino acids may have simply been too reactive. For example, amino acids such as homoserine and homocysteine tend to form five-membered cyclic forms that limit their use in proteins (Figure 2.11); the alternative amino acids that are found in proteins — serine and cysteine — do not readily cyclize, because the rings in their cyclic forms are too small to be stable.

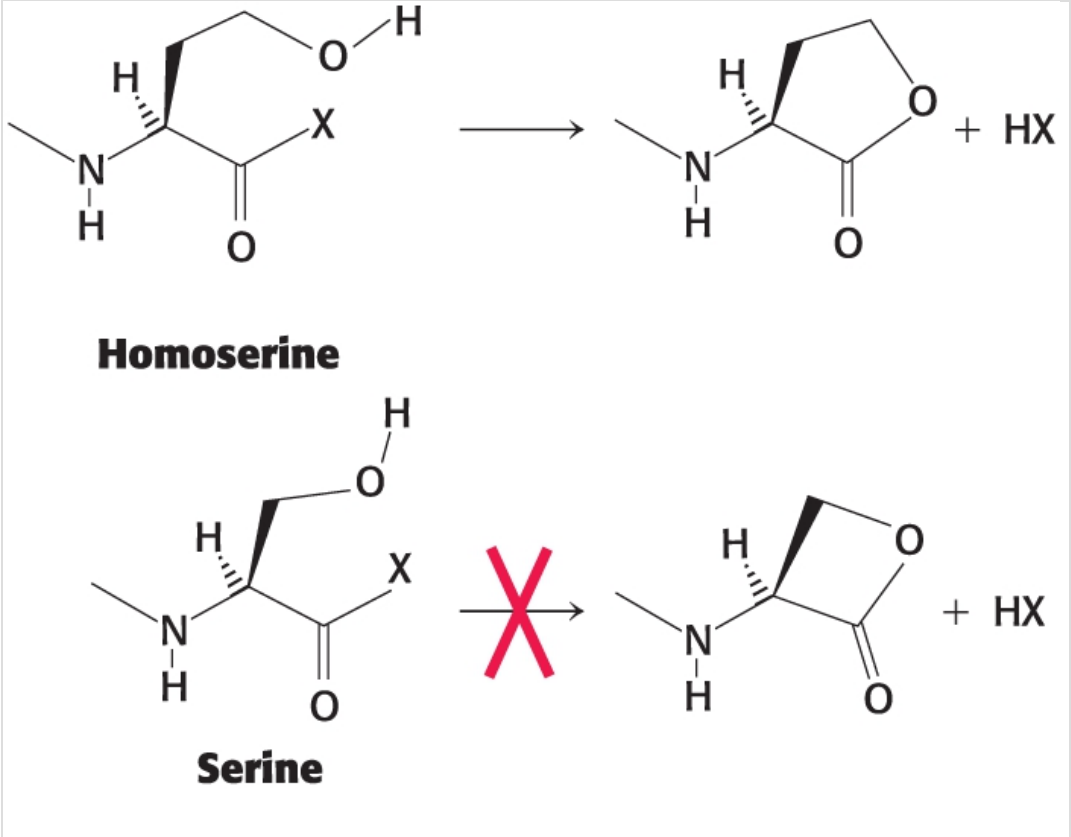


FIGURE 2.11 Some amino acids are not found in proteins because they are too reactive. Homoserine readily cyclizes to form a stable, five-membered ring, potentially resulting in peptide-bond cleavage. In contrast, serine cyclizes to a four-membered ring, which is significantly less stable.



Self-Check Question



Which two amino acids have additional chiral centers besides their α-carbon atoms?

2.3 Primary Structure: Amino Acids Are Linked by Peptide Bonds to Form Polypeptide Chains

Proteins are linear polymers formed by linking the α-carboxyl group of one amino acid to the α-amino group of another amino acid. This type of linkage is called a **peptide bond** (or an **amide bond**). The formation of a dipeptide from two amino acids is accompanied by the loss of a water molecule (**Figure 2.12**). Under most conditions, the equilibrium of this reaction lies on the side of hydrolysis rather than synthesis. Hence, the biosynthesis of peptide bonds requires an input of free energy. Nonetheless, peptide bonds are quite stable kinetically because the rate of hydrolysis is extremely slow; the lifetime of a peptide bond in aqueous solution in the absence of a catalyst approaches 1000 years.

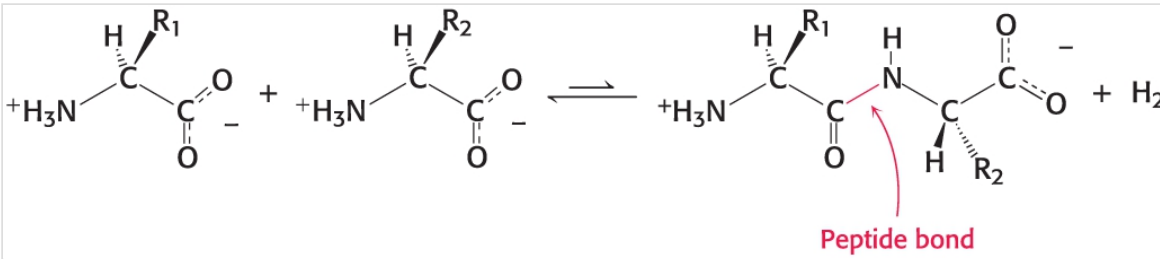


FIGURE 2.12 The formation of the peptide bond linking two amino acids is accompanied by t loss of a molecule of water.

A series of amino acids joined by peptide bonds forms a polypeptide chain, and each amino acid unit in a polypeptide is called a **residue**. A polypeptide chain has directionality because its ends are different: an α-amino group is present at one end and an α-carboxyl group at the other.

The amino end is taken to be the beginning of a polypeptide chain; by convention, the sequence of amino acids in a polypeptide chain is written starting with the amino-terminal residue. Thus, in the polypeptide Tyr-Gly-Gly-Phe-Leu (YGGFL), tyrosine is the amino-terminal (N-terminal) residue and leucine is the carboxyl-terminal (C-terminal) residue (Figure 2.13). Leu-Phe-Gly-Gly-Tyr (LFGGY) is a different polypeptide, with different chemical properties.

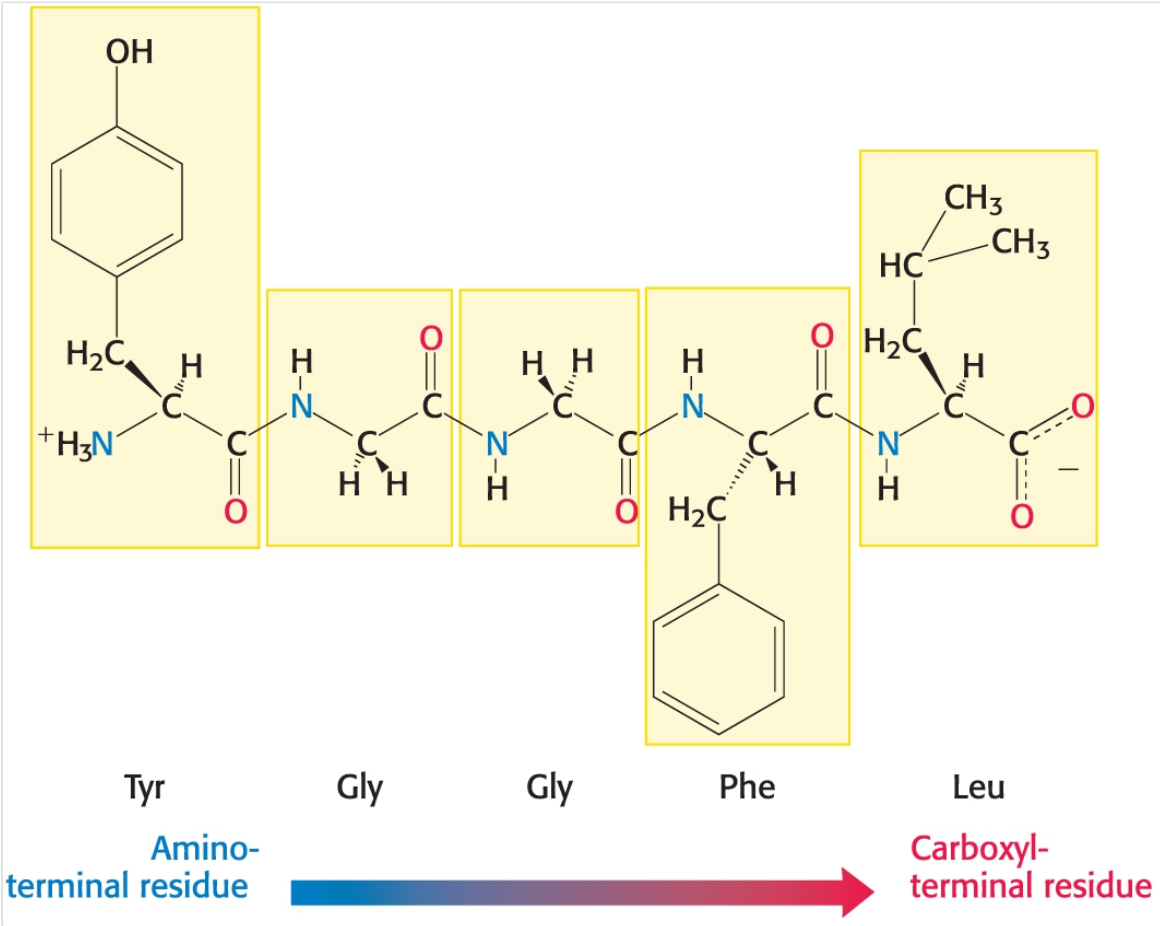


FIGURE 2.13 Amino acid sequences have direction. This illustration of the pentapeptide Tyr-Gl Gly-Phe-Leu (YGGFL) shows the sequence from the amino terminus to the carboxyl terminus. Th pentapeptide, Leu-enkephalin, is an opioid peptide that modulates the perception of pain. The reverse pentapeptide, Leu-Phe-Gly-Gly-Tyr (LFGGY), is a different molecule and has no such effects.

A polypeptide chain consists of a regularly repeating part, called the **main chain** (or **backbone**), and a variable part, comprising the distinctive side chains (**Figure 2.14**). The polypeptide backbone is rich in hydrogen-bonding potential. Each residue contains a carbonyl group (C=O), which is a good hydrogen-bond acceptor, and, with the exception of proline, an NH group, which is a good hydrogen-bond donor. These groups interact with each other and with functional groups from side chains to stabilize particular structures, as we will discuss shortly.

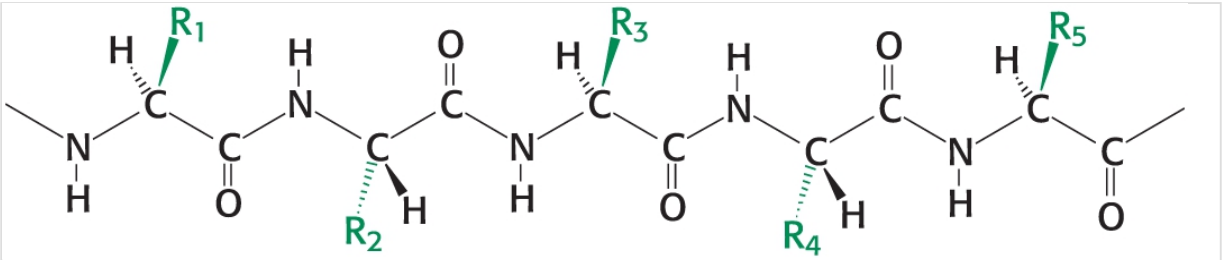


FIGURE 2.14 A polypeptide chain consists of a constant backbone and variable side chains. The side chains are shown in green.

Most natural polypeptide chains contain between 50 and 2000 amino acid residues and are commonly referred to as **proteins**. The largest single polypeptide known is the muscle protein titin, which consists of more than 27,000 amino acids. Polypeptide chains made of small numbers of amino acids are called **oligopeptides** (or, simply, **peptides**). The mean molecular weight of an amino acid residue is about $110\ \text{g mol}^{-1}$, and so the molecular weights of most proteins are between 5500 and $220{,}000\ \text{g mol}^{-1}$. We can also refer to the *molecular mass*, or the weight of a single molecule, of a protein in units of **daltons**; one dalton is equal to one atomic mass unit. A protein with a molecular weight of $50{,}000\ \text{g mol}^{-1}$ has a molecular mass of 50,000 daltons, or 50 kDa (kilodaltons).

In some proteins, the linear polypeptide chain is cross-linked. The most common cross-links are **disulfide bonds**, formed by the oxidation of a pair of cysteine residues (Figure 2.15). The resulting unit of two linked cysteines is called *cystine*. Extracellular proteins often have several disulfide bonds, whereas intracellular proteins usually lack them. Rarely, nondisulfide cross-links derived from other side chains are present in proteins. For example, collagen fibers in connective tissue are strengthened in this way, as are fibrin blood clots.

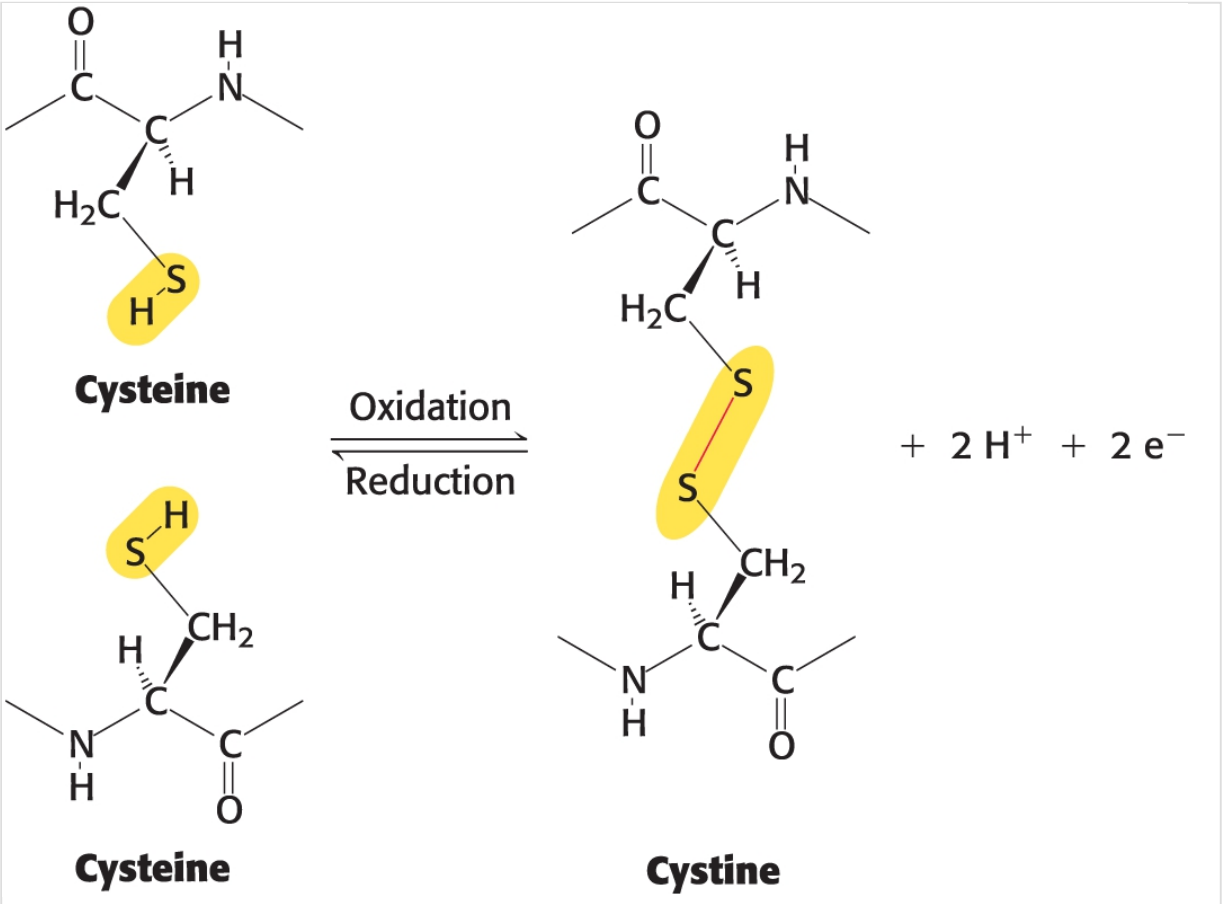


FIGURE 2.15 The formation of a disulfide bond from two cysteine residues is an oxidation reaction.

Proteins have unique amino acid sequences specified by genes

In 1953, Frederick Sanger determined the amino acid sequence of insulin, a protein hormone (**Figure 2.16**). This work is a landmark in biochemistry because it showed for the first time that a protein has a precisely defined amino acid sequence consisting only of L amino acids linked by peptide bonds. This accomplishment inspired other scientists to carry out sequence studies of a variety of proteins. Currently, the complete amino acid sequences of millions of proteins are known. The amino acid sequence of a protein is referred to as its **primary structure**.

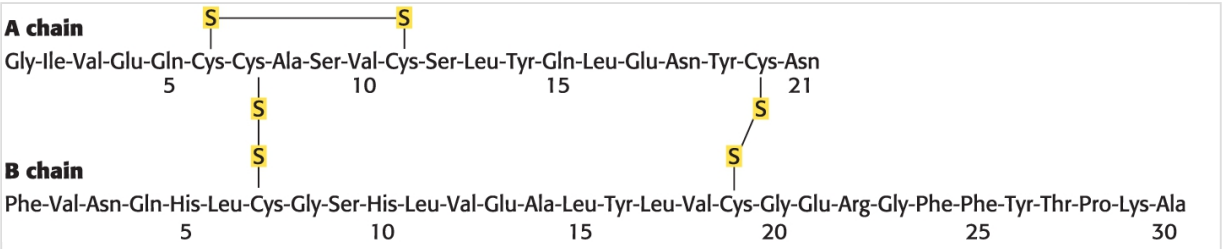


FIGURE 2.16 The primary structure of bovine insulin is its amino acid sequence. The cross links between the polypeptide chains, formed by disulfide bonds, are also shown.

A series of incisive studies in the late 1950s and early 1960s revealed that the amino acid sequences of proteins are determined by the nucleotide sequences of genes. The sequence of nucleotides in DNA specifies a complementary sequence of nucleotides in RNA, which in turn specifies the amino acid sequence of a protein. In particular, each of the 20 amino acids of the repertoire is encoded by one or more specific sequences of three nucleotides (Section 8.6).

Knowing amino acid sequences is important for several reasons:

- *Knowledge of the sequence of a protein is usually essential to elucidating its function (e.g., the catalytic mechanism of an enzyme)*. In fact, proteins with novel properties can be generated by varying the sequence of known proteins.

- *Amino acid sequences determine the three-dimensional structures of proteins*. The amino acid sequence is the link between the genetic message in DNA and the three-dimensional structure that performs a protein's biological function. Analyses of the relationships between amino acid sequences and three-dimensional structures of proteins are uncovering the rules that govern the folding of polypeptide chains.

- *Alterations in amino acid sequence can lead to abnormal protein function and disease*. Severe and sometimes fatal diseases, such as sickle-cell anemia and cystic fibrosis, can result from a change in a single amino acid within a protein.

- *The sequence of a protein reveals much about its evolutionary history*. Proteins resemble one another in amino acid sequence only if they have a common ancestor. Consequently, molecular events in evolution can be traced from amino acid sequences; molecular paleontology is a flourishing area of research.

Polypeptide chains are flexible yet conformationally restricted

Examination of the geometry of the protein backbone reveals several important features:

- *The peptide bond is essentially planar* (**Figure 2.17**). Thus, for a pair of amino acids linked by a peptide bond, six atoms lie in the same plane: the α-carbon atom and CO group of the first amino acid and

the NH group and α-carbon atom of the second amino acid. The nature of the chemical bonding within a peptide accounts for the bond's planarity.

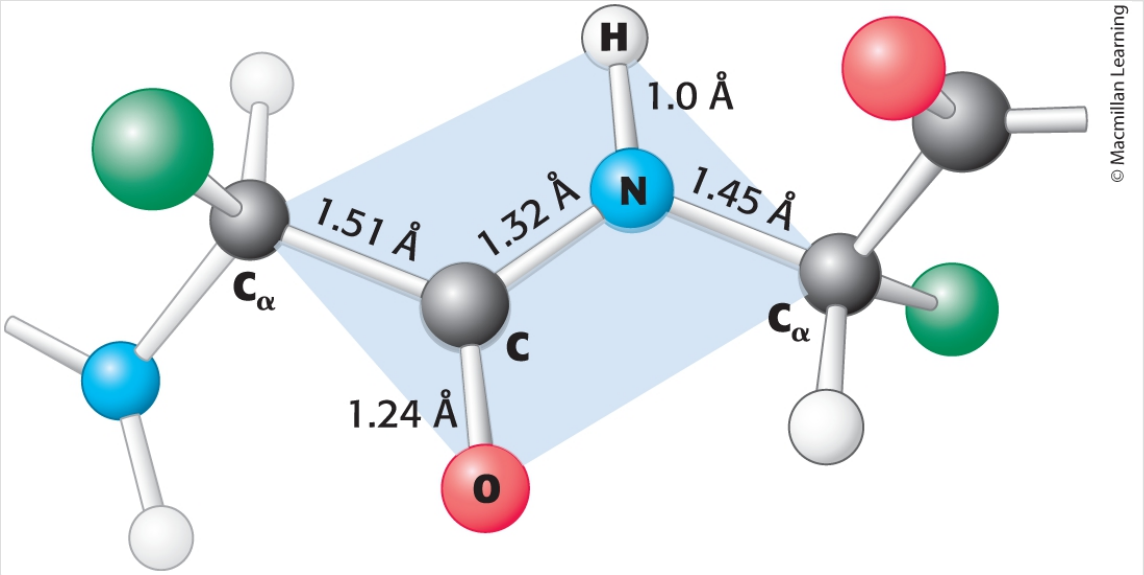
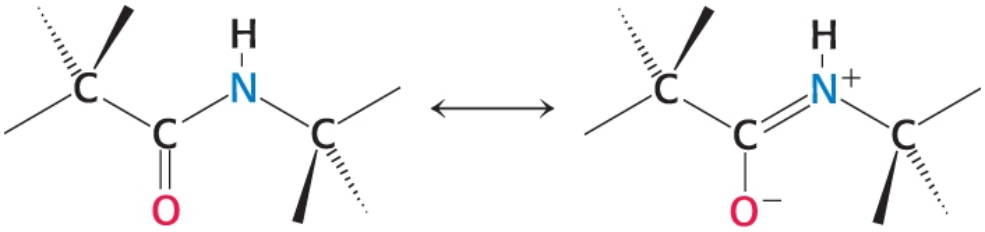


FIGURE 2.17 Peptide bonds are planar and have partial double-bond character. In a pair of linked amino acids, six atoms (C_α, C, O, N, H, and C_α) lie in a plane. Side chains are shown as green balls. The length of the peptide bond (1.32 Å) is between the expected values for a single bond and a double bond.

- *The peptide bond resonates between a single bond and a double bond.* Because of this partial double-bond character, rotation about this bond is prevented, and conformation of the peptide backbone is constrained.



Peptide-bond resonance structures

The partial double-bond character is also expressed in the length of the bond between the CO and the NH groups. As shown in Figure 2.17, the $C-N$ distance in a peptide bond is typically $1.32\ \text{Å}$, which is between the values expected for a $C-N$ single bond ($1.49\ \text{Å}$) and a $C=N$ double bond ($1.27\ \text{Å}$). Finally, the peptide bond is uncharged, allowing polymers of amino acids linked by peptide bonds to form tightly packed globular structures.

- *Almost all peptide bonds have a trans configuration*. In the trans configuration, the two α-carbon atoms are on opposite sides of the peptide bond. In the cis configuration, these groups are on the same side of the peptide bond. The preference for trans over cis can be explained by *steric repulsion*, the fact that two atoms will strongly oppose being brought together closer than their van der Waals contact distance (Section 1.3). Steric repulsion between groups attached to the α-carbon atoms hinders the formation of the cis configuration but does not arise in the trans configuration (**Figure 2.18**). By far the most common cis peptide bonds are found between proline and its preceding amino acid. Because the nitrogen of proline is bonded to two tetrahedral carbon atoms, the steric differences between the trans and cis forms are minimal, and both forms occur (**Figure 2.19**).

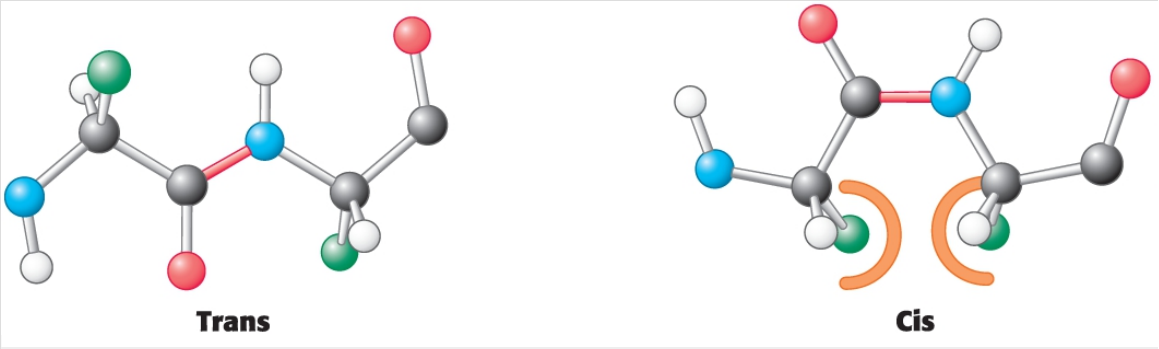


FIGURE 2.18 For most amino acids, the trans configuration of the peptide bond is strongly favored because of steric clashes that arise in the cis isomer. Steric clashes are indicated by orange semicircles. The exception to this rule is found in the next figure.

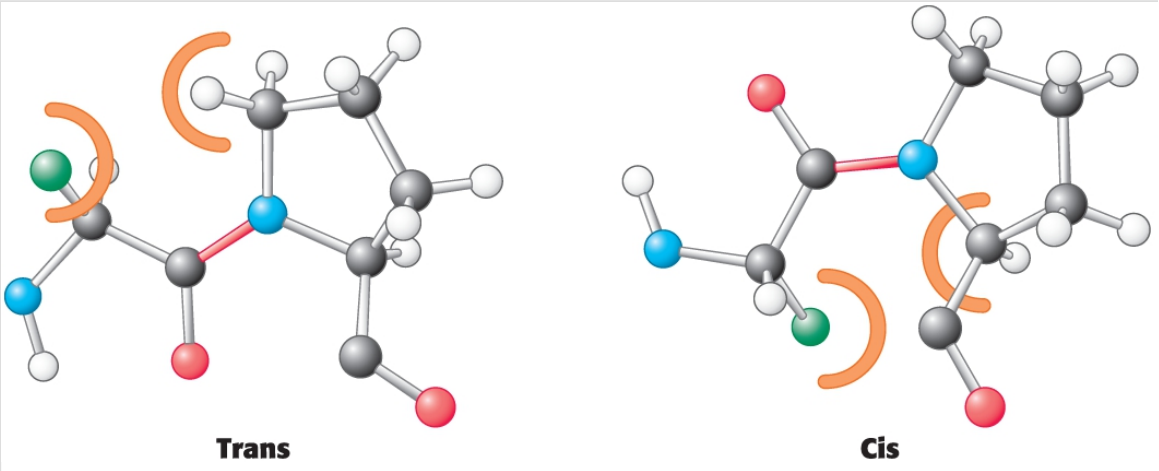


FIGURE 2.19 For peptide bonds between proline and its preceding residue, cis bonds are as likely as trans bonds. Neither configuration is favored because steric clashes exist for both the cis and trans forms.

- *The main chain bonds connected to the α carbon have rotational flexibility*. In contrast with the peptide bond, the bonds between the amino group and the α-carbon atom and between the α-carbon atom and the carbonyl group are pure single bonds. The two

adjacent rigid peptide units can rotate about these bonds, taking on various orientations. The freedom of rotation about these two bonds of each amino acid allows proteins to fold in many different conformations.

The rotations about these bonds can be specified by **torsion angles**, or **dihedral angles** (Figure 2.20). The angle of rotation about the bond between the nitrogen and the α-carbon atoms is called *phi* (ϕ). The angle of rotation about the bond between the α-carbon and the carbonyl carbon atoms is called *psi* (ψ). A clockwise rotation about either bond as viewed from the nitrogen atom toward the α-carbon atom or from the α-carbon atom toward the carbonyl group corresponds to a positive value. The ϕ and ψ angles determine the path of the polypeptide chain.

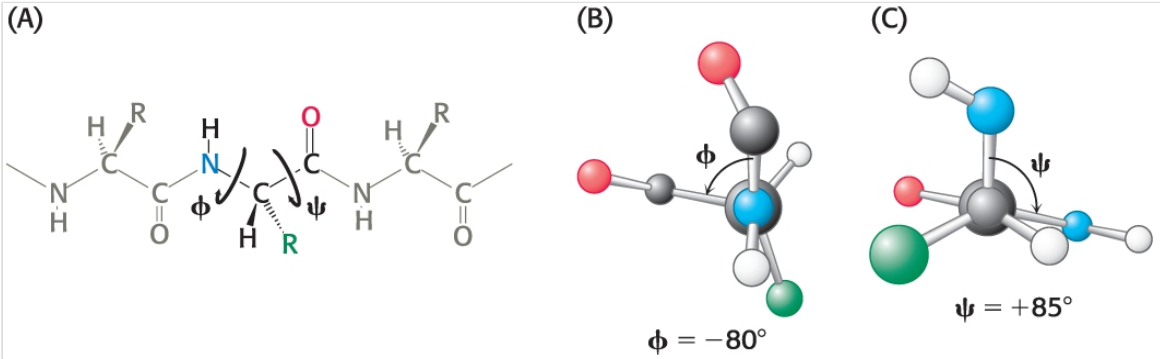


FIGURE 2.20 The structure of each amino acid in a polypeptide adjusts by rotation about two single bonds. (A) Phi (ϕ) is the angle of rotation about the bond between the nitrogen and the α carbon atoms, whereas psi (ψ) is the angle of rotation about the bond between the α-carbon ar the carbonyl carbon atoms. (B) A view down the bond between the nitrogen and the α-carbon atoms shows how φ is measured. (C) A view down the bond between the α-carbon and the carbonyl carbon atoms shows how ψ is measured.

Despite their rotational flexibility, not all values of ϕ and ψ are possible. In 1963, Gopalasamudram Ramachandran demonstrated that many combinations of ϕ and ψ are forbidden because of steric collisions between atoms. The allowed values can be visualized on a two-

dimensional plot called a **Ramachandran plot** (**Figure 2.21**). Three-quarters of the possible (ϕ, ψ) combinations are excluded simply by local steric clashes. Steric exclusion, the fact that two atoms cannot be in the same place at the same time, can be a powerful organizing principle.

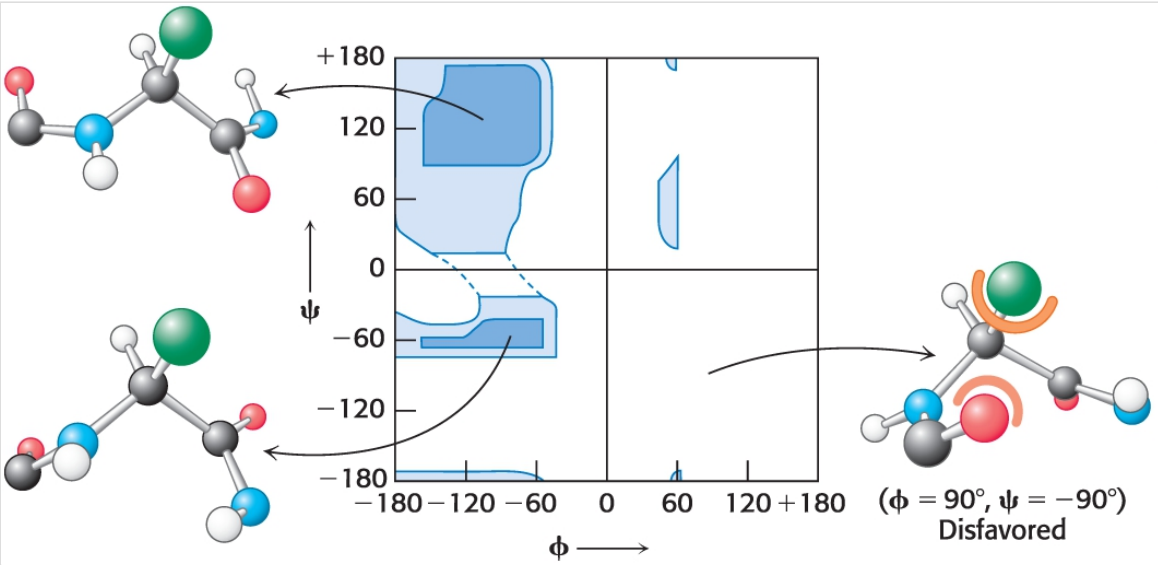


FIGURE 2.21 A Ramachandran plot shows that not all ϕ and ψ values are possible without collisions between atoms. The most favorable regions are shown in dark blue; borderline regions are shown in light blue. The structure on the right is disfavored because of steric clashes

The ability of biological polymers such as proteins to fold into well-defined structures is remarkable thermodynamically. An unfolded polymer exists as a random coil: each copy of an unfolded polymer will have a different conformation, yielding a mixture of many possible conformations. The favorable entropy associated with a mixture of many conformations opposes folding and must be overcome by interactions favoring the folded form. Thus, highly flexible polymers with a large number of possible conformations do not fold into unique structures. The rigidity of the peptide unit and the restricted set of

allowed ϕ and ψ angles limits the number of structures accessible to the unfolded form sufficiently to allow protein folding to take place.

Self-Check Question



Ramachandran plots of 18 amino acids exhibit allowed regions similar to those shown in Figure 2.21. However, the plots for two amino acids exhibit strikingly different patterns. Which two, and why?

2.4 Secondary Structure: Polypeptide Chains Can Fold into Regular Structures

Ramachandran demonstrated that many conformations of a polypeptide backbone are disallowed on the basis of steric exclusion. Do the allowed conformations permit a polypeptide chain to fold into a regularly repeating structure? In 1951, Linus Pauling, Robert Corey, and Herman Branson defined two periodic structures, the α helix (alpha helix) and the β pleated sheet (beta pleated sheet). Subsequently, other structures such as the β turn and loop were identified. Although not periodic, these common turn or loop structures are well-defined and contribute with α helices and β sheets to form the final protein structure. Alpha helices, β strands, and turns are formed by a regular pattern of hydrogen bonds between the peptide $N-H$ and $C=O$ groups of amino acids that are near one another in the linear sequence. Such folded segments are called **secondary structure**.

The alpha helix is a coiled structure stabilized by intrachain hydrogen bonds

In evaluating potential structures, Pauling, Corey, and Branson considered which conformations of peptides were sterically allowed and which most fully exploited the hydrogen-bonding capacity of the backbone NH and CO groups. The first of their proposed structures, the **α helix**, is a rodlike structure (Figure 2.22). A tightly coiled backbone forms the inner part of the rod and the side chains extend outward in a helical array.

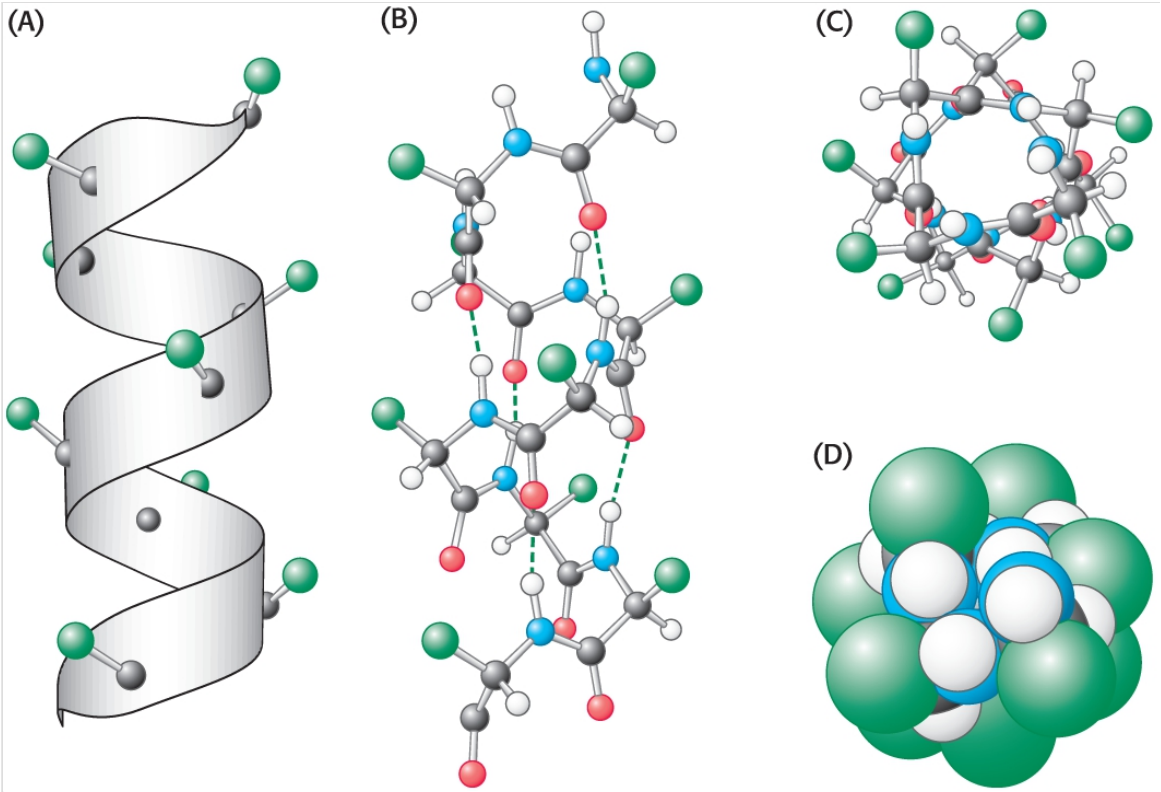


FIGURE 2.22 Various depictions of an α helix reveal several of its key features. (A) A ribbon depiction shows the α-carbon atoms and side chains (green). (B) A side view of a ball-and-stick version depicts the hydrogen bonds (dashed lines) between NH and CO groups. (C) An end view shows the coiled backbone as the inside of the helix and the side chains (green) projecting outward. (D) A space-filling view of part C shows the tightly packed interior core of the helix.



Photo provided by AIP Emilio Segrè Visual Archives, Physics Today Collection

HERMAN BRANSON While Pauling and Corey often receive the most recognition for the discovery of the α helix, a third scientist, Herman Branson, also made key contributions to the discovery and was a coauthor on the seminal paper. Dr. Branson, a physics professor at Howard University who was a visiting scientist in Linus Pauling's lab at the California Institute of Technology in 1948, performed computational analysis using Pauling's x-ray measurements to narrow the possible structures down to the α helix and a looser structure called the gamma helix.

Following this work, his scientific career continued for two more decades, after which he served as the president at two historically Black universities, Central State University from 1968 to 1970, and Lincoln University from 1970 to 1985.

The α helix is stabilized by hydrogen bonds between the NH and CO groups of the main chain. In particular, the CO group of each amino acid forms a hydrogen bond with the NH group of the amino acid that is situated four residues ahead in the sequence (Figure 2.23). Thus, except for amino acids near the ends of an α helix, all the main-chain CO and NH groups are hydrogen bonded.

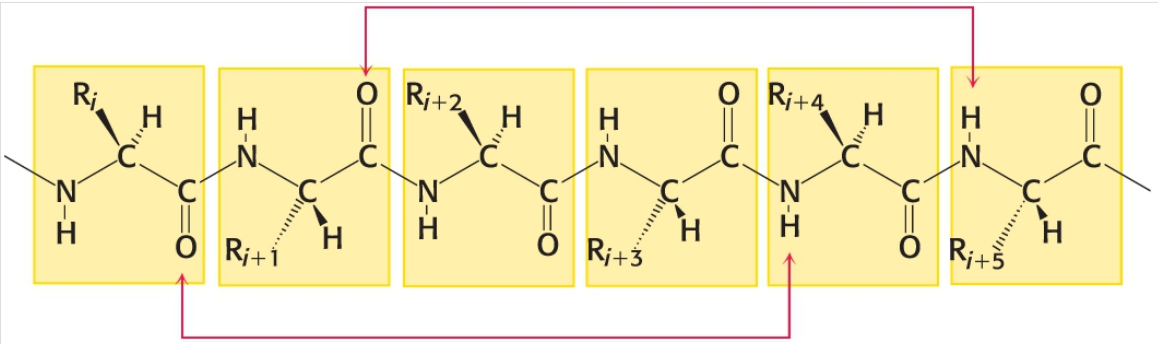


FIGURE 2.23 In an α helix, hydrogen bonds form between the CO group of residue *i* and the N group of residue $i + 4$.

Each residue in an α helix is related to the next one by a *rise* (or *translation*) of $1.5\ \text{Å}$ along the helix axis and a rotation of 100 degrees; this gives 3.6 amino acid residues per turn of the helix. Therefore, amino acids spaced three and four apart in the sequence are spatially quite close to one another in an α helix. In contrast, amino acids spaced two apart in the sequence are situated on opposite sides of the helix and so are unlikely to make contact. The *pitch* of the α helix is the length of one complete turn along the helix axis and is equal to the product of the rise ($1.5\ \text{Å}$) and the number of residues per turn (3.6), or $5.4\ \text{Å}$.

The direction of rotation about the axis of an α helix (called *screw sense*) can be right-handed (clockwise) or left-handed (counterclockwise). While the Ramachandran plot reveals that both the right-handed and the left-handed helices are among allowed conformations (Figure 2.24), essentially all α helices found in proteins are right-handed. Right-handed helices are energetically more favorable because there is less steric clash between the side chains and the backbone. In schematic representations of proteins, α helices are depicted as twisted ribbons or rods (Figure 2.25).

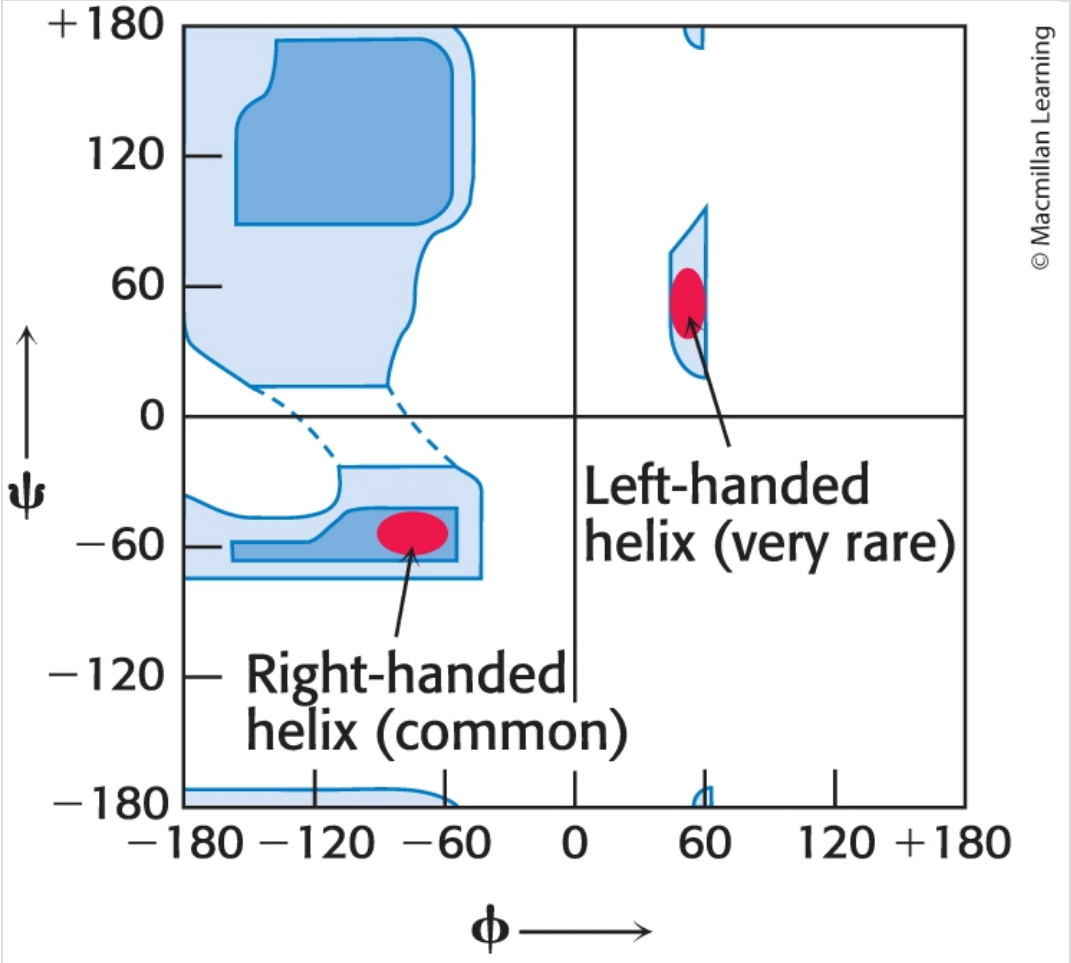


FIGURE 2.24 Both right- and left-handed helices lie in regions of allowed conformations in the Ramachandran plot. However, essentially all α helices in proteins are right-handed.

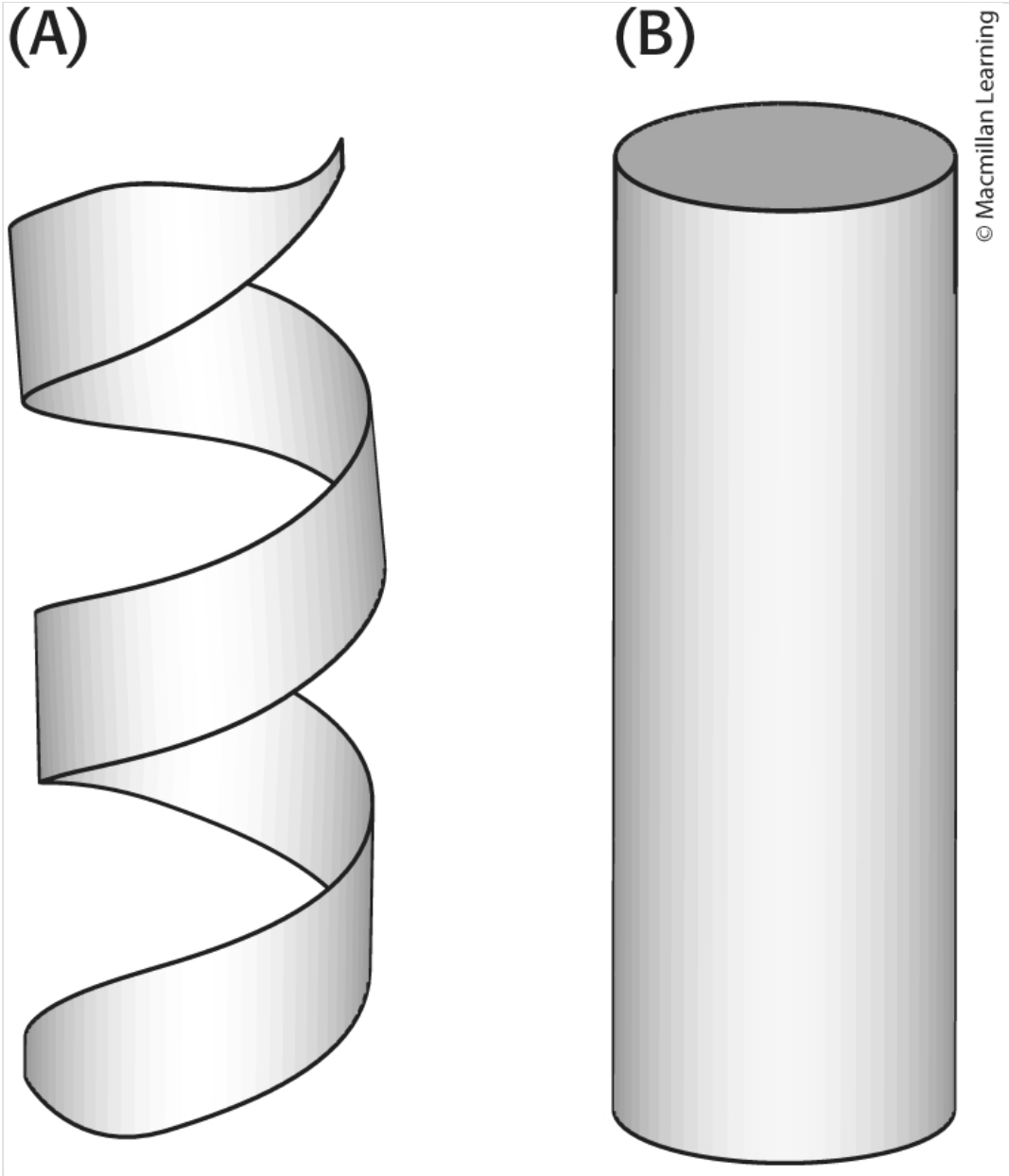


FIGURE 2.25 There are two common ways to draw α helices. (A) A ribbon depiction. (B) A cylindrical (rod) depiction.

Not all amino acids can be readily accommodated in an α helix. Branching at the β-carbon atom — the side chain carbon atom bonded to the α carbon — as in valine, threonine, and isoleucine, tends to destabilize α helices because of steric clashes. Serine, aspartate, and asparagine also tend to disrupt α helices because their side chains contain hydrogen-bond donors or acceptors in close proximity to the main chain, where they compete for main-chain NH and CO groups. Proline also is a helix breaker because it lacks an NH group and because its ring structure prevents it from assuming the Φ value to fit into an α helix.

The α-helical content of proteins ranges widely, from none to almost 100%. For example, about 75% of the residues in ferritin, a protein that helps store iron, are in α helices (Figure 2.26). Indeed, about 25% of all soluble proteins are composed of α helices connected by loops and turns of the polypeptide chain. Single α helices are usually less than 45 Å long. Many proteins that span biological membranes also contain α helices.

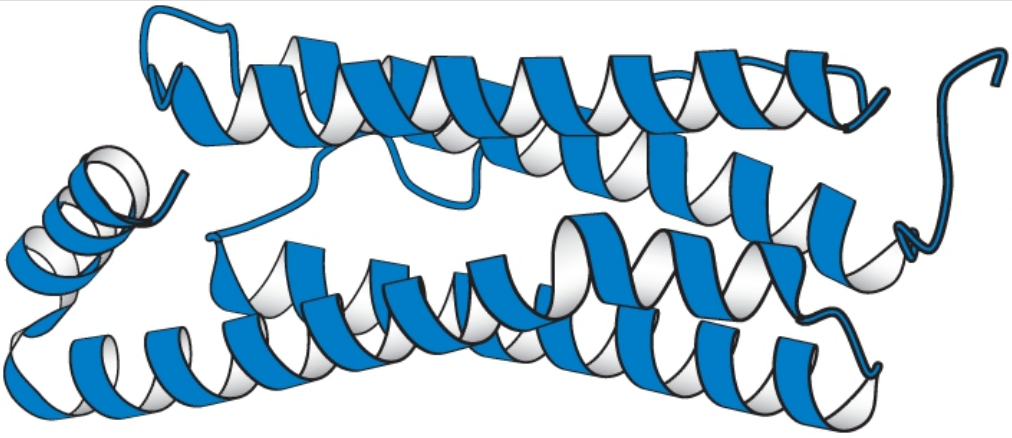


FIGURE 2.26 Ferritin, an iron-storage protein, is composed largely of α helices.

[Drawn from 1AEW.pdb.]

INTERACT with this model in Achieve

Beta sheets are stabilized by hydrogen bonding between polypeptide strands

Pauling and Corey proposed another periodic structural motif, which they named the **β pleated sheet** (β because it was the second structure they elucidated, the α helix having been the first). The β pleated sheet (or, more simply, the β sheet) differs markedly from the rodlike α helix. It is composed of two or more polypeptide chains called **β strands**. A β strand is almost fully extended rather than being tightly coiled as in the α helix. A range of extended structures are sterically allowed (Figure 2.27).

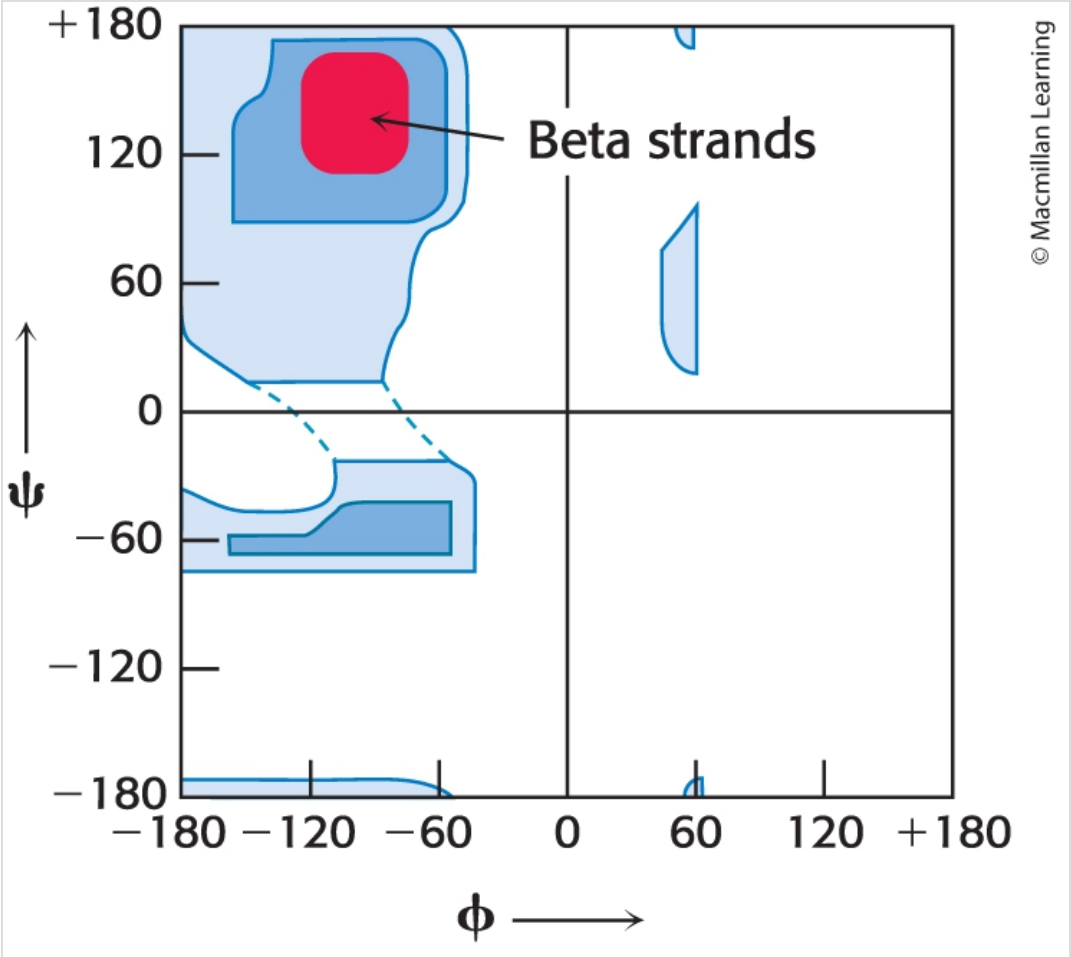


FIGURE 2.27 β strands occupy an allowed region of the Ramachandran plot.

The distance between adjacent amino acids along a β strand is approximately 3.5 Å, in contrast with a distance of 1.5 Å along an α helix. The side chains of adjacent amino acids point in opposite directions (Figure 2.28). A β sheet is formed by linking two or more β strands lying next to one another through hydrogen bonds. Adjacent strands in a β sheet can run in opposite directions (antiparallel β sheet) or in the same direction (parallel β sheet). In the antiparallel arrangement, the NH group and the CO group of each amino acid are respectively hydrogen bonded to the CO group and the NH group of a partner on the adjacent chain (Figure 2.29). In the parallel arrangement, the hydrogen-bonding scheme is slightly more complicated. For each amino acid, the NH group is hydrogen bonded to the CO group of one amino acid on the adjacent strand, whereas the CO group is hydrogen bonded to the NH group on the amino acid two residues farther along the chain (Figure 2.30). Many strands, typically 4 or 5 but as many as 10 or more, can come together in β sheets. Such β sheets can be purely antiparallel, purely parallel, or mixed (Figure 2.31).

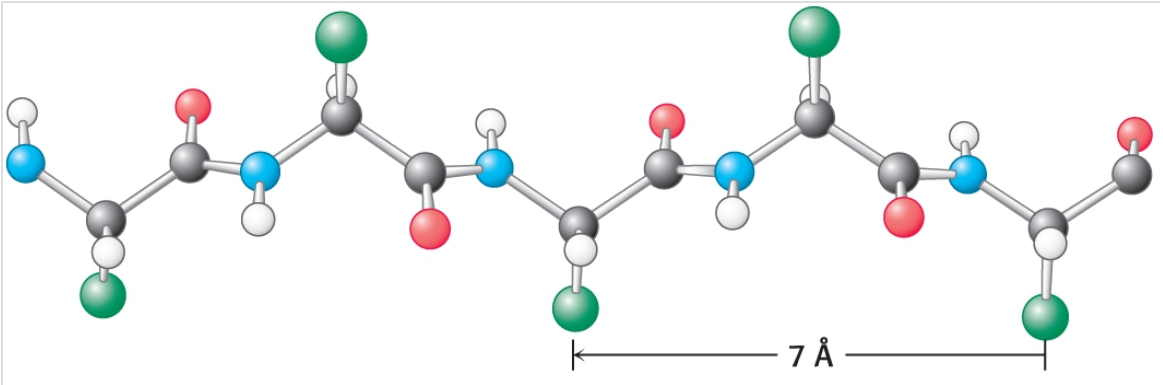


FIGURE 2.28 The side chains of a β strand project alternately above and below the plane of tl strand. In this extended conformation, the side chains (shown in green) on the same face of the strand are positioned about 7 Å apart.

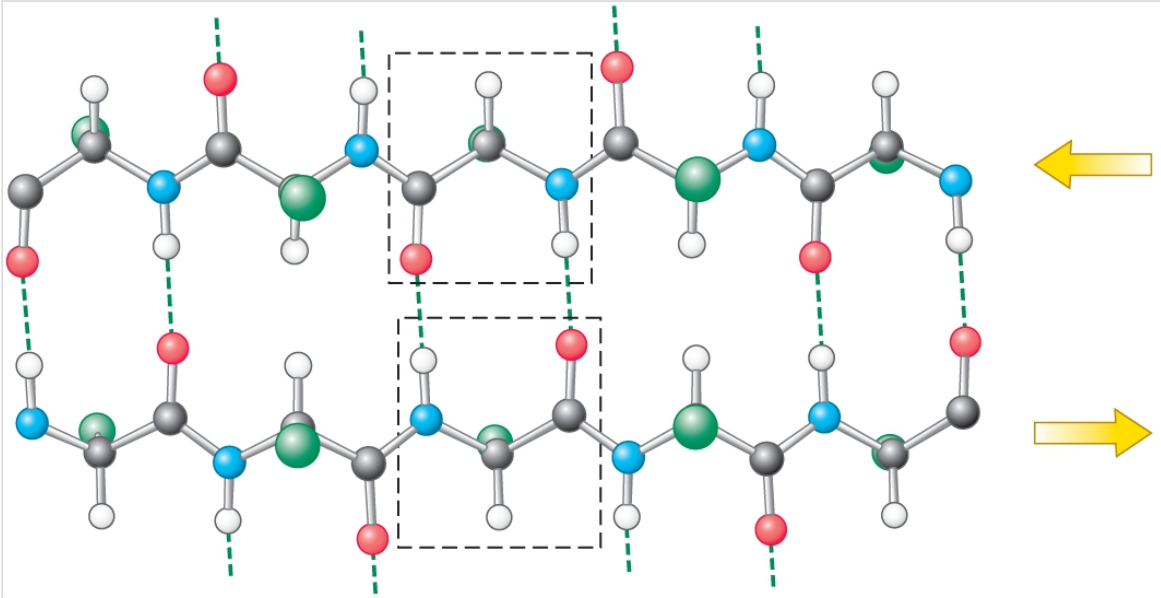


FIGURE 2.29 In an antiparallel β sheet, adjacent β strands run in opposite directions. Note th hydrogen bonds between NH and CO groups connect each amino acid to a single amino acid or an adjacent strand, stabilizing the structure.

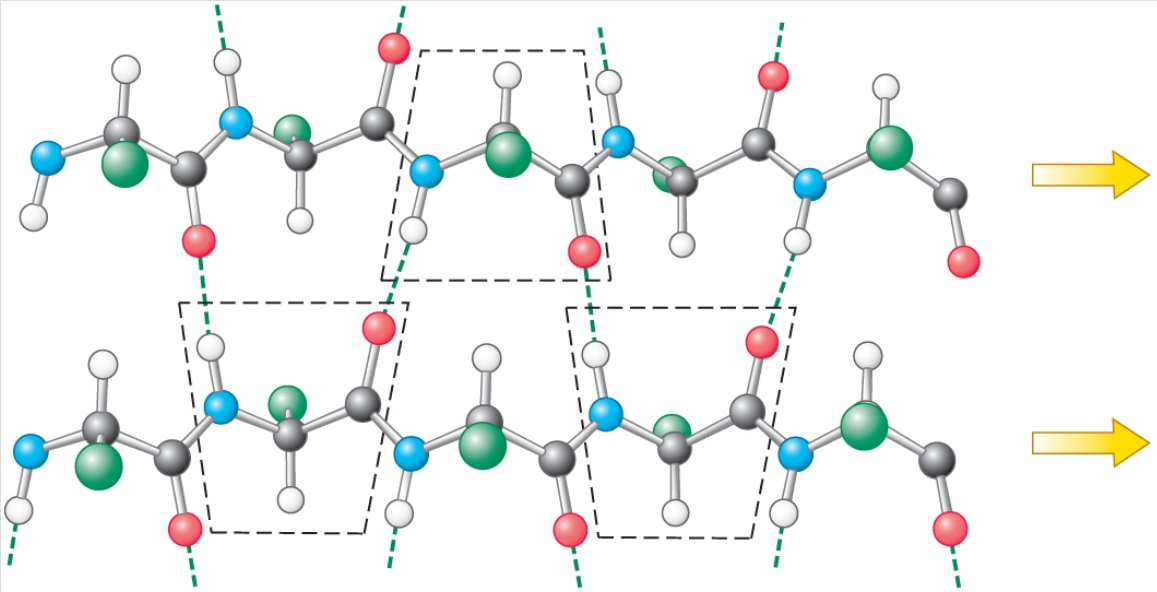


FIGURE 2.30 In a parallel β sheet, adjacent β strands run in the same direction. Note that hydrogen bonds connect each amino acid on one strand with two different amino acids on the adjacent strand.

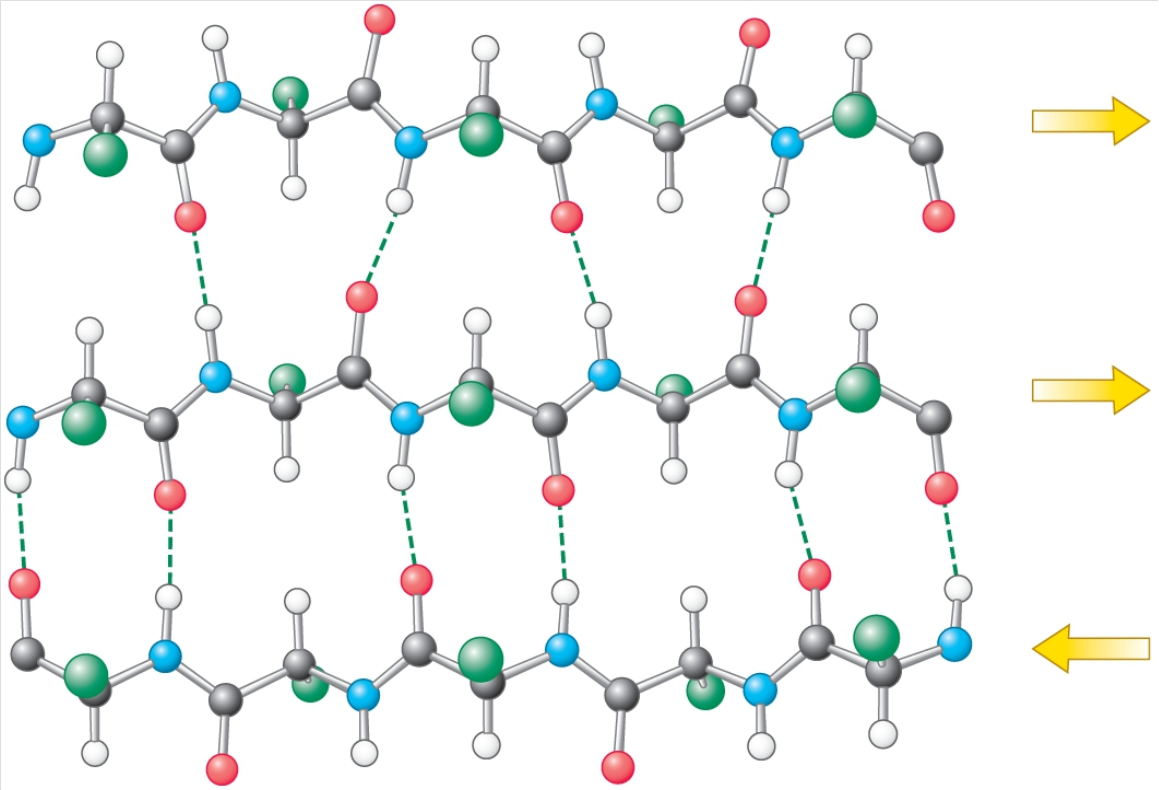


FIGURE 2.31 In a mixed β sheet, the β strands have a combination of parallel and antiparalle pairings.

In schematic representations, β strands are usually depicted by broad arrows pointing in the direction of the carboxyl-terminal end to indicate the type of β sheet formed — parallel or antiparallel. More structurally diverse than α helices, β sheets can be almost flat, but most adopt a somewhat twisted shape (Figure 2.32). The β sheet is an important structural element in many proteins. For example, fatty acid-binding proteins, important for lipid metabolism, are built almost entirely from β sheets (Figure 2.33).

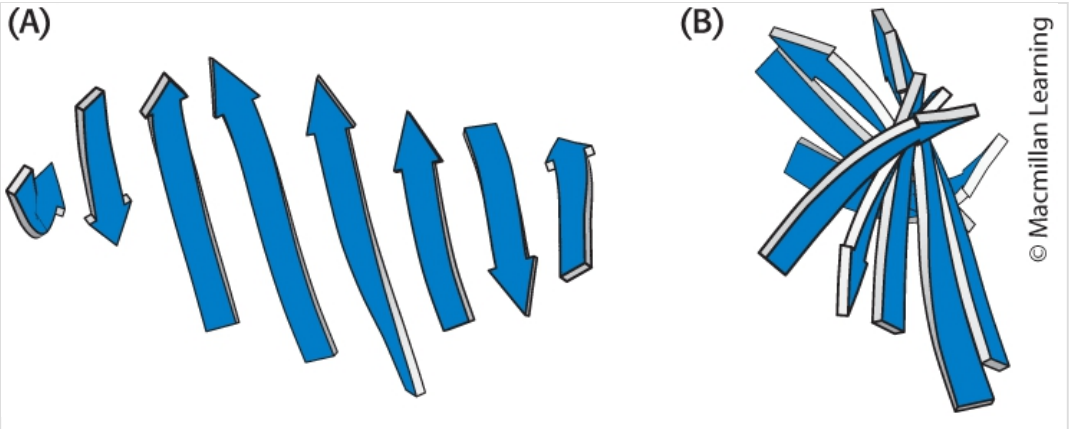
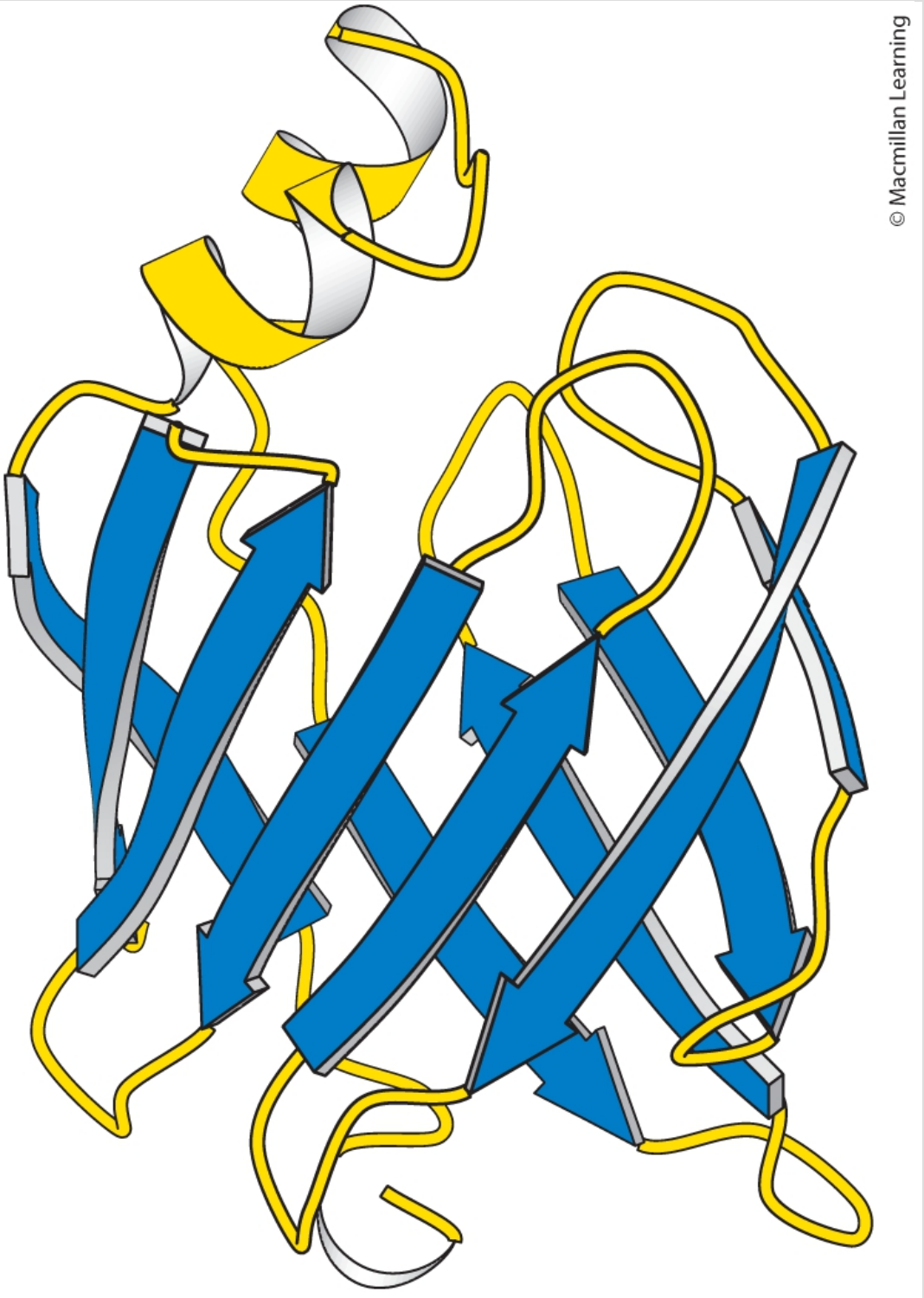


FIGURE 2.32 The twisted shape of some β sheets is more evident in a schematic depiction of β strands. (A) β strands are represented by broad arrows pointing towards their carboxy-terminal end. (B) When rotated by 90 degrees, the schematic view more clearly illustrates the twist in the β sheet.



© Macmillan Learning

FIGURE 2.33 Fatty acid-binding protein is rich in β sheets.

[Drawn from 1FTP.pdb.]

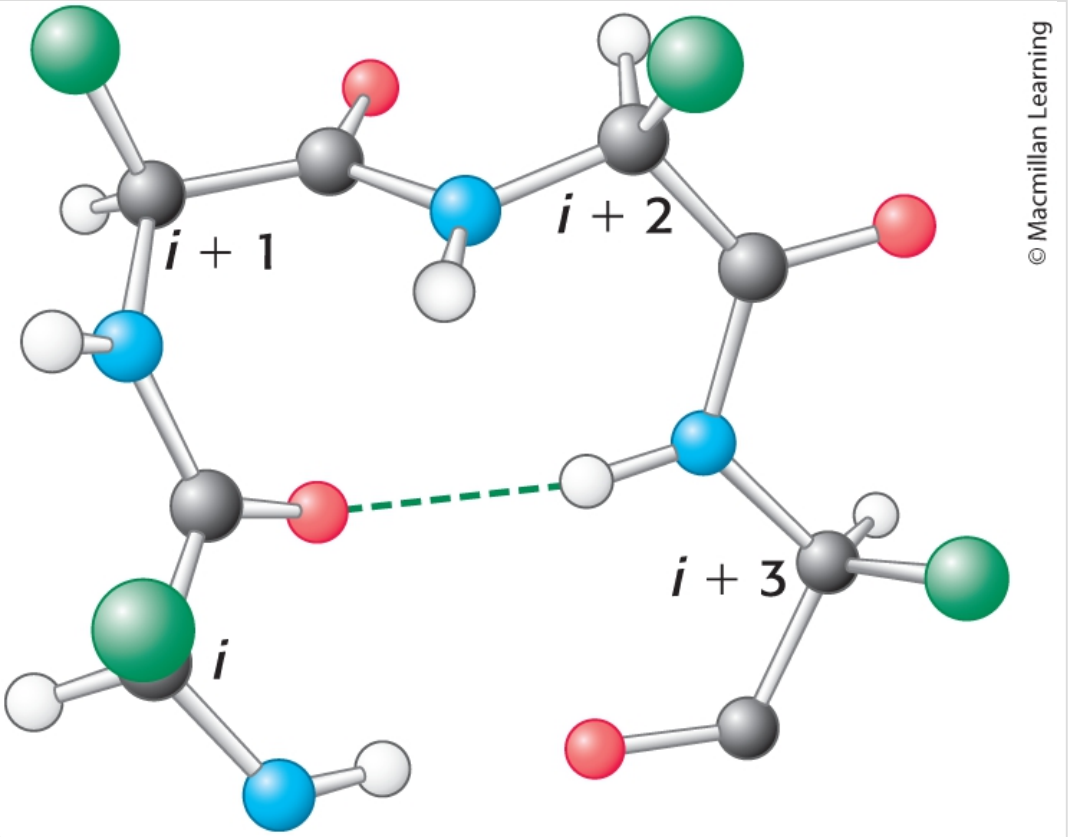
Self-Check Question



How far apart are residues that appear on the same face of an α helix? What about on a β strand?

Polypeptide chains can change direction by making reverse turns and loops

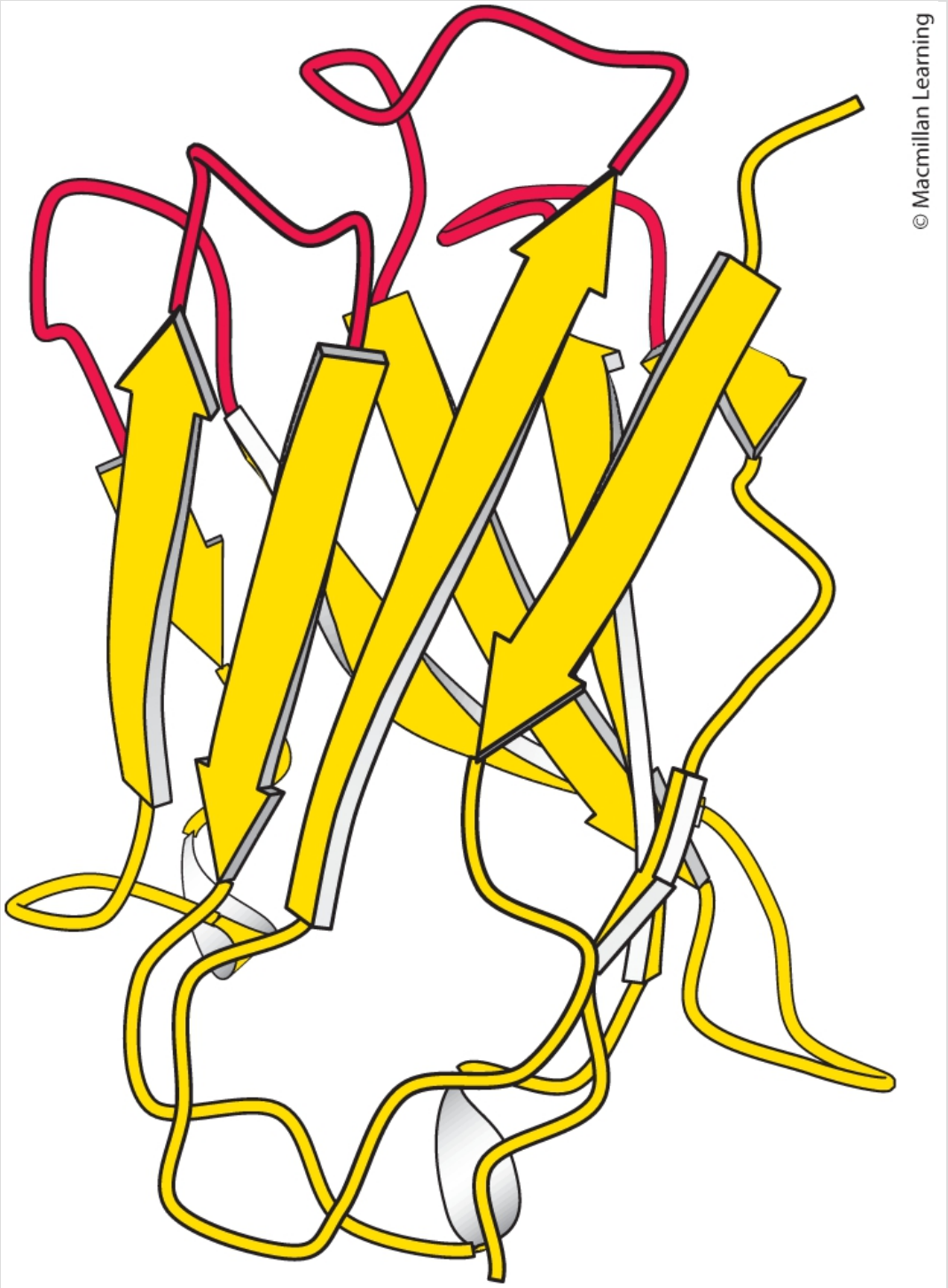
As we will explore in Section 2.5, most proteins have compact, globular shapes owing to reversals in the direction of their polypeptide chains. Many of these reversals are accomplished by a common structural element called the **reverse turn** (also known as the **β turn** or **hairpin turn**), illustrated in **Figure 2.34**. In many reverse turns, the CO group of residue *i* of a polypeptide is hydrogen bonded to the NH group of residue $i + 3$. This interaction stabilizes abrupt changes in direction of the polypeptide chain.



© Macmillan Learning

FIGURE 2.34 In a reverse turn, the CO group of residue *i* of the polypeptide chain is hydrogen bonded to the NH group of residue $i + 3$. This hydrogen bond stabilizes the turn.

In other cases, more-elaborate structures are responsible for chain reversals. These structures are called **loops**. Unlike α helices and β strands, loops do not have regular, periodic structures. Nonetheless, loop structures are often rigid and well-defined (Figure 2.35). Turns and loops invariably lie on the surfaces of proteins and often participate in interactions between proteins and other molecules.



© Macmillan Learning

FIGURE 2.35 Loops are found on protein surfaces. A part of an antibody molecule has surface loops (shown in red) that mediate interactions with other molecules.

[Drawn from 7FAB.pdb.]



2.5 Tertiary Structure: Proteins Can Fold into Globular or Fibrous Structures

Let us now examine how amino acids are grouped together in a complete protein. X-ray crystallographic, nuclear magnetic resonance (NMR), and cryo-electron microscopic (cryo-EM) studies (Section 4.5) have revealed the detailed three-dimensional structures of thousands of proteins. We begin here with an examination of myoglobin, the first protein to be seen in atomic detail, in work reported by John Kendrew and colleagues in 1958. Myoglobin, the oxygen storage protein in muscle, is a single polypeptide chain of 153 amino acids (Chapter 3) that forms an extremely compact molecule. Its overall dimensions are $45 \times 35 \times 25$ Å, an order of magnitude less than if it were fully stretched out (**Figure 2.36**). About 70% of the main chain is folded into eight α helices, and much of the rest of the chain forms turns and loops between helices.

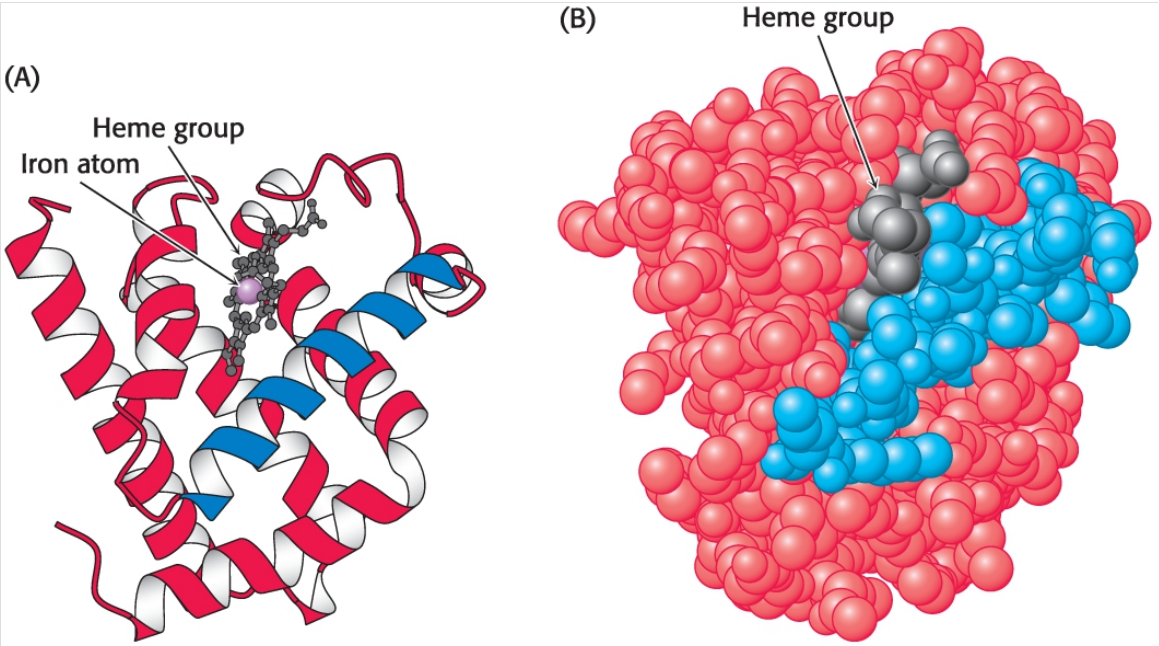


FIGURE 2.36 Myoglobin folds into a compact structure. (A) A ribbon diagram shows that the protein consists largely of α helices. (B) A space-filling model in the same orientation shows hov tightly packed the folded protein is. Notice that the heme group is nestled into a crevice in the compact protein with only an edge exposed. One helix is blue to allow comparison of the two structural depictions.

[Drawn from 1A6N.pdb.]

The folding of the main chain of myoglobin, like that of most other proteins, is complex and devoid of symmetry. The overall course of the polypeptide chain of a protein is referred to as its **tertiary structure**. A unifying principle emerges from the distribution of side chains. Strikingly, the interior consists almost entirely of nonpolar residues such as leucine, valine, methionine, and phenylalanine (Figure 2.37). Charged residues such as aspartate, glutamate, lysine, and arginine are absent from the inside of myoglobin. The only polar residues inside are two histidine residues, which play critical roles in binding iron and oxygen. The outside of myoglobin, on the other hand, consists of both polar and nonpolar residues. The space-filling model shows that there is very little empty space inside.

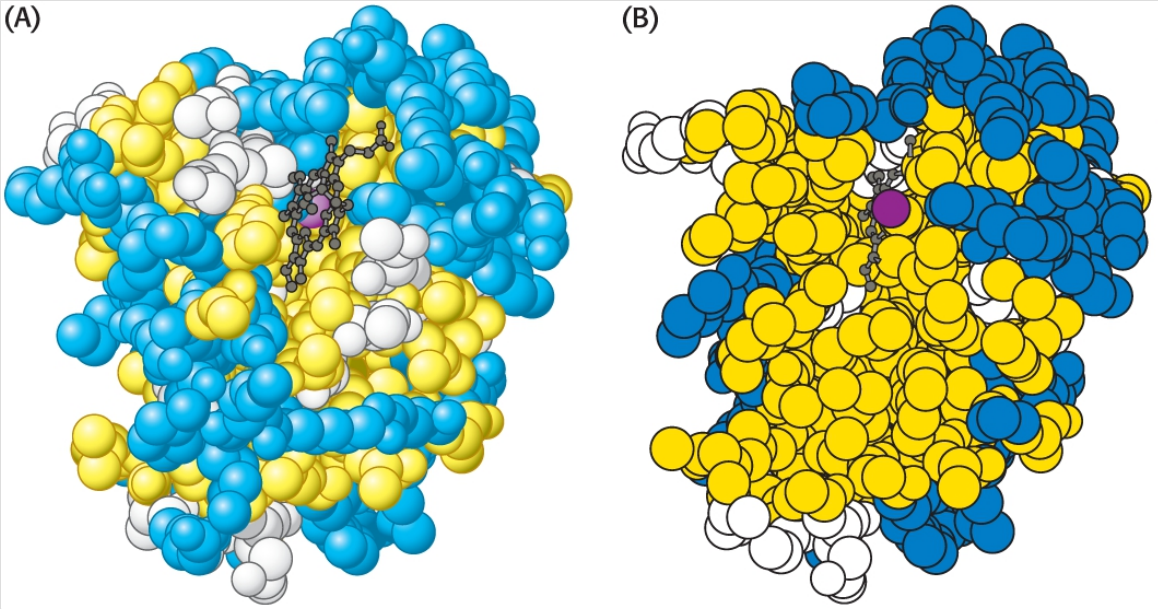


FIGURE 2.37 Hydrophobic amino acids are preferentially distributed in the interior of myoglobin. (A) A space-filling model of myoglobin with hydrophobic amino acids shown in yellow, charged amino acids shown in blue, and others shown in white. Notice that the surface of the molecule has many charged amino acids, as well as some hydrophobic amino acids. (B) In this cross-sectional view, notice that mostly hydrophobic amino acids are found on the inside of the structure, whereas the charged amino acids are found on the protein surface.

[Drawn from 1MBD.pdb.]

Globular proteins form tightly packed structures

The tight packing of myoglobin into a highly compact structure, its lack of symmetry, and its solubility in water are characteristics of **globular proteins** which perform a wide array of important functions, including regulatory, signaling, and enzymatic activities.

The contrasting distribution of polar and nonpolar residues reveals a key facet of protein architecture: in an aqueous environment, protein folding is driven by the strong tendency of hydrophobic residues to be

excluded from water. Recall that a system is more thermodynamically stable when hydrophobic groups are clustered rather than extended into the aqueous surroundings (the hydrophobic effect). The polypeptide chain therefore folds so that its hydrophobic side chains are buried and its polar, charged chains are on the surface.

Many α helices and β strands are amphipathic; that is, the α helix or β strand has a hydrophobic face, which points into the protein interior, and a more polar face, which points into solution. The fate of the main chain accompanying the hydrophobic side chains is important, too. An unpaired peptide NH or CO group markedly prefers water to a nonpolar milieu. The secret of burying a segment of main chain in a hydrophobic environment is to pair all the NH and CO groups by hydrogen bonding. This pairing is neatly accomplished in an α helix or β sheet.

Van der Waals interactions between tightly packed hydrocarbon side chains also contribute to the stability of proteins. We can now understand why the set of 20 amino acids contains several that differ subtly in size and shape. They provide a palette from which to choose to fill the interior of a protein neatly and thereby maximize van der Waals interactions, which require intimate contact.

Some proteins that span biological membranes are “the exceptions that prove the rule” because they have the reverse distribution of hydrophobic and hydrophilic amino acids. For example, consider porins — proteins found in the outer membranes of many bacteria (**Figure 2.38**). Membranes are built largely of hydrophobic chains. Thus, porins are covered on the outside largely with hydrophobic residues that interact with the neighboring alkane chains. In contrast, the center of the protein contains many charged and polar amino acids that surround a water-filled channel running through the middle of the protein. Because porins function in hydrophobic environments, they are “inside out” relative to proteins that function in aqueous solution.

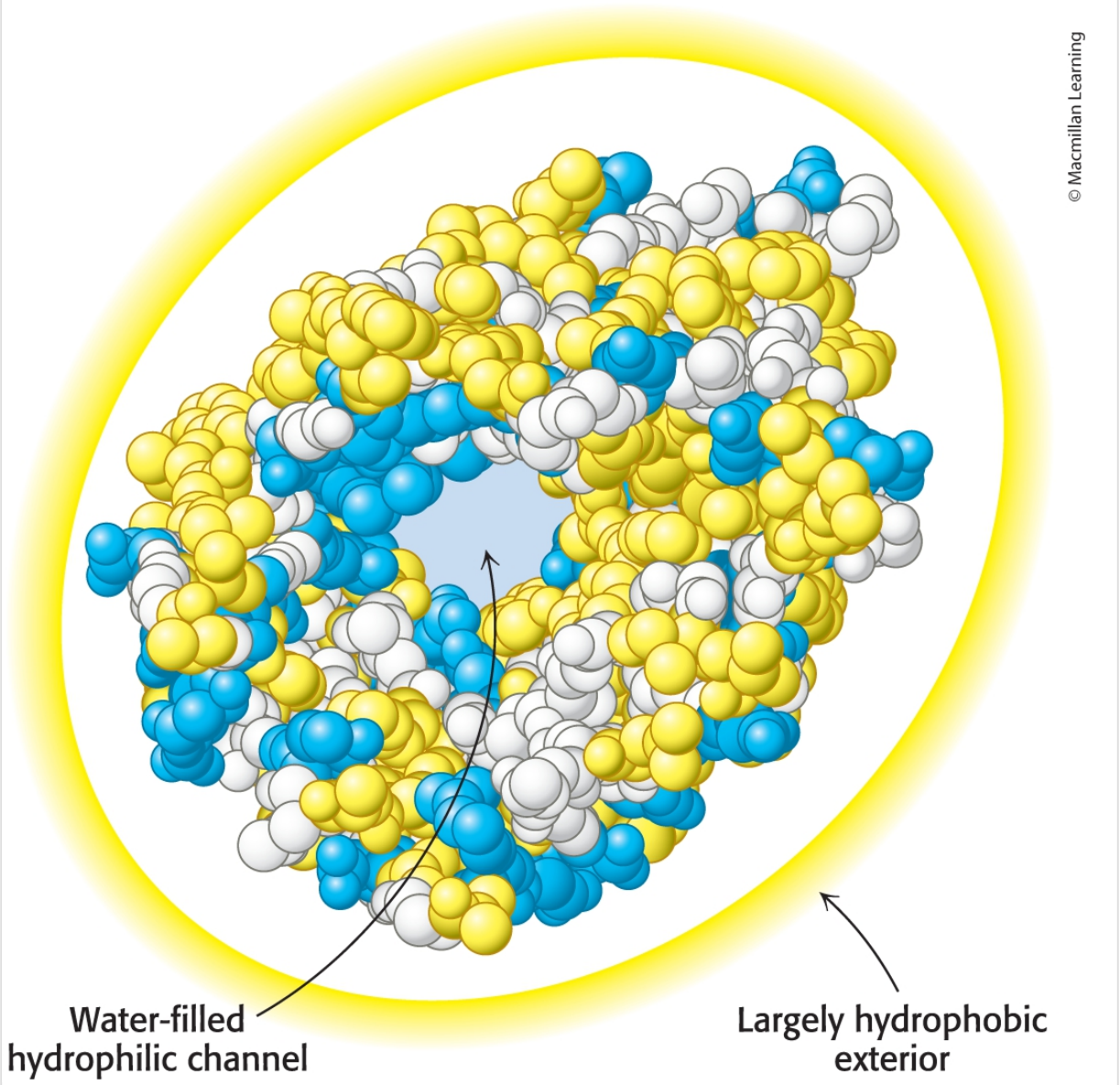


FIGURE 2.38 Porin, found in the hydrophobic environment of the membrane, exhibits an "inside out" amino acid distribution. The outside of porin (which contacts hydrophobic groups in membranes) is covered largely with hydrophobic residues, whereas the center includes a water-filled channel lined with charged and polar amino acids.

[Drawn from 1PRN.pdb.]

Certain combinations of secondary structure are present in many proteins and frequently exhibit similar functions. These combinations

are called **motifs** (or **supersecondary structures**). For example, an α helix separated from another α helix by a turn, called a *helix-turn-helix* motif, is found in many proteins that bind DNA (**Figure 2.39**).

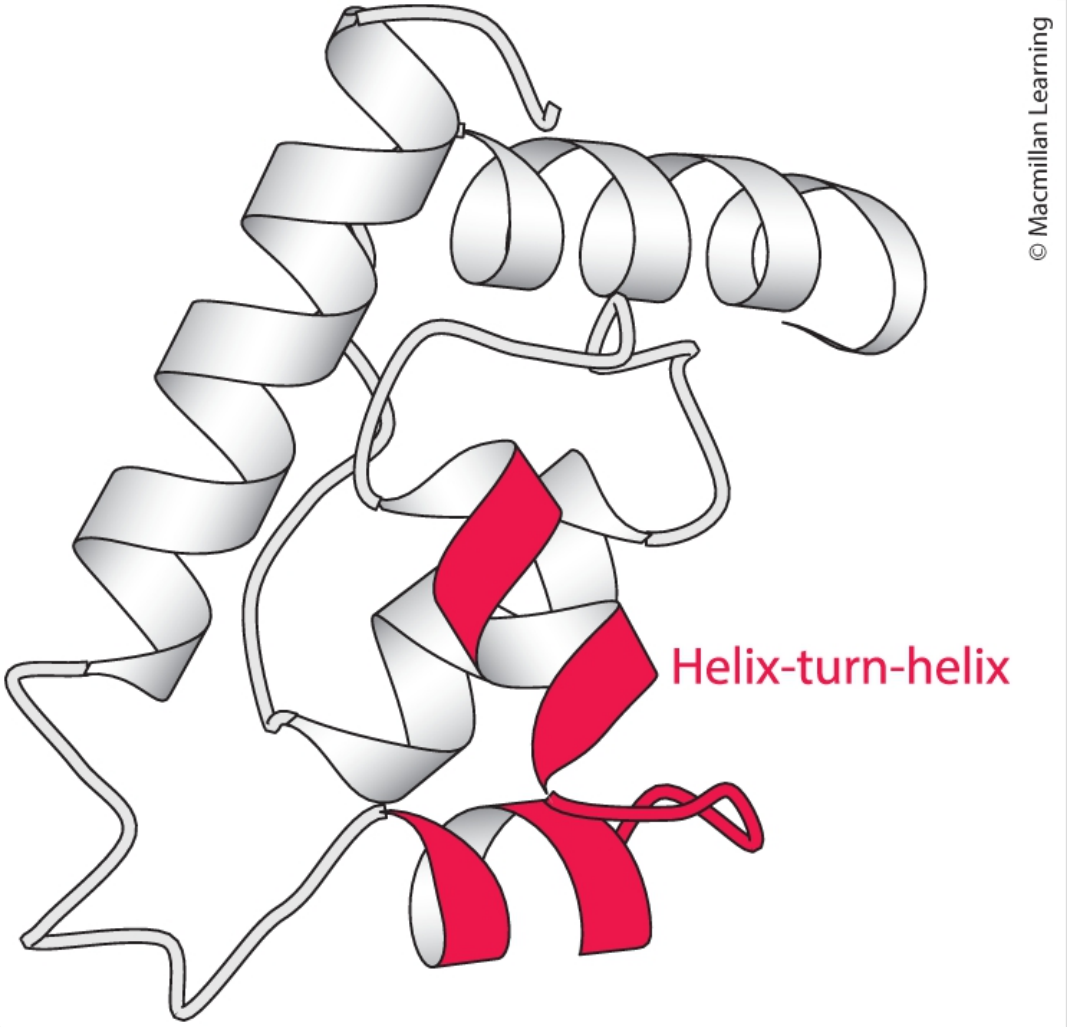


FIGURE 2.39 The helix-turn-helix motif is a supersecondary structural element found in many DNA-binding proteins.

[Drawn from 1LMB.pdb.]

Some polypeptide chains fold into two or more compact regions that may be connected by a flexible segment of polypeptide chain, rather

like pearls on a string. These compact globular units, called **domains**, range in size from about 30 to 400 amino acid residues. For example, the extracellular part of CD4, a protein on the surface of certain cells of the immune system, comprises four similar domains of approximately 100 amino acids each (**Figure 2.40**). Proteins may have domains in common even if their overall tertiary structures are different.

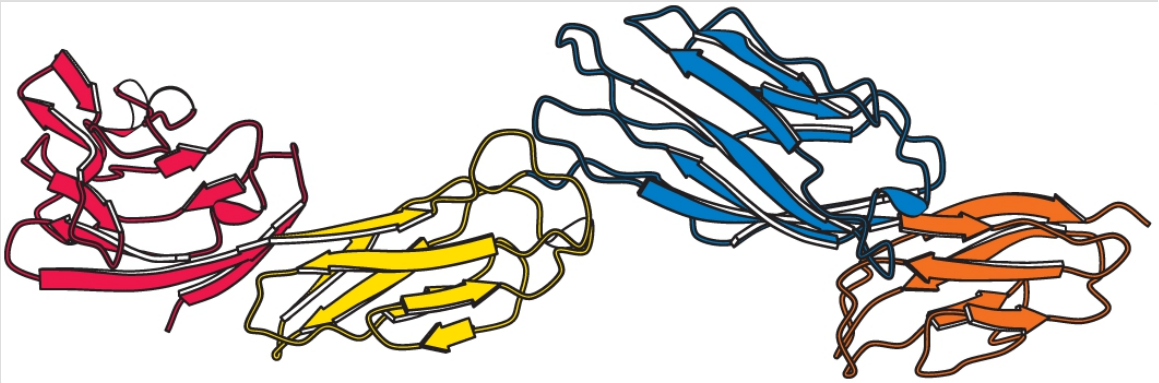


FIGURE 2.40 Domains are compact regions within proteins that are connected by flexible polypeptide segments. The cell-surface protein CD4 consists of four similar domains.

[Drawn from 1WIO.pdb.]

Self-Check Question

Proteins that span biological membranes often contain α helices. Given that the insides of membranes are highly hydrophobic, predict what type of amino acids would be in such an α helix. Why is an α helix particularly suited to existence in the hydrophobic environment of a membrane interior?

Fibrous proteins form extended structures that provide support for cells and tissues

In contrast to globular proteins, **fibrous proteins** form long, extended structures that feature repeated sequences. These proteins, such as α-keratin and collagen, use special types of helices that facilitate the formation of long fibers that serve a structural role.

α-Keratin, which is an essential component of wool, hair, and skin, consists of two right-handed α helices intertwined to form a type of left-handed superhelix called an α-*helical coiled coil*. α-Keratin is a member of a superfamily of proteins referred to as *coiled-coil proteins* (**Figure 2.41**). In these proteins, two or more α helices can entwine to form a very stable structure, which can have lengths of 1000 Å (100 nm, or 0.1 μm) or more. There are approximately 60 members of this family in humans, including intermediate filaments, proteins that contribute to the cell cytoskeleton (internal scaffolding in a cell), and the muscle proteins myosin and tropomyosin. Members of this family are characterized by a central region of 300 amino acids that contains imperfect repeats of a sequence of 7 amino acids called a *heptad repeat*.

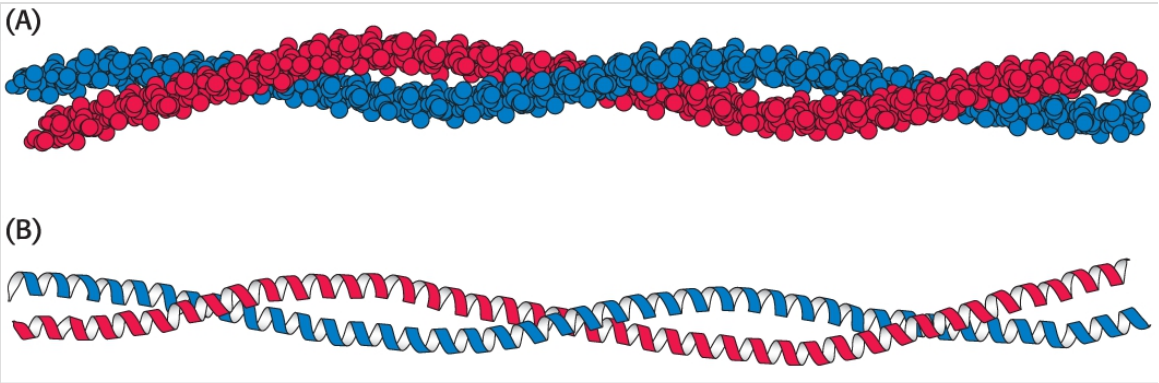


FIGURE 2.41 The α-helical coiled coil adopts an extended structure. (A) A space-filling model. (B) A ribbon diagram. The two helices wind around one another to form a superhelix. Such structures are found in many proteins, including keratin in hair, quills, claws, and horns.

[Drawn from 1C1G.pdb.]

The two helices in α-keratin associate with each other by weak interactions such as van der Waals forces and ionic interactions. The left-handed supercoil alters the two right-handed α helices such that there are 3.5 residues per turn instead of 3.6. As a result, the pattern of side-chain interactions can be repeated every seven residues, forming the heptad repeats. Two helices with such repeats are able to interact with one another if the repeats are complementary (Figure 2.42). For example, the repeating residues may be hydrophobic, allowing van der Waals interactions, or have opposite charge, allowing ionic interactions. In addition, the two helices may be linked by disulfide bonds formed by neighboring cysteine residues.

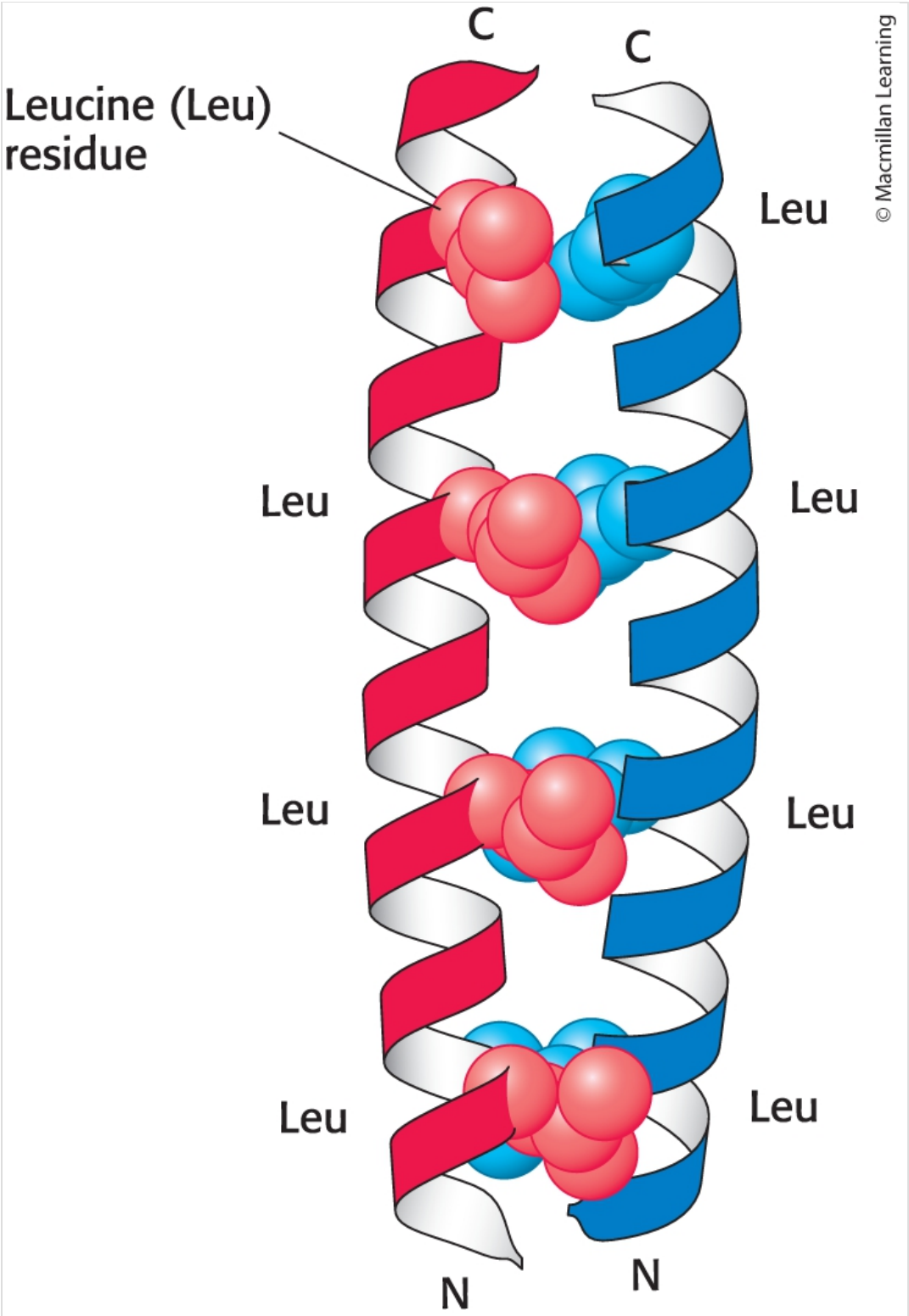


FIGURE 2.42 Heptad repeats from each helix in a coiled-coil protein interact with one another. Every seventh residue in each helix is leucine. The two helices are held together by van der Waals interactions primarily between the leucine residues.

[Drawn from 2ZTA.pdb.]

INTERACT with the models shown in Figure 2.33 and Figures 2.35–2.42 in Achieve

The bonding of the helices accounts for the physical properties of wool, an example of an α-keratin. Wool is extensible and can be stretched to nearly twice its length because the α helices stretch, breaking the weak interactions between neighboring helices. However, the covalent disulfide bonds resist breakage and return the fiber to its original state once the stretching force is released. The number of disulfide bond cross-links further defines the fiber's properties. Hair and wool, having fewer cross-links, are flexible. Horns, claws, and hooves, having more cross-links, are much harder.

A different type of helix is present in collagen, the most abundant protein of mammals. Collagen is the main fibrous component of skin, bone, tendon, cartilage, and teeth. This extracellular protein is a rod-shaped molecule, about $3000\ \text{Å}$ long and only $15\ \text{Å}$ in diameter. It contains three helical polypeptide chains, each nearly 1000 residues long. Glycine appears at every third residue in the amino acid sequence, and the sequence glycine-proline-hydroxyproline recurs frequently (**Figure 2.43**). Hydroxyproline is a derivative of proline that has a hydroxyl group in place of one of the hydrogen atoms on the pyrrolidine ring.

13
-Gly-Pro-Met-Gly-Pro-Ser-Gly-Pro-Arg-
22
-Gly-Leu-Hyp-Gly-Pro-Hyp-Gly-Ala-Hyp-
31
-Gly-Pro-Gln-Gly-Phe-Gln-Gly-Pro-Hyp-
40
-Gly-Glu-Hyp-Gly-Glu-Hyp-Gly-Ala-Ser-
49
-Gly-Pro-Met-Gly-Pro-Arg-Gly-Pro-Hyp-
58
-Gly-Pro-Hyp-Gly-Lys-Asn-Gly-Asp-Asp-

© Macmillan Learning

FIGURE 2.43 The amino acid sequence of a part of a collagen chain reveals that every third residue is a glycine. Proline and hydroxyproline (Hyp) also are abundant.

The collagen helix has properties different from those of the α helix. Hydrogen bonds within a strand are absent, and each strand adopts an extended conformation (Figure 2.44). The helix is stabilized by steric repulsion of the pyrrolidine rings of the proline and hydroxyproline residues. The pyrrolidine rings keep out of each other's way when the polypeptide chain assumes its helical form, which has about three residues per turn. Three strands wind around one another to form what is called a *superhelical cable*, a structure that is stabilized by hydrogen bonds between strands. The hydrogen bonds form between the peptide NH groups of glycine residues and the CO groups of residues on the other chains. The hydroxyl groups of hydroxyproline residues also participate in hydrogen bonding.

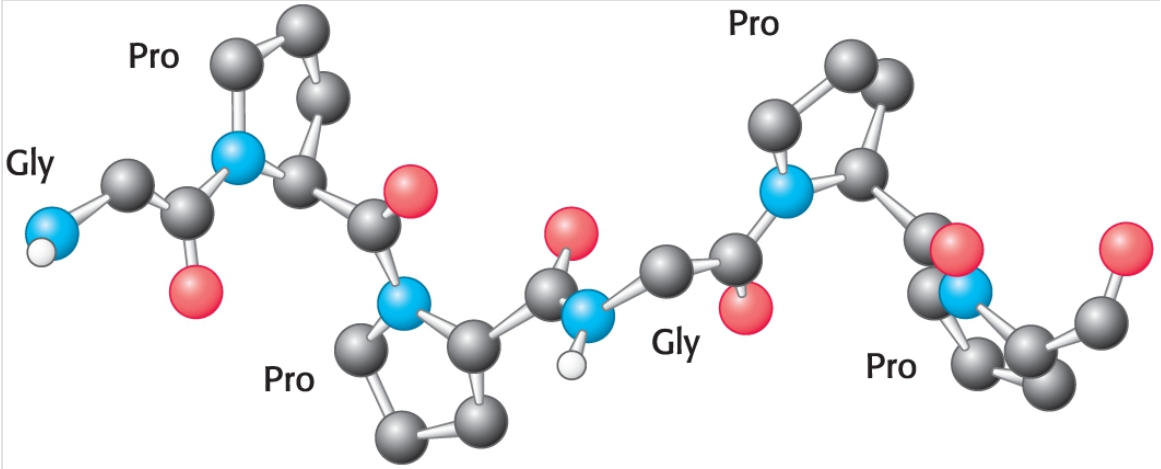


FIGURE 2.44 A single strand of a collagen triple helix adopts an extended conformation.

The inside of the triple-stranded helical cable is very crowded and accounts for the requirement that glycine be present at every third position on each strand (Figure 2.45A). The only residue that can fit in an interior position is glycine. The amino acid residue on either side of glycine is located on the outside of the cable, where there is room for the bulky rings of proline and hydroxyproline residues (Figure 2.45B).

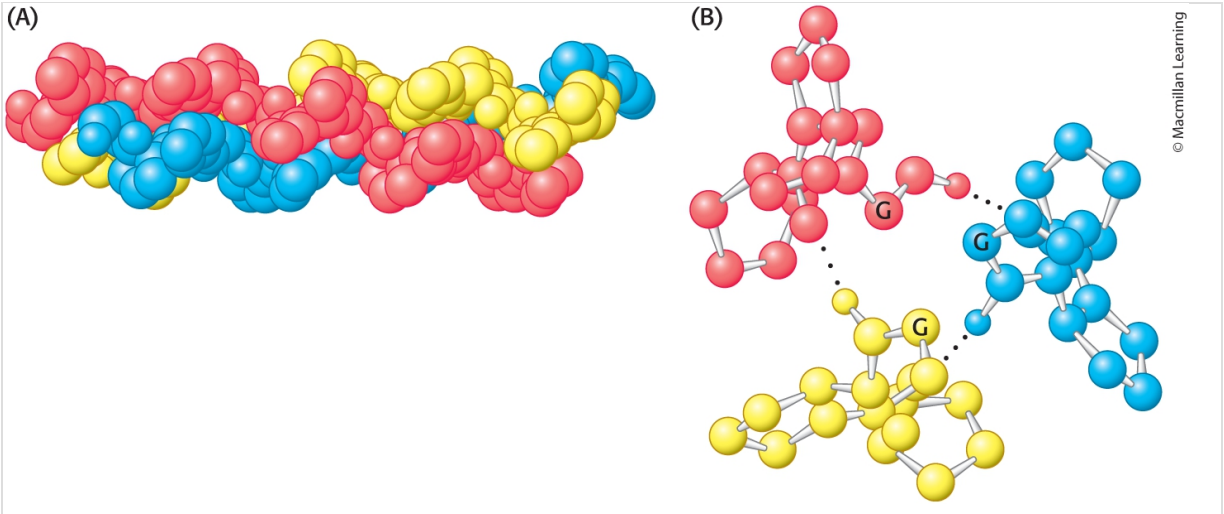


FIGURE 2.45 Glycine residues form the interior of the collagen triple helix. (A) In this space-filling model of collagen, each strand is shown in a different color. (B) In this cross section of a

model of collagen, each strand is hydrogen bonded to the other two strands. The α-carbon atom of a glycine residue is identified by the letter G. Every third residue must be glycine because there is no space in the center of the helix. Notice that the pyrrolidine rings of the proline residues are on the outside.



The importance of the positioning of glycine inside the triple helix is illustrated in the disorder osteogenesis imperfecta, also known as brittle bone disease. In this condition, which can vary from mild to very severe, other amino acids replace the internal glycine residue. This replacement leads to a delayed and improper folding of collagen. The most serious symptom is severe bone fragility. Defective collagen in the eyes causes the whites of the eyes, or *sclera*, to have a blue tint.

2.6 Quaternary Structure: Polypeptide Chains Can Assemble into Multisubunit Structures

Four levels of structure are cited in discussions of protein architecture. So far, we have considered three: primary, secondary, and tertiary. We now turn to proteins containing more than one polypeptide chain. Such proteins exhibit a fourth level of structural organization. Each polypeptide chain in such a protein is called a **subunit**. The spatial arrangement of subunits and the nature of their interactions is called **quaternary structure**.

The simplest sort of quaternary structure is a **homodimer**, consisting of two identical subunits. For example, this organization is present in the DNA-binding protein Cro, found in a bacterial virus called *bacteriophage λ* (**Figure 2.46**). However, more-complicated quaternary structures are also common. More than one type of subunit can be present, often in variable numbers. For example, human hemoglobin, the oxygen-carrying protein in blood, consists of two subunits of one type (designated α) and two subunits of another type (designated β), as illustrated in **Figure 2.47**. Thus, the hemoglobin molecule exists as an $\alpha_2\beta_2$ tetramer. Subtle changes in the arrangement of subunits within the hemoglobin molecule allow it to carry oxygen from the lungs to tissues with great efficiency (Chapter 3).



FIGURE 2.46 Quaternary structure refers to the arrangement of multiple polypeptide chains. The Cro protein of bacteriophage λ adopts the simplest type of quaternary structure, a homodimer (two identical subunits).

[Drawn from 5CRO.pdb.]

INTERACT with the models shown in Figure 2.46 and 2.47 in Achieve

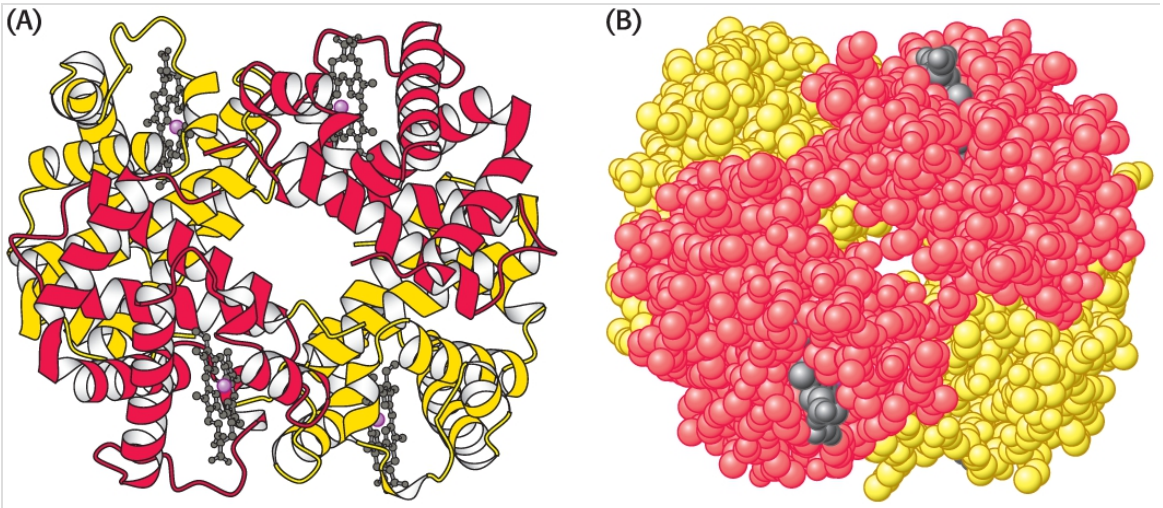
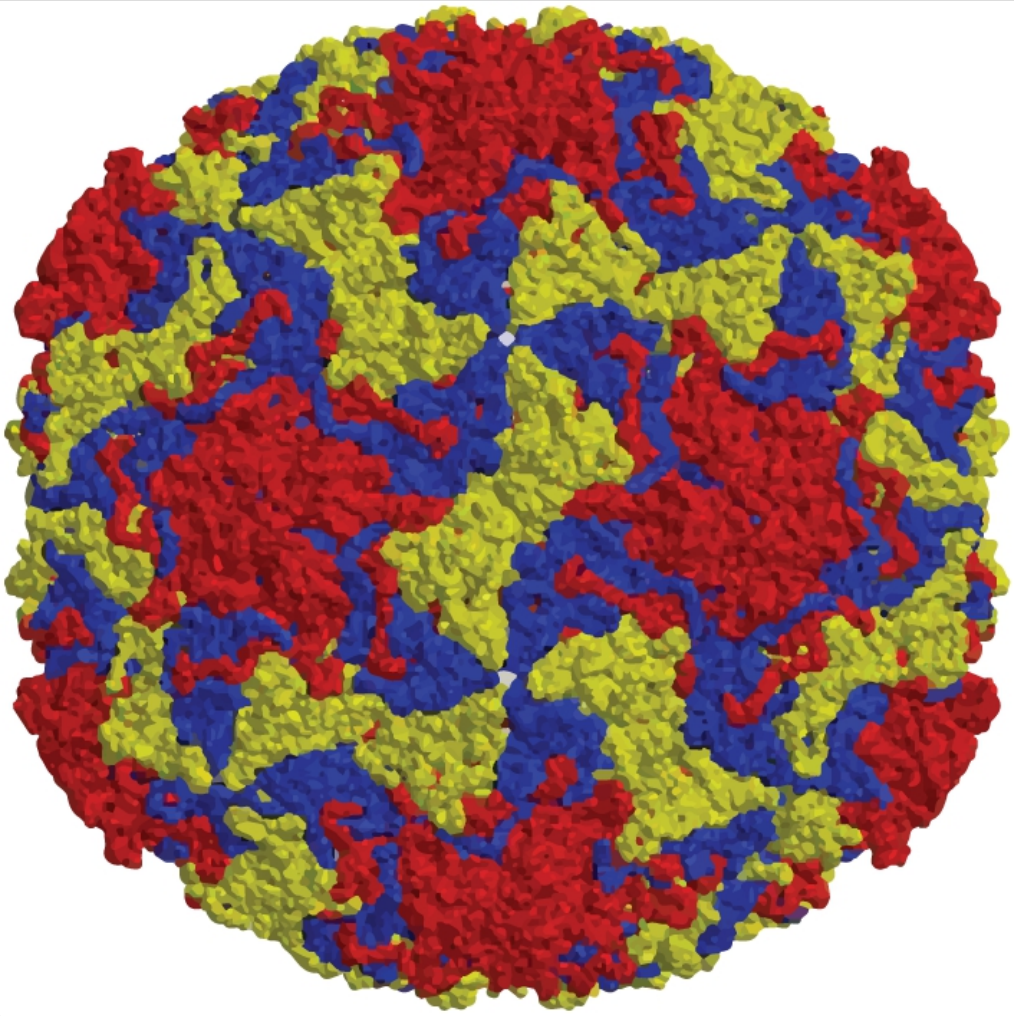


FIGURE 2.47 Human hemoglobin is composed of a $\alpha_2\beta_2$ tetramer. The structure of the two α subunits (red) is similar but not identical to that of the two β subunits (yellow). The molecule contains four heme groups (gray with the iron atom shown in purple). (A) The ribbon diagram highlights the similarity of the subunits and shows they are composed mainly of α helices. (B) The space-filling model illustrates how the heme groups occupy crevices in the protein.

[Drawn from 1A3N.pdb.]

Viruses make the most of a limited amount of genetic information by forming coats that use the same kind of subunit repetitively in a symmetric array. For example, the coat of rhinovirus, the virus that causes the common cold, includes 60 copies of each of four subunits (**Figure 2.48**). The subunits come together to form a nearly spherical shell that encloses the viral genome. Although the rhinovirus coat ultimately requires 240 polypeptide chains, the symmetry achieved by its quaternary structure enables this structure to form from only four distinct sequences.



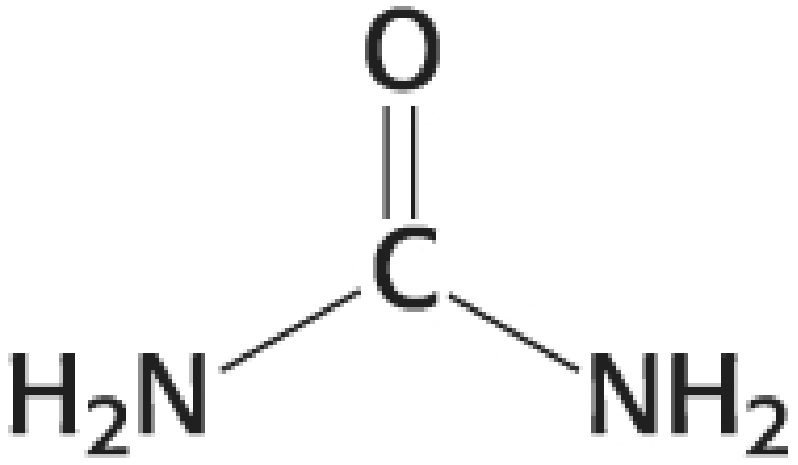
© Macmillan Learning

FIGURE 2.48 Viral coat proteins adopt complex quaternary structures with many copies of relatively few unique subunits. The coat of human rhinovirus, the cause of the common cold, comprises 240 individual polypeptide chains, 60 copies of each of four subunits. The three most prominent subunits are shown as different colors.

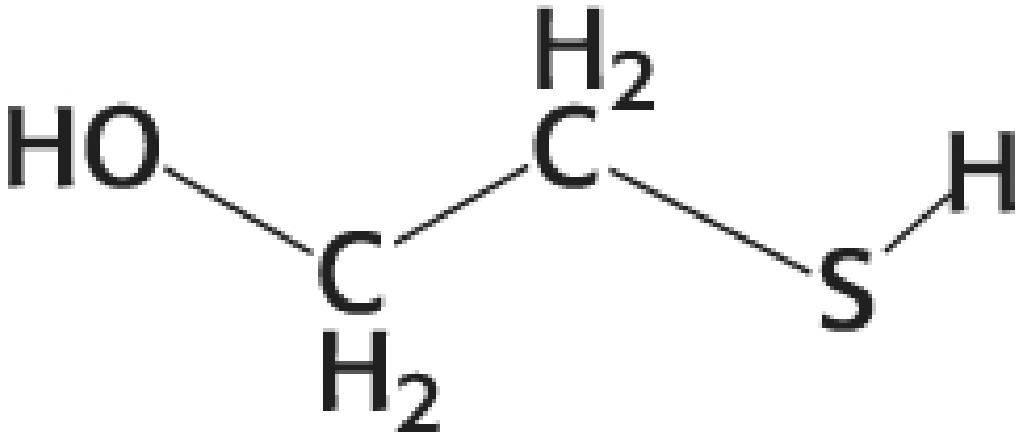
2.7 The Amino Acid Sequence of a Protein Determines Its Three-Dimensional Structure

Thus far, we have seen that proteins can adopt a wide variety of structures, ranging from highly compact to fully extended. These structures reflect the broad diversity of protein functions and represent a theme we will encounter numerous times throughout this book. How polypeptide chains achieve these elaborate tertiary structures has been the focus of decades of research that still continues today.

The classic work of Christian Anfinsen in the 1950s on the enzyme ribonuclease revealed the relationship between the amino acid sequence of a protein and its conformation. Ribonuclease is a single polypeptide chain consisting of 124 amino acid residues cross-linked by four disulfide bonds (**Figure 2.49**). Anfinsen's plan was to destroy the three-dimensional structure of the enzyme and to then determine what conditions were required to restore the structure. In order to unfold ribonuclease, he used a high concentration (8 M) of urea, which effectively disrupts a protein's noncovalent interactions. Complete unfolding of ribonuclease also requires the cleavage, or reduction, of its four disulfide bonds (Figure 2.15). Using a large excess of β-mercaptoethanol, Anfinsen fully reduced the disulfides (cystines) into sulfhydryls (cysteines) (**Figure 2.50**).



Urea



β-Mercaptoethanol

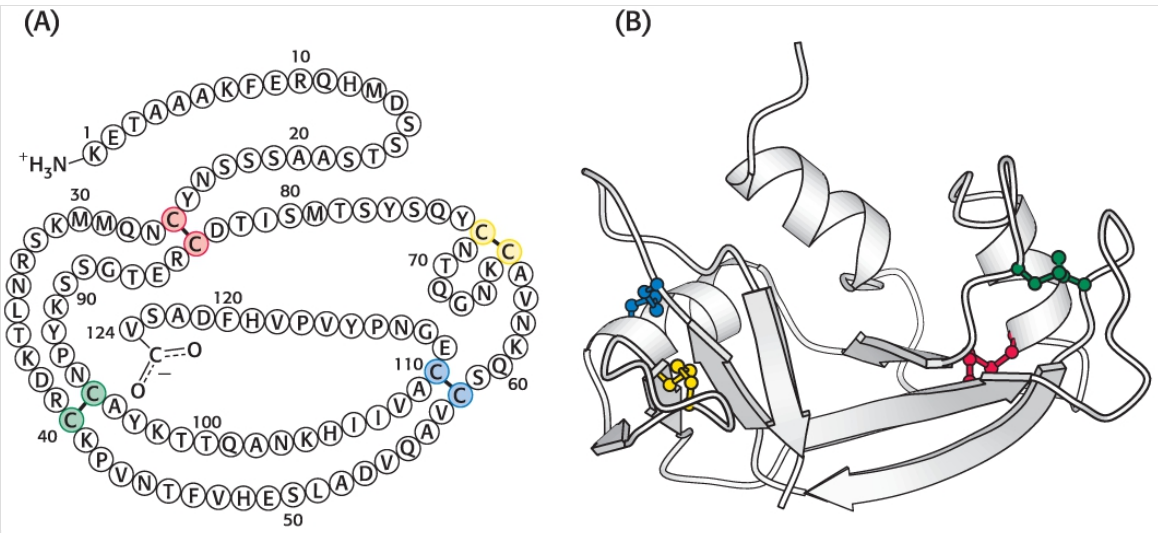


FIGURE 2.49 Bovine ribonuclease is a single polypeptide chain with four intramolecular disulfide bonds. (A) The primary structure of ribonuclease with the four disulfide bonds shown color. (B) Three-dimensional structure of ribonuclease with the same four disulfide bonds highlighted.

[(A) After C. H. W. Hirs, S. Moore, and W. H. Stein, *J. Biol. Chem*. 235:633–647, 1960; (B) Drawn from 1RBX.pdb.]

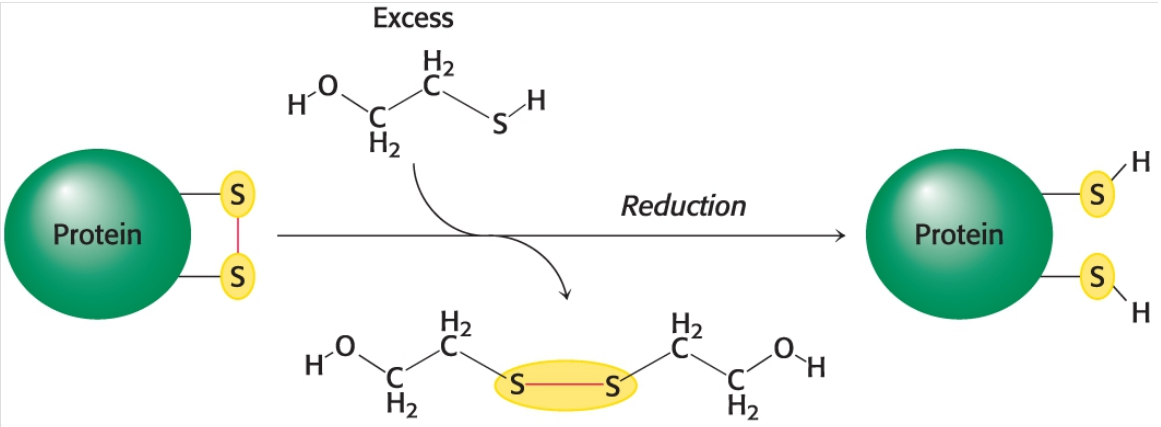


FIGURE 2.50 β-Mercaptoethanol disrupts disulfide bonds. Notice as the disulfides are disrupte (reduced), the β-mercaptoethanol is oxidized and forms dimers.

Most polypeptide chains devoid of cross-links assume a random-coil conformation in 8 M urea. When ribonuclease was treated with β-mercaptoethanol in 8 M urea, the product was a fully reduced, randomly coiled polypeptide chain devoid of enzymatic activity. When a protein is converted into a randomly coiled peptide without its normal activity, it is referred to as a **denatured protein** (**Figure 2.51**).

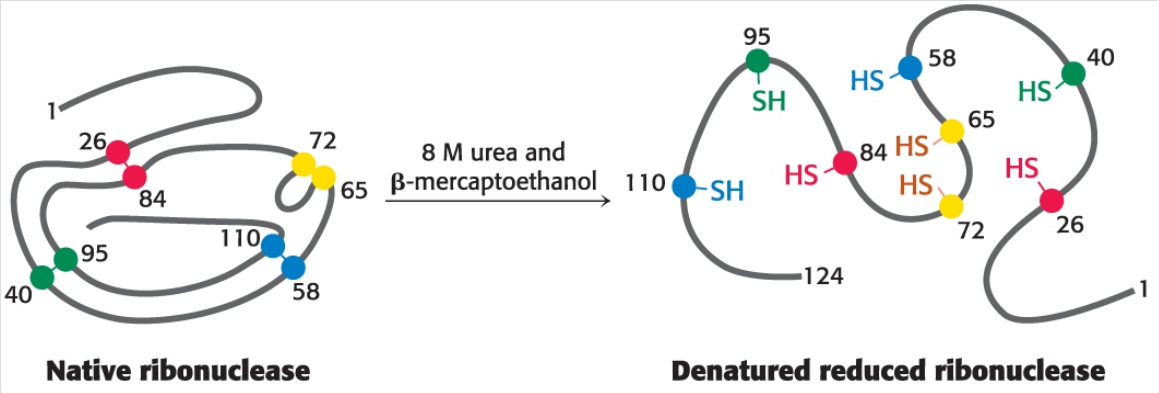
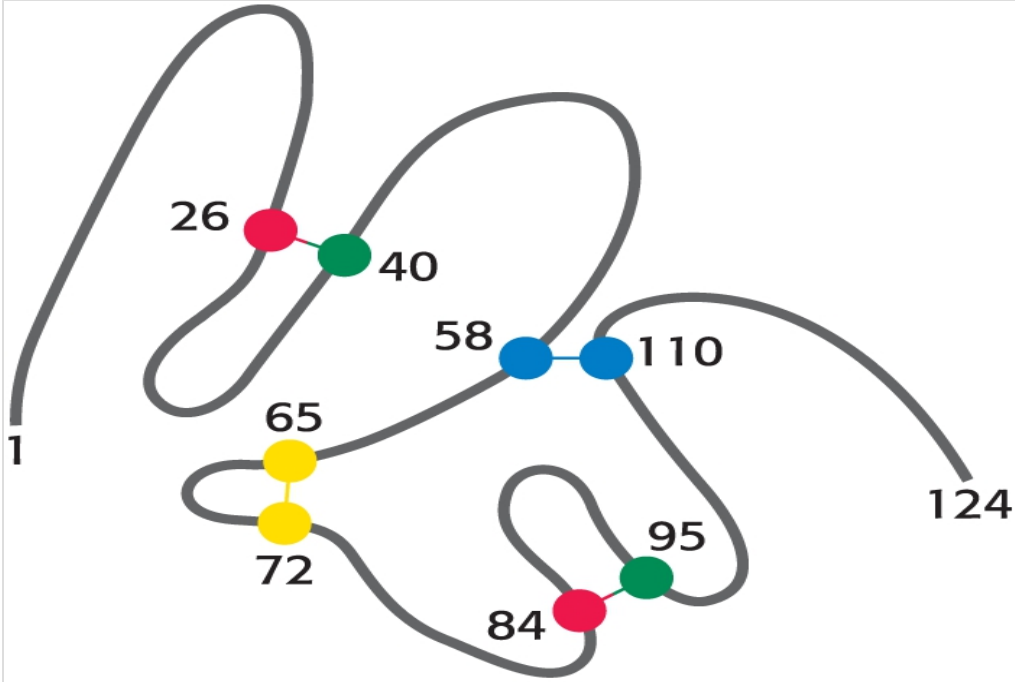


FIGURE 2.51 Ribonuclease is denatured with urea and β-mercaptoethanol.

Anfinsen then made the critical observation that the denatured ribonuclease, introduced into a solution without urea and β-mercaptoethanol by a technique known as *dialysis* (Section 4.1), slowly regained enzymatic activity. He perceived the significance of this chance finding: the sulfhydryl groups of the denatured enzyme re-form disulfide bonds when exposed to air. Detailed studies then showed that nearly all the original enzymatic activity was regained if the disulfide bonds were oxidized under suitable conditions. All the measured physical and chemical properties of the refolded enzyme were virtually identical with those of the **native protein**; that is, the protein as it was originally isolated. These experiments showed that the information needed to specify the catalytically active structure of ribonuclease is contained in its amino acid sequence. Subsequent studies have

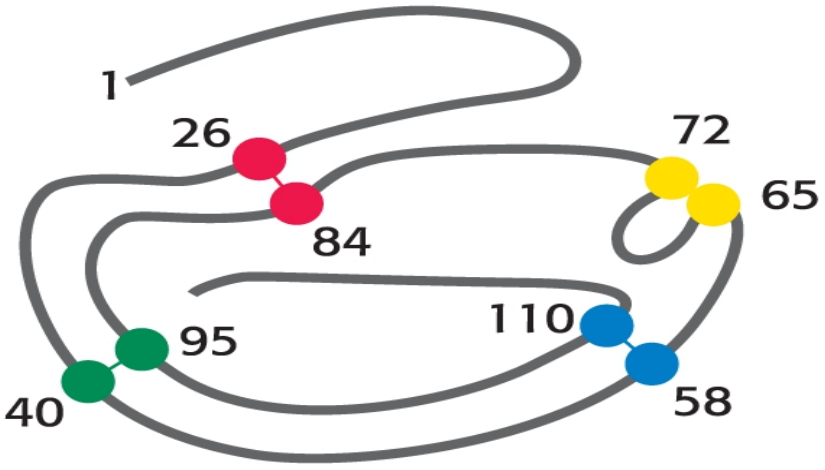
established the generality of this central principle of biochemistry: sequence specifies conformation.

A quite different result was obtained when ribonuclease was reoxidized while it was still in 8 M urea, followed by the removal of the urea. Ribonuclease treated in this way had only 1% of the enzymatic activity of the native protein. Why were the outcomes so different when reduced ribonuclease was reoxidized in the presence and absence of urea? The reason is that the wrong disulfides formed pairs in urea. There are 105 different ways of pairing eight cysteine molecules to form four disulfides; only one of these combinations is enzymatically active. The 104 wrong pairings have been picturesquely termed “scrambled” ribonuclease. Anfinsen found that scrambled ribonuclease spontaneously converted into fully active, native ribonuclease when trace amounts of β-mercaptoethanol were added to an aqueous solution of the protein (**Figure 2.52**). The added β-mercaptoethanol catalyzed the rearrangement of disulfide pairings until the native structure was regained in about 10 hours. This process was driven by the decrease in free energy as the scrambled conformations were converted into the stable, native conformation of the enzyme. The native disulfide pairings of ribonuclease thus contribute to the stabilization of the thermodynamically preferred structure.



Scrambled ribonuclease

Trace of
β-mercaptoethanol



Native ribonuclease

© Macmillan Learning

FIGURE 2.52 Native ribonuclease can be re-formed from scrambled ribonuclease in the presence of a trace of β-mercaptoethanol.



Similar refolding experiments have been performed on many other proteins. In many cases, the native structure can be generated under suitable conditions. For other proteins, however, refolding does not proceed efficiently. In these cases, the unfolded protein molecules usually become tangled up with one another to form aggregates. Inside cells, proteins called *chaperones* block such undesirable interactions. Additionally, it is now evident that some proteins do not assume a defined structure until they interact with molecular partners.

Self-Check Question



In his renaturation experiments, Anfinsen used a concentration of ribonuclease around $1\ \text{mg ml}^{-1}$. Inside a cell, the protein concentration is estimated to be around $100\ \text{mg ml}^{-1}$. Predict the outcome of Anfinsen's experiments had he used $100\ \text{mg ml}^{-1}$ ribonuclease.

Amino acids have different propensities for forming α helices, β sheets, and turns

How does the amino acid sequence of a protein specify its three-dimensional structure? How does an unfolded polypeptide chain acquire the form of the native protein? These fundamental questions in

biochemistry can be approached by first asking a simpler one: What determines whether a particular sequence in a protein forms an α helix, a β strand, or a turn? One source of insight is to examine the frequency of occurrence of particular amino acid residues in these secondary structures (Table 2.3). Residues such as alanine, glutamate, and leucine tend to be present in α helices, whereas valine and isoleucine tend to be present in β strands. Glycine, asparagine, and proline are more commonly observed in turns.

TABLE 2.3 Relative frequencies of amino acid residues in secondary structures

Amino acid	α helix	β sheet	Reverse turn
Glu	1.59	0.52	1.01
Ala	1.41	0.72	0.82
Leu	1.34	1.22	0.57
Met	1.30	1.14	0.52
Gln	1.27	0.98	0.84
Lys	1.23	0.69	1.07
Arg	1.21	0.84	0.90
His	1.05	0.80	0.81
Val	0.90	1.87	0.41
Ile	1.09	1.67	0.47

Tyr	0.74	1.45	0.76
Cys	0.66	1.40	0.54
Trp	1.02	1.35	0.65
Phe	1.16	1.33	0.59
Thr	0.76	1.17	0.96
Gly	0.43	0.58	1.77
Asn	0.76	0.48	1.34
Pro	0.34	0.31	1.32
Ser	0.57	0.96	1.22
Asp	0.99	0.39	1.24

Note: The amino acids are grouped according to their preference for α helices (top group), β sheets (middle group), or turns (bottom group).
Source: T. E. Creighton, *Proteins: Structures and Molecular Properties*, 2nd ed. (W. H. Freeman and Company, 1992), p. 256.

Studies of proteins and synthetic peptides have revealed some reasons for these preferences. Branching at the β-carbon atom, as in valine, threonine, and isoleucine, tends to destabilize α helices because of steric clashes. These residues are readily accommodated in β strands, where their side chains project out of the plane containing the main chain. Serine and asparagine tend to disrupt α helices because their side chains contain hydrogen-bond donors or acceptors in close proximity to the main chain, where they compete for main-chain NH and CO groups. Proline tends to disrupt both α helices and β strands because it lacks an NH group and because its ring structure restricts its φ value to near 60

degrees. Glycine readily fits into all structures, but its conformational flexibility renders it well-suited to reverse turns.

Can we predict the secondary structure of a protein by using this knowledge of the conformational preferences of amino acid residues? Accurate predictions of secondary structure adopted by even a short stretch of residues have proved to be difficult. Note that the conformational preferences of amino acid residues are not tipped all the way to one structure (Table 2.3). For example, glutamate, one of the strongest helix formers, prefers α helix to β strand by only a factor of three. The preference ratios of most other residues are smaller. Indeed, some penta- and hexapeptide sequences have been found to adopt one structure in one protein and an entirely different structure in another (**Figure 2.53**). Hence, some amino acid sequences do not uniquely determine secondary structure.

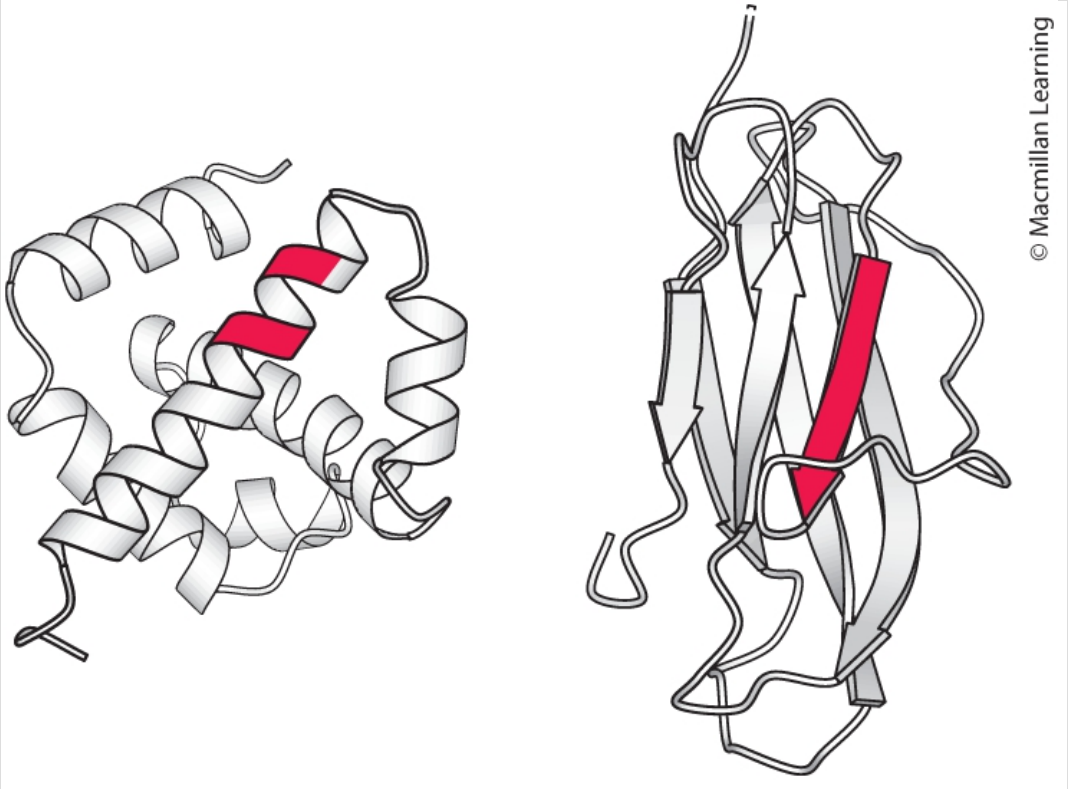


FIGURE 2.53 Many sequences can adopt alternative conformations in different proteins. Here the sequence VDLLKN shown in red assumes an α helix in one protein context (left) and a β strand in another (right).

[Drawn from (left) 3WRP.pdb and (right) 2HLA.pdb.]



Tertiary interactions — interactions between residues that are far apart in the sequence — may be decisive in specifying the secondary structure of some segments. Context is often crucial: the conformation of a protein has evolved to work in a particular environment. Nevertheless, substantial improvements in secondary structure prediction have been achieved by using families of related sequences, each of which adopts the same structure.

Protein folding is a highly cooperative process

Proteins can be denatured by any treatment that disrupts the weak bonds stabilizing tertiary structure, such as heating or chemical denaturants such as urea or guanidinium chloride. For many proteins, a comparison of the degree of unfolding as the concentration of denaturant increases reveals a sharp transition from the folded, or native, form to the unfolded, or denatured form, suggesting that only these two conformational states are present to any significant extent (Figure 2.54). A similar sharp transition is observed if denaturants are removed from unfolded proteins, allowing the proteins to refold.

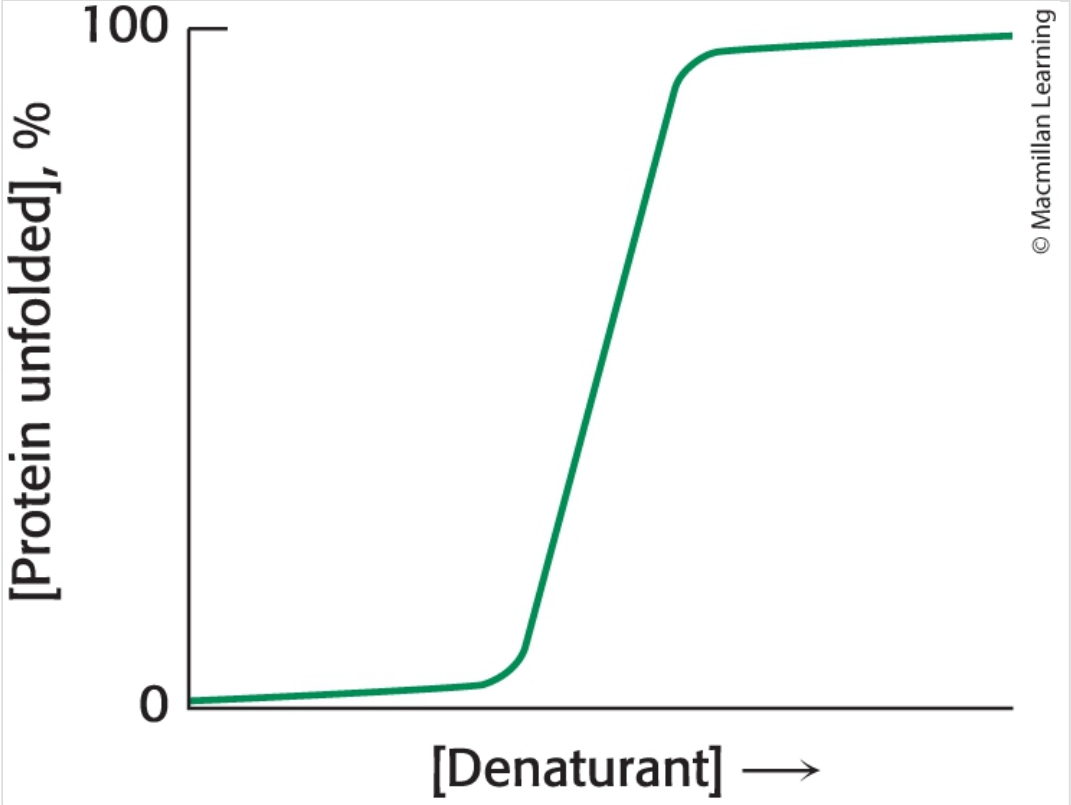


FIGURE 2.54 The transition from folded to unfolded state is abrupt. Most proteins show a sharp transition from the folded to the unfolded form on treatment with increasing concentrations of denaturants.

The sharp transition seen in Figure 2.54 suggests that protein folding and unfolding is an "all or none" process that results from a **cooperative transition**. Consider this example: suppose that a protein is placed in conditions under which some part of the protein structure is thermodynamically unstable. As this part of the folded structure is disrupted, the interactions between it and the remainder of the protein will be lost. The loss of these interactions, in turn, will destabilize the remainder of the structure. Thus, conditions that lead to the disruption of any part of a protein structure are likely to unravel the protein completely. The structural properties of proteins provide a clear rationale for the cooperative transition.

The consequences of cooperative folding can be illustrated by considering the contents of a protein solution under conditions corresponding to the middle of the transition between the folded and the unfolded forms. Under these conditions, the protein is "half folded." Yet the solution will appear to have no partly folded molecules but, instead, look as if it is a 50/50 mixture of fully folded and fully unfolded molecules (Figure 2.55). Although the protein may appear to behave as if it exists in only two states, this simple two-state existence is an impossibility at a molecular level. Even simple reactions go through reaction intermediates, and so a complex molecule such as a protein cannot simply switch from a completely unfolded state to the native state in one step. Unstable, transient intermediate structures must exist between the native and denatured state. Determining the nature of these intermediate structures is an area of intense biochemical research.

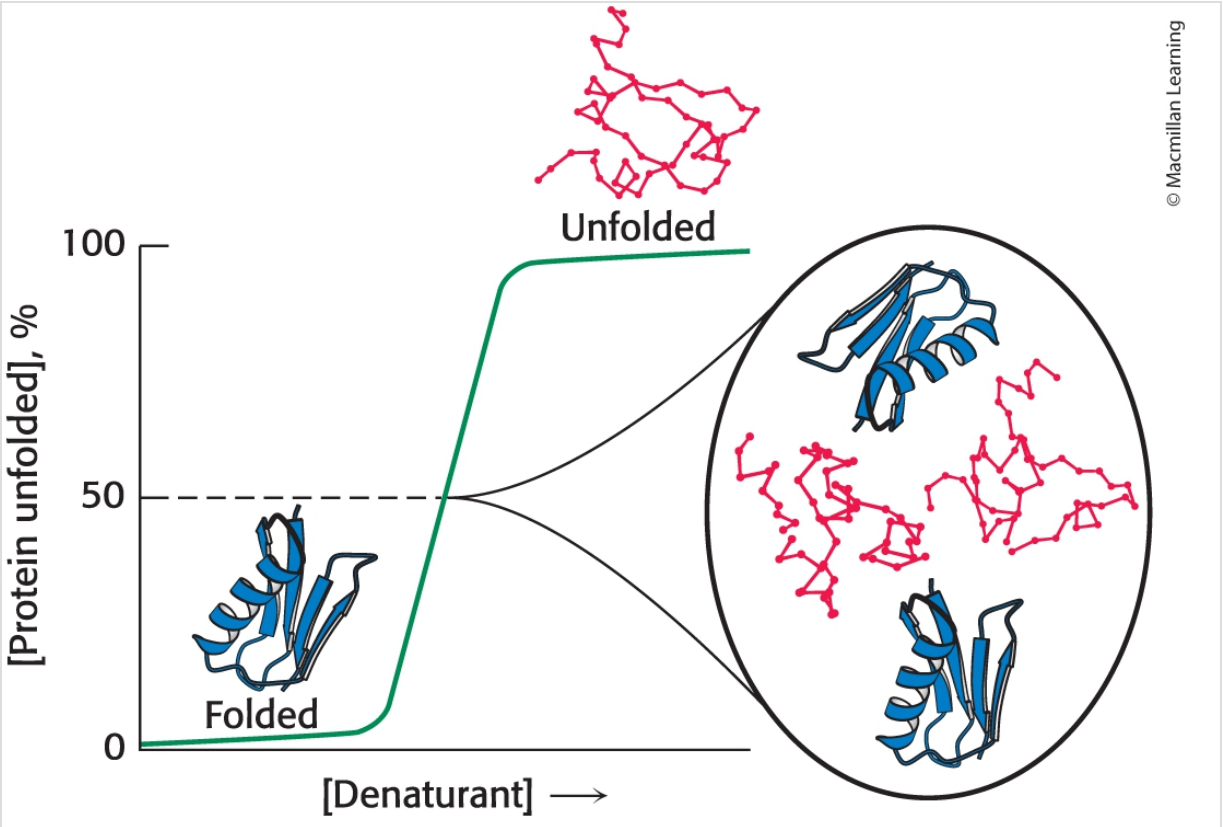


FIGURE 2.55 At the denaturation midpoint, half the molecules are fully folded and half are fully unfolded.

Proteins fold by progressive stabilization of intermediates rather than by random search

How does a protein make the transition from an unfolded structure to a unique conformation in the native form? One theoretical possibility would be that all possible conformations are sampled to find the energetically most favorable one. How long would such a random search take? Consider a small protein with 100 residues. In 1969, Cyrus Levinthal calculated that, if each residue can assume three different conformations, the total number of structures would be 3^{100}, which is equal to 5×10^{47}. If it takes 10^{-13} s to convert one structure into another, the total search time would be $5 \times 10^{47} \times 10^{-13}$ s, which is equal to 5×10^{34} s, or 1.6×10^{27} years. In reality, small proteins can fold in less than a second. Clearly, it would take much too long for even a small protein to fold properly by randomly trying out all possible conformations. The enormous difference between calculated and actual folding times is called *Levinthal's paradox*. This paradox clearly reveals that proteins do not fold by trying every possible conformation; instead, they must follow at least a partly defined folding pathway consisting of intermediates between the fully denatured protein and its native structure.

The way out of this paradox is to recognize the power of cumulative selection. Richard Dawkins, in *The Blind Watchmaker*, asked how long it would take a monkey poking randomly at a typewriter to reproduce Hamlet's remark to Polonius, "Methinks it is like a weasel" (**Figure 2.56**).

An astronomically large number of keystrokes, on the order of 10^{40}, would be required. However, suppose that we preserved each correct character and allowed the monkey to retype only the wrong ones. In this case, only a few thousand keystrokes, on average, would be needed. The crucial difference between these cases is that the first employs a completely random search, whereas, in the second, partly correct intermediates are retained.

```
 200 ?T(\G{+s x[A.N5~,#ATxSGpn`e□@
 400 oDr'Jh7s DFR:W41'u+^v6zpJseOi
 600 e2ih'8zs n527x8l8d_ih=H1dseb.
 800 S#dh>}/s ]tZqC%lP%DK<|!^aseZ.
1000 V0th>nLs ut/is]l_kwojjwMasef.
1200 juth+nvs it is[lukh?SCw=ase5.
1400 Iithdn4s it is0l/ks/IxwLase~.
1600 M?thinrs it is lXk?T"_woasel.
1800 MSthinWs it is lwkN7□Kw(asel.
2000 Mhthin`s it is likv,aww_asel.
2200 MMthinns it is lik+5avw1asel.
2400 MethinXs it is likydaqw)asel.
2600 Methin4s it is lik2daseasel.
2800 MethinHs it is like□aTweasel.
2883 Methinks it is like a weasel.
```

```
 200 )z~hg)W4{{cu!kO{d6jS!N1EyUx}p
 400 "W hi\kR.<&CfA%4-Y1G!iT$6({|6
 600 .L=hinkm4(uMGP^lAWoE6k1wW=yiS
 800  AthinkaPa_vYH liR\Hb,Uo4\-"(
1000 OFthinksP)@fZO li8v] /+Eln26B
1200 6ithinksMVt -V likm+gl#K~)BFk
1400 vxthinksaEt □w like.S1Geutks.
1600 :Othinks<it MC likesN2[eaVe4.
1800 uxthinksqit 0r likeQh)weaoeW.
2000 Y/thinks it id like7a1wea)e&.
2200 Methinks it iW like a[weaWel.
2400 Methinks it is like a:weasel.
2431 Methinks it is like a weasel.
```

© Macmillan Learning

FIGURE 2.56 In the analogy of the typing monkey, the desired result is achieved more rapidly if individual correct keystrokes are retained. In the two computer simulations shown, the cumulative number of keystrokes required to write a line from Shakespeare's *Hamlet* is given at the left of each line.



The essence of protein folding is the tendency to retain partly correct intermediates. However, the protein-folding problem is much more difficult than the one presented to our simian Shakespeare. First, the criterion of correctness is not a residue-by-residue scrutiny of conformation by an omniscient observer but rather the total free energy of the transient species. Second, proteins are only marginally stable. The free-energy difference between the folded and the unfolded states of a typical 100-residue protein is $42\ \text{kJ mol}^{-1}$ $(10\ \text{kcal mol}^{-1})$, and thus each residue contributes on average only $0.42\ \text{kJ mol}^{-1}$ $(0.1\ \text{kcal mol}^{-1})$ of energy to maintain the folded state. This amount is less than the amount of thermal energy, which is $2.5\ \text{kJ mol}^{-1}$ $(0.6\ \text{kcal mol}^{-1})$ at room temperature. This meager stabilization energy means that correct intermediates, especially those formed early in folding, can be lost. The analogy is that the monkey would be somewhat free to undo its correct keystrokes. Nonetheless, the interactions that lead to cooperative folding can stabilize intermediates as structure builds up. Thus, local regions that have significant structural preference, though not necessarily stable on their own, will tend to adopt their favored structures and, as they form, can interact with one other, leading to increasing stabilization. This conceptual framework is often referred to as the *nucleation-condensation model*.

A simulation of the folding of a protein, based on the nucleation-condensation model, is shown in **Figure 2.57**. This model suggests that certain pathways may be preferred. Although Figure 2.57 suggests a discrete pathway, each of the intermediates shown represents an

ensemble of similar structures, and thus a protein follows a general rather than a precise pathway in its transition from the unfolded to the native state. The energy surface for the overall process of protein folding can be visualized as a funnel (Figure 2.58). The wide rim of the funnel represents the wide range of structures accessible to the ensemble of denatured protein molecules. As the free energy of the population of protein molecules decreases, the proteins move down into narrower parts of the funnel, and fewer conformations are accessible. At the bottom of the funnel is the folded state with its well-defined conformation. Many paths can lead to this same energy minimum.

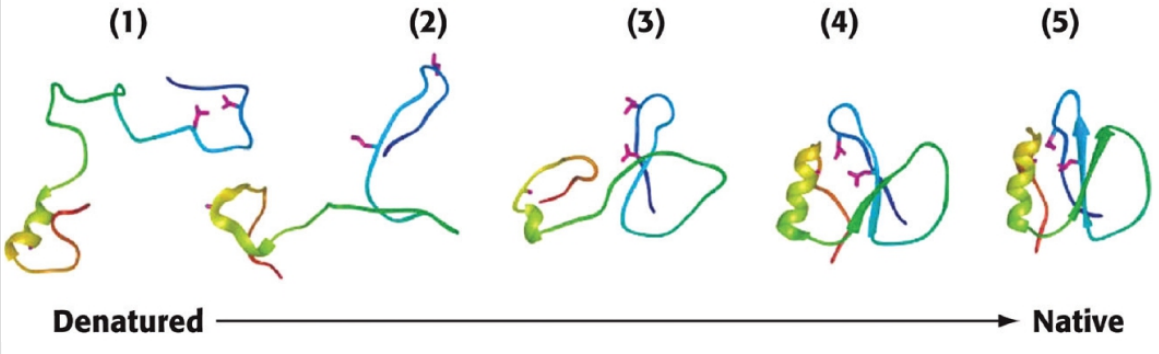


FIGURE 2.57 The proposed folding pathway of chymotrypsin inhibitor-2 demonstrates the nucleation-condensation model. Local regions with sufficient structural preference tend to adopt their favored structures initially (1). These structures come together to form a nucleus wi a nativelike, but still mobile, structure (4). This structure then fully condenses to form the native more rigid structure (5).

[From A. R. Fersht and V. Daggett. *Cell* 108:573–582, 2002; with permission from Elsevier.]

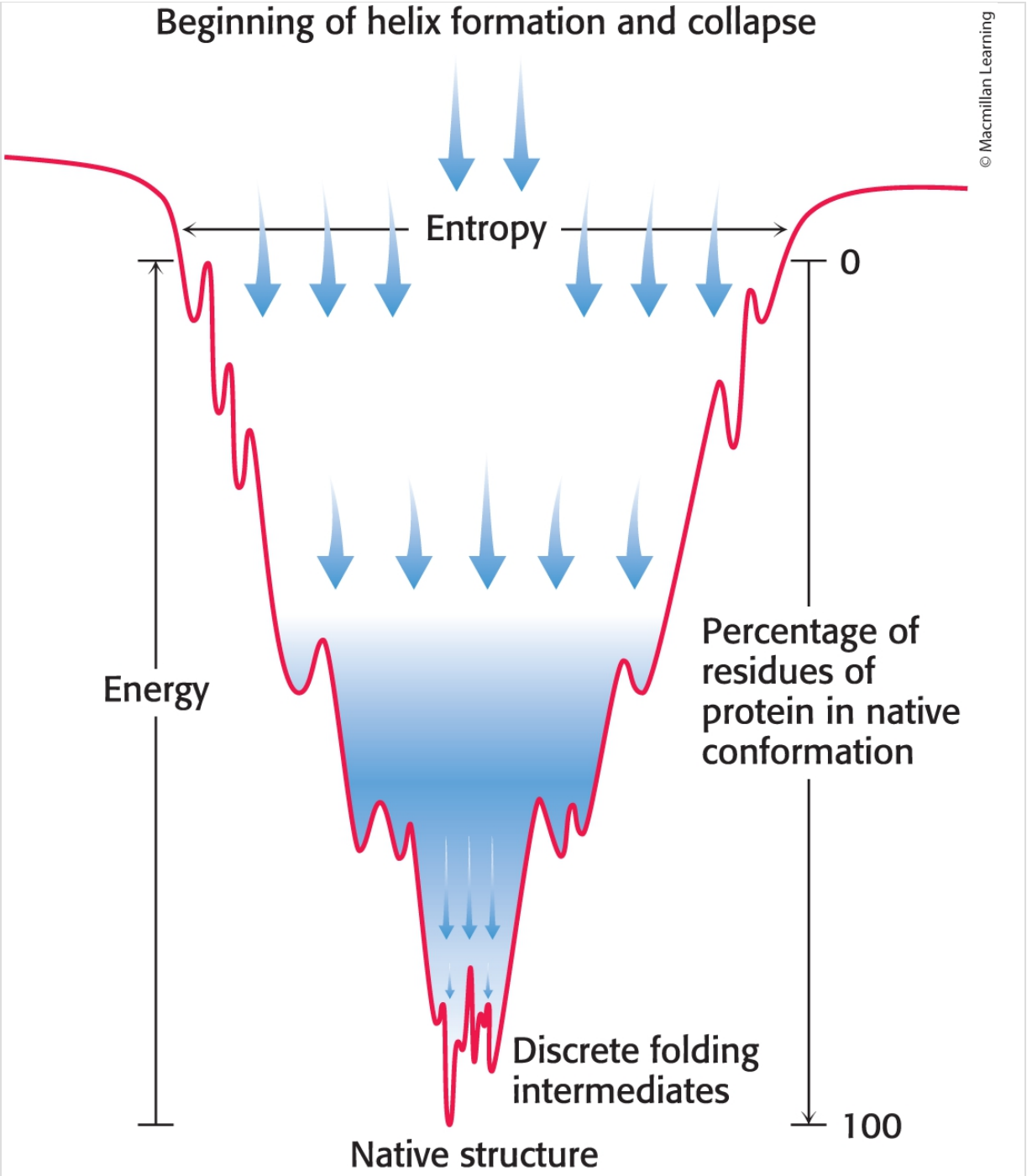


FIGURE 2.58 The folding funnel depicts the thermodynamics of protein folding. The top of the funnel represents all possible denatured conformations — that is, maximal conformational entropy. Depressions on the sides of the funnel represent semistable intermediates that can facilitate or hinder the formation of the native structure, depending on their depth. Secondary structures, such as helices, form and collapse onto one another to initiate folding.

[After D. L. Nelson and M. M. Cox, *Lehninger Principles of Biochemistry*, 5th ed. (W. H. Freeman and Company, 2008), p. 143.]

Prediction of three-dimensional structure from sequence remains a great challenge

The prediction of three-dimensional structure from sequence has proved to be extremely difficult. The local sequence appears to determine only between 60% and 70% of the secondary structure; long-range interactions are required to stabilize the full secondary structure and the tertiary structure.

Investigators are exploring two fundamentally different approaches to predicting three-dimensional structure from amino acid sequence:

1. Ab initio *predictions attempt to predict the folding of an amino acid sequence without prior knowledge about similar sequences in known protein structures*. (*Ab initio*, from the Latin, means "from the beginning.") Computer-based calculations are employed that attempt to minimize the free energy of a structure with a given amino acid sequence or to simulate the folding process. The utility of these methods is limited by the vast number of possible conformations, the marginal stability of proteins, and the subtle energetics of weak interactions in aqueous solution.

2. *Knowledge-based methods take advantage of our growing knowledge of the three-dimensional structures of many proteins*. The amino acid sequence of unknown structure is examined for compatibility with known protein structures or fragments therefrom. If a significant match is detected, the known structure can be used as an initial model. Knowledge-based methods have been a source of many

insights into the three-dimensional conformation of proteins of known sequence but unknown structure.

The prediction of protein folding from sequence information is a formidable task, one that has compelled the scientific community to explore creative methods for achieving progress. In 1994, John Moult and Krzysztof Fidelis organized the first protein-structure prediction challenge called Critical Assessment of Structure Prediction (CASP). In this competition, contestants are provided with sequences of proteins whose structures had been recently solved but not yet published, and are asked to submit their structural predictions. The submissions are then graded based on how well their predictions match the experimentally determined structures. Importantly, the entire process is *blinded*: the entrants have no prior knowledge of the experimentally solved structures, and the judges have no information about the identity of the competitors and their prediction methods.

Since its inception, CASP competitions have been conducted every two years, with participation from over 200 groups in the most recent event in 2020. Highlighting the difficulty of the task, improvements in structure prediction have been modest, with the results largely reaching a plateau in the early 2010s. However, significant improvement has been achieved in the most recent two events, largely based on the advancement of artificial intelligence (AI) methods developed by the company DeepMind. Their algorithm, AlphaFold, recently achieved an average accuracy of nearly 90%, almost equivalent to what would be expected from experimental methods. For example, their best structural prediction of the protein ORF8 from the SARS-CoV-2 virus was 89% accurate, far exceeding the competition (**Figure 2.59**). Their success suggests that the accurate computational prediction of protein folding may very well be within reach. Additionally, these results serve as evidence of the achievements made possible through collaborative research.

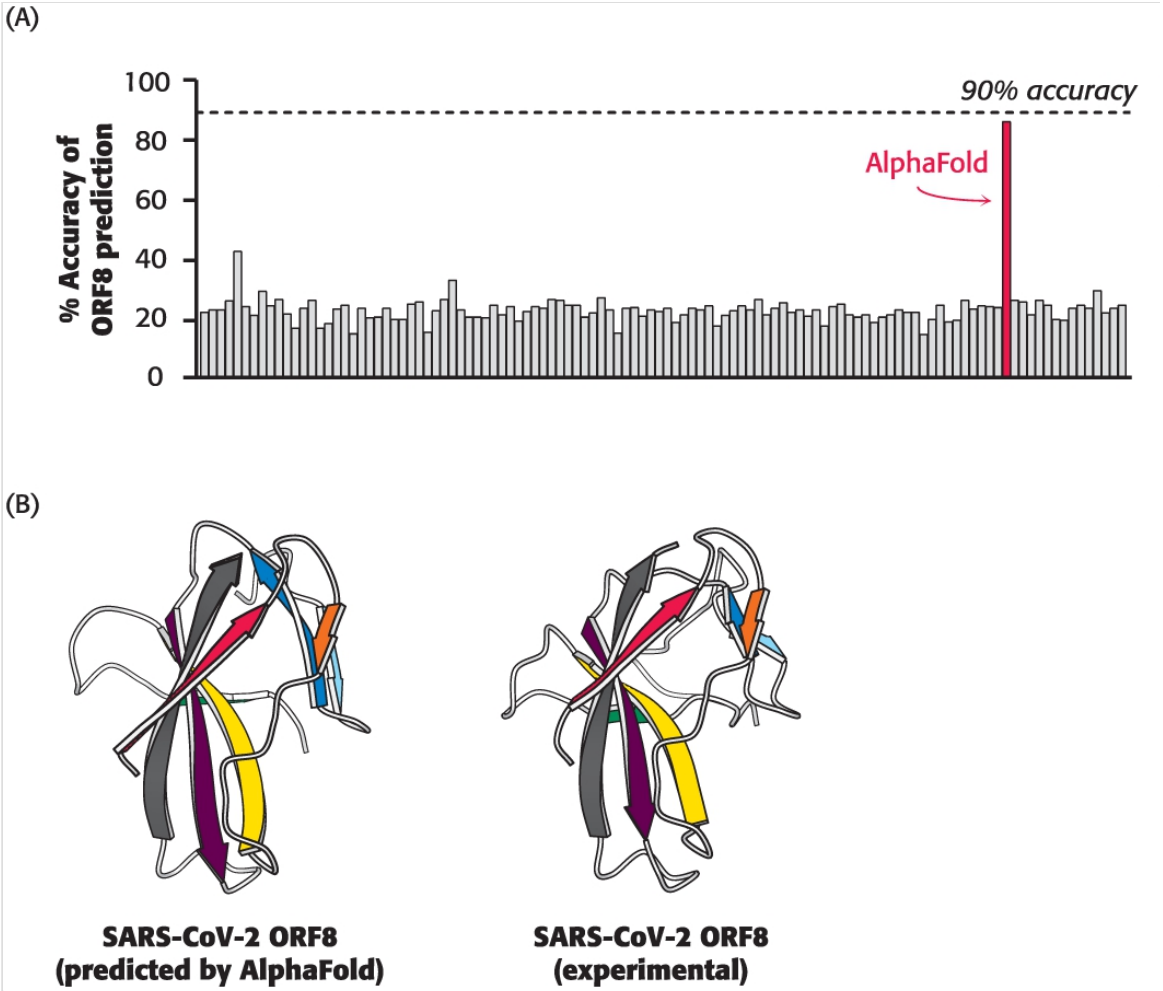


FIGURE 2.59 AlphaFold represents a significant step forward in protein folding prediction. On of the targets from the most recent CASP competition was the ORF8 protein from the SARS-CoV virus. (A) The AlphaFold algorithm (red bar) predicted the structure with nearly 90% accuracy (dashed line), far better than the other competitors (gray bars). (B) Comparison of the predicted structure with the experimentally determined structure shows the extensive similarity.

[(A) Drawn from data obtained from predictioncenter.org/casp14/ and (B) 7JTL.pdb.]

Protein misfolding and aggregation are associated with some neurological diseases



Understanding protein folding and misfolding is of more than academic interest. A host of neurological diseases, including Alzheimer disease, Parkinson disease, and Huntington disease are associated with improperly folded proteins. All of these diseases result in the deposition of protein aggregates, called **amyloid fibrils** or **amyloid plaques**. A common feature of such diseases is that normally soluble proteins are converted into insoluble fibrils rich in β sheets. The correctly folded protein is only marginally more stable than the incorrect form. But the incorrect form aggregates, pulling more correct forms into the incorrect form. For example, the brains of patients with Alzheimer disease contain amyloid plaques that consist primarily of a single polypeptide termed Aβ Polypeptide Aβ is prone to form insoluble aggregates. As expected, the structure is rich in β strands, which come together to form extended parallel β-sheet structures (**Figure 2.60**).

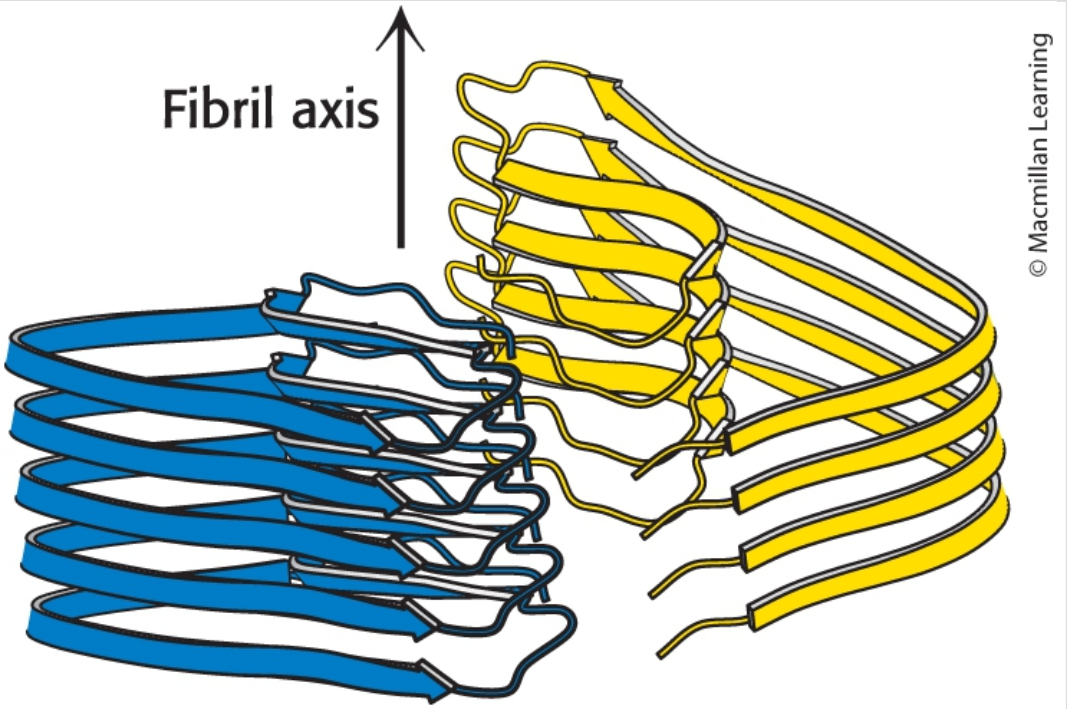


FIGURE 2.60 The structure of the Aβ amyloid fibril reveals its extensive β sheet network. The Aβ amyloid fibril structure shows that protein aggregation is due to the formation of large parallel β sheets. The black arrow indicates the long axis of the fibril.

[Drawn from 5OQV.pdb].

How do such aggregates lead to the death of the cells that harbor them? The answer is still controversial. One hypothesis is that the large aggregates themselves are not toxic but, instead, smaller aggregates of the same proteins may be the culprits, perhaps damaging cell membranes. Nevertheless, the amount of fibrillar Aβ deposited in the brain is correlated with the severity of disease. In fact, the extent of amyloid fibril accumulation can be measured in patients using a technique called *positron emission tomography* (PET) scanning. These images can be used to anticipate the progressive worsening of neurological function (**Figure 2.61**).

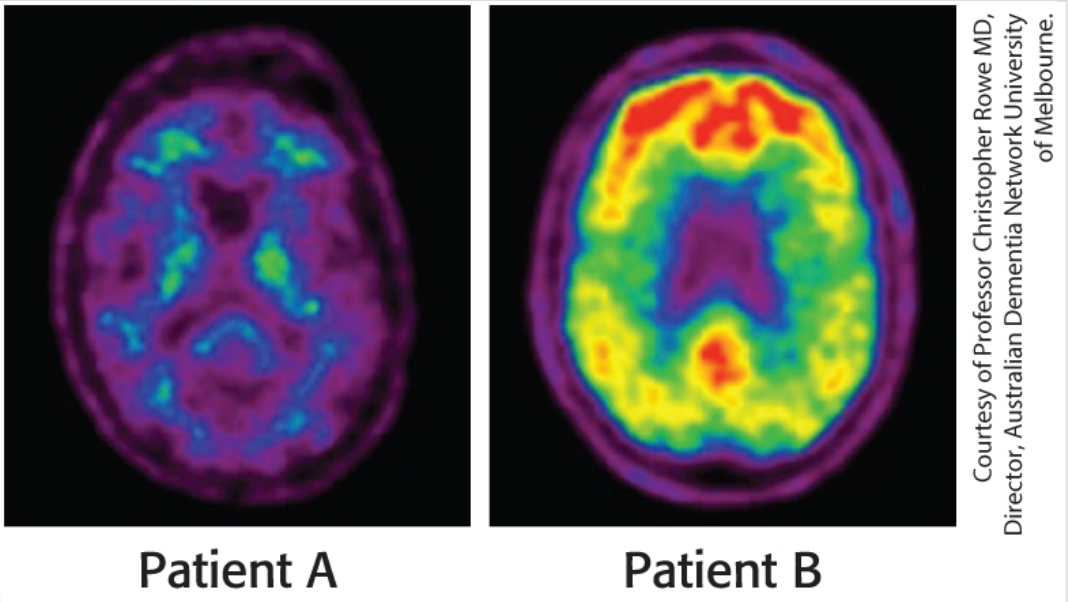


FIGURE 2.61 The extent of amyloid fibril aggregation in the brain can predict the progression of Alzheimer disease. With the aid of a molecule that binds Aβ fibrils, positron emission tomography scanning can measure the extent of amyloid aggregation in the brains of Alzheimer disease patients. The scan of Patient A (low) exhibited a relatively low signal, while the scan of Patient B (right) revealed a high degree of labeling throughout the brain. The mild impairment exhibited by Patient A remained stable for more than 4.5 years after the scan was taken, while Patient B progressed to dementia 3 years after the scan.

Posttranslational modifications confer new capabilities to proteins

Proteins are able to perform numerous functions that rely solely on the versatility of their 20 amino acids. This array of functions can be expanded even further by the incorporation of **posttranslational modifications**, alterations in the structure of a protein after its synthesis in the cell. These modifications may include the covalent attachment of groups to amino acid side chains (Figure 2.62) or the cleavage or modification of the polypeptide backbone.

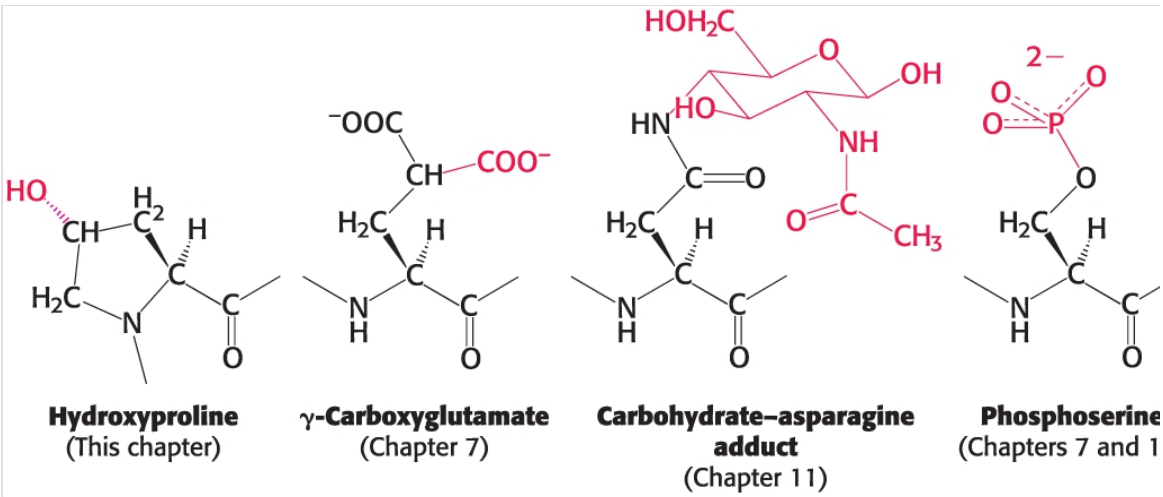


FIGURE 2.62 Posttranslational modifications to proteins include covalent attachments. Examples of common and important covalent modifications of amino acid side chains are show in red. These will be discussed in the indicated chapters.

One example of a posttranslational modification is hydroxylation. As discussed in Section 2.5, the addition of hydroxyl groups to many proline residues stabilizes fibers of newly synthesized collagen. The biological significance of this modification is evident in the disease scurvy: a deficiency of vitamin C results in insufficient hydroxylation of collagen, and the abnormal collagen fibers that result are unable to maintain normal tissue strength. Other covalent modifications shown in Figure 2.62 will be discussed in future chapters.

Other special groups are generated by chemical rearrangements of side chains and, sometimes, the peptide backbone. For example, the jellyfish *Aequorea victoria* produces green fluorescent protein (GFP), which emits green light when stimulated with blue light. The source of the fluorescence is a group formed by the spontaneous rearrangement and oxidation of the sequence Ser-Tyr-Gly within the center of the protein (**Figure 2.63A**). Since the discovery of GFP, a number of mutants have been engineered which absorb and emit light across the entire visible

spectrum (Figure 2.63B). These proteins are of great service to researchers as markers within cells (Figure 2.63C).

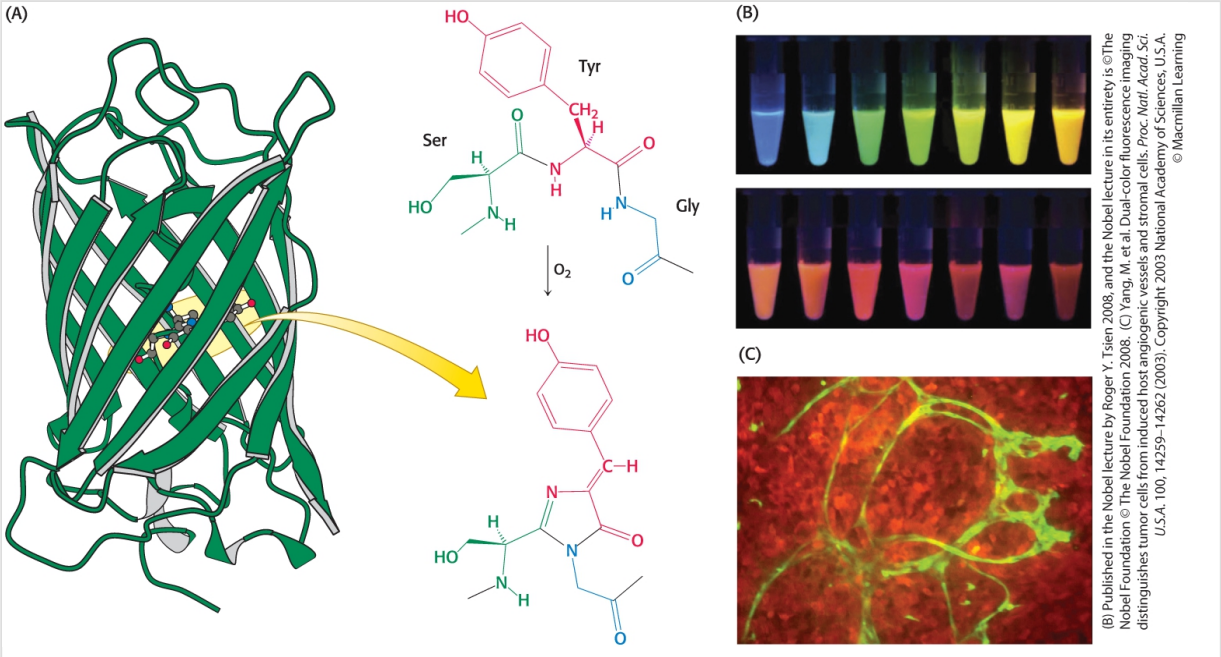


FIGURE 2.63 GFP is modified posttranslationally by the chemical rearrangement of three amino acids. (A) The rearrangement and oxidation of the sequence Ser-Tyr-Gly in green fluorescent protein (GFP) is the source of its fluorescence. (B) Mutants of GFP emit light across the visible spectrum. (C) A melanoma cell line engineered to express one of these GFP mutants, red fluorescent protein (RFP), was injected into a mouse whose blood vessels express GFP. In this fluorescence micrograph, the formation of new blood vessels (green) in the tumor (red) is readily apparent.

[(A) Drawn from 1GFL.pdb;]

Finally, many proteins are cleaved and trimmed after synthesis. For example, digestive enzymes are synthesized as inactive precursors that can be stored safely in the pancreas. After release into the intestine, these precursors become activated by peptide-bond cleavage (Section 7.4). In blood clotting, peptide-bond cleavage converts soluble fibrinogen into insoluble fibrin. A number of polypeptide hormones, such as adrenocorticotropic hormone, arise from the splitting of a single large precursor protein. Likewise, many viral proteins are

produced by the cleavage of large polyprotein precursors. We shall encounter many more examples of modification and cleavage as essential features of protein formation and function. Indeed, these finishing touches account for much of the versatility, precision, and elegance of protein action and regulation.

Chapter 2 Summary

2.1 Several Properties of Protein Structure Are Key to Their Functional Versatility

- Proteins are linear polymers built of amino acids.
- Proteins contain a wide range of functional groups.
- Proteins interact with each other to form assemblies.
- Proteins can vary from rigid to highly flexible.

2.2 Proteins Are Built from a Repertoire of 20 Amino Acids

- Proteins are polymers of L amino acids which can be classified on the properties of their side chains.
- Hydrophobic amino acids with nonpolar R groups include: glycine, alanine, valine, leucine, isoleucine, methionine, proline, phenylalanine, and tryptophan.
- Polar amino acids include: serine, threonine, tyrosine, asparagine, glutamine, cysteine, and histidine.
- Positively charged amino acids include: lysine and arginine.
- Negatively charged amino acids include: aspartate and glutamate.

2.3 Primary Structure: Amino Acids Are Linked by Peptide Bonds to Form Polypeptide Chains

- Amino acids are linked together into polypeptides by peptide bonds.
- The sequence of amino acids in a protein is called its primary structure.
- Polypeptide chains are directional, in that the ends of the chain are different: by convention, polypeptide sequences are written

from the amino-terminal residue to the carboxyl-terminal residue.
- Each protein has its own unique primary structure.
- Peptide bonds have a planar geometry due to their partial double-bond character.
- The main chain bonds preceding and following the α carbon have rotational flexibility, which can be depicted in a Ramachandran plot.

2.4 Secondary Structure: Polypeptide Chains Can Fold into Regular Structures

- Secondary structure refers to the formation of regular structures near one another in the protein sequence.
- The α helix is a tightly packed rod where the CO group from one amino acid is hydrogen bonded to the NH group four residues further along the chain.
- The β sheet features a series of fully extended polypeptide chains (β strands) hydrogen-bonded to each other.
- Turns and loops are shorter, less-regular secondary structures that enable the polypeptide chain to change direction.

2.5 Tertiary Structure: Proteins Can Fold into Globular or Fibrous Structures

- Tertiary structure refers to the fully folded structure of a single polypeptide chain.
- The formation of tertiary structure in water-soluble proteins is largely driven by packing hydrophobic residues in the interior of the protein and exposing hydrophilic resides on the surface.
- Proteins can fold into highly compact and asymmetric globular proteins or fully extended fibrous proteins.

2.6 Quaternary Structure: Polypeptide Chains Can Assemble into Multisubunit Structures

- Quaternary structure refers to the organization of multiple polypeptide chains (subunits) into an organized complex.
- These assemblies can range from simple dimers to highly complicated viral coats with hundreds of subunits.
- Quaternary structures are held together by numerous noncovalent bonds.

2.7 The Amino Acid Sequence of a Protein Determines Its Three-Dimensional Structure

- The amino acid sequence determines the three-dimensional structure and, hence, all other properties of a protein.
- Protein folding does not occur by random searching, but by progressive stabilization of intermediate structural elements.
- Protein folding is a highly cooperative process; structural intermediates between the unfolded and folded forms do not accumulate.
- The versatility of proteins is further increased by posttranslational modifications, including the chemical modification or rearrangement of side chains and the cleavage of the peptide backbone.

Key Terms

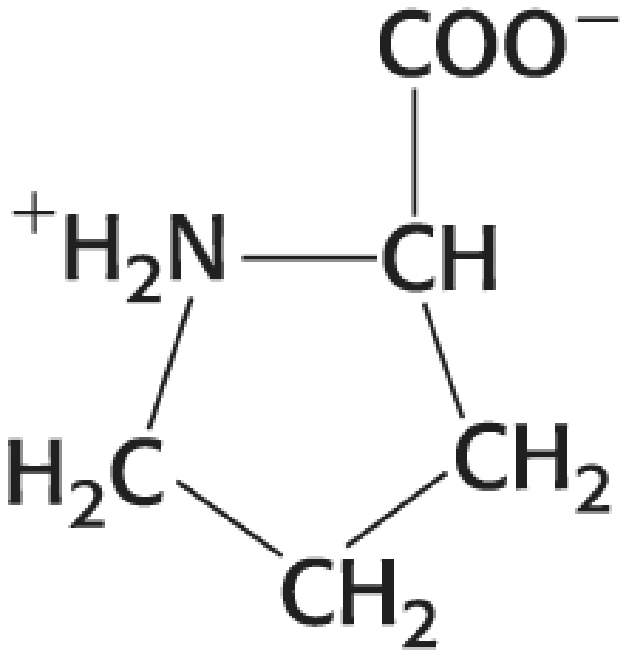
enzymes
amino acid
α carbon
side chain (R group)
chiral
dipolar ion (zwitterion)
peptide bond (amide bond)
residue
main chain (backbone)

proteins
oligopeptides (peptides)
dalton
disulfide bond
primary structure
torsion angle (dihedral angle)
Ramachandran plot
secondary structure
α helix
β pleated sheet (β sheet)
β strand
reverse turn (β turn; hairpin turn)
loop
tertiary structure
globular protein
motif (supersecondary structure)
domain
fibrous protein
subunit
quaternary structure
homodimer
denatured protein
native protein
cooperative transition
amyloid fibrils (amyloid plaques)
posttranslational modification

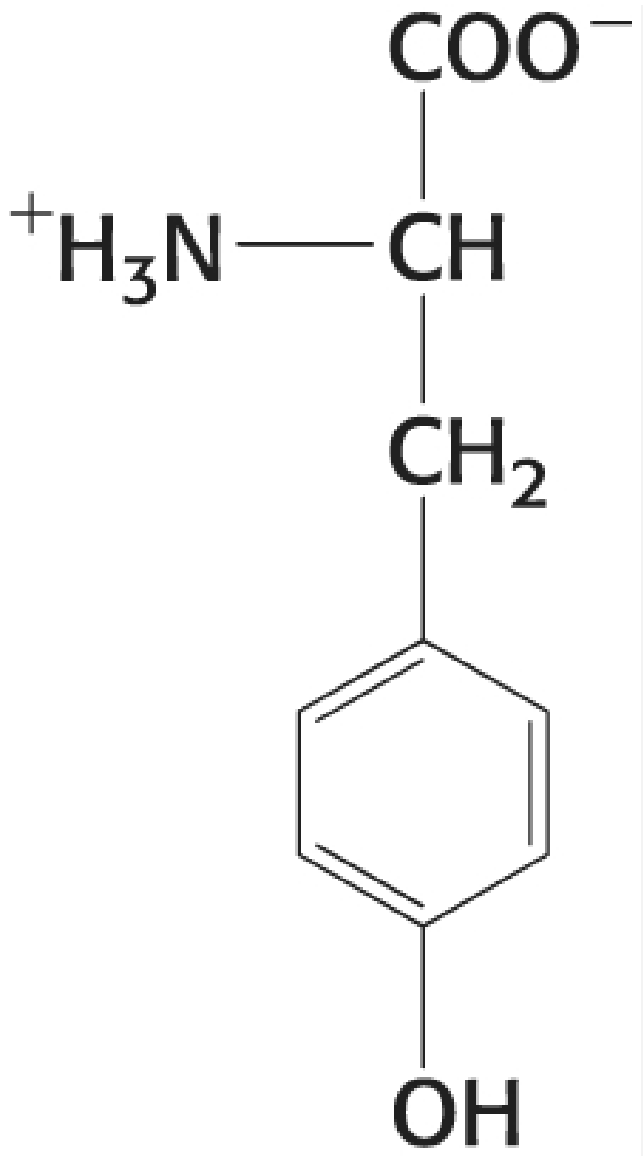
Problems

1. Examine the following four amino acids (A–D):

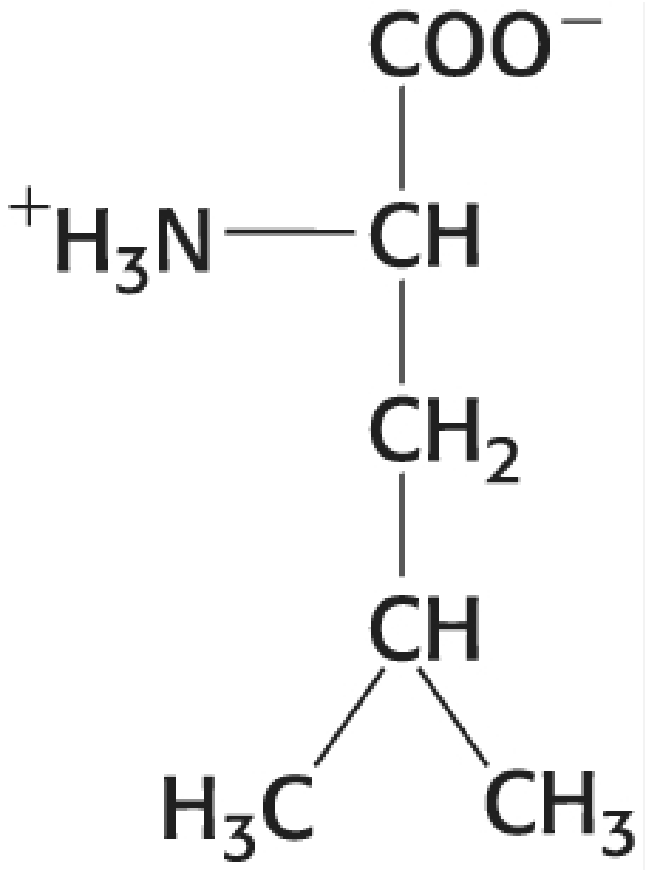
A.



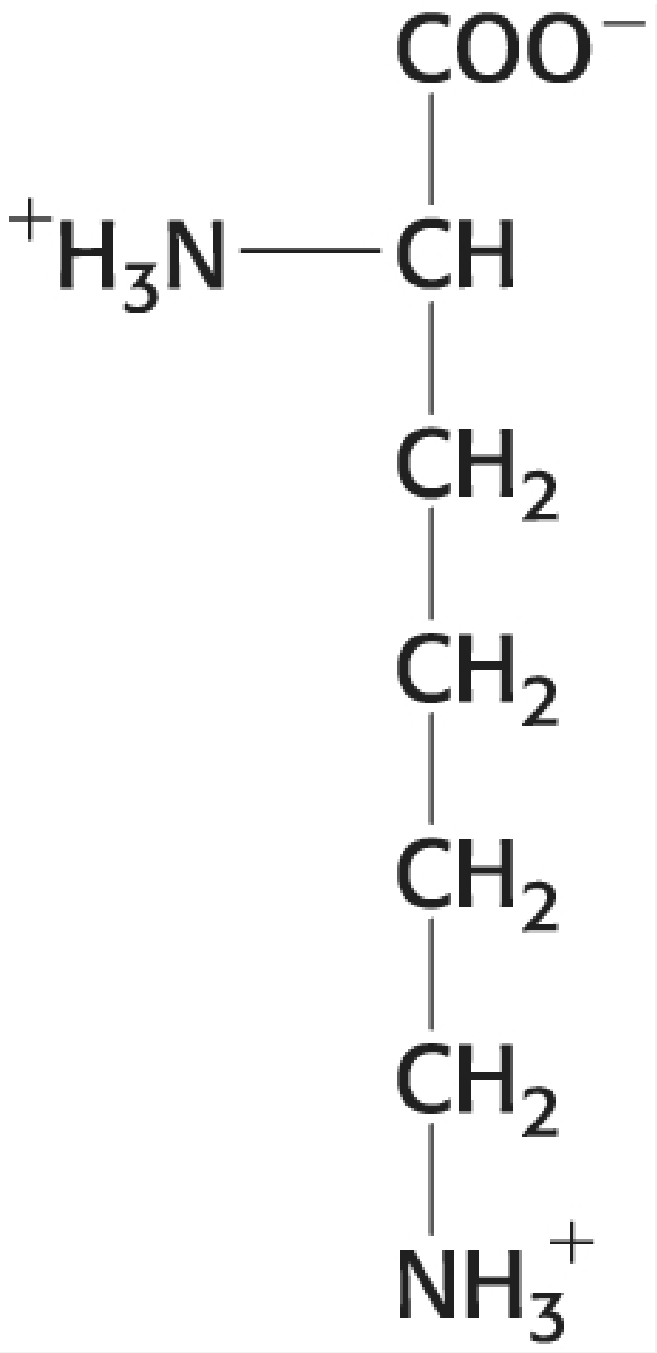
B.



C.



D.



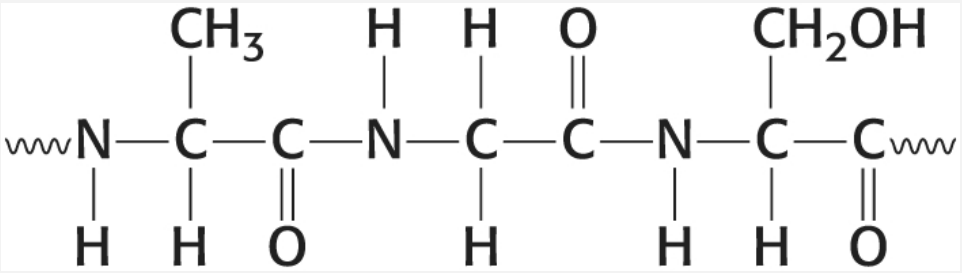
What are their names, three-letter abbreviations, and one-letter symbols? 1

2. Sort the amino acids shown in problem 1 according to the category in which it fits. 1

a. Basic side chain _____
b. Acidic side chain _____
c. Neutral polar side chain _____
d. Hydrophobic side chain _____

3. Which of the following amino acids have R groups that have hydrogen-bonding potential? Ala, Gly, Ser, Phe, Glu, Tyr, Ile, and Thr. 1

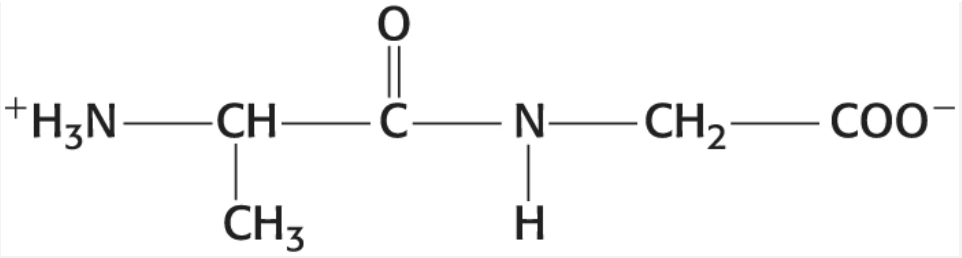
4. Examine the segment of a protein shown here.



a. What three amino acids are present?
b. Of the three, which is the N-terminal amino acid?
c. How many peptide bonds are explicitly shown in this peptide?

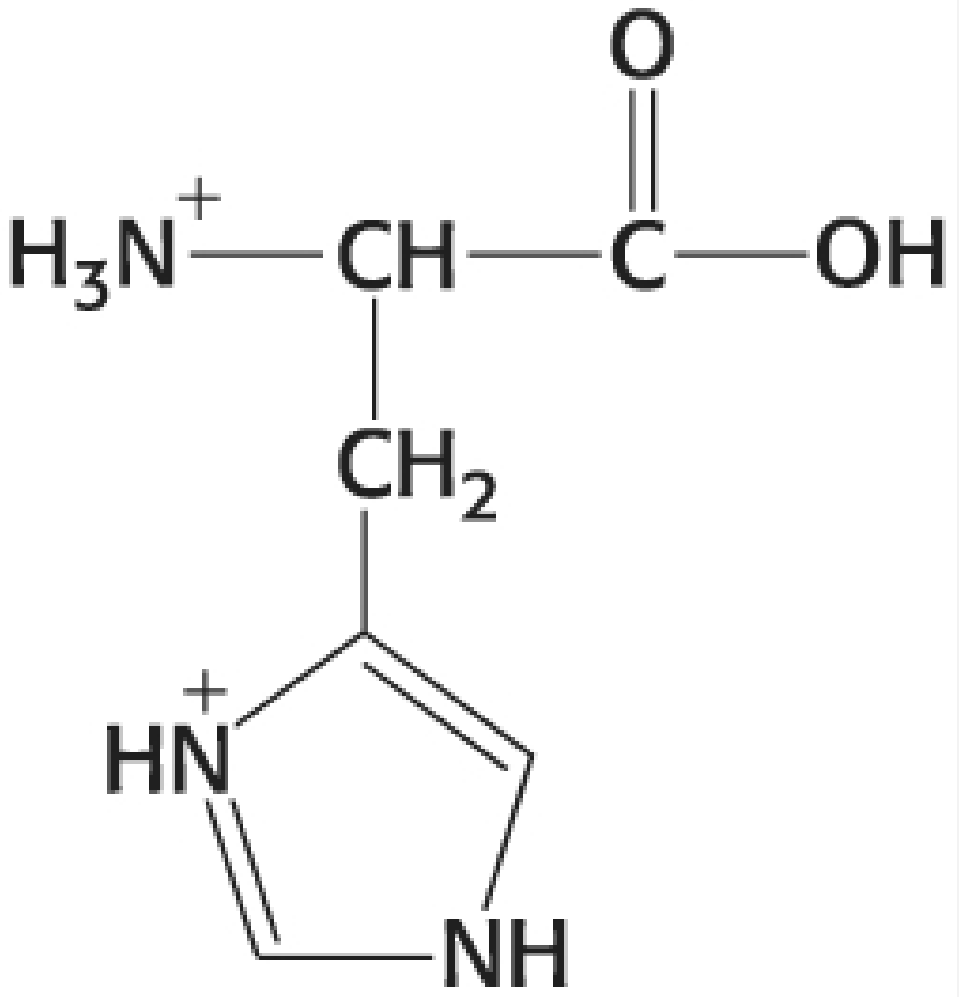
5. Draw the structure of the dipeptide Gly-His. What is the charge on the peptide at pH 5.5? pH 7.5? 1

6. Draw the resonance structure for the peptide bond shown in the image.



7. On Figure 2.5, indicate the pH value at which a solution of this amino acid would have no net charge.

8. All amino acids have two ionizable functional groups: an α-amino group (typical pK_a of 8.0) and an α-carboxylic acid group (typical pK_a of 3.1). Histidine also has an ionizable side chain (R group) with a pK_a of about 6.0. One of the possible ionization states of histidine is shown in the image.



a. At what pH would the structure be the predominant ionization state? Consider the ionization state of all three of the functional groups.

pH 11.6 pH 8.4 pH 7.0 pH 6.0 pH 3.1 pH 1.5

b. The protonated form of the R group of histidine is shown in the structure. The ratio of the charged

(protonated) form to the deprotonated form depends on the pK_a of the R group and the pH of the solution. At which of these pH values would the charged form of the R group predominate?

pH 3.0 pH 4.9 pH 6.0 pH 11.1

9.

a. Tropomyosin, a 70-kDa muscle protein, is a two-stranded α-helical coiled coil. Estimate the length of the molecule.
b. Suppose that a 40-residue segment of a protein folds into a two-stranded antiparallel β structure with a 4-residue hairpin turn. What is the longest dimension of this motif? 3

10. Poly-L-leucine in an organic solvent such as dioxane is α helical, whereas poly-L-isoleucine is not. Why do these amino acids with the same number and kinds of atoms have different helix-forming tendencies? 3

11. An enzyme that catalyzes disulfide–sulfhydryl exchange reactions, called protein disulfide isomerase (PDI), has been isolated. PDI rapidly converts inactive scrambled ribonuclease into enzymatically active ribonuclease. In contrast, insulin is rapidly inactivated by PDI. What does this important observation imply about the relationship between the amino acid sequence of insulin and its three-dimensional structure?

12. What is the length of a 12 kDa single-stranded α-helical protein segment? Assume a mean residue mass of 110 daltons. 3

13. Which of these four peptides is most likely to form a β sheet?

a. Lys-Thr-Val-Ile-Trp-Pro-Phe-Tyr-Ile-Gln-Ile-Gly
b. Met-Leu-Lys-Ala-Ser-Ala-Leu-Glu-Lys-Leu-Ser-Glu
c. Arg-Ser-Tyr-Glu-Gly-Leu-Lys-Arg-Ile-Ala-Glu-Ser
d. Ala-Glu-Met-Leu-Gln-Lys-Arg-Gly-Cys-Gly-Asp-Glu

14. Consider the Ramachandran plots in Figures 2.21, 2.24, and 2.27.

a. Which observation most likely describes part of an observed α helix? (choose one) 3
   1. $\varphi = -60^\circ$; $\psi = -47^\circ$; many Ala residues
   2. $\varphi = -140^\circ$; $\psi = +130^\circ$; many Val residues
   3. $\varphi = -59^\circ$; $\psi = +150^\circ$; many Ser residues
   4. $\varphi = +60^\circ$; $\psi = +40^\circ$; many Gly residues
   5. $\varphi = -57^\circ$; $\psi = -47^\circ$; many Pro residues

b. Which observations would not likely occur in a β sheet? (may be more than one)
   1. $\varphi = -57^\circ$; $\psi = -49^\circ$; many Ala residues
   2. $\varphi = +60^\circ$; $\psi = +60^\circ$; many Gly residues
   3. $\varphi = -51^\circ$; $\psi = +153^\circ$; many Gly and Pro residues
   4. $\varphi = -139^\circ$; $\psi = +135^\circ$; many Val residues
   5. $\varphi = -120^\circ$; $\psi = +120^\circ$; many Tyr residues

15. Classify each phrase as a description of α helices, β sheets, reverse turns, or all: 3

a. Contains —NH hydrogen bonded to C=O

b. Successive R groups point in opposite directions
c. All —NH groups point in the same direction
d. First residue hydrogen bonded to fourth residue (i.e., residue *i* is H-bonded to residue $i + 3$)
e. First residue hydrogen bonded to fifth residue (i.e., residue *i* is H-bonded to residue $i + 4$)

16. The α and β subunits of hemoglobin bear a remarkable structural similarity to myoglobin. However, certain residues that are hydrophilic in myoglobin are hydrophobic in the subunits of hemoglobin. Why might this be the case?

17. For an amino acid such as alanine, the major species in solution at pH 7 is the zwitterionic form. Assume a pK_a value of 8 for the amino group and a pK_a value of 3 for the carboxylic acid. Estimate the ratio of the concentration of the neutral amino acid species (with the carboxylic acid protonated and the amino group neutral) to that of the zwitterionic species at pH 7 (Section 1.3).

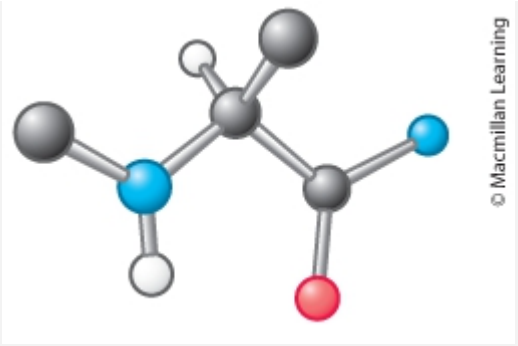
18. Translate the following amino acid sequence into one-letter code: Glu-Leu-Val-Ile-Ser-Ile-Ser-Leu-Ile-Val-Ile-Asn-Gly-Ile-Asn-Leu-Ala-Ser-Val-Glu-Gly-Ala-Ser. 1

19. Would you expect Pro—X peptide bonds to tend to have cis conformations like those of X—Pro bonds? Why or why not?

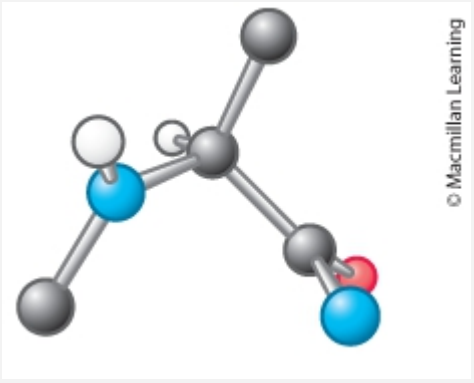
20. For each of the amino acid derivatives shown here (A–E), find the matching set of ϕ and ψ values (a–e).

(A)

(a)
$\phi = 120$,
$\psi = 120$



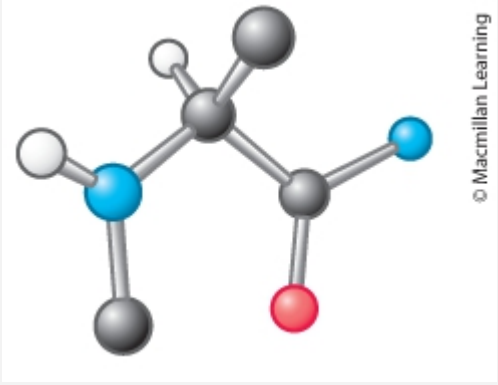
(B)



(b)
$\phi = 180$,
$\psi = 0$

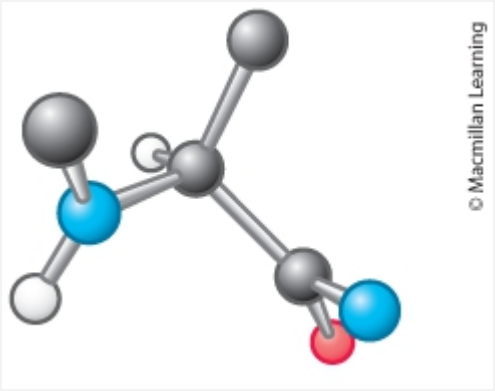
(C)

(c)
$\phi = 180$,
$\psi = 180$



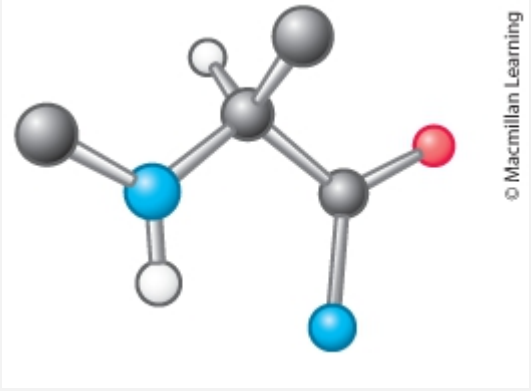
(D)

(d)
$\phi = 0$,
$\psi = 180$



(E)

(e)
$\phi = -60$,
$\psi = -40$



21. In the 1950s, Christian Anfinsen demonstrated the renaturation of the protein ribonuclease *in vitro*. After reduction and the addition of urea, the protein was in an unfolded state. After removing the urea and then the reducing agent, the protein oxidized and refolded, with greater than 90% activity. If reducing agent removal occurs before removing the urea, the protein showed less than 5% activity. Why does ribonuclease refold incorrectly if the reducing agent is removed before urea removal?

Chapter 3
Binding and Molecular Recognition





Stefan Christmann/naturepl.com
© Macmillan Learning

Penguins can recognize and find their mates even in a crowd of quite similar-looking and sounding birds. At the level of molecules, recognition plays a hugely important role in biochemical interactions. The complex shown above involves a protein that recognizes and binds extended amino acid sequences on other proteins and helps target them to the proper cellular compartment. The receptor protein can readily distinguish even minor differences in its target, such as the substitution of an isoleucine for a leucine.

Outline

3.1 Binding Is a Fundamental Process in Biochemistry
3.2 Myoglobin Binds and Stores Oxygen
3.3 Hemoglobin Is an Efficient Oxygen Carrier
3.4 The Immune System Depends on Key Binding Proteins

3.5 Quantitative Terms Can Describe Binding Propensity

Learning Goals



By the end of this chapter, you should be able to:

1. Explain in qualitative terms how the interaction between a receptor and a ligand that it binds depends on the concentration of the ligand.
2. Describe the key principles for the binding of oxygen by myoglobin and hemoglobin.
3. Discuss the concept of binding cooperativity and how it applies to hemoglobin, and how cooperativity enhances the ability of hemoglobin to function as a highly effective oxygen carrier.
4. Describe some key binding proteins in the immune system, including toll-like receptors, immunoglobulins, and major histocompatibility complex proteins, and how binding reactions involving these proteins function in the immune system.
5. Calculate parameters of binding reactions using the concentrations of the reactants and the characteristics such as the dissociation constant and kinetic rate constants.

Organisms and cells are packed with different kinds of small molecules, including building blocks and metabolites, as well as macromolecules including proteins and nucleic acids, all bustling around due to thermal motion. Yet, out of this chaos, order emerges with intricately organized assemblies on a range of scales and specific biochemical pathways that are the subject of much of this book. The key process that enables this organization is specific molecular binding. The ability of many biological macromolecules to bind a specific set of molecules out of extremely complicated mixtures is very unusual compared to the capacity of non-biological molecules and can seem astounding, but it is the consequence of chemical principles and the selective power of molecular evolution.

3.1 Binding Is a Fundamental Process in Biochemistry

Sets of molecules stick together so that they spend much more time together than they would without this binding, and this occurs despite the fact that there are many other potential binding partners around them. This ability for certain molecules to bind to one another in the face of many alternatives is often referred to as **molecular recognition**. Furthermore, this binding is specific in another way: the structures of the complexes formed have particular three-dimensional shapes. This enables the complexes to have well-defined properties including participating in other binding events and, in some cases, playing key roles in processes such as the transmission of information within and between cells.

In this chapter, we will focus primarily on two examples, likely familiar in some aspects of everyday life, to illustrate these principles. These are the oxygen storage and carrier proteins myoglobin and hemoglobin, and important proteins from the immune system, including antibodies. **Myoglobin** binds oxygen and stores it for use when muscles expend energy and need to convert molecules from food into useable forms. Myoglobin, by virtue of bound **heme**, is responsible for the color of red meat. **Hemoglobin** is a related heme-containing protein found in blood that acts as oxygen carrier, transporting oxygen that it binds in the lungs to tissues throughout the body. Hemoglobin is remarkably efficient in fulfilling this role. It binds and releases oxygen in a manner that is quite sensitive to the amount of available oxygen in its environment and also to pH and the presence of carbon dioxide. These binding properties allow hemoglobin to deliver oxygen specifically to tissues where it is most needed due to ongoing metabolic activity.

Our immune systems must respond to pathogens such as viruses and bacteria, even those to which we have never previously been exposed. Remarkably, our immune systems can generate proteins called *antibodies* that bind specifically to components of these pathogens. Each antibody has a set of polypeptide loops on its surface that are selected to facilitate binding to a particular pathogen component. The ability to generate an essentially infinite set of binding proteins by combining a limited set of component loops has kept members of our and other species protected in the face of an ever-evolving set of potentially deadly pathogens.

We begin with a discussion of some of the general characteristics of binding processes. For this, we will use examples related to the estrogen receptor, a key protein that functions physiologically by binding certain steroid hormones and is also the target of some important drugs and environmental pollutants.

Binding depends on the concentrations of the binding partners

Suppose we start with a receptor R, typically a protein, and add a potential binding partner, often referred to as a **ligand**, L. These might come together to form a complex, RL.

$$\mathrm{R} + \mathrm{L} \rightleftharpoons \mathrm{RL} \tag{1}$$

If R and L have a very strong tendency to bind to one another, then every molecule of L that is added will combine with a molecule of R, if one is available, to form a complex. As we add more L, this will continue until all of the R molecules are now in the RL form. On the other hand, if R and L have little tendency to combine, then, even if R and L collide, no complex will form as thermal motions will dominate. In between

these two limiting cases, some of the added L will combine with R to form RL while the remainder remains free. These cases are summarized in Figure 3.1.

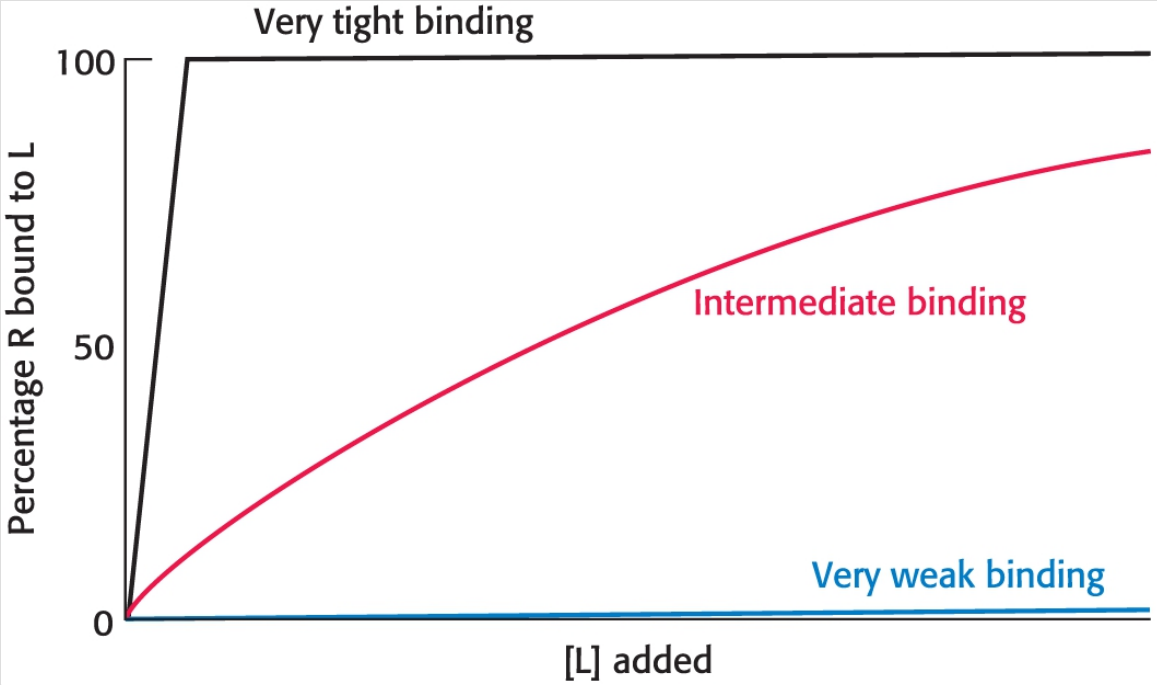


FIGURE 3.1 Comparing the percentage of receptor R bound to ligand L with the concentration of added L reveals how tightly R binds L.

Let us examine the case of intermediate binding in more detail. As more L is added, the probability that a given receptor molecule is bound to L gradually increases. A parameter that is useful for characterizing such curves is the concentration of L at which half of the receptor is bound to L and half is free. This is designated as $L_{1/2}$ in Figure 3.2. This parameter is useful because it reveals the concentration range of L around which the receptor makes the transition from being mostly free to mostly bound. We will explore these curves in more quantitative terms later in this chapter.

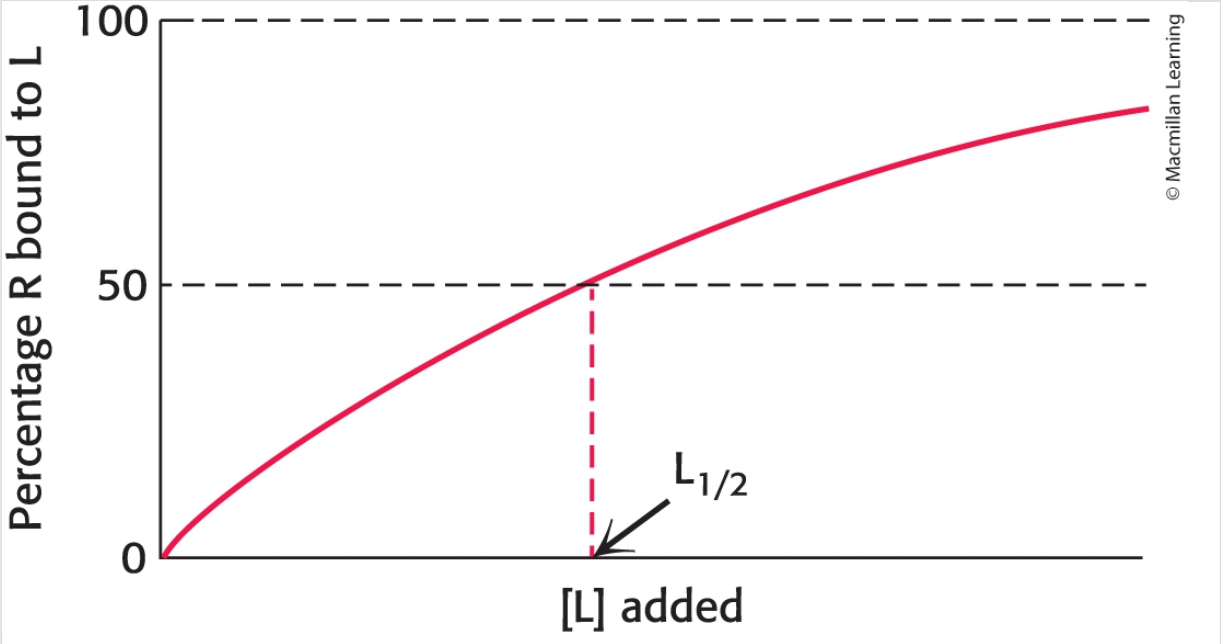


FIGURE 3.2 The binding of L to R can be characterized by $L_{1/2}$. The parameter $L_{1/2}$ is the concentration of L at which half (50%) of the total amount of R is bound to L.

Proteins can selectively bind certain small molecules

To put the importance of binding within biochemical systems in context, let us consider the estrogen receptor and its ligands. Estrogens are steroid hormones that play primary roles in the development of the female reproductive system and secondary sex characteristics. The most prevalent estrogen is β-estradiol or, more simply, estradiol (Figure 3.3). The first step in estrogen exerting its biological activity is binding to estrogen receptors. These receptors are present in tissues such as mammary glands and the endometrium. Estradiol binds to these receptors with an $L_{1/2}$ of approximately $1\ \text{nM}\ (10^{-9}\ \text{M})$. The amount of

estradiol in blood serum varies with age and time within the menstrual cycle, but on average it is around 1.1 nM, just in the range likely to trigger substantial receptor occupancy and activity.

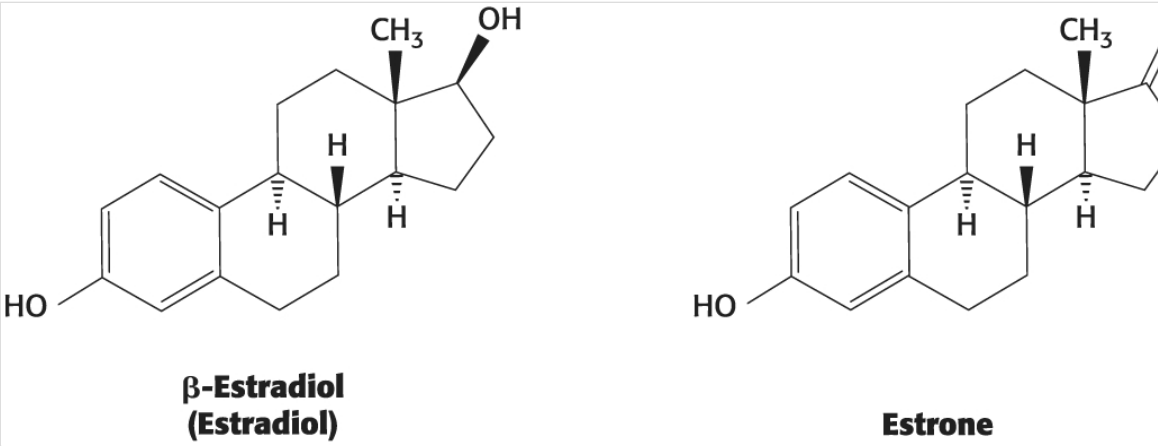


FIGURE 3.3 Estrogens are hormones that are bound by estrogen receptors. β-Estradiol is the most prevalent and potent estrogen, and estrone is one of a number of other estrogens that pla somewhat different biological roles.

This binding occurs despite the fact that serum contains thousands of different small molecules, many of which are present at concentrations higher than that for estradiol. For example, testosterone, a steroid hormone associated with the development of the male reproductive system and secondary sex characteristics, is present at concentrations comparable to or even higher than those for estradiol, even in women. However, the binding of testosterone to the estrogen receptor is very weak with $L_{1/2} > 1\mu M$, more than 1000 times larger than that for estradiol.

The ability of the estrogen receptor to recognize estradiol, that is, to discriminate between estradiol and testosterone, is impressive given the similarities in their structures (**Figure 3.4**). Both structures are based on the same four-ring framework characteristic of steroids. However, one six-membered ring (the A ring shown in Figure 3.4) in estrogens such as

estradiol is aromatic and, therefore, planar, whereas the corresponding ring in testosterone is not aromatic and is bonded to an additional methyl group absent in estrogens. Examination of the three-dimensional structure of the estrogen receptor bound to estradiol reveals that this protein has a narrow binding pocket lined with hydrophobic residues such as leucine and phenylalanine that fits neatly around the ligand but would likely sterically clash with thicker ligands such as testosterone. Moreover, the pocket includes groups that recognize both the oxygen and the hydrogen of the hydroxyl group in estradiol (Figure 3.5).

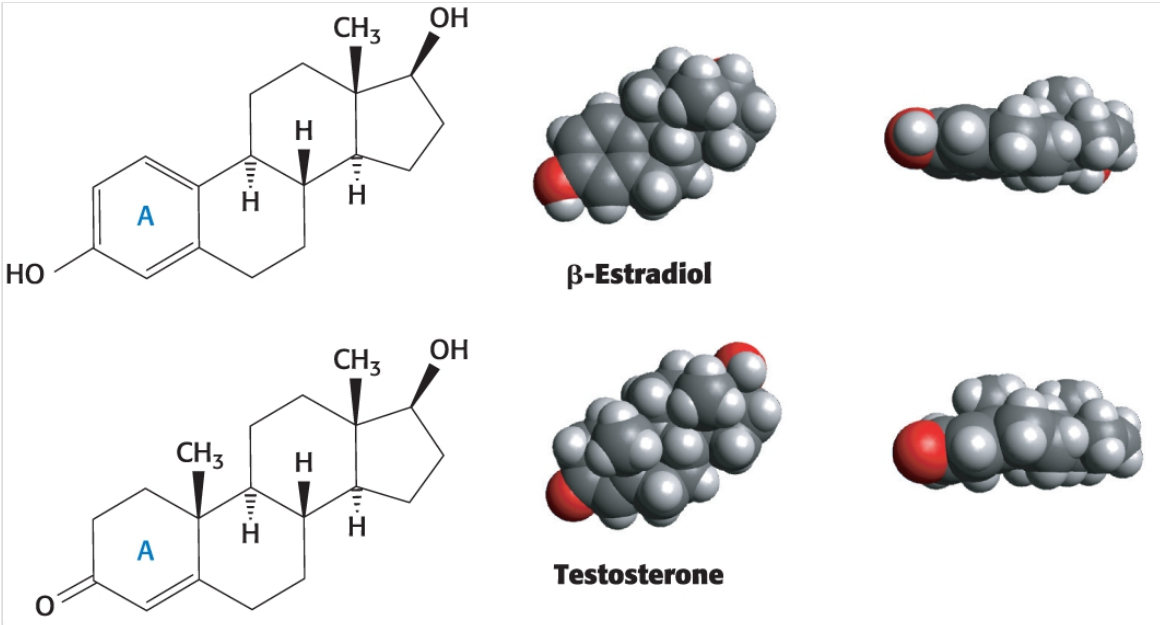


FIGURE 3.4 The steroid hormones β-estradiol and testosterone appear quite similar, yet receptors recognize the molecules as distinct. Their chemical structures are shown together with space-filling depictions from two orientations. The side views on the right reveal key differences in thickness that aid molecular recognition. The ring marked "A" is aromatic (and therefore planar) in β-estradiol, but not in testosterone.

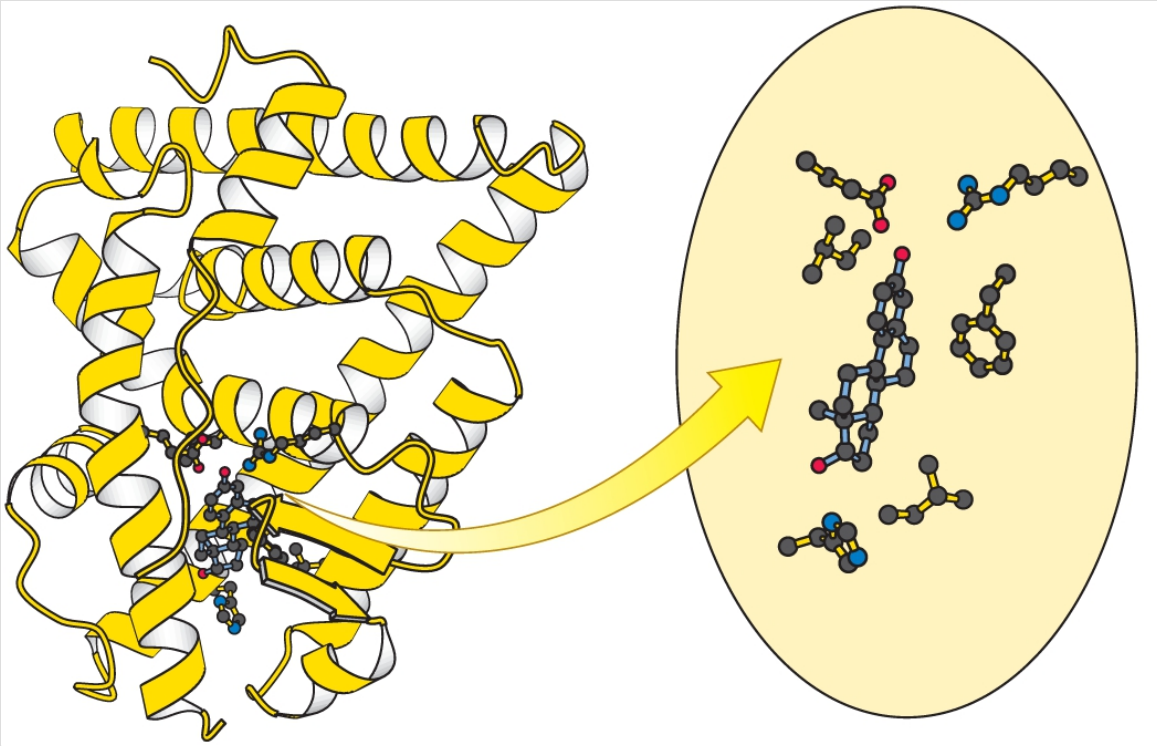


FIGURE 3.5 Proteins such as estrogen receptors include binding pockets that are complementary to the shapes of specific ligands. This enables the proteins to bind these ligands while rejecting ligands with even subtly different shapes. In the case of estrogen receptors, and some but not all proteins, some conformational changes occur upon ligand binding.

This ability of proteins such as the estrogen receptor to bind ligands selectively has been probed further through the use of synthetic compounds that share some characteristics with estrogens. For example, the two compounds in **Figure 3.6** are mirror images of each other by virtue of the orientation of a single methyl group. Despite this relatively small change in structure, these compounds are bound by the estrogen receptor with $\downarrow_{1/2}$ values that differ from one another by a factor of more than 20.

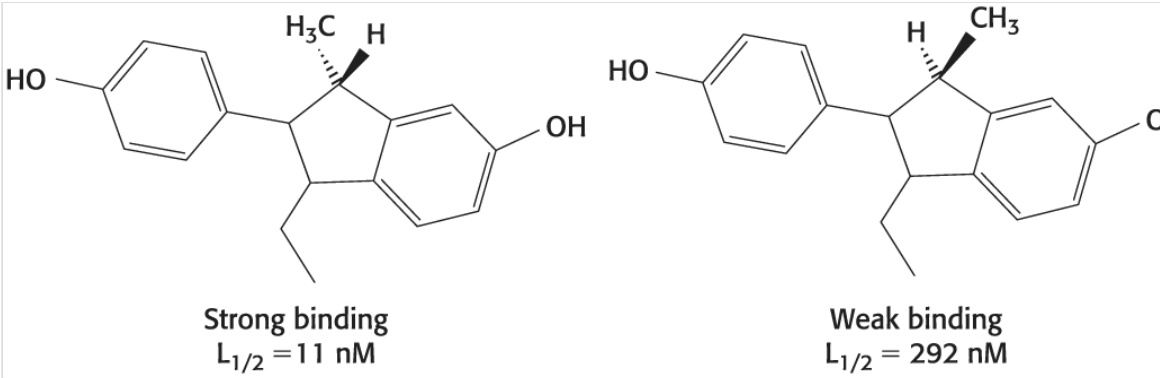


FIGURE 3.6 Even subtle features of ligands can be recognized. These two synthetic ligands for estrogen receptors are mirror images of one another, differing in the orientation of a single methyl group, yet they show substantial differences in how tightly they are bound by estrogen receptors.

This example of ligand binding by the estrogen receptor is typical of a great many proteins that we will encounter throughout this book. The ability to bind small molecules with selectivity allows proteins to pick particular molecules out of complicated mixtures to facilitate sensing of the presence of these molecules and, in some cases, to use the bound molecules for other purposes.

Self-Check Question

Human growth hormone is a protein with a molecular weight of approximately 22,000 grams/mol and a concentration in the bloodstreams of children in the range of 50 nanograms/ml. What is its molar concentration? What range would you anticipate for its $L_{1/2}$ value for the growth hormone receptor?

Binding is a dynamic process involving association and dissociation

At a given ligand concentration at equilibrium, the concentrations of receptor and receptor-ligand complex are constant. For example, when the ligand concentration is $L_{1/2}$, the concentrations of the receptor and the receptor-ligand complex are equal to one another and, therefore, equal to half of the total receptor concentration. Yet, each receptor is constantly releasing one ligand molecule and, subsequently, rebinding another (Figure 3.7). Thus, at equilibrium where the concentrations of all species are constant, underlying processes of association and dissociation occur.

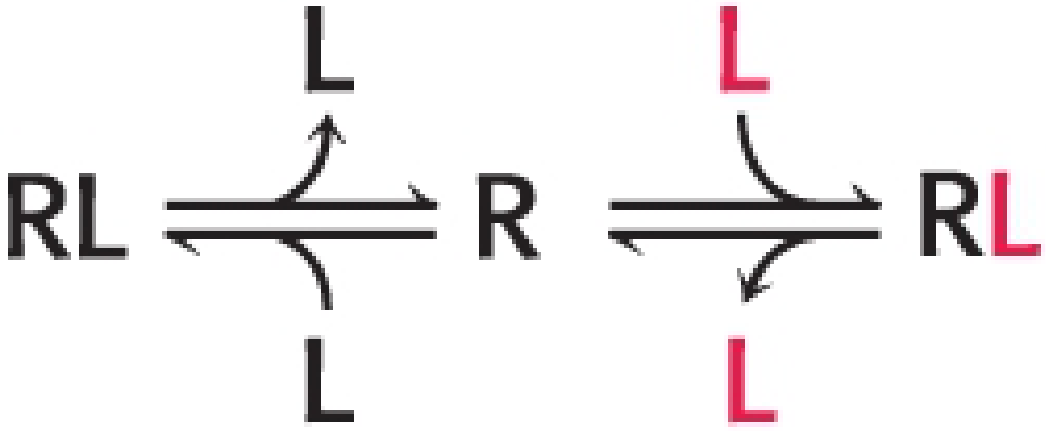


FIGURE 3.7 Dissociation and association are constantly occurring, even at equilibrium where the concentrations of all species are constant.

Returning to the estrogen receptor, experiments reveal that each receptor-estradiol complex releases its ligand on average once every 10 minutes. This relatively slow dissociation rate is related to the tight binding of estradiol to its receptor. At equilibrium, the dissociation and association rates must balance. Thus, if the estradiol concentration is

$1\ nM\ (L_{1/2})$, the rate of association between an unoccupied receptor and an estradiol molecule is also once every 10 minutes.

Self-Check Question



A testosterone derivative has been found to bind to the estrogen receptor with an $L_{1/2}$ of approximately $5\ \mu M$. When this compound is present at this concentration, the association rate with the estrogen receptor is estimated to be $5\ s^{-1}$. What is the expected dissociation rate?

3.2 Myoglobin Binds and Stores Oxygen

Myoglobin is a fairly abundant protein representing about 0.5% by weight in our muscles, and up to nearly 10% by weight in species such as sperm whales. This protein functions to bind and store oxygen, picking it up from the bloodstream and storing in muscle for use when needed. The abundance of myoglobin in sperm whale muscles is one of the adaptations that allows these marvelous creatures to dive very deep and to stay under water for up to two hours.

More myoglobin binds oxygen as the oxygen partial pressure is increased

We can characterize the oxygen-binding properties of myoglobin by observing its oxygen-binding curve, a plot of the fractional saturation versus the concentration of oxygen. The **fractional saturation** (Y) is defined as the fraction of possible binding sites that contain bound oxygen. The value of Y can range from 0 (all sites empty) to 1 (all sites filled). The concentration of oxygen is most conveniently measured by its partial pressure, pO_2. For myoglobin, a binding curve indicating a simple chemical equilibrium is observed (**Figure 3.8**). Notice that the curve rises sharply as pO_2 increases and then levels off. Half-saturation of the binding sites, referred to as P_{50} (analogous to $L_{1/2}$ introduced previously) occurs at approximately 2 torr (mm Hg) for human myoglobin. For context, the partial pressure of oxygen at sea level is around 150 torr. Thus, a P_{50} value of 2 torr reveals that myoglobin binds oxygen with high affinity.

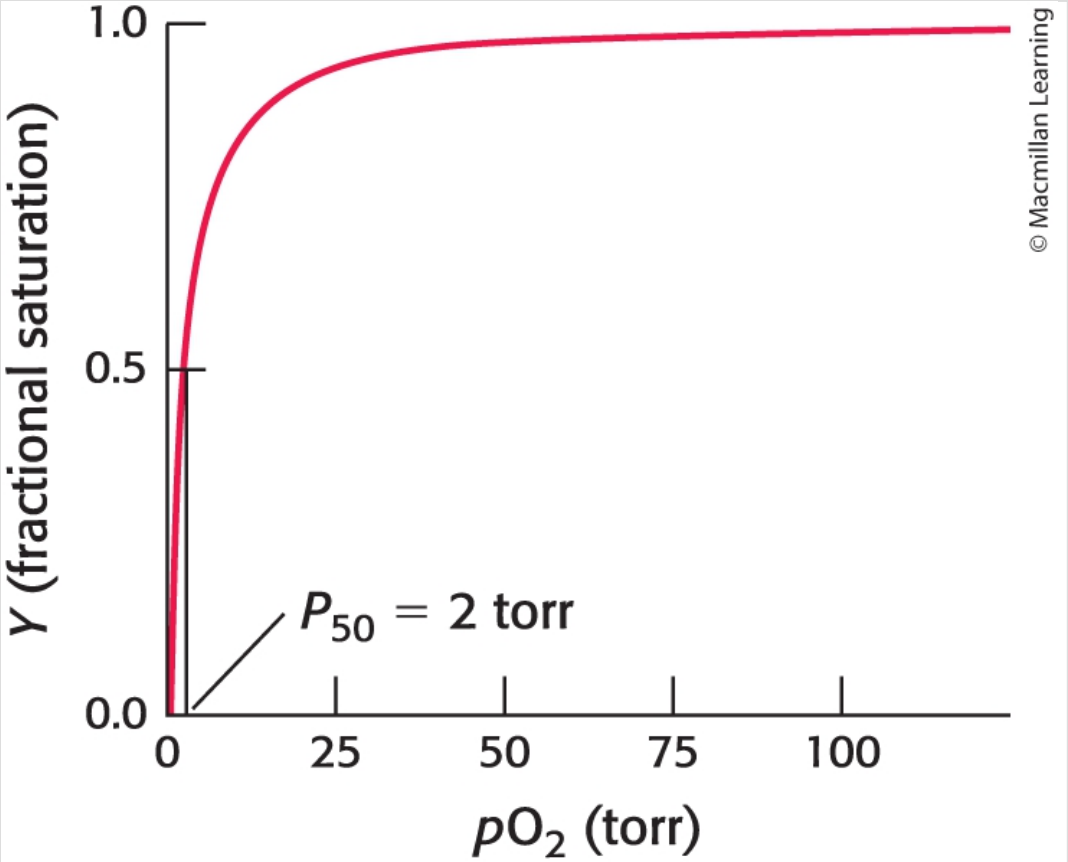


FIGURE 3.8 Half saturation of human myoglobin occurs when the partial pressure of oxygen is 2 torr. This point is revealed by plotting the fraction of myoglobin molecules that have oxygen bound (fractional saturation) as a function of the partial pressure of oxygen (pO_2).

A bond is formed between oxygen and iron in heme

Sperm whale myoglobin was the first protein for which the three-dimensional structure was determined (Figure 3.9). Myoglobin consists largely of α helices that are linked to one another by turns to form a globular structure. The ability of myoglobin to bind oxygen depends on

the presence of a *heme* molecule (Figure 3.10). The heme group consists of an organic component and a central iron atom. The organic component, called protoporphyrin IX, is made up of four linked pyrrole rings. The iron atom lies in the center of the protoporphyrin, bonded to the four pyrrole nitrogen atoms. The iron ion in myoglobin can form two additional bonds, one on each side of the heme plane. These binding sites are referred to as the fifth and sixth coordination sites. The fifth coordination site is occupied by the imidazole ring of a histidine residue from the protein, known as the **proximal histidine**.

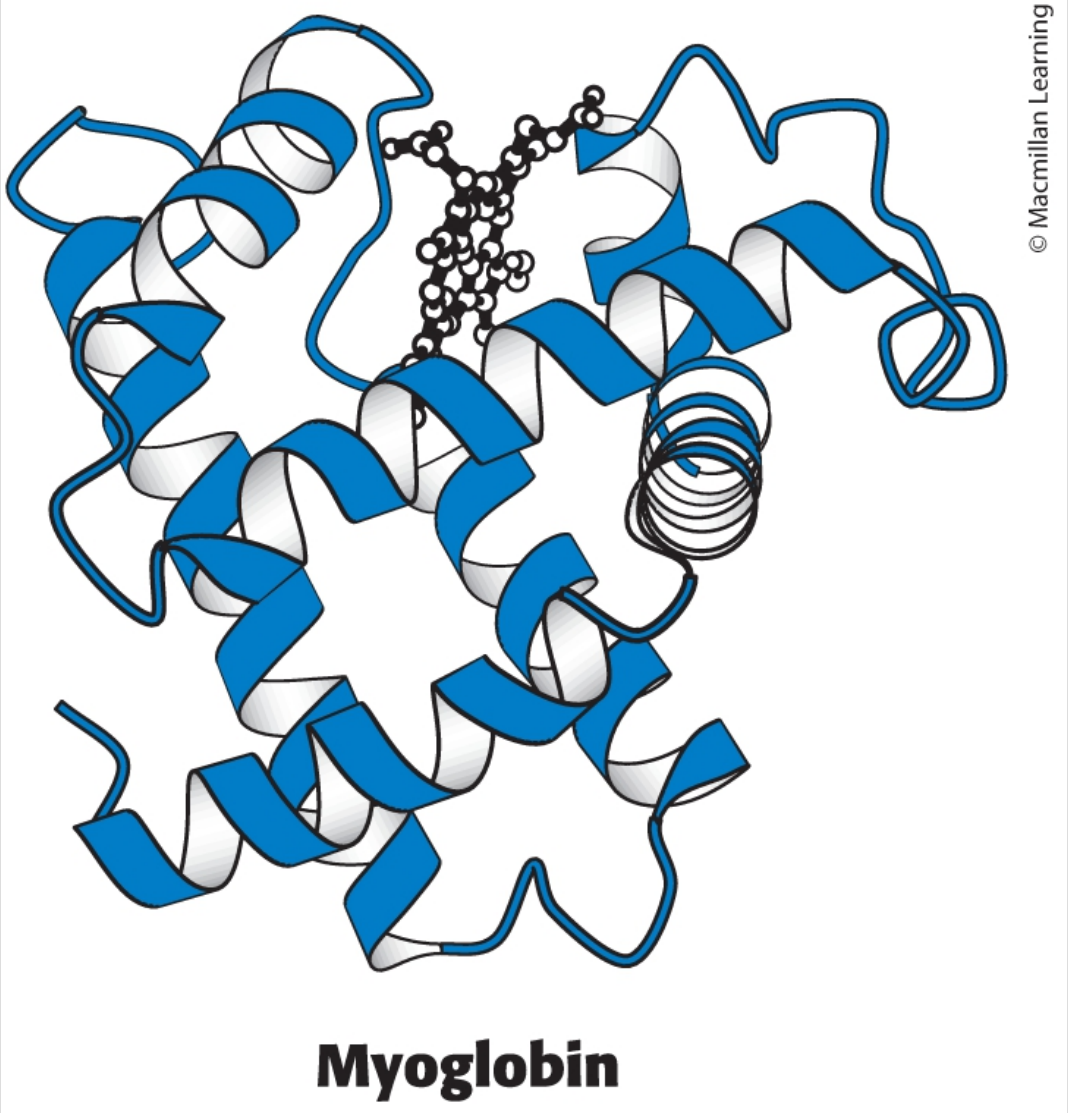


FIGURE 3.9 The structure of myoglobin consists primarily of α helices surrounding a heme molecule. The heme molecule functions as the oxygen-binding site.

INTERACT with this model in Achieve

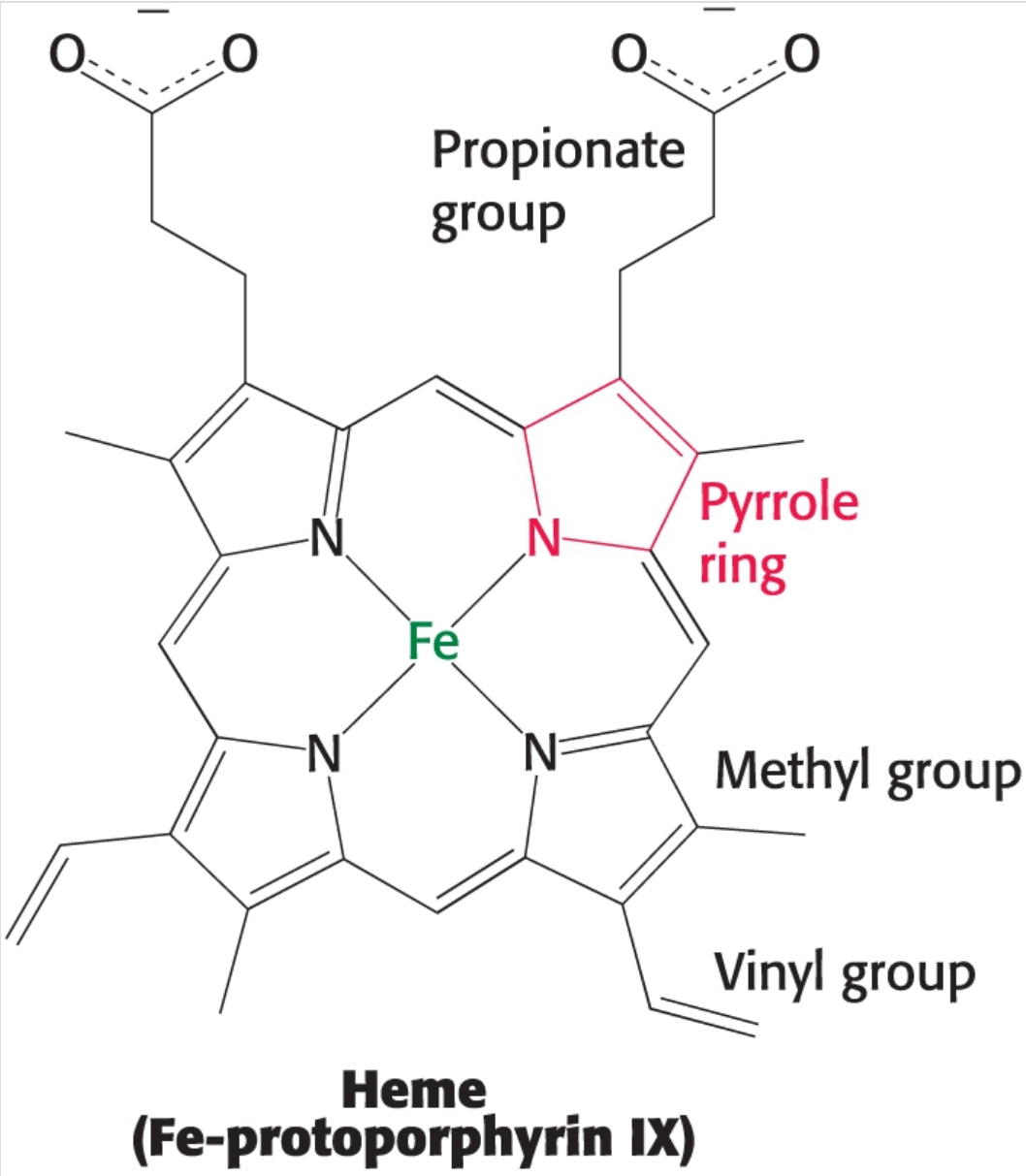


FIGURE 3.10 The structure of heme comprises four pyrrole rings that use their nitrogen atoms to bind to a central iron atom. Four methyl groups, two vinyl groups, and two propionate side chains are attached to the central tetrapyrrole.

Myoglobin can exist in an oxygen-free form called **deoxymyoglobin** or in a form with an oxygen molecule bound called **oxymyoglobin**. In deoxymyoglobin, the iron is in the ferrous (Fe^{2+}) oxidation state, and the sixth site remains unoccupied. The ferrous iron ion is slightly too large to fit into the well-defined hole within the porphyrin ring; it lies approximately $0.4\ \text{Å}$ outside the porphyrin plane (**Figure 3.11**).

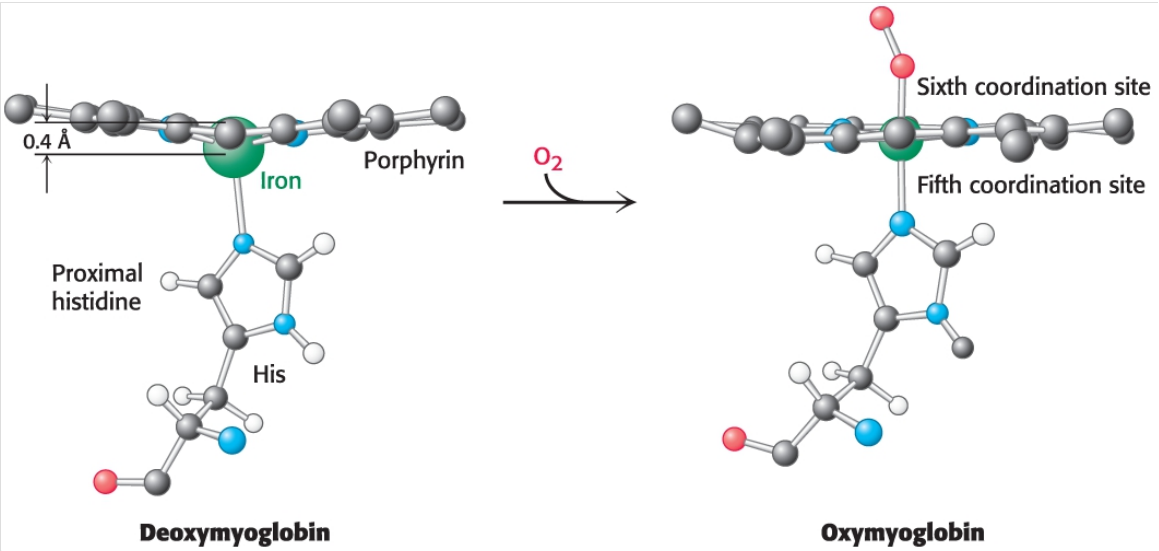


FIGURE 3.11 Oxygen binding changes the position of the heme iron ion. In deoxymyoglobin, t iron ion lies slightly outside the plane of the porphyrin and moves into the plane of the porphyr upon oxygen binding.

Oxymyoglobin forms when oxygen binding occurs at the sixth coordination site. This oxygen binding substantially rearranges the electrons within the iron so that the ion becomes effectively smaller, allowing it to move into the plane of the porphyrin (Figure 3.11, above).

Oxygen binding to iron in heme is accompanied by the partial transfer of an electron from the ferrous ion to oxygen. In many ways, the structure is best described as a complex between ferric ion (Fe^{3+}) and superoxide anion O_2^- (Figure 3.12).



FIGURE 3.12 The complex between iron and oxygen in myoglobin can be described by two resonance structures. One resonance structure has Fe^{2+} bound to dioxygen, and the other has Fe^{3+} bound to superoxide ion.

The structure of myoglobin prevents the release of reactive oxygen species

It is crucial that oxygen, when it is released, leaves as dioxygen rather than superoxide ion, for two important reasons. First, superoxide ion and other species generated from it are reactive oxygen species that can be damaging to many biological materials. Second, release of superoxide would leave the iron ion in the ferric state, producing a species, termed *metmyoglobin*, that does not bind oxygen. Thus, potential oxygen-storage capacity would be lost.

Features of myoglobin stabilize the oxygen complex such that superoxide is less likely to be released. In particular, the binding pocket

of myoglobin includes an additional histidine residue (termed the **distal histidine**) that donates a hydrogen bond from its imidazole group to the bound oxygen molecule (**Figure 3.13**).

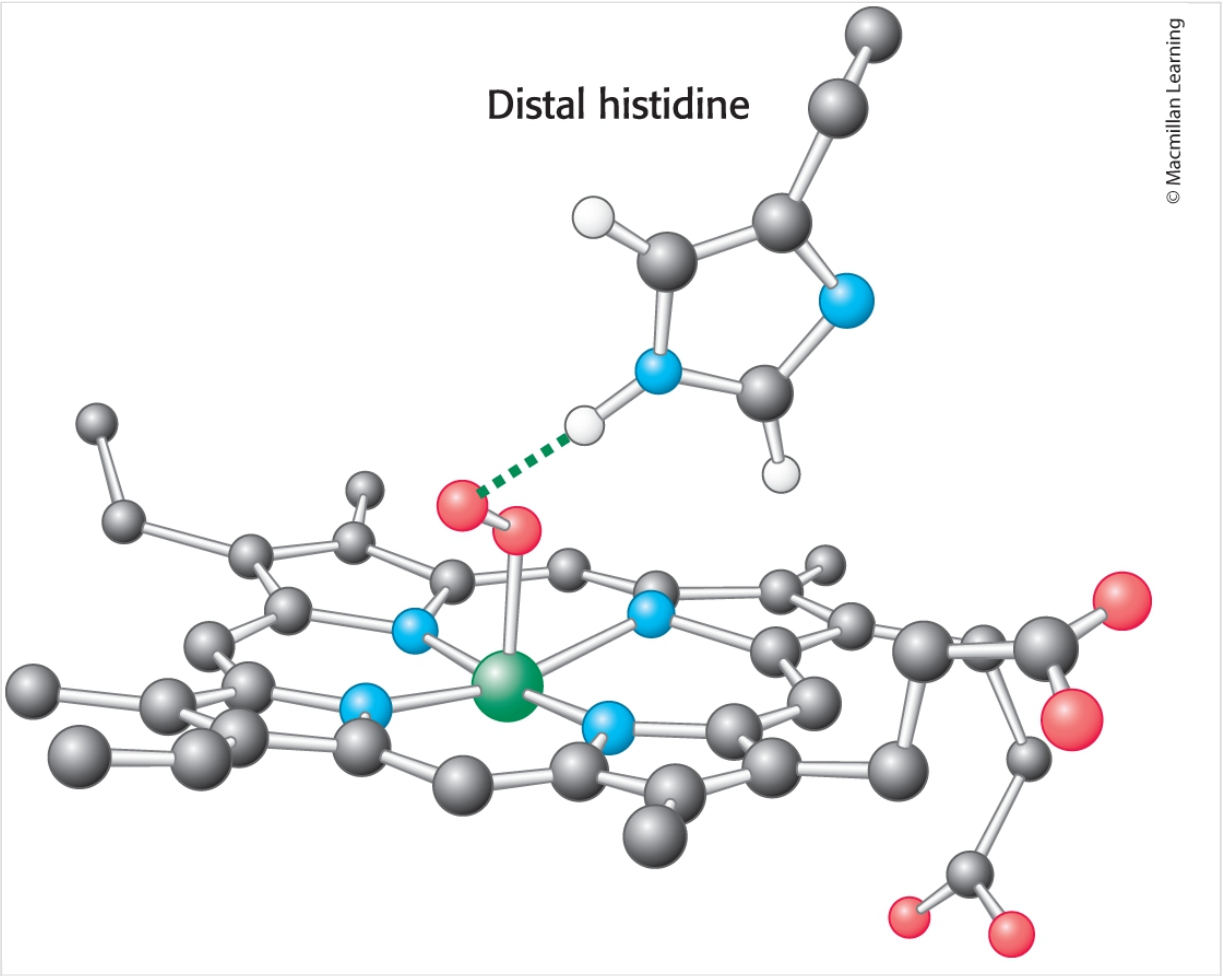


FIGURE 3.13 Bound oxygen is stabilized through a hydrogen bond between the distal histidine and one of the oxygen atoms. The hydrogen bond is shown as a dotted green line. The superoxide character of the bound oxygen species strengthens this interaction. Thus, the protein component of myoglobin controls the intrinsic reactivity of heme, making it more suitable for reversible oxygen binding.

Compared with model compounds, myoglobin discriminates between oxygen and carbon monoxide

While the available site on deoxymyoglobin allows oxygen binding, it also has the potential to enable combination with other molecules of similar size and binding characteristics. In particular, **carbon monoxide** (CO) is a potential competitor for this site. Indeed, this odorless gas can be deadly due to its ability to bind myoglobin and hemoglobin. Binding studies indicate that deoxymyoglobin binds CO very tightly, with a P_{50} of approximately 0.02 torr, a hundredfold tighter than oxygen (**Figure 3.14**). This is a potential problem, since oxygen cannot bind if CO is occupying the site. Environmental exposure to CO can result in blocking and inactivating both myoglobin and hemoglobin, the oxygen-carrying protein in the blood to be discussed shortly. In addition, some CO is produced by the body, ironically during the breakdown of heme, and this, too, can compete for oxygen-binding sites.

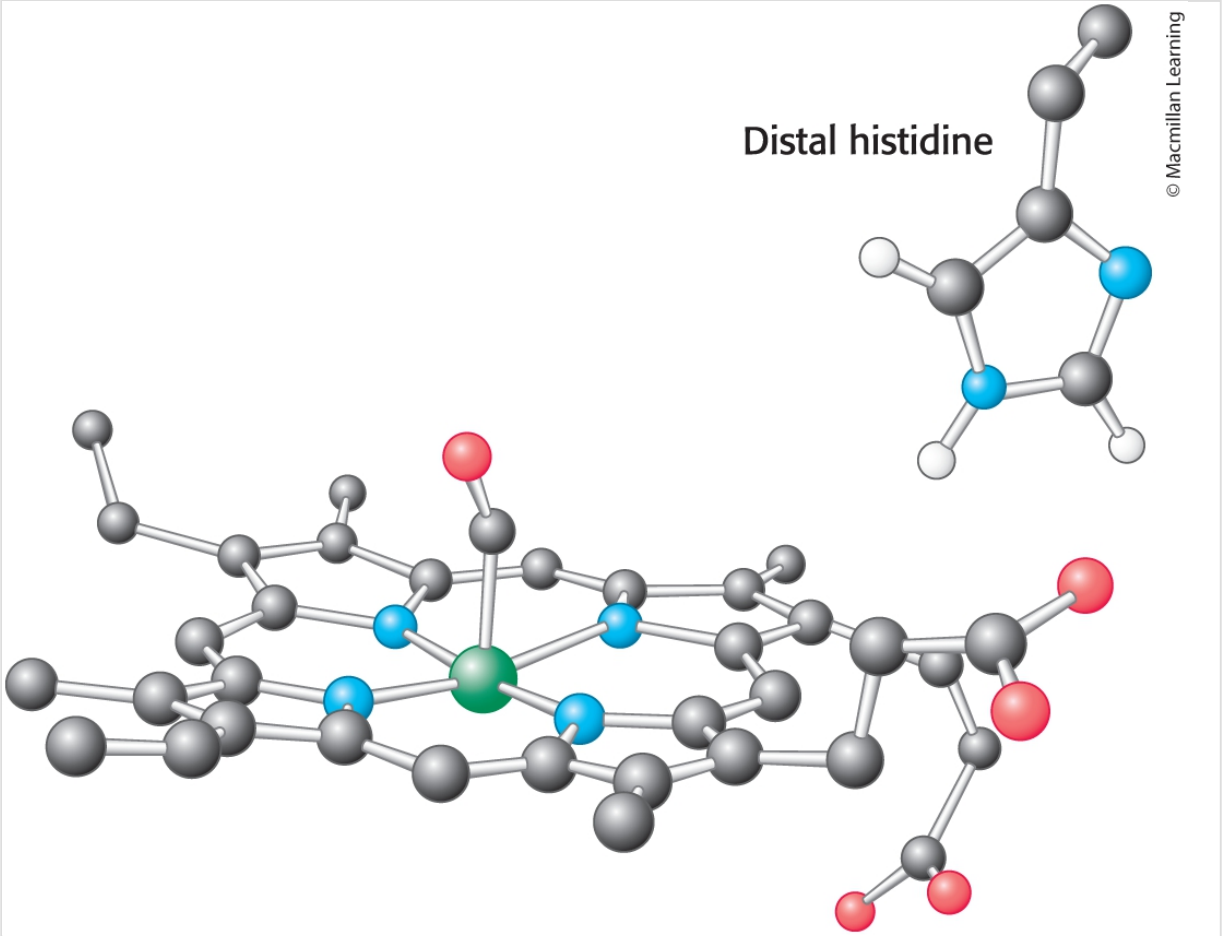


FIGURE 3.14 Carbon monoxide can bind to the iron ion in myoglobin, blocking the oxygen-binding site.

It may seem surprising that myoglobin does not discriminate better against CO given the potential risks of CO poisoning. Scientists have probed the chemical basis underlying this phenomenon using synthetic heme model compounds that mimic the essential characteristics of the myoglobin ligand-binding site. Some of these model compounds have affinities for oxygen similar to that for myoglobin, with a P_{50} of 0.6 torr. However, these model compounds bind CO with a P_{50} of 0.00002 torr; their affinity for CO is 30,000 times higher than that for oxygen. This suggests that myoglobin has evolved to show enhanced recognition of

oxygen versus CO but is limited by the much higher intrinsic affinity of iron for CO.

Site-directed mutagenesis studies of sperm whale myoglobin support this conclusion and highlight an important role of the distal histidine. Removal of the imidazole group by the replacement of histidine with glycine results in a protein that binds oxygen approximately 13 times less tightly than does the wide-type protein but binds CO five times more tightly. This combination decreases the recognition of oxygen over CO by a factor of 65. Other substitutions can increase this factor further. These results reveal a major mechanism by which myoglobin has evolved to improve recognition of a key ligand.

3.3 Hemoglobin Is an Efficient Oxygen Carrier

As we have seen, myoglobin functions as an oxygen storage protein. Hemoglobin serves a more complicated role as an oxygen carrier. This role requires considerable sophistication, as this protein must bind oxygen in the lungs and then release as much oxygen as possible to tissues, particularly where it is most needed. We shall see that the oxygen-binding properties of hemoglobin differ from those of simpler proteins like myoglobin, and how additional ligands including carbon dioxide and hydrogen ions can influence these binding properties. Hemoglobin serves as an archetype for many other proteins with complicated properties that we will encounter throughout the book.

Human hemoglobin is an assembly of four myoglobin-like subunits

The three-dimensional structure of hemoglobin from horse heart was solved by Max Perutz and colleagues shortly after the determination of myoglobin's structure. Since then, the structures of hemoglobins from other species, including humans, have been determined. Hemoglobin consists of four polypeptide chains, two identical α chains, and two identical β chains (**Figure 3.15**). Each of the subunits consists of a set of α helices in the same arrangement as the α helices in myoglobin. The recurring structural motif is called a globin fold.

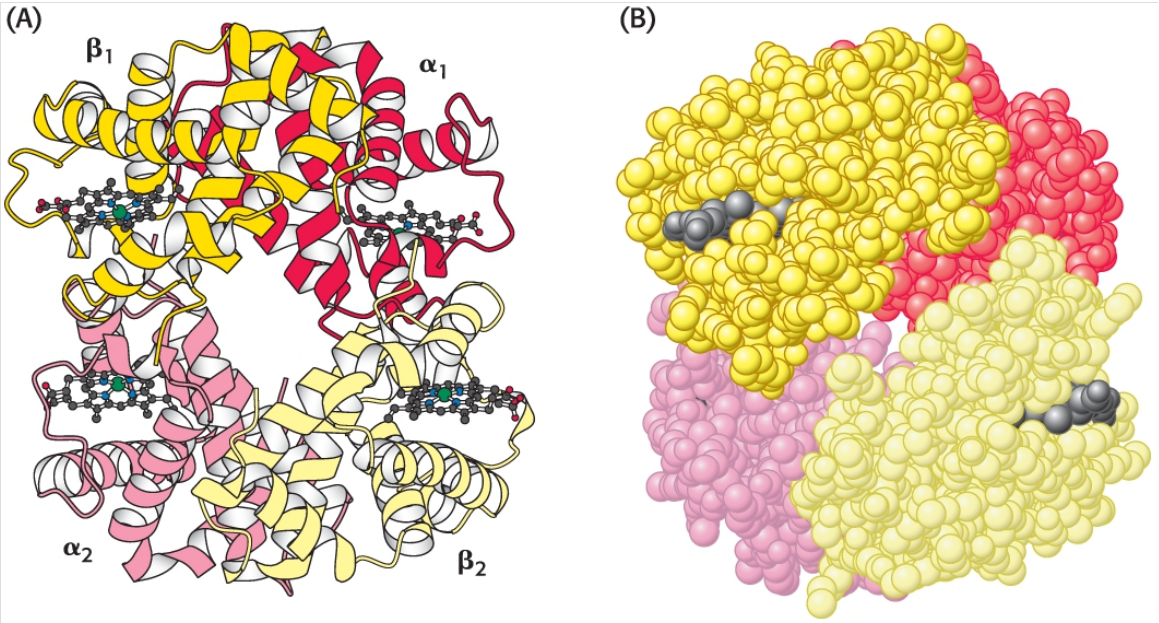


FIGURE 3.15 Hemoglobin is an assembly of four subunits, each of which is very similar to myoglobin. There are two α subunits and two β subunits that come together to form two αβ dimers. (A) A ribbon diagram. (B) A space-filling model.

INTERACT with this model in Achieve

The hemoglobin tetramer, referred to as hemoglobin A (HbA), is best described as a homodimer of heterodimers, that is, a pair of identical αβ dimers ($\alpha_1\beta_1$ and $\alpha_2\beta_2$) that associate to form the tetramer. In deoxyhemoglobin, these αβ dimers are linked by an extensive interface, which includes the carboxyl terminus of each chain. The heme groups are well separated in the tetramer by iron–iron distances ranging from 24 to 40 Å.

Hemoglobin binds oxygen cooperatively

The oxygen-binding curve for hemoglobin in red blood cells shows some remarkable features (Figure 3.16). It does not look like a simple binding curve such as that for myoglobin; instead, it resembles an "S." Such curves are described as **sigmoid** for their S-like shape. In addition, oxygen binding for hemoglobin $(P_{50} = 26\ \text{torr})$ is significantly weaker than that for myoglobin. Note that this binding curve is derived from hemoglobin in red blood cells.

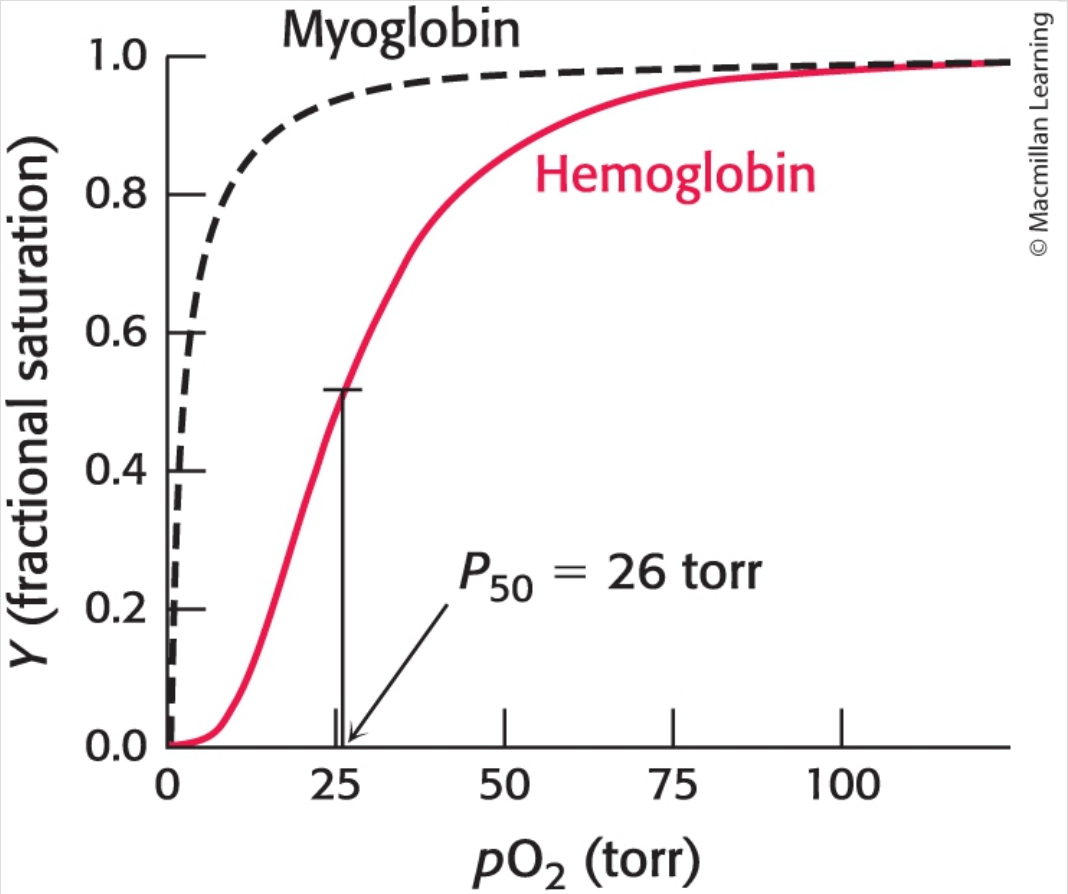


FIGURE 3.16 The oxygen-binding curve for hemoglobin, with its sigmoid (S-like) shape, is markedly different from that for myoglobin. The P_{50} value for hemoglobin is 26 torr compared with 2 torr for myoglobin.

A sigmoid binding curve indicates that a protein exhibits a particular binding behavior. For hemoglobin, the sigmoid shape suggests that the binding of oxygen at one site within the hemoglobin tetramer increases the likelihood that oxygen binds at the remaining unoccupied sites. Conversely, the unloading of oxygen at one heme facilitates the unloading of oxygen at the others. This sort of binding behavior is referred to as *cooperative*, because the binding reactions at individual sites in each hemoglobin molecule are not independent of one another. We have seen cooperativity in a different context, protein folding, where folding of one part of a protein is not independent of the folding of other parts. We will return to the mechanism of oxygen-binding cooperativity shortly.

What is the physiological significance of the cooperative binding of oxygen by hemoglobin?

- *Cooperative binding leads to efficient oxygen transport*. Oxygen must be transported in the blood from the lungs, where the partial pressure of oxygen is relatively high (approximately 100 torr), to the actively metabolizing tissues, where the partial pressure of oxygen is much lower (typically, 20 torr). Let us consider how the cooperative behavior indicated by the sigmoid curve leads to efficient oxygen transport (**Figure 3.17**). In the lungs, hemoglobin becomes nearly saturated with oxygen such that 98% of the oxygen-binding sites are occupied. When hemoglobin moves to the tissues and releases oxygen, the saturation level drops to 32%. Thus, a total of 66% (98% − 32%) of the potential oxygen-binding sites contribute to oxygen transport.

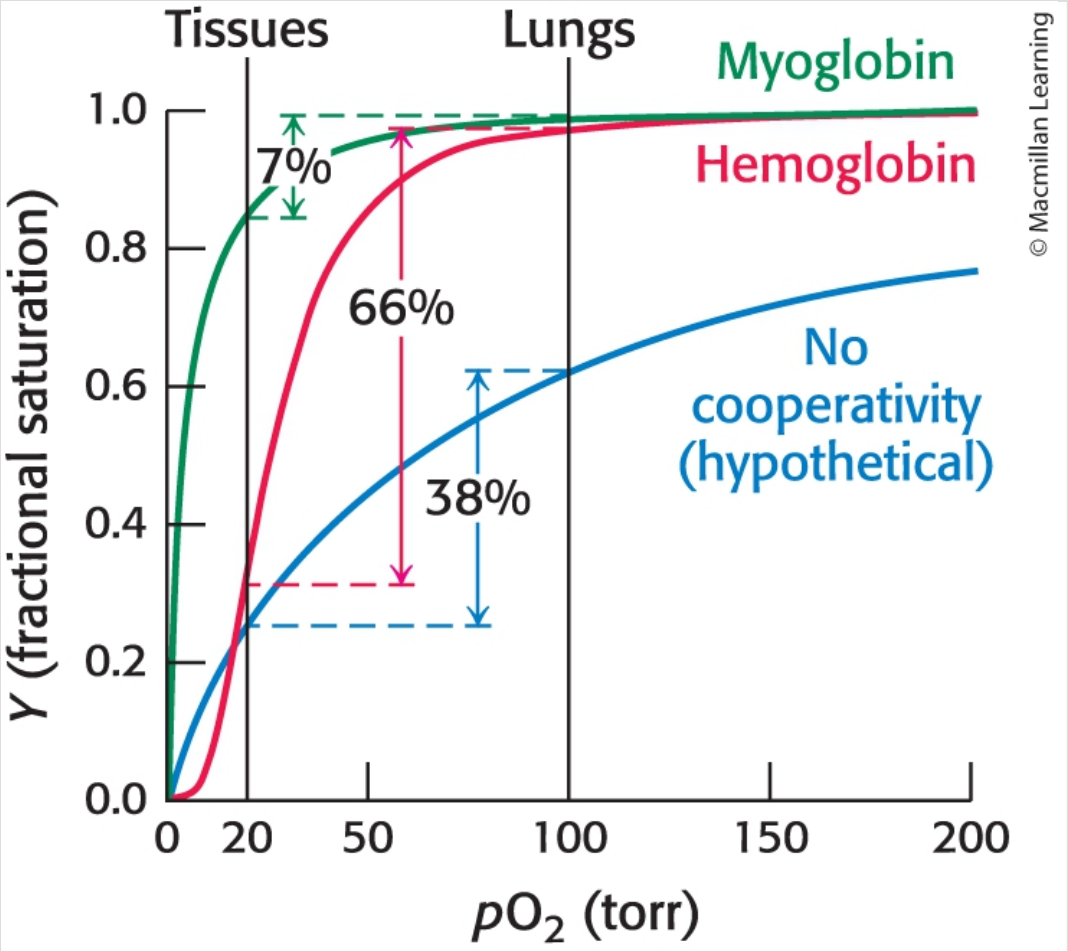


FIGURE 3.17 Cooperativity enhances oxygen delivery by hemoglobin. Because of cooperativity between oxygen-binding sites, hemoglobin delivers more oxygen to actively metabolizing tissues than would myoglobin or, indeed, any noncooperative protein, even with an optimized oxygen affinity.

- *Cooperative release of oxygen favors more complete delivery to tissues.* The cooperative release of oxygen favors a more complete unloading of oxygen in the tissues. If myoglobin were employed for oxygen transport, it would be 98% saturated in the lungs but would remain 91% saturated in the tissues, and so only 7% of the sites would contribute to oxygen transport; myoglobin binds oxygen too tightly to be useful in oxygen transport. Nature might have solved this problem by weakening the affinity of myoglobin for oxygen to

maximize the difference in saturation between 20 and 100 torr. However, for such a protein, the most oxygen that could be transported from a region in which pO_2 is 100 torr to one in which it is 20 torr is 38% (63% − 25%), as indicated by the blue curve in Figure 3.17. Thus, the cooperative binding and release of oxygen by hemoglobin enables it to deliver nearly 10 times as much oxygen as could be delivered by myoglobin and more than 1.7 times as much as could be delivered by an optimized noncooperative protein.

- *Oxygen is delivered to tissues where it is most needed.* Closer examination of oxygen concentrations in tissues at rest and during exercise underscores the effectiveness of hemoglobin as an oxygen carrier (**Figure 3.18**). Under resting conditions, the oxygen concentration in muscle is approximately 40 torr, but during exercise the concentration is reduced to 20 torr. In the decrease from 100 torr in the lungs to 40 torr in resting muscle, the oxygen saturation of hemoglobin is reduced from 98% to 77%, and so 21% of the oxygen is released over a drop of 60 torr. In a decrease from 40 torr to 20 torr, the oxygen saturation is reduced from 77% to 32%, corresponding to an oxygen release of 45% over a drop of 20 torr. Thus, because the change in oxygen concentration from rest to exercise corresponds to the steepest part of the oxygen-binding curve, oxygen is effectively delivered to tissues where it is most needed. Later, we shall examine other properties of hemoglobin that enhance its physiological responsiveness.

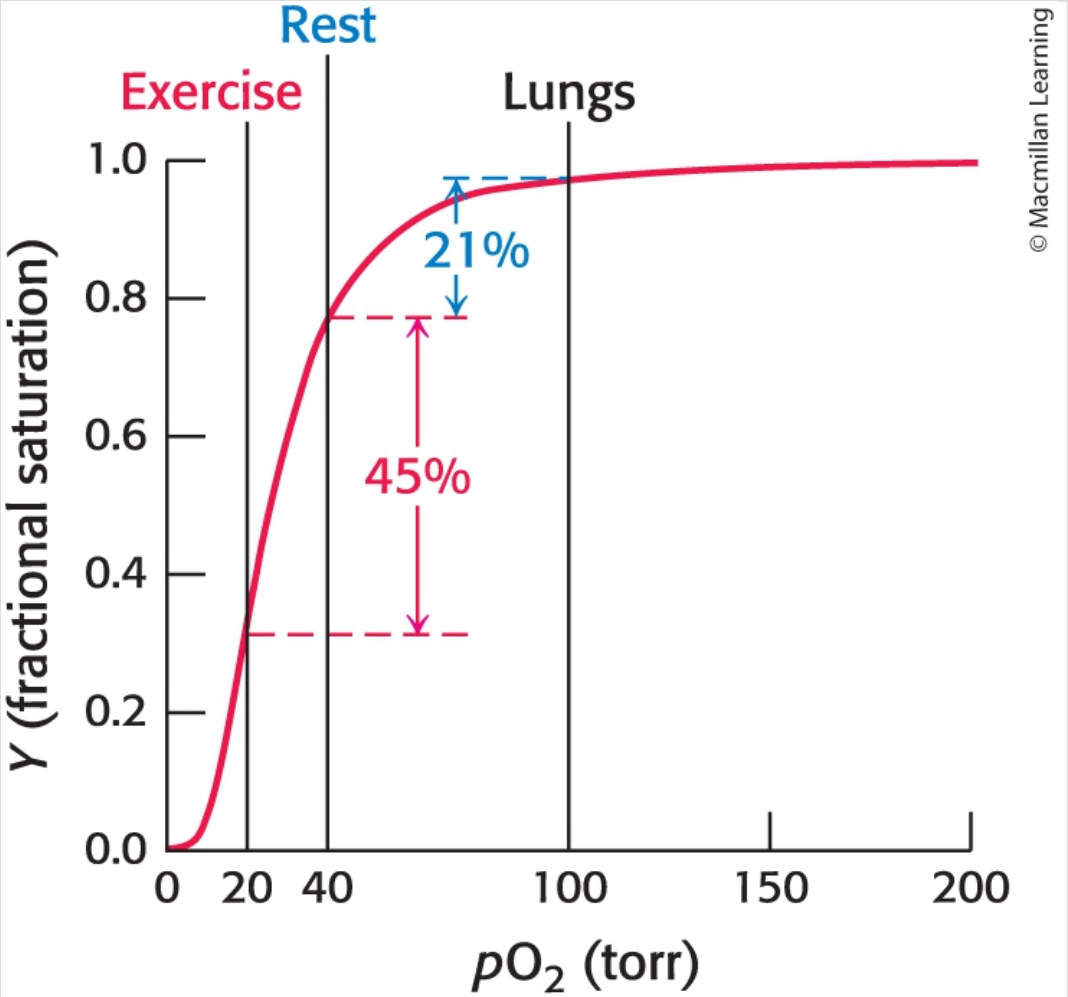


FIGURE 3.18 Oxygen delivery by hemoglobin responds to exercise. The drop in oxygen concentration from 40 torr in resting tissues to 20 torr in exercising tissues corresponds to the steepest part of the oxygen-binding curve. This allows a substantial quantity of oxygen to be released to exercising tissues.

Oxygen binding markedly changes the quaternary structure of hemoglobin

The cooperative binding of oxygen by hemoglobin requires that the binding of oxygen at one site in the hemoglobin tetramer influences the

oxygen-binding properties at the other sites. Given the large separation between the iron sites, direct interactions are not possible. Thus, indirect mechanisms for coupling the sites must be at work. These mechanisms are intimately related to the quaternary structure of hemoglobin.

Hemoglobin undergoes substantial changes in quaternary structure on oxygen binding: the $\alpha_1\beta_1$ and $\alpha_2\beta_2$ dimers rotate approximately 15 degrees with respect to one another (Figure 3.19). The dimers themselves are relatively unchanged, although there are localized conformational shifts. Thus, the interface between the $\alpha_1\beta_1$ and $\alpha_2\beta_2$ dimers is most affected by this structural transition. In particular, the $\alpha_1\beta_1$ and $\alpha_2\beta_2$ dimers are more free to move with respect to one another in the oxygenated state than they are in the deoxygenated state.

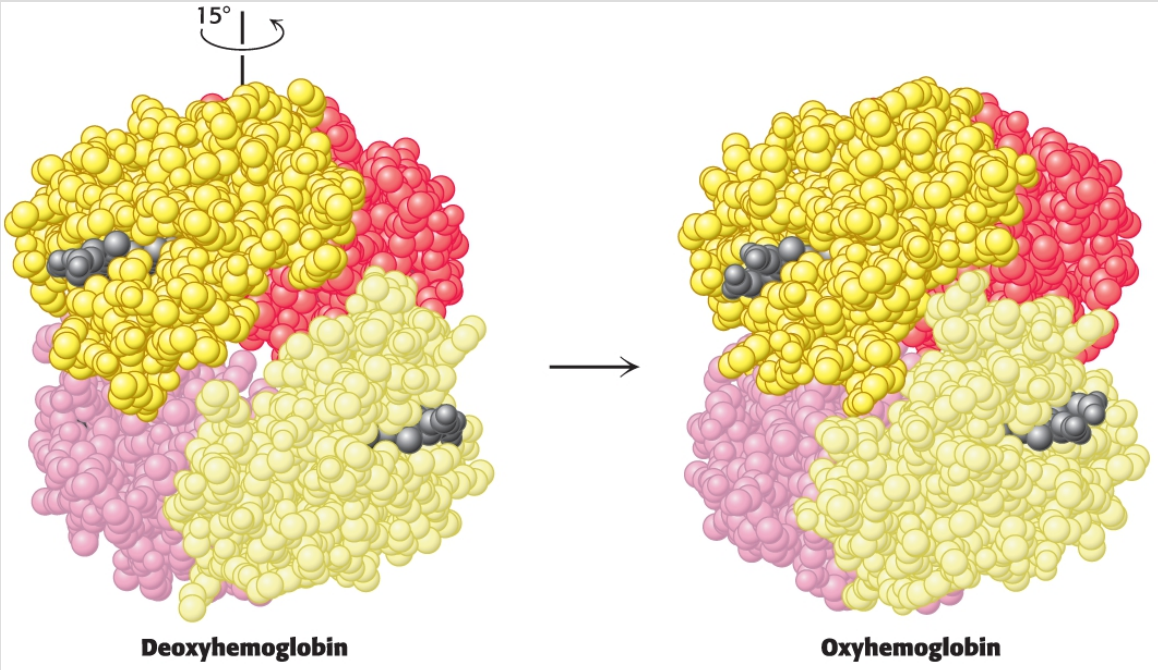


FIGURE 3.19 Substantial quaternary structural changes occur in hemoglobin upon oxygen binding. Comparing the structures of deoxyhemoglobin and oxyhemoglobin reveals that one α
dimer has rotated by 15 degrees relative to the other.

INTERACT with this model in Achieve

The quaternary structure observed in the deoxy form of hemoglobin, **deoxyhemoglobin**, is often referred to as the **T state** (T for *tense*), because it is quite constrained by subunit–subunit interactions. In contrast, the quaternary structure of the fully oxygenated form, **oxyhemoglobin**, is referred to as the **R state** (R for *relaxed*). In light of the observation that the R form of hemoglobin is less constrained, the tense and relaxed designations seem particularly apt. Importantly, in the R state, the oxygen-binding sites are free of strain and are capable of binding oxygen with higher affinity than are the sites in the T state. By triggering the shift of the hemoglobin tetramer from the T state to the R state, the binding of oxygen to one site increases the binding affinity of other sites.

Hemoglobin cooperativity can be potentially explained by several models

Two limiting models have been developed to explain the cooperative binding of ligands to a multisubunit assembly such as hemoglobin. In the **concerted model**, also known as the MWC model after Jacques Monod, Jeffries Wyman, and Jean-Pierre Changeux, who first proposed it, the overall assembly can exist only in two forms: the T state and the R state. The binding of ligands simply shifts the equilibrium between these two states (**Figure 3.20**). Thus, as a hemoglobin tetramer binds each oxygen molecule, the probability that the tetramer is in the R state increases. Deoxyhemoglobin tetramers are almost exclusively in the T state. However, the binding of oxygen to one site in the molecule shifts the equilibrium toward the R state. If a molecule assumes the R quaternary structure, the oxygen affinity of its sites increases.

Additional oxygen molecules are now more likely to bind to the three unoccupied sites. Thus, the binding curve for hemoglobin can be seen as a combination of the binding curves that would be observed if all molecules remained in the T state or if all of the molecules were in the R state. As oxygen molecules bind, the hemoglobin tetramers convert from the T state into the R state, yielding the sigmoid binding curve so important for efficient oxygen transport (Figure 3.21).

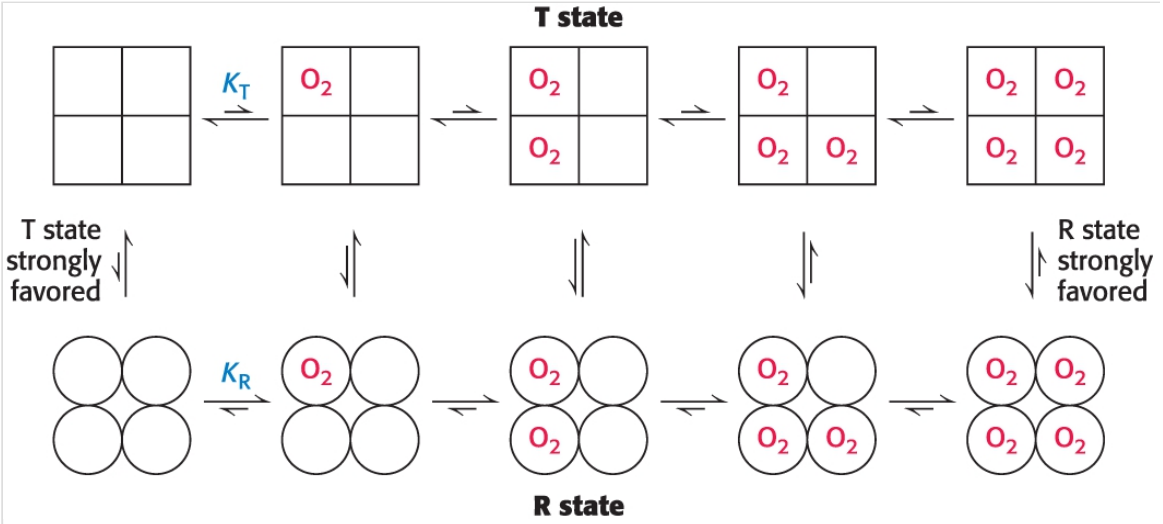


FIGURE 3.20 A concerted model can explain cooperative oxygen binding by hemoglobin. The hemoglobin tetramer can exist in the T state or the R state. With no oxygen bound, the equilibrium between these states strongly favors the T state. As each oxygen binds, the equilibrium shifts so that when all four sites have oxygen bound, the equilibrium strongly favors the R state. Binding sites in the R state have a higher affinity for oxygen than those in the T state

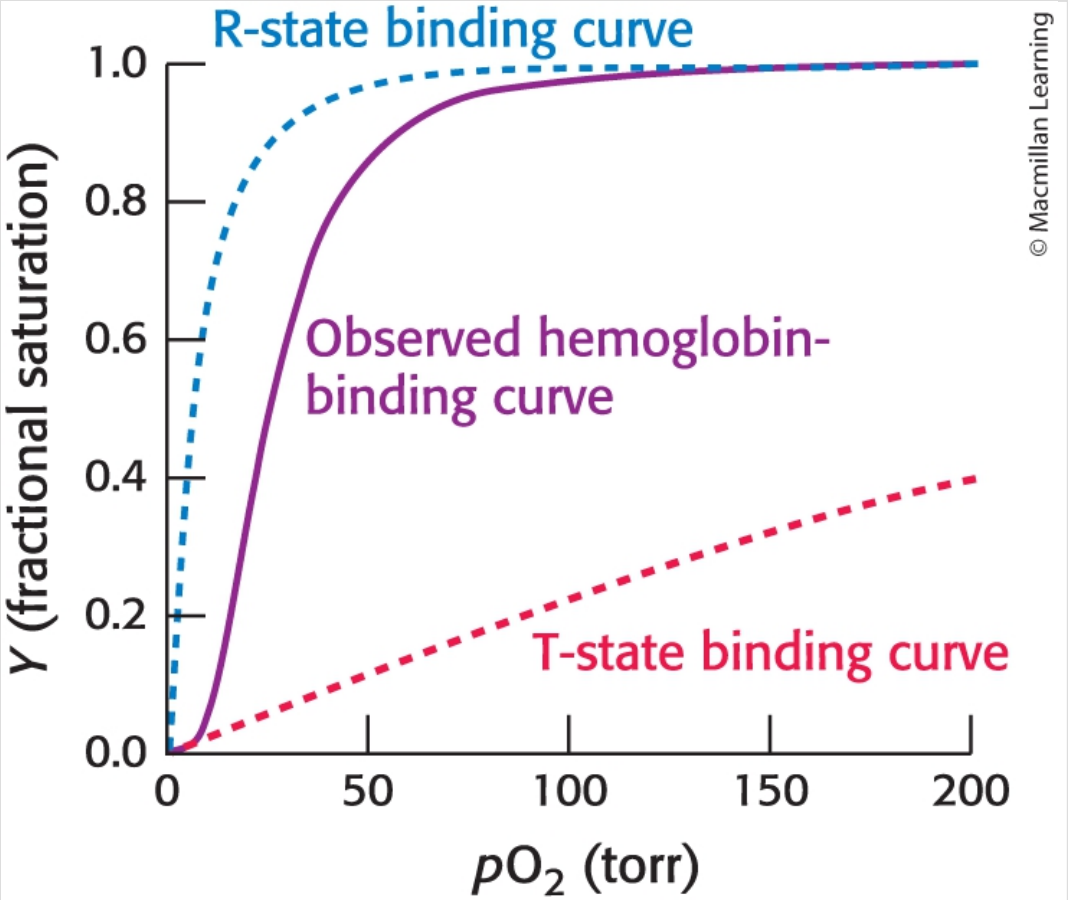


FIGURE 3.21 The sigmoid oxygen-binding curve of hemoglobin can be seen as a combination of the T state binding curve and the R state binding curve. As oxygen binds, more hemoglobin tetramers are converted from the T state to the R state, increasing the oxygen affinity of the available binding sites.

In the concerted model, each tetramer can exist in only two states—the T state and the R state. In an alternative model, the **sequential model**, the binding of a ligand to one site in an assembly increases the binding affinity of neighboring sites without inducing a full conversion from the T into the R state (**Figure 3.22**).

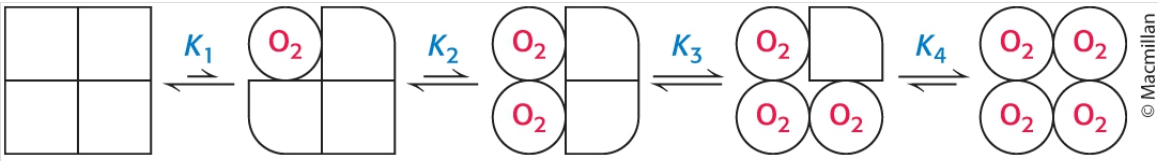


FIGURE 3.22 A sequential model can account for oxygen-binding cooperativity. As each oxyge molecule binds to one site in the hemoglobin tetramer, the affinities of the remaining sites increase, resulting in a sigmoidal binding curve.

Is the cooperative binding of oxygen by hemoglobin better described by the concerted or the sequential model? Neither model in its pure form fully accounts for all of the behavior of hemoglobin. Instead, a combined model is required. Hemoglobin behavior is concerted in that the tetramer with three sites occupied by oxygen is almost always in the quaternary structure associated with the R state. The remaining open binding site has an affinity for oxygen more than 20-fold greater than that of fully deoxygenated hemoglobin binding its first oxygen. However, the behavior is not fully concerted, because hemoglobin with oxygen bound to only one of four sites remains primarily in the T-state quaternary structure. Yet, this molecule binds oxygen three times as strongly as does fully deoxygenated hemoglobin, an observation consistent only with a sequential model. These results highlight the fact that the concerted and sequential models represent idealized limiting cases, which real systems may approach but rarely attain.

Self-Check Question

Which is higher: (a) the affinity of a deoxyhemoglobin molecule for its first oxygen, or (b) the affinity of a hemoglobin molecule with three bound oxygens for its last oxygen?

Structural changes at the heme groups are transmitted to the $\alpha_1\beta_1$-$\alpha_2\beta_2$ interface

We will now examine how oxygen binding at one site is able to shift the equilibrium between the T and R states of the entire hemoglobin tetramer. As in myoglobin, oxygen binding causes each iron atom in hemoglobin to move from outside the plane of the porphyrin into the plane. When the iron atom moves, the proximal histidine residue moves with it. This histidine residue is part of an α helix, which also moves (Figure 3.23). The carboxyl terminal end of this α helix lies in the interface between the two αβ dimers. The change in position of the carboxyl terminal end of the helix favors the T-to-R transition. Consequently, the structural transition at the iron ion in one subunit is directly transmitted to the other subunits. The rearrangement of the dimer interface provides a pathway for communication between subunits, enabling the cooperative binding of oxygen.

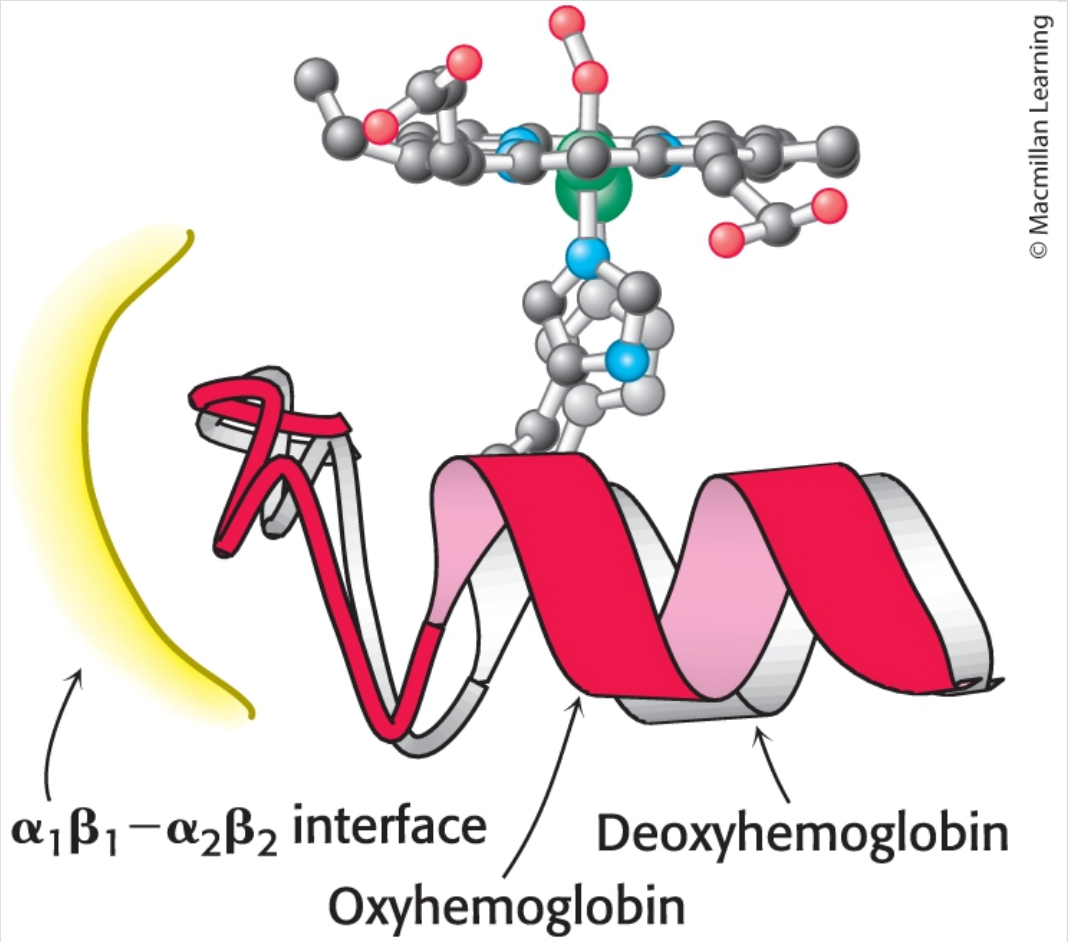


FIGURE 3.23 Oxygen binding causes the iron to move into the porphyrin. The motion of the iron pulls the proximal histidine and the associated helix, transmitting the structure change to the $\alpha_1\beta_1-\alpha_2\beta_2$ interface. The structure of oxyhemoglobin is shown in red on top of that for deoxyhemoglobin, in gray.

This mechanism predicts that if the bonds connecting the proximal histidines to the α helices were to be severed, then the resulting hemoglobin molecules would bind oxygen with relatively high affinity, retain the T quaternary structure even upon oxygen binding, and show no or substantially less cooperativity. This thought experiment has actually been realized by replacing the proximal histidines with glycines and adding free imidazole, which binds to the iron ion in place of the histidine side chain (Figure 3.24). Such binding studies, along with

structural studies, have confirmed this prediction, although some cooperativity remains, indicating that some other pathways for inter-subunit communication must be present.

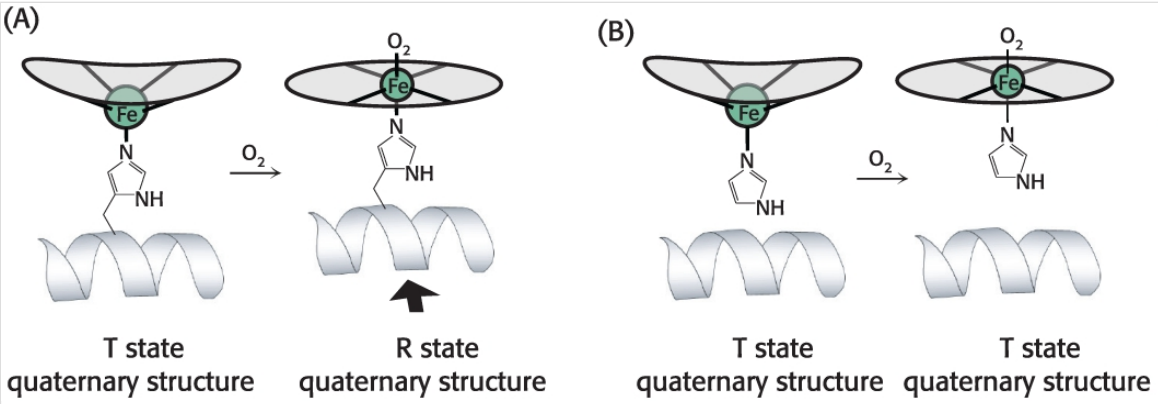


FIGURE 3.24 The movement of the proximal histidine and its associated α helix upon oxygen binding drives cooperativity. (A) In normal hemoglobin, the structural changes at iron upon oxygen binding in normal hemoglobin result in motion of the α helix that includes the proximal histidine, indicated by the arrow. (B) In hemoglobin, with the proximal histidine replaced with glycine with added imidazole bound to iron, oxygen binding results in the same changes at iron but the motion of the α helix does not occur.

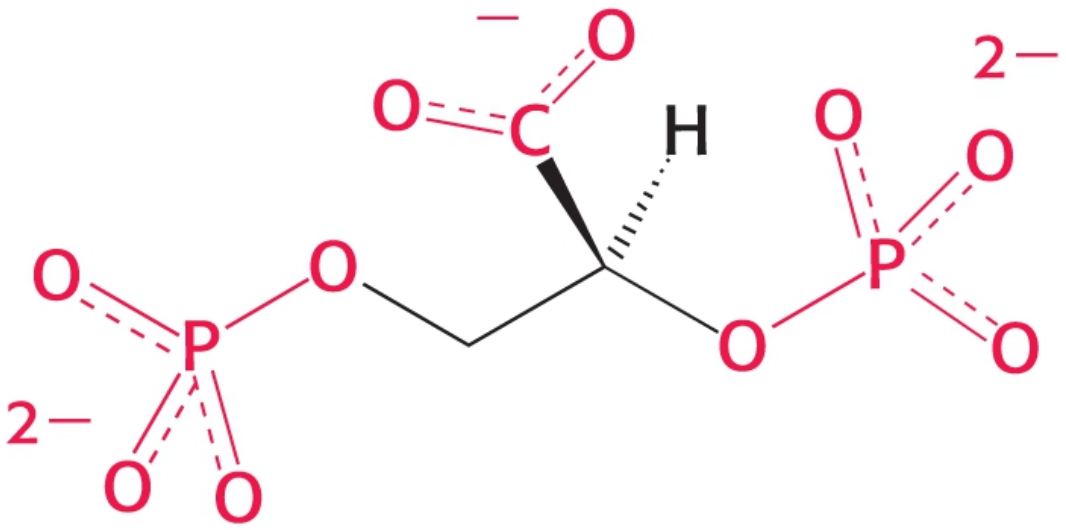
Self-Check Question

Why is the oxygen affinity of the hemoglobin variant with the proximal histidines detached (as shown in Figure 3.24) relatively high?

2,3-Bisphosphoglycerate in red blood cells is crucial in determining the oxygen affinity of

hemoglobin

The oxygen-binding curves for hemoglobin shown up to this point have been for hemoglobin in red blood cells. Surprisingly, highly purified hemoglobin binds oxygen much more tightly than does hemoglobin in red blood cells (Figure 3.25). This dramatic difference is due to the presence within red blood cells of 2,3-bisphosphoglycerate (2,3-BPG).



2,3-Bisphosphoglycerate (2,3-BPG)

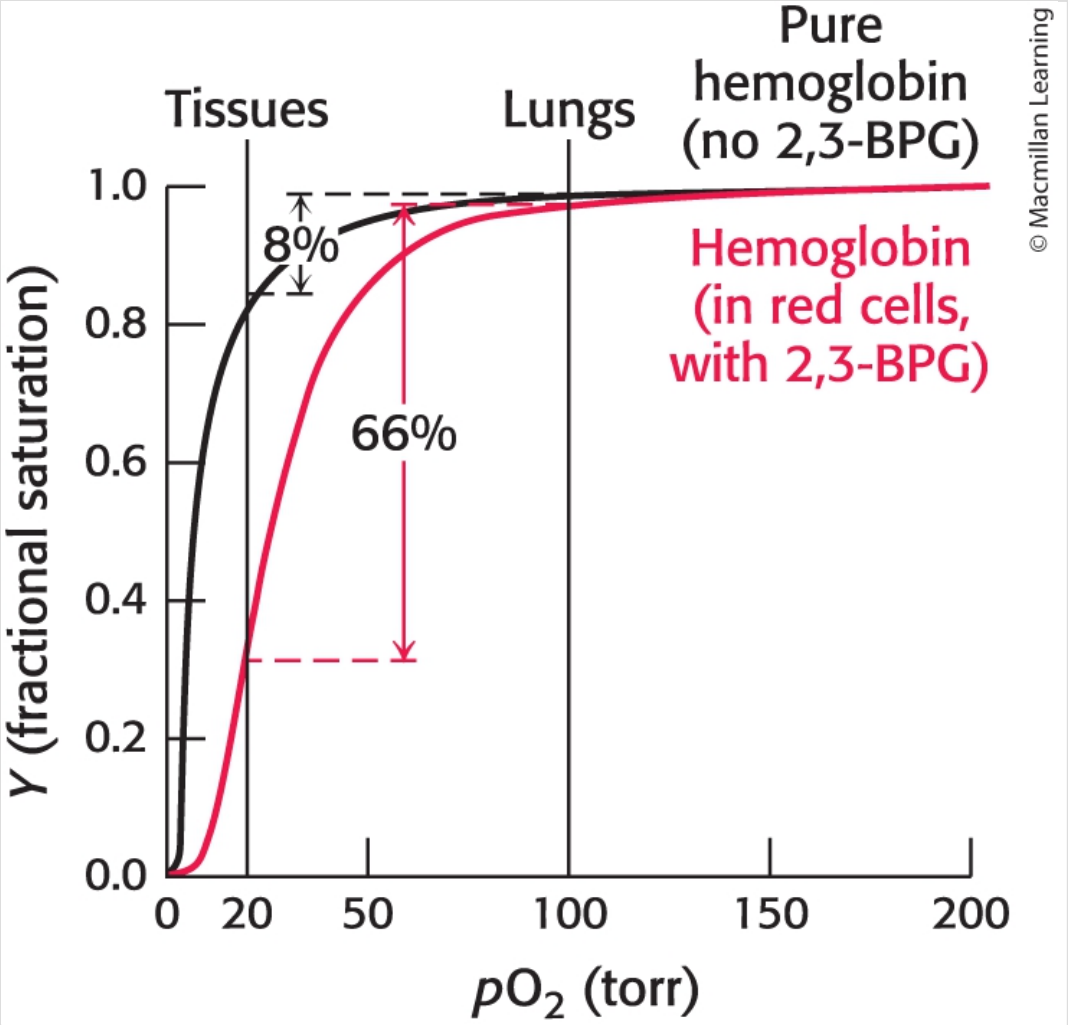


FIGURE 3.25 The oxygen-binding curves for pure hemoglobin and hemoglobin in red blood are markedly different. Hemoglobin in red blood cells shows a lower oxygen affinity than does pure hemoglobin due to the presence of 2,3-bisphosphoglycerate in red blood cells.

This highly anionic compound is present in red blood cells at approximately the same concentration as that of hemoglobin (~2 mM). Without 2,3-BPG, hemoglobin would be an extremely inefficient oxygen transporter, releasing only 8% of its cargo in the tissues.

How does 2,3-BPG lower the oxygen affinity of hemoglobin so significantly? Examination of the crystal structure of deoxyhemoglobin in the presence of 2,3-BPG reveals that a single molecule of 2,3-BPG binds in the center of the tetramer, in a pocket present only in the T state (Figure 3.26). During the T-to-R transition, this pocket collapses, and 2,3-BPG is released. Thus, in order for the structural transition from T to R to take place, the interactions between hemoglobin and 2,3-BPG must be disrupted. In the presence of 2,3-BPG, more oxygen-binding sites within the hemoglobin tetramer must be occupied in order to induce the T-to-R transition, and so hemoglobin remains in the lower-affinity T state until higher oxygen concentrations are reached.

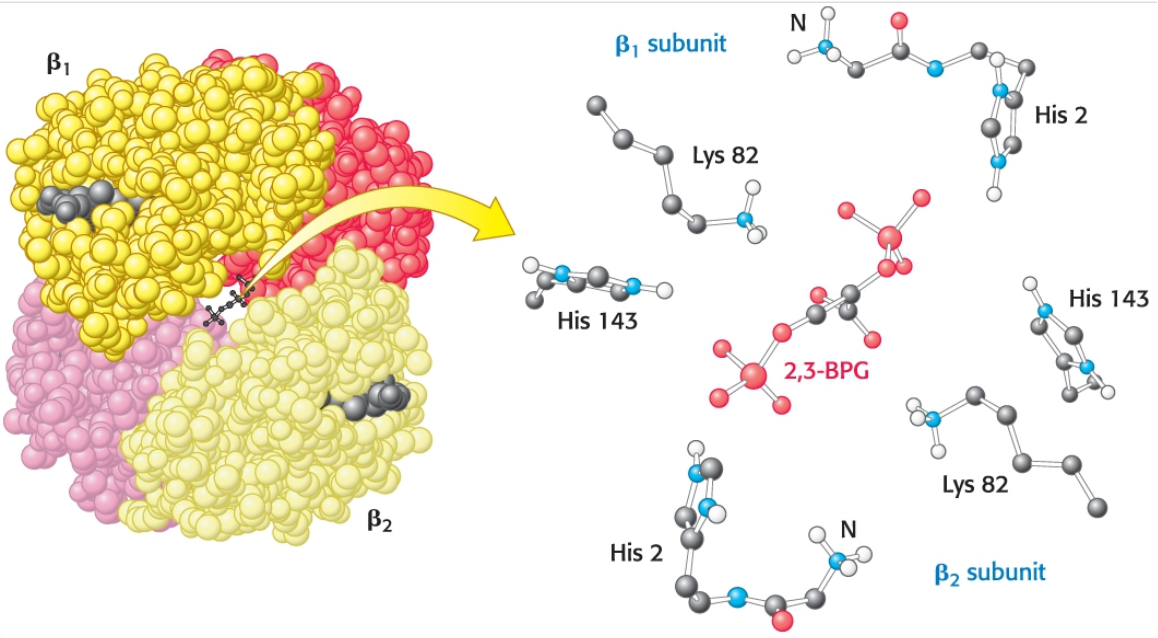


FIGURE 3.26 2,3-Bisphosphoglycerate binds in the central cavity within deoxyhemoglobin. Within the cavity, the negatively charged molecule interacts with three positively charged side chains from each β chain.

INTERACT with this model in Achieve

This mechanism of regulation is remarkable because 2,3-BPG does not in any way resemble oxygen, the molecule on which hemoglobin carries out its primary function. 2,3-BPG is referred to as an **allosteric effector** (from the Greek *allos*, "other," and *stereos*, "structure"), a molecule that affects the binding of another molecule from a distance. Because they bind in sites other than the active site, allosteric effector molecules can have structures that are completely different from the other molecules to which a protein binds. We will encounter allosteric effectors again when we consider enzyme regulation in Chapter 5. The binding of 2,3-BPG by deoxyhemoglobin but not by oxyhemoglobin is another illustration of the utility of molecular recognition.



The binding of 2,3-BPG to hemoglobin has other crucial physiological consequences. For example, the hemoglobin produced by human fetuses is different from that produced by adults. The differences are relatively subtle, but one of their consequences is that fetal hemoglobin has a lower affinity for 2,3-BPG than does adult hemoglobin. Consequently, the oxygen affinity of fetal red blood cells is higher than that for maternal (adult) red blood cells (**Figure 3.27**). This difference in oxygen affinity allows oxygen to be effectively transferred from maternal to fetal red blood cells, helping to ensure that the fetus receives an adequate oxygen supply.

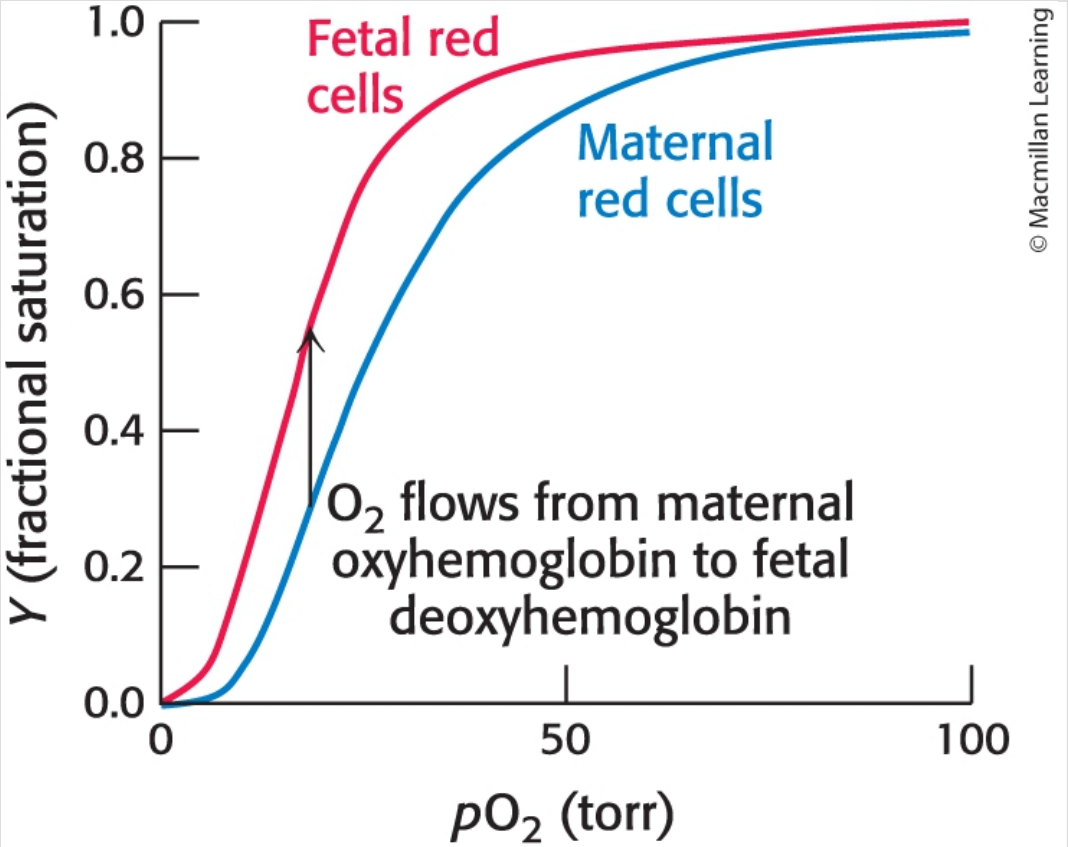


FIGURE 3.27 Fetal red blood cells obtain oxygen from maternal red blood cells by virtue of fetal hemoglobin's lower affinity for 2,3-BPG. This results in fetal hemoglobin having a higher affinity for oxygen.

Hydrogen ions and carbon dioxide promote the release of oxygen

We have seen how cooperative release of oxygen from hemoglobin helps deliver oxygen to where it is most needed: tissues exhibiting low oxygen partial pressures. This ability is enhanced by the facility of hemoglobin to respond to other cues in its physiological environment that signal the need for oxygen. For example, consider rapidly metabolizing tissues, such as contracting muscle, which generate large

amounts of hydrogen ions and carbon dioxide. To release oxygen where the need is greatest, hemoglobin has evolved to respond to higher levels of these substances. Like 2,3-BPG, hydrogen ions and carbon dioxide are allosteric effectors of hemoglobin that bind to sites on the molecule that are distinct from the oxygen-binding sites. The regulation of oxygen binding by hydrogen ions and carbon dioxide is called the **Bohr effect** after Christian Bohr, who described this phenomenon in 1904.

The effect of hydrogen ions

The oxygen affinity of hemoglobin decreases as pH decreases from a value of 7.4 (**Figure 3.28**). Consequently, as hemoglobin moves into a region of lower pH, its tendency to release oxygen increases. For example, transport from the lungs, with pH 7.4 and an oxygen partial pressure of 100 torr, to active muscle, with a pH of 7.2 and an oxygen partial pressure of 20 torr, results in a release of oxygen amounting to 77% of total carrying capacity. Only 66% of the oxygen would be released in the absence of any change in pH.

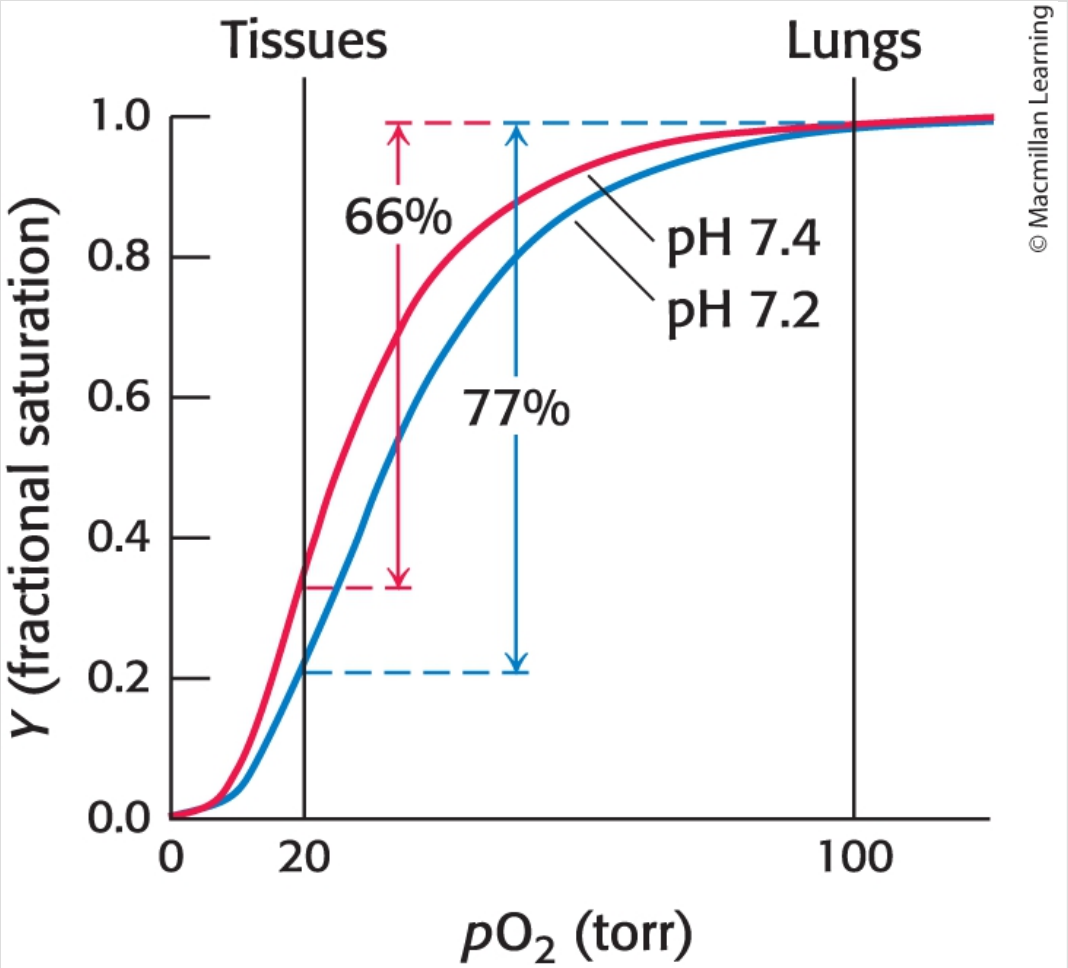


FIGURE 3.28 Lowering the pH decreases the oxygen affinity of hemoglobin and facilitates the release of oxygen into metabolically active tissues. The oxygen-binding curve at pH 7.2 (blue curve) is compared with that at pH 7.4 (red curve).

Structural and chemical studies have revealed much about the chemical basis of the Bohr effect. Several chemical groups within the hemoglobin tetramer are important for sensing changes in pH; all of these have pK_a values near pH 7. Consider histidine $\beta 146$, the residue at the C terminus of the β chain. In its protonated form, the histidine sidechain participates in an ionic interaction with the negatively charged aspartate $\beta 94$ in the same chain. This interaction locks the terminal

carboxylate group of β^{146} in a position where it can interact electrostatically with a lysine residue from the α subunit of the other αβ dimer in the T-state conformation (Figure 3.29).

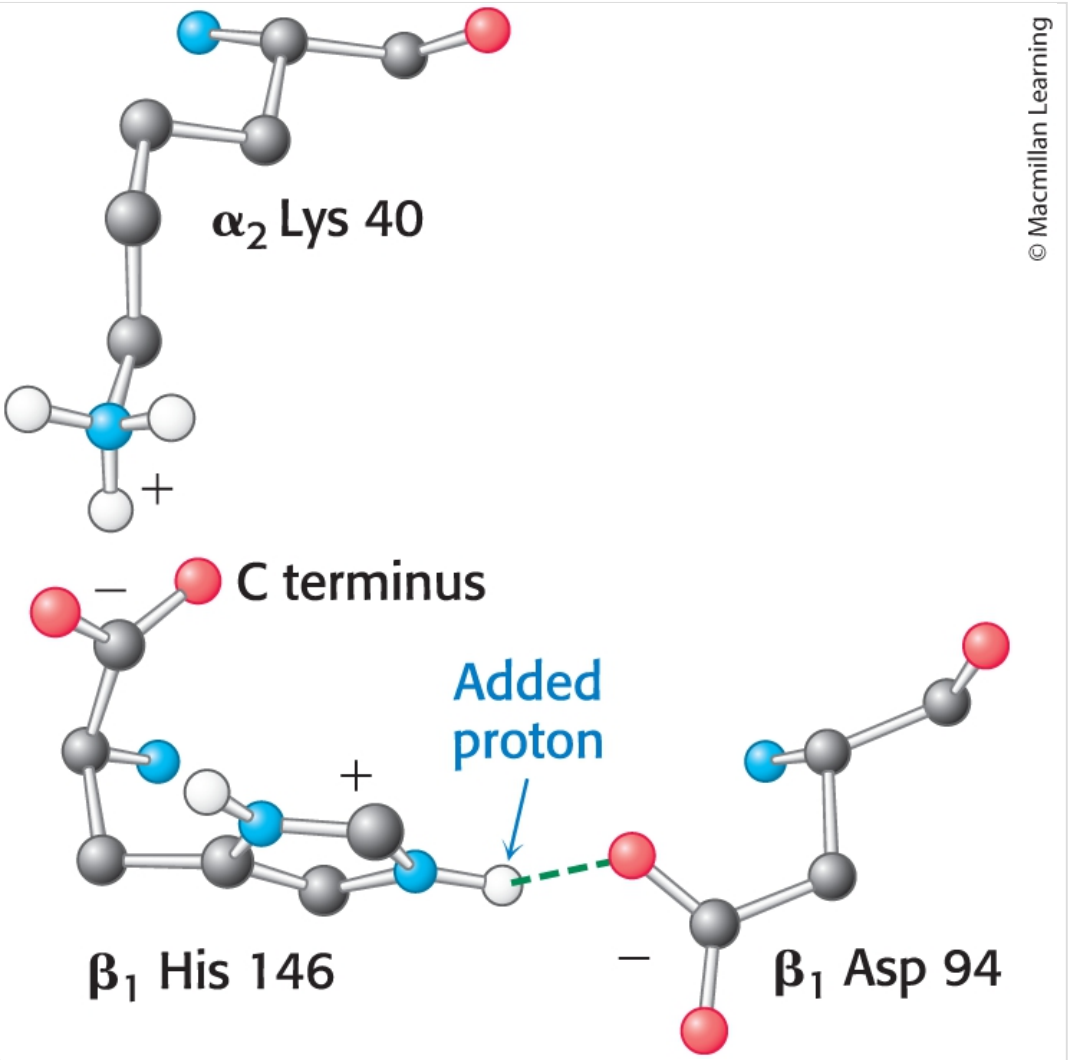


FIGURE 3.29 Ionic interactions involving the β chain C-terminal histidine are responsible for some of the pH sensitivity of hemoglobin oxygen affinity. As the pH decreases, the likelihood that the imidazole side chain of His β^{146} is protonated increases. This promotes an ionic interaction between the terminal carboxylate and a lysine side chain from the other αβ dimer, stabilizing the T state.

In addition to His $\beta 146$, the α-amino groups at the amino termini of the α chains and the side chain of histidine $\alpha 122$ also participate in ionic interactions in the T state. The formation of these ionic interactions stabilizes the T state, leading to a greater tendency for oxygen to be released.

The effect of carbon dioxide

Carbon dioxide stimulates oxygen release by two mechanisms. First, carbon dioxide reacts with water to form to form bicarbonate ion, HCO_3^- and H^+, resulting in a drop in pH that stabilizes the T state by the mechanism discussed previously. Second, a direct chemical interaction between carbon dioxide and hemoglobin stimulates oxygen release.

The effect of carbon dioxide on oxygen affinity can be seen by comparing oxygen-binding curves in the absence and in the presence of carbon dioxide at a constant pH (**Figure 3.30**). In the presence of carbon dioxide at a partial pressure of 40 torr at pH 7.2, the amount of oxygen released increases to 88% of the maximum carrying capacity.

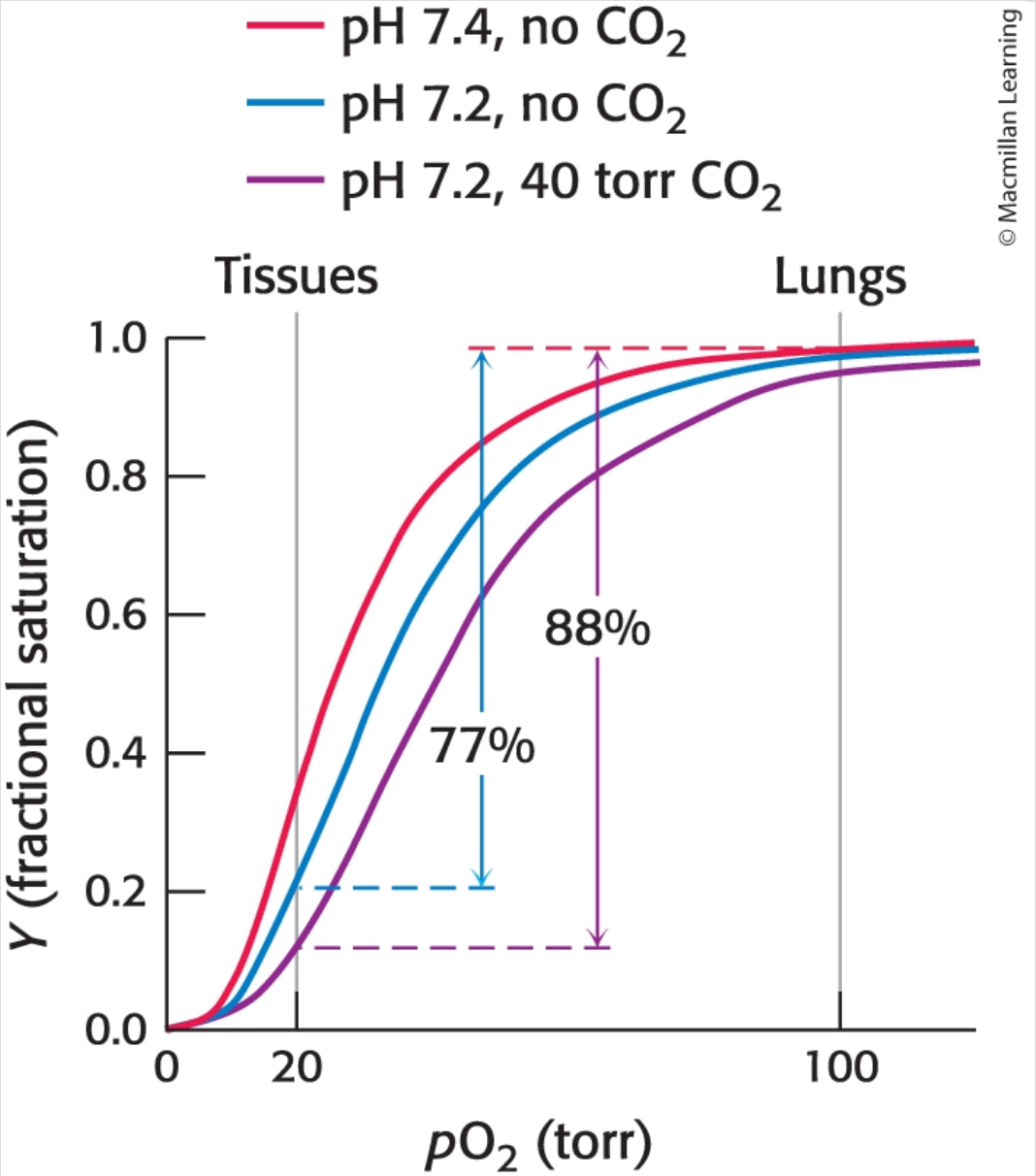
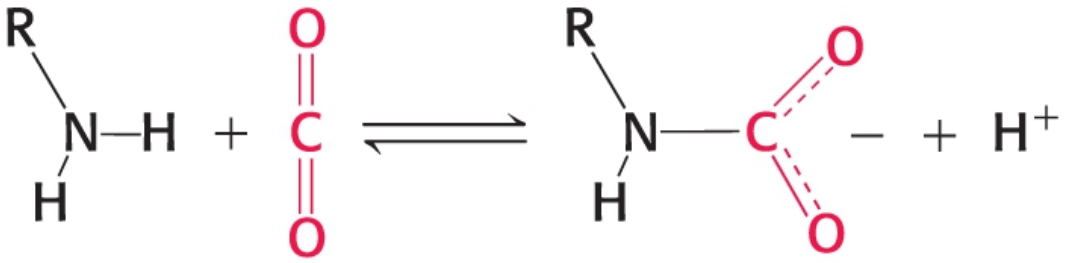


FIGURE 3.30 The presence of carbon dioxide decreases the oxygen affinity of hemoglobin, even beyond the effect due to a decrease in pH. At a constant pH 7.2, the presence of CO_2 at a level of 40 torr decreases the oxygen affinity of hemoglobin and increases the amount of oxygen delivered from 77% to 88%.

Carbon dioxide stabilizes deoxyhemoglobin by reacting with the terminal amino groups to form carbamate groups, which are negatively

charged, in contrast with the neutral or positive charges on the free amino groups.



Carbamate

The amino termini lie at the interface between the αβ dimers, and these negatively charged carbamate groups participate in ionic interactions that stabilize the T state, favoring the release of oxygen. The binding of hydrogen ions and carbon dioxide by hemoglobin illustrate another example of molecular recognition based on chemical reactivity.

The binding mode of carbon dioxide is very different from the binding mode for carbon monoxide. Just as for myoglobin, carbon monoxide binds to the heme irons in hemoglobin and competes with oxygen for binding. Carbon monoxide poisoning from burning materials with inadequate ventilation is a frequent cause of emergency department visits and deaths in many countries.

A variant of neuroglobin, a monomeric protein evolutionarily and structurally related to myoglobin and hemoglobin, is being developed as a potential treatment for carbon monoxide that could be administered by first responders. In the course of studying neuroglobin, scientists replaced the distal histidine with glutamine. This substitution resulted in a protein with an extremely high affinity for oxygen and, most importantly, for carbon monoxide. With three additional changes to

improve the solubility, a protein termed Ngb-H64Q was generated which binds carbon monoxide 500 times more tightly that does hemoglobin. When carboxyhemoglobin was mixed with free Ngb-H64Q, CO transfer was very rapid, with almost complete conversion in less than one minute (Figure 3.31)! The discovery of this mutant neuroglobin revealed an exciting potential therapeutic option for the treatment of carbon monoxide poisoning, which has since been directly tested in animal studies.

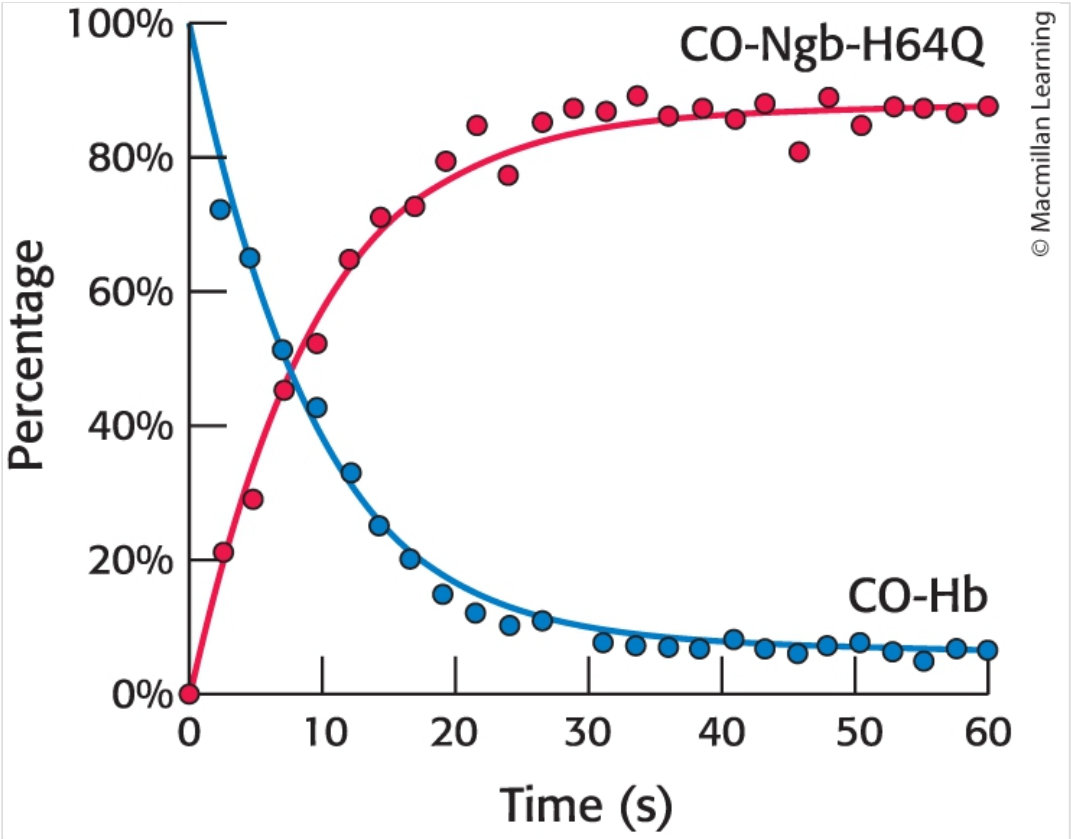


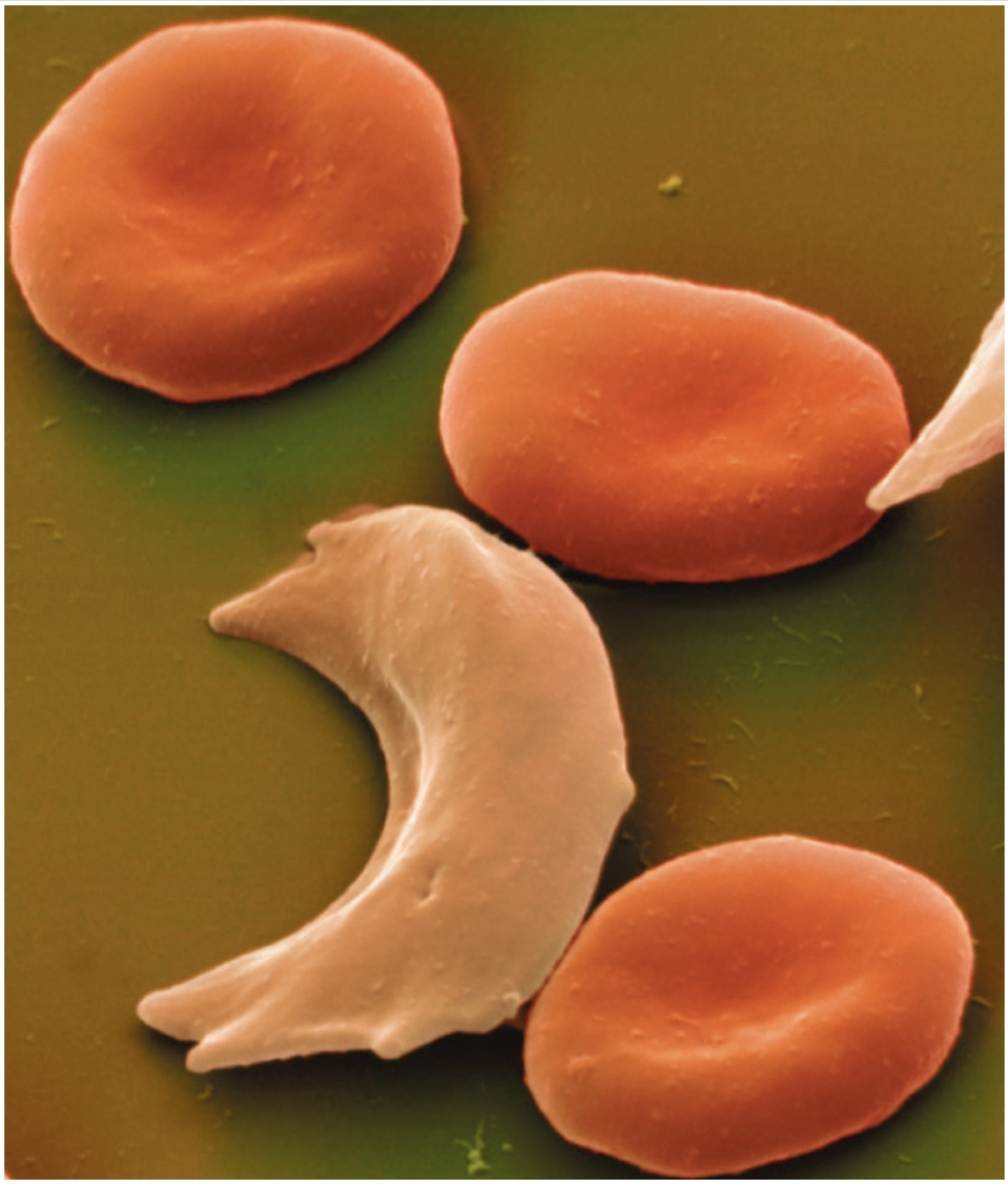
FIGURE 3.31 Carbon monoxide is rapidly transferred from carboxyhemoglobin to Ngb-H64Q. When carboxyhemoglobin (CO-Hb) is mixed with ligand-free Ngb-H64Q, CO is rapidly transferred away from hemoglobin, with exchange complete in less than one minute.

[Information from I. Azarov et al., 2016, *Sci. Trans. Med*. 8:368ra173, Fig. 2c.]

Mutations in genes encoding hemoglobin subunits can result in disease



In modern times, particularly after the sequencing of the human genome, it is routine to think of genetically encoded variations in protein sequence as a factor in specific diseases. But this was not always the case. In 1949, four years prior to the proposal of the structure of the DNA double helix, the notion that diseases might be caused by molecular defects was proposed by Linus Pauling, Harvey Itano, and colleagues to explain the blood disease **sickle-cell anemia**. The name of the disorder comes from the abnormal sickle shape of red blood cells deprived of oxygen in people suffering from this disease (**Figure 3.32**). Based on experimental studies, they proposed that sickle-cell anemia might be caused by a specific variation in the amino acid sequence of one hemoglobin chain. Today, we know that this bold hypothesis is correct.

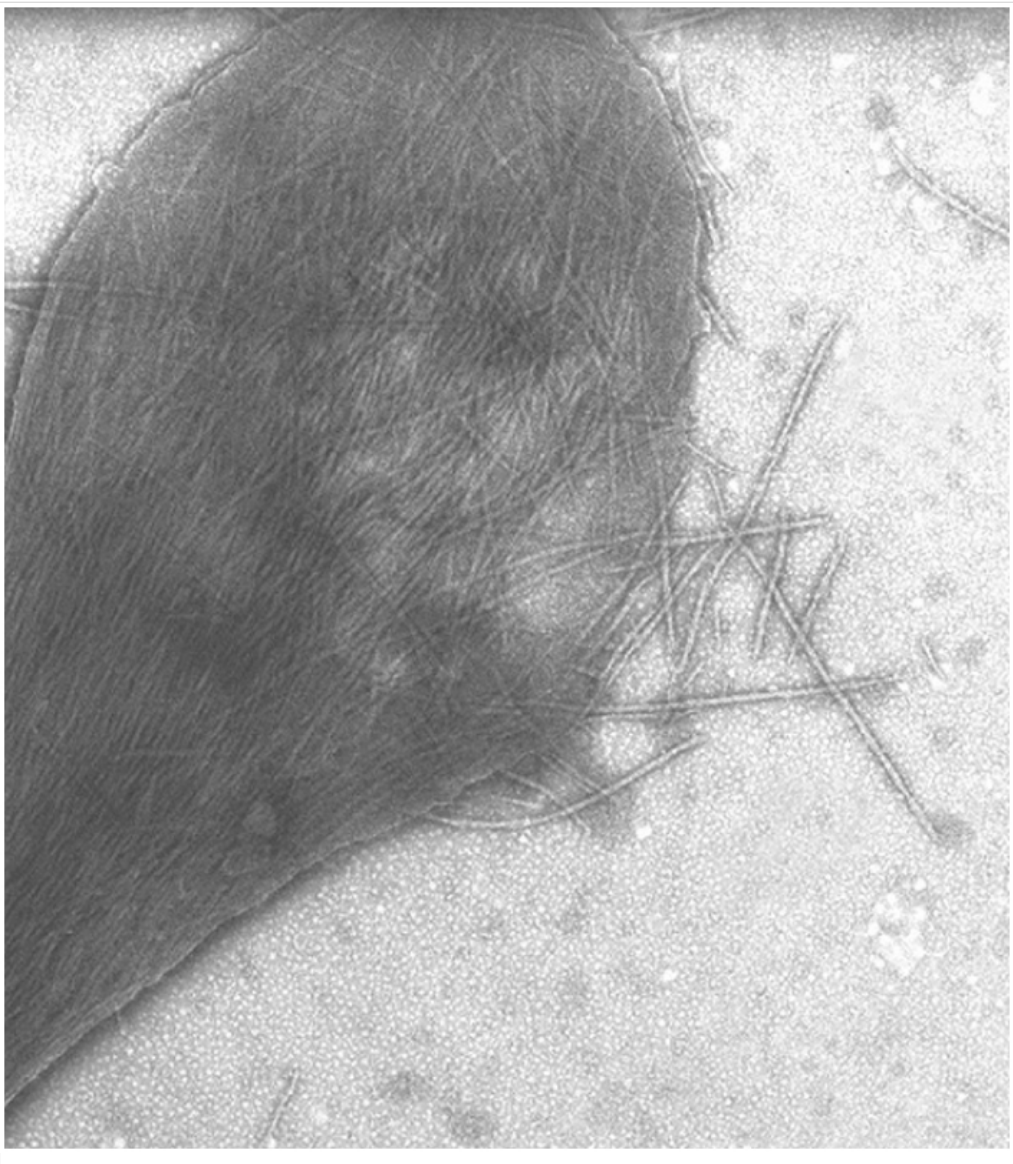


Eye of Science/Science Source

FIGURE 3.32 Red blood cells in patients with sickle-cell anemia adopt a sickle shape when oxygen levels are low. The micrograph shows a sickled red blood cell adjacent to normally shaped red blood cells

People with sickled red blood cells experience a number of dangerous symptoms. Examination of the contents of these cells reveals that the hemoglobin molecules have formed large fibrous aggregates (Figure 3.33). These fibers extend across the red blood cells, distorting them so that they clog small capillaries and impair blood flow. In addition, red blood cells from sickle-cell patients adhere more readily to the walls of

blood vessels than those from normal individuals, prolonging the opportunity to block capillaries. The results may be painful swelling of the extremities and a higher risk of stroke or bacterial infection, due to poor circulation. The sickled red blood cells also do not remain in circulation as long as normal cells do, in part because even a single event when sickling occurs can increase the tendency of the cells to break open, or lyse, leading to anemia.



Courtesy of Robert Josephs and Thomas E. Wellems, University of Chicago.

FIGURE 3.33 Hemoglobin in individuals with sickle-cell disease forms long fibers. An electron micrograph depicting a ruptured sickled red blood cell is shown with fibers of sickle-cell hemoglobin emerging.

What is the molecular defect associated with sickle-cell anemia? Vernon Ingram and coworkers demonstrated in 1956 that a single amino acid substitution in the β chain of hemoglobin is responsible—namely, the replacement of a glutamate residue with valine in position 6. The mutated form is referred to as hemoglobin S (HbS). In people with sickle-cell anemia, both alleles (one from the mother and one from the father) of the hemoglobin β-chain gene are mutated. The HbS substitution substantially decreases the solubility of deoxyhemoglobin, although it does not markedly alter the properties of oxyhemoglobin.

Examination of the structure of hemoglobin S reveals that the new valine residue lies on the surface of the T-state molecule (**Figure 3.34**). This new hydrophobic patch interacts with another hydrophobic patch formed by Phe 85 and Leu 88 of the β chain of a neighboring molecule to initiate the aggregation process. Why do these aggregates not form when hemoglobin S is oxygenated? When oxyhemoglobin S is in the R state, residues Phe 85 and Leu 88 on the β chain are largely buried inside the hemoglobin assembly. In the absence of a partner with which to interact, the surface Val residue in position 6 is benign. While these interactions are generally not very specific, hemoglobin S fibers illustrate how many such interactions can work together to form a specific oligomeric structure.

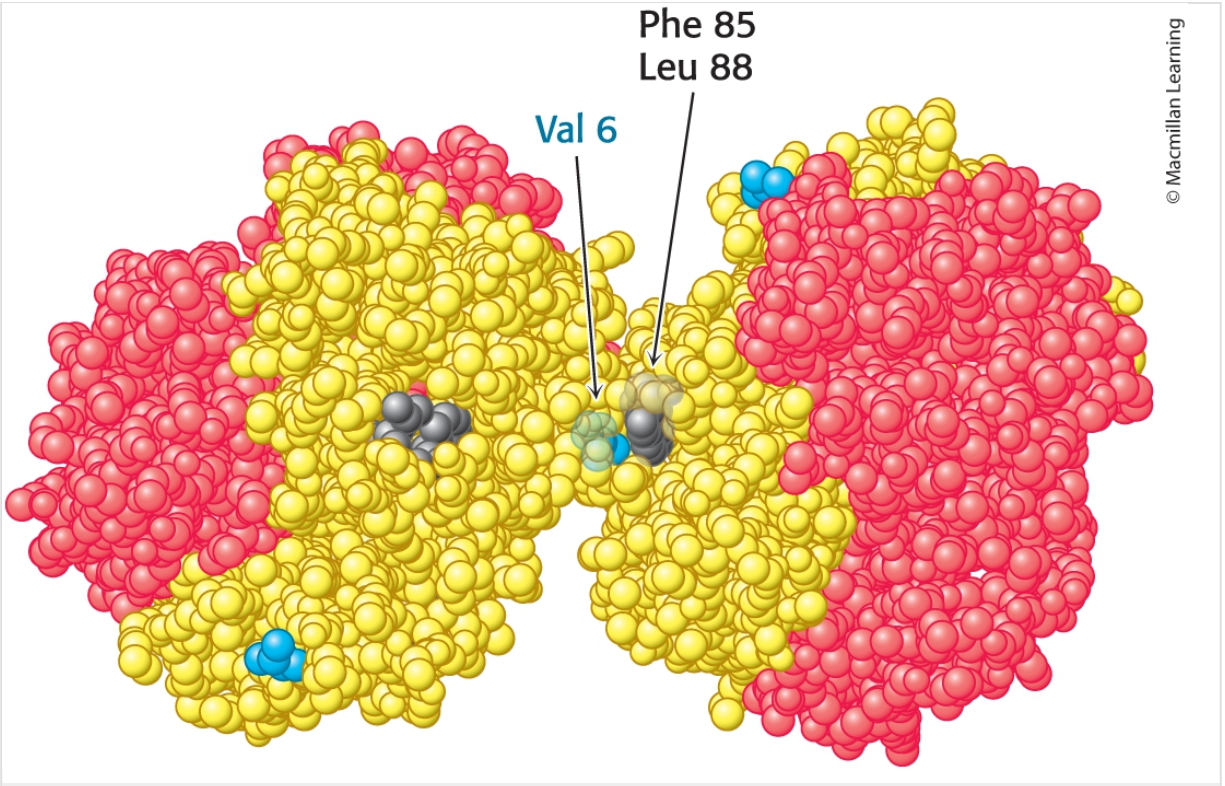


FIGURE 3.34 Two molecules of hemoglobin S interact through hydrophobic patches. These patches involve the Val $\beta 6$ residue characteristic of hemoglobin S, and Phe $\beta 85$ and Leu $\beta 88$ on an adjacent hemoglobin tetramer. This interaction drives the formation of hemoglobin S fibers.

INTERACT with this model in Achieve

3.4 The Immune System Depends on Key Binding Proteins

The immune system faces a daunting challenge in molecular recognition, namely the ability to identify and respond to signs of invading foreign pathogens such as bacteria and viruses in the presence of vast numbers of highly similar molecules from normal cells. Several elaborate and elegant systems have evolved that address the problem of recognition of non-self in the context of self. Here, the term "non-self" can refer to pathogens such as viruses and bacteria but also to tissue from another individual in the case of organ transplantation.

The **innate immune system** is an evolutionarily ancient defense system found, at least in some form, in all multicellular plants and animals. The innate immune system represents a first line of defense against foreign pathogens. It relies on the recognition of classes of molecules common to invading organisms to identify and eliminate these threats.

Because intracellular pathogens do not leave markings on the exteriors of infected cells, vertebrates have evolved mechanisms to display components of interior contents, both self and foreign, on the cell surface. Some internal proteins are broken into peptides, which are then bound to proteins encoded by the **major histocompatibility complex (MHC)**. T cells continually scan the bound peptides to find and kill cells that display foreign motifs on their surfaces. In all of these systems, molecular recognition processes are fundamental, facilitating the detection of components of foreign pathogens and then elimination of the invaders.

The innate immune system recognizes molecules characteristic of pathogens

Perhaps the most important components of the innate immune system are members of a family of receptors that can recognize specific classes of molecules present in many pathogens but normally absent in the host. The best-understood of these receptors are the Toll-like receptors (TLRs). The name "Toll-like" is derived from a receptor known as Toll encoded in the genome of the fruit fly *Drosophila melanogaster*. The TLRs, which are present on the outer surfaces of cells, have a common C-shaped three-dimensional structure (**Figure 3.35**). Each receptor consists of a large domain that sits on the outside of cells and is built primarily from imperfectly repeated amino acid sequences termed leucine-rich repeats (LRRs). Each LRR typically contains 20–30 residues, including 6 that are usually leucine. The human TLRs have from 18 to 27 LRR repeats. In addition to the LRR domains, each TLR has additional domains that anchor the protein to the cell surface and participate in signaling processes inside the cell.

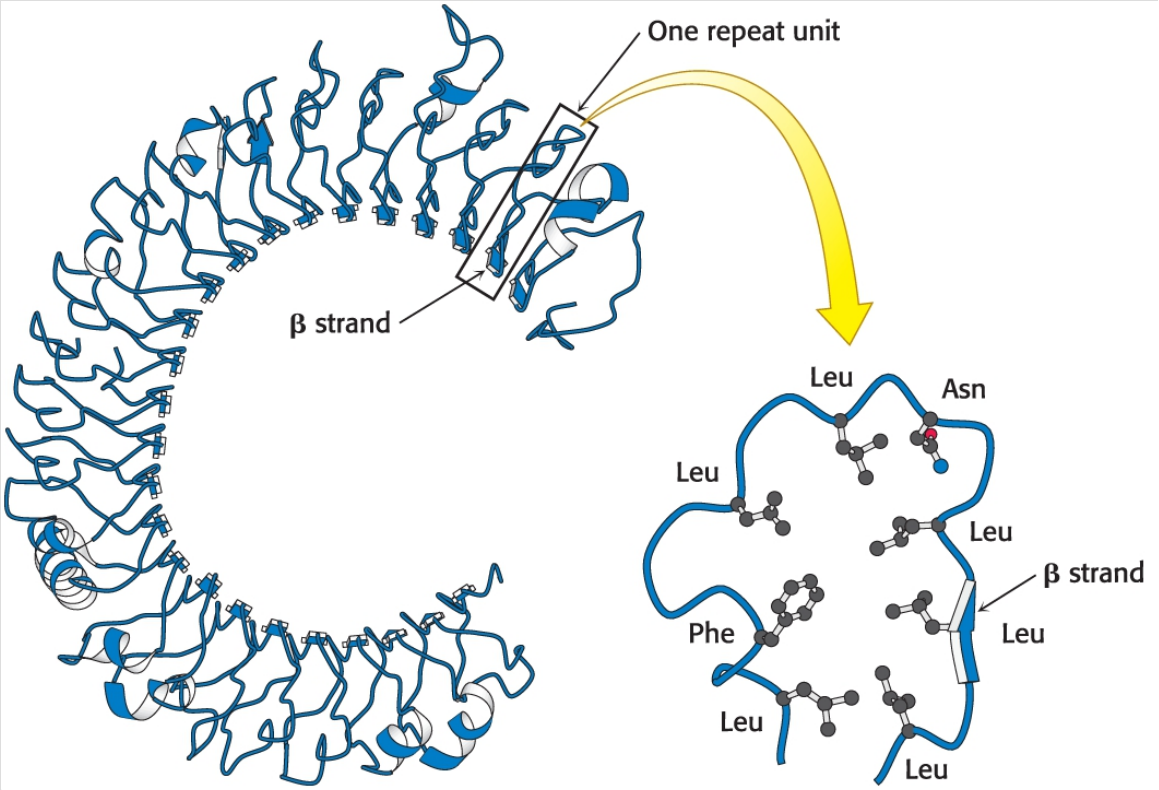
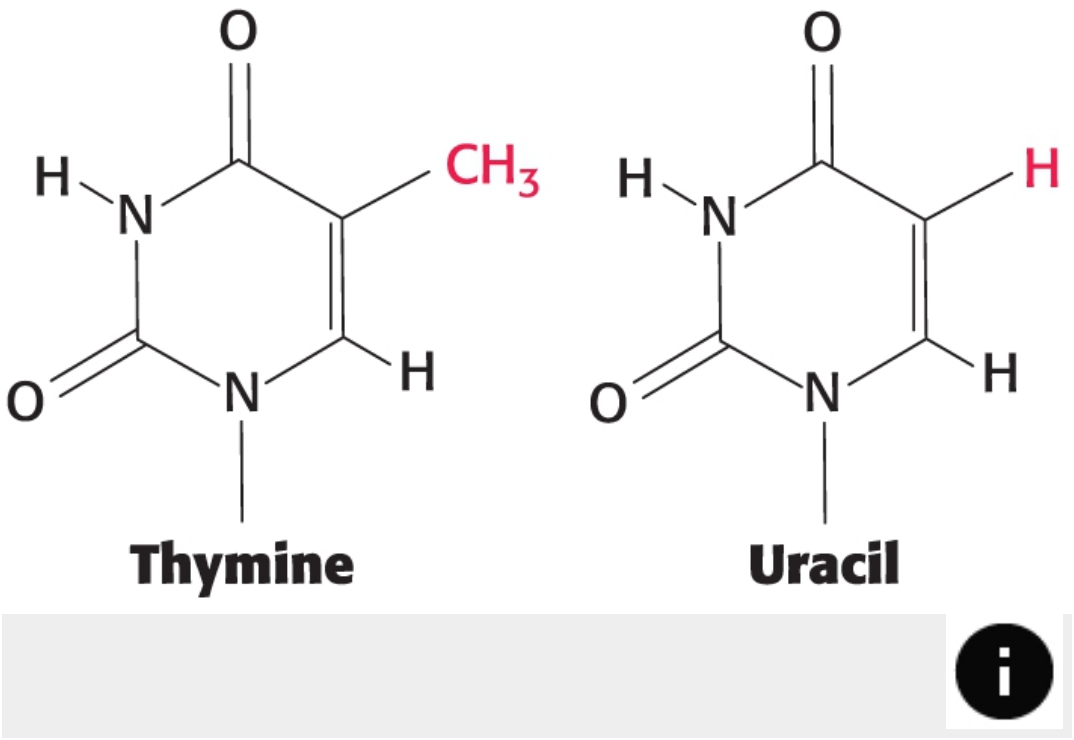


FIGURE 3.35 The structure of the LRR domain from TLR3 reveals how many LRR units come together to form a structure with binding surfaces for potential partners. Each LRR has a sing β strand and included leucine residues that come together to form a hydrophobic core. The interior and the two sides of the C-like structure are surfaces that recognize potential partners.

Each TLR targets a specific molecular class, often called a *pathogen-associated molecular pattern (PAMP)*, found primarily on invading organisms. Typically, a PAMP is a critical and widespread component of the pathogen. Examples include certain key molecules found on bacterial cell surfaces and certain classes of nucleic acids, including double-stranded RNAs. RNA is a relative of DNA that has an additional hydroxyl group on each backbone sugar unit and has uracil instead of thymine, present in DNA. Uracil lacks the methyl group in thymine.



RNA molecules are present inside normal cells in single-stranded forms. However, many viruses utilize RNA as their genomes; RNAs outside cells are therefore markers of infections or cellular damage. The difference between uracil and thymine as well as differences in the backbone conformation due to the additional hydroxyl group present opportunities for recognition of RNA versus DNA.

How do TLRs recognize PAMPs? The hook-like structures from the extracellular domains of TLRs have surfaces that are capable of recognizing a variety of a ligands in a wide array of binding modes. For example, the PAMPs for TLR3 are double-stranded RNA molecules of appropriate lengths which fit in the cavity between two monomers (Figure 3.36). As might be anticipated from this structure, RNA molecules that are much shorter than 46 base pairs are bound less tightly, as they cannot interact with the two TLR3 molecules optimally at the same time. In addition, studies show that more than 1000 times the concentration of double-stranded DNA molecules are required to achieve the same level of binding as for double-stranded RNA. This can be explained by the fact that double-stranded RNA molecules have a

somewhat different double-helical structure from those of double-stranded DNA molecules.

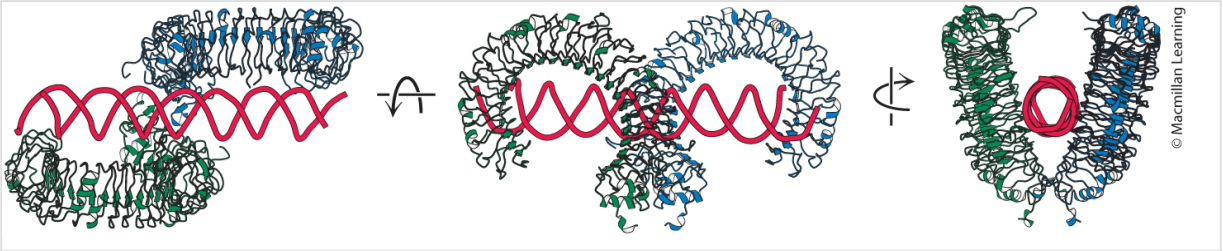


FIGURE 3.36 The innate immunity component TLR3 recognizes its PAMP, a double-stranded RNA. The structure of the complex between two molecules of the extracellular domain of TLR3 and a 46-base-pair double-stranded RNA molecule is shown from three perspectives showing how the receptor recognizes the structure and length of the RNA molecule.

Because the TLRs and other components of the innate immune system are always present on the surfaces of appropriate cells, they provide the host organism with a rapid response to resist attack by pathogens. However, many pathogens have evolved the ability to escape detection by the innate immune system. How does the host defend itself in these instances?

Antibodies bind specific molecules through specific hypervariable loops

For protection against novel pathogens, the host relies on the **adaptive immune system**, which is able to target specific pathogens, even those that it has never encountered in the course of evolution. The adaptive immune system comprises two parallel but interrelated responses: humoral and cellular immune responses. In the humoral immune response, soluble proteins called **antibodies** (or **immunoglobulins**) function to recognize foreign molecules and mark them, signaling

foreign invasion. In the cellular immune response, cells called **cytotoxic T lymphocytes** (also commonly called **killer T cells**) destroy cells that have been invaded by a pathogen.

How does a system capable of recognizing essentially any foreign molecule function? A clue emerged from comparison of the amino acid sequences of a large number of antibodies of a type referred to as *immunoglobulin G* (IgG). For most proteins, the amino acid sequences from many different individuals, and even across species such as human beings and mice, show only minor variations. However, for portions of these IgG molecules, especially three stretches of approximately 7 to 12 amino acids within each chain, these sequences are highly variable (**Figure 3.37**). These segments are referred to as the *hypervariable regions*.

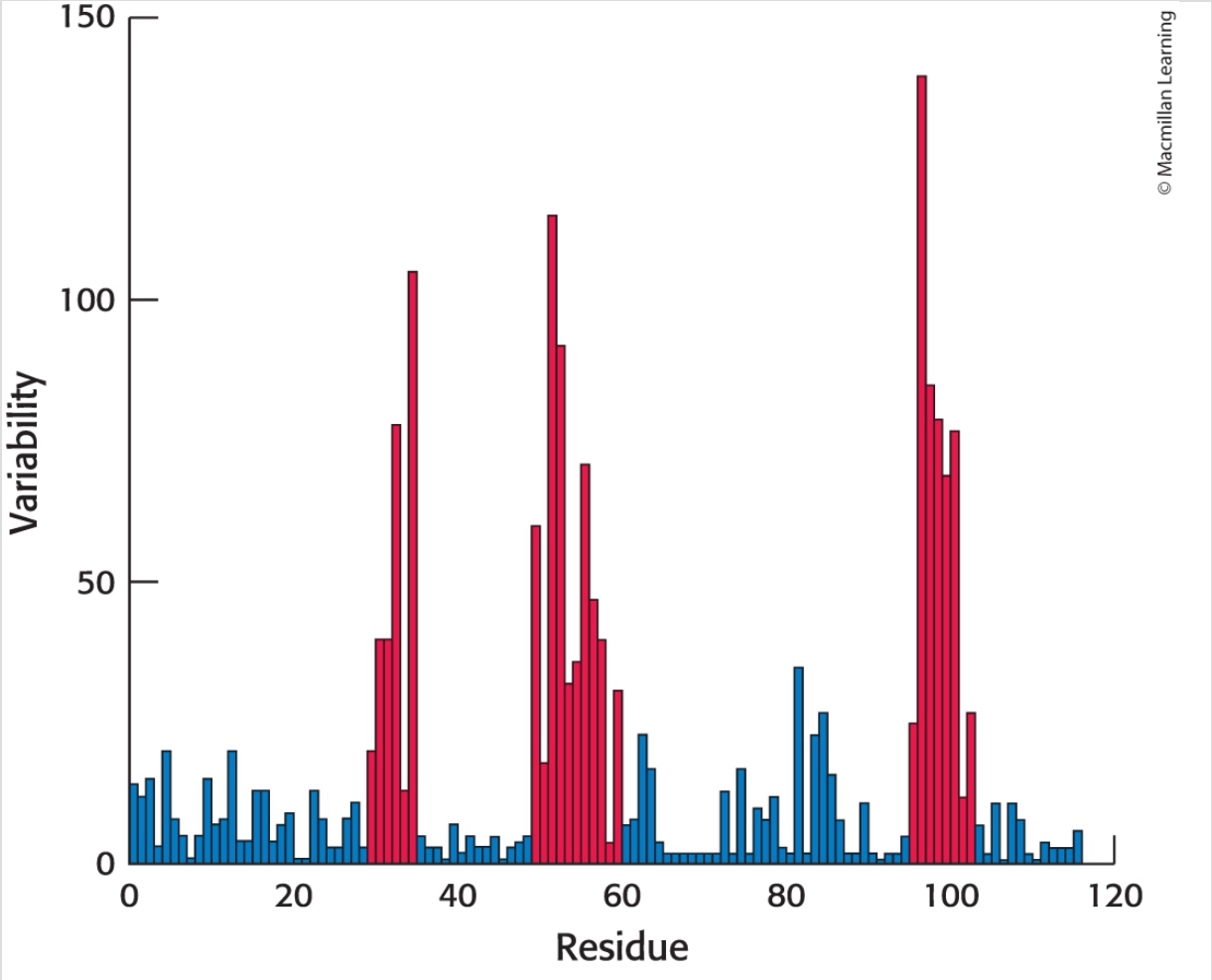


FIGURE 3.37 Immunoglobulin sequences include regions of extensive sequence variability. A plot of sequence variability in a portion of immunoglobulins as a function of position reveals three regions (red) with much greater variability than the rest of the sequence (blue). Sequence variability is measured by the number of different amino acids that were observed within a set of immunoglobulin sequences.

[After R. A. Goldsby, T. J. Kindt, and B. A. Osborne, *Kuby Immunology*, 4th ed. (W. H. Freeman and Company, 2000), p. 91.]



Based on this observation, one could envisage a process involving a vast collection of potential binding proteins, each of which is constructed with a relatively constant scaffold with other regions that vary substantially from one member of the collection to another. If the collection is large and varied enough, then the odds are that one or more members of the collection have a surface that will recognize any foreign molecule. Molecules that induce immune responses are referred to as **antigens**. The challenge is to find the "needle in the haystack" for the given antigen and then produce the antibody at adequate levels to be of use. This is, indeed, the principle by which the adaptive immune system operates.

Let us look carefully at the structure of IgG to examine this adaptive ability in more detail. An IgG molecule consists of 12 structural domains. These domains have many sequence features in common and adopt a common structure, the **immunoglobulin fold** (**Figure 3.38**). The immunoglobulin fold consists of a pair of β sheets, each built of antiparallel β strands, that surround a central hydrophobic core. A single disulfide bond bridges the two sheets. Two aspects of this structure are particularly important for its function. First, three loops at one end of the structure that contain hypervariable regions form a potential binding surface. These loops are referred to as **hypervariable loops** or **complementarity-determining regions (CDRs)**. Second, the amino terminus and the carboxyl terminus are at opposite ends of the

structure, which allows structural domains to be strung together to form chains.

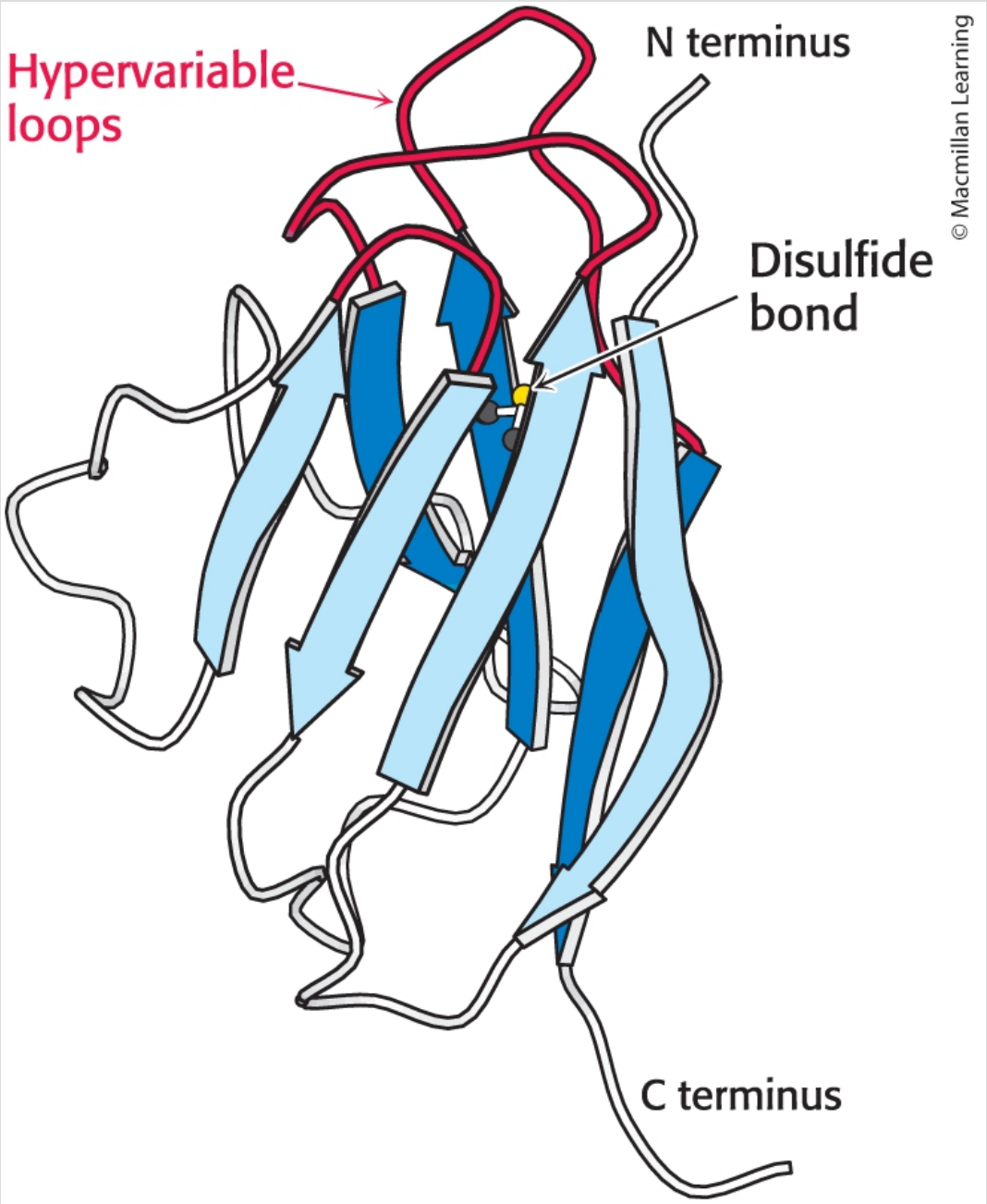


FIGURE 3.38 The immunoglobulin fold consists of a pair of β sheets linked by a disulfide bond. Hydrophobic interactions occur with three hypervariable loops at one end of the structure.

INTERACT with this model in Achieve

The 12 immunoglobulin fold domains in an IgG molecule are arranged to form a Y-shaped structure (Figure 3.39). Each IgG molecule consists of four chains: two so-called *heavy chains*, each of which has four immunoglobulin domains; and two *light chains*, each of which has two immunoglobulin domains. The two heavy chains are linked together by a disulfide bond, and each heavy chain is also linked to one light chain by an additional disulfide bond. The positions of the CDRs are striking. These hypervariable sequences, present in three loops of each domain, come together so that all six loops come together at the end of each arm.

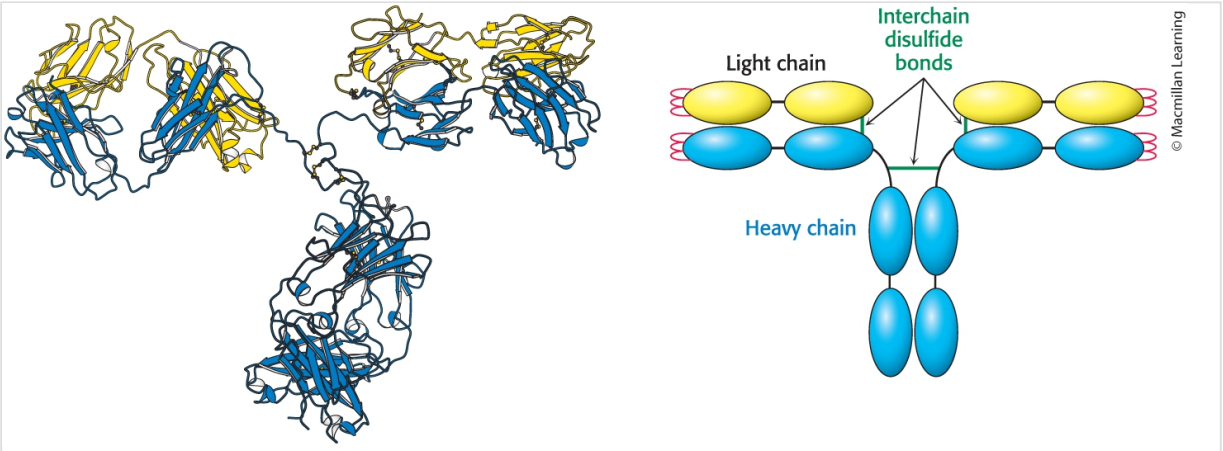
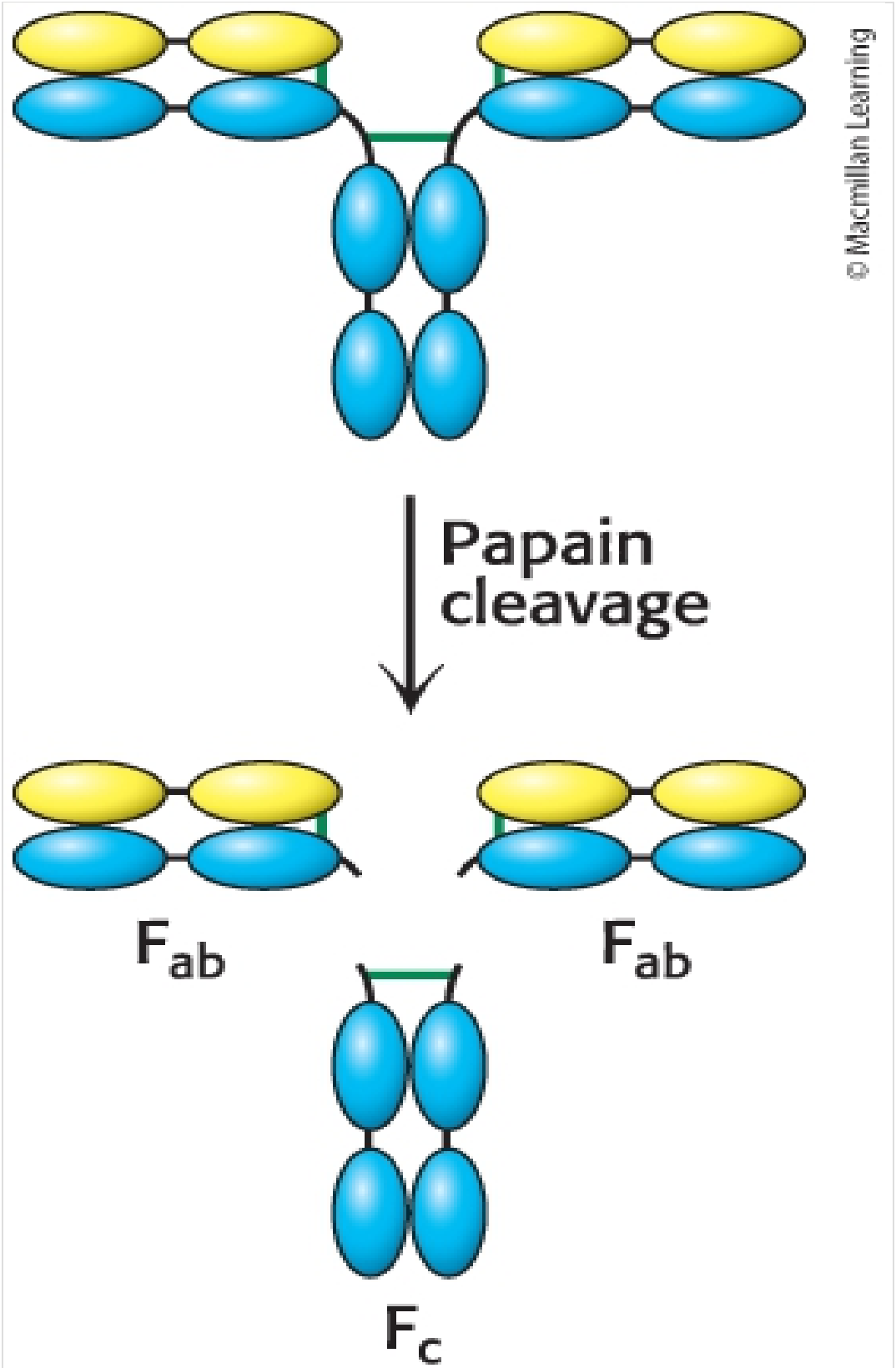


FIGURE 3.39 An IgG molecule has a Y-shaped structure comprising two identical arms with hypervariable regions at the end. The heavy chains are shown in blue, the light chains in yellow, and the hypervariable loops at the end of the two arms in red. The positions of intrachain disulfide bonds are indicated.

INTERACT with this model in Achieve

Biochemists have dissected IgG using a protein called papain, isolated from papaya fruit (**Figure 3.40**). Papain catalyzes the cleavage of certain exposed peptide binds; treatment of an IgG molecule with papain results in two products in a 2:1 ratio. The first products are F_{ab} fragments, which comprise a light chain as well as a portion of the heavy chain; the second product, termed F_c, comprises two disulfide-linked portions of the heavy chain. This dissection allows the binding and structural properties of IgG molecules to be studied more easily; the three-dimensional structure of an F_{ab} fragment shows how the CDRs come together to form a binding surface (**Figure 3.41**).



© Macmillan Learning

FIGURE 3.40 Immunoglobulin G molecules can be cleaved into two F_{ab} fragments and one F_c fragment by treatment with papain. The F_{ab} fragments include the antigen binding sites.



FIGURE 3.41 The structure of an F_{ab} fragment reveals how the six hypervariable loops come together to form a binding surface. (A) Side view. (B) End view looking down on the binding surface.

Let us now examine in detail the interactions in one representative complex between an antibody F_{ab} fragment and a typical protein: lysozyme from egg whites. This antibody binds two polypeptide segments of lysozyme that are widely separated in the primary structure. All six CDRs of the antibody participate directly in molecular recognition. The region of contact is quite extensive (about 30×20 Å), and the apposed surfaces are rather flat. The only exception is the side chain of glutamine 121 of lysozyme, which penetrates deeply into the antibody's binding site, where it forms a hydrogen bond with a main-chain carbonyl oxygen atom and is surrounded by three aromatic side chains (Figure 3.42).

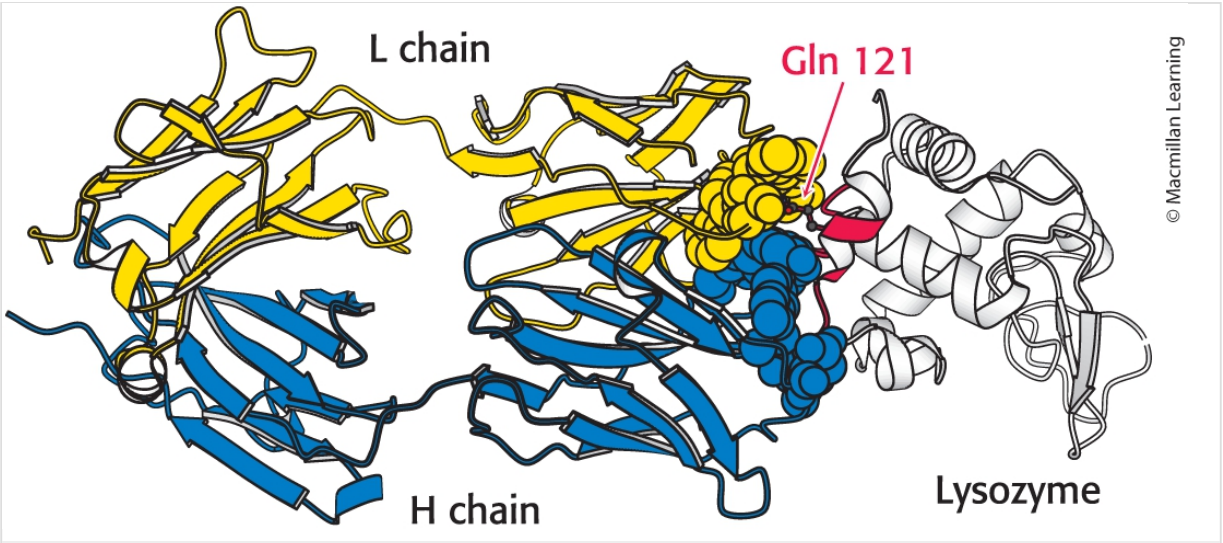


FIGURE 3.42 The structure of a complex between lysozyme and a specific F_{ab} fragment reveals how the binding surface on the F_{ab} interacts with the antigen. The hypervariable loops are shown as space-filling models. A single residue from lysozyme, glutamine 121, penetrates relatively deeply into the antibody.

INTERACT with this model in Achieve

The formation of 12 hydrogen bonds and numerous van der Waals interactions contributes to the high affinity ($L_{1/2} = 20$ nM) of this antibody–antigen interaction. Examination of the F_{ab} molecule without bound protein reveals that the structures of the immunoglobulin domains change little on binding, although they slide 1 Å apart to allow more intimate contact with lysozyme.

Studies of thousands of large and small antigens bound to F_{ab} molecules have been sources of much insight into the structural basis of molecular recognition by antibodies. The interaction between complementary shapes results in numerous contacts between amino acids at the binding surfaces of both molecules. Many hydrogen bonds, ionic

interactions, and van der Waals interactions, reinforced by hydrophobic interactions, combine to give specific and strong binding.

Self-Check Question



How many total hypervariable loops does an immunoglobulin G molecule have? Not counting duplicates more than once, how many unique loops does it have?

Antibodies possess distinct antigen-binding and effector units

The major antibody in the serum is immunoglobulin G. As noted previously, IgG molecules have Y-shaped structures with two F_{ab} arms that participate in antigen binding and one F_c arm (Figure 3.39). The F_c arm is not merely a scaffold but is a target for molecular recognition itself, as it is recognized by specific proteins on the surfaces of certain cells. This allows the IgG molecule to act as an adaptor, linking an antigen bound by the F_{ab} arms to cells expressing the F_c receptor, initiating other steps that can help destroy the pathogen.

Why does an IgG have more than one F_{ab} arm? Many invaders such as viruses and bacteria have surfaces with repeating structures. Having two F_{ab} arms joined by a flexible hinge allows the IgG to bind to such a surface, with each F_{ab} binding to a different instance of the structural repeat. This allows the IgG to stick more avidly to the surface with a longer dissociation time. The polyvalent interactions are analogous to Velcro®, in which many hooks and loops interact relatively weakly but together can produce a strong interaction.

Recall that an IgG protein is a heterotetramer with two heavy chains and two light chains. Five different classes of antibody—IgG, IgM, IgA, IgD, and IgE—differ in their heavy chains and, hence, in their effector functions (Figure 3.43). By virtue of their different effector domains and, hence, different interaction partners, each of these classes can participate in different physiological processes. For example, IgM has a noteworthy pentameric structure with ten potential antigen-binding sites. IgMs are the first class of antibody produced after an infection; in general, each IgM antigen-binding site has a relatively modest affinity for antigen, but the overall affinity is higher due to the large number of connected potential binding sites.

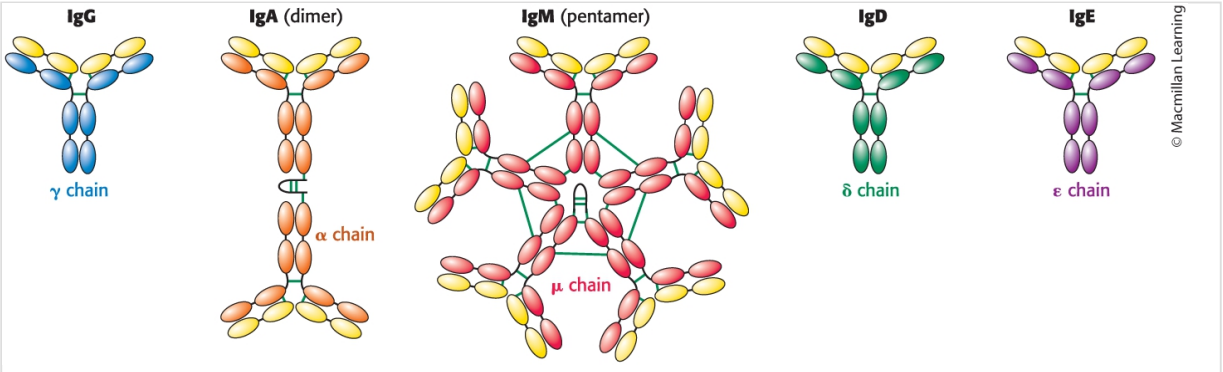


FIGURE 3.43 Five classes of immunoglobulin have the same light chain combined with a different heavy chain (γ, α, μ, δ, or ε). The light chains are shown in yellow, and disulfide bonds are indicated by green lines.

Recombination events equip the adaptive immune system with millions of unique antibodies

The genes that encode immunoglobulin light and heavy chains undergo fascinating recombination events that introduce different combinations

of CDRs, resulting in more than 300 possible light chains and more than 8000 possible IgG heavy chains. As each light chain can come together with each heavy chain, this produces more than $300 \times 8000 = 2{,}400{,}000$ potential antibodies. This explains how the adaptive immune system can respond to unknown invaders; it is prepared with many potential molecular recognition templates, some of which will adequately match any new threat.

 Through the use of vaccines, the adaptive immune system can be primed for agents known to be potential threats. Vaccines, which expose the immune system to molecules associated with a potential infection without causing serious disease, are perhaps the most powerful public health measures ever developed. Vaccines can be complete bacteria or viruses that have been rendered relatively harmless by various means, or they may be molecular components that trigger protective immune responses. The development of several vaccines against the so-called “spike” protein found on the surface of SARS-CoV-2, the virus that causes COVID-19, were hugely important advances. The vaccines can induce antibodies that bind to the spike protein and block its ability to bind to and infect cells (**Figure 3.44**).

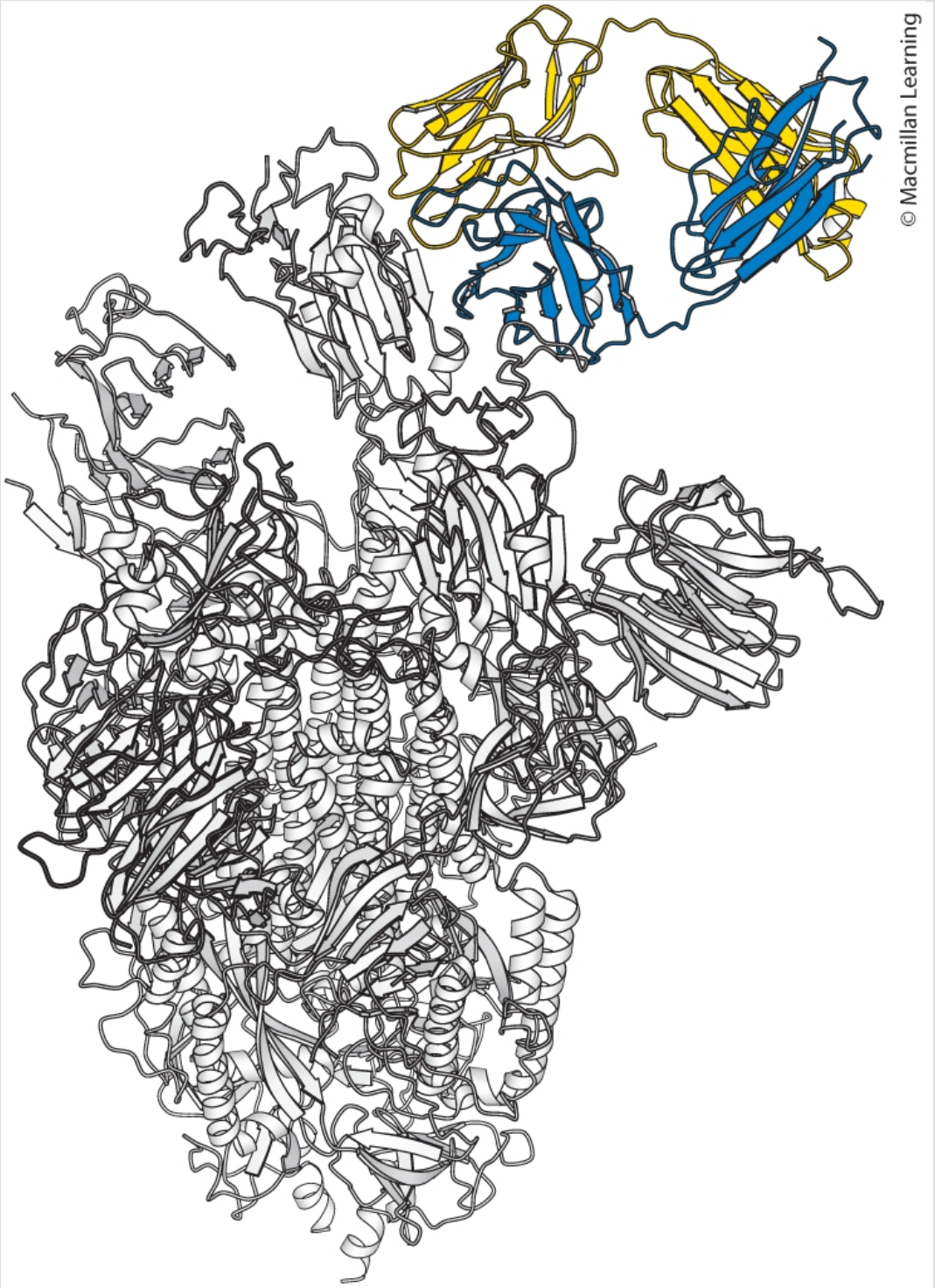


FIGURE 3.44 Antibodies elicited against the spike protein of SARS-CoV-2 can bind to this protein and block the ability of the virus to infect cells. The structure shows the trimeric spike protein targeted by an F_{ab} fragment from one specific antibody.

Major-histocompatibility-complex proteins present peptide antigens on cell surfaces for recognition by T-cell receptors

Soluble antibodies are highly effective against extracellular pathogens, but they confer little protection against microorganisms that are predominantly intracellular, such as some viruses and mycobacteria (which cause tuberculosis and leprosy). These pathogens are shielded from antibodies by the host-cell membrane. A different and more subtle strategy, **cell-mediated immunity**, evolved in response to the damaging properties of intracellular pathogens. The task is not simple; intracellular microorganisms are not so obliging as to leave telltale traces on the cell surfaces of their host without assistance. Quite the contrary, successful pathogens are masters of the art of camouflage. However, vertebrates use an elaborate mechanism—cut and display—to reveal the presence of stealthy intruders. The process starts in the cytoplasm with the cutting step; self-proteins as well as those of pathogens are cleaved into short peptides. Nearly all vertebrate cells exhibit on their surfaces a sample of peptides derived from the digestion of proteins in their cytoplasm. These peptides are then displayed by proteins embedded in the cell membrane that are encoded by the major histocompatibility complex (MHC); they are called **class I MHC proteins**. These cell-surface proteins tightly grip their bound peptides, which are then touched and scrutinized by other cells.

The three-dimensional structure of a large extracellular fragment of a human MHC class I protein termed HLA-A2, solved in 1987 by Don Wiley, Pamela Bjorkman, and colleagues, reveals a deep groove that

serves as the binding site for the presentation of peptides (**Figure 3.45**). The groove can be filled by a peptide from 8 to 10 residues long in an extended conformation (**Figure 3.46**). An individual typically has six distinct MHC class I proteins with different peptide specificities, and these vary from individual to individual across the population.

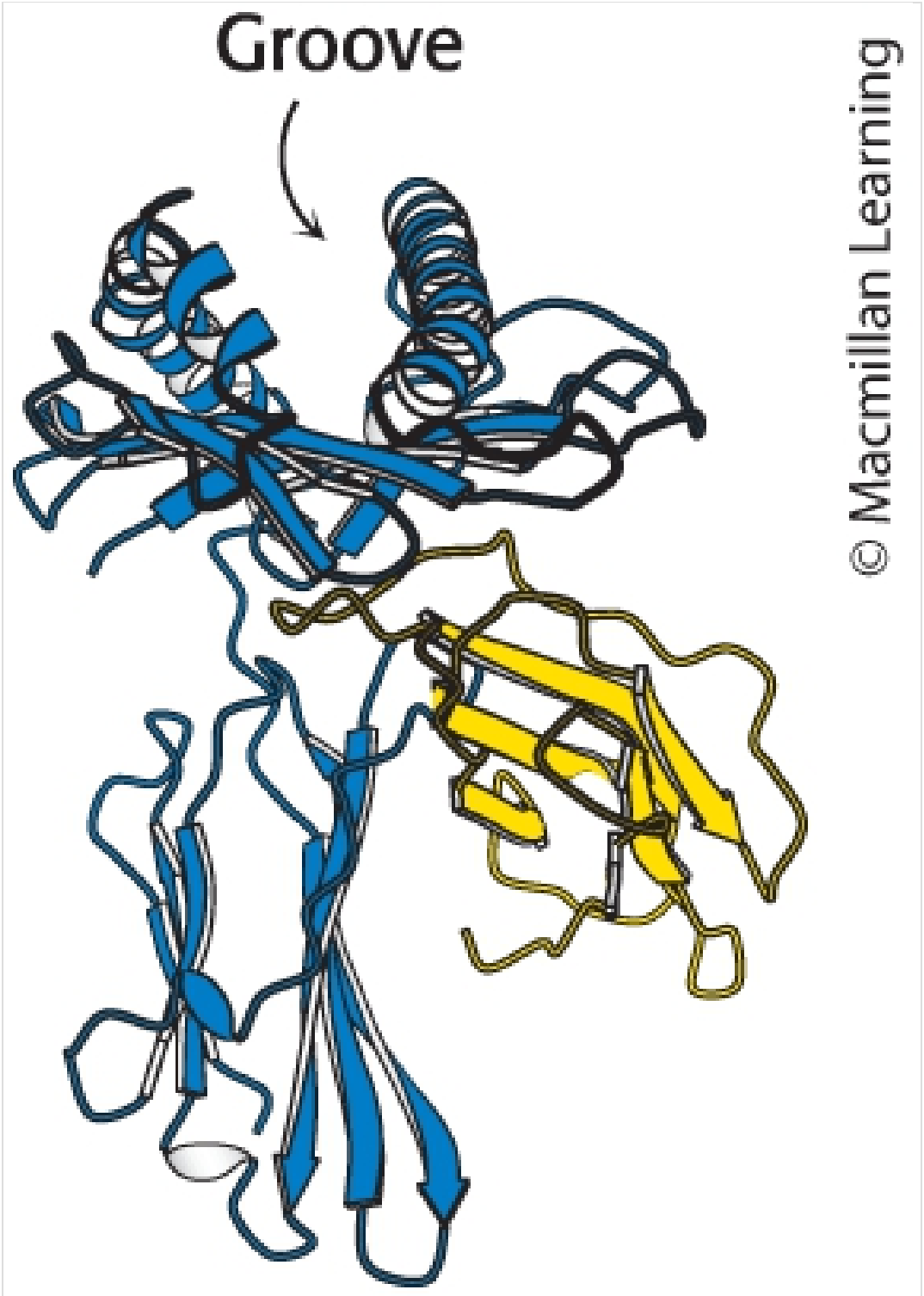


FIGURE 3.45 The structure of the extracellular domain of a class I MHC protein reveals a deep groove. The domain is a complex between two different polypeptide chains, shown in blue and yellow.

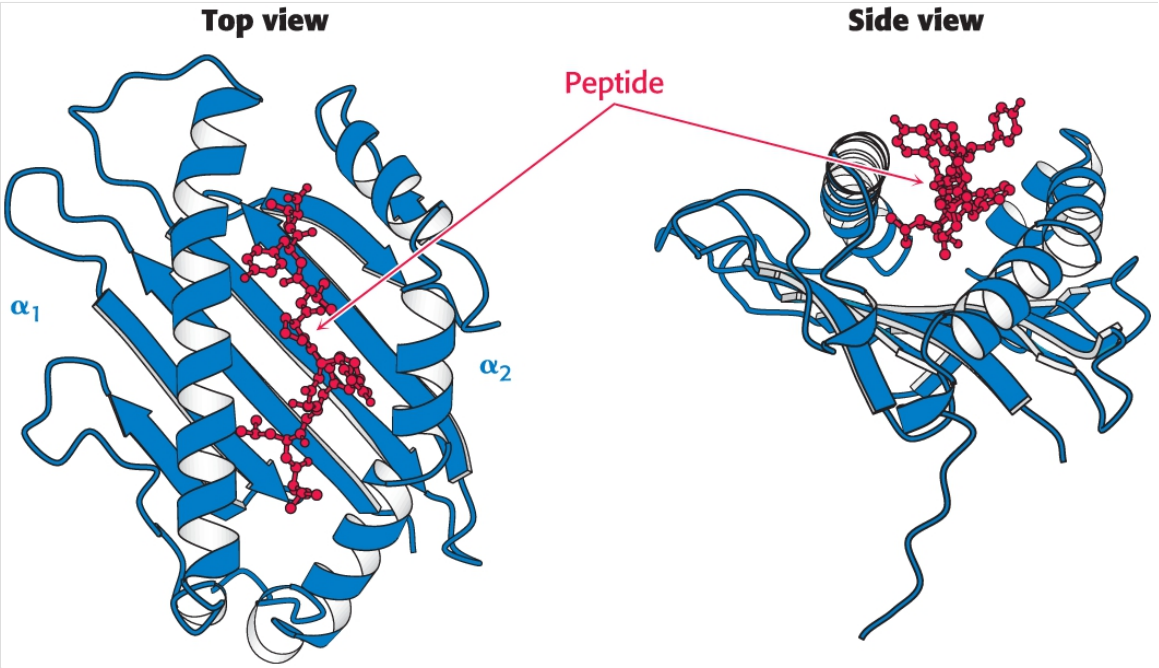


FIGURE 3.46 In class I MHC proteins, peptides can bind in the groove. The peptide (shown in red) binds in a relatively extended conformation.

The first class I MHC protein to have its structure determined binds peptides that almost always have leucine in the second position and valine in the last position (Figure 3.47). Side chains from the MHC molecule interact with the amino and carboxyl termini and with amino acids in these two key positions. These two residues are often referred to as the *anchor residues*. The other residues are highly variable. Thus, many millions of different peptides can be presented by this particular class I MHC protein; the identities of only two of the nine residues are crucial for binding to the MHC protein. Each different MHC molecule

recognizes a unique set of anchor residues, so a tremendous range of peptides can be presented by these molecules.

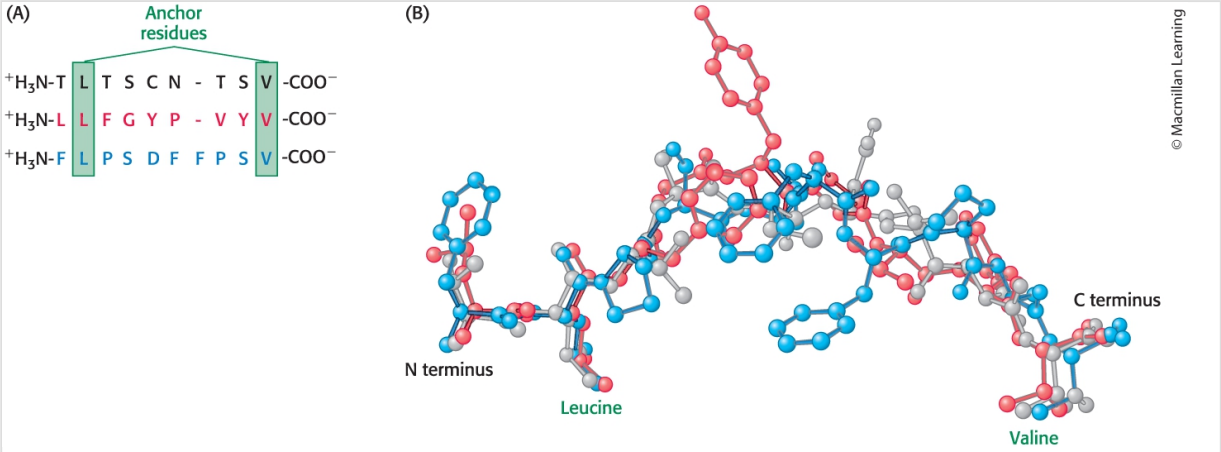


FIGURE 3.47 Each MHC class I protein presents peptides with some recurring features. (A) The amino acid sequences of three peptides that bind to the class I MHC protein HLA-A2 are shown. Each of these peptides has leucine in the second position and valine in the carboxyl-terminal position. (B) Comparison of the structures of these peptides reveals that the amino and carboxyl termini, as well as the side chains of the leucine and valine residues, are in essentially the same positions in each peptide, whereas the remainder of the structures are quite different.

One face of the bound peptide is exposed to solution, where it can be examined by other molecules, particularly receptors on the surfaces of T cells. These T-cell receptors have a structure that is closely related to the F_{ab} portion of an antibody, comprising two chains with immunoglobulin folds and hypervariable loops. Each T-cell receptor is, in principle, capable of recognizing an MHC-peptide complex by forming a structure analogous to an antibody–antigen complex (Figure 3.48).

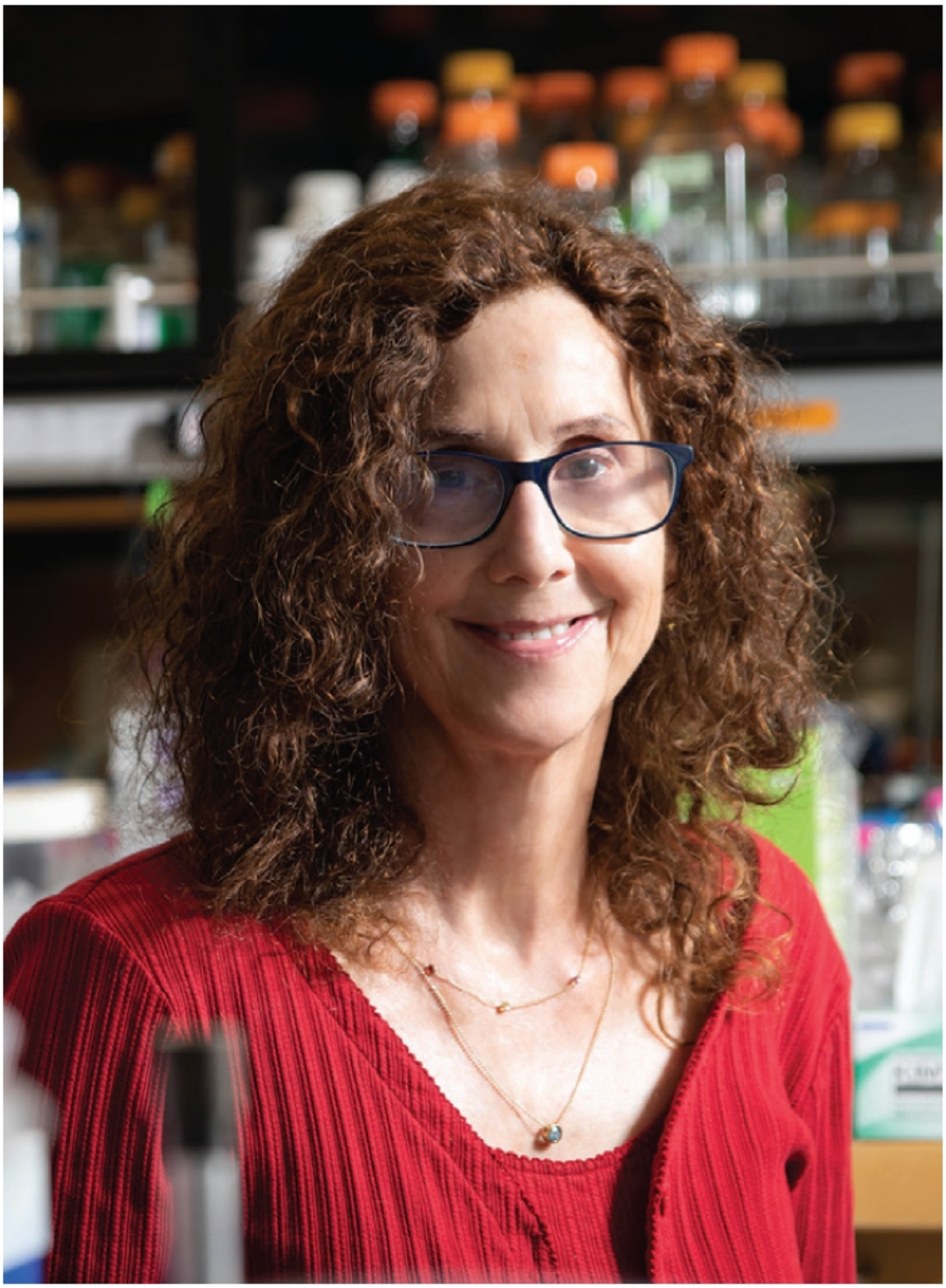

T-cell receptor
MHC class I
© Macmillan Learning

FIGURE 3.48 The T-cell receptor recognizes specific class I MHC complexes, contacting both the MHC protein and the bound peptide. The bound peptide is shown in red.

INTERACT with the models shown in Figures 3.45, 3.46, and 3.48 in Achieve

Neither the foreign peptide alone nor the MHC protein alone forms a complex with the T-cell receptor. Molecular recognition depends on the complete structure identifying fragments of an intracellular pathogen, after they are presented in a context that allows their detection and an appropriate response. An assembly consisting of the foreign peptide-MHC complex, the T-cell receptor, and some additional proteins triggers a cascade that induces death of the infected cell.

We close this section by considering an essential biological aspect of molecular recognition in the immune system; namely, the ability to distinguish between self and non-self. How is this achieved? There is no special molecular characteristic of self-proteins that pathogen proteins lack. Instead, the answer lies in developmental biology: antibody-producing cells and T cells that react to self-proteins are identified and blocked before they are released into the circulation, preventing dangerous immune responses to normal tissues. This process can fail, however, as revealed by the occurrence of autoimmune diseases such as type 1 diabetes, rheumatoid arthritis, and dozens of other conditions.



Lance Hayashida/Caltech

PAMELA BJORKMAN Soon after entering graduate school with a strong background in chemistry, Pamela Bjorkman was intrigued by a presentation by Assistant Professor Don Wiley, who was trying to determine the three-dimensional structures of an important viral protein. She also learned that another graduate student in Professor Jack Strominger's laboratory had painstakingly purified substantial amounts of an MHC protein. She convinced the two professors that she should try to solve the MHC structure for her PhD dissertation project. She was stymied in solving the structure by what turned out to be unexpected peptides bound in the groove, but she completed the structure as a postdoctoral fellow. The elucidation of this MHC-

peptide structure represents a key milestone in immunology. Dr. Bjorkman has gone on to an extremely productive career at the California Institute of Technology, where she works with students, fellows, and staff to reveal other important structures of the immune system, with an aim to developing interventions that improve human health.

3.5 Quantitative Terms Can Describe Binding Propensity

Molecular recognition is not a “yes or no” process. The tendency of a receptor to bind a particular ligand depends on the ligand concentration. We have thus far used parameters such as $L_{1/2}$ and P_{50} to capture this concentration dependence. In order to describe binding propensity in more quantitative terms, we will now apply concepts from chemical equilibrium for ligand-binding reactions.

Dissociation constants are useful in describing binding reactions quantitatively

Recall the ligand-binding reaction (equation 1)

$$\mathrm{R} + \mathrm{L} \rightleftharpoons \mathrm{RL}$$

The equilibrium constant for this reaction is

$$K = \{\mathrm{RL}\}/\{\mathrm{R}\}\{\mathrm{L}\}$$

where {X} is the thermodynamic activity for component X. These activities are ratios of the concentrations of the components relative to standard states; they are unitless quantities and, therefore, so is *K*. The standard states are usually defined as concentrations of 1 M. With certain assumptions, the equilibrium constant can be written in terms of concentration as

$$K = [RL]/[R][L]$$

where [X] is the concentration of component X in molarity. Since each concentration has units of molarity, the equilibrium constant has units of M^{-1}; the appearance of units of molarity reflects the choice of standard states.

The equilibrium constant for this reaction is often written as K_a, where the subscript "a" refers to the fact this this is an association reaction. (This K_a should not be confused with K_a related to acidity and pH.) An equivalent but generally more useful quantity is the equilibrium constant for the reaction written as a dissociation process:

$$RL \rightleftharpoons R + L$$

$$K_d = [R][L]/[RL]$$

K_d has units of concentration (in molarity with standard states of 1 M). These units are easier to understand intuitively than are units of inverse concentration.

Suppose that $[L] = L_{1/2}$. Recall that under these conditions, half of the receptor is bound and half is unbound, therefore, $[R] = [RL]$. Making these two substitutions for [L] and [R] in the equation for K_d above gives us:

$$K_d = [RL][L_{1/2}]/[RL] \text{ or } K_d = L_{1/2}$$

In many experiments, the concentration of the receptor-ligand complex, RL, is measured as the concentration of added L is increased. In general, the concentrations of free R and free L are not measured, but rather the total concentrations of R and L are known. We can use these parameters in the equilibrium constant expression:

$$R_{total} = [R] + [RL] \text{ so } [R] = R_{total} - [RL]$$

$$\text{and } L_{total} = [L] + [RL] \text{ so } [L] = L_{total} - [RL]$$

$$\text{Thus, } K_d = (R_{total} - [RL])(L_{total} - [RL])/[RL]$$

Except for ligands that are bound very tightly, the concentration of [RL] is usually much lower than the total concentration of L added, that is, $L_{total} - [RL] \approx L_{total}$.

Then, $K_d = (R_{total} - [RL])(L_{total} - [RL])/[RL] \approx (R_{total} - [RL])(L_{total})/[RL]$

$$= R_{total}L_{total}/[RL] - L_{total}$$

Rearranging, we find that $K_d + L_{total} = R_{total}L_{total}/[RL]$ so that

$$[RL]/R_{total} = L_{total}/(K_d + L_{total})$$

(2)

Now, suppose that the total added ligand concentration is equal to K_d.

$$[RL]/R_{total} = L_{total}/(K_d + L_{total}) = L_{total}/(L_{total} + L_{total}) = 1/2$$

At this point, the one half of the total receptor concentration is bound to L. Therefore, the dissociation constant K_d is equivalent to $L_{1/2}$. Also notice that $[RL]/R_{total}$ is the fraction of the total receptor bound to a ligand; thus, the degree of saturation of the receptor with a ligand can be found from equation 2 once the K_d value is known (**Figure 3.49**).

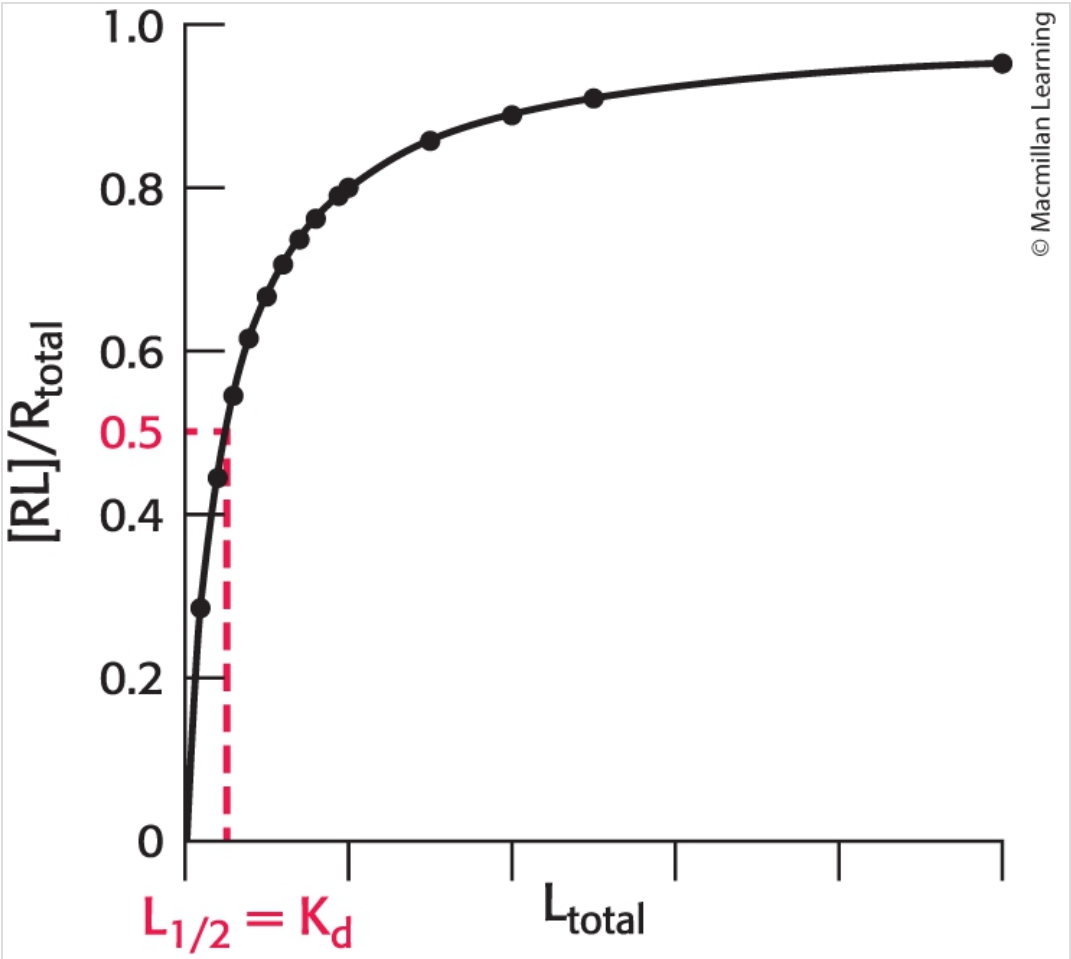


FIGURE 3.49 Binding can be monitored by measuring the fraction of receptors with ligand bound as a function of the amount of ligand added. The data curve is characterized by the value of K_d, which is the same as $L_{1/2}$.

Example

Determining the Fraction of Bound Receptors

Problem:

What fraction of receptors are occupied with ligand at a ligand concentration of $5\ \mu M$, given that half of the receptors are occupied with ligand at a total ligand concentration of $20\ \mu M$?

Getting Started:

Equation 2 gives the relationship between the fraction of receptors occupied with ligands as a function of the total ligand concentration and the dissociation constant:

$$[RL]/R_{total} = L_{total}/(K_d + L_{total})$$

We are interested in what happens at a total ligand concentration of $5\ \mu M$. In order to use equation 2, we need to know the dissociation constant.

Solve:

We showed that the half of the receptors are occupied with ligands when the total ligand concentration is equal to the dissociation constant. Since half of the receptors are occupied when the ligand concentration is $20\ \mu M$, we know that $K_d = 20\ nM$. Substituting this and $L_{total} = 5\ \mu M$ into equation 2, we find that

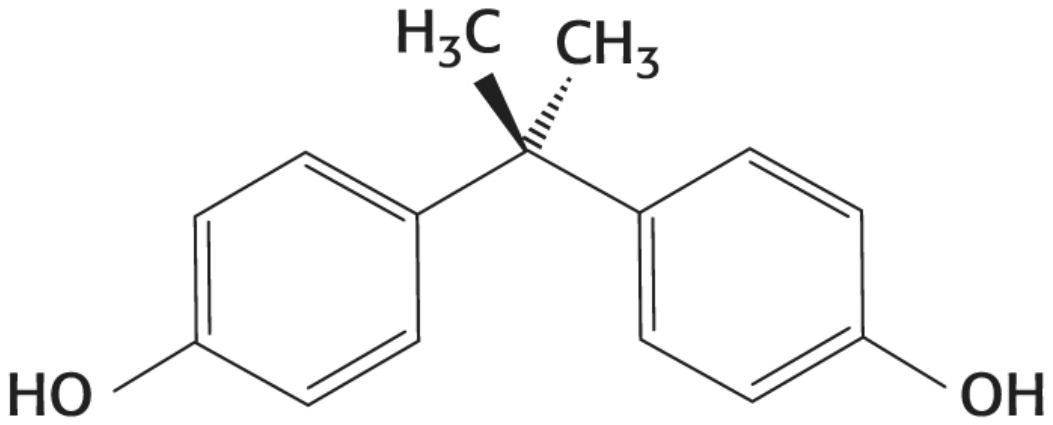
$$[RL]/R_{total} = 5\ \mu M/(20\ \mu M + 5\ \mu M) = 0.20$$

Reflect:

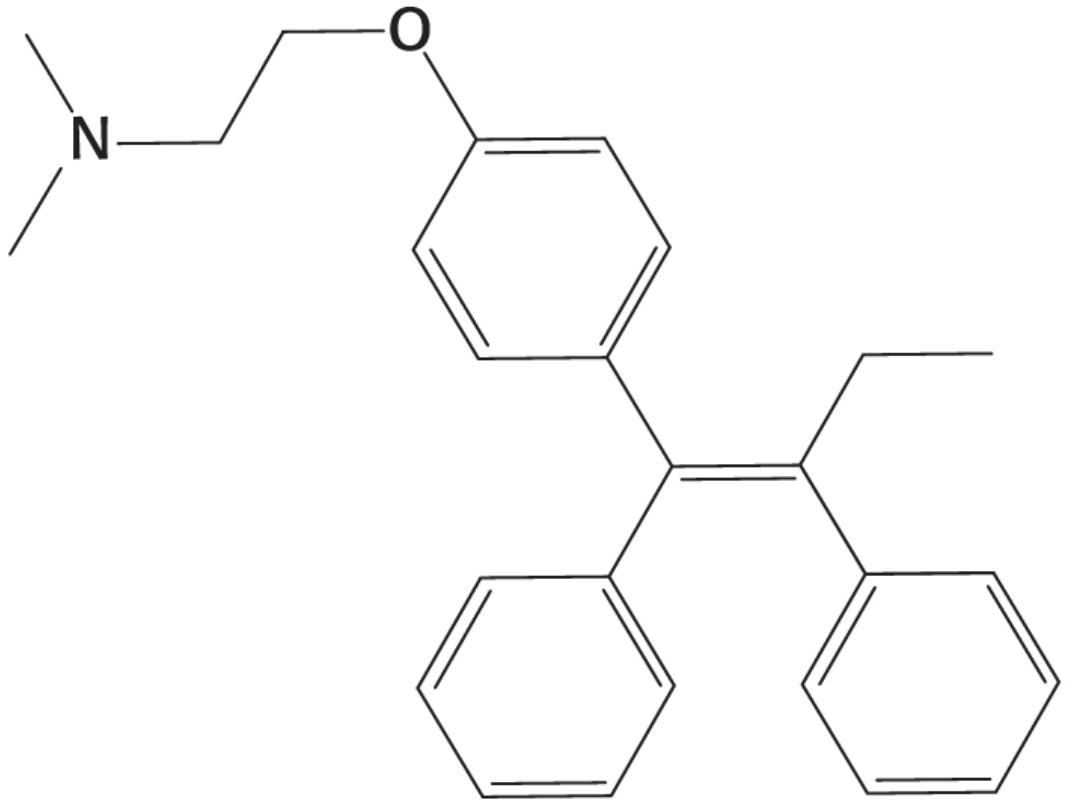
This result makes sense since the total ligand concentration is somewhat less than $20\ \mu M$, the ligand concentration at which half (0.50) of the receptors are occupied.

Specificity can be quantified by comparing dissociation constants

Molecular recognition is reflected not just in the affinity of a protein for its preferred ligands, but also in the affinities of the protein for other potentially competitor ligands. For example, estrogen receptors can bind ligands such as estradiol but also competitor ligands such as bisphenol A (BPA), a precursor used in the manufacture of some types of plastics, and tamoxifen, a cancer drug that is bound without receptor activation.



Bisphenol A (BPA)



Tamoxifen

For estradiol, the $L_{1/2}$, which we now know is equal to the dissociation constant K_d, is 1 nM. Thus, if the estradiol concentration is 1 nM, the fraction of receptors that will be occupied by estradiol is 0.5. For BPA, $L_{1/2} = K_d = 200\ \text{nM}$. If we assume that BPA is present at a concentration of 1 nM, we can apply equation 2 to find that the fraction of receptors occupied is $1\ \text{nM} / (200\ \text{nM} + 1\ \text{nM}) = 0.005$. The concentration of BPA must be increased to 200 nM in order for the fraction of receptors to be occupied with BPA to reach 0.5.

Suppose we have estrogen receptors in the presence of 1 nM estradiol and then add $1\ \mu\text{M}$ BPA (**Figure 3.50**). We cannot simply use equation 2 for each ligand, because this equation was derived assuming that $R_{total} = [R] + [RL]$ without any other species present. But with two ligands, say L_1 and L_2, R_{total} must be replaced with $[R] + [RL_1] + [RL_2]$, since the receptor can be unoccupied or bound to either ligand. Using this expression, we can derive the concentrations of RL_1 and RL_2 as a function of the concentrations of L_1 and L_2, although we will not go through this derivation here. With 1 nM estradiol and $1\ \mu\text{M}$ BPA, we find that the fraction of receptors occupied with estradiol is 0.14 and the fraction of receptors occupied with BPA is 0.71. Thus, the fraction of receptors bound to estradiol drops due to the addition of substantial concentrations of BPA. Conceptually, we can understand this in the following way. Initially, half of the receptors are bound to estradiol and half are unoccupied. As the concentration of BPA increases, BPA will bind to the free receptors. This will drive the equilibrium

$$\text{Receptor} + \text{estradiol} \rightleftharpoons \text{Receptor-estradiol}$$

away from the receptor-estradiol complex as the occupied receptor concentration drops.

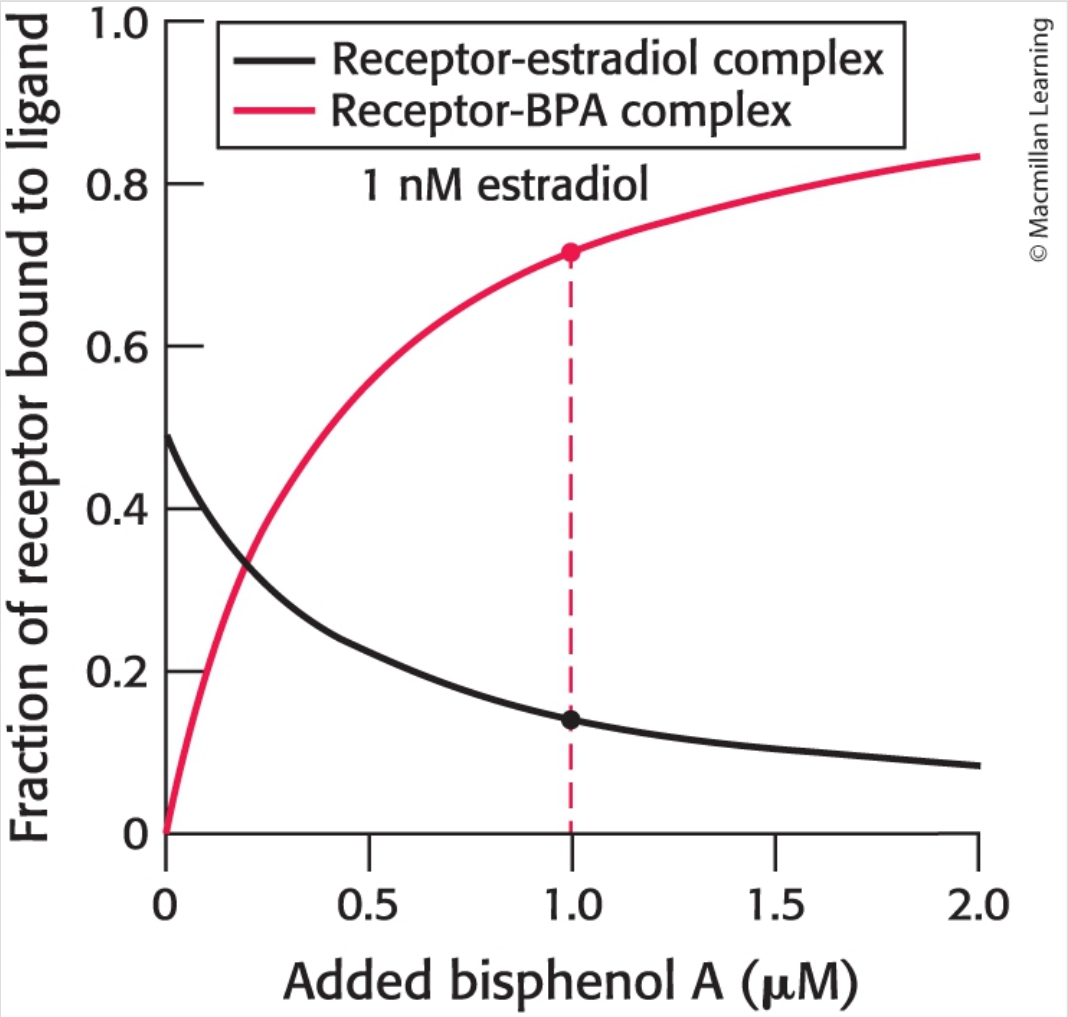


FIGURE 3.50 At high enough concentrations, ligands with lower affinity for a receptor can compete for binding with high-affinity ligands. The curves show the concentrations of an estrogen receptor-estradiol complex (black) and an estrogen receptor-BPA complex (red) as a function of increasing concentrations of BPA. At a BPA concentration of $1\ \mu M$, the fraction of estrogen receptor bound to estradiol is reduced from 0.5 to 0.14.

This analysis provides a quantitative measure of how well estrogen receptors recognize estradiol compared with BPA as an alternative ligand based on their different K_d values; if the two ligands are present at the same concentration, then a much larger fraction of receptors will bind estradiol; a much higher concentration of BPA is required for BPA to successfully compete with estradiol for the receptor-binding sites.

Kinetic parameters can also describe binding processes

Equilibria can also be viewed from the perspective of the rates of forward and reverse reactions.

$$R + L \underset{k_{-1}}{\overset{k_1}{\rightleftharpoons}} RL$$

The forward reaction, the association of R and L to form RL, is a second-order reaction, meaning that its rate depends on the concentrations of two species, R and L. The rate of the forward reaction is given by

$$\text{Rate}_{\text{forward}} = k_1[R][L]$$

The forward rate constant, k_1, has units $M^{-1}s^{-1}$. The reverse reaction, the dissociation of RL, is a first-order reaction, depending only on the concentration of RL. The rate of the reverse reaction is given by

$$\text{Rate}_{\text{revserse}} = k_{-1}[RL]$$

The reverse rate constant, k_{-1}, has units s^{-1}.

At equilibrium, the concentrations of all species are unchanging. The rates of the forward and reverse reactions must be the same even though both reactions are still continuing (Figure 3.51). $\text{Rate}_{\text{forward}} = \text{Rate}_{\text{reverse}}$, so that $k_1[R][L] = k_{-1}[RL]$; therefore, $k_{-1}/k_1 = [R][L]/[RL] = K_d$. Thus, we can also determine the dissociation constant of a complex, K_d, by examining the ratio of the reverse rate constant to the forward rate constant.

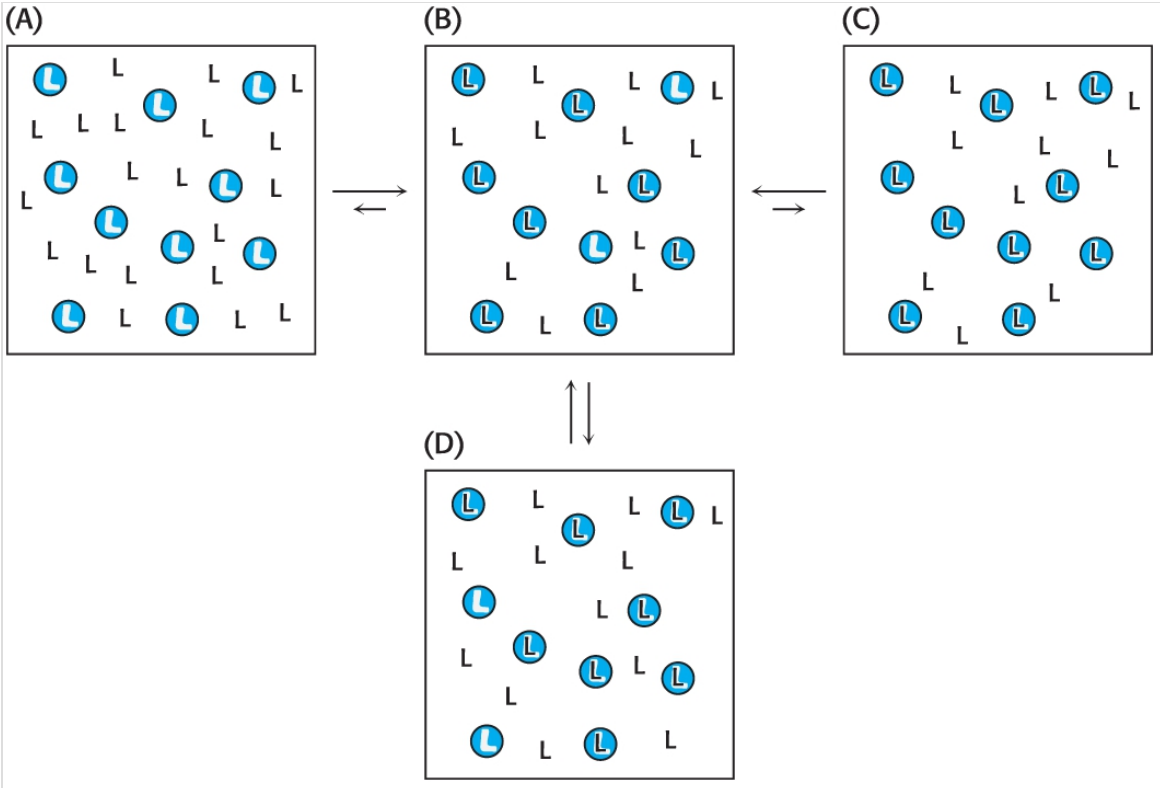


FIGURE 3.51 At equilibrium, the rates of the forward and reverse reactions are the same. A ligand-binding reaction is shown. In (A), no ligands are bound and the forward reaction will proceed faster than the reverse reaction to reach the equilibrium distribution in (B). In (C), all receptor sites are filled and the reverse reaction will proceed faster to reach (B). At equilibrium,

the forward and reverse reactions can proceed at the same rates to interconvert the distributio
in (B) and (D), which have the same fraction of receptors filled.

Self-Check Question

A receptor binds a ligand L with a rate of $10^4\ s^{-1}$ when the ligand concentration is 1 mM. The dissociation rate is $50\ s^{-1}$. What is the dissociation constant for the receptor-ligand complex?

Let us consider again the complex between the estrogen receptor and estradiol. The forward rate constant is found to be approximately $1.2 \times 10^6\ M^{-1}s^{-1}$, and the reverse rate constant is found to be $1.2 \times 10^{-3}\ s^{-1}$, consistent with $K_d = (1.2 \times 10^{-3}\ s^{-1})/(1.2 \times 10^6\ M^{-1}s^{-1}) = 10^{-9}\ M = 1\ nM$. For comparison, for BPA, the forward rate constant is found to be approximately $1.3 \times 10^6\ M^{-1}s^{-1}$ and the reverse rate constant is $2.7 \times 10^{-1}\ s^{-1}$, consistent with $K_d = (2.7 \times 10^{-1}\ s^{-1})/(1.3 \times 10^6\ M^{-1}s^{-1}) = 2 \times 10^{-7}\ M = 210\ nM$.

Notice that the forward rate constants are quite similar to one another, at approximately $1 \times 10^6\ M^{-1}s^{-1}$. There is a limit for such forward rate constants, as two molecules cannot form a complex any faster than they can diffuse together and collide. The rate constants for such

diffusion processes for proteins and small molecules in solution are approximately $10^9\,M^{-1}s^{-1}$. Of course, not all collisions result in complex formation. The ratio of the observed rate constant to the diffusion limit of $10^6\,M^{-1}s^{-1}/10^9\,M^{-1}s^{-1} = 0.001$ indicates that approximately 1 in 1000 collisions is productive.

Empirically, many forward rate constants for biochemical binding reactions are found to fall in the $10^6 - 10^7\,M^{-1}s^{-1}$ range, providing a useful tool for estimating such rate constants in the absence of other information, although there are exceptions. For example, the drug tamoxifen binds to the estrogen receptor with a forward rate constant of only $4.5 \times 10^3\,M^{-1}s^{-1}$. However, the reverse rate constant for the estrogen-tamoxifen complex is $1.0 \times 10^{-3}\,s^{-1}$, consistent with $K_d = (1.0 \times 10^{-3}\,s^{-1})/(4.5 \times 10^3\,M^{-1}s^{-1}) = 22 \times 10^{-7}\,M = 220\,nM$. The strikingly low forward rate constant indicates that only a small number of collusions result in complex formation, consistent with a substantial conformational change being necessary for binding.

We close the chapter with a reminder that rate constants are ensemble properties and, as such, represent the average behavior of the single molecules within the ensemble. For instance, for the estrogen receptor-tamoxifen complex the dissociation rate constant is $1.0 \times 10^{-3}\,s^{-1}$, but if we were to examine such complexes at the single molecule level, we would see a distribution of dissociation times (**Figure 3.52**). The histogram of these dissociation times can be fit to an exponential equation of the form

$$RL(t) = RL_0 e^{-k_{-1}t}$$

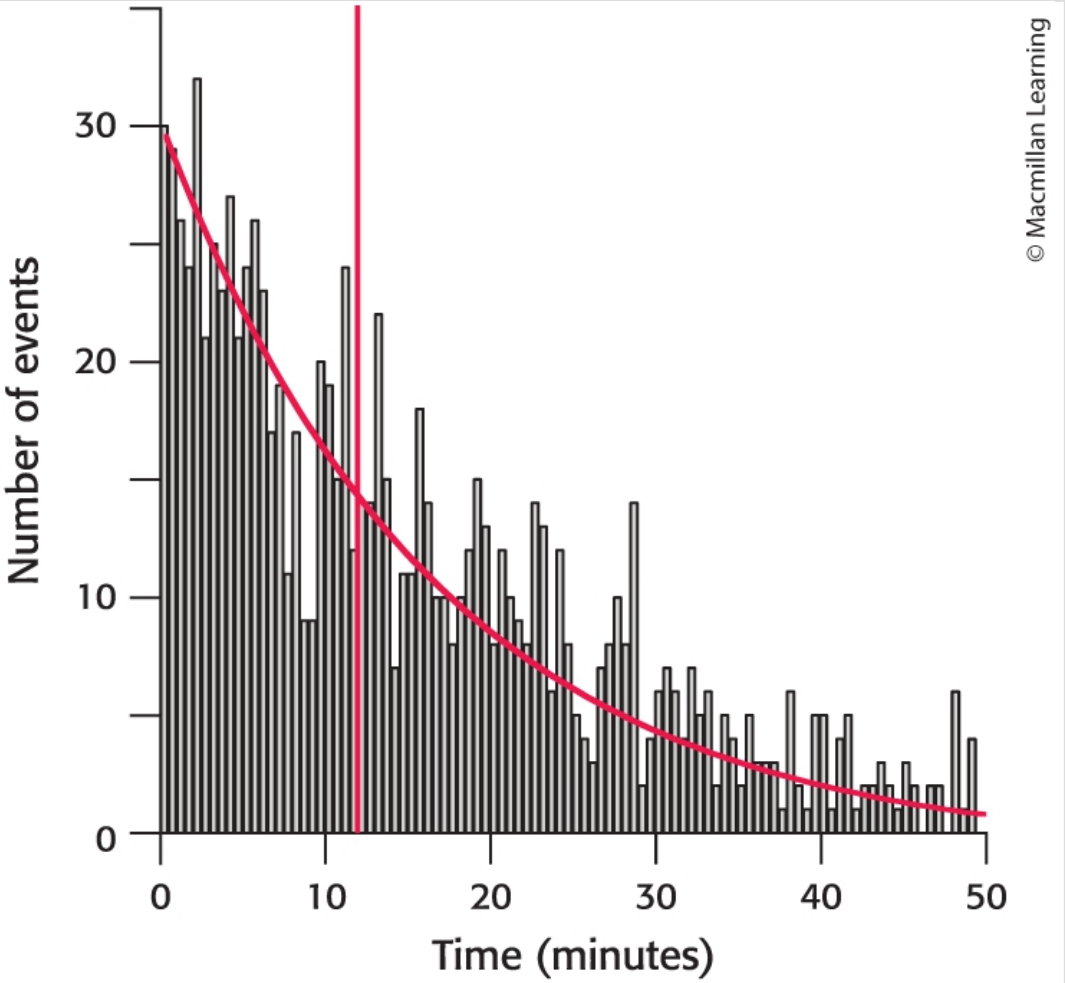


FIGURE 3.52 A rate constant reflects the distribution of reaction times at the single molecule level. The results of a simulation with 1000 events of dissociation times for an estrogen receptor–tamoxifen complex are shown, with dissociation times ranging from nearly zero to more than 50 minutes, with an average of 12 minutes. The rate constant of $1.0 \times 10^{-3}\ s^{-1}$ characterizes the exponential decline in this distribution, shown in red.

The average dissociation time in this distribution is approximately 12 minutes, a duration that is quite long in the context of the biochemical timescale. This may be important for the role of tamoxifen as a drug since, once bound, it remains bound to the receptor and blocks estradiol binding for a substantial period of time.

Chapter 3 Summary

3.1 Binding Is a Fundamental Process in Biochemistry

- Many biochemical macromolecules form specific complexes with other macromolecules or metabolites, and these molecular recognition processes facilitate the organization and specificity of binding.
- The tendency of molecules to form complexes increases as the concentration of the partners rises, with the key concentrations required for substantial complex formation varying greatly from one complex to another.
- The concentrations of many biomolecules fall in the range required to drive substantial complex formation.

3.2 Myoglobin Binds and Stores Oxygen

- The muscle protein myoglobin binds oxygen via a bound heme group with a central iron atom.
- Myoglobin binds oxygen via a simple binding reaction; myoglobin is half-saturated with oxygen at a partial pressure of 2 torr, corresponding to a high oxygen affinity.

3.3 Hemoglobin Is an Efficient Oxygen Carrier

- Human hemoglobin consists of four myoglobin-like subunits of two types, forming a homodimer of heterodimeric structures.
- Hemoglobin binds oxygen cooperatively, with relatively low affinity when no oxygen is bound, but higher affinity as each hemoglobin tetramer has already bound an increasing number of oxygen molecules.
- This cooperativity together with changes in the oxygen affinity in response to pH and the presence of carbon dioxide make

hemoglobin quite efficient in delivering oxygen to tissues where it is most needed.
- Sickle-cell disease illustrates how the change of a single amino acid in a large protein can lead to disease through the formation of an unusual macromolecular complex.

3.4 The Immune System Depends on Key Binding Proteins

- The immune system includes two components: an innate system that stands ready to respond immediately to signs of pathogens; and an adaptive system that develops specific components tailored to new pathogens encountered by the host.
- Antibodies, also known as immunoglobulins, have structures comprising a conserved framework with hypervariable loops that form binding surfaces able to recognize almost any foreign antigen.
- Class I major compatibility complex proteins include a deep binding groove that presents peptides from foreign proteins on surfaces where they can be sensed by T-cell receptors, leading to an immune response.

3.5 Quantitative Terms Can Describe Binding Propensity

- Binding reactions are chemical equilibria that can be described in quantitative terms, allowing the calculation of the concentrations of various species based on a small number of parameters, including the dissociation constant and kinetic rate constants.
- Different molecules (ligands) can compete for binding to the same receptor site; the relative occupancies depend on the binding affinities and concentrations of these ligands.

Key Terms

molecular recognition
myoglobin
heme
hemoglobin
ligand
fractional saturation
proximal histidine
deoxymyoglobin
oxymyoglobin
distal histidine
carbon monoxide
sigmoid
deoxyhemoglobin
T state
oxyhemoglobin
R state
concerted model
sequential model
allosteric effector
Bohr effect
sickle-cell anemia
innate immune system
major histocompatibility complex (MHC)
adaptive immune system
antibodies (immunoglobulins)
cytotoxic T lymphocytes (killer T cells)
antigen
immunoglobulin fold
hypervariable loops (complementarity-determining regions, CDRs)
cell-mediated immunity

class I MHC proteins

Problems

1. What fraction of estrogen receptors is expected to be free in the presence of an estradiol concentration of 1 nM assuming no other ligands are present? 1

2. The molecular weight of sperm whale myoglobin is 17.8 kDa. The myoglobin content of sperm whale muscle is about $80.0\ g \cdot kg^{-1}$. In contrast, the myoglobin content of some human muscles is about $8.00\ g \cdot kg^{-1}$.

a. Compare the amounts of O_2 bound to myoglobin in human muscle and in sperm whale muscle. Assume that the myoglobin is saturated with O_2, and that the molecular weights of human and sperm whale myoglobin are the same. 2
b. The amount of oxygen dissolved in tissue water at 37°C is about $3.5 \times 10^{-5}\ M$. What is the ratio of myoglobin–bound oxygen to dissolved oxygen in the tissue water of sperm whale muscle?

3. Suppose myoglobin is prepared with Zn^{2+} in the place of Fe^{2+} in the porphyrin. Would you expect this modified myoglobin to bind oxygen? 2

4. Does myoglobin exhibit a Bohr effect? Why or why not? 3

5. Alkyl isocyanides, R-NC, are bound by myoglobin and hemoglobin.



Would you expect that n-hexyl isocyanide would be bound more or less tightly than methyl isocyanide? Briefly explain. 2

6. The pK_a of an acid depends partly on its environment. Predict the effect of each of the following environmental changes on the pK_a of a glutamic acid side chain. 3

a. If a lysine side chain is brought into proximity, the pK_a of the glutamic acid chain is _____.
b. If the terminal carboxyl group of the protein is brought into proximity to the glutamic acid side chain, the pK_a of the side chain is _____.
c. If the glutamic acid side chain is shifted from the outside of the protein to a nonpolar site inside of the protein, the pK_a is _____.

7. In 1913, Archibald Hill described an alternative formulation for cooperative processes such as the binding of oxygen by hemoglobin by considering the hypothetical equilibrium

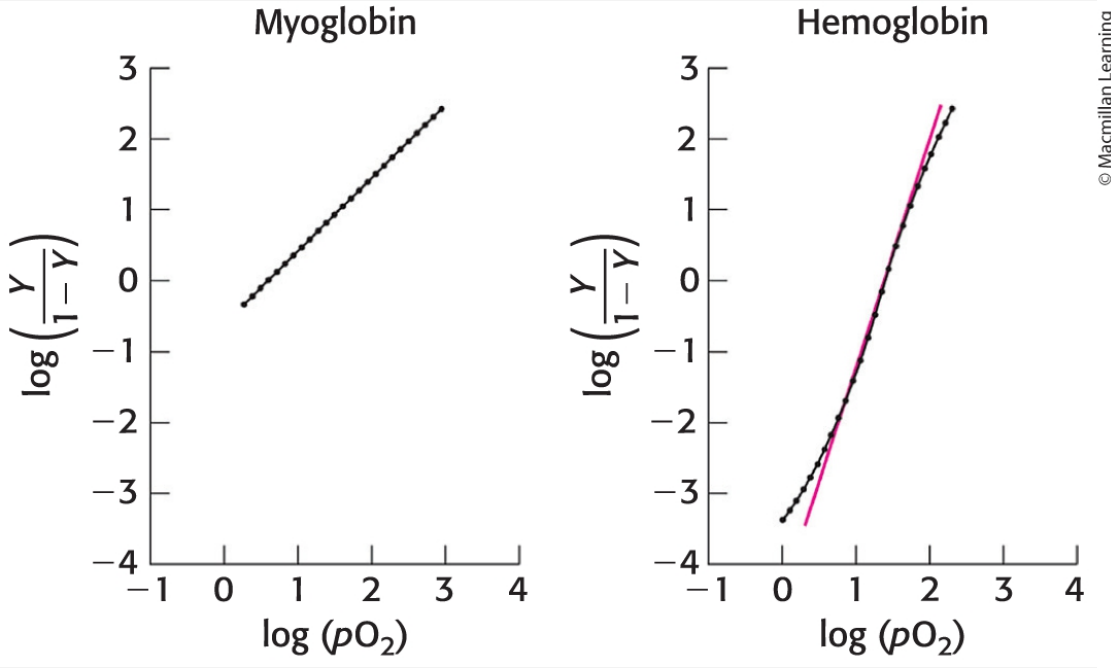
$$Hb + nO_2 \rightleftharpoons Hb(O_2)_n$$

Analysis leads to the Hill equation:

$$\log(Y/1-Y) = \log(pO_2{}^n / P_{50}{}^n) = n\log(pO_2) - n\log(P_{50})$$

where Y is the fractional saturation. This equation suggests that a plot of $\log(Y/1-Y)$ versus $\log(pO_2)$ should yield a line with slope n.

Plots for myoglobin and hemoglobin are shown below:



© Macmillan Learning

a. Estimate the apparent slope of the plot for myoglobin and comment on the value.
b. Estimate the apparent slope in the center of the plot for hemoglobin and comment on the value. 3

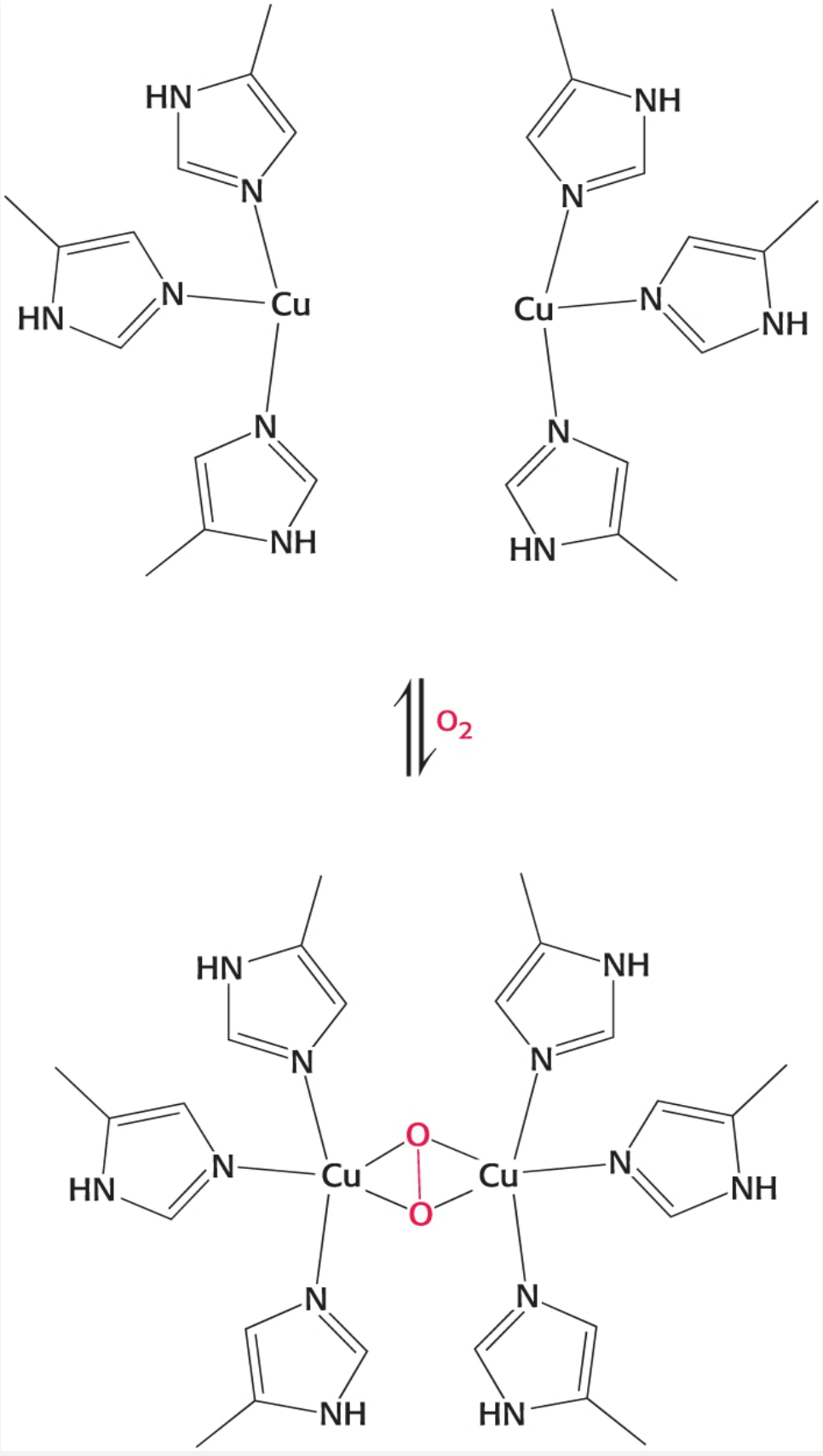
8. Suppose Gina climbs a high mountain where the oxygen partial pressure in the air decreases to 70 torr. Assume that the pH of her tissues and lungs is 7.4 and the oxygen concentration in her tissues is 20 torr. The P_{50} of hemoglobin is 26 torr. The degree of cooperativity of hemoglobin (n) based on the Hill equation in problem 7 is 2.8.

a. Estimate the percentage of the oxygen–carrying capacity that she utilizes. Calculate your answer to one decimal place.

After Gina spends a day at the mountaintop, where the oxygen partial pressure is 70 torr, the concentration of 2,3–bisphosphoglycerate (2,3–BPG) in her red blood cells increases.

b. Why does increasing the concentration of 2,3–BPG in Gina's blood cells help her function well at high altitudes?
 3

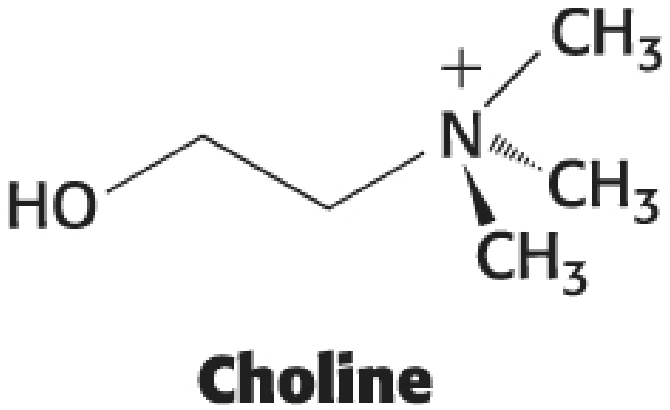
9. Arthropods such as lobsters have oxygen carriers quite different from those of hemoglobin. The oxygen-binding sites do not contain heme but, instead, are based on two copper (Cu) ions. The structural changes that accompany oxygen binding are shown below.


HN
N
N
HN
Cu
N
NH
NH
N
Cu
N
NH
N
HN
O2
HN
NH
N
N
N
HN
Cu
O
O
Cu
N
NH
N
NH
N
HN

How might these changes be used to facilitate cooperative oxygen binding? 3

10. Blood cells from some birds do not contain 2,3-bisphosphoglycerate but, instead, contain one of the compounds shown below, which plays an analogous functional role. Which compound do you think is most likely to play this role? Explain briefly. 3

a.



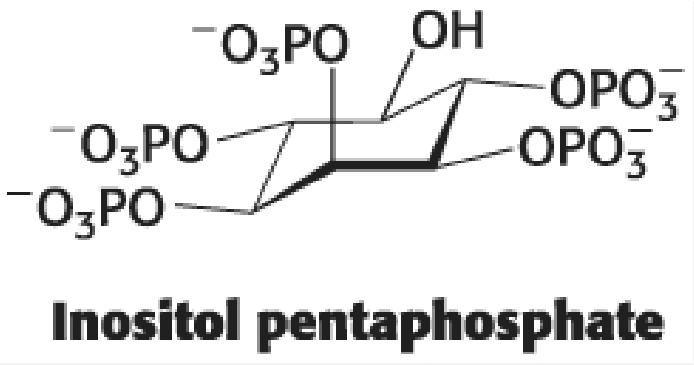
Choline

b.



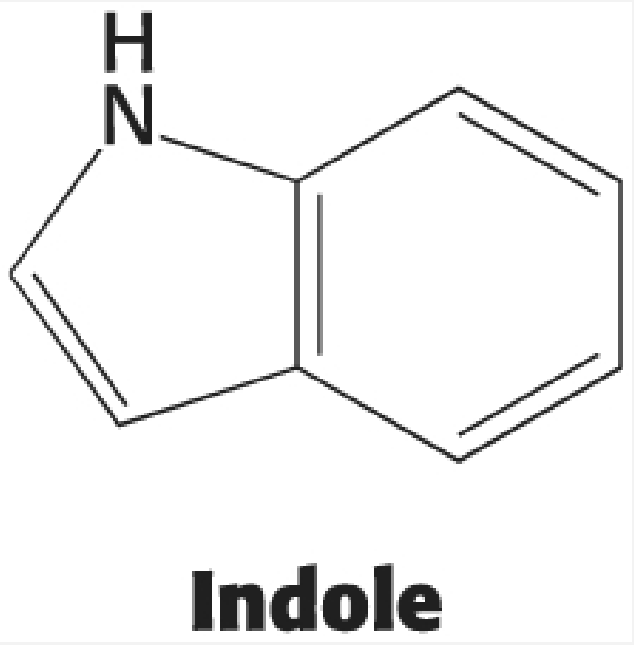
Spermine

c.



Inositol pentaphosphate

d.



Indole

11. Some Toll-like receptors bind nucleic acids that contain uracil, but not thymine or similar bases. What is the biological rationale for this binding preference? 4

12. Some of the first vaccines against COVID-19 are based on RNA molecules that lead to the production of the SARS-CoV-2 spike protein. The RNA molecules are modified so that one base is replaced with an alternative. What base is most likely to need to be replaced? 4

13. Addition of an IgG molecule specific for hemoglobin to a solution of hemoglobin results in the formation of a red precipitate. In contrast, addition of the F_{ab} fragments from this antibody to myoglobin results in no such precipitate. Propose an explanation. 4

14. The amino acid sequence of a small protein is MSRLASKNLIRSDHAGGLLQATYSAVSSIKNTMSFGAWSNAALNDS RDA. Which peptide would most likely be presented by the class I MHC molecule HLA–A2? 4

a. LLQATYSAV
b. MSRLASKNLIRSD
c. NLIRS
d. SSIKNTMSF

15. A receptor-ligand complex has a dissociation constant of $5\ \mu M$. What is the ratio of the receptor-ligand complex to total receptor when the total receptor concentration is 10 nM with total added ligand concentrations of $1\ \mu M$, $10\ \mu M$, $100\ \mu M$, and 1 mM. 5

16. Recall that when we calculated that estrogen receptors with 1 nM estradiol and $1\ \mu M$ BPA, the fraction of receptors occupied with estradiol was 0.14 and the fraction of receptors occupied with BPA was 0.71.

a. Calculate the concentration of free receptor in terms of the total concentration of receptor, R_{total}.

b. Calculate the concentration of free estradiol in terms of the total concentration of receptor, R_{total}.
c. Calculate the concentration of free BPA in terms of the total concentration of receptor, R_{total}.
d. Confirm the approximate values for the dissociation constants for the estrogen receptor-estradiol and estrogen receptor-BPA complexes. 5

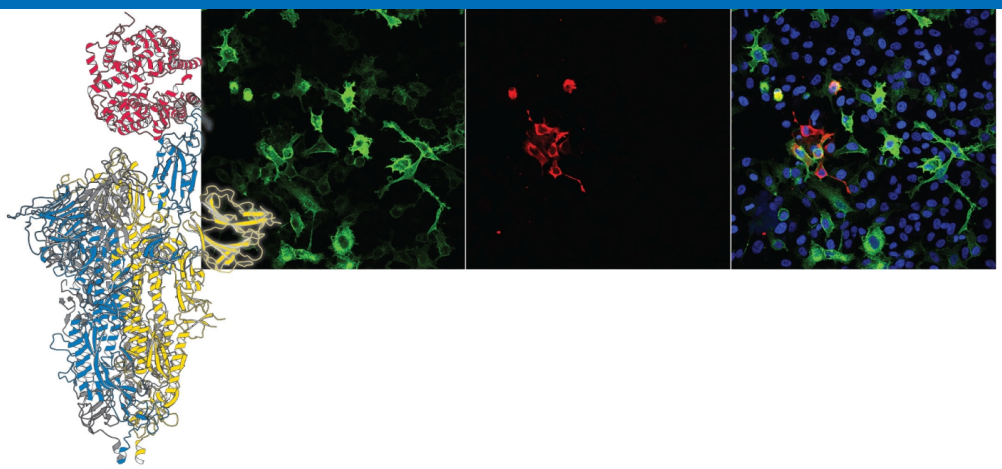
17. A receptor-ligand complex has a dissociation constant of $K_d = 20\ nM$. The rate of receptor-ligand complex formation with an added ligand concentration of $10\ \mu M$ is $5 \times 10^3\ s^{-1}$. What is the value of the reverse rate constant, k_{-1}? 5

18. An F_{ab} fragment binds to lysozyme with a dissociation constant of $K_D = 10^{-11}\ M$. A $1\ nM\ (10^{-9}\ M)$ solution of lysozyme is treated with increasing concentrations of the F_{ab} fragment. At what concentration of added F_{ab} will half of the lysozyme be bound to F_{ab}? 5

19. A different F_{ab} fragment binds to lysozyme with a dissociation constant of $K_D = 10^{-6}$ M. A 1 nM solution of lysozyme is treated with increasing concentrations of this F_{ab} fragment. At what concentration of added F_{ab} will half of the lysozyme be bound to this F_{ab}? 5

20. Deoxyhemoglobin is treated with a 1:1 mixture of oxygen and carbon monoxide under conditions where essentially all of the iron atoms in hemoglobin are bound to a ligand. Approximately what percentage of the irons will be bound to oxygen? 2, 5

Chapter 4
Protein Methods



Courtesy of Dr. Peng Zhou, Principle Investigator, Bat virus infection and immunity group, Wuhan Institute of Virology, Chinese Academy of Sciences. © Macmillan Learning

In 2019, researchers in China identified a new strain of coronavirus that caused acute respiratory syndrome in several thousand individuals in the city of Wuhan. Using antibodies labeled with fluorescent tags, they showed that the virus (center, labeled red) preferentially infected cells that expressed angiotensin-converting enzyme 2 (ACE2, left, labeled green). Note that the signals overlap in the combined image (right; cell nuclei are stained in blue). These data suggested that ACE2 served as the target for the virus particles. Less than a year later, the structure of the SARS-CoV-2 spike protein bound to ACE2 (shown at left) was solved by cryo-electron microscopy. These experiments were critical in understanding how the virus functions and developing effective vaccines.

[Drawn from 7DF4.pdb.]

Outline

4.1 The Purification of Proteins Is an Essential First Step in Understanding Their Function
4.2 Immunology Provides Important Techniques for Investigating Proteins
4.3 Mass Spectrometry Is a Powerful Technique for the Identification of Peptides and Proteins
4.4 Peptides Can Be Synthesized by Automated Solid-Phase Methods
4.5 Three-Dimensional Protein Structures Can Be Determined Experimentally

Learning Goals



By the end of this chapter, you should be able to:

1. Explain the importance of protein purification and how it can be quantified.
2. Describe the different types of chromatography used to purify proteins.
3. Describe the different methods available for determining the mass of a protein.
4. Explain how antibodies can be used as tools for protein identification, purification, and quantitation.
5. Describe how proteins are sequenced, and explain why sequence determination is important.
6. Distinguish between the commonly used methods for protein structure determination, and describe the advantages and disadvantages of each.

A major goal of the biochemist is to understand how individual proteins adopt their unique structures and perform their functions. The first step in these experiments is usually the purification of the protein of interest so as to avoid confounding effects from contaminants. Once purified, a protein's molecular mass and amino acid sequence can be precisely determined. Many protein sequences are now available in vast sequence databases. Such a protein might

be identified by matching its mass to those deduced for proteins in these databases.

After a protein has been purified and its identity confirmed, the challenge remains to determine its function and its three-dimensional structure within a physiologically relevant context. Throughout this chapter, we will discuss some of the more commonly used — and still rapidly improving — methods to achieve the purification, functional evaluation, and structural determination of a given protein. The exploration of proteins by this array of physical and chemical techniques has greatly enriched our understanding of the molecular basis of life. These techniques make it possible to tackle some of the most challenging questions of biology in molecular terms.

4.1 The Purification of Proteins Is an Essential First Step in Understanding Their Function

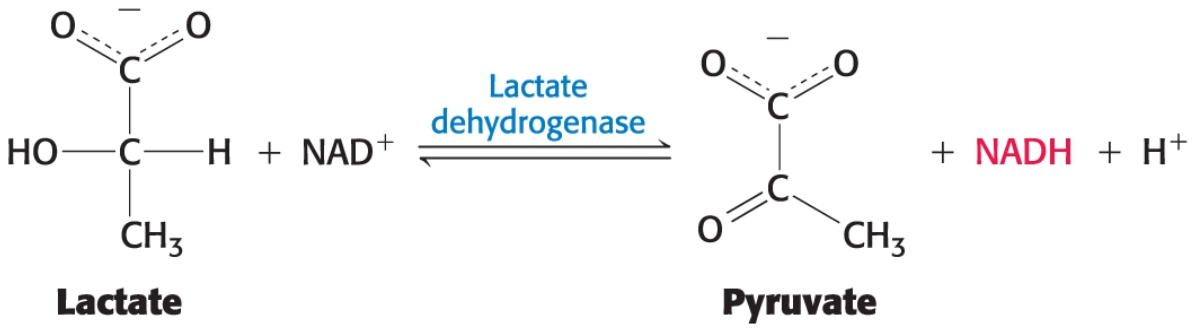
An adage of biochemistry is "never waste pure thoughts on an impure protein." Starting from pure proteins, we can determine amino acid sequences and investigate biochemical functions. From the amino acid sequences, we can map evolutionary relationships between proteins in diverse organisms (Chapter 10). By using crystals grown from pure protein, we can obtain x-ray data that will provide us with a picture of the protein's tertiary structure — the shape that determines function.

The assay: How do we recognize the protein we are looking for?

Purification should yield a sample containing only one type of molecule — the protein in which the biochemist is interested. This protein sample may be only a fraction of 1% of the starting material, whether that starting material consists of one type of cell in culture or a particular organ from a plant or animal. How is the biochemist able to isolate a particular protein from a complex mixture of proteins?

A protein can be purified by subjecting the impure mixture of the starting material to a series of separations based on physical properties such as size and charge. To monitor the success of this purification, the biochemist needs a test, called an **assay**, for some unique identifying property of the protein. A positive result on the assay indicates that the protein is present.

Although assay development can be a challenging task, the more specific the assay, the more effective the purification. For enzymes, the assay usually measures catalytic activity — that is, the ability of the enzyme to promote a particular chemical reaction. This activity is often measured indirectly. Consider the enzyme lactate dehydrogenase, which catalyzes the following reaction in the synthesis of glucose:



Reduced nicotinamide adenine dinucleotide (NADH, Section 15.4) absorbs light at 340 nm, whereas oxidized nicotinamide adenine dinucleotide (NAD^+) does not. Consequently, we can follow the progress of the reaction by examining how much light-absorbing ability is developed by a sample in a given period of time — for instance, within 1 minute after the addition of the enzyme. Our assay for enzyme activity during the purification of lactate dehydrogenase is thus the increase in the absorbance of light at 340 nm observed in 1 minute.

To analyze how our purification scheme is working, we need one additional piece of information — the amount of total protein present in the mixture being assayed. There are various rapid and reasonably accurate means of determining protein concentration. With these two experimentally determined numbers — enzyme activity and protein concentration — we then calculate the **specific activity**, the ratio of enzyme activity to the amount of protein in the mixture. Ideally, the specific activity will rise as the purification proceeds, and the protein

mixture will contain the protein of interest to a greater extent. For a pure enzyme, the specific activity will have a constant value. In essence, the overall goal of the purification is to maximize the specific activity.

Proteins must be released from the cell to be purified

Having found an assay and chosen a source of protein, we now fractionate the cell into components and determine which component is enriched in the protein of interest. In the first step, a **homogenate** is formed by disrupting the cell membrane, and the mixture is fractionated by centrifugation, yielding a dense pellet of heavy material at the bottom of the centrifuge tube and a lighter supernatant above (**Figure 4.1**). The supernatant is again centrifuged at a greater force to yield yet another pellet and supernatant. This procedure, called *differential centrifugation*, yields several fractions of decreasing density, each still containing hundreds of different proteins. The fractions are each separately assayed for the desired activity. Usually, one fraction will be enriched for such activity, and it then serves as the source of material to which more-discriminating purification techniques are applied.

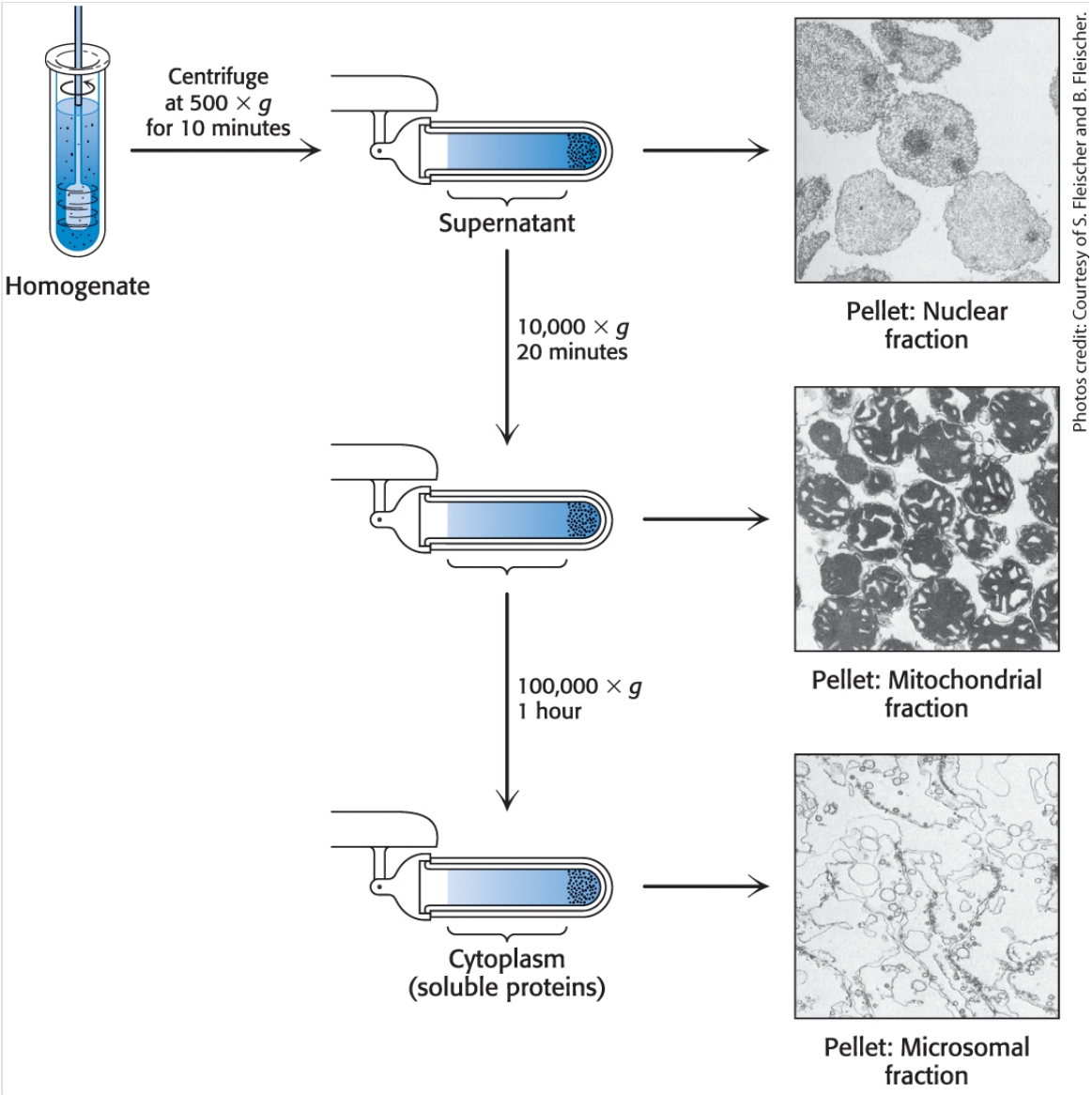


FIGURE 4.1 Differential centrifugation separates the contents of cells based on their density. Cells are disrupted in a homogenizer and the resulting mixture is centrifuged in a step-by-step fashion of increasing centrifugal force. Centrifugal forces are represented as multipliers of *g*, the force of gravity. The denser material will form a pellet at lower centrifugal force than will the less dense material. The isolated fractions can be used for further purification.

Proteins can be purified according to solubility, size, charge, and binding affinity

Thousands of proteins have been purified in active form on the basis of such characteristics as solubility, size, charge, and binding affinity. Usually, protein mixtures are subjected to a series of separations, each based on a different property. At each step in the purification, the preparation is assayed and its specific activity is determined. A variety of purification techniques are available.

Salting out

Most proteins are less soluble at high salt concentrations, an effect called *salting out*. The salt concentration at which a protein falls out of solution, or precipitates, differs from one protein to another. Hence, salting out can be used to fractionate proteins. For example, 0.8 M ammonium sulfate precipitates fibrinogen, a blood-clotting protein, whereas a concentration of 2.4 M is needed to precipitate serum albumin. Salting out is also useful for concentrating dilute solutions of proteins, including active fractions obtained from other purification steps. Dialysis can be used to remove the salt, if necessary.

Dialysis

Proteins can be separated from small molecules such as salt by **dialysis** through a semipermeable membrane, such as a cellulose membrane with pores (**Figure 4.2**). The protein mixture is placed inside the dialysis bag, which is then submerged in a buffer solution that is devoid of the small molecules to be separated away. Molecules having dimensions significantly greater than the pore diameter remain inside the dialysis bag. Smaller molecules and ions capable of passing through the pores of the membrane diffuse down their concentration gradients and emerge in the solution outside the bag. This technique is useful for removing a

salt or other small molecule from a cell fractionate, but it does not distinguish between proteins effectively.

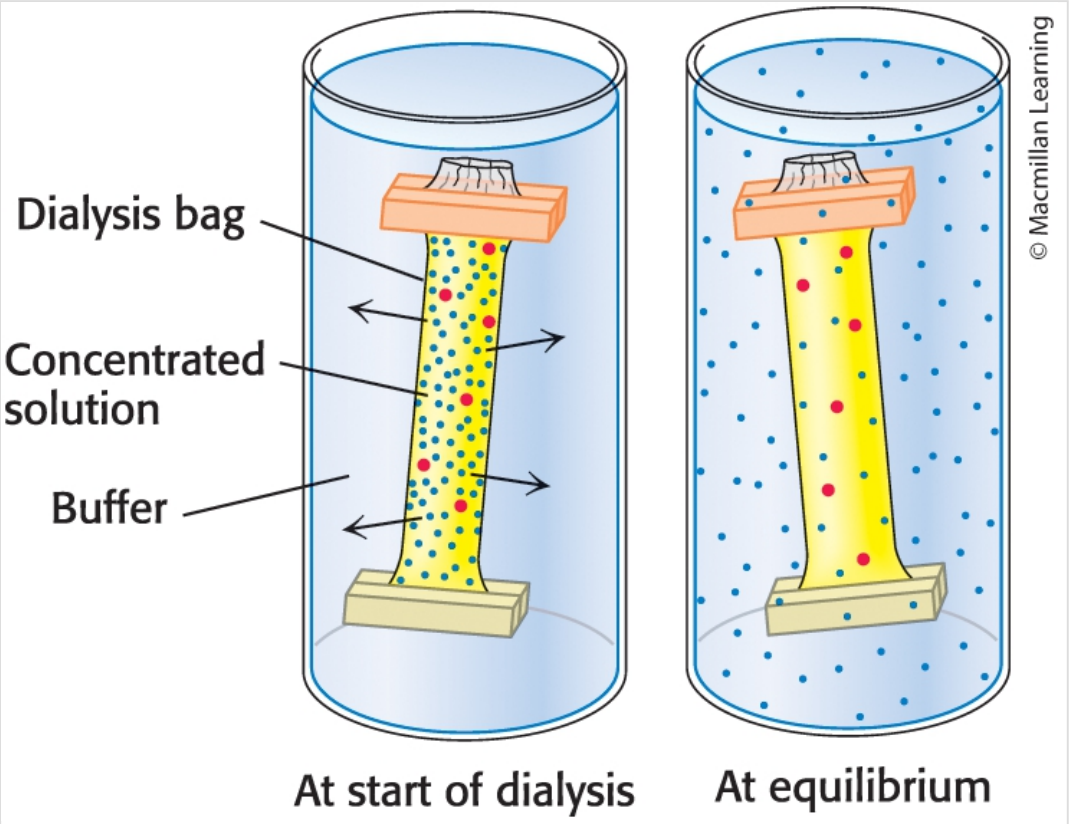


FIGURE 4.2 Dialysis separates proteins from smaller molecules. Protein molecules (red) are retained within the dialysis bag, whereas small molecules (blue) diffuse down their concentration gradient into the surrounding medium.

Gel-filtration chromatography

More precise separations on the basis of size can be achieved by the technique of **gel-filtration chromatography**, also known as molecular exclusion chromatography (Figure 4.3). The sample is applied to the top of a column consisting of porous beads made of an insoluble but highly hydrated polymer such as dextran or agarose (carbohydrates) or

polyacrylamide. Sephadex, Sepharose, and Biogel are commonly used commercial preparations of these beads, which are typically 100 μm (0.1 mm) in diameter. Small molecules can enter these beads; large ones cannot.

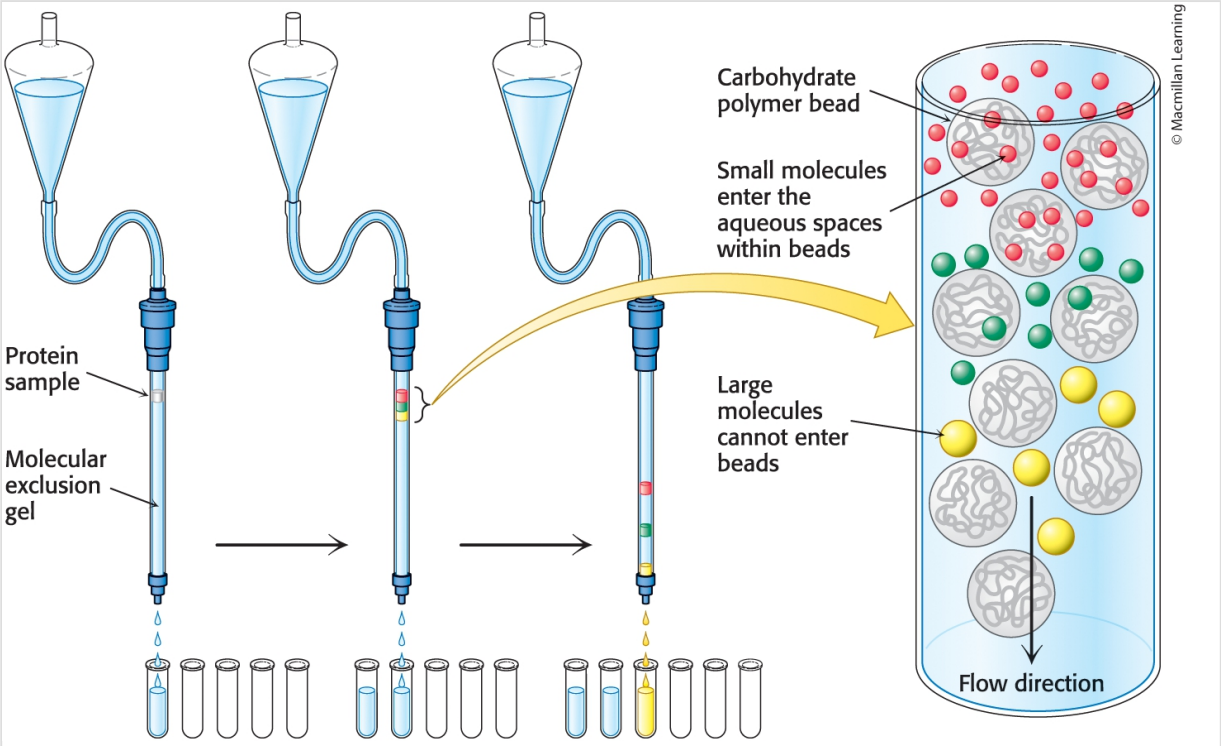


FIGURE 4.3 Gel-filtration chromatography separates proteins based on size. A mixture of proteins in a small volume is applied to a column filled with porous beads. Because large proteins cannot enter the internal volume of the beads, they emerge sooner than do small ones.

VIEW an animation of this technique in Achieve

The result is that small molecules are distributed in the aqueous solution both inside the beads and between them, whereas large molecules are located only in the solution between the beads. Large molecules flow more rapidly through this column and emerge first because a smaller volume is accessible to them. Molecules of medium size occasionally enter the beads and will flow from the column at an

intermediate position, while small molecules, which take a longer path through the beads, will exit last.

Ion-exchange chromatography

To obtain a protein of high purity, one chromatography step is usually not sufficient. For example, other proteins in the crude mixture of similar size as the desired protein will likely pass through the column together during a separation using gel filtration chromatography. Additional purity can be achieved by performing sequential separations based on distinct molecular properties.

For example, in addition to size, proteins can be separated on the basis of their net charge by **ion-exchange chromatography**. If a protein has a net positive charge at pH 7, it will usually bind to a column of beads containing carboxylate groups, whereas a negatively charged protein will not (**Figure 4.4**). The bound protein can then be eluted, or released, from the column by increasing the concentration of sodium chloride or another salt in the eluting buffer; sodium ions compete with positively charged groups on the protein for binding to the column. Proteins that have a low density of net positive charge will tend to emerge first, followed by those having a higher charge density.

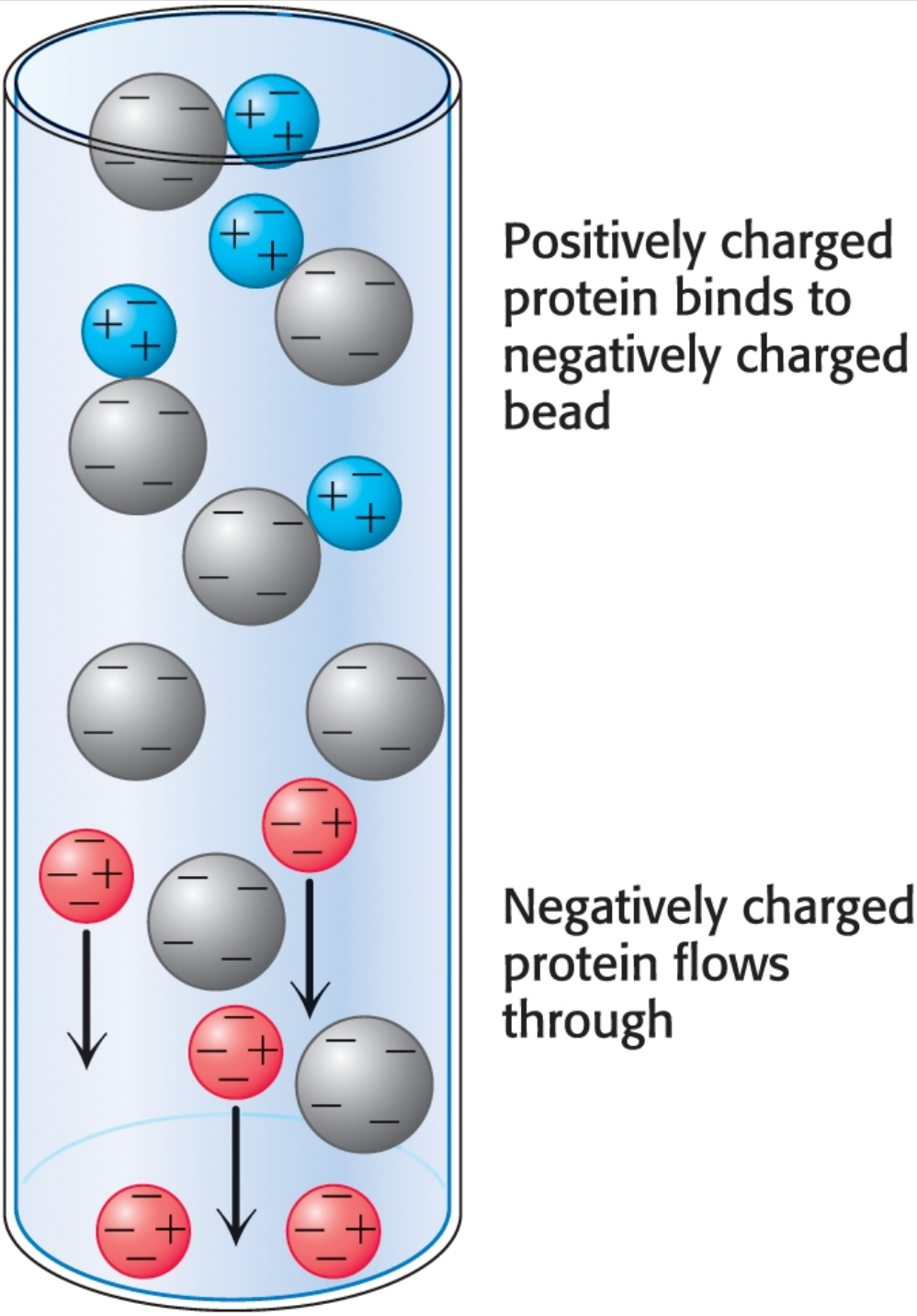
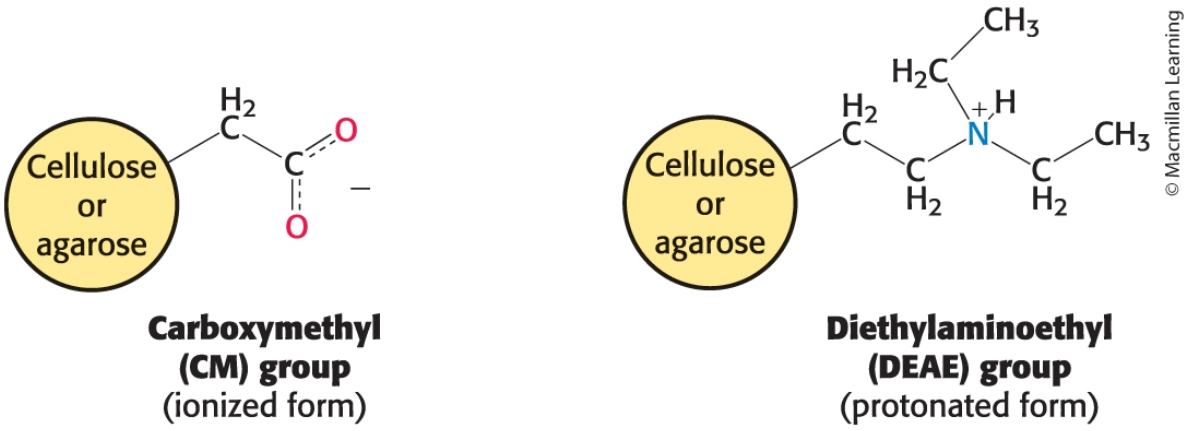


FIGURE 4.4 Ion-exchange chromatography separates proteins based on their net charge. As shown here, proteins with a net positive charge will bind to a column in which the beads are coated with negatively charged groups. Proteins with a net negative charge will pass through much more quickly. This is an example of cation exchange.

This procedure is also referred to as **cation exchange** to indicate that positively charged groups will bind to the anionic beads. Positively charged proteins (cationic proteins) can be separated by chromatography on negatively charged carboxymethylcellulose (CM-cellulose) columns. Conversely, negatively charged proteins (anionic proteins) can be separated by **anion exchange** on positively charged diethylaminoethylcellulose (DEAE-cellulose) columns.



Affinity chromatography

Another powerful means of purifying proteins that is highly selective for the protein of interest is **affinity chromatography**. This technique takes advantage of the high affinity of many proteins for specific molecules, called *ligands*. For example, the plant protein concanavalin A is a carbohydrate-binding protein that has affinity for glucose. When a crude extract is passed through a column of beads containing covalently attached glucose residues, concanavalin A binds to the beads, whereas

most other proteins do not (Figure 4.5). The bound concanavalin A can then be eluted from the column by adding a concentrated solution of glucose. At a high concentration, the added glucose will replace the bead-bound glucose as the ligand for concanavalin A, releasing it from the column.

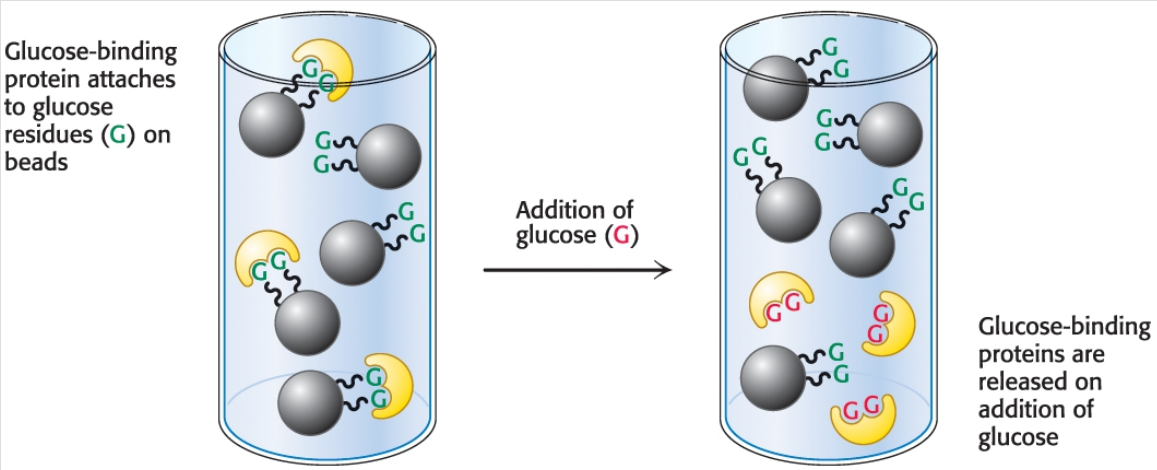


FIGURE 4.5 Affinity chromatography enables the separation of proteins that can bind to a specific ligand. In this example, concanavalin A (shown in yellow), a glucose-binding protein, ca be retained on a column composed of beads with covalently attached glucose residues (G). Afte washing away proteins that cannot bind the ligand, concanavalin can be eluted by adding a concentrated solution of glucose.

Affinity chromatography is a powerful means of isolating transcription factors — proteins that regulate gene expression by binding to specific DNA sequences. A protein mixture is passed through a column containing specific DNA sequences attached to a matrix; proteins with a high affinity for the sequence will bind and be retained. In this instance, the transcription factor is released by washing with a solution containing a high concentration of salt.

In general, affinity chromatography can be effectively used to isolate a protein that recognizes a particular ligand X by (1) covalently attaching X or a derivative of it to a column; (2) adding a mixture of proteins to

this column, which is then washed with buffer to remove unbound proteins; and (3) eluting the desired protein by adding a high concentration of a soluble form of X or altering the conditions to decrease binding affinity. Affinity chromatography is most effective when the interaction between the protein and its ligand is highly specific.

Affinity chromatography can also be applied to proteins that do not have an identified ligand using the power of recombinant DNA technology (Section 9.2). Simply put, the desired protein is attached to a polypeptide that can bind to a highly specific, known ligand. For example, repeats of the amino acid histidine may be added such that the expressed protein has a string of histidine residues (called a *His tag*) on one end. The tagged proteins are then passed through a column of beads containing covalently attached, immobilized nickel(II). The His tag binds tightly to the immobilized metal ion, capturing the desired protein, while other proteins flow through the column. The tagged protein can then be eluted from the column by the addition of imidazole that binds to the metal ions and displaces the protein.

High-performance liquid chromatography

A technique called **high-performance liquid chromatography (HPLC)** is an enhanced version of the column techniques already discussed. The solid beads within the column have a much smaller diameter, and, as a consequence, possess a greater surface area that yields more interaction sites. With this increase in surface area, HPLC results in greater resolving power. Because the column is made of finer material, pressure must be applied to the column to obtain adequate flow rates. The net result is both sharper separations between proteins and a more rapid separation.

In a typical HPLC setup, the presence of protein emerging from the column is measured in real time. Since the peptide bond absorbs light at

a wavelength of 220 nm, a detector that monitors light absorbance at this wavelength is placed immediately after the column. In the sample HPLC elution profile shown in **Figure 4.6**, proteins emerging from the column are readily noted by the presence of sharp peaks measured by the detector. In a short span of 10 minutes, a number of individual proteins can be readily identified.

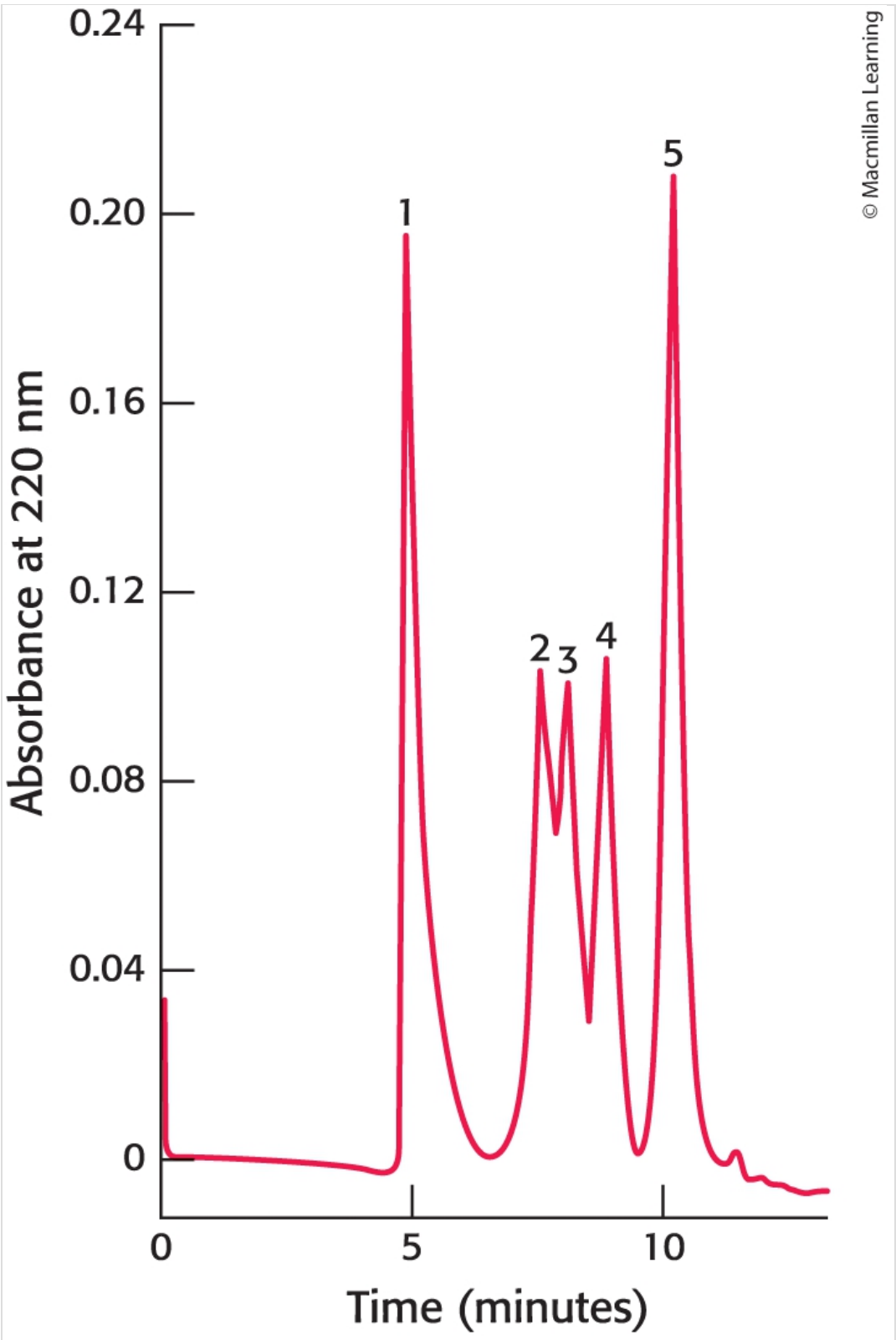


FIGURE 4.6 High-performance liquid chromatography (HPLC) can separate proteins with high resolving power over short elution times. Gel filtration by HPLC

clearly defines the individual proteins because of its greater resolving power: (1) thyroglobulin (669 kDa), (2) catalase (232 kDa), (3) bovine serum albumin (67 kDa), (4) ovalbumin (43 kDa), and (5) ribonuclease (13.4 kDa).

[Data from K. J. Wilson and T. D. Schlabach. In *Current Protocols in Molecular Biology*, vol. 2, suppl. 41, F. M. Ausubel, R. Brent, R. E. Kingston, D. D. Moore, J. G. Seidman, J. A. Smith, and K. Struhl, Eds. (Wiley, 1998), p. 10.14.1.]

Proteins can be separated by gel electrophoresis and displayed

How can we tell that a purification scheme is effective? One way is to ascertain that the specific activity rises with each purification step. Another is to determine that the number of different proteins in each sample declines at each step. The technique of electrophoresis makes the latter method possible.

Gel electrophoresis

A molecule with a net charge, such as a protein or a nucleic acid, will move in an electric field. This phenomenon, termed *electrophoresis*, offers a powerful means of separating mixtures of proteins or nucleic acids. Electrophoretic separations are nearly always carried out in porous gels (or on solid supports such as paper) because the gel serves as a molecular sieve that enhances separation (**Figure 4.7**). Molecules that are small compared with the pores in the gel readily move through the gel, whereas molecules much larger than the pores are almost immobile. Intermediate-size molecules move through the gel with various degrees of facility. The electric field is applied such that proteins migrate from the negative to the positive electrodes, typically from top to bottom. **Gel electrophoresis** is performed in a thin, vertical slab of a

gel composed of the polymer polyacrylamide (Figure 4.8). Polyacrylamide gels are choice supporting media for electrophoresis because they are chemically inert and readily formed by the polymerization of acrylamide with a small amount of a cross-linking agent to make a three-dimensional mesh.

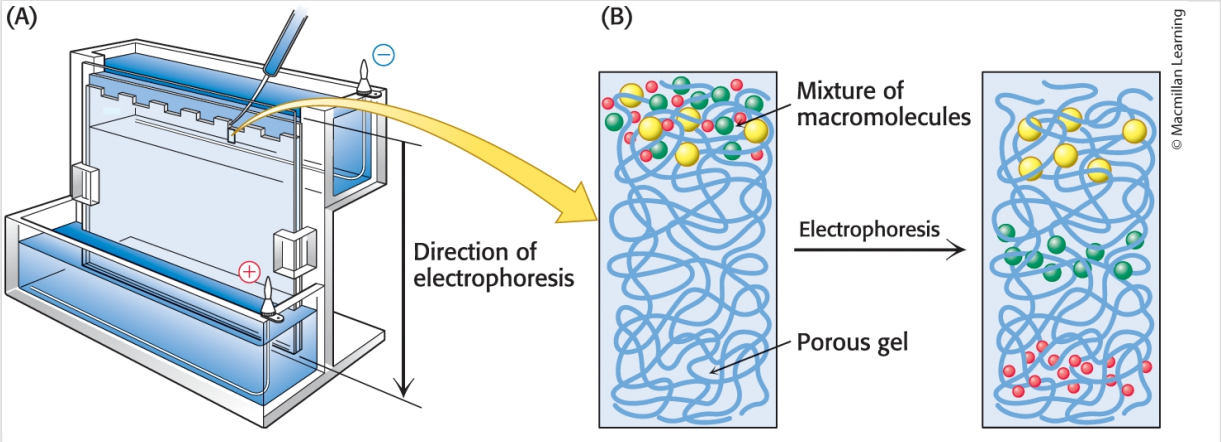


FIGURE 4.7 Polyacrylamide gel electrophoresis can be used to separate and visualize mixtures of proteins. (A) A microliter pipette is used to place solutions of proteins in the wells of the slab. A cover is then placed over the gel chamber and voltage is applied. The negatively charged SDS (sodium dodecyl sulfate)–protein complexes migrate in the direction of the anode, at the bottom of the gel. (B) The sieving action of a porous gel separates proteins according to size, with the smallest moving most rapidly.

VIEW animations of the techniques shown in Figure 4.5 and Figure 4.7 in Achieve

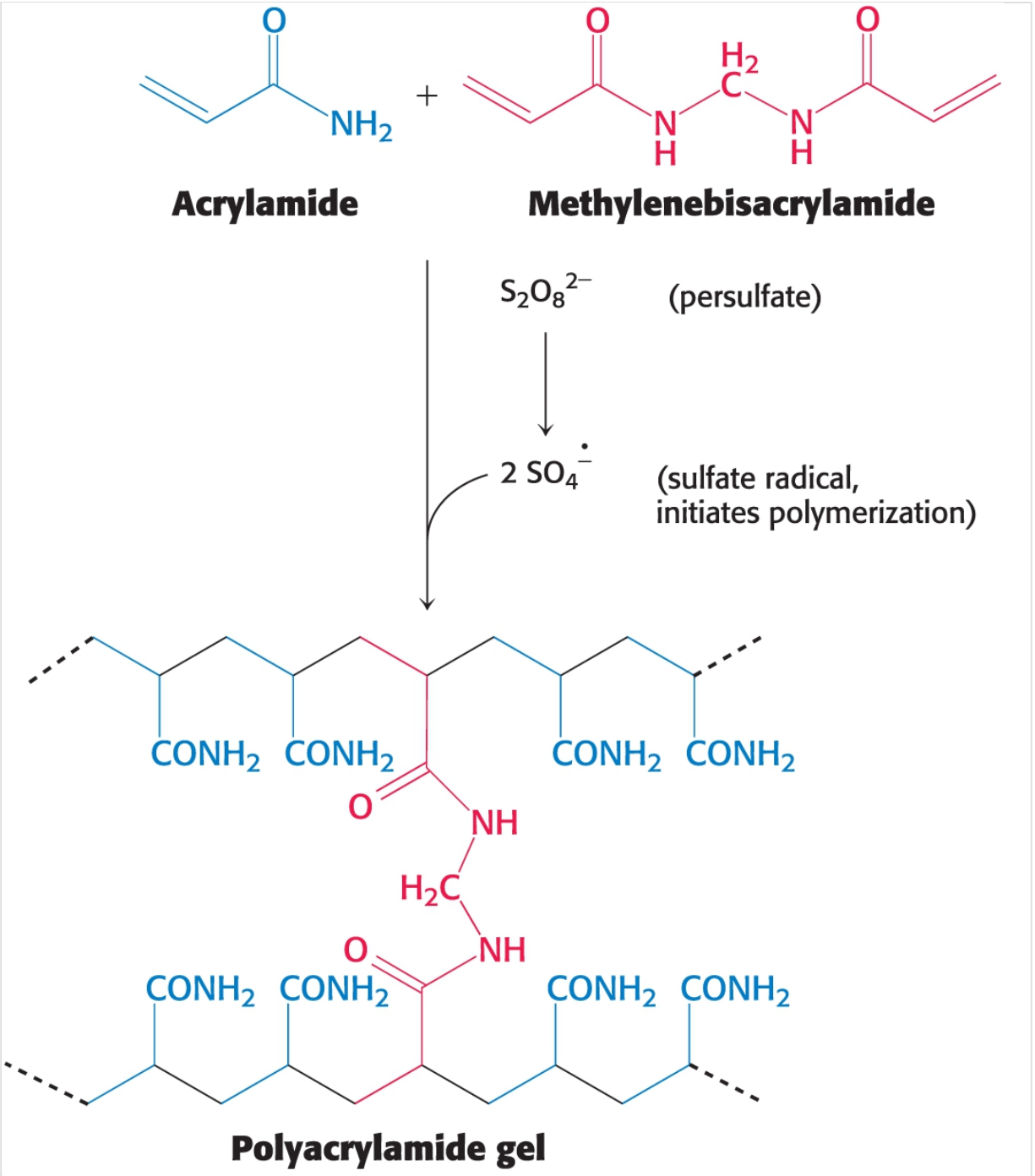
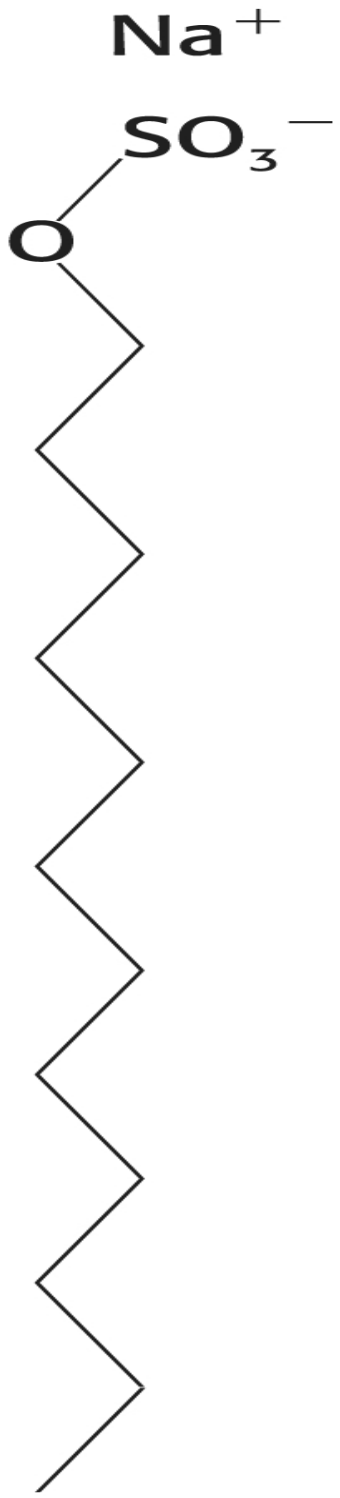


FIGURE 4.8 A polyacrylamide gel is a highly cross-linked three-dimensional mesh. The gel is formed by polymers of acrylamide with intermittently spaced cross-linker (red).

Proteins can be separated largely on the basis of mass by electrophoresis in a polyacrylamide gel under denaturing conditions. The mixture of proteins is first dissolved in a solution of sodium dodecyl sulfate (SDS), an anionic detergent that disrupts nearly all noncovalent interactions in native proteins. Then, β-mercaptoethanol (2-thioethanol) or dithiothreitol is added to reduce disulfide bonds. Anions of SDS bind to main chains at a ratio of about one SDS anion for every two amino acid residues. The negative charge acquired on binding SDS is usually much greater than the charge on the native protein; the contribution of the protein to the total charge of the SDS–protein complex is thus rendered insignificant. As a result, this complex of SDS with a denatured protein has a large net negative charge roughly proportional to the mass of the protein.



Sodium dodecyl sulfate (SDS)

The SDS–protein complexes are then subjected to electrophoresis. When the electrophoresis is complete, the proteins in the gel can be visualized by staining them with silver nitrate or a dye such as Coomassie blue, which reveals a series of bands (Figure 4.9). Small proteins move rapidly through the gel, whereas large proteins stay at the top, near the point of application of the mixture. The mobility of most polypeptide chains under these conditions is linearly proportional to the logarithm of their mass (Figure 4.10). Some carbohydrate-rich proteins and membrane proteins do not obey this empirical relation, however.

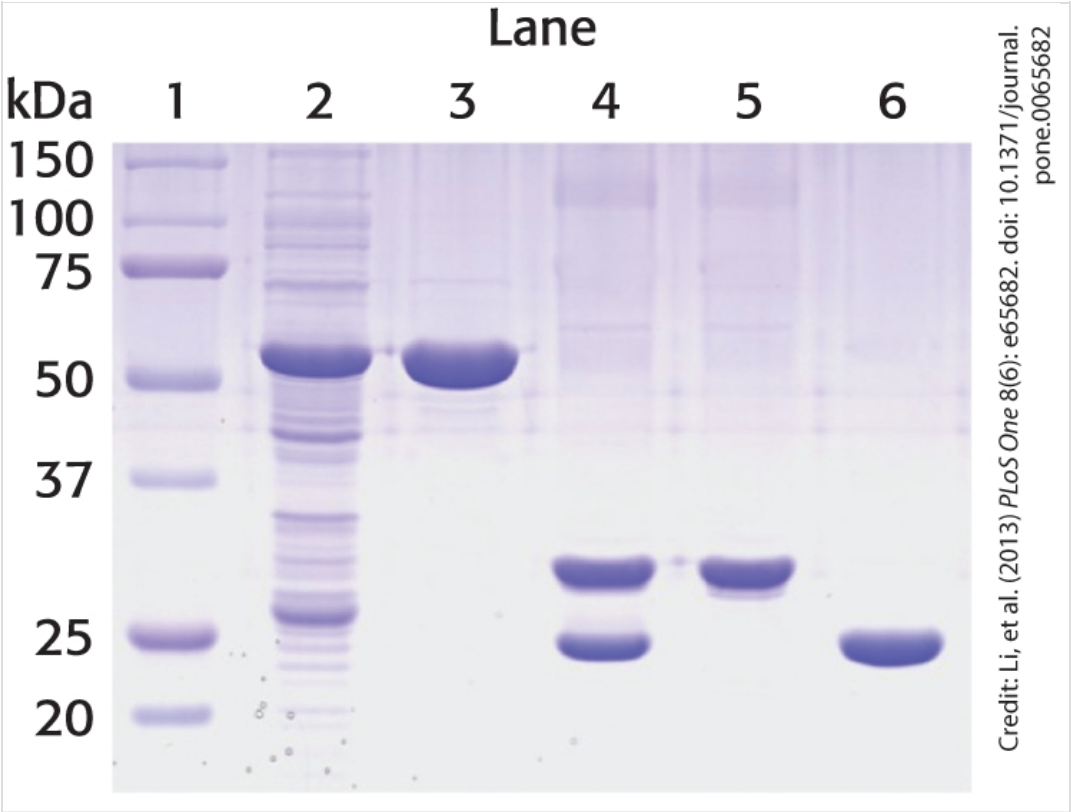


FIGURE 4.9 Staining of the polyacrylamide after electrophoresis enables visualization of the protein bands. Mixtures of proteins subjected to electrophoresis on an SDS–polyacrylamide gel can be visualized by staining with Coomassie blue. The first lane contains a mixture of proteins of known molecular weights, which can be used to estimate the sizes of the bands in the samples.

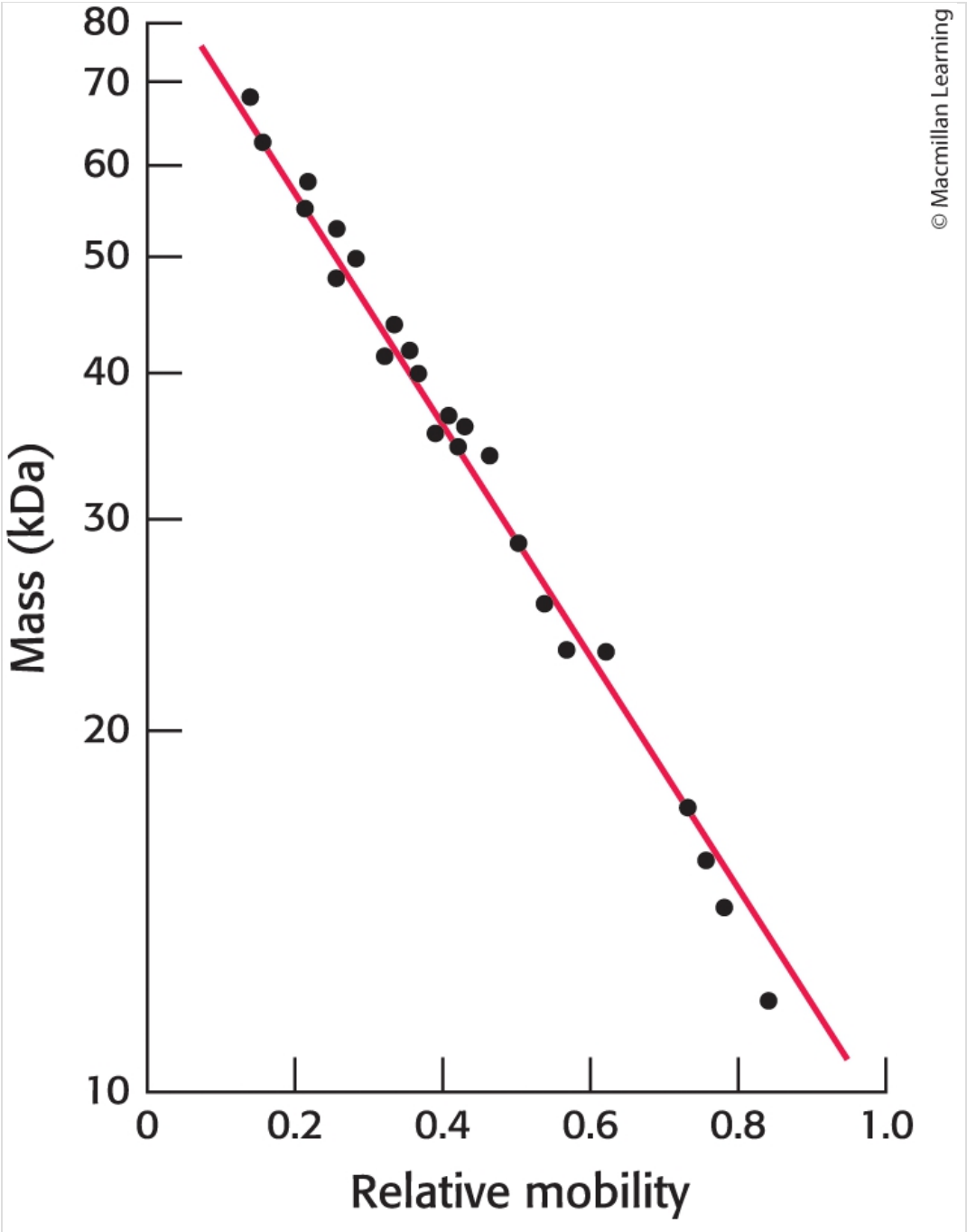


FIGURE 4.10 Electrophoresis can determine the mass of a protein. The electrophoretic mobility of many proteins in SDS–polyacrylamide gels is inversely proportional to the logarithm of their mass.

[Data from K. Weber and M. Osborn, *The Proteins*, vol. 1, 3rd ed. (Academic Press, 1975), p. 179.]

This technique, **SDS–polyacrylamide gel electrophoresis** (often referred to as SDS-PAGE), is rapid, sensitive, and capable of a high degree of resolution. As little as $0.1\ \mu g\ (\sim 2\ pmol)$ of a protein gives a distinct band when stained with Coomassie blue, and even less $(\sim 0.02\ \mu g)$ can be detected with a silver stain. Proteins that differ in mass by about 2% (e.g., 50 and 51 kDa, arising from a difference of about 10 amino acids) can usually be distinguished with SDS-PAGE.

We can examine the efficacy of a purification scheme by analyzing a part of each fraction by SDS-PAGE. The initial fractions will display dozens to hundreds of proteins. As the purification progresses, the number of bands will diminish, and the prominence of one of the bands should increase (**Figure 4.11**). This band should correspond to the protein of interest.

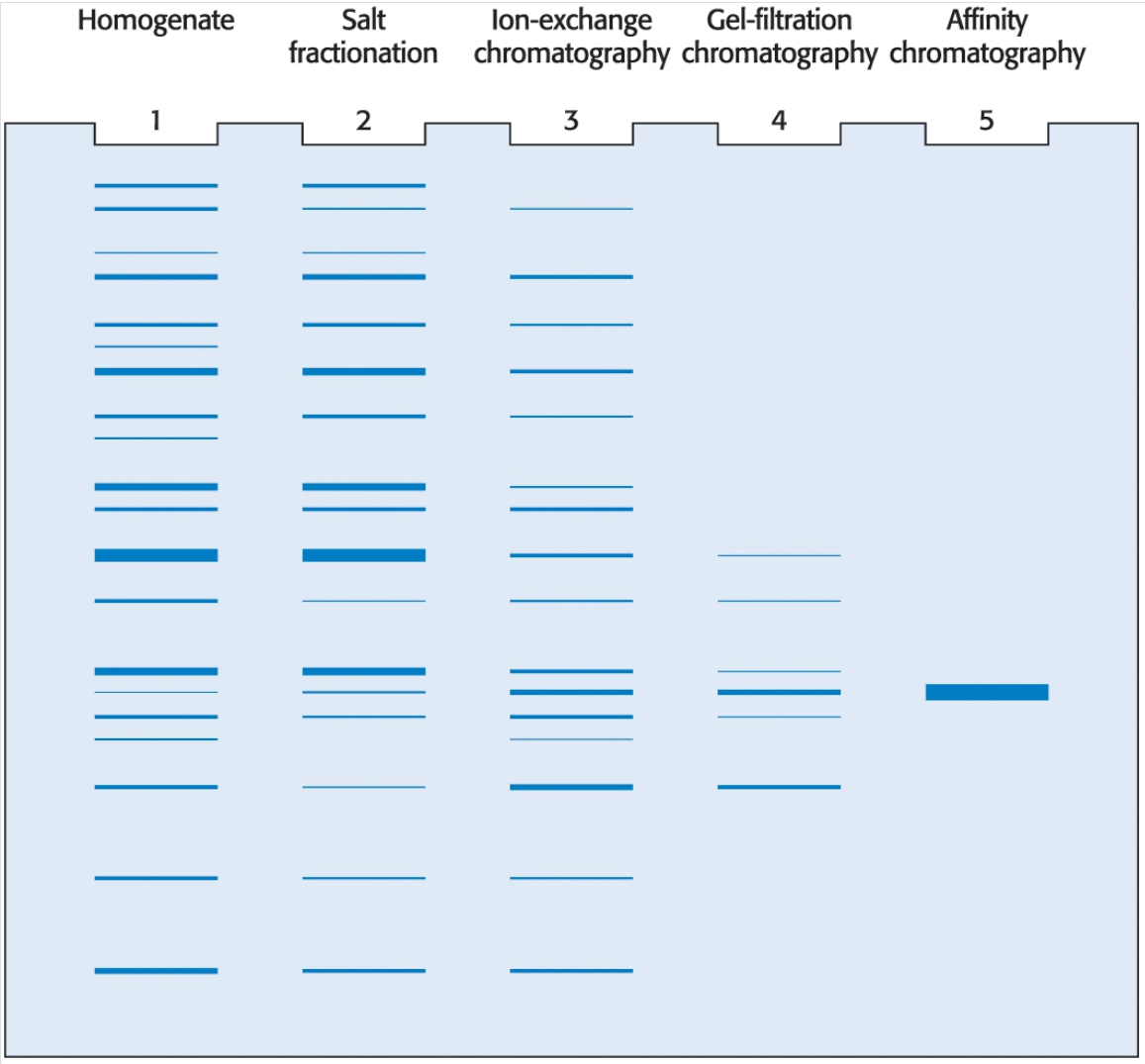


FIGURE 4.11 Electrophoretic analysis can be used to monitor the progress of protein purification. At each step of a protein purification scheme, the sample was analyzed by SDS-PAGE. Each lane contained 50 µg of sample. The effectiveness of the purification can be seen as the band for the protein of interest becomes more prominent relative to other bands.

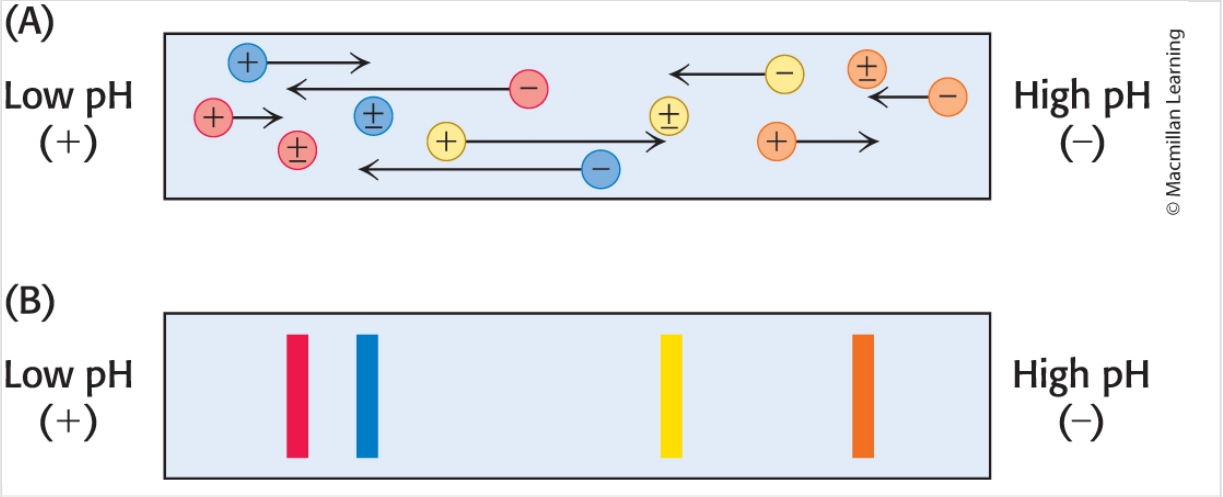
Self-Check Question

The relative electrophoretic mobilities of a 30-kDa protein and a 92-kDa protein used as standards on an SDS–polyacrylamide gel are 0.80 and 0.41, respectively. What is the apparent mass of a protein having a mobility of 0.62 on this gel?

Isoelectric focusing

Proteins can also be separated electrophoretically on the basis of their relative contents of acidic and basic residues. The **isoelectric point** (pI) of a protein is the pH at which its net charge is zero. At this pH, its electrophoretic mobility is zero. For example, the pI of cytochrome *c*, a highly basic electron-transport protein found primarily in mitochondria, is 10.6, whereas that of serum albumin, an acidic protein in blood, is 4.8.

Suppose that a mixture of proteins undergoes electrophoresis in a pH gradient in a gel in the absence of SDS. Each protein will move until it reaches a position in the gel at which the pH is equal to the pI of the protein. This method of separating proteins according to their isoelectric point is called **isoelectric focusing**. The pH gradient in the gel is formed first by subjecting a mixture of small multicharged polymers having many different pI values to electrophoresis. Isoelectric focusing can readily resolve proteins that differ in pI by as little as 0.01, which means that proteins differing by one net charge can be separated (**Figure 4.12**).



© Macmillan Learning

FIGURE 4.12 Isoelectric focusing separates proteins based on their isoelectric point (pI). A pH gradient is established in a gel before loading the sample. (A) Each protein, represented by the different-colored circles, will possess a net positive charge in the regions of the gel where the pH is lower than its respective pI value and a net negative charge where the pH is greater than its pI. When voltage is applied to the gel, each protein will migrate to its pI, the location at which it has no net charge. (B) The proteins form bands that can be excised and used for further experimentation.

Two-dimensional electrophoresis

Isoelectric focusing can be combined with SDS-PAGE to obtain very high-resolution separations by **two-dimensional electrophoresis**. A single sample is first subjected to isoelectric focusing. This single-lane gel is then placed horizontally across the top of an SDS–polyacrylamide slab. The proteins are thus spread across the top of the polyacrylamide gel according to how far they migrated during isoelectric focusing. They then undergo electrophoresis again in a perpendicular direction (vertically) to yield a two-dimensional pattern of spots (**Figure 4.13A**). In such a gel, proteins have been separated in the horizontal direction on the basis of isoelectric point and in the vertical direction on the basis of mass. Remarkably, more than a thousand different proteins in the

bacterium *Escherichia coli* can be resolved in a single experiment by two-dimensional electrophoresis (**Figure 4.13B**).

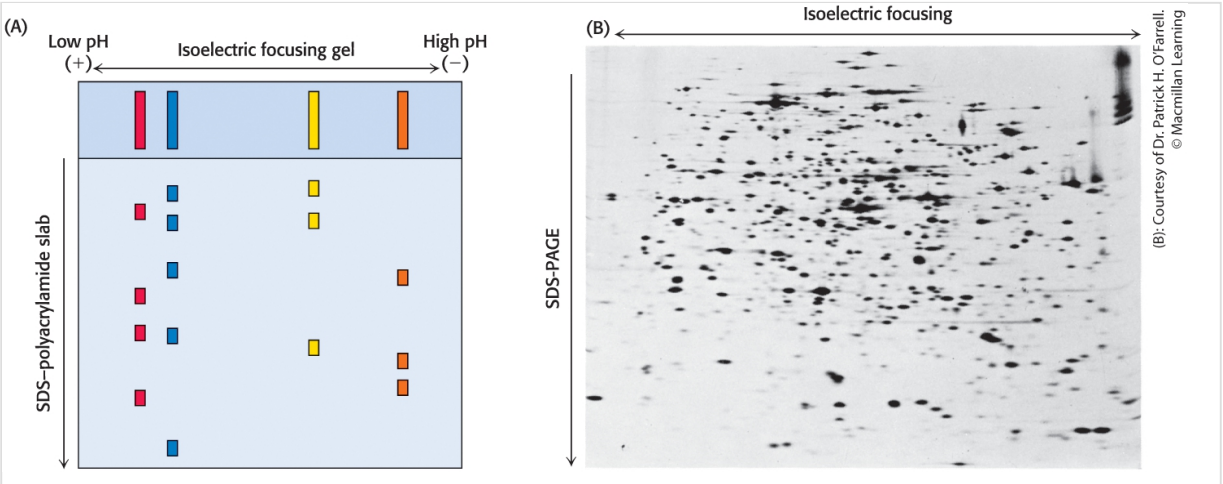
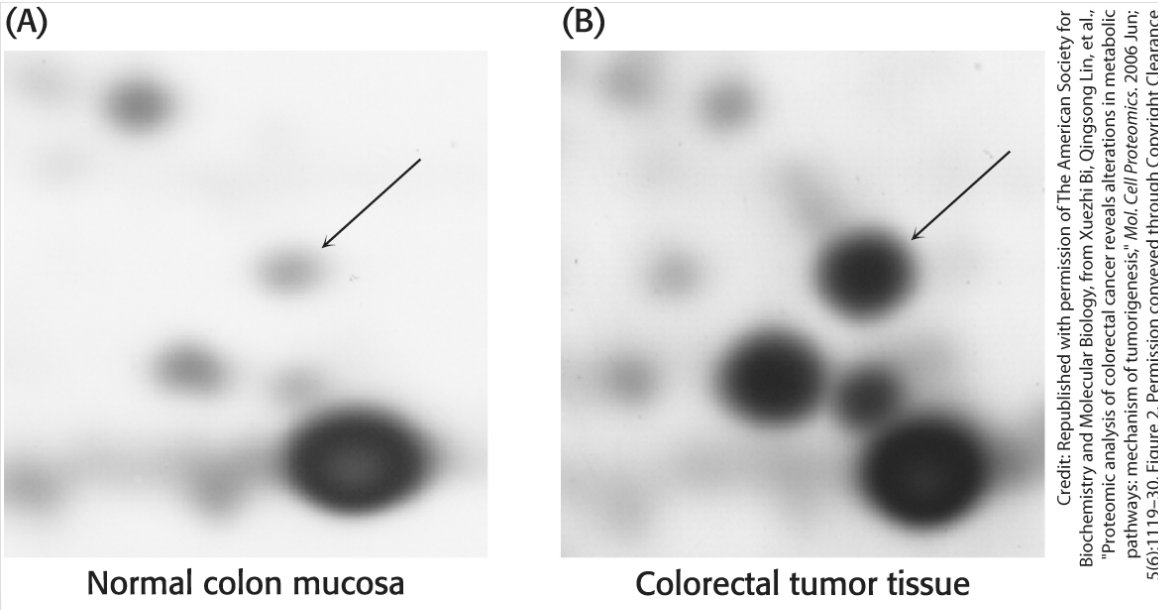


FIGURE 4.13 Two-dimensional electrophoresis uses isoelectric focusing and polyacrylamide gel electrophoresis to separate complex mixtures of proteins. (A) A protein sample is initially fractionated in one dimension by isoelectric focusing as described in Figure 4.12. The isoelectric focusing gel is then attached to an SDS–polyacrylamide gel, and electrophoresis is performed in the second dimension, perpendicular to the original separation. Proteins with the same pI are now separated on the basis of mass. (B) Proteins from *E. coli* were separated by two-dimensional gel electrophoresis, resolving more than a thousand different proteins.

VIEW animations of the techniques shown in Figure 4.12 and Figure 4.13 in Achieve

Two-dimensional electrophoresis can be used to resolve proteins isolated from cells under different physiological conditions. The intensities of individual spots on the gels can then be compared, with any differences indicating that the concentrations of specific proteins have changed in response to the physiological state (**Figure 4.14**). How can we discover the identity of a protein that is showing such responses? Although many proteins are displayed on a two-dimensional gel, they are not identified. We will examine how it is possible to identify proteins by coupling two-dimensional gel electrophoresis with mass spectrometric techniques (Section 4.3).



Credit: Republished with permission of The American Society for Biochemistry and Molecular Biology, from Xuezhi Bi, Qingsong Lin, et al., "Proteomic analysis of colorectal cancer reveals alterations in metabolic pathways: mechanism of tumorigenesis," *Mol. Cell Proteomics*. 2006 Jun; 5(6):1119–30. Figure 2. Permission conveyed through Copyright Clearance

FIGURE 4.14 Alterations in protein levels under differing cellular conditions can be detected b two-dimensional gel electrophoresis. Samples of (A) normal colon mucosa and (B) colorectal tumor tissue from the same person were analyzed by two-dimensional gel electrophoresis. In th gel section shown, changes in the intensity of several spots are evident, including a dramatic increase in levels of the protein indicated by the arrow, corresponding to the enzyme glyceraldehyde-3-phosphate dehydrogenase.

A protein purification scheme can be quantitatively evaluated

To determine the success of a protein purification scheme, we monitor each step of the procedure by determining the specific activity of the protein mixture and by subjecting it to SDS-PAGE analysis. Consider the results for the purification of a fictitious enzyme, summarized in **Table 4.1** and Figure 4.11. At each step, the following parameters are measured:

- *Total Protein.* The quantity of protein present in a fraction is obtained by determining the protein concentration of a part of each fraction and multiplying by the fraction's total volume.
- *Total Activity.* The total activity for the fraction is obtained by measuring the enzyme activity in the volume of fraction used in the assay and multiplying by the fraction's total volume.
- *Specific Activity.* This parameter is obtained by dividing total activity by total protein.
- *Yield.* This parameter is a measure of the activity retained after each purification step as a percentage of the activity in the crude extract. The amount of activity in the initial extract is taken to be 100%.
- *Purification Level.* This parameter is a measure of the increase in purity and is obtained by dividing the specific activity, calculated after each purification step, by the specific activity of the initial extract.

TABLE 4.1 Quantification of a purification protocol for a fictitious enzyme

Step	Total protein (mg)	Total activity (units)	Specific activity (units mg^{-1})	Yield (%)	Purification level
Homogenization	15,000	150,000	10	100	1
Salt fractionation	4600	138,000	30	92	3
Ion-exchange chromatography	1278	115,500	90	77	9

Gel-filtration chromatography	68.8	75,000	1100	50	110
Affinity chromatography	1.75	52,500	30,000	35	3000

As we see in Table 4.1, the first purification step, salt fractionation, leads to an increase in purity of only 3-fold, but we recover nearly all the target protein in the original extract, given that the yield is 92%. After dialysis to lower the high concentration of salt remaining from the salt fractionation, the fraction is passed through an ion-exchange column. The purification now increases to 9-fold compared with the original extract, whereas the yield falls to 77%. Gel-filtration chromatography brings the level of purification to 110-fold, but the yield is now at 50%. The final step is affinity chromatography with the use of a ligand specific for the target enzyme. This step, the most powerful of these purification procedures, results in a purification level of 3000-fold but lowers the yield to 35%. The SDS-PAGE analysis in Figure 4.11 shows that, if we load a constant amount of protein onto each lane after each step, the number of bands decreases in proportion to the level of purification, and the amount of protein of interest increases as a proportion of the total protein present.

A good purification scheme takes into account both purification levels and yield. A high degree of purification and a poor yield leave little protein with which to experiment. A high yield with low purification leaves many contaminants (proteins other than the one of interest) in the fraction and complicates the interpretation of subsequent experiments.

Example

Calculating the Effectiveness of Protein Purification

Problem:

In the final column chromatography step of a protein purification sequence, the total protein drops from 50 mg to 11 mg, and the total activity goes from 11,000 units to 1040 units. Was this final purification step effective?

Getting Started:

The problem provides us with the data for only one purification step within a scheme, the total protein and the total activity before and after the column. Recall that the goal of protein purification is to maximize specific activity. How do we calculate specific activity given the values provided?

Solve:

The specific activity of a protein sample is simply the activity (usually in units) divided by the total amount of protein present. Before the column, the specific activity of the sample was:

$$\text{Specific activity} = \frac{11{,}000 \text{ units}}{50 \text{ mg}} = 220 \text{ units mg}^{-1}$$

After the purification step, the specific activity is now:

$$\text{Specific activity} = \frac{1040 \text{ units}}{11 \text{ mg}} = 94.5 \text{ units mg}^{-1}$$

Another helpful equation for assessing efficacy is the purification level. Usually, this is determined by dividing the specific activity of the current sample with the specific activity of the crude extract. The problem does not provide any data about the crude extract, but we can measure the purification level for this particular step:

$$\text{Purification level} = \frac{94.5 \text{ units mg}^{-1}}{220 \text{ units mg}^{-1}} = 0.43$$

Reflect:

What is the significance of this result? In a single purification step, the amount of total protein has decreased, but this is always the case (notice, for example, that in Table 4.1, the amount of total protein drops with each step). More importantly, however, the specific activity of the sample has *decreased* after this column step, resulting in a purification level of less than one. Clearly, this final chromatography step was not effective in the purification of our protein.

Ultracentrifugation is valuable for separating biomolecules and determining their masses

We have already seen that centrifugation is a powerful and generally applicable method for separating a crude mixture of cell components. At higher velocities, this technique, referred to as **ultracentrifugation**, is also valuable for the analysis of the physical properties of biomolecules. Using ultracentrifugation, we can determine such parameters as mass and density, learn about the shape of a molecule, and investigate the interactions between molecules.

A particle will move through a liquid medium when subjected to a centrifugal force. A convenient means of quantifying the rate of movement is the sedimentation coefficient of a particle. Sedimentation coefficients are usually expressed in Svedberg units (S). The smaller the S value, the more slowly a molecule moves in a centrifugal field. The S values for a number of biomolecules are listed in **Table 4.2**. In general, a more massive particle sediments more rapidly than does a less-massive particle of the same shape and density. Also, elongated particles sediment more slowly than do spherical ones of the same mass.

TABLE 4.2 S values and molecular weights of sample proteins

Protein	S value (Svedberg units)	Molecular weight
Pancreatic trypsin inhibitor	1	6520
Cytochrome *c*	1.83	12,310
Ribonuclease A	1.78	13,690
Myoglobin	1.97	17,800

Trypsin	2.5	23,200
Carbonic anhydrase	3.23	28,800
Concanavalin A	3.8	51,260
Malate dehydrogenase	5.76	74,900
Lactate dehydrogenase	7.54	146,200

Source: T. Creighton, *Proteins*, 2nd ed. (W. H. Freeman and Company, 1993), Table 7.1.

The mass of a protein can be directly determined by sedimentation equilibrium, in which a sample is centrifuged at low speed such that a concentration gradient of the sample is formed. However, this sedimentation is counterbalanced by the diffusion of the sample from regions of high to low concentration. When equilibrium has been achieved, the shape of the final gradient depends solely on the mass of the sample.

The sedimentation-equilibrium technique for determining mass is very accurate and can be applied without denaturing the protein. Thus, the native quaternary structure of multimeric proteins is preserved. In contrast, SDS–polyacrylamide gel electrophoresis provides only an estimate of the mass of dissociated polypeptide chains under denaturing conditions. Note that, if we know the mass of the dissociated components of a multimeric protein as determined by SDS–polyacrylamide analysis and the mass of the intact multimer as determined by sedimentation-equilibrium analysis, we can determine the number of copies of each polypeptide chain present in the protein complex.

Recombinant DNA technology can make protein purification easier

In Chapter 9, we shall consider the widespread effect of recombinant DNA technology on all areas of biochemistry and molecular biology. The application of recombinant methods to the overproduction of proteins has enabled dramatic advances in our understanding of their structure and function. Before the advent of this technology, proteins were isolated solely from their native sources, often requiring a large amount of tissue to obtain a sufficient amount of protein for analytical study. For example, the purification of bovine deoxyribonuclease in 1946 required nearly ten pounds of beef pancreas to yield one gram of protein. As a result, biochemical studies on purified material were often limited to abundant proteins.

Recombinant DNA technology affords a number of advantages in the production and purification of proteins:

- *Proteins can be expressed in large quantities.* For recombinant systems, a host organism that is amenable to genetic manipulation, such as the bacterium *E. coli* or the yeast *Pichia pastoris*, is utilized to express a protein of interest. The biochemist can exploit the short doubling times and ease of genetic manipulation of such organisms to produce large amounts of protein from manageable amounts of culture. As a result, purification can begin with a homogenate that is often highly enriched with the desired molecule. Moreover, a protein can be easily obtained regardless of its natural abundance or its species of origin.

- *Affinity tags can be fused to proteins.* As described above, affinity chromatography can be a highly selective step within a protein purification scheme. Recombinant DNA technology enables the attachment of any one of a number of possible affinity tags to a protein (such as the “His tag” mentioned earlier). Hence, the benefits of affinity chromatography can be realized even for those

proteins for which a binding partner is unknown or not easily determined.

- *Proteins with modified primary structures can be readily generated.* Recombinant DNA technology gives biochemists the ability to manipulate genes to generate variants of a native protein sequence. Recall from Section 2.5 that many proteins consist of compact domains connected by flexible linker regions. With the use of recombinant DNA technology, fragments of a protein that encompass single domains can be generated, an advantageous approach when expression of the entire protein is limited by its size or solubility. Additionally, amino acid substitutions can be introduced into a protein to precisely probe the significance of these residues.

4.2 Immunology Provides Important Techniques for Investigating Proteins

The purification of a protein enables the biochemist to explore its function and structure within a precisely controlled environment. However, the isolation of a protein removes it from its native context within the cell, where its activity is most physiologically relevant. Advances in the field of immunology have enabled the use of antibodies as critical reagents for exploring the functions of proteins within the cell. The exquisite specificity of antibodies for their target proteins provides a means to tag a specific protein so that it can be isolated, quantified, or visualized.

Antibodies to specific proteins can be generated

Immunological techniques begin with the generation of antibodies to a particular protein. Recall from Section 3.4 that antibodies have specific and high affinity for the antigens — foreign proteins, polysaccharides, and nucleic acids — that stimulated their production. Small foreign molecules, such as synthetic peptides, also can elicit antibodies, provided that the small molecule is attached to a macromolecular carrier. An antibody recognizes a specific group or cluster of amino acids on the target molecule called an **antigenic determinant** or **epitope**.

Animals have a very large repertoire of antibody-producing cells, each producing an antibody that contains a unique surface for antigen recognition. When an antigen is introduced into an animal, it is recognized by a select few cells from this population, stimulating the

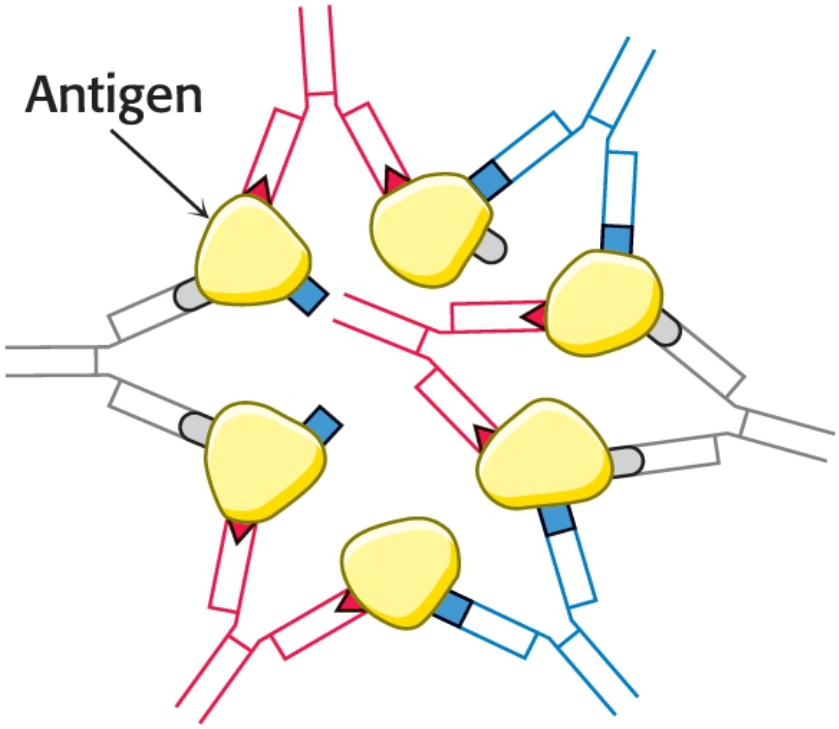
proliferation of these cells. This process ensures that more antibodies of the appropriate specificity are produced.

Immunological techniques depend on the ability to generate antibodies to a specific antigen. To obtain antibodies that recognize a particular protein, a biochemist injects the protein into a rabbit or other lab mammal. The injected protein acts as an antigen, stimulating the reproduction of cells producing antibodies that recognize it. Blood is drawn from the immunized rabbit several weeks later and centrifuged to separate blood cells from the supernatant. This supernatant contains antibodies to all antigens to which the rabbit has been exposed, and is therefore called *antiserum*.

Only some of the antibodies in the antiserum will react with the injected protein. Moreover, antibodies that recognize a particular antigen are not a single molecular species. For instance, when 2,4-dinitrophenol (DNP) is used as an antigen to generate antibodies, the dissociation constants of individual anti-DNP antibodies range from about 0.1 nM to $1\ \mu M$. Correspondingly, a large number of bands are evident when the anti-DNP antibody mixture is subjected to isoelectric focusing.

These results indicate that cells are producing many different antibodies, each recognizing a different surface feature of the same antigen. These antibodies are termed **polyclonal antibodies**, referring to the fact that they are derived from multiple antibody-producing cell populations (**Figure 4.15**). The heterogeneity of polyclonal antibodies can be advantageous for certain applications, such as the detection of a protein of low abundance, because each protein molecule can be bound by more than one antibody at multiple distinct antigenic sites.

Polyclonal antibodies



© Macmillan Learning

Monoclonal antibodies

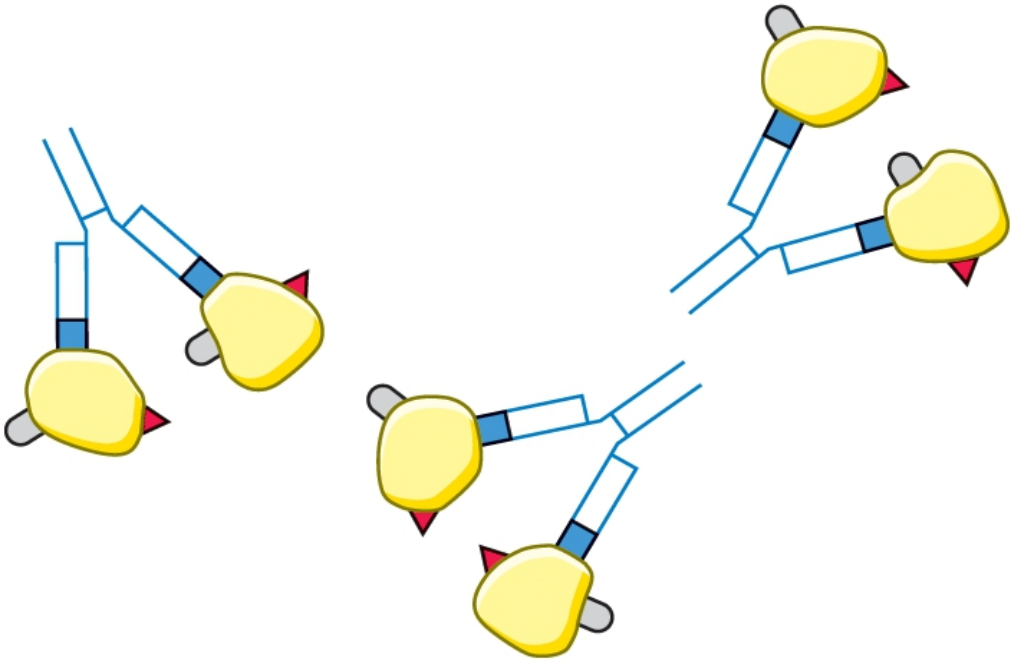


FIGURE 4.15 Polyclonal and monoclonal antibodies differ in the number of epitopes they recognize. Most antigens have several epitopes. Polyclonal antibodies are heterogeneous mixtures of antibodies, each specific for one of the various epitopes on an antigen. Monoclonal antibodies are all identical, produced by clones of a single antibody-producing cell. They recognize one specific epitope.

[Information from R. A. Goldsby, T. J. Kindt, and B. A. Osborne, *Kuby Immunology*, 4th ed. (W. H. Freeman and Company, 2000), p. 154.]



Monoclonal antibodies with virtually any desired specificity can be readily prepared

The discovery of a means of producing **monoclonal antibodies** of virtually any desired specificity was a major breakthrough that intensified the power of immunological approaches. As when working with impure proteins, working with a mixture of different antibodies makes it difficult to interpret data. Ideally, biochemists would isolate a clone of cells producing a single, identical antibody. The problem is that antibody-producing cells isolated from an organism have short life spans.

Immortal cell lines that produce monoclonal antibodies do exist. These cell lines are derived from a type of cancer called *multiple myeloma*, which is a malignant disorder of antibody-producing cells. In this cancer, a single transformed plasma cell (a type of white blood cell) divides uncontrollably, generating a very large number of cells of a single kind. Such a group of cells is called a *clone* because the cells are descended from the same cell and have identical properties. The identical cells of the myeloma secrete large amounts of a single immunoglobulin generation after generation. While these antibodies have proven useful for elucidating antibody structure, nothing is known

about their specificity. Hence, they have little utility for the immunological methods described in the next pages.

César Milstein and Georges Köhler discovered that large amounts of antibodies of nearly any desired specificity can be obtained by fusing a short-lived antibody-producing cell with an immortal myeloma cell. An antigen is injected into a mouse, and its spleen is removed several weeks later (**Figure 4.16**). A mixture of plasma cells from this spleen is then fused in vitro with myeloma cells. Each of the resulting hybrid cells, called **hybridoma** cells, indefinitely produces the identical antibody specified by the parent cell from the spleen. Hybridoma cells can then be screened by a specific assay for the antigen–antibody interaction to determine which ones produce antibodies of the preferred specificity. Collections of cells shown to produce the desired antibody are subdivided and assayed again. This process is repeated until a pure cell line, a clone producing a single antibody, is isolated. These positive cells can be grown in culture medium or injected into mice to induce myelomas. Alternatively, the cells can be frozen and stored for long periods.

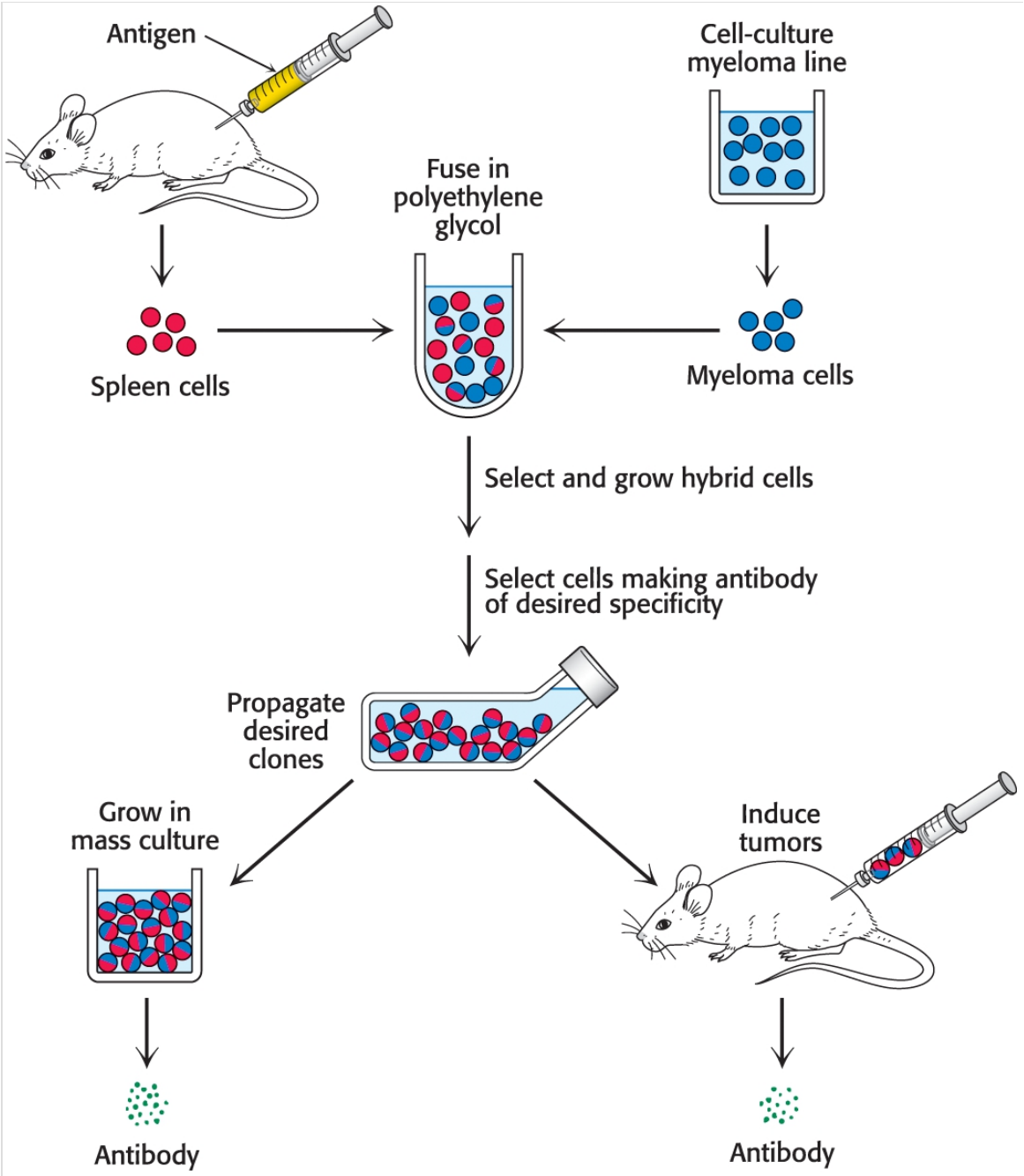


FIGURE 4.16 Monoclonal antibodies are produced by hybridoma cells formed by the fusion o antibody-producing cells and myeloma cells. The hybrid cells are allowed to proliferate by growing them in selective medium. They are then screened to determine which ones produce antibody of the desired specificity.

[Information from C. Milstein. Monoclonal antibodies. Copyright © 1980 by Scientific American, Inc. All rights reserved.]

The hybridoma method of producing monoclonal antibodies has had a dramatic impact on biology and medicine. Biochemists can now readily prepare large amounts of identical antibodies with tailor-made specificities and use them to gather insight into the relationship between antibody structure and specificity. Monoclonal antibodies attached to solid supports can be used as affinity columns to purify scarce proteins. For example, this method has been used to purify interferon (an antiviral protein) 5000-fold from a crude mixture. Moreover, as we shall see below, biologists can use monoclonal antibodies as precise analytical and preparative reagents.

 Clinical laboratories use monoclonal antibodies in many assays. For example, the detection in blood of proteins that are normally localized in the heart points to a heart attack. Blood transfusions have been made safer by antibody screening of donor blood for viruses that cause AIDS (acquired immune deficiency syndrome), hepatitis, and other infectious diseases. Monoclonal antibodies can also be used as therapeutic agents (Chapter 32). For example, trastuzumab (Herceptin) is a monoclonal antibody useful for treating some forms of breast cancer.

Proteins can be detected and quantified by using an enzyme-linked immunosorbent assay

Antibodies can be used as exquisitely specific analytic reagents to quantify the amount of a protein or other antigen present in a biological

sample. The **enzyme-linked immunosorbent assay (ELISA)** makes use of an enzyme, such as horseradish peroxidase or alkaline phosphatase, that reacts with a colorless substrate to produce a colored product. The enzyme is covalently linked to a specific antibody that recognizes a target antigen. If the antigen is present, the antibody–enzyme complex will bind to it and, on addition of the substrate, the enzyme will catalyze the reaction, generating the colored product. Thus, the presence of the colored product indicates the presence of the antigen. Rapid and convenient, ELISAs can detect less than a nanogram $(10^{-9}\ g)$ of a specific protein. ELISAs can be performed with either polyclonal or monoclonal antibodies, but the use of monoclonal antibodies yields more-reliable results.

Of the several types of ELISA that exist, we will further examine two types:

- *The indirect ELISA is used to detect the presence of antibodies.* This method is the basis of the test for HIV infection. The HIV test detects the presence of antibodies that recognize viral core protein antigens. Viral core proteins are coated on the bottom of a well. Antibodies from the person being tested are then added to the coated well. Only someone infected with HIV will have antibodies that bind to the antigen. Finally, enzyme-linked antibodies to human antibodies (e.g., enzyme-linked goat antibodies that recognize human antibodies) are allowed to react in the well, and unbound antibodies are removed by washing. Substrate is then applied. An enzyme reaction yielding a colored product suggests that the enzyme-linked antibodies were bound to human antibodies, which in turn implies that the patient has antibodies to the viral antigen (**Figure 4.17A**). This assay is quantitative: the rate of the color-formation reaction is proportional to the amount of antibody originally present.

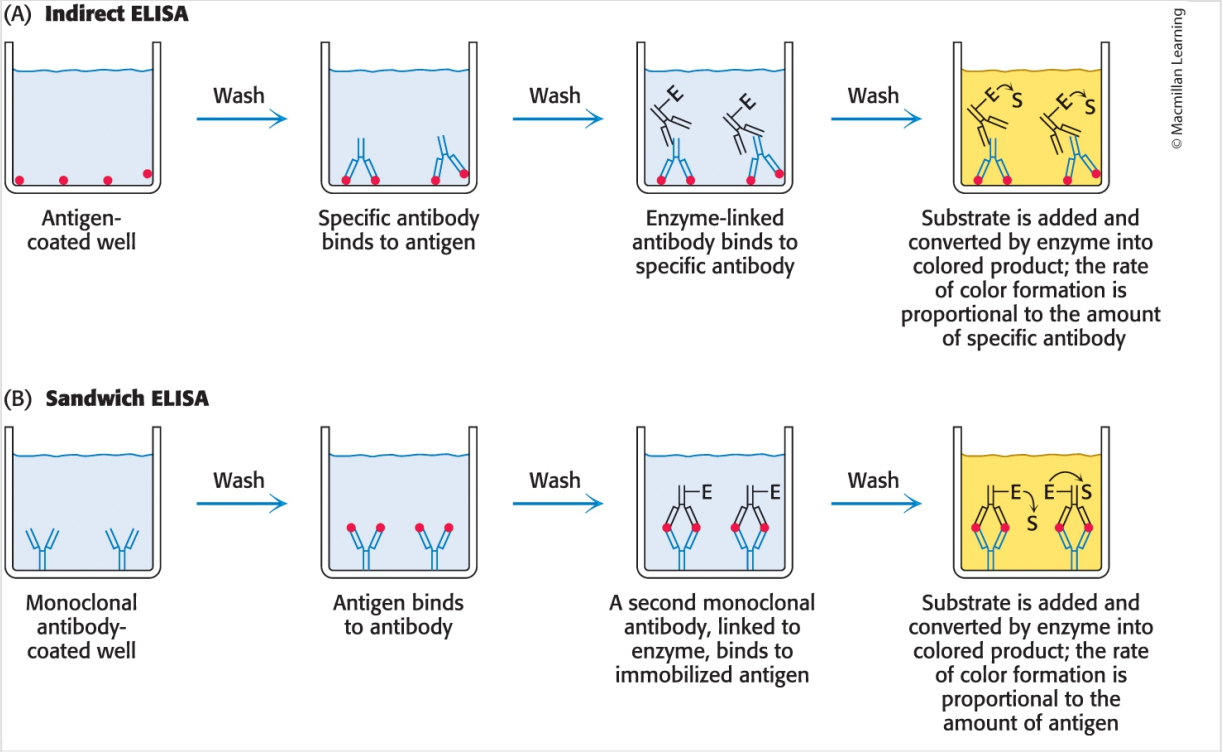


FIGURE 4.17 Indirect ELISA and sandwich ELISA are sensitive methods for detecting the presence of antigen or antibody in a sample. (A) In indirect ELISA, the production of color indicates the amount of an antibody to a specific antigen. (B) In sandwich ELISA, the production of color indicates the quantity of antigen.

[Information from R. A. Goldsby, T. J. Kindt, and B. A. Osborne, *Kuby Immunology*, 4th ed. (W. H. Freeman and Company, 2000), p. 162.]

- *The sandwich ELISA is used to detect an antigen rather than an antibody*. An antibody to a particular antigen — the capture antibody — is first coated on the bottom of a well. Next, solution containing the antigen (such as blood or urine, in medical diagnostic tests) is added to the well and binds to the antibody. Finally, a second antibody — the detection antibody — that also recognizes the antigen is added. Importantly, this antibody binds to the antigen in a region distinct from, and thus does not displace, the first antibody. This antibody is enzyme-linked and is processed as described for indirect ELISA. In this case, the rate of color formation is directly proportional to the amount of antigen present.

Consequently, it permits the measurement of small quantities of antigen (Figure 4.17B).

Self-Check Question



Suppose in a sandwich ELISA experiment, the antibody coated on the bottom of the well recognized the same epitope as the antibody used for antigen detection. Will this experiment work? Why or why not?

Western blotting permits the detection of proteins separated by gel electrophoresis

Very small quantities of a protein of interest in a cell or in body fluid can be detected by an immunoassay technique called **western blotting** (Figure 4.18). A sample is subjected to electrophoresis on an SDS–polyacrylamide gel. A polymer sheet is pressed against the gel, transferring the resolved proteins on the gel to the sheet, which makes the proteins more accessible for reaction. An antibody that is specific for the protein of interest, called the *primary antibody*, is added to the sheet and reacts with the antigen. The antibody–antigen complex on the sheet can then be detected by rinsing the sheet with a second antibody, called the *secondary antibody*, that is specific for the primary antibody (e.g., a goat antibody that recognizes mouse antibodies). Typically, the secondary antibody is fused to an enzyme that produces a chemiluminescent or colored product or contains a fluorescent tag, enabling the identification and quantitation of the protein of interest.

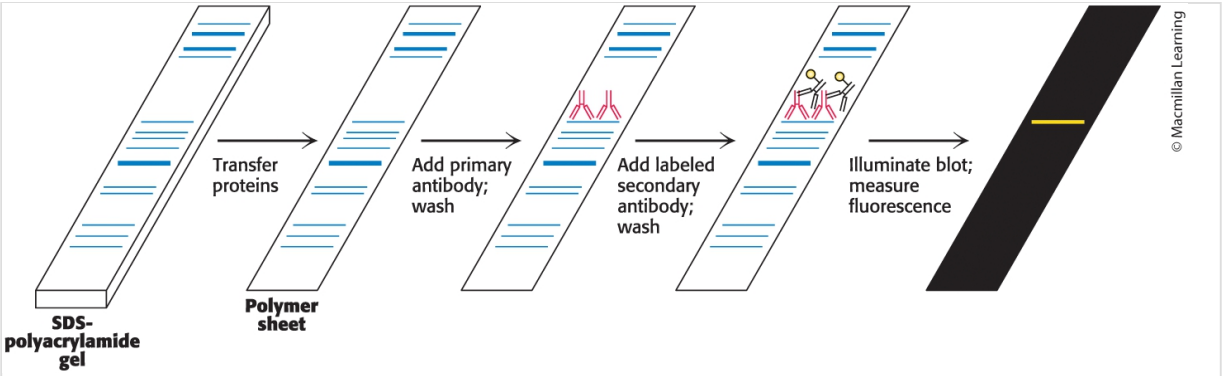


FIGURE 4.18 Western blotting uses antibodies to detect specific proteins after gel electrophoresis. Proteins on an SDS–polyacrylamide gel are transferred to a polymer sheet. The sheet is first treated with a primary antibody, which is specific for the protein of interest, and then washed to remove unbound antibody. Next, the sheet is treated with a secondary antibody, which recognizes the primary antibody, and washed again. Since the secondary antibody is labeled (here, with a fluorescent tag indicated by the yellow circle), the band containing the protein of interest can be identified.

VIEW an animation of this technique in Achieve

Western blotting makes it possible to find a protein in a complex mixture, the proverbial needle in a haystack. It is the basis for the test for infection by hepatitis C, where it is used to detect a core protein of the virus. This technique is also very useful in monitoring protein purification and in the cloning of genes.

Co-immunoprecipitation enables the identification of binding partners of a protein

With a monoclonal antibody against a specific protein, it is also possible to determine the binding partners of that protein under a specific set of conditions. In this technique, known as co-immunoprecipitation, the

sample of interest — an extract prepared from cultured cells or isolated tissue, for example — is incubated with the specific antibody. Then, agarose beads coated with an antibody-binding protein (such as Protein A from the bacterium *Staphylococcus aureus*) are added to the mixture. Protein A recognizes a portion of the antibody that is separate from the antigen-binding region (e.g., the F_c domain, Figure 3.40), and thus does not disrupt the protein-antibody complex. After centrifugation at low speed, the antibody, now bound to the beads, aggregates at the bottom of the tube. Under optimal buffer conditions, the antibody-protein complex will also precipitate any additional proteins that are bound to the original protein (**Figure 4.19**). Subsequent analysis of the precipitate by SDS-PAGE, followed by either western blot or mass spectrometric fingerprinting (Section 4.3), enables the identification of the binding partners.

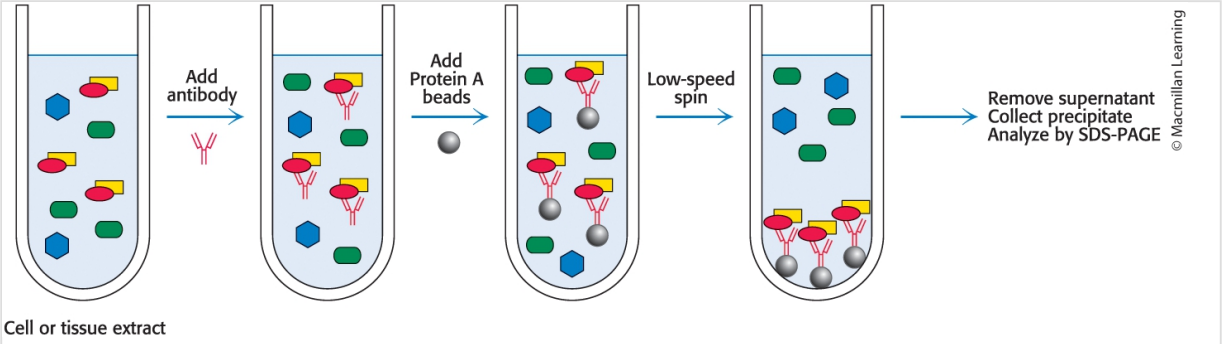
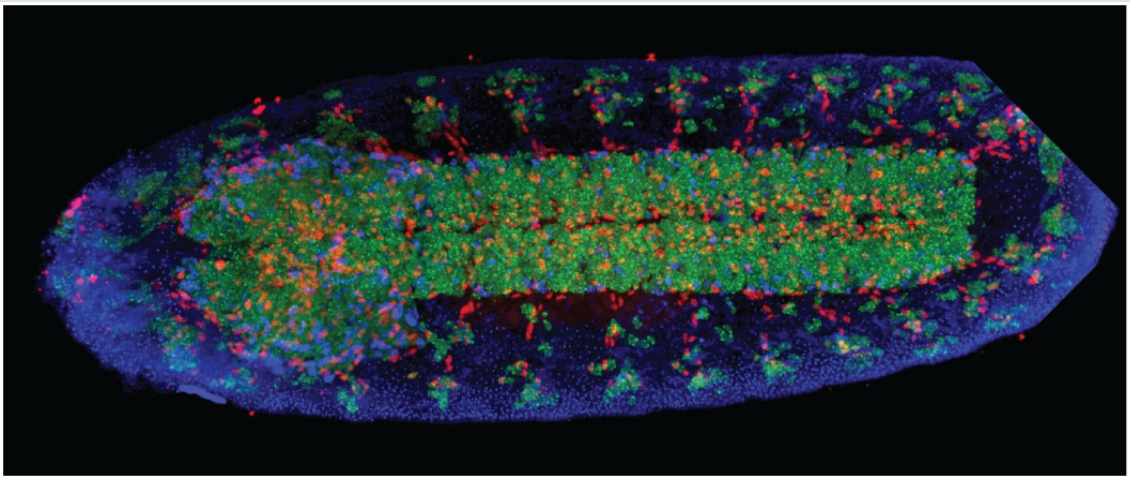


FIGURE 4.19 Co-immunoprecipitation can identify binding partners to a specific protein. An antibody specific for a particular protein (here, the red oval) is added to an extract isolated from cells or tissue. After an incubation period, agarose beads coated with Protein A are added, and the mixture is subjected to low-speed centrifugation. The beads bind to the antibody-protein complex and precipitate. Any additional proteins that interact with the target protein (here, the yellow rectangle) will also precipitate and can be identified by SDS-PAGE followed by western blotting or mass spectrometry.

Fluorescent markers make the visualization of proteins in the cell possible

Fluorescent markers provide a powerful means of examining proteins in their biological context. Cells can be stained with fluorescence-labeled antibodies and examined by **fluorescence microscopy** to reveal the location of a protein of interest. For example, proteins that play key roles in embryonic development have been identified with the use of monoclonal antibodies as tags (**Figure 4.20**).

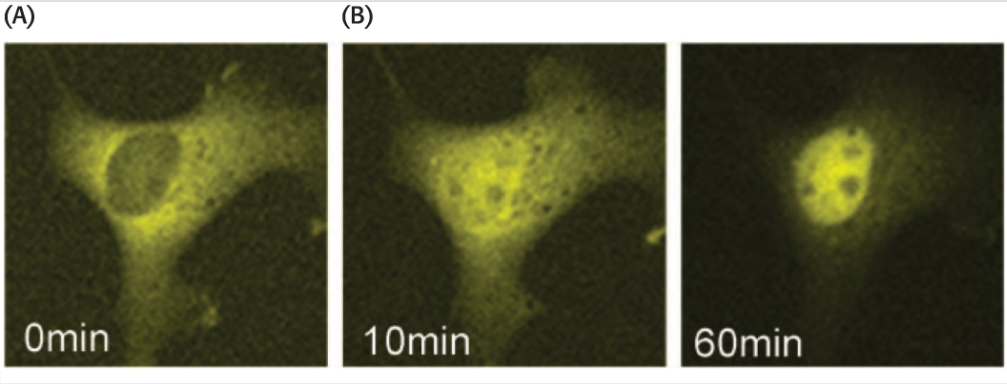


Credit: Laurina Manning, Chris Doe Lab, HHMI at University of Oregon.

FIGURE 4.20 Fluorescence-labeled monoclonal antibodies can detect proteins in a multicellular embryo imaged by microscopy. Here, a developing *Drosophila* embryo was stained with three different fluorescence-labeled monoclonal antibodies (red, green, and blue), each directed against a different protein important for gene regulation.

By tracking protein location, fluorescent markers also provide clues to protein function. For instance, the mineralocorticoid receptor protein binds to steroid hormones, including cortisol. The receptor was linked to a yellow variant of green fluorescent protein (GFP), a naturally fluorescent protein isolated from the jellyfish *Aequorea victoria* (Section 2.7). Fluorescence microscopy revealed that, in the absence of the hormone, the receptor is located in the cytoplasm (**Figure 4.21A**). On addition of the steroid, the receptor is translocated to the nucleus, where it binds to DNA (**Figure 4.21B**). These results indicate that the

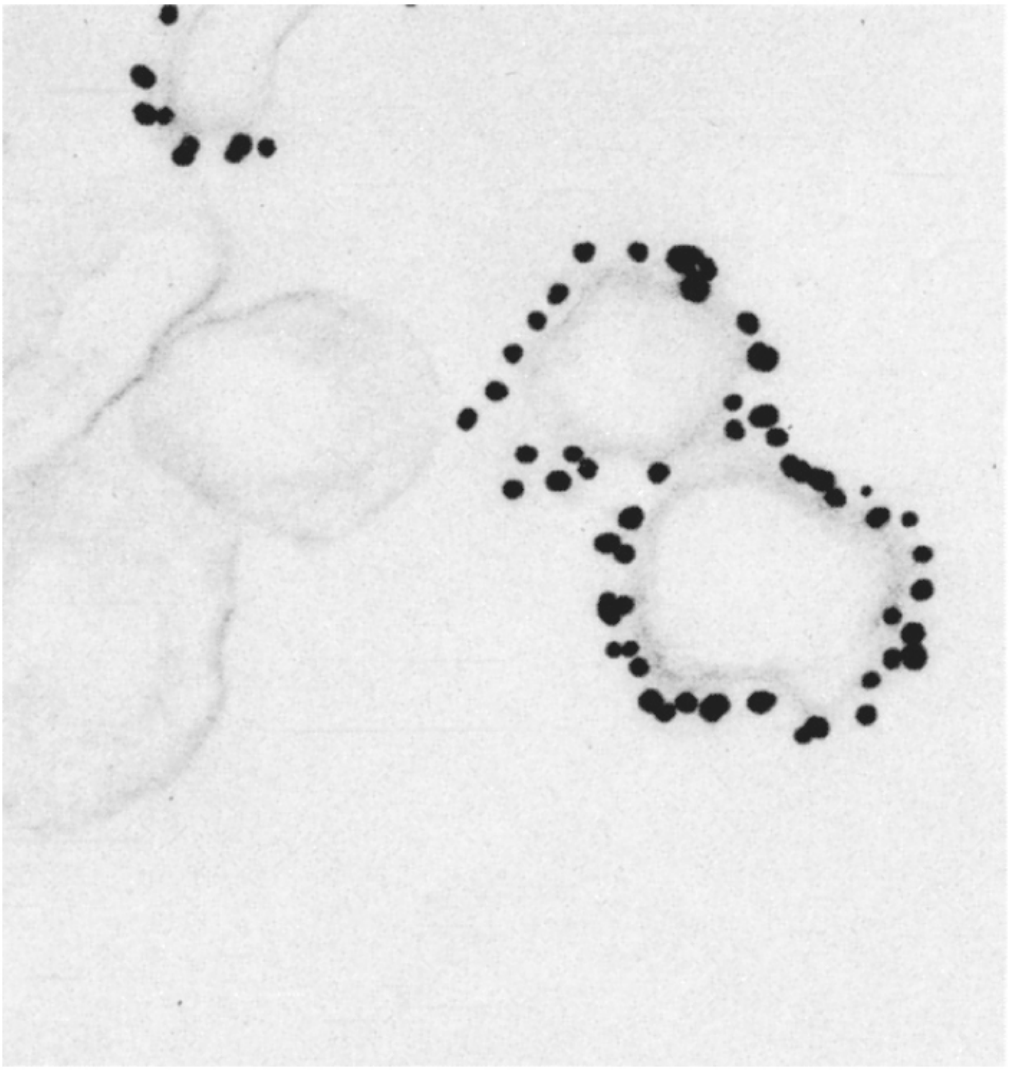
mineralocorticoid receptor protein is a transcription factor that controls gene expression.



Credit: Republished with permission of Society for Neuroscience, from Nishi, M. et al., "Visualization of Glucocorticoid Receptor and Mineralocorticoid Receptor Interactions in Living Cells with GFP-Based Fluorescence Resonance Energy Transfer," *The Journal of Neuroscience*, 24, 21, 2004, 4918-27, Figure 7. Permission conveyed through Copyright Clearance Center, Inc.

FIGURE 4.21 Fluorescence microscopy can detect changes in protein localization within the cell. (A) The mineralocorticoid receptor, made visible by attachment to a yellow variant of GFP, is located predominantly in the cytoplasm of the cultured cell. (B) Subsequent to the addition of corticosterone (a glucocorticoid steroid that also binds to the mineralocorticoid receptor), the receptor moves into the nucleus.

The highest resolution of fluorescence microscopy is about $0.2\ \mu m$ (200 nm, or $2000\ Å$), the wavelength of visible light. Finer spatial resolution can be achieved by electron microscopy if the antibodies are tagged with electron-dense markers. For example, antibodies attached to clusters of gold or to ferritin (which has an electron-dense core rich in iron) are highly visible under the electron microscope. This technique, called *immunoelectron microscopy*, can define the position of antigens to a resolution of 10 nm $(100\ Å)$ or finer (**Figure 4.22**).



Courtesy of Dr. Peter Sargent.

FIGURE 4.22 Immunoelectron microscopy can detect proteins at very high spatial resolution. The opaque particles (150–Å, or 15-nm, diameter) in this electron micrograph are clusters of gold atoms bound to antibody molecules. A gold-labeled antibody against a channel protein (Section 13.1) identifies membrane vesicles at the termini of neurons that contain this protein.

4.3 Mass Spectrometry Is a Powerful Technique for the Identification of Peptides and Proteins

In several of the techniques described in the previous section, identification of the proteins present in the sample is often critical. For example, we may use co-immunoprecipitation to discover an unexpected protein that interacts with our sample protein. The identity of this unknown protein must be determined to advance our understanding of how our protein works. Antibody-based techniques, such as ELISA, can be very helpful toward this goal. However, these techniques are limited to the detection of proteins for which an antibody is already available.

Mass spectrometry enables the highly precise and sensitive measurement of the atomic composition of a particular molecule, or *analyte*, without prior knowledge of its identity. Originally, this method was relegated to the study of the chemical composition and molecular mass of gases or volatile liquids. However, technological advances have dramatically expanded the utility of mass spectrometry to the study of proteins, even those found at very low concentrations within highly complex mixtures, such as the contents of a particular cell type.

Mass spectrometers operate by converting analyte molecules into gaseous, charged forms (called *gas-phase ions*). Through the application of electrostatic potentials, the ratio of the mass of each ion to its charge (termed the *mass-to-charge ratio*, or m/z) can be measured. Although a wide variety of techniques employed by mass spectrometers are used in current practice, each of them comprises three essential components: the ion source, the mass analyzer, and the detector. Let us consider the

first two in greater detail, because improvements in them have contributed most significantly to the analysis of biological samples:

1. *The ion source achieves the first critical step in mass spectrometric analysis: ionization, or the conversion of the analyte into gas-phase ions.* Proteins are difficult to ionize efficiently because of their high molecular weights and low volatility. However, the development of two techniques in particular has enabled the clearing of this significant hurdle.

    - In **matrix-assisted laser desorption/ionization (MALDI)**, the analyte is evaporated to dryness in the presence of a volatile, aromatic compound (the matrix) that can absorb light at specific wavelengths. A laser pulse tuned to one of these wavelengths excites and vaporizes the matrix, converting some of the analyte into the gas phase. Subsequent gaseous collisions enable the intermolecular transfer of charge, ionizing the analyte.

    - In **electrospray ionization (ESI)**, a solution of the analyte is passed through an electrically charged nozzle. Droplets of the analyte, now charged, emerge from the nozzle into a chamber of very low pressure, evaporating the solvent and ultimately yielding the ionized analyte.

2. *In the second step, the newly formed analyte ions then enter the mass analyzer, where they are distinguished on the basis of their mass-to-charge ratios.* There are a number of different types of mass analyzers. For this discussion, we will consider one of the simplest, the **time-of-flight (TOF) mass analyzer**, in which ions are accelerated through an elongated chamber under a fixed electrostatic potential. Given two ions of identical net charge, the smaller ion will require less time to traverse the chamber than will the larger ion. The mass of each ion can be determined by measuring the time required for each ion to pass through the chamber.

The sequential action of the ion source and the mass analyzer enables the highly sensitive measurement of the mass-to-charge ratios of very large ions, such as the charged forms of proteins. Consider an example of a MALDI ion source coupled to a TOF mass analyzer: the MALDI-TOF mass spectrometer (Figure 4.23). Gas-phase ions generated by the MALDI ion source pass directly into the TOF analyzer, where the mass-to-charge ratios are recorded. In Figure 4.24, the MALDI-TOF mass spectrum of a mixture of 5 pmol (5×10^{-12} mol) each of insulin and lactoglobulin is shown. The masses determined by MALDI-TOF are 5733.9 and 18,364, respectively. A comparison with the calculated values of 5733.5 and 18,388 reveals that MALDI-TOF is clearly an accurate means of determining protein mass.

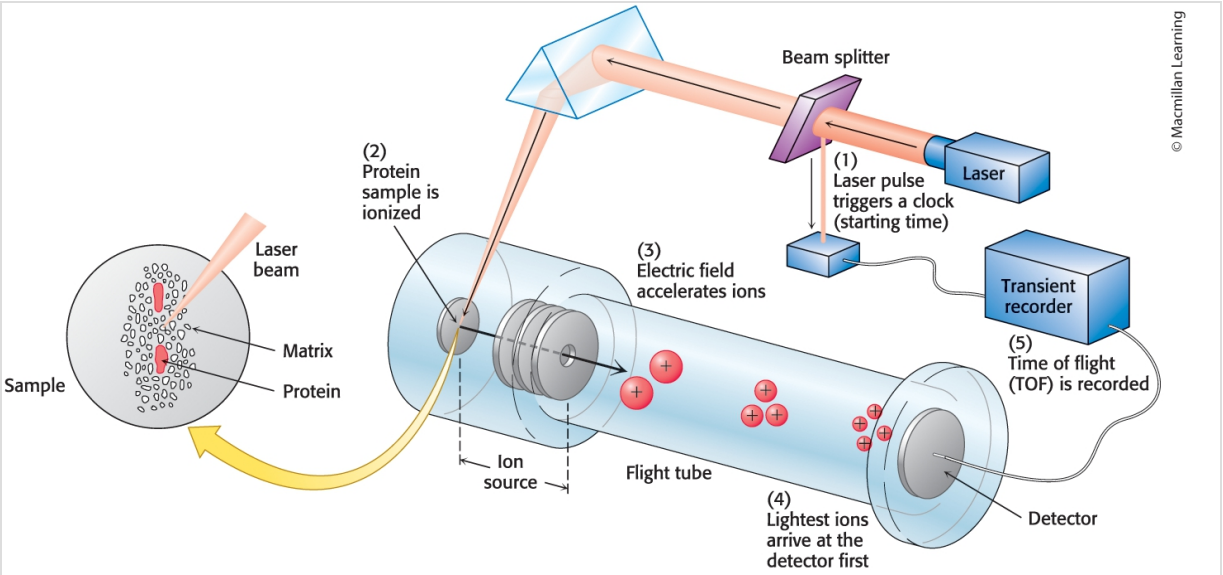


FIGURE 4.23 The MALDI-TOF mass spectrometer measures ionized samples based on their mass-to-charge ratio. (1) A laser pulse simultaneously starts a clock and is directed toward the sample. (2) The protein sample, embedded in an appropriate matrix, is ionized by the application of the laser pulse. (3) An electric field accelerates the ions through the flight tube toward the detector. (4) The lightest ions arrive first. (5) Based on the clock reading initiated in Step 1, the time of flight (TOF) for the ions can be measured.

[Information from J. T. Watson, *Introduction to Mass Spectrometry*, 3rd ed. (Lippincott-Raven, 1997), p. 279.]

VIEW an animation of this technique in Achieve

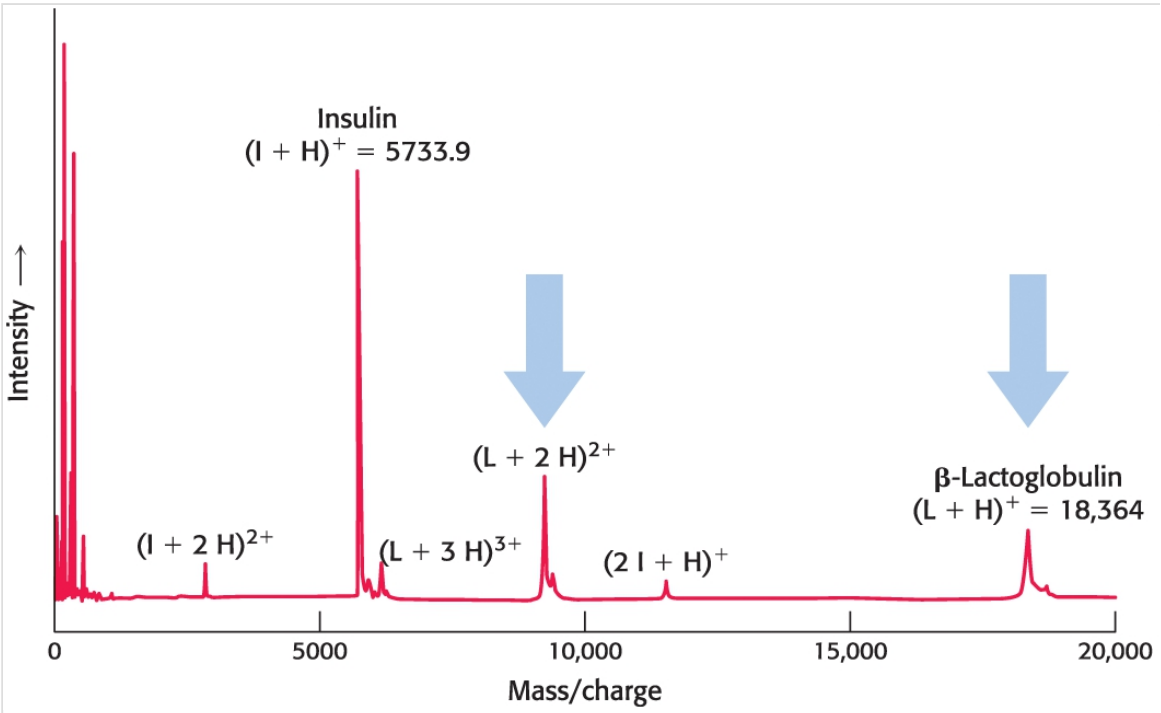


FIGURE 4.24 MALDI-TOF mass spectrometry can detect molecular masses with a high degree sensitivity and accuracy. A mixture of 5 pmol each of insulin (I) and β-lactoglobulin (L) was ionized by MALDI, which produces predominantly singly charged molecular ions from peptides and proteins — the insulin ion $(I+H)^+$ and the lactoglobulin ion $(L+H)^+$. Peaks corresponding to β-lactoglobulin but carrying different total net charges are indicated by the blue arrows, as well as small quantities of a singly charged dimer of insulin $(2\,I+H)^+$ also ar produced.

[Data from J. T. Watson, *Introduction to Mass Spectrometry*, 3rd ed. (Lippincott-Raven, 1997), p. 282.]

In the ionization process, a family of ions, each of the same mass but carrying different total net charges, is formed from a single analyte. Because the mass spectrometer detects ions on the basis of their mass-

to-charge ratio, these ions will appear as separate peaks in the mass spectrum. For example, in the mass spectrum of β-lactoglobulin shown in Figure 4.24, peaks near $m/z = 18{,}364$ (corresponding to the $+1$ charged ion) and $m/z = 9183$ (corresponding to the $+2$ charged ion) are visible (indicated by the blue arrows). Although multiple peaks for the same ion may appear to be a nuisance, they enable the spectrometrist to measure the mass of an analyte ion more than once in a single experiment, improving the overall precision of the calculated result.

Peptides can be sequenced by mass spectrometry

For many years, chemical methods were the primary means for peptide sequencing. In the most common of these methods, called *Edman degradation*, the N-terminal amino acid of a polypeptide is labeled with phenyl isothiocyanate. Subsequent cleavage yields the phenylthiohydantoin (PTH)-amino acid derivative, which can be identified by chromatographic methods, and the polypeptide chain, now shortened by one residue (**Figure 4.25**). This procedure can then be repeated on the shortened peptide, yielding another PTH–amino acid, which can again be identified by chromatography.

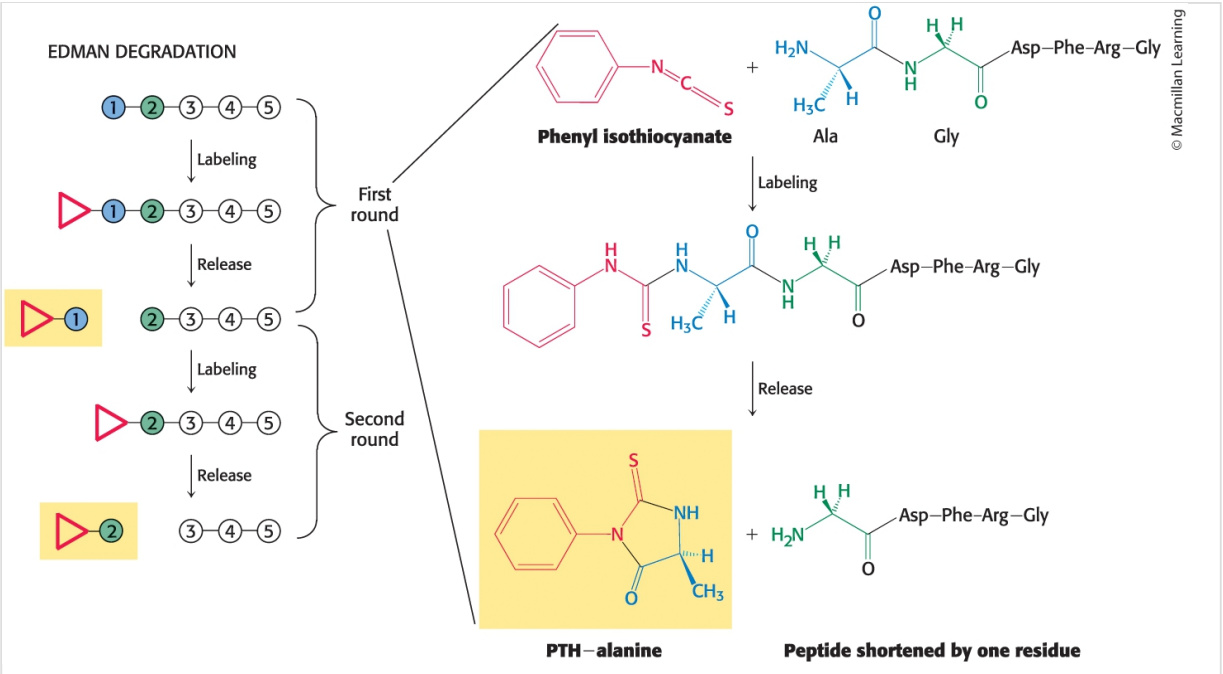


FIGURE 4.25 The Edman degradation is a chemical method for peptide sequencing. The labeled amino-terminal residue (PTH–alanine in the first round) can be released without hydrolyzing the rest of the peptide. Hence, the amino-terminal residue of the shortened peptide (Gly-Asp-Phe-Arg-Gly) can be determined in the second round. Three more rounds of the Edman degradation reveal the complete sequence of the original peptide.

While technological advancements have improved the speed and sensitivity of the Edman degradation, these parameters have largely been surpassed by the application of mass spectrometric methods. The use of mass spectrometry for protein sequencing takes advantage of the fact that ions of proteins that have been analyzed by a mass spectrometer, called *precursor ions*, can be broken into smaller peptide chains by bombardment with atoms of an inert gas such as helium or argon. These new fragments, called *product ions*, can be passed through a second mass analyzer for further mass characterization.

Using two mass analyzers arranged in this manner is referred to as **tandem mass spectrometry**. Importantly, the product-ion fragments are formed in chemically predictable ways that can provide clues to the

amino acid sequence of the precursor ion. For polypeptide analytes, disruption of individual peptide bonds will yield two smaller peptide ions, containing the sequences before and after the cleavage site. Hence, a family of ions can be detected; each ion represents a fragment of the original peptide with one or more amino acids removed from one end (**Figure 4.26A**). For simplicity, only the carboxyl-terminal peptide fragments are shown in Figure 4.26A. **Figure 4.26B** depicts a representative mass spectrum from a fragmented peptide. The mass differences between the peaks in this fragmentation experiment indicate the amino acid sequence of the precursor peptide ion.

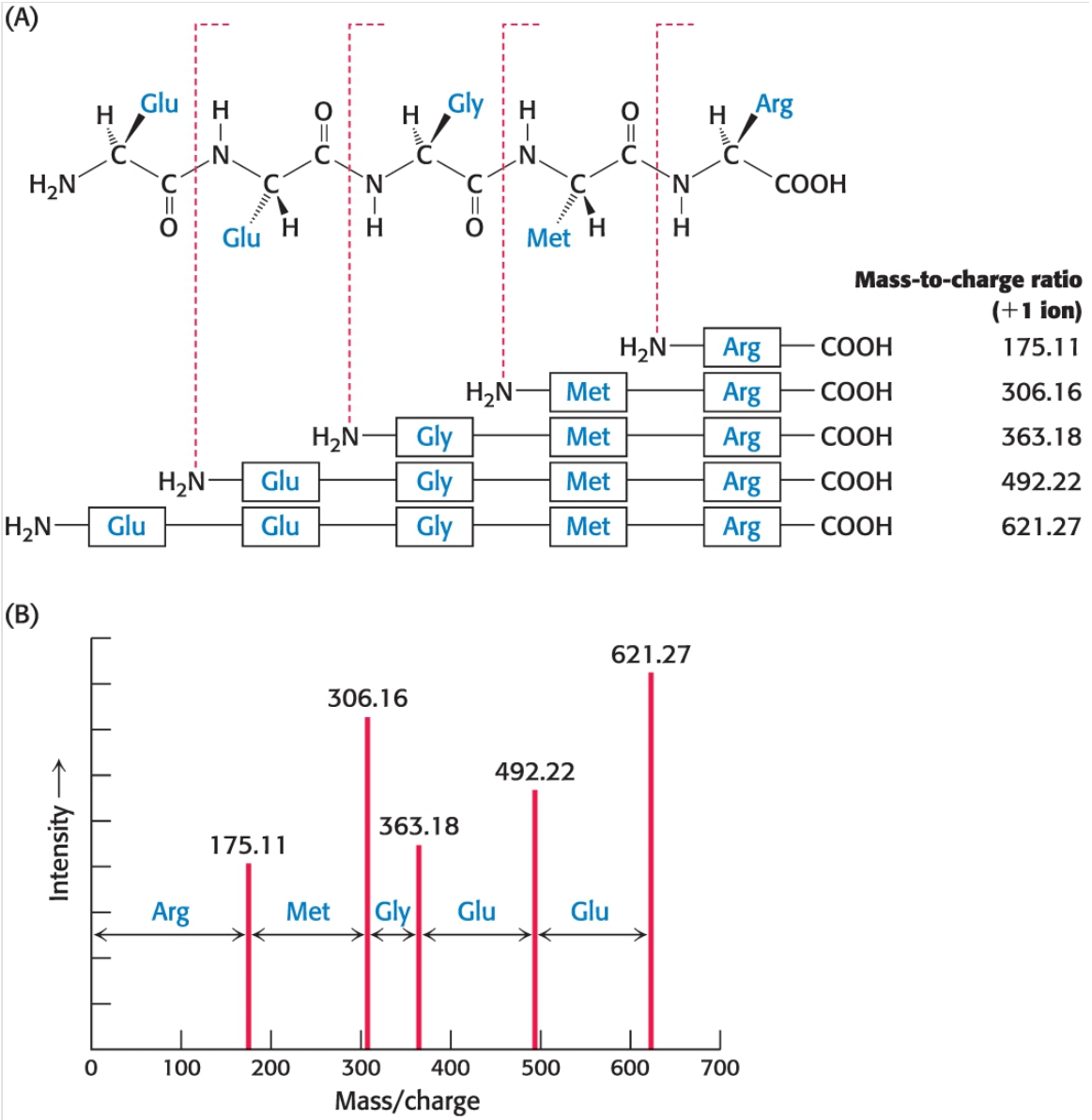


FIGURE 4.26 Peptides can be sequenced by tandem mass spectrometry. (A) Within the mass spectrometer, peptides can be fragmented by bombardment with inert gaseous ions to generat a family of product ions in which individual amino acids have been removed from one end. In th example, the carboxyl fragment of the cleaved peptide bond is ionized. (B) The product ions are detected in the second mass analyzer. The mass differences between the peaks indicate the sequence of amino acids in the precursor ion.

[Data from H. Steen and M. Mann, *Nat. Rev. Mol. Cell Biol.* 5:699–711, 2004.]

VIEW an animation of this technique in Achieve

Self-Check Question



Which two amino acids are indistinguishable by tandem mass spectrometry as described above, and why?

Proteins can be specifically cleaved into small peptides to facilitate analysis

In principle, it should be possible to sequence an entire protein using the Edman degradation or mass spectrometric methods. In practice, the Edman degradation is limited to peptides of 50 residues, because not all peptides in the reaction mixture release the amino acid derivative at each step. For instance, if the efficiency of release for each round were 98%, the proportion of "correct" amino acid released after 60 rounds would be (0.98^{60}), or 0.3 — a hopelessly impure mix.

Similarly, sequencing of long peptides by mass spectrometry yields a mass spectrum that can be complex and difficult to interpret. This obstacle can be overcome by cutting the protein into smaller peptides that can be sequenced. **Table 4.3** lists several ways of cleaving polypeptide chains, with either chemical reagents or proteolytic (protein-breaking) enzymes. Note that these methods are sequence specific: they disrupt the protein backbone at particular amino acid residues in a predictable manner. The peptides obtained by these methods are separated by some type of chromatography. The sequence of each purified peptide can then be more easily determined. At this point, the amino acid sequences of segments of the protein are known, but the order of these segments is not yet defined.

TABLE 4.3 Specific cleavage of polypeptides

Reagent	Cleavage site
Chemical cleavage	
Cyanogen bromide	Carboxyl side of methionine residues
O-Iodosobenzoate	Carboxyl side of tryptophan residues
Hydroxylamine	Asparagine–glycine bonds
2-Nitro-5-thiocyanobenzoate	Amino side of cysteine residues
Enzymatic cleavage	
Trypsin	Carboxyl side of lysine and arginine residues
Clostripain	Carboxyl side of arginine residues
Staphylococcal protease	Carboxyl side of aspartate and glutamate residues (glutamate only under certain conditions)
Thrombin	Carboxyl side of arginine
Chymotrypsin	Carboxyl side of tyrosine, tryptophan, phenylalanine, leucine, and methionine
Carboxypeptidase A	Amino side of C-terminal amino acid (not arginine, lysine, or proline)

How can we order the peptides to obtain the primary structure of the original protein? The necessary additional information is obtained from **overlap peptides** (Figure 4.27). A second enzyme is used to split the polypeptide chain at different linkages. For example, chymotrypsin

cleaves preferentially on the carboxyl side of aromatic and some other bulky nonpolar residues, while trypsin cleaves on the carboxyl side of positively charged residues (Table 4.3). Because these chymotryptic peptides overlap two or more tryptic peptides, they can be used to establish the order of the peptides. The entire amino acid sequence of the polypeptide chain is then known.

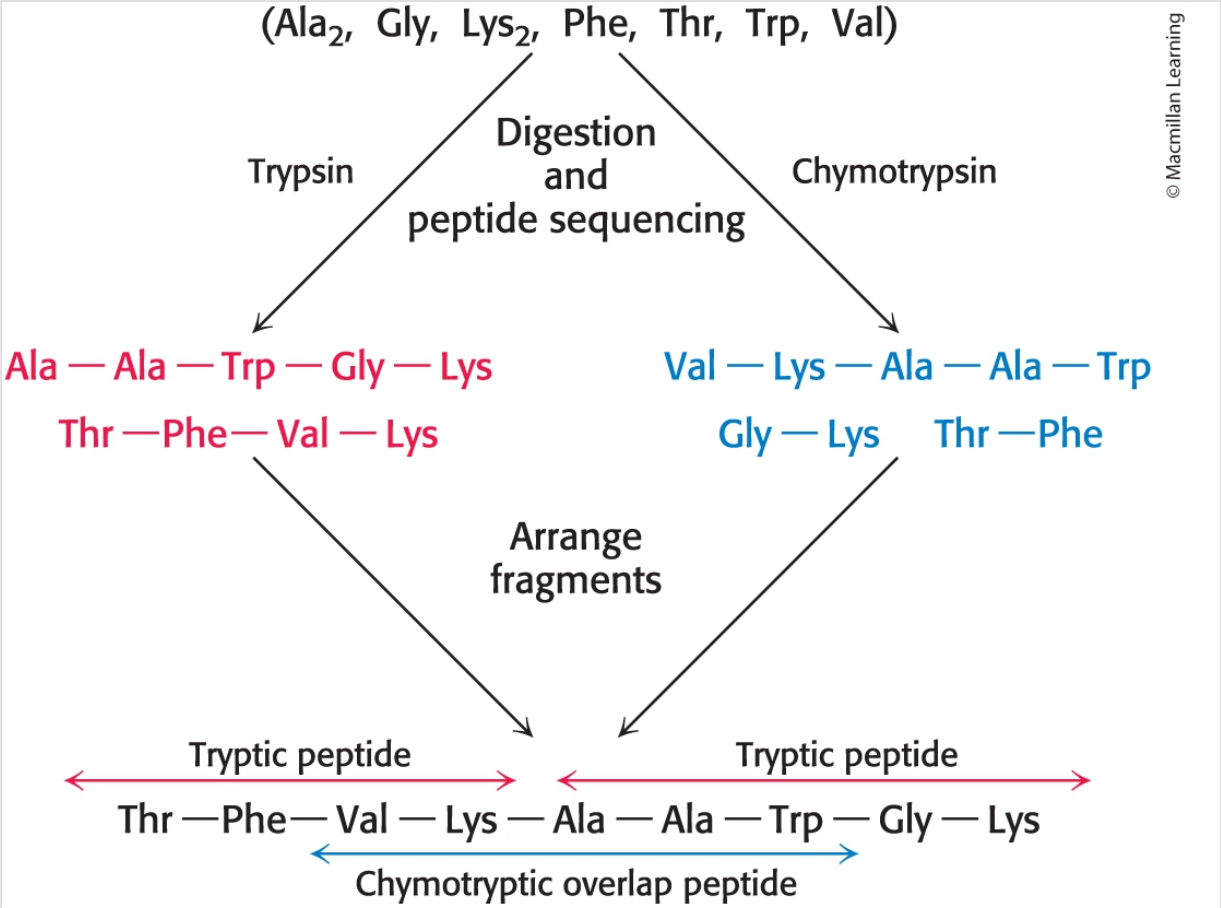


FIGURE 4.27 Overlap peptides are used to establish the order of sequenced peptides. The peptide obtained by chymotryptic digestion overlaps two tryptic peptides, establishing their order.

Additional steps are necessary if the initial protein sample is actually several polypeptide chains. SDS-PAGE under reducing conditions should

display the number of chains. Alternatively, the number of distinct N-terminal amino acids could be determined. After a protein has been identified as being made up of two or more polypeptide chains, the chains must be separated from one another first. Denaturing agents, such as urea or guanidine hydrochloride, are used to dissociate chains held together by noncovalent interactions; polypeptide chains linked by covalent disulfide bonds are separated by reduction with thiols such as β-mercaptoethanol or dithiothreitol. To prevent the cysteine residues from recombining, they are alkylated with iodoacetate to form stable *S*-carboxymethyl derivatives (**Figure 4.28**).

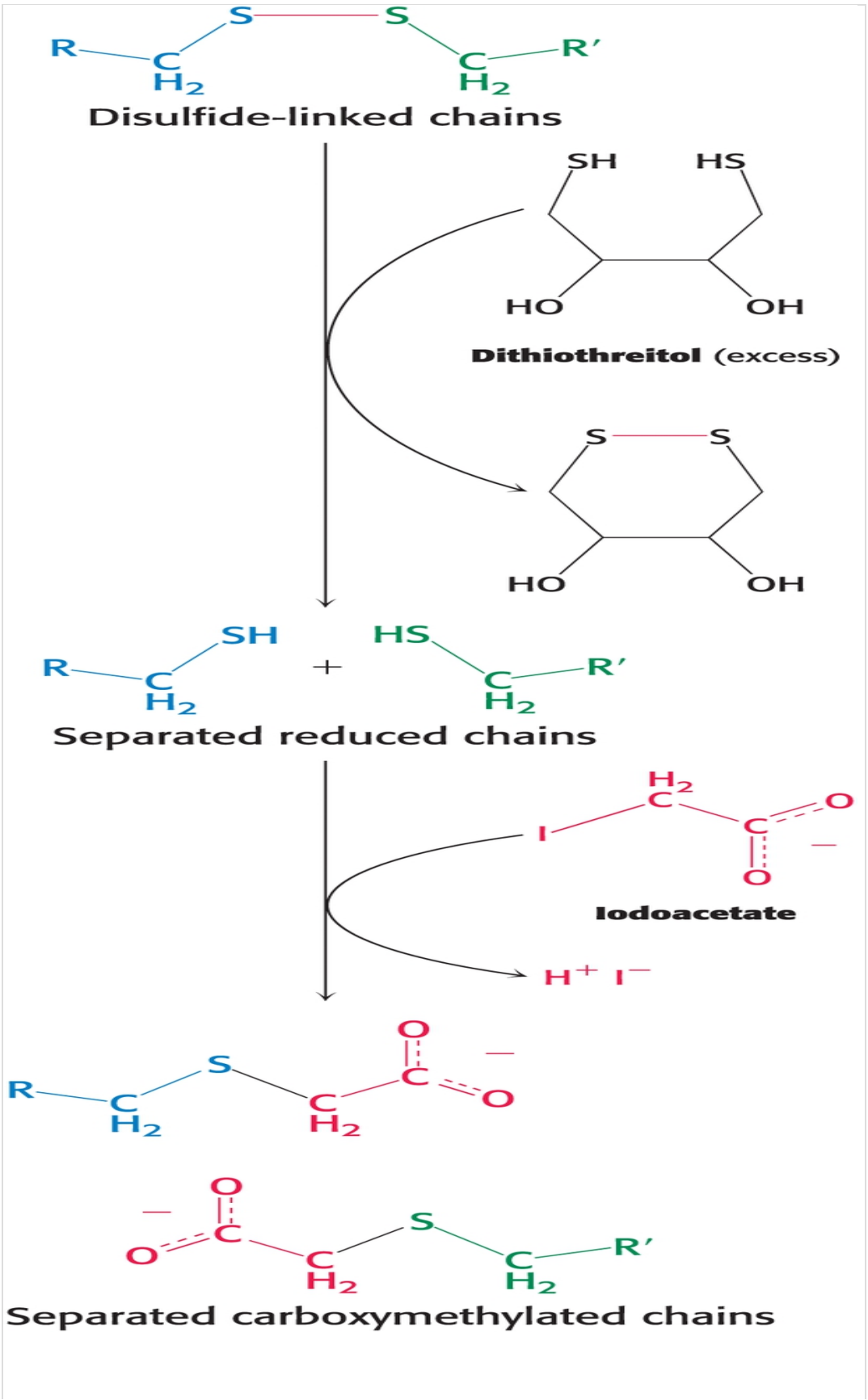

Disulfide-linked chains
Dithiothreitol (excess)
Separated reduced chains
Iodoacetate
Separated carboxymethylated chains

FIGURE 4.28 Reduction and alkylation are used to separate disulfide-linked polypeptides prior to sequencing. Polypeptides linked by disulfide bonds can be separated by reduction with dithiothreitol followed by alkylation to prevent them from re-forming.



Genomic and proteomic methods are complementary approaches to deducing protein structure and function

Despite the technological advancements in both chemical and mass spectrometric methods of peptide sequencing, heroic effort is required to elucidate the sequence of large proteins, those with more than 1000 residues. For sequencing such proteins, a complementary experimental approach based on recombinant DNA technology is often more efficient. As will be discussed in Chapter 9, long stretches of DNA can be cloned and sequenced, and the nucleotide sequence can be translated to reveal the amino acid sequence of the protein encoded by the gene. Recombinant DNA technology has generated a wealth of amino acid sequence information at a remarkable rate.

Even with the use of the DNA base sequence to determine primary structure, however, there is still a need to work with isolated proteins. The amino acid sequence deduced by reading the DNA sequence is that of the nascent protein, the direct product of the translational machinery. However, many proteins undergo posttranslational modifications after their syntheses (Section 2.7). Some have their ends trimmed, and others arise by cleavage of a larger initial polypeptide chain. Cysteine residues in some proteins are oxidized to form disulfide links, connecting either parts within a chain or separate polypeptide chains. Specific side chains of some proteins are altered. Amino acid

sequences derived from DNA sequences are rich in information, but they do not disclose these modifications. Chemical analyses of proteins in their mature form are needed to delineate the nature of these changes, which are critical for the biological activities of most proteins.

The amino acid sequence of a protein provides valuable information

Regardless of the method used for its determination, the amino acid sequence of a protein provides the biochemist with a wealth of information as to the protein's structure, function, and history.

- *The sequence of a protein of interest can be compared with all other known sequences to determine whether significant similarities exist.* A search for kinship between a newly sequenced protein and the millions of previously sequenced ones takes only a few seconds on a personal computer (Chapter 10). If the newly isolated protein is a member of an established class of protein, we can begin to infer information about the protein's structure and function. For instance, chymotrypsin and trypsin are members of the serine protease family, a clan of proteolytic enzymes that have a common catalytic mechanism based on a reactive serine residue (Chapter 6). If the sequence of the newly isolated protein shows sequence similarity with trypsin or chymotrypsin, the result suggests that it, too, may be a serine protease.

- *Comparison of sequences of the same protein in different species yields information about evolutionary pathways.* Evolutionary relationships between species can be inferred from sequence differences between their proteins. If we assume that the random mutation rate of proteins over time is constant, then careful sequence comparison of related proteins between two organisms can provide an estimate for when these two evolutionary lines diverged. For

example, a comparison of serum albumins found in primates indicates that human beings and African apes diverged 5 million years ago, not 30 million years ago as was once thought. Sequence analyses have opened a new perspective on the fossil record and the pathway of human evolution.

- *Amino acid sequences can be searched for the presence of internal repeats*. Such internal repeats can reveal the history of an individual protein itself. Many proteins apparently have arisen by duplication of primordial genes followed by their diversification. For example, calmodulin, a ubiquitous eukaryotic calcium sensor, contains four similar calcium-binding modules that arose by gene duplication (**Figure 4.29**).

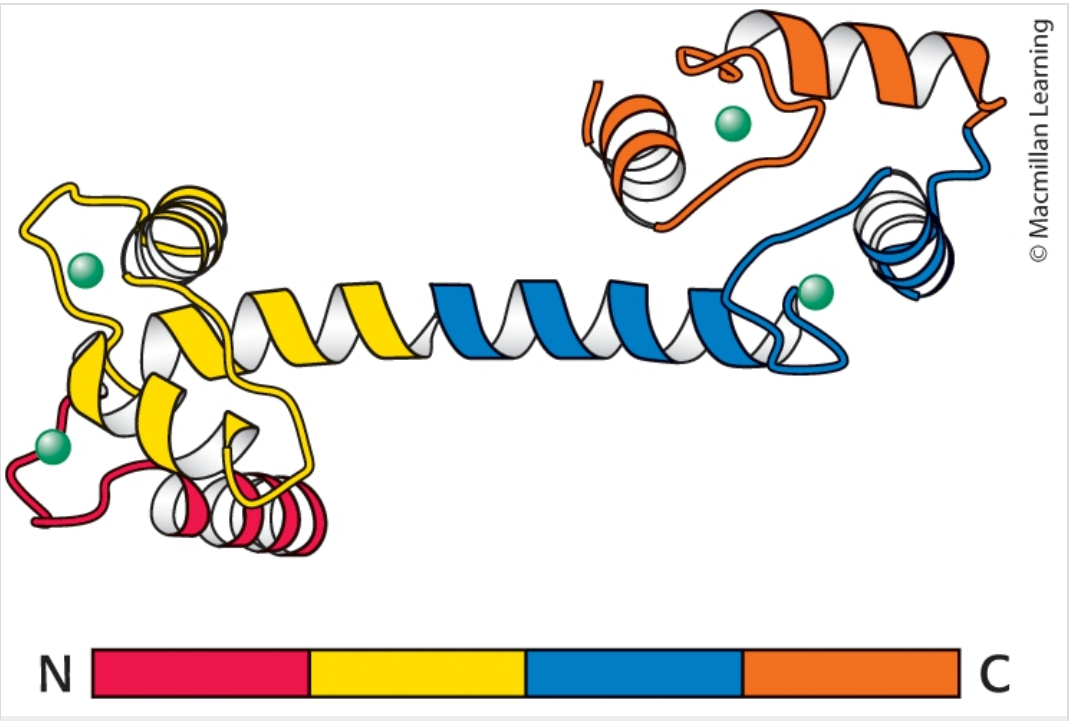
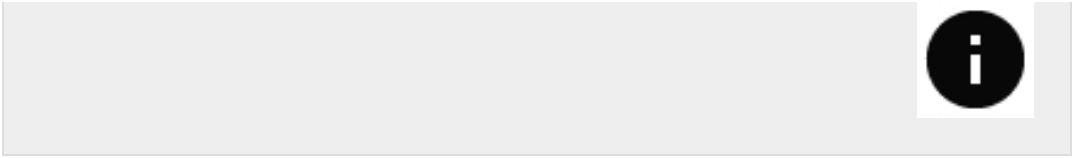


FIGURE 4.29 Many proteins contain internal repeats within their sequences. Calmodulin, a calcium sensor, contains four similar units (shown in red, yellow, blue, and orange) in a single polypeptide chain. Each unit binds a calcium ion (shown in green).

[Drawn from 1CLL.pdb.]

INTERACT with this model in Achieve



- *Many proteins contain amino acid sequences that serve as signals designating their destinations or controlling their processing*. For example, a protein destined for export from a cell or for location in a membrane contains a signal sequence — a stretch of about 20 hydrophobic residues near the amino terminus that directs the protein to the appropriate membrane. Another protein may contain a stretch of amino acids that functions as a nuclear localization signal, directing the protein to the nucleus. Identification of these sequences within a protein provides clues to its function within the cell.

- *Sequence data provide a basis for preparing antibodies specific for a protein of interest*. One or more parts of the amino acid sequence of a protein will elicit an antibody when injected into a mouse or rabbit. These specific antibodies can be very useful in determining the amount of a protein present in solution or in the blood, ascertaining its distribution within a cell, or cloning its gene (Section 4.2).

- *Amino acid sequences are valuable for making DNA probes that are specific for the genes encoding the corresponding proteins*. Knowledge of a protein's primary structure means that DNA sequences corresponding to a part of the amino acid sequence can be constructed on the basis of the genetic code. These DNA sequences can be used as probes to isolate the gene encoding the protein so that the entire sequence of the protein can be determined. The gene in turn can provide valuable information about the physiological regulation of the protein. Protein sequencing is an integral part of molecular genetics, just as DNA cloning is central to the analysis of protein structure and function. We will revisit some of these topics in more detail in Chapter 9.

Individual proteins can be identified by mass spectrometry

The combination of mass spectrometry with chromatographic and peptide-cleavage techniques enables highly sensitive protein identification in complex biological mixtures. When a protein is cleaved by chemical or enzymatic methods (Table 4.3), a specific and predictable family of peptide fragments is formed. We learned in Chapter 2 that each protein has a unique, precisely defined amino acid sequence. Hence, the identity of the individual peptides formed from this cleavage reaction — and, importantly, their corresponding masses — is a distinctive signature for that particular protein. Protein cleavage, followed by chromatographic separation and mass spectrometry, enables rapid identification and quantitation of these signatures, even if they are present at very low concentrations. This technique for protein identification is referred to as **peptide mass fingerprinting**.

The speed and sensitivity of mass spectrometry has made this technology critical for the study of proteomics. Let us consider the analysis of the nuclear pore complex from yeast, which facilitates the transport of large molecules into and out of the nucleus. This huge macromolecular complex — around 100,000 kDa! — was purified from yeast cells, then fractionated by HPLC followed by gel electrophoresis. Individual bands from the gel were isolated, cleaved with trypsin, and analyzed by MALDI-TOF mass spectrometry. The fragments produced were compared with amino acid sequences deduced from the DNA sequence of the yeast genome, as shown in **Figure 4.30**. A total of 174 nuclear pore proteins were identified in this manner.

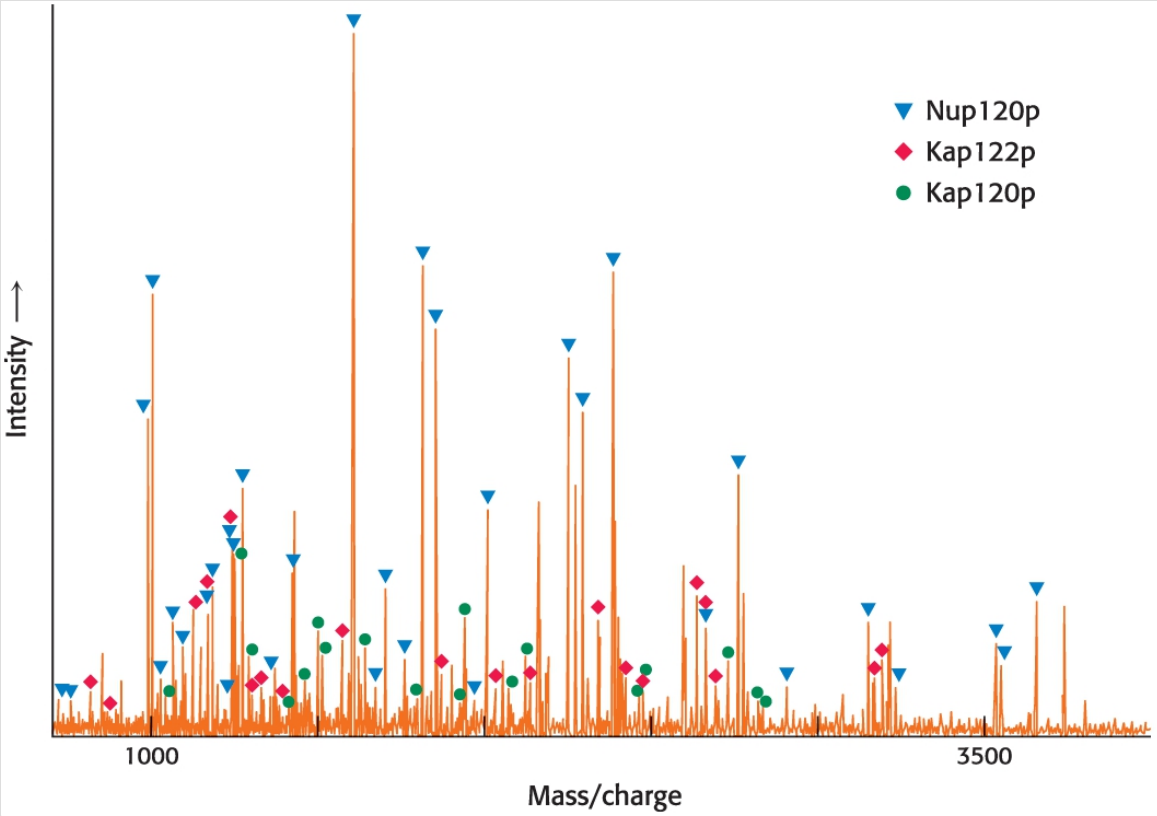


FIGURE 4.30 Peptide mass fingerprinting can identify individual proteins within complex mixtures. This mass spectrum was obtained by analyzing a trypsin-treated band in a gel derive from a yeast nuclear-pore sample. Many of the peaks were found to match the masses predicte for peptide fragments from three proteins (Nup120p, Kap122p, and Kap120p) within the yeast genome.

[Data from M. P. Rout, J. D. Aitchison, A. Suprapto, K. Hjertaas, Y. Zhao, and B. T. Chait, *J. Cell Biol*. 148:635–651, 200

Many of the proteins found in this experiment had not previously been identified as being associated with the nuclear pore despite years of study. Furthermore, mass spectrometric methods are sensitive enough to detect essentially all components of the pore if they are present in the samples used. Thus, a complete list of the components constituting this macromolecular complex could be obtained in a straightforward manner.

The proteome is the functional representation of the genome

Thus far, we have discussed several techniques, including two-dimensional electrophoresis and peptide mass fingerprinting, which allow for the rapid and scalable detection and quantitation of large numbers of proteins in a single experiment. These methods can be used to (1) explore the compete catalog of proteins expressed in a cell under a specific set of conditions, and (2) investigate how this inventory changes when these conditions are altered. These studies, referred to as *proteomics*, can be very powerful in understanding the mechanisms by which cells adapt to changing environments.

As will be discussed in Chapter 9, the complete DNA base sequences, or genomes, of many organisms are now available. For example, the roundworm *Caenorhabditis elegans* has a genome of 97 million bases and about 19,000 protein-encoding genes, whereas that of the fruit fly *Drosophila melanogaster* contains 180 million bases and about 14,000 genes. The completely sequenced human genome contains 3 billion bases and about 23,000 genes. However, these genomes are simply inventories of the genes that could be expressed within a cell under specific conditions. Only a subset of the proteins encoded by these genes will actually be present in a given biological context. The **proteome** — derived from proteins expressed by the genome — of an organism signifies a more complex level of information content, encompassing the types, functions, and interactions of proteins within its biological environment.

The proteome is not a fixed characteristic of the cell. Because it represents the functional expression of information, it varies with cell type, developmental stage, and environmental conditions. The proteome is much larger than the genome because almost all gene products are proteins that can be chemically modified in a variety of ways. Furthermore, these proteins do not exist in isolation; they often

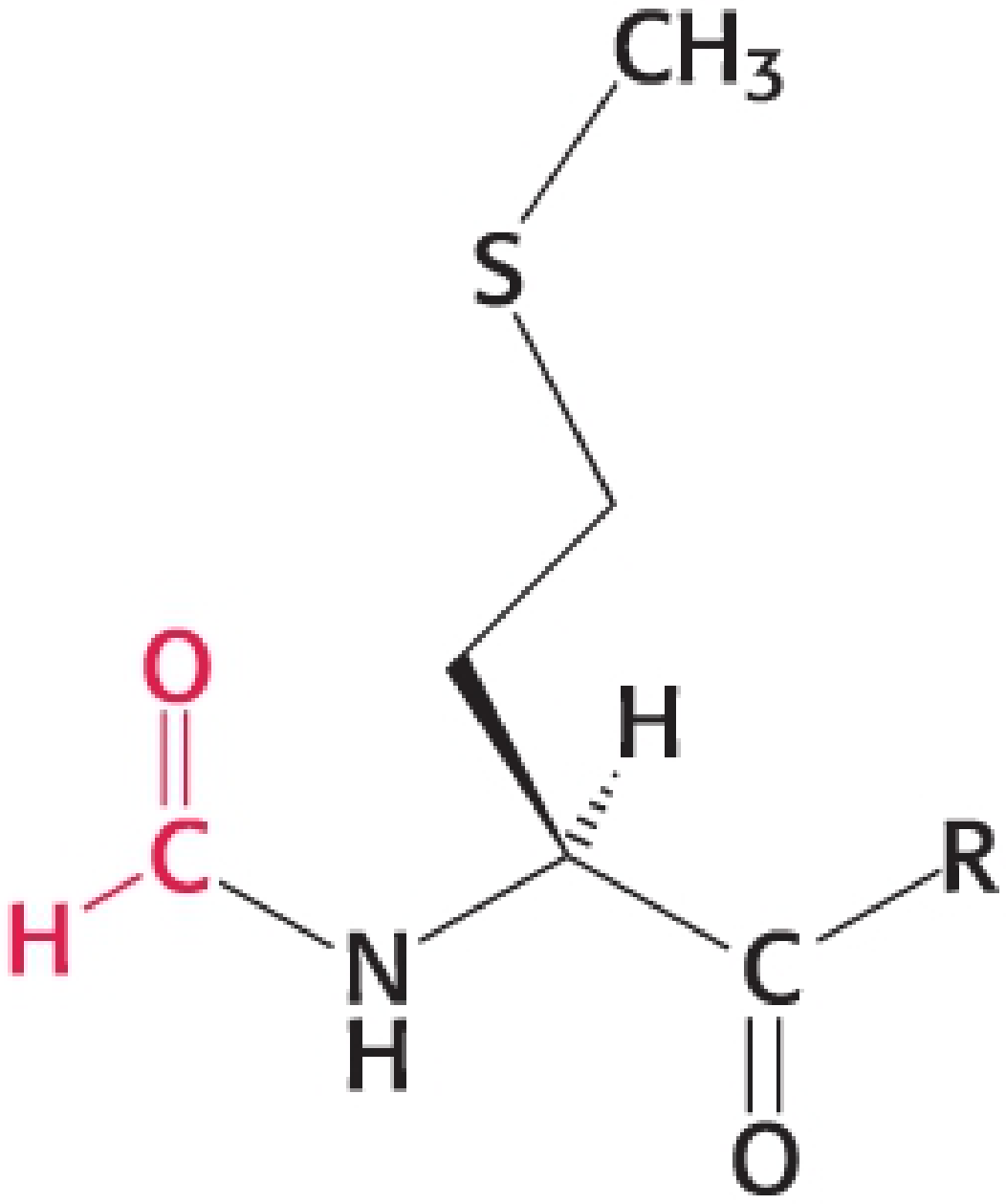
interact with one another to form complexes with specific functional properties. Whereas the genome is “hard wired,” the proteome is highly dynamic. The techniques we have described in this section enable the understanding of the proteome by providing a means of investigating, characterizing, and cataloging proteins.

4.4 Peptides Can Be Synthesized by Automated Solid-Phase Methods

Peptides of defined sequence can be synthesized to assist in biochemical analysis. These peptides are valuable tools for several purposes.

- *Synthetic peptides can serve as antigens to stimulate the formation of specific antibodies*. Suppose we want to isolate the protein expressed by a specific gene. Peptides can be synthesized that match the translation of part of the gene's nucleic acid sequence, and antibodies can be generated that target these peptides. These antibodies can then be used to isolate the intact protein or localize it within the cell.

- *Synthetic peptides can be used to isolate receptors for many hormones and other signal molecules*. For example, white blood cells are attracted to bacteria by formylmethionyl (fMet) peptides released in the breakdown of bacterial proteins. Synthetic formylmethionyl peptides have been useful in identifying the cell-surface receptor for this class of peptide. Moreover, synthetic peptides can be attached to agarose beads to prepare affinity chromatography columns for the purification of receptor proteins that specifically recognize the peptides.



fMet peptide

- *Synthetic peptides enable the study of the effects of nonproteinogenic amino acids on protein structure and function.* Recall from Section 2.2 that proteins synthesized within the cell are composed from a repertoire of 20 natural, or *proteinogenic*, amino acids. Chemical synthesis of peptides provides a convenient method for inserting *nonproteinogenic* amino acids — that is, those not directly coded into the genome — into peptides. Examples of nonproteinogenic amino acids include the D isomers of the proteinogenic amino acids (e.g., D-alanine) and amino acids that contain posttranslational modifications (Section 2.7), such as hydroxyproline. Peptides containing these amino acids are valuable tools in the study of protein structure and function.

- *Synthetic peptides can serve as drugs.* Vasopressin is a peptide hormone that stimulates the reabsorption of water in the kidney, leading to the formation of more-concentrated urine. Patients with diabetes insipidus are deficient in vasopressin (also called *antidiuretic hormone*), and so they excrete large volumes of dilute urine (more than 5 liters per day) and are continually thirsty. This defect can be treated by administering 1-desamino-8-D-arginine vasopressin (also called desmopressin), a synthetic analog of the missing hormone (**Figure 4.31**). This synthetic peptide is degraded in the body much more slowly than vasopressin and does not increase blood pressure.

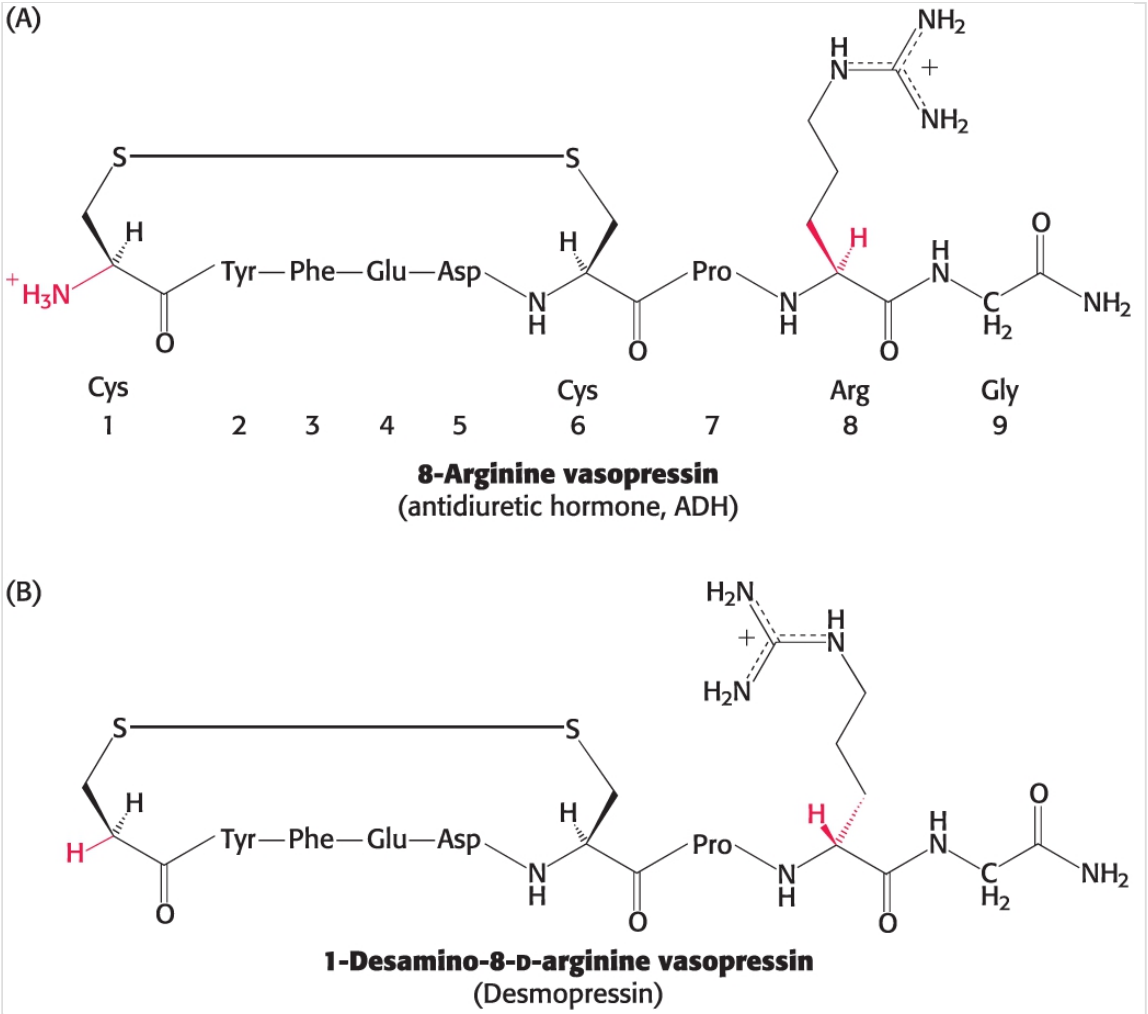


FIGURE 4.31 Desmopressin, a synthetic vasopressin analog, can be used to treat patients deficient in vasopressin. Structural formulas of (A) vasopressin, a peptide hormone that stimulates water resorption, and (B) 1-desamino-8-D-arginine vasopressin (desmopressin), a more stable synthetic analog of this antidiuretic hormone.

- *Studying synthetic peptides can help define the rules governing the three-dimensional structure of proteins.* We can ask whether a particular sequence by itself tends to fold into an α helix, a β strand, or a hairpin turn, or behaves as a random coil (Section 2.4). The peptides created for such studies can incorporate amino acids not

normally found in proteins, allowing greater variation in chemical structure than is possible with the use of only 20 amino acids.

How are these peptides constructed? The **solid-phase method**, first developed by R. Bruce Merrifield, provides a highly efficient approach to the synthesis of polypeptides (**Figure 4.32**). Recall that the amino group of one amino acid can link to the carboxyl group of any another. However, a unique product will form if only a single amino group and a single carboxyl group are available for reaction. To achieve this, it is necessary to block some groups and to activate others to prevent unwanted reactions:

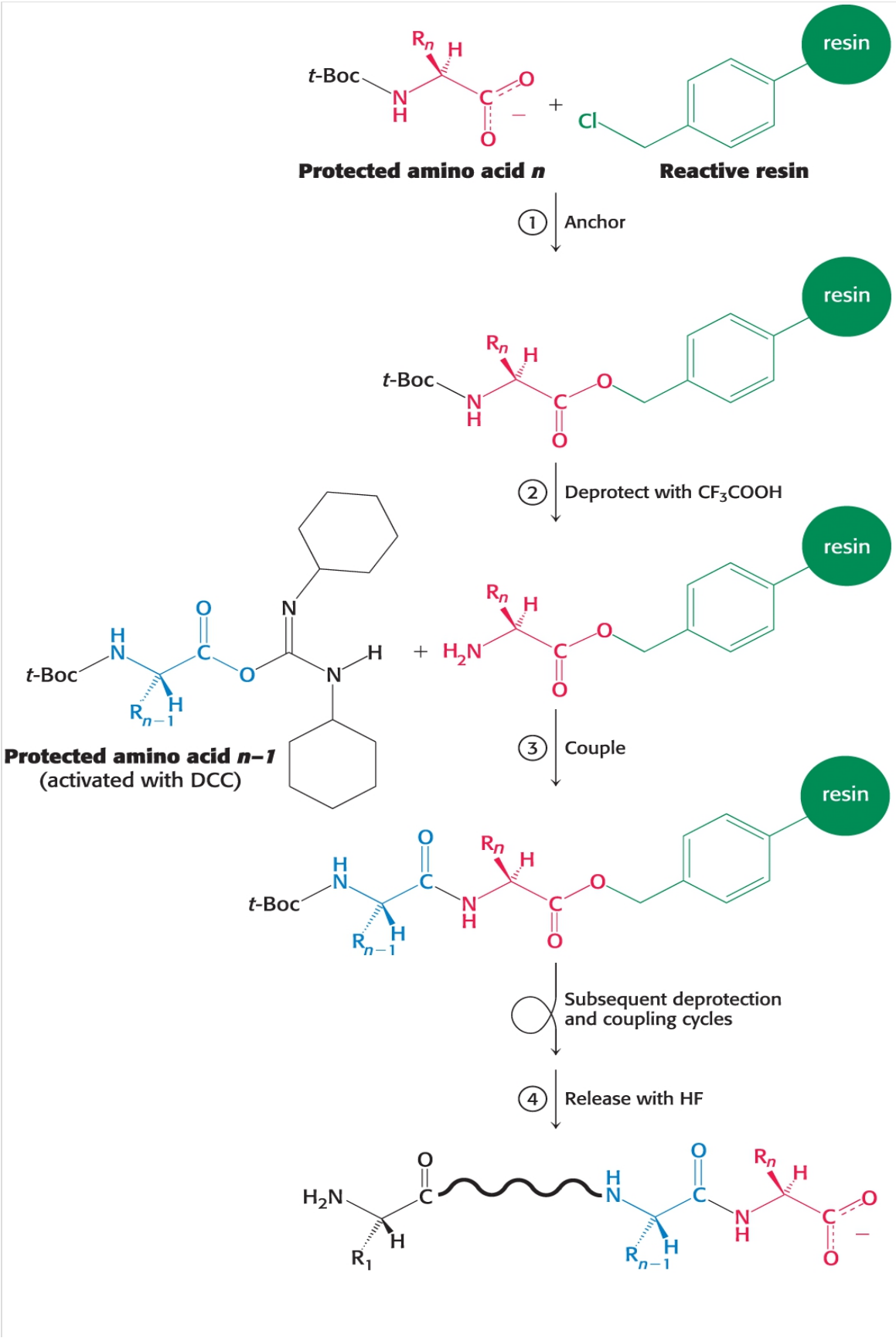
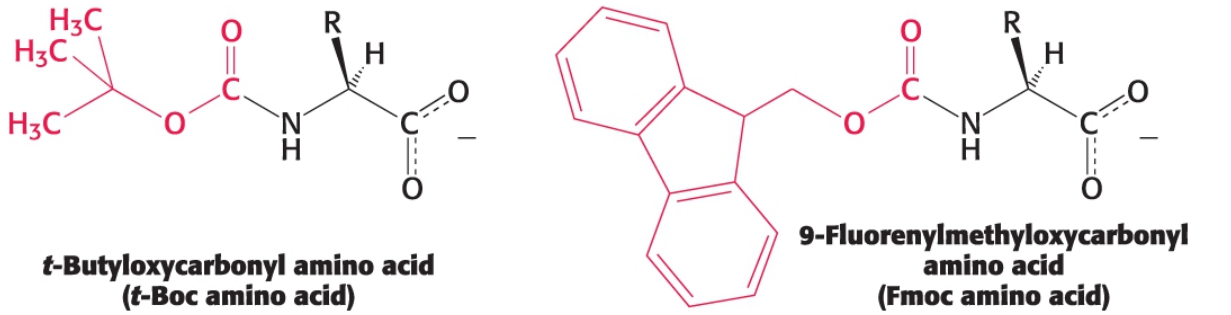

t-Boc
Protected amino acid n
Cl
resin
Reactive resin
1 Anchor
2 Deprotect with CF3COOH
Protected amino acid n–1
(activated with DCC)
3 Couple
Subsequent deprotection
and coupling cycles
4 Release with HF

FIGURE 4.32 Solid-phase peptide synthesis is achieved by repeated coupling and deprotectic steps. The sequence of steps in solid-phase synthesis is: (1) anchoring of the *t*-Boc-protected C-terminal amino acid to a solid resin, (2) deprotection of the amino terminus, and (3) coupling of the free amino terminus with the DCC-activated carboxyl group of the next *t*-Boc-protected amino acid. Steps 2 and 3 are repeated for each added amino acid. Finally, in step 4, the completed peptide is released from the resin.

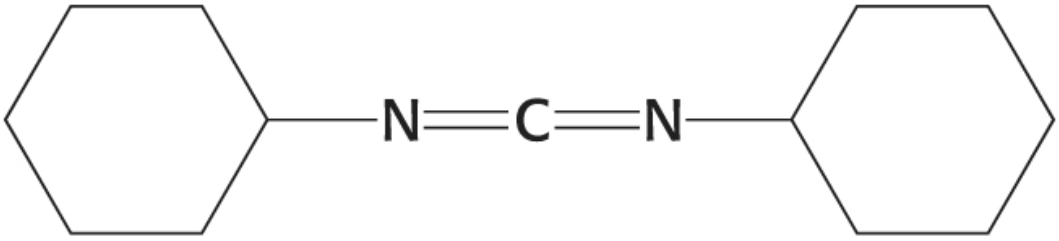
1. First, the carboxyl-terminal amino acid (shown in red in Figure 4.32) is anchored to an insoluble resin, usually beads, by its carboxyl group, effectively protecting it from further peptide-bond-forming reactions. The α-amino group of this amino acid is blocked with a protecting group such as the *tert*-butyloxycarbonyl (*t*-Boc) or the 9-fluorenylmethyloxycarboyl (Fmoc) group. In this example, we will use the *t*-Boc protecting groups.



2. The *t*-Boc protecting group of this amino acid is then removed with trifluoroacetic acid, freeing the α-amino group for the next coupling reaction.

3. The next amino acid (in the protected *t*-Boc form, shown in blue in Figure 4.32) and dicyclohexylcarbodiimide (DCC) are added together. At this stage, only the carboxyl group of the incoming amino acid and the amino group of the resin-bound amino acid are

free to form a peptide bond. DCC reacts with the carboxyl group of the incoming amino acid, activating it for the peptide-bond-forming reaction. After the peptide bond has formed, excess reagents are washed away, leaving the desired dipeptide product attached to the beads. Additional amino acids are linked by repeating Steps 2 and 3.



Dicyclohexylcarbodiimide (DCC)

4. At the end of the synthesis, the peptide is released from the beads by the addition of hydrofluoric acid (HF), which cleaves the carboxyl ester anchor without disrupting peptide bonds. Protecting groups on potentially reactive side chains, such as that of lysine, also are removed at this time.

A major advantage of the solid-phase method is that the desired product at each stage is bound to beads that can be rapidly filtered and washed. Hence, there is no need to purify intermediates. Additionally, all reactions are carried out in a single vessel, eliminating losses caused by repeated transfers of products, and the cycle of reactions can be readily automated, which makes it feasible to routinely synthesize peptides containing about 50 residues in good yield and purity.

Even larger peptides can be synthesized using a technique called *native chemical ligation*. In this approach, two synthetic peptide fragments can

be linked together provided the C-terminus of one peptide features a thioester and the N-terminal residue of the other peptide is a cysteine residue (Figure 4.33). In the first step, a trans-thioesterification reaction occurs, where the side-chain sulfur of the cysteine residue displaces the thiol group of the incoming thioester. This is followed by the rapid, irreversible rearrangement of the new thioester, yielding a new peptide bond. Native chemical ligation can be used to link together multiple peptide fragments, allowing for the synthesis of fully active proteins over 100 residues in length.

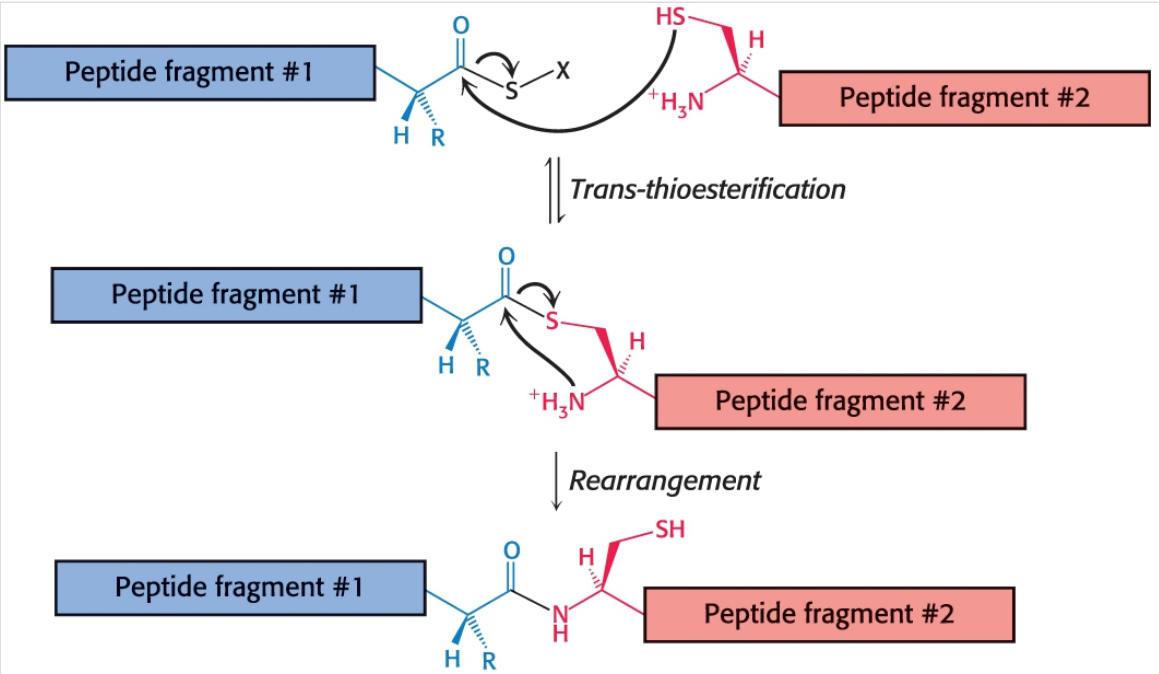


FIGURE 4.33 Native chemical ligation can be used to link two synthetic peptides. The sulfur atom of the N-terminal cysteine of one synthetic peptide ("Peptide fragment #2") undergoes a trans-thioesterification reaction with the C-terminal thioester of the other peptide ("Peptide fragment #1"). A rapid, irreversible rearrangement leads to the formation of a peptide bond between the two fragments.

4.5 Three-Dimensional Protein Structures Can Be Determined Experimentally

Elucidating the three-dimensional structure of a protein can provide a tremendous amount of insight into its corresponding function. For example, the precise atomic arrangements within active sites and binding sites provide clues to their specificities. Knowing a protein's structure enables the biochemist to predict its mechanism of action, the effects of mutations on its function, and the desired features of drugs that may inhibit or augment its activity. X-ray crystallography, nuclear magnetic resonance spectroscopy, and cryo-electron microscopy are the most important techniques for elucidating the conformation of proteins.



Universal Images Group Editorial/Getty Images

ROSALIND FRANKLIN Today, Rosalind Franklin is known as the x-ray crystallographer who generated clear diffraction patterns for DNA. Her data were used by James Watson and Francis Crick to develop their proposed structural model of the DNA double helix. However, the importance of her contributions to this landmark achievement were not fully appreciated or acknowledged at the time. Dr. Franklin had completed her PhD in physical chemistry, studying the density and porosity of coal, and she then learned x-ray crystallography to examine structural changes in carbon upon heating. She was a very skilled experimentalist and began to apply x-ray crystallographic techniques to the structure of DNA two years before the structural proposal by Watson and Crick. She subsequently did outstanding work on the structures of viruses. Her structural analysis of the polio virus was abruptly cut short by her untimely death from ovarian cancer at the age of 37. The subsequent

publication of the polio virus structure by John Finch and Aaron Klug was dedicated to her memory.

X-ray crystallography reveals three-dimensional structure in atomic detail

The first method developed to determine protein structure in atomic detail was **x-ray crystallography**. This technique provides the clearest visualization of the precise three-dimensional positions of most atoms within a protein. Of all forms of radiation, x-rays provide the best resolution for the determination of molecular structures because their wavelength approximately corresponds to the length of a covalent bond. While the details of crystallography can be technically challenging, there are several fundamental steps required in an x-ray crystallographic experiment (**Figure 4.34**):

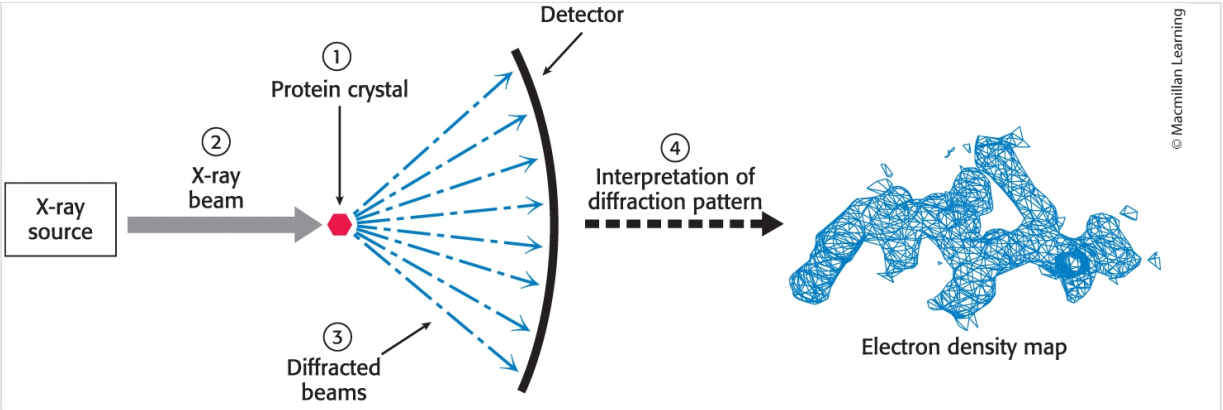


FIGURE 4.34 An x-ray crystallographic experiment is composed of several fundamental steps. (1) A crystal of the protein is prepared, then (2) placed within the path of an x-ray beam. (3) The crystal diffracts the beam, and the resulting pattern is collected on a detector. (4) The diffraction pattern is interpreted using computational methods to generate an electron density map, which enables the determination of the atomic positions of the protein.

VIEW an animation of this technique in Achieve

1. *Preparing a protein crystal.* X-ray crystallography first requires the preparation of a protein or protein complex in crystal form, in which all protein molecules are oriented in a fixed, repeated arrangement with respect to one another. Slowly adding ammonium sulfate or another salt to a concentrated solution of protein to reduce its solubility favors the formation of highly ordered crystals — the process of salting out discussed in Section 4.1.

   Protein crystallization can be challenging: a concentrated solution of highly pure material is required, and it is often difficult to predict which experimental conditions will yield the most-effective crystals. Typically, hundreds of conditions must be tested to obtain crystals fully suitable for crystallographic studies. Nevertheless, increasingly large and complex proteins have been crystallized. For example, poliovirus, an 8500-kDa assembly of 240 protein subunits surrounding an RNA core, has been crystallized and its structure solved by x-ray methods. Crucially, proteins frequently crystallize in their biologically active configuration, and thus enzyme crystals may display catalytic activity if the crystals are suffused with substrate.

2. *Exposing the crystal to a source of x-rays.* After a suitably pure crystal of protein has been obtained, a source of x-rays is required. A beam of x-rays of wavelength 1.54 Å is produced by accelerating electrons against a copper target. Alternatively, x-rays can be produced by the acceleration of electrons in circular orbits at speeds close to the speed of light, a phenomenon referred to as *synchrotron radiation*. Synchrotron-generated x-ray beams are much more intense than those generated by electrons hitting copper. The higher intensity allows high-quality data to be gathered from smaller crystals over a shorter exposure time. There are around 100 facilities across the world that generate synchrotron radiation.

3. *Detecting the diffraction of the x-ray by the crystal.* When a narrow beam of x-rays is directed at the protein crystal, most of the beam

passes directly through the crystal while a small part is scattered in various directions. These scattered, or diffracted, x-rays can be detected by x-ray film or by a solid-state electronic detector.

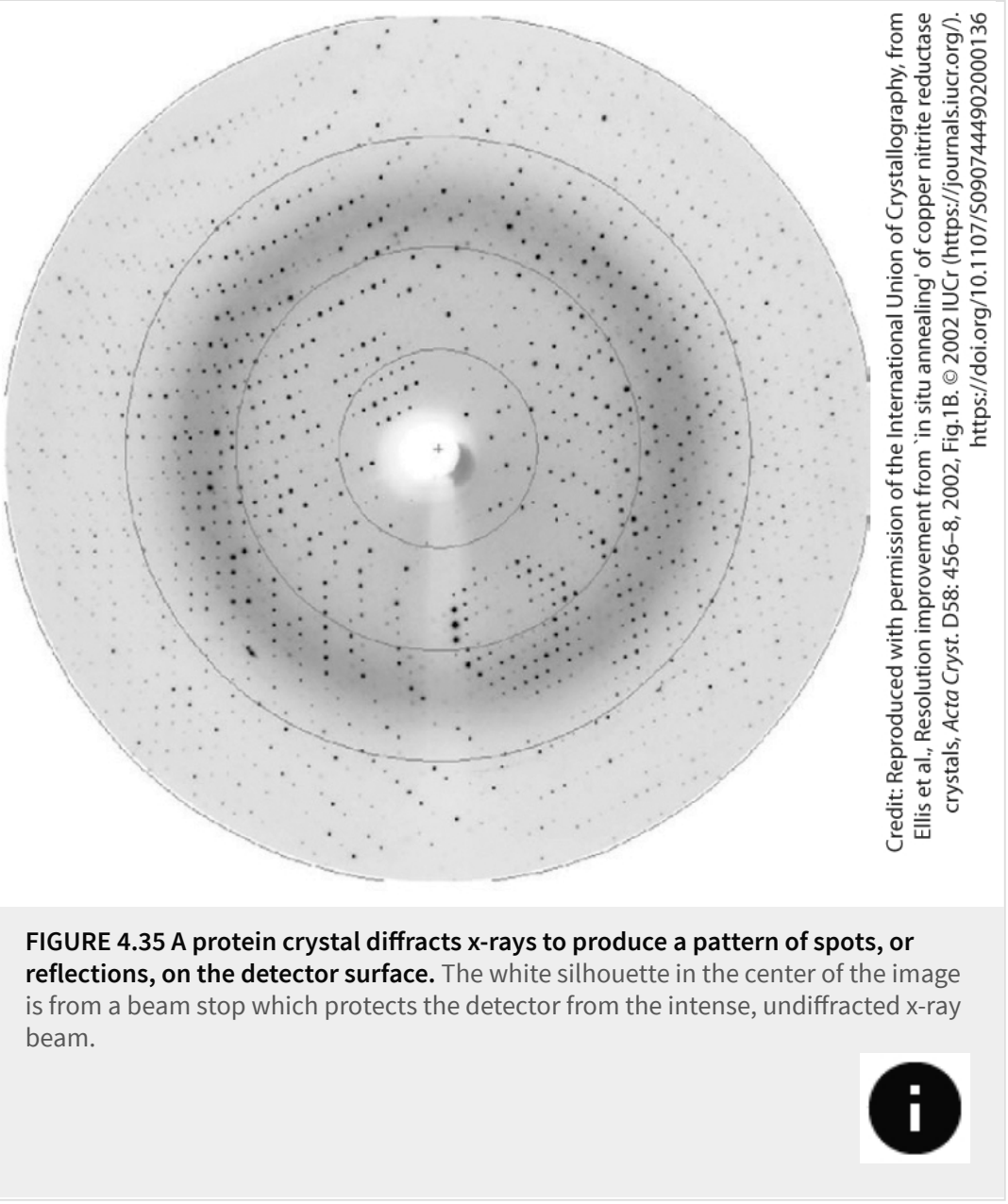
The scattering pattern produced by the diffracted x-rays provides abundant information about protein structure. The basic physical principles underlying the technique are:

- *Electrons scatter x-rays*. The amplitude of the wave scattered by an atom is proportional to its number of electrons. Thus, a carbon atom scatters six times as strongly as a hydrogen atom does.

- *The scattered waves recombine*. Each diffracted beam comprises waves scattered by each atom in the crystal. The scattered waves reinforce one another at the film or detector if they are in phase — that is, they are aligned — and they cancel one another if they are out of phase.

- *The way in which the scattered waves recombine depends only on the atomic arrangement*. The protein crystal is mounted and positioned in a precise orientation with respect to the x-ray beam and the film. The crystal is rotated so that the beam can strike the crystal from many directions. This rotational motion results in an x-ray photograph consisting of a regular array of spots called *reflections*.

The intensities and positions of these reflections are the basic experimental data of an x-ray crystallographic analysis. The x-ray photograph shown in **Figure 4.35** is a two-dimensional section through a three-dimensional array of tens of thousands of reflections. Each reflection is formed from a wave with an amplitude proportional to the square root of the observed intensity of the spot. Each wave also has a phase — that is, the timing of its crests and troughs relative to those of other waves. Additional experiments or calculations must be performed to determine the phases corresponding to each reflection.



Credit: Reproduced with permission of the International Union of Crystallography, from Ellis et al., Resolution improvement from `in situ annealing' of copper nitrite reductase crystals, *Acta Cryst.* D58: 456–8, 2002, Fig.1B. © 2002 IUCr (https://journals.iucr.org/). https://doi.org/10.1107/S0907444902000136

FIGURE 4.35 A protein crystal diffracts x-rays to produce a pattern of spots, or reflections, on the detector surface. The white silhouette in the center of the image is from a beam stop which protects the detector from the intense, undiffracted x-ray beam.

4. *Interpreting the diffraction pattern into an electron density map.* The next step is to reconstruct an image of the protein from the observed reflections. In light microscopy or electron microscopy, the diffracted beams are focused by lenses to directly form an image. However, appropriate lenses for focusing x-rays do not exist. Instead, the image is formed by applying a mathematical calculation called a *Fourier transform* to the measured amplitudes and calculated phases of every observed reflection. The image

obtained is referred to as the **electron-density map**. This map is a three-dimensional graphic representation of where the electrons are most densely localized and it is used to determine the positions of the atoms in the crystallized molecule (Figure 4.36).

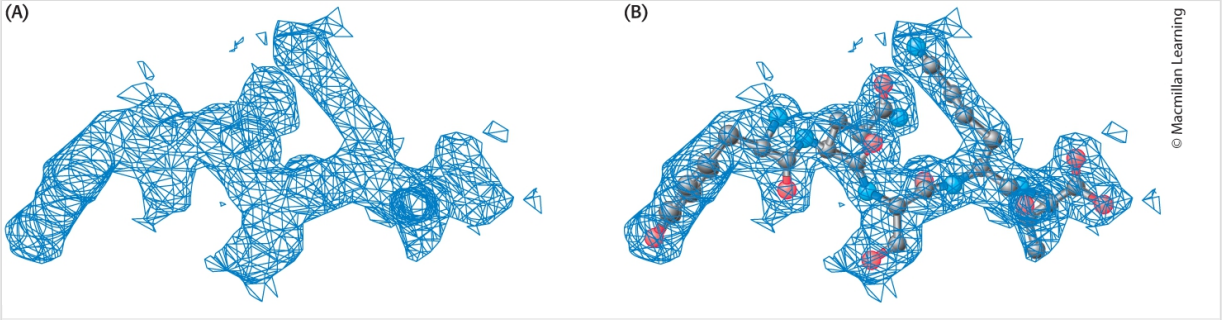


FIGURE 4.36 The electron-density map enables the determination of atomic positions of the crystallized protein. (A) A segment of an electron-density map is drawn as a three-dimensional contour plot, in which the regions inside the "cage" represent the regions of highest electron density. (B) A model of the protein is built into this map so as to maximize the placement of atoms within this density.

[Drawn from 1FCH.pdb.]

Critical to the interpretation of the electron-density map is its resolution, which is established by the number of scattered intensities used in the Fourier transform. The fidelity of the image depends on this resolution. A resolution of $6\ \text{Å}$ reveals the course of the polypeptide chain but few other structural details. The reason is that polypeptide chains pack together so that their centers are between $5\ \text{Å}$ and $10\ \text{Å}$ apart. Maps at higher resolution are needed to delineate groups of atoms, which lie between $2.8\ \text{Å}$ and $4.0\ \text{Å}$ apart, and individual atoms, which are between $1.0\ \text{Å}$ and $1.5\ \text{Å}$ apart (Figure 4.37). The ultimate resolution of an x-ray analysis is determined by the degree of perfection

of the crystal. For proteins, this limiting resolution is often about $2\ \text{Å}$; however, in exceptional cases, resolutions of $1.0\ \text{Å}$ have been obtained.

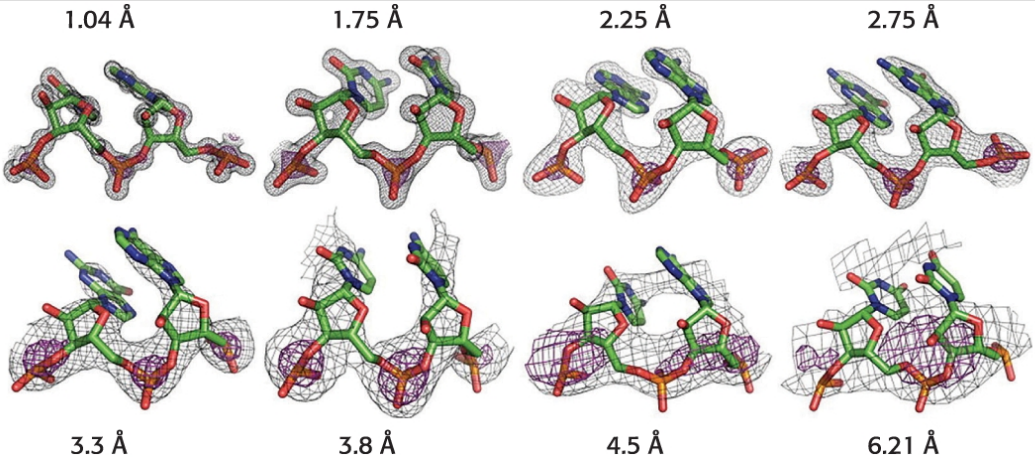


FIGURE 4.37 Resolution affects the quality of the electron density map. Electron density maps at six different resolution levels are shown. At the low resolution levels ($4.5\ \text{Å}$ and $6.21\ \text{Å}$) only a poorly defined area of density is visible, whereas at the higher resolutions, individual atoms are distinguishable.

Self-Check Question

Structures of proteins comprising domains separated by flexible linker regions can be quite difficult to solve by x-ray crystallographic methods. Why might this be the case?

Nuclear magnetic resonance spectroscopy can reveal the structures of proteins in solution

While x-ray crystallography is a powerful method for determining protein structures, some proteins do not readily crystallize. Furthermore, nonphysiological conditions (such as pH and added salts) are often required for successful crystallization. In addition, crystallized proteins adopt conformations that may be influenced by constraints imposed by the crystalline environment. However, since most proteins function not in crystalline form but in solution under physiological conditions, greater insight into protein function may be gained by other methods.

Nuclear magnetic resonance (NMR) spectroscopy is unique in being able to reveal the atomic structure of macromolecules in solution, provided that highly concentrated solutions ($\sim 1\ \text{mM}$, or $15\ \text{mg ml}^{-1}$ for a 15-kDa protein) can be obtained. This technique depends on the fact that certain atomic nuclei are intrinsically magnetic. Only a limited number of isotopes display this property, called *spin*; Table 4.4 lists those most important to biochemistry.

TABLE 4.4 Biologically important nuclei giving NMR signals

Nucleus	Natural abundance (% by weight of the element)
^{1}H	99.984
^{2}H	0.016
^{13}C	1.108

^{14}N	99.635
^{15}N	0.365
^{17}O	0.037
^{23}Na	100.0
^{25}Mg	10.05
^{31}P	100.0
^{35}Cl	75.4
^{39}K	93.1

The simplest example of an isotope with spin is the hydrogen nucleus (^{1}H), which is a proton. The spinning of a proton generates a property called a *magnetic moment*. This moment can take either of two orientations, called *spin states* (α and β), when an external magnetic field is applied (**Figure 4.38**). The energy difference between these states is proportional to the strength of the imposed magnetic field. The α state has a slightly lower energy because it is aligned with this applied field. Hence, in a given population of nuclei, slightly more will occupy the α state (by a factor of the order of 1.00001 in a typical experiment). A spinning proton in an α state can be raised to an excited state (β state) by applying a pulse of electromagnetic radiation (a radio-frequency, or RF, pulse), provided that the frequency corresponds to the energy difference between the α and the β states. In these circumstances, the

spin will change from α to β; in other words, resonance will be obtained.

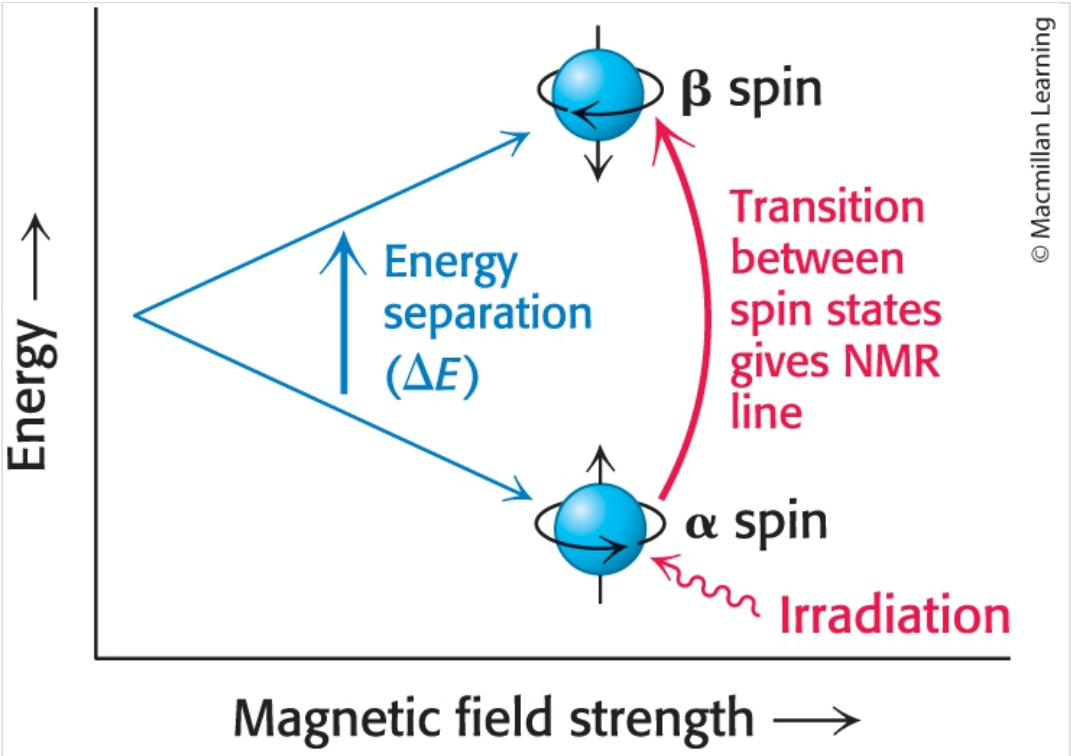


FIGURE 4.38 The transition between spin states forms the basis of NMR spectroscopy. The energies of the two orientations of an intrinsically magnetic nucleus depend on the strength of the applied magnetic field. Absorption of electromagnetic radiation of appropriate frequency induces a transition from the lower to the upper level.

VIEW an animation of NMR spectroscopy in Achieve

These properties can be used to examine the chemical surroundings of the hydrogen nucleus. The flow of electrons around a magnetic nucleus generates a small, local magnetic field that opposes the applied field. The degree of such shielding depends on the surrounding electron density. Consequently, nuclei in different environments will change states, or resonate, at slightly different field strengths or radiation frequencies.

One-dimensional NMR

Most protons in many proteins can be resolved by using a technique called *one-dimensional NMR*, in which a resonance spectrum for a molecule is obtained by keeping the magnetic field constant and varying the frequency of the electromagnetic radiation. The nuclei of the perturbed sample absorb electromagnetic radiation at a measurable frequency. The different frequencies, termed **chemical shifts**, are expressed in fractional units δ (parts per million, or ppm) relative to the shifts of a standard compound, such as a water-soluble derivative of tetramethylsilane, that is added with the sample. For example, a $-CH_3$ proton typically exhibits a chemical shift (δ) of 1 ppm, compared with a chemical shift of 7 ppm for an aromatic proton. The chemical shifts of most protons in protein molecules fall between 0 and 9 ppm (**Figure 4.39**). With this information, we can then deduce changes to a particular chemical group under different conditions, such as the conformational change of a protein from a disordered structure to an α helix in response to a change in pH.

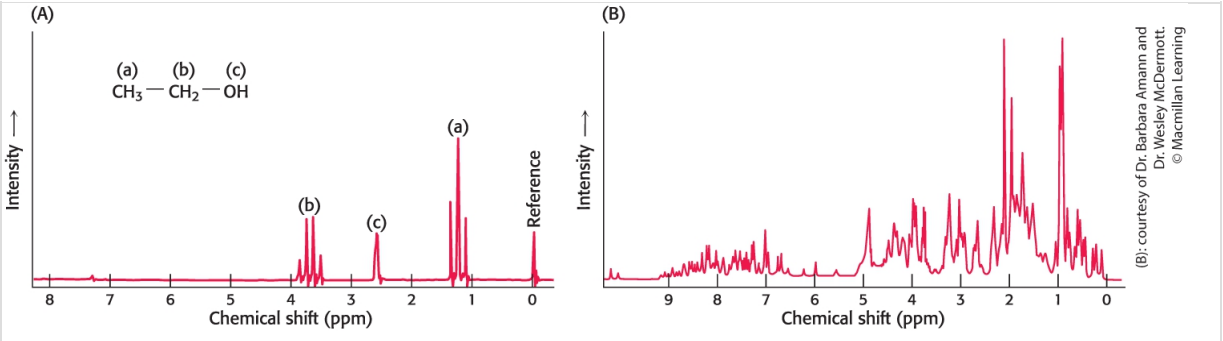


FIGURE 4.39 One-dimensional ^1H NMR spectra reveal the chemical shifts of protons within the sample. (A) ^1H-NMR spectrum of ethanol (CH_3CH_2OH) shows that the chemical shifts for the hydrogen are clearly resolved. (B) ^1H-NMR spectrum of a 55 amino acid fragment of a protein having a role in RNA splicing shows a greater degree of complexity. A large number of peaks are present, and many overlap.

[(A) Data from C. Branden and J. Tooze, *Introduction to Protein Structure* (Garland, 1991), p. 280.]

Two-dimensional NMR

We can garner even more information by examining how the spins on different protons affect their neighbors. Through the application of a radio-frequency pulse to briefly induce magnetization in the sample, we can alter the spin on one nucleus and examine the effect on the spin of a neighboring nucleus. Especially revealing is a two-dimensional spectrum obtained by nuclear Overhauser enhancement spectroscopy (NOESY), which graphically displays pairs of protons that are in close proximity, even if they are not close together in the primary structure. The basis for this technique is the **nuclear Overhauser effect**, an interaction between nuclei that is proportional to the inverse sixth power of the distance between them. Magnetization is transferred from an excited nucleus to an unexcited one if the two nuclei are less than about 5 Å apart (**Figure 4.40A**).

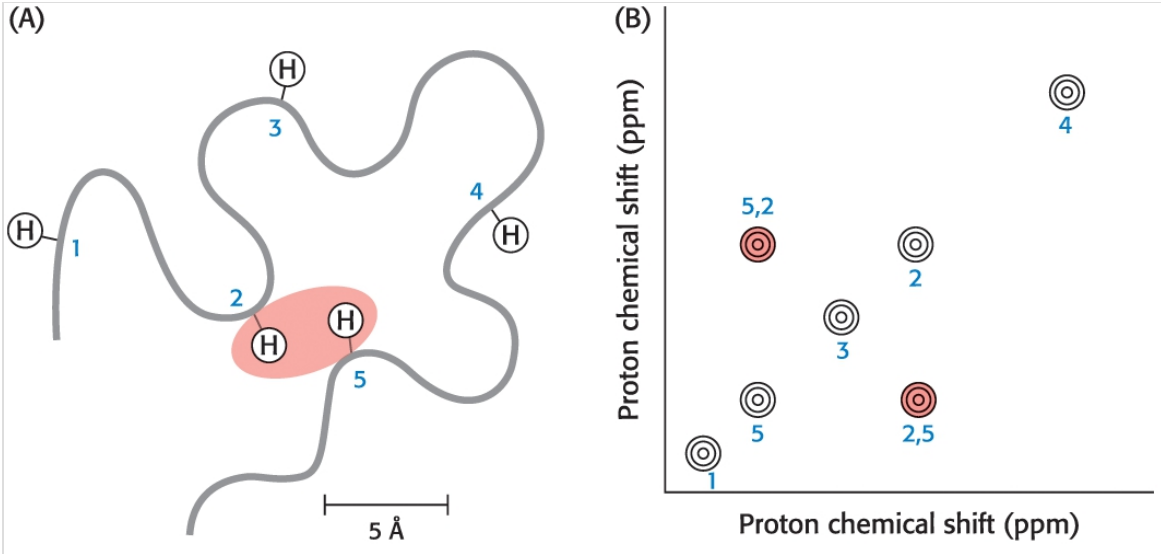


FIGURE 4.40 The nuclear Overhauser effect identifies pairs of protons that are in close proximity. (A) Schematic representation of a polypeptide chain highlighting five particular

protons. Protons 2 and 5 are in close proximity (~ 4 Å apart), whereas other pairs are farther apart. (B) A highly simplified NOESY spectrum. The diagonal shows five peaks corresponding to the five protons in part A. The peak above the diagonal and the symmetrically related one belo reveal that proton 2 is close to proton 5.



In other words, the nuclear Overhauser effect provides a means of detecting the location of atoms relative to one another in the three-dimensional structure of the protein. The peaks that lie along the diagonal of a NOESY spectrum (shown in white in **Figure 4.40B**) correspond to those present in a one-dimensional NMR experiment. The peaks apart from the diagonal (shown in red in Figure 4.40B), referred to as *off-diagonal peaks* or *cross-peaks*, provide crucial new information: they identify pairs of protons that are less than 5 Å apart.

A two-dimensional NOESY spectrum for a protein comprising 55 amino acids is shown in **Figure 4.41**. The large number of off-diagonal peaks reveals short proton–proton distances. The three-dimensional structure of a protein can be reconstructed with the use of such proximity relationships. Structures are calculated such that proton pairs identified by NOESY cross-peaks must be separated by less than 5 Å in the three-dimensional structure (**Figure 4.42**). If a sufficient number of distance constraints are applied, the three-dimensional structure can nearly be determined uniquely.

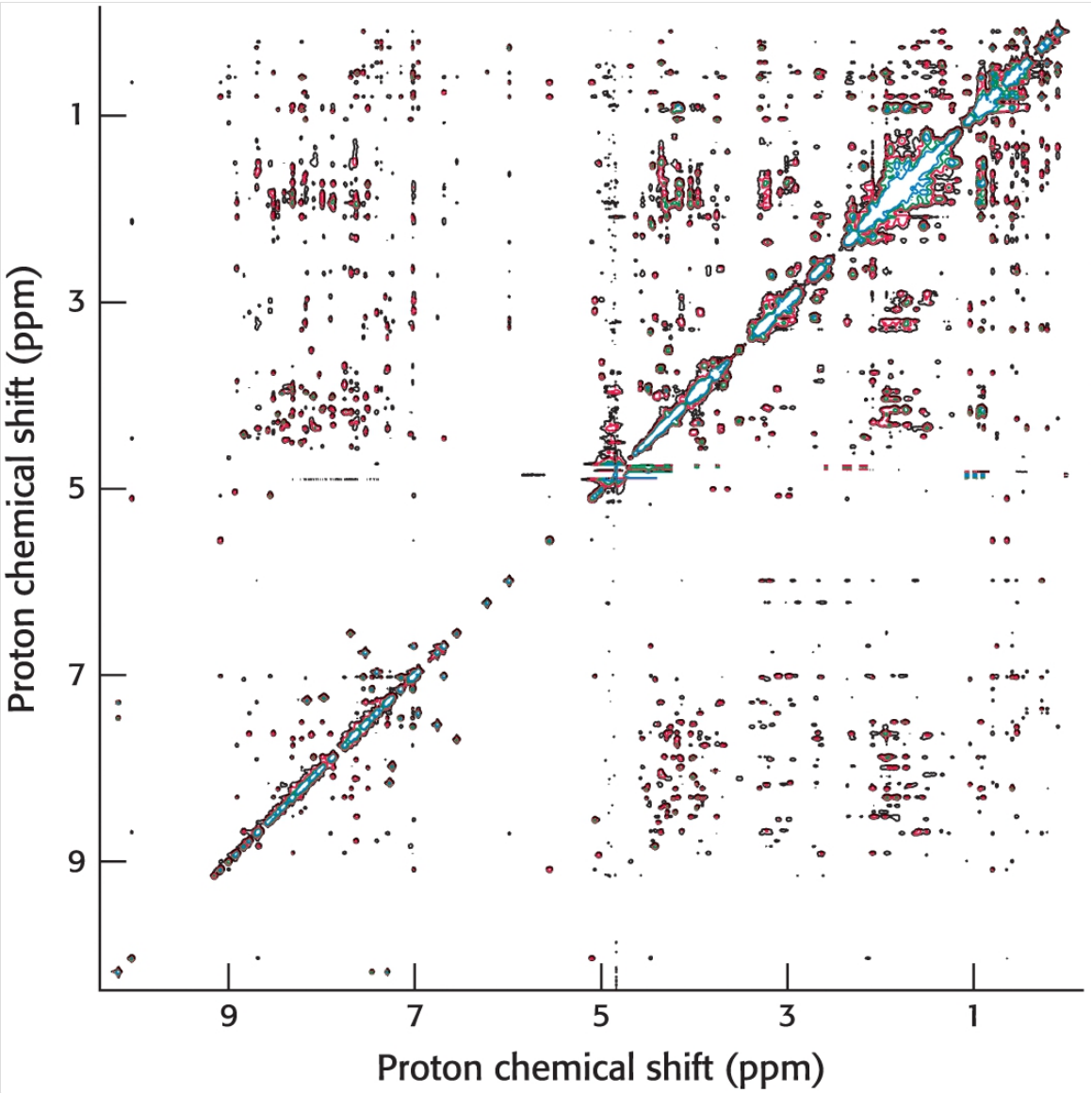


FIGURE 4.41 The NOESY spectrum for a protein reveals many short proton–proton distances. Each off-diagonal peak corresponds to a short proton–proton separation. This spectrum, obtained from a 55-amino-acid protein domain, reveals hundreds of such short proton–proton distances, which can be used to determine the three-dimensional structure of this domain.

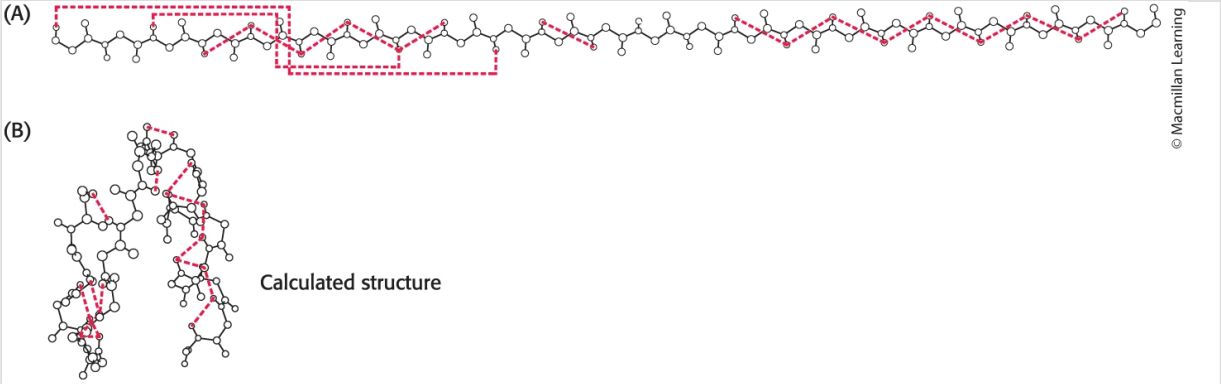
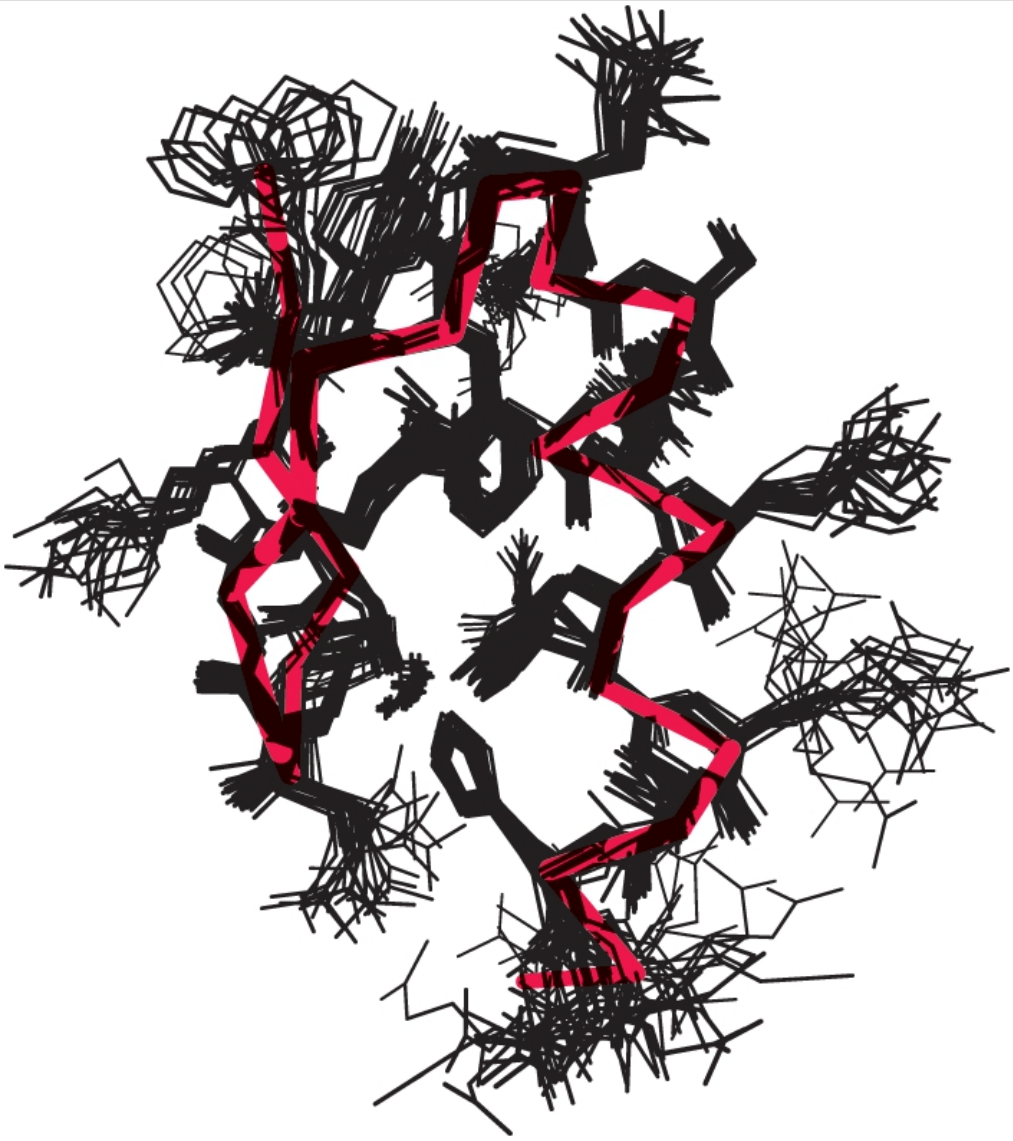


FIGURE 4.42 Structures are calculated on the basis of NMR constraints. (A) NOESY observations show that protons (connected by dotted red lines) are close to one another in space. (B) A three-dimensional structure calculated with these proton pairs constrained to be close together.

In practice, a family of related structures is generated by two-dimensional NMR spectroscopy for three reasons (Figure 4.43). First, not enough constraints may be experimentally accessible to fully specify the structure. Second, the distances obtained from analysis of the NOESY spectrum are only approximate. Finally, the experimental observations are made not on single molecules but on a large number of molecules in solution that may have slightly different structures at any given moment. Thus, the family of structures generated from NMR structure analysis indicates the range of conformations for the protein in solution. With the ability of recombinant DNA technology to produce proteins labeled uniformly or at specific sites with ^{13}C, ^{15}N, and ^{2}H, structural determination by NMR spectroscopy can be applied to proteins up to 50 kDa. While solving the structure of proteins above this limit remains challenging, creative approaches have allowed NMR spectroscopy to address many important questions relating to very large proteins.



Courtesy of Dr. Barbara Amann

FIGURE 4.43 NMR spectroscopy generates a family of related structures. A set of 25 structures placed on top of each other for a 28-amino-acid domain from a DNA-binding protein. The red line traces the average course of the protein backbone. Each of these structures is consistent with hundreds of constraints derived from NMR experiments. The differences between the individual structures are due to a combination of imperfections in the experimental data and the dynamic nature of proteins in solution.

Cryo-electron microscopy can be used to determine the structures of large proteins and macromolecular complexes

As we shall see throughout this book, the structures determined by x-ray crystallography and NMR spectroscopy have illuminated much of our understanding of protein function. However, certain proteins, especially those that form large macromolecular complexes or are embedded within lipid membranes, represent a unique challenge. While crystallographic methods have been developed to enable structure determination of such proteins, these techniques can be quite complex and are not always reliable. An additional method for protein structure determination, **cryo-electron microscopy (cryo-EM)**, has emerged as a viable alternative.

In order to perform cryo-EM, a thin layer of the protein solution is prepared in a fine grid and then frozen very quickly, trapping the molecules in an ensemble of orientations. The sample is then placed in a transmission electron microscope under vacuum conditions and exposed to an incident electron beam. Each protein interacts with the beam to produce a two-dimensional projection on the image capture device, or detector. Many projections are detected, each capturing a molecule in a different orientation (**Figure 4.44A**). Using a process called *single-particle analysis*, these projections are assembled to build a three-dimensional representation of the protein (**Figure 4.44B**).

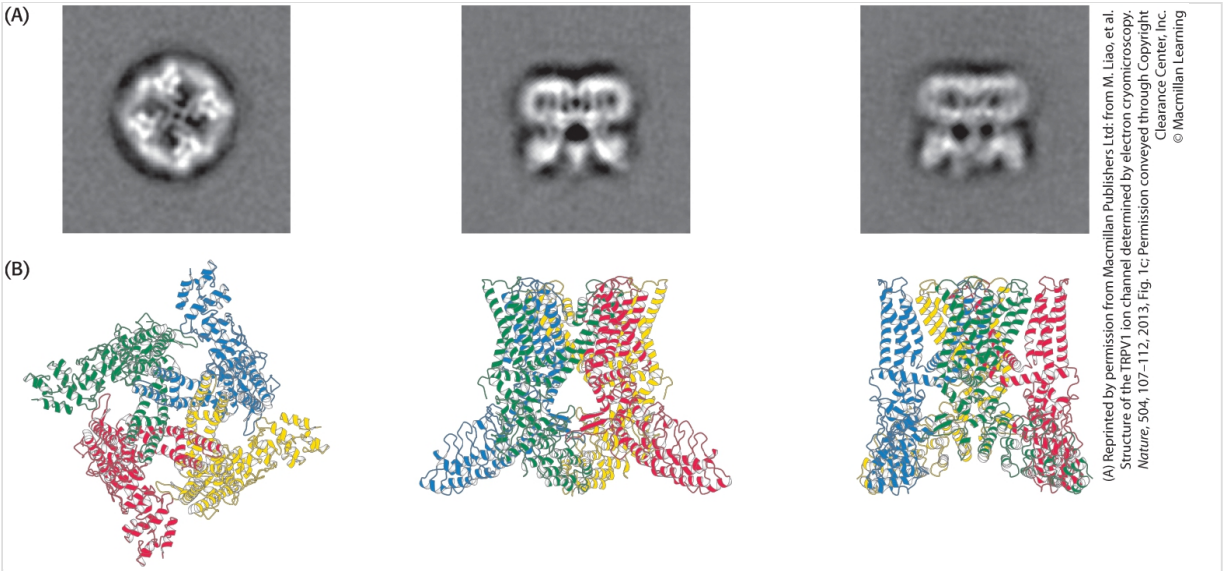


FIGURE 4.44 Cryo-EM captures numerous projections of a protein complex. The projections detected in a cryo-EM experiment represent two-dimensional images of the protein trapped in various orientations. Three such projections of the tetrameric protein TRPV1 are shown in (A). Collection of many such projections enables the reconstruction of a three-dimensional model of the protein, as depicted in (B).

[(B) Drawn from 3J5P.pdb.]

With improvements in image quality and sample preparation, cryo-EM is delivering structures at resolutions approaching $3\ \text{Å}$ or better. At this level, details of atomic groups emerge. For example, cryo-EM studies were able to identify the location and structure of small molecules within the structure of TRPV1, the tetrameric protein present in the plasma membranes of pain-sensing neurons and depicted in Figure 4.44. At this resolution, cryo-EM can be used to aid the discovery and optimization of drug molecules (Chapter 32).

In addition, cryo-EM enables the visualization of very large molecular complexes. Consider the spliceosome, a complex of 4 oligonucleotide chains and over 30 protein subunits that plays an important role in the processing of eukaryotic messenger RNA (Chapter 29). While x-ray

crystallographic methods have been unable to determine the structure of this massive complex, it has been solved to nearly $3.5\ \text{Å}$ resolution by cryo-EM.

By the end of 2020, x-ray crystallography, NMR spectroscopy, and cryo-EM had revealed the structures of over 170,000 proteins. Several new structures are now determined each day. The coordinates are collected at the Protein Data Bank (www.pdb.org), and the structures can be accessed for visualization and analysis. Knowledge of the detailed molecular architecture of proteins has provided insight into how proteins recognize and bind other molecules, how they function as enzymes, how they fold, and how they have evolved. This extraordinarily rich harvest is continuing at a rapid pace and is greatly influencing the entire field of biochemistry as well as other biological and physical sciences.

Chapter 4 Summary

4.1 The Purification of Proteins Is an Essential First Step in Understanding Their Function

- Effective protein purification relies on the development of an assay, used to determine the specific activity of a sample.
- The starting point for protein purification is the homogenate, in which the cellular membranes have been disrupted.
- Chromatography can separate proteins on the basis of size (gel-filtration chromatography), charge (ion-exchange chromatography), and specific binding to a ligand (affinity chromatography).
- Proteins can be separated and easily visualized by gel electrophoresis.
- Isoelectric focusing separates proteins on the basis of their isoelectric points.
- Two-dimensional electrophoresis combines isoelectric focusing and gel electrophoresis to separate complex mixtures of proteins.

4.2 Immunology Provides Important Techniques for Investigating Proteins

- Antibodies against a specific protein can be generated by injecting the protein, or a fragment of the protein, into an animal and collecting the antiserum.
- Monoclonal antibodies can be obtained by the hybridoma method.
- Using antibodies, proteins can be sensitively detected using enzyme-linked immunosorbent assays and western blotting.
- Labeled antibodies can be used to visualize proteins within cells and tissues.

4.3 Mass Spectrometry Is a Powerful Technique for the Identification of Peptides and Proteins

- Tandem mass spectrometry enables the rapid and highly accurate sequencing of peptides.
- Knowledge of a sequence provides valuable clues to the conformation, function, and evolutionary history of a protein.
- Peptide mass fingerprinting can be used to identify proteins, even in complex mixtures and at very low concentrations.
- Mass spectrometric techniques are central to proteomics because they make it possible to analyze the constituents of large macromolecular assemblies or other collections of proteins.

4.4 Peptides Can Be Synthesized by Automated Solid-Phase Methods

- Synthetic peptides have many important applications, including as antigens for the generation of antibodies.
- In the solid phase method, repeated cycles of peptide coupling and deprotection of a growing peptide attached to resin enables rapid synthesis without isolation of intermediates.

4.5 Three-Dimensional Protein Structures Can Be Determined Experimentally

- X-ray crystallography uses diffracted x-rays from a protein crystal to generate an electron density map, which indicates the atomic positions of the protein.
- Nuclear magnetic resonance spectroscopy reveals the structure and dynamics of proteins in solution by identifying protons in close proximity to one another.
- Cryo-electron microscopy is a rapidly developing method that can elucidate the structures of large multimeric complexes at increasingly higher resolutions.

- The three-dimensional structures of over 170,000 proteins are now known in atomic detail.

Key Terms

assay
specific activity
homogenate
dialysis
gel-filtration chromatography
ion-exchange chromatography
cation exchange
anion exchange
affinity chromatography
high-performance liquid chromatography (HPLC)
gel electrophoresis
SDS–polyacrylamide gel electrophoresis (SDS-PAGE)
isoelectric point
isoelectric focusing
two-dimensional electrophoresis
ultracentrifugation
antigenic determinant (epitope)
polyclonal antibodies
monoclonal antibody
hybridoma
enzyme-linked immunosorbent assay (ELISA)
western blotting
co-immunoprecipitation
fluorescence microscopy
mass spectrometry
matrix-assisted laser desorption/ionization (MALDI)
electrospray ionization (ESI)

time-of-flight (TOF) mass analyzer
tandem mass spectrometry
overlap peptides
peptide mass fingerprinting
proteome
solid-phase method
x-ray crystallography
electron-density map
nuclear magnetic resonance (NMR) spectroscopy
chemical shift
nuclear Overhauser effect
cryo-electron microscopy (cryo-EM)

Problems

1. Which of the following statements about SDS-PAGE under reducing conditions is true? Select all that apply. 3

a. Smaller proteins migrate faster through the polyacrylamide gel.
b. Protein-SDS complexes migrate toward the negative electrode.
c. Proteins are separated in a polyacrylamide gel matrix.
d. Protein-SDS complexes have similar mass-to-charge ratios; therefore, separation is by size.
e. Proteins are visualized using a dye that binds to the gel matrix, but not to proteins.
f. Sodium dodecyl sulfate binds proteins, resulting in protein-SDS complexes that are similar in size.

2. Complete the following table. 1

Purification procedure	Total protein (mg)	Total activity (units)	Specific activity (units mg^{-1})	Purification level	Yield (%)
Crude extract	20,000	4,000,000		1	100
$(NH_4)_2SO_4$ precipitation	5000	3,000,000			
DEAE-cellulose chromatography	1500	1,000,000			
Gel-filtration chromatography	500	750,000			
Affinity chromatography	45	675,000			

3.

a. A purified protein is in a buffer solution at pH 7 with 800 mM NaCl. A 1 mL sample of the protein solution is placed in a dialysis membrane and dialyzed against 2.0 L of the same buffer with 0 mM NaCl. Small molecules and ions, such as Na, Cl, and the buffer, can diffuse across the membrane, but the protein cannot. Once the dialysis has come to equilibrium, what is the concentration of NaCl in the protein sample (assuming no change in volume inside the membrane)?
b. If the original 1 mL sample were dialyzed twice, successively, against 200 mL of the same buffer in 0 mM

NaCl, what would be the final NaCl concentration in the sample?

4. Fluorescence-activated cell sorting (FACS) is a powerful technique for separating cells according to their content of particular molecules. For example, a fluorescence-labeled antibody specific for a cell-surface protein can be used to detect cells containing such a molecule. Suppose that you want to isolate cells that possess a receptor enabling them to detect bacterial degradation products. However, you do not yet have an antibody directed against this receptor. Which fluorescence-labeled molecule would you prepare to identify such cells?

5.

a. The octapeptide AVGWRVKS was digested with the enzyme trypsin. Which method would be most appropriate for separating the products: ion-exchange or gel-filtration chromatography? Explain.
b. Suppose that the peptide was digested with chymotrypsin. What would be the optimal separation technique? Explain.  2

6. Your frustrated colleague hands you a mixture of four proteins with the following properties:

	Isoelectric point (pI)	Molecular weight (in kDa)
Protein A	4.1	80
Protein B	9.0	81
Protein C	8.8	37

Protein D	3.9	172

a. Propose a method for the isolation of Protein B from the other proteins.
b. If Protein B also carried a His tag at its N-terminus, how could you revise your method? 2

7. The amide hydrogen atoms of peptide bonds within proteins can exchange with protons in the solvent. In general, amide hydrogen atoms in buried regions of proteins and protein complexes exchange more slowly than those on the solvent-accessible surface do. Determination of these rates can be used to explore the protein-folding reaction, probe the tertiary structure of proteins, and identify the regions of protein–protein interfaces. These exchange reactions can be followed by studying the behavior of the protein in solvent that has been labeled with deuterium (^2H), a stable isotope of hydrogen. What two methods described in this chapter could be readily applied to the study of hydrogen–deuterium exchange rates in proteins?

8. In this chapter, we described co-immunoprecipitation as a method for identifying binding partners to a protein of interest. A simpler variation of this method can also be used to isolate proteins of low abundance in a complex mixture. Arrange the steps in sequential order to use this technique for this purpose: 4

a. The antibody-protein complexes become insoluble.
b. Protein A beads are added to the mixture.
c. An antibody against the protein of interest is added to the mixture.

d. The protein mixture is centrifuged, the supernatant is removed, and the pellet is washed.
e. The antibody binds to the protein of interest.

9. You have isolated a protein from the bacterium *E. coli* and seek to confirm its identity by trypsin digestion and mass spectrometry. Determination of the masses of several peptide fragments has enabled you to deduce the identity of the protein. However, there is a discrepancy with one of the peptide fragments, which you believe should have the sequence MLNSFK and an $(M + H)^+$ value of 739.38. In your experiments, you repeatedly obtain an $(M + H)^+$ value of 767.38. What is the cause of this discrepancy, and what does it tell you about the region of the protein from which this peptide is derived? 5

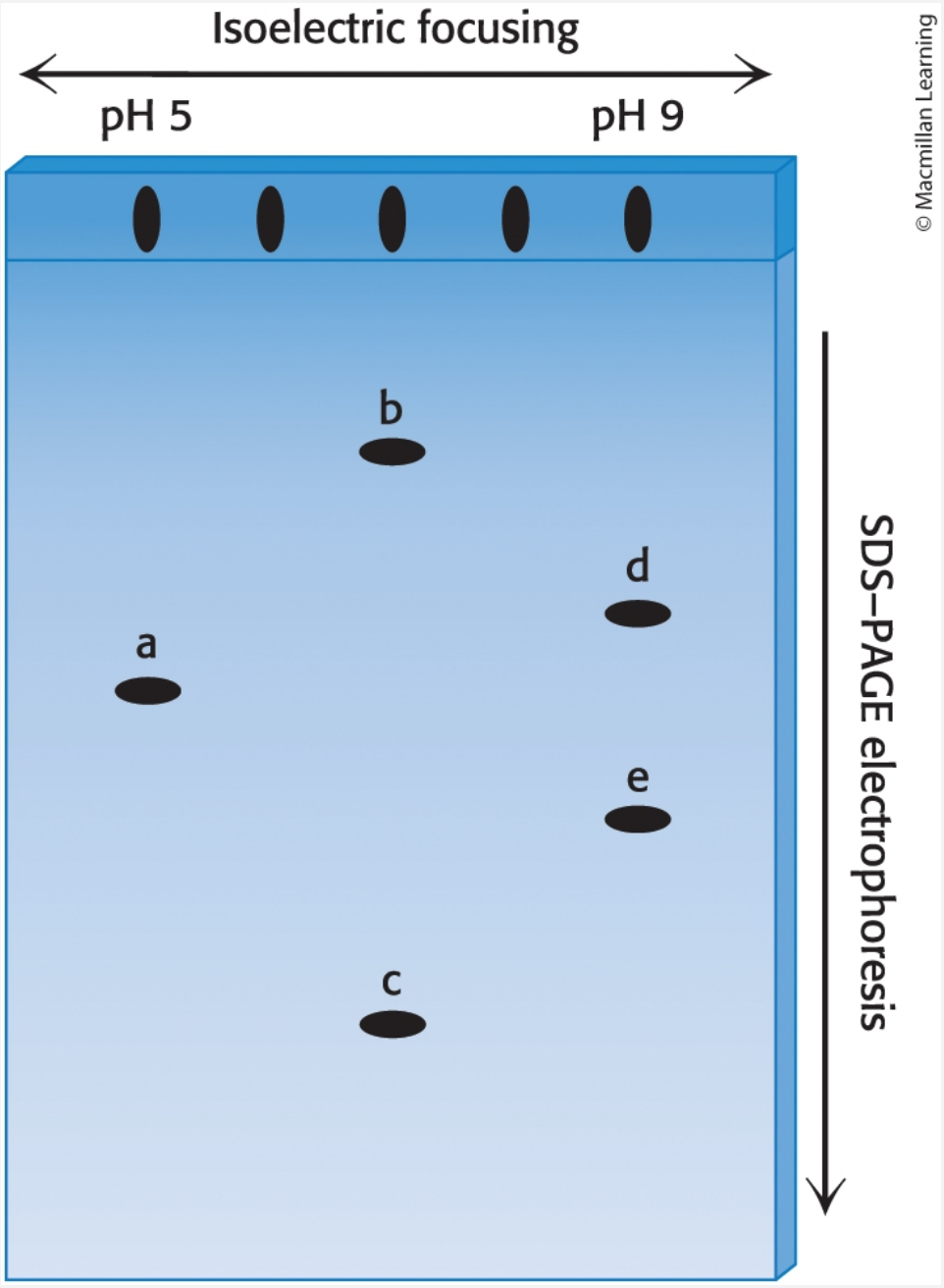
10. Which solution conditions would be best used for eluting a transcription factor from a DNA affinity column? 2

a. High imidazole concentration
b. High salt concentration
c. High glucose concentration
d. A mixture of free DNA nucleotides

11. A peptide has the sequence Gly-Ser-Lys-Ala-Gly-Arg-Ser-Arg.

a. How many fragments would result from cleaving the sequence with trypsin? What is the sequence of the smallest fragment?
b. How many fragments result from chymotrypsin cleavage? What is the sequence of the largest fragment?

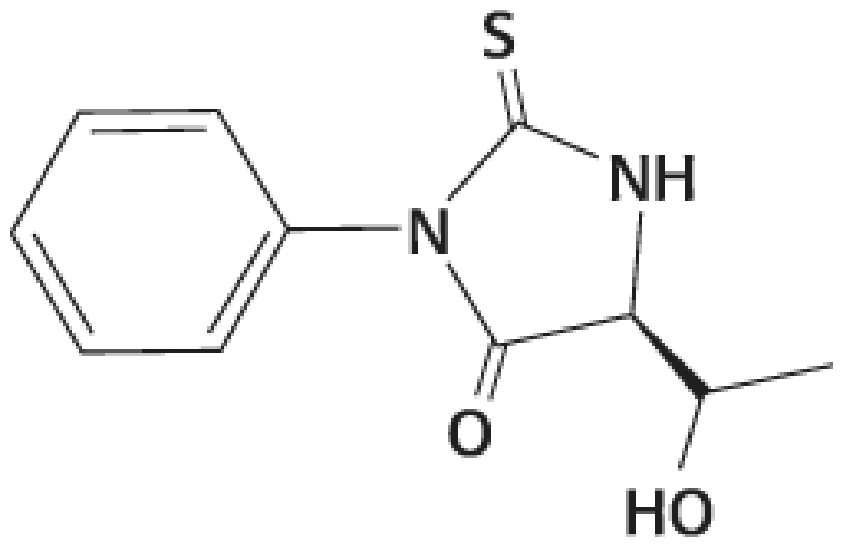
12. The results of a separation using two-dimensional electrophoresis are:



a. Which protein(s) have the highest pI value?
b. Which protein has the highest molecular weight? 3

13. A protein has been isolated, but now one needs to determine its amino acid sequence. The results are shown:

- After one cycle of Edman degradation, the following phenylthiohydantoin (PTH) derivative was produced:



- Treatment with cyanogen bromide gave the fragments: KPAM, PD, LICWM, and TRM.
- One of the fragments produced after treatment with chymotrypsin was MPD.

What is the sequence of the peptide? 5

14. Determine the sequence of decapeptide on the basis of the following data.

Trysin digestion gave two fragments with multiple residues (not in order):

T1: Ala, Arg, Phe, Gly, Thr, Trp, Tyr
T2: Lys, Met, Val

Chymotrypsin digestion gave four fragments with multiple residues (not in order):

CT1: Ala, Phe
CT2: Thr, Trp
CT3: Lys, Met, Tyr, Val
CT4: Arg, Gly

Treatment with cyanogen bromide yielded a single amino acid, methionine, and a nonapeptide.

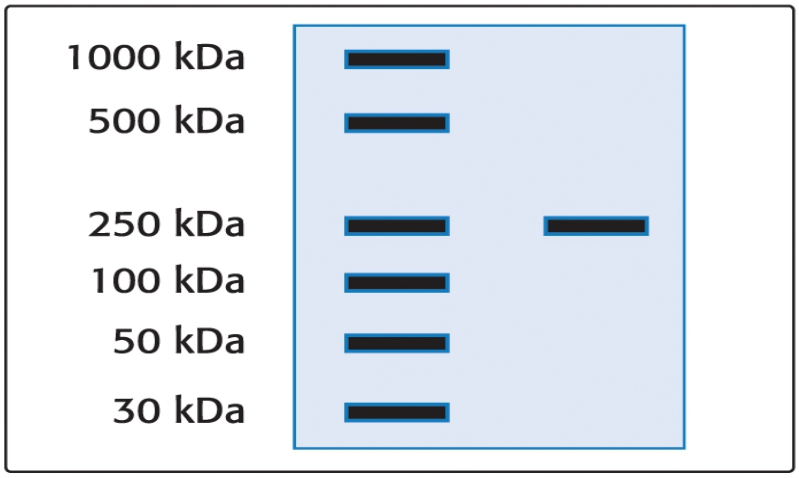
What is the sequence of this decapeptide? 5

15. Polyacrylamide gel electrophoresis experiments can be run under different sample preparation conditions, with informative results. Native PAGE does not include SDS. Reducing SDS-PAGE uses both SDS and a reducing agent, such as β-mercaptoethanol. Nonreducing SDS-PAGE uses SDS, but no reducing agent.

a. A protein sample complex consists of two proteins, a smaller protein X, and a larger protein Y. Protein X is composed of two polypeptide chains lined by disulfide bonds. Protein Y is composed of three polypeptide chains linked by disulfide bonds.

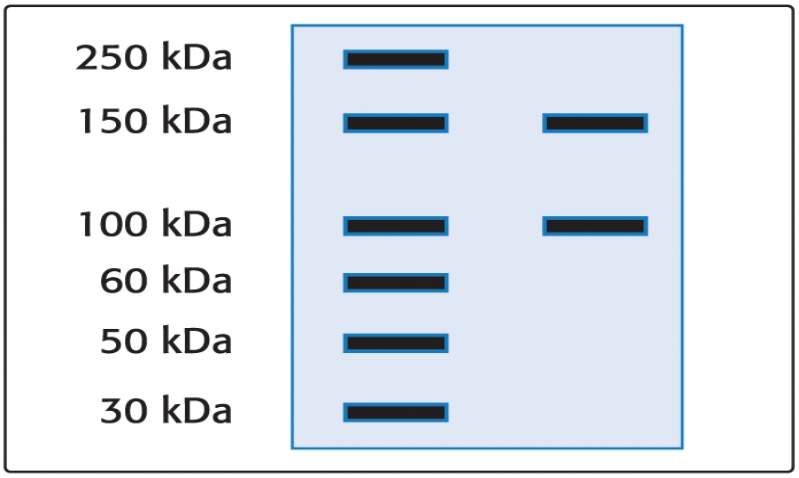
   Which type of PAGE was used to generate the each of the gels below?

(A)

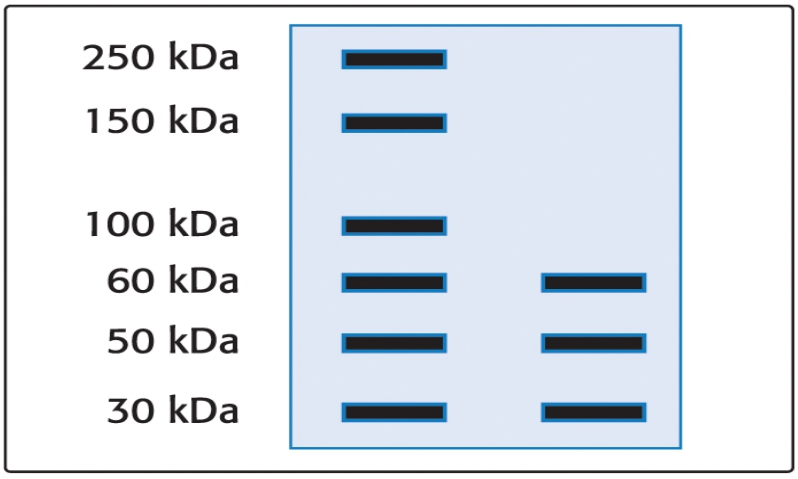


© Macmillan Learning

(B)

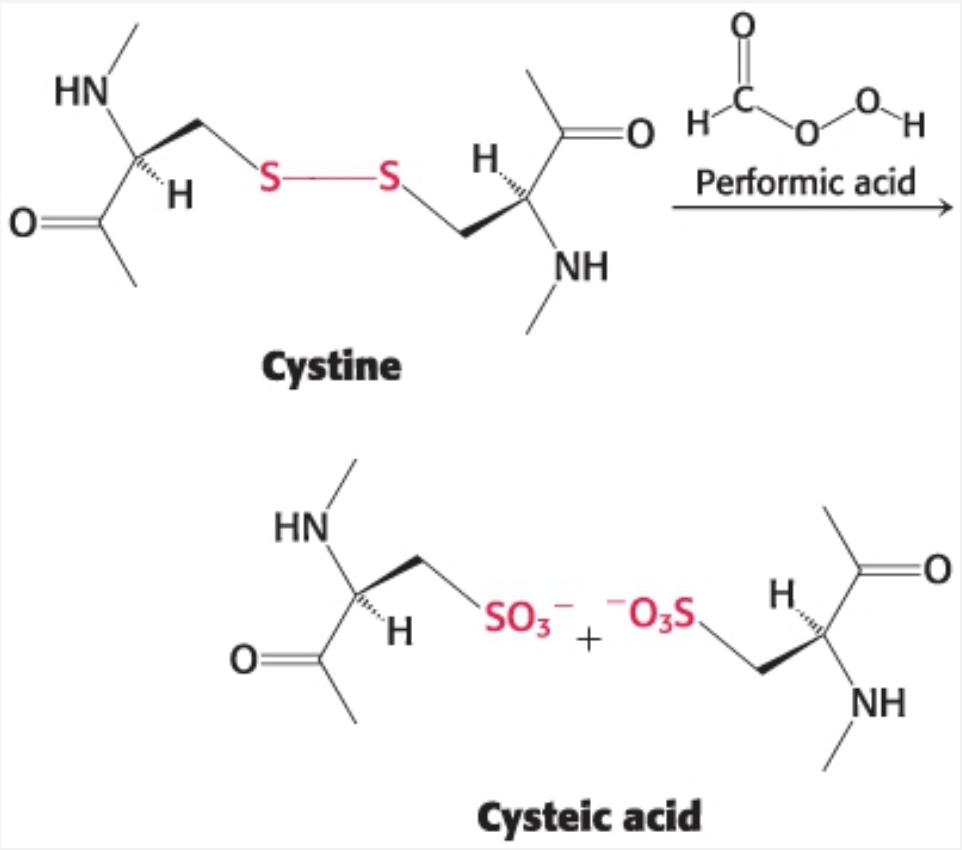


(C)



b. What are the molecular weights of the protein X polypeptides?
c. What are the molecular weights of the protein Y polypeptides? 3

16. Performic acid cleaves the disulfide linkage of cystine and converts the sulfhydryl groups into cysteic acid residues, which are then no longer capable of disulfide-bond formation.



Consider the following experiment: You suspect that a protein containing three cysteine residues has a single disulfide bond. You digest the protein with trypsin and subject the mixture to electrophoresis along one end of a sheet of paper. After treating the paper with performic acid, you subject the sheet to electrophoresis in the perpendicular direction and stain it with a reagent that detects proteins. How would the paper appear if the protein did not contain any disulfide bonds? If the protein contained a single disulfide bond? Propose an experiment to identify which cysteine residues form the disulfide bond.

17. If the proteins listed in the following table were subjected to SDS-PAGE, give the order of migration from the top (where the proteins are applied to the gel) to the bottom.

Protein	Isoelectric point (pI)	Molecular weight (daltons)
(a) Aldolase	10.1	40,000
(b) Cytochrome *c*	9.2	14,000
(c) Lactate dehydrogenase	8.5	18,000
(d) Ornithine decarboxylase	4.1	75,000
(e) Phosphoenolpyruvate carboxylase	5.0	74,000
(f) Pyruvate kinase	6.0	62,000

18. If the same proteins listed in Problem 17 were separated by isoelectric focusing, indicate their distribution in the gradient

from low pH to high pH.

Chapter 5
Enzymes: Core Concepts and Kinetics



John Lamb/Getty Images
© Macmillan Learning

Much of life is motion, whether at the macroscopic level of our daily life or at the molecular level of a cell. Stop-motion photography captures the motion of this dancer in frames separated by only about a quarter of a second. In biochemistry, kinetics (derived from the Greek *kinesis*, meaning "movement") is used to measure the extremely fast dynamics of enzyme activity. The enzyme carbonic anhydrase, one of the fastest known, can catalyze 250,000 reactions in the time elapsed between each frame shown in the image of the dancer.

Outline

5.1 Enzymes Are Powerful and Highly Specific Catalysts
5.2 Gibbs Free Energy Is a Useful Thermodynamic Function for Understanding Enzymes
5.3 Enzymes Accelerate Reactions by Facilitating the Formation of the Transition State

5.4 The Michaelis–Menten Model Accounts for the Kinetic Properties of Many Enzymes
5.5 Enzymes Can Be Studied One Molecule at a Time
5.6 Enzymes Can Be Inhibited by Specific Molecules

Learning Goals



By the end of this chapter, you should be able to:

1. Explain the thermodynamics of catalyzed and uncatalyzed reactions using Gibbs free energy diagrams.
2. Describe the central role of the formation of the transition state in enzyme catalysis.
3. Explain how reaction velocity is determined and used to characterize enzyme activity in terms of the fundamental kinetic parameters of an enzyme, K_M and k_{cat}.
4. Differentiate between types of reversible and irreversible inhibitors by mechanisms of action and using kinetics data.

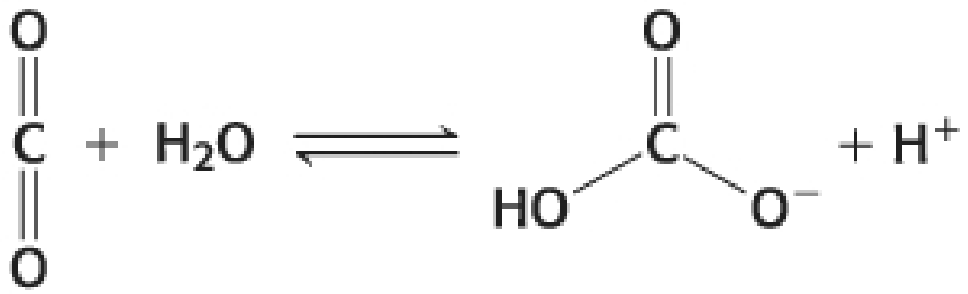
Enzymes like carbonic anhydrase are biological catalysts that determine the patterns of chemical transformations and mediate the transformation of one form of energy into another. Enzymes are also the target of many drugs; in fact, the majority of all pharmaceuticals ever created have been molecules that reduce enzyme function. For instance, a host of drugs used to manage pain, inflammation, and fever are inhibitors of a class of enzymes called cyclooxygenases. One of the most widely used medications in the world, acetylsalicylic acid, commonly known as aspirin, is among this group. About a quarter of the genes in the human genome encode enzymes, a testament to their importance to life. In this chapter, you will learn how enzymes accelerate reactions, how the

speed of their effects is measured, and how their action can be inhibited.

5.1 Enzymes Are Powerful and Highly Specific Catalysts

Agents called **catalysts** speed up chemical reactions without being consumed by them. **Enzymes** are powerful biological catalysts — made by all living organisms — that dramatically enhance and control the rates of chemical reactions. Almost all enzymes are proteins, which are highly effective catalysts for an enormous diversity of chemical reactions because of their capacity to specifically bind a very wide range of molecules. Using the full repertoire of intermolecular forces, enzymes optimally orient reactant molecules to make and break chemical bonds. However, proteins do not have an absolute monopoly on catalysis; the discovery of catalytically active RNA molecules, called **ribozymes**, provides compelling evidence that RNA was a biocatalyst early in evolution. Two remarkable properties of enzymes to consider from the start are their speed and their specificity.

- *Speed*. Enzymes can accelerate reactions by factors of a billion or more (**Table 5.1**). Indeed, most reactions in biological systems do not take place at perceptible rates in the absence of enzymes. Even a reaction as simple as the hydration of carbon dioxide is catalyzed by an enzyme — namely, carbonic anhydrase.



The transfer of CO_2 from the tissues to the blood and then to the air in the alveolae of the lungs would be less complete in the absence of this enzyme. In fact, carbonic anhydrase is one of the fastest enzymes known. Each enzyme molecule can hydrate 10^6 molecules of CO_2 per second. This catalyzed reaction is 10^7 times as fast as the uncatalyzed one. We will consider the mechanism of carbonic anhydrase catalysis in Chapter 6.

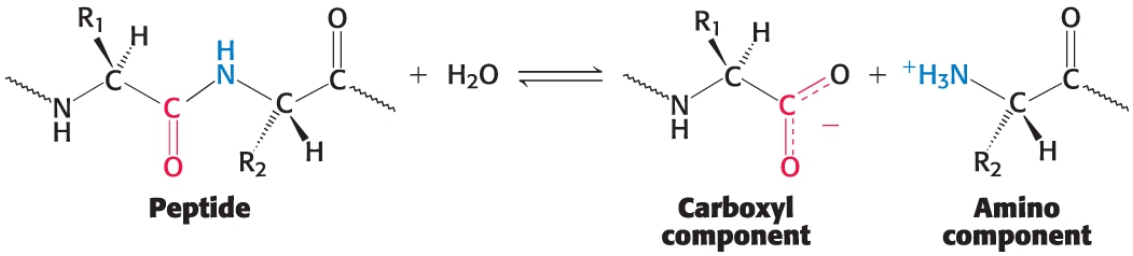
TABLE 5.1 Rate enhancement by selected enzymes

Enzyme	Nonenzymatic half-life	Uncatalyzed rate $(k_{un}s^{-1})$	Catalyzed rate $(k_{cat}s^{-1})$	Rate enhancement $(k_{cat}s^{-1}/k_{un}s^{-1})$
OMP decarboxylase	78,000,000 years	2.8×10^{-16}	39	1.4×10^{17}
Staphylococcal nuclease	130,000 years	1.7×10^{-13}	95	5.6×10^{14}
AMP nucleosidase	69,000 years	1.0×10^{-11}	60	6.0×10^{12}
Carboxypeptidase A	7.3 years	3.0×10^{-9}	578	1.9×10^{11}
Ketosteroid isomerase	7 weeks	1.7×10^{-7}	66,000	3.9×10^{11}

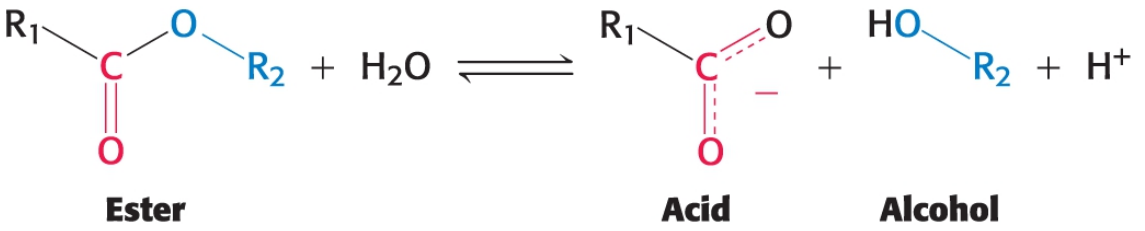
Triose phosphate isomerase	1.9 days	4.3×10^{-6}	4300	1.0×10^{9}
Chorismate mutase	7.4 hours	2.6×10^{-5}	50	1.9×10^{6}
Carbonic anhydrase	5 seconds	1.3×10^{-1}	1×10^{6}	7.7×10^{6}

Abbreviations: OMP, orotidine monophosphate; AMP, adenosine monophosphate.
Source: After A. Radzicka and R. Wolfenden, *Science* 267:90–93, 1995.

- *Specificity*. Enzymes are highly specific both in the reactions that they catalyze and in the reactants they bind, which are called **substrates**. An enzyme usually catalyzes a single chemical reaction or a set of closely related reactions. For example, enzymes known as **proteases** catalyze proteolysis, the hydrolysis of a peptide bond.



Most proteolytic enzymes also catalyze a different but related reaction in vitro — namely, the hydrolysis of an ester bond. Such reactions are more easily monitored than is proteolysis and are useful in experimental investigations of these enzymes.



Proteolytic enzymes differ markedly in their degree of substrate specificity. Papain, which is found in papaya plants, is quite undiscriminating: it will cleave any peptide bond with little regard to the identity of the adjacent side chains. The digestive enzyme trypsin, on the other hand, is quite specific and catalyzes the splitting of peptide bonds only on the carboxyl side of lysine and arginine residues (**Figure 5.1A**). Thrombin, an enzyme that participates in blood clotting (Section 10.4), is even more specific than trypsin. It catalyzes the hydrolysis of Arg–Gly bonds in particular peptide sequences only (**Figure 5.1B**). The specificity of an enzyme is due to the precise interaction of the substrate with the enzyme, which is a result of the intricate three-dimensional structure of the enzyme.

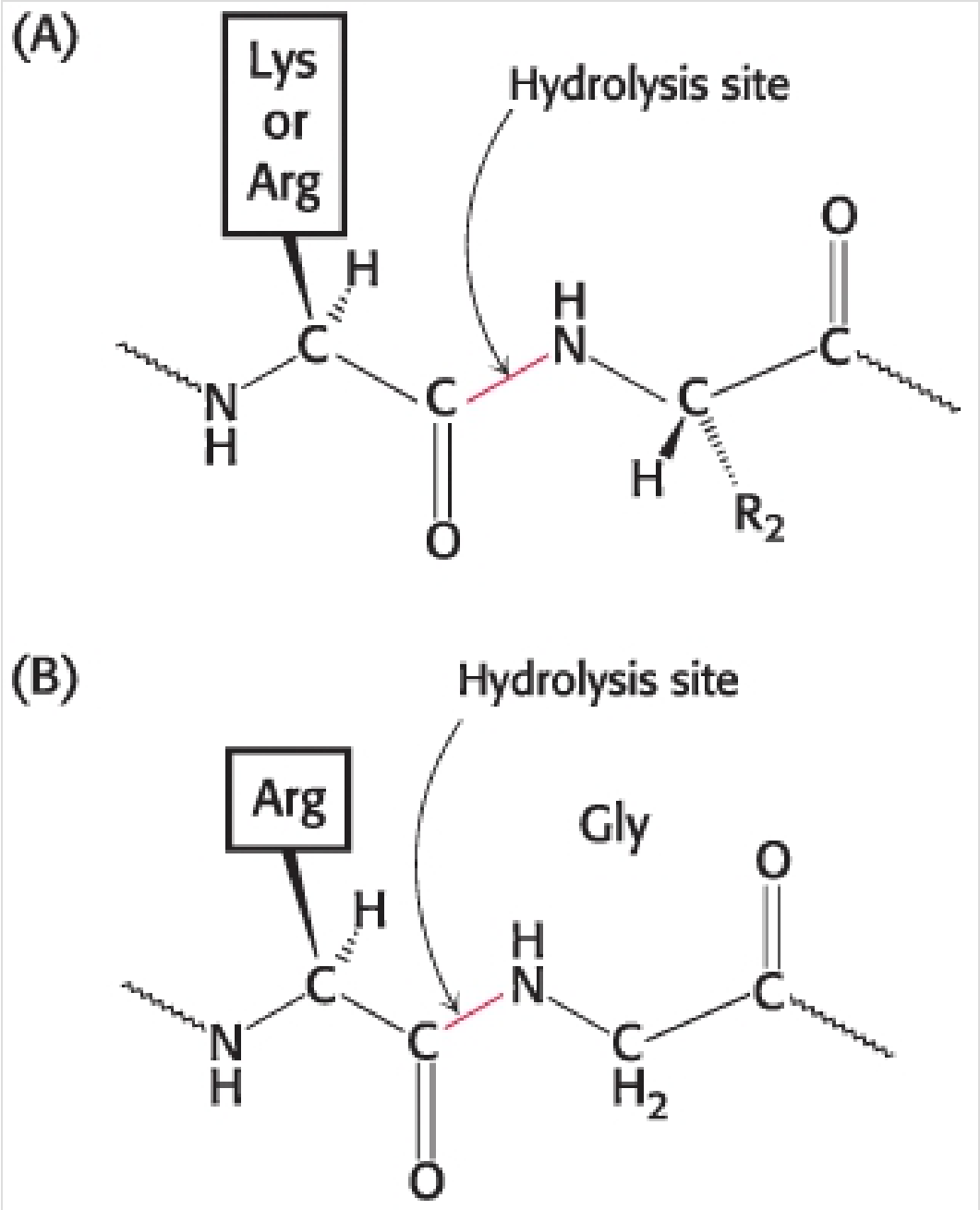


FIGURE 5.1 Enzymes are highly specific to particular substrates and chemical reactions. (A) Trypsin cleaves on the carboxyl side of arginine and lysine residues, whereas (B) thrombin cleaves Arg–Gly bonds in particular sequences only.

Most enzymes are classified by the types of reactions they catalyze

While some enzymes have common names — like papain, trypsin, and thrombin — that provide little information regarding their function, most enzymes are named for one of their substrates and for the reactions that they catalyze, with the suffix "-ase" added. Thus, a peptide hydrolase is an enzyme that hydrolyzes peptide bonds, whereas ATP synthase is an enzyme that synthesizes ATP. It is important to note, however, that enzymes catalyze chemical reactions in both the forward and reverse directions, yet only one direction of the reaction is typically denoted in the name.

To bring some consistency to enzyme nomenclature, a classification system for enzymes — developed by the International Union of Biochemistry — divides reactions into seven major groups (**Table 5.2**). These groups are further subdivided so that a four-number code preceded by the letters *EC* could precisely identify all enzymes. Consider as an example nucleoside monophosphate (NMP) kinase, an enzyme that we will examine in detail in Section 9.4. It catalyzes the following reaction:

$$\text{ATP} + \text{NMP} \rightleftharpoons \text{ADP} + \text{NDP}$$



NMP kinase transfers a phosphoryl group from ATP to any NMP to form a nucleoside diphosphate (NDP) and ADP. Consequently, it is a transferase, or member of group 2. Transferases that shift a phosphoryl group are designated 2.7. If a phosphate is the acceptor,

the transferase is designated 2.7.4, and most precisely EC 2.7.4.4 if a nucleoside monophosphate is the acceptor. Although the common names are used routinely, the classification number is used when the precise identity of the enzyme is not clear from the common name alone.

TABLE 5.2 Seven major classes of enzymes

Class	Type of reaction	Example	Chapter
1. Oxidoreductases	Oxidation–reduction	Lactate dehydrogenase	16
2. Transferases	Group transfer	Nucleoside monophosphate kinase (NMP kinase)	6
3. Hydrolases	Hydrolysis reactions (transfer of functional groups to water)	Chymotrypsin	6
4. Lyases	Addition or removal of groups to form double bonds	Fumarase	17
5. Isomerases	Isomerization (intramolecular group transfer)	Triose phosphate isomerase	16
6. Ligases	Ligation of two substrates at the expense of ATP hydrolysis	Aminoacyl-tRNA synthetase	30
7. Translocases	Movement of ions or molecules across membranes	Na^+–K^+ATPase	12

	or within membranes

Many enzymes require cofactors for activity

The catalytic activity of many enzymes depends on the presence of small molecules termed **cofactors**, although the precise role varies with the cofactor and the enzyme. Generally, these cofactors are able to execute chemical reactions that cannot be performed by the standard set of twenty amino acids. An enzyme without its cofactor is referred to as an **apoenzyme**; the complete, catalytically active enzyme is called a **holoenzyme**.

$$\text{apoenzyme} + \text{cofactor} = \text{holoenzyme}$$

Cofactors can be subdivided into two groups: (1) metals, whose importance to enzymatic activity we will explore in Chapter 6, and (2) small organic molecules called **coenzymes** (**Table 5.3**). Often derived from vitamins, coenzymes either can be tightly or loosely bound to the enzyme.

TABLE 5.3 Enzyme cofactors

Cofactor	Enzyme
Coenzyme	
Thiamine pyrophosphate	Pyruvate dehydrogenase

Flavin adenine nucleotide	Monoamine oxidase
Nicotinamide adenine dinucleotide	Lactate dehydrogenase
Pyridoxal phosphate	Glycogen phosphorylase
Coenzyme A (CoA)	Acetyl CoA carboxylase
Biotin	Pyruvate carboxylase
$5'$-Deoxyadenosylcobalamin	Methylmalonyl mutase
Tetrahydrofolate	Thymidylate synthase
Metal	
Zn^{2+}	Carbonic anhydrase
Zn^{2+}	Carboxypeptidase
Mg^{2+}	*Eco*RV
Mg^{2+}	Hexokinase
Ni^{2+}	Urease
Mo	Nitrogenase
Se	Glutathione peroxidase

Mn	Superoxide dismutase
K^+	Acetyl CoA thiolase

Tightly bound coenzymes are called **prosthetic groups**. Prosthetic groups are catalytic in that they are unchanged in the overall chemical reaction. In contrast, loosely associated coenzymes often behave more like second substrates (cosubstrates) because they bind to the enzyme, are changed by it, and then are released from it. Thus, these are also sometimes called *stoichiometric coenzymes* because they must be present in stoichiometric ratios with other substrates. The use of the same loosely associated coenzyme by a variety of enzymes sets these coenzymes apart from normal substrates, however, as does their source in vitamins (Table 5.3 and Section 15.4). Enzymes that use the same coenzyme usually perform catalysis by similar mechanisms. Throughout the book, we will see how coenzymes and their enzyme partners operate in their biochemical context.

Self-Check Question



Which terms (cofactor, coenzyme, and/or prosthetic group) correctly describe the heme from cytochrome c oxidase, which doesn't dissociate from the protein?

Enzymes can transform energy from one form into another

A key activity in all living systems is the conversion of one form of energy into another. For example, in photosynthesis, light energy is converted into chemical potential energy. In cellular respiration, which takes place in mitochondria, the free energy contained in small molecules derived from food is converted first into the free energy of an ion gradient and then into a different currency — the free energy of adenosine triphosphate. Given their centrality to life, it should come as no surprise that enzymes play vital roles in energy transformation.

After enzymes perform fundamental roles in photosynthesis and cellular respiration, other enzymes can then use the chemical potential energy of ATP in diverse ways. For instance, the enzyme myosin converts the energy of ATP into the mechanical energy of contracting muscles (Section 6.5). Pumps in the membranes of cells and organelles, which can be thought of as enzymes that move substrates rather than chemically alter them, use the energy of ATP to transport molecules and ions across the membrane (Chapter 13). The chemical and electrical gradients resulting from the unequal distribution of these molecules and ions are themselves forms of potential energy that can be used for a variety of purposes, such as sending nerve impulses (Section 13.4).

Recent developments show that the power of enzymes may be harnessed to generate energy for entire communities, as well as reducing landfill. Unsorted municipal waste can be treated with a cocktail of enzymes that includes an array of proteases as well as carbohydrate- and lipid-degrading enzymes, turning much of the waste into a bioliquid of sugars, amino acids, and other biomolecules. The bioliquid can then be used to fuel the growth of

methane-producing bacteria, and the methane harvested and burned to generate electricity. Any waste not degraded by the enzyme cocktail is recycled or incinerated to produce electricity.

5.2 Gibbs Free Energy Is a Useful Thermodynamic Function for Understanding Enzymes

Enzymes speed up the rate of chemical reactions, but the properties of the reaction — whether it can take place at all and the degree to which the enzyme accelerates the reaction — depend on energy differences between reactants (the initial state) and products (the final state). Gibbs free energy (G), which was discussed in Section 1.3, is a thermodynamic property that is a measure of useful energy, or the energy that is capable of doing work. To understand how enzymes operate, we need to consider only two thermodynamic properties of the reaction: (1) the free-energy difference (ΔG) between the products and reactants; and (2) the energy required to initiate the conversion of reactants into products. The former determines whether the reaction will take place spontaneously, whereas the latter determines the rate of the reaction. Enzymes affect only the rate.

The free-energy change provides information about the spontaneity but not the rate of a reaction

The free-energy change of a reaction (ΔG) tells us if the reaction can take place spontaneously:

- *A reaction can take place spontaneously only if* ΔG *is negative*. Such reactions are said to be *exergonic*.
- *A system is at equilibrium and no net change can take place if* ΔG *is zero*.
- *A reaction cannot take place spontaneously if* ΔG *is positive*. An input of free energy is required to drive such a reaction. These reactions are termed *endergonic*.
- *The* ΔG *of a reaction depends only on the free energy of the products minus the free energy of the reactants*. The ΔG of a reaction is independent of the molecular mechanism of the transformation. For example, the ΔG for the oxidation of glucose to CO_2 and H_2O is the same whether it takes place by combustion or by a series of enzyme-catalyzed steps in a cell.
- *The* ΔG *provides no information about the rate of a reaction*. A negative ΔG indicates that a reaction can take place spontaneously, but it does not signify whether it will proceed at a perceptible rate.

The standard free-energy change of a reaction is related to the equilibrium constant

As for any reaction, we need to be able to determine ΔG for an enzyme-catalyzed reaction to know whether the reaction is spontaneous or requires an input of energy, measured in kilojoules (kJ) or kilocalories (kcal); one kilojoule is equivalent to 0.239

kilocalories. To determine this important thermodynamic parameter, we need to take into account the nature of both the reactants and the products as well as their concentrations.

Consider the reaction

$$A + B \rightleftharpoons C + D$$

The ΔG of this reaction is given by

$$\Delta G = \Delta G^\circ + RT \ln \frac{[C][D]}{[A][B]} \quad \textbf{(1)}$$

in which ΔG° is the standard free-energy change, R is the gas constant, T is the absolute temperature, and [A], [B], [C], and [D] are the molar concentrations (more precisely, the activities) of the reactants. ΔG° is the free-energy change for this reaction under standard conditions — that is, when each of the reactants A, B, C, and D is present at a concentration of 1.0 M (for a gas, the standard state is usually chosen to be 1 bar, which is very close to 1 atmosphere). Thus, the ΔG of a reaction depends on the nature of the reactants (expressed in the ΔG° term of equation 1) and on their concentrations (expressed in the logarithmic term of equation 1).

A convention has been adopted to simplify free-energy calculations for biochemical reactions, in which the standard state is defined as having a pH of 7. Consequently, when H^+ is a reactant, its activity has the value 1 (corresponding to a pH of 7) in equations 1 and 2. The activity of water also is taken to be 1 in these equations. The standard free-energy change at pH 7, denoted by the symbol $\Delta G^{\circ\prime}$, will be used throughout this book. A simple way to determine $\Delta G^{\circ\prime}$ is to measure the concentrations of reactants and products when the reaction has reached equilibrium. At equilibrium, there is no net change in reactants and products; in essence, the reaction has stopped and $\Delta G = 0$. At equilibrium, equation 1 then becomes

$$0 = \Delta G^{\circ\prime} + RT \ln \frac{[C]_{eq}[D]_{eq}}{[A]_{eq}[B]_{eq}}$$

and so

$$\Delta G^{\circ\prime} = -RT \ln \frac{[C]_{eq}[D]_{eq}}{[A]_{eq}[B]_{eq}} \quad \textbf{(2)}$$

The equilibrium constant under standard conditions, K'_{eq}, is defined as

$$K'_{eq} = \frac{[C]_{eq}[D]_{eq}}{[A]_{eq}[B]_{eq}}$$

(3)

Substituting equation 3 into equation 2 gives

$$\Delta G^{\circ\prime} = -RT \ln K'_{eq}$$

(4)

which can be rearranged to give

$$K'_{eq} = e^{-\Delta G^{\circ\prime}/RT}$$

Substituting $R = 8.315 \times 10^{-3}\ \text{kJ mol}^{-1}\ \text{K}^{-1}$ and $T = 298\ \text{K}$ (corresponding to 25°C) gives

$$K'_{eq} = e^{-\Delta G^{\circ\prime}/2.48}$$

(5)

where $\Delta G^{\circ\prime}$ is here expressed in kilojoules per mole because of the choice of the units for *R* in equation 4. Thus, the standard free energy and the equilibrium constant of a reaction are related by a simple expression. For example, an equilibrium constant of 10 gives

a standard free-energy change of $-5.69\ \text{kJ mol}^{-1}$ or $-1.36\ \text{kcal mol}^{-1}$ at 25°C (Table 5.4). Note that, for each 10-fold change in the equilibrium constant, the $\Delta G^{\circ\prime}$ changes by $5.69\ \text{kJ mol}^{-1}$ or $1.36\ \text{kcal mol}^{-1}$.

TABLE 5.4 Relationship between $\Delta G^{\circ\prime}$ and K'_{eq} (at 25°C)

	$\Delta G^{\circ\prime}$	
K'_{eq}	kJ mol^{-1}	kcal mol^{-1}
10^{-5}	28.53	6.82
10^{-4}	22.84	5.46
10^{-3}	17.11	4.09
10^{-2}	11.42	2.73
10^{-1}	5.69	1.36
1	0.00	0.00
10	−5.69	−1.36
10^{2}	−11.42	−2.73

10^3	−17.11	−4.09
10^4	−22.84	−5.46
10^5	−28.53	−6.82

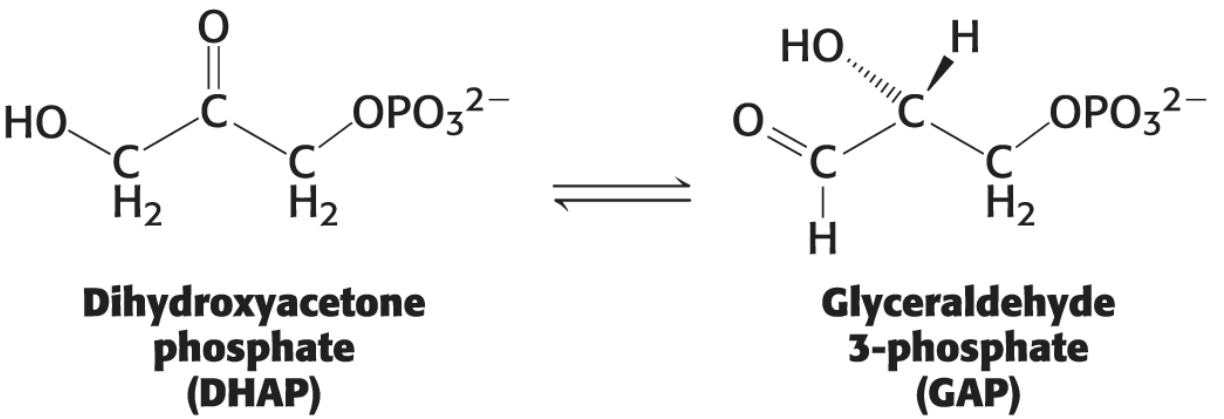
It is important to stress that whether the ΔG for a reaction is larger, smaller, or the same as $\Delta G^{\circ\prime}$ depends on the concentrations of the reactants and products. The criterion of spontaneity for a reaction under real conditions is ΔG, not $\Delta G^{\circ\prime}$. This point is important because reactions that are not spontaneous based on $\Delta G^{\circ\prime}$ can be made spontaneous by adjusting the concentrations of reactants and products. This principle is commonly observed in enzyme-catalyzed reactions in metabolic pathways (Chapter 15).

Example

Calculating and Comparing $\Delta G^{\circ\prime}$ and ΔG

Problem:

Calculate $\Delta G^{\circ\prime}$ and ΔG for a specific reaction that occurs during glucose metabolism:



Dihydroxyacetone phosphate (DHAP)

Glyceraldehyde 3-phosphate (GAP)

At equilibrium, the ratio of GAP to DHAP is 0.0475 at 25°C (298 K) and pH 7; hence, $K'_{eq} = 0.0475$. Typical concentrations in the cell are $2 \times 10^{-4}\ \text{M}$ for DHAP and $3 \times 10^{-6}\ \text{M}$ for GAP.

Getting Started:

Locate the equations used to calculate $\Delta G^{\circ\prime}$ and ΔG (equations 1 and 4). Besides the values given in the problem, is there anything else we need to know to solve these equations? Recall that the gas constant, *R*, is $8.315 \times 10^{-3}\ \text{kJ mol}^{-1}\ \text{K}^{-1}$

Calculate:

Let's begin by calculating $\Delta G^{\circ\prime}$, the standard free-energy change for this reaction, using equation 4 and substituting in the values for

R, the temperature in Kelvin, and the value of K'_{eq}:

$$\begin{aligned}\Delta G^{\circ\prime} &= -RT \ln K'_{eq} \\ &= -8.315 \times 10^{-3} \times 298 \times \ln (0.0475) \\ &= +7.53 \text{ kJ mol}^{-1} \text{or} +1.80 \text{ kcal mol}^{-1}\end{aligned}$$

What does $\Delta G^{\circ\prime}$ tell us? We can see from this result that under standard conditions the reaction is endergonic and DHAP will not spontaneously convert into GAP. However, this pertains only to standard conditions, not actual physiological conditions. For those we need to calculate ΔG, by substituting the real cellular concentrations into the equation for ΔG (equation 1):

$$\begin{aligned}\Delta G &= 7.53 \text{ kJ mol}^{-1} - RT \ln \frac{3 \times 10^{-6} \text{ M}}{2 \times 10^{-4} \text{ M}} \\ &= 7.53 \text{ kJ mol}^{-1} - (10.42 \text{ kJ mol}^{-1}) \\ &= -2.89 \text{ kJ mol}^{-1} \text{ or } -0.69 \text{ kcal mol}^{-1}\end{aligned}$$

Reflect:

What is the significance of the difference between ΔG and $\Delta G^{\circ\prime}$? Note that ΔG for this reaction is negative, even though $\Delta G^{\circ\prime}$ is positive. The negative value for ΔG indicates that the conversion of

DHAP to GAP is exergonic and can take place spontaneously when these species are present at the concentrations given.

Enzymes alter only the reaction rate and not the reaction equilibrium

We have established that enzymes are excellent catalysts, but it is equally important to understand what they cannot do: an enzyme cannot alter the laws of thermodynamics and consequently cannot alter the equilibrium of a chemical reaction. Consider an enzyme-catalyzed reaction, the conversion of substrate, S, into product, P. **Figure 5.2** shows the rate of product formation with time in the presence and absence of enzyme. Note that the amount of product formed is the same whether or not the enzyme is present but, in the current example, the amount of product formed in seconds when the enzyme is present might take hours (or centuries; see Table 5.1) to form if the enzyme were absent.

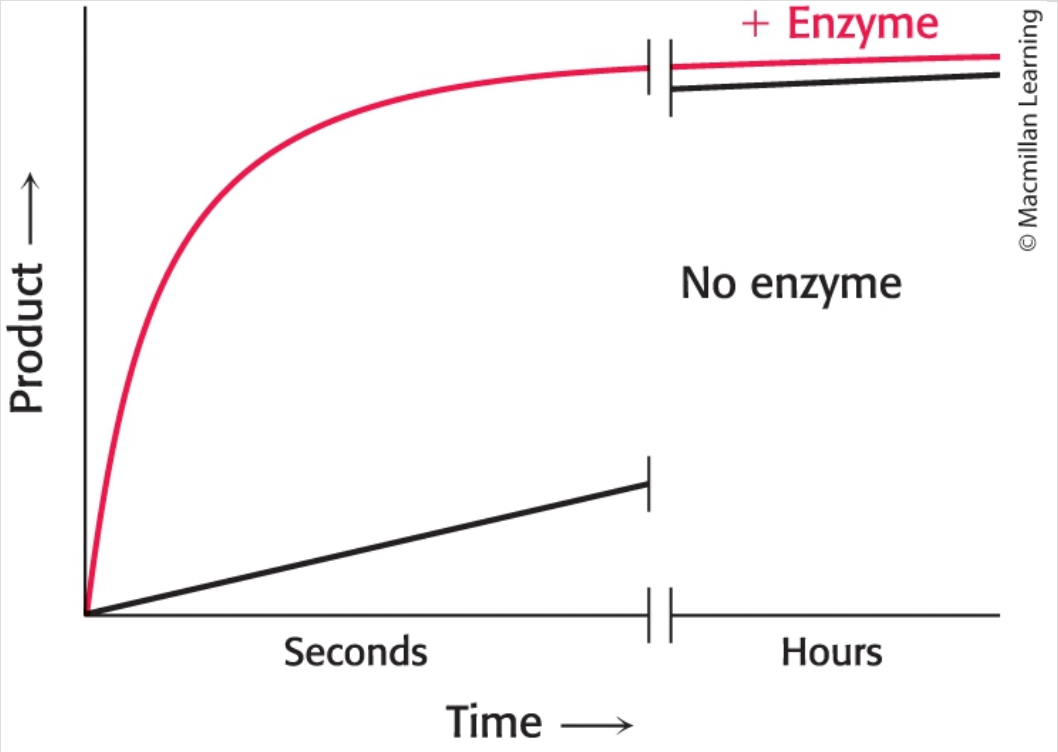


FIGURE 5.2 Enzymes do not affect thermodynamics and therefore do not change the equilibrium point. The same equilibrium point is reached much more quickly in the presence of an enzyme.

Why does the rate of product formation level off with time? The reaction has reached equilibrium. Substrate S is still being converted into product P, but P is being converted into S at a rate such that the amount of P present stays the same.

Let us examine the equilibrium in a more quantitative way. Suppose that, in the absence of enzyme, the forward rate constant (k_F) for the conversion of S into P is $10^{-4}\ s^{-1}$ and the reverse rate constant (k_R) for the conversion of P into S is $10^{-6}\ s^{-1}$. Remember: enzymes accelerate the rate of both the forward and reverse reactions. So,

also suppose that in the presence of an enzyme these values are $10^5\ s^{-1}$ and $10^3\ s^{-1}$ for k_F and k_R, respectively. The equilibrium constant *K* is given by the ratio of these rate constants in either case:

$$S \underset{10^{-6}\,s^{-1}}{\overset{10^{-4}\,s^{-1}}{\rightleftharpoons}} P \qquad S \underset{10^{3}\,s^{-1}}{\overset{10^{5}\,s^{-1}}{\rightleftharpoons}} P$$

$$K_{Uncatalyzed} = \frac{[P]}{[S]} = \frac{k_F}{k_R} = \frac{10^{-4}}{10^{-6}} = 100 \qquad K_{Catalyzed} = \frac{[P]}{[S]} = \frac{k_F}{k_R} = \frac{10^{5}}{10^{3}} = 100$$



Notice that the equilibrium concentration of P is 100 times that of S, whether or not enzyme is present. However, it might take a very long time to approach this equilibrium without enzyme, whereas equilibrium would be attained rapidly in the presence of a suitable enzyme (Table 5.1).

By catalyzing both the forward and reverse directions of reactions, enzymes accelerate the attainment of equilibria but do not shift their positions. The equilibrium position is a function only of the free-energy difference between reactants and products.

5.3 Enzymes Accelerate Reactions by Facilitating the Formation of the Transition State

The free-energy difference between reactants and products accounts for the equilibrium of the reaction, but enzymes accelerate how quickly this equilibrium is attained. How can we explain the rate enhancement in terms of thermodynamics? To do so, we have to consider not the end points of the reaction, but the chemical pathway between the end points.

A chemical reaction of substrate S to form product P goes through a **transition state** $X^{\ddagger}$ that has a higher free energy than does either S or P.

$$S \rightarrow X^{\ddagger} \rightarrow P$$

The double dagger $(\ ^{\ddagger})$ denotes the transition state. The transition state is a transitory molecular structure that is no longer the substrate but is not yet the product. The transition state is the least-stable and most-seldom-occupied species along the reaction pathway because it is the one with the highest free energy. The difference in free energy between the transition state and the substrate is called the **Gibbs free energy of activation** or simply the **activation energy**, symbolized by $\Delta G^{\ddagger}$ (**Figure 5.3**).

$$\Delta G^{\ddagger} = G_{X}{}^{\ddagger} - G_{S}$$

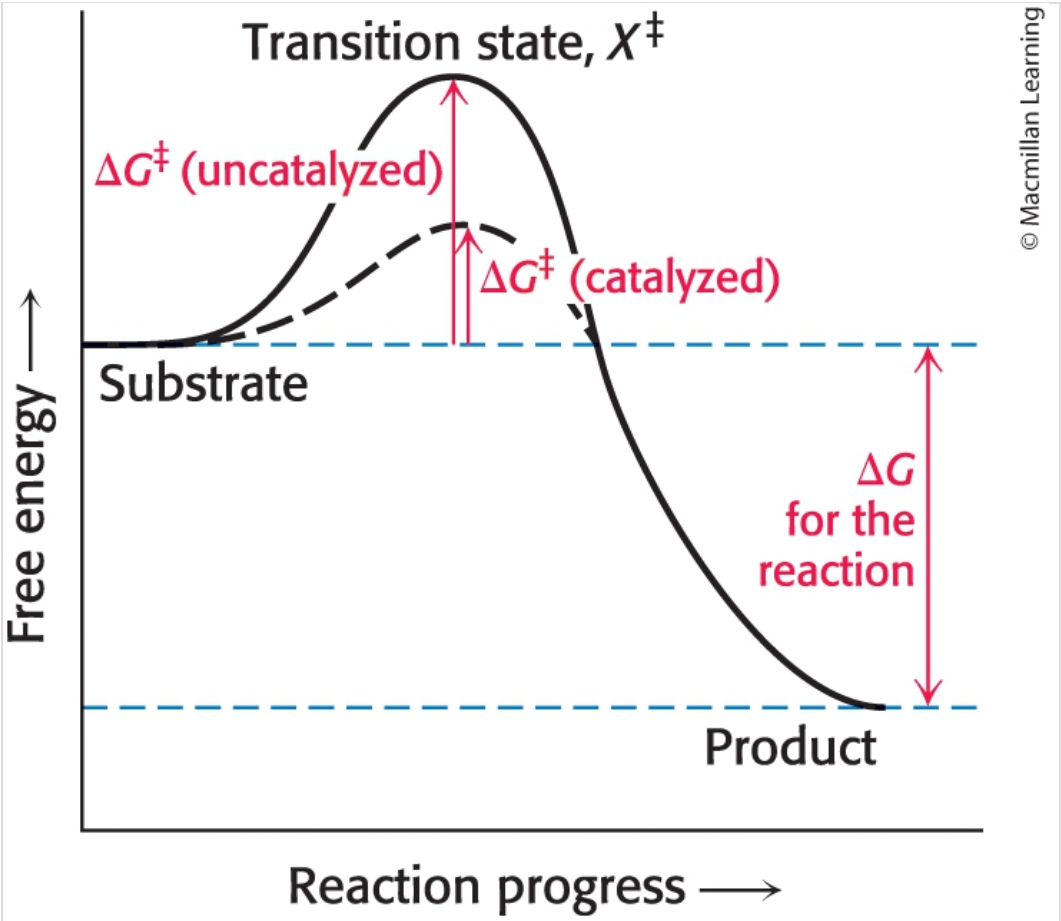


FIGURE 5.3 Enzymes accelerate reactions by decreasing $\Delta G^{\ddagger}$, the free energy of activation.

Note that $\Delta G^{\ddagger}$ does not enter into the final ΔG calculation for the reaction, because the energy required to generate the transition state is released when the transition state forms the product. This is also true when we consider the reaction from the reverse direction.

The activation-energy barrier immediately suggests how an enzyme enhances the reaction rates in both directions without altering ΔG of the reaction: enzymes accelerate reactions by decreasing $\Delta G^{\ddagger}$, the activation energy, thus facilitating the formation of the transition state from either substrate or product.

The combination of substrate and enzyme creates a reaction pathway whose transition-state energy is lower than that of the reaction in the absence of enzyme (Figure 5.3). Because the activation energy is lower, more molecules have the energy required to reach the transition state. Decreasing the activation barrier is analogous to lowering the height of a high-jump bar; more athletes will be able to clear the bar.

The formation of an enzyme–substrate complex is the first step in enzymatic catalysis

Much of the catalytic power of enzymes comes from their binding to and then altering the structure of the substrate to promote the formation of the transition state. Thus, the first step in catalysis is the formation of an enzyme–substrate (ES) complex. Substrates bind to a specific region of the enzyme called the **active site**. Most enzymes are highly selective in the substrates that they bind. Indeed, the catalytic specificity of enzymes depends in part on the specificity of binding.

What is the evidence for the existence of an enzyme–substrate complex?

- The first clue was the observation that, at a constant concentration of enzyme, the reaction rate increases with increasing substrate concentration until a maximal velocity is reached (Figure 5.4), suggesting that a discrete ES complex has formed. In contrast, uncatalyzed reactions do not show this saturation effect. At a sufficiently high substrate concentration, all the catalytic sites are filled, or saturated, and so the reaction rate cannot increase. Although indirect, the ability to saturate an enzyme with substrate is the most general evidence for the existence of ES complexes.

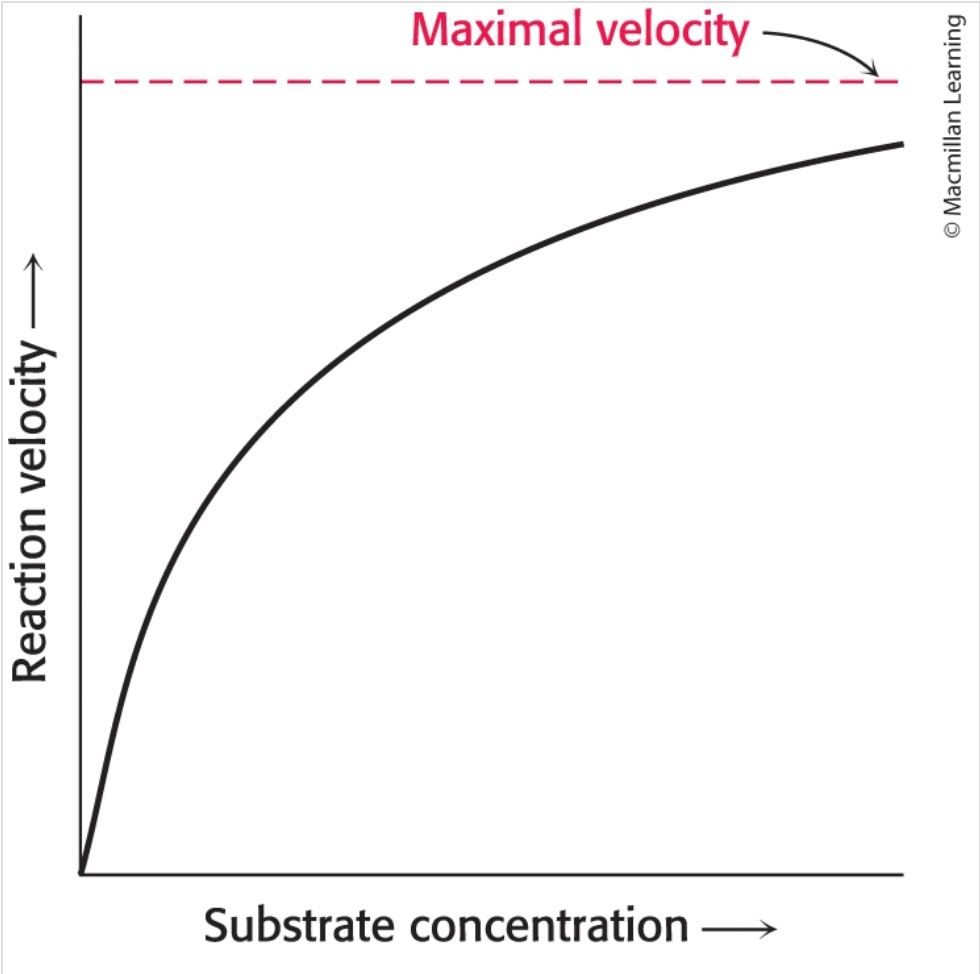


FIGURE 5.4 As substrate concentration increases, an enzyme-catalyzed reaction asymptotically approaches a maximal velocity.

- The spectroscopic characteristics of many enzymes and substrates change on the formation of an ES complex. These changes are particularly striking if the enzyme contains a colored prosthetic group.
- X-ray crystallography has provided high-resolution images of substrates and substrate analogs bound to the active sites of many enzymes (**Figure 5.5**). In Chapter 6, we will take a close look at several of these complexes.

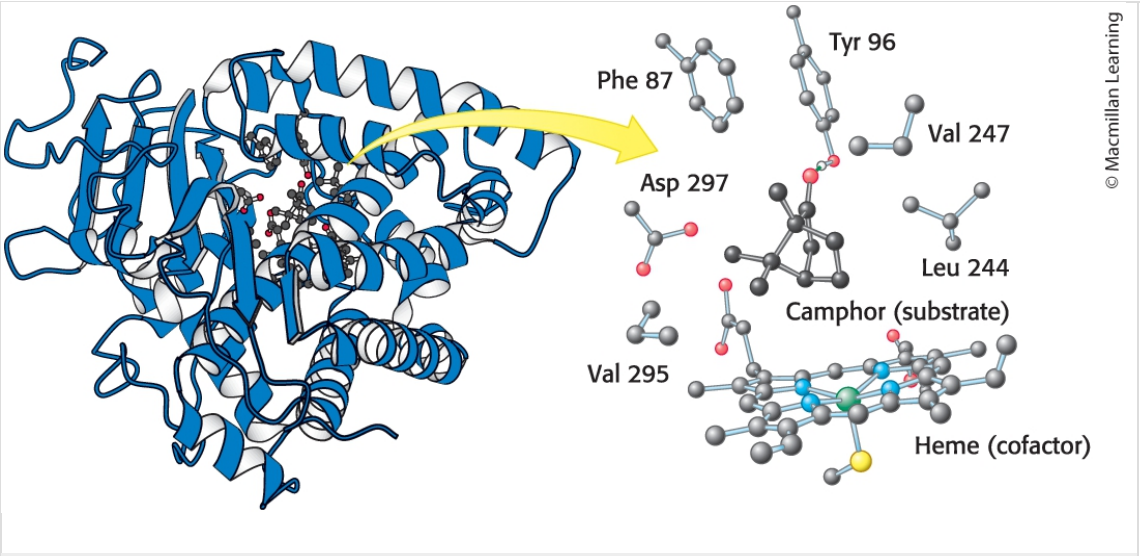


FIGURE 5.5 In the active site, substrates are surrounded by enzyme residues and sometimes cofactors. (Left) The structure of the complex between the enzyme cytochrome P450 and its substrate camphor. (Right) The substrate sits in the active site, which is a cavity formed by residues from the enzyme and the heme prosthetic group.

[Drawn from 2CPP.pdb.]

INTERACT with this model in Achieve

The active sites of enzymes have some common features

Recall from Chapter 2 that proteins are not rigid structures, but are flexible and exist in an array of conformations. Thus, the interaction of the enzyme and substrate at the active site and the formation of the transition state is a dynamic process. Although enzymes differ widely in structure, specificity, and mode of catalysis, at least five generalizations can be made concerning their active sites:

1. *The active site is a three-dimensional cleft, or crevice, formed by groups that come from different parts of the amino acid sequence*. Indeed, residues far apart in the amino acid sequence may interact more strongly than adjacent residues in the sequence, which may be sterically constrained from interacting with one another. For example, in the enzyme lysozyme, the residues that contribute important groups to the active site are numbered 35, 52, 62, 63, 101, and 108 in the sequence of 129 amino acids (**Figure 5.6**). Lysozyme, found in a variety of organisms and tissues, including human tears, degrades the cell walls of some bacteria.

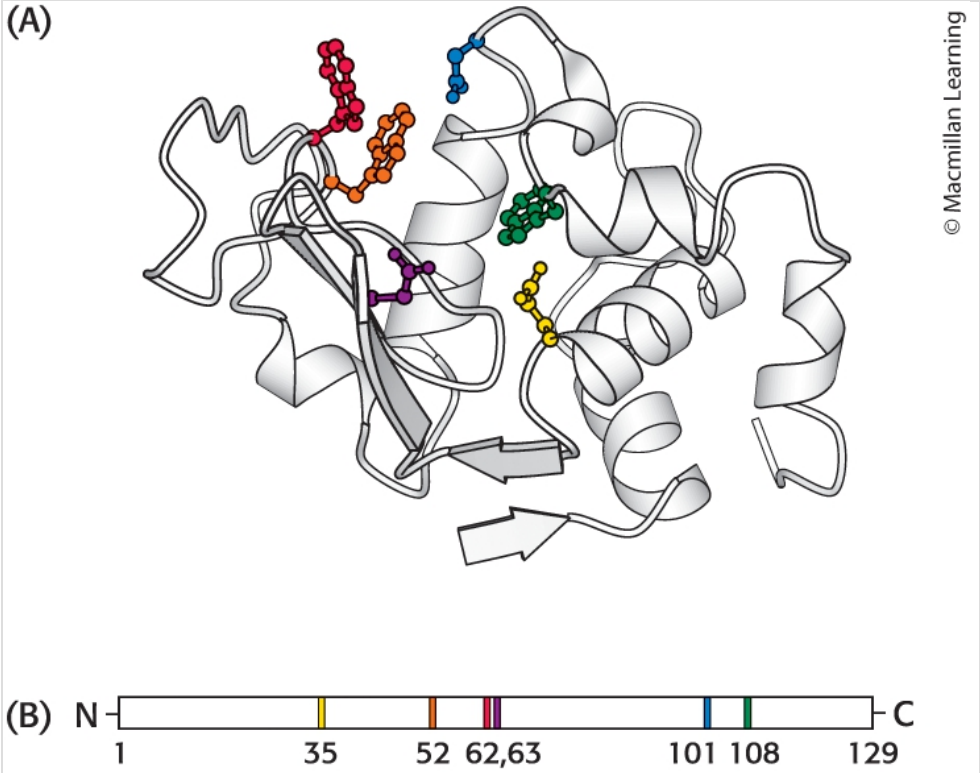


FIGURE 5.6 Amino acids that are far apart in sequence can be close together in the active site of the folded protein. (A) A ribbon diagram of the enzyme lysozyme with several components of the active site shown in color. (B) A schematic representation of the primary structure of lysozyme shows that the active site is composed of residues that come from different parts of the polypeptide chain.

[Drawn from 6LYZ.pdb.]

INTERACT with this model in Achieve

2. *The active site takes up a small part of the total volume of an enzyme*. Although residues in an enzyme are not in contact with the substrate, the cooperative motions of the entire enzyme help to correctly position the catalytic residues at the active site. Experimental attempts to reduce the size of a catalytically active enzyme show that the minimum size requires about 100

residues. In fact, nearly all enzymes are larger than this, which gives them a mass normally greater than 10 kDa and a diameter of more than $25\ \text{Å}$, suggesting that all residues in a protein, not just those at the active site, are ultimately required to form a functional enzyme.

3. *Active sites are unique microenvironments*. Water is usually excluded from the active site cleft unless it is a reactant. Often a nonpolar microenvironment in the cleft enhances the binding of substrates as well as catalysis. The cleft may also contain polar residues, some of which may acquire special properties essential for substrate binding or catalysis. The internal positions of these polar residues are biologically crucial exceptions to the general rule that polar residues are located on the surface of proteins, exposed to water.

4. *Substrates are bound to enzymes by multiple weak attractions*. The noncovalent interactions in ES complexes are much weaker than covalent bonds, which have energies between -210 and $-460\ \text{kJ mol}^{-1}$ (between -50 and $-110\ \text{kcal mol}^{-1}$). In contrast, ES complexes usually have equilibrium constants that range from 10^{-2} to $10^{-8}\ \text{M}$ corresponding to free energies of interaction ranging from about -13 to $-50\ \text{kJ mol}^{-1}$ (from -3 to $-12\ \text{kcal mol}^{-1}$). As discussed in Section 1.3, these weak reversible contacts are mediated by ionic interactions, hydrogen bonds, van der Waals forces, and the hydrophobic effect. Van der Waals forces become significant in binding only when numerous substrate and enzyme atoms simultaneously come into close contact. Hence, the enzyme and substrate should have complementary shapes. The directional character of hydrogen bonds between enzyme and substrate often

enforces a high degree of specificity, as seen in the RNA-degrading enzyme ribonuclease (Figure 5.7).

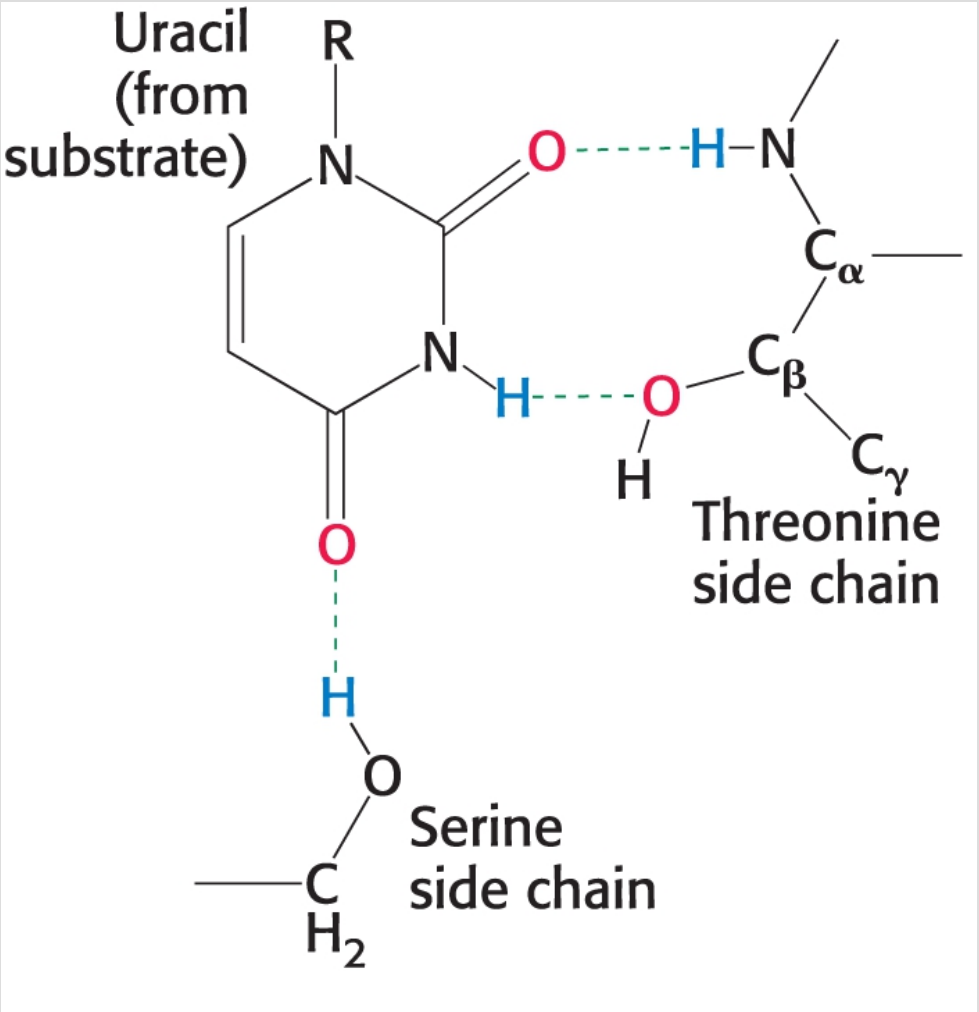


FIGURE 5.7 The geometry of hydrogen bonds often creates specificity between an enzyme and its substrate. The enzyme ribonuclease forms hydrogen bonds with the uridine component of the substrate.

[Information from F. M. Richards, H. W. Wyckoff, and N. Allewell, In *The Neurosciences: Second Study Program*, F. O. Schmidt, Ed. (Rockefeller University Press, 1970), p. 970.]

5. *The specificity of binding depends on the precisely defined arrangement of atoms in an active site*. Because the enzyme and

the substrate interact by means of short-range forces that require close contact, a substrate must have a matching shape to fit into the site. Emil Fischer proposed the lock-and-key analogy in 1890, which was the model for enzyme–substrate interaction for several decades (**Figure 5.8A**). We now know that enzymes are flexible and that the shapes of the active sites can be markedly modified by the binding of substrate, a process of dynamic recognition called **induced fit** (**Figure 5.8B**). Moreover, the substrate may bind to only certain conformations of the enzyme, in what is called *conformation selection*. Thus, the mechanism of catalysis is dynamic, involving structural changes in both the substrates and the enzyme until the substrate reaches the transition state.

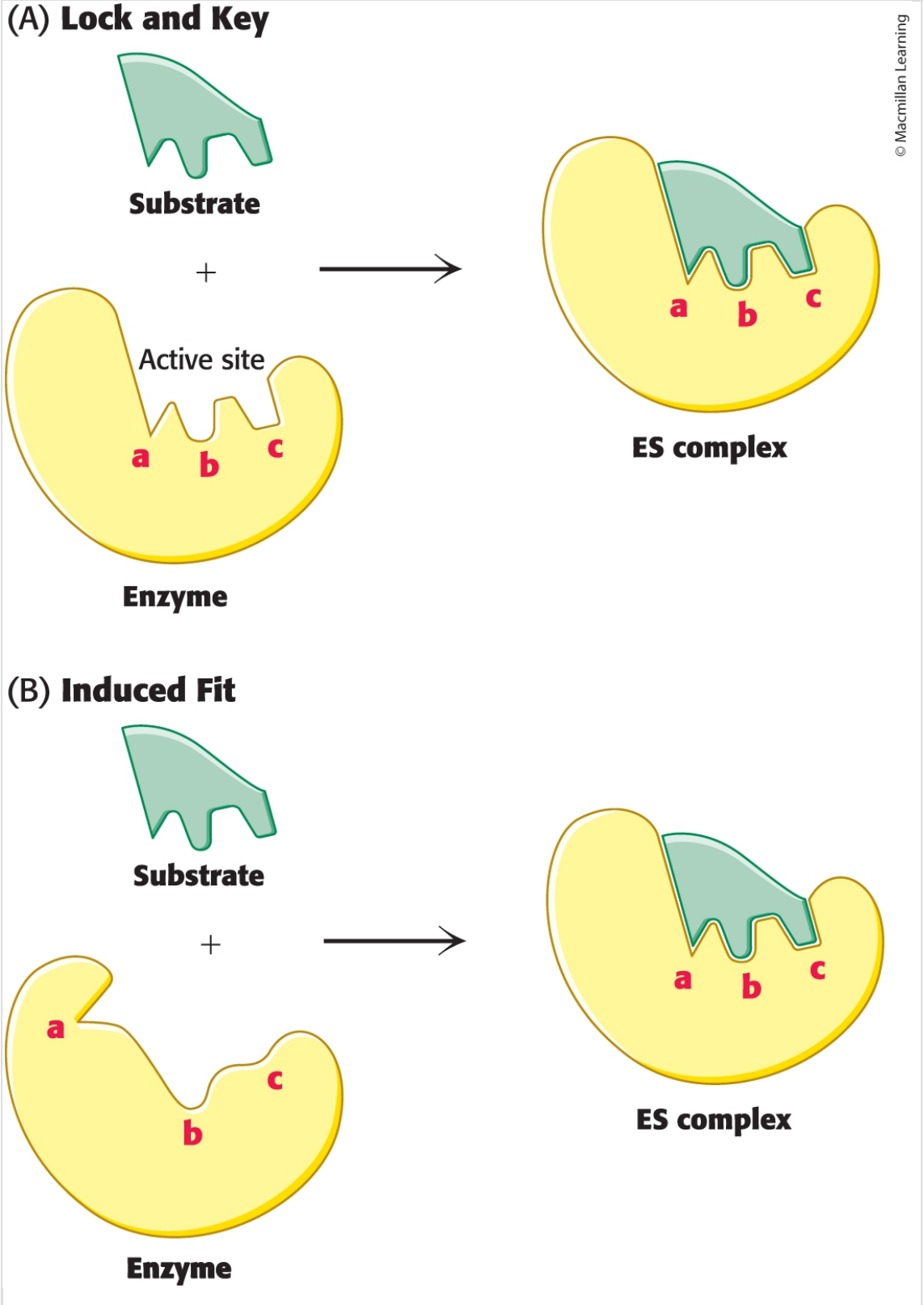


FIGURE 5.8 The old lock-and-key model of enzyme binding has been replaced by an induced-fit model. (A) In the lock-and-key model of enzyme–substrate binding, the

active site of the unbound enzyme was proposed to be complementary in shape to the substrate, whereas in (B) the current induced-fit model of enzyme–substrate binding, the enzyme changes shape on substrate binding, with the active site forming a shape complementary to the substrate only after the substrate has been bound. The enzyme then continues to change shape as it induces changes in the substrate, converting it into the transition state.

The binding energy between enzyme and substrate is important for catalysis

Enzymes lower the activation energy, but where does the energy to lower the activation energy come from? Free energy is released by the formation of a large number of weak interactions between a complementary enzyme and its substrate. The free energy released on binding is called the **binding energy**. Only the correct substrate can participate in most or all of the interactions with the enzyme and thus maximize binding energy, accounting for the exquisite substrate specificity exhibited by many enzymes. Furthermore, the full complement of such interactions is formed — and the maximal binding energy is released — only when the substrate is converted into the transition state. The energy released by the interaction between the enzyme and the substrate can be thought of as lowering the activation energy.

Because the transition state collapses randomly, the activation energies

determine the accumulation of either product or substrate

Molecular movements resulting in the optimal alignment of functional groups at the active site occur fleetingly. The transition state is too unstable to exist for long, collapsing randomly to either substrate or product. A consideration of the biochemical timescale, in which molecule motion is occurring on the order of microseconds to nanoseconds, is once again illuminating: a substrate may reach the transition state and collapse back to substrate again many times in a single active site within a fraction of a second before collapsing to product.

Whether substrate or product ultimately accumulates is determined only by the energy difference between the substrate and the product — that is, by the ΔG of the reaction, but why? If the direction of the collapse from the transition state is random, then the accumulation of either product or substrate can be explained by the activation energy in either direction because it dictates how frequently substrates or products reach the transition state. By lowering this activation energy, enzymes accelerate reactions in both directions by increasing the rate at which both products and substrates reach the transition state.

5.4 The Michaelis–Menten Model Accounts for the Kinetic Properties of Many Enzymes

The study of the rates of chemical reactions is called *kinetics*, and the study of the rates of enzyme-catalyzed reactions is called *enzyme kinetics*. A kinetic description of enzyme activity will help us understand how enzymes function.

Kinetics is the study of reaction rates

What do we mean when we say the "rate" of a chemical reaction? Consider a simple reaction:

$$A \rightarrow P$$

The rate V is the quantity of A that disappears in a specified unit of time. It is equal to the rate of the appearance of P, or the quantity of P that appears in a specified unit of time.

$$V = -d[A]/dt = d[P]/dt$$

If A is yellow and P is colorless, we can follow the decrease in the concentration of A by measuring the decrease in the intensity of yellow color with time. Consider only the change in the

concentration of A for now. The rate of the reaction is directly related to the concentration of A by a proportionality constant, *k*, called the *rate constant*.

$$V = k[A]$$

Reactions that are directly proportional to the reactant concentration are first-order reactions. First-order rate constants have the units of s^{-1}.

Many important biochemical reactions include two reactants. For example,

$$2A \rightarrow P$$

or

$$A + B \rightarrow P$$

They are called *bimolecular reactions*, and the corresponding rate equations often take the form

$$V = k[A]^2$$

and

$$V = k[A][B] \quad \textbf{(6)}$$

The rate constants, called second-order rate constants, have the units $M^{-1}\,s^{-1}$.

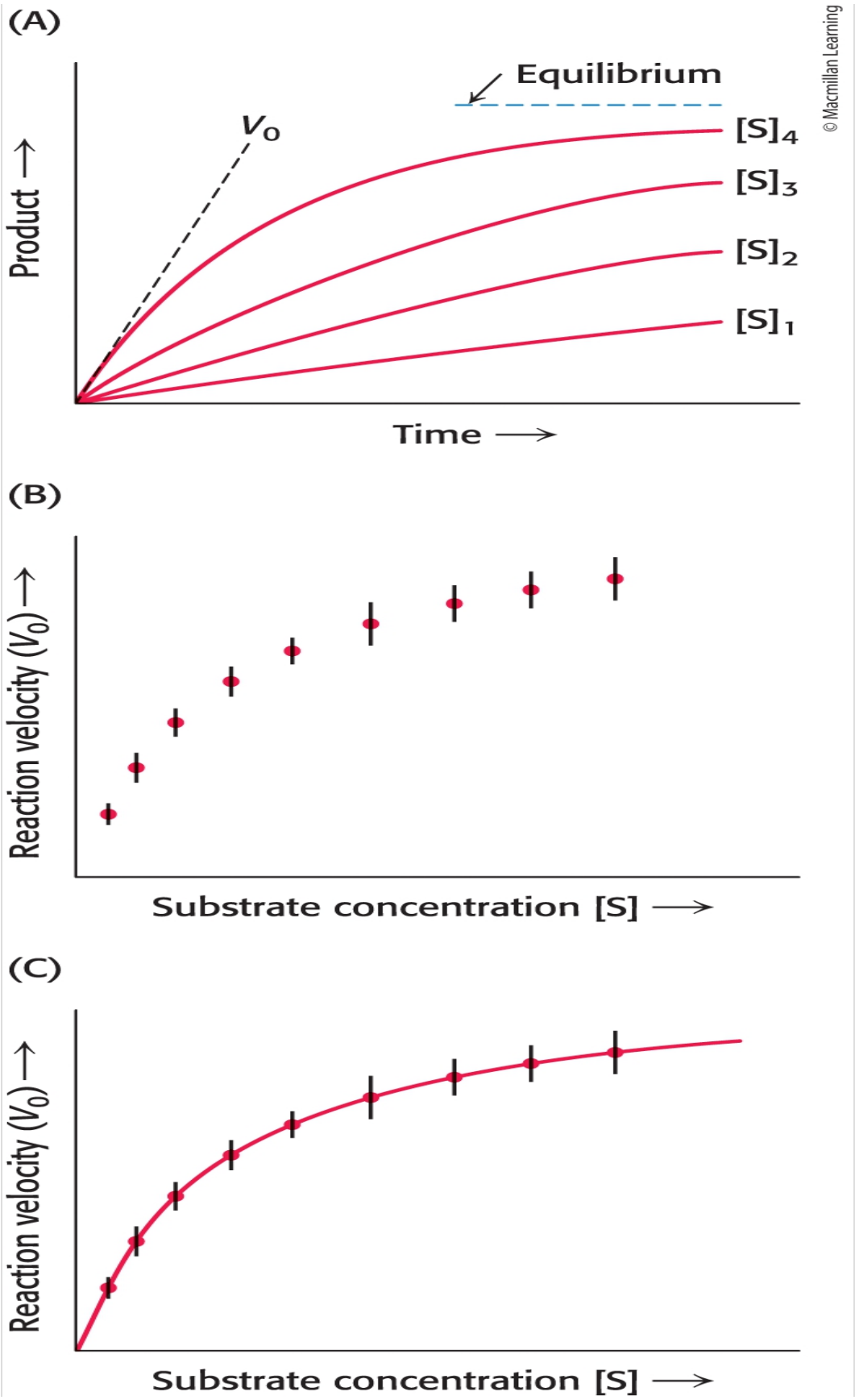
Sometimes, second-order reactions can appear to be first-order reactions. For instance, in the reaction described by equation 6, if B is present in excess and A is present at low concentrations, the reaction rate will be first order with respect to A and will not appear to depend on the concentration of B. These reactions are called *pseudo-first-order reactions*, and we will see them a number of times in our study of biochemistry.

Interestingly, under some conditions, a reaction can be zero order. In these cases the rate is independent of reactant concentrations. Enzyme-catalyzed reactions can approximate zero-order reactions under some circumstances, as we will soon see.

The steady-state assumption aids a description of enzyme kinetics

The simplest way to investigate the reaction rate is to follow the increase in reaction product as a function of time. First, the extent of product formation is determined as a function of time for a series of substrate concentrations (**Figure 5.9A**). As expected, in each case, the amount of product formed increases with time, although eventually a time is reached when there is no net change in the concentration of S or P. The enzyme is still actively converting

substrate into product and vice versa, but the reaction equilibrium has been attained.



© Macmillan Learning

FIGURE 5.9 The relation between initial velocity and substrate concentration can be determined by a series of assays. (A) The amount of product formed at different substrate concentrations is plotted as a function of time. The initial velocity (V_0) for each substrate concentration is determined from the slope of the curve at the beginning of a reaction, when the reverse reaction is insignificant. (B) The values for initial velocity determined in part A are then plotted, with error bars, against substrate concentration. (C) The data points are connected to clearly reveal the relationship of initial velocity to substrate concentration.



However, enzyme kinetics is more readily comprehended if we consider only the forward reaction, which is most closely described by the initial rates of the reaction. Note that the rate of the reaction (the slope of the tangent line in Figure 5.9A) decreases over time. Additionally, only at the beginning of the reaction is the exact concentration of the substrate known because it is being converted to product as the reaction progresses. For these two reasons, it is often most useful to focus on initial rate enzyme kinetics. We can define the rate of catalysis V_0, or the initial rate of catalysis, as the number of moles of product formed per second when the reaction is just beginning — that is, when $t \approx 0$ and $[P] \approx 0$, so the rate of the reverse reaction is negligible (Figure 5.9A). These experiments are repeated three to five times with each substrate concentration to ensure the accuracy of and assess the variability of the values attained.

Next, we plot V_0 versus the initial substrate concentration used in each experiment, [S], assuming a constant amount of enzyme and showing the data points with error bars (**Figure 5.9B**). Finally, the data points are connected, yielding the results shown in **Figure 5.9C**. The rate of catalysis rises linearly as substrate concentration increases and then begins to level off and approach a maximum at

higher substrate concentrations. For convenience, we will show idealized data without error bars throughout the text, but it is important to keep in mind that in reality, all experiments are repeated multiple times.

The Michaelis–Menten model explains many observations of enzyme kinetics

In 1913, Leonor Michaelis and Maud Menten proposed a simple model to account for these kinetic characteristics. The critical feature in their treatment is that a specific ES complex is a necessary intermediate in catalysis. The model they proposed is

$$E + S \underset{k_{-1}}{\overset{k_1}{\rightleftharpoons}} ES \underset{k_{-2}}{\overset{k_2}{\rightleftharpoons}} E + P$$



An enzyme E (here representing the “free enzyme”) combines with substrate S (“free substrate”) to form an ES complex, with a rate constant k_1.

The ES complex has two possible fates. It can dissociate to E and S, with a rate constant k_{-1}, or it can proceed to form product P, with a rate constant k_2. The ES complex can also be reformed from E and P by the reverse reaction with a rate constant k_{-2}. However, as before, we can simplify these reactions by considering the rate of

reaction at times close to zero (hence, V_0) when there is negligible product formation and thus no back reaction $(k_{-2}[E][P] \approx 0)$.

$$E + S \underset{k_{-1}}{\overset{k_1}{\rightleftharpoons}} ES \xrightarrow{k_2} E + P$$

(7)

Thus, for the graph in **Figure 5.10**, V_0 is determined for each substrate concentration by measuring the rate of product formation at early times before P accumulates (Figure 5.9A).

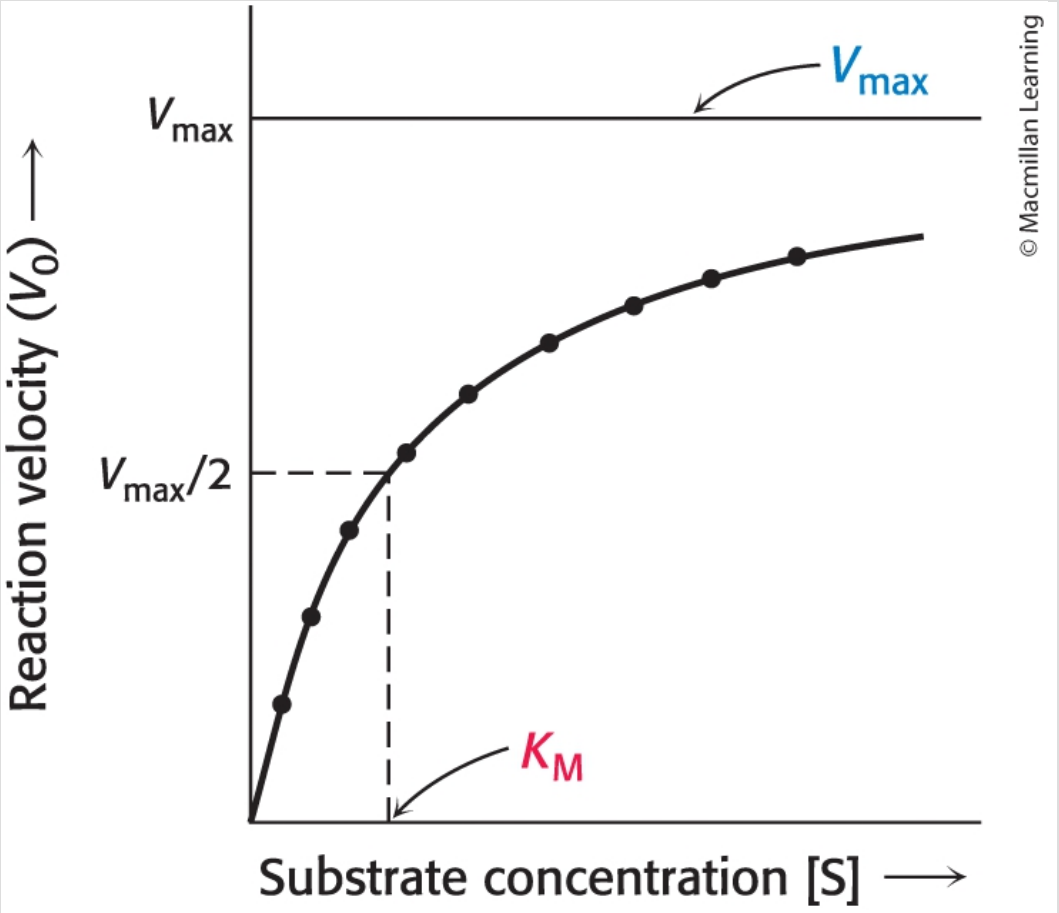


FIGURE 5.10 Michaelis–Menten kinetics are marked by a hyperbolic relationship between initial velocity and substrate concentration. A plot of the reaction velocity (V_0) as a function of the substrate concentration [S] for an enzyme that obeys Michaelis–Menten kinetics shows that the maximal velocity (V_{max}) is approached asymptotically, which is to say, V_{max} will be attained only at an infinite substrate concentration. The Michaelis constant (K_M) is the substrate concentration yielding a velocity of $V_{max}/2$.

The Michaelis–Menten equation describes the relationship between initial velocity and substrate concentration

We want an expression that relates the rate of catalysis to the concentrations of substrate and enzyme and the rates of the individual steps. For any chemical reaction, the overall reaction rate is determined only by the slowest, or rate-determining step. Thus, our starting point is the assumption that catalysis, resulting from the ES complex, is slow relative to the rate of substrate binding, i.e., the formation of the ES complex. Thus, the overall reaction rate can be expressed solely as the rate of this one step, which is the product of the concentration of the ES complex and k_2.

$$V_0 = k_2[\mathrm{ES}]$$

(8)

Now we need to express [ES] in terms of known quantities. The rates of formation and breakdown of ES are given by

$$\text{Rate of formation of ES} = k_1[\mathrm{E}][\mathrm{S}]$$

(9)

$$\text{Rate of breakdown of ES} = (k_{-1} + k_2)[\mathrm{ES}]$$

(10)

We will use what biochemists term the *steady-state assumption* to simplify matters. In a steady-state system, the concentrations of intermediates — in this case, [ES] — stay the same even though the concentrations of starting materials and products are changing and the system is not in equilibrium. An analogy is a sink filled with water that has the tap open just enough to match the loss of water down the drain: the level of the water in the sink never changes even though water is constantly flowing from the faucet through the sink and out through the drain. This steady state is reached when the rates of formation and breakdown of the ES complex are equal. Setting the right-hand sides of equations 9 and 10 equal gives

$$k_1[E][S] = (k_{-1} + k_2)[ES]$$

(11)

By rearranging equation 11, we obtain

$$[E][S]/[ES] = (k_{-1} + k_2)/k_1$$

(12)

Equation 12 can be simplified by defining a new constant, K_M, called the **Michaelis constant**:

$$K_M = \frac{k_{-1} + k_2}{k_1}$$

(13)

Note that K_M has the units of concentration and is independent of enzyme and substrate concentrations. As will be explained, K_M is an important characteristic of enzyme–substrate interactions.

Inserting equation 13 into equation 12 and solving for [ES] yields

$$[ES] = \frac{[E][S]}{K_M} \tag{14}$$

Now let us examine the numerator of equation 14. Because the substrate is usually present at a much higher concentration than that of the enzyme, the concentration of uncombined (free) substrate [S] is very nearly equal to the total substrate concentration. The concentration of uncombined (free) enzyme [E] is equal to the total enzyme concentration $[E]_T$ minus the concentration of the ES complex:

$$[E] = [E]_T - [ES]$$

Substituting this expression for [E] in equation 14 gives

$$[ES] = \frac{([E]_T - [ES])[S]}{K_M}$$

Solving the above equation for [ES] gives

$$[ES] = \frac{[E]_T[S]/K_M}{1 + [S]/K_M}$$

or

$$[ES] = [E]_T \frac{[S]}{[S] + K_M}$$

By substituting this expression for [ES] into equation 8, we obtain

$$V_0 = k_2[E]_T \frac{[S]}{[S] + K_M}$$

(15)

The **maximal rate**, V_{max}, is attained when the catalytic sites on the enzyme are saturated with substrate — that is, when $[ES] = [E]_T$. Thus,

$$V_{max} = k_2[E]_T$$

(16)

Substituting equation 16 into equation 15 yields the **Michaelis–Menten equation**:

$$V_0 = V_{max} \frac{[S]}{[S] + K_M}$$

(17)

This equation accounts for the kinetic data given in Figure 5.10. At very low substrate concentration, when [S] is much less than K_M, $V_0 = (V_{max} / K_M)[S]$; that is, the reaction is first order with the rate directly proportional to the substrate concentration. At high substrate concentration, when [S] is much greater than K_M, $V_0 = V_{max}$; that is, the rate is maximal. The reaction is zero order, independent of substrate concentration.

Notice that because V_0 is a function of [S], then if the K_M value is known, the equation gives the velocity as a fraction of V_{max} at any concentration of substrate. Thus, the velocity can be calculated at any [S], using the Michaelis–Menten equation, and expressed either in real units (if V_{max} is known) or as a fraction of V_{max}. Likewise, if the fraction of V_{max} is known, then the relationship between [S] and K_M can be calculated.

The significance of K_M is clear when we set $[S] = K_M$ in equation 17. When $[S] = K_M$, then $V_0 = V_{max}/2$. Thus, K_M is equal to the substrate concentration at which the reaction rate is half its maximal value. As we will see, K_M is an important characteristic of an enzyme-catalyzed reaction and is significant for its biological function.



Smithsonian Institution Archives, Accession 90-105, Science Service Records, Image No. SIA2008-5999

MAUD MENTEN Paving new career paths for women at the dawn of the 20th century, Maud Menten was among the first Canadian women to obtain an MD degree, in 1911; she then earned a PhD in 1916. Although she is most famous for her groundbreaking work on enzyme kinetics as a graduate student, she had a long and productive scientific career at the University of Pittsburgh and the British Columbia Medical Research Institute, teaching and publishing over 70 papers on a variety of subjects. She invented a still-used histochemical assay for

alkaline phosphatase, characterized bacterial toxins and early vitamin C deficiency, and pioneered the use of electrophoresis for the study of proteins.

Example

Applying the Michaelis–Menten Equation

Problem:

Assume that the initial velocity of an enzyme is 80% of V_{max}. What is the ratio of [S] to K_M under these conditions?

Getting Started:

The Michaelis–Menten equation relates the three terms discussed in the problem, so let's begin with it:

$$V_0 = V_{max} \frac{[S]}{[S] + K_M}$$

What do we already know? The question states the $V_0 = 80\%\ V_{max}$. This is the only value we are provided, so we should be able to solve the problem with that value and the equation.

SOLVE:

First, for convenience, let's convert 80% to 0.8 and substitute the $0.8\ V_{max}$ for V_0 in the equation:

$$0.8V_{max} = V_{max}\frac{[S]}{[S] + K_M}$$

Now we see that we can divide both sides of the equation by V_{max}, which yields

$$0.8 = \frac{[S]}{[S] + K_M}$$

Now we can solve the equation for $[S]/K_M$.

$$\begin{aligned} 0.8[S] + 0.8K_M &= [S] \\ 0.8K_M &= [S] - 0.8[S] \\ 0.8K_M &= 0.2[S] \\ 4 &= \frac{[S]}{K_M} \end{aligned}$$

Thus, when [S] is fourfold greater than K_M, $V_0 = 0.8\ V_{max} = 80\%\ V_{max}$.

Reflect:

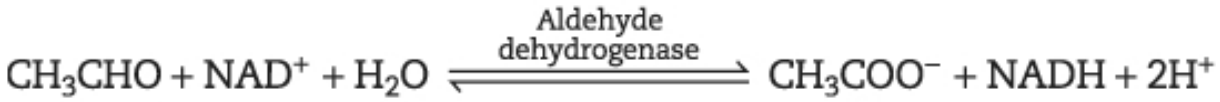
You can confirm this answer by solving the Michaelis–Menten equation using $[S] = 4K_M$ and solving for V_0 as a fraction of V_{max}.

Variations in K_M can have physiological consequences

The physiological consequence of K_M is illustrated by the sensitivity of some persons to ethanol. Such persons exhibit facial flushing and rapid heart rate (tachycardia) after ingesting even small amounts of alcohol. In the liver, alcohol dehydrogenase converts ethanol (CH_3CH_2OH) into acetaldehyde (CH_3CHO).

$$CH_3CH_2OH + NAD^+ \underset{}{\overset{\text{Alcohol dehydrogenase}}{\rightleftharpoons}} CH_3CHO + NADH + H^+$$

Normally, the acetaldehyde, which is the cause of the symptoms when present at high concentrations, is processed to acetate by aldehyde dehydrogenase.



Most people have two forms of the aldehyde dehydrogenase, a low K_M mitochondrial form and a high K_M cytoplasmic form. In susceptible persons, the mitochondrial enzyme is less active owing to the substitution of a single amino acid, and acetaldehyde is processed only by the cytoplasmic enzyme. Because this enzyme has a high K_M, it achieves a high rate of catalysis only at very high concentrations of acetaldehyde. Consequently, less acetaldehyde is converted into acetate; excess acetaldehyde escapes into the blood and accounts for the physiological effects.

K_M and V_{max} values can be determined by several means

K_M is equal to the substrate concentration that yields $V_{max}/2$; however, like perfection, V_{max} is approached but never attained. How, then, can we experimentally determine K_M and V_{max}, and how do these parameters enhance our understanding of enzyme-catalyzed reactions? The Michaelis constant, K_M, and the maximal rate, V_{max}, can be readily derived from rates of catalysis measured at a variety of substrate concentrations if an enzyme operates according to the simple scheme given in equation 17. The derivation of K_M and V_{max} is most commonly achieved with the use of curve-fitting programs on a computer. However, an older method,

although rarely used because the data points at high and low concentrations are weighted differently and thus sensitive to errors, is a source of further insight into the meaning of K_M and V_{max}.

Before the availability of computers, the determination of K_M and V_{max} values required algebraic manipulation of the Michaelis–Menten equation. The Michaelis–Menten equation is transformed into one that gives a straight-line plot that yields values for V_{max} and K_M. Taking the reciprocal of both sides of equation 17 gives

$$\frac{1}{V_0} = \frac{K_M}{V_{max}} \times \frac{1}{[S]} + \frac{1}{V_{max}} \quad \textbf{(18)}$$

A plot of $1/V_0$ versus $1/[S]$, called a **Lineweaver–Burk plot** or sometimes just called a *double-reciprocal plot*, yields a straight line with a *y*-intercept of $1/V_{max}$ and a slope of K_M/V_{max} (**Figure 5.11**). The intercept on the *x*-axis is $-1/K_M$.

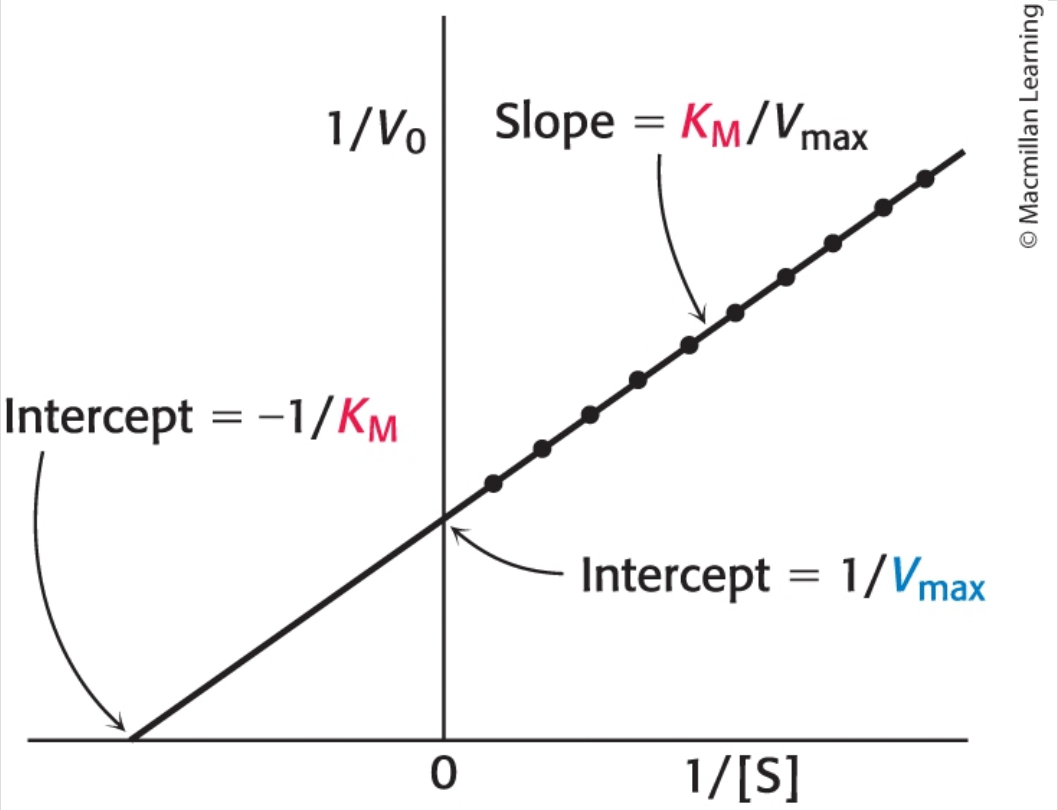


FIGURE 5.11 A Lineweaver–Burk plot shows $1/V_0$ as a function of $1/[S]$. The slope is K_M/V_{max}, the intercept on the vertical axis is $1/V_{max}$, and the intercept on the horizontal axis is $-1/K_M$.

K_M and k_{cat} values are important enzyme characteristics

The K_M values of enzymes range widely (Table 5.5). For most enzymes, K_M lies between 10^{-1} and 10^{-7} M. The K_M value for an enzyme depends on the particular substrate and on environmental

conditions such as pH, temperature, and ionic strength. The Michaelis constant, being equal to the concentration of substrate at which half the active sites are filled, thus provides a measure of the substrate concentration required for significant catalysis to take place.

TABLE 5.5 K_M values of some enzymes

Enzyme	Substrate	K_M (μM)
Chymotrypsin	Acetyl-L-tryptophanamide	5000
Lysozyme	Hexa-*N*-acetylglucosamine	6
β-Galactosidase	Lactose	4000
Threonine deaminase	Threonine	5000
Carbonic anhydrase	CO_2	8000
Penicillinase	Benzylpenicillin	50
Pyruvate carboxylase	Pyruvate	400
	HCO_3^-	1000
	ATP	60
Arginine-tRNA synthetase	Arginine	3
	tRNA	0.4

For many enzymes, experimental evidence suggests that the K_M value provides an approximation of the substrate concentration in vivo, which in turn suggests that most enzymes evolved to have a K_M approximately equal to the substrate concentration commonly available. Why might it be beneficial to have a K_M value approximately equal to the commonly available substrate concentration? If the normal concentration of substrate is near K_M, the enzyme will display significant activity, and yet the activity will be sensitive to changes in environmental conditions — that is, changes in substrate concentration. This property is known as **elasticity**. At values below K_M, enzymes are very sensitive to changes in substrate concentration — in other words, they are elastic — but display little activity. At substrate values well above K_M, enzymes have greater catalytic activity but are insensitive — or inelastic — to changes in substrate concentration. Thus, with the normal substrate concentration being approximately K_M, the enzymes have significant activity ($1/2\ V_{max}$) but are still elastic to changes in substrate concentration.

Under certain circumstances, K_M reflects the strength of the enzyme–substrate interaction. In equation 13, K_M is defined as $(k_{-1} + k_2)/k_1$. Consider a case in which k_{-1} is much greater than k_2. Under such circumstances, the ES complex dissociates to E and S much more rapidly than product is formed. Under these conditions, ($k_{-1} \gg k_2$)

$$K_M \approx \frac{k_{-1}}{k_1}$$

(19)

Equation 19 describes the dissociation constant, K_d (Chapter 3), of the ES complex.

$$K_{ES} = \frac{[E][S]}{[ES]} = \frac{k_{-1}}{k_1}$$

In other words, K_M is equal to the dissociation constant (K_d) of the ES complex if k_2 is much smaller than k_{-1}. When this condition is met, K_M is a measure of the strength of the ES complex: a high K_M indicates weak binding; a low K_M indicates strong binding. It must be stressed that K_M indicates the affinity of the ES complex only when k_{-1} is much greater than k_2.

The maximal rate, V_{max}, reveals the **turnover number** of an enzyme, which is the number of substrate molecules converted into product by an enzyme molecule in a unit time when the enzyme is fully saturated with substrate. For a single active site, it is equal to the rate constant k_2, which is also called k_{cat}. The maximal rate, V_{max}, reveals the turnover number of an enzyme if the concentration of active sites $[E]_T$ is known, because

$$V_{max} = k_{cat}[E]_T$$

and thus

$$k_{cat} = V_{max} / [E]_T \tag{20}$$

For example, a 10^{-6} M solution of carbonic anhydrase catalyzes the formation of 0.6 M H_2CO_3 per second when the enzyme is fully saturated with substrate. Hence, k_{cat} is 6×10^5 s^{-1}. This turnover number is one of the largest known. Each catalyzed reaction takes place in a time equal to, on average, $1/k_{cat}$, which is 1.7 μs for carbonic anhydrase. The turnover numbers of most enzymes with their physiological substrates range from 1 to 10^6 per second (Table 5.6).

TABLE 5.6 Turnover numbers of some enzymes

Enzyme	Turnover number (per second)
Carbonic anhydrase	600,000
3-Ketosteroid isomerase	280,000
Acetylcholinesterase	25,000
Penicillinase	2000
Lactate dehydrogenase	1000
Chymotrypsin	100

DNA polymerase I	15
Tryptophan synthetase	2
Lysozyme	0.5

K_M and V_{max} also permit the determination of f_{ES}, the fraction of active sites filled. This relation of f_{ES} to K_M and V_{max} is given by the following equation:

$$f_{ES} = \frac{V_0}{V_{max}} = \frac{[S]}{[S] + K_M}$$

(21)

Self-Check Question



Explain why K_M is an intrinsic property of an enzyme while V_{max} is not?

k_{cat}/K_M is a measure of catalytic efficiency

Recall that when the substrate concentration is much greater than K_M, the rate of catalysis is equal to V_{max}, which is a function of k_{cat}, the turnover number. However, most enzymes are not normally

saturated with substrate. Under physiological conditions, the $[S]/K_M$ ratio is typically between 0.01 and 1.0. When $[S] = K_M$, the enzymatic rate is much less than k_{cat} because most of the active sites are unoccupied.

Is there a number that characterizes the kinetics of an enzyme under these more typical cellular conditions? Indeed there is, as can be shown by combining equations 8 and 14 to give

$$V_0 = \frac{k_{cat}}{K_M}[E][S]$$

When $[S] \ll K_M$, the concentration of free enzyme [E], is nearly equal to the total concentration of enzyme $[E]_T$; so

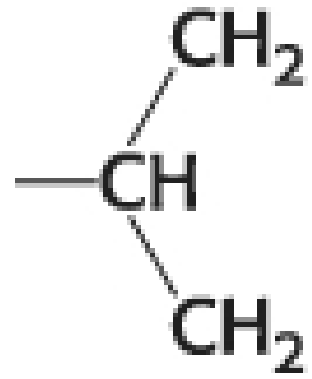
$$V_0 = \frac{k_{cat}}{K_M}[S][E]_T$$

Thus, when $[S] \ll K_M$, the enzymatic velocity depends on the values of k_{cat}/K_M, [S], and $[E]_T$. Under these conditions, k_{cat}/K_M is the rate constant for the interaction of S and E.

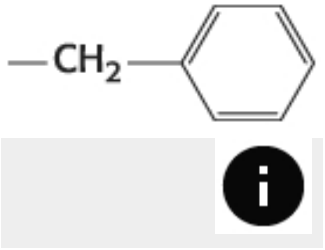
The rate constant $\boldsymbol{k_{cat}/K_M}$, called the **specificity constant**, is a measure of catalytic efficiency because it takes into account both the rate of catalysis with a particular substrate (k_{cat}) and the nature of the enzyme–substrate interaction (K_M). For instance, by using

k_{cat}/K_M values, we can compare an enzyme's preference for different substrates. Table 5.7 shows the k_{cat}, K_M, and k_{cat}/K_M values for several different substrates of chymotrypsin. Chymotrypsin clearly has a preference for cleaving next to bulky, hydrophobic side chains.

TABLE 5.7 Substrate preferences of chymotrypsin

Amino acid in ester	Amino acid side chain	k_{cat}/K_M ($s^{-1}\,M^{-1}$)
Glycine	—H	1.3×10^{-1}
Valine		2.0
Norvaline	$-CH_2CH_2CH_3$	3.6×10^{2}
Norleucine	$-CH_2CH_2CH_2CH_3$	3.0×10^{3}

Phenylalanine	1.0×10^5



Source: Information from A. Fersht, *Structure and Mechanism in Protein Science: A Guide to Enzyme Catalysis and Protein Folding* (W. H. Freeman and Company, 1999), Table 7.3.

How efficient can an enzyme be? We can approach this question by determining whether there are any physical limits on the value of k_{cat}/K_M. Note that the k_{cat}/K_M ratio depends on k_1, k_{-1}, and k_{cat}, as can be shown by substituting for K_M.

$$k_{cat}/K_M = \frac{k_{cat}k_1}{k_{-1}+k_{cat}} = \left(\frac{k_{cat}}{k_{-1}+k_{cat}}\right)k_1 < k_1$$

Note that the value of k_{cat}/K_M is always less than k_1. Suppose that the rate of formation of product (k_{cat}) is much faster than the rate of dissociation of the ES complex (k_{-1}). The value of k_{cat}/K_M then approaches k_1. Thus, the ultimate limit on the value of k_{cat}/K_M is set by k_1, the rate of formation of the ES complex, which is limited by the diffusion-controlled encounter of an enzyme and its substrate. Because diffusion limits the value of k_1, it cannot be higher than between 10^8 and $10^9\ s^{-1}M^{-1}$.

Enzymes that have k_{cat}/K_M ratios in the range of these upper limits, such as superoxide dismutase, acetylcholinesterase, and triose phosphate isomerase, have attained what is called *kinetic perfection*. Their catalytic velocity is restricted only by the rate at which they encounter substrate in the solution (Table 5.8). Any further gain in catalytic rate can come only by decreasing the time for diffusion of the substrate into the enzyme's immediate environment.

TABLE 5.8 Enzymes with k_{cat}/K_M near the diffusion-controlled limit

Enzyme	k_{cat}/K_M ($s^{-1}\,M^{-1}$)
Acetylcholinesterase	1.6×10^8
Carbonic anhydrase	8.3×10^7
Catalase	4×10^7
Crotonase	2.8×10^8
Fumarase	1.6×10^8
Triose phosphate isomerase	2.4×10^8
β-Lactamase	1×10^8
Superoxide dismutase	7×10^9

Source: Information from A. Fersht, *Structure and Mechanism in Protein Science: A Guide to Enzyme Catalysis and Protein Folding* (W. H. Freeman and Company, 1999), Table 4.5.

Remember that the active site is only a small part of the total enzyme structure. Yet, for catalytically perfect enzymes, every encounter between enzyme and substrate is productive. In these cases, there may be attractive electrostatic forces on the enzyme that entice the substrate to the active site. These forces are sometimes referred to poetically as *Circe effects*, named for the figure from Greek mythology known for her powers of seduction and transformation.

The diffusion of a substrate throughout a solution can also be partly overcome by confining substrates and products in the limited volume of a multienzyme complex, such that the product of one enzyme is very rapidly found by the next enzyme. In effect, products are channeled from one enzyme to the next, much as in an assembly line.

Self-Check Question



If a mutation occurs in the gene encoding an enzyme which decreases k_{cat} for a specific substrate by a factor of 2 and decreases K_M for that substrate by a factor of 3, did the mutation make the enzyme a more or less efficient catalyst with respect to that substrate?

Most biochemical reactions include multiple substrates

Most reactions in biological systems are bisubstrate reactions, which start with two substrates and yield two products, represented by:

$$A + B \rightleftharpoons P + Q$$

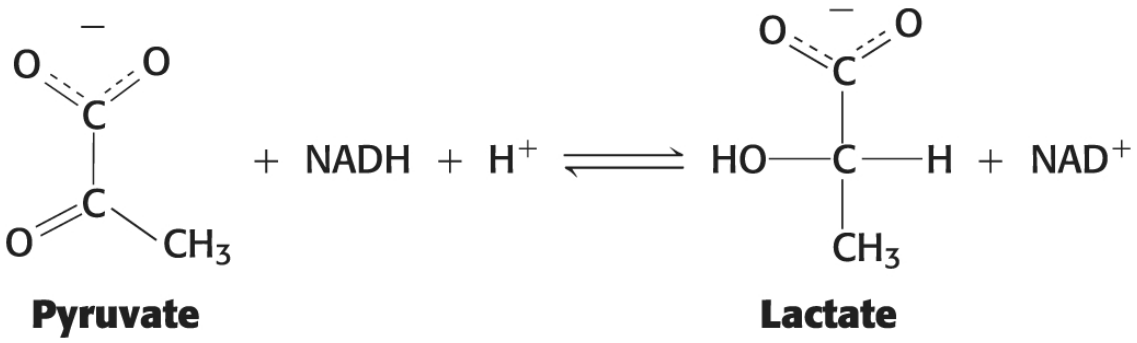
Many bisubstrate reactions transfer a functional group, such as a phosphoryl or an ammonium group, from one substrate to the other. Those that are oxidation–reduction reactions transfer electrons between substrates. Multiple substrate reactions can be divided into two classes: sequential reactions and double-displacement reactions.

Sequential reactions

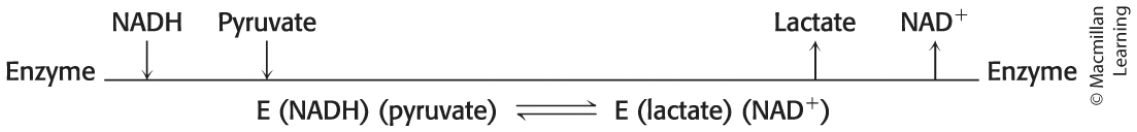
In **sequential reactions**, all substrates must bind to the enzyme before any product is released. Specifically, in a bisubstrate reaction, a ternary complex — composed of the enzyme and both substrates — forms.

- *In ordered sequential mechanisms, the substrates bind the enzyme in a defined sequence*. For example, many enzymes that have NAD^+ or NADH as a substrate exhibit the ordered sequential mechanism. Consider lactate dehydrogenase, an important

enzyme in glucose metabolism (Section 16.1). This enzyme reduces pyruvate to lactate while oxidizing NADH to NAD^+.

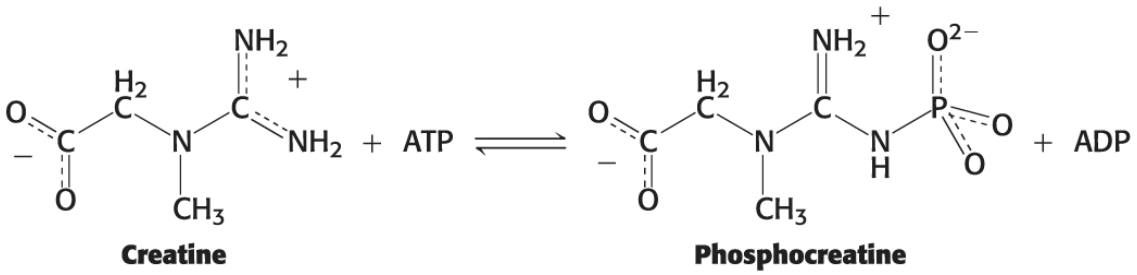


In the ordered sequential mechanism, the coenzyme always binds first, and the lactate is always released first. This sequence can be represented by using a notation developed by W. Wallace Cleland:

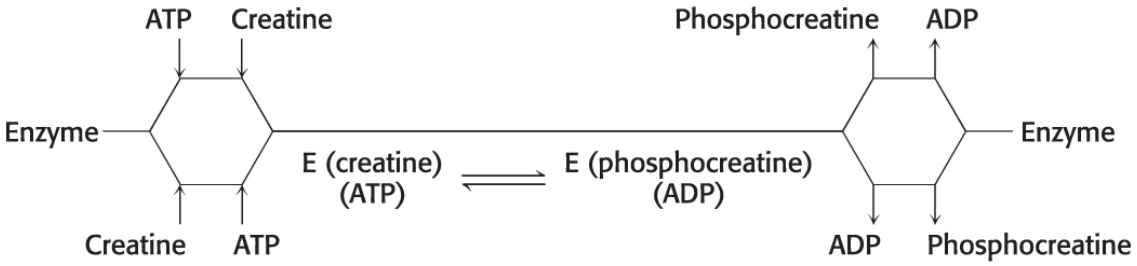


The enzyme exists as a ternary complex consisting of, first, the enzyme and substrates and, after catalysis, the enzyme and products.

- *In the random sequential mechanism, the order of the addition of substrates and the release of products is arbitrary*. An example of a random sequential reaction is the formation of phosphocreatine and ADP from creatine and ATP which is catalyzed by creatine kinase (Section 15.2).



Either creatine or ATP may bind first, and either phosphocreatine or ADP may be released first. Phosphocreatine is an important energy source in muscle. Random sequential reactions also can be depicted in the Cleland notation.

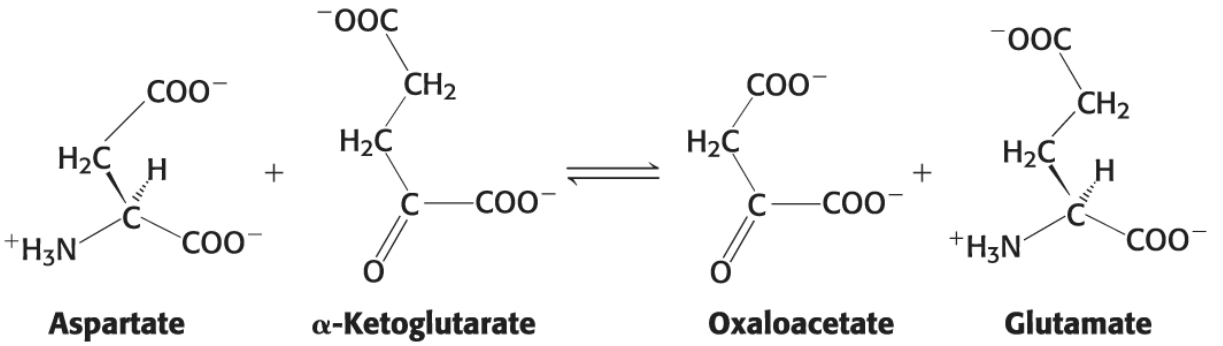


Although the order of certain events is random, the reaction still passes through the ternary complexes, including the substrates first and then the products.

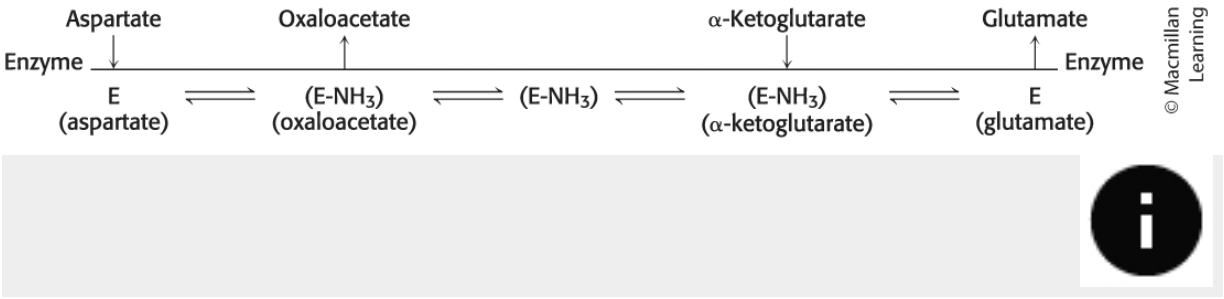
Double-displacement reactions

In **double-displacement reactions** (also called **Ping-Pong reactions**), one or more products are released before all substrates bind the enzyme. The defining feature of double-displacement reactions is the existence of an enzyme intermediate in which the enzyme is temporarily modified.

Reactions that shuttle amino groups between amino acids and α-ketoacids are classic examples of double-displacement mechanisms. The enzyme aspartate aminotransferase catalyzes the transfer of an amino group from aspartate to α-ketoglutarate.



The sequence of events can be portrayed as the following Cleland notation:



After aspartate binds to the enzyme, the enzyme accepts aspartate's amino group to form the substituted enzyme intermediate. The first product, oxaloacetate, subsequently departs. The second substrate, α-ketoglutarate, binds to the enzyme, accepts the amino group from the modified enzyme, and is then released as the final product, glutamate. In the Cleland notation, the substrates appear to bounce on and off the enzyme much as a Ping-Pong ball bounces on a table. Note that for double-displacement reactions, substrate binding order is always fixed (ordered) and never random.

Allosteric enzymes often do not obey Michaelis–Menten kinetics

The Michaelis–Menten model has greatly assisted the development of enzymology. Its virtues are simplicity and broad applicability. However, the Michaelis–Menten model cannot account for the kinetic properties of many enzymes. An important group of enzymes that often do not obey Michaelis–Menten kinetics are **allosteric enzymes**, which consist of multiple subunits and multiple active sites. The binding of substrate to one active site can alter the properties of other active sites in the same enzyme molecule (an effect known as *allostery*, Chapter 3). Allosteric enzymes often display sigmoidal plots of the reaction velocity V_0 versus substrate

concentration [S] (**Figure 5.12**), rather than the hyperbolic plots predicted by the Michaelis–Menten equation (see Figure 5.10).

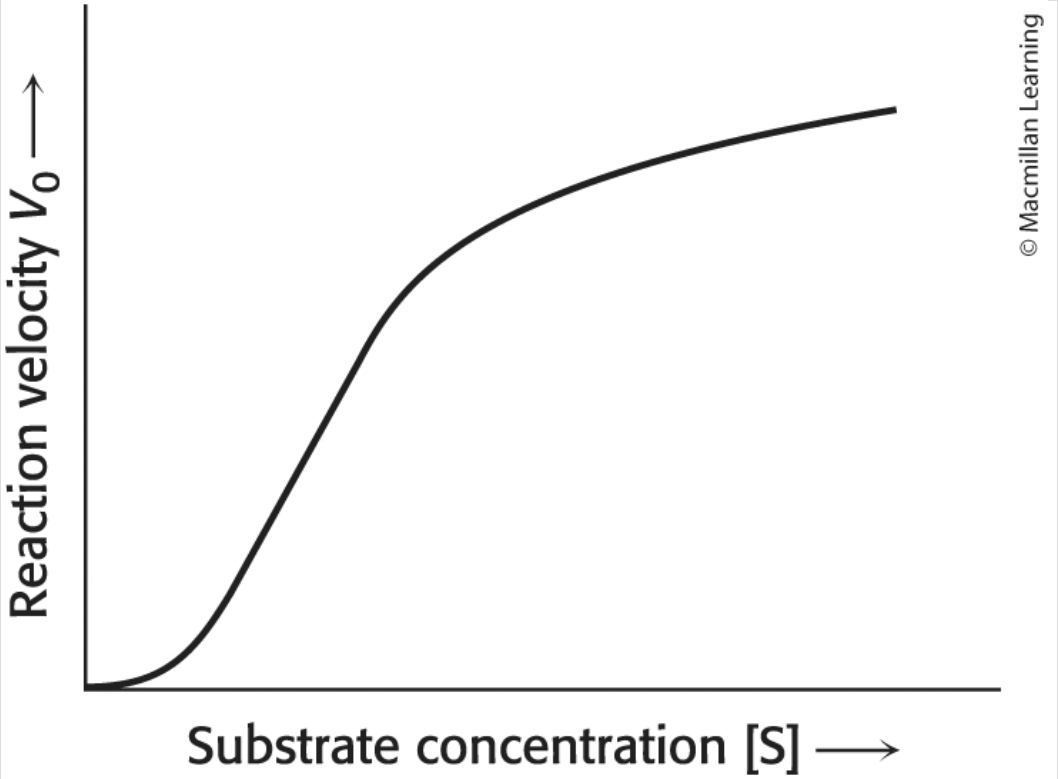


FIGURE 5.12 Allosteric enzymes often display a sigmoidal dependence of reaction velocity on substrate concentration. Shown are the kinetics for an allosteric enzyme exhibiting positive cooperativity.

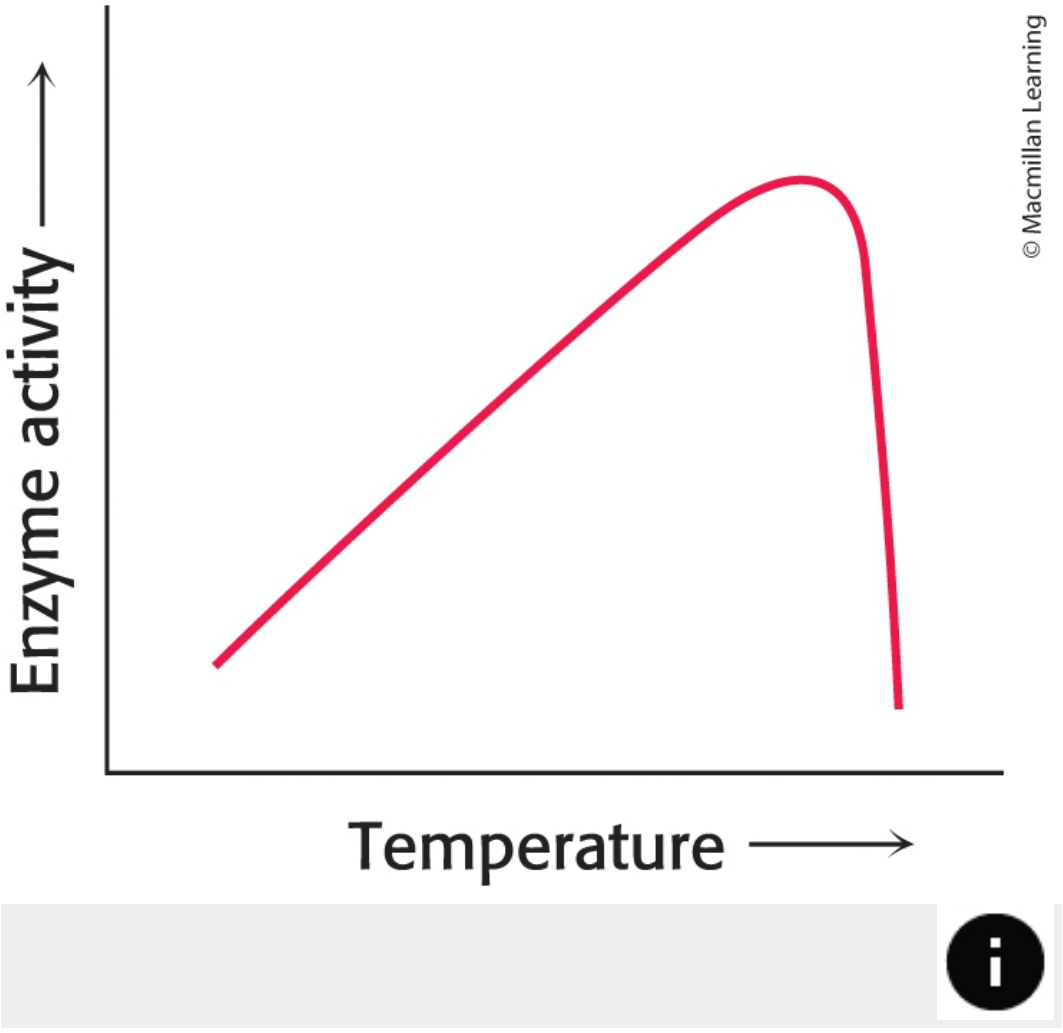
The interaction between an allosteric enzyme's multiple subunits can exhibit positive cooperativity. In other words, the binding of substrate to one active site facilitates the binding of substrate to the other active sites, akin to the behavior of oxygen binding to the multiple subunits of the allosteric protein hemoglobin (see Section 3.3). Such positive cooperativity results in a sigmoidal plot of V_0 versus [S]. In addition, the activity of an allosteric enzyme may be altered by regulatory molecules that reversibly bind to specific sites

other than the catalytic sites. Furthermore, the enzymes themselves can often interconvert between more- or less-active quaternary states, typically denoted as “R” and “T,” respectively, by the conventions established for hemoglobin.

The complexities of allosteric enzymes often require more-elaborate models than the Michaelis–Menten model to account for multiple active sites and quaternary state transitions. The catalytic properties of allosteric enzymes make them key regulators of metabolic pathways in ways we will explore more fully in Chapter 7.

Temperature affects enzymatic activity

As the temperature rises, the rate of most reactions, including enzyme-catalyzed reactions, increases. For most enzymes, there is a temperature at which the increase in catalytic activity ceases and there is a precipitous loss of activity.

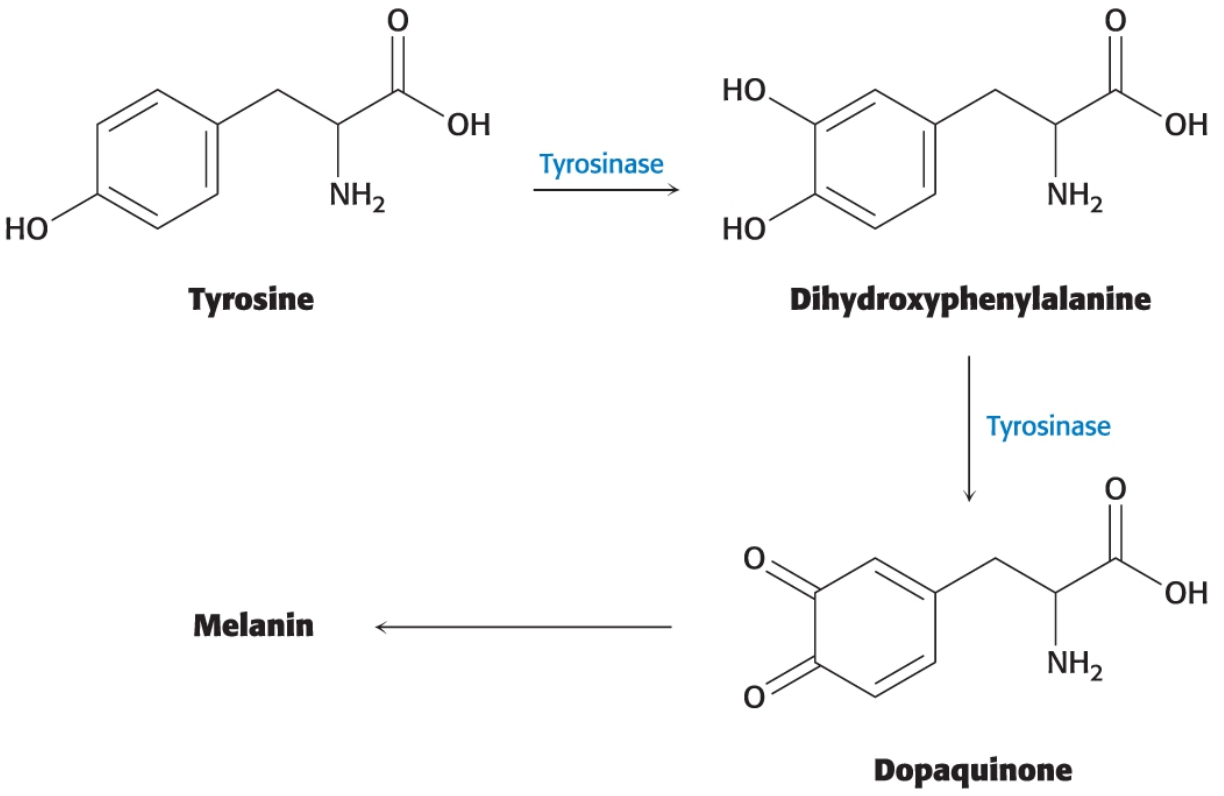


What is the basis of this loss of activity? Recall from Chapter 2 that proteins have a complex three-dimensional structure that is held together by weak interactions. When the temperature increases beyond a certain point, the favorable interactions maintaining the three-dimensional structure are not strong enough to withstand the polypeptide chain's thermal jostling, and the protein loses the structure required for activity. The protein is said to be *denatured* (Section 2.7).

In endotherms, organisms such as ourselves that maintain a constant body temperature, the effect of outside temperature on enzyme activity is minimized. However, in ectotherms, organisms

that assume the temperature of their environment, temperature is an important regulator of biochemical and, indeed, biological activity. Lizards, for instance, are most active in warmer temperatures — a behavioral manifestation of biochemical activity.

Although endotherms are not as sensitive to ambient temperature as ectotherms, slight tissue temperature alterations are sometimes important and can even have dramatic effects. For example, the characteristic coloration of Siamese cats can be explained by variation in enzyme sensitivity due to temperature. Their fur color is due to the presence of the pigment melanin, the same pigment that is responsible for human skin color. The first steps in the synthesis of melanin are catalyzed by the enzyme tyrosinase:



Most Siamese cats are born with very little coloration; sometimes they are even white. As they mature, their extremities — tips of the ears, snout, paws, and end of the tail — darken to black. A hint to understanding this phenomenon comes from the knowledge that a cat's skin temperature is coolest at the extremities. Biochemists have established that there is a mutation in the Siamese tyrosinase that results in a loss of activity above 37-39°C. The temperature of a Siamese kitten is too warm for the enzyme to be active, but as the kitten grows, the temperature at its extremities cools enough to allow the enzyme to become active and pigment to form. The core of the cat's body remains above the threshold temperature, however, and thus remains pale in color.

5.5 Enzymes Can Be Studied One Molecule at a Time

Most experiments performed to determine an enzyme's characteristics use an enzyme preparation in a buffered solution. Even a few microliters of such a solution will contain millions of enzyme molecules. Experiments on this scale, called *ensemble studies*, make the basic assumption that all of the enzyme molecules are the same or very similar. For example, when we determine an enzymatic property such as the value of K_M in ensemble studies, we assume that value is an average value of all of the enzyme molecules present.

Keep in mind, however, that individual enzyme molecules behave stochastically, as we saw for DNA double helix formation in Chapter 1. New methods, dubbed *single-molecule experiments*, now allow one individual molecule to be examined at a time, yielding a great deal of new information but with a potential pitfall: how can we be certain that the molecule is representative and not an outlier? We can overcome this challenge by studying enough individuals to satisfy statistical analysis for validity.

Let us consider a biochemical situation. **Figure 5.13A** shows a hypothetical enzyme that displays molecular heterogeneity, with three active forms that catalyze the same reaction but at different rates. These forms have slightly different stabilities, but thermal motion is sufficient to interconvert them. Each form is present as a fraction of the total enzyme population, as indicated. If we were to perform an ensemble method experiment to determine enzyme activity under a particular set of conditions, we would get a single

value, which would represent the average of the heterogeneous assembly (Figure 5.13B). However, were we to perform a sufficient number of single-molecule experiments, we would discover that the enzyme has three different molecular forms with very different activities (Figure 5.13C). Moreover, these different forms would most likely correspond to important biochemical differences.

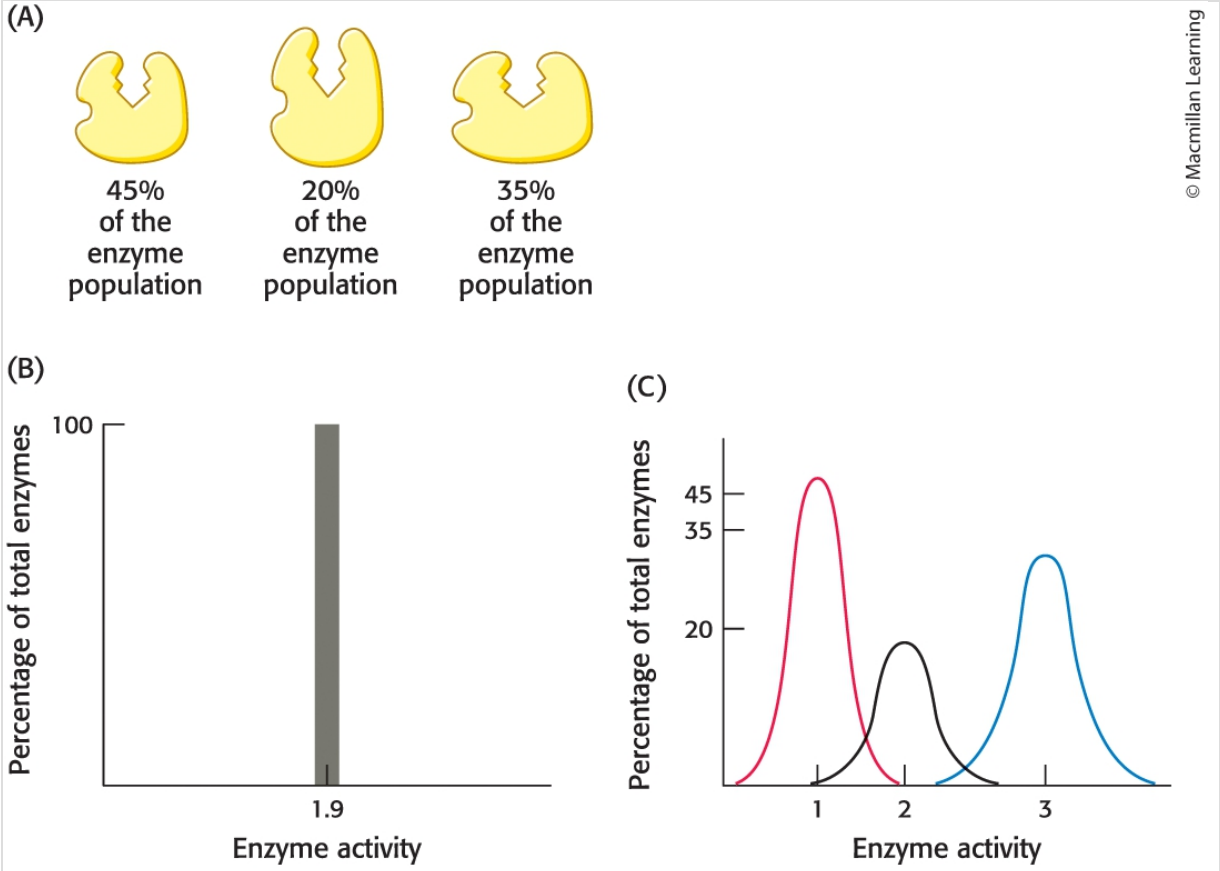


FIGURE 5.13 Single-molecule studies can reveal molecular heterogeneity. (A) Complex biomolecules, such as enzymes, display molecular heterogeneity. (B) When measuring an enzyme property using ensemble methods, an average value of all of the enzymes present can be obtained. (C) Single-enzyme studies reveal molecular heterogeneity, with the various forms showing different properties.

Single-molecule kinetics confirm results obtained from ensemble studies

Now suppose that we watch an individual enzyme molecule in action, monitoring every time it produces a molecule of product. **Figure 5.14** illustrates what we would expect to see, with each line representing a single reaction event. Because individual enzyme molecules behave stochastically, the time between consecutive reaction events appears to vary randomly. However, if we watch an individual enzyme molecule turn over many thousands of times, we find a pattern in the distribution of the time intervals separating consecutive events that allows us to state the anticipated relationship between the average time increments at different substrate concentrations as

$$1/(\text{Time increment})_{\text{average}} = k_2[S]/([S] + K_M)$$

The output from this equation, called the *single-molecule Michaelis–Menten equation*, reveals the same saturation behavior for reaction rates that we observe for ensemble studies of enzymes. In fact, plotting the reciprocal of the average time increment at different substrate concentrations produces a Michaelis–Menten saturation curve, which can also be visualized as a Lineweaver–Burk plot, as we will see shortly. This illustrates a reassuring finding of single-molecule methods: they often reaffirm observations made by ensemble methods.

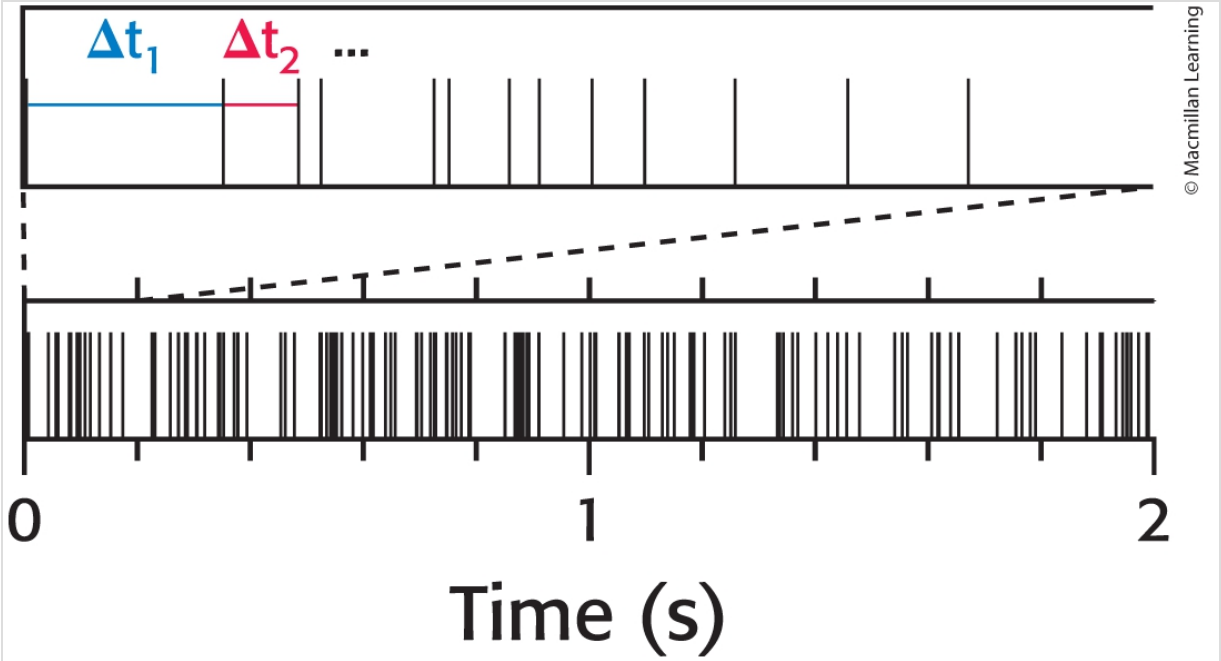
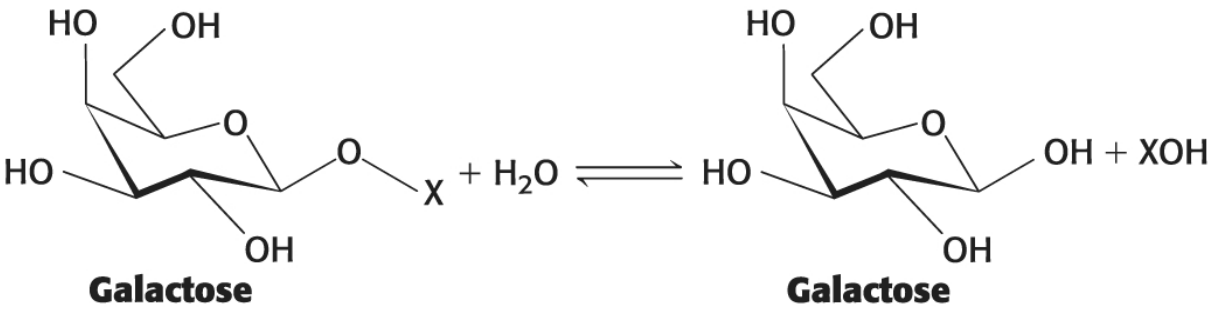


FIGURE 5.14 An anticipated time course for a single-enzyme molecule reveals stochastic behavior. Each line represents an enzyme molecule turning a substrate molecule into product. These events occur stochastically, with variable time increments between consecutive events.

Up to this point, we have discussed monitoring hypothetical enzymes. We now turn to a real example, the enzyme β-galactosidase from *E. coli*, which allows this bacterium to utilize certain sugars. Studies of this enzyme played a central role in elucidating fundamental mechanisms in gene regulation, to be discussed in Chapter 31. This enzyme catalyzes reactions of the form



While the enzyme is quite specific for the carbohydrate galactose (to be discussed in Chapter 11), substantial variations in the other half of the substrate can be accommodated, permitting the binding of probe substrates such as Substrate G-R (**Figure 5.15**). Cleavage of this substrate by β-galactosidase releases a fluorescent product.

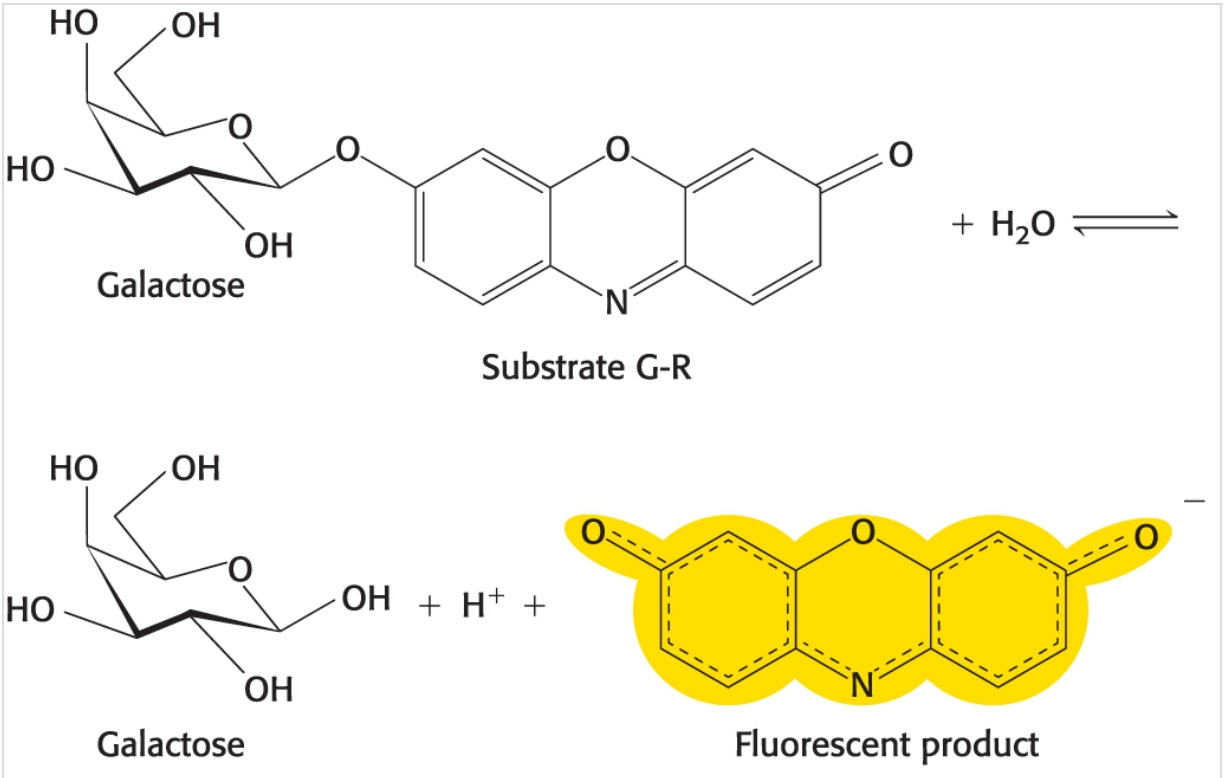


FIGURE 5.15 Upon reaction with β-galactosidase, Substrate G-R produces a highly fluorescent product. The formation of individual molecules of this product can be detected,

allowing for the observation of single-enzyme turnovers to be tracked.



Using immobilized enzyme molecules and a fluorescence microscope, product release (and, hence, enzyme activity) can be monitored directly at the single-molecule level. With this system, experiments were performed at a range of substrate concentrations and the results compared with those obtained from ensemble studies using the same enzyme and substrate (**Figure 5.16**).

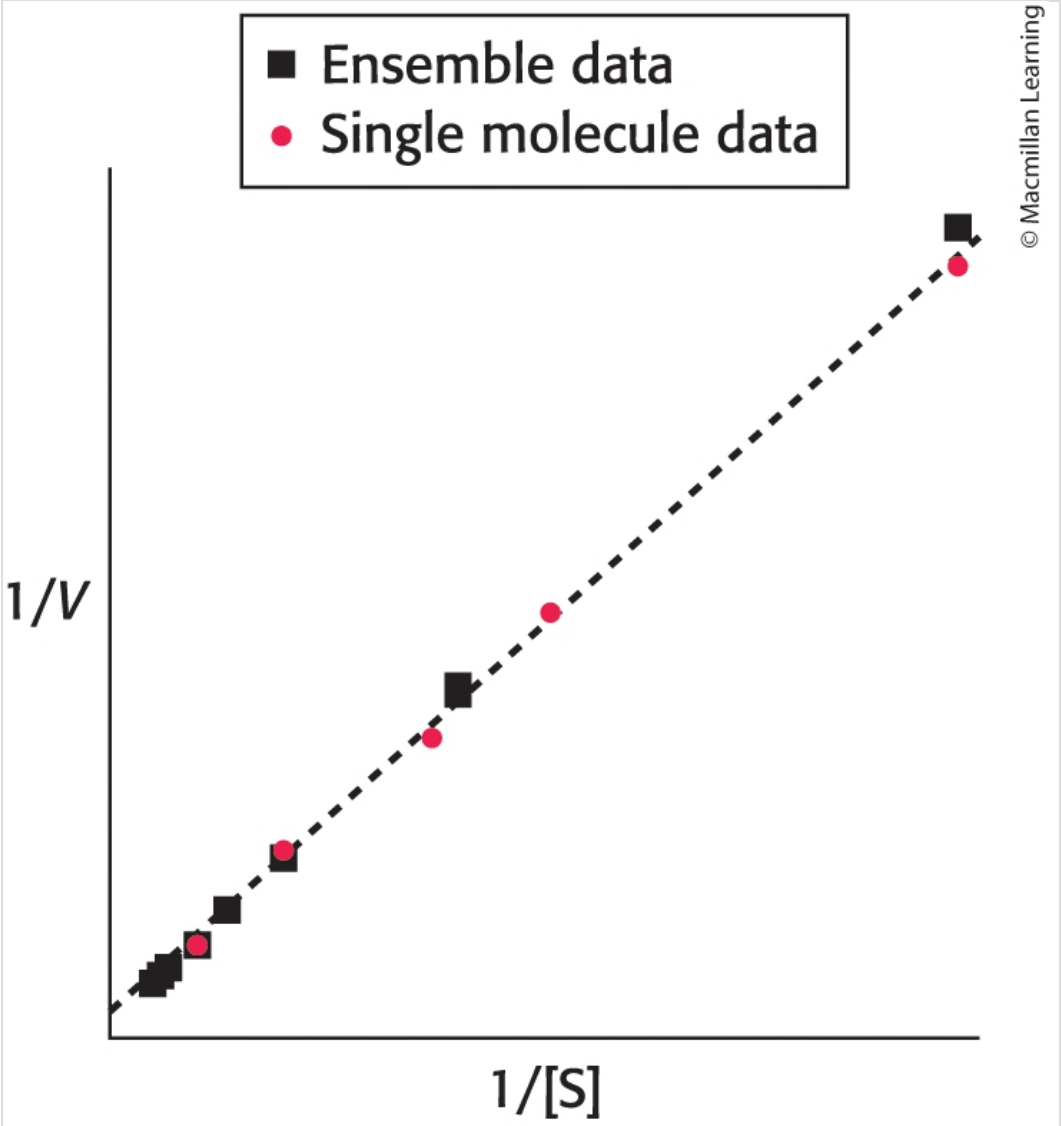


FIGURE 5.16 Lineweaver–Burk plots of single-molecule data compare favorably to those from ensemble studies. The results from single-molecule kinetic studies of β-galactosidase (red) are nearly indistinguishable from those from ensemble studies of the same enzyme at the same substrate concentration (black).

[Adapted from B. P. English et al., *Nature Chemical Biology* 2:87–94, 2006.]

Single-molecule studies continue to reveal new information about enzyme molecular dynamics

While it is quite reassuring to see in a real example that the results of technically challenging single-molecule studies agree so well with those of ensemble studies, the single-molecule results don't tell us anything new about enzyme behavior. However, depicting the distribution of time increments on a log plot does reveal an important new insight (**Figure 5.17**). At a low substrate concentration of $10\ \mu M$, this plot is relatively linear. However, at a higher concentration of $100\ \mu M$, this plot is decidedly nonlinear, changing from a relatively steep slope at short time increments to a more gradual slope at longer time increments.

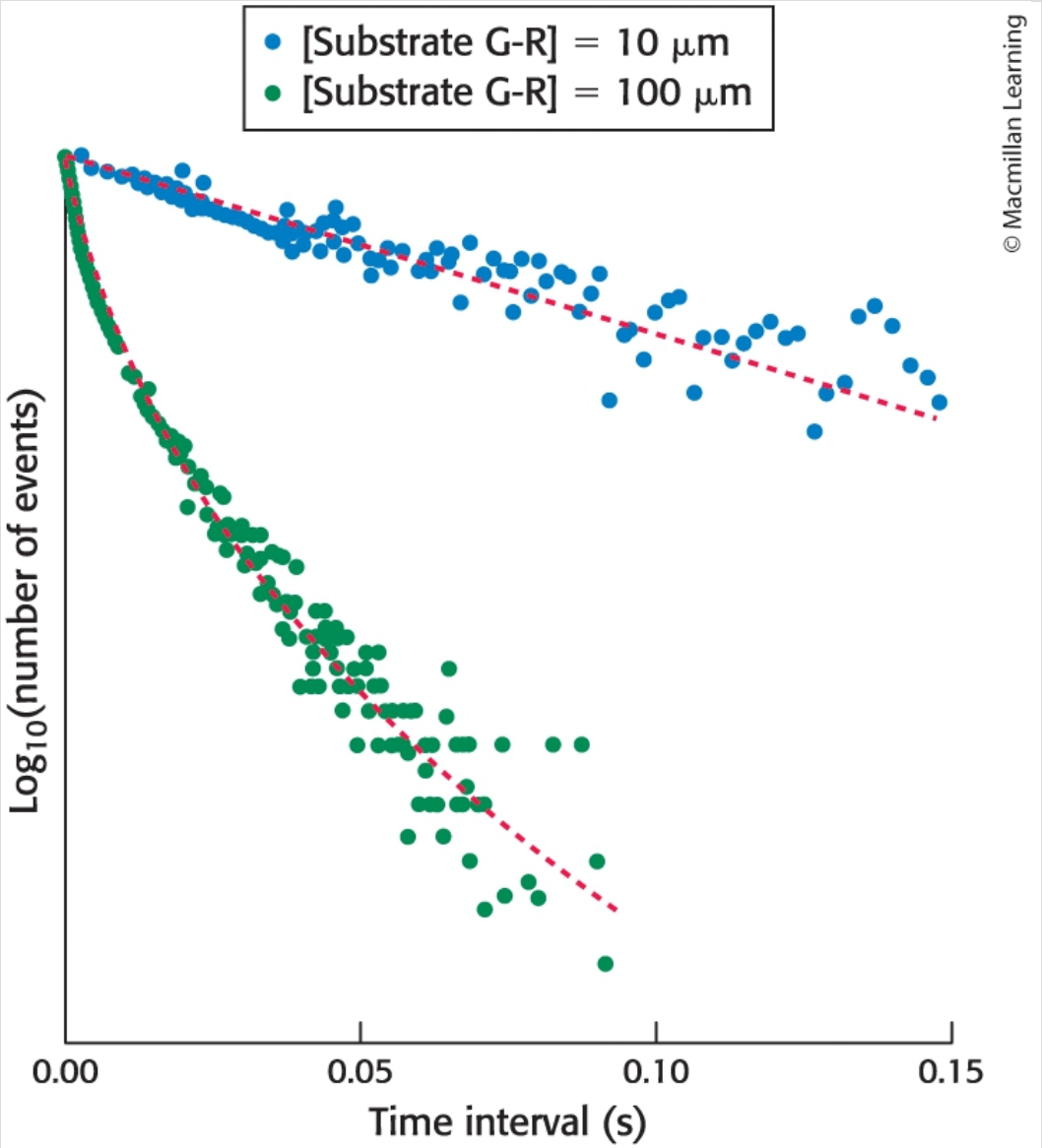


FIGURE 5.17 Details of single-molecule time increment distributions for β-galactosidase indicate heterogeneity at the molecular level. At a relatively high substrate concentration (100 μM), a plot of the logarithm of the number of events in each time interval is not linear, indicated by the distribution not following a simple exponential fall off. This observation reveals that the enzyme cannot be modeled as a single species at the single-molecule level.

[Adapted from B. P. English et al., *Nature Chemical Biology* 2:87–94, 2006.]

We can explain this observation in terms of the dynamic nature of individual enzyme molecules. Each molecule can exist and convert between multiple conformational states, as we envisioned hypothetically in Figure 5.13, each conformation having distinct catalytic properties. The structural differences of these conformational states could be as simple as the orientations of particular side chains or as complex as large, interdomain movements. Further studies are required to gain such structural information, but regardless of the structural details, single-molecule experiments provide direct evidence for a critical aspect of enzymes: their dynamic nature.

Using the many powerful single-molecule techniques that now exist, we can observe events at a molecular level to reveal rare or transient structures and fleeting events in a reaction sequence, as well as to measure mechanical forces affecting or generated by an enzyme. Single-molecule studies open a new vista on the function of enzymes in particular and all large biomolecules in general. We will examine additional single-molecule studies in future chapters.

5.6 Enzymes Can Be Inhibited by Specific Molecules

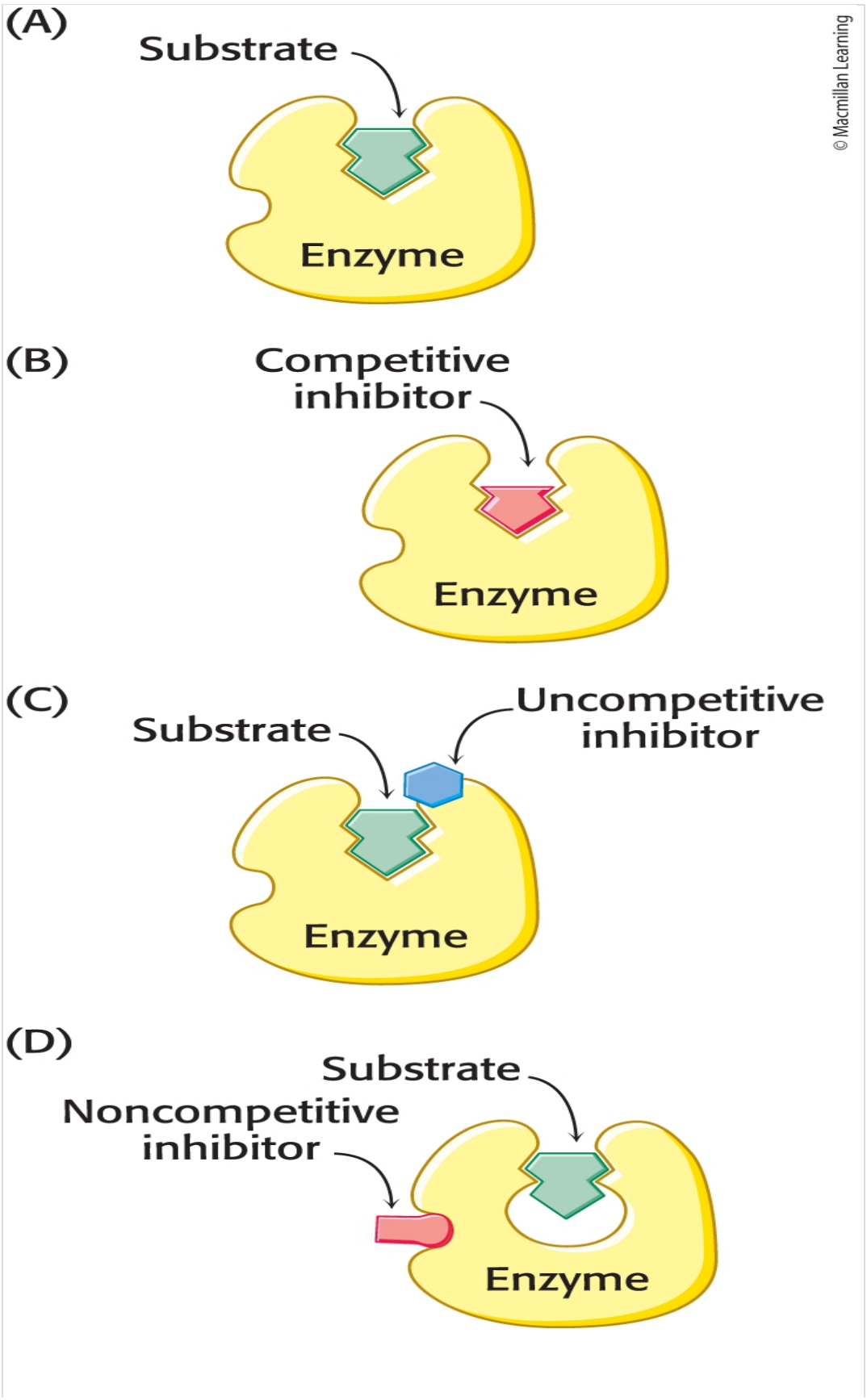
The activity of many enzymes can be inhibited by the binding of specific small molecules and ions. Enzyme inhibition serves as a major control mechanism in biological systems, especially by regulating the activity of allosteric enzymes. In addition, many drugs and toxic agents act by inhibiting enzymes (Chapter 32). These inhibitors are often designed by scientists or result from a chance discovery of an inhibitory molecule. Examining inhibition can give insight into the mechanism of enzyme action; for example, specific inhibitors are often used to identify residues critical for catalysis. Enzyme inhibition can be either irreversible or reversible.

- *An irreversible inhibitor covalently bonds to its target enzyme and thus does not dissociate at any appreciable rate*. The mode of action of some important drugs is irreversible inhibition. For example, as we will discuss shortly, penicillin acts by covalently modifying the enzyme transpeptidase, thereby preventing the synthesis of bacterial cell walls and thus killing the bacteria. Aspirin acts by covalently modifying the enzyme cyclooxygenase, reducing the synthesis of signaling molecules in inflammation.

- *Reversible inhibition is characterized by the dissociation of the enzyme–inhibitor complex, which is formed by noncovalent interactions*. Depending on their target and their effect, reversible inhibitors are classified as competitive, uncompetitive, or noncompetitive.

In **competitive inhibition**, the inhibitor competes with the substrate for binding to the enzyme and thus reduces the proportion of enzyme molecules bound to substrate. The enzyme can bind the substrate (**Figure 5.18A**) or an inhibitor (**Figure 5.18B**), but not both at the same time. Competitive inhibitors can bind anywhere on the enzyme, but

they most often resemble the substrate and bind to the active site. The substrate is thereby prevented from binding to the same active site. At any given inhibitor concentration, competitive inhibition can be relieved by increasing the substrate concentration. Under these conditions, the substrate successfully competes with the inhibitor for the enzyme.

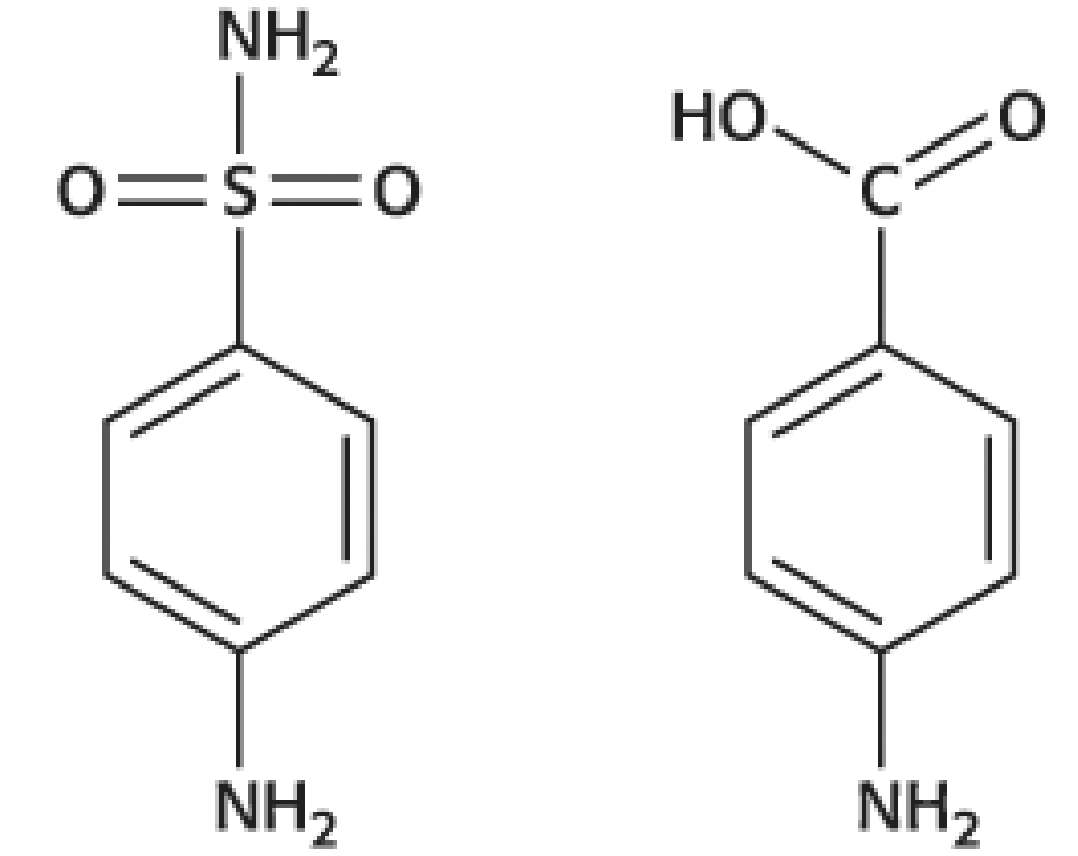


© Macmillan Learning

FIGURE 5.18 Reversible inhibitors can be distinguished by whether they bind to the enzyme with or without the substrate present. (A) An enzyme–substrate complex; (B) competitive inhibitors prevent the substrate from binding, usually by themselves binding at the active site; (C) an uncompetitive inhibitor binds only to the enzyme–substrate complex; (D) a pure noncompetitive inhibitor does not affect the binding of substrate.



Many competitive inhibitors are useful drugs. Drugs such as ibuprofen are competitive inhibitors of enzymes that participate in signaling pathways in the inflammatory response. Statins are drugs that reduce high cholesterol levels by competitively inhibiting a key enzyme in cholesterol biosynthesis (Section 26.3). One of the earliest examples was the use of sulfanilamide as an antibiotic. Sulfanilamide is an example of a sulfa drug, a sulfur-containing antibiotic. Structurally, sulfanilamide mimics *p*-aminobenzoic acid (PABA), a metabolite required by bacteria for the synthesis of the coenzyme folic acid. Sulfanilamide binds to the enzyme that normally metabolizes PABA and competitively inhibits it, preventing folic acid synthesis. Human beings, unlike bacteria, absorb folic acid from the diet and are thus unaffected by the sulfa drug.



In **uncompetitive inhibition**, the inhibitor binds not to the enzyme itself but to the enzyme–substrate complex; it is therefore substrate-dependent. The binding site of an uncompetitive inhibitor is created only on interaction of the enzyme and substrate (**Figure 5.18C**). Uncompetitive inhibitors inhibit catalysis, rather than prevent substrate binding, and cannot be overcome by the addition of more substrate. The herbicide glyphosate, also known as Roundup, is an uncompetitive inhibitor of an enzyme in the biosynthetic pathway for aromatic amino acids.

In **pure noncompetitive inhibition**, the inhibitor and substrate can bind simultaneously to an enzyme molecule at two different binding sites (**Figure 5.18D**). Unlike competitive or uncompetitive inhibition, a noncompetitive inhibitor can bind free enzyme or the enzyme–substrate complex, but in either case it decreases the rate catalysis.

Noncompetitive inhibitors can be either pure or mixed. A pure noncompetitive inhibitor binds equally well to the enzyme with or without substrate bound, and the effect is that only turnover number is decreased. Thus, pure noncompetitive inhibitors act by decreasing the concentration of functional enzyme rather than by altering the proportion of enzyme molecules that are bound to substrate. Noncompetitive inhibition, like uncompetitive inhibition, cannot be overcome by increasing the substrate concentration. **Mixed noncompetitive inhibition** is more complex in that the inhibitor binds preferentially to either the free enzyme or the enzyme–substrate complex, resulting in a pattern of inhibition that alters both substrate binding and turnover number simultaneously. The commonly prescribed antibiotic doxycycline, which is used to treat periodontal disease, functions at low concentrations as a noncompetitive inhibitor of a proteolytic enzyme (collagenase).

The different types of reversible inhibitors are kinetically distinguishable

How can we determine whether a reversible inhibitor acts by competitive, uncompetitive, or noncompetitive inhibition? Considering only enzymes that exhibit Michaelis–Menten kinetics, we can use measurements of the rates of catalysis at different concentrations of substrate and inhibitor and Lineweaver–Burk plots as clues to which type of reversible inhibition is occurring.

Competitive inhibition

In competitive inhibition, where the inhibitor competes with the substrate for the enzyme, the dissociation constant for the inhibitor is given by

$$K_i = [E][I]/[EI]$$

The smaller the K_i, the more potent the inhibition. The hallmark of competitive inhibition is that it can be overcome by a sufficiently high concentration of substrate (**Figure 5.19**). The effect of a competitive inhibitor is to increase the apparent value of K_M, meaning that more substrate is needed to obtain the same reaction rate. This new apparent value of K_M, called K_M^{app}, is numerically equal to

$$K_M^{app} = K_M(1 + [I]/K_i)$$

where [I] is the concentration of inhibitor and K_i is the dissociation constant for the enzyme–inhibitor complex. In the presence of a competitive inhibitor, an enzyme will have the same V_{max} as in the absence of an inhibitor. At a sufficiently high concentration, virtually all the active sites are filled with substrate, and the enzyme is fully operative.

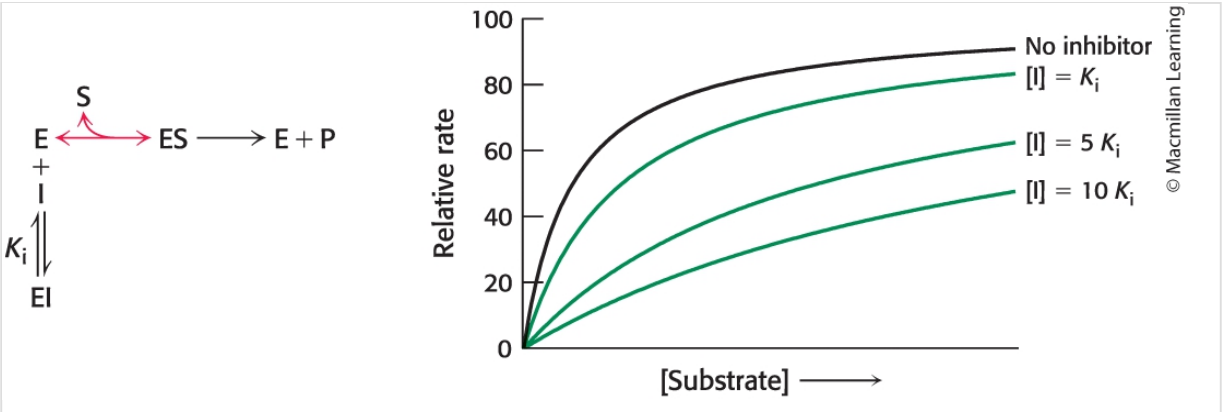


FIGURE 5.19 Michaelis–Menten plots of a competitive inhibitor reveal changes in the apparent K_M but not V_{max}. As the concentration of a competitive inhibitor increases, higher concentrations of substrate are required to attain a particular reaction velocity. The reaction pathway suggests how sufficiently high concentrations of substrate can completely relieve competitive inhibition resulting in the same V_{max} value at infinite substrate concentration.

A Lineweaver–Burk plot can also reveal competitive inhibition. In competitive inhibition, the intercept on the *y*-axis of the plot of $1/V_0$ versus $1/[S]$ is the same in the presence and in the absence of inhibitor, although the slope is increased (Figure 5.20).

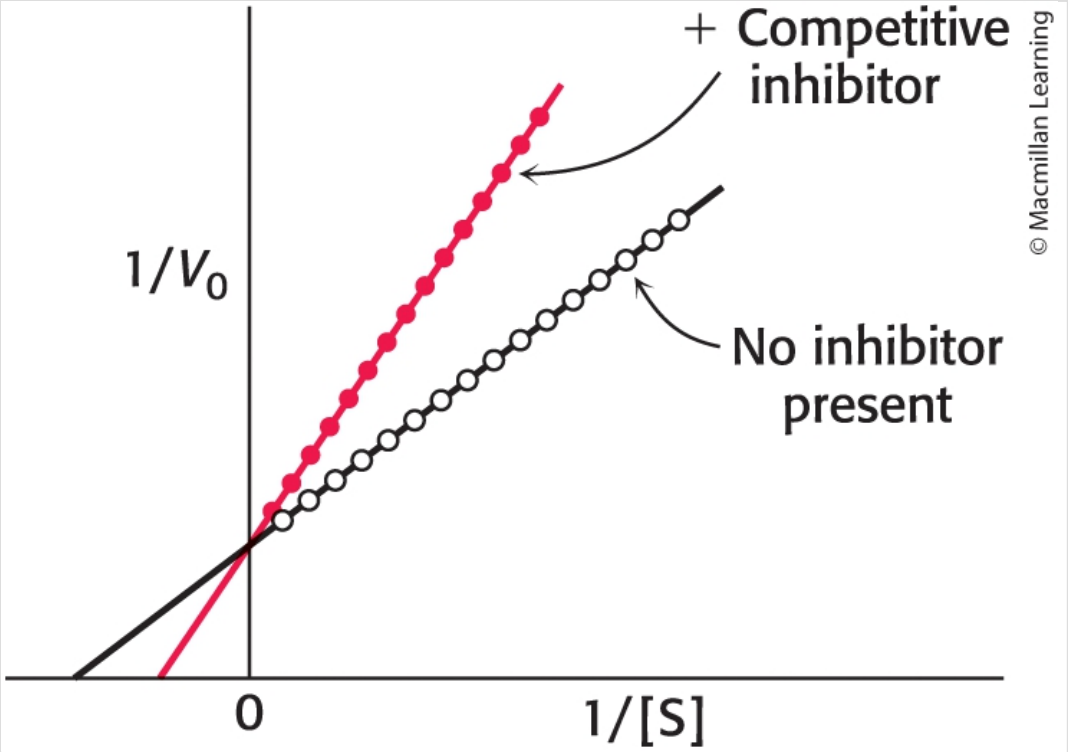


FIGURE 5.20 Competitive inhibition is easily recognized using a Lineweaver–Burk plot. A Lineweaver–Burk plot of enzyme kinetics in the presence and absence of a competitive inhibitor illustrates that the inhibitor has no effect on V_{max} but increases the apparent K_M.

The intercept is unchanged because a competitive inhibitor does not alter V_{max}. The increase in the slope of the $1/V_0$ versus $1/[S]$ plot indicates the strength of binding of a competitive inhibitor. In the presence of a competitive inhibitor, equation 18 is replaced by

$$\frac{1}{V_0} = \frac{1}{V_{max}} + \frac{K_M}{V_{max}}\left(1 + \frac{[I]}{K_i}\right)\left(\frac{1}{[S]}\right) \quad \textbf{(22)}$$

In other words, the slope of the plot is increased by the factor $(1 + [I]/K_i)$ in the presence of a competitive inhibitor. Consider an enzyme with a K_M of 10^{-4} M. In the absence of inhibitor, when $V_0 = V_{max}/2$, $[S] = 10^{-4}$ M. In the presence of a 2×10^{-3} M competitive inhibitor that is bound to the enzyme with a K_i of 10^{-3} M, the apparent K_M (K_M^{app}) will be equal to $K_M(1 + [I]/K_i)$, or 3×10^{-4} M. Substitution of these values into equation 22 gives $V_0 = V_{max}/4$, when $[S] = 10^{-4}$ M. Thus, the presence of the competitive inhibitor cuts the reaction rate in half at this substrate concentration.

Uncompetitive inhibition

In uncompetitive inhibition, where the inhibitor binds only to the ES complex, the resulting enzyme–substrate–inhibitor (ESI) complex does not go on to form any product. Because some unproductive ESI complex will always be present, V_{max} will be lower in the presence of inhibitor than in its absence (**Figure 5.21**). The uncompetitive inhibitor lowers the apparent value of K_M because the inhibitor binds to ES to form ESI, depleting ES. To maintain the equilibrium between E and ES, more S binds to E, increasing the apparent value of k_1 and thereby reducing the apparent value of K_M (see equation 13). Thus, a lower concentration of S is required to form half of the maximal concentration of ES.

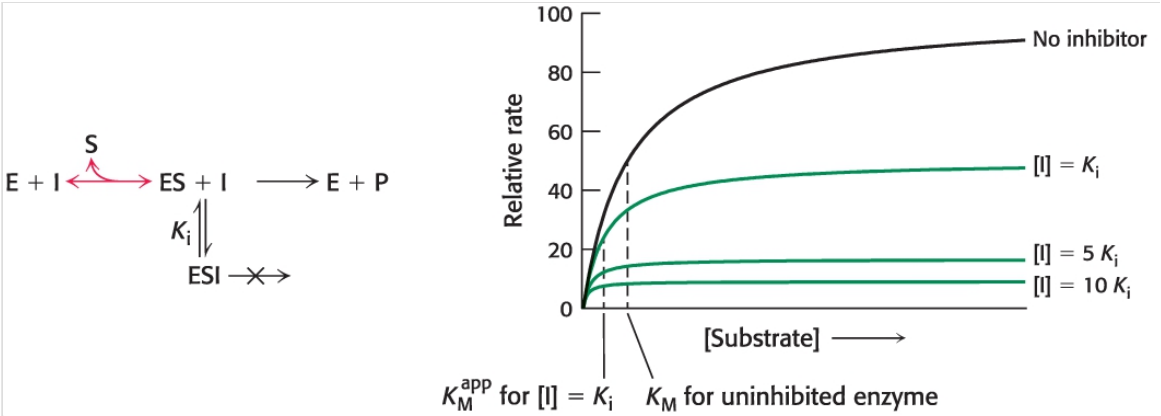


FIGURE 5.21 Michaelis–Menten plots of an uncompetitive inhibitor reveal decreases in both the apparent K_M and V_{max}. The reaction pathway shows that the inhibitor binds only to the enzyme–substrate complex. Consequently, V_{max} cannot be attained, even at high substrate concentrations. The apparent value for K_M is lowered, becoming smaller as more inhibitor is added.

The equation that describes the Lineweaver–Burk plot for an uncompetitive inhibitor is

$$\frac{1}{V_0} = \frac{K_M}{V_{max}}\left(\frac{1}{[S]}\right) + \frac{1}{V_{max}}\left(1 + \frac{[I]}{K_i}\right)$$

The slope of the line, K_M / V_{max}, is the same as that for the uninhibited enzyme, but the intercept on the *y*-axis will be increased by $1 + [I]/K_i$. Consequently, the lines in Lineweaver–Burk plots will be parallel (Figure 5.22).

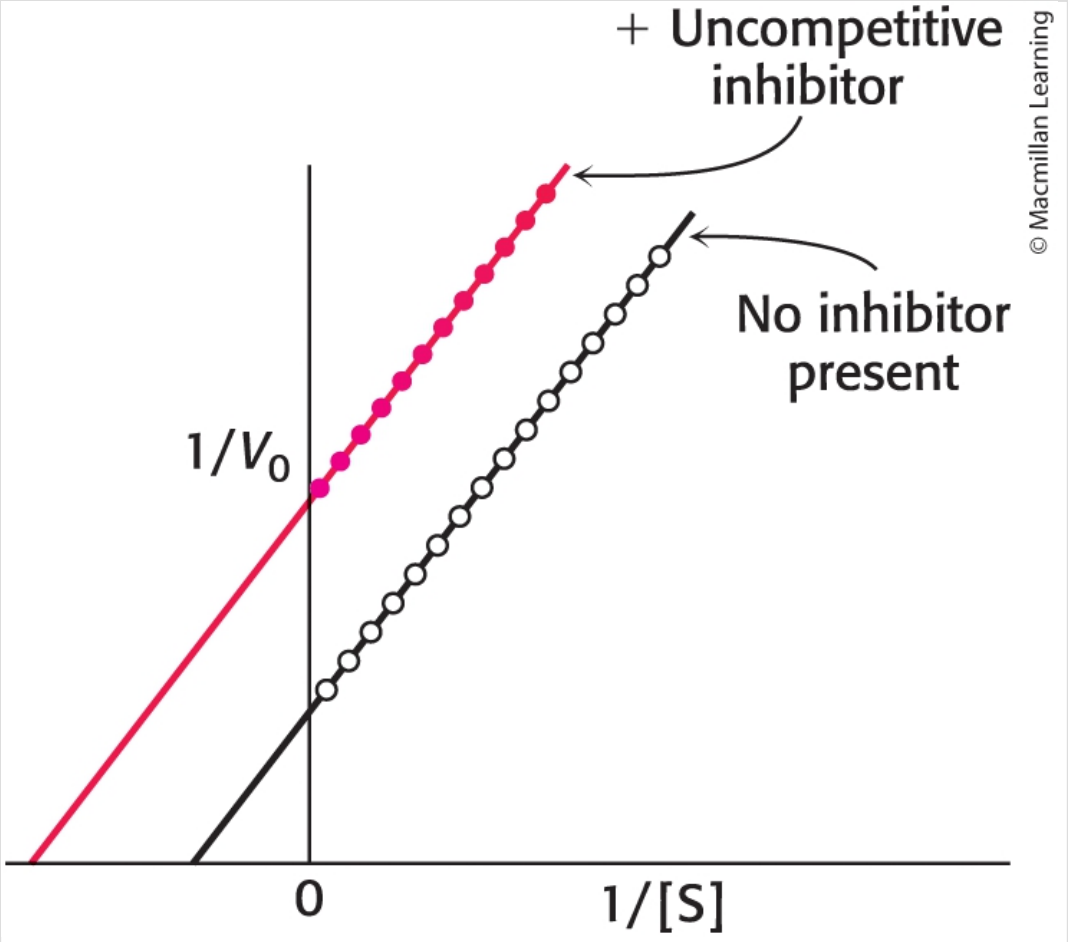


FIGURE 5.22 Uncompetitive inhibition is easily distinguished by parallel lines in a Lineweaver–Burk plot. An uncompetitive inhibitor does not affect the slope of the Lineweaver–Burk plot. V_{max} and K_M are reduced by equivalent amounts.

Noncompetitive inhibition

Recall that in noncompetitive inhibition, the inhibitor can bind at a different site from the substrate either the enzyme or the enzyme–substrate complex; in either case, the enzyme–inhibitor–substrate complex does not proceed to form product. In pure noncompetitive

inhibition, the K_i for the inhibitor binding to E is the same as for binding to ES complex (Figure 5.23).

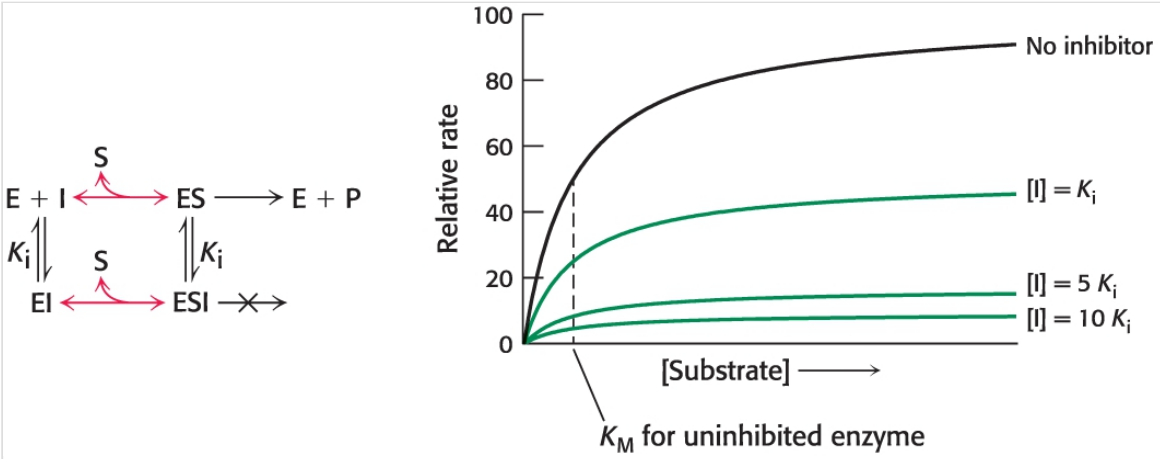


FIGURE 5.23 Michaelis–Menten plots of a pure noncompetitive inhibitor reveal a decrease in V_{max}, while K_M remains unchanged. The reaction pathway shows that the inhibitor binds both to free enzyme and to an enzyme–substrate complex. Consequently, as with uncompetitiv inhibition, V_{max} cannot be attained. In pure noncompetitive inhibition, K_M remains unchanged, and so the reaction rate increases more slowly at low substrate concentrations tha is the case for uncompetitive competition.

The apparent value of V_{max} is decreased to a new value called V_{max}^{app}, whereas the value of K_M is unchanged. The maximal velocity in the presence of a pure noncompetitive inhibitor, V_{max}^{app}, is given by

$$V_{max}^{app} = \frac{V_{max}}{1 + [I]/K_i} \quad (23)$$

Why is V_{max} lowered though K_M remains unchanged? In essence, the inhibitor simply lowers the concentration of functional enzyme because some quantity of enzyme is always bound to the inhibitor and inactive at any given moment, regardless of the substrate concentration. Because the inhibitor and the substrate do not affect the binding of one another, pure noncompetitive inhibition cannot be overcome by increasing the substrate concentration.

In the Lineweaver–Burk plot for pure noncompetitive inhibition (**Figure 5.24**), the value of V_{max} is decreased to the new value V_{max}^{app}, and so the intercept on the vertical axis is increased (equation 23). The new slope, which is equal to K_M / V_{max}^{app}, is larger by the same factor. In contrast with V_{max}, K_M is not affected by pure noncompetitive inhibition.

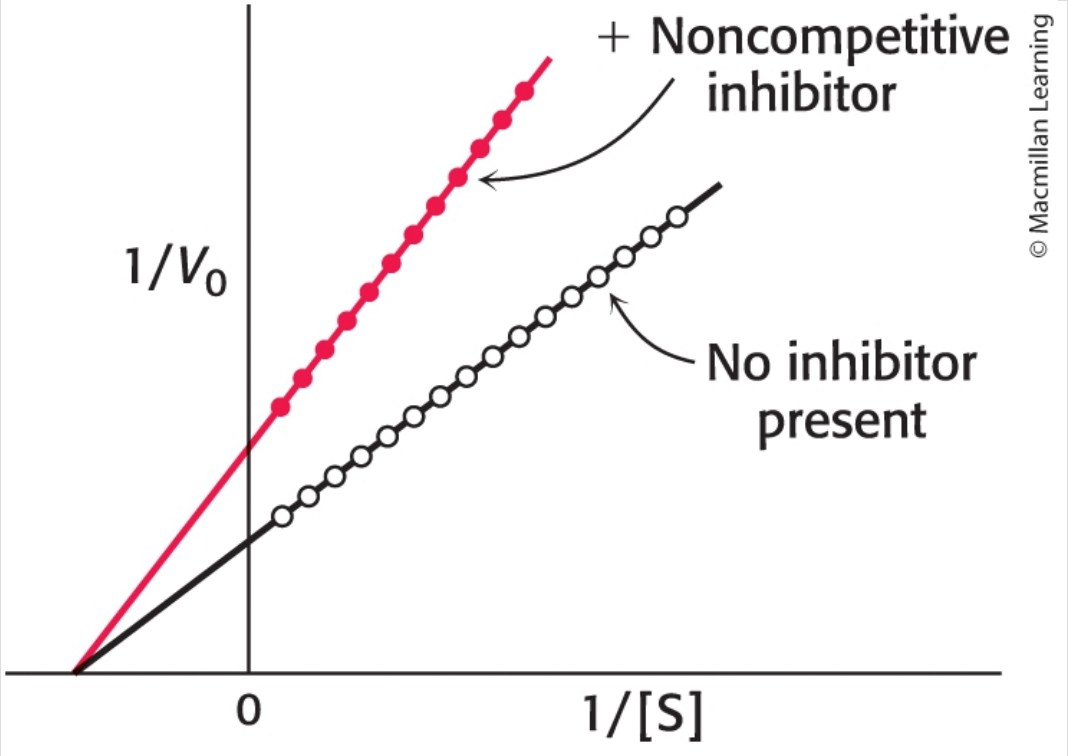


FIGURE 5.24 Pure noncompetitive inhibition can be distinguished on a Lineweaver–Burk plot by lines converging at the *x*-axis. A Lineweaver–Burk plot of enzyme kinetics in the presence and absence of a pure noncompetitive inhibitor shows that K_M is unaltered and V_{max} is decreased.

Finally, in mixed noncompetitive inhibition, the inhibitor binds preferentially to either E or ES, but still binds both, and thus behaves as a blend of a noncompetitive inhibitor and either a competitive or an uncompetitive inhibitor, depending upon the binding preference. Thus, for a mixed noncompetitive inhibitor V_{max} always decreases but the apparent value of K_M can either increase or decrease; the Lineweaver–Burk plot resembles that of a pure noncompetitive inhibitor but with lines converging either above or below the *x*-axis.

Transition-state analogs are potent competitive inhibitors

We turn now to compounds that provide the most intimate views of the catalytic process itself. Linus Pauling proposed in 1948 that compounds resembling the transition state of a catalyzed reaction should be very effective inhibitors of enzymes. These mimics are called **transition-state analogs**.

The inhibition of proline racemase is an instructive example. The racemization of proline proceeds through a transition state in which the tetrahedral α-carbon atom has become trigonal (**Figure 5.25**). In the trigonal form, all three bonds are in the same plane; C_α also carries a net negative charge. This symmetric carbanion can be reprotonated on one side to give the L isomer or on the other side to give the D isomer. Pauling's hypothesis was supported by the finding that the inhibitor pyrrole 2-carboxylate binds to the racemase active site 160 times as

tightly as does proline. The α-carbon atom of this inhibitor, like that of the transition state, is trigonal.

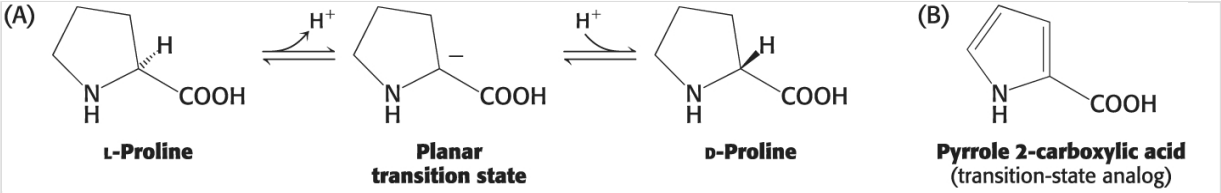


FIGURE 5.25 Transition-state analogs are potent competitive inhibitors because they structurally resemble the transition state of a catalyzed reaction. (A) The isomerization of L-proline to D-proline by proline racemase proceeds through a planar transition state in which the α-carbon atom is trigonal rather than tetrahedral. (B) Pyrrole 2-carboxylic acid, a transition-state analog because of its trigonal geometry, is a potent competitive inhibitor of proline racemase. An analog that also carries a negative charge on C_α would be expected to bind even more tightly.

In general, highly potent and specific competitive inhibitors of enzymes can be produced by synthesizing compounds that more closely resemble the transition state than the substrate itself. Because only molecules that are structurally similar to the real transition state will bind tightly to the active site, potent competitive inhibition — or its absence — by these molecules can be used to support or refute hypotheses regarding the structure of the transition state for a given enzyme-catalyzed reaction, providing evidence for particular chemical mechanisms. The inhibitory power of transition-state analogs underscores the essence of enzyme catalysis: catalysis is accomplished by selective binding of the transition state structure by the active site.

Self-Check Question

An inhibitor binds noncovalently to an allosteric site and induces a change in protein structure such that the enzyme can no longer bind substrate in the active site. Conversely,

when the substrate is bound in the active site, the allosteric site for the inhibitor is closed such that the inhibitor cannot bind. What type of inhibition is being described here?

Irreversible inhibitors can be used to map the active site

The first step in obtaining the chemical mechanism of an enzyme is to determine what functional groups are required for enzyme activity. How can we ascertain what these functional groups are? X-ray crystallography of the enzyme bound to its substrate or substrate analog provides one approach. Irreversible inhibitors that covalently bond to the enzyme provide an alternative and often complementary approach: the inhibitors modify the functional groups, which can then be identified. Irreversible inhibitors can be divided into three categories: group-specific reagents, affinity labels, and suicide inhibitors.

- **Group-specific reagents** inhibit enzymes by reacting with specific side chains of the enzyme's amino acids. An example of a group-specific reagent is diisopropylphosphofluoridate (DIPF). DIPF modifies only 1 of the 28 serine residues in the proteolytic enzyme chymotrypsin and yet inhibits the enzyme, implying that this serine residue is especially reactive. We will see in Chapter 6 that this serine residue is indeed located at the active site. DIPF also revealed a reactive serine residue in acetylcholinesterase, an enzyme important in the transmission of nerve impulses (**Figure 5.26**). Thus, DIPF and similar compounds that bind and inactivate acetylcholinesterase are potent nerve gases. Most group-specific reagents do not display the exquisite specificity shown by DIPF. Consequently, more specific means of modifying the active site are required.

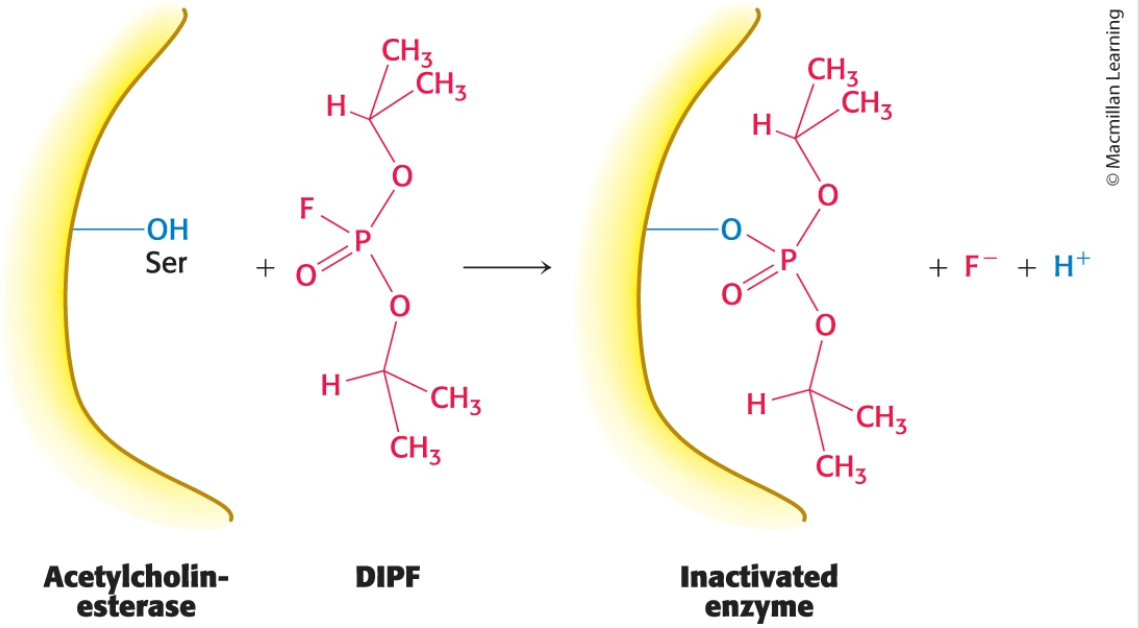


FIGURE 5.26 A group-specific reagent irreversibly inhibits enzymes by reacting with specific side chains. For example, DIPF can inhibit an enzyme by covalently modifying a crucial serine residue.

- **Affinity labels (reactive substrate analogs)** inhibit enzymes by being structurally similar to the substrate and covalently bonding to active-site residues. They are thus more specific for the enzyme's active site than are group-specific reagents. Tosyl-L-phenylalanine chloromethyl ketone (TPCK) is a substrate analog for chymotrypsin (Figure 5.27). TPCK binds at the active site and then reacts irreversibly with a histidine residue at that site, inhibiting the enzyme.

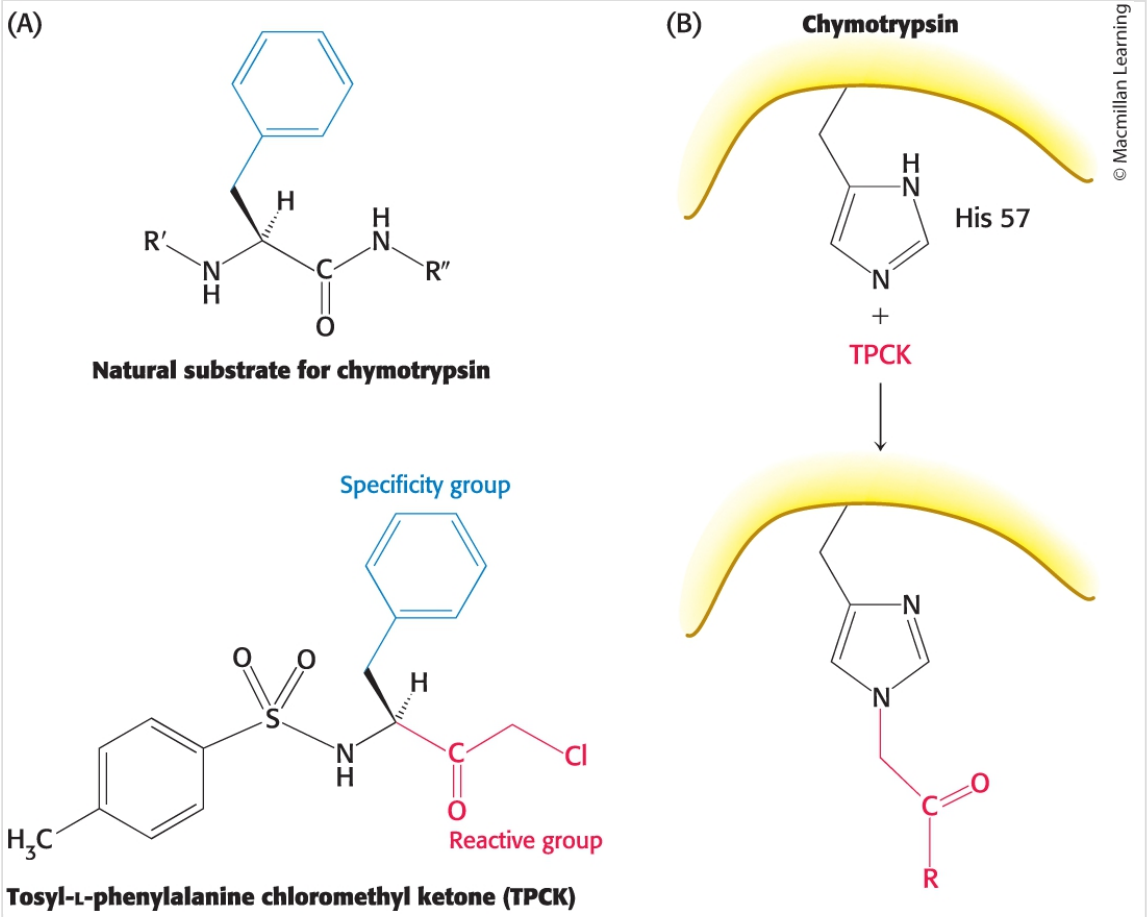


FIGURE 5.27 Affinity labels are highly specific irreversible inhibitors because they are structurally similar to the enzyme substrate. (A) Tosyl-L-phenylalanine chloromethyl ketone (TPCK) is a reactive analog of the normal substrate for the enzyme chymotrypsin. (B) TPCK binds at the active site of chymotrypsin and modifies an essential histidine residue.

- **Mechanism-based (suicide) inhibitors** are modified substrates that provide the most specific means for modifying an enzyme's active site. The inhibitor binds to the enzyme as a substrate and is initially processed by the normal catalytic mechanism. The mechanism of catalysis then generates a chemically reactive intermediate that inactivates the enzyme through covalent modification. The fact that

the enzyme participates in its own irreversible inhibition strongly suggests that the covalently modified group on the enzyme is vital for catalysis.

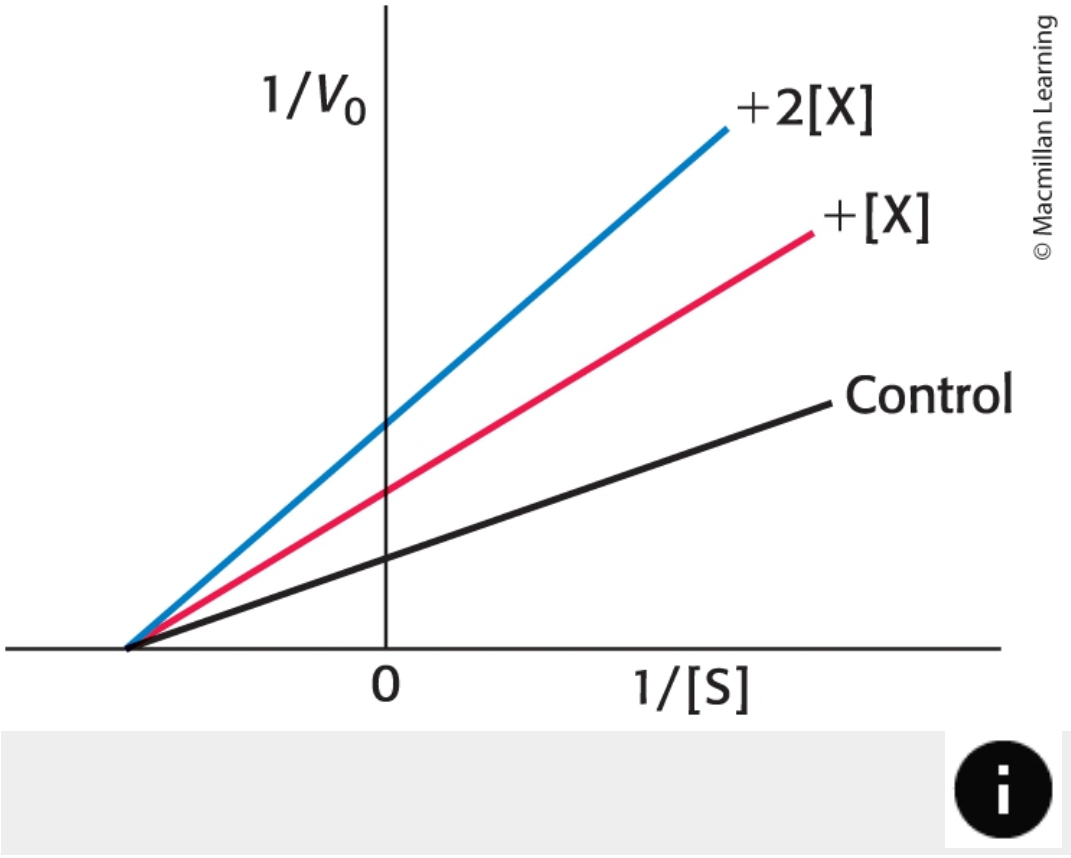
How would a molecule like TPCK — or other types of irreversible inhibitors, for that matter — affect the kinetic parameters V_{max} and K_M that we have discussed throughout this chapter? We will address that question in the context of all the inhibitors discussed in this chapter in the example below.

Example

Determining Inhibitor Type from Data

Problem:

The graph shows the effect of two different concentrations of a molecule X on an enzyme. What kind of molecule is X, and how is it affecting enzyme activity?



Getting Started:

What kind of plot is this? The first step is to examine the axes: the *x*-axis shows 1/[S], while the *y*-axis displays $1/V_0$. Note that these are two reciprocal values, so this is a double reciprocal plot, specifically a Lineweaver–Burk plot. Next, consider what we know about these plots: they can reveal how molecules affect the apparent values of the kinetic parameters K_M and V_{max} based on where the line crosses the two axes. Recall that the point where the line crosses the *y*-axis is $1/V_{max}$, while the intersection with the *x*-axis is $-1/K_M$.

Analyze:

How is the molecule affecting the enzyme? If we first consider the *x*-axis, we see that all of the lines converge there. Therefore, the apparent K_M is not altered in the presence of X. However, when X is present, the lines cross the *y*-axis at increasing values, indicating that $1/V_{max}$ increases with increasing amounts of X. If $1/V_{max}$ increases in the presence of X, then the apparent V_{max} must be decreasing.

Let's summarize these effects and then consider the possibilities. The apparent K_M is unchanged, but the apparent V_{max} is reduced. This latter observation means that X must be some type of an inhibitor of the enzyme. Let's consider some possibilities: competitive inhibitors, including transition-state analogs, alter the apparent K_M but don't affect V_{max}. Uncompetitive inhibitors decrease both the apparent values of K_M and V_{max}. Finally, mixed noncompetitive inhibitors may raise or lower the apparent value of K_M but do not leave it unchanged. None of these descriptions fit the data. The only type of reversible inhibitor that affects an enzyme this way is a pure noncompetitive inhibitor. Recall that pure noncompetitive inhibitors lower the apparent V_{max} without altering K_M.

However, this is not the end of the problem! One more possibility exists that we have not considered: irreversible inhibitors. Because irreversible inhibitors permanently inactivate enzyme molecules, essentially removing a stoichiometric amount of them from pool of active enzyme molecules involved in the observed reaction, the effect is the same as if there were less enzyme originally added to the reaction mixture. That is, the apparent V_{max} is lowered because there are fewer active enzyme molecules, but the K_M is unaffected because those excess enzyme molecules which do not react with the inhibitor are completely unaffected by it.

Reflect:

All irreversible inhibitors give rise to the same pattern as a pure noncompetitive inhibitor with respect to the observed changes to the apparent values of K_M and V_{max}; so, in this case, additional information is required to distinguish whether molecule X is an irreversible or a pure noncompetitive inhibitor. The effects of various types of inhibitors are summarized in Table 5.9.

Table 5.9 Summary of effects of enzyme inhibitors on kinetic parameters

Type of inhibition	K_M	V_{max}
Competitive	Increased	Unchanged
Uncompetitive	Decreased	Decreased
Pure noncompetitive	Unchanged	Decreased
Mixed noncompetitive	Increased or decreased	Decreased
Irreversible	Unchanged	Decreased

Penicillin irreversibly inactivates a key enzyme in bacterial cell-wall synthesis

Penicillin, the first antibiotic ever discovered, is a clinically useful suicide inhibitor. Penicillin consists of a thiazolidine ring fused to a β-*lactam* ring to which a variable R group is attached by a peptide bond (Figure 5.28A). In benzylpenicillin, for example, R is a benzyl group (Figure 5.28B). The β-lactam ring is very labile due to significant strain in the four-membered ring; this instability is closely tied to the antibiotic action of penicillin.

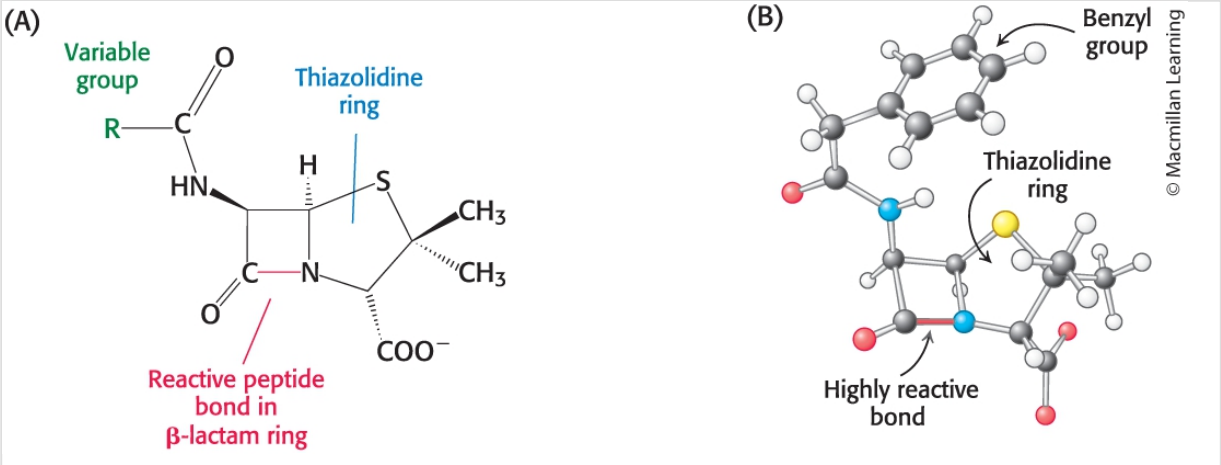


FIGURE 5.28 The reactive site of penicillin is the peptide bond of its β-lactam ring. (A) Structural formula of penicillin. (B) Representation of benzylpenicillin.

How does penicillin inhibit bacterial growth? Let us consider *Staphylococcus aureus*, the most common cause of staph infections. Like the vast majority of all bacteria, the cell wall of *S. aureus* is made up of a macromolecule, called *peptidoglycan* (Figure 5.29), which consists of linear polysaccharide chains that are cross-linked by short peptides. The enormous peptidoglycan molecule provides a continuous, covalently linked mesh that confers mechanical support and prevents bacteria from bursting in response to their high internal osmotic pressure. Glycopeptide transpeptidase catalyzes the formation of the cross-links that make the peptidoglycan so stable. Note that bacterial

cell walls are distinctive in containing D amino acids, which form cross-links by a mechanism different from that used to synthesize proteins.

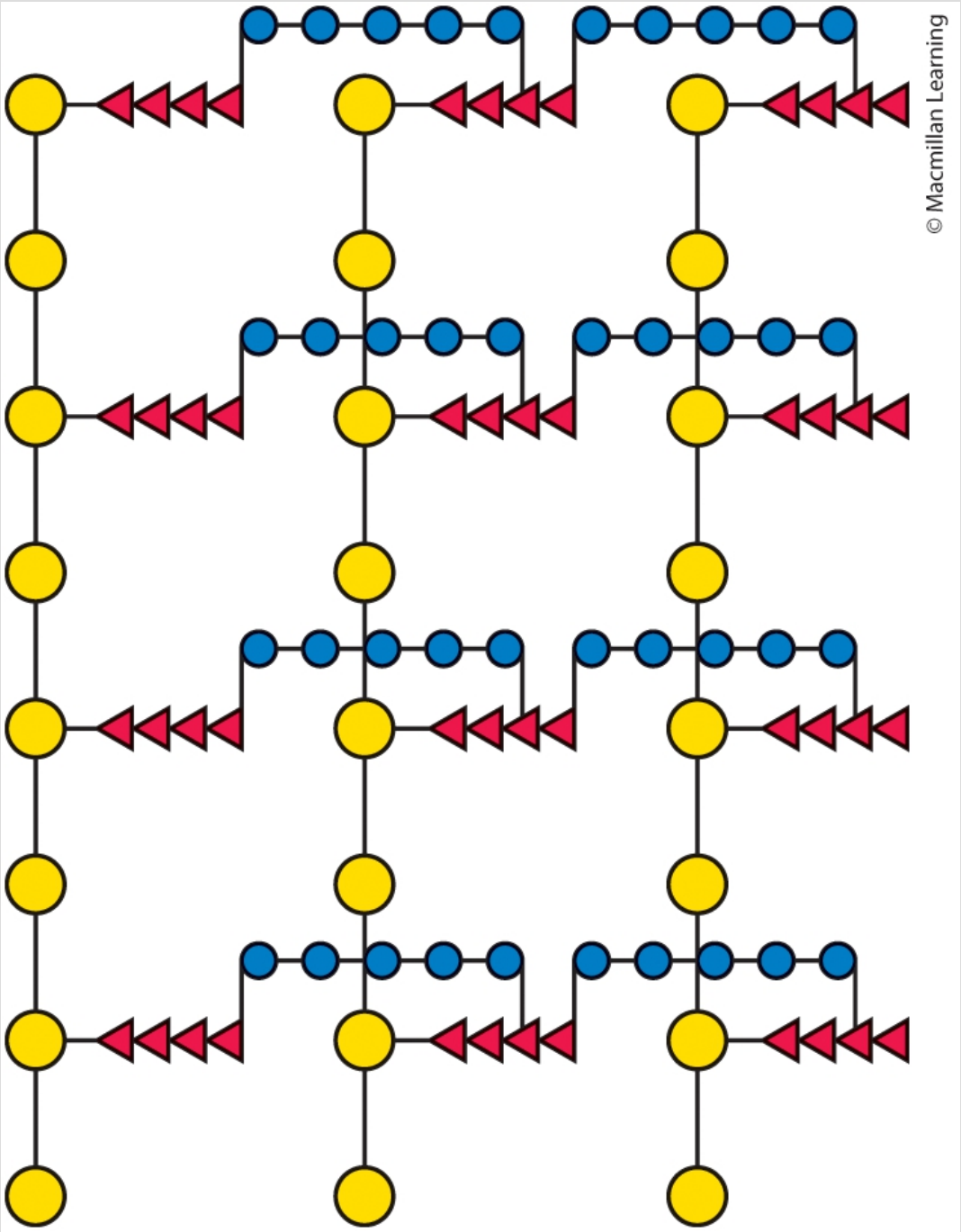


FIGURE 5.29 A schematic representation of a peptidoglycan section in *S. aureus* shows the crosslinking between sugar fibers. The sugars are shown in yellow, the tetrapeptides in red, and the pentaglycine bridges in blue. Only a small section is represented; the cell wall is a single, enormous, bag-shaped macromolecule because of extensive crosslinking.

Penicillin is an effective antibiotic because it interferes with the synthesis of the bacterial cell wall by irreversibly inhibiting the cross-linking transpeptidase. The transpeptidase normally forms an acyl intermediate with the penultimate D-alanine residue of the D-Ala-D-Ala peptide, which then reacts with the amino group of the terminal glycine in another peptide to form the cross-link. But penicillin can be accepted into the active site of the transpeptidase instead, because it mimics the D-Ala-D-Ala moiety of the normal substrate (Figure 5.30). Bound penicillin then forms a covalent bond with an active-site serine, permanently inactivating the enzyme and preventing the completion of cell-wall synthesis.

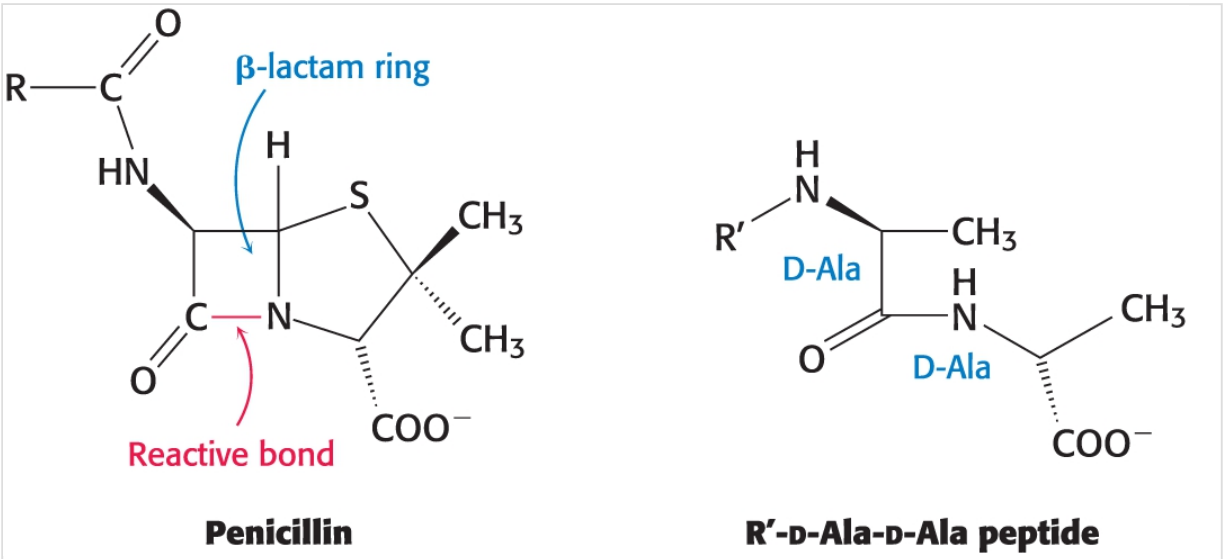


FIGURE 5.30 Penicillin resembles the transition state of the transpeptidase reaction. In the vicinity of its reactive peptide bond, the conformation of penicillin resembles the postulated conformation of the transition state of R'-D-Ala-D-Ala in the transpeptidation reaction.

[Information from B. Lee, *J. Mol. Biol.* 61:463–469, 1971.]

Why is penicillin such an effective inhibitor of the transpeptidase? The highly strained, four-membered β-lactam ring of penicillin makes it especially reactive. On binding to the transpeptidase, the serine residue at the active site attacks the carbonyl carbon atom of the lactam ring to form the penicilloyl-serine derivative (Figure 5.31). Because the peptidase participates in its own inactivation, penicillin acts as a suicide inhibitor.

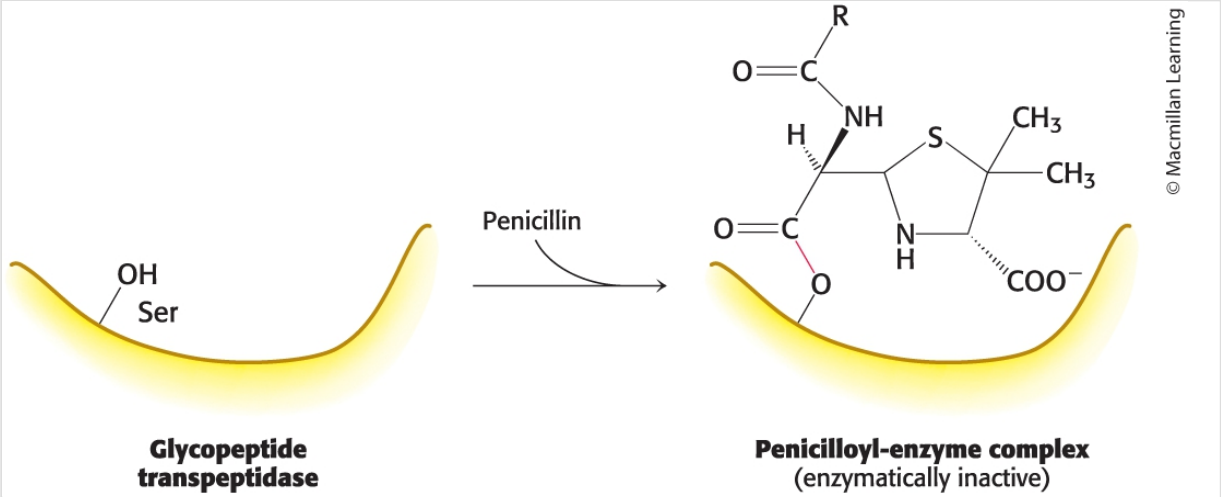


FIGURE 5.31 The formation of a penicilloyl-enzyme derivative is irreversible. Penicillin reacts irreversibly with the transpeptidase to inactivate the enzyme.

Chapter 5 Summary

5.1 Enzymes Are Powerful and Highly Specific Catalysts

- Enzymes are biological catalysts, most of which are proteins.
- Enzymes are highly specific and can enhance reaction rates by factors as great as 10^{17}.
- Many enzymes require cofactors for activity which can be metal ions or small, vitamin-derived organic molecules called coenzymes.

5.2 Gibbs Free Energy Is a Useful Thermodynamic Function for Understanding Enzymes

- A reaction can take place spontaneously only if the change in free energy (ΔG) is negative.
- The free-energy change of a reaction under standard conditions is called the standard free-energy change (ΔG°) while biochemists use $\Delta G^{\circ\prime}$, the standard free-energy change at pH 7.
- Enzymes do not alter reaction equilibria; rather, they increase the rate at which equilibrium is attained.

5.3 Enzymes Accelerate Reactions by Facilitating the Formation of the Transition State

- Enzymes decrease the free energy of activation of a chemical reaction by providing a reaction pathway in which the transition state (the highest-energy species) has a lower free energy and hence is more rapidly formed than in the uncatalyzed reaction; the result is that the reaction is accelerated in both directions.
- The first step in catalysis is the formation of an enzyme–substrate complex in which substrates are bound at active-site

clefts from which water is largely excluded.
- The specificity of enzyme–substrate interactions arises mainly from weak reversible contacts mediated by ionic interactions, hydrogen bonds, and van der Waals forces, and from the shape of the active site, which rejects molecules that do not have a sufficiently complementary shape and charge.
- Enzymes facilitate formation of the transition state by a dynamic process in which the substrate binds to specific conformations of the enzyme, accompanied by conformational changes at active sites that result in catalysis.

5.4 The Michaelis–Menten Model Accounts for the Kinetic Properties of Many Enzymes

- The kinetic properties of many enzymes are described by the Michaelis–Menten model in which an enzyme (E) combines with a substrate (S) to form an enzyme–substrate (ES) complex, which can proceed to form a product (P) or to dissociate into E and S.

$$E + S \underset{k_{-1}}{\overset{k_1}{\rightleftharpoons}} ES \xrightarrow{k_2} E + P$$



- The rate of formation of product V_0 is given by the Michaelis–Menten equation:

$$V_0 = V_{max} \frac{[S]}{[S] + K_M}$$

in which V_{max} is the reaction rate when the enzyme is fully saturated with substrate and K_M, the Michaelis constant, is the

substrate concentration at which the reaction rate is half maximal.
- The kinetic constant k_{cat}, called the turnover number, is the number of substrate molecules converted into product per unit time at a single catalytic site when the enzyme is fully saturated with substrate. The ratio of k_{cat}/K_M provides a measure of enzyme efficiency and specificity.
- Allosteric enzymes constitute an important class of enzymes whose catalytic activity can be regulated. These enzymes have multiple active sites which often display cooperativity, as evidenced by a sigmoidal dependence of reaction velocity on substrate concentration.

5.5 Enzymes Can Be Studied One Molecule at a Time

- Single-molecule methods reaffirm the key findings from ensemble studies but also reveal a distribution of enzyme characteristics rather than an average value.

5.6 Enzymes Can Be Inhibited by Specific Molecules

- Irreversible inhibitors bind covalently to enzymes and can provide a means of mapping the enzyme's active site, while reversible inhibition is characterized by a more rapid and less stable interaction between enzyme and inhibitor.
- Competitive inhibitors prevent the substrate from binding to the active site and thereby reduce the reaction velocity by diminishing the proportion of enzyme molecules that are bound to substrate. Competitive inhibition can be overcome by raising the substrate concentration.
- Uncompetitive inhibitors bind only to the enzyme–substrate complex, decreasing both the turnover number and the apparent K_M.
- Pure noncompetitive inhibitors decrease only the turnover number, while mixed noncompetitive inhibitors can have a

variety of effects.
- Transition-state analogs are stable compounds that mimic key features of the transition state and are potent and specific competitive inhibitors of enzymes.

Key Terms

catalyst
enzyme
ribozyme
substrate
protease
cofactor
apoenzyme
holoenzyme
coenzyme
prosthetic group
transition state
Gibbs free energy of activation (activation energy)
active site
induced fit
binding energy
K_M (Michaelis constant)
V_{max} (maximal rate)
Michaelis–Menten equation
Lineweaver–Burk plot
elasticity
turnover number
k_{cat}/K_M (specificity constant)
sequential reaction
double-displacement (Ping-Pong) reaction
allosteric enzyme

competitive inhibition
uncompetitive inhibition
pure noncompetitive inhibition
mixed noncompetitive inhibition
transition-state analog
group-specific reagent
affinity label (reactive substrate analog)
mechanism-based (suicide) inhibitor

Problems

1. What does an apoenzyme require to become a holoenzyme?

2. Consider the reaction: $S \rightleftharpoons P$. Which of the following

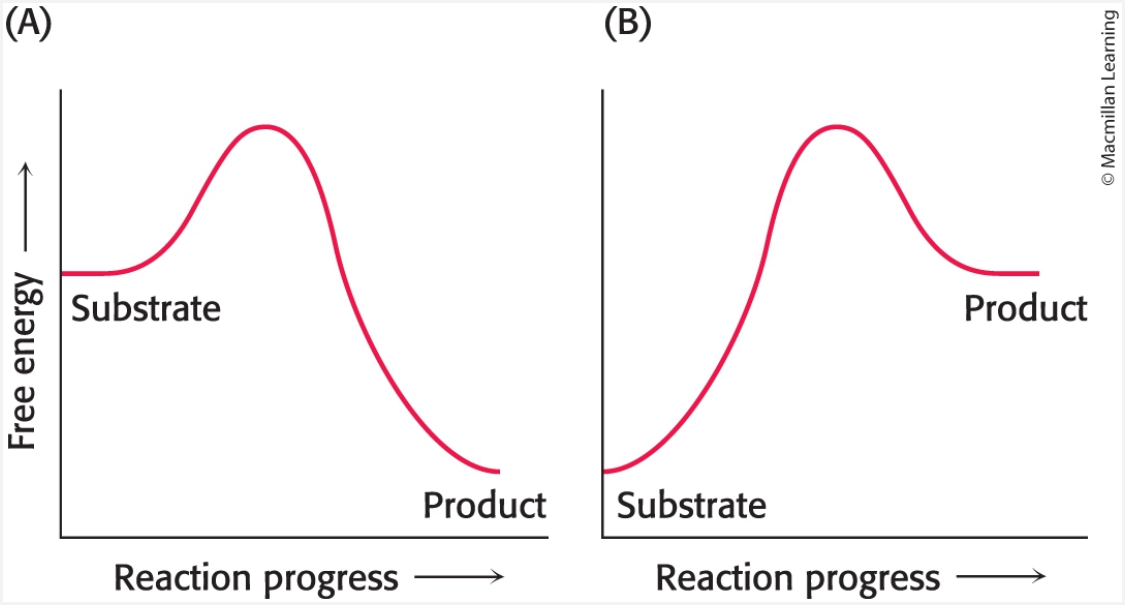
effects are produced by an enzyme on the general reaction?
1, 2

a. The reaction equilibrium is shifted away from the products.
b. The concentration of the products is increased.
c. ΔG for the reaction increases.
d. The activation energy for the reaction is lowered.
e. The formation of the transition state is promoted.
f. The rate constant for the forward reaction increases.

3. Why does the activation energy of a reaction not appear in the final ΔG of the reaction? 1

4. The illustrations below show the reaction-progress curves for two different reactions. Indicate the activation energy as well as

the ΔG for each reaction. Which reaction is endergonic? Exergonic? 1



5. Suppose that, in the absence of enzyme, the forward rate constant (k_F) for the conversion of S into P is $10^{-4}\ s^{-1}$ and the reverse rate constant (k_R) for the conversion of P into S is $10^{-6}\ s^{-1}$. 1, 2

$$S \underset{10^{-6}\ s^{-1}}{\overset{10^{-4}\ s^{-1}}{\rightleftharpoons}} P$$

a. What is the equilibrium for the reaction? What is the $\Delta G^{\circ\prime}$?

b. Suppose an enzyme enhances the rate of the reaction 100-fold. What are the rate constants for the enzyme-catalyzed reaction? What is the equilibrium constant? The $\Delta G^{\circ\prime}$?

6. What would be the result of an enzyme having a greater binding energy for the substrate than for the transition state?

2

7. Match the K'_{eq} values with the appropriate $\Delta G^{\circ\prime}$ values.

1

K'_{eq}	$\Delta G^{\circ\prime}$ (kJ mol^{-1})
1. 1	28.53
2. 10^{-5}	−11.42
3. 10^{4}	5.69
4. 10^{2}	0

-22.84

5. 10^{-1}

---

8. Assume that you have a solution of 0.1 M glucose 6-phosphate (G 6-P). To this solution, you add the enzyme phosphoglucomutase, which catalyzes the following reaction:

$$\text{G 6-P} \underset{}{\overset{\text{Phosphoglucomutase}}{\rightleftharpoons}} \text{G 1-P}$$

The $\Delta G^{\circ\prime}$ for the reaction is $+7.5\ \text{kJ mol}^{-1}\ (+1.8\ \text{kcal mol}^{-1})$. 1

a. Does the reaction proceed as written? If so, what are the final concentrations of G 6-P and G 1-P?
b. Under what cellular conditions could you produce G 1-P at a high rate?

9. Consider the following reaction:

$$\text{G 6-P} \underset{}{\overset{\text{Phosphoglucomutase}}{\rightleftharpoons}} \text{G 1-P}$$

After reactant and product were mixed and allowed to reach equilibrium at 25°C, the concentration of each compound was measured:

$$[\text{Glucose 1-phosphate}]_{eq} = 0.01\ \text{M}$$
$$[\text{Glucose 6-phosphate}]_{eq} = 0.19\ \text{M}$$

Calculate K_{eq} and $\Delta G^{\circ\prime}$. 1

10. The affinity between a protein and a molecule that binds to the protein is frequently expressed in terms of a dissociation constant K_d. 3

$$\text{Protein} + \text{small molecule} \rightleftharpoons \text{Protein} - \text{small molecule complex}$$

$$K_d = \frac{[\text{protein}][\text{small molecule}]}{[\text{protein} - \text{small molecule complex}]}$$

Does K_M measure the affinity of the enzyme complex? Under what circumstances might K_M approximately equal K_d?

11. Match the term with the description or compound. 3, 4

1. Competitive inhibition _____
2. Uncompetitive inhibition _____
3. Noncompetitive inhibition _____

1. Inhibitor and substrate can bind simultaneously
2. V_{max} remains the same but the K_M^{app} increases
3. Sulfanilamide
4. Binds to the enzyme–substrate complex only
5. Lowers V_{max} and K_M^{app}

6. Roundup

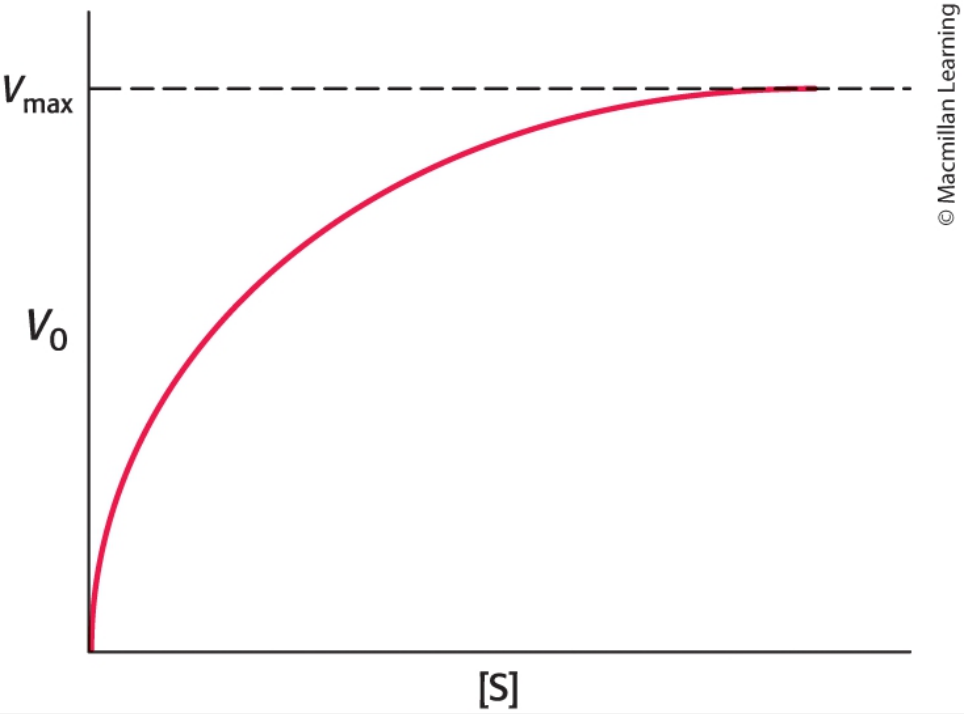
7. K_M remains unchanged but V_{max} is lower

8. Doxycycline

9. Prevents S from binding to the active site

---

12. Many biochemists go bananas, and justifiably, when they see a Michaelis–Menten plot like the one shown below. To see why, determine the V_0 as a fraction of V_{max} when the substrate concentration is equal to 10 K_M and 20 K_M. Please control your outrage. 3



13. The hydrolysis of pyrophosphate to orthophosphate is important in driving forward biosynthetic reactions such as the synthesis of DNA. This hydrolytic reaction is catalyzed in *E. coli* by a pyrophosphatase that has a mass of 120 kDa and consists of six identical subunits. For this enzyme, a unit of activity is defined as the amount of enzyme that hydrolyzes 10 μmol of pyrophosphate in 15 minutes at 37°C under standard assay conditions. The purified enzyme has a V_{max} of 2800 units per milligram of enzyme. 3

a. How many moles of substrate are hydrolyzed per second per milligram of enzyme when the substrate concentration is much greater than K_M?
b. How many moles of active sites are there in 1 mg of enzyme? Assume that each subunit has one active site.
c. What is the turnover number of the enzyme? Compare this value with others mentioned in this chapter.

14. Penicillin is hydrolyzed and thereby rendered inactive by penicillinase (also known as β-lactamase), an enzyme present in some penicillin-resistant bacteria. The mass of this enzyme in *Staphylococcus aureus* is 29.6 kDa. The amount of penicillin hydrolyzed in 1 minute in a 10-ml solution containing 10^{-9} g of purified penicillinase was measured as a function of the concentration of penicillin. Assume that the concentration of penicillin does not change appreciably during the assay. 3

[Penicillin] μM	Amount hydrolyzed (nmol)

1	0.11
3	0.25
5	0.34
10	0.45
30	0.58
50	0.61

a. Plot V_0 versus [S] and $1/V_0$ versus 1/[S] for these data. Does penicillinase appear to obey Michaelis–Menten kinetics? If so, what is the value of K_M?
b. What is the value of V_{max}?
c. What is the turnover number of penicillinase under these experimental conditions? Assume one active site per enzyme molecule.

15. The kinetics of an enzyme is measured as a function of substrate concentration in the presence and absence of $100\ \mu M$ inhibitor. 3, 4

	Velocity $(\mu mol\ minute^{-1})$	
[S] (μM)	**No inhibitor**	**Inhibitor**
3	10.4	2.1

5	14.5	2.9
10	22.5	4.5
30	33.8	6.8
90	40.5	8.1

a. What are the values of V_{max} and K_M in the presence of this inhibitor?
b. What type of inhibition is it?
c. What is the dissociation constant of this inhibitor?
d. If $[S] = 30\ \mu M$, what fraction of the enzyme molecules has a bound substrate in the presence and in the absence of $100\ \mu M$ inhibitor?

16. The plot of $1/V_0$ versus 1/[S] is sometimes called a Lineweaver–Burk plot. Another way of expressing the kinetic data is to plot V_0 versus $V_0/[S]$, which is known as an Eadie–Hofstee plot. 3, 4

a. Rearrange the Michaelis–Menten equation to give V_0 as a function of $V_0/[S]$.
b. What is the significance of the slope, the *y*-intercept, and the *x*-intercept in a plot of V_0 versus $V_0/[S]$?
c. Sketch a plot of V_0 versus $V_0/[S]$ in the absence of an inhibitor, in the presence of a competitive inhibitor, and in the presence of a noncompetitive inhibitor.

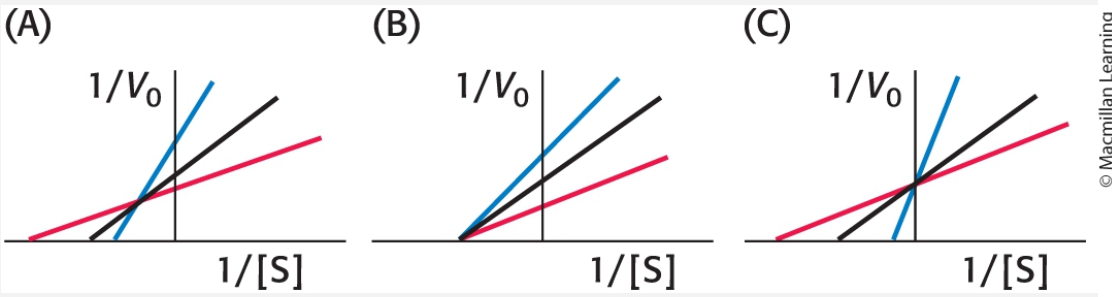
17. What is the defining characteristic for an enzyme catalyzing a sequential reaction? A double-displacement reaction?

18. You have isolated two versions of the same enzyme, a wild type and a mutant differing from the wild type at a single amino acid. Working carefully but expeditiously, you then establish the following kinetic characteristics of the enzymes. 1, 3

	Maximum velocity	K_M
Wild type	100 μmol/min	10 mM
Mutant	1 μmol/min	0.1 mM

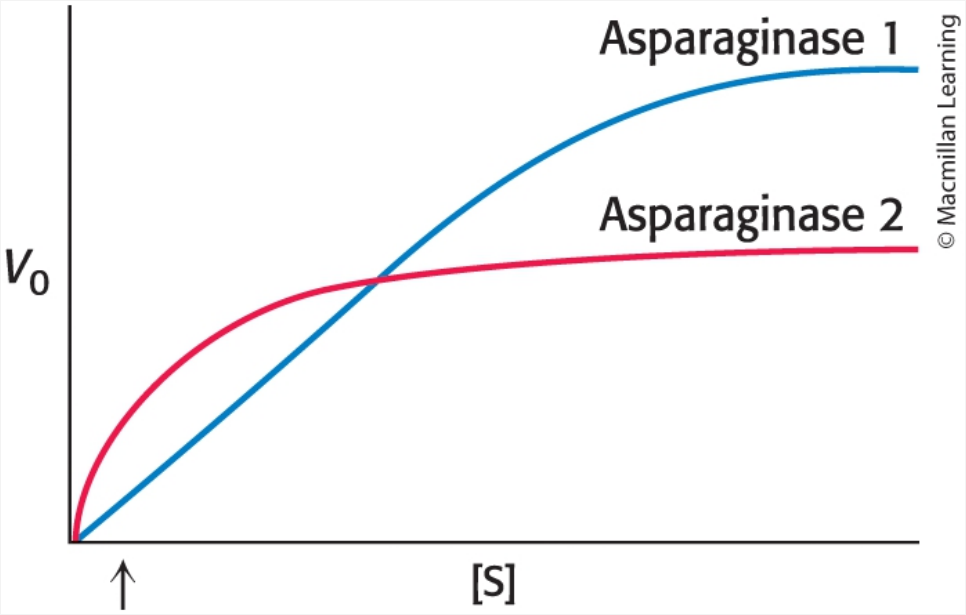
a. With the assumption that the reaction occurs in two steps in which k_{-1} is much larger than k_2, which enzyme has the higher affinity for substrate?
b. What is the initial velocity of the reaction catalyzed by the wild-type enzyme when the substrate concentration is 10 mM?
c. Which enzyme alters the equilibrium more in the direction of product?

19. For a one-substrate, enzyme-catalyzed reaction, double-reciprocal plots were determined for three different enzyme concentrations. Which of the following three families of curve would you expect to be obtained? Explain. 3



© Macmillan Learning

20. The amino acid asparagine is required by cancer cells to proliferate. Treating patients with the enzyme asparaginase is sometimes used as a chemotherapy treatment. Asparaginase hydrolyzes asparagine to aspartate and ammonia. The below illustration shows the Michaelis–Menten curves for two asparaginases from different sources, as well as the concentration of asparagine in the environment (indicated by the arrow). Which enzyme would make a better chemotherapeutic agent? 3



21. Picture in your mind the velocity-versus-substrate concentration curve for a typical Michaelis–Menten enzyme.

Now, imagine that the experimental conditions are altered as described below. For each of the conditions described, fill in the table indicating precisely (when possible) the effect on V_{max} and K_M of the imagined Michaelis–Menten enzyme. 3, 4

Experimental condition	V_{max}	K_M
1. Twice as much enzyme is used.		
2. Half as much enzyme is used.		
3. A competitive inhibitor is present.		
4. An uncompetitive inhibitor is present.		
5. A pure noncompetitive inhibitor is present.		

---

22. In the conversion of A into D in the following biochemical pathway, enzymes E_A, E_B, and E_C have the K_M values indicated under each enzyme. If all of the substrates and products are present at a concentration of 10^{-4} M and the enzymes have approximately the same V_{max}, which step will be rate limiting and why? 3

$$A \underset{E_A}{\rightleftharpoons} B \underset{E_B}{\rightleftharpoons} C \underset{E_C}{\rightleftharpoons} D$$

$K_M =$ 10^{-2} M 10^{-4} M 10^{-6} M

23. Proteins are thermodynamically unstable. The ΔG of the hydrolysis of proteins is quite negative, yet proteins can be quite

stable. Explain this apparent paradox. What does it tell you about protein synthesis? 1

24. Transition-state analogs, which can be used as enzyme inhibitors and to generate catalytic antibodies, are often difficult to synthesize. Suggest a reason. 2

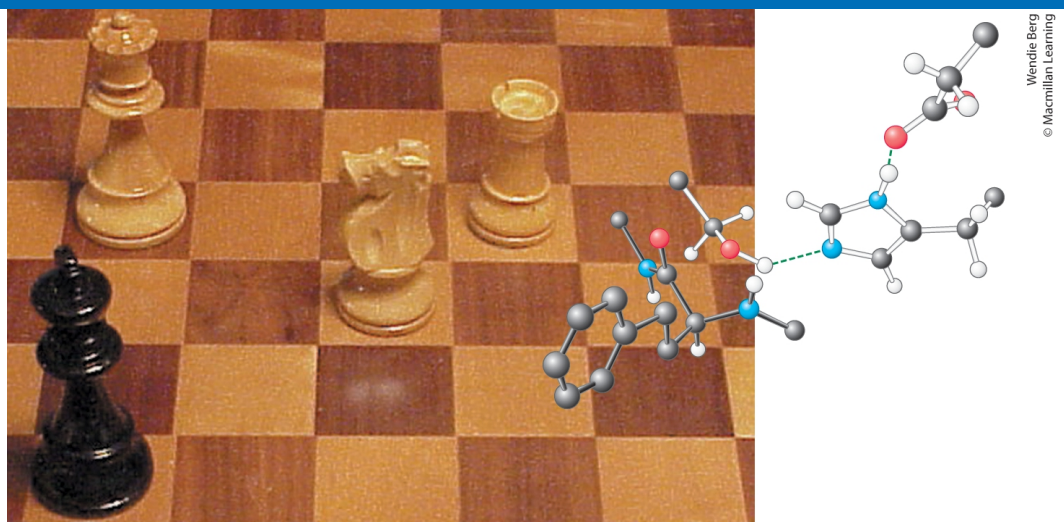
25. What is the biochemical advantage of having a K_M approximately equal to the substrate concentration normally available to an enzyme? 3

26. Succinylcholine is a fast-acting, short-duration muscle relaxant that is used when a tube is inserted into a patient's trachea or when a bronchoscope is used to examine the trachea and bronchi for signs of cancer. Within seconds of the administration of succinylcholine, the patient experiences muscle paralysis and is placed on a respirator while the examination proceeds. Succinylcholine is a competitive inhibitor of acetylcholinesterase, a nervous system enzyme, and this inhibition causes paralysis. However, succinylcholine is hydrolyzed by blood-serum cholinesterase, which shows a broader substrate specificity than does the nervous system enzyme. Paralysis lasts until the succinylcholine is hydrolyzed by the serum cholinesterase, usually several minutes later. 3

a. As a safety measure, serum cholinesterase is measured before the examination takes place. Explain why this measurement is good idea.
b. What would happen to the patient if the serum cholinesterase activity were only 10 units of activity per liter rather than the normal activity of about 80 units?
c. Some patients have a mutant form of the serum cholinesterase that displays a K_M of 10 mM, rather than

the normal 1.4 mM. What will be the effect of this mutation on the patient?

Chapter 6
Enzyme Catalytic Strategies



Chess and enzymes have in common the use of strategy, consciously thought out in the game of chess and selected by evolution for the action of an enzyme. The three amino acid residues at the right, denoted by the white bonds, represent a particular chemical strategy for catalyzing a reaction that is normally very slow. This strategy relies on the properties of the different amino acids, much as chess strategy relies on different rules for moving each type of piece.

Outline

6.1 Enzymes Use a Core Set of Catalytic Strategies
6.2 Proteases Facilitate a Fundamentally Difficult Reaction
6.3 Carbonic Anhydrases Make a Fast Reaction Faster

6.4 Restriction Enzymes Catalyze Highly Specific DNA-Cleavage Reactions
6.5 Molecular Motor Proteins Harness Changes in Enzyme Conformation to Couple ATP Hydrolysis to Mechanical Work

Learning Goals



By the end of this chapter, you should be able to:

1. Discuss four general strategies used by enzymes to accelerate particular reactions.
2. Give examples of specific chemical features of enzyme active sites that facilitate increasing the rates of specific reactions.
3. Give an example of when high absolute rate acceleration is physiologically important and how an enzyme achieves this acceleration.
4. Understand when high specificity is important for an enzyme and how this specificity is achieved.
5. Describe an example of when large conformational changes that occur during an enzymatic reaction cycle are used to drive other processes.
6. Discuss some of the experimental approaches biochemists use to elucidate enzymatic mechanisms.

What are the sources of the catalytic power and specificity of enzymes? This chapter presents the catalytic strategies used by four classes of enzymes, each of which catalyze reactions that involve the addition of water to a substrate. Scientists have revealed the mechanisms of these enzymes using incisive experimental probes, including protein structure determination, site-directed mutagenesis, detailed kinetic studies, and the use of isotope labels.

Each of the four classes of enzymes addresses a different challenge. Serine proteases promote a reaction that is almost immeasurably slow at neutral pH in the absence of a catalyst; carbonic anhydrases

achieve a high absolute rate of reaction, suitable for integration with other rapid physiological processes; and restriction enzymes attain a high degree of specificity. Finally, molecular motor proteins such as myosin harness the free energy associated with the hydrolysis of ATP to drive other processes.

6.1 Enzymes Use a Core Set of Catalytic Strategies

In Chapter 5, we learned that enzymatic catalysis begins with substrate binding. The **binding energy** is the free energy released in the formation of a large number of weak interactions between the enzyme and the substrate. The use of this binding energy is the first common strategy used by enzymes. This binding energy serves two purposes: it establishes substrate specificity and increases catalytic efficiency. Often only the correct substrate can participate in most or all of the interactions with the enzyme and thus optimize binding energy, accounting for the exquisite substrate specificity exhibited by many enzymes.

Furthermore, the full complement of such interactions is formed only when the combination of enzyme and substrate is in the transition state. Thus, interactions between the enzyme and the substrate stabilize the transition state, thereby lowering the free energy of activation. The binding energy can also promote structural changes in both the enzyme and the substrate that facilitate catalysis, a process referred to as **induced fit**.

In addition to the first strategy involving binding energy, enzymes commonly employ one or more of the following four additional strategies to catalyze specific reactions:

1. *Covalent catalysis*. In **covalent catalysis**, the active site contains a reactive group that becomes temporarily covalently attached to a part of the substrate in the course of catalysis. The proteolytic enzyme chymotrypsin provides an excellent example of this strategy (Section 6.2).

2. *General acid–base catalysis*. In **general acid–base catalysis**, a molecule other than water plays the role of a proton donor or acceptor. These include histidine residues in chymotrypsin and carbonic anhydrase, an aspartate residue in EcoRV, and a phosphate group of the ATP substrate for myosin and kinesin.

3. *Catalysis by approximation*. Many reactions have two distinct substrates, including all four classes of hydrolases considered in detail in this chapter. In such cases, the reaction rate may be considerably enhanced by bringing the two substrates together along a single binding surface on an enzyme, a process called **catalysis by approximation**. For example, carbonic anhydrase binds carbon dioxide and water in adjacent sites to facilitate their reaction.

4. *Metal ion catalysis*. In **metal ion catalysis**, metal ions function catalytically in several ways. For instance, a metal ion may facilitate the formation of reactive species such as hydroxide ion by direct coordination. A zinc(II) ion serves this purpose in catalysis by carbonic anhydrase. Alternatively, a metal ion may serve to stabilize a negative charge on a reaction intermediate, a role played by magnesium(II) ion in EcoRV. Finally, a metal ion may serve as a bridge between enzyme and substrate, increasing the binding energy and holding the substrate in a conformation appropriate for catalysis. This strategy is used by myosin and kinesin and, indeed, by essentially all enzymes that use ATP as a substrate.

Although we shall not consider catalytic RNA molecules explicitly in this chapter, the principles described for protein enzymes also apply to these catalysts.

Self-Check Question

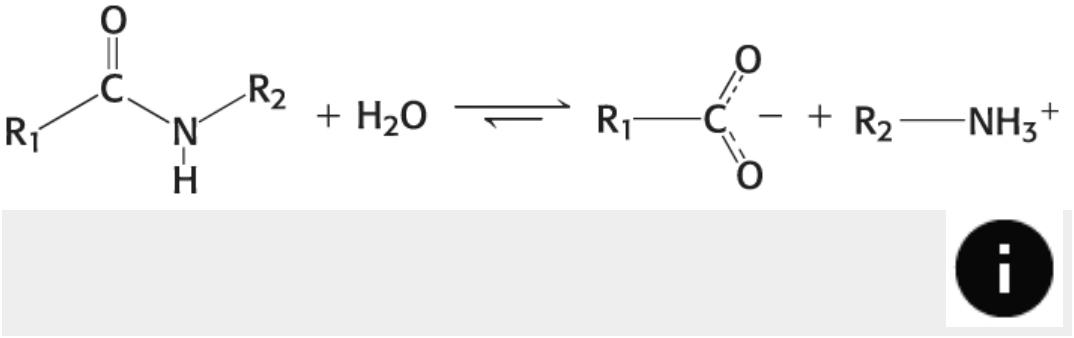


The enzyme adenylate kinase can convert two molecules of ADP to one molecule of AMP and one molecule of ATP. Suggest at least one catalytic strategy likely used by this enzyme.

6.2 Proteases Facilitate a Fundamentally Difficult Reaction

Peptide bond hydrolysis is an important process in living systems. Proteins that have served their purpose must be degraded so that their constituent amino acids can be recycled for the synthesis of new proteins; for example, proteins ingested in the diet must be broken down into small peptides and amino acids for absorption in the gut. Furthermore, as described in detail in Chapter 7, proteolytic reactions are important in regulating the activity of certain enzymes and other proteins.

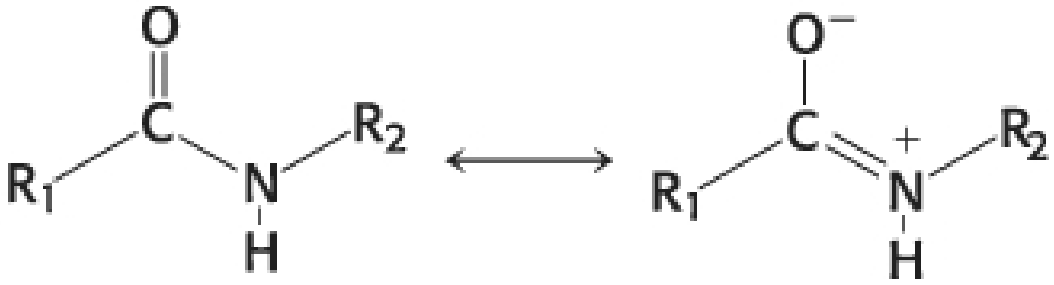
Proteases cleave proteins by a hydrolysis reaction — the addition of a molecule of water to a peptide bond:



Although the hydrolysis of peptide bonds is thermodynamically favorable, such reactions are extremely slow. In the absence of a catalyst, the half-life for the hydrolysis of a typical peptide at neutral pH is estimated to be between 10 and 1000 years. Yet, peptide bonds must be hydrolyzed within milliseconds in some biochemical processes.

The chemical nature of peptide bonds is responsible for their kinetic stability. Specifically, the resonance structure that accounts for the

planarity of peptide bonds also makes them resistant to hydrolysis. This resonance structure endows them with partial double-bond character:



The carbon–nitrogen bond is strengthened by its double-bond character. More importantly, the carbonyl carbon atom is less **electrophilic** and less susceptible to **nucleophilic** attack than are the carbonyl carbon atoms in more reactive compounds such as carboxylate esters. Consequently, to promote peptide-bond cleavage, an enzyme must facilitate nucleophilic attack at a normally unreactive carbonyl group.

Chymotrypsin possesses a highly reactive serine residue

A number of proteolytic enzymes participate in the breakdown of proteins in the digestive systems of mammals and other organisms. One such enzyme, chymotrypsin, cleaves peptide bonds selectively on the carboxyl-terminal side of the large hydrophobic amino acids such as tryptophan, tyrosine, phenylalanine, and methionine (**Figure 6.1**). Chymotrypsin is a good example of the use of covalent catalysis. The enzyme employs a powerful nucleophile to attack the unreactive carbonyl carbon atom of the substrate. This nucleophile becomes covalently attached to the substrate transiently in the course of catalysis.

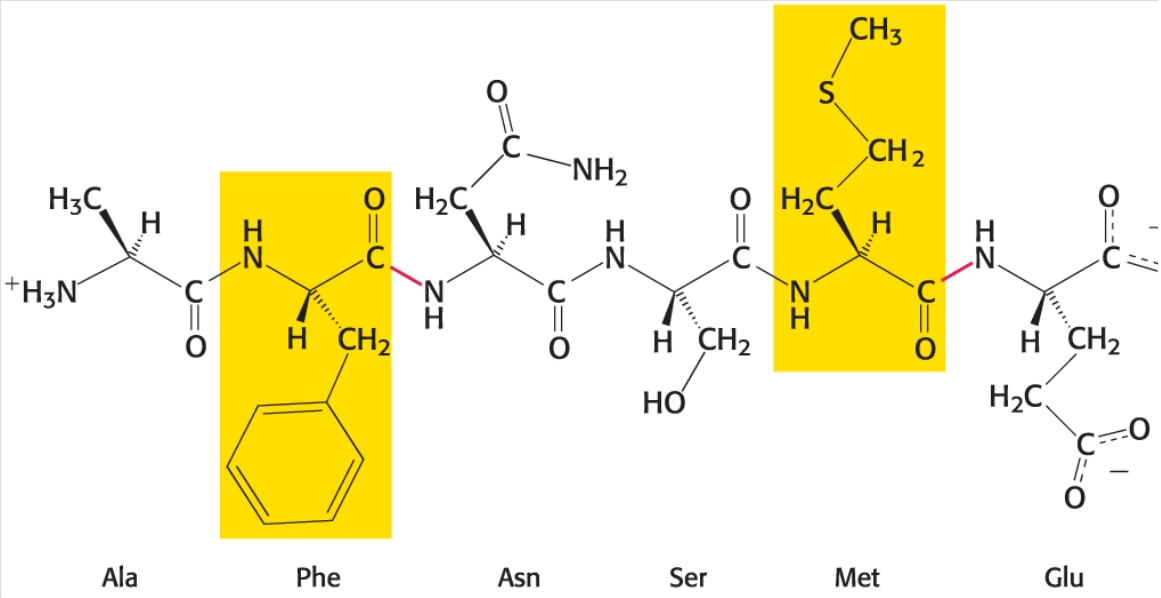


FIGURE 6.1 Chymotrypsin cleaves proteins specifically on the carboxyl side of aromatic or large hydrophobic amino acids. The targeted amino acids are highlighted, and the bonds cleaved by chymotrypsin are indicated in red.

What is the nucleophile that chymotrypsin employs to attack the substrate carbonyl carbon atom? A clue comes from the fact that chymotrypsin contains an extraordinarily reactive serine residue. Chymotrypsin molecules treated with organofluorophosphates such as diisopropylphosphofluoridate (DIPF) lose all activity irreversibly (Figure 6.2). Only a single residue, serine 195, is modified. This chemical modification reaction suggests that this unusually reactive serine residue plays a central role in the catalytic mechanism of chymotrypsin.

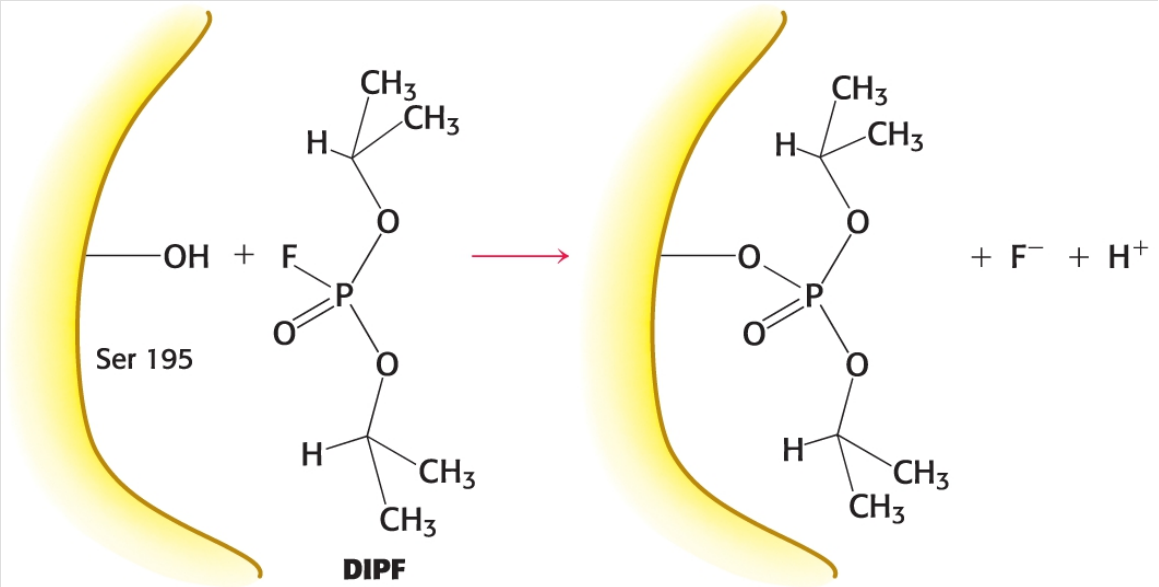
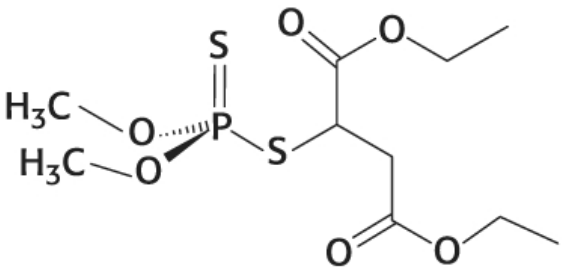
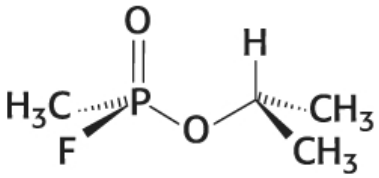


FIGURE 6.2 Chymotrypsin is inactivated by treatment with diisopropylphosphofluoridate (DIPF). DIPF reacts only with one serine among 28 possible serine residues, revealing the unusu reactivity of serine 195.

Phosphorus-based agents that modify reactive serine residues can be potent toxins. Compounds such as malathion, used to kill pest insects, and nerve agents such as sarin, developed as a chemical weapon, each modify a reactive serine residue in a key enzyme in the nervous system and disrupt nerve function.



Malathion



Sarin

Chymotrypsin action proceeds in two steps linked by a covalently bound intermediate

A study of the kinetics of chymotrypsin provides a second clue to its catalytic mechanism. Enzyme kinetics is often monitored by having the enzyme act on a substrate analog, called a **chromogenic substrate**, that forms a colored product. For chymotrypsin, one such substrate is *N*-acetyl-L-phenylalanine *p*-nitrophenyl ester. You might notice that this substrate is an ester rather than an amide, but many proteases will also hydrolyze esters. One of the products formed cleavage of this substrate by chymotrypsin is *p*-nitrophenolate, which has a yellow color (**Figure 6.3**). Measurements of the absorbance of light reveal the amount of *p*-nitrophenolate being produced.

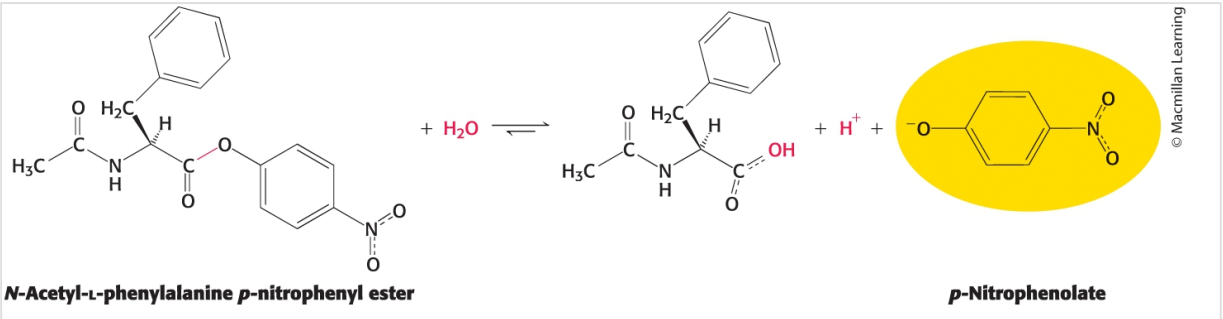


FIGURE 6.3 The action of chymotrypsin can be monitored by using a substrate that forms a colored product. The substrate *N*-Acetyl-L-phenylalanine *p*-nitrophenyl ester is cleaved to produce a yellow-colored product, *p*-nitrophenolate. *p*-Nitrophenolate forms by deprotonation of *p*-nitrophenol at pH 7.

Under steady-state conditions, the cleavage of this substrate obeys Michaelis–Menten kinetics with K_M of $20\ \mu M$ and k_{cat} of $77\ s^{-1}$. More insight into the mechanism can be gained by monitoring the initial phase of the reaction by using the stopped-flow method, which makes it possible to mix enzyme and substrate and monitor the results within a millisecond. This method reveals an initial rapid burst of colored product, followed by its slower formation as the reaction reached the steady state (Figure 6.4), confirming that hydrolysis proceeds in two phases. In the first reaction cycle that takes place on each enzyme molecule immediately after mixing, only the first phase must take place before the colored product is released. In subsequent reaction cycles, both phases must take place. Note that the burst is observed because the first phase is substantially more rapid than the second phase for this substrate.

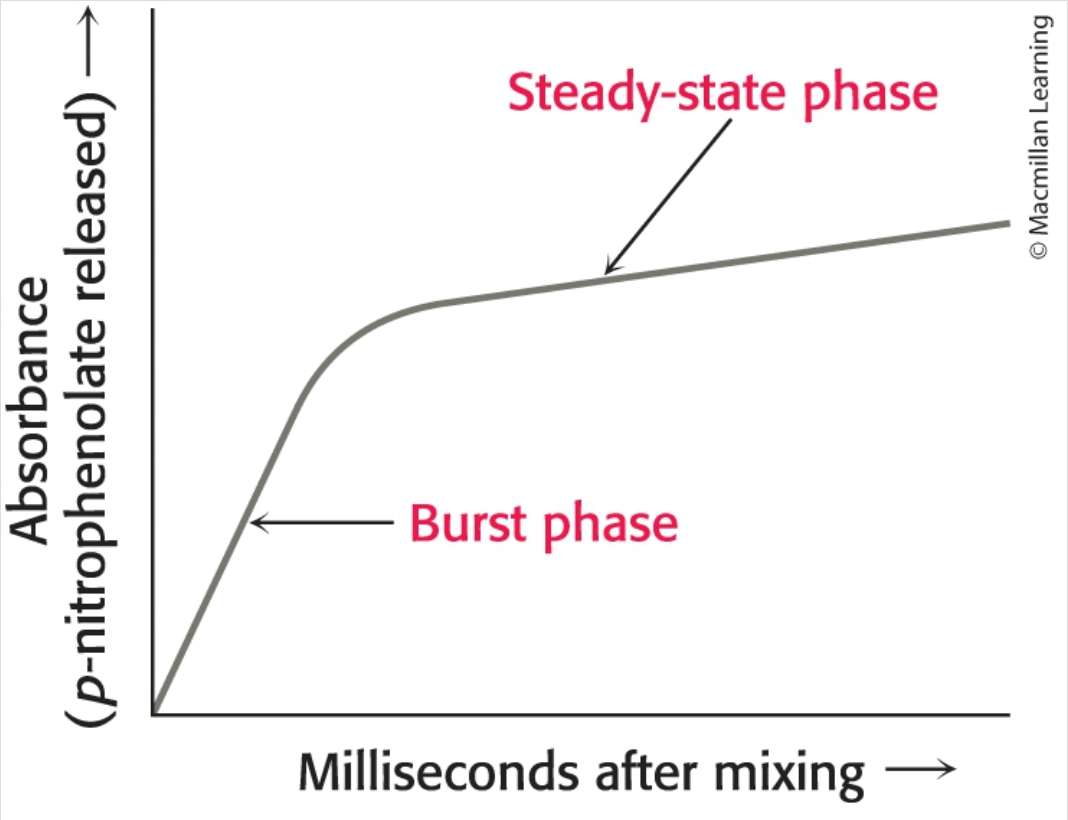


FIGURE 6.4 Two kinetic phases are evident by monitoring the initial action of chymotrypsin. When chymotrypsin is rapidly mixed with a solution of *N*-acetyl-L-phenylalanine *p*-nitrophenyl ester, a rapid burst phase of colored product is

observed followed by a steady-state phase. This observation provides insight into the chymotrypsin mechanism.

The two phases are explained by the formation of a covalent enzyme–substrate intermediate (Figure 6.5). First, the acyl group of the substrate becomes covalently attached to the enzyme as *p*-nitrophenolate (or an amine if the substrate is an amide rather than an ester) is released. The enzyme–acyl group complex is called the acyl-enzyme intermediate. Second, the acyl-enzyme intermediate is hydrolyzed to release the carboxylic acid component of the substrate and regenerate the free enzyme. Thus, one molecule of *p*-nitrophenolate is produced rapidly from each enzyme molecule as the acyl-enzyme intermediate is formed. However, it takes longer for the enzyme to be reset by the hydrolysis of the acyl-enzyme intermediate, and both phases are required for enzyme turnover.

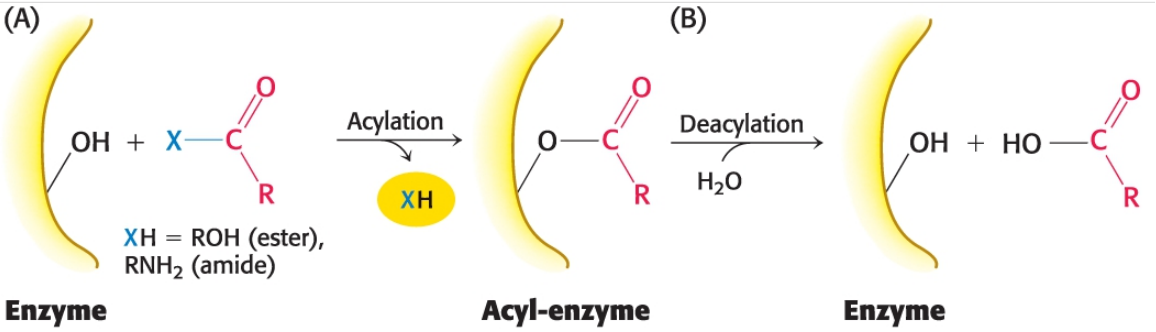


FIGURE 6.5 Hydrolysis by chymotrypsin involves covalent catalysis. In step (A), the enzyme is covalently modified to form an acyl-enzyme intermediate. In step (B), the enzyme is freed by deacylation.

Serine is part of a catalytic triad that also includes histidine and aspartate

The three-dimensional structure of chymotrypsin reveals that this enzyme is roughly spherical and comprises three polypeptide chains, linked by disulfide bonds (Figure 6.6). Note that the active site of chymotrypsin, marked by serine 195, lies in a cleft on the surface of the enzyme. The structure of the active site explains the special reactivity of serine 195 (Figure 6.7). The side chain of serine 195 is hydrogen bonded to the imidazole ring of histidine 57. The —NH group of this imidazole ring is, in turn, hydrogen bonded to the carboxylate group of aspartate 102. This constellation of residues is referred to as the **catalytic triad**.

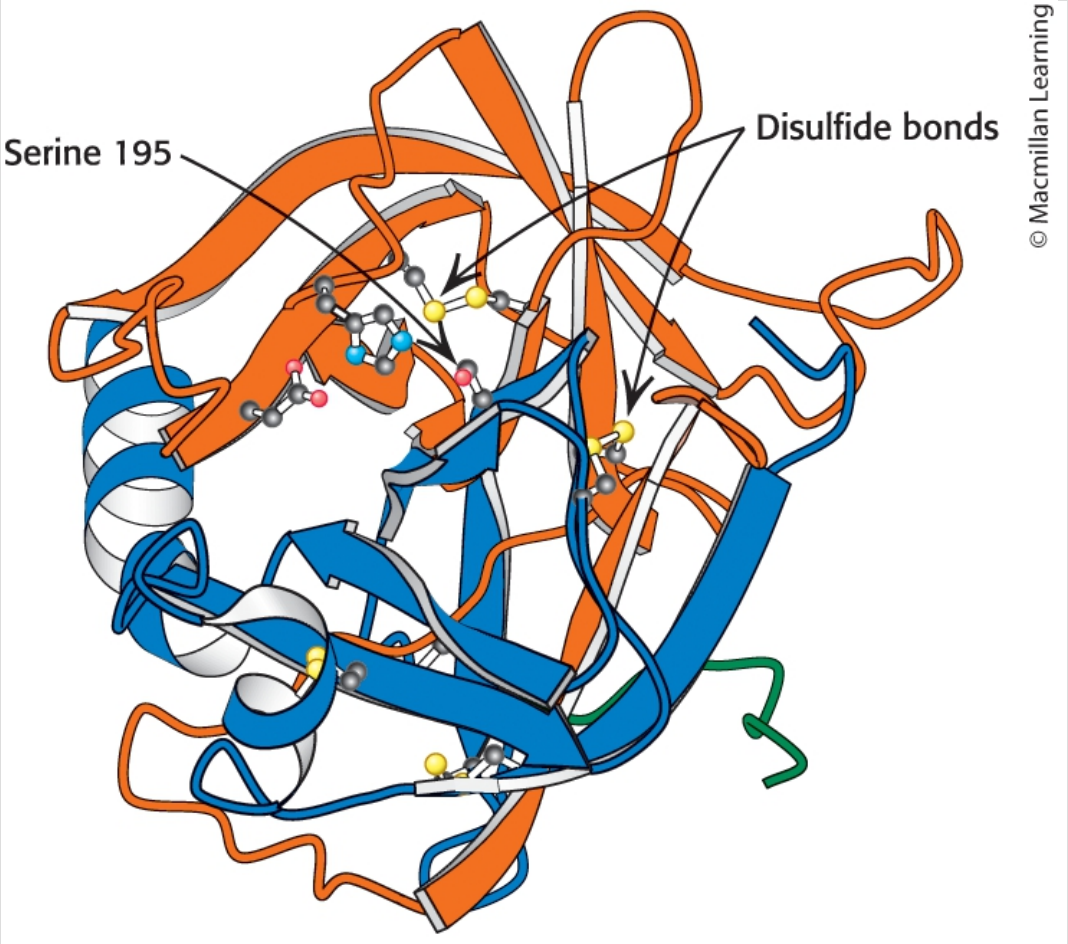


FIGURE 6.6 The active site serine 195 sits in a cleft on the surface of chymotrypsin. In the ribbon diagram shown here, chymotrypsin's three chains are indicated in

orange, blue, and green. Two intrastrand and two interstrand disulfide bonds are also shown.

[Drawn from 1GCT.pdb.]

INTERACT with this model in Achieve

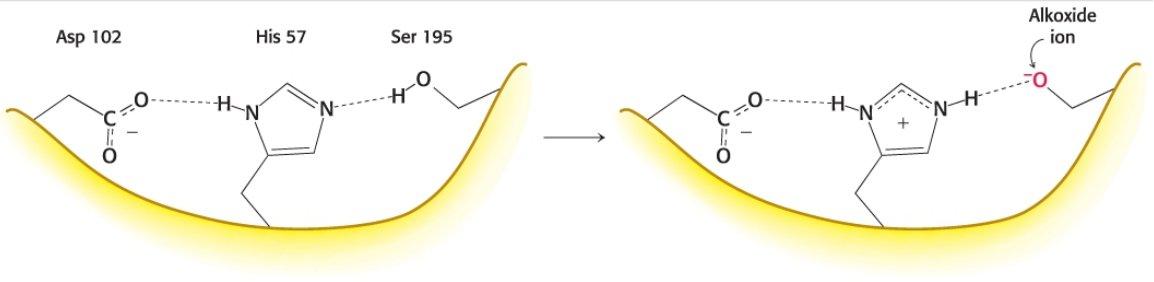


FIGURE 6.7 The catalytic triad increases the reactivity of serine 195. The catalytic triad poises this residue for formation of an alkoxide ion, a much stronger nucleophile than a hydroxyl grou

How does this arrangement of residues lead to the high reactivity of serine 195? The histidine residue serves to position the serine side chain and to polarize its hydroxyl group so that it is poised for deprotonation. In the presence of the substrate, the histidine residue accepts the proton from the serine 195 hydroxyl group. In doing so, the histidine acts as a general base catalyst. The withdrawal of the proton from the hydroxyl group generates an alkoxide ion, which is a much more powerful nucleophile than is an alcohol. The aspartate residue helps orient the histidine residue and make it a better proton acceptor through hydrogen bonding and electrostatic effects.

These observations suggest a mechanism for peptide hydrolysis (Figure 6.8). After substrate binding (step 1), the reaction begins with the oxygen atom of the side chain of serine 195 making a nucleophilic attack on the carbonyl carbon atom of the target peptide bond (step 2).

There are now four atoms bonded to the carbonyl carbon, arranged as a tetrahedron, instead of three atoms in a planar arrangement. This inherently unstable tetrahedral intermediate bears a formal negative charge on the oxygen atom derived from the carbonyl group. This charge is stabilized by interactions with NH groups from the protein in a site termed the **oxyanion hole** (**Figure 6.9**). These interactions also help stabilize the transition state that precedes the formation of the tetrahedral intermediate. This tetrahedral intermediate collapses to generate the acyl-enzyme (step 3), facilitated by the transfer of the proton being held by the positively charged histidine residue to the amino group formed by cleavage of the peptide bond. The amine component is now free to depart from the enzyme (step 4), completing the first stage of the hydrolytic reaction — acylation of the enzyme. Such acyl-enzyme intermediates have been observed using x-ray crystallography by trapping them through adjustment of conditions such as the nature of the substrate, pH, or temperature.

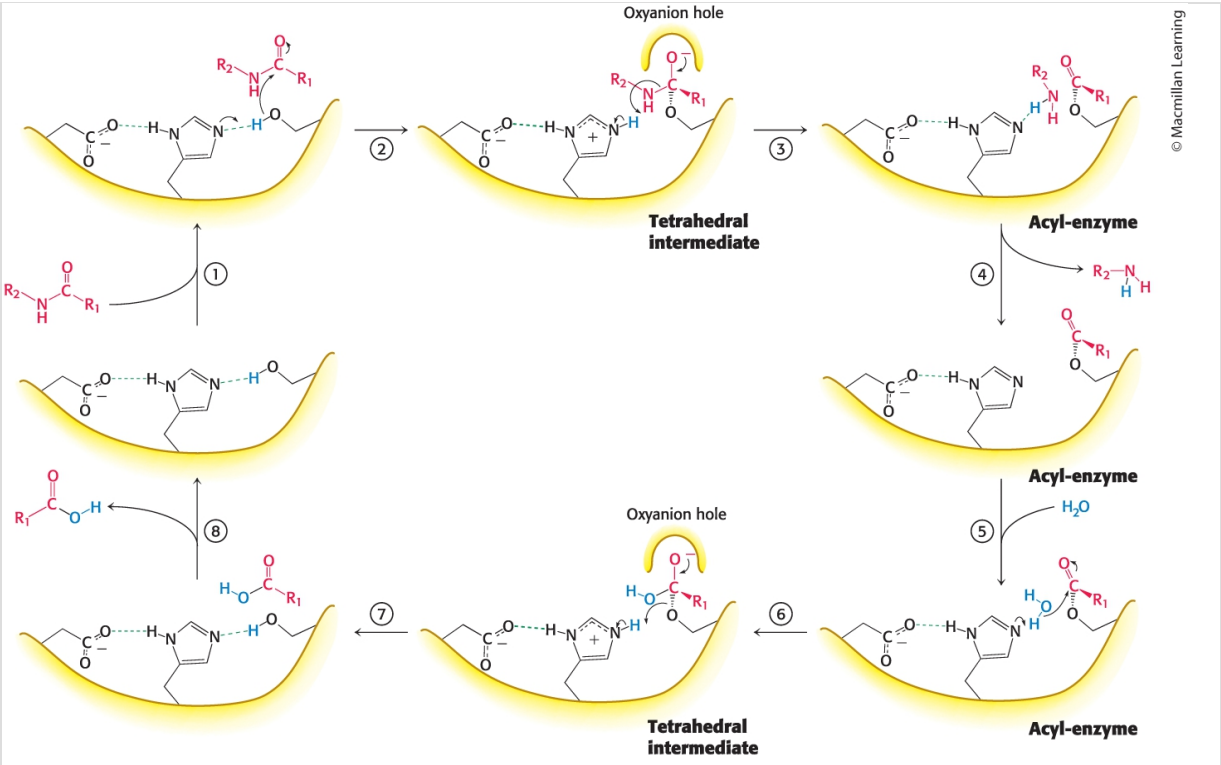


FIGURE 6.8 The mechanism of peptide hydrolysis illustrates the principles of covalent and acid–base catalysis. The mechanism proceeds in eight steps: (1) substrate binding, (2) nucleophilic attack of serine on the peptide carbonyl group, (3) collapse of the tetrahedral

intermediate, (4) release of the amine component, (5) water binding, (6) nucleophilic attack of water on the acyl-enzyme intermediate, (7) collapse of the tetrahedral intermediate, and (8) release of the carboxylic acid component. The dashed green lines represent hydrogen bonds.

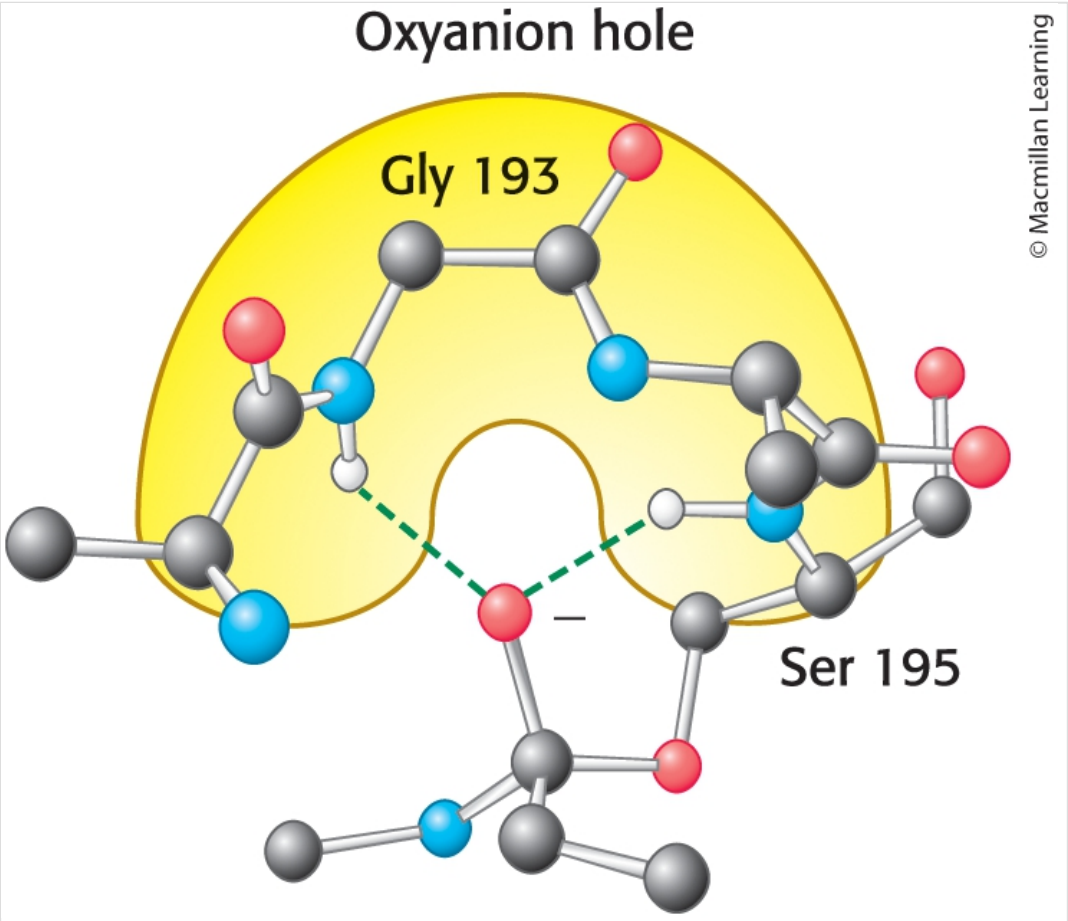


FIGURE 6.9 The oxyanion hole stabilizes the tetrahedral intermediates that occur during the chymotrypsin reaction. Note the hydrogen bonds (shown in green) that link peptide NH groups and the negatively charged oxygen atom of the intermediate.

The next stage — deacylation — begins when a water molecule takes the place occupied earlier by the amine component of the substrate (step 5).

The ester group of the acyl-enzyme is now hydrolyzed by a process that essentially repeats steps 2 through 4. Again acting as a general base catalyst, histidine 57 draws a proton away from the water molecule. The resulting OH^- ion attacks the carbonyl carbon atom of the acyl group, forming a tetrahedral intermediate (step 6). This structure breaks down to form the carboxylic acid product (step 7). Finally, the release of the carboxylic acid product (step 8) readies the enzyme for another round of catalysis.

This mechanism accounts for all characteristics of chymotrypsin action except the observed preference for cleaving the peptide bonds just past residues with large, hydrophobic side chains. Examination of the three-dimensional structure of chymotrypsin with substrate analogs and enzyme inhibitors reveals the presence of a deep hydrophobic pocket, called the S_1 pocket, into which the long, uncharged side chains of residues such as phenylalanine and tryptophan can fit. The binding of an appropriate side chain into this pocket positions the adjacent peptide bond into the active site for cleavage (**Figure 6.10**). The bond to be cleaved is called the **scissile bond**.

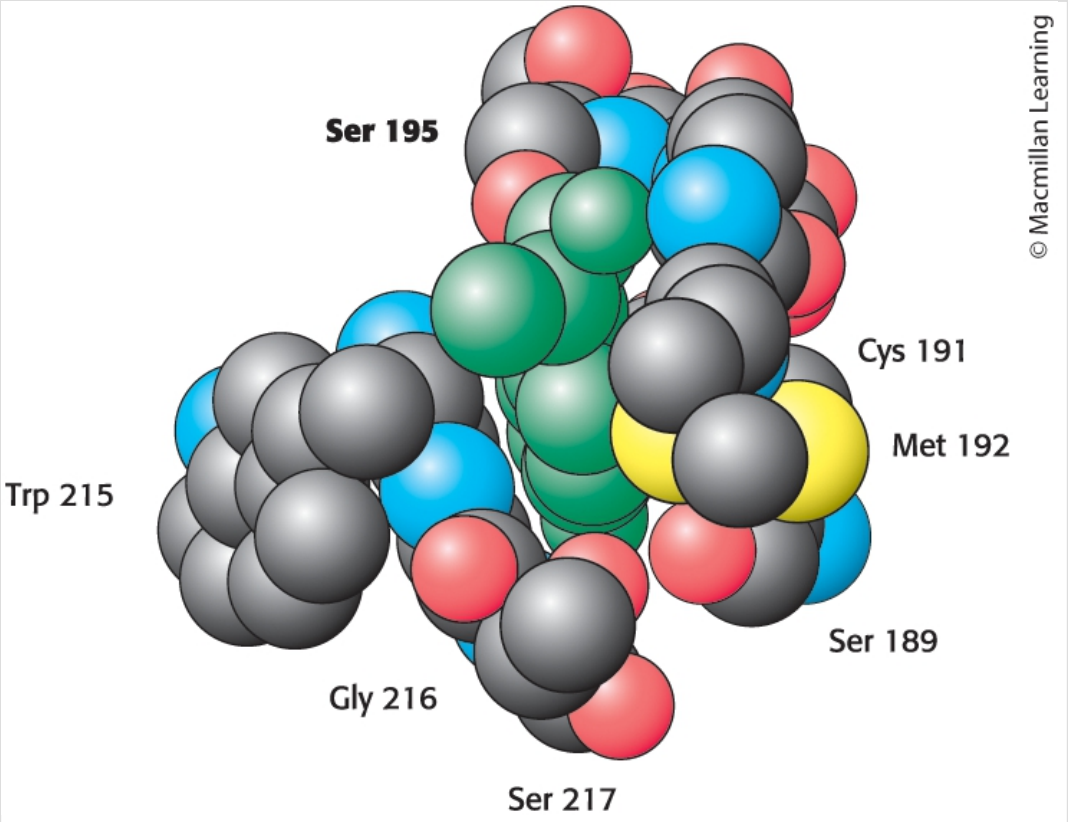


FIGURE 6.10 The specificity pocket of chymotrypsin favors the binding of residues with long hydrophobic side chains. The pocket is deep and lined with hydrophobic residues, with active-site serine residue (serine 195) positioned to cleave the peptide backbone between the residue bound in the pocket (in this case, phenylalanine, shown in green) and the next residue in the sequence.

The specificity of chymotrypsin depends almost entirely on which amino acid is directly on the amino-terminal side of the peptide bond to be cleaved, but other proteases have more-complex specificity patterns. Such enzymes have additional pockets on their surfaces for the recognition of other residues in the substrate. Figure 6.11 shows a generic example of the nomenclature used in diagramming protease-substrate interactions. Residues on the amino-terminal side of the scissile bond are labeled P_1, P_2, P_3, and so forth, heading away from the scissile bond. Likewise, residues on the carboxyl side of the scissile

bond are labeled P_1', P_2', P_3', and so forth. The corresponding sites on the enzyme are referred to as S_1, S_2 or S_1', S_2', and so forth.

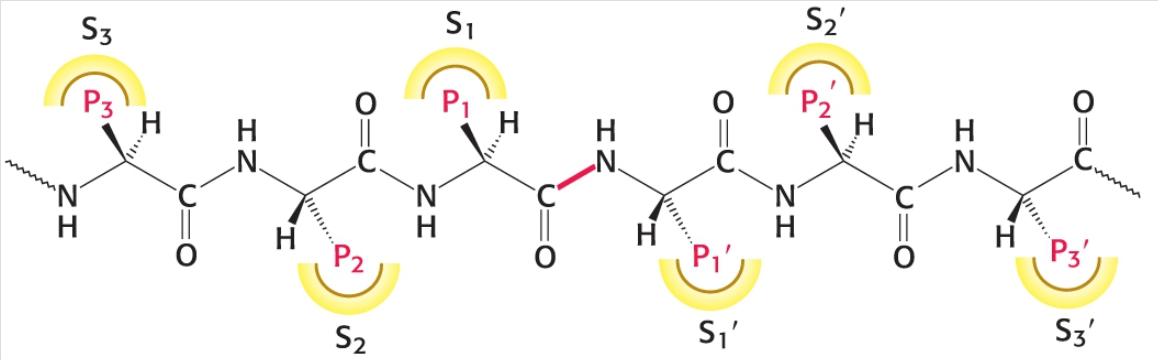


FIGURE 6.11 The specificity nomenclature for protease–substrate interactions shows the potential sites of interaction. The protease site is designated P, and the corresponding binding sites on the enzyme are designated S. The scissile bond (shown in red) is the reference point.

Catalytic triads are found in other hydrolytic enzymes

Many other peptide-cleaving proteins have subsequently been found to contain catalytic triads similar to that discovered in chymotrypsin. Some, such as trypsin and elastase, are obvious homologs of chymotrypsin; that is, they clearly evolved from a common ancestor. The sequences of these proteins are approximately 40% identical with that of chymotrypsin, and their overall structures are quite similar (Figure 6.12). These proteins operate by mechanisms identical with that of chymotrypsin. However, the three enzymes differ markedly in substrate specificity. Chymotrypsin cleaves at the peptide bond after residues with an aromatic or long, nonpolar side chain. Trypsin cleaves at the peptide bond after residues with long, positively charged side

chains — namely, arginine and lysine. Elastase cleaves at the peptide bond after amino acids with small side chains — such as alanine and serine.

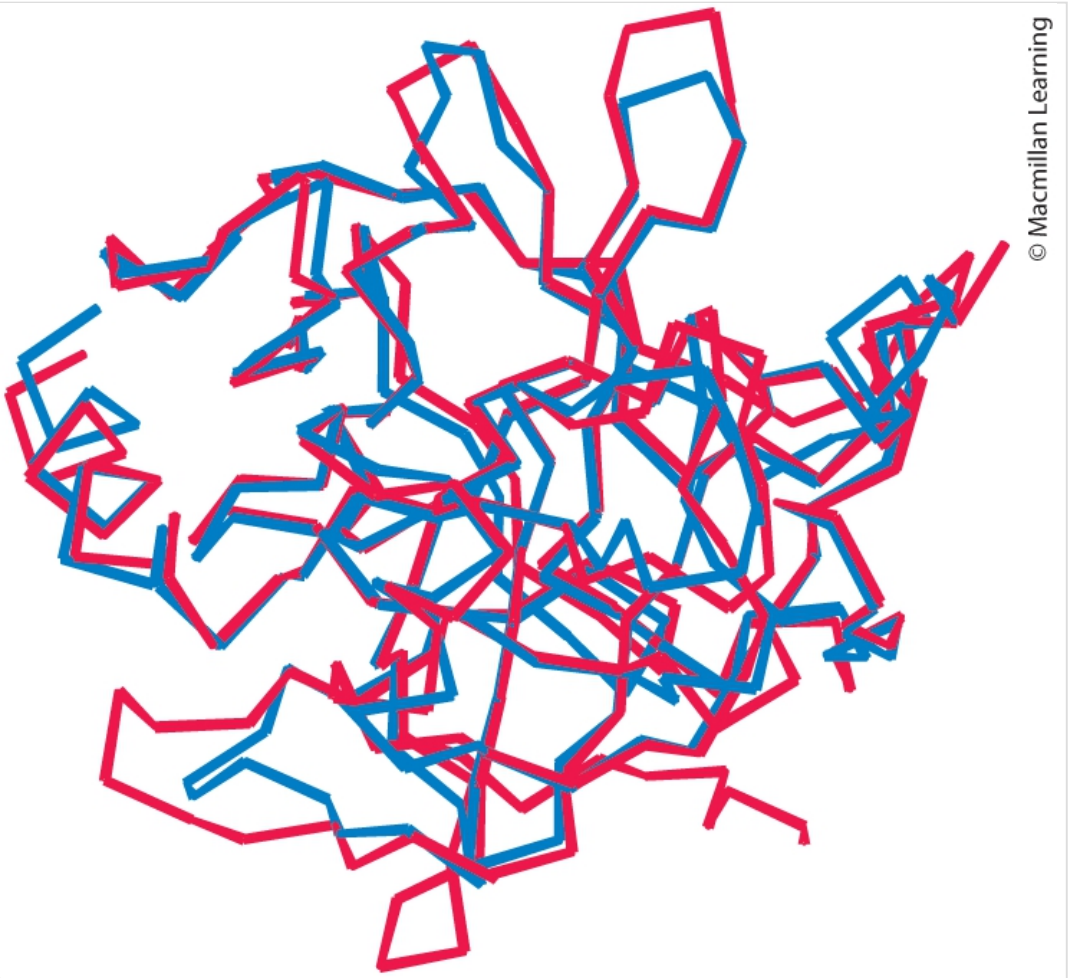


FIGURE 6.12 Chymotrypsin and trypsin are structurally similar. This similarity is revealed by overlaying the structures of chymotrypsin (red) and trypsin (blue). Only α-carbon-atom positions are shown. The mean deviation in position between corresponding α-carbon atoms is quite small, only 1.7 Å.

[Drawn from 5PTP.pdb and 1GCT.pdb.]

INTERACT with this model in Achieve

Comparison of the S_1 pockets of these enzymes reveals that these different specificities are due to small structural differences. In trypsin, an aspartate residue (Asp 189) is present at the bottom of the S_1 pocket in place of a serine residue in chymotrypsin. The aspartate residue attracts and stabilizes a positively charged arginine or lysine residue in the substrate. In elastase, two residues at the top of the pocket in chymotrypsin and trypsin are replaced by much bulkier valine residues (Val 190 and Val 216). These residues close off the mouth of the pocket so that only small side chains can enter (Figure 6.13).

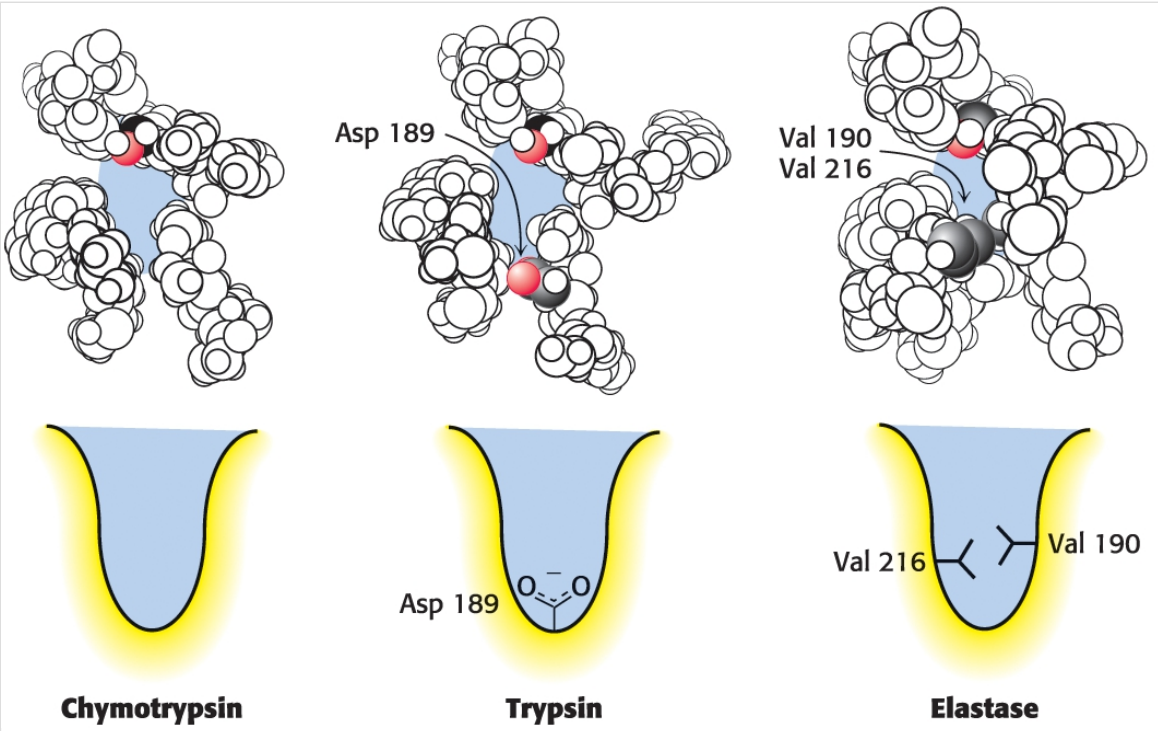


FIGURE 6.13 The S_1 pockets of chymotrypsin, trypsin, and elastase show the residues that play key roles in determining enzyme specificity. The side chains of these residues, as well as those of the active-site serine residues, are shown in color, and schematic depictions are shown below.

Other members of the chymotrypsin family include a collection of proteins that take part in blood clotting, to be discussed in Chapter 7, as well as the tumor marker protein prostate-specific antigen (PSA). In addition, a wide range of proteases found in bacteria, viruses, and plants belong to this clan.

Other enzymes that are not homologs of chymotrypsin have been found to contain very similar active sites to that of chymotrypsin, not because of a shared common ancestor, but because a similar active evolved independently. Subtilisin, a protease in bacteria such as *Bacillus amyloliquefaciens*, is a particularly well-characterized example. The active site of this enzyme includes both the catalytic triad and the oxyanion hole. However, one of the NH groups that forms the oxyanion hole comes from the side chain of an asparagine residue rather than from the peptide backbone (**Figure 6.14**). Subtilisin is the founding member of another large family of proteases. Still other proteases have been discovered that contain an active-site serine or threonine residue that is activated not by a histidine–aspartate pair but by a primary amino group from the side chain of lysine or by the N-terminal amino group of the polypeptide chain.

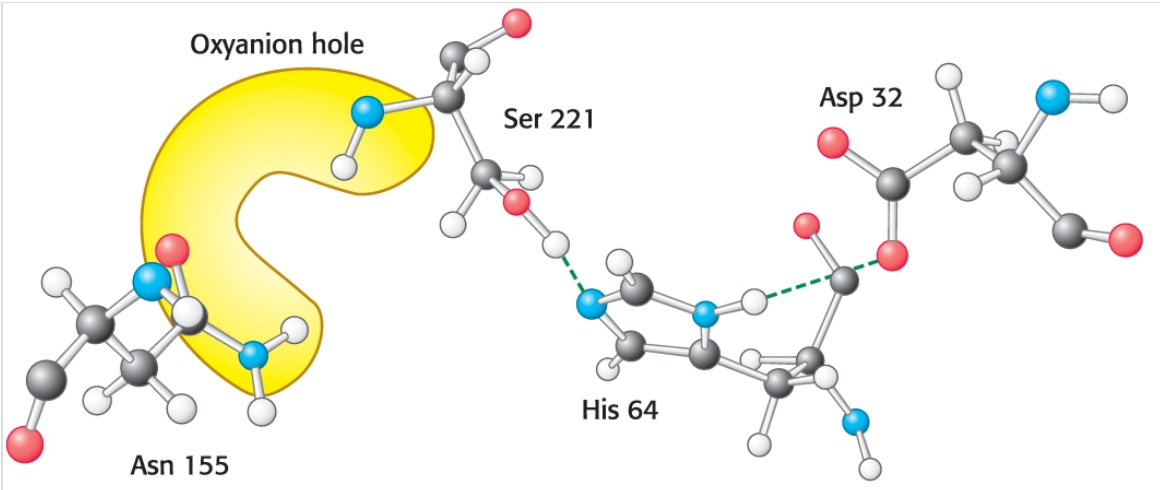


FIGURE 6.14 The catalytic triad and oxyanion hole of subtilisin includes two NH groups, one from the backbone and one from the side chain of Asn 155. The NH groups will stabilize a negative charge that develops on the peptide bond attacked by nucleophilic serine 221 of the catalytic triad.

The catalytic triad in proteases has clearly emerged several times in the course of evolution. We can conclude that this catalytic strategy must be an especially effective approach to the hydrolysis of peptides and related bonds.

Scientists have dissected the catalytic triad using site-directed mutagenesis

How can we test the validity of the mechanism proposed for the catalytic triad? One way is to test the contribution of individual amino acid residues to the catalytic power of a protease by using site-directed mutagenesis. Subtilisin has been extensively studied by this method. Each of the residues within the catalytic triad, consisting of aspartic acid 32, histidine 64, and serine 221, has been individually converted into alanine, and the ability of each mutant enzyme to cleave a model substrate has been examined (**Figure 6.15**).

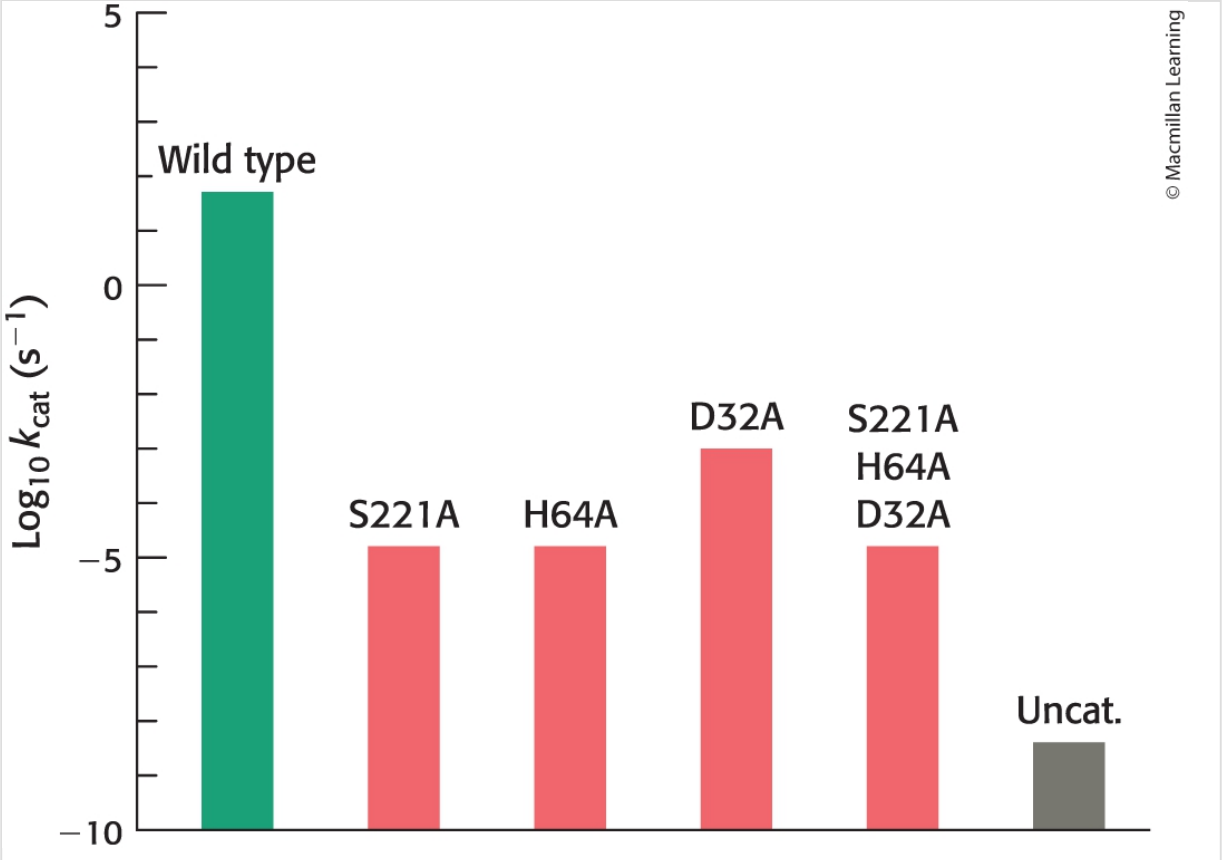


FIGURE 6.15 Mutating the residues of the catalytic triad to alanine allows the importance of each residue for catalytic activity to be quantified. Note that the activities are displayed on a logarithmic scale. The mutations are identified as follows: the first letter is the one-letter abbreviation for the amino acid being altered; the number identifies the position of the residue in the primary structure; and the second letter is the one-letter abbreviation for the amino acid replacing the original one. *Uncat.* refers to the estimated rate for the uncatalyzed reaction.

As expected, the conversion of active-site serine 221 into alanine dramatically reduces catalytic power; the value of k_{cat} falls to less than one millionth of its value for the wild-type enzyme. The value of K_M is essentially unchanged; its increase by no more than a factor of two indicates that substrate continues to bind normally. The mutation of histidine 64 to alanine reduces catalytic power to a similar degree. The conversion of aspartate 32 into alanine reduces catalytic power by less, although the value of k_{cat} still falls to less than 0.005% of its wild-type

value. The simultaneous conversion of all three residues into alanine is no more deleterious than the conversion of serine or histidine alone. These observations support the notion that the catalytic triad and, particularly, the serine–histidine pair act together to generate a nucleophile of sufficient power to attack the carbonyl carbon atom of a peptide bond. Despite the reduction in their catalytic power, the mutated enzymes still hydrolyze peptides a thousand times as fast as buffer at pH 8.6.

Site-directed mutagenesis also offers a way to probe the importance of the oxyanion hole for catalysis. The mutation of asparagine 155 to glycine eliminates the side-chain NH group from the oxyanion hole of subtilisin. The elimination of the NH group reduces the value of k_{cat} to 0.2% of its wild-type value but increases the value of K_M by only a factor of two. These observations demonstrate that the NH group of the asparagine residue plays a significant role in stabilizing the tetrahedral intermediate and the transition state leading to it.

Some proteases cleave peptides at other locations besides serine residues

Not all proteases use strategies based on activated serine residues. Classes of proteins have been discovered that employ three alternative approaches to peptide-bond hydrolysis. In each case, the strategy is to generate a nucleophile that attacks the peptide carbonyl group (**Figure 6.16**).

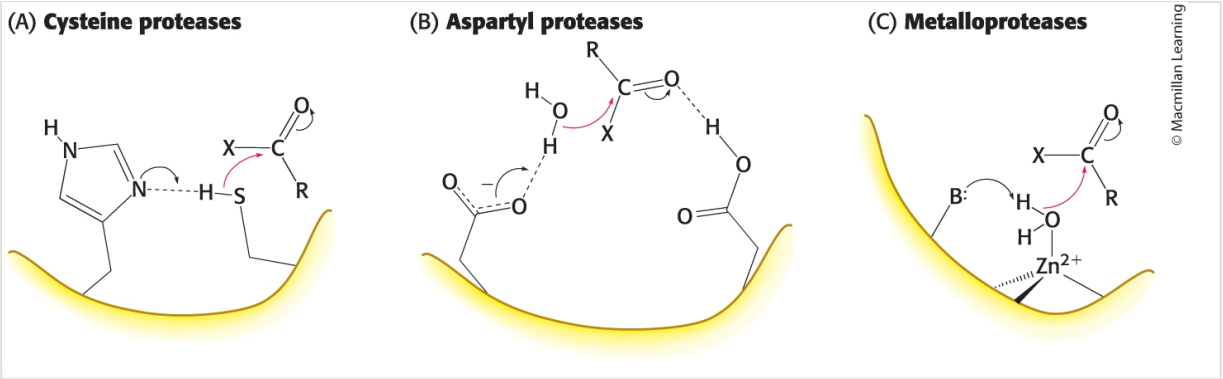


FIGURE 6.16 The key steps employed by the three classes of proteases reveal three different catalytic strategies. The peptide carbonyl group is attacked by (A) a histidine-activated cysteine in the cysteine proteases, (B) an aspartate-activated water molecule in the aspartyl proteases, and (C) a metal-activated water molecule in the metalloproteases. For the metalloproteases, the letter B represents a base (often glutamate) that helps deprotonate the metal-bound water.

Cysteine proteases

The strategy used by the cysteine proteases is most similar to that used by the chymotrypsin family. In these enzymes, a cysteine residue, activated by a histidine residue, plays the role of the nucleophile that attacks the peptide bond in a manner quite analogous to that of the serine residue in serine proteases (Figure 6.16). Because the sulfur atom in cysteine is inherently a better nucleophile than is the oxygen atom in serine, cysteine proteases appear to require only this histidine residue in addition to cysteine and not the full catalytic triad.

Aspartyl proteases

The central feature of the active sites in aspartyl proteases is a pair of aspartic acid residues that act together to allow a water molecule to attack the peptide bond. One aspartic acid residue (in its deprotonated form) activates the attacking water molecule by poising it for deprotonation. The other aspartic acid residue (in its protonated form)

polarizes the peptide carbonyl group so that it is more susceptible to attack (Figure 6.16).

Metalloproteases

The active site of a metalloprotease contains a bound metal ion, most often zinc, that activates a water molecule to act as a nucleophile to attack the peptide carbonyl group. In each of these three classes of enzymes, the active site includes features that act to (1) activate a water molecule or another nucleophile, (2) polarize the peptide carbonyl group, and (3) stabilize a tetrahedral intermediate (Figure 6.16).

Self-Check Question



Write out a mechanism for a cysteine protease analogous with that for chymotrypsin.

Protease inhibitors are important drugs



Because of the fundamental biological roles of proteases, these enzymes are important drug targets. Drugs that block protease activity are called **protease inhibitors**. For example, captopril, a drug used to regulate blood pressure, is one of many inhibitors of the angiotensin-converting enzyme (ACE), a metalloprotease. Indinavir (Crixivan), retrovir, and many other compounds used in the treatment of AIDS are inhibitors of HIV protease, an aspartyl protease. HIV protease cleaves multidomain

viral proteins into their active forms; blocking this process completely prevents the virus from being infectious. HIV protease inhibitors, in combination with inhibitors of other key HIV enzymes, have dramatically reduced deaths due to AIDS, assuming that the cost of the treatment could be covered. In many cases, these drugs have converted AIDS from a death sentence to a treatable chronic disease.

Indinavir, one of the first HIV protease inhibitors developed but not one that is widely used at present, reveals an important strategy for developing enzyme inhibitors. Indinavir was designed to resemble a peptide substrate of the enzyme. X-ray crystallographic studies revealed that indinavir adopts a confirmation that approximates the twofold symmetry of the enzyme (Figure 6.17). The active site of HIV protease is covered by two flexible flaps that fold down on top of the bound inhibitor. The OH group of the central alcohol interacts with the two aspartate residues of the active site and was intended to mimic a water molecule observed in crystal structures of HIV protease but generally absent in cellular aspartyl proteases. This OH group was intended to contribute to the specificity of indinavir for HIV protease. To prevent side effects, enzyme inhibitors used as drugs should be relatively specific for one enzyme, minimally inhibiting other similar enzymes within the body.

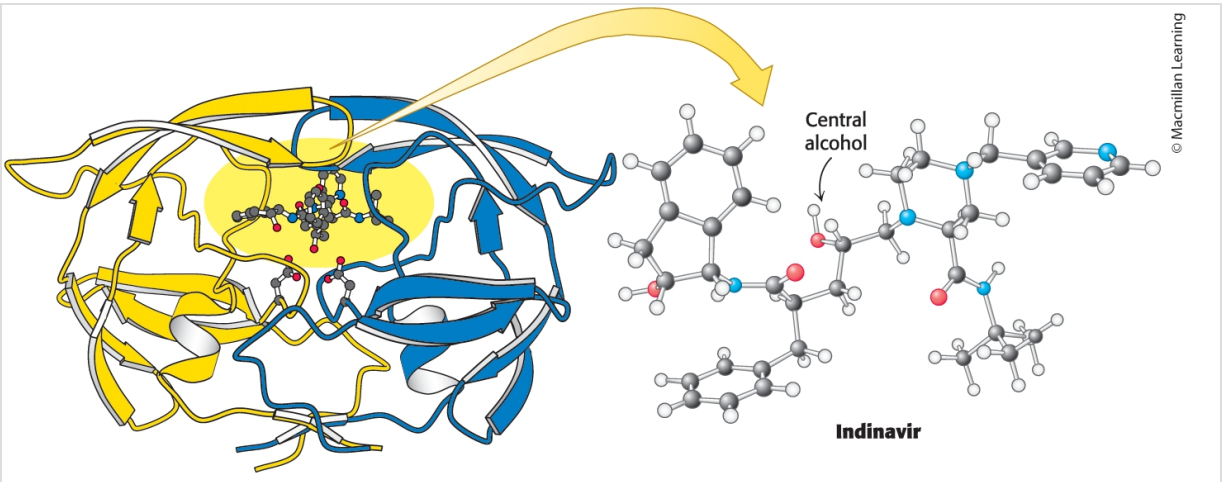


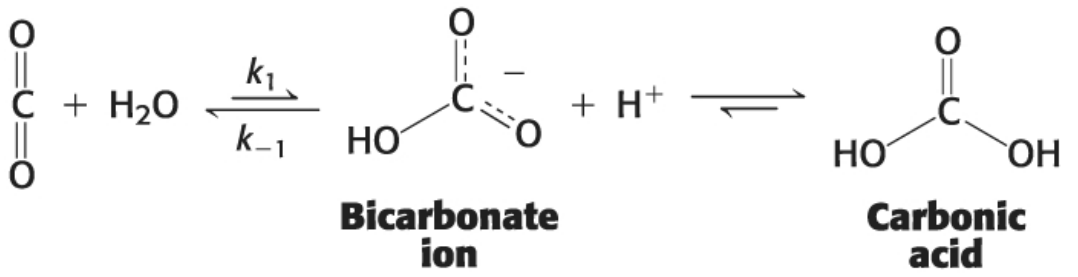
FIGURE 6.17 HIV protease has twofold symmetry. (Left) The three-dimensional structure of HIV protease is shown with the inhibitor indinavir bound in the active site. (Right) The drug has been rotated to reveal its approximately twofold symmetric conformation.

[Drawn from 1HSH.pdb.]

INTERACT with this model in Achieve

6.3 Carbonic Anhydrases Make a Fast Reaction Faster

Carbon dioxide is a major end product of aerobic metabolism. In mammals, this carbon dioxide is released into the blood and transported to the lungs for exhalation. While in the red blood cells, carbon dioxide reacts with water. The products of this reaction are bicarbonate ion (HCO_3^-) and a proton. These are a form of carbonic acid, H_2CO_3, a moderately strong acid, with $pK_a = 3.5$.



Even in the absence of a catalyst, this hydration reaction proceeds at a moderately fast pace. At 37°C near neutral pH, the second-order rate constant k_1 is $0.0027\ M^{-1}\ s^{-1}$. This value corresponds to an effective first-order rate constant of $0.15\ s^{-1}$ in water $([H_2O] = 55.5\ M)$. The reverse reaction, the dehydration of HCO_3^-, is even more rapid, with a rate constant of $k_{-1} = 50\ s^{-1}$. These rate constants correspond to an equilibrium constant of $K_1 = 5.4 \times 10^{-5}$ and a ratio of $[CO_2]$ to $[H_2CO_3]$ of 340:1 at equilibrium.

Carbon dioxide hydration and HCO_3^- dehydration are often coupled to rapid processes, particularly transport processes. Thus, almost all organisms contain enzymes, referred to as **carbonic anhydrases**, that increase the rate of reaction beyond the already relatively high spontaneous rate. For example, carbonic anhydrases dehydrate HCO_3^- in the blood to form CO_2 for exhalation as the blood passes through the lungs. Conversely, they convert CO_2 into HCO_3^- to generate the aqueous humor of the eye and other secretions. For this reason, one of the drugs used for treating glaucoma, a condition associated with too much pressure inside the eye, acts by inhibiting carbonic anhydrase. Furthermore, both CO_2 and HCO_3^- are substrates and products for a variety of enzymes, and the rapid interconversion of these species may be necessary to ensure appropriate substrate levels.

Carbonic anhydrases accelerate CO_2 hydration dramatically. The most-active enzymes hydrate CO_2 at rates as high as $k_{cat} = 10^6\ s^{-1}$, or a million times a second per enzyme molecule. Fundamental physical processes such as diffusion and proton transfer ordinarily limit the rate of hydration, and so the enzymes employ special strategies to attain such high rates.

Carbonic anhydrase contains a bound zinc ion essential for catalytic activity

Less than 10 years after the discovery of carbonic anhydrase in 1932, this enzyme was found to contain a bound zinc ion. Moreover, the zinc ion appeared to be necessary for catalytic activity. This discovery, remarkable at the time, made carbonic anhydrase the first known zinc-containing enzyme. At present, thousands of enzymes are known to contain zinc. In fact, more than one-third of all enzymes either contain bound metal ions or require the addition of such ions for activity.

Metal ions have several properties that increase chemical reactivity: their positive charges, their ability to form strong yet kinetically labile bonds, and, in some cases, their capacity to be stable in more than one oxidation state. The chemical reactivity of metal ions explains why catalytic strategies that employ metal ions have been adopted throughout evolution.

X-ray crystallographic studies have supplied the most detailed and direct information about the zinc site in carbonic anhydrase. At least seven carbonic anhydrases, each with its own gene, are present in human beings. They are all clearly homologous, as revealed by substantial sequence identity. Carbonic anhydrase II, a major protein component of red blood cells, has been the most extensively studied (Figure 6.18). It is also one of the most active carbonic anhydrases.

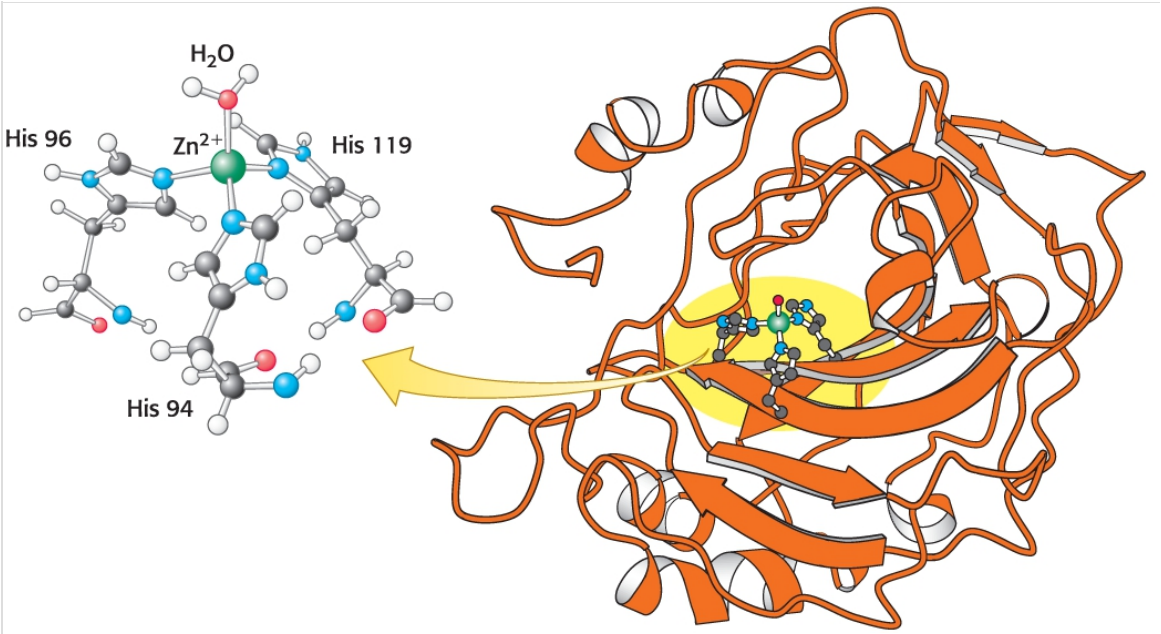


FIGURE 6.18 The active site of human carbonic anhydrase II includes a bound zinc ion. The active site includes a zinc ion that is bound to the imidazole rings of three histidine residues as well as to a water molecule in a cleft near the center of the enzyme.

[Drawn from 1CA2.pdb.]

INTERACT with this model in Achieve

Zinc is found only in the $^{+2}$ state in biological systems. A zinc atom is essentially always bound to four or more specific molecules or groups, called **ligands**. In carbonic anhydrase, three coordination sites are occupied by nitrogen ligands from the imidazole rings of three histidine residues, and an additional coordination site is occupied by a water molecule (or a hydroxide ion, depending on pH). Because the ligands occupying the coordination sites are neutral, the overall charge on the $Zn(His)_3$ unit remains $^{+2}$.

Catalysis involves zinc activation of a water molecule

How does this zinc complex facilitate carbon dioxide hydration? A major clue comes from the pH profile of enzymatically catalyzed carbon dioxide hydration (**Figure 6.19**). At pH 8, the reaction proceeds near its maximal rate. As the pH decreases, the rate of the reaction drops. The midpoint of this transition is near pH 7, suggesting that a group that loses a proton at pH 7 $(pK_a = 7)$ plays an important role in the activity of carbonic anhydrase. Moreover, the curve suggests that the deprotonated (high pH) form of this group participates more effectively in catalysis. Although some amino acids, notably histidine, have pK_a values near 7, a variety of evidence suggests that the group responsible for this transition is not an amino acid but is the zinc-bound water molecule.

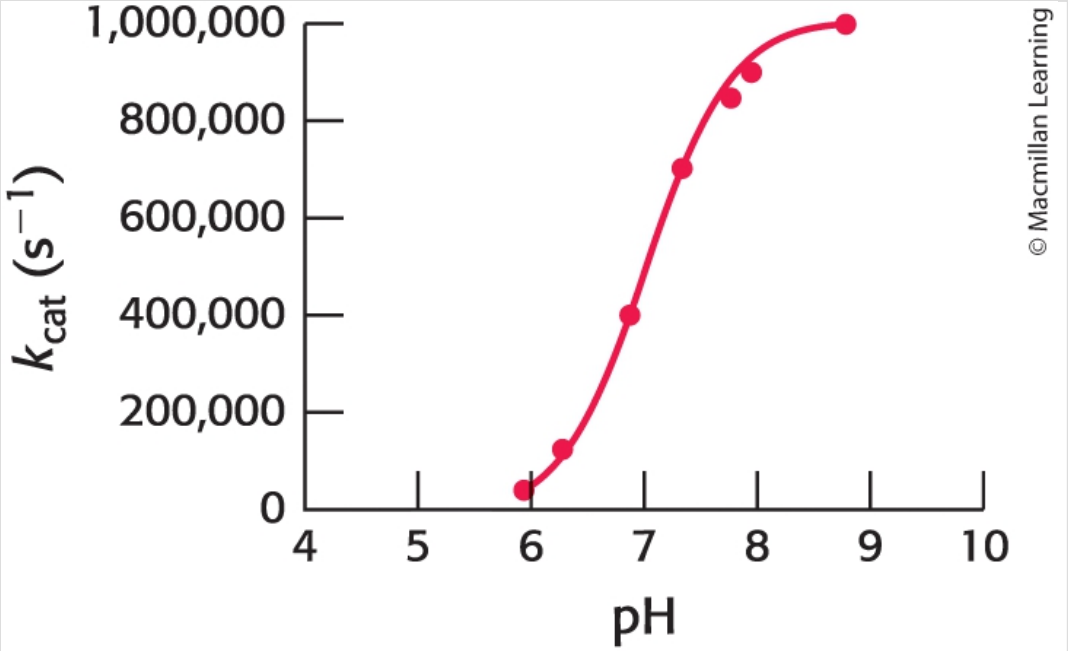


FIGURE 6.19 The activity of carbonic anhydrase varies with pH. The enzyme is maximally active at pH values near 9.

The binding of a water molecule to the positively charged zinc center reduces the pK_a of the water molecule from 15.7 to 7 (Figure 6.20). With the pK_a lowered, the water molecule can more easily lose a proton at neutral pH, generating a substantial concentration of hydroxide ion (bound to the zinc atom). A zinc-bound hydroxide ion (OH^-) is a potent nucleophile able to attack carbon dioxide much more readily than water does. Adjacent to the zinc site, carbonic anhydrase also possesses a hydrophobic patch that serves as a binding site for carbon dioxide (Figure 6.21). Based on these observations, a simple mechanism for carbon dioxide hydration can be proposed (Figure 6.22):

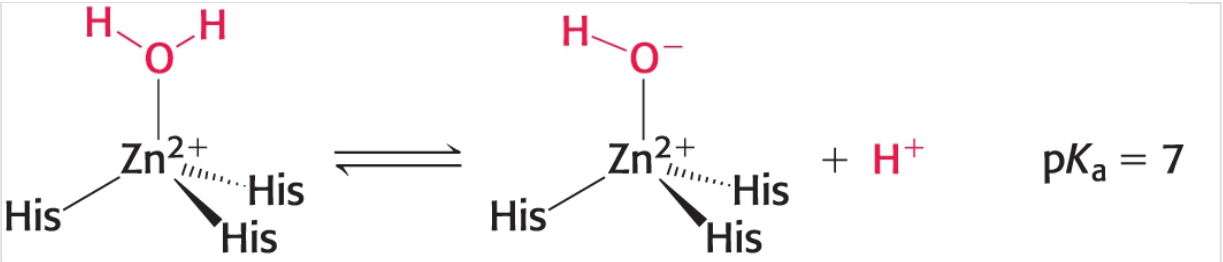


FIGURE 6.20 Upon binding to zinc in carbonic anhydrase, the pK_a of water decreases from 15.7 to approximately 7.

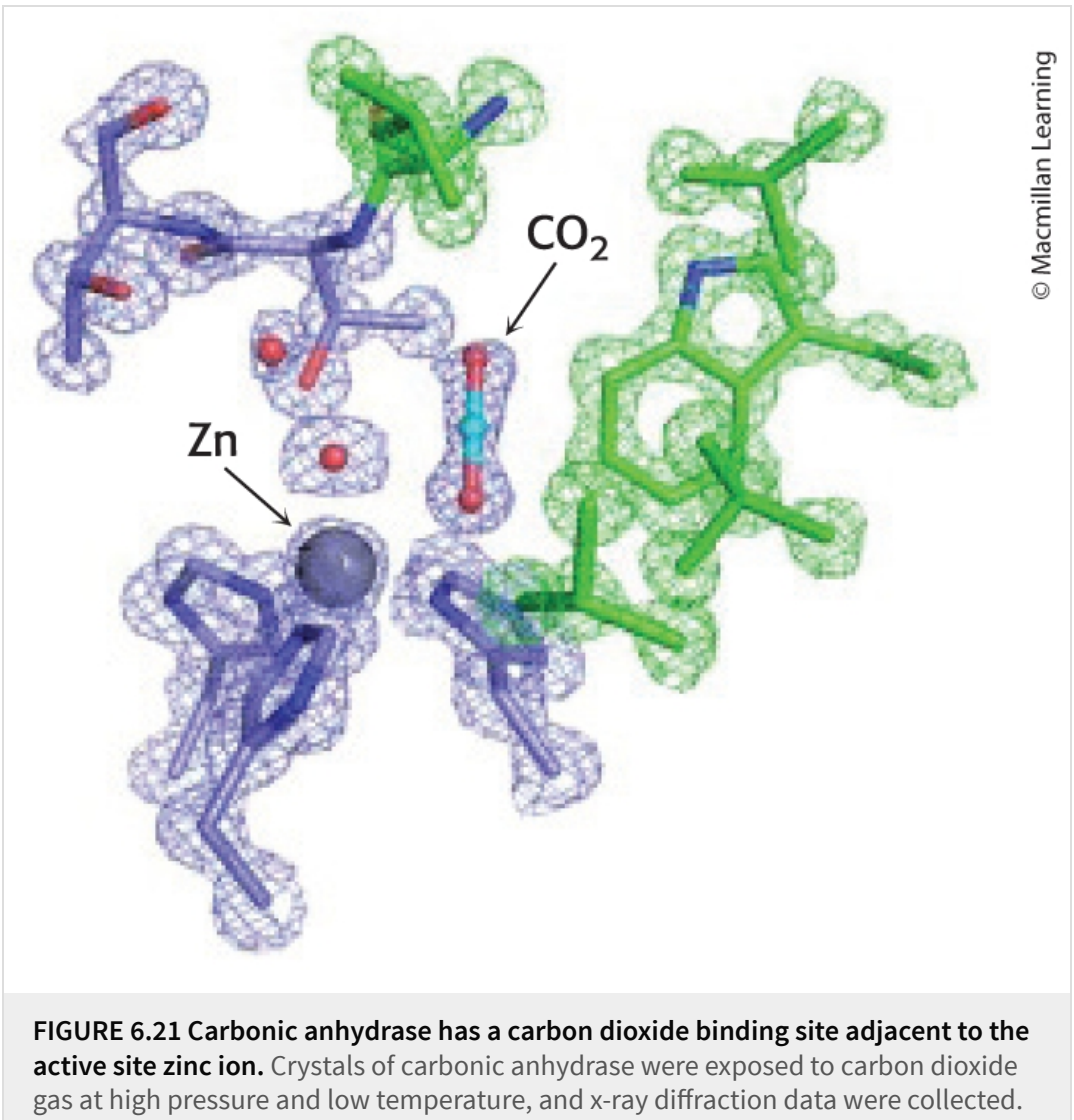


FIGURE 6.21 Carbonic anhydrase has a carbon dioxide binding site adjacent to the active site zinc ion. Crystals of carbonic anhydrase were exposed to carbon dioxide gas at high pressure and low temperature, and x-ray diffraction data were collected.

The electron density (shown as cages) for carbon dioxide, clearly visible adjacent to the zinc and its bound water, reveals the carbon dioxide binding site. Hydrophobic amino acids are shaded green, and the purple ones are hydrophilic.

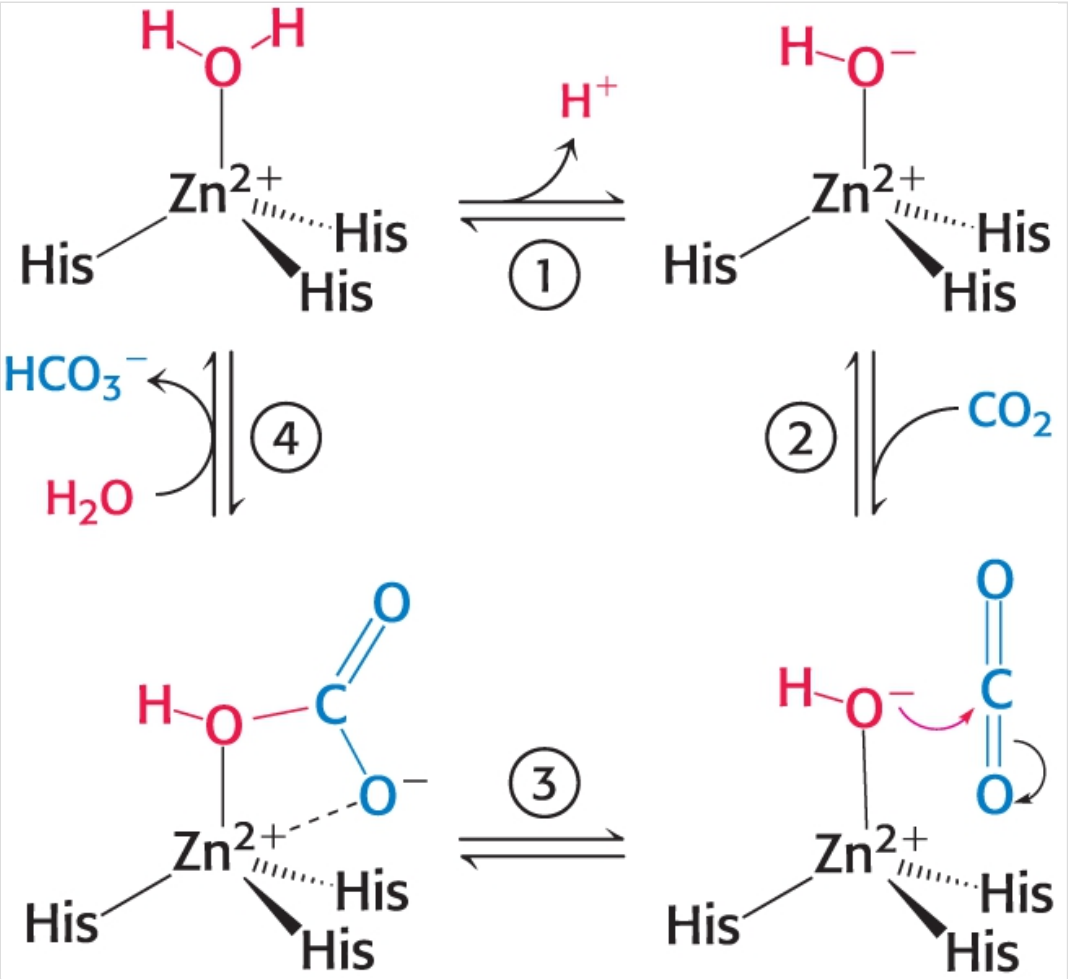


FIGURE 6.22 The zinc-bound hydroxide mechanism for the hydration of carbon dioxide proceeds in four steps. These are (1) water deprotonation, (2) carbon dioxide binding, (3) nucleophilic attack by hydroxide on carbon dioxide, and (4) displacement of bicarbonate ion by water. This mechanism provides a good example of one type of metal ion catalysis.

1. The zinc ion facilitates the release of a proton from a water molecule, which generates a hydroxide ion.
2. The carbon dioxide substrate binds to the enzyme's active site and is positioned to react with the hydroxide ion.
3. The hydroxide ion attacks the carbon dioxide, converting it into bicarbonate ion, HCO_3^-.
4. The catalytic site is regenerated with the release of HCO_3^- and the binding of another molecule of water.

Thus, the binding of a water molecule to the zinc ion favors the formation of the transition state by facilitating proton release and by positioning the water molecule to be in close proximity to the other reactant.

Rapid regeneration of the active form of carbonic anhydrase depends on proton availability

In the first step of a carbon dioxide hydration reaction, the zinc-bound water molecule must lose a proton to regenerate the active form of the enzyme (Figure 6.23). Let use consider this in detail:

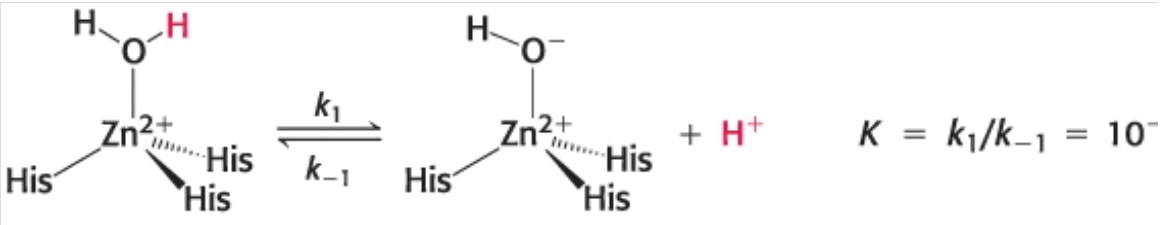


FIGURE 6.23 The ratio of the rate constant for water deprotonation to that for hydroxide protonation must equal 10^{-7}. This is true since the pK_a of this water molecule in carbonic anhydrase is 7.

- The equilibrium constant for this process is $K = 10^{-7}\ \mathrm{M}$ (since $\mathrm{p}K_a = 7$) and $K = k_1 / k_{-1}$.
- The rate of the reverse reaction, the protonation of the zinc-bound hydroxide ion, is limited by the rate of proton diffusion. Protons diffuse very rapidly with second-order rate constants near $10^{11}\ \mathrm{M}^{-1}\,\mathrm{s}^{-1}$.
- The forward rate constant is given by $k_1 = K \times k_{-1}$. Since $k_{-1} \leq 10^{11}\ \mathrm{M}^{-1}\,\mathrm{s}^{-1}$, k_1 must be less than or equal to $10^4\ \mathrm{s}^{-1}$.

As noted earlier, some carbonic anhydrases can hydrate carbon dioxide at rates as high as a million times a second $(10^6\ \mathrm{s}^{-1})$. This rate is so high that it seems to violate the analysis above. If carbon dioxide is hydrated at a rate of $10^6\ \mathrm{s}^{-1}$, then every step in the mechanism (Figure 6.22) must take place at least this fast. How is this apparent paradox resolved?

The role of buffers

The answer became clear with the observation that the highest rates of carbon dioxide hydration require the presence of buffer, suggesting that the buffer components participate in the reaction. The buffer can bind or release protons. The advantage is that, whereas the concentrations of protons and hydroxide ions are limited to $10^{-7}\ \mathrm{M}$ at neutral pH, the concentration of buffer components can be much higher, of the order of several millimolar. Let us consider the role of buffer components in more detail:

- If the buffer component BH^+ has a pK_a of 7 (matching that for the zinc-bound water molecule), then the equilibrium constant for the reaction in Figure 6.24 is 1.

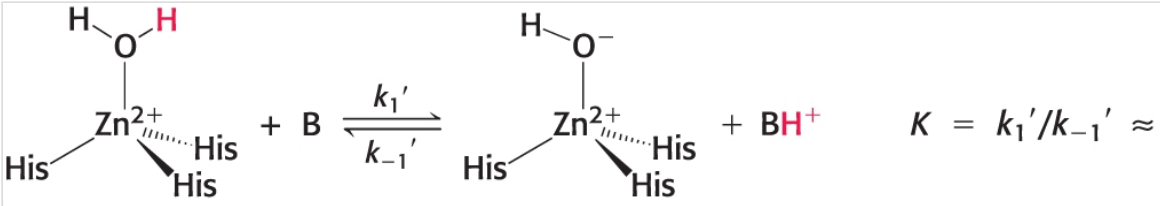


FIGURE 6.24 The deprotonation of the zinc-bound water molecule in carbonic anhydrase can be aided by buffer component B. This is optimized if the pK_a of the buffer is near 7 and if the buffer is present at a sufficiently high concentration.

- The second-order rate constants k_1' and k_{-1}' will be limited by buffer diffusion to values less than approximately $10^9\ M^{-1}\ s^{-1}$.
- The rate of proton abstraction is given by $k_1' \times [B]$.
- If buffer concentrations greater than $[B] = 10^{-3}\ M$ (or 1 mM) are used, then carbon dioxide hydration rates $\geq 10^6\ M^{-1}\ s^{-1}$ may be possible because

$$k_1' \times [B] = (10^9\ M^{-1}\ s^{-1}) \times (10^{-3}\ M) = 10^6\ s^{-1}$$

The prediction that the rate increases with increasing buffer concentration has been confirmed experimentally (Figure 6.25).

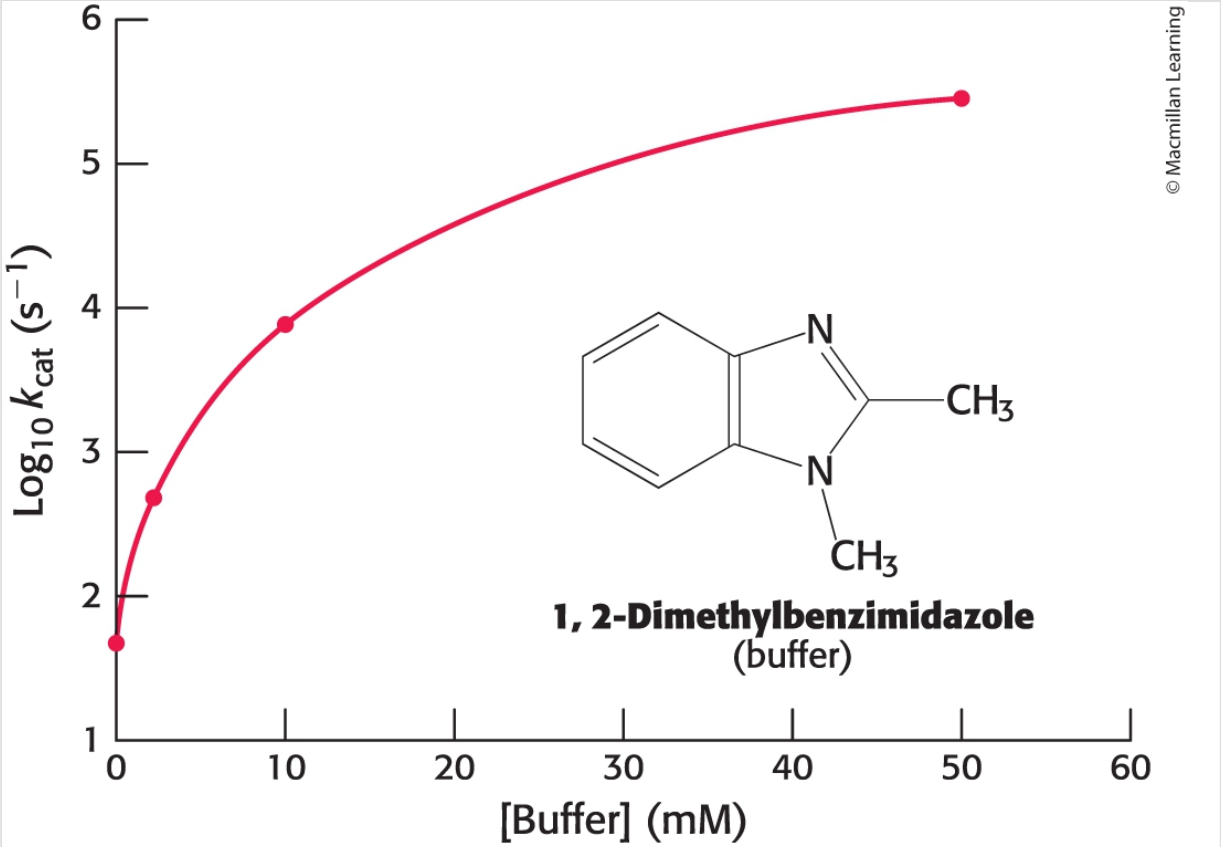


FIGURE 6.25 The rate of carbon dioxide hydration by carbonic anhydrase increases with the concentration of the buffer 1,2-dimethylbenzimidazole. If present at high enough concentrations, such buffers enable the enzyme to achieve its highest catalytic rates.

Self-Check Question

Suppose that the rate of CO_2 hydration is measured in 1 mM buffer at pH 7.0. What is the maximum expected rate?

A “proton shuttle” for large buffers

The molecular components of many buffers are too large to reach the active site of carbonic anhydrase. Carbonic anhydrase II has evolved a **proton shuttle** to allow buffer components to participate in the reaction from solution. The primary component of this shuttle is histidine 64. This residue transfers protons from the zinc-bound water molecule to the protein surface and then to the buffer (Figure 6.26). Thus, catalytic function has been enhanced through the evolution of an apparatus for controlling proton transfer from and to the active site. Because protons participate in many biochemical reactions, the manipulation of the proton inventory within active sites is crucial to the function of many enzymes and explains the prominence of acid–base catalysis.

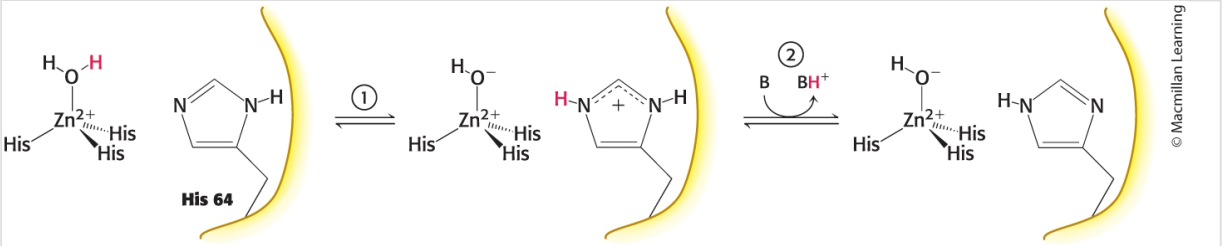


FIGURE 6.26 Histidine 64 acts as a proton shuttle. Histidine 64 (1) removes a proton from the zinc-bound water molecule and (2) transfers the proton to buffer molecules in solution.

6.4 Restriction Enzymes Catalyze Highly Specific DNA-Cleavage Reactions

We next consider a hydrolytic reaction that results in the cleavage of DNA. Bacteria and archaea have evolved mechanisms to protect themselves from viral infections. Many viruses inject their DNA genomes into cells; once inside, the viral DNA hijacks the cell's machinery to drive the production of viral proteins and, eventually, of progeny virus. Often, a viral infection results in the death of the host cell.

A major protective strategy for the host is to use **restriction enzymes** (also called **restriction endonucleases**) to degrade the viral DNA on its introduction into a cell. These enzymes recognize particular base sequences, called **recognition sequences** or recognition sites, in DNA molecules and cleave such molecules (hereafter referred to as *cognate DNA*) at defined positions. Restriction enzymes are best known because they are powerful tools for characterizing and manipulating DNA molecules, and their discovery was a key step that led to a revolution in molecular biology and genetic engineering. The most well-studied class of restriction enzymes comprises the type II restriction enzymes, which cleave DNA within their recognition sequences. Other types of restriction enzymes cleave DNA at positions somewhat distant from their recognition sites.

Restriction enzymes must show tremendous specificity at two levels:

1. *Restriction enzymes must cleave only DNA molecules that contain recognition sites, without cleaving DNA molecules that lack these sites.* Suppose that a recognition sequence is six base-pairs long. Because

there are 4^6, or 4096, sequences having six base pairs, the concentration of sites that must not be cleaved will be approximately 4000-fold higher than the concentration of sites that should be cleaved. Thus, to keep from damaging host DNA, restriction enzymes must cleave cognate DNA molecules much more than 4000 times as efficiently as they cleave nonspecific sites. We shall return to the mechanism used to achieve the necessary high specificity after considering the chemistry of the cleavage process.

2. *Restriction enzymes must not degrade host DNA containing the recognition sequences.* How do these enzymes manage to degrade viral DNA while sparing their own? In *E. coli*, the restriction endonuclease EcoRV cleaves double-stranded viral DNA molecules that contain the sequence $5'-GATATC-3'$, but it leaves intact host DNA containing hundreds of such sequences. We shall return to the strategy by which host cells protect their own DNA at the end of this section.

Cleavage is by direct displacement of $3'$-oxygen from phosphorus by magnesium-activated water

A restriction enzyme catalyzes the hydrolysis of the phosphodiester backbone of DNA. Specifically, the bond between the $3'$-oxygen atom and the phosphorus atom is broken. The products of this reaction are DNA strands with a free $3'$-hydroxyl group and a $5'$-phosphoryl group at the cleavage site (**Figure 6.27**). This reaction proceeds by nucleophilic attack at the phosphorus atom. We will consider two alternative mechanisms, suggested by analogy with the proteases.

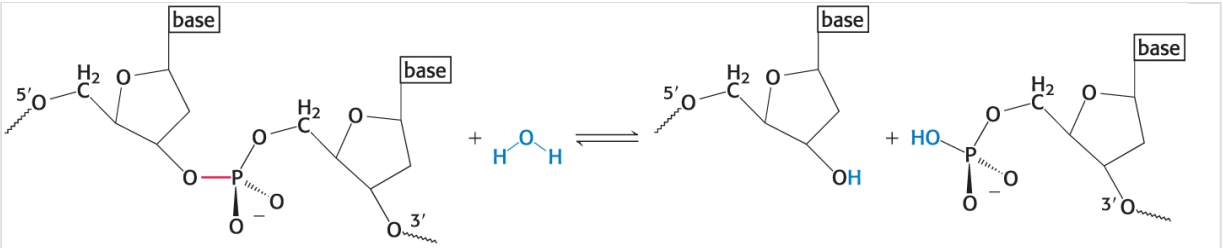
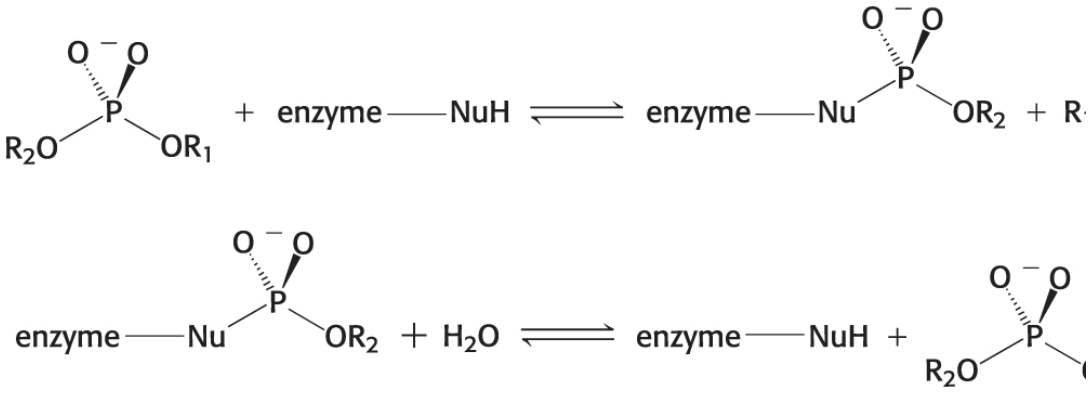
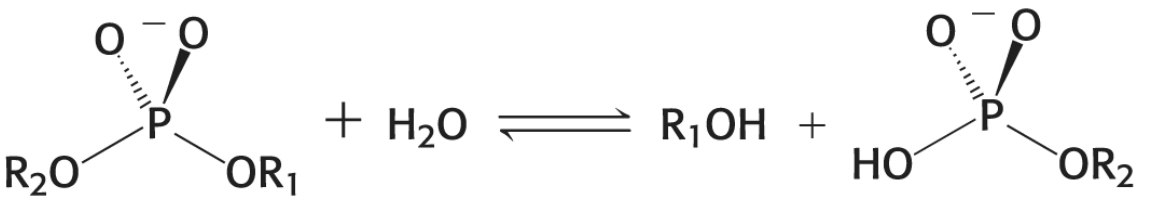


FIGURE 6.27 Restriction enzymes catalyze the hydrolysis of DNA phosphodiester bonds. The reaction leaves a hydroxyl group at the 3′ end of one product fragment and a phosphoryl group attached to the 5′ end of the other. The bond that is cleaved is shown in red.

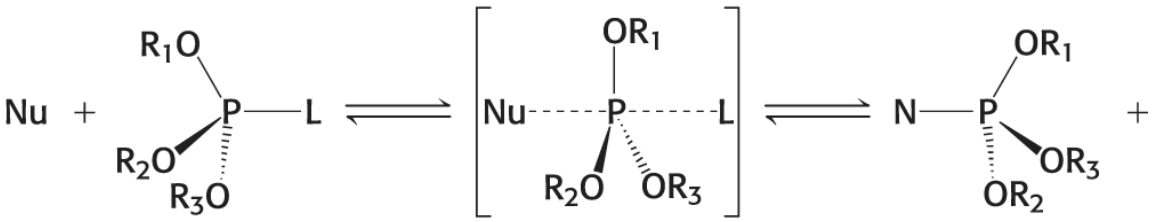
1. The restriction enzyme might cleave DNA through a covalent intermediate, employing a potent nucleophile (Nu):
   Mechanism 1 (covalent intermediate)



2. Alternatively, the restriction enzyme might cleave DNA through direct hydrolysis:
   Mechanism 2 (direct hydrolysis)



Each mechanism postulates a different nucleophile to attack the phosphorus atom. In either case, each reaction takes place by in-line displacement, in which the incoming nucleophile attacks the phosphorus atom, and a pentacoordinate transition state is formed:



The transition state has a trigonal bipyramidal geometry centered at the phosphorus atom, with the incoming nucleophile at one apex of the two pyramids and the group that is displaced (the leaving group, L) at the other apex. Note that the displacement inverts the stereochemical conformation at the tetrahedral phosphorous atom, analogous to the interconversion of stereoisomers around a tetrahedral carbon center.

The two mechanisms differ in the number of times that the displacement takes place in the course of the reaction:

1. In the first type of mechanism, a nucleophile in the enzyme (analogous to serine 195 in chymotrypsin) attacks the phosphate

group to form a covalent intermediate. Next, this intermediate is hydrolyzed to produce the final products. In this case, two displacement reactions take place at the phosphorus atom. Consequently, the stereochemical configuration at the phosphorus atom would be inverted and then inverted again, and the overall configuration would be retained.

2. In the second type of mechanism, analogous to that used by the aspartyl- and metalloproteases, an activated water molecule attacks the phosphorus atom directly. In this mechanism, a single displacement reaction takes place at the phosphorus atom. Hence, the stereochemical configuration at the phosphorus atom is inverted after cleavage.

One approach to determine which mechanism is correct involves examining potential changes in the stereochemistry at the phosphorus atom over the course of cleavage. However, this stereochemical change is not easily observed, because two of the groups bound to the phosphorus atom are simply oxygen atoms, identical with each other. This challenge can be overcome by replacing one oxygen atom with sulfur (producing a species called a phosphorothioate).

Let us consider EcoRV endonuclease. This enzyme cleaves the phosphodiester bond between the T and the A at the center of the recognition sequence $5'-GATATC-3'$. The first step is to synthesize an appropriate substrate for EcoRV containing phosphorothioates at the sites of cleavage (**Figure 6.28**). The reaction is then performed in water that has been greatly enriched in ^{18}O to allow the incoming oxygen atom to be tagged. The location of the ^{18}O label with respect to the sulfur atom indicates whether the reaction proceeds with inversion or retention of stereochemistry. This experiment reveals that the stereochemical configuration at the phosphorus atom is inverted only once with cleavage. This result is consistent with a direct attack by

water at the phosphorus atom and rules out the formation of any covalently bound intermediate (Figure 6.29).

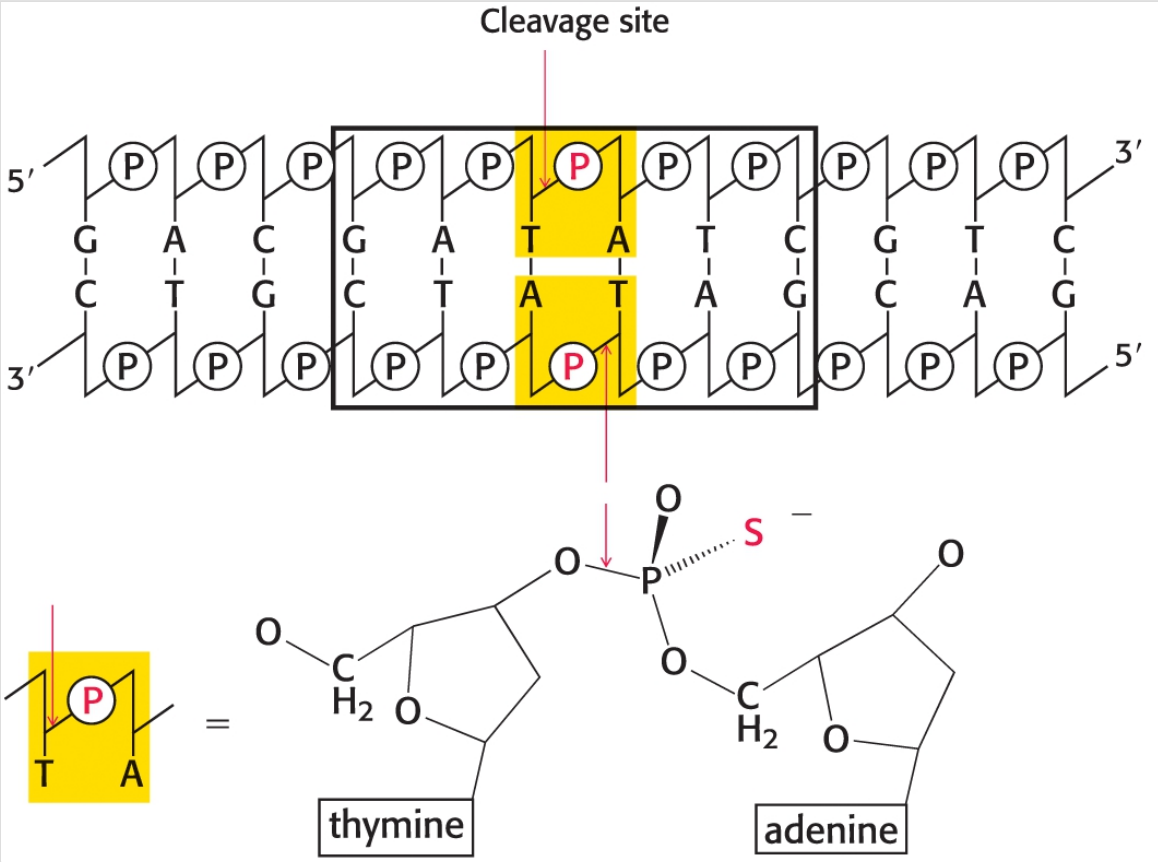


FIGURE 6.28 Phosphorothioate groups can be used to determine the overall stereochemical course of a displacement reaction. A phosphorothioate group has one of the nonbridging oxygen atoms replaced by a sulfur atom. Here, a phosphorothioate is placed at sites of cleavage by EcoRV endonuclease.

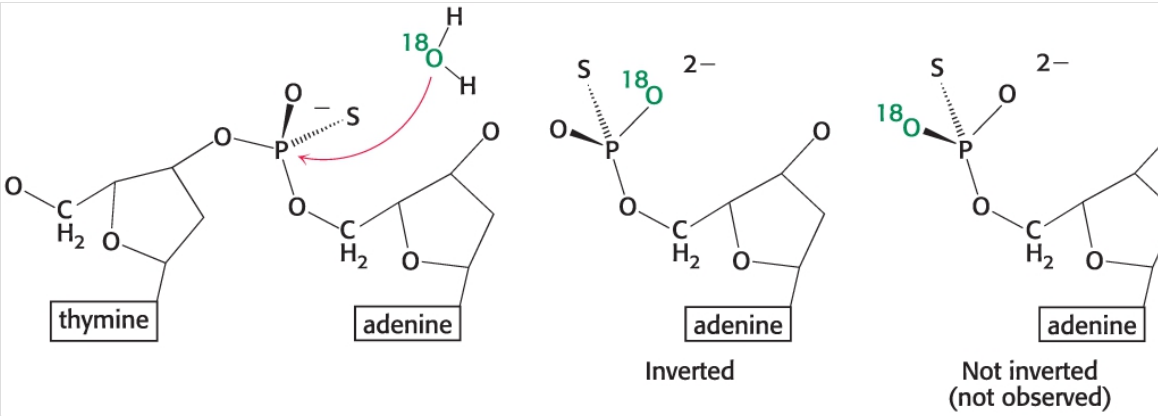


FIGURE 6.29 Cleavage of DNA by EcoRV endonuclease results in overall inversion of the stereochemical configuration at the phosphorus atom. This is indicated by the stereochemistr of the phosphorus atom bound to one bridging oxygen atom, one ^{16}O, one ^{18}O, and one sulfur atom. Two possible products are shown, only one of which is observed, indicating direct attack of water at the phosphorous atom.

Restriction enzymes require magnesium for catalytic activity

Many enzymes that act on phosphate-containing substrates require Mg^{2+} or some other similar divalent cation for activity. One or more Mg^{2+} (or similar) cations are essential to the function of restriction endonucleases. What are the functions of these metal ions?

Direct visualization of the complex between EcoRV endonuclease and cognate DNA molecules in the presence of Mg^{2+} by crystallization has been challenging, because the enzyme cleaves the substrate under these circumstances. Nonetheless, metal ion complexes can be visualized through several approaches. In one approach, crystals of

EcoRV endonuclease are prepared bound to oligonucleotides that contain the enzyme's recognition sequence. These crystals are grown in the absence of magnesium to prevent cleavage; after their preparation, the crystals are soaked in solutions containing the metal ion. Alternatively, crystals have been grown with the use of a mutated form of the enzyme that is less active. Finally, Mg^{2+} can be replaced by metal ions such as Ca^{2+} that bind but do not result in much catalytic activity. In all cases, no cleavage takes place, and so the locations of the metal ion-binding sites are readily determined.

As many as three metal ions per active site have been found. One ion-binding site is occupied in essentially all structures. This metal ion is coordinated to the protein through two aspartate residues and to one of the phosphate-group oxygen atoms at the site of cleavage. This metal ion binds the water molecule that attacks the phosphorus atom, helping to position and activate the water molecule in a manner similar to that for the Zn^{2+} ion of carbonic anhydrase (**Figure 6.30**).

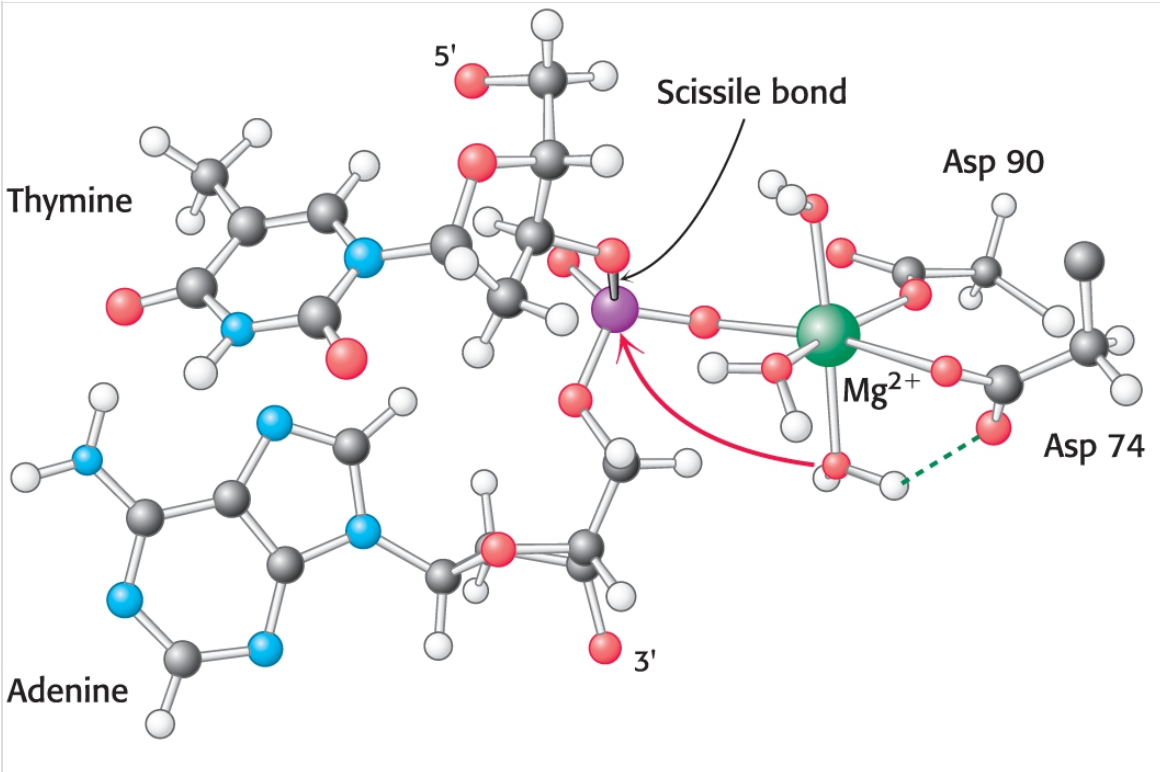


FIGURE 6.30 A magnesium ion forms a bridge between the enzyme and the DNA substrate. In this position, the ion helps activate a water molecule and position it so that it can attack the phosphorus atom at the cleavage site.

The complete catalytic apparatus is assembled only within complexes of cognate DNA molecules, ensuring specificity

We now return to the question of cleavage site-specificity, the defining feature of restriction enzymes.

The recognition sequences for most restriction enzymes are inverted repeats, giving the three-dimensional structure of the recognition site a twofold rotational symmetry, meaning that the structure is the same if rotated by $360^\circ/2 = 180^\circ$ (Figure 6.31). The restriction enzymes display a corresponding symmetry: they are dimers whose two subunits are related by an appropriate 180° rotation. The matching symmetry of the recognition sequence and the enzyme facilitates the recognition of cognate DNA by the enzyme. This similarity in structure has been confirmed by the determination of the structure of the complex between EcoRV endonuclease and DNA fragments containing its recognition sequence (Figure 6.32). The enzyme surrounds the DNA in a tight embrace.

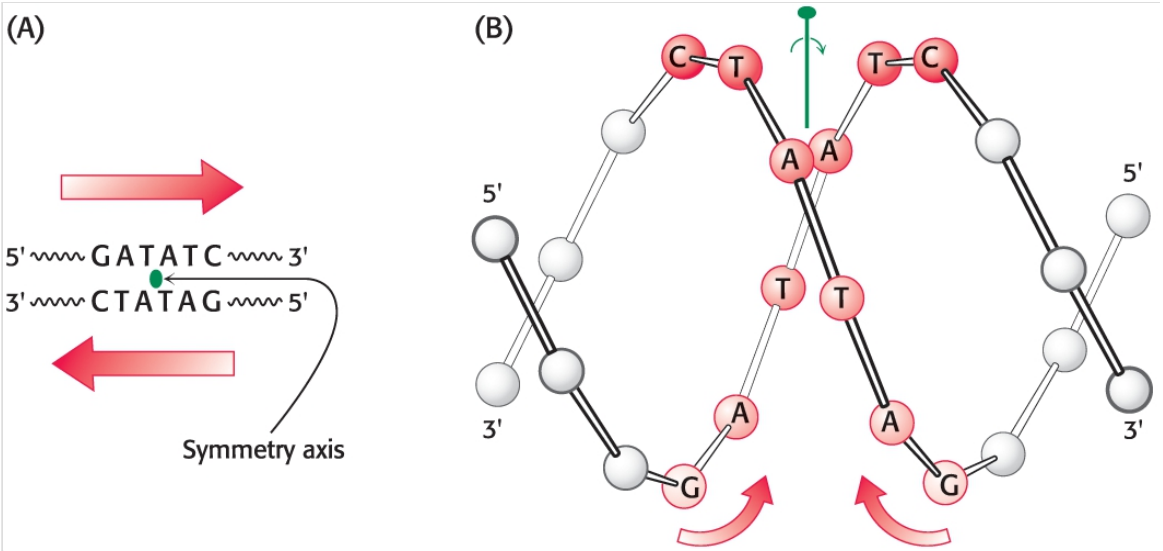


FIGURE 6.31 The recognition site for EcoRV displays twofold rotational symmetry. (A) The sequence of the recognition site, which is symmetric around the axis of rotation designated in green. (B) The inverted repeat within the recognition sequence of EcoRV (and most other restriction endonucleases) endows the DNA site with twofold rotational symmetry.

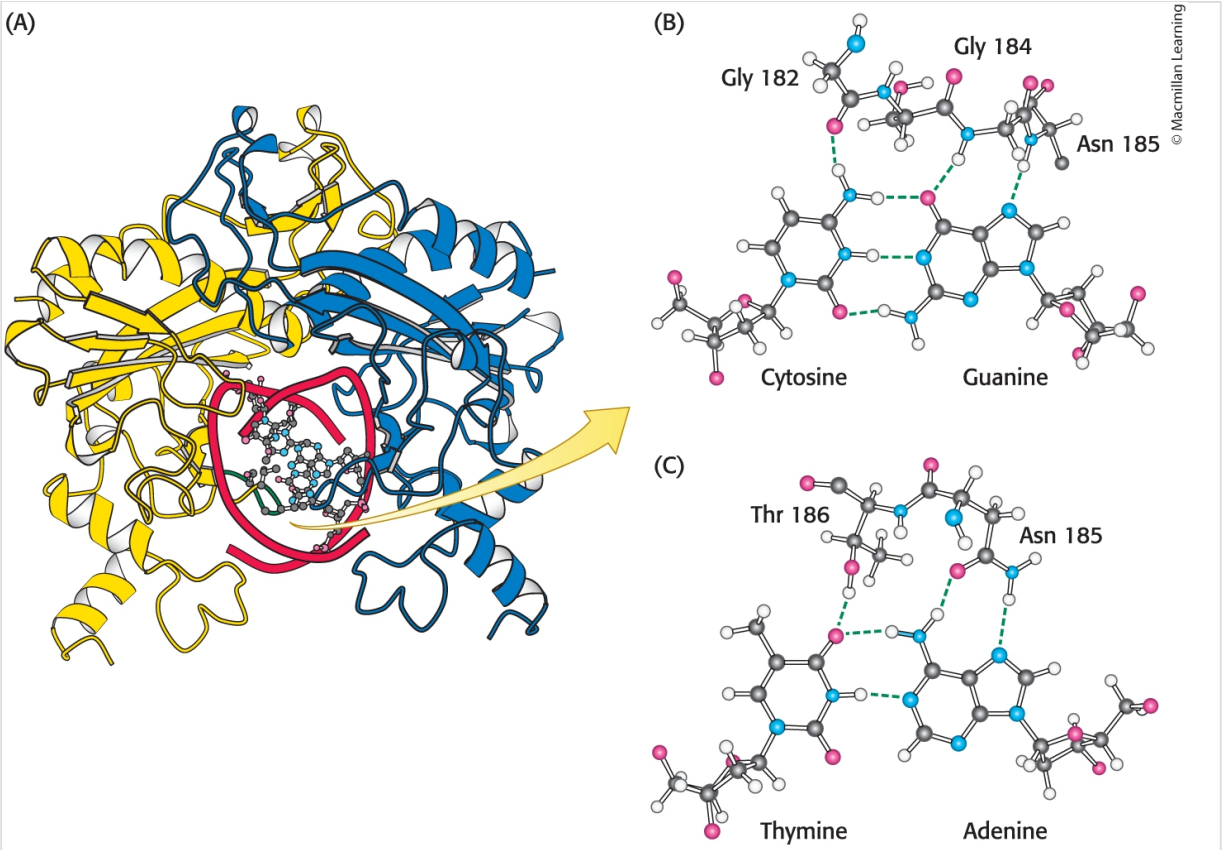


FIGURE 6.32 The three-dimensional structure of the complex between EcoRV and a cognate DNA molecule reveals interactions responsible for the sequence specificity. (A) This view of the structure of EcoRV endonuclease bound to a cognate DNA fragment is down the helical axis of the DNA. The two protein subunits are in yellow and blue, and the DNA backbone is in red. One of the DNA-binding loops of EcoRV endonuclease is shown interacting with the base pairs of its cognate DNA-binding site. Key amino acid residues are shown hydrogen-bonding with (B) a CG base pair and (C) an AT base pair.

[Drawn from 1RVB.pdb.]

INTERACT with this model in Achieve

Surprisingly, binding studies performed in the absence of magnesium have demonstrated that the EcoRV endonuclease binds to all sequences, both cognate and noncognate, with approximately equal affinity. Why, then, does the enzyme cleave only cognate sequences? The answer lies in a unique set of interactions between the enzyme and a cognate DNA

sequence. Within the $5'-GATATC-3'$ sequence, the G and A bases at the $5'$ end of each strand (and their Watson–Crick partners) directly contact the enzyme via hydrogen bonds with residues that are located in two loops, one projecting from the surface of each enzyme subunit (Figure 6.32). The most striking feature of this complex is the distortion of the DNA, which is substantially kinked in the center (**Figure 6.33**), whereas double-stranded DNA is normally straight. The central two TA base pairs in the recognition sequence play a key role in allowing the kink. They do not make contact with the enzyme but appear to be required because of their ease of distortion. The $5'-TA-3'$ sequence is known to be among the most easily deformed base-pair steps.

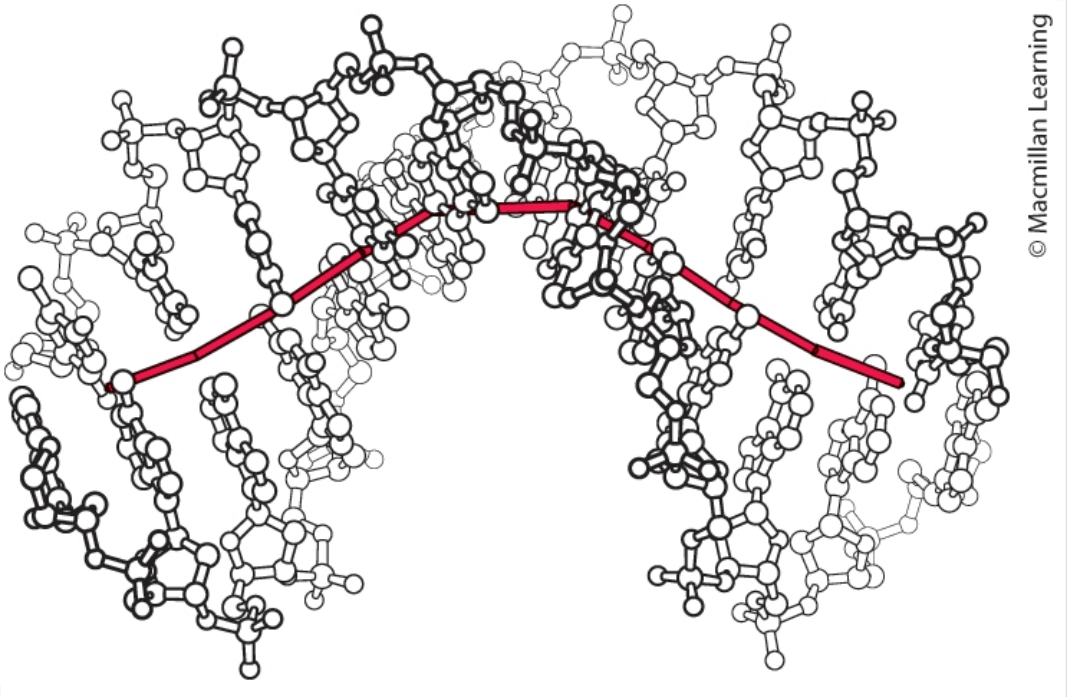

© Macmillan Learning

FIGURE 6.33 The cognate DNA from the EcoRV complex is substantially bent. The DNA is represented as a ball-and-stick model. The path of the DNA helical axis, shown in red, is substantially distorted on binding to the enzyme. For B form DNA, the axis is normally straight (not shown).

The structures of complexes formed with noncognate DNA fragments are strikingly different from those formed with cognate DNA; the noncognate DNA conformation is not substantially distorted (**Figure 6.34**). This lack of distortion has important consequences with regard to catalysis. No phosphate is positioned sufficiently close to the active-site aspartate residues to complete a magnesium ion-binding site (Figure 6.30). Hence, the nonspecific complexes do not bind the magnesium ions and the complete catalytic apparatus is never assembled. The distortion of the substrate and the subsequent binding of the magnesium ion account for the catalytic specificity of more than a million-fold that is observed for EcoRV endonuclease. Thus, enzyme specificity may be determined not by the specificity of substrate binding but rather by the specificity of forming a structure capable of DNA cleavage.

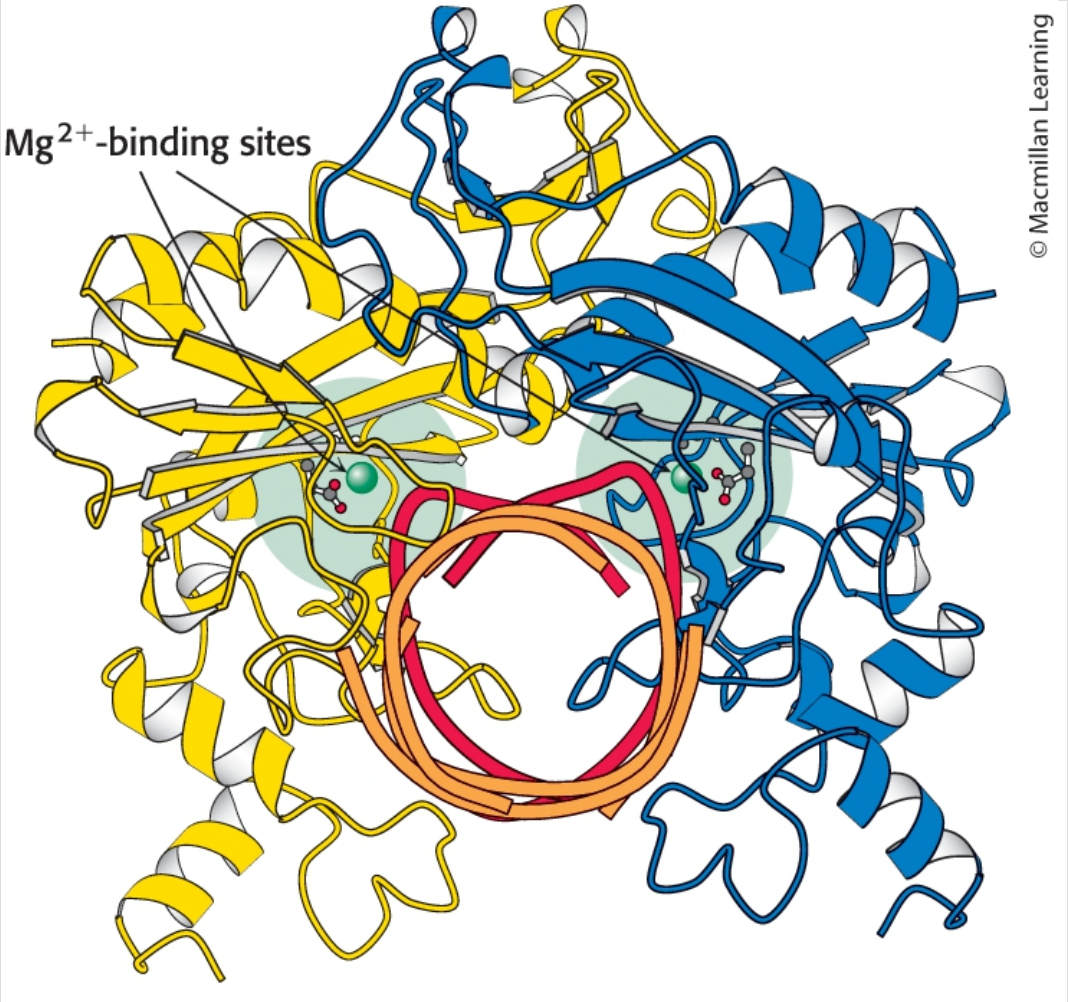


FIGURE 6.34 A comparison of the positions of the nonspecific and the cognate DNA within EcoRV shows the absence and presence of substantial DNA distortion. Note that, in the nonspecific complex (shown in orange compared to the specific complex in red), the DNA backbone is too far from the enzyme to complete the magnesium ion-binding sites required for DNA cleavage.

[Drawn from 1RVB.pdb.]

INTERACT with this model in Achieve

We can now see the role of binding energy in this strategy for attaining catalytic specificity. The distorted DNA makes additional contacts with the enzyme, increasing the binding energy, but the increase in binding energy is canceled by the energetic cost of distorting the DNA from its relaxed conformation into one that is catalytically competent, that is, into a conformation that allows DNA cleavage to proceed (Figure 6.35). Thus, for EcoRV endonuclease, there is little difference in binding affinity for cognate and nonspecific DNA fragments. However, the distortion in the cognate complex dramatically affects DNA hydrolysis by completing the magnesium ion-binding site. This example illustrates how enzymes can use available binding energy to deform substrates and position them for chemical transformation. Interactions that take place within the distorted substrate complex stabilize the transition state leading to DNA hydrolysis.

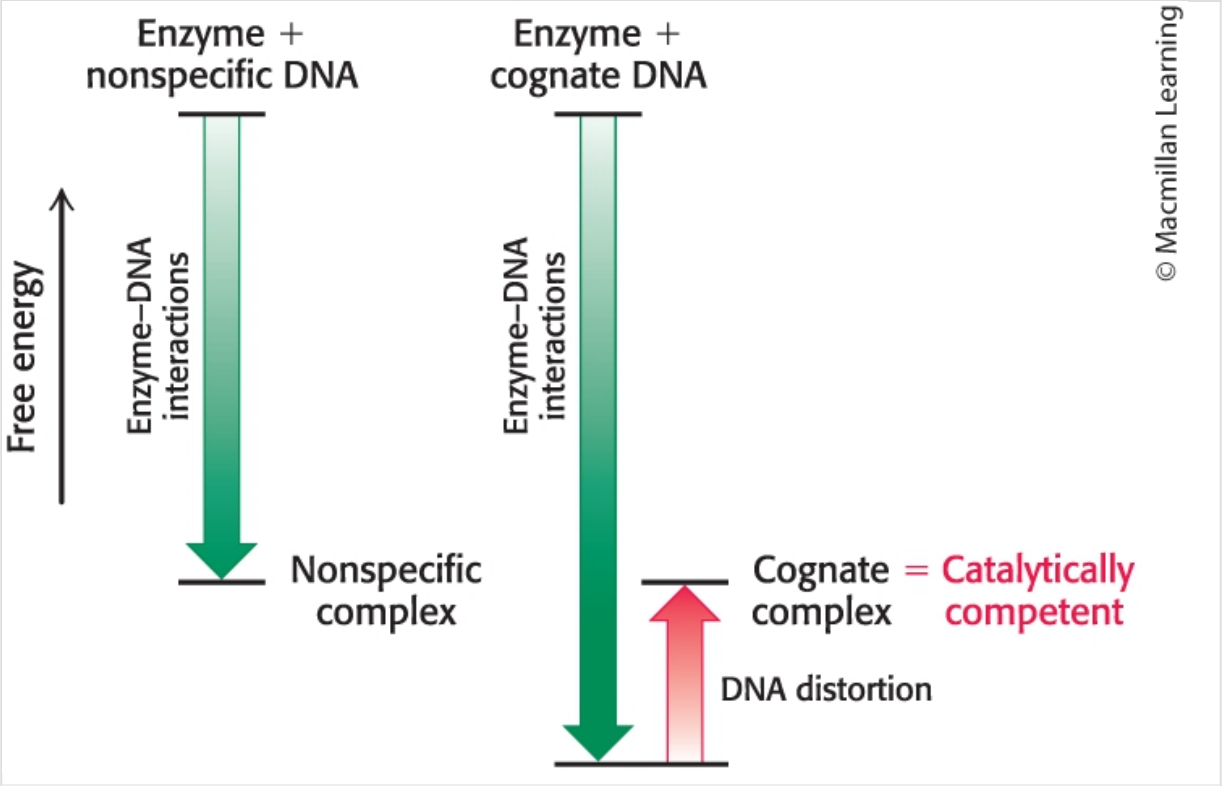


FIGURE 6.35 The binding energy drives DNA distortion. The additional interactions between EcoRV endonuclease and cognate DNA increase the binding energy, driving distortions that form a complex that is catalytically competent for DNA cleavage.

Self-Check Question

The restriction enzyme EcoRI binds DNA fragments containing its recognition site very tightly and specifically; changing even a single base results is a loss of approximately 1000-fold in binding affinity. How does this compare with EcoRV?

Host-cell DNA is protected by the addition of methyl groups to specific bases

How does a host cell harboring a restriction enzyme protect its own DNA? The host DNA is methylated on specific adenine bases within host recognition sequences by other enzymes called **DNA methylases** (**Figure 6.36**). A restriction enzyme will not cleave DNA if its recognition sequence is methylated. For each restriction enzyme, the host cell produces a corresponding methylase that marks the host DNA at the appropriate methylation site. These pairs of enzymes are referred to as **restriction-modification systems**.



FIGURE 6.36 Methylation of recognition sequences for EcoRV endonuclease protects these DNA sites from cleavage by EcoRV. The specific sites are indicated by asterisks; the structure of a methylated adenine is shown on the right.

The distortion of the DNA explains how methylation blocks catalysis and protects host-cell DNA. The host *E. coli* adds a methyl group to the amino group of the adenine nucleotide at the 5′ end of the recognition sequence for EcoRV endonuclease. The presence of the methyl group blocks the formation of a hydrogen bond between the amino group and the side-chain carbonyl group of asparagine 185 in the endonuclease

(Figure 6.37). This asparagine residue is closely linked to the other amino acids that would form specific contacts with the DNA. The absence of the hydrogen bond disrupts other interactions between the enzyme and the DNA substrate, and the distortion necessary for cleavage will not take place. Thus, these added methyl groups prevent cleavage and protect the host DNA; the methylation reactions are slower than the DNA-cleavage reactions so that injected viral DNA is cleaved before it can be protected.

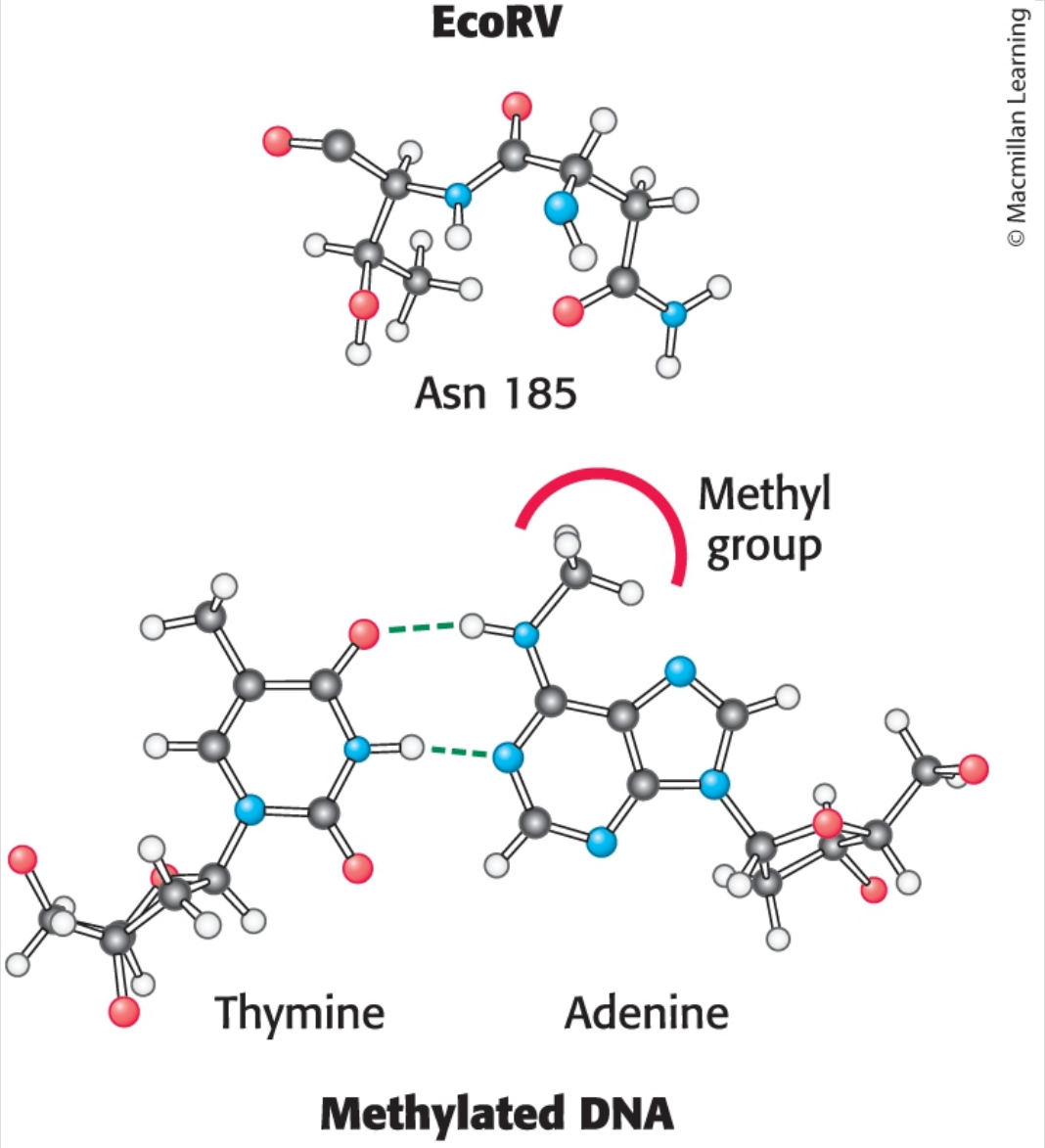


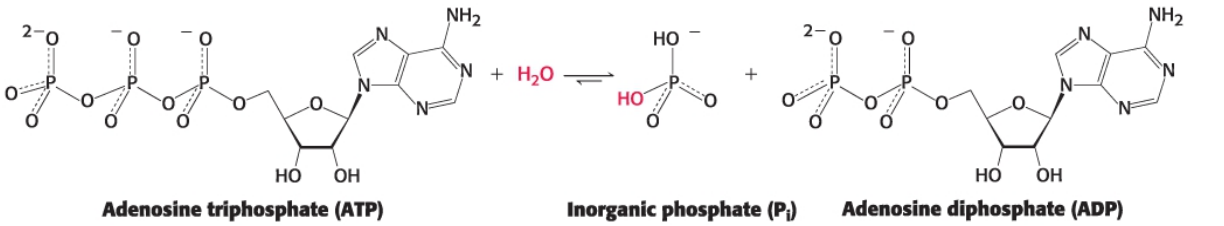
FIGURE 6.37 The methylation of adenine blocks the formation of hydrogen bonds between EcoRV endonuclease and cognate DNA molecules. This blockage prevents

the hydrolysis of methylated DNA.



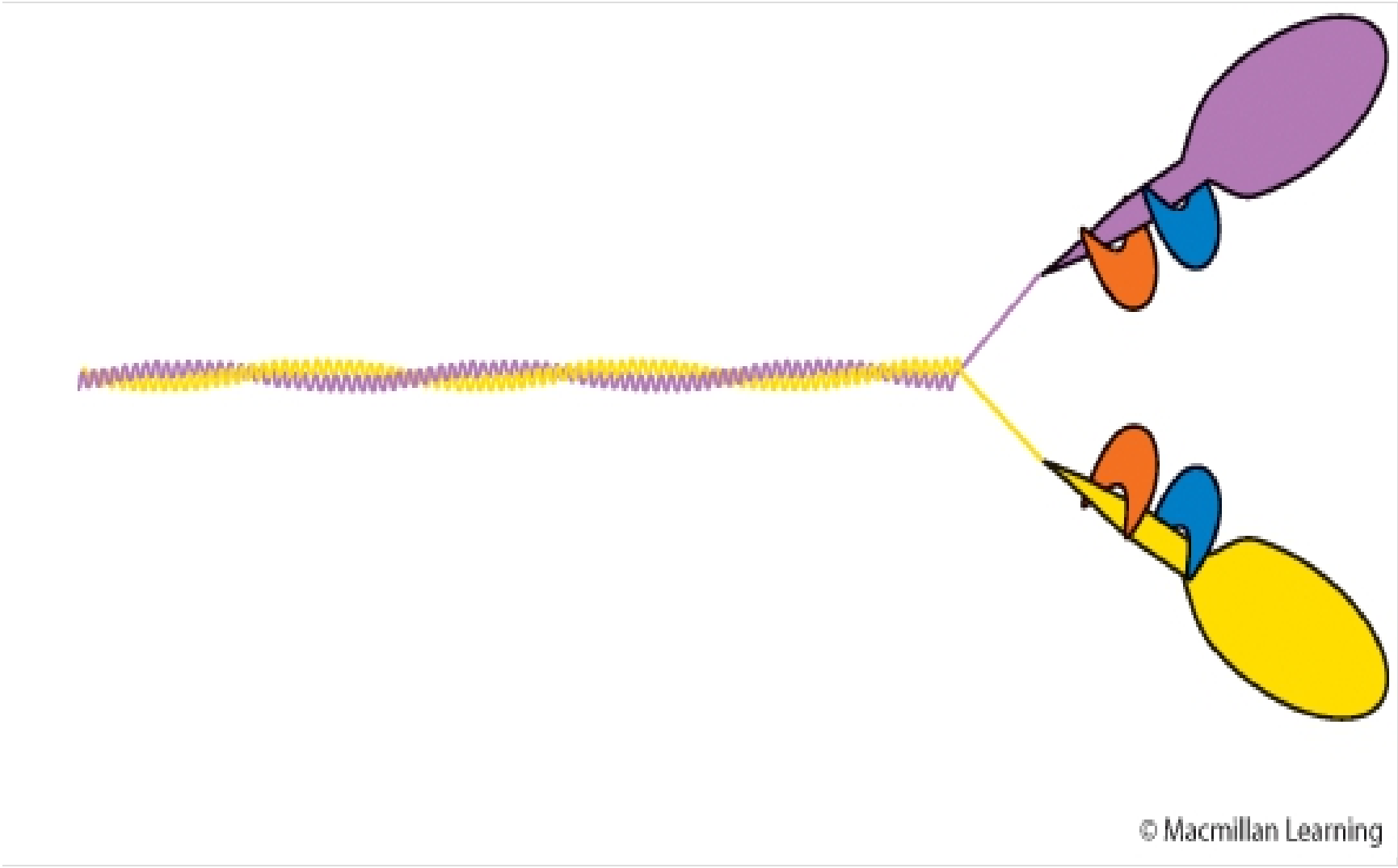
6.5 Molecular Motor Proteins Harness Changes in Enzyme Conformation to Couple ATP Hydrolysis to Mechanical Work

The final enzymes that we will consider are a class of molecular motor proteins called **myosins**. These enzymes catalyze the hydrolysis of adenosine triphosphate (ATP) to form adenosine diphosphate (ADP) and inorganic phosphate (P_i) and use the energy associated with this thermodynamically favorable reaction to drive the motion of molecules within cells.



For example, when we lift a book, the energy required comes from ATP hydrolysis catalyzed by myosin in our muscles. Myosins are found in all eukaryotes, and the human genome encodes more than 40 different myosins, defined by large proteins termed myosin heavy chains. Myosins have elongated structures with globular domains that actually carry out ATP hydrolysis at one end, extended α-helical structures that promote dimer formation, and ancillary associate proteins termed light chains (**Figure 6.38**). We will focus on the globular **ATPase** domains, particularly the strategies that allow myosins to hydrolyze ATP in a

controlled manner and to use the free energy associated with this reaction to promote substantial conformational changes within the myosin molecule. These conformational changes are amplified by other structures in the elongated myosin molecules to transport proteins or other cargo substantial distances within cells.



© Macmillan Learning

FIGURE 6.38 A schematic view of a myosin molecule reveals an elongated dimeric structure. The two heavy chains are shown in purple and yellow, and the light chains are shown in blue and orange.



ATP is used as the major currency of energy inside cells. Many enzymes use ATP hydrolysis to drive other reactions and processes. In almost all cases, an enzyme that hydrolyzed ATP without coupling the reaction to other processes would simply drain the energy reserves of a cell without benefit.

ATP hydrolysis proceeds by the attack of water on the gamma phosphoryl group

In our examination of the mechanism of restriction enzymes, we learned that an activated water molecule performs a nucleophilic attack on phosphorus to cleave the phosphodiester backbone of DNA. The cleavage of ATP by myosins follows an analogous mechanism. To understand the myosin mechanism in more detail, we must first examine the structure of the myosin ATPase domain.

The structures of the ATPase domains of several different myosins have been examined. One such domain, that from the soil-living amoeba *Dictyostelium discoideum*, an organism that has been extremely useful for studying cell movement and molecular-motor proteins, has been studied in great detail. The crystal structure of this protein fragment in the absence of nucleotides reveals a single globular domain comprising approximately 750 amino acids. A water-filled pocket is present toward the center of the structure, suggesting a possible nucleotide-binding active site (**Figure 6.39**). However, when crystals of this protein were soaked in a solution containing ATP, the resulting structure reveals intact ATP bound in the proposed active site, but with very little change

in the overall structure and without evidence of significant hydrolysis. The ATP is also bound to a Mg^{2+} ion.

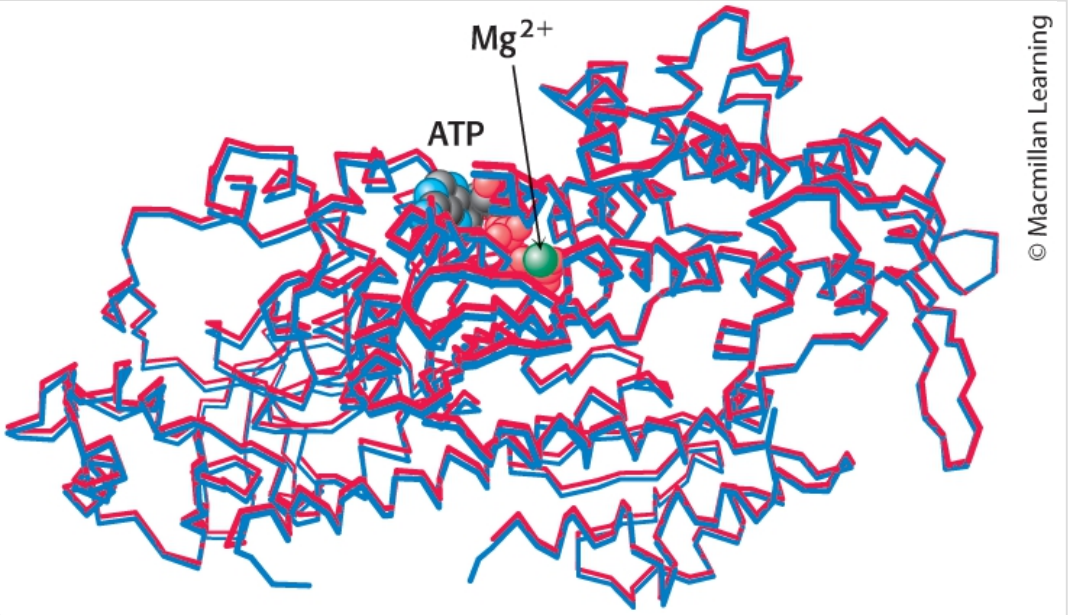


FIGURE 6.39 ATP binding to myosin does not dramatically alter its structure. An overlay of the structures of the ATPase domain from *Dictyostelium discoideum* myosin with nothing bound (blue) and the complex of this protein with ATP and magnesium bound (red) reveals that these two structures are quite similar to one another.

[Drawn from 1FMV.pdb and 1FMW.pdb.]

INTERACT with this model in Achieve

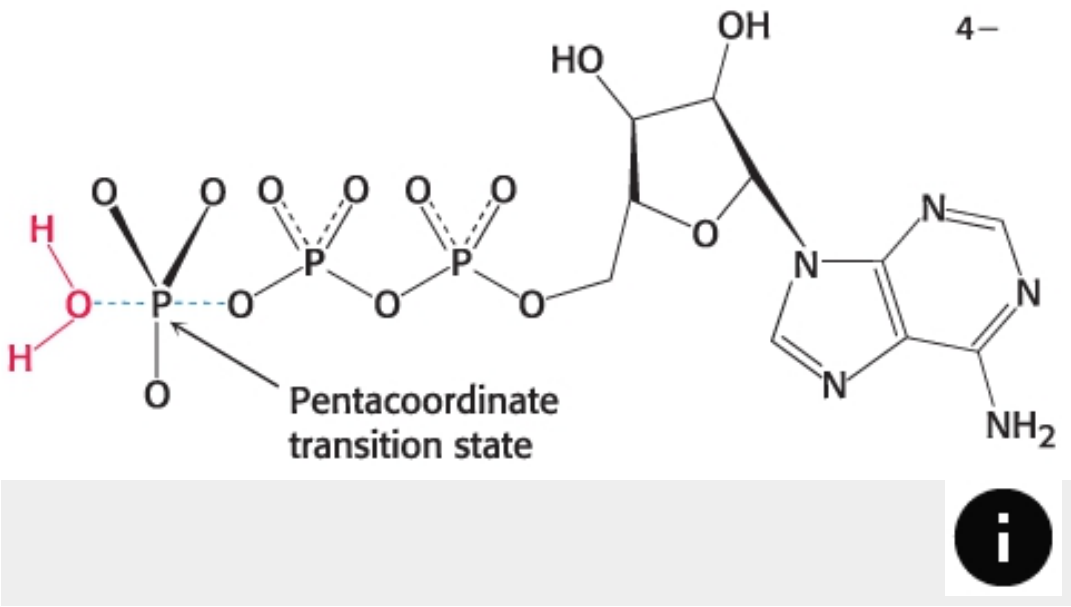
Kinetic studies of myosins, as well as many other enzymes having ATP or other nucleoside triphosphates as a substrate, reveal that these enzymes are essentially inactive in the absence of divalent metal ions such as magnesium (Mg^{2+}) or manganese (Mn^{2+}) but acquire activity on the addition of these ions. In contrast with the enzymes discussed so far, the metal is not a component of the active site. Rather, nucleotides such as ATP bind these ions, and it is the metal ion–nucleotide complex that is the true substrate for the enzymes. The dissociation constant for

the ATP–Mg^{2+} complex is approximately 0.1 mM, and thus, given that intracellular Mg^{2+} concentrations are typically in the millimolar range, essentially all nucleoside triphosphates (NTP) are present as NTP–Mg^{2+} complexes. Magnesium or manganese complexes of nucleoside triphosphates are the true substrates for essentially all NTP-dependent enzymes.

Since the ATP–Mg^{2+} complex was present in the crystallography study discussed above, why was there no evidence for hydrolysis? The nucleophilic attack by a water molecule on the γ-phosphoryl group requires some mechanism to activate the water, such as a basic residue or a bound metal ion. Examination of the myosin–ATP complex structure shows no basic residue in an appropriate position and reveals that the bound Mg^{2+} ion is too far away from the phosphoryl group to play this role. These observations suggest why the ATP complex is relatively stable: The enzyme is not in a conformation that is suitable for promoting the ATP-hydrolysis reaction. This conclusion suggests that the domain must undergo a conformational change in order to carry out catalysis.

Formation of the transition state for ATP hydrolysis is associated with a substantial conformational change

The catalytically competent conformation of the myosin ATPase domain must bind and stabilize the transition state of the reaction. In analogy with restriction enzymes, we expect that ATP hydrolysis includes a pentacoordinate transition state.



Such pentacoordinate structures based on phosphorus are too unstable to be readily observed. However, transition-state analogs in which other atoms replace phosphorus are more stable. The transition metal vanadium, in particular, forms similar structures. After crystallizing the myosin ATPase domain in the presence of ADP and vanadate, VO_4^{3-}, a complex forms that closely matches the expected transition-state structure (Figure 6.40).

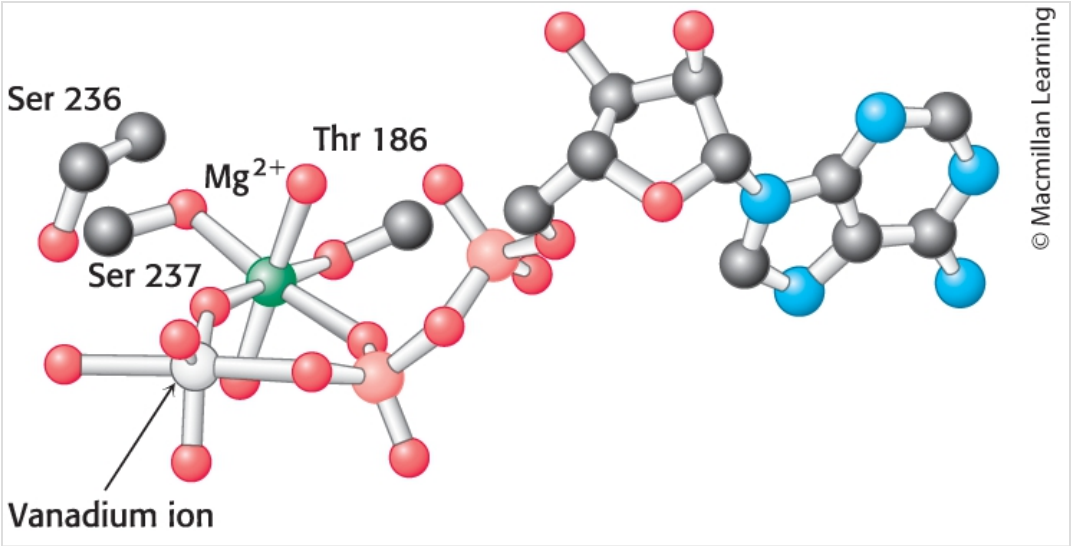


FIGURE 6.40 A stable structural analog of the myosin transition state can be prepared. The transition-state analog formed by treating the myosin ATPase domain

with ADP and vanadate (VO_4^{3-}) in the presence of magnesium shows the vanadium ion (analogous to phosphorus) coordinated to five oxygen atoms including one from ADP. The positions of two residues that bind magnesium as well as Ser 236, a residue that appears to play a direct role in catalysis, are shown.

[Drawn from 1VOM.pdb.]

As expected, the vanadium atom is coordinated to five oxygen atoms, including one oxygen atom from ADP diametrically opposite an oxygen atom that is analogous to the attacking water molecule in the transition state. The Mg^{2+} ion is coordinated to one oxygen atom from the vanadate, one oxygen atom from the ADP, two hydroxyl groups from the enzyme, and two water molecules. In this position, this ion does not appear to play any direct role in activating the attacking water. However, an additional residue from the enzyme, Ser 236, is well positioned to play a role in catalysis (Figure 6.41).

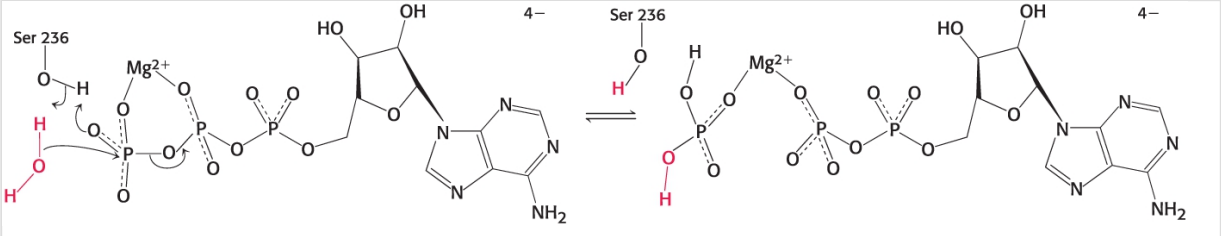


FIGURE 6.41 Water attack is facilitated by Ser 236. The attack of the water molecule on the γ-phosphoryl group of ATP is facilitated by Ser 236, which helps to deprotonate the water molecule. The serine sidechain, in turn, is deprotonated by one of the oxygen atoms of the γ-phosphoryl group forming the $H_2PO_4^-$ product.

In the proposed mechanism of ATP hydrolysis based on this structure, the water molecule attacks the γ-phosphoryl group, with the hydroxyl

group of Ser 236 facilitating the transfer of a proton from the attacking water to the hydroxyl group of Ser 236, which, in turn, is deprotonated by one of the oxygen atoms of the γ-phosphoryl group. Thus, in effect, the ATP serves as a base to promote its own hydrolysis.

Comparison of the overall structures of the myosin ATPase domain complexed with ATP and with the ADP–vanadate reveals some remarkable differences. Relatively modest structural changes occur in and around the active site. In particular, a stretch of amino acids moves closer to the nucleotide by approximately 2 Å and interacts with the oxygen atom that corresponds to the attacking water molecule. These changes aid the hydrolysis reaction by stabilizing the transition state. However, examination of the overall structure shows even more striking changes.

A region comprising approximately 60 amino acids at the carboxyl-terminus of the domain adopts a different configuration in the ADP–vanadate complex, displaced by as much as 25 Å from its position in the ATP complex (**Figure 6.42**). This displacement tremendously amplifies the relatively subtle changes that take place in the active site, and it even affects locations beyond from the ATPase domain, because the carboxyl-terminus is connected to other atoms within the elongated structures typical of myosin molecules (Figure 6.38). Thus, the conformation that is capable of promoting the ATP hydrolysis reaction is substantially different from other conformations that are present in the course of the catalytic cycle.

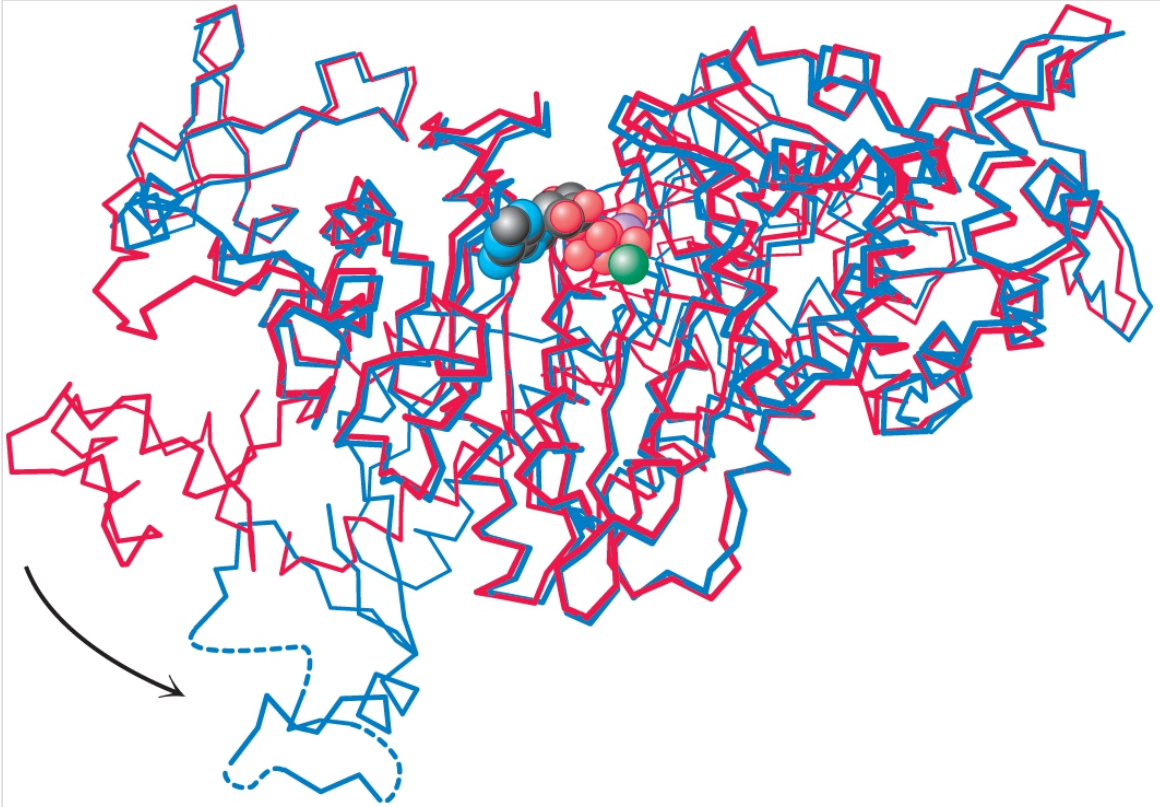


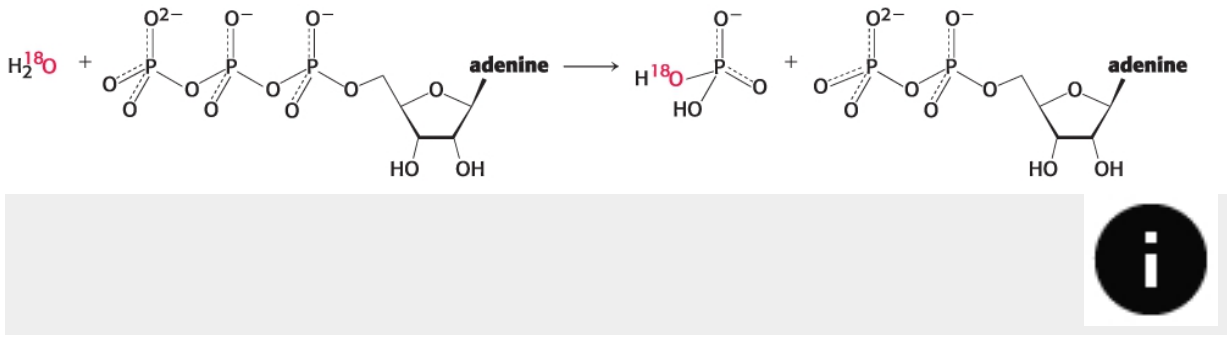
FIGURE 6.42 A substantial conformation change is associated with the formation of the myosin transition state. A comparison of the overall structures of the myosin ATPase domain with ATP bound (shown in red) and that with the transition-state analog ADP–vanadate (shown blue) reveals dramatic conformational changes of a region at the carboxyl-terminus of the domain (see arrow), some parts of which move as much as 25 Å.

[Drawn from 1FMW.pdb and 1VOM.pdb.]

The altered conformation of myosin persists for a substantial period of time

Myosins are slow enzymes, typically turning over approximately once per second. What steps limit the rate of turnover? In a particularly revealing experiment, the hydrolysis of ATP was catalyzed by the

myosin ATPase domain from mammalian muscle. The reaction took place in water labeled with ^{18}O to track the incorporation of solvent oxygen into the reaction products; then the fraction of oxygen in the phosphate product was analyzed. In the simplest case, the phosphate would be expected to contain one oxygen atom derived from water and three initially present in the terminal phosphoryl group of ATP. Instead, between two and three of the oxygen atoms in the phosphate were found, on average, to be derived from water. These observations indicate that the ATP hydrolysis reaction within the enzyme active site is reversible. Each molecule of ATP is cleaved to ADP and P_i and then re-formed from these products several times before the products are released from the enzyme (Figure 6.43).



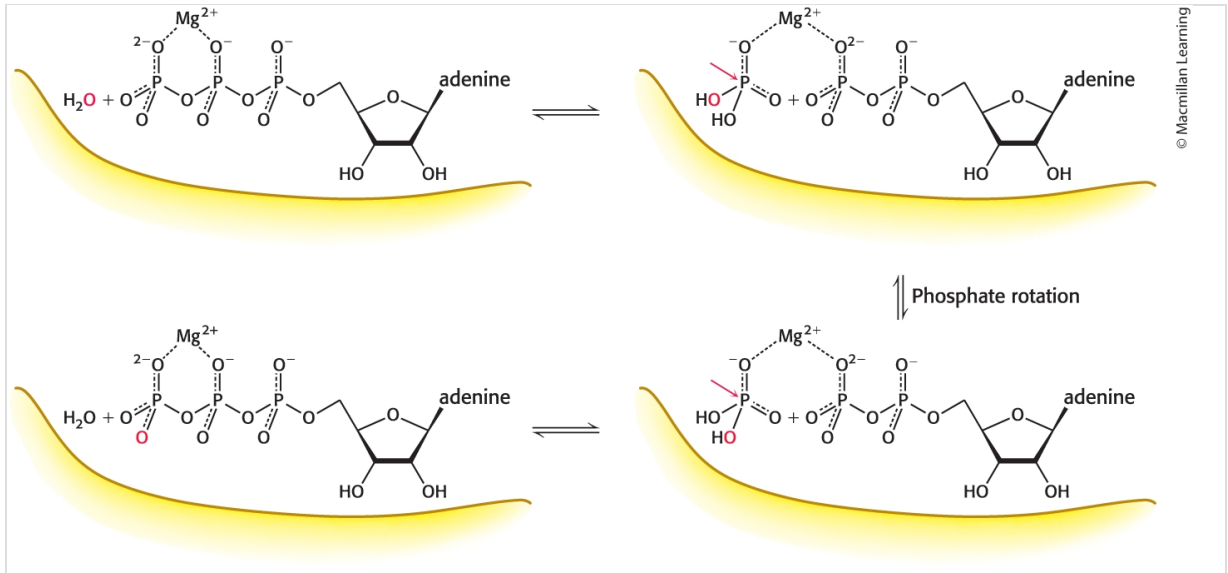


FIGURE 6.43 The hydrolysis of ATP is reversible within the active site of myosin. This is revealed by the fact that more than one atom of oxygen from water is incorporated in inorganic

phosphate. The oxygen atoms are incorporated in cycles of hydrolysis of ATP to ADP and inorganic phosphate, phosphate rotation within the active site, and reformation of ATP now containing oxygen from water.



At first glance, this observation is startling because ATP hydrolysis is a very favorable reaction with an equilibrium constant of approximately 140,000. However, this equilibrium constant applies to the molecules free in solution, not within the active site of an enzyme. Indeed, further analysis suggests that this equilibrium constant on the enzyme is approximately 10.

This result illustrates a general strategy used by enzymes: Enzymes catalyze reactions by stabilizing the transition state. The structure of this transition state is intermediate between the enzyme-bound reactants and the enzyme-bound products. Many of the interactions that stabilize the transition state will help equalize the stabilities of the reactants and the products. Thus, the equilibrium constant between enzyme-bound reactants and products usually 10 or below and is often close to 1, regardless of the equilibrium constant for the reactants and products free in solution.

These observations reveal that the hydrolysis of ATP to ADP and P_i is not the rate-limiting step for the reaction catalyzed by myosin. Instead, the release of the products, particularly P_i, from the enzyme is rate limiting. The fact that a conformation of myosin with ATP hydrolyzed but still bound to the enzyme persists for a significant period of time is critical for coupling conformational changes that take place in the course of the reaction to other processes.

Self-Check Question



Myosin is treated with ATP in the presence of water labelled with $H_2{}^{18}O$. After a period of time, the remaining ATP is isolated and found to contain ^{18}O. Explain.

Actin forms filaments along which myosin can move

Myosin molecules use the free energy of hydrolysis of ATP to drive their own macroscopic movement along a filamentous protein termed *actin*, a 42-kDa protein that very abundant in eukaryotic cells, typically accounting for as much as 10% of the protein. Actin monomers come together to form actin filaments (**Figure 6.44**). Actin filaments have helical structures; each monomer is related to the preceding one by a translation of $27.5\ \text{Å}$ and a rotation of 166 degrees around the helical axis. Because the rotation is nearly 180 degrees, F-actin resembles a two-stranded cable. Note that each actin monomer is oriented in the same direction along the actin filament, and so the structure is polar, with discernibly different ends. One end is called the barbed (plus) end, and the other is called the pointed (minus) end. Each actin monomer contains a bound nucleotide, ATP or ADP.

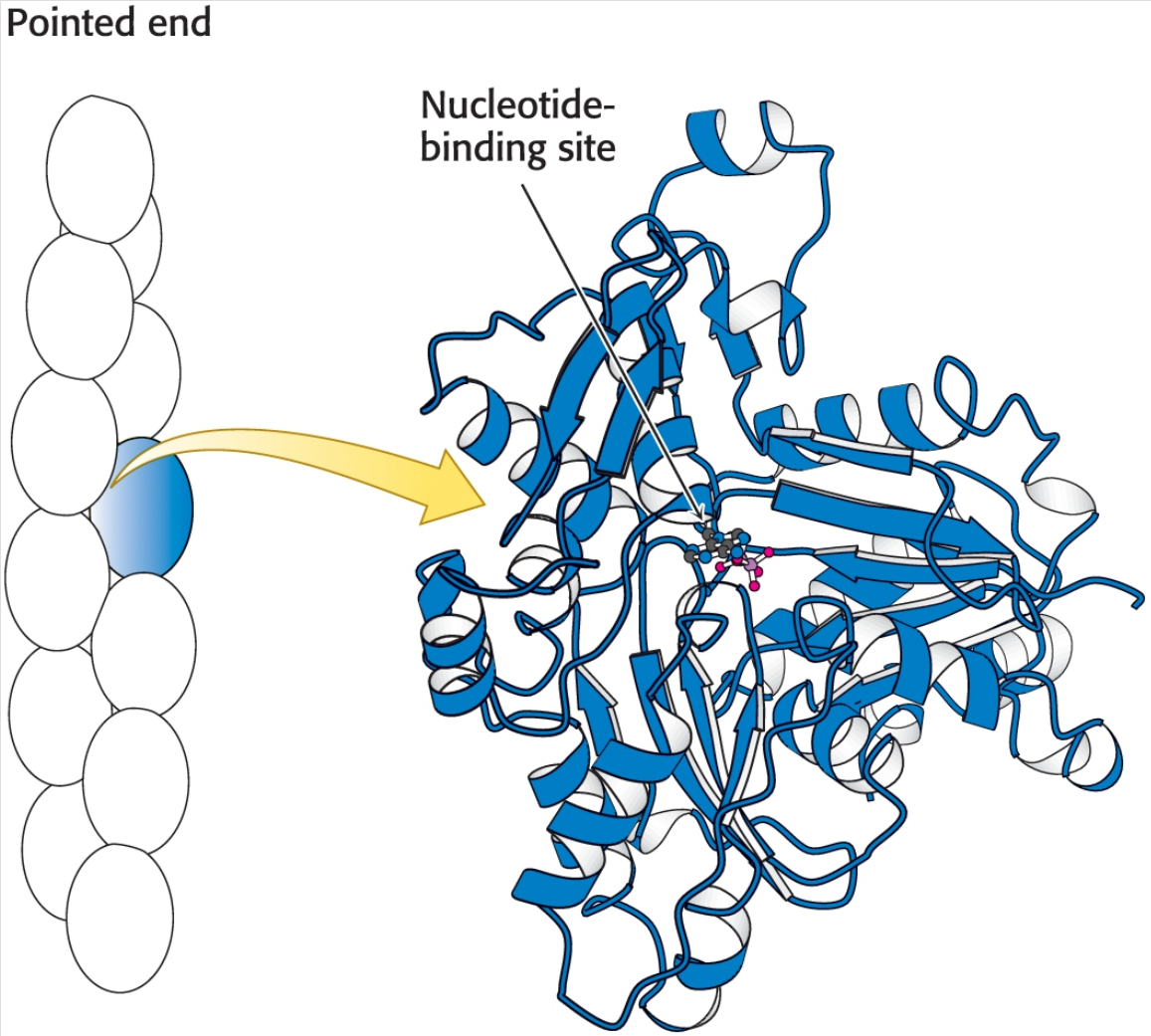


FIGURE 6.44 An actin filament has a polymeric structure. In the schematic view at left, actin monomers are depicted as ovals. The detailed structure of one actin monomer (blue) is shown a right.

[Drawn from 1J6Z.pdb.]

INTERACT with this model in Achieve

Using a variety of physical methods, scientists have been able to watch single myosin molecules moving along actin filaments. For example, a myosin family member termed myosin V can be labeled with

fluorescent tags so that it can be localized when fixed on a surface with a precision of less than 15 Å. When this myosin in the absence of ATP is placed on a surface coated with actin filaments, each molecule remains in a fixed position. However, when ATP is added, each molecule moves along the surface. Tracking individual molecules reveals that each moves in steps of approximately 74 nm (Figure 6.45). The observation of steps of a fixed size as well as the determination of this step size helps reveal details of the mechanism of action of these tiny molecular machines.

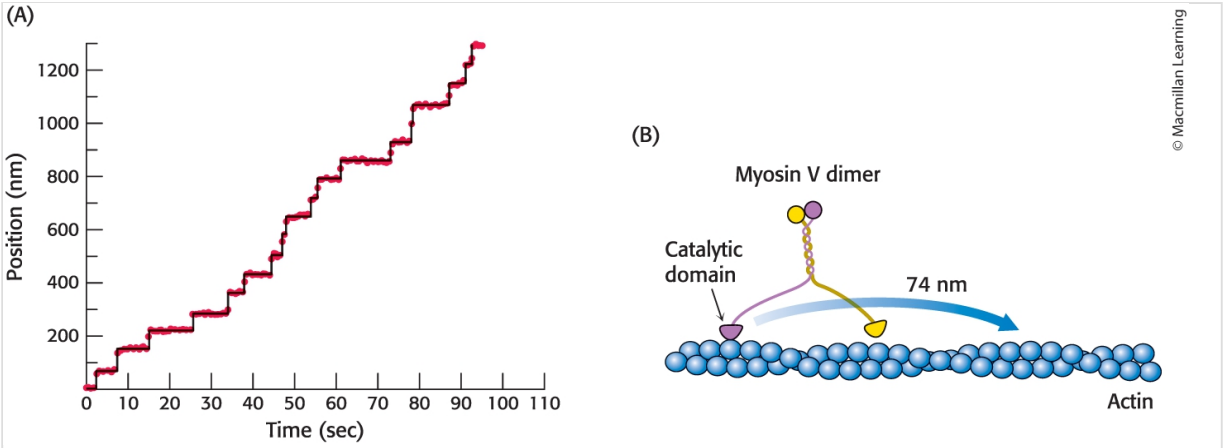


FIGURE 6.45 A molecular motor such as myosin V moves in discrete steps. (A) A trace of the position of a single dimeric myosin V molecule as it moves across a surface coated with actin filaments. (B) A model of how the dimeric molecule moves in discrete steps with an average size of 74 ± 5 nm.

How does ATP hydrolysis drive this motion? A key observation is that the addition of ATP to a complex of myosin and actin results in the dissociation of the complex. Thus, ATP binding and hydrolysis cannot be directly responsible for the power stroke. We can combine this fact with observations from three-dimensional structures of myosin in various forms to construct a mechanism for the motion of myosin along actin (Figure 6.46).

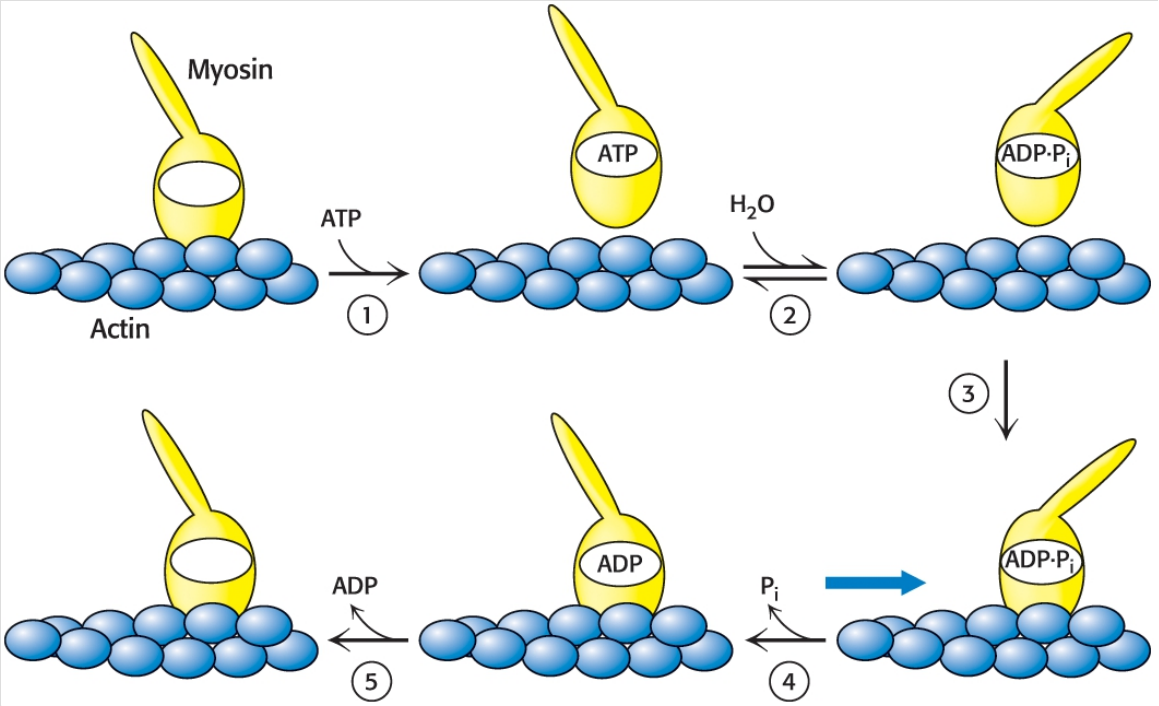


FIGURE 6.46 The mechanism by which myosin moves along an actin filament involves five steps. The binding of ATP (1) results in the release of myosin (yellow) from actin (blue). The reversible hydrolysis of ATP bound to myosin (2) can result in the reorientation of the lever arm. With ATP hydrolyzed but still bound to actin, myosin can bind actin (3). The release of P_i (4) results in the reorientation of the lever arm and the concomitant motion of actin relative to myosin. The release of ADP (5) completes the cycle.

Let us begin with nucleotide-free myosin bound to actin. The binding of ATP to actin results in the dissociation of myosin from actin. With ATP bound and free of actin, the myosin domain can undergo the conformational change associated with the formation of the transition state for ATP hydrolysis. This conformational change results in the reorientation of the lever arm. In this form, the myosin head can dock onto the actin filament; phosphate is released with an accompanying motion of the lever arm. This conformational change represents the power stroke and moves the body of the myosin molecule relative to the actin filament. The release of ADP completes the cycle.

The most well-studied actin-myosin motor system is that from skeletal muscle (Figure 6.47). Muscle contains organized assemblies of actin molecules, referred to as thin filaments, together with multiheaded assemblies of myosin molecules that form thick filaments. Upon activation, the myosin motors move along the actin filaments to cause the combined assembly to contract.

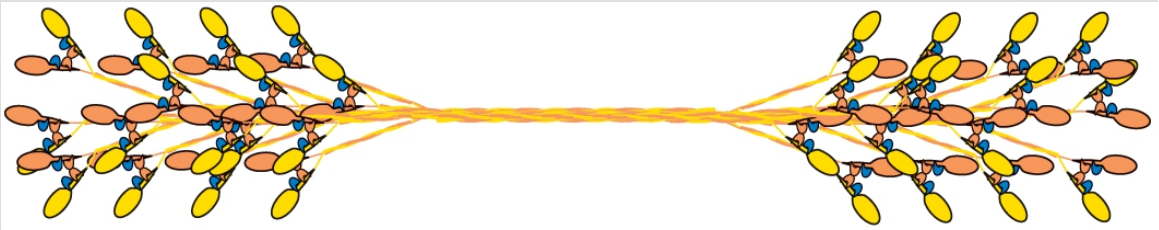


FIGURE 6.47 A myosin assembly from muscle has a two-headed structure. A schematic view shows how multiple myosin molecules come together to form the thick filament.

Other cells contain elaborate meshworks of actin filaments that form an internal cellular skeleton or cytoskeleton, which plays a major role in determining cell shape. Two techniques for observing the cytoskeleton have traditionally been used, but each has shortcomings: Electron microscopy can produce clear images but cannot be performed on living cells, whereas light microscopy that visualizes fluorescent tags attached to actin can be performed on living cells, but the clarity of the images is limited by the relatively long wavelengths of visible light.

Recently, scientists have developed new microscopic methods based on the principle that the position of an isolated fluorescent molecule can be determined much more precisely than the image produced by monitoring the fluorescence. These methods have produced beautiful pictures of the intricate tracks inside living cells along which molecular motors can move (Figure 6.48). With these new tools, scientists can now ask new questions about the elaborate movements that occur within living cells driven by molecular motors.

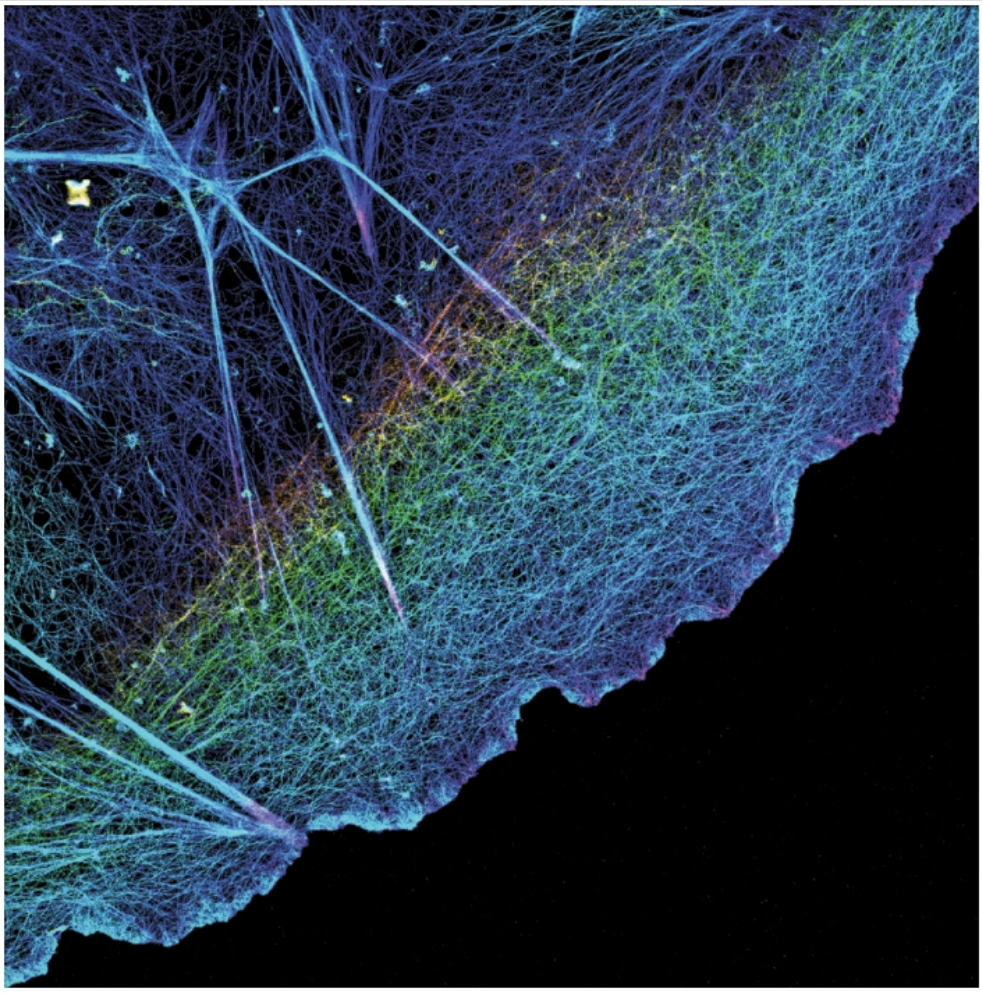


Image Courtesy of Ke Xu, University of California, Berkeley, and Xiaowei Zhuang, Harvard University

FIGURE 6.48 Actin networks can be imaged in great detail using modern fluorescence microscopy methods. A section of a live mammalian fibroblast cell with tagged actin clearly reveals individual actin filaments.

Chapter 6 Summary

6.1 Enzymes Use a Core Set of Catalytic Strategies

- Enzymes adopt conformations that are structurally and chemically complementary to the transition states of the reactions that they catalyze.
- Enzymes use five basic strategies to form and stabilize the transition state: the use of binding energy to promote both specificity and catalysis, covalent catalysis, general acid–base catalysis, catalysis by approximation, and metal ion catalysis.

6.2 Proteases Facilitate a Fundamentally Difficult Reaction

- The cleavage of peptide bonds by chymotrypsin is initiated by the attack by a serine residue on the peptide carbonyl group with the serine activated by a catalytic triad of Ser-His-Asp.
- The product of this initial reaction is a covalent intermediate formed by the enzyme and an acyl group derived from the bound substrate that is subsequently hydrolyzed.
- Tetrahedral intermediates that occur during these reactions have a negative charge on the peptide carbonyl oxygen atom that is stabilized by interactions with peptide NH groups in a region on the enzyme termed the oxyanion hole.
- Some other proteases employ the same catalytic strategy based on a similar catalytic triad, including homologs of chymotrypsin such as trypsin and elastase and other proteins such as subtilisin that evolved the same catalytic apparatus independently.

6.3 Carbonic Anhydrases Make a Fast Reaction Faster

- Carbonic anhydrases catalyze the reaction of water with carbon dioxide at rates as high as 1 million times per second to generate bicarbonate ion which can be protonated to form carbonic acid.
- A tightly bound zinc ion binds a water molecule, promotes its deprotonation to generate a hydroxide ion at neutral pH, and uses this nucleophile to attack carbon dioxide.
- To overcome limitations imposed by the rate of proton transfer from the zinc-bound water, the most-active carbonic anhydrases have evolved a proton shuttle to transfer protons to buffer components in solution.

6.4 Restriction Enzymes Catalyze Highly Specific DNA-Cleavage Reactions

- Restriction enzymes that cleave DNA at specific recognition sequences discriminate between molecules that contain these recognition sequences and those that do not.
- Restriction enzymes use magnesium ions to bind and activate a water molecule to attacks the phosphodiester backbone and facilitate DNA cleavage.
- EcoRV distorts DNA molecules containing the proper sequence are in a manner that allows magnesium ion binding and, hence, DNA cleavage.
- Restriction enzymes are prevented from acting on the DNA of a host cell by the methylation of key sites within its recognition sequences, blocking specific interactions between the enzymes and the DNA.

6.5 Molecular Motor Proteins Harness Changes in Enzyme Conformation to Couple ATP Hydrolysis to Mechanical Work

- Molecular motors called myosins catalyze the hydrolysis of adenosine triphosphate, using the free energy generated to drive large-scale molecular movement.

- Myosin associated with the transition state for ATP hydrolysis has a distinct structure indicating a large-scale conformational change.
- The rate of ATP hydrolysis by myosin is relatively low and is limited by the rate of product release from the enzyme.
- Myosins move along a filamentous protein called actin, binding and releasing actin filaments over the course of its catalytic cycle to facilitate movement.
- Actin filaments occur in muscle and also form a cytoskeleton inside eukaryotic cells along which myosins can move; the cytoskeleton also functions like scaffolding, giving the cell its shape.

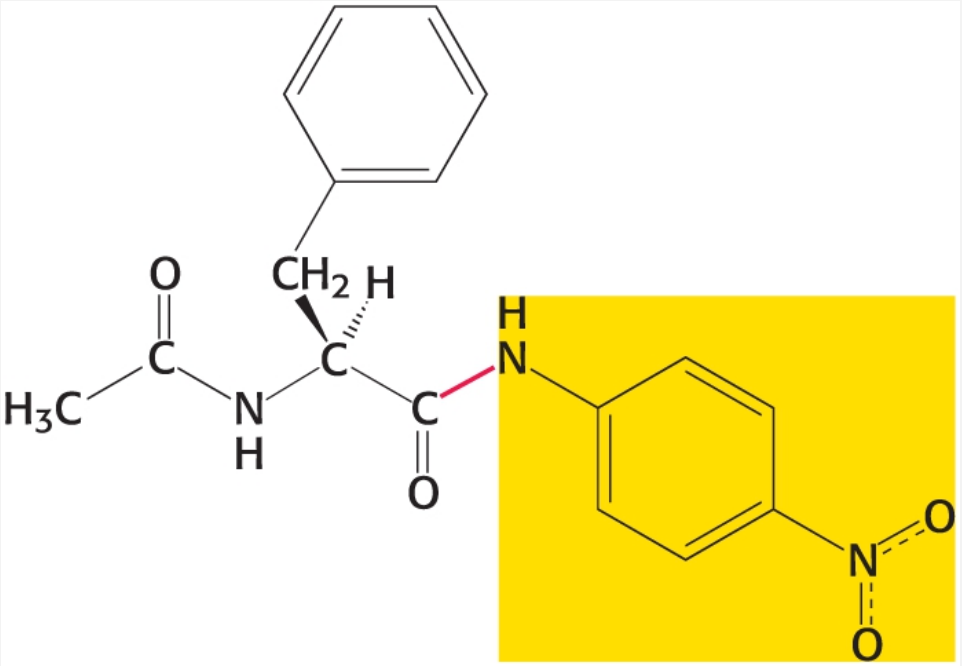
Key Terms

binding energy
induced fit
covalent catalysis
general acid–base catalysis
catalysis by approximation
metal ion catalysis
protease
electrophilic
nucleophilic
chemical modification reaction
chromogenic substrate
catalytic triad
oxyanion hole
scissile bond
protease inhibitor
carbonic anhydrase
ligand

proton shuttle
restriction enzyme (restriction endonuclease)
recognition sequence
DNA methylase
restriction-modification system
myosin
ATPase
cytoskeleton

Problems

1. Examination of the cleavage of the amide substrate, A, by chymotrypsin with the use of stopped-flow kinetic methods reveals no burst. The reaction is monitored by noting the color produced by the release of the amino part of the substrate (highlighted in orange). Why is no burst observed? 1, 6



2. Consider the subtilisin substrates A and B.

Phe-Ala-Gln-Phe-X	Phe-Ala-His-Phe-X
A	B

These substrates are cleaved (between Phe and X) by native subtilisin at essentially the same rate. However, the His 64-to-Ala mutant of subtilisin cleaves substrate B more than 1000-fold as rapidly as it cleaves substrate A. Propose an explanation. 2

3. Consider the following argument. In subtilisin, mutation of Ser 221 to Ala results in a 10^6-fold decrease in activity. Mutation of His 64 to Ala results in a similar 10^6-fold decrease. Therefore, simultaneous mutation of Ser 221 to Ala and His 64 to Ala should result in a $10^6 \times 10^6 = 10^{12}$-fold reduction in activity. Is this correct? Why or why not?

4. In chymotrypsin, a mutant was constructed with Ser 189, which is in the bottom of the substrate-specificity pocket, changed to Asp. What effect would you predict for this mutation?

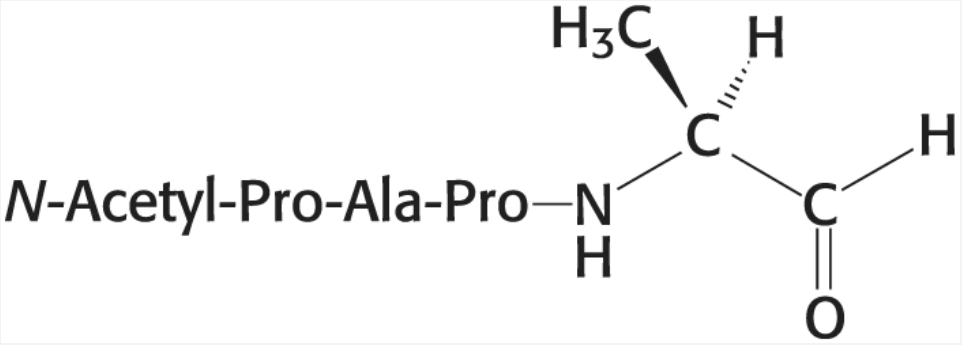
5. In carbonic anhydrase II, mutation of the proton-shuttle residue His 64 to Ala was expected to result in a decrease in the maximal catalytic rate. However, in buffers such as imidazole

with relatively small molecular components, no rate reduction was observed. In buffers with larger molecular components, significant rate reductions were observed. Propose an explanation.

6. Restriction endonucleases are, in general, quite slow enzymes with typical turnover numbers of $1\ s^{-1}$. Suppose that endonucleases were faster, with turnover numbers similar to those for carbonic anhydrase such that they act faster than do methylases. Would this increased rate be beneficial to host cells, assuming that the fast enzymes have similar levels of specificity?

7. Treatment of carbonic anhydrase with high concentrations of the metal chelator EDTA (ethylenediaminetetraacetic acid) results in the loss of enzyme activity. Propose an explanation.
2, 3

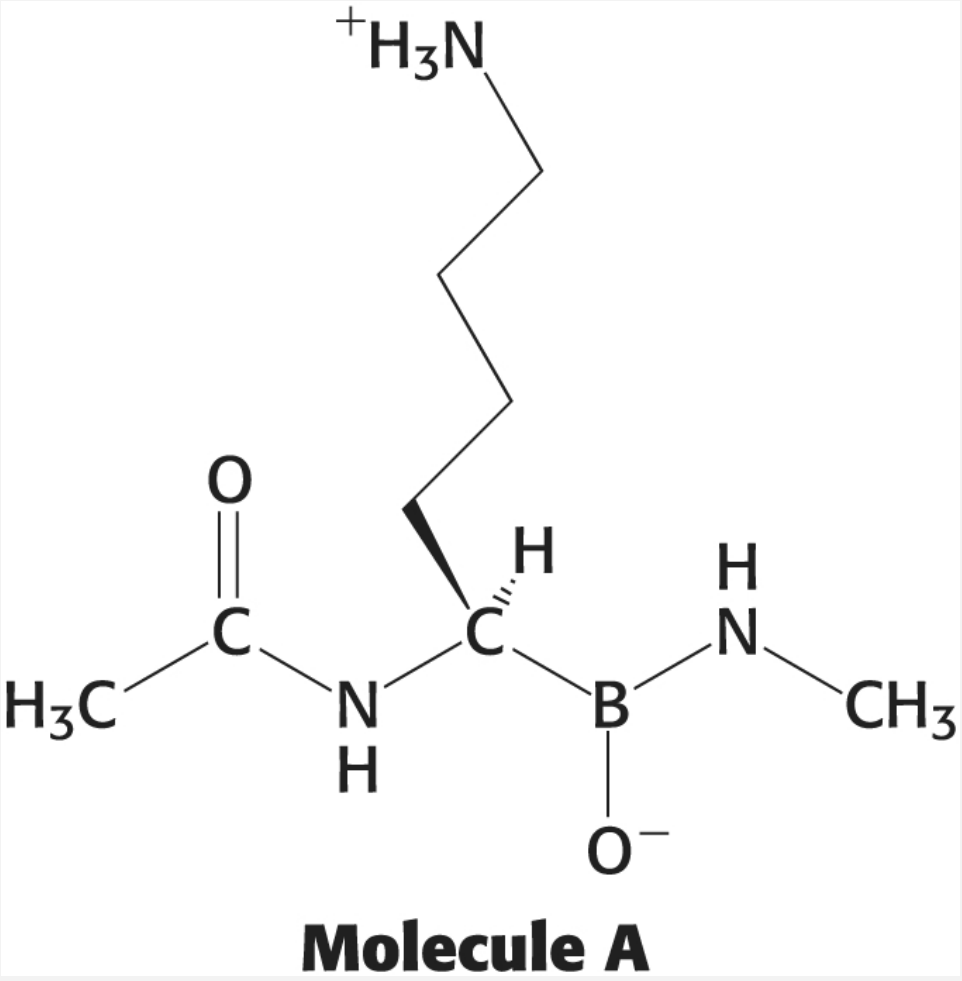
8. Elastase is specifically inhibited by an aldehyde derivative of one of its substrates:



a. Which residue in the active site of elastase is most likely to form a covalent bond with this aldehyde?
b. What type of covalent link would be formed?

9. Use the provided structure of molecule A to complete the passage.

Molecule A contains a side chain similar to that of _____. Molecule A effectively inhibits _____ ___ by binding to the _____ residue in the enzyme's S_1 pocket.
2



Molecule A

10. At pH 7.0, carbonic anhydrase exhibits a k_{cat} of $60{,}000\ s^{-1}$. Estimate the value expected for k_{cat} at pH 6.0.

11. To terminate a reaction in which a restriction enzyme cleaves DNA, researchers often add high concentrations of the metal chelator EDTA (ethylenediaminetetraacetic acid). Why does the addition of EDTA terminate the reaction?

12. Many patients become resistant to HIV protease inhibitors with the passage of time, owing to mutations in the HIV gene that encodes the protease. Mutations are not found in the aspartate residue characteristic of aspartyl proteases. Why not? 1, 2

13. Serine 236 in *Dictyostelium discoideum* myosin has been mutated to alanine. The mutated protein showed modestly reduced ATPase activity. Analysis of the crystal structure of the mutated protein revealed that a water molecule occupied the position of the hydroxyl group of the serine residue in the wild-type protein. Propose a mechanism for the ATPase activity of the mutated enzyme. 1, 2, 6

14. The catalytic power of an enzyme can be defined as the ratio of the rate of the enzyme catalyzed reaction to that for the uncatalyzed reaction. Using the information in Figure 6.15 for subtilisin and in Figure 6.19 for carbonic anhydrase, calculate the catalytic powers for these two enzymes.

15. Would a reaction catalyzed by a version of subtilisin with all three residues in the catalytic triad mutated have less or more

activity compared to the uncatalyzed reaction (see Figure 6.15)? Propose an explanation for any remaining catalytic power.

16. On the basis of the information provided in Figure 6.16, complete the mechanisms for peptide-bond cleavage by

a. a cysteine protease,
b. an aspartyl protease, and
c. a metalloprotease. 1, 2

17. Most enzymes are quite specific, catalyzing a particular reaction on a set of substrates that are structurally quite similar to one another. Discuss why this is advantageous from a biological perspective. Suggest why this is likely to be true from a chemical perspective. Why would it be difficult to evolve an enzyme with high catalytic activity but low specificity? 4

18. In the absence of actin, myosin will hydrolyze ATP, but very slowly. Based on the mechanism shown in Figure 6.46, propose an explanation for this slow rate.

Chapter 7
Enzyme Regulatory Strategies



Photo: LeManna/Getty Images
© Macmillan Learning

Like motor traffic, metabolic pathways flow more efficiently when regulated by signals. Cytidine triphosphate (CTP), the final product of a multistep pathway, controls flux through the pathway by inhibiting the committed step catalyzed by aspartate transcarbamoylase (ATCase).

Outline

7.1 Allosteric Regulation Enables Control of Metabolic Pathways
7.2 Isozymes Provide a Means of Regulation Specific to Distinct Tissues and Developmental Stages
7.3 Covalent Modification Is a Means of Regulating Enzyme Activity
7.4 Many Enzymes Are Activated by Specific Proteolytic Cleavage

7.5 Enzymatic Cascades Allow Rapid Responses Such as Blood Clotting

---

Learning Goals



By the end of this chapter, you should be able to:

1. Explain how the kinetic properties of allosteric enzymes differ from Michaelis–Menten enzymes.
2. Describe the role of feedback inhibition in the regulation of enzymes.
3. Differentiate between homotropic and heterotropic effects and explain how they modify the equilibrium between the T and R forms of an allosteric enzyme.
4. Explain the role of isozymes in the regulation of metabolism.
5. Describe the activity of protein kinases and protein phosphatases.
6. Explain why phosphorylation is an effective means of regulating the activities of target proteins.
7. Explain why the mechanism of zymogen activation is important physiologically and how it differs from the other control mechanisms discussed in this chapter.

The activity of enzymes must often be regulated so that they function at the proper time and place. This control is essential for coordination of the vast array of biochemical processes taking place at any instant in an organism. While numerous regulatory mechanisms have been elucidated, this chapter explores four commonly utilized methods: (1) allosteric control by regulatory molecules, (2) alternate enzymes that catalyze the same reactions but exhibit different catalytic and regulatory properties, (3) reversible covalent modifications, and (4) irreversible proteolytic cleavage to yield an active enzyme product. Another method, adjusting the amount of enzyme present, usually takes place at the level of gene transcription and will be discussed in Chapter 31.

7.1 Allosteric Regulation Enables Control of Metabolic Pathways

As we shall discuss in Section 8.1, pyrimidines and purines are the aromatic groups that compose the unique bases found in DNA and RNA. Aspartate transcarbamoylase (ATCase) catalyzes the first step in the biosynthesis of pyrimidines: the condensation of aspartate and carbamoyl phosphate to form *N*-carbamoylaspartate and orthophosphate (**Figure 7.1**). This reaction is the **committed step** in the pathway, which consists of 10 reactions that will ultimately yield the pyrimidine nucleotides uridine triphosphate (UTP) and cytidine triphosphate (CTP). The committed step means that the products of the reaction are committed to ultimate synthesis of the end products of the pathway, in this case UTP and CTP. The committed step, in any pathway, is irreversible under cellular conditions and is the reaction catalyzed by allosteric enzymes. How is ATCase regulated to generate precisely the amount of pyrimidines needed by the cell?

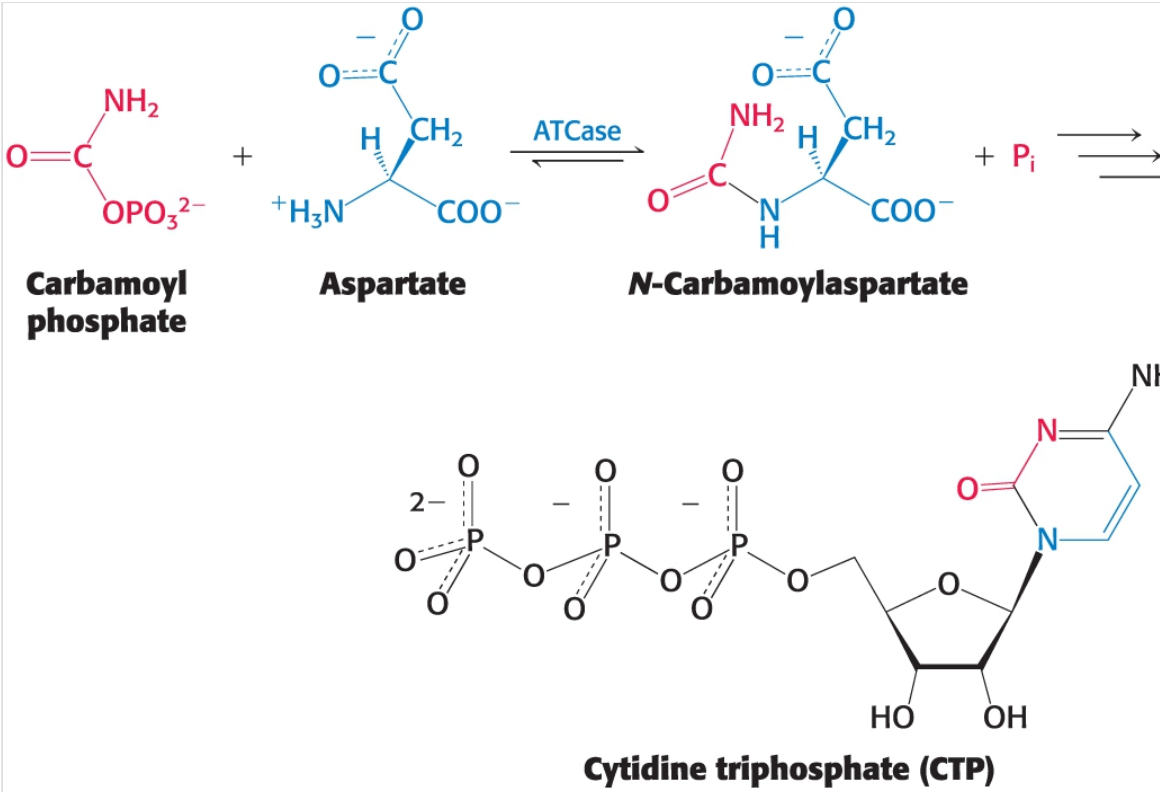


FIGURE 7.1 Aspartate transcarbamoylase (ATCase) catalyzes the committed step in pyrimidir synthesis. The reaction is the condensation of aspartate and carbamoyl phosphate to form *N*-carbamoylaspartate.

ATCase is inhibited by CTP, the final product of the ATCase-initiated pathway. The rate of the reaction catalyzed by ATCase is fast at low concentrations of CTP but slows as CTP concentration increases (Figure 7.2). Thus, the pathway continues to make new pyrimidines until sufficient quantities of CTP have accumulated. The inhibition of ATCase by CTP is an example of **feedback inhibition**, the inhibition of an enzyme by the end product of the pathway. Feedback inhibition by CTP ensures that *N*-carbamoylaspartate and subsequent intermediates in the pathway are not needlessly formed when pyrimidines are abundant.

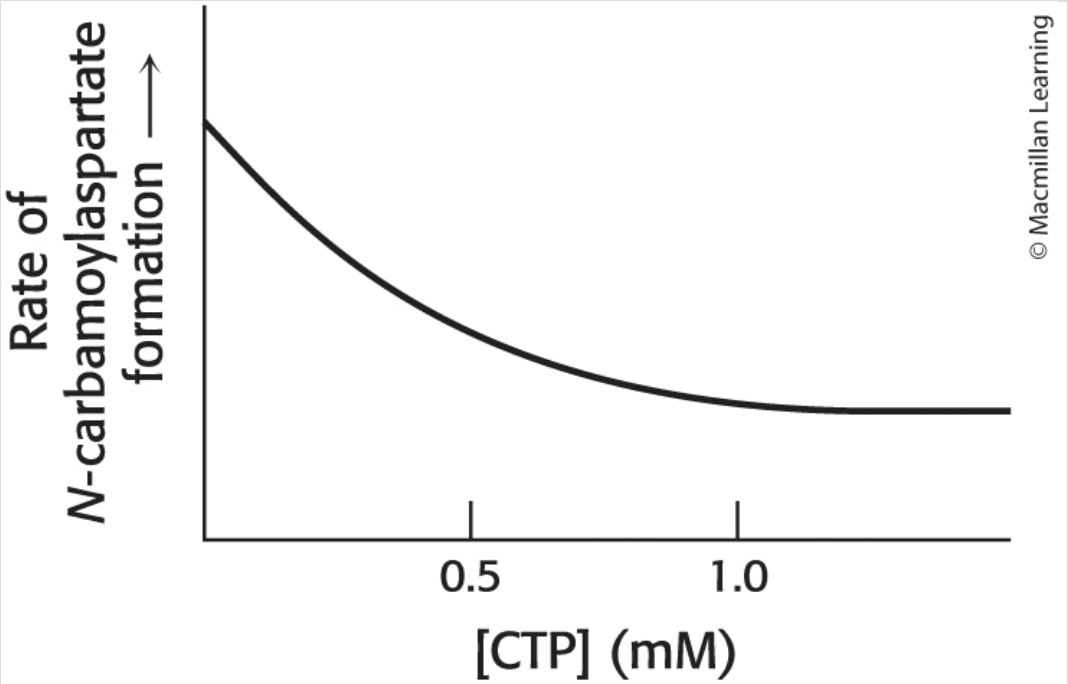


FIGURE 7.2 CTP inhibits ATCase. Cytidine triphosphate, an end product of the pyrimidine-synthesis pathway, inhibits aspartate transcarbamoylase despite having little structural similarity to reactants or products.

The inhibitory ability of CTP is remarkable because CTP is structurally quite different from the substrates of the reaction (Figure 7.1). Thus, CTP must bind to a site distinct from the active site at which substrate binds. Such sites are called **allosteric** (or **regulatory**) **sites**. CTP is an example of an allosteric inhibitor. In ATCase (but not all allosterically regulated enzymes), the catalytic sites and the regulatory sites are on separate polypeptide chains.

Many allosterically regulated enzymes do not follow Michaelis–Menten kinetics

Allosteric enzymes are distinguished by their response to changes in substrate concentration in addition to their susceptibility to regulation

by other molecules. Let us examine the rate of product formation as a function of substrate concentration for ATCase (**Figure 7.3**). The curve differs from that expected for an enzyme that follows Michaelis–Menten kinetics. The observed curve is referred to as sigmoidal because it resembles the letter "S." The vast majority of allosteric enzymes display sigmoidal kinetics. Recall from the discussion of hemoglobin (Chapter 3) that sigmoidal curves result from cooperation between subunits: the binding of substrate to one active site in a molecule increases the likelihood that substrate will bind to other active sites. To understand the basis of sigmoidal enzyme kinetics and inhibition by CTP, we need to examine the structure of ATCase.

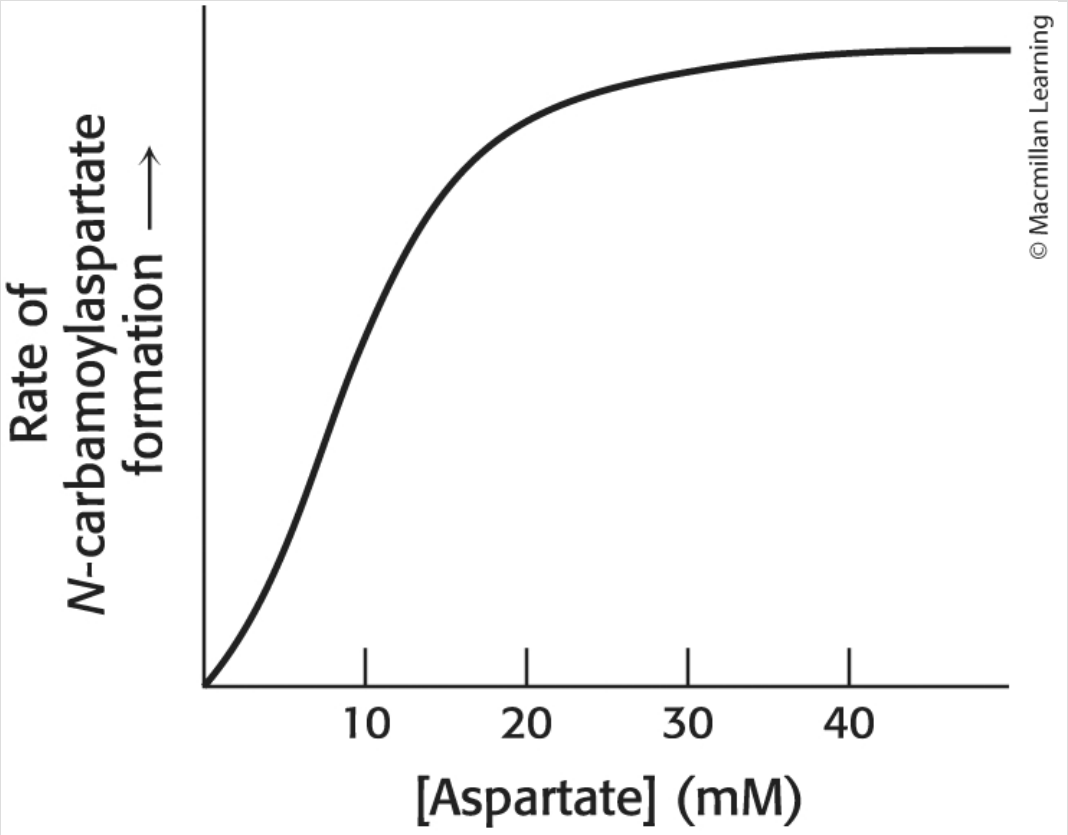


FIGURE 7.3 ATCase displays sigmoidal kinetics. A plot of product formation as a function of substrate concentration produces a sigmoidal curve because the binding of substrate to one active site increases the activity at the other active sites. Thus, the enzyme shows cooperativity.

ATCase consists of separable catalytic and regulatory subunits

What is the evidence that ATCase has distinct regulatory and catalytic sites? ATCase can be separated into regulatory (r) and catalytic (c) subunits by treatment with a mercurial compound such as *p*-hydroxymercuribenzoate, which reacts with sulfhydryl groups and prevents them from re-forming disulfide bonds (**Figure 7.4**). The larger subunit is called the *catalytic subunit.* This subunit has catalytic activity, but when tested by itself, it displays the hyperbolic kinetics of Michaelis–Menten enzymes rather than sigmoidal kinetics. Furthermore, the isolated catalytic subunit is unresponsive to CTP. The isolated smaller subunit can bind CTP but has no catalytic activity. Hence, that subunit is called the *regulatory subunit*. The catalytic subunit (c_3) consists of three c chains (34 kDa each), and the regulatory subunit (r_2) consists of two r chains (17 kDa each).

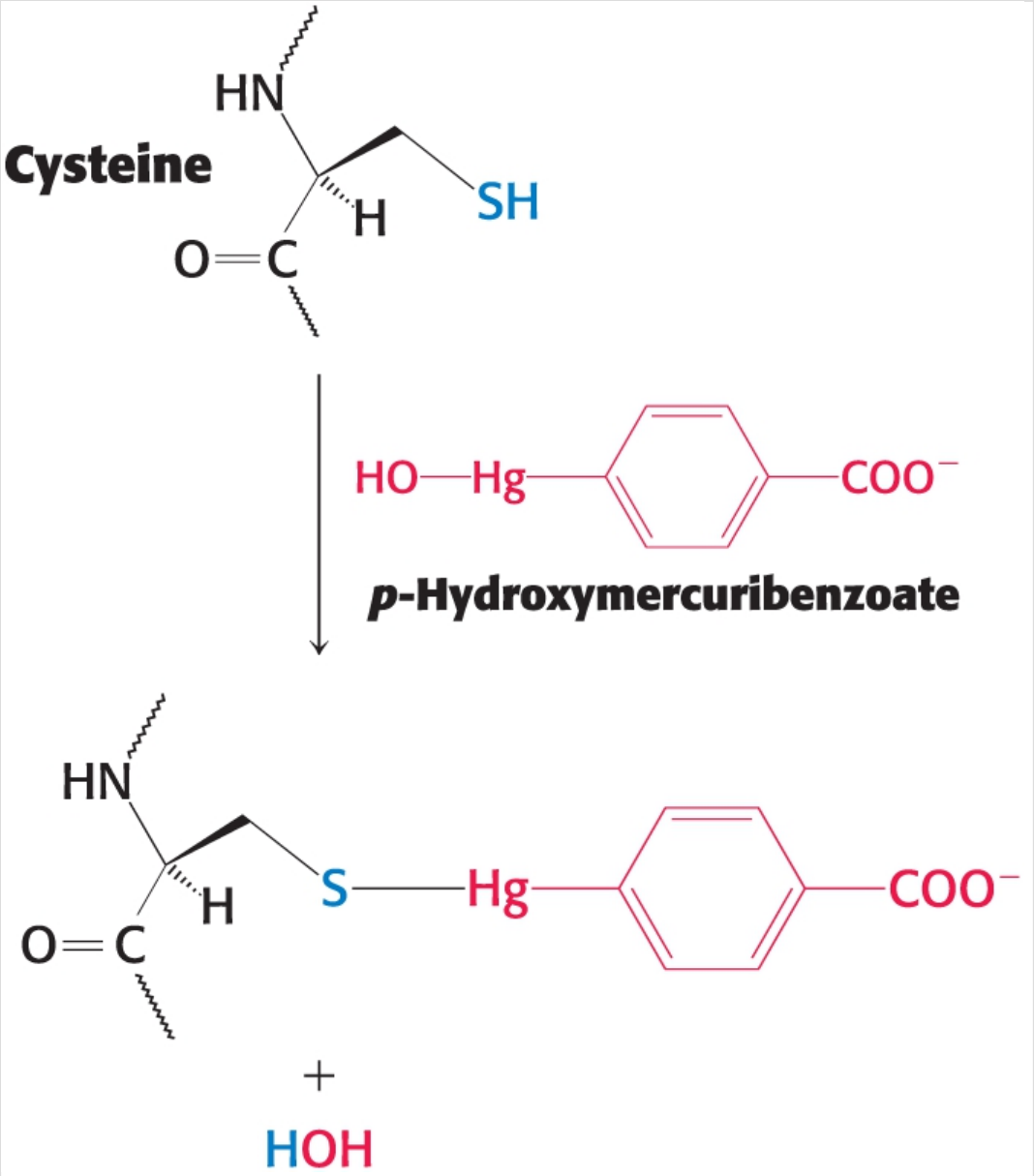


FIGURE 7.4 *p*-Hydroxymercuribenzoate reacts with crucial cysteine residues in aspartate transcarbamoylase. Treatment of ATCase with *p*-hydroxymercuribenzoate separates the enzyme into its regulatory and catalytic subunits.

The catalytic and regulatory subunits combine rapidly when they are mixed. The resulting complex has the same structure, c_6r_6, as the native enzyme: two catalytic trimers and three regulatory dimers.

$$2c_3 + 3r_2 \longrightarrow c_6r_6$$

Most strikingly, the reconstituted enzyme has the same allosteric and kinetic properties as those of the native enzyme. Thus, ATCase is composed of discrete catalytic and regulatory subunits, and the interaction of the subunits in the native enzyme produces its regulatory and catalytic properties. The fact that the enzyme can be separated into isolated catalytic and regulatory subunits, which can be reconstituted back to the functional enzyme, allows for a variety of experiments to characterize the allosteric properties of the enzyme.

Allosteric interactions in ATCase are mediated by large changes in quaternary structure

What are the subunit interactions that account for the properties of ATCase? Significant clues have been provided by the three-dimensional structure of various forms of ATCase (**Figure 7.5**). Two catalytic trimers are stacked one on top of the other, linked by three dimers of the regulatory chains. There are significant contacts between the catalytic and the regulatory subunits: each r chain within a regulatory dimer interacts with a c chain within a catalytic trimer. The c chain makes contact with a structural domain in the r chain that is stabilized by a zinc ion bound to four cysteine residues. The zinc ion is critical for the interaction of the r chain with the c chain. *p*-Hydroxymercuribenzoate is able to dissociate the catalytic and regulatory subunits because mercury binds strongly to the cysteine residues, displacing the zinc and preventing interaction with the c chain.

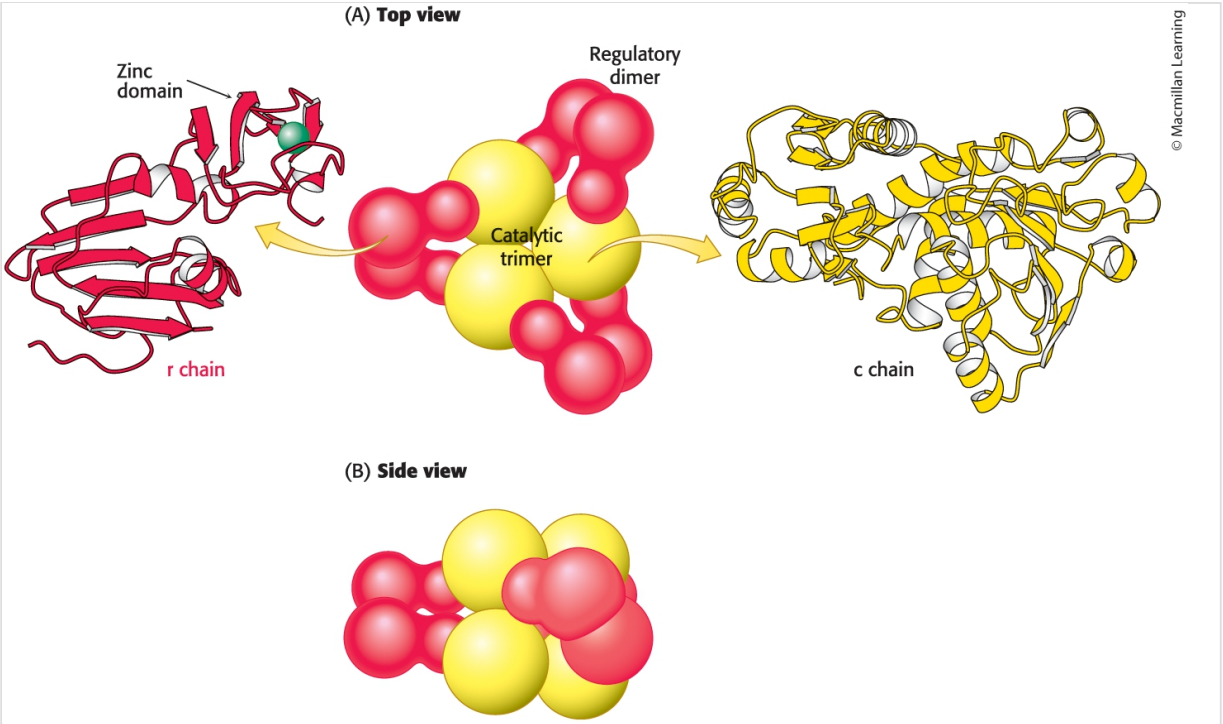


FIGURE 7.5 ATCase consists of a pair of catalytic subunit trimers surrounded by three regulatory subunit dimers. (A) The quaternary structure of aspartate transcarbamoylase as viewed from the top. The drawing in the center is a simplified representation of the relations between subunits. A single catalytic trimer [catalytic (c) chains, shown in yellow] is visible; in this view, the second trimer is hidden below the visible one. Each r chain (red) interacts with a c chain through the zinc domain. (B) A side view of the complex.

[Drawn from 1RAI.pdb.]

INTERACT with this model in Achieve

To locate the active sites, the enzyme has been crystallized in the presence of *N*-(phosphonacetyl)-L-aspartate (PALA), a *bisubstrate analog* (an analog of the two substrates) that resembles an intermediate along the pathway of catalysis (Figure 7.6). PALA is a potent competitive inhibitor of ATCase that binds to and blocks the active sites. The structure of the ATCase–PALA complex reveals that PALA binds at sites lying at the boundaries between pairs of c chains within a catalytic

trimer (Figure 7.7). Each catalytic trimer contributes three active sites to the complete enzyme.

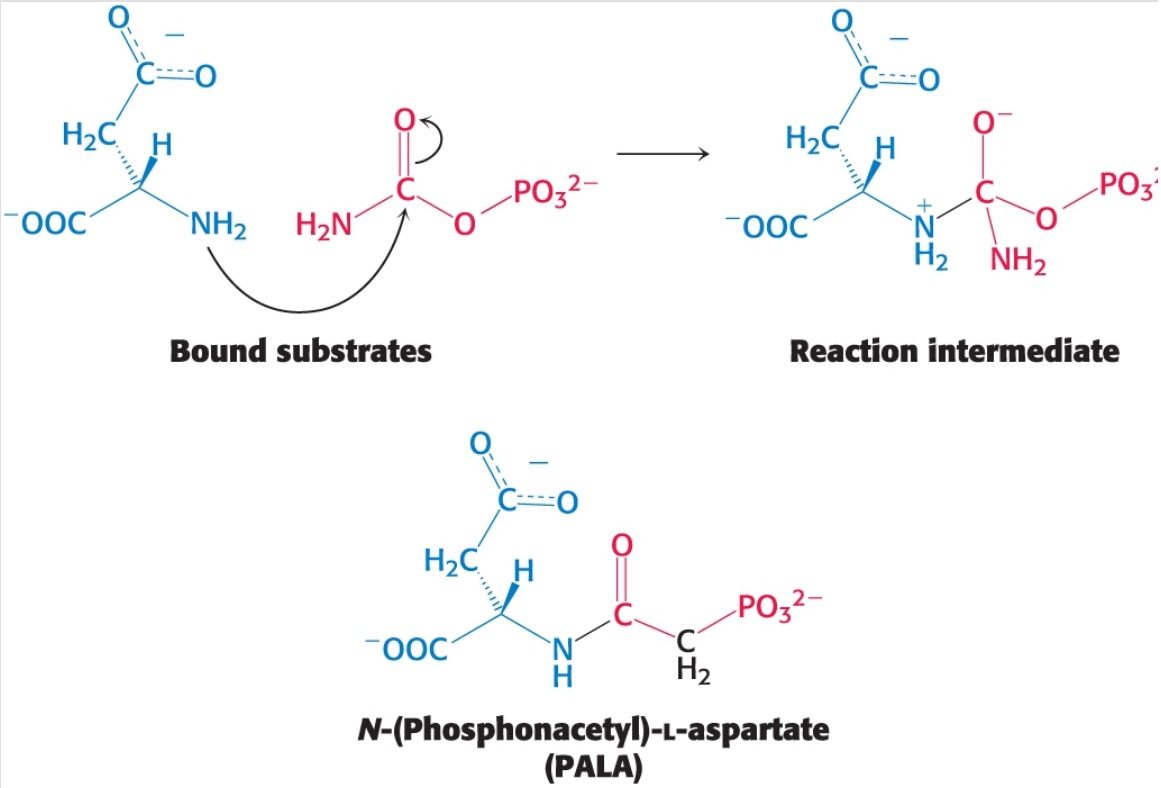


FIGURE 7.6 PALA is a bisubstrate analog representing an intermediate along the ATCase catalytic pathway. (Top) Nucleophilic attack by the amino group of aspartate on the carbonyl carbon atom of carbamoyl phosphate generates an intermediate on the pathway to the formation of *N*-carbamoylaspartate. (Bottom) *N*-(Phosphonacetyl)-L-aspartate (PALA) is an analog of the reaction intermediate and a potent competitive inhibitor of aspartate transcarbamoylase.

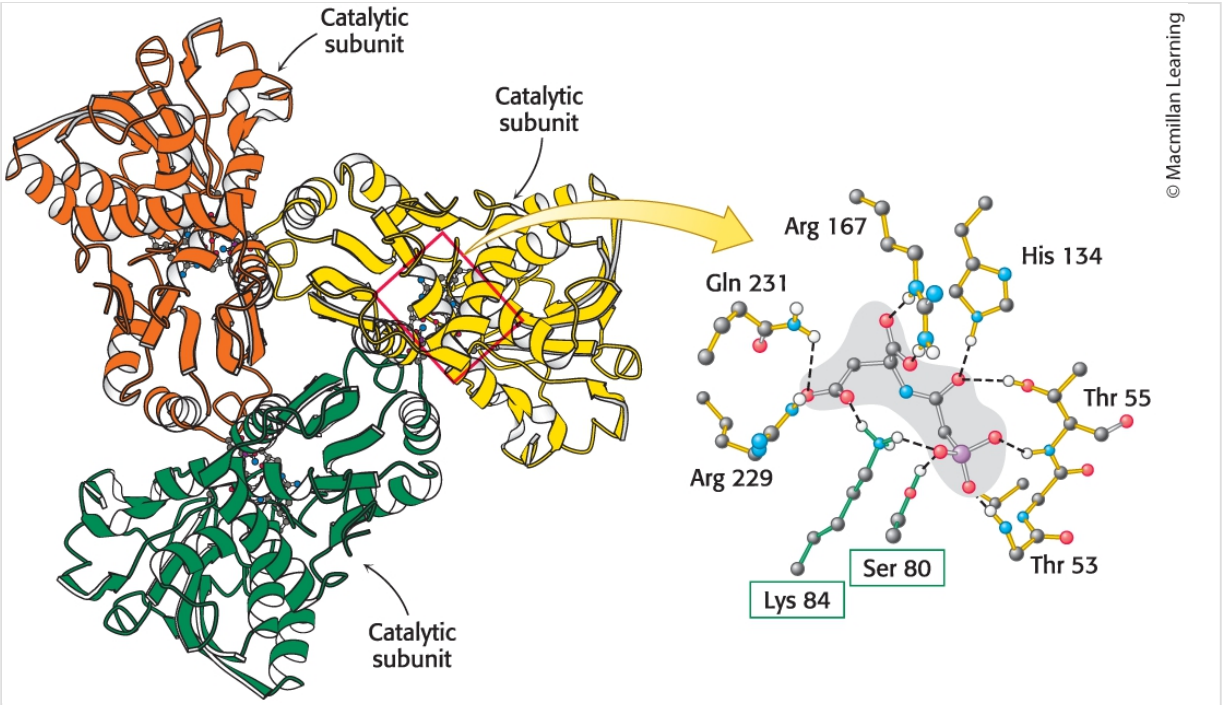


FIGURE 7.7 The structure of PALA bound to ATCase identifies the active site. The catalytic trimer, C_3, of ATCase contains three active sites, each shown bound to a PALA molecule. Some of the crucial active-site residues are shown binding to the inhibitor PALA (shaded gray) via hydrogen bonds (black dotted lines). Notice that an active site is composed mainly of residues from one c chain (yellow bonds), but an adjacent c chain also contributes important residues (green bonds and boxed in green).

[Drawn from 1EKX.pdb.]

INTERACT with this model in Achieve

Further examination of the ATCase–PALA complex reveals a remarkable change in quaternary structure on binding of PALA. The two catalytic trimers move 12 Å farther apart and rotate approximately 10 degrees about their common threefold axis of symmetry. Moreover, the regulatory dimers rotate approximately 15 degrees to accommodate this motion (Figure 7.8). The enzyme literally expands on PALA binding. In essence, ATCase has two distinct quaternary forms: one that predominates in the absence of substrate or substrate analogs, and another that predominates when substrates or analogs are bound. We

call these forms the T (for tense) state and the R (for relaxed) state, respectively, as we did for the two quaternary states of hemoglobin.

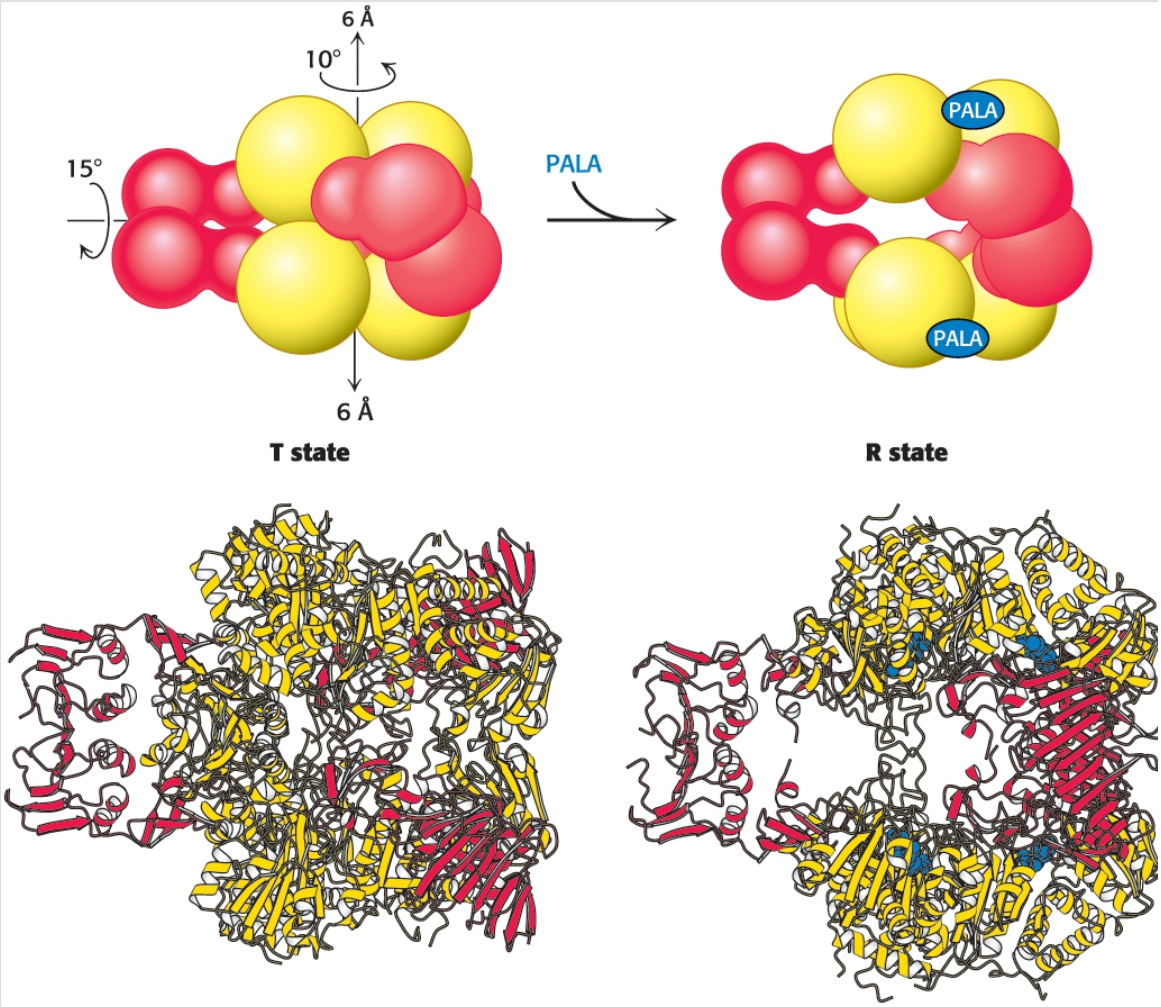


FIGURE 7.8 ATCase exists in two conformations: the tense (T) state and the relaxed (R) state. The structure of ATCase changes dramatically in the transition from the compact, relatively inactive T state to the expanded, active R state. PALA (blue) binding stabilizes the R state.

[Drawn from 6AT1.pdb and 8ATC.pdb.]

How can we explain the enzyme's sigmoidal kinetics in light of the structural observations? Like hemoglobin, the enzyme exists in an equilibrium between the T state and the R state.



In the absence of substrate, almost all the enzyme molecules are in the T state because the T state is energetically more stable than the R state. The ratio of the concentration of enzyme in the T state to that in the R state is called the *allosteric coefficient* (L). For most allosteric enzymes, L is on the order of 10^2 to 10^3.

$$L = \frac{T}{R}$$

The T state has a low affinity for substrate and hence exhibits low catalytic activity. The occasional binding of a substrate molecule to one active site in an enzyme increases the likelihood that the entire enzyme shifts to the R state with its higher binding affinity for substrate.

The addition of more substrate has two effects. First, it increases the probability that each enzyme molecule will bind at least one substrate molecule. Second, it increases the average number of substrate molecules bound to each enzyme. The presence of additional substrate will increase the fraction of enzyme molecules in the more active R state because the position of the equilibrium depends on the number of active sites that are occupied by substrate. We considered this property, called *cooperativity* because the subunits cooperate with one another, when we discussed the sigmoidal oxygen-binding curve of hemoglobin in Chapter 3. The cooperative effects of substrates on allosteric enzymes are also referred to as **homotropic effects** (from the Greek *homós*, "same"), as they reflect the effects of the binding in one site on the

affinity at the comparable site elsewhere in the enzyme. In the case of substrate cooperativity, these homotropic effects act on the enzyme active sites.

Recall that in Chapter 3, we discussed two limiting models for cooperativity: the *concerted* and the *sequential* models (Section 3.3). The mechanism for allosteric regulation of ATCase presented here is best described by the concerted model, as the change in the enzyme is "all or none"; the entire enzyme is converted from T into R, affecting all of the catalytic sites equally. In contrast, the sequential model assumes that the binding of ligand to one site on the complex increases the affinity of neighboring sites without causing a full T-to-R transition of all the sites. Although the concerted model explains the behavior of ATCase well, most other allosteric enzymes exhibit features of both models.

The sigmoidal curve for ATCase can be pictured as a composite of two Michaelis–Menten curves, one corresponding to the less-active T state and the other to the more-active R state. At low concentrations of substrate, the curve closely resembles that of the T state enzyme. As the substrate concentration is increased, the curve progressively shifts to resemble that of the R state enzyme (**Figure 7.9**).

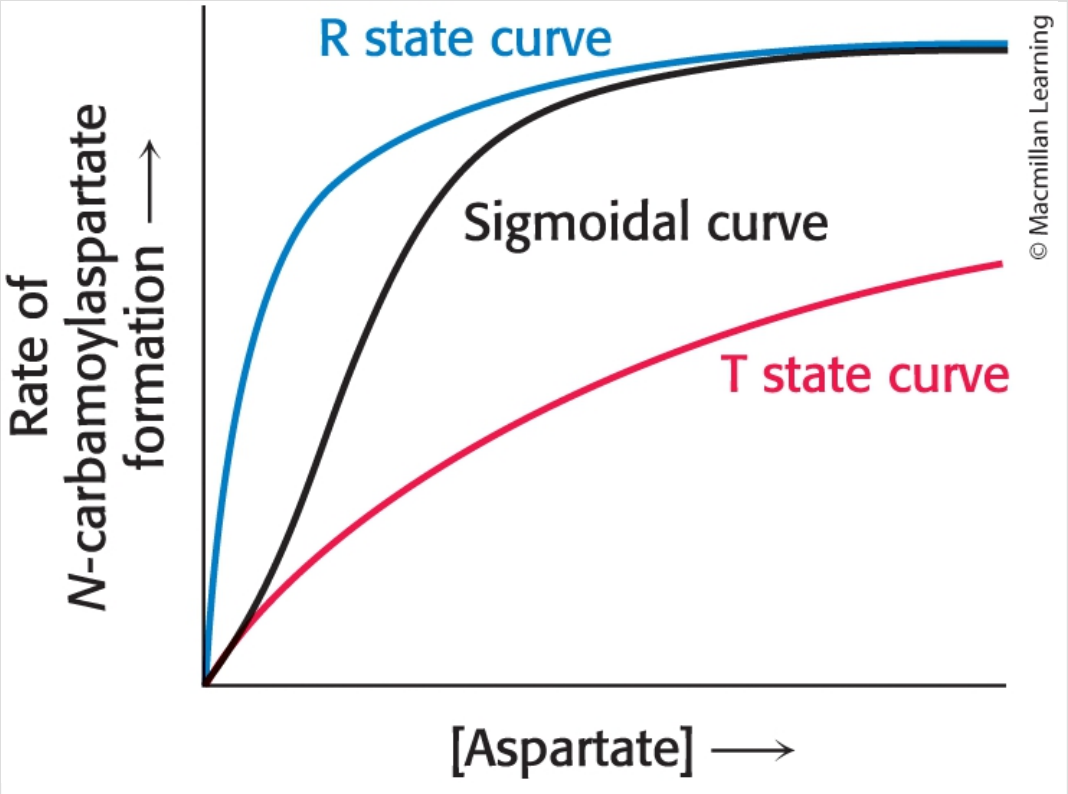


FIGURE 7.9 The sigmoidal curve in cooperative enzymes can be understood as the combination of two Michaelis–Menten enzymes. The first enzyme corresponds to the T state, with a high K_M value, while the second enzyme corresponds to the R state, with a low K_M value. As the concentration of substrate is increased, the equilibrium shifts from the T state to the R state, which results in a steep rise in activity with respect to substrate concentration.

What is the biochemical advantage of sigmoidal kinetics? Allosteric enzymes transition from a less active state to a more active state within a narrow range of substrate concentration. The benefit of this behavior is illustrated in **Figure 7.10**, which compares the kinetics of a Michaelis–Menten enzyme (blue curve) to that of an allosteric enzyme (red curve). In this example, the Michaelis–Menten enzyme requires an approximately 27-fold increase in substrate concentration to increase V_0 from $0.1\ V_{max}$ to $0.8\ V_{max}$. In contrast, the allosteric enzyme requires only about a fourfold increase in substrate concentration to attain the

same increase in velocity. Simply put, the activity of allosteric enzymes is more sensitive to changes in substrate concentration near K_M than are Michaelis–Menten enzymes with the same V_{max}. This sensitivity is called a *threshold effect*: below a certain substrate concentration, there is little enzyme activity. However, after the threshold has been reached, enzyme activity increases rapidly. In other words, much like an "on/off" switch, cooperativity ensures that most of the enzyme is either on (R state) or off (T state). The vast majority of allosteric enzymes display sigmoidal kinetics.

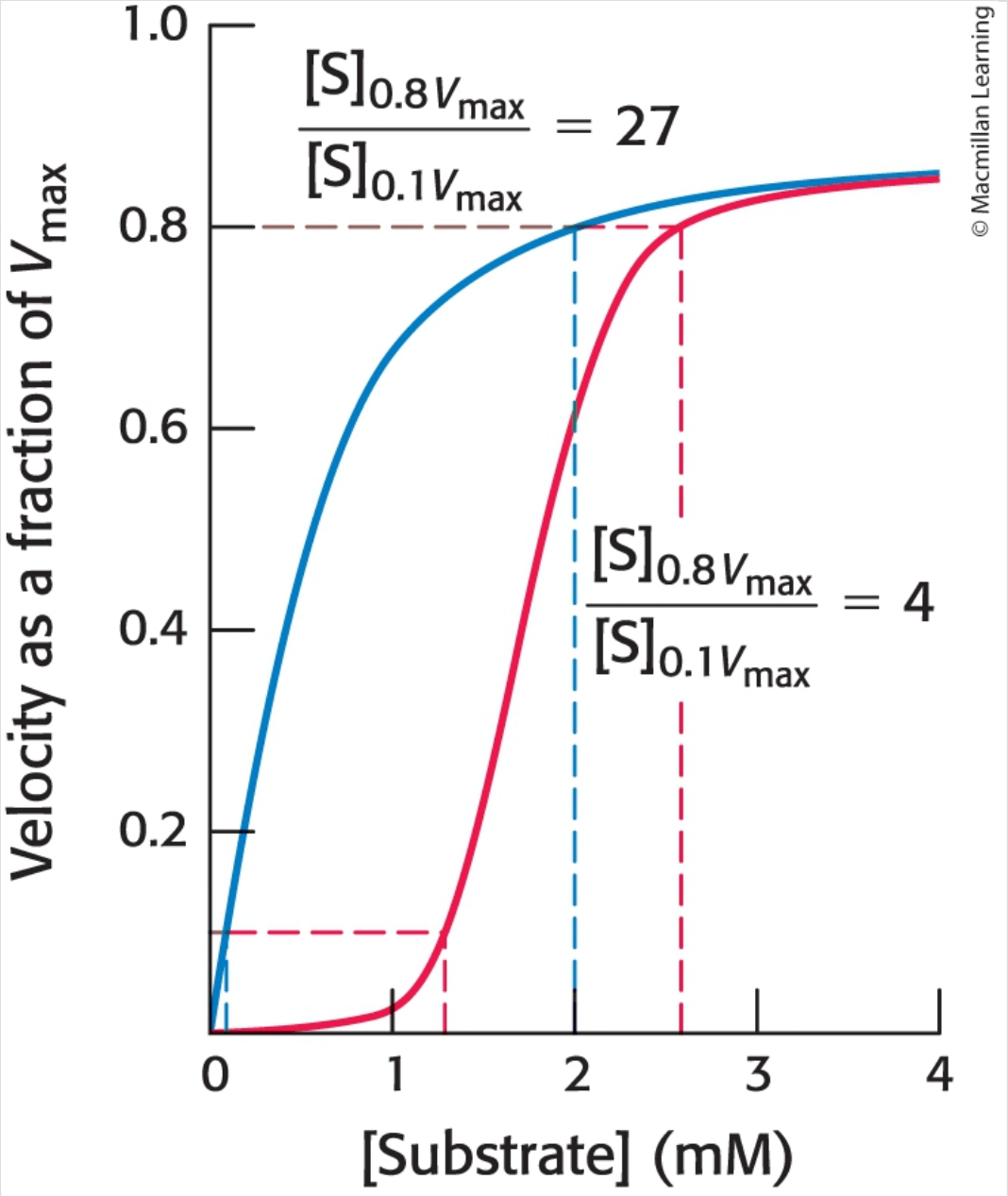


FIGURE 7.10 Allosteric enzymes display threshold effects. As the T-to-R transition occurs, the velocity increases over a narrower range of substrate concentration for an allosteric enzyme (red curve) than for a Michaelis–Menten enzyme (blue curve).

Self-Check Question



What would be the effect of a mutation in an allosteric enzyme that resulted in an allosteric coefficient of 0?

Allosteric regulators modulate the T-to-R equilibrium

We now turn our attention to the effects of pyrimidine nucleotides on ATCase activity. As noted earlier, CTP inhibits the action of ATCase. X-ray studies of ATCase in the presence of CTP reveal (1) that the enzyme is in the T state when bound to CTP and (2) that a binding site for this nucleotide exists in each regulatory chain in a domain that does not interact with the catalytic subunit (**Figure 7.11**). Each active site is more than 50 Å from the nearest CTP-binding site. The question naturally arises: how can CTP inhibit the catalytic activity of the enzyme when it does not interact with the catalytic chain?

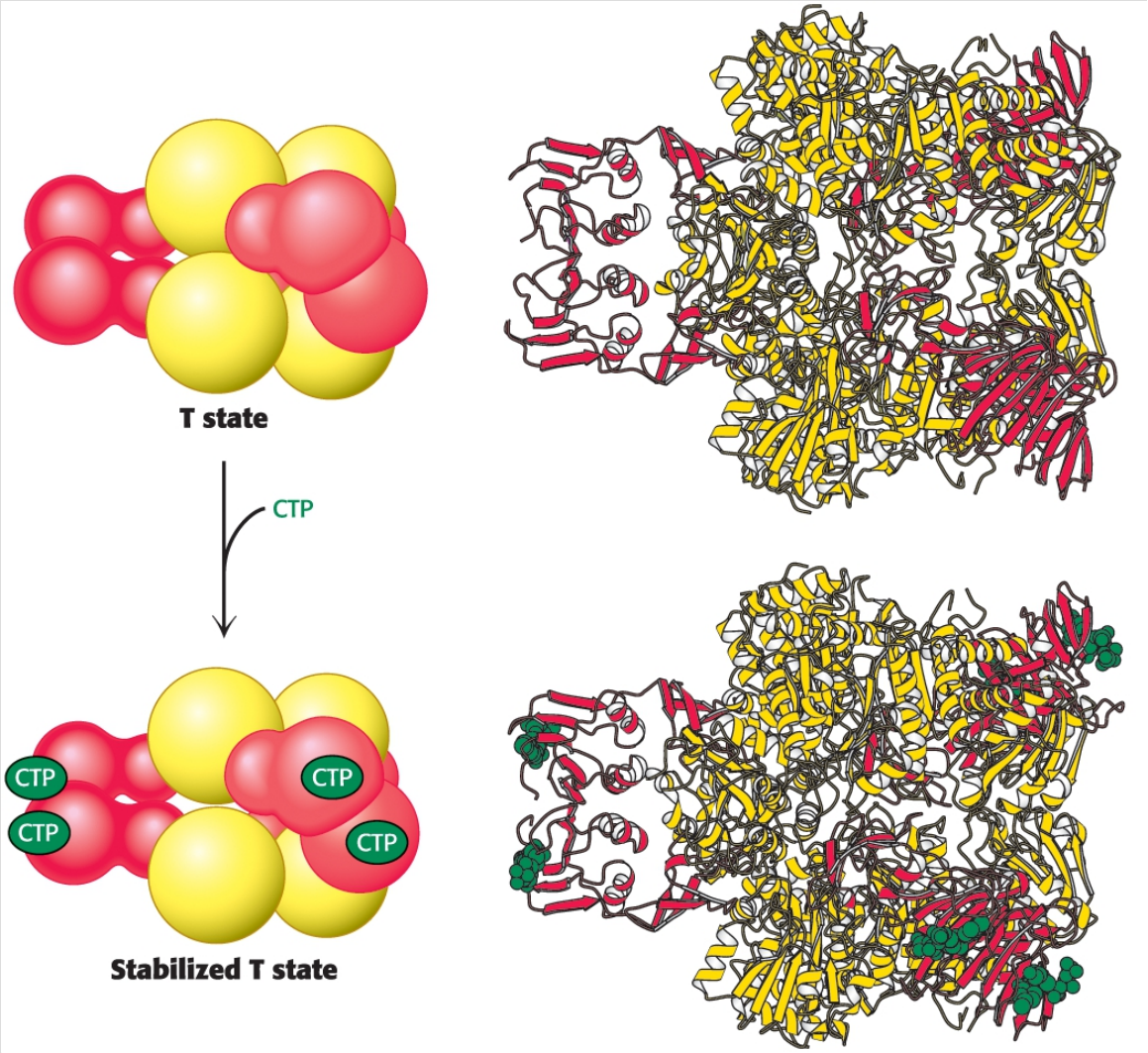


FIGURE 7.11 CTP stabilizes the T state. The binding of CTP (green) to the regulatory subunit of ATCase stabilizes the T state.

[Drawn from 6AT1.pdb and 5AT1.pdb.]

The quaternary structural changes observed on substrate-analog binding suggest a mechanism for inhibition by CTP (Figure 7.12). The binding of the inhibitor CTP to the T state shifts the T-to-R equilibrium in favor of the T state, decreasing net enzyme activity. CTP increases the allosteric coefficient from 200 in its absence to 1250 when all of the regulatory sites are occupied by CTP. Because the binding of CTP makes

it more difficult for substrate binding to convert the enzyme into the R state, CTP increases the initial phase of the sigmoidal curve (Figure 7.13). More substrate is required to attain a given reaction rate. UTP, the immediate precursor to CTP, also regulates ATCase. While unable to inhibit the enzyme alone, UTP synergistically inhibits ATCase in the presence of CTP.

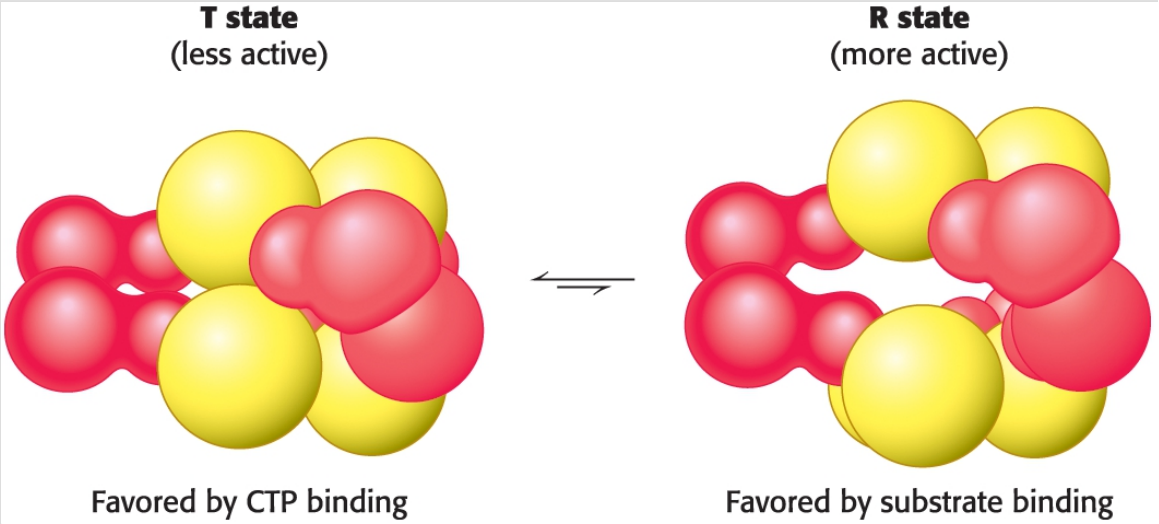


FIGURE 7.12 The R state and the T state are in equilibrium. Even in the absence of any substra or regulators, ATCase exists in equilibrium between the R and the T states. Under these conditions, the T state is favored by a factor of approximately 200.

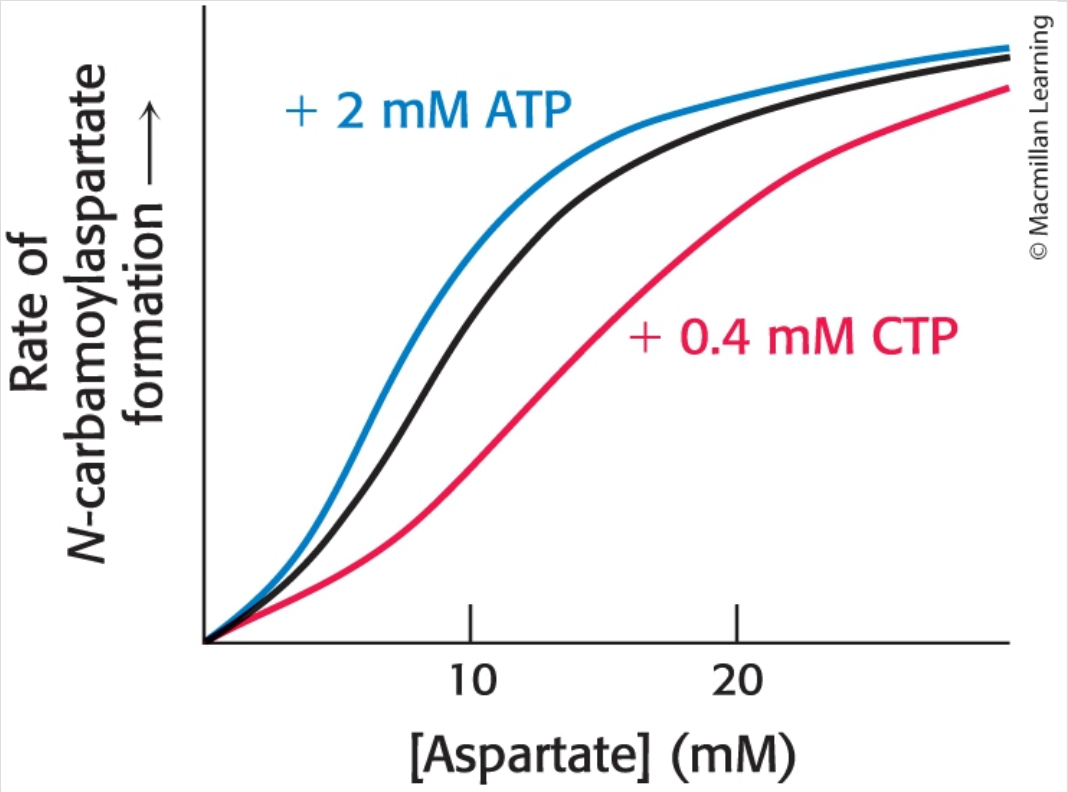


FIGURE 7.13 CTP and ATP impact ATCase kinetics differently. CTP stabilizes the T state of ATCase, making it more difficult for substrate binding to convert the enzyme into the R state. As a result, the curve is shifted to the right, as shown in red. ATP is an allosteric activator of ATCase because it stabilizes the R state, making it easier for substrate to bind. As a result, the curve is shifted to the left, as shown in blue.

Interestingly, ATP, too, is an allosteric effector of ATCase, binding to the same site as CTP. However, ATP binding stabilizes the R state, lowering the allosteric coefficient from 200 to 70 and thus *increasing* the reaction rate at a given aspartate concentration (Figure 7.13). Hence, ATP is an allosteric activator of ATCase, while CTP is an allosteric inhibitor. In the presence of sufficient ATP, the kinetic profile shows a less-pronounced sigmoidal behavior. Because ATP and CTP bind at the same site, high levels of ATP prevent CTP from inhibiting the enzyme. The effects of nonsubstrate molecules on allosteric enzymes (such as those of CTP and ATP on ATCase) are referred to as **heterotropic effects** (from the Greek

héteros, "different"), since they bind at sites distinct from the sites that they affect. In the case of ATCase, CTP and ATP binding at their corresponding site acts on the enzyme active site. In summary, substrates generate the sigmoidal curve (homotropic effects), whereas regulators shift the K_M (heterotropic effects). Note, however, that both types of effects impact ATCase activity by altering the T/R ratio.

The increase in ATCase activity in response to increased ATP concentration has two potential physiological ramifications. First, high ATP concentration signals a high concentration of purine nucleotides in the cell; the increase in ATCase activity will tend to balance the purine and pyrimidine pools. As we shall see in Chapter 8, this balance is important for the structure and synthesis of DNA. Second, a high concentration of ATP indicates that energy is available for mRNA synthesis and DNA replication and leads to the synthesis of pyrimidines needed for these processes.

7.2 Isozymes Provide a Means of Regulation Specific to Distinct Tissues and Developmental Stages

Enzymes that differ in amino acid sequence yet catalyze the same reaction are called **isozymes**, or **isoenzymes**. Typically, these enzymes display different kinetic parameters, such as K_M, or respond to different regulatory molecules. They are encoded by different genes, which usually arise through gene duplication and divergence. Isozymes can often be distinguished from one another by physical properties such as electrophoretic mobility. *Isoform* is a more generic term used when the protein in question is not an enzyme.

The existence of isozymes permits the fine-tuning of metabolism to meet the needs of a given tissue or developmental stage. Consider the example of lactate dehydrogenase (LDH), an enzyme that catalyzes a step in anaerobic glucose metabolism and glucose synthesis. Human beings have two isozymic polypeptide chains for this enzyme: the H protein is highly expressed in heart muscle, and the M protein is highly expressed in skeletal muscle. The amino acid sequences are 75% identical. Each functional enzyme is tetrameric, and many different combinations of the two isozymic polypeptide chains are possible. The H_4 isozyme, found in the heart, has a higher affinity for substrates than does the M_4 isozyme. In addition, high levels of pyruvate allosterically inhibit the H_4 but not the M_4 isozyme. The other combinations, such as H_3M, have intermediate properties. We will consider these isozymes in their biological context in Chapter 16.

The M_4 isozyme functions optimally in the anaerobic environment of hardworking skeletal muscle, whereas the H_4 isozyme does so in the aerobic environment of heart muscle. Indeed, the proportions of these isozymes change throughout the development of the rat heart as the tissue switches from an anaerobic environment to an aerobic one (Figure 7.14A). The distribution of tissue-specific forms of lactate dehydrogenase in adult rat tissues is shown in Figure 7.14B. Essentially all of the enzymes that we will encounter in later chapters, including allosteric enzymes, exist in isozymic forms.

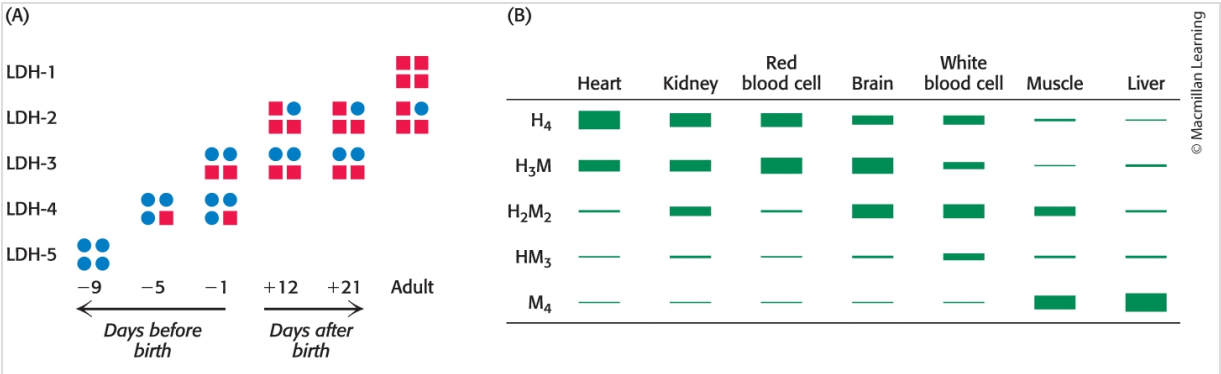


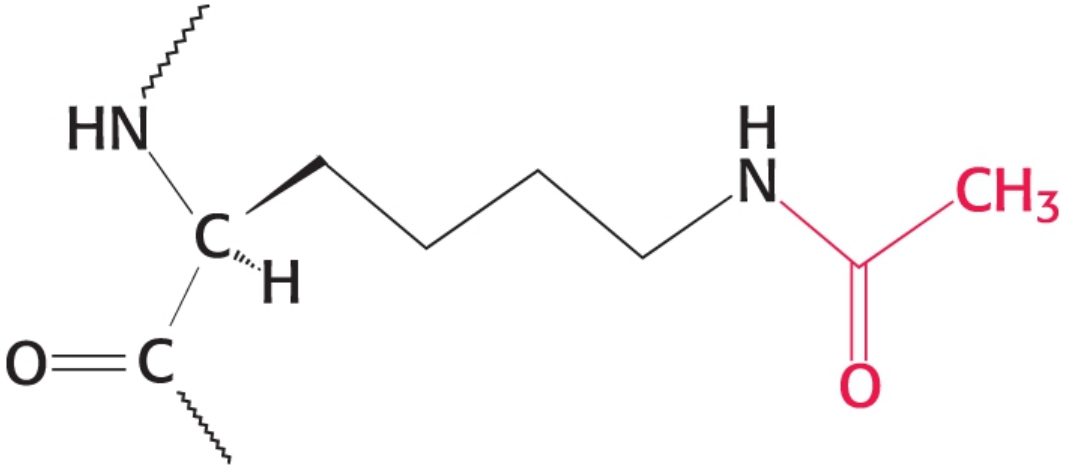
FIGURE 7.14 The five isozymes of lactate dehydrogenase differ in their timing of expression during development and their tissue specificity. (A) The rat heart lactate dehydrogenase (LDH) isozyme profile changes in the course of development. The H isozyme is represented by squares and the M isozyme by circles. (B) LDH isozyme content varies by tissue. The thickness of the green bars represents the relative amounts of the isozymes.

[(A) Data from W.-H. Li, *Molecular Evolution* (Sinauer, 1997), p. 283; (B) Source: K. Urich, *Comparative Animal Biochemistry* (Springer Verlag, 1990), p. 542.]

7.3 Covalent Modification Is a Means of Regulating Enzyme Activity

For many enzymes, the covalent attachment of a modifying functional group can markedly alter its catalytic activity. Most covalent modifications are reversible. Phosphorylation and dephosphorylation are common means of reversible covalent modification, which we discuss in detail below.

The attachment of acetyl groups to lysine residues by acetyltransferases and their removal by deacetylases are another example of reversible covalent modifications. Histones — proteins that are packaged with DNA into chromosomes — are extensively acetylated and deacetylated in vivo on lysine residues (Section 31.5). More heavily acetylated histones are associated with genes that are being actively transcribed. Although protein acetylation was originally discovered as a modification of histones, we now know that it is a major means of regulation, with more than 2000 different proteins in mammalian cells regulated by acetylation. Protein acetylation appears to be especially important in the regulation of metabolism. The acetyltransferase and deacetylase enzymes are themselves regulated by phosphorylation, showing that the covalent modification of a protein can be controlled by the covalent modification of the modifying enzymes.



Acetylated lysine

In some cases, the covalent modification is not reversible. The irreversible attachment of a lipid group causes some proteins in signal-transduction pathways, such as Ras (a GTPase), to become affixed to the cytoplasmic face of the plasma membrane. Fixed in this location, the proteins are better able to receive and transmit information that is being passed along their signaling pathways (Section 14.4). Mutations in Ras are seen in a wide array of cancers.

Virtually all metabolic processes are regulated in part by covalent modification. Indeed, the allosteric properties of many enzymes are altered by covalent modification. **Table 7.1** lists some common covalent modifications.

TABLE 7.1 Common covalent modifications of protein activity

Modification	Donor molecule	Example of modified protein	Protein function

Phosphorylation	ATP	Glycogen phosphorylase	Glucose homeostasis; energy transduction
Acetylation	Acetyl CoA	Histones	DNA packing; transcription
Myristoylation	Myristoyl CoA	Src	Signal transduction
ADP ribosylation	NAD^+	RNA polymerase	Transcription
Farnesylation	Farnesyl pyrophosphate	Ras	Signal transduction
γ-Carboxylation	HCO_3^-	Thrombin	Blood clotting
Sulfation	$3'$-Phosphoadenosine-$5'$-phosphosulfate	Fibrinogen	Blood clot formation
Ubiquitination	Ubiquitin	Cyclin	Control of cell cycle

Kinases and phosphatases control the extent of protein phosphorylation

Phosphorylation is a regulatory mechanism in virtually every metabolic process in eukaryotic cells. Indeed, as much as 30% of eukaryotic proteins are phosphorylated. The enzymes catalyzing the phosphorylation of protein substrates are called **protein kinases**. These enzymes constitute one of the largest protein families known: there are

more than 500 homologous protein kinases in human beings. This multiplicity of enzymes allows regulation to be fine-tuned according to a specific tissue, time, or substrate.

ATP is the most common donor of phosphoryl groups. The terminal (γ) phosphoryl group of ATP is transferred to a specific amino acid of the acceptor protein or enzyme. In eukaryotes, the acceptor residue is commonly one of the three containing a hydroxyl group in its side chain. Transfers to serine and threonine residues are handled by one class of protein kinases and transfers to tyrosine residues by another. Tyrosine kinases, which are unique to multicellular organisms, play pivotal roles in growth regulation, and mutations in these enzymes are commonly observed in cancer cells (Section 14.3).

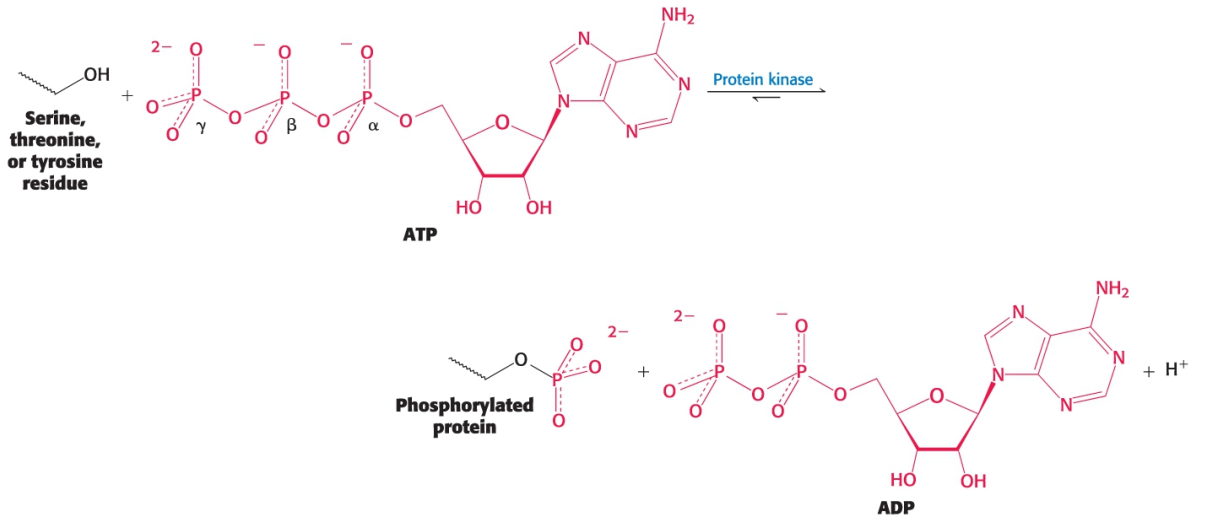


Table 7.2 lists a few of the known serine and threonine protein kinases. Proteins that undergo protein-phosphorylation reactions are located inside cells, where the phosphoryl-group donor ATP is abundant. Proteins that are entirely extracellular are not regulated by reversible phosphorylation.

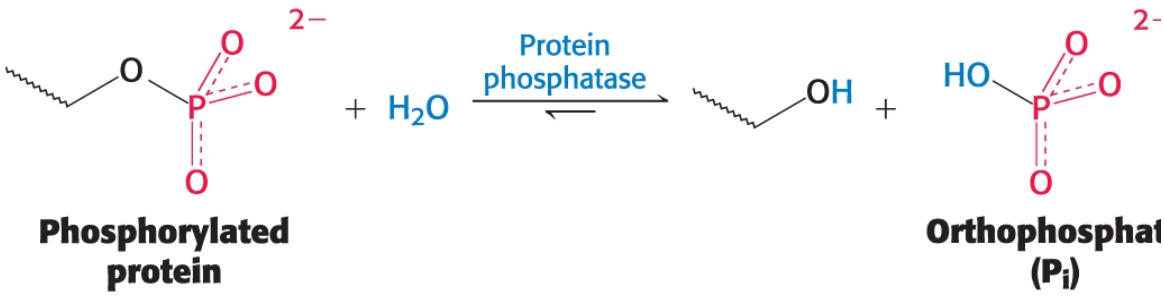
TABLE 7.2 Examples of serine and threonine kinases and their activating signals

Signal	Enzyme
Cyclic nucleotides	Cyclic AMP-dependent protein kinase Cyclic GMP-dependent protein kinase
Ca^{2+} and calmodulin	Calmodulin-dependent protein kinase Phosphorylase kinase Glycogen synthase kinase
AMP	AMP-activated kinase
Diacylglycerol	Protein kinase C
Metabolic intermediates and other "local" effectors	Many target-specific enzymes, such as pyruvate dehydrogenase kinase and branched-chain ketoacid dehydrogenase kinase

Source: Information from D. Fell, *Understanding the Control of Metabolism* (Portland Press, 1997), Table 7.2.

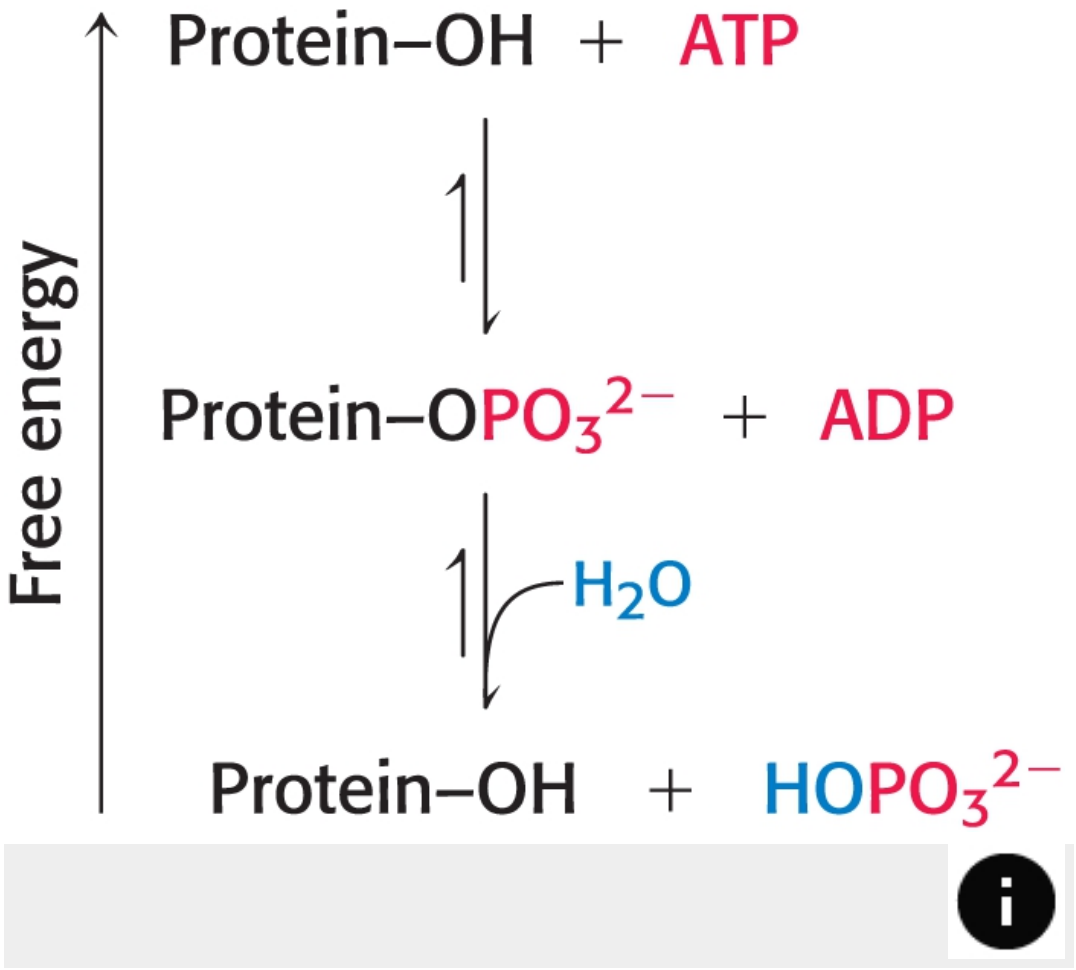
Comparisons of amino acid sequences of many phosphorylation sites show that an individual kinase may recognize many related sequences. For example, the **consensus sequence** recognized by protein kinase A is Arg-Arg-X-*Ser*-Z or Arg-Arg-X-*Thr*-Z, in which X is a small residue, Z is a large hydrophobic one, and *Ser* or *Thr* is the site of phosphorylation. However, this sequence is not absolutely required. Lysine, for example, can substitute for one of the arginine residues but with some loss of affinity. Thus, the primary determinant of specificity is the amino acid sequence surrounding the serine or threonine phosphorylation site. However, distant residues can contribute to specificity. For instance, a change in protein conformation can open or close access to a possible phosphorylation site.

Protein phosphatases reverse the effects of kinases by catalyzing the removal of phosphoryl groups attached to proteins. The enzyme hydrolyzes the bond attaching the phosphoryl group.



The unmodified hydroxyl-containing side chain is regenerated and orthophosphate (P_i) is produced. These enzymes, of which there are about 200 members in human beings, play a vital role in cells because they turn off the signaling pathways that are activated by kinases. One class of highly conserved phosphatases called PP2A suppresses the cancer-promoting activity of certain kinases.

Importantly, the phosphorylation and dephosphorylation reactions are not the reverse of one another; each is essentially irreversible under physiological conditions. Furthermore, both reactions take place at negligible rates in the absence of enzymes. Thus, phosphorylation of a protein substrate will take place only through the action of a specific protein kinase and at the expense of ATP cleavage, and dephosphorylation will take place only through the action of a phosphatase. The result is that target proteins cycle between unphosphorylated and phosphorylated forms. The rate of cycling between the phosphorylated and the unphosphorylated states depends on the relative activities of the specific kinases and phosphatases.



Phosphorylation is a highly effective means of regulating the activities of target proteins

Phosphorylation is a common covalent modification of proteins in all forms of life, which leads to the question: What makes protein phosphorylation so valuable in regulating protein function that its use is ubiquitous? Phosphorylation is a highly effective means of controlling the activity of proteins for several reasons:

- *The free energy of phosphorylation is large.* Of the $-50\ \text{kJ mol}^{-1}\ (-12\ \text{kcal mol}^{-1})$ provided by ATP, about half is consumed in making phosphorylation irreversible; the other half is

conserved in the phosphorylated protein. A free-energy change of $5.69\ \text{kJ mol}^{-1}$ $(1.36\ \text{kcal mol}^{-1})$ corresponds to a factor of 10 in an equilibrium constant. Hence, phosphorylation can change the conformational equilibrium between different functional states by a large factor, of the order of 10^4. In essence, the energy expenditure allows for a stark shift from one conformation to another.

- *A phosphoryl group adds two negative charges to a protein.* These new charges may disrupt electrostatic interactions present in the unmodified protein and allow new electrostatic interactions to be formed. Such structural changes can markedly alter substrate binding and catalytic activity.

- *A phosphoryl group can form three or more hydrogen bonds.* The tetrahedral geometry of a phosphoryl group makes these bonds highly directional, allowing for specific interactions with hydrogen-bond donors.

- *Phosphorylation and dephosphorylation can take place in less than a second or over a span of hours*. The kinetics can be adjusted to meet the timing needs of a particular physiological process.

- *Phosphorylation often evokes highly amplified effects.* A single activated kinase can phosphorylate hundreds of target proteins in a short interval. If the target protein is an enzyme, it can in turn transform a large number of substrate molecules.

- *ATP is the cellular energy currency*. The use of this compound as a phosphoryl-group donor links the energy status of the cell to the regulation of metabolism (Section 15.2).

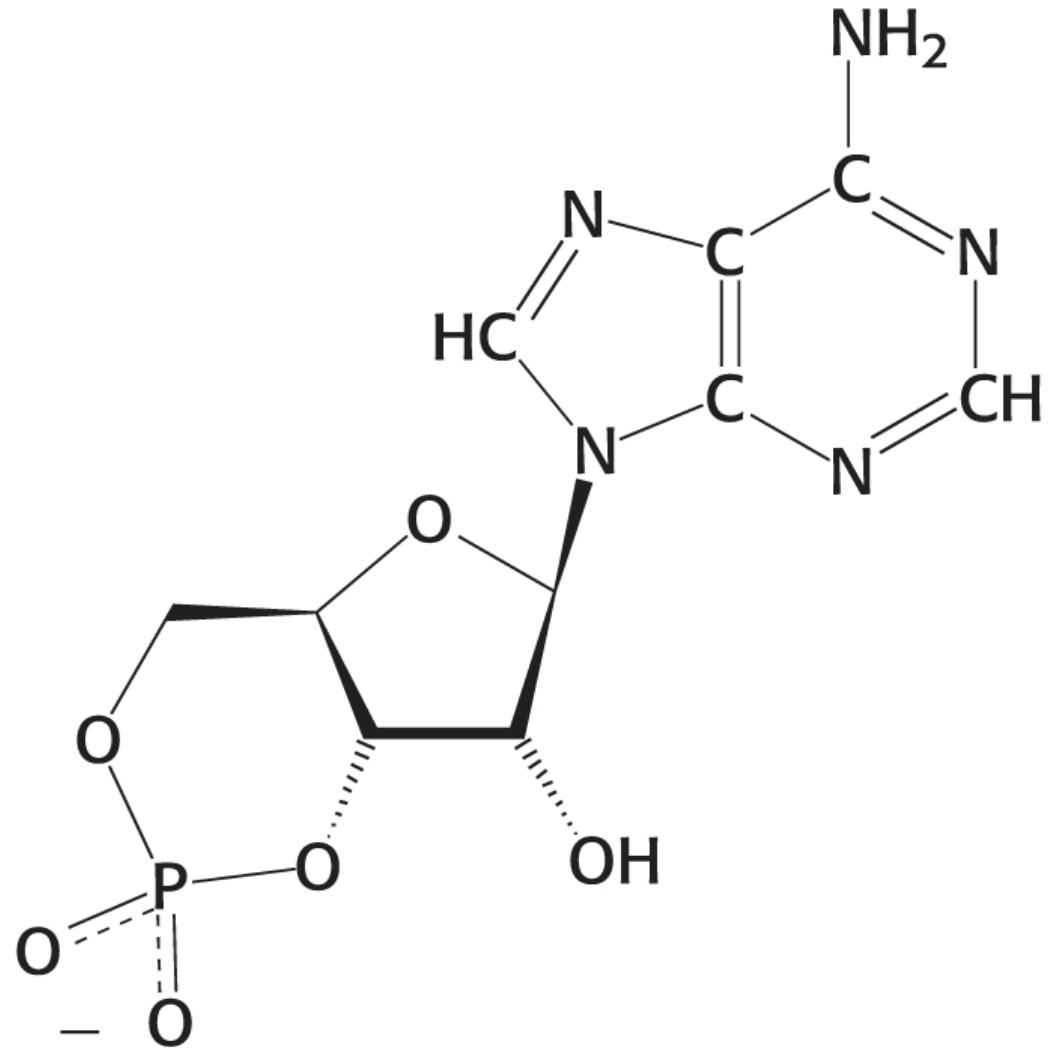
Self-Check Question



What is the energy cost associated with a single cycle of phosphorylation by a protein kinase and dephosphorylation by a protein phosphatase?

Cyclic AMP activates protein kinase A by altering the quaternary structure

Let us examine a specific protein kinase that helps animals, including humans, cope with stressful situations. As we shall see in Section 14.2, the "fight-or-flight" response — including an increase in heart rate, dilation of the airway muscles, and constriction of the blood vessels in muscle — is common to many animals presented with a dangerous or exciting situation. This response is the result of the activity of the hormone epinephrine (also called adrenaline), which triggers the formation of cyclic AMP (cAMP), an intracellular messenger formed by the cyclization of ATP. Cyclic AMP subsequently activates a key enzyme, protein kinase A (PKA). This kinase alters the activities of target proteins by phosphorylating specific serine or threonine residues. The striking finding is that most effects of cAMP in eukaryotic cells are achieved through the activation of PKA by cAMP.



Cyclic adenosine monophosphate (cAMP)

Similar to ATCase, PKA provides an example of allosteric regulation of enzyme activity. In fact, the quaternary structure of PKA is reminiscent of that of ATCase in that it is comprised of distinct regulatory and catalytic subunits. In the absence of cAMP, the 49-kDa regulatory (R) and 38-kDa catalytic (C) subunits of PKA in muscle form an R_2C_2

complex that is enzymatically inactive (Figure 7.15). The binding of two molecules of cAMP to each of the regulatory subunits leads to the dissociation of R_2C_2 into an R_2 subunit and two C subunits. These free catalytic subunits are enzymatically active. Thus, the binding of cAMP to the regulatory subunit relieves its inhibition of the catalytic subunit. PKA, like most other kinases, exists in isozymic forms for fine-tuning regulation to meet the needs of a specific cell or developmental stage. In mammals, four isoforms of the R subunit and three of the C subunit are encoded in the genome.

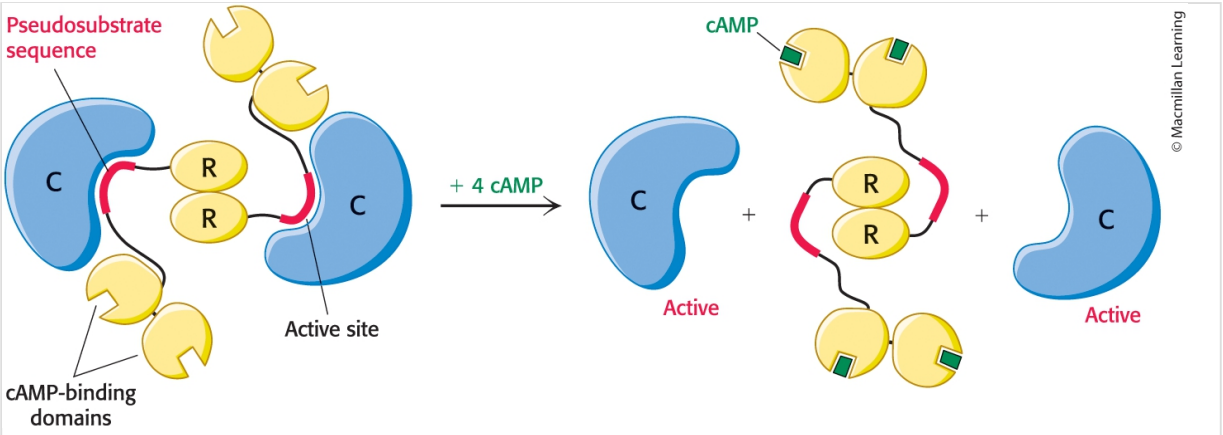


FIGURE 7.15 The binding of cAMP to the regulatory subunits of PKA activates the kinase. The binding of four molecules of cAMP activates protein kinase A by dissociating the inhibited holoenzyme (R_2C_2) into a regulatory subunit (R_2) and two catalytically active subunits (C). Each R chain includes cAMP-binding domains and a pseudosubstrate sequence.

INTERACT with this model in Achieve

How does the binding of cAMP activate the kinase? All four isoforms of the R chain contain an inhibitor site sequence which binds in the active site pocket of the C chains. Two of these R chains contain the sequence Arg-Arg-Gly-*Ala*-Ile, which matches the consensus sequence for phosphorylation except for the presence of alanine in place of serine. In the R_2C_2 complex, this **pseudosubstrate sequence** of R occupies the

catalytic site of C, thereby preventing the entry of protein substrates (Figure 7.15). The remaining two R chains contain the sequence Arg-Arg-Gly-Ser-Ile. In the tetrameric complex, these sequences are packed into the catalytic site of the C chain such that ATP cannot bind, keeping these sequences unphosphorylated. In either case, the binding of cAMP to the R chains allosterically moves the inhibitor site sequences out of the catalytic domains.

Kinetic studies of the activated form of PKA indicate that cAMP enhances the dissociation rate of the C chain from the R chain by almost 700-fold. The released C chains are then free to bind and phosphorylate substrate proteins. However, even after this rate enhancement, the binding affinity between the R and C chains is still significant, and R chains are present in the cell in large molar excess. The net result is that while C chains are free to exert their cellular effects, they are probably re-captured quite rapidly by the R subunits. Hence, the activation mechanism of PKA has evolved to enable control over the active form of kinase.

Mutations in protein kinase A can cause Cushing's syndrome



As we have just seen, the allosteric regulation of kinases such as PKA enables precise timing for the activation and the inhibition of their catalytic activities. The significance of this control is emphasized by disease states in which these mechanisms fail. For example, Cushing's syndrome, a collection of diseases resulting from excess cortisol secretion by the adrenal cortex, is a metabolic disorder characterized by a variety of symptoms such as muscle weakness, thinning skin that is easily bruised, and osteoporosis. Cortisol, a steroid hormone (Section 27.4), has a number of physiological effects including stimulation of

glucose synthesis, suppression of the immune response, and inhibition of bone growth.

The most common cause of Cushing's syndrome, called Cushing's disease, is a tumor of the pituitary gland that overstimulates cortisol secretion by the adrenal cortex. Mutations within the catalytic subunit of PKA have been identified in a number of patients with these tumors. These mutations disrupt the interaction between the R and C subunits. Thus, the enzyme is active even in the absence of cAMP, with the ultimate result being unregulated secretion of cortisol. In Section 14.5, we will discuss other instances where dysregulation of enzymes can lead to disease.

The phosphorylation states of the proteome can be measured

In Section 4.3, we introduced the concept of the proteome, the array of proteins expressed within a cell at a given time under specific conditions. The techniques used to study the proteome have been expanded to include the analysis of protein phosphorylation under specific conditions. The **phosphoproteome** is the name given to all proteins that are modified by phosphorylation. Through study of the phosphoproteome, termed *phosphoproteomics*, one can elucidate the pathways switched on or off under a specific set of conditions.

For example, as we will see more clearly in later chapters, exercise is fundamental to sustaining good health, in part by regulating energy metabolism and maintaining whole-body insulin sensitivity. Given the prominence of phosphorylation in biological regulation, it should come as no surprise that exercise modifies the phosphoproteome. Recent research has shown that exercise results in the phosphorylation of more than 1000 potential phosphorylation sites on almost 600 different proteins. Protein kinase A and AMP-activated kinase (AMPK, Section

22.7) as well as other kinases catalyze these modifications. These modifications alter a number of biological functions, most notably an increase in the ability to process fuels aerobically (Chapters 17 and 18). Determining the functions of the modified proteins will surely keep exercise biochemists engaged for many years.

7.4 Many Enzymes Are Activated by Specific Proteolytic Cleavage

While many enzymes acquire full enzymatic activity as they spontaneously fold into their characteristic three-dimensional forms, the folded forms of other enzymes are inactive until one or a few specific peptide bonds are cleaved. The inactive precursor is called a **zymogen** (or **proenzyme**). Since an energy source such as ATP is not needed for specific proteolytic cleavage, even extracellular proteins can be activated by this means. This contrasts with reversible enzyme regulation by phosphorylation, which requires ATP. Another noteworthy difference is that proteolytic activation, unlike allosteric control and reversible covalent modification, is irreversible, taking place just once in the life of an enzyme molecule.

Specific proteolysis is a common means of activating enzymes and other proteins in biological systems. For example:

- The digestive enzymes that hydrolyze foodstuffs are synthesized as zymogens in the stomach and pancreas (Table 7.3).
- Blood clotting is mediated by a cascade of proteolytic activations that ensures a rapid and amplified response to trauma.
- Some protein hormones are synthesized as inactive precursors. For example, *insulin* is derived from *proinsulin* by proteolytic removal of a peptide.
- The fibrous protein collagen, the major constituent of skin and bone, is derived from procollagen, a soluble precursor.

TABLE 7.3 Zymogens of the stomach and pancreas

Site of synthesis	Zymogen	Active enzyme
Stomach	Pepsinogen	Pepsin
Pancreas	Chymotrypsinogen	Chymotrypsin
Pancreas	Trypsinogen	Trypsin
Pancreas	Procarboxypeptidase	Carboxypeptidase

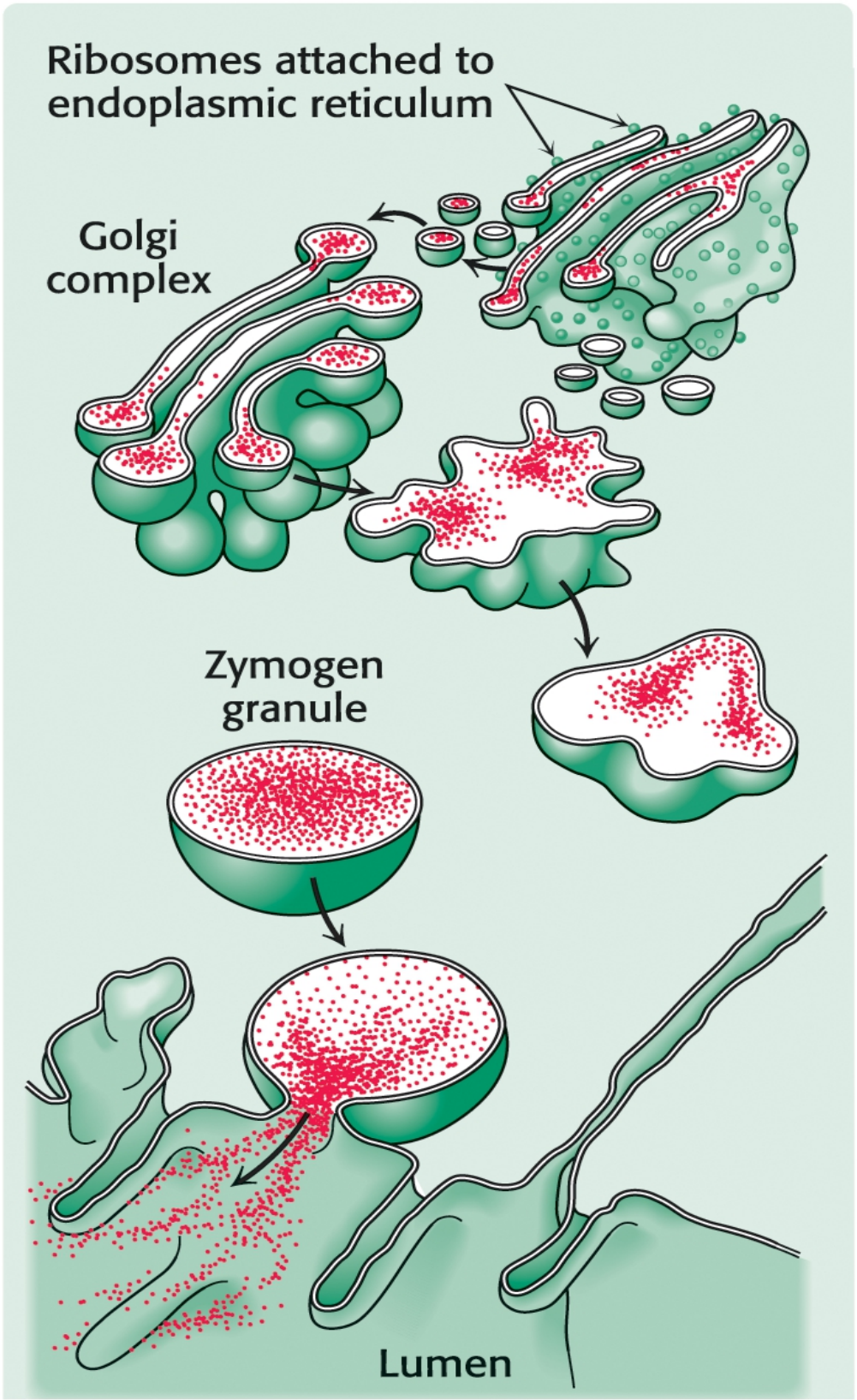
Many developmental processes are controlled by the activation of zymogens. For example, in the metamorphosis of a tadpole into a frog, large amounts of collagen are resorbed from the tail in the course of a few days. Likewise, much collagen is broken down in a mammalian uterus after delivery. The conversion of procollagenase into collagenase, the active protease responsible for collagen breakdown, is precisely timed in these remodeling processes.

Programmed cell death, also called *apoptosis,* is mediated by proteolytic enzymes called *caspases,* which are synthesized in precursor form as *procaspases*. When activated by various signals, caspases function to cause cell death in most organisms, ranging from *C. elegans* to human beings. Apoptosis provides a means of sculpting the shapes of body parts in the course of development and is a means of eliminating damaged or infected cells.

Chymotrypsinogen is activated by specific cleavage of a single peptide bond

Let us examine the activation and control of zymogens, using enzymes responsible for digestion. Chymotrypsin is a member of a large family of serine proteases whose mechanism of action was described in detail in Section 6.2. Specifically, it is a digestive enzyme that cleaves peptide

bonds on the carboxyl side of amino acid residues with large, hydrophobic R groups (Table 5.7). Its inactive precursor, chymotrypsinogen, is synthesized in the pancreas, as are several other zymogens and digestive enzymes. Indeed, the pancreas is one of the most active organs in synthesizing and secreting proteins. The enzymes and zymogens are synthesized in the acinar cells of the pancreas and stored inside membrane-bounded granules (**Figure 7.16**). The zymogen granules accumulate at the apex of the acinar cell; when the cell is stimulated by a hormonal signal or a nerve impulse, the contents of the granules are released into a duct leading into the duodenum, the first segment of the small intestine into which the stomach empties.



© Macmillan Learning

FIGURE 7.16 The acinar cells of the pancreas secrete zymogens. Zymogens are synthesized on ribosomes attached to the endoplasmic reticulum. They are subsequently processed in the Golgi apparatus and packaged into zymogen or secretory granules. With the proper signal, the granules fuse with the plasma membrane, discharging their contents into the interior (lumen) of the pancreatic ducts. Cell cytoplasm is depicted as pale green. Membranes and lumen are shown as dark green.



Chymotrypsinogen, a single polypeptide chain consisting of 245 amino acid residues, is virtually devoid of enzymatic activity. It is converted into a fully active enzyme when the peptide bond joining arginine 15 and isoleucine 16 is cleaved by trypsin (Figure 7.17). The resulting active enzyme, called π-chymotrypsin, then acts on other π-chymotrypsin molecules by removing two dipeptides to yield α-chymotrypsin, the stable form of the enzyme. The three resulting chains in α-chymotrypsin remain linked to one another by two interchain disulfide bonds. The striking feature of this activation process is that cleavage of a single specific peptide bond transforms the protein from a catalytically inactive form into one that is fully active.

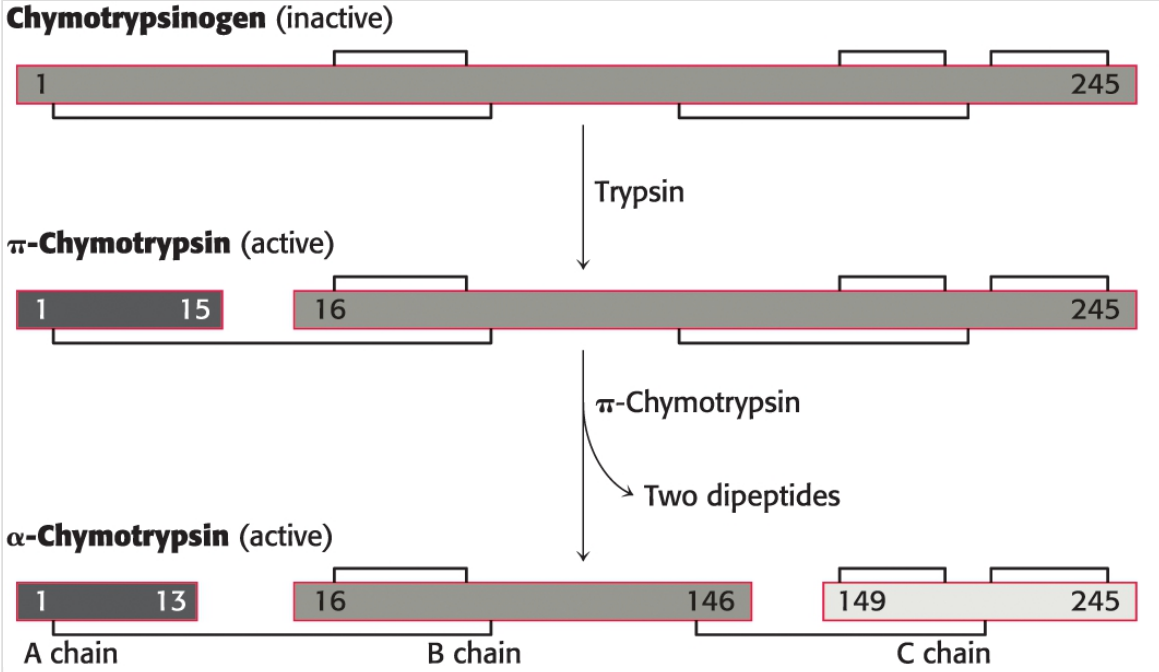


FIGURE 7.17 Proteolysis activates chymotrypsinogen. The three chains of α-chymotrypsin are linked by two interchain disulfide bonds (A to B and B to C). The approximate positions of both inter- and intrachain disulfide bonds are shown.

Proteolytic activation of chymotrypsinogen leads to the formation of a substrate-binding site

How does cleavage of a single peptide bond activate the zymogen? The cleavage of the peptide bond between amino acids 15 and 16 triggers key conformational changes, which were revealed by the elucidation of the three-dimensional structure of chymotrypsinogen.

- The newly formed amino-terminal group of isoleucine 16 turns inward and forms an ionic bond with aspartate 194 in the interior of the chymotrypsin molecule (Figure 7.18).

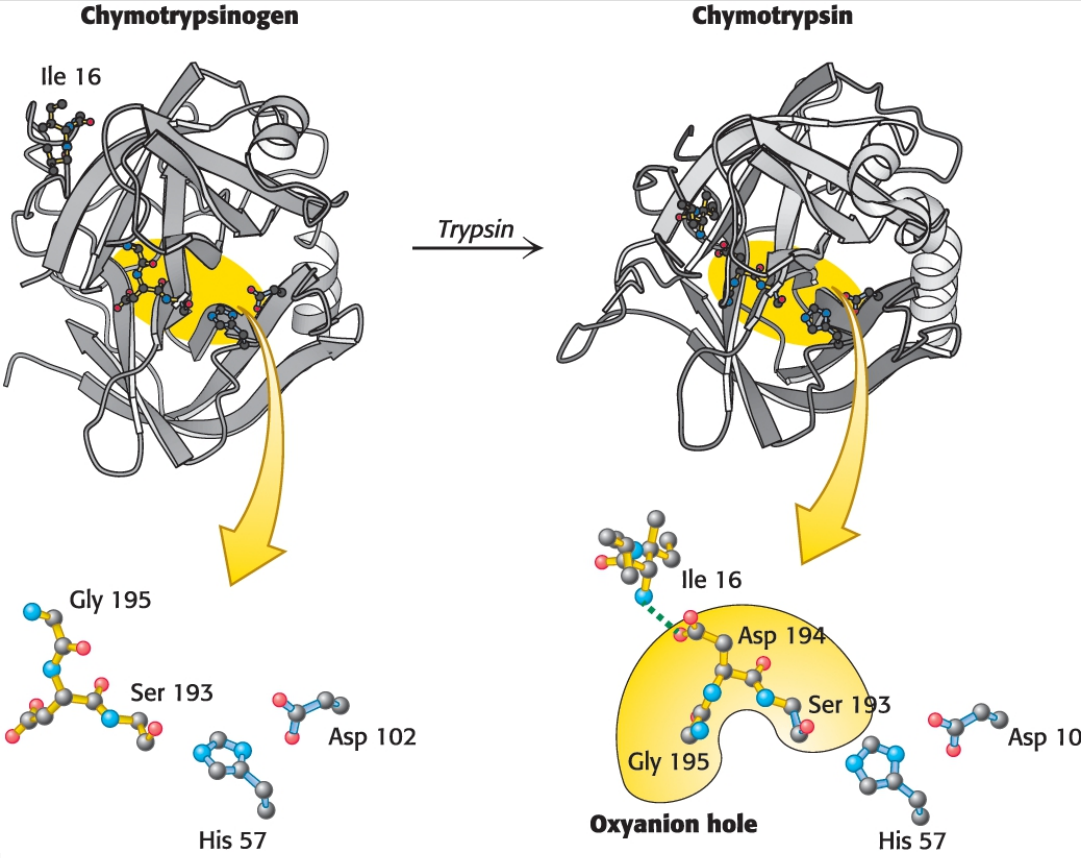


FIGURE 7.18 Cleavage of chymotrypsinogen by trypsin initiates the conformational transition into active chymotrypsin. In chymotrypsinogen, isoleucine 16 is positioned fa away from the active site. Upon cleavage by trypsin, the newly formed α-amino group of isoleucine 16 forms an electrostatic interaction with the carboxylate of aspartate 194 yielding the proper conformation of the oxyanion hole (yellow half-circle) and the formation of the substrate specificity pocket (not shown).

[Drawn from 1CHG.pdb and 5CHA.pdb.]

- This electrostatic interaction triggers a number of conformational changes. Methionine 192 moves from a deeply buried position in the zymogen to the surface of the active enzyme, and residues 187 and 193 move farther apart from each other. These changes result in the formation of the substrate-specificity site for aromatic and bulky nonpolar groups. One side of this site is made up of residues

189 through 192 (Figure 6.10). This cavity for binding part of the substrate is not fully formed in the zymogen.

- The repositioning of aspartate 194 also rearranges the main chain amino group of glycine 195. Recall that the tetrahedral transition state generated by chymotrypsin has an oxyanion (a negatively charged carbonyl oxygen atom) that is stabilized by hydrogen bonds with two NH groups of the main chain of the enzyme (the oxyanion hole, Figure 6.9). The new position of the NH group of glycine 195 enables the proper formation of the oxyanion hole (Figure 7.18).

The conformational changes elsewhere in the molecule are very small. For example, the positions of the residues forming the catalytic triad (Ser 193, His 57, and Asp 102) are essentially the same in both structures (Figure 7.18). Thus, the switching on of enzymatic activity in a protein can be accomplished by discrete, highly localized conformational changes that are triggered by the hydrolysis of a single peptide bond.

The generation of trypsin from trypsinogen leads to the activation of other zymogens

The structural changes accompanying the activation of trypsinogen, the precursor of the proteolytic enzyme trypsin, another serine protease, are different from those in the activation of chymotrypsinogen. Four regions of the polypeptide are very flexible in the zymogen, whereas they have a well-defined conformation in trypsin. The resulting structural changes also complete the formation of the oxyanion hole.

The digestion of proteins and other molecules in the duodenum requires the concurrent action of several enzymes, because each is specific for a limited number of side chains. Thus, the zymogens must be switched on at the same time. Coordinated control is achieved by the action of trypsin as the common activator of all the pancreatic zymogens — trypsinogen, chymotrypsinogen, proelastase,

procarboxypeptidase, and prolipase, the inactive precursor of a lipid-degrading enzyme.

To produce active trypsin, the cells that line the duodenum display a membrane-embedded enzyme, enteropeptidase, which hydrolyzes a unique lysine–isoleucine peptide bond in trypsinogen as the zymogen enters the duodenum from the pancreas. The small amount of trypsin produced in this way activates more trypsinogen and the other zymogens (Figure 7.19). Thus, the formation of trypsin by enteropeptidase is the master activation step.

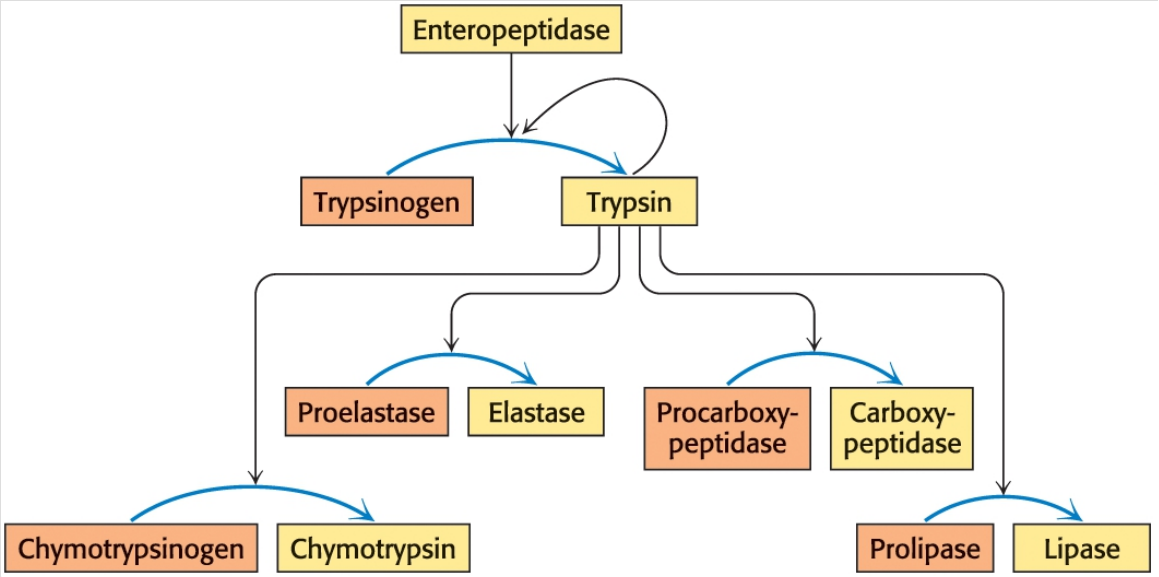


FIGURE 7.19 Enteropeptidase initiates the activation of the pancreatic zymogens by activatir trypsin, which then activates other zymogens. Active enzymes are shown in yellow; zymogens are shown in orange.

Self-Check Question

Predict the physiological effects of a mutation that resulted in a deficiency of enteropeptidase.

Some proteolytic enzymes have specific inhibitors

The conversion of a zymogen into a protease by cleavage of a single peptide bond is a precise means of switching on enzymatic activity. However, this activation step is irreversible, and so a different mechanism is needed to terminate proteolysis. Specific protease inhibitors accomplish this task.

Inhibitors called *serpins*, shorthand for serine protease inhibitors, are an example of one such family of inhibitors. For example, pancreatic trypsin inhibitor, a 6-kDa serpin, inhibits trypsin by binding very tightly to its active site. The dissociation constant of the complex is 0.1 pM, which corresponds to a standard free energy of binding of about $-75\ \text{kJ mol}^{-1}\ (-18\ \text{kcal mol}^{-1})$. In contrast with nearly all known protein assemblies, this complex is not dissociated into its constituent chains by treatment with denaturing agents such as 8 M urea (Section 2.7).

The reason for the exceptional stability of the complex is that pancreatic trypsin inhibitor is a very effective substrate analog. X-ray analyses show that the inhibitor lies in the active site of the enzyme, positioned such that the side chain of lysine 15 of this inhibitor interacts with the aspartate side chain in the specificity pocket of trypsin. In addition, there are many hydrogen bonds between the main chain of trypsin and that of its inhibitor. Furthermore, the carbonyl group of lysine 15 and the surrounding atoms of the inhibitor fit snugly in the active site of the enzyme.

Comparison of the structure of the inhibitor bound to the enzyme with that of the free inhibitor reveals that the structure is essentially unchanged on binding to the enzyme (Figure 7.20). Thus, the inhibitor is preorganized into a structure that is highly complementary to the enzyme's active site. Indeed, the peptide bond between lysine 15 and alanine 16 in pancreatic trypsin inhibitor is cleaved but at a very slow rate: the half-life of the trypsin–inhibitor complex is several months. In essence, the inhibitor is a substrate, but its intrinsic structure is so nicely complementary to the enzyme's active site that it binds very tightly, rarely progressing to the transition state, and is turned over slowly.

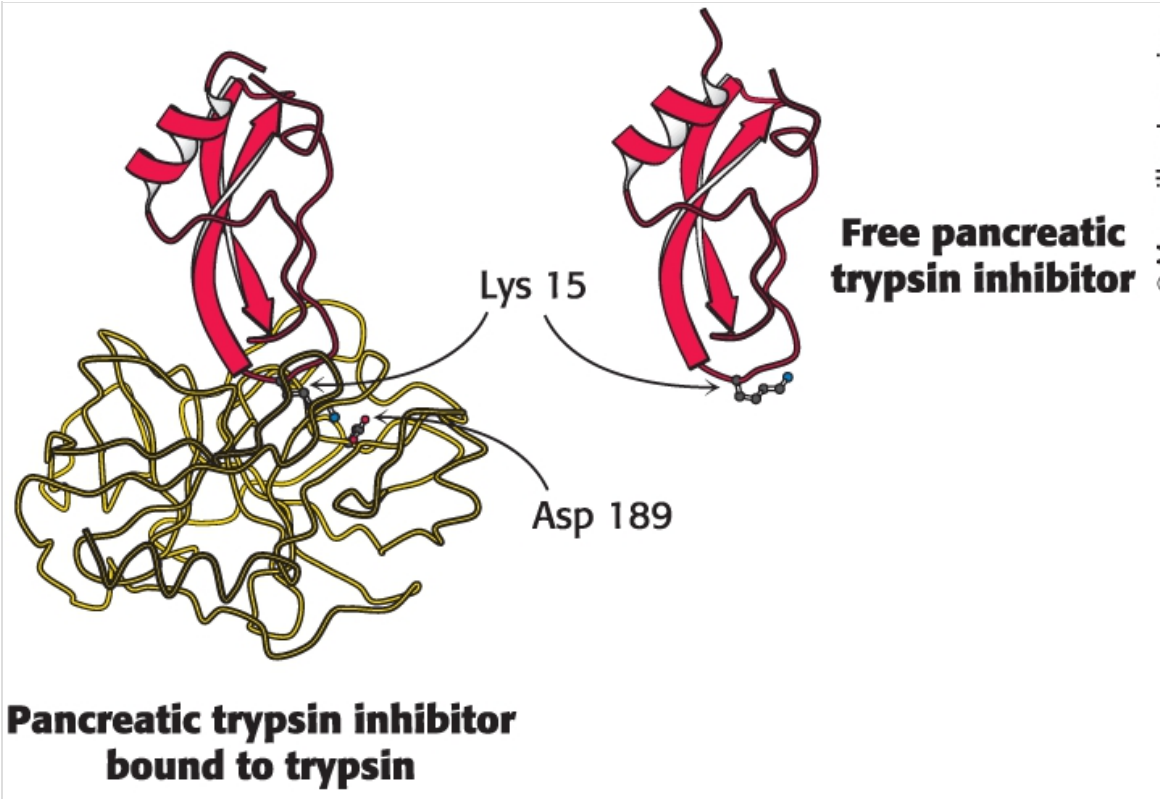


FIGURE 7.20 Trypsin binds very tightly to pancreatic trypsin inhibitor, a serpin. In the structu of a complex of trypsin (yellow) and pancreatic trypsin inhibitor (red), lysine 15 of the inhibitor penetrates into the active site of the enzyme. There it forms an ionic bond with aspartate 189 in the active site. Notice that bound inhibitor and the free inhibitor are almost identical in structu

[Drawn from 2PTC.pdb and 1BPI.pdb.]

INTERACT with this model in Achieve

Why does trypsin inhibitor exist? Recall that trypsin activates other zymogens. Consequently, preventing even small amounts of trypsin from initiating the cascade while the zymogens are still in the pancreas or pancreatic ducts is vital. Trypsin inhibitor binds to any prematurely activated trypsin molecules in the pancreas or pancreatic ducts. This inhibition prevents severe damage to those tissues, which could lead to acute pancreatitis.

Pancreatic trypsin inhibitor is not the only important protease inhibitor. A 53-kDa plasma protein, α_1-antitrypsin (also called α_1-*antiproteinase*), protects tissues from digestion by elastase, a secretory product of neutrophils (white blood cells that engulf bacteria). Antielastase would be a more accurate name for this inhibitor, because it blocks elastase much more effectively than it blocks trypsin. Like pancreatic trypsin inhibitor, α_1-antitrypsin blocks the action of target enzymes by binding nearly irreversibly to their active sites.

 Genetic disorders leading to a deficiency of α_1-antitrypsin illustrate the physiological importance of this inhibitor. For example, the substitution of lysine for glutamate at residue 53 in the type Z mutant slows the secretion of this inhibitor from liver cells. Serum levels of the inhibitor are about 15% of normal in people homozygous for this defect. The consequence is that excess elastase destroys alveolar walls in the lungs by digesting elastic fibers and other connective-tissue proteins.

The resulting clinical condition is called *emphysema*. People with emphysema must breathe much harder than normal people to exchange the same volume of air because their alveoli are much less resilient than

7.5 Enzymatic Cascades Allow Rapid Responses Such as Blood Clotting

Biochemical systems often use a series of zymogen activations, called an **enzymatic cascade**, to achieve a rapid response. In a cascade, a signal initiates a series of steps, each of which is catalyzed by an enzyme. At each step, the signal is amplified. For instance, if a signal molecule activates an enzyme that in turn activates 10 enzymes, and each of the 10 enzymes in turn activates 10 additional enzymes, after four steps the original signal will have been amplified 10,000-fold.

In the previous section, we discussed the cascade of proteolytic enzymes that accompanies digestion of a meal. Another physiological process that requires enzymatic cascades is **hemostasis**, the process of blood clot formation and dissolution. Because the activated form of one clotting factor catalyzes the activation of the next (**Figure 7.22**), a very small amount of the initial factors suffice to trigger the cascade, ensuring a rapid response to trauma.

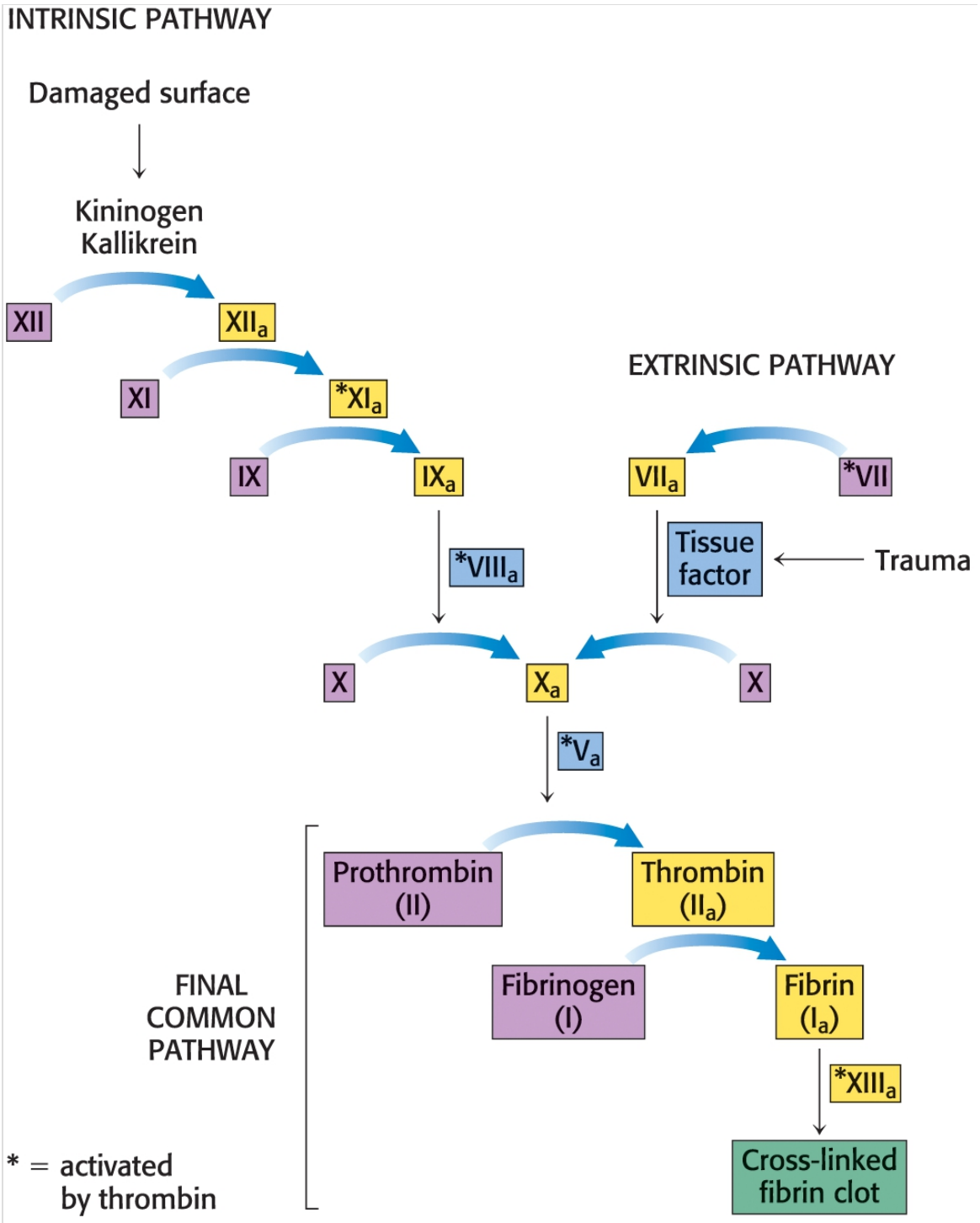


FIGURE 7.22 Blood clotting is the result of an enzymatic cascade. A fibrin clot is formed by the interplay of the intrinsic, extrinsic, and final common pathways. The intrinsic pathway begins with the activation of factor XII (Hageman factor) by contact with abnormal surfaces produced b injury. The extrinsic pathway is triggered by trauma, which releases tissue factor (TF). TF forms complex with VII, which initiates a cascade-activating thrombin. Inactive forms of clotting facto are shown in purple; their activated counterparts (indicated by the subscript "a") are in yellow. Stimulatory proteins that are not themselves enzymes are shown in blue boxes. A striking featu

of this process is that the activated form of one clotting factor catalyzes the activation of the ne
factor.

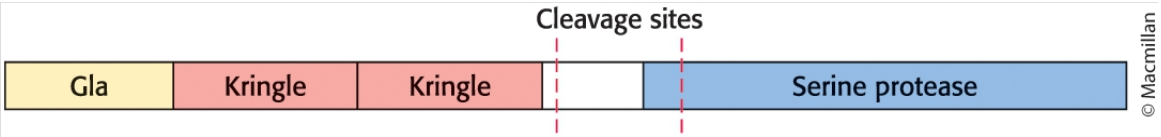


Two means of initiating blood clotting have been elucidated. The *intrinsic pathway* is activated by exposure of anionic surfaces upon rupture of the endothelial lining of the blood vessels. The *extrinsic pathway*, which appears to be most crucial in blood clotting, is initiated when trauma exposes tissue factor (TF), an integral membrane glycoprotein. Upon exposure to the blood, tissue factor binds to factor VII to activate factor X. Both the intrinsic and extrinsic pathways lead to the activation of factor X (a serine protease), which in turn converts prothrombin into thrombin, the key protease in clotting. Thrombin then amplifies the clotting process by activating enzymes and factors that lead to the generation of yet more thrombin, an example of positive feedback. Note that the active forms of the clotting factors are designated with a subscript "a," whereas factors that are enzymes or enzyme cofactors activated by thrombin are designated with an asterisk.

Prothrombin must bind to Ca^{2+} to be converted to thrombin

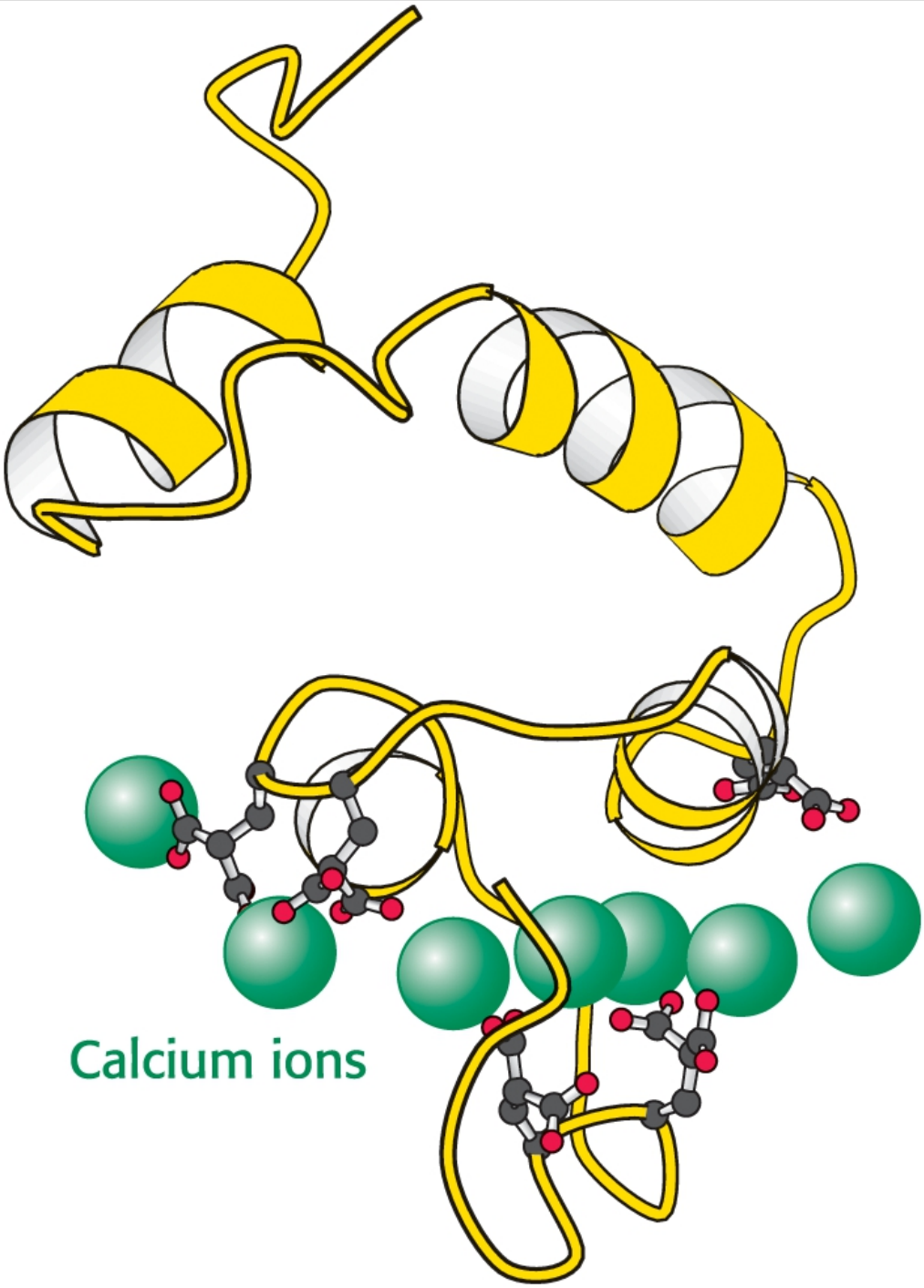
Thrombin is synthesized as a zymogen called prothrombin. The inactive molecule is comprised of four major domains, with the serine protease domain at its carboxyl terminus (Figure 7.23). The first domain, called the *gla domain*, is rich in γ-carboxyglutamate residues (abbreviation gla), and the second and third domains are called *kringle domains* (named after a Danish pastry that they resemble). These three domains work in concert to keep prothrombin in an inactive form. Moreover, because it is rich in γ-carboxyglutamate, the gla domain is able to bind

Ca^{2+} (Figure 7.24). What is the effect of this binding? The binding of Ca^{2+} by prothrombin anchors the zymogen to phospholipid membranes derived from blood platelets after injury. This binding is crucial because it brings prothrombin into close proximity to two clotting proteins, factor X_a and factor V_a (a stimulatory protein), that catalyze its conversion into thrombin. Factor X_a cleaves the bond between arginine 274 and threonine 275 to release a fragment containing the first three domains. Factor X_a also cleaves the bond between arginine 323 and isoleucine 324 to yield active thrombin.



© Macmillan

FIGURE 7.23 Prothrombin contains four distinct protein domains. Cleavage of two peptide bonds yields active thrombin. All the γ-carboxyglutamate residues are in the gla domain.



© Macmillan Learning

FIGURE 7.24 The gla domain of prothrombin contains a calcium-binding region.
Prothrombin binds calcium ions with the carboxyl groups of the modified amino acid γ-carboxyglutamate (red).

[Drawn from 2PF2.pdb.]

INTERACT with this model in Achieve

Fibrinogen is converted by thrombin into a fibrin clot

The best-characterized part of the clotting process is the final step in the cascade: the conversion of fibrinogen into fibrin by thrombin. Fibrinogen is a large glycoprotein composed of three nonidentical chains, Aα, Bβ, and γ, and is found in the blood plasma of all vertebrates. The overall composition of this 340-kDa protein is $(A\alpha)_2(B\beta)_2\,\gamma_2$. Three globular units are connected by two rods, and the rod regions are triple-stranded α-helical coiled coils, a recurring motif in proteins (Section 2.5; **Figure 7.25A**). Thrombin cleaves four arginine–glycine peptide bonds in the central globular region of fibrinogen (**Figure 7.25B**). On cleavage, an A peptide of 18 residues is released from each of the two Aα chains, as is a B peptide of 20 residues from each of the two Bβ chains. These A and B peptides are called *fibrinopeptides* (**Figure 7.26**). A fibrinogen molecule devoid of these fibrinopeptides is called a *fibrin monomer* and has the subunit structure $(\alpha\beta\gamma)_2$.

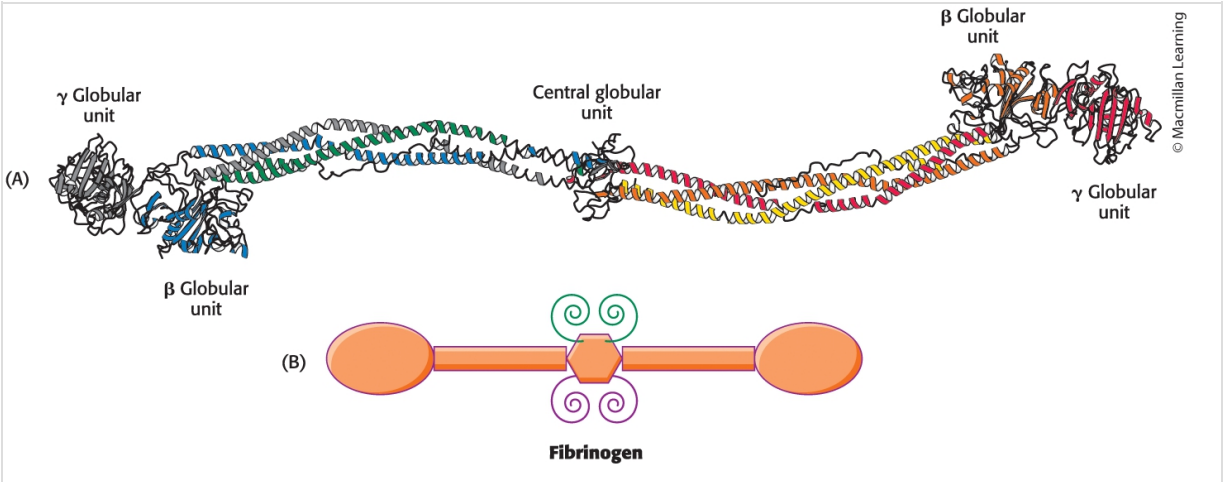


FIGURE 7.25 Fibrinogen contains three globular regions connected by rod-shaped structures. (A) A ribbon diagram. The two rod regions are α-helical coiled coils, connected to the three globular regions. (B) A schematic representation showing the positions of the fibrinopeptides (green and purple) in the central globular region.

[Part A drawn from 1M1J.pdb.]

INTERACT with this model in Achieve

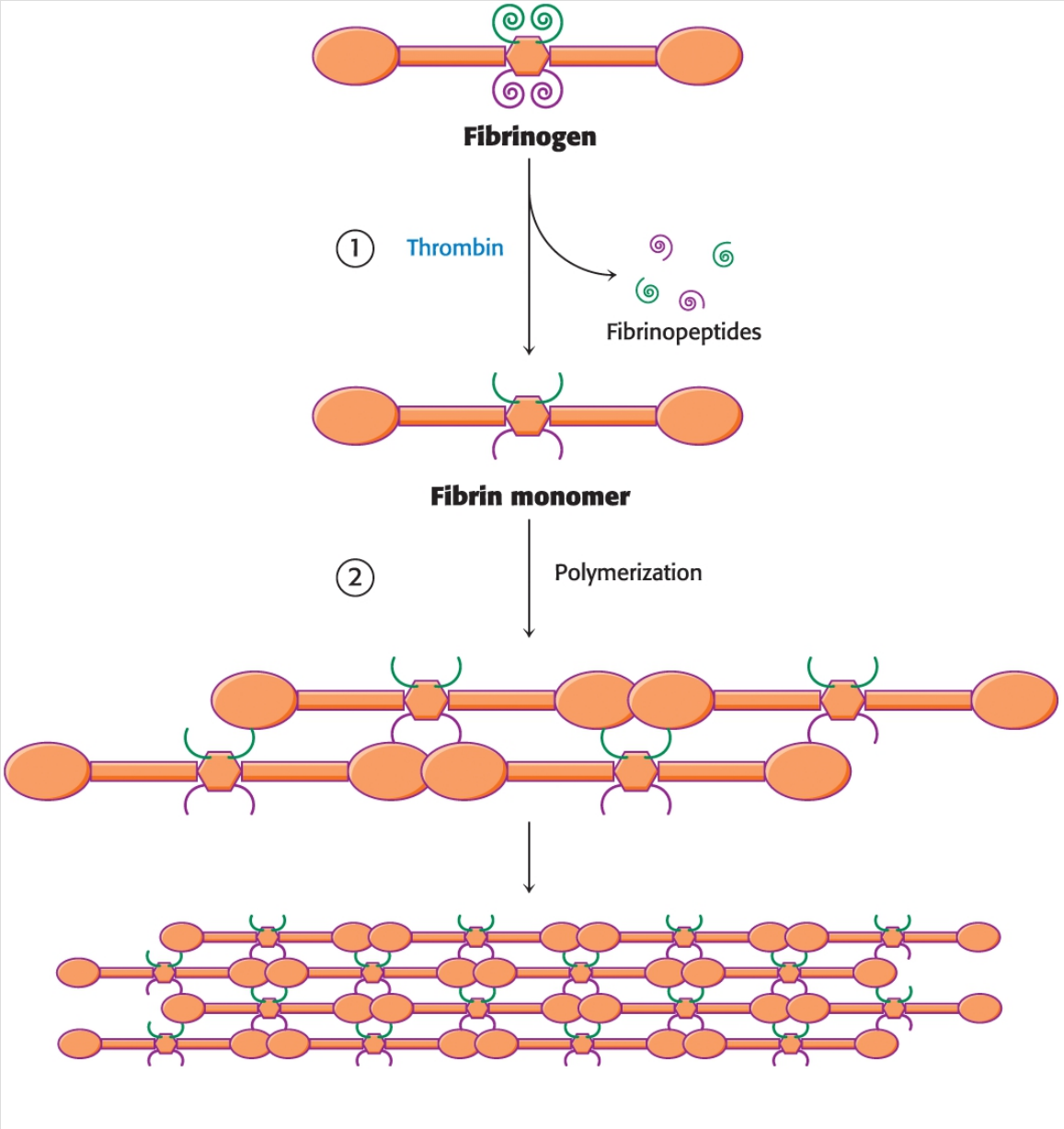
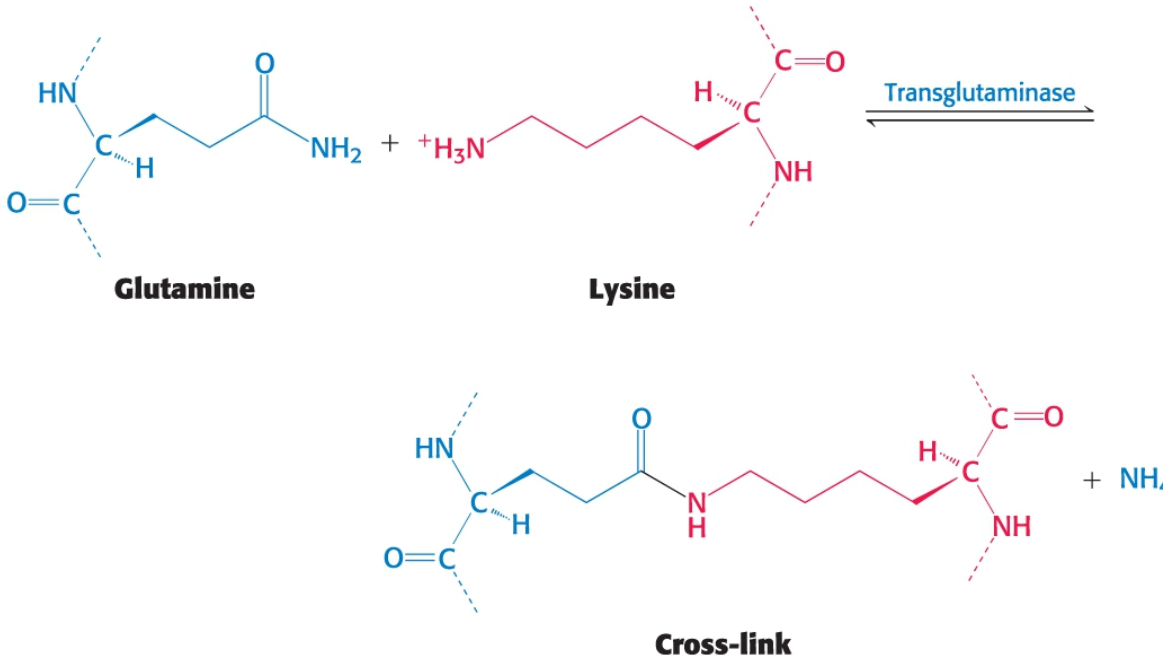


FIGURE 7.26 The cleavage of fibrinogen by thrombin initiates fibrin clot formation. (1) Thrombin cleaves fibrinopeptides from the central globule of fibrinogen. (2) Globular domains a the carboxyl-terminal ends of the β and γ chains interact with the peptides exposed upon thrombin cleavage.

Upon thrombin cleavage, amino acid sequences are exposed in the central globular unit that interact with the γ and β subunits of other monomers. Polymerization occurs as more fibrin monomers interact with one another (Figure 7.26). Thus, analogous to the activation of chymotrypsinogen, peptide-bond cleavage exposes new amino termini that can participate in specific interactions. The newly formed "soft clot" is stabilized by the formation of amide bonds between the side chains of lysine and glutamine residues in different monomers. This cross-linking reaction is catalyzed by transglutaminase (factor $XIII_a$), which itself is activated from its protransglutaminase form by thrombin.



Vitamin K is required for the formation of γ-carboxyglutamate

Vitamin K (Figure 7.27) has been known for many years to be essential for the synthesis of prothrombin and several other clotting factors. Indeed, it is called vitamin K because a deficiency in this vitamin results in defective blood koagulation (Scandinavian spelling). After ingestion, vitamin K is reduced to a dihydro derivative that is required by γ-glutamyl carboxylase to convert the first 10 glutamate residues in the amino-terminal region of prothrombin into γ-carboxyglutamate (Figure 7.28). Recall from above that γ-carboxyglutamate, a strong chelator of Ca^{2+}, is required for the activation of prothrombin.

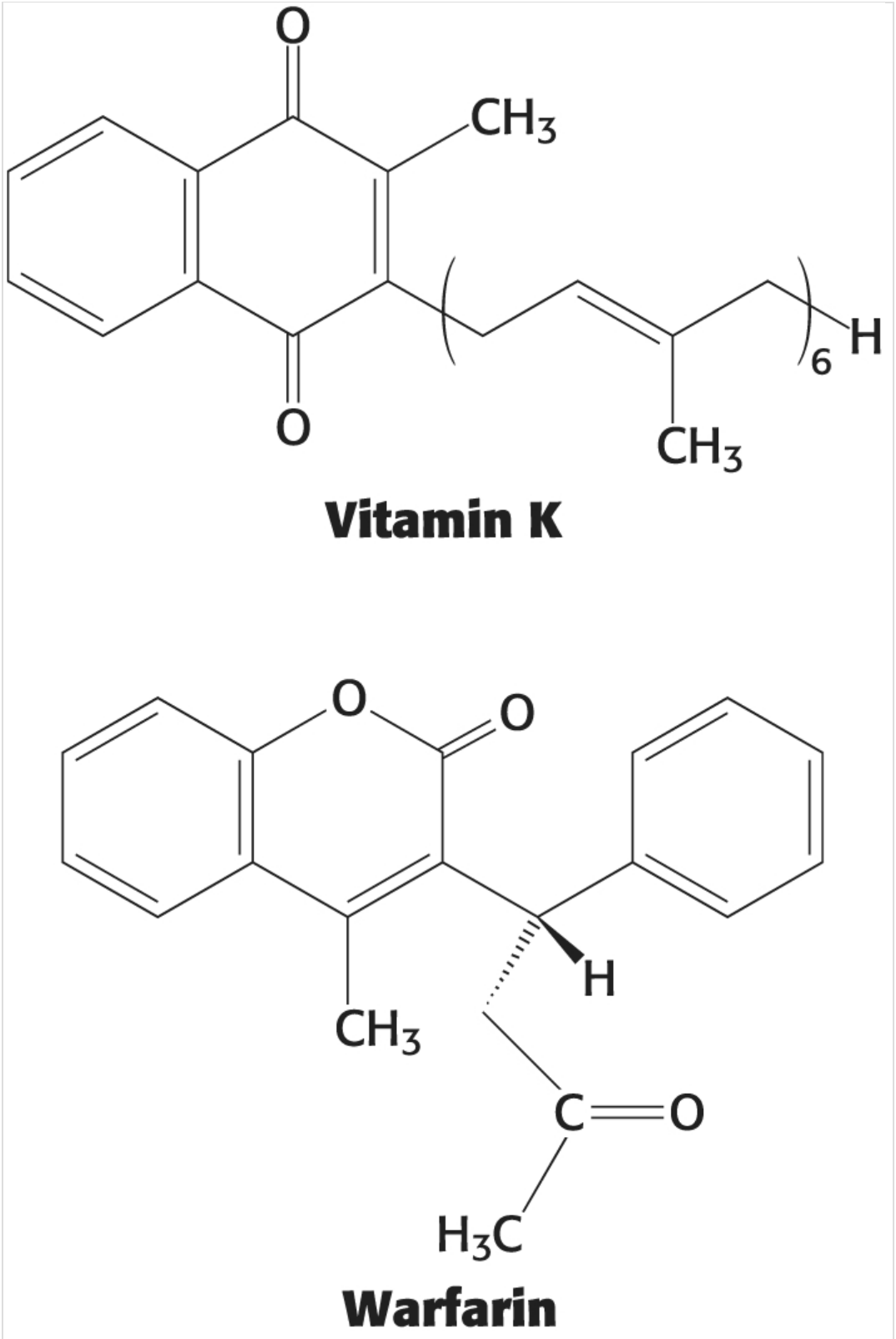


FIGURE 7.27 Vitamin K and the anticoagulant warfarin share structural features.

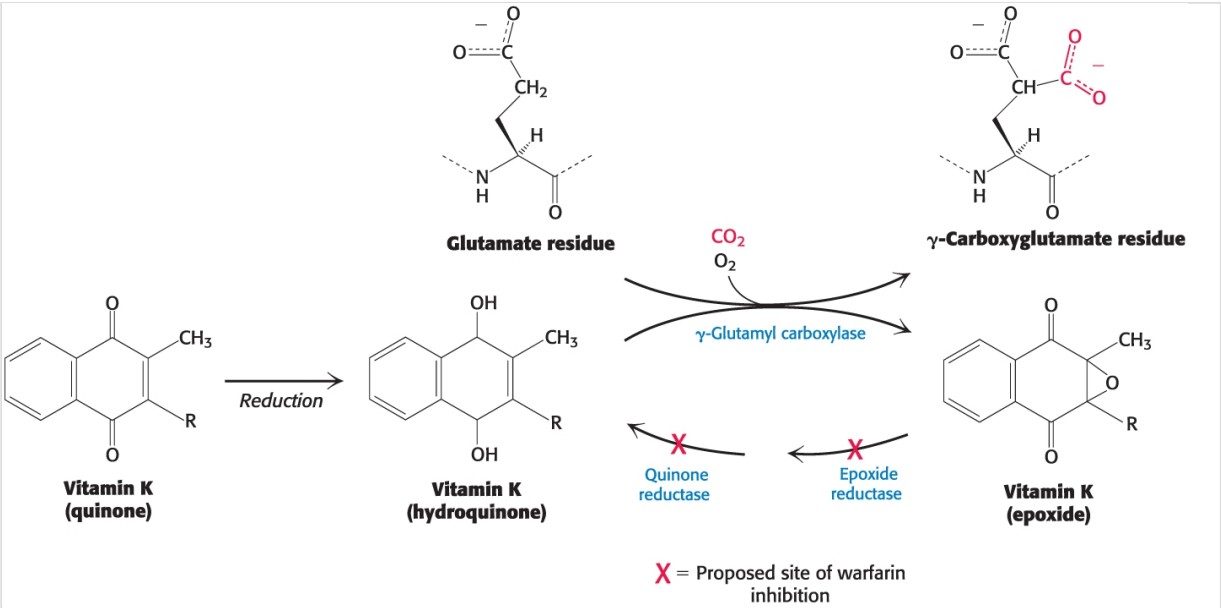


FIGURE 7.28 Vitamin K is required for the synthesis of γ-carboxyglutamate by γ-glutamyl carboxylase. The formation of γ-carboxyglutamate requires the hydroquinone (reduced) derivative of vitamin K, which is then regenerated from the epoxide derivative by the sequential action of epoxide reductase and quinone reductase, both of which are inhibited by warfarin.

Medicines that reduce blood clot formation, known as anticoagulant drugs, play an important role in the prevention of stroke, myocardial infarction (heart attack), and pulmonary embolism in patients with increased clotting risk. One most commonly prescribed anticoagulants is warfarin, a vitamin K antagonist sold under the name of coumadin (Figure 7.27). Warfarin appears to inhibit the epoxide reductase and quinone reductase that are required to regenerate the dihydro derivative of vitamin K (Figure 7.28). Newer anticoagulants have also entered the market, including inhibitors of factor X_a and thrombin.

The clotting process must be precisely regulated

There is a fine line between hemorrhage and thrombosis, the formation of blood clots in blood vessels. Clots must form rapidly yet remain confined to the area of injury. What are the mechanisms that normally limit clot formation to the site of injury? The lability of clotting factors contributes significantly to the control of clotting. Activated factors are short-lived because they are diluted by blood flow, removed by the liver, and degraded by proteases. For example, the stimulatory protein factors V_a and $VIII_a$ are digested by protein C, a protease that is switched on by the action of thrombin. Thus, thrombin has a dual function: it catalyzes the formation of fibrin, and it initiates the deactivation of the clotting cascade.

Specific inhibitors of clotting factors are also critical in the termination of clotting. For instance, tissue factor pathway inhibitor (TFPI) inhibits the complex of $TF-VII_a-X_a$ that activates thrombin. Another key inhibitor is antithrombin III, a member of the serpin family of protease inhibitors that forms an irreversible inhibitory complex with thrombin. Antithrombin III resembles α_1-antitrypsin except that it inhibits thrombin much more strongly than it inhibits elastase (Figure 7.20). Antithrombin III also blocks other serine proteases in the clotting cascade — namely, factors XII_a, XI_a, IX_a, and X_a.

The inhibitory action of antithrombin III is enhanced by the glycosaminoglycan *heparin*, a negatively charged polysaccharide (Section 11.3) found in mast cells near the walls of blood vessels and on the surfaces of endothelial cells. Heparin acts as an anticoagulant by increasing the rate of formation of irreversible complexes between antithrombin III and the serine protease clotting factors.

Self-Check Question



Antithrombin III forms an irreversible complex with thrombin but not with prothrombin. What is the most likely reason for this difference in reactivity?

Chapter 7 Summary

7.1 Allosteric Regulation Enables Control of Metabolic Pathways

- Allosteric proteins constitute an important class of proteins whose biological activity can be altered by binding to distinct regulatory sites.
- Aspartate transcarbamoylase (ATCase), one of the best-understood allosteric enzymes, catalyzes the synthesis of *N*-carbamoylaspartate, the first and committed step in the synthesis of pyrimidines.
- ATCase is feedback inhibited by CTP, the final product of the pathway, and is stimulated by ATP and the bisubstrate analog PALA.
- The inhibitory effect of CTP, the stimulatory action of ATP, and the cooperative binding of substrates to ATCase are mediated by the interconversion between the T (low-affinity for substrate) to the R (high-affinity) states.
- The sigmoidal kinetics exhibited by ATCase can be pictured as a composite of the Michaelis–Menten curves for the T and R states.

7.2 Isozymes Provide a Means of Regulation Specific to Distinct Tissues and Developmental Stages

- Isozymes differ in structural characteristics but catalyze the same reaction.
- Typically, isozymes display different kinetic parameters or respond to different regulatory molecules.
- Isozymic forms of an enzyme can vary by tissue or developmental stage, providing a means of fine-tuning metabolism.

7.3 Covalent Modification Is a Means of Regulating Enzyme Activity

- Reversible and irreversible covalent modifications are powerful means of controlling enzyme activity.
- Phosphorylation is a common type of reversible covalent modification in all forms of life.
- Kinases are the enzymes responsible for protein phosphorylation, while phosphatases catalyze the hydrolysis of attached phosphoryl groups.
- Protein kinase A (PKA) is a kinase whose activity is controlled by allosteric regulation. Cyclic AMP switches on PKA by binding to the regulatory subunit of the enzyme, thereby releasing the active catalytic subunits of PKA.

7.4 Many Enzymes Are Activated by Specific Proteolytic Cleavage

- The activation of an enzyme by the proteolytic cleavage of one or a few peptide bonds is a recurring irreversible control mechanism.
- The inactive precursors of these enzymes are called zymogens.
- Proteolytic cleavage plays an important role in the digestive enzymes, where control over activation prevents tissue damage.
- Trypsinogen is activated by enteropeptidase or trypsin, and trypsin then activates a host of other zymogens, leading to the digestion of foodstuffs.
- Specific inhibitors of proteolytic enzymes, including the serpins, also provide an additional layer of regulatory control.

7.5 Enzymatic Cascades Allow Rapid Responses Such as Blood Clotting

- Blood clotting is an example of a process that utilizes an enzymatic cascade to achieve a rapid response.
- The activated form of one clotting factor, often a serine protease, catalyzes the activation of the next precursor.
- In the final step of clot formation, fibrinogen, a highly soluble molecule in the plasma, is converted by thrombin into fibrin by

the hydrolysis of four arginine–glycine bonds.

Key Terms

committed step
feedback inhibition
allosteric (regulatory) site
homotropic effect
heterotropic effect
isozymes (isoenzymes)
protein kinase
consensus sequence
protein phosphatase
pseudosubstrate sequence
phosphoproteome
zymogen (proenzyme)
enzymatic cascade
hemostasis
anticoagulant drugs

Problems

1. Suppose you have a dimeric allosteric enzyme that follows the concerted model. Which of the following statements are true? 3

a. The equilibrium between the T state and R state favors the T state.
b. The enzyme can exist as a RR dimer.
c. The enzyme can exist as an RT dimer.

d. The RR form of the enzyme is most active.

2. An allosteric enzyme that follows the concerted model has an allosteric coefficient (T/R) of 300 in the absence of substrate. Suppose that a mutation reversed the ratio. Select all of the effects this mutation will have on the relationship between the rate of the reaction (*V*) and substrate concentration, [S]. 3

a. The enzyme would be more active.
b. The enzyme would mostly be in the T form.
c. The enzyme would likely follow Michaelis–Menten kinetics.
d. The plot of *V* versus [S] would be shaped like a hyperbola.
e. The plot of *V* versus [S] would be sigmoidal.

3. Differentiate between homotropic and heterotropic effectors. 3

4. As shown in Figure 7.2, CTP inhibits ATCase; however, the inhibition is not complete. Can you suggest another molecule that might enhance the inhibition of ATCase? Hint: See Figure 26.2. 1

5. Classify the following phrases as describing a kinase, a phosphatase, neither, or both. 5

a. May use ATP as a phosphoryl group donor
b. PKA is an example.
c. Removes phosphoryl groups from proteins
d. Catalyzes reactions that are the reverse of dephosphorylation reactions
e. Regulates the activity of other proteins
f. Catalyzes phosphorylation reactions
g. Turns off signaling reactions triggered by kinases
h. In eukaryotes, transfers phosphoryl groups to acidic amino acids

6. Which statements about isozymes are true? 4

a. Isozymes are encoded by the same gene.
b. Isozymes may be expressed in different tissues.
c. Isozymes catalyze different reactions.
d. Isozymes have different amino acid sequences.
e. Isozymes have identical regulatory properties.
f. Lactate dehydrogenase is an example.

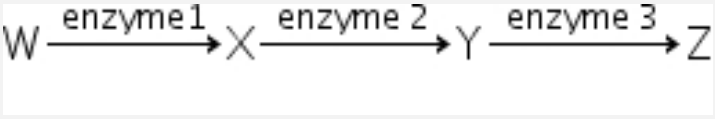
7. Consider the following molecules: ATP, CTP, UTP, cAMP, and PALA. With respect to ATCase, which of these molecules is … 2

a. … a feedback inhibitor?
b. … a bisubstrate analog?
c. … an allosteric activator?

8. Order the steps below for the activation of PKA by cAMP.

a. The free catalytic subunits interact with proteins to phosphorylate Ser and Thr residues.
b. The regulatory subunits move out of the active sites of the catalytic subunits, and the R_2C_2 complex dissociates.
c. Cytosolic cAMP concentration increases.
d. The cAMP molecules bind to each PKA regulatory subunit.

9. Consider the following reaction scheme:

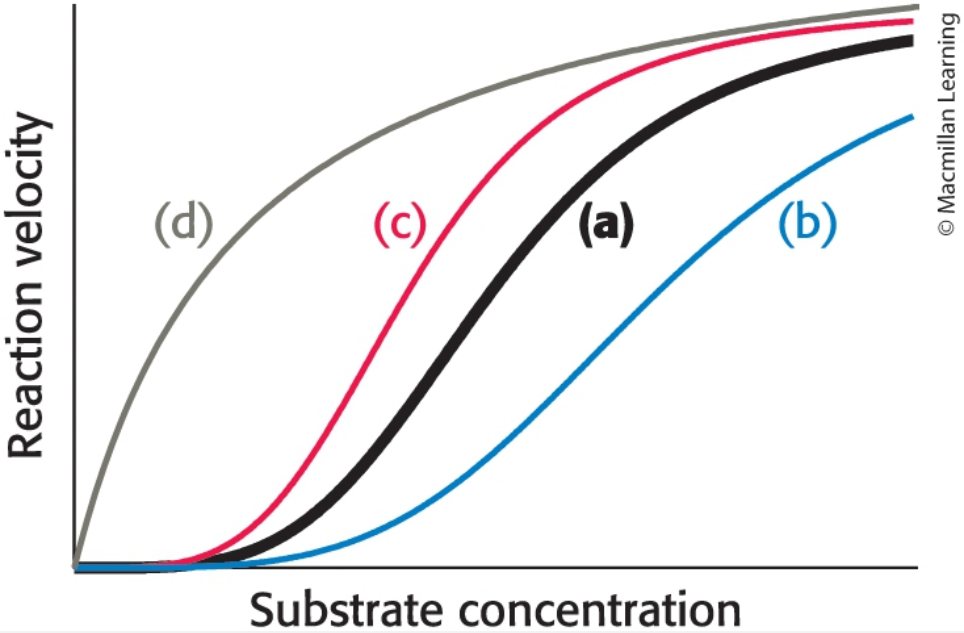


Product Z is a feedback inhibitor of enzyme 1. Assuming Z eventually diffuses out of the cell, in the presence of a high concentration of Z: 2

a. Would the concentration of X increase, decrease, or stay the same?
b. Would the concentration of Y increase, decrease, or stay the same?
c. Would the concentration of Z increase, decrease, or stay the same?
d. What happens to the activity of enzyme 1 if the concentration of Z decreases?

10. A drug company has decided to use recombinant DNA methods to prepare a modified α_1-antitrypsin that will be more resistant to oxidation than is the naturally occurring inhibitor. Which single amino acid substitution would you recommend?

11. Consider the velocity curve of an allosteric enzyme, the thick black curve labeled "(a)" in the graph below.



Which of the four depicted curves correctly illustrates the effect of a negative modifier? 1

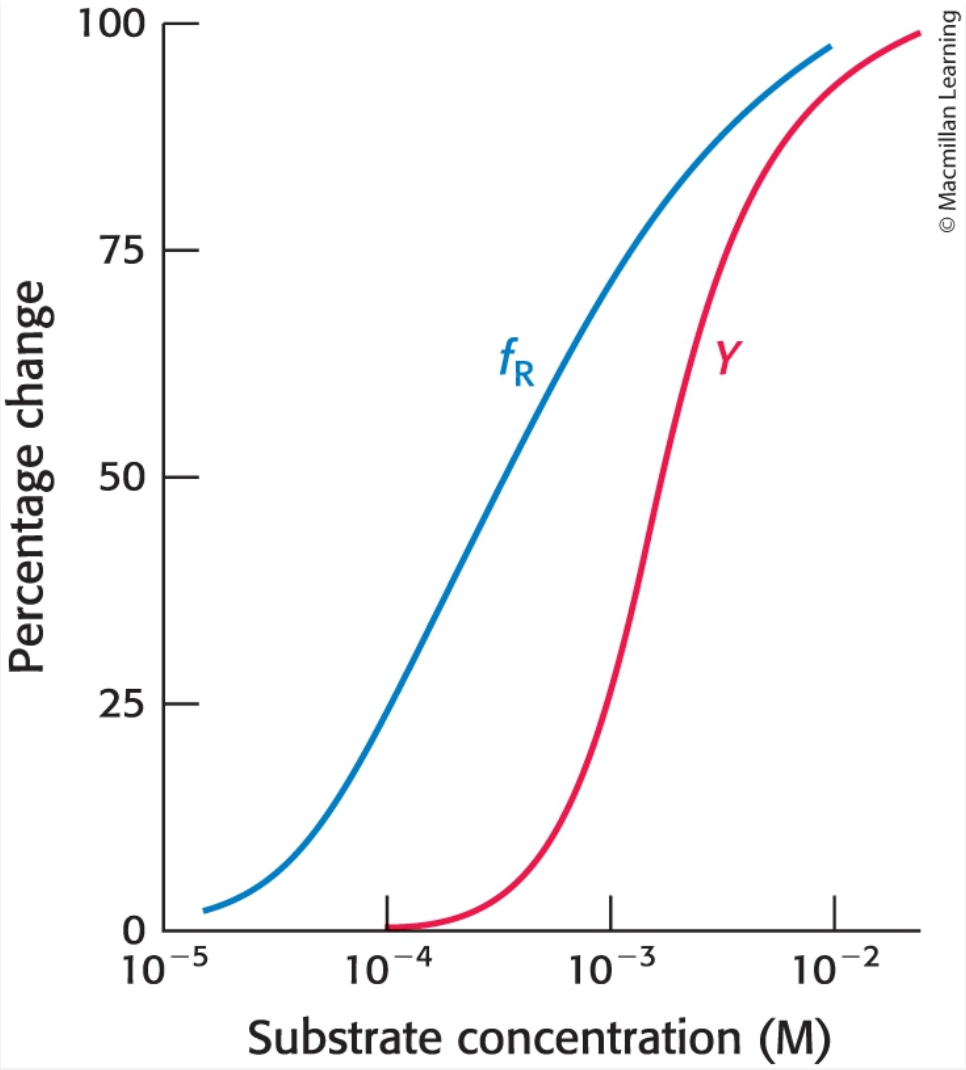
12. The proteolytic enzyme trypsin is produced in the pancreas as the zymogen trypsinogen. Trypsinogen is cleaved to yield active trypsin, which, in turn, activates other pancreatic zymogens.

a. Which of the following enzymes is used in the activation of trypsinogen: chymotrypsin, enteropeptidase, fibrin, trypsin?
b. Which of the following zymogens is directly activated by trypsin: chymotrypsinogen, proelastase, procarboxypeptidase, prolipase?

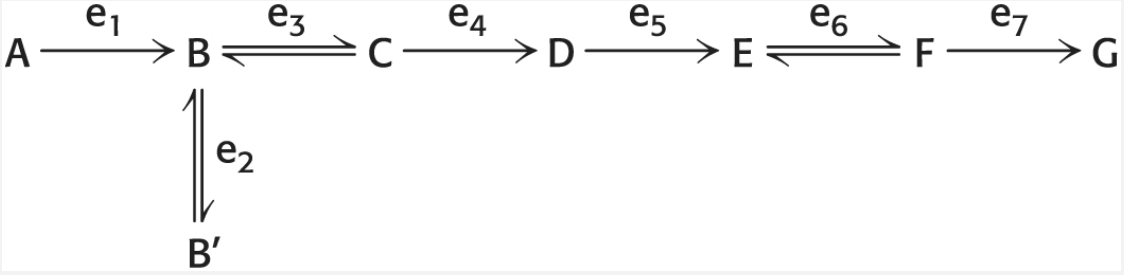
13. Arrange the events of blood clot formation in the correct order:

a. Fibrinogen is converted to fibrin.
b. Trauma releases tissue factor (TF).
c. Transglutaminase cross-links fibrin, yielding a stabilized clot.
d. TF activates factor X to factor X_a.
e. Fibrin threads align, forming a “soft clot.”
f. Prothrombin is converted to thrombin.

14. The following graph shows the fraction of an allosteric enzyme in the R state (f_R) and the fraction of active sites bound to substrate (Y) as a function of substrate concentration. Which model, the concerted or sequential, best explains these results? 1



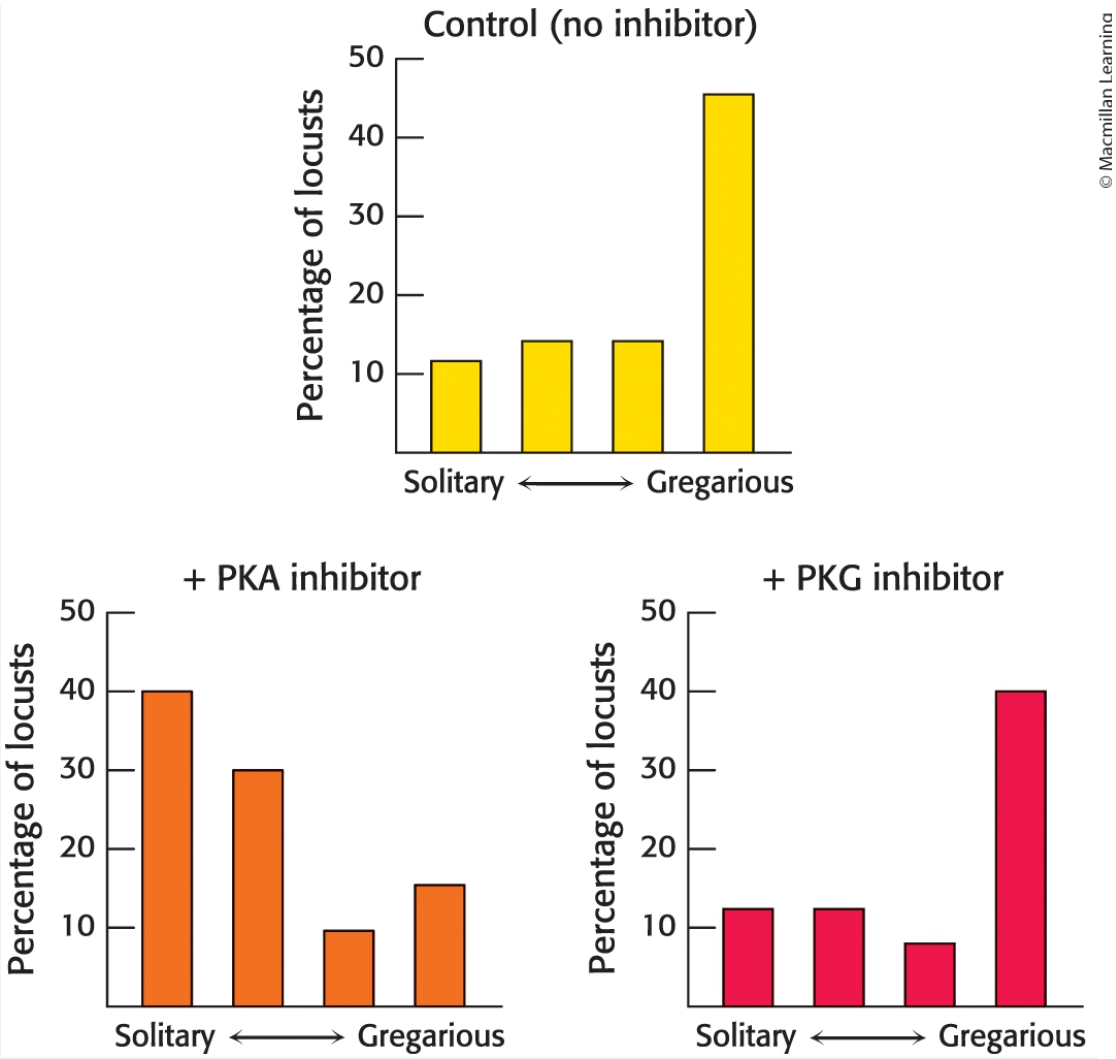
15. Examine the following metabolic pathway:



a. Which enzymes catalyze irreversible reactions?
b. Which of the enzymes, identified as “e” with a numeric subscript, is likely to be the allosteric enzyme that controls the synthesis of G?

16. Recent studies have suggested that protein kinase A may be important in establishing behaviors in many organisms, including humans. One study investigated the role of PKA in locust behavior. Certain species of locust live solitary lives until crowded, at which point they become gregarious — they prefer the crowded life.

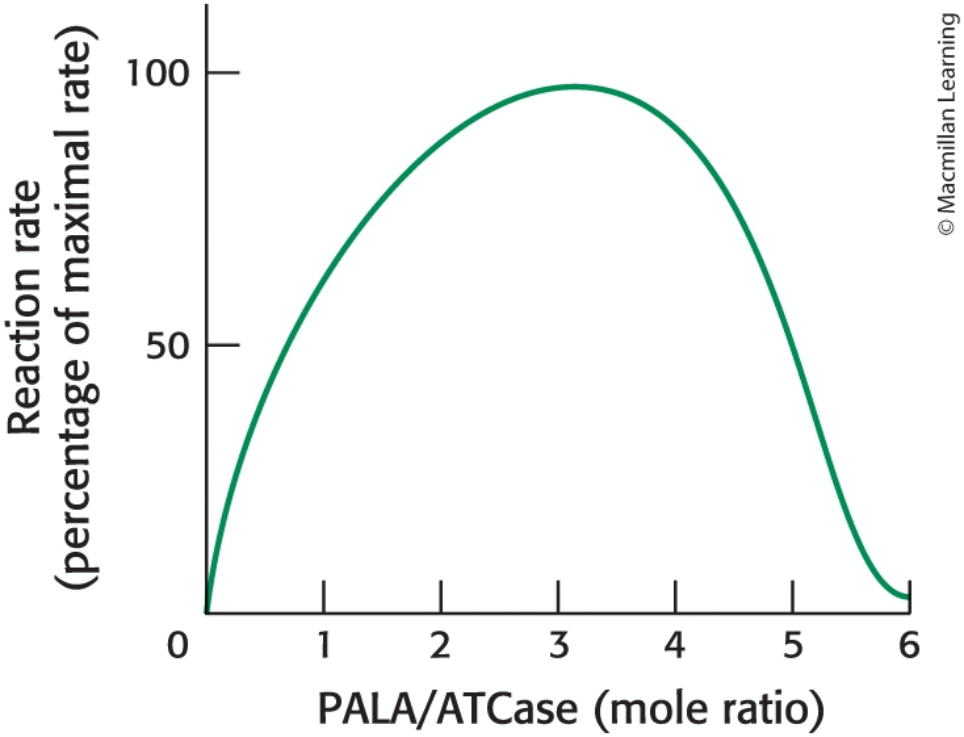
Locusts were grouped together for one hour, and then allowed to stay with the group or move away. Prior to crowding, some insects were injected with a PKA inhibitor, a cyclic GMP-dependent kinase inhibitor, or no inhibitor, as indicated. The results are shown here: 5



© Macmillan Learning

a. What is the response of the control group to crowding?
b. What is the result if the insects are first treated with PKA inhibitor? PKG inhibitor?
c. What was the purpose of the experiment with the PKG inhibitor?
d. What do these results suggest about the role of PKA in the transition from a solitary to a gregarious lifestyle?

17. Recall that PALA is a potent inhibitor of ATCase because it mimics the two physiological substrates. However, in the presence of substrates, low concentrations of this unreactive bisubstrate analog *increase* the reaction velocity. On the addition of PALA, the reaction rate increases until an average of three molecules of PALA are bound per molecule of enzyme. This maximal velocity is 17-fold greater than it is in the absence of PALA. The reaction rate then decreases to nearly zero on the addition of three more molecules of PALA per molecule of enzyme. Why do low concentrations of PALA activate ATCase?



18. According to the concerted model, the relationship between the concentrations of the T and R states in the presence of substrates can be expressed as:

$$\frac{[T_i]}{[R_i]} = c^i L$$

where c is the ratio of the dissociation constants of the substrate for the R state to the T state, that is:

$$c = \frac{K_d^R}{K_d^T},$$

L is the ratio of [T] to [R] *in the absence of substrate,* and i is the number of substrate molecules bound.

Assume we have an allosteric enzyme for which a substrate binds 100 times as tightly to the R state as to its T state.

a. By what factor does the binding of one substrate molecule per enzyme molecule alter the ratio of the concentrations of enzyme molecules in the R and T states?
b. Suppose that L, the ratio of [T] to [R] in the absence of substrate, is 10^7 and that the enzyme contains four binding sites for substrate. What is the ratio of enzyme molecules in the R state to those in the T state in the presence of saturating amounts of substrate, assuming that the concerted model is obeyed? 3

Chapter 8
DNA, RNA, and the Flow of Genetic Information

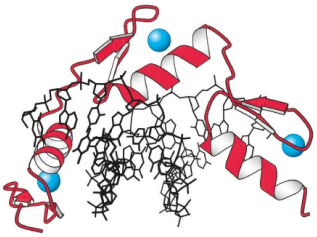




Photo: Lelusy/Shutterstock
© Macmillan Learning

Family resemblance, shown here in the likeness of a puppy to its parents, results from having genes in common. Genes must be expressed to exert an effect, and proteins regulate such expression. One such regulatory protein, a zinc-finger protein (zinc ions are blue, protein is red), is shown bound to a control region of DNA (black).

[Drawn from 1AAY.pdb.]

Outline

8.1 A Nucleic Acid Consists of Four Kinds of Bases Linked to a Sugar–Phosphate Backbone
8.2 A Pair of Nucleic Acid Strands with Complementary Sequences Can Form a Double-Helical Structure

8.3 The Double Helix Facilitates the Accurate Transmission of Hereditary Information
8.4 DNA Is Replicated by Polymerases That Take Instructions from Templates
8.5 Gene Expression Is the Transformation of DNA Information into Functional Molecules
8.6 Amino Acids Are Encoded by Groups of Three Bases Starting from a Fixed Point
8.7 Most Eukaryotic Genes Are Mosaics of Introns and Exons

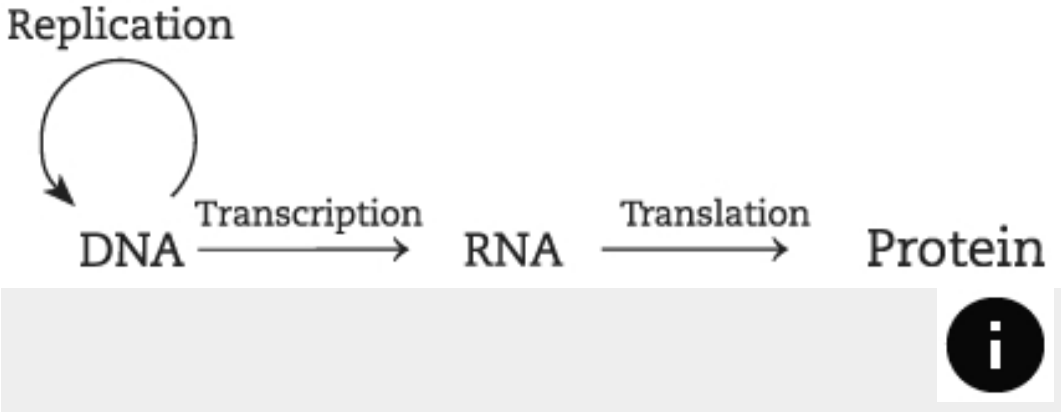
Learning Goals



By the end of this chapter, you should be able to:

1. Identify the bases for DNA and RNA and distinguish between nucleosides and nucleotides.
2. Distinguish between DNA and RNA in both structure and function.
3. Explain how DNA is replicated.
4. Explain how information flows from DNA to protein.
5. Identify some key differences between bacterial and eukaryotic genes.

DNA and RNA are long linear polymers, called nucleic acids, that carry information in a form that can be passed from one generation to the next. Due to its remarkable long-term stability and double-helical structure, DNA polymers are well-suited for the storage and replication of the genetic information for all cells and many viruses. However, DNA is not the direct template for protein synthesis. Rather, a DNA strand is copied into a class of RNA molecules called messenger RNA (mRNA). The scheme that underlies information processing at the level of gene expression was first proposed by Francis Crick in 1958.



Crick called this scheme the *central dogma*. The basic tenets of this dogma are true, but, as we will see later, this scheme is not as simple as depicted. This flow of information depends on the genetic code, which defines the relation between the sequence of bases in DNA and the sequence of amino acids in a protein.

8.1 A Nucleic Acid Consists of Four Kinds of Bases Linked to a Sugar–Phosphate Backbone

The nucleic acids **deoxyribonucleic acid (DNA)** and **ribonucleic acid (RNA)** are well suited to function as the carriers of genetic information by virtue of their covalent structures. These macromolecules are linear polymers built from similar units connected end to end (**Figure 8.1**). Each monomer unit within the polymer is a **nucleotide**. A single nucleotide unit consists of three components: a sugar, a phosphate, and one of four bases. The sequence of bases in the polymer uniquely characterizes a nucleic acid and constitutes a form of linear information — information analogous to the letters that spell a person's name.

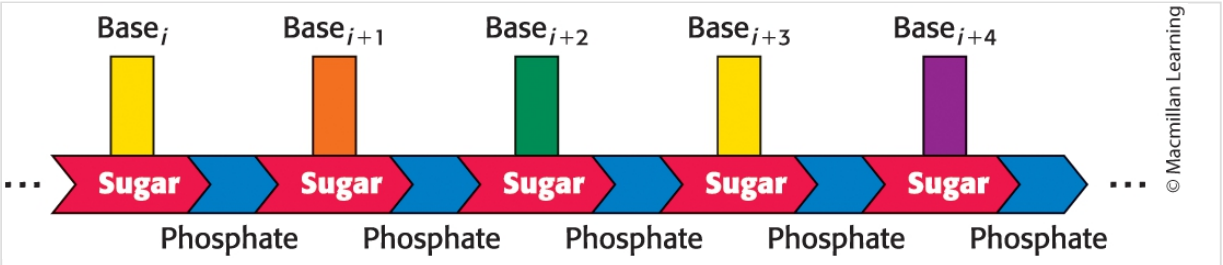


FIGURE 8.1 Nucleic acids are linear polymers of nucleotides. Each nucleotide contains three components: a sugar, a phosphate, and a base.

RNA and DNA differ in the sugar component and one of the bases

The sugar in DNA is **deoxyribose**. The prefix deoxy- indicates that the $2'$-carbon atom of the sugar lacks the oxygen atom that is linked to the $2'$-carbon atom of **ribose**, as shown in **Figure 8.2**. Note that sugar carbons are numbered with primes to differentiate them from atoms in the bases. The sugars in both nucleic acids are linked to one another by phosphodiester bridges. Specifically, the $3'$-hydroxyl ($3'-OH$) group of the sugar moiety of one nucleotide is esterified to a phosphate group, which, in turn, is joined to the $5'$-hydroxyl group of the adjacent sugar.

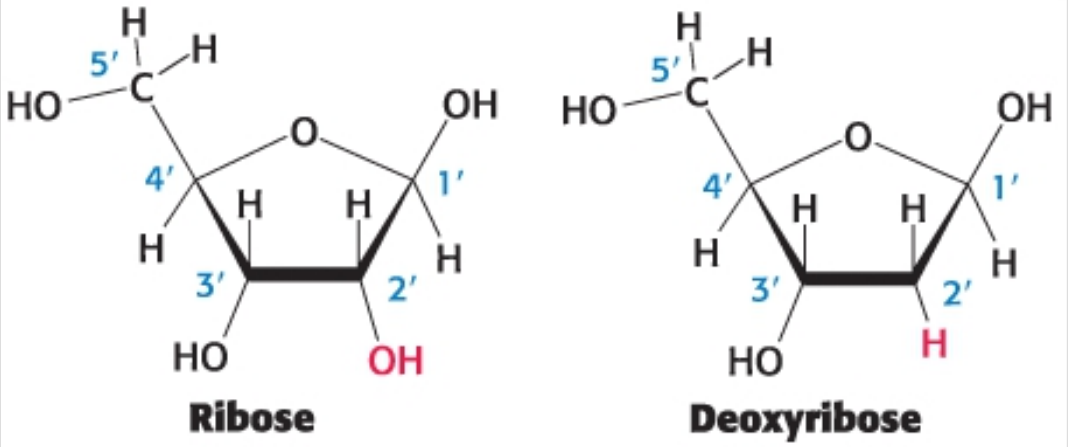


FIGURE 8.2 Ribose and deoxyribose are the sugars found in RNA and DNA, respectively. Atoms in sugar units are numbered with primes to distinguish them from atoms in bases (see Figure 8.4).

The chain of sugars linked by phosphodiester bridges is referred to as the *backbone* of the nucleic acid (**Figure 8.3**). Whereas the backbone is constant in a nucleic acid, the bases vary from one monomer to the

next. Two of the bases of DNA are derivatives of **purine** — adenine (A) and guanine (G) — and two of **pyrimidine** — cytosine (C) and thymine (T), as shown in **Figure 8.4**.

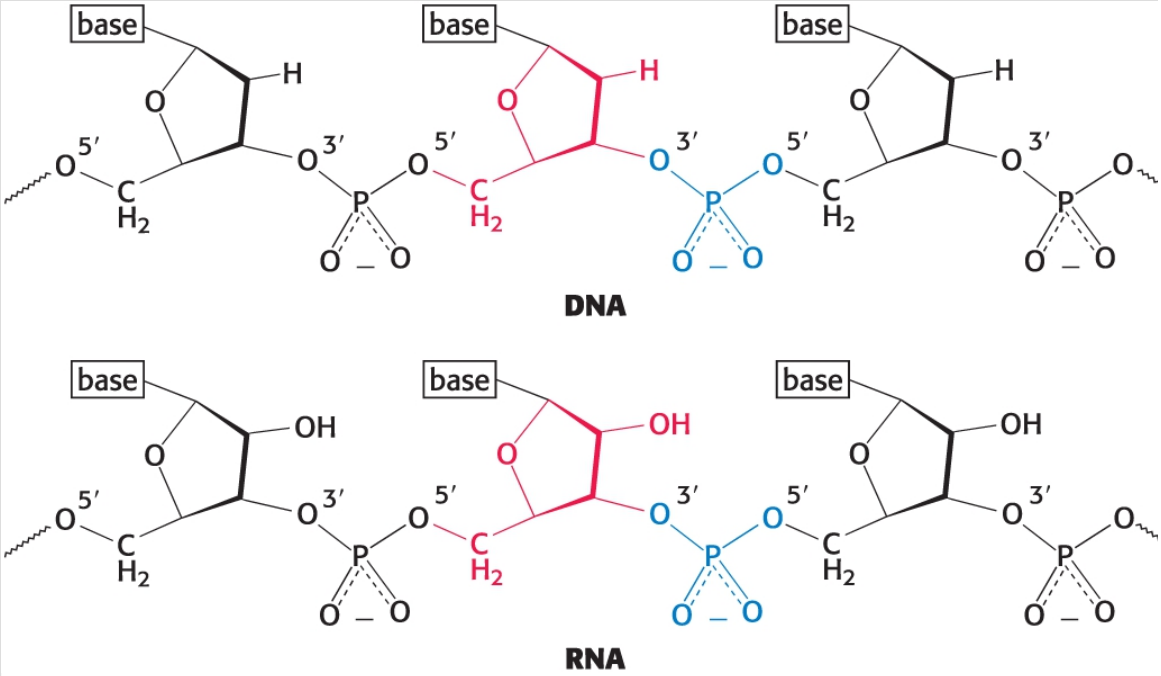


FIGURE 8.3 The sugar–phosphate backbones of nucleic acids are formed by 3′-to-5′ phosphodiester linkages. For each nucleic acid, a sugar unit is highlighted in red and a phosphate group in blue.

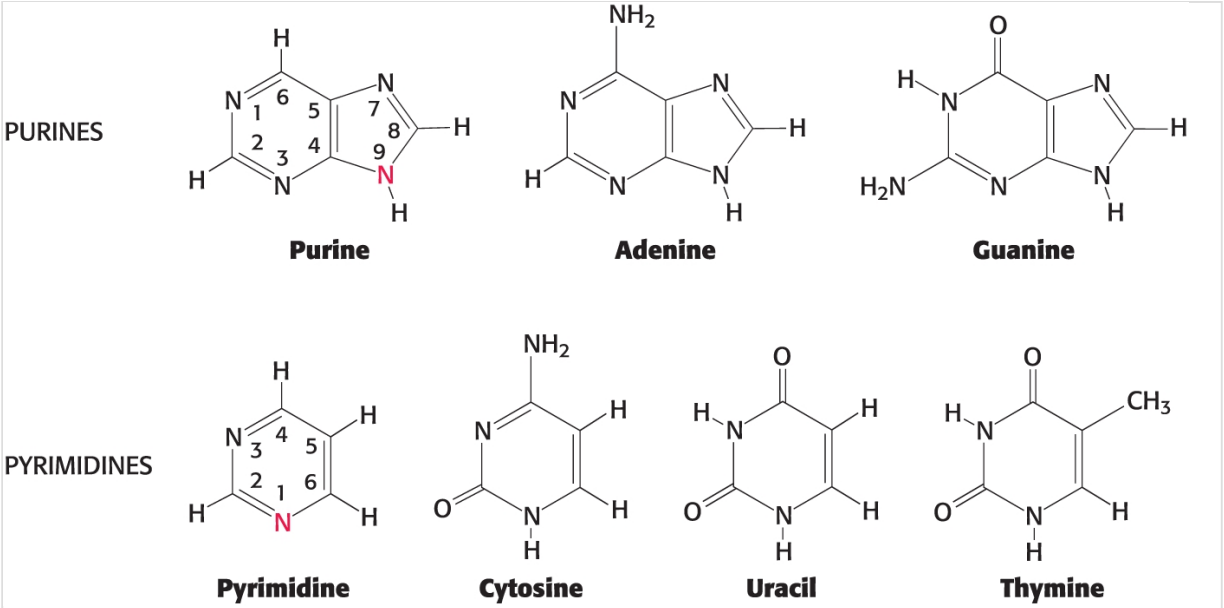


FIGURE 8.4 The bases in nucleic acids are either purines or pyrimidines. Atoms within bases are numbered without primes. Uracil is present in RNA instead of thymine. N-9 in purines and N-1 in pyrimidines form a bond with the sugar (see Figure 8.5).

RNA, like DNA, is a long, unbranched polymer consisting of nucleotides joined by $3'$-to-$5'$ phosphodiester linkages (Figure 8.3). The covalent structure of RNA differs from that of DNA in two respects. First, the sugar units in RNA are riboses rather than deoxyriboses. Ribose contains a $2'$-hydroxyl group not present in deoxyribose (Figure 8.2). Second, one of the four major bases in RNA is uracil (U) instead of thymine (T) (Figure 8.4).

Note that each phosphodiester bridge has a negative charge (Figure 8.3). This negative charge repels nucleophilic species such as hydroxide ions, which are capable of hydrolytic attack on the phosphate backbone. This resistance is crucial for maintaining the integrity of information stored in nucleic acids. The absence of the $2'$-hydroxyl group in DNA further

increases its resistance to hydrolysis. The greater stability of DNA probably accounts for its use rather than RNA as the hereditary material in all modern cells and in many viruses.

Nucleotides are the monomeric units of nucleic acids

The building blocks of nucleic acids and the precursors of these building blocks play many other roles throughout the cell — for instance, as energy currency and as molecular signals. Consequently, it is important to be familiar with the nomenclature of nucleotides and their precursors. A unit consisting of a base bonded to a sugar is referred to as a **nucleoside**. The four nucleoside units in RNA are called *adenosine*, *guanosine*, *cytidine*, and *uridine*, whereas those in DNA are called *deoxyadenosine*, *deoxyguanosine*, *deoxycytidine*, and *thymidine*. (Thymidine contains deoxyribose, and by convention, the prefix deoxy- is not added because thymine-containing nucleosides are only rarely found in RNA.)

In each nucleoside, N-9 of a purine or N-1 of a pyrimidine is attached to $C-1'$ of the sugar by an *N*-β-glycosidic linkage (**Figure 8.5**). The base lies above the plane of the sugar when the structure is written in the standard orientation; that is, the configuration of the *N*-glycosidic linkage is β (Section 11.1).

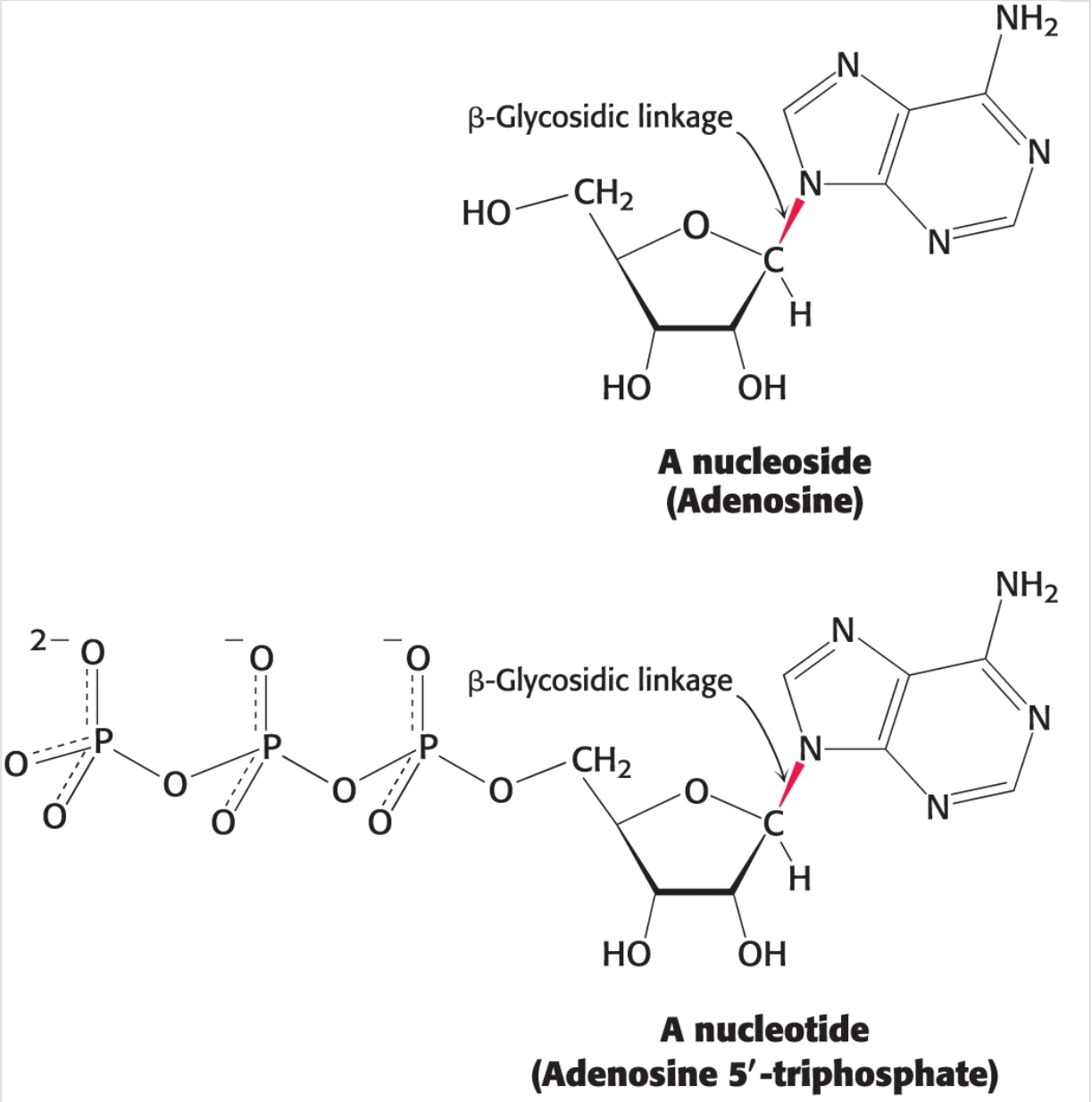


FIGURE 8.5 Nucleosides and nucleotides are distinguished by the presence of phosphoryl groups. A nucleoside contains a sugar and a base joined by an *N*-β-glycosidic linkage. A nucleotide contains a nucleoside linked to one or more phosphoryl groups.

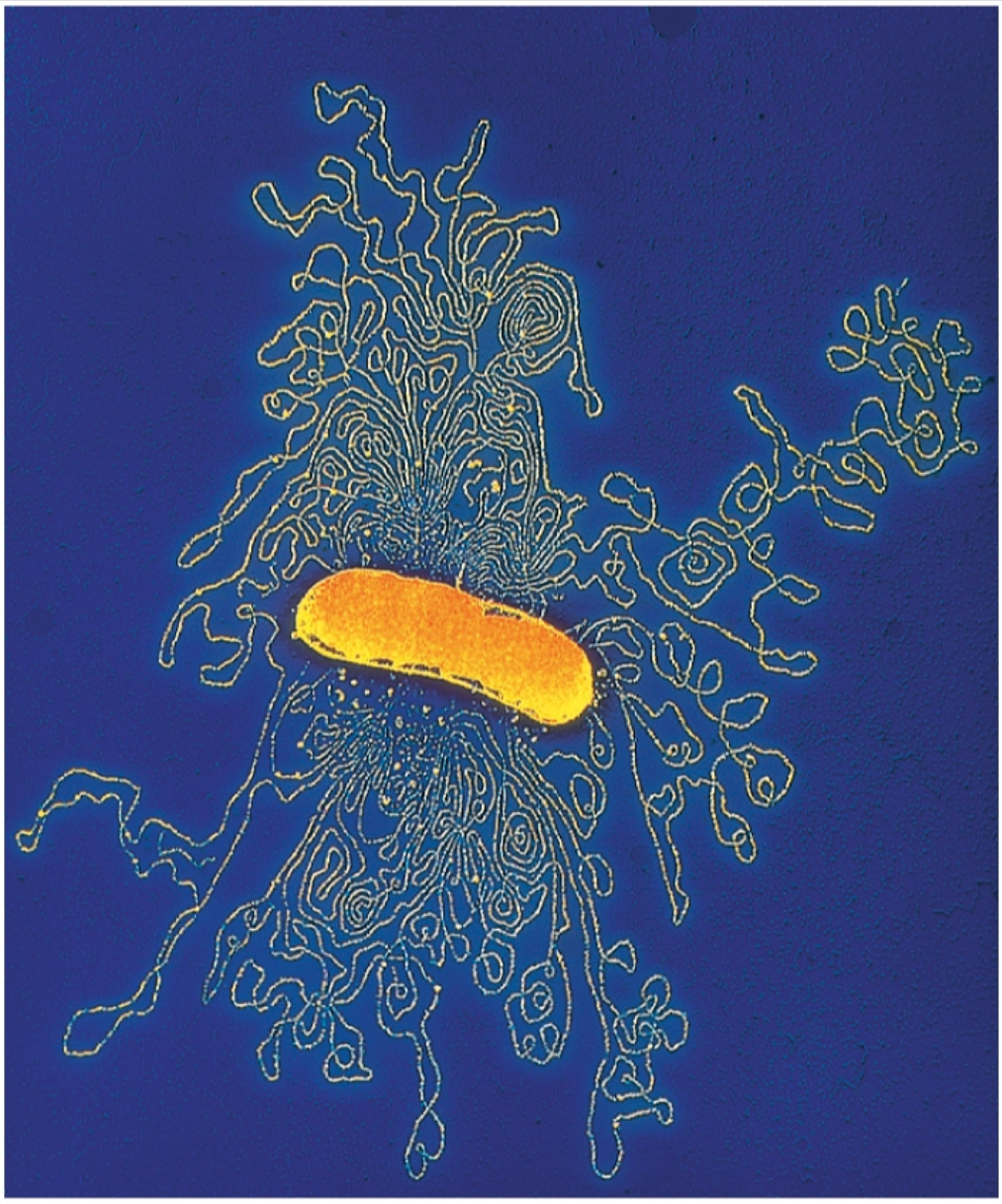
A nucleotide is a nucleoside joined to one or more phosphoryl groups by an ester linkage (Figure 8.5). Nucleoside triphosphates, nucleotides

containing three phosphoryl groups, are the precursors that form RNA and DNA. The four nucleotide units that comprise DNA are nucleoside monophosphates called *deoxyadenylate*, *deoxyguanylate*, *deoxycytidylate*, and *thymidylate*. Note that a pyrophosphate is released when the nucleotides are linked (Section 8.4). Similarly, the most common nucleotides found in RNA are nucleoside monophosphates: *adenylate*, *guanylate*, *cytidylate*, and *uridylate*.

A more precise nomenclature is commonly used to describe the number of phosphoryl groups and the site of attachment to carbon of the ribose. Consider the structure of ATP (Figure 8.5). This compound is formed by the attachment of a phosphoryl group to $C-5'$ of a nucleoside sugar (the most common site of phosphate esterification). In this naming system for nucleotides, the number of phosphoryl groups and the attachment site are designated. Hence, ATP is short for adenosine $5'$-triphosphate. ATP is tremendously important because, in addition to being a building block for RNA, it is the most commonly used energy currency. The energy released from cleavage of the triphosphate group is used to power many cellular processes (Chapter 15).

DNA molecules are very long and have directionality

A striking characteristic of naturally occurring DNA molecules is their length. A DNA molecule must comprise many nucleotides to carry the genetic information necessary for even the simplest organisms. For example, the DNA of a virus such as polyoma, which can cause cancer in certain organisms, consists of two paired strands of DNA, each 5100 nucleotides in length. The *E. coli* genome is a single DNA molecule consisting of two strands of 4.6 million nucleotides each (**Figure 8.6**).



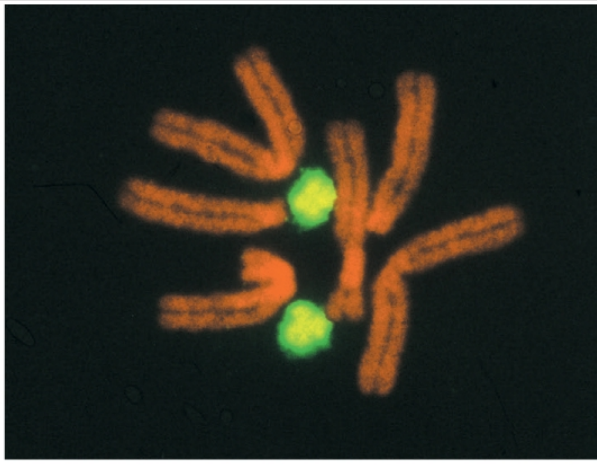
Dr. Gopal Murti/Science Source

FIGURE 8.6 The *E. coli* genome is composed of two paired nucleic acid strands, each with more than 4.5 million nucleotides. As shown by this electron micrograph, the DNA must be tightly compacted in order to fit in such a small volume.

The DNA molecules of higher organisms can be much larger. The human genome comprises approximately 3 billion nucleotides in each strand of DNA, divided among 24 distinct molecules of DNA called

chromosomes (22 autosomal chromosomes plus the X and Y sex chromosomes) of different sizes. One of the largest known DNA molecules is found in the Indian muntjac, an Asiatic deer; its genome is nearly as large as the human genome but is distributed on only 3 chromosomes (**Figure 8.7**). The largest of these chromosomes has two strands of more than 1 billion nucleotides each. If such a DNA molecule could be fully extended, it would stretch more than 1 foot in length. Some plants contain even larger DNA molecules.





Credits: (Left) Super Prin/Shutterstock; (Right) Reprinted by permission from Macmillan Publishers Ltd: *Nature Genetics*, J-Y Lee, M. Koi, E.J. Stanbridge, M. Oshimura, A.T. Kumamoto, & A.P. Feinberg, Simple purification of human chromosomes to homogeneity using muntjac hybrid cells, vol. 7, pp. 29–33, ©1994, Figure 2b. Permission conveyed through Copyright Clearance Center, Inc.

FIGURE 8.7 The Indian muntjac genome is about as large as a human's but is divided among three chromosome pairs. In cells from a female Indian muntjac (left), the three pairs of very lar chromosomes are stained orange in the right image. The image also shows a pair of human chromosomes (stained green) for comparison.

Note that, like a polypeptide (Section 2.3), a DNA chain has directionality, commonly called polarity. One end of the chain has a free $5'-OH$ group or a $5'-OH$ group attached to a phosphoryl group, and the other end has a free $3'-OH$ group, neither of which is linked to another nucleotide (**Figure 8.8**). When presenting very long sequences

of nucleotides, only the identity of the bases are written, given that these bases represent the genetic information. However, it is important to remember that even if only the bases are presented, the base sequence is written in the $5'$-to-$3'$ direction. Thus, ACG indicates that the unlinked $5'-OH$ group is on deoxyadenylate, whereas the unlinked $3'-OH$ group is on deoxyguanylate. Because of this polarity, ACG and GCA correspond to different compounds.

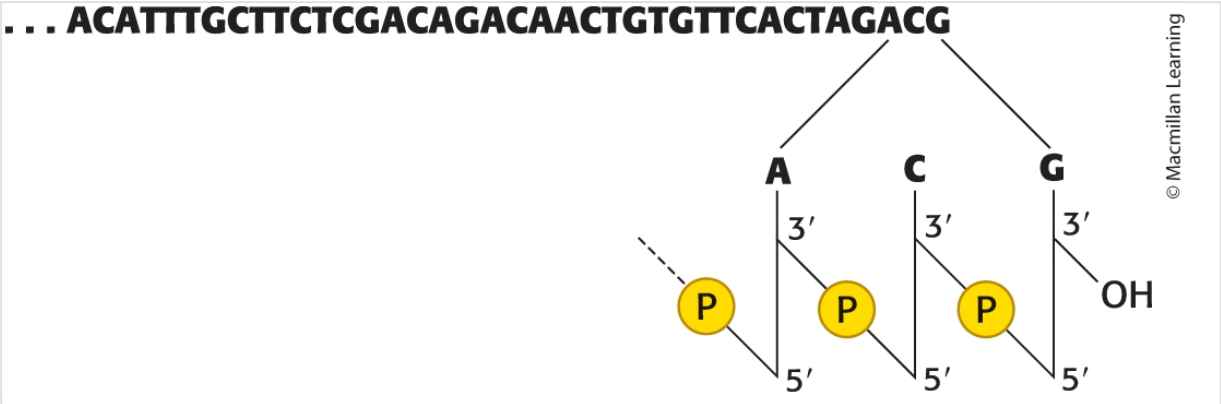


FIGURE 8.8 The structure of a nucleic acid strand can be simplified to the identity of its bases.

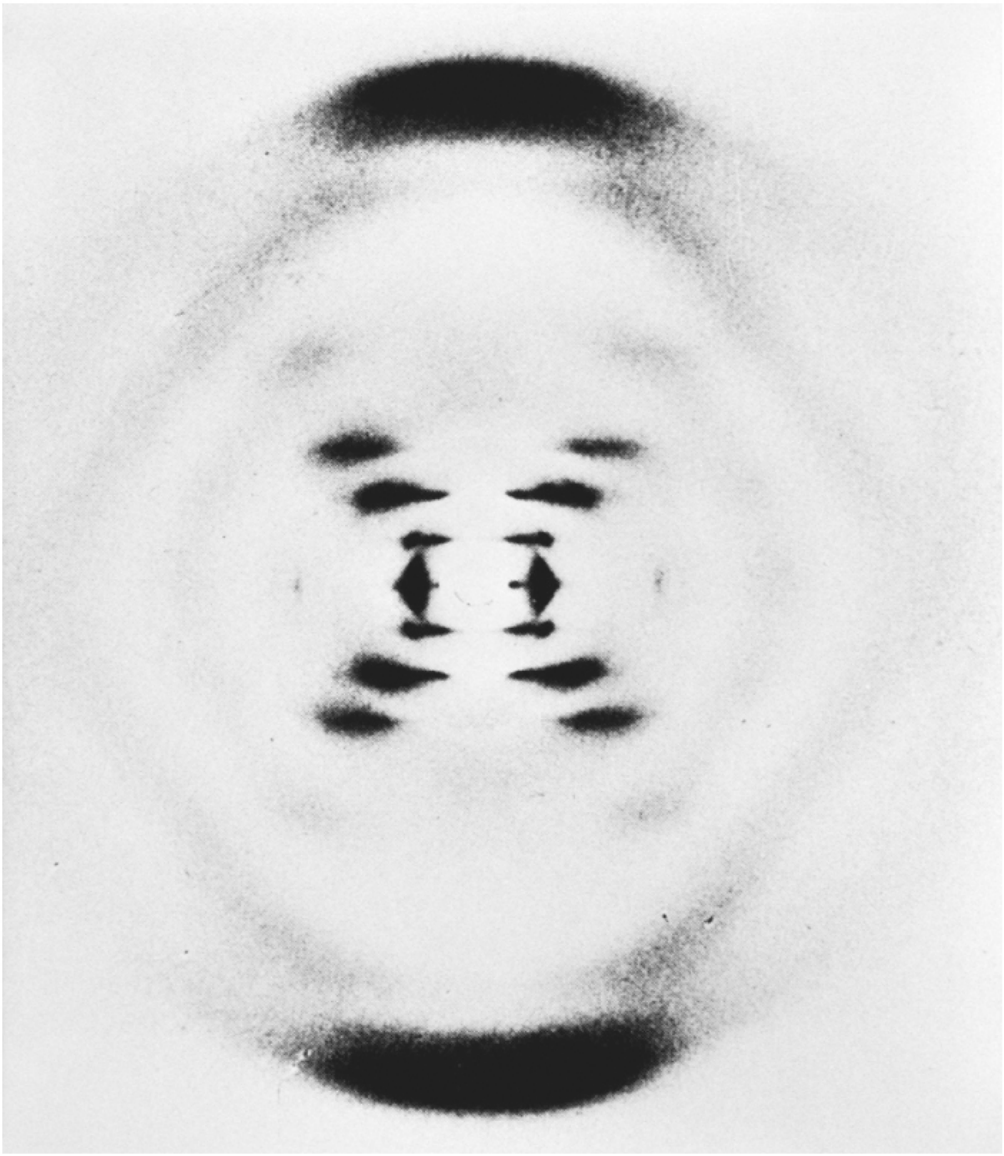
A simplified depiction of a nucleic acid (compare with Figure 8.3). The strand has a $5'$ end, which is usually attached to a phosphoryl group, and a $3'$ end, which is usually a free hydroxyl group.

8.2 A Pair of Nucleic Acid Strands with Complementary Sequences Can Form a Double-Helical Structure

As discussed in Section 1.2, the covalent structure of nucleic acids accounts for their ability to carry information in the form of a sequence of bases along a nucleic acid strand. The bases on the two separate nucleic acid strands form specific base pairs in such a way that a helical structure is formed. The double-helical structure of DNA facilitates the replication of the genetic material — that is, the generation of two copies of a nucleic acid from one.

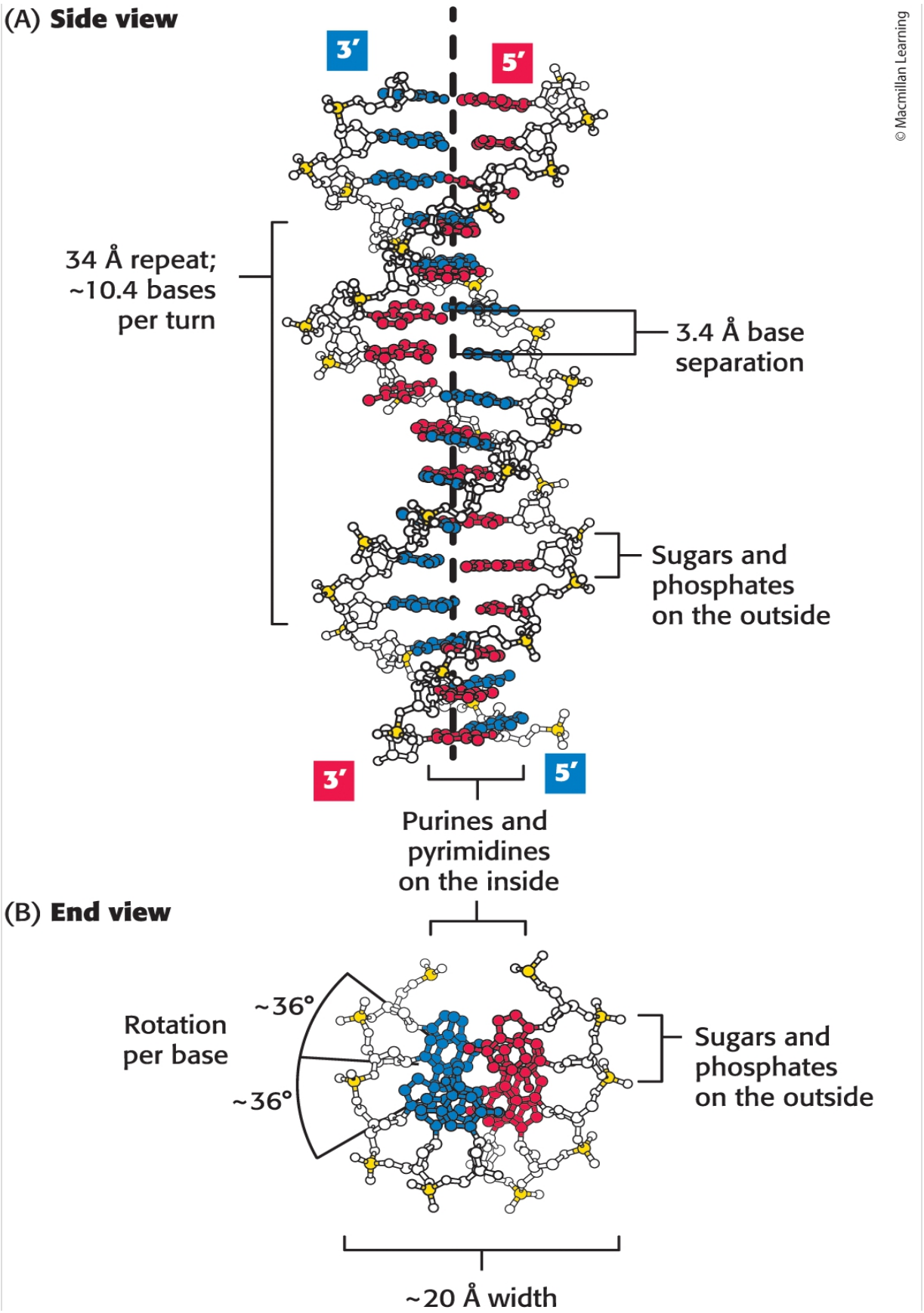
The double helix is stabilized by hydrogen bonds and van der Waals interactions

The ability of nucleic acids to form specific base pairs was discovered in the course of studies directed at determining the three-dimensional structure of DNA. Maurice Wilkins and Rosalind Franklin obtained x-ray diffraction photographs of fibers of DNA (**Figure 8.9**). The characteristics of these diffraction patterns indicated that DNA is formed of two strands that wind in a regular helical structure. From these data and others, James Watson and Francis Crick deduced a structural model for DNA that accounted for the diffraction pattern and was the source of some remarkable insights into the functional properties of nucleic acids (**Figure 8.10**).



Omikron/Science Source

FIGURE 8.9 The x-ray diffraction photograph of a hydrated DNA fiber provided experimental evidence of DNA's three-dimensional structure. When crystals of a biomolecule are irradiated with x-rays, the x-rays are diffracted, and these diffracted x-rays are seen as a series of spots, called reflections, on a screen behind the crystal. The structure of the molecule can be determined by the pattern of the reflections (Section 4.5). In regard to DNA crystals, the central cross is diagnostic of a helical structure. The strong arcs on the meridian arise from the stack of nucleotide bases, which are 3.4 Å apart.



© Macmillan Learning

FIGURE 8.10 The Watson–Crick model of double-helical DNA reveals critical structural features. In this figure, the bases of the individual strands are colored red and blue, while the phosphates are colored yellow. (A) The side view reveals that adjacent bases are separated by 3.4 Å. The structure repeats along the helical axis (vertical) at intervals of 34 Å, which corresponds to approximately 10 nucleotides on each chain. (B) The end view, looking down the helix axis, reveals a rotation of 36° per base and shows that the bases are stacked on top of one another.

[Drawn from 3BSE.pdb.]



The features of the Watson–Crick model of DNA deduced from the diffraction patterns are:

- Two helical polynucleotide strands are coiled around a common axis with a right-handed screw sense (Section 2.4). The strands are antiparallel, meaning that they have opposite directionality.
- The sugar–phosphate backbones are on the outside and the purine and pyrimidine bases lie on the inside of the helix.
- The bases are nearly perpendicular to the helix axis, and adjacent bases are separated by approximately 3.4 Å. The helical structure repeats on the order of every 34 Å, with about 10.4 bases per turn of helix. There is a rotation of nearly 36 degrees per base (360 degrees per full turn/10.4 bases per turn).
- The diameter of the helix is about 20 Å.

How is such a regular structure able to accommodate an arbitrary sequence of bases, given the different sizes and shapes of the purines and pyrimidines? In attempting to answer this question, Watson and Crick discovered that guanine can be paired with cytosine and adenine with thymine to form base pairs that have essentially the same shape (**Figure 8.11**). These base pairs are held

together by specific hydrogen bonds, which, although weak ($4\text{–}21\ \text{kJ mol}^{-1}$, or $1\text{–}5\ \text{kcal mol}^{-1}$), stabilize the helix because of their large numbers in a DNA molecule. These base-pairing rules account for the observation originally made by biochemist Erwin Chargaff in the 1940s — and subsequently referred to as *Chargaff's rules* — that the ratios of adenine to thymine and of guanine to cytosine are nearly the same in all species studied, whereas the adenine-to-guanine ratio varies considerably (**Table 8.1**).

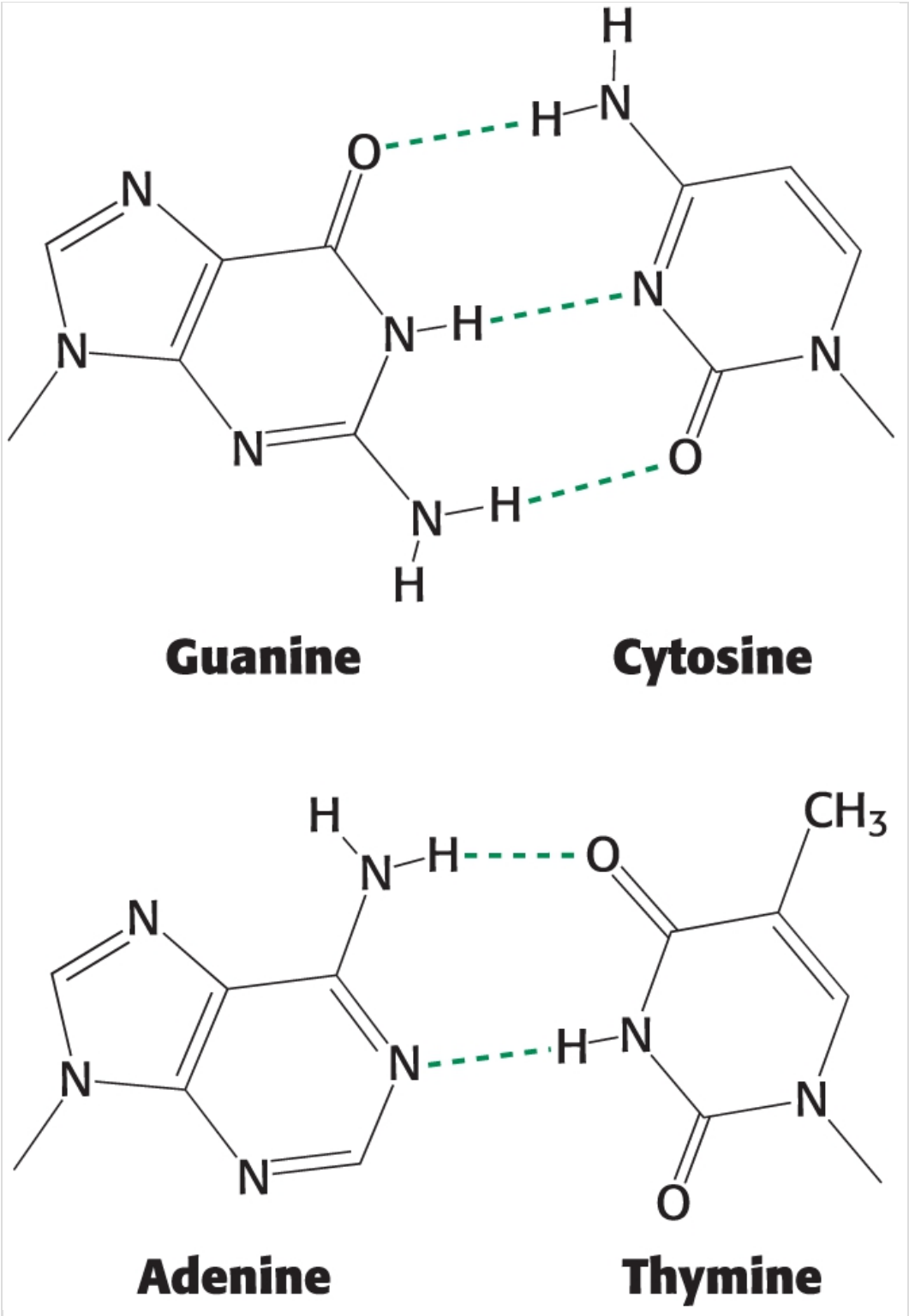


FIGURE 8.11 Watson and Crick proposed two base pairs. In their model, guanine paired with cytosine and adenine paired with thymine.

TABLE 8.1 Base compositions experimentally determined for a variety of organisms

Organism	A : T	G : C	A : G
Human being	1.00	1.00	1.56
Salmon	1.02	1.02	1.43
Wheat	1.00	0.97	1.22
Yeast	1.03	1.02	1.67
Escherichia coli	1.09	0.99	1.05
Serratia marcescens	0.95	0.86	0.70

Inside the helix, the bases are essentially stacked one on top of another (Figure 8.10B). Recall from Section 1.3 that the stacking of base pairs contributes to the stability of the double helix in two ways:

- *The formation of the double helix is facilitated by the hydrophobic effect.* The hydrophobic bases cluster in the interior of the helix away from the surrounding water, whereas the more polar surfaces are exposed to water. This arrangement is reminiscent of protein folding, where hydrophobic amino acids are in the protein's interior and the hydrophilic amino acids are on the exterior (Section 2.5).

- *The stacked base pairs attract one another through van der Waals forces.* These forces, appropriately referred to as *stacking forces*, further contribute to stabilization of the helix (**Figure 8.12**). The energy associated with a single van der Waals interaction is quite small, typically from 2 to $4\ \text{kJ mol}^{-1}$ $(0.5\text{–}1.0\ \text{kcal mol}^{-1})$. In the double helix, however, a large number of atoms are in van der Waals contact, and the net effect, summed over these atom pairs, is substantial. In addition, base stacking in DNA is favored by the conformations of the somewhat rigid five-membered rings of the backbone sugars.

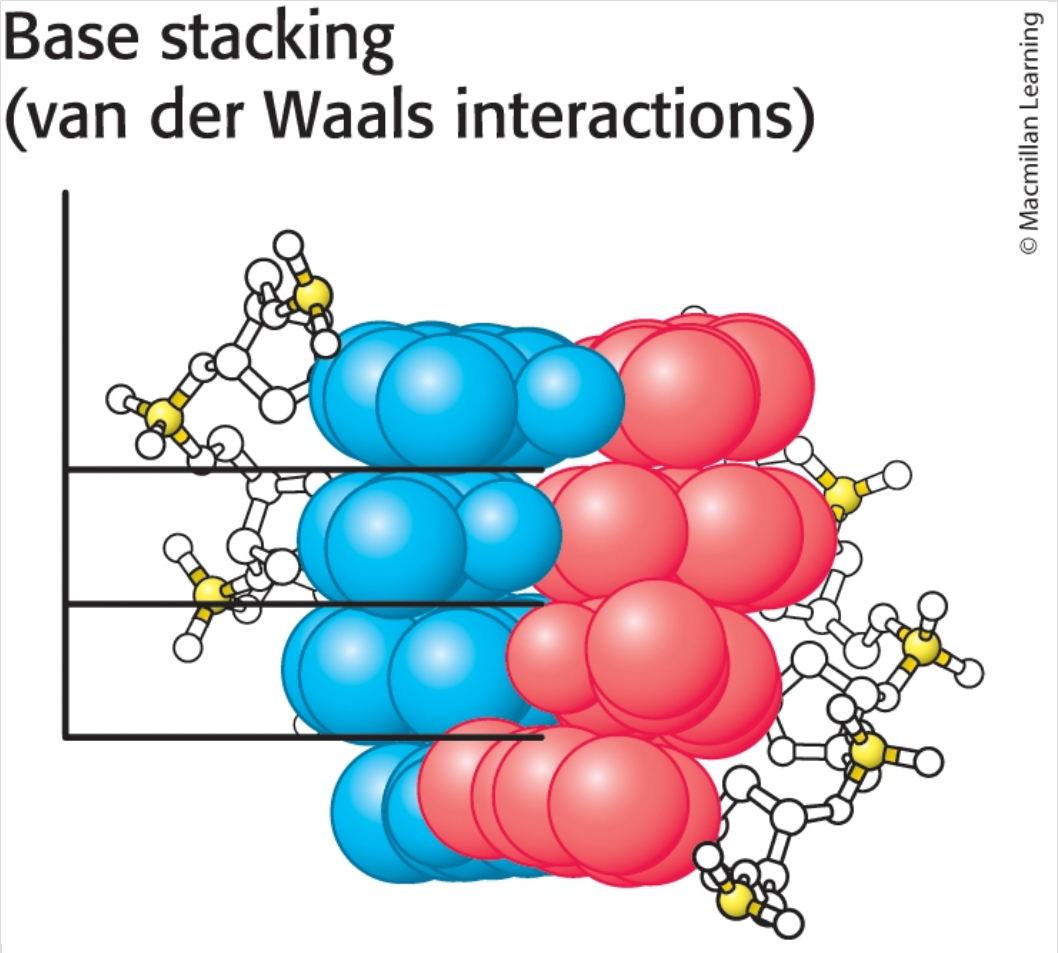


FIGURE 8.12 A side view of DNA reveals the stacking of base pairs within the double helix. The stacked bases interact via van der Waals forces. Such stacking

forces help stabilize the double helix.

[Drawn from 3BSE.pdb.]

Self-Check Question

DNA in the form of a double helix must be associated with cations, usually Mg^{2+}. Why is this requirement the case?

DNA can assume a variety of structural forms

Watson and Crick based their model on x-ray diffraction patterns of highly hydrated DNA fibers, which provided information about properties of the double helix that are averaged over its constituent residues. It is now known that DNA helices can take different forms under different conditions.

Under physiological conditions, most DNA is in the form that Watson and Crick modeled. This form, called *B-DNA*, is a right-handed double helix made up of antiparallel strands held together by Watson–Crick base-pairing. X-ray diffraction studies of less-hydrated DNA fibers have revealed a different form called *A-DNA*. Like B-DNA, A-DNA is a right-handed double helix made up of antiparallel strands held together by Watson–Crick base-pairing.

The A-form helix is wider and shorter than the B-form helix, and its base pairs are tilted rather than perpendicular to the helix axis (Figure 8.13).

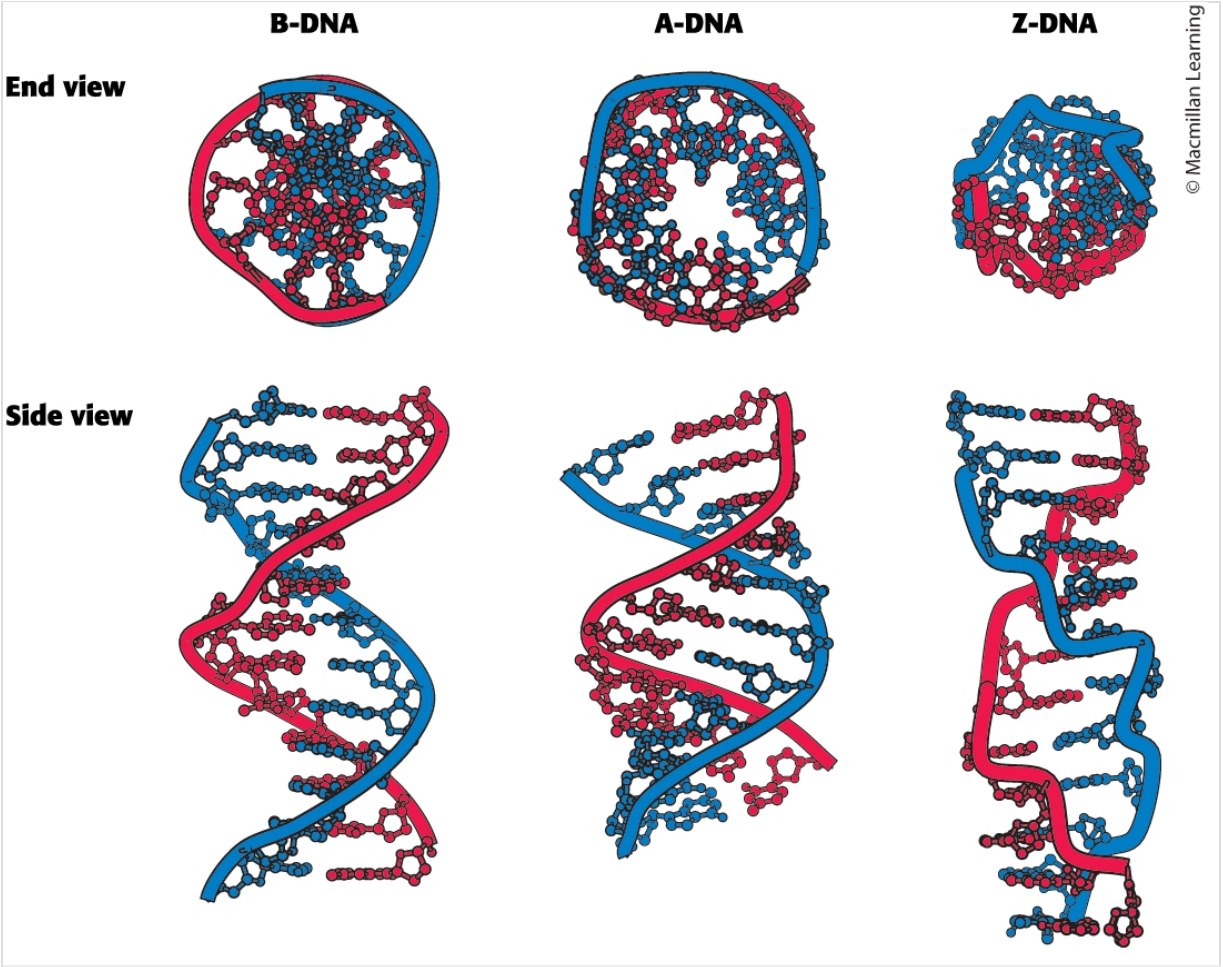


FIGURE 8.13 DNA can adopt different structural forms. Models of B-form and A-form DNA depict their right-handed helical structures. The B-form helix is longer and narrower than the A-form helix. Z-DNA is a left-handed helix in which the phosphoryl groups zigzag along the backbone.

[Drawn from 3BSE.pdb, 3V9D.pdb, and 4OCB.pdb.]

INTERACT with these models Achieve

If the A-form helix were simply a property of dehydrated DNA, it would be of little significance. However, double-stranded regions of RNA and at least some RNA–DNA hybrids adopt a double-helical form very similar to that of A-DNA. What is the biochemical basis for differences between the two forms of DNA? Many of the structural differences between B-DNA and A-DNA arise from different puckerings of their ribose units (Figure 8.14). In A-DNA, C–3′ lies out of the plane (a conformation referred to as C–3′ *endo*) formed by the other four atoms of the ring; in B-DNA, C–2′ lies out of the plane (a conformation called C–2′ *endo*). The C–3′-endo puckering in A-DNA leads to an 11-degree tilting of the base pairs away from being perpendicular to the helix.

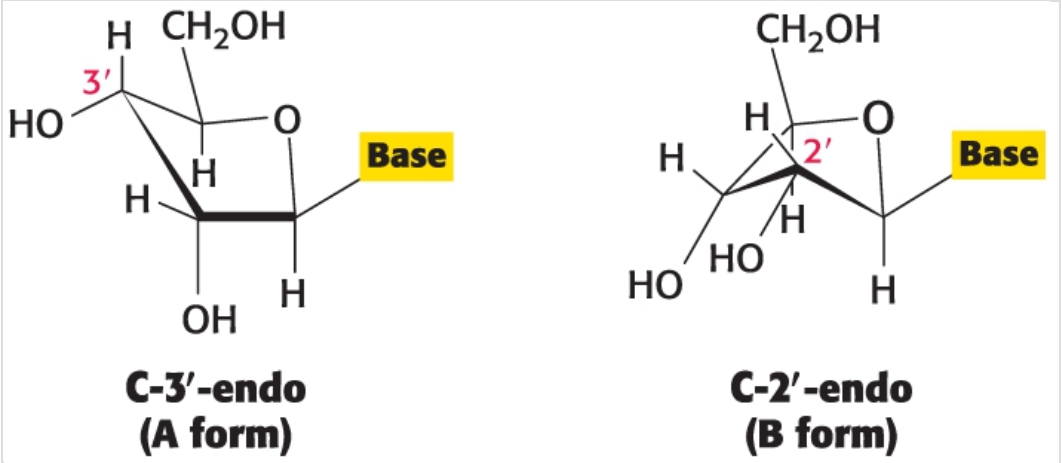


FIGURE 8.14 Sugar pucker explains many of the structural differences between the B-form and A-form of DNA. In A-form DNA, the C–3′ carbon atom lies above the approximate plane defined by the four other sugar nonhydrogen atoms (called C–3′ endo). In B-form DNA, each deoxyribose is in a C–2′-endo conformation, in which C–2′ lies out of the plane.

RNA helices are further induced to take the A-DNA form because of steric hindrance from the $2'$-hydroxyl group: the $2'$-oxygen atom would be too close to three atoms of the adjoining phosphoryl group and to one atom in the next base. In an A-form helix, in contrast, the $2'$-oxygen atom projects outward, away from other atoms. The phosphoryl and other groups in the A-form helix bind fewer H_2O molecules than do those in B-DNA. Hence, dehydration favors the A form.

A third type of double helix is left-handed, in contrast with the right-handed screw sense of the A and B helices. Furthermore, the phosphoryl groups in the backbone are zigzagged; hence, this form of DNA is called *Z-DNA* (Figure 8.13). Although the biological role of Z-DNA is still under investigation, Z-DNA-binding proteins have been isolated, one of which is required for viral pathogenesis of poxviruses, including variola, the agent of smallpox. The existence of Z-DNA shows that DNA is a flexible, dynamic molecule whose parameters are not as fixed as depictions suggest. The properties of B-, A-, and Z-DNA are compared in **Table 8.2**.

TABLE 8.2 Comparison of B-, A-, and Z-DNA

	B	A	Z
Shape	Intermediate	Broadest	Narrowest
Rise per base pair	3.4 Å	2.3 Å	3.8 Å

Helix diameter	~20 Å	~26 Å	~18 Å
Screw sense	Right-handed	Right-handed	Left-handed
Glycosidic bond*	*anti*	*anti*	Alternating *anti* and *syn*
Base pairs per turn of helix	10.4	11	12
Pitch per turn of helix	35.4 Å	25.3 Å	45.6 Å
Tilt of base pairs from perpendicular to helix axis	1 degree	19 degrees	9 degrees

**Syn* and *anti* refer to the orientation of the *N*-glycosidic bond between the base and deoxyribose. In the *anti* orientation, the base extends away from the deoxyribose. In the *syn* orientation, the base is above the deoxyribose. Pyrimidines can be in *anti* orientations only, whereas purines can be *anti* or *syn*.

The major and minor grooves are lined by sequence-specific hydrogen-bonding groups

An examination of the DNA molecule in the B form, as shown in Figure 8.13, reveals the presence of two distinct grooves, called the major groove and the minor groove. These grooves arise because the glycosidic bonds of a base pair are not diametrically opposite each other (**Figure 8.15A**). In B-DNA, the major groove is wider (12 Å versus 6 Å) and deeper (8.5 Å versus 7.5 Å) than the minor groove (**Figure 8.15B**).

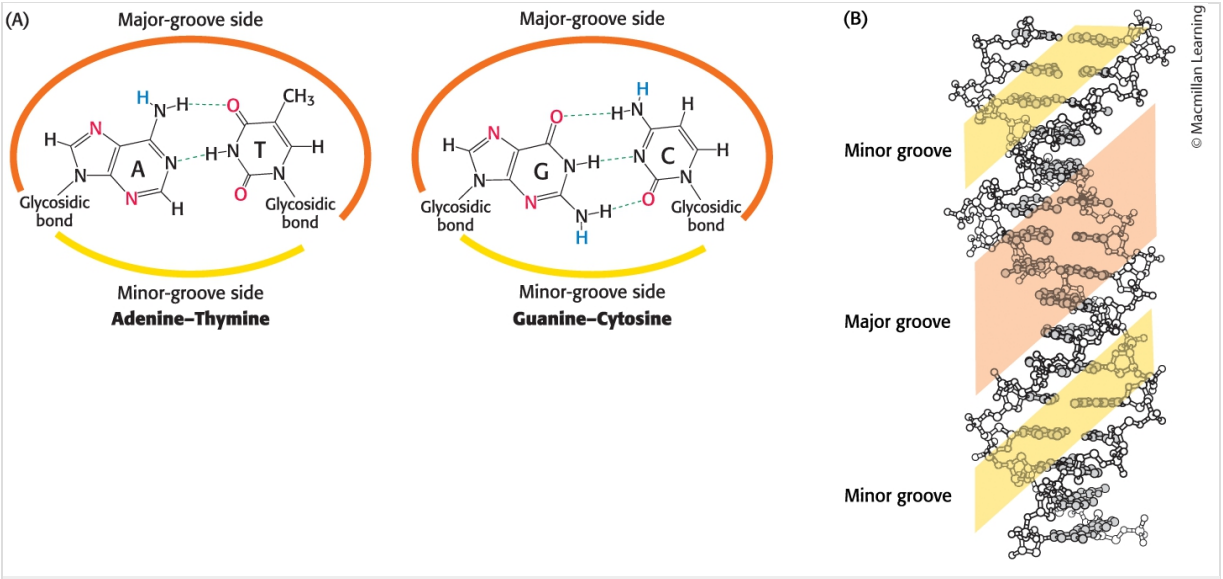


FIGURE 8.15 The DNA double helix features a major and a minor groove. (A) Because the two glycosidic bonds are not directly opposite each other, each base pair has a larger side that defines the major groove and a smaller side that defines the minor groove. The grooves are lined by potential hydrogen-bond donors (blue) and acceptors (red). (B) In a side view of the double helix, the major (orange) and the minor (yellow) grooves alternate with each other.

Each groove is lined by potential hydrogen-bond donor and acceptor atoms that enable interactions with proteins. These interactions are essential for replication and transcription because particular proteins bind to DNA, recognizing specific hydrogen-bond donors and acceptors on the surfaces of the grooves, to catalyze these processes (Chapters 28, 29, and 31).

In the minor groove, N-3 of adenine or guanine and O-2 of thymine or cytosine can serve as hydrogen acceptors, and the amino group attached to C-2 of guanine can be a hydrogen donor. In the major groove, N-7 of guanine or adenine is a potential acceptor, as are O-4 of thymine and O-6 of guanine. The amino groups attached to C-6 of adenine and C-4 of cytosine can serve as hydrogen donors. The

methyl group of thymine also lies in the major groove. Note that the major groove displays more features that distinguish one base pair from another than does the minor groove. The larger size of the major groove in B-DNA makes it more accessible for interactions with proteins that recognize specific DNA sequences.

Some DNA molecules are circular and supercoiled

The DNA molecules in human chromosomes are linear. However, electron microscopic and other studies have shown that intact DNA molecules from bacteria and archaea are circular (**Figure 8.16A**). DNA molecules inside cells necessarily have a very compact shape. Note that the *E. coli* chromosome, fully extended, would be about 1000 times as long as the greatest diameter of the bacterium.

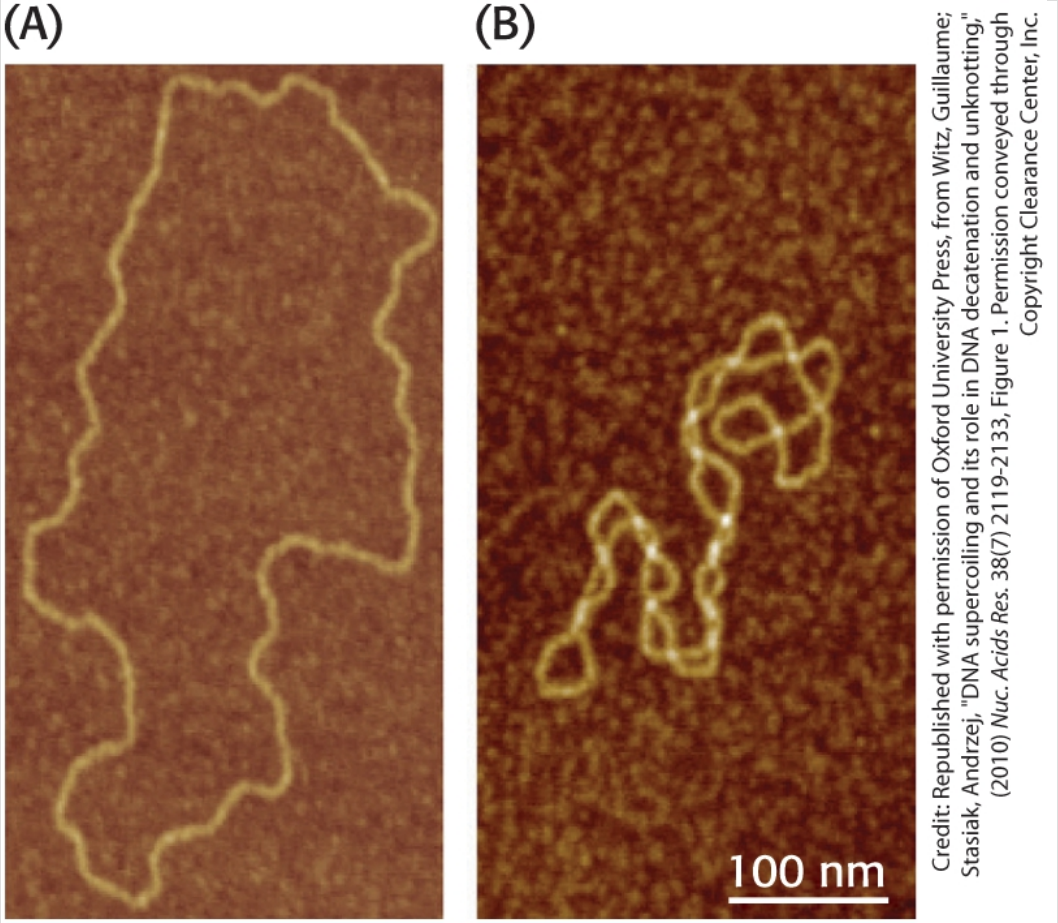


FIGURE 8.16 Atomic force microscopy of circular DNA from bacteria reveals both relaxed and supercoiled forms. (A) Relaxed form. (B) Supercoiled form

A closed DNA molecule has a property unique to circular DNA. The axis of the double helix can itself be twisted into a *superhelix*, where the helix is wound about itself, in a process known as *supercoiling* (**Figure 8.16B**). A circular DNA molecule without any superhelical turns is known as a *relaxed molecule*. Supercoiling is biologically important for two reasons that will be considered further in Chapter 28:

- A supercoiled DNA molecule is more compact than its relaxed counterpart.
- Supercoiling may hinder or favor the capacity of the double helix to unwind and thereby affect the interactions between DNA and other molecules.

Single-stranded nucleic acids can adopt elaborate structures

Single-stranded nucleic acids often fold back on themselves to form well-defined structures. Such structures are especially prominent in RNA and RNA-containing complexes such as the ribosome — a large complex of RNAs and proteins on which proteins are synthesized.

The simplest and most-common structural motif formed is a **stem-loop**, created when two complementary sequences within a single strand come together to form double-helical structures (**Figure 8.17**). In many cases, these double helices are made up entirely of Watson–Crick base pairs. In other cases, however, the structures include mismatched base pairs or unmatched bases that bulge out from the helix. Such mismatches destabilize the local structure but introduce deviations from the standard double-helical structure that can be important for higher-order folding and for function (**Figure 8.18**).

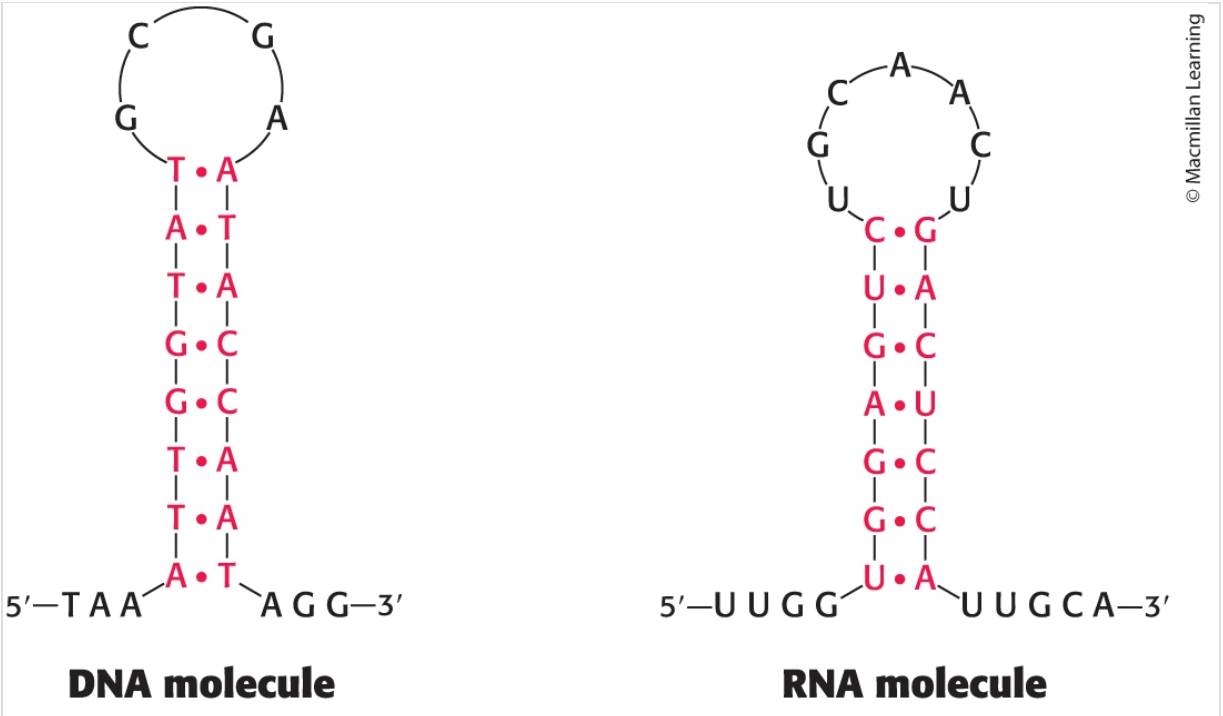


FIGURE 8.17 Stem-loop structures can be formed from single-stranded DNA and RNA molecules.

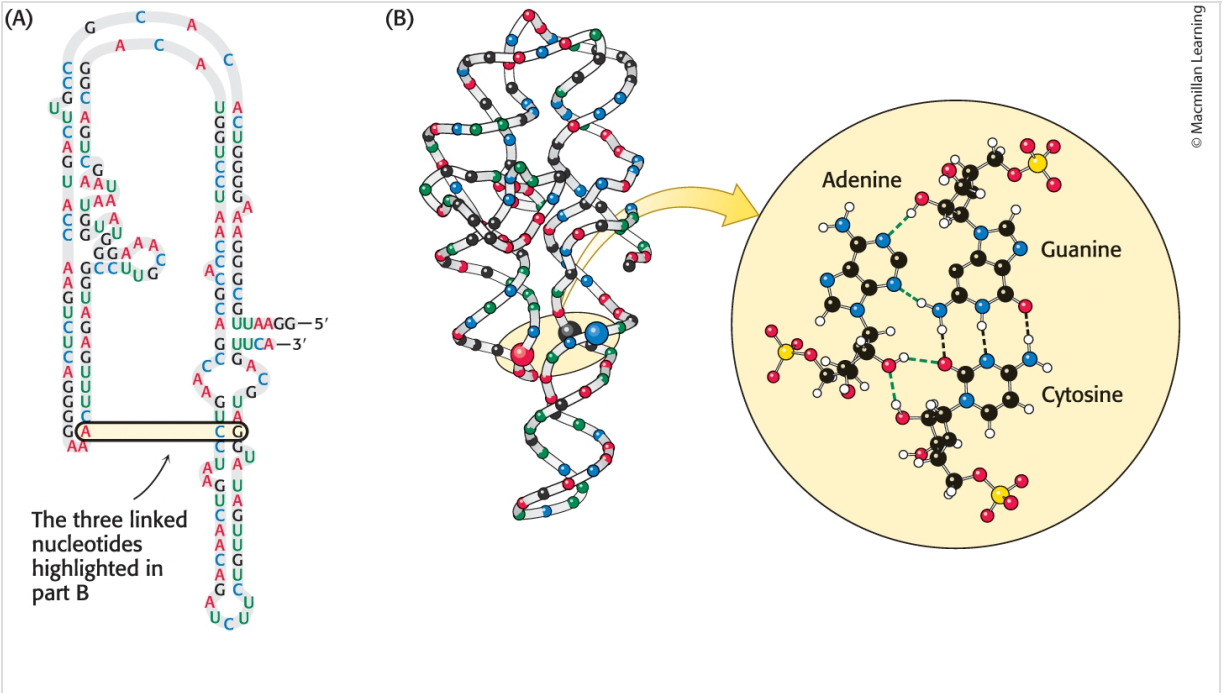


FIGURE 8.18 RNA molecules can adopt complex structures. In this example, a single-stranded RNA molecule folds back on itself. (A) The nucleotide sequence shows Watson–Crick base pairs and other nonstandard base pairings in stem-loop structures. (B) In the three-dimensional structure at the left, cytidine nucleotides are shown in blue, adenosine in red, guanosine in black, and uridine in green. The detailed projection at the right shows an important long-range interaction between three of the bases. Hydrogen bonds within the Watson–Crick base pair are shown as dashed black lines; additional hydrogen bonds are shown as dashed green lines.



Single-stranded nucleic acids can adopt complex structures through the interaction of more widely separated bases. Often, three or more bases interact to stabilize these structures. In such cases, hydrogen-bond donors and acceptors that do not participate in Watson–Crick base pairs participate in hydrogen bonds to form nonstandard pairings (Figure 8.18B). Metal ions such as magnesium ion (Mg^{2+}) often assist in the stabilization of these more elaborate structures. These complex structures allow RNA to perform a host of functions that the double-stranded DNA molecule cannot. Indeed, the complexity of some RNA molecules rivals that of proteins, and these RNA molecules perform a number of functions that had formerly been thought the exclusive domain of proteins.

8.3 The Double Helix Facilitates the Accurate Transmission of Hereditary Information

The double-helical model of DNA proposed by Watson and Crick, and in particular the specific base pairing of adenine with thymine and guanine with cytosine, immediately suggested to them how the genetic material might replicate: The sequence of bases of one strand of the double helix precisely determines the sequence of the other strand. A guanine on one strand is always paired with a cytosine on the other strand, and so on. Thus, separation of a double helix into its two component strands would yield two single-stranded templates onto which new double helices could be constructed, each of which would have the same sequence of bases as the parent double helix. The hypothesis was that as DNA is replicated, one of the strands of each daughter DNA molecule is newly synthesized, whereas the other is passed unchanged from the parent DNA molecule. This distribution of parental atoms is called **semiconservative replication**.

Differences in DNA density established the validity of the semiconservative replication hypothesis

Matthew Meselson and Franklin Stahl carried out a critical test of this hypothesis in 1958. They labeled the parent DNA with ^{15}N, a heavy isotope of nitrogen, to make it denser than ordinary DNA. The labeled DNA was generated by growing *E. coli* for many generations in a medium that contained $^{15}NH_4Cl$ as the sole nitrogen source. After the

incorporation of heavy nitrogen was complete, the bacteria were abruptly transferred to a medium that contained only ^{14}N, the ordinary isotope of nitrogen. The question asked was: What is the distribution of ^{14}N and ^{15}N in the DNA molecules after successive rounds of replication?

The distribution of ^{14}N and ^{15}N was revealed by the technique of density-gradient equilibrium sedimentation. A small amount of the *E. coli* DNA was dissolved in a concentrated solution of cesium chloride. This solution was centrifuged until it was nearly at equilibrium. At that point, the opposing processes of sedimentation and diffusion created a stable density gradient in the concentration of cesium chloride across the sample. The DNA molecules in this density gradient were driven by centrifugal force into the region where the solution's density was equal to their own. The DNA yielded a narrow band or bands that were detected by absorption of ultraviolet light by the DNA. A mixture of ^{14}N DNA and ^{15}N DNA molecules gave clearly separate bands because they differ in density by about 1% (**Figure 8.19**).

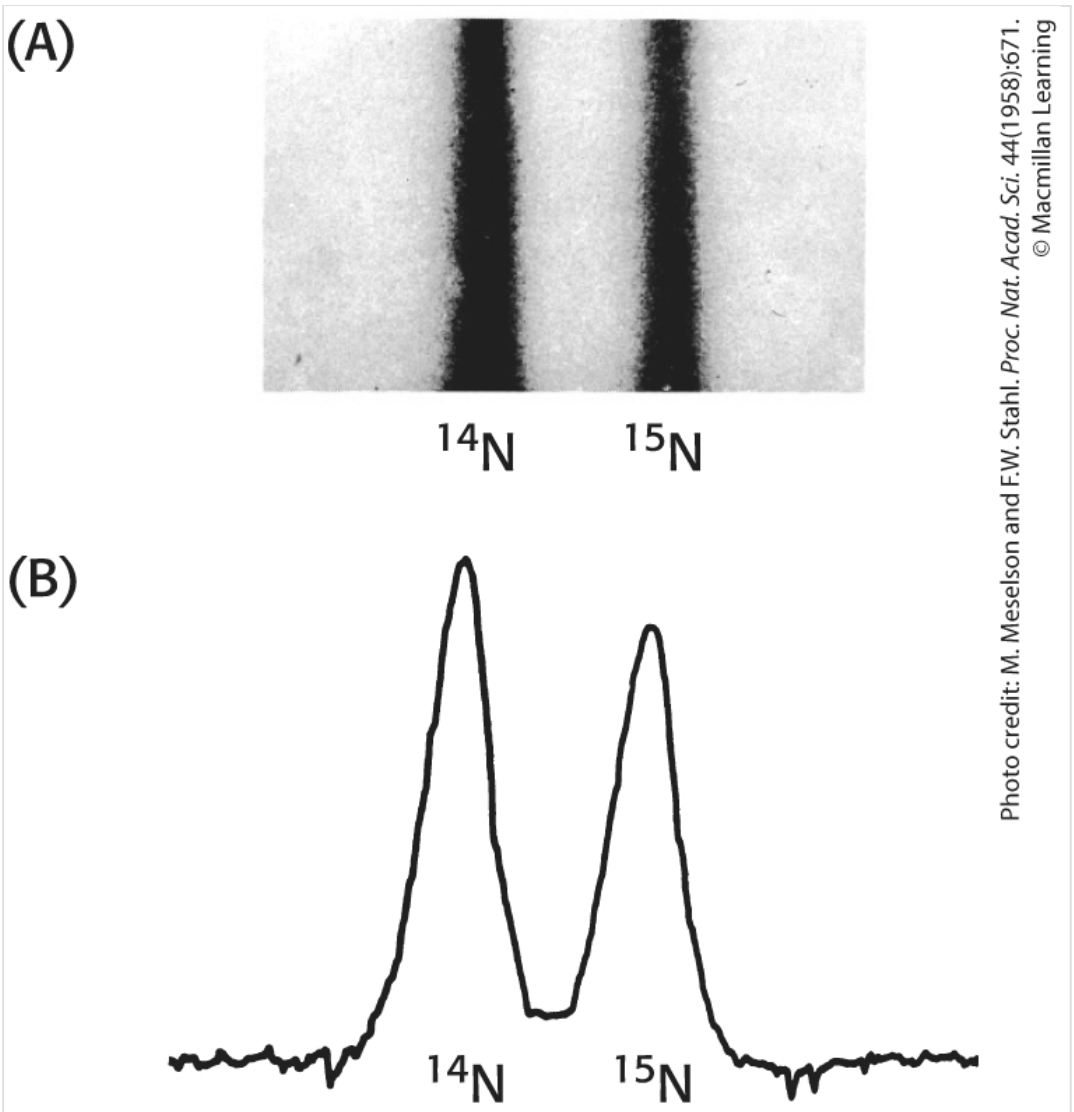


FIGURE 8.19 Meselson and Stahl resolved ^{14}N DNA and ^{15}N DNA by density-gradient centrifugation. (A) An ultraviolet-absorption photograph of a special centrifuged tube shows the two distinct bands of DNA. (B) Densitometric tracing of the absorption photograph.

In their experiment, Meselson and Stahl extracted DNA from the bacteria at various times after the bacteria were transferred from ^{15}N-containing to ^{14}N-containing medium and subjected the samples to

density-gradient equilibrium sedimentation. Figure 8.20 shows that all of the DNA is labeled with ^{15}N at the start of the experiment (generation 0). After one generation, all of the DNA is still in a single band, but the band has shifted. The density of this band (called *hybrid DNA*) is precisely halfway between the densities of the ^{14}N DNA and ^{15}N DNA bands. After two generations, there are equal amounts of two bands of DNA. One is hybrid DNA, and the other is ^{14}N DNA. After three rounds of replication, the positions of the two bands remain unchanged, but there is three times the amount of ^{14}N DNA as there is hybrid DNA.

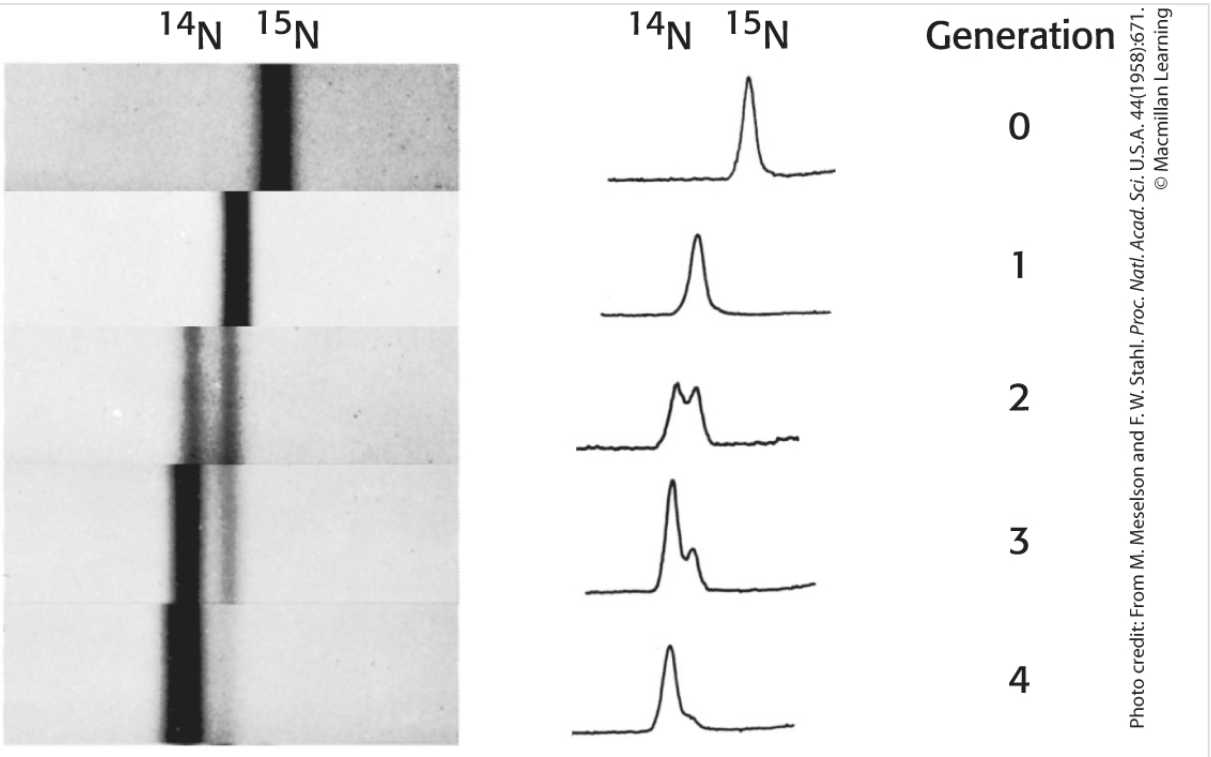
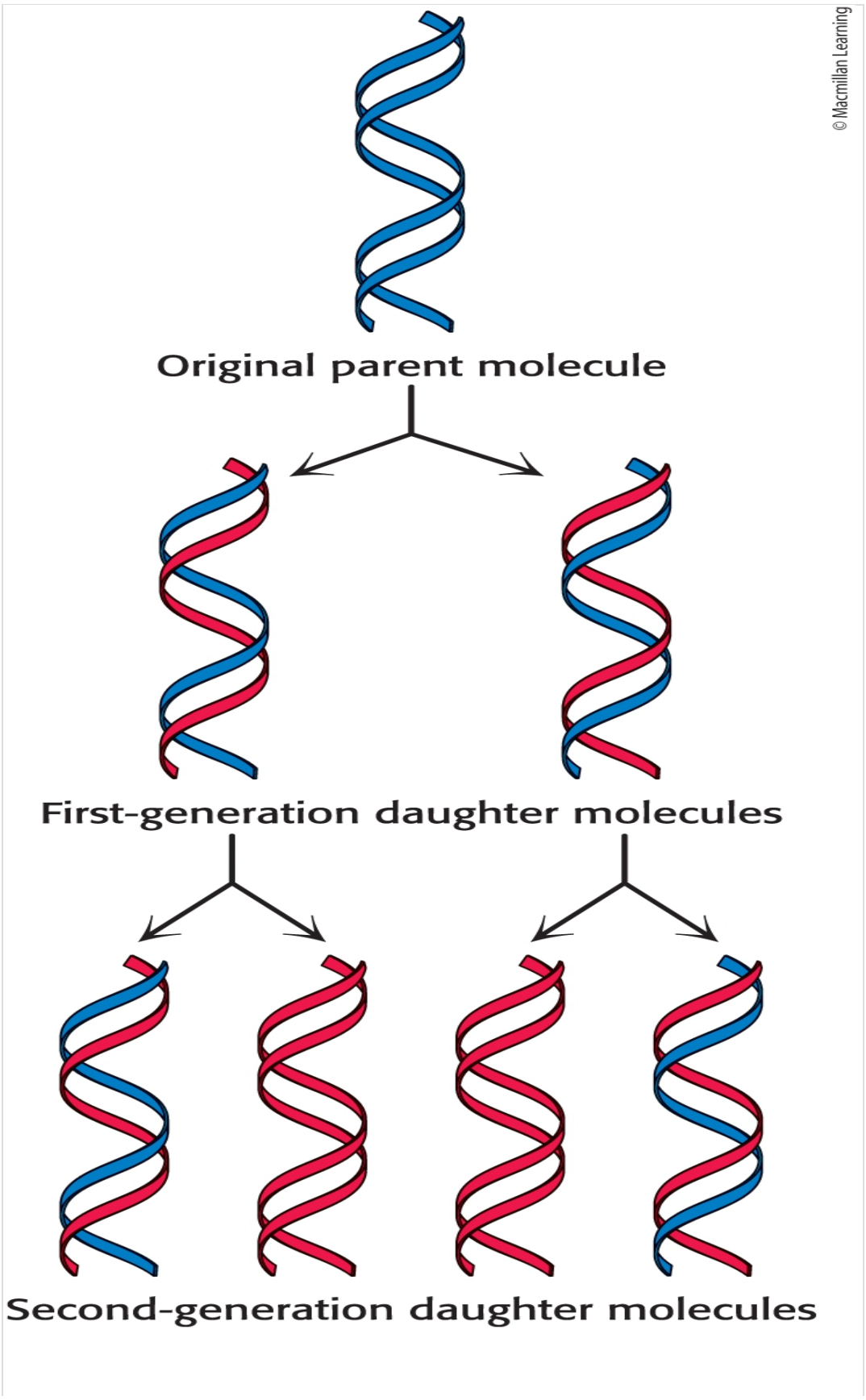


FIGURE 8.20 Semiconservative replication of *E. coli* DNA was detected by density-gradient centrifugation after incubation over several generations. The position of a band of DNA depends on its content of ^{14}N and ^{15}N.

The absence of ^{15}N DNA indicated that parental DNA was not preserved as an intact unit after replication. The absence of ^{14}N DNA in generation 1 indicated that all of the daughter DNA derived some of their atoms from the parent DNA. Additionally, the proportion of atoms derived from the parent had to be half because the density of the hybrid DNA band was halfway between the densities of the ^{14}N DNA and ^{15}N DNA bands.

Meselson and Stahl concluded from these incisive experiments that replication was indeed semiconservative: each new double helix contains a parent strand and a newly synthesized strand. Their results agreed perfectly with the Watson–Crick model for DNA replication (**Figure 8.21**).



© Macmillan Learning

FIGURE 8.21 In semiconservative replication, each daughter DNA molecule contains one parental strand and one newly synthesized strand. Original parental DNA is shown in blue and newly synthesized DNA in red.

[Information from M. Meselson and F. W. Stahl, *Proc. Natl. Acad. Sci. U.S.A.* 44: 671–682, 1958.]



The double helix can be reversibly melted

During DNA replication and transcription, the two strands of the double helix must be separated from each other, at least in a local region. The two strands of a DNA helix readily come apart when the hydrogen bonds between base pairs are disrupted. In the laboratory, the double helix can be disrupted by heating a solution of DNA or by adding acid or alkali to ionize its bases.

The dissociation of the double helix is called *melting* because it occurs abruptly at a certain temperature. The **melting temperature** (T_m) of DNA is defined as the temperature at which half the helical structure is lost. Inside cells, however, the double helix is not melted by the addition of heat. Instead, proteins called *helicases* use chemical energy (from ATP) to disrupt the helix (Chapter 29).

Stacked bases in nucleic acids absorb less ultraviolet light at a wavelength of 260 nm than do unstacked bases, an effect called *hypochromism* (**Figure 8.22A**). Thus, as a sample of DNA is heated, the strands separate, increasing the proportion of single-stranded DNA, which is monitored by measuring the increase in absorption of 260 nm light (**Figure 8.22B**).

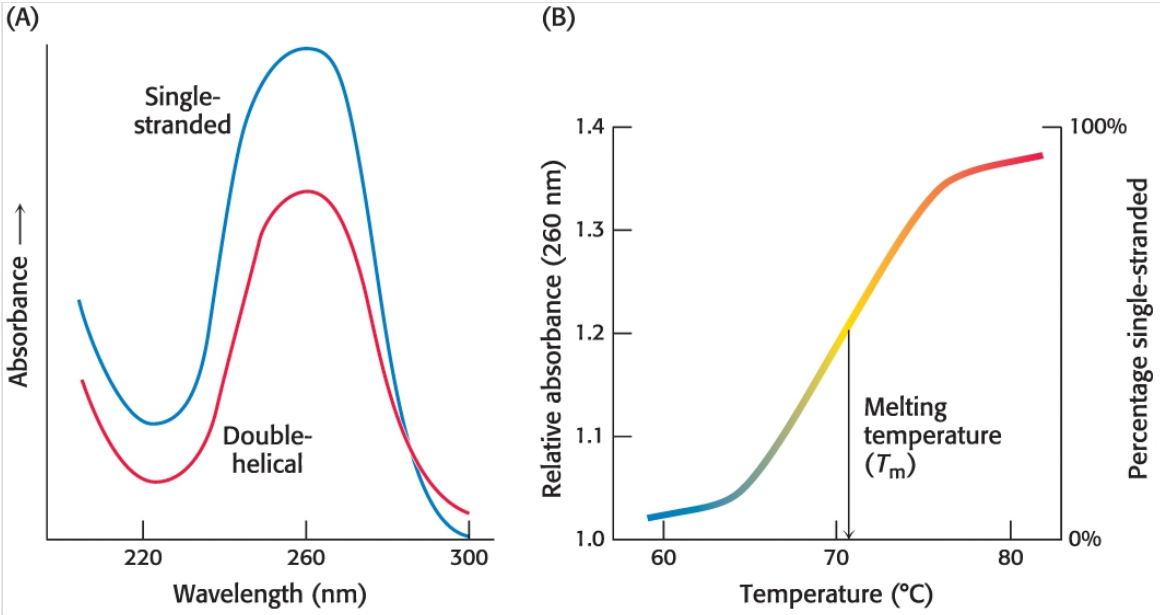


FIGURE 8.22 Single-stranded DNA absorbs light more effectively than does double-helical DNA. (A) The absorbance spectrum of similar quantities of single-stranded and double-helical DNA reveals a lower peak at around 260 nm for the double-helical sample. (B) The absorbance o a DNA solution at a wavelength of 260 nm increases when the double helix is melted into single strands.

Separated complementary strands of nucleic acids spontaneously reassociate to form a double helix when the temperature is lowered below T_m. This renaturation process is called *annealing*. The facility with which double helices can be melted and then reassociated is crucial for the biological functions of nucleic acids. The ability to melt and reanneal DNA reversibly in the laboratory provides a powerful tool for investigating sequence similarity. We will return to this important technique in Chapter 9.

Self-Check Question

In general, the greater the percentage of GC base pairs within a region of DNA, the higher the melting temperature. **(a)** What are the chemical forces that stabilize the double helix? **(b)** Based on your answers to (a), what are some possible explanations for the relationship between GC content and T_m?

8.4 DNA Is Replicated by Polymerases That Take Instructions from Templates

We now turn to the molecular mechanism of DNA replication. The full replication machinery in a cell comprises more than 20 proteins engaged in intricate and coordinated interplay. The primary catalytic components of the replication machinery are enzymes, called *DNA polymerases*, that promote the formation of the bonds joining units of the DNA backbone. *E. coli* has a number of DNA polymerases that participate in DNA replication and repair (Chapter 28).

DNA polymerase catalyzes phosphodiester-bridge formation

DNA polymerases catalyze the step-by-step addition of deoxyribonucleotide units to a DNA strand (**Figure 8.23**). The reaction catalyzed, in its simplest form, is

$$(\mathrm{DNA})_n + \mathrm{dNTP} \rightleftharpoons (\mathrm{DNA})_{n+1} + \mathrm{PP_i}$$

where dNTP stands for any deoxyribonucleotide and $\mathrm{PP_i}$ is a pyrophosphate ion.

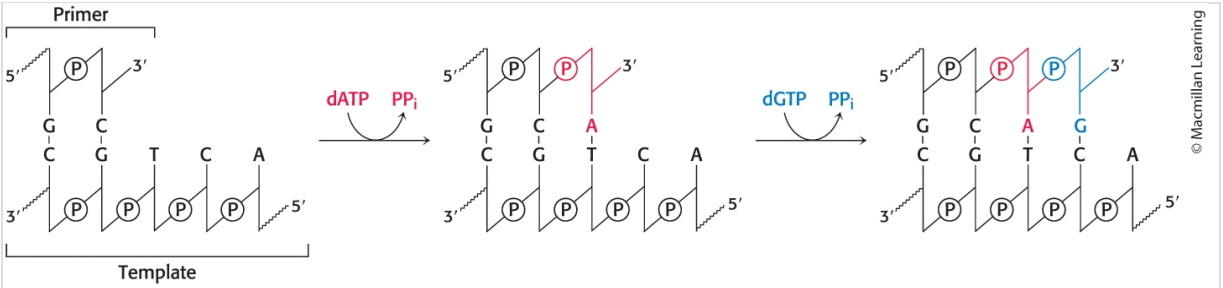


FIGURE 8.23 DNA polymerase catalyzes the polymerization reaction using nucleotide 5′-triphosphates as substrates. The reaction requires a preexisting DNA template and a primer with a free $3'-OH$ group.

DNA synthesis has the following characteristics:

- *The reaction requires all four activated precursors* — that is, the deoxynucleoside $5'$-triphosphates dATP, dGTP, dCTP, and TTP — as well as Mg^{2+} ion.

- *The new DNA strand is assembled directly on a preexisting DNA template*. DNA polymerases catalyze the formation of a phosphodiester linkage efficiently only if the base on the incoming nucleoside triphosphate is complementary to the base on the **template strand**. Thus, DNA polymerase is a template-directed enzyme that synthesizes a product with a base sequence complementary to that of the template.

- *DNA polymerases require a primer to begin synthesis*. A short single-stranded oligonucleotide having a free $3'-OH$ group, called a **primer**, must be already bound to the template strand.

The chain-elongation reaction catalyzed by DNA polymerases is a nucleophilic attack by the $3'-OH$ terminus of the growing strand on the innermost phosphorus atom of the deoxynucleoside triphosphate (Figure 8.24). A phosphodiester bridge is formed and pyrophosphate is released.

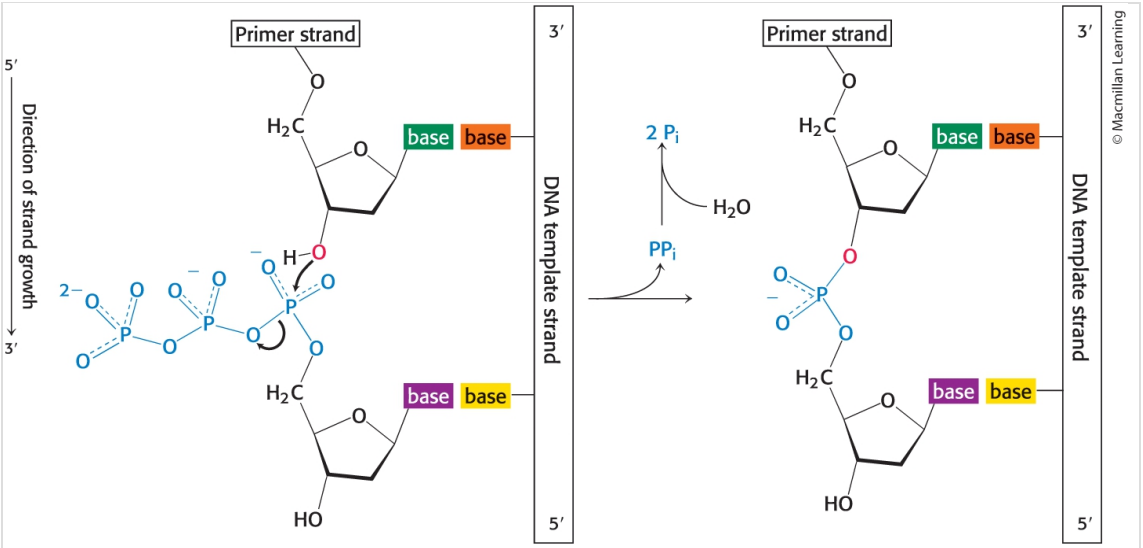


FIGURE 8.24 DNA polymerases catalyze the strand-elongation reaction in the $5'$-to-$3'$ direction. The product of the reaction is the formation of a phosphodiester bridge.

[Source: J. L. Tymoczko, J. Berg, and L. Stryer, *Biochemistry: A Short Course*, 2nd ed. (W. H. Freeman and Company, 2013), Fig. 34.2.]

At this point, the reaction is readily reversible. The subsequent hydrolysis of pyrophosphate to yield two ions of orthophosphate (P_i) by pyrophosphatase, an irreversible reaction under cellular conditions, helps drive the polymerization forward. This is an example of coupled

reactions, where a second reaction provides the energy to drive the first reaction forward, a common occurrence in biochemical pathways (Section 15.1).

- *Elongation of the DNA chain proceeds in the* $5'$ *-to-* $3'$ *direction.*

- *Many DNA polymerases are able to correct mistakes in DNA by removing mismatched nucleotides.* These polymerases have a distinct nuclease activity that allows them to excise incorrect bases by a separate reaction. This nuclease activity contributes to the remarkably high fidelity of DNA replication, which has an error rate of less than 10^{-8} per base pair.

The genes of some viruses are made of RNA

Genes in all cellular organisms are made of DNA. The same is true for some viruses, but for others, the genetic material is RNA. Viruses are genetic elements enclosed in protein coats that can move from one cell to another but are not capable of independent growth. A well-studied example of an RNA virus is the tobacco mosaic virus, which infects the leaves of tobacco plants. This virus consists of a single strand of RNA (6390 nucleotides) surrounded by a protein coat of 2130 identical subunits. An RNA polymerase that takes direction from an RNA template, called an *RNA-directed RNA polymerase*, copies the viral RNA. The infected cells die because of virus-instigated programmed cell death; in essence, the virus instructs the cell to commit suicide. Cell death results in discoloration in the tobacco leaf in a variegated pattern, hence the name mosaic virus.

Another important class of RNA virus comprises the **retroviruses**, so called because the genetic information flows from RNA to DNA rather than from DNA to RNA. This class includes human immunodeficiency virus 1 (HIV-1), the cause of acquired immunodeficiency syndrome (AIDS), as well as a number of RNA viruses that produce tumors in susceptible animals. Retrovirus particles contain two copies of a single-stranded RNA molecule. On entering the cell, the RNA is copied into DNA through the action of a viral enzyme called *reverse transcriptase*, which acts as both a DNA polymerase and an RNase (**Figure 8.25**). The resulting double-helical DNA version of the viral genome can become incorporated into the chromosomal DNA of the host and is replicated along with the normal cellular DNA. At a later time, the integrated viral genome is expressed to form viral RNA and viral proteins, which assemble into new virus particles.

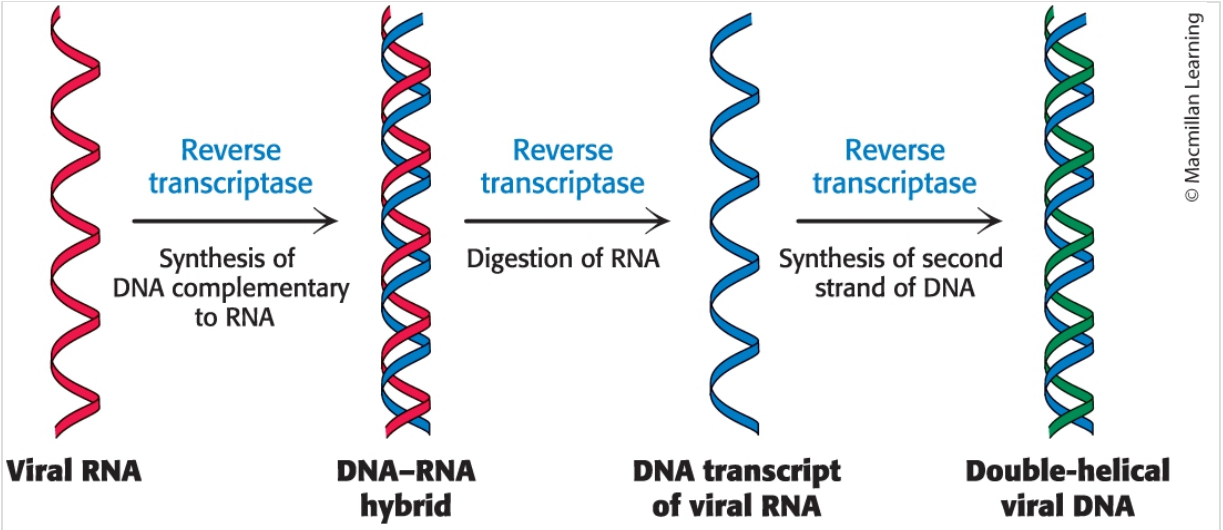


FIGURE 8.25 In retroviruses, information flows from RNA to DNA. The single-stranded RNA genome of a retrovirus is converted into double-stranded DNA by reverse transcriptase, an enzyme brought into the cell by the infecting virus particle. Reverse transcriptase possesses several activities and catalyzes the synthesis of a complementary DNA strand, the digestion of the RNA, and the subsequent synthesis of the second DNA strand.

8.5 Gene Expression Is the Transformation of DNA Information into Functional Molecules

The information stored as DNA becomes useful when it is expressed in the production of RNA and proteins. This rich and complex topic is the subject of several chapters later in this book, but here we introduce the basics of gene expression.

DNA can be thought of as archival information, stored and manipulated in ways that minimize damage (mutations). It is expressed in two steps. First, an RNA copy is made that encodes directions for protein synthesis. This messenger RNA can be thought of as a temporary photocopy of the original information; it can be made in multiple copies, used, and then disposed of. Second, the information in messenger RNA is translated to synthesize functional proteins. Other types of RNA molecules exist to facilitate this translation.

Several kinds of RNA play key roles in gene expression

RNA is more than a passive conveyor of information during gene expression. Scientists have demonstrated that RNA plays a variety of roles, from catalysis to regulation. Cells contain three major kinds of RNA that are involved in gene expression (**Table 8.3**):

1. **Messenger RNA (mRNA)** is the template for protein synthesis. An mRNA molecule may be produced for each gene or group of

genes that is to be expressed in bacteria, whereas a distinct mRNA is produced for each gene in eukaryotes. Consequently, mRNA is a heterogeneous class of molecules. The average length of an mRNA molecule is about 1.2 kilobases (kb) in bacteria and about 2.2 kb in mammals. The mRNA of all organisms has structural features, such as stem-loop structures, that regulate its efficiency of translation and lifetime. Such structural features are more prominent in eukaryotic mRNA (Chapters 29 and 31).

2. **Transfer RNA (tRNA)** carries amino acids in an activated form to the ribosome for peptide-bond formation, in a sequence dictated by the mRNA template. There is at least one kind of tRNA for each of the 20 amino acids. Transfer RNA consists of about 75 nucleotides (having a mass of about 25 kDa).

3. **Ribosomal RNA (rRNA)** is the major component of ribosomes (Chapter 30). In bacteria, there are three kinds of rRNA, called 23S, 16S, and 5S RNA because of their sedimentation behavior (Section 4.1). One molecule of each of these species of rRNA is present in each ribosome. As we shall discuss in Chapter 30, eukaryotic rRNAs, as well as their corresponding ribosomes, are larger. Ribosomal RNA was once thought to play only a structural role in ribosomes. We now know that rRNA is the actual catalyst for protein synthesis.

TABLE 8.3 RNA molecules in *E. coli*

Type	Relative amount (%)	Sedimentation coefficient (*S*)	Mass (kDa)	Number of nucleotides
Ribosomal RNA (rRNA)	80	23	1.2×10^3	3700

		16	0.55×10^3	1700
		5	3.6×10^1	120
Transfer RNA (tRNA)	15	4	2.5×10^1	75
Messenger RNA (mRNA)	5		Heterogeneous	

Ribosomal RNA is the most abundant of these three types of RNA. Transfer RNA comes next, followed by messenger RNA, which constitutes only 5% of the total RNA. Eukaryotic cells contain additional small RNA molecules that play a variety of roles including the regulation of gene expression, the processing of RNA, and the synthesis of proteins. We will examine these small RNAs in later chapters. In this chapter, we will consider rRNA, mRNA, and tRNA.

All cellular RNA is synthesized by RNA polymerases

The synthesis of RNA from a DNA template is called **transcription** and is catalyzed by the enzyme *RNA polymerase* (**Figure 8.26**). RNA polymerase catalyzes the initiation and elongation of RNA chains. The reaction catalyzed by this enzyme is

$$(\text{RNA})_{n\ \text{residues}} + \text{ribonucleoside triphosphate} \rightleftharpoons (\text{RNA})_{n+1\ \text{residues}} + \text{PP}_\text{i}$$

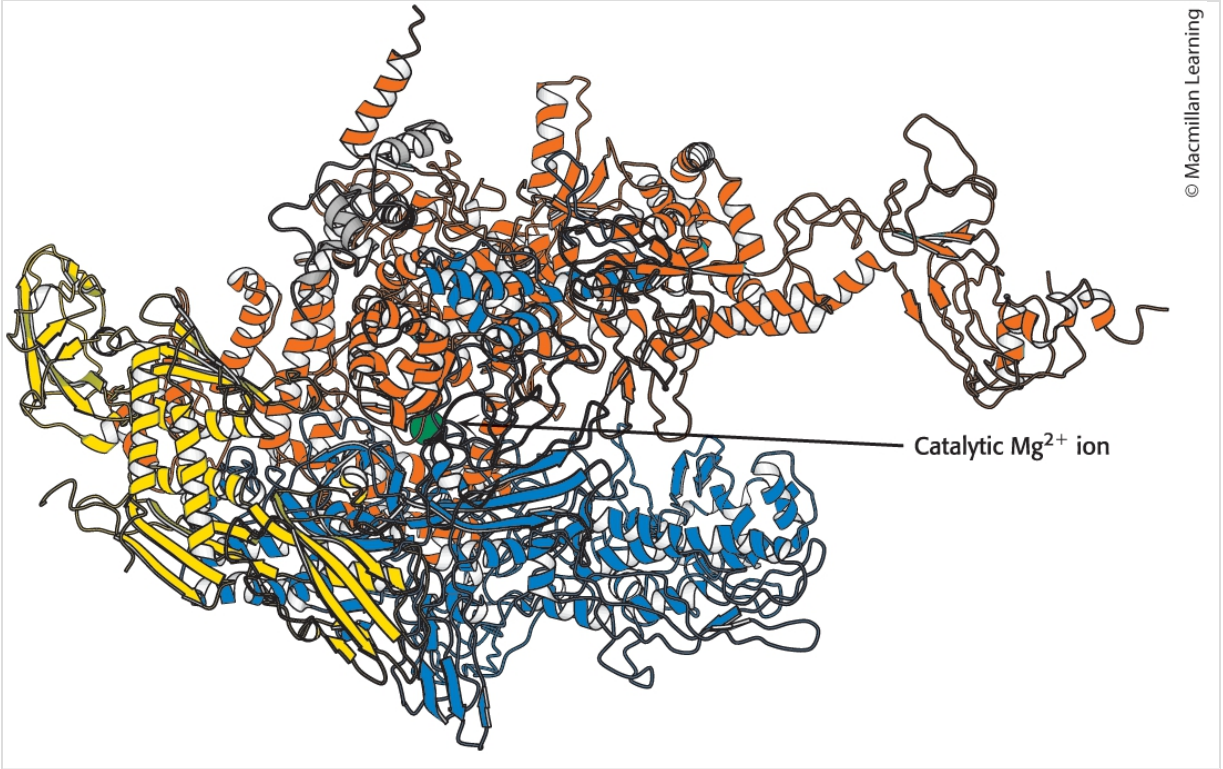


FIGURE 8.26 RNA polymerase is a multisubunit enzyme that catalyzes the synthesis of RNA from a DNA template. This large enzyme comprises many subunits, including β (blue) and β' (orange), which form a "claw" that holds the DNA to be transcribed. The active site includes a Mg^{2+} ion (green) at the center of the structure.

[Drawn from 1IW7.pdb.]

INTERACT with this model in Achieve

RNA polymerase requires the following components:

1. *A template.* The preferred template is double-stranded DNA. Single-stranded DNA also can serve as a template. RNA, whether single or double stranded, is not an effective template, nor are RNA–DNA hybrids.

2. *Activated precursors.* All four ribonucleoside triphosphates — ATP, GTP, UTP, and CTP — are required.

3. *A divalent metal ion.* Either Mg^{2+} or Mn^{2+} is effective.

The synthesis of RNA is like that of DNA in several respects (**Figure 8.27**). First, the direction of synthesis is $5' \rightarrow 3'$. Second, the mechanism of elongation is similar: the $3'-OH$ group at the terminus of the growing chain makes a nucleophilic attack on the innermost phosphoryl group of the incoming nucleoside triphosphate. Third, the synthesis is driven forward by the hydrolysis of pyrophosphate. In contrast with DNA polymerase, however, RNA polymerase does not require a primer. In addition, the ability of RNA polymerase to correct mistakes is not as extensive as that of DNA polymerase.

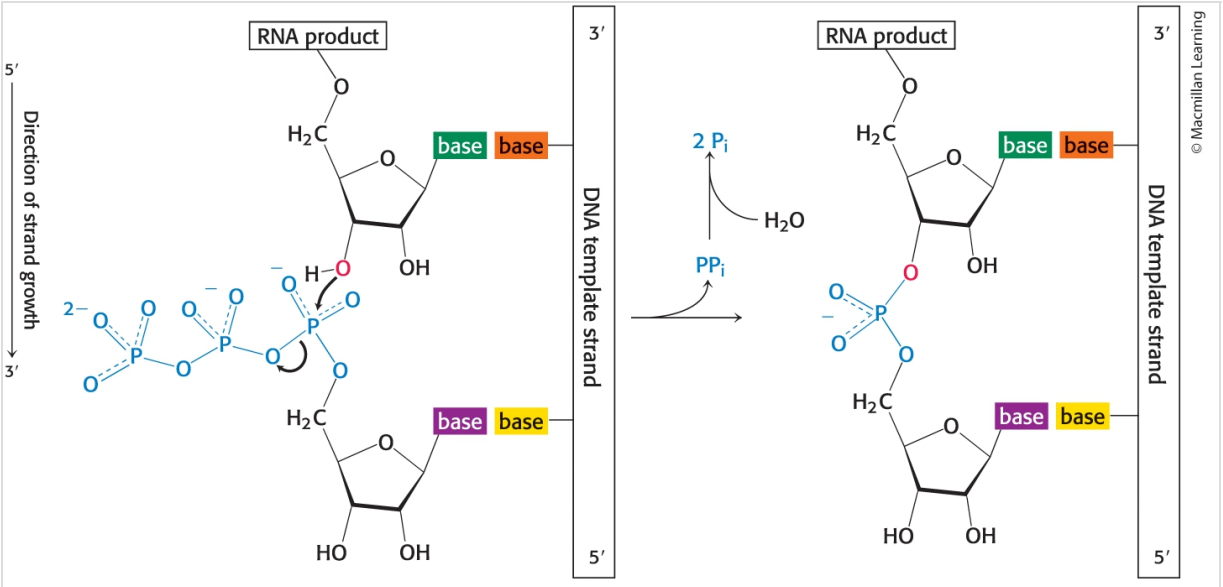


FIGURE 8.27 RNA polymerase catalyzes the strand-elongation reaction in the $5'$-to-$3'$ direction. Note the similarity in mechanism to that of DNA polymerase shown in Figure 8.24.

[Source: J. L. Tymoczko, J. Berg, and L. Stryer, *Biochemistry: A Short Course*, 2nd ed. (W. H. Freeman and Company, 2013), Fig. 36.3.]

All three types of cellular RNA — mRNA, tRNA, and rRNA — are synthesized in *E. coli* by the same RNA polymerase according to instructions given by a DNA template. In mammalian cells, there is a division of labor among several different kinds of RNA polymerases. We shall return to these RNA polymerases in Chapter 29.

RNA polymerases take instructions from DNA templates

RNA polymerase, like the DNA polymerases described earlier, takes instructions from a DNA template. The earliest evidence supporting this conclusion was the finding that the base composition of newly synthesized RNA is the complement of that of the DNA template strand (the plus or coding strand), as exemplified by the RNA synthesized from a template of single-stranded DNA from the ϕX174 virus (**Table 8.4**).

TABLE 8.4 Base composition of RNA synthesized from a viral DNA template

DNA template (plus, or coding, strand of ϕX174)		RNA product	
A	25%	U	25%
T	33%	A	32%

G	24%	C	23%
C	18%	G	20%

The strongest evidence for the fidelity of transcription came from base-sequence studies. For instance, the nucleotide sequence of a segment of the gene encoding the enzymes required for tryptophan synthesis was determined with the use of DNA-sequencing techniques (Section 9.1). Likewise, the sequence of the mRNA for the corresponding gene was determined. The results showed that the RNA sequence is the precise complement of the DNA template (**Figure 8.28**).

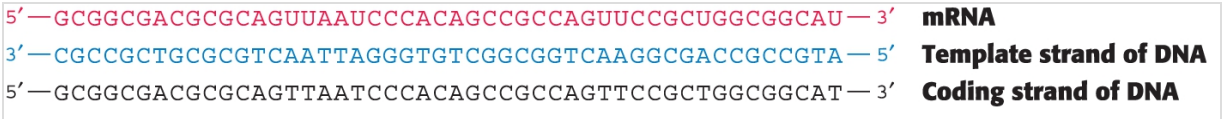


FIGURE 8.28 The sequences of the template DNA strand and its corresponding mRNA are complementary. The base sequence of mRNA (red) is the complement of that of the DNA template strand (blue). The sequence shown here is from the tryptophan operon, a segment of DNA containing the genes for five enzymes that catalyze the synthesis of tryptophan. The other strand of DNA (black) is called the coding strand because it has the same sequence as the RNA transcript except for thymine (T) in place of uracil (U).

Transcription begins near promoter sites and ends at terminator sites

RNA polymerase must detect and transcribe discrete genes from within large stretches of DNA. What marks the beginning of the unit to be transcribed? DNA templates contain regions called **promoter**

sites that specifically bind RNA polymerase and determine where transcription begins. While not every promoter site of a given type carries the exact same sequence, they typically vary from an idealized single sequence, or *consensus sequence*, by only one or two residues. In prokaryotes, two sequences on the $5'$ (upstream) side of the first nucleotide to be transcribed function as promoter sites (Figure 8.29A). One of them, called the *Pribnow box*, has the consensus sequence TATAAT and is centered at -10 (10 nucleotides on the $5'$ side of the first nucleotide transcribed, which is denoted by $+1$). The other, called the -35 *region*, has the consensus sequence TTGACA. The first nucleotide transcribed is usually a purine.

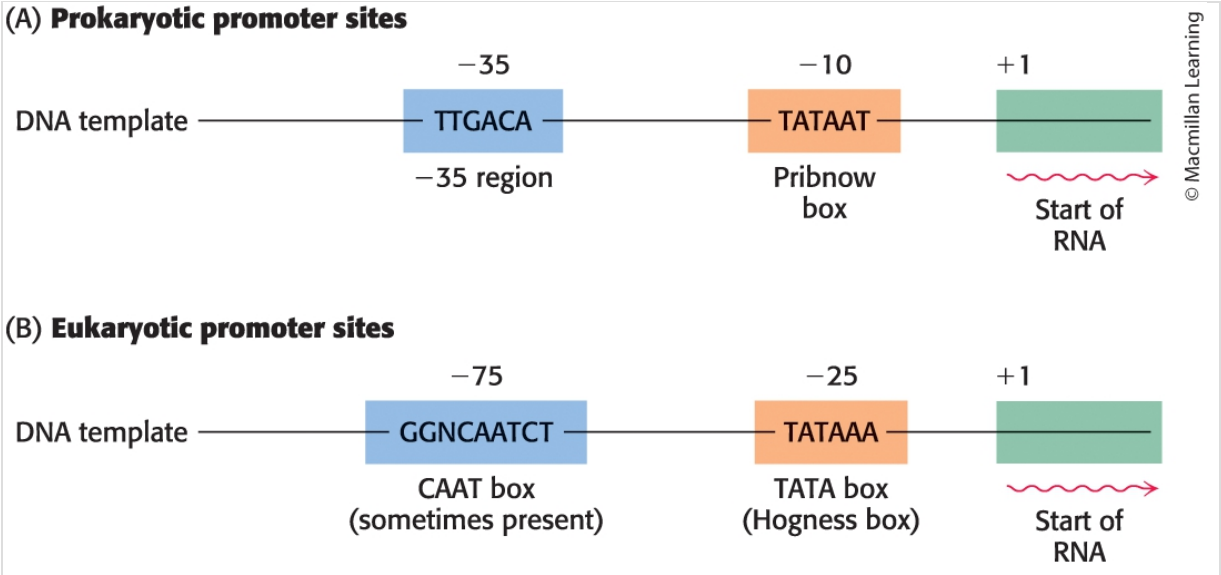
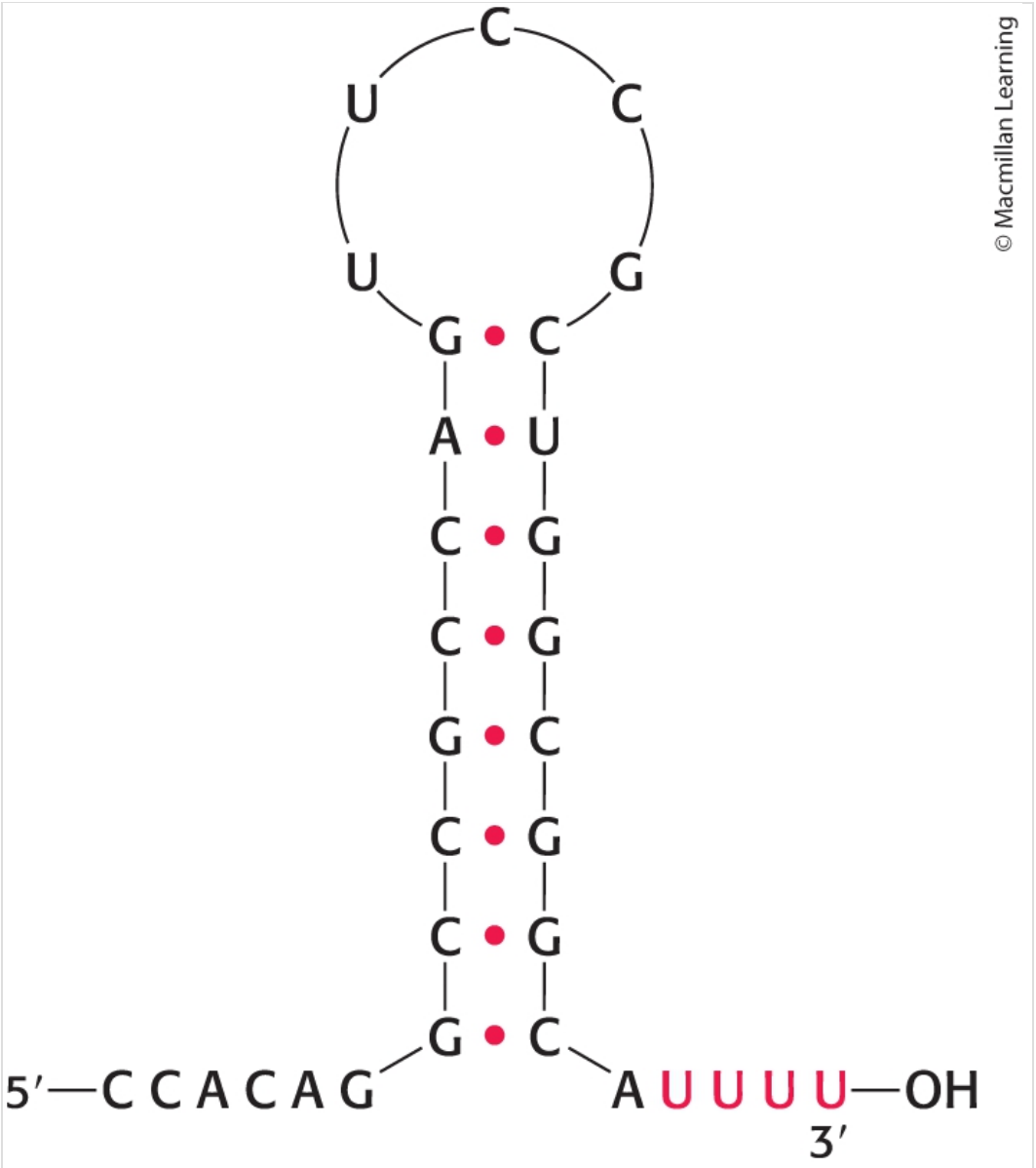


FIGURE 8.29 Promoter sites for transcription initiation differ between prokaryotes and eukaryotes. Consensus sequences are shown for (A) prokaryotic and (B) eukaryotic promoters. The first nucleotide to be transcribed is numbered $+1$. The adjacent nucleotide on the $5'$ side is numbered -1. The sequences shown are those of the coding strand of DNA.

Eukaryotic genes encoding proteins have promoter sites with a TATAAA consensus sequence, called a *TATA box* or a *Hogness box*, centered at about -25 (**Figure 8.29B**). Many eukaryotic promoters also have a *CAAT box* with a GGNCAATCT consensus sequence centered at about -75. The transcription of eukaryotic genes is further stimulated by enhancer sequences, which can be quite distant (as many as several kilobases) from the start site, on either its $5'$ or its $3'$ side.

In *E. coli*, RNA polymerase proceeds along the DNA template, transcribing one of its strands until it synthesizes a terminator sequence. This sequence encodes a termination signal, which is a stem-loop structure on the newly synthesized RNA molecule (**Figure 8.30**). This structure is formed by base-pairing of self-complementary sequences that are rich in G and C. The newly synthesized RNA spontaneously dissociates from RNA polymerase when this stem-loop is followed by a string of U residues. Alternatively, RNA synthesis in *E.coli* can be terminated by the action of the protein rho. Less is known about the termination of transcription in eukaryotes. A more detailed discussion of the initiation and termination of transcription will be given in Chapter 30. The important point now is that discrete start and stop signals for transcription are encoded in the DNA template.



© Macmillan Learning

FIGURE 8.30 The base sequence of the 3′ end of an mRNA transcript in *E. coli* forms a stem-loop structure. This structure is followed by a sequence of uridine (U) residues.

In eukaryotes, the messenger RNA is modified after transcription (Figure 8.31). A “cap” structure — a guanosine nucleotide with an

unusual $5'$-$5'$ triphosphate linkage — is attached to the $5'$ end, and a poly(A) "tail" — a sequence of adenylates — is added to the $3'$ end. These modifications will be presented in detail in Chapter 30.

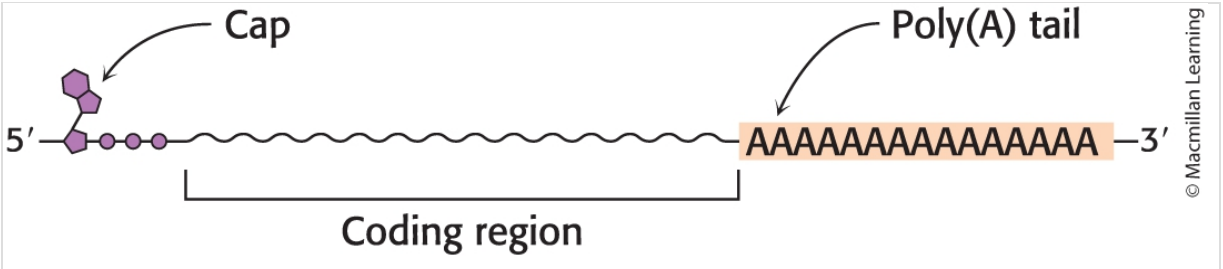


FIGURE 8.31 mRNA in eukaryotes is modified after transcription. A nucleotide "cap" structure is added to the $5'$ end, and a poly(A) tail is added at the $3'$ end.

Transfer RNAs are the adaptor molecules in protein synthesis

We have seen that mRNA is the template for protein synthesis. How then does it direct amino acids to become joined in the correct sequence to form a protein? Specific adaptor RNA molecules called transfer RNAs (tRNAs) bring the amino acids to the mRNA. The structure and reactions of these remarkable molecules will be considered in detail in Chapter 30. For the moment, it suffices to note that tRNAs contain an amino acid-attachment site and a template-recognition site.

Each tRNA molecule is composed of around 75 nucleotides and contains an amino acid-attachment site and a template-recognition site. Within the tRNA structure are several regions of base-paired segments in multiple stem-loops (**Figure 8.32**). The tRNA recognizes the mRNA template via three base pairs at the end of one of the stem-loops. Since the three coding bases on the mRNA template are known as the **codon**, the three complementary bases on the tRNA are referred to as the **anticodon**.

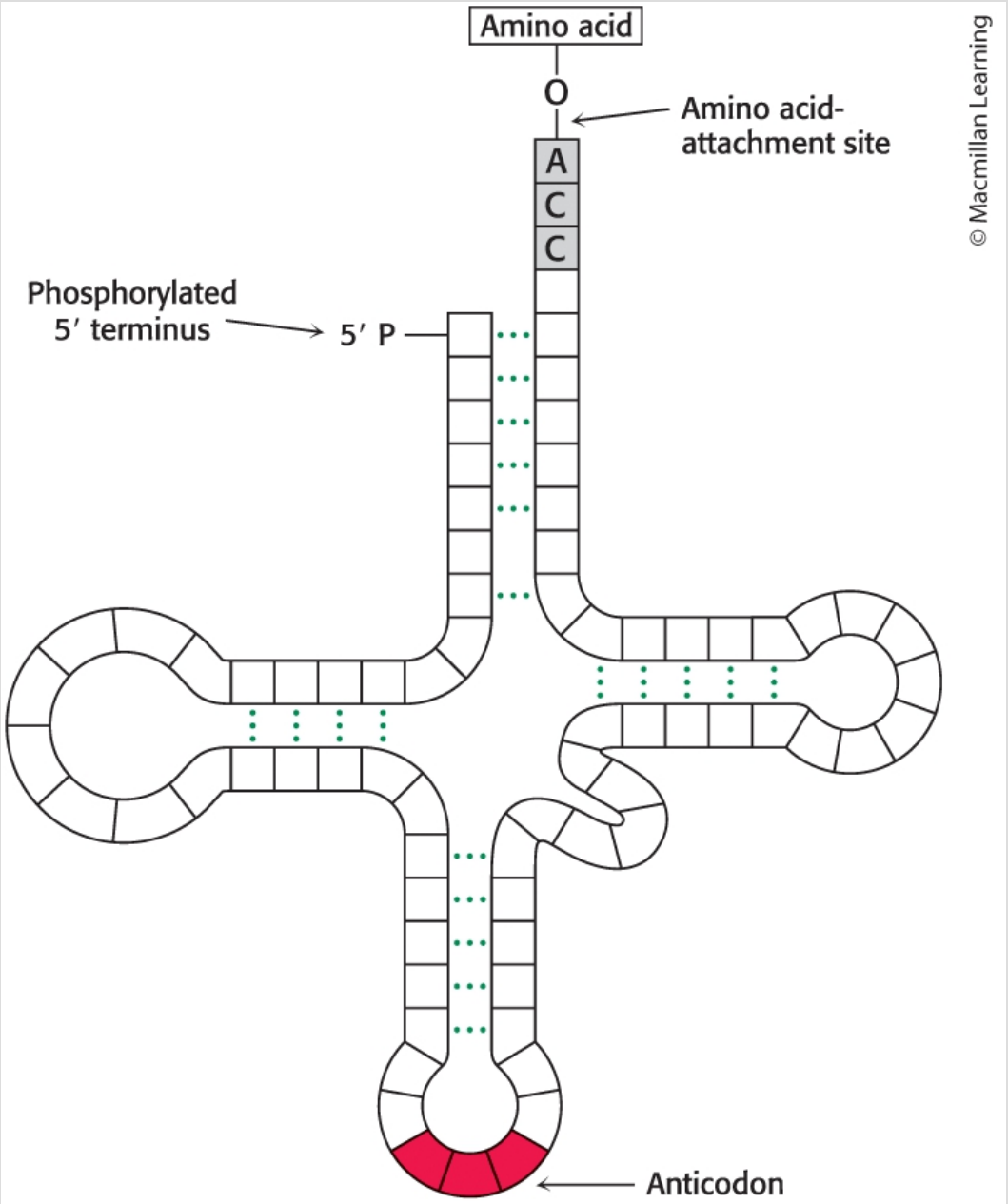


FIGURE 8.32 A tRNA molecule contains multiple stem-loop structures. The amino acid is attached at the 3′ end of the RNA. The anticodon (shown in red) is the template-recognition site. The tRNA has a cloverleaf structure with many hydrogen bonds (green dots) between bases.

Initially, the amino acid is attached to the either the $3'$- or $2'$-hydroxyl group of the ribose at the $3'$ end of the tRNA molecule. However, the amino acid can rapidly equilibrate between the two positions; ultimately, the $3'$-hydroxyl-bound form is the substrate for peptide bond formation. The sequence at the $3'$ end of the tRNA invariably contains two cytidylates followed by an adenylate, yielding what is referred to as the *CCA terminal region* or *CCA terminus* (**Figure 8.33**). The joining of an amino acid to a tRNA molecule to form an **aminoacyl-tRNA** is catalyzed by a specific enzyme called an *aminoacyl-tRNA synthetase*. There is at least one specific synthetase for each of the 20 amino acids.

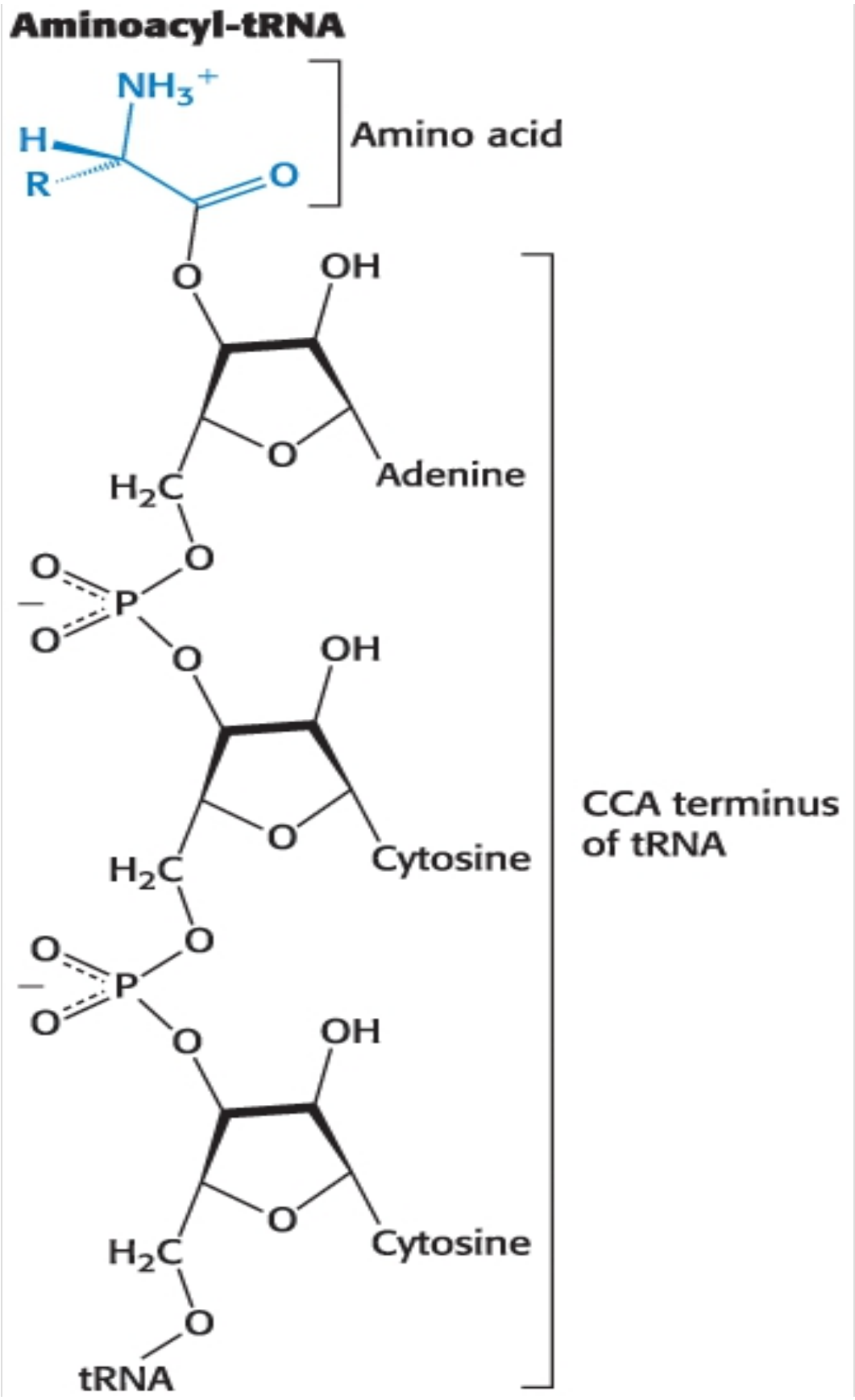

Aminoacyl-tRNA
NH3+
H
R
O
Amino acid
O
OH
O
Adenine
H2C
O
O
P
O
O
OH
O
Cytosine
H2C
O
O
P
O
O
OH
O
Cytosine
H2C
O
tRNA
CCA terminus
of tRNA

FIGURE 8.33 An amino acid is attached to the 3′ end of a tRNA molecule. The amino acid (shown in blue) is esterified to the 3′-hydroxyl group of the terminal adenylate of tRNA. The two bases preceding the 3′ adenylate are cytidylates; hence, this region of the tRNA is often called the CCA terminus.

[Source: J. L. Tymoczko, J. Berg, and L. Stryer, *Biochemistry: A Short Course*, 2nd ed. (W. H. Freeman and Company, 2013), Fig. 39.3.]

8.6 Amino Acids Are Encoded by Groups of Three Bases Starting from a Fixed Point

The **genetic code** is the relation between the sequence of bases in DNA (or its RNA transcripts) and the sequence of amino acids in proteins. Numerous experiments established the following features of the genetic code by 1961:

- *Three nucleotides encode an amino acid*. Proteins are built from a basic set of 20 amino acids, but there are only four bases. Simple calculations show that a minimum of three bases is required to encode at least 20 amino acids. Genetic experiments showed that an amino acid is in fact encoded by a group of three bases, or codon.

- *The code is nonoverlapping*. Consider a base sequence ABCDEF. In an overlapping code, ABC specifies the first amino acid, BCD the next, CDE the next, and so on. In a nonoverlapping code, ABC designates the first amino acid, DEF the second, and so forth. Genetic experiments again established the code to be nonoverlapping.

- *The code has no "punctuation."* In principle, one base (denoted as Q) might serve as a "comma" between groups of three bases.

  ...QABCQDEFQGHIQJKLQ ...

  However, this is not the case. Rather, the sequence of bases is read sequentially from a fixed starting point, without

punctuation.

- *The code has directionality*. The code is read from the $5'$ end of the messenger RNA to its $3'$ end.

- *The genetic code is degenerate, in that most amino acids are encoded by more than one codon.* There are 64 possible base triplets and only 20 amino acids; 61 of the 64 possible triplets specify particular amino acids. The remaining three triplets (called **stop codons**) designate the termination of translation.



University of Wisconsin-Madison Archives Collections

HAR GOBIND KHORANA Born in 1922 in a small village in Punjab in British India, Har Gobind Khorana completed his master's degree in India and his PhD at the University of Liverpool. In 1952, he began his independent career at the University of British Columbia (UBC). He synthesized RNA polymers with repeating sequences of two, three, or four nucleotides and used these synthetic RNAs to guide protein synthesis. This work contributed greatly to the elucidation of the genetic code for which he shared the Nobel Prize in 1968. The ability to synthesize oligonucleotides, developed by him and his coworkers,

fueled the development of PCR and many other methods. His work at UBC, the University of Wisconsin, and the Massachusetts Institute of Technology demonstrated his mastery of one of the pillars of chemistry: the powerful ability to synthesize even very complex molecules for a range of applications.

Major features of the genetic code

All 64 codons have been deciphered (Table 8.5). Because the code is highly degenerate, only tryptophan and methionine are encoded by just one triplet each. Each of the other 18 amino acids is encoded by two or more. Indeed, leucine, arginine, and serine are specified by six codons each.

TABLE 8.5 The genetic code

First position	Second position				Third position
(5′ end)	U	C	A	G	(3′ end)
U	Phe	Ser	Tyr	Cys	U
	Phe	Ser	Tyr	Cys	C
	Leu	Ser	Stop	Stop	A
	Leu	Ser	Stop	Trp	G

C	Leu	Pro	His	Arg	U
	Leu	Pro	His	Arg	C
	Leu	Pro	Gln	Arg	A
	Leu	Pro	Gln	Arg	G
A	Ile	Thr	Asn	Ser	U
	Ile	Thr	Asn	Ser	C
	Ile	Thr	Lys	Arg	A
	Met	Thr	Lys	Arg	G
G	Val	Ala	Asp	Gly	U
	Val	Ala	Asp	Gly	C
	Val	Ala	Glu	Gly	A
	Val	Ala	Glu	Gly	G

Note: This table identifies the amino acid encoded by each triplet. For example, the codon $5'$-AUG-$3'$ on mRNA specifies methionine, whereas CAU specifies histidine. UAA, UAG, and UGA are

termination signals. AUG is part of the initiation signal, in addition to coding for internal methionine residues.

Codons that specify the same amino acid are called *synonyms*. For example, CAU and CAC are synonyms for histidine. Note that synonyms are not distributed haphazardly throughout the genetic code. In Table 8.5, an amino acid specified by two or more synonyms occupies a single box (unless it is specified by more than four synonyms). The amino acids in a box are specified by codons that have the same first two bases but differ in the third base, as exemplified by GUU, GUC, GUA, and GUG. Thus, most synonyms differ only in the last base of the triplet. Inspection of the code shows that XYC and XYU always encode the same amino acid, and XYG and XYA usually encode the same amino acid as well. The structural basis for these equivalences of codons becomes evident when we consider the nature of the anticodons of tRNA molecules (Section 30.1).

What is the biological significance of the extensive degeneracy of the genetic code? If the code were not degenerate, 20 codons would designate amino acids and 44 would lead to chain termination. The probability of mutating to chain termination would therefore be much higher with a nondegenerate code. Chain-termination mutations usually lead to inactive proteins, whereas substitutions of one amino acid for another are usually rather harmless. Moreover, the code is constructed such that a change in any single nucleotide base of a codon results in a synonym or an amino acid with similar chemical properties. Thus, degeneracy minimizes the deleterious effects of mutations.

As we will see many times in our study of biochemistry, often things are not as straightforward as they first appear. Recent research has revealed a nonrandom use of synonymous codons in genes in different organisms, a phenomenon called *codon bias*. In other

words, different organisms prefer different sets of synonymous codons. For example, there are six codons that encode arginine, but the most commonly used codons vary widely, from the bacterium *E. coli* to the yeast *S. cerevisiae* to humans (**Figure 8.34**). The biochemical benefit of codon bias is not yet clearly established, but codon bias may help regulate translation. From an experimental perspective, codon bias can have a significant impact on the efficacy of expressing a human protein within bacteria or yeast using recombinant DNA technology, as we shall discuss in Section 9.2. By adjusting the codon usage within the gene to be expressed to match the host organism, a process called *codon optimization*, one can express the protein at a higher yield without altering the protein sequence.

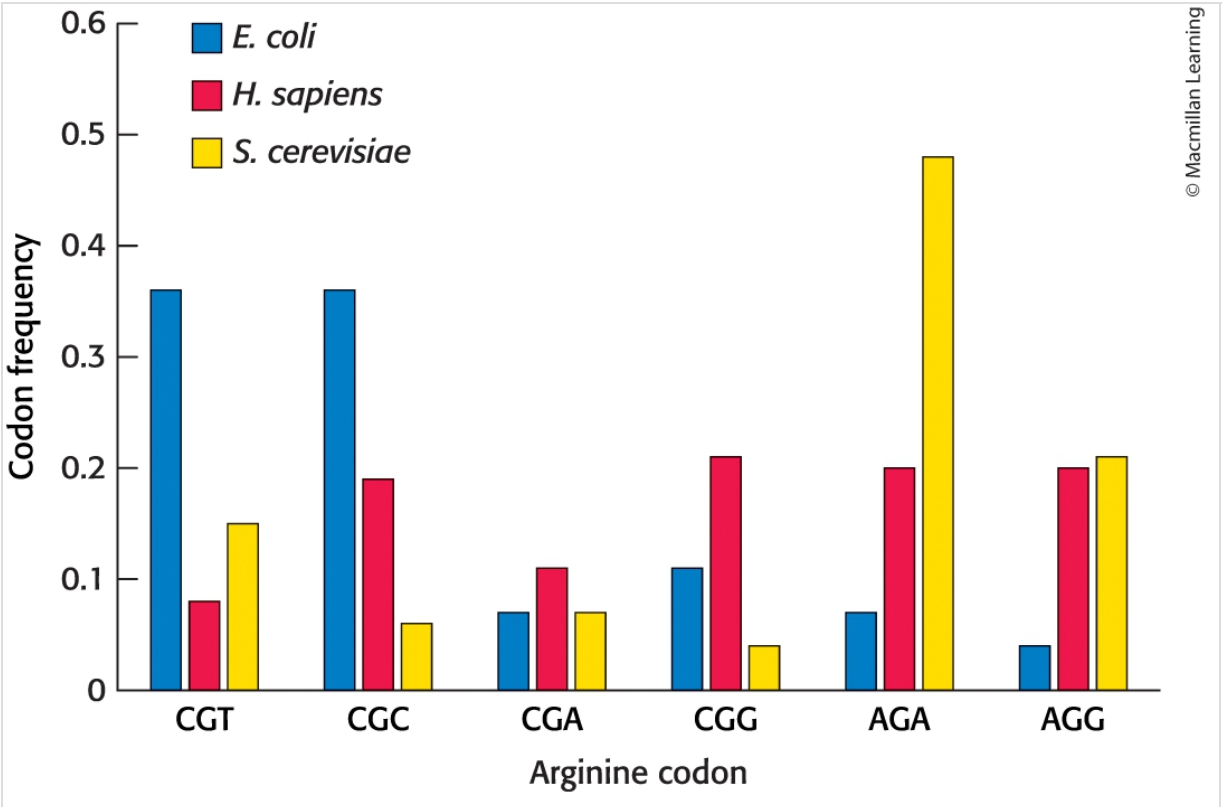


FIGURE 8.34 Different species exhibit different codon usage preferences. The relative preferences for the different arginine-encoding codons across three species — *E. coli* (blue), humans (red), and *S. cerevisiae* (yellow) — are shown. Although all of these codons encode the same amino acid, each organism exhibits a unique set of preferences, or codon bias.

[Source: https://www.genscript.com/tools/codon-frequency-table.]

Self-Check Question

The amino acid sequences of a yeast protein and a human protein having the same function are found to be 60% identical. However, the corresponding DNA sequences are only 45% identical. Account for this differing degree of identity.

Messenger RNA contains start and stop signals for protein synthesis

Messenger RNA is translated into proteins on **ribosomes** — large molecular complexes assembled from proteins and ribosomal RNA. How is mRNA interpreted by the translation apparatus?

The start signal for protein synthesis in bacteria is complex. Polypeptide chains start with a modified amino acid — namely, formylmethionine (fMet). A specific tRNA, called the *initiator tRNA*, carries fMet and recognizes the codon AUG. However, AUG is also the codon for an internal methionine residue. Hence, the signal for the first amino acid in a bacterial polypeptide chain must be more complex than that for all subsequent ones. In fact, the AUG codon is only part of the initiation signal (**Figure 8.35A**). The initiating AUG codon is preceded several nucleotides away by a purine-rich sequence, called the **Shine–Dalgarno sequence** (named after John

Shine and Lynn Dalgarno, who first described the sequence), that base-pairs with a complementary sequence in a ribosomal RNA molecule (Section 30.3).

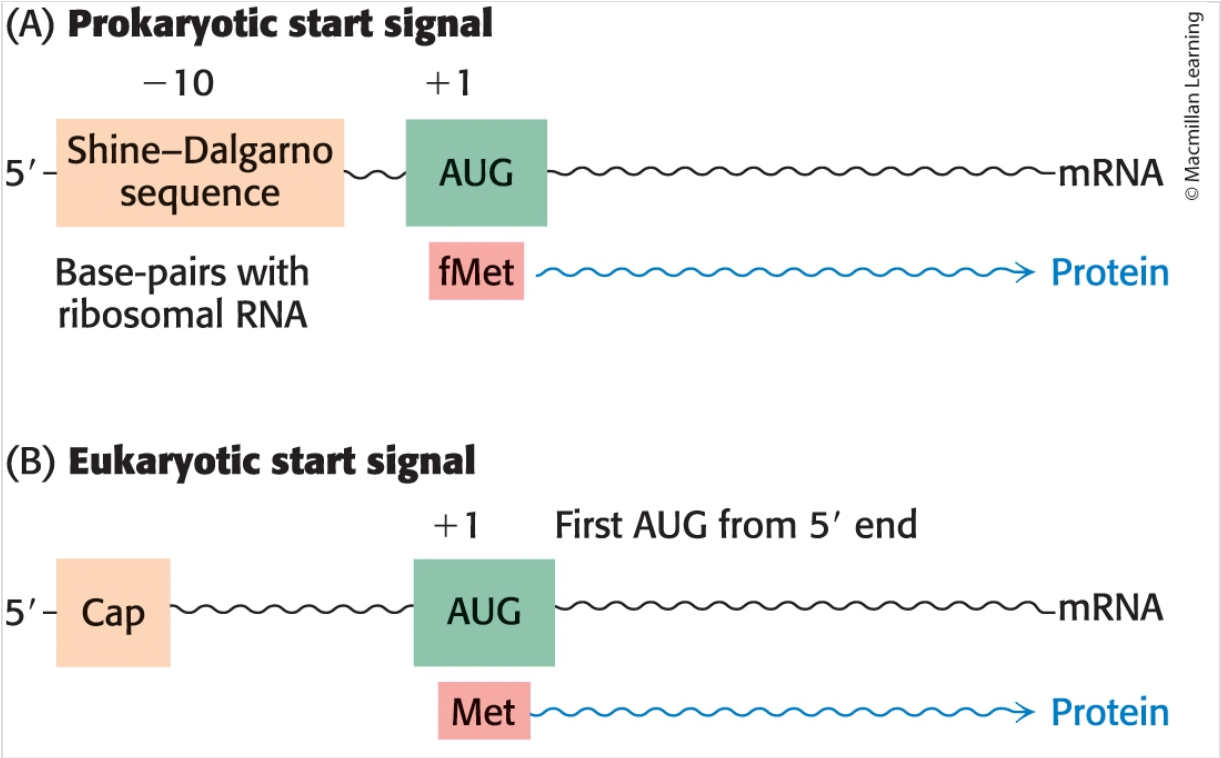


FIGURE 8.35 Initiation of protein synthesis differs between prokaryotes and eukaryotes. In prokaryotes (A), protein synthesis starts at the AUG codon about 10 bases downstream of a Shine–Dalgarno sequence, while in eukaryotes (B), the AUG closest to the 5′ end of the mRNA is usually the start signal.

In eukaryotes, the AUG closest to the 5′ end of an mRNA molecule is usually the start signal for protein synthesis (**Figure 8.35B**). This particular AUG is read by an initiator tRNA conjugated to methionine. After the initiator AUG has been located, the order of

the three nonoverlapping nucleotides, or *reading frame*, is established.

As already mentioned, UAA, UAG, and UGA designate chain termination in most species. These codons are read not by tRNA molecules but rather by specific proteins called *release factors* (Section 30.3). Binding of a release factor to the ribosome releases the newly synthesized protein.

The genetic code is nearly universal

Most organisms use the same genetic code. This universality accounts for the fact that human proteins, such as insulin, can be synthesized in the bacterium *E. coli* and harvested from it for the treatment of diabetes. However, genome-sequencing studies have shown that not all genomes are translated by the same code. Ciliated protozoa, for example, differ from most organisms in that UAA and UAG are read as codons for amino acids rather than as stop signals; UGA is their sole termination signal.

The first variations in the genetic code were found in mitochondria from a number of species, including human beings (**Table 8.6**). As we shall see later (Section 18.1), mitochondria possess their own circular DNA which encodes proteins important for cellular respiration. The genetic code of mitochondria can differ from that of the rest of the cell because mitochondrial DNA also encodes a distinct set of tRNAs that recognize the alternative codons.

TABLE 8.6 Distinctive codons of human mitochondria

Codon	Standard Code	Mitochondrial code

UGA	Stop	Trp
UGG	Trp	Trp
AUA	Ile	Met
AUG	Met	Met
AGA	Arg	Stop
AGG	Arg	Stop

Why has the code remained nearly invariant through billions of years of evolution, from bacteria to human beings? A mutation that altered the reading of mRNA would change the amino acid sequence of most, if not all, proteins synthesized by that particular organism. Many of these changes would undoubtedly be deleterious, and so there would be strong selection against a mutation with such pervasive consequences.

8.7 Most Eukaryotic Genes Are Mosaics of Introns and Exons

In bacteria, polypeptide chains are encoded by a continuous array of triplet codons in DNA. For many years, genes in higher organisms were assumed to be organized in the same manner. This view was unexpectedly shattered in 1977, when investigators discovered that most eukaryotic genes are *discontinuous*. For example, the gene for the β chain of hemoglobin is interrupted within its amino acid-coding sequence by a short stretch of 120 noncoding base pairs and a long one of 550 base pairs. Thus, the β-globin gene is split into three coding sequences (Figure 8.36). Noncoding regions are called **introns** (for intervening sequences), whereas coding regions are called **exons** (for expressed sequences). The average human gene has 8 introns, and some have more than 100. Intron size ranges from 50 to 10,000 nucleotides.

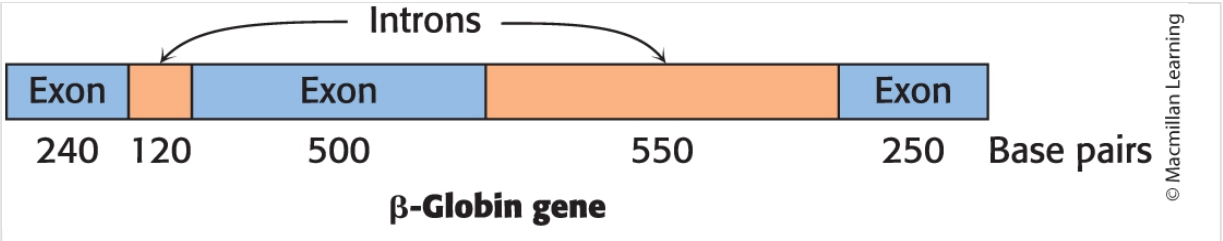


FIGURE 8.36 The β-globin gene is discontinuous. The coding regions, or exons (in blue), are interrupted by noncoding regions, or introns (in orange). This figure does not include regulatory regions (or transcribed but not translated regions) of the gene.

RNA processing generates mature RNA

At what stage in gene expression are introns removed? Newly synthesized RNA molecules (called *pre-mRNAs* or *primary transcripts*) isolated from nuclei are much larger than the mRNA molecules derived from them. In regard to β-globin RNA, the primary transcript consists of approximately 1600 nucleotides, and the processed mRNA (called *mature mRNA*) consists of approximately 900 nucleotides, which includes nontranslated regions of the mRNA. The primary transcript of the β-globin gene contains two regions, corresponding to the introns described above, that are not present in the mRNA. These regions in the primary transcript are excised, and the coding sequences are simultaneously linked by a precise splicing complex to form the mature mRNA (**Figure 8.37**). A common feature in the expression of discontinuous, or split, genes is that their exons are ordered in the same sequence in mRNA as in DNA. Thus, the codons in split genes, like continuous genes, are in the same linear order as the amino acids in the polypeptide products.

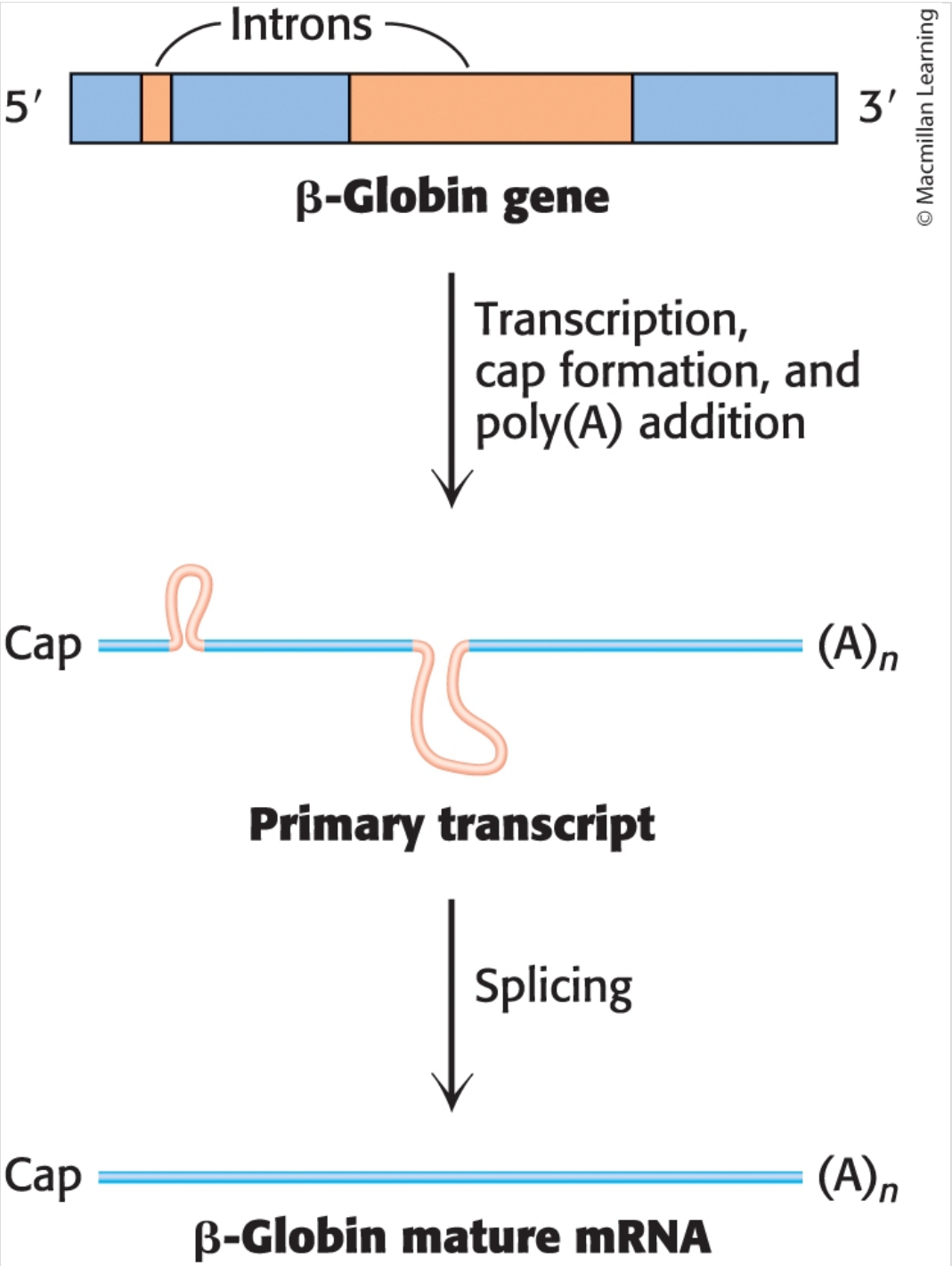


FIGURE 8.37 Transcription and processing of the β-globin gene includes an intermediate step where introns are removed. The gene is transcribed to yield the primary transcript, which is modified by cap and poly(A) addition. The introns in the primary RNA transcript are then removed to form the mature mRNA.

Splicing is a complicated series of reactions carried out by complexes called *spliceosomes*, which are assemblies of proteins and small nuclear RNA molecules (snRNAs). RNA plays the catalytic role (Section 29.4). Spliceosomes recognize signals in the primary transcript that specify the splice sites. Introns nearly always begin with GU and end with an AG that is preceded by a pyrimidine-rich tract (**Figure 8.38**). This consensus sequence is part of the signal for splicing.

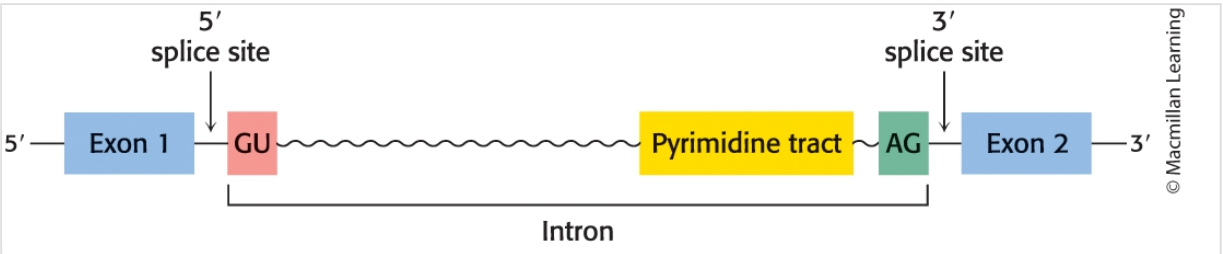


FIGURE 8.38 A consensus sequence ensures that splicing occurs at the correct locations. The introns typically begin with a GU pair and end with an AG pair that is preceded by a pyrimidine-rich tract.

Many exons encode protein domains

Most genes of higher eukaryotes, such as birds and mammals, are split. Lower eukaryotes, such as yeast, have a much higher proportion of continuous genes. In bacteria, split genes are extremely rare. From an evolutionary perspective, this raises the question: have introns been inserted into genes in the evolution of higher organisms or have they been removed from genes to form the streamlined genomes of bacteria and simple eukaryotes? Comparisons of the DNA sequences of genes

encoding evolutionarily conserved proteins suggest that introns were present in ancestral genes and were lost in the evolution of organisms that have become optimized for very rapid growth, such as bacteria. The positions of introns in some genes are at least 1 billion years old. Furthermore, the hypothesis that a common mechanism of splicing developed before the divergence of fungi, plants, and vertebrates is supported by the finding that mammalian cell extracts can splice yeast RNA.

What advantages might split genes confer? An attractive hypothesis is that new proteins arose in evolution by the rearrangement of exons encoding discrete structural elements, binding sites, and catalytic sites, a process called **exon shuffling**. Because it preserves functional units but allows them to interact in new ways, exon shuffling is a rapid and efficient means of generating novel genes. **Figure 8.39** shows the composition of a gene that was formed in part by exon shuffling. DNA can break and recombine in introns with no deleterious effect on encoded proteins. In contrast, the exchange of sequences within different exons usually leads to loss of protein function.

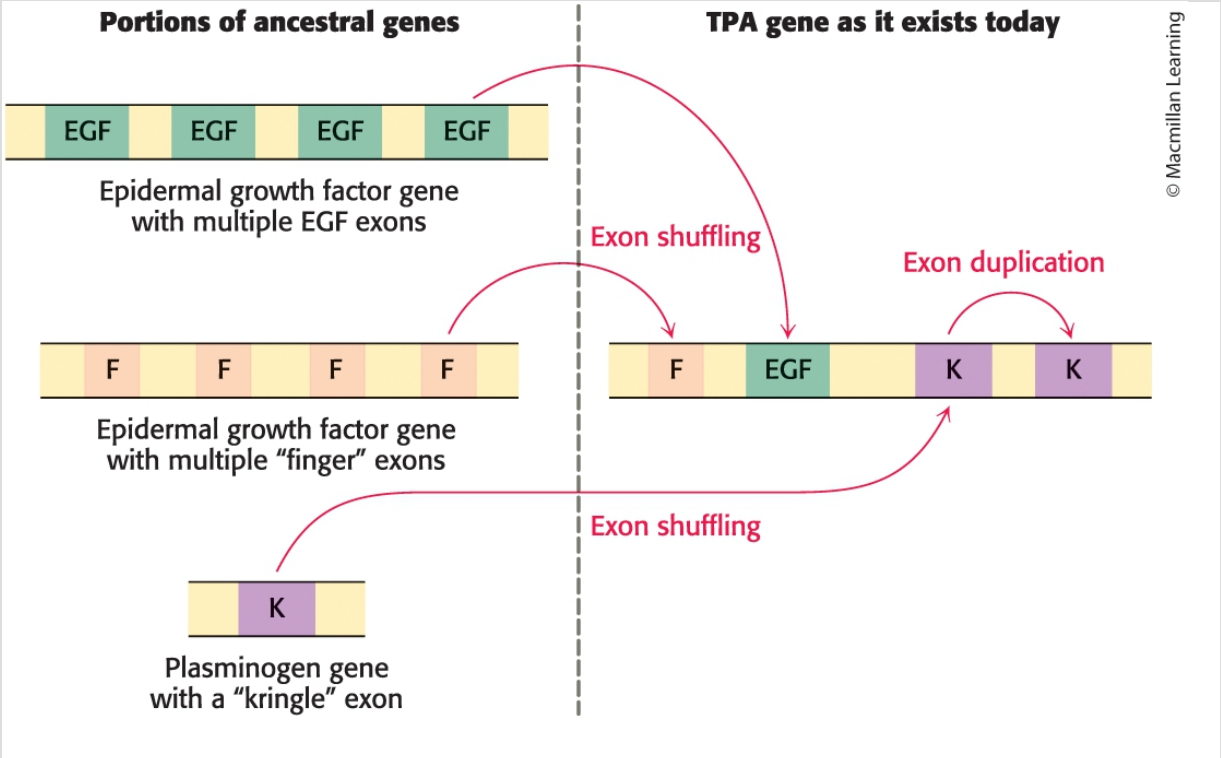


FIGURE 8.39 The tissue plasminogen activator (TPA) gene was generated by exon shuffling. The gene for TPA encodes an enzyme that functions in hemostasis (Section 7.4). This gene consists of 4 exons, one (F) derived from the fibronectin gene which encodes an extracellular matrix protein, one from the epidermal growth factor gene (EGF), and two from the plasminogen gene (K, Section 7.4), the substrate of the TPA protein. The K domain appears to have arrived by exon shuffling and then to have been duplicated to generate the TPA gene that exists today.

[Information from: www.ehu.es/ehusfera/genetica/2012/10/02/demostracion-molecular-de-microevolucion/.]

Another advantage of split genes is the potential for generating a series of related proteins by **alternative splicing** of the primary transcript. For example, a precursor of an antibody-producing cell forms an antibody that is anchored in the cell's plasma membrane (**Figure 8.40**). The attached antibody recognizes a specific foreign antigen, an event that leads to cell differentiation and proliferation. The activated antibody-producing cells then splice their primary transcript in an alternative manner to form soluble antibody molecules that are secreted rather than retained on the cell surface. Alternative splicing is a facile means of forming a set of proteins that are variations of a basic motif without requiring a gene for each protein. Due in large part to alternative splicing, the proteome is more diverse than the genome in eukaryotes.

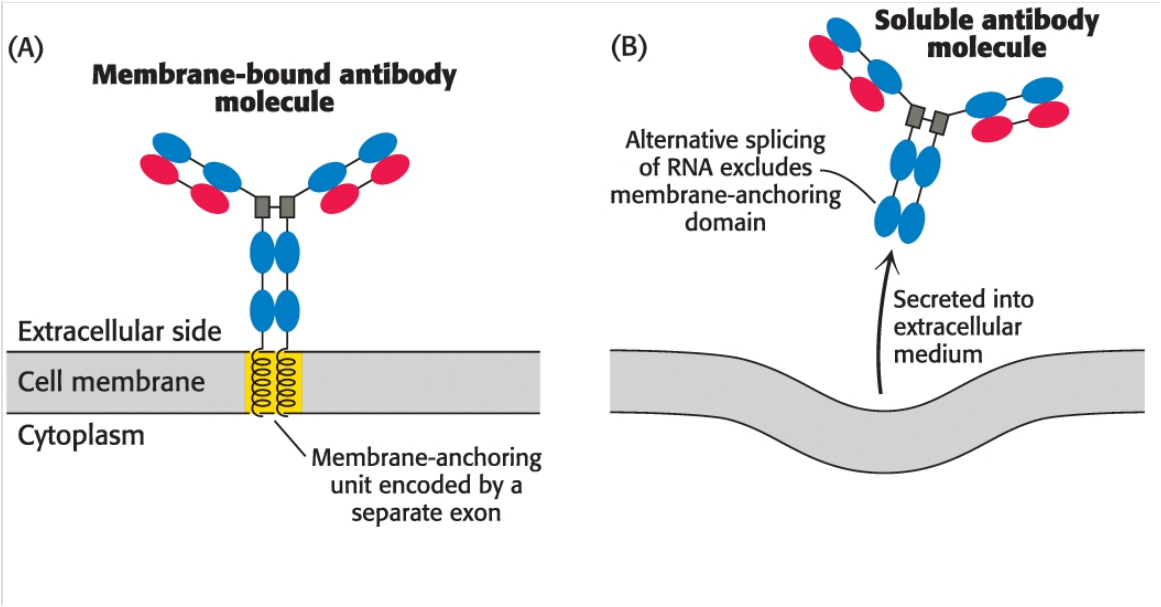


FIGURE 8.40 Alternative splicing generates mRNAs that are templates for different forms of a protein. For example, (A) a membrane-bound antibody on the surface of a lymphocyte and (B) i soluble counterpart, exported from the cell, are products of alternative splicing of the same transcript. The membrane-bound antibody is anchored to the plasma membrane by a helical segment (highlighted in yellow) that is encoded by its own exon.



Chapter 8 Summary

8.1 A Nucleic Acid Consists of Four Kinds of Bases Linked to a Sugar–Phosphate Backbone

- DNA and RNA are linear polymers of a limited number of nucleotide monomers. Each nucleotide contains a sugar, a phosphate, and a base.
- In DNA, the sugar is deoxyribose, and the bases are adenine (A), thymine (T), guanine (G), and cytosine (C). In RNA, the sugar is ribose, and thymine is replaced with uracil (U).
- Nucleic acids have directionality and are written in the $5'$-to-$3'$ direction.

8.2 A Pair of Nucleic Acid Strands with Complementary Sequences Can Form a Double-Helical Structure

- Cellular DNA consists of two very long, helical polynucleotide strands coiled around a common axis: the double helix.
- The sugar–phosphate backbone of each strand is on the outside of the double helix, whereas the purine and pyrimidine bases are on the inside stabilized by stacking forces.
- The two strands run in opposite directions and are held together by hydrogen bonds between pairs of bases: adenine is always paired with thymine, and guanine is always paired with cytosine. Hence, one strand of a double helix is the complement of the other.
- DNA can exist in a variety of helical forms. including B-DNA (the classic Watson–Crick double helix), A-DNA, and Z-DNA. Most of the DNA in a cell is in the B-form.
- Single-stranded nucleic acids, most notably RNA, can form complicated three-dimensional structures.

8.3 The Double Helix Facilitates the Accurate Transmission of Hereditary Information

- In DNA replication, the strands of the helix separate, and a new strand complementary to each of the original strands is synthesized. This mode of replication is called semiconservative because each new helix retains one of the parental strands.
- In order for replication to take place, the strands of the double helix must be separated, or melted.
- In the laboratory, the double helix can be melted by heating the solution above its melting temperature. This process is reversible, and the strands will reassemble spontaneously below the melting temperature.

8.4 DNA Is Replicated by Polymerases That Take Instructions from Templates

- The replication of DNA is a complex process carried out by many proteins, including several DNA polymerases.
- Replication by DNA polymerase requires: all four activated precursors (deoxynucleotide $5'$-triphosphates), a DNA template, and a primer with a free $3'-OH$ group.
- The new strand is synthesized in the $5' \rightarrow 3'$ direction.
- DNA polymerases catalyze the formation of a phosphodiester linkage only if the base on the incoming nucleotide is complementary to the base on the template strand.

8.5 Gene Expression Is the Transformation of DNA Information into Functional Molecules

- The flow of genetic information in normal cells is from DNA to RNA to protein.

- Transcription is the synthesis of RNA from a DNA template, and translation is the synthesis of a protein from an RNA template.
- Cells contain several kinds of RNA, among which are messenger RNA (mRNA), transfer RNA (tRNA), and ribosomal RNA (rRNA), which vary in size from 75 to more than 5000 nucleotides.
- As with DNA polymerases, RNA polymerases synthesize cellular RNA in the $5'$-to-$3'$ direction according to instructions given by DNA templates. RNA polymerase differs from DNA polymerase in not requiring a primer.

8.6 Amino Acids Are Encoded by Groups of Three Bases Starting from a Fixed Point

- The genetic code is the relationship between the sequence of bases in DNA (or its RNA transcript) and the sequence of amino acids in proteins.
- Amino acids are encoded by codons — groups of three bases — starting from a fixed point known as the start codon.
- Sixty-one of the 64 possible codons specify particular amino acids, whereas the other 3 codons (UAA, UAG, and UGA) are signals for chain termination. Thus, for most amino acids, there is more than one code word.
- Natural mRNAs contain start and stop signals for translation.

8.7 Most Eukaryotic Genes Are Mosaics of Introns and Exons

- Most genes in higher eukaryotes are discontinuous: coding sequences (exons) are separated by noncoding sequences (introns).
- Introns are removed in the conversion of the primary transcript into mature mRNA by a process known as splicing.
- A striking feature of many exons is that they encode functional domains in proteins. New proteins probably arose in the course of evolution by the shuffling of exons.

Key Terms

deoxyribonucleic acid (DNA)
ribonucleic acid (RNA)
nucleotide
deoxyribose
ribose
purine
pyrimidine
nucleoside
stem-loop
semiconservative replication
melting temperature (T_m)
template strand
primer
retrovirus
messenger RNA (mRNA)
transfer RNA (tRNA)
ribosomal RNA (rRNA)
transcription
promoter site
codon
anticodon
aminoacyl-tRNA
genetic code
stop codon
ribosome
Shine–Dalgarno sequence
intron
exon
splicing
exon shuffling

alternative splicing

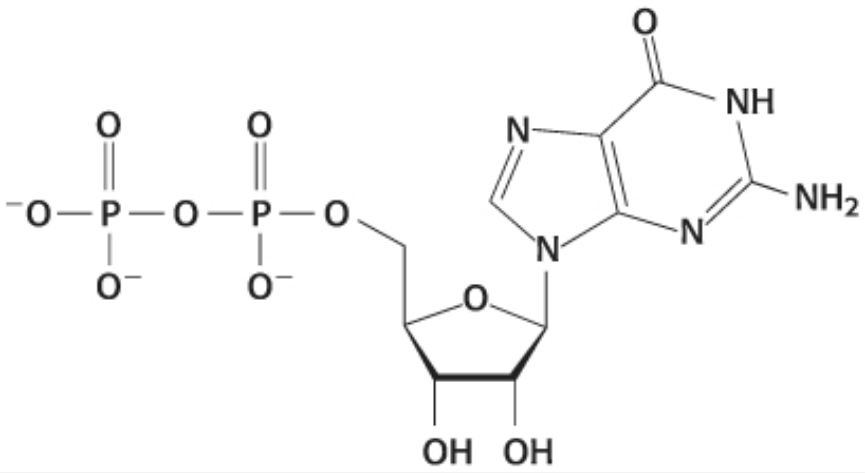
Problems

1. Classify the following descriptions as pertaining to nucleosides, nucleotides, or both nucleosides and nucleotides: 1

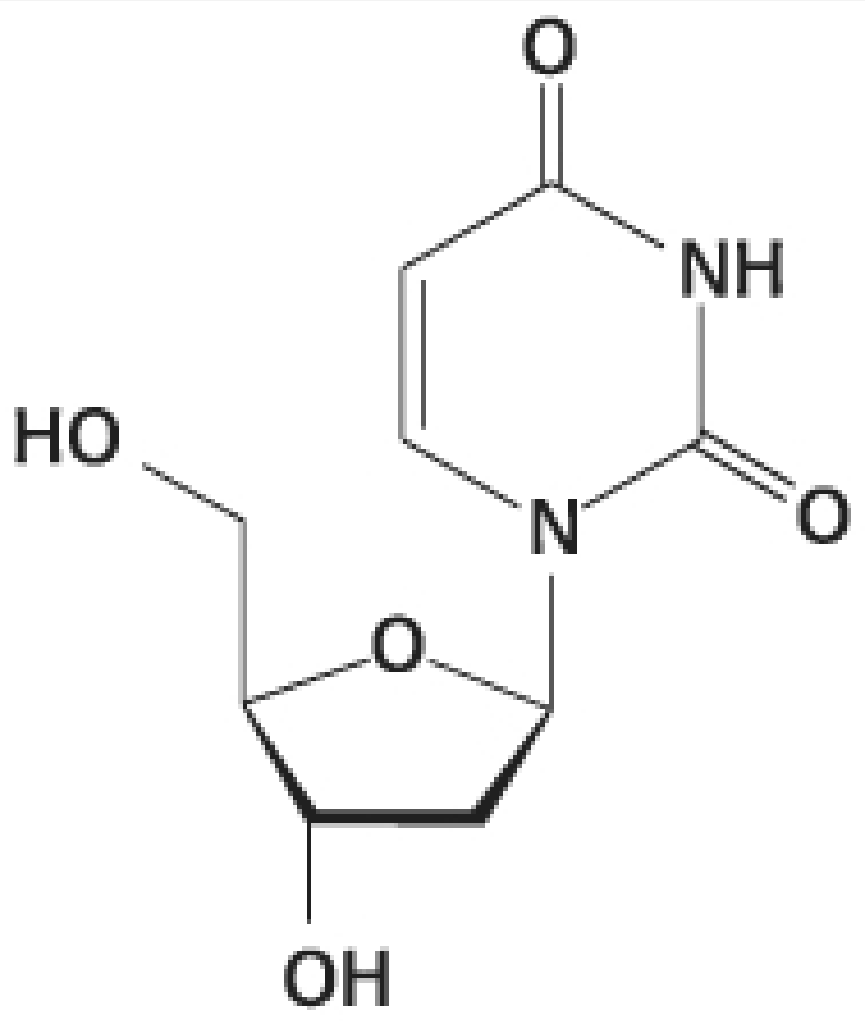
a. Contain a base, a sugar, and a phosphate group
b. Are found in RNA and DNA
c. Do not contain a phosphate group
d. May contain either a purine or a pyrimidine
e. One example is adenosine 5′-monophosphate
f. Are the product when a base bonds at C1 of ribose or deoxyribose
g. Are the monomers of nucleic acids
h. Contain a base and a sugar

2. Name the following nucleosides/nucleotides: 1

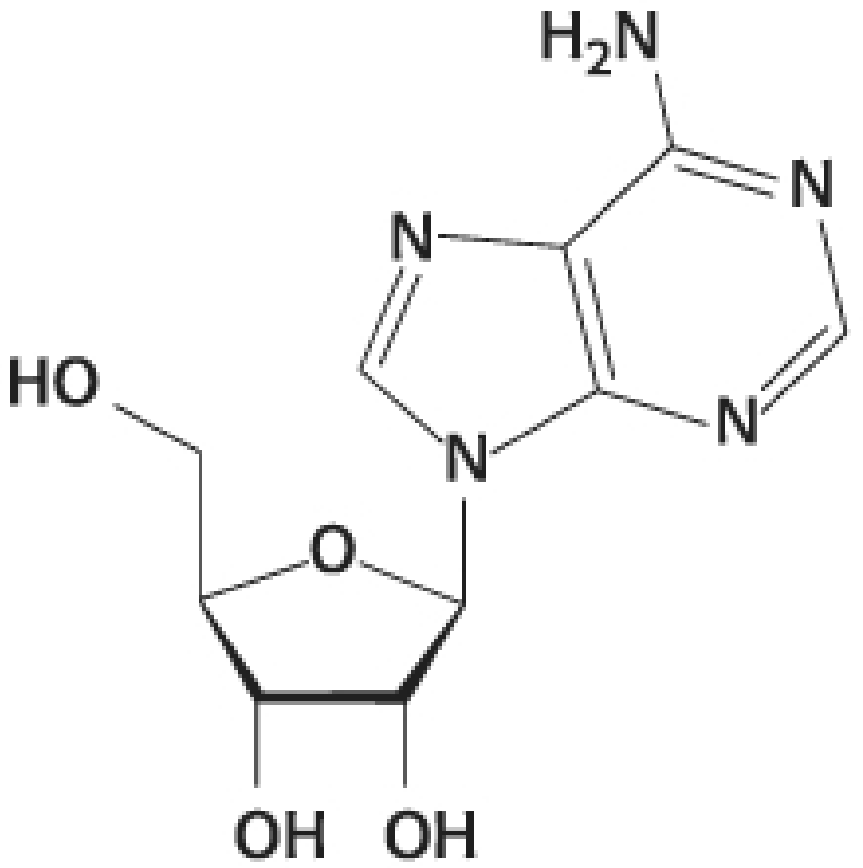
a.



b.



c.



3. Biochemist Erwin Chargaff was the first to note that, in DNA, $[A] = [T]$ and $[G] = [C]$. Using this rule, determine the percentages of all the bases in DNA that is 20% thymine.
1, 2

4. Write the complementary sequence (in the standard $5' \rightarrow 3'$ notation) for

a. GATCAA
b. TCGAAC
c. ACGCGT

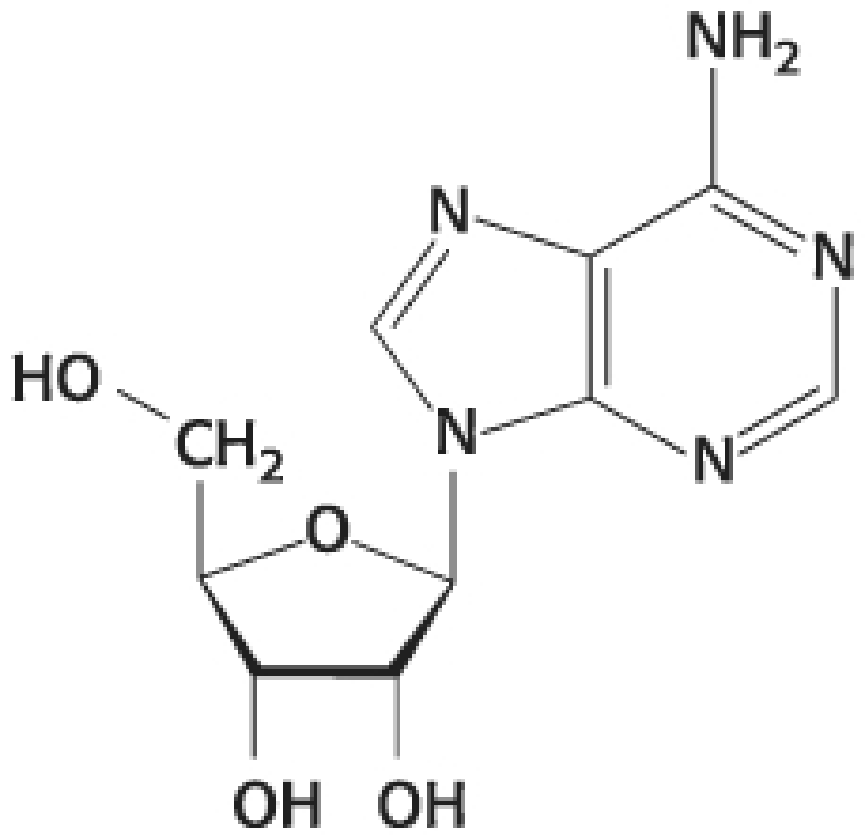
d. TACCAT

5. Classify the following statements as describing DNA or RNA: 2

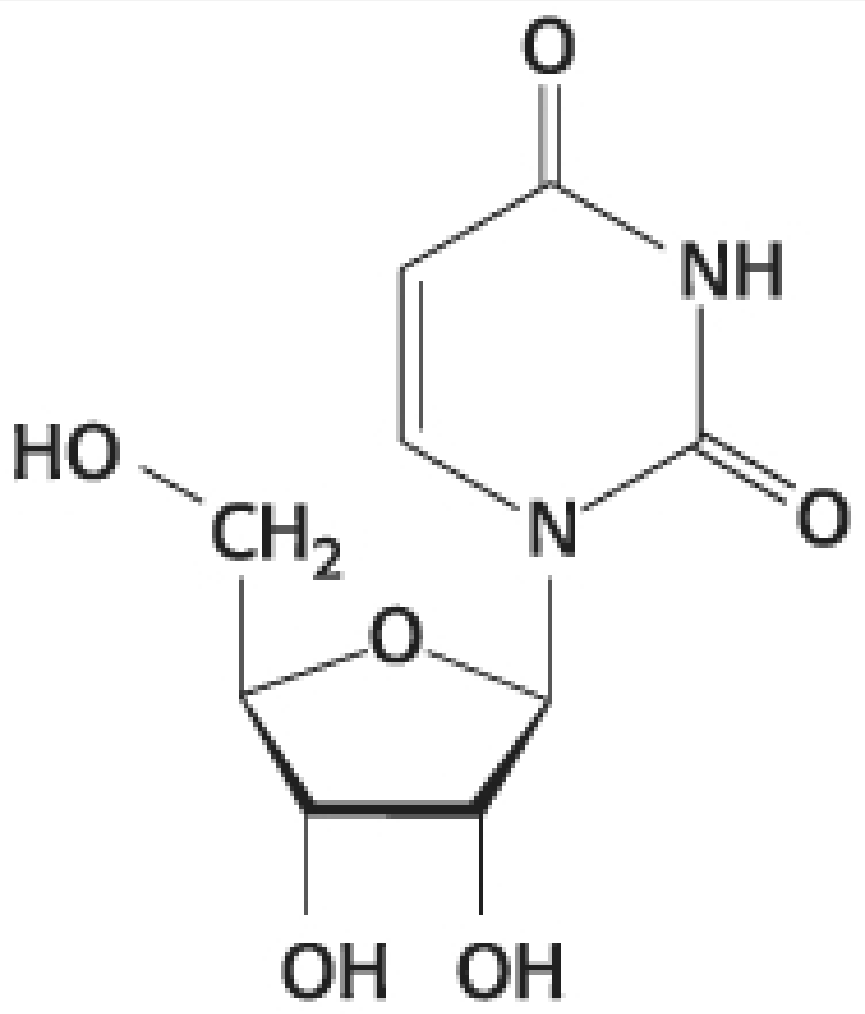
a. Is usually single-stranded
b. Is the genome for prokaryotic organisms
c. Includes the sugar deoxyribose
d. Includes the base uracil
e. Can form a complex secondary structures
f. Is usually double-stranded
g. Can be translated into a protein

6. Classify each nucleotide or nucleoside by the type of base (purine vs. pyrimidine) and the type of sugar (ribose vs. deoxyribose) 2

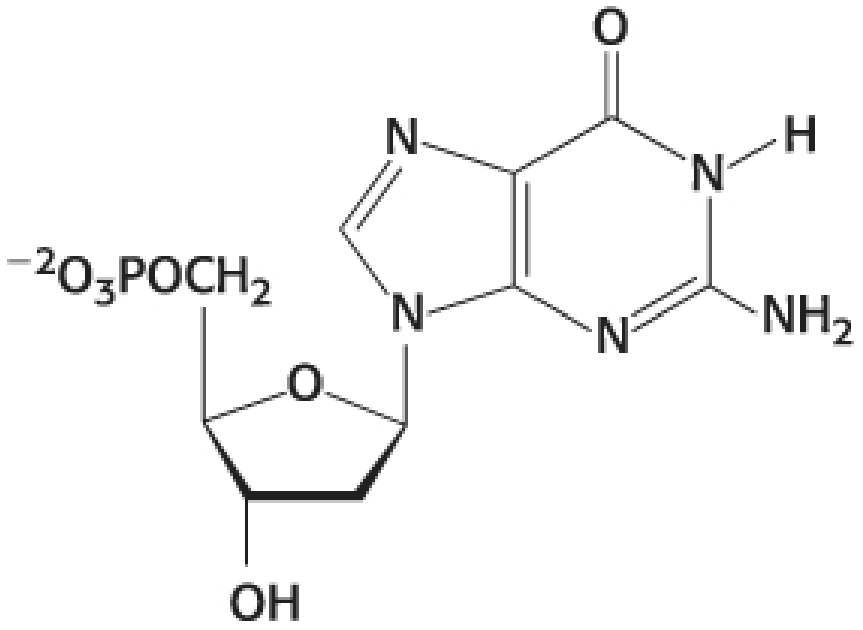
a.



b.



c.



7. Classify the following statements as describing B-DNA, A-DNA, Z-DNA, or all three. 2

a. Widest helix diameter
b. Has a helix diameter of ~20 Å
c. C−3′ of deoxyribose is out of the plane of the other sugar ring atoms
d. Left-handed
e. Antiparallel strands
f. Most stable under physiological conditions
g. Narrowest helix diameter
h. G pairs with C; A pairs with T
i. More likely observed in dehydrated DNA fibers

8.

a. Suppose that you want to radioactively label DNA but not RNA in dividing and growing bacterial cells. Which radioactive molecule would you add to the culture medium? 3
b. Suppose that you want to prepare DNA in which the backbone phosphorus atoms are uniformly labeled with ^{32}P. Which precursors should be added to a solution containing DNA polymerase and primed template DNA? Specify the position of radioactive atoms in these precursors.

9. A solution contains DNA polymerase and the Mg^{2+} salts of dATP, dGTP, dCTP, and TTP. The following DNA molecules are added to aliquots of this solution. Which of them would lead to DNA synthesis? Explain your answer. 3

a. A single-stranded closed circle containing 1000 nucleotide units
b. A double-stranded closed circle containing 1000 nucleotide pairs
c. A single-stranded closed circle of 1000 nucleotides base-paired to a linear strand of 500 nucleotides with a free $3'$ -OH terminus
d. A double-stranded linear molecule of 1000 nucleotide pairs with a free $3'-OH$ group at each end

10. In their famous experiment, Matthew Meselson and Franklin Stahl grew *E. coli* cells in a medium containing only the "heavy" isotope of nitrogen, ^{15}N. These cells were then transferred to a medium with the "light" isotope of nitrogen,

^{14}N. The results of the experiment supported the hypothesis of semiconservative replication. 3

a. Heavy DNA (^{15}N DNA), hybrid DNA, and light DNA (^{14}N DNA) can be separated by centrifugation. If cells containing ^{15}N DNA are transferred to a medium with only $^{14}NH_4Cl$ as a nitrogen source, what percentage of daughter molecules are composed of hybrid DNA after 2 generations?
b. Predict what percentage of daughter molecules would be composed of hybrid DNA if DNA exhibited conservative replication (i.e., if a daughter DNA molecule were composed of newly synthesized DNA only).

11. What is the axial ratio (length:diameter) of a DNA molecule $20\ \mu m$ long?

12. The DNA of a deletion mutant of λ bacteriophage has a length of $15\ \mu m$ instead of the $17\ \mu m$ found in the wild type phage. How many base pairs are missing from this mutant? 2

13. Match the components in the right-hand column with the appropriate process in the left-hand column. Terms in the left-hand column may be used more than once. 4

1. Replication _____	1. RNA polymerase
2. Transcription _____	2. DNA polymerase
3. Translation _____	3. Ribosome

4. dNTP

5. tRNA

6. NTP

7. mRNA

8. Primer

9. rRNA

10. Promoter

14.

a. Write the sequence of the mRNA molecule synthesized from a DNA template strand having the following sequence: 4

$$5' - ATCGTACCGTTA - 3'$$

b. What amino acid sequence is encoded by the following base sequence of an mRNA molecule? Assume that the reading frame starts at the $5'$ end.

$$5' - UUGCCUAGUGAUUGGAUG - 3'$$

c. What is the sequence of the polypeptide formed on addition of poly(UUAC) to a cell-free protein-synthesizing system?

15. Compare DNA polymerase and RNA polymerase from *E. coli* in regard to each of the following features: 4

a. Activated precursors
b. Direction of chain elongation
c. Conservation of the template
d. Need for a primer

16. What are the key characteristics of the genetic code? 4

17. Classify the following terms on whether they are associated with tRNA, mRNA, or rRNA. 4

a. Codon
b. Combines with protein to form ribosomes
c. Transports amino acids
d. Product of transcription
e. Anticodon

18. Do the following phrases describe prokaryotic promoters, eukaryotic promoters, or both? 5

a. Includes two conserved sequences at -35 and -10
b. Contains highly conserved DNA sequences that specify the start of transcription
c. Includes a TATA, or Hogness, box upstream of the transcription start site
d. Includes a Pribnow box upstream of the transcription start site
e. May by further stimulated by enhancer sequences

19. What is the significance of the fact that human mRNA can be accurately translated in *E. coli*? 5

20. Match the components in the right-hand column with the appropriate process in the left-hand column. 5

1. fMet _____
2. Shine–Dalgarno _____
3. Introns _____
4. Exons _____
5. Pre-mRNA _____
6. mRNA _____
7. Spliceosome _____

1. Continuous message
2. Removed during processing
3. The first of many amino acids
4. Joins exons
5. Joined to make the final message
6. Locates the start site
7. Discontinuous message

Chapter 9
Nucleic Acid Methods

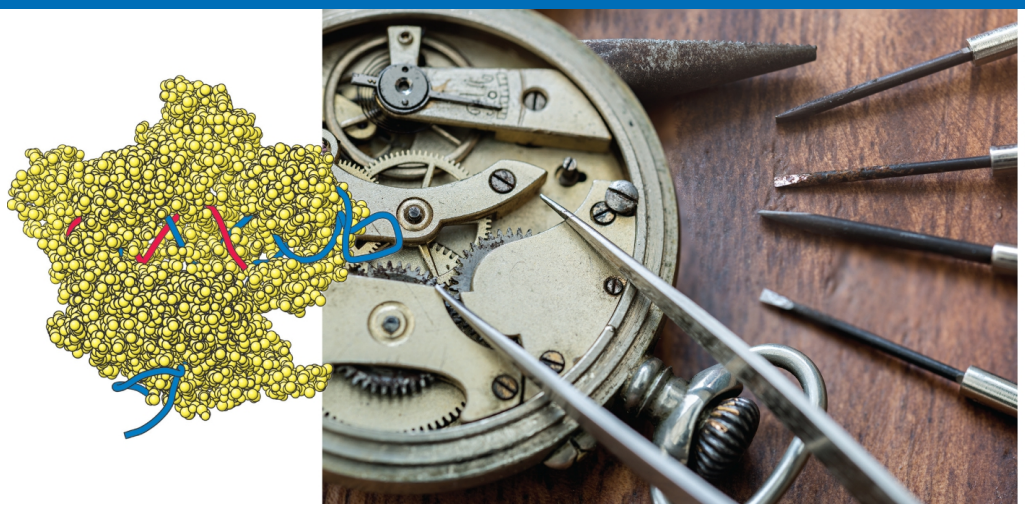


Photo: Gitanna/Shutterstock
© Macmillan Learning

The repair of delicate machinery, such as an old pocket watch, requires a steady hand, considerable experience, and the right tools for the job. Likewise, the advent of recombinant DNA technology has unlocked the potential to disrupt and repair DNA sequences with considerable precision. More recent developments have given us the tools such as the Cas9 endonuclease (left) to make directed changes to genomic DNA sequences with a high degree of specificity.

Outline

9.1 The Exploration of Genes Relies on Key Tools
9.2 Recombinant DNA Technology Has Revolutionized All Aspects of Biology
9.3 Complete Genomes Have Been Sequenced and Analyzed

[9.4 Eukaryotic Genes Can Be Quantitated and Manipulated with Considerable Precision]

Learning Goals



By the end of this chapter, you should be able to:

1. Explain how restriction enzymes work and their importance to recombinant DNA technology.
2. Describe several methods commonly used for the sequencing of DNA.
3. List the fundamental steps of the polymerase chain reaction.
4. Describe the various types of vectors used in DNA cloning, and explain the difference between a cloning vector and an expression vector.
5. Describe some commonly used methods to introduce mutations into DNA.
6. Explain how genes can be altered in living organisms, and describe some of the applications of these techniques.

Recombinant DNA technology is the fruit of several decades of basic research on DNA, RNA, and viruses. These methods are rapidly evolving in terms of their speed, precision, and complexity. Nevertheless, even the more complex processes can be distilled to their essential biochemical principles, which we explore in this chapter.

The impact of recombinant DNA technology, generally referred to as *biotechnology*, cannot be overstated. In addition to the dramatic expansion of our understanding of human disease, these methods have enabled wide-ranging advancements across a broad spectrum of disciplines, including agriculture, environmental science, forensics, and evolutionary biology.

9.1 The Exploration of Genes Relies on Key Tools

The rapid progress in biotechnology — indeed, its very existence — is a result of a few key techniques.

- *Restriction-enzyme analysis.* Restriction enzymes are precise molecular scalpels that allow an investigator to manipulate DNA segments.

- *Blotting techniques.* Southern and northern blots are used to separate and identify DNA and RNA sequences, respectively. The western blot, which uses antibodies to characterize proteins, was described in Chapter 4.

- *DNA sequencing.* The exact nucleotide sequence of a molecule of DNA can be determined. Sequencing has yielded a wealth of information concerning gene architecture, the control of gene expression, and protein structure.

- *Solid-phase synthesis of nucleic acids.* Specific sequences of nucleic acids can be synthesized de novo and used to identify or amplify other nucleic acids.

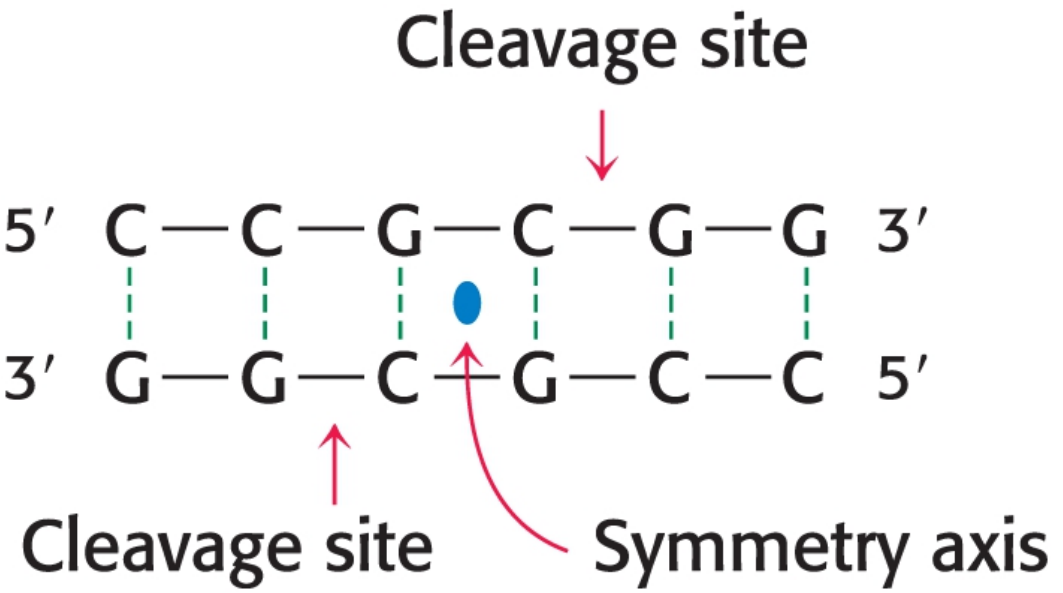
- *The polymerase chain reaction* (PCR). The polymerase chain reaction leads to a billionfold amplification of a segment of DNA. One molecule of DNA can be amplified to quantities that permit characterization and manipulation. This powerful technique can be used to detect pathogens and genetic diseases, determine the source of a hair left at the scene of a crime, and resurrect genes from the fossils of extinct organisms.

- *Bioinformatics.* A final set of techniques relies on the computer, without which it would be impossible to catalog, access, and characterize the abundant information generated by the methods outlined above. Such uses of the computer, referred to as *bioinformatics,* will be presented in Chapter 10.

Restriction enzymes split DNA into specific fragments

As discussed in Chapter 6, **restriction enzymes**, also called **restriction endonucleases**, recognize specific base sequences in double-helical DNA and cleave both strands of that duplex at specific places. To biochemists, these exquisitely precise scalpels are marvelous gifts of nature. They are indispensable for analyzing chromosome structure, sequencing very long DNA molecules, isolating genes, and creating new DNA molecules that can be cloned.

Restriction enzymes are found in a wide variety of prokaryotes. Their biological role is to cleave foreign DNA molecules, providing the host organism with a primitive immune system. Many restriction enzymes recognize specific sequences of four to eight base pairs and hydrolyze a phosphodiester bond in each strand in this region. A striking characteristic of these cleavage sites is that they almost always possess twofold rotational symmetry. In other words, the recognized sequence is a palindrome, that is, a sequence that reads the same forwards or backwards. As a consequence of this symmetry, the cleavage sites are also symmetrically positioned. For example, the sequence recognized by a restriction enzyme from *Streptomyces achromogenes* is



In each strand, the enzyme cleaves the C–G phosphodiester bond on the 3′ side of the symmetry axis. As we saw in Chapter 6, this symmetry corresponds to that of the structures of the restriction enzymes themselves.

Several thousand restriction enzymes have been purified and characterized. Their names consist of a three-letter abbreviation for the host organism (e.g., Eco for *Escherichia coli,* Hin for *Haemophilus influenzae,* Hae for *Haemophilus aegyptius*) followed by a strain designation, if needed, and a roman numeral to distinguish multiple enzymes from the same strain. The specificities of several of these enzymes are shown in **Figure 9.1**.

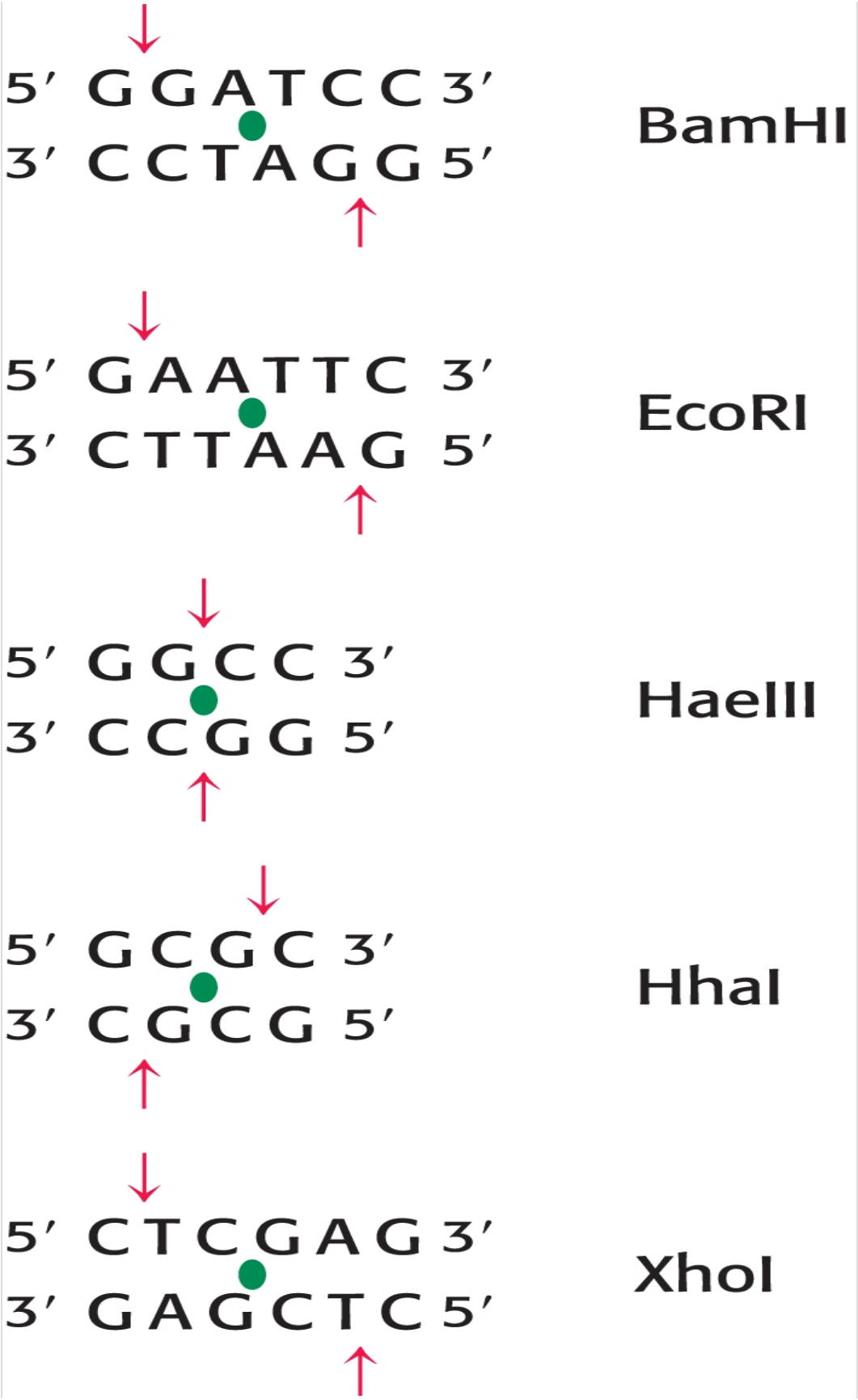

5′ G G A T C C 3′
3′ C C T A G G 5′
BamHI
5′ G A A T T C 3′
3′ C T T A A G 5′
EcoRI
5′ G G C C 3′
3′ C C G G 5′
HaeIII
5′ G C G C 3′
3′ C G C G 5′
HhaI
5′ C T C G A G 3′
3′ G A G C T C 5′
XhoI

FIGURE 9.1 Restriction endonucleases vary in their sequence specificity and sites of cleavage. The sequences that are recognized by these enzymes contain a twofold axis of symmetry. The two strands in these regions are related by a 180-degree rotation about the axis marked by the green symbol. The cleavage sites are denoted by red arrows. The abbreviated name of each restriction enzyme is given at the right of the sequence that it recognizes. Note that the cuts may be staggered or even.

VIEW an animation of a restriction digest and gel electrophoresis in Achieve

Restriction enzymes are used to cleave DNA molecules into specific fragments that are more readily analyzed and manipulated than the entire parent molecule. For example, the 5.1-kilobase circular duplex DNA of the tumor-producing SV40 virus is cleaved at one site by EcoRI, at four sites by HpaI, and at 11 sites by HindIII. A piece of DNA, called a restriction fragment, produced by the action of one restriction enzyme can be specifically cleaved into smaller fragments by another restriction enzyme. The pattern of such fragments can serve as a fingerprint of a DNA molecule. Indeed, complex chromosomes containing hundreds of millions of base pairs can be mapped by using a series of restriction enzymes.

Self-Check Question

The restriction enzyme AluI cleaves at the sequence $5'-AGCT-3'$, and NotI cleaves at $5'-GCGGCCGC-3'$. What would be the average distance between cleavage

sites for each enzyme on digestion of double-stranded DNA? Assume that the DNA contains equal proportions of A, C, G, and T.

Restriction fragments can be separated by gel electrophoresis and visualized

In Chapter 4, we considered the use of gel electrophoresis to separate protein molecules (Section 4.1). Because the phosphodiester backbone of DNA is highly negatively charged, this technique is also suitable for the separation of nucleic acid fragments. Among the many applications of DNA electrophoresis are the detection of mutations that affect restriction fragment size (such as insertions and deletions) and the isolation, purification, and quantitation of a specific DNA fragment.

For most gels, the shorter the DNA fragment, the farther the migration. Polyacrylamide gels are used to separate, by size, fragments containing as many as 1000 base pairs, whereas more-porous agarose gels are used to resolve mixtures of larger fragments (as large as 20 kilobases, kb). An important feature of these gels is their high resolving power. In certain kinds of gels, fragments differing in length by just one nucleotide out of several hundred can be distinguished. Individual bands or spots of DNA that have been labeled with radioactivity can be visualized by autoradiography after gel electrophoresis. Alternatively, a gel can be stained with a dye such as ethidium bromide, which fluoresces an intense orange under irradiation with ultraviolet light when bound to a double-helical DNA molecule (**Figure 9.2**). A band containing only 10 ng of DNA can be readily seen.

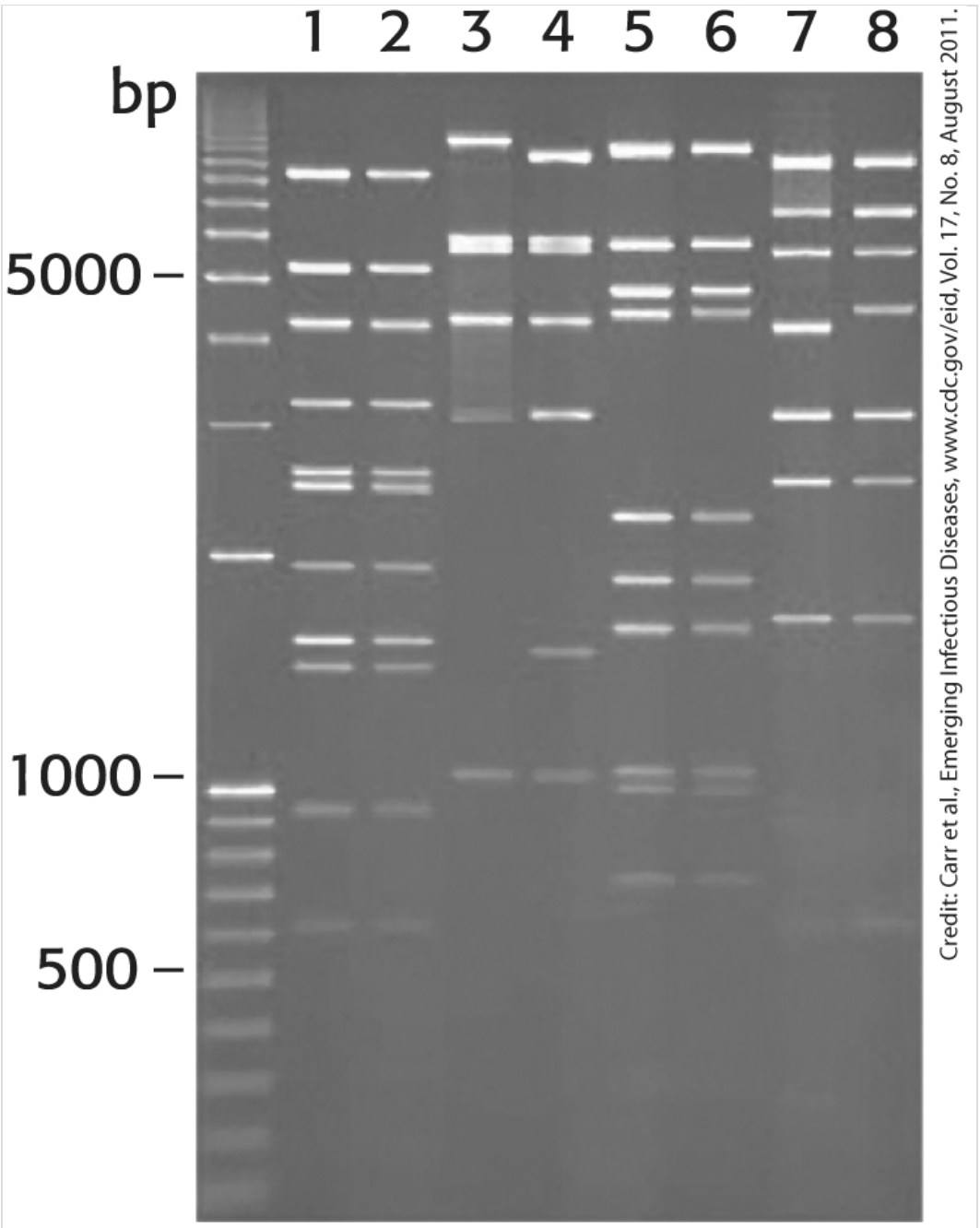


FIGURE 9.2 Gel-electrophoresis separates DNA fragments on the basis of their sizes. This gel shows the fragments produced by cleaving DNA from two viral strains (odd- vs. even-numbered lanes) with each of four restriction enzymes. These fragments were made fluorescent by staining the gel with ethidium bromide.

It is often necessary to determine if a particular base sequence is represented in a given DNA sample. For example, one may wish to confirm the presence of a specific mutation in genomic DNA isolated from patients known to be at risk for a particular disease. This specific sequence can be identified by hybridizing it with a labeled complementary DNA strand using a powerful technique named **Southern blotting**, for its inventor Edwin Southern (**Figure 9.3**).

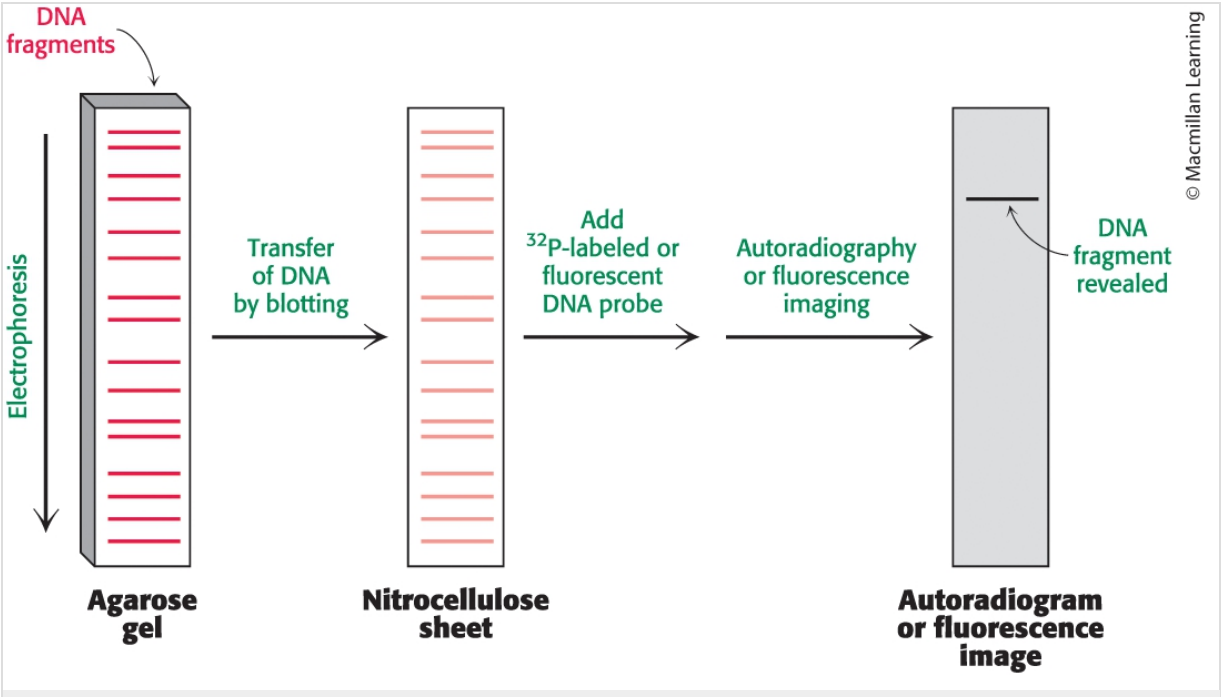


FIGURE 9.3 Southern blotting is used to detect the presence of a particular DNA sequence within a mixture of DNA molecules. A DNA fragment containing a specific sequence can be identified by separating a mixture of fragments by electrophoresis, transferring them to nitrocellulose, and hybridizing with a labeled probe complementary to the sequence. The fragment containing the sequence is then visualized by autoradiography or fluorescence imaging.

1. A mixture of restriction fragments is separated by electrophoresis through an agarose gel, denatured to form

single-stranded DNA, and transferred to a membrane composed of nitrocellulose or nylon. The positions of the DNA fragments in the gel are preserved during the transfer.

2. The membrane is then exposed to a ^{32}P-labeled or fluorescently tagged **DNA probe**, a short stretch of single-stranded DNA which contains a known base sequence.

3. The probe hybridizes with a restriction fragment having a complementary sequence.

4. Autoradiography or fluorescence imaging then reveals the position of the restriction-fragment–probe duplex.

A particular fragment amid a million others can be readily identified in this way.

In a similar manner, RNA molecules of a specific sequence can also be readily identified. After separation by gel electrophoresis and transfer to nitrocellulose, specific sequences can be detected by DNA probes. This analogous technique for the analysis of RNA has been whimsically termed **northern blotting**.

DNA can be sequenced by controlled termination of replication

The analysis of DNA structure and its role in gene expression has been markedly facilitated by the development of powerful techniques for the sequencing of DNA molecules. One of the first and most widely used techniques for DNA sequencing is **controlled termination of replication**, also referred to as the **Sanger dideoxy method** for its pioneer, Frederick Sanger. The key to this approach is

the generation of DNA fragments whose length is determined by the last base in the sequence (**Figure 9.4**).

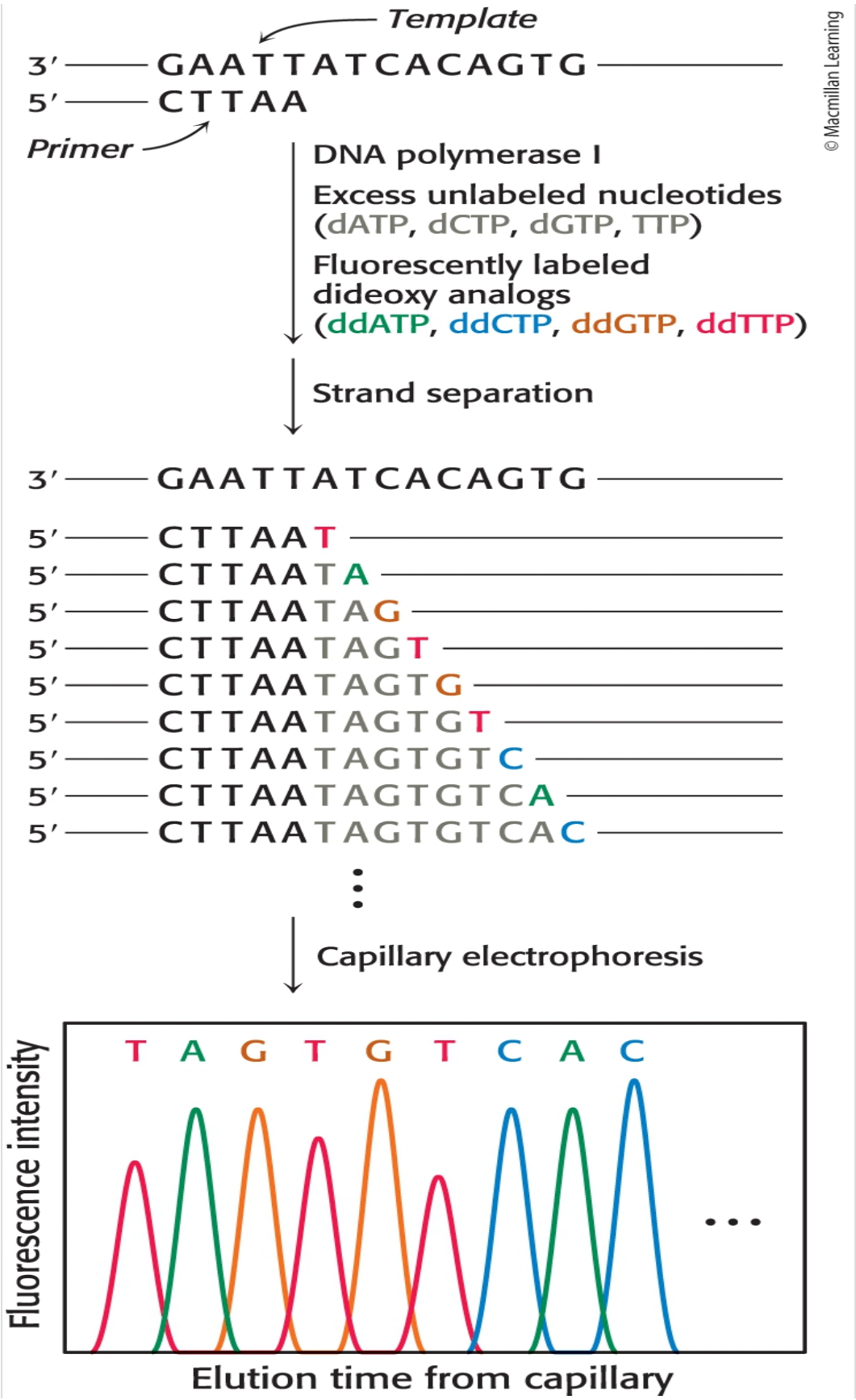
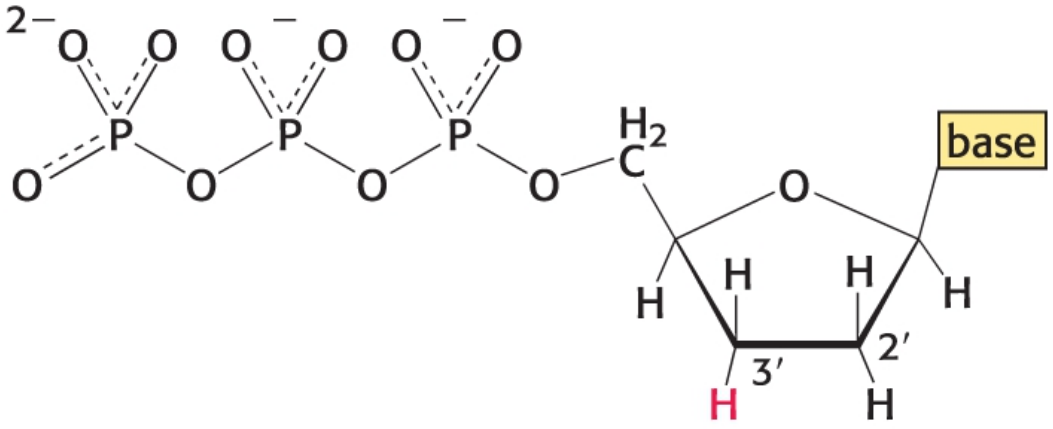

Template
3′ GAATTATCACAGTG
5′ CTTAA
Primer
DNA polymerase I
Excess unlabeled nucleotides
(dATP, dCTP, dGTP, TTP)
Fluorescently labeled
dideoxy analogs
(ddATP, ddCTP, ddGTP, ddTTP)
Strand separation
3′ GAATTATCACAGTG
5′ CTTAAT
5′ CTTAATA
5′ CTTAATAG
5′ CTTAATAGT
5′ CTTAATAGTG
5′ CTTAATAGTGT
5′ CTTAATAGTGTC
5′ CTTAATAGTGTCA
5′ CTTAATAGTGTCAC
Capillary electrophoresis
T A G T G T C A C
Fluorescence intensity
Elution time from capillary
© Macmillan Learning

FIGURE 9.4 Controlled termination of replication uses the separation of fluorescently labeled oligonucleotide fragments to determine an overall sequence. A sequencing reaction is performed with four chain-terminating dideoxy nucleotides, each labeled with a tag that fluoresces at a different wavelength, with the color of each fragment indicating the identity of the last base in the chain. The fragments are separated by size using capillary electrophoresis, and the fluorescence at each of the four wavelengths indicates the sequence of the complement of the original DNA template.

VIEW an animation of the dideoxy sequencing method in Achieve

In the current application of this method, a DNA polymerase is used to make the complement of a particular sequence within a single-stranded DNA molecule. The synthesis is primed by a chemically synthesized fragment that is complementary to a part of the sequence known from other studies. In addition to the four deoxyribonucleoside triphosphates, the reaction mixture contains a small amount of the 2′,3′-dideoxy analog of each nucleotide, each

carrying a different fluorescent label attached to the base (e.g., a green emitter for termination at A and a red one for termination at T).



2′, 3′-Dideoxy analog

The incorporation of the dideoxy nucleotide blocks further growth of the new chain because this analog lacks the $3'$-hydroxyl terminus needed to form the next phosphodiester bond. The concentration of the dideoxy analog is low enough that chain termination will take place only occasionally. The polymerase will insert the correct nucleotide sometimes and the dideoxy analog other times, stopping the reaction. For instance, if the dideoxy analog of dATP is present, fragments of various lengths are produced, but all will be terminated by the dideoxy analog. Importantly, this dideoxy analog of dATP will be inserted only where a T was located in the DNA being sequenced. Thus, the fragments of different length will correspond to the positions of T.

The resulting fragments are separated by a technique known as *capillary electrophoresis*, in which the mixture is passed through a very narrow tube containing a gel matrix at high voltage to achieve efficient separation within a short time. As the DNA fragments emerge from the capillary, they are detected by their fluorescence; the sequence of their colors directly gives the base sequence. Sequences of as many as 1000 bases can be determined in this way. Indeed, automated Sanger sequencing machines can read more than 1 million bases per day.

DNA probes and genes can be synthesized by automated solid-phase methods

DNA strands, like polypeptides (Section 4.4), can be synthesized by the sequential addition of activated monomers to a growing chain that is linked to a solid support (resin). The activated monomers are protected deoxyribonucleoside $3'$-phosphoramidites. The synthesis of specific sequences proceeds by the repetition of the following cycle (**Figure 9.5**).

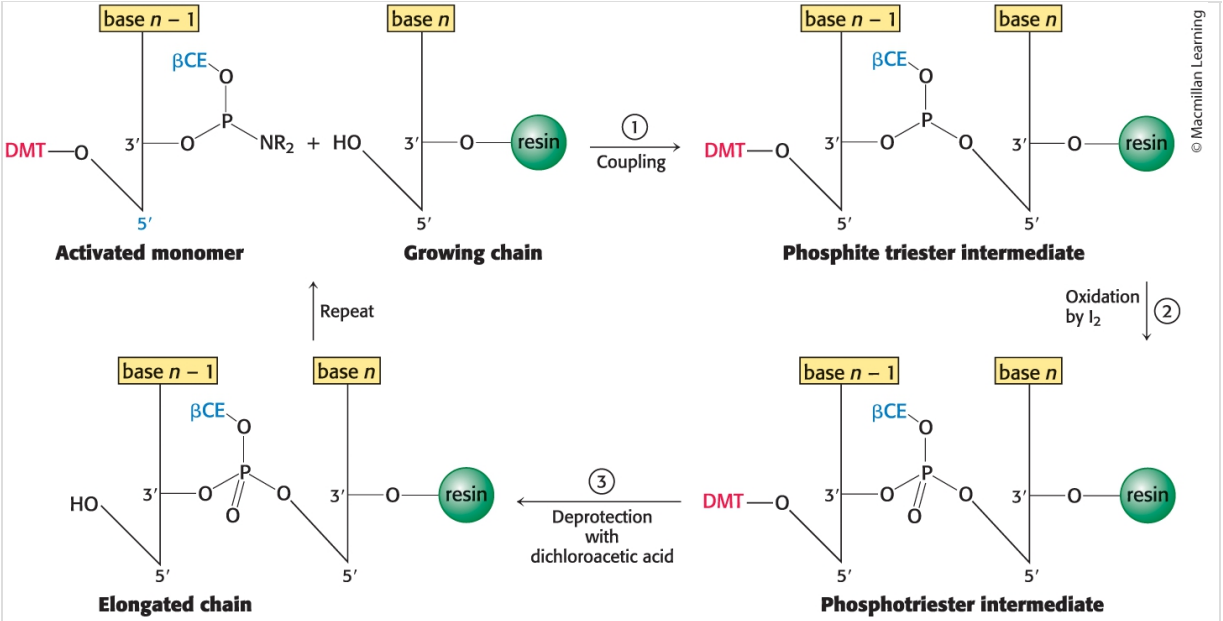
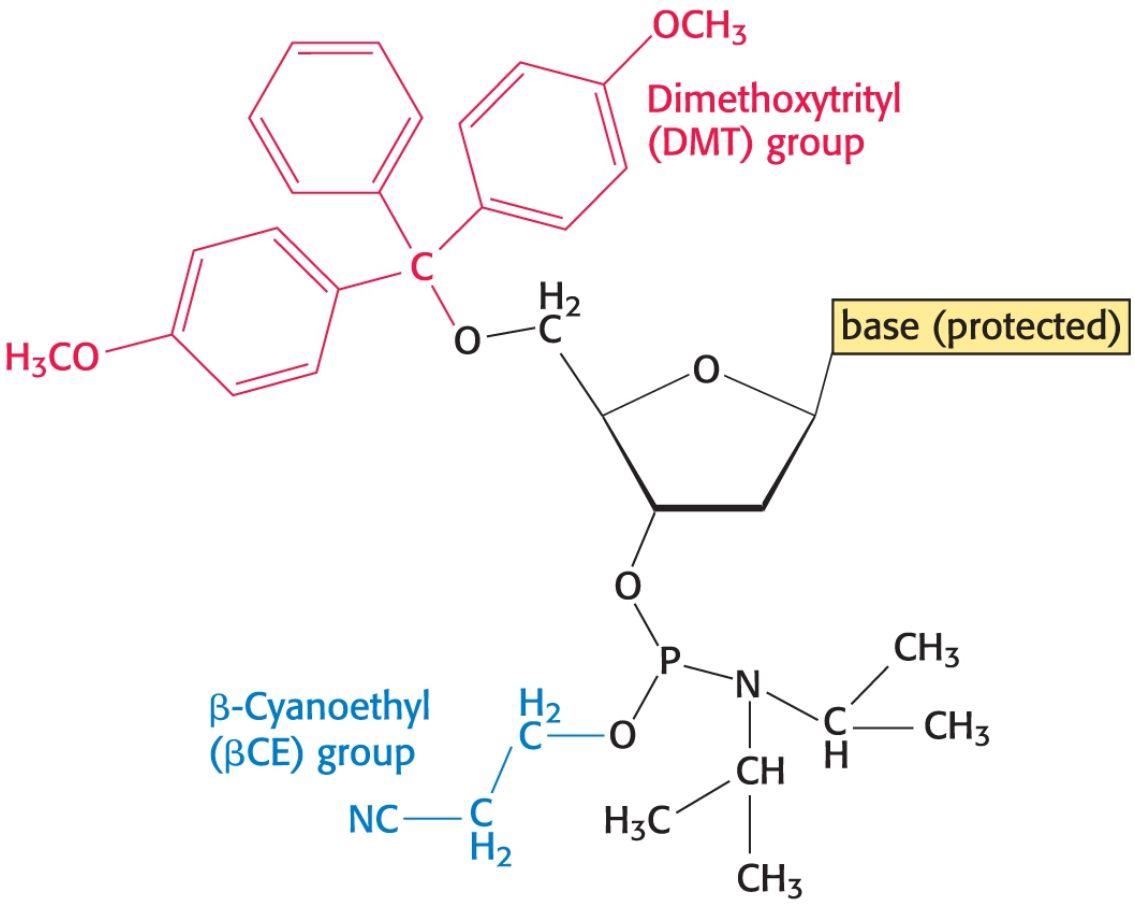


FIGURE 9.5 Oligonucleotides are synthesized in the solid-phase by the phosphite triester method. The activated monomer added to the growing chain is a deoxyribonucleoside $3'$-phosphoramidite containing a dimethoxytrityl (DMT) protecting group on its $5'$-oxygen atom, a β-cyanoethyl (βCE) protecting group on its $3'$-phosphoryl oxygen atom, and a protecting group on the base.



1. The $3'$-phosphorus atom of the incoming unit is joined to the $5'$-oxygen atom of the growing chain to form a phosphite triester. The $5'$-OH group of the activated monomer is unreactive because it is blocked by a dimethoxytrityl (DMT) protecting group, and the $3'$-phosphoryl oxygen atom is rendered unreactive by attachment of the β-cyanoethyl (βCE) group. Likewise, amino groups on the purine and pyrimidine bases are blocked. This step, called *coupling*, is carried out under anhydrous conditions because water reacts with phosphoramidites.



A deoxyribonucleoside 3′-phosphoramidite with DMT and βCE attached

2. The phosphite triester (in which P is trivalent) is oxidized by iodine to form a phosphotriester (in which P is pentavalent).

3. The DMT protecting group on the $5'$-OH group of the growing chain is removed by the addition of dichloroacetic acid, which leaves other protecting groups intact. The DNA chain is now elongated by one unit and ready for another cycle of addition.

Each cycle takes only about 10 minutes and usually elongates more than 99% of the chains that are linked to the solid support resin.

This solid-phase approach is ideal for the synthesis of DNA, as it is for polypeptides, because the desired product stays on the insoluble support until the final release step. All the reactions take place in a single vessel, and excess soluble reagents can be added to drive reactions to completion. At the end of each step, soluble reagents and by-products are washed away from the resin that bears the growing chains.

At the end of the synthesis, NH_3 is added to remove all protecting groups and release the oligonucleotide from the solid support. Because elongation is never 100% complete, the new DNA chains are of diverse lengths — the desired chain is the longest one. The sample can be purified by high-performance liquid chromatography or by electrophoresis on polyacrylamide gels. DNA chains of as many as 100 nucleotides can be readily synthesized by this automated method.

The ability to rapidly synthesize DNA chains of any selected sequence opens many experimental avenues. For example, a synthesized DNA probe labeled at one end with ^{32}P or a fluorescent tag can be used to search for a complementary sequence in a very long DNA molecule or even in a genome consisting of many chromosomes. Such a probe can be used as a primer to initiate the replication of neighboring DNA by DNA polymerase.

Another application of the solid-phase approach is the synthesis of new tailor-made genes. New proteins with novel properties can now be produced in abundance by the expression of synthetic genes. Finally, the synthesis described in the steps above can be slightly modified for the solid-phase synthesis of RNA oligonucleotides,

which can be very powerful reagents for the degradation of specific mRNA molecules in living cells by a technique known as RNA interference (Section 9.4).

Selected DNA sequences can be greatly amplified by the polymerase chain reaction

In 1984, Kary Mullis devised an ingenious method called the **polymerase chain reaction (PCR)** for amplifying specific DNA sequences. Consider a DNA duplex consisting of a target sequence surrounded by nontarget DNA. Millions of copies of the target sequences can be readily obtained by PCR if the sequences flanking the target are known. PCR is carried out by adding the following components to a solution containing the target sequence: (1) a pair of primers that hybridize with the flanking sequences of the target, (2) all four deoxyribonucleoside triphosphates (dNTPs), and (3) a heat-stable DNA polymerase. A PCR cycle consists of three steps (**Figure 9.6**).

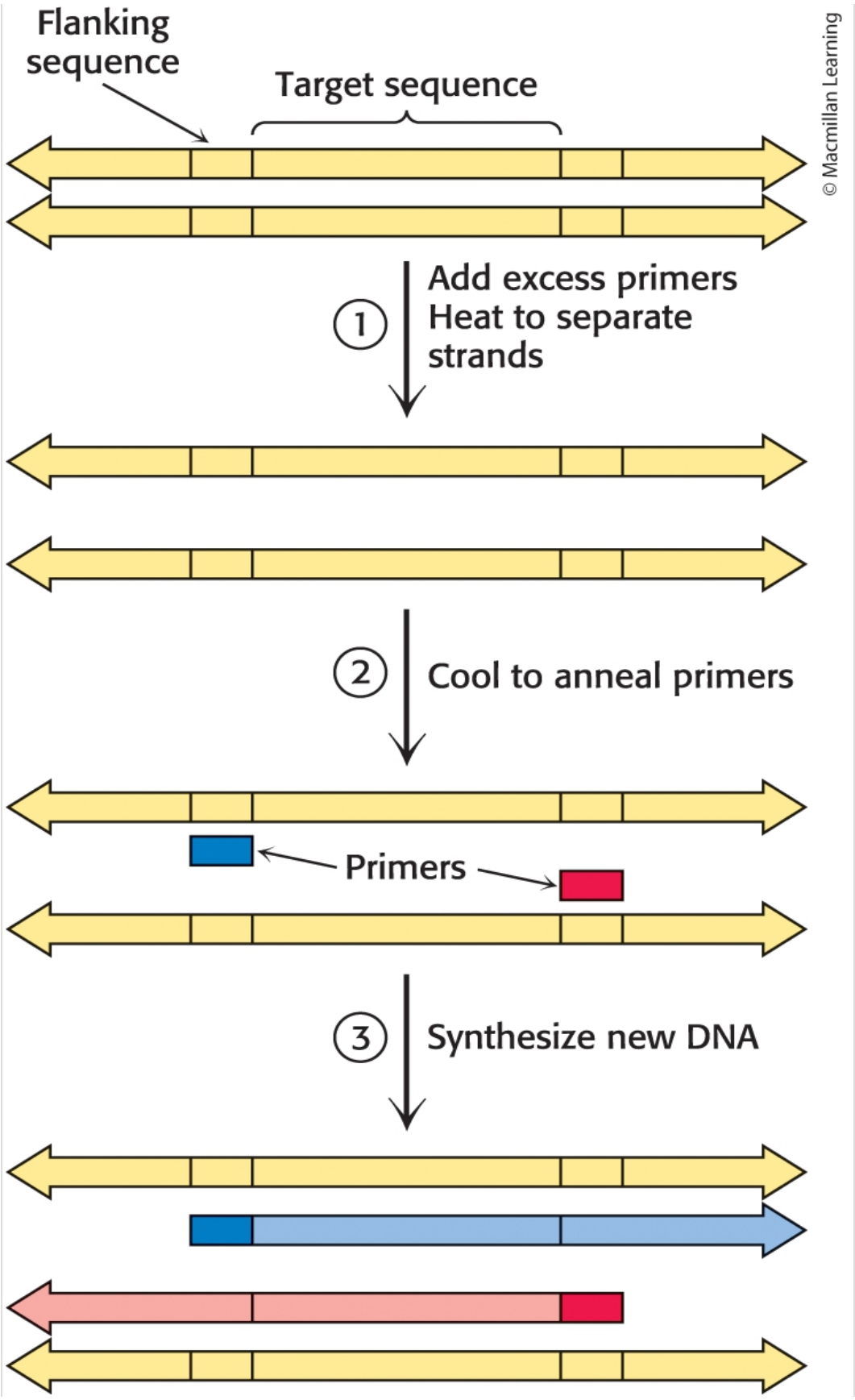

Flanking sequence
Target sequence
© Macmillan Learning
1
Add excess primers
Heat to separate strands
2
Cool to anneal primers
Primers
3
Synthesize new DNA

FIGURE 9.6 The first cycle in the polymerase chain reaction (PCR) generates two double-stranded DNA molecules. A cycle consists of three steps: DNA double-strand separation, the hybridization of primers, and the extension of primers by DNA synthesis.



1. *Strand separation.* The two strands of the parent DNA molecule are separated by heating the solution to 95°C for 15 s.

2. *Annealing of primers.* The solution is then abruptly cooled to 54°C to allow each primer to hybridize to a DNA strand, a process called *annealing*. One primer hybridizes to the $3'$ end of the target on one strand, and the other primer hybridizes to the $3'$ end on the complementary target strand. Parent DNA duplexes do not form, because the primers are present in large excess. Primers are typically from 20 to 30 nucleotides long.

3. *DNA synthesis.* The solution is then heated to 72°C, the optimal temperature for heat-stable polymerases. One such enzyme is *Taq* DNA polymerase, which is derived from *Thermus aquaticus*, a thermophilic bacterium that lives in hot springs. The polymerase elongates both primers in the direction of the target sequence because DNA synthesis is in the $5'$-to-$3'$ direction. DNA synthesis takes place on both strands but extends beyond the target sequence in this initial round.

These three steps — strand separation, annealing of primers, and DNA synthesis — constitute one cycle of the PCR amplification and can be carried out repetitively just by changing the temperature of the reaction mixture. The thermostability of the polymerase makes it feasible to carry out PCR in a closed container; no reagents are

added after the first cycle. At the completion of the second cycle, four duplexes containing the target sequence have been generated (**Figure 9.7**). Of the eight DNA strands comprising these duplexes, two short strands constitute only the target sequence — the sequence including and bounded by the primers. Subsequent cycles will amplify the target sequence exponentially. Ideally, after n cycles, the desired sequence is amplified 2^n-fold. The amplification is a millionfold after 20 cycles and a billionfold after 30 cycles, which can be carried out in less than an hour.

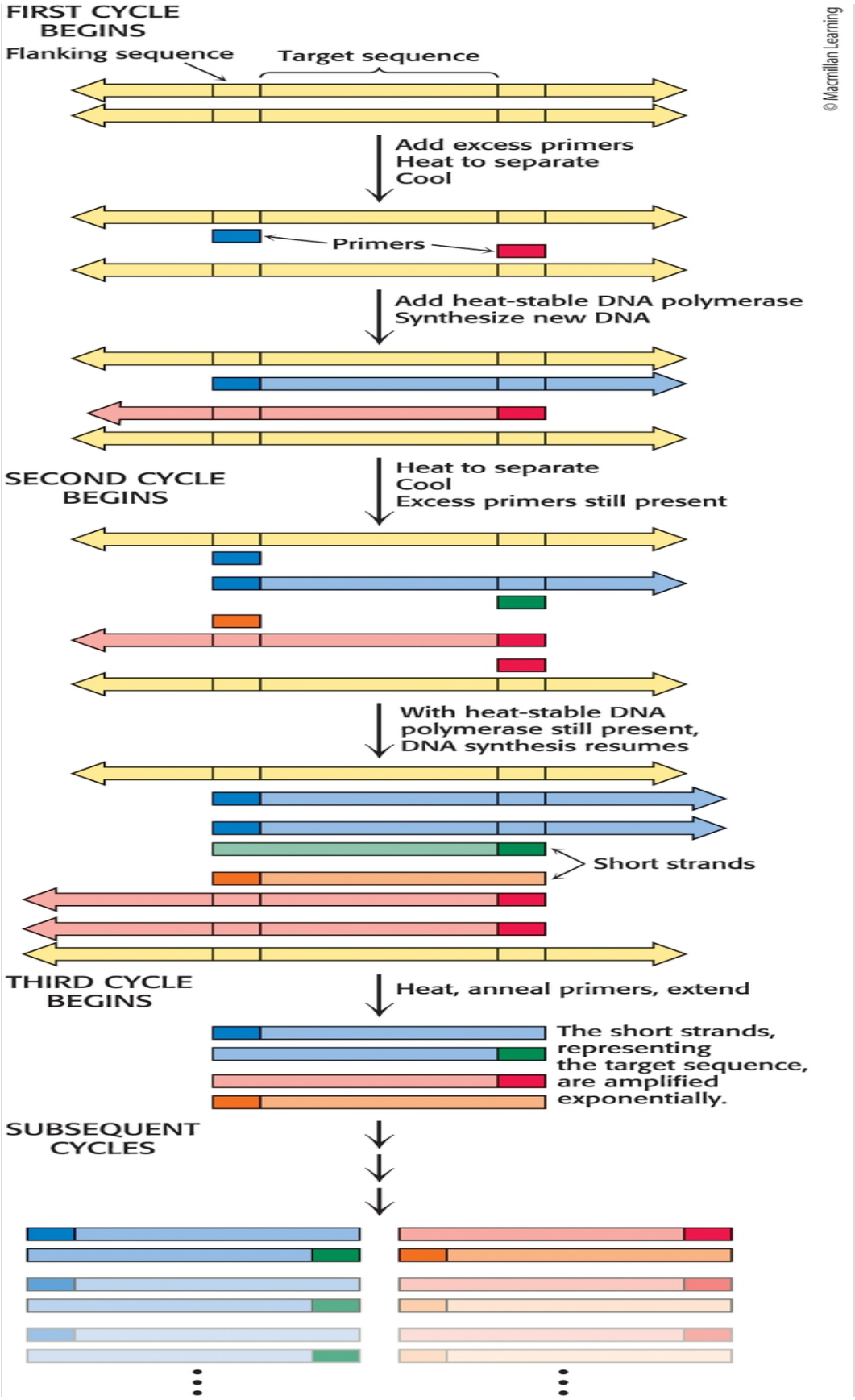

FIRST CYCLE BEGINS
Flanking sequence
Target sequence
Add excess primers
Heat to separate
Cool
Primers
Add heat-stable DNA polymerase
Synthesize new DNA
SECOND CYCLE BEGINS
Heat to separate
Cool
Excess primers still present
With heat-stable DNA polymerase still present, DNA synthesis resumes
Short strands
THIRD CYCLE BEGINS
Heat, anneal primers, extend
The short strands, representing the target sequence, are amplified exponentially.
SUBSEQUENT CYCLES
© Macmillan Learning

FIGURE 9.7 Multiple cycles of the polymerase chain reaction generate numerous copies of the amplified fragment. The two short double-stranded fragments produced at the end of the third cycle represent the target sequence. Subsequent cycles will amplify the target sequence exponentially and the parent sequence (yellow) arithmetically.

VIEW an animation of this technique in Achieve

Several features of this remarkable method for amplifying DNA are noteworthy. First, the sequence of the target need not be known. All that is required is knowledge of the flanking sequences so that complementary primers can be synthesized. Second, the target can be much larger than the primers. Targets larger than 10 kb have been amplified by PCR. Third, primers do not have to be perfectly matched to flanking sequences to amplify targets. With the use of primers derived from a gene of known sequence, it is possible to search for variations on the theme. In this way, families of genes are being discovered by PCR. Fourth, PCR is highly specific because of the stringency of hybridization at relatively high temperature. *Stringency* is the required closeness of the match between primer and target, which can be controlled by temperature and salt. At high temperatures, only the DNA between hybridized primers is amplified. A gene constituting less than a millionth of the total DNA of a higher organism is accessible by PCR. Fifth, PCR is exquisitely sensitive. A single DNA molecule can be amplified and detected.

Self-Check Question

How would altering the stringency (for example, by changing the temperature of hybridization) affect PCR amplification? Suppose that you have a particular yeast gene

A and that you wish to see if it has a counterpart in humans. How would controlling the stringency of the hybridization help you?

PCR is a powerful technique in medical diagnostics, forensics, and studies of molecular evolution

PCR has been utilized in a wide variety of applications across many different disciplines:

- *Diagnosing certain infections caused by viruses and bacteria.* With the use of specific primers, PCR can reveal the presence of small amounts of DNA from the human immunodeficiency virus (HIV) in persons who have not yet mounted an immune response to this pathogen. In these patients, assays designed to detect antibodies against the virus would yield a false negative test result. Similarly, in patients suspected of having tuberculosis, PCR can be used to rapidly detect as few as 10 tubercle bacilli per million human cells, whereas finding *Mycobacterium tuberculosis* bacilli in tissue specimens would be slow and laborious.

- *Detecting certain cancers early and monitoring chemotherapy.* PCR can identify mutations of certain growth-control genes, such as the *ras* genes (Chapter 14). PCR is also ideal for detecting leukemias caused by chromosomal rearrangements. In addition, tests using PCR can detect when cancerous cells have been eliminated and treatment can be stopped; they can also detect a relapse and the need to immediately resume treatment.

- *Solving forensics cases.* An individual DNA profile is highly distinctive because many genetic loci are highly variable within a population. For example, each chromosome contains regions which vary in length from individual to individual. The pattern of DNA fragment sizes from PCR amplification across these regions provides a unique fingerprint for that individual. Numerous assault and rape cases rely on analyses of blood stains and semen samples by PCR (**Figure 9.8**). The root of a single shed hair found at a crime scene contains enough DNA for typing by PCR.



Martin Shields/Science Source

FIGURE 9.8 PCR can be applied to forensic cases. DNA isolated from sperm obtained during the examination of a rape victim was amplified by PCR, then compared with DNA from the victim and two potential suspects using gel electrophoresis and autoradiography. Sperm DNA matched the pattern of Suspect 1, but not that of Suspect 2.

- *Studying molecular evolution.* DNA is a remarkably stable molecule, particularly when shielded from air, light, and water. Under such circumstances, large fragments of DNA can remain intact for thousands of years or longer. PCR provides an ideal method for amplifying such ancient DNA molecules so that they can be detected and characterized. As will be discussed in Chapter 10, sequences from these PCR products can be sources of considerable insight into evolutionary relationships between organisms.

The tools for recombinant DNA technology have been used to identify disease-causing mutations

Let us consider how the techniques just described have been used to study the molecular underpinning of human disease. Amyotrophic lateral sclerosis (ALS) was first described clinically in 1869 as a fatal neurodegenerative disease of progressive weakening and atrophy of voluntary muscles. ALS is commonly referred to as *Lou Gehrig's disease,* for the baseball legend whose career and life were

prematurely cut short as a result of this devastating disease. For many years, little progress had been made in the study of the mechanisms underlying ALS.

Five percent of all patients suffering from ALS have family members who also have been diagnosed with the disease. A heritable disease pattern is indicative of a strong genetic component of disease causation. To identify these disease-causing genetic alterations, researchers identify **polymorphisms** (instances of genetic variation) within an affected family that correlate with the emergence of disease. These polymorphisms may themselves cause disease or be closely linked to the responsible genetic alteration. **Restriction-fragment-length polymorphisms (RFLPs)** are polymorphisms within restriction sites that change the sizes of DNA fragments produced by the appropriate restriction enzyme. Using restriction digests and Southern blots of the DNA from members of ALS-affected families, researchers identified RFLPs that were found preferentially in those family members diagnosed with the disease. For some of these families, strong evidence was obtained for the disease-causing mutation within a specific region of chromosome 21.

After the probable location of one disease-causing gene had been identified, this same research group compared the locations of the ALS-associated RFLPs with the known sequence of chromosome 21. They noted that this chromosomal locus contains the *SOD1* gene, which encodes the Cu/Zn superoxide dismutase protein SOD1, an enzyme important for the protection of cells against oxidative damage (Section 18.3). PCR amplification of regions of the *SOD1* gene from the DNA of affected family members, followed by Sanger dideoxy sequencing of the targeted fragment, enabled the identification of 11 disease-causing mutations from 13 different families. This work was pivotal for focusing further inquiry into the

roles that superoxide dismutase and its corresponding mutant forms play in the pathology of some forms of ALS.

9.2 Recombinant DNA Technology Has Revolutionized All Aspects of Biology

The development of recombinant DNA technology has taken biology from an exclusively analytical science to a synthetic one. New combinations of unrelated genes can be constructed in the laboratory by applying recombinant DNA techniques. These novel combinations can be cloned — amplified many-fold — by introducing them into suitable cells, where they are replicated by the DNA-synthesizing machinery of the host. The inserted genes are often transcribed and translated in their new setting. What is most striking is that the genetic endowment of the host can be permanently altered in a designed way.

Restriction enzymes and DNA ligase are key tools in forming recombinant DNA molecules

Let us begin by exploring how novel DNA molecules can be constructed in the laboratory. An essential tool for the manipulation of recombinant DNA is a **vector**, a DNA molecule that can replicate autonomously in an appropriate host organism. Vectors are designed to enable the rapid, covalent insertion of DNA fragments of interest. **Plasmids**, naturally occurring circles of DNA that act as accessory chromosomes in bacteria, and the virus **bacteriophage lambda (λ phage)** are choice vectors for cloning in *E. coli*. DNA fragments can be inserted into these vectors in several steps.

- *The vector is cut by restriction enzymes, creating sticky ends.* A vector can be prepared for accepting a new DNA fragment by cleaving it at a single specific site with a restriction enzyme. For example, the plasmid pSC101, a 9.9-kb double-helical circular DNA molecule, is split at a unique site by the EcoRI restriction enzyme. The staggered cuts made by this enzyme produce complementary single-stranded ends, which have specific affinity for each other and hence are known as **cohesive** or **sticky ends**. Any DNA fragment can be inserted into this plasmid if it has the same cohesive ends. Such a fragment can be extracted from a larger piece of DNA by using the same restriction enzyme as was used to open the plasmid DNA (**Figure 9.9**).

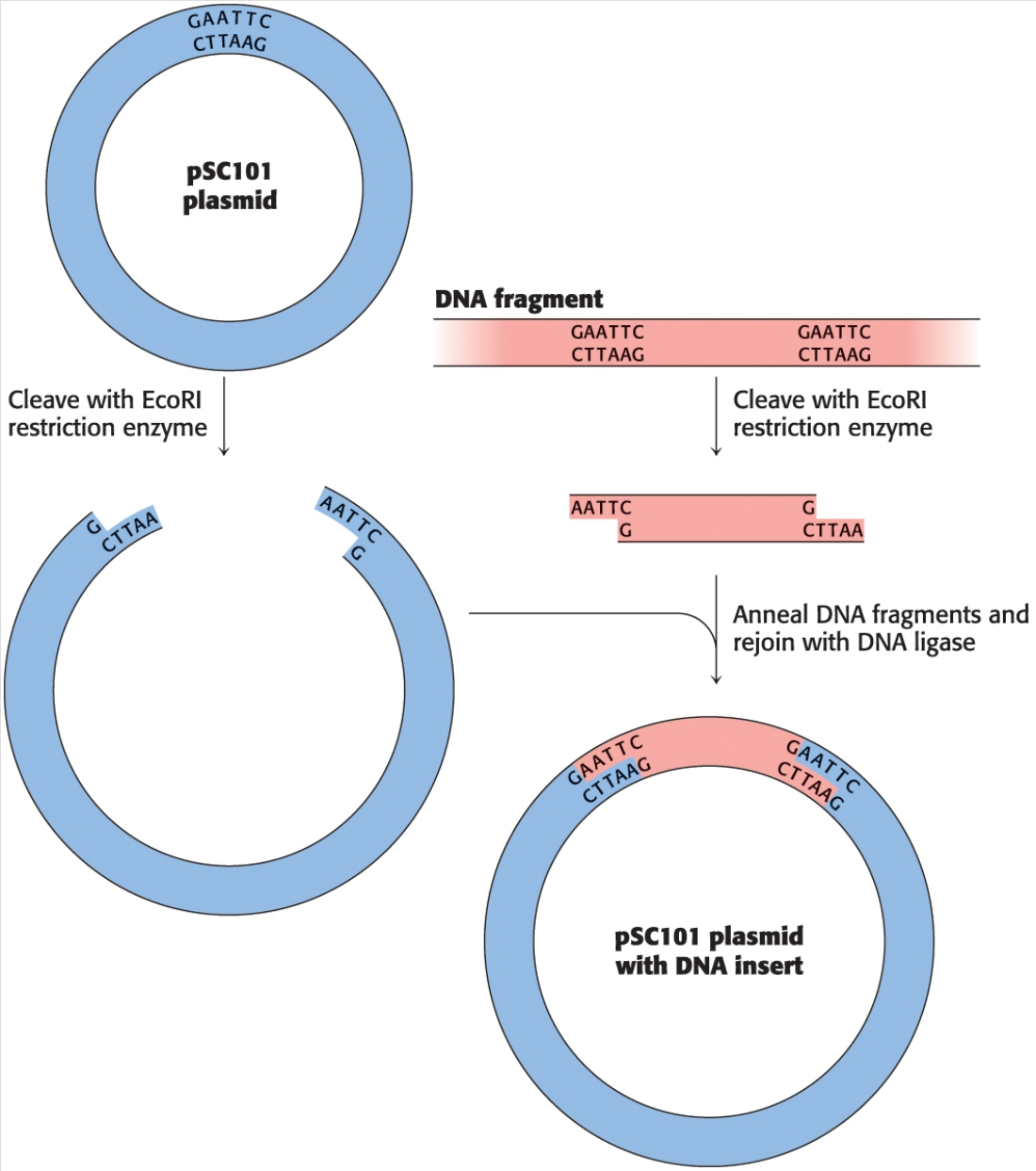


FIGURE 9.9 Different DNA molecules can be joined by the cohesive-end method. The pSC101 plasmid (blue) is cleaved once by EcoRI to yield a pair of cohesive ends. A fragment of DNA (red), also cleaved with EcoRI, can be ligated to the cut plasmid to form a new plasmid with the DNA fragment inserted.

- *DNA ligase inserts the DNA fragment within the cut vector.* The single-stranded ends of the fragment are complementary to those of the cut plasmid. The sticky ends of the DNA fragment and the cut plasmid can base pair with each other, or *anneal,* and then joined by *DNA ligase,* which catalyzes the formation of a phosphodiester bond at a break in a DNA chain. DNA ligase requires a free $3'$-hydroxyl group and a $5'$-phosphoryl group. Furthermore, the chains joined by ligase must be in a double helix. An energy source such as ATP or NAD^+ is required for the joining reaction, as will be discussed in Chapter 28.

- *When necessary, linkers can be added to DNA fragments to yield cohesive ends.* What if the target DNA is not naturally flanked by the appropriate restriction sites? How is the fragment cut and annealed to the vector? The cohesive-end method for joining DNA molecules can still be used in these cases by adding a short, chemically synthesized DNA linker that can be cleaved by restriction enzymes. First, the linker is covalently joined to the ends of a DNA fragment. For example, the $5'$ ends of a decameric linker and a DNA molecule are phosphorylated by polynucleotide kinase and then joined by the ligase from T4 phage (**Figure 9.10**). This particular ligase can form a covalent bond between blunt-ended double-helical DNA molecules. Finally, cohesive ends are produced when these terminal extensions are cut by an appropriate restriction enzyme. Thus, cohesive ends corresponding to the product of a particular restriction enzyme can be added to virtually any DNA molecule. We see here the fruits of combining enzymatic and synthetic chemical approaches in crafting new DNA molecules.

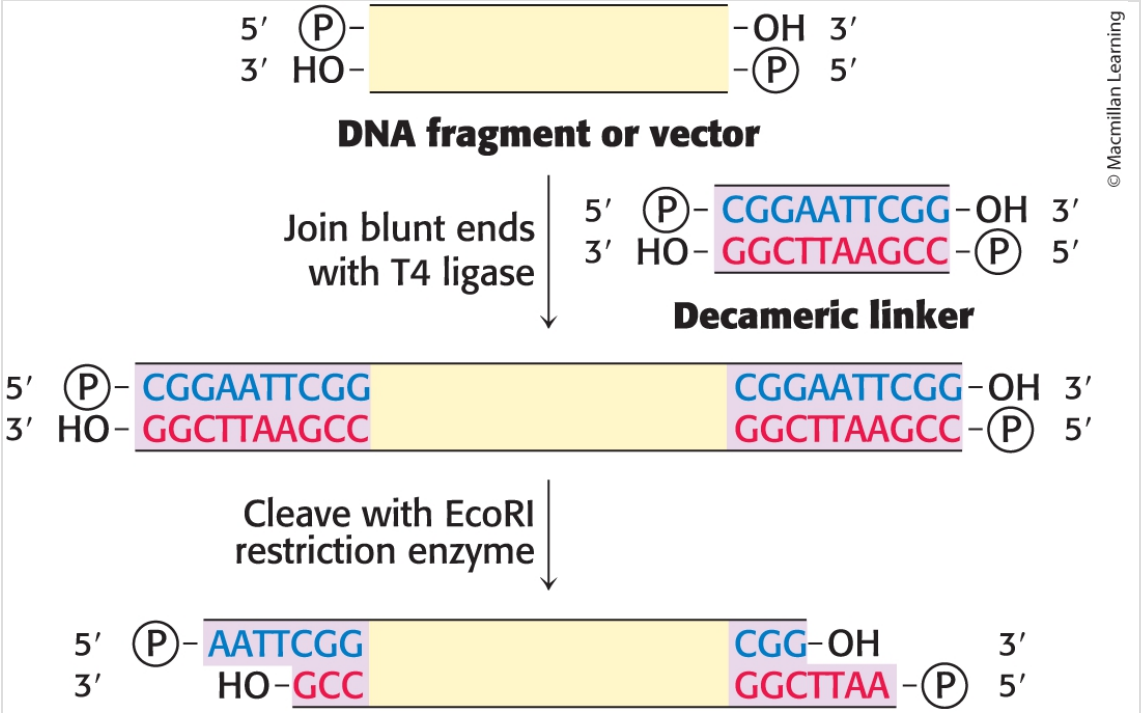


FIGURE 9.10 Cohesive ends can be added to any DNA fragment. A chemically synthesized linker containing a specific restriction site is joined to the ends of the fragment by T4 ligase. Subsequent cleavage by the restriction enzyme yields the new cohesive ends.

Plasmids and λ phage are choice vectors for DNA cloning in bacteria

Many plasmids and bacteriophages have been ingeniously modified by researchers to both enhance the delivery of recombinant DNA molecules into bacteria and to facilitate the genetic selection of bacteria harboring these vectors.

Plasmids

These circular DNA molecules found in bacteria range in size from two to several hundred kilobases and carry genes for the inactivation of antibiotics, the production of toxins, and the breakdown of natural products. As accessory chromosomes, they can replicate independently of the host chromosome and, in contrast with the host genome, are dispensable under certain conditions. A bacterial cell may have no plasmids at all, or it may house as many as 20 copies of a naturally occurring plasmid.

Many plasmids have been optimized for a particular experimental task. Some engineered plasmids, for example, can achieve nearly a thousand copies per bacterial cell. One class of plasmids, known as **cloning vectors**, is particularly suitable for the facile insertion and replication of a collection of DNA fragments. These vectors often feature a **polylinker** region that includes many unique restriction sites within its sequence. This polylinker can be cleaved with a variety of restriction enzymes or combinations of enzymes, providing great versatility in the DNA fragments that can be inserted. In addition, these plasmids contain **reporter genes**, which encode easily detectable markers such as antibiotic-resistance enzymes or fluorescent proteins. Creative placement of these reporter genes within these plasmids enables the rapid identification of those vectors that harbor the desired DNA insert.

For example, let us consider the cloning vector pUC18 (**Figure 9.11**). This plasmid contains three essential components: an origin of replication, so that the plasmid can be replicated when the host bacterium divides; a gene encoding ampicillin resistance, which enables the selection of bacteria that harbor the plasmid; and the *lacZ* gene, which encodes an essential fragment of the enzyme *β-galactosidase*, an enzyme which naturally cleaves the milk sugar lactose (Section 11.2). Insertion of a DNA fragment into the

polylinker region disrupts the *lacZ* gene, an effect called *insertional inactivation*. β-Galactosidase also cleaves the synthetic substrate X-gal, releasing a blue dye. Bacterial cells containing a DNA insert within the polylinker will no longer produce the dye in the presence of X-gal. Hence, bacteria harboring vectors that have received an insert are readily identified by their white color (Figure 9.12).

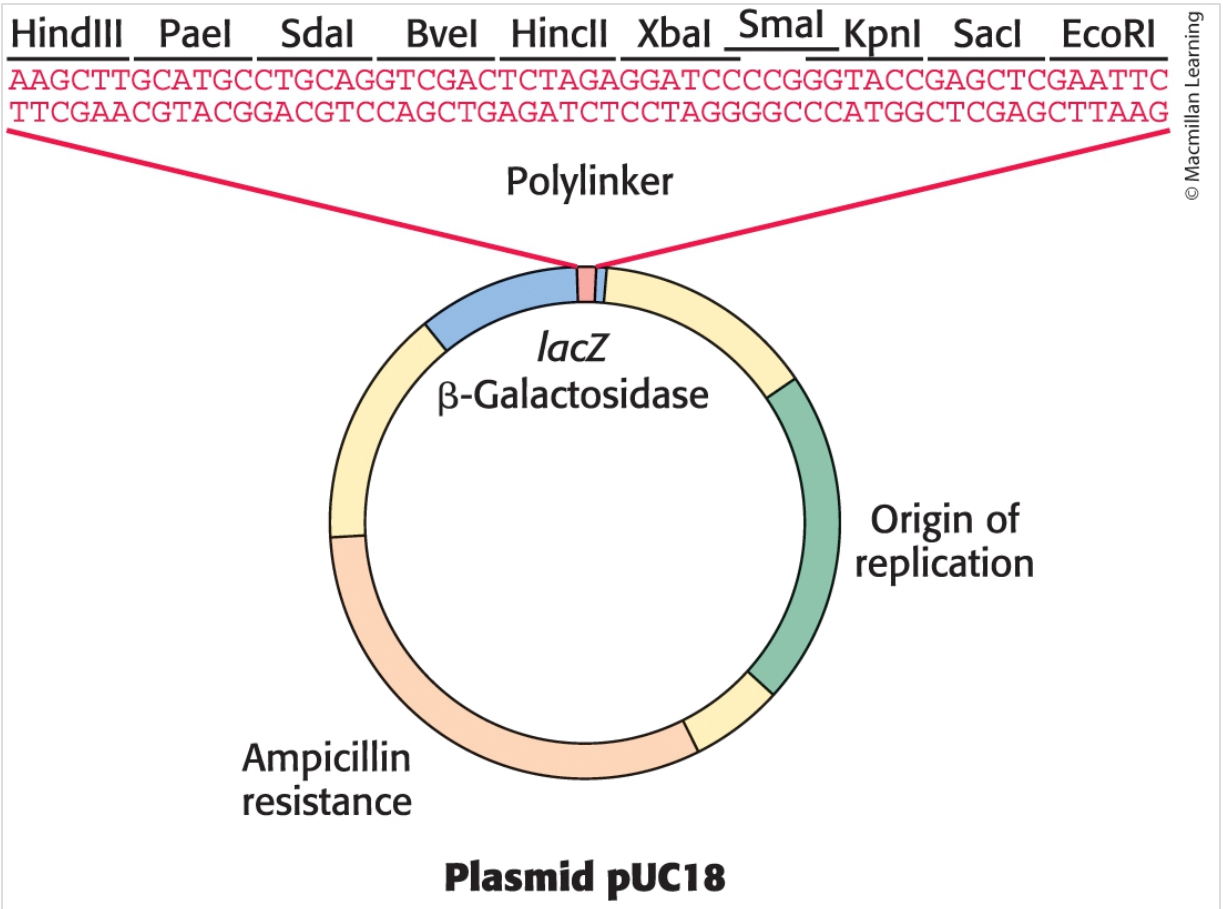
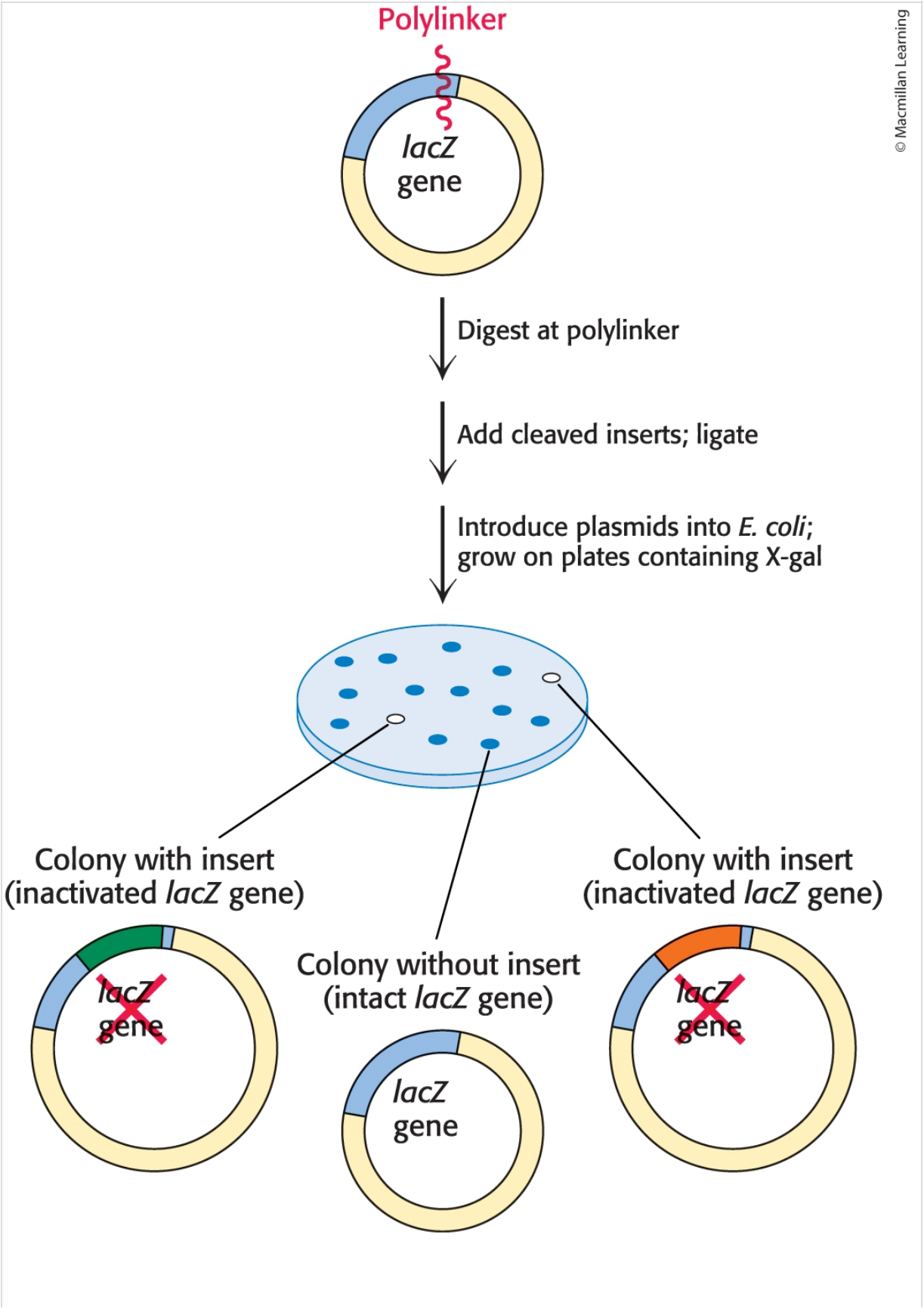


FIGURE 9.11 A polylinker contains multiple unique restriction sites. In addition to an origin of replication and a gene encoding ampicillin resistance, the plasmid pUC18 includes a polylinker within an essential fragment of the β-galactosidase gene (often called the *lacZ* gene).



© Macmillan Learning

FIGURE 9.12 Insertional inactivation allows for the rapid identification of colonies that have new insertions. Successful insertion of DNA fragments into the polylinker region of pUC18 will result in the disruption of the β-galactosidase gene. Bacterial colonies that harbor such plasmids will no longer convert the substrate X-gal into a colored product, and will appear white on the plate.



Another class of plasmids has been optimized for use as **expression vectors** for the production of large amounts of protein. Many different expression vectors are currently in use. **Figure 9.13** depicts the typical elements of a vector designed to express a protein in prokaryotes. In addition to an antibiotic-resistance gene and an origin of replication, an expression vector contains promoter and terminator sequences specifically designed to drive the transcription of large amounts of a protein-coding DNA sequence. As in the cloning vectors, these plasmids also contain a polylinker region, which often contain sequences flanking the cloning site that simplify the addition of fusion tags to the protein of interest (Section 4.1), greatly facilitating purification of the overexpressed protein. Many expression vectors also possess transcriptional repressor and operator sequences (Section 31.2), which enable the precise control of when production of the protein will be turned on.

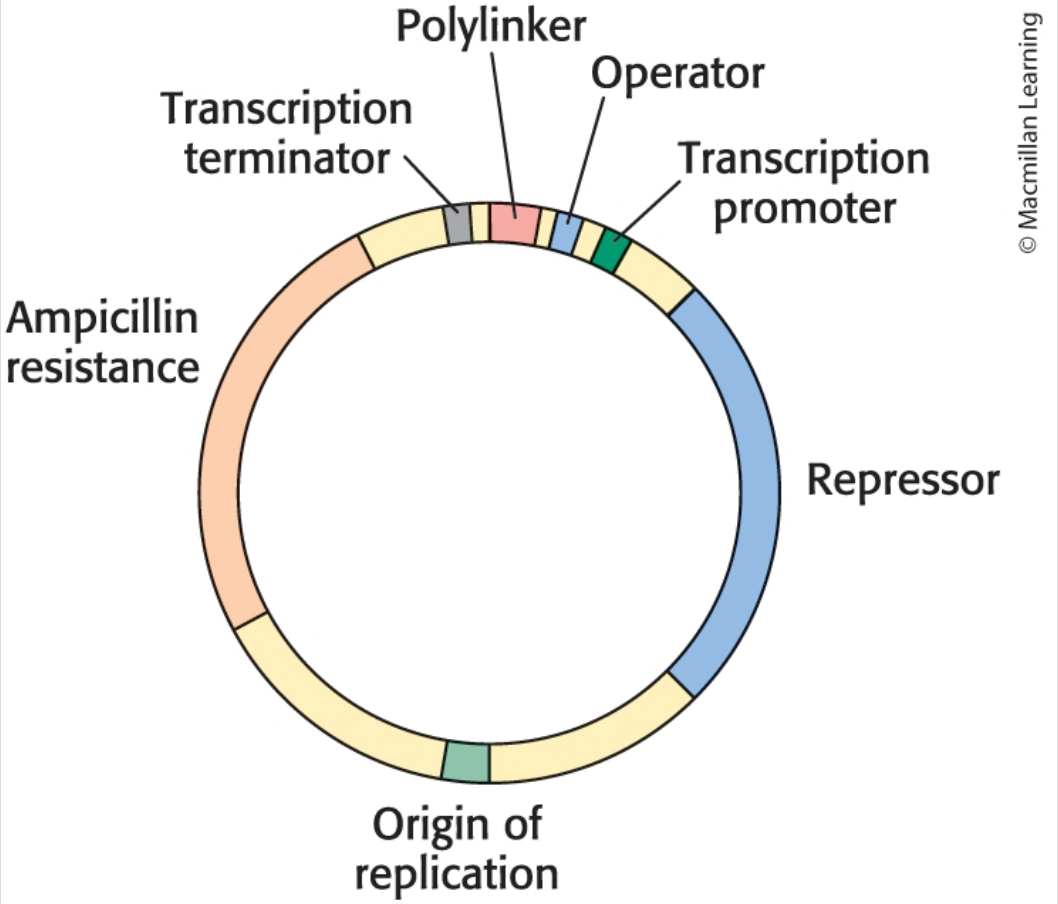


FIGURE 9.13 Expression vectors are designed to generate protein product. As with the cloning vector (Figure 9.11), the prokaryotic expression vector shown here contains an origin of replication and an antibiotic-resistance gene. In addition, these plasmids include transcription initiation (promoter) and termination sequences, required for the expression of a protein-coding gene inserted in the polylinker. Many expression plasmids also contain repressor and operator sequences which allow for the control of the timing of protein production.

λ phage

Another widely used vector is the bacteriophage lambda, or λ phage. Bacteriophages are viruses that infect and replicate within bacteria.

The λ phage enjoys a choice of lifestyles: it can destroy its host or become part of its host (Figure 9.14). In the *lytic pathway*, viral functions are fully expressed: viral DNA and proteins are quickly produced and packaged into virus particles, leading to the lysis (destruction) of the host cell and the sudden appearance of about 100 progeny virus particles, also called *virions*. In contrast, in the *lysogenic pathway*, the phage DNA becomes inserted into the host-cell genome and can be replicated together with host-cell DNA for many generations, remaining inactive. Certain environmental changes can trigger the expression of this dormant viral DNA, which leads to the formation of progeny viruses and lysis of the host. Large segments of the 48-kb DNA genome of λ phage are not essential for productive infection and can be replaced by foreign DNA, thus making λ phage an ideal vector.

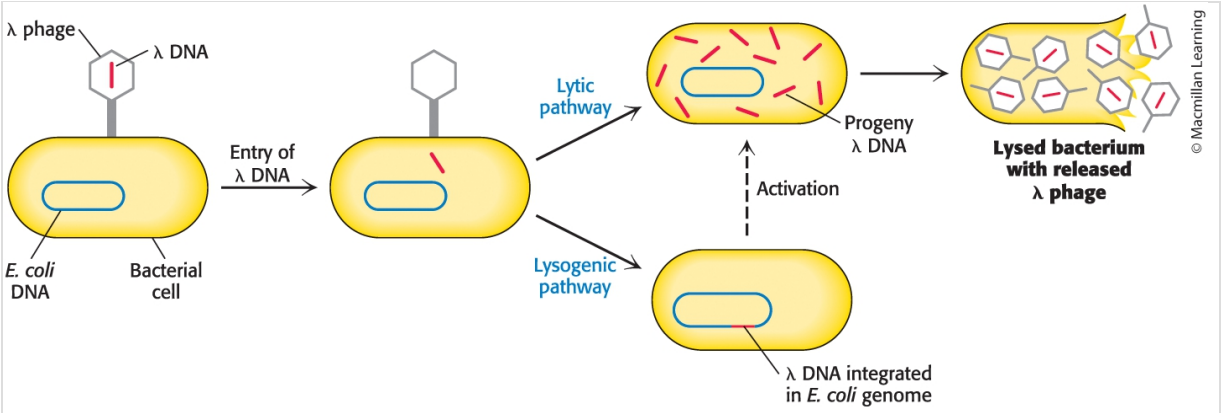


FIGURE 9.14 λ phage alternates between two infection modes. λ phage can multiply within a host and lyse it (lytic pathway), or its DNA can become integrated into the host genome (lysogenic pathway), where it is dormant until activated.

Scientists have constructed mutant λ phages that are well-suited for cloning. An especially useful one called λgt-λβ contains only two EcoRI cleavage sites instead of the five normally present (Figure

9.15). After cleavage, the middle segment of this λ DNA molecule can be removed. The two remaining pieces of DNA (called arms) have a combined length equal to 72% of a normal genome length. This amount of DNA is too little to be packaged into a λ particle, which can take up only DNA measuring from 78% to 105% of a normal genome. However, a suitably long DNA insert (such as 10 kb) between the two ends of λ DNA enables such a recombinant DNA molecule (93% of normal length) to be packaged. Nearly all infectious λ particles formed in this way will contain an inserted piece of foreign DNA. An advantage of using these modified viruses as vectors is that they enter bacteria much more easily than do plasmids.

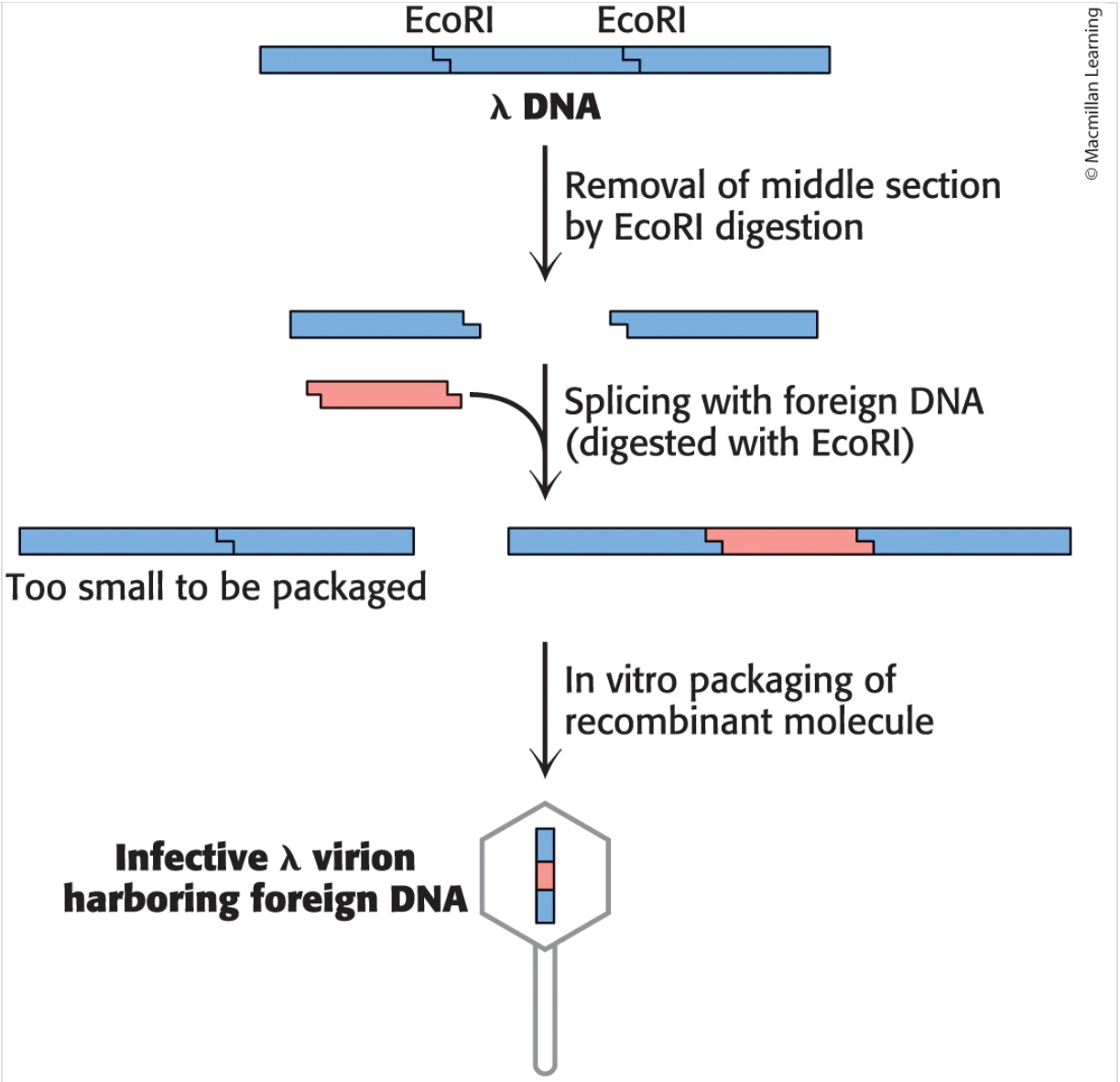


FIGURE 9.15 Mutant λ phage can be used as a cloning vector. The packaging process selects DNA molecules that contain an insert (colored red). DNA molecules that have resealed without an insert are too small to be efficiently packaged.

Specific genes can be cloned from digests of genomic DNA

Ingenious cloning and selection methods have made it possible to isolate small stretches of DNA in a genome containing more than 3×10^6 kb (i.e., 3×10^9 bases). The approach is to prepare a large collection, called a **genomic library**, of DNA fragments and then to identify those members of the collection that have the gene of interest. Hence, to clone a gene that is present just once in an entire genome, two critical components must be available: a specific oligonucleotide probe for the gene of interest, and a DNA library that can be screened rapidly.

How is a specific probe obtained? In one method, a probe for a gene can be prepared if a part of the amino acid sequence of the protein encoded by the gene is known. Peptide sequencing of a purified protein (Chapter 4) or knowledge of the sequence of a homologous protein from a related species (Chapter 10) are two potential sources of such information. However, a problem arises because a single peptide sequence can be encoded by a number of different oligonucleotides (**Figure 9.16**). Thus, for this purpose, peptide sequences containing tryptophan and methionine are preferred, because these amino acids are specified by a single codon, whereas other amino acid residues have between two and six codons (Table 8.5). All the possible DNA sequences (or their complements) that encode the targeted peptide sequence are synthesized by the solid-phase method and made radioactive by phosphorylating their $5'$ ends with ^{32}P.

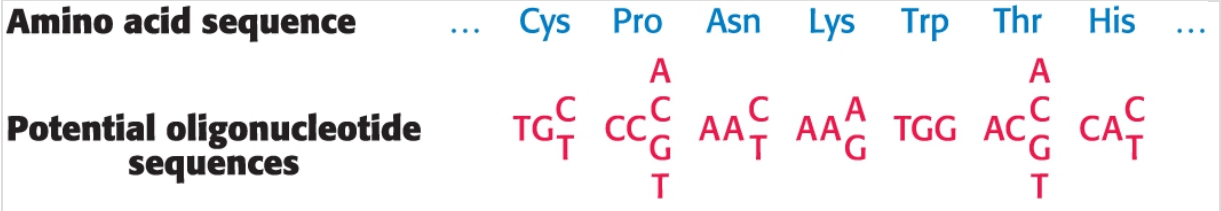


FIGURE 9.16 Oligonucleotide probes can be designed from the target protein sequence. A probe can be generated by synthesizing all possible oligonucleotides encoding a particular sequence of amino acids. Because of the degeneracy of the genetic code, 256 distinct oligonucleotides must be synthesized to ensure that the probe matching the sequence of seven amino acids in this example is present.

To prepare the DNA library, a sample containing many copies of total genomic DNA is first mechanically sheared or partly digested by restriction enzymes into large fragments (Figure 9.17). This process yields a nearly random population of overlapping DNA fragments. These fragments are then separated by gel electrophoresis to isolate the set of all fragments that are about 15 kb long. Synthetic linkers are attached to the ends of these fragments, cohesive ends are formed, and the fragments are then inserted into a vector, such as λ phage DNA, prepared with the same cohesive ends. *E. coli* bacteria are then infected with these recombinant phages. These phages replicate themselves and then lyse their bacterial hosts. The resulting lysate contains fragments of genomic DNA housed in a sufficiently large number of virus particles to ensure that nearly the entire genome is represented in the library. Phages can be propagated indefinitely such that the library can be used repeatedly over long periods.

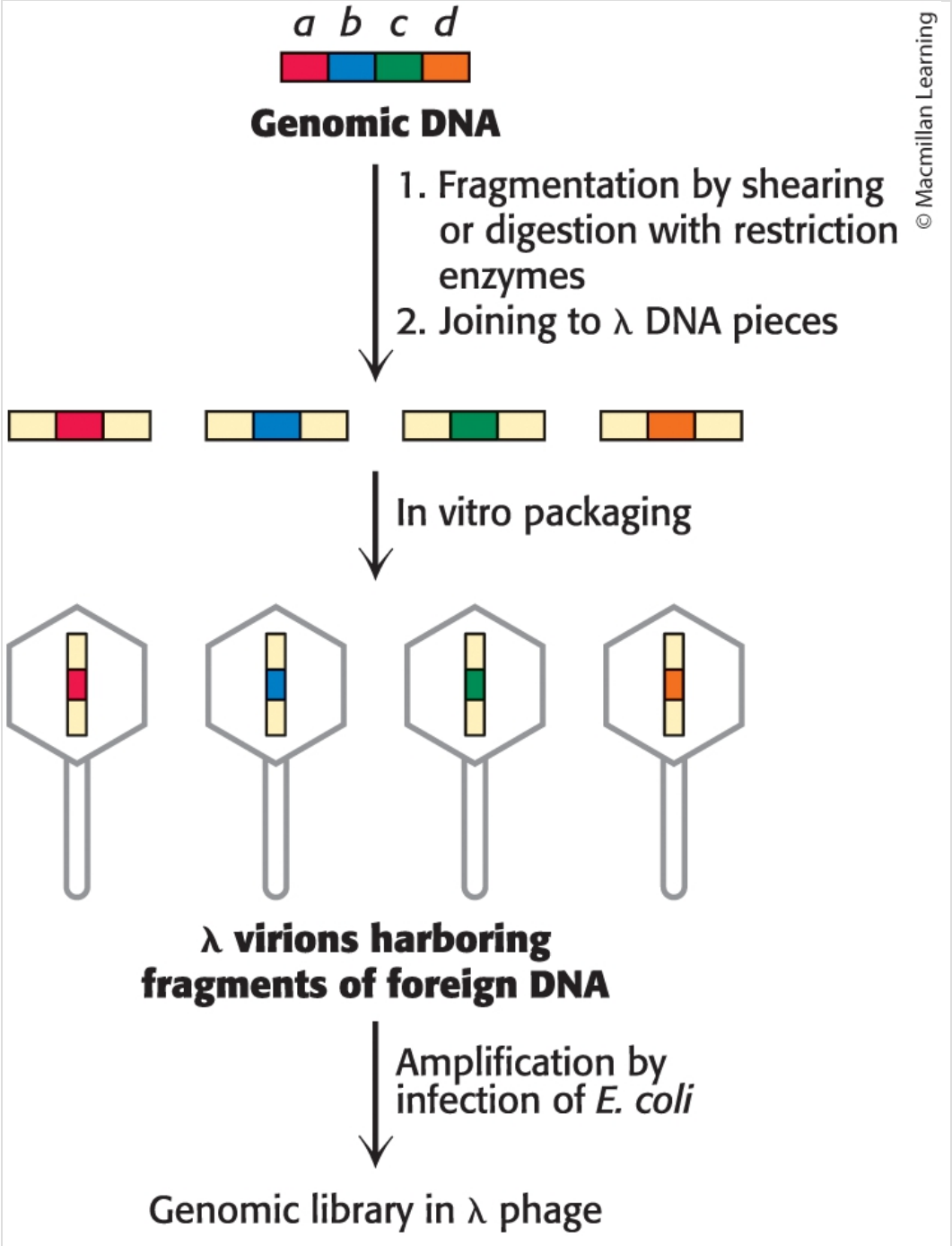
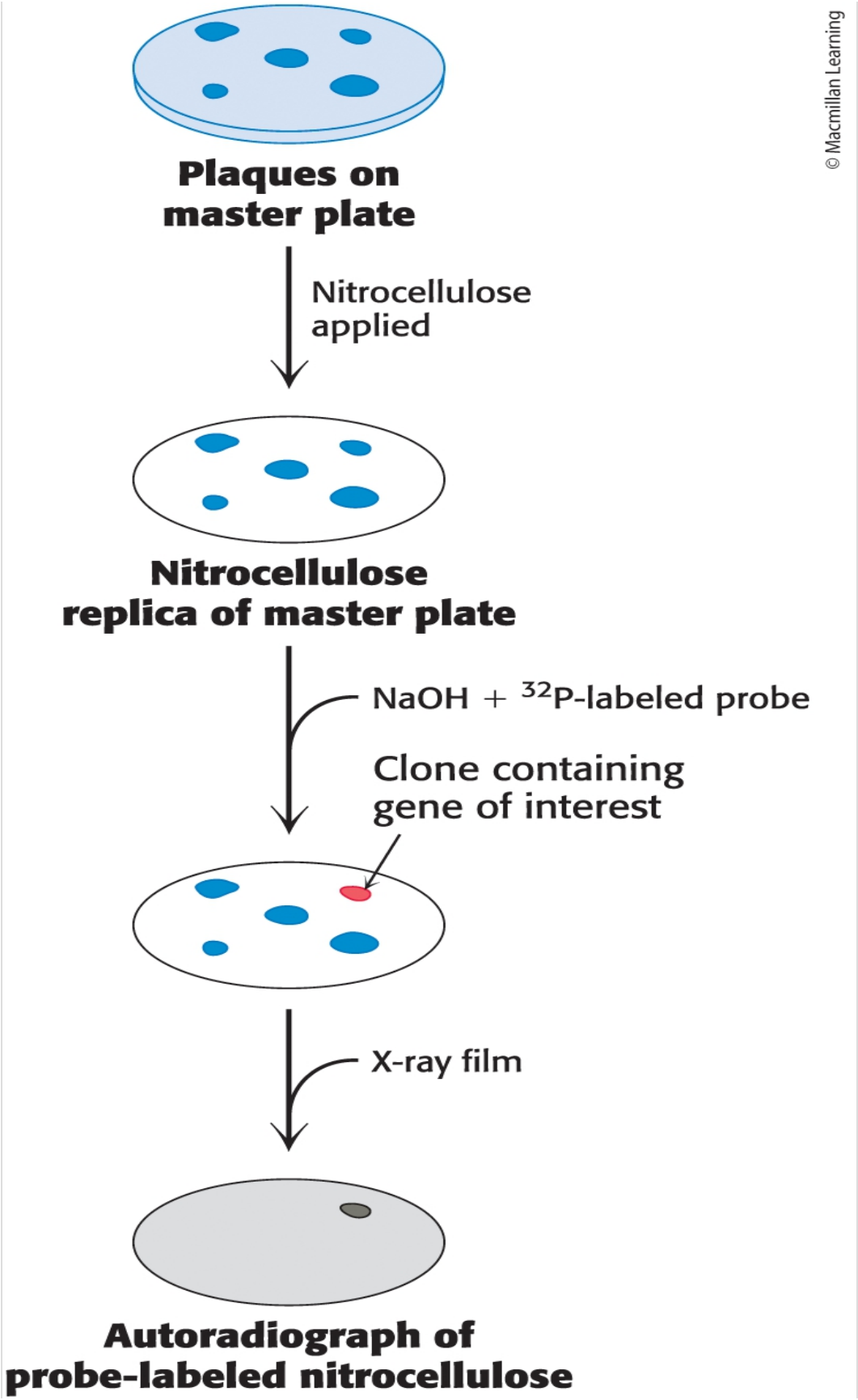


FIGURE 9.17 A genomic library can be created from a digest of a whole genome. After fragmentation of the genomic DNA into overlapping segments, the DNA is inserted into the λ phage vector (shown in yellow). Packaging into virions and amplification by infection in *E. coli* yields a genomic library.

This genomic library is then screened to find the very small number of phages harboring the gene of interest. For the human genome, a calculation shows that a 99% probability of success requires screening about 500,000 clones; hence, a very rapid and efficient screening process is essential. Rapid screening can be accomplished by DNA hybridization.

A dilute suspension of the recombinant phages is first plated on a lawn of bacteria (**Figure 9.18**). Where each phage particle has landed and infected a bacterium, a *plaque* containing identical phages develops on the plate. A replica of this master plate is then made by applying a sheet of nitrocellulose. Infected bacteria and phage DNA released from lysed cells adhere to the sheet in a pattern of spots corresponding to the plaques. Intact bacteria on this sheet are lysed with sodium hydroxide, which also serves to denature the DNA so that it becomes accessible for hybridization with a ^{32}P-labeled probe. The presence of a specific DNA sequence in a single spot on the replica can be detected by using a radioactive complementary DNA or RNA molecule as a probe. Autoradiography then reveals the positions of spots harboring recombinant DNA. The corresponding plaques are picked out of the intact master plate and grown. A single investigator can readily screen a million clones in a day. This method makes it possible to isolate virtually any gene, provided that a probe is available.



© Macmillan Learning

FIGURE 9.18 A genomic library is screened for a specific gene using a labeled DNA probe. Here, a plate is tested for plaques containing gene *a* of Figure 9.17.



Self-Check Question



Suppose that a human genomic library is prepared by exhaustive digestion of human DNA with the EcoRI restriction enzyme. What is the average fragment length generated by this enzyme? Is this procedure suitable for cloning large genes? Why or why not?

Complementary DNA prepared from mRNA can be expressed in host cells

The preparation of eukaryotic genomic libraries presents unique challenges, especially if the researcher is interested primarily in the protein-coding region of a particular gene. Recall that most mammalian genes are mosaics of introns and exons. These interrupted genes cannot be expressed by bacteria, which lack the machinery to splice introns out of the primary transcript. However, this difficulty can be circumvented by causing bacteria to take up recombinant DNA that is complementary to mRNA, where the introns have been removed.

The key to forming **complementary DNA**, or **cDNA**, is the enzyme reverse transcriptase. As discussed in Section 8.4, a retrovirus uses this enzyme to form a DNA–RNA hybrid in replicating its genomic

RNA. Reverse transcriptase synthesizes a DNA strand complementary to an RNA template if the transcriptase is provided with a DNA primer that is base-paired to the RNA and contains a free $3'-OH$ group. We can use a simple sequence of linked thymidine [oligo(T)] residues as the primer. This oligo(T) sequence pairs with the poly(A) sequence at the $3'$ end of most eukaryotic mRNA molecules (Section 4.5), as shown in **Figure 9.19**.

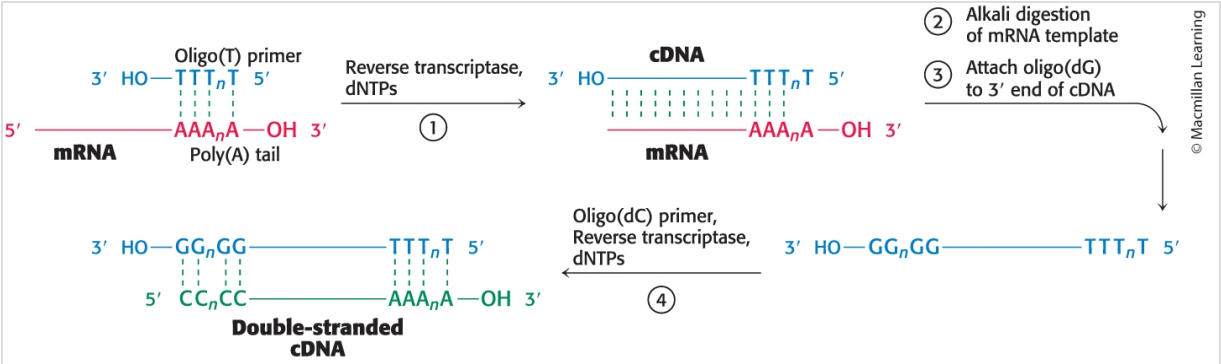


FIGURE 9.19 Double-stranded cDNA is prepared from mRNA using reverse transcriptase. A complementary DNA (cDNA) duplex is created from mRNA by (1) use of reverse transcriptase to synthesize a cDNA strand, (2) digestion of the original RNA strand, (3) addition of several G bases to the DNA by terminal transferase, and (4) synthesis of a complementary DNA strand using the newly synthesized cDNA strand as a template.

1. The reverse transcriptase synthesizes the rest of the cDNA strand in the presence of the four deoxyribonucleoside triphosphates (dNTPs).

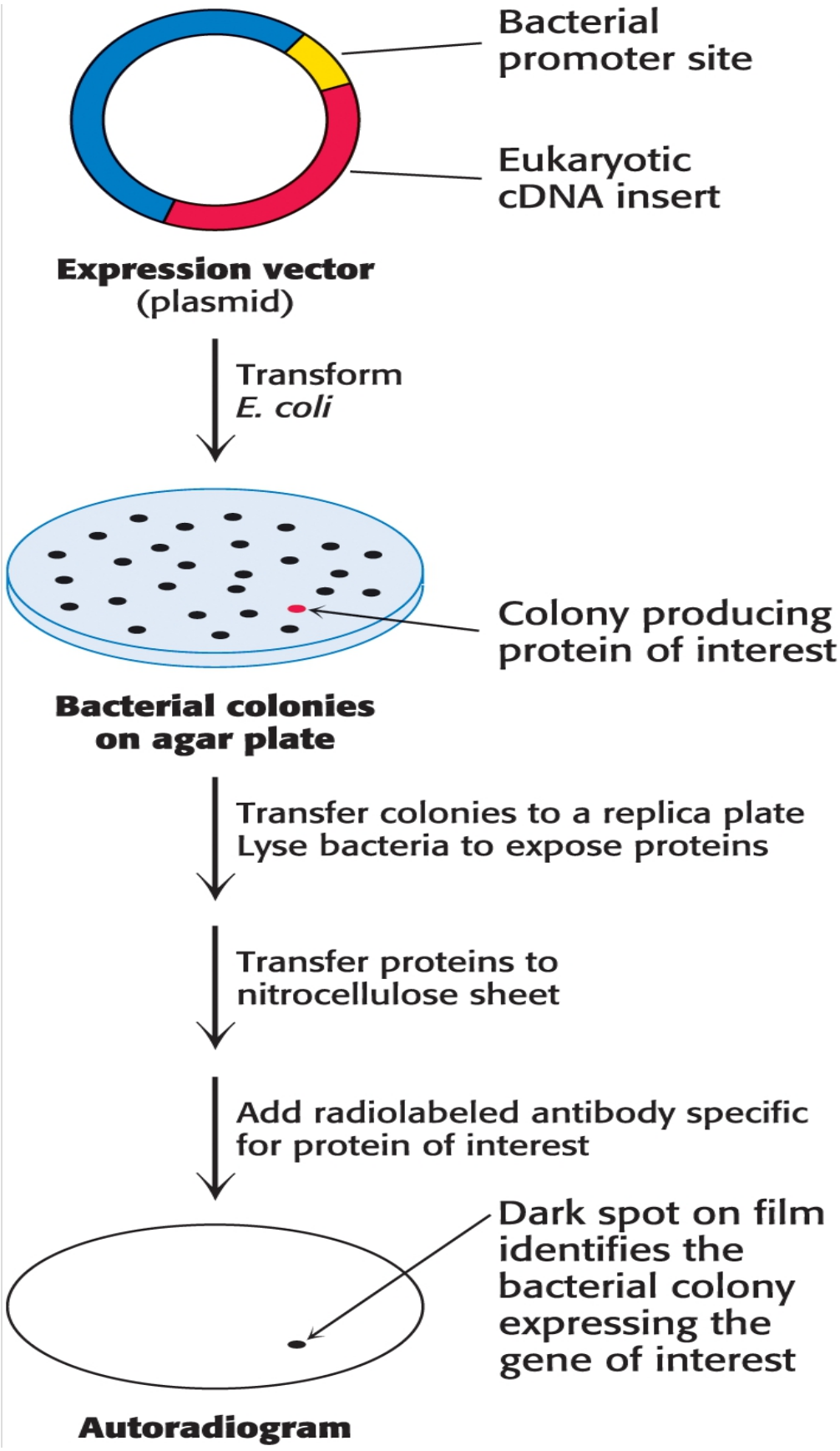
2. The template RNA strand of this RNA–DNA hybrid is hydrolyzed by raising the pH (also called *alkali digestion*). Unlike RNA, DNA is resistant to alkaline hydrolysis.

3. The enzyme terminal transferase adds nucleotides — for instance, several residues of dG — to the $3'$ end of DNA.

4. Oligo(dC) can bind to dG residues and prime the synthesis of the second DNA strand. Synthetic linkers can be added to this double-helical DNA for ligation to a suitable vector.

Complementary DNA for all mRNA that a cell contains can be made, inserted into vectors, and then inserted into bacteria. Such a collection is called a **cDNA library**.

cDNA libraries can be prepared in expression vectors to enable the production of the corresponding protein of interest. Clones are then screened on the basis of their capacity to direct the synthesis of a foreign protein in bacteria, a technique referred to as *expression cloning*. A labeled antibody specific for the protein of interest can be used to identify colonies of bacteria that express the corresponding protein product (**Figure 9.20**). As described earlier, spots of bacteria on a replica plate are lysed to release proteins, which bind to an applied nitrocellulose filter. With the addition of labeled antibody specific for the protein of interest, the location of the desired colonies on the master plate can be readily identified. This immunochemical screening approach can be used whenever a protein is expressed and corresponding antibody is available.



© Macmillan Learning

FIGURE 9.20 Expression cloning identifies colonies in a cDNA library that express the protein of interest. Protein products are identified by staining with antibody specific to the desired protein.

Complementary DNA has many applications beyond the generation of genomic libraries. The overproduction and purification of most eukaryotic proteins in prokaryotic cells necessitates the insertion of cDNA into plasmid vectors. For example, proinsulin, a precursor of insulin, is synthesized by bacteria-harboring plasmids that contain DNA complementary to mRNA for proinsulin (Figure 9.21) to produce much of the insulin used today by millions of diabetics.

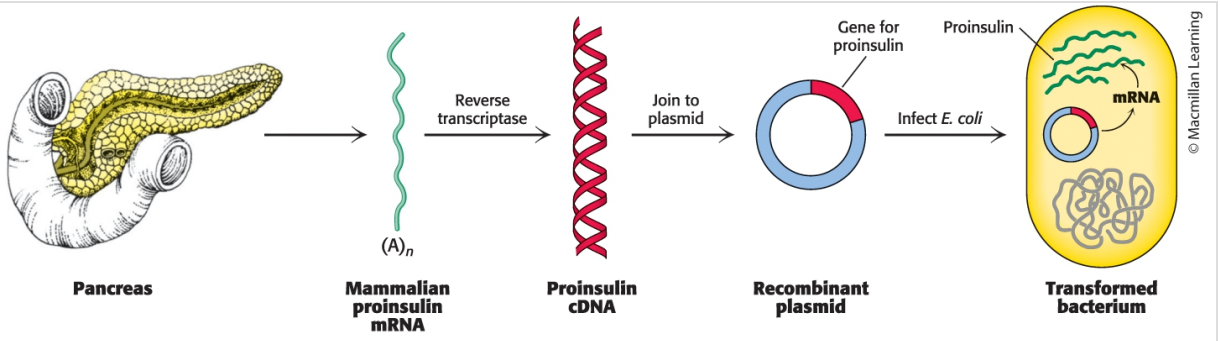


FIGURE 9.21 Bacteria infected with proinsulin cDNA can express the eukaryotic protein. Proinsulin, a precursor of insulin, can be synthesized by transformed (genetically altered) clones of *E. coli.* The clones contain the mammalian proinsulin gene.

Proteins with new functions can be created through directed changes in DNA

Many insights about genes and proteins can be gained by analyzing the effects of genetic mutations on protein structure and function. In the classic genetic approach, mutations are generated randomly throughout the genome of a host organism, and those individuals exhibiting a phenotype of interest are selected. Analysis of these mutants then reveals which genes are altered, and DNA sequencing identifies the precise nature of the changes. Recombinant DNA technology makes the creation of specific mutations feasible in vitro. We can construct new genes with designed properties by making three types of directed changes: deletions, insertions, and substitutions. A variety of methods can be used to introduce these mutations.

Site-directed mutagenesis

Mutant proteins with single amino acid substitutions can be readily produced by **site-directed mutagenesis**. Suppose that we want to replace a particular serine residue with cysteine. This mutation can be made if (1) we have a plasmid containing the gene or cDNA for the protein and (2) we know the base sequence around the site to be altered. If the serine of interest is encoded by TCT, mutation of the central base from C to G yields the TGT codon, which encodes cysteine. This type of mutation is called a *point mutation* because only one base is altered. One method for introducing this mutation into our plasmid is shown in **Figure 9.22**.

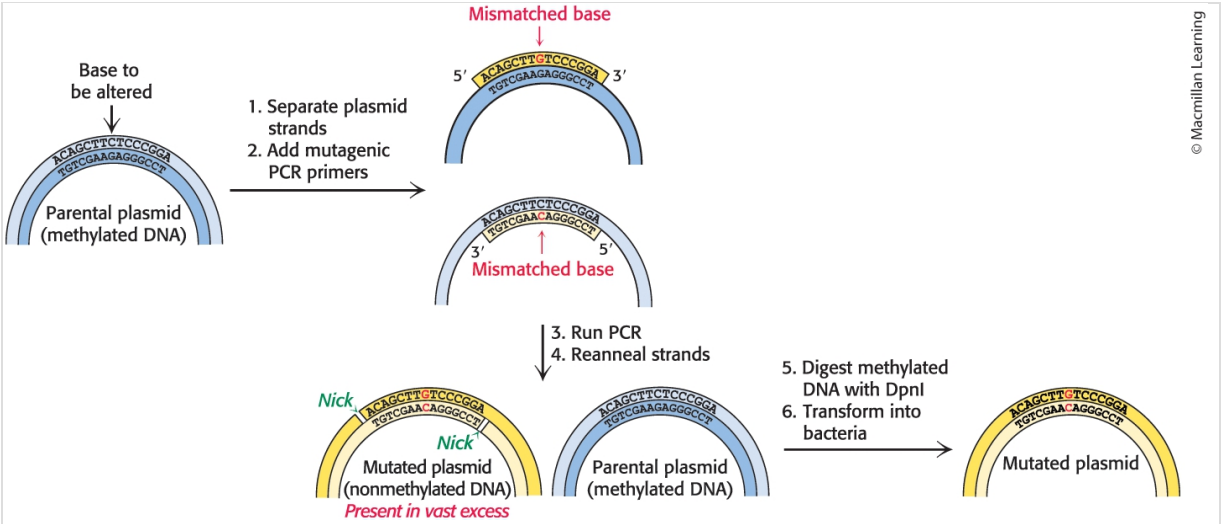


FIGURE 9.22 Site-directed mutagenesis uses mismatched primers in a polymerase chain reaction. The products will be linear strands complementary to the original plasmid strands, except for the desired single base change encoded in the PCR primers. Subsequent cleavage of the methylated parental DNA, using DpnI, and transformation into bacteria will yield the altered plasmid.

1. The two strands of the plasmid are separated by raising the temperature.

2. Mutagenic PCR primers are added to the mixture. These oligonucleotides contain the desired base change but are otherwise complementary to the neighboring sequence. The single mismatch is tolerable if the annealing is carried out at an appropriate temperature.

3. Using these two primers and the original plasmid as a template, a PCR is run. With each subsequent cycle, new DNA is synthesized that is identical to the parental plasmid, except the single base change is incorporated. Because there is no DNA ligase in the reaction mixture, the product strands are linear.

4. At the completion of the PCR, the strands are reannealed. Since the newly synthesized strands are linear, they contain two single nicks at either side of the PCR primer site. Importantly, the newly mutated DNA product is present in vast excess relative to the parental plasmid.

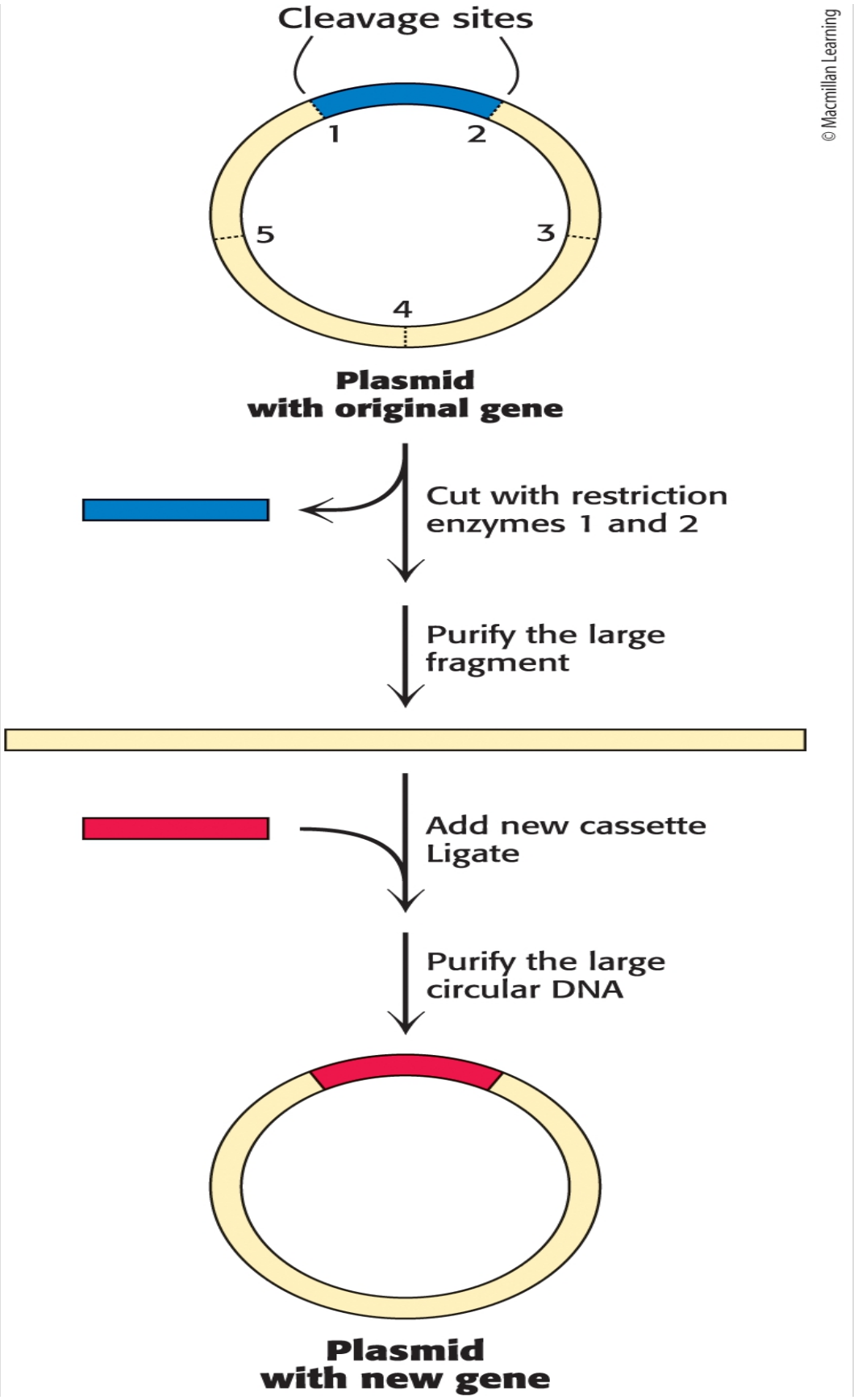
5. As we have seen in Section 6.3, DNA in bacterial cells is methylated to protect itself from cleavage by its own restriction endonucleases. The *Diplococcus pneumoniae* restriction enzyme DpnI is unique in that it specifically cleaves methylated sequences over a 4 bp recognition site. Since the newly mutated plasmid generated by PCR is not methylated — it has never been inside a living cell — we can use DpnI to cleave any remaining parental plasmid DNA.

6. The mutated plasmid is then transformed into bacteria, where the nicks are sealed.

We will encounter many examples of the use of site-directed mutagenesis to precisely alter regulatory regions of genes and to produce proteins with tailor-made features.

Cassette mutagenesis

In **cassette mutagenesis**, a variety of mutations, including insertions, deletions, and multiple point mutations, can be introduced into the gene of interest. A plasmid harboring the original gene is cut with a pair of restriction enzymes to remove a short segment (**Figure 9.23**). A synthetic double-stranded oligonucleotide — the *cassette* — carrying the genetic alterations of interest is prepared with cohesive ends that are complementary to the ends of the cut plasmid. Ligation of the cassette into the plasmid yields the desired mutated gene product.



© Macmillan Learning

FIGURE 9.23 In cassette mutagenesis, a synthetic DNA fragment is swapped into the plasmid using compatible restriction sites. DNA is cleaved at a pair of unique restriction sites by two different restriction enzymes. A synthetic oligonucleotide with ends that are complementary to these sites (the cassette) is then ligated to the cleaved DNA. The method is highly versatile because the inserted DNA can have any desired sequence.



Mutagenesis by PCR

A number of methods have been developed that use the creative design of PCR primers (Section 9.1) to introduce specific insertions, deletions, and substitutions into a particular sequence. One such method, called *inverse PCR*, introduces deletions into plasmid DNA (**Figure 9.24**). In this approach, primers are designed to flank the sequence to be deleted. However, these primers are oriented in the opposite direction, such that they direct the amplification of the entire plasmid, minus the region to be deleted. If each of the primers contains a $5'$ phosphate group, the amplified product can be recircularized with DNA ligase, yielding the desired deletion mutation.

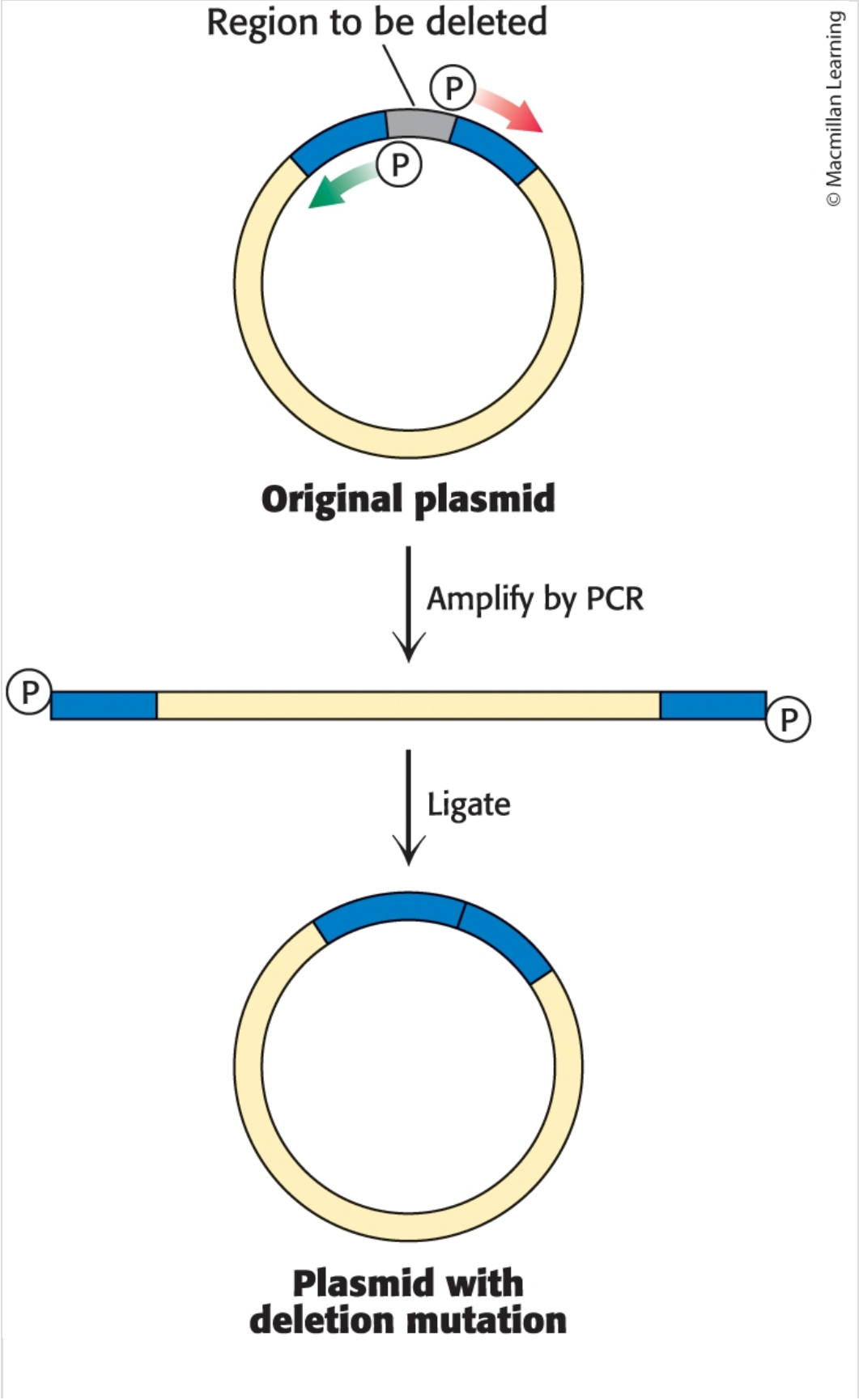

Region to be deleted
P
P
Original plasmid
Amplify by PCR
P
P
Ligate
Plasmid with deletion mutation
© Macmillan Learning

FIGURE 9.24 PCR can be used to generate mutations. In this example of inverse PCR, a deletion can be introduced into a plasmid with primers that flank this region but are oriented away from the segment to be removed. PCR amplification yields a linear product that contains the entire plasmid minus the unwanted sequence. If the primers contained a 5′ phosphate group, this product can be recircularized using DNA ligase, generating a plasmid with the desired mutation.



Designer genes

Novel proteins can also be created by splicing together gene segments that encode domains that are not associated in nature. For example, a gene for an antibody can be joined to a gene encoding a toxic protein, yielding a chimeric protein that kills any cells that are recognized by the antibody. These *immunotoxins* are being evaluated as anticancer agents. Furthermore, noninfectious coat proteins of viruses can be produced in large amounts by recombinant DNA methods. They can serve as *synthetic vaccines* that are safer than conventional vaccines prepared by inactivating pathogenic viruses. For example, a subunit of the hepatitis B virus produced in yeast is proving to be an effective vaccine against this debilitating viral disease. Finally, entirely new genes can be synthesized de novo by the solid-phase method described above. These genes can encode proteins with no known counterparts in nature.

9.3 Complete Genomes Have Been Sequenced and Analyzed

The methods just described are extremely effective for the isolation and characterization of fragments of DNA. However, the genomes of organisms ranging from viruses to human beings contain considerably longer sequences, arranged in very specific ways that are crucial for their integrated functions. Is it possible to sequence complete genomes and analyze them?

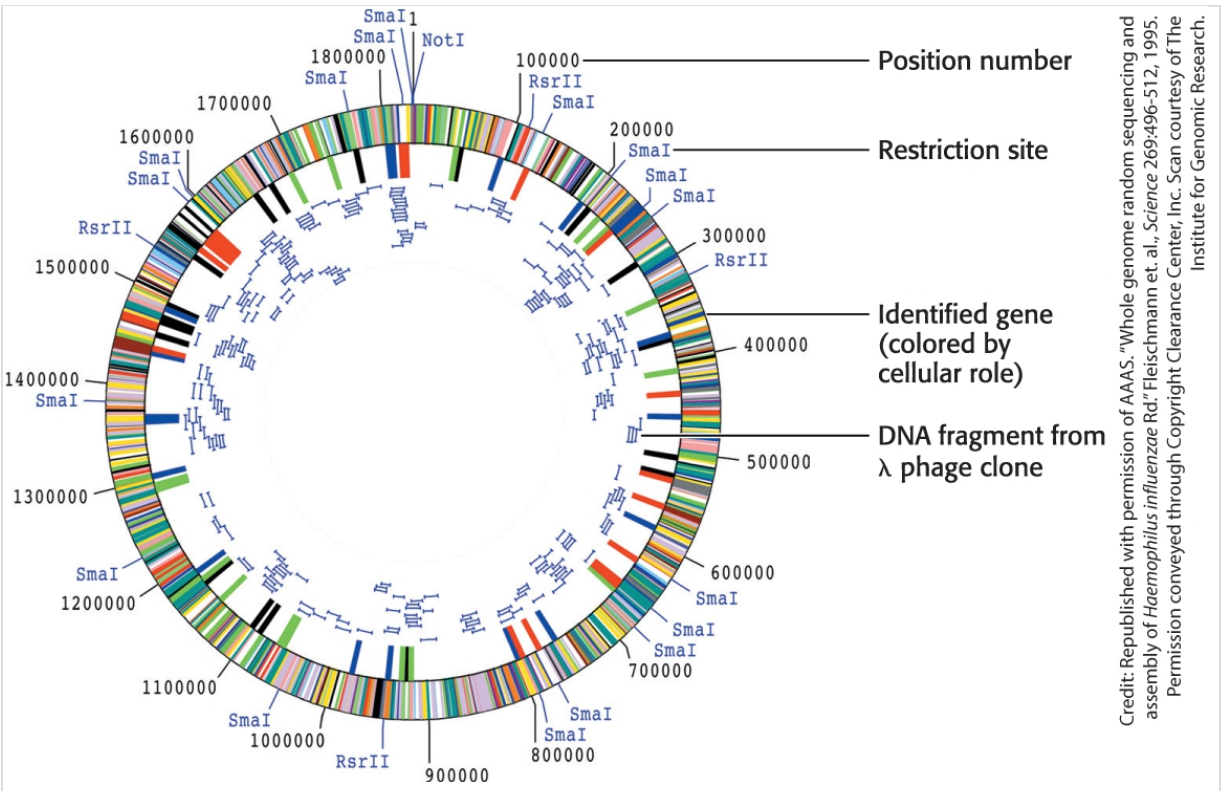
For small genomes, complete sequencing was accomplished soon after DNA-sequencing methods were developed. Sanger and his coworkers determined the complete sequence of the 5386 bases in the genome of the φX174 DNA virus in 1977, just a quarter century after Sanger's pioneering elucidation of the amino acid sequence of a protein. This tour de force was followed several years later by the determination of the sequence of human mitochondrial DNA, a double-stranded circular DNA molecule containing 16,569 base pairs that encodes 2 ribosomal RNAs, 22 transfer RNAs, and 13 proteins. Many other viral genomes were sequenced in subsequent years.

However, the genomes of free-living organisms present a much greater challenge because even the simplest comprises more than 1 million base pairs. Thus, sequencing projects require both rapid sequencing techniques and efficient methods for assembling many short stretches of 300 to 500 base pairs into a complete sequence.

The genomes of organisms ranging from bacteria to multicellular eukaryotes have

been sequenced

With the development of automatic DNA sequencers based on fluorescent dideoxynucleotide chain terminators, high-volume, rapid DNA sequencing became a reality. The genome sequence of the bacterium *Haemophilus influenzae* was determined in 1995 using a "shotgun" approach in which the genomic DNA was sheared randomly into fragments that were then sequenced. Computer programs then assembled the complete sequence by matching up overlapping regions between fragments. The *H. influenzae* genome comprises 1,830,137 base pairs and encodes approximately 1740 proteins (**Figure 9.25**). Using similar approaches, as well as more advanced methods described below, investigators have determined the sequences of more than 10,000 bacterial and archaeal species, including key model organisms such as *E. coli*, *Salmonella typhimurium*, and *Archaeoglobus fulgidus*, as well as pathogenic organisms such as *Yersinia pestis* (bubonic plague) and *Bacillus anthracis* (anthrax).



Credit: Republished with permission of AAAS. "Whole genome random sequencing and assembly of *Haemophilus influenzae* Rd." Fleischmann et. al., *Science* 269:496-512, 1995. Permission conveyed through Copyright Clearance Center, Inc. Scan courtesy of The Institute for Genomic Research.

FIGURE 9.25 The genome of *Haemophilus influenzae* was the first of a free-living organism to be completely sequenced. The genome encodes more than 1700 proteins (indicated by the colored bars in the outer circle) and 70 RNA molecules. The likely function of approximately one-half of the proteins was determined by comparisons with sequences of proteins already characterized in other species. Gaps in the final sequence were filled by sequencing genomic DNA inserts from 300 phage clones (indicated by the blue bars in the inner circle), many of these overlap one another.

The first eukaryotic genome to be completely sequenced was that of baker's yeast, *Saccharomyces cerevisiae*, in 1996. This yeast genome comprises approximately 12 million base pairs, distributed on 16 chromosomes, and encodes more than 6000 proteins. This achievement was followed in 1998 by the first complete sequencing of the genome of a multicellular organism, the nematode *Caenorhabditis elegans*, which contains 97 million base pairs and includes more than 19,000 genes. The genomes of many organisms

widely used in biological and biomedical research have now been sequenced, including those of the fruit fly *Drosophila melanogaster*, the model plant *Arabidopsis thaliana*, the mouse, the rat, and the dog. However, note that even after a genome sequence has been considered complete, some sections, such as the repetitive sequences that make up heterochromatin, may be missing because these DNA sequences are very difficult to manipulate with the use of standard techniques.

The sequence of the human genome has been completed

The ultimate goal of much of genomics research has been the sequencing and analysis of the human genome. Given that the human genome comprises approximately 3 billion base pairs of DNA distributed among 24 chromosomes (**Figure 9.26**), the challenge of producing a complete sequence was daunting. However, through an organized international effort of academic laboratories and private companies, the human genome progressed from a draft sequence first reported in 2001 to a finished sequence reported in late 2004.

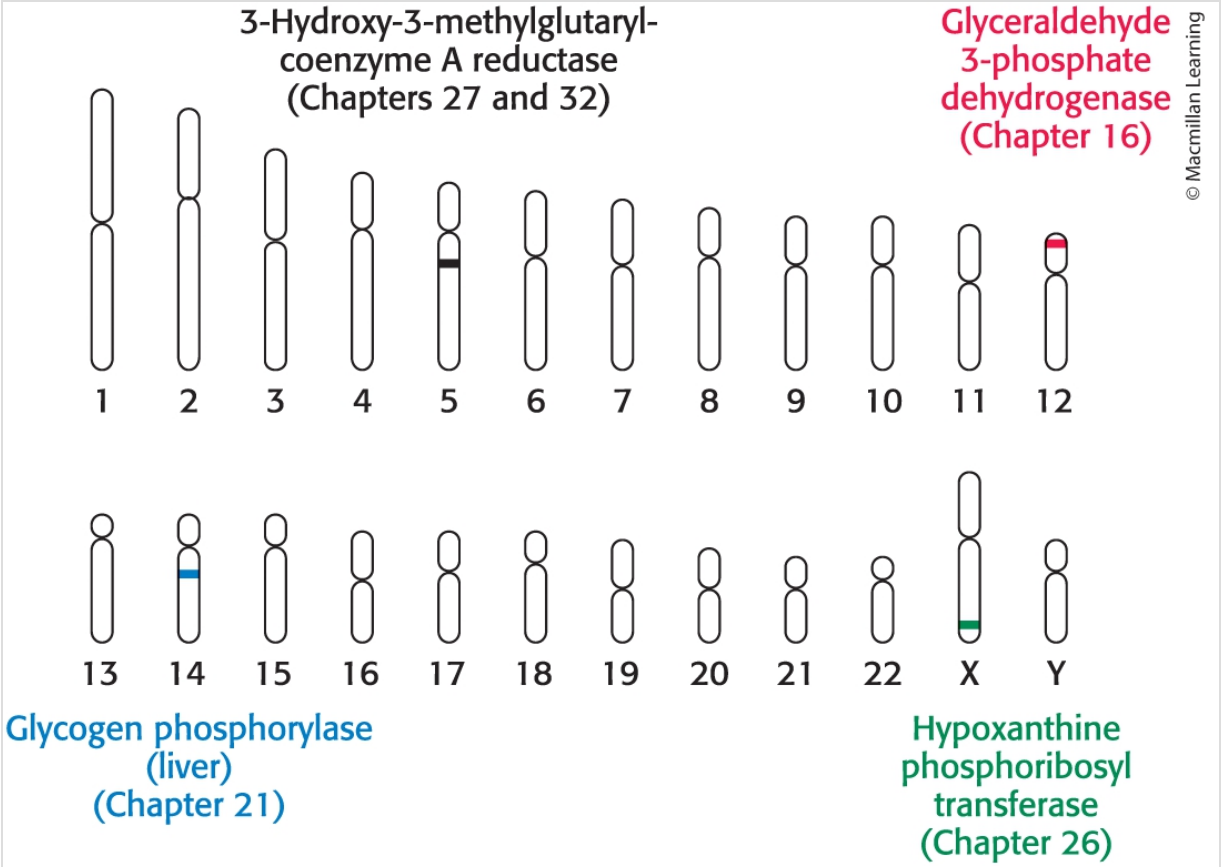


FIGURE 9.26 The human genome has been completely sequenced. The human genome is arrayed on 46 chromosomes — 22 pairs of autosomes and the X and Y sex chromosomes. The locations of several genes associated with important pathways in biochemistry are highlighted.

The human genome is a rich source of information about many aspects of humanity, including our biochemistry and evolution. Analysis of the genome will continue for many years to come. Developing an inventory of protein-encoding genes was one of the first tasks. At the beginning of the genome-sequencing project, the number of such genes was estimated to be approximately 100,000. With the availability of the completed (but not finished) genome, this estimate was reduced to between 30,000 and 35,000. With the

finished sequence, the estimate fell to between 20,000 and 25,000. We will use the estimate of 23,000 throughout this book.

The reduction in this estimate is due, in part, to the realization that there are a large number of **pseudogenes**, formerly functional genes that have accumulated mutations such that they no longer produce proteins. For example, more than half of the genomic regions that correspond to olfactory receptors — key molecules responsible for our sense of smell — are pseudogenes (Section 14.6). In contrast, the corresponding regions in the genomes of other primates and rodents encode functional olfactory receptors.

Nonetheless, the surprisingly small number of genes belies the complexity of the human proteome. Many genes encode more than one protein through mechanisms such as alternative splicing of mRNA and posttranslational modifications of proteins. The different proteins encoded by a single gene often display important variations in functional properties.

The human genome contains a large amount of DNA that does not encode proteins. A great challenge in modern biochemistry and genetics is to elucidate the roles of this noncoding DNA. Much of this DNA is present because *mobile genetic elements*, which are related to retroviruses (Section 8.4), have inserted themselves throughout the genome over time. Most of these elements have accumulated mutations and are no longer functional. For example, more than 1 million *Alu sequences*, each approximately 300 bases in length, are present in the human genome. *Alu* sequences are examples of SINEs, or short interspersed elements. The human genome also includes nearly 1 million LINEs, or long interspersed elements, sequences that can be as long as 10 kilobases (kb). The roles of these elements as neutral genetic parasites or instruments of genome evolution are under current investigation.

Next-generation sequencing methods enable the rapid determination of a complete genome sequence

Since the introduction of the Sanger dideoxy method in the mid-1970s, significant advances have been made in DNA-sequencing technologies, enabling the readout of progressively longer sequences with higher fidelity and shorter run times. The development of **next-generation sequencing (NGS)** platforms has extended this capability to formerly unforeseen levels. By combining technological breakthroughs in the handling of very small amounts of liquid, high-resolution optics, and computing power, these methods have already made a significant impact on the ability to obtain whole genome sequences rapidly and cheaply (Section 1.4).

Next-generation sequencing refers to a family of technologies, each of which uses a unique approach for the determination of a DNA sequence. All of these methods are highly parallel: from 1 million to 1 billion DNA fragment sequences are individually acquired in a single experiment. How are NGS methods capable of determining such a high number of sequences in parallel? Individual DNA fragments are amplified by PCR on a solid support — a single bead or a small region of a glass slide — such that clusters of identical DNA fragments are distinguishable by high-resolution imaging. These fragments then serve as templates for DNA polymerase, where the addition of nucleotide triphosphates is converted to a signal that can be detected in a highly sensitive manner.

The technique used to detect individual base incorporation varies among the variety of NGS methods. Let us consider one of these methods, called **pyrosequencing**, in greater detail (**Figure 9.27**). In

this method, a single-stranded fragment of DNA tethered to a solid support serves as the sequencing template. A solution containing one of the four deoxyribonucleoside triphosphates (dATP in Figure 9.27A) is then added to the reaction. If the nucleotide base is not complementary to the next available base on the template strand, no reaction occurs.

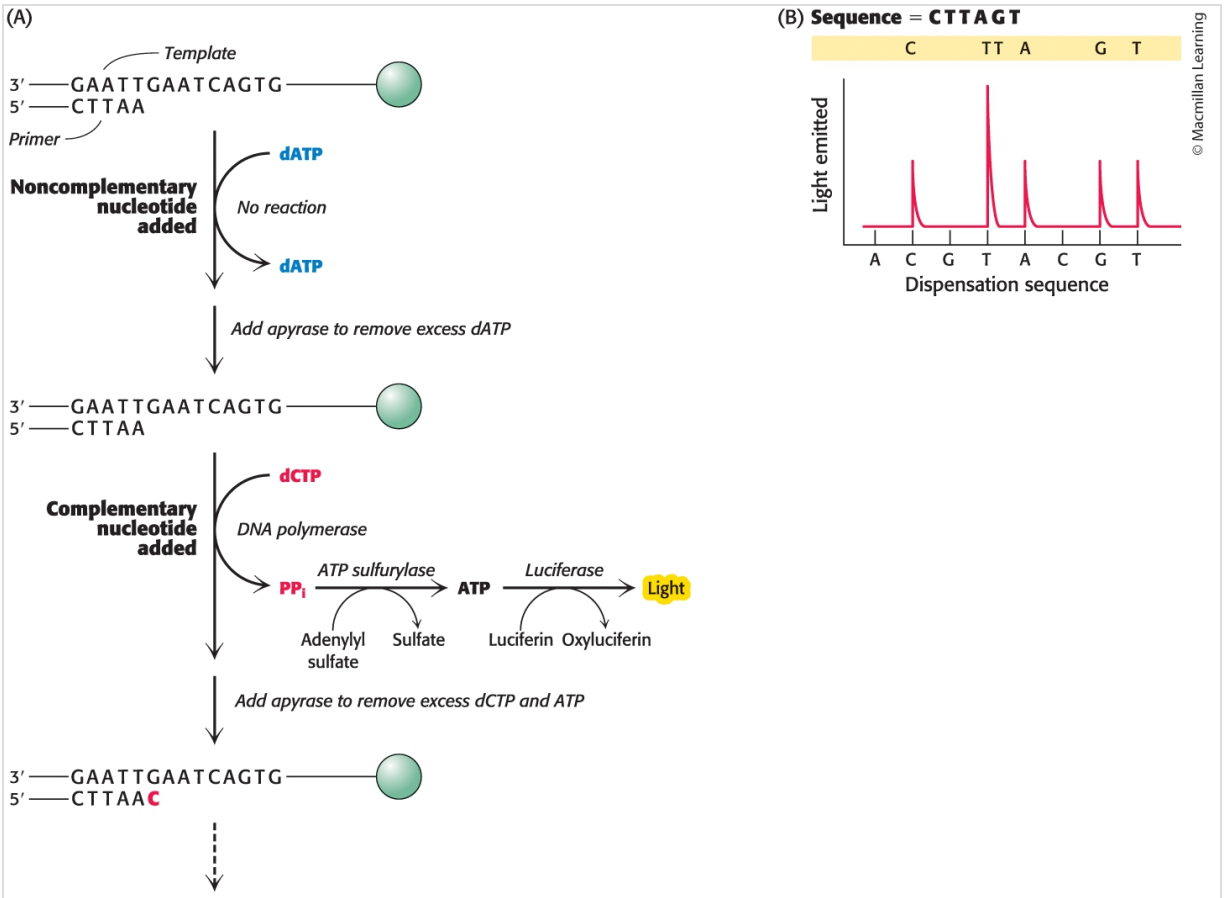
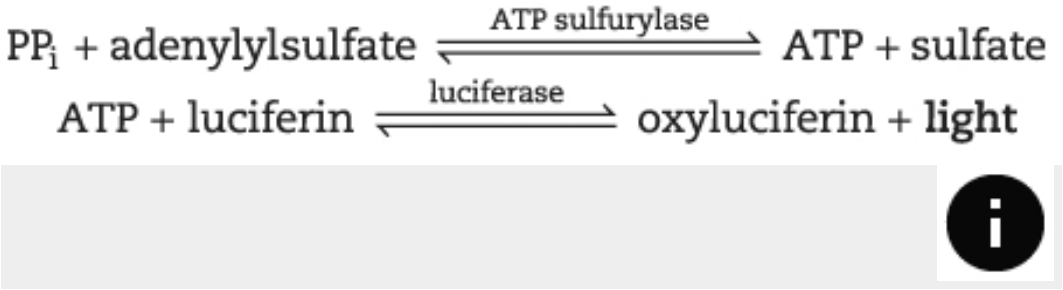


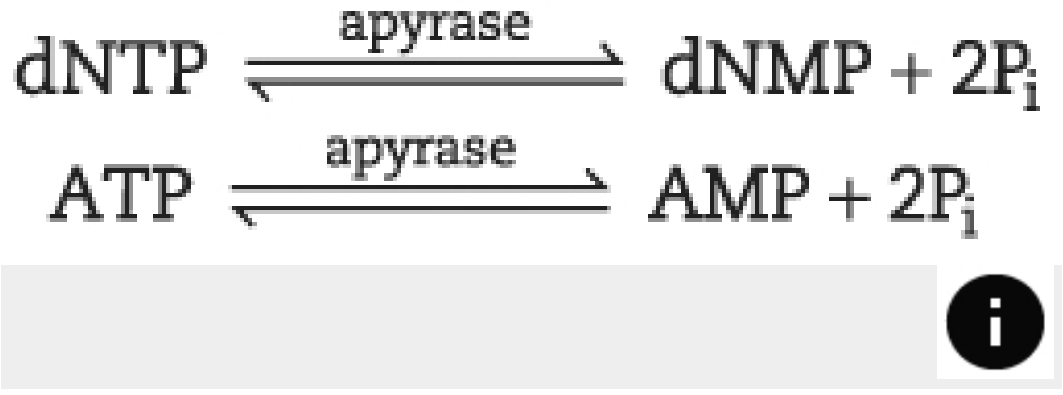
FIGURE 9.27 Pyrosequencing is an example of next-generation sequencing. (A) If a nucleotide is successfully incorporated into the growing duplex, the newly produced pyrophosphate is enzymatically converted into light. (B) Light is measured at each deoxynucleotide addition. A peak indicates the next base in the sequence, and the height of the peak indicates how many of the same deoxynucleotide were incorporated in a row.

However, if the nucleotide base is complementary, and thus incorporated, the released pyrophosphate is coupled to the production of light by the sequential action of the enzymes ATP sulfurylase and luciferase:



The emitted light is measured, indicating that a reaction has occurred, thus revealing the identity of the base at that position (Figure 9.27B). If the template contains a run of one particular base, then multiple consecutive additions will take place in a single reaction; the length of this run can be determined by the intensity of the emitted light.

After each nucleotide addition, the remaining deoxynucleotide and ATP are removed by the enzyme apyrase.



The next nucleotide is added, and the steps are repeated. Nucleotides are added in a defined order, referred to as the

dispensation sequence, and the pattern of peaks that emerge reveals the sequence of the template strand (Figure 9.27B).

Other NGS methods are also commonly used. These methods can be understood simply by considering the overall reaction of chain elongation catalyzed by DNA polymerase (**Figure 9.28**). In the reversible terminator method, the four nucleotides are added to the template DNA, with each base tagged with a unique fluorescent label and a reversibly blocked 3′ end. The blocked end assures that only one phosphodiester linkage will form. Once the nucleotide is incorporated into the growing strand, it is identified by its fluorescent tag, the blocking agent is removed, and the process is repeated. The protocol for ion semiconductor sequencing is similar to pyrosequencing, except that nucleotide incorporation is detected by sensitively measuring the very small changes in pH of the reaction mixture due to the release of a proton upon nucleotide incorporation.

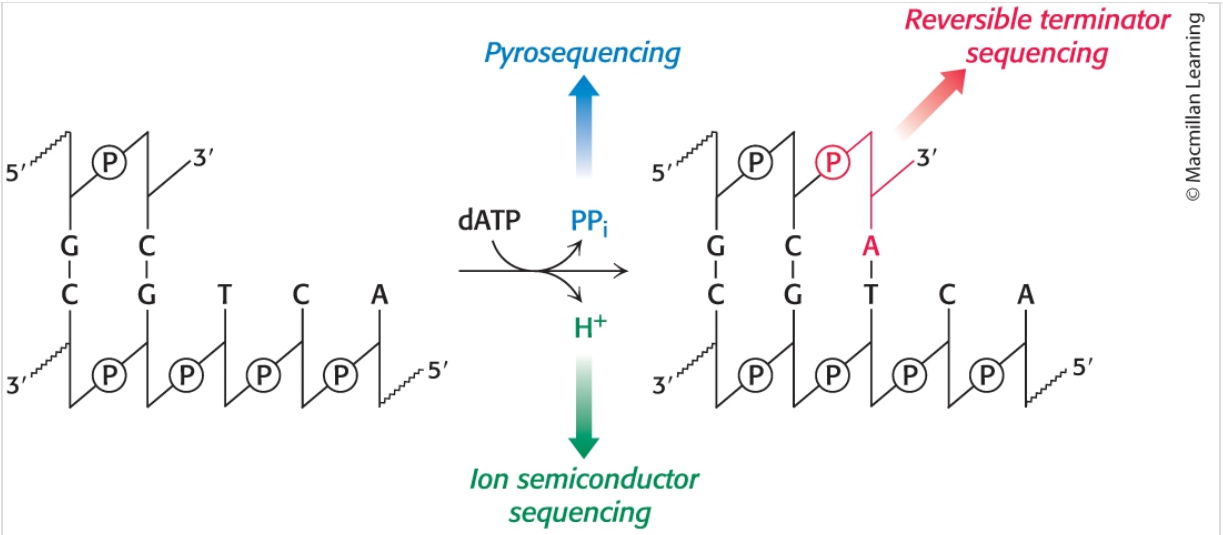


FIGURE 9.28 Next-generation sequencing methods use different approaches to measure nucleotide incorporation. Measurement of base incorporation in next-generation sequencing methods relies on the detection of the various products of the DNA polymerase reaction. Reversible terminator sequencing measures the nucleotide incorporation in a

manner similar to Sanger dideoxy sequencing, while pyrosequencing and ion semiconductor sequencing detect the release of pyrophosphate and protons, respectively.



Regardless of the sequencing method, the technology exists to quantify the signal produced by millions of DNA fragment templates simultaneously. However, for many approaches, as few as 50 bases are read per fragment. Hence, significant computing power is required to both store the massive amounts of sequence data and perform the necessary alignments required to assemble a completed sequence.

NGS methods are being used to answer an ever-growing number of questions in many areas, including genomics, the regulation of gene expression, and evolutionary biology. Additionally, individual genome sequences will provide information about genetic variation within populations and may usher in an era of personalized medicine, when these data can be used to guide treatment decisions.

Comparative genomics is a powerful research tool

Comparisons with genomes from other organisms are sources of insight into the human genome. The sequencing of the genome of the chimpanzee, our closest living relative, as well as that of other mammals that are widely used in biological research, such as the mouse and the rat, has been completed. Comparisons reveal that an astonishing 99% of human genes have counterparts in mouse and rat genomes. However, these genes have been substantially

reassorted among chromosomes in the estimated 75 million years of evolution since humans and these rodents had a common ancestor (Figure 9.29).

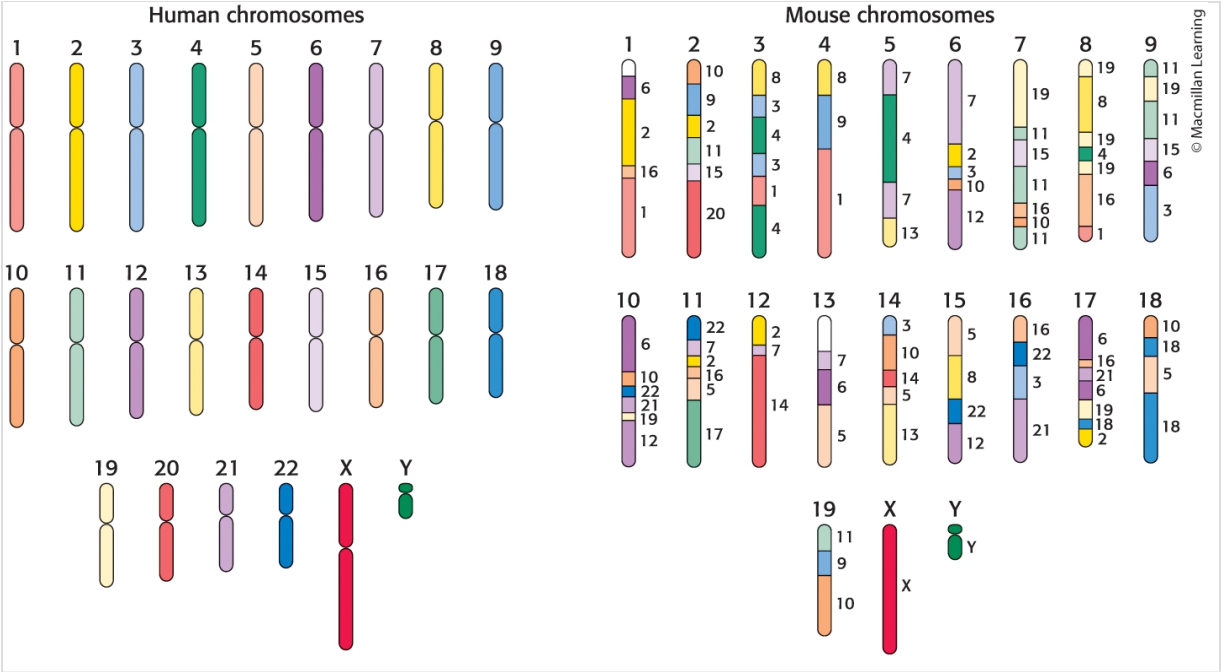


FIGURE 9.29 The human and mouse genomes are closely related, although they have been rearranged relative to each other. A schematic comparison of the human genome and the mouse genome shows reassortment of large chromosomal fragments. The small numbers to the right of the mouse chromosomes indicate the human chromosome to which each region is most closely related.

The genomes of other organisms also have been determined specifically for use in comparative genomics. For example, the genomes of two species of puffer fish, *Takifugu rubripes* and *Tetraodon nigroviridis*, have been determined. These genomes were selected because they are very small and lack much of the noncoding DNA present in such abundance in the human genome. The puffer fish genomes include fewer than 400 megabase pairs (Mbp), one-eighth of the number in the human genome, yet the

puffer fish and human genomes contain essentially the same number of genes.

Comparison of the genomes of these puffer fish species with that of humans revealed more than 1000 formerly unrecognized human genes. Furthermore, comparison of the two species of puffer fish, which had a common ancestor approximately 25 million years ago, is a source of insight into more-recent events in evolution. Comparative genomics is a powerful tool, both for interpreting the human genome and for understanding major events in the origin of genera and species (Section 10.3).

9.4 Eukaryotic Genes Can Be Quantitated and Manipulated with Considerable Precision

After a gene of interest has been identified, cloned, and sequenced, it is often desirable to understand how that gene and its corresponding protein product function in the context of a whole cell or organism. It is now possible to determine how the expression of a particular gene is regulated, how mutations in the gene affect the function of the corresponding protein product, and how the behavior of an entire cell or model organism is altered by the introduction of mutations within specific genes. In addition, levels of transcription of large families of genes within cells and tissues can be readily quantified and compared across a range of environmental conditions.

Gene-expression levels can be comprehensively examined

Most genes are present in the same quantity in every cell — namely, one copy per haploid cell or two copies per diploid cell. However, the level at which a gene is expressed, as indicated by mRNA quantities, can vary widely, ranging from no expression to hundreds of mRNA copies per cell. Gene-expression patterns vary from cell type to cell type, distinguishing, for example, a muscle cell from a nerve cell. Even within the same cell, gene-expression levels may vary as the cell responds to changes in physiological circumstances. Although mRNA levels sometimes correlate with the levels of proteins expressed, this correlation does not always hold. Thus, care

must be exercised when interpreting the results of mRNA levels alone.

Quantitative PCR

The quantity of individual mRNA transcripts can be determined by **quantitative PCR (qPCR)**, or real-time PCR. RNA is first isolated from the cell or tissue of interest. With the use of reverse transcriptase, cDNA is prepared from this RNA sample. In one qPCR approach, the transcript of interest is PCR amplified with the appropriate primers in the presence of the dye SYBR Green I, which fluoresces brightly when bound to double-stranded DNA. In the initial PCR cycles, not enough duplex is present to allow a detectable fluorescence signal. However, after repeated PCR cycles, the fluorescence intensity exceeds the detection threshold and continues to rise as the number of duplexes corresponding to the transcript of interest increases (**Figure 9.30A**).

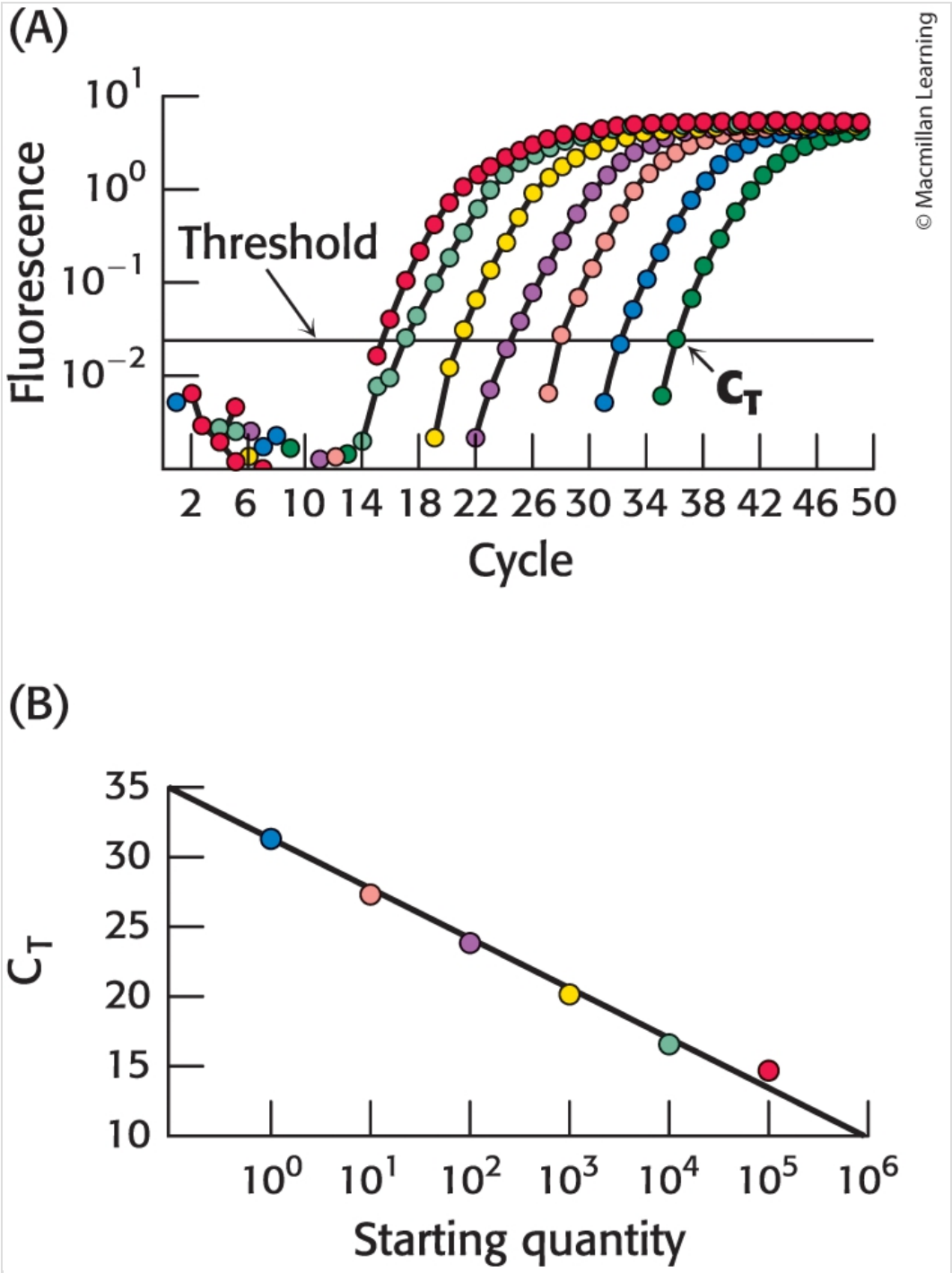


FIGURE 9.30 Quantitative PCR detects the amount of a particular transcript in a sample. (A) In qPCR, fluorescence is monitored in the course of PCR amplification to determine C_T, the cycle at which this signal exceeds a defined threshold. Each color represents a different starting quantity of cDNA. (B) C_T values are inversely proportional to the number of copies of the original cDNA template.

[Data from N. J. Walker, *Science* 296:557–559, 2002.]

Importantly, the cycle number at which the fluorescence becomes detectable over a defined threshold (or C_T) is inversely proportional to the number of copies of the original template (**Figure 9.30B**). After the relation between the original copy number and the C_T has been established with the use of a known standard, subsequent qPCR experiments can be used to determine the number of copies of any desired transcript in the original sample, provided the appropriate primers are available.

DNA microarrays

Although qPCR is a powerful technique for quantitation of a small number of transcripts in any given experiment, we can now use our knowledge of complete genome sequences to investigate an entire **transcriptome**, the pattern and level of expression of all genes in a particular cell or tissue. One of the most powerful methods for this purpose is based on hybridization. Single-stranded oligonucleotides whose sequences correspond to coding regions of the genome are affixed to a solid support such as a microscope slide, creating a **DNA microarray**. Importantly, the position of each sequence within the array is known. **Figure 9.31** outlines the steps in the creation of a DNA microarray.

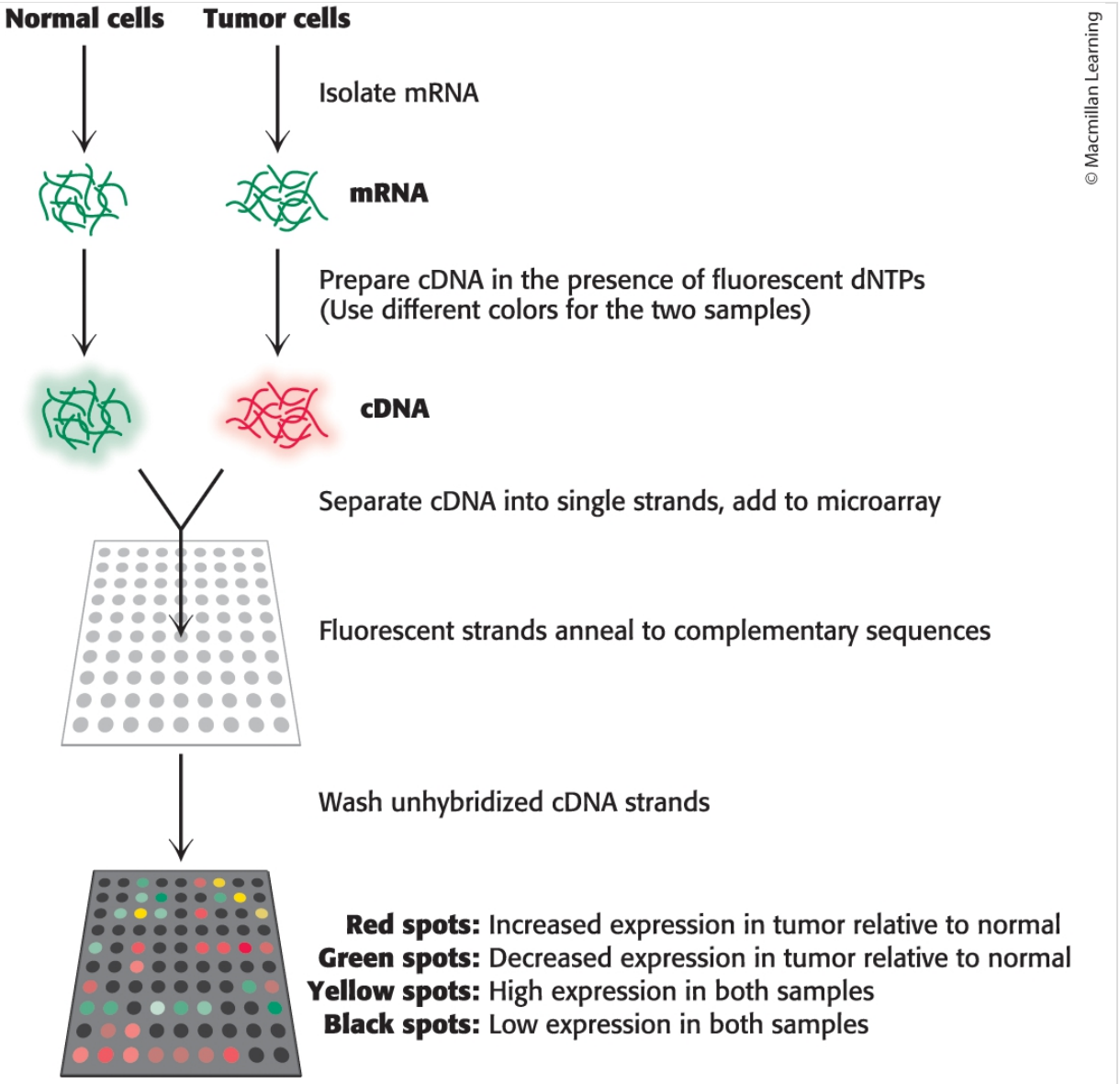


FIGURE 9.31 DNA microarrays can measure gene expression changes in a tumor. mRNA is isolated from two samples, tumor cells and a control sample. From these transcripts, cDNA is prepared in the presence of a fluorescent nucleotide, with a red label for the tumor sample and a green label for the control sample. Spots that are red indicate genes that are expressed more highly in the tumor, while the green spots indicate reduced expression relative to control. Spots that are black or yellow indicate comparable expression at either low or high levels, respectively.

[Information from D. L. Nelson and M. M. Cox, *Lehninger Principles of Biochemistry*, 6th ed. (W. H. Freeman and Company, 2013).]

1. mRNA is isolated from the cells of interest (a tumor, for example) as well as a control sample.
2. From this mRNA, cDNA is prepared (Section 9.2) in the presence of fluorescent nucleotides using different labels, usually green and red, for the two samples.
3. The samples are combined, separated into single strands, and added to the microarray.
4. The fluorescent strands anneal their complementary sequences.
5. Any unhybridized cDNA strands are washed off, leaving an array in which relative levels of green and red fluorescence at each spot indicate the differences in expression for each gene.

DNA microarrays have been prepared such that thousands of transcript levels can be assessed in a single experiment. Hence, over several arrays, the differences in expression of many genes across a number of different cell types or conditions can be measured (**Figure 9.32**).

Credit: Kao J, Salari K, Bocanegra M, Choi YL, Girard L, Gandhi J, Kwei KA, Hernandez-Boussard T, Wang P, Gazdar AF, Minna JD, Pollack JR. Molecular profiling of breast cancer cell lines defines relevant tumor models and provides a resource for cancer gene discovery. February 2009. *PLoS One* 4(7):e6146, Figure 1B. DOI:10.1371/journal. pone.0006146.

FIGURE 9.32 Microarrays detect numerous expression changes in a single experiment. The expression levels of thousands of genes can be simultaneously analyzed with DNA microarrays. Here, an analysis of 8750 genes in 50 breast cancer cell lines reveals that these samples can be divided into distinct classes (basal-A, basal-B, and luminal) based on their gene-expression patterns. In this "heat map" representation, each row represents a different gene, and each column represents a different breast cancer cell line (i.e., a separate microarray experiment). Red corresponds to gene induction, and green corresponds to gene repression.



RNA-seq

One disadvantage of the qPCR and microarray methods is that the transcript sequences must be known prior to the experiment, in order to design primers or microarray probes. However, the emergence of next-generation sequencing techniques, such as those described in the previous section, has enabled the detection of the presence and quantitation of virtually all the RNA molecules in a cell under specific conditions. This method, termed **RNA-seq**, consists of several essential steps:

1. *Isolation of RNA from the cells or tissue of interest.* Deoxyribonuclease (DNase), an enzyme which specifically cleaves DNA, can be used at this step to degrade any unwanted genomic DNA.

2. *RNA selection.* At this step, mRNA can be selectively enriched by filtering for sequences that contain poly(A) tails. This step allows for the removal of the abundant rRNAs from the sample.

3. *cDNA synthesis.* cDNA is prepared from the RNA sample using reverse transcriptase, as described earlier in the chapter.

4. *Sequencing and assembly.* The cDNA molecules within the sample are then sequenced using an NGS method, such as pyrosequencing. Each sequencing run is typically quite short, yielding only 50–100 bases, but millions of sequences are generated in a single experiment. Computational algorithms are then used to assemble the sequencing data into a comprehensive understanding of the transcripts present within the sample.

RNA-seq is more sensitive than microarray methods, enabling the detection of very low abundance transcripts. This sensitivity has led to the application of RNA-seq to the determination of transcript profiles of individual cells (called *single-cell RNA-seq*, or *scRNA-seq*). These single-cell experiments have broad application across a variety of disciplines, yielding insight on the variability of cancer cells within a single tumor or the changes within individual cell lineages during embryonic development.

New genes inserted into eukaryotic cells can be efficiently expressed

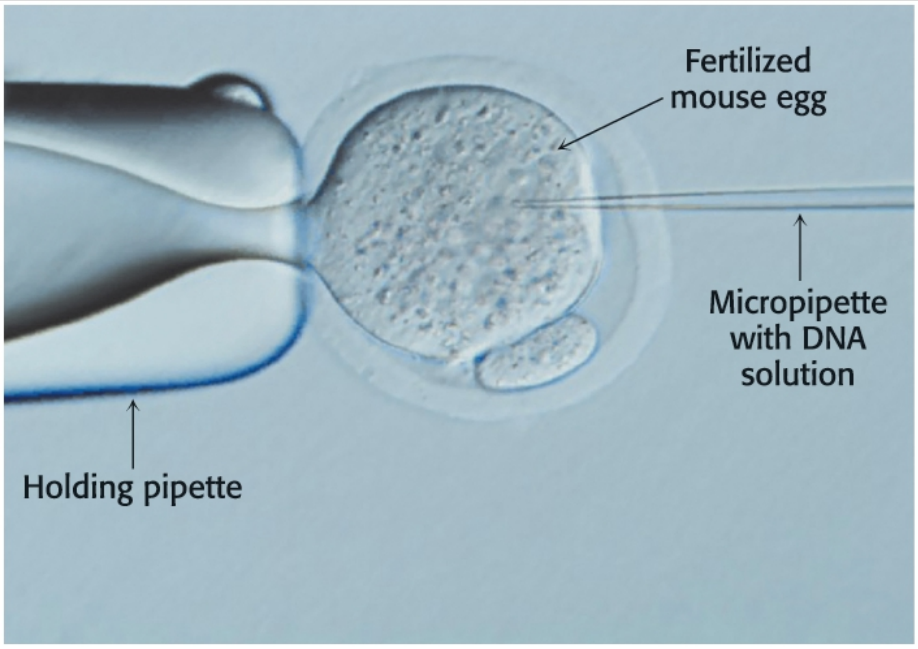
We have seen how bacteria can be turned into factories for the production of a wide range of prokaryotic and eukaryotic proteins. However, bacteria lack the necessary enzymes to carry out posttranslational modifications unique to these proteins, such as the specific cleavage of polypeptides and the attachment of carbohydrate units. Thus, many eukaryotic genes can be expressed correctly only in eukaryotic host cells.

Moreover, the introduction of recombinant DNA molecules into cells of higher organisms can be a source of insight into how their genes

are organized and expressed. How are genes turned on and off in embryological development? How does a fertilized egg give rise to an organism with highly differentiated cells that are organized in space and time? These central questions of biology can now be fruitfully approached by expressing foreign genes in mammalian cells.

Recombinant DNA molecules can be introduced, or *transformed*, into animal cells in several ways:

- Foreign DNA molecules precipitated by calcium phosphate can be taken up by animal cells by a process known as *transfection*. A small fraction of the imported DNA becomes stably integrated into the chromosomal DNA. While the efficiency of incorporation is low, this method is useful because it is easy to apply.
- DNA can be microinjected into cells. A fine-tipped glass micropipette containing a solution of foreign DNA is inserted into the nucleus (**Figure 9.33**). A skilled investigator can inject hundreds of cells per hour.
- Viruses can be used to introduce new genes into animal cells through a process called *transduction*. The most effective vectors are retroviruses, whose genomes are encoded by RNA and replicate through DNA intermediates. The retroviruses used for this purpose typically do not harm their hosts.



Credit: Marh et al, Hyperactive self-inactivating piggyBac for transposase-enhanced pronuclear microinjection transgenesis, PNAS, Vol 109, no. 47, pp. 19184–19189. Copyright 2012 National Academy of Sciences.

FIGURE 9.33 Cloned plasmid DNA is microinjected into a fertilized mouse egg.

A striking feature of the life cycle of a retrovirus is that the double-helical DNA form of its genome, produced by the action of reverse transcriptase, becomes randomly incorporated into host chromosomal DNA. This DNA version of the viral genome, called *proviral DNA*, can be efficiently expressed by the host cell and replicated along with normal cellular DNA. Foreign genes have been efficiently introduced into mammalian cells by infecting them with vectors derived from the Moloney murine leukemia virus, a retrovirus which can accept inserts as long as 6 kb. Some genes introduced by this vector into the genome of a transformed host cell are efficiently expressed.

Two other vectors based on two large-genome viruses have been engineered to express DNA inserts efficiently. *Vaccinia* virus, a large DNA-containing virus, replicates in the cytoplasm of mammalian

cells, where it shuts down host-cell protein synthesis. *Baculovirus* infects insect cells, which can be conveniently cultured. Insect larvae infected with this virus can serve as efficient protein factories.

Transgenic animals harbor and express genes introduced into their germ lines

As shown in Figure 9.33, plasmids harboring foreign genes can be microinjected into the male pronucleus of fertilized mouse eggs, which are then inserted into the uterus of a foster-mother mouse. A subset of the resulting embryos in this host will then harbor the foreign gene; these embryos may develop into mature animals. Southern blotting or PCR analysis of DNA isolated from the progeny can be used to determine which offspring carry the introduced gene. These **transgenic mice** are a powerful means of exploring the role of a specific gene in the development, growth, and behavior of an entire organism. Transgenic animals often serve as useful models for a particular disease process, enabling researchers to test the efficacy and safety of a newly developed therapy.

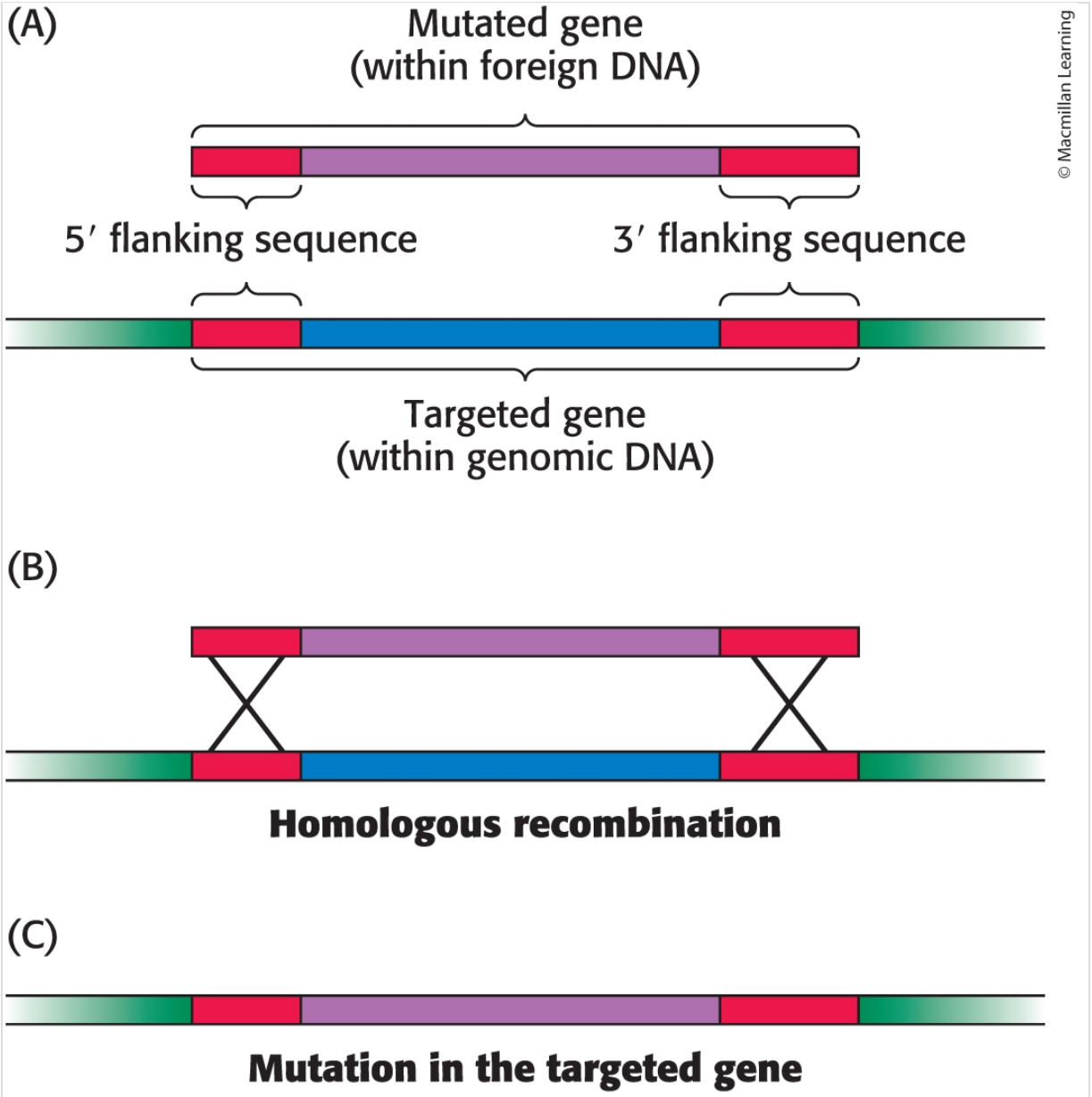
Consider the example of ALS, introduced in Section 9.1. Research groups have generated transgenic mouse lines that express forms of human superoxide dismutase that harbor mutations matching those identified in earlier genetic analyses. Many of these strains exhibit a clinical picture similar to that observed in ALS patients: progressive weakness of voluntary muscles and eventual paralysis, motor-neuron loss, and rapid progression to death. Since their first characterization in 1994, these strains continue to serve as valuable sources of information for the exploration of the mechanism and potential treatment of ALS.

Gene disruption and genome editing provide clues to gene function and opportunities for new therapies

The function of a gene can also be probed by inactivating or editing it and looking for resulting abnormalities.

Gene knockouts

Powerful methods have been developed for accomplishing such **gene disruption** (or **gene knockout**) in organisms such as yeast and mice. These methods rely on the process of **homologous recombination** (Section 28.5), in which two DNA molecules with strong sequence similarity exchange segments. If a region of foreign DNA is flanked by sequences that have high homology to a particular region of genomic DNA, two recombination events will yield the transfer of the foreign DNA into the genome (**Figure 9.34**). In this manner, specific genes can be targeted if their flanking nucleotide sequences are known.



© Macmillan Learning

FIGURE 9.34 Foreign DNA can be inserted into the host genome by homologous recombination. (A) A mutated version (purple) of the gene to be disrupted (blue) is constructed, maintaining some regions of homology with the normal gene (red). When the foreign mutated gene is introduced into an embryonic stem cell, (B) recombination takes place at regions of homology and (C) the normal (targeted) gene is replaced, or "knocked out," by the foreign gene. The cell is inserted into embryos, and mice lacking the gene (knockout mice) are produced.

For example, the gene-knockout approach has been applied to the genes encoding gene-regulatory proteins (also called *transcription factors*; Section 29.3) that control the differentiation of muscle cells. When both copies of the gene for the regulatory protein myogenin are disrupted in mice, the animals lack functional skeletal muscle. The impaired formation of respiratory muscles, such as the diaphragm, leads to the inability to breathe and death shortly after birth. Microscopic inspection reveals that the tissues from which muscle normally forms contain precursor cells that have failed to differentiate fully (**Figure 9.35A**). Heterozygous mice containing one normal myogenin gene and one disrupted gene appear normal, suggesting that a reduced level of myogenin gene expression is still sufficient for normal muscle development. The generation and characterization of this knockout mouse provided strong evidence that functional myogenin is essential for proper development of skeletal muscle tissue (**Figure 9.35B**).

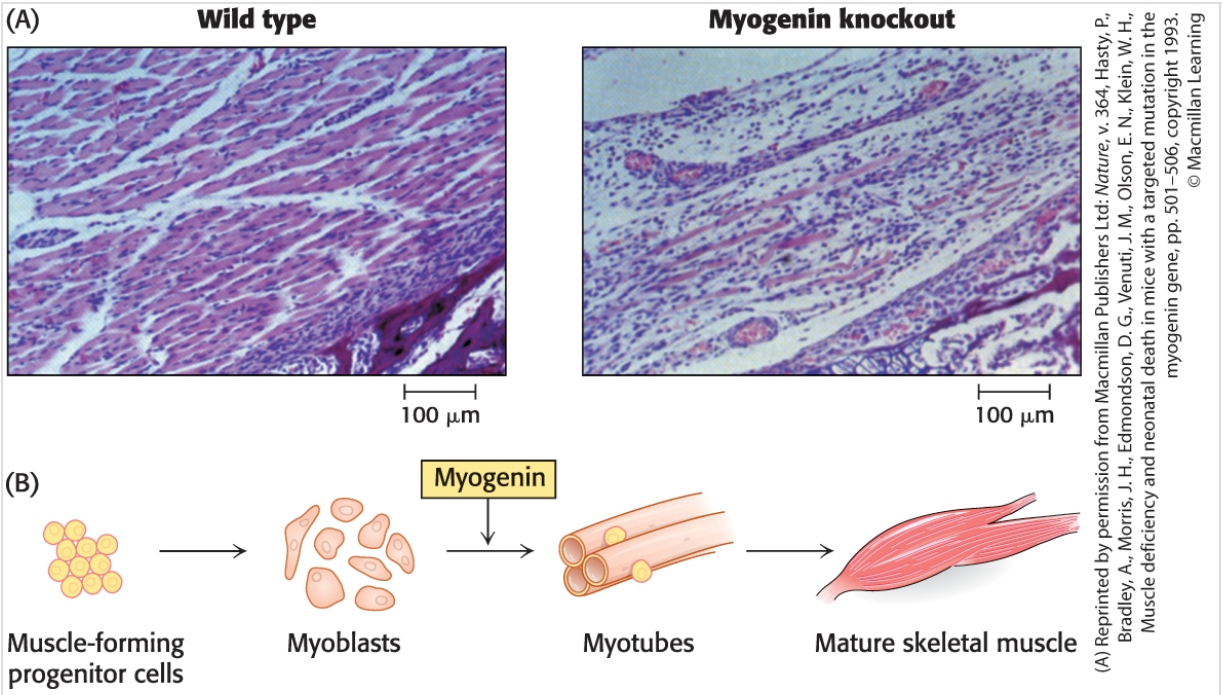


FIGURE 9.35 In knockout mice, gene disruption can have dramatic consequences. (A) Sections of muscle from normal (left) and myogenin-knockout (right) mice, as viewed under the light microscope. Muscles do not develop properly in mice having both myogenin genes

disrupted. (B) Through the gene-disruption studies in (A), myogenin was identified as an essential component of the development of mature skeletal muscle.

[(B) Information from S. Hettmer and A. J. Wagers, *Nat. Med*. 16:171–173, 2010, Fig. 1.]



Analogous studies have probed the function of many other genes in the context of a living organism. Furthermore, mice harboring gene knockouts can be used as animal models for known human genetic diseases, enabling the assessment of new potential therapies for treatment. However, manipulation of genomic DNA using homologous recombination, while a powerful tool, has limitations. Recombination at the desired site can be inefficient and time-consuming. In addition, this method is generally limited to specific model organisms, such as yeast, mice, and fruit flies.

Genome editing

Over the past 10 years, new methods for the highly specific modification of genomic DNA, or **genome editing**, have emerged. These approaches rely on the introduction of double-strand breaks at precisely determined sequences within genomic DNA. The resulting cleavage site is repaired by the DNA repair machinery of the host cell in one of two ways (Section 28.4) If no template is provided, the cell will repair the break using a process known as *non-homologous end joining* (NHEJ; **Figure 9.36**). However, this process is error-prone, and a variety of insertions or deletions will be introduced into the repair site. It is likely that a subset of these modifications will introduce a premature stop codon into the targeted gene, resulting in a gene knockout. Alternatively, if a DNA template containing the desired sequence change is simultaneously introduced with the nucleases, the repair machinery will use this

donor template to introduce these changes directly into the genomic sequence, in a process known as *homology directed repair* (HDR; Figure 9.36).

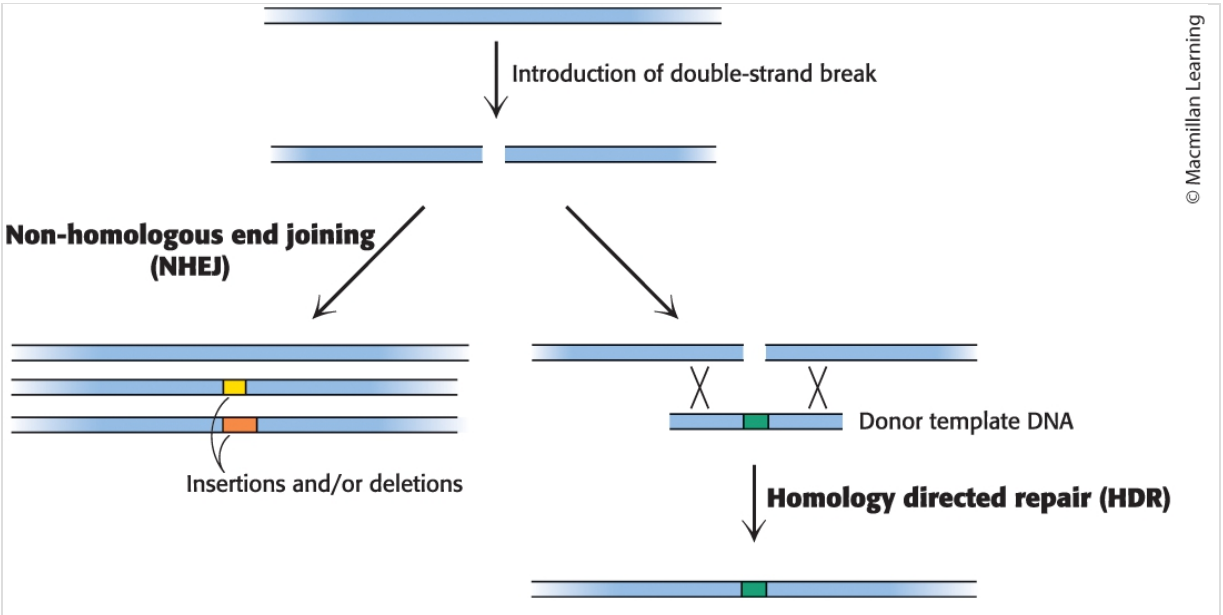


FIGURE 9.36 Genome editing starts with the introduction of precisely generated double-strand breaks in host DNA. These breaks are repaired in the cell by two possible mechanisms. One is non-homologous end joining (NHEJ), a process that is error-prone and may lead to the introduction of insertions or deletions. Such errors may introduce frameshift mutations that ultimately knock out the entire gene. Alternatively, if a donor template DNA fragment is also provided, the break can be repaired by homology directed repair (HDR), which results in the incorporation of the desired modifications (green) into the targeted gene.

How are double-stranded breaks introduced specifically into the gene of interest? In one approach, a sequence-specific nuclease is engineered by fusing the nonspecific nuclease domain of the restriction enzyme FokI to a DNA-binding domain designed to bind to a particular DNA sequence. Two examples of this strategy are in common usage:

- **Zinc-finger nucleases (ZFNs)** are formed by combining the FokI nuclease domain with the DNA-binding domain that contains a series of zinc-finger domains, small zinc-binding motifs that each recognize a sequence of three base pairs. The preferred DNA-binding sequence can be altered by changing the identity of only four contact residues within each finger.

- **Transcription activator-like effector nucleases (TALENs)** are formed from the fusion of the FokI nuclear domain with an array of TALE repeats. Each repeat contains 34 amino acids and two α-helices, yet only two of these residues (at positions 12 and 13) are responsible for the unique recognition of a single nucleotide within the double helix (**Figure 9.37**). Mutation of these residues within an array of repeats enables the recognition of a vast number of possible DNA target sequences with a high degree of specificity.

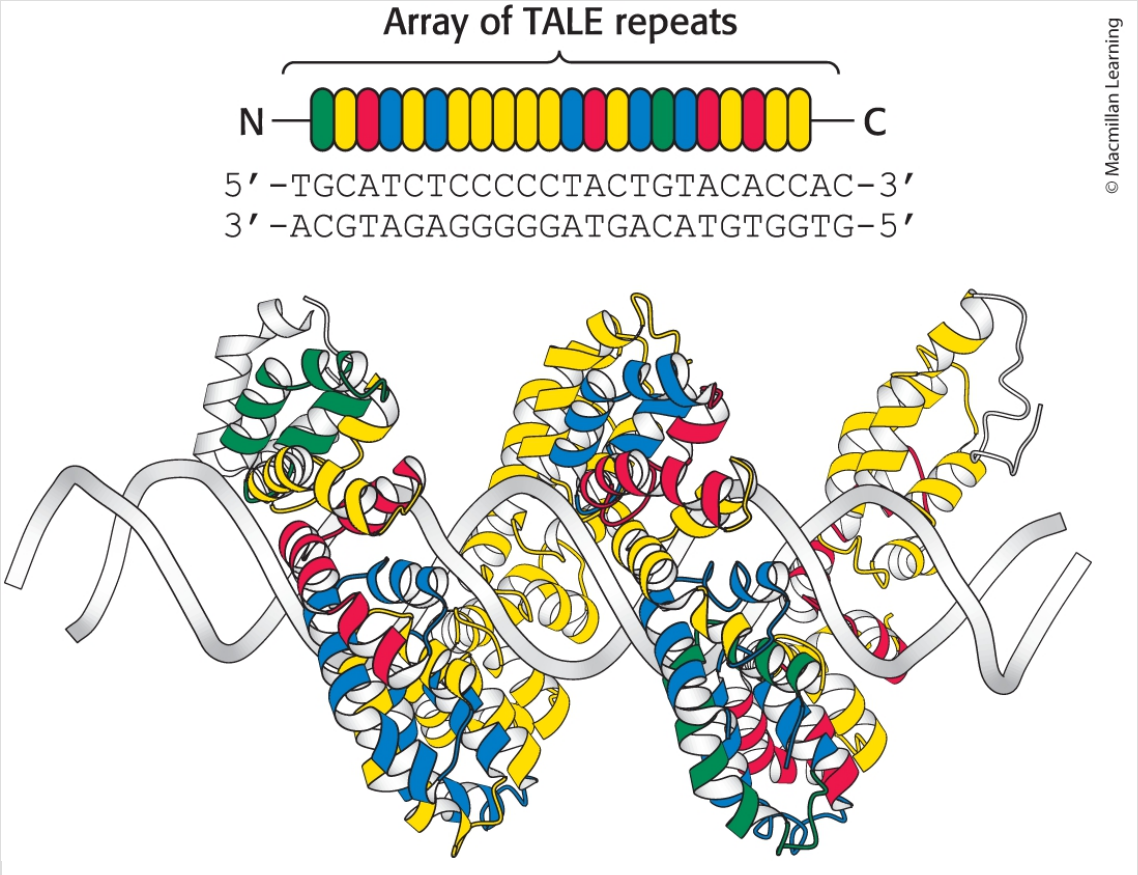


FIGURE 9.37 TALE repeats recognize individual bases in DNA. Each TALE repeat contains 34 amino acids, two of which specify its nucleotide binding partner. In this figure, the identity of these residues is indicated by the color of the repeat. TALE proteins can be designed to uniquely recognize extended oligonucleotide sequences. In this example, a 22 base-pair sequence is bound by a single TALE protein, the bacterial effector PthXo1.

[Drawn from 3UGM.pdb.]

Since the FokI nuclease functions as a dimer, two ZFN/TALEN constructs are necessary to generate a double-stranded break, one for each strand of DNA (Figure 9.38).

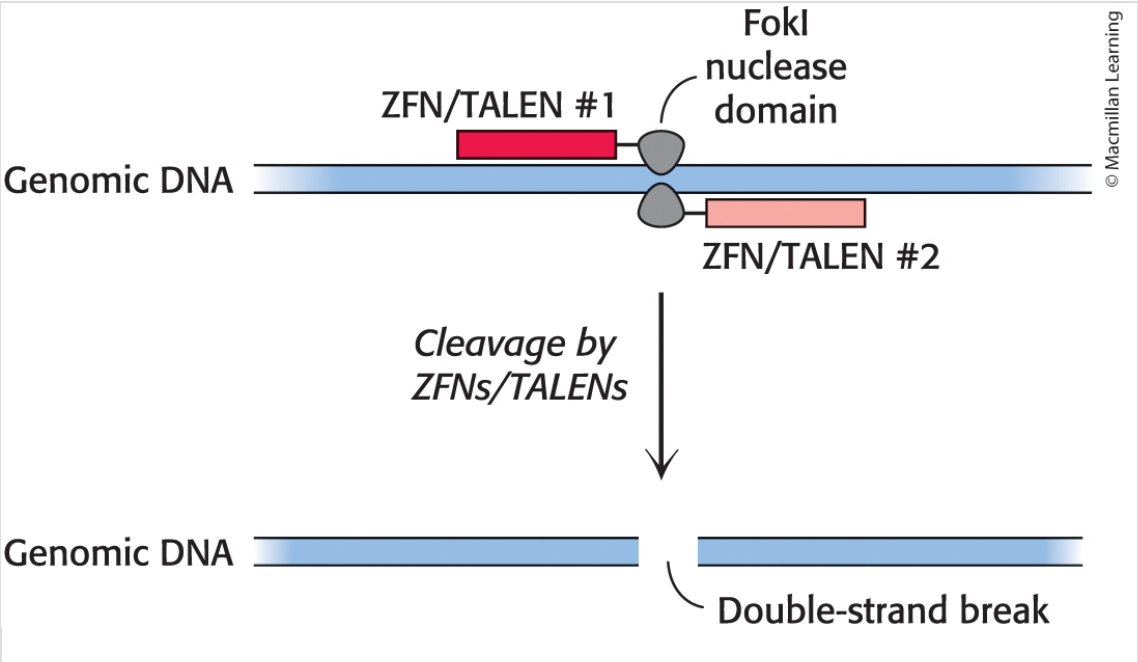


FIGURE 9.38 A pair ZFNs or TALENs introduce double-strand breaks into DNA. The nuclease domain of FokI functions as a dimer. Thus, in order to achieve a sequence-specific double-strand break, two ZFNs or TALENs are required, one for each DNA strand.

- The **CRISPR-Cas system** enables even greater diversity and potential for customization in the generation of precise double-strand DNA breaks. Clustered regularly interspaced palindromic repeats (or CRISPRs) were first discovered in the late 1980s in the genome of the bacterium *E. coli*, then subsequently identified in numerous bacterial and archaeal species. Near these repeats are clusters of genes encoding CRISPR-associated, or *Cas*, proteins, which were predicted to function as enzymes that bind to and cleave DNA. Twenty years later, it was confirmed that these loci constitute a prokaryotic immune system, enabling the cleavage of foreign DNA sequences. Since this discovery, CRISPR-Cas systems have been cleverly adapted to enable customized sequence-specific DNA cleavage.

How do CRISPR-Cas systems achieve sequence-specific double-strand breaks in DNA? Cleavage of target DNA by the CRISPR-Cas system of the bacterium *Streptococcus pyogenes* requires only a single protein, the nuclease Cas9, and an engineered, single-stranded **single guide RNA**, or **sgRNA**. At its $5'$ end, the sgRNA contains approximately 20 nucleotides that can be customized to complement the desired target site, followed by multiple stem-loop structures at its $3'$ end, which are required for binding to the nuclease (**Figure 9.39**). Cas9 is a large, 158 kDa protein which contains two lobes: a REC lobe, which binds to the duplex formed between the sgRNA and the target strand of DNA; and a NUC lobe, which contains the two

nuclease domains that are responsible for cleavage of the two strands of the target DNA (Figure 9.40A).

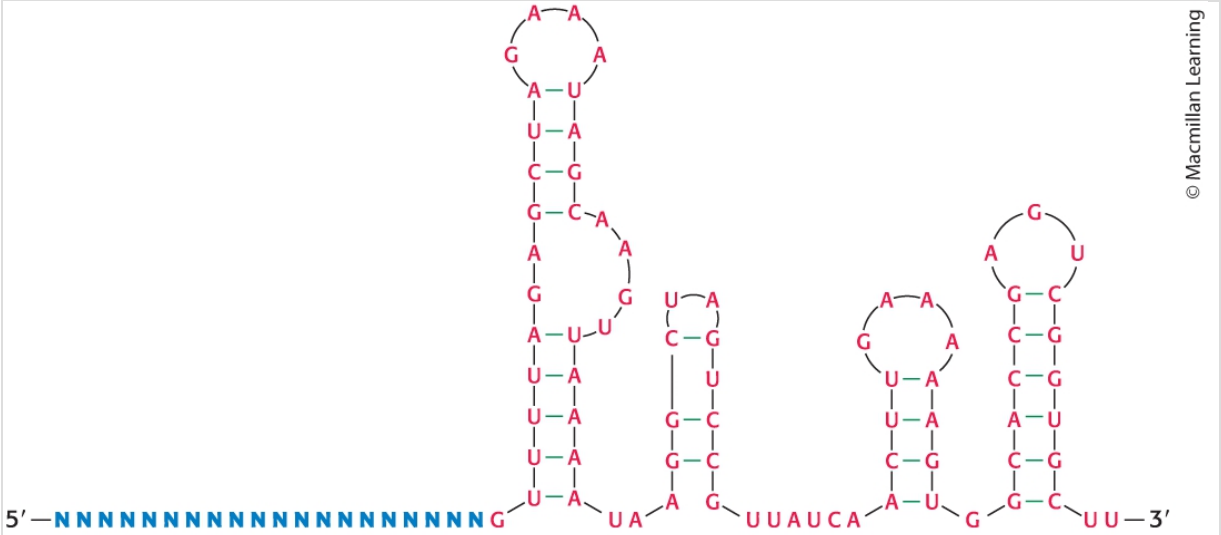


FIGURE 9.39 The single guide RNA contains the sequence that will drive site-specific cleavage. A single guide RNA (sgRNA) contains 20 nucleotides at its 5′ end (blue) which specify the target sequence, followed by multiple stem-loop structures (red) which mediate the interaction with Cas9.

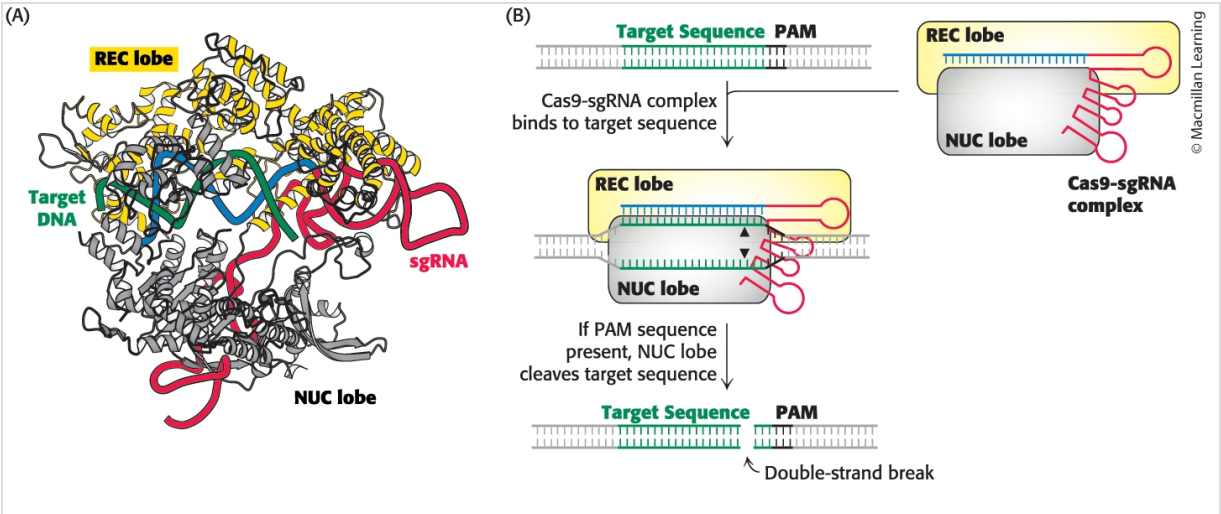


FIGURE 9.40 DNA is cleaved by the CRISPR-Cas system. (A) The structure of a Cas9-sgRNA complex reveals the two lobes of Cas9: the REC lobe (yellow) and the NUC lobe (gray). The REC lobe mediates the interaction with the sgRNA, shown in blue and red as in Figure 9.39. The NUC lobe contains the nuclease domain that will cleave the target DNA (green). (B) If the target DNA sequence contains an adjacent PAM sequence, the sgRNA-Cas9 complex will bind and cleave both strands of the target, at the sites indicated by the black triangles, yielding a double-strand break.

[Part (A) Drawn from 4OO8.pdb.]

VIEW an animation of this technique in Achieve

Cas9 also contains a region that recognizes a short (usually three- or four-nucleotide) sequence of DNA known as the *protospacer-adjacent motif* (PAM). If the target DNA sequence complementary to the sgRNA is adjacent to a PAM, the Cas9 complex cleaves both target strands using the two nuclease domains of the NUC lobe (**Figure 9.40B**). As the specificity of this nuclease is driven by a complementary sequence of RNA, the CRISPR-Cas system can be engineered to cleave virtually any DNA sequence, provided it is adjacent to a PAM, without the need for designing new protein recognition domains such as those required for ZFNs or TALENs.

Site-specific nuclease-based genome editing methods have now been applied to a variety of species, including model organisms used in the laboratory (rat, zebrafish, and fruit fly), various forms of livestock (pig, cow), and a number of plants. In addition, their use as therapeutic tools in humans is currently under investigation. For example, a ZFN that inactivates the human CCR5 gene, a coreceptor for cellular invasion of human immunodeficiency virus (HIV), is currently in clinical trials for the treatment of patients infected with HIV.



dpa picture alliance/Alamy

EMMANUELLE CHARPENTIER AND JENNIFER DOUDNA French microbiologist and biochemist Emmanuelle Charpentier (right) has spent much of her career investigating bacterial pathogens and the factors that contribute to their virulence. In 2011, then working at Umeå University in Sweden, she and her research team published a detailed study on the CRISPR-Cas9 system of *Streptococcus pyogenes*, including characterization of the RNA components that determine the sequence specificity of the Cas9 nuclease enzyme. While presenting her work at a conference later that year, she met Jennifer Doudna (left), a biochemist at the University of California, Berkeley, and a world leader in the structure and function of RNA molecules, who had recently developed an interest in the CRISPR-Cas9 system. Their mutual and complementary interests formed the basis for a collaboration, and the following year they together published a landmark paper demonstrating how an engineered single guide RNA could direct the Cas9-mediated cleavage of almost any DNA sequence. Their work has transformed the field of genome editing and underscores the power of collaboration in the scientific endeavor. In 2020, Charpentier and Doudna shared the Nobel Prize in Chemistry for their discovery.

Self-Check Question



Targeting a DNA sequence for editing by the CRISPR-Cas9 system requires that a PAM sequence be present just downstream of the target sequence. For *S. pyogenes* Cas9, this PAM is $5'-NGG-3'$, where N represents any nucleotide. Mutants of this Cas9 enzyme have been developed which recognize different PAM sequences, such as $5'-NGAN-3'$. Why might these mutants be useful for genome editing studies?

RNA interference enables disruption of gene expression and presents new therapeutic opportunities

An extremely powerful tool for disrupting gene expression was serendipitously discovered in the course of studies that required the introduction of RNA into a cell. The introduction of a specific double-stranded RNA molecule into a cell was found to suppress the transcription of genes that contained sequences present in the double-stranded RNA molecule. Thus, the introduction of a specific RNA molecule can interfere with the expression of a specific gene.

The mechanism of this process, called **RNA interference (RNAi)**, has been largely established (**Figure 9.41**):

1. When a double-stranded RNA molecule is introduced into an appropriate cell, the RNA is cleaved by the enzyme Dicer into

fragments approximately 21 nucleotides in length. Each fragment, termed a small interfering RNA (siRNA), consists of 19 bp of double-stranded RNA and 2 bases of unpaired RNA on each 5′ end.

2. The siRNA is loaded into an assembly of several proteins referred to as the *RNA-induced silencing complex* (RISC).

3. The RISC unwinds the RNA duplex and cleaves one of the strands, the so-called *passenger strand*. The uncleaved single-stranded RNA segment, the *guide strand*, remains incorporated into the enzyme.

4. The fully assembled RISC cleaves mRNA molecules that contain exact complements of the guide-strand sequence. Thus, levels of such mRNA molecules are dramatically reduced.

The technique of RNA interference is called *gene knockdown*, because the expression of the gene is reduced but not eliminated, as is the case with gene knockouts.

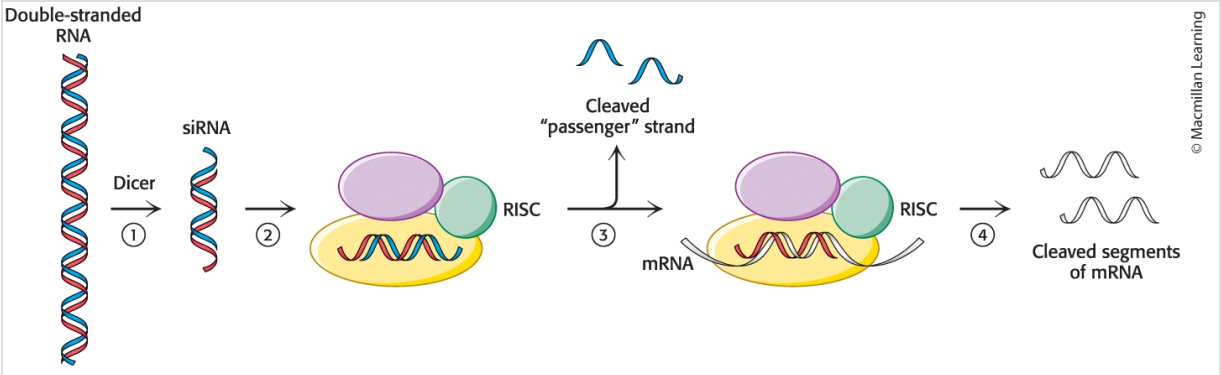


FIGURE 9.41 Specific mRNA transcripts are degraded by RNA interference. A double-stranded RNA molecule is cleaved into 21-bp fragments by the enzyme Dicer to produce siRNAs. These siRNAs are incorporated into the RNA-induced silencing complex (RISC), where the single-stranded RNAs guide the cleavage of mRNAs that contain complementary sequences.

The machinery necessary for RNA interference is found in many cells. In some organisms such as *C. elegans*, RNA interference is quite efficient. Indeed, RNA interference can be induced simply by feeding *C. elegans* strains of *E. coli* that have been engineered to produce appropriate double-stranded RNA molecules. Although not as efficient in mammalian cells, RNA interference has emerged as a powerful research tool for reducing the expression of specific genes. Moreover, in 2017, an siRNA targeting the protein transthyretin achieved positive results in a Phase III clinical trial for the treatment of familial amyloid polyneuropathy.

Foreign DNA can be introduced into plants

Several methods have been developed to introduce foreign DNA into plant cells.

Ti plasmids

The common soil bacterium *Agrobacterium tumefaciens* infects plants and introduces foreign genes into plant cells, causing a lump of tumor tissue called a *crown gall* to grow at the site of infection (**Figure 9.42**). Crown galls synthesize opines, a group of amino acid derivatives that are metabolized by the infecting bacteria. In essence, the bacterium hijacks the metabolism of the plant cells to satisfy its highly distinctive appetite. **Tumor-inducing plasmids (Ti plasmids)** that are carried by *A. tumefaciens* carry instructions for

the switch to the tumor state and the synthesis of opines. A small part of the Ti plasmid becomes integrated into the genome of infected plant cells; this 20-kb segment is called *T-DNA*, for transferred DNA.



Credit: Matthew A. Escobar, Edwin L. Civerolo, Kristin R. Summerfelt, and Abhaya M. Dandekar. RNAi-mediated oncogene silencing confers resistance to crown gall tumorigenesis. *PNAS* 2001 98 (23) 13437–13442. Copyright 2001 National Academy of Sciences, U.S.A.

FIGURE 9.42 Crown gall, a plant tumor, is caused by the bacterium *Agrobacterium tumefaciens*. This bacterial species introduces a tumor-inducing plasmid (Ti plasmid) into the plant host.

Ti-plasmid derivatives can be used as vectors to deliver foreign genes into plant cells. First, a segment of foreign DNA is inserted into the T-DNA region of a small plasmid through the use of restriction enzymes and ligases. This synthetic plasmid is added to

A. tumefaciens colonies harboring naturally occurring Ti plasmids, and, by recombination, Ti plasmids containing the foreign gene are formed. These Ti vectors are valuable tools for exploring the genomes of plant cells and modifying plants to improve their agricultural value and crop yield.

Electroporation

Foreign DNA can also be introduced into plants by applying intense electric fields, a technique called **electroporation** (**Figure 9.43**). First, the cellulose wall surrounding plant cells is removed by adding cellulase; this treatment produces protoplasts, plant cells with exposed plasma membranes. Electric pulses are then applied to a suspension of protoplasts and plasmid DNA. Because high electric fields make membranes transiently permeable to large molecules, plasmid DNA molecules enter the cells. The cell wall is then allowed to re-form, and the plant cells are again viable. Moreover, the transfected cells efficiently express the plasmid DNA. Corn and carrot cells have been stably transfected in this way with the use of plasmid DNA that includes genes for resistance to herbicides. Electroporation is also an effective means of delivering foreign DNA into mammalian and bacterial cells.

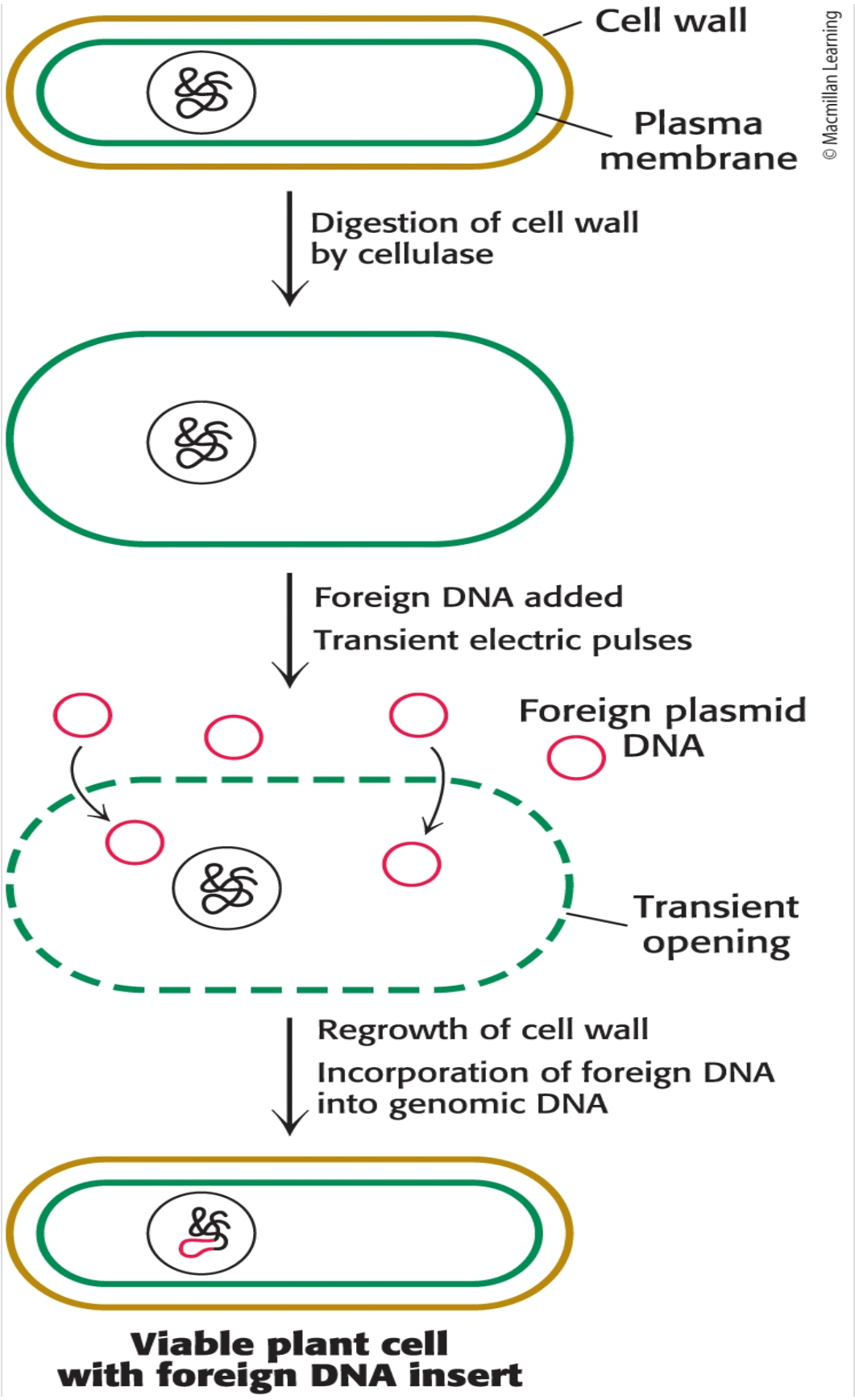

Cell wall
Plasma membrane
Digestion of cell wall by cellulase
Foreign DNA added
Transient electric pulses
Foreign plasmid DNA
Transient opening
Regrowth of cell wall
Incorporation of foreign DNA into genomic DNA
Viable plant cell with foreign DNA insert
© Macmillan Learning

FIGURE 9.43 Foreign DNA can be introduced into plant cells by electroporation. In this technique, the application of intense electric fields makes the plant plasma membranes transiently permeable to large molecules, such as plasmid DNA.



Gene guns

The most effective means of transforming plant cells is through the use of so-called *gene guns*, or *bombardment-mediated transformation*. DNA is coated onto $1\text{-}\mu\text{m}\text{-}\text{diameter}$ tungsten pellets, and these microprojectiles are fired at the target cells with a velocity greater than $400\ \text{m}\ \text{s}^{-1}$. Despite its apparent crudeness, this technique is an effective way of transforming plants, especially important crop species such as soybean, corn, wheat, and rice.

The aforementioned techniques afford an opportunity to develop genetically modified organisms (GMOs) with beneficial characteristics, such as the ability to grow in poor soils, resistance to natural climatic variation, resistance to pests, and fortified nutritional content. These crops might be most useful in regions where malnutrition is prevalent. However, the use of GMOs is highly controversial, as some fear that their safety risks have not been adequately addressed.

The first GMO to come to market was a tomato characterized by delayed ripening. This was achieved by disrupting the gene for the enzyme that breaks down pectin, the polysaccharide that gives tomatoes their firmness. During ripening, pectin is destroyed, and the tomatoes soften, making shipment difficult; by disrupting

production of the pectin-destroying enzyme, the tomatoes stayed firm longer. However, the tomato's poor taste hindered its commercial success. An especially successful result of the use of Ti plasmid to modify crops is golden rice. Golden rice is a variety of genetically modified rice that contains the genes for β-carotene synthesis, a required precursor for vitamin A synthesis in humans. Consumption of this rice has the potential to benefit regions of the world where rice is a dietary staple and vitamin A deficiency is common.

Chapter 9 Summary

9.1 The Exploration of Genes Relies on Key Tools

- Restriction enzymes recognize specific base sequences in double-helical DNA and cleave both strands of the duplex, forming specific fragments of DNA.
- A DNA fragment containing a particular sequence can be identified by hybridizing it with a labeled single-stranded DNA probe (Southern blotting).
- DNA can be sequenced by controlled interruption of replication. The fragments produced are separated by capillary electrophoresis and visualized by fluorescent tags at their $5'$ ends.
- DNA probes for hybridization reactions, as well as new genes, can be synthesized by the automated solid-phase method.
- The polymerase chain reaction makes it possible to greatly amplify specific segments of DNA in vitro. The region amplified is determined by the placement of a pair of primers that are added to the target DNA along with a thermostable DNA polymerase and deoxyribonucleoside triphosphates.

9.2 Recombinant DNA Technology Has Revolutionized All Aspects of Biology

- Novel DNA molecules are made by joining fragments that have complementary cohesive ends produced by the action of a restriction enzyme. DNA ligase seals breaks in DNA chains.
- Vectors for propagating the DNA include plasmids and λ phage. Two broad categories of plasmids include cloning vectors, used for easy insertion and replication of DNA fragments, and

expression vectors, for generating protein product in large quantities.
- Specific genes can be cloned from a genomic library with the use of a DNA or RNA probe.
- Complementary DNA (cDNA) is produced by reverse transcription of mRNA, yielding DNA corresponding to expressed genes. Because cDNA is generated from mature mRNA, all introns have been removed.
- Mutations can be generated in vitro to engineer novel proteins using site-directed mutagenesis, cassette mutagenesis, and mutagenesis by PCR.

9.3 Complete Genomes Have Been Sequenced and Analyzed

- More than 50,000 bacterial, archaeal, and eukaryotic genomes have been sequenced, including those from key model organisms and important pathogens.
- The sequence of the human genome has now been completed with nearly full coverage and high precision.
- Only from 20,000 to 25,000 protein-encoding genes appear to be present in the human genome, a substantially smaller number than earlier estimates.
- Next-generation sequencing methods have greatly accelerated the pace at which large genomes can be sequenced and analyzed.
- Comparative genomics has become a powerful tool for analyzing individual genomes and for exploring evolution.

9.4 Eukaryotic Genes Can Be Quantitated and Manipulated with Considerable Precision

- Changes in gene expression can be readily determined in cells and tissues by such techniques as quantitative PCR, microarrays, and RNA-seq.

- Transgenic mice, in which a gene has been inserted into the host organism, and knockout mice, in which a gene has been removed, have been a source of considerable insight into disease mechanisms and possible therapies.
- Genome editing techniques, such as those enabled by the CRISPR-Cas system and ZFNs/TALENs, involve the introduction of precise double-strand breaks into the host genome. Repair of these breaks can yield insertions and deletions, often disrupting the target gene, or the template-based replacement of the target gene with a new sequence.
- Another method of disrupting the expression of a particular gene is through RNA interference, which depends on the introduction of specific double-stranded RNA molecules into eukaryotic cells.
- DNA can be transformed into plant cells by the Ti plasmids of the soil bacterium *Agrobacterium tumefaciens*, or by other techniques such as electroporation or gene guns.

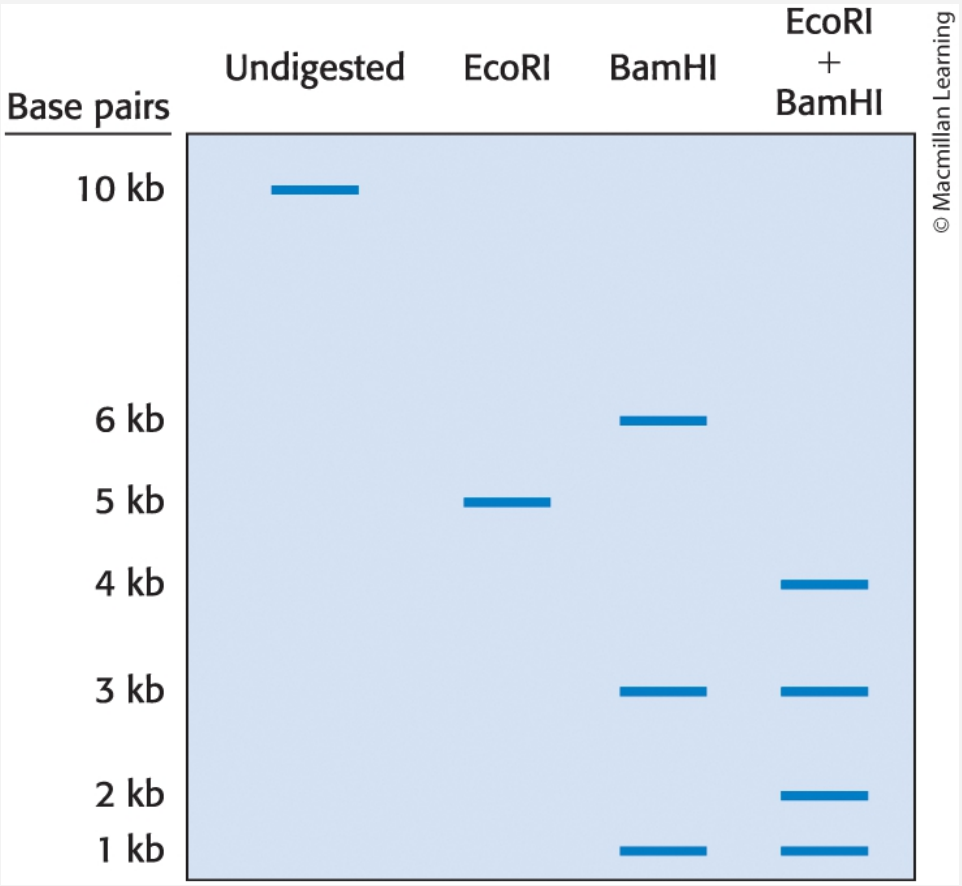
Key Terms

restriction enzyme (restriction endonuclease)
Southern blotting
DNA probe
northern blotting
controlled termination of replication (Sanger dideoxy method)
polymerase chain reaction (PCR)
polymorphism
restriction-fragment-length polymorphism (RFLP)
vector
plasmid
bacteriophage lambda (λ phage)
cohesive (sticky) ends

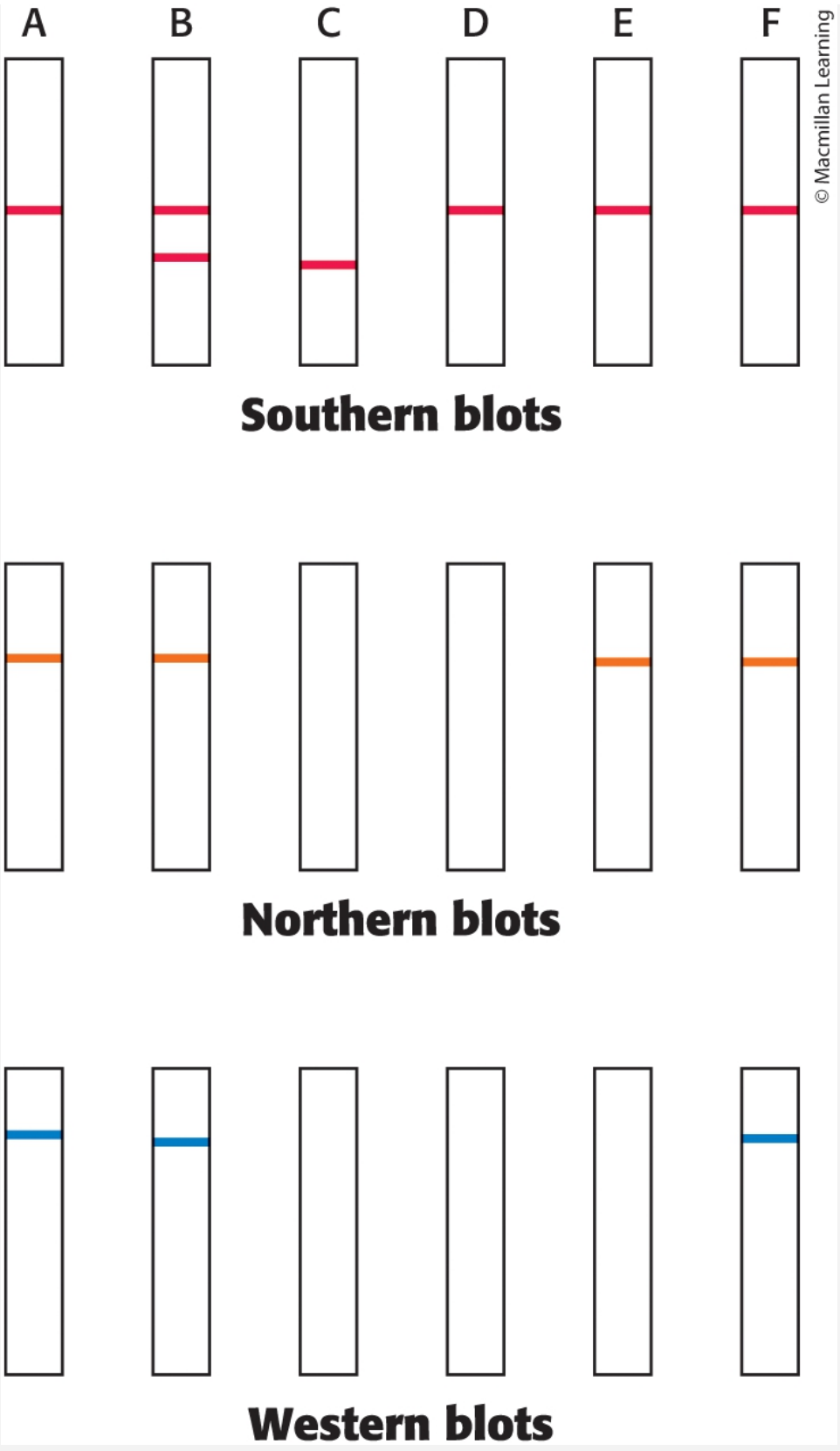
cloning vector
polylinker
reporter gene
expression vector
genomic library
complementary DNA (cDNA)
cDNA library
site-directed mutagenesis
cassette mutagenesis
pseudogene
next-generation sequencing (NGS)
pyrosequencing
quantitative PCR (qPCR)
transcriptome
DNA microarray
RNA-seq
transgenic mouse
gene disruption (gene knockout)
homologous recombination
genome editing
zinc-finger nuclease (ZFN)
transcription activator-like effector nuclease (TALEN)
CRISPR-Cas system
single guide RNA (sgRNA)
RNA interference (RNAi)
tumor-inducing plasmid (Ti plasmid)
electroporation

Problems

1. Samples of a linear segment of unknown DNA are digested using the restriction enzymes EcoRI, BamHI, and a combination of EcoRI and BamHI. The digests are then run on an agarose gel in order to separate the resulting fragments by size. Use the results of the gel electrophoresis shown in the image to draw a restriction map, indicating the locations of the restriction sites and the distances between them. 1

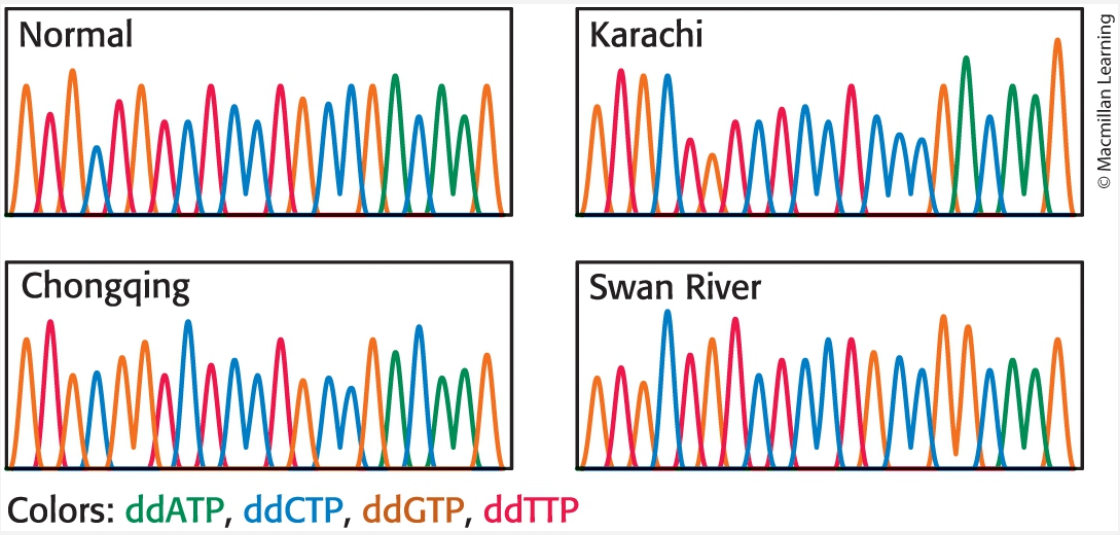


2. A series of people are found to have difficulty eliminating certain types of drugs from their bloodstreams. The problem has been linked to a gene X, which encodes an enzyme Y. Six people were tested with the use of various techniques of molecular biology. Person A is a normal control, person B is asymptomatic but some of his children have the metabolic problem, and persons C through F display the trait. Tissue samples from each person were obtained. Southern analysis was performed on the DNA after digestion with the restriction enzyme HindIII. Northern analysis of mRNA also was done. In both types of analysis, the gels were probed with labeled X cDNA. Finally, a western blot with an enzyme-linked monoclonal antibody was used to test for the presence of protein Y. The results are shown below. Why is person B without symptoms? Suggest possible mutations in the other people.  1



© Macmillan Learning

3. Representations of sequencing chromatograms for variants of the α chain of human hemoglobin are shown here. What is the nature of the amino acid change in each of the variants? The first triplet encodes valine. 2



4. You wish to amplify a 250 bp segment of DNA from a plasmid template by PCR with the use of the following primers: $5'-GGATCGATGCTCGCGA-3'$ and $5'-AGGATCGGGTCGCGAG-3'$. Despite repeated attempts, you fail to observe a PCR product of the expected length after electrophoresis on an agarose gel. Instead, you observe a

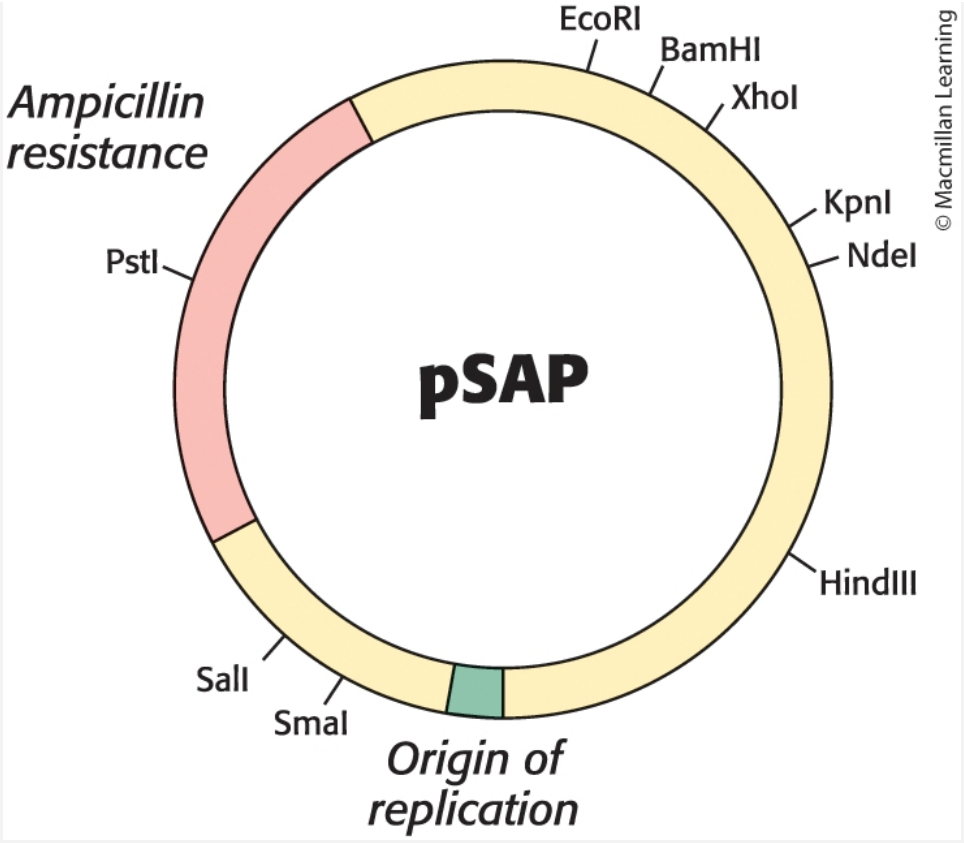
bright smear on the gel with an approximate length of 25 to 30 base pairs. Explain these results. 3

5. A gel pattern displaying PCR products shows four strong bands. The four pieces of DNA have lengths that are approximately in the ratio of 1:2:3:4. The largest band is cut out of the gel, and PCR is repeated with the same primers. Again, a ladder of four bands is evident in the gel. What does this result reveal about the structure of the encoded protein? 3

6. A young investigator would like to express and purify a newly discovered gene. She decides to clone the gene into an expression plasmid that contains the sequence for a hexahistidine tag. Order the steps for construction of the expression plasmid and generation of the protein. (The gene of interest will be inserted between the NotI and HindIII sites.) 4

a. Ligate the cut plasmid and DNA fragment.
b. Introduce NotI and HindIII restriction sites at the ends of the gene of interest.
c. Transfect the modified plasmid into *E. coli* for expression.
d. Digest the plasmid and the gene insert with NotI and HindIII.

7. The map of a hypothetical plasmid, pSAP, is shown here:



Suppose you have a DNA fragment you would like to insert into pSAP. The fragment has PstI and EcoRI restriction endonuclease sites near the $5'$ end, and HindIII and SmaI restriction endonuclease sites near the $3'$ end. What are the best restriction enzymes to use to digest both the DNA fragment and pSAP? 4

8. You have identified a gene that is located on human chromosome 20 and wish to identify its location within the mouse genome. On which chromosome would you be most likely to find the mouse counterpart of this gene?

9. Which of the following amino acid sequences would yield the most optimal oligonucleotide probe?

Ala-Met-Ser-Leu-Pro-Trp
Gly-Trp-Asp-Met-His-Lys
Cys-Val-Trp-Asn-Lys-Ile
Arg-Ser-Met-Leu-Gln-Asn

How many unique oligonucleotides would be required to detect all sequence possibilities for the optimal probe?

10. Suppose a researcher previously cloned gene *Y* into M13 bacteriophage vector. Gene *Y* encodes a product called peptide Y. A region of gene *Y* contains the DNA sequence ATG–CGC–GAA–CTG–GTG–AAC–TAA. The researcher wishes to change a Val residue to an Ala residue in this region of peptide Y using site-directed mutagenesis. What should be the sequence of the mutant oligonucleotide primer in this region? 5

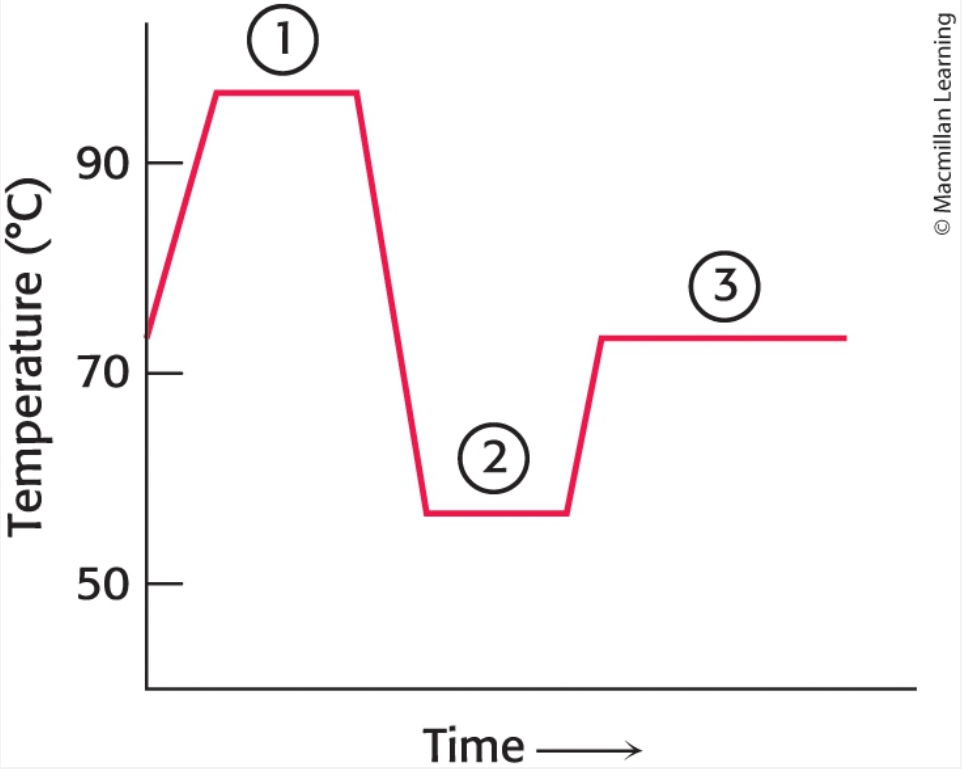
11. Targeting a DNA sequence for editing by the CRISPR-Cas9 system requires that a PAM sequence be present just downstream of the target sequence. For *S. pyogenes* Cas9, this PAM is $5'-NGG-3'$, where N represents any nucleotide. Assuming a fragment of DNA includes equal amounts of A, C, G, and T bases, how far apart would one expect to find these PAMs? 6

12.

a. Using RNA interference, it is possible to significantly reduce homologous mRNA transcripts and thereby reduce the expression level of a specific gene of interest. What methods could be used to confirm that an RNAi knockdown experiment has been successful?

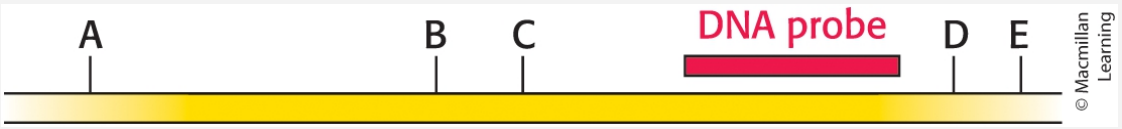
b. The relative ease of RNAi studies means that large-scale screens can be performed to assess a wide array of targets. What source would produce the most functional RNAi library for conducting genome-wide screens: whole-genome DNA, whole-genome proteins, or whole-genome cDNA?

13. The image below shows a time versus temperature plot for one cycle of PCR. Match the events below with the indicated regions (1, 2, and 3) on the plot. 3

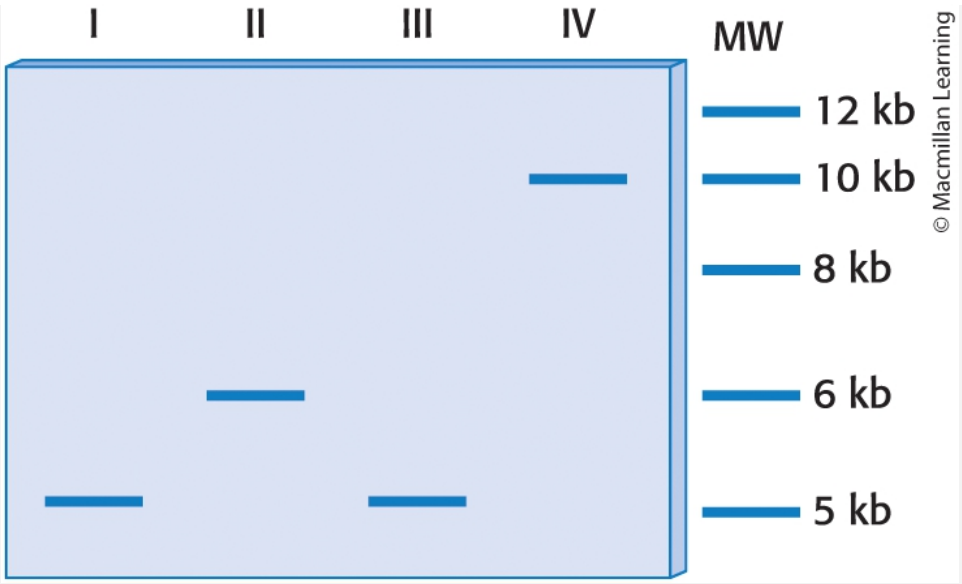


a. DNA polymerase extends primers.
b. DNA separates into single strands.
c. Primers anneal to single-stranded DNA.

14. You are interested in identifying mutations in a region of DNA that, in most individuals, has 5 cleavage sites for EcoRI. In the figure below, these sites are labeled A through E. You also have a probe that is complementary to the region between sites C and D:

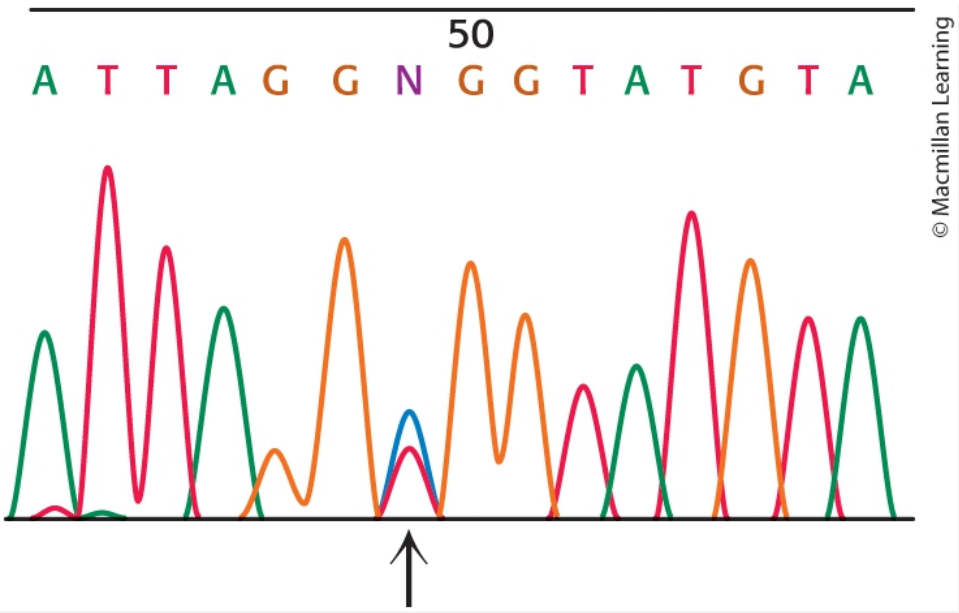


DNA samples from four individuals were cleaved with EcoRI. The DNA fragments were separated by gel electrophoresis, transferred to a membrane, and hybridized with your DNA probe. The image of the Southern blot shows the labeled DNA bands and molecular weight (MW) markers. The lane labels I, II, III, and IV correspond to individuals I, II, III, and IV. Assume that fragments such as C–D and C–E are clearly resolved in this gel system. Fragment sizes are as given: A–B is 4 kb, B–C is 1 kb, C–D is 5 kb, and D–E is 650 bp. Individual I represents the positive control, and has all five EcoRI sites intact.

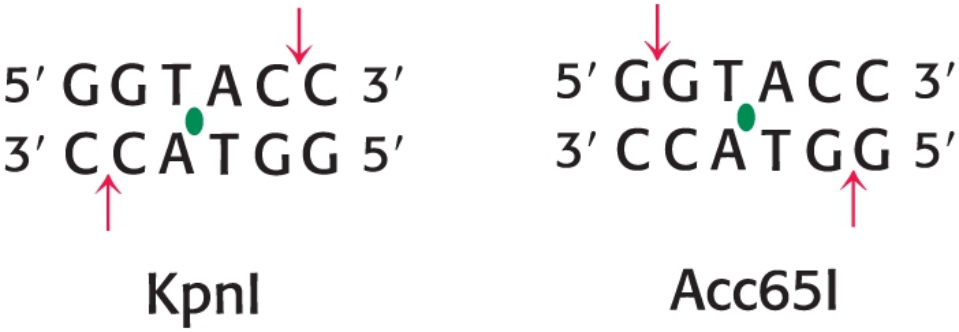


a. Which individual has at least one point mutation that eliminates restriction site C?
b. Which individual has mutation(s) that eliminate restriction sites B and C?
c. Which individual has at least one point mutation that eliminates restriction site A?

15. In the course of studying a gene and its possible mutation in humans, you obtain genomic DNA samples from a collection of persons and PCR amplify a region of interest within this gene. For one of the samples, you obtain the sequencing chromatogram shown here. Provide an explanation for the appearance of these data at position 49 (indicated by the arrow):



16. The restriction enzymes KpnI and Acc65I recognize and cleave the same 6-bp sequence. However, the sticky end formed from KpnI cleavage cannot be ligated directly to the sticky end formed from Acc65I cleavage. Explain why.

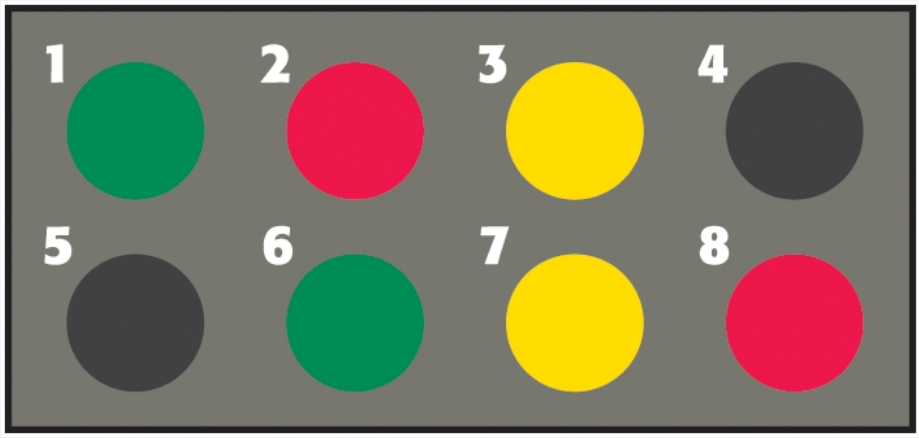


17. Suppose a single linear molecule of double-stranded DNA is amplified by PCR. How many molecules of double-stranded DNA will there be after 1 cycle? After 3 cycles? After 30 PCR cycles (a typical cycle count used in PCR experiments)? 3

18. Which of the following reagents are needed for a typical PCR? 3

a. DNA ligase
b. Four nucleotides (A, U, C, G)
c. *Taq* DNA polymerase
d. Template DNA
e. Two primers
f. *E. coli* DNA polymerase
g. Four nucleotides (A, T, C, G)

19. In preparation for a microarray experiment, cDNA was isolated from tumor tissue and labeled with a red fluorescent probe, while the cDNA from normal tissue was labeled with a green fluorescent probe. A small segment of the resulting microarray data is shown below.



© Macmillan Learning

Classify the individual genes (numbered on the array) based on the following descriptions:

a. Primarily expressed in tumor tissue
b. Primarily expressed in normal tissue
c. Expressed in both tissues
d. Not expressed in either tissue.

20. As RNA-seq becomes cheaper and less computationally intensive, many researchers are replacing microarray analysis with RNA-seq as the preferred method to measure cellular transcript levels. What are some advantages of RNA-seq over microarray analysis?

Chapter 10
Exploring Evolution and Bioinformatics



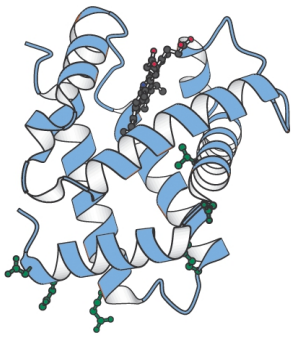


Photo: The Picture Art Collection/Alamy Stock Photo
© Macmillan Learning

Evolutionary relationships are clear in protein sequences. The now-extinct woolly mammoth (*Mammuthus primigenius*) coexisted with early humans, as evidenced by Late Stone Age cave paintings such as those at the Rouffignac Cave in France. Using samples obtained from frozen preserved tissue, researchers used recombinant DNA technology to determine the complete sequence of the woolly mammoth genome and the structural and functional adaptations of its proteins. In the case of α-hemoglobin (right), only six residues (shown in green) are nonidentical and dissimilar between the woolly mammoth and human sequences. Amino acid sequence comparisons with living species and functional expression of these extinct proteins have provided new insights into how this species adapted to very cold environments.

[Drawn from 3VRE.pdb.]

Outline

10.1 Homologs Are Descended from a Common Ancestor and Can Be Detected by Sequence Alignments
10.2 Examination of Three-Dimensional Structure Enhances Our Understanding of Evolutionary Relationships

10.3 Evolutionary Trees Can Be Constructed on the Basis of Sequence Information
10.4 Modern Techniques Make the Experimental Exploration of Evolution Possible

Learning Goals



By the end of this chapter, you should be able to:

1. Distinguish between homologs, paralogs, and orthologs.
2. Describe how two protein sequences are aligned, and how one can determine whether that alignment is significant.
3. Explain how substitution matrices can be used to facilitate the identification of related protein sequences.
4. Distinguish between divergent and convergent evolution.
5. Describe one way the evolution of biomolecules can be demonstrated in the laboratory.

Like members of a human family, members of molecular families often have features in common. Such family resemblance is most easily detected by comparing three-dimensional structure, the aspect of a molecule most closely linked to function. However, such structures have been determined for only a small proportion of the total number of proteins. In contrast, gene sequences and the corresponding amino acid sequences are available for a great number of proteins, largely owing to the tremendous power of DNA cloning and sequencing techniques, including complete-genome sequencing (Section 9.3). As we will discuss in this chapter, sequence databases can be probed for matches to a newly elucidated sequence to identify related molecules, providing considerable insight into the function, mechanism, and evolutionary history of the molecule encoded by that sequence.

10.1 Homologs Are Descended from a Common Ancestor and Can Be Detected by Sequence Alignments

The exploration of biochemical evolution consists largely of an attempt to determine how proteins, other molecules, and biochemical pathways have been transformed through time. Sequence comparisons can often reveal pathways of evolutionary descent and estimated dates of specific evolutionary landmarks. This information can be used to construct evolutionary trees that trace the evolution of a particular protein or nucleic acid, in many cases from Archaea and Bacteria through Eukarya, including human beings.

Orthologs and paralogs are two different classes of homologous proteins

The most fundamental relationship between two entities is *homology*; two molecules are said to be *homologous* if they are derived from a common ancestor. Homologous molecules, or **homologs**, can be divided into two classes (**Figure 10.1**):

- **Orthologs** are homologs that are present within different species and have very similar or identical functions. In Section 2.6, we discussed the structure of ribonuclease from cows (Figure 10.1; yellow). This protein is highly similar in structure to human ribonuclease (Figure 10.1; red). Both proteins share very similar functions, namely, the hydrolytic cleavage of RNA molecules.

- **Paralogs** are homologs that are present within one species. Paralogs often differ in their detailed biochemical functions. For example, angiogenin (Figure 10.1; blue), a protein that stimulates

the growth of new blood vessels, is also structurally similar to ribonuclease — so similar that both angiogenin and ribonuclease are clearly members of the same protein family. Paralogs such as angiogenin and ribonuclease strongly suggest a common ancestor at some earlier stage of evolution.

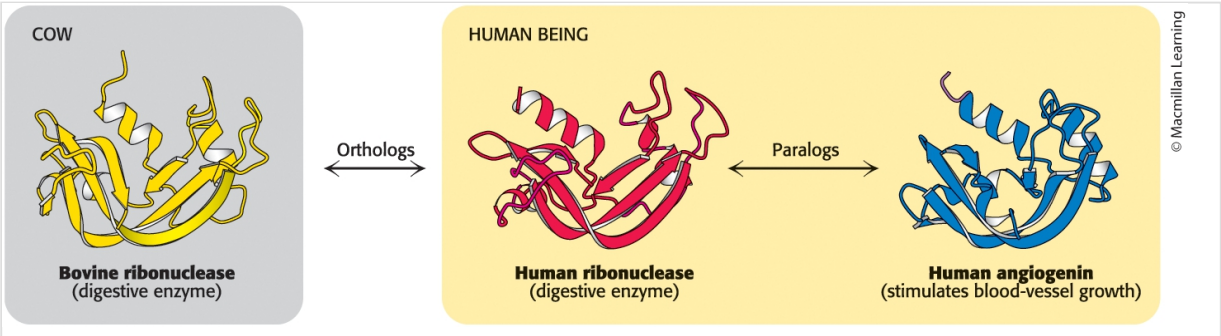


FIGURE 10.1 Homologs can be divided into two classes. Homologs that perform identical or very similar functions in different species are called orthologs, whereas homologs that perform different functions within one species are called paralogs.

[Drawn from 8RAT.pdb, 2RNF.pdb, and 2ANG.pdb.]

Understanding the homology between molecules can reveal the evolutionary history of the molecules as well as information about their function; if a newly sequenced protein is homologous to an already characterized protein, we have a strong indication of the new protein's biochemical function.

Statistical analysis of sequence alignments can detect homology

How can we tell whether two human proteins are paralogs or whether a yeast protein is the ortholog of a human protein? A significant sequence similarity between two molecules implies that they are likely to have the

same evolutionary origin and, therefore, similar three-dimensional structures, functions, and mechanisms. Both nucleic acid and protein sequences can be compared to detect homology. However, the possibility exists that the observed agreement between any two sequences is solely a product of chance. Because nucleic acids are composed of fewer building blocks than proteins (4 bases versus 20 amino acids), the likelihood of random agreement between two DNA or RNA sequences is significantly greater than that for protein sequences. For this reason, detection of homology between protein sequences is typically far more effective.

To illustrate sequence-comparison methods, let us consider the globins, the critical oxygen carrying proteins which we first encountered in Chapter 3. Recall that myoglobin is a monomer, while each human hemoglobin molecule is composed of four heme-containing polypeptide chains, two identical α chains and two identical β chains. Here, we shall consider only the α chain. To examine the similarity between the amino acid sequence of the human α chain of hemoglobin and that of human myoglobin (**Figure 10.2**), we apply a method, referred to as a **sequence alignment**, in which the two sequences are systematically aligned with respect to each other to identify regions of significant overlap.

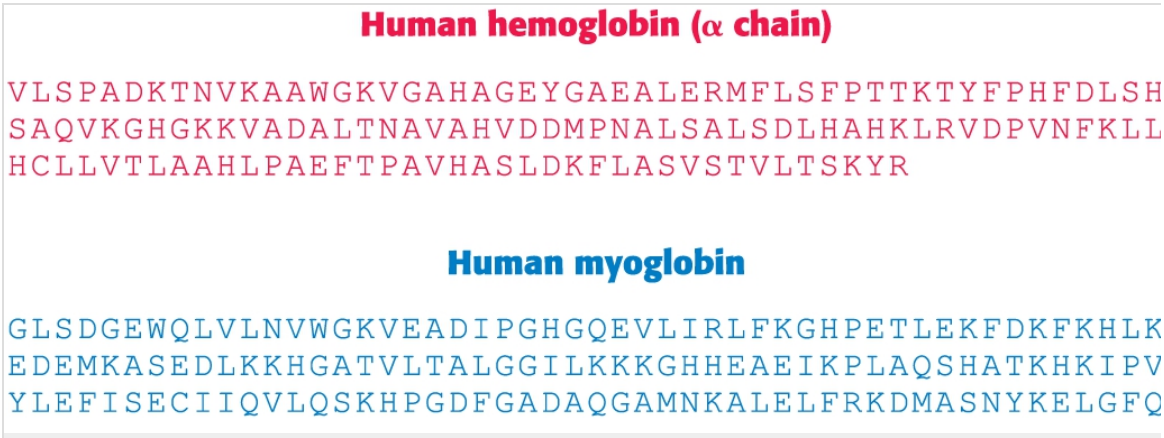


FIGURE 10.2 The amino acid sequences of human hemoglobin (α chain) and human myoglob will be used to demonstrate sequence alignments. α-Hemoglobin is composed of 141 amino acids; myoglobin consists of 153 amino acids. (One-letter abbreviations designating amino acic are used; see Table 2.2.)

How can we tell where to align the two sequences? In the course of evolution, the sequences of two proteins that have an ancestor in common will have diverged in a variety of ways. Insertions and deletions may have occurred at the ends of the proteins or within the functional domains themselves. Individual amino acids may have been mutated to other residues of varying degrees of similarity. To understand how the methods of sequence alignment take these potential sequence variations into account, let us first consider the simplest approach, where we slide one sequence past the other, one amino acid at a time, and count the number of matched residues, or sequence **identities** (**Figure 10.3**). For α-hemoglobin and myoglobin, the best alignment reveals 23 sequence identities spread throughout the central parts of the sequences.

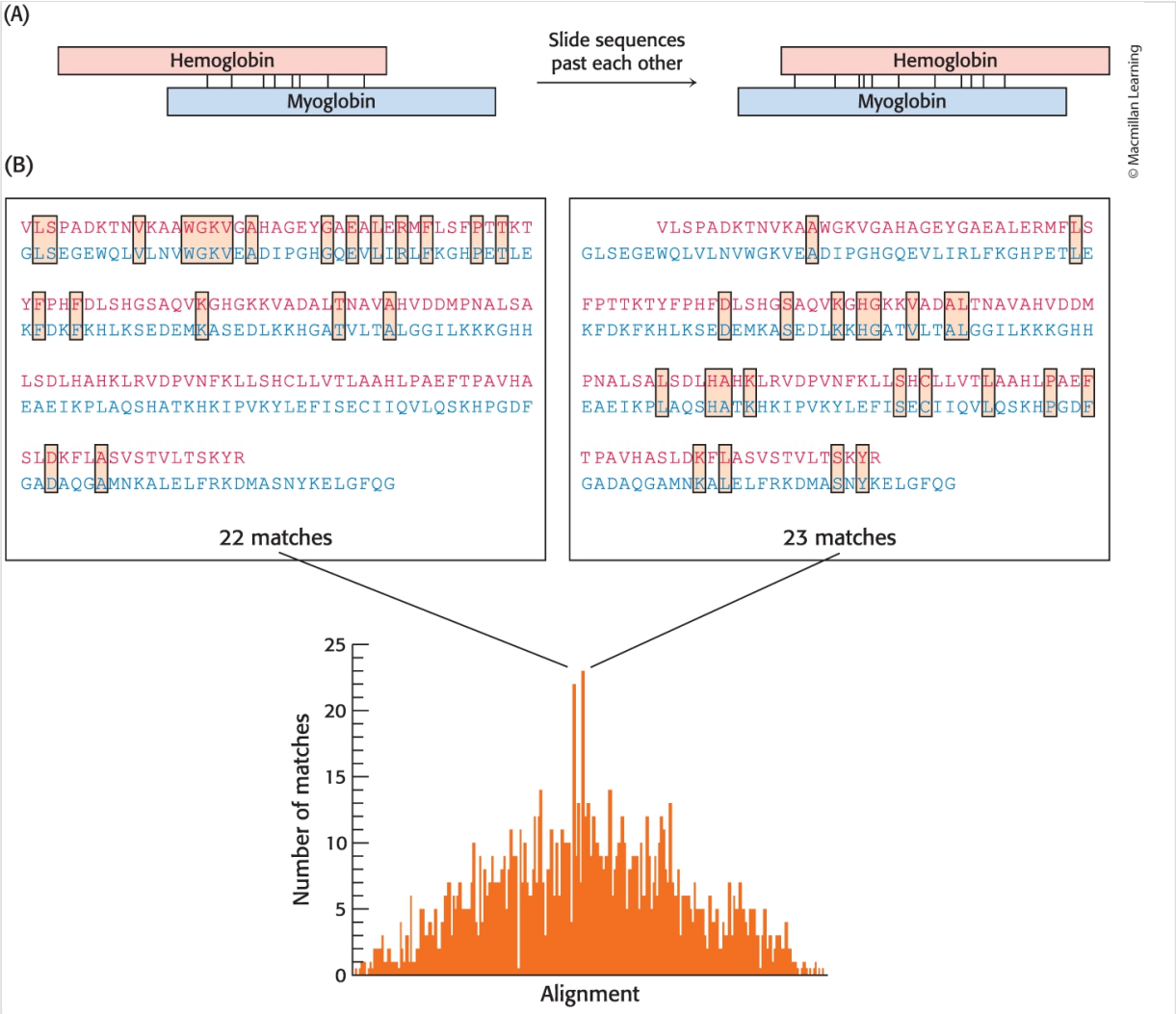


FIGURE 10.3 Amino acid sequences are compared by sliding one sequence past the other, one amino acid at a time. (A) At each step, we count the number of amino acid identities between the two proteins. Shown are representations of just two of the > 100 possible alignments. (B) The two alignments with the largest number of matches are shown above the graph, which plots the matches as a function of alignment.

However, careful examination of all the possible alignments and their scores suggests that important information regarding the relationship between myoglobin and hemoglobin α has been lost with this method. In particular, we see that another alignment, featuring 22 identities, is

nearly as good (Figure 10.3). This alignment is shifted by six residues relative to the preceding alignment and yields identities that are concentrated toward the amino-terminal end of the sequences. By introducing a gap into one of the sequences, the identities found in both alignments will be represented (**Figure 10.4**). The insertion of gaps allows the alignment method to compensate for the insertions or deletions of nucleotides that may have taken place in the gene for one molecule but not the other in the course of evolution.

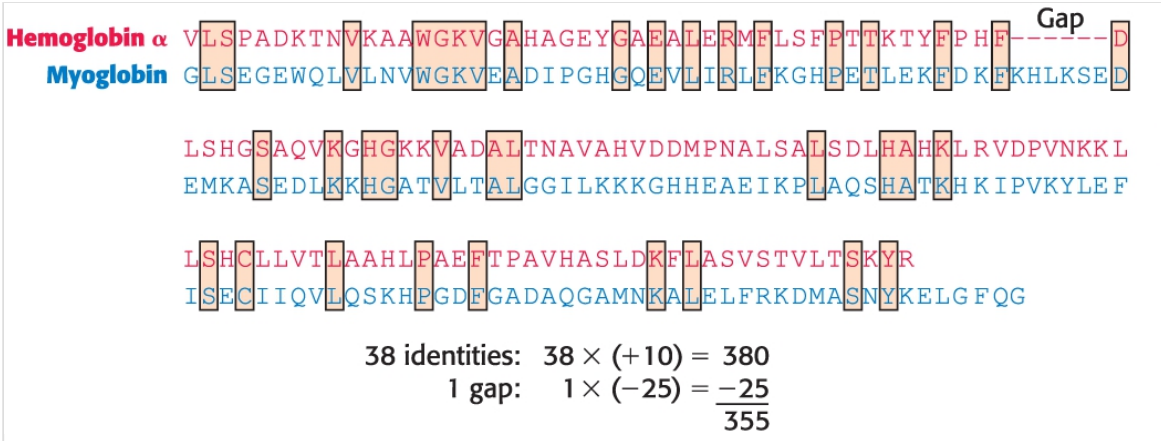


FIGURE 10.4 Addition of a gap improves the alignment between myoglobin and α-hemoglobi
In the scoring method shown in this figure, a penalty is applied for the gap introduced.

The use of gaps substantially increases the complexity of sequence alignment because a vast number of possible gaps, varying in both position and length, must be considered throughout each sequence. Moreover, the introduction of an excessive number of gaps can yield an artificially high number of identities. Nevertheless, methods have been developed for the insertion of gaps in the automatic alignment of sequences. These methods use scoring systems to compare different alignments, including penalties for gaps to prevent the insertion of an unreasonable number of them. For example, in one scoring system, each identity between aligned sequences is counted as $+10$ points,

whereas each gap introduced, regardless of size, counts for -25 points. For the alignment shown in Figure 10.4, there are 38 identities ($38 \times 10 = 380$) and 1 gap ($1 \times -25 = -25$), producing a score of ($380 + -25 = 355$). Overall, there are 38 matched amino acids in an average length of 147 residues; thus, the sequences are 25.9% identical.

Alignments such as the one just described inform us as to the percent identity between two sequences. However, the question remains: how do we interpret this value? For example, we have determined that α-hemoglobin and myoglobin, when allowing for the insertion of gaps, are 25.9% identical. Is this value sufficiently high to suggest a relationship between these two proteins? To answer these questions, we must determine the significance of alignment scores and percent identities.

Self-Check Question



Why is it important to assess penalties for the placement of gaps when scoring an alignment?

The statistical significance of alignments can be estimated by shuffling

The sequence similarities in Figure 10.4 appear striking, yet there remains the possibility that a grouping of sequence identities has occurred by chance alone. Because proteins are composed of the same set of 20 amino acid monomers, the alignment of any two unrelated proteins will yield some identities, particularly if we allow the introduction of gaps. Even if two proteins have identical amino acid composition, they may not be linked by evolution. It is the order of the

residues within their sequences that implies a relationship between them.

We can assess the significance of our alignment by "shuffling," or randomly rearranging, one of the sequences (Figure 10.5), performing the sequence alignment, and determining a new alignment score. This process is repeated many times to yield a histogram showing, for each possible score, the number of shuffled sequences that received that score (Figure 10.6). If the original score is appreciably different from the scores from the shuffled alignments, then it is unlikely that the original alignment is merely a consequence of chance.

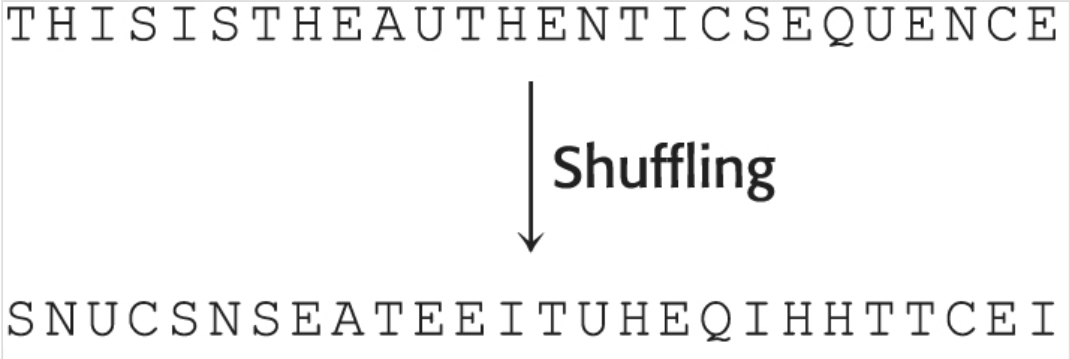


FIGURE 10.5 The individual amino acids are scrambled to generate a shuffled sequence.

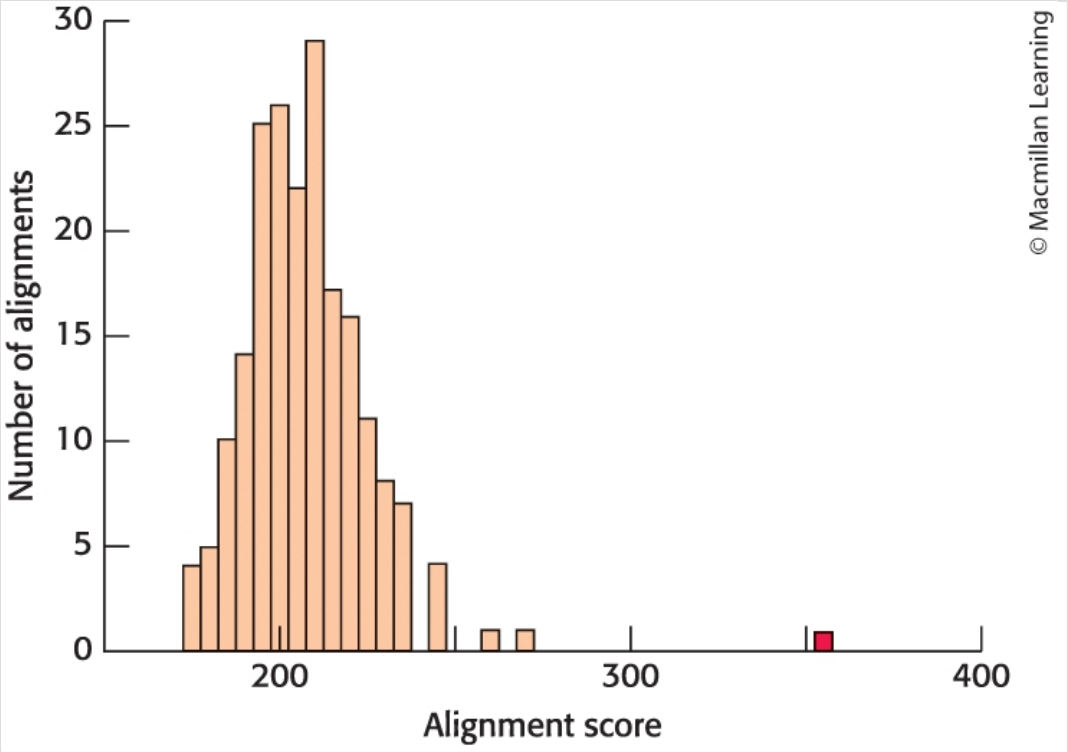


FIGURE 10.6 Comparison of alignment scores reveals the statistical significance of an unshuffled alignment. Alignment scores are calculated for many shuffled sequences, and the number of sequences generating a particular score is plotted against the score. The resulting plot is a distribution of alignment scores occurring by chance. The alignment score for unshuffled α-hemoglobin and myoglobin (shown in red) is substantially greater than any of these scores, strongly suggesting that the sequence similarity is significant.

When this procedure is applied to the sequences of myoglobin and α-hemoglobin, the authentic alignment (indicated by the red bar in Figure 10.6) clearly stands out. Its score is far above the mean for the alignment scores based on shuffled sequences. The probability that such a deviation occurred by chance alone is approximately 1 in 10^{20}.

Thus, we can comfortably conclude that the two sequences are genuinely similar; the simplest explanation for this similarity is that these sequences are homologous — that is, the two molecules have descended from a common ancestor.

Distant evolutionary relationships can be detected through the use of substitution matrices

The scoring scheme described above assigns points only to positions occupied by identical amino acids in the two sequences. No credit is given for any pairing that is not an identity. However, as already discussed, two proteins related by evolution undergo amino acid substitutions as they diverge. A scoring system based solely on amino acid identity cannot account for these changes. To add greater sensitivity to the detection of evolutionary relationships, methods have been developed to compare two amino acids and assess their degree of *similarity*.

Not all substitutions are equivalent. For example, amino acid changes can be classified as structurally conservative or nonconservative. A **conservative substitution** replaces one amino acid with another that is similar in size and chemical properties. Conservative substitutions may have only minor effects on protein structure and often can be tolerated without compromising protein function. In contrast, in a **nonconservative substitution**, an amino acid is replaced by one that is structurally dissimilar. Amino acid changes can also be classified by the fewest number of nucleotide changes necessary to achieve the corresponding amino acid change. Some substitutions arise from the replacement of only a single nucleotide in the gene sequence, whereas others require two or three replacements. Conservative and single-nucleotide substitutions are likely to be more common than are substitutions with more radical effects.

How can we account for the type of substitution when comparing sequences? We can approach this problem by first examining the substitutions that have been observed in proteins known to be evolutionarily related. From an examination of appropriately aligned sequences, substitution matrices have been deduced. A **substitution**

matrix describes a scoring system for the replacement of any amino acid with each of the other 19 amino acids. In these matrices, a large positive score corresponds to a substitution that occurs relatively frequently, whereas a large negative score corresponds to a substitution that occurs only rarely.

One commonly used substitution matrix, the Blosum-62 (for Blocks of amino acid substitution matrix), is illustrated in **Figure 10.7**. In this depiction, each column in this matrix represents 1 of the 20 amino acids, whereas the position of the single-letter codes within each column specifies the score for the corresponding substitution. Notice that scores corresponding to identity (the boxed codes at the top of each column) are not the same for each residue, owing to the fact that less frequently occurring amino acids such as cysteine (C) and tryptophan (W) will align by chance less often than the more common residues. Furthermore, structurally conservative substitutions such as lysine (K) for arginine (R) and isoleucine (I) for valine (V) have relatively high scores, whereas nonconservative substitutions such as lysine for tryptophan result in negative scores (**Figure 10.8**).

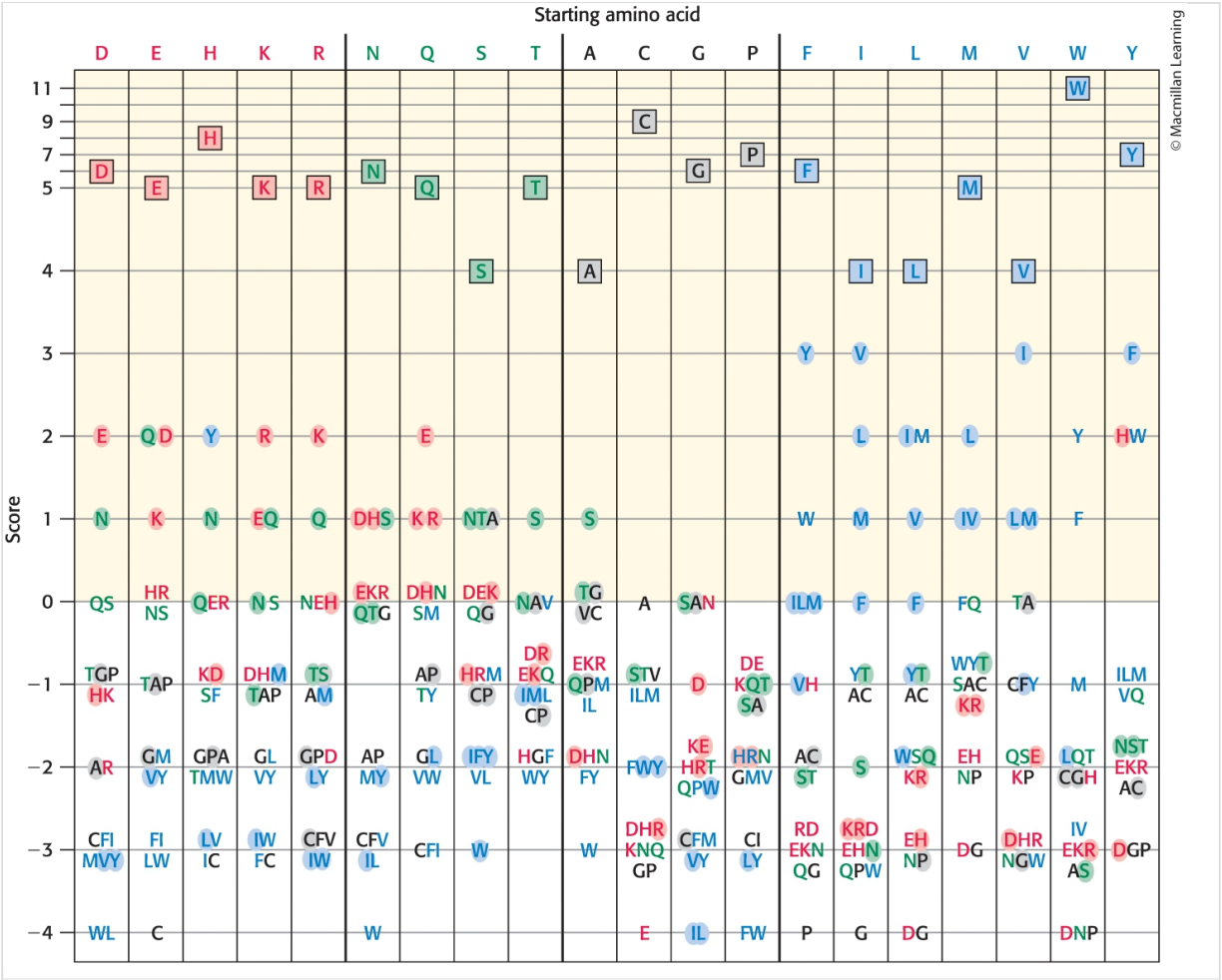


FIGURE 10.7 The Blosum-62 substitution matrix enables scoring based on amino acid similarity. This matrix was derived by examining substitutions within aligned sequence blocks in related proteins. In this graphical view, amino acids are classified into four groups (charged, red; polar, green; large and hydrophobic, blue; other, black). Substitutions that require the change of only a single nucleotide are shaded. Identities are boxed. To find the score for a substitution of, for instance, a Y for an H, you find the Y in the column having H at the top and check the number at the left. In this case, the resulting score is 2.

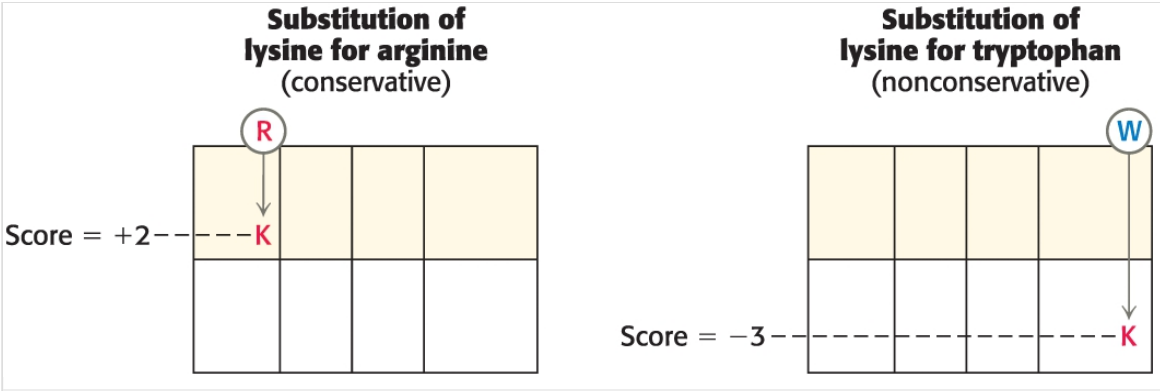


FIGURE 10.8 Conservative and nonconservative substitutions yield very different scores in th Blosum-62 matrix. A conservative substitution (lysine for arginine) receives a positive score, whereas a nonconservative substitution (lysine for tryptophan) is scored negatively. The matrix depicted as an abbreviated form of Figure 10.7.

When two sequences are compared, each pair of aligned residues is assigned a score based on the matrix. In addition, gap penalties are often assessed. For example, the introduction of a single-residue gap lowers the alignment score by 12 points, and the extension of an existing gap costs 2 points per residue. With the use of the Blosum-62 scoring system, the alignment between human α-hemoglobin and human myoglobin shown in Figure 10.4 receives a score of 115. In many regions, most substitutions are conservative (defined as those substitutions with scores greater than 0), and relatively few are strongly disfavored (**Figure 10.9**).



FIGURE 10.9 Counting conservative substitutions reveals strong similarity between α-hemoglobin and myoglobin. Conservative substitutions are indicated by yellow shading and

identities by the orange boxes.

This scoring system detects homology between less obviously related sequences with greater sensitivity than would a comparison of identities only. Consider, for example, the protein leghemoglobin, an oxygen-binding protein found in the roots of leguminous plants. The amino acid sequence of leghemoglobin from the lupine plant can be aligned with that of human myoglobin and scored by using either the simple scoring scheme based on identities only or the Blosum-62 (Figure 10.7). Repeated shuffling and scoring provides a distribution of alignment scores, as shown in **Figure 10.10**.

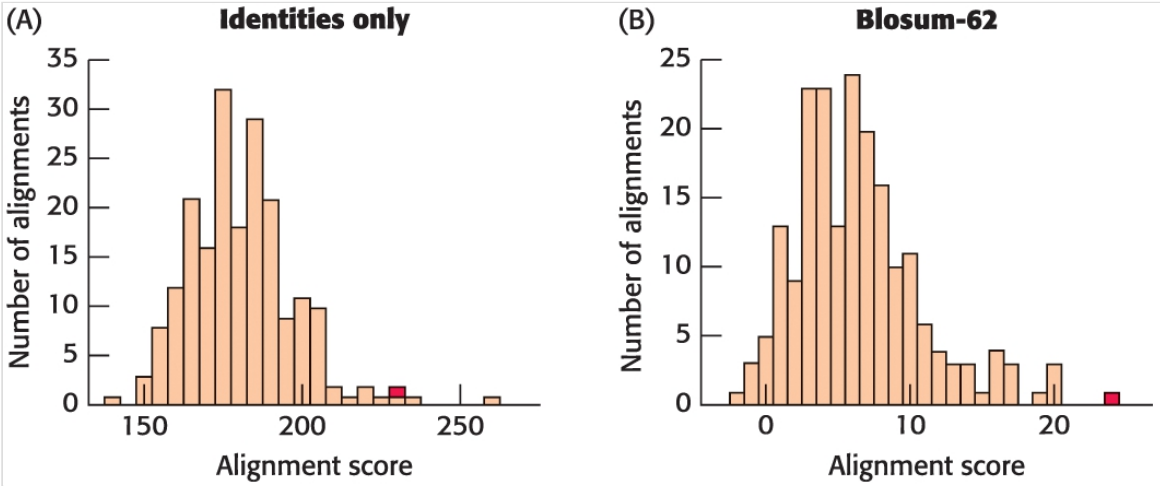


FIGURE 10.10 Alignment using Blosum-62 can uncover more distant evolutionary relationships. Repeated shuffling and scoring reveal the significance of sequence alignment for human myoglobin versus lupine leghemoglobin with the use of either (A) the simple, identity-based scoring system or (B) the Blosum-62. The scores for the alignment of the authentic sequences are shown in red. Accounting for amino acid similarity in addition to identity reveals greater separation between the authentic alignment and the population of shuffled alignments. (Note that these two scoring systems use different scales on their respective *x*-axes, so the raw scores cannot be directly compared.)

Scoring based solely on identities (Figure 10.10A) indicates that the probability of the alignment between myoglobin and leghemoglobin occurring by chance alone is 1 in 20. Thus, although the level of similarity suggests a relationship, there is a 5% chance that the similarity is accidental on the basis of this analysis. In contrast, scoring based on the substitution matrix, which accounts for conservative substitutions, determines that the odds of the alignment occurring by chance are calculated to be approximately 1 in 300 (Figure 10.10B). Thus, an analysis performed with the substitution matrix reaches a much firmer conclusion about the evolutionary relationship between these proteins (**Figure 10.11**).

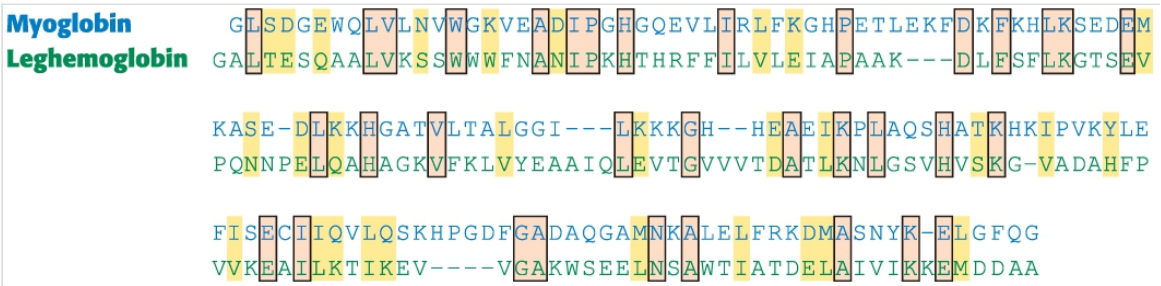


FIGURE 10.11 Alignment of human myoglobin and lupine leghemoglobin reveals many conservative substitutions. The use of Blosum-62 yields the alignment shown between human myoglobin and lupine leghemoglobin, illustrating identities (orange boxes) and conservative substitutions (yellow). These sequences are 23% identical.

Experience with sequence analysis has led to the development of simpler rules of thumb. For sequences longer than 100 amino acids, sequence identities greater than 25% are almost certainly not the result of chance alone; such sequences are probably homologous. In contrast, if two sequences are less than 15% identical, their alignment alone is unlikely to indicate statistically significant similarity. For sequences that are between 15% and 25% identical, further analysis is necessary to determine the statistical significance of the alignment.

It must be emphasized that the lack of a statistically significant degree of sequence similarity does not rule out homology. The sequences of many proteins that have descended from common ancestors have diverged to such an extent that the relationship between the proteins can no longer be detected from their sequences alone. As we will see, such homologous proteins can often be identified by examining their three-dimensional structures.

Databases can be searched to identify homologous sequences

When the sequence of a protein is first determined, comparing it with all previously characterized sequences can provide tremendous insight into its evolutionary relatives and, hence, its structure and function. Indeed, an extensive sequence comparison is almost always the first analysis performed on a newly elucidated sequence. The sequence-alignment methods just described are used to compare an individual sequence with all members of a database of known sequences.

Database searches for homologous sequences are most often accomplished by using resources available on the Internet at the National Center for Biotechnology Information (www.ncbi.nlm.nih.gov). The procedure used is referred to as a **basic local alignment search tool (BLAST) search**. An amino acid sequence is entered into a browser (blast.ncbi.nlm.nih.gov), and a search is performed, most often against a nonredundant database of all known sequences. In 2021, this database included more than 400 million sequences. A BLAST search yields a list of sequence alignments, each accompanied by an estimate giving the likelihood that the alignment occurred by chance (**Figure 10.12**).

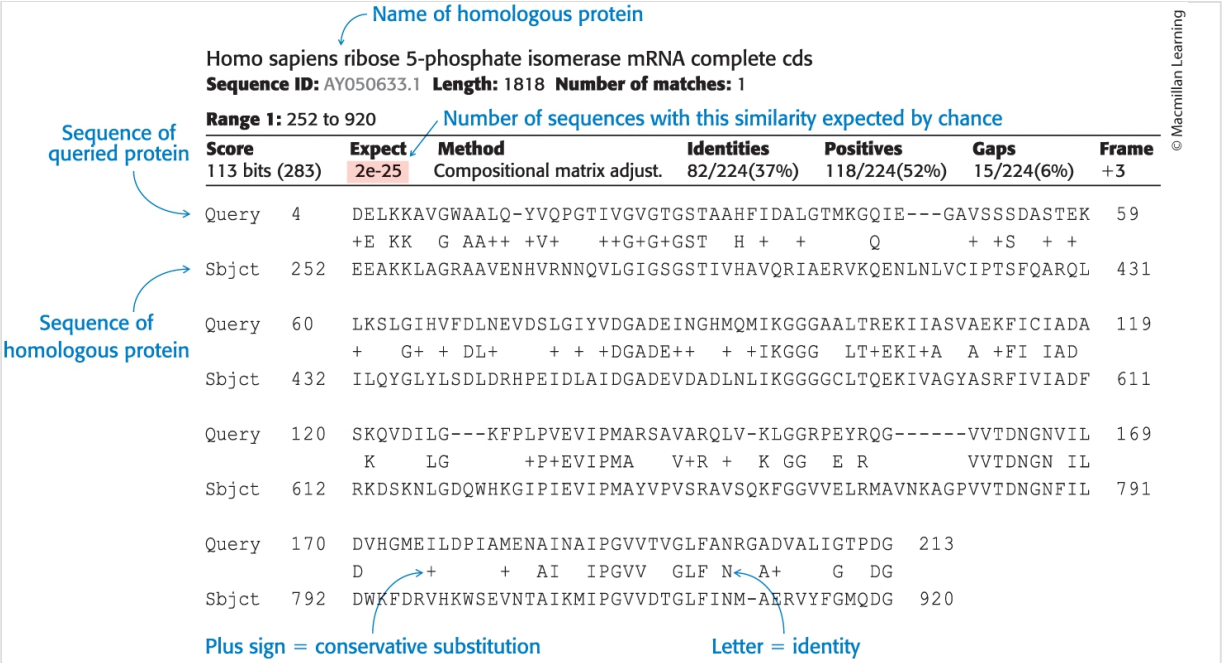


FIGURE 10.12 Related protein sequences can be rapidly identified using online BLAST searches. Part of the results from a BLAST search of the nonredundant (nr) protein sequence database using the sequence of ribose 5-phosphate isomerase (also called phosphopentose isomerase, Chapter 20) from *E. coli* as a query. Among the thousands of sequences found is the orthologous sequence from humans, and the alignment between these sequences is shown. The number of sequences with this level of similarity expected to be in the database by chance is 2×10^{-25} as shown by the E value (highlighted in red). Because this value is much less than 1, we can confidently conclude that the observed sequence alignment is highly significant.

In 1995, investigators reported the first complete sequence of the genome of a free-living organism, the bacterium *Haemophilus influenzae* (Figure 9.25). With the sequences available, they performed a BLAST search with each deduced protein sequence. Of 1743 identified protein-coding regions, also referred to as **open reading frames (ORFs)**, 1007 (58%) could be linked to some protein of known function that had been previously characterized in another organism. An additional 347 ORFs could be linked to sequences in the database for which no function had yet been assigned ("hypothetical proteins"). The remaining 389 sequences did not match any sequence present in the database at that

time. Thus, investigators were able to identify likely functions for more than half the proteins within this organism solely by sequence comparisons.

Self-Check Question



Using the National Center for Biotechnology Information website (www.ncbi.nlm.nih.gov), find the sequences of the enzyme triose phosphate isomerase from *E. coli* strain K-12 and from *Homo sapiens* (use isoform #1). Use the Global Align tool on the NCBI BLAST website to align these two sequences. What is the percent identity between these two proteins?

10.2 Examination of Three-Dimensional Structure Enhances Our Understanding of Evolutionary Relationships

Sequence comparison is a powerful tool for extending our knowledge of protein function and kinship. However, biomolecules generally function as intricate three-dimensional structures rather than as linear polymers. Mutations occur at the level of sequence, but the effects of the mutations are at the level of function, and function is directly related to tertiary structure. Consequently, to gain a deeper understanding of evolutionary relationships between proteins, we must examine three-dimensional structures, especially in conjunction with sequence information. The techniques of structural determination were presented in Section 4.5.

Tertiary structure is more conserved than primary structure

Because three-dimensional structure is much more closely associated with function than is sequence, tertiary structure is more evolutionarily conserved than is primary structure. This conservation is apparent in the tertiary structures of the globins (**Figure 10.13**), which are extremely similar even though the similarity between human myoglobin and lupine leghemoglobin is weakly detectable at the sequence level (Figure 10.10) and that between human α-hemoglobin and lupine leghemoglobin is not statistically significant (15% identity). This structural similarity firmly establishes that the framework that binds

the heme group and facilitates the reversible binding of oxygen has been conserved over a long evolutionary period.

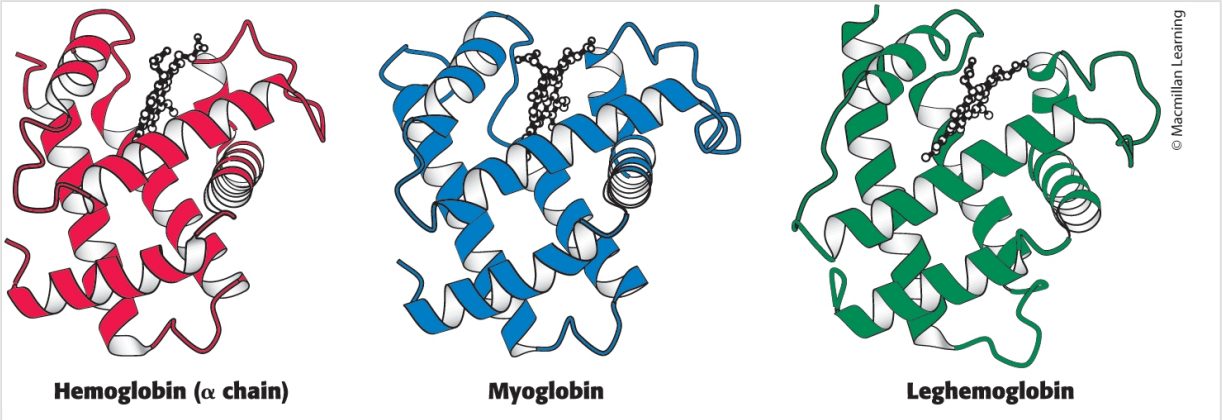


FIGURE 10.13 Three-dimensional structure is more conserved than primary structure. The tertiary structures of human hemoglobin (α chain), human myoglobin, and lupine leghemoglobin are conserved. Each heme group contains an iron atom to which oxygen binds.

[Drawn from 1HBB.pdb, 1MBD.pdb, and 1GDJ.pdb.]

INTERACT with these models in Achieve

Anyone aware of the similar biochemical functions of hemoglobin, myoglobin, and leghemoglobin could expect the structural similarities. In a growing number of other cases, however, a comparison of three-dimensional structures has revealed striking similarities between proteins that were *not* expected to be related, on the basis of their diverse functions. A case in point is the protein actin, a major component of the cytoskeleton (Section 6.5) and heat shock protein 70 (Hsp70), which assists protein folding inside cells. These two proteins were found to be noticeably similar in structure despite only 16% sequence identity (**Figure 10.14**). On the basis of their three-dimensional structures, actin and Hsp70 are paralogs. The level of structural similarity strongly suggests that, despite their different biological roles in modern organisms, these proteins descended from a common ancestor.

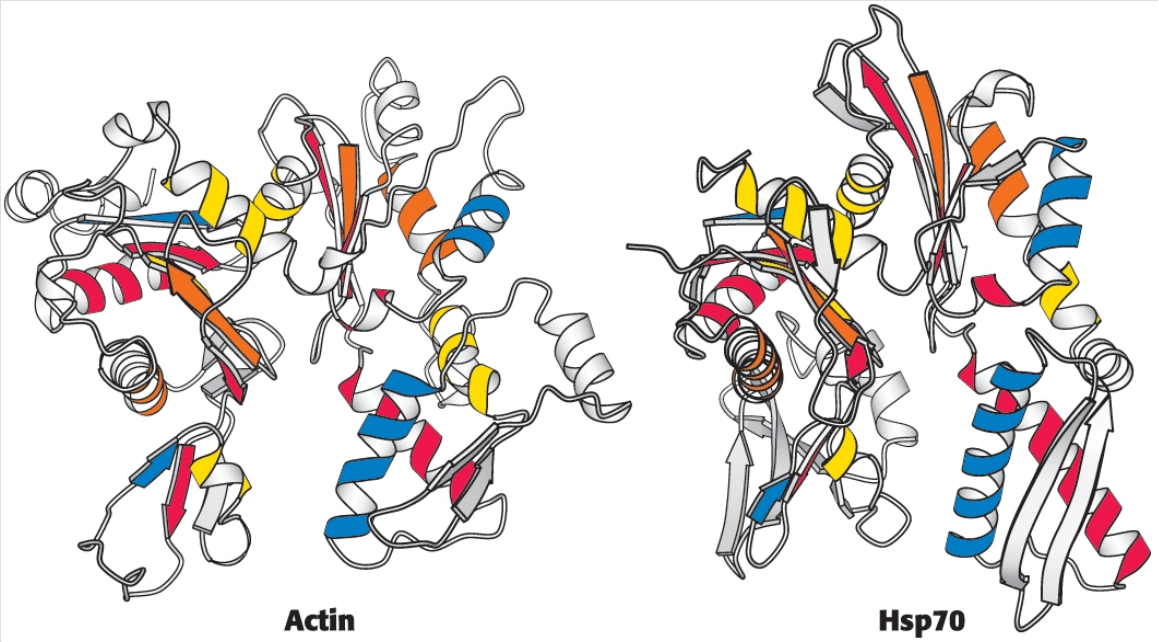


FIGURE 10.14 The structures of actin and a large fragment of heat shock protein 70 (Hsp70) reveal an unexpected relationship. A comparison of the identically colored elements of secondary structure reveals the overall similarity in structure despite the difference in biochemical activities.

[Drawn from 1ATN.pdb and 1ATR.pdb.]

INTERACT with these models in Achieve

As the three-dimensional structures of more proteins are determined, such unexpected kinships are being discovered with increasing frequency. The search for such kinships relies ever more frequently on computer-based searches that are able to compare the three-dimensional structure of any protein with all other known structures.

Knowledge of three-dimensional structures can aid in the evaluation of sequence

alignments

The sequence-comparison methods described thus far treat all positions within a sequence equally. However, we have learned from examining families of homologous proteins for which at least one three-dimensional structure is known that regions and residues critical to protein function are more strongly conserved than are other residues. For example, each type of globin contains a bound heme group with an iron atom at its center. A histidine residue that interacts directly with this iron atom (Section 3.2) is conserved in all globins.

After we have identified key residues or highly conserved sequences within a family of proteins, we can generate a **sequence template** — a map of conserved residues that are structurally and functionally important and are characteristic of particular families of proteins. By preferentially scoring residues known to be important for structure or function, we can sometimes identify other family members even when the overall level of sequence similarity is below statistical significance and might be undetectable by other means.

Still other methods are able to identify conserved residues within a family of homologous proteins, even without a known three-dimensional structure. These methods often use substitution matrices that differ at each position within a family of aligned sequences. Such methods can often detect quite distant evolutionary relationships.

Repeated motifs can be detected by aligning sequences with themselves

As discussed in Section 2.5, domains are compact regions of structure that can be found in a wide variety of proteins. In fact, more than 10% of all proteins contain sets of two or more domains that are similar to

one another. Sequence search methods can often detect these internally repeated sequences that have been characterized in other proteins.

Often, however, internally repeated sequences do not correspond to previously identified domains. In these cases, their presence can be detected by attempting to align a given sequence with itself. The statistical significance of such repeats can be tested by aligning the regions in question as if these regions were sequences from separate proteins. Of course, in a self-alignment, there will be one "hit" that will yield a perfect score. However, additional regions where internal alignment achieves significance may indicate the presence of repeated domains within a given protein.

Consider, for example, the TATA-box-binding protein, a key protein in controlling eukaryotic gene transcription (Section 29.3). Alignment of this protein with itself reveals a significant region of homology between the N-terminal half of the protein with its C-terminal half (**Figure 10.15A**). Comparison of two 65-residue segments from these regions reveals that 40% of the amino acids are identical (**Figure 10.15B**). The estimated probability of such an alignment occurring by chance is less than 1 in 10^{10}. The determination of the three-dimensional structure of the TATA-box-binding protein confirmed the presence of repeated structures; the protein is formed of two nearly identical domains (**Figure 10.15C**). The evidence is convincing that the gene encoding this protein evolved by duplication of a gene encoding a single domain.

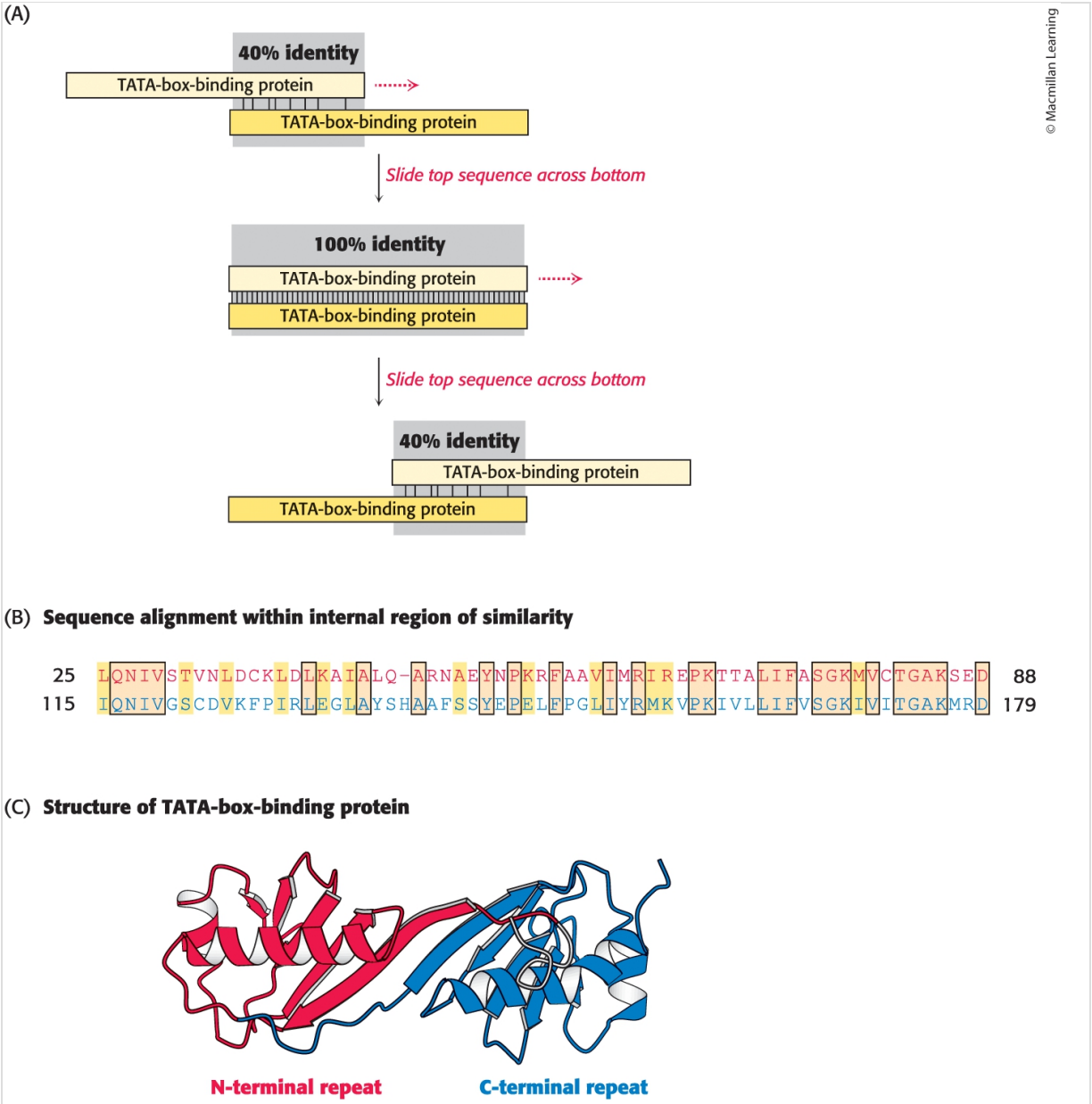


FIGURE 10.15 Internal repeats can be identified using a self-alignment. (A) When the TATA-box-binding protein is aligned against itself, a region of significant identity between the N-terminal and C-terminal halves is revealed. (B) Alignment of these N-terminal and C-terminal sequences shows 40% identity and considerable similarity. The N-terminal region is shown in red and the C-terminal region in blue. (C) Consistent with the sequence alignment data, the three-dimensional structure of the TATA-box-binding protein reveals the presence of two structurally similar repeats. The N-terminal domain is shown in red and the C-terminal domain in blue.

[Drawn from 1VOK.pdb.]

INTERACT with this model in Achieve

Convergent evolution illustrates common solutions to biochemical challenges

Thus far, we have been using sequence analysis methods to identify occurrences of **divergent evolution**, the process by which proteins derived from a common ancestor accumulate differences over time, potentially acquiring new functions. In other examples, proteins have been identified that are structurally similar in important ways but are not descended from a common ancestor. How might two unrelated proteins come to resemble each other structurally? Two proteins evolving independently may have converged on similar structural features to perform a similar biochemical activity. Perhaps that structure was an especially effective solution to a biochemical problem. The process by which very different evolutionary pathways lead to the same solution is called **convergent evolution**.

An example of convergent evolution is found among the serine proteases. Recall that these enzymes cleave peptide bonds by hydrolysis (Section 6.2). The active sites for two such enzymes, mammalian chymotrypsin and bacterial subtilisin, are remarkably similar (**Figure 10.16, top**). In each case, the catalytic triad of a serine residue, a histidine residue, and an aspartate residue is positioned in space in nearly identical arrangements. This conserved spatial arrangement is critical for the activity of these enzymes and affords the same mechanistic solution to the problem of peptide bond hydrolysis.

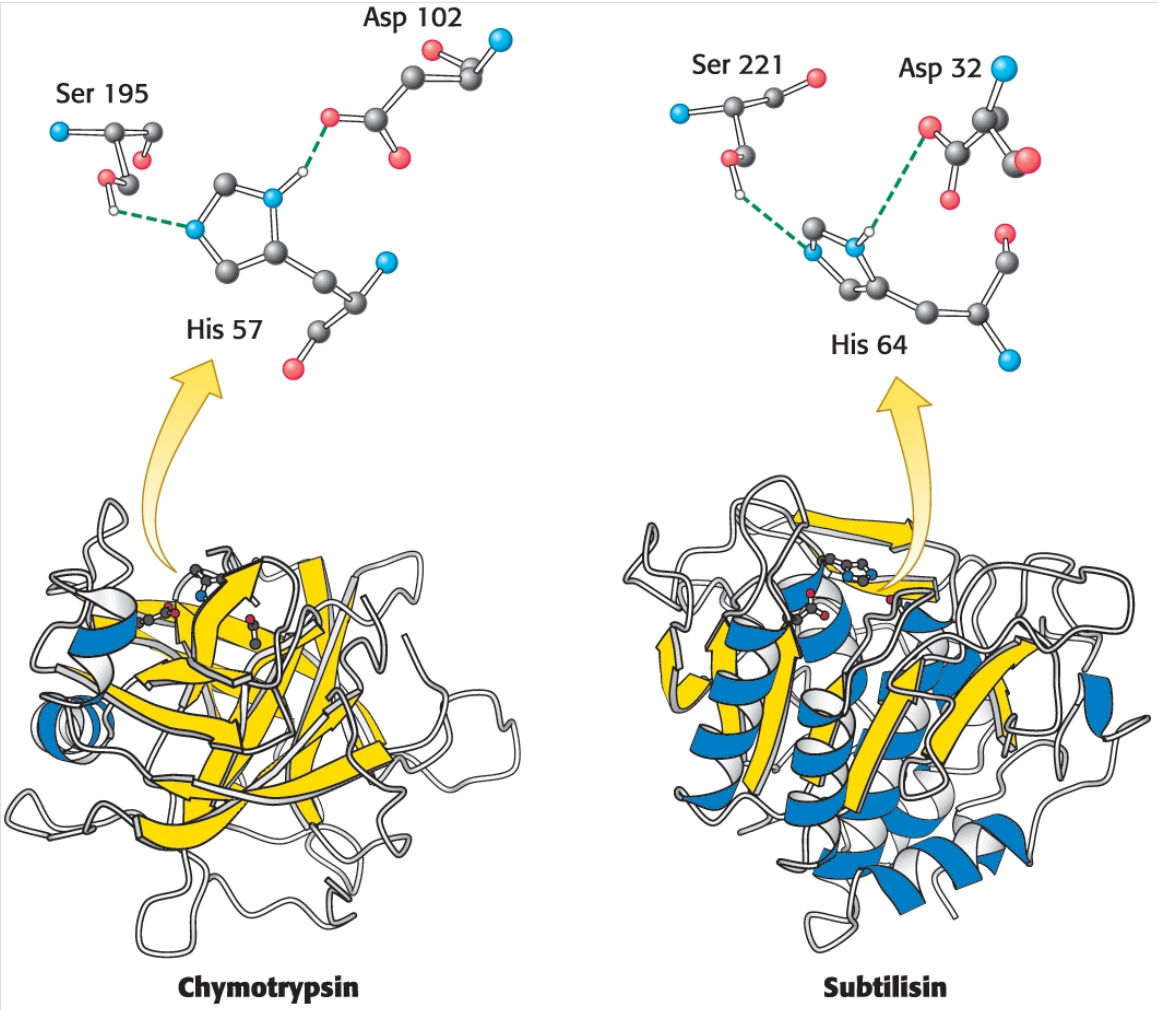


FIGURE 10.16 Mammalian chymotrypsin and bacterial subtilisin are examples of convergent evolution. The relative positions of the three key catalytic residues are nearly identical in the active sites of the serine proteases chymotrypsin and subtilisin. Yet, the overall protein structur are quite dissimilar, suggesting that although these proteins derived from different ancestors, they arrived at a similar solution to the challenge of peptide bond hydrolysis.

[Drawn from 1GCT.pdb and 1SUP.pdb.]

INTERACT with these models in Achieve

At first glance, this similarity between chymotrypsin and subtilisin might suggest that these proteins are homologous. However, striking differences in the overall structures of these proteins make an

evolutionary relationship extremely unlikely (**Figure 10.16, bottom**). Whereas chymotrypsin consists almost entirely of β sheets, subtilisin contains extensive α-helical structure. Moreover, the key serine, histidine, and aspartic acid residues do not even appear in the same order within the two sequences. It is extremely unlikely that two proteins evolving from a common ancestor could have retained similar active-site structures while other aspects of the structure changed so dramatically.

Comparison of RNA sequences can be a source of insight into RNA secondary structures

The methods and interpretation of sequence alignments described above are not limited to proteins. Homologous RNA sequences can also be similarly studied, yielding important insights into evolutionary relationships. Additionally, these analyses provide clues to the three-dimensional structure of the RNA itself. As noted in Chapter 8, single-stranded nucleic acid molecules fold back on themselves to form elaborate structures held together by Watson–Crick base-pairing and other noncovalent interactions. In a family of sequences that form similar base-paired structures, base sequences may vary, but base-pairing ability is conserved.

Consider, for example, a region from a large RNA molecule present in the ribosomes of all organisms (**Figure 10.17**). In the region shown, the *E. coli* sequence has a guanine (G) residue in position 9 and a cytosine (C) residue in position 22, whereas the human sequence has uracil (U) in position 9 and adenine (A) in position 22. Examination of the six sequences shown in Figure 10.17A reveals that the bases in positions 9 and 22, as well as several of the neighboring positions, retain the ability to form Watson–Crick base pairs even though the identities of the bases

in these positions vary. We can deduce that two segments with paired mutations that maintain base-pairing ability are likely to form a double helix (Figure 10.17B), a prediction that was confirmed when the three-dimensional structure of this particular rRNA was determined (Section 30.3). Where sequences are known for several homologous RNA molecules, this type of sequence analysis can often suggest complete secondary structures as well as interactions that do not follow the standard Watson–Crick base-pairing rules (Section 8.2).

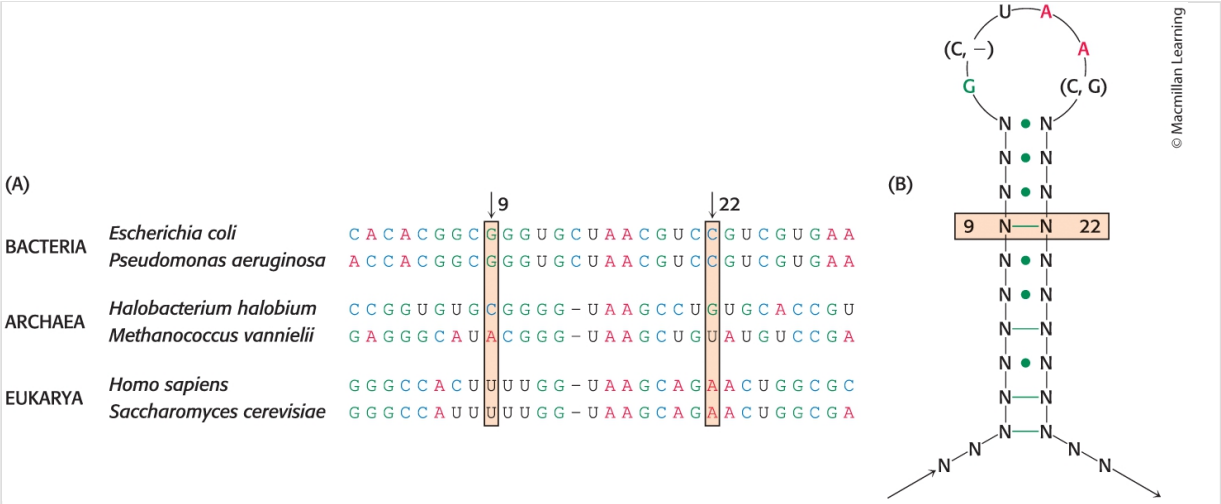


FIGURE 10.17 RNA sequence alignments provide insights into structure based on conservation of base-pairing. (A) A comparison of sequences in a part of ribosomal RNA taken from a variety of species. (B) The implied secondary structure. Green lines indicate positions at which Watson–Crick base-pairing is completely conserved in the sequences shown, whereas dots indicate positions at which Watson–Crick base-pairing is conserved in most cases.

Self-Check Question

When RNA alignments are used to determine secondary structure, it is advantageous to have many sequences representing a wide variety of species. Why?

Example

Interpreting an RNA Alignment

Problem:

Sequences of an RNA fragment from five species have been determined and aligned. Propose a likely secondary structure for these fragments:

(1) UUGGAGAUUCGGUAGAAUCUCCC
(2) GCCGGGAAUCGACAGAUUCCCCG
(3) CCCAAGUCCCGGCAGGGACUUAC
(4) CUCACCUGCCGAUAGGCAGGUCA
(5) AAUACCACCCGGUAGGGUGGUUC

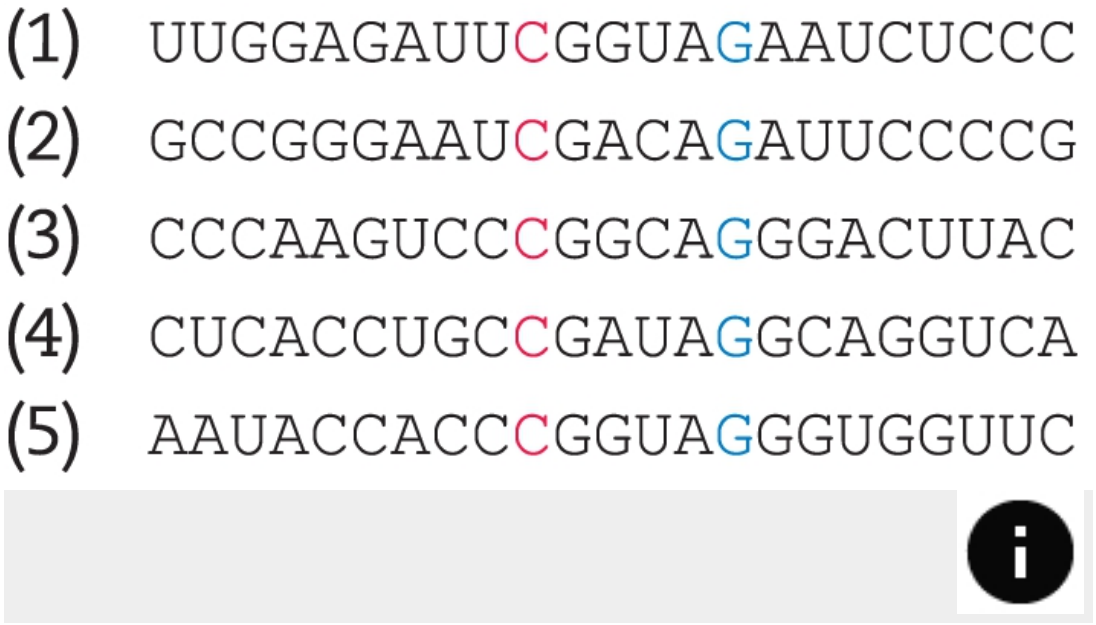


Getting Started:

For a simple alignment over a short RNA fragment such as the one featured in this problem, the trick is to look for two positions that could form a base pair in each of the aligned sequences. If the possibility of a

base pair is conserved through all the sequences, then it is likely that this pairing is a component of the predicted secondary structure.

Of particular interest in this alignment is the base highlighted in red:

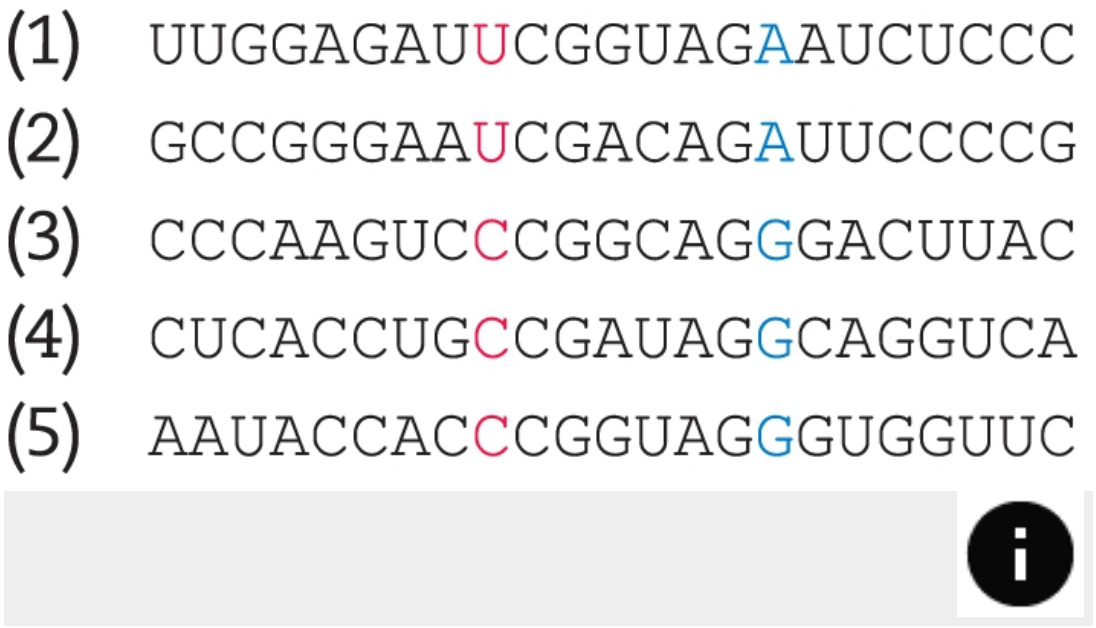


In all five sequences, this is an absolutely conserved cytosine. In this alignment, there are only two absolutely conserved guanine bases. One is immediately 3′ to this cytosine, and we know from oligonucleotide

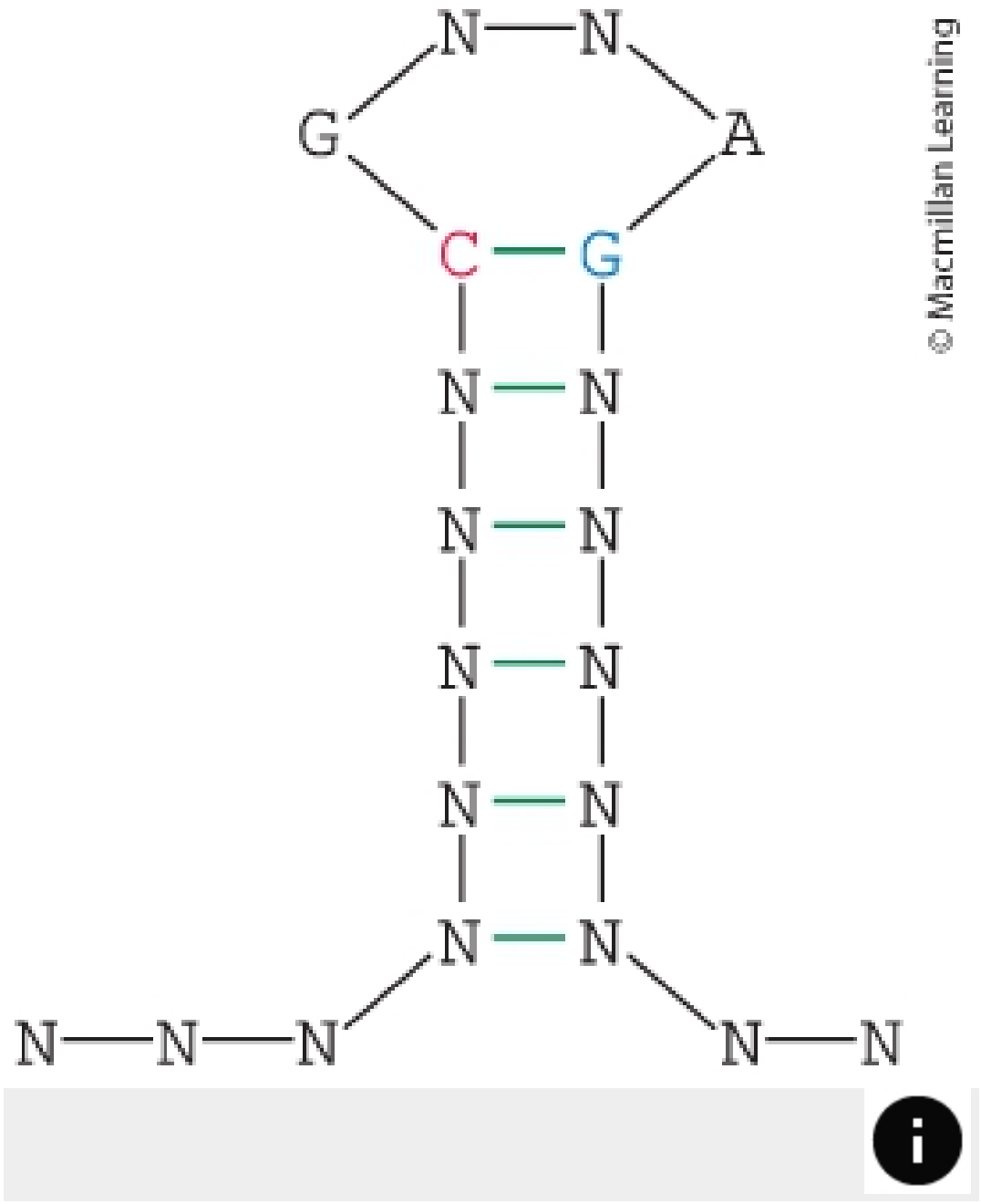
structure that a base pair between adjacent positions is highly unlikely. The other is the guanine highlighted in blue, which is separated from the cytosine by four nucleotides. An intriguing possibility!

SOLVE:

Now, we have an “anchor” from which we can continue looking for additional pairings. In order for this red–blue pairing to form, the RNA fragment would need to fold on itself. Hence, we should look outward from this pair to identify additional base pairs:



Again, we have a conserved pairing. In sequences (1) and (2), the red and blue positions feature a U–A pair, while in sequences (3), (4), and (5), these positions form a C–G pair. If we continue to "walk" along the sequence in this manner, a clear stretch of base-pairing emerges. Moreover, since several of these positions are absolutely conserved, we can include them in our proposed structure (shown at right, with the original C–G base pair in red/blue).



Reflect:

Determining secondary structure predictions from oligonucleotide sequences can appear difficult at first. There are only four possible bases, so patterns may not be easily discernible. The key strategy is to look for potential base pairs and work one's way in either direction from

that point. For structure-forming base pairs, while the identities of the bases may not be conserved across the sequence alignments, the possibility of forming a base pair will be absolutely conserved.

10.3 Evolutionary Trees Can Be Constructed on the Basis of Sequence Information

We have discussed previously how measurement of sequence similarity can provide us with information about the evolutionary relationship between two proteins. This concept suggests that by comparing multiple sequences within a protein family, we can deduce their evolutionary history. As we introduced in Section 1.4, this approach is based on the *molecular clock hypothesis*: the notion that sequences that are more similar to one another have had less evolutionary time to diverge than have sequences that are less similar.

This method can be illustrated by using the three globin sequences in Figures 10.9 and 10.11, as well as the sequence for the human hemoglobin β chain. These sequences can be aligned with the additional constraint that gaps, if present, should be at the same positions in all of the proteins. These aligned sequences can be used to construct an **evolutionary tree** in which the length of the branch connecting each pair of proteins is proportional to the number of amino acid differences between the sequences (**Figure 10.18**).

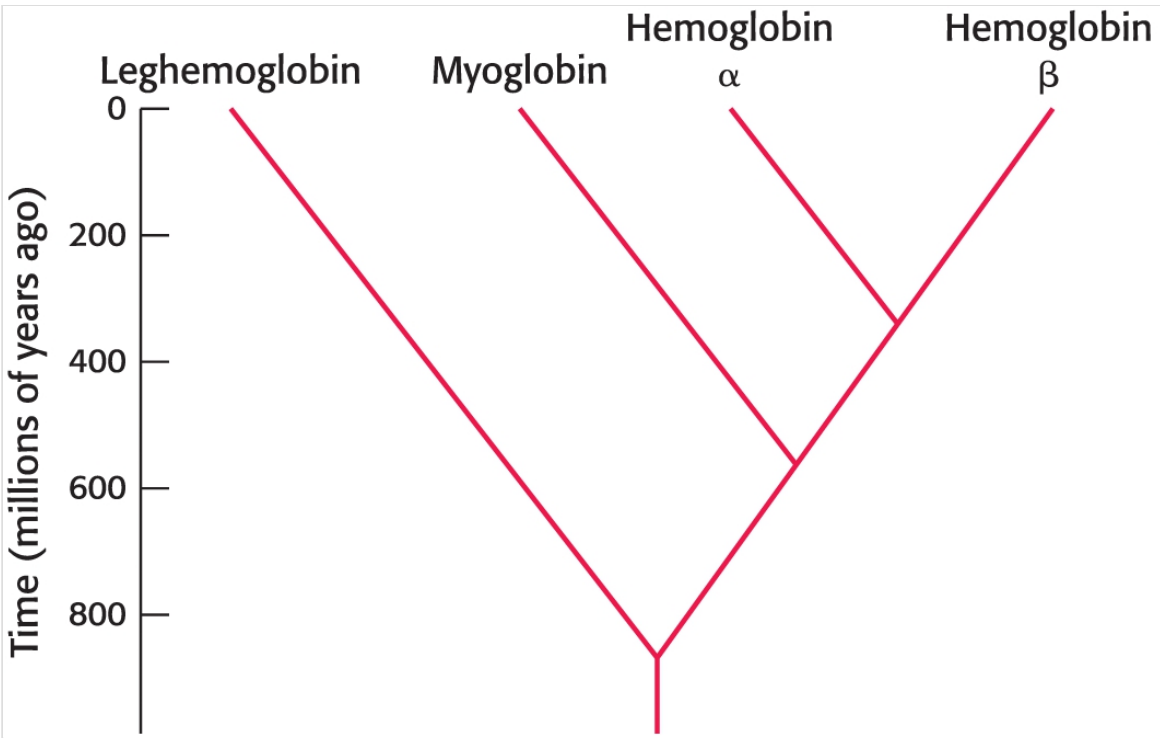


FIGURE 10.18 Sequence alignments enable the construction of an evolutionary tree. In the case of the globins, the branching structure was deduced by sequence comparison, whereas th results of fossil studies provided the overall time scale showing when divergence occurred.

Evolutionary trees can be calibrated using fossil record data

Such comparisons reveal only the relative divergence times — for example, that myoglobin diverged from hemoglobin twice as long ago as the α chain diverged from the β chain. How can we estimate the approximate dates of gene duplications and other evolutionary events? Evolutionary trees can be calibrated by comparing the deduced branch points with divergence times determined from the fossil record. For example, the duplication leading to the two chains of hemoglobin appears to have occurred 350 million years ago. This estimate is supported by the fossil records on the divergence of jawless fish from

bony fish. Jawless fish, such as the lamprey (**Figure 10.19**), contain hemoglobin built from a single subunit. If the fossil record and our globin evolutionary trees are in agreement, jawless fish should have diverged from bony fish at roughly the same time. This is, in fact, the case, as the fossil record suggests this point of divergence was approximately 400 million years ago.



A Hartl/AGE Fotostock

FIGURE 10.19 The lamprey is a jawless fish whose ancestors diverged from bony fishes approximately 400 million years ago. Lamprey hemoglobin molecules contain only a single type of polypeptide chain.

These methods can be applied to both relatively modern and very ancient molecules, such as the ribosomal RNAs that are found in all organisms. Indeed, such an RNA sequence analysis led to the realization that Archaea are a distinct group of organisms that diverged from Bacteria very early in evolutionary history (Figure 1.3).



Russell F. Doolittle, UCSD Chemistry Dept., July 6, 1988, SIO Photographic Laboratory records. SAC 0044. Special Collections & Archives, UC San Diego. https://library.ucsd.edu/dc/object/bb3038569z

RUSSELL DOOLITTLE A pioneer in bioinformatics and the study of molecular evolution, Russell Doolittle compared the sequences of fibrinopeptides (Section 7.5) across animal species and described how this information could illuminate evolutionary relationships during his postdoctoral fellowship in Sweden. Then, as a faculty member at the University of California, San Diego, Doolittle collected blood samples from a variety of mammals at the San Diego Zoo and constructed a detailed evolutionary tree from their fibrinopeptide sequences. Additionally, well before the existence of online sequence databases, Prof. Doolittle established a compendium of known amino acid sequences, single-handedly compiling sequence data from the scientific literature. With his colleagues, he was able to search this information, perform sequence alignments, and construct phylogenetic trees. Prof. Doolittle made numerous additional seminal contributions throughout his career, including the

assessment of sequences for their hydrophobic character (the hydropathy plot, Section 12.4).

Horizontal gene transfer events may explain unexpected branches of the evolutionary tree

Evolutionary trees that encompass orthologs of a particular protein across a range of species can lead to unexpected findings. Consider the unicellular red alga *Galdieria sulphuraria*, a remarkable eukaryote that can thrive in extreme environments, including at temperatures up to 56°C, at pH values between 0 and 4, and in the presence of high concentrations of toxic metals (**Figure 10.20**). *G. sulphuraria* belongs to the order Cyanidiales, clearly within the eukaryotic branch of the evolutionary tree (**Figure 10.21A**). However, the complete genome sequence of this organism revealed that nearly 5% of the *G. sulphuraria* ORFs encode proteins that are more closely related to bacterial or archaeal, not eukaryotic, orthologs. Furthermore, the proteins that exhibited these unexpected evolutionary relationships possess functions that are likely to confer a survival advantage in extreme environments, such as the removal of metal ions from inside the cell (**Figure 10.21B**).



FIGURE 10.20 The unicellular red alga *Galdieria sulphuraria* is a eukaryote that can survive extreme environments. This species has been isolated from hot springs such as the Grand Prismatic Spring in Yellowstone National Park, pictured here.

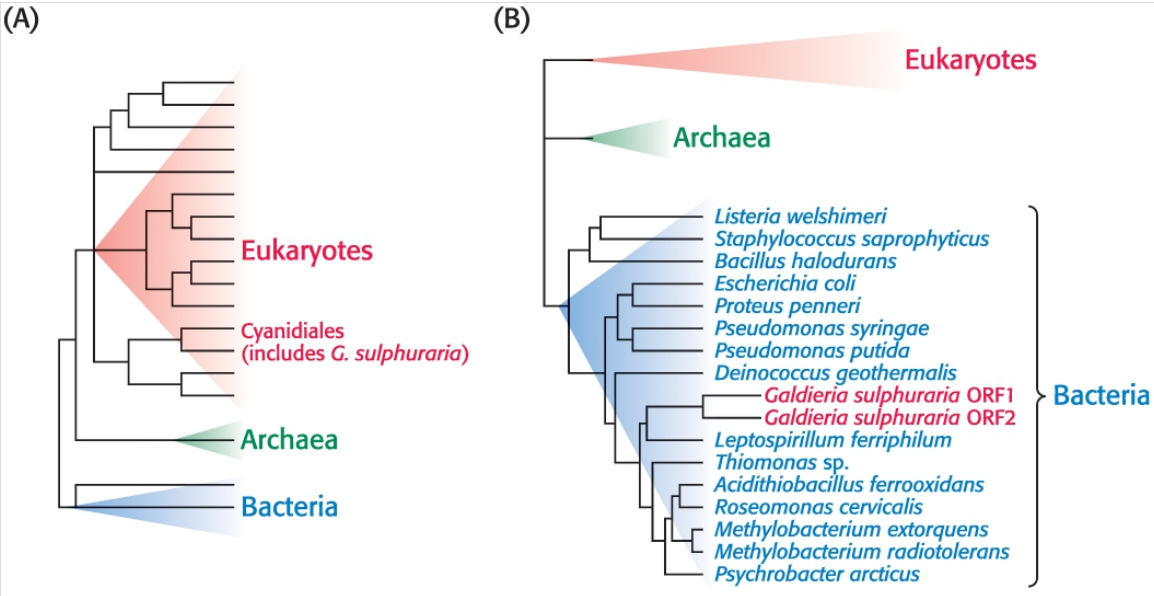


FIGURE 10.21 Proteins encoded within the *G. sulphuraria* genome with high homology to prokaryotic sequences are suggestive of horizontal gene transfer. (A) *Galdieria sulphuraria* belongs to the order Cyanidiales, clearly within the eukaryotic branch of the evolutionary tree. (B) Within the completely sequenced *G. sulphuraria* genome, two ORFs encode proteins involve in transport of arsenate ions across membranes. Alignment of these ORFs against orthologs fro

a variety of species reveals that these pumps are most closely related to their bacterial counterparts, suggesting that a horizontal gene transfer event occurred during the evolution of this species.

[(A) Information from Dr. Gerald Schönknecht; (B) Information from G. Schönknecht et al., *Science* 339:1207–1210, 2013, Fig. 3.]

One likely explanation for these observations is **horizontal gene transfer**, or the exchange of DNA between species that provides a selective advantage to the recipient. Amongst prokaryotes, horizontal gene transfer is a well-characterized and important evolutionary mechanism. For example, exchange of plasmid DNA between bacterial species likely enabled the transfer of genes encoding restriction endonucleases between bacterial species (Section 6.3). For example, EcoRI (from *E. coli*) and RsrI (from *Rhodobacter sphaeroides*) are 50% identical in sequence over 266 amino acids, clearly indicating a close evolutionary relationship. However, these species of bacteria are not as closely related. These species appear to have obtained the gene for these restriction endonucleases from a common source more recently than the time of their evolutionary divergence.

Recent studies such as those on *G. sulphuraria* described above were made possible by the expansive growth of complete genome sequence information. The results of such studies suggest that horizontal gene transfer from prokaryotes to eukaryotes — that is, between different domains of life — may also have led to evolutionarily significant events.

10.4 Modern Techniques Make the Experimental Exploration of Evolution Possible

Two techniques of biochemistry have made it possible to examine the course of evolution directly and not simply by inference. (1) The polymerase chain reaction (Section 9.1) allows the direct amplification and examination of ancient DNA sequences. If DNA samples can be obtained from preserved remains, we can explore genomes from species that are no longer living. (2) Molecular evolution may also be investigated through the process of synthesizing highly diverse populations of molecules and selecting for a biochemical property. The combination of these two techniques provides a glimpse into the types of molecules that may have existed very early in evolution.

Ancient DNA can sometimes be amplified and sequenced

The tremendous chemical stability of DNA makes the molecule well-suited to its role as the storage site of genetic information. So stable is the molecule that samples of DNA have survived for many thousands of years under appropriate conditions. With the development of PCR and advanced DNA-sequencing methods, such ancient DNA can be amplified and sequenced. This approach was first applied to mitochondrial DNA isolated from a Neanderthal humerus bone estimated at 38,000 years of age. Comparison of the complete Neanderthal mitochondrial sequence with those from human beings (*Homo sapiens*) revealed between 201 and 234 nucleotide substitutions, considerably fewer than the approximately 1500 differences between human beings and chimpanzees over the same region of mitochondrial DNA.

Since the initial sequencing of Neanderthal mitochondrial DNA, the complete genome sequences of a Neanderthal and a closely related hominin known as a Denisovan have been obtained using DNA isolated from nearly 50,000-year-old fossils. Comparison of these sequences suggests that the common ancestor of modern human beings and Neanderthals lived approximately 570,000 years ago, while the common ancestor between Neanderthals and Denisovans lived nearly 380,000 years ago. An evolutionary tree constructed from these data revealed that the Neanderthal was not an intermediate between chimpanzees and human beings but, instead, was an evolutionary "dead end" that became extinct (**Figure 10.22**). Further analysis of these sequences has enabled researchers to determine the extent of interbreeding between these groups, map the geographic history of these populations, and make inferences about additional ancestors whose DNA has not yet been sequenced.

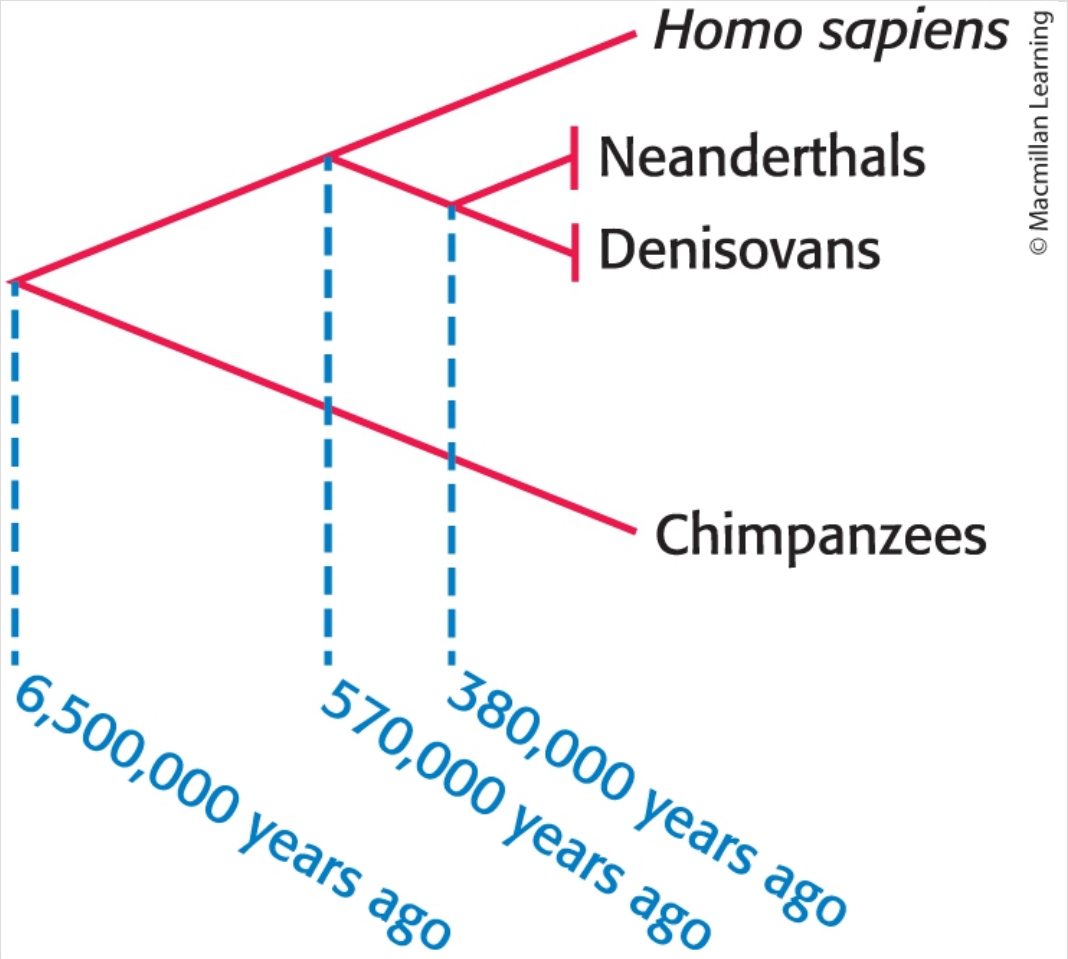


FIGURE 10.22 DNA sequence comparisons enable the placement of Neanderthals and Denisovans on an evolutionary tree. Sequence data suggest that neither Neanderthals nor the Denisovans are on the line of direct descent leading to *Homo sapiens* but, instead, branched off earlier and then became extinct.

A few earlier studies claimed to determine the sequences of far more ancient DNA such as that found in insects trapped in amber, but these studies appear to have been flawed. The source of these sequences turned out to be contaminating modern DNA. Successful sequencing of ancient DNA requires sufficient DNA for reliable amplification and the rigorous exclusion of all sources of contamination.

Molecular evolution can be examined experimentally

For a population to evolve, the following conditions must be met: (1) the generation of a diverse population, (2) the selection of members based on some criterion of fitness, and (3) the reproduction of that population to subsequent generations. This last condition determines, in part, the time under which evolution can occur: organisms with long generation times (such as humans) will evolve much more slowly than those that reproduce rapidly (such as bacteria).

With the advancement of the methods of molecular biology, such as those described in Chapter 9, it is possible to meet these evolutionary conditions using nucleic acid molecules in a controlled experimental setting under convenient time-scales. The results of such studies enable us to glimpse how evolutionary processes might have generated catalytic activities and specific binding abilities — important biochemical functions in all living systems.

Biochemists can synthesize a large, diverse population of nucleic acid molecules in the laboratory using **combinatorial chemistry**, a process by which millions of compounds are synthesized in a single process. A population of molecules of a given size can be generated randomly so that many or all possible sequences are present in the mixture. Once an initial population has been prepared, it is subjected to a selection process that isolates specific molecules with desired binding or reactivity properties. Finally, molecules that have survived the selection process are replicated through the use of PCR; primers are directed toward specific sequences included at the ends of each member of the population. Errors that occur naturally in the course of the replication process introduce additional variation into the population in each generation.

Let us consider an application of this approach. Scientists hypothesize that early in evolution of life, before the emergence of proteins, RNA

molecules may have played all major roles in biological catalysis. To understand the properties of potential RNA catalysts, researchers have used the methods described above to create an RNA molecule capable of binding adenosine triphosphate and related nucleotides.

First, an initial population of RNA molecules 169 nucleotides long was created. In this pool of RNA molecules, 120 of the positions differed randomly, with equimolar mixtures of adenine, cytosine, guanine, and uracil. The initial synthetic pool that was used contained approximately 10^{14} unique RNA molecules — a huge number, but still a very small fraction of the total possible pool of random 120-base sequences. From this pool, affinity chromatography (Section 4.1) was used to select those molecules that bound to ATP (**Figure 10.23**).

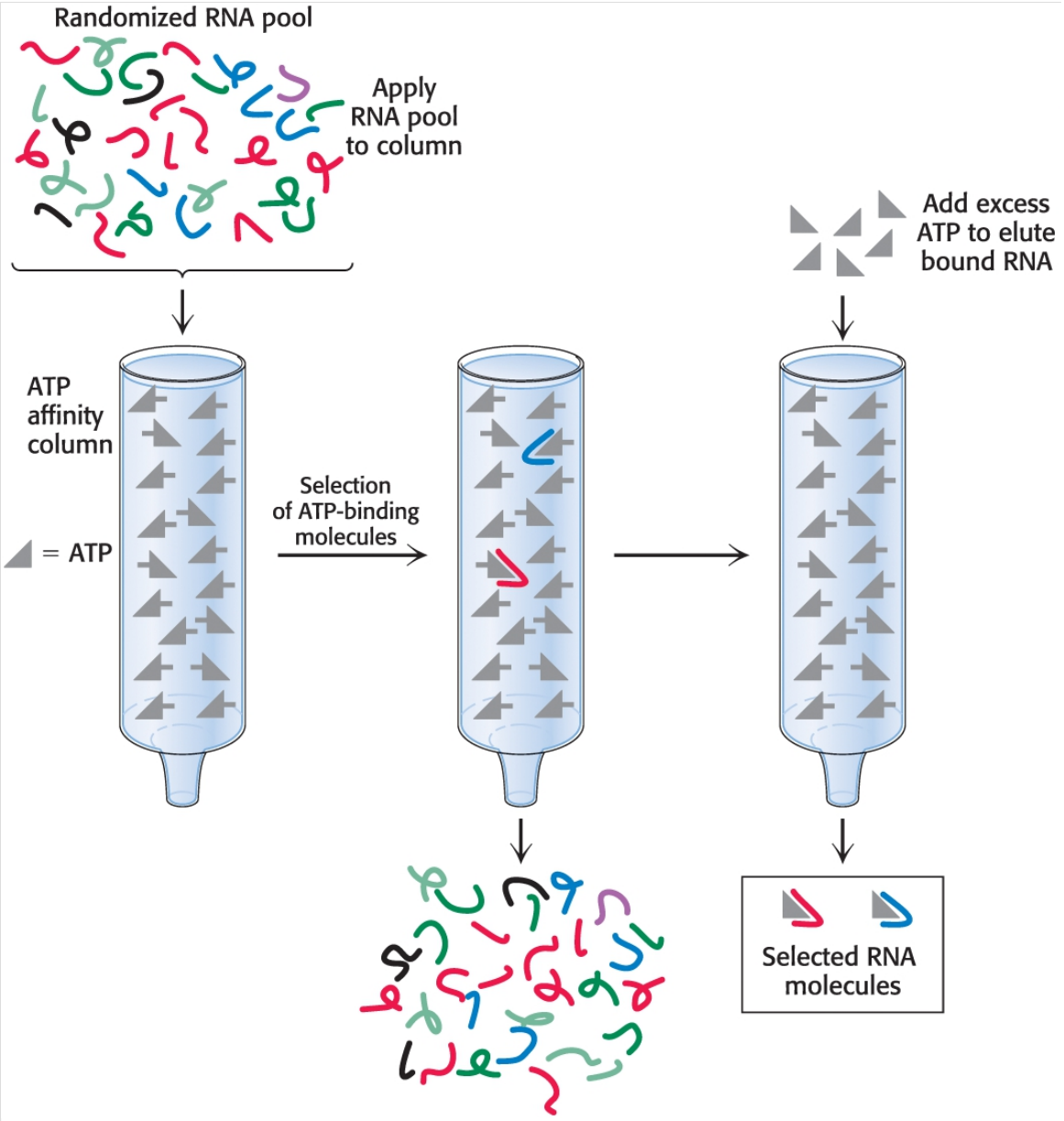


FIGURE 10.23 Evolution can be studied in the laboratory setting. A collection of RNA molecule of random sequences is synthesized by combinatorial chemistry. This collection is selected for the ability to bind ATP by passing the RNA through an ATP affinity column (Section 4.1). The ATP binding RNA molecules are released from the column by washing with excess ATP and then replicated. The process of selection and replication is then repeated several times. The final RN products with significant ATP-binding ability are isolated and characterized.

The molecules that bound well to the ATP affinity column were replicated by reverse transcription into DNA, amplified by PCR, and transcribed back into RNA. Additional diversity was introduced into the pool by the use of a somewhat error-prone reverse transcriptase, which introduces additional mutations into the population during each cycle. The new population was subjected to additional rounds of selection for ATP-binding activity, and after eight generations, members of the selected population were characterized by sequencing. Seventeen different sequences were obtained, 16 of which could form the structure shown in **Figure 10.24**. Each of these molecules bound ATP with dissociation constants less than 50 μM.

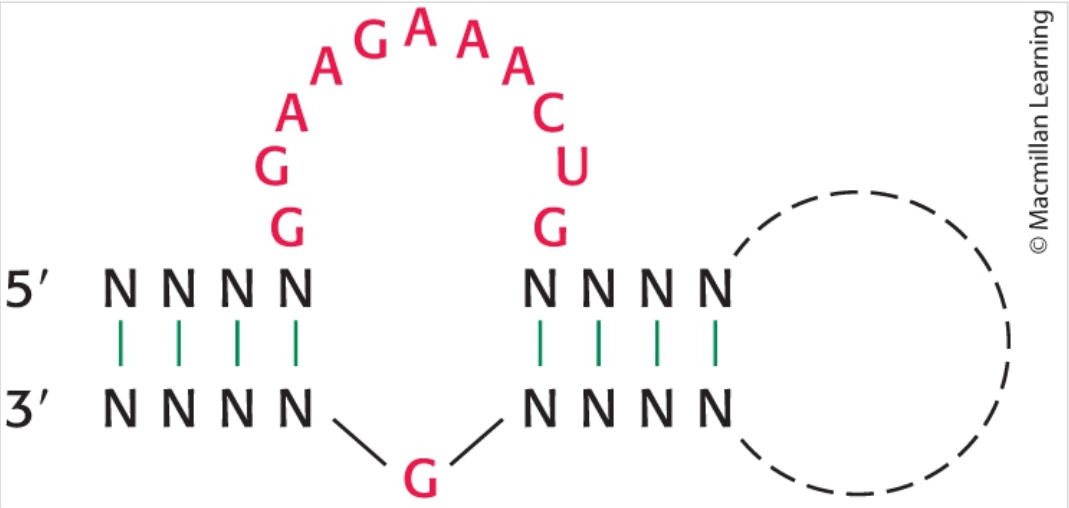


FIGURE 10.24 A conserved secondary structure is common to RNA molecules selected for ATP binding. Bases important for ATP recognition are shown in red. The dashed line indicates a region which varied in length among the various RNA products.

The folded structure of the ATP-binding region from one of these RNAs was determined by nuclear magnetic resonance (NMR) methods (Section 4.5). As expected, this 40-nucleotide molecule is composed of two Watson–Crick base-paired helical regions separated by an 11-nucleotide loop (**Figure 10.25A**). This loop folds back on itself in an

intricate way (Figure 10.25B) to form a deep pocket into which the adenine ring can fit (Figure 10.25C). Thus, a structure had evolved in vitro that was capable of a specific interaction.

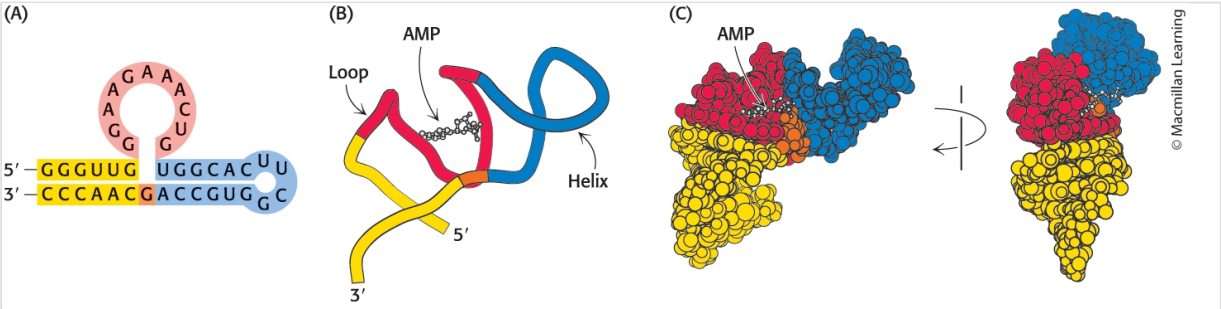


FIGURE 10.25 Experimental molecular evolution yields an ATP-binding RNA molecule. (A) The Watson–Crick base-pairing pattern of an RNA molecule selected to bind adenosine nucleotides is shown. (B) The NMR structure of this RNA molecule reveals how the nucleotide molecule (here, AMP) binds largely to the loop region (red). (C) In this representation, the tight pocket into which the AMP molecule binds is quite clear.

[Drawn from 1RAW.pdb.]

Synthetic oligonucleotides that can specifically bind ligands, such as the ATP-binding RNA molecules described above, are referred to as **aptamers**. In addition to their role in understanding molecular evolution, aptamers have shown promise as versatile tools for biotechnology and medicine. For example, they have been developed for diagnostic applications, serving as sensors for ligands ranging from small organic molecules, such as cocaine, to larger proteins, such as thrombin. Several aptamers are also being tested in clinical trials as therapies for diseases ranging from leukemia to diabetes. Macugen (pegaptanib sodium), an aptamer which binds to and inhibits the protein vascular endothelial growth factor, has been approved for the treatment of age-related macular degeneration.

Chapter 10 Summary

10.1 Homologs Are Descended from a Common Ancestor and Can Be Detected by Sequence Alignments

- Two molecules are homologous if they are derived from a common ancestor.
- Paralogs are homologous molecules that are found in one species and have acquired different functions through evolutionary time.
- Orthologs are homologous molecules that are found in different species and have similar or identical functions.
- Sequences can be aligned to maximize their similarity, and the significance of these alignments can be judged by statistical tests.
- Sequence alignments can be scored based on the number of identities or by the degree of similarity, using a substitution matrix such as Blosum-62.

10.2 Examination of Three-Dimensional Structure Enhances Our Understanding of Evolutionary Relationships

- Comparison of three-dimensional structure may reveal evolutionary relationships not detectable by sequence alignments.
- Alignment of a protein sequence against itself may reveal internal repeats, which suggests a gene duplication event occurred in its evolutionary history.
- Proteins may be related by convergent evolution: they evolved from distinct ancestors but use similar structural features to solve biochemical challenges.
- Nucleic acid sequence alignments enable structural predictions through the identification of base-pairing relationships.

10.3 Evolutionary Trees Can Be Constructed on the Basis of Sequence Information

- Evolutionary trees can be constructed with the assumption that the number of sequence differences corresponds to the time since the two sequences diverged.
- Comparison of evolutionary trees based on sequence alignments with those based on fossil records provides a clearer understanding of the timeline of divergences.
- Horizontal gene transfer events can appear as unexpected branches on the evolutionary tree.

10.4 Modern Techniques Make the Experimental Exploration of Evolution Possible

- Recombinant DNA technology now allows for the exploration of evolution as a laboratory science.
- In favorable cases, PCR amplification of well-preserved samples allows the determination of nucleotide sequences from extinct organisms. These sequences can help authenticate parts of an evolutionary tree constructed by other means.
- Molecular evolutionary experiments performed in the laboratory can examine how molecules such as ligand-binding RNA molecules might evolve over time.

Key Terms

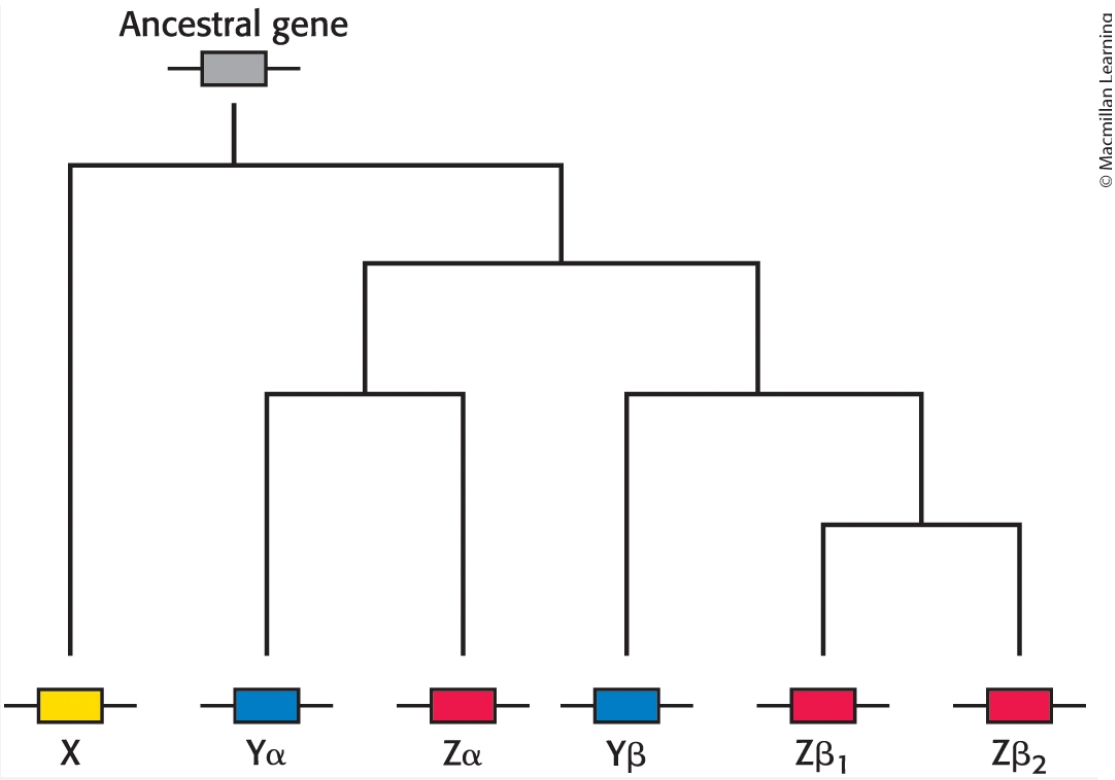
homologs
orthologs
paralogs
sequence alignment
identity
conservative substitution

nonconservative substitution
substitution matrix
basic local alignment search tool (BLAST) search
open reading frame (ORF)
sequence template
divergent evolution
convergent evolution
evolutionary tree
horizontal gene transfer
combinatorial chemistry
aptamers

Problems

1. Distinguish between paralogs and orthologs. 1

2. A evolutionary tree is shown in the image. Similar genes are represented by boxes. The letters X, Y, and Z represent different species. Similarly colored genes designate genes present in the same species (species X, Y, or Z).



© Macmillan Learning

Indicate whether the following pairs of genes are orthologs or paralogs: 1

a. Zα and $Z\beta_2$
b. X and $Z\beta_2$
c. Yα and Yβ
d. $Z\beta_1$ and $Z\beta_2$
e. Yα and Zα
f. X and Yα

3. Using the identity-based scoring system applied in Figure 10.4, calculate the score for the following alignment. What is the

percent identity between the two sequences? Do you think these two proteins are related? 2

```
(1) WYLGKITRMDAEVLLKKPTVRDGHFLVTQCESSPGEF
(2) WYFGKITRRESERLLLNPENPRGTFLVRESETTKGAY

    SISVRFGDSVQ-----HFKVLRDQNGKYYLWAVK-FN
    CLSVSDFDNAKGLNVKHYKIRKLDSGGFYITSRTQFS

    SLNELVAYHRTASVSRTHTILLSDMNV
    SSLQQLVAYYSKHADGLCHRLTNV
```

4. Explain why protein shuffling is a helpful tool for predicting the significance of homology between two protein sequences. 2

5. Using the identity-based scoring system (Section 10.1), calculate the alignment score for the alignment of the following two short sequences:

```
(1) ASNFLDKAGK

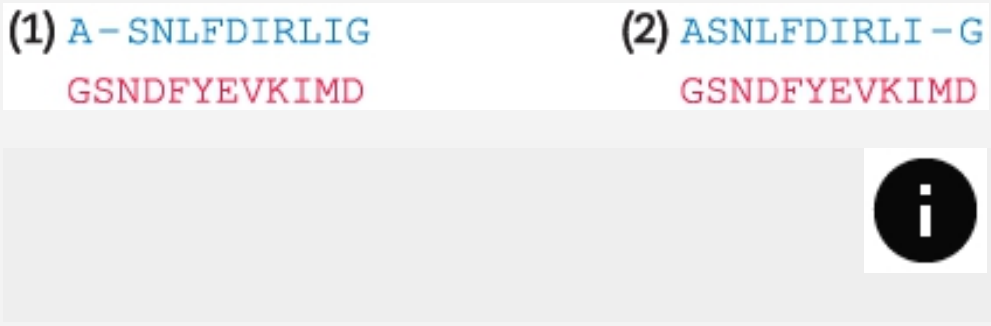
(2) ATDYLEKAGK
```

Generate a shuffled version of sequence 2 by randomly reordering these 10 amino acids. Align your shuffled sequence with sequence 1 without allowing gaps, and calculate the alignment score between sequence 1 and your shuffled sequence. 2

6. Consider the Blosum-62 matrix in Figure 10.7. Replacement of which three amino acids never yields a positive score? What features of these residues might contribute to this observation? 3

7. The protein sequence of myoglobin has aspartate (D) in a certain position, whereas the α chain of hemoglobin has glutamate (E) in the same position. How would this substitution be scored in the Blosum-62 matrix? 3

8. Consider the following two sequence alignments:



Which alignment has a higher score if the identity-based scoring system (Figure 10.4) is used? Which alignment has a higher score if the Blosum-62 substitution matrix (Figure 10.7) is used? For the Blosum scoring, you need not apply a gap penalty. 3

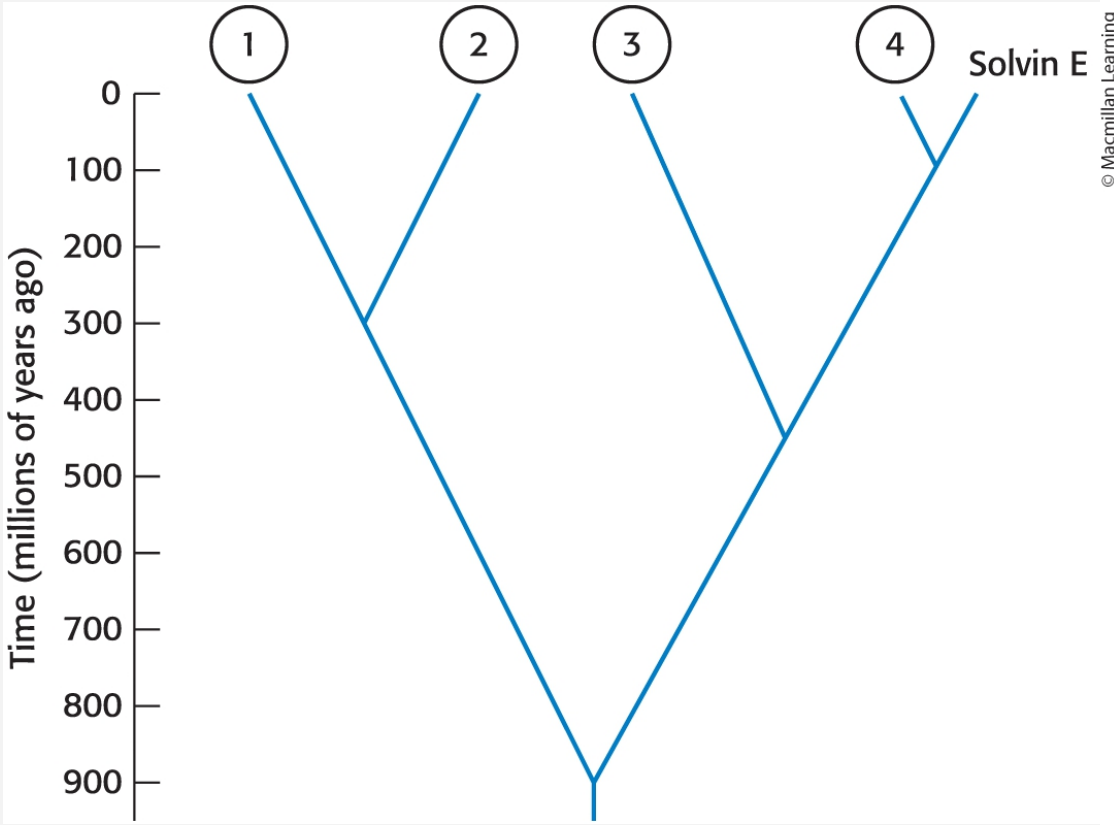
9. Suppose that the sequences of two proteins each consisting of 200 amino acids are aligned and that the percentage of identical residues has been calculated. How would you interpret each of

the following results in regard to the possible divergence of the two proteins from a common ancestor? 4

a. 80%
b. 50%
c. 20%
d. 10%

10. Suppose that you wish to synthesize a pool of RNA molecules that contain all four bases at each of 40 positions. How much RNA must you have in grams if the pool is to have at least a single molecule of each sequence? The average molecular weight of a nucleotide is $330\ g\ mol^{-1}$. 5

11. Below is an evolutionary tree for a fictitious protein family, the Solvins. The location of Solvin E is shown.



© Macmillan Learning

Place Solvins A, B, C, and D on the tree in the numbered positions according to the following statements: 1

- The Solvin family results from divergent evolution.
- Solvin A diverged from Solvin E three times as long ago as Solvin D evolved from Solvin A.
- Solvin C diverged from Solvin E 500 million years ago.
- Solvin B is not a direct descendent of Solvin A.

Which two Solvins are most similar? When did Solvin B diverge from Solvin E?

12. Classify the following statements as describing convergent evolution, divergent evolution, or both: 4

a. Proteins with similar functions that are derived from unrelated ancestors
b. May result in proteins with similar functions
c. Change in protein sequence over time
d. Results in homologous proteins
e. Proteins with similar functions that are derived from a common ancestor
f. Chymotrypsin and trypsin are an example.
g. Chymotrypsin and subtilisin are an example.

13. Classify the following evolutionary processes as examples of either convergent of divergent evolution:

a. The gene encoding malate dehydrogenase mutates in a way that confers increased specificity for lactate rather than malate.

b. Coffee and tea plants both have genes to produce caffeine, whereas their most recent common ancestor does not.
c. Some members of the β-helix fold superfamily of proteins are iron-dependent, whereas others are not.

14. The sequences of three proteins (A, B, and C) are compared with one another, yielding the following levels of identity:

	A	B	C
A	100%	65%	15%
B	65%	100%	55%
C	15%	55%	100%

Assume that the sequence matches are distributed uniformly along each aligned sequence pair. Would you expect protein A and protein C to have similar three-dimensional structures? Explain.

15. You have discovered a mutant form of a thermostable DNA polymerase with significantly reduced fidelity in adding the appropriate nucleotide to the growing DNA strand, compared with wild-type DNA polymerase. How might this mutant be useful in the molecular-evolution experiments described in Section 10.4? 5

Chapter 11
Carbohydrates and Glycoproteins

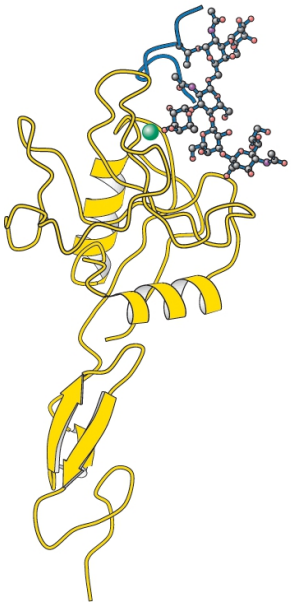




Photo: Shutterstock

Carbohydrates are important fuel molecules, but they play many other biochemical roles. Carbohydrate attachments on proteins fit into the binding sites of other proteins like a key into lock and can act as an ID code that can be read by other proteins, much like a QR code can be read by a phone. The model at left shows the protein P-selectin binding its ligand, a glycoprotei with specific carbohydrates attached.

[Drawn from 1G1S.pdb.]

Outline

11.1 Monosaccharides Are the Simplest Carbohydrates
11.2 Monosaccharides Are Linked to Form Complex Carbohydrates
11.3 Carbohydrates Can Be Linked to Proteins to Form Glycoproteins
11.4 Lectins Are Specific Carbohydrate-Binding Proteins

Learning Goals



By the end of this chapter, you should be able to:

1. Describe the structure and main roles of carbohydrates in nature.
2. Describe how simple carbohydrates are linked to form complex carbohydrates.
3. Explain how carbohydrates are linked to proteins and what functions the linked carbohydrates play.
4. Describe the three main classes of glycoproteins and explain their biochemical roles.
5. Define what lectins are and outline their biochemical functions.

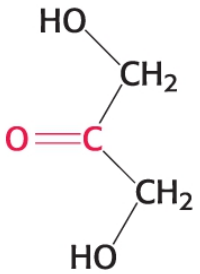
For decades, carbohydrates were recognized as important fuels and structural components but were thought to be peripheral to most key activities of the cell. This view has changed dramatically in recent years, as we now know that cells of all organisms are coated in a dense and complex coat of carbohydrates — frequently attached to lipids and proteins — that are essential to cell survival and cell-to-cell interactions and communication. The attachment of a carbohydrate to a protein is the most common post-translational modification of proteins — typically determining where a protein will be localized — and secreted proteins are often extensively decorated with carbohydrates. The extracellular matrix in higher eukaryotes — the environment in which the cells live — is also rich in secreted carbohydrates. Indeed, rather than being mere energy and infrastructure components, carbohydrates supply details and enhancements to the biochemical architecture of the cell, helping to define the functionality and uniqueness of the cell.

11.1 Monosaccharides Are the Simplest Carbohydrates

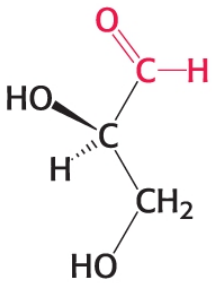
Carbohydrates are carbon-based molecules that are rich in hydroxyl groups; the empirical formula for many carbohydrates is $(CH_2O)_n$ — literally, a carbon hydrate. However, many carbohydrates have additional groups or modifications that deviate from this simple empirical formula. Thus, a better definition for carbohydrates is that they are polyhydroxy aldehydes and ketones, and their derivatives.

There are many monosaccharides but they are structurally similar

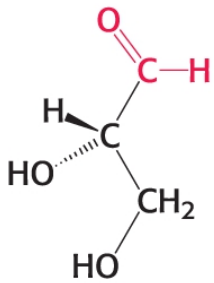
Simple carbohydrates are **monosaccharides**, also commonly called *sugars*, which are three to seven carbons in length. These simple sugars serve not only as fuel molecules but also as fundamental constituents of living systems. For instance, DNA has a backbone consisting of alternating phosphoryl groups and deoxyribose, the cyclic form of a five-carbon aldehyde sugar. The smallest monosaccharides, composed of three carbon atoms, are dihydroxyacetone and D- and L-glyceraldehyde.



Dihydroxyacetone
(a ketose)



D-Glyceraldehyde
(an aldose)



L-Glyceraldehyd
(an aldose)

Nomenclature

Monosaccharides are typically classified based upon both carbon-chain length and the identity of the most oxidized group. Dihydroxyacetone is called a *ketose* because it contains a keto group (in red, above), whereas glyceraldehyde is called an *aldose* because it contains an aldehyde group (also in red). Both these molecules are referred to as *trioses* (tri- for three, referring to the three carbon atoms that they contain). Similarly, simple monosaccharides with four, five, six, and seven carbon atoms are called *tetroses*, *pentoses*, *hexoses*, and *heptoses*, respectively. Perhaps the monosaccharides of which we are most aware are the hexoses, such as glucose and fructose. Glucose is an essential energy source for virtually all forms of life, and fructose is found commonly in many foods and used as a sweetener; fructose is converted into glucose derivatives inside the cell.

Isomers

Carbohydrates can exist in a dazzling variety of isomeric forms (**Figure 11.1**). Dihydroxyacetone and glyceraldehyde are *constitutional isomers* because they have identical molecular formulas but differ in how the atoms are ordered. These are in contrast to *stereoisomers*, which differ in spatial arrangement but not bonding order. Recall from the discussion of amino acids (Section 2.2) that stereoisomers are designated as having either D or L configuration. Glyceraldehyde has a single asymmetric carbon atom and, thus, there are two stereoisomers of this sugar: D-glyceraldehyde and L-glyceraldehyde. These molecules are a type of stereoisomer called *enantiomers*, which are mirror images of each other. Most monosaccharides from vertebrates have the D configuration.

According to convention, the D and L isomers are determined by the configuration of the asymmetric carbon atom farthest from the aldehyde or keto group. Dihydroxyacetone is the only monosaccharide without at least one asymmetric carbon atom.

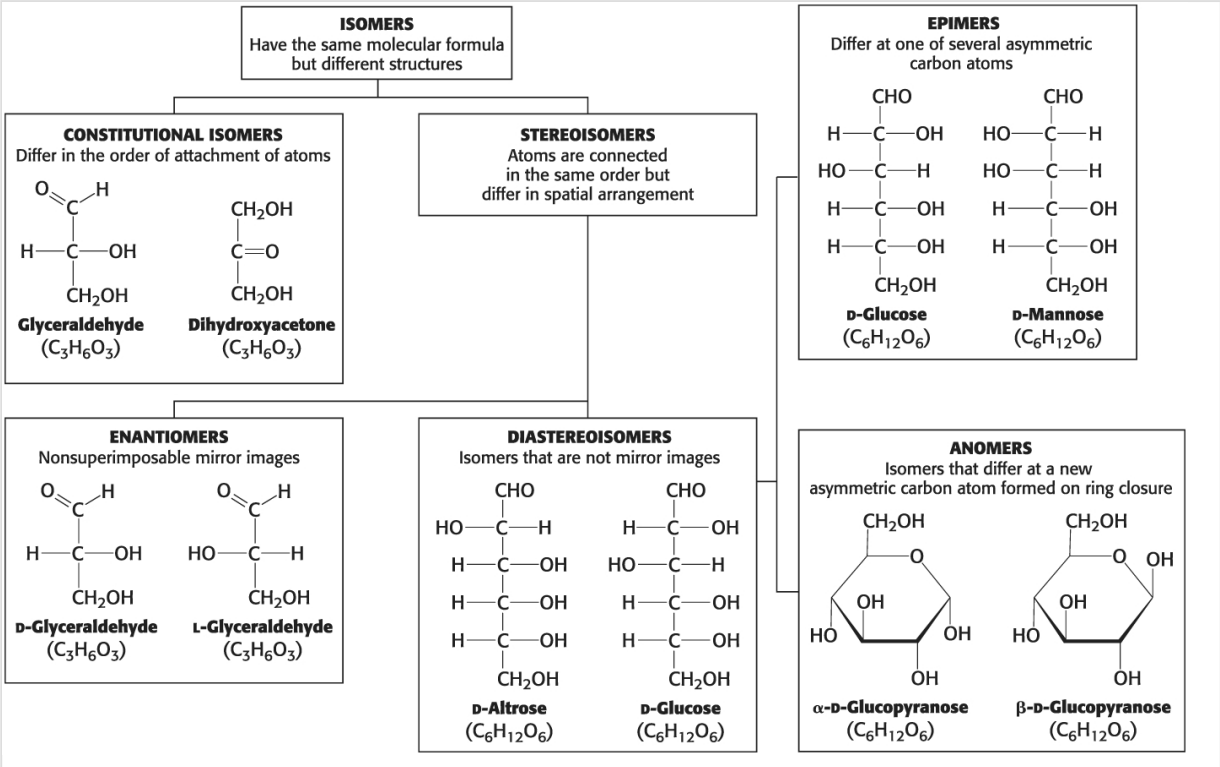


FIGURE 11.1 The complexity of carbohydrate structures results in many different types of isomeric forms.

Monosaccharides made up of more than three carbon atoms have multiple asymmetric carbons, and so they can exist not only as enantiomers but also as *diastereoisomers*, stereoisomers that are not mirror images of each other. The number of possible stereoisomers equals 2^n, where n is the number of asymmetric carbon atoms. Thus, a six-carbon aldose with four asymmetric carbon atoms can exist as eight possible diastereoisomers, each of which can exist in two different

enantiomeric forms, for a total of 16 stereoisomers. D-Glucose is one such aldohexose. Note that ketoses have one less asymmetric center than aldoses with the same number of carbon atoms. D-Fructose is the most abundant ketohexose.

Common monosaccharides

The monosaccharides that we will see most frequently in our study of biochemistry are shown in **Figure 11.2**. D-Ribose, the carbohydrate component of RNA, is a five-carbon aldose, as is deoxyribose, the monosaccharide component of deoxynucleotides. D-Glucose, D-mannose, and D-galactose are abundant six-carbon aldoses. Note that D-glucose and D-mannose differ in configuration only at C-2, the carbon atom in the second position. Sugars that are diastereoisomers differing in configuration at only a single asymmetric center are **epimers**. Thus, D-glucose and D-mannose are epimeric at C-2; D-glucose and D-galactose are epimeric at C-4.

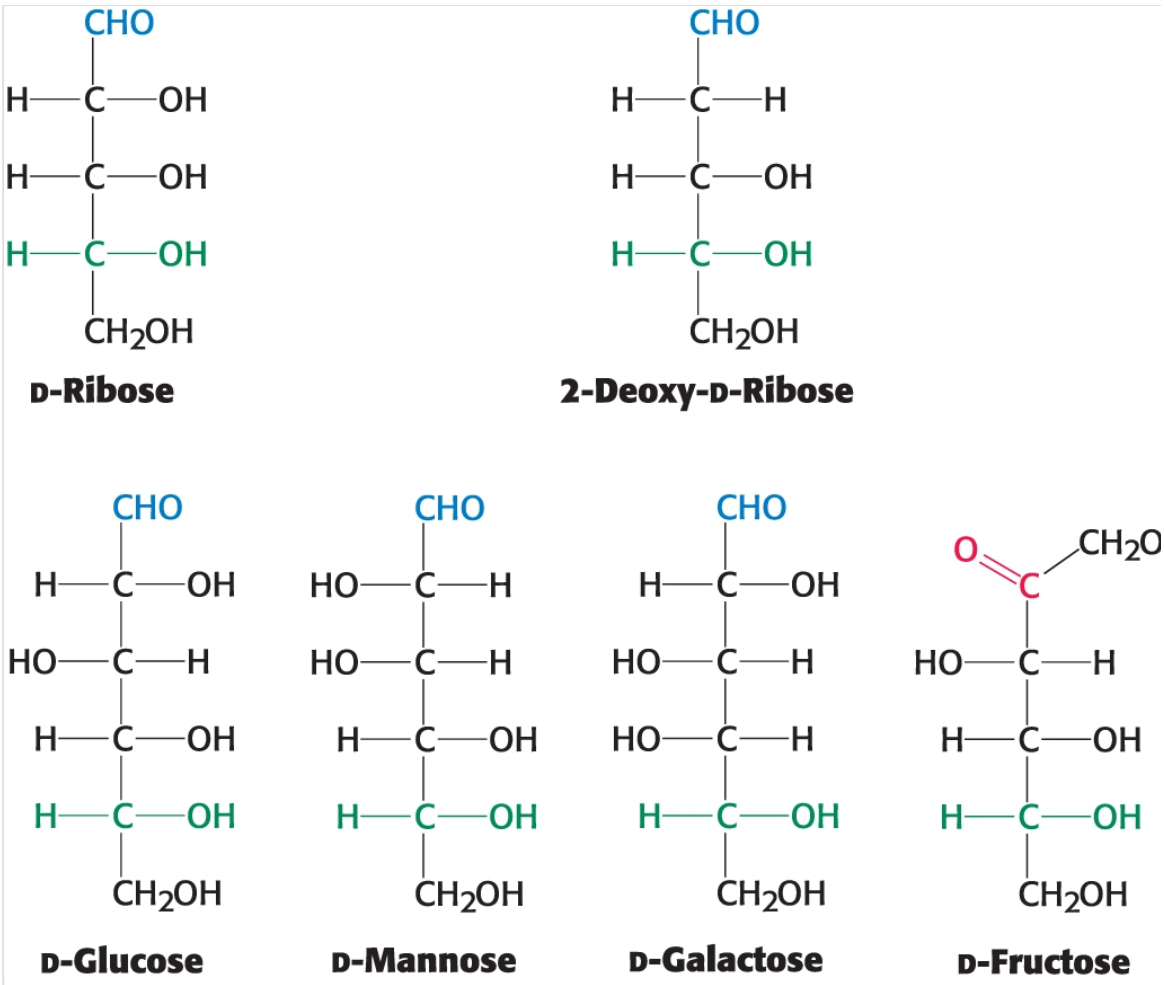
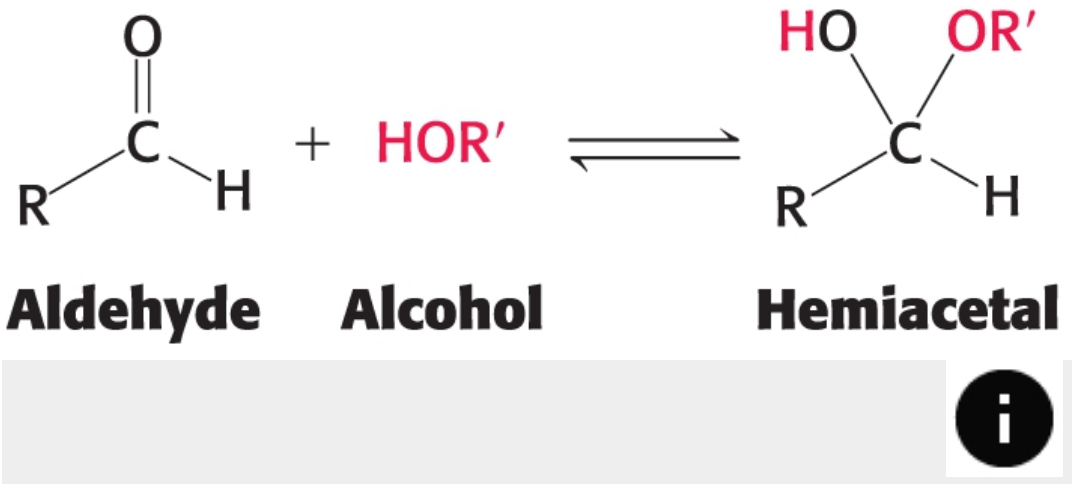


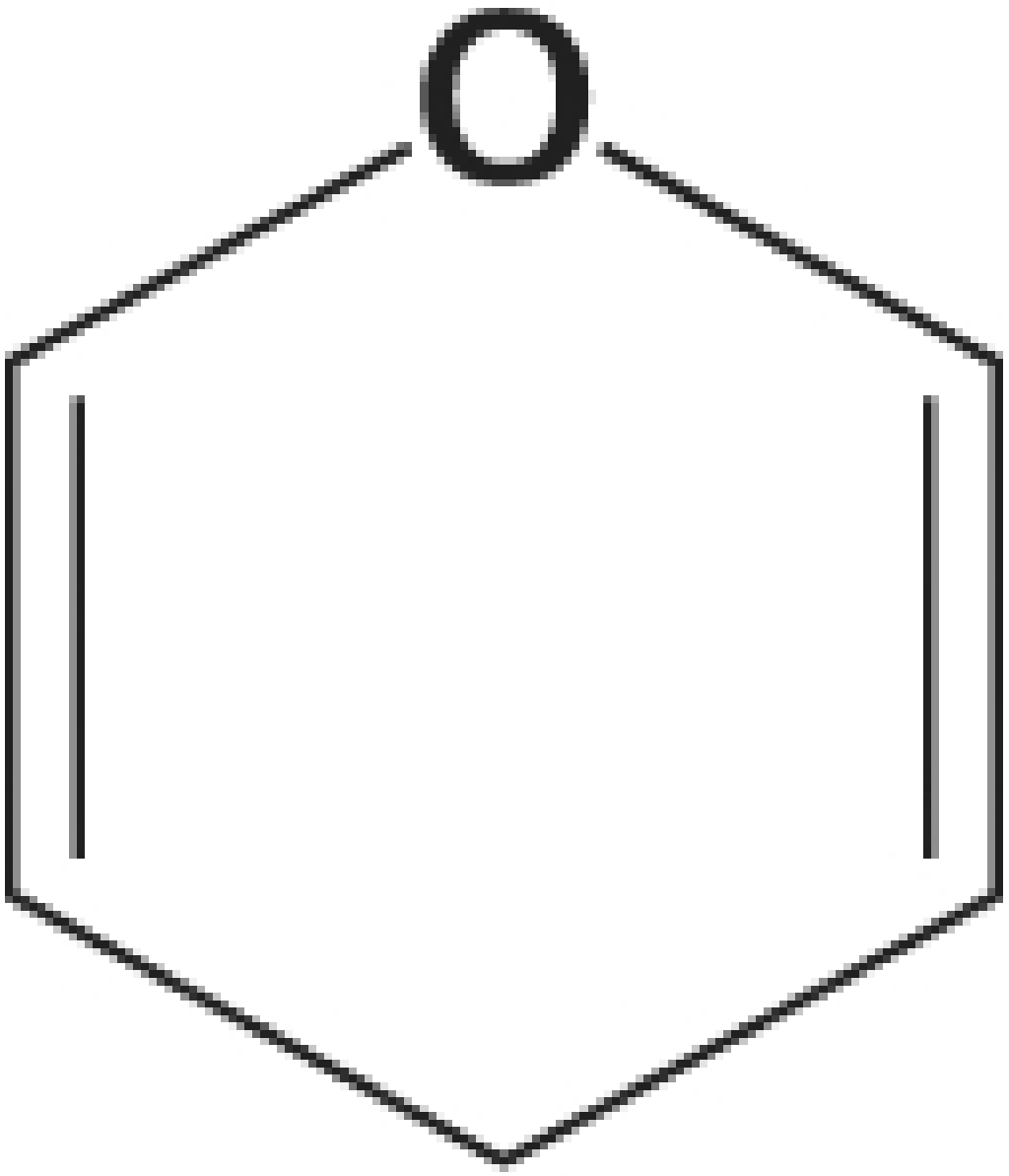
FIGURE 11.2 The most common monosaccharides are pentoses and hexoses. Aldoses contain an aldehyde group (shown in blue), whereas ketoses, such as D-fructose, contain a keto group (shown in red). The asymmetric carbon atom (shown in green) farthest from the aldehyde or ke group designates the structures as being in the D configuration.

Most monosaccharides exist as interchanging cyclic forms

The predominant forms of ribose, glucose, fructose, and many other sugars in solution, as is the case inside the cell, are not open chains. Rather, the open-chain forms of these sugars cyclize into rings. The chemical basis for ring formation is that an aldehyde can react with an alcohol to form a *hemiacetal*.



For an aldohexose such as glucose, a single molecule provides both the aldehyde and the alcohol: the C-1 aldehyde in the open-chain form of glucose reacts with the C-5 hydroxyl group to form an intramolecular hemiacetal (**Figure 11.3**). The resulting cyclic hemiacetal, a six-membered ring, is called *pyranose* because of its similarity to the cyclic molecule *pyran*.



Pyran

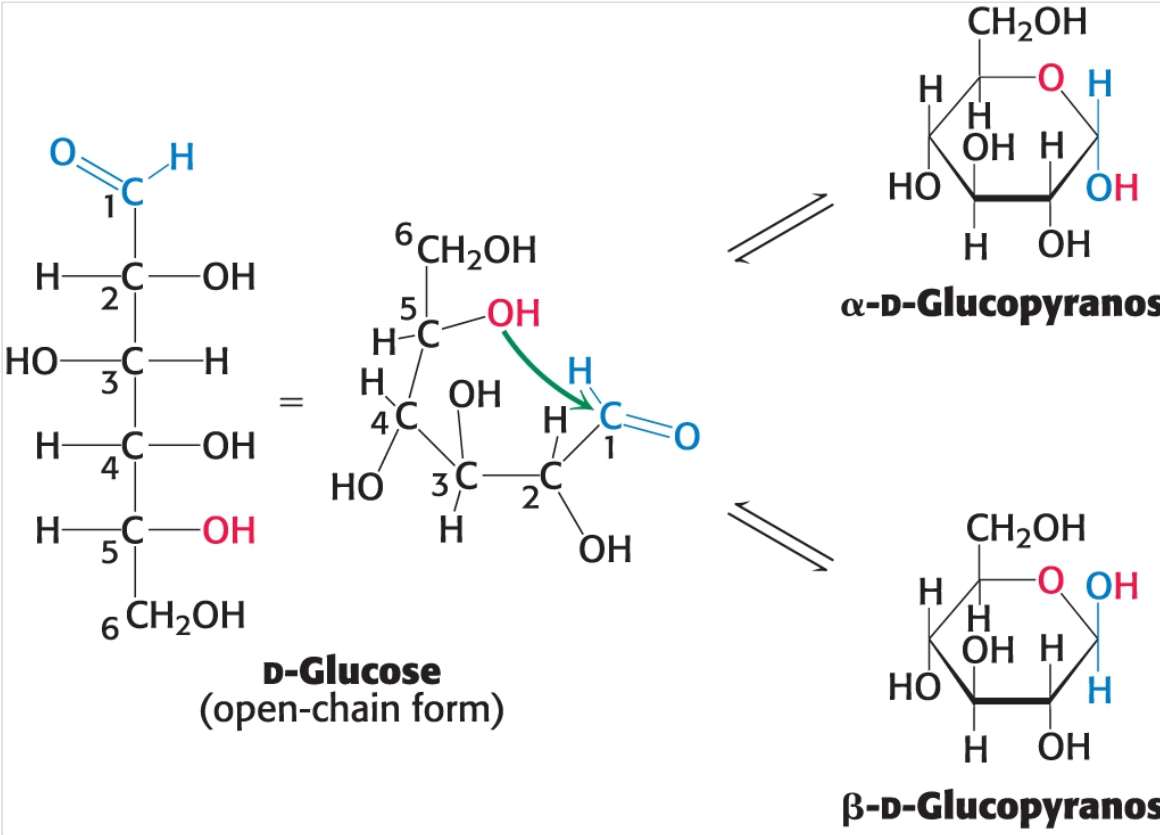
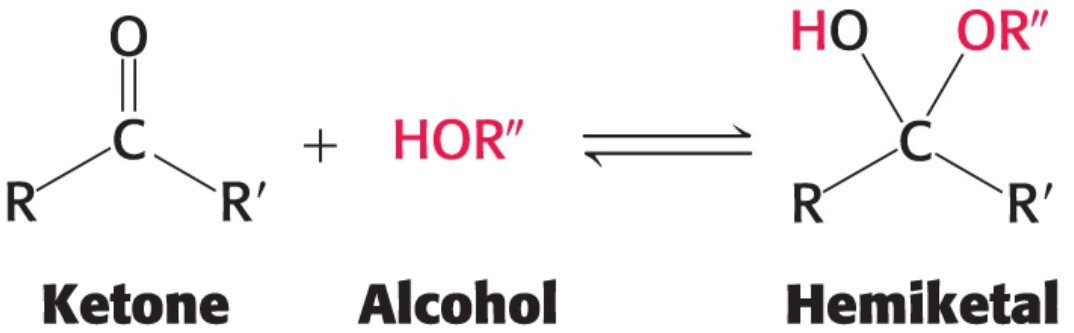
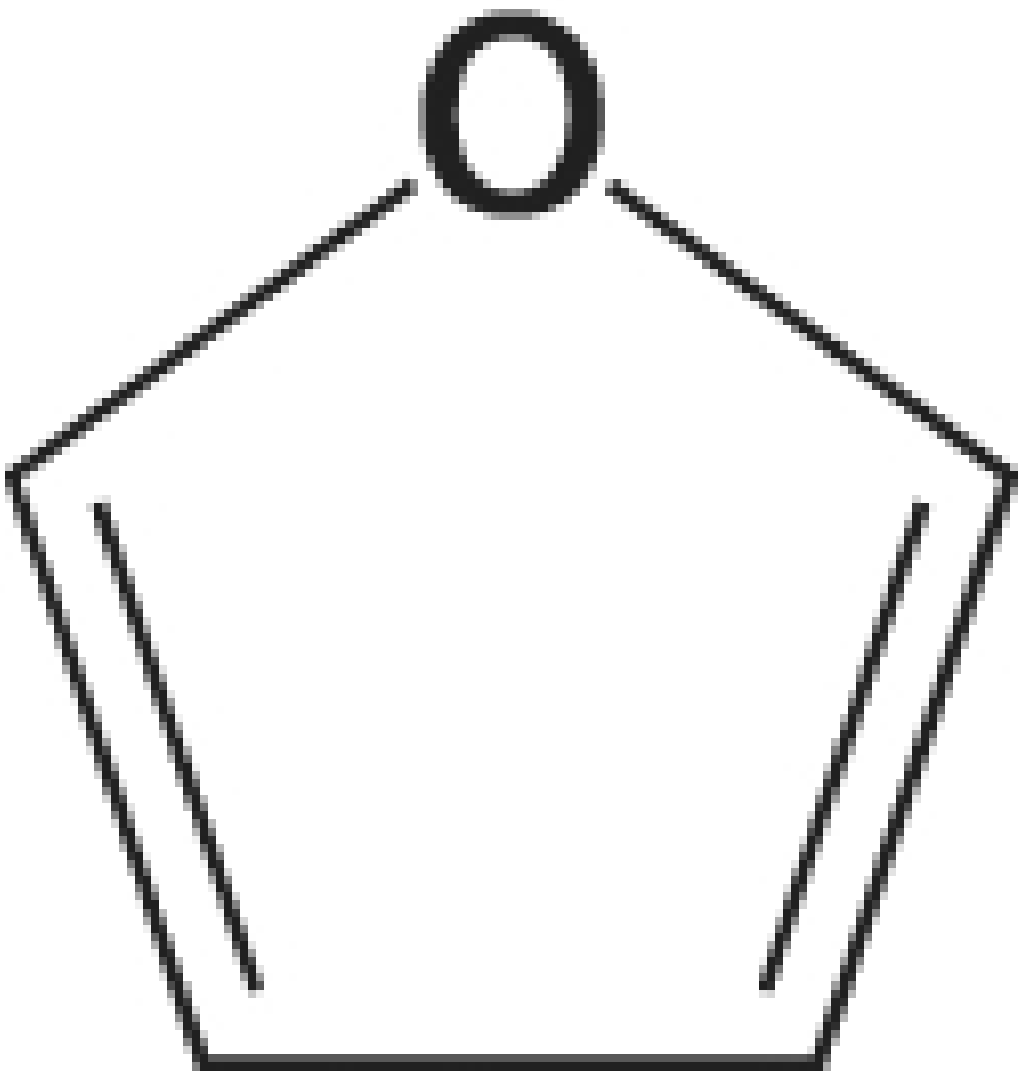


FIGURE 11.3 D-Glucose and other monosaccharides can temporarily form a pyranose ring. Th open-chain form of glucose cyclizes when the C-5 hydroxyl group attacks the oxygen atom of th C-1 aldehyde group to form an intramolecular hemiacetal. Two interchanging anomeric forms c the pyranose ring, designated α and β, can result; both in rapid equilibrium with the open-chair (linear) form.

Similarly, a ketone can react with an alcohol to form a *hemiketal*.



The C-2 keto group in the open-chain form of a ketohexose, such as fructose, can form an intramolecular hemiketal by reacting with either the C-6 hydroxyl group to form a six-membered cyclic hemiketal or the C-5 hydroxyl group to form a five-membered cyclic hemiketal (**Figure 11.4**). The five-membered ring is called a *furanose* because of its similarity to the five-membered heterocycle *furan*.



Furan

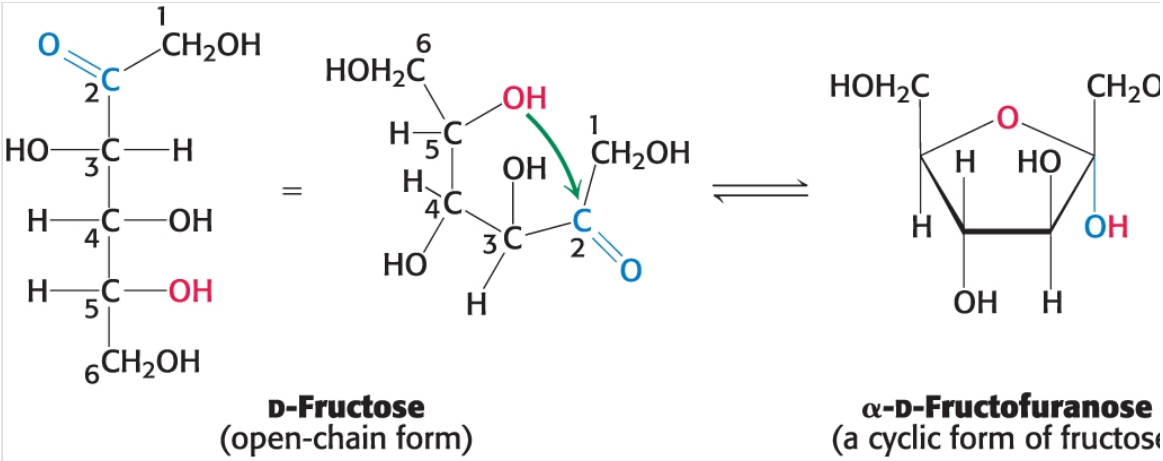


FIGURE 11.4 D-Fructose and other monosaccharides can temporarily form a furanose ring. Th
open-chain form of fructose cyclizes to a five-membered ring when the C-5 hydroxyl group attacks the C-2 ketone to form an intramolecular hemiketal. Two interchanging anomers are formed, but only the α anomer is shown.

The depictions of glucopyranose (glucose) and fructofuranose (fructose) shown in Figures 11.3 and 11.4 are examples of Haworth projections. In such projections, the carbon atoms in the ring are not written out. The approximate plane of the ring is perpendicular to the plane of the paper, with the heavy line on the ring projecting toward the reader.

We have seen that carbohydrates can contain many asymmetric carbon atoms. An additional asymmetric center is created when a cyclic hemiacetal is formed, generating yet another diastereoisomeric form of sugars called an **anomer**. In glucose, C-1 (the carbonyl carbon atom in the open-chain form) becomes an asymmetric center. Thus, two ring structures are formed: α-D-glucopyranose and β-D-glucopyranose (Figure 11.3). For D sugars drawn as Haworth projections in the standard orientation, as shown in Figure 11.3, the designation α means that the hydroxyl group attached to C-1 is on the opposite side of the ring as C-6; β means that the hydroxyl group is on the same side of the ring as C-6. The C-1 carbon atom is called the *anomeric carbon atom.* An equilibrium

mixture of glucose contains approximately one-third α anomer, two-thirds β anomer, and $< 1\%$ of the open-chain form. Note that these structures are constantly interconverting by opening to the linear structure and reclosing again, a process referred to as *mutarotation*. Here again, the biochemical timescale can be illuminating to consider: while the interconversion of epimers is best measured in years, anomers rapidly interconvert in seconds, reaching equilibrium in a matter of minutes. Below we will also consider conformations of sugars, which change in a matter of milliseconds.

The furanose-ring form of fructose also has anomeric forms, in which α and β refer to the hydroxyl groups attached to C-2, the anomeric carbon atom (Figure 11.4). Fructose forms both pyranose and furanose rings. The pyranose form predominates in fructose that is free in solution, due to reduced steric hindrances; the furanose form predominates in many fructose derivatives where additional groups attached to the sugar disfavor or prevent the pyranose ring form (**Figure 11.5**).

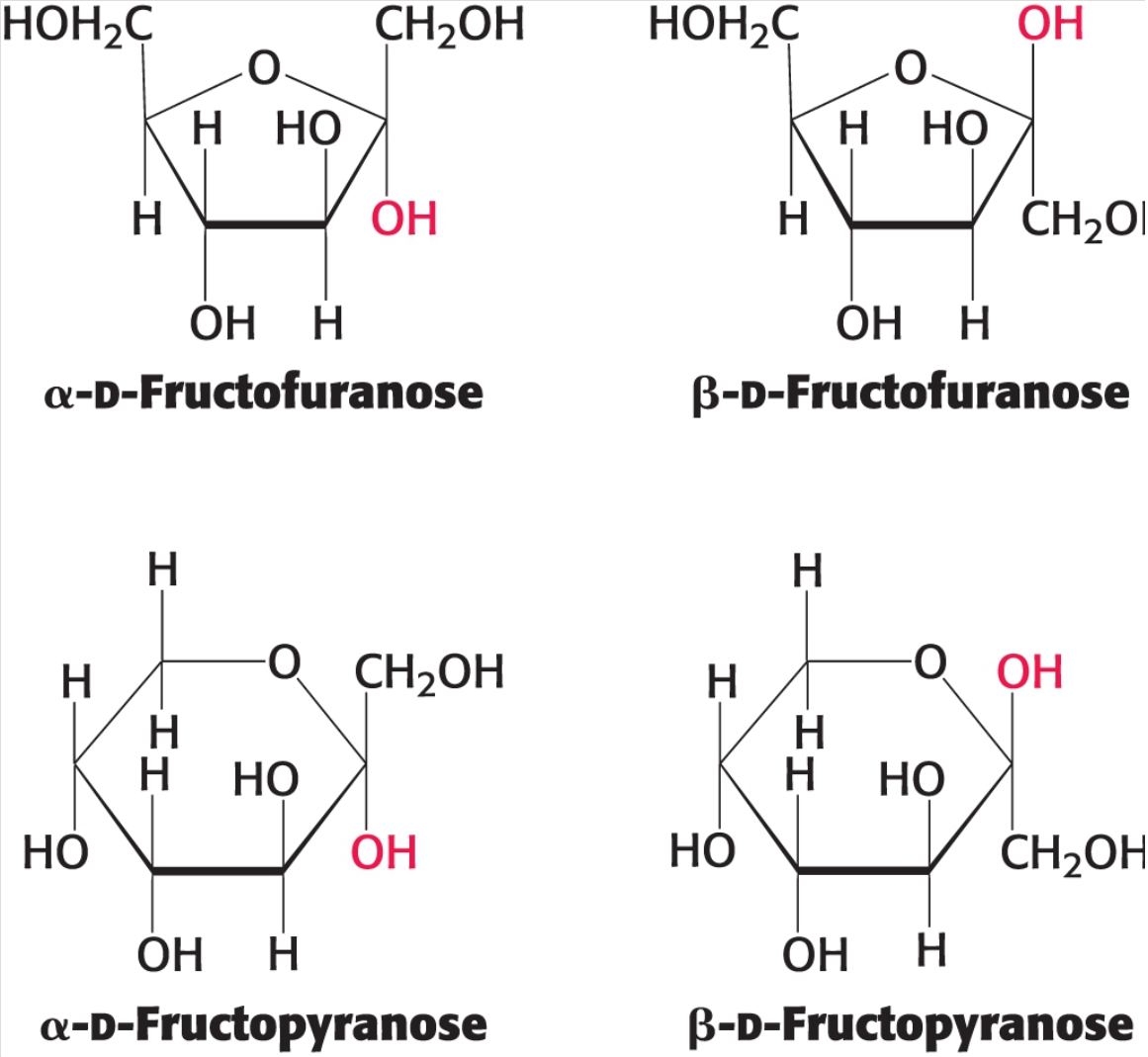


FIGURE 11.5 D-Fructose rapidly interchanges between four distinct ring structures in solutio
D-Fructose can form both five-membered furanose (top) and six-membered pyranose (bottom) rings. In each case, both α and β anomers are possible and all are in rapid equilibrium with the open-chain form.

β-D-Fructopyranose, found in honey and many fruits, is the sweetest common monosaccharide, while the β-D-fructofuranose form is not nearly as sweet. Because heating converts β-fructopyranose into the β-fructofuranose form, corn syrup with a high concentration of fructose

in the β-D-pyranose form is used as a sweetener in cold, but not hot, drinks. Figure 11.6 shows common sugars in their ring forms.

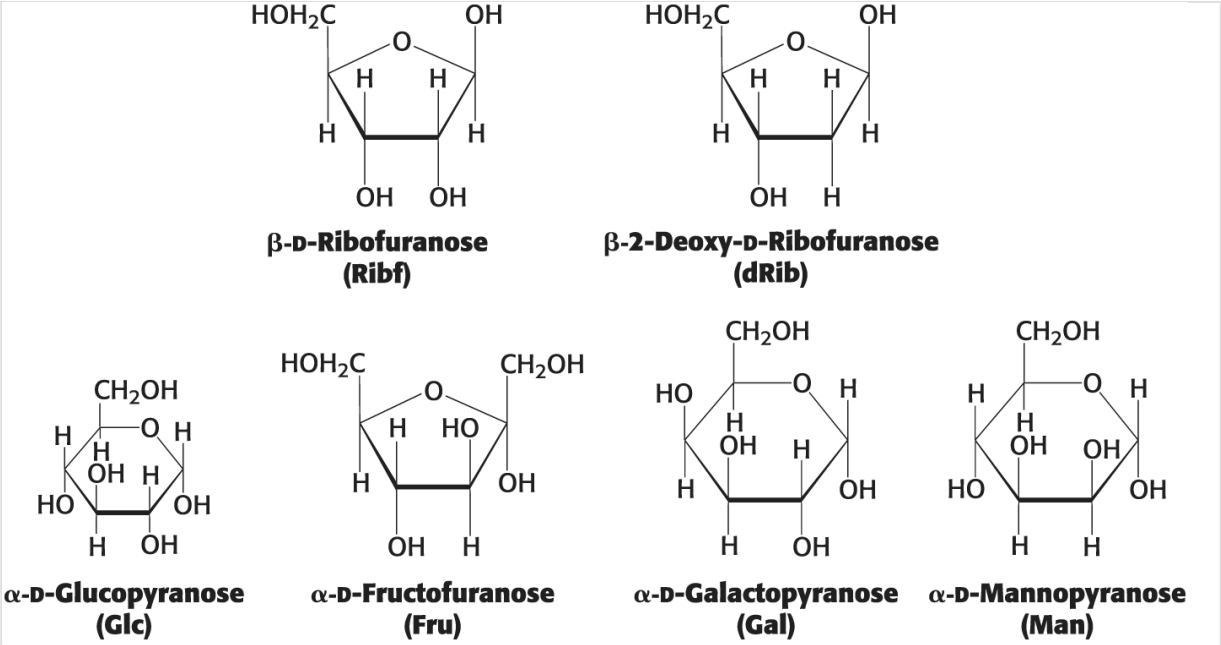


FIGURE 11.6 The most common monosaccharides exist primarily in their ring forms. Only one anomer of each is shown. The shorthand carbohydrate code for each sugar is given in parentheses.

Pyranose and furanose rings can assume different conformations

The six-membered pyranose ring is not planar because of the tetrahedral geometry of its saturated carbon atoms. Instead, pyranose rings adopt two classes of conformations, termed *chair* and *boat* because of the resemblance to these objects (Figure 11.7). In the chair form, the substituents on the ring carbon atoms have two orientations: axial and equatorial. *Axial* bonds are nearly perpendicular to the average plane of

the ring, whereas *equatorial* bonds are nearly parallel to this plane. Axial substituents sterically hinder each other if they emerge on the same side of the ring (e.g., 1,3-diaxial groups). In contrast, equatorial substituents are less crowded.

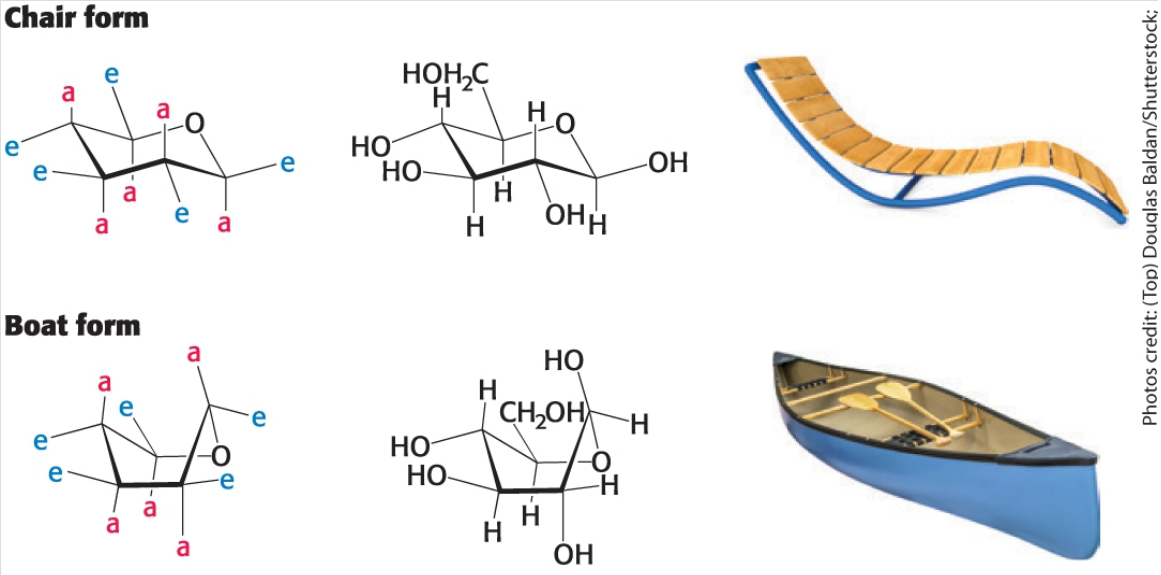
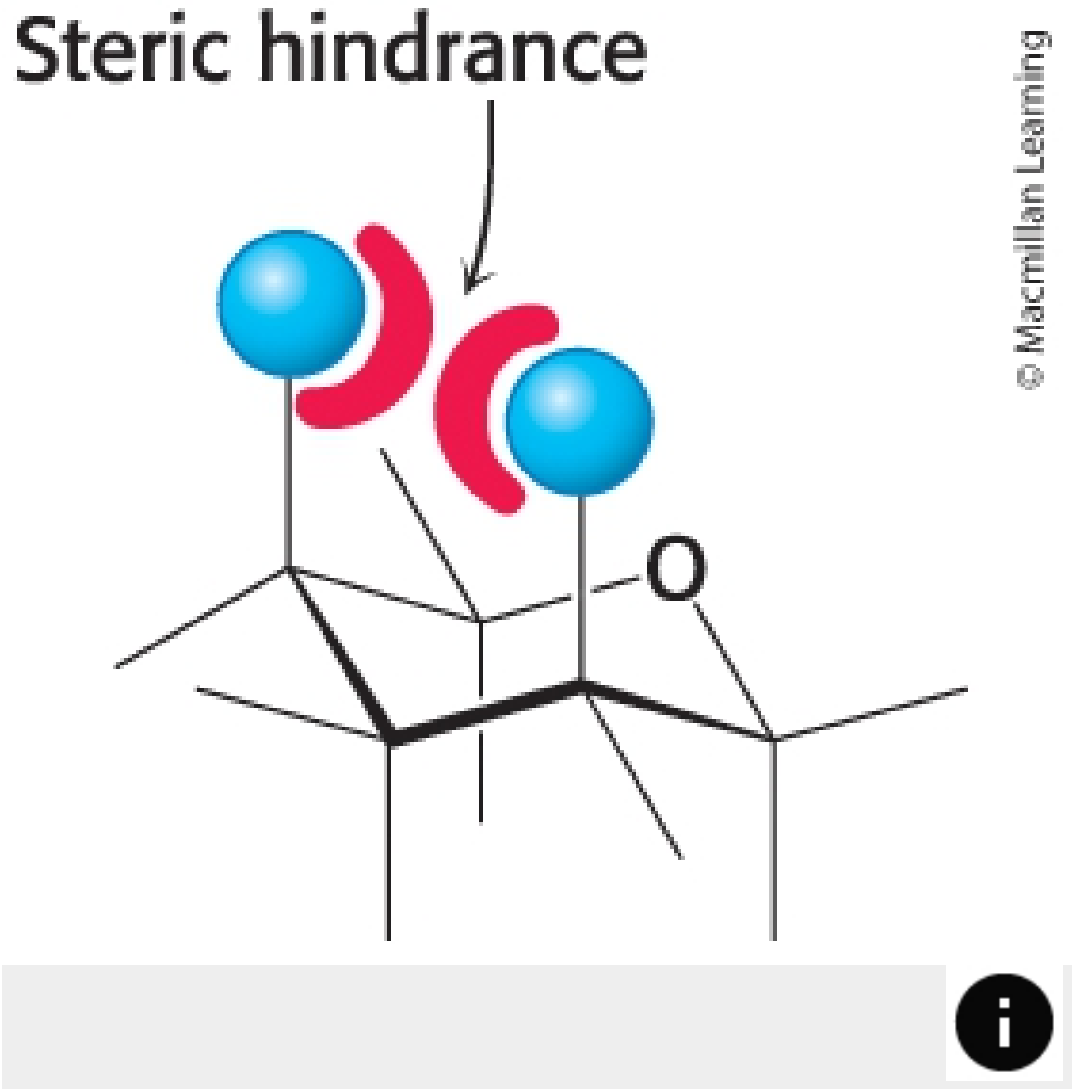


FIGURE 11.7 Pyranose rings like β-D-glucopyranose are not actually planar but adopt chair and boat forms. The chair form is more stable because the less bulky hydrogen atoms occupy a of the axial positions, resulting in less steric hindrance. Abbreviations: a, axial; e, equatorial.

The chair form of β-D-glucopyranose predominates because all axial positions are occupied by hydrogen atoms. The bulkier $-OH$ and $-CH_2OH$ groups emerge at the less-hindered periphery. The boat form of glucose is disfavored because it is quite sterically hindered.



Furanose rings, like pyranose rings, are not planar. They can be puckered so that four atoms are nearly coplanar and the fifth is about 0.5 Å away from this plane (**Figure 11.8**). This conformation is called an *envelope form* because the structure resembles an opened envelope with the back flap raised. In the ribose moiety of most biomolecules, either C-2 or C-3 is out of the plane on the same side as C-5. These conformations are called *C-2-endo* and *C-3-endo*, respectively.

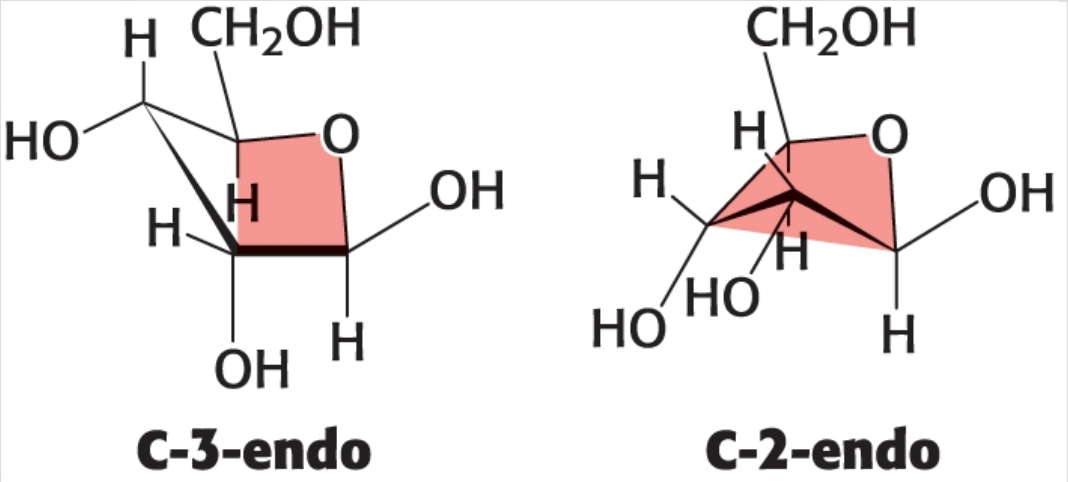


FIGURE 11.8 Furanose rings like β-D-ribofuranose are nonplanar and adopt alternative envelope conformations. The shading indicates the four atoms that lie approximately in a plane.

D-Glucose is an important fuel for most organisms

D-Glucose is a common and important fuel molecule in nearly all organisms. In mammals, D-glucose is the predominant form of carbohydrate circulated in the blood — commonly called *blood sugar* — and is the only fuel that the brain uses under non-starvation conditions, and the only fuel used by red blood cells. Why is D-glucose, instead of any of the many other monosaccharides, such a prominent biological fuel molecule? We can speculate on the reasons. First, glucose is one of several monosaccharides formed from formaldehyde under prebiotic conditions, and so it may have been available as a fuel source for primitive biochemical systems. Second, glucose is relatively non-reactive (inert) compared to other monosaccharides and is therefore less likely to react nonenzymatically with proteins, potentially rendering them nonfunctional.

A consideration of glucose's specific chemical structure holds the key to understanding why its selection as life's primary sugar was not arbitrary. From the perspective of chemical stability, six-membered rings are preferable to five-membered rings due to decreased ring strain. Likewise, as noted above, the chair conformation is preferable for a six-membered ring, and the most stable chair conformation will have all bulky groups ($-OH$ and $-CH_2OH$) in the equatorial positions. Of all possible monosaccharides, the most stable six-membered ring structure that can be formed is that of D-glucose in the pyranose form with the anomeric carbon in the β orientation, as this is the only six-membered ring with all five bulky groups in the equatorial positions. This structural observation also explains the roughly 2:1 ratio of β-to-α anomer conformations for D-glucose in an equilibrium solution. Because glucose has such a strong tendency to exist in this stable ring conformation, it consequently has relatively little tendency to modify proteins in a reaction that results from the linear form compared to other sugars, though these reactions do still occur, as described in the next section.

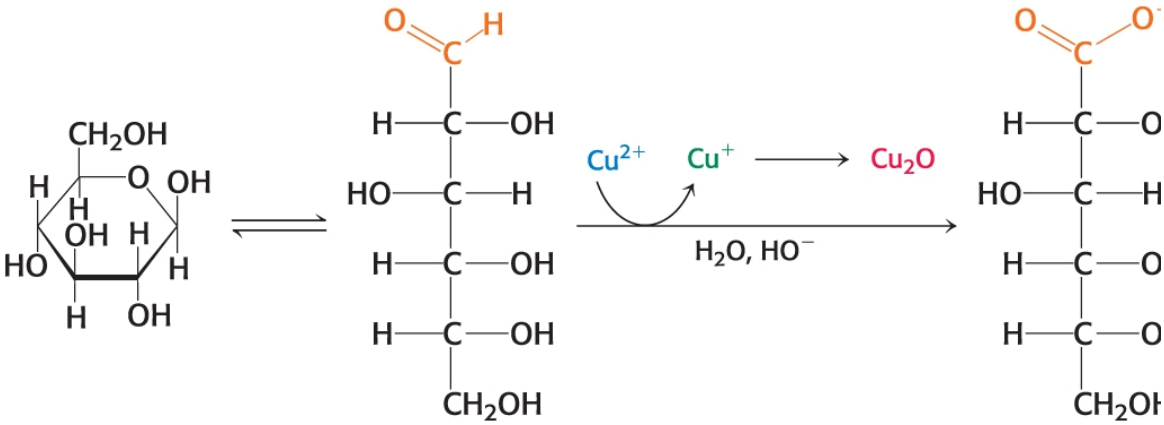
Self-Check Question



Based on ring strain and steric clashes, which is the more stable structure in each pair: D-fructopyranose or D-fructofuranose; boat or chair conformations of D-fructopyranose; bulky groups in axial or equatorial positions about a ring structure; β or α anomer of D-glucopyranose?

Glucose is a reducing sugar and reacts nonenzymatically with hemoglobin

Although 99% of D-glucose molecules in solution are in the pyranose ring forms at any given moment, the α and β anomers of glucose are in an equilibrium that passes through the open-chain form. Thus, glucose has some of the chemical properties of other aldehydes, such as the ability to react with oxidizing agents. For example, glucose in its linear form can react with cupric ion (Cu^{2+}), reducing it to cuprous ion (Cu^{+}), while being oxidized to gluconic acid.



Solutions of cupric ion (known as *Fehling's solution*) provide a simple test for the presence of sugars, such as D-glucose, that at least temporarily adopt an open structure. Sugars that react are called **reducing sugars**. Because ketose sugars can tautomerize to a small degree into temporary structures that have aldehydes, all monosaccharides that can access their open (linear) structures in solution are reducing sugars.

Reducing sugars often nonspecifically react with free amino groups on proteins, usually at a lysine or arginine residue, to form a stable

covalent bond. This nonenzymatic (random) addition of a carbohydrate to another molecule is called *glycation*, as opposed to *glycosylation*, which is enzyme catalyzed. As emphasized above, D-glucose has a low tendency to glycate proteins; however, when the concentrations of both the sugar and the protein are very high for long periods of time — as is the case with both D-glucose and hemoglobin in red blood cells — even unlikely reactions can occur at an appreciable rate. As such, the reducing sugar D-glucose reacts with hemoglobin to form glycated hemoglobin (called *hemoglobin A1c* or often just A1C).

 Monitoring changes in A1C levels — that is, the amount of *glycated hemoglobin* (often incorrectly called *glycosylated hemoglobin*) in the blood — is an especially useful means of assessing the effectiveness of treatments for diabetes mellitus, a serious condition in which insulin, a key hormone in regulating glucose homeostasis, is either absent (type 1 diabetes) or ineffective (type 2 diabetes), resulting in high levels of blood glucose (Section 24.3). Because the glycated hemoglobin remains in circulation, the amount of the modified hemoglobin corresponds to the long-term regulation — over several months — of glucose levels. This kind of measurable sign of an illness that correlates with a disease regardless of whether it is actually mechanistically involved is called a *biomarker*. In nondiabetic individuals, less than 6% of hemoglobin is glycated, whereas in patients with uncontrolled diabetes, almost 10% of hemoglobin is glycated. Thus, glycated hemoglobin (A1C) is a widely used biomarker for the early onset and treatment of diabetes, among other disorders.

Although the glycation of hemoglobin has no effect on oxygen binding and is thus benign, similar reducing reactions with other proteins such as collagen are often detrimental, because the glycations alter the normal biochemical function of the modified proteins. Following the primary modification, cross-linking may occur between the site of the first modification and elsewhere in the protein, further compromising function. These modifications, known as *advanced glycation end products*

(AGEs), have been implicated in aging, arteriosclerosis, and diabetes, as well as other pathological conditions.

Monosaccharides are joined to alcohols and amines through glycosidic linkages by specific enzymes

The biochemical properties of monosaccharides can by modified by reaction with other molecules. These modifications increase the biochemical versatility of carbohydrates, enabling them to serve as signal molecules or facilitating their metabolism. Three common reactants are alcohols, amines, and phosphates.

The covalent linkage formed between the anomeric carbon atom of a carbohydrate and the oxygen atom of an alcohol is called a **glycosidic linkage** — specifically, an O-*glycosidic linkage* (**Figure 11.9A**). *O*-Glycosidic linkages are prominent when carbohydrates are joined together to form long polymers. In addition, the anomeric carbon atom of a sugar can be linked to the nitrogen atom of an amine to form an N-*glycosidic linkage*, such as when nitrogenous bases are attached to ribose units to form nucleotides (**Figure 11.9B**). Both types of linkages are used to attach carbohydrates to proteins. Carbohydrates can also be modified by the attachment of functional groups to carbons other than the anomeric carbon (**Figure 11.10**). For example, *N*-acetylgalactosamine is called an *amino sugar*, so named because an amino group replaces a hydroxyl group.

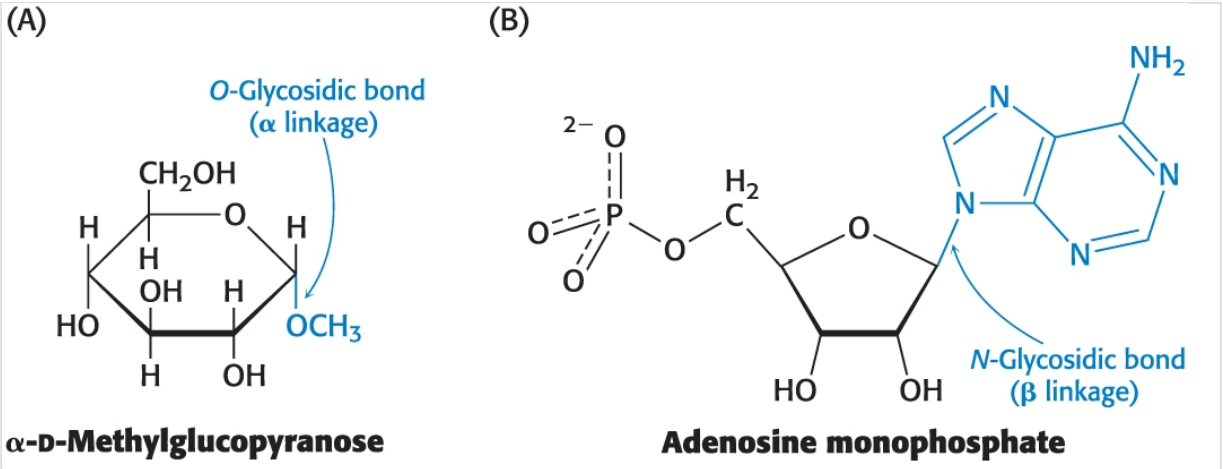


FIGURE 11.9 Carbohydrates are often attached to other molecules through *O*- and *N*-glycosidic linkages. (A) An *O*-glycosidic linkage connects glucose to a methyl group in α-D-methylglucopyranose. (B) An *N*-glycosidic linkage joins ribose to the base adenine in adenosine monophosphate.

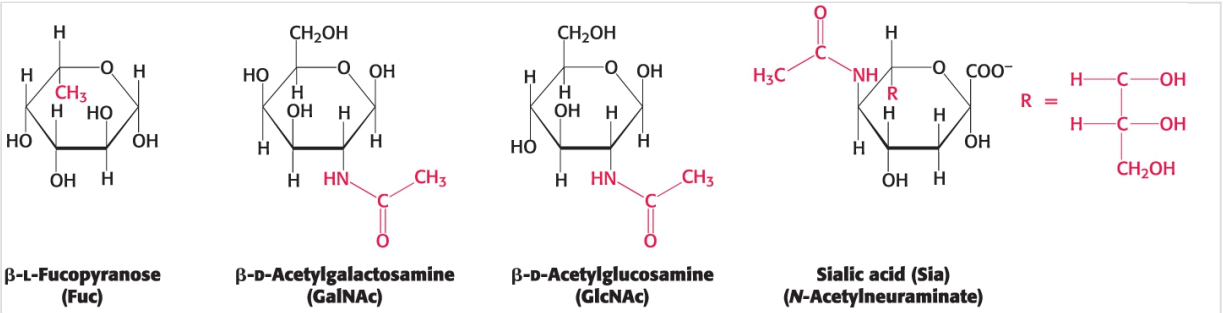
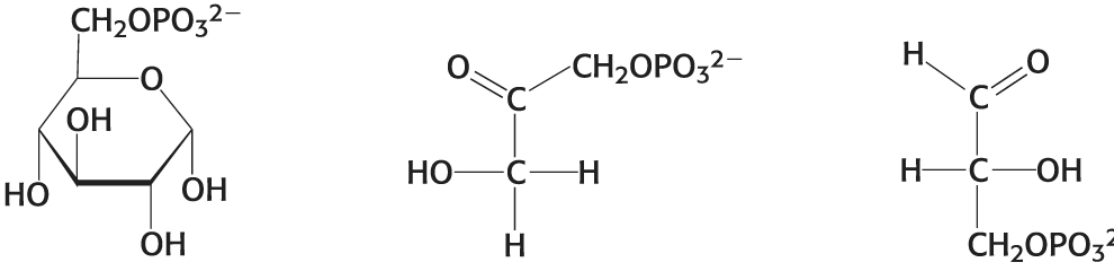


FIGURE 11.10 Monosaccharides can be modified by the addition of substituents other than hydroxyl groups. Additional substituents are shown in red.

Phosphorylated sugars are key intermediates in metabolism

The addition of phosphoryl groups is a common modification of sugars in metabolic reactions. For instance, the first step in the breakdown of glucose to obtain energy is its conversion into glucose 6-phosphate. Several subsequent intermediates in this metabolic pathway, such as dihydroxyacetone phosphate and glyceraldehyde 3-phosphate, are phosphorylated sugars.



Glucose 6-phosphate (G-6P)

Dihydroxyacetone phosphate (DHAP)

Glyceraldehyde 3-phosphate (GAP)

By making sugars anionic (negatively charged), phosphorylation not only prevents these sugars from spontaneously leaving the cell by crossing lipid-bilayer membranes but also prevents them from interacting with transporters of the unmodified sugar. Moreover, phosphorylation blocks the formation of alternative ring conformations; for example, phosphorylation of fructose at C-6 prevents the formation of both pyranose anomers, effectively increasing the concentration of the furanose forms. Finally, phosphorylation creates reactive intermediates that will more readily undergo metabolism. For example, a multiply phosphorylated derivative of ribose plays key roles in the biosyntheses of purine and pyrimidine nucleotides (Chapter 25).

Self-Check Question



Which of the following — D-fructose, D-galactose, β-D-ribofuranose — are reducing sugars like D-glucose?

11.2 Monosaccharides Are Linked to Form Complex Carbohydrates

Because sugars contain hydroxyl groups, glycosidic linkages can join one monosaccharide to another. **Oligosaccharides** are built by the linkage of two or more monosaccharides by *O*-glycosidic bonds (**Figure 11.11**). In the disaccharide maltose, for example, two D-glucose residues are joined by a glycosidic linkage between the α-anomeric form of C-1 on one sugar and the hydroxyl oxygen atom on C-4 of the adjacent sugar. This is called an α-*1,4-glycosidic linkage*.

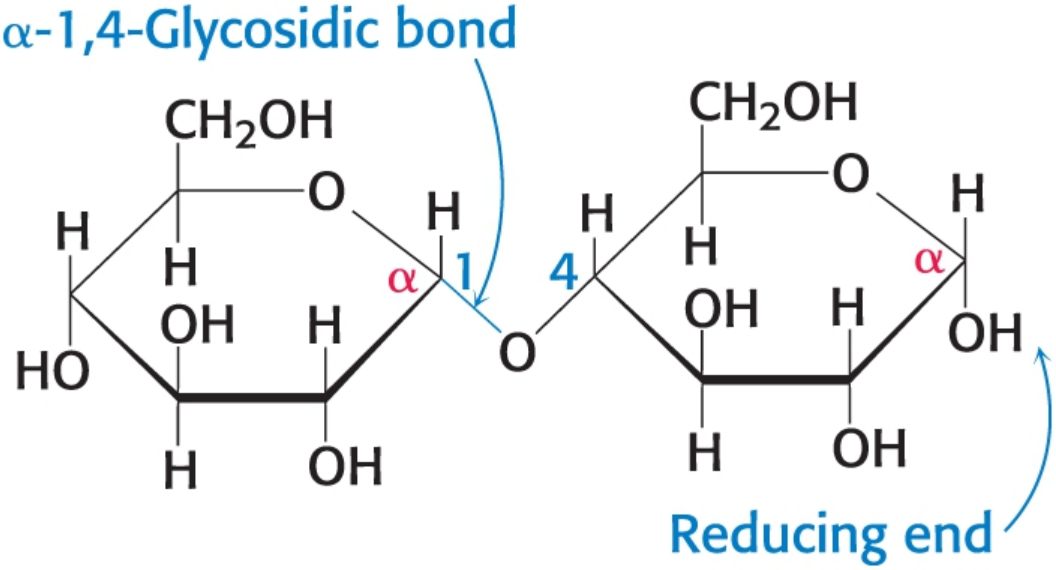


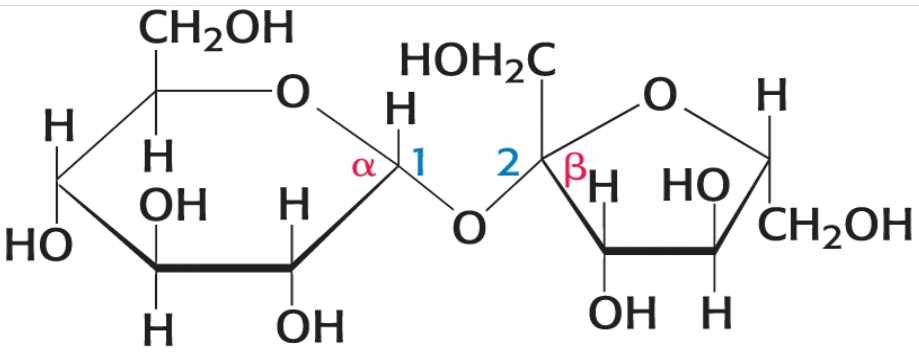
FIGURE 11.11 Maltose is a disaccharide of only D-glucose. Two molecules of glucose are linked by an α-1,4-glycosidic linkage to form the disaccharide maltose. The glucose molecule on the right is capable of assuming the open-chain form, which can act as a reducing agent. The glucose molecule on the left cannot assume the open-chain form, because the C-1 carbon atom is bound to another molecule.

Just as proteins have a directionality defined by the amino and carboxyl ends, oligosaccharides have a directionality defined by their reducing and nonreducing ends. Anomeric carbons in glycosidic linkages are locked in their specific anomeric form and can no longer convert to the open-chain form, or mutarotate. However, the sugar at the reducing end has a free anomeric carbon atom that has reducing activity because it can form the open-chain form. By convention, this end of the oligosaccharide is still called the *reducing end* even when it is bound to another molecule such as a protein and thus no longer has reducing properties.

The fact that monosaccharides have multiple hydroxyl groups means that many different glycosidic linkages are possible. For example, consider three monosaccharides: glucose, mannose, and galactose. In principle, these molecules could be linked together to form more than 12,000 structures differing in the order of the monosaccharides and the hydroxyl groups participating in the glycosidic linkages. In this section, we will look at some of the most common oligosaccharides that actually occur in nature.

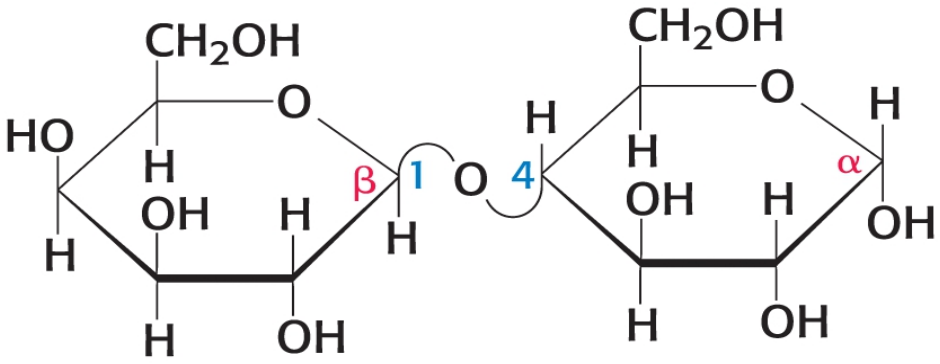
Sucrose, lactose, and maltose are common disaccharides

A **disaccharide** consists of two sugars joined by an *O*-glycosidic linkage. Figure 11.12 illustrates three abundant disaccharides.



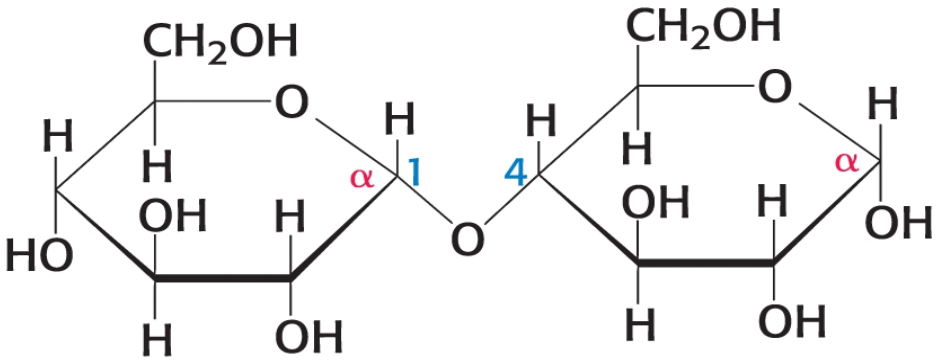
Sucrose

(α-D-Glucopyranosyl-(1→2)-β-D-Fructofuranose)



α-Lactose

(β-D-Galactopyranosyl-(1→4)-α-D-Glucopyranose)



α-Maltose

(α-D-Glucopyranosyl-(1→4)-α-D-Glucopyranose)

FIGURE 11.12 Sucrose, lactose, and maltose are common dietary disaccharides. In sucrose, neither sugar can access the open chain form since both anomeric carbons are in the glycosidic linkage; hence, sucrose is not a reducing sugar, and there are no anomeric forms. For lactose and maltose, only one anomer is shown. In lactose, the curved lines indicate the connectivity of the atoms but are normal covalent bonds. One sugar is upside down with respect to the other in the structure; however, for viewing convenience both sugars here are shown in the normal orientation for a Haworth projection, necessitating curved lines.



- In *sucrose*, obtained commercially from sugar cane or sugar beets and refined into table sugar, both the anomeric carbons of a glucose unit and a fructose unit are joined; the configuration of this glycosidic linkage is α for glucose and β for fructose. Note that because both anomeric carbons are involved in the glycosidic linkage, sucrose is not a reducing sugar. Sucrose can be cleaved into its component monosaccharides by the enzyme *sucrase*, also called *invertase*.

- The disaccharide found in milk, *lactose*, consists of galactose joined to glucose by a β-1,4-glycosidic linkage. Lactose is hydrolyzed to these monosaccharides by *lactase* in human beings and by *β-galactosidase* in bacteria.

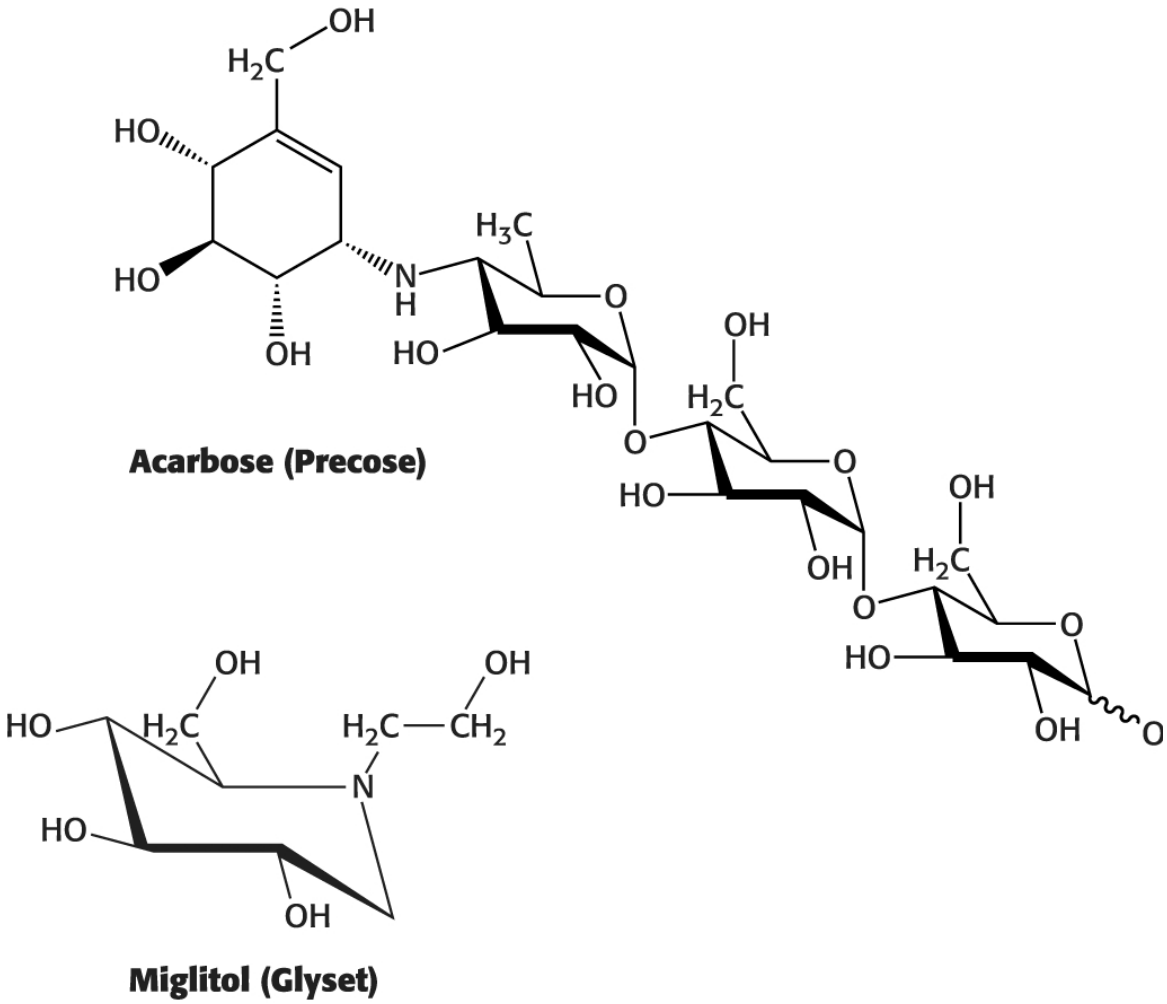
- In *maltose*, two glucose units are joined by an α-1,4-glycosidic linkage. Maltose comes from the hydrolysis of large polymeric oligosaccharides such as starch and glycogen and is in turn hydrolyzed to glucose by *maltase* (α-glucosidase). Maltase will also degrade oligosaccharides linked by α-1,4-glycosidic linkages.

The enzymes sucrase, lactase, and maltase are located on the outer surfaces of epithelial cells lining the small intestine. The cleavage products of sucrose, lactose, and maltose can be further processed to provide energy in the form of ATP.

Maltase inhibitors can help to maintain blood glucose homeostasis



Maintaining the proper concentration of glucose in the blood (3.9–5.5 mM) — glucose homeostasis — is vital, since glucose can form advanced glycation products. Moreover, as we noted earlier, elevated blood glucose (hyperglycemia) is characteristic of diabetes. Pharmacological intervention is sometimes required, including the administration of insulin or other drugs that control blood glucose, and maltase is one potential drug target. Following a meal, starch and glycogen are initially degraded by α-amylase secreted by the salivary glands and pancreas. The oligosaccharides generated by α-amylase are further digested by α-glucosidase. Two drugs commonly used to inhibit maltase are acarbose (Precose) and miglitol (Glyset):



Both acarbose and miglitol are competitive inhibitors (Section 5.6) of maltase and are usually ingested at the start of a meal to slow postprandial (after a meal) glucose absorption in the treatment of diabetes.

Human milk oligosaccharides protect newborns from infection



In addition to the disaccharide lactose, more than 150 different oligosaccharides have been identified in human milk; the amount and composition of these sugars vary among lactating women. Interestingly, these carbohydrates are not digested by breastfed infants but play a significant role in protecting them against bacterial infection. In particular, they may protect infants from infections caused by certain types of *Streptococcus* bacteria that are sometimes transmitted during vaginal childbirth. How the protection arises is not firmly established, but the oligosaccharides may serve as a fuel source for beneficial bacteria. Alternatively, or in addition, these carbohydrates may prevent the attachment of microbial pathogens to the intestinal wall of the newborn. Biochemists continue to explore the therapeutic potential of these oligosaccharides.

Glycogen and starch are storage polysaccharides of glucose

As we know, glucose is an important energy source in virtually all life forms. However, free glucose molecules cannot be stored; in high concentrations, glucose will disturb the osmotic balance of the cell, potentially resulting in cell death. The solution is to store glucose as units in a large polymer, which is less osmotically active.

Large polymeric oligosaccharides, formed by the linkage of multiple monosaccharides, are called **polysaccharides**, or *glycans*, and play vital roles in energy storage and in maintaining the structural integrity of an

organism. If all of the monosaccharide units in a polysaccharide are the same, the polymer is called a *homopolymer*.

The most common homopolymer in animal cells is **glycogen**, the storage form of glucose. Glycogen is present in most of our tissues but is most abundant in muscle and liver. As will be considered in detail in Chapter 21, glycogen is a large, branched polymer of glucose residues. Most of the glucose units in glycogen are linked by α-1,4-glycosidic linkages. The branches are formed by α-1,6-glycosidic linkages, present about once in 12 units (**Figure 11.13**). The great degree of branching in glycogen increases the surface area of a glycogen particle, allowing better access for enzymes to rapidly break it down when glucose is needed in animal cells.

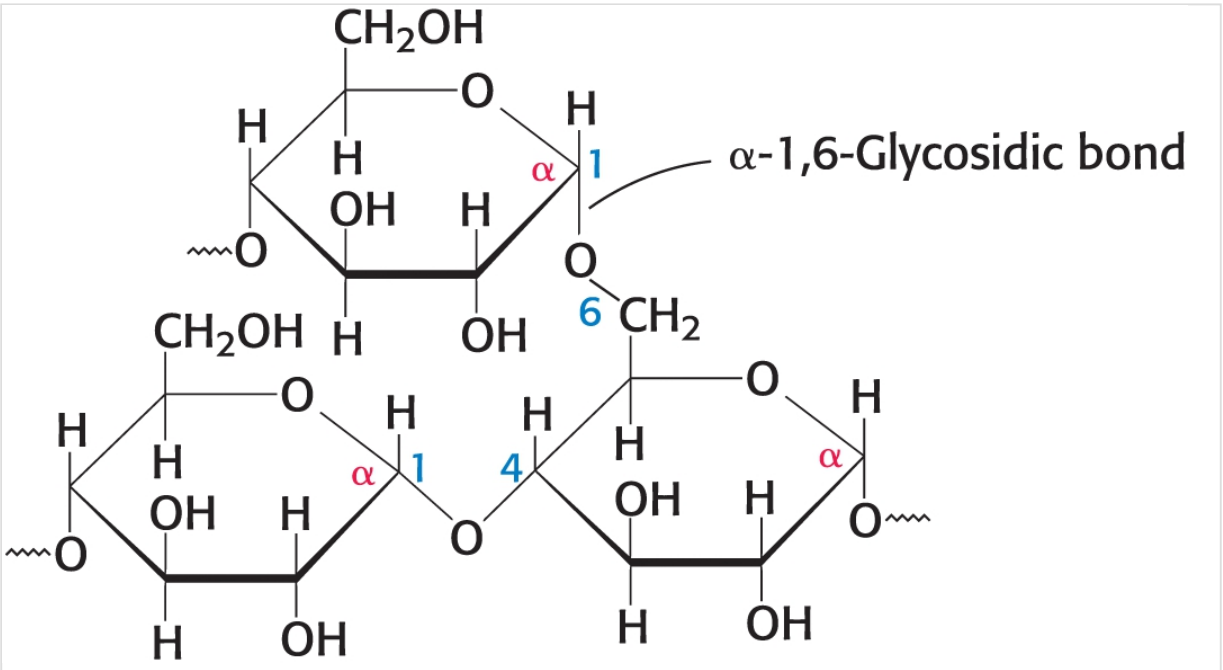


FIGURE 11.13 Glycogen consists of linear polymers with many branch points. Two chains of glucose molecules joined by α-1,4-glycosidic linkages are joined by an α-1,6-glycosidic linkage to create a branch point. Such an α-1,6-glycosidic linkage forms at approximately every 12 glucose units, making glycogen a highly branched molecule.

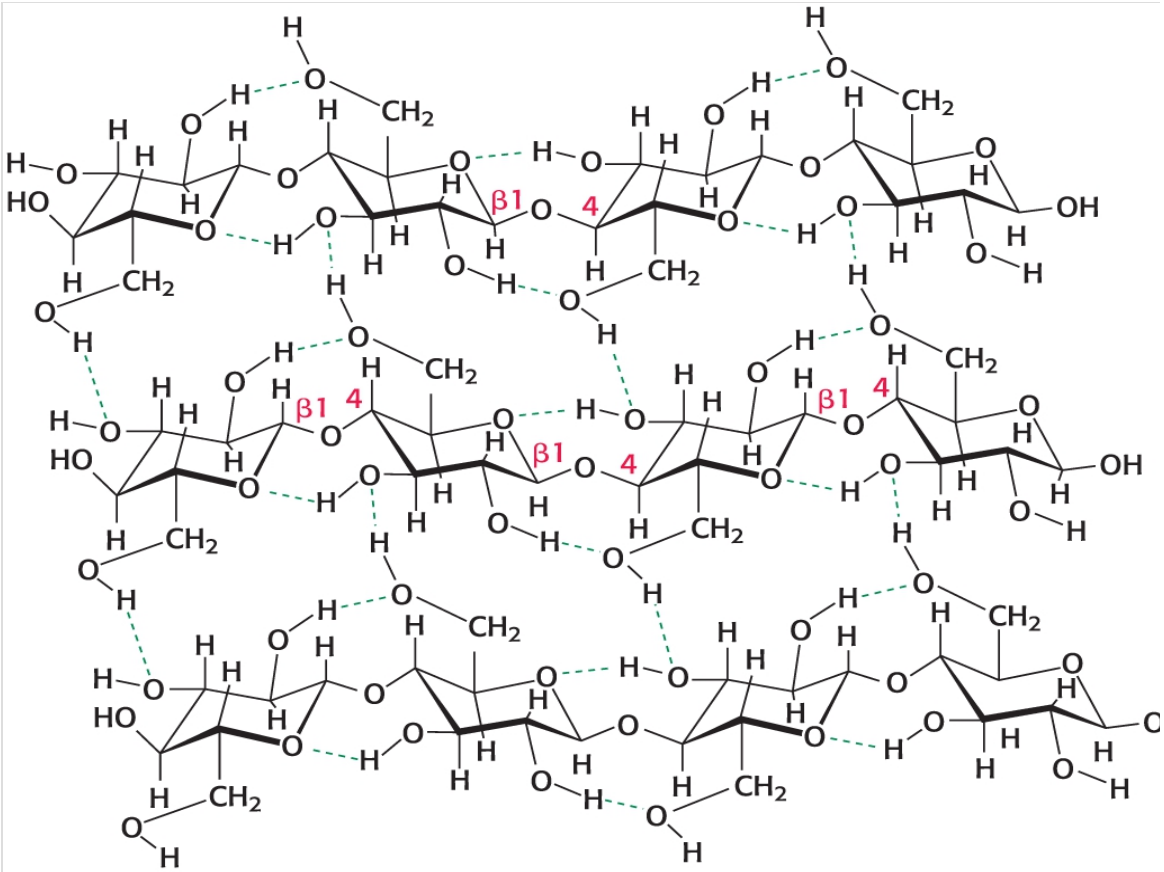
The nutritional reservoir in plants is the homopolymer **starch**, of which there are two forms. *Amylose*, the unbranched type of starch, consists of glucose residues in α-1,4 linkage. *Amylopectin*, the branched form, has about one α-1,6 linkage per 30 α-1,4 linkages. The structure of amylopectin is therefore identical to that of glycogen except for its lower degree of branching, which results in a more compacted structure known as a starch granule. Plants do not need to break down starch as quickly as animals need to degrade glycogen. More than half the carbohydrate ingested by human beings is starch, which is found in wheat, potatoes, rice, and other plant sources. Amylopectin, amylose, and glycogen are all hydrolyzed by α-*amylase*, an enzyme secreted by the salivary glands and the pancreas that can cleave the α-1,4 linkages common to all three glucose-storing homopolymers.

Cellulose is the main structural polysaccharide of plants

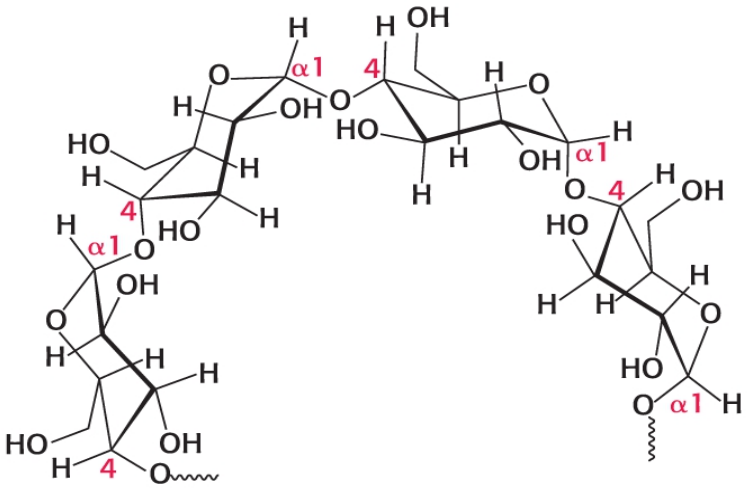
Another major polysaccharide of glucose found in plants, **cellulose**, serves a structural rather than a nutritional role as an important component of the plant cell wall. As one of the most abundant organic compounds in the biosphere, some 10^{15} kg of cellulose is synthesized and degraded on Earth each year, an amount 1000 times as great as the combined weight of the total human population.

Cellulose is an unbranched polymer of glucose residues joined by β-1,4 linkages, in contrast with the α-1,4 linkage seen in starch and glycogen. This simple difference in stereochemistry creates two molecules with very different properties and biological functions. The β configuration allows cellulose to form very long, straight chains. Fibrils of cellulose are formed by parallel chains that interact with one another through hydrogen bonds, generating a rigid, supportive structure (**Figure 11.14, top**). The straight chains formed by β linkages are optimal for the

construction of fibers having a high tensile strength. In contrast, the α-1,4 linkages in glycogen and starch produce a very different molecular architecture: a hollow helix is formed instead of a straight chain (**Figure 11.14, bottom**). The hollow helix formed by α linkages is well suited to the formation of a more compact, accessible store of sugar.



Cellulose
(β-1,4 linkages)

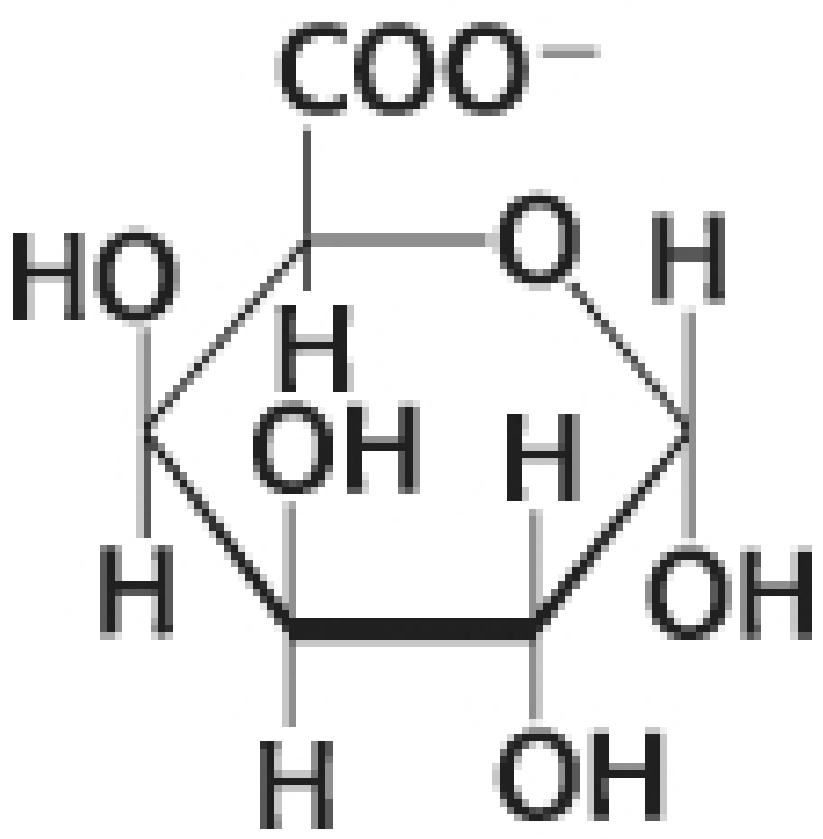


Starch and glycogen
(α-1,4 linkages)

FIGURE 11.14 Glycosidic linkages determine polysaccharide structure. The β-1,4 linkages favo straight chains, which are optimal for structural purposes. The α-1,4 linkages favor bent, helical structures, which are more suitable for storage.



Although animals lack cellulases and therefore cannot digest wood and vegetable fibers, cellulose and other plant fibers are still an important constituent of the mammalian diet as a component of dietary fiber. Soluble fiber such as pectin (polygalacturonic acid) slows the movement of food through the gastrointestinal tract, allowing improved digestion and the absorption of nutrients. Insoluble fibers, such as cellulose, increase the rate at which digestion products pass through the large intestine, softening stools and making them easier to pass.



Galacturonic acid

Chitin is the main structural polysaccharide of fungi and arthropods

Likely the second most abundant polysaccharide on the planet, chitin is found in the cell walls of fungi, in the exoskeletons and shells of arthropods such as insects, arachnids, mollusks, and crustaceans, and in numerous other organisms. The structure of chitin is very similar to cellulose with the exception that each glucose sugar has the C-2

hydroxyl replaced with an amino group which is acetylated such that chitin is a homopolymer of β -1,4 linked *N*-acetylglucosamine, rather than glucose (Figure 11.15). Chitin fibers are also often crosslinked to one another and composited with minerals and proteins to further increase its rigidity and strength. For example, cephalopods such as squid use their razor-sharp beaks, which are made of extensively cross-linked chitin, to disable and consume prey.

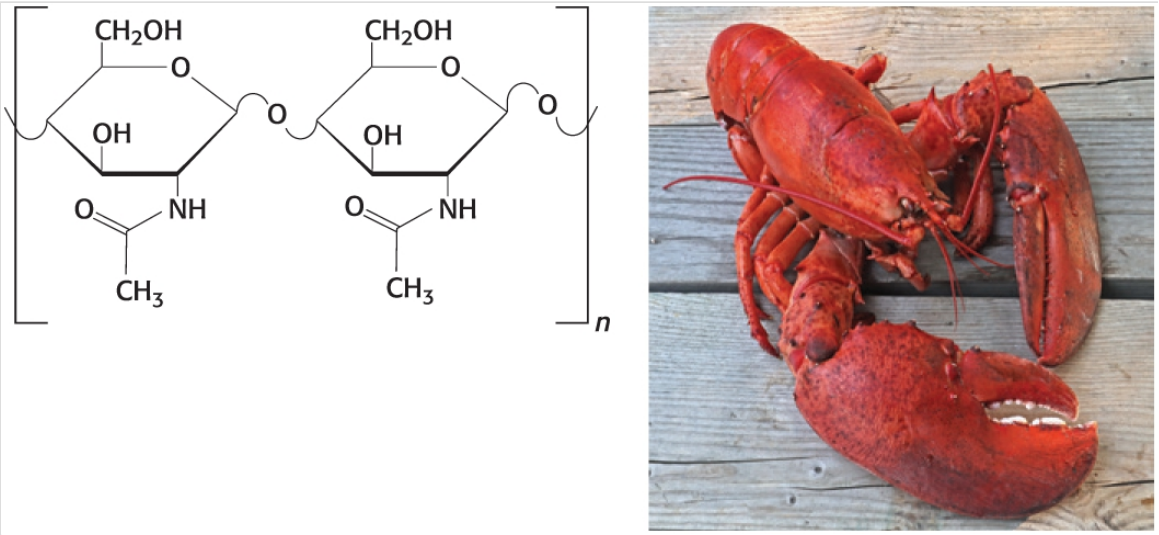


FIGURE 11.15 Chitin, a homopolymer of *N*-Acetylglucosamine, is a structural glycan found in insect wings and the exoskeletons of arthropods, including lobster shells.

Chitin can be processed to a molecule with a variety of uses

We are all aware, in one way or another, of the many uses of the polysaccharide cellulose. It is a major constituent of paper, bioadhesives, and the clothes you are wearing. Less obvious to most of us are uses of chitin. Estimates are that 10,000 tons of chitin could be

recovered from the shellfishing industry by processing the shells into a more versatile molecule called *chitosan.*

Chitosan has a variety of uses. For instance, it is used as a carrier to assist in drug delivery, as surgical stitches, and as a component of cosmetic and food products. Recent research shows that chitosan can be used as a component of an adhesive that strongly adheres to wet tissues, allowing the adhesive to be used as a surgical dressing.

One way to process chitin, which is water-insoluble, to water-soluble chitosan is with a series of microbial/enzymatic processes. First, shells are washed and ground to a fine powder, which is then exposed to lactic acid-generating bacteria. The lactic acid removes minerals from the chitin. Following demineralization, the chitin is treated with protease-secreting bacteria to degrade the protein components. Finally, chitin is treated with chitin deacetylase to remove approximately half of the acetyl groups, generating the more versatile chitosan.

Self-Check Question



Which of these carbohydrates — sucrose, maltose, lactose, cellulose, starch, amylose, glycogen, chitin — are composed entirely of D-glucose monomers? Which are structural (rather than storage) glycans?

11.3 Carbohydrates Can Be Linked to Proteins to Form Glycoproteins

A carbohydrate group can be covalently attached to a protein to form a **glycoprotein**. Such modifications are common; 50% of the human proteome consists of glycoproteins. Many of the proteins secreted from cells are glycosylated, or modified by the attachment of carbohydrates, including most proteins present in the serum component of blood.

Glycosylation greatly increases the complexity of the proteome. A given protein with several potential glycosylation sites can have many different glycosylated forms, called *glycoforms*. Like protein isoforms (Section 7.2), each is typically generated only in a specific cell type or developmental stage.

In this section, we will examine three classes of glycoproteins:

1. In members of the first class, simply referred to as *glycoproteins*, the protein constituent is the largest component by weight. This versatile class plays a variety of biochemical roles. Many glycoproteins are components of cell membranes, where they take part in processes such as cell adhesion, including the binding of sperm to eggs. Other glycoproteins are formed by linking carbohydrates to soluble proteins.

2. In **proteoglycans**, the protein component of the glycoprotein is conjugated to a particular type of polysaccharide called a **glycosaminoglycan**. Carbohydrates make up a much larger percentage by weight of the proteoglycan compared with simple glycoproteins. Proteoglycans function as structural components and lubricants.

3. **Mucins** (or **mucoproteins**) are, like proteoglycans, predominantly carbohydrate, and they are a key component of mucus. In mucins, the protein component is extensively glycosylated at serine or threonine residues, typically by *N*-acetylgalactosamine (Figure 11.10). Mucins serve as lubricants.

Carbohydrates can be linked to proteins through asparagine (*N*-linked) or through serine or threonine (*O*-linked) residues

Sugars in glycoproteins are attached either to the amide nitrogen atom in the side chain of asparagine (termed an N-*linkage*) or to the oxygen atom in the side chain of serine or threonine (termed an O-*linkage*), as shown in **Figure 11.16**. An asparagine residue can accept an oligosaccharide only if the residue is part of an Asn-X-Ser or Asn-X-Thr sequence, in which X can be any residue, except proline.

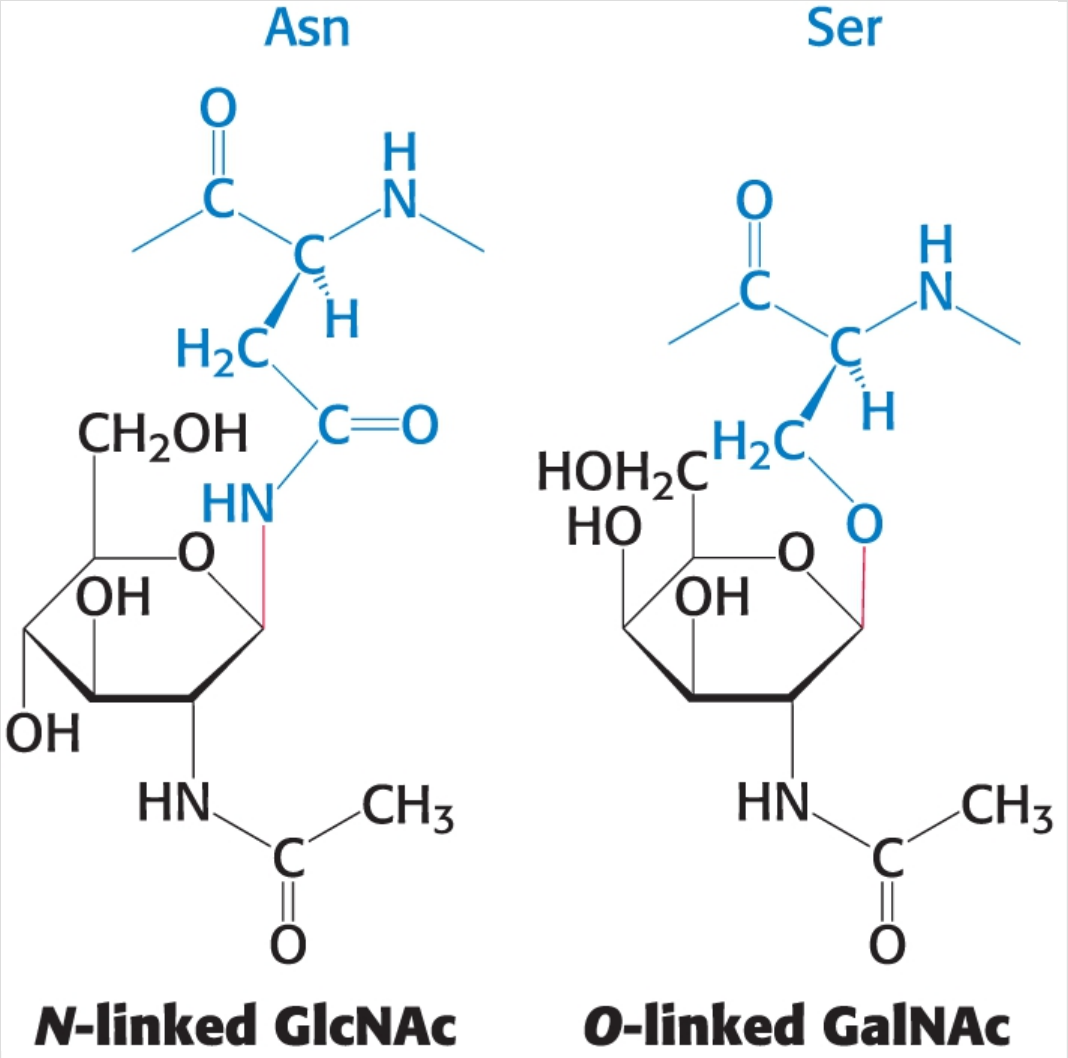


FIGURE 11.16 Glycosidic linkages connect proteins and carbohydrates. A glycosidic linkage connects a carbohydrate to the side chain of asparagine (*N*-linked) or to the side chain of serine or threonine (*O*-linked). The glycosidic linkages are shown in red.

However, not all potential sites are glycosylated. Which sites are glycosylated depends on other aspects of the protein structure and on the cell type in which the protein is expressed. All *N*-linked oligosaccharides have a pentasaccharide core consisting of three mannose and two *N*-acetylglucosamine residues. Additional sugars are

attached to this core to form the great variety of oligosaccharide patterns found in glycoproteins (Figure 11.17).

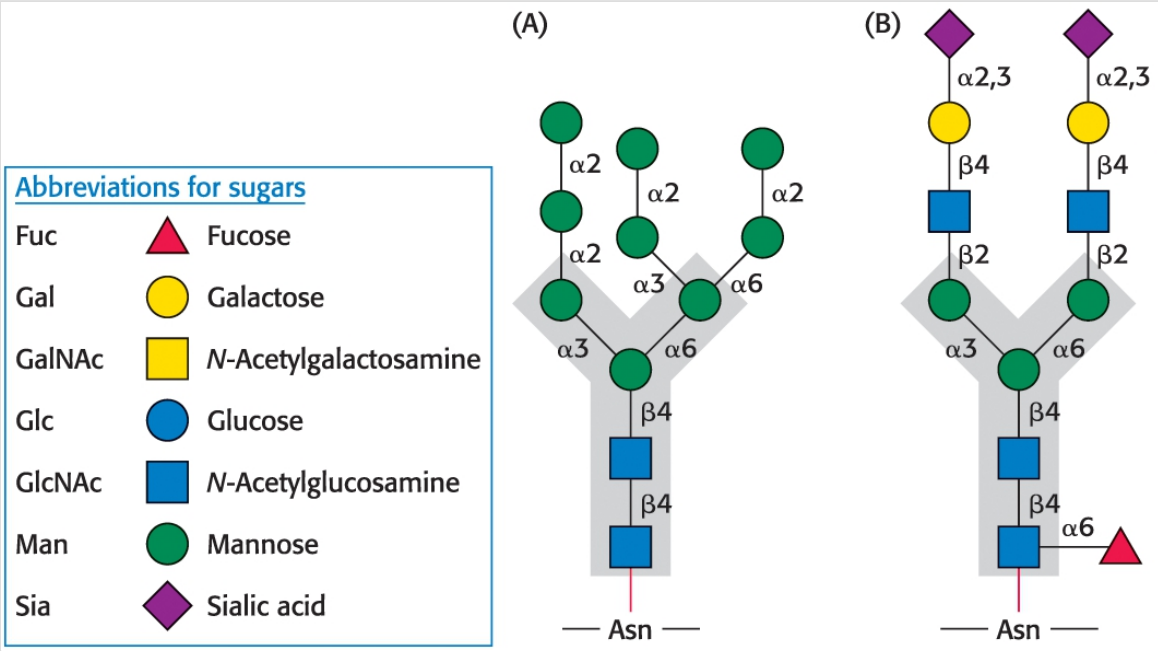


FIGURE 11.17 *N*-linked oligosaccharides have a common core but diverse structures. A pentasaccharide core (shaded gray) is common to all *N*-linked oligosaccharides and serves as th foundation for a wide variety of *N*-linked oligosaccharides, two of which are illustrated: (A) high mannose type; (B) complex type. The carbohydrate structures are depicted symbolically with a scheme widely used by biochemists.

The glycoprotein erythropoietin is a vital hormone

Let us look at a glycoprotein present in the blood serum called *erythropoietin* (EPO), whose cloned recombinant form has dramatically

improved treatment for anemia, particularly that induced by cancer chemotherapy. EPO, which is secreted by the kidneys and stimulates the production of red blood cells, is composed of 165 amino acids and is *N*-glycosylated at three asparagine residues and *O*-glycosylated on a serine residue, resulting in a mature protein that is 40% carbohydrate by weight (**Figure 11.18**). Glycosylation enhances the stability of the protein in the blood; unglycosylated protein has only about 10% of the bioactivity of the glycosylated form because the protein is rapidly removed from the blood by the kidneys.

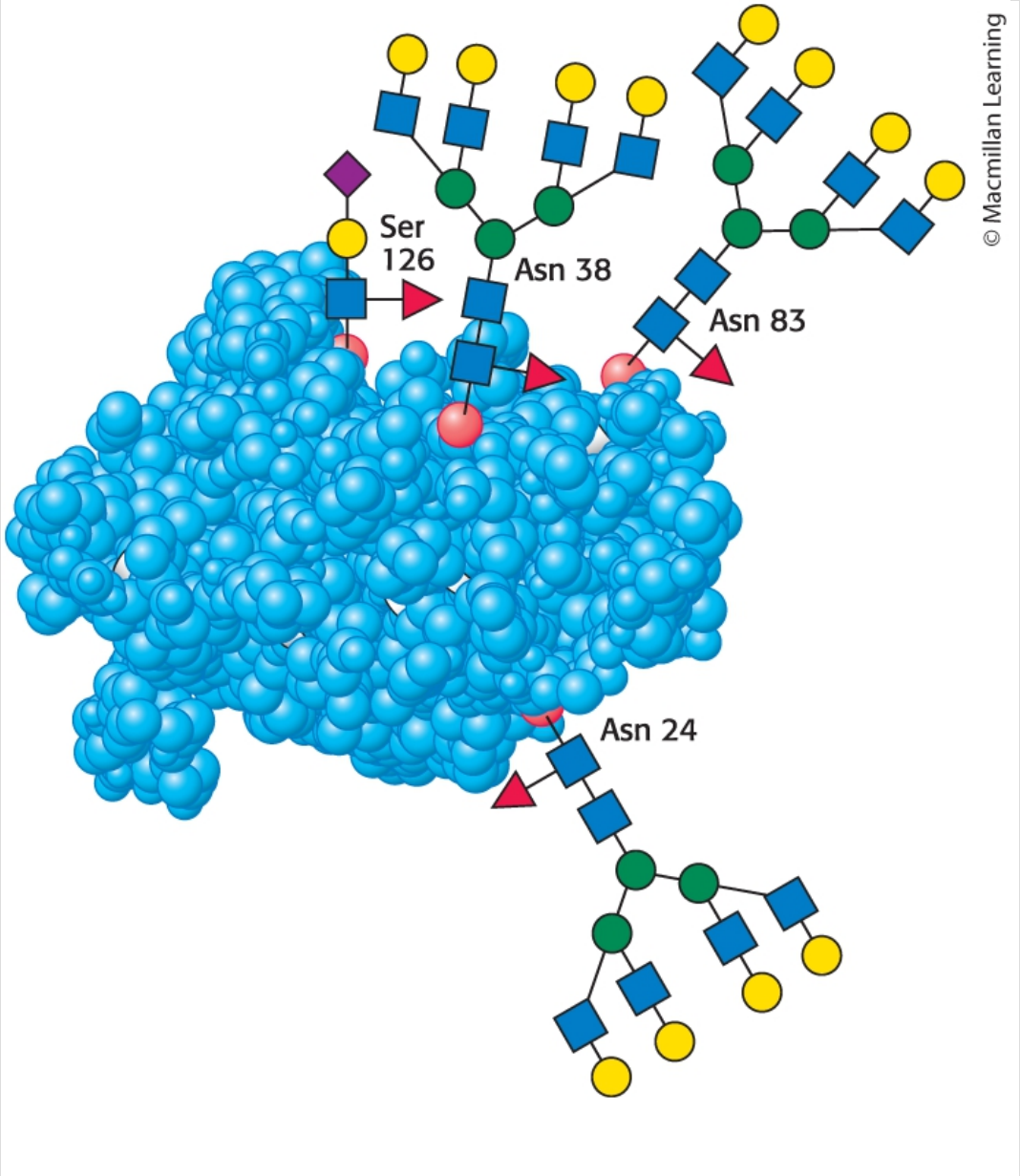


FIGURE 11.18 Erythropoietin has large oligosaccharides linked to three asparagine residues and one serine residue. The structures shown are approximately to scale. See Figure 11.17 for the carbohydrate key.

[Drawn from 1BUY.pdb.]

INTERACT with this model in Achieve

Although the availability of recombinant human EPO has greatly aided the treatment of anemias, some endurance athletes have abused recombinant human EPO to increase the red-blood-cell count and hence their oxygen-carrying capacity. Drug-testing laboratories are able to distinguish some forms of prohibited human recombinant EPO from natural EPO in athletes by detecting differences in their glycosylation patterns.

Glycosylation functions in nutrient sensing

An especially important glycosylation reaction is the covalent attachment of a single *N*-acetylglucosamine (GlcNAc) to serine or threonine residues of cytoplasmic, nuclear, and mitochondrial proteins. The reaction, one of the most common post-translational modifications, is catalyzed by *O*-GlcNAc transferase, a highly conserved enzyme found in all multicellular animals. The concentration of GlcNAc reflects the active metabolism of carbohydrates, amino acids, and fats, indicating that nutrients are abundant (**Figure 11.19**).

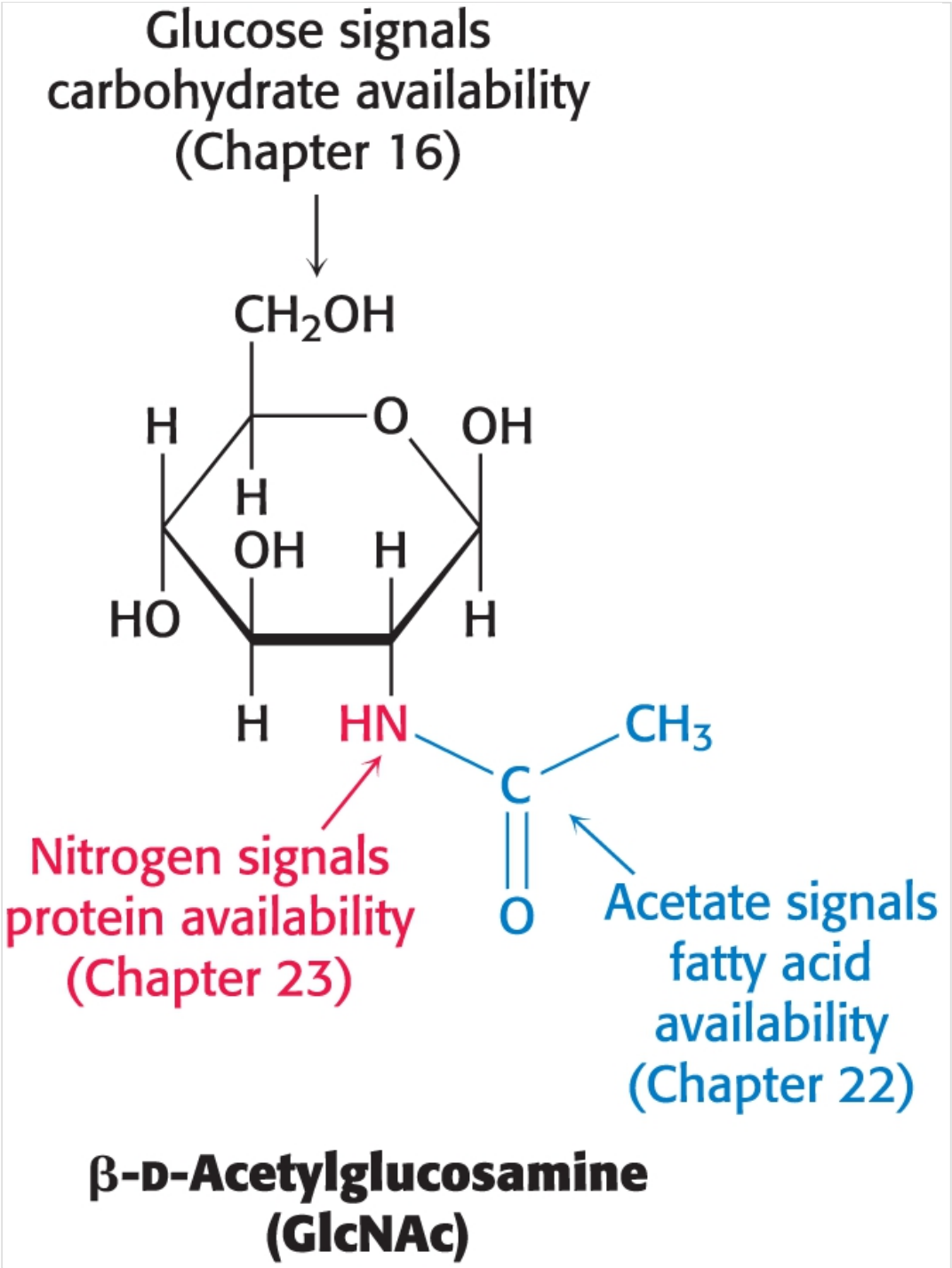


FIGURE 11.19 Glycosylation can serve as a nutrient sensor. *N*-Acetylglucosamine is attached to proteins when nutrients are abundant.

More than 4000 proteins are modified by GlcNAcylation, including transcription factors and components of signaling pathways. Interestingly, because the GlcNAcylation sites are also potential phosphorylation sites, *O*-GlcNAc transferase and protein kinases may be involved in cross talk to modulate one another's signaling activity. Like phosphorylation, GlcNAcylation is reversible, with another enzyme, called *GlcNAcase,* catalyzing the removal of the carbohydrate. Dysregulation of GlcNAc transferase has been linked to insulin resistance, diabetes, cancer, and neurological pathologies.

Proteoglycans have important structural roles

The glycosaminoglycan component of a proteoglycan makes up as much as 95% of the biomolecule by weight, and so a proteoglycan resembles a polysaccharide more than a protein. Proteoglycans not only function as lubricants and structural components in connective tissue but also mediate the adhesion of cells to the extracellular matrix and bind factors that regulate cell proliferation.

The properties of proteoglycans are determined primarily by the glycosaminoglycan component. Many glycosaminoglycans are made of repeating units of disaccharides containing a derivative of an amino sugar, either glucosamine or galactosamine (**Figure 11.20**). At least one of the two sugars in the repeating unit has a negatively charged carboxylate or sulfate group. The major glycosaminoglycans in animals are chondroitin sulfate, keratan sulfate, heparin, dermatan sulfate, and hyaluronate. Recall that heparin acts as an anticoagulant to assist the termination of blood clotting (Section 7.5). The inability to degrade glycosaminoglycans is the cause of a collection of diseases marked by skeletal deformities and reduced life expectancies.

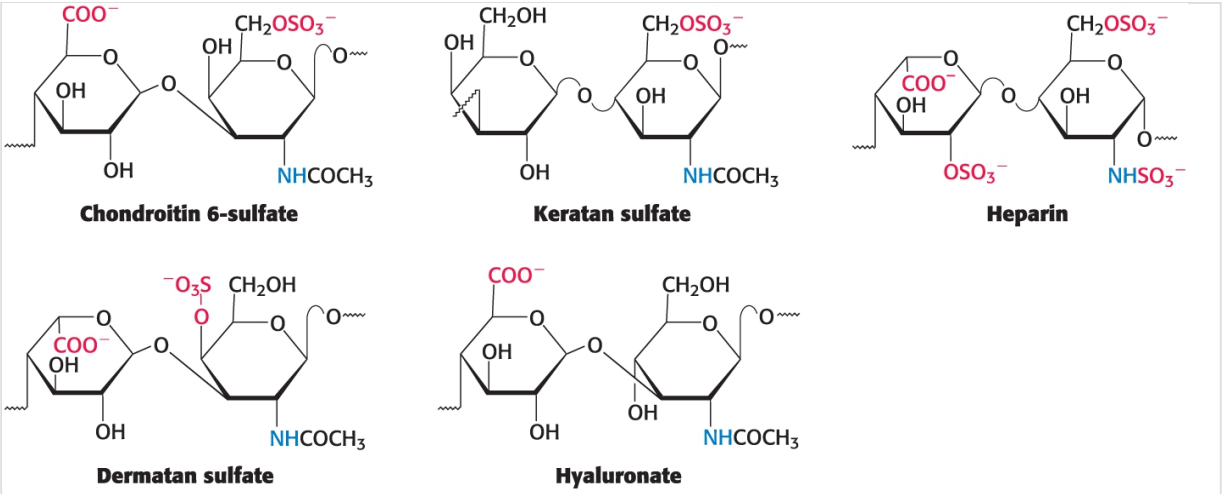


FIGURE 11.20 Glycosaminoglycans are made of repeating units. Structural formulas for five repeating units of important glycosaminoglycans illustrate the variety of possible modifications and linkages. Amino groups are shown in blue and negatively charged groups in red, with hydrogen atoms omitted for clarity. For each molecule shown, the right-hand hexose is a glucosamine derivative.

Proteoglycans are important components of cartilage

Among the best-characterized proteoglycans are those found in the extracellular matrix of cartilage, where they complement the functions of proteins. For example, the triple helix of collagen protein (Section 2.5) provides structure and tensile strength, whereas the proteoglycan aggrecan serves as a shock absorber. The protein component of aggrecan is a large molecule composed of 2397 amino acids with three globular domains (G1, G2, and G3), and the site of glycosaminoglycan attachment is in the extended region between G2 and G3 (**Figure 11.21**). This linear region contains highly repetitive amino acid sequences, which are sites for the attachment of keratan sulfate and chondroitin sulfate. Many molecules of aggrecan are in turn noncovalently bound

through the first globular domain to a very long filament formed by linking together molecules of the sugar component of aggrecan, the glycosaminoglycan hyaluronate (Figure 11.21). In addition, water is bound to the glycosaminoglycans, attracted by the many negative charges.

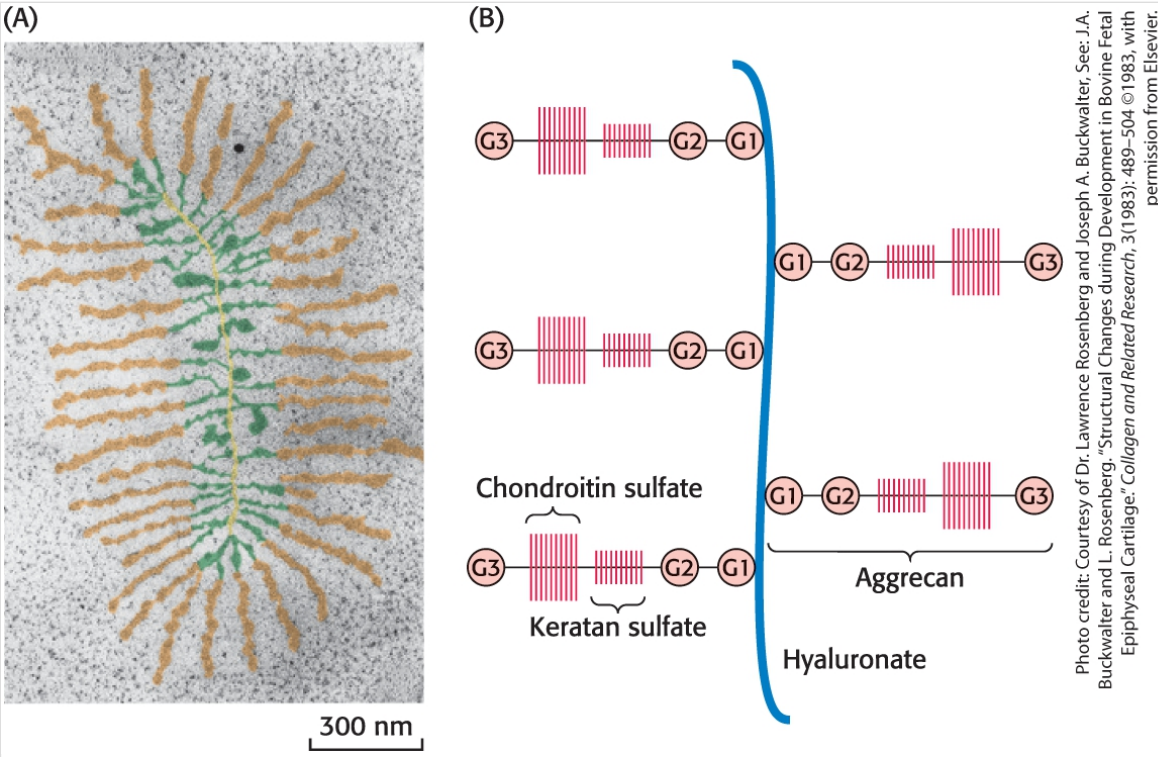


FIGURE 11.21 The proteoglycan from cartilage has an enormous and complex structure. (A) In this electron micrograph of a proteoglycan from cartilage (with false color added), proteoglycan monomers emerge laterally at regular intervals from opposite sides of a central filament of hyaluronate. (B) A schematic representation. The G1 globular domains of multiple aggrecan proteins bind noncovalently to a central polymer of hyaluronate. Multiple polymers of keratan sulfate and chondroitin sulfate glycosaminoglycans are attached to the extended region betwe globular domains G2 and G3 of each aggrecan molecule.

Aggrecan can cushion compressive forces acting on cartilage because the adsorbed water enables it to spring back after having been deformed. When pressure is exerted, as when the foot hits the ground

while walking, water is squeezed from the glycosaminoglycan, cushioning the impact. When the pressure is released, the water rebinds. Osteoarthritis, the most common form of arthritis, results when water is lost from proteoglycan with aging. Other forms of arthritis can result from the proteolytic degradation of aggrecan and collagen in the cartilage.

Mucins are glycoprotein components of mucus

Mucins form large polymeric structures that serve as lubricants in mucous and salivary secretions. These glycoproteins are synthesized by specialized cells in the tracheobronchial, gastrointestinal, and genitourinary tracts.

A model of a mucin is shown in Figure 11.22A. The defining feature of the mucins is a region of the protein backbone termed the *variable number of tandem repeats* (VNTR) region, which is rich in serine and threonine residues that are *O*-glycosylated. Indeed, the carbohydrate moiety can account for as much as 80% of the molecule by weight. A number of core carbohydrate structures are conjugated to the protein component of mucin; Figure 11.22B shows one example.

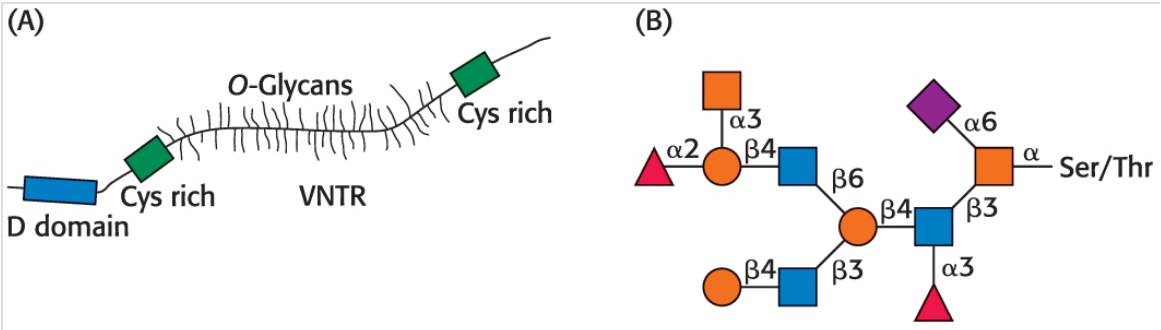


FIGURE 11.22 Mucins have common regions that are heavily *O*-glycosylated. (A) A schematic representation of a mucoprotein. The VNTR region is highly glycosylated, forcing the molecule into an extended conformation. The Cys-rich domains and the D domain facilitate the

polymerization of many such molecules. (B) An example of an oligosaccharide that is bound to the VNTR region of the protein. See Figure 11.17 for the carbohydrate key.

[Data from A. Varki et al. (Eds.), *Essentials of Glycobiology*, 2nd ed. (Cold Spring Harbor Press, 2009), pp. 117, 118.]



Mucins adhere to epithelial cells and act as a protective barrier; they also hydrate the underlying cells. In addition to protecting cells from environmental insults, such as stomach acid, inhaled chemicals in the lungs, and bacterial infections, mucins have roles in fertilization, the immune response, and cell adhesion. Mucins are overexpressed in bronchitis and cystic fibrosis, and the overexpression of mucins is characteristic of adenocarcinomas — cancers of the glandular cells of epithelial origin.

Protein glycosylation takes place in the lumen of the endoplasmic reticulum and in the Golgi complex

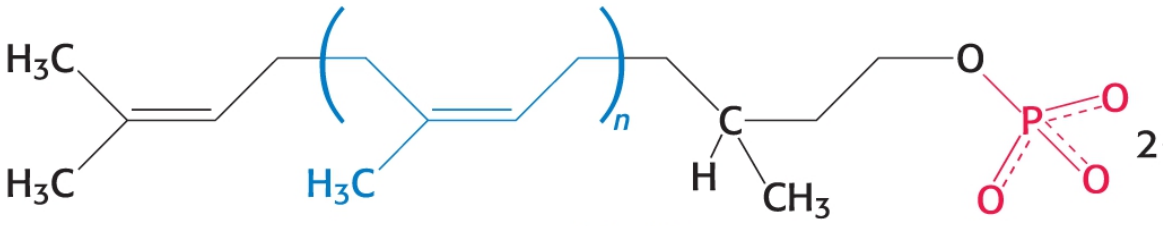
The major pathway for protein glycosylation takes place inside the lumen of the **endoplasmic reticulum (ER)** and in the **Golgi complex**, organelles that play central roles in protein trafficking (**Figure 11.23**). The protein is synthesized by ribosomes attached to the cytoplasmic face of the ER membrane, and the peptide chain is inserted into the lumen of the ER (Section 30.4). The *N*-linked glycosylation begins in the ER and continues in the Golgi complex, whereas the *O*-linked glycosylation takes place exclusively in the Golgi complex.



FIGURE 11.23 The Golgi complex and endoplasmic reticulum are the sites of protein glycosylation. The electron micrograph shows the Golgi complex and adjacent endoplasmic reticulum. The black dots on the cytoplasmic surface of the ER membrane are ribosomes.

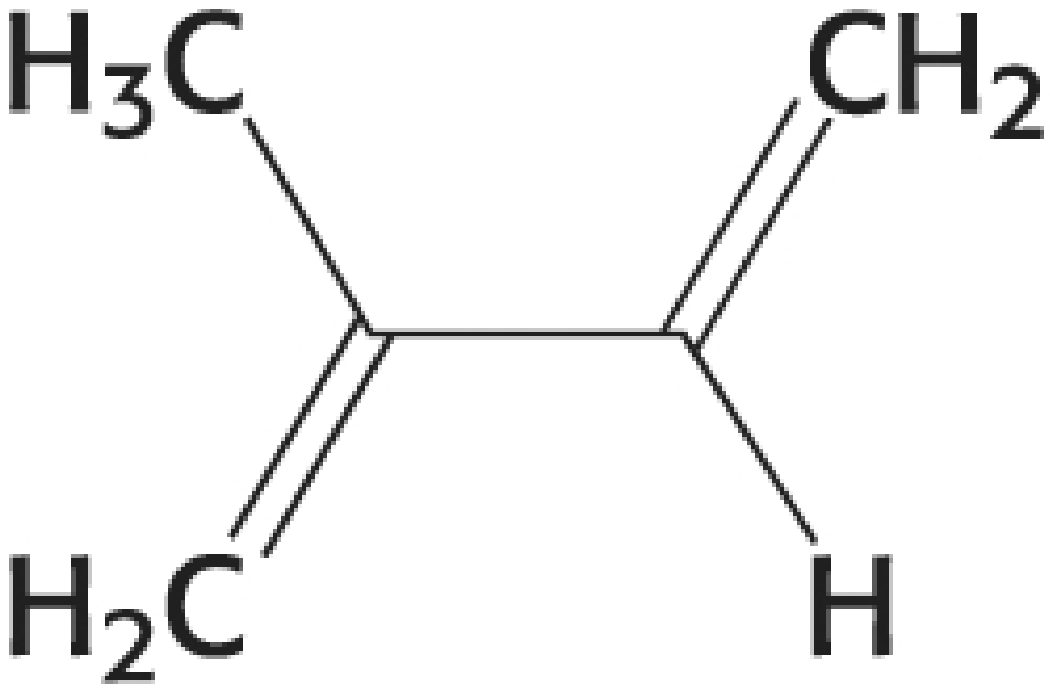
A large oligosaccharide destined for attachment to the asparagine residue of a protein is assembled on a specialized lipid molecule called

dolichol phosphate, located in the ER membrane and containing about 20 isoprene (C_5) units.



$n = 15–19$

Dolichol phosphate



Isoprene

The terminal phosphate group of the dolichol phosphate is the site of attachment of the oligosaccharide. This activated (energy-rich) form of the oligosaccharide is subsequently transferred to a specific asparagine residue of the growing polypeptide chain by an enzyme located on the lumenal (interior) side of the ER.

Proteins in the lumen of the ER and in the ER membrane are transported to the Golgi complex, which is a stack of flattened membranous sacs that are the major sorting center of the cell. The *O*-linked sugar units are fashioned there, and the *N*-linked sugars, arriving from the ER as a component of a glycoprotein, are modified in many different ways. Proteins proceed from the Golgi complex to lysosomes, secretory granules, or the plasma membrane, according to signals encoded within their amino acid sequences and three-dimensional structures (**Figure 11.24**).

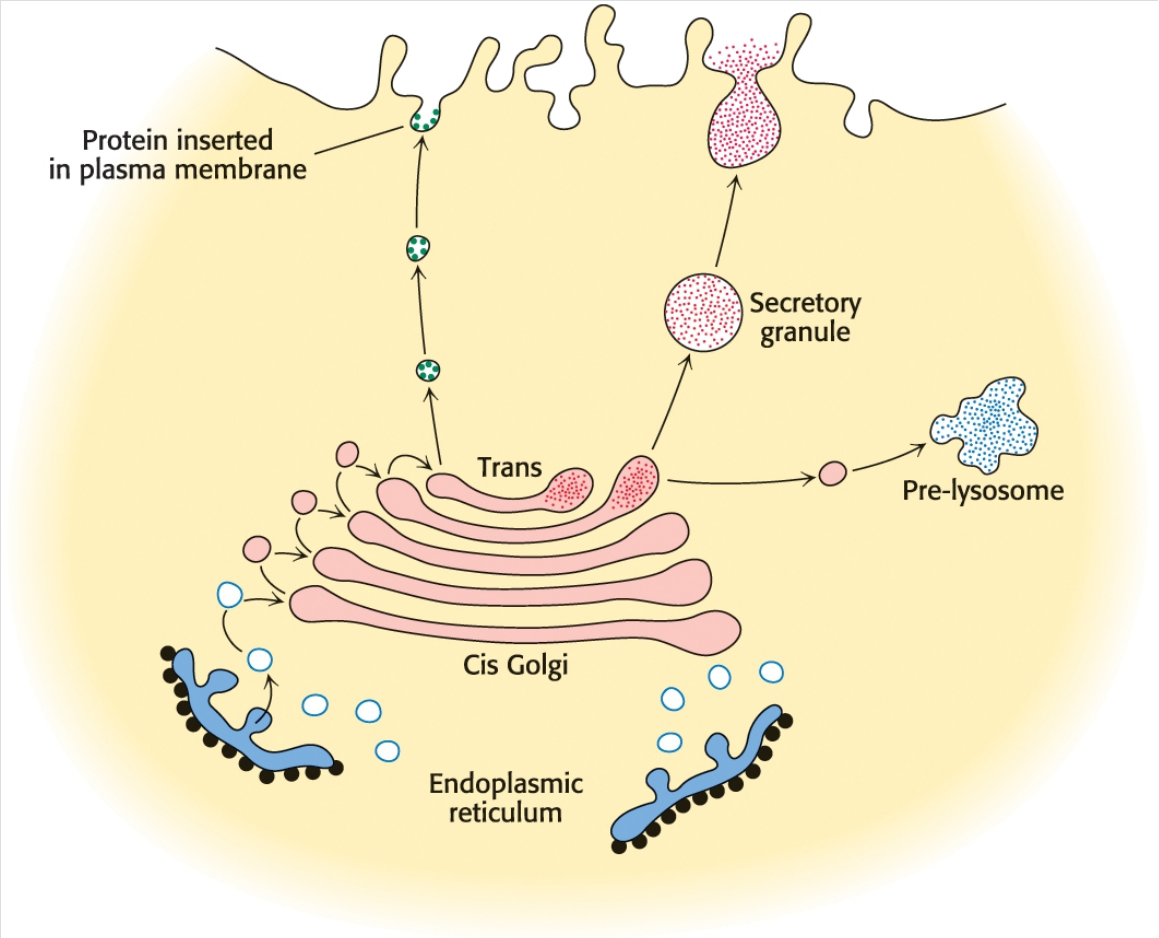


FIGURE 11.24 The Golgi complex is a sorting center. The Golgi complex is the sorting center in the targeting of proteins to lysosomes, secretory vesicles, and the plasma membrane. The cis face of the Golgi complex receives vesicles from the endoplasmic reticulum, and the trans face sends a different set of vesicles to target sites. Vesicles also transfer proteins from one compartment of the Golgi complex to another.

[Courtesy of Dr. Marilyn Farquhar.]

Specific enzymes are responsible for oligosaccharide assembly

Complex carbohydrates are synthesized through the action of specific enzymes called **glycosyltransferases**, which catalyze the formation of glycosidic linkages. Given the diversity of known glycosidic linkages, many different enzymes are required. Indeed, glycosyltransferases account for 1% to 2% of gene products in all organisms examined.

While dolichol phosphate-linked oligosaccharides are substrates for some glycosyltransferases, the most common carbohydrate donors for glycosyltransferases are activated sugar nucleotides, such as UDP-glucose (UDP is the abbreviation for uridine diphosphate; **Figure 11.25**). The attachment of a nucleotide to enhance the energy content of a molecule is a common strategy in biosynthesis that we will see many times in our study of biochemistry. The acceptor substrates for glycosyltransferases are quite varied and include carbohydrates, serine, threonine, and asparagine residues of proteins, lipids, and even nucleic acids.

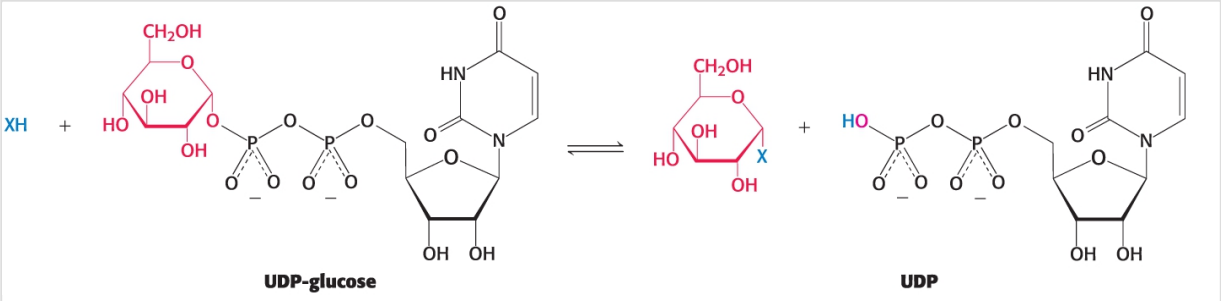


FIGURE 11.25 Glycosyltransferase reactions follow a general form. The sugar to be added comes from a sugar nucleotide — in this case, UDP-glucose. The acceptor, designated X in this illustration, can be one of a variety of biomolecules, including other carbohydrates or proteins.

Blood groups are based on protein glycosylation patterns

The human ABO blood groups illustrate the effects of glycosyltransferases on the formation of glycoproteins. Each blood group is designated by the presence of one of the three different carbohydrates — termed A, B, or O — attached to glycoproteins and glycolipids on the surfaces of red blood cells (Figure 11.26). These structures have in common an oligosaccharide foundation called the O (or sometimes H) antigen. The A and B antigens differ from the O antigen by the addition of one extra monosaccharide, either *N*-acetylgalactosamine (for A) or galactose (for B) through an α-1,3 linkage to a galactose moiety of the O antigen.

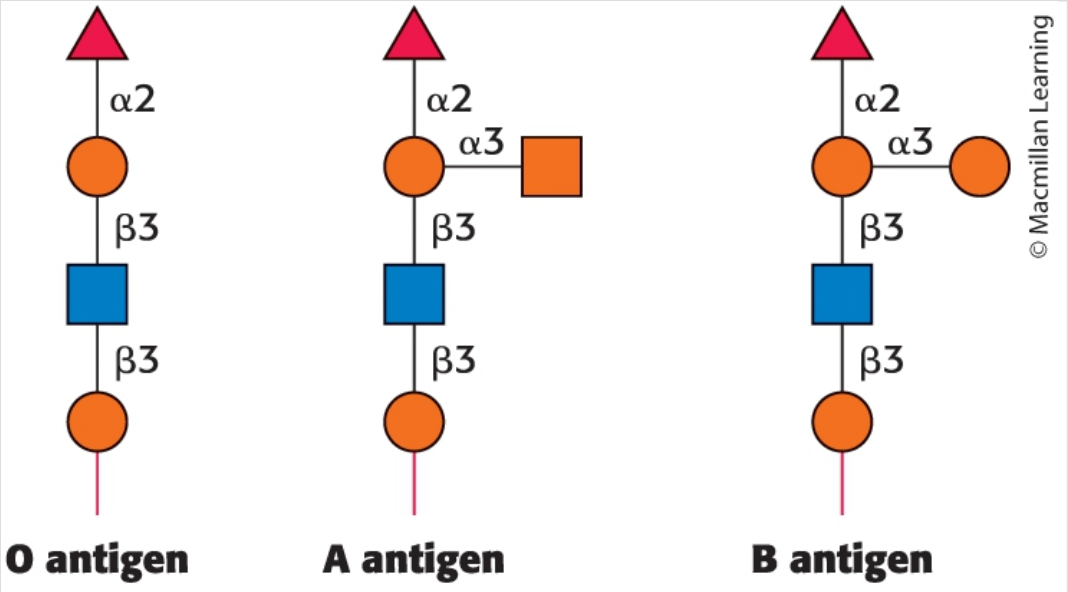


FIGURE 11.26 The A, B, and O oligosaccharide antigens share a common core structure, the O antigen. Different glycosylation patterns account for the different human blood groups.

Specific glycosyltransferases add the extra monosaccharide to the O antigen. Each person inherits the gene for one glycosyltransferase of this type from each parent. The type A transferase specifically adds *N*-acetylgalactosamine, whereas the type B transferase adds galactose. These enzymes are identical in all but 4 of 354 positions. In the AB blood group, both enzymes are present, whereas the O phenotype results if both enzymes are absent.

These structures have important implications for blood transfusions and other transplantation procedures. If an antigen not normally present in a person is introduced, the person's immune system recognizes it as foreign. Red-blood-cell lysis occurs rapidly, leading to a severe drop in blood pressure (hypotension), shock, kidney failure, and death from circulatory collapse.

Why are different blood types present in the human population? Suppose that a pathogenic organism such as a parasite expresses on its cell surface a carbohydrate antigen similar to one of the blood-group antigens. Since this antigen is not detected as foreign in a person whose blood type matches the parasite antigen, the parasite may flourish. However, other people with different blood types will be protected. Hence, there will be selective pressure on human beings to vary blood type to prevent parasitic mimicry and a corresponding selective pressure on parasites to enhance mimicry. The constant "arms race" between pathogenic microorganisms and human beings drives the evolution of diversity of surface antigens within the human population.

 One example of a disease affected by blood type is cholera. Millions of cases of this disease, caused by the organism *Vibrio cholerae*, occur around the world each year, leading to tens of thousands of deaths. Blood type does not appear to influence the likelihood of contracting cholera, but individuals with blood type O are approximately eight times more likely to have severe disease. Biochemical studies show that the O antigen binds more tightly to the

toxin responsible for disease symptoms than do the other blood type antigens (Figure 11.27). The impact of these interactions on human society is revealed by the observation that the frequency of blood type O is notably low in regions where cholera has been endemic for centuries.

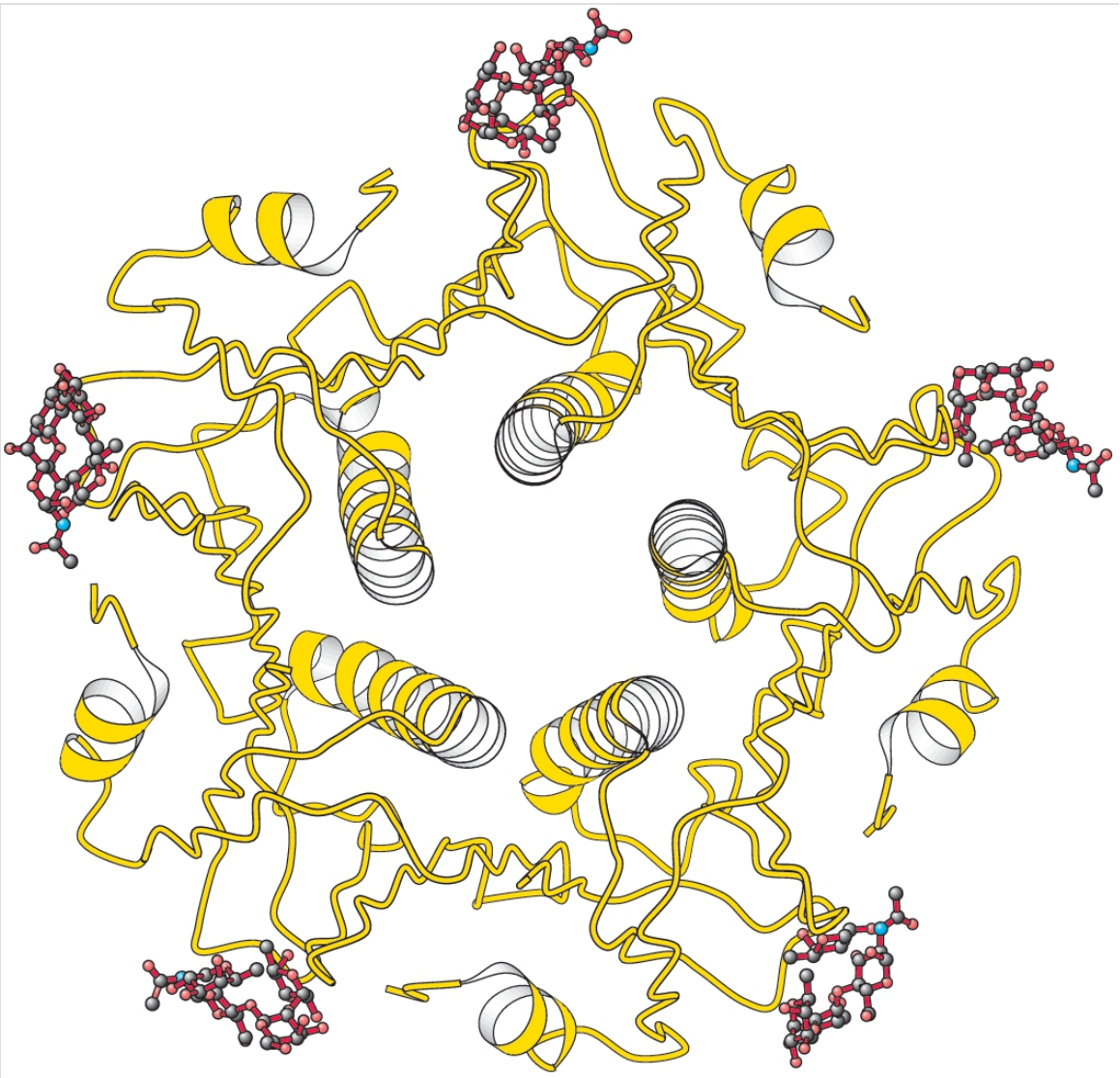


FIGURE 11.27 Cholera toxin makes specific noncovalent interactions with the O antigen, resulting in higher affinity binding. Cholera toxin is shown in yellow and the O antigen as a bal and-stick model.

Errors in glycosylation can result in pathological conditions



Protein function is often compromised when proteins are improperly glycosylated, sometimes resulting in disease. For instance, certain types of muscular dystrophy can be traced to improper glycosylation of dystroglycan, a membrane protein that links the extracellular matrix with the cytoskeleton. Indeed, an entire family of severe inherited human diseases called *congenital disorders of glycosylation* has been identified. These pathological conditions reveal the importance of proper modification of proteins by carbohydrates and their derivatives.

An especially clear example of the role of glycosylation is provided by I-cell disease, a lysosomal storage disease. Normally, a carbohydrate marker directs certain digestive enzymes from the Golgi complex to organelles called *lysosomes*, which degrade and recycle damaged cellular components or material brought into the cell by endocytosis. In patients with I-cell disease, affected lysosomes contain large inclusions of undigested glycosaminoglycans and glycolipids — hence the "I" in the name of the disease — because the enzymes normally responsible for the degradation of glycosaminoglycans are missing. Remarkably, the enzymes are present at very high levels in the blood and urine. Thus, active enzymes are synthesized, but, in the absence of appropriate glycosylation, they are exported instead of being sequestered in lysosomes.

In other words, in I-cell disease, a whole series of enzymes are incorrectly addressed and delivered to the wrong location. Normally, these enzymes contain a mannose 6-phosphate residue as a component of an *N*-oligosaccharide that serves as the marker directing the enzymes from the Golgi complex to lysosomes. In I-cell disease, however, the attached mannose lacks a phosphate. I-cell patients are deficient in the

N-acetylglucosamine phosphotransferase catalyzing the first step in the addition of the phosphoryl group; the consequence is the mistargeting of eight essential enzymes (**Figure 11.28**). I-cell disease causes the patient to suffer severe psychomotor impairment and skeletal deformities. Interestingly, mutations in the phosphotransferase have also been linked to stuttering. Why some mutations cause stuttering while others cause I-cell disease is a mystery.

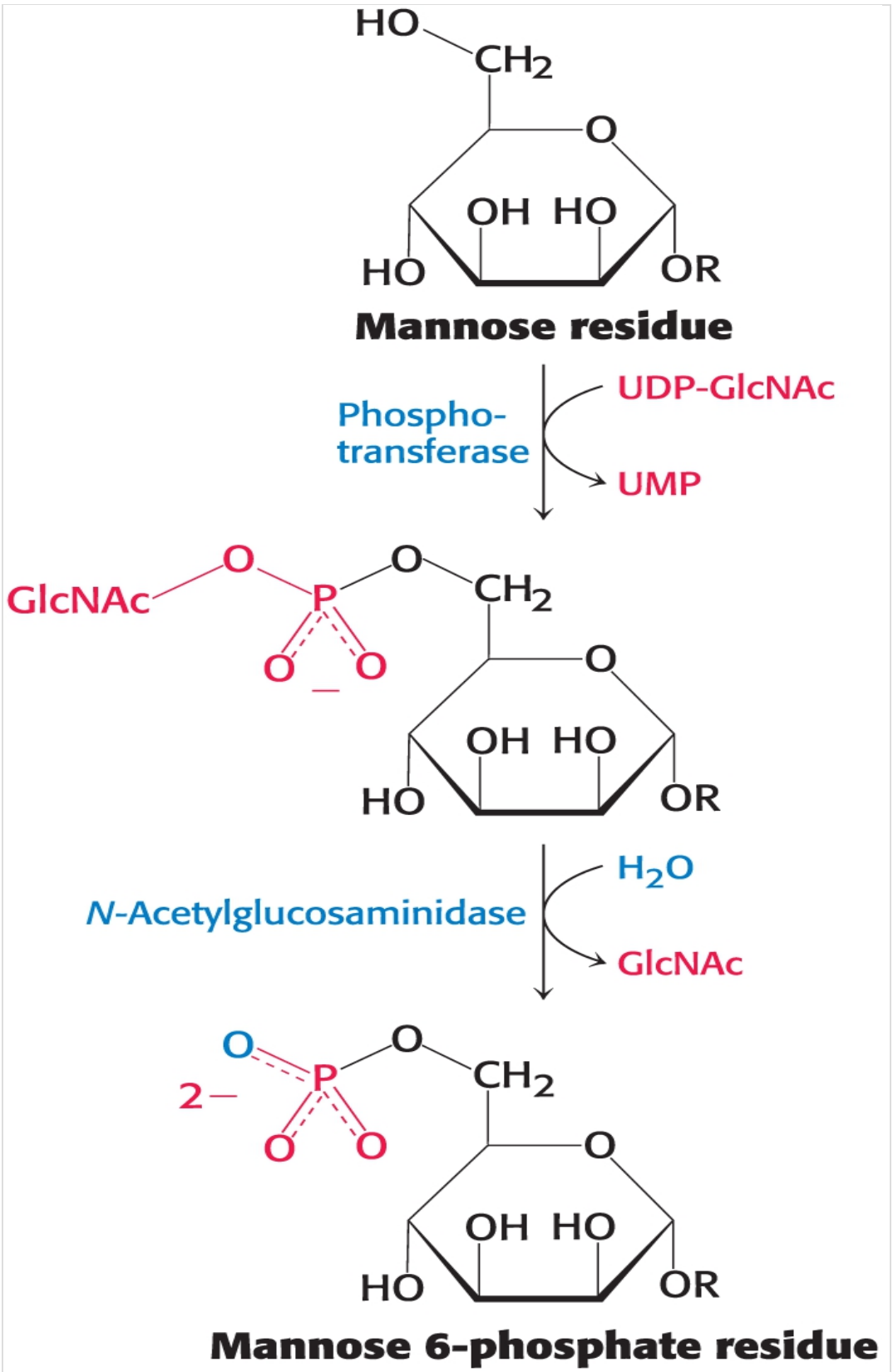

HO
CH2
O
OH HO
HO
OR
Mannose residue
Phospho-
transferase
UDP-GlcNAc
UMP
GlcNAc
O
P
O
O
O
O
CH2
O
OH HO
HO
OR
N-Acetylglucosaminidase
H2O
GlcNAc
2—
O
P
O
O
O
O
CH2
O
OH HO
HO
OR
Mannose 6-phosphate residue

FIGURE 11.28 In a two-step process, a glycoprotein destined for delivery to lysosomes acquires a mannose 6-phosphate marker in the Golgi compartment. First, GlcNAc phosphotransferase adds a phospho-*N*-acetylglucosamine unit to the 6-OH group of a mannose; second, an *N*-acetylglucosaminidase removes the added sugar to generate a mannose 6-phosphate residue in the core oligosaccharide.



Biochemists use several techniques to analyze the oligosaccharide components of glycoproteins

How is it possible to determine the structure of a glycoprotein — the oligosaccharide structures and their points of attachment? Most approaches make use of enzymes that cleave oligosaccharides at specific types of linkages.

The first step is to detach the oligosaccharide from the protein. For example, *N*-linked oligosaccharides can be released from proteins by an enzyme such as peptide *N*-glycosidase F, which cleaves the *N*-glycosidic linkages connecting the oligosaccharide to the protein. The oligosaccharides can then be isolated and analyzed.

Matrix-assisted laser desorption/ionization/time-of-flight (MALDI-TOF) or other mass spectrometric techniques (Section 4.3) provide the mass of an oligosaccharide fragment; however, many possible oligosaccharide structures are consistent with a given mass. More complete information can be obtained by cleaving the oligosaccharide with enzymes of varying specificities. For example, β-1,4-galactosidase cleaves β-glycosidic linkages exclusively at galactose residues. The products can again be analyzed by mass spectrometry (**Figure 11.29**). The repetition of this process with the use of an array of enzymes of

different specificity will eventually reveal the structure of the oligosaccharide.

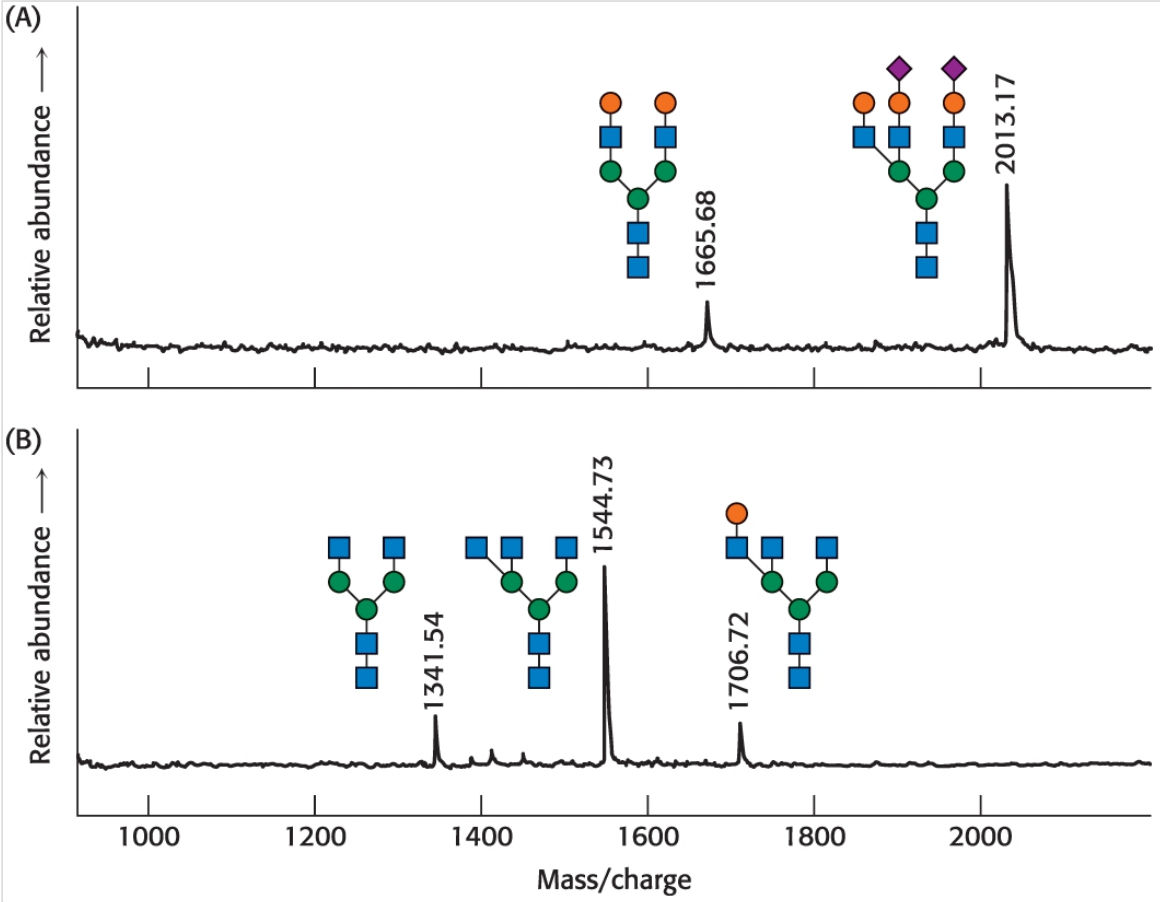


FIGURE 11.29 Oligosaccharides can be characterized by mass spectrometry. Carbohydrate-cleaving enzymes were used to release and specifically cleave the oligosaccharide component c the glycoprotein fetuin. Parts A and B show the masses obtained with MALDI-TOF spectrometry as well as the corresponding structures of the oligosaccharide-digestion products: (A) digestion with peptide *N*-glycosidase F (to release the oligosaccharide from the protein) and neuraminidase (which cleaves at sialic acid residues); (B) digestion with peptide *N*-glycosidase neuraminidase, and β-1,4-galactosidase. Knowledge of the enzyme specificities and the masses of the products permits the characterization of the oligosaccharide. See Figure 11.17 for the carbohydrate key.

[Data from A. Varki, R. D. Cummings, J. D. Esko, H. H. Freeze, G. W. Hart, and J. Marth (Eds.), *Essentials of Glycobiolo* (Cold Spring Harbor Laboratory Press, 1999), p. 596.]

Biochemists can also locate the points of oligosaccharide attachment by applying proteases to glycoproteins. Cleavage by a specific protease yields a characteristic pattern of peptide fragments that can be analyzed chromatographically. Fragments attached to oligosaccharides can be picked out because their chromatographic properties will change on glycosidase treatment. Mass spectrometric analysis or direct peptide sequencing can reveal the identity of the peptide in question and, with additional effort, the exact site of oligosaccharide attachment.

Self-Check Question



Just as all the proteins made by an organism at any given moment are called the *proteome*, all the carbohydrates and carbohydrate-associated molecules can be called the *glycome.* Compare the amount of information inherent in the genome, the proteome, and the glycome.

11.4 Lectins Are Specific Carbohydrate-Binding Proteins

The diversity and complexity of the carbohydrate units and the variety of ways in which they can be joined in oligosaccharides and polysaccharides attest to their biochemical importance. Evolution rarely results in complex patterns when simpler ones are equally effective, so why all this intricacy and diversity? It is now clear that these carbohydrate structures are the recognition sites for a distinct class of proteins. Such proteins, termed *glycan-binding proteins*, bind specific carbohydrate structures on neighboring cell surfaces. Originally discovered in plants, glycan-binding proteins are ubiquitous, and no living organisms have been found that lack these key proteins.

We will focus on a particular class of glycan-binding proteins termed **lectins** (from Latin *legere*, "to select"). The interaction of lectins with their carbohydrate partners is another example of carbohydrates being information-rich molecules that guide many biological processes. The diverse carbohydrate structures displayed on cell surfaces are well-suited to serving as sites of interaction between cells and their environments. Interestingly, the partners for lectin binding are often the carbohydrate moiety of glycoproteins.

Lectins promote interactions between cells and within cells

Cell–cell contact is a vital interaction in a host of biochemical functions, ranging from building a tissue from isolated cells to facilitating the transmission of information. The chief function of lectins is to facilitate cell–cell contact. A lectin usually contains two or more carbohydrate-binding sites, whereby the lectins on the surface of one cell interact

with arrays of carbohydrates displayed on the surface of another cell. Lectins and carbohydrates are linked by a number of weak noncovalent interactions that ensure specificity yet permit unlinking as needed. The weak interactions between one cell surface and another resemble the action of Velcro; each interaction is weak, but the composite is strong.

We have already met a lectin in this chapter, although we didn't name it as such. Recall that, in I-cell disease, lysosomal enzymes lack the appropriate mannose 6-phosphate, a molecule that directs the enzymes to the lysosome. Under normal circumstances, the mannose 6-phosphate receptor, a lectin, binds the enzymes in the Golgi apparatus and directs them to the lysosome. Not surprisingly, I-cell disease can also be caused by a loss of the mannose 6-phosphate receptor.

Lectins are organized into two large classes

Lectins can be divided into two large classes on the basis of their amino acid sequences and biochemical properties.

C-type lectins

C-type (for calcium-requiring) lectins are found in animals. These proteins each have a homologous domain of 120 amino acids that is responsible for carbohydrate binding. The structure of one such domain bound to a carbohydrate target is shown in **Figure 11.30**.

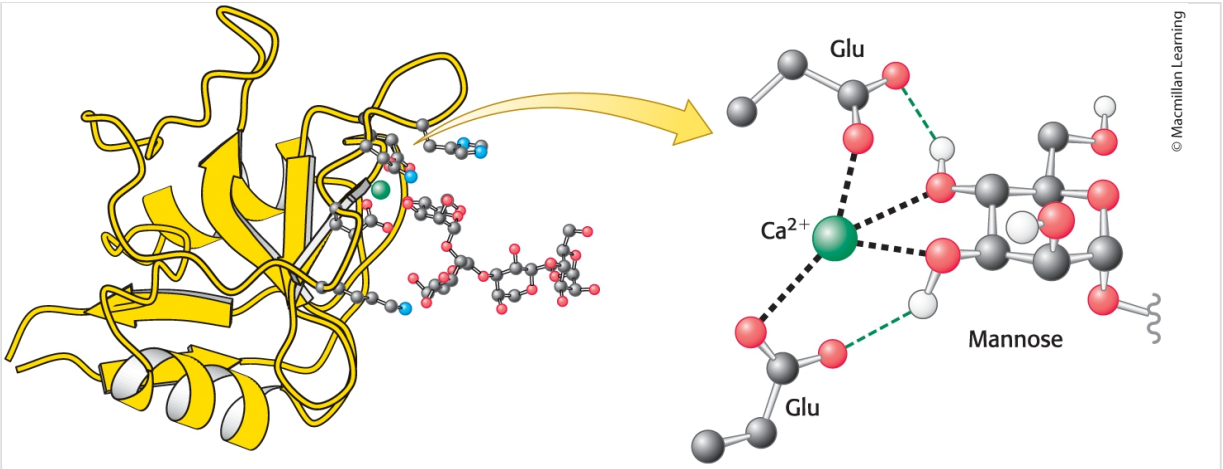


FIGURE 11.30 C-type lectins use calcium ions to bind carbohydrates. Selected interactions of the carbohydrate-binding domain of an animal C-type lectin are shown, with some hydrogen atoms omitted for clarity. A calcium ion tightly bound to two Glu residues of the lectin binds to a mannose residue of the carbohydrate moiety.

[Drawn from 2MSB.pdb.]

INTERACT with this model in Achieve

A calcium ion on the protein acts as a bridge between the protein and the sugar through direct interactions with sugar OH groups. In addition, two glutamate residues in the protein bind to both the calcium ion and the sugar, and other protein side chains form hydrogen bonds with other OH groups on the carbohydrate. The carbohydrate-binding specificity of a particular lectin is determined by the amino acid residues that bind the carbohydrate. C-type lectins function in a variety of cellular activities, including receptor-mediated endocytosis — a process by which soluble molecules are bound to the cell surface and subsequently internalized (Section 27.3) — and cell–cell recognition.

C-type proteins known as **selectins** bind immune-system cells to sites of injury in the inflammatory response. The L, E, and P forms of selectins bind specifically to carbohydrates on lymph-node vessels, endothelium, or activated blood platelets, respectively. Selectins play central roles in

recruiting leukocytes (white blood cells) to sites of inflammation. By participating in a large set of interactions, each of which is relatively weak, selectins can bring cells together where other molecules of the surfaces of the two cells are positioned to interact if they have appropriate affinities for one another.

L-type lectins

The other large class of lectins comprises the L-type lectins. These lectins are especially rich in the seeds of leguminous plants such as beans and peas; many of the initial biochemical characterizations of lectins were performed on these particular lectins because they are so readily available. Although the exact role of lectins in plants is unclear, they can serve as potent toxins to herbivorous insects. Other L-type lectins, such as calnexin and calreticulin, are prominent chaperones in the eukaryotic endoplasmic reticulum. Recall that chaperones are proteins that facilitate the folding of other proteins (Section 2.7).



JAMES TENSUAN/The New York Times/Redux

CAROLYN BERTOZZI Chemist Carolyn Bertozzi is a leader in developing the field of glycobiology and communicating its exciting possibilities. Initially planning to go to medical school, her interest in chemistry developed in college, and she went on to complete a PhD focused on synthesizing carbohydrate-containing molecules and using them as probes for biological systems. After postdoctoral training, she joined the faculty at the University of California, Berkeley, where her training as a synthetic chemist allowed her to think about how to make new molecules with desired properties. She and her coworkers invented new tools for probing the roles of carbohydrates in biology, including those that allow the synthesis of new molecules in living organisms. Her talent was recognized with a MacArthur “genius” grant early in her career. In addition to winning research grants from various governmental agencies, she has been supported by the Howard Hughes Medical Institute, a leading funder of cutting-edge biomedical research since 2000. She now teaches and does research at Stanford University.

Influenza virus binds to sialic acid residues

Many pathogens gain entry into specific host cells by adhering to cell-surface carbohydrates. For example, influenza virus recognizes sialic acid residues (Figure 11.10) linked to galactose residues that are present on cell-surface glycoproteins. The viral protein that binds to these sugars is a lectin called *hemagglutinin* (**Figure 11.31A**).

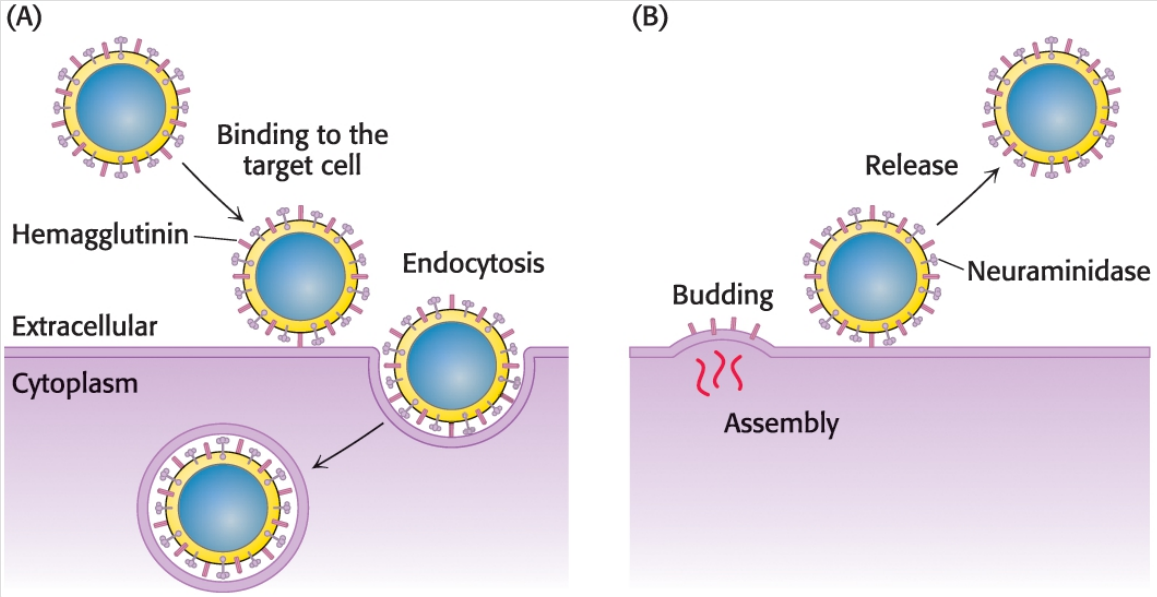


FIGURE 11.31 Influenza virus uses a lectin for specific cell binding. (A) Influenza virus targets cells by binding to sialic acid residues located at the termini of oligosaccharides present on cell-surface glycoproteins and glycolipids. These carbohydrates are bound by the lectin hemagglutinin, one of the major proteins expressed on the surface of the virus. (B) When viral replication is complete, the components (red lines) assemble and the viral particle buds from th cell. The other major viral-surface protein, neuraminidase, cleaves oligosaccharide chains to release the viral particle.

After binding hemagglutinin, the virus is engulfed by the cell and begins to replicate. Viral assembly concludes with the budding of the viral particle from the cell (**Figure 11.31B**). Upon complete assembly, the viral particle is still attached to sialic acid residues of the cell membrane

by hemagglutinin on the surface of the new virions. Another viral protein, neuraminidase (sialidase), cleaves the glycosidic linkages between the sialic acid residues and the rest of the cellular glycoprotein, freeing the virus to infect new cells, and thus spreading the infection throughout the respiratory tract. Inhibitors of this enzyme such as oseltamivir (Tamiflu) and zanamivir (Relenza) are important anti-influenza agents.

Viral hemagglutinin's carbohydrate-binding specificity may play an important role in species specificity of infection and ease of transmission. For instance, avian influenza H5N1 (bird flu) is especially lethal and is readily spread between birds. Although human beings can be infected by this virus, infection is rare and human-to-human transmission rarer still. The biochemical basis of these characteristics is that the avian virus hemagglutinin recognizes a different carbohydrate moiety from that recognized by human influenza hemagglutinin. Although human beings have carbohydrate residues that the avian virus might recognize and bind, they are located deep in the lungs. Infection by the avian virus is thus difficult, and, when it does occur, the avian virus is not readily transmitted by sneezing or coughing.

Chapter 11 Summary

11.1 Monosaccharides Are the Simplest Carbohydrates

- Carbohydrates are aldoses or ketoses that are rich in hydroxyl groups, and their derivatives. The simplest are monosaccharides — sugars that are three to seven carbons in length.
- Pentoses and hexoses can close into five-membered furanose rings or six-membered pyranose rings. Pyranose rings usually adopt the chair conformation, and furanose rings usually adopt the envelope conformation. These ring structures are in rapid equilibrium with the linear forms in aqueous solutions.
- In sugars undergoing cyclization, an additional asymmetric center is formed, resulting in α and β anomer forms that differ by the position of the hydroxyl group on the anomeric carbon. In monosaccharides, these anomers rapidly interchange via the linear form.
- D-Glucose is the most common sugar in living organisms and is the human "blood sugar" most likely because it can form a six-membered ring with all bulky groups in the equatorial positions. As a reducing sugar, it can nonenzymatically react with hemoglobin to form glycated hemoglobin, an important biomarker for diabetes.
- Sugars are joined to alcohols and amines by glycosidic linkages from the anomeric carbon atom. For example, *N*-glycosidic linkages connect sugars to purines and pyrimidines in nucleotides, RNA, and DNA.

11.2 Monosaccharides Are Linked to Form Complex Carbohydrates

- Sugars are linked to one another in disaccharides and polysaccharides by *O*-glycosidic linkages.
- Sucrose, lactose, and maltose are common disaccharides.
- Sucrose (table sugar) consists of α-glucose and β-fructose joined by a glycosidic linkage between their anomeric carbon atoms.
- Lactose (in milk) consists of galactose joined to glucose by a β-1,4 linkage.
- Maltose (from starch) consists of two glucoses joined by an α-1,4 linkage.
- Starch is a storage homopolymer of glucose in plants; glycogen serves a similar role in animals. Glucose units in starch and glycogen are in α-1,4 linkages with α-1,6 linked branches.
- Cellulose, the major structural polymer of plant cell walls, consists of glucose units joined by β-1,4 linkages, which give rise to long straight chains that form fibrils with high tensile strength.
- Chitin is the major structural polymer of fungal cell walls and the exoskeletons and shells of arthropods. Like cellulose, it is a homopolymer composed of β-1,4 linkages, but the monomeric unit is GlcNAc rather than glucose.

11.3 Carbohydrates Can Be Linked to Proteins to Form Glycoproteins

- Carbohydrates are commonly conjugated to proteins; in glycoproteins, the protein component is predominant.
- Most secreted proteins, such as the signal molecule erythropoietin, are glycoproteins that are prominent on the external surface of the plasma membrane.
- Glycosaminoglycans are polymers of repeating disaccharides with a derivative of glucosamine or galactosamine and a high density of carboxylate or sulfate groups.
- Proteoglycans — proteins bearing covalently linked glycosaminoglycans — are found in the extracellular matrices of

animals and are key components of cartilage.
- Mucoproteins, like proteoglycans, serve as lubricants and are predominantly carbohydrate by weight, with the protein component heavily *O*-glycosylated with *N*-acetylgalactosamine joining the oligosaccharide to the protein.
- Glycosyltransferases link the oligosaccharide units on proteins in the lumen of the endoplasmic reticulum. Additional sugars are attached in the Golgi complex to form diverse patterns.

11.4 Lectins Are Specific Carbohydrate-Binding Proteins

- Carbohydrates on cell surfaces are recognized by proteins called lectins. In animals, the interplay of lectins and their sugar targets guides cell–cell contact as well as viral entry.
- Lectins also play a role inside the cell, such as directing proteins to their proper cellular locations and assisting in protein folding.

Key Terms

monosaccharide
epimers
anomers
reducing sugar
glycosidic linkage
oligosaccharide
disaccharide
polysaccharide
glycogen
starch
cellulose
glycoprotein
proteoglycan

glycosaminoglycan
mucin (mucoprotein)
endoplasmic reticulum (ER)
Golgi complex
glycosyltransferase
lectin
selectin

Problems

1. Which of the following are aldoses? 1

a. glyceraldehyde
b. glucose
c. fucose
d. fructose

2. Which of the following are reducing sugars? 1

a. sucrose
b. ribose
c. fructose
d. glucose
e. lactose

3. Which of the following is found in glycogen and starch? 2

a. fructose
b. β-D-glucose
c. mannose
d. α-D-glucose

4. How many different oligosaccharides can be made by linking one glucose, one mannose, and one galactose? Assume that each sugar is in its pyranose form. Compare this number with the number of tripeptides that can be made from three different amino acids. 2

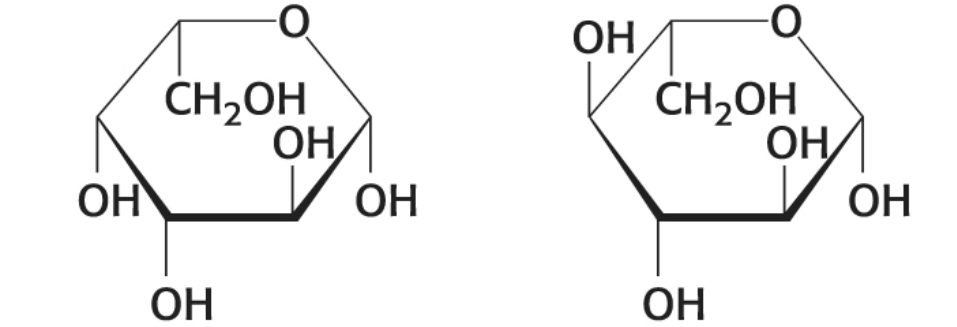
5. Match each term with its description. 1, 2

1. Enantiomers	1. Has the molecular formula $(CH_2O)_n$
2. Cellulose	2. Monosaccharides that differ at a single asymmetric carbon atom
3. Lectins	3. The storage form of glucose in animals
4. Glycosyltransferases	4. The storage form of glucose in plants
5. Epimers	5. Glycoprotein containing glycosaminoglycans
6. Starch	6. The most abundant organic molecule in the biosphere
7. Carbohydrates	7. *N*-Acetylgalactosamine is a key component of this glycoprotein
8. Proteoglycan	8. Carbohydrate-binding proteins
9. Mucoprotein	9. Enzymes that synthesize oligosaccharides
10. Glycogen	10. Stereoisomers that are mirror images of each other

6. Indicate whether each of the following pairs of sugars consists of anomers, epimers, or an aldose–ketose pair: 1

a. D-glyceraldehyde and dihydroxyacetone
b. D-glucose and D-mannose
c. D-glucose and D-fructose
d. α-D-glucose and β-D-glucose
e. D-ribose and D-ribulose
f. D-galactose and D-glucose

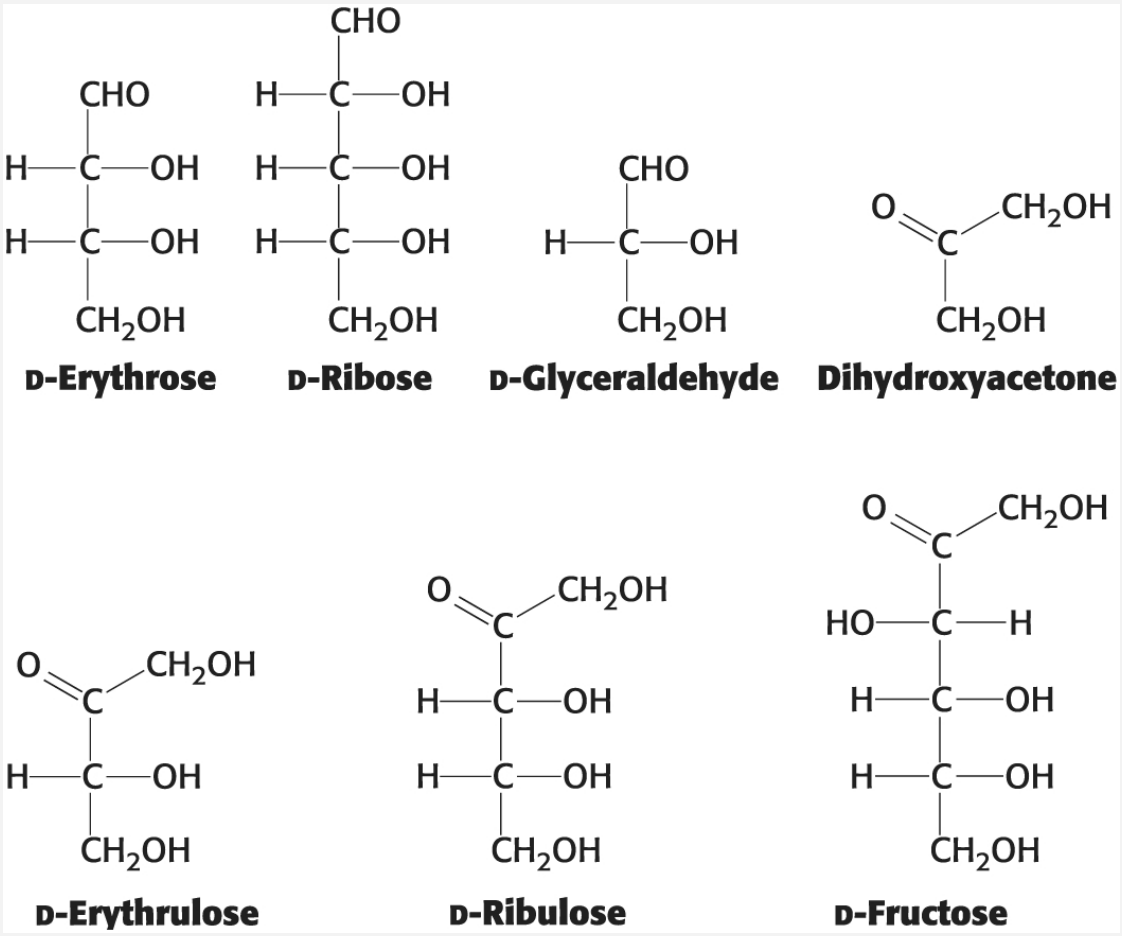
7. Analyze the pair of compounds. 1



Which of the terms explains the relationship between the two compounds?

a. Anomers
b. Epimers
c. Diastereomers
d. Enantiomers

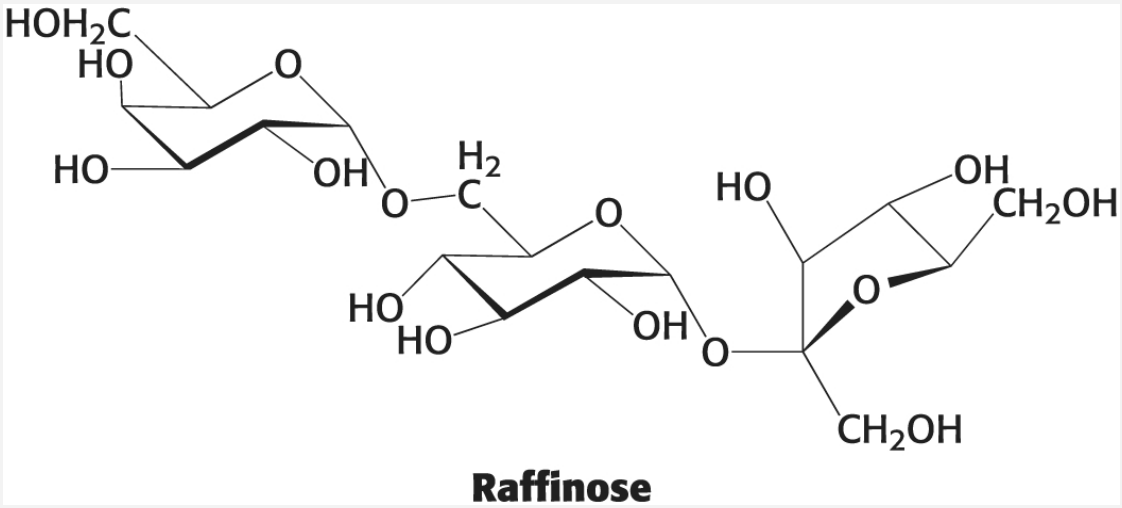
8. To which classes of sugars do the monosaccharides shown here belong? 1



9. The specific rotations of the α and β anomers of D-glucose are $+112$ degrees and $+18.7$ degrees, respectively. Specific rotation, $[\alpha]_D$, is defined as the observed rotation of light of wavelength 589 nm (the D line of a sodium lamp) passing through 10 cm of a $1\ g\ ml^{-1}$ solution of a sample. When a crystalline sample of α-D-glucose is dissolved in water, the

specific rotation decreases from 112 degrees to an equilibrium value of 52.7 degrees. On the basis of this result, what are the proportions of the α and β anomers at equilibrium? Assume that the concentration of the open-chain form is negligible. 1

10. Raffinose is a trisaccharide and a minor constituent in sugar beets. 2



Raffinose

a. Is raffinose a reducing sugar? Explain.
b. What are the monosaccharides that compose raffinose?
c. α-Galactosidase is an enzyme that will remove galactose residues from an oligosaccharide. What are the products of α-galactosidase treatment of raffinose?

11.

a. Compare the number of reducing ends to nonreducing ends in a molecule of glycogen.

b. As we will see in Chapter 21, glycogen is an important fuel-storage form that is rapidly mobilized. At which end — the reducing or nonreducing — would you expect most metabolism to take place? 2

12. Glucose and fructose are reducing sugars. Sucrose, or table sugar, is a disaccharide consisting of both fructose and glucose. Is sucrose a reducing sugar? Which statements about reducing sugars are true? 1, 2

a. A reducing sugar will not react with the Cu^{2+} in Fehling's reagent.
b. D-Arabinose (an aldose) is a reducing sugar.
c. The oxidation of a reducing sugar forms a carboxylic acid sugar.
d. Reducing sugars contain ketone groups instead of aldehyde groups.
e. A disaccharide with its anomeric carbons joined by the glycosidic linkage (like sucrose) cannot be a reducing sugar.

13. For each statement below, write which polymers apply from the following list: chitin, glycogen, cellulose, starch. 2

a. Provides structural support for plants
b. Consists of *N*-acetylglucosamine monomers
c. Is a storage form of carbohydrate in animal cells
d. Is a homopolymer
e. Is branched

14. List the key classes of glycoproteins, their defining characteristics, and their biological functions. 1, 4

15. Proteoglycans are part of the extracellular matrix; they provide structure, viscosity and lubrication, and adhesiveness.

They are composed of proteins conjugated to carbohydrate components called glycosaminoglycans. The glycosaminoglycan component makes up the majority of the mass of a proteoglycan. Which statements about glycosaminoglycans are true? 3, 4

a. β-D-Fructofuranose and amylose are possible components of glycosaminoglycans.
b. Glycosaminoglycans are heteropolysaccharides composed of repeating disaccharide units.
c. Chondroitin sulfate and heparin are examples of glycosaminoglycans.
d. Glycosaminoglycans are homopolysaccharides composed of repeating glucosamine or galactosamine residues.
e. Because glycosaminoglycans consist of only two residues, they generally have low molecular weights.

16. Which amino acids are used for the attachment of carbohydrates to proteins? 3

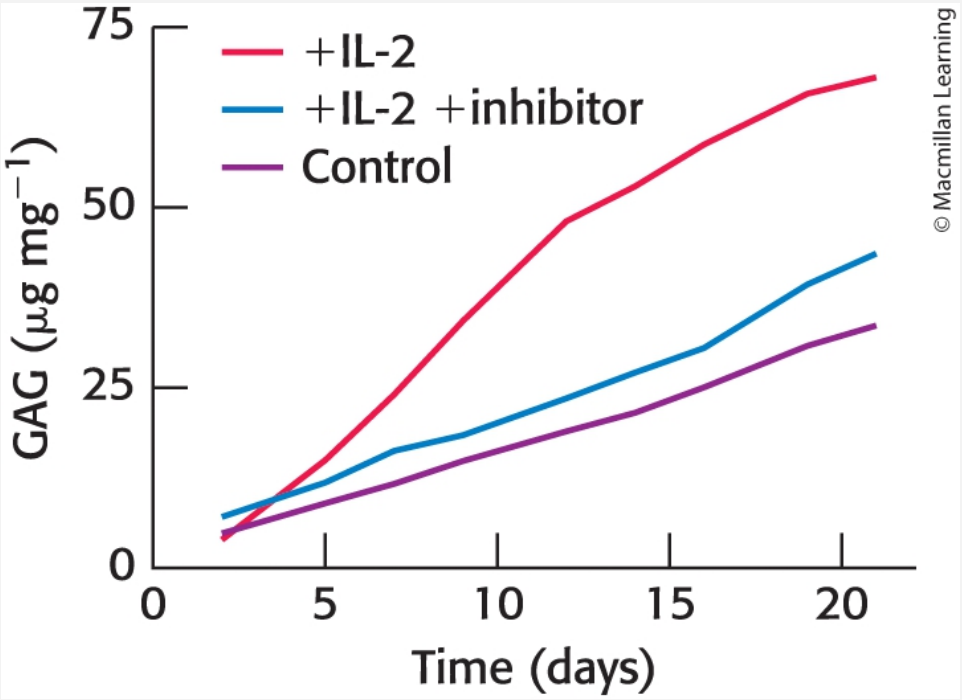
17. Differentiate between a glycoprotein and a lectin. 4, 5

18. Suppose that a protein contains six potential *N*-linked glycosylation sites. How many possible proteins can be generated, depending on which of these sites is actually glycosylated? Do not include the effects of diversity within the carbohydrate added. 3

19. How might the technique of affinity chromatography be used to purify lectins? 5

20. A contributing factor to the development of arthritis is the inappropriate proteolytic destruction of the aggrecan component of cartilage by the proteolytic enzyme aggrecanase.

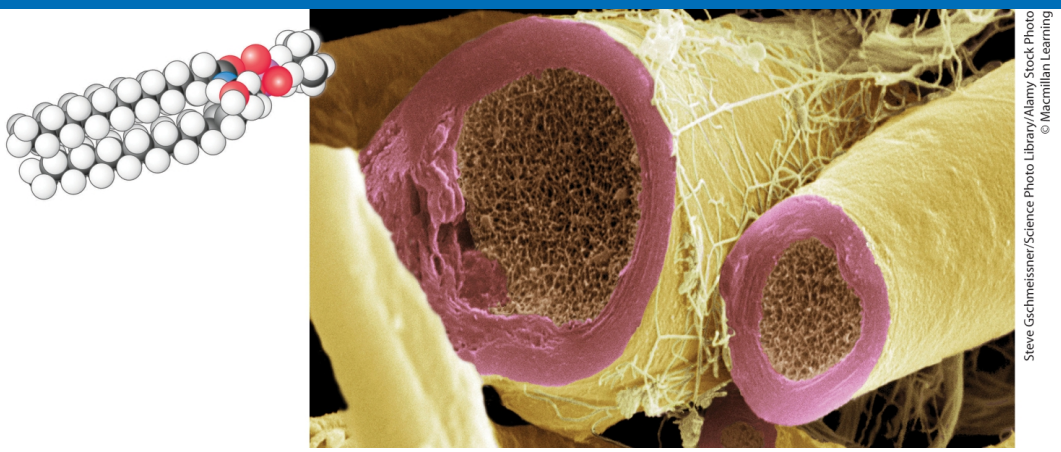
The immune-system signal molecule interleukin 2 (IL-2) activates aggrecanase; in fact, IL-2 blockers are sometimes used to treat arthritis. Studies were undertaken to determine whether inhibitors of aggrecanase could counteract the effects of IL-2. Pieces of cartilage were incubated in media with various additions, and the amount of aggrecan destruction was measured as a function of time.



a. Aggrecan degradation was measured by the release of glycosaminoglycan. What is the rationale for this assay?
b. Why might glycosaminoglycan release not indicate aggrecan degradation?
c. What is the purpose of the control (cartilage incubated with no additions)?
d. What is the effect of adding IL-2 to the system?

e. What is the response when an aggrecanase inhibitor is added in addition to IL-2?
f. Why is there some aggrecan destruction in the control with the passage of time?

Chapter 12
Lipids and Biological Membranes



Steve Gschmeissner/Science Photo Library/Alamy Stock Photo
© Macmillan Learning

Myelin sheaths, such as those seen in this scanning electron micrograph (in pink), enable rapid transmission of electrical impulses in neurons. These membranes, rich in phospholipids such as sphingomyelin (above), wrap around nerve fibers multiple times to create the biological equivalent of an insulated wire. The importance of these structures is emphasized by the existence of demyelination disorders, such as multiple sclerosis, where the myelin sheaths degrade over time.

Outline

12.1 Fatty Acids Are Key Constituents of Lipids
12.2 Biological Membranes Are Composed of Three Common Types of Membrane Lipids
12.3 Phospholipids and Glycolipids Readily Form Bimolecular Sheets in Aqueous Media

12.4 Proteins Carry Out Most Membrane Processes
12.5 Lipids and Many Membrane Proteins Diffuse Rapidly in the Plane of the Membrane
12.6 Prokaryotes and Eukaryotes Differ in Their Use of Biological Membranes

Learning Goals



By the end of this chapter, you should be able to:

1. Describe the structure of a fatty acid and explain how it is named.
2. Define the three most common types of membrane lipids.
3. Explain how membrane lipids self-assemble into bimolecular sheets.
4. Distinguish between integral and peripheral membrane proteins.
5. Describe how proteins interact with membranes and how membrane-spanning motifs within proteins may be identified.
6. Explain the properties of membrane fluidity and its dependence upon lipid composition.
7. Explain the importance of membranes in eukaryotic cells.

The boundaries of all cells are defined by biological membranes, dynamic structures in which proteins float in a sea of lipids. The lipid component prevents molecules generated inside the cell from leaking out and unwanted molecules from diffusing in, while the protein components act as transport systems that allow the cell to take up specific molecules and remove unwanted ones. In addition to an external cell membrane, eukaryotic cells also contain internal membranes that form the boundaries of organelles such as mitochondria, chloroplasts, peroxisomes, and lysosomes.

Biological membranes serve several additional functions indispensable for life, such as energy storage and information

transduction. The proteins associated with the membrane define these functions for any given cell. In this chapter, we will examine the properties of membrane proteins that enable them to exist in the hydrophobic environment of the membrane while connecting two hydrophilic environments. In the next chapter, we will discuss the functions of these proteins.

12.1 Fatty Acids Are Key Constituents of Lipids

By definition, **lipids** are water-insoluble biomolecules that are highly soluble in organic solvents such as chloroform. The hydrophobic properties of lipids are essential to their ability to form membranes. Most lipids owe their hydrophobic properties to one component, their fatty acids.

Fatty acid names are based on their parent hydrocarbons

Let us first consider how fatty acids are named and distinguished from one another. **Fatty acids** are long hydrocarbon chains of various lengths and numbers of double bonds that terminate with carboxylic acid groups. The systematic name for a fatty acid is derived from the name of its parent hydrocarbon by the substitution of *oic* for the final *e.* For example, the C_{18} saturated fatty acid — that is, containing no double bonds — is called *octadecanoic acid* because the parent hydrocarbon is octadecane. A C_{18} fatty acid with one double bond is called octadec*enoic* acid; with two double bonds, octadeca*dienoic* acid; and with three double bonds, octadeca*trienoic* acid. The notation 18:0 denotes a C_{18} fatty acid with no double bonds, whereas 18:2 signifies that there are two double bonds. The structures of the ionized forms of two common fatty acids — palmitic acid (16:0) and oleic acid (18:1) — are shown in **Figure 12.1**.

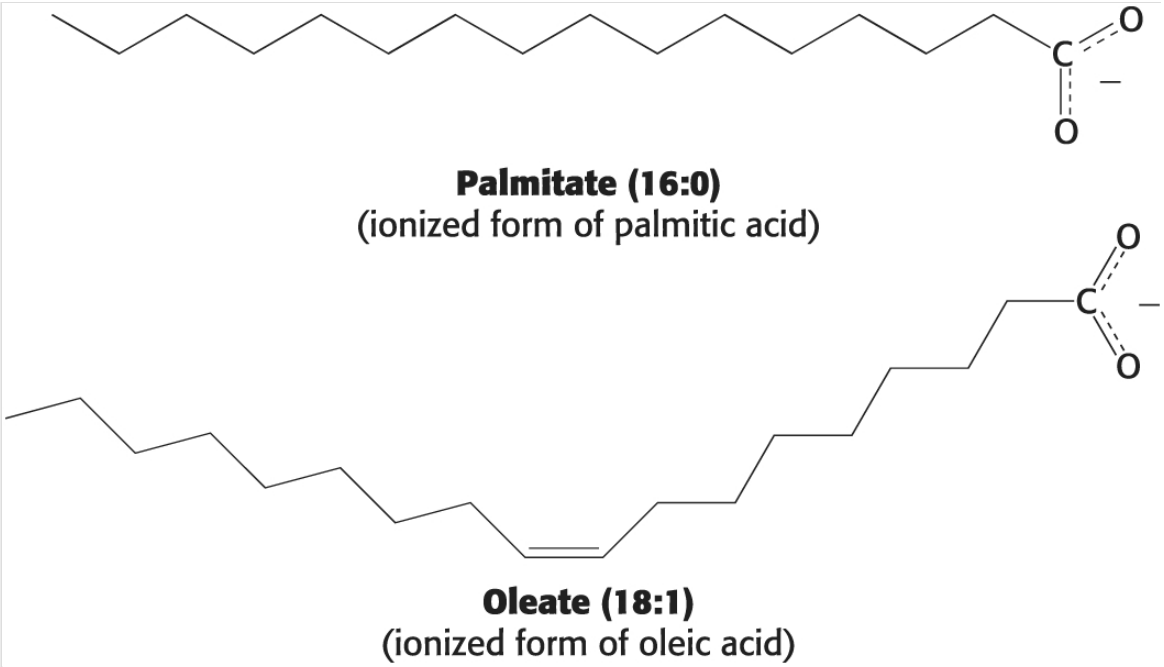


FIGURE 12.1 Fatty acids vary in their chain length and degree of saturation. For example, palmitate is a 16-carbon, saturated fatty acid (16:0), while oleate is an 18-carbon fatty acid with a single cis double bond (18:1).

Fatty acid carbon atoms are numbered starting at the carboxyl terminus (Figure 12.2). Carbon atoms 2 and 3 are often referred to as α and β, respectively. The methyl carbon atom at the distal end of the chain is called the *ω-carbon atom.* The position of a double bond is represented by the symbol Δ followed by a superscript number. For example, *cis*-Δ^9 means that there is a cis double bond between carbon atoms 9 and 10; *trans*-Δ^2 means that there is a trans double bond between carbon atoms 2 and 3. Alternatively, the position of a double bond can be denoted by counting from the distal end, with the ω-carbon atom (the methyl carbon) as number 1. Fatty acids are ionized at physiological pH, and so it is appropriate to refer to them according to their carboxylate form; for example, palmitate or hexadecanoate.

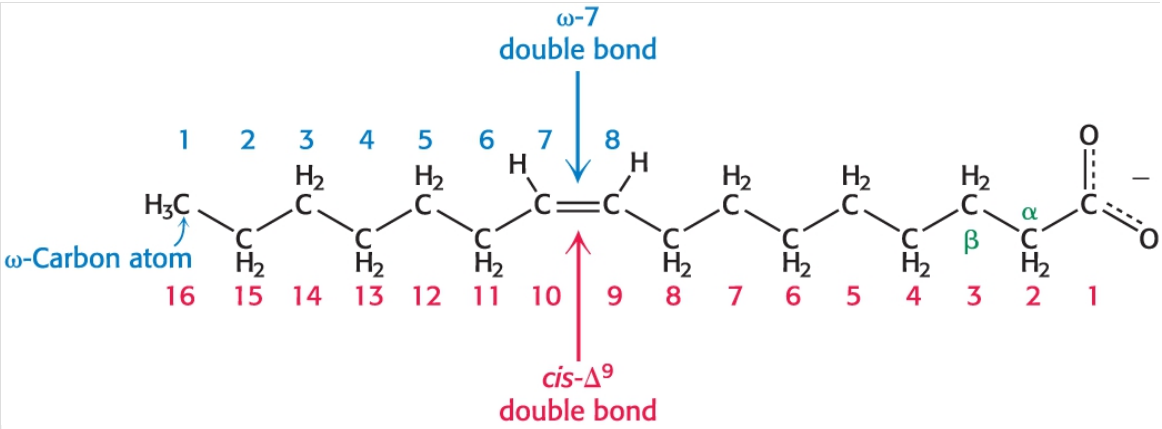
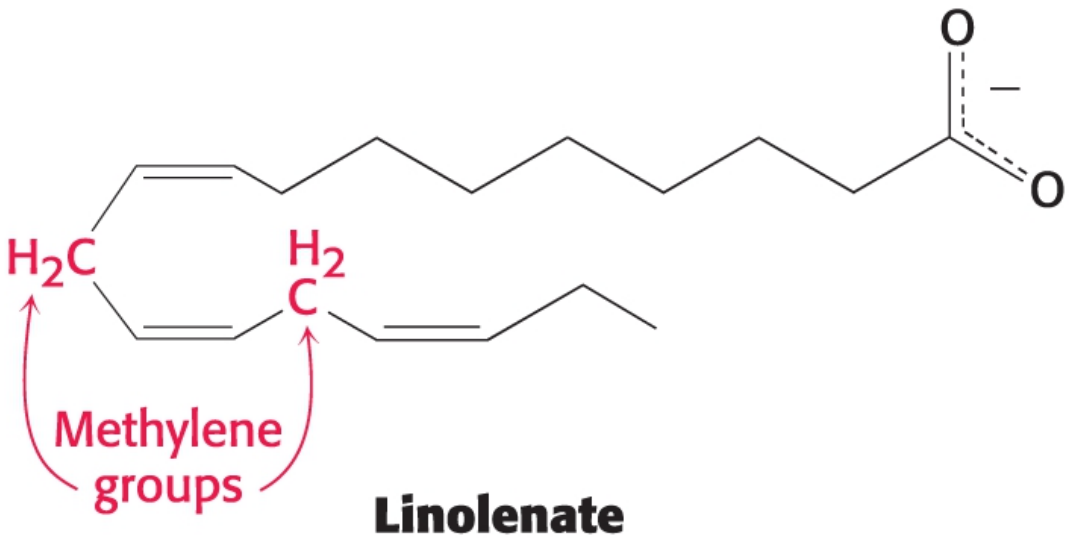


FIGURE 12.2 Fatty acid carbon atoms can be numbered in two ways. In one method (red), the carbon atoms are numbered starting with the carbonyl carbon. Carbon atoms numbered 2 and 3 are often referred to as α and β, respectively (green). The position of a double bond is indicated by the number of the carbon closest to carbon atom 1. Alternatively, carbons can be counted from the distal end, or the ω carbon (blue). For example, a double bond between the ω-7 and ω-8 carbons would be called a ω-7 double bond, as shown.

Chain length and degree of unsaturation affect fatty acid properties

Fatty acids in biological systems usually contain an even number of carbon atoms, typically between 14 and 24 (**Table 12.1**), with the 16- and 18-carbon fatty acids being the most common. The dominance of fatty acid chains containing an even number of carbon atoms reflects the manner in which fatty acids are biosynthesized (Chapter 27). The hydrocarbon chain is almost invariably unbranched in animal fatty acids. The alkyl chain may be saturated, or it may contain one or more double bonds. The configuration of the double bonds in most unsaturated fatty acids is cis. The double bonds in polyunsaturated fatty acids are separated by at least one methylene group.



Linolenate

TABLE 12.1 Some naturally occurring fatty acids in animals

Number of carbons	Number of double bonds	Common name	Systematic name	Formula
12	0	Laurate	*n*-Dodecanoate	$CH_3(CH_2)_{10}COO^-$
14	0	Myristate	*n*-Tetradecanoate	$CH_3(CH_2)_{12}COO^-$
16	0	Palmitate	*n*-Hexadecanoate	$CH_3(CH_2)_{14}COO^-$
18	0	Stearate	*n*-Octadecanoate	$CH_3(CH_2)_{16}COO^-$
20	0	Arachidate	*n*-Eicosanoate	$CH_3(CH_2)_{18}COO^-$

22	0	Behenate	*n*-Docosanoate	$CH_3(CH_2)_{20}COO^-$
24	0	Lignocerate	*n*-Tetracosanoate	$CH_3(CH_2)_{22}COO^-$
16	1	Palmitoleate	*cis*-Δ^9-Hexadecenoate	$CH_3(CH_2)_5CH=CH(CH_2)_7COO^-$
18	1	Oleate	*cis*-Δ^9-Octadecenoate	$CH_3(CH_2)_7CH=CH(CH_2)_7COO^-$
18	2	Linoleate	*cis, cis*-Δ^9, Δ^{12}-Octadecadienoate	$CH_3(CH_2)_4(CH=CHCH_2)_2(CH)_6COO^-$
18	3	Linolenate	all-*cis*-$\Delta^9, \Delta^{12}, \Delta^{15}$-Octadecatrienoate	$CH_3CH_2(CH=CHCH_2)_3(CH_2)_6COO^-$
20	4	Arachidonate	all-*cis* $\Delta^5, \Delta^8, \Delta^{11}, \Delta^{14}$-Eicosatetraenoate	$CH_3(CH_2)_4(CH=CHCH_2)_4(CH_2)_2COO^-$

The properties of fatty acids and of lipids derived from them are markedly dependent on chain length and degree of saturation. Unsaturated fatty acids have lower melting points than do saturated fatty acids of the same length. For example, the melting point of stearic acid is 69.6°C, whereas that of oleic acid (which contains one cis double bond) is 13.4°C. The melting points of polyunsaturated fatty acids of the C_{18} series are even lower. Chain length also affects the melting point, as illustrated

by the fact that the melting temperature of palmitic acid (C_{16}) is 6.5 degrees lower than that of stearic acid (C_{18}). Thus, short chain length and unsaturation enhance the fluidity of fatty acids and of their derivatives.

12.2 Biological Membranes Are Composed of Three Common Types of Membrane Lipids

Lipids have a variety of biological roles: they serve as fuel molecules, highly concentrated energy stores, signal molecules and messengers in signal-transduction pathways, and components of membranes. The first three roles of lipids will be considered in later chapters. Here, we will explore the role of lipids as the essential component of biological membranes.

In order to appreciate the structural and chemical properties of membrane lipids, let us first consider the membranes themselves. While biological membranes are as diverse in structure as they are in function, they do have in common a number of important attributes:

- Membranes are sheetlike structures, only two molecules thick, that form closed boundaries between different compartments. The thickness of most membranes is between 60 Å (6 nm) and 100 Å (10 nm).
- Membranes consist mainly of lipids and proteins. The mass ratio of lipids to proteins ranges from 1:4 to 4:1. Membranes also contain carbohydrates that are linked to lipids and proteins.
- Membrane lipids are small molecules that have both hydrophilic and hydrophobic moieties. These lipids spontaneously form closed bimolecular sheets in aqueous media. These sheets, called *lipid bilayers*, are barriers to the flow of polar molecules.
- Specific proteins mediate distinctive functions of membranes. Proteins serve as pumps, channels, receptors, energy transducers,

and enzymes. Membrane proteins are embedded in lipid bilayers, which create suitable environments for their action.

- Membranes are noncovalent assemblies. The constituent protein and lipid molecules are held together by many noncovalent interactions, which act cooperatively.
- Membranes are asymmetric. The two faces of biological membranes always differ from each other.
- Membranes are fluid structures. Lipid molecules diffuse rapidly in the plane of the membrane, as do proteins, unless they are anchored by specific interactions. In contrast, lipid molecules and proteins do not readily rotate across the membrane. Membranes can be regarded as two-dimensional solutions of oriented proteins and lipids.
- Most cell membranes are electrically polarized, such that the inside is negatively charged. Membrane potential plays a key role in transport, energy conversion, and excitability (Chapter 13).

Here, our focus is on the principal lipids found in the membranes of eukaryotes and bacteria: *phospholipids*, *glycolipids*, and *cholesterol*. While the membrane lipids of archaea are distinct, they have many features related to membrane formation in common with lipids of other organisms.

Phospholipids are the major class of membrane lipids

Phospholipids are abundant in all biological membranes. A **phospholipid** molecule is constructed from four components (**Figure 12.3**):

- One or more fatty acids

- A platform to which the fatty acids are attached
- A phosphate
- An alcohol attached to the phosphate

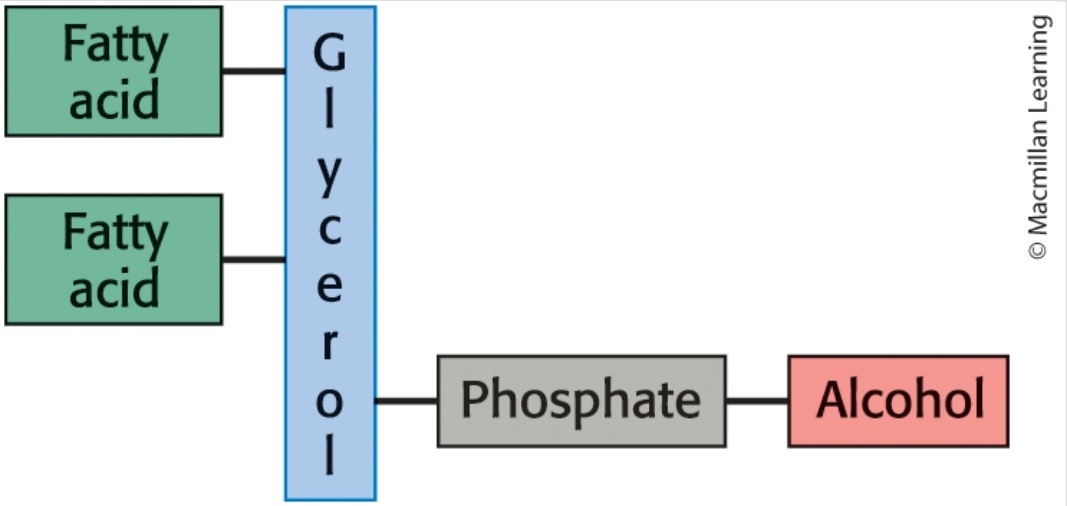


FIGURE 12.3 A phospholipid molecule contains four components. These components are shown here in schematic form: (1) fatty acids (green), (2) a platform for fatty acid attachment (here, glycerol, shown in blue), (3) a phosphate (gray), and (4) an alcohol (red).

The fatty acid components provide a hydrophobic barrier, whereas the remainder of the molecule has hydrophilic properties that enable interaction with the aqueous environment.

The platform on which phospholipids are built may be glycerol, a three-carbon alcohol, or sphingosine, a more complex alcohol. Phospholipids derived from glycerol are called **phosphoglycerides**. A phosphoglyceride consists of a glycerol backbone to which are attached two fatty acid chains and a phosphorylated alcohol.

In phosphoglycerides, the hydroxyl groups at C-1 and C-2 of glycerol are esterified to the carboxyl groups of the two fatty acid chains (**Figure 12.4**). The C-3 hydroxyl group of the glycerol backbone is esterified to phosphoric acid. When no further additions are made, the resulting compound is phosphatidate (diacylglycerol 3-phosphate), the simplest phosphoglyceride. Although only small amounts of phosphatidate are present in membranes, it is a key intermediate in the biosynthesis of the other phosphoglycerides (Section 27.1). The absolute configuration of the glycerol 3-phosphate moiety of membrane lipids is shown in Figure 12.4.

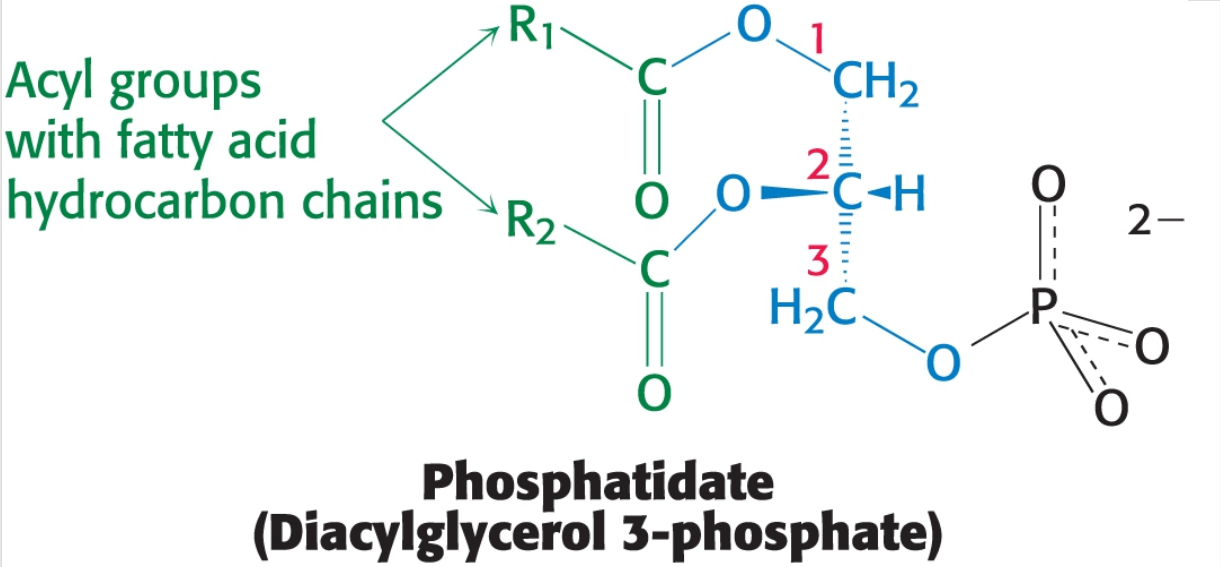


FIGURE 12.4 Phosphatidate, the simplest phosphoglyceride, does not contain an alcohol component. The absolute configuration of the center carbon (C-2) is shown.

The major phosphoglycerides are derived from phosphatidate by the formation of an ester bond between the phosphate group of phosphatidate and the hydroxyl group of one of several alcohols (**Figure 12.5**).

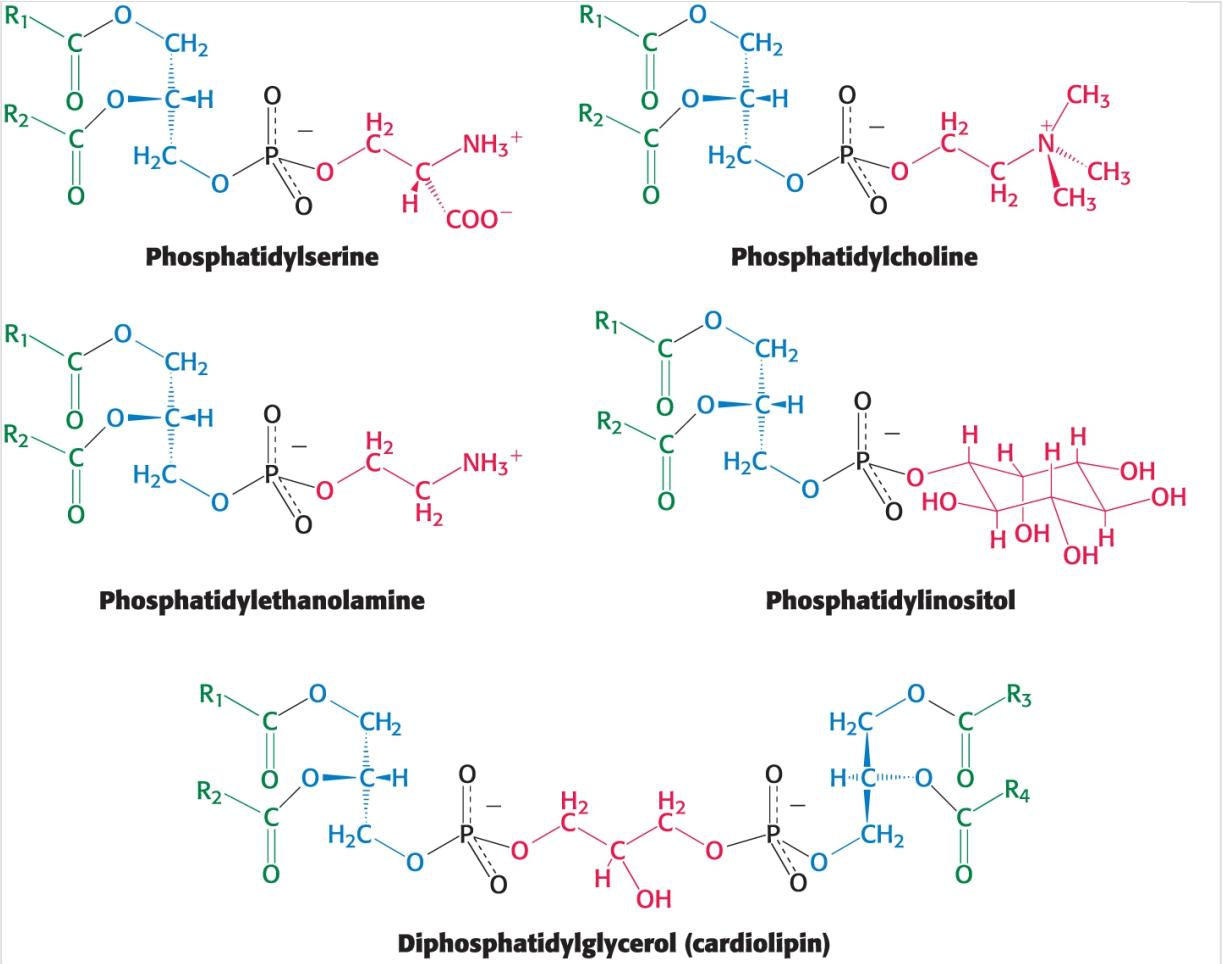
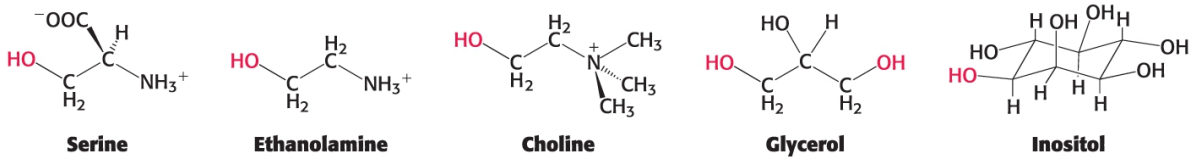


FIGURE 12.5 The common phosphoglycerides found in membranes contain an ester bond between phosphatidate and an alcohol. These structures are colored to match the four phospholipid components depicted in Figure 12.3.

The common alcohol moieties of phosphoglycerides are the amino acid serine, ethanolamine, choline, glycerol, and inositol.



Sphingomyelin is a phospholipid found in membranes that is not derived from glycerol. Instead, the backbone in sphingomyelin is **sphingosine**, an amino alcohol that contains a long, unsaturated hydrocarbon chain (**Figure 12.6**). In sphingomyelin, the amino group of the sphingosine backbone is linked to a fatty acid by an amide bond. In addition, the primary hydroxyl group of sphingosine is esterified to phosphorylcholine.

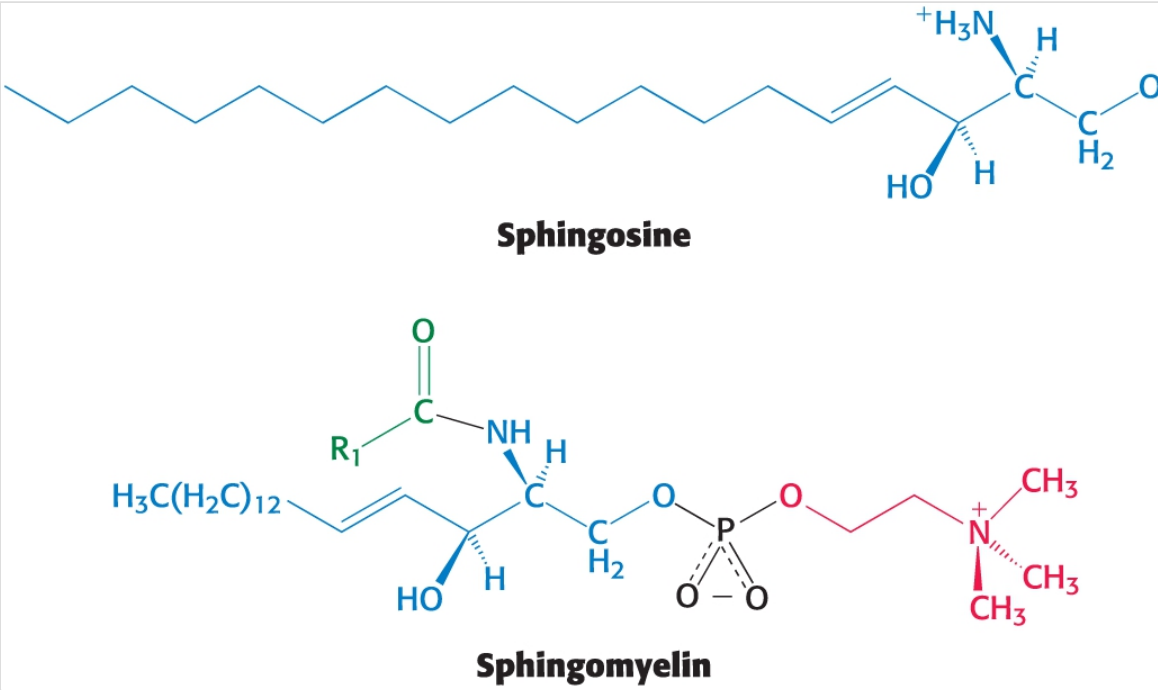
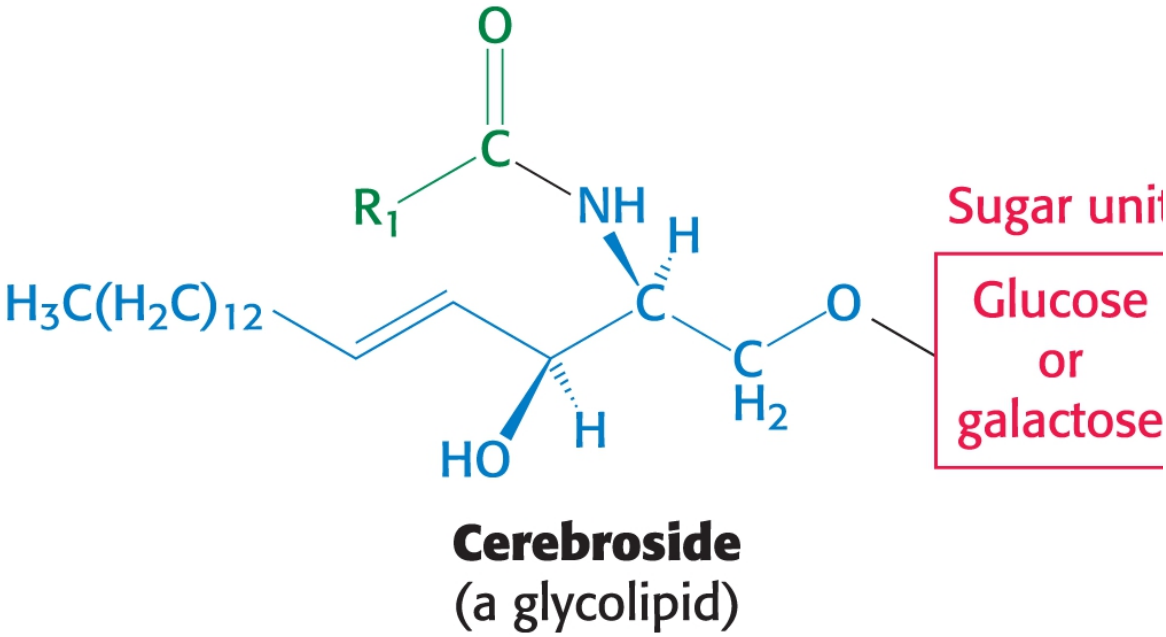


FIGURE 12.6 Sphingosine forms the backbone of the phospholipid sphingomyelin. The sphingosine moiety of sphingomyelin is highlighted in blue.

Glycolipids include carbohydrate moieties

The second major class of membrane lipids, **glycolipids**, are sugar-containing lipids. Like sphingomyelin, the glycolipids in animal cells are derived from sphingosine. The amino group of the sphingosine backbone is acylated by a fatty acid, as in sphingomyelin. Glycolipids differ from sphingomyelin in the identity of the unit that is linked to the primary hydroxyl group of the sphingosine backbone. In glycolipids, one or more sugars (rather than phosphorylcholine) are attached to this group. The simplest glycolipid, called a *cerebroside*, contains a single sugar residue, either glucose or galactose.



Cerebroside
(a glycolipid)

More complex glycolipids contain a branched chain of as many as seven sugar residues. Glycolipids are oriented in a completely asymmetric fashion with the sugar residues always on the extracellular side of the membrane.



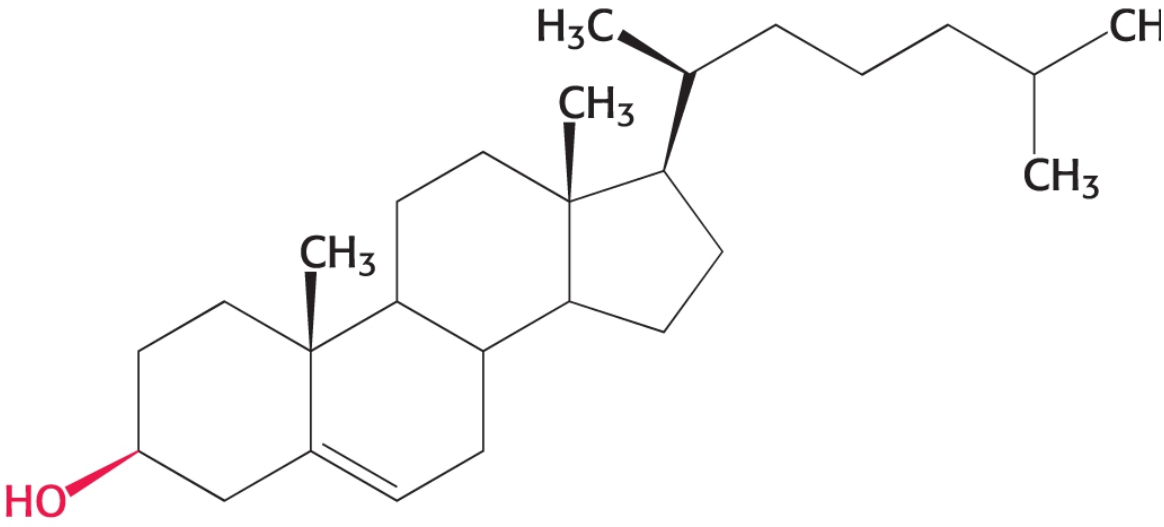
Archives of the Albert Einstein College of Medicine, Ted Burrows, photographer

MARIE M. DALY In 1947, Marie M. Daly became the first Black woman in the United States to earn a PhD in chemistry. Soon after, she worked with others at Columbia University to examine the role of dietary cholesterol in contributing to hypertension in an animal model system. Later, in an independent faculty position at Albert Einstein College of Medicine, where she remained for more than 25 years, she continued her work on lipids and heart disease and other topics. Dr. Daly demonstrated an interest in promoting the careers of minority women in science. In

1975, she participated in a groundbreaking meeting that led to a report — *The Double Bind: The Price of Being a Minority Woman in Science* — that laid out challenges faced at different career stages. Her energetic pursuit of important scientific questions and her commitment to help others follow in her footsteps illustrate some of the many dimensions of a productive scientific career.

Cholesterol is a lipid based on a steroid nucleus

The third major type of membrane lipid, **cholesterol**, has a structure that is quite different from that of phospholipids. It is a steroid, built from four linked hydrocarbon rings.



Cholesterol

A hydrocarbon tail is linked to the steroid at one end, and a hydroxyl group is attached at the other end. In membranes, the orientation of the molecule is parallel to the fatty acid chains of the phospholipids, and the hydroxyl group interacts with the nearby phospholipid head groups. Cholesterol is absent from prokaryotes but is found to varying degrees

in virtually all animal membranes. It constitutes almost 25% of the membrane lipids in certain nerve cells but is essentially absent from some intracellular membranes.

Archaeal membranes are built from ether lipids with branched chains

The membranes of archaea differ in composition from those of eukaryotes or bacteria in three important ways. The first two of these differences clearly relate to the hostile living conditions of many archaea (**Figure 12.7**):

1. The nonpolar chains are joined to a glycerol backbone by ether rather than ester linkages. The ether linkage is more resistant to hydrolysis.

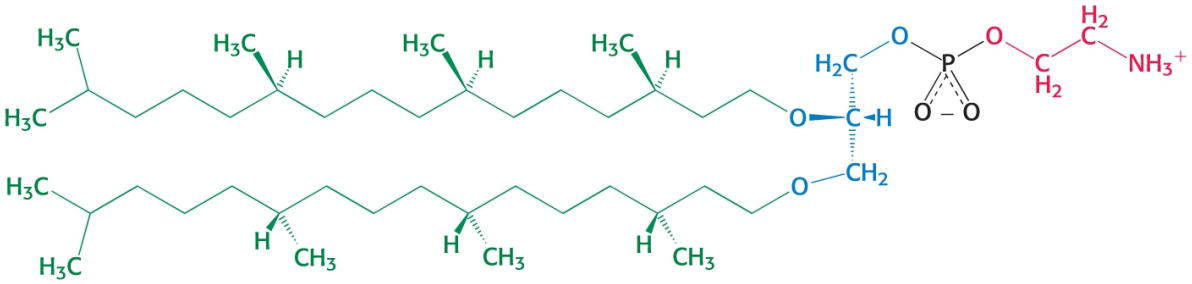
2. The alkyl chains are branched rather than linear. They are built up from repeats of a fully saturated five-carbon fragment. These branched, saturated hydrocarbons are more resistant to oxidation than the unbranched chains of eukaryotic and bacterial membrane lipids. The ability of archaeal lipids to resist hydrolysis and oxidation may help these organisms to withstand the extreme conditions, such as high temperature, low pH, or high salt concentration, under which some of these archaea grow.

3. The stereochemistry of the central glycerol is inverted compared with that shown in Figure 12.4.



Daniel Viñé Garcia/Getty Images

FIGURE 12.7 Archaea can thrive in harsh habitats. Here, thermophilic archaea are responsible, in part, for the bright colors of the Morning Glory Pool hot spring in Yellowstone National Park.



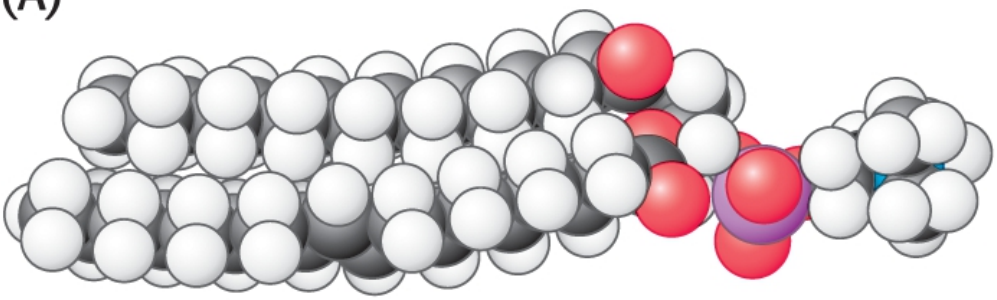
Membrane lipid from the archaeon *Methanococcus jannaschii*

A membrane lipid is an amphipathic molecule containing a hydrophilic and a hydrophobic moiety

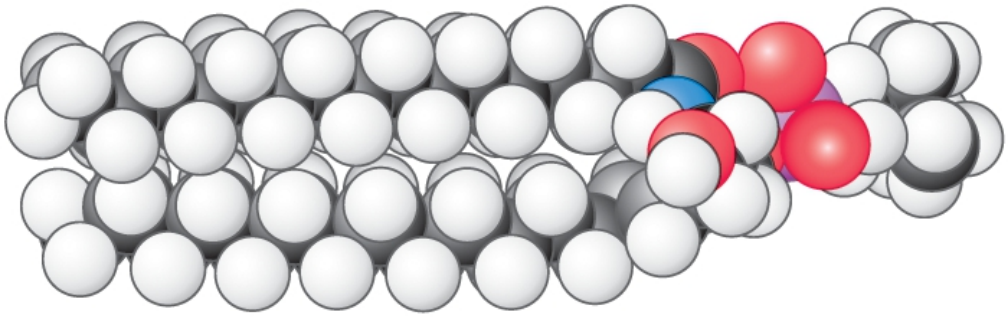
The repertoire of membrane lipids is extensive. However, these lipids possess a critical common structural theme: membrane lipids are **amphipathic molecules (amphiphilic molecules)**, that is, they contain both a hydrophilic and a hydrophobic moiety.

Let us look at a model of a phosphoglyceride, such as phosphatidylcholine. Its overall shape is roughly rectangular (**Figure 12.8A**). The hydrophilic phosphorylcholine moiety lies at one end of the molecule, while the two hydrophobic fatty acid chains project approximately parallel to each other. Sphingomyelin has a similar conformation, as does the archaeal lipid depicted. Therefore, the following shorthand has been adopted to represent these membrane lipids: the hydrophilic unit, also called the *polar head group,* is represented by a circle, and the hydrocarbon tails are depicted by straight or wavy lines (**Figure 12.8B**).

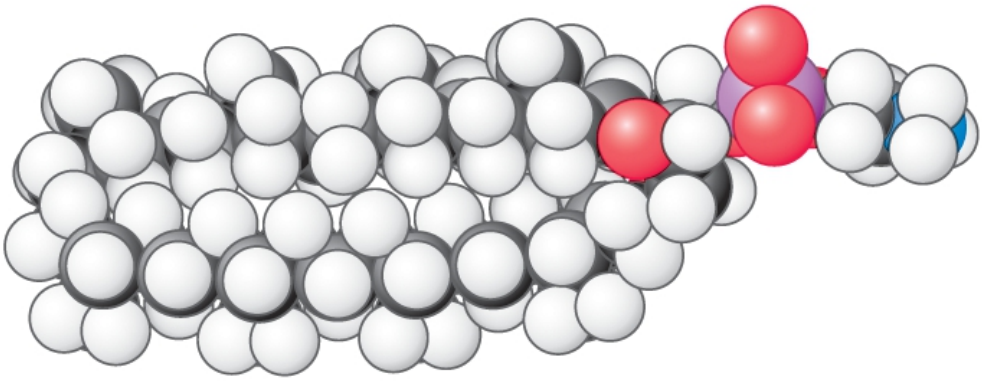
(A)



Phosphoglyceride

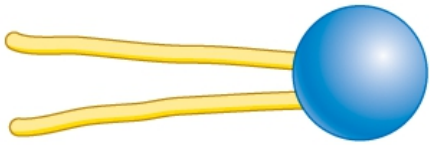


Sphingomyelin



Archaeal lipid

(B)



© Macmillan Learning

FIGURE 12.8 The structures of membrane lipids can be drawn using a shorthand depiction. (A) Space-filling models of a phosphoglyceride, sphingomyelin, and an archaeal lipid show their overall rectangular shapes and distribution of hydrophilic and hydrophobic moieties. (B) A shorthand depiction of a membrane lipid.

Self-Check Question

What are the three primary types of membrane lipids? What are some molecules that form the polar head groups of phospholipids?

12.3 Phospholipids and Glycolipids Readily Form Bimolecular Sheets in Aqueous Media

What properties enable phospholipids to form membranes? Membrane formation is a consequence of the amphipathic nature of the molecules. Their polar head groups favor contact with water, whereas their hydrocarbon tails interact with one another in preference to water. How can molecules with these preferences arrange themselves in aqueous solutions? One way is to form a globular structure called a **micelle**. The polar head groups form the outside surface of the micelle, which is surrounded by water, and the hydrocarbon tails are sequestered inside, interacting with one another (**Figure 12.9**).

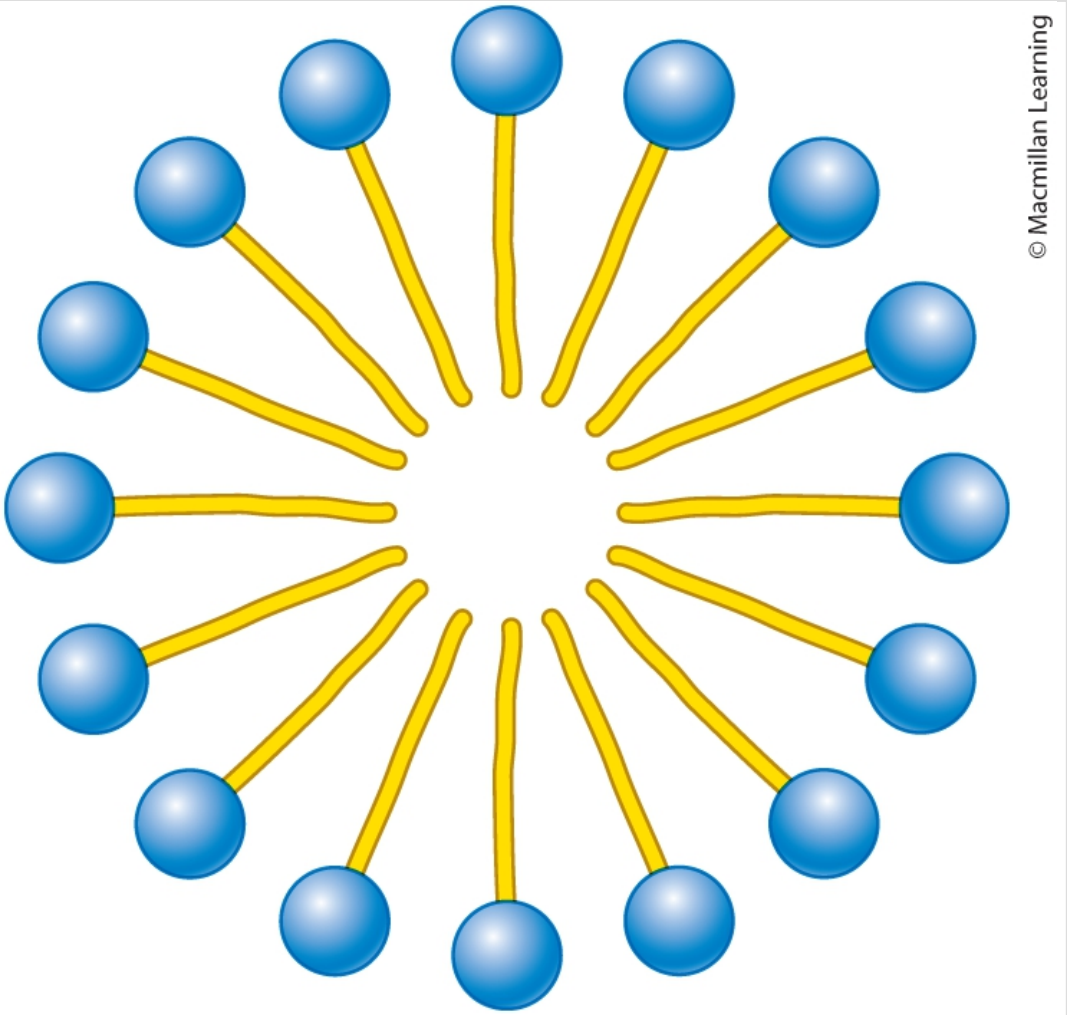


FIGURE 12.9 Micelles are globular structures formed from ionized fatty acids with single tails. Ionized fatty acids readily form such structures, but most phospholipids do not.

Alternatively, the strongly opposed preferences of the hydrophilic and hydrophobic moieties of membrane lipids can be satisfied by forming a **lipid bilayer**, composed of two lipid sheets (**Figure 12.10**). A lipid bilayer is also called a *bimolecular sheet*. The hydrophobic tails of each individual sheet interact with one another, forming a hydrophobic interior that acts as a permeability barrier. The hydrophilic head groups

interact with the aqueous medium on each side of the bilayer. The two opposing sheets are called leaflets.

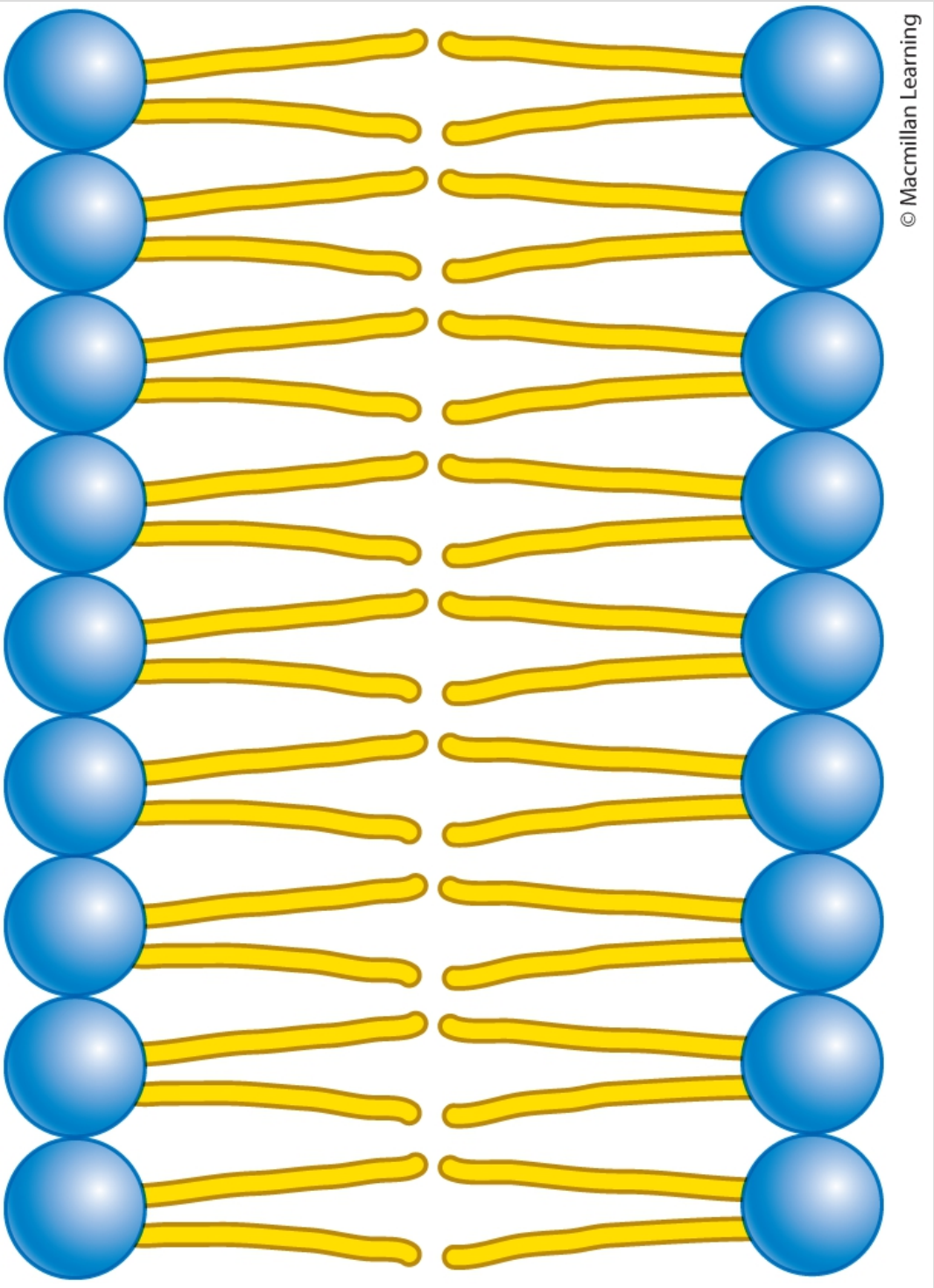


FIGURE 12.10 A lipid bilayer is formed from two opposing lipid sheets.

The favored structure for most phospholipids and glycolipids in aqueous media is a bimolecular sheet rather than a micelle. The reason is that the two fatty acid chains of a phospholipid or a glycolipid are too bulky to fit into the interior of a micelle. In contrast, salts of fatty acids (such as sodium palmitate, a constituent of soap) readily form micelles because they contain only one chain. The formation of bilayers instead of micelles by phospholipids is of critical biological importance. A micelle is a limited structure, usually less than 200 Å (20 nm) in diameter. In contrast, a bimolecular sheet can extend to macroscopic dimensions, as much as a millimeter (10^7 Å, or 10^6 nm) or more. Phospholipids and related molecules are important membrane constituents because they readily form extensive bimolecular sheets.

Lipid bilayers form spontaneously by a self-assembly process. In other words, the structure of a bimolecular sheet is inherent in the structure of the constituent lipid molecules. The growth of lipid bilayers from phospholipids is rapid and spontaneous in water. Bimolecular sheets are stabilized by the full array of forces that mediate molecular interactions in biological systems:

- Hydrophobic interactions are the major driving force for the formation of lipid bilayers. We have already encountered the dominant role that hydrophobic interactions play in the stabilization of double-helical DNA and the folding of proteins (Sections 1.3 and 2.4). Water molecules are released from the hydrocarbon tails of membrane lipids as these tails become sequestered in the nonpolar interior of the bilayer.

- van der Waals attractive forces between the hydrocarbon tails favor close packing of the tails.

- Electrostatic and hydrogen-bonding attractions between the polar head groups and water molecules.

Because lipid bilayers are held together by many reinforcing, noncovalent interactions (predominantly hydrophobic), they are cooperative structures. These hydrophobic interactions have three significant biological consequences: (1) lipid bilayers have an inherent tendency to be extensive; (2) lipid bilayers will tend to close on themselves so that there are no edges with exposed hydrocarbon chains, and so they form compartments; and (3) lipid bilayers are self-sealing because a hole in a bilayer is energetically unfavorable.

Self-Check Question



Phospholipids form lipid bilayers in water. What structure might form if phospholipids were placed in an organic solvent?

Lipid vesicles can be formed from phospholipids

The propensity of phospholipids to form membranes has been used to create important experimental and clinical tools. **Lipid vesicles**, or **liposomes**, are aqueous compartments enclosed by a lipid bilayer (**Figure 12.11**), which can be used to study membrane permeability or to deliver chemicals to cells.

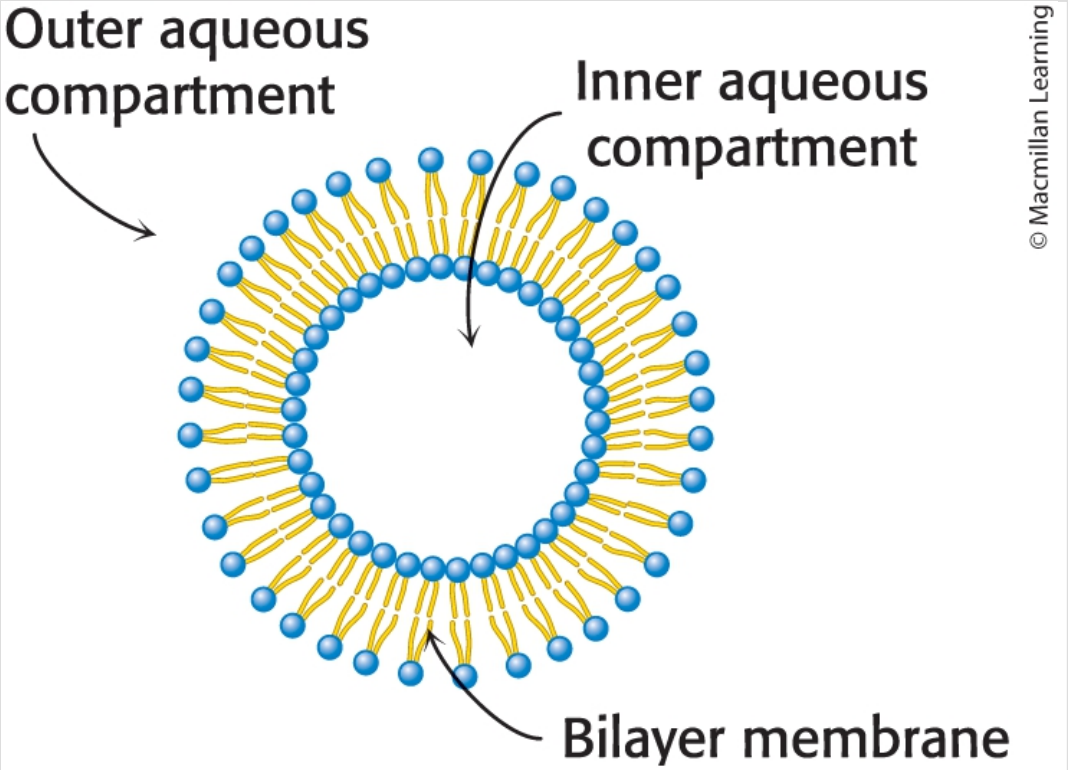


FIGURE 12.11 A liposome is a small aqueous compartment surrounded by a lipid bilayer.

Liposomes are formed by suspending a suitable lipid, such as phosphatidylcholine, in an aqueous medium, and then sonicating (i.e., agitating by high-frequency sound waves) to give a dispersion of closed vesicles that are quite uniform in size (Figure 12.12). Vesicles formed by this method are nearly spherical and have a diameter of about 500 Å (50 nm). Larger vesicles (of the order of $1\ \mu m$ or 10^4 Å in diameter) can be prepared by slowly evaporating the organic solvent from a suspension of phospholipid in a mixed-solvent system.

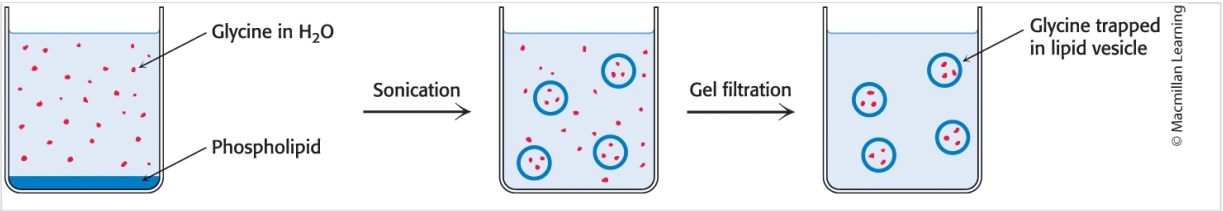


FIGURE 12.12 Liposomes containing trapped ions or molecules can be synthesized. Liposomes containing glycine are formed by the sonication of phospholipids in the presence of glycine. Free glycine is removed by gel filtration.

Ions or molecules can be trapped in the aqueous compartments of lipid vesicles by forming the vesicles in the presence of these substances, as shown in Figure 12.12. For example, 500-Å-diameter vesicles formed in a 0.1 M glycine solution will trap about 2000 molecules of glycine in each inner aqueous compartment. These glycine-containing vesicles can be separated from the surrounding solution of glycine by dialysis or by gel-filtration chromatography (Section 4.1). The permeability of the bilayer membrane to glycine can then be determined by measuring the rate of efflux of glycine from the inner compartment of the vesicle to the ambient solution.

Liposomes can be formed with specific membrane proteins embedded in them by solubilizing the proteins in the presence of detergents and then adding them to the phospholipids from which liposomes will be formed. Protein–liposome complexes provide valuable experimental tools for examining a range of membrane-protein functions.

Therapeutic applications for liposomes are currently under active investigation. For example, liposomes containing drugs or DNA can be injected into patients. These liposomes fuse with the plasma membrane of many kinds of cells, introducing into the cells the molecules they contain. Drug delivery with liposomes often lessens its toxicity. Less of the drug is distributed to normal tissues because long-circulating liposomes concentrate in regions of increased blood circulation, such as solid tumors and sites of inflammation. Moreover, the selective fusion of lipid vesicles with particular kinds of cells is a promising means of controlling the delivery of drugs to target cells.

Another well-defined synthetic membrane adopts the structure of a planar bilayer. This membrane can be formed across a 1-mm hole in a partition between two aqueous compartments by dipping a fine paintbrush into a membrane-forming solution, such as phosphatidylcholine in decane, and stroking the tip of the brush across the hole. The lipid film across the hole thins spontaneously into a lipid bilayer. The electrical conduction properties of this macroscopic bilayer membrane are readily studied by inserting electrodes into each aqueous compartment (**Figure 12.13**). For example, the permeability of the membrane to ions is determined by measuring the current across the membrane as a function of the applied voltage.

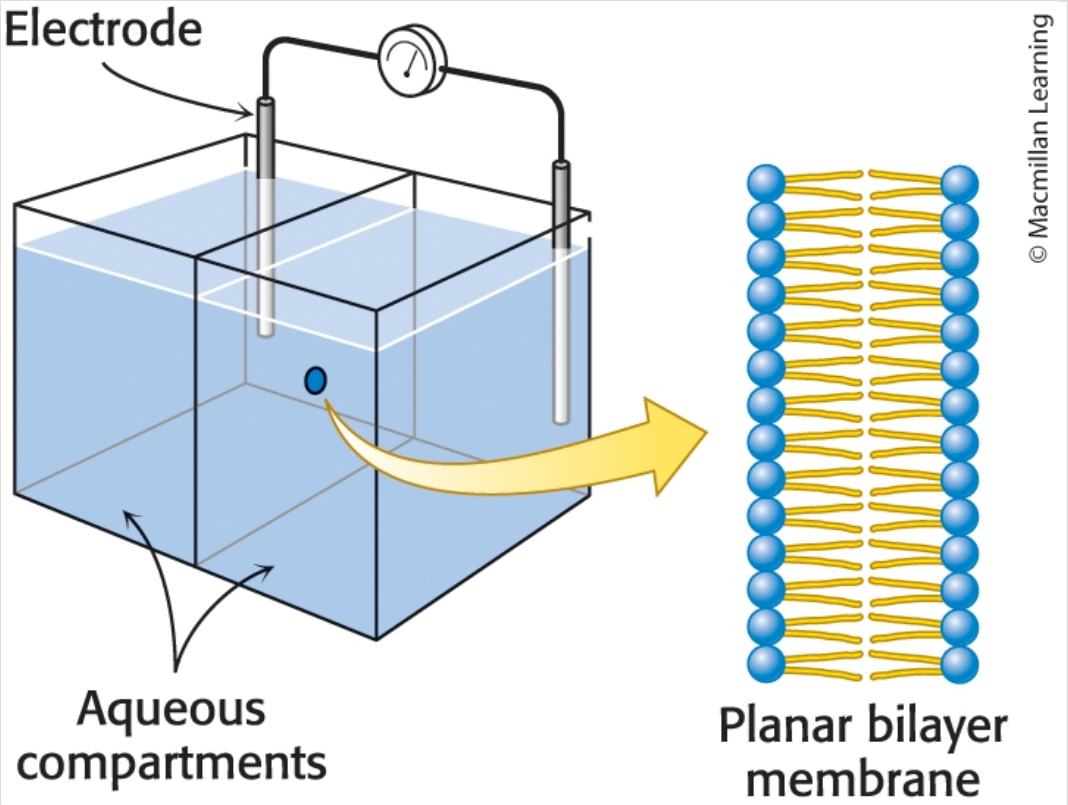


FIGURE 12.13 The properties of planar bilayer membranes can be studied experimentally. A bilayer membrane is formed across a 1-mm hole in a septum that separates two aqueous compartments. This arrangement permits measurements of the permeability and electrical conductance of lipid bilayers.

Lipid bilayers are highly impermeable to ions and most polar molecules

Permeability studies of lipid vesicles and electrical-conductance measurements of planar bilayers have revealed several important properties:

- *Lipid bilayer membranes have a very low permeability for ions and most polar molecules.* Water is a conspicuous exception to this

generalization; it traverses such membranes relatively easily because of its low molecular weight, high concentration, and lack of a complete charge.

- *The range of measured permeability coefficients is very wide* (**Figure 12.14**). For example, Na^+ and K^+ traverse lipid bilayer membranes 10^9 times as slowly as does H_2O. Tryptophan, a zwitterion at pH 7, crosses the membrane 10^3 times as slowly as does indole, a structurally related molecule that lacks ionic groups.

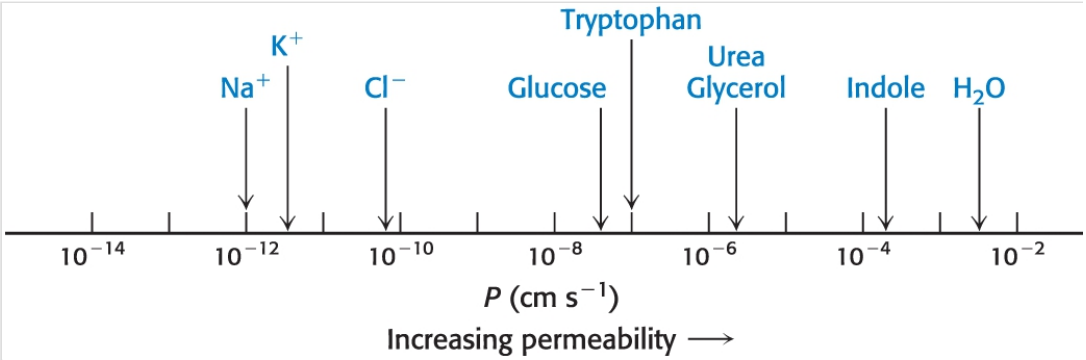


FIGURE 12.14 The permeability coefficients (*P*) of ions and molecules in a lipid bilayer span a wide range of values.

- *The permeability of small molecules is correlated with their solubility in a nonpolar solvent relative to their solubility in water.* This relationship suggests that a small molecule might traverse a lipid bilayer membrane in the following way: first, it sheds any interacting water molecules (Section 1.3); then, it is dissolved in the hydrocarbon core of the membrane; finally, it diffuses through this core to the other side of the membrane, where it becomes resolvated by water. An ion such as Na^+ traverses membranes very slowly because the

replacement of its numerous interactions with polar water molecules by nonpolar interactions with the membrane interior is highly unfavorable energetically.

12.4 Proteins Carry Out Most Membrane Processes

We now turn to membrane proteins, which are responsible for most of the dynamic processes carried out by membranes. Whereas membrane lipids form a permeability barrier and thereby establish compartments, specific proteins mediate nearly all other membrane functions. In particular, proteins transport chemicals and information across a membrane. Membrane lipids create the appropriate environment for the action of such proteins.

Membranes differ in their protein content. For example, relatively pure lipids are well suited for insulation. **Myelin**, a membrane that serves as an electrical insulator around certain nerve fibers, has a low content of protein (18%). As such, myelin plays a critical role in enabling the rapid transmission of nerve impulses, or action potentials (Section 13.4). Its structure is quite unique: the cells that generate myelin wrap their plasma membranes multiple times around the axon, the part of the neuron that conducts the electrical signal (**Figure 12.15**).

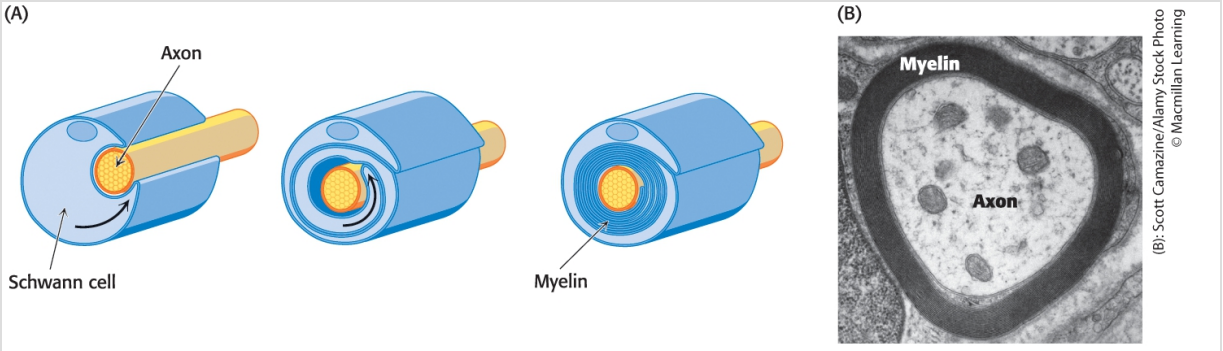


FIGURE 12.15 The lipid-rich membranes of myelin form an electrical insulator around some nerve fibers. (A) Myelin is comprised of the lipid-rich plasma membrane of a Schwann cell in peripheral nerves or the oligodendrocyte in the brain that has wrapped multiple times around the axon, or the portion of the neuron that conducts electrical impulses. [https://biologydictionary.net/myelin-sheath] (B) The myelin sheath around an axon is readily apparent by electron microscopy.

Significant myelination of neurons in the brain occurs during infancy but persists throughout adolescence, a reminder that the brain is an actively developing organ throughout childhood. The importance of myelination is further underscored by the existence of demyelinating diseases, such as multiple sclerosis, where myelin assembly is impaired or existing myelin is damaged.

In contrast to myelin, the plasma membranes, or exterior membranes, of most other cells are much more metabolically active. They contain many pumps, channels, receptors, and enzymes. The protein content of these plasma membranes is typically 50%. Energy-transduction membranes, such as the internal membranes of mitochondria and chloroplasts, have the highest content of protein, around 75%.

The protein components of a membrane can be readily visualized by SDS–polyacrylamide gel electrophoresis. As we discussed in Section 4.1, the electrophoretic mobility of many proteins in SDS-containing gels depends on the mass rather than on the net charge of the protein. The gel-electrophoresis patterns of three membranes are shown in **Figure 12.16**. It is evident that each of these three membranes contains many proteins but has a distinct protein composition. In general, membranes performing different functions contain different repertoires of proteins.

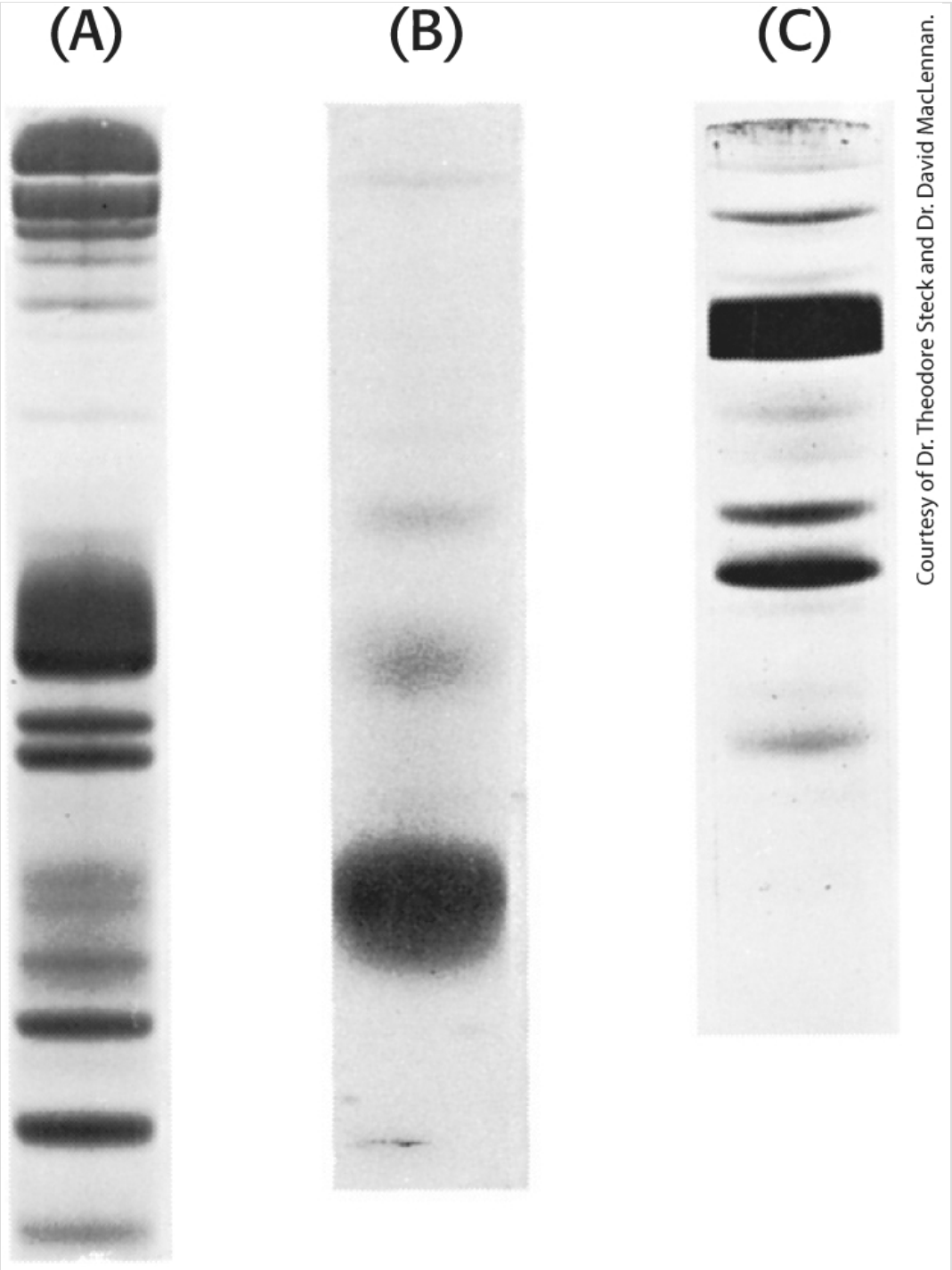


FIGURE 12.16 The protein composition of plasma membranes varies with cell type. Here, the SDS–acrylamide gel patterns of membrane proteins from three different cell types are shown: (A) The plasma membrane of red blood cells. (B) The photoreceptor membranes of retinal rod cells. (C) The sarcoplasmic reticulum membrane of muscle cells.

Proteins associate with the lipid bilayer in a variety of ways

The ease with which a protein can be dissociated from a membrane indicates how intimately it is associated with the membrane. Some membrane proteins can be solubilized by relatively mild means, such as extraction by a solution of high ionic strength (e.g., 1 M NaCl). Other membrane proteins are bound much more tenaciously; they can be solubilized only by using a detergent or an organic solvent. Membrane proteins can be classified as being either peripheral or integral on the basis of their difference in dissociability (**Figure 12.17**):

- **Integral membrane proteins** interact extensively with the hydrocarbon chains of membrane lipids, and they can be released only by agents that compete for these nonpolar interactions. In fact, most integral membrane proteins span the lipid bilayer.

- **Peripheral membrane proteins** are bound to membranes primarily by electrostatic and hydrogen-bond interactions with the head groups of lipids. These polar interactions can be disrupted by adding salts or by changing the pH. Many peripheral membrane proteins are bound to the surfaces of integral proteins, on either the cytoplasmic or the extracellular side of the membrane. Others are anchored to the lipid bilayer by a covalently attached hydrophobic chain, such as a fatty acid.

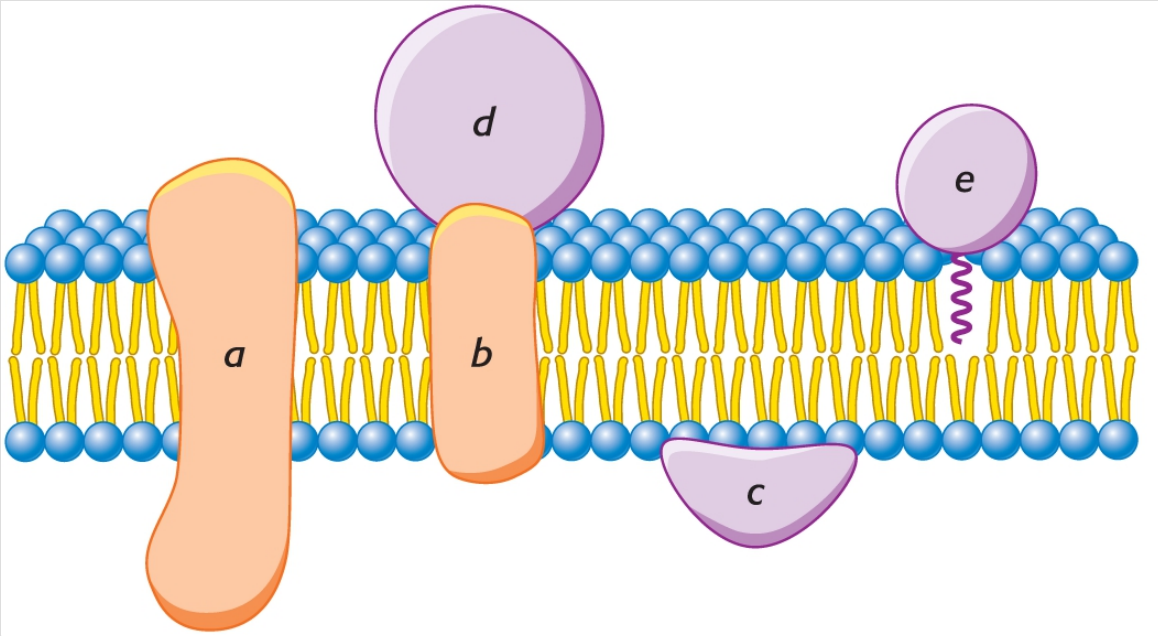


FIGURE 12.17 Membrane proteins interact with lipid bilayers in different ways. Integral membrane proteins (*a* and *b*) interact extensively with the hydrocarbon region of the bilayer. Most known integral membrane proteins traverse the lipid bilayer. Peripheral membrane protei interact with the polar head groups of the lipids (*c*) or bind to the surfaces of integral proteins (*d* Other proteins are tightly anchored to the membrane by a covalently attached lipid molecule (*e*

Proteins interact with membranes in a variety of ways

Membrane proteins are more difficult to purify and crystallize than are water-soluble proteins. Nonetheless, researchers using x-ray crystallography or cryo-electron microscopy have determined the three-dimensional structures of more than 4000 such proteins at sufficiently high resolution to discern the molecular details. As noted in Chapter 2, membrane proteins differ from soluble proteins in the distribution of hydrophobic and hydrophilic groups. We will consider the structures of three membrane proteins in some detail.

- *Membrane-spanning alpha helices are the most common structural motif in membrane proteins.* The first membrane protein that we consider is the archaeal protein bacteriorhodopsin (**Figure 12.18**). We will discuss the function of this important protein in Section 19.1. Bacteriorhodopsin is built almost entirely of α helices; seven closely packed α helices, nearly perpendicular to the plane of the cell membrane, span its 45-Å width. Examination of the primary structure of bacteriorhodopsin reveals that most of the amino acids in these membrane-spanning α helices are nonpolar and only a very few are charged (**Figure 12.19**). This distribution of nonpolar amino acids is sensible because these residues are either in contact with the hydrocarbon core of the membrane or with one another. As will be considered in Section 12.5, membrane-spanning α helices can often be detected by examining amino acid sequence alone.

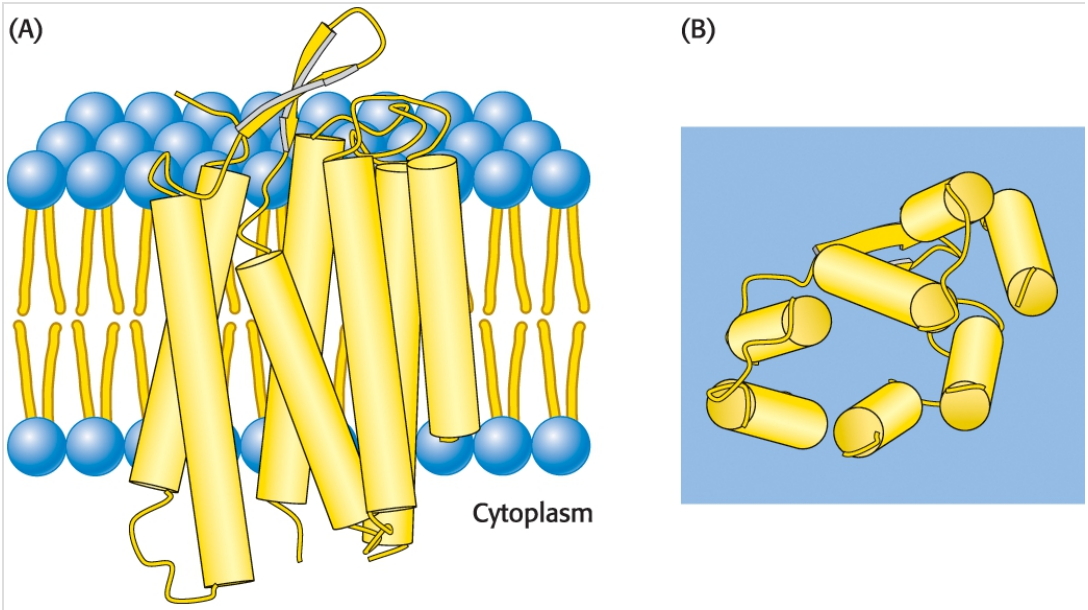


FIGURE 12.18 Bacteriorhodopsin is an integral membrane protein that contains membrane-spanning α helices. These helices are represented by yellow cylinders. (A) Vie through the membrane bilayer. (B) View from the cytoplasmic side of the membrane.

[Drawn from 1BRX.pdb.]

INTERACT with this model in Achieve



FIGURE 12.19 The membrane-spanning helices of bacteriorhodopsin contain predominantly nonpolar amino acids. The seven helical regions are highlighted in yellow and the charged residues in red.

- *A channel protein can be formed from beta strands.* Porin, a protein from the outer membranes of bacteria such as *E. coli* and *Rhodobacter capsulatus*, represents a class of membrane proteins with a completely different type of structure from bacteriorhodopsin. Structures of this type are built from β strands and contain essentially no α helices (Figure 12.20). The arrangement of β strands is quite simple: each strand is hydrogen bonded to its neighbor in an antiparallel arrangement, forming a single β sheet. The β sheet curls up to form a hollow cylinder that, as its name suggests, forms a pore, or channel, in the membrane. The outside surface of porin is appropriately nonpolar, given that it interacts with the hydrocarbon core of the membrane. In contrast, the inside of the channel is quite hydrophilic and is filled with water. This arrangement of nonpolar and polar surfaces is accomplished by the alternation of hydrophobic and hydrophilic amino acids along each β strand (Figure 12.21).

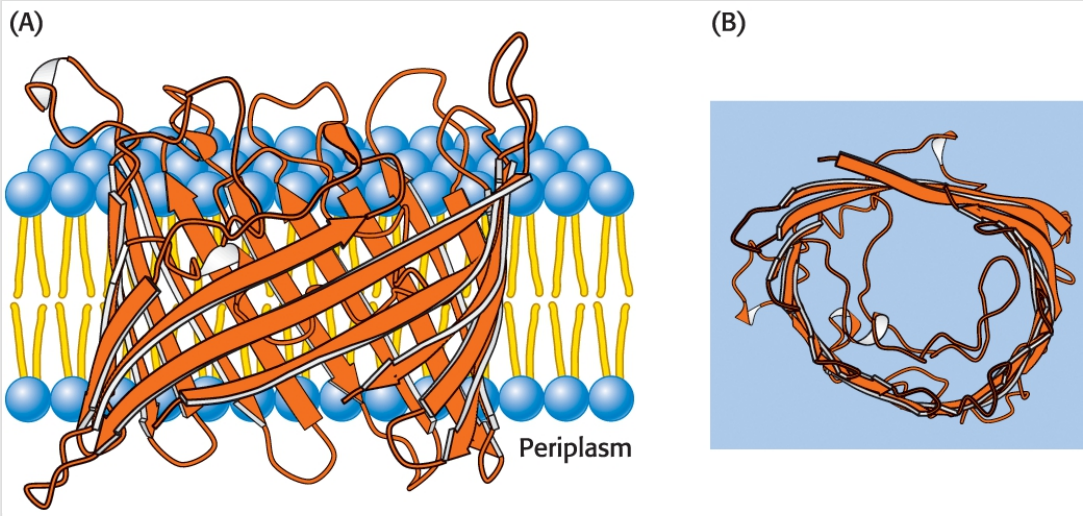


FIGURE 12.20 The bacterial integral membrane protein porin from *Rhodopseudomonas blastica* is built entirely of β strands. (A) Side view. (B) View from the periplasmic space. Only one monomer of the trimeric protein is shown.

[Drawn from 1PRN.pdb.]

INTERACT with this model in Achieve

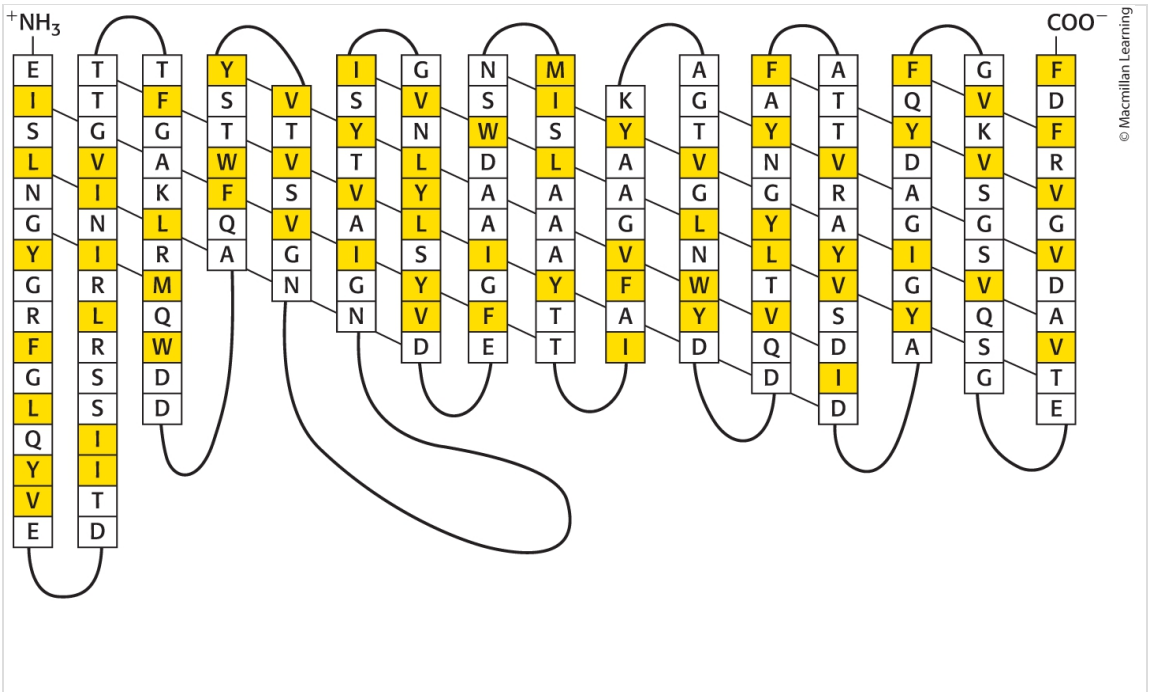


FIGURE 12.21 Porin contains alternating hydrophobic and hydrophilic amino acids along each β strand. The secondary structure of porin from *Rhodopseudomonas blastica* is shown, with the diagonal lines indicating the direction of hydrogen bonding along the β sheet. Hydrophobic residues (F, I, L, M, V, W, and Y) are shown in yellow. These residues tend to lie on the outside of the structure, in contact with the hydrophobic core of the membrane.



- *Embedding part of a protein in a membrane can link the protein to the membrane surface*. The structure of the endoplasmic reticulum membrane-bound enzyme prostaglandin H_2 synthase-1 reveals a rather different role for α helices in protein–membrane associations. This enzyme is a homodimer with a complicated structure consisting primarily of α helices. Unlike bacteriorhodopsin, this protein is not largely embedded in the membrane. Instead, it lies along the outer surface of the membrane, firmly bound by a set of α helices with hydrophobic surfaces that extend from the bottom of the protein into the membrane (Figure 12.22). This linkage is sufficiently strong that only the action of detergents can release the protein from the membrane. Thus, this enzyme is classified as an integral membrane protein, although it does not span the membrane.

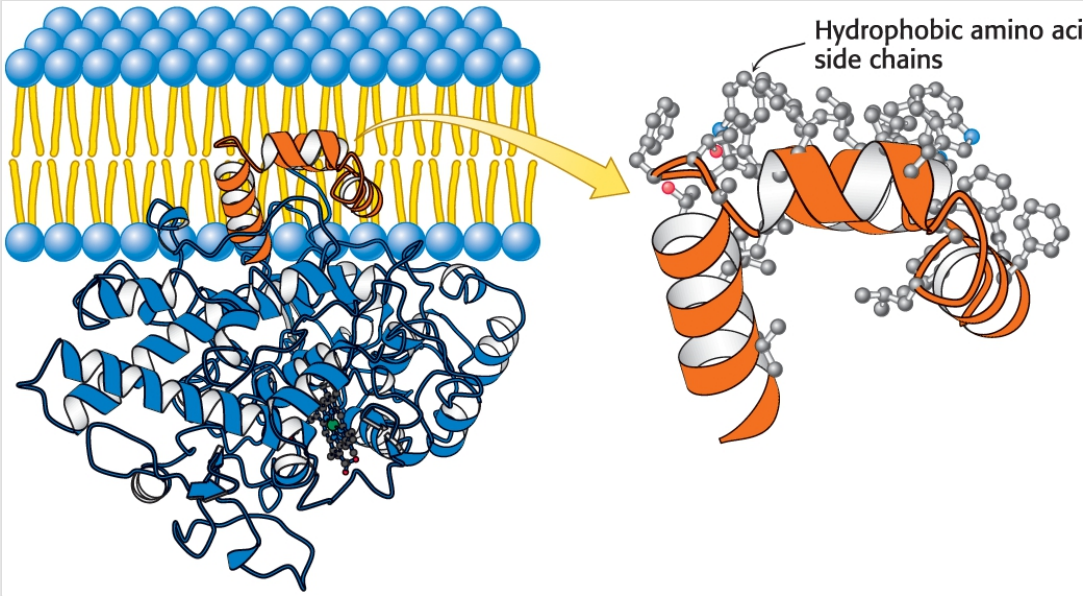


FIGURE 12.22 Prostaglandin H_2 synthase-1 is an integral membrane protein attached the membrane surface. This enzyme is held in the membrane by a set of α helices (orang coated with hydrophobic side chains. One monomer of the dimeric enzyme is shown.

[Drawn from 1PTH.pdb.]

INTERACT with this model in Achieve

The localization of prostaglandin H_2 synthase-1 in the membrane is crucial to its function. This enzyme catalyzes the conversion of arachidonic acid into prostaglandin H_2 in two steps: (1) a cyclooxygenase reaction, and (2) a peroxidase reaction (Figure 12.23). The substrate for this enzyme, arachidonic acid, is a hydrophobic molecule generated by the hydrolysis of membrane lipids. Arachidonic acid reaches the active site of the enzyme from the membrane without entering an aqueous environment by traveling through a hydrophobic channel in the protein (Figure 12.24). The reaction product, prostaglandin H_2, promotes inflammation and modulates gastric acid secretion.

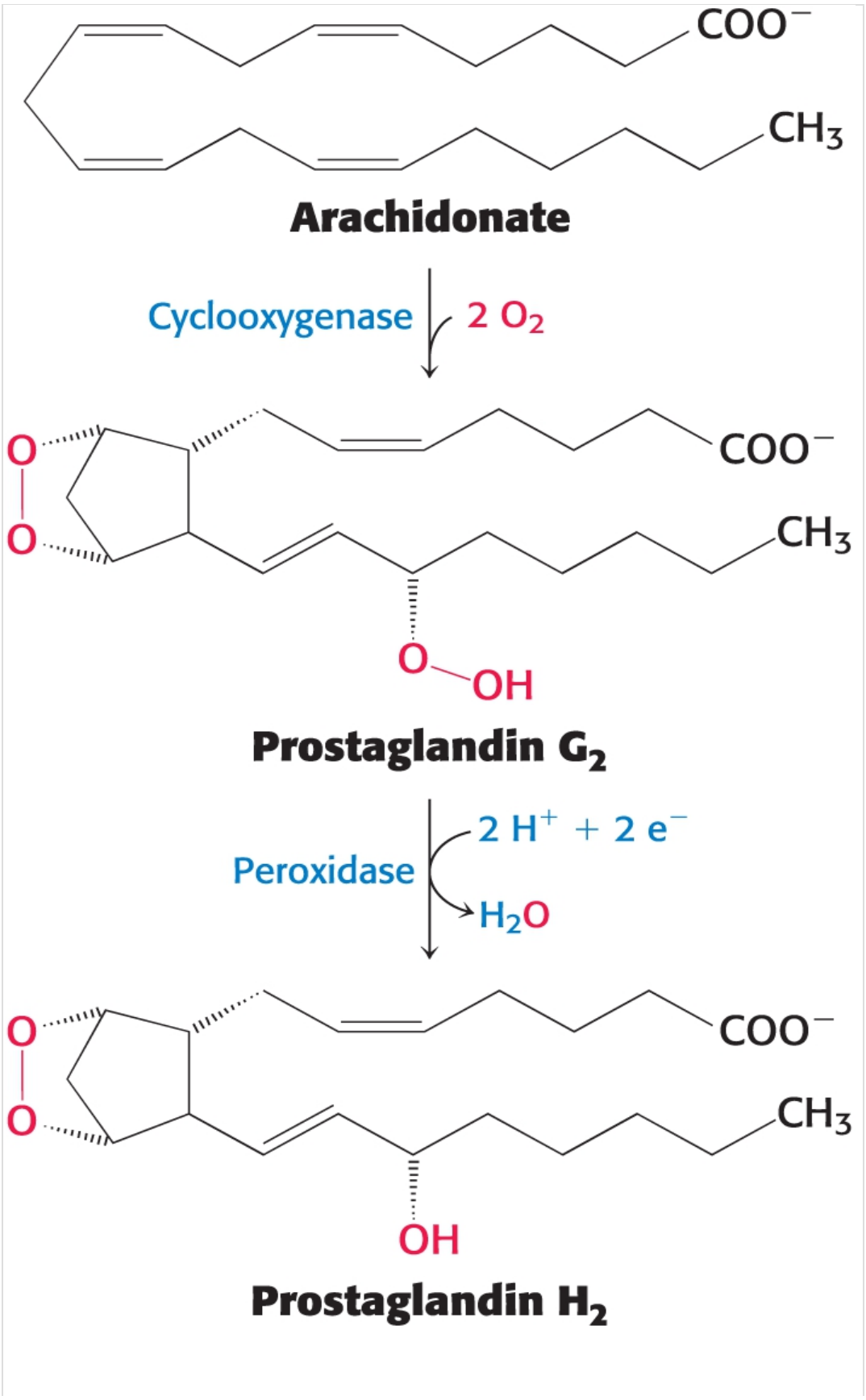

COO⁻
CH3
Arachidonate
Cyclooxygenase
2 O2
O
O
COO⁻
CH3
O
OH
Prostaglandin G2
Peroxidase
2 H+ + 2 e⁻
H2O
O
O
COO⁻
CH3
OH
Prostaglandin H2

FIGURE 12.23 Prostaglandin H_2 synthase-1 catalyzes the formation of prostaglandin H_2 from arachidonic acid in two steps.

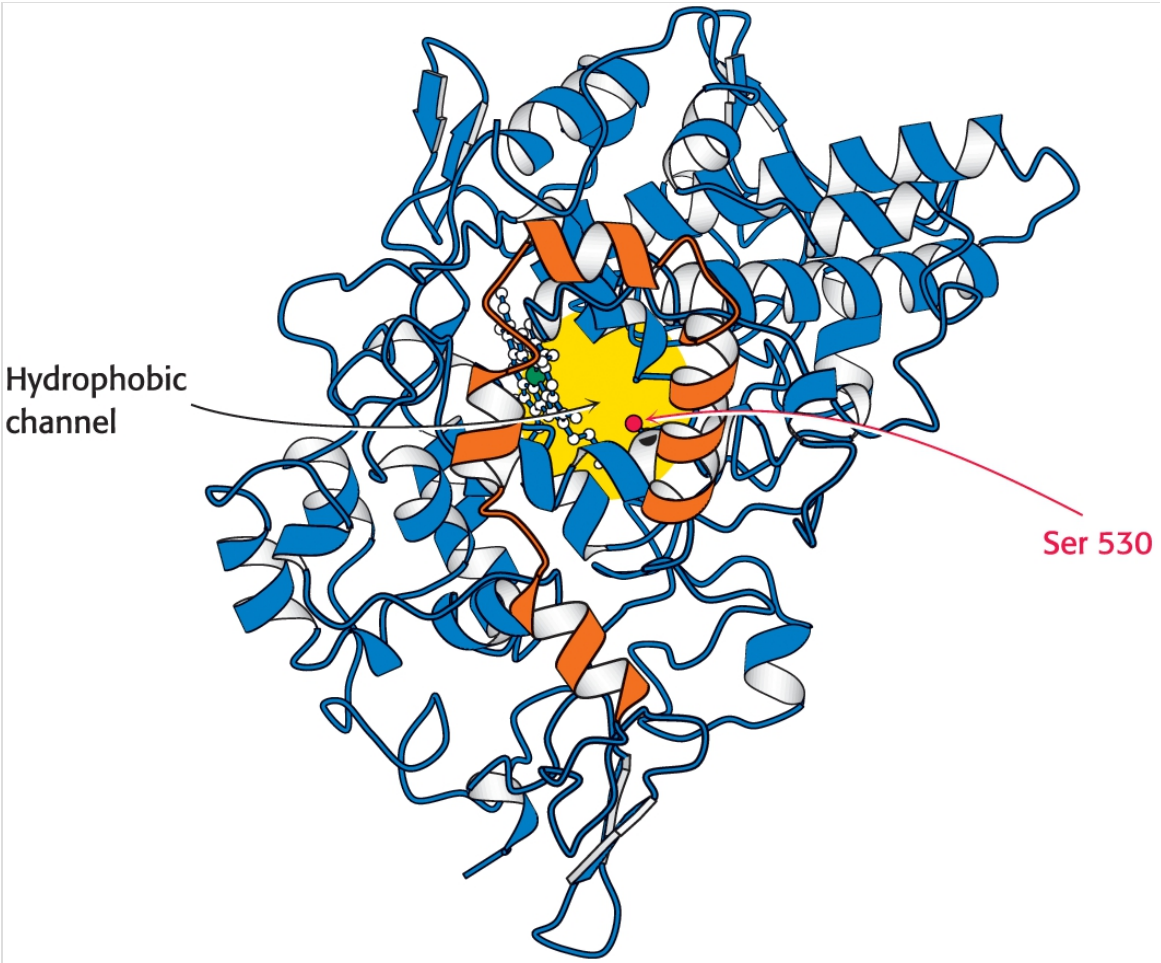


FIGURE 12.24 Arachidonic acid reaches the prostaglandin H_2 synthase-1 active site through hydrophobic channel. A view of prostaglandin H_2 synthase-1 from the membrane-facing side shows this channel more clearly. The membrane-anchoring helices are shown in orange. [Drawn from 1PTH.pdb.]

INTERACT with this model in Achieve

Indeed, nearly all of us have experienced the importance of this channel: drugs such as aspirin and ibuprofen block the channel and prevent prostaglandin synthesis by inhibiting the cyclooxygenase activity of the synthase. In particular, aspirin acts through the transfer of its acetyl group to a serine residue (Ser 530) that lies along the path to the active site (Figure 12.25). In response to an injury or infection, prostaglandins promote the inflammatory response, which includes swelling, pain, and fever. Cyclooxygenase inhibitors blunt this response, providing pain relief and fever reduction.

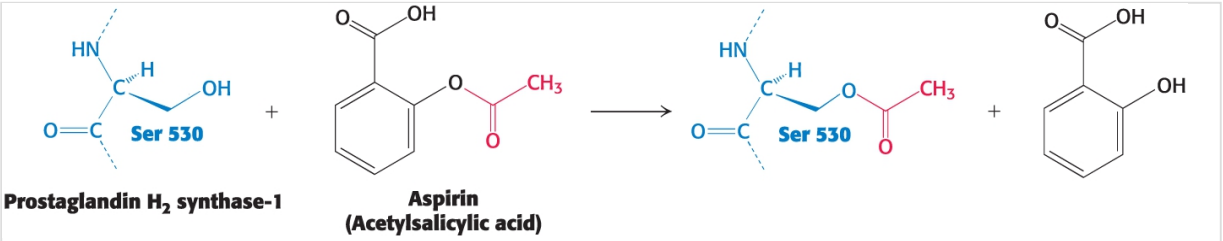


FIGURE 12.25 Aspirin acts by transferring an acetyl group to a serine residue in prostaglandin H_2 synthase-1.

Two important features emerge from our examination of these three examples of membrane-protein structure. First, the parts of the protein that interact with the hydrophobic parts of the membrane are coated with nonpolar amino acid side chains, whereas those parts that interact with the aqueous environment are much more hydrophilic. Second, the structures positioned within the membrane are quite regular and, in particular, all backbone hydrogen-bond donors and acceptors participate in hydrogen bonds. Breaking a hydrogen bond within a

membrane is quite unfavorable, because little or no water is present to compete for the polar groups.

Some proteins associate with membranes through covalently attached hydrophobic groups

The membrane proteins considered thus far associate with the membrane through surfaces generated by hydrophobic amino acid side chains. However, even otherwise soluble proteins can associate with membranes if hydrophobic groups are attached to the proteins. Three such groups are shown in Figure 12.26: (1) a palmitoyl group attached to a specific cysteine residue by a thioester bond, (2) a farnesyl group attached to a cysteine residue at the carboxyl terminus, and (3) a glycolipid structure termed a glycosylphosphatidylinositol (GPI) anchor attached to the carboxyl terminus. These modifications are attached by enzyme systems that recognize specific signal sequences near the attachment site.

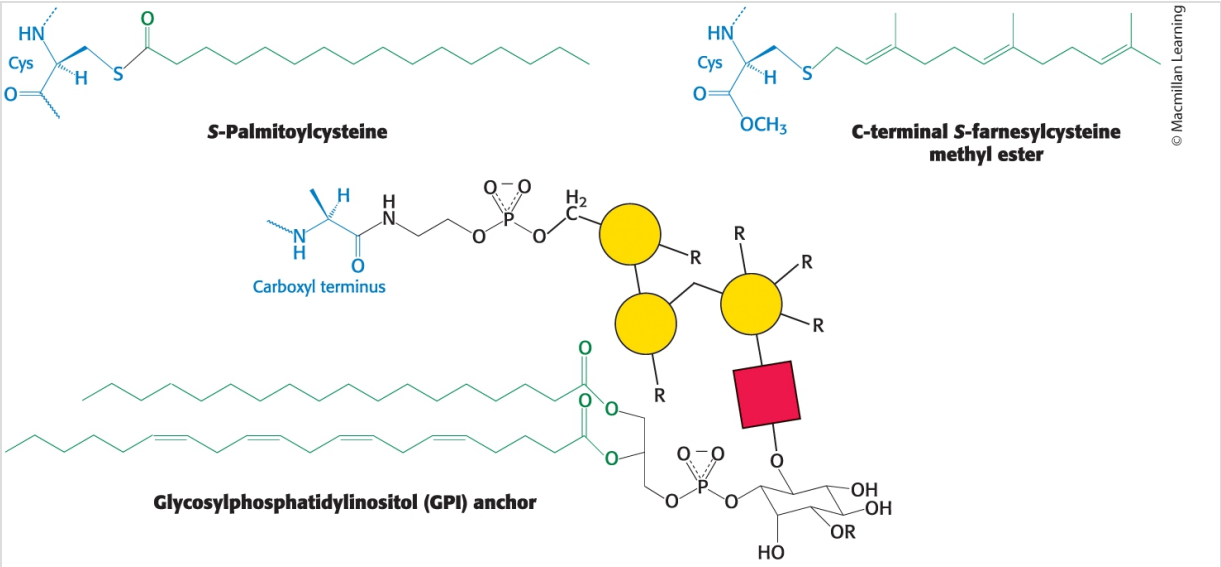


FIGURE 12.26 Membrane anchors are hydrophobic groups that tether proteins to the membrane. The anchors are attached to the proteins (blue) by covalent bonds. The yellow circles

and red square correspond to mannose and β-D-acetylglucosamine (GlcNAc), respectively. R groups represent points of additional modification.



Transmembrane helices can be accurately predicted from amino acid sequences

Many membrane proteins, like bacteriorhodopsin, employ α helices to span the hydrophobic part of a membrane. As noted earlier, most of the residues in these α helices are nonpolar and almost none of them are charged. Can we use this information to identify likely membrane-spanning regions from sequence data alone?

One approach to identifying transmembrane helices is to ask whether a postulated helical segment is likely to be more stable in a hydrocarbon environment or in water. Specifically, we want to estimate the free-energy change when a helical segment is transferred from the interior of a membrane to water. Free-energy changes for the transfer of individual amino acid residues from a hydrophobic to an aqueous environment are given in **Table 12.2**. For example, the transfer of a helix formed entirely of L-arginine residues — a positively charged amino acid — from the interior of a membrane to water would be highly favorable, with a negative transfer free energy of $-51.5\ \text{kJ mol}^{-1}\ (-12.3\ \text{kcal mol}^{-1})$ per arginine residue in the helix. In contrast, the transfer of a helix formed entirely of L-phenylalanine — a hydrophobic amino acid — would be unfavorable, with a positive transfer free energy value of $+15.5\ \text{kJ mol}^{-1}\ (+3.7\ \text{kcal mol}^{-1})$ per phenylalanine residue in the helix.

TABLE 12.2 Polarity scale for identifying transmembrane helices

Amino acid residue	Transfer free energy in $kJ\ mol^{-1}$ $(kcal\ mol^{-1})$
Phe	15.5 (3.7)
Met	14.3 (3.4)
Ile	13.0 (3.1)
Leu	11.8 (2.8)
Val	10.9 (2.6)
Cys	8.4 (2.0)
Trp	8.0 (1.9)
Ala	6.7 (1.6)
Thr	5.0 (1.2)
Gly	4.2 (1.0)
Ser	2.5 (0.6)
Pro	−0.8 (−0.2)
Tyr	−2.9 (−0.7)
His	−12.6 (−3.0)

Gln	−17.2 (−4.1)
Asn	−20.2 (−4.8)
Glu	−34.4 (−8.2)
Lys	−37.0 (−8.8)
Asp	−38.6 (−9.2)
Arg	−51.7 (−12.3)

Source: Data from D. M. Engelman, T. A. Steitz, and A. Goldman. *Annu. Rev. Biophys. Biophys. Chem.* 15(1986):321–353.
Note: The free energies are for the transfer of an amino acid residue in an α helix from the membrane interior (assumed to have a dielectric constant of 2) to water.

The hydrocarbon core of a membrane is typically 30 Å wide, a length that can be traversed by an α helix of about 20 residues. We can take the amino acid sequence of a protein and estimate the free-energy change that takes place when a hypothetical α helix formed of residues 1 through 20 is transferred from the membrane interior to water. The same calculation can be made for residues 2 through 21, 3 through 22, and so forth, until we reach the end of the sequence. The span of 20 residues chosen for this calculation is called a *window*. The free-energy change for each window, termed the *hydropathy index*, is plotted against the first amino acid at the window to create a **hydropathy plot** (**Figure 12.27A**).

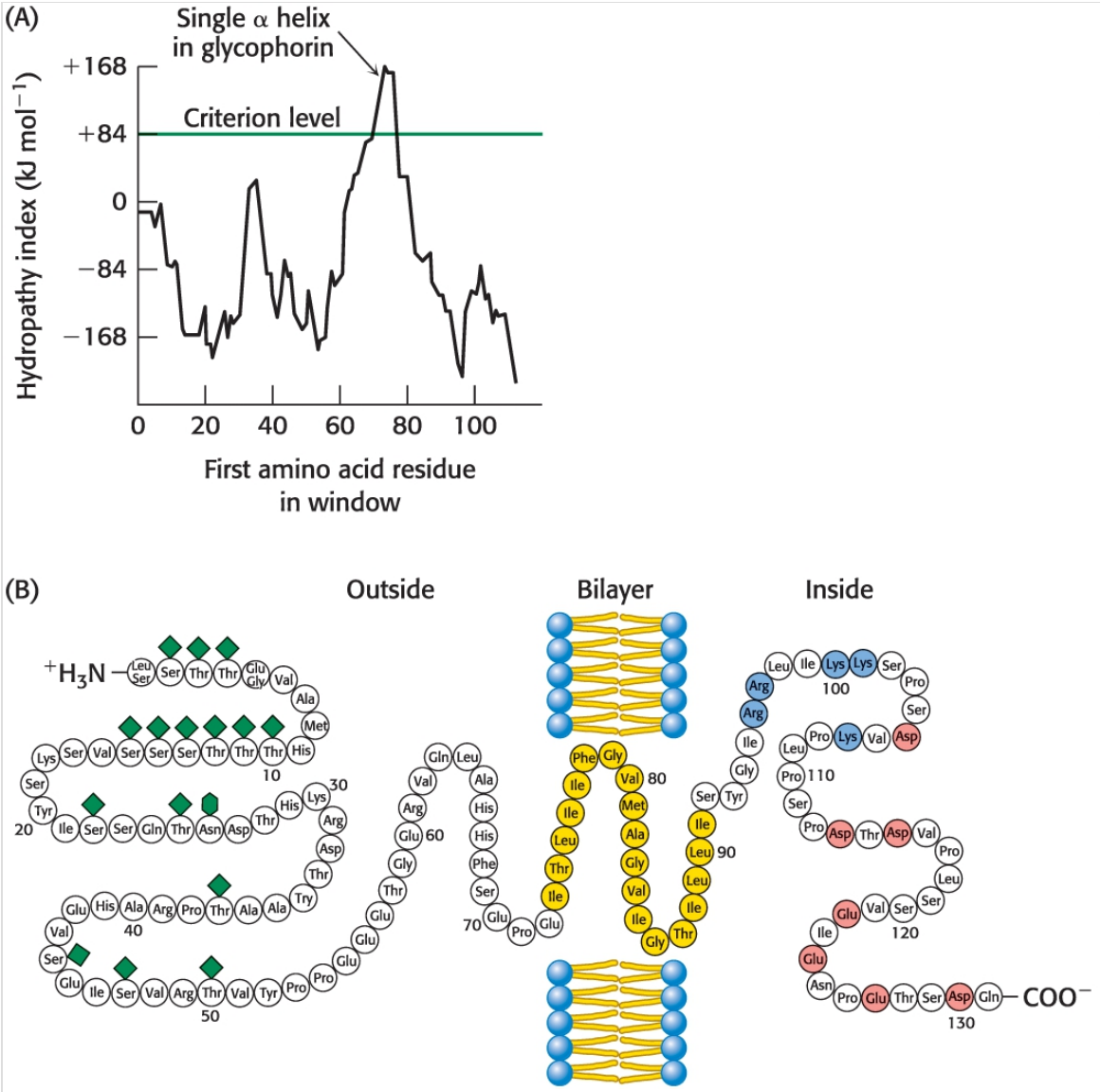


FIGURE 12.27 Hydropathy plots can be used to locate the membrane-spanning helices from protein sequences. (A) The hydropathy plot for glycophorin A is shown. Peaks of greater than $+84\ \text{kJ mol}^{-1}\ (+20\ \text{kcal mol}^{-1})$ in hydropathy plots are indicative of potential transmembrane helices. (B) The amino acid sequence and transmembrane disposition of glycophorin A from the red-blood-cell membrane are shown. Sites of glycosylation are indicated by the green shapes. The hydrophobic residues (yellow) buried in the bilayer form a transmembrane α helix. The negatively charged (red) and positively charged (blue) residues on the interior side of the membrane are indicated.

[(A) Information from Dr. Vincent Marchesi; (B) Data from D. M. Engelman, T. A. Steitz, and A. Goldman, *Annu. Rev. Biophys. Biophys. Chem*. 15:321–353, 1986. Copyright © 1986 by Annual Reviews, Inc. All rights reserved.]

Empirically, a peak of $+84\ \text{kJ mol}^{-1}\ (+20\ \text{kcal mol}^{-1})$ or more in a hydropathy plot based on a window of 20 residues indicates that a polypeptide segment could be a membrane-spanning α helix. For example, glycophorin — a protein found in the membranes of red blood cells — is predicted by this criterion to have one membrane-spanning helix, in agreement with experimental findings (**Figure 12.27B**). Note, however, that a peak in the hydropathy plot does not prove that a segment is a transmembrane helix. Even soluble proteins may have highly nonpolar regions. Conversely, some membrane proteins contain membrane-spanning features (such as a set of cylinder-forming β strands) that escape detection by these plots (**Figure 12.28**).

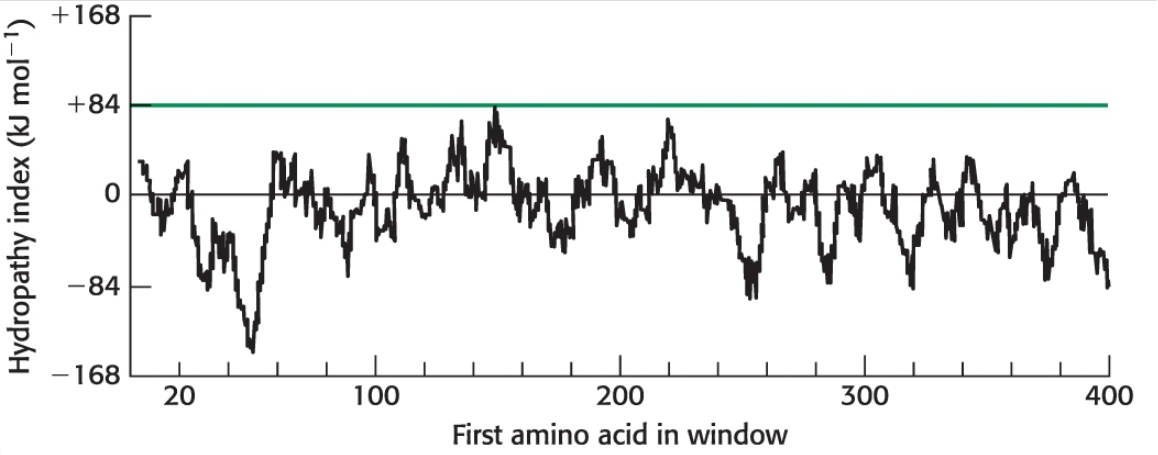


FIGURE 12.28 No strong peaks are observed in the hydropathy plot for porin. Porin is constructed from membrane-spanning β strands rather than α helices (Figure 12.20); hence, it escapes detection using this method.

Self-Check Question



Would a homopolymer of alanine be more likely to form an α helix in water or in a hydrophobic medium? Explain.

12.5 Lipids and Many Membrane Proteins Diffuse Rapidly in the Plane of the Membrane

Biological membranes are not rigid, static structures. On the contrary, lipids and many membrane proteins are constantly in lateral motion, a process called **lateral diffusion**. The rapid lateral movement of membrane proteins has been visualized by means of fluorescence microscopy using the technique of fluorescence recovery after photobleaching (FRAP; **Figure 12.29**):

1. A cell-surface component is specifically labeled with a fluorescent chromophore, and a small region of the cell surface $(\sim 3\ \mu m^2)$ is viewed through a fluorescence microscope.

2. The fluorescent molecules in this region are then destroyed (bleached) by a very intense light pulse from a laser, as indicated by the pale spot in Figure 12.29A. The fluorescence of this region is subsequently monitored as a function of time by using a light level sufficiently low to prevent further bleaching.

3. If the labeled component is mobile, bleached molecules leave and unbleached molecules enter the illuminated region, resulting in an increase in the fluorescence intensity, a process called *recovery*. The rate of recovery depends on the lateral mobility of the fluorescence-labeled component, which can be expressed in terms of a diffusion coefficient, *D*. The average distance *S* traversed in time *t* depends on *D* according to the expression

$$S = (4Dt)^{1/2}$$

The diffusion coefficient of lipids in a variety of membranes is about $1\ \mu m^2\ s^{-1}$. Thus, a phospholipid molecule diffuses an average distance of $2\ \mu m$ in 1 s. This rate means that a lipid molecule can travel from one end of a bacterium to the other in a second. The magnitude of the observed diffusion coefficient indicates that the viscosity of the membrane is about 100 times that of water, rather like that of olive oil.

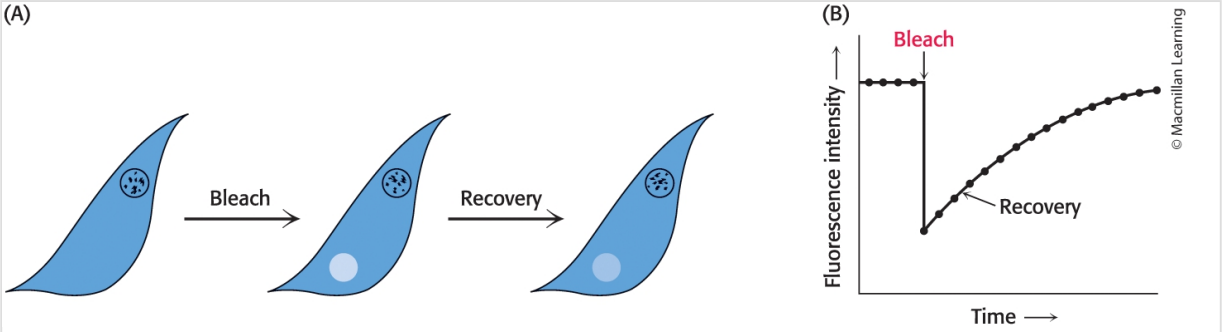


FIGURE 12.29 Lateral diffusion rates within a membrane can be measured using fluorescence recovery after photobleaching (FRAP). (A) The cell surface fluoresces because of a labeled surface component. The fluorescent molecules of a small part of the surface are bleached by an intense light pulse; then the fluorescence intensity recovers as bleached molecules diffuse out of the region and unbleached molecules diffuse into it. (B) The rate of recovery depends on the diffusion coefficient.

In contrast, proteins vary markedly in their lateral mobility. Some proteins are nearly as mobile as lipids, whereas others are virtually immobile. For example, the photoreceptor protein rhodopsin (Section 14.6), a very mobile protein, has a diffusion coefficient of $0.4\ \mu m^2\ s^{-1}$. The rapid movement of rhodopsin is essential for fast signaling. At the other extreme is fibronectin, a peripheral glycoprotein that interacts with the extracellular matrix. For fibronectin, *D* is less than $10^{-4} \mu m^2\ s^{-1}$. Fibronectin has a very low mobility because it is anchored to actin filaments on the inside of the plasma membrane

through integrin, a transmembrane protein that links the extracellular matrix to the cytoskeleton.

The fluid mosaic model allows lateral movement but not rotation through the membrane

On the basis of the mobility of proteins in membranes, in 1972 S. Jonathan Singer and Garth Nicolson proposed a **fluid mosaic model** to describe the overall organization of biological membranes. The essence of their model is that membranes are two-dimensional solutions of oriented lipids and globular proteins. The lipid bilayer has a dual role: it is both a solvent for integral membrane proteins and a permeability barrier. Membrane proteins are free to diffuse laterally in the lipid matrix unless restricted by special interactions.

Although the lateral diffusion of membrane components can be rapid, the spontaneous rotation of lipids from one face of a membrane to the other is a very slow process. The transition of a molecule from one membrane surface to the other is called *transverse diffusion* or *flip-flop* (**Figure 12.30**). The flip-flop of phospholipid molecules in phosphatidylcholine vesicles has been directly measured by electron spin resonance techniques, which show that a phospholipid molecule flip-flops once in several hours. Thus, a phospholipid molecule takes about 10^9 times as long to flip-flop across a membrane as it takes to diffuse a distance of 50 Å in the lateral direction. The free-energy barriers to flip-flopping are even larger for protein molecules than for lipids because proteins have more-extensive polar regions. In fact, the flip-flop of a protein molecule has not been observed. Hence, membrane asymmetry can be preserved for long periods.

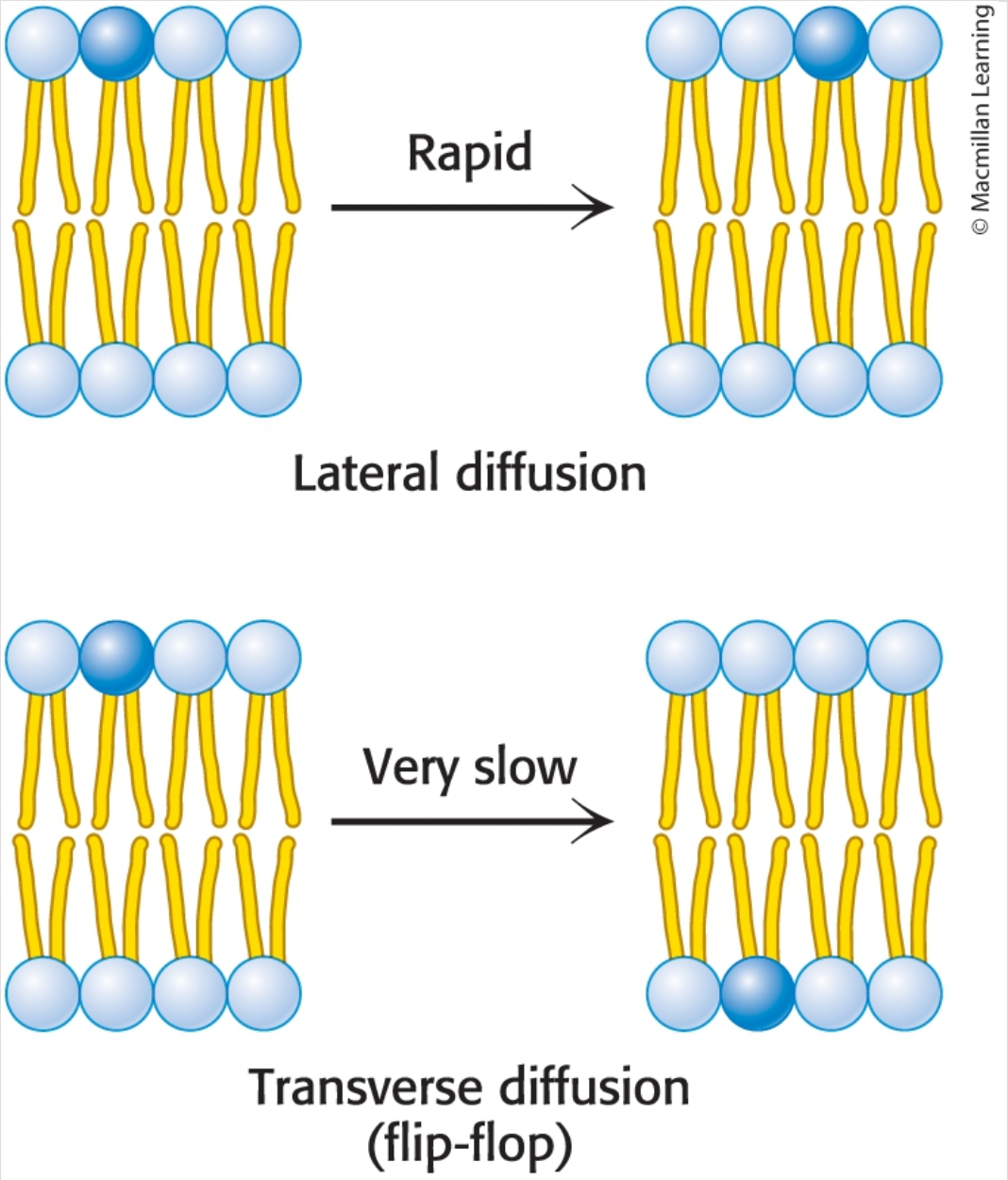


FIGURE 12.30 Lateral diffusion of lipids in membranes is much more rapid than transverse diffusion (flip-flop).

Membrane fluidity is controlled by fatty acid composition and cholesterol content

Many membrane processes, such as transport or signal transduction, depend on the fluidity of the membrane lipids, which in turn depends on the properties of fatty acid chains. Fatty acid chains in membrane bilayers can exist in an ordered, rigid state or in a relatively disordered, fluid state. The transition from the rigid to the fluid state takes place abruptly as the temperature is raised above T_m, the melting temperature (Figure 12.31).

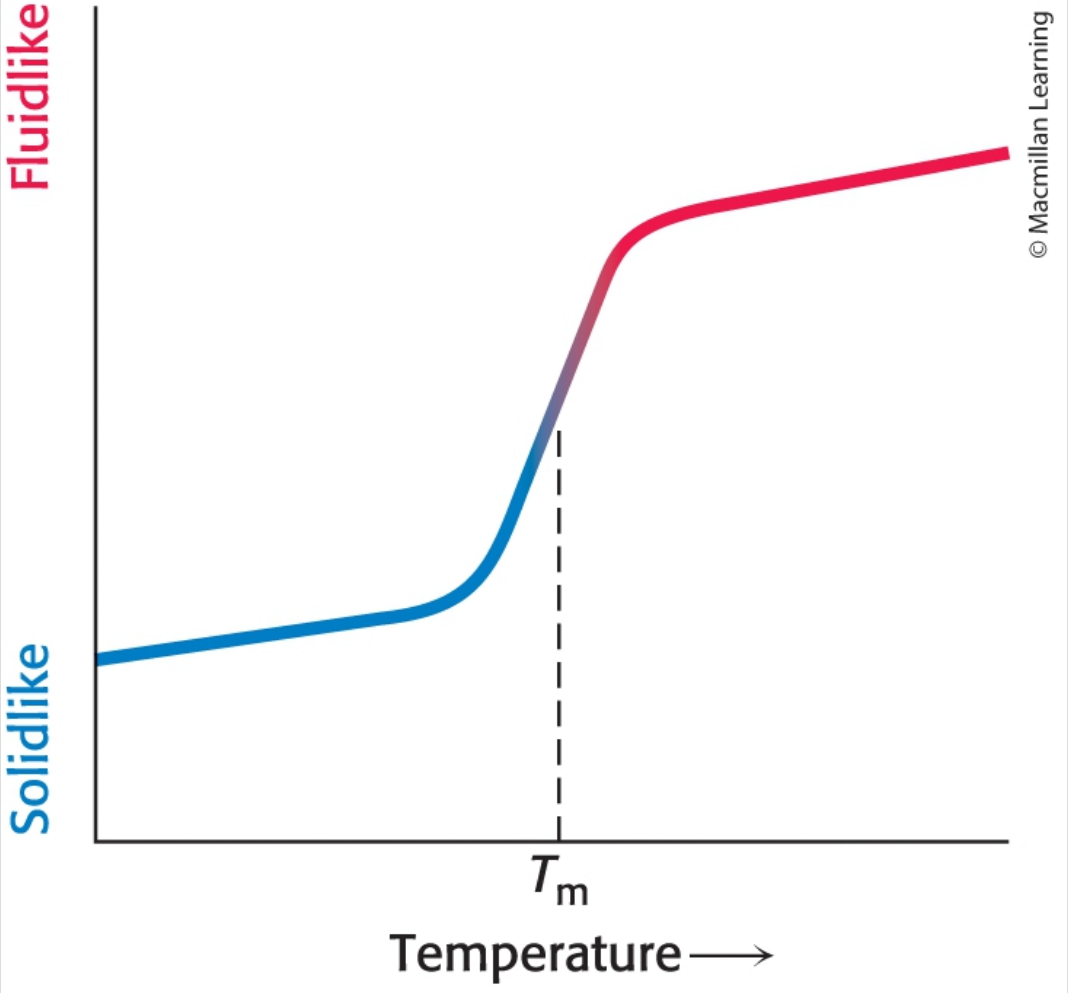


FIGURE 12.31 The melting temperature (T_m) for a phospholipid membrane represents the midpoint along the phase-transition curve. As the temperature is

raised, the phospholipid membrane changes from a packed, ordered state to a more random one.



The melting temperature of a fluid membrane depends on the length of the fatty acid chains and on their degree of unsaturation (Table 12.3). The presence of saturated fatty acid residues favors the rigid state because their straight hydrocarbon chains interact very favorably with one another. On the other hand, a cis double bond produces a bend in the hydrocarbon chain that interferes with a highly ordered packing of fatty acid chains, and so T_m is lowered (Figure 12.32). The length of the fatty acid chain also affects the transition temperature. Long hydrocarbon chains interact more strongly than do short ones. Specifically, each additional $-CH_2-$ group makes a favorable contribution of about $-2\ kJ\ mol^{-1}\ (-0.5\ kcal\ mol^{-1})$ to the free energy of interaction of two adjacent hydrocarbon chains.

TABLE 12.3 The melting temperature of phosphatidylcholine containing different pairs of identical fatty acid chains

		Fatty acid		
Number of carbons	**Number of double bonds**	**Common name**	**Systematic name**	**T_m (°C**
22	0	Behenate	*n*-Docosanoate	75
18	0	Stearate	*n*-Octadecanoate	58
16	0	Palmitate	*n*-Hexadecanoate	41
14	0	Myristate	*n*-Tetradecanoate	24

18	1	Oleate	*cis*-Δ^9-Octadecenoate	−22

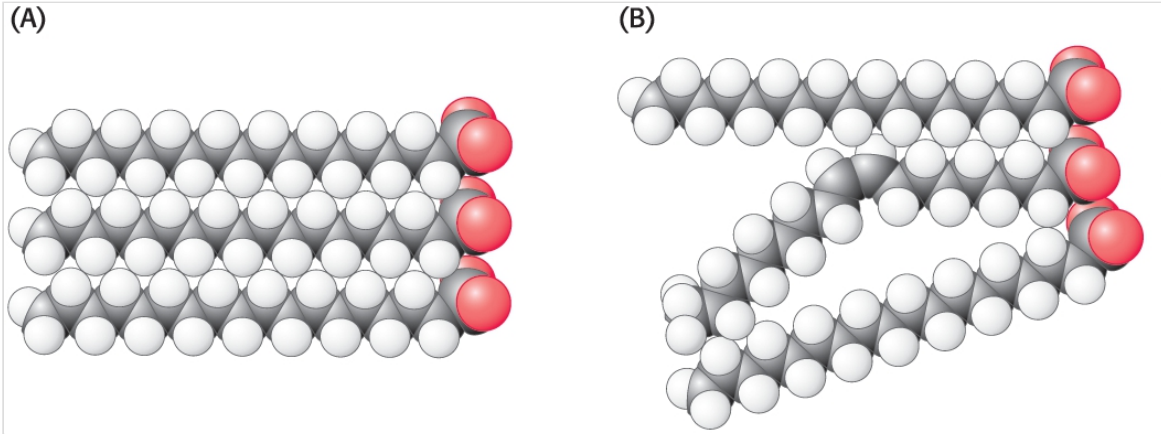


FIGURE 12.32 The highly ordered packing of fatty acid chains in a membrane is disrupted by the presence of cis double bonds. The space-filling models show the packing of (A) three molecules of stearate (C_{18}, saturated) and (B) a molecule of oleate (C_{18}, unsaturated) between two molecules of stearate.

Bacteria regulate the fluidity of their membranes by varying the number of double bonds and the length of their fatty acid chains. For example, the ratio of saturated to unsaturated fatty acid chains in the *E. coli* membrane decreases from 1.6 to 1.0 as the growth temperature is lowered from 42°C to 27°C. This decrease in the proportion of saturated residues prevents the membrane from becoming too rigid at the lower temperature.

In animals, cholesterol is the key regulator of membrane fluidity. Cholesterol contains a bulky steroid nucleus with a hydroxyl group at one end and a flexible hydrocarbon tail at the other end. Cholesterol inserts into bilayers with its long axis perpendicular to the plane of the membrane. The hydroxyl group of cholesterol forms a hydrogen bond

with a carbonyl oxygen atom of a phospholipid head group, whereas the hydrocarbon tail of cholesterol is located in the nonpolar core of the bilayer. The different shape of cholesterol compared with that of phospholipids disrupts the regular interactions between fatty acid chains (Figure 12.33).

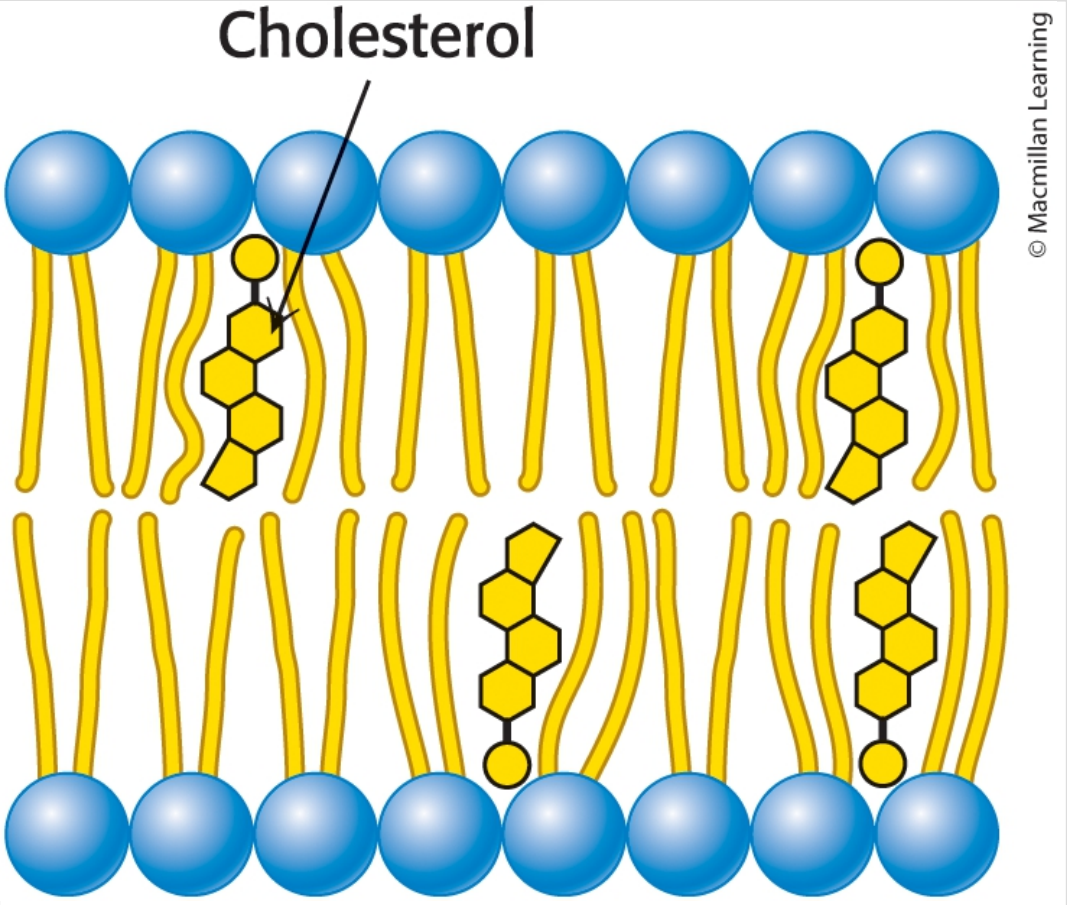


FIGURE 12.33 Cholesterol disrupts the tight packing of the fatty acid chains.

[Information from S. L. Wolfe, *Molecular and Cellular Biology* (Wadsworth, 1993).]

Self-Check Question

Explain why oleic acid (18 carbons, one cis bond) has a lower melting point than stearic acid, which has the same number of carbon atoms but is saturated. How would you expect the melting point of *trans*-oleic acid to compare with that of *cis*-oleic acid? Why might most unsaturated fatty acids in phospholipids be in the cis rather than the trans conformation?

Lipid rafts are highly dynamic complexes formed between cholesterol and specific lipids

In addition to its nonspecific effects on membrane fluidity, cholesterol can form complexes with lipids that contain the sphingosine backbone, including sphingomyelin and certain glycolipids, and with lipid-anchored membrane proteins. These complexes concentrate within small (10–200 nm) and highly dynamic regions within membranes, which have the potential to cluster into larger domains of greater than 300 nm. These structures are referred to as **lipid rafts** (**Figure 12.34A**).

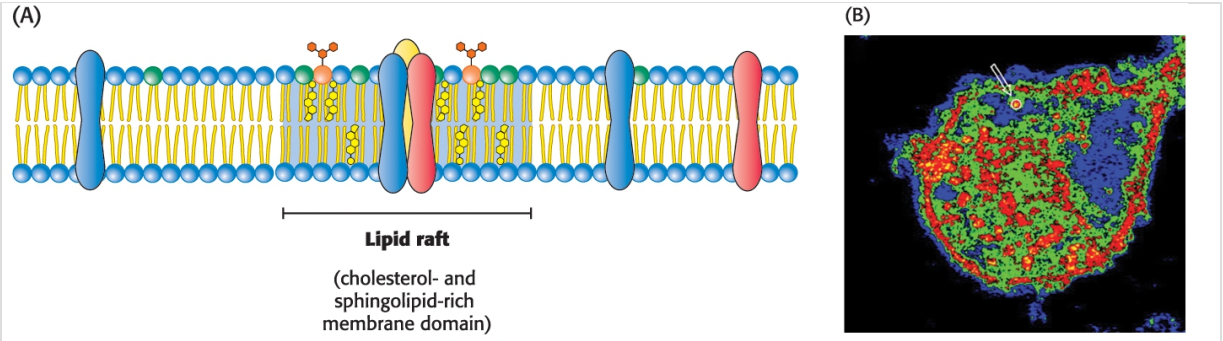


Photo credit: Katharina Gaus, Enrico Gratton, Eleanor P. W. Kable, et al., "Visualizing lipid structure and raft domains in living cells with two-photon microscopy." PNAS December 23, 2003 100 (26) 15554–15559; https://doi.org/10.1073/pnas.2534386100, Figure 1B. Copyright (2003) National Academy of Sciences, U.S.A.
© Macmillan Learning

FIGURE 12.34 Lipid rafts are membrane domains exhibiting reduced fluidity. (A) Cholesterol molecules, sphingomyelin (green head groups), and glycolipids (orange head groups) tend to be concentrated within the lipid rafts. These regions (shaded blue) provide the opportunity for changes in protein structure and oligomerization that may have significant functional consequences. (B) Image of a human monocytic cell, stained with a fluorescent dye sensitive to the level of disorder in its environment. Highly ordered regions have been colored red/yellow. Small regions of increased order, consistent with the presence of lipid raft domains, are apparent.

One result of these interactions is the moderation of membrane fluidity, making membranes less fluid but at the same time less subject to phase transitions. The presence of lipid rafts thus represents a modification of the original fluid mosaic model for biological membranes. Although their small size and dynamic nature have made them very difficult to study, recent developments in microscopy have significantly improved the ability to study these domains (**Figure 12.34B**).

What are the functions of lipid rafts? By segregation of certain lipid and protein species into smaller domains, lipid rafts may induce conformational changes in membrane proteins, regulating their functional activities. In addition, lipid rafts provide an environment favorable for specific protein–protein interactions, which can be used to promote signal transduction events (Chapter 14). Furthermore, it appears that pathogens, such as viruses, preferentially bind to lipid rafts to obtain entry into the cell and use lipid rafts to induce membrane budding and subsequent cellular escape. As technology advances, our appreciation of the importance of these membrane domains will likely expand.

All biological membranes are asymmetric

Membranes are structurally and functionally asymmetric: the outer and inner surfaces of all known biological membranes have different components and different enzymatic activities. A clear-cut example is the pump that regulates the concentration of Na^+ and K^+ ions in cells (**Figure 12.35**). This transport protein is located in the plasma membrane of nearly all cells in higher organisms. The $Na^+ - K^+$ pump

is oriented so that it pumps Na^+ out of the cell and K^+ into it. Furthermore, ATP must be on the inside of the cell to drive the pump. Ouabain, a specific inhibitor of the pump, is effective only if it is located outside. We shall consider the mechanism of this important and fascinating family of pumps in Chapter 13.

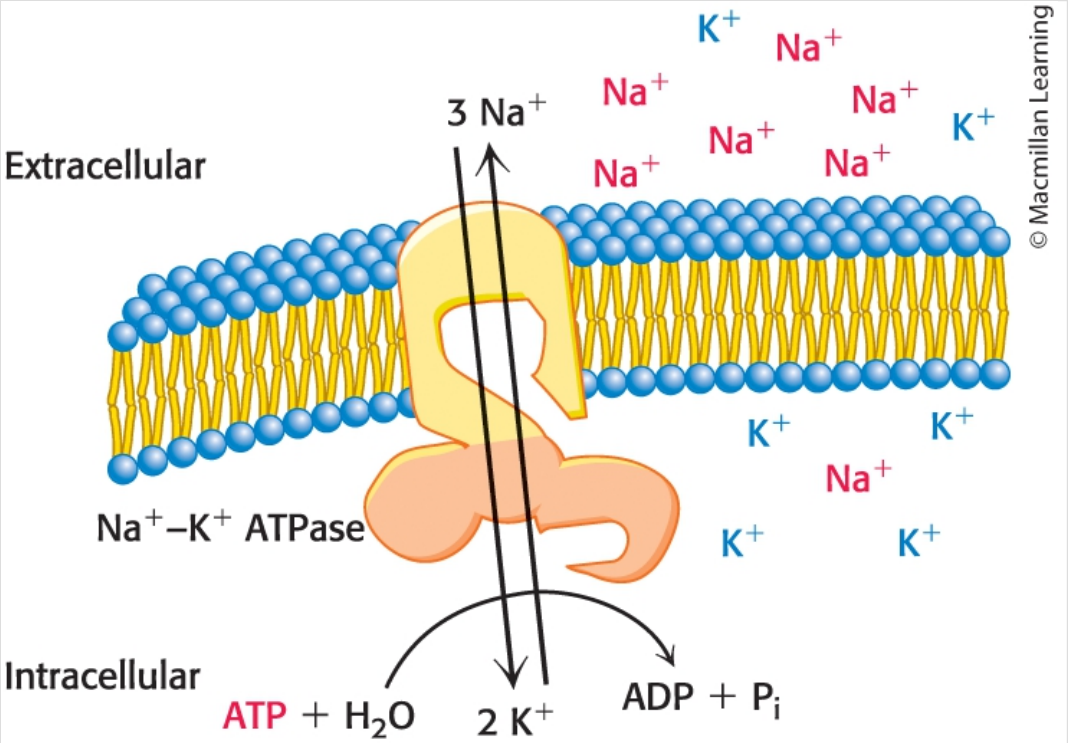


FIGURE 12.35 The orientation of the Na^+-K^+ transport system in the lipid bilayer exemplifies membrane asymmetry. The Na^+-K^+ transport system pumps Na^+ out of the cell and K^+ into the cell by hydrolyzing ATP on the intracellular side of the membrane.

Membrane proteins have a unique orientation because, after synthesis, they are inserted into the membrane in an asymmetric manner. This absolute asymmetry is preserved because membrane proteins do not

rotate from one side of the membrane to the other and because membranes are always synthesized by the growth of preexisting membranes.

Lipids, too, are asymmetrically distributed between the two membrane leaflets. For example, in the red-blood-cell membrane, sphingomyelin and phosphatidylcholine are preferentially located in the outer leaflet of the bilayer, whereas phosphatidylethanolamine and phosphatidylserine are located mainly in the inner leaflet. Large amounts of cholesterol are present in both leaflets.

12.6 Prokaryotes and Eukaryotes Differ in Their Use of Biological Membranes

Thus far, we have considered only the plasma membrane of eukaryotic cells. Some bacteria and archaea have only this single membrane, surrounded by a thick cell wall (Figure 12.36A). Other bacteria, such as *E. coli*, have two membranes separated by a cell wall (made of proteins, peptides, and carbohydrates) lying between them (Figure 12.36B). The inner membrane acts as the permeability barrier, and the outer membrane and the cell wall provide additional protection. The outer membrane is quite permeable to small molecules, owing to the presence of porins. The region between the two membranes containing the cell wall is called the *periplasm*.

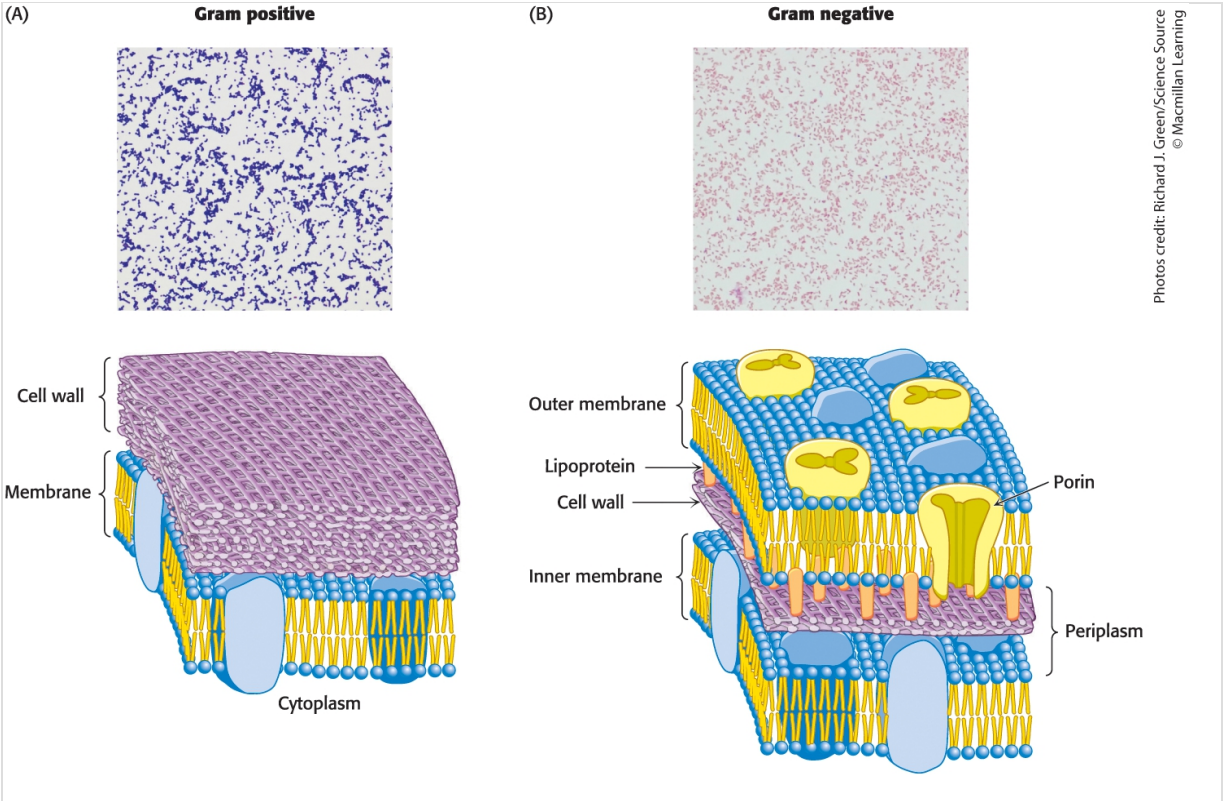


FIGURE 12.36 Bacteria can be classified based on their plasma membranes. (A) Some bacteria are surrounded by a single lipid bilayer encased in a thick cell wall. These bacteria are termed Gram positive since they retain the crystal violet stain in their cell walls. (B) Other bacteria are surrounded by two separate lipid bilayers. These bacteria are termed Gram negative because they do not retain crystal violet stain and appear pink.



The two types of bacterial membranes depicted in Figure 12.36 can be distinguished microscopically using a technique known as **Gram staining**, named for its inventor Hans Christian Gram. The dye called *crystal violet* is added to a fixed sample of bacteria, followed by iodine to trap the dye in the cell. Then, alcohol is used to wash out the dye. In those cells with a thick cell wall, as shown in Figure 12.36A, the trapped dye binds quite tightly and does not wash out. These bacteria stain dark purple, and are referred to as *Gram positive*. In those cells where the cell wall is very thin, the dye washes out quickly; these bacteria appear pink (due to the addition of a second stain at the conclusion of the experiment) and are referred to as *Gram negative* (Figure 12.36B). Gram staining is an important method for the initial classification of a bacterial sample, particularly in fluid samples from an infected patient, where rapid identification of bacterial type is critical for the selection of antibiotic treatment.

Eukaryotic cells contain compartments bounded by internal membranes

Eukaryotic cells, with the exception of plant cells, do not have cell walls, and their plasma membranes consist of a single lipid bilayer. In plant cells, the cell wall is on the outside of the plasma membrane. Eukaryotic cells are distinguished from prokaryotic cells by the presence of membranes inside the cell that form internal compartments. For

example, peroxisomes, organelles that play a major role in the oxidation of fatty acids for energy conversion, are defined by a single membrane. The nucleus is surrounded by a double membrane, the *nuclear envelope*, that consists of a set of closed membranes that come together at structures called *nuclear pores* (Figure 12.37). These pores regulate transport into and out of the nucleus. The nuclear envelope is linked to another membrane-defined structure, the *endoplasmic reticulum*, which plays a host of cellular roles, including drug detoxification and the modification of proteins for secretion.

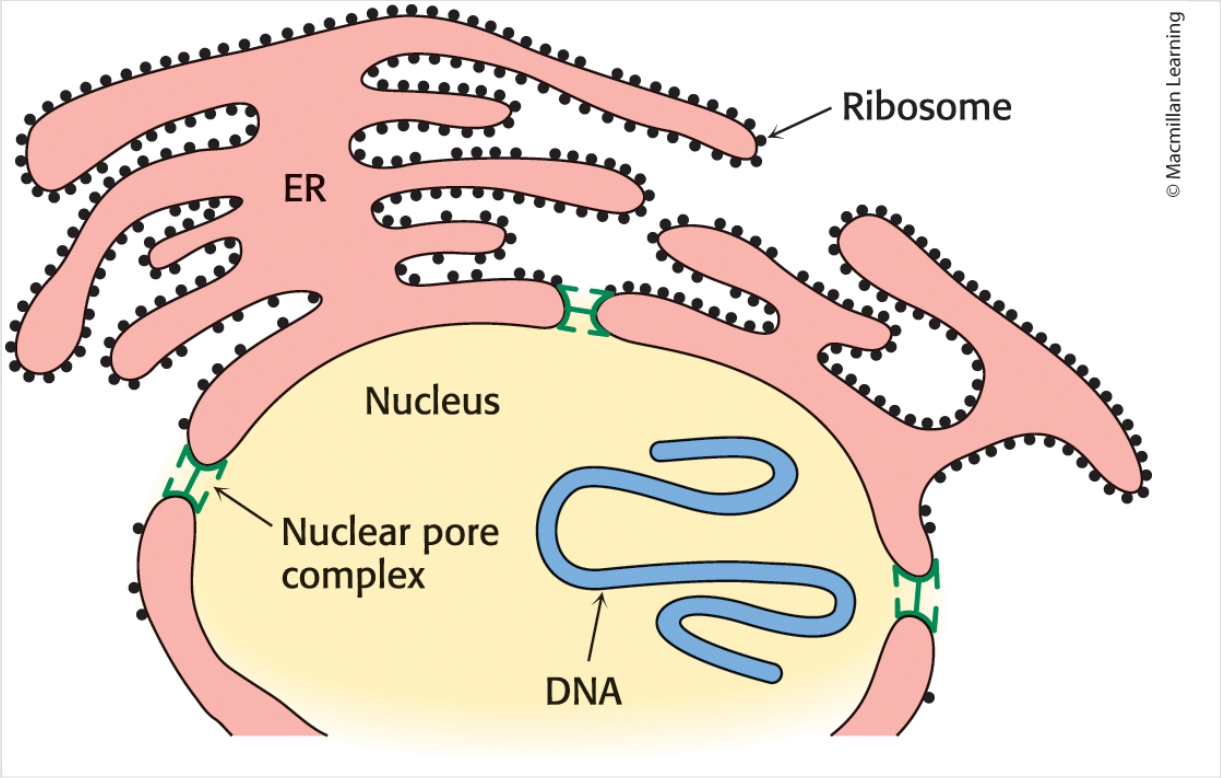


FIGURE 12.37 The nuclear envelope is a double membrane connected to another membrane system of eukaryotes, the endoplasmic reticulum.

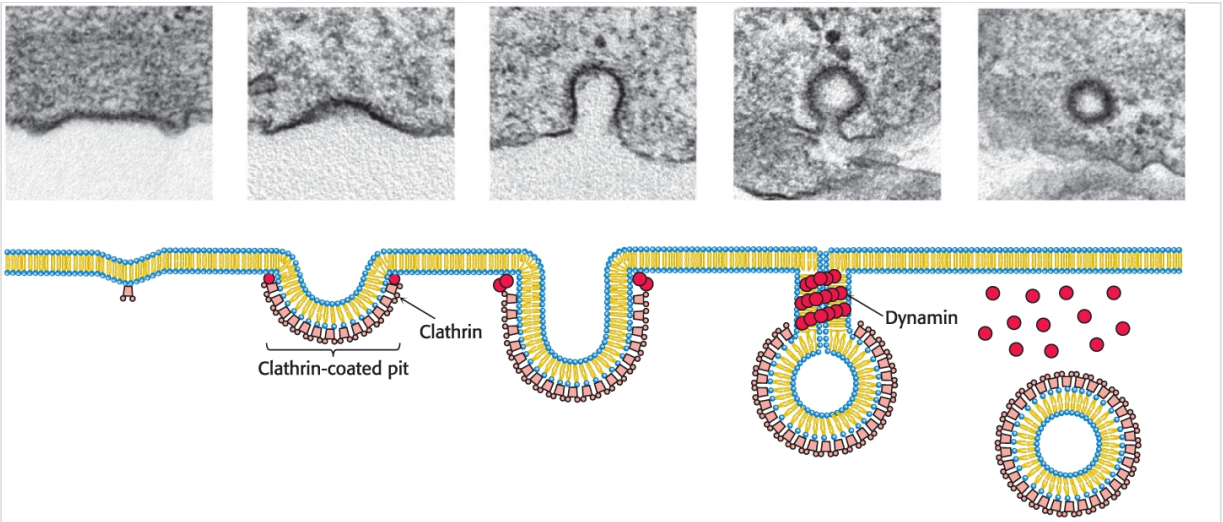
[Information from E. C. Schirmer and L. Gerace, *Genome Biol*. 3(4):1008.1–1008.4, 2002, reviews, Fig.1.]

Mitochondria, the organelles in which ATP is synthesized, are also surrounded by two membranes. As in the case for a bacterium, the

outer membrane is quite permeable to small molecules, whereas the inner membrane is not. Indeed, considerable evidence now indicates that mitochondria evolved from bacteria by endosymbiosis (Section 18.1).

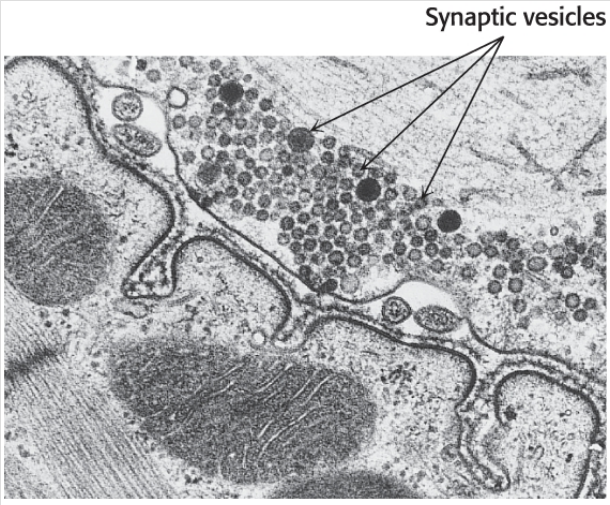
Membrane budding and fusion are highly controlled processes

Membranes must be able to separate (by budding) or join together (by fusion) so that cells and compartments may take up, transport, and release molecules. Let us consider an example of membrane budding using an example at the plasma membrane. Many cells take up molecules through the process of **receptor-mediated endocytosis**. Here, a protein or larger complex initially binds to a receptor on the cell surface. After the receptor is bound, specialized proteins act to cause the membrane in this region to invaginate. One of these specialized proteins is clathrin, which polymerizes into a lattice network around the growing membrane bud, often referred to as a *clathrin-coated pit* (**Figure 12.38**). Through the action of a GTPase enzyme called *dynamin*, the invaginated membrane eventually breaks off and fuses to form a vesicle. Various hormones, transport proteins, and antibodies employ receptor-mediated endocytosis to gain entry into a cell. A less-advantageous consequence is that this pathway is available to viruses and toxins as a means of invading cells. The reverse process — the fusion of a vesicle to a membrane — is a key step in the release of neurotransmitters from a neuron into the synaptic cleft (**Figure 12.39**).



Credit: *Top*: Republished with permission of Company of Biologists, from Membrane remodeling in clathrin-mediated endocytosis. Volker Haucke, Michael M. Kozlov, J Cell Sci (2018) 131 (17): jcs216812. Figure 1. Permission conveyed through Copyright Clearance Center, Inc.; *Bottom*: Schmid SL. Reciprocal regulation of signaling and endocytosis: Implications for the evolving cancer cell. J Cell Biol. 2017 Sep 4;216(9):2623-2632. doi: 10.1083/jcb.201705017. Epub 2017 Jul 3. PMID: 28674108; PMCID: PMC5584184. Copyright © 2017 Schmid. Illustration by Marcel Mettlen. Used with permission.

FIGURE 12.38 Many cells take up molecules by receptor-mediated endocytosis. Receptor binding on the surface of the cell induces the membrane to invaginate, with the assistance of specialized intracellular proteins such as clathrin and dynamin. The process results in the formation of a vesicle within the cell.



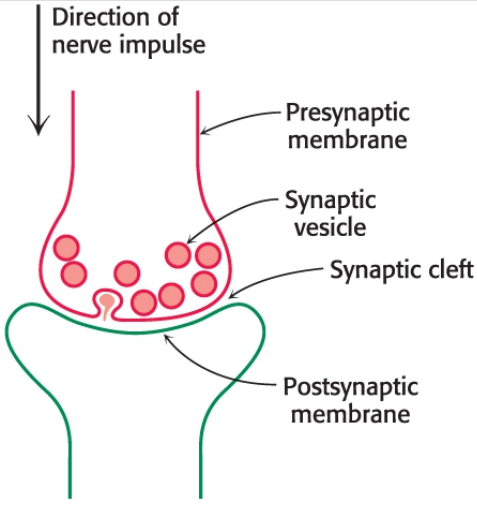


Photo: Don W. Fawcett/T. Reese/Science Source

FIGURE 12.39 Vesicle fusion to the plasma membrane is critical for neurotransmitter release. Neurotransmitter-containing synaptic vesicles (indicated by the arrows on the micrograph at le are arrayed near the plasma membrane of a nerve cell. Synaptic vesicles fuse with the plasma membrane, releasing the neurotransmitter into the synaptic cleft.

Let's consider one example of receptor-mediated endocytosis. Iron is a critical element for the function and structure of many proteins, including hemoglobin and myoglobin (Chapter 3). However, free iron ions are highly toxic to cells, owing to their ability to catalyze the formation of free radicals. Hence, the transport of iron atoms from the digestive tract to the cells where they are most needed must be tightly controlled. In the bloodstream, iron is bound very tightly by the protein transferrin, which can bind two Fe^{3+} ions with a dissociation constant of $10^{-23}\ M$ at neutral pH. Cells requiring iron express the transferrin receptor in their plasma membranes (Section 31.6).

Formation of a complex between the transferrin receptor and iron-bound transferrin initiates receptor-mediated endocytosis, internalizing these complexes within vesicles called **endosomes** (**Figure 12.40**). As the endosomes mature, proton pumps within the vesicle membrane lower the lumenal pH to about 5.5. Under these conditions, the affinity of iron ions for transferrin is reduced; these ions are released and are free to pass through channels in the endosomal membranes into the cytoplasm. The iron-free transferrin complex is recycled to the plasma membrane, where transferrin is released back into the bloodstream and the transferrin receptor can participate in another uptake cycle.

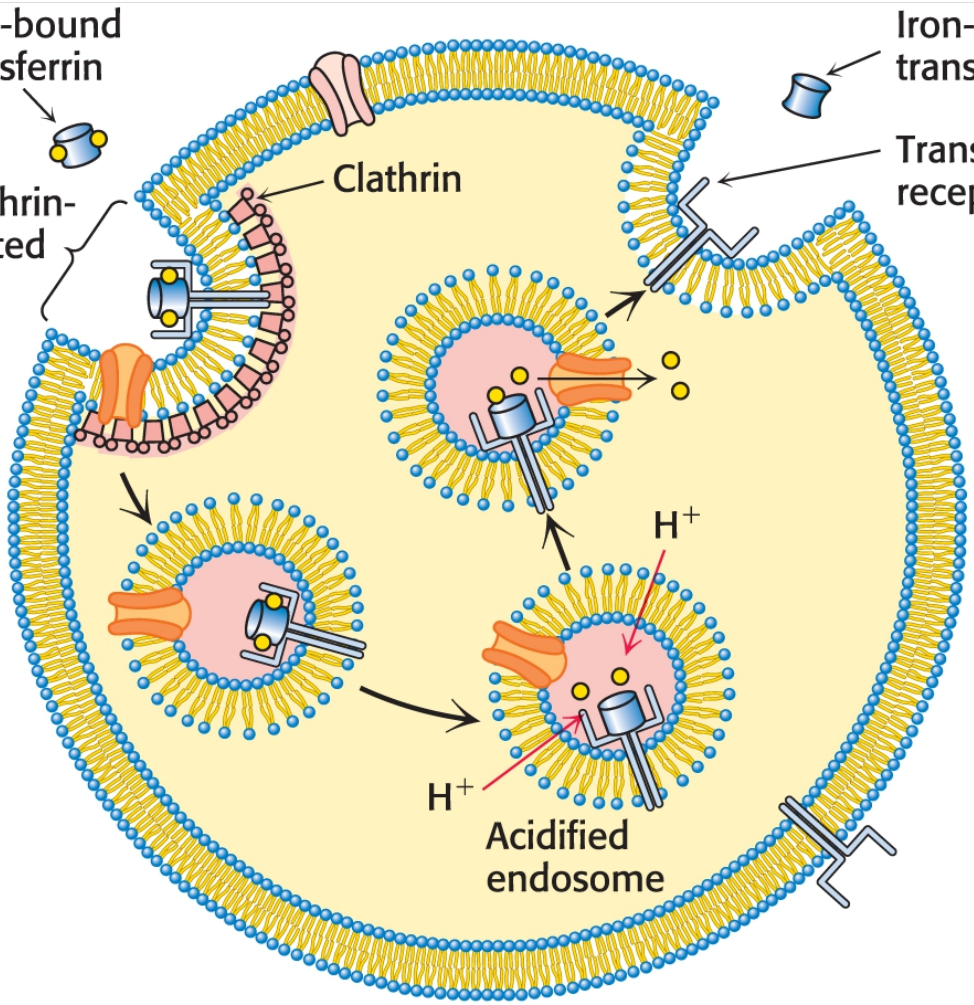


FIGURE 12.40 Receptor-mediated endocytosis of the transferrin receptor mediates cellular uptake of iron. Iron-bound transferrin binds to the transferrin receptor (TfR) on the surface of cells. Receptor-mediated endocytosis occurs, leading to the formation of a vesicle called an endosome. As the lumen of the endosome is acidified by the action of proton pumps, iron is released from transferrin, passes through channels in the membrane, and is used by the cell. Th complex between iron-free transferrin and the transferrin receptor is returned to the plasma membrane for another cycle.

[Information from L. Zecca et al., *Nat. Rev. Neurosci*. 5:863–873, 2004, Fig.1.]

Membrane budding and fusion events throughout the cell must be highly specific in order to prevent incorrect membrane fusion events. The structures of the intermediates in these processes and the detailed

mechanisms remain ongoing areas of investigation. Researchers have identified *SNARE proteins* — short for soluble *N*-ethylmaleimide-sensitive-factor attachment protein receptor — as essential to these processes. SNARE proteins guide membrane fusion by drawing appropriate lipid bilayers together through the formation of tightly coiled four-helical bundles (Figure 12.41). Once these membranes are brought into close proximity with one another, the fusion process can proceed. In addition, SNARE proteins, which are encoded by gene families in all eukaryotic cells, largely determine the compartment with which a vesicle will fuse. The specificity of membrane fusion ensures the orderly trafficking of membrane vesicles and their cargos through eukaryotic cells.

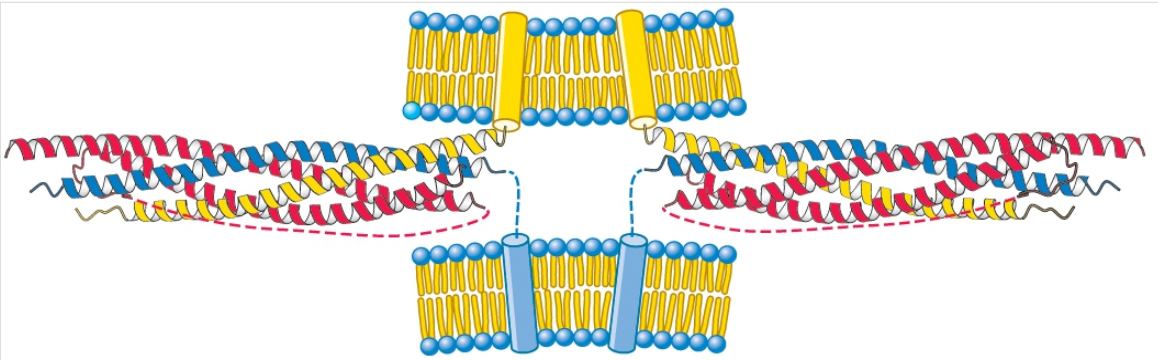


FIGURE 12.41 SNARE complexes initiate membrane fusion. The SNARE protein synaptobrevin (yellow) from one membrane forms a tight four-helical bundle with the corresponding SNARE proteins syntaxin-1 (blue) and SNAP25 (red) from a second membrane. The complex brings the membranes close together, initiating the fusion event.

[Drawn from 1SFC.pdb.]

Chapter 12 Summary

12.1 Fatty Acids Are Key Constituents of Lipids

- Fatty acids are hydrocarbon chains of various lengths and degrees of unsaturation that terminate with a carboxylic acid group.
- The fatty acid chains in membranes usually contain between 14 and 24 carbon atoms; they may be saturated or unsaturated.
- Short chain length and unsaturation enhance the fluidity of fatty acids and their derivatives by lowering the melting temperature.

12.2 Biological Membranes Are Composed of Three Common Types of Membrane Lipids

- The major types of membrane lipids are phospholipids, glycolipids, and cholesterol.
- Phosphoglycerides, a type of phospholipid, consist of a glycerol backbone, two fatty acid chains, and a phosphorylated alcohol.
- Phosphatidylcholine, phosphatidylserine, and phosphatidylethanolamine are major phosphoglycerides.
- Sphingomyelin, a different type of phospholipid, contains a sphingosine backbone instead of glycerol.
- Glycolipids are sugar-containing lipids derived from sphingosine.
- Cholesterol, which modulates membrane fluidity, is constructed from a steroid nucleus.

12.3 Phospholipids and Glycolipids Readily Form Bimolecular Sheets in Aqueous Media

- Membrane lipids spontaneously form extensive bimolecular sheets in aqueous solutions.
- The driving force for membrane formation is the hydrophobic interactions among the fatty acid tails of membrane lipids. The

hydrophilic head groups interact with the aqueous medium.
- Lipid bilayers are cooperative structures, held together by many weak bonds.
- These lipid bilayers are highly impermeable to ions and most polar molecules, yet they are quite fluid, which enables them to act as a solvent for membrane proteins.

12.4 Proteins Carry Out Most Membrane Processes

- Biological membranes vary in their protein content, which reflects the diverse functions of various cell types.
- Integral membrane proteins interact extensively with the hydrocarbon chains of membrane lipids, and they can be released only by agents that compete for these nonpolar interactions.
- Peripheral membrane proteins are bound to membranes primarily by electrostatic and hydrogen-bond interactions with the head groups of lipids and can be released by adding salt or changing the pH.
- Membrane-spanning proteins have regular structures, including β strands, although the α helix is most common.
- Membrane-spanning α helices can often be predicted from amino acid sequence using a hydropathy plot.

12.5 Lipids and Many Membrane Proteins Diffuse Rapidly in the Plane of the Membrane

- Membranes are dynamic structures in which proteins and lipids diffuse rapidly in the plane of the membrane.
- The rotation of lipids from one face of a membrane to the other is usually very slow.
- Proteins do not rotate across bilayers; hence, membrane asymmetry can be preserved.
- The degree of fluidity of a membrane depends on the chain length of its lipids and on the extent to which their constituent

fatty acids are unsaturated.
- In animals, cholesterol content also regulates membrane fluidity.

12.6 Prokaryotes and Eukaryotes Differ in Their Use of Biological Membranes

- Most bacteria exhibit one of two types of membranes: a single membrane surrounded by a cell wall, or a double membrane, where the inner membrane serves as the permeability barrier.
- An extensive array of internal membranes in eukaryotes creates compartments within a cell for distinct biochemical functions.
- The budding and fusion of membranes are highly controlled processes.
- Receptor-mediated endocytosis enables the formation of intracellular vesicles when ligands bind to their corresponding receptor proteins in the plasma membrane.
- The reverse process — the fusion of a vesicle to a membrane — is a key step in the release of signaling molecules outside the cell.

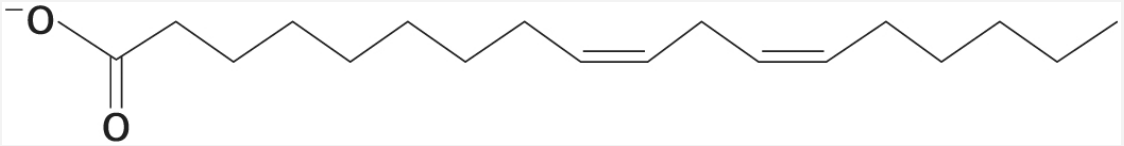
Key Terms

lipids
fatty acid
phospholipid
phosphoglyceride
sphingomyelin
sphingosine
glycolipid
cholesterol
amphipathic (amphiphilic) molecule
micelle
lipid bilayer
liposome (lipid vesicle)

myelin
integral membrane protein
peripheral membrane protein
hydropathy plot
lateral diffusion
fluid mosaic model
lipid rafts
Gram staining
receptor-mediated endocytosis
endosomes

Problems

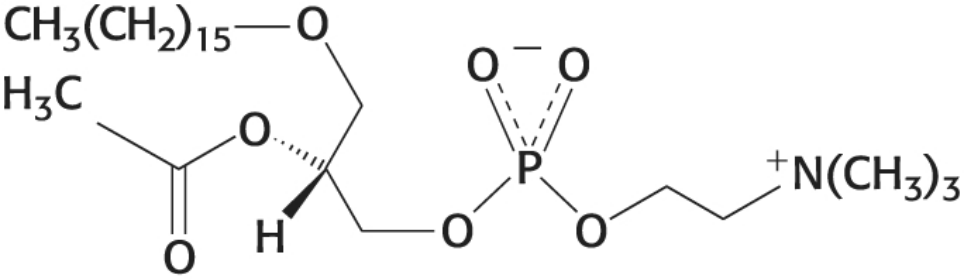
1. Consider the following fatty acid:



What is an accurate designation of this structure that indicates the length, degree of unsaturation, and location of double bonds? What is the common name for this fatty acid (see Table 12.1)? What are the positions of the double bonds expressed in relation to the distal carbon atom? 1

2. Draw the chemical structure of cis-Δ^9-hexadecenoic acid. What is the common name for this fatty acid? 1

3. Platelet-activating factor (PAF) is a phospholipid that plays a role in allergic and inflammatory responses, as well as in toxic shock syndrome. The structure of PAF is shown here. How does it differ from the structures of the phospholipids discussed in this chapter? 2



Platelet-activating factor (PAF)

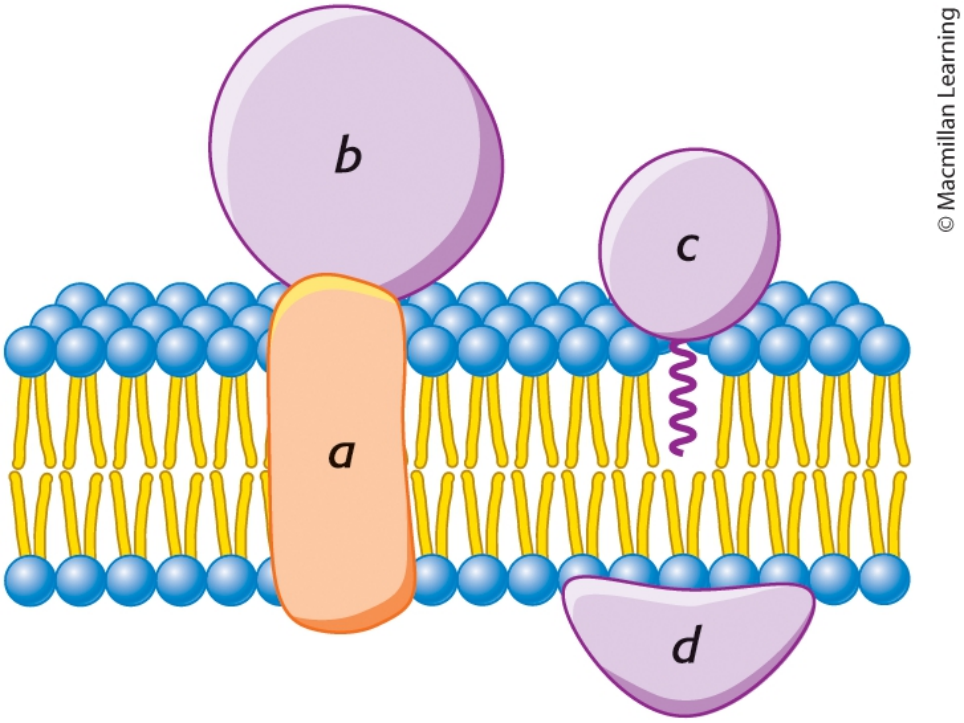
4. Match the following statements with the type of lipid it best describes: phospholipids, sphingolipids, glycolipids, archaeal lipids, or cholesterol. Some statements may describe more than one lipid type: 2

a. Includes two fatty acids joined to glycerol by ester linkages
b. Does not contain glycerol
c. Is a steroid
d. Contains a sphingosine backbone
e. Contains one or more sugars
f. Usually have branched alkyl chains

5. What is the average distance traversed by a membrane lipid in $1\ \mu s$, 1 ms, and 1 s? Assume a diffusion coefficient of $10^{-8}\ cm^2\ s^{-1}$. 6

6. Which of the following molecules could align side-by-side to form a lipid bilayer: phospholipids, fatty acids, triacylglycerol, sphingolipids, cholesterol? 3

7. Label the molecules in the diagram below as either integral membrane proteins, peripheral membrane proteins, or lipid-anchored membrane proteins: 4

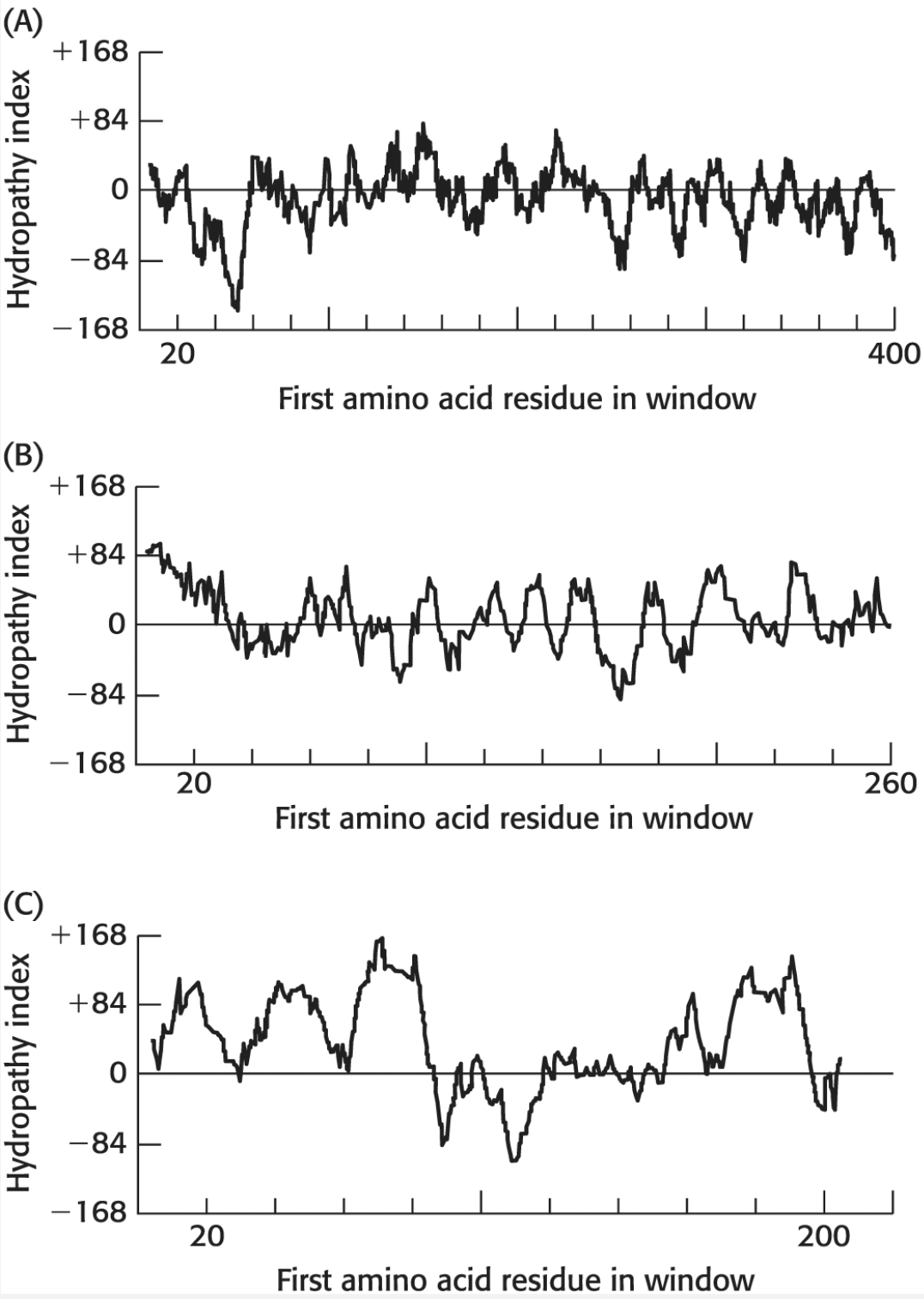


8. Match each statement to the category of membrane-associated protein it describes: membrane-spanning α helix,

membrane spanning β strands, lipid-anchored membrane protein, or peripheral membrane protein: 4

a. Contains residue(s) with covalently attached fatty acyl groups
b. Often tethered to the membrane via a membrane-embedded protein
c. Composed of about 20 hydrophobic residues
d. Can usually be released from the membrane with concentrated salt solutions
e. Features a pattern of alternating nonpolar and polar side chains

9. On the basis of the following hydropathy plots for three proteins (A–C), predict which would be membrane proteins. What are the ambiguities with respect to using such plots to determine if a protein is a membrane protein? 5



© Macmillan Learning

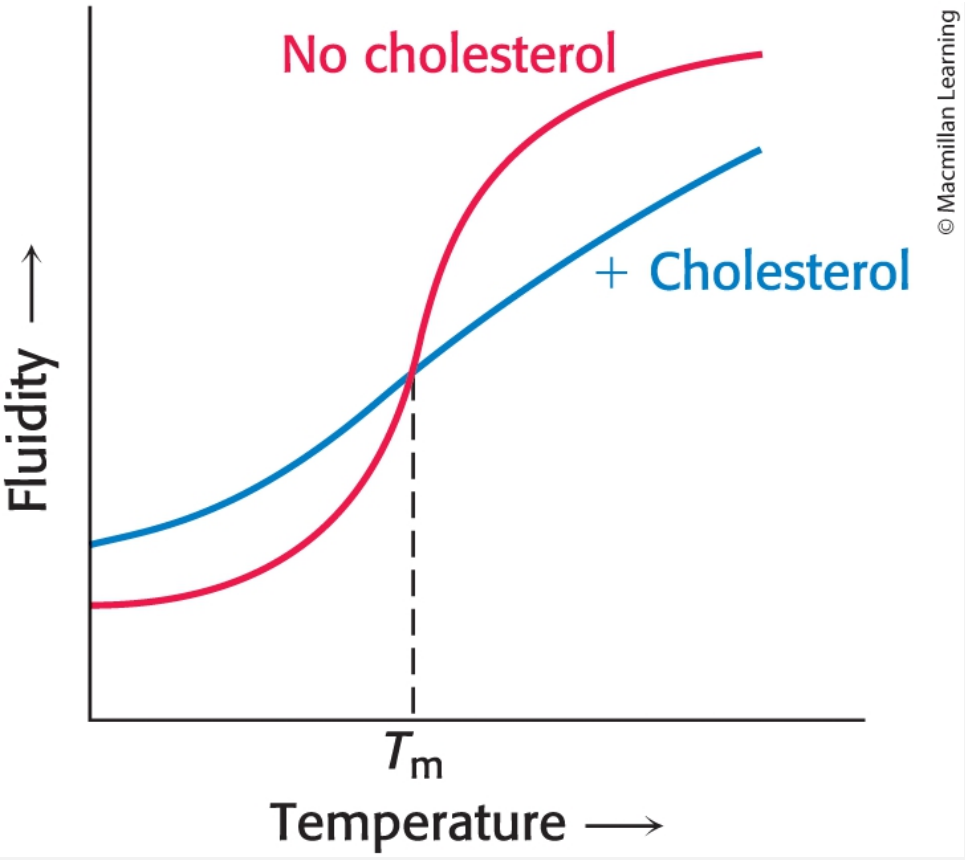
10. Hydropathy plot analysis of your protein of interest reveals a single, prominent hydrophobic peak. However, you later discover that this protein is soluble and not membrane associated. Explain how the hydropathy plot may have been misleading. 5

11. The diffusion coefficient, *D*, of a rigid spherical molecule is given by

$$D = kT/6\pi\eta r$$

in which η is the viscosity of the solvent, *r* is the radius of the sphere, *k* is the Boltzmann constant $(1.38 \times 10^{-16} \text{erg degree}^{-1})$, and *T* is the absolute temperature. What is the diffusion coefficient at 37°C of a 100-kDa protein in a membrane that has an effective viscosity of 1 poise $(1 \text{ poise} = 1 \text{ erg s}^{-1} \text{ cm}^{-3})$? What is the average distance traversed by this protein in $1\ \mu s$, 1 ms, and 1 s? Assume that this protein is an unhydrated, rigid sphere with a density of 1.35 g cm^{-3}. 5

12. The red curve on the following graph shows the fluidity of the fatty acids of a phospholipid bilayer as a function of temperature. The blue curve shows the fluidity in the presence of cholesterol. 6



a. What is the effect of cholesterol?
b. Why might this effect be biologically important?

13. Calculate the distance olive oil (a lipid) could move in a membrane in 13 seconds assuming the diffusion coefficient is $1\ \mu m^2\ s^{-1}$. Use the equation $S = (4Dt)^{1/2}$ where S is the distance traveled, t is time, and D is the diffusion coefficient. 6

14. Arrange the fatty acids in order of increasing melting point:

a. Stearic acid (18:0)

b. Oleic acid (18:1)
c. Palmitoleic acid (16:1)
d. α-Linoleic acid (18:3)
e. Palmitic acid (16:0)

15. Each intracellular fusion of a vesicle with a membrane requires a SNARE protein on the vesicle (called the v-SNARE) and a SNARE protein on the target membrane (called the t-SNARE). Assume that a genome encodes 21 members of the v-SNARE family and 7 members of the t-SNARE family. With the assumption of no specificity, how many potential v-SNARE–t-SNARE interactions could take place? 7

16. Some antibiotics act as carriers that bind an ion on one side of a membrane, diffuse through the membrane, and release the ion on the other side. The conductance of a lipid-bilayer membrane containing a carrier antibiotic decreased abruptly when the temperature was lowered from 40°C to 36°C. In contrast, there was little change in conductance of the same bilayer membrane when it contained a channel-forming antibiotic. Why?

17. Of the following pairs of ions and/or molecules, identify which one is more permeable across a lipid bilayer:

a. K^+ vs. H_2O
b. Tryptophan vs. indole
c. H_2O vs. Cl^-

In general the permeability coefficient is most directly correlated with which property: size, flexibility, solubility in nonpolar solvents, or interaction with polar head groups?

18. Small mammalian hibernators can withstand body temperatures of 0 – 5°C without injury. However, the body fats of

most mammals have melting temperatures of approximately 25°C. Predict how the composition of the body fat of hibernators might differ from that of their nonhibernating cousins. 6

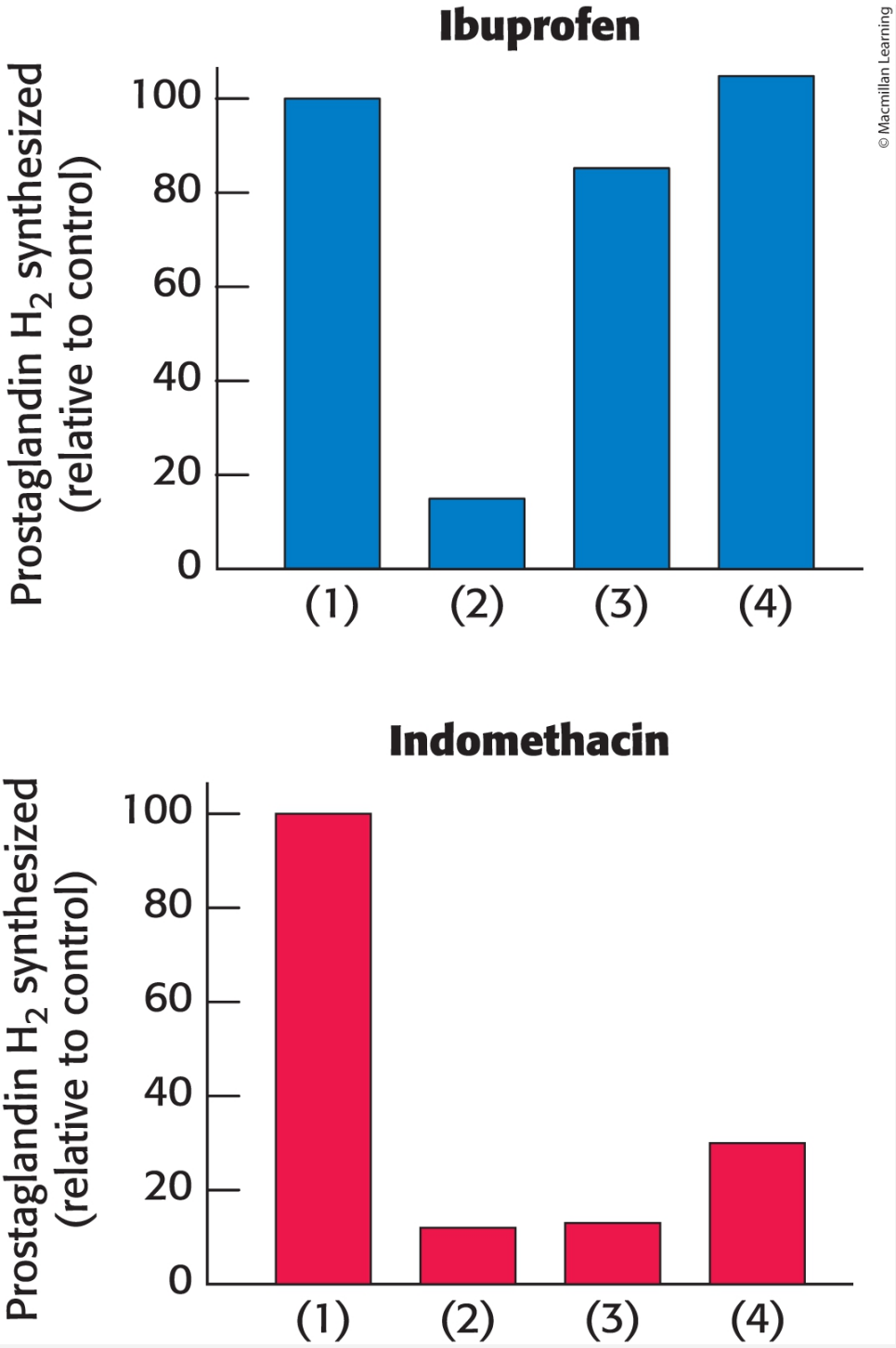
19. Classify each of these statements as to whether they describe saturated phospholipids, unsaturated phospholipids, or both:

a. Contain one or more double bonds within their fatty acid tails
b. Are built upon a glycerol backbone
c. Produce a fairly inflexible membrane at low temperatures
d. Have bent fatty acid tails

20. Ibuprofen and indomethacin are clinically important inhibitors of prostaglandin H_2 synthase-1. Cells expressing this enzyme were incubated under the following conditions, after which the activity of the enzyme was measured by adding radiolabeled arachidonic acid and detecting newly produced prostaglandin H_2:

1. 40 min *without* inhibitor (control)
2. 40 min with inhibitor
3. 40 min with inhibitor, after which the cells were resuspended in medium *without* inhibitor
4. 40 min with inhibitor, after which the cells were resuspended in medium *without* inhibitor and incubated for an additional 30 minutes

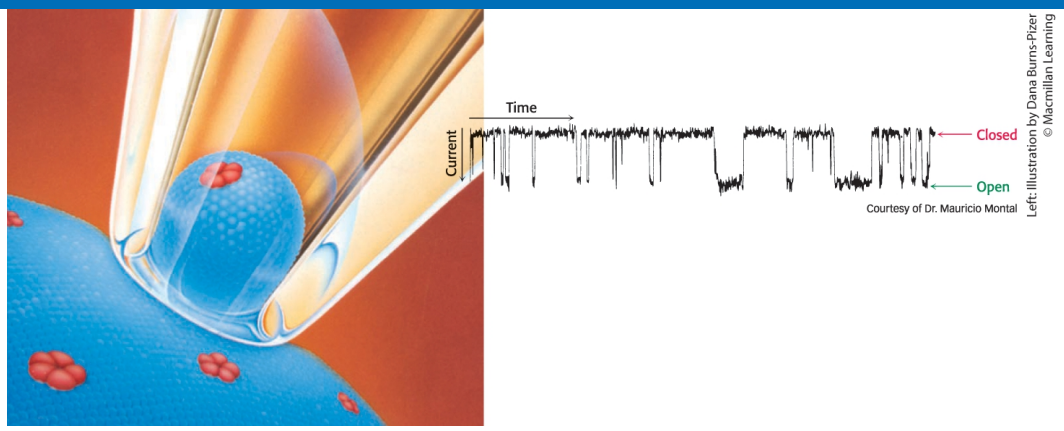
The results are shown below:



© Macmillan Learning

a. Provide a hypothesis explaining the different results for these two inhibitors.
b. How would these results look if aspirin were tested in a similar fashion?

Chapter 13
Membrane Channels and Pumps



The flow of ions through a single membrane channel (channels are shown in red in the illustration at the left) can be detected by the patch-clamp technique, which records current changes as the channel alternates between open and closed states.

Outline

13.1 The Transport of Molecules Across a Membrane May Be Active or Passive
13.2 Two Families of Membrane Proteins Use ATP Hydrolysis to Pump Ions and Molecules Across Membranes
13.3 Lactose Permease Is an Archetype of Secondary Transporters That Use One Concentration Gradient to Power the Formation of Another
13.4 Specific Channels Can Rapidly Transport Ions Across Membranes
13.5 Gap Junctions Allow Ions and Small Molecules to Flow Between Communicating Cells

[13.6 Specific Channels Increase the Permeability of Some Membranes to Water]

Learning Goals



By the end of this chapter, you should be able to:

1. Distinguish between passive and active transport.
2. Calculate the free energy stored in a concentration or electrochemical gradient.
3. Compare the mechanisms of the P-type ATPase pump and the ABC transporter pump.
4. Contrast primary and secondary active transport.
5. Explain how channels are able to rapidly and selectively move ions across membranes.
6. Describe two mechanisms by which ion channels are gated.
7. Explain the steps that lead to the formation of an action potential.

The lipid bilayer of biological membranes is intrinsically impermeable to ions and polar molecules, yet these species must be able to cross these membranes for normal cell function. As we will discuss in this chapter, permeability is conferred by three classes of membrane transporter proteins: pumps, carriers, and channels. These proteins are critical for many basic cellular functions, including access to ions and solutes for metabolism, conduction of nerve impulses, contraction of muscles, and communication of signals within cells.

Consider, for example, the rhythmic beating of the heart: the coordinated movement of ions across cardiac cellular membranes can sustain the contraction of heart muscle for, on average, 60 times each minute for over 70 years — a total of over 2.2 billion

contractions! The remarkable consistency of cardiac contraction is just one example of the importance of these protein classes.

13.1 The Transport of Molecules Across a Membrane May Be Active or Passive

We will first consider some general principles of membrane transport. Two factors determine whether a molecule will cross a membrane: (1) the permeability of the molecule in a lipid bilayer and (2) the availability of an energy source.

Many molecules require protein transporters to cross membranes

As stated in Chapter 12, some molecules can pass through cell membranes because they dissolve in the lipid bilayer. Such molecules are called *lipophilic molecules*. The steroid hormones provide a physiological example. These cholesterol relatives can pass through a membrane, but what determines the direction in which they will move? Such molecules will pass through a membrane down their concentration gradient in a process called **simple diffusion**. In accord with the Second Law of Thermodynamics, molecules spontaneously move from a region of higher concentration to one of lower concentration.

Matters become more complicated when the molecule is highly polar. For example, sodium ions are present at 143 mM outside a typical cell and at 14 mM inside the cell. However, sodium does not freely enter the cell, because the charged ion cannot pass through the hydrophobic membrane interior. In some circumstances, as

during a nerve impulse, sodium ions must enter the cell. How are they able to do so? Sodium ions pass through specific channels in the hydrophobic barrier formed by membrane proteins. This means of crossing the membrane is called **facilitated diffusion** because the diffusion across the membrane is facilitated by the channel. It is also called **passive transport** because the energy driving the ion movement originates from the ion gradient itself, without any contribution by the transport system. Channels, like enzymes, display substrate specificity in that they facilitate the transport of some ions, but not other, even closely related, ions.

How is the sodium gradient established in the first place? In this case, sodium must move, or be pumped, *against* a concentration gradient. Because moving the ion from a low concentration to a higher concentration results in a decrease in entropy, it requires an input of free energy. Protein transporters embedded in the membrane are capable of using an energy source to move the molecule up a concentration gradient. Because an input of energy from another source is required, this means of crossing the membrane is called **active transport**.

Free energy stored in concentration gradients can be quantified

An unequal distribution of molecules is an energy-rich condition because free energy is minimized when all concentrations are equal. Consequently, to attain such an unequal distribution of molecules requires an input of free energy. How can we quantify the amount of energy required to generate a concentration gradient (**Figure 13.1**)?

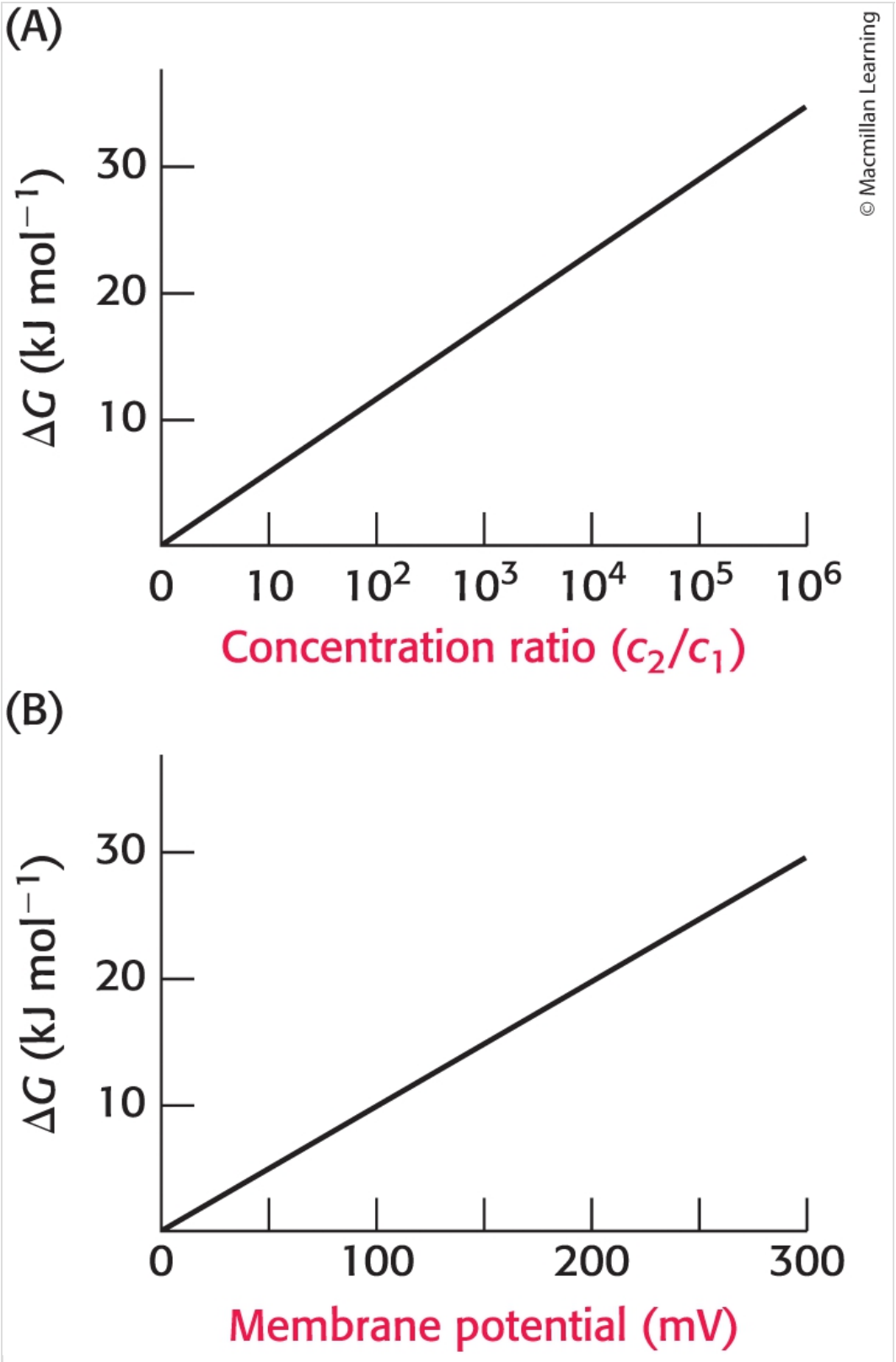


FIGURE 13.1 Transport of solutes and ions across a membrane imposes an energetic cost. The free-energy change in transporting (A) an uncharged solute

from a compartment at concentration c_1 to one at c_2 and (B) a singly charged species across a membrane to the side having the same charge as that of the transported ion are shown. The free-energy change imposed by a membrane potential of 59 mV is equivalent to that imposed by a concentration ratio of 10 for a singly charged ion at 25°C.



Consider an *uncharged* solute molecule. The free-energy change in transporting this species from side 1, where it is present at a concentration of c_1, to side 2, where it is present at concentration c_2, is

$$\Delta G = RT \ln (c_2 / c_1)$$

where R is the gas constant (8.315×10^{-3} kJ mol^{-1} deg^{-1}, or 1.987×10^{-3} kcal mol^{-1} deg^{-1}) and T is the temperature in kelvins. A transport process must be active when ΔG is positive, whereas it can be passive when ΔG is negative. For example, consider the transport of an uncharged molecule from $c_1 = 10^{-3}$ M to $c_2 = 10^{-1}$ M at 25°C (298 K).

$$\begin{aligned}\Delta G &= RT \ln (10^{-1} / 10^{-3}) \\ &= (8.315 \times 10^{-3}) \times 298 \times \ln (10^2) \\ &= +11.4 \text{ kJ mol}^{-1} (+2.7 \text{ kcal mol}^{-1})\end{aligned}$$

The ΔG is $+11.4\ \text{kJ mol}^{-1}\ (+2.7\ \text{kcal mol}^{-1})$, indicating that this transport process requires an input of free energy.

For a *charged* species, the unequal distribution across the membrane generates an electrical potential that also must be considered because the ions will be repelled by like charges. The sum of the concentration and electrical terms is called the **electrochemical potential** or **membrane potential**. The free-energy change is then given by

$$\Delta G = RT \ln (c_2 / c_1) + ZF\Delta V$$

in which Z is the electrical charge of the transported species, ΔV is the potential in volts across the membrane (expressed as $V_{\text{side 2}} - V_{\text{side 1}}$), and F is the Faraday constant ($96.5\ \text{kJ V}^{-1}\ \text{mol}^{-1}$, or $23.1\ \text{kcal V}^{-1}\ \text{mol}^{-1}$).

Example

Calculating the Energetic Cost of Ion Transport

Problem:

Suppose that the concentrations of Na^+ outside and inside the cell are 143 and 14 mM, respectively, and the corresponding values for K^+ are 4 and 157 mM. At a membrane potential of $-50\ \text{mV}$ and a

temperature of 37°C what are the energetic costs of transporting a K^+ ion into the cell and a Na^+ ion out of the cell?

Getting Started:

Since potassium and sodium ions are both charged species, we must use the electrochemical potential equation described in this section to determine the free energy change. As both ions carry a single positive charge, *Z* will be $+1$ for each calculation. Applying the equation is rather straightforward, as long as we make sure we're keeping each side of the membrane and the direction of transport consistent. It is important to remember that, by convention, the membrane potential ΔV is expressed as the voltage of the inside of the cell minus the voltage of the outside of the cell ($V_{inside} - V_{outside}$).

Calculate:

For K^+ transport, the problem asks us to move the ion into the cell.

Hence, the inside of the cell will be side 2 and the outside of the cell will be side 1.

$$\Delta G = RT \ln (c_2/c_1) + ZF\Delta V = RT \ln(c_2/c_1) + ZF(V_2 - V_1)$$

$$\Delta G = (8.315 \times 10^{-3}\ \text{kJ mol}^{-1}\ \text{deg}^{-1}) \times (310\ \text{deg}) \times \ln(157/4) + (1) \times (96.5\ \text{kJ mol}^{-1}\ \text{V}^{-1}) \times (-0.05\ \text{V})$$

$$\Delta G = 4.64\ \text{kJ mol}^{-1}$$

For Na^+ transport, we are calculating the cost of moving the ion out of the cell, so the *outside* of the cell is side 2 and the *inside* is side 1. Thus, the sign of the ΔV term is opposite that of the first part of the question.

$$\Delta G = RT\ \ln(c_2/c_1) + ZF\Delta V = RT\ln(c_2/c_1) + ZF(V_2 - V_1)$$

$$\Delta G = (8.315 \times 10^{-3}\ \text{kJ mol}^{-1}\ \text{deg}^{-1}) \times (310\ \text{deg}) \times \ln(143/14) + (1) \times (96.5\ \text{kJ mol}^{-1}\ \text{V}^{-1}) \times (0.05\ \text{V})$$

$$\Delta G = 10.82\ \text{kJ mol}^{-1}$$

Reflect:

For both ions, moving the charge against its concentration gradient is energetically unfavorable. However, the cost is significantly greater for Na^+ than K^+. Why is this the case? Note that while that the chemical term is positive (unfavorable) for both ions, the electrical term is favorable for K^+ (ΔV is negative) and unfavorable for Na^+ (ΔV is positive) as the membrane has net negative charge on its inner surface. Essentially, transporting Na^+ out of the cell requires movement against its chemical gradient and in an electrically unfavorable direction.

13.2 Two Families of Membrane Proteins Use ATP Hydrolysis to Actively Transport Ions and Molecules Across Membranes

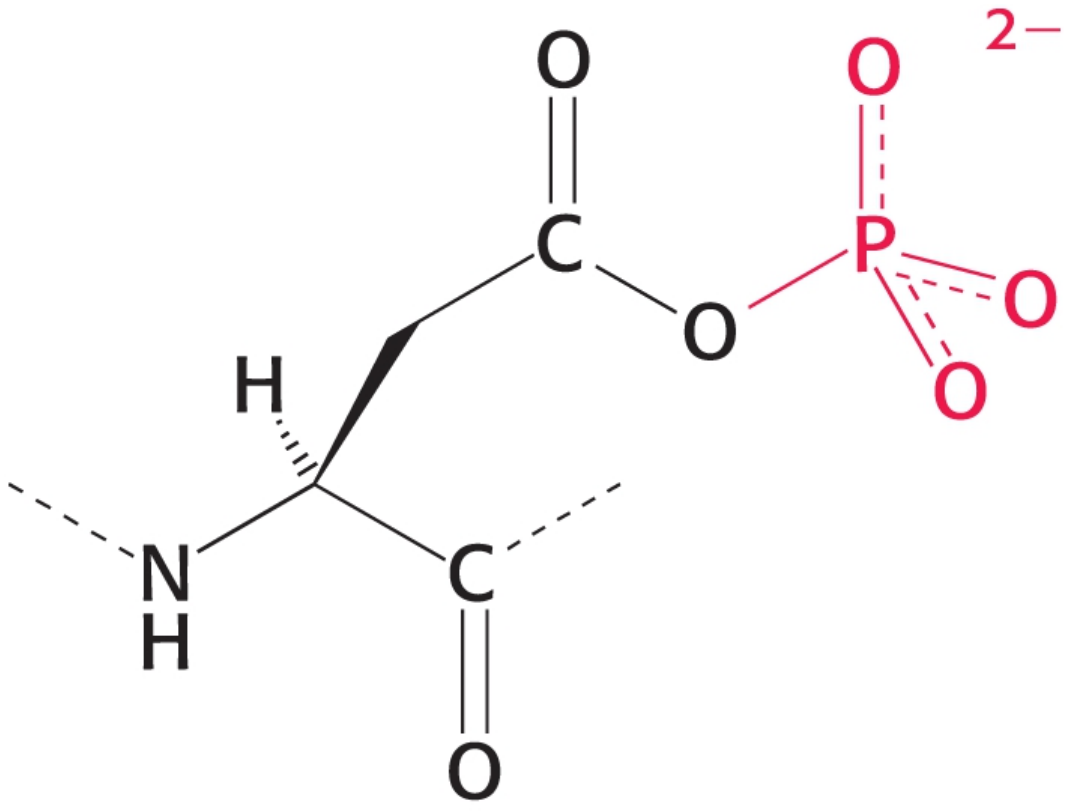
The extracellular fluid of animal cells has a salt concentration similar to that of seawater. However, cells must control their intracellular salt concentrations to facilitate specific processes, such as signal transduction and action potential propagation, and prevent unfavorable interactions with high concentrations of ions such as Ca^{2+}. For instance, most animal cells contain a high concentration of K^+ and a low concentration of Na^+ relative to the external medium. To generate these gradients, energy expenditure is required. **Pumps** are membrane proteins that catalyze the active transport of ions against their electrochemical gradients. The sodium and potassium gradients across the plasma membrane are generated by a specific transport system, an enzyme that is called the Na^+-K^+ *pump*, or the Na^+-K^+ *ATPase*. The hydrolysis of ATP by the pump provides the energy needed for the active transport of Na^+ out of the cell and K^+ into the cell, generating the gradients. The pump is called the Na^+-K^+ ATPase because the hydrolysis of ATP takes place only when Na^+ and K^+ are present. This ATPase, like all such enzymes, requires Mg^{2+}.

The Na^+-K^+ ATPase transports ions with a stoichiometry of $3\ Na^+$ ions and $2\ K^+$ ions per catalytic cycle. In the example at the end of the last

section, we calculated change in free energy accompanying the transport of Na^+ and K^+. Taking into account the transport of $3\ Na^+$ ions and $2\ K^+$ ions for every transport cycle, the free energy required to operate the pump is:

$$\Delta G = 3 \times (10.82\ \text{kJ mol}^{-1}) + 2 \times (4.64\ \text{kJ mol}^{-1})$$
$$\Delta G = 41.7\ \text{kJ mol}^{-1}$$

Under typical cellular conditions, the hydrolysis of a single ATP molecule per transport cycle provides sufficient free energy, about $-50\ \text{kJ mol}^{-1}\ (-12\ \text{kcal mol}^{-1})$ to drive the uphill transport of these ions. The active transport of Na^+ and K^+ is of great physiological significance. Indeed, more than a third of the ATP consumed by a resting animal is used to pump these ions. The Na^+-K^+ gradient in animal cells controls cell volume, renders neurons and muscle cells electrically excitable, and drives the active transport of sugars and amino acids. The purification of other ion pumps has revealed a large family of evolutionarily related ion pumps including proteins from bacteria, archaea, and all eukaryotes. Each of these pumps is specific for a particular ion or set of ions. Two are of particular interest: the *sarcoplasmic reticulum* Ca^{2+} *ATPase* (or SERCA) transports Ca^{2+} out of the cytoplasm and into the sarcoplasmic reticulum of muscle cells, and the *gastric* H^+-K^+ *ATPase* is the enzyme responsible for pumping sufficient protons into the stomach to lower the pH to 1.0. These enzymes and the hundreds of known homologs, including the Na^+-K^+ ATPase, are referred to as **P-type ATPases** because they form a key phosphorylated intermediate. In the formation of this intermediate, a phosphoryl group from ATP is linked to the side chain of a specific conserved aspartate residue in the ATPase to form phosphorylaspartate.



Phosphorylaspartate

P-type ATPases couple phosphorylation and conformational changes to pump calcium ions across membranes

Membrane pumps function by mechanisms that are simple in principle but often complex in detail. Fundamentally, each pump protein can exist in two principal conformational states, one with ion-binding sites open to one side of the membrane and the other with ion-binding sites open to the other side (Figure 13.2). To pump ions in a single direction

across a membrane, the free energy of ATP hydrolysis must be coupled to the interconversion between these conformational states.

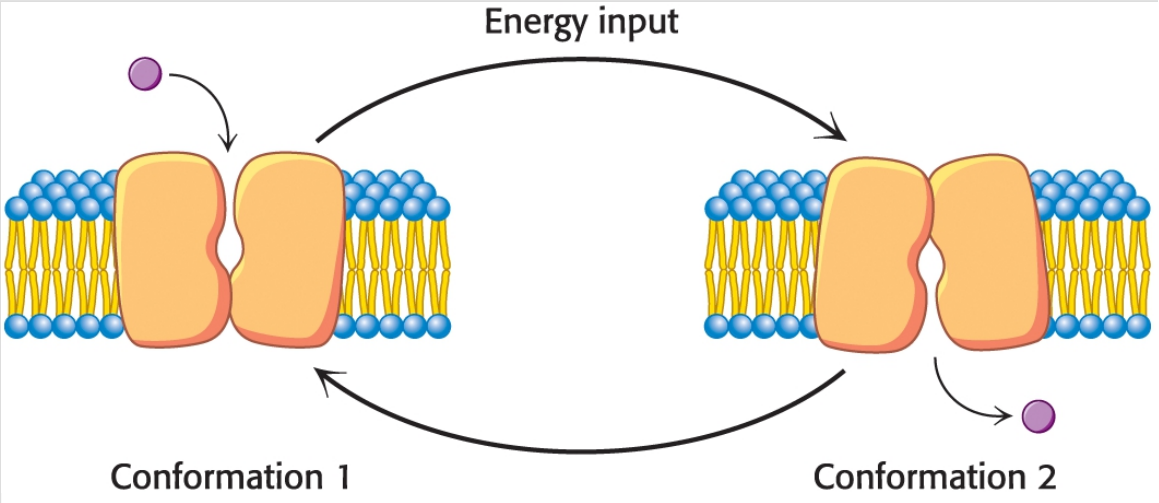


FIGURE 13.2 Pumps use the input of energy to transport ions across a membrane. This simple scheme illustrates the pumping of a molecule across a membrane. The pump interconverts between two conformational states, each with a binding site accessible to a different side of the membrane.

We will consider the structural and mechanistic features of P-type ATPases by examining SERCA. The properties of this P-type ATPase have been established in great detail by relying on crystal structures of the pump in five different states. This enzyme, which constitutes 80% of the total protein in the sarcoplasmic reticulum membrane, plays an important role in relaxation of contracted muscle. Muscle contraction is triggered by an abrupt rise in the cytoplasmic calcium ion level. Subsequent muscle relaxation depends on the rapid removal of Ca^{2+} from the cytoplasm into the sarcoplasmic reticulum, a specialized compartment for Ca^{2+} storage, by SERCA. This pump maintains a Ca^{2+} concentration of approximately $0.1\ \mu M$ in the cytoplasm, compared to nearly 1.5 mM in the sarcoplasmic reticulum.

The first structure of SERCA to be determined had Ca^{2+} bound, but no nucleotides present (Figure 13.3). SERCA is a single 110-kDa polypeptide with a transmembrane domain consisting of 10 α helices. The transmembrane domain includes sites for binding two calcium ions. Each calcium ion is coordinated to seven oxygen atoms coming from a combination of side-chain glutamate, aspartate, threonine, and asparagine residues, backbone carbonyl groups, and water molecules. A large cytoplasmic headpiece constitutes nearly half the molecular weight of the protein and consists of three distinct domains, each with a distinct function. One domain (N) binds the ATP nucleotide, another (P) accepts the phosphoryl group on a conserved aspartate residue, and the third (A) serves as an actuator, linking changes in the N and P domains to the transmembrane part of the enzyme.

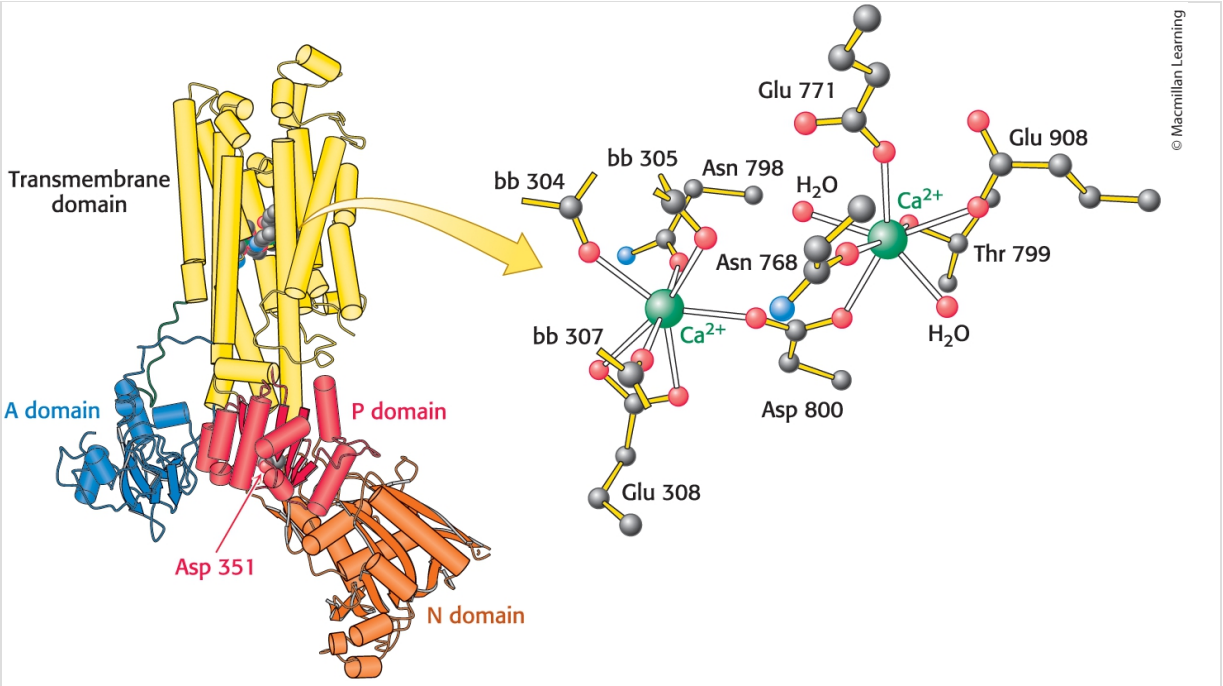


FIGURE 13.3 SERCA is a well-characterized example of a P-type ATPase pump. The overall structure of the SERCA P-type ATPase with calcium, but no nucleotide, bound is shown. Notice the two calcium ions (green) that lie in the center of the transmembrane domain. A conserved aspartate residue (Asp 351) that binds a phosphoryl group lies in the P domain. The designation bb refers to backbone carbonyl groups.

[Drawn from 1SU4.pdb.]

INTERACT with this model in Achieve

SERCA is a remarkably dynamic protein. For example, the structure of SERCA without bound Ca^{2+}, but with a phosphorylaspartate analog present in the P domain, is shown in **Figure 13.4**. The N and P domains are now closed around the phosphorylaspartate analog, and the A domain has rotated substantially relative to its position in SERCA with Ca^{2+} bound and without the phosphoryl analog. Furthermore, the transmembrane part of the enzyme has rearranged significantly and the well-organized Ca^{2+}-binding sites are disrupted. These sites are now accessible from the side of the membrane opposite the N, P, and A domains.

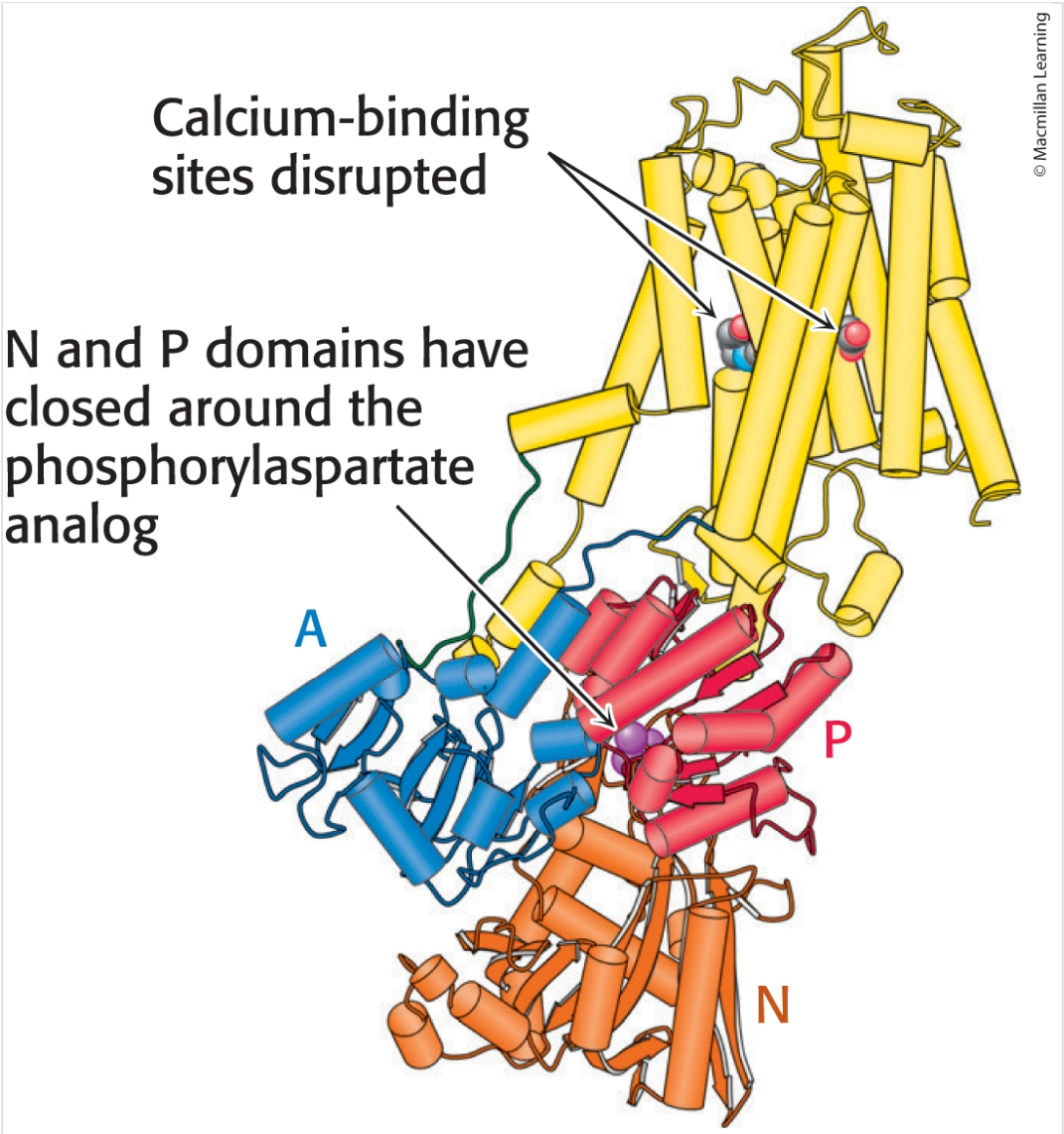


FIGURE 13.4 SERCA undergoes dynamic conformational changes. This structure was determined in the absence of bound calcium but with a phosphorylaspartate analog present in the P domain. Notice how different this structure is from the calcium-bound form shown in Figure 13.3: both the transmembrane part (yellow) and the A, P, and N domains have substantially rearranged.

[Drawn from 1WPG.pdb.]

INTERACT with this model in Achieve

The structural results can be combined with other studies to construct a detailed mechanism for Ca^{2+} pumping by SERCA (Figure 13.5):

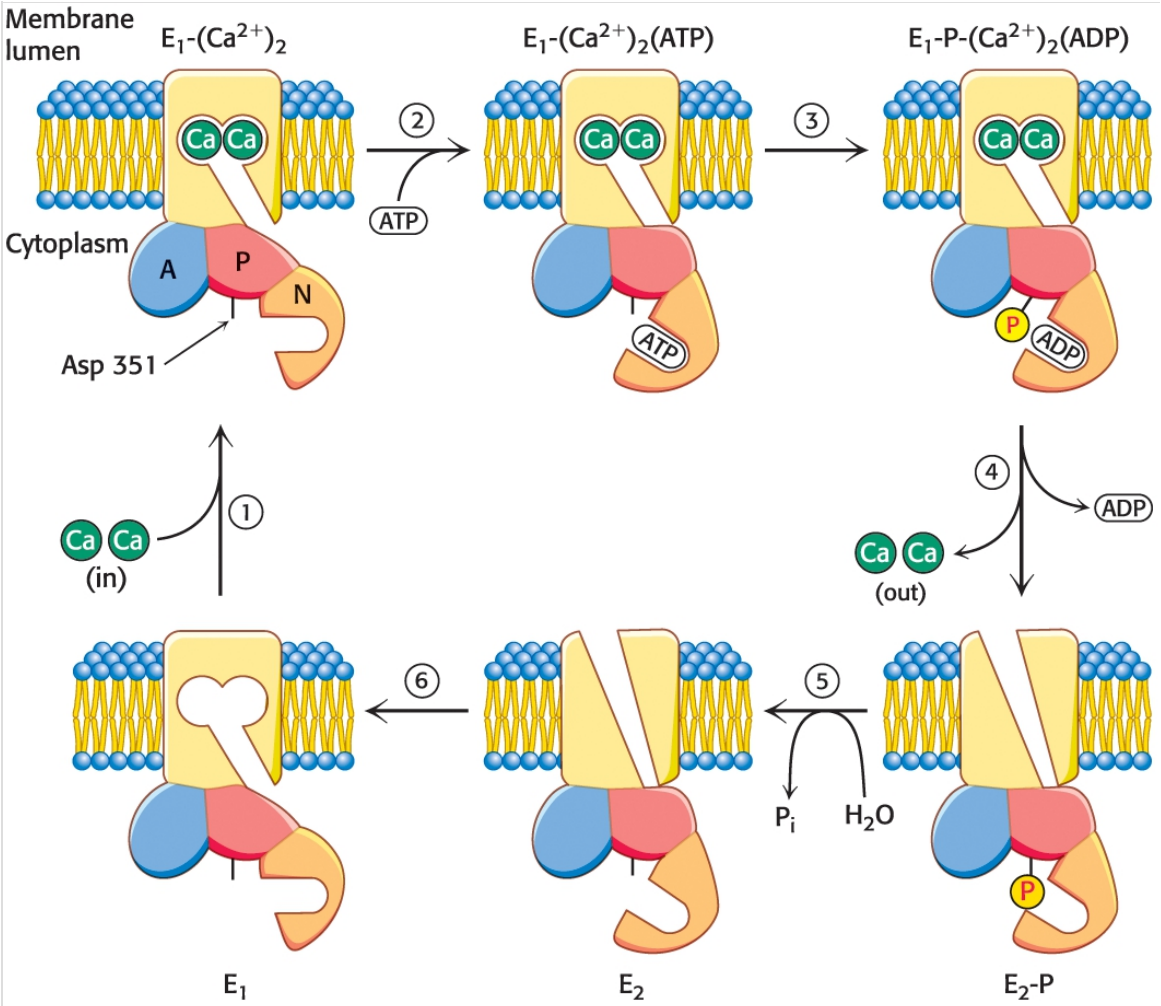


FIGURE 13.5 SERCA interconverts between E_1 and E_2 conformations during a catalytic cycl

Ca^{2+} ATPase transports Ca^{2+} through the membrane by a mechanism that includes (1) Ca^{2+} binding from the cytoplasm, (2) ATP binding, (3) ATP cleavage with the transfer of a phosphoryl group to Asp 351 on the enzyme, (4) ADP release and eversion of the enzyme to release Ca^{2+} on the opposite side of the membrane, (5) hydrolysis of the phosphorylaspartat residue, and (6) eversion to prepare for the binding of Ca^{2+} from the cytoplasm.

1. The catalytic cycle begins with the enzyme in its unphosphorylated state with two calcium ions bound. We will refer to the overall enzyme conformation in this state as E_1; with Ca^{2+} bound, it is E_1-$(Ca^{2+})_2$. In this conformation, SERCA can bind calcium ions only on the cytoplasmic side of the membrane. This conformation is shown in Figure 13.3.

2. In the E_1 conformation, the enzyme can bind ATP. The N, P, and A domains undergo substantial rearrangement as they close around the bound ATP, but there is no substantial conformational change in the transmembrane domain. The calcium ions are now trapped inside the enzyme.

3. The phosphoryl group is then transferred from ATP to Asp 351.

4. Upon ADP release, the enzyme again changes its overall conformation, including the membrane domain this time. This new conformation is referred to as E_2 or E_2-P in its phosphorylated form. The process of interconverting the E_1 and E_2 conformations is sometimes referred to as **eversion**. In the E_2-P conformation, the Ca^{2+}-binding sites become disrupted and the calcium ions are released to the side of the membrane opposite that at which they entered; ion transport has been achieved. This conformation is shown in Figure 13.4.

5. The phosphorylaspartate residue is hydrolyzed to release inorganic phosphate.

6. With the release of phosphate, the interactions stabilizing the E_2 conformation are lost, and the enzyme everts to the E_1

conformation. The binding of two calcium ions from the cytoplasmic side of the membrane completes the cycle.

This mechanism likely applies to other P-type ATPases. For example, Na^+-K^+ ATPase is an $\alpha_2\beta_2$ tetramer. Its α subunit is homologous to SERCA and includes a key aspartate residue analogous to Asp 351. The β subunit does not directly take part in ion transport. A mechanism analogous to that shown in Figure 13.5 applies, with three Na^+ ions binding from the inside of the cell to the E_1 conformation and two K^+ ions binding from outside the cell to the E_2 conformation.

Digoxin specifically inhibits the Na^+-K^+ pump by blocking its dephosphorylation



Certain steroids derived from plants are potent inhibitors $(K_i \approx 10\ nM)$ of the Na^+-K^+ pump. Digoxin and ouabain are members of this class of inhibitors, which are known as *cardiotonic steroids* because of their strong effects on the heart (**Figure 13.6**). These compounds inhibit the dephosphorylation of the E_2-P form of the ATPase when applied on the extracellular face of the membrane.

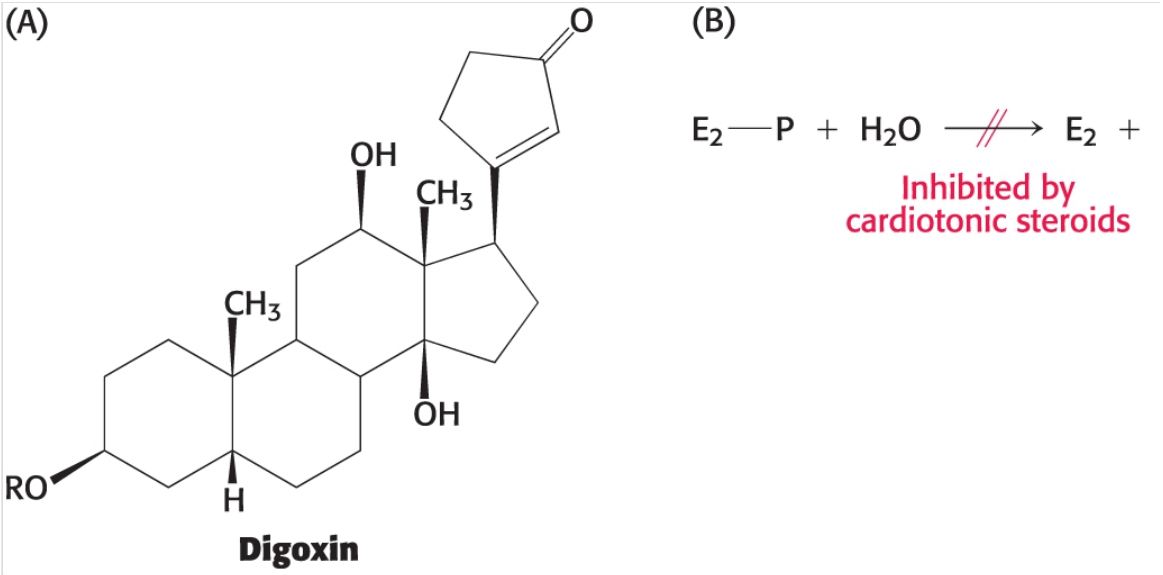


FIGURE 13.6 Digoxin is an example of a cardiotonic steroid. (A) The chemical structure of the cardiotonic steroid digoxin is shown. (B) Cardiotonic steroids inhibit the Na^+–K^+ pump by blocking the dephosphorylation of E_2-P.

Digoxin is one of the cardiotonic steroids derived from the dried leaf of the foxglove plant, *Digitalis purpurea* (**Figure 13.7**). The compound increases the force of contraction of heart muscle and is consequently administered for the treatment of congestive heart failure. Inhibition of the Na^+–K^+ pump by digoxin leads to a higher level of Na^+ inside the cell. As we shall see (Section 13.3), the diminished Na^+ gradient results in slower removal of Ca^{2+} from the cytoplasm. The subsequent increase in the intracellular level of Ca^{2+} enhances the ability of cardiac muscle to contract.



Roger Hall/Shutterstock

FIGURE 13.7 Foxglove (*Digitalis purpurea*) is a naturally occurring source of digoxin.

It is interesting to note that cardiotonic steroids were used effectively long before the discovery of the Na^+-K^+ ATPase. In 1785, William

Withering, a British physician, heard tales of an elderly woman, known as "the old woman of Shropshire," who cured people of "dropsy" (which today would be recognized as congestive heart failure) with an extract of foxglove. Withering conducted the first scientific study of the effects of foxglove on congestive heart failure and documented its effectiveness.

P-type ATPases are evolutionarily conserved and play a wide range of roles

Analysis of the complete yeast genome revealed the presence of 16 proteins that clearly belong to the P-type ATPase family. More-detailed sequence analysis suggests that two of these proteins transport H^+ ions, two transport Ca^{2+}, three transport Na^+, and two transport metals such as Cu^{2+}. In addition, five members of this family appear to participate in the transport of phospholipids with amino acid head groups. These five proteins help maintain membrane asymmetry by transporting lipids such as phosphatidylserine from the outer to the inner leaflet of the bilayer membrane. Such enzymes have been termed *flippases*. Remarkably, the human genome encodes 70 P-type ATPases. All members of this protein family employ the same fundamental mechanism: the free energy of ATP hydrolysis drives membrane transport by means of conformational changes, which are induced by the addition and removal of a phosphoryl group at an analogous aspartate site in each protein.

Multidrug resistance highlights a family of membrane pumps with ATP-binding cassette

domains

Studies of human disease have revealed another large and important family of active-transport proteins, with structures and mechanisms quite different from those of the P-type ATPase family. These pumps were identified from studies on tumor cells in culture that developed resistance to drugs that had been initially quite toxic to the cells. Remarkably, the development of resistance to one drug had made the cells less sensitive to a range of other compounds, a phenomenon known as **multidrug resistance**.

In a significant discovery, the onset of multidrug resistance was found to correlate with the expression and activity of a membrane protein with an apparent molecular mass of 170 kDa. This protein acts as an ATP-dependent pump that extrudes a wide range of small molecules from cells that express it. The protein is called the *multidrug-resistance (MDR) protein* or *P-glycoprotein* ("glyco" because it includes a carbohydrate moiety). Thus, when cells are exposed to a drug, the MDR pumps the drug out of the cell before the drug can exert its effects.

Analysis of the amino acid sequences of MDR and homologous proteins revealed a common architecture (**Figure 13.8A**). Each protein comprises four domains: two membrane-spanning domains and two ATP-binding domains. The ATP-binding domains of these proteins are called **ATP-binding cassettes (ABCs)** and are homologous to domains in a large family of transport proteins in bacteria and archaea. Transporters that include these domains are called **ABC transporters**. With 79 members, the ABC transporters are the largest single family identified in the *E. coli* genome. The human genome includes more than 150 ABC transporter genes.

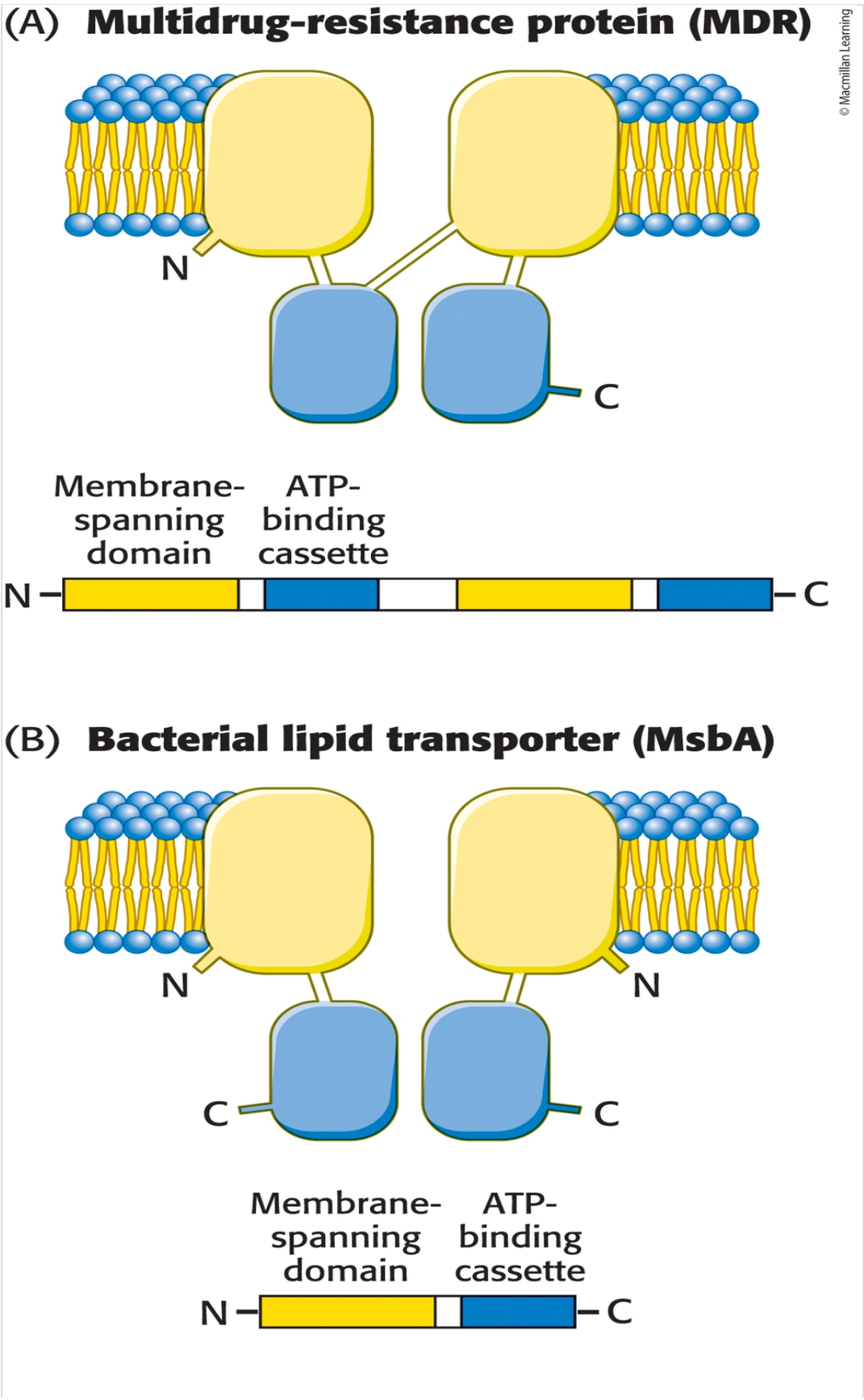

(A) Multidrug-resistance protein (MDR)
© Macmillan Learning
N
C
Membrane-spanning domain
ATP-binding cassette
N
C
(B) Bacterial lipid transporter (MsbA)
N
N
C
C
Membrane-spanning domain
ATP-binding cassette
N
C

FIGURE 13.8 ABC transporter are a large family of membrane pumps that share a common architecture. These proteins are composed of two transmembrane domains and two ATP-binding domains called ATP-binding cassettes (ABCs). (A) The multidrug-resistance protein is a single polypeptide chain containing all four domains, whereas (B) the bacterial lipid transporter MsbA consists of a dimer of two identical chains, containing one of each domain.

The three-dimensional structures of several members of the ABC transporter family have now been determined, including that of the bacterial lipid transporter MsbA. In contrast with the eukaryotic MDR protein, this protein is a dimer of 62-kDa chains: the amino-terminal half of each protein contains the membrane-spanning domain, and the carboxyl-terminal half contains the ATP-binding cassette (Figure 13.8B). Prokaryotic ABC proteins are often made up of multiple subunits, such as a dimer of identical chains, or as a heterotetramer of two membrane-spanning domain subunits and two ATP-binding-cassette subunits. The two ATP-binding cassettes are in contact, but they do not interact strongly in the absence of bound ATP (Figure 13.9A). The consolidation of the enzymatic activities of several polypeptide chains in prokaryotes to a single chain in eukaryotes is a theme that we will see again.

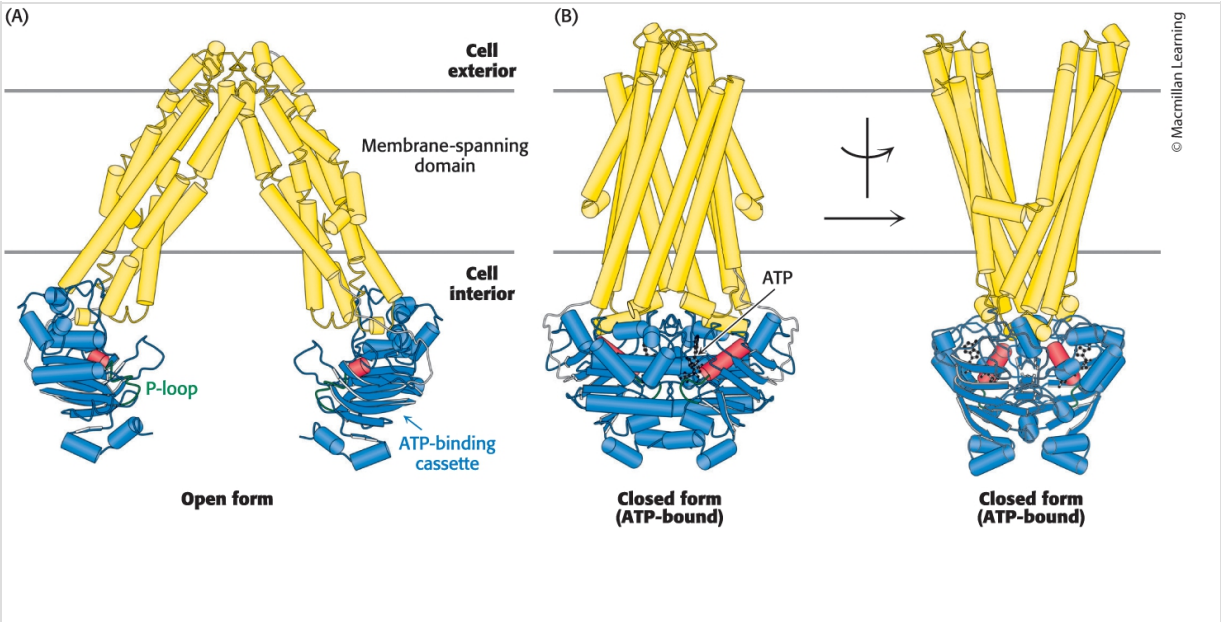


FIGURE 13.9 ABC transporters undergo significant conformational change upon ATP binding. Two structures of the bacterial lipid transporter MsbA, a representative ABC transporter: (A) The nucleotide-free, inward-facing form and (B) the ATP-bound, outward-facing form is shown in two views (rotated by 90 degrees). Upon nucleotide binding, the two ATP-binding cassettes (blue) interact strongly with one another, resulting in reorientation of the substrate binding site. The gray lines indicate the extent of the plasma membrane.

[Drawn from 3B5W.pdb and 3B60.pdb.]

INTERACT with this model in Achieve

On the basis of several solved structures of ABC transporters, combined with data from other experiments, a mechanism for active transport by these proteins has been proposed (Figure 13.10):

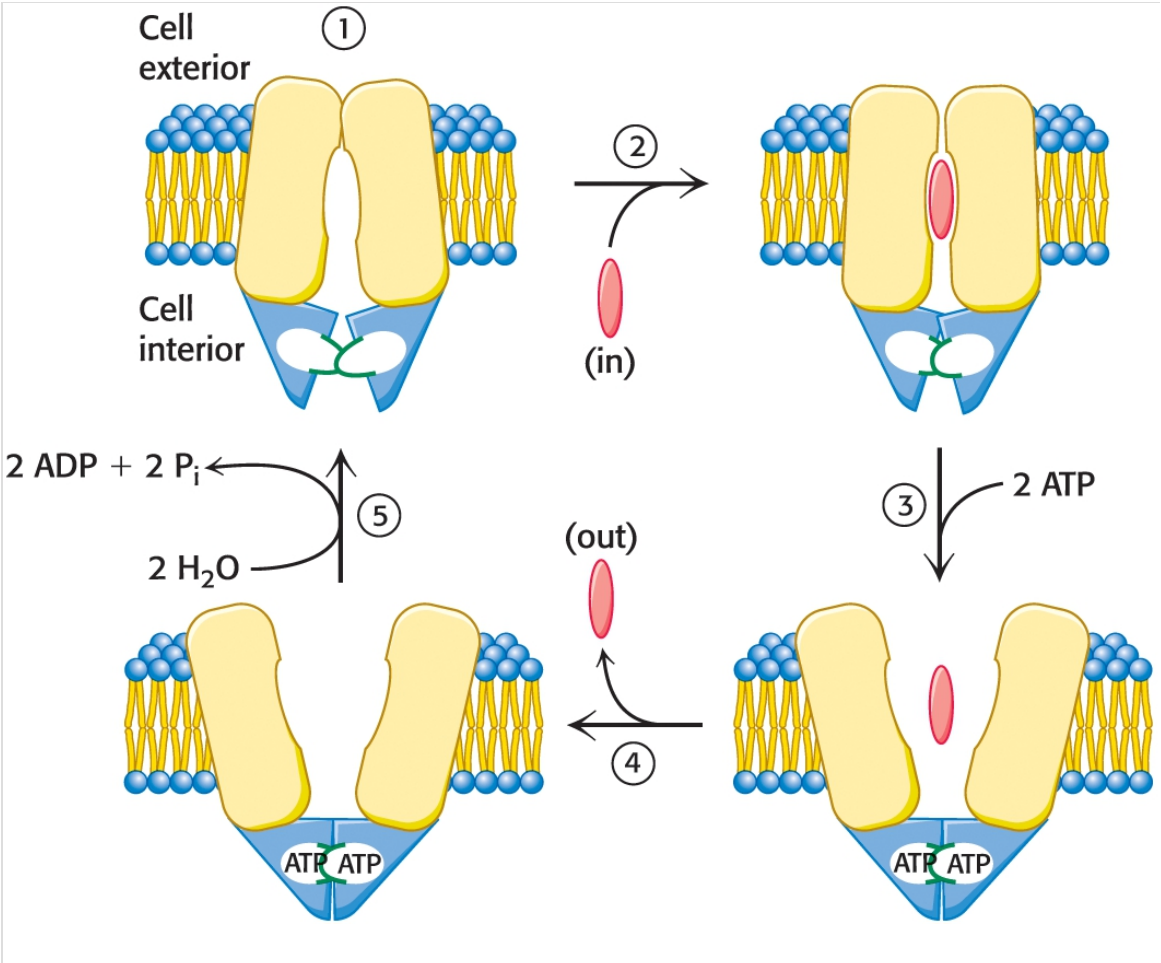


FIGURE 13.10 The open surface of ABC transporters alternates between conformations based on the presence of bound nucleotide. The mechanism includes the following steps: (1) opening of the channel toward the inside of the cell, (2) substrate binding and conformational changes in the ATP-binding cassettes, (3) ATP binding and opening of the channel to the opposite face of the membrane, (4) release of the substrate to the outside of the cell, and (5) ATP hydrolysis to reset the transporter to its initial state.



1. The catalytic cycle begins with the transporter free of both ATP and substrate. While the distance between the ATP-binding cassettes in this form may vary with the individual transporter, the substrate binding region of the transporter faces inward.

2. Substrate enters the central cavity of the transporter from inside the cell. Substrate binding induces conformational changes in the ATP-binding cassettes that increase their affinity for ATP.

3. ATP binds to the ATP-binding cassettes, changing their conformations so that the two domains interact strongly with one another. The close interaction of the ABCs reorients the transmembrane helices such that the substrate binding site is now facing outside the cell (**Figure 13.9B**).

4. The outward facing conformation of the transporter has reduced affinity for the substrate, enabling the release of the substrate on the opposite face of the membrane.

5. The hydrolysis of ATP and the release of ADP and inorganic phosphate reset the transporter for another cycle.

Whereas eukaryotic ABC transporters generally act to export molecules from inside the cell, prokaryotic ABC transporters often act to import specific molecules from *outside* the cell. A specific binding protein acts in concert with the bacterial ABC transporter, delivering the substrate to the transporter and stimulating ATP hydrolysis inside the cell. These binding proteins are present in the periplasm, the compartment

between the two membranes that surround some bacterial cells (Figure 12.36B).

Thus, ABC transporters use a substantially different mechanism from the P-type ATPases to couple the ATP hydrolysis reaction to conformational changes. Nonetheless, the net result is the same: The transporters are converted from one conformation capable of binding substrate from one side of the membrane to another that releases the substrate on the other side.

Self-Check Question



When SERCA is incubated with $[\gamma-{}^{32}P]$ ATP (in which the terminal phosphate is radiolabeled) and calcium, and then analyzed by gel electrophoresis, a radioactive band is observed at the molecular weight corresponding to full-length SERCA. Explain the result. Would you expect a similar band if you were performing a similar assay, with a suitable substrate, for the MDR protein?

13.3 Lactose Permease Is an Archetype of Secondary Transporters That Use One Concentration Gradient to Power the Formation of Another

Carriers are proteins that transport ions or molecules across the membrane without hydrolysis of ATP. The mechanism of carriers involves both large conformational changes and the interaction of the protein with only a few molecules per transport cycle, limiting the maximum rate at which transport can occur. Although carriers cannot mediate primary active transport — owing to their inability to hydrolyze ATP — they can couple the thermodynamically unfavorable flow of one species of ion or molecule *up* a concentration gradient to the favorable flow of a different species *down* a concentration gradient, a process referred to as **secondary active transport**. Carriers that move ions or molecules "uphill" by this means are termed **secondary transporters** or **cotransporters**.

Secondary transporters can be classified as either antiporters or symporters. **Antiporters** couple the downhill flow of one species to the uphill flow of another in the *opposite direction* across the membrane; **symporters** use the flow of one species to drive the flow of a different species in the *same direction* across the membrane. **Uniporters**, another class of carriers, are able to transport a specific species in either direction governed only by concentrations of that species on either side of the membrane (**Figure 13.11**).

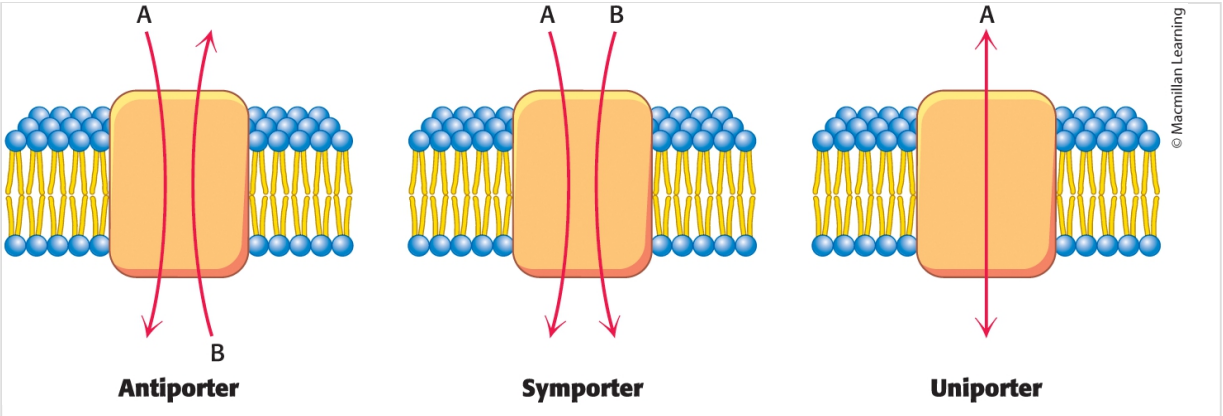


FIGURE 13.11 The three classes of secondary transporters are antiporters, symporters, and uniporters. Secondary transporters can transport two substrates in opposite directions (antiporters), two substrates in the same direction (symporters), or one substrate in either direction (uniporter).

Secondary transporters are ancient molecular machines, common today in bacteria and archaea as well as in eukaryotes. For example, approximately 160 (of around 4000) proteins encoded by the *E. coli* genome are secondary transporters. Sequence comparison and hydropathy analysis suggest that members of the largest family have 12 transmembrane helices that appear to have arisen by duplication and fusion of a membrane protein containing 6 transmembrane helices.

Lactose permease, an *E. coli* symporter, uses the H^+ gradient across the *E. coli* membrane (outside has higher H^+ concentration) generated by the oxidation of fuel molecules to drive the uptake of lactose and other sugars against a concentration gradient. This transporter has been extensively studied for many decades and is a useful archetype for this family. As expected from the sequence analysis, the lactose permease consists of two domains, each of which comprises six membrane-spanning α helices (Figure 13.12). The two domains are well separated and are joined by a single polypeptide. In this structure, a sugar

molecule lies in a pocket in the center of the protein and is accessible from a path that leads from the interior of the cell.

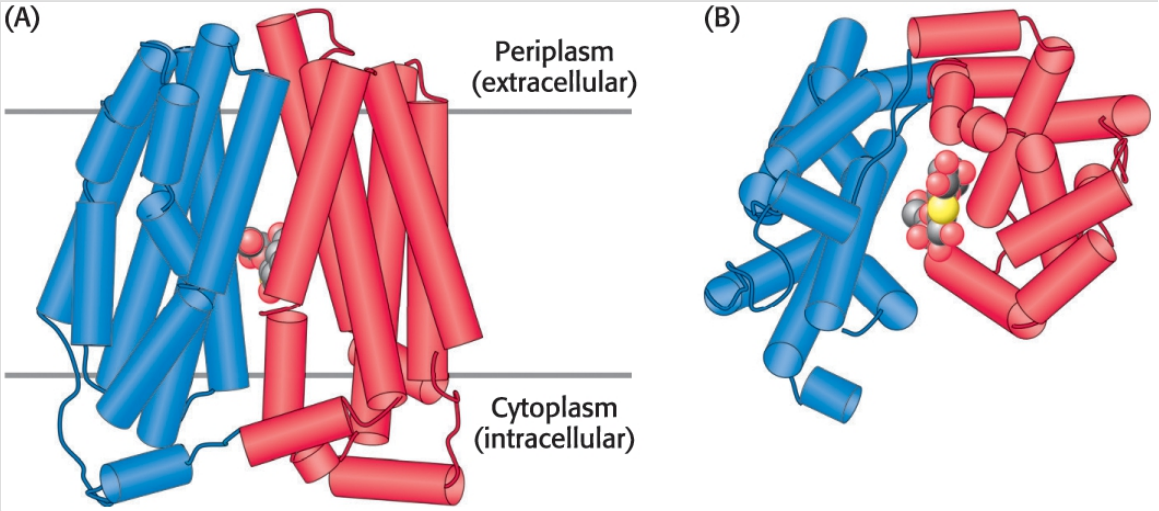


FIGURE 13.12 Lactose permease from *E. coli* is a well-studied example of a secondary transporter. The amino-terminal half of the protein is shown in blue and the carboxyl-terminal half in red. (A) Side view. The gray lines indicate the extent of the plasma membrane. (B) Botton view (from inside the cell). The protein consists of two halves that surround the sugar and are linked to one another by only a single stretch of polypeptide.

[Drawn from 1PV7.pdb.]

INTERACT with this model in Achieve

On the basis of this structure and a wide range of other experiments, a mechanism for symporter action has been developed. This mechanism (Figure 13.13) has many features similar to those for P-type ATPases and ABC transporters:

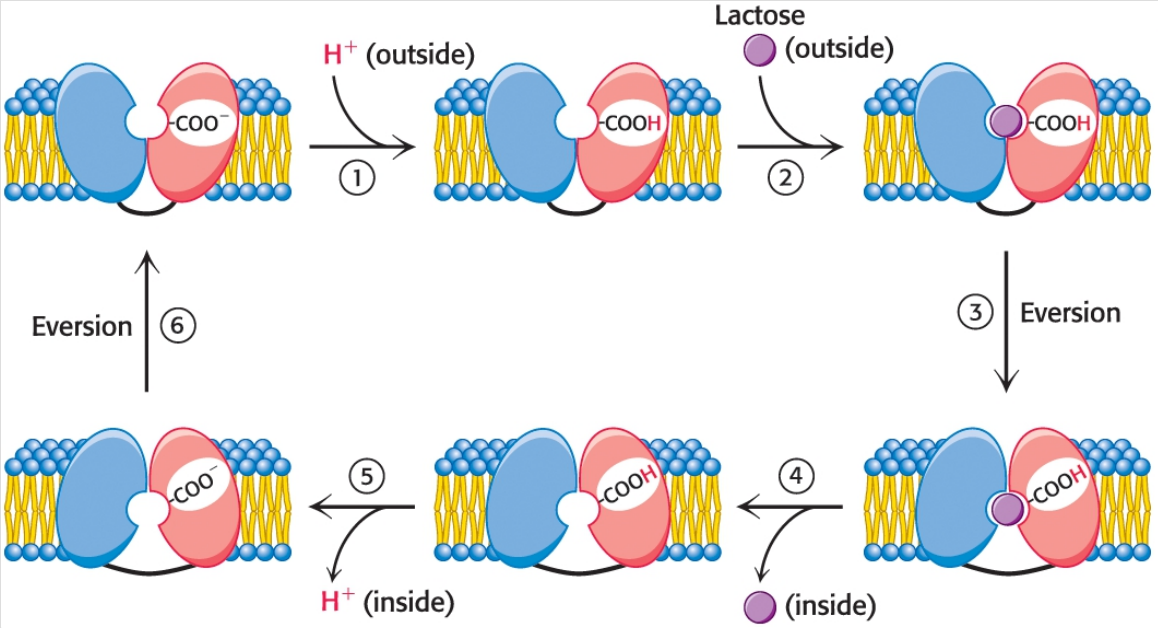


FIGURE 13.13 Lactose permease catalyzes the symport of a proton and lactose across the membrane. The mechanism begins with the permease open to the outside of the cell (upper left). The permease binds a proton from the outside of the cell (1) and then binds its substrate (2 The permease everts (3) and then releases its substrate (4) and a proton (5) to the inside of the cell. It then everts (6) to complete the cycle.

1. The cycle begins with the two domains oriented so that the opening to the binding pocket faces outside the cell, in a conformation different from that observed in the structures solved to date. A proton from outside the cell binds to a residue in the permease, quite possibly Glu 325. Although not shown in the figure, the site of protonation likely changes in the course of this cycle.

2. In the protonated form, the permease binds lactose from outside the cell.

3. The structure everts to the form observed in the crystal structure (Figure 13.12).

4. The permease releases lactose to the inside of the cell.

5. The permease releases a proton to the inside of the cell.
6. The permease everts to complete the cycle.

It is thought that this eversion mechanism applies to all classes of secondary transporters, which resemble the lactose permease in overall architecture.

Self-Check Question



Carbonyl cyanide 4-(trifluoromethoxy) phenylhydrazone (FCCP) is a proton ionophore: it enables protons to pass freely through membranes. Treatment of *E. coli* with FCCP prevents the accumulation of lactose in these cells. Explain.

13.4 Specific Channels Can Rapidly Transport Ions Across Membranes

Pumps and carriers can move ions and substrates across the membrane at rates approaching several thousand molecules per second. Other membrane proteins, the passive-transport systems called **ion channels**, are capable of ion-transport rates that are more than 1000 times as fast. These rates of transport through ion channels are close to rates expected for ions diffusing freely through aqueous solution. Yet ion channels are not simply tubes that span membranes through which ions can rapidly flow. Instead, they are highly sophisticated molecular machines that respond to chemical and physical changes in their environments and undergo precisely timed conformational changes.

Action potentials are mediated by transient changes in Na^+ and K^+ permeability

One of the most important manifestations of ion-channel action is the nerve impulse, which is the fundamental means of communication in the nervous system. A **nerve impulse**, or **action potential**, is an electrical signal produced by the flow of ions across the plasma membrane of a neuron. The interior of a neuron, like that of most other cells, contains a high concentration of K^+ and a low concentration of Na^+. These ionic gradients are generated by the Na^+-K^+ ATPase. The cell membrane has an electrical potential determined by the ratio of the internal to the external concentration of ions. In the resting state, the membrane potential is typically $-60\ mV$. An action potential is generated when the membrane potential is depolarized beyond a critical threshold value (e.g., from -60 to $-40\ mV$). The membrane potential becomes positive within about a millisecond and attains a

value of about $+30\ mV$ before turning negative again (repolarization). This amplified depolarization is propagated along the nerve terminal (Figure 13.14).

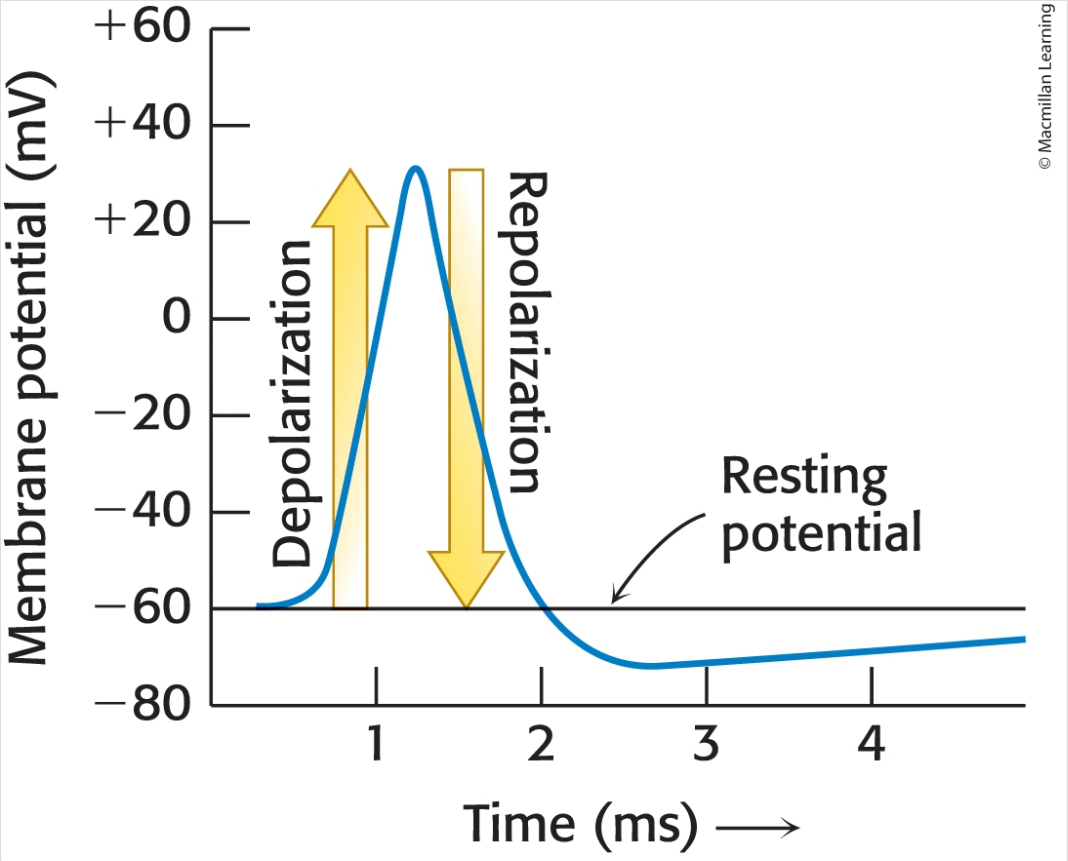


FIGURE 13.14 The action potential is a rapid electrical signal across a plasma membrane. Signals are sent along neurons by the transient depolarization and repolarization of the membrane.

Ingenious experiments carried out by Alan Hodgkin and Andrew Huxley revealed that action potentials arise from large, transient changes in the permeability of the axon membrane to Na^+ and K^+ ions. Depolarization of the membrane beyond the threshold level leads to an increase in permeability to Na^+. Sodium ions begin to flow into the cell because of

the large electrochemical gradient across the plasma membrane. The entry of Na^+ further depolarizes the membrane, leading to an added increase in Na^+ permeability. This positive feedback yields the very rapid and large change in membrane potential described above and shown in Figure 13.14.

The membrane spontaneously becomes less permeable to Na^+ and more permeable to K^+. Consequently, K^+ flows outward, and so the membrane potential returns to a negative value. The resting level of $-60\ mV$ is restored in a few milliseconds as the K^+ conductance decreases to the value characteristic of the unstimulated state. The wave of depolarization followed by repolarization moves rapidly along a nerve cell. The propagation of these waves allows a touch at the tip of your toe to be detected in your brain in a few milliseconds.

The proposal that action potentials arise from changes in Na^+ and K^+ membrane permeability postulated the existence of channels specific for these ions. These channels must open in response to changes in membrane potential and then close after having remained open for a brief period of time. The bold hypotheses of Hodgkin and Huxley predicted the existence of molecules with a well-defined set of properties long before tools existed for their direct detection and characterization.

Patch-clamp conductance measurements reveal the activities of single channels

Direct evidence for the existence of these channels was elucidated using the **patch-clamp technique**. This powerful method enables the measurement of the ion conductance through a small patch of cell

membrane (Figure 13.15). A clean glass pipette with a tip diameter of about $1\ \mu m$ is pressed against an intact cell to form a seal. Slight suction leads to the formation of a very tight seal so that the resistance between the inside of the pipette and the bathing solution is many gigaohms (1 gigaohm is equal to 10^9 ohms). Thus, a gigaohm seal (called a *gigaseal*) ensures that an electric current flowing through the pipette is identical with the current flowing through the membrane covered by the pipette. The gigaseal makes possible high-resolution current measurements while a known voltage is applied across the membrane.

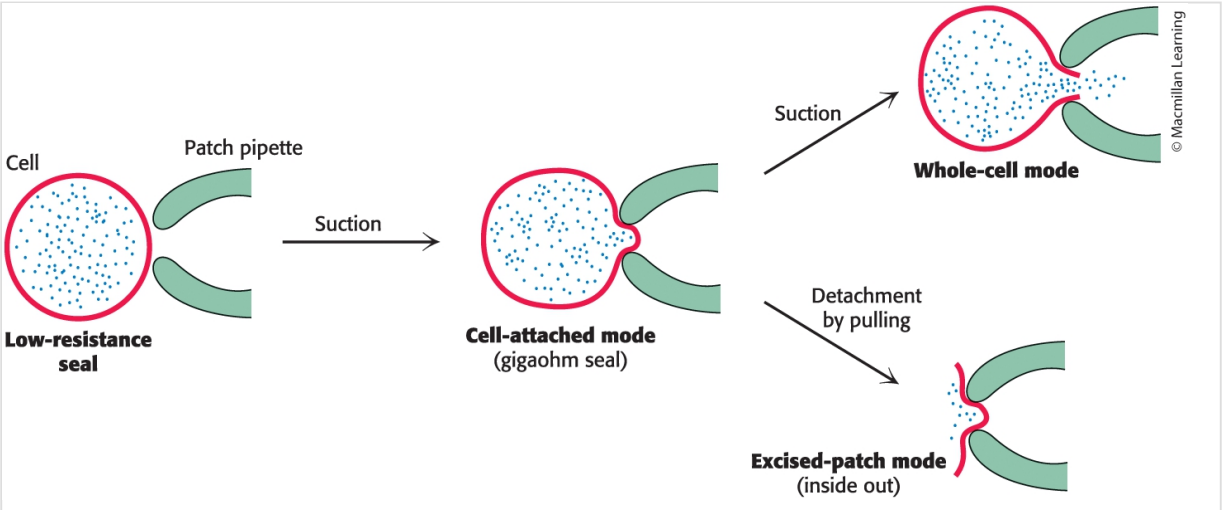


FIGURE 13.15 The patch-clamp technique for monitoring channel activity is highly versatile. A high-resistance seal (gigaseal) is formed between the pipette and a small patch of plasma membrane. This configuration is called the *cell-attached mode*. The breaking of the membrane patch by increased suction produces a low-resistance pathway between the pipette and the interior of the cell. The activity of the channels in the entire plasma membrane can be monitored in this *whole-cell mode*. To prepare a membrane in the *excised-patch mode*, the pipette is pulled away from the cell. A piece of plasma membrane with its cytoplasmic side now facing the medium is monitored by the patch pipette.

Remarkably, the flow of ions through a single channel and transitions between the open and closed states of a channel can be monitored with a time resolution of microseconds (Figure 13.16). Furthermore, the

activity of a channel in its native membrane environment, even in an intact cell, can be directly observed. Patch-clamp methods provided one of the first views of single biomolecules in action. Subsequently, other methods for observing single molecules were invented, opening new vistas on biochemistry at its most fundamental level.

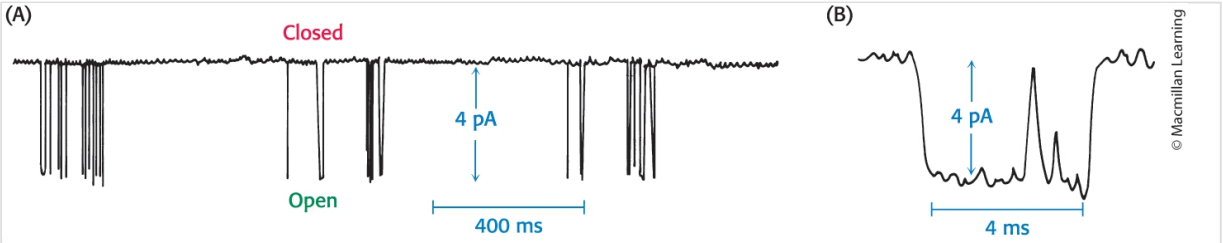
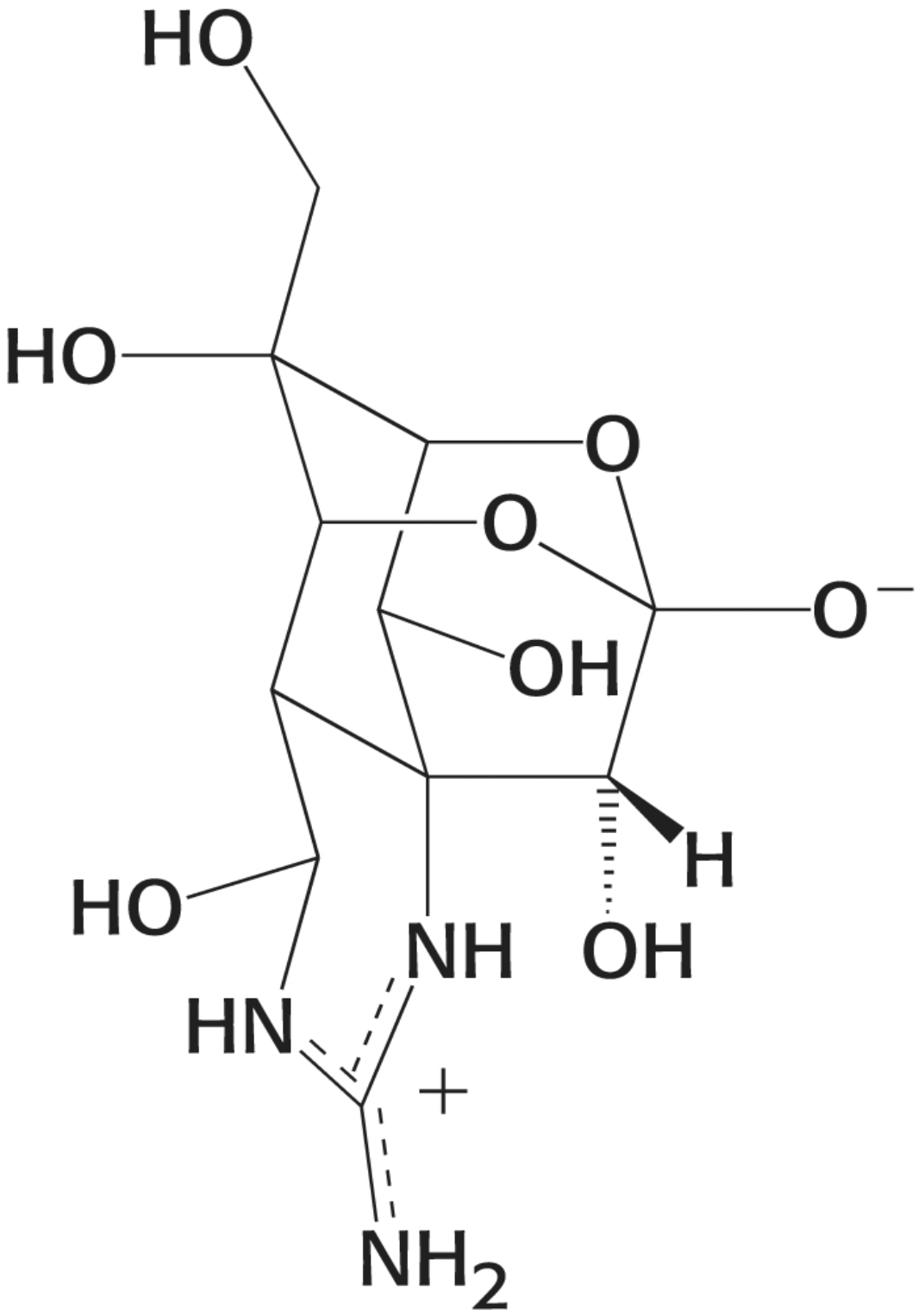


FIGURE 13.16 Patch-clamp methods enable the observation of ion movement across single channels. (A) The results of a patch-clamp experiment reveal the small amount of current, measured in picoamperes (pA, 10^{-12} amperes), passing through a single ion channel. The downward spikes indicate transitions between closed and open states. (B) Closer inspection of one of the spikes in (A) reveals the length of time the channel is in the open state.

The structure of a potassium ion channel is an archetype for many ion-channel structures

With the existence of ion channels firmly established by patch-clamp methods, scientists sought to identify the molecules that form ion channels. The Na^+ channel was first purified from the electric organ of the electric eel, which is a rich source of the protein forming this channel. The channel was purified on the basis of its ability to bind tetrodotoxin, a neurotoxin from the puffer fish that binds to Na^+

channels very tightly ($K_i \approx 1$ nM). The lethal dose of this poison for an adult human being is about 10 ng.



Tetrodotoxin

The isolated Na^+ channel is a single 260-kDa chain. Cloning and sequencing of cDNAs encoding Na^+ channels revealed that the channel contains four internal repeats, each having a similar amino acid sequence, suggesting that gene duplication and divergence have produced the gene for this channel (Figure 13.17A). Hydrophobicity profiles indicate that each repeat contains five hydrophobic segments (S1, S2, S3, S5, and S6). Each repeat also contains a highly positively charged S4 segment; positively charged arginine or lysine residues are present at nearly every third residue. It was proposed that segments S1 through S6 are membrane-spanning α helices, while the positively charged residues in S4 act as the voltage sensors of the channel. Ca^{2+} channels also share the same sequence pattern as Na^+ channels.

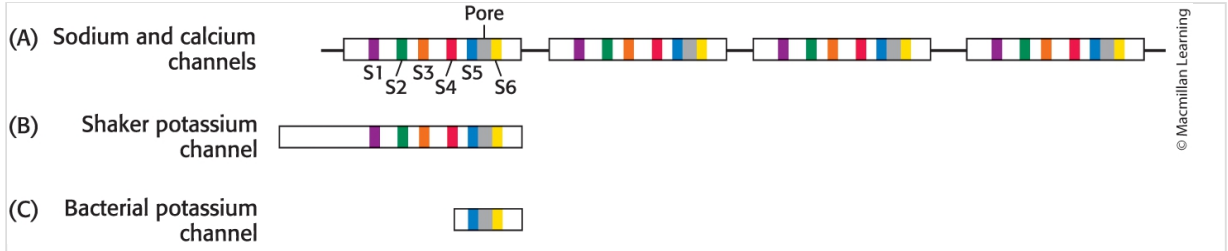


FIGURE 13.17 Ion channels share structural features. Like colors indicate structurally similar regions of the (A) sodium and calcium channels, (B) the Shaker potassium channel, and (C) the bacterial potassium channel. Each of these channels exhibits approximate fourfold symmetry, either within one chain (sodium, calcium channels) or by forming tetramers (potassium channels).

The purification of K^+ channels proved to be much more difficult because of their low abundance and the lack of known high-affinity

ligands comparable to tetrodotoxin. The breakthrough came in studies of mutant fruit flies that shake violently when anesthetized with ether. The mapping and cloning of the gene, termed *Shaker*, responsible for this phenotype revealed the amino acid sequence encoded by a K^+-channel gene. The *Shaker* gene encodes a 70-kDa protein that contains sequences corresponding to segments S1 through S6 in one of the repeated units of the Na^+ channel (**Figure 13.17B**). Thus, a K^+-channel subunit is homologous to one of the repeated units of Na^+ channels. Consistent with this homology, four Shaker polypeptides come together to form a functional channel. Bacterial K^+ channels have also been discovered that contain only the two membrane-spanning regions corresponding to segments S5 and S6 (**Figure 13.17C**). This and other information suggested that S5 and S6 — including the region between them — form the actual pore in the K^+ channel and that segments S1 through S4 contain the apparatus that opens the pore.

In 1998, Roderick MacKinnon and coworkers determined the structure of a K^+ channel from the bacterium *Streptomyces lividans* by x-ray crystallography. This channel contains only the pore-forming segments S5 and S6. As expected, the K^+ channel is a tetramer of identical subunits, each of which includes two membrane-spanning α helices (**Figure 13.18**). The four subunits come together to form a pore in the shape of a cone that runs through the center of the structure.

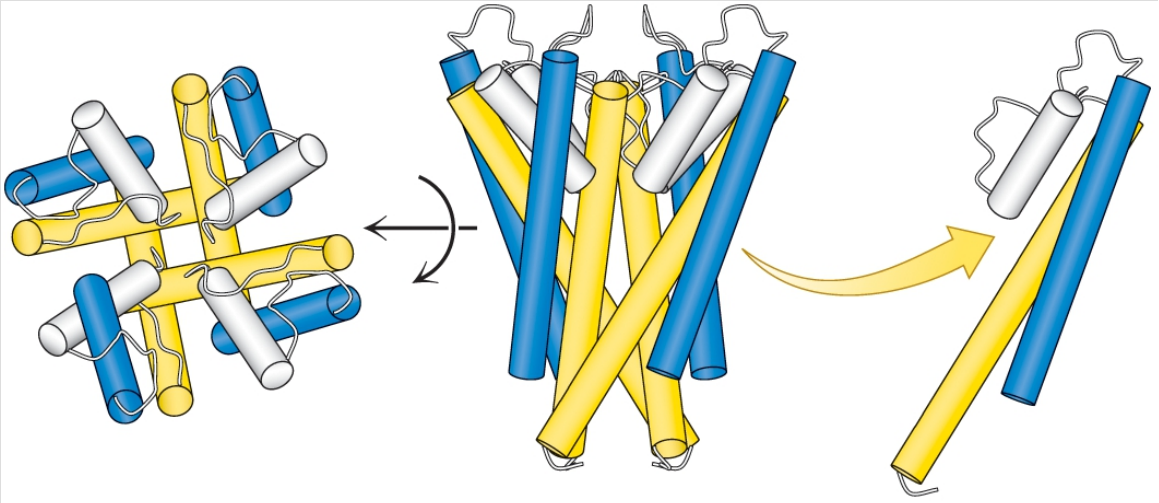


FIGURE 13.18 The bacterial potassium ion channel forms a pore at the center of a tetrameric complex. The K^+ channel, composed of four identical subunits, is cone shaped, with the large opening facing the inside of the cell (center). A view down the pore, looking toward the outside the cell, shows the relations of the individual subunits (left). One of the four identical subunits c the pore is illustrated at the right, with the pore-forming region shown in gray.

[Drawn from 1K4C.pdb.]



University of Utah

BALDOMERO OLIVERA After completing his PhD and postdoctoral training in the United States, Dr. Baldomero "Toto" Olivera returned to his native Philippines to start a faculty position. There, he began studying toxins from readily available cone snails, with which he was familiar from shell-collecting as a child. Cone snails deploy these potent toxins to paralyze their prey. Using chromatography, Dr. Olivera and his coworkers separated the toxins into hundreds of components that they then injected directly into the nervous system of mice. They discovered that each component could induce specific behavioral responses, and subsequent studies revealed that many components can bind and inhibit a single ion channel or pump in a highly specific manner. The different peptide toxins, now called *conotoxins*, are powerful tools, and

one has been developed into a drug to treat intractable pain. In the mid-1970s, Dr. Olivera moved to the University of Utah, where he is now Distinguished Professor of Biology.

The structure of the potassium ion channel reveals the basis of ion specificity

The structure of the bacterial potassium channel revealed much about how these proteins efficiently and selectively transport ions across a membrane. Beginning from the inside of the cell, the pore starts with a diameter of approximately 10 Å and then constricts to a smaller cavity with a diameter of 8 Å (**Figure 13.19**). Both the opening to the outside and the central cavity of the pore are filled with water, and a K^+ ion can fit in the pore without losing its shell of bound water molecules. Approximately two-thirds of the way through the membrane, the pore becomes more constricted (3-Å diameter, shaded yellow in **Figure 13.19**), and at that point, any K^+ ions must give up their water molecules and interact directly with groups from the protein. The channel structure effectively reduces the thickness of the membrane from 34 Å to 12 Å by allowing the solvated ions to penetrate into the membrane before the ions must directly interact with the channel.

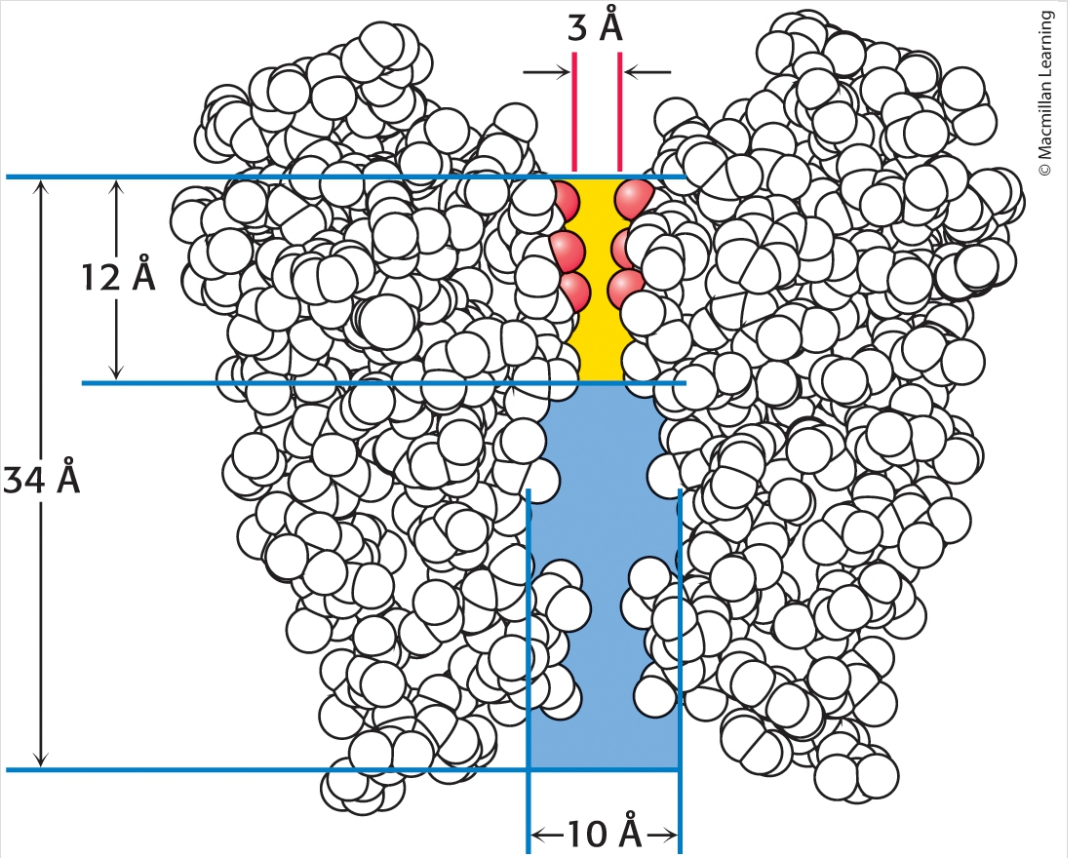


FIGURE 13.19 The path through the potassium channel features only a short region where the ion must be desolvated. A potassium ion entering the K^+ channel can pass a distance of 22 Å into the membrane while remaining solvated with water (blue). At this point, the pore diameter narrows to 3 Å (yellow), and potassium ions must shed their water and interact with carbonyl groups (red) of the pore amino acids.

The restricted part of the pore is built from residues contributed by the two transmembrane α helices. In particular, a five-amino-acid stretch within this region functions as the **selectivity filter** that determines the preference for K^+ over other ions (Figure 13.20). The stretch has the sequence Thr-Val-Gly-Tyr-Gly (TVGYG), and is nearly completely conserved in all K^+ channels. The region of the strand containing the conserved sequence lies in an extended conformation and is oriented

such that the peptide carbonyl groups are directed into the channel, in good position to interact with the desolvated potassium ions.

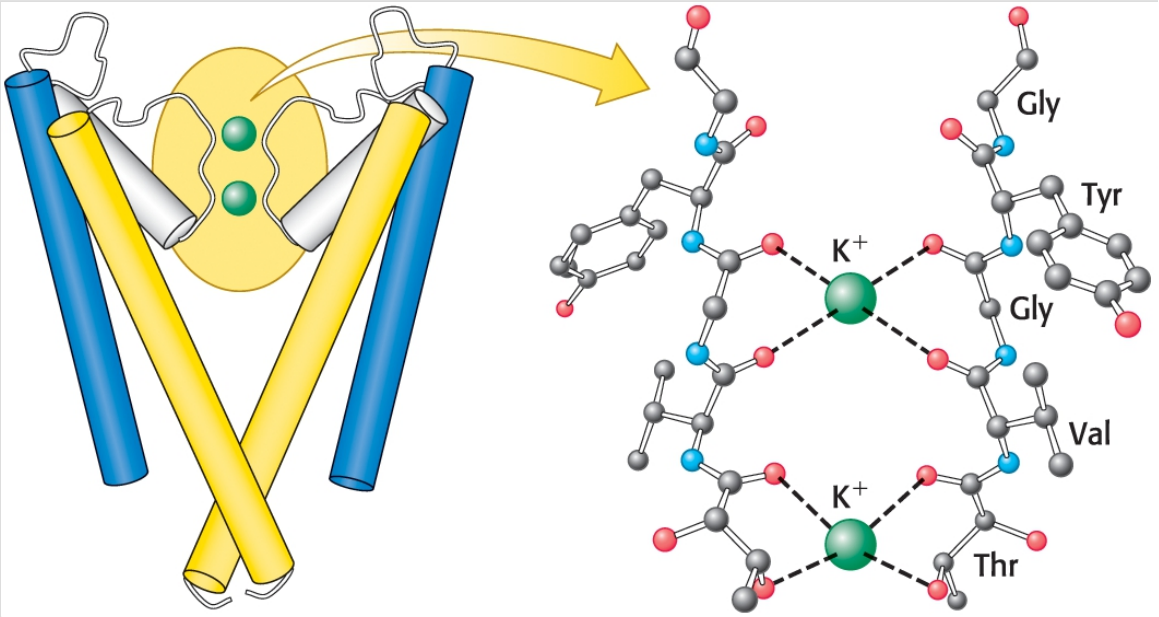


FIGURE 13.20 The selectivity filter determines the preference of the channel for K^+ over oth

ions. Potassium ions interact with the carbonyl groups of the TVGYG sequence of the selectivity filter, located at the 3-Å-diameter pore of the K^+ channel. Only two of the four channel subuni are shown.

Potassium ion channels are 100-fold more permeable to K^+ than to Na^+. How is this high degree of selectivity achieved? Ions having a radius larger than 1.5 Å cannot pass into the narrow diameter (3 Å) of the selectivity filter of the K^+ channel. However, a desolvated Na^+ is small enough (Table 13.1) to pass through the pore. Indeed, the ionic radius of Na^+ is substantially smaller than that of K^+. How then is Na^+ rejected?

TABLE 13.1 Properties of alkali cations

Ion	Ionic radius (Å)	Hydration free energy in $kJ\ mol^{-1}(kcal\ mol^{-1})$
Li^+	0.60	−410(−98)
Na^+	0.95	−301(−72)
K^+	1.33	−230(−55)
Rb^+	1.48	−213(−51)
Cs^+	1.69	−197(−47)

The key point is that the free-energy costs of dehydrating ions are considerable. For example, Table 13.1 reveals that the cost of dehydrating Na^+ is $301\ kJ\ mol^{-1}$($72\ kcal\ mol^{-1}$), while that of K^+ is $230\ kJ\ mol^{-1}$ ($55\ kcal\ mol^{-1}$). The channel pays the cost of desolvating K^+ by providing optimal compensating interactions with the carbonyl oxygen atoms lining the selectivity filter. Careful studies of the potassium channel, enabled by the determination of its three-dimensional structure, have revealed that the interior of the pore is a highly dynamic, fluid environment. The favorable resolvation interactions between the carbonyl oxygen atoms, which carry a partial negative charge, with the cation are balanced by the repulsion of these oxygen atoms from one another. For this channel, the ideal balance is achieved with K^+, but not with Na^+ (**Figure 13.21**). Hence, sodium ions are rejected because the higher energetic cost of dehydrating them would not be recovered.

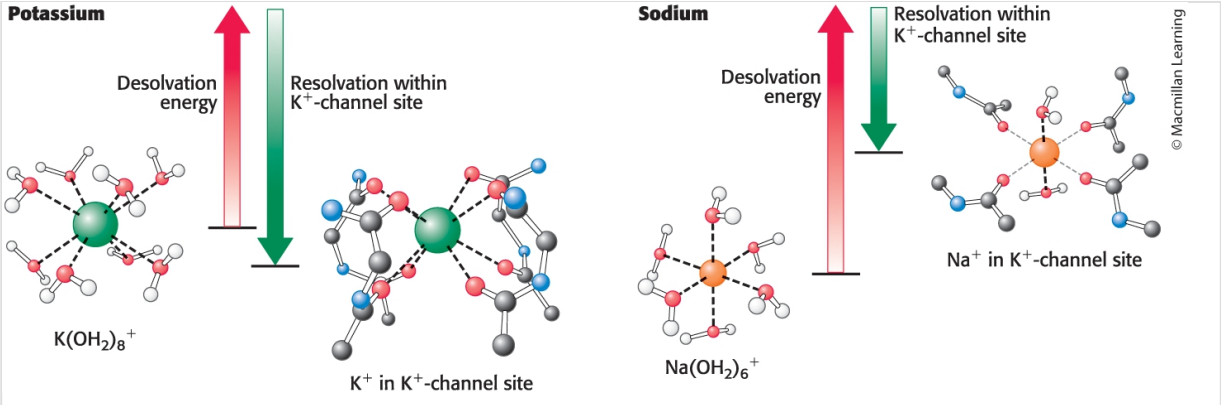


FIGURE 13.21 Ion selectivity is driven by the energetic balance between ion desolvation and coordination within the selectivity filter. The energy cost of dehydrating a potassium ion is compensated by favorable interactions with the selectivity filter. Because a sodium ion is too small to interact favorably with the selectivity filter, the free energy of desolvation cannot be compensated and the sodium ion does not pass through the channel.

The K^+ channel structure enables a clearer understanding of the structure and function of Na^+ and Ca^{2+} channels because of their homology to K^+ channels (Figure 13.17). Sequence comparisons and the results of mutagenesis experiments have implicated the region between segments S5 and S6 in ion selectivity in the Ca^{2+} channel. In Ca^{2+} channels, one glutamate residue of this region in each of the four repeated units plays a major role in determining ion selectivity (**Figure 13.22**). Residues in the positions corresponding to the glutamate residues in Ca^{2+} channels are major components of the selectivity filter of the Na^+ channel. These residues — aspartate, glutamate, lysine, and alanine — are located in each of the internal repeats of the Na^+ channel, forming a region termed the DEKA locus. Thus, the potential fourfold symmetry of the channel is clearly broken in this region, which explains why Na^+ channels consist of a single large polypeptide chain

rather than a noncovalent assembly of four identical subunits. The preference of the Na^+ channel for Na^+ over K^+ depends on ionic radius; the diameter of the pore determined by these residues and others is sufficiently restricted that small ions such as Na^+ and Li^+ can pass through the channel, but larger ions such as K^+ are significantly hindered.

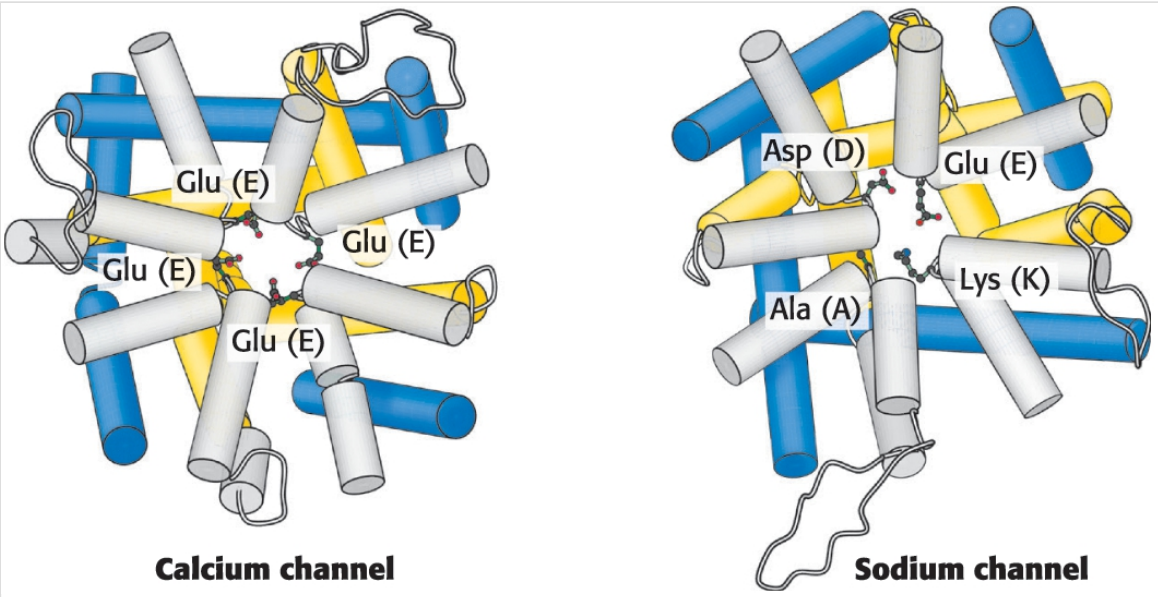


FIGURE 13.22 The amino acids defining the selectivity filter differ between calcium and sodium channels. The pores of eukaryotic calcium and sodium channels are comprised of sing polypeptide chains. In these views, we are looking down the pore; for simplicity, only the S5 (blue), S6 (yellow), and pore-forming (white) regions are drawn. The selectivity filter for the calcium channel contains four glutamate (E) residues, while the filter for the sodium channel contains four different residues (the DEKA locus): aspartate (D), glutamate (E), lysine (K), and alanine (A).

[Drawn from 5GJV.pdb and 5X0M.pdb.]

The structure of the potassium ion channel explains its rapid rate of transport

The tight binding sites required for ion selectivity should slow the progress of ions through a channel, yet ion channels achieve rapid rates of ion transport. How is this paradox resolved? A structural analysis of the channel at high resolution provides an appealing explanation. Consider the process of ion conductance starting from inside the cell (Figure 13.23). Four K^+-binding sites crucial for rapid ion flow are present in the constricted region of the K^+ channel. A hydrated potassium ion proceeds into the channel and through the relatively unrestricted part of the channel. The ion then gives up its coordinated water molecules and binds to a site within the selectivity-filter region. The ion can move between the four sites within the selectivity filter because they have similar ion affinities. As each subsequent potassium ion moves into the selectivity filter, its positive charge will repel the potassium ion at the nearest site, causing it to shift to a site farther up the channel and in turn push upward any potassium ion already bound to a site farther up. Thus, each ion that binds anew favors the release of an ion from the other side of the channel. This multiple-binding-site mechanism solves the paradox of high ion selectivity and rapid flow.

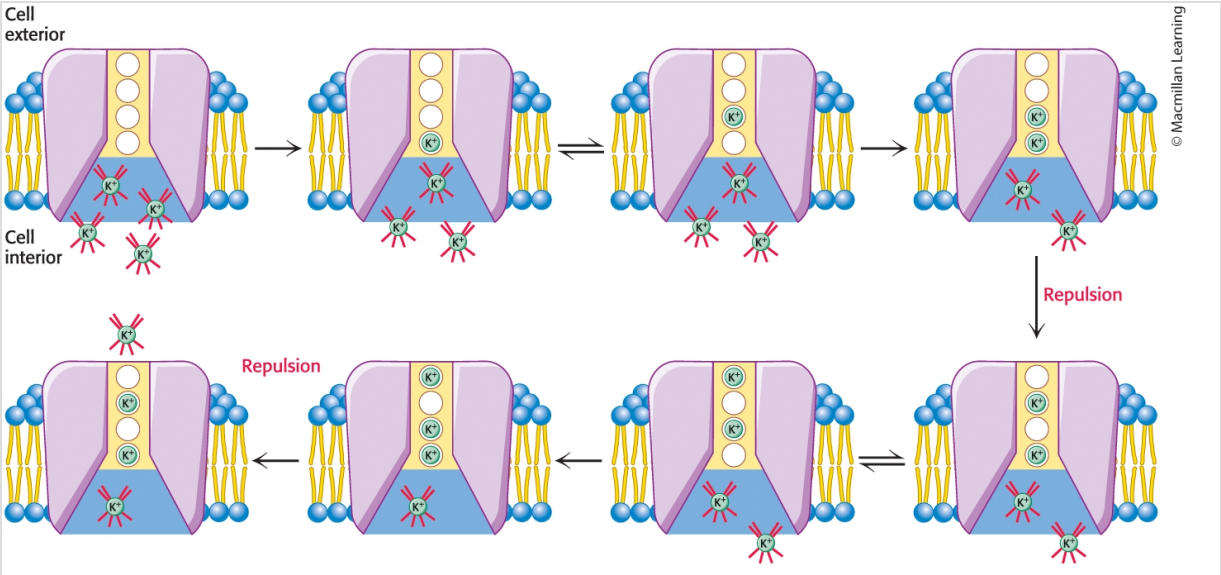


FIGURE 13.23 The model for K^+-channel ion transport relies on multiple ion binding sites within the pore. The selectivity filter has four binding sites. Hydrated potassium ions can enter these sites, one at a time, losing their hydration shells. When two ions occupy adjacent sites, electrostatic repulsion forces them apart. Thus, as ions enter the channel from one side, other ions are pushed out the other side.



Self-Check Question



The K^+ channel and the Na^+ channel have similar structures and are arranged in the same orientation in the cell membrane. Yet the Na^+ channel allows sodium ions to flow into the cell and the K^+ channel allows potassium ions to flow out of the cell. Explain.

Voltage gating requires substantial conformational changes in specific ion-channel domains

Na^+ and K^+ channels are gated by membrane potential; that is, they change conformation to a highly conducting form in response to changes in voltage across the membrane. As already noted, these voltage-gated channels include segments S1 through S4 in addition to the pore itself formed by S5 and S6. The structure of a voltage-gated K^+ channel from *Aeropyrum pernix* reveals that the segments S1 through S4

form domains, termed *paddles*, that extend from the core of the channel (Figure 13.24). These paddles include the segment S4, the voltage sensor itself. Segment S4 forms an α helix lined with positively charged residues. In contrast with expectations, segments S1 through S4 are not enclosed within the protein but, instead, are positioned to lie in the membrane itself.

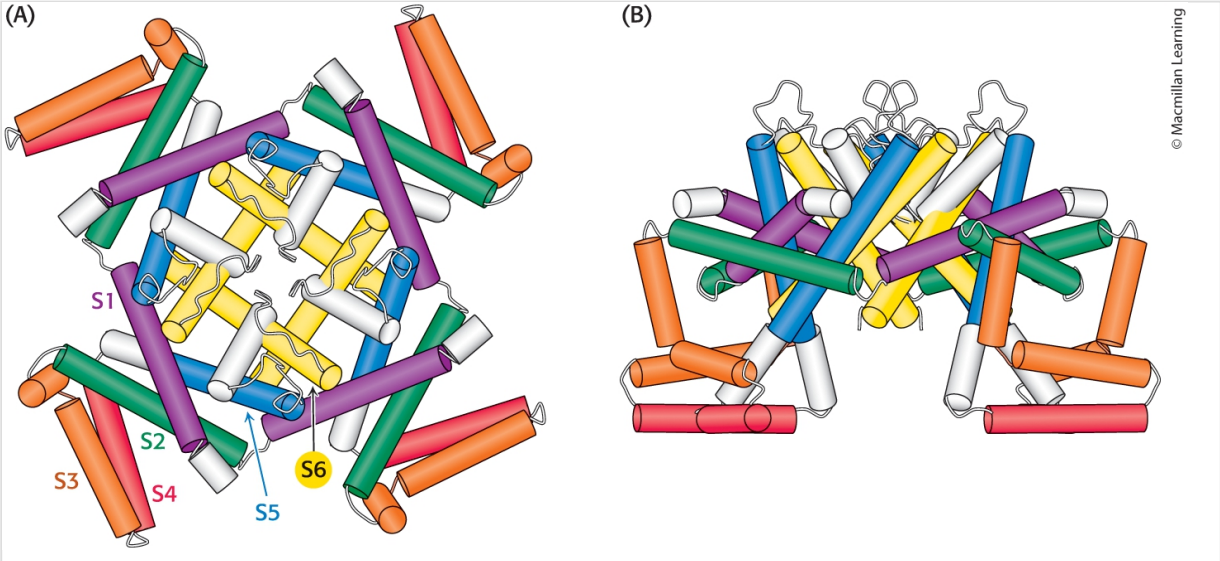


FIGURE 13.24 The S4 region lies on the outer surface of the voltage-gated potassium channel. (A) A view looking down through the pore and (B) a side view of the structure are shown. The positively charged S4 region (red) lies on the outside of the structure at the bottom of the pore.

[Drawn from 1ORQ.pdb.]

A model for voltage gating has been proposed by Roderick MacKinnon and coworkers on the basis of this structure and a range of other experiments (Figure 13.25). In the closed state, the paddles lie in a "down" position. On membrane depolarization, the cytoplasmic side of the membrane becomes more positively charged, repelling the paddles through the membrane into an "up" position. In this position, they pull the four sides of the base on the pore apart, increasing access to the selectivity filter and opening the channel.

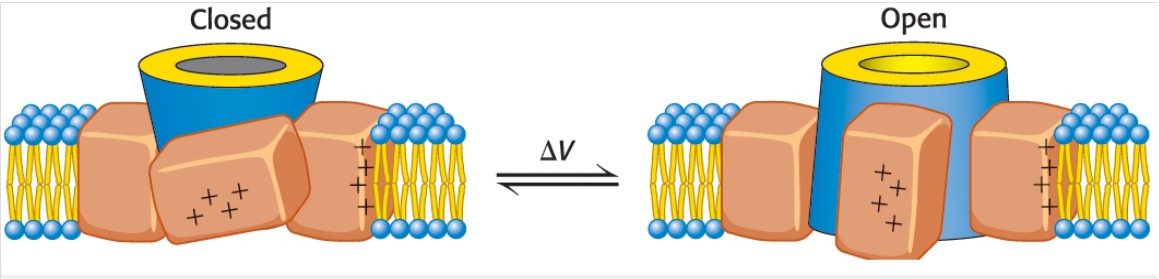


FIGURE 13.25 Movement of the S4 region controls the opening of the voltage-gated potassiu channel. The voltage-sensing paddles lie in the "down" position below the closed channel (left) Membrane depolarization pulls these paddles through the membrane. The motion pulls the ba of the channel apart, opening the channel (right).

A channel can be inactivated by occlusion of the pore: the ball-and-chain model

The K^+ channel and the Na^+ channel undergo inactivation within milliseconds of opening (Figure 13.26A). A first clue to one mechanism of inactivation came from exposing the cytoplasmic side of either channel to the protease trypsin. Cleavage by trypsin produced trimmed channels that stayed persistently open after depolarization, suggesting that a flexible (i.e., accessible to protease) region of the protein was responsible for inactivation. Furthermore, a mutant Shaker channel lacking 42 amino acids near the amino terminus opened in response to depolarization but did not inactivate (Figure 13.26B). Remarkably, inactivation was restored by adding a synthetic peptide corresponding to the first 20 residues of the native channel (Figure 13.26C).

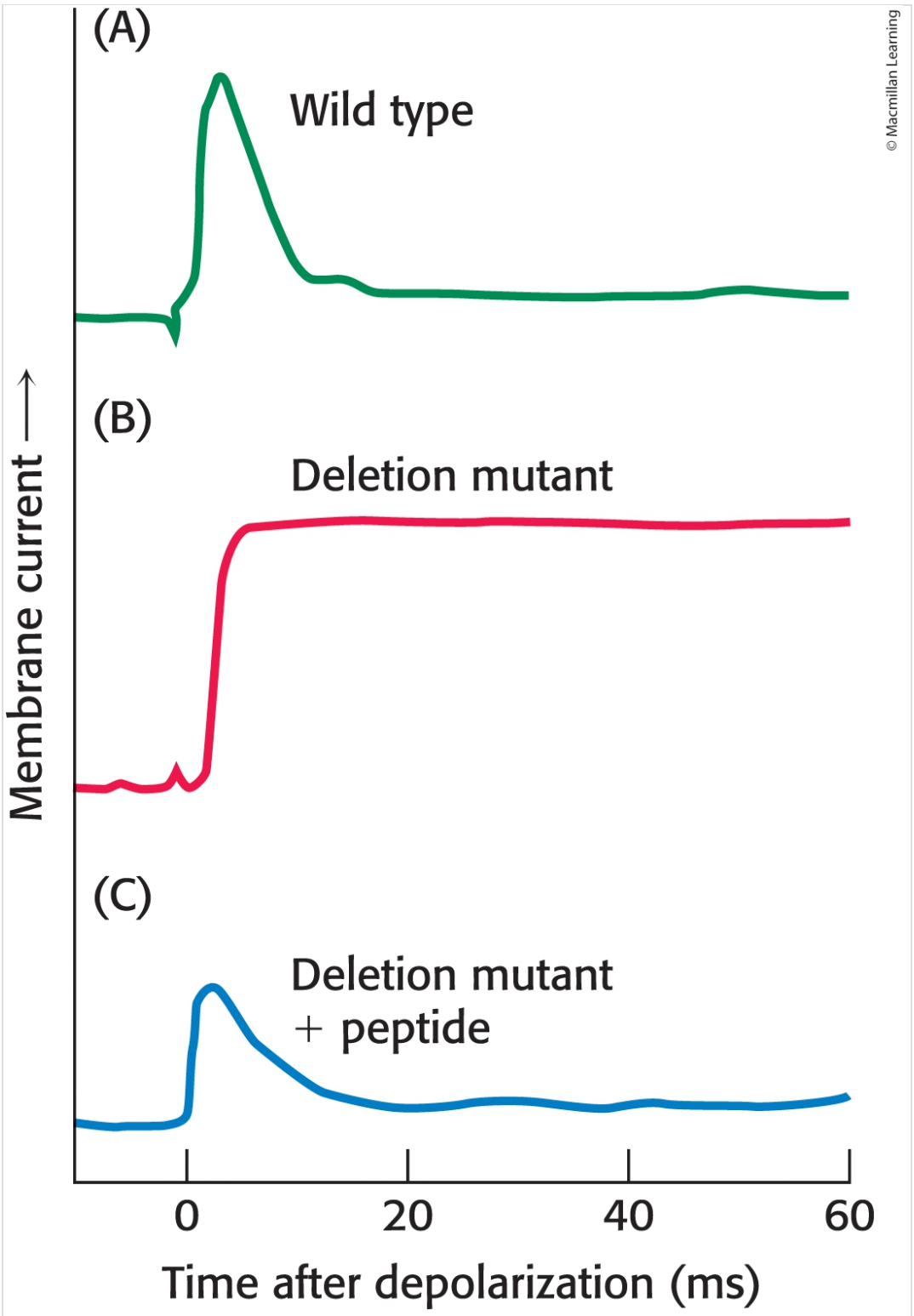


FIGURE 13.26 The amino-terminal region of the K^+ channel is critical for inactivation. (A) The wild-type Shaker K^+ channel displays rapid inactivation after

opening. (B) A mutant channel lacking residues 6 through 46 does not inactivate. (C) Inactivation can be restored by adding a peptide consisting of residues 1 through 20 at a concentration of $100\ \mu M$.

[Data from W. N. Zagotta, T. Hoshi, and R. W. Aldrich, *Science* 250:568–571, 1990.]

These experiments strongly support the **ball-and-chain model** for channel inactivation that had been proposed years earlier (**Figure 13.27**). According to this model, the first 20 residues of the K^+ channel form a cytoplasmic unit (the *ball*) that is attached to a flexible segment of the polypeptide (the *chain*). When the channel is closed, the ball rotates freely in the aqueous solution. When the channel opens, the ball quickly finds a complementary site in the open pore and occludes it. Hence, the channel opens for only a brief interval before it undergoes inactivation by occlusion. Shortening the chain speeds inactivation because the ball finds its target more quickly. Conversely, lengthening the chain slows inactivation. Thus, the duration of the open state can be controlled by the length and flexibility of the tether. In some senses, the "ball" domains, which include substantial regions of positive charge, can be thought of as large, tethered cations that are pulled into the open channel but get stuck and block further ion conductance.

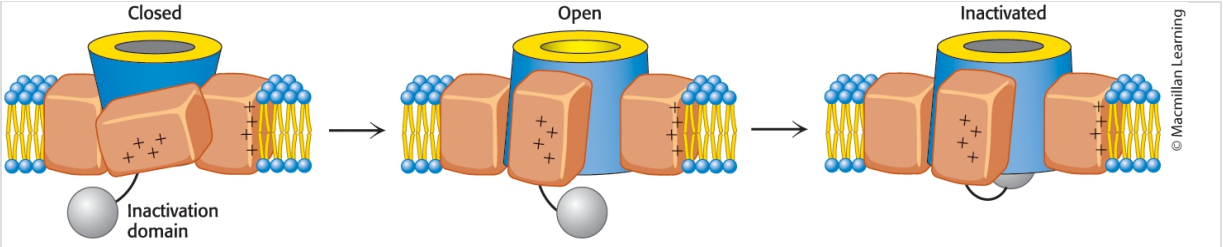
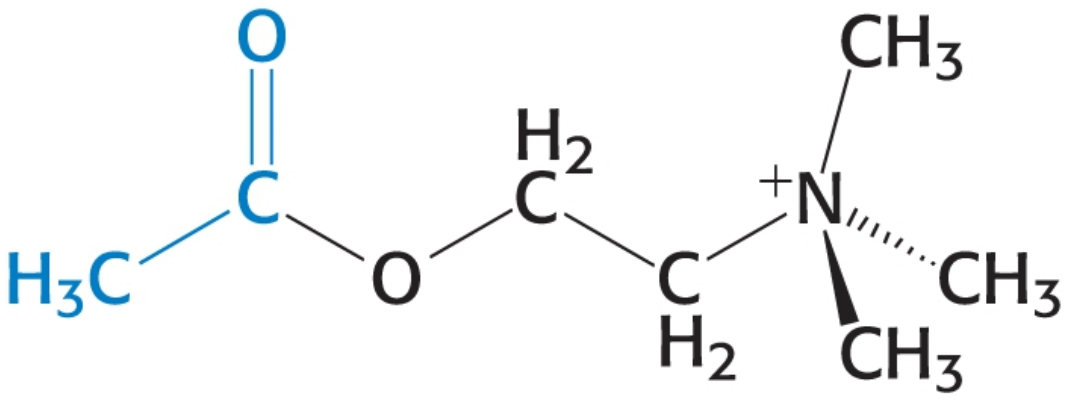


FIGURE 13.27 The ball-and-chain model provides a mechanism for channel inactivation. The inactivation domain, or "ball" (gray), is tethered to the channel by a flexible "chain." In the closed state, the ball is located in the cytoplasm. Depolarization opens the channel and creates a binding site for the positively charged ball in the mouth of the pore. Movement of the ball into this site inactivates the channel by occluding it.

It is apparent from the example in Figure 13.27 that the closed and inactivated states of the ion channel are not identical. The process of returning the inactivated channel to its initial closed state, termed **recovery**, requires disengagement of the ball domain from the pore opening as well as realignment of the voltage-sensing paddles. Depending upon the mechanism of inactivation, recovery can take milliseconds to seconds. Importantly, while inactivated, the channel cannot be opened by further membrane depolarization. As we shall see, the time needed for channel recovery has implications for repeated action potential generation.

The acetylcholine receptor is an archetype for ligand-gated ion channels

Nerve impulses are communicated across synapses by small, diffusible molecules called **neurotransmitters**. For example, one function of the neurotransmitter acetylcholine is to stimulate skeletal muscle contraction when released by contacting neurons. The presynaptic membrane of a synapse is separated from the postsynaptic membrane by a gap of about 50 nm called the **synaptic cleft**. The arrival of a nerve impulse at the end of an axon leads to the synchronous export of the contents of some 300 membrane-bound compartments, or vesicles, of acetylcholine into the cleft (**Figure 13.28**). The binding of acetylcholine to the postsynaptic membrane markedly changes its ionic permeability, triggering an action potential. Acetylcholine opens a single kind of cation channel, called the *acetylcholine receptor*, which is almost equally permeable to Na^+ and K^+.



Acetylcholine

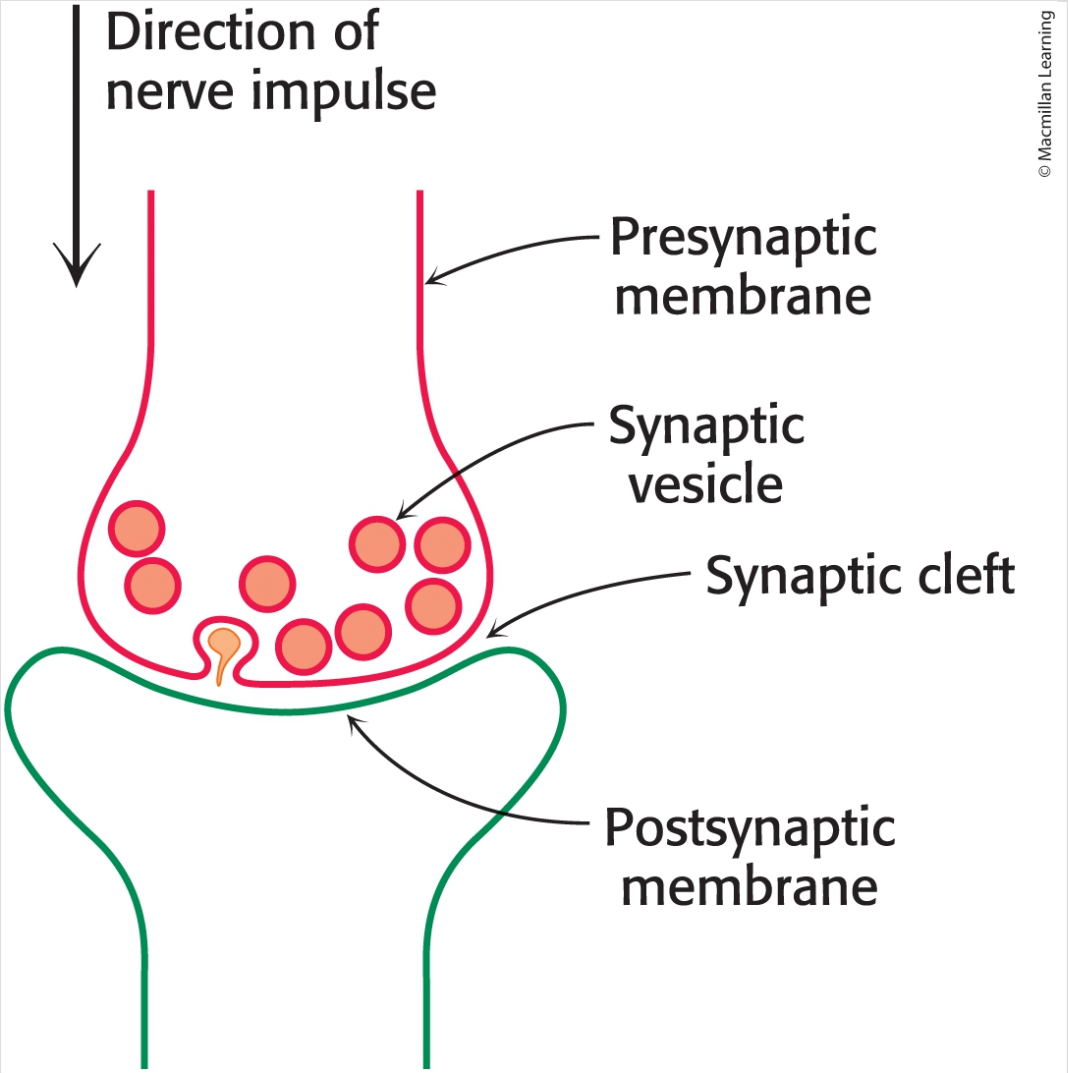


FIGURE 13.28 The synapse is the gap between cells where nerve impulses are transmitted.

The acetylcholine receptor is the best-understood **ligand-gated channel**, a channel that is gated not by voltage but by the presence of specific ligands. The binding of acetylcholine to the channel is followed by its transient opening. The electric organ of *Torpedo marmorata*, an electric ray (**Figure 13.29**), is a choice source of acetylcholine receptors for study because its electroplaxes (voltage-generating cells) are very rich in postsynaptic membranes densely packed with acetylcholine

receptors $(\sim 20{,}000\ \mu m^{-2})$ and therefore highly responsive to this neurotransmitter.



A. Martin UW Photography/Moment/Getty Images

FIGURE 13.29 The marbled electric ray (*Torpedo marmorata*) has an electric organ rich in acetylcholine receptors. These organs, called electroplaxes, can deliver a shock of as much as 200 V for approximately 1 second.

In order to study the acetylcholine receptor in molecular detail, biochemists solubilized the protein by adding a nonionic detergent to a postsynaptic membrane preparation from the electric organ and purified it by affinity chromatography on a column bearing covalently attached cobratoxin, a small protein toxin from snakes that has a high affinity for acetylcholine receptors. With the use of techniques presented in Chapter 4, the 268-kDa receptor was identified as a pentamer of four kinds of membrane-spanning subunits — α_2, β, γ, and δ. The cloning and sequencing of the cDNAs for the four kinds of subunits (50–58 kDa) showed that they have clearly similar sequences; the genes for the α, β, γ, and δ subunits arose by duplication and

divergence of a common ancestral gene. Each subunit has a large extracellular domain, followed at the carboxyl end by four predominantly hydrophobic segments that span the bilayer membrane.

Using cryo-EM and x-ray crystallographic methods (Section 4.5), the structure of purified acetylcholine receptors has been determined to have approximate fivefold symmetry, in harmony with the similarity of its five constituent subunits (**Figure 13.30A**). The subunits are arranged in the form of a ring that creates a pore through the membrane. Acetylcholine binds at the $\alpha-\gamma$ and $\alpha-\delta$ interfaces (**Figure 13.30B**).

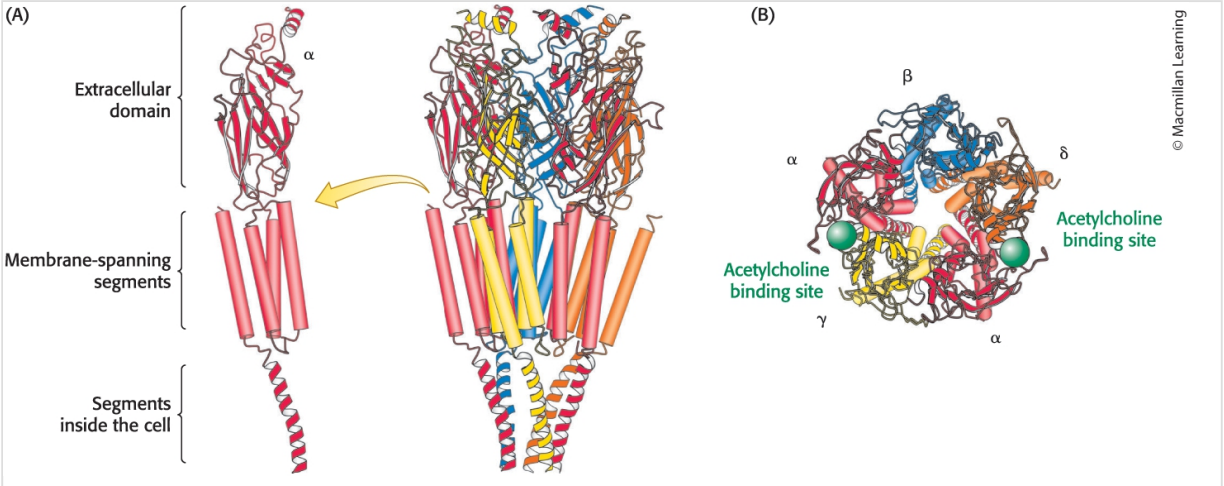


FIGURE 13.30 The acetylcholine receptor is a pentamer formed from four different subunit proteins. A model for the structure of the acetylcholine receptor deduced from high-resolution electron microscopic studies reveals that each subunit consists of a large extracellular domain consisting primarily of β strands, four membrane-spanning α helices, and a final α helix inside the cell. (A) A side view shows the pentameric receptor with each subunit type in a different color. One copy of the α subunit is shown in isolation. (B) A view down the channel from outside the cell shows the pore opening as well as the binding sites for the acetylcholine ligand, indicated in green.

[Drawn from 2BG9.pdb.]

INTERACT with this model in Achieve

What is the basis of channel opening in the acetylcholine receptor? A high-resolution answer to this question has remained elusive, but the details of this mechanism are becoming apparent. Cryo-EM images of the receptor in the open and closed states have been determined, albeit at low resolution. These structures indicate that the binding of acetylcholine to the extracellular domain ultimately leads to the straightening of the α-helices from the α and δ subunits that line the pore (Figure 13.31). In the closed state, the region of narrowest diameter in the pore (the "gate") is located about midway through the membrane. This region is lined with nonpolar residues, which cannot form favorable interactions with K^+ and Na^+ ions. However, once the helices are straightened, the region of narrowest diameter shifts closer to the inner membrane leaflet. This region is lined with polar residues and can conduct K^+ and Na^+ ions freely.

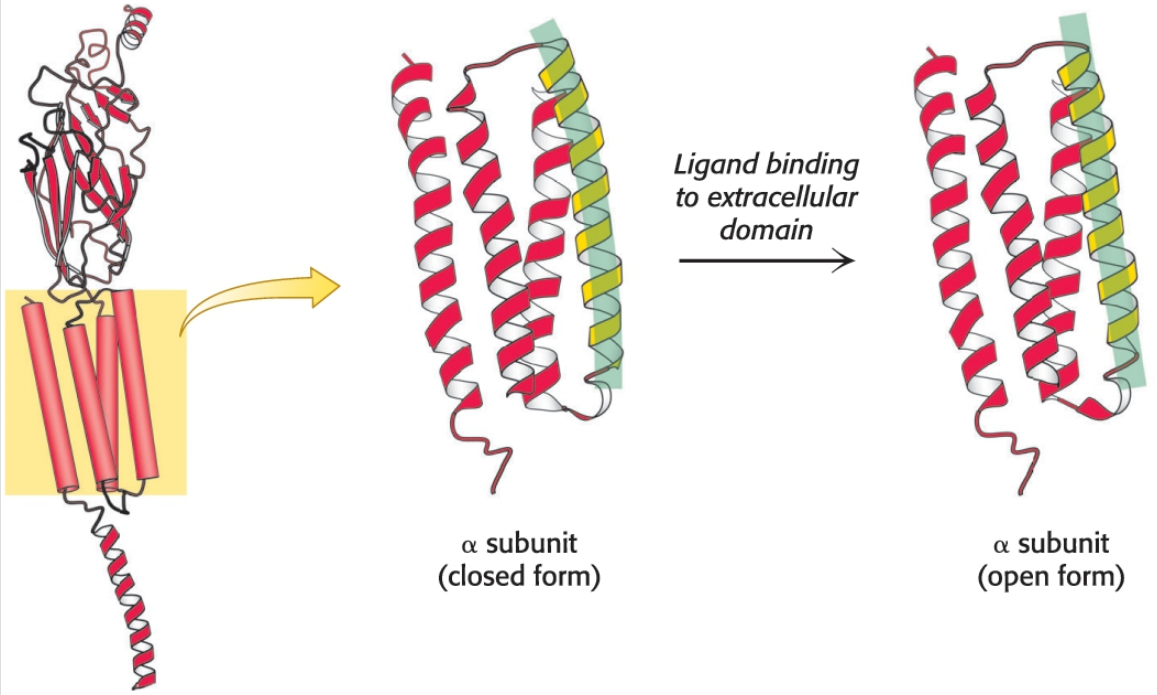


FIGURE 13.31 Ligand binding induces the opening of the acetylcholine receptor. Binding of acetylcholine to the extracellular region of the receptor leads to a series of conformational changes that are transmitted to the pore-lining helices. Notice that upon ligand binding, the pore-lining helix of the α subunit straightens (green bar). This subtle structural adjustment changes the gating properties of the pore, enabling cations to pass through.

[Drawn from 4AQ5.pdb and 4AQ9.pdb.]

Action potentials integrate the activities of several ion channels working in concert

To see how ligand-gated and voltage-gated channels work together to generate a sophisticated physiological response, we now revisit the action potential introduced at the beginning of this section. First, we need to introduce the concept of **equilibrium potential**. Suppose that a membrane separates two solutions that contain different concentrations of some cation X^+, as well as an equivalent amount of anions to balance the charge in each solution (**Figure 13.32**).

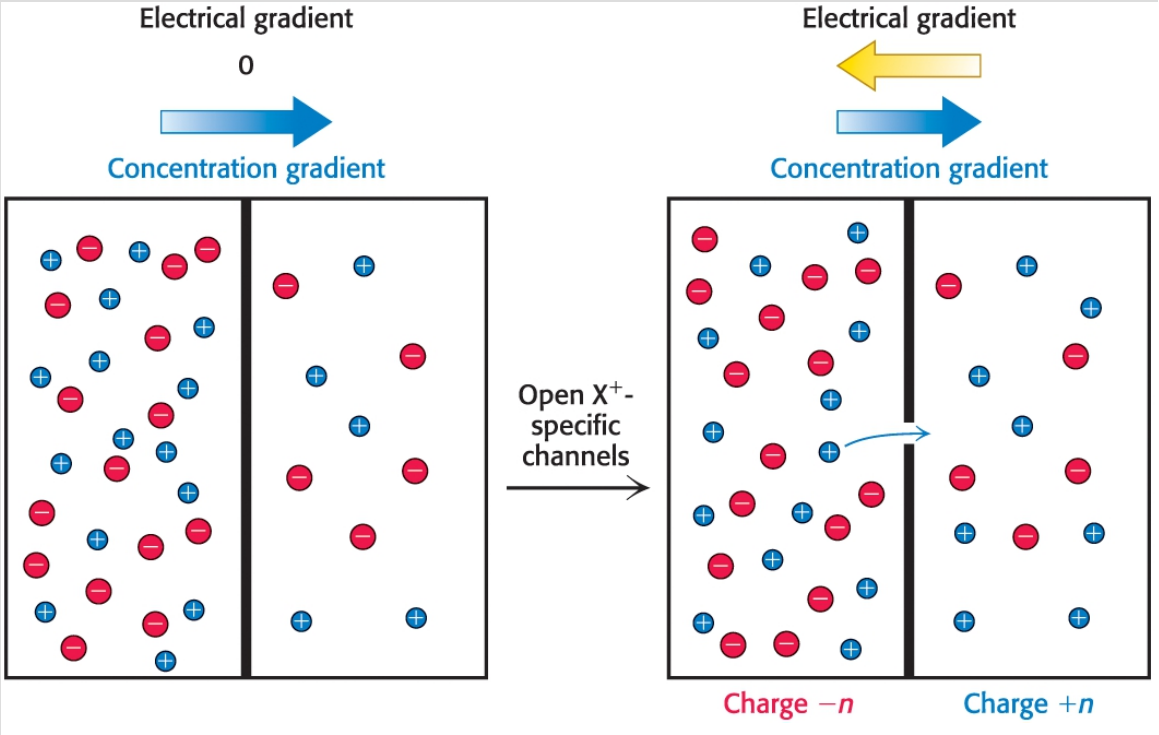


FIGURE 13.32 The equilibrium potential represents the balance between chemical and electrical gradients. The membrane potential reaches equilibrium when the driving force due t

the concentration gradient is exactly balanced by the opposing force due to the repulsion of like charges.



Let $[X^+]_{in}$ be the concentration of X^+ on one side of the membrane (corresponding to the inside of a cell) and $[X^+]_{out}$ be the concentration of X^+ on the other side (corresponding to the outside of a cell). Now let us assume that an ion channel opens that allows X^+ to move across the membrane. What will happen? It seems clear that X^+ will move through the channel from the side with the higher concentration to the side with the lower concentration. However, positive charges will start to accumulate on the side with the lower concentration, making it more difficult to move each additional positively charged ion. An equilibrium will be achieved when the driving force due to the concentration gradient is balanced by the electrostatic force resisting the motion of an additional charge. In these circumstances, the membrane potential is given by the Nernst equation:

$$V_{eq} = -(RT/zF)\ln([X]_{in}/[X]_{out})$$

where R is the gas constant and F is the Faraday constant ($96.5\ \text{kJ V}^{-1}\text{mol}^{-1}$, or $23.1\ \text{kcal V}^{-1}\text{mol}^{-1}$) and z is the charge on the ion X (e.g., $+1$ for X^+).

The membrane potential at equilibrium is called the equilibrium potential for a given ion at a given concentration ratio across a membrane. For sodium with $[Na^+]_{in} = 14\ \text{mM}$ and $[Na^+]_{out} = 143\ \text{mM}$,

the equilibrium potential is $+62\ \text{mV}$ at $37°\text{C}$. Similarly, for potassium with $[K^+]_{in} = 157\ \text{mM}$ and $[K^+]_{out} = 4\ \text{mM}$, the equilibrium potential is $-98\ \text{mV}$. In the absence of stimulation, the resting potential for a typical neuron is $-60\ \text{mV}$. This value is close to the equilibrium potential for K^+ owing to the fact that a small number of K^+ channels are open.

Example

Calculating Equilibrium Potentials

Problem:

For a typical mammalian cell, the intracellular and extracellular concentrations are of the calcium ion (Ca^{2+}) are $0.2\ \mu\text{M}$ and 1.8 mM, respectively. Calculate the equilibrium potential at 37° for Ca^{2+}.

Getting Started:

This problem represents a fairly straightforward application of the Nernst equation:

$$V_{eq} = -(RT/zF)\ln([X]_{in}/[X]_{out})$$

The most common pitfalls made in the application of this equation are mixing up the inside and outside concentrations and applying the incorrect ion charge (z). The calcium ion is a divalent cation, so $z = +2$.

Calculate:

Using the concentrations given (note that the two concentrations are given in different units!), substitute into the Nernst equation:

$$V_{eq} = -(RT/zF)\ln([X]_{in}/[X]_{out})$$

$$V_{eq} = -\left(\frac{(8.315 \times 10^{-3}\ \text{kJ mol}^{-1}\ \text{deg}^{-1}) \times (310\ \text{deg})}{(+2) \times (96.5\ \text{kJ V}^{-1}\ \text{mol}^{-1})}\right)\ln\left(\frac{0.0002\ \text{mM}}{1.8\ \text{mM}}\right)$$

$$V_{eq} = +122\ \text{mV}$$

Reflect:

Calcium ions are maintained at a very low intracellular concentration, owing to the activity of Ca^{2+} pumps such as SERCA. Hence, the equilibrium potential is quite high, over 120 millivolts. Cells are highly sensitive to changes in intracellular Ca^{2+}, which can be exploited by signal transduction pathways (Section 14.2).

We are now prepared to consider what happens in the generation of an action potential (**Figure 13.33**):

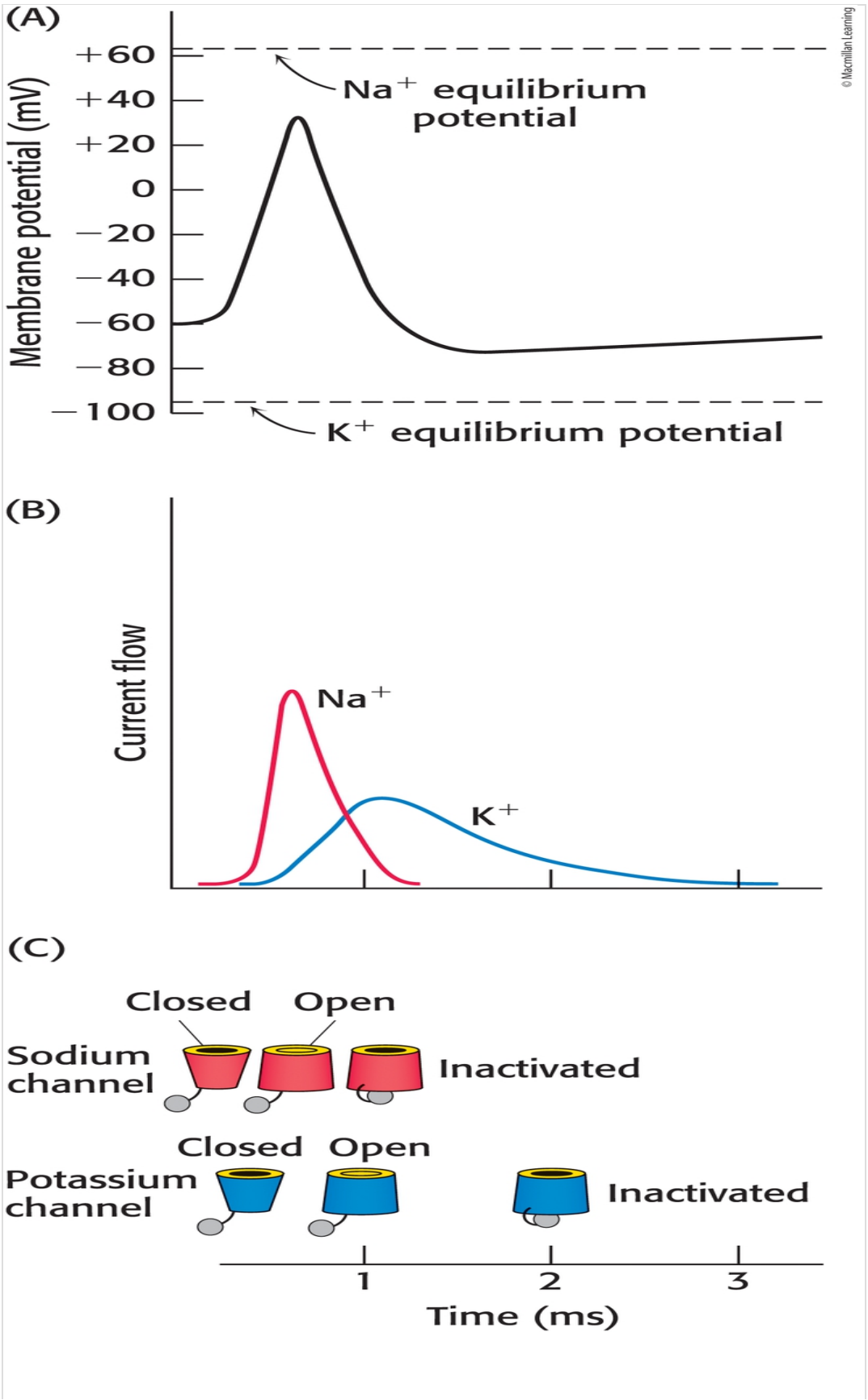

(A)
Membrane potential (mV)
+60
+40
+20
0
−20
−40
−60
−80
−100
Na+ equilibrium potential
K+ equilibrium potential
© Macmillan Learning
(B)
Current flow
Na+
K+
(C)
Closed
Open
Sodium channel
Inactivated
Closed
Open
Potassium channel
Inactivated
1
2
3
Time (ms)

FIGURE 13.33 The action potential is generated by the coordinated opening, closing, and inactivation of Na^+ and K^+ channels. (A) On the initiation of an action potential, the membrane potential moves from the resting potential upward toward the Na^+ equilibrium potential and then downward toward the K^+ equilibrium potential. (B) The currents through the Na^+ and K^+ channels underlying the action potential. (C) The states of the Na^+ and K^+ channels during the action potential.



- Initially, a neurotransmitter such as acetylcholine is released into the synaptic cleft from a presynaptic membrane (Figure 13.28). The released acetylcholine binds to the acetylcholine receptor on the postsynaptic membrane, causing it to open within less than a millisecond. The acetylcholine receptor is a nonspecific cation channel. Sodium ions flow into the cell and potassium ions flow out of the cell. Without any further events, the membrane potential would move to a value corresponding to the average of the equilibrium potentials for Na^+ and K^+, approximately $-2\ mV$.

- As the membrane potential approaches $-40\ mV$, the voltage-sensing paddles of Na^+ channels are pulled into the membrane, opening the Na^+ channels. With these channels open, sodium ions flow rapidly into the cell and the membrane potential rises rapidly toward the Na^+ equilibrium potential (Figure 13.33B, red curve).

- The voltage-sensing paddles of K^+ channels also are pulled into the membrane by the changed membrane potential, but more slowly than Na^+ channel paddles. Nonetheless, after approximately 1 ms, many K^+ channels start to open.

- As the K^+ channels open, inactivation "ball" domains plug the open Na^+ channels, decreasing the Na^+ current. The acetylcholine receptors that initiated these events are also inactivated on this time scale.
- With the Na^+ channels inactivated and only the K^+ channels open, the membrane potential drops rapidly toward the K^+ equilibrium potential (Figure 13.33B, blue curve). The open K^+ channels are susceptible to inactivation by their "ball" domains, and these K^+ currents, too, are blocked.
- With the membrane potential returned to close to its initial value, the inactivation domains are released and the channels undergo recovery to return to their original closed states. During the time preceding this recovery, the Na^+ channels cannot be reopened by membrane depolarization. Hence, a new action potential cannot be induced for a short interval, termed the **refractory period**, which usually lasts around one millisecond in neurons.

These events propagate along the neuron as the depolarization of the membrane opens channels in nearby patches of membrane. Note that the refractory period ensures that an action potential does not recur in parts of the membrane that were just depolarized. The net result is that the action potential travels along the membrane in one direction.

How much current actually flows across the membrane over the course of an action potential? Consider that a typical nerve cell contains $100\ Na^+$ channels per square micrometer. At a membrane potential of $+20\ mV$, each channel conducts 10^7 ions per second. Thus, in a period of 1 millisecond, approximately 10^5 ions flow through each square micrometer of membrane surface. Assuming a cell volume of $10^4\ \mu m^3$

and a surface area of $10^4\ \mu m^2$, this rate of ion flow corresponds to an increase in the Na^+ concentration of less than 1%. How can this be? A robust action potential is generated because the membrane potential is very sensitive to even a slight change in the distribution of charge. This sensitivity makes the action potential a very efficient means of signaling over long distances and with rapid repetition rates.

Disruption of ion channels by mutations or chemicals can be potentially life-threatening

The generation of an action potential requires the precise coordination of gating events of a collection of ion channels. Perturbation of this timing can have devastating effects. For example, the rhythmic generation of action potentials by the heart is absolutely essential to maintain delivery of oxygenated blood to the peripheral tissues. **Long QT syndrome (LQTS)** is a genetic disorder in which the recovery of the action potential from its peak potential to the resting equilibrium potential is delayed. The term *QT* refers to a specific feature of the cardiac electrical activity pattern as measured by electrocardiography. LQTS can lead to brief losses of consciousness (syncope), disruption of normal cardiac rhythm (arrhythmia), and sudden death. The most common mutations identified in LQTS patients inactivate K^+ channels or prevent the proper trafficking of these channels to the plasma membrane. The resulting loss in potassium permeability slows the repolarization of the membrane and delays the induction of the subsequent cardiac contraction, rendering the cardiac tissue susceptible to arrhythmias.

 Prolongation of the cardiac action potential in this manner can also be a potentially dangerous side effect of certain therapeutic drugs.

In particular, the K^+ channel hERG (for human *ether-a-go-go*-related gene, named for its ortholog in *Drosophila melanogaster*) is highly susceptible to interactions with certain drugs. The hydrophobic regions of these drugs can block hERG by binding to two nonconserved aromatic residues on the internal surface of the channel cavity. In addition, this cavity is predicted to be wider than other K^+ channels because of the absence of a conserved Pro-X-Pro motif within the S6 hydrophobic segment. Inhibition of hERG by these drugs can lead to an increased risk of cardiac arrhythmias and sudden death. Accordingly, a number of these agents, such as the antihistamine terfenadine, have been withdrawn from the market. Screening for the inhibition of hERG is now a critical safety hurdle for the pharmaceutical advancement of a molecule to an approved drug.

Hyperpolarization-activated ion channels enable pacemaker activity in the heart

The heart utilizes coordinated changes in the membrane potential to facilitate the efficient muscular contractions necessary to pump blood throughout the body effectively. However, the heart can beat spontaneously, without the use of a neurotransmitter such as acetylcholine. How does the heart initiate an action potential without such an input?

The answer lies within a collection of cardiac cells known as the pacemaker. While there are several pacemakers in the human heart, the most important of these is the sinoatrial (SA) node, located on the posterior wall of the right atrium. The cells of the SA node spontaneously generate action potentials at rates from 60 to 100 per second. Researchers have known for many years that these cells possess an unusual capacity for mixed Na^+/K^+ conductance when their membranes are hyperpolarized. This membrane permeability has been

referred to as the *funny current* (I_f). At rest, this current is active, leading to a gradual depolarization of the membrane to a level that triggers the initiation of an action potential. During the action potential, this current shuts off. However, once the action potential is complete and the membrane returns to its resting potential, the funny current turns back on, repeating the cycle. The action potential propagates from the SA node to the rest of the cardiac tissue in a highly organized manner, stimulating muscle contraction and the movement of blood.

The channels responsible for the funny current have been identified. The hyperpolarization-activated cyclic nucleotide-gated (HCN) channels comprise four isoforms. Functional channels are composed of tetramers of these isoforms, either all of the same type (homotetramers) or of a combination of types (heterotetramers). HCN4 is the most prominently expressed in the SA node. These channels are unusual in that they are opened by hyperpolarization, and close when the membrane is depolarized. Moreover, these channels are responsive to changing levels of intracellular cyclic AMP (cAMP), as expected: while the heart can beat spontaneously, neuronal and hormonal input can affect this rate to accommodate the body's changing energetic needs.

Mutations in the *HCN4* gene have been identified in patients with sick sinus syndrome, a condition where patients exhibit an abnormally low heart rate (bradycardia) that may manifest with symptoms of dizziness, fainting, headaches, and fatigue. In one family, the identified mutation resulted in a greater hyperpolarization required to achieve HCN4 opening (**Figure 13.34**) when these channels were expressed in cultured cells. In a patient carrying this mutation, fewer HCN4 channels are open at a given resting potential, leading to a slower depolarization and a reduced heart rate.

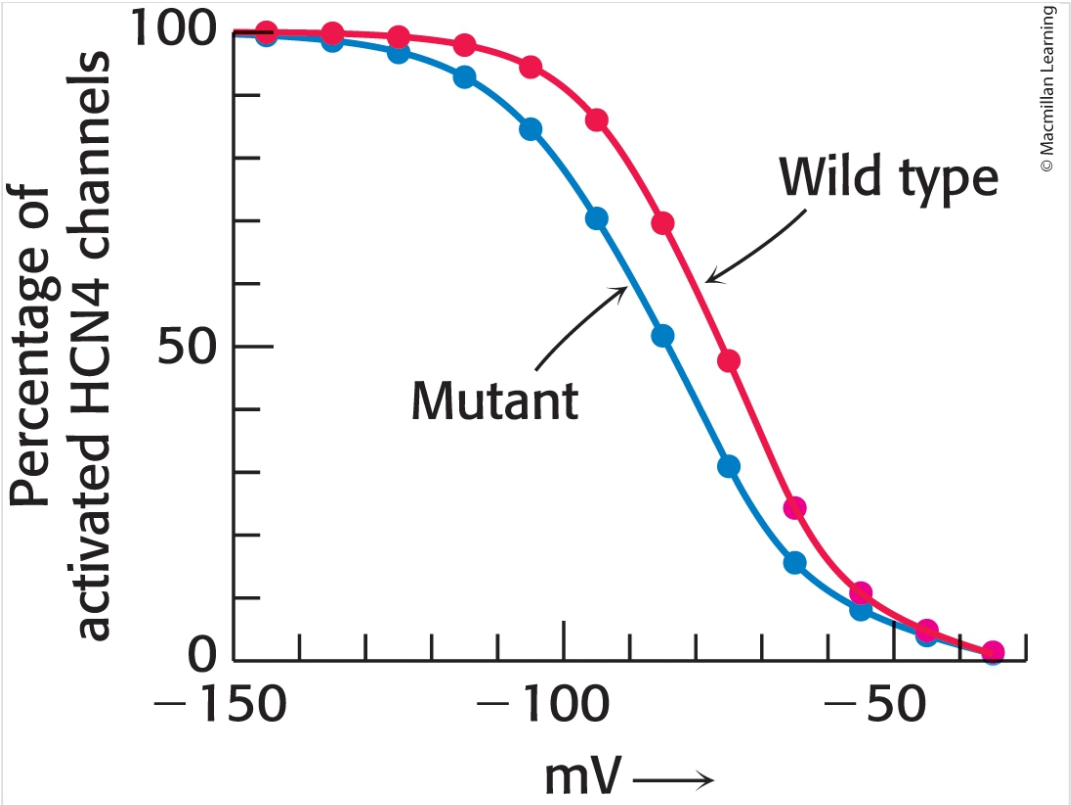
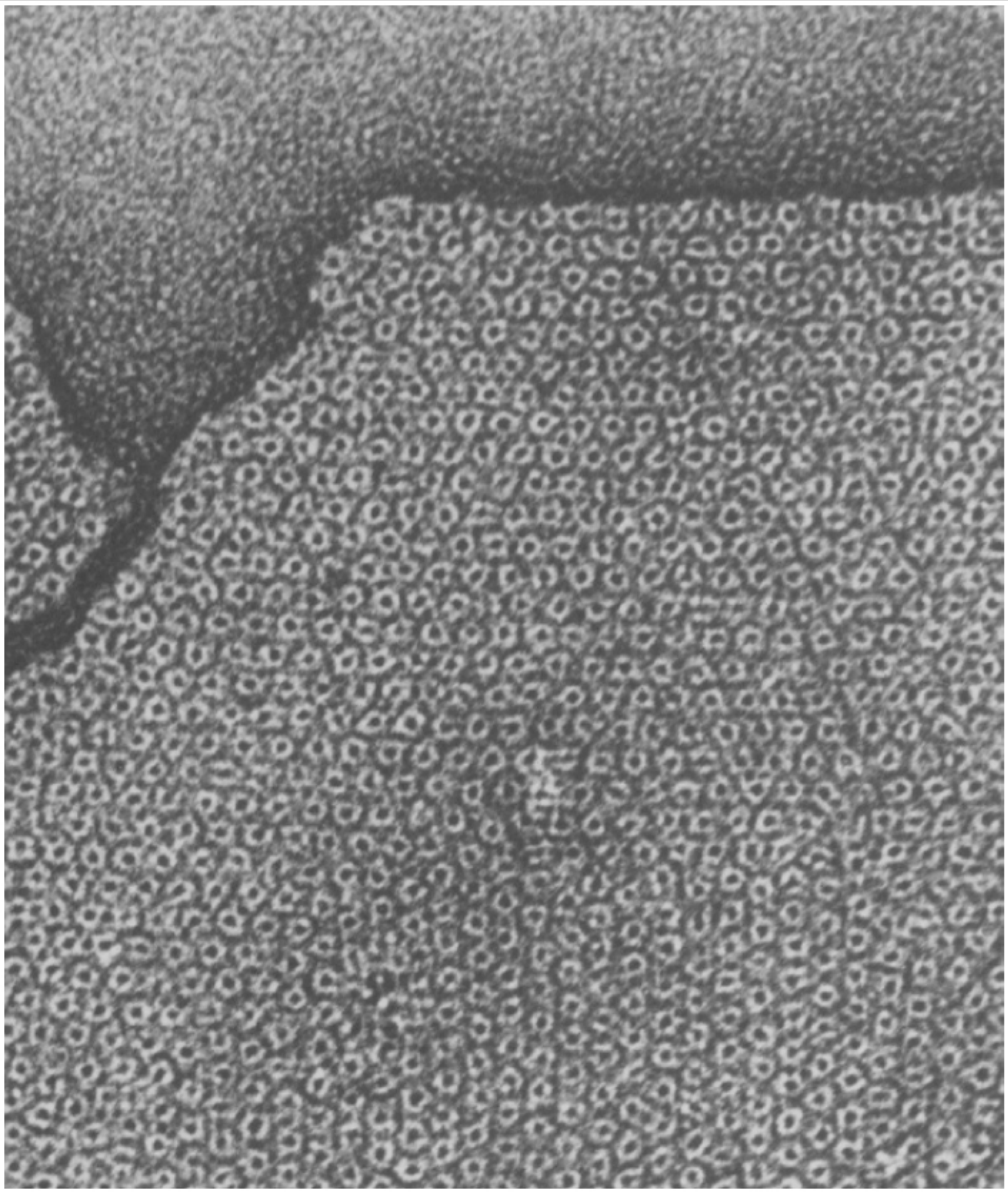


FIGURE 13.34 A disease-causing HCN4 mutant requires greater membrane hyperpolarization to open the channel. This graph shows the percentage of open channels at a given membrane potential. HCN4 channels are open at hyperpolarized membrane potentials, and close as the membrane depolarizes. For the mutant HCN4 channels (blue circles), the channel requires a more hyperpolarized state to be open to the same extent as the wild-type channels (red circles). [R. Milanese, M. Baruscotti, T. Gnecchi-Ruscone, and D. DiFrancesco, *New Eng. J. Med.* 354:151–157, 2006, Fig. 3A.]

13.5 Gap Junctions Allow Ions and Small Molecules to Flow Between Communicating Cells

The ion channels we have considered thus far have narrow pores and are moderately to highly selective in the ions they allow to pass through them. They are closed in the resting state and have short lifetimes in the open state, typically a millisecond, that enable them to transmit frequent neural signals. Let us turn now to a channel with a very different role. **Gap junctions**, also known as **cell-to-cell channels**, serve as passageways between the interiors of contiguous cells. Gap junctions are clustered in discrete regions of the plasma membranes of apposed cells. Electron micrographs of sheets of gap junctions show them tightly packed in a regular hexagonal array (**Figure 13.35**). An approximately 20-Å central hole, the lumen of the channel, is prominent in each gap junction. These channels span the intervening space, or gap, between apposed cells (hence, the name *gap junction*).



Don W. Fawcett/Science Source

FIGURE 13.35 Gap junctions form tightly packed arrays. This electron micrograph shows a sheet of isolated gap junctions. The cylindrical connexons form a hexagonal lattice having a unit-cell length of 85 Å. The densely stained central hole has a diameter of about 20 Å.

Small hydrophilic molecules as well as ions can pass through gap junctions. The pore size of the junctions was determined by microinjecting a series of fluorescent molecules into cells and observing their passage into adjoining cells. All polar molecules with a mass of less than about 1 kDa can readily pass through these

cell-to-cell channels. Thus, inorganic ions and most metabolites (e.g., sugars, amino acids, and nucleotides) can flow between the interiors of cells joined by gap junctions. In contrast, proteins, nucleic acids, and polysaccharides are too large to traverse these channels.

Gap junctions are important for intercellular communication. Cells in some excitable tissues, such as heart muscle, are coupled by the rapid flow of ions through these junctions, which ensures a speedy and synchronous response to stimuli. Gap junctions are also essential for the nourishment of cells that are distant from blood vessels, as in bone and the lens of the eye. Moreover, communicating channels are important in development and differentiation. For example, the quiescent (calm) uterus transforms to a forcefully contracting organ at the onset of labor; the formation of functional gap junctions at that time creates a syncytium of muscle cells that contract in synchrony.

A gap junction is made of 12 molecules of connexin, one of a family of transmembrane proteins with molecular masses ranging from 30 to 42 kDa. Each connexin molecule contains four membrane-spanning helices (**Figure 13.36A**). Six connexin molecules are hexagonally arrayed to form a half-channel, called a **connexon** or **hemichannel**. Two connexons join end to end in the intercellular space to form a functional channel between the communicating cells (**Figure 13.36B**). Each connexon adopts a funnel shape: At the cytoplasmic face, the inner diameter of the channel is 35 Å, while at its innermost point, the pore narrows to a diameter of 14 Å (**Figure 13.36C**). Cell-to-cell channels differ from other membrane channels in three respects:

1. They traverse *two* membranes rather than one.

2. They connect cytoplasm to cytoplasm, rather than to the extracellular space or the lumen of an organelle.

3. The connexons forming a channel are synthesized by different cells.

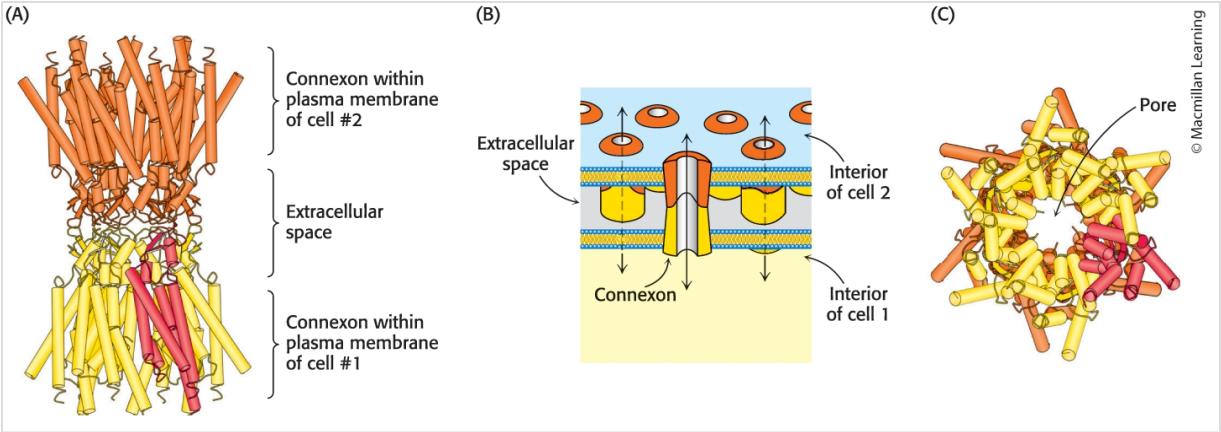


FIGURE 13.36 Gap junctions are formed from connexons of neighboring cells. (A) Six connexins join to form a connexon, or hemichannel, within the plasma membrane (yellow). A single connexin monomer is highlighted in red. The extracellular region of one connexon binds to the same region of a connexon from another cell (orange), forming a complete gap junction. (B) A schematic view of the gap junction, oriented in the same direction as in (A). (C) A bottom-up view looking through the pore of a gap junction. This perspective is visualized in Figure 13.35.

[(A) and (C) Drawn from 2ZW3.pdb; (B) Information from Dr. Werner Loewenstein.]

Gap junctions form readily when cells are brought together. A cell-to-cell channel, once formed, tends to stay open for seconds to minutes. They are closed by high concentrations of calcium ion and by low pH. The closing of gap junctions by Ca^{2+} and H^{+} serves to seal normal cells from injured or dying neighbors. Gap junctions are also controlled by membrane potential and by hormone-induced phosphorylation.

Self-Check Question



The human genome contains more than 20 connexin-encoding genes. Several of these genes are expressed in high levels in the heart. Why are connexins so highly expressed in cardiac tissue?

13.6 Specific Channels Increase the Permeability of Some Membranes to Water

One more important class of channels does not take part in ion transport at all. Instead, these channels increase the rate at which water flows through membranes. As noted in Section 12.3, membranes are reasonably permeable to water. Why, then, are water-specific channels required? In certain tissues, in some circumstances, rapid water transport through membranes is necessary. In the kidney, for example, water must be rapidly reabsorbed into the bloodstream after filtration. Similarly, in the secretion of saliva and tears, water must flow quickly through membranes. These observations suggested the existence of specific water channels, but initially the channels could not be identified.

The channels, now called **aquaporins**, were discovered serendipitously. Peter Agre (pictured at the beginning of Chapter 1) noticed a protein present at high levels in red-blood-cell membranes that had not been previously identified because the protein does not stain well with Coomassie blue, the stain commonly used in protein SDS-PAGE (Section 4.1). In addition to red blood cells, this protein was found in large quantities in tissues such as the kidney and the cornea, precisely the tissues hypothesized to contain water channels. On the basis of this observation, further studies were designed, revealing that this 24-kDa membrane protein is, indeed, a water channel.

The structure of aquaporin consists of six membrane-spanning α helices (**Figure 13.37**). Two loops containing hydrophilic residues line the actual channel. Water molecules pass through in single file at a rate of 10^6 molecules per second. Importantly, specific positively charged

residues toward the center of the channel prevent the transport of protons through aquaporin. Thus, aquaporin channels will not disrupt proton gradients, which play fundamental roles in energy transduction, as we will see in Chapter 18. Remarkably, the aquaporins are channels that have evolved specifically to conduct uncharged substrates.

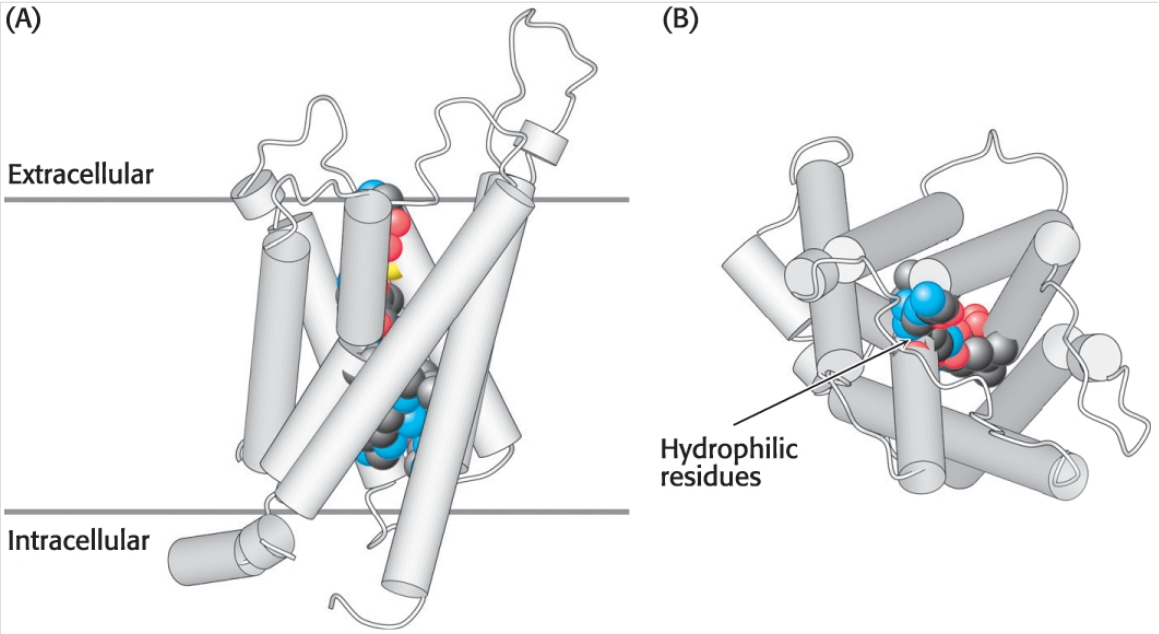


FIGURE 13.37 Aquaporins are channels specifically permeable to water. The structure of aquaporin viewed (A) from the side and (B) from the top. Notice the hydrophilic residues (shown as space-filling models) that line the water channel. The gray lines in (A) indicate the extent of the plasma membrane.

[Drawn from 1J4N.pdb.]

INTERACT with this model in Achieve

Chapter 13 Summary

13.1 The Transport of Molecules Across a Membrane May Be Active or Passive

- Lipophilic molecules can pass through a membrane's hydrophobic interior by simple diffusion.
- Passive transport or facilitated diffusion takes place when an ion or polar molecule moves down its concentration gradient with the assistance of a channel.
- Active transport uses an input of energy to move molecules against a concentration gradient.
- The electrochemical potential measures the combined ability of a concentration gradient and an uneven distribution of charge to drive species across a membrane.

13.2 Two Families of Membrane Proteins Use ATP Hydrolysis to Actively Transport Ions and Molecules Across Membranes

- Pumps are membrane proteins that catalyze the active transport of ions against their electrochemical gradients.
- P-type ATPases are pumps that are transiently phosphorylated on an aspartic acid residue during the transport cycle.
- ABC transporters are pumps that use ATP-binding cassettes to control protein conformation.

13.3 Lactose Permease Is an Archetype of Secondary Transporters That Use One Concentration Gradient to Power the Formation of Another

- Carriers are proteins that transport ions or molecules across the membrane without hydrolysis of ATP.
- Uniporters transport a substrate in either direction, determined by the concentration gradient.

- Antiporters couple the downhill flow of one substrate in one direction to the uphill flow of another in the opposite direction.
- Symporters couple the downhill flow of one substrate in one direction to the uphill flow of another in the same direction.

13.4 Specific Channels Can Rapidly Transport Ions Across Membranes

- Ion channels allow the rapid movement of ions across the hydrophobic barrier of the membrane.
- Ions must transiently lose their coordinated water molecules as they move to the narrowest part of an ion channel — the selectivity filter — which determines the specificity of the ion channel.
- Voltage-gated ion channels are opened by changes in membrane potential.
- Many channels spontaneously inactivate after having been open for a short period of time.
- Ligand-gated channels are opened or closed by the binding of ligands.
- Nerve impulses, or action potentials, are electrical signals produced by the coordinated flow of K^+ and Na^+ ions through their respective ion channels.

13.5 Gap Junctions Allow Ions and Small Molecules to Flow Between Communicating Cells

- Gap junctions, or cell-to-cell channels, serve to connect the interiors of contiguous groups of cells.
- Gap junctions are important for intercellular communication, enabling the coordinated contraction of the heart during a beat or the uterus during labor.

13.6 Specific Channels Increase the Permeability of Some Membranes to Water

- Aquaporin, a water-channel-forming protein, consists of six membrane-spanning α helices and a central channel lined with hydrophilic residues that allow water molecules to pass in single file.
- Aquaporins do not transport protons, and thus do not disrupt protein gradients across membranes.

Key Terms

simple diffusion
facilitated diffusion (passive transport)
active transport
electrochemical potential (membrane potential)
pumps
P-type ATPase
eversion
multidrug resistance
ATP-binding cassette (ABC)
ABC transporter
carrier
secondary active transport
secondary transporter (cotransporter)
antiporter
symporter
uniporter
ion channel
nerve impulse (action potential)
patch-clamp technique
selectivity filter
voltage-gated channel
ball-and-chain model
recovery
neurotransmitters

[synaptic cleft]
[ligand-gated channel]
[equilibrium potential]
[refractory period]
[long QT syndrome (LQTS)]
[gap junction (cell-to-cell channels)]
[connexon (hemichannel)]
[aquaporin]

Problems

1. Differentiate between simple diffusion and facilitated diffusion. 1

2. Distinguish the mechanisms by which uniporters and channels transport ions or molecules across the membrane. 1, 4

3. Which of the following statements applies to passive transport or active transport? 1

a. Moves substances from an area of low concentration to an area of higher concentration
b. Does not require energy
c. Requires energy
d. Moves substances from an area of high concentration to an area of lower concentration

4. For a typical mammalian cell, the intracellular and extracellular concentrations of the chloride ion (Cl^-) are $4\ \mu M$ and 150 mM, respectively. Calculate the equilibrium potential at 37°C for the chloride ion. 2

5. Intestinal epithelial cells pump glucose into the cell against its concentration gradient using the Na^+–glucose symporter. The symporter couples the "downhill" transport of two Na^+ ions into the cell to the "uphill" transport of glucose into the cell.

a. If the Na^+ concentration outside the cell is 155 mM and that inside the cell is 17 mM, and the membrane potential is $-55\ mV$, what is the maximum energy available for pumping a mole of glucose into the cell?
b. What is the maximum ratio of $[glucose]_{in} / [glucose]_{out}$ that could theoretically be produced if the energy coupling were 100% efficient? 2

6. If the pH of the interior of the stomach is pH 2, what is the amount of energy required for the transport of protons from the interior of the cell (pH 7.4) into the stomach lumen? Assume the membrane potential across this membrane is $-70\ mV$ and the temperature is 37°C. 2

7. Classify each phrase as a descriptor of ABC transporters, P-type ATPases, or both: 3

a. Substrate binds before ATP
b. The multidrug resistance protein is an example.
c. An aspartate residue in the membrane pump is phosphorylated.
d. The gastric H^+-K^+ ATPase is an example.
e. ATP-dependent
f. Two ATP-binding domains

8. Which of the following binding states are present in the SERCA catalytic cycle? For each state, assume that only the species mentioned are bound. 3

a. AMP bound
b. 2 Ca^{2+}, ADP, and P_i bound
c. 2 Ca^{2+} bound
d. 2 Ca^{2+} and ADP bound
e. ADP bound
f. 2 Ca^{2+} and ATP bound
g. P_i bound

9. To study the mechanism of SERCA, you prepare membrane vesicles containing this protein oriented such that its ATP binding site is on the outer surface of the vesicle. To measure pump activity, you use an assay that detects the formation of inorganic phosphate in the medium. When you add calcium and ATP to the medium, you observe phosphate production for only a short period of time. Only after the addition of calcimycin, a molecule that makes membranes selectively permeable to calcium, do you observe sustained phosphate production. Explain. 3

10. Name the three types of carrier proteins. Which of these can mediate secondary active transport? 4

11. Classify each description as characterizing facilitated diffusion, primary active transport, secondary active transport, or both primary and secondary active transport:

a. Requires ATP
b. Includes the Na^+-K^+ ATPase pump
c. Uses energy stored in electrochemical gradients generated by pumps
d. Always moves more than one substance at a time
e. Does not require energy input

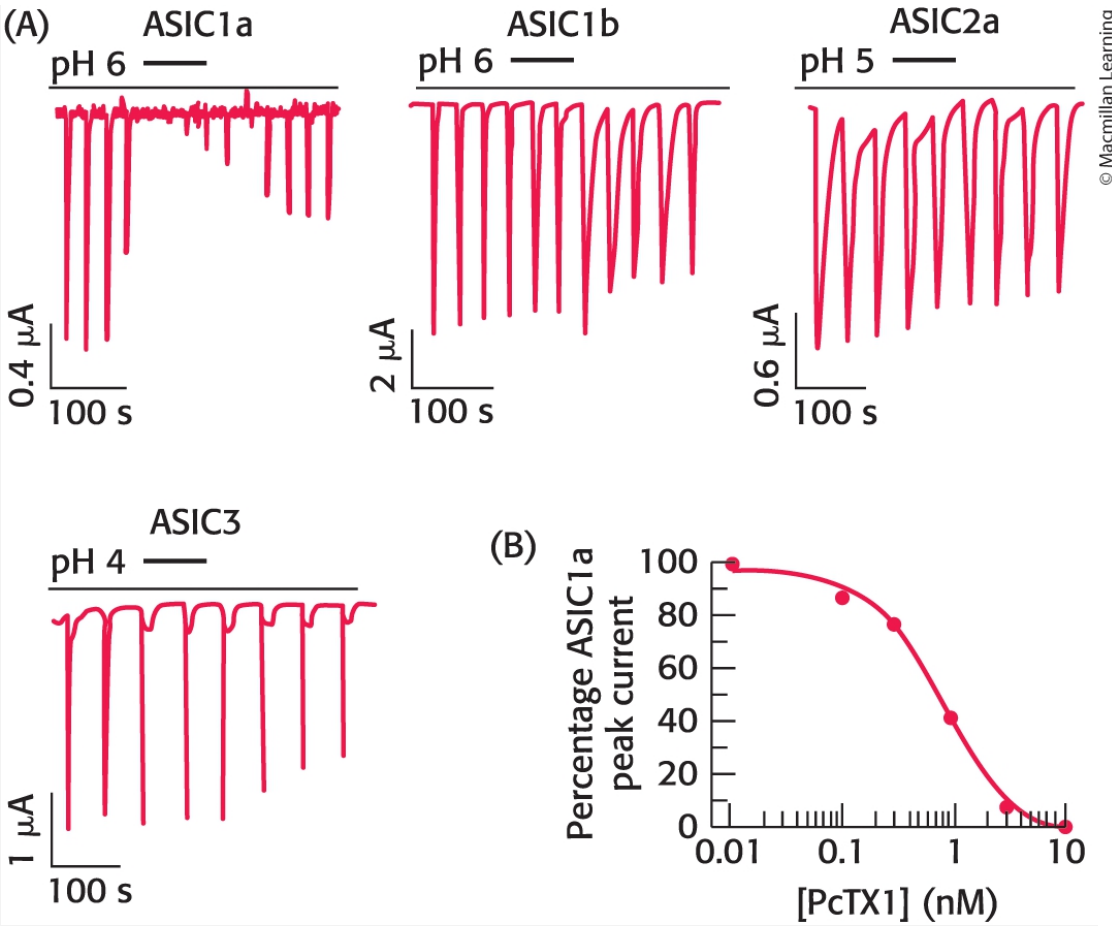
f. Moves substances against a chemical gradient
g. Directly uses ATP hydrolysis to pump substances across the membrane
h. Includes lactose permease
i. Includes uniporters

12. In energetic terms, why do K^+ channels not enable Na^+ ions to cross the membrane? 5

13. How might a mutation in a cardiac voltage-dependent sodium channel cause long QT syndrome? 7

14. Batrachotoxin (BTX) is a steroidal alkaloid from the skin of *Phyllobates terribilis*, a poisonous Colombian frog (the source of the poison used on blowgun darts). In the presence of BTX, Na^+ channels in an excised patch stay persistently open when the membrane is depolarized. They close when the membrane is repolarized. Which transition is blocked by BTX?

15. Acid sensing is associated with pain, tasting, and other biological activities. Acid sensing is carried out by a ligand-gated channel that permits Na^+ influx in response to H^+. This family of acid-sensitive ion channels (ASICs) includes a number of members. Psalmotoxin 1 (PcTX1), a venom from the tarantula, inhibits some members of this family. The following electrophysiological recordings of cells containing several members of the ASIC family were made in the presence of the toxin at a concentration of 10 nM. The channels were opened by changing the pH from 7.4 to the indicated values. The PcTX1 was present for a short time (indicated by the black bar above the recordings below), after which time it was rapidly washed from the system.



© Macmillan Learning

a. Which member of the ASIC family — ASIC1a, ASIC1b, ASIC2a, or ASIC3 — is most sensitive to the toxin?
b. Is the effect of the toxin reversible? Explain.
c. What concentration of PcTX1 yields 50% inhibition of the sensitive channel?

16. Cone snails are carnivores that inject a powerful set of toxins into their prey, leading to rapid paralysis. Many of these toxins are found to bind to specific ion-channel proteins. Why are such

molecules so toxic? How might such toxins be useful for biochemical studies? 7

17. Determine whether each phrase describes ligand-gated ion channels, voltage-gated ion channels, or both: 6

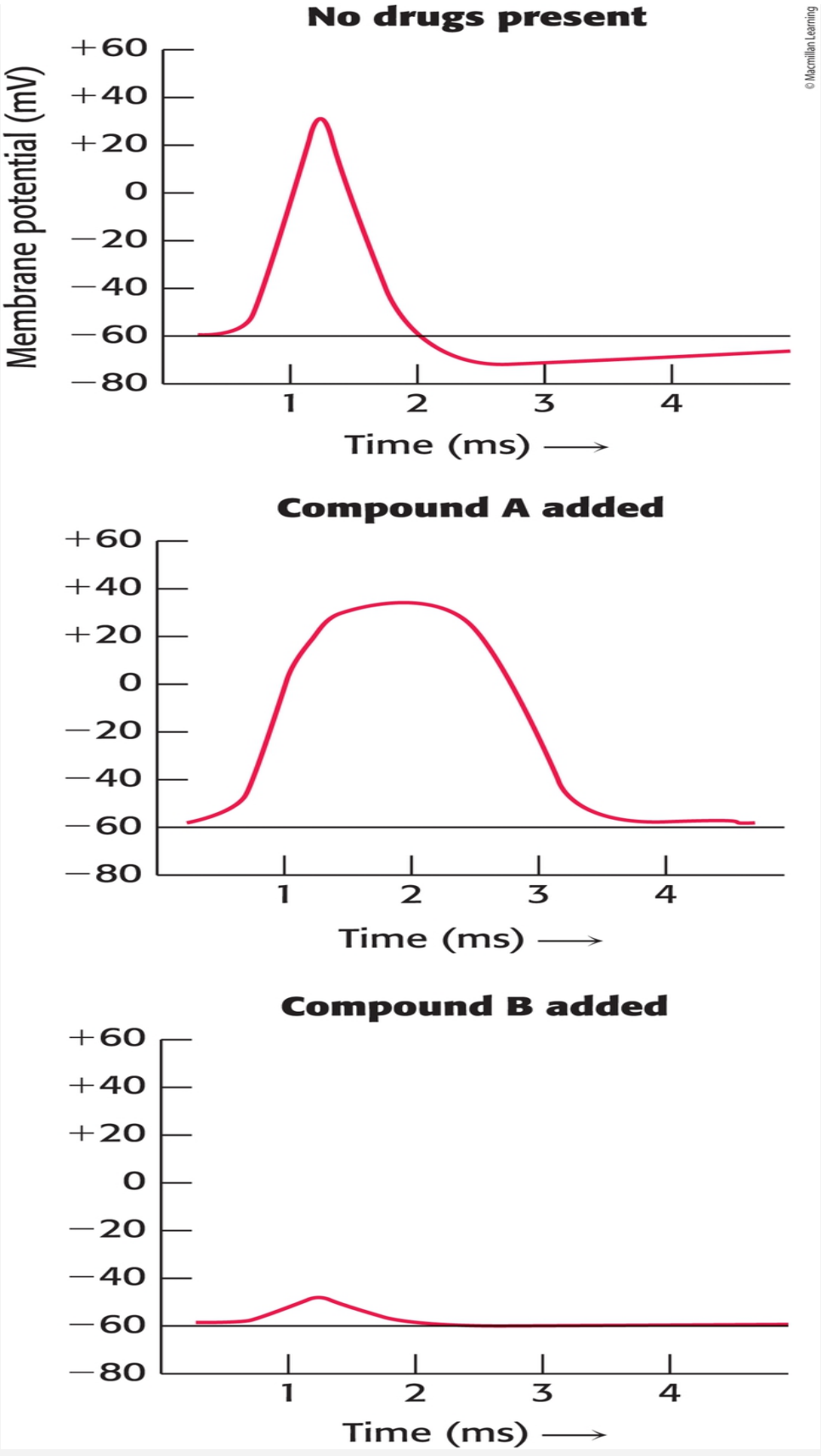
a. Change conformation in response to changing membrane potential
b. May participate in an action potential
c. An example is the acetylcholine receptor
d. Is a form of passive transport
e. Change conformation in response to a signal-molecule binding

18. Immediately after the repolarization phase of an action potential, the neuronal membrane is temporarily unable to respond to the stimulation of a second action potential, a phenomenon referred to as the *refractory period*. What is the mechanistic basis for the refractory period? 7

19. Place the events of an action potential in order, starting and ending with a cell at its resting membrane potential. 7

a. K^+ rushes out of the cell, causing repolarization.
b. Ligand activation of the acetylcholine receptor depolarizes the membrane.
c. K^+ channels fully open, and Na^+ channels are inactivated.
d. Fast Na^+ and slow K^+ channels are activated.
e. Na^+ rushes into the cell, causing membrane depolarization.
f. K^+ channels close slowly, resulting in hyperpolarization. Na^+ channel gates reset.

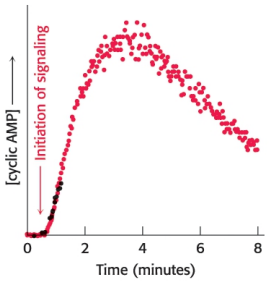
20. Drugs like tetrodotoxin (TTX) and tetraethylammonium (TEA) alter action potentials in neurons. TTX is able to block voltage-gated sodium (Na^+) channels, whereas TEA is able to block voltage-gated potassium (K^+) channels. The first graph shows an action potential in the absence of any of these drugs. The next two graphs show the effect of either TTX or TEA on the action potential. Match these graphs with the likely drug that was used. 7



© Macmillan Learning



Chapter 14
Signal-Transduction Pathways



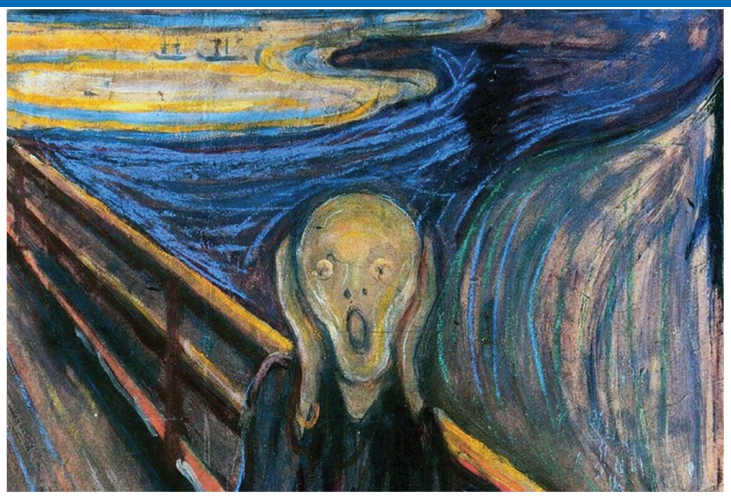


Photo12/Universal Images Group/Getty Images
© Macmillan Learning

Many biological processes involve biochemical signaling. The "fight-or-flight" response triggered by fear or shock is mediated by the release of the hormone adrenaline (epinephrine). Information about the arrival of this molecule at specific receptors on cell surfaces is converted rapidly into increases in the concentration of cyclic adenosine monophosphate (cAMP) inside cells. This, in turn, drives other biochemical responses.

Outline

14.1 Many Signal-Transduction Pathways Share Common Themes
14.2 Epinephrine Signaling: Heterotrimeric G Proteins Transmit Signals and Reset Themselves
14.3 Insulin Signaling: Phosphorylation Cascades Are Central to Many Signal-Transduction Processes

14.4 Epidermal Growth Factor: Receptor Dimerization Can Drive Signaling
14.5 Defects in Signal-Transduction Pathways Can Lead to Cancer and Other Diseases
14.6 Sensory Systems Are Based on Specialized Signal-Transduction Pathways

Learning Goals



By the end of this chapter, you should be able to:

1. Describe the essential features of a signal-transduction circuit.
2. Define what is meant by a second messenger and give several examples.
3. Compare and contrast how the adrenergic receptors, the insulin receptor, and the epidermal growth factor receptors transmit a ligand-binding event across the plasma membrane to initiate an intracellular signaling cascade.
4. Give examples of how mutations in signaling proteins can result in cancer.
5. Discuss the signal-transduction pathways that are central to the senses of smell, vision, and hearing.

Imagine you and a group of friends are sitting around a firepit, waiting to finish cooking your dinner. Unexpectedly, you hear a rustling sound and fear that you may have an uninvited animal visitor. Your heart pounds, your eyes grow wide, and you turn pale, as you and your friends quickly run away from the sound. After 15 minutes, when you have calmed down and return to the fire; everything seems untouched. The same cannot be said for your leg, however, which sustained a deep scratch as you made your escape. After your friends help you clean and dress your wound, your thoughts return to dinner. The food smells, looks, and tastes delicious. After enjoying a nice meal, you feel satisfied.

Many of the steps in this encounter involve biochemical signaling processes within your cells. These chains of events, termed *signal-transduction pathways*, convert molecular messages into a range of physiological responses. In this chapter, we will focus on sets of signal-transduction pathways that affect circulation, metabolism, cell growth and division, and sensory perception.

14.1 Many Signal-Transduction Pathways Share Common Themes

The conversion of information of the presence or concentration of a signal molecule into other forms is called **transduction**. Signal-transduction pathways often include many components and branches. Moreover, they show variations that are used in different tissues and cell types. They can be immensely complicated and confusing. Nonetheless, the logic of signal transduction can be simplified by examining the common strategies and classes of molecules that recur in these pathways. These principles of signal-transduction pathways introduced here are at play in essentially all the metabolic pathways we will be exploring throughout the rest of the book.

Signal transduction depends on molecular circuits

Signal-transduction pathways follow a broadly similar course that can be viewed as a molecular circuit (**Figure 14.1**).

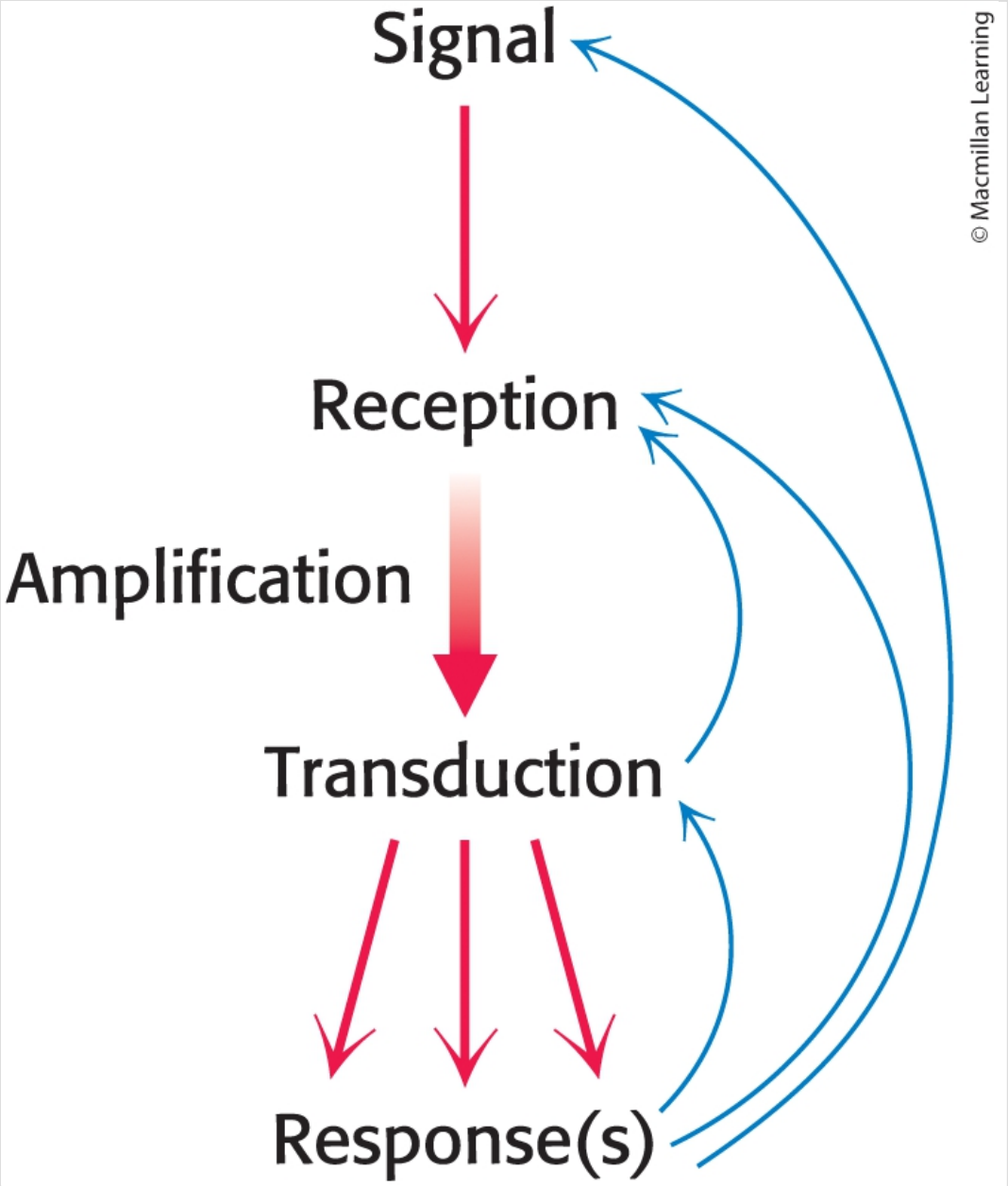


FIGURE 14.1 Signals such as changes in hormone levels lead to responses through signal-transduction pathways. An environmental signal is first received by interaction with a cellular component, most often a cell-surface receptor. Typically, the transduction process comprises many steps. The signal is often amplified before evoking one or more responses. Feedback pathways regulate the entire signaling process.

All such circuits contain certain key steps:

1. *Release of the primary messenger ("signal")*. A stimulus such as stress, a wound, or a digested meal triggers the release of the signal molecule, also called the **primary messenger**.

2. *Reception of the primary messenger*. Most signal molecules do not enter cells. Instead, proteins in the cell membrane act as **receptors** that convert signal molecule binding on the cell surface to a structural change within the cell's interior. Receptors span the cell membrane and thus have both extracellular and intracellular components. A binding site on the extracellular side specifically recognizes the signal molecule. Such binding sites are analogous to enzyme active sites except that no catalysis takes place within them. The interaction of the ligand and the receptor alters the tertiary or quaternary structure of the receptor to induce a structural change on the intracellular side.

3. *Delivery of the message inside the cell by the second messenger*. Other small molecules, called **second messengers**, are used to relay information from receptor–ligand complexes. Second messengers are intracellular molecules that change in concentration in response to environmental signals and mediate the next step in the molecular information circuit. Some particularly important second messengers are cyclic AMP (cAMP) and cyclic GMP (cGMP), calcium ion, inositol 1,4,5-trisphosphate (IP_3), and diacylglycerol (DAG), shown in **Figure 14.2**.

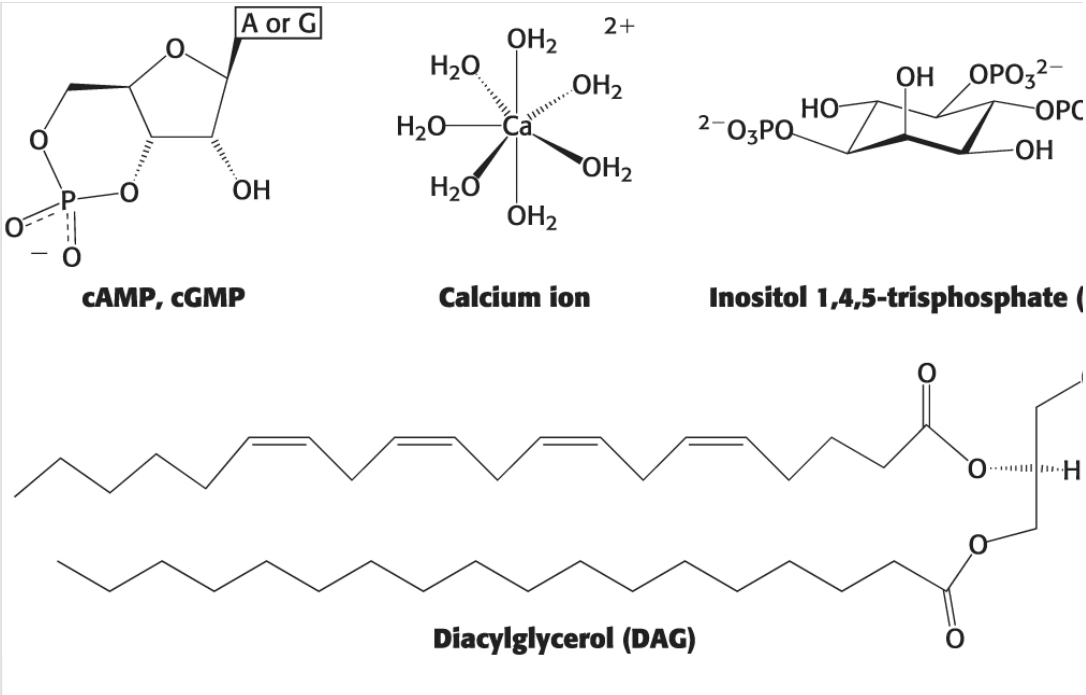


FIGURE 14.2 Several molecules function as second messengers common to many signa transduction pathways. As intracellular molecules that change in concentration in response to environmental signals, second messengers convey information inside the cel

The use of second messengers has several consequences. First, the signal may be amplified significantly: Only a small number of receptor molecules may be activated by the direct binding of signal molecules, but each activated receptor molecule can lead to the generation of many second messengers. Thus, a low concentration of signal in the environment, even as little as a single molecule, can yield a large intracellular signal and response. Second, these messengers are often free to diffuse so that they can influence processes throughout the cell. Third, the use of common second messengers in multiple signaling pathways creates both opportunities and potential challenges. Input from several signaling pathways, often called cross talk, may alter the concentration of a common second messenger. Cross talk permits

more finely tuned regulation of cell activity than would the action of individual independent pathways. However, inappropriate cross talk has the potential for misinterpretation of changes in second-messenger concentration.

4. *Activation of other molecules that directly alter the physiological response*. The ultimate effect of the signal pathway is to activate (or inhibit) the enzymes, ion channels, pumps, and transcription factors that directly control metabolic pathways, the permeability of membranes to specific ions, and gene expression.

5. *Termination of the signal.* After a cell has completed its response to a signal, the signaling process must be terminated or the cell would lose its responsiveness to incoming signals. Moreover, signaling processes that fail to terminate properly can have highly undesirable consequences. Many cancers are associated with signal-transduction processes that are overly active, especially processes that control cell growth.

We will examine components of the three signal-transduction pathways shown in **Figure 14.3**. In doing so, we will encounter many classes of proteins and other molecules that are present in many other signal-transduction pathways as well as some common strategies. It is important to keep in mind that each specific example reveals components present in many other pathways.

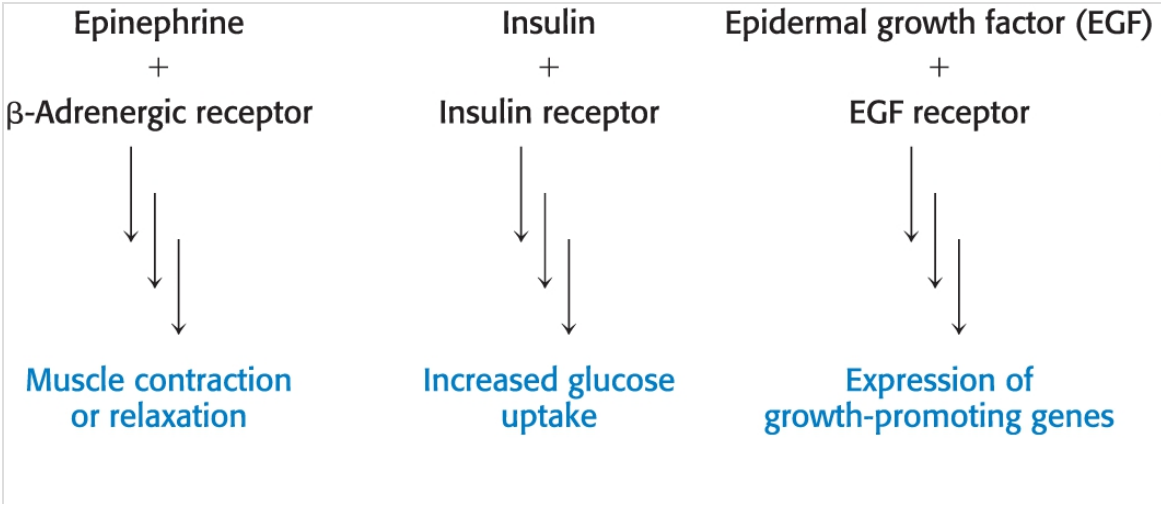
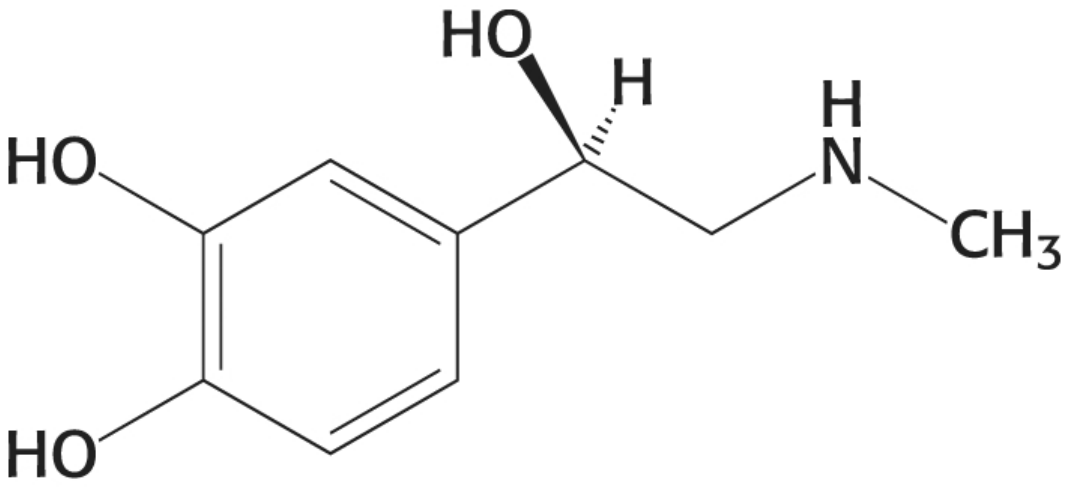


FIGURE 14.3 Three pathways illustrate many of the principles of signal transduction. The binding of signaling molecules to their receptors initiates pathways that lead to important physiological responses.



14.2 Epinephrine Signaling: Heterotrimeric G Proteins Transmit Signals and Reset Themselves

Your fear at hearing a potentially menacing sound triggers the release of a chemical signal that begins a coordinated response. The hormone **epinephrine** is one such signal, secreted by the adrenal glands of mammals in response to internal and external stressors. The molecule is often called **adrenaline**.



Epinephrine (Adrenaline)

Epinephrine exerts a wide range of effects — collectively referred to as the fight-or-flight response — that help organisms anticipate the need for rapid muscular activity, including acceleration of heart rate, dilation of the smooth muscle of the airways and constriction of blood vessels in

the skin and skeletal muscles, and initiation of the breakdown of glycogen (Chapter 21) and fatty acids (Chapter 22).

Epinephrine signaling begins with ligand binding to cell-surface proteins called **adrenergic receptors**. Nine adrenergic receptors are encoded within the human genome, and they fall into two classes: α-adrenergic receptors and β-adrenergic receptors. These initiate analogous and, in many ways, complementary signaling pathways, as we shall see shortly. These receptors are members of the largest class of cell-surface receptors, called the **seven-transmembrane-helix (7TM) receptors**. Members of this family are responsible for transmitting information initiated by signals as diverse as hormones, neurotransmitters, odorants, and even light. Tens of thousands of such receptors are now known, including nearly 1000 encoded in the human genome. Furthermore, about one-third of the marketed therapeutic drugs target receptors of this class. As the name indicates, these receptors contain seven helices that span the membrane bilayer, as originally deduced from the patterns of hydrophobic residues in the amino acid sequences of these receptors (**Figure 14.4**).

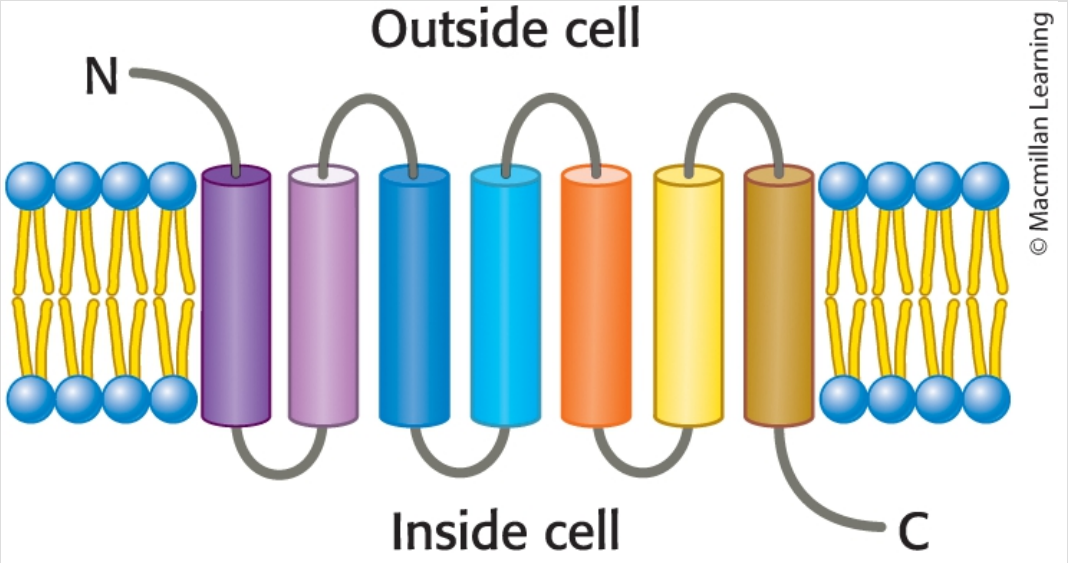


FIGURE 14.4 A large and important family of receptors share a common structure with seven transmembrane (7TM) helices. This schematic representation of a 7TM helix receptor shows its passage through the membrane seven times.

We begin our more-detailed discussion of 7TM receptors with the β-adrenergic receptors that are typically present in tissues such as the heart and the airways. The three-dimensional structure of human β-adrenergic receptors (β-AR) have been determined in a variety of forms by x-ray crystallography. As anticipated, the receptor structure consists of a bundle of seven membrane-spanning alpha helices, with helices adjacent in the sequence next to one another, circling in a counterclockwise direction when viewed from the extracellular side (Figure 14.5).

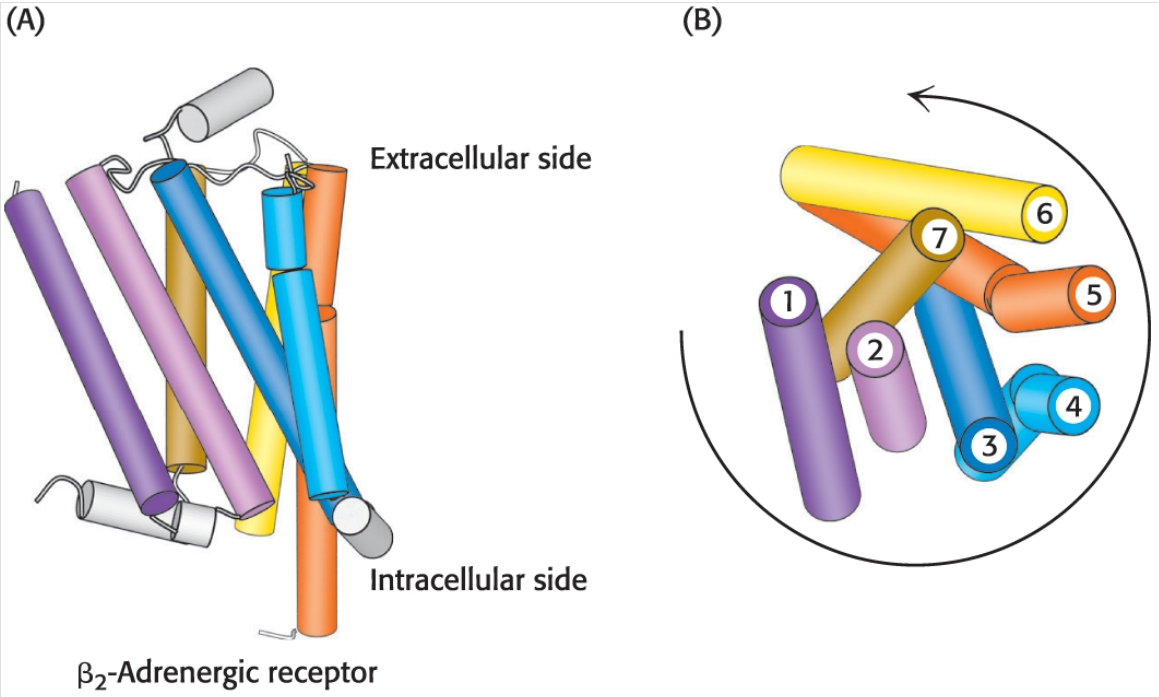


FIGURE 14.5 The three-dimensional structure of the β-adrenergic receptor reveals the arrangement of helices in 7TM receptors. (A) A side view shows the 7TM helices spanning the membrane. (B) A top view from the extracellular side shows the 7TM helices arranged in a counterclockwise manner.

The binding site for ligands such as epinephrine that activate the receptor as well as other compounds that block this site and prevent activation is present toward the center of the bundle of helices, about 20% of the way into the receptor from the extracellular side. Ligands that activate receptors are referred to as **agonists**. The presence of a bound agonist stabilizes a modified conformation of the receptor (**Figure 14.6**). Most notably, helix 5 extends deeper into the cell, and helix 6 moves outward from the center of the receptor. This change in conformational preference is crucial since it represents the transmission of information from a ligand increasing in concentration outside the cell to structural changes inside the cell.

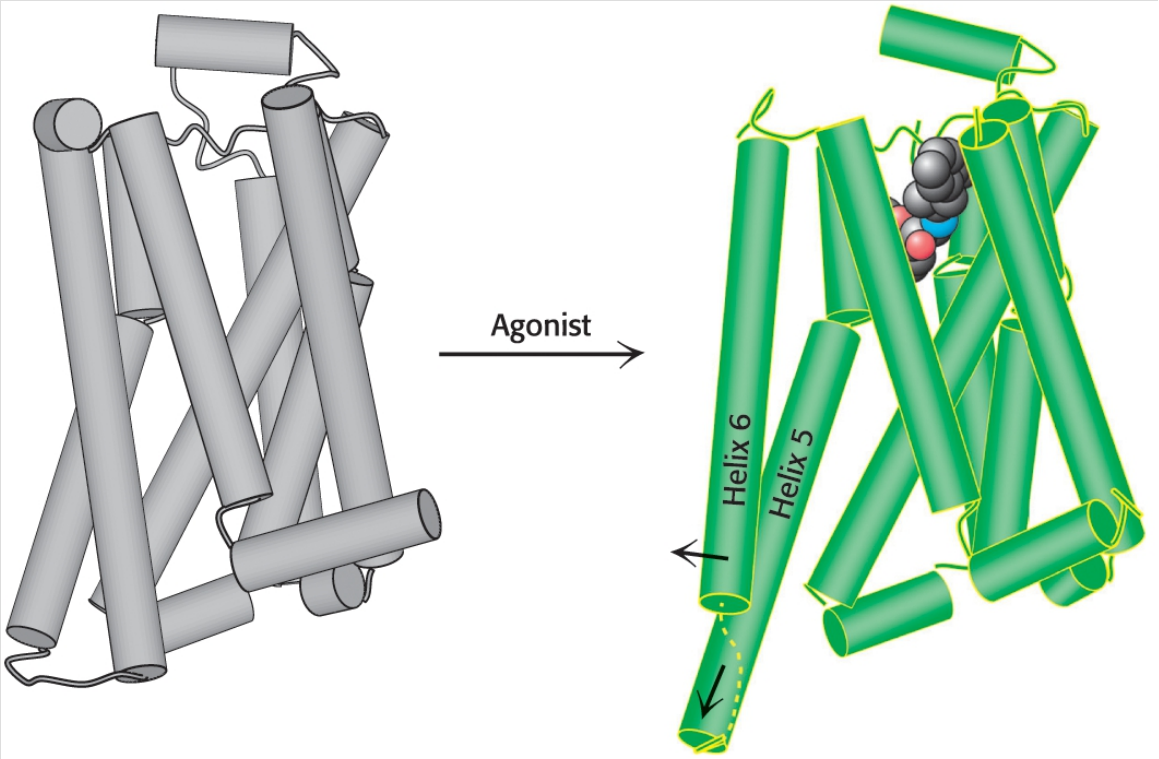


FIGURE 14.6 The binding of an agonist to the β-adrenergic receptor results in stabilization of an activated conformation of the receptor. The largest changes involve the movement of helix away from the center of the receptor and the extension of helix 5 deeper into the cell.

Ligand binding to 7TM receptors leads to the activation of heterotrimeric G proteins

What are the next steps in signaling after the binding of epinephrine? Biochemical studies had revealed that this signaling process required a specific nucleotide, GTP. The conformational change on the cytoplasmic side of the receptor activates a protein called a **G protein**, named for its requirement for guanyl nucleotides. We will examine this process in three types of muscle cells: cardiac muscle cells, cells of the constrictor muscle that controls dilation of the pupil of the eye, and smooth muscle cells in the small blood vessels.

Let us begin with cardiac muscles, which express β-adrenergic receptors. Here, the associated G protein, when activated, stimulates the activity of adenylate cyclase, an enzyme that catalyzes the conversion of ATP into cAMP. The G protein and adenylate cyclase remain attached to the membrane, whereas cAMP, a second messenger, can travel throughout the cell carrying the signal originally brought by the binding of epinephrine. **Figure 14.7** provides a broad overview of these steps.

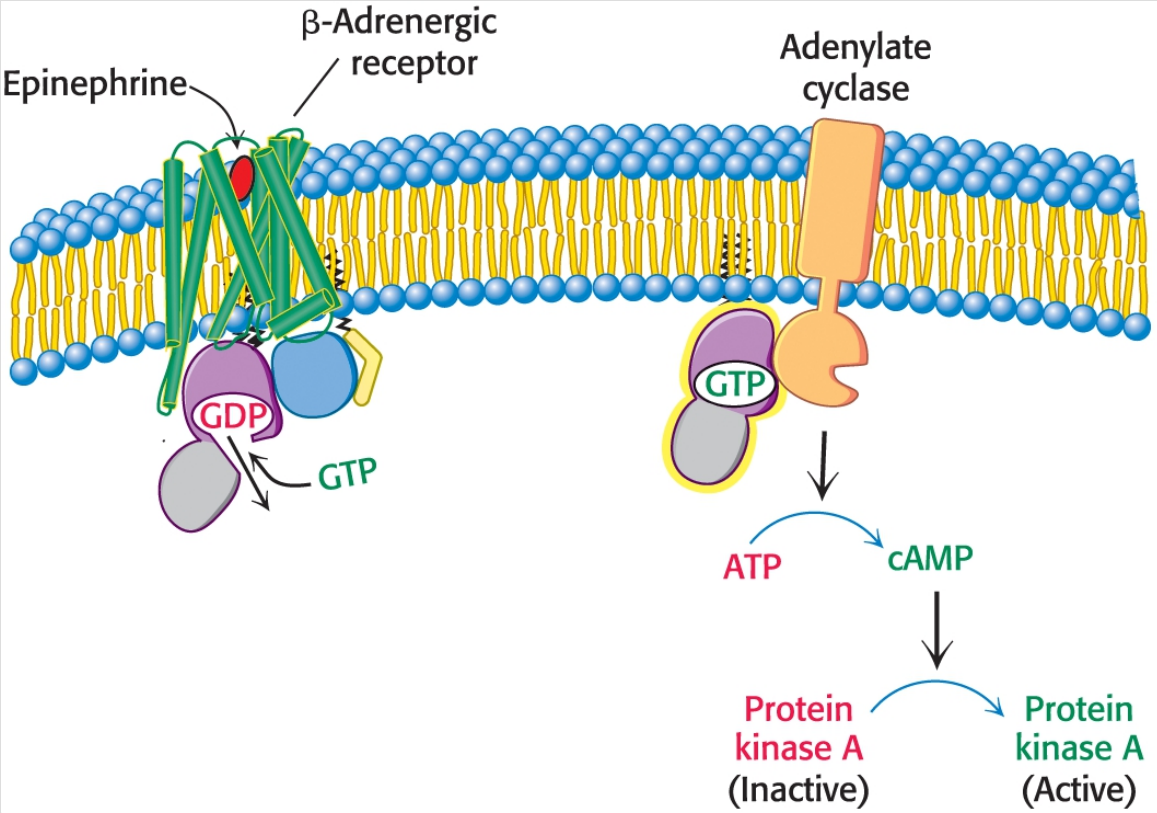


FIGURE 14.7 The signal-transduction pathway initiated by epinephrine in cardiac muscle cell results in an increase in cAMP concentration, increasing contraction. Epinephrine binding to the 7TM receptor initiates a signal-transduction pathway that acts through a G protein and cAM to activate protein kinase A. Phosphorylation of certain muscle proteins promotes muscle contraction.

- *The role of the hormone-bound receptor is to catalyze the exchange of GTP for bound GDP.* Let us consider the role of the G protein in this signaling pathway in more detail. In its inactive state, the G protein is bound to GDP. In this form, the G protein exists as a heterotrimer consisting of α, β, and γ subunits; the α subunit (referred to as G_α) binds the nucleotide at the interface between two domains (Figure 14.8). The α and γ subunits are usually anchored to the membrane by covalently attached fatty acids.

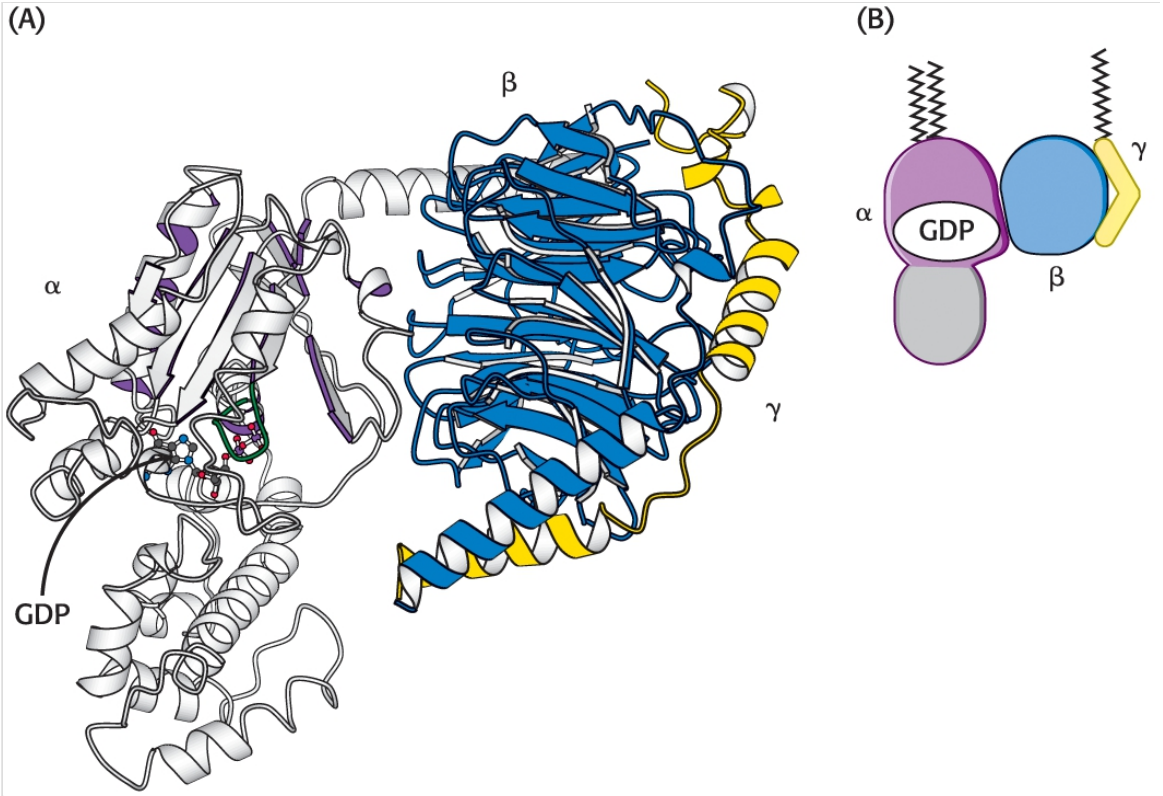


FIGURE 14.8 An inactive G protein exists as a heterotrimer consisting of α, β, and γ subunits. (A) A ribbon diagram shows the relation between the three subunits. In this complex, GDP is bound to the α subunit (gray and purple) in a pocket close to the surface through which the α subunit interacts with the βγ dimer. (B) A schematic representation of the heterotrimeric G protein is shown.

[Drawn from 1GOT.pdb.]

INTERACT with this model in Achieve

- *Analysis of the hormone-G-protein complex structure reveals its mechanism.* The structure of the complex between the hormone–β_2_AR complex and the heterotrimeric G protein shows that the G_α subunit interacts with the surface of the receptor, primarily with the two helices (helix 5 and helix 6) that changes most dramatically upon agonist binding (Figure 14.9). When bound to the receptor, the two domains of the G protein are relatively free to move with

respect to one another, allowing G_α to open substantially, enabling the replacement of GDP with GTP from solution.

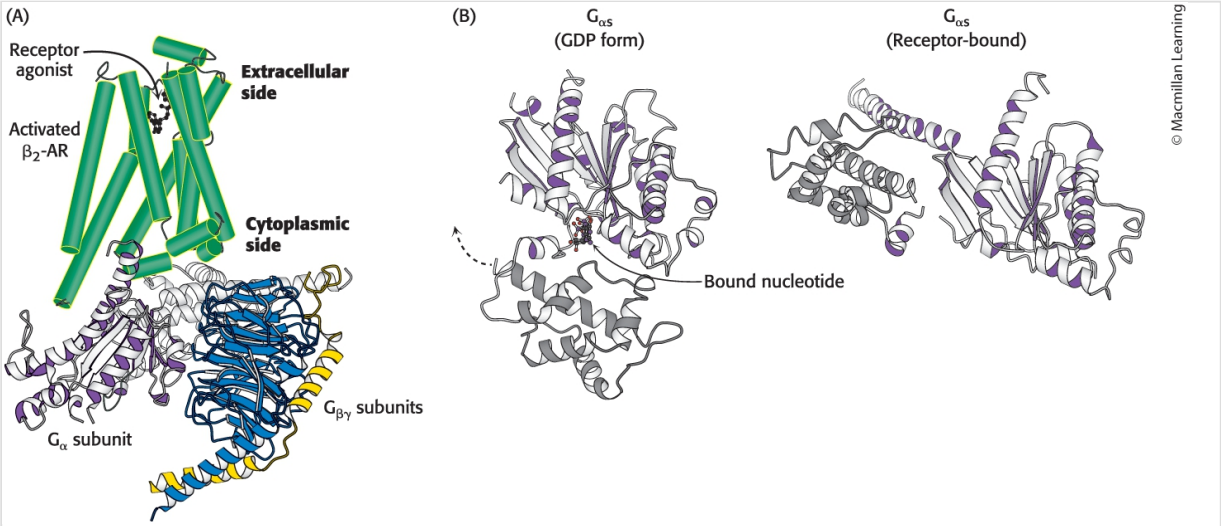


FIGURE 14.9 The activated β_2-AR activates a heterotrimeric G protein by allowing the α subunit to open and release GDP and bind GTP. (A) When the β_2-AR (green) binds a receptor agonist, the cytoplasmic face of the receptor forms an interaction surface with the G_α subunit of a heterotrimeric G protein. (B) The interaction with the activated receptor leads to a substantial conformational change in the G_α protein, in which the guanine nucleotide binding site is opened, enabling nucleotide exchange.

[Drawn from 3SN6.pdb and 1AZT.pdb.]

- *A single hormone–receptor complex can stimulate nucleotide exchange in many G-protein heterotrimers.* On GTP binding, the α subunit dissociates from the βγ dimer $(G_{\beta\gamma})$ and from the receptor. The freed receptor is available to bind other G-protein heterotrimers and to catalyze the exchange of GTP for GDP. Thus, hundreds of G_α molecules can be converted from their GDP form into their GTP form for each bound molecule of hormone, amplifying the

response. Because they signal through G proteins, 7TM receptors are often called G-protein-coupled receptors (GPCRs).

Activated G proteins transmit signals by binding to other proteins

In the GTP form, the surface of G_{α} that had been bound to $G_{\beta\gamma}$ has changed its conformation from the GDP form so that it no longer has a high affinity for $G_{\beta\gamma}$. This surface is now exposed for binding to other proteins. In the β-AR pathway, the new binding partner is adenylate cyclase, the enzyme that converts ATP into cAMP. This enzyme includes 12 membrane-spanning helices with two cytoplasmic domains that come together to form the catalytic part of the enzyme (Figure 14.10).

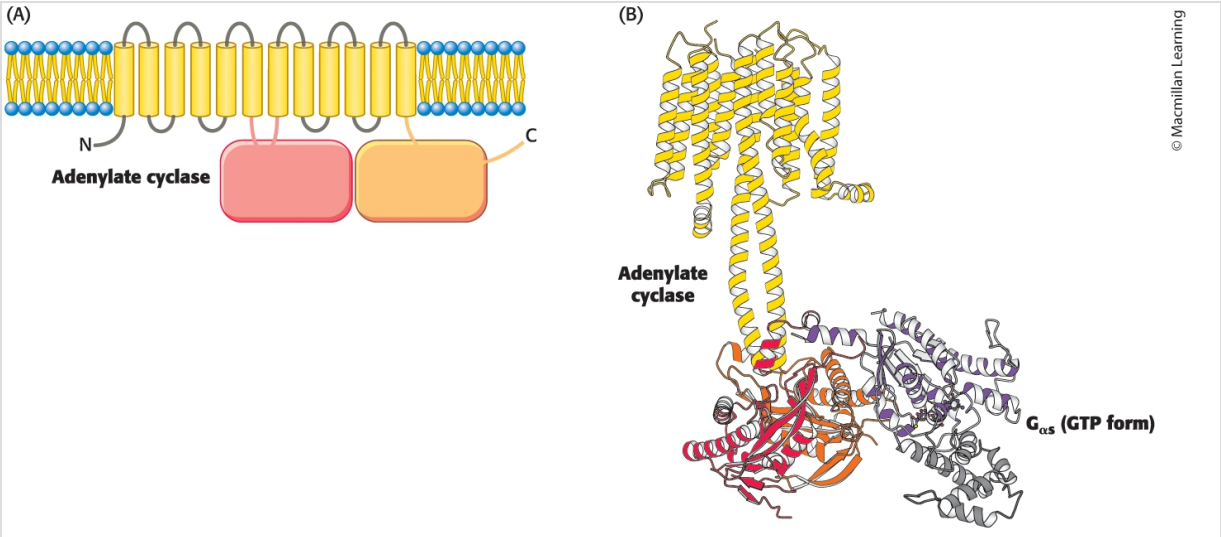


FIGURE 14.10 Adenylate cyclase is activated by binding of $G_{\alpha s}$ (GTP). (A) Adenylate cyclase is a membrane protein with two intracellular domains that come together to form the catalytic apparatus. (B) The structure of a complex between G_{α} in its GTP form bound to a adenylate cyclase is shown. The surface of $G_{\alpha s}$ that had been bound to the βγ dimer now binds adenylate cyclase.

[Drawn from 1AZS.pdb.]

INTERACT with this model in Achieve

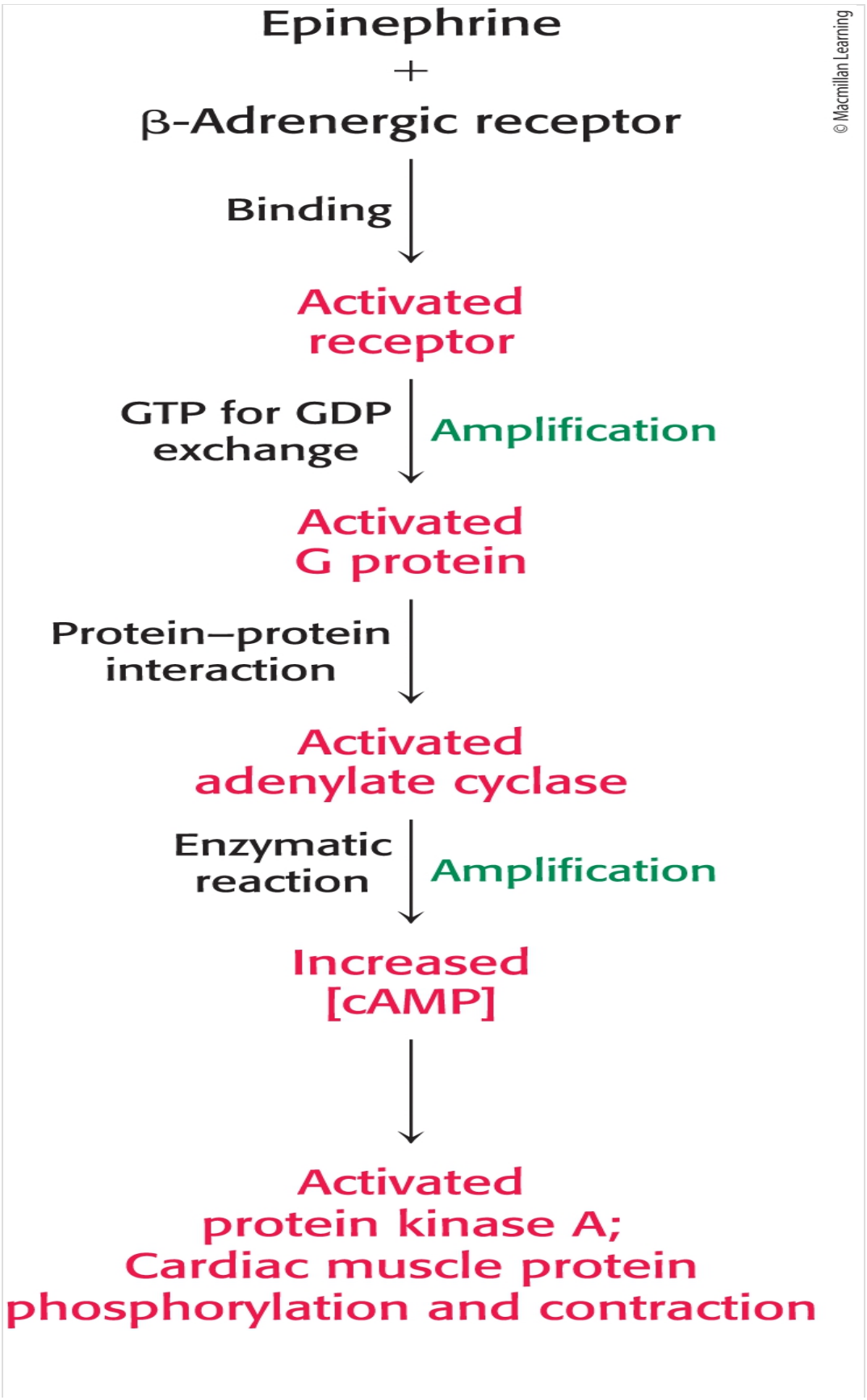
The interaction of G_α with adenylate cyclase favors a more catalytically active conformation of the enzyme, thus stimulating cAMP production. Indeed, the G_α subunit that participates in the β-AR pathway is called $G_{\alpha s}$, where "s" stands for *stimulatory*. The generation of cAMP by adenylate cyclase provides a second level of amplification because each activated adenylate cyclase molecule can convert ATP into cAMP at a rate of approximately $100\ s^{-1}$. The net result is that the binding of epinephrine to the receptor on the cardiac muscle cell surface increases the level of cAMP inside the cell rapidly.

Cyclic AMP stimulates the phosphorylation of many target proteins by activating protein kinase A

In all eukaryotic cells, most effects of cAMP are mediated by the activation of a single protein kinase, protein kinase A (PKA). As described in Chapter 7, PKA consists of two regulatory (R) chains and two catalytic (C) chains (R_2C_2). In the absence of cAMP, the R_2C_2 complex is catalytically inactive. The binding of cAMP to the regulatory chains decreases their affinity for the catalytic chains, which are catalytically active when freed. Activated PKA then phosphorylates specific serine and threonine residues in many targets to alter their activity.

In cardiac muscle cells, increases in cAMP levels leads to increased contraction. In these cells, one of these PKA substrates is troponin I.

This protein is part of the troponin complex found in cardiac and skeletal muscle but not smooth muscle. The troponin complex blocks the ability of myosin to bind to actin, preventing muscle contraction (see Chapter 6). Upon phosphorylation of troponin I, the binding of troponin to actin is weakened and myosin is more likely to bind to actin, driving muscle contraction. PKA also phosphorylates certain calcium-specific ion channels and activates them. The increased level of calcium ions binds to another troponin subunit and stimulates muscle contraction. The signal-transduction pathway initiation by epinephrine with the β-adrenergic receptor is summarized in **Figure 14.11**.



© Macmillan Learning

FIGURE 14.11 Epinephrine binding promotes cardiac muscle contraction. The binding of epinephrine to the β-adrenergic receptor initiates the signal-transduction pathway. The process in each step is indicated in black at the left of each arrow. Steps that have the potential for signal amplification are indicated at the right in green. The final step is phosphorylation of key cardiac muscle proteins, promoting muscle contraction.



G proteins spontaneously reset themselves through GTP hydrolysis

How is the signal initiated by epinephrine switched off? G_α subunits have intrinsic GTPase activity, that is, by themselves they can promote the hydrolysis of bound GTP to GDP and P_i. This hydrolysis reaction is slow, however, requiring from seconds to minutes. Thus, the GTP form of G_α is able to activate downstream components of the signal-transduction pathway before it is deactivated by GTP hydrolysis. In essence, the bound GTP acts as a built-in clock that spontaneously resets the G_α subunit after a short time. After GTP hydrolysis and the release of P_i, the GDP-bound form of G_α then reassociates with $G_{\beta\gamma}$ to re-form the inactive heterotrimeric protein (Figure 14.12). The GTP hydrolysis step also provides an additional opportunity for regulation; Some G-protein signaling pathways include additional components called GTPase-activating proteins that increase the rate of GTP hydrolysis by G-protein α subunits.

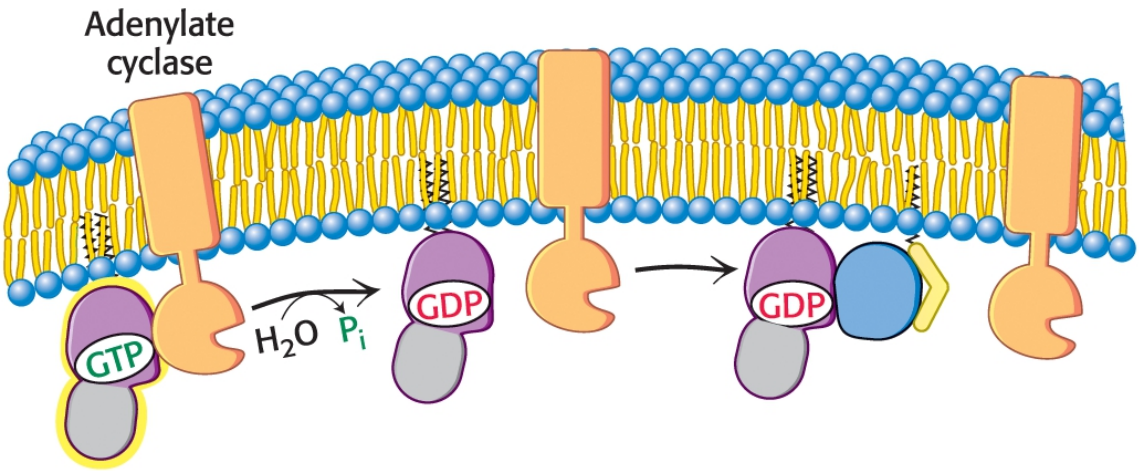


FIGURE 14.12 G proteins reset themselves by GTP hydrolysis. On hydrolysis of the bound GTP promoted by the GTPase activity of G_α, G_α dissociates from adenylate cyclase, reversing its stimulation. G_α in its GDP form then reassociates with the βγ dimer to reform the heterotrimer G protein.

The hormone-bound activated receptor must be reset as well to prevent the continuous activation of G proteins. This resetting is accomplished by two processes (Figure 14.13). First, the hormone can dissociate, returning the receptor to its initial inactive state. The likelihood that the receptor remains in its unbound state depends on the extracellular concentration of hormone. Second, members of a specialized family of enzymes, the G-protein receptor kinases, are bound by activated receptors and phosphorylates serine and threonine residues in their carboxyl-terminal tails. Finally, proteins called β-arrestins bind to the phosphorylated receptors and block their ability to activate G proteins.

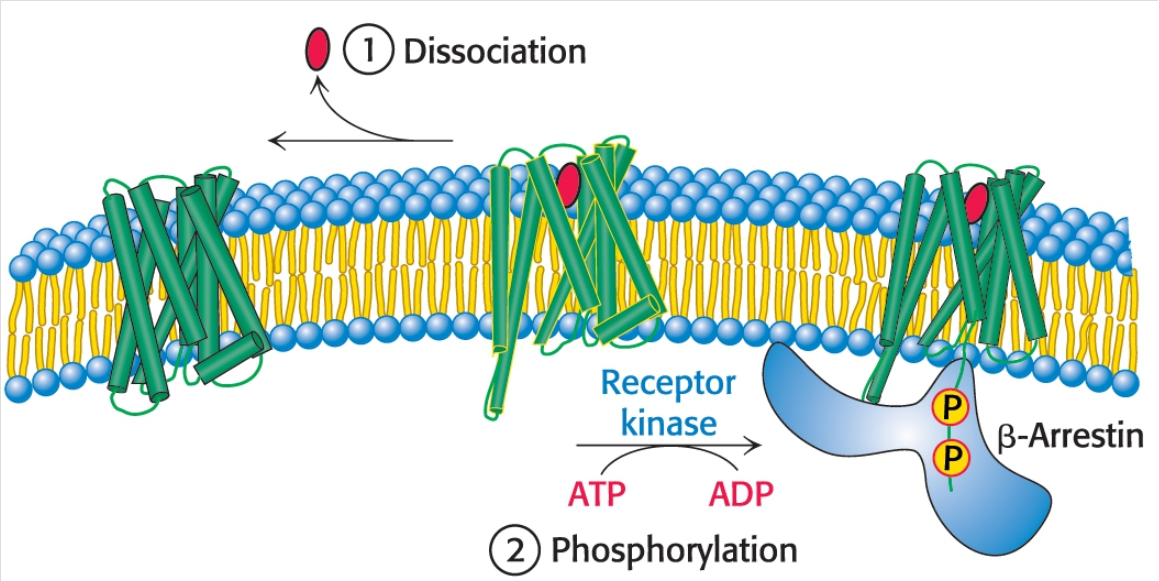


FIGURE 14.13 β-Adrenergic receptor signaling is terminated by two processes. Signal transduction by the 7TM receptor is halted (1) by dissociation of the signal molecule from the receptor and (2) by phosphorylation of the cytoplasmic C-terminal tail of the receptor and the subsequent binding of β-arrestin.

Some 7TM receptors activate the phosphoinositide cascade

We now turn to the muscle cells that control dilation of the pupils of our eyes and those that line small blood vessels in our skin. These cells express α1-adrenergic receptors rather than β-adrenergic receptors. α-Adrenergic receptors are homologous to β-adrenergic receptors, also bind epinephrine, and have very similar three-dimensional structures. They differ, however, in the G proteins to which they are coupled in their signal-transduction pathway by virtue of differences in parts of the intracellular face of the receptors. α1-Adrenergic receptors activate a G protein called $G_{\alpha q}$. In its GTP form, $G_{\alpha q}$ binds to and activates a form of the enzyme phospholipase C.

Phospholipase C catalyzes the cleavage of a phospholipid present in cell membranes, phosphatidylinositol 4,5-bisphosphate (PIP_2), into the two second messengers — inositol 1,4,5-trisphosphate (IP_3) and diacylglycerol (DAG; **Figure 14.14**). IP_3 is soluble and diffuses away from the membrane. This second messenger causes the rapid release of Ca^{2+} from the intracellular stores in the endoplasmic reticulum (ER), which accumulates a reservoir of Ca^{2+} through the action of transporters such as the Ca^{2+} ATPase (Section 13.2). On binding IP_3, specific IP_3-gated Ca^{2+}–channel proteins in the ER membrane open to allow calcium ions to flow from the ER into the cytoplasm. Calcium ion is itself a signaling molecule: it can bind proteins, including a ubiquitous signaling protein called **calmodulin (CaM)**, and enzymes such as protein kinase C.

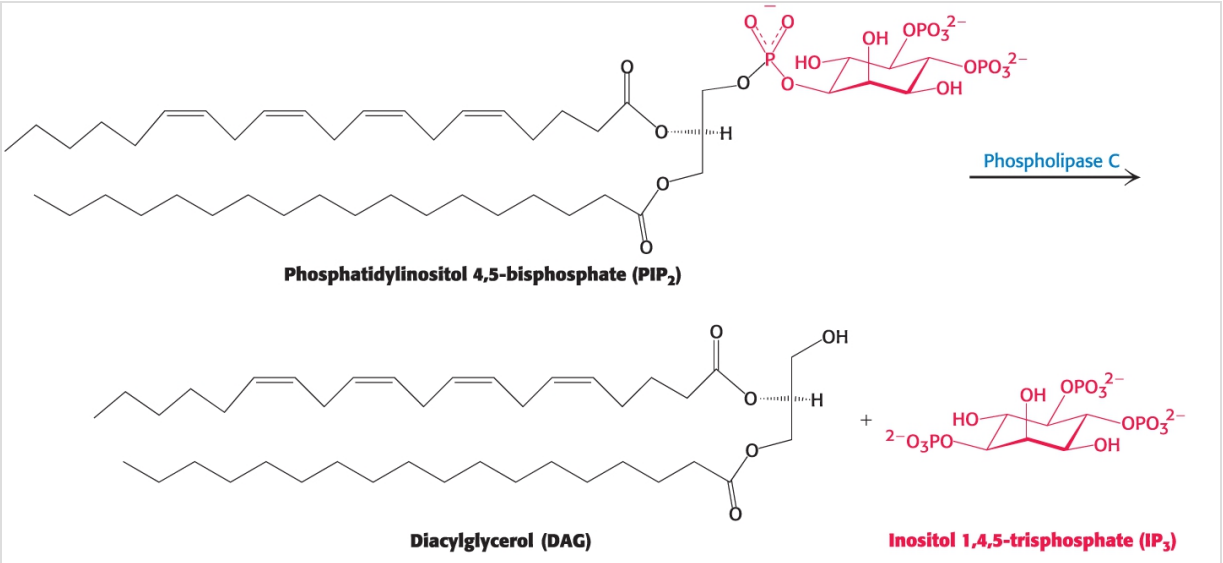


FIGURE 14.14 Phospholipase C cleaves the membrane lipid phosphatidylinositol 4,5-bisphosphate (PIP_2) into two second messengers. The two messengers are diacylglycerol (DAG) and inositol 1,4,5-trisphosphate (IP_3). DAG remains in the membrane while IP_3 is free to diffuse away.

DAG remains in the plasma membrane where it binds and activates protein kinase C (PKC), a protein kinase that phosphorylates serine and threonine residues in many target proteins. Specialized domains of this kinase bind DAG and require bound calcium to do so. Thus, DAG and IP_3 work in tandem: IP_3 increases the Ca^{2+} concentration, and Ca^{2+} facilitates the DAG-mediated activation of protein kinase C. Like PKA (Chapter 7), activation involves removal of a pseudo-substrate in a regulatory domain from the active site. The overall signal-transduction pathway, referred to as the phosphoinositide cascade, is summarized in **Figure 14.15**. Both IP_3 and DAG act transiently because they are converted into other species by phosphorylation or other processes.

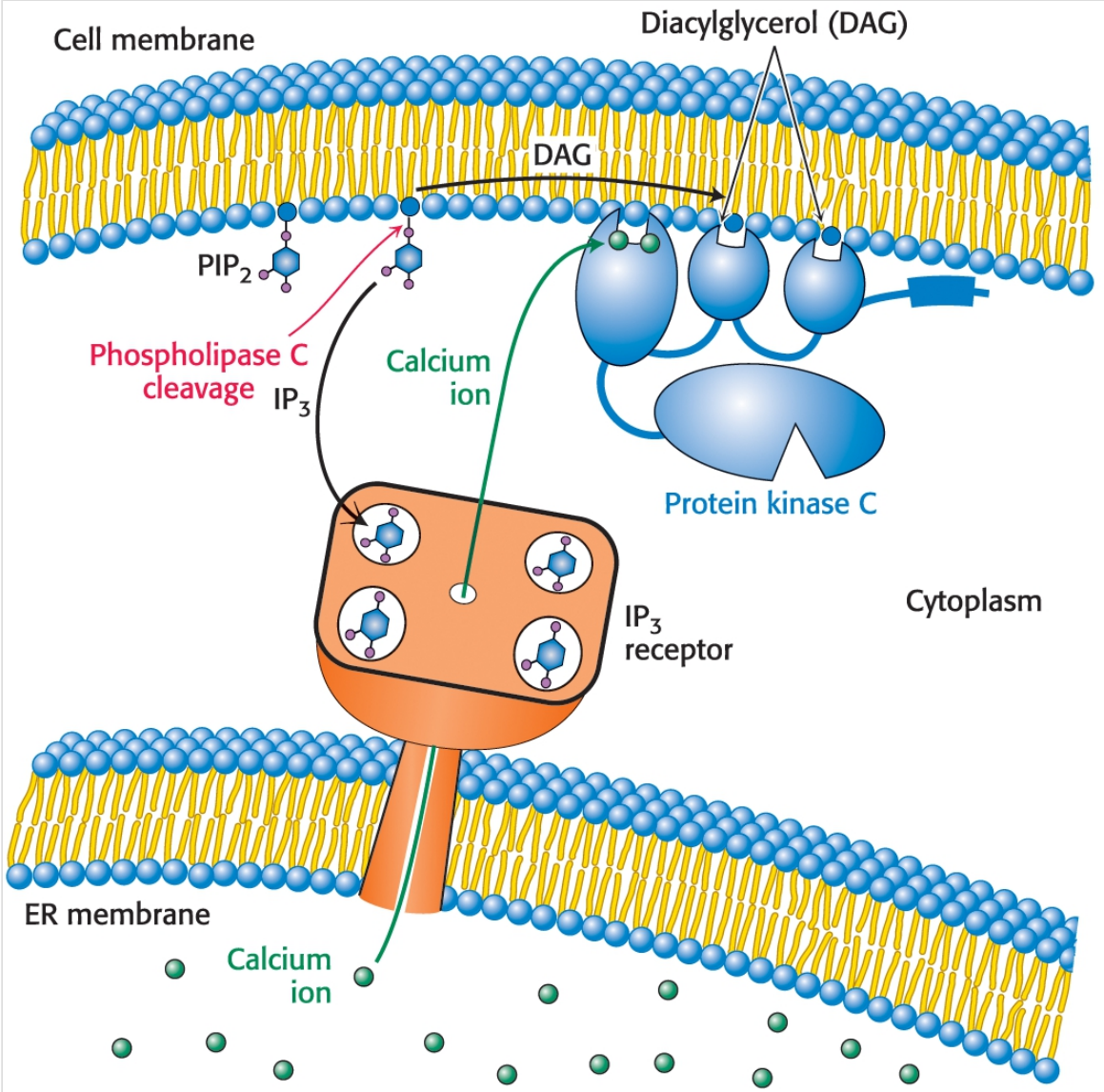


FIGURE 14.15 The phosphoinositide cascade results in protein kinase C activation.
Phospholipase C cleaves PIP_2 into IP_3 and DAG. IP_3 release results in the influx of calcium ions (owing to the opening of the IP_3 receptor ion channels), and DAG accumulation results in the activation of protein kinase C when protein kinase C binds to DAG in the membrane. Calciur ions bind to domains in protein kinase C and help facilitate its binding to DAG.

Calcium ion is a widely used second messenger

Calcium ion participates in many signaling processes in addition to the phosphoinositide cascade. Two properties of this ion account for its widespread use as an intracellular messenger:

- *Fleeting changes in Ca^{2+} concentration are readily detected.* At steady state, intracellular levels of Ca^{2+} must be kept low to prevent the precipitation of carboxylated and phosphorylated compounds, which form poorly soluble salts with Ca^{2+}. Transport systems extrude Ca^{2+} from the cytoplasm, maintaining the cytoplasmic concentration of Ca^{2+} at approximately 100 nM — several orders of magnitude lower than that of the extracellular medium. Given this low steady-state level, transient increases in Ca^{2+} concentration produced by signaling events can be readily sensed.
- *Ca^{2+} can bind tightly to proteins and induce substantial structural rearrangements.* A second property of Ca^{2+} that makes it a highly suitable intracellular messenger is its ability to interact with protein through many points of contact. Calcium ions bind well to negatively charged oxygen atoms (from the side chains of glutamate and aspartate) and uncharged oxygen atoms (main-chain carbonyl groups and side-chain oxygen atoms from glutamine and asparagine; **Figure 14.16**). The capacity of Ca^{2+} to be coordinated to multiple ligands — from six to eight oxygen atoms — enables it to cross-link different segments of a protein and induce significant conformational changes.

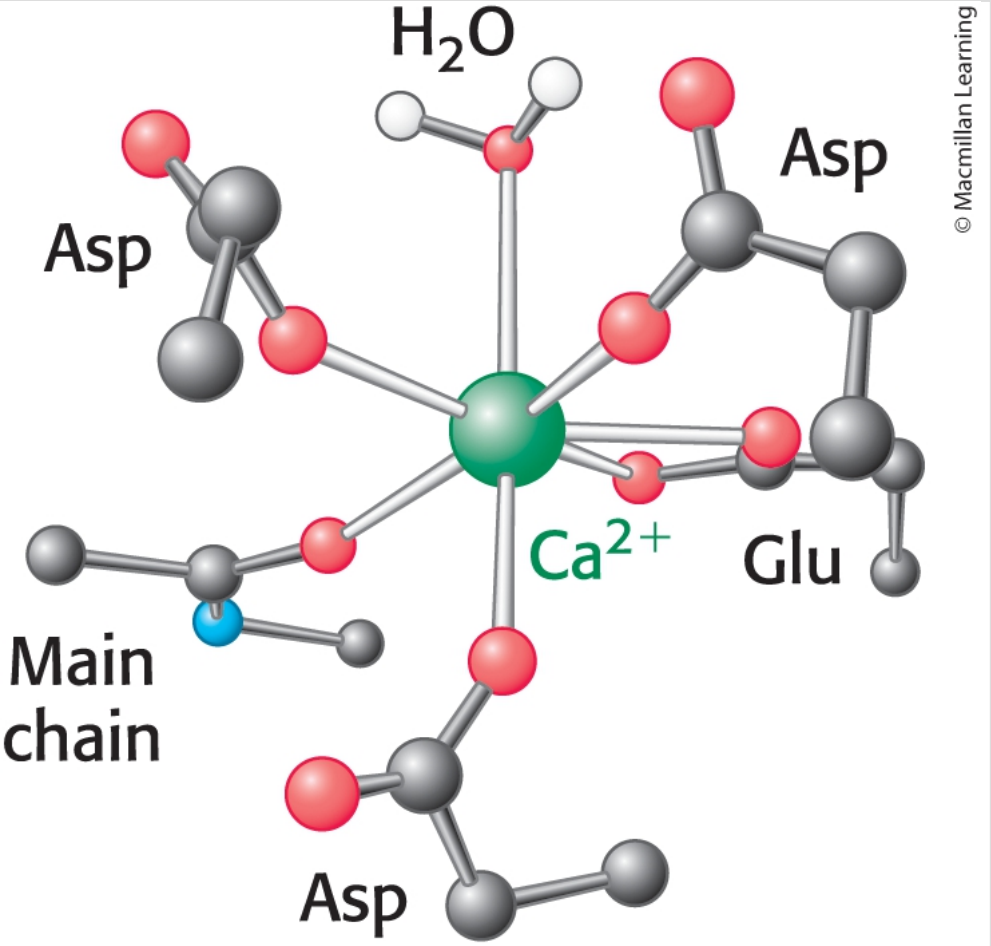
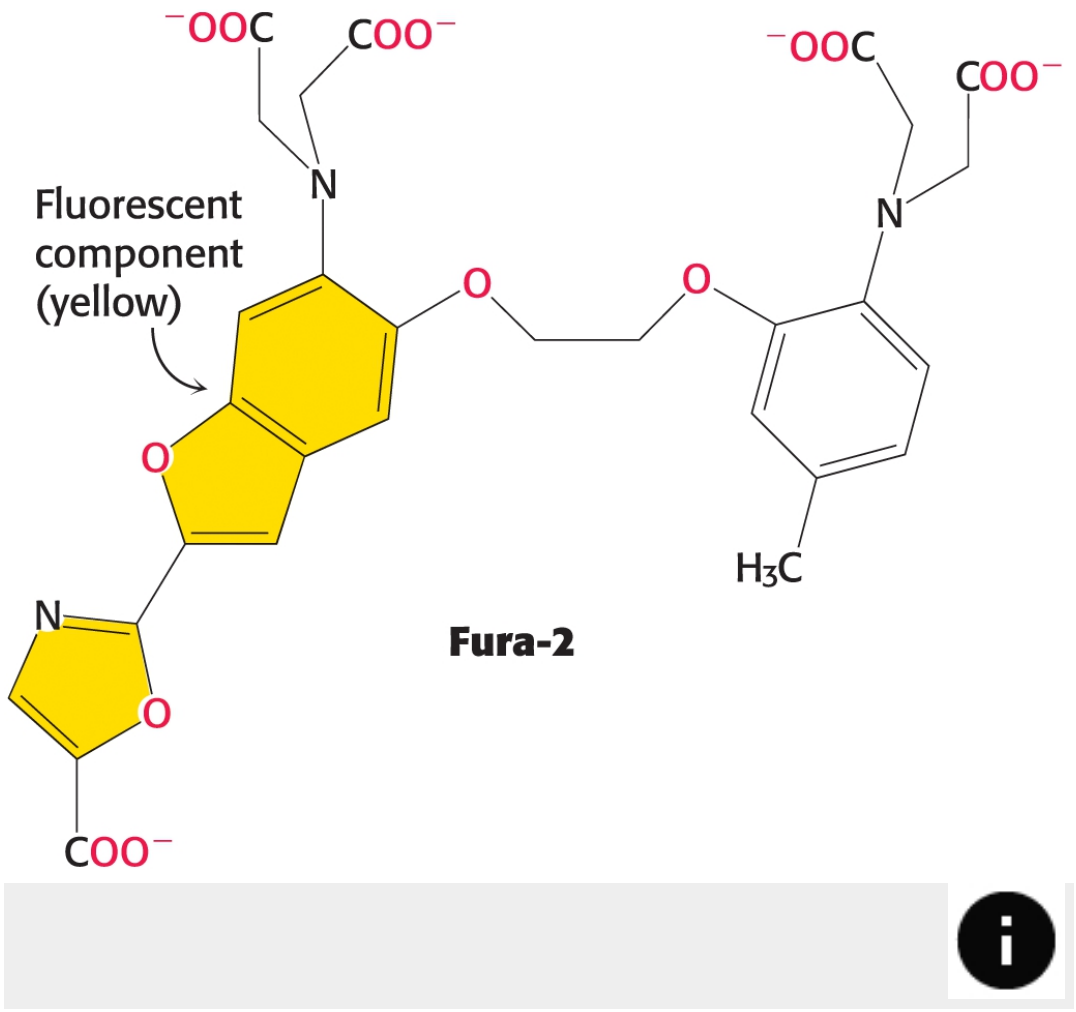


FIGURE 14.16 Calcium-binding sites typically include seven oxygen atoms. In one common mode of binding, calcium is coordinated to six oxygen atoms from a protein and one from water. The multiple protein-based ligands allow calcium ions to stabilize particular protein structures.

Our understanding of the role of Ca^{2+} in cellular processes has been greatly enhanced by our ability to detect changes in Ca^{2+} concentrations inside cells and even monitor these changes in real time. In Section 4.2, we discussed how intact proteins can be detected in live cells using fluorescence microscopy. A similar approach can be used for

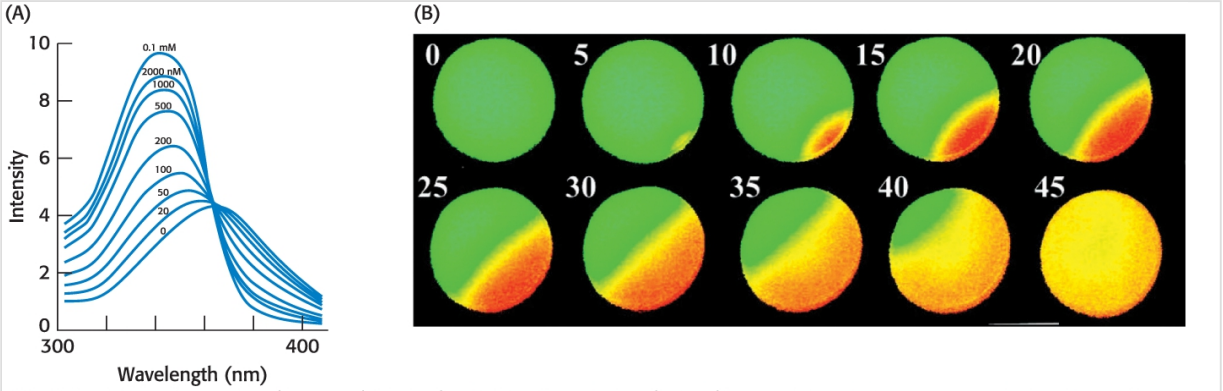
the visualization of changes in Ca^{2+} concentrations. This ability depends on the use of specially designed dyes such as Fura-2 that bind Ca^{2+} and change their fluorescent properties on Ca^{2+} binding. Fura-2 binds Ca^{2+} through appropriately positioned oxygen atoms (shown in red) within its structure:



Fura-2

When such a dye is introduced into cells, changes in available Ca^{2+} concentration can be monitored with microscopes capable of detecting changes in fluorescence (Figure 14.17). Following pioneering work on calcium sensors, probes for sensing other second messengers such as

cAMP also have been developed. These molecular-imaging agents are greatly enhancing our understanding of signal-transduction processes.



(B) Credit: Republished with permission of Company of Biologists, from Exploring the mechanism of action of the sperm-triggered calcium-wave pacemaker in ascidian zygotes, Carroll, M. et al., December 15, 2003, *J Cell Sci* 116: 4997–5004; permission conveyed through Copyright Clearance Center, Inc. Courtesy Alex McDougall.
© Macmillan Learning

FIGURE 14.17 Free calcium ion concentrations inside cells can be imaged using fluorescence microscopy with appropriate dyes. (A) The fluorescence spectra of the calcium-binding dye Fura-2 can be used to measure available calcium ion concentrations in solution and in cells. (B) A series of images show Ca^{2+} spreading across an egg cell following fertilization by sperm, with the numbers indicating time elapsed in seconds. These images were obtained through the use of Fura-2. The images are false colored: orange represents high Ca^{2+} concentrations, and green represents low Ca^{2+} concentrations.

[(A) Information from S. J. Lippard and J. M. Berg, *Principles of Bioinorganic Chemistry* (University Science Books, 1994), p. 193.]

Calcium ion often activates the regulatory protein calmodulin

Calmodulin (CaM), a 17-kDa protein with four Ca^{2+}-binding sites, serves as a calcium sensor in nearly all eukaryotic cells. At cytoplasmic

concentrations above about 500 nM, Ca^{2+} binds to and activates calmodulin. Calmodulin is a member of the EF-hand protein family. The **EF hand** is a Ca^{2+}-binding motif that consists of a helix, a loop, and a second helix. This motif was named the *EF hand* because the two key helices designated *E* and *F* in parvalbumin, the first protein where the motif was observed, are positioned like the forefinger and thumb of the right hand (**Figure 14.18**). The two helices and the intervening loop of the EF hand form the Ca^{2+}-binding motif. Seven oxygen atoms are coordinated to each Ca^{2+}, six from the protein and one from a bound water molecule. Calmodulin is made up of four EF-hand motifs, each of which can bind a single Ca^{2+} ion.

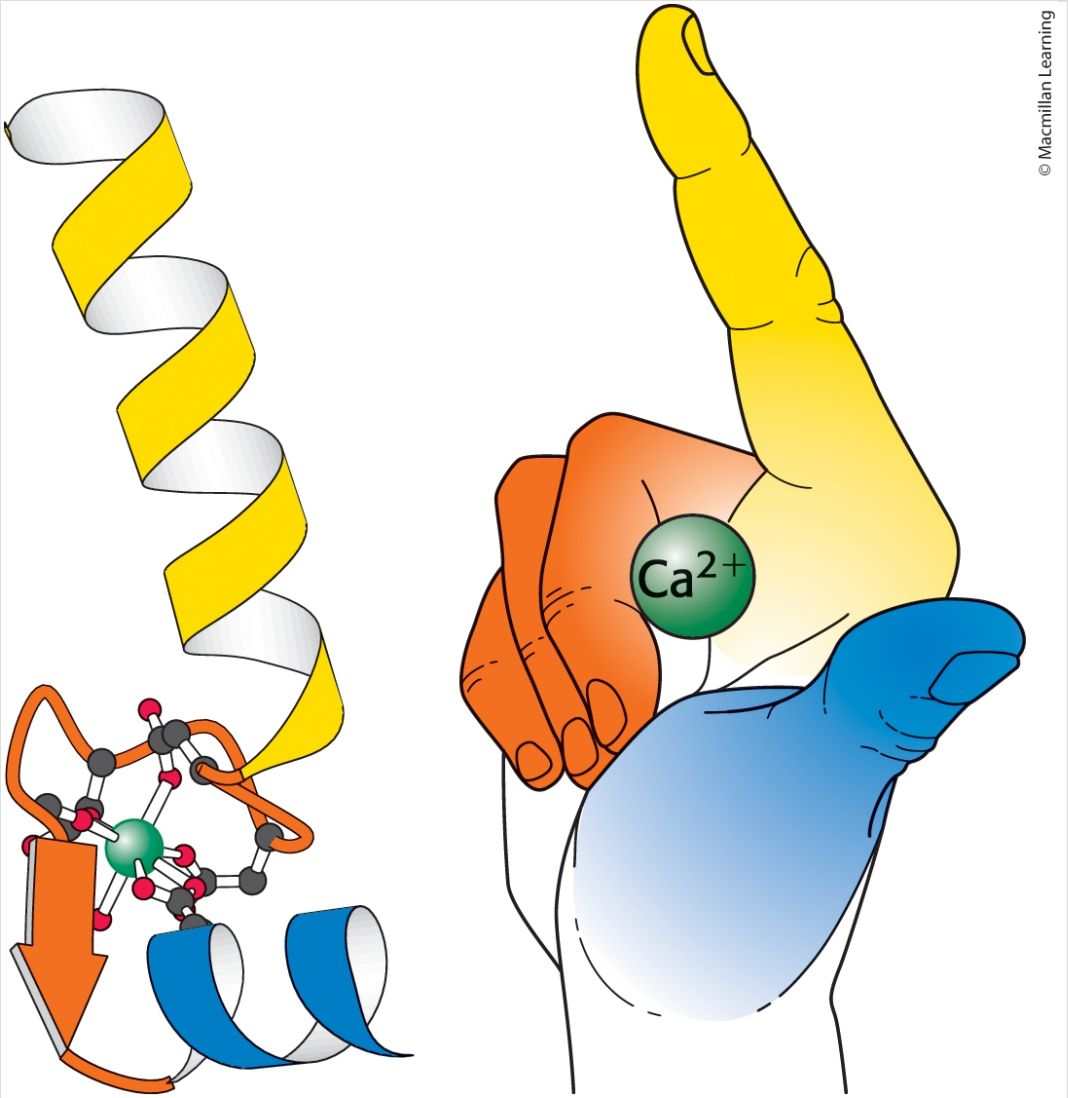


FIGURE 14.18 An EF hand is a binding site for Ca^{2+} in many calcium-sensing proteins. The structure, resembling a hand, is formed by a helix-loop-helix unit with the E helix is yellow, the loop in red, the F helix is blue, and calcium is represented by the green sphere.

[Drawn from 1CLL.pdb.]

The binding of Ca^{2+} to calmodulin induces substantial conformational changes in its EF hands, exposing hydrophobic surfaces that can be

used to bind other proteins. Using its two sets of two EF hands, calmodulin clamps down around specific regions of target proteins — usually exposed α helices with appropriately positioned hydrophobic and charged groups (Figure 14.19). Some protein kinases, for example, are activated when calmodulin binds to a target α helix and removes it from a position when it inhibits kinase function.

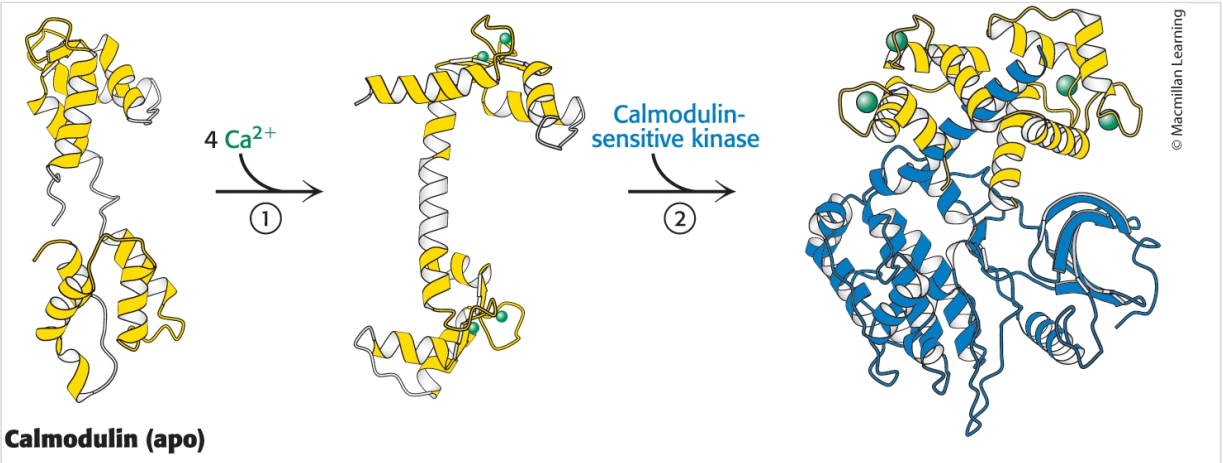


FIGURE 14.19 Calmodulin binds calcium and activates some protein kinases. On Ca^{2+} binding to the apo, or calcium-free, form of calmodulin, the two halves of calmodulin change conformation. Calmodulin can then clamp down around an α helix through surfaces that are exposed. Some kinases have an α helix that inhibits enzyme activity and calmodulin binding can relieve this inhibition.

[Drawn from 1CFD.pdb, 1CLL.pdb, and 6PAW.pdb.]

INTERACT with the models shown in Figure 14.18 and 14.19 in Achieve

How, then, does initiation of the phosphoinositide cascade lead to smooth muscle contraction? Smooth muscle does not contain the troponin complex. However, myosin binding to actin and subsequent contraction is stimulated by phosphorylation of a component of myosin, the regulatory light chain. The increased level of calcium activates calmodulin, which, in turn, binds to and activates myosin light chain kinase. The activated kinase phosphorylates the myosin light chain and

facilitates contraction. This signal-transduction-pathway-induced contraction leads to pupil dilation and pale skin as blood flow is restricted.

Some receptors signal through G proteins that inhibit rather than stimulate adenylate cyclase

Some blood vessel smooth muscle cells express a different class of 7TM receptors termed α_2-adrenergic receptors. These receptors are quite similar to the α_1- and β-adrenergic receptors, but signal through a third class of G protein, $G_{\alpha i}$. Like $G_{\alpha s}$, this G-protein α subunit binds adenylate cyclase, but $G_{\alpha i}$-binding inhibits cyclase activity rather than simulating it. Thus, activation of this signaling pathway results in a decrease in cAMP levels. Such lower cAMP levels influence a protein kinase cascade (**Figure 14.20**). The net result is increased smooth muscle contraction.

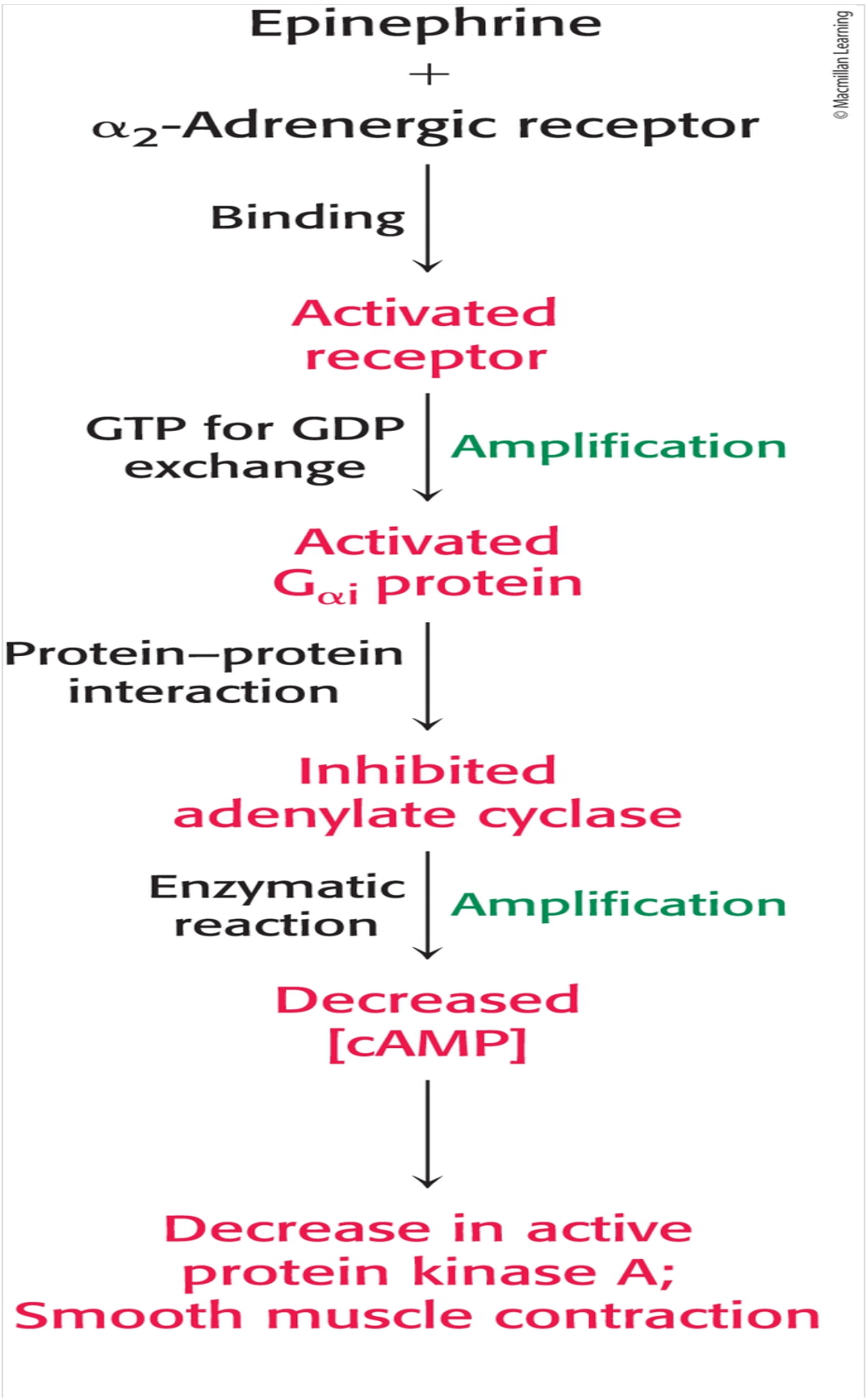

Epinephrine
+
α2-Adrenergic receptor
Binding
Activated receptor
GTP for GDP exchange
Amplification
Activated Gαi protein
Protein–protein interaction
Inhibited adenylate cyclase
Enzymatic reaction
Amplification
Decreased [cAMP]
Decrease in active protein kinase A; Smooth muscle contraction
© Macmillan Learning

FIGURE 14.20 α2-Adrenergic receptors signal through the G protein $G_{\alpha i}$, which inhibits adenylate cyclase. The signal-transduction pathway from epinephrine binding to α2-adrenergic receptors results in smooth muscle contraction. This is achieved through a decrease in cAMP concentration and the associated reduction in protein kinase A activity.



Self-Check Question



Why is increased cardiac muscle contraction favored by increased cAMP levels but increased smooth muscle contraction favored by reduced cAMP levels?

G-protein βγ-dimers can also directly participate in signaling

When a heterotrimeric G protein is activated, it dissociates into a G_{α} subunit and a $G_{\beta\gamma}$ dimer. It was widely believed that the only role of the $G_{\beta\gamma}$ dimer was to sequester G_{α} subunits. However, through studies using purified G-protein subunits led to the discovery that the $G_{\beta\gamma}$ dimer was the active component in activating a key ion channel in the heart (Figure 14.21). Subsequent studies have revealed that these subunits play active roles in a wide range of signaling pathways, revealing an additional level of complexity and control.

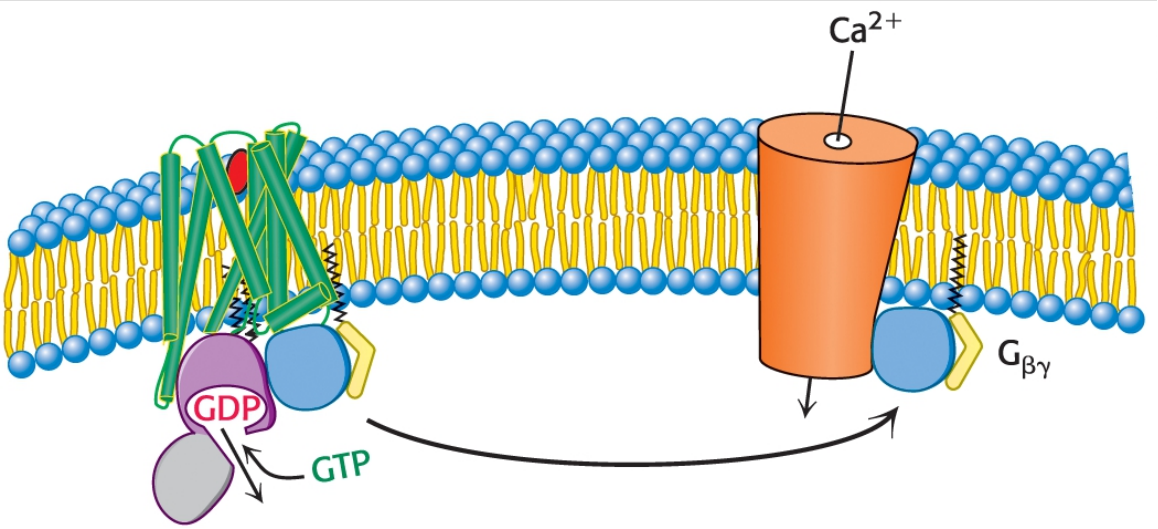


FIGURE 14.21 The G protein βγ dimer actively participates in some signal-transduction pathways. When released from the G protein α subunit, the βγ dimer can bind to other proteins and, for example, open certain ion channels.



Barbara Steiner

EVA NEER Born in Poland in 1938, Eva Neer escaped from the Nazis at the age of one, hiding under her mother's skirt. Her family emigrated first to Brazil, then to the United States. After completing her MD degree, she began research purifying the membrane protein adenylate cyclase; this was an enzyme of much interest, given research by Earl Sutherland, Martin Rodbell, and Alfred Gilman implicating cAMP as a key intracellular messenger. Dr. Neer continued her career as a faculty member, working on many aspects of G-protein signaling and sharing some of her partially

purified G_{as} with David Clapham, a colleague interested in ion-channel activation. Her preparation potently activated the ion channels, but subsequent studies revealed that this was due not to $G_{\alpha s}$ but to contaminating $G_{\beta\gamma}$ that was present. This serendipitous discovery revealed the active role $G_{\beta\gamma}$ plays in some signaling systems and laid the foundation for many future studies. Dr. Neer was known for her great integrity; she trained many graduate students and postdoctoral fellows before she died prematurely of breast cancer at the age of 62.

7TM receptors trigger signaling through G proteins in many other cell types

We noted earlier that the human genome encodes nearly 1000 7TM receptors. Approximately 1/3 of these participate in our sense of smell, and a few others are central to vision. We will explore these specialized receptors at the end of this chapter. The others participate in one or more processes in almost all aspects of physiology.

This array of signaling molecules, receptors, and pathways can be dizzyingly complex. However, once we know that a pathway involves a 7TM receptor and we identify the participating G protein, we can deduce the participating second messengers and key steps in the pathway (**Figure 14.22**).

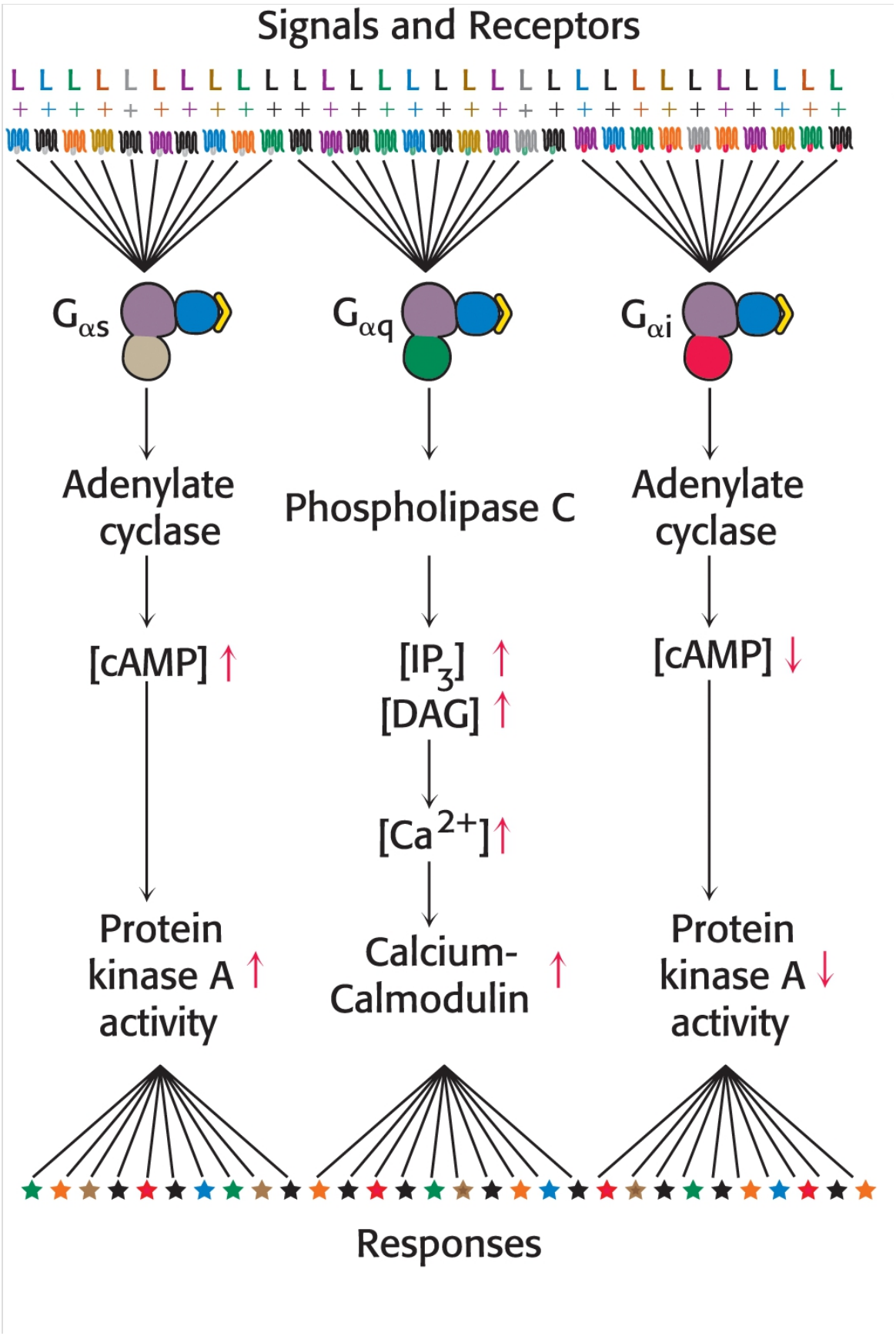
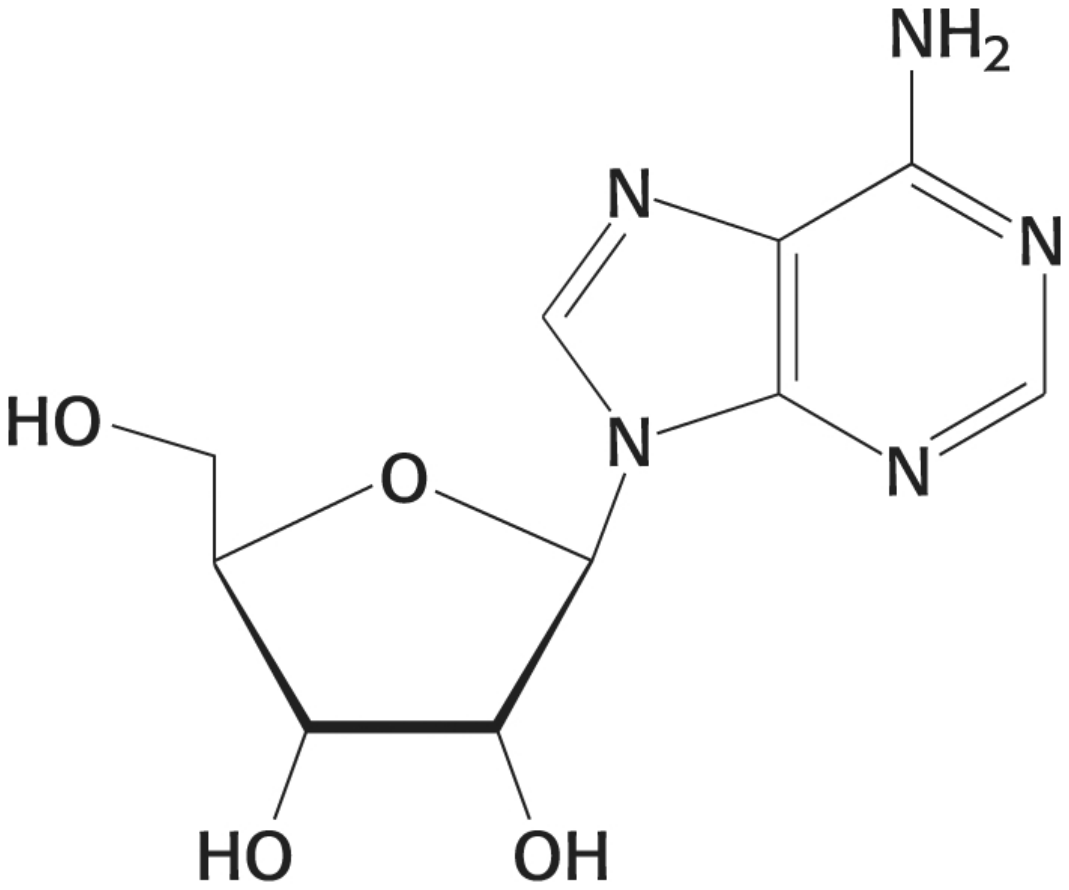

Signals and Receptors
$G_{\alpha s}$
$G_{\alpha q}$
$G_{\alpha i}$
Adenylate cyclase
Phospholipase C
Adenylate cyclase
[cAMP] ↑
$[IP_3]$ ↑
[DAG] ↑
[cAMP] ↓
$[Ca^{2+}]$ ↑
Protein kinase A activity ↑
Calcium-Calmodulin ↑
Protein kinase A activity ↓
Responses

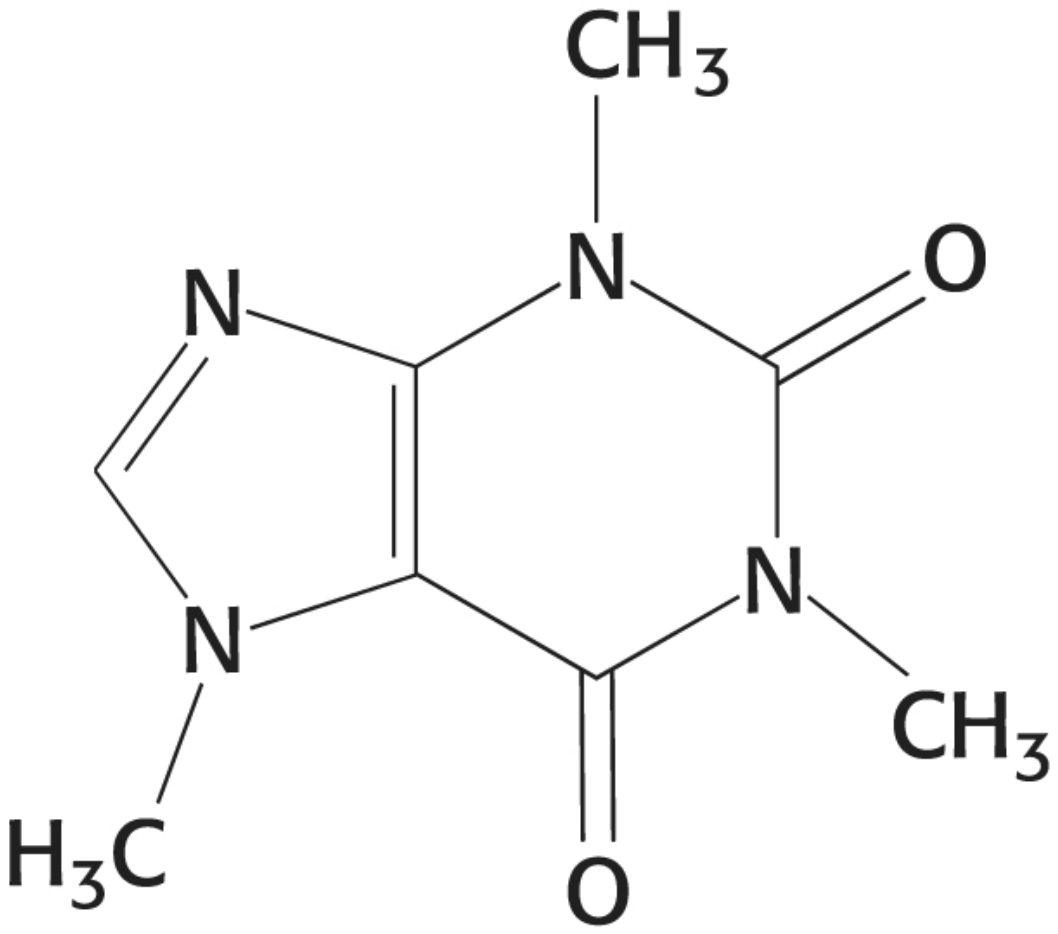
FIGURE 14.22 Common pathways recur in many different signaling processes involving G proteins. A very large number of 7TM receptors and their associated ligands signal through the three classes of G protein α subunits: $G_{\alpha s}$, $G_{\alpha q}$, and $G_{\alpha i}$. The occurrence of these α subunits in the pathways dictate several steps in the pathways. After these steps, a wide variety of responses can occur.



For example, the peptide hormone glucagon, which plays a central role in control of metabolism during fasting, has a receptor that signals through $G_{\alpha s}$. We can deduce that cAMP levels will rise in cells that express the receptor, and this will activate PKA. PKA phosphorylates two enzymes that lead to the breakdown of glycogen, the polymeric store of glucose, and the inhibition of further glycogen synthesis (Section 21.4). Our genome encodes four receptors for the nucleoside adenosine that are expressed throughout the body, including the heart and the brain. One of these, the adenosine A_1 receptor, signals through $G_{\alpha i}$. The A_1 pathway slows the heartbeat as we would anticipate due to a decreased level of cAMP. In the brain, it decreases the release of certain neurotransmitters. Compounds that block receptors without activating them are referred to as **antagonists**. You are likely familiar with the actions of a widely occurring adenosine receptor antagonist, caffeine.



Adenosine



Caffeine

14.3 Insulin Signaling: Phosphorylation Cascades Are Central to Many Signal-Transduction Processes

We now turn to a signaling pathway that comes into play after you return to complete your meal after your quick retreat. The maintenance of blood glucose levels with a relatively narrow range in the face of substantial changes in food intake and activity is a major challenge that we will explore extensively later in the book. For now, we will explore the signal-transduction pathway initiated by **insulin**, the hormone released in response to increased blood-glucose levels after a meal (**Figure 14.23**). In all of its detail, this multifaceted pathway is quite complex. Hence, we will focus solely on the major branch, which leads to the movement of glucose transporters to the surfaces of fat and muscle cells. These transporters allow these cells to take up the glucose that is plentiful in the bloodstream after a meal. We will discuss the mechanisms by which pancreatic β-cells sense glucose levels and release insulin in Chapter 15.

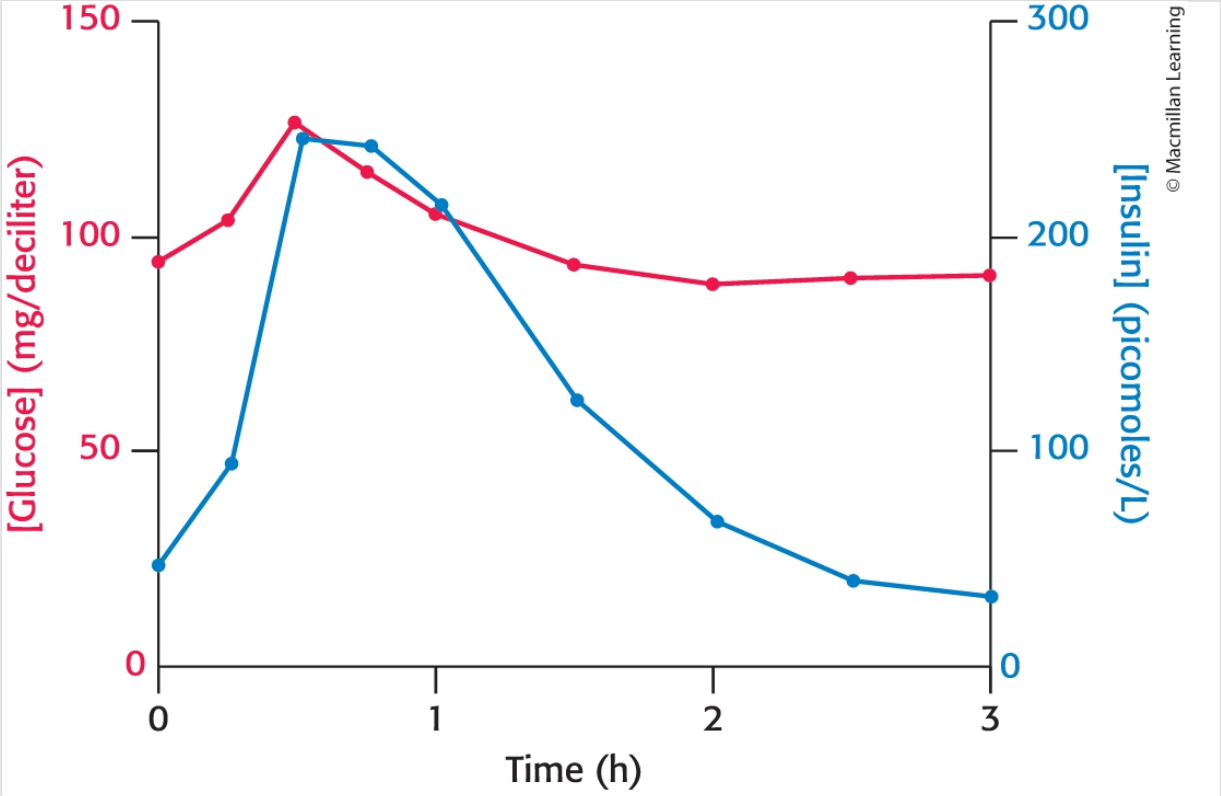


FIGURE 14.23 Glucose and insulin levels increase and then decrease following a meal. Shortly after eating, glucose levels in the bloodstream increase. These increased levels are sensed and insulin is released into the bloodstream from the pancreas. Insulin then stimulates absorption of glucose by muscle and fat cells, decreasing the glucose levels.

The signaling pathways we have examined so far have activated protein kinases as downstream components. The receptor for insulin is a member of a large family of receptors that include protein kinases as a key part of their covalent structures that are inactive under resting conditions. The activation of these protein kinases sets in motion other processes that ultimately modify the effectors of these pathways.

The insulin receptor is a protein kinase that is autoinhibited prior to insulin binding

Insulin is a peptide hormone, consisting of two chains that are linked by three disulfide bonds (Figure 14.24).

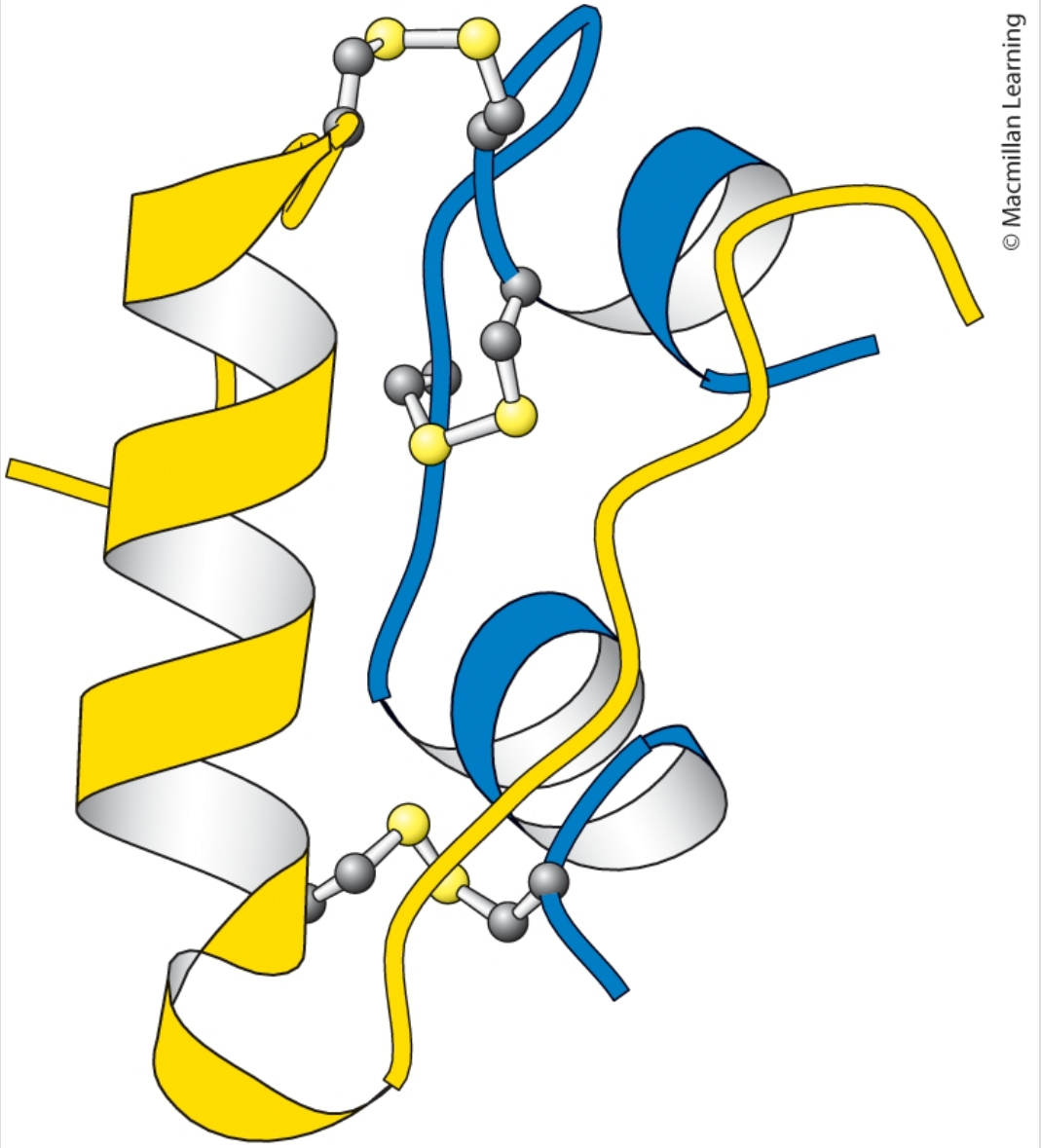


FIGURE 14.24 Insulin comprises two chains linked by two interchain disulfide bonds. The α chain (blue) also has an intrachain disulfide bond. The β chain is shown in yellow.

[Drawn from 1B2F.pdb.]

Its receptor has a quite different structure from that of the β-AR. The insulin receptor is a homodimer of heterodimers. Each component of the homodimer consists of one α chain and one β chain (Figure 14.25). The α chain has an elaborate structure with six domains while the β chain has two domains in addition to a protein kinase domain. Each α chain lies completely outside the cell, whereas each β chain lies primarily inside the cell, spanning the membrane with a single transmembrane segment.

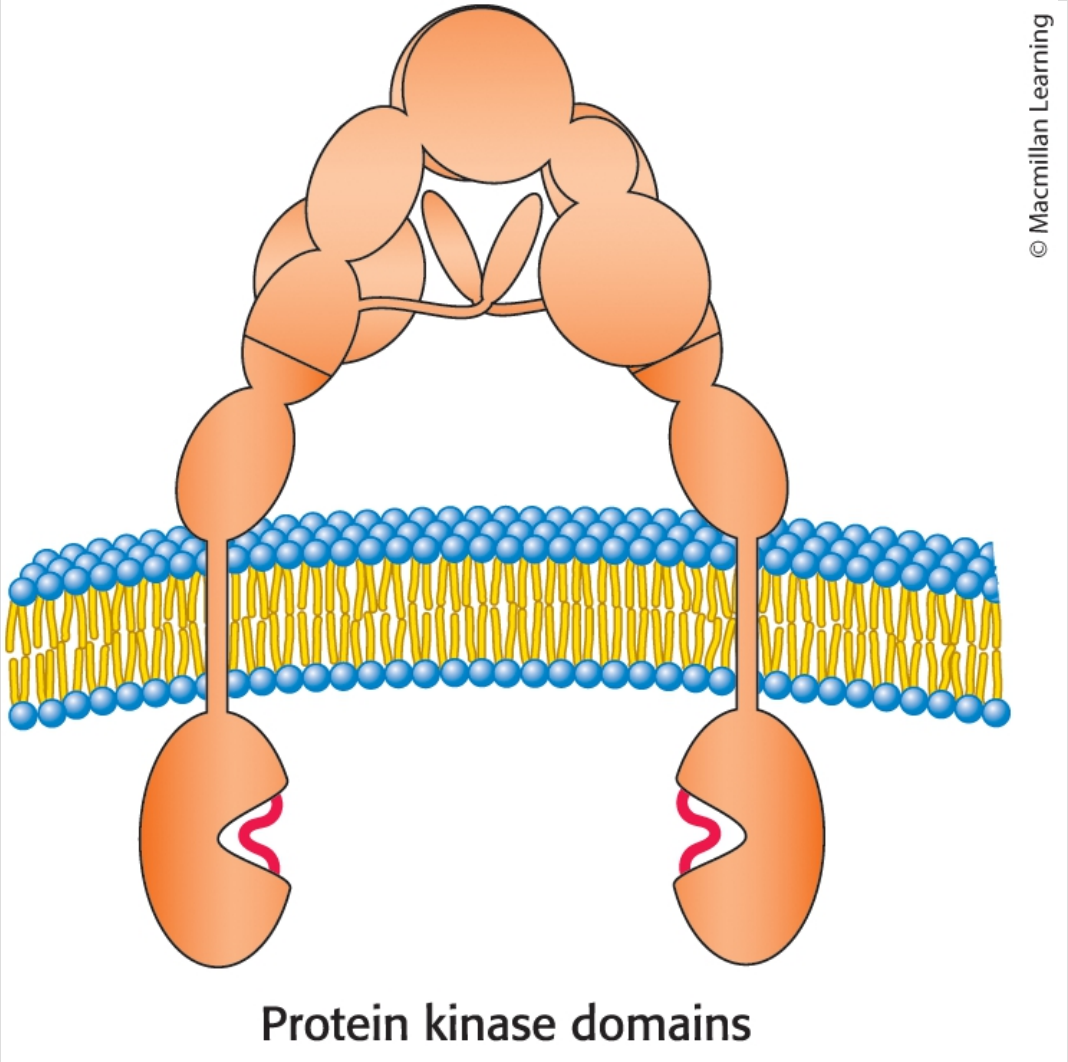
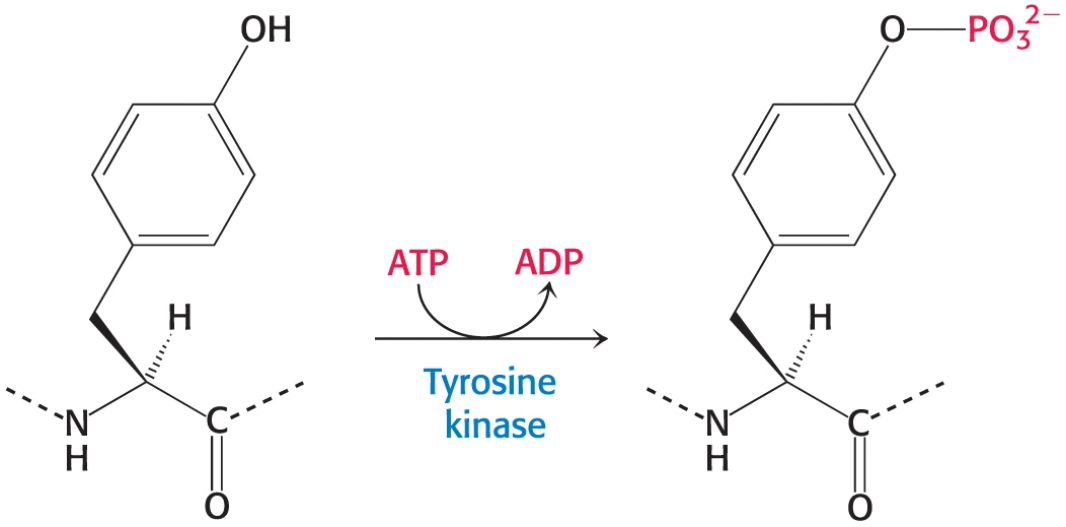


FIGURE 14.25 The insulin receptor consists of two subunits, each of which consists of an α chain and a β chain with protein kinase domains inside the cell. The two α chains are depicted in a lighter shade of orange than are the β chains. Each α chain is entirely outside the cell, while each β chain lies primarily inside the cell and includes a protein kinase domain.

The kinase domain in the β chain is homologous to that from protein kinase A but differs in two important ways. First, the insulin-receptor kinase is a tyrosine kinase; that is, it catalyzes the transfer of a phosphoryl group from ATP to the hydroxyl group of tyrosine, rather than serine or threonine.



Because this tyrosine kinase is a component of the receptor itself, the insulin receptor is referred to as a receptor tyrosine kinase. Second, the insulin receptor kinase is in an inactive conformation when the domain is not covalently modified.

The structure of this inactive form reveals an intricate mechanism for maintaining this inactivity. The key element is a relatively unstructured region termed the **activation loop**. Tyrosine kinases have two substrates, a peptide containing a tyrosine residue and ATP. The binding sites for these two substrates, determined from the active form of the enzyme, are shown in **Figure 14.26**. In the inactive form, one of the tyrosine residues that is to be phosphorylated as part of the activation process and is part of the activation loop is bound in the active site. However, ATP cannot bind because the ATP binding site is occupied by another part of the activation loop with the sequence Asp-Phe-Gly (DFG). The phenylalanine sidechain mimics the adenine ring of ATP while the aspartate provides a negative charge. Thus, even though a potential substrate is the active site, no reaction can take place as the DFG sequence is tethered closely enough to the protein structure that it cannot move out of the way. This is analogous to the impossibility of scratching your right elbow with your right hand.

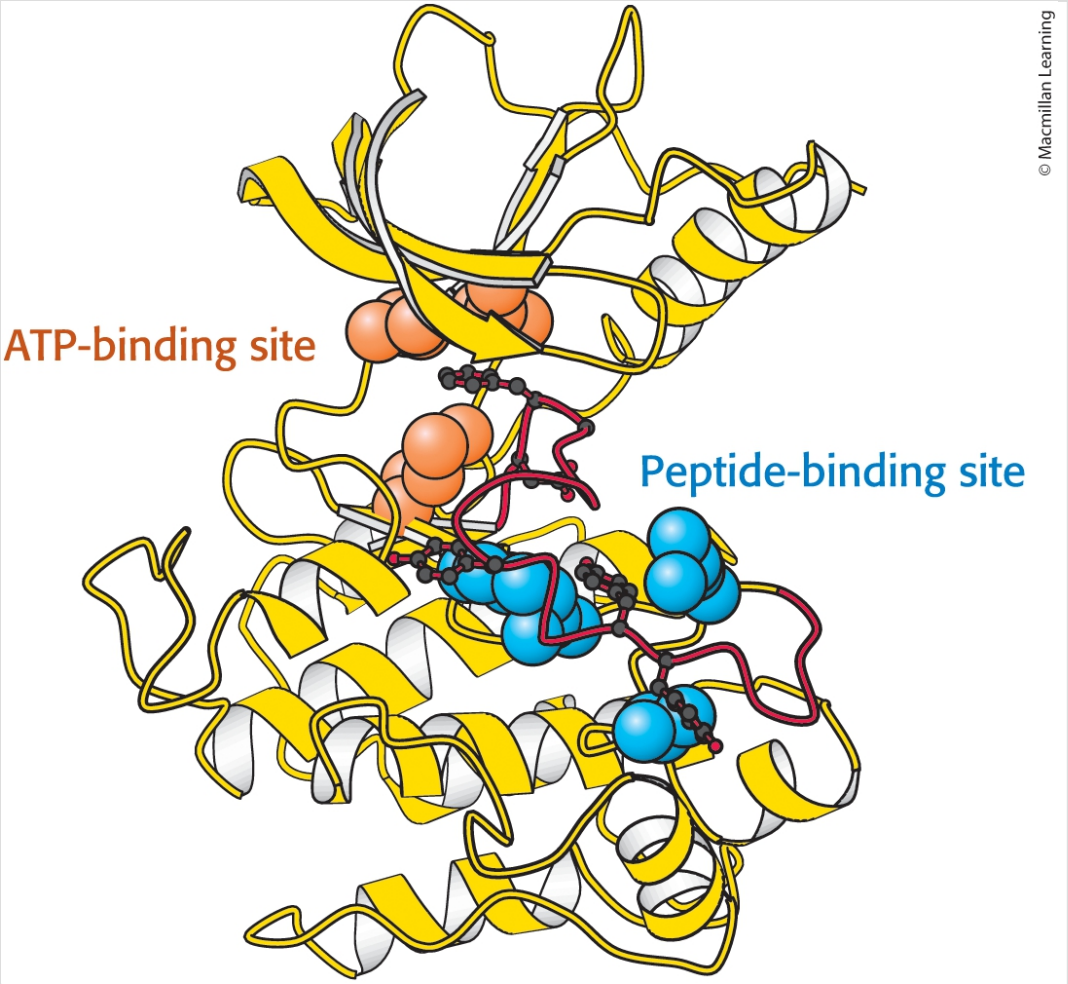


FIGURE 14.26 The insulin receptor kinase is inactive due to part of the activation loop blocking the ATP-binding site. The structure of the unactivated form of the insulin receptor kinase is shown with residues from the ATP-binding site in orange and residues from the peptide substrate binding site in blue. The activation loop, shown in red, has a tyrosine residue in the active site, but it cannot be phosphorylated because the ATP-binding site is blocked.

[Drawn from 1IRK.pdb.]

Insulin binding results in the cross-phosphorylation and activation of the

insulin receptor

In the absence of bound insulin, the insulin receptor dimer has an inverted “V”-like structure. Most importantly, this structure holds the kinase domains apart so that they cannot interact with one another. Insulin binds first to a site that includes elements from both subunits with a substantial conformation change induced upon binding. Overall, each receptor can bind up to four insulin molecules, and the final dimer has a “T”-like structure (Figure 14.27).

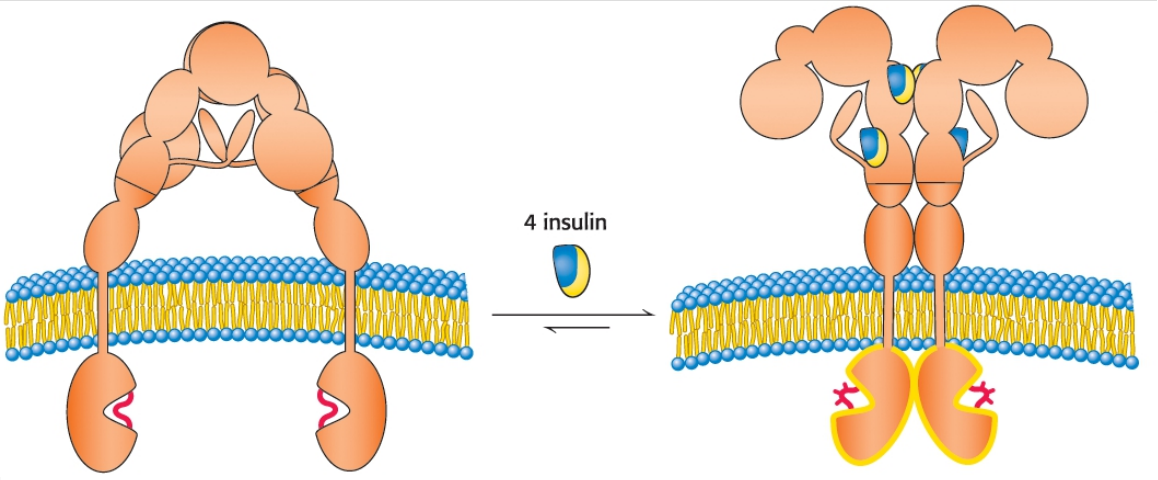


FIGURE 14.27 The insulin receptor dramatically changes conformation when it binds insulin. Upon binding insulin, the extracellular domains of the insulin receptor change conformation, causing the overall receptor to convert from an inverted “V” shape to a “T” shape. This allows th protein kinase domains to come together. The receptor dimer can bind up to four insulin molecules.

In this structure, the two protein kinase domains inside of the cell are pushed together. The flexible activation loop of one kinase subunit can fit into the active site of the other kinase subunit within the dimer in place of the domain’s own activation loop, opening up an ATP-binding site, and allowing the phosphorylation reaction to occur. When these tyrosine residues are phosphorylated, they can no longer fit into the

active site and the activation loops swings out into a different conformation with both the ATP- and peptide-binding sites available to phosphorylated additional substrates. Three tyrosine residues in each activation loop are phosphorylated (Figure 14.28). The net result of this overall process is that insulin binding on the outside of the cell results in the activation of a membrane-associated kinase within the cell.

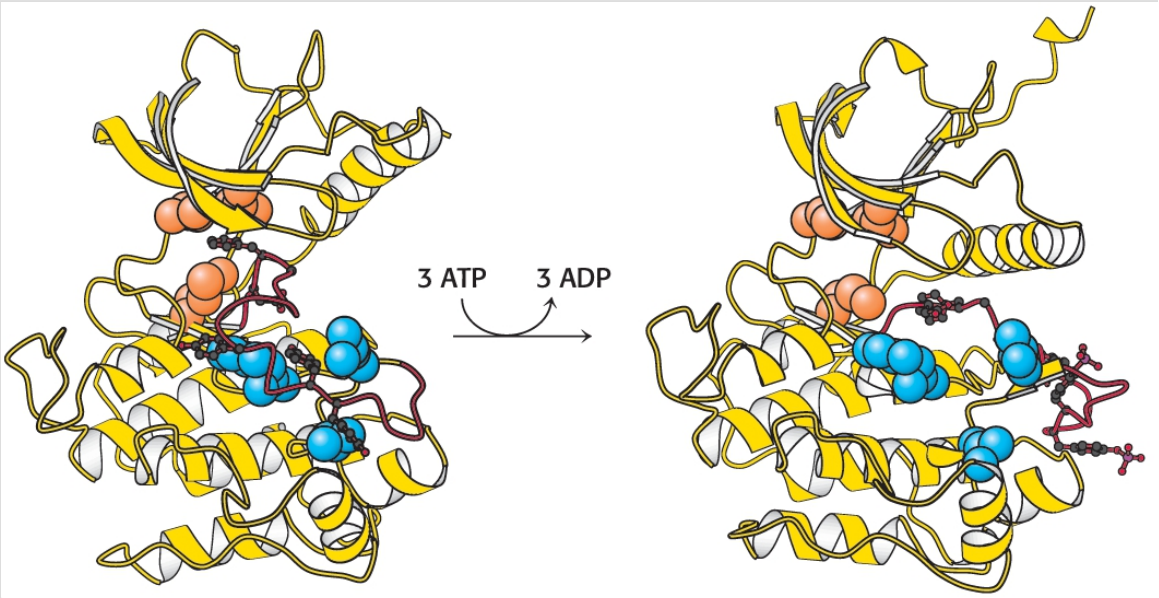


FIGURE 14.28 Activation of the insulin receptor involves phosphorylation of tyrosine residues in the kinase domain. One kinase domain phosphorylates tyrosine residues in the other. When tyrosine residues in the activation loop are phosphorylated, they can no longer fit into the activ site; the activation loop is released, opening up the ATP-binding site and activating the kinase.

[Drawn from 1IRK.pdb and 1IR3.pdb.]

The activated insulin-receptor kinase initiates a kinase cascade

With the kinase activated, additional sites within the receptor are also as the two subunits of the receptor are in close proximity to one

another. These phosphorylated sites act as docking sites for other substrates, including a class of molecules referred to as insulin-receptor substrates (IRS). IRS-1 and IRS-2 are two homologous proteins with a common modular structure (Figure 14.29). The amino-terminal part includes a **pleckstrin homology domain**, which binds phosphoinositide, and a phosphotyrosine-binding domain. These domains act together to anchor the IRS protein to the insulin receptor and the associated membrane.

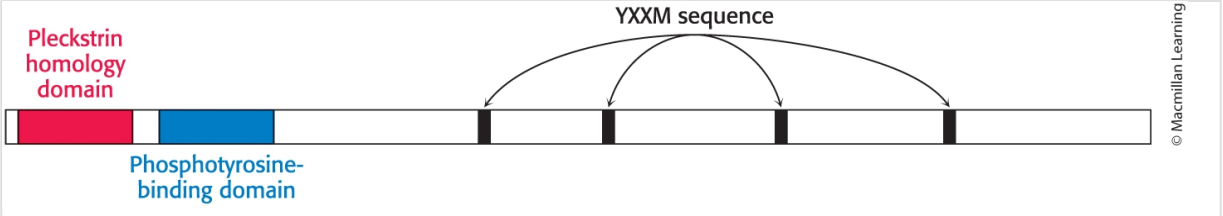


FIGURE 14.29 Insulin-receptor substrates IRS-1 and IRS-2 have modular structures. This schematic view represents the amino acid sequence common to IRS-1 and IRS-2. Each protein contains a pleckstrin homology domain (which binds phosphoinositide lipids), a phosphotyrosine-binding domain, and four sequences that approximate Tyr-X-X-Met (YXXM). The four sequences are phosphorylated by the insulin-receptor tyrosine kinase.

Each IRS protein contains four sequences of the form Tyr-X-X-Met. These sequences are also substrates for the activated insulin-receptor kinase. When the tyrosine residues within these sequences are phosphorylated, IRS molecules can act as adaptors, bringing additional components of this signaling pathway together at the membrane. The most important proteins that bind to the phosphorylated IRS molecules are specific lipid kinases, called phosphoinositide 3-kinases (PI3Ks), that add a phosphoryl group to the 3-position of inositol in phosphatidylinositol 4,5-bisphosphate (PIP_2) to form phosphatidylinositol 3,4,5-trisphosphate (PIP_3) (Figure 14.30). These enzymes are dimers of 110-kDa catalytic subunits and 85-kDa regulatory subunits. These enzymes bind to the phosphorylated IRS proteins and are drawn to the membrane where they can phosphorylate PIP_2 to form

PIP_3. The PIP_3 molecules serve as gathering points for other proteins, continuing a kinase cascade (Figure 14.31).

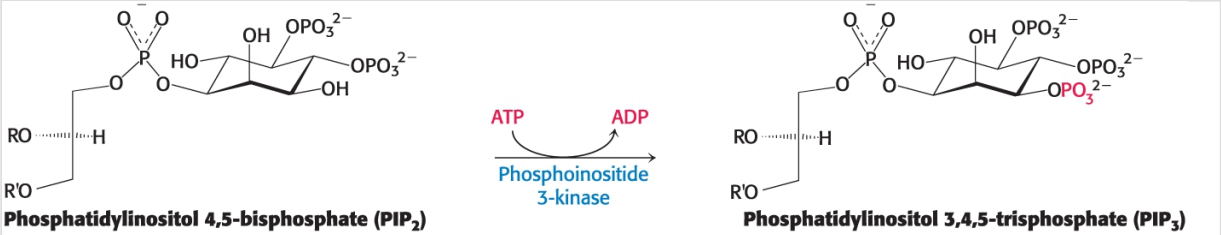


FIGURE 14.30 Phosphoinositide 3-kinase adds a phosphoryl group to PIP_2, forming PIP_3.

This generates a modified lipid headgroup that can be recognized by other enzymes.

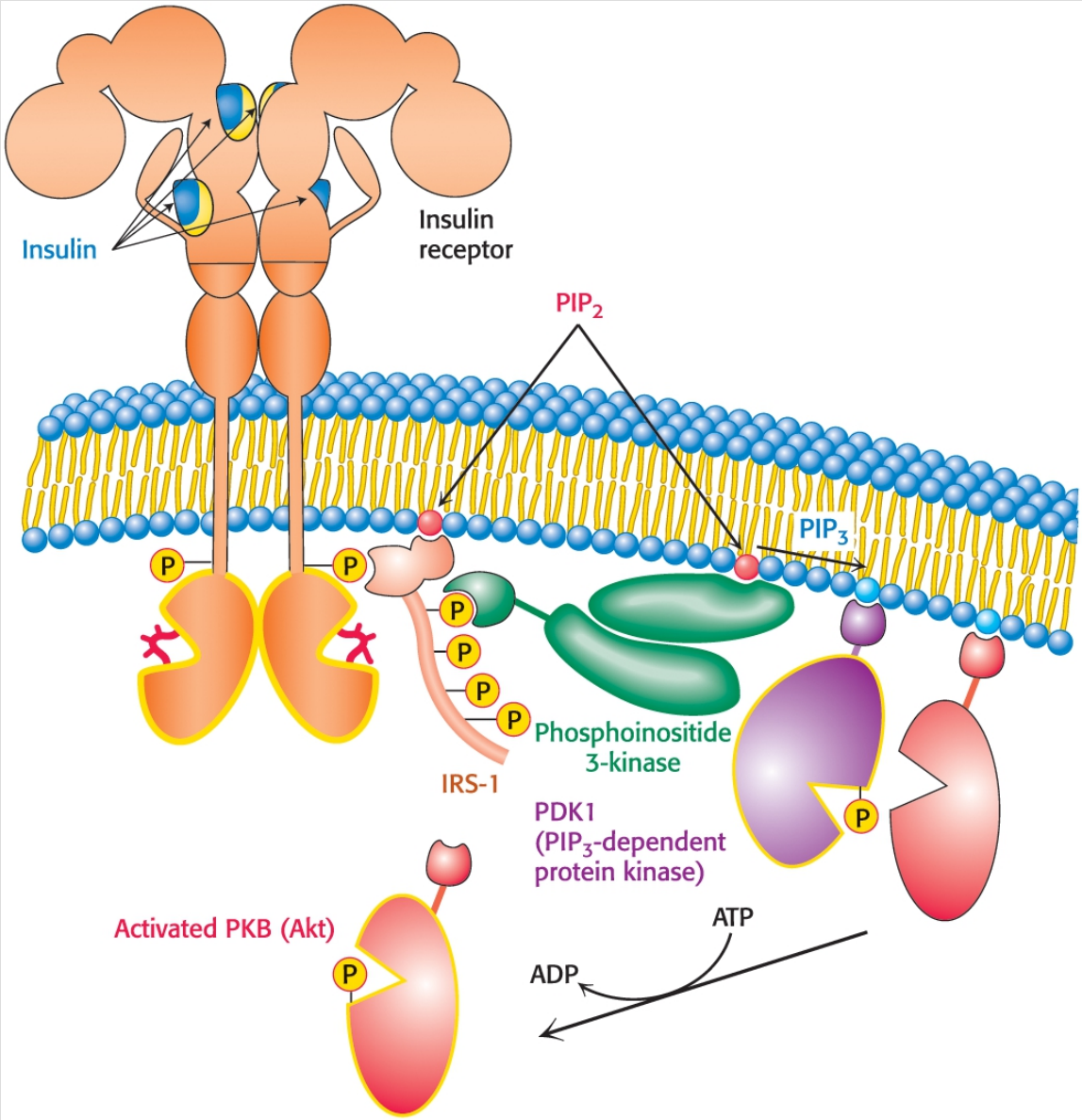


FIGURE 14.31 The insulin signaling pathway results in protein kinase activation. The binding insulin results in the cross-phosphorylation and activation of the insulin receptor. Phosphorylated sites on the receptor act as binding sites for insulin-receptor substrates such as IRS-1. The lipid kinase phosphoinositide 3-kinase binds to phosphorylated sites on IRS-1 through its regulatory domain and converts PIP_2 into PIP_3. PIP_3 then serves as a binding site for PIP_3-dependent protein kinase (PDK1), which phosphorylates and activates kinases such as PKB. Activated PKB can then diffuse throughout the cell to continue the signal-transduction pathway.

The first protein recruited to the PIP_3 molecules is phosphoinositide-dependent kinase-1 (PDK1). PDK1 is a member of a large class of serine/threonine-specific kinases that require phosphorylation on their activation loops in a manner similar to the insulin-receptor kinase. However, the activation mechanism is different. For the serine-threonine kinases, the enzymes adapt an inactivate conformation even through the ATP- and peptide-binding sites are accessible. Phosphorylation results in a change to an active conformation (**Figure 14.32**).

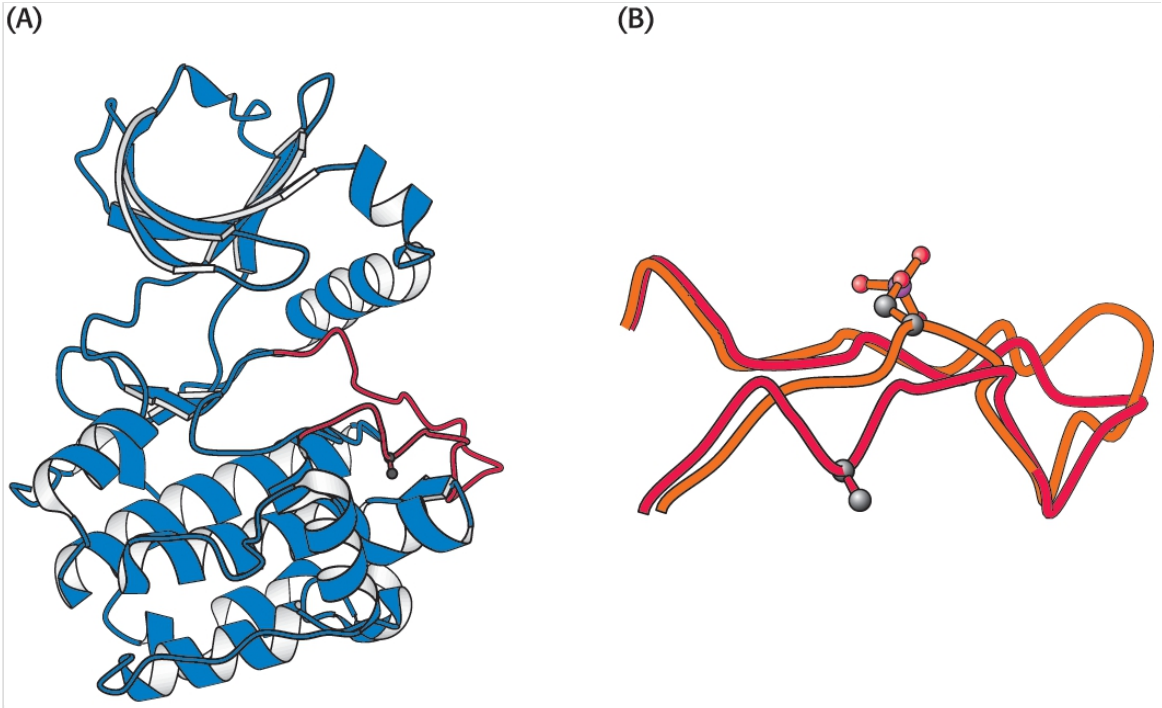


FIGURE 14.32 Phosphorylation activates phosphoinositide-dependent protein kinase. (A) The structure of phosphoinositide-dependent protein kinase (PDK1) is shown in an inactive conformation (with an alanine replacing a key serine to prevent self-activation). (B) A comparis of the structures of the activation loops of PDK1, in inactive and active forms, shows the conformation change associated with activation.

[Drawn from 2BIY.pdb and 3HRF.pdb.]

The most important characteristics of a protein kinase are its substrate sequence preferences and the sequence around its activation site. For PDK1, its substrates approximate the sequence -XXTX(**S,T**)FCGT-, where X represents relatively variable positions. Its activation site has the sequence -QARAN**S**FGVTA-, where the underlined residues match the preferred substrate sequence. The match between this sequence and the substrate preference indicates that PDK1 can activate itself by cross-phosphorylation. PDK1 also includes a pleckstrin homology domain that is specific for PIP_3 and, thus, PDK1 is concentrated at PIP_3-rich sites generated by PI3K (Figure 14.31).

Other kinases that include pleckstrin homology domains are also concentrated at these sites including Protein Kinase B (PKB, also known as Akt). The activation loop of this kinase has the sequence -GATMK**T**FCGTPE-, which matches the substrate preference for PDK1. The substrate preference for PKB is quite different with the form -RRRXX(**S,T**)XSXSX-. Thus, PKB can be activated by PDK1 but is not capable of self-activation. Once activated, PKB can leave the membrane and move throughout the cell to phosphorylate other targets. These include components that control the trafficking of the glucose receptor GLUT4 to the cell surface. This completes the part of the insulin-signaling pathway we have been considering after our meal, namely, the process from an increase in insulin concentration in the bloodstream to enhanced glucose uptake.

The cascade initiated by the binding of insulin to the insulin receptor is summarized in **Figure 14.33**. The signal is amplified at several stages along this pathway. Because the activated insulin receptor itself is a protein kinase, each activated receptor can phosphorylate multiple IRS molecules. Activated enzymes further amplify the signal in at least two of the subsequent steps. Thus, a small increase in the concentration of circulating insulin can produce a robust intracellular response.

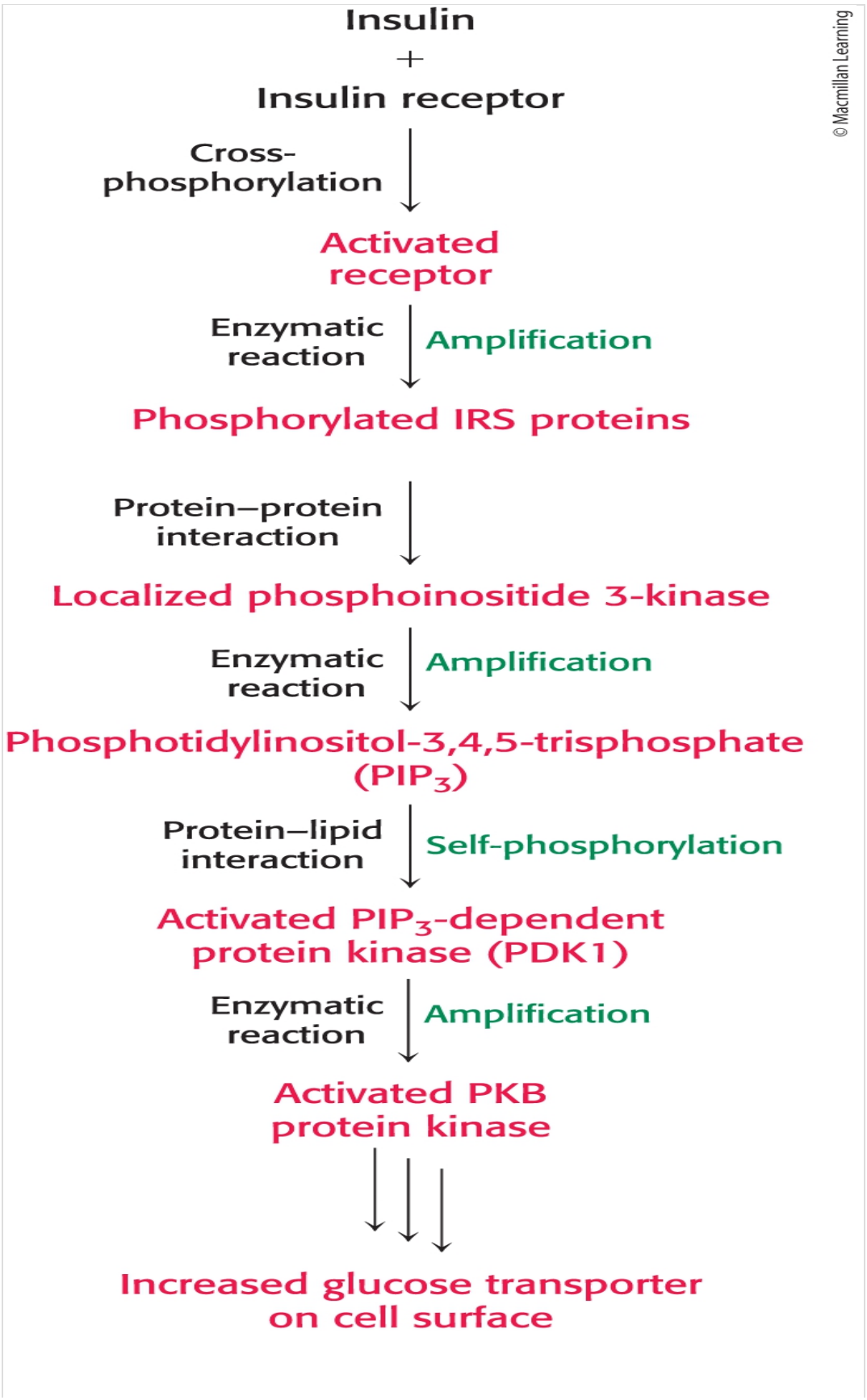

Insulin
+
Insulin receptor
Cross-phosphorylation
Activated receptor
Enzymatic reaction
Amplification
Phosphorylated IRS proteins
Protein–protein interaction
Localized phosphoinositide 3-kinase
Enzymatic reaction
Amplification
Phosphotidylinositol-3,4,5-trisphosphate (PIP_3)
Protein–lipid interaction
Self-phosphorylation
Activated PIP_3-dependent protein kinase (PDK1)
Enzymatic reaction
Amplification
Activated PKB protein kinase
Increased glucose transporter on cell surface
© Macmillan Learning

FIGURE 14.33 Insulin binding initiates a signaling pathway leading to a protein kinase cascade. Key steps in the signal-transduction pathway are shown. The result is activation of protein kinases that phosphorylate targets, leading to an increase in glucose transporters on cell surfaces, among other effects.



Self-Check Question



Can a kinase with substrate preference XXXPX(**S,T**)PXXXX and an activation loop sequence of -HTGFL**T**EYVAT- activate itself?

Insulin signaling is terminated by the action of phosphatases

We have seen that the activated G protein promotes its own inactivation by the catalytic release of a phosphoryl group from GTP. In contrast, proteins phosphorylated on serine, threonine, or tyrosine residues are extremely stable kinetically. Specific enzymes, called protein phosphatases, are required to hydrolyze these phosphorylated proteins and return them to their initial states. Similarly, enzymes called lipid phosphatases are required to remove phosphoryl groups from inositol lipids that had been activated by lipid kinases.

In insulin signaling, three classes of enzymes are of particular importance in shutting off the signaling pathway:

1. Protein tyrosine phosphatases that remove phosphoryl groups from tyrosine residues on the insulin receptor and the IRS adaptor

proteins

2. Lipid phosphatases that hydrolyze PIP_3 to PIP_2

3. Protein serine phosphatases that remove phosphoryl groups from activated protein kinases such as PKB

Many of these phosphatases are activated or recruited as part of the response to insulin. Thus, the binding of the initial signal sets the stage for the eventual termination of the response.

14.4 Epidermal Growth Factor: Receptor Dimerization Can Drive Signaling

Next, we will look at the signaling that takes place shortly after you are wounded. Within a few hours, signaling molecules such as epidermal growth factor (EGF) are released into the affected region. EGF is a 6-kDa polypeptide that stimulates the growth of epidermal and epithelial cells (**Figure 14.34**).

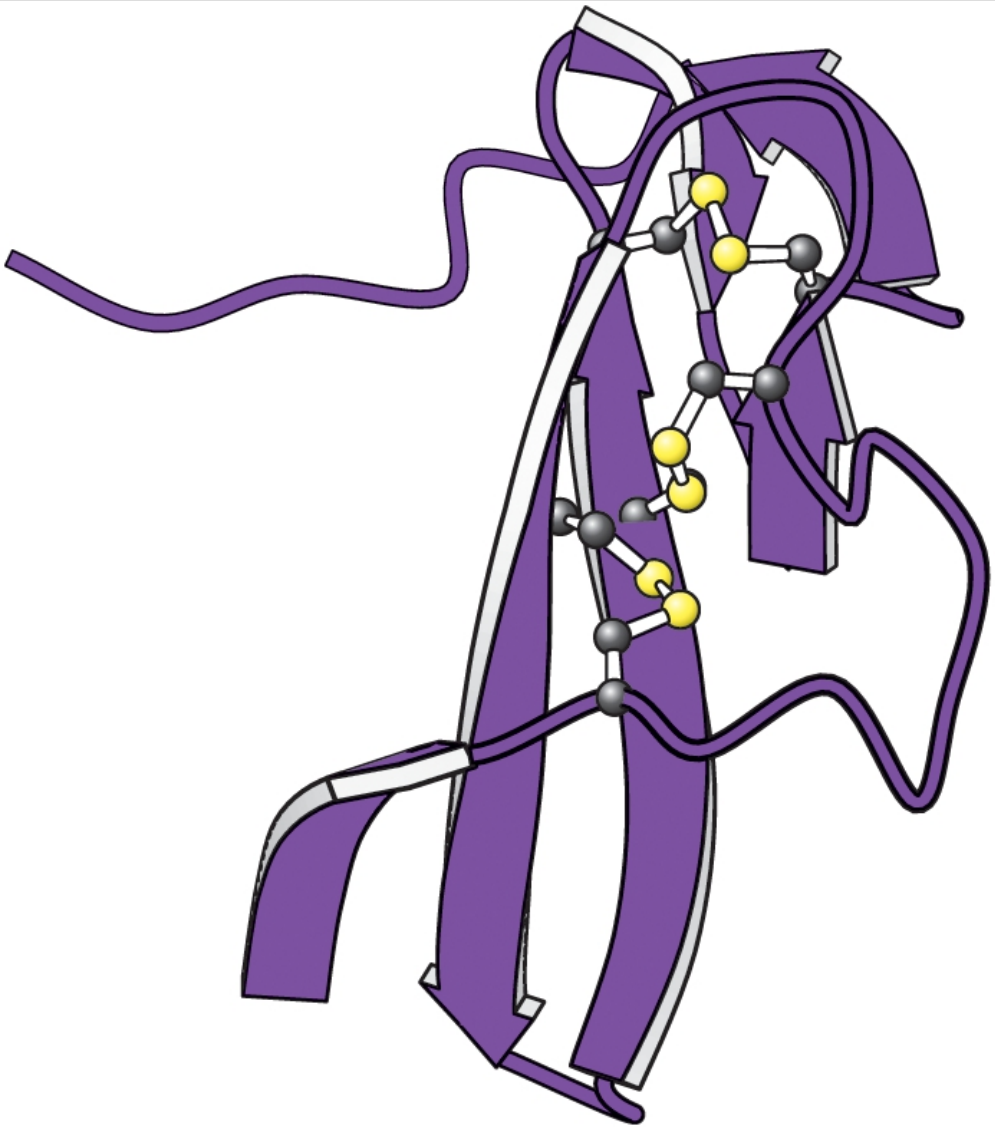


FIGURE 14.34 Epidermal growth factor consists of a single polypeptide chain stabilized by three disulfide bonds.

[Drawn from 1EGF.pdb.]

INTERACT with this model in Achieve

EGF is bound by a family of receptor tyrosine kinases, similar in some ways to the insulin receptor, but quite different in others. Unlike those of the insulin receptor, however, these receptors exist as monomers. Each EGF receptor monomer binds a single molecule of EGF in its extracellular domain. EGF binding results in a substantial rearrangement of the extracellular domain (Figure 14.35). After this rearrangement, the receptors dimerize, stabilized by a structure termed the *dimerization arm* from each monomer. This arm is buried within the monomer structure prior to EGF binding but inserts into a binding pocket on the other monomer after EGF binding.

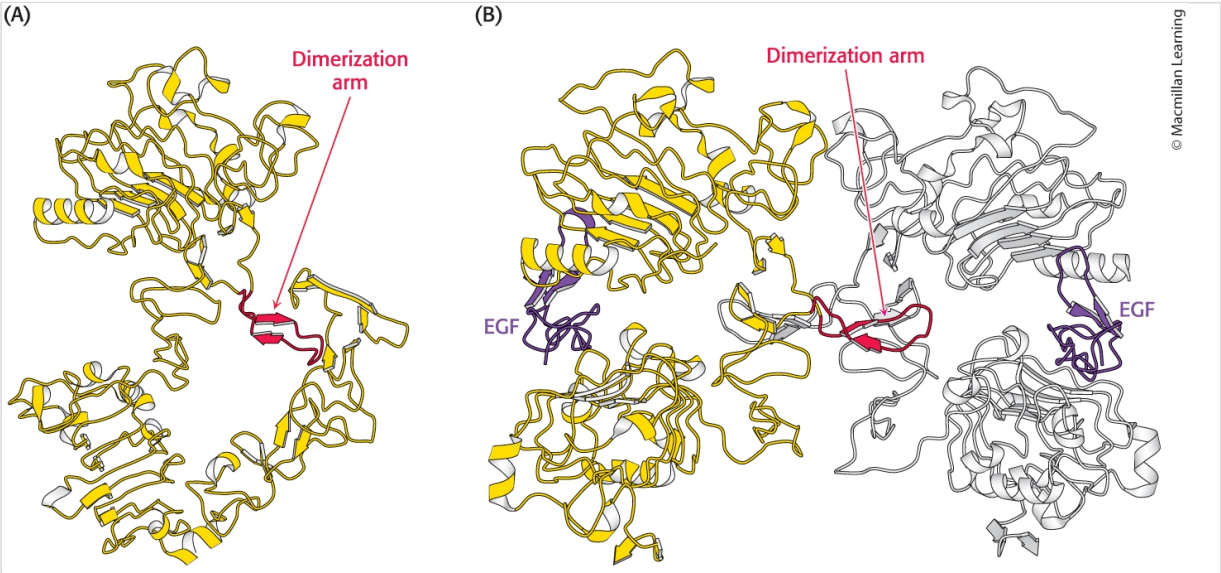


FIGURE 14.35 EGF binding to the EGF receptor results in a substantial rearrangement and facilitates receptor dimerization. (A) The structure of the extracellular domain of the EGF receptor is folded so that a region termed the dimerization loop is facing toward the interior of the structure. (B) Upon EGF binding, the structure rearranges so that the dimerization arm points outward and participates with dimerization with another receptor molecule.

[Drawn from 1NQL.pdb and 1IVO.pdb.]

INTERACT with this model in Achieve

The EGF receptor undergoes phosphorylation of its carboxyl-terminal tail

Like the insulin receptor, the kinase domains of the EGF receptor are inactive prior to dimerization. When an EGF receptor dimerizes, the kinase domains come together to form an asymmetric dimer with one kinase domain functioning as an allosteric activator of the other, stabilizing an active conformation. This active kinase phosphorylates tyrosine residues on the other subunit, but in a region that lies on the C-terminal side of the kinase domain, rather in an activation loop. As many as five tyrosine residues in this region are phosphorylated.

EGF signaling leads to the activation of Ras, a small G protein

The phosphotyrosines on the EGF receptors act as docking sites for phosphotyrosine-binding domains on other proteins. The intracellular signaling cascade begins with the binding of Grb2, a key adaptor protein that contains one phosphotyrosine-binding domain and two domains that recognize extended, proline-rich sequences. On phosphorylation of the receptor, Grb2 binds to the phosphotyrosine residues of the EGF receptor. Through its other domains, Grb2 then binds polyproline-rich polypeptides within a protein called Sos. Sos, in turn, binds to a protein called Ras and activates it.

A very prominent signal-transduction component, Ras is a member of a class of proteins called the small G proteins. These proteins have many key mechanistic and structural motifs in common with the G_{α} subunit of the heterotrimeric G proteins and are related by divergent evolution. In keeping with this relationship, Ras contains bound GDP in its unactivated form. Sos opens up the nucleotide-binding pocket of Ras, allowing GDP to escape and GTP to enter in its place. Because of its

effect on Ras, Sos is referred to as a guanine-nucleotide-exchange factor (GEF). Thus, the binding of EGF to its receptor leads to the conversion of Ras into its GTP form through the intermediacy of Grb2 and Sos (Figure 14.36). This occurs on the membrane surface as Ras is anchored via covalently attached lipids.

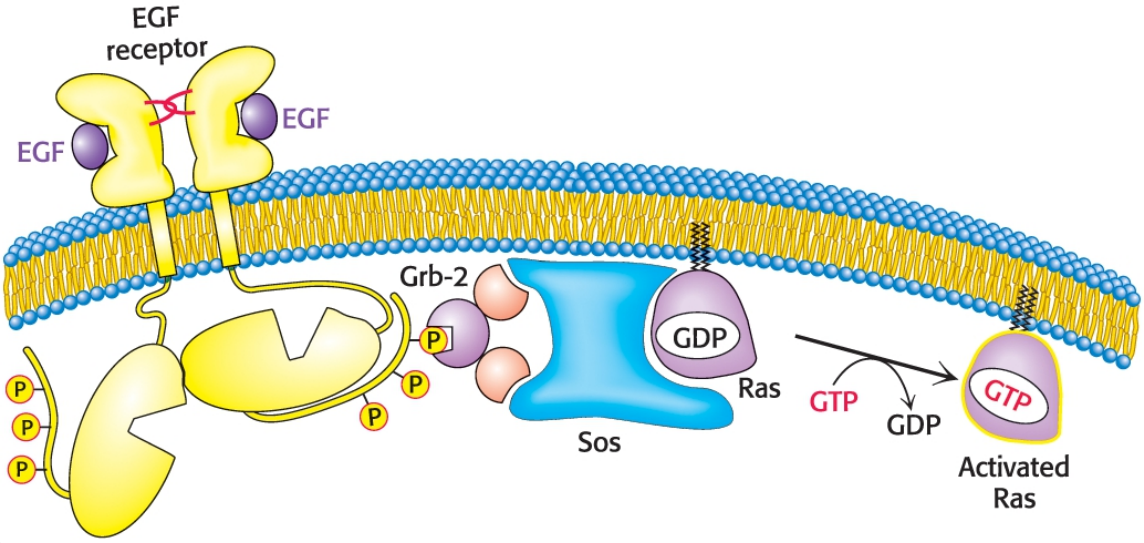


FIGURE 14.36 The binding of EGF to the EGF receptor results in the activation of Ras. The dimerization of the EGF receptor due to EGF binding leads to the phosphorylation of the C-terminal tails of the receptor. This, in turn, results in the recruitment of Grb2 and Sos, and the exchange of GTP for GDP in Ras. This signal-transduction pathway results in the conversion of Ras into its activated GTP-bound form.

Activated Ras initiates a protein kinase cascade

Ras changes conformation when it is transformed from its GDP into its GTP form. In the GTP form, Ras binds other proteins, including a membrane-anchored protein kinase termed Raf. When bound to Ras, Raf undergoes a conformational change that activates the Raf protein

kinase. Activated Raf then phosphorylates other proteins, including protein kinases termed MEKs. In turn, MEKs activate kinases called extracellular signal-regulated kinases (ERKs). ERKs then phosphorylate numerous substrates, including transcription factors in the nucleus as well as other protein kinases. The flow of information from the arrival of EGF at the cell surface to changes in gene expression is summarized in **Figure 14.37**.

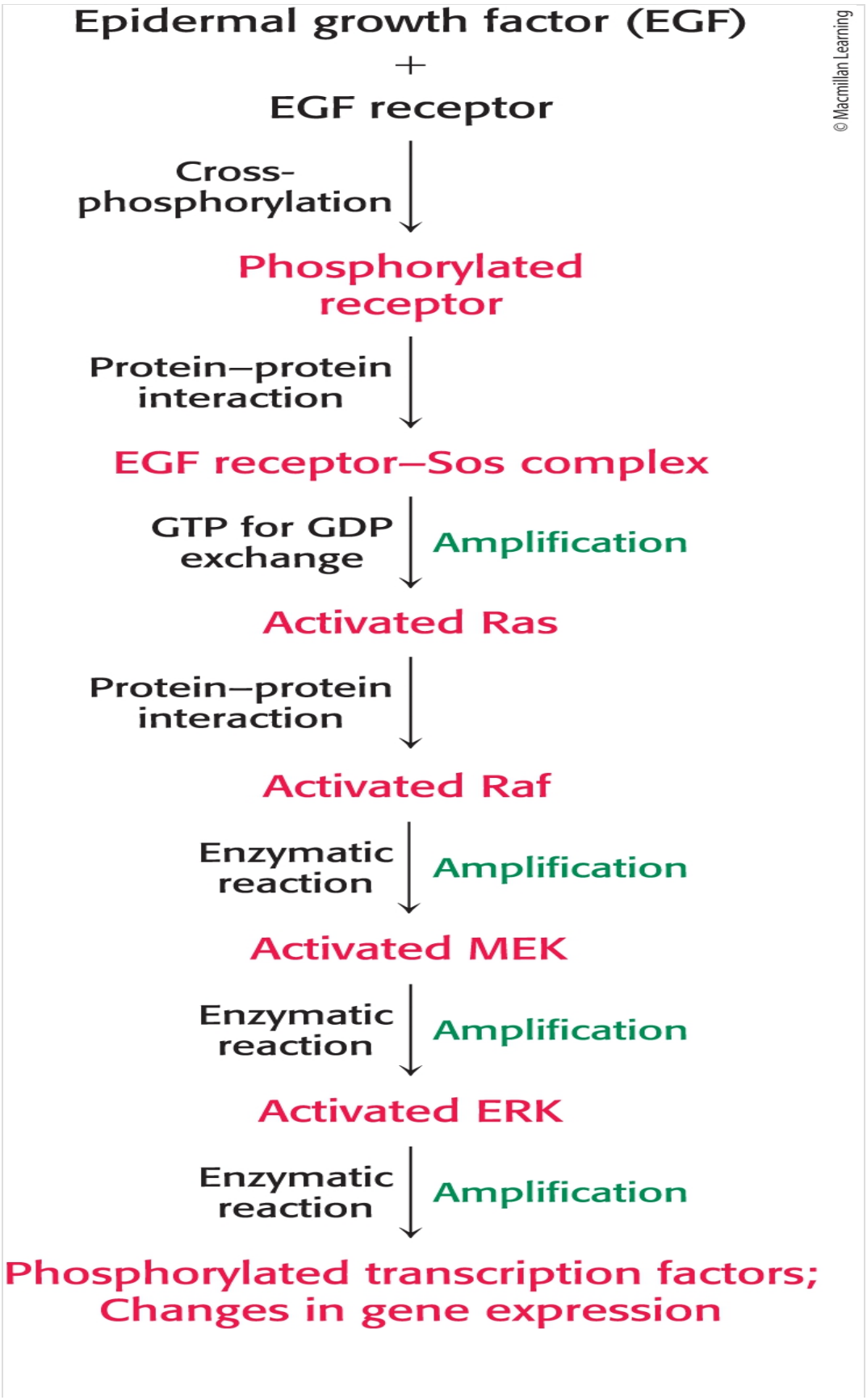

Epidermal growth factor (EGF)
+
EGF receptor
Cross-phosphorylation
Phosphorylated receptor
Protein–protein interaction
EGF receptor–Sos complex
GTP for GDP exchange
Amplification
Activated Ras
Protein–protein interaction
Activated Raf
Enzymatic reaction
Amplification
Activated MEK
Enzymatic reaction
Amplification
Activated ERK
Enzymatic reaction
Amplification
Phosphorylated transcription factors; Changes in gene expression
© Macmillan Learning

FIGURE 14.37 The EGF signaling pathway results in a protein kinase cascade. The key steps in the pathway are shown. A kinase cascade leads to the phosphorylation of transcription factors and concomitant changes in gene expression.



EGF signaling is terminated by protein phosphatases and the intrinsic GTPase activity of Ras

Because so many components of the EGF signal-transduction pathway are activated by phosphorylation, we can expect protein phosphatases to play key roles in the termination of EGF signaling. Indeed, crucial phosphatases remove phosphoryl groups from tyrosine residues on the EGF receptor and from serine, threonine, and tyrosine residues in the protein kinases that participate in the signaling cascade. The signaling process itself sets in motion the events that activate many of these phosphatases. Consequently, signal activation also initiates signal termination.

Like the G proteins activated by 7TM receptors, Ras possesses intrinsic GTPase activity. Thus, the activated GTP form of Ras spontaneously converts into the inactive GDP form. The rate of conversion can be accelerated in the presence of GTPase-activating proteins (GAPs), which interact with small G proteins in the GTP form and facilitate GTP hydrolysis. Thus, the lifetime of activated Ras is regulated by accessory proteins in the cell.

Self-Check Question



List one important similarity and one important difference between Ras and a heterotrimeric G protein.

14.5 Defects in Signal-Transduction Pathways Can Lead to Cancer and Other Diseases



In light of their complexity, it comes as no surprise that signal-transduction pathways occasionally fail, leading to disease states. Cancer, a set of diseases characterized by uncontrolled or inappropriate cell growth, is strongly associated with defects in signal-transduction proteins, particularly those that play key roles in growth-control pathways. Indeed, the study of cancer — particularly cancers caused by certain viruses — has contributed greatly to our understanding of signal-transduction proteins and pathways.

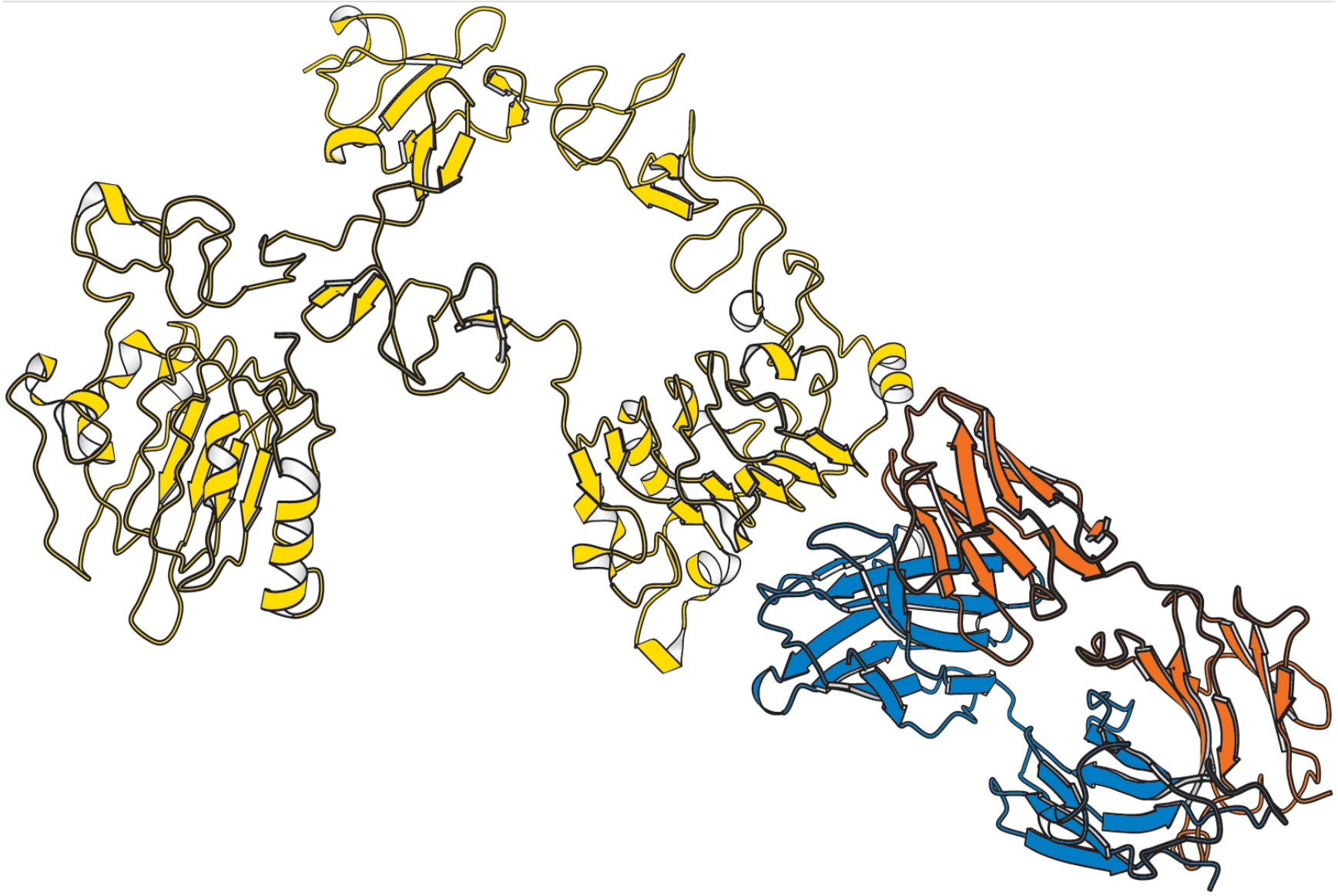
Mammalian cells may contain three distinct Ras proteins (H-, K-, and N-Ras), each of which cycles between inactive GDP and active GTP forms. The genes encoding members of the Ras family are among the most commonly mutated in human tumors. The most common mutations in tumors lead to a loss of the ability to hydrolyze GTP. Thus, the Ras protein is trapped in the "on" position and continues to stimulate cell growth, even in the absence of a continuing signal. Genes such as these mutated Ras genes are referred to **oncogenes** because they can induce cancer under appropriate circumstances. Unmutated Ras genes are referred to as **proto-oncogenes** since they can be converted into oncogenes through mutation.

Other genes can contribute to cancer development only when both copies of the gene normally present in a cell are deleted or otherwise damaged. Such genes are called **tumor-suppressor genes**. For example, genes for some of the phosphatases that participate in the termination of EGF signaling are tumor suppressors. Without any functional phosphatase present, EGF signaling persists once initiated, stimulating inappropriate cell growth.

Monoclonal antibodies can be used to inhibit signal-transduction pathways activated in tumors

Mutated or overexpressed receptor tyrosine kinases are frequently observed in tumors. For instance, the epidermal-growth-factor receptor (EGFR) is overexpressed in some human epithelial cancers, including breast, ovarian, and colorectal cancer. Because some small amount of the receptor can dimerize and activate the signaling pathway even without binding to EGF, overexpression of the receptor increases the likelihood that a "grow and divide" signal will be inappropriately sent to the cell.

This understanding of cancer-related signal-transduction pathways has led to a therapeutic approach that targets the EGFR. The strategy is to produce monoclonal antibodies to the extracellular domains of the offending receptors. One such antibody, cetuximab (Erbitux), has effectively targeted the EGFR in colorectal cancers. Cetuximab inhibits the EGFR by competing with EGF for the binding site on the receptor (**Figure 14.38**). Because the antibody sterically blocks the change in conformation that exposes the dimerization arm, the antibody itself cannot induce dimerization. The result is that the EGFR-controlled pathway is not initiated.



© Macmillan Learning

FIGURE 14.38 The monoclonal antibody drug cetuximab binds to the EGF receptor and prevents receptor signaling. The structure of the complex between the extracellular domain of the EGF receptor and an F_{ab} fragment from cetuximab reveals that the antibody binds in a manner that blocks the conformational changes necessary for productive dimerization and signaling.

[Drawn from 1YY9.pdb.]

Cetuximab is not the only monoclonal antibody that has been developed to target a receptor tyrosine kinase. Trastuzumab (Herceptin) inhibits another EGFR family member, HER2, that is overexpressed in approximately 30% of breast cancers (**Figure 14.39**). HER2 normally forms heterodimers with other members of the EGFR family, but it can signal even in the absence of ligand when it homodimerizes. Thus, overexpression of HER2 can stimulate cell proliferation. Breast tumors are now routinely screened for HER2 overexpression, and patients showing such overexpression may be treated with Herceptin if appropriate. Thus, this cancer treatment is tailored to the genetic characteristics of the tumor.

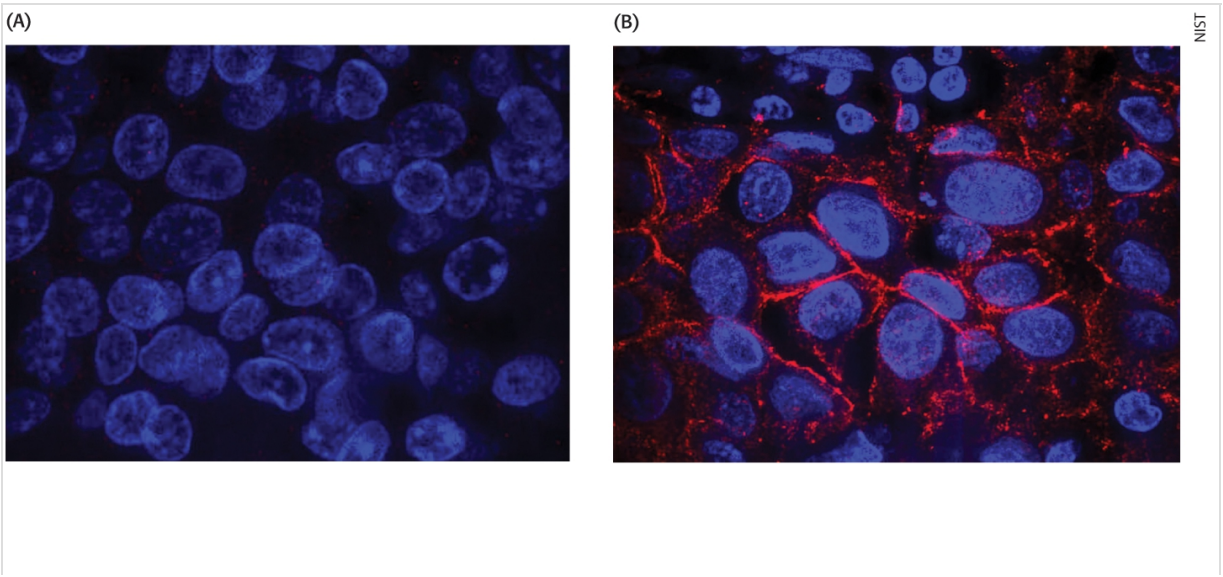


FIGURE 14.39 The EGF receptor family member HER2 is overexpressed in some breast cancer cells. (A) A panel of breast cancer cells expressing HER2 at normal levels. Cell nuclei are blue, and HER2 would be red if detectable. (B) A panel of breast cancer cells overexpressing HER2. The overexpression is due to amplification of the *HER2* gene such that many more than the normal two copies are present.



Protein kinase inhibitors can be effective anticancer drugs

The widespread occurrence of overactive protein kinases in cancer cells suggests that molecules that inhibit these enzymes might act as antitumor agents. For example, more than 90% of patients with chronic myelogenous leukemia (CML) show a specific chromosomal defect in cancer cells (**Figure 14.40**). The translocation of genetic material between chromosomes 9 and 22 causes the c-*abl* gene, which encodes a tyrosine kinase of the Src family, to be inserted into the *bcr* gene on chromosome 22. The result is the production of a fusion protein called Bcr-Abl that consists primarily of sequences for the c-Abl kinase. However, the *bcr-abl* gene is not regulated appropriately; it is expressed at higher levels than that of the gene encoding the normal c-Abl kinase, stimulating a growth-promoting pathway.

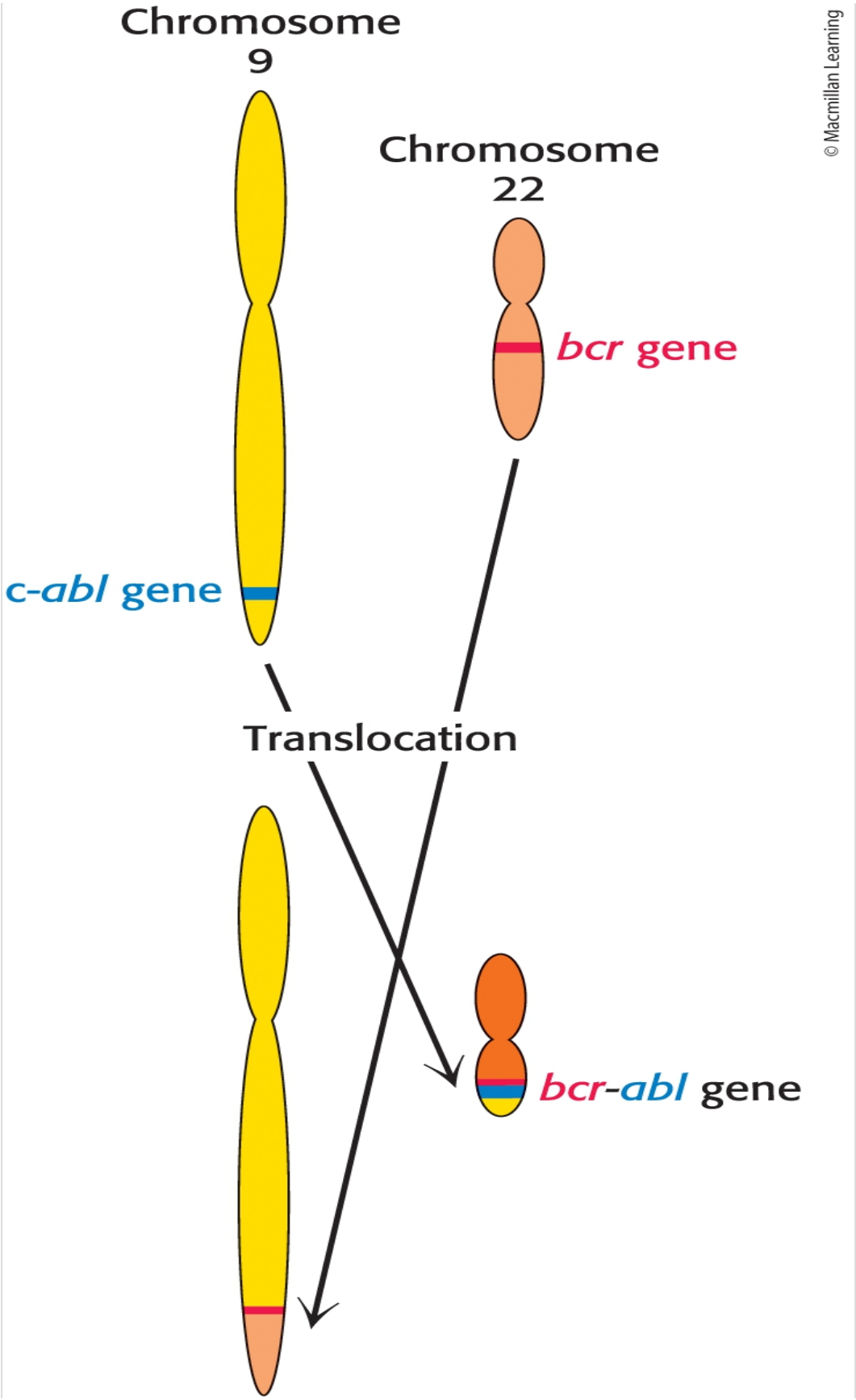
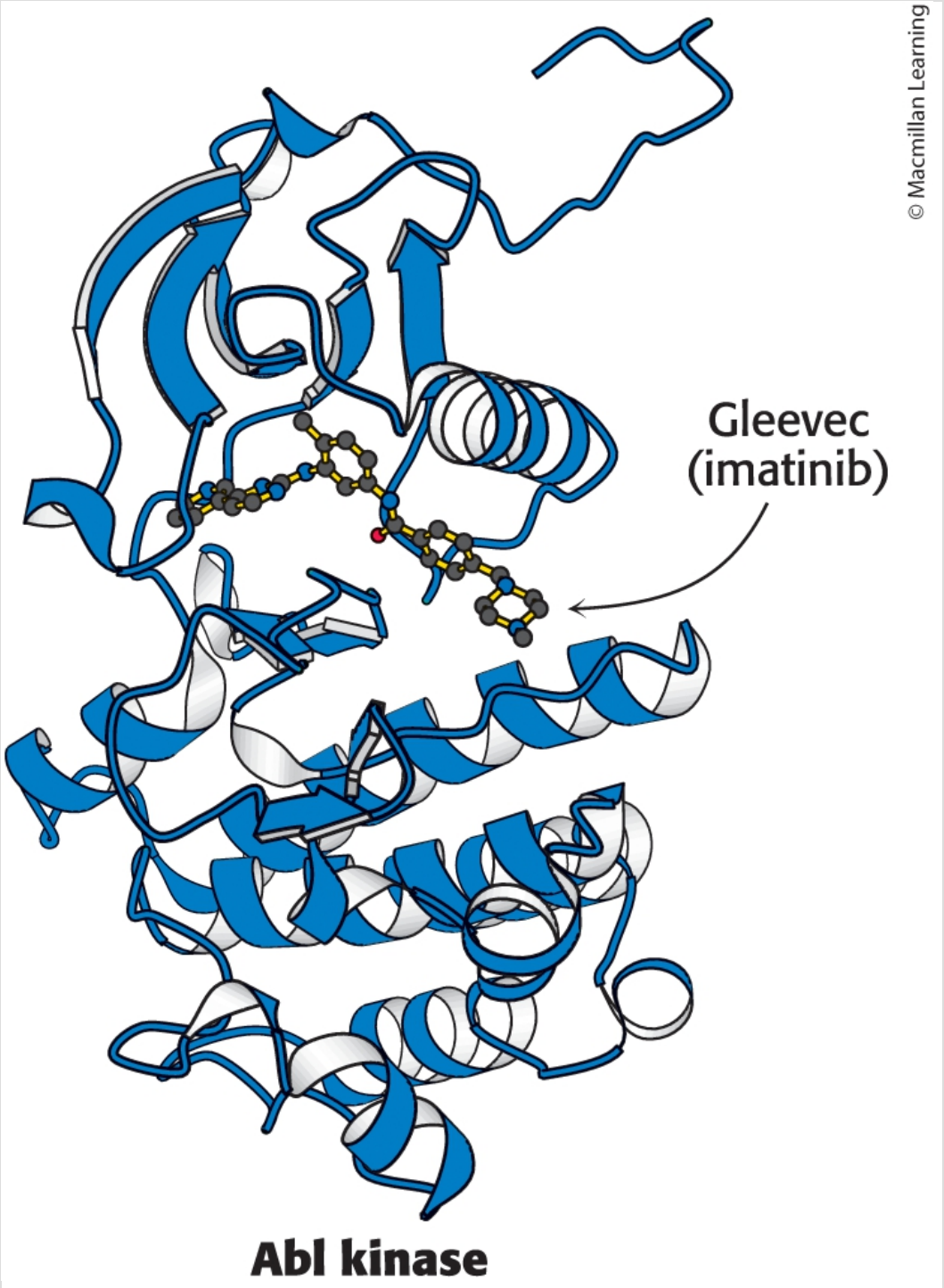

Chromosome 9
Chromosome 22
bcr gene
c-abl gene
Translocation
bcr-abl gene
© Macmillan Learning

FIGURE 14.40 Translocation of DNA from one chromosome to another results in the formation of the *bcr-abl* gene. In chronic myelogenous leukemia, parts of chromosomes 9 and 22 are reciprocally exchanged, causing the *bcr* and *abl* genes to fuse. The protein kinase encoded by the *bcr-abl* gene is expressed at higher levels in tumor cells than is the c-*abl* gene in normal cells, leading to inappropriate cell proliferation.



Because of this overexpression, leukemia cells express a unique target for chemotherapy. A specific inhibitor of the Bcr-Abl kinase, Gleevec (STI-571, imatinib mesylate), has proved to be a highly effective treatment for patients with CML (**Figure 14.41**). This approach to cancer chemotherapy is fundamentally distinct from most approaches, which target all rapidly growing cells, including normal ones. Because Gleevec targets tumor cells specifically, side effects caused by the impairment of normal dividing cells can be minimized. Subsequently, drugs that target other protein kinases have been developed for treatment of other cancer types. Thus, our understanding of signal-transduction pathways has enabled conceptually new disease treatment strategies.



© Macmillan Learning

FIGURE 14.41 The drug imatinib inhibits Abl kinase by blocking the ATP-binding site. The structure of the kinase domain of Abl with imatinib (Gleevec) bound is shown. The inhibitor occupies the ATP-binding site in the kinase.

[Drawn from 1IEP.pdb.]

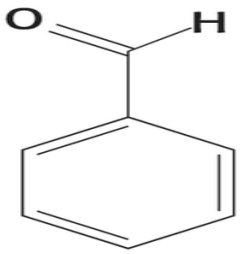


14.6 Sensory Systems Are Based on Specialized Signal-Transduction Pathways

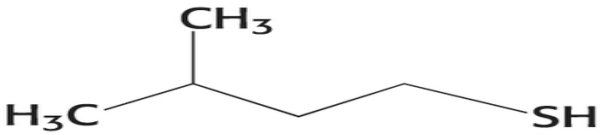
Recall once again the scene you imagined at the start of this chapter. One enticement to eating dinner after your return to the campfire was the delicious smell of the cooked food. Many organic compounds can evaporate from the surface of food, and both the number and amount of these increases as food is heated. How are these compounds sensed and distinguished from one another? In this section, we will explore the signal-transduction pathways behind smell and other senses as well, including vision and hearing.

A huge family of 7TM receptors detect a wide variety of organic compounds

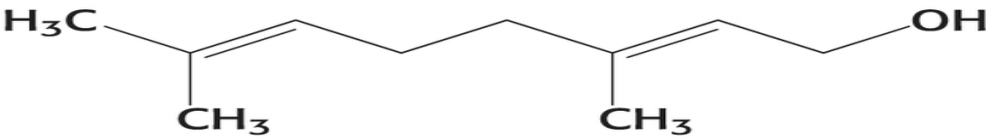
Human beings can detect and distinguish thousands of different compounds by smell, often with considerable sensitivity and specificity. Most odorants are small organic compounds with sufficient volatility that they can be carried as vapors into the nose. For example, a major component responsible for the odor of almonds is the simple aromatic compound benzaldehyde, whereas the sulfhydryl compound 3-methylbutane-1-thiol is a major component of the odor of skunks.



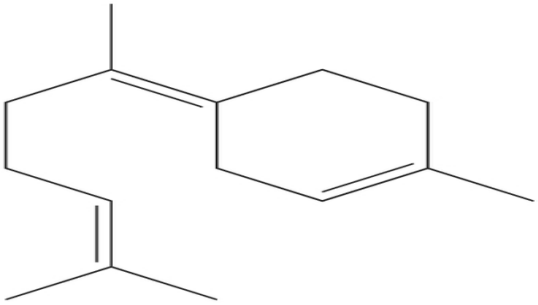
Benzaldehyde
(Almond)



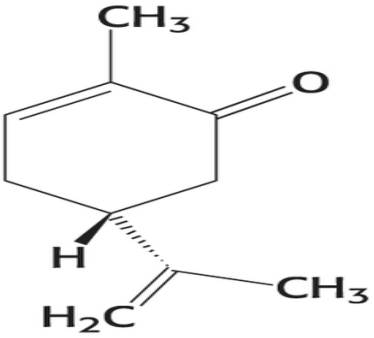
3-Methylbutane-1-thiol
(Skunk)



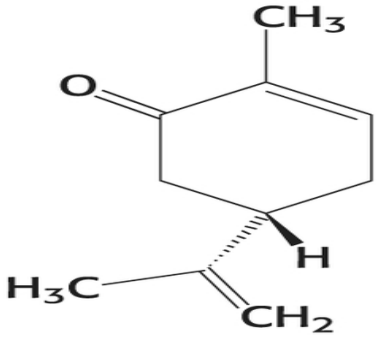
Geraniol
(Rose)



Zingiberene
(Ginger)



***R*-Carvone**
(Spearmint)



***S*-Carvone**
(Caraway)



What properties of these molecules are responsible for their odors? First, the shape of the molecule rather than its other physical properties is crucial. We can most clearly see the importance of shape by comparing molecules such as those responsible for the odors of spearmint and caraway. These compounds are identical in essentially all physical properties such as hydrophobicity because they are exact mirror images of one another. Thus, the odor produced by an odorant depends not on a physical property but on the compound's interaction with specific receptors.

Investigations revealed that olfaction depends on cAMP and GTP, and a G-protein α subunit, termed $G_{(olf)}$, was discovered that is uniquely expressed in the olfactory system. From our knowledge, these factors should strongly suggest the involvement of 7TM receptors. Complementary DNAs were sought that (1) were expressed primarily in the sensory neurons lining the nasal epithelium, (2) encoded members of the 7TM-receptor family, and (3) were present as a large and diverse family to account for the range of odorants. Based on these criteria, cDNAs for odorant receptors from rats were identified in 1991 by Richard Axel and Linda Buck.

The odorant receptor (OR) family is even larger than expected: more than 1000 OR genes are present in the mouse and the rat, whereas the human genome encodes approximately 400 ORs. The OR proteins are typically 20% identical in sequence with the β-adrenergic receptor and from 30% to 60% identical with one another.

Interestingly, each olfactory neuron expresses only a single OR gene, among the hundreds available. The binding of an odorant to an OR on the neuronal surface initiates a signal-transduction cascade, quite similar to that from the β-adrenergic receptor, that results in an action

potential (Figure 14.42). The ligand-bound OR activates $G_{(olf)}$, which releases GDP, binds GTP, and dissociates its βγ subunits. The α subunit then binds to and stimulates a specific adenylate cyclase, increasing the intracellular concentration of cAMP. The rise in the intracellular concentration of cAMP activates a nonspecific cation channel that allows calcium and other cations into the cell. The flow of cations through the channel depolarizes the neuronal membrane and initiates an action potential. This action potential, combined with those from other olfactory neurons, leads to the perception of a specific odor.

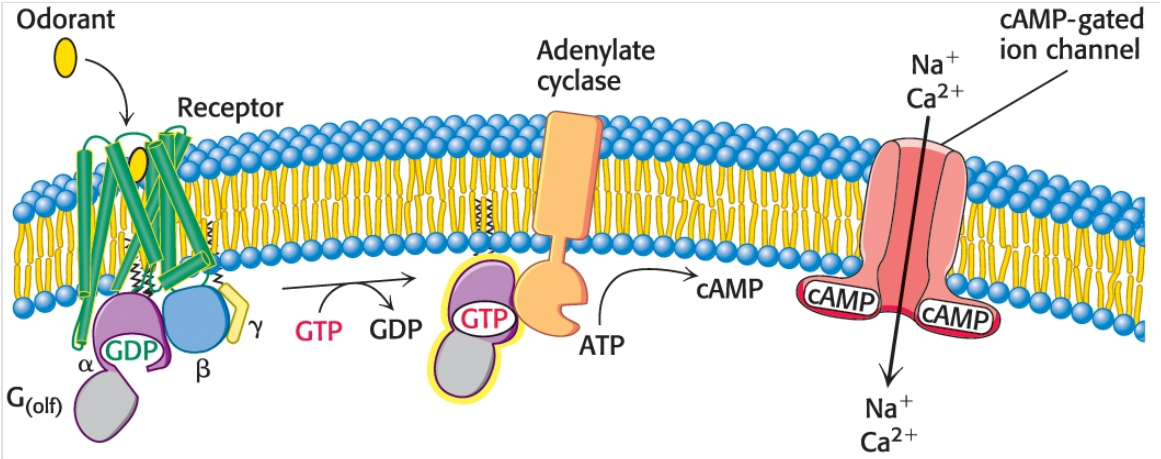


FIGURE 14.42 The olfactory signal-transduction cascade is similar to that for the β-adrenergi receptor. The binding of odorant to an olfactory receptor results in stimulating the activity of adenylate cyclase. The final result is the opening of cAMP-gated ion channels and the initiation an action potential.

An obvious challenge presented to an investigator by the large size of the OR family is to match each OR with the one or more odorant molecules to which it binds. Dramatic progress was made by taking advantage of our knowledge of the OR signal-transduction pathway. A section of nasal epithelium from a mouse was loaded with the calcium-sensitive dye Fura-2. The tissue was then treated with different odorants, one at a time, at a specific concentration (Figure 14.43). If the odorant had bound to an OR and activated it, that neuron could be

detected under a microscope by the change in fluorescence caused by the influx of calcium that takes place as part of the signal-transduction process.

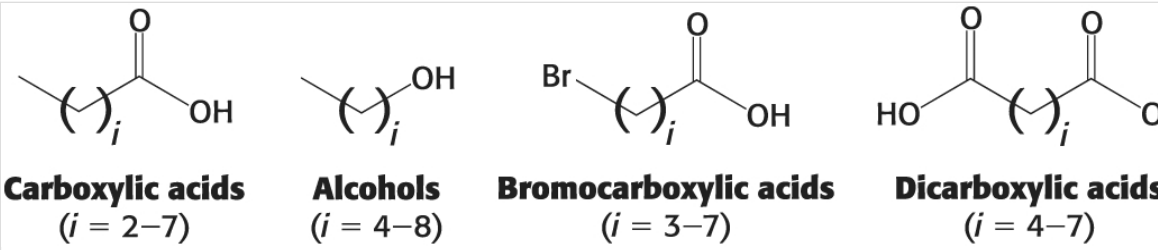


FIGURE 14.43 Olfactory-receptor activation has been tested with sets of closely related compounds. The structures of four series of compounds are shown.

To determine which OR was responsible for the response, cDNA was generated from mRNA that had been isolated from single identified neurons, and cDNAs were produced that encoded ORs. These studies revealed there is not a simple 1:1 correspondence between odorants and receptors. Almost every odorant activates a number of receptors (usually to different extents) and almost every receptor is activated by more than one odorant (Figure 14.44). Note, however, that each odorant activates a unique combination of receptors. This combinatorial mechanism allows even a small array of receptors to distinguish a vast number of odorants.

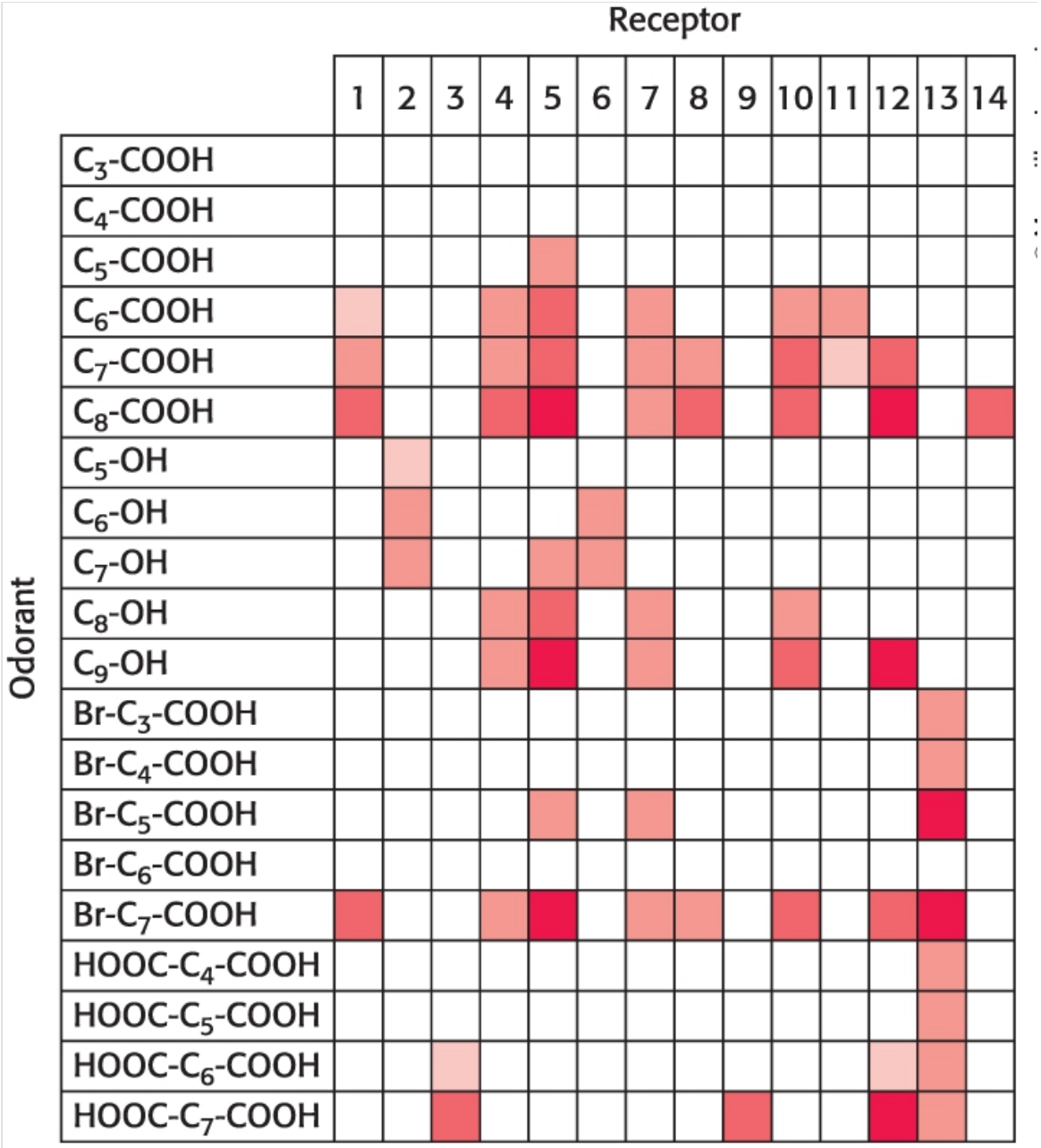


FIGURE 14.44 Different compounds result in distinct patterns of olfactory-receptor activation
Fourteen different receptors were tested for responsiveness to the compounds shown in Figure 14.43. A colored box indicates that the receptor at the top responded to the compound at the le Darker colors indicate that the receptor was activated at a lower concentration of odorant.

One of the manifestations of COVID-19 in many people is a loss of the sense of smell. While the cause of this is still under investigation, a clue has come from genomic studies of populations of individuals who either have or have not lost their sense of smell. These studies have suggested that enzymes that add sugars to some odorants to help terminate olfactory signaling may differ in these two groups of people. This example highlights another mechanism for signal termination, but also another role of carbohydrates that we will see again when we discuss drug metabolism.

Self-Check Question

What symptoms would you expect if an individual had a mutation that disrupted an olfactory receptor gene?

Vision relies on a specialized 7TM receptor to signal in response to absorbed light

We now turn from olfaction to vision. Vision is based on the absorption of light by photoreceptor cells in the eye. These cells are sensitive to light in a narrow region of the electromagnetic spectrum — the region with wavelengths between 390 and 750 nm (Figure 14.45). Vertebrates have two kinds of photoreceptor cells, called rods and cones because of their distinctive shapes. Cones function in bright light and are responsible for color vision, whereas rods function in dim light but do not perceive color. A human retina contains about 3 million cones and 100 million rods. Remarkably, a rod cell can respond to a single photon,

and the brain requires fewer than 10 such responses to register the sensation of a flash of light.

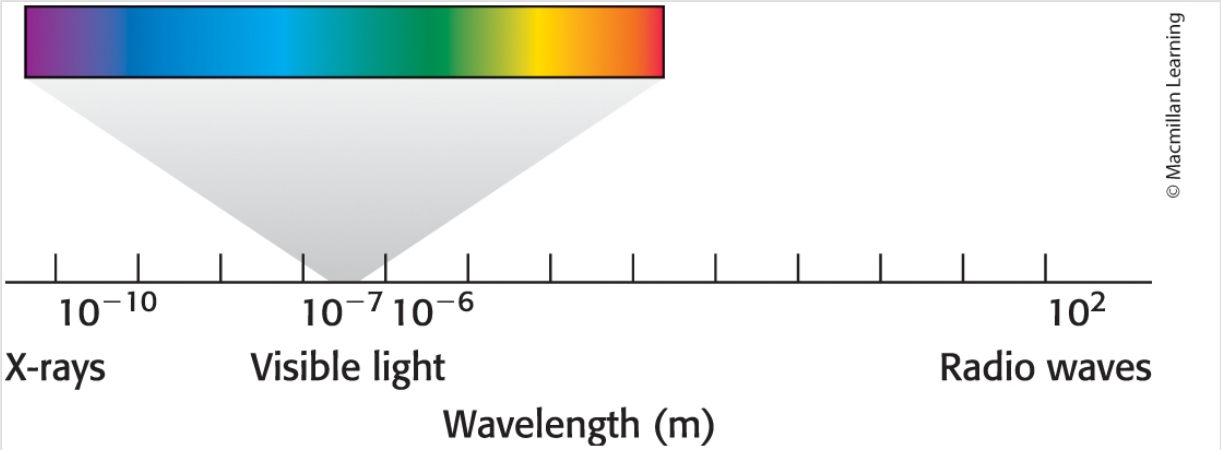
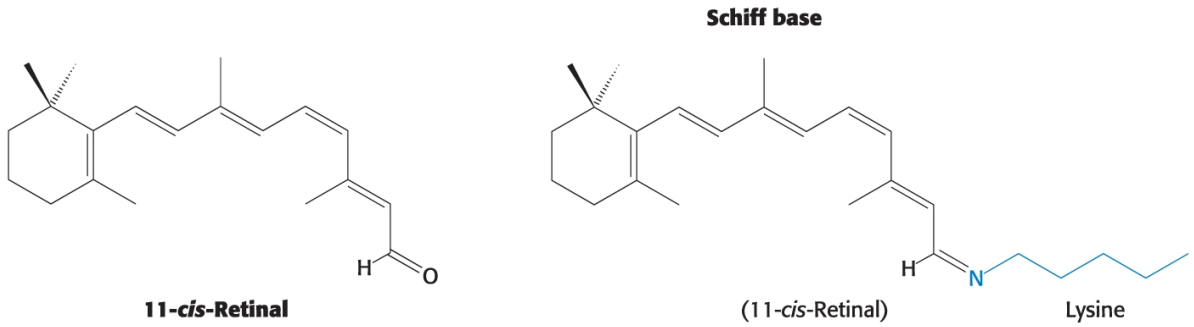


FIGURE 14.45 Visible light represents a small region of the electromagnetic spectrum. Visible light has wavelengths between 390 and 750 nm.

Rods are slender, elongated structures; the outer segment is specialized for photoreception (Figure 14.46). It contains a stack of about 1000 discs, which are membrane-enclosed sacs densely packed with photoreceptor molecules. The photosensitive molecule is often called a visual pigment because it is highly colored owing to its ability to absorb light. The photoreceptor molecule in rods is rhodopsin, which consists of the protein opsin linked to 11-*cis*-retinal, a prosthetic group, via a lysine residue.



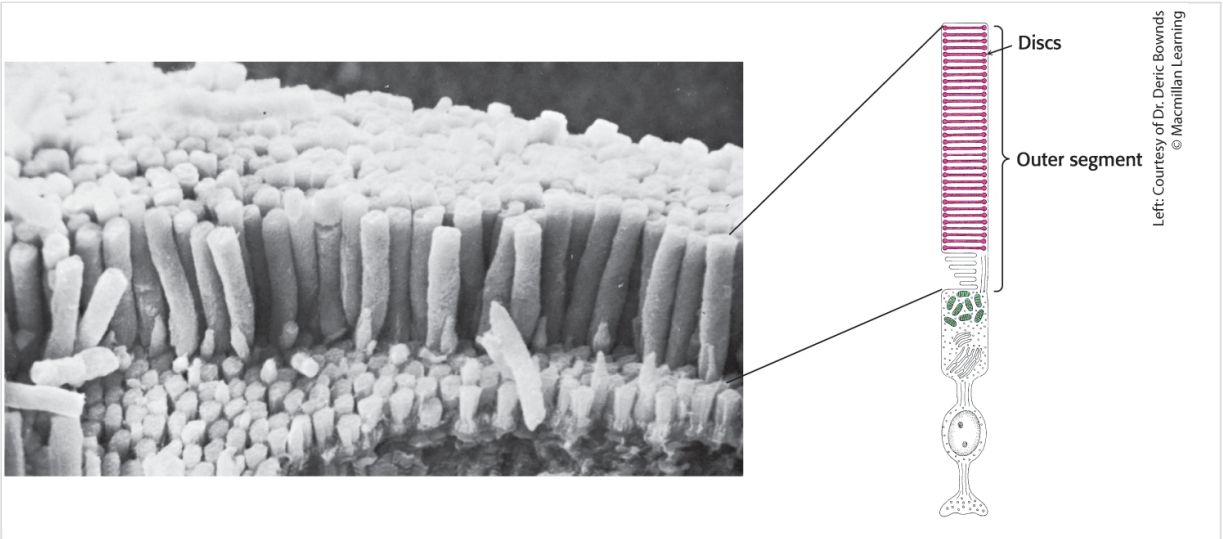


FIGURE 14.46 Rod cells have elongated structures including stacked discs where light absorption occurs. (Left) A scanning electron micrograph of retinal rod cells. (Right) A schematic representation of a rod cell.

Rhodopsin absorbs light very efficiently in the middle of the visible spectrum, its absorption being centered on 500 nm, which nicely matches the solar output (Figure 14.47). A rhodopsin molecule will absorb a high percentage of the photons of the correct wavelength that strike it. Opsin is a member of the 7TM-receptor family. Indeed, rhodopsin was the first member of this family to be purified, its gene was the first to be cloned and sequenced, and its three-dimensional structure was the first to be determined. The color of rhodopsin and its responsiveness to light depend on the presence of the light-absorbing group 11-*cis*-retinal.

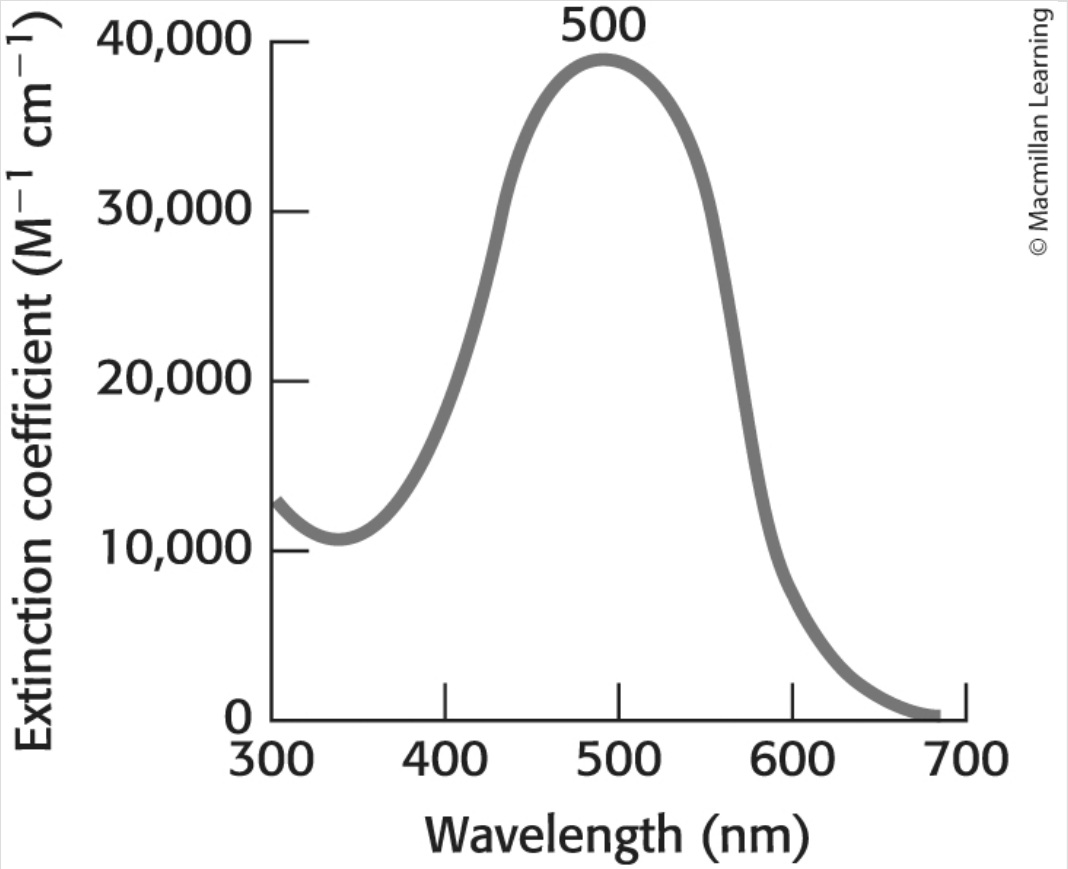


FIGURE 14.47 Rhodopsin absorbs light quite effectively toward the blue end of the visible spectrum. The absorption spectrum of rhodopsin is shown. The large ($> 10{,}000\ M^{-1}\ cm^{-1}$) extinction coefficients reveal that most of the light striking a rhodopsin molecule is absorbed.

Light absorption induces a specific isomerization of bound 11-*cis*-retinal

How does the absorption of light by retinal generate a signal? George Wald and his coworkers discovered that light absorption results in the isomerization of the 11-*cis*-retinal group of rhodopsin to its all-trans

form (Figure 14.48). This isomerization causes the nitrogen atom from the linked lysine residue to move approximately 5Å, assuming that the cyclohexane ring of the retinal group remains fixed. In essence, the light energy of a photon is converted into atomic motion. The change in atomic positions, like the binding of a ligand to other 7TM receptors, sets in motion a series of events that lead to the closing of ion channels and the generation of a nerve impulse.

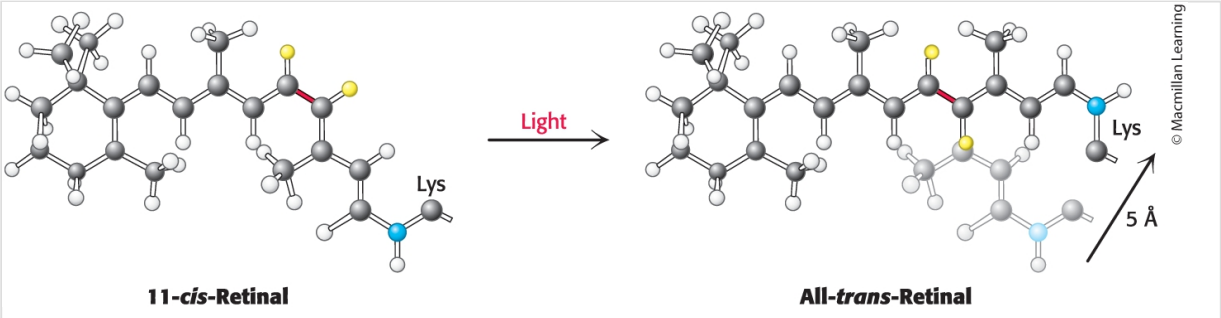


FIGURE 14.48 Isomerization of retinal results in a substantial motion. The nitrogen atom of the lysine residue linked to retinal moves 5Å as a consequence of the light-induced isomerization of 11-*cis*-retinal to all-*trans*-retinal by rotation about the bond shown in red.

Like these receptors, this form of rhodopsin activates a heterotrimeric G protein that propagates the signal. The G protein associated with rhodopsin is called transducin. Light absorption and retinal isomerization triggers the exchange of GDP for GTP by the α subunit of transducin (Figure 14.49). On the binding of GTP, the βγ subunits of transducin are released and the GTP form of the α subunit is free to bind to its target. The target for transducing is not adenylate cyclase, but rather a specific cGMP phosphodiesterase. Transducin binds to an inhibitory subunit of this enzyme and removes it. The activated phosphodiesterase is a potent enzyme that rapidly hydrolyzes cGMP to GMP. The reduction in cGMP concentration causes cGMP-gated ion channels to close, leading to the hyperpolarization of the membrane and neuronal signaling. At each step in this process, the initial signal —

the absorption of a single photon — is amplified so that it leads to sufficient membrane hyperpolarization to result in signaling. For a multistep, enzyme-based process, the visual signal-transduction system is strikingly fast, responding in approximately 1 ms.

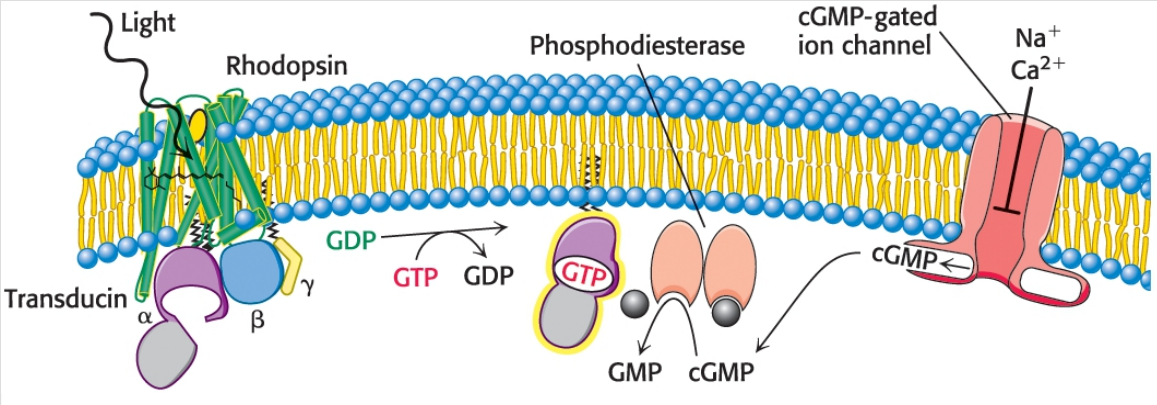


FIGURE 14.49 Visual signal transduction involves G-protein activation of cGMP phosphodiesterase. The light-induced activation of rhodopsin activates a novel G protein, transducin, which leads to the hydrolysis of cGMP. This, in turn, leads to ion-channel closing and the initiation of an action potential.

Color vision is mediated by three cone receptors that are homologs of rhodopsin

Cone cells, like rod cells, contain visual pigments. Like rhodopsin, these photoreceptor proteins are members of the 7TM-receptor family and use 11-*cis*-retinal as their chromophore. In human cone cells, there are three distinct photoreceptor proteins with absorption maxima at 426, 530, and ~560 nm (Figure 14.50). These absorbances correspond to the blue, green, and yellow-green regions of the spectrum. Recall that the absorption maximum for rhodopsin is 500 nm. The photoreceptor protein with its absorption maximum near 560 nm absorbs red light

(with wavelength > 620 nm), whereas the other two photoreceptors do not. These three proteins are often referred to as the blue, green, and red photoreceptors. The cone photoreceptors signal through pathways that are identical to that used by rhodopsin.

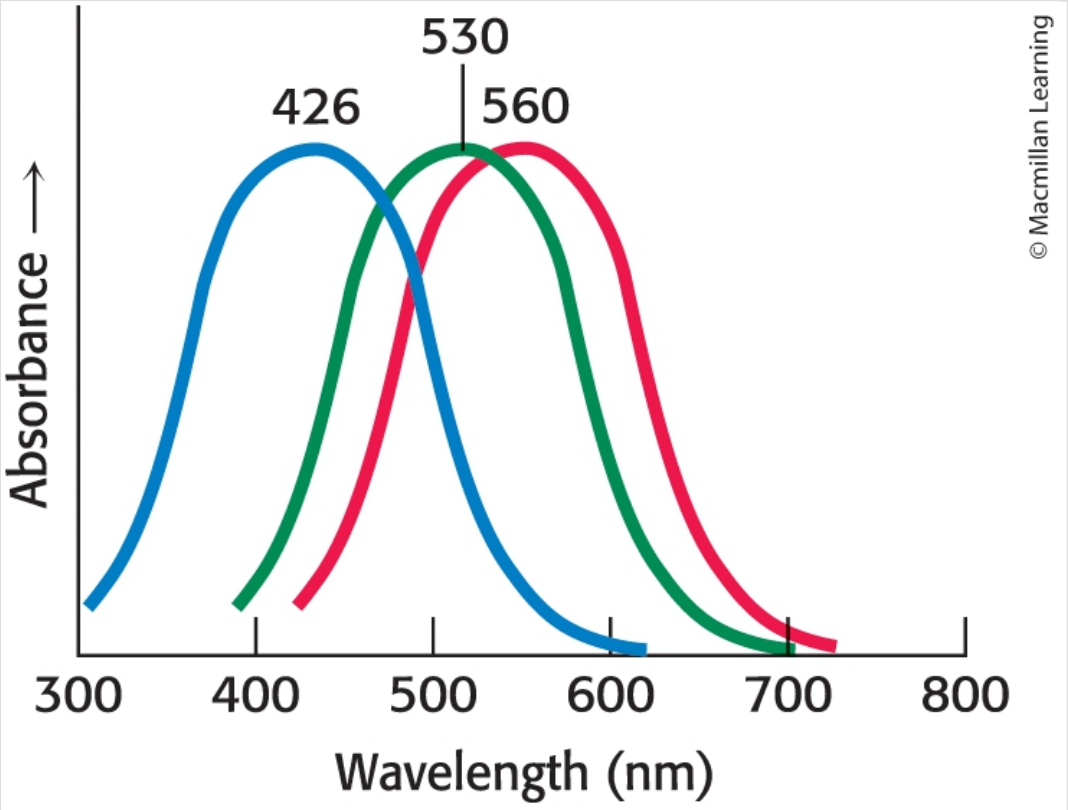


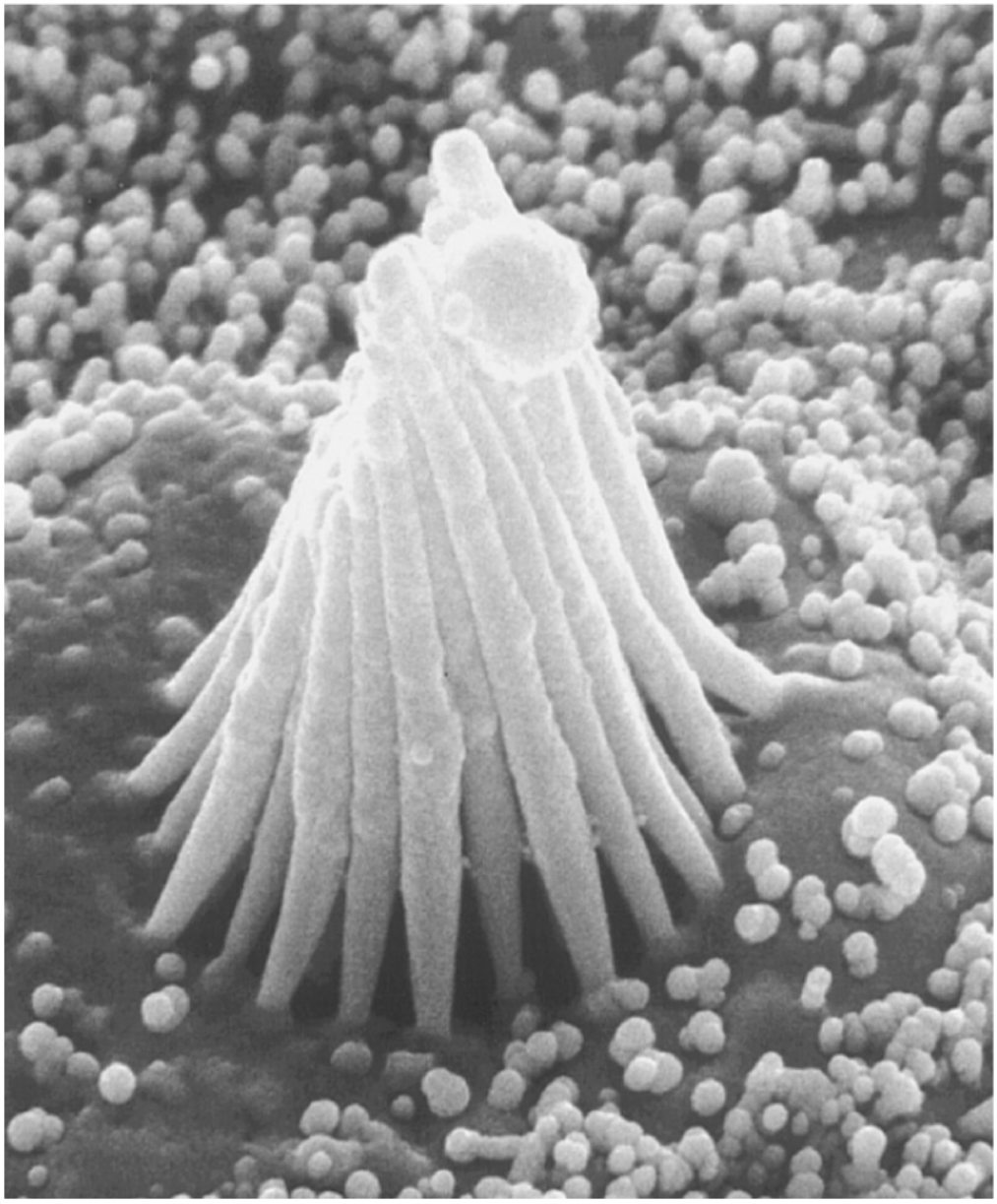
FIGURE 14.50 Color vision is mediated by visual pigments that absorb light of different colors. The absorption spectra of the three types of light receptors from human cone cells are shown.

The decoding of color vision is analogous to olfaction. Each cone expresses only one of the photoreceptors, but most wavelengths of light activate more than one type of photoreceptor. Our brains compare the signals from the three classes of cones to assign a color to an object in our field of view based on the light that it reflects.

Hearing depends on hair cells that use mechanosensitive ion channels to detect tiny motions

The first indications that we had about our animal intruder were the sounds we heard coming from behind us. Our sense of hearing operates at a remarkable speed. We hear frequencies ranging from 200 to 20,000 Hz (cycles per second), corresponding to times of 5 to 0.05 ms. Furthermore, our ability to locate sound sources — one of the most important functions of hearing — depends on the ability to detect the time delay between the arrival of a sound at one ear and its arrival at the other. Given the separation of our ears and the speed of sound, we must be able to accurately sense time differences of 0.7 ms. In fact, human beings can locate sound sources associated with temporal delays as short as 0.02 ms. This high time resolution implies that hearing depends on direct transduction mechanisms that do not use enzymes or second messengers.

Sound waves are detected inside the cochlea of the inner ear. The cochlea is a fluid-filled, membranous sac that is coiled like a snail shell. The primary detection is accomplished by specialized neurons inside the cochlea called hair cells. Each cochlea contains approximately 16,000 hair cells, and each hair cell contains a hexagonally shaped bundle of 20 to 300 hairlike projections called stereocilia (**Figure 14.51**). These stereocilia are graded in length across the bundle. Mechanical deflection of the hair bundle, as takes place when a sound wave arrives at the ear, creates a change in the membrane potential of the hair cell.



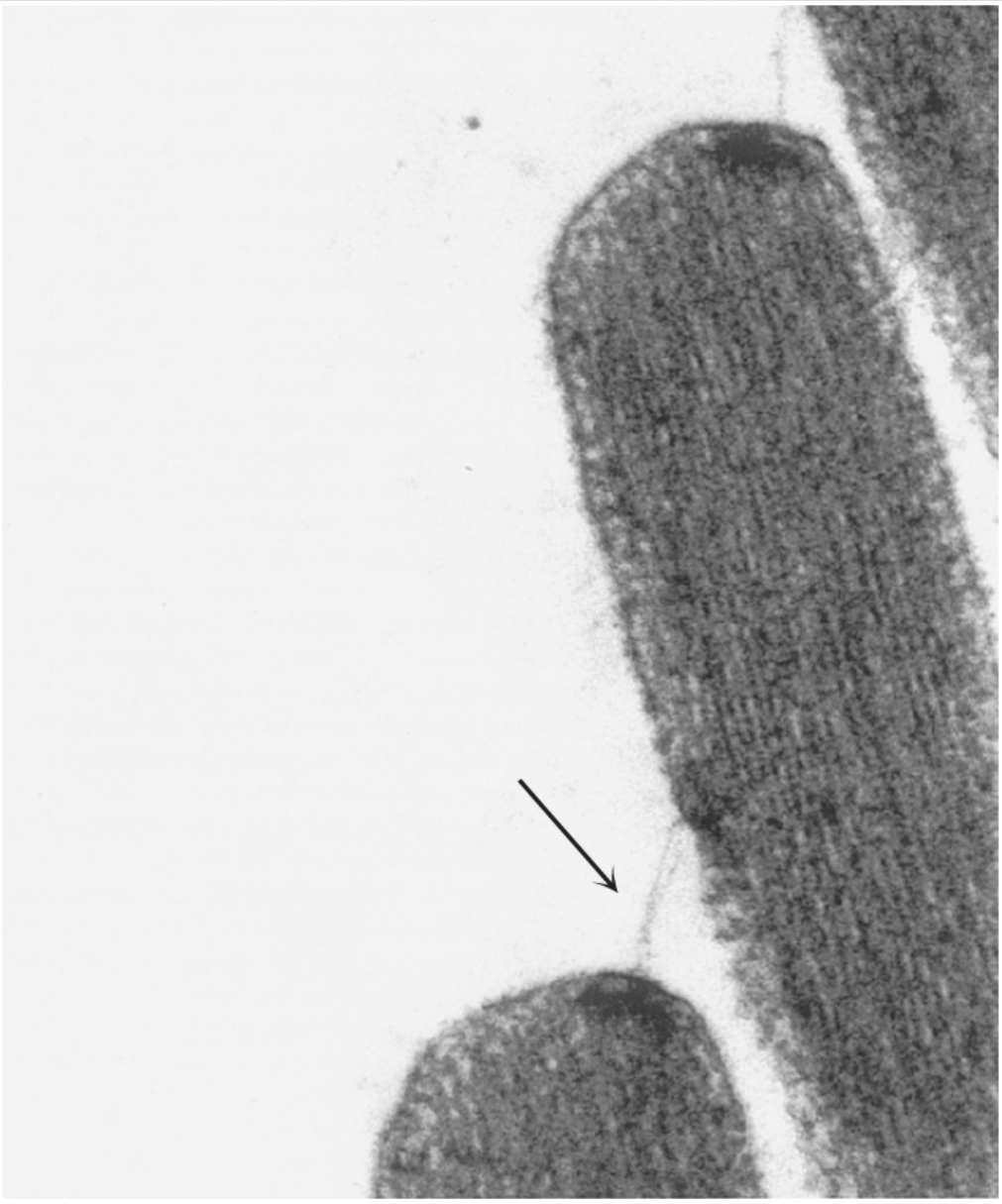
Courtesy of R. Jacobs and A.J. Hudspeth

FIGURE 14.51 Hearing is mediated by bundles of stereocilia on hair cells. An electron micrograph of a stereocilia bundle is shown.

Micromanipulation experiments have directly probed the connection between mechanical stimulation and membrane potential. Displacement toward the direction of the tallest part of the hair bundle results in the depolarization of the hair cell, whereas displacement in

the opposite direction results in its hyperpolarization. Remarkably, displacement of the hair bundle by as little as 3Å (0.3 nm) results in a measurable (and functionally important) change in membrane potential. This motion of 0.001 degree corresponds to a 0.3-inch movement of the top of a 100-story building.

The rapid response, within microseconds, suggests that the movement of the hair bundle acts on ion channels directly. An important observation is that adjacent stereocilia are linked by individual filaments called tip links (**Figure 14.52**). The presence of these tip links suggests a simple mechanical model for transduction by hair cells (**Figure 14.53**). The tip links are coupled to ion channels in the membranes of the stereocilia that are gated by mechanical stress. In the absence of a stimulus, approximately 15% of these channels are open. When the hair bundle is displaced toward its tallest part, the stereocilia slide across one another and the tension on the tip links increases, causing additional channels to open. The flow of ions through the newly opened channels depolarizes the membrane. Conversely, if the displacement is in the opposite direction, the tension on the tip links decreases, the open channels close, and the membrane hyperpolarizes. Thus, the mechanical motion of the hair bundle is directly converted into current flow across the hair-cell membrane. Many of the molecular components of this elegant micromechanical system have now been identified, including those from the mechanosensitive ion channel and the tip link filaments, as well as specialized myosin motors that maintain appropriation tension in the system.



Courtesy of R. Jacobs and A.J. Hudspeth

FIGURE 14.52 Tip links that connect adjacent stereocilia are crucial for signal detection in hearing. An electron micrograph of tip links is shown. The tip link between two stereocilia is marked by an arrow.

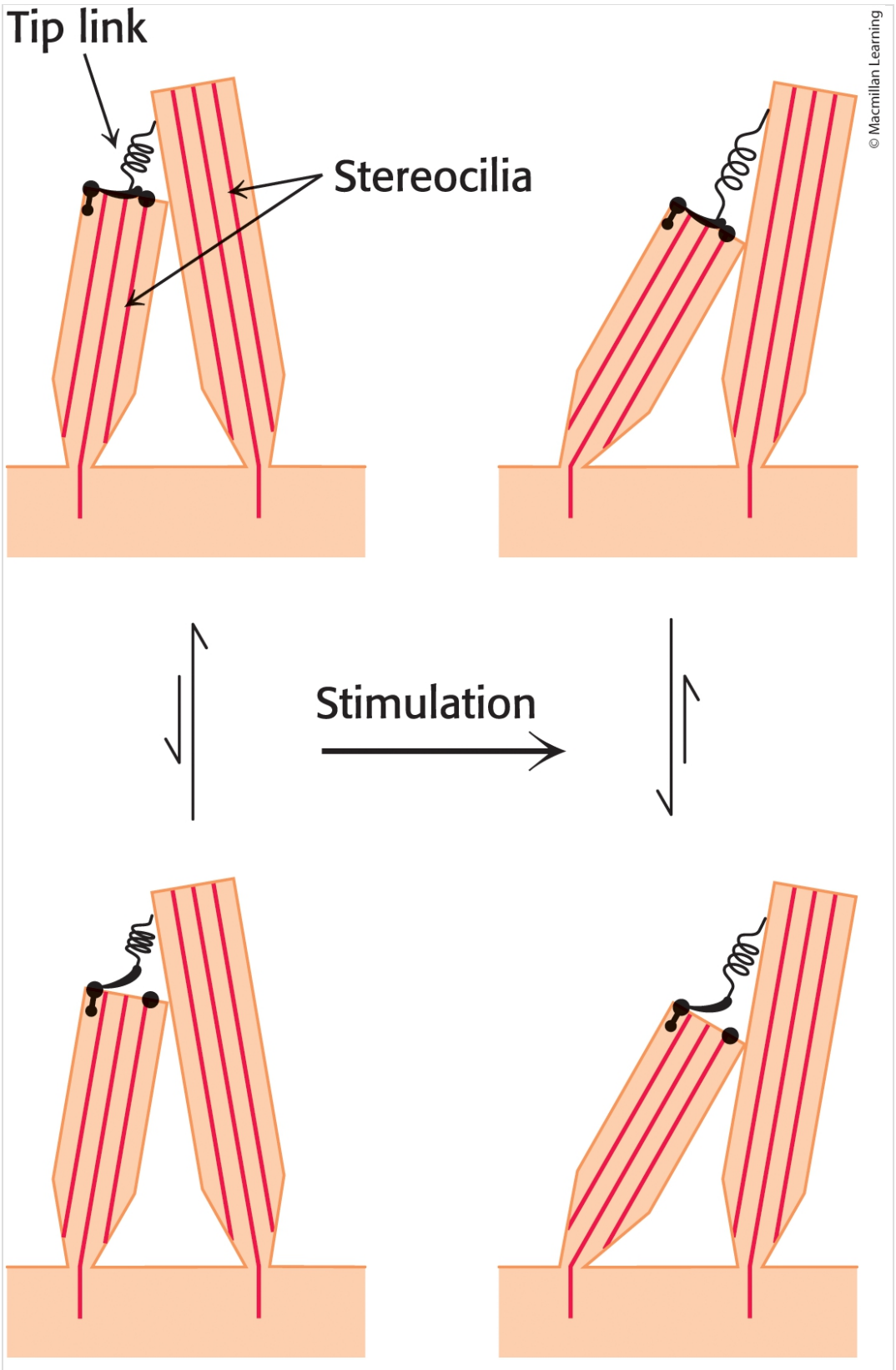


FIGURE 14.53 Hair cell signal detection involves ion-channel opening in response to small displacements of stereocilia bundles. When the hair bundle is tipped

toward the tallest part, the tip link pulls on an ion channel and opens it. Movement in the opposite direction relaxes the tension in the tip link, increasing the probability that any open channels will close.

[Information from A. J. Hudspeth, *Nature* 341:397–404, 1989 and M. Beurg, R. Fettiplace, J. H. Nam, and A. J. Ricci, *Nature Neuroscience* 12:553–558, 2009.]



Self-Check Question



What are the primary signals in olfaction, vision, and hearing? Compare the mechanisms by which these primary signals are first detected in the three sensory systems.

Comparison of different organisms yields insights into sensory system evolution

In addition to representing instructive examples of applying the knowledge we have gained about signal-transduction pathways, sensory systems also provide compelling glimpses into evolution at the molecular level. As we noted, rodents have more than 1000 ORs, whereas our genomes only include only approximately 400 functional genes. Further examination reveals that our genomes contain hundreds of OR pseudogenes, DNA segments that encode ORs but have one or more defects so that they will not produce functional receptors. Examination of other organisms reveals a steady conversion from functional OR genes into pseudogenes over the course of the primate evolution (Figure 14.54).

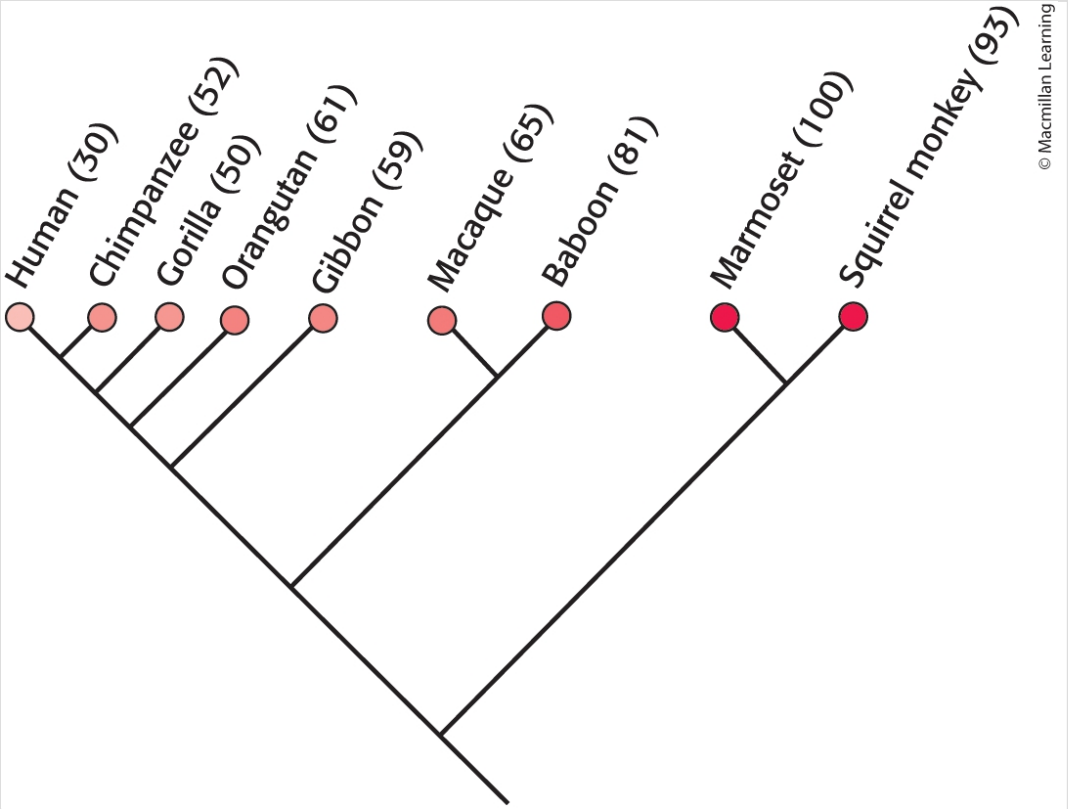
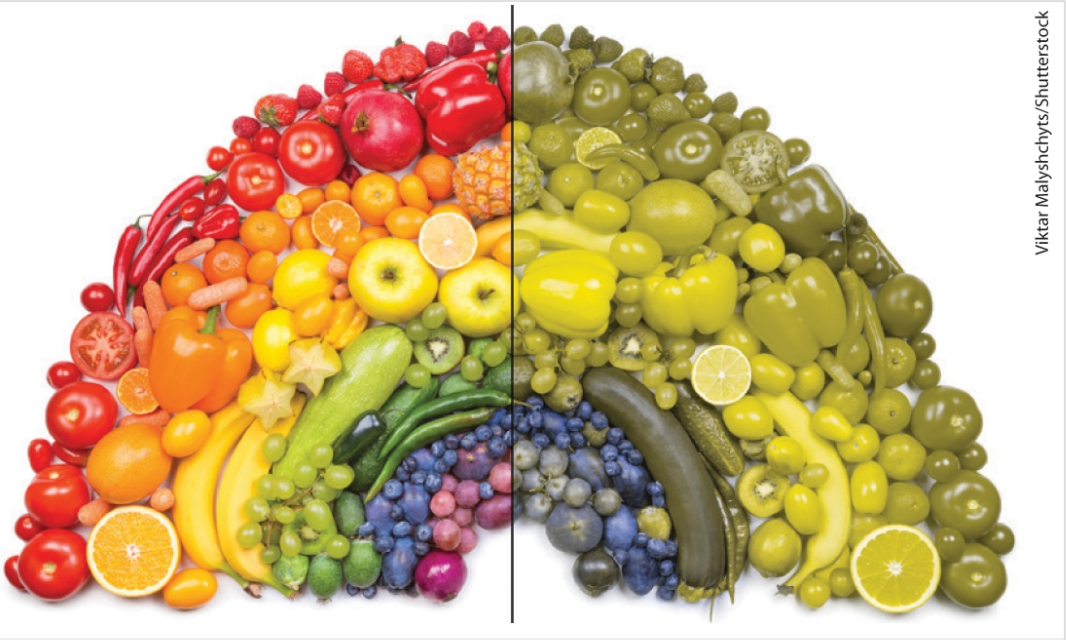


FIGURE 14.54 Functional odorant receptor genes have been lost over the course of primate evolution. Odorant receptors appear to have lost function through conversion into pseudogenes during primate evolution. The percentage of OR genes that appear to be functional for each species is given in parentheses.

The opposite has occurred with regard to color vision. Human beings and many other primates have three cone receptors. Most other placental mammals have only two. Thus, rodents as well as organisms such as dogs do sense color but are not capable of distinguishing color such as red and green as well as we are. Indeed, some human beings have variations in their visual pigments (so-called “color blindness”) so that they see colors differently (Figure 14.55). Earlier ancestors of all animals had four cone pigments as do some modern organisms such as many birds. In addition to better color discrimination, the absorption spectra extend further into the ultraviolet region so that they can sense colors that we cannot. These differences provide vivid examples of how

signal-transduction pathways have a profound influence on how we experience the world.



Viktar Malyshchyts/Shutterstock

FIGURE 14.55 More colors can be distinguished with three versus two cone pigments. The left side of the image shows its appearance with three cone pigments, while the right side show its appearance with two. Most human beings have three functional pigments, whereas mammals such as rodents and dogs have two.

Chapter 14 Summary

14.1 Many Signal-Transduction Pathways Share Common Themes

- Most signal-transduction pathways involve a common set of steps: Binding of a primary messenger to a receptor on the cell surface; transduction of the information across the cell membrane to the interior of the cell; a change in the concentration of one or more second messenger molecules inside the cell; initiation of other processes by the second messenger; and termination of the signaling.
- Signal-transduction processes can be very intricate as they occur with variation in different biological contexts and cell types, but common themes and classes of molecules do occur.

14.2 Epinephrine Signaling: Heterotrimeric G Proteins Transmit Signals and Reset Themselves

- Hormones such as epinephrine bind to members of a large family of cell-surface receptors that have a common structure of seven transmembrane (7TM) helices.
- When activated by ligand binding, these 7TM helix receptors bind to specific heterotrimeric G proteins and stimulate the release of bound GDP and the binding of GTP in the α subunit of the G protein.
- When activated by GTP binding, the α subunit of the G protein releases the heterodimer consisting of the β and γ subunits and then binds to other targets such as the enzyme adenylate cyclase.
- Stimulation of adenylate cyclase increases the concentration of the second messenger cyclic AMP, which, in turn, activates protein kinase A.
- Some 7TM receptors signal through different heterotrimeric G proteins that inhibit the activity of adenylate cyclase or activate

the phosphoinositide pathway, starting with the activation of phospholipase C, which cleaves a membrane lipid to produce two secondary messengers, diacylglycerol and inositol 1,4,5-trisphosphate.
- G-protein signaling is terminated by the hydrolysis of the bound GTP to GDP.

14.3 Insulin Signaling: Phosphorylation Cascades Are Central to Many Signal-Transduction Processes

- Protein kinases are key components in many signal-transduction pathways, including some for which the protein kinase is an integral component of the initial receptor.
- Insulin binds to a dimeric receptor that includes an intracellular tyrosine kinase as part of its structure that is activated by the kinase domain of one subunit of the dimer phosphorylating certain tyrosine residues on the other subunit.
- The activated receptor kinase initiates a signaling cascade that includes both lipid kinases and protein kinases that eventually leads to the mobilization of glucose transporters to the cell surface, increasing glucose uptake.
- Insulin signaling is terminated through the action of phosphatases.

14.4 Epidermal Growth Factor: Receptor Dimerization Can Drive Signaling

- Epidermal growth factor also signals through a receptor tyrosine kinase, but this receptor is a monomer prior to EGF binding.
- EGF binding induces a conformational change that allows receptor dimerization and cross-phosphorylation.
- The phosphorylated receptor binds adaptor proteins that mediate the activation of Ras, a small G protein that initiates a protein kinase cascade that eventually leads to the

phosphorylation of transcription factors and changes in gene expression.
- EGF signaling is terminated by the action of phosphatases and the hydrolysis of GTP by Ras.

14.5 Defects in Signal-Transduction Pathways Can Lead to Cancer and Other Diseases

- Genes encoding components of signal-transduction pathways that control cell growth are often mutated in cancer.
- Some genes can be mutated to forms called oncogenes that are active regardless of appropriate signals.
- Monoclonal antibodies directed against cell-surface receptors that participate in signaling have been developed for use in cancer treatment.
- Our understanding of the molecular basis of cancer has enabled the development of anticancer drugs directed against specific targets, such as specific protein kinase inhibitors.

14.6 Sensory Systems Are Based on Specialized Signal-Transduction Pathways

- Olfaction involves a large family of 7TM receptors that signal through a pathway involving adenylate cyclase, leading to ion-channel opening.
- Vision uses a specialized 7TM receptor called rhodopsin that includes a covalently bound ligand, 11-*cis*-retinal, that isomerizes upon absorbing light, activating the receptor.
- Color vision is mediated by a set of three receptors similar to rhodopsin that tune the absorption of light to different wavelengths.
- Hearing involves specialized cells called hair cells that have bundles of stereocilia that move subtly in response to sound waves in the air.

- Signal transduction is very fast, depending on the direct coupling of stereocilia motion to ion-channel opening, without any chemical steps.

Key Terms

transduction
primary messenger
receptor
second messenger
epinephrine (adrenaline)
adrenergic receptor
seven-transmembrane-helix (7TM) receptor
agonist
G protein
G-protein-coupled receptor (GPCR)
adenylate cyclase
calmodulin (CaM)
EF hand
antagonist
insulin
activation loop
pleckstrin homology domain
oncogene
proto-oncogene
tumor-suppressor gene

Problems

1. Place the steps of the insulin-signaling pathway in the correct order: 1

a. Phosphorylation of IRS proteins
b. Alteration of glucose metabolism in response to insulin
c. Binding of insulin to the α subunit of the insulin receptor
d. Activation of insulin receptor tyrosine kinase
e. Activation of PKB by PDK1
f. Recruitment of PI3K to the cell membrane
g. Conversion of PIP_2 to PIP_3

2. Glucagon is a hormone that is released when the level of circulating glucose in the blood is low. Glucagon signals the cell via a $G_{\alpha s}$ signaling pathway. Put the steps of the glucagon signal-transduction pathway in order. 1

a. Adenylate cyclase converts ATP to cAMP.
b. $G_{\alpha s}$ releases GDP and binds GTP.
c. Glucagon binds extracellularly to the G-protein-coupled receptor.
d. Activated $G_{\alpha s}$ activates adenylate cyclase.
e. cAMP activates protein kinase A (PKA).
f. PKA activates enzymes needed for glucose release.

3. Suppose that each β-adrenergic receptor bound to epinephrine converts 100 molecules of $G_{\alpha s}$ into their GTP forms and that each molecule of activated adenylate cyclase produces 1000 molecules of cAMP per second. With the assumption of a full response, how many molecules of cAMP will be produced in 10 s after the formation of a single complex between

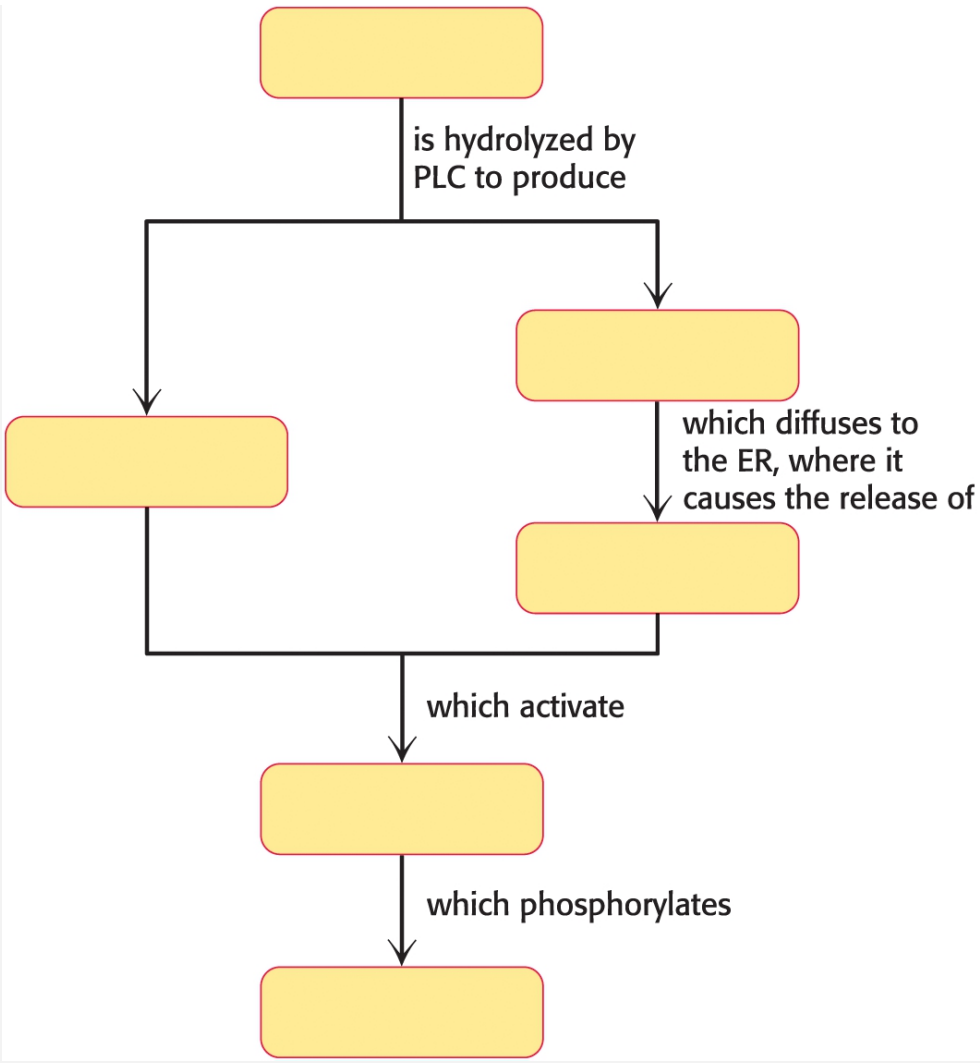
epinephrine and the β-adrenergic receptor? Assume the pathway is fully responsive. 1

4. A mutated form of the α subunit of the heterotrimeric G protein has been identified; this form readily exchanges nucleotides even in the absence of an activated receptor. What would be the effect on a signaling pathway containing the mutated α subunit? 5

5. Glucose is mobilized for ATP generation in muscle in response to epinephrine, which activates $G_{\alpha s}$. Cyclic AMP phosphodiesterase is an enzyme that converts cAMP into AMP. How would inhibitors of cAMP phosphodiesterase affect glucose mobilization in muscle? 2

6. Some G-protein-coupled receptors are sensitive to hormones such as angiotensin II and oxytocin and act through molecules such as phospholipase C (PLC) and IP_3. 1

a. Complete the flowchart showing the cleavage of a membrane lipid to form compounds that ultimately cause the phosphorylation of specific proteins. Use the following terms to complete the steps: IP_3, Ser/Thr residues, DAG, PIP_3, PKC, Ca^{2+}.



© Macmillan Learning

b. Of the terms you used to complete the chart, which can be considered second messengers?

7. Consider the structure of calmodulin (Figure 14.19). Which of the following statements are correct?

a. Calmodulin contains two Ca^{2+} binding sites.

b. Binding of Ca^{2+} activates calmodulin.

c. Each calcium-binding domain in calmodulin is formed from a helix-loop-helix motif.
d. Calmodulin is a structural subunit of proteins such as CaM kinase.
e. Calmodulin contains a central, flexible β sheet that enables it to wrap around another protein, inhibiting the protein's activity.
f. A calcium ion is bound in the loop of an EF hand.

8. Classify each statement as describing G-protein-coupled receptors, receptor tyrosine kinases, both, or neither: 3

a. An example is the insulin receptor.
b. They transport some ligands through the membrane.
c. Their structure contains seven transmembrane helices.
d. An example is the adrenergic receptor.
e. Receptor activation causes phosphorylation of their cytosolic subunits.
f. Ligand binding induces conformational change in these receptors.
g. They activate heterotrimeric G proteins directly.
h. Autophosphorylation of these receptors can initiate signal.
i. Phosphorylation of these receptors can terminate signal.

9. Drugs like imatinib (Gleevec) and cetuximab (Erbitux) are approved for the treatment of various types of cancer. Contrast these two drugs based on their mechanism of action. 4

10. Which of the following events contribute to the termination of a response in a GPCR signaling pathway? 1

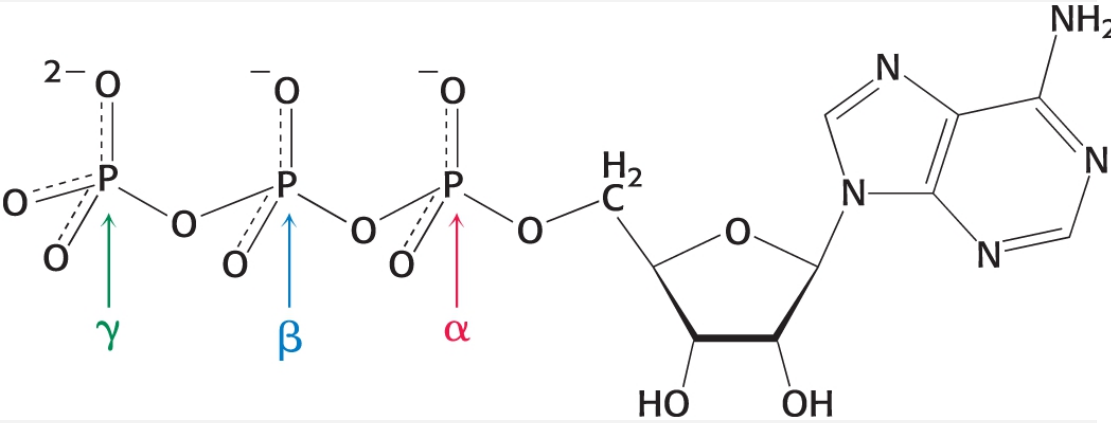
a. The ligand dissociates from the receptor, which resumes its inactive conformation.

b. G_α dissociates from the $G_{\beta\gamma}$ subunits.
c. G_α releases GDP and binds GTP.
d. G_α hydrolyzes GTP to GDP and P_i.
e. The receptor is inactivated by phosphorylation of Ser and other residues on its intracellular domain.

11. The structure of adenylate cyclase is similar to the structures of some types of DNA polymerases, suggesting that these enzymes derived from a common ancestor. Compare the reactions catalyzed by these two enzymes. In what ways are they similar?

12. Suppose you were investigating a newly discovered growth-factor signal-transduction pathway, involving a G-protein-coupled receptor system. When you add $GTP_{\gamma S}$, a nonhydrolyzable analog of GTP, the duration of the hormonal response increased. Why does the response last longer in the presence of $GTP_{\gamma S}$? 2

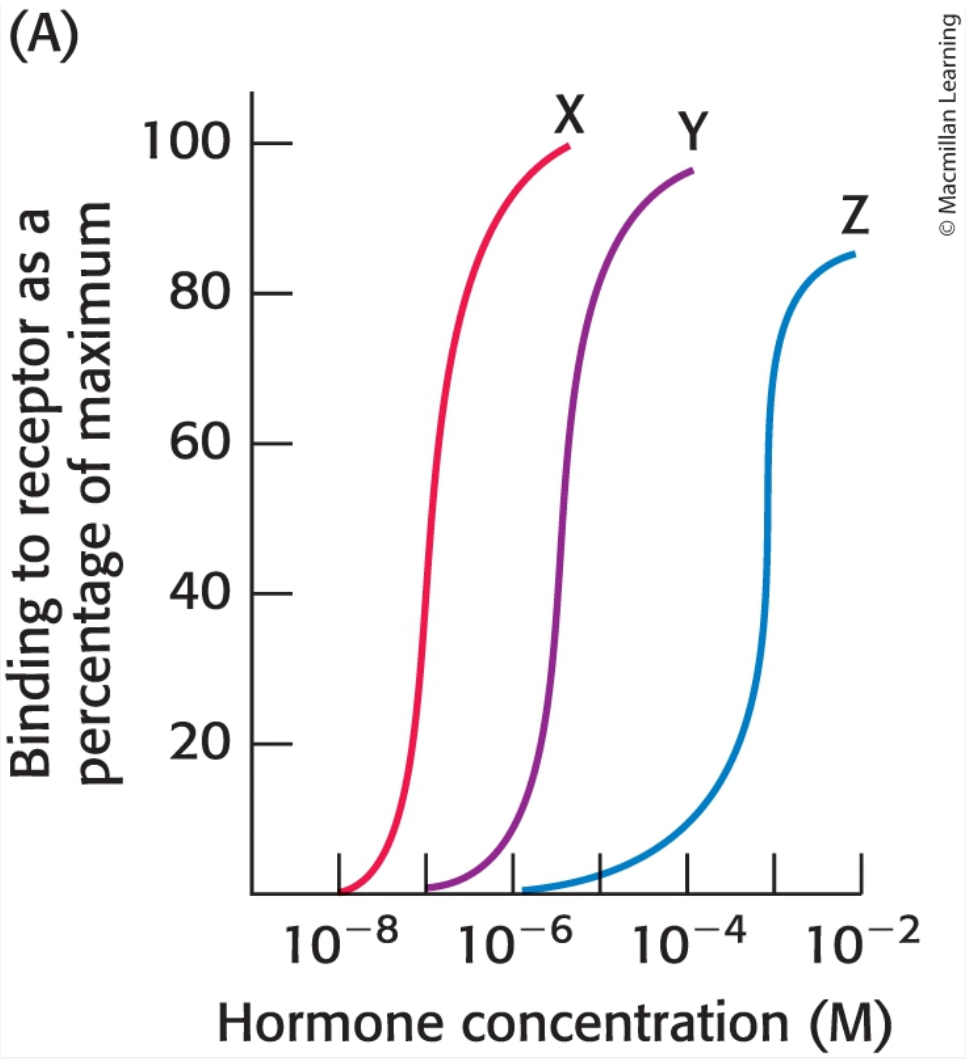
13. Consider the structure of ATP, and the identification of the individual phosphate groups.



a. If you wanted to identify the substrates of a particular kinase in a signaling pathway, you should use a version of ATP with ^{33}P-labeling at which phosphate?

b. If you wanted to generate a labeled form of cAMP by the enzymatic action of adenylate cyclase, you should use a version of ATP with ^{33}P labeling at which phosphate?

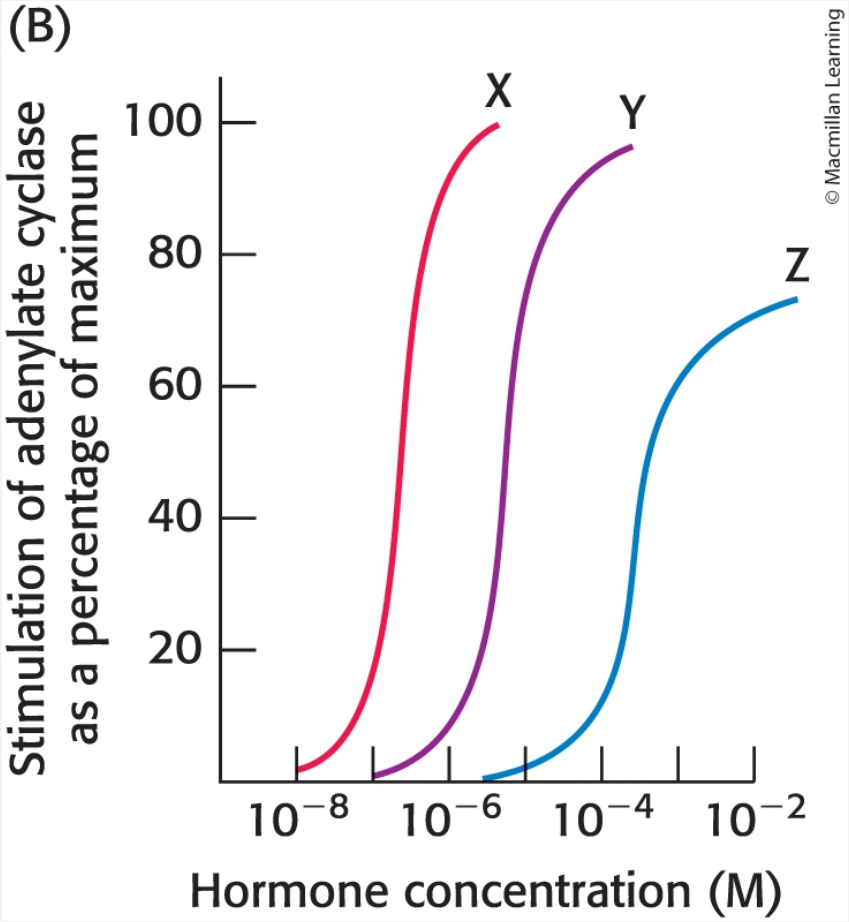
14. You wish to determine the hormone-binding specificity of a newly identified membrane receptor. Three different hormones, X, Y, and Z, were mixed with the receptor in separate experiments, and the percentage of binding capacity of the receptor was determined as a function of hormone concentration, as shown in graph A.



a. What concentrations of each hormone yield 50% maximal binding?
b. Which hormone shows the highest binding affinity for the receptor?

You next wish to determine whether the hormone–receptor complex stimulates the adenylate cyclase cascade. To do so, you measure adenylate cyclase activity

as a function of hormone concentration, as shown in graph B.



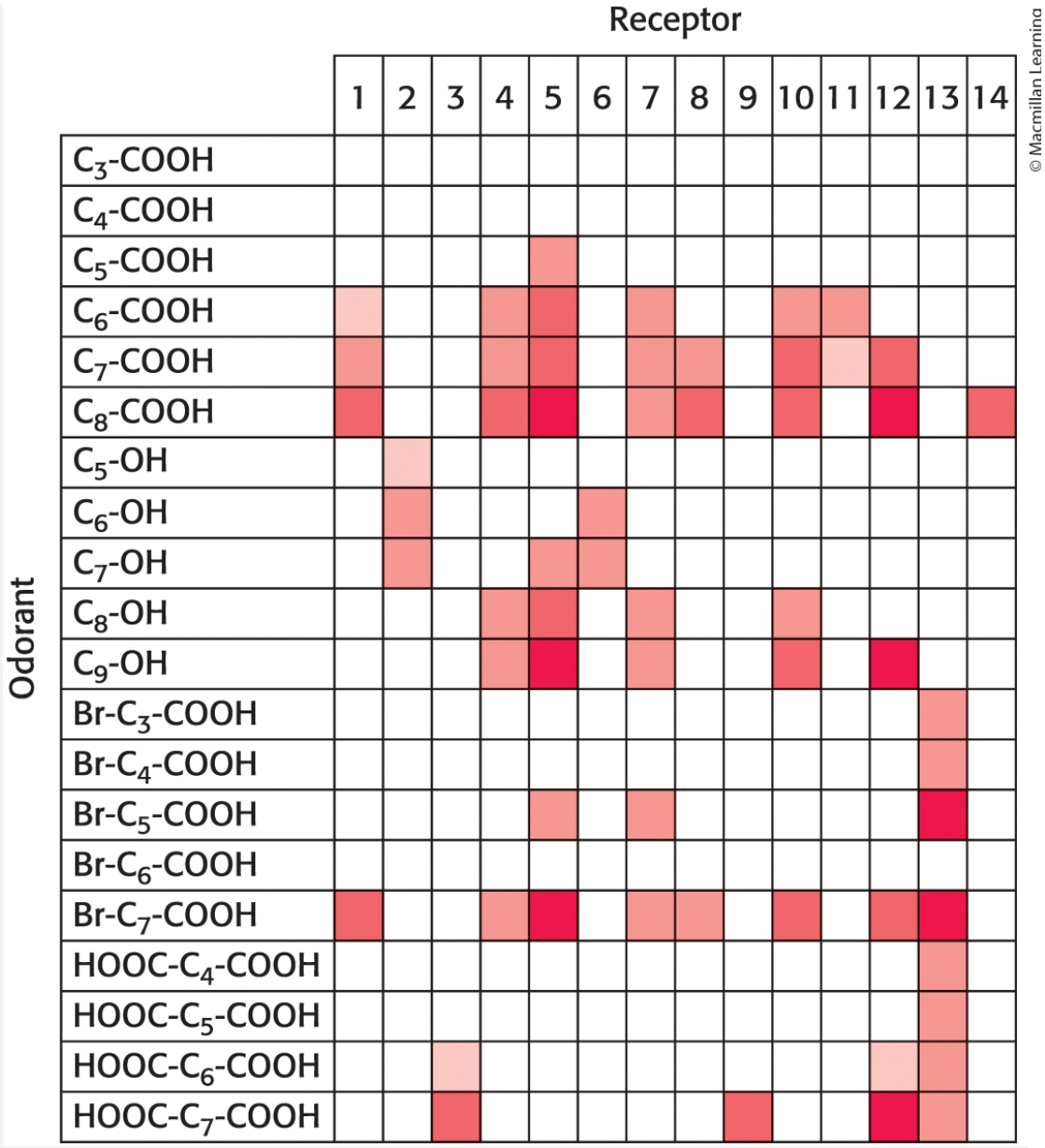
c. What is the relationship between the binding affinity of the hormone–receptor complex and the ability of the hormone to enhance adenylate cyclase activity? What can you conclude about the mechanism of action of the hormone–receptor complex?

d. Suggest experiments that would determine whether a $G_{\alpha s}$ protein is a component of the signal-transduction

pathway.

15. Unlike the olfactory neurons in the mammalian systems discussed herein, olfactory neurons in the nematode *C. elegans* express multiple olfactory receptors. In particular, one neuron (called AWA) expresses receptors for compounds to which the nematode is attracted, whereas a different neuron (called AWB) expresses receptors for compounds that the nematode avoids. Suppose that a transgenic nematode is generated such that one of the receptors for an attractant is expressed in AWB rather than AWA. What behavior would you expect in the presence of the corresponding attractant? 5

16. A mixture of two compounds is applied to a section of olfactory epithelium. Only receptors 3, 5, 9, 12, and 13 are activated. Using the figure, identify the likely compounds in the mixture. 5



© Macmillan Learning

17. Our ability to determine the direction from which a sound is coming is partly based on the difference in time at which our two ears detect the sound. Given the speed of sound $(350\ ms^{-1})$

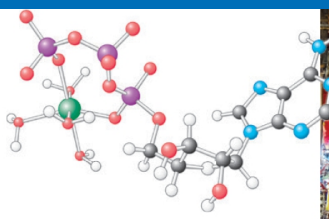
and the separation between our ears (0.15 m), what difference is expected in the times at which a sound arrives at our two ears? How does this difference compare with the time resolution of the human hearing system? Would a sensory system that utilized 7TM receptors and G proteins be capable of adequate time resolution? 5

18. Suppose humans have 380 different odorant receptors.

a. How many different odorants could a person distinguish if each odorant is bound by a single type of receptor and each receptor binds only a single odorant? 5
b. How many if each odorant binds to two different odorant receptors?
c. How many if each odorant binds to three different odorant receptors?

19. Describe the effect of light absorption on 11-*cis*-retinal bound within rhodopsin. 5

Chapter 15
Metabolism: Basic Concepts and Themes





Dani Salvà/VWPics/Alamy
© Macmillan Learning

Currencies are used as a "go-between" in the exchange of labor and resources: people first earn money and later exchange it for goods and services. In an analogous way, organisms extract and store energy and later use it to power almost all biological processes requiring the input of energy, including homeostasis, biosynthesis, and motion. Within all organisms, this exchange is accomplished during cellular metabolism using a single energy currency: ATP.

Outline

15.1 Metabolism Is Composed of Many Interconnected Reactions
15.2 ATP Is the Universal Currency of Free Energy in Biological Systems
15.3 The Oxidation of Carbon Fuels Is an Important Source of Cellular Energy
15.4 Metabolic Pathways Contain Many Recurring Motifs

Learning Goals



By the end of this chapter, you should be able to:

1. Explain what is meant by metabolism in terms of both catabolic and anabolic processes.
2. Identify the factors that make ATP a useful molecule for capturing and transferring chemical energy.
3. Explain how ATP can power reactions that would otherwise not take place.
4. Describe the relationship between the oxidation state of a carbon molecule and its usefulness as a fuel.
5. Summarize the recurring motifs in metabolic pathways.

The concepts of conformation and dynamics developed in this book so far — especially those dealing with enzymatic activity and the transport of molecules and ions across membranes — are fundamental tools for understanding biochemistry. In this chapter, you will be introduced to the recurring themes of metabolism that together form the foundation for many of the concepts in the rest of this book. The distinct combinations of a limited selection of enzymes and cofactors can perform a vast array of biochemical feats using the universal energy currency of life, ATP. Combining knowledge of this currency and the themes of metabolism with the concepts of the previous chapters will allow us to tackle two of the fundamental questions of biochemistry:

1. How does a cell extract energy and reducing power from its environment?

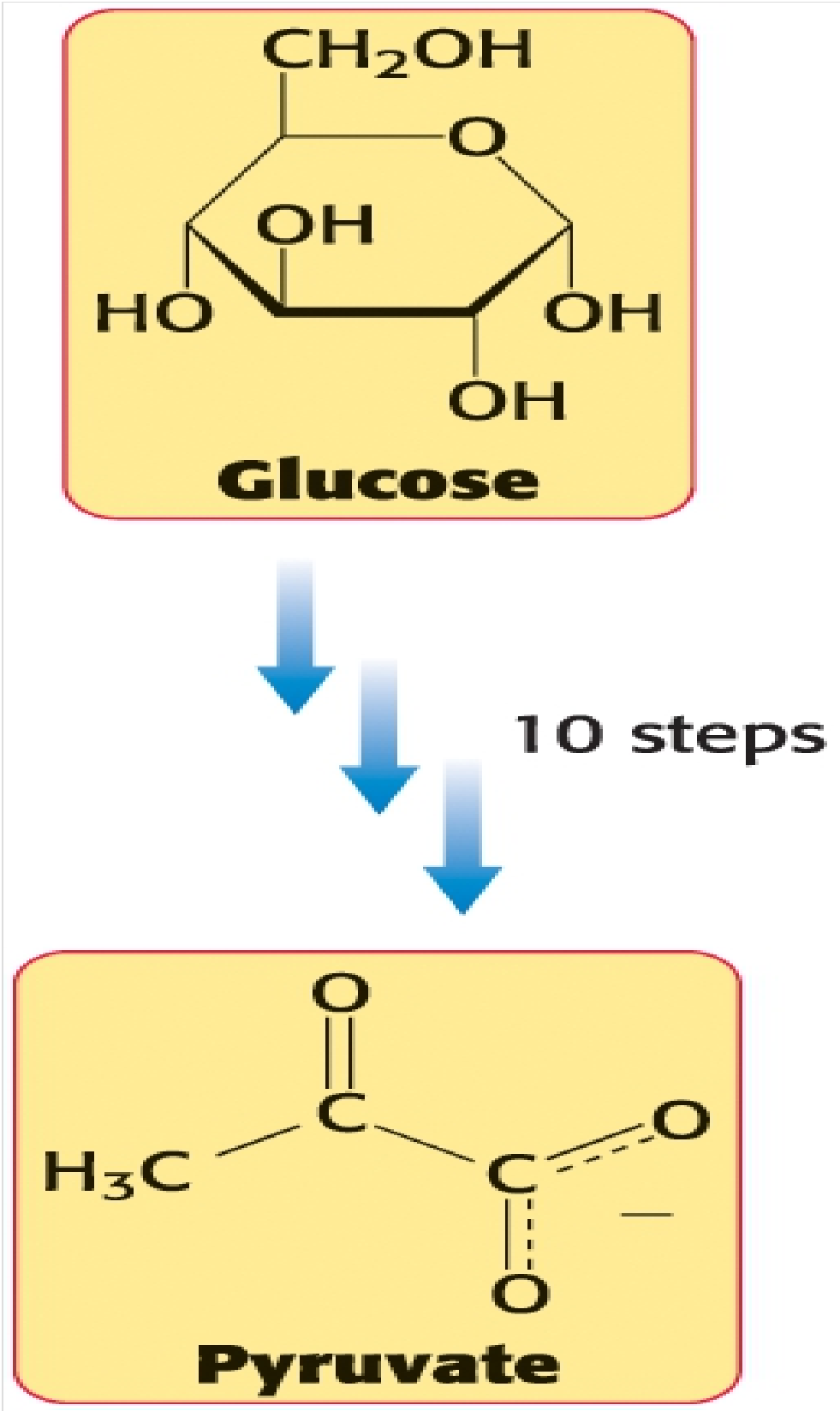
2. How does a cell synthesize the building blocks of its macromolecules and then the macromolecules themselves?

While this chapter gives many specific examples of reaction classes and patterns, it's important to first focus on familiarizing yourself with the broad patterns; the examples will be covered in greater depth in subsequent chapters.

15.1 Metabolism Is Composed of Many Interconnected Reactions

Living organisms require a continual input of free energy for three major purposes: (1) mechanical work in muscle contraction and cellular movements, (2) the active transport of molecules and ions, and (3) the synthesis of macromolecules and other biomolecules from simple precursors. The free energy used in these processes, which maintain an organism in a steady state that is far from equilibrium, is derived from the environment. **Phototrophs**, which include all photosynthetic organisms, capture energy from sunlight, whereas **chemotrophs**, which include all animals, capture energy through the oxidation of chemicals, often generated by phototrophs. Despite this difference, all living organisms share a tremendous number of metabolic reactions to utilize and produce lipids, proteins, nucleic acids, and common carbohydrates like glucose.

The fundamental cellular processes of extracting energy and synthesizing new material are carried out by a highly integrated network of chemical reactions collectively known as **metabolism** (or **intermediary metabolism**). Metabolism is essentially a sequence of chemical reactions that begins with a particular molecule and results in the formation of some other molecule or molecules in a carefully defined fashion (**Figure 15.1**). There are many such defined pathways in the cell (**Figure 15.2**), and we will examine a few of them in some detail later. Advances in analytical techniques such as mass spectrometry (Section 4.3) have greatly facilitated the study of metabolism and generated yet another "omics" — metabolomics.



© Macmillan Learning

FIGURE 15.1 Glucose metabolism in human beings starts with glycolysis. Glycolysis is a metabolic pathway consisting of 10 linked reactions (steps) transforming the molecules into pyruvate.

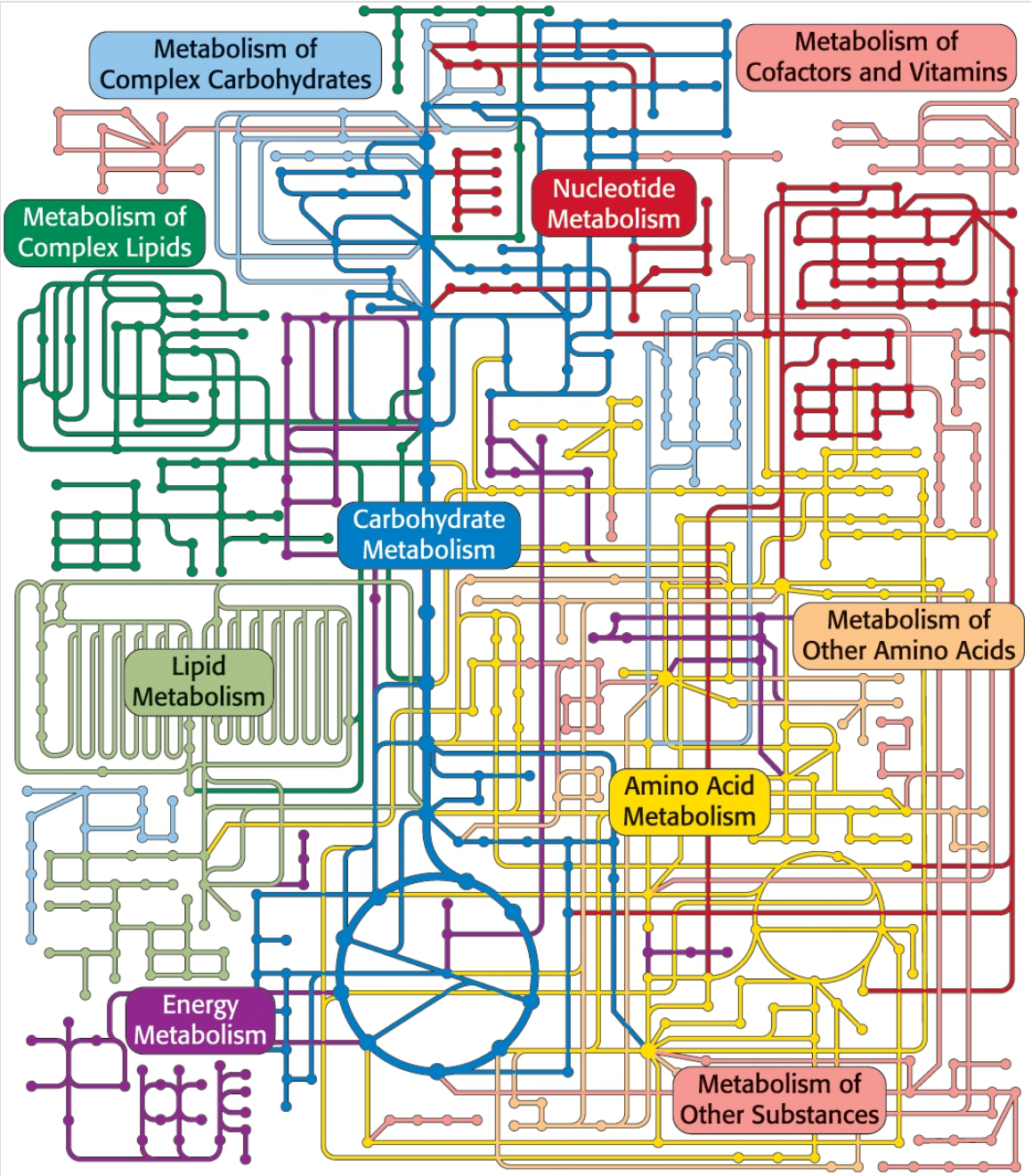


FIGURE 15.2 Metabolic pathways are interconnected series of enzyme-catalyzed reactions. Each node in the diagram represents a specific metabolite, whereas lines connecting nodes represent enzyme-catalyzed reactions. These reactions and the pathways they make up form a deeply integrated network in which reactions communicate with one another through multiple modes of regulation. The details of this figure will be explored over the next 12 chapters.

[From the Kyoto Encyclopedia of Genes and Genomes (www.genome.ad.jp/kegg).]

EXPLORE this pathway further in the Metabolic Map in Achieve

This chapter highlights unifying themes common to all metabolic reactions:

- *Metabolism is a coherent network containing many common motifs.* More than a thousand chemical reactions take place in even as simple an organism as *Escherichia coli*. The array of reactions may seem overwhelming at first glance, but closer scrutiny reveals common motifs. One motif across all life forms is the use of a common energy currency, **adenosine triphosphate (ATP)**, which links energy-releasing (exergonic) pathways with energy-requiring (endergonic) pathways. In all organisms, either sunlight or the oxidation of chemical fuels powers the formation of ATP. Another motif is the repeated appearance of a limited number of activated intermediates; about 100 molecules play central roles in all forms of life.

- *While metabolism involves many different reactions, it uses only a few kinds of mechanisms.* Furthermore, these mechanisms are usually quite simple.

- *Metabolic reactions are highly regulated.* Fuels are degraded and large molecules are constructed step by step in a series of linked reactions called *metabolic pathways*. The total number of intricately connected metabolic pathways taking place in your cells is mind-boggling (Figure 15.2); for obvious reasons, a high degree of

coordination is required to keep all the reactions running smoothly. Metabolic pathways are interdependent, and their activity is carefully coordinated by exquisitely sensitive means of communication in which allosteric enzymes are regulated by small molecules (Chapter 7) as well as being subject to external hormonal control (Chapter 14).

- *Many of the enzymes involved in metabolism are organized into large complexes.* This arrangement increases speed and efficiency by facilitating substrate and product movement between the individual enzymes of the complex. Furthermore, the arrangement allows efficient processing of unstable or even toxic intermediates that are often produced or consumed in metabolic pathways.

Metabolism consists of destructive and constructive reactions that typically yield or require energy

We can divide metabolic pathways into two broad classes: (1) those that convert energy from fuels into biologically useful forms, and (2) those that require inputs of energy to proceed. Although this division is often imprecise, it is nonetheless a useful distinction in an examination of metabolism. Reactions that break down complex molecules, like fuels, into simpler ones are called *catabolic reactions* or, more generally, **catabolism**. Catabolism allows energy to be captured in useful forms, such as the oxidation of carbohydrates and fats which generates ATP along with the waste products carbon dioxide and water.

$$\text{Fuel (carbohydrates, fats)} \xrightarrow{\text{Catabolism}} CO_2 + H_2O + \text{useful energy}$$

Reactions that construct a more complex molecule from simpler components are called *anabolic reactions* or **anabolism**. These reactions — such as the synthesis of glucose, fats, or DNA — usually require energy. Useful forms of energy that are produced in catabolism are employed in anabolism to generate complex structures from simple ones, or energy-rich states from energy-poor ones.

$$\text{Useful energy} + \text{simple precursors} \xrightarrow{\text{Anabolism}} \text{complex molecules}$$

cnding on the energy conditions in the cell. These pathways are referred to as **amphibolic pathways**.

An important general principle of metabolism is that biosynthetic and degradative pathways are almost always distinct. This separation is necessary for energetic reasons, as will be evident in subsequent chapters. It also facilitates the control of metabolism.

A thermodynamically unfavorable reaction can be driven by a favorable reaction

How are specific pathways constructed from individual reactions? A pathway must satisfy minimally two criteria: (1) the individual reactions must be specific, and (2) each of the reactions that constitutes the pathway must be thermodynamically favored under real, rather than standard, conditions. A reaction that is specific will yield only one particular product or set of products from its reactants. As discussed in Section 5.1, enzymes provide this specificity.

The thermodynamics of metabolism are most readily approached in relation to free energy, which was discussed in Sections 1.3 and 5.2. A reaction can occur spontaneously only if ΔG, the change in free energy,

is negative. Recall that ΔG for the formation of products C and D from substrates A and B is given by

$$\Delta G = \Delta G^{\circ\prime} + RT \ln \frac{[C][D]}{[A][B]}$$

Thus, the ΔG of a reaction depends on the nature of the reactants and products (expressed by the $\Delta G^{\circ\prime}$ term, the standard free-energy change) and on their concentrations (expressed by the second term). In a metabolic pathway, reactions with a positive $\Delta G^{\circ\prime}$ can proceed under physiological conditions because the concentrations of reactants and products are far from standard conditions, such that the ΔG of the reaction is negative. Another important thermodynamic fact is that the overall free-energy change for a chemically coupled series of reactions is equal to the sum of the free-energy changes of the individual steps. Consider the following reactions:

$A \rightleftharpoons B + C$	$\Delta G^{\circ\prime} = +21$ kJ mol^{-1} (+5 kcal mol^{-1})
$B \rightleftharpoons D$	$\Delta G^{\circ\prime} = -34$ kJ mol^{-1} (–8 kcal mol^{-1})
$A \rightleftharpoons C + D$	$\Delta G^{\circ\prime} = -13$ kJ mol^{-1} (–3 kcal mol^{-1})

Under standard conditions, A cannot be spontaneously converted into B and C, because $\Delta G^{\circ\prime}$ is positive. However, the conversion of B into D under standard conditions is thermodynamically feasible; if the two reactions are coupled such that one cannot occur without the other, then the free-energy changes are additive. Thus, the conversion of A

into C and D has a $\Delta G^{\circ\prime}$ of $-13\ \text{kJ mol}^{-1}\ (-3\ \text{kcal mol}^{-1})$, which means that it can occur spontaneously under standard conditions.

Thus, a thermodynamically unfavorable reaction can be driven by a thermodynamically favorable reaction to which it is coupled. This kind of coupling occurs in the active sites of enzymes; in this example, the reactions are coupled by the shared chemical intermediate B, which is both formed and destroyed in the course of the reaction. Metabolic pathways often employ the coupling of thermodynamically favorable reactions to unfavorable reactions to create new enzymatically catalyzed reactions that have an overall negative change in free energy.

Self-Check Question



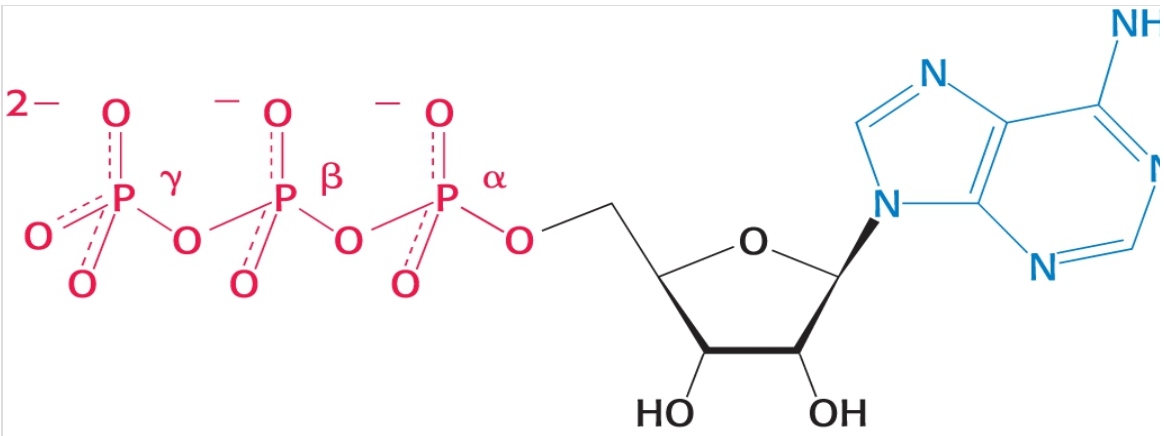
Imagine that a cell needs to produce a compound B, but the reaction converting A into B has a positive $\Delta G^{\circ\prime}$ value. There are two ways that A can still be converted to B; one involves changing the reaction itself, and the other does not. What are they?

15.2 ATP Is the Universal Currency of Free Energy in Biological Systems

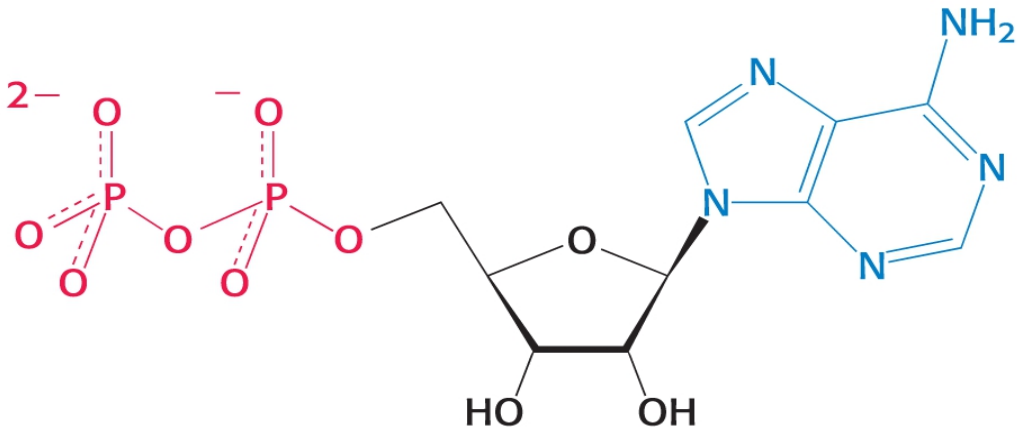
Just as commerce is facilitated by the use of a common currency, the commerce of the cell — metabolism — is facilitated by the use of a common energy currency, adenosine triphosphate (ATP). Part of the free energy derived from light or the oxidation of food is transformed into this highly accessible molecule, which acts as the free-energy donor in most energy-requiring processes such as motion, active transport, and biosynthesis. Indeed, most of catabolism consists of reactions that extract energy from fuels such as carbohydrates and fats and capture it through the production of ATP.

ATP hydrolysis is exergonic

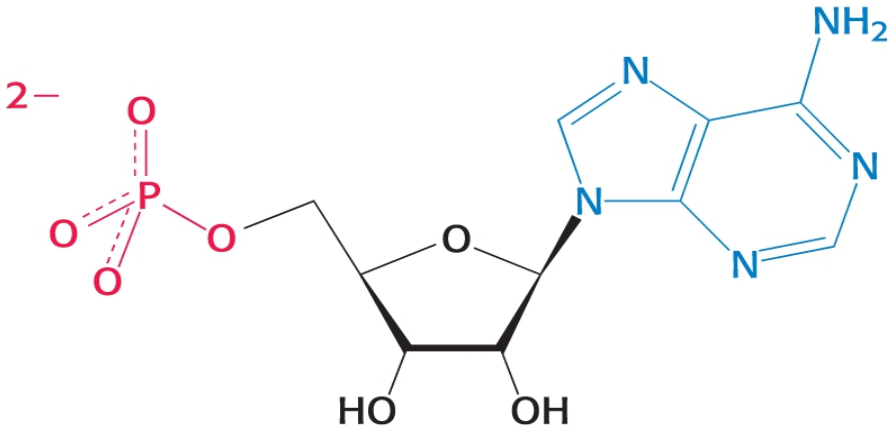
ATP is a nucleotide consisting of adenine, a ribose, and a triphosphate unit (**Figure 15.3**). The active form of ATP is usually a complex of ATP with Mg^{2+} or Mn^{2+}. In considering the role of ATP as an energy carrier, we can focus on its triphosphate moiety.



Adenosine triphosphate (ATP)



Adenosine diphosphate (ADP)



Adenosine monophosphate (AMP)

FIGURE 15.3 Structures of ATP, ADP, and AMP differ only by the number of phosphates. These adenylates consist of adenine (blue), a ribose (black), and a tri-, di-, or monophosphate unit (red). The innermost phosphorus atom of ATP is designated P_α, the middle one P_β, and the outermost one P_γ.

- *ATP is an energy-rich molecule because its triphosphate unit contains two phosphoanhydride linkages*. A large amount of free energy is released when ATP is hydrolyzed to adenosine diphosphate (ADP) and orthophosphate (P_i), or when ATP is hydrolyzed to adenosine monophosphate (AMP) and pyrophosphate (PP_i).

$$ATP + H_2O \rightleftharpoons ADP + P_i$$
$$\Delta G^{\circ\prime} = -30.5 \text{ kJ mol}^{-1} (-7.3 \text{ kcal mol}^{-1})$$

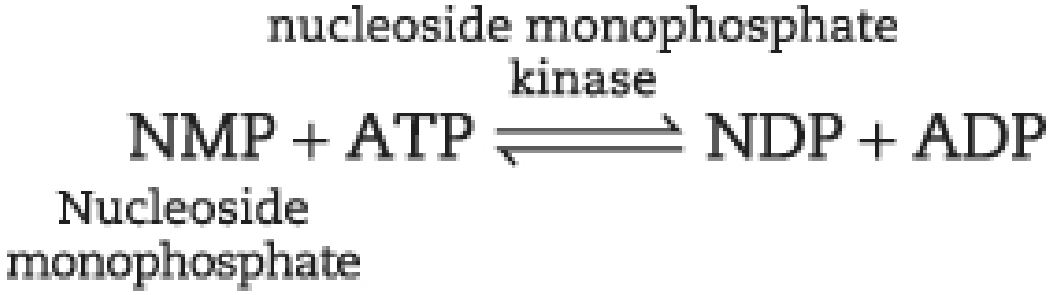
$$ATP + H_2O \rightleftharpoons AMP + PP_i$$
$$\Delta G^{\circ\prime} = -45.6 \text{ kJ mol}^{-1} (-10.9 \text{ kcal mol}^{-1})$$

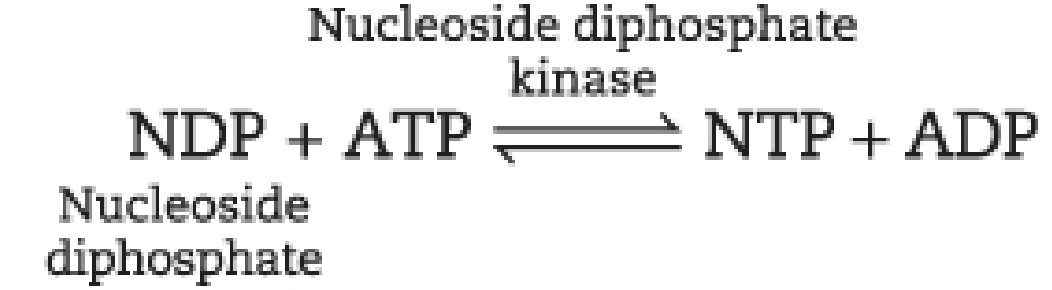
However, this hydrolysis reaction is frequently misunderstood. It is imperative to note that this release of free energy does *not* derive from the cleavage of the any of the covalent bonds in ATP, as it requires energy to break a covalent bond. Instead, the energy is released by the formation of new covalent bonds and noncovalent interactions with water, and from the increase in entropy of the products relative to the reactants. Furthermore, the precise ΔG for these reactions depends on the ionic strength of the medium and on the concentrations of Mg^{2+} and other metal ions. Under typical

cellular concentrations, the ΔG for these hydrolyses is approximately $-50\ \text{kJ mol}^{-1}(-12\ \text{kcal mol}^{-1})$.

- *The ATP–ADP cycle is the fundamental mode of energy exchange in biological systems.* The free energy released in the hydrolysis of ATP is harnessed to drive reactions that require an input of free energy, such as muscle contraction. In turn, ATP is formed from ADP and P_i when fuel molecules are oxidized in chemotrophs or when light is trapped by phototrophs.

- *Enzymes catalyze the exchange of phosphoryl groups from one nucleotide to another.* Some biosynthetic reactions are driven not by ATP, but by guanosine triphosphate (GTP), uridine triphosphate (UTP), and cytidine triphosphate (CTP). The diphosphate forms of these nucleotides are denoted by GDP, UDP, and CDP, and the monophosphate forms by GMP, UMP, and CMP. The phosphorylation of nucleoside monophosphates is catalyzed by a family of nucleoside monophosphate kinases. The phosphorylation of nucleoside diphosphates is catalyzed by nucleoside diphosphate kinase, an enzyme with broad specificity.





- *Although all of the nucleoside triphosphates are energetically equivalent, ATP is nonetheless the primary cellular energy carrier and therefore the energy currency.* In addition, two important electron carriers — NAD^+ and FAD — as well the acyl group carrier, coenzyme A, are derivatives of ATP. It is intriguing to consider why evolution selected adenosine derivatives, but it may be due to differences in the stability of adenine compared to the other bases in prebiotic conditions. Regardless of the reason, the role of adenosine phosphates — particularly ATP — in energy metabolism is paramount.

ATP hydrolysis drives metabolism by shifting the equilibrium of coupled reactions

An otherwise unfavorable reaction can be made possible by coupling to ATP hydrolysis. Consider a reaction that is thermodynamically unfavorable without an input of free energy, a situation common to most biosynthetic reactions. Suppose that the standard free energy of the B is $+16.7\ \text{kJ mol}^{-1}$ or $+4.0\ \text{kcal mol}^{-1}$

$$\text{A} \rightleftharpoons \text{B} \quad \Delta G^{\circ\prime} = +16.7\ \text{kJ mol}^{-1}\ (+4.0\ \text{kcal mol}^{-1})$$

The equilibrium constant K'_{eq} of this reaction at 25°C is related to $\Delta G^{\circ\prime}$ (in units of kilojoules per mole) by

$$K'_{eq} = [\text{B}]_{eq}/[\text{A}]_{eq} = e^{-\Delta G^{\circ\prime}/2.47} = 1.15 \times 10^{-3}$$

Thus, net conversion of A into B cannot take place when the molar ratio of B to A is equal to or greater than 1.15×10^{-3}.

However, A can be converted into B under these conditions if the reaction is coupled to the hydrolysis of ATP. Under standard conditions, the $\Delta G^{\circ\prime}$ of hydrolysis is approximately $-30.5\ \text{kJ mol}^{-1}$ or $-7.3\ \text{kcal mol}^{-1}$. The new overall reaction is

$$\text{A} + \text{ATP} + \text{H}_2\text{O} \rightleftharpoons \text{B} + \text{ADP} + \text{P}_i$$
$$\Delta G^{\circ\prime} = -13.8\ \text{kJ mol}^{-1}\ (-3.3\ \text{kcal mol}^{-1})$$

Its free-energy change of $-13.8\ \text{kJ mol}^{-1}$ or $-3.3\ \text{kcal mol}^{-1}$ is the sum of the value of $\Delta G^{\circ\prime}$ for the conversion of A into B ($+16.7\ \text{kJ mol}^{-1}$ or $+4.0\ \text{kcal mol}^{-1}$) and the value of $\Delta G^{\circ\prime}$ for the hydrolysis of ATP ($-30.5\ \text{kJ mol}^{-1}$ or $-7.3\ \text{kcal mol}^{-1}$). At pH 7, the equilibrium constant of this coupled reaction is

$$K'_{eq} = \frac{[B]_{eq}}{[A]_{eq}} \times \frac{[ADP]_{eq}[P_i]_{eq}}{[ATP]_{eq}} = e^{13.8/2.47} = 2.67 \times 10^2$$

At equilibrium, the ratio of [B] to [A] is given by

$$\frac{[B]_{eq}}{[A]_{eq}} = K'_{eq} \frac{[ATP]_{eq}}{[ADP]_{eq}[P_i]_{eq}}$$

which means that the hydrolysis of ATP enables A to be converted into B until the [B]/[A] ratio reaches a value of 2.67×10^2.

This equilibrium ratio is strikingly different from the value of 1.15×10^{-3} for the reaction $A \rightarrow B$ in the absence of ATP hydrolysis. In other words, coupling the hydrolysis of ATP with the conversion of A into B under standard conditions has changed the equilibrium ratio of B to A by a factor of about 10^5. If we were to use the ΔG of hydrolysis of

ATP under cellular conditions ($-50.2\ \text{kJ mol}^{-1}$ or $-12\ \text{kcal mol}^{-1}$) in our calculations instead of $\Delta G^{\circ\prime}$, the change in the equilibrium ratio would be even more dramatic, on the order of 10^8.

We see here the thermodynamic essence of ATP's action as an energy-coupling agent. Cells maintain ATP levels by using oxidizable substrates or light as sources of free energy for synthesizing the molecule. In the cell, the hydrolysis of an ATP molecule in a coupled reaction then changes the equilibrium ratio of products to reactants by a very large factor, of the order of 10^8. More generally, the hydrolysis of *n* ATP molecules changes the equilibrium ratio of a coupled reaction (or sequence of reactions) by a factor of 10^{8n}. For example, the theoretical hydrolysis of three ATP molecules in a coupled reaction changes the equilibrium ratio by a factor of 10^{24}. Thus, a thermodynamically unfavorable process can be converted into a favorable one by coupling it to the hydrolysis of a sufficient number of ATP molecules in a new reaction.

It should also be emphasized that A and B in the preceding coupled reaction may be interpreted very generally, not only as different chemical species. For example, A and B may represent activated and unactivated conformations of a protein that is activated by phosphorylation with ATP. Through such changes in protein conformation, molecular motors such as myosin, kinesin, and dynein convert the chemical energy of ATP into mechanical energy (Section 6.5). Indeed, this conversion is the basis of muscle contraction.

Alternatively, A and B may refer to the concentrations of an ion or molecule on the outside and inside of a cell, as in the active transport of a nutrient. The active transport of Na^+ and K^+ across membranes is

driven by the phosphorylation of the sodium–potassium pump by ATP and its subsequent dephosphorylation (Section 13.2).

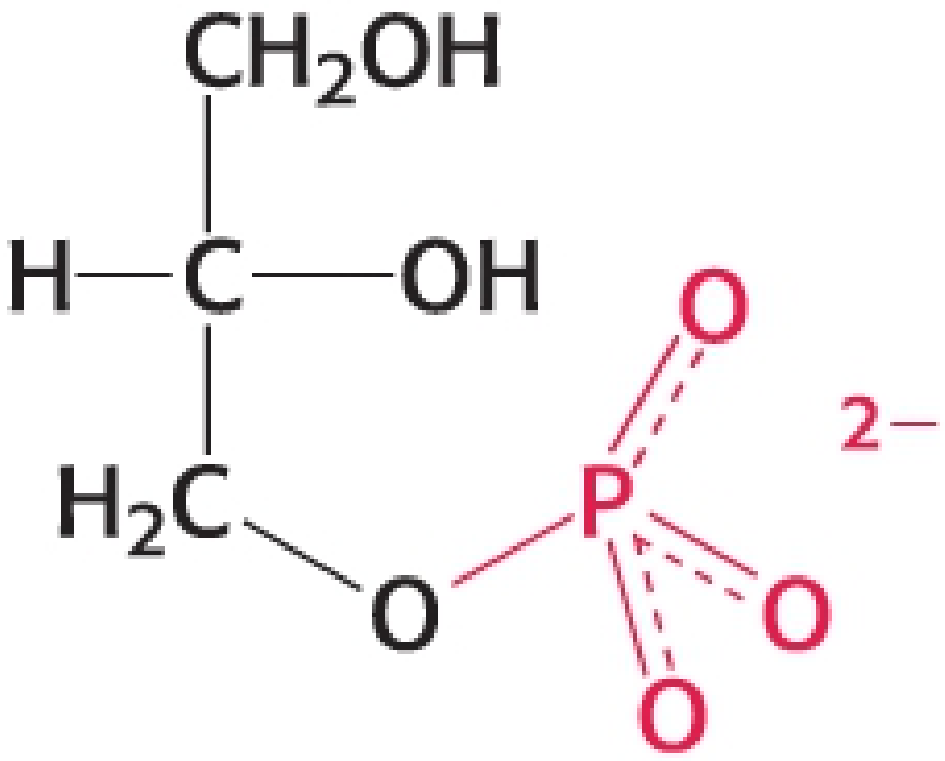
The high phosphoryl potential of ATP results from structural differences between ATP and its hydrolysis products

What makes ATP an efficient phosphoryl-group donor? Let us compare the standard free energy of hydrolysis of ATP with that of a phosphate ester, such as glycerol 3-phosphate:

$$\text{ATP} + \text{H}_2\text{O} \rightleftharpoons \text{ADP} + \text{P}_\text{i}$$
$$\Delta G^{\circ\prime} = -30.5 \text{ kJ mol}^{-1} (-7.3 \text{ kcal mol}^{-1})$$

$$\text{Glycerol 3-phosphate} + \text{H}_2\text{O} \rightleftharpoons \text{glycerol} + \text{P}_\text{i}$$
$$\Delta G^{\circ\prime} = -9.2 \text{ kJ mol}^{-1} (-2.2 \text{ kcal mol}^{-1})$$





Glycerol 3-phosphate

The magnitude of $\Delta G^{\circ\prime}$ for the hydrolysis of glycerol 3-phosphate is much smaller than that of ATP, which means that ATP has a stronger tendency to transfer its terminal phosphoryl group to water than does glycerol 3-phosphate. In other words, ATP has a higher **phosphoryl-transfer potential** than glycerol 3-phosphate.

The high phosphoryl-transfer potential of ATP can be explained by features of the ATP structure. Because $\Delta G^{\circ\prime}$ depends on the difference in free energies of the products and reactants, we need to examine the

structures of both ATP and its hydrolysis products, ADP and P_i, to answer this question. Four factors are important:

1. *Resonance stabilization*. Orthophosphate (P_i), one of the products of ATP hydrolysis, has greater resonance stabilization than do any of the ATP phosphoryl groups. Orthophosphate has several resonance forms of similar energy (**Figure 15.4**), whereas the γ phosphoryl group of ATP has a smaller number.

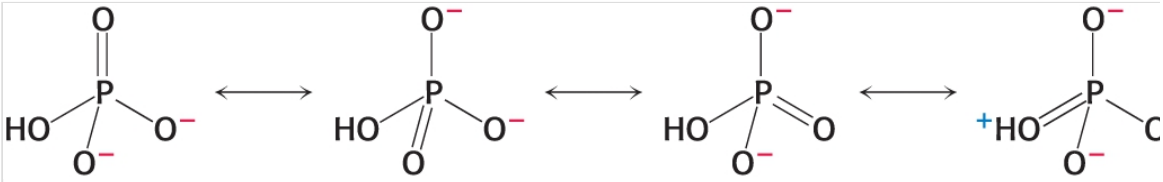


FIGURE 15.4 Orthophosphate has four favorable resonance structures.

2. *Electrostatic repulsion.* At pH 7, the triphosphate unit of ATP carries about four negative charges. These charges repel one another because they are in close proximity. The repulsion between them is reduced when ATP is hydrolyzed.

3. *Increase in entropy*. The entropy of the products of ATP hydrolysis is greater, in that there are now two molecules instead of a single ATP molecule. We disregard the molecule of water used to hydrolyze the ATP; given the high concentration (55.5 M), there is effectively no change in the concentration of water during the reaction.

4. *Stabilization due to hydration.* Water binds to ADP and P_i, stabilizing these molecules, and rendering the reverse reaction — the synthesis of ATP — more unfavorable.

ATP is often called a high-energy phosphate compound, and its phosphoanhydride linkages are sometimes referred to as high-energy

bonds. Indeed, a “squiggle” $(\sim P)$ is often used to indicate the bonds that can be broken in ATP hydrolysis. This is a misnomer, however, as there is nothing special about the bonds themselves. The phosphoanhydride linkages are high-energy in the sense that much free energy is released when they are hydrolyzed — a reaction with water — for the reasons listed above, but the energy release comes from entropy and new bond formation, rather than bond cleavage.

Phosphoryl-transfer potential is an important form of cellular energy transformation

The standard free energies of hydrolysis provide a convenient means of comparing the phosphoryl-transfer potential of phosphorylated compounds. Such comparisons reveal that ATP is not the only compound with a high phosphoryl-transfer potential. In fact, some compounds in biological systems have a higher phosphoryl-transfer potential than that of ATP. These compounds include phosphoenolpyruvate (PEP), 1,3-bisphosphoglycerate (1,3-BPG), and creatine phosphate (**Figure 15.5**).

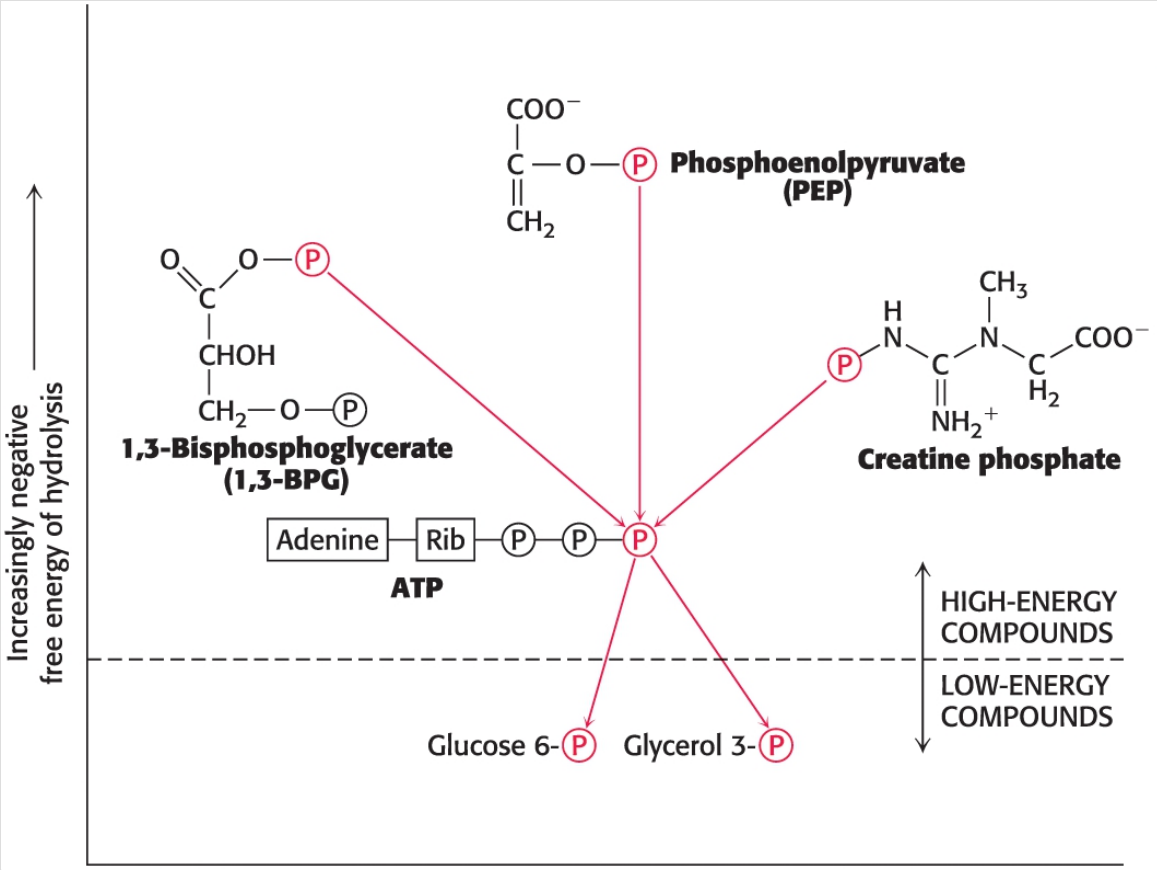


FIGURE 15.5 Compounds with high phosphoryl-transfer potential can be used to make ATP from ADP. The role of ATP as the cellular energy currency is illustrated by its relation to other phosphorylated compounds. ATP has a phosphoryl-transfer potential that is intermediate among the biologically important phosphorylated molecules. High-phosphoryl-transfer-potential compounds (1,3-BPG, PEP, and creatine phosphate) derived from the metabolism of fuel molecules are used to power ATP synthesis. In turn, ATP donates a phosphoryl group to other biomolecules to facilitate their metabolism.

[Data from D. L. Nelson and M. M. Cox, *Lehninger Principles of Biochemistry*, 5th ed. (W. H. Freeman and Company, 2009), Fig. 13-19.]

PEP can transfer its phosphoryl group to ADP to form ATP. Indeed, this transfer is one of the ways in which ATP is generated in the breakdown of sugars (Section 16.1). It is significant that ATP has a phosphoryl-transfer potential that is intermediate among the biologically important phosphorylated molecules (**Table 15.1**). This intermediate position enables ATP to function efficiently as a carrier of phosphoryl groups.

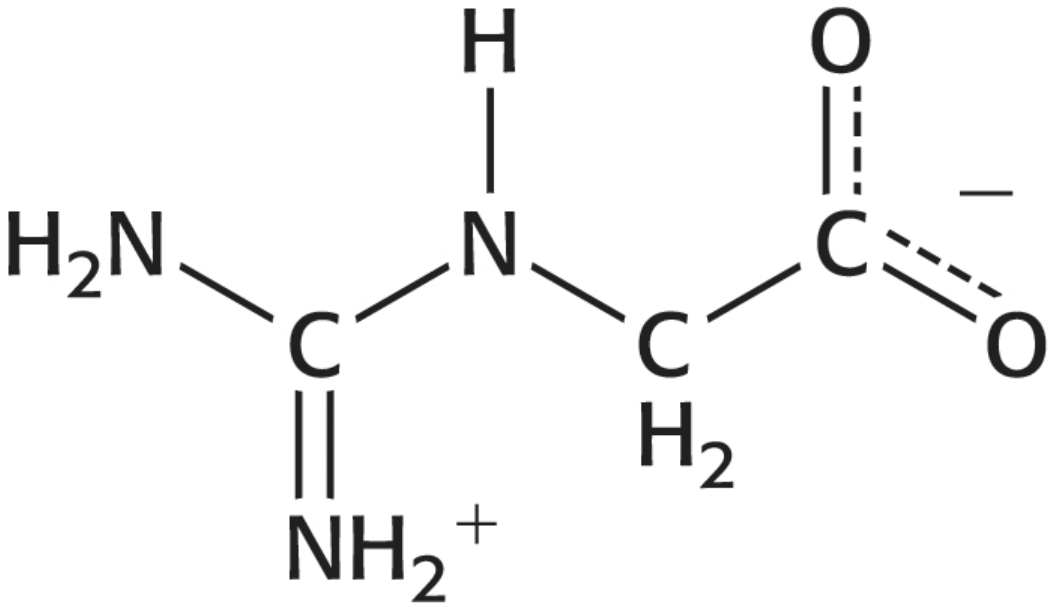
TABLE 15.1 Standard free energies of hydrolysis of some phosphorylated compounds

Compound	$kJ\ mol^{-1}$	$kJ\ mol^{-1}$
Phosphoenolpyruvate	−61.9	−14.8
1,3-Bisphosphoglycerate	−49.4	−11.8
Creatine phosphate	−43.1	−10.3
ATP (to ADP)	−30.5	−7.3
Glucose 1-phosphate	−20.9	−5.0
Pyrophosphate	−19.3	−4.6
Glucose 6-phosphate	−13.8	−3.3
Glycerol 3-phosphate	−9.2	−2.2

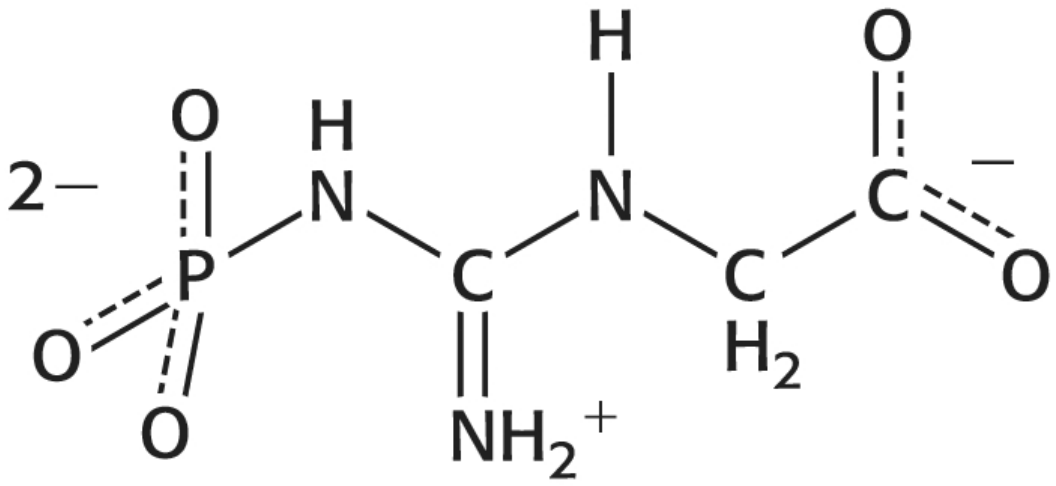
The amount of ATP in muscle suffices to sustain contractile activity for less than a second. Creatine phosphate in vertebrate muscle serves as a reservoir of high-potential phosphoryl groups that can be readily transferred to ADP. Indeed, we use creatine phosphate to regenerate ATP from ADP every time we exercise strenuously. This reaction is catalyzed by creatine kinase.

$$\text{Creatine phosphate} + \text{ADP} \xrightleftharpoons{\text{creatine kinase}} \text{ATP} + \text{creatine}$$

At pH 7, the standard free energy of hydrolysis of creatine phosphate is $-43.1\ \text{kJ mol}^{-1}\ (-10.3\ \text{kcal mol}^{-1})$ compared with $-30.5\ \text{kJ mol}^{-1}\ (-7.3\ \text{kcal mol}^{-1})$ for ATP.



Creatine



Creatine phosphate

As illustrated in the next boxed example, there is a large amount of creatine phosphate present in resting muscle. Because of its abundance and high phosphoryl-transfer potential relative to that of ATP, creatine phosphate is a highly effective phosphoryl buffer. Indeed, creatine phosphate is the major source of phosphoryl groups for ATP regeneration for a runner during the first 4 seconds of a 100-meter sprint. The fact that creatine phosphate can replenish ATP pools is the basis of the use of creatine as a dietary supplement by athletes in sports requiring short bursts of intense activity. After the creatine phosphate pool is depleted, ATP must be generated through anaerobic or aerobic metabolism (Figure 15.6).

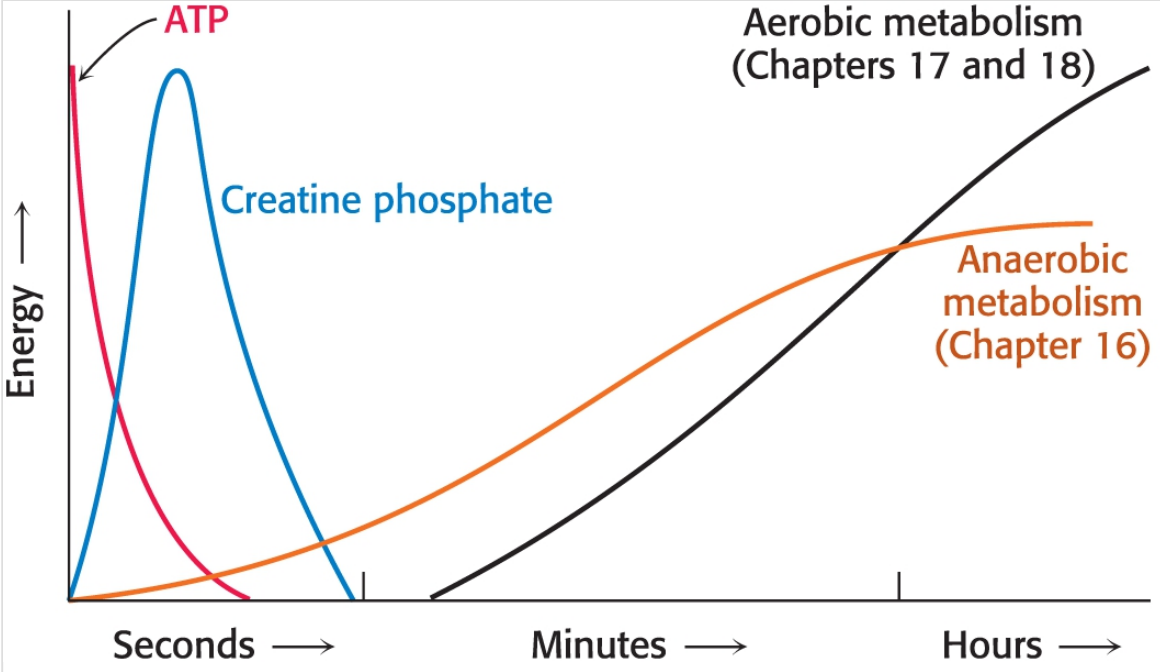


FIGURE 15.6 The sources of ATP change as exercise duration increases, even within the first few seconds. In the initial seconds of exertion, power is generated by existing high-phosphoryl-transfer compounds (ATP and creatine phosphate). Subsequently, the ATP must be regenerated by metabolic pathways.

EXAMPLE

Calculating ΔG for a Coupled Reaction Under Real Conditions

PROBLEM:

Creatine phosphate is used as a phosphoryl donor for ATP synthesis in muscle in the following reaction:

$$\text{Creatine phosphate} + \text{ADP} \overset{\text{creatine kinase}}{\rightleftharpoons} \text{ATP} + \text{creatine}$$

When muscles are at rest, the reaction proceeds in the reverse direction, synthesizing creatine phosphate. As noted above, for a skeletal muscle at rest, the following metabolites are present at the indicated concentrations.

$$[\text{ATP}] = 4\ \text{mM}; \text{ADP} = 0.013\ \text{mM}$$
$$[\text{creatine phosphate}] = 25\ \text{mM}; [\text{creatine}] = 13\ \text{mM}$$

Calculate the ΔG for the creatine kinase reaction as written above for a muscle at rest assuming body temperature is 37°C.

Getting Started:

What formula do we need to calculate ΔG, and what information are we missing to complete this calculation?

$$\Delta G = \Delta G^{\circ\prime} + RT \ln \frac{[C][D]}{[A][B]}$$

Analyze:

The values necessary for the right-hand term are provided, but we need to know $\Delta G^{\circ\prime}$ for the kinase reaction. How do we determine $\Delta G^{\circ\prime}$? Recall from this chapter that two component parts of a reaction have

additive $\Delta G^{\circ\prime}$ values. We need to dissect the creatine kinase reaction into its two component reactions and look up the $\Delta G^{\circ\prime}$ values for each of the component reactions. These are:

$$ADP + P_i \rightarrow ATP + H_2O$$
$$\text{Creatine phosphate} + H_2O \rightarrow \text{creatine} + P_i$$

Using Table 15.1, we can determine the $\Delta G^{\circ\prime}$ values for both reactions.

For ATP synthesis, $\Delta G^{\circ\prime} = +30.5\ \text{kJ mol}^{-1}$. For creatine phosphate hydrolysis, $\Delta G^{\circ\prime} = -43.1\ \text{kJ mol}^{-1}$.

Calculate:

What is the $\Delta G^{\circ\prime}$ of the overall creatine kinase reaction in the direction written?

$\Delta G^{\circ\prime}$ values are additive, so the $\Delta G^{\circ\prime}$ for the kinase reaction is $-43.1\ \text{kJ mol}^{-1} + 30.5\ \text{kJ mol}^{-1} = -12.6\ \text{kJ mol}^{-1}$.

Now, having determined $\Delta G^{\circ\prime}$, we can use the equation above and the values provided to determine ΔG.

$$\Delta G = -12.6\ \text{kJ mol}^{-1} + RT \ln\left(\frac{[\text{ATP}][\text{creatine}]}{[\text{ADP}][\text{creatine phosphate}]}\right)$$

$$= -12.6\ \text{kJ mol}^{-1} + (0.0083\ \text{kJ K}^{-1}\ \text{mol}^{-1})(310\ \text{K}) \ln\left(\frac{[4\ \text{mM}][13\ \text{mM}]}{[0.013\ \text{mM}][25\ \text{mM}]}\right)$$

$$= -12.6\ \text{kJ mol}^{-1} + (2.573\ \text{kJ mol}^{-1}) \ln(160)$$

$$= 0.5\ \text{kJ mol}^{-1}$$

Reflect:

Note that this value is close to zero, indicating that the reaction is very near equilibrium. Does this make sense to you, for resting muscle? Consider that upon sudden muscle contraction during exercise, the depletion of ATP shifts the reaction toward creatine and ATP. Conversely, during the recovery from exercise, the replenishment of ATP from oxidative phosphorylation shifts the reaction back toward the formation of creatine phosphate. Once replenished, and when the muscle is at rest, we should expect that the reaction will eventually settle at equilibrium concentrations and, therefore, ΔG should be near zero.

15.3 The Oxidation of Carbon Fuels Is an Important Source of Cellular Energy

ATP serves as the principal immediate donor of free energy in biological systems rather than as a long-term storage form of free energy. In a typical cell, an ATP molecule is consumed within a minute of its formation.

- *Having mechanisms for regenerating ATP is vital.* Although the total quantity of ATP in the body is limited to approximately 100 g, the turnover of this small quantity of ATP is very high. For example, a resting human being consumes about 40 kg (88 pounds) of ATP in 24 hours. During strenuous exertion, the rate of utilization of ATP may be as high as 0.5 kg/minute. For a 2-hour run, 60 kg (132 pounds) of ATP is utilized. Of course, this is essentially the same 100 g of ATP being used and regenerated again and again.

- *The regeneration of ATP is one of the primary roles of catabolism.* Motion, active transport, signal amplification, and biosynthesis can take place only if ATP is continually regenerated from ADP (**Figure 15.7**). In most aerobic organisms, the carbon in fuel molecules — such as glucose and fats — is oxidized to CO_2. The resulting electrons are captured and their energy is used to regenerate ATP from ADP and P_i.

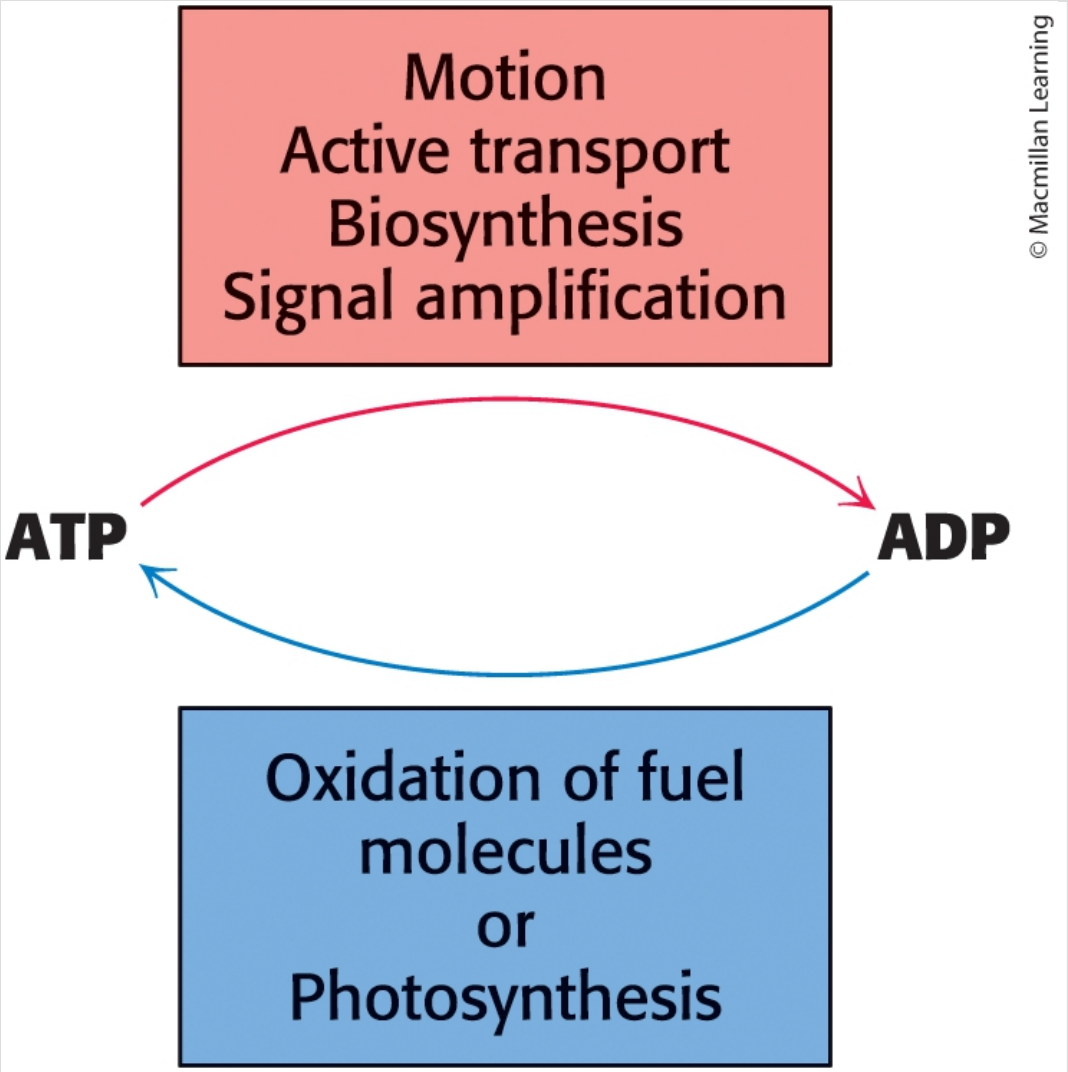
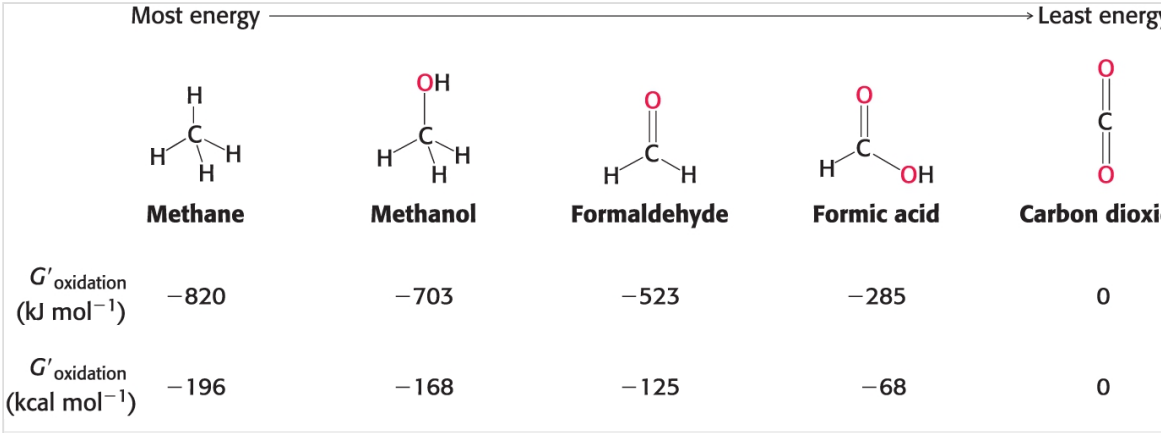


FIGURE 15.7 The ATP–ADP cycle is the fundamental mode of energy exchange in biological systems.

- *Oxidation of fuels takes place one carbon at a time.* The ultimate electron acceptor for the aerobic oxidation of carbon is O_2, which is reduced to water, and the oxidation product is CO_2. Consequently, the more reduced a carbon is to begin with, the more free energy is released by its oxidation. Figure 15.8 shows the $\Delta G^{\circ\prime}$ of oxidation for one-carbon compounds. While fuel molecules are more

complex (Figure 15.9) than these single-carbon compounds, their oxidation nevertheless takes place one carbon at a time. The carbon-oxidation energy is used in some cases to create a compound with high phosphoryl-transfer potential and in other cases to create an ion gradient. In either case, the end point is the formation of ATP.



	Methane	Methanol	Formaldehyde	Formic acid	Carbon dioxi
$G'_{oxidation}$ (kJ mol^{-1})	−820	−703	−523	−285	0
$G'_{oxidation}$ (kcal mol^{-1})	−196	−168	−125	−68	0

FIGURE 15.8 The free energy of oxidation of single-carbon compounds increases with the degree of hydrogen saturation.

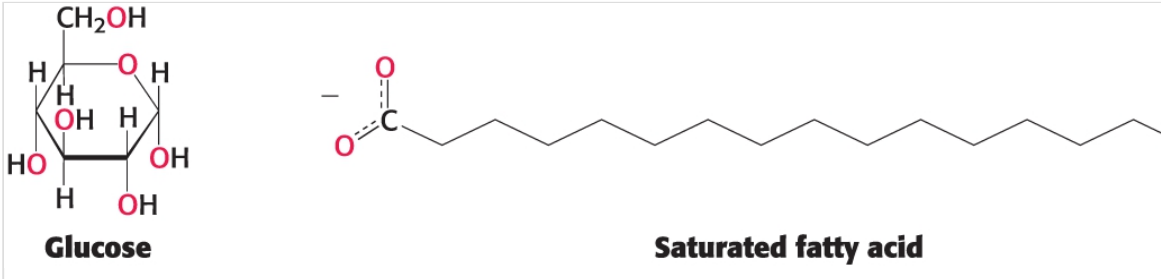
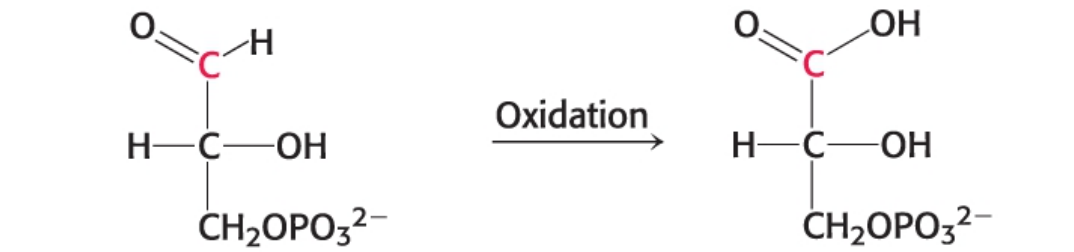


FIGURE 15.9 Fats are a more efficient fuel source than carbohydrates such as glucose becaus the carbon in fats is more reduced.

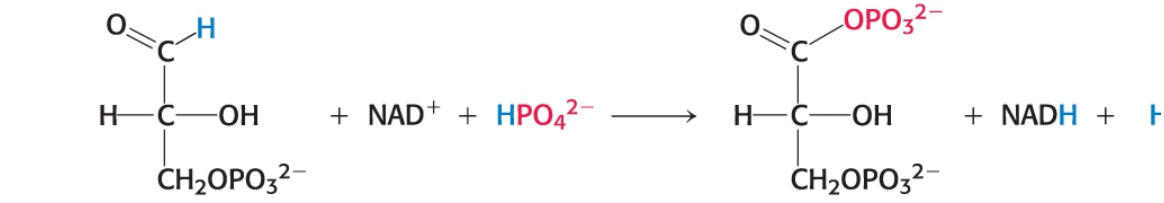
Compounds with high phosphoryl-transfer potential can couple carbon oxidation to ATP synthesis

How is the energy released from the oxidation of a carbon compound captured in ATP? As an example, consider glyceraldehyde 3-phosphate (shown below), which is a metabolite of glucose formed during the oxidation of that sugar. The C-1 carbon (shown in red) is at the aldehyde-oxidation level and is not in its most oxidized state. Oxidation of the aldehyde to an acid will release energy.



Glyceraldehyde 3-phosphate **3-Phosphoglyceric acid**

However, the oxidation does not take place directly. Instead, the carbon oxidation generates an acyl phosphate, 1,3-bisphosphoglycerate (1,3-BPG). The electrons released are captured by NAD^+,forming NADH, in a process that we will consider shortly.



Glyceraldehyde 3-phosphate (GAP) **1,3-Bisphosphoglycerate (1,3-BPG)**

For reasons similar to those discussed for ATP, 1,3-BPG has a high phosphoryl-transfer potential that is, in fact, greater than that of ATP. Thus, the hydrolysis of 1,3-BPG can be coupled to the synthesis of ATP.



1,3-Bisphosphoglycerate **3-Phosphoglyceric acid**

The energy of oxidation is initially trapped as a high-phosphoryl-transfer-potential compound and then used to form ATP. The oxidation energy of a carbon atom is transformed into phosphoryl-transfer potential, first as 1,3-BPG and ultimately as ATP. We will consider these reactions in mechanistic detail in Chapter 16.

Ion gradients across membranes provide an important form of cellular energy that can be coupled to ATP synthesis

As described in Section 13.1, electrochemical potential is an effective means of storing free energy. In fact, the electrochemical potential of ion gradients across membranes — produced by the oxidation of fuel molecules or by phototrophy — ultimately powers the synthesis of most

of the ATP in cells. In general, ion gradients are versatile means of coupling thermodynamically unfavorable reactions to favorable ones.

In animals, proton gradients generated by the oxidation of carbon fuels account for more than 90% of ATP generation (**Figure 15.10**). This process, called *oxidative phosphorylation,* will be explored in depth in Chapter 18. ATP hydrolysis can then be used to form ion gradients of different types and functions. The electrochemical potential of a Na^+ gradient, for example, can be tapped to pump Ca^{2+} out of cells or to transport nutrients such as sugars and amino acids into cells.

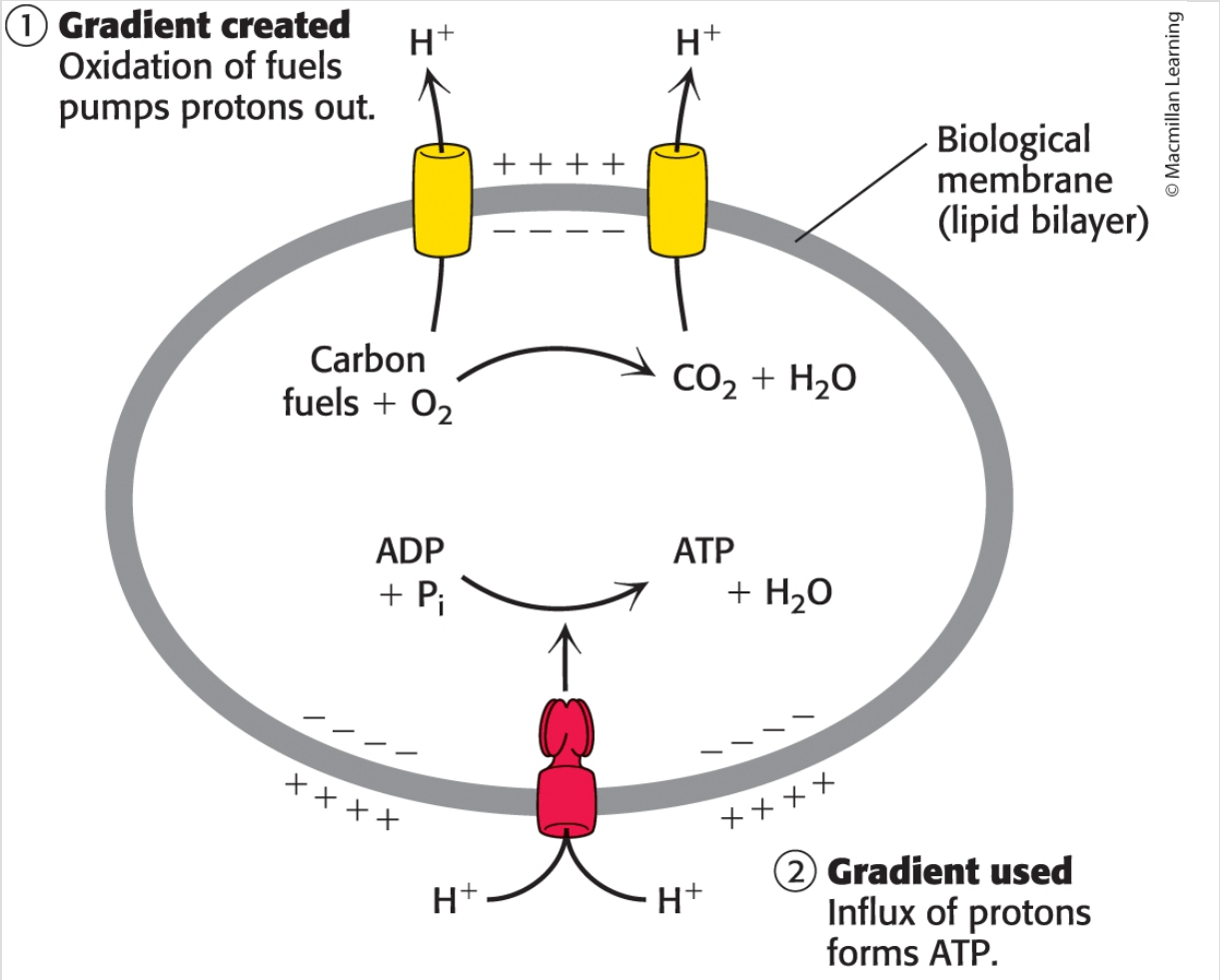


FIGURE 15.10 Proton gradients formed using the energy from either sunlight or chemical oxidation can power ATP synthesis. Either the oxidation of fuels or the capture of the energy from sunlight can power the formation of proton gradients by the action of specific proton

pumps (yellow cylinders). These proton gradients can in turn drive the synthesis of ATP when the protons flow through an ATP-synthesizing enzyme (red complex).



Phosphates play a prominent role in biochemical processes

We have seen in Chapter 14 and in this chapter the prominence of phosphoryl group transfer from ATP to acceptor molecules. How is it that phosphate came to play such a prominent role in biology? Phosphate and its esters have several characteristics that render them useful for biochemical systems:

- *The energy release from phosphate esters can be manipulated by enzymes, making them ideal regulatory molecules.* Phosphate esters have an important chemical characteristic by being thermodynamically unstable yet kinetically stable in water. Phosphate esters are thus molecules whose energy release can be manipulated by enzymes. The kinetic stability of phosphate esters is due to the negative charges that make them resistant to hydrolysis in the absence of enzymes. This accounts for the presence of phosphate in the backbone of DNA and explains why they are ideal regulatory molecules; protein structure and function can be reliably controlled through the stable addition and removal of phosphates. Because both phosphate ester formation and hydrolysis are both very slow in free solution, these changes are not readily reversed without the action of an enzyme: protein kinases normally add phosphates to proteins while protein phosphatases typically remove them, as we explored in Section 7.3.

- *The addition of a phosphate group changes molecule conformation and behavior.* Phosphates are also frequently added to metabolites that might otherwise diffuse through the cell membrane. Even when transporters exist for unphosphorylated forms of a metabolite, the addition of a phosphate changes the geometry and polarity of the molecules so that they no longer fit in the binding sites of the transporters.

- *All other ions fall short.* No other ions have the chemical characteristics of phosphate. Citrate is not sufficiently charged to prevent hydrolysis. Arsenate forms esters that are unstable and susceptible to spontaneous hydrolysis. Indeed, arsenate is poisonous to cells because it can replace phosphate in reactions required for ATP synthesis, generating unstable compounds and preventing ATP synthesis. Silicate is more abundant than phosphate, but silicate salts are virtually insoluble and are used for biomineralization, as in diatoms and certain sponges. Only phosphate has the chemical properties to meet the needs of living systems.

Energy from food is extracted in three stages

Let us take an overall view of the processes of energy conversion in animals before considering them in detail in subsequent chapters. Hans Krebs described three stages in the generation of energy from the oxidation of food (**Figure 15.11**).

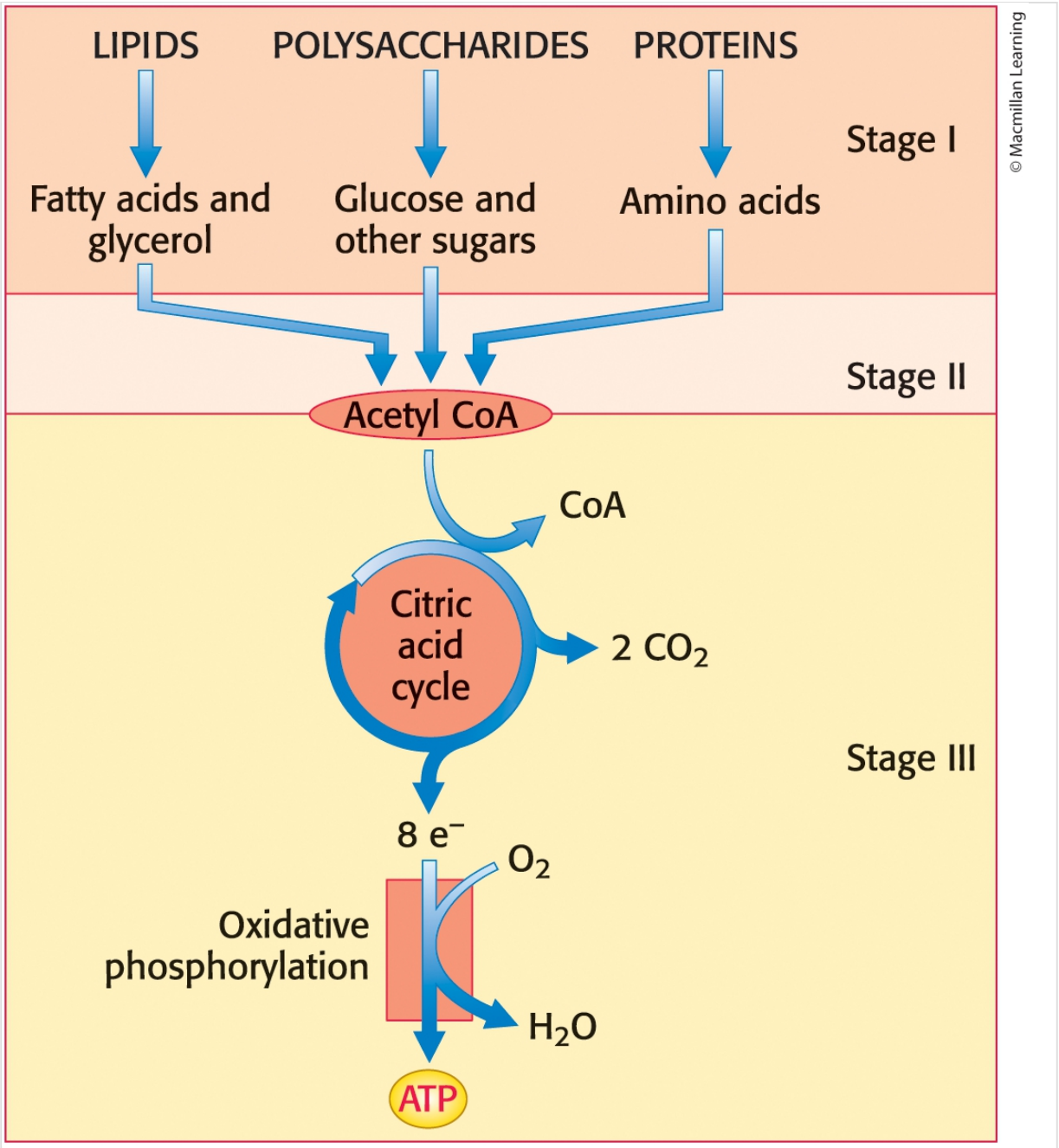


FIGURE 15.11 The extraction of energy from food molecules by aerobic organisms can be described as taking place in three stages.

1. *Large molecules in food are broken down into smaller units in the process of digestion*. Proteins are hydrolyzed to their 20 different amino acids, polysaccharides are hydrolyzed to simple sugars such as glucose, and lipids are hydrolyzed to glycerol and fatty acids. The degradation products are then absorbed by the cells of the intestine and distributed throughout the body. This stage is strictly a preparation stage; no useful energy is captured in this phase.

2. *Numerous small molecules resulting from digestion are degraded to a few simple units that play a central role in metabolism*. In fact, most of them — sugars, fatty acids, glycerol, and several amino acids — are converted into the acetyl unit of acetyl CoA. Some ATP is generated in this stage, but the amount is small compared with that obtained in the third stage.

3. *ATP is produced from the complete oxidation of the acetyl unit of acetyl CoA*. The third stage consists of the citric acid cycle and oxidative phosphorylation, which are the final common pathways in the oxidation of fuel molecules. Acetyl CoA brings acetyl units into the citric acid cycle — also called the CAC, the tricarboxylic acid (TCA) cycle, or the Krebs cycle — where they are completely oxidized to CO_2. Four pairs of electrons are transferred (three to NAD^+ and one to FAD) for each acetyl group that is oxidized (Chapter 17). Then, a proton gradient is generated as electrons flow from the reduced forms of these carriers to O_2. This gradient is used to synthesize ATP (Chapter 18).

Self-Check Question



Which of the following statements is/are true? (1) Energy is released when the covalent bond linking two phosphates in ATP is broken. (2) ATP is the cellular energy currency because it has the highest phosphoryl transfer potential of any biological molecule. (3) ATP has two

phosphoanhydride linkages, each of which can be hydrolyzed to provide useable energy for an organism.

15.4 Metabolic Pathways Contain Many Recurring Motifs

The sheer number of reactants and reactions of metabolism makes it seem very complex. Fortunately, we can look to several unifying themes to help make sense of it all. These themes include common metabolites, reactions, and regulatory schemes that stem from a common evolutionary heritage.

Activated carriers exemplify the modular structure and economy of metabolism

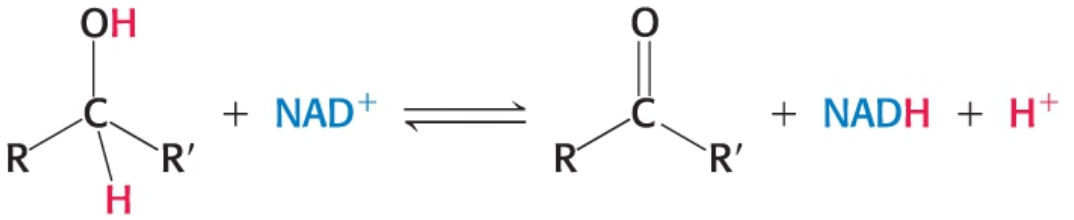
We have seen that phosphoryl transfer can be used to drive otherwise endergonic reactions, alter the conformation energy of a protein, or serve as a signal to alter the activity of a protein. The phosphoryl-group donor in all these reactions is ATP. In summary, ATP is an **activated carrier** of phosphoryl groups because phosphoryl transfer from ATP is an exergonic process. Activated carriers are small molecules to which a chemical group or electrons have been added, which can then be donated to another molecule; they frequently act as coenzymes or cosubstrates in enzyme-catalyzed reactions.

The use of ATP and other activated carriers is a recurring motif in biochemistry. Here we introduce the activated carriers that will appear repeatedly in the next several chapters, often functioning as coenzymes. Next, we provide an overview of their key roles.

NADH and $FADH_2$: Activated carriers of electrons for fuel oxidation

In aerobic organisms, the ultimate electron acceptor in the oxidation of fuel molecules is O_2. However, electrons are not transferred directly from the fuel molecule to O_2. Instead, fuel molecules transfer electrons to carriers, which then transfer their high-potential electrons to O_2.

One of the major electron carriers in the oxidation of fuel molecules is nicotinamide adenine dinucleotide (NAD^+; Figure 15.12). The reactive part of NAD^+ is its nicotinamide ring, derived from vitamin B_3 (niacin). In the oxidation of a substrate, the nicotinamide ring of NAD^+ accepts a proton and two electrons, which are equivalent to a hydride ion $(H:^-)$. The reduced form of this carrier is NADH. In the oxidized form, the nitrogen atom carries a positive charge, as indicated by NAD^+. NAD^+ is the electron acceptor in many reactions of the type



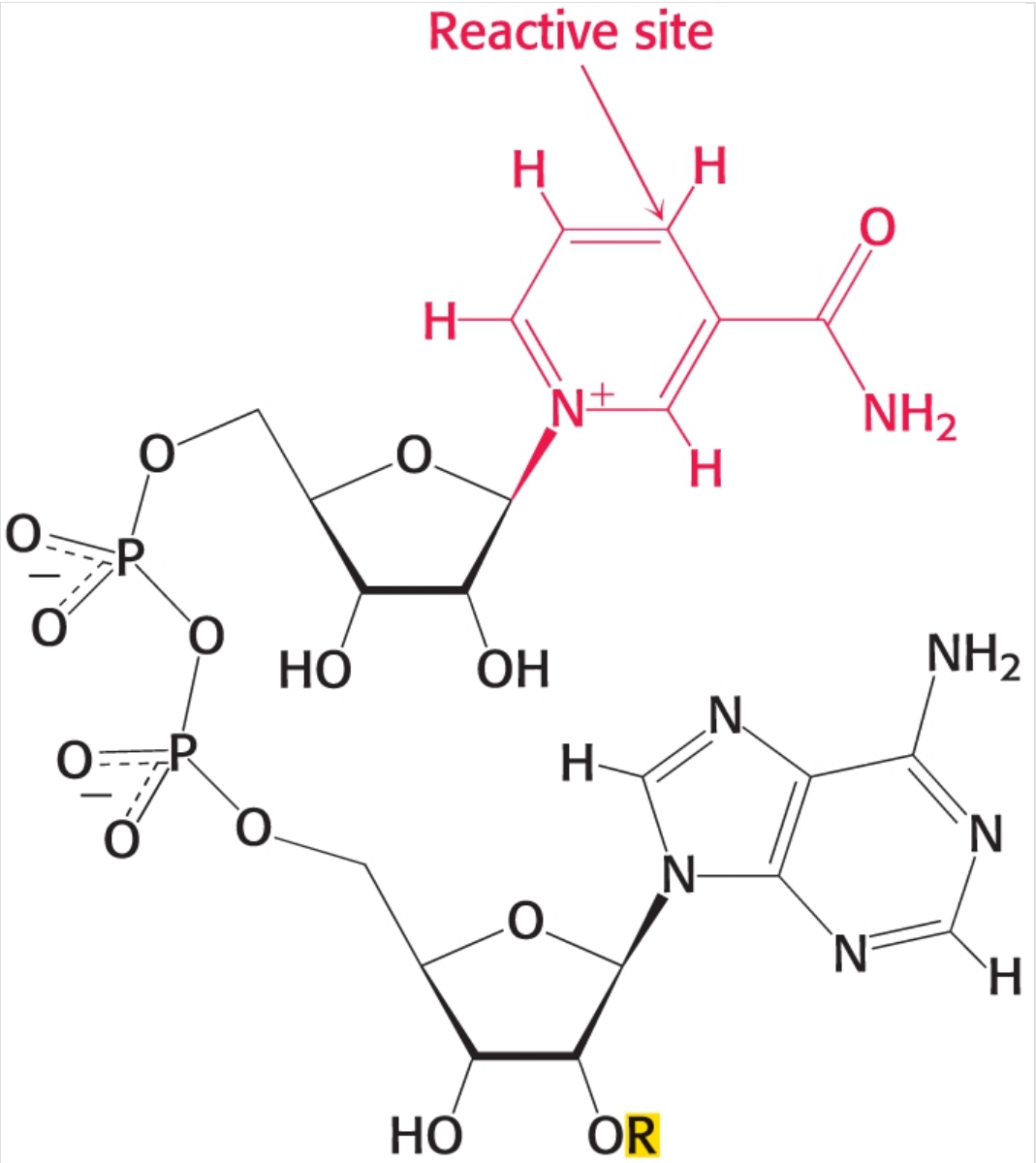
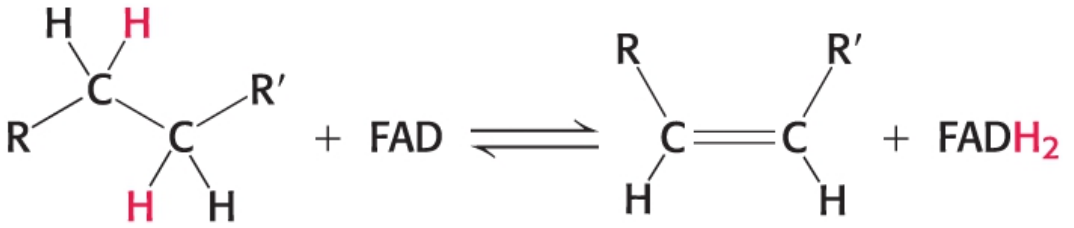


FIGURE 15.12 Nicotinamide adenine dinucleotide (NAD^+) and nicotinamide adenine dinucleotide phosphate $(NADP^+)$ are prominent carriers of high-energy electrons. The oxidized forms are shown; in NAD^+, $R = H$; in $NADP^+$, $R = PO_3^{2-}$. A hydride ion (H^-) can be accepted by the nicotinamide ring (shown in red).

In this dehydrogenation, one hydrogen atom of the substrate is directly transferred to NAD^+, whereas the other appears in the solvent as a proton. Both electrons lost by the substrate are transferred to the nicotinamide ring.

The other major electron carrier in the oxidation of fuel molecules is the coenzyme flavin adenine dinucleotide (FAD; **Figure 15.13**). The abbreviations for the oxidized and reduced forms of this carrier are FAD and $FADH_2$, respectively. FAD is the electron acceptor in reactions of this type:



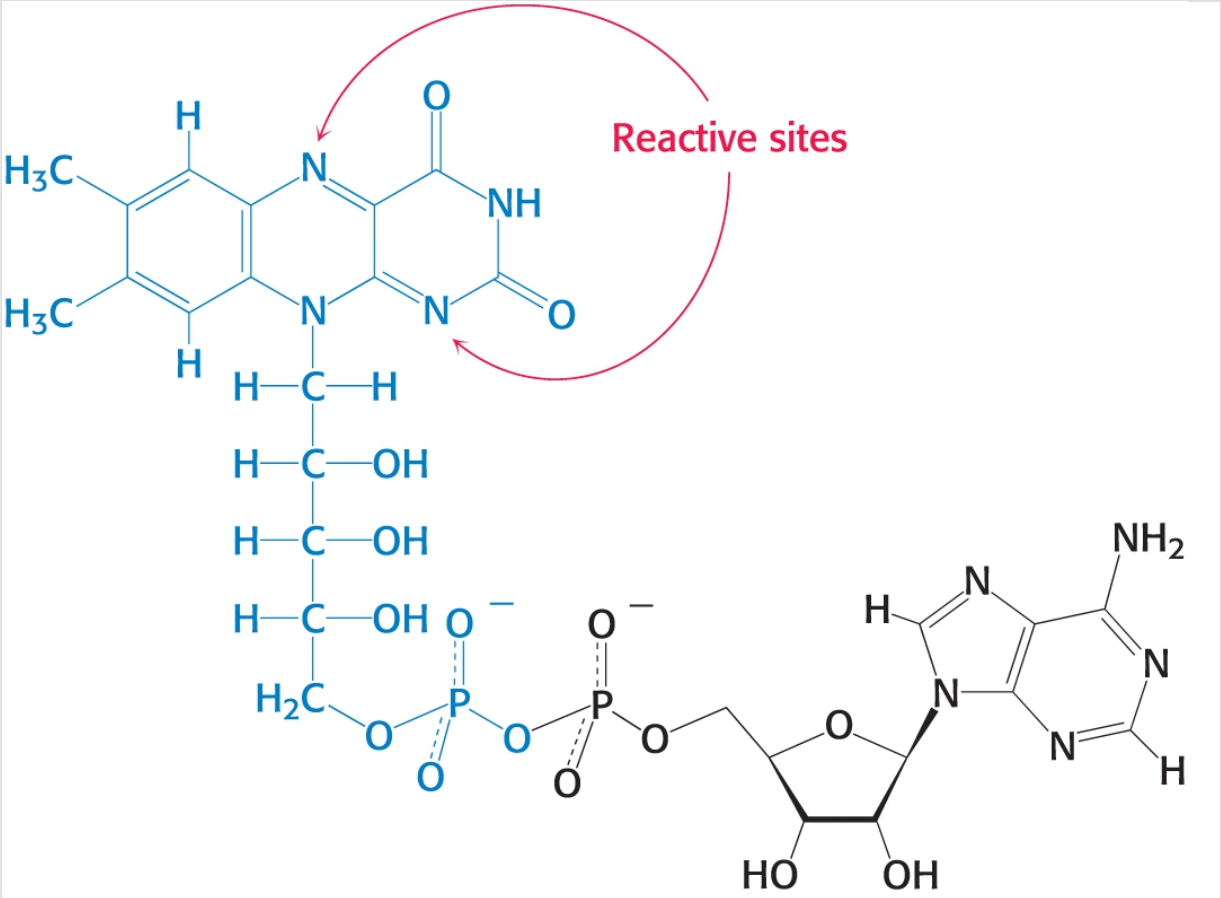


FIGURE 15.13 The oxidized form of flavin adenine dinucleotide (FAD) consists of two units. FAD has a flavin mononucleotide (FMN) unit (shown in blue) and an AMP unit (shown in black).

The reactive part of FAD is its isoalloxazine ring, a derivative of the vitamin riboflavin (**Figure 15.14**). FAD, like NAD^+, can accept two electrons. In doing so, FAD, unlike NAD^+, takes up two protons; its reduced form is $FADH_2$. These carriers of high-potential electrons as well as flavin mononucleotide (FMN) — an electron carrier similar to FAD but lacking the adenine nucleotide — will be considered further in Chapter 18.

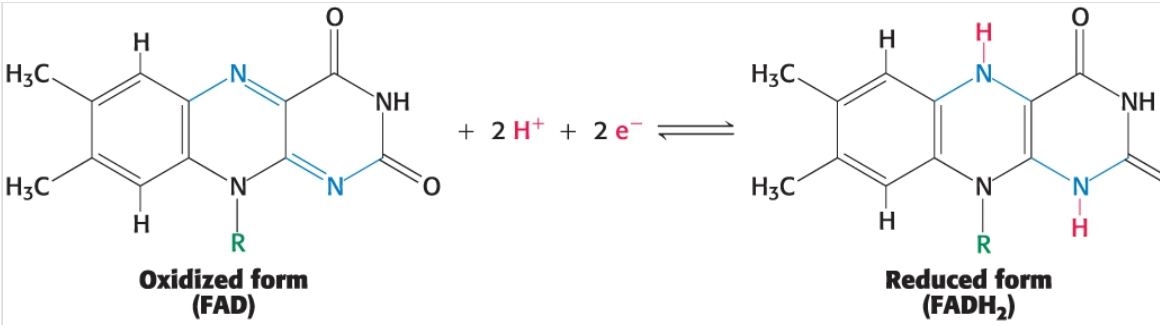
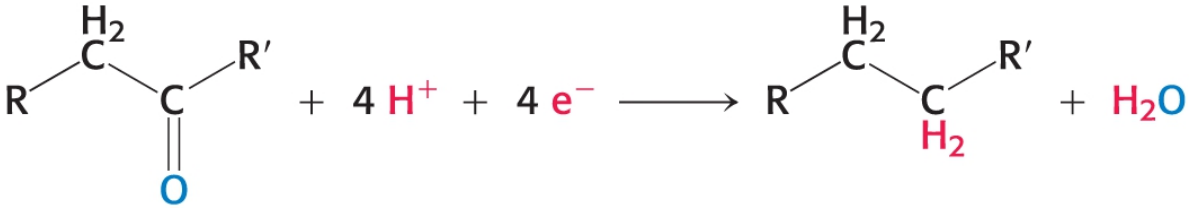


FIGURE 15.14 Structures of the reactive components of FAD and $FADH_2$ reveal that electrons and protons are carried by the reactive isoalloxazine ring component.

NADPH: Activated carrier of electrons for reductive biosynthesis

High-potential electrons are required in most biosyntheses because the precursors are more oxidized than the products. Hence, reducing power is needed in addition to ATP. For example, in the biosynthesis of fatty acids, a keto group is reduced to a methylene group in several steps. This sequence of reactions requires an input of four electrons.

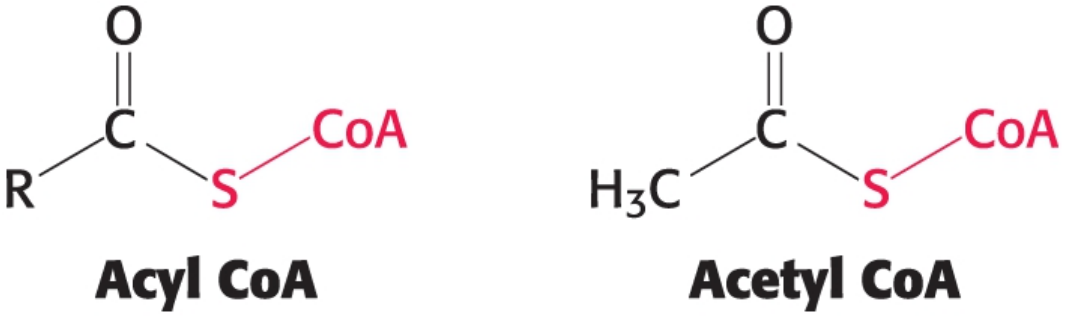


The electron donor in most reductive biosyntheses is NADPH, the reduced form of nicotinamide adenine dinucleotide phosphate (Figure

15.12). Its oxidized form is $NADP^+$. NADPH differs from NADH in that the $2'$–hydroxyl group of its adenosine moiety is esterified with phosphate. NADPH carries electrons in the same way as NADH. However, NADPH is used almost exclusively for reductive biosyntheses, whereas NADH is used primarily for the generation of ATP. The extra phosphoryl group on NADPH is a tag that enables enzymes to distinguish between high-potential electrons to be used in anabolism and those to be used in catabolism.

Coenzyme A: Activated carrier of two-carbon fragments

Coenzyme A (CoA), another central molecule in metabolism, is a carrier of acyl groups that is derived from vitamin B_5 (pantothenate) (**Figure 15.15**). The terminal sulfhydryl group in CoA is the reactive site. Acyl groups are linked to CoA by thioester bonds. The resulting derivative is called an *acyl CoA*. An acyl group often linked to CoA is the acetyl unit; this derivative is called *acetyl CoA*.



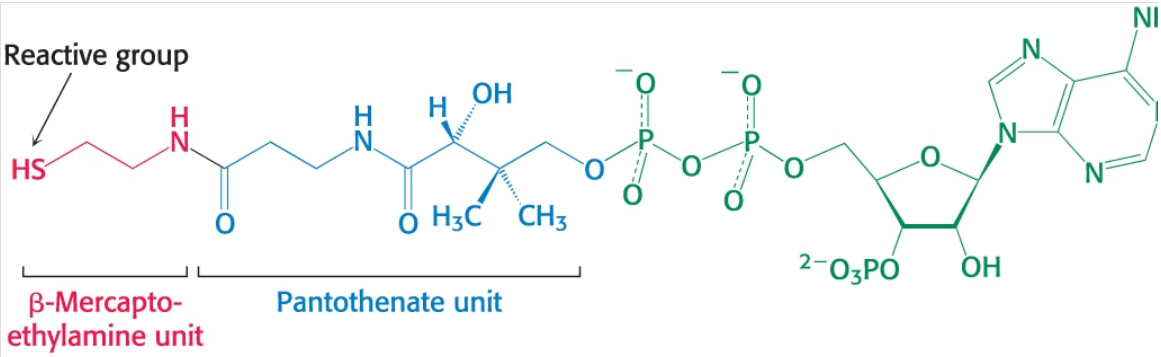


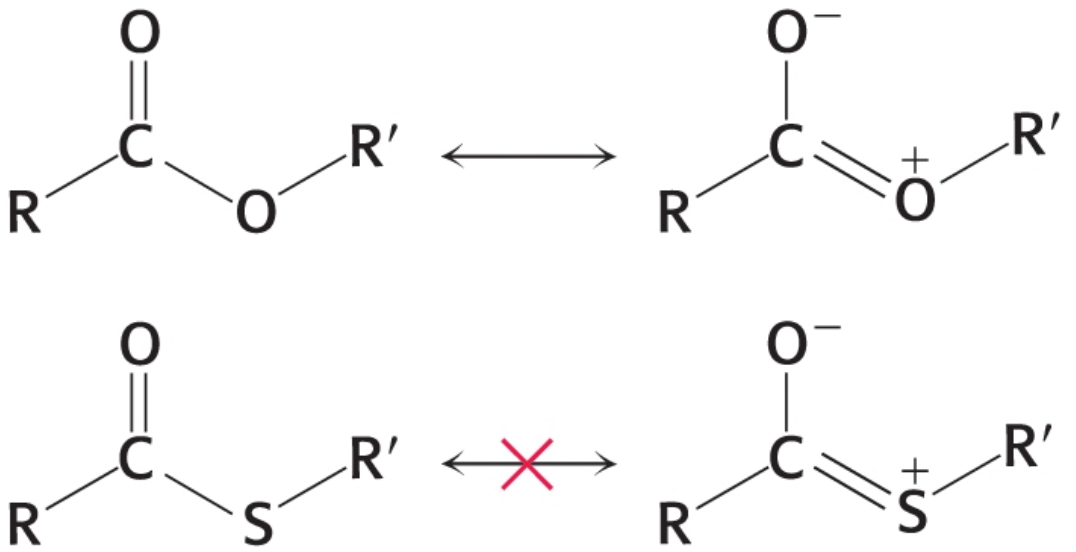
FIGURE 15.15 Structure of coenzyme A (CoA) reveals its derivation from both ADP and the vitamin pantothenate.

Acyl groups are important constituents both in catabolism, as in the oxidation of fatty acids, and in anabolism, as in the synthesis of membrane lipids.

The $\Delta G^{\circ\prime}$ for the hydrolysis of acetyl CoA has a large negative value:

$$\text{Acetyl CoA} + H_2O \rightleftharpoons \text{acetate} + \text{CoA} + H^+$$
$$\Delta G^{\circ\prime} = -31.4 \text{ kJ mol}^{-1} \ (-7.5 \text{ kcal mol}^{-1})$$

A thioester is thermodynamically more unstable than an oxygen ester because the electrons of the $C{=}O$ bond cannot form resonance structures with the $C{-}S$ bond that are as stable as those that they can form with the $C{-}O$ bond.



Consequently, acetyl CoA has a high acetyl-group-transfer potential because transfer of the acetyl group is exergonic. Acetyl CoA carries an activated acetyl group, just as ATP carries an activated phosphoryl group.

The use of activated carriers illustrates two key aspects of metabolism:

1. *Kinetic stability allows enzymatic control over the flow of energy.* First, NADH, NADPH, and $FADH_2$ react slowly with O_2 in the absence of a catalyst. Likewise, ATP and acetyl CoA are hydrolyzed slowly (over many hours or even days) in the absence of a catalyst. These molecules are kinetically quite stable in the face of a large thermodynamic driving force for reaction with O_2 (in regard to the electron carriers) and H_2O (for ATP and acetyl CoA). The kinetic stability of these molecules in the absence of specific catalysts is

essential for their biological function because it enables enzymes to control the flow of free energy and reducing power.

2. *A small set of carriers accomplishes the majority of the exchanges of activated groups in metabolic pathways* (Table 15.2). The existence of a recurring "cast of characters" — a small set of activated carriers in all organisms — illustrates the modular design of metabolism. A small set of molecules carries out a very wide range of tasks.

TABLE 15.2 Some activated carriers in metabolism

Carrier molecule in activated form	Group carried	Vitamin precursor
ATP	Phosphoryl	
NADH and NADPH	Electrons	Nicotinate (niacin) (vitamin B_3)
$FADH_2$ and $FMNH_2$	Electrons	Riboflavin (vitamin B_2)
Coenzyme A	Acyl	Pantothenate (vitamin B_5)
Lipoamide	Acyl	
Thiamine pyrophosphate	Aldehyde	Thiamine (vitamin B_1)
Biotin	CO_2	Biotin (vitamin B_7)
Tetrahydrofolate	One-carbon units	Folate (vitamin B_9)
S-Adenosylmethionine	Methyl	

Uridine diphosphate glucose	Glucose
Cytidine diphosphate diacylglycerol	Phosphatidate
Nucleoside triphosphates	Nucleotides

Note: Many of the activated carriers are coenzymes that are derived from water-soluble vitamins.

Many activated carriers are derived from vitamins

As noted in Table 15.2, most activated carriers that act as coenzymes are derived from **vitamins**, organic molecules that are needed in small amounts in the diets of some higher animals. In all cases, a vitamin must be modified before it can serve its function. **Table 15.3** lists the vitamins that act as coenzymes, and **Figure 15.16** shows the structures of some of B group vitamins.

TABLE 15.3 The B vitamins

Vitamin	Coenzyme	Typical reaction Type	Consequences of Deficiency
Thiamine (B_1)	Thiamine pyrophosphate (TPP)	Aldehyde transfer	Beriberi (weight loss, heart problems, neurological dysfunction)
Riboflavin (B_2)	Flavin adenine dinucleotide (FAD)	Oxidation–reduction	Lesions of the mouth, dermatitis

Pyridoxine (B_6)	Pyridoxal phosphate (PLP)	Group transfer to or from amino acids	Depression, confusion, convulsions
Nicotinic acid (niacin) (B_3)	Nicotinamide adenine dinucleotide (NAD^+)	Oxidation–reduction	Pellagra (dermatitis, depression, diarrhea)
Pantothenic acid (B_5)	Coenzyme A (CoA)	Acyl-group transfer	Hypertension
Biotin (B_7)	Biotin–lysine adducts (biocytin)	ATP-dependent carboxylation and carboxyl-group transfer	Rash about the eyebrows, muscle pain, fatigue (rare)
Folic acid (B_9)	Tetrahydrofolate (THF)	Transfer of one-carbon components; thymine synthesis	Anemia, neural-tube defects in development
Cobalamin (B_{12})	5′-Deoxyadenosyl-cobalamin	Transfer of methyl groups; intramolecular rearrangements	Anemia, pernicious anemia, methylmalonic acidosis

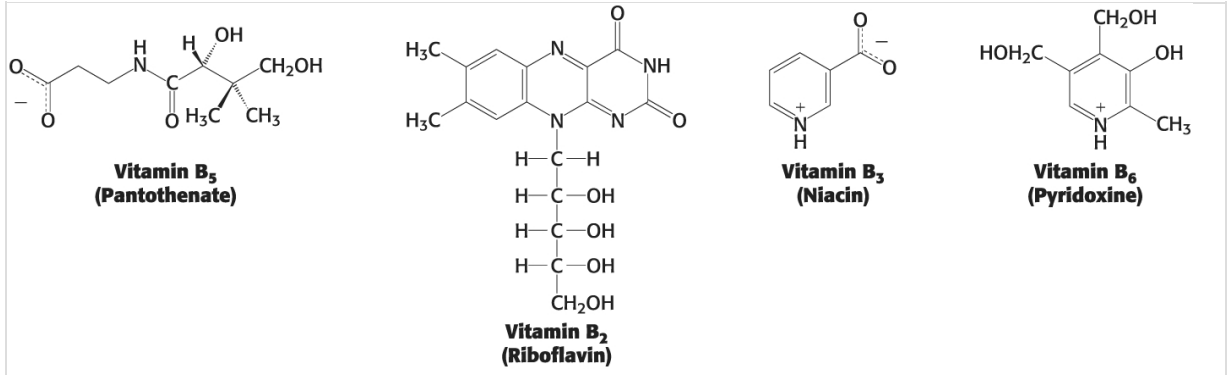


FIGURE 15.16 The B vitamins are a diverse group of small, water-soluble molecules. These vitamins, along with vitamin C, are often referred to as water-soluble vitamins because of the

ease with which they dissolve in water.



Not all vitamins function as coenzymes; vitamins designated by the letters A, C, D, E, and K (Table 15.4) have a diverse array of functions that we will encounter, along with the B vitamins, in our study of biochemistry.

TABLE 15.4 Noncoenzyme vitamins

Vitamin	Function	Deficiency
A	Roles in vision, growth, reproduction	Night blindness, cornea damage, damage to respiratory tract and gastrointestinal tract
C	Antioxidant, essential for collagen production	Scurvy (swollen and bleeding gums, subdermal hemorrhaging)
D	Regulation of calcium and phosphate metabolism	Rickets (children): skeletal deformities, impaired growth Osteomalacia (adults): soft, bending bones
E	Antioxidant	Lesions in muscles and nerves (rare)
K	Blood coagulation	Subdermal and cerebral hemorrhaging



Vitamins serve the same roles in nearly all forms of life, but higher animals lost the capacity to synthesize them in the course of evolution. For instance, whereas *E. coli* can thrive on glucose and organic salts, human beings require at least 12 vitamins in their diet. The biosynthetic pathways for vitamins can be complex; thus, it is

biologically more efficient to ingest vitamins than to synthesize the enzymes required to construct them from simple molecules. This efficiency comes at the cost of dependence on other organisms for chemicals essential for life. Indeed, vitamin deficiency can generate diseases in all organisms requiring these molecules (Tables 15.3 and 15.4).

Key reactions are reiterated throughout metabolism

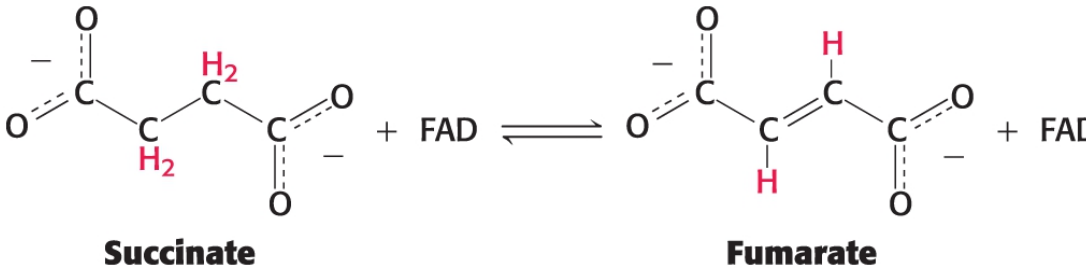
Just as there is an economical use of the same small set of activated carriers, there is also an economical use of a small set of biochemical reactions. In fact, the thousands of metabolic reactions can be subdivided into just six types (**Table 15.5**). These six types of reactions correspond to the six major classes of enzymes discussed in Section 5.1. Specific reactions of each type appear repeatedly.

TABLE 15.5 Types of chemical reactions in metabolism

Type of reaction	Description
Oxidation–reduction	Electron transfer
Group transfer	Transfer of a functional group from one molecule to another
Hydrolytic	Cleavage of bonds by the addition of water
Carbon bond cleavage by means other than hydrolysis or oxidation	Two substrates yielding one product or vice versa. When H_2O or CO_2 are a product, a double bond is formed.

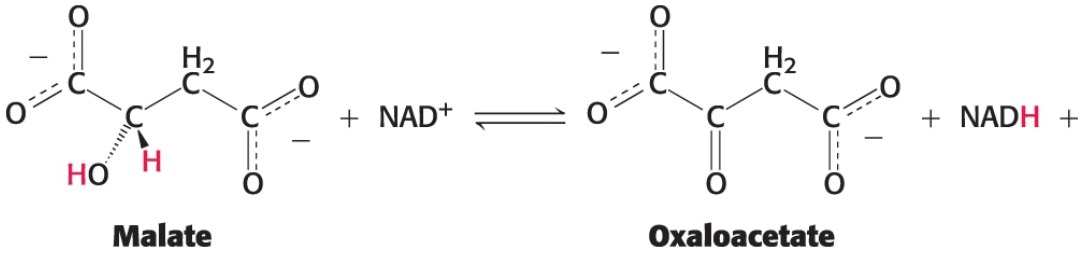
Isomerization	Rearrangement of atoms to form isomers
Ligation requiring ATP cleavage	Formation of covalent bonds (i.e., carbon–carbon bonds)

1. *Oxidation–reduction reactions are essential components of many pathways.* Useful energy is often derived from the oxidation of carbon compounds. Consider the following two reactions:



Succinate **Fumarate**

(1)

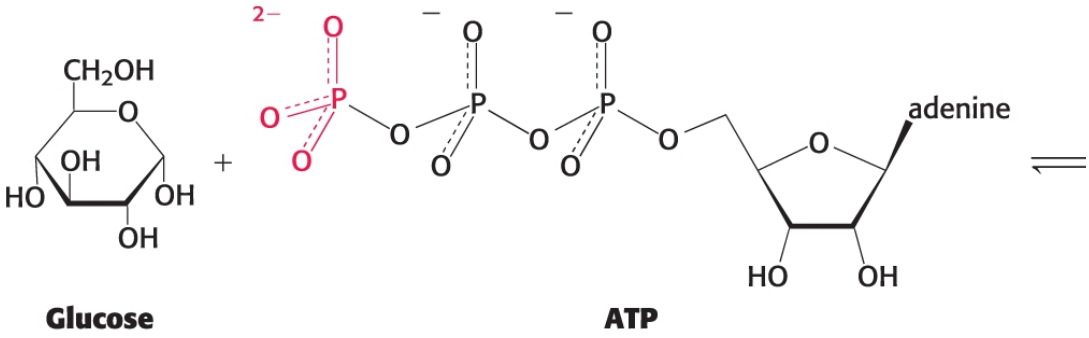


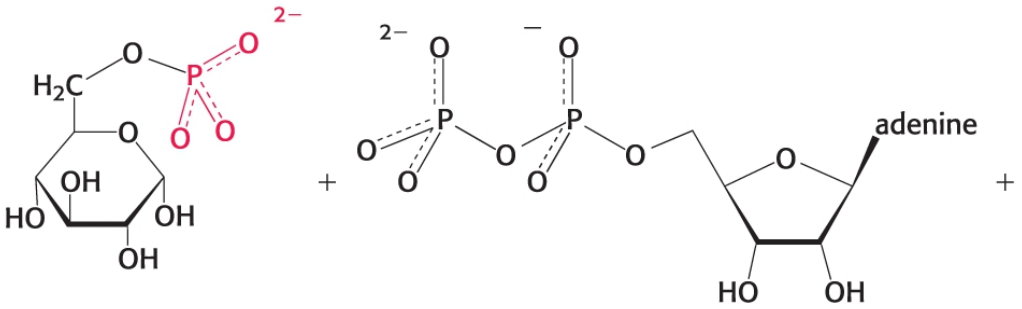
Malate **Oxaloacetate**

(2)

These two oxidation–reduction reactions are components of the citric acid cycle (Chapter 17), which completely oxidizes the activated two-carbon fragment of acetyl CoA to two molecules of CO_2. In reaction 1, $FADH_2$ carries the electrons, whereas in reaction 2, electrons are carried by NADH.

2. *Group-transfer reactions play a variety of roles.* Phosphoryl group transfer is representative of such a reaction:



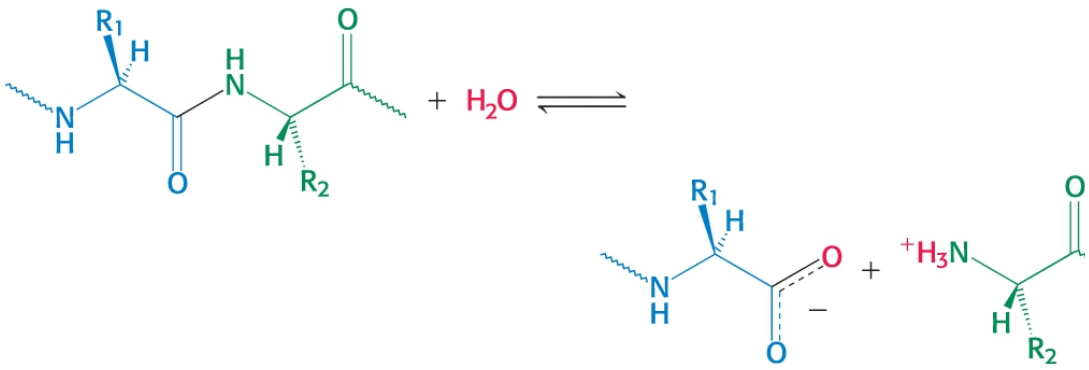


(3)

A phosphoryl group is transferred from the activated phosphoryl-group carrier, ATP, to glucose in the initial step in glycolysis, a key pathway for extracting energy from glucose (Chapter 16). This

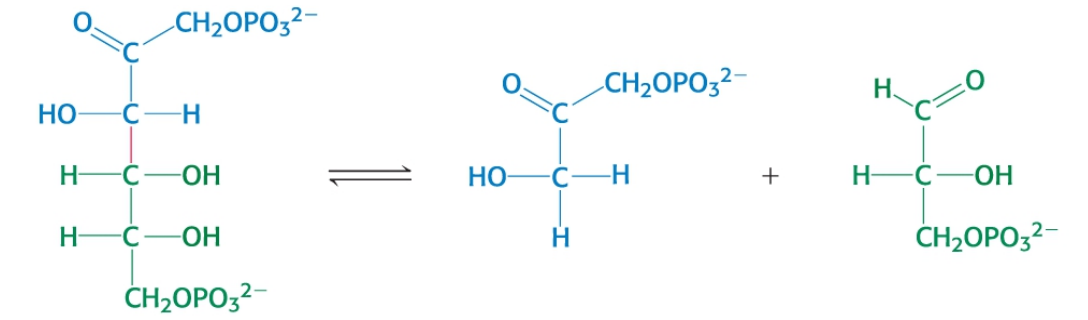
reaction traps glucose in the cell so that further catabolism can take place. As stated earlier, group-transfer reactions are used to synthesize ATP. We also saw examples of their use in signaling pathways (Chapter 14).

3. *Hydrolytic reactions cleave bonds by the addition of water.* Hydrolysis is a common means of degrading large molecules, either to facilitate further metabolism or to reuse some of the components for biosynthetic purposes. For example, recall from Section 6.1 that proteins are digested by hydrolytic cleavage:



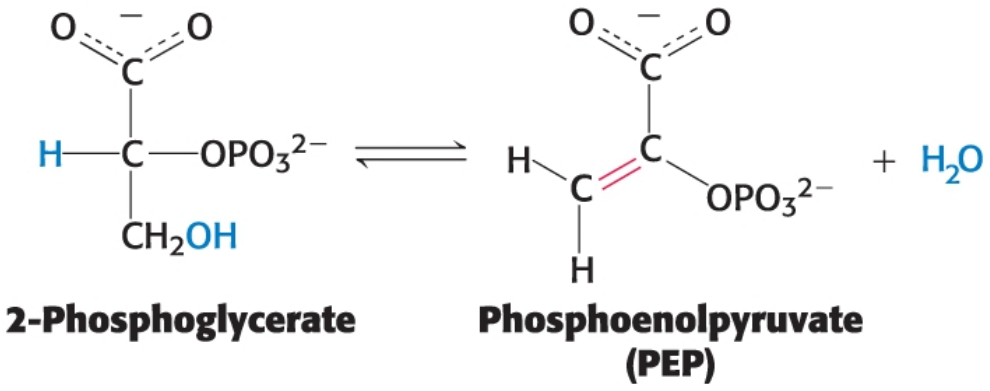
(4)

4. *Carbon bonds can be cleaved by means other than hydrolysis or oxidation.* When CO_2 or H_2O is released, a double bond is formed. The enzymes that catalyze these types of reactions are classified as *lyases*. An important example is the conversion of the six-carbon molecule fructose 1,6-bisphosphate into two three-carbon fragments:



(5)

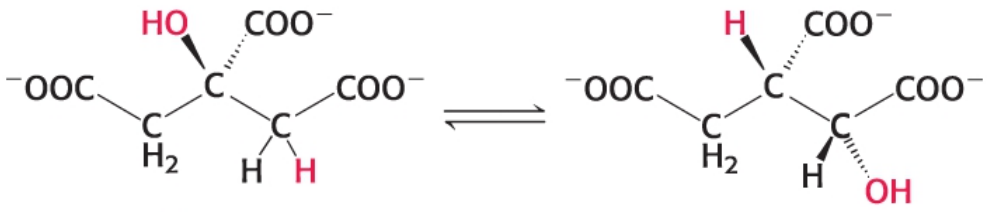
This reaction is a critical step in glycolysis (Chapter 16). In addition, the formation of double bonds through dehydration — such as generating phosphoenolpyruvate (Figure 15.5) from 2-phosphoglycerate — is an important subclass of this reaction type:



(6)

This dehydration sets up the next step in the pathway, a group-transfer reaction that uses the high phosphoryl-transfer potential of the product PEP to form ATP from ADP.

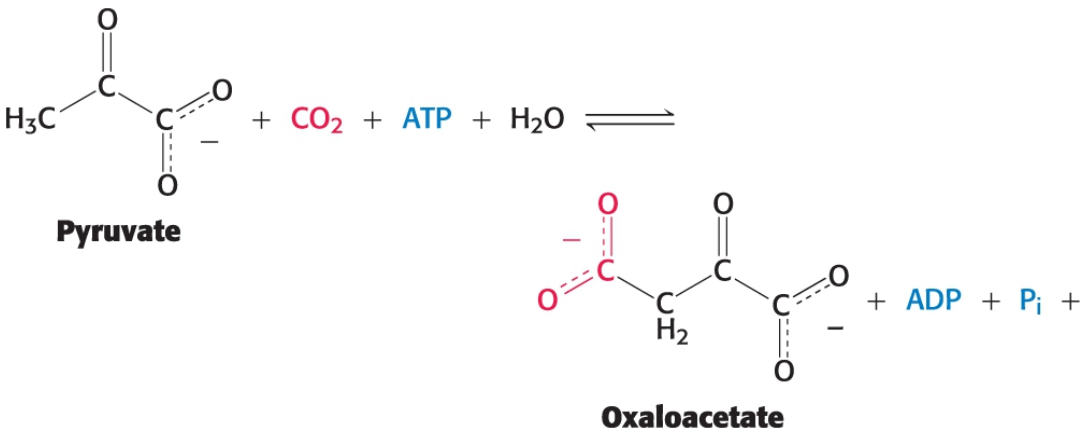
5. *Isomerization reactions rearrange particular atoms within a molecule.* The role of these reactions is often to prepare the molecule for subsequent reactions such as the oxidation–reduction reactions described above.



(7)

The reaction above is an essential component of the citric acid cycle, analyzed in detail in Chapter 17.

6. *Ligation reactions form bonds by using free energy from ATP hydrolysis.* In many cases, the free energy from ATP hydrolysis is necessary to combine smaller molecules to form larger ones. For example, oxaloacetate is formed from pyruvate and CO_2, using energy from ATP to form the carbon–carbon bond.



(8)

The oxaloacetate can be used in the citric acid cycle, or converted into glucose or amino acids such as aspartic acid.

These six fundamental reaction types are the basis of metabolism; you will encounter them repeatedly in the next few chapters. Remember, all six types can proceed in either direction, depending on the standard free energy for the specific reaction and the concentrations of the reactants and products inside the cell.

Metabolic processes are regulated in three principal ways

Because the network of metabolic reactions is so complex, it must be rigorously regulated. Cells have feedback mechanisms that monitor and adjust levels of available nutrients and the activity of metabolic pathways to create *homeostasis*, a stable biochemical environment. At the same time, metabolic control must be flexible, able to adjust to the

constantly changing external environments of cells. Metabolism is regulated through three principal mechanisms:

1. *The amounts of enzymes can be altered.* The amount of a particular enzyme depends on both its rate of synthesis and its rate of degradation. For many enzymes, their abundance is principally adjusted by a change in the rate of transcription of the genes encoding them (Section 29.3). In *E. coli,* for example, within minutes the presence of lactose induces a more-than-50-fold increase in the rate of synthesis of β-galactosidase, the enzyme required for the breakdown of this disaccharide.

2. *The accessibility of substrates by enzymes can be restricted.* Limiting the availability of substrates is another means of regulating metabolism in all organisms. For instance, glucose breakdown can take place in many cells only if insulin is present to promote the entry of glucose into the cell. In eukaryotes, access to substrates is regulated in part by compartmentalization. For example, fatty acid oxidation takes place in mitochondria, whereas fatty acid synthesis takes place in the cytoplasm. Compartmentalization often segregates opposed reactions.

3. *The catalytic activity of enzymes can be internally regulated or externally controlled.* The catalytic activity of enzymes is continuously adjusted in several ways. Allosteric regulation is especially important; for example, the first reaction in many biosynthetic pathways is allosterically inhibited by the ultimate product of the pathway, called *feedback inhibition,* which can be almost instantaneous. A well-understood example is the inhibition of aspartate transcarbamoylase (ATCase) by cytidine triphosphate (Section 7.1). Another recurring mechanism is reversible covalent modification (Section 7.3). Hormones like adrenaline externally control the catalytic rates of enzymes often by inducing reversible covalent modification of key enzymes or by changing the concentrations of allosteric activators and inhibitors, as we explored in Chapter 14. Finally, many reactions are regulated by the

energy status of the cell. One useful concept that can serve as an index of the energy status is the **energy charge**, which is proportional to the mole fraction of ATP plus half the mole fraction of ADP, given that ATP contains two anhydride bonds, whereas ADP contains one. Hence, the energy charge is defined as

$$\text{Energy charge} = \frac{[\text{ATP}] + \frac{1}{2}[\text{ADP}]}{[\text{ATP}] + [\text{ADP}] + [\text{AMP}]}$$

The energy charge can have a value ranging from 0 (all AMP) to 1 (all ATP). ATP-generating pathways are inhibited under conditions of high-energy charge, whereas ATP-utilizing pathways are often stimulated under those same conditions. In plots of the reaction rates of such pathways versus the energy charge, the curves are steep near an energy charge of 0.9, where they usually intersect (**Figure 15.17**). Regulation of these pathways has evolved to maintain the energy charge within rather narrow limits. In other words, the energy charge, like the pH of a cell, is buffered. The energy charge of most cells ranges from 0.90 to 0.95, but can fall to less than 0.7 in muscle during high-intensity exercise. However, energy charge itself does not directly regulate pathways; rather, enzymes regulating these pathways are allosterically inhibited or activated by binding to ATP or AMP, specifically.

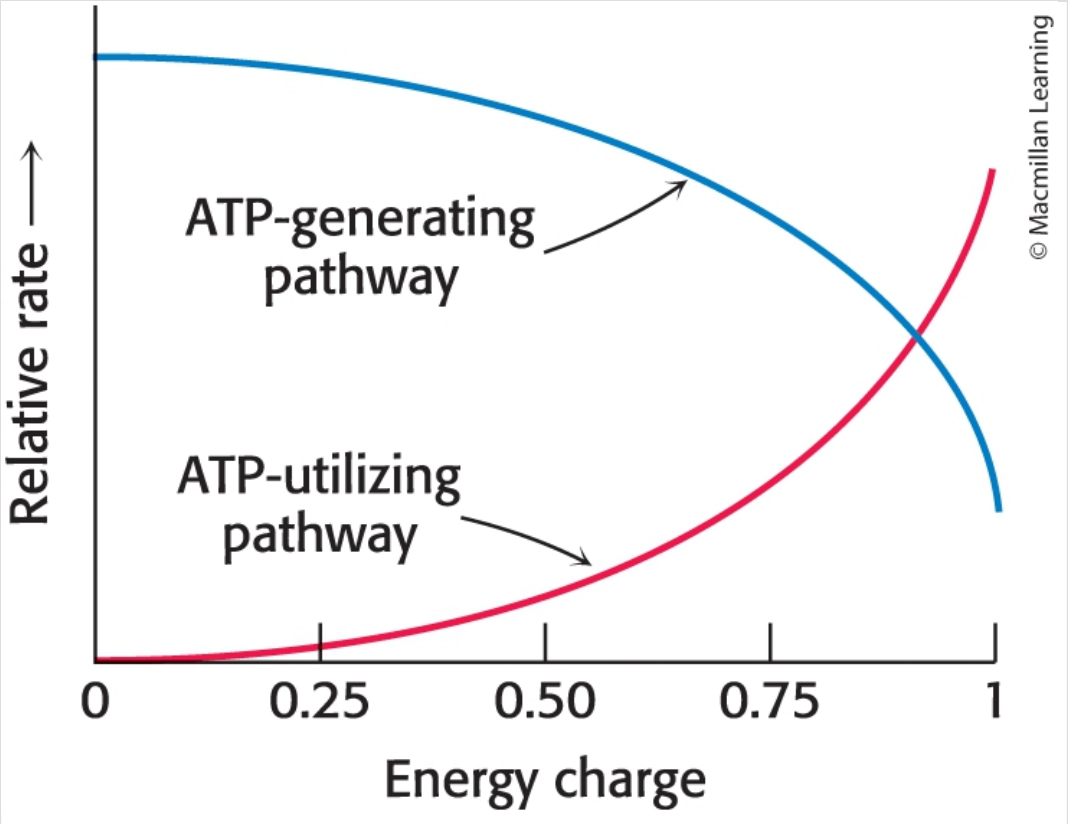


FIGURE 15.17 Energy charge is a useful concept for understanding how metabolism is regulated. When the energy charge is high, ATP commonly inhibits the relative rates of a typical ATP-generating pathway and stimulates the typical ATP-utilizing pathway, while AMP has the opposite effects.

EXPLORE this pathway further in the Metabolic Map in Achieve

Looking at the commonalities in diverse metabolic pathways exposes a chemical logic that renders the complexity of the chemistry of living systems more manageable and reveals its elegance. As you delve into any of the next 12 chapters, you might find it useful to return to this chapter to review the common themes.

Self-Check Question



Name the common cellular carrier of activated two-carbon fragments, and name the common carrier of electrons for biosynthesis. Both these molecules have parts derived from which group of small organic molecules that are precursors to coenzymes?

Chapter 15 Summary

15.1 Metabolism Is Composed of Many Interconnected Reactions

- All cells transform energy. They extract energy from their environment and use this energy to convert simple molecules into cellular components.
- The process of energy transduction takes place through metabolism, a highly integrated network of chemical reactions.
- Metabolism can be subdivided into catabolism (processes that break complex things into simpler ones and typically extract energy from fuels) and anabolism (biosynthetic processes that typically require energy).
- The most valuable thermodynamic concept for understanding bioenergetics is free energy. A reaction can occur spontaneously only if the change in free energy (ΔG) is negative.
- A thermodynamically unfavorable reaction can be driven by a thermodynamically favorable one, which is the hydrolysis of ATP in many cases.

15.2 ATP Is the Universal Currency of Free Energy in Biological Systems

- The energy derived from catabolism is captured in the form of adenosine triphosphate (ATP).
- ATP hydrolysis is exergonic and the energy released can be used to power cellular processes, including motion, active transport, and biosynthesis.
- ATP, the universal currency of energy in biological systems, is an energy-rich molecule because it contains two kinetically

stable, but thermodynamically unstable, phosphoanhydride linkages.

15.3 The Oxidation of Carbon Fuels Is an Important Source of Cellular Energy

- ATP formation is coupled to the oxidation of chemicals, either directly or through the formation of ion gradients in chemotrophs. Phototrophic organisms, including all photosynthetic organisms, can use light to generate such gradients.
- The extraction of energy from food by aerobic organisms comprises three stages: (1) large molecules are catabolized into smaller ones, such as amino acids, sugars, and fatty acids; (2) these small molecules are degraded to a few simple units, such as acetyl CoA; (3) the citric acid cycle and oxidative phosphorylation generate ATP as electrons flow to O_2, the ultimate electron acceptor, and fuels are completely oxidized to CO_2.

15.4 Metabolic Pathways Contain Many Recurring Motifs

- Metabolism is characterized by common motifs. A small number of recurring activated carriers, such as ATP, NADH, and acetyl CoA, transfer activated groups in many metabolic pathways. Many activated carriers are derived from vitamins — small organic molecules required in the diets of many higher organisms.
- NADPH, which carries two electrons at a high potential, provides reducing power for reductive biosynthesis of cell components.
- Key reaction types are used repeatedly in metabolic pathways. Metabolism is regulated in a variety of ways: the amounts of enzymes are altered, the catalytic activities of many enzymes

are regulated by allosteric interactions and controlled by covalent modification, and the availability of many substrates is also limited.
- The energy charge, which is a measure of the relative amounts of ATP, ADP, and AMP, is a useful concept for approximating the energy status of a cell. ATP generally inhibits ATP-generating pathways and stimulates ATP-utilizing pathways, while AMP often has the opposite effects.

Key Terms

phototroph
chemotroph
metabolism (intermediary metabolism)
adenosine triphosphate (ATP)
catabolism
anabolism
amphibolic pathway
phosphoryl-transfer potential
activated carrier
vitamin
energy charge

Problems

1. Differentiate between anabolism and catabolism. 1

2. Distinguish between a phototroph and a chemotroph. 1

3. What are the three major stages in the energy extraction from food? Assess the contribution of each stage to ATP synthesis. 1

4. What are the three primary uses for cellular energy?

5. What factors account for the high phosphoryl-transfer potential of nucleoside triphosphates? 2

6. The standard free energy of hydrolysis for ATP is $-30.5\ \text{kJ mol}^{-1}\ (-7.3\ \text{kcal mol}^{-1})$.

$$\text{ATP} + \text{H}_2\text{O} \rightleftharpoons \text{ADP} + \text{P}_i$$

How might physiological conditions, such as rest, intense exercise, or an alteration of intracellular ionic environment, alter the free energy of hydrolysis? 3

7. What is the direction of each of the following reactions when the reactants are initially present in equimolar amounts? Use the data given in Table 15.1. 3

a. $\text{ATP} + \text{creatine} \rightleftharpoons \text{creatine phosphate} + \text{ADP}$

b. $\text{ATP} + \text{glycerol} \rightleftharpoons \text{glycerol 3-phosphate} + \text{ADP}$

c. $\text{ATP} + \text{pyruvate} \rightleftharpoons \text{phosphoenolpyruvate} + \text{ADP}$

d. $\text{ATP} + \text{glucose} \rightleftharpoons \text{glucose 6-phosphate} + \text{ADP}$

8. Consider the following reaction:

$$\text{ATP} + \text{pyruvate} \rightleftharpoons \text{phosphoenolpyruvate} + \text{ADP}$$

a. Calculate $\Delta G^{\circ\prime}$ and K'_{eq} at 25°C for this reaction by using the data given in Table 15.1.
b. What is the equilibrium ratio of pyruvate to phosphoenolpyruvate if the ratio of ATP to ADP is 10? 3

9. Using the information in Table 15.1, calculate $\Delta G^{\circ\prime}$ for the isomerization of glucose 6-phosphate to glucose 1-phosphate. What is the equilibrium ratio of glucose 6-phosphate to glucose 1-phosphate at 25°C?

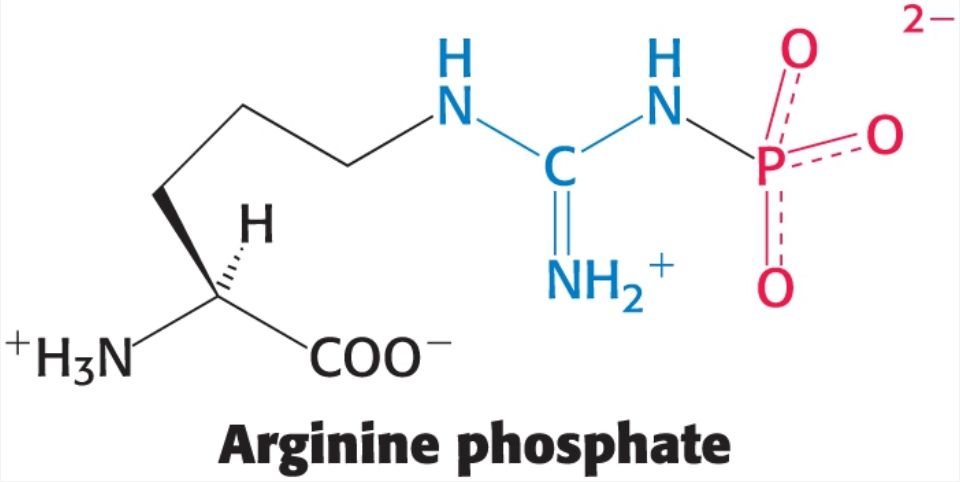
10. The formation of acetyl CoA from acetate is an ATP-driven reaction:

$$\text{Acetate} + \text{ATP} + \text{CoA} \rightleftharpoons \text{acetyl CoA} + \text{AMP} + \text{PP}_i$$

3

a. Calculate $\Delta G^{\circ\prime}$ for this reaction by using data given in this chapter.
b. The PP_i formed in the preceding reaction is rapidly hydrolyzed in vivo because of the ubiquity of inorganic pyrophosphatase. The $\Delta G^{\circ\prime}$ for the hydrolysis of PP_i is $-19.2\ \text{kJ mol}^{-1}(-4.6\ \text{kcal mol}^{-1})$. Calculate the $\Delta G^{\circ\prime}$ for the overall reaction, including pyrophosphate hydrolysis. What effect does the hydrolysis of PP_i have on the formation of acetyl CoA? 3, 5

11. The muscles of some invertebrates are rich in arginine phosphate (phosphoarginine). Propose a function for this amino acid derivative. 2



Arginine phosphate

12. What is the structural feature common to ATP, FAD, NAD^+, and CoA? 5

13. Creatine is a popular dietary supplement.

a. What is the biochemical rationale for the use of creatine?
b. What type of exercise would benefit most from creatine supplementation? 3

14. The enzyme aldolase catalyzes the following reaction in the glycolytic pathway:

$$\text{Fructose 1, 6-bisphosphate} \xrightleftharpoons{\text{Aldolase}} \text{dihydroxyacetone phosphate} + \text{glyceraldehyde 3-phosphate}$$

The $\Delta G^{\circ\prime}$ for the reaction is $+23.8\ \text{kJ mol}^{-1}\ (+5.7\ \text{kcal mol}^{-1})$, whereas the ΔG in the cell is $-1.3\ \text{kJ mol}^{-1}\ (-0.3\ \text{kcal mol}^{-1})$. Calculate the ratio of reactants to products under equilibrium and intracellular conditions. Using your results, explain how the reaction can be endergonic under standard conditions and exergonic under intracellular conditions.

15. The concentrations of ATP, ADP, and P_i differ with cell type. Consequently, the release of free energy with the hydrolysis of ATP will vary with cell type. Using the following table, calculate the ΔG for the hydrolysis of ATP in liver, muscle, and brain cells. In which cell type is the free energy of ATP hydrolysis most negative? 2

	ATP (mM)	ADP (mM)	P_i (mM)
Liver	3.5	1.8	5.0
Muscle	8.0	0.9	8.0

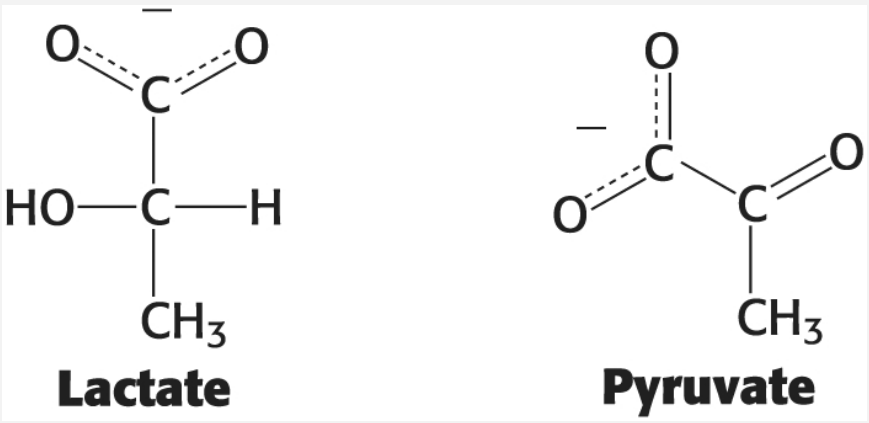
Brain	2.6	0.7	2.7

16. Examine the pairs of molecules and identify the more-reduced molecule in each pair. 4

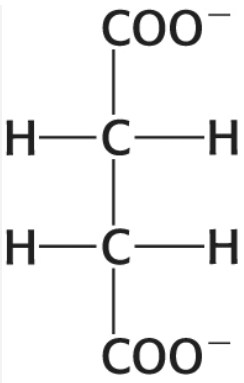
a.



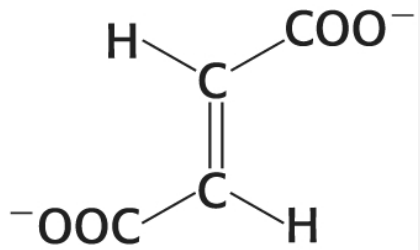
b.



c.

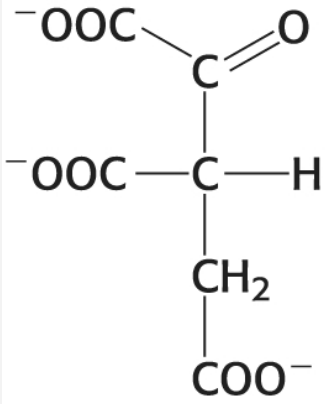


Succinate

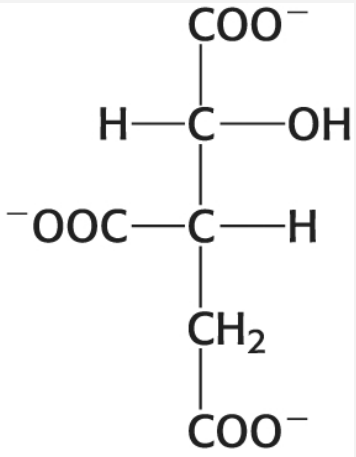


Fumarate

d.

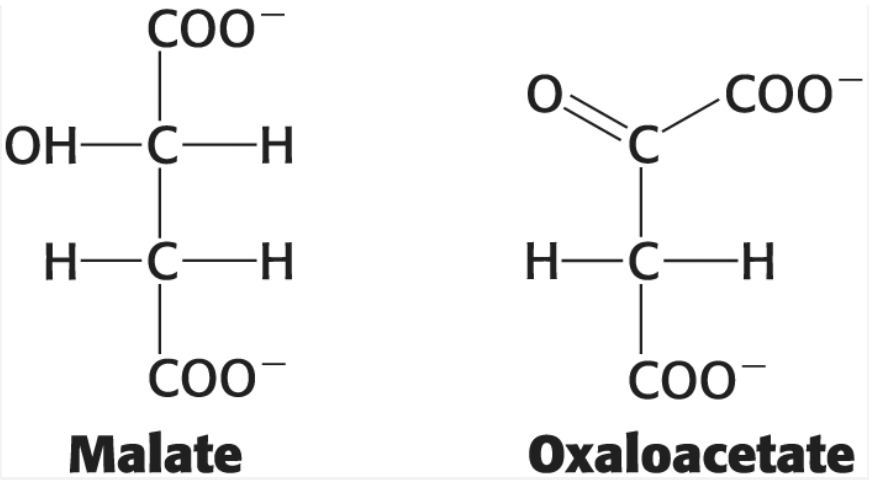


Oxalosuccinate



Isocitrate

e.

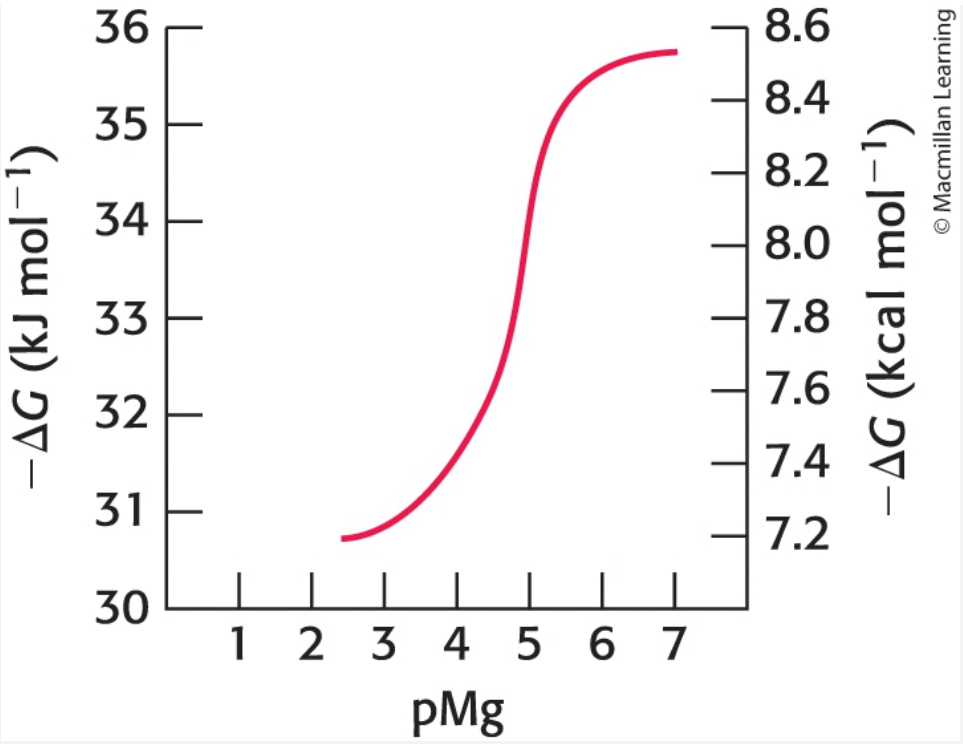


17. What are the activated electron carriers for catabolism? For anabolism? 5

18. What are the six common types of reactions seen in biochemistry? 5

19. What are the three principal means of controlling metabolic reactions described in this chapter? 5

20. The following graph shows how the ΔG for the hydrolysis of ATP varies as a function of the Mg^{2+} concentration, $pMg = -\log[Mg^{2+}]$. 2



a. How does decreasing $[Mg^{2+}]$ affect the ΔG of hydrolysis for ATP?
b. Explain this effect.

Chapter 16
Glycolysis and Gluconeogenesis



Glucose metabolism can generate the ATP to power muscle contraction. During a sprint, when the ATP needs outpace oxygen delivery, glucose is metabolized to lactate (pathway A). When oxygen delivery is adequate, glucose is metabolized more efficiently to carbon dioxide and water (pathway B).

Outline

16.1 Glycolysis Is an Energy-Conversion Pathway in Most Organisms
16.2 Glycolysis Can Be Divided into Two Parts
16.3 The Glycolytic Pathway Is Tightly Controlled
16.4 Glucose Can Be Synthesized from Noncarbohydrate Precursors
16.5 Gluconeogenesis and Glycolysis Are Reciprocally Regulated

Learning Goals



By the end of this chapter, you should be able to:

1. Describe how ATP is generated in glycolysis.
2. Explain why the regeneration of NAD^+ is crucial to fermentations.

3. Describe how gluconeogenesis is powered in the cell.
4. Describe the coordinated regulation of glycolysis and gluconeogenesis.

Our understanding of carbohydrate metabolism has a rich history. Indeed, the development of biochemistry and the delineation of the metabolic pathways that begin with glucose went hand in hand. A key discovery was made in 1897 by a pair of biochemist brothers, Hans and Eduard Buchner, quite by accident. The Buchners were interested in manufacturing cell-free extracts of baker's yeast for possible therapeutic use. These extracts had to be preserved without the use of antiseptics such as phenol, and so they decided to try sucrose, a commonly used preservative in kitchen chemistry. They obtained a startling result: sucrose was rapidly fermented into ethanol by the yeast juice. The Buchners demonstrated for the first time that fermentation could take place outside living cells.

The significance of this finding was immense. The accepted view of their day, asserted by Louis Pasteur in 1860, was that fermentation is inextricably tied to living cells. The chance discovery by the Buchners refuted this dogma. The Buchners' discovery inspired the search for the biochemicals that catalyze the conversion of sucrose into alcohol and opened the door to modern biochemistry.

16.1 Glycolysis Is an Energy-Conversion Pathway in Most Organisms

The first metabolic pathway that we encounter is glycolysis, an ancient energy-conversion pathway employed by a host of organisms. **Glycolysis** is the sequence of reactions that metabolizes one molecule of glucose to two molecules of pyruvate with the concomitant net production of two molecules of ATP. This process is anaerobic, meaning that it does not require O_2, because it evolved before substantial amounts of oxygen accumulated in the atmosphere. Glycolysis is common to virtually all cells, both prokaryotic and eukaryotic. The complete glycolytic pathway is also known as the *Embden-Meyerhof-Parnas pathway*, named after three pioneers of research on glycolysis. As observed accidentally by the Buchners, pyruvate can be further processed anaerobically by fermentation to lactic acid, ethanol, or a variety of other final products depending on the organism. Under aerobic conditions, pyruvate can be completely oxidized to CO_2, generating much more ATP, as will be described in Chapters 17 and 18. **Figure 16.1** shows a few possible fates of pyruvate produced by glycolysis.

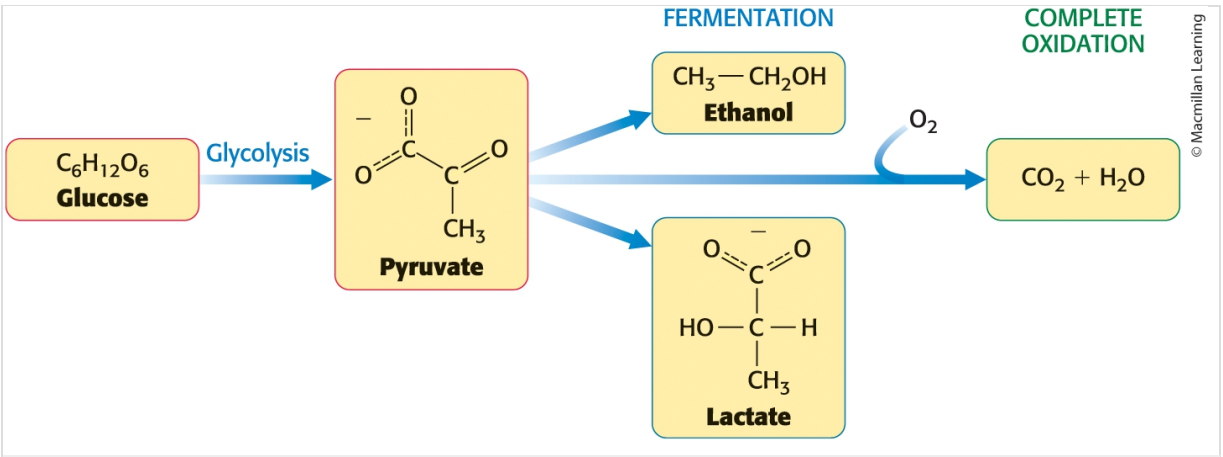


FIGURE 16.1 Glucose can be metabolized to different products depending on the organism and the presence or absence of oxygen.

Recall from Chapter 11 that glucose is a common but yet precious fuel for almost all organisms. In mammals, it is the only fuel that the brain uses under nonstarvation conditions and the only fuel that red blood cells can use at all. Because glucose is such a precious fuel, metabolic products, such as pyruvate and lactate, are salvaged to synthesize glucose in the process of **gluconeogenesis**, but the majority of glucose circulating in our blood each day originates directly from our diet.

Glucose is generated from dietary carbohydrates

In our diets, we typically consume a generous amount of glucose in the form of starch and a smaller amount as glycogen. These complex carbohydrates must be converted into simpler carbohydrates for absorption by the intestine and transport in the blood. Starch and glycogen are digested primarily by the pancreatic

and salivary enzyme α-*amylase*. Amylase cleaves the α-1,4 bonds of starch and glycogen, but not the α-1,6 bonds. The products are the di- and trisaccharides maltose and maltotriose. The material not digestible because of the α-1,6 bonds is called the *limit dextrin*.

α-Glucosidase (maltase) cleaves maltose and maltotriose, as well as any other α-1,4-linked oligosaccharides that may have escaped digestion by the amylase, into glucose molecules. α-Dextrinase further digests the limit dextrin. α-Glucosidase is located on the surface of the intestinal cells, as are sucrase and lactase. Sucrase degrades ingested sucrose to fructose and glucose, while lactase is responsible for degrading the milk sugar lactose into glucose and galactose. The monosaccharides are transported into the endothelial cells lining the intestine by the action of active transporters. Glucose then moves passively down its concentration gradient out of endothelial cells and into the bloodstream, and again passively into cells that will finally utilize it. How is this directional movement from one tissue to another accomplished?

A family of transporters enables glucose to enter and leave animal cells

Several glucose transporters (named GLUT1 to GLUT5) mediate the thermodynamically downhill movement of glucose across the plasma membranes of animal cells. Although all have a 12-transmembrane-helix structure similar to that of lactose permease (Section 13.3), the members of this family have distinctive roles, summarized in **Table 16.1**. GLUT1 and GLUT3, present in nearly all mammalian cells, are responsible for basal glucose uptake. Their K_M value for glucose is about 1 mM, significantly less than the normal blood serum-glucose range of 4–8 mM. Hence, GLUT1 and GLUT3

continually transport glucose into cells at an essentially constant rate.

TABLE 16.1 Family of glucose transporters

Name	Tissue location	K_M	Comments
GLUT 1	All mammalian tissues	1 mM	Basal glucose uptake
GLUT 2	Liver and pancreatic β cells	15–20 mM	In the pancreas, plays a role in the regulation of insulin In the liver, removes excess glucose from the blood
GLUT 3	All mammalian tissues	1 mM	Basal glucose uptake
GLUT 4	Muscle and fat cells	5 mM	Amount in muscle plasma membrane increases with endurance training and in response to insulin
GLUT 5	Small intestine	—	Primarily a fructose transporter

As described in Section 14.3, the number of GLUT4 transporters in the plasma membrane of muscle and fat cells increases rapidly in the presence of insulin, which signals the fed state. Thus, insulin promotes the uptake of glucose by muscle and fat. Endurance exercise training also increases the amount of this transporter

present in muscle membranes. GLUT2 is present in liver and pancreatic β cells but is distinctive in having a very high K_M value for glucose (15–20 mM). Because of this, glucose enters these tissues at a biologically significant rate only when there is much glucose in the blood. The pancreas can sense the glucose level and accordingly adjust the rate of insulin secretion. Lastly, while GLUT5 can also transport glucose, it functions primarily as a fructose transporter in the small intestine. Once finally in the cytoplasm of a glycolytically active cell, glucose and other monosaccharides are ready to enter the glycolytic pathway.

16.2 Glycolysis Can Be Divided into Two Parts

The 10 enzyme-catalyzed reactions that make up the glycolytic pathway can be thought of as comprising two stages (Figure 16.2). Stage 1 is the trapping and preparation phase. No ATP is generated in this stage. In stage 1, glucose is converted into fructose 1,6-bisphosphate in three steps: a phosphorylation, an isomerization, and a second phosphorylation reaction. The strategy of these initial steps in glycolysis is to trap the glucose in the cell and form a compound that can be readily cleaved into phosphorylated three-carbon units (Figure 16.3). Stage 1 is completed with the cleavage of the fructose 1,6-bisphosphate into two three-carbon fragments. These resulting three-carbon units are readily interconvertible. In stage 2, ATP is harvested when the three-carbon fragments are oxidized to pyruvate.

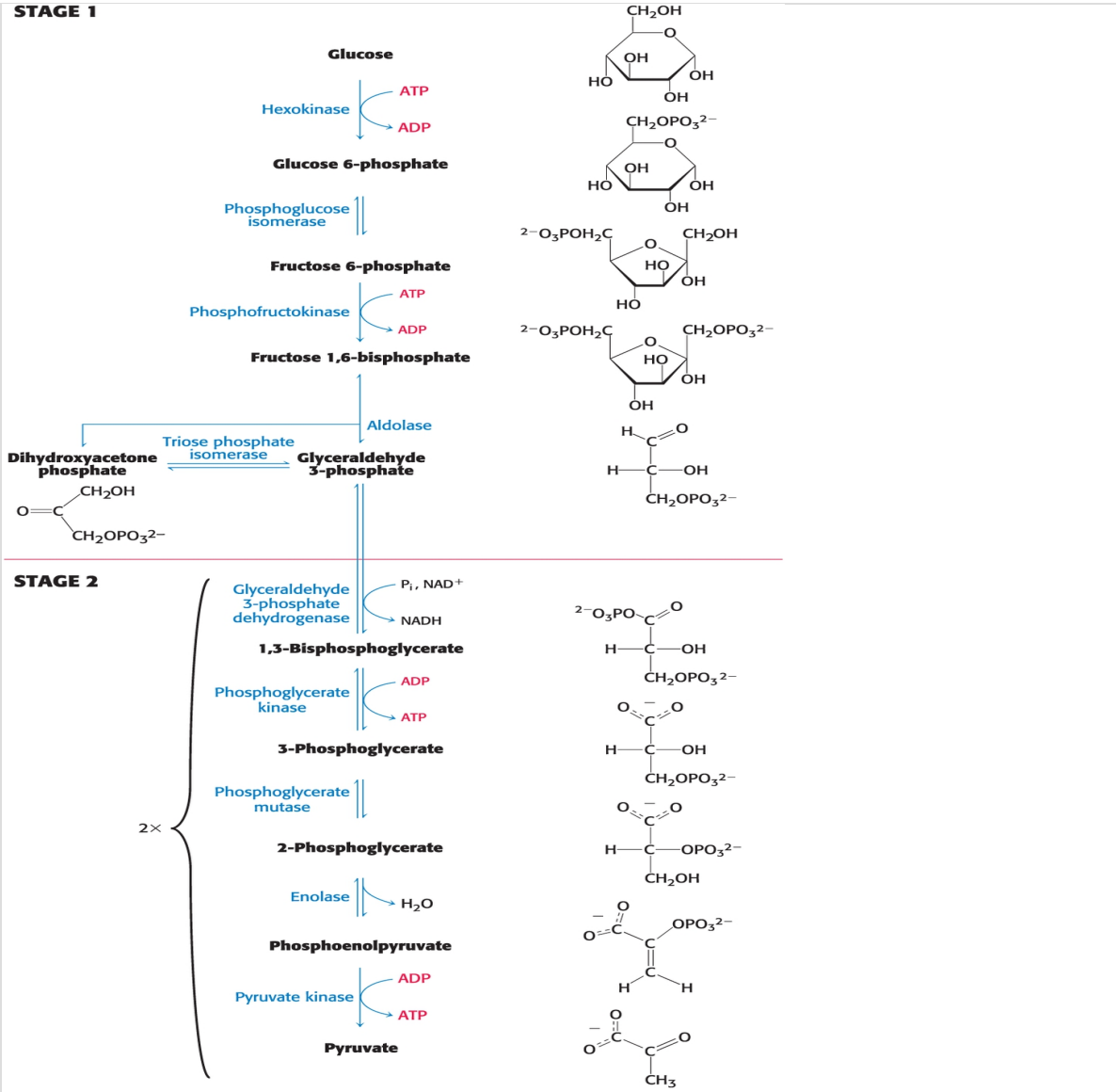


FIGURE 16.2 The glycolytic pathway can be divided into two stages. In Stage 1, glucose is trapped, destabilized, and cleaved into two interconvertible three-carbon molecules generated by cleavage of six-carbon fructose; and in Stage 2, ATP is generated.

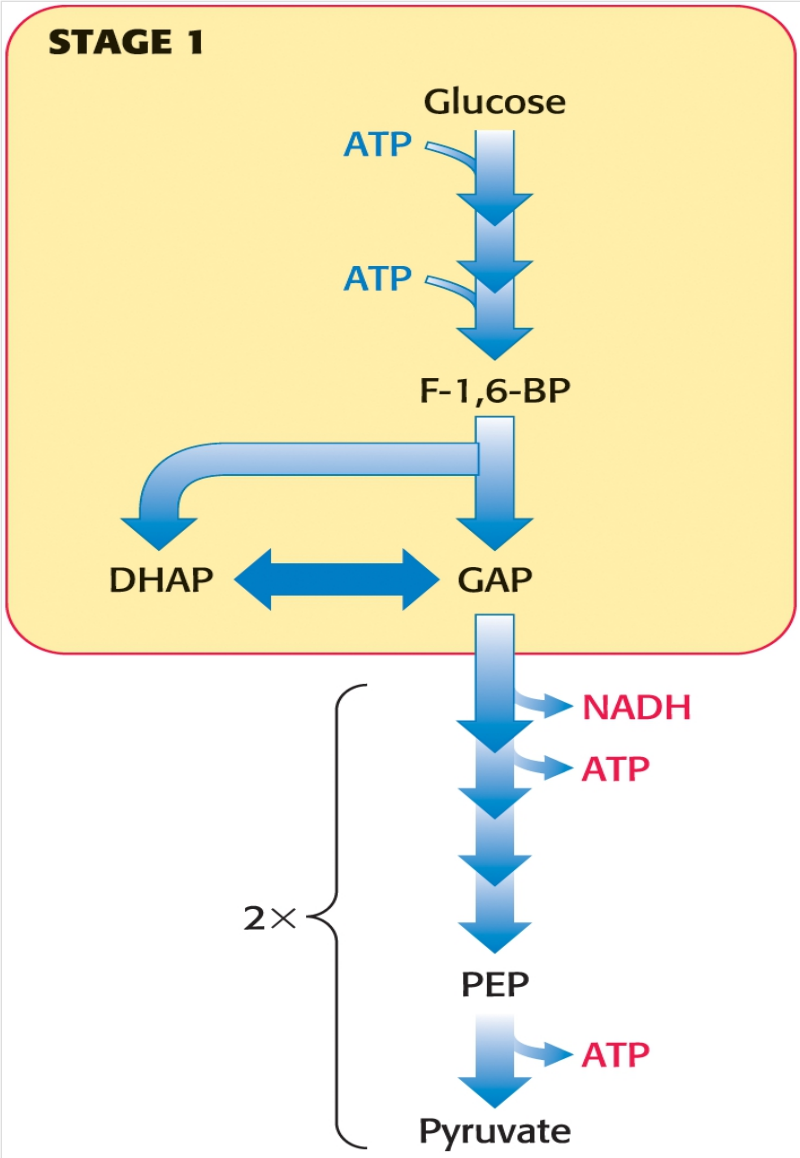
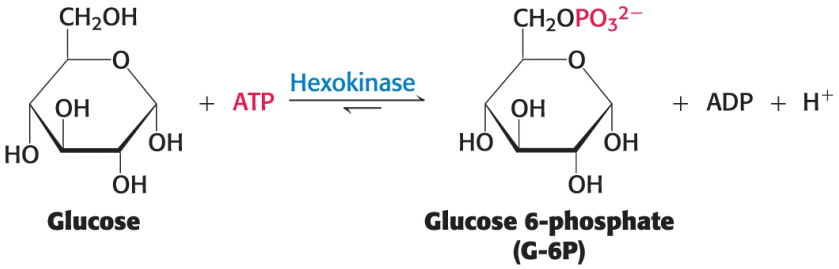


FIGURE 16.3 The first or "investment" stage of glycolysis uses the energy from two molecules of ATP. The products of this stage are two molecules of GAP for every molecule of glucose entering the pathway.

Stage 1 begins: Hexokinase traps glucose in the cell and begins glycolysis

Glucose entering a glycolytically active cell has one principal fate: it is phosphorylated by ATP to form glucose 6-phosphate. This step is notable for several reasons. Glucose 6-phosphate cannot pass through the membrane because of the negative charges on the phosphoryl groups, and it is not a substrate for glucose transporters. Also, the addition of the phosphoryl group facilitates the eventual metabolism of glucose into three-carbon molecules with high phosphoryl-transfer potential. The transfer of the phosphoryl group from ATP to the hydroxyl group on carbon 6 of glucose is catalyzed by hexokinase.



Phosphoryl transfer is a fundamental reaction in biochemistry. **Kinases** are enzymes that catalyze the transfer of a phosphoryl group from ATP to an acceptor, or to ADP from a phosphoryl donor. Hexokinase, then, catalyzes the transfer of a phosphoryl group from ATP to a variety of six-carbon sugars (hexoses), such as glucose and mannose. Hexokinase, like adenylate kinase (Section 6.1) and all other kinases, requires Mg^{2+} (or another divalent metal ion such as Mn^{2+}) for activity. The divalent metal ion forms a complex with ATP.

X-ray crystallographic studies of yeast hexo-kinase revealed that the binding of glucose induces a large conformational change in the enzyme. Hexokinase consists of two lobes, which move toward each other when glucose is bound (**Figure 16.4**). On glucose binding, one lobe rotates 12 degrees with respect to the other, resulting in movements of the polypeptide backbone of as much as 8 Å. The cleft between the lobes closes, and the bound glucose becomes surrounded by protein, except for the hydroxyl group of carbon 6, which will accept the phosphoryl group from ATP. The closing of the cleft in hexokinase is a striking example of the role of induced fit in enzyme action (Section 5.3).

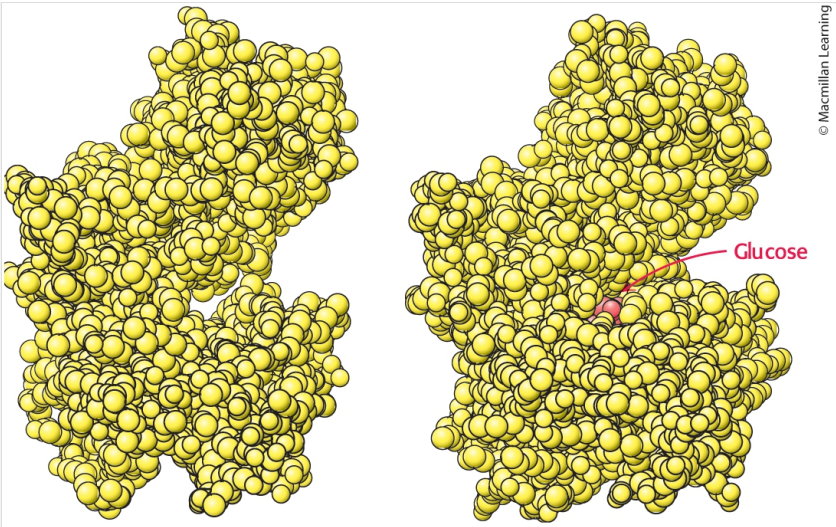


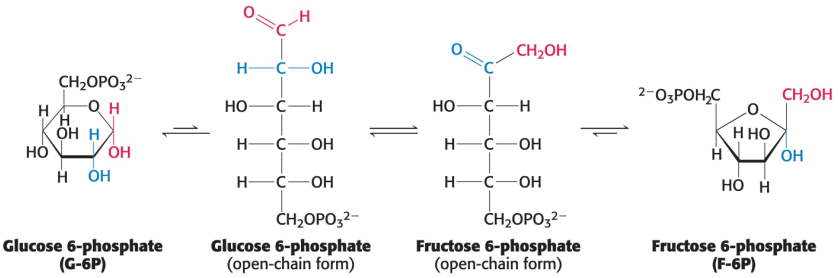
FIGURE 16.4 The induced fit of hexokinase is due to large structural changes upon binding the first of its two substrates. The two lobes of hexokinase are separated in the absence of glucose (left). The conformation of hexokinase changes markedly on binding glucose as the two lobes of the enzyme come together, creating the necessary environment for catalysis (right).

[Drawn from 2YHX.pdb and 1HKG.pdb.]

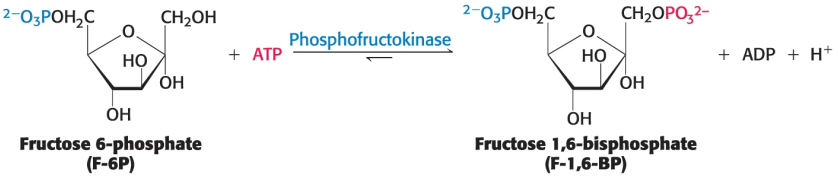
The glucose-induced structural changes are significant in two respects. First, the environment around the glucose becomes more nonpolar, which favors reaction between the hydrophilic hydroxyl group of glucose and the terminal phosphoryl group of ATP. Second, the conformational changes enable the kinase to discriminate against H_2O as a substrate. The closing of the cleft keeps water molecules away from the active site. If hexokinase were rigid, a molecule of H_2O occupying the binding site for the $-CH_2OH$ of glucose could attack the γ phosphoryl group of ATP, forming ADP and P_i. In other words, a rigid kinase would likely also be an ATPase.

Fructose 1,6-bisphosphate is generated from glucose 6-phosphate

A crucial step toward completion of the first phase of glycolysis — the formation of fructose 1,6-bisphosphate — is the isomerization of glucose 6-phosphate to fructose 6-phosphate. Recall that the open-chain form of glucose has an aldehyde group at carbon 1, whereas the open-chain form of fructose has a keto group at carbon 2. Thus, the isomerization of glucose 6-phosphate to fructose 6-phosphate is a conversion of an aldose into a ketose. The reaction catalyzed by phosphoglucose isomerase takes several steps because both glucose 6-phosphate and fructose 6-phosphate are present primarily in the cyclic forms. The enzyme must first open the six-membered ring of glucose 6-phosphate, catalyze the isomerization, and then promote the formation of the five-membered ring of fructose 6-phosphate.



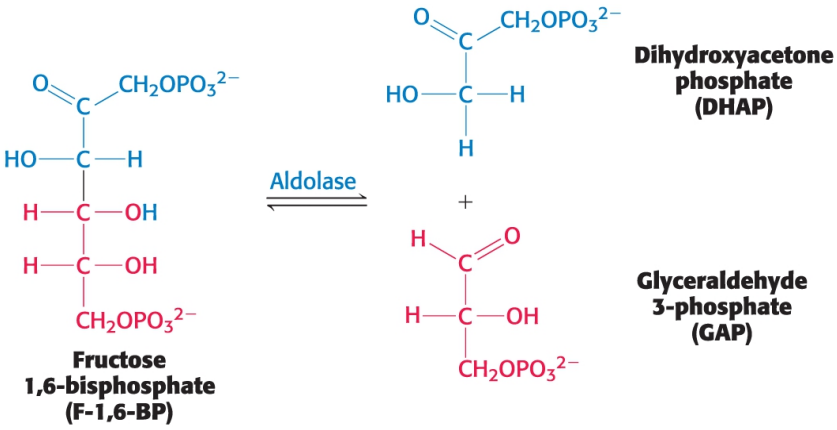
A second phosphorylation reaction follows the isomerization step. Fructose 6-phosphate is phosphorylated at the expense of ATP to fructose 1,6-bisphosphate (F-l,6-BP). The prefix *bis-* in bisphosphate means that two separate monophosphoryl groups are present, whereas the prefix *di-* in diphosphate (as in adenosine diphosphate) means that two phosphoryl groups are present and are connected by an anhydride linkage.



This reaction is catalyzed by phosphofructokinase (PFK), an allosteric enzyme that sets the pace of glycolysis. As we will learn, this enzyme plays a central role in the metabolism of many molecules in all parts of the body.

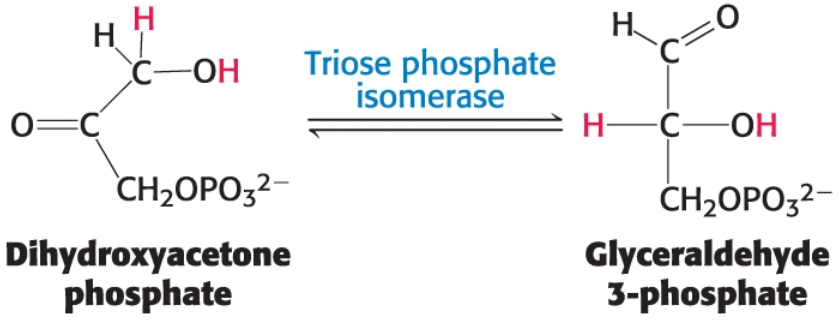
The six-carbon sugar is cleaved into two three-carbon fragments

The newly formed fructose 1,6-bisphosphate is cleaved into glyceraldehyde 3-phosphate (GAP) and dihydroxyacetone phosphate (DHAP), completing stage 1 of glycolysis. The products of the remaining steps in glycolysis consist of three-carbon units rather than six-carbon units. This reaction, which is readily reversible, is catalyzed by aldolase. This enzyme derives its name from the nature of the reverse reaction, an aldol addition.



What is the biochemical rationale for the isomerization of glucose 6-phosphate to fructose 6-phosphate and its subsequent phosphorylation to form fructose 1,6-bisphosphate? First, phosphorylation of the fructose 6-phosphate to fructose 1,6-bisphosphate prevents the reformation of glucose 6-phosphate. Second, and perhaps more important, had the aldol cleavage taken place in the aldose glucose, a two-carbon and a four-carbon fragment would have resulted. Two different metabolic pathways — one to process the two-carbon fragment and one for the four-carbon fragment — would have been required to extract energy. Instead, the cleavage of fructose 1,6-bisphosphate yields two phosphorylated interconvertible three-carbon fragments that will be oxidized in the later steps of glycolysis to capture energy in the form of ATP.

Glyceraldehyde 3-phosphate is on the direct pathway of glycolysis, whereas dihydroxyacetone phosphate is not. Unless a means exists to convert dihydroxyacetone phosphate into glyceraldehyde 3-phosphate, a three-carbon fragment useful for generating ATP will be lost. These compounds are isomers that can be readily interconverted: dihydroxyacetone phosphate is a ketose, whereas glyceraldehyde 3-phosphate is an aldose. The isomerization of these three-carbon phosphorylated sugars is catalyzed by triose phosphate isomerase (TPI, sometimes abbreviated TIM).



This reaction is rapid and reversible. At equilibrium, 96% of the triose phosphate is dihydroxyacetone phosphate. However, the reaction proceeds readily from dihydroxyacetone phosphate to glyceraldehyde 3-phosphate because the subsequent reactions of glycolysis remove this product.

Mechanism: Triose phosphate isomerase salvages a three-carbon fragment

Much is known about the catalytic mechanism of triose phosphate isomerase (Figure 16.5). TPI catalyzes the transfer of a hydrogen atom from carbon 1 to carbon 2, an intramolecular oxidation–reduction. This isomerization of a ketose into an aldose proceeds through an enediol intermediate (Figure 16.6).

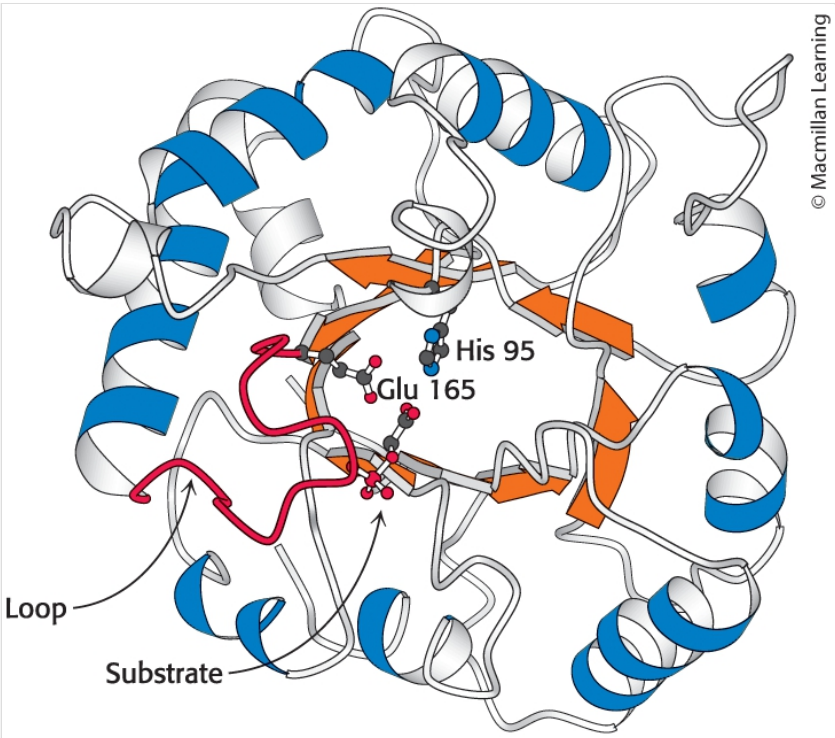


FIGURE 16.5 Triose phosphate isomerase is an example of a common "barrel" motif, with the active site buried in the center. This enzyme consists of a central core of eight parallel β strands (orange) surrounded by eight α helices (blue). This structural motif, called an αβ barrel or a TIM barrel because of this enzyme, is also found in the glycolytic enzymes aldolase, enolase, and pyruvate kinase. Notice that histidine 95 and glutamate 165, essential components of the active site of triose phosphate isomerase, are located in the barrel. A loop (red) closes off the active site on substrate binding.

[Drawn from 2YPI.pdb.]

INTERACT with this model in Achieve

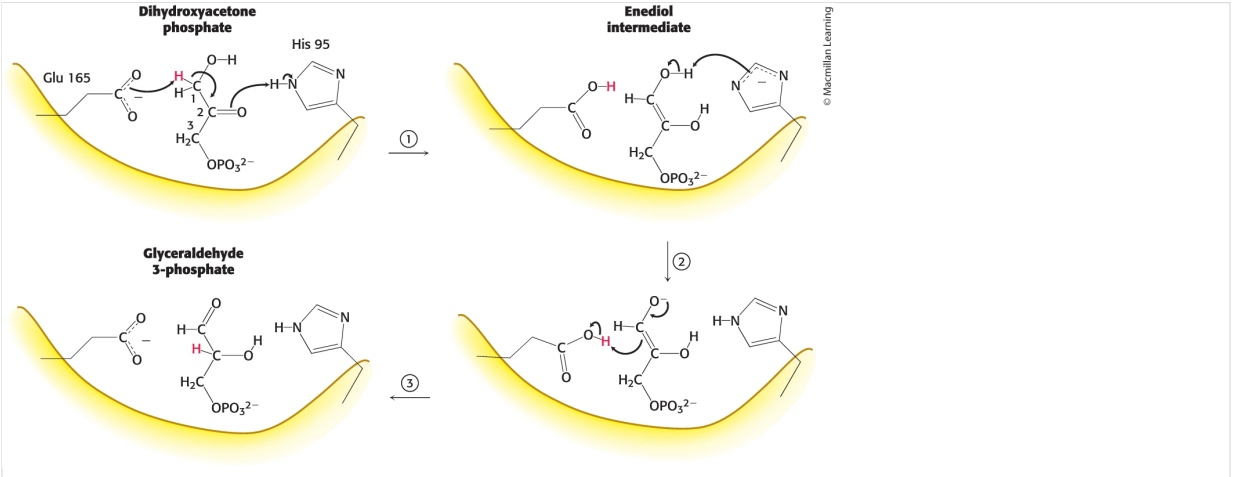
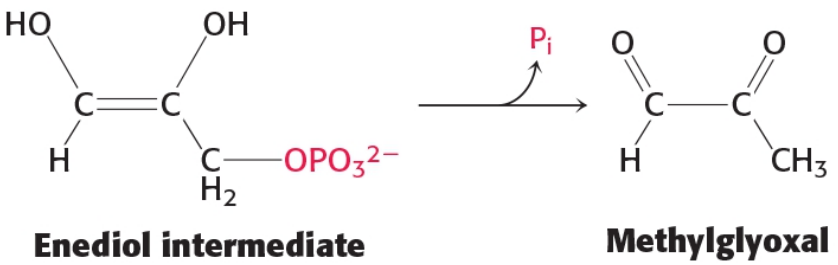


FIGURE 16.6 The catalytic mechanism of triose phosphate isomerase is an acid/base mechanism proceeding through an enediol intermediate. (1) Glutamate 165 acts as a general base by abstracting a proton (H^+) from carbon 1. Histidine 95, acting as a general acid, donates a proton to the oxygen atom bonded to carbon 2, forming the enediol intermediate. (2) Glutamic acid, now acting as a general acid, donates a proton to C-2, while histidine removes a proton from the OH group of C-1. (3) The product is formed, and glutamate and histidine are returned to their ionized and neutral forms, respectively.

X-ray crystallographic and other studies showed that glutamate 165 plays the role of a general acid–base catalyst: it abstracts a proton (H^+) from carbon 1 and then donates it to carbon 2. However, the carboxylate group of glutamate 165 by itself is not basic enough to pull a proton away from a carbon atom adjacent to a carbonyl group. Histidine 95 assists catalysis by donating a proton to stabilize the negative charge that develops on the C-2 carbonyl group.

Two features of this enzyme are noteworthy. First, TPI displays great catalytic prowess. It accelerates isomerization by a factor of 10^{10} compared with the rate obtained with a simple base catalyst such as acetate ion. Indeed, the k_{cat}/K_M ratio for the isomerization of glyceraldehyde 3-phosphate is $2 \times 10^8\ M^{-1}\,s^{-1}$, which is close to the diffusion-controlled limit. In other words, catalysis takes place every time that enzyme and substrate meet. The diffusion-controlled encounter of substrate and enzyme is thus the rate-limiting step in catalysis. TPI is an example of a kinetically perfect enzyme (Section 5.4). Second, TPI suppresses an undesired side reaction, the decomposition of the enediol intermediate into methylglyoxal and orthophosphate.



In solution, this physiologically useless reaction is 100 times as fast as isomerization. Moreover, methylglyoxal is a highly reactive compound that can modify the structure and function of a variety of biomolecules, including proteins and DNA. The reaction of methylglyoxal with a biomolecule is an example of deleterious reactions called advanced glycation end products, discussed earlier (AGEs, Section 11.1). Hence, TPI must prevent the enediol from leaving the enzyme. This labile intermediate is trapped in the active site by the movement of a loop of 10 residues (Figure 16.5). This loop serves as a lid on the active site, shutting it when the enediol is present and reopening it when isomerization is completed. We see here a striking example of one means of preventing an undesirable alternative reaction: the active site is kept closed until the desirable reaction takes place.

Thus, two molecules of glyceraldehyde 3-phosphate are formed from one molecule of fructose 1,6-bisphosphate by the sequential action of aldolase and triose phosphate isomerase. The economy of metabolism is evident in this reaction sequence. The isomerase funnels dihydroxyacetone phosphate into the main glycolytic pathway; a separate set of reactions is not needed.

Stage 2 begins: The oxidation of an aldehyde powers the formation of a compound with high phosphoryl-transfer potential

The preceding steps in glycolysis have transformed one molecule of glucose into two molecules of glyceraldehyde 3-phosphate, but no energy has yet been extracted. On the contrary, thus far, two molecules of ATP have been invested. We come now to the second stage of glycolysis — a series of steps that harvest some of the energy contained in glyceraldehyde 3-phosphate as ATP (**Figure 16.7**).

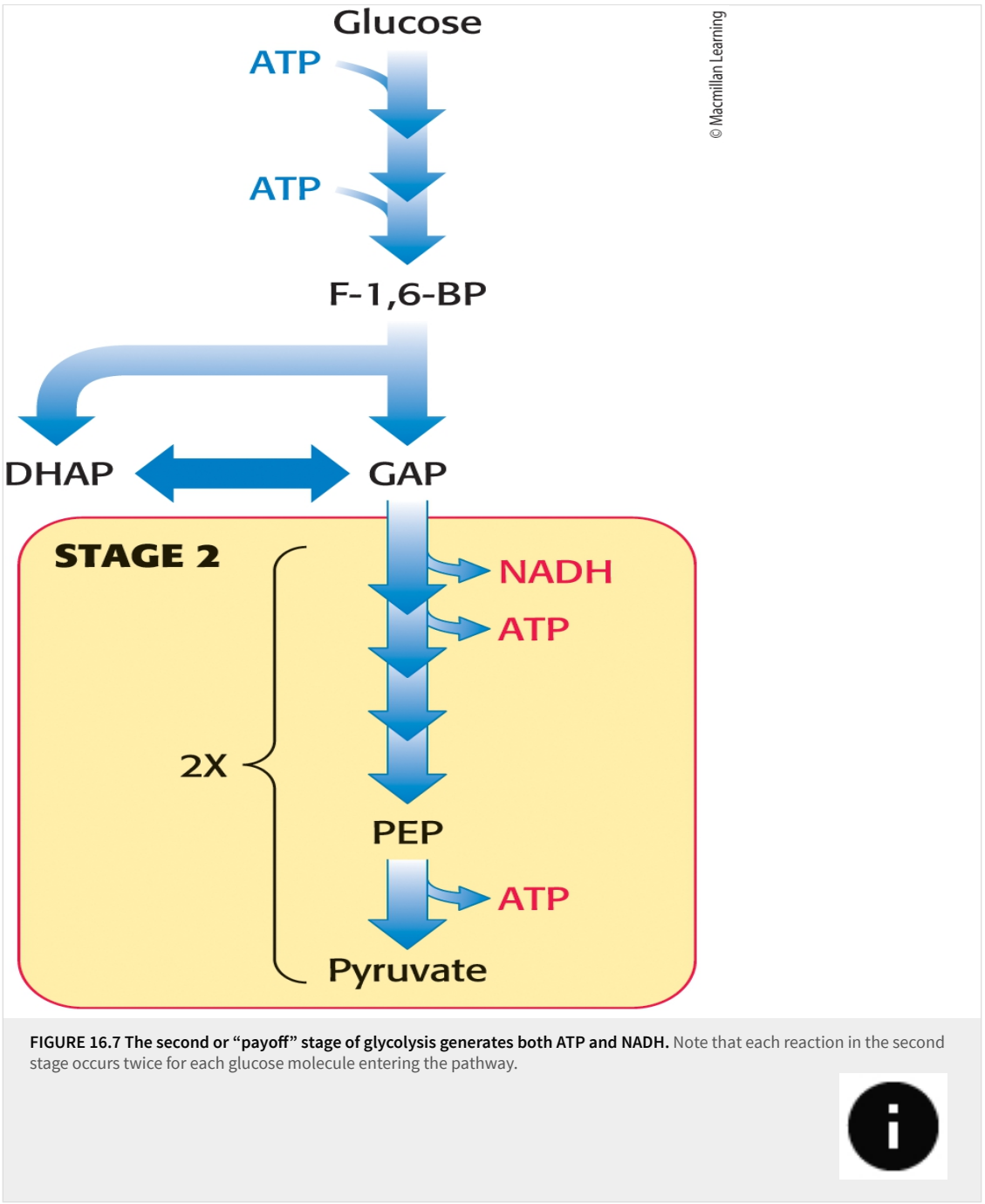
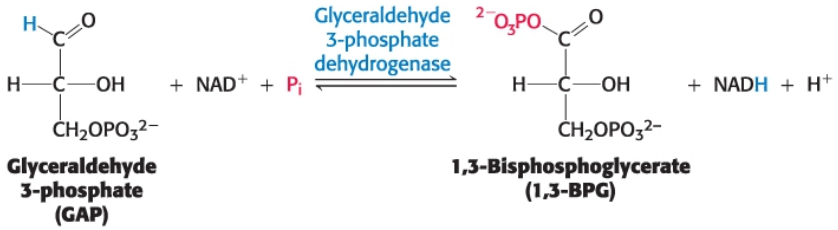


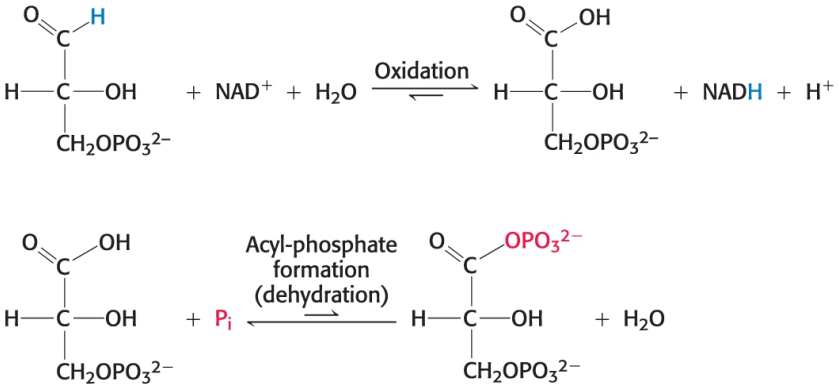
FIGURE 16.7 The second or "payoff" stage of glycolysis generates both ATP and NADH. Note that each reaction in the second stage occurs twice for each glucose molecule entering the pathway.

The initial reaction in this sequence is the conversion of glyceraldehyde 3-phosphate into 1,3-bisphosphoglycerate (1,3-BPG), a reaction catalyzed by glyceraldehyde 3-phosphate dehydrogenase (GAPDH).



1,3-Bisphosphoglycerate is an acyl phosphate, which is a mixed anhydride of phosphoric acid and a carboxylic acid. Such compounds have a high phosphoryl-transfer potential (Section 15.2); one of its phosphoryl groups is transferred to ADP in the next step in glycolysis.

The reaction catalyzed by GAPDH can be viewed as the sum of two processes: the oxidation of the aldehyde to a carboxylic acid by NAD^+, and the joining of the carboxylic acid and orthophosphate to form the acyl-phosphate product.



The first reaction is thermodynamically quite favorable, with a standard free-energy change, $\Delta G^{\circ\prime}$, of approximately $-50\ \text{kJ mol}^{-1}\ (-12\ \text{kcal mol}^{-1})$, whereas the second reaction is quite unfavorable, with a standard free-energy change of the same magnitude but the opposite sign. If these two reactions simply took place in succession, the second reaction would have a very large activation energy and thus not take place at a biologically significant rate. These two processes must be coupled so the favorable aldehyde oxidation can be used to drive the formation of the acyl phosphate.

How are these reactions coupled? The key is an intermediate, formed as a result of the aldehyde oxidation, that is connected to the enzyme by a thioester linkage (Section 15.4). The thioester intermediate, which is higher in free energy than the free carboxylic acid is, couples the favorable oxidation and the unfavorable phosphorylation reactions. This coupling preserves much of the free

energy released in the oxidation reaction. The thioester intermediate reacts with orthophosphate to form the high-energy compound 1,3-bisphosphoglycerate.

We see here the use of a covalent enzyme-bound intermediate as a mechanism of energy coupling. A free-energy profile of the GAPDH reaction, compared with a hypothetical process in which the reaction proceeds without this intermediate, reveals how this intermediate allows a favorable process to drive an unfavorable one (Figure 16.8).

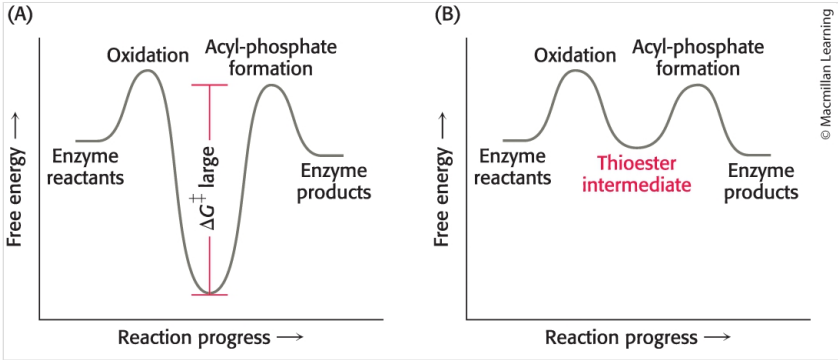


FIGURE 16.8 Free-energy profiles for glyceraldehyde oxidation followed by acyl-phosphate formation demonstrate the importance of the reaction coupling. (A) A hypothetical case with no coupling between the two processes. The second step would have a very large activation barrier, making the reaction very slow. (B) The actual case with the two reactions coupled through a thioester intermediate vastl accelerates the reaction and allows a favorable reaction to drive an unfavorable one.

Mechanism: Phosphorylation is coupled to the oxidation of glyceraldehyde 3-phosphate by a thioester intermediate

The active site of GAPDH includes a reactive cysteine residue, as well as NAD^+ and a crucial histidine (Figure 16.9).

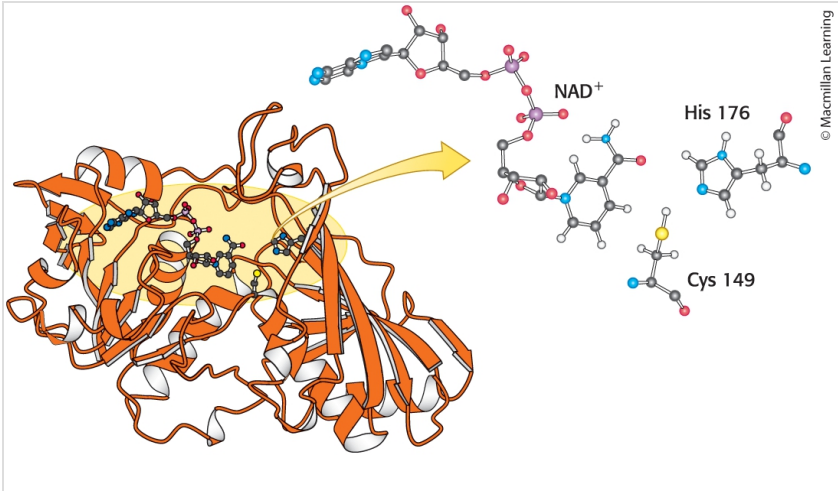


FIGURE 16.9 The active site of GAPDH includes cysteine and histidine residues adjacent to a bound NAD^+ molecule. The sulfur atom of cysteine will react with the substrate to form a transitory thioester intermediate.

[Drawn from 1GAD.pdb.]

INTERACT with this model in Achieve

Let's consider in detail how these components cooperate in the reaction mechanism (Figure 16.10) in the following four steps:

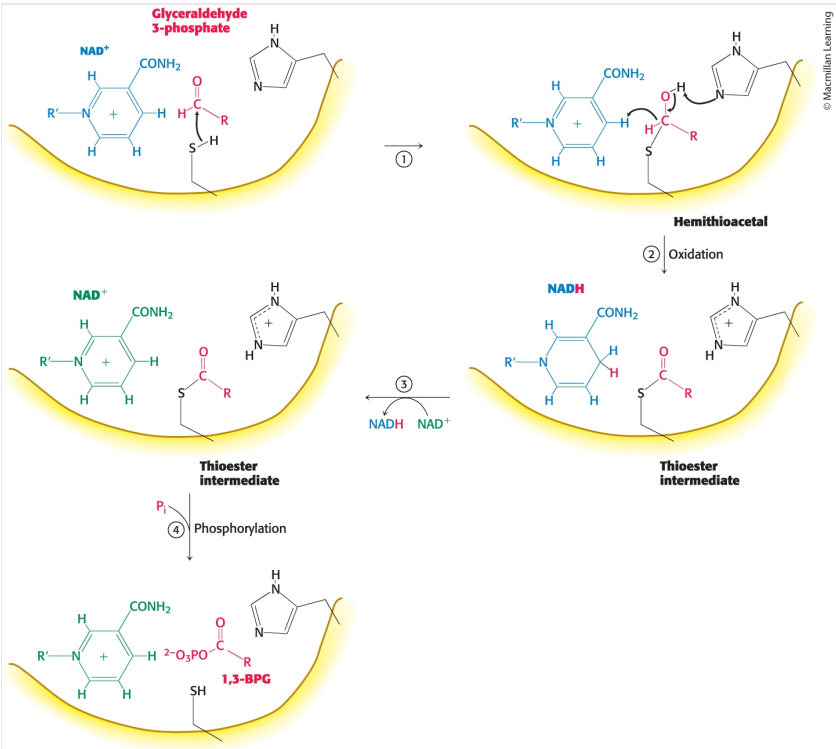


FIGURE 16.10 The catalytic mechanism of GAPDH is an example of covalent catalysis to form a key intermediate. The reaction proceeds through a thioester intermediate, which allows the oxidation of glyceraldehyde to be coupled to the phosphorylation of 3-phosphoglycerate. (1) Cysteine reacts with the aldehyde group of the substrate, forming a hemithioacetal. (2) An oxidation takes place with the transfer of a hydride ion to NAD^+, forming a thioester. This reaction is facilitated by the transfer of a proton to histidine. (3) The reduced NADH is exchanged for an NAD^+ molecule. (4) Orthophosphate attacks the thioester, forming the product 1,3-BPG.

1. The aldehyde substrate reacts with the sulfhydryl group of cysteine 149 on the enzyme to form a hemithioacetal.

2. The hydride ion is transferred to a molecule of NAD^+ that is bound to the enzyme and is adjacent to the cysteine residue. This reaction is favored by the deprotonation of the hemithioacetal by histidine 176. The products are the reduced coenzyme NADH and a thioester intermediate. This thioester intermediate has a free energy close to that of the reactants (Figure 16.8).

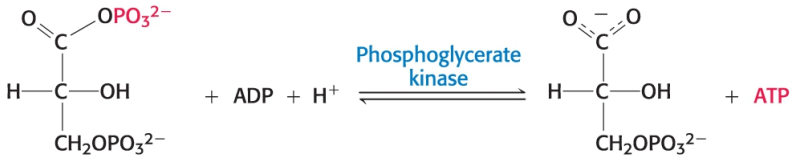
3. The NADH formed from the aldehyde oxidation leaves the enzyme and is replaced by a second molecule of NAD^+. This step is important because the positive charge on NAD^+ polarizes the thioester intermediate to facilitate the attack by orthophosphate.

4. The orthophosphate attacks the thioester to form 1,3-BPG and free the cysteine residue.

This example illustrates the essence of energy transformations and of metabolism itself: energy released by carbon oxidation is converted into high phosphoryl-transfer potential.

ATP is formed by phosphoryl transfer from 1,3-bisphosphoglycerate

1,3-Bisphosphoglycerate is an energy-rich molecule with a greater phosphoryl-transfer potential than that of ATP (Section 15.2). Thus, 1,3-BPG can be used to power the synthesis of ATP from ADP. Phosphoglycerate kinase catalyzes the transfer of the phosphoryl group from the acyl phosphate of 1,3-bisphosphoglycerate to ADP; ATP and 3-phosphoglycerate are the products.



1,3-Bisphosphoglycerate **3-Phosphoglycerate**

The formation of ATP in this manner is referred to as **substrate-level phosphorylation** because the phosphate donor, 1,3-BPG, is a substrate with high phosphoryl-transfer potential. We will contrast this manner of ATP formation with the formation of ATP from ionic gradients in Chapters 18 and 19.

Thus, the outcomes of the reactions catalyzed by glyceraldehyde 3-phosphate dehydrogenase and phosphoglycerate kinase are:

1. Glyceraldehyde 3-phosphate, an aldehyde, is oxidized to 3-phosphoglycerate, a carboxylic acid.

2. NAD^+ is concomitantly reduced to NADH.

3. ATP is formed from P_i and ADP at the expense of carbon-oxidation energy.

In essence, the energy released during the oxidation of glyceraldehyde 3-phosphate to 3-phosphoglycerate is temporarily trapped as 1,3-bisphosphoglycerate. This energy powers the transfer of

a phosphoryl group from 1,3-bisphosphoglycerate to ADP to yield ATP. Keep in mind that, because of the actions of aldolase and triose phosphate isomerase, two molecules of glyceraldehyde 3-phosphate were formed, and hence two molecules of ATP were generated. These ATP molecules make up for the two molecules of ATP consumed in the first stage of glycolysis.

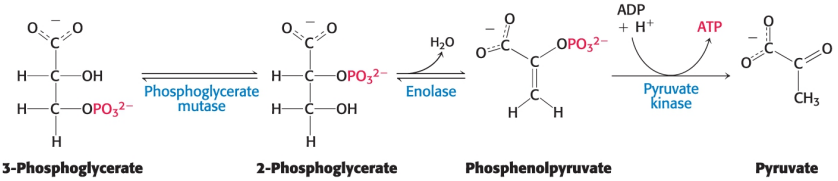
Self-Check Question



Arsenate (AsO_4^{3-}) resembles P_i in structure and reactivity closely enough that GAPDH can incorporate arsenate instead of phosphate. The product, 1-arseno-3-phosphoglycerate, is highly unstable and rapidly hydrolyzed by the surrounding water molecules producing 3-phosphoglycerate and arsenate. Based on this information, what would be the effect of arsenate on ATP generation in a cell?

Additional ATP is generated with the formation of pyruvate

In the remaining steps of glycolysis, 3-phosphoglycerate is converted into pyruvate, and a second molecule of ATP is formed from ADP.



The first reaction is a rearrangement. The position of the phosphoryl group shifts in the conversion of 3-phosphoglycerate into 2-phosphoglycerate, a reaction catalyzed by phosphoglycerate mutase. In general, a mutase is an enzyme that catalyzes the intramolecular shift of a chemical group, such as a phosphoryl group. The phosphoglycerate mutase reaction has an interesting mechanism: the phosphoryl group is not simply moved from one carbon atom to another. This enzyme requires catalytic amounts of 2,3-bisphosphoglycerate (2,3-BPG) to maintain an active-site histidine residue in a phosphorylated form. This phosphoryl group is transferred to 3-phosphoglycerate to reform 2,3-bisphosphoglycerate.

Enz-His-phosphate + 3-phosphoglycerate $\rightleftharpoons$ Enz-His + 2,3-bisphosphoglycerate

The mutase then functions as a phosphatase: it converts 2,3-bisphosphoglycerate into 2-phosphoglycerate. The mutase retains the phosphoryl group to regenerate the modified histidine.

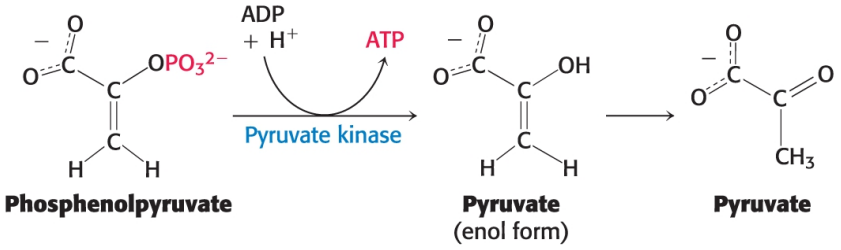
Enz-His + 2,3-bisphosphoglycerate $\rightleftharpoons$ Enz-His-phosphate + 2-phosphoglycerate

The sum of these reactions yields the mutase reaction:

3-Phosphoglycerate $\rightleftharpoons$ 2-phosphoglycerate

In the next reaction, the dehydration of 2-phosphoglycerate introduces a double bond, creating an enol. Enolase catalyzes this formation of the enol phosphate phosphoenolpyruvate (PEP). This dehydration markedly elevates the transfer potential of the phosphoryl group. An enol phosphate has a high phosphoryl-transfer potential, whereas the phosphate ester of an ordinary alcohol, such as 2-phosphoglycerate, has a low one. The $\Delta G^{\circ\prime}$ of the hydrolysis of a phosphate ester of an ordinary alcohol is $-13\ \text{kJ mol}^{-1}\ (-3\ \text{kcal mol}^{-1})$, while that of phosphoenolpyruvate is $-62\ \text{kJ mol}^{-1}\ (-15\ \text{kcal mol}^{-1})$.

Why does phosphoenolpyruvate have such a high phosphoryl-transfer potential? The phosphoryl group traps the molecule in its unstable enol form. When the phosphoryl group has been donated to ATP, the enol undergoes a conversion into the more stable ketone — namely, pyruvate.



Thus, the high phosphoryl-transfer potential of phosphoenolpyruvate arises primarily from the large driving force of the subsequent enol–ketone conversion. Hence, pyruvate is formed, and ATP is generated concomitantly. The virtually irreversible transfer of a phosphoryl group from phosphoenolpyruvate to ADP is catalyzed by pyruvate kinase.

What is the energy source for the formation of phosphoenolpyruvate? The answer to this question becomes clear when we compare the structures of 2-phosphoglycerate and pyruvate. The formation of pyruvate from 2-phosphoglycerate is, in essence, an internal oxidation–reduction reaction; carbon 3 takes electrons from carbon 2 in the conversion of 2-phosphoglycerate into pyruvate. Compared with 2-

phosphoglycerate, C-3 is more reduced in pyruvate, whereas C-2 is more oxidized. Once again, carbon oxidation powers the synthesis of a compound with high phosphoryl-transfer potential, phosphoenolpyruvate here and 1,3-bisphosphoglycerate earlier, which allows the synthesis of ATP.

Because the molecules of ATP used in forming fructose 1,6-bisphosphate have already been regenerated, the two molecules of ATP generated from phosphoenolpyruvate are "profit."

Two ATP molecules are formed in the conversion of glucose into pyruvate

The net reaction in the transformation of glucose into pyruvate is

$$\text{Glucose} + 2\ P_i + 2\ \text{ADP} + 2\ \text{NAD}^+ \rightarrow 2\ \text{pyruvate} + 2\ \text{ATP} + 2\ \text{NADH} + 2\ \text{H}^+ + 2\ \text{H}_2\text{O}$$

Thus, two molecules of ATP are generated in the conversion of glucose into two molecules of pyruvate. The reactions of glycolysis are summarized in Table 16.2.

TABLE 16.2 Reactions of glycolysis

Step	Reaction	Enzyme	Reaction type	$\Delta G^{\circ\prime}$ in kJ mol^{-1} (kcal mol
1	Glucose + ATP → glucose 6–phosphate + ADP + H^+	Hexokinase	Phosphoryl transfer	−16.7 (−4.0)
2	Glucose 6-phosphate ⇌ fructose 6-phosphate	Phosphoglucose isomerase	Isomerization	+1.7 (+0.4)
3	Fructose 6–phosphate + ATP → fructose 1,6–bisphosphate + ADP + H^+	Phosphofructokinase	Phosphoryl transfer	−14.2 (−3.4)
4	Fructose 1,6-bisphosphate ⇌ dihydroxyacetone phosphate + glyceraldehyde 3-phosphate	Aldolase	Aldol cleavage	+23.8 (+5.7)
5	Dihydroxyacetone phosphate ⇌ glyceraldehyde 3-phosphate	Triose phosphate isomerase	Isomerization	+7.5 (+1.8)

TABLE 16.2 Reactions of glycolysis

Step	Reaction	Enzyme	Reaction type	$\Delta G^{\circ\prime}$ in kJ mol^{-1} (kcal mol^{-1})
6	Glyceraldehyde 3-phosphate + P_i + NAD^+ ⇌ 1,3-bisphosphoglycerate + NADH + H^+	Glyceraldehyde 3-phosphate dehydrogenase	Phosphorylation coupled to oxidation	+6.3 (+1.5)
7	1,3-Bisphosphoglycerate + ADP ⇌ 3-phosphoglycerate + ATP	Phosphoglycerate kinase	Phosphoryl transfer	−18.8 (−4.5)
8	3-Phosphoglycerate ⇌ 2-phosphoglycerate	Phosphoglycerate mutase	Phosphoryl shift	+4.6 (+1.1)
9	2-Phosphoglycerate ⇌ phosphoenolpyruvate + H_2O	Enolase	Dehydration	+1.7 (+0.4)
10	Phosphoenolpyruvate + ADP + H^+ → pyruvate + ATP	Pyruvate kinase	Phosphoryl transfer	−31.4 (−7.5)

Note: ΔG, the actual free-energy change, has been calculated from $\Delta G^{\circ\prime}$ and known concentrations of reactants under typical physiological conditions. Glycolysis can proceed only if the ΔG values of all reactions are negative. The small positive ΔG values of three of the above reactions indicate that the concentrations of metabolites in vivo in cells undergoing glycolysis are not precisely known.

The energy released in the anaerobic conversion of glucose into two molecules of pyruvate is about $-90\ \text{kJ mol}^{-1}$ ($-22\ \text{kcal mol}^{-1}$). We shall see in Chapters 17 and 18 that much more energy can be released from glucose in the presence of oxygen.

Self-Check Question

The conversion of one molecule of fructose 1,6-bisphosphate into two molecules of pyruvate results in the net synthesis of how many molecules each of NADH and ATP?

NAD^+ is regenerated from the metabolism of pyruvate

The conversion of glucose into two molecules of pyruvate has resulted in the net synthesis of ATP. However, an energy-converting pathway that stops at pyruvate will not proceed for long, because redox balance has not been maintained. As we have seen, the activity of glyceraldehyde 3-phosphate dehydrogenase, in addition to generating a compound with high phosphoryl-transfer potential, reduces NAD^+ to NADH. In the cell, there are limited amounts of NAD^+, which is derived from the vitamin niacin (B_3), a dietary requirement for human beings. Consequently, NAD^+ must be regenerated for glycolysis to proceed. Thus, the final process in the pathway is the regeneration of NAD^+ through the metabolism of pyruvate.

The sequence of reactions from glucose to pyruvate is similar in most organisms and most types of cells. In contrast, the fate of pyruvate is variable. Three reactions of pyruvate are of primary importance: conversion into ethanol, lactate, or carbon dioxide (Figure 16.11). The first two reactions are fermentations that take place in the absence of oxygen. A **fermentation** is an ATP-generating process in which organic compounds act both as the donor and as the acceptor of electrons; thus, they are redox neutral pathways for the production of ATP from an organic fuel molecule. In contrast, in the presence of oxygen — the most common situation in multicellular organisms and in many unicellular ones — pyruvate is oxidized to carbon dioxide and water through the citric acid cycle and the electron-transport chain, with oxygen serving as the final electron acceptor. We now take a closer look at these three examples of possible fates of pyruvate.

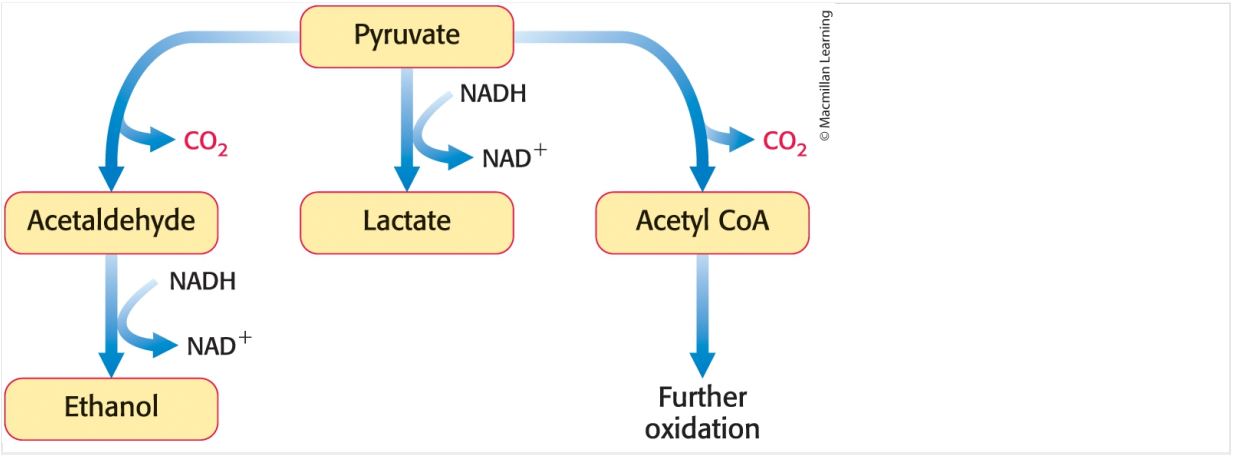
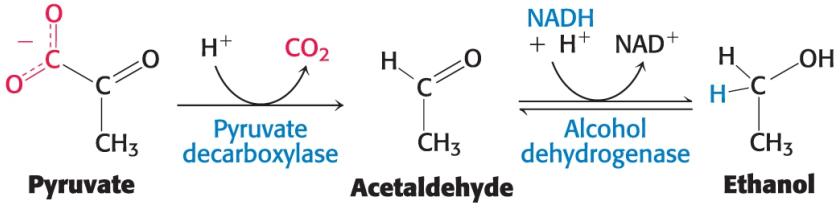


FIGURE 16.11 Pyruvate has many possible fates. Shown are just three possible fates, but many others exist. Ethanol and lactate can be formed by reactions that include NADH. Alternatively, a two-carbon unit from pyruvate can be coupled to coenzyme A (Chapter 17) to form acetyl CoA.

Ethanol fermentation

Ethanol is formed from pyruvate in yeast and several other microorganisms. The conversion of glucose into ethanol in anerobic conditions is called **ethanol fermentation**. The first step is the decarboxylation of pyruvate. This reaction is catalyzed by pyruvate decarboxylase, which requires the coenzyme

thiamine pyrophosphate that is derived from the vitamin thiamine (B_1). The second step is the reduction of acetaldehyde to ethanol by NADH, in a reaction catalyzed by alcohol dehydrogenase. This reaction regenerates NAD^+.



The active site of alcohol dehydrogenase contains a zinc ion that is coordinated to the sulfur atoms of two cysteine residues and a nitrogen atom of histidine (Figure 16.12). This zinc ion polarizes the carbonyl group of the substrate to favor the transfer of a hydride from NADH.

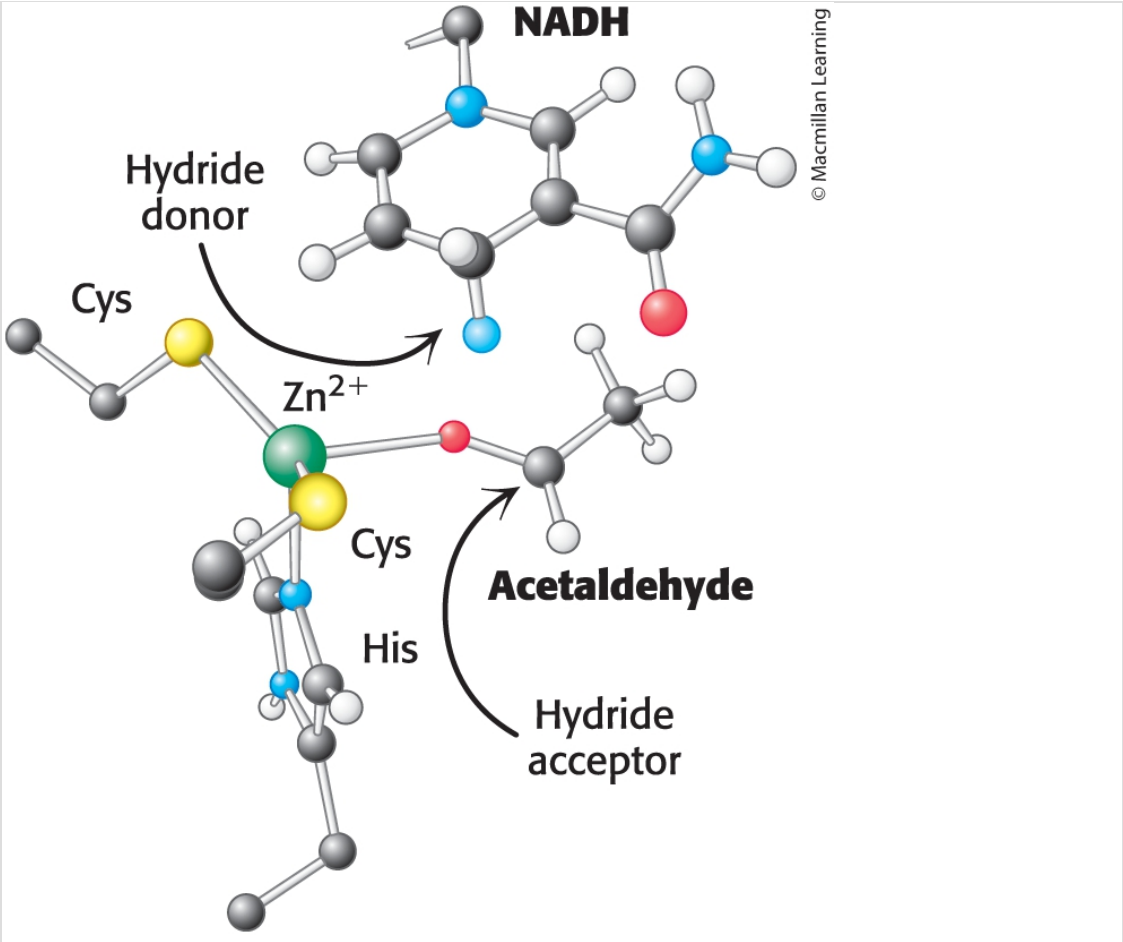


FIGURE 16.12 The active site of alcohol dehydrogenase contains a critical zinc ion bound to two cysteine residues and one histidine residue. The zinc ion binds the acetaldehyde substrate through its oxygen atom, polarizing the substrate so that it more easily accepts a hydride from NADH. Only the nicotinamide ring of NADH is shown.

The net result of this anaerobic process is

$$\text{Glucose} + 2\ P_i + 2\ \text{ADP} + 2\ H^+ \rightarrow 2\ \text{ethanol} + 2\ CO_2 + 2\ \text{ATP} + 2\ H_2O$$

Note that NAD^+ and NADH do not appear in this equation, even though they are crucial for the overall process. NADH generated by the oxidation of glyceraldehyde 3-phosphate is consumed in the reduction of acetaldehyde to ethanol. Thus, there is no net oxidation–reduction in the conversion of glucose into ethanol (**Figure 16.13**). The ethanol formed during fermentation provides a key ingredient for brewing and winemaking.

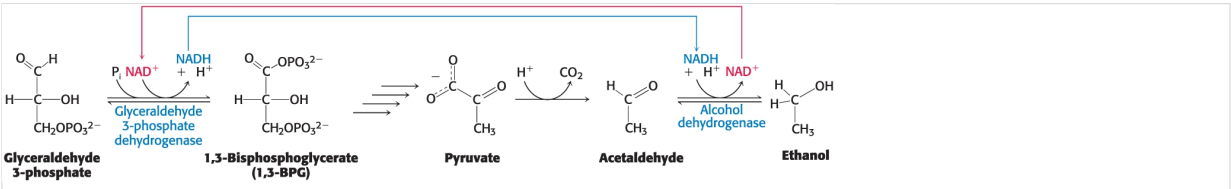
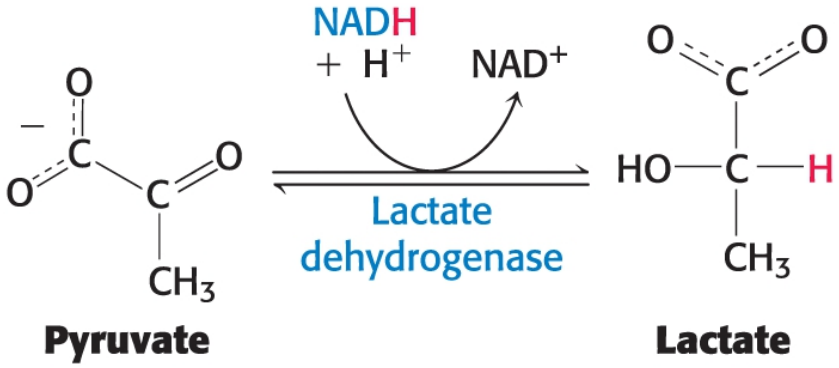


FIGURE 16.13 The NADH produced in glycolysis must be reoxidized to NAD^+ for the glycolytic pathway to continue. NADH is constantly generated by the glyceraldehyde 3-phosphate dehydrogenase reaction. In ethanol fermentation, alcohol dehydrogenase oxidizes NADH and generates ethanol.

Lactic acid fermentation

Lactate is formed from pyruvate under anaerobic conditions in a variety of microorganisms and in a variety of animal tissues. The conversion of glucose to lactate in anaerobic conditions is called **lactic acid fermentation**. After the Buchners' original discovery of ethanol fermentation by yeast, studies of muscle extracts later showed that many of the reactions of lactic acid fermentation were the same as those of ethanol fermentation. This second exciting discovery revealed an underlying unity in biochemistry. Lactic acid fermentation occurs regularly in the retina of the eye and in erythrocytes (red blood cells), even in the presence of oxygen, as well as in tissues like the outer layers of the skin that are perpetually limited in oxygen availability. Additionally, certain types of skeletal muscles in most animals can also function anaerobically for short periods. For example, lactic acid fermentation occurs when a specific type of muscle fiber, called fast-twitch or type IIb fibers, performs short bursts of intense exercise because the ATP needs rise faster than the ability of the body to provide oxygen to the muscle. The muscle functions anaerobically until fatigue sets in, which is caused, in part, by lactate buildup. Indeed, the pH of resting type IIb muscle fibers, which is about 7.0, may fall to as low as 6.3 during the bout of exercise. The drop in pH inhibits phosphofructokinase, as we will discuss shortly. A

$lactate/H^+$ symporter allows the exit of lactate from the muscle cell. The reduction of pyruvate by NADH to form lactate is catalyzed by lactate dehydrogenase.



The overall reaction in the conversion of glucose into lactate is

$$\text{Glucose} + 2\ P_i + 2\ \text{ADP} \rightarrow 2\ \text{lactate} + 2\ \text{ATP} + 2\ H_2O$$

As in ethanol fermentation, there is no net oxidation–reduction. The NADH formed in the oxidation of glyceraldehyde 3-phosphate is consumed in the reduction of pyruvate. The regeneration of NAD^+ in the reduction of pyruvate to lactate or ethanol sustains the continued process of glycolysis under anaerobic conditions (**Figure 16.14**).

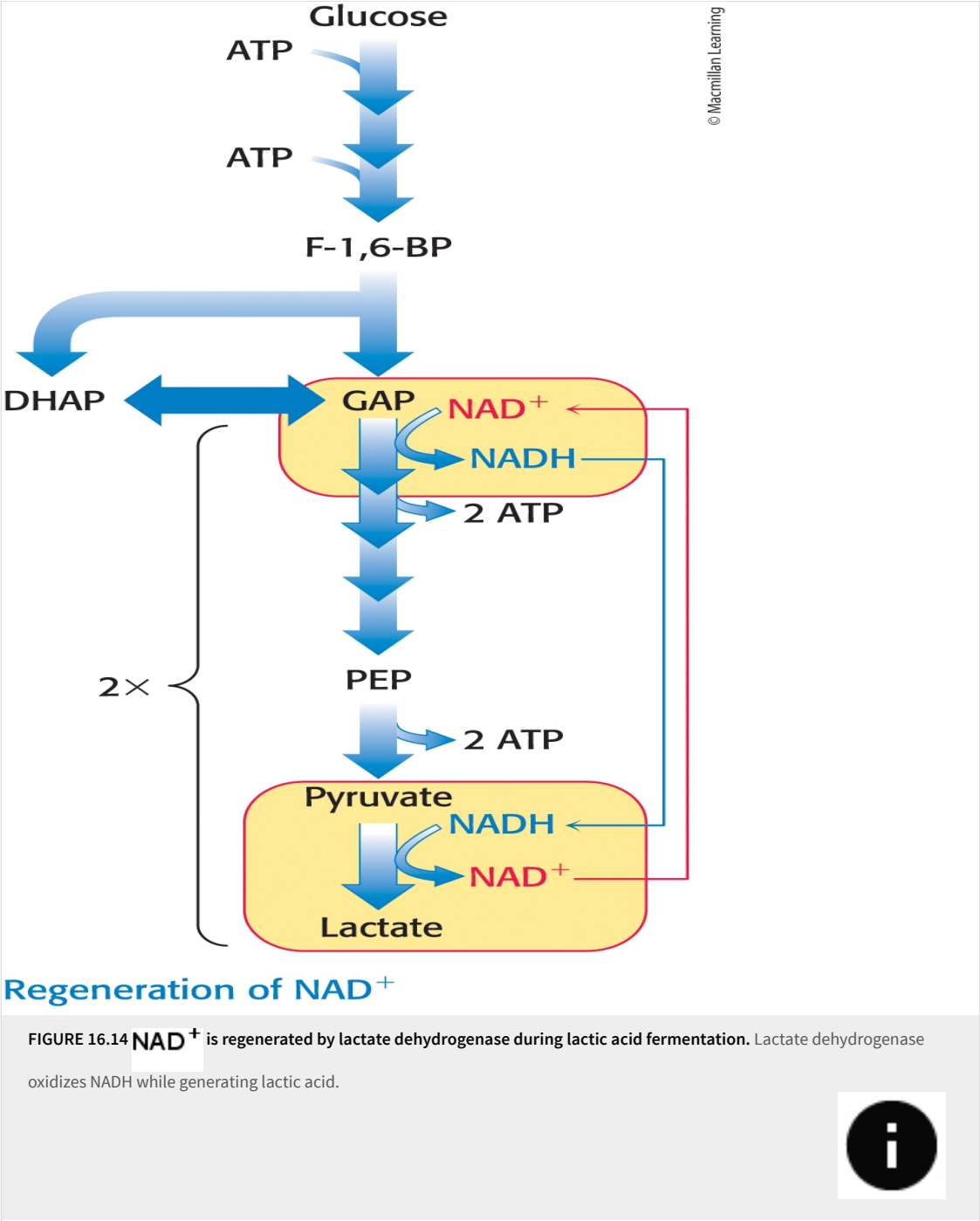


FIGURE 16.14 NAD^+ is regenerated by lactate dehydrogenase during lactic acid fermentation. Lactate dehydrogenase oxidizes NADH while generating lactic acid.

Oxidation by the citric acid cycle and the electron transport chain

Carbon dioxide and water are formed, and a great deal of energy extracted, when pyruvate is metabolized under aerobic conditions by means of the citric acid cycle and the electron-transport chain. In contrast, only a fraction of the energy of glucose is released in its anaerobic conversion into ethanol or lactate. The entry point to this oxidative pathway is acetyl coenzyme A (acetyl CoA), which is formed inside mitochondria by the oxidative decarboxylation of pyruvate.

$$\text{Pyruvate} + \text{NAD}^+ + \text{CoA} \rightarrow \text{acetyl CoA} + \text{CO}_2 + \text{NADH} + \text{H}^+$$

This reaction, which is catalyzed by the pyruvate dehydrogenase complex, will be considered in detail in Chapter 17. The NAD^+ required for this reaction and for the oxidation of glyceraldehyde 3-phosphate is regenerated when NADH ultimately transfers its electrons to O_2 through the electron-transport chain in mitochondria.

Fermentations provide usable energy in the absence of oxygen

Fermentations yield only a fraction of the energy available from the complete combustion of glucose. Why is a relatively inefficient metabolic pathway so extensively used? The fundamental reason is that oxygen is not required. The ability to survive without oxygen affords a host of living accommodations such as soils, deep water, and skin pores. Some organisms, called **obligate anaerobes**, cannot survive in the presence of O_2, a highly reactive compound. The bacterium *Clostridium perfringens*, the cause of gangrene, is an example of an obligate anaerobe. Other pathogenic obligate anaerobes are listed in **Table 16.3**. Some organisms, such as yeast, are **facultative anaerobes** that metabolize glucose aerobically when oxygen is present and perform fermentation when oxygen is absent.

TABLE 16.3 Examples of pathogenic obligate anaerobes

Bacterium	Result of infection
Clostridium tetani	Tetanus (lockjaw)
Clostridium botulinum	Botulism (an especially severe type of food poisoning)
Clostridium perfringens	Gas gangrene (gas is produced as an end point of the fermentation, distorting and destroying the tissue)
Bartonella hensela	Cat-scratch fever (flu-like symptoms)
Bacteroides fragilis	Abdominal, pelvic, pulmonary, and blood infections

Many food products, including sour cream, yogurt, various cheeses, beer, wine, and sauerkraut, result from fermentation. Yogurt is produced by the fermentation of lactose in milk to lactate by a mixed culture of *Lactobacillus acidophilus* and *Streptococcus thermophilus*. Sour cream begins with pasteurized light cream, which is fermented to lactate by *Streptococcus lactis*. The lactate is further fermented to ketones and aldehydes by *Leuconostoc citrovorum*. The second fermentation adds to the taste and aroma of sour cream. Yeast, *Saccharomyces cerevisiae*, ferments carbohydrates to ethanol and carbon dioxide, providing some of the ingredients for an array of alcohol beverages. Although we have considered only lactic acid and ethanol fermentation, microorganisms are capable of generating a wide array of molecules as end points of fermentation (**Table 16.4**).

TABLE 16.4 Starting and ending points of various fermentations

Glucose	→	Lactate
Lactate	→	Acetate
Glucose	→	Ethanol
Ethanol	→	Acetate
Purines	→	Formate
Ethylene glycol	→	Acetate
Threonine	→	Propionate
Leucine	→	2-Alkylacetate
Phenylalanine	→	Propionate

Note: The products of some fermentations are the substrates for others.

Self-Check Question



The conversion of one molecule of glucose into two molecules of lactate results in the net synthesis of how many ATP and how many NADH molecules?

Fructose is converted into glycolytic intermediates by fructokinase

Although glucose is the most widely used monosaccharide, others also are important fuels. Let us consider how fructose is funneled into the glycolytic pathway (Figure 16.15). There is no separate catabolic pathway for metabolizing fructose, and so the strategy is to convert this sugar into a metabolite of glucose.

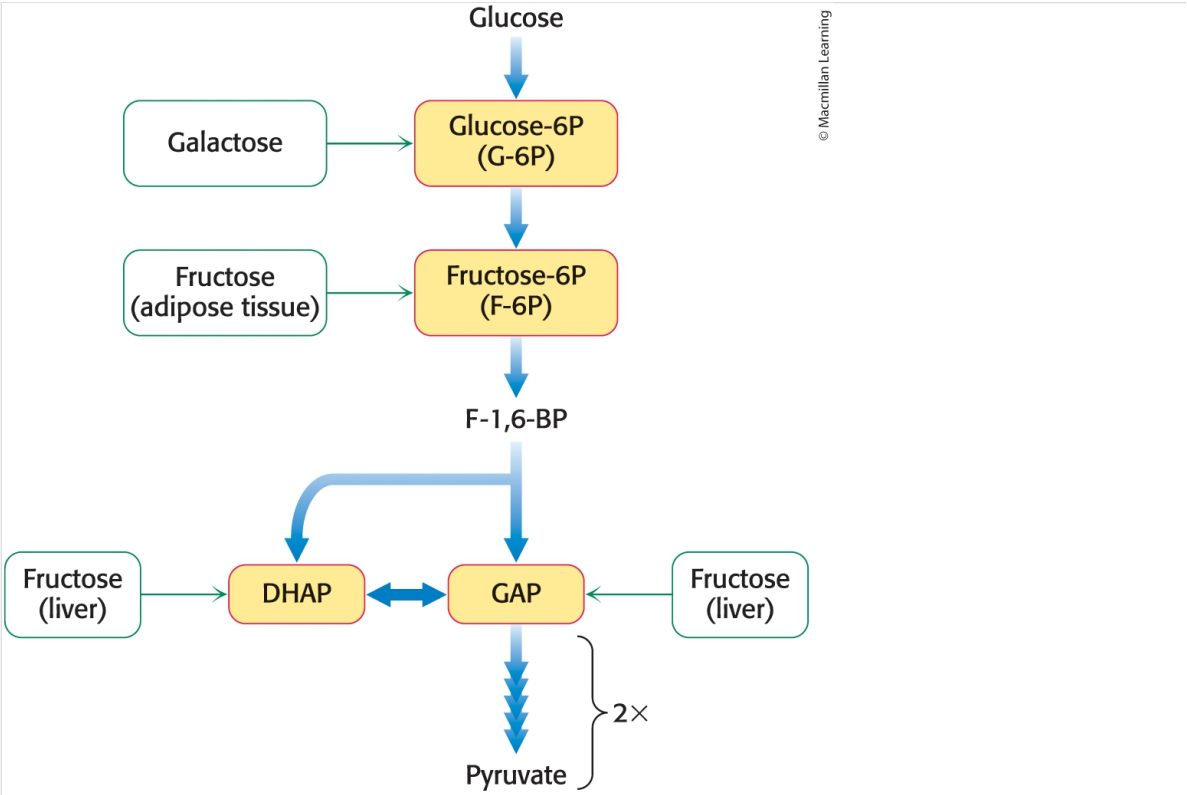


FIGURE 16.15 Additional sugars such as fructose and galactose can enter glycolysis at a variety of points.

The main site of fructose metabolism is the liver, using the fructose 1-phosphate pathway (Figure 16.16). The first step is the phosphorylation of fructose to fructose 1-phosphate by fructokinase. Fructose 1-phosphate is then split into glyceraldehyde and dihydroxyacetone phosphate, an intermediate in glycolysis. This aldol cleavage is catalyzed by a specific fructose 1-phosphate aldolase. Glyceraldehyde is then phosphorylated to glyceraldehyde 3-phosphate, a glycolytic intermediate, by triose kinase. In other tissues, such as adipose tissue, fructose can be phosphorylated to fructose 6-phosphate by hexokinase.

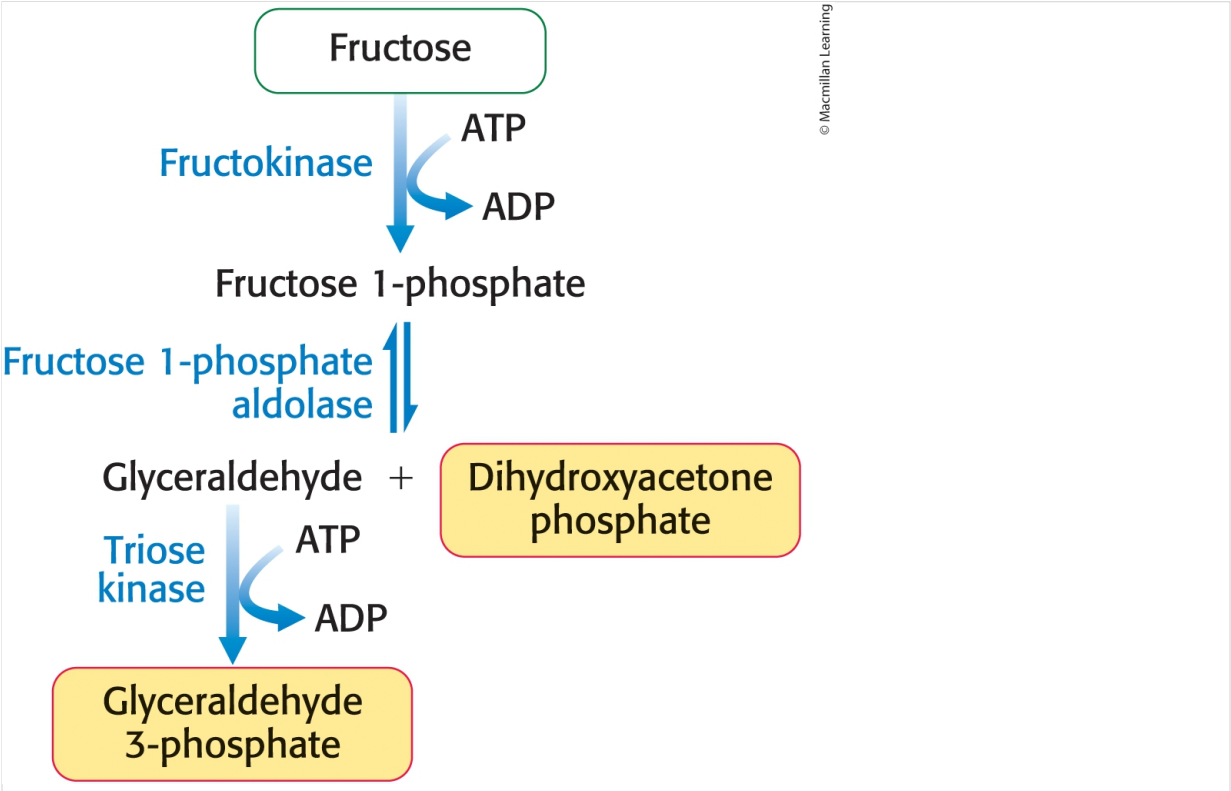


FIGURE 16.16 In the liver, fructose enters the glycolytic pathway through the fructose 1-phosphate pathway.

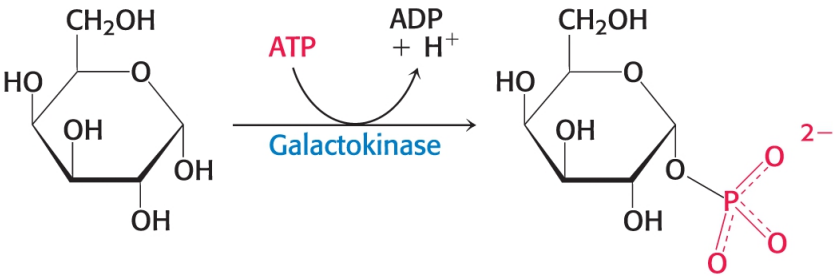
Fructose consumption, previously associated with pathological conditions, is likely inconsequential relative to caloric intake. Fructose, a commonly used sweetener, is a component of sucrose and high fructose corn syrup (which contains approximately 55% fructose and 45% glucose). Epidemiological as well as clinical studies previously linked excessive fructose consumption to fatty liver, insulin insensitivity, and obesity, while other studies found negligible or even beneficial effects of fructose consumption, relative to calorically equivalent quantities of other sugars like glucose and sucrose. Recent meta-analyses, large studies which methodically evaluate the results of many other experiments collectively, now indicate that the widely held belief in the negative effects of fructose is no longer supported by the current literature. Interestingly, the hypothesis that overconsumption of fructose, specifically, contributed to poor health outcomes has a biochemical underpinning.

Note that, as shown in Figure 16.16, the actions of fructokinase and triose kinase bypass the most important regulatory step in glycolysis, the phosphofructokinase-catalyzed reaction. Thus, the fructose-derived glyceraldehyde 3-phosphate and dihydroxyacetone phosphate are produced in an unregulated fashion. However, it is likely that additional regulatory enzymes prevent any further unregulated metabolism of the downstream product pyruvate. Although the type of sugar may be unimportant, the overconsumption of sugars and fats is still strongly associated with fatty liver, insulin insensitivity, and obesity, conditions that may eventually result in type 2 diabetes (Chapter 24). Excess pyruvate produced in glycolysis, from any source, is metabolized to acetyl CoA. As we will see in Chapter 22, this excess

acetyl CoA is converted to fatty acids, which can be transported to adipose tissue and result in obesity. The liver also begins to accumulate fatty acids, resulting in fatty liver. We will return to the topic of obesity and caloric homeostasis in Chapter 24.

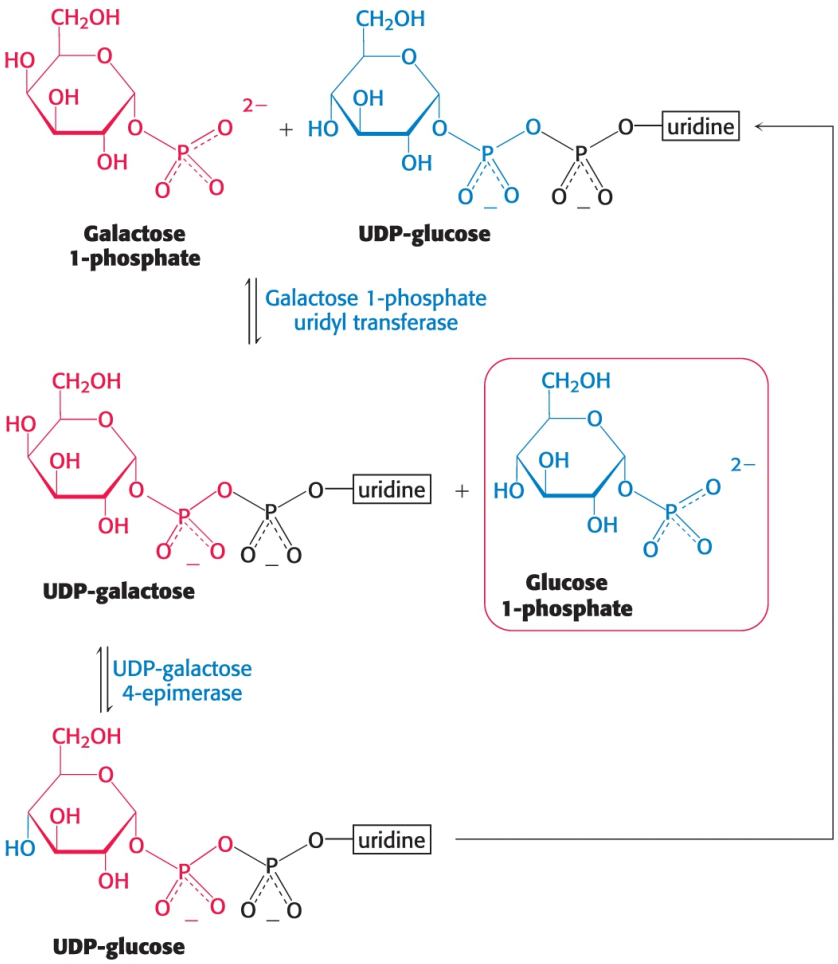
Galactose is converted into glucose 6-phosphate

Like fructose, galactose is an abundant sugar common in dairy products that must be converted into metabolites of glucose (Figure 16.15). Galactose is converted into glucose 6-phosphate in four steps. The first reaction in the galactose–glucose interconversion pathway is the phosphorylation of galactose to galactose 1-phosphate by galactokinase.



Galactose **Galactose 1-phosphate**

Galactose 1-phosphate then acquires a uridyl group from uridine diphosphate glucose (UDP-glucose), an activated intermediate in the synthesis of carbohydrates (Section 21.4).



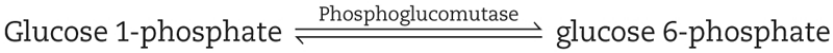
The products of this reaction, which is catalyzed by galactose 1-phosphate uridyl transferase, are UDP-galactose and glucose 1-phosphate. The galactose moiety of UDP-galactose is then epimerized to glucose. The configuration of the hydroxyl group at carbon 4 is inverted by UDP-galactose 4-epimerase.

The sum of the reactions catalyzed by galactokinase, the transferase, and the epimerase is

$$\text{Galactose} + \text{ATP} \rightarrow \text{glucose 1-phosphate} + \text{ADP} + \text{H}^+$$

Note that UDP-glucose is not consumed in the conversion of galactose into glucose, because it is regenerated from UDP-galactose by the epimerase. This reaction is reversible, and the product of the reverse direction also is important. The conversion of UDP-glucose into UDP-galactose is essential for the synthesis of galactosyl residues in complex polysaccharides and glycoproteins if the amount of galactose in the diet is inadequate to meet these needs.

Finally, glucose 1-phosphate, formed from galactose, is isomerized to glucose 6-phosphate by phosphoglucomutase.



We shall return to this reaction when we consider the synthesis and degradation of glycogen, which proceeds through glucose 1-phosphate, in Chapter 21.

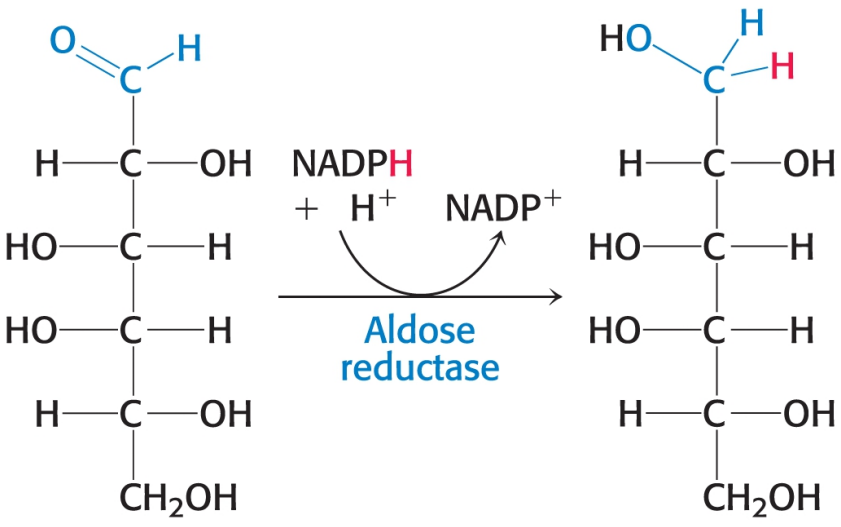
Galactose can be highly toxic with a defective metabolic pathway



Rare disorders that interfere with the metabolism of galactose are collectively referred to as *galactosemias.* The most common form, called classic galactosemia, is an inherited deficiency in galactose 1-phosphate uridyl transferase activity. Afflicted infants fail to thrive; they vomit or have diarrhea after consuming milk, and enlargement of the liver and jaundice are common, sometimes progressing to cirrhosis. Cataracts will form, and lethargy and delayed neurological development also are common. The blood-galactose level is markedly elevated, and galactose is found in the urine.

The most common treatment is to remove galactose (and lactose) from the diet. An enigma of galactosemia is that, although elimination of galactose from the diet prevents liver disease and cataract development, the majority of patients still suffer from central nervous system malfunction, most commonly a delayed acquisition of language skills. Female patients also display ovarian failure.

Cataract formation is better understood. A cataract is the clouding of the normally clear lens of the eye due to pathological protein aggregation (**Figure 16.17**). If the transferase is not active in the lens of the eye, the presence of aldose reductase causes the accumulating galactose to be reduced to galactitol.



Galactose **Galactitol**

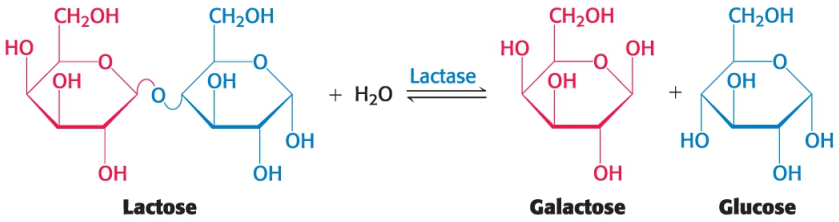


FIGURE 16.17 Cataracts are evident as the clouding of the lens. (A) A healthy eye. (B) An eye with a cataract.

Galactitol is poorly metabolized and accumulates in the lens. Water will diffuse into the lens to maintain osmotic balance, triggering the formation of cataracts. In fact, there is a high incidence of cataract formation with age in populations that consume substantial amounts of milk into adulthood.

Many adults worldwide are intolerant of milk because they are deficient in lactase

Many adults are unable to metabolize the milk sugar lactose and experience gastrointestinal disturbances if they drink milk. Lactose intolerance is most commonly caused by a deficiency of the enzyme lactase, which cleaves lactose into glucose and galactose.



"Deficiency" is not quite the appropriate term, because a decrease in lactase is normal in the course of development in all mammals. As children are weaned and milk becomes less prominent in their diets, lactase activity normally declines to about 5% to 10% of the level at birth. This decrease is not as pronounced with some groups of people, and people from these groups can continue to ingest milk without gastrointestinal difficulties.

How did this tolerance evolve? With the development of dairy farming, an adult with active lactase would have a selective advantage in being able to consume calories from the readily available milk. Indeed, estimates suggest that people with the mutation would have produced almost 20% more fertile offspring. Some form of lactose tolerance evolved independently at least four different times in different human populations in the last 10,000 years, indicating that the evolutionary selective pressure on lactase persistence must have been substantial, attesting to the biochemical value of being able to use milk as an energy source into adulthood.

What happens to the lactose in the intestine of a lactase-deficient person? The lactose is a good energy source for microorganisms in the colon (Figure 16.18), which ferment it to lactic acid while generating methane (CH_4) and hydrogen gas (H_2). The gas produced creates the uncomfortable feeling of gut distension and the annoying problem of flatulence. The lactate produced by these microorganisms is osmotically active and draws water into the intestine, as does any undigested lactose, resulting in diarrhea. If severe enough, the gas and diarrhea hinder the absorption of other nutrients such as fats and proteins. The simplest treatment is to avoid the consumption of products containing much lactose. Alternatively, the enzyme lactase can be ingested with milk products.



SPL/Science Source

FIGURE 16.18 *Lactobacillus* is one example of an industrially useful anaerobic bacterium. A scanning electron micrograph of an anaerobic bacterial species from the genus *Lactobacillus* is shown. As suggested by its name, this genus ferments glucose into lactic acid. *Lactobacillus* is widely used in the food industry and is an important component of the normal human bacterial flora of the urogenital tract, where it prevents the growth of harmful organisms by creating an acid environment.

Self-Check Question



Which condition is more detrimental to human health: lactose intolerance or classic galactosemia? Also, if a person were galactosemic, would it be better to be lactose tolerant or intolerant?

16.3 The Glycolytic Pathway Is Tightly Controlled

The glycolytic pathway has a dual role: it degrades glucose to generate ATP, and it provides building blocks for biosynthetic reactions. The rate of conversion of glucose into pyruvate is regulated to meet these two major cellular needs. In metabolic pathways, enzymes catalyzing essentially irreversible reactions are potential sites of control. In glycolysis, the reactions catalyzed by hexokinase, phosphofructokinase, and pyruvate kinase are virtually irreversible, and each of them serves as a control site. These enzymes become more active or less so in response to the reversible binding of allosteric effectors or to covalent modification. In addition, the amounts of these important enzymes are varied by the regulation of transcription to meet changing metabolic needs. The time required for allosteric regulation, control by phosphorylation, and transcriptional change is measured typically in milliseconds, seconds, and hours, respectively. We will consider the control of glycolysis in two different tissues — skeletal muscle and liver.

Glycolysis in muscle is regulated to meet the need for ATP

Glycolysis in skeletal muscle provides ATP primarily to power contraction. Consequently, the primary regulation of muscle glycolysis is the ratio of ATP to AMP. Let's examine how each of the key regulatory enzymes responds to changes in the amounts of ATP and AMP present in the cell.

Phosphofructokinase

Phosphofructokinase is the most important control site in the mammalian glycolytic pathway (Figure 16.19). High levels of ATP allosterically inhibit the enzyme (a 340-kDa tetramer). ATP binds to a specific regulatory site that is distinct from the catalytic site.

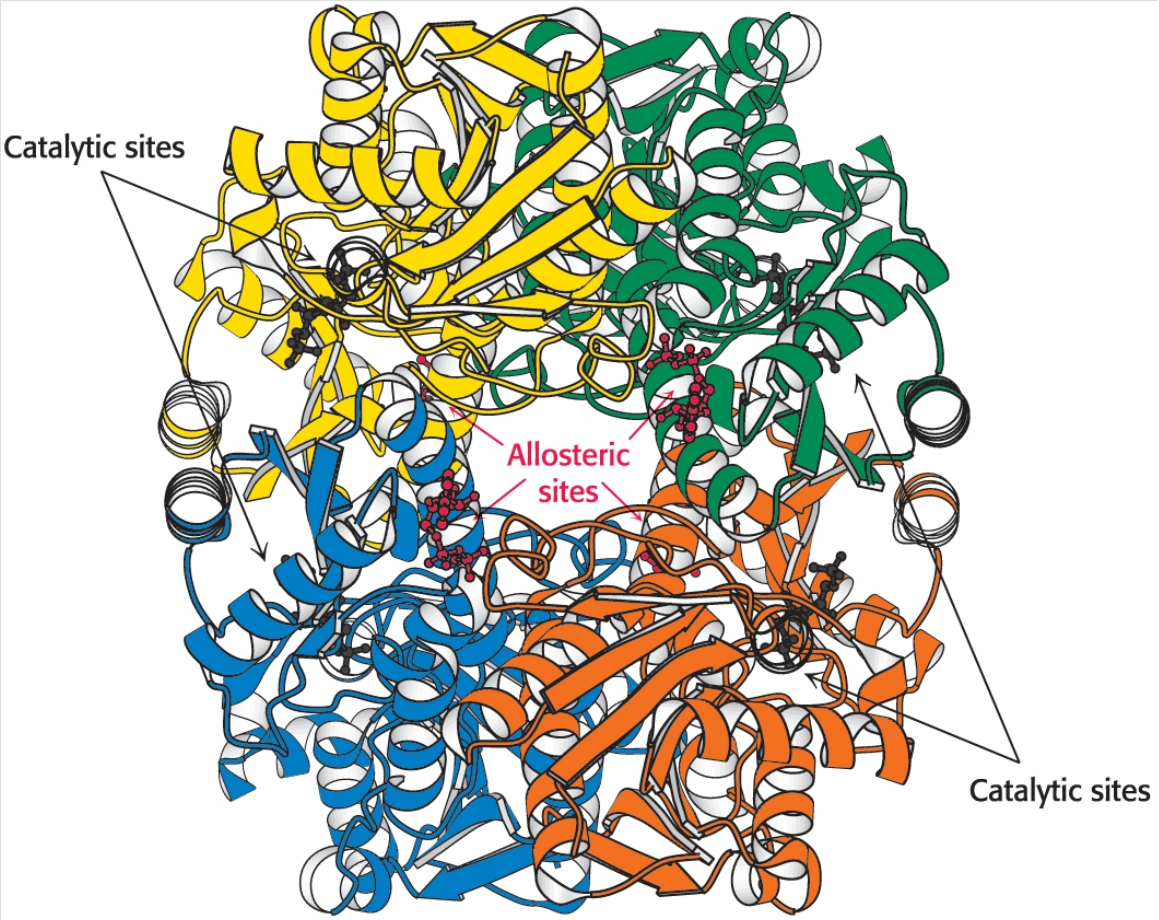


FIGURE 16.19 Phosphofructokinase from *E. coli* is comprised of four identical subunits with separate catalytic and allosteric sites. Each subunit of the human liver enzyme consists of two domains that are similar to the *E. coli* enzyme.

[Drawn from 1PFK.pdb.]

The binding of ATP lowers the enzyme's affinity for fructose 6-phosphate. Thus, a high concentration of ATP converts the hyperbolic binding curve of fructose 6-phosphate into a sigmoidal one (**Figure 16.20**). AMP reverses the inhibitory action of ATP, and so the activity of the enzyme increases when the ATP/AMP ratio is lowered. A decrease in pH also inhibits phosphofructokinase activity by augmenting the inhibitory effect of ATP. The pH might fall when fast-twitch muscle is functioning anaerobically, producing excessive quantities of lactic acid. The inhibitory effect protects the muscle from damage that would result from the accumulation of too much acid.

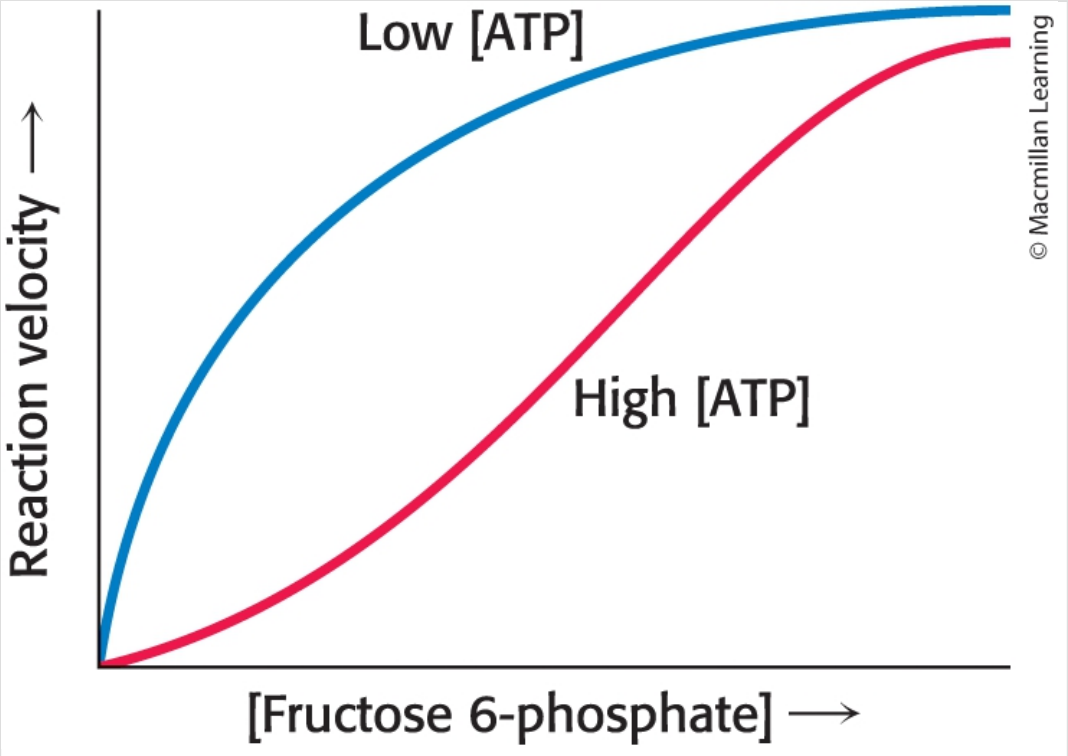


FIGURE 16.20 A high level of ATP allosterically inhibits phosphofructokinase by decreasing its affinity for fructose 6-phosphate.

Why is AMP and not ADP the positive regulator of phosphofructokinase? When ATP is being utilized rapidly, the enzyme adenylate kinase can

form ATP from ADP by the following reaction:

$$\mathrm{ADP} + \mathrm{ADP} \rightleftharpoons \mathrm{ATP} + \mathrm{AMP}$$

Thus, some ATP is salvaged from ADP, and AMP becomes the signal for the low-energy state.

Moreover, the use of AMP as an allosteric effector provides an especially sensitive regulation. We can understand why by considering the following. First, the total adenylate pool ([ATP], [ADP], [AMP]) in a cell is constant over the short term. Second, the concentration of ATP is greater than that of ADP, and the concentration of ADP is, in turn, greater than that of AMP. Consequently, small percentage changes in [ATP] result in larger percentage changes in the concentrations of the other adenylate nucleotides. This magnification of small changes in [ATP] to larger changes in [AMP] leads to tighter regulation by increasing the range of sensitivity of phosphofructokinase.

Hexokinase

Phosphofructokinase is the most prominent regulatory enzyme in glycolysis, but it is not the only one. Hexokinase, the enzyme catalyzing the first step of glycolysis, is inhibited by its product, glucose 6-phosphate. High concentrations of this molecule signal that the cell no longer requires glucose for energy or for the synthesis of glycogen, a storage form of glucose (Chapter 21), and the glucose will be left in the blood. A rise in glucose 6-phosphate concentration is a means by which phosphofructokinase communicates with hexokinase. When phosphofructokinase is inactive, the concentration of fructose 6-phosphate rises. In turn, the level of glucose 6-phosphate rises because it is in equilibrium with fructose 6-phosphate. Hence, the inhibition of phosphofructokinase leads to the inhibition of hexokinase.

Why is phosphofructokinase rather than hexokinase the pacemaker of glycolysis? The reason becomes evident on noting that glucose 6-phosphate is not solely a glycolytic intermediate. In muscle, glucose 6-phosphate can also be converted into glycogen. The first irreversible reaction unique to the glycolytic pathway, the **committed step**, is the phosphorylation of fructose 6-phosphate to fructose 1,6-bisphosphate. Thus, it is highly appropriate for phosphofructokinase to be the primary control site in glycolysis. In general, the enzyme catalyzing the committed step in a metabolic sequence is the most important control element in the pathway.

Pyruvate kinase

Pyruvate kinase, the enzyme catalyzing the third irreversible step in glycolysis, controls the outflow from this pathway. This final step yields ATP and pyruvate, a central metabolic intermediate that can be oxidized further or used as a building block. ATP allosterically inhibits pyruvate kinase to slow glycolysis when the energy charge is high. When the pace of glycolysis increases, fructose 1,6-bisphosphate — the product of the preceding irreversible step in glycolysis — activates the kinase to enable it to keep pace with the oncoming high flux of intermediates. Such a process is called **feedforward stimulation** or **feedforward activation**. A summary of the regulation of glycolysis in resting and active muscle is shown in **Figure 16.21**.

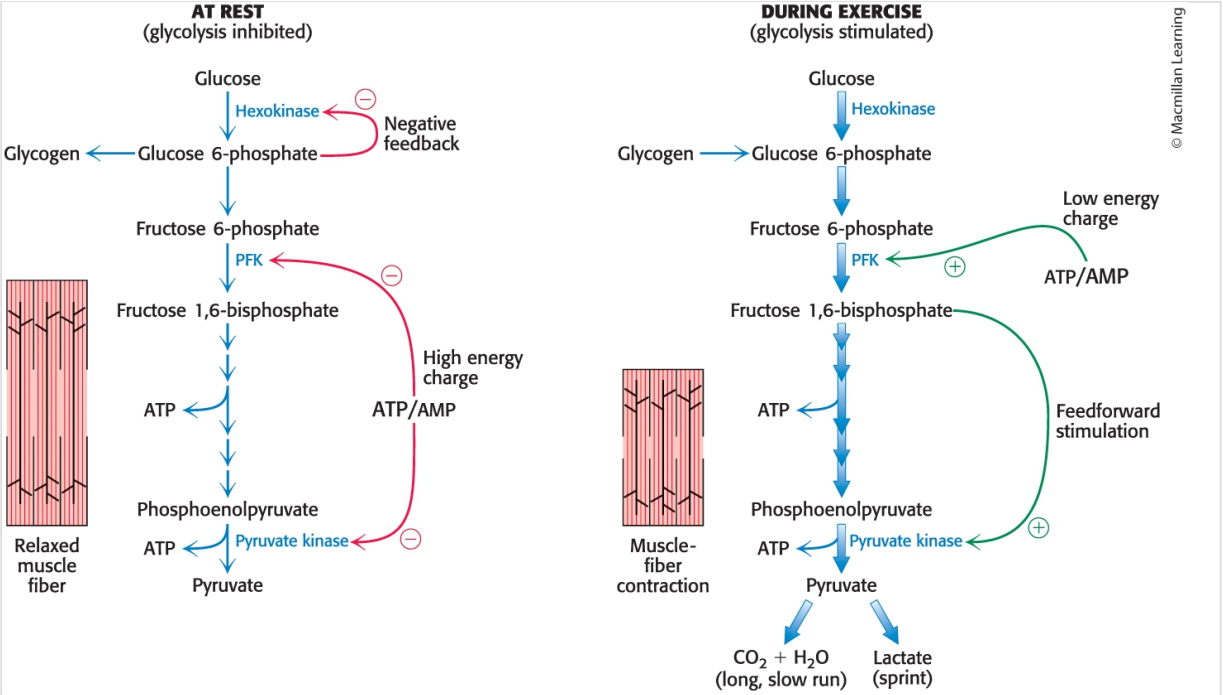


FIGURE 16.21 Regulation of glycolysis in muscle. At rest (left), glycolysis is not very active (thin arrows). The high concentration of ATP inhibits phosphofructokinase (PFK), pyruvate kinase, and hexokinase. Glucose 6-phosphate is converted into glycogen (Chapter 21). During exercise (right), the decrease in the ATP/AMP ratio resulting from muscle contraction activates phosphofructokinase and hence glycolysis. The flux down the pathway is increased, as represented by the thick arrows.

The regulation of glycolysis in the liver illustrates the biochemical versatility of the liver

The liver has more diverse biochemical functions than does muscle. Significantly, the liver maintains blood-glucose concentration: it stores glucose as glycogen when glucose is plentiful, and it releases glucose when supplies are low. It also uses glucose to generate reducing power

for biosynthesis (Section 20.3) as well as to synthesize a host of biochemicals. So, although the liver has many of the regulatory features of muscle glycolysis, the regulation of glycolysis in the liver is more complex.

Phosphofructokinase

Liver phosphofructokinase can be regulated by ATP as in muscle, but such regulation is not as important since the liver does not experience the sudden ATP needs that a contracting muscle does. Likewise, low pH is not an important metabolic signal for the liver enzyme, because lactate is not normally produced in the liver. Indeed, as we will see, lactate is converted into glucose in the liver.

Glycolysis in the liver furnishes carbon skeletons for biosyntheses, and so a signal indicating whether building blocks are abundant or scarce should also regulate phosphofructokinase. In the liver, phosphofructokinase is inhibited by citrate, an early intermediate in the citric acid cycle (Chapter 17). A high level of citrate in the cytoplasm means that biosynthetic precursors are abundant, and so there is no need to degrade additional glucose for this purpose. Citrate inhibits phosphofructokinase by enhancing the inhibitory effect of ATP.

The key means by which glycolysis in the liver responds to changes in blood glucose is through the signal molecule fructose 2,6-bisphosphate (F-2,6-BP), a potent activator of phosphofructokinase. In the liver, the concentration of fructose 6-phosphate rises when blood-glucose concentration is high, and the abundance of fructose 6-phosphate accelerates the synthesis of F-2,6-BP (**Figure 16.22**). Hence, an abundance of fructose 6-phosphate leads to a higher concentration of F-2,6-BP.

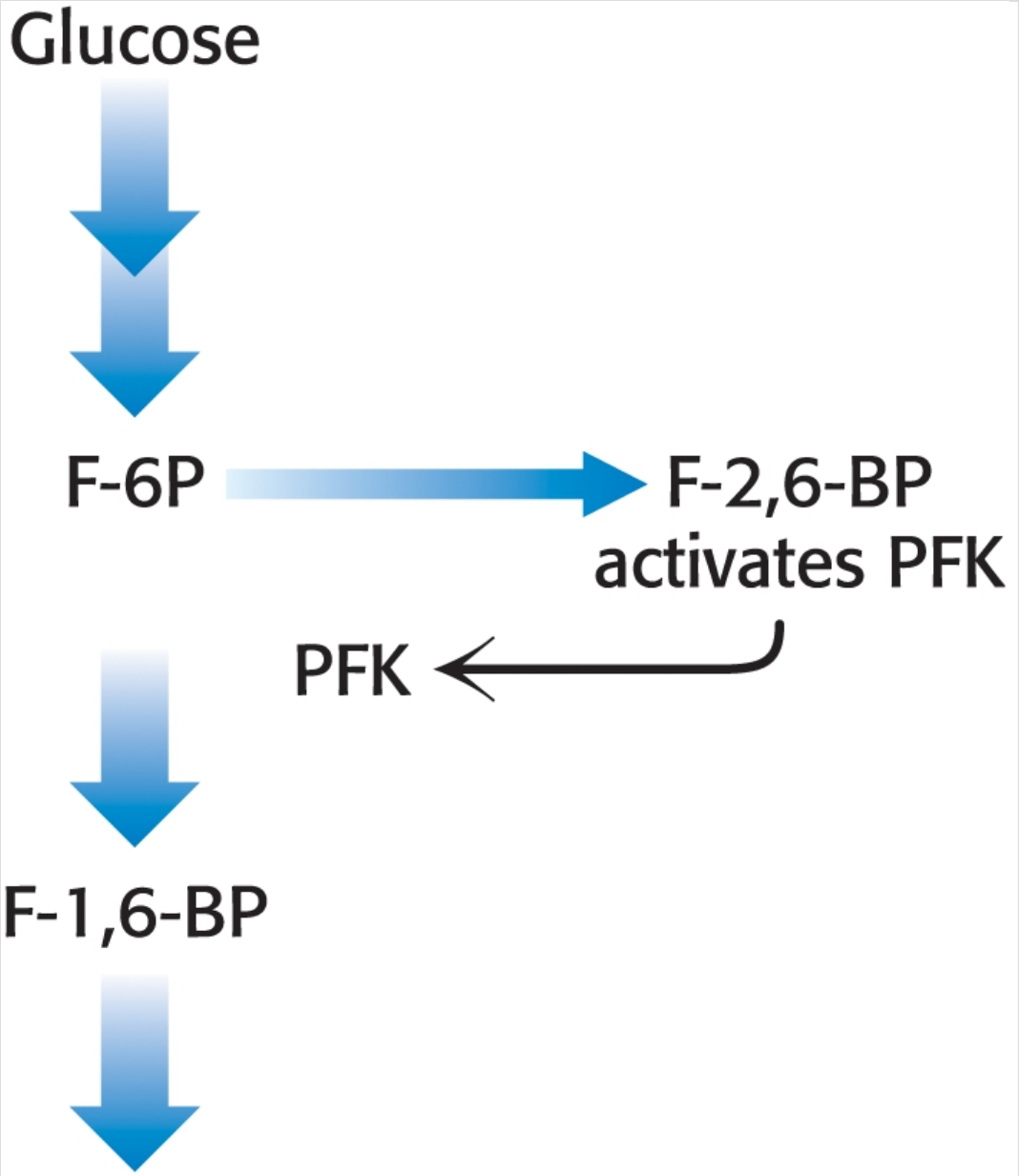
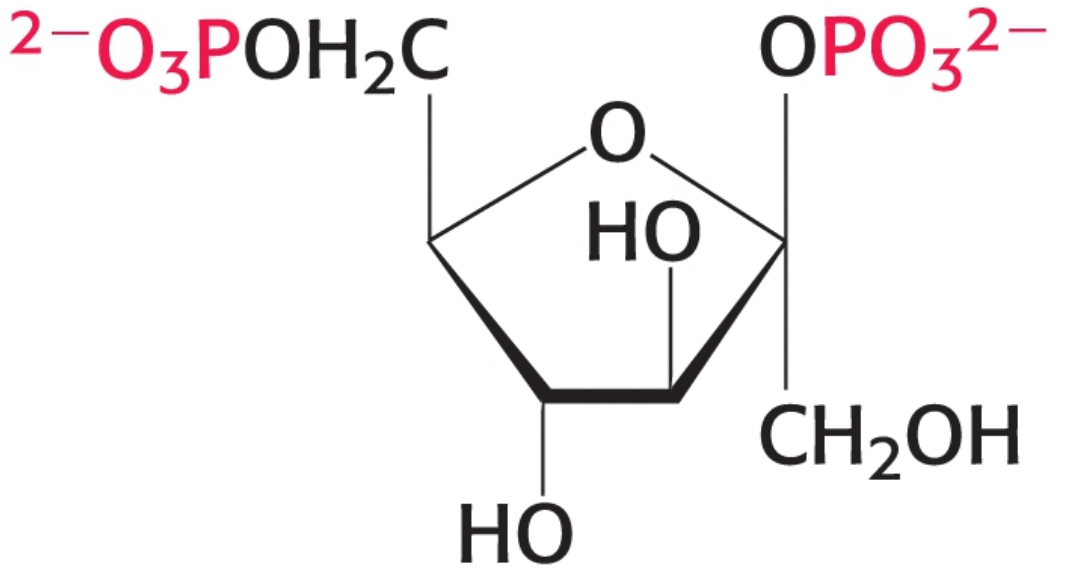


FIGURE 16.22 Fructose 2,6-bisphosphate allosterically activates phosphofructokinase. In high concentrations, fructose 6-phosphate (F-6P) activates the enzyme phosphofructokinase (PFK) through an intermediary, fructose 2,6-bisphosphate (F-2,6-BP).

The binding of fructose 2,6-bisphosphate increases the affinity of phosphofructokinase for fructose 6-phosphate and diminishes the

inhibitory effect of ATP (Figure 16.23). Glycolysis is thus accelerated when glucose is abundant. We will further explore the additional hormonal control over the synthesis and degradation of this important regulatory molecule after we have considered gluconeogenesis.



Fructose 2,6-bisphosphate (F-2,6-BP)

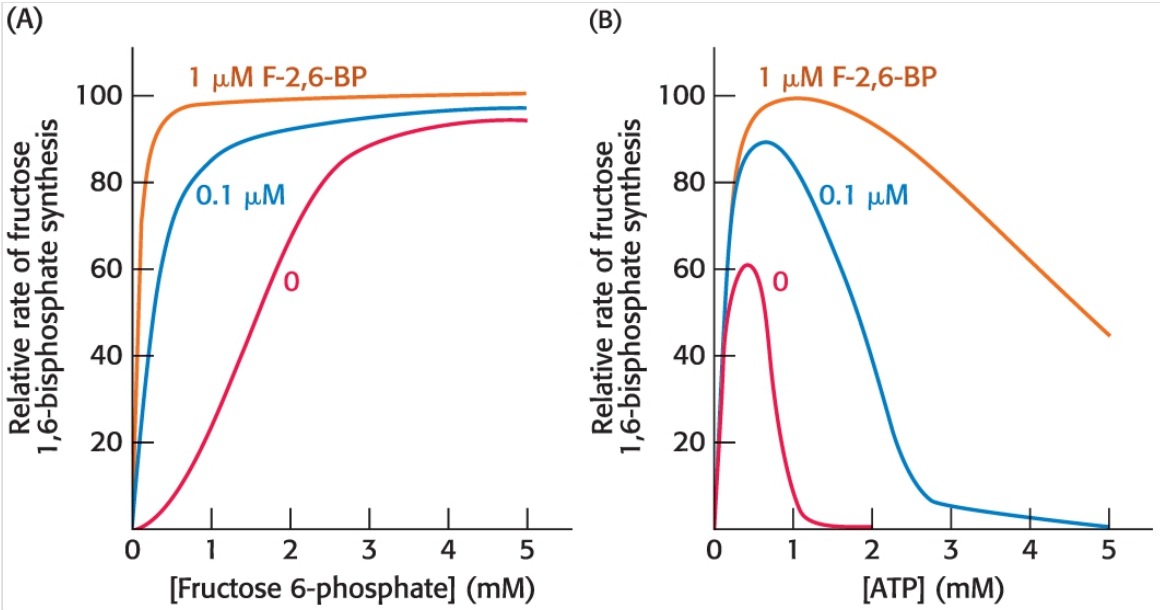


FIGURE 16.23 Activation of phosphofructokinase by fructose 2,6-bisphosphate changes the properties of the enzyme and counteracts inhibition by ATP. (A) The sigmoidal dependence of velocity on substrate concentration becomes hyperbolic in the presence of 1 μM fructose 2,6-bisphosphate. (B) ATP, acting as a substrate, initially stimulates the reaction. As the concentration of ATP increases, it acts as an allosteric inhibitor. The inhibitory effect of ATP is reversed by fructose 2,6-bisphosphate.

[Data from E. Van Schaftingen, M. F. Jett, L. Hue, and H. G. Hers, *Proc. Natl. Acad. Sci. U.S.A.* 78:3483–3486, 1981.]

Hexokinase and glucokinase

The hexokinase reaction in the liver is regulated as in the muscle. However, the liver, in keeping with its role as monitor of blood-glucose levels, possesses another specialized isozyme of hexokinase, called *glucokinase*, which is not inhibited by glucose 6-phosphate. The role of glucokinase is to provide glucose 6-phosphate for the synthesis of glycogen and for the formation of fatty acids (Chapter 22).

Remarkably, glucokinase displays the sigmoidal kinetics characteristic of an allosteric enzyme even though it functions as a monomer.

Glucokinase phosphorylates glucose only when glucose is abundant because the affinity of glucokinase for glucose is about 50-fold lower than that of hexokinase. Moreover, when glucose concentration is low, glucokinase is inhibited by the liver-specific glucokinase regulatory protein (GKRP), which sequesters the kinase in the nucleus until the glucose concentration increases. The low affinity of glucokinase for glucose gives the brain and muscles first call on glucose when its supply is limited, and it ensures that glucose will not be wasted when it is abundant.

 Glucokinase is also present in the β cells of the pancreas, which secrete the hormone insulin in response to the increased formation of glucose 6-phosphate by glucokinase when blood-glucose levels are elevated. Insulin signals the need to remove glucose from the blood for storage as glycogen or conversion into fat. Drugs that activate liver glucokinase or disrupt its interaction with GKRP are being evaluated as a treatment for type 2 diabetes, in which the sensitivity to natural levels of insulin has decreased.

Pyruvate kinase

Several isozymic forms of pyruvate kinase (a tetramer of 57-kDa subunits) encoded by different genes are present in mammals: The L type predominates in the liver, and the M type in muscle and the brain. The L and M forms of pyruvate kinase have many properties in common. Indeed, the liver enzyme behaves much like the muscle enzyme with regard to allosteric regulation, except that the liver enzyme is also inhibited by alanine (synthesized in one step from pyruvate), a signal that building blocks are available. Moreover, the isozymic forms differ in their susceptibility to covalent modification. The catalytic properties of the L form — but not of the M form — are also controlled by reversible phosphorylation (**Figure 16.24**). When the blood-glucose level is low, the glucagon-triggered cyclic AMP cascade

(Section 14.2) leads to the phosphorylation of pyruvate kinase, which diminishes its activity. This hormone-triggered phosphorylation prevents the liver from consuming glucose when it is more urgently needed by the brain and muscle. We see here a clear-cut example of how isoenzymes contribute to the metabolic diversity of different organs.

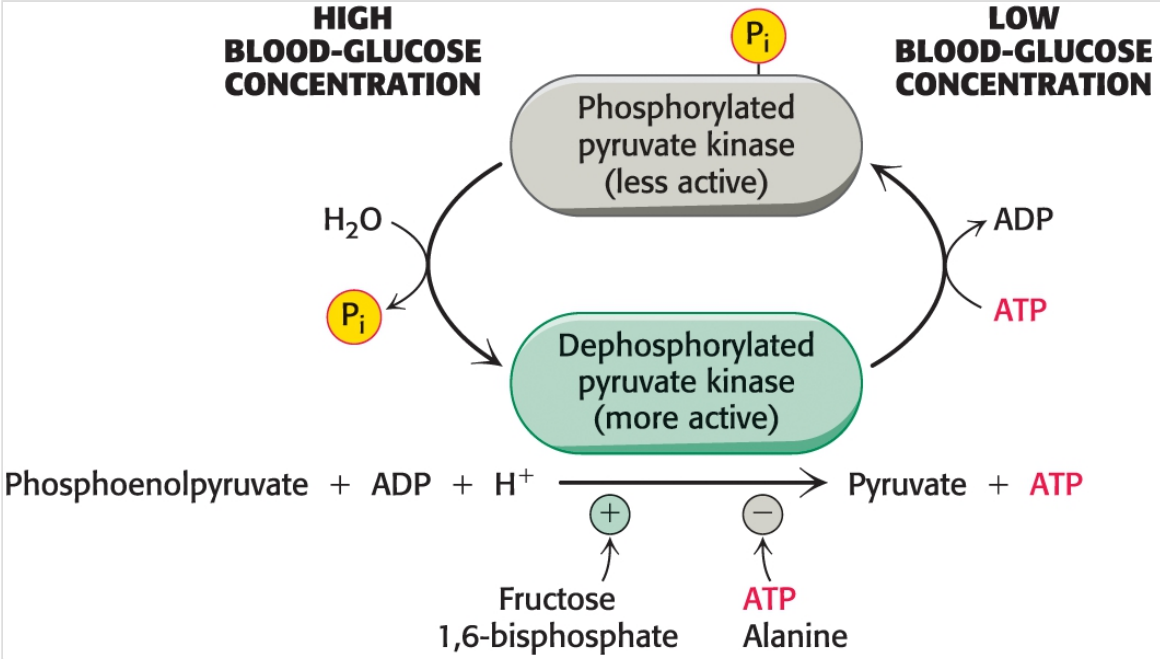


FIGURE 16.24 Pyruvate kinase activity is controlled by phosphorylation and dephosphorylation. Pyruvate kinase is automatically regulated by allosteric effectors but controlled by extracellular signals through reversible covalent modification. Fructose 1,6-bisphosphate allosterically stimulates the enzyme, while ATP and alanine are allosteric inhibitors. Glucagon, secreted in response to low blood glucose, promotes phosphorylation and inhibition of the enzyme. When blood glucose concentration is adequate, the enzyme is dephosphorylated and activated.

The enzymes of glycolysis are physically associated with one another

Evidence has accumulated that the enzymes of glycolysis in eukaryotes are organized into complexes. For example, in yeast, the glycolytic enzymes are associated with the mitochondria, while in mammalian erythrocytes, the enzymes are found bound to the inner surface of the cell membrane. Indeed, some level of organization appears to occur in all cell types. This arrangement increases enzyme efficiency by facilitating movement of substrates and products between enzymes — a process called **substrate channeling** — and prevents the release of any toxic intermediates. We will see that the organization of metabolic pathways into large complexes is a common occurrence inside the cell.

Aerobic glycolysis is a property of tumor cells and other rapidly growing cells



Tumors have been known for decades to display enhanced rates of glucose uptake and glycolysis. Indeed, rapidly growing tumor cells will metabolize glucose to lactate even in the presence of oxygen, a process called **aerobic glycolysis** or the *Warburg effect*, after Otto Warburg, the biochemist who first noted this characteristic of cancer cells in the 1920s. In fact, tumors with a high glucose uptake are particularly aggressive, and the cancer is likely to have a poor prognosis. A nonmetabolizable glucose analog, 2-^{18}F-2-D-deoxyglucose, detectable by a combination of positron emission tomography (PET) and computer-aided tomography (CAT), easily visualizes tumors and allows monitoring of treatment effectiveness (**Figure 16.25**).

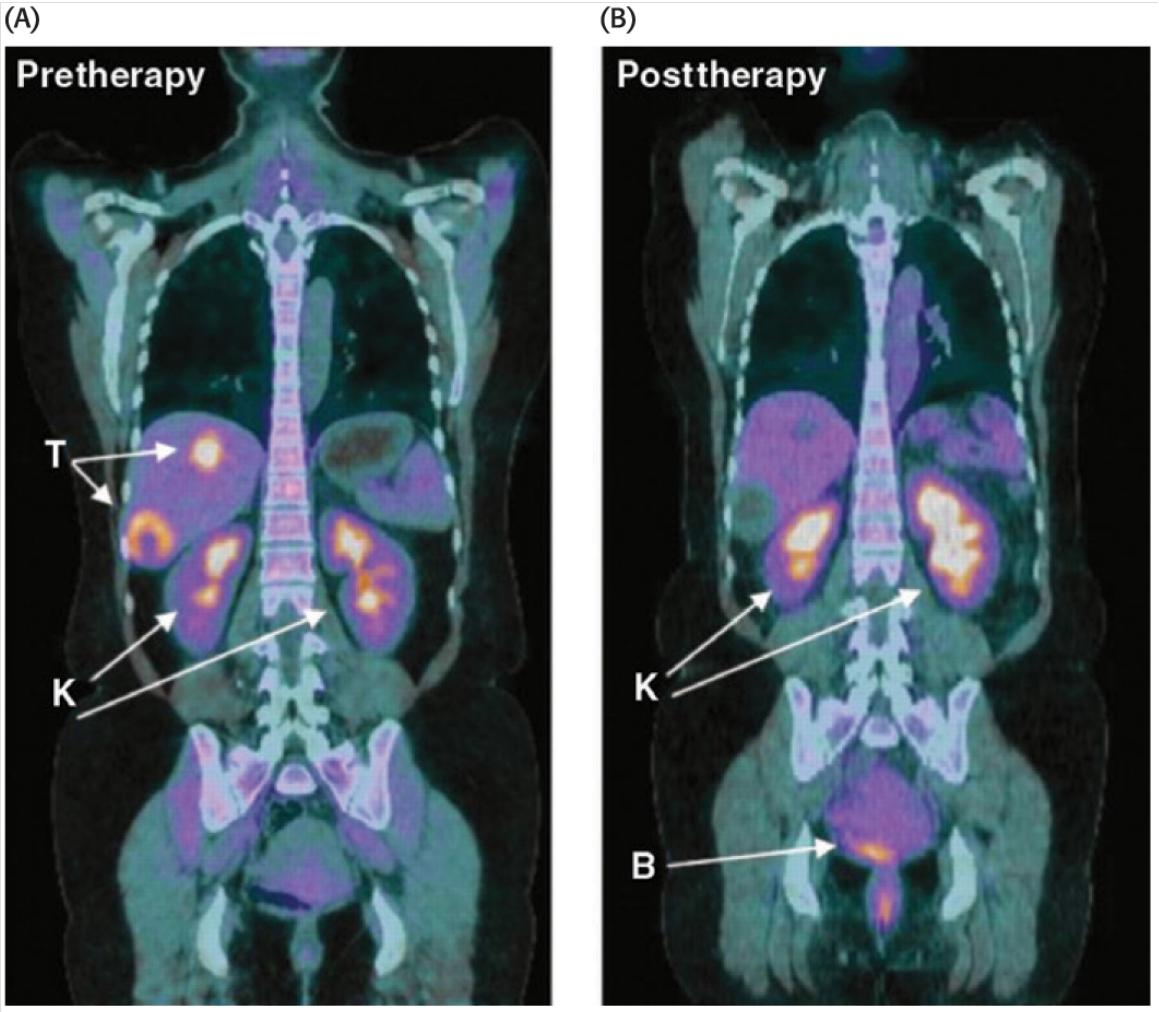


FIGURE 16.25 Tumors can be visualized with 2-^{18}F-2-D-deoxyglucose (FDG) and positron emission tomography. (A) A nonmetabolizable glucose analog infused into a patient and detected by a combination of positron emission and computer-aided tomography reveals the presence of a malignant tumor (T). (B) After 4 weeks of treatment with a tyrosine kinase inhibitc (Section 14.5), the tumor shows no uptake of FDG, indicating decreased metabolism. Excess FD which is excreted in the urine, also visualizes the kidneys (K) and bladder (B).

What selective advantage does aerobic glycolysis offer the tumor over the energetically more efficient oxidative phosphorylation? Researchers are actively pursuing the answer to this question, but we can speculate on the benefits. First, aerobic glycolysis generates lactic acid that is then

secreted. Acidification of the tumor environment has been shown to facilitate tumor invasion. Moreover, lactate impairs the activation of $CD8^+$ T and NK immune system cells that normally attack the tumor. However, even leukemias perform aerobic glycolysis, and leukemia is not an invasive cancer. Second, and perhaps more importantly, the increased uptake of glucose and formation of glucose 6-phosphate provides substrates for another metabolic pathway — the pentose phosphate pathway (Section 20.3) — that generates biosynthetic reducing power, NADPH. Finally, cancer cells grow more rapidly than the blood vessels that nourish them; thus, as solid tumors grow, the oxygen concentration in their environment falls. In other words, they begin to experience a deficiency of oxygen, called *hypoxia*. The use of aerobic glycolysis reduces the dependence of cell growth on oxygen.

What biochemical alterations facilitate the switch to aerobic glycolysis? Again, the answers are not complete, but changes in gene expression of isozymic forms of two glycolytic enzymes may be crucial. Tumor cells express an isozyme of hexokinase that binds to mitochondria. There, the enzyme has ready access to any ATP generated by oxidative phosphorylation and is not susceptible to feedback inhibition by its product, glucose 6-phosphate. More importantly, an embryonic isozyme of pyruvate kinase, pyruvate kinase M, is also expressed. Remarkably, this isozyme has a lower catalytic rate than normal pyruvate kinase and creates a bottleneck, allowing the use of glycolytic intermediates for biosynthetic processes required for cell proliferation. The need for biosynthetic precursors is greater than the need for ATP, suggesting that even glycolysis at a reduced rate produces sufficient ATP to allow cell proliferation. Although originally observed in cancer cells, the Warburg effect is also seen in noncancerous, rapidly dividing cells.

Cancer and endurance training affect glycolysis in a similar fashion



The hypoxia that some tumors experience with rapid growth activates a transcription factor, hypoxia-inducible transcription factor (HIF-1). HIF-1 increases the expression of most glycolytic enzymes and the glucose transporters GLUT1 and GLUT3 (Table 16.5). These adaptations by the cancer cells enable a tumor to survive until blood vessels can grow. HIF-1 also increases the expression of signal molecules, such as vascular endothelial growth factor (VEGF), that facilitate the growth of blood vessels that will provide nutrients to the cells (Figure 16.26). Without new blood vessels, a tumor would cease to grow and either die or remain harmlessly small.

TABLE 16.5 Proteins in glucose metabolism encoded by genes regulated by hypoxia-inducible factor

GLUT1
GLUT3
Hexokinase
Phosphofructokinase
Aldolase
Glyceraldehyde 3-phosphate dehydrogenase
Phosphoglycerate kinase

Enolase
Pyruvate kinase

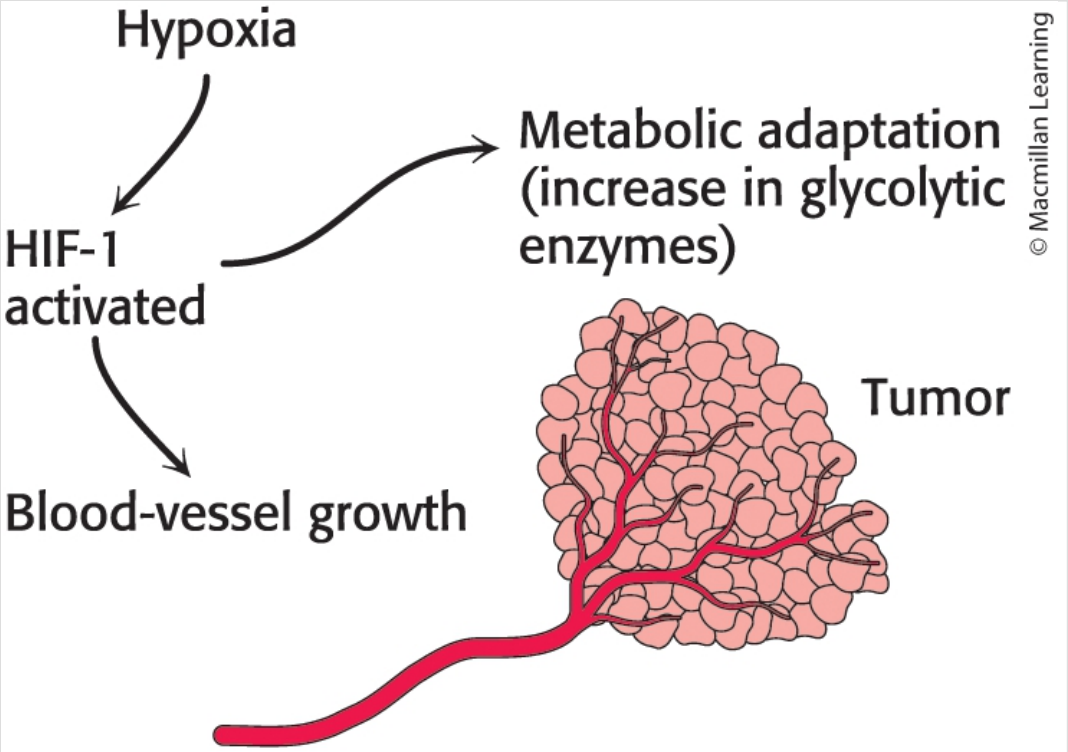


FIGURE 16.26 Hypoxia alters gene expression in tumors. The hypoxic conditions inside a tumor mass lead to the activation of the hypoxia-inducible transcription factor (HIF-1), which induces metabolic adaptation (an increase in glycolytic enzymes) and activates angiogenic factors that stimulate the growth of new blood vessels.

[Information from C. V. Dang and G. L. Semenza, *Trends Biochem. Sci.* 24:68–72, 1999.]

Efforts are underway to develop drugs that inhibit the growth of blood vessels in tumors. Indeed, bevacizumab, a monoclonal antibody that binds to VEGF and prevents activation of angiogenesis, has been approved for treatment of glioblastomas, which are fast-growing cancers of the central nervous system derived from glial cells.

Interestingly, anaerobic exercise training — forcing muscles to rely on lactic acid fermentation for ATP production — also activates HIF-1, producing the same effects as those seen in the tumor — enhanced ability to generate ATP anaerobically and a stimulation of blood-vessel growth. These biochemical effects account for the improved athletic performance that results from training and demonstrate how behavior can affect biochemistry. Other signals from sustained muscle contraction trigger muscle mitochondrial biogenesis, allowing for more efficient aerobic energy generation and forestalling the need to resort to lactic acid fermentation for ATP synthesis.

Self-Check Question



Muscle phosphofructokinase activity increases as a function of ATP concentration, but only up to a point, and then it falls rapidly. Explain these results and how they relate to the role of phosphofructokinase in glycolysis.

16.4 Glucose Can Be Synthesized from Noncarbohydrate Precursors

We now turn to the synthesis of glucose from noncarbohydrate precursors, a process called *gluconeogenesis.* Maintaining levels of glucose is important because the brain depends on glucose as its primary fuel and red blood cells use glucose as their only fuel. The daily glucose requirement of the brain in a typical adult human being is about 120 g, which accounts for most of the 160 g of glucose needed daily by the whole body. The amount of glucose present in body fluids is about 20 g, and that readily available from glycogen is approximately 190 g. Thus, the direct glucose reserves are sufficient to meet glucose needs for about a day. Gluconeogenesis is especially important during a longer period of fasting or starvation (Section 24.2) and to constantly remove and recycle lactate, which is always being produced by some tissues.

The gluconeogenic pathway converts pyruvate into glucose. The major noncarbohydrate precursors of glucose — lactate, amino acids, and glycerol — are first converted into pyruvate or enter the pathway at later intermediates such as oxaloacetate and dihydroxyacetone phosphate (**Figure 16.27**). Lactate is readily converted into pyruvate by the action of lactate dehydrogenase (Section 16.2). Amino acids are derived from proteins in the diet and, during starvation, from the breakdown of proteins in skeletal muscle (Section 23.1).

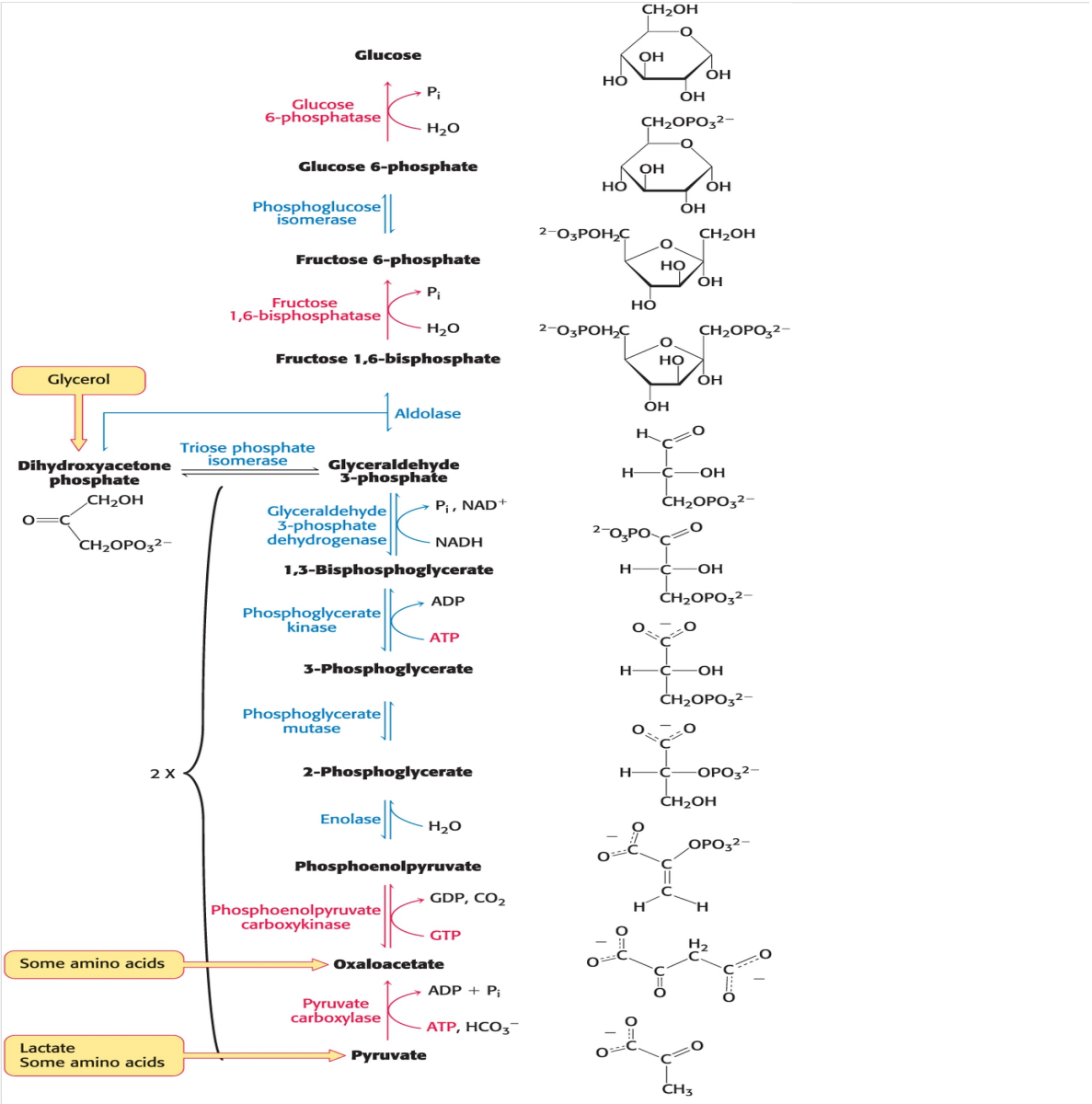
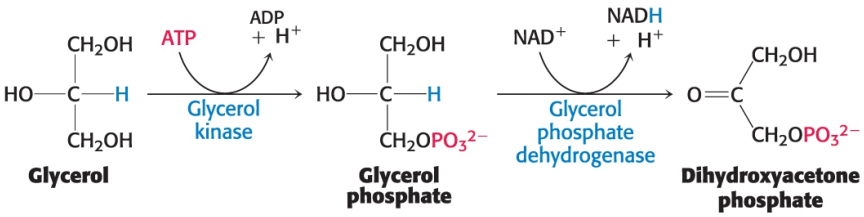


FIGURE 16.27 Gluconeogenesis shares many enzymatic steps with glycolysis. The reactions and enzymes unique to gluconeogenesis are shown in red. The other shared reactions are in black. The enzymes for gluconeogenesis are located in the cytoplasm, except for pyruvate carboxylase (in the mitochondria) and glucose 6-phosphatase (membrane bound in the lumen of the endoplasmic reticulum). The entry points for lactate, glycerol, and amino acids are shown.

The hydrolysis of triacylglycerols (Section 22.2) in fat cells yields glycerol and fatty acids. Glycerol is a precursor of glucose, but animals cannot convert fatty acids into glucose, for reasons that will be discussed in Chapter 17. Glycerol may enter either the gluconeogenic or the glycolytic pathway as dihydroxyacetone phosphate.



The major site of gluconeogenesis is the liver, with a small amount also taking place in the kidney and other tissues. Gluconeogenesis in the liver and kidney helps to maintain the glucose concentration in the blood so that the brain and muscle can extract sufficient glucose from it to meet their metabolic demands.

Gluconeogenesis is not a reversal of glycolysis

In glycolysis, glucose is converted into pyruvate; in gluconeogenesis, pyruvate is converted into glucose. However, gluconeogenesis is not a reversal of glycolysis. Several reactions must differ because the equilibrium of glycolysis lies far on the side of pyruvate formation. The actual free-energy change for the formation of pyruvate from glucose is about $-90\ \text{kJ mol}^{-1}\ (-22\ \text{kcal mol}^{-1})$ under typical cellular conditions. Most of the decrease in free energy in glycolysis takes place in the three essentially irreversible steps catalyzed by hexokinase, phosphofructokinase, and pyruvate kinase.

$$\text{Glucose} + \text{ATP} \xrightarrow{\text{Hexokinase}} \text{glucose 6-phosphate} + \text{ADP} \qquad \Delta G = -33\ \text{kJ mol}^{-1}\ (-8.0\ \text{kcal mol}^{-1})$$

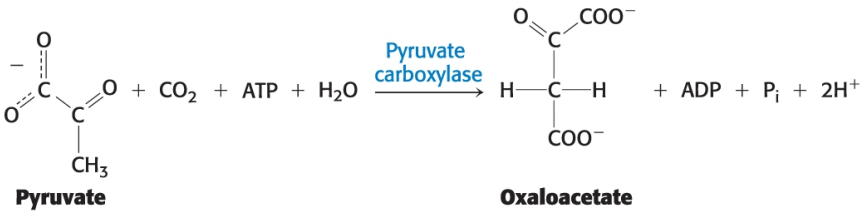
$$\text{Fructose 6-phosphate} + \text{ATP} \xrightarrow{\text{Phosphofructokinase}} \text{fructose 1,6-bisphosphate} + \text{ADP} \qquad \Delta G = -22\ \text{kJ mol}^{-1}\ (-5.3\ \text{kcal mol}^{-1})$$

$$\text{Phosphoenolpyruvate} + \text{ADP} \xrightarrow{\text{Pyruvate kinase}} \text{pyruvate} + \text{ATP} \qquad \Delta G = -17\ \text{kJ mol}^{-1}\ (-4.0\ \text{kcal mol}^{-1})$$

In gluconeogenesis, these virtually irreversible reactions of glycolysis must be bypassed.

The conversion of pyruvate into phosphoenolpyruvate begins with the formation of oxaloacetate

The first step in gluconeogenesis is the carboxylation of pyruvate to form oxaloacetate at the expense of a molecule of ATP, a reaction catalyzed by pyruvate carboxylase. This reaction occurs in the mitochondria.



Pyruvate carboxylase requires biotin, a covalently attached prosthetic group, which serves as the carrier of activated CO_2. The carboxylate group of biotin is linked to the ε-amino group of a specific lysine residue by an amide bond (**Figure 16.28**). Recall that, in aqueous solutions, CO_2 exists primarily as HCO_3^- with the aid of carbonic anhydrase (Section 6.2).

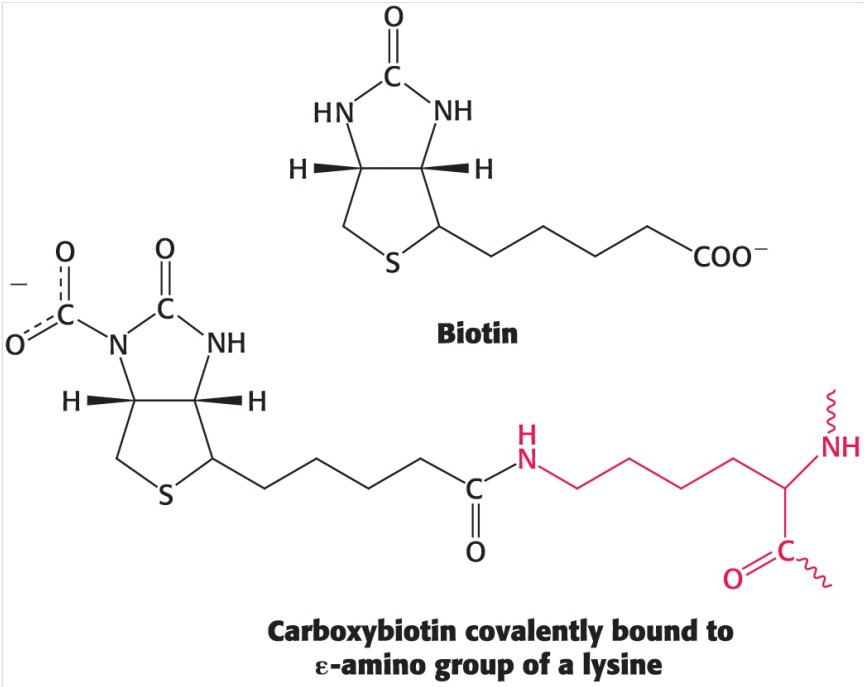


FIGURE 16.28 Carboxybiotin linked to lysine can act as a movable "arm" carrying activated CO_2 groups. Notice the great distance between the bound CO_2 group and where the lysine connects to the rest of the protein. This allows the lysyl-carboxybiotin moiety to act like a long lever arm to move CO_2 from one location in a protein to another. This movement is usually from one distinct active site to a second active site within the same or, in the case of pyruvate carboxylase, in a different subunit.

The carboxylation of pyruvate takes place in three stages:

$$HCO_3^- + ATP \rightleftharpoons HOCO_2 - PO_3^{2-} + ADP$$

$$\text{Biotin–enzyme} + HOCO_2 - PO_3^{2-} \rightarrow CO_2 - \text{biotin–enzyme} + P_i$$

$$CO_2 - \text{biotin-enzyme} + \text{pyruvate} \rightleftharpoons \text{biotin-enzyme} + \text{oxaloacetate}$$

Pyruvate carboxylase functions as a tetramer composed of four identical subunits, and each subunit consists of four domains (Figure 16.29). The biotin carboxylase domain (BC) catalyzes the formation of carboxyphosphate and the subsequent attachment of CO_2 to the second domain, the biotin carboxyl carrier protein (BCCP) — the site of the covalently attached biotin. Once bound to CO_2, BCCP leaves the biotin carboxylase active site and swings almost the entire length of the subunit (≈ 75 Å) to the active site of the carboxyl transferase domain (CT), which transfers the CO_2 to pyruvate to form oxaloacetate. BCCP in one subunit interacts with the active sites on an adjacent subunit. The fourth domain (PT) facilitates the formation of the tetramer and is the binding site for acetyl CoA, a required allosteric activator.

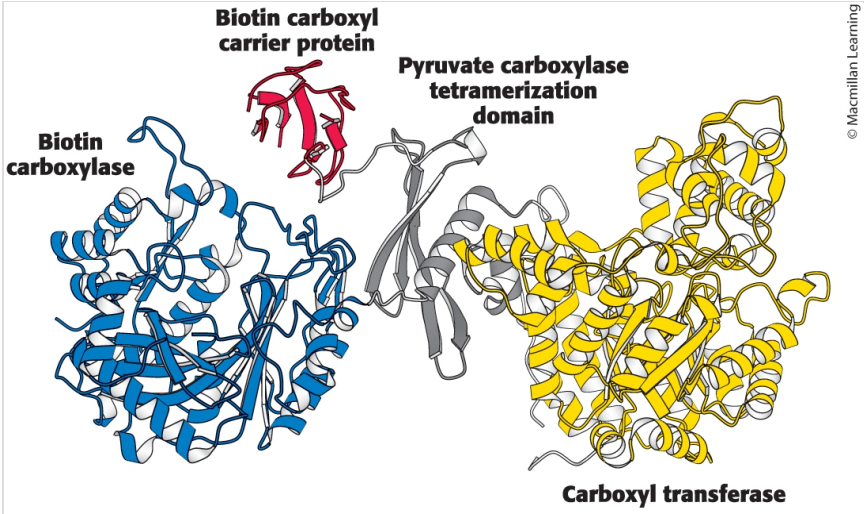


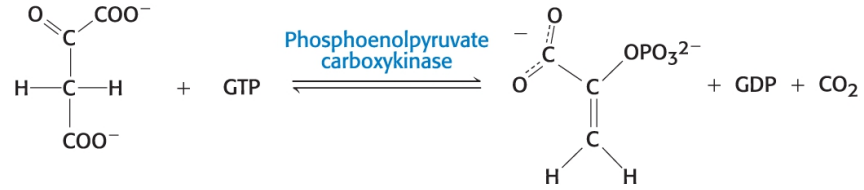
FIGURE 16.29 A subunit of pyruvate carboxylase shows the complexity of the enzyme. The functional enzyme is a tetramer compose of these complex subunits which each have four distinct domains as shown. Biotin, covalently attached to the biotin carboxyl carrier protein, transports CO_2 from the biotin carboxylase active site to the carboxyl transferase active site.

[Information from G. Lasso, L. P. C. Yu, D. Gil, S. Xiang, L. Tong, and M. Valle, *Structure* 18:1300–1310, 2010.]

How acetyl CoA facilitates the carboxylase reaction is under investigation. Recent research suggests that by binding to the enzyme, acetyl CoA enhances conformational communication between the BC and CT domains that enables the movement of the BCCP domain between two catalytic sites. The allosteric activation of pyruvate carboxylase by acetyl CoA is also an important physiological control mechanism that will be discussed in Section 17.5.

Oxaloacetate is shuttled into the cytoplasm and converted into phosphoenolpyruvate

Oxaloacetate must thus be transported to the cytoplasm to complete the synthesis of phosphoenolpyruvate. Oxaloacetate is first reduced to malate by malate dehydrogenase. Malate is transported across the mitochondrial membrane and reoxidized to oxaloacetate by a cytoplasmic NAD^+-linked malate dehydrogenase (**Figure 16.30**). The formation of oxaloacetate from malate also provides NADH for use in subsequent steps in gluconeogenesis. Finally, oxaloacetate is simultaneously decarboxylated and phosphorylated by phosphoenolpyruvate carboxykinase (PEPCK) to generate phosphoenolpyruvate. The phosphoryl donor is GTP. The CO_2 that was added to pyruvate by pyruvate carboxylase comes off in this step.



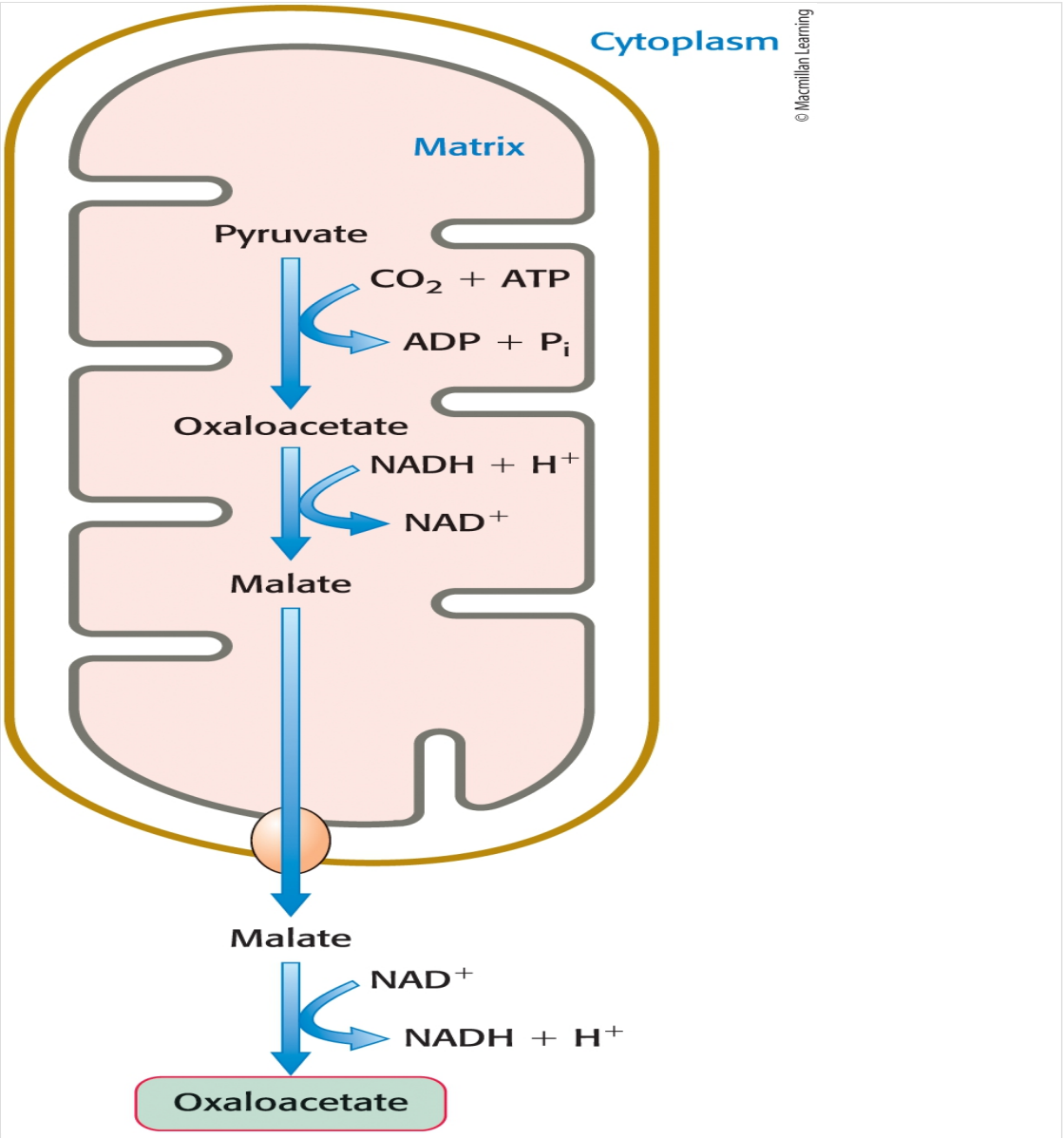


FIGURE 16.30 Oxaloacetate used in the cytoplasm for gluconeogenesis is formed in the mitochondrial matrix. Pyruvate is carboxylated to form oxaloacetate that then leaves the mitochondrion by a specific transport system (oval structure in the mitochondrial membranes) in the form of malate. Malate is reoxidized to oxaloacetate in the cytoplasm.

The sum of the reactions catalyzed by pyruvate carboxylase and phosphoenolpyruvate carboxykinase is

$$\text{Pyruvate} + \text{ATP} + \text{GTP} + H_2O \rightarrow \text{phosphoenolpyruvate} + \text{ADP} + \text{GDP} + P_i + 2H^+$$

This pair of reactions bypasses the irreversible reaction catalyzed by pyruvate kinase in glycolysis.

Why is a carboxylation and a decarboxylation required to form phosphoenolpyruvate from pyruvate? Recall that, in glycolysis, the presence of a phosphoryl group traps the unstable enol isomer of pyruvate as phosphoenolpyruvate (Section 16.2). However, the addition of a phosphoryl group to pyruvate is a highly unfavorable reaction: the $\Delta G^{\circ\prime}$ of the reverse of the glycolytic reaction catalyzed by pyruvate kinase is $+31\ \text{kJ mol}^{-1}\ (+7.5\ \text{kcal mol}^{-1})$. In gluconeogenesis, the use of the carboxylation and decarboxylation steps results in a much more favorable $\Delta G^{\circ\prime}$. The formation of phosphoenolpyruvate from pyruvate in the gluconeogenic pathway has a $\Delta G^{\circ\prime}$ of $+\ 0.8\ \text{kJ mol}^{-1}\ (+0.2\ \text{kcal mol}^{-1})$. A molecule of ATP is used to power the addition of a molecule of CO_2 to pyruvate in the carboxylation step. That CO_2 is then removed to power the formation of phosphoenolpyruvate in the decarboxylation step.

Decarboxylations often drive reactions that are otherwise highly endergonic. This metabolic motif is used in the citric acid cycle (Chapter 17), the pentose phosphate pathway (Chapter 20), and fatty acid synthesis (Section 22.4).

The conversion of fructose 1,6-bisphosphate into fructose 6-phosphate and orthophosphate is an irreversible step

On formation, phosphoenolpyruvate is metabolized by the enzymes of glycolysis but in the reverse direction. These reactions are near equilibrium under intracellular conditions; so, when conditions favor gluconeogenesis, the reverse reactions will take place until the next irreversible step is reached. This step is the hydrolysis of fructose 1,6-bisphosphate to fructose 6-phosphate and P_i.

$$\text{Fructose 1,6–bisphosphate} + H_2O \xrightarrow{\text{Fructose 1,6–bisphosphatase}} \text{fructose 6–phosphate} + P_i$$

The enzyme responsible for this step is fructose 1,6-bisphosphatase (FBPase). Like its glycolytic counterpart, it is an allosteric enzyme that participates in the regulation of gluconeogenesis. It is also an example of a **phosphatase**, an enzyme that catalyzes the hydrolysis of a phosphate to form inorganic phosphate and the reverse reaction. Note that the difference between kinases and phosphatases is not the physiologically relevant direction of the reaction but whether the phosphate is transferred to water or ADP.

The generation of free glucose occurs only in some tissues and is an important control point

The fructose 6-phosphate generated by fructose 1,6-bisphosphatase is readily converted into glucose 6-phosphate. The final step in the generation of free glucose takes place primarily in the liver, a

tissue whose metabolic duty is to maintain adequate glucose concentration in the blood for use by other tissues. Free glucose is not formed in the cytoplasm. Rather, glucose 6-phosphate is transported into the lumen of the endoplasmic reticulum, where it is hydrolyzed to glucose by glucose 6-phosphatase, which is bound to the ER membrane (**Figure 16.31**). Glucose and P_i are then shuttled back to the cytoplasm by a pair of transporters.

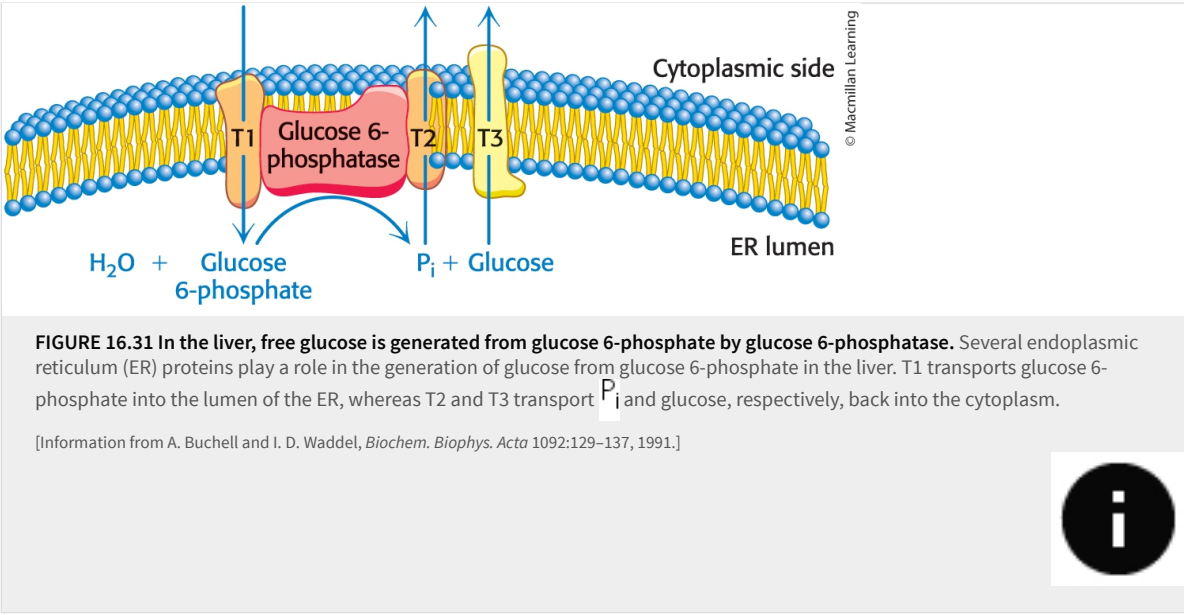


FIGURE 16.31 In the liver, free glucose is generated from glucose 6-phosphate by glucose 6-phosphatase. Several endoplasmic reticulum (ER) proteins play a role in the generation of glucose from glucose 6-phosphate in the liver. T1 transports glucose 6-phosphate into the lumen of the ER, whereas T2 and T3 transport P_i and glucose, respectively, back into the cytoplasm.

[Information from A. Buchell and I. D. Waddel, *Biochem. Biophys. Acta* 1092:129–137, 1991.]

In most tissues, gluconeogenesis ends with the formation of glucose 6-phosphate. Free glucose is not generated because most tissues lack glucose 6-phosphatase. Rather, the glucose 6-phosphate is commonly converted into glycogen, the storage form of glucose (Chapter 21).

Six high-transfer-potential phosphoryl groups are spent in synthesizing glucose from pyruvate

The formation of glucose from pyruvate is energetically unfavorable unless it is coupled to reactions that are favorable. Compare the stoichiometry of gluconeogenesis with that of the reverse of glycolysis.

The stoichiometry of gluconeogenesis is

$$2\ \text{Pyruvate} + 4\ \text{ATP} + 2\ \text{GTP} + 2\ \text{NADH} + 6\ H_2O \rightarrow \text{glucose} + 4\ \text{ADP} + 2\ \text{GDP} + 6\ P_i + 2\ NAD^+ + 2\ H^+$$

$$\Delta G^{\circ\prime} = -48\ \text{kJ mol}^{-1}\ (-11\ \text{kcal mol}^{-1})$$

In contrast, the stoichiometry for the reversal of glycolysis is

$$2\ \text{Pyruvate} + 2\ \text{ATP} + \text{NADH} + 2\ H_2O \rightarrow \text{glucose} + 2\ \text{ADP} + 2\ P_i + 2\ NAD^+ + 2\ H^+$$
$$\Delta G^{\circ\prime} = +90\ \text{kJ mol}^{-1}\ (+22\ \text{kcal mol}^{-1})$$

Note that *six* nucleoside triphosphate molecules are hydrolyzed to synthesize glucose from pyruvate in gluconeogenesis, whereas only *two* molecules of ATP are generated in glycolysis in the conversion of glucose into pyruvate. Thus, the extra cost of gluconeogenesis is four high-phosphoryl-transfer-potential molecules for each molecule of glucose synthesized from pyruvate. The four additional molecules having high phosphoryl-transfer potential are needed to turn an energetically unfavorable process (the reversal of glycolysis) into a favorable one (gluconeogenesis). Here we have a clear example of the coupling of reactions: NTP hydrolysis is used to power an energetically unfavorable reaction. The reactions of gluconeogenesis are summarized in Table 16.6.

TABLE 16.6 Reactions of gluconeogenesis

Step	Reaction	Enzyme	Reaction type	$\Delta G^{\circ\prime}$ in kJ mol^{-1}
1	$\text{Pyruvate} + CO_2 + \text{ATP} + H_2O \rightarrow \text{oxaloacetate} + \text{ADP} + P_i + 2H^+$	Pyruvate carboxylase	Phosphoryl transfer	−2.1
2	$\text{Oxaloacetate} + \text{GTP} \rightleftharpoons \text{phosphoenolpyruvate} + \text{GDP} + CO_2$	Phosphoenolpyruvate carboxykinase	Phosphoryl-coupled oxidation	+2.9
3	$\text{Phosphoenolpyruvate} + H_2O \rightleftharpoons \text{2-phosphoglycerate}$	Enolase	Hydration	−1.7
4	$\text{2-Phosphoglycerate} \rightleftharpoons \text{3-phosphoglycerate}$	Phosphoglycerate mutase	Phosphoryl shift	−4.6
5	$\text{3-Phosphoglycerate} + \text{ATP} \rightleftharpoons \text{1,3-bisphosphoglycerate} + \text{ADP}$	Phosphoglycerate kinase	Phosphoryl transfer	+18.8
6	$\text{1,3-Bisphosphoglycerate} + \text{NADH} + H^+ \rightleftharpoons \text{glyceraldehyde 3-phosphate} + NAD^+ + P_i$	Glyceraldehyde 3-phosphate dehydrogenase	Phosphoryl-coupled reduction	−6.3

7	Glyceraldehyde 3-phosphate $\rightleftharpoons$ dihydroxyacetonephosphate	Triose phosphate isomerase	Isomerization	−7.5
8	Glyceraldehyde 3-phosphate + dihydroxyacetone phosphate $\rightleftharpoons$ fructose 1,6-bisphosphate	Aldolase	Aldol addition	−23.8
9	$\text{Fructose 1,6–bisphosphate} + H_2O \rightarrow \text{fructose 6–phosphate} + P_i$	Fructose 1,6-bisphosphatase	Phosphoryl transfer	−16.3
10	Fructose 6-phosphate $\rightleftharpoons$ glucose 6-phosphate	Phosphoglucose isomerase	Isomerization	−1.7
11	$\text{Glucose 6–phosphatase} + H_2O \rightarrow \text{glucose} + P_i$	Glucose 6-phosphatase	Phosphoryl transfer	−12.1

16.5 Gluconeogenesis and Glycolysis Are Reciprocally Regulated

Gluconeogenesis and glycolysis are coordinated so that, within a cell, one pathway is relatively inactive while the other is highly active. If both sets of reactions were highly active at the same time, the net result would be the hydrolysis of four nucleoside triphosphates (two ATP molecules plus two GTP molecules) per reaction cycle. Both glycolysis and gluconeogenesis are highly exergonic under cellular conditions, and so there is no thermodynamic barrier to such simultaneous activity. However, the amounts and activities of the distinctive enzymes of each pathway are controlled so that both pathways are not highly active at the same time. The rate of glycolysis is also determined by the concentration of glucose, and the rate of gluconeogenesis by the concentrations of lactate and other precursors of glucose. The basic premise of the reciprocal regulation is that, when energy is needed or glycolytic intermediates are needed for biosynthesis, glycolysis will predominate. When there is a surplus of energy and glucose precursors, gluconeogenesis will take over.

Glycolysis and gluconeogenesis are regulated by adenosine nucleotides and other metabolic intermediates

The first important regulation site is the interconversion of fructose 6-phosphate and fructose 1,6-bisphosphate (**Figure 16.32**). Consider first a situation in which energy is needed, as in active muscle. In this case, the concentration of AMP is high. Under this condition, AMP stimulates phosphofructokinase but inhibits fructose 1,6-bisphosphatase. Thus, glycolysis is turned on and gluconeogenesis is inhibited. Conversely, high levels of ATP and citrate, and therefore low levels of AMP, indicate

that the energy charge is high and that biosynthetic intermediates are abundant. ATP and citrate both inhibit phosphofructokinase, whereas the decrease in AMP relieves inhibition of fructose 1,6-bisphosphatase. Under these conditions, glycolysis is nearly switched off and gluconeogenesis is promoted. Why does citrate take part in this regulatory scheme? As we will see in Chapter 17, citrate reports on the status of the citric acid cycle, the primary pathway for oxidizing fuels in the presence of oxygen. High levels of citrate indicate an energy-rich situation and the presence of precursors for biosynthesis.

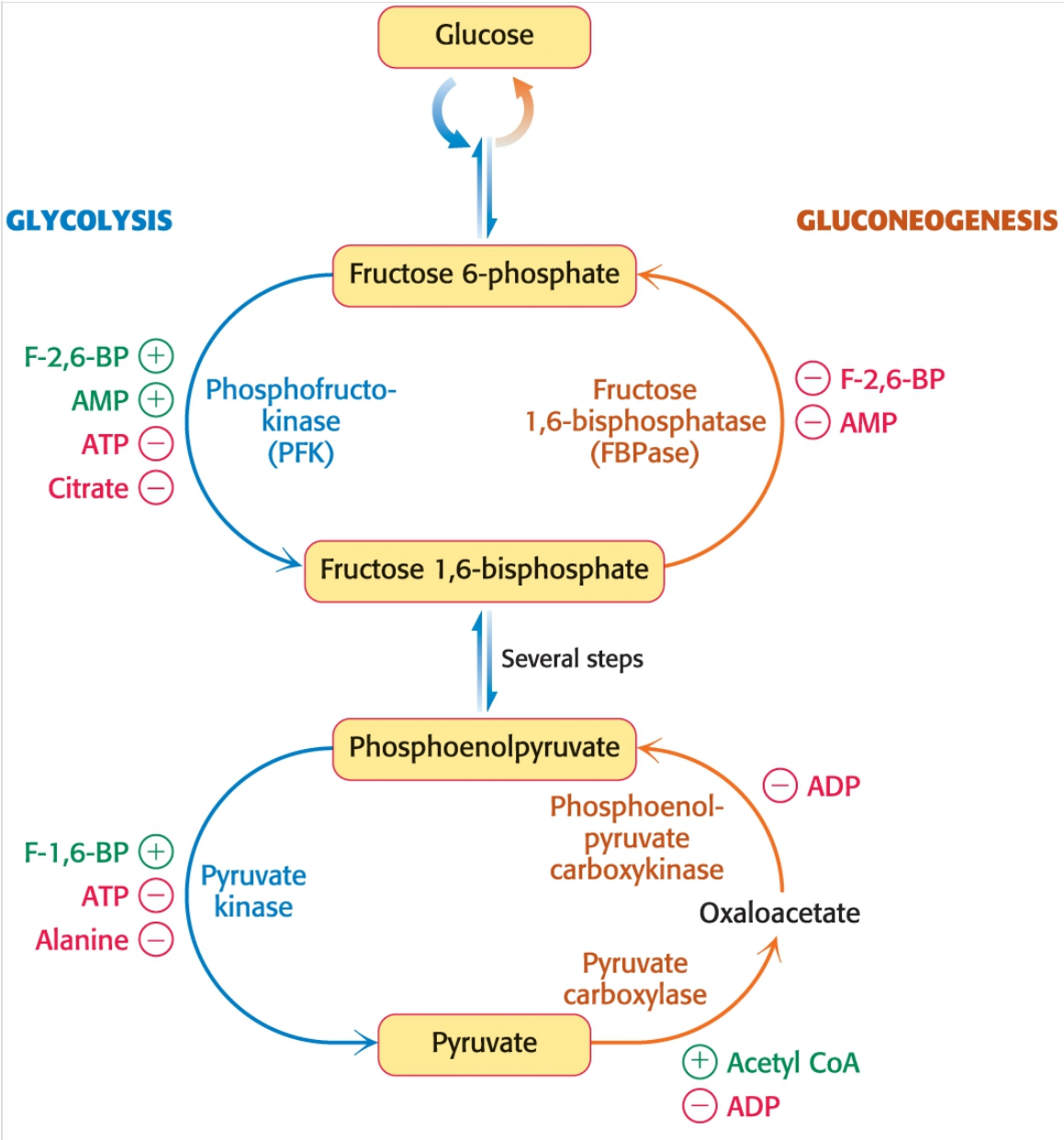


FIGURE 16.32 Gluconeogenesis and glycolysis in the liver are under reciprocal regulation. The concentration of fructose 2,6-bisphosphate is high in the fed state and low in starvation. Another important control is the inhibition of pyruvate kinase by phosphorylation during starvation.



Glycolysis and gluconeogenesis are also reciprocally regulated at the interconversion of phosphoenolpyruvate and pyruvate in the liver. The glycolytic enzyme pyruvate kinase is inhibited by allosteric effectors ATP and alanine, which signal that the energy charge is high and that building blocks are abundant. Conversely, pyruvate carboxylase and phosphoenolpyruvate carboxykinase, which catalyze the first two steps of gluconeogenesis from pyruvate, are inhibited by ADP. Pyruvate carboxylase is also activated by acetyl CoA, which, like citrate, indicates that the citric acid cycle is producing energy and biosynthetic intermediates (Chapter 17). Hence, gluconeogenesis is favored when the cell is rich in biosynthetic precursors and ATP.

In mammals, glycolysis and gluconeogenesis in the liver are controlled by hormones sensitive to blood-glucose concentration

In the liver, rates of glycolysis and gluconeogenesis are adjusted to maintain the blood-glucose concentration. The signal molecule fructose 2,6-bisphosphate strongly stimulates phosphofructokinase (PFK) and inhibits fructose 1,6-bisphosphatase (FBPase). When blood glucose is low, fructose 2,6-bisphosphate (F-2,6-BP) loses a phosphoryl group to form fructose 6-phosphate, which is not an allosteric effector of either PFK or FBPase.

How is the concentration of fructose 2,6-bisphosphate controlled to rise and fall with blood-glucose levels?

- *A bifunctional enzyme determines fructose 2,6-bisphosphate levels.* Two enzyme activities regulate the concentration of F-2,6-BP: one phosphorylates fructose 6-phosphate to form F-2,6-BP, and the other dephosphorylates F-2,6-BP, converting it back to fructose 6-phosphate. The formation reaction is catalyzed by phosphofructokinase 2 (PFK2), a different enzyme from phosphofructokinase. F-2,6-BP is degraded by a specific phosphatase, fructose bisphosphatase 2 (FBPase2).

  The striking finding is that both PFK2 and FBPase2 are present in a single 55-kDa polypeptide chain (**Figure 16.33**). This **bifunctional enzyme**, PFK2/FBPase2, contains an N-terminal regulatory domain, followed by a kinase domain and a phosphatase domain. PFK2 resembles adenylate kinase, whereas FBPase2 resembles phosphoglycerate mutase (Section 16.2). Recall that the mutase is essentially a phosphatase. In the bifunctional enzyme, the phosphatase activity evolved to become specific for F-2,6-BP. The bifunctional enzyme itself probably arose by the fusion of genes encoding the kinase and phosphatase domains.

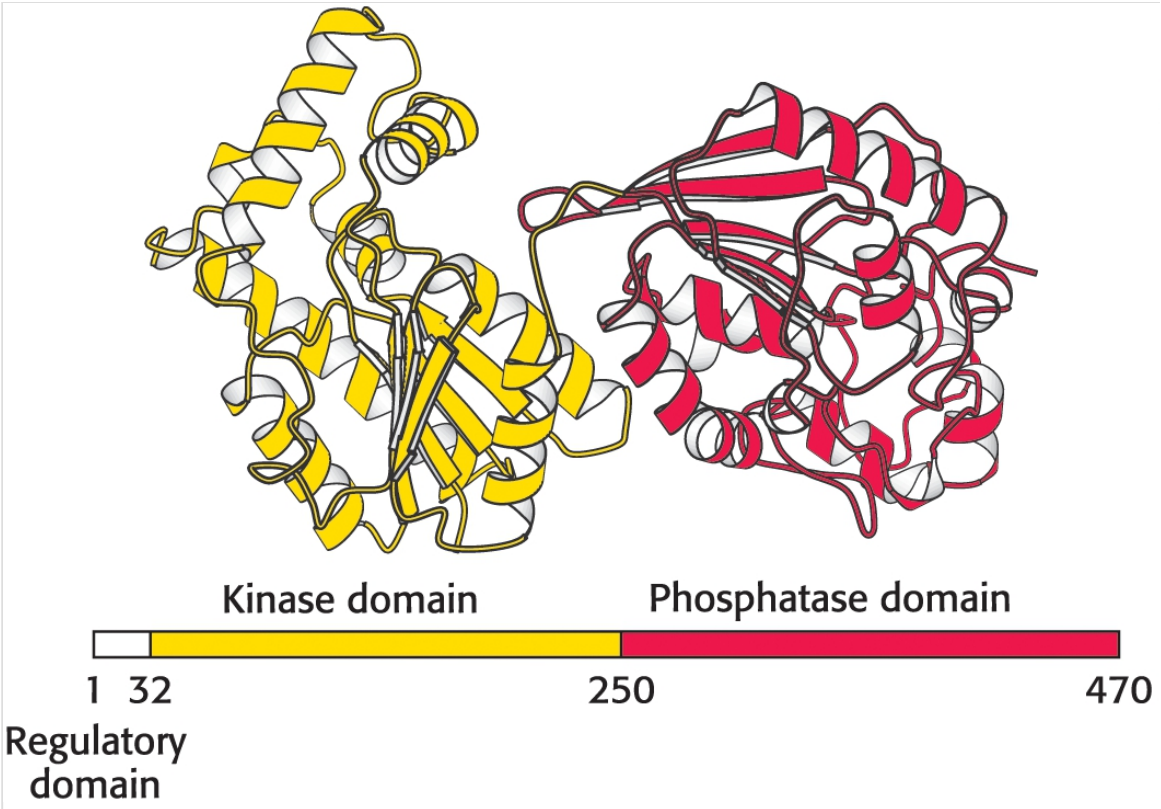


FIGURE 16.33 The bifunctional enzyme PFK2/FBPase2 has two distinct domains. The kinase domain (yellow) is fused to the phosphatase domain (red). The bar represents the amino acid sequence of the enzyme.

[Drawn from 1BIF.pdb.]

INTERACT with this model in Achieve

- *The bifunctional enzyme is controlled by reversible phosphorylation.* What controls whether PFK2 or FBPase2 dominates the bifunctional enzyme's activities in the liver? The activities of PFK2 and FBPase2 are reciprocally controlled by phosphorylation of a single serine residue. When glucose is scarce, such as during a night's fast, a rise in the blood concentration of the hormone glucagon triggers a cyclic AMP signal cascade (Section 14.2), leading to the phosphorylation of this bifunctional enzyme by protein kinase A (**Figure 16.34**). This covalent modification

activates FBPase2 and inhibits PFK2, lowering the level of F-2,6-BP. Gluconeogenesis predominates. Glucose formed by the liver under these conditions is essential for the viability of the brain. Glucagon stimulation of protein kinase A also inactivates pyruvate kinase in the liver.

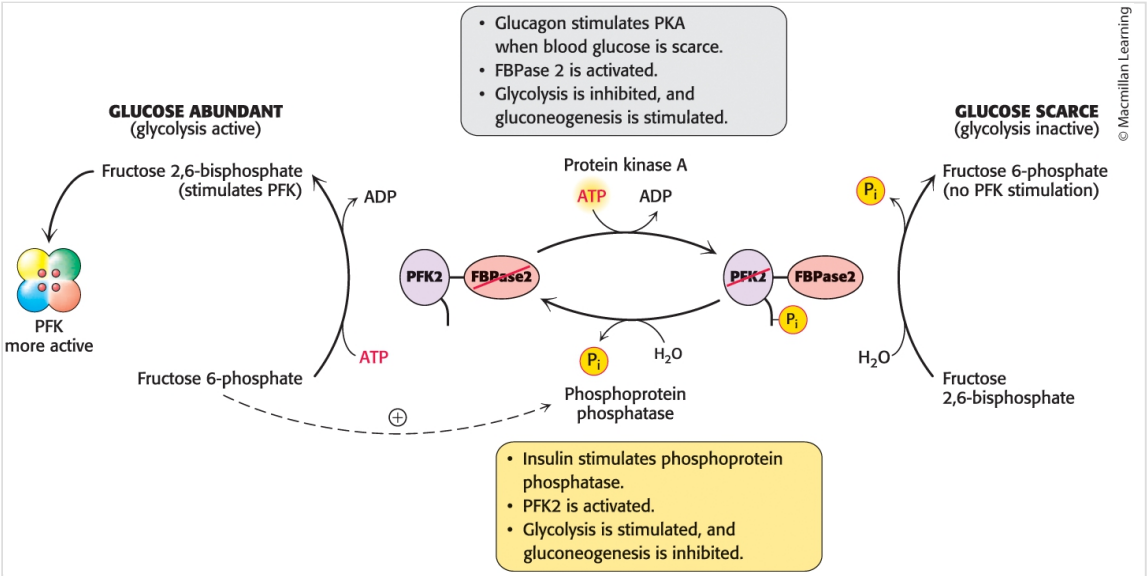


FIGURE 16.34 The synthesis and degradation of fructose 2,6-bisphosphate is hormonally controlled. A low blood-glucose concentration as signaled by glucagon leads to the phosphorylation of the bifunctional enzyme and hence to a lower concentration of fructose 2,6-bisphosphate, slowing glycolysis. Insulin accelerates the formation of fructose 2,6-bisphosphate by facilitating the dephosphorylation of the bifunctional enzyme.

Conversely, when the blood-glucose concentration is high, such as after a meal, gluconeogenesis is not needed. Insulin is secreted and initiates a signal pathway that activates a protein phosphatase, which removes the phosphoryl group from the bifunctional enzyme. This covalent modification activates PFK2 and inhibits FBPase2. The resulting rise in the level of F-2,6-BP accelerates glycolysis. In liver, a key role of glycolysis is to generate metabolites for biosynthesis. The coordinated control of glycolysis and

gluconeogenesis is facilitated by the location of the kinase and phosphatase domains on the same polypeptide chain as the regulatory domain.

- *The bifunctional enzyme is also under transcriptional control by glucagon and insulin.* The hormones glucagon and insulin also regulate the amounts of essential enzymes by altering gene expression, primarily by changing the rate of transcription. Transcriptional control in eukaryotes is much slower than allosteric control, taking hours or days instead of seconds to minutes.

  Glucagon rises during fasting, when gluconeogenesis is needed to replace scarce glucose. To encourage gluconeogenesis, glucagon inhibits the expression of the three regulated glycolytic enzymes and stimulates instead the production of two key gluconeogenic enzymes, phosphoenolpyruvate carboxykinase and fructose 1,6-bisphosphatase.

  In contrast, insulin levels rise subsequent to eating, when there is plenty of glucose for glycolysis. To encourage glycolysis, insulin stimulates the expression of phosphofructokinase, pyruvate kinase, and the bifunctional enzyme that makes and degrades F-2,6-BP.

Self-Check Question



Why is the regulation of phosphofructokinase by ATP and AMP not as important in the liver as it is in muscle?

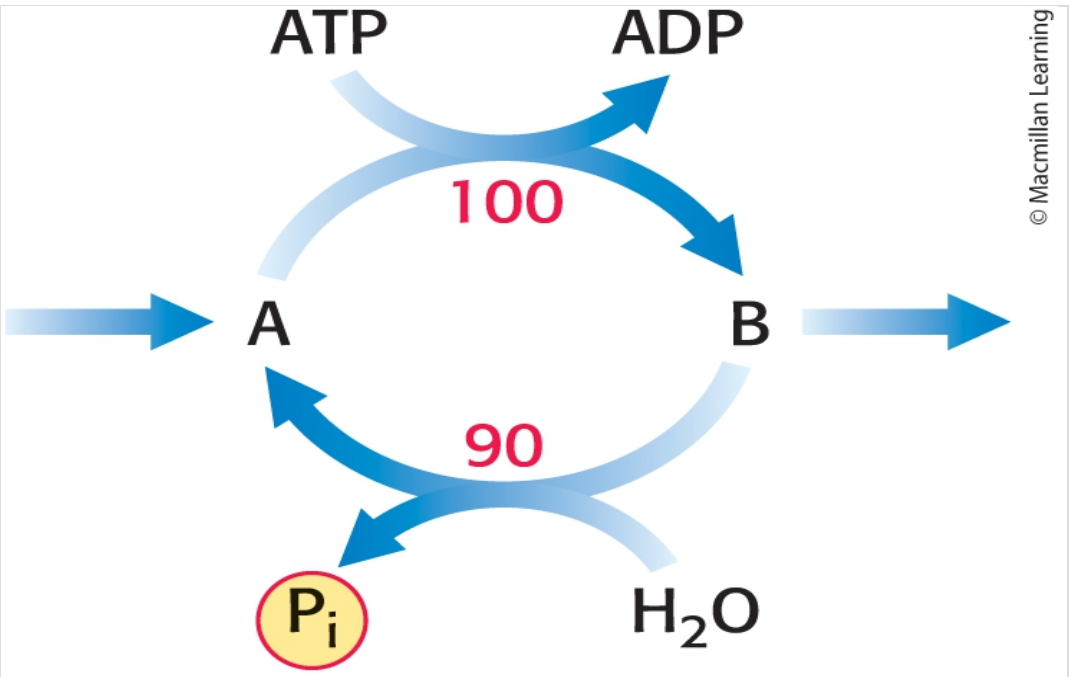
Substrate cycles amplify metabolic signals and produce heat

A pair of reactions such as the phosphorylation of fructose 6-phosphate to fructose 1,6-bisphosphate and its hydrolysis back to fructose 6-phosphate is called a **substrate cycle**. As already mentioned, both reactions are not fully active at the same time because of reciprocal regulation. However, isotope-labeling studies have shown that some fructose 6-phosphate is phosphorylated to fructose 1,6-bisphosphate even during gluconeogenesis. There also is a limited degree of cycling in other pairs of opposed irreversible reactions. This cycling was regarded as an imperfection in metabolic control, and so substrate cycles have sometimes been called *futile cycles*.

 Pathological conditions may result from futile cycles. A clear example is malignant hyperthermia, which occurs predominantly in muscle tissue. Susceptible individuals are sensitive to certain anesthetics which cause uncontrolled calcium release from the sarcoplasmic reticulum through the calcium channel. The rapid rise in cytoplasmic calcium activates the sarcoplasmic reticulum calcium pump, the Ca^{2+} ATPase, a P-type ATPase, in an attempt to remove the calcium from the cytoplasm. The constant release and reuptake of calcium, and the consequent rapid hydrolysis of ATP, raises the body temperature to 44°C (111°F) and depletes muscle ATP. Muscle damage and death may occur if untreated with an inhibitor of the calcium channel.

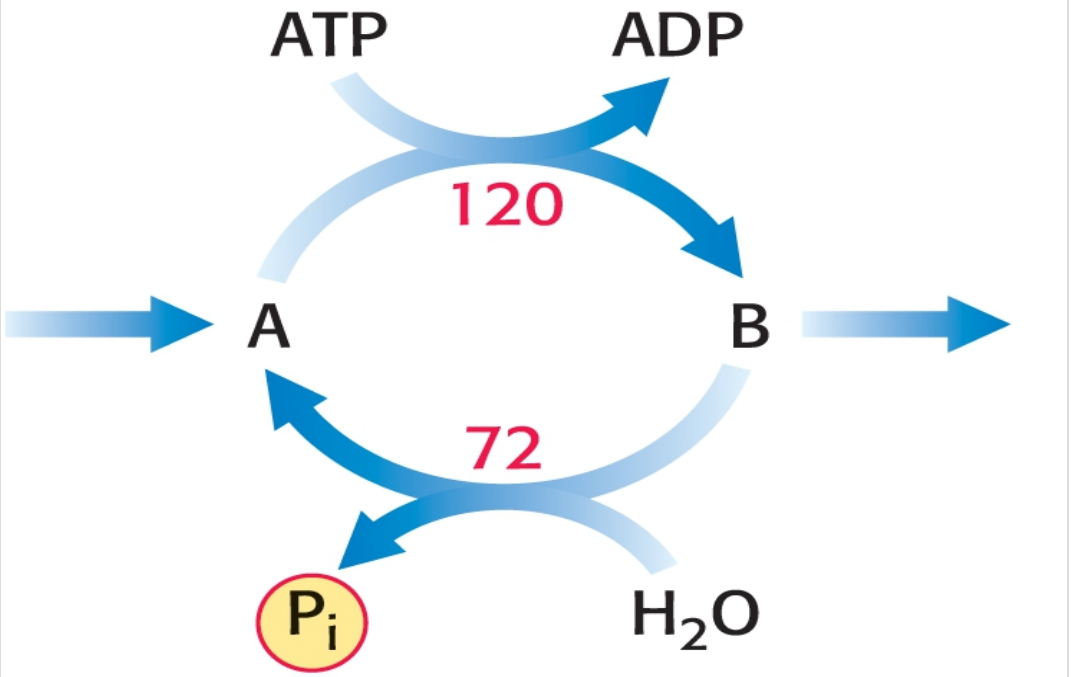
Despite such extraordinary circumstances, substrate cycles now seem likely to be biologically important. One possibility is that substrate cycles amplify metabolic signals. Suppose that the rate of conversion of A into B is 100 and of B into A is 90, giving an initial net flux of 10. Assume that an allosteric effector increases the $A \rightarrow B$ rate by 20% to

120 and reciprocally decreases the $B \rightarrow A$ rate by 20% to 72. The new net flux is 48, and so a 20% change in the rates of the opposing reactions has led to a 380% increase in the net flux. In the example shown in **Figure 16.35**, this amplification is made possible by the rapid hydrolysis of ATP. The flux down the glycolytic pathway has been suggested to increase as much as 1000-fold at the initiation of intense exercise. Because the allosteric activation of enzymes alone seems unlikely to explain this increased flux, the existence of substrate cycles may partly account for the rapid rise in the rate of glycolysis.



© Macmillan Learning

Net flux of B = 10



Net flux of B = 48

FIGURE 16.35 Substrate cycles can have advantages. This ATP-driven cycle operates at two different rates. A small change in the rates of the two opposing reactions results in a large change in the *net* flux of product B.



Lactate and alanine formed by contracting muscle and peripheral tissues are used by other organs

Lactate produced by active skeletal muscle, erythrocytes, skin, and other tissues is a source of energy for other organs. Erythrocytes lack mitochondria and can never oxidize glucose completely, whereas other tissues like the skin remain largely anaerobic at all times due to the distance from the arterial blood supply. In contracting fast-twitch skeletal muscle fibers during vigorous exercise, the rate at which glycolysis produces pyruvate exceeds the rate at which the citric acid cycle oxidizes it. In these cells, lactate dehydrogenase reduces excess pyruvate to lactate to restore redox balance (Section 16.2). However, lactate is a dead-end in metabolism. It must be converted back into pyruvate before it can be metabolized. Both pyruvate and lactate diffuse out of these cells through carriers into the blood. In contracting skeletal muscle, the formation and release of lactate lets the muscle generate ATP in the absence of oxygen and shifts the burden of metabolizing lactate from muscle to other organs.

The pyruvate and lactate in the bloodstream have two fates. In one fate, the plasma membranes of some cells — particularly cells in cardiac muscle and slow-twitch (type 1) skeletal muscle — contain carriers that make the cells highly permeable to lactate and pyruvate. These molecules diffuse from the blood into such permeable cells. Once inside these well-oxygenated cells, lactate can be reverted back to pyruvate

and metabolized through the citric acid cycle and oxidative phosphorylation to generate ATP. The use of lactate in place of glucose by these cells makes more circulating glucose available to the active muscle cells. In the other fate, excess lactate enters the liver and is converted first into pyruvate and then into glucose by the gluconeogenic pathway. Contracting skeletal muscle supplies lactate to the liver, which uses it to synthesize and release glucose. Thus, the liver restores the level of glucose necessary for active muscle cells, which derive ATP from the glycolytic conversion of glucose into lactate. Because this multi-tissue cooperation was elucidated by Gerty and Carl Cori, it is known as the **Cori cycle** (**Figure 16.36**).

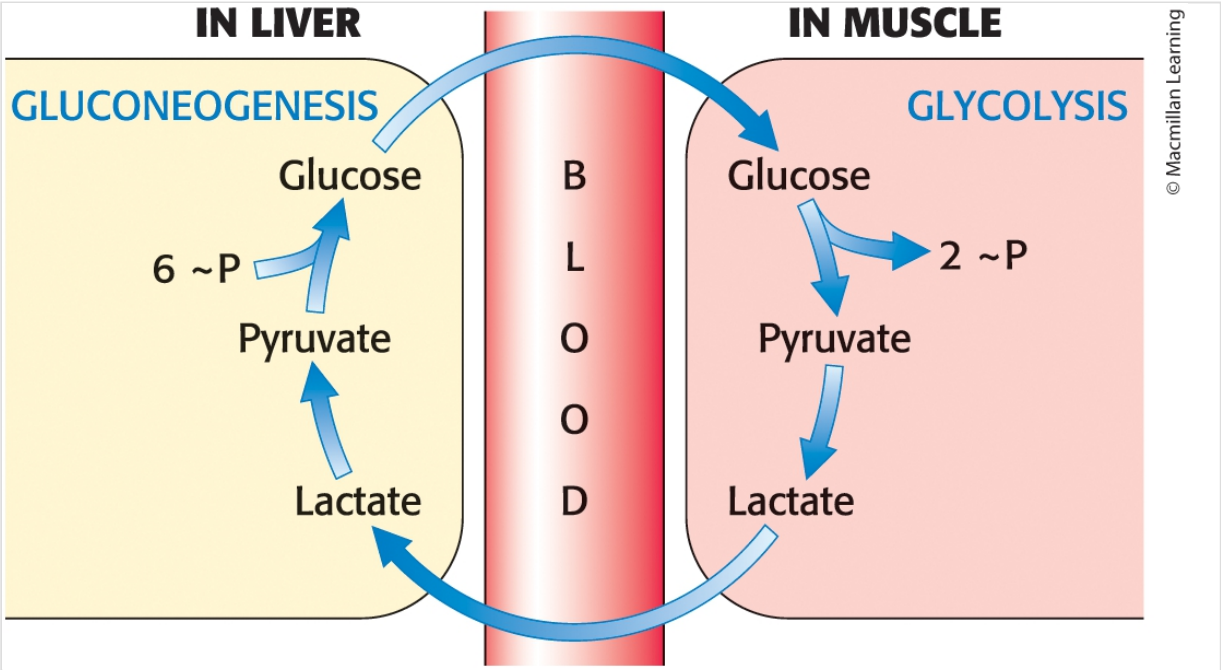


FIGURE 16.36 The Cori cycle allows the liver to better support other tissues, such as skeletal muscle. Lactate formed by active muscle is converted into glucose by the liver. This cycle shifts part of the metabolic burden of active muscle to the liver. The symbol, ~P represents nucleoside triphosphates.

EXPLORE this pathway further in the Metabolic Map in Achieve



Alfred Eisenstaedt/The LIFE Picture Collection/Shutterstock

GERTY CORI After growing up in a Jewish family in Austria-Hungary, Gerty Cori (*née* Radnitz) attended medical school at the German University of Prague. During medical school she met Carl Cori, and the two were married and became lifelong research partners, working together as equals. Despite this, Carl often received more recognition than Gerty due to gender discrimination, something he ardently opposed his entire career. They relocated to the United States in 1922 due to rising anti-Semitism in Europe. Dr. Cori published numerous papers with Carl, and independently, on tumor and carbohydrate metabolism. She became the first woman to win the Nobel Prize in Physiology or Medicine, which she shared with Carl for their work on glycogen metabolism and the elaboration of the Cori Cycle. Notably, six other scientists who were mentored by the Coris also went on to win Nobel Prizes.

Studies have shown that alanine, like lactate, is a major precursor of glucose in the liver. The alanine is generated in muscle when the carbon skeletons of some amino acids are used as fuels. The nitrogens from these amino acids are transferred to pyruvate to form alanine; the reverse reaction takes place in the liver. This process also helps maintain nitrogen balance. The interplay between glycolysis and gluconeogenesis is summarized in Figure 16.37, which shows how these pathways help meet the energy needs of different cell types.

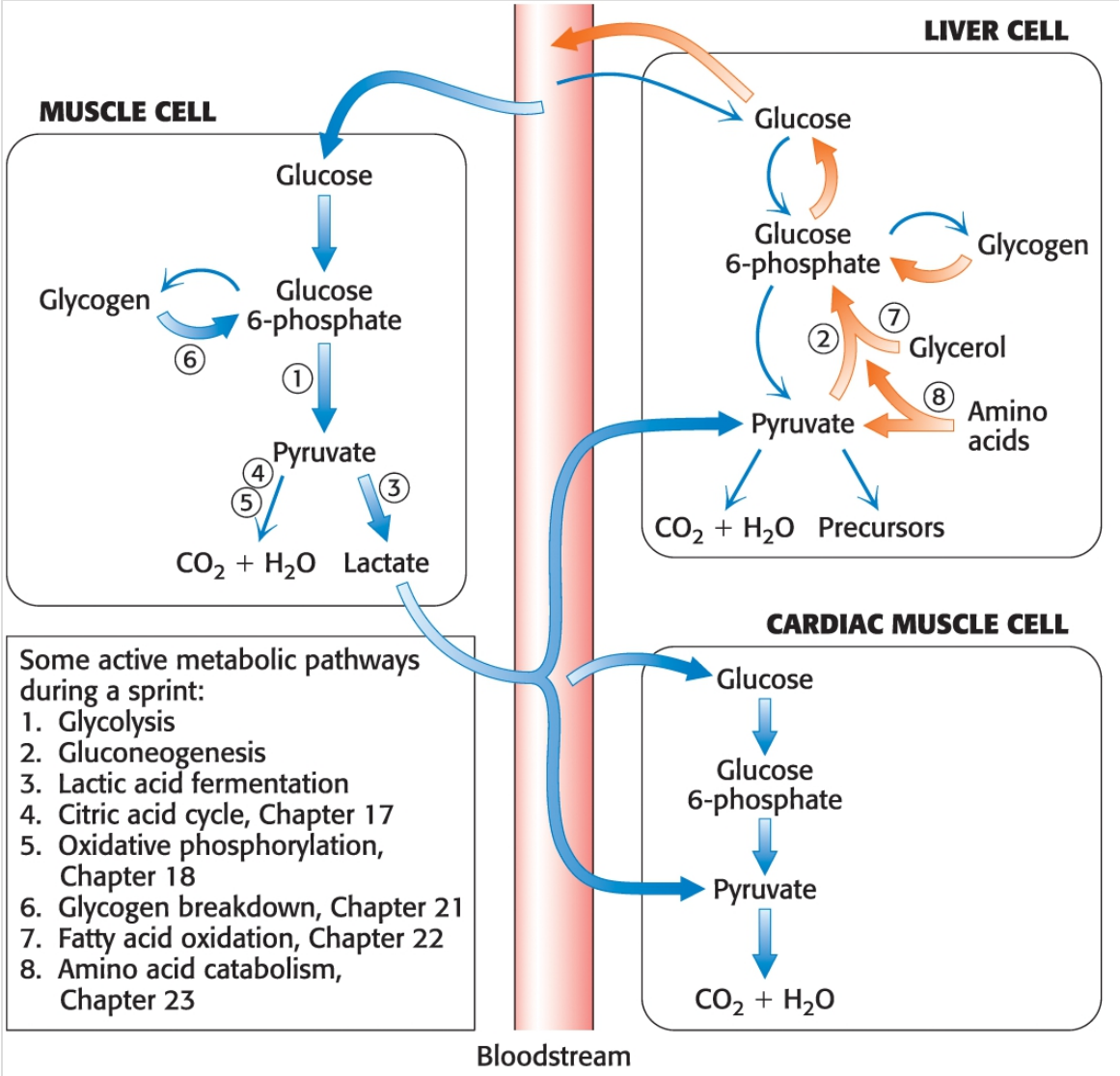


FIGURE 16.37 During a sprint, cooperation between glycolysis and gluconeogenesis occurs within multiple tissues. Glycolysis and gluconeogenesis are coordinated, in a tissue-specific fashion, to ensure the energy needs of all cells are met. Consider a sprinter. In skeletal leg musc

glucose will be metabolized aerobically to CO_2 and H_2O or, more likely (thick arrows) during a sprint, anaerobically to lactate. In cardiac muscle, the lactate can be converted into pyruvate and used as a fuel, along with glucose, to power the heartbeats to keep the sprinter's blood flowing. Gluconeogenesis, a primary function of the liver, will be taking place rapidly (thick arrows) to ensure that enough glucose is present in the blood for skeletal and cardiac muscle, as well as for other tissues. Glycogen, glycerol, and amino acids are other sources of energy that will learn about in later chapters.

EXPLORE this pathway further in the Metabolic Map in Achieve

Self-Check Question

If lactate is a dead-end product in that its sole fate is to be converted back into glucose, then why do cells bother to form lactate at all?

Deficiencies in glycolytic or gluconeogenic enzymes are rare genetic disorders

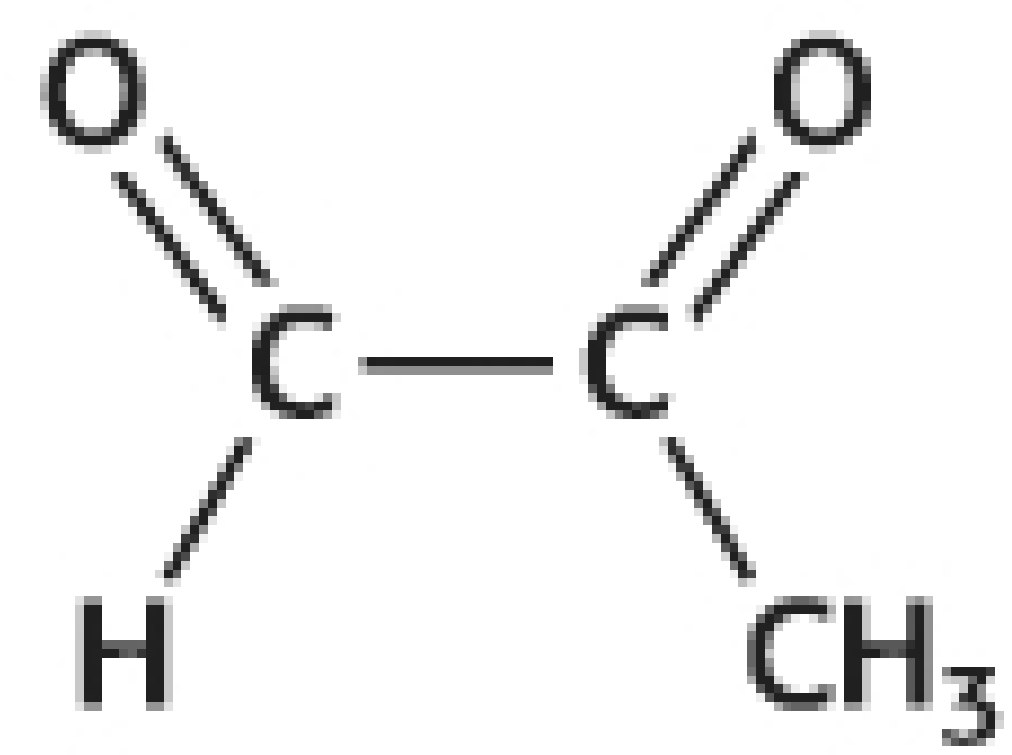
Genetically inherited deficiencies in the activity or regulation of specific enzymes are sometimes called *inborn errors of metabolism*. Because the enzymes of glycolysis and gluconeogenesis are so central to human metabolism, nonlethal deficiencies in these enzymes are rare but do still occur. Here we will briefly discuss two:

Triose phosphate isomerase deficiency

TPID is a multisystem disorder presenting in early childhood. Symptoms include congenital hemolytic anemia (deficiency of red cells due to premature destruction of the cell that is present at birth) and progressive neuromuscular disorder, including cardiomyopathy (inflammation and damage to the heart muscle). In severe cases, TPID can lead to death in early childhood. Dihydroxyacetone phosphate accumulates in cells, especially red blood cells. TPID is rare, so the causal relationship between the biochemical defect and the clinical features remains to be established. Let's consider a hypothesis regarding the pathologies of TPID.

First of all, recall that central nervous system and red blood cells rely on glucose metabolism exclusively for energy. Thus, any disruption in glycolysis would impact these tissues. Also, though resting skeletal muscles utilize fats as fuels, rapidly contracting muscle quickly becomes reliant on glucose for lactic acid fermentation.

Consider the consequences of TPID by reviewing its role in glycolysis in Figure 16.2. If the isomerase activity is missing, then half of the carbons of glucose cannot be metabolized to yield ATP. These observations account for the nature of the symptoms: without adequate ATP, neuromuscular function would be compromised. However, research suggests that disruption of energy metabolism is not the cause of the more serious consequences of TPID. Even if the cells try to compensate for lack of isomerase activity by processing more glucose, there will be an unavoidable buildup of dihydroxyacetone phosphate. Strong evidence now exists that this buildup of dihydroxyacetone phosphate is to blame, as it can be converted into methylglyoxal.



Methylglyoxal

Methylglyoxal, a highly reactive molecule, covalently binds to available amino groups on proteins, yielding advanced glycation end products (AGEs) (Section 11.1). These modifications inhibit protein function. Extensive loss of protein function would then contribute to the pathologies observed in TPID, including early death. AGEs have also been implicated in aging, arteriosclerosis (thickening and hardening of artery walls), and diabetes. Clearly establishing the causes of all TPID pathologies awaits further research.

Pyruvate carboxylase deficiency

PCD is another rare disorder of carbohydrate metabolism. Several types vary in the seriousness of clinical outcomes, but all are characterized to some extent by hypoglycemia (low concentration of blood glucose) and lactic acidosis (excessive lactic acid in the blood). Symptoms include lethargy, seizures, and, in severe cases, death in the first few months of life. In this case the two primary biochemical characteristics, hypoglycemia and lactic acidosis, are reasonably easy to explain. Again, as with TPID, lack of glucose would impair neuromuscular functions.

Because pyruvate carboxylase is a key regulatory enzyme in gluconeogenesis, which occurs primarily in the liver, we can surmise that the lack of the pyruvate carboxylase would account for the hypoglycemia. Lacking this enzyme, the liver cannot serve its role in maintaining adequate blood glucose concentration for tissues that depend on glucose. Likewise, an important role of liver is to remove lactic acid from the blood and use it as a gluconeogenic precursor. However, lactic acid can't be used to form glucose due to the lack of pyruvate carboxylase, causing it to remain in the blood, leading to a fall in blood pH (acidosis). In later chapters we will see that the oxaloacetate formed by pyruvate carboxylase is an important and versatile molecule, so the lack of carboxylase activity has greater effects than discussed here.

Glycolysis and gluconeogenesis are evolutionarily intertwined

The metabolism of glucose has ancient origins. Organisms living in the early biosphere depended on the anaerobic generation of energy until significant amounts of oxygen began to accumulate 2 billion years ago. Glycolytic enzymes were most likely derived independently rather than

by gene duplication, because glycolytic enzymes with similar properties do not have similar amino acid sequences. Although there are four kinases and two isomerases in the pathway, sequence and structural comparisons suggest that these sets of enzymes are not related to one another by divergent evolution.

We can speculate on the relationship between glycolysis and gluconeogenesis if we think of glycolysis as consisting of two segments: the metabolism of hexoses (the upper segment of Figure 16.2) and the metabolism of trioses (the lower segment of Figure 16.2). The enzymes of the upper segment are different in some species and are missing entirely in some archaea, whereas enzymes of the lower segment are quite conserved. In fact, four enzymes of the lower segment are present in all species. The lower part of the glycolytic pathway is used by gluconeogenesis, too. This common part of the two pathways may be the oldest part, constituting the core to which the other steps were added. The upper part would have varied according to the sugars that were available to evolving organisms in particular niches. Interestingly, this core part of carbohydrate metabolism can generate triose precursors for ribose sugars, a component of RNA and a critical requirement for the RNA world. Thus, we are left with the unanswered question: Was the original core pathway used for energy conversion or biosynthesis?

Self-Check Question



What are the likely consequences of a genetic disorder rendering fructose 1,6-bisphosphatase in the liver less sensitive to regulation by fructose 2,6-bisphosphate?

Chapter 16 Summary

16.1 Glycolysis Is an Energy-Conversion Pathway in Most Organisms

- Glycolysis is a highly common pathway among most organisms; it consists of a set of 10 cytoplasmic reactions that convert glucose into pyruvate.
- Glucose and other monosaccharides are generated from the breakdown of dietary starch, glycogen, sucrose, and other nutrients.
- A family of glucose transporters facilitates the movement of glucose throughout the body.

16.2 Glycolysis Can Be Divided into Two Parts

- The first stage consumes two molecules of ATP as glucose is converted into dihydroxyacetone phosphate and glyceraldehyde 3-phosphate, which are readily interconvertible.
- In the second stage, glyceraldehyde 3-phosphate is oxidized and ultimately converted into pyruvate, generating two molecules of ATP.
- There is a net gain of two molecules of ATP in the formation of two molecules of pyruvate from one molecule of glucose because each of the ATP-generating second stage steps occur twice for each molecule of glucose metabolized.
- The electron acceptor in the oxidation of glyceraldehyde 3-phosphate is NAD^+, which must be regenerated for glycolysis to continue.
- In aerobic organisms, the NADH formed in glycolysis transfers its electrons to O_2 through the electron-transport chain, which thereby regenerates NAD^+.

- Under anaerobic conditions and in some microorganisms, NAD^+ is regenerated by the reduction of pyruvate to lactate. In other microorganisms, NAD^+ is regenerated by the reduction of pyruvate to ethanol. These two processes are examples of fermentations.

16.3 The Glycolytic Pathway Is Tightly Controlled

- The rate of conversion of glucose into pyruvate is tightly regulated at specific steps.
- Phosphofructokinase — the most important control element in glycolysis — is inhibited by high levels of ATP and citrate and activated by AMP and fructose 2,6-bisphosphate.
- Hexokinase is inhibited by glucose 6-phosphate, which accumulates when phosphofructokinase is inactive.
- ATP and alanine allosterically inhibit pyruvate kinase, whereas fructose 1,6-bisphosphate activates it.

16.4 Glucose Can Be Synthesized from Noncarbohydrate Precursors

- Gluconeogenesis, which occurs primarily in the liver, is the synthesis of glucose from noncarbohydrate sources, such as lactate, amino acids, glycerol, and alanine produced from pyruvate by active skeletal muscle.
- Gluconeogenesis requires four new reactions to bypass the essential irreversibility of three reactions in glycolysis.
- In two of the new reactions, pyruvate is carboxylated in mitochondria to oxaloacetate, which in turn is decarboxylated and phosphorylated in the cytoplasm to phosphoenolpyruvate, at the expense of one ATP and one GTP.
- The other distinctive reactions of gluconeogenesis are the hydrolyses of fructose 1,6-bisphosphate and glucose 6-phosphate, which are catalyzed by specific phosphatases.

16.5 Gluconeogenesis and Glycolysis Are Reciprocally Regulated

- Gluconeogenesis and glycolysis are reciprocally regulated so that one pathway is relatively inactive while the other is highly active.
- Phosphofructokinase and fructose 1,6-bisphosphatase are key control elements of gluconeogenesis and glycolysis.
- Fructose 2,6-bisphosphate, an intracellular signal molecule present at higher levels when glucose is abundant, activates glycolysis and inhibits gluconeogenesis by regulating these enzymes.
- Pyruvate kinase and pyruvate carboxylase are regulated by other effectors so that both are not maximally active at the same time.
- Allosteric regulation and reversible phosphorylation, which are rapid, are complemented by transcriptional control, which takes place in hours or days.

Key Terms

glycolysis
gluconeogenesis
kinase
substrate-level phosphorylation
fermentation
ethanol fermentation
lactic acid fermentation
obligate anaerobe
facultative anaerobe
committed step
feedforward stimulation (feedforward activation)
substrate channeling
aerobic glycolysis
phosphatase
bifunctional enzyme
substrate cycle

[Cori cycle]

Problems

1. Select all the steps of glycolysis in which ATP is produced.

a. 1,3-bisphosphoglycerate → 3-phosphoglycerate
b. Glyceraldehyde 3-phosphate → 1,3-bisphosphoglycerate
c. Fructose 6-phosphate → fructose 1,6-bisphosphate
d. Glucose → glucose 6-phosphate
e. Phosphoenolpyruvate → pyruvate

2. Which of the following statements is (are) true for a muscle performing lactic acid fermentation?

a. The process is inhibited by AMP.
b. The process is inhibited by ATP.
c. There is a net synthesis of NADH.
d. The process is exergonic.

3. Match each term with its description.  1

1. Hexokinase
2. Phosphoglucose isomerase
3. Phosphofructokinase
4. Aldolase
5. Triose phosphate isomerase
6. Glyceraldehyde 3-phosphate dehydrogenase

1. Forms fructose 1,6-bisphosphate
2. Generates the first high-phosphoryl-transfer-potential compound that is not ATP
3. Converts glucose 6-phosphate into fructose 6-phosphate
4. Phosphorylates glucose
5. Generates the second molecule of ATP
6. Cleaves fructose 1, 6-bisphosphate
7. Generates the second high-phosphoryl-transfer-potential

7. Phosphoglycerate kinase
8. Phosphoglycerate mutase
9. Enolase
10. Pyruvate kinase

compound that is not ATP
8. Catalyzes the interconversion of three-carbon isomers
9. Converts 3-phosphoglycerate into 2-phosphoglycerate
10. Generates the first molecule of ATP

---

4. Lactic acid fermentation and ethanol fermentation are oxidation–reduction reactions. Identify the ultimate electron donor and electron acceptor. 2

5. Why is it advantageous for the liver to have both hexo-kinase and glucokinase to phosphorylate glucose?

6. The interconversion of DHAP and GAP greatly favors the formation of DHAP at equilibrium. Yet the conversion of DHAP by triose phosphate isomerase proceeds readily. Why?

7. Although both hexokinase and phosphofructokinase catalyze irreversible steps in glycolysis and the hexokinase-catalyzed step is first, phosphofructokinase is nonetheless the pacemaker of glycolysis. What does this information tell you about the fate of the glucose 6-phosphate formed by hexokinase?

8. What reactions of glycolysis are not readily reversible under intracellular conditions? 4

9. Why is it physiologically advantageous for the pancreas to use GLUT2, with a high K_M, as the transporter that allows glucose entry into β cells?

10. Suppose that a microorganism that was an obligate anaerobe suffered a mutation that resulted in the loss of triose phosphate isomerase activity. How would this loss affect the ATP yield of fermentation? Could such an organism survive? 1

11. What are the equilibrium concentrations of fructose 1,6-bisphosphate, dihydroxyacetone phosphate, and glyceraldehyde 3-phosphate when 1 mM fructose 1,6-bisphosphate is incubated with aldolase under standard conditions?

12. Indicate which of the conditions listed in the right-hand column increase the activity of the glycolytic and gluconeogenic pathway in the liver. 4

1. Glycolysis 2. Gluconeogenesis	1. Increase in ATP 2. Increase in AMP 3. Increase in fructose 2,6-bisphosphate 4. Increase in citrate 5. Increase in acetyl CoA 6. Increase in insulin 7. Increase in glucagon 8. Fasting 9. Fed

---

13. Why does the lack of glucose 6-phosphatase activity in the brain and muscle make good physiological sense?

14. How many NTP molecules are required for the synthesis of one molecule of glucose from two molecules of pyruvate? How many NADH molecules? 3

15. Suppose 25 glucose molecules are formed during gluconeogenesis. Calculate the amount of pyruvate, ATP, and NADH molecules required.

16. Predict the effect of each of the following mutations on the pace of glycolysis in liver cells: 4

a. Loss of the allosteric site for ATP in phosphofructokinase

b. Loss of the binding site for citrate in phosphofructokinase
c. Loss of the phosphatase domain of the bifunctional enzyme that controls the level of fructose 2,6-bisphosphate
d. Loss of the binding site for fructose 1,6-bisphosphate in pyruvate kinase

17. Avidin, a 70-kDa protein in egg white, has very high affinity for biotin. In fact, it is a highly specific inhibitor of biotin enzymes. Which of the following conversions would be blocked by the addition of avidin to a cell homogenate?

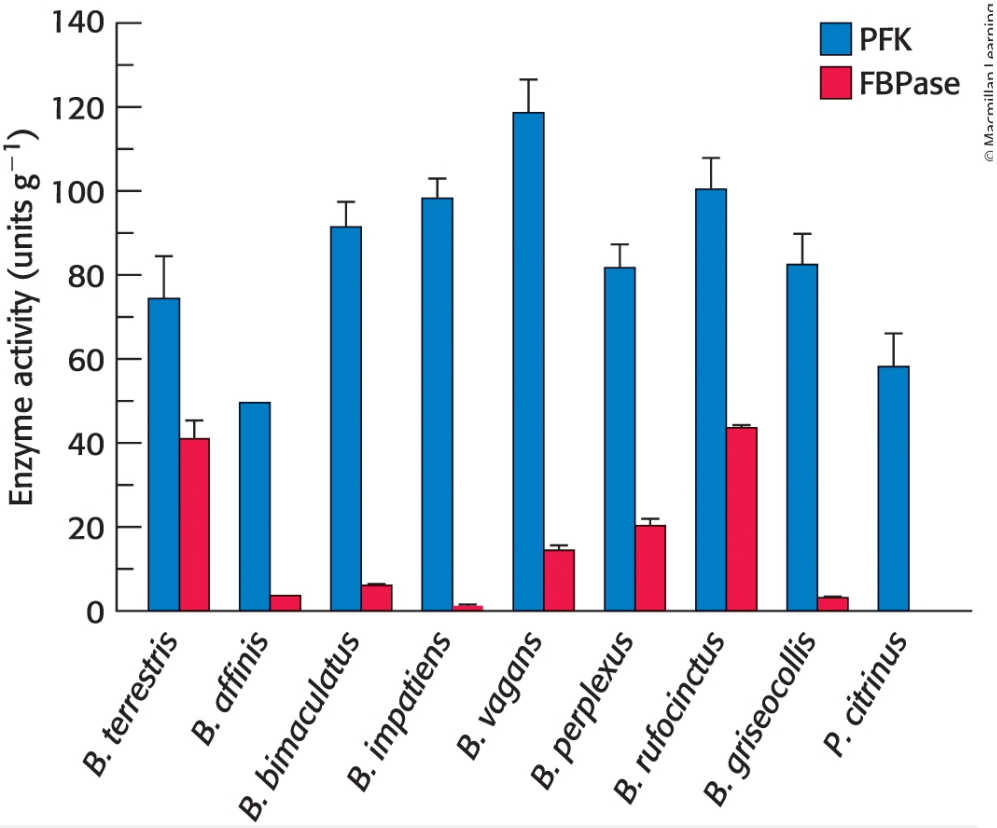
a. Glucos → pyruvate
b. Pyruvate → glucose
c. Oxaloacetate → glucose
d. Malate → oxaloacetate
e. Pyruvate → oxaloacetate
f. Glyceraldehyde 3 → fructose 1,6-bisphosphate

18. In the conversion of glucose into two molecules of lactate, the NADH generated earlier in the pathway is oxidized to NAD^+. Why is it not to the cell's advantage to simply make more NAD^+ so that the regeneration would not be necessary? After all, the cell would save much energy because it would no longer need to synthesize lactic acid dehydrogenase. 2

19. Hexokinase in red blood cells has a K_M of approximately $50\ \mu M$. Because life is hard enough as it is, let's assume that the hexokinase displays Michaelis–Menten kinetics. What concentration of blood glucose would yield V_0 equal to 90% V_{max}? What does this result tell you if normal blood glucose levels range between approximately 3.6 and 6.1 mM?

20. In principle, a futile cycle that includes phosphofructokinase and fructose 1,6-bisphosphatase could be used to generate heat. The heat could be used to warm tissues. For instance, certain bumblebees have been reported to use such a futile cycle to warm their flight muscles on cool mornings. Scientists undertook a series of experiments to determine if a number of species of bumblebee use this futile cycle. Their approach was to measure the activity of PFK and F-1,6-BPase in flight muscle.

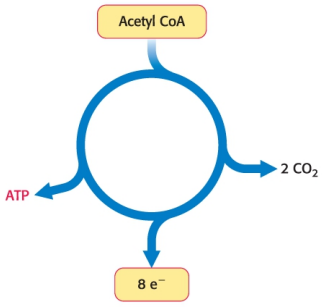
a. What was the rationale for comparing the activities of these two enzymes?
b. The data below show the activities of both enzymes for a variety of bumblebee species (genera *Bombus* and *Psithyrus*). Do these results support the notion that bumblebees use futile cycles to generate heat? Explain.
c. In which species might futile cycling take place? Explain your reasoning.
d. Do these results prove that futile cycling does not participate in heat generation?



© Macmillan Learning

Chapter 17
Pyruvate Dehydrogenase and the Citric Acid Cycle





Chalermkiat Seedokmai/Getty Images
© Macmillan Learning

Roundabouts, or traffic circles, function as hubs to facilitate traffic flow. Likewise, the citric acid cycle is the biochemical hub of the cell, oxidizing carbon fuels, usually in the form of acetyl CoA, as well as serving as a source of precursors for biosynthesis.

Outline

17.1 The Citric Acid Cycle Harvests High-Energy Electrons
17.2 The Pyruvate Dehydrogenase Complex Links Glycolysis to the Citric Acid Cycle
17.3 The Citric Acid Cycle Oxidizes Two-Carbon Units
17.4 Entry to the Citric Acid Cycle and Metabolism Through It Are Controlled

17.5 The Citric Acid Cycle Is a Source of Biosynthetic Precursors
17.6 The Glyoxylate Cycle Enables Plants and Bacteria to Grow on Acetate

Learning Goals



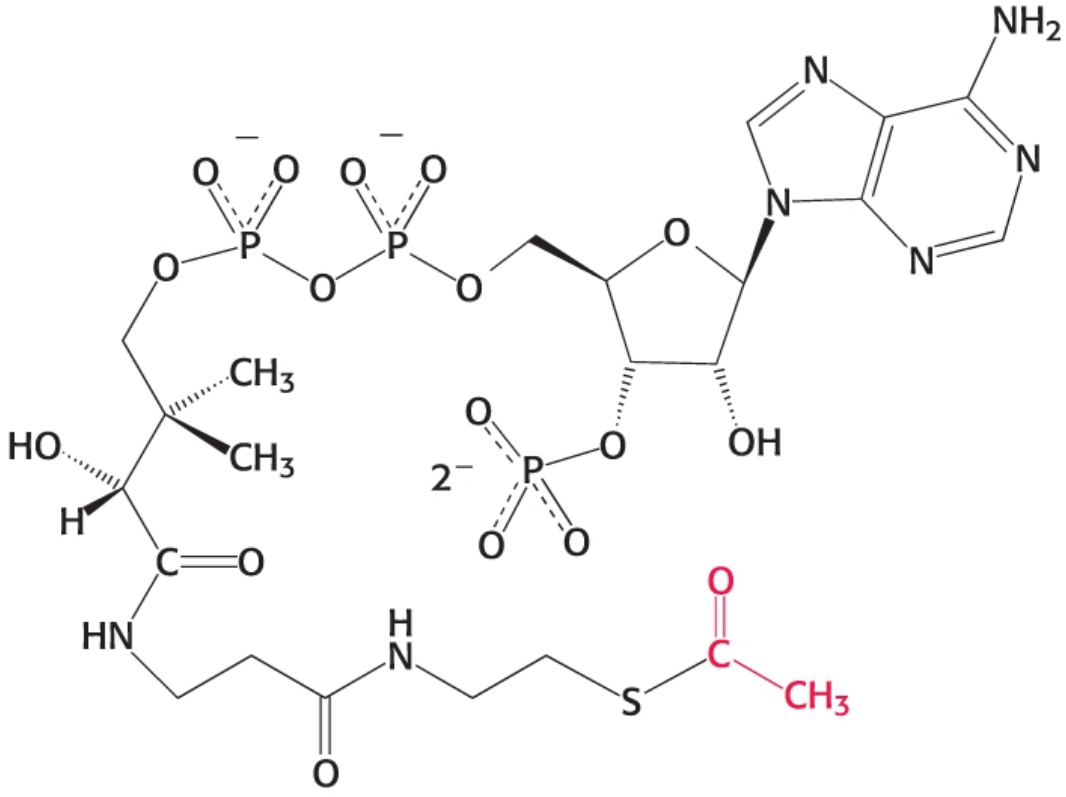
By the end of this chapter, you should be able to:

1. Explain why the reaction catalyzed by the pyruvate dehydrogenase complex is a crucial juncture in metabolism.
2. Identify the means by which the pyruvate dehydrogenase complex is regulated.
3. Identify the primary catabolic purpose of the citric acid cycle.
4. Explain the efficiency of using the citric acid cycle to oxidize acetyl CoA.
5. Describe how the citric acid cycle is regulated.
6. Describe the role of the citric acid cycle in biosynthesis.
7. Identify the biochemical advantages that the glyoxylate cycle provides.

The metabolism of glucose to pyruvate in glycolysis, an anaerobic process, harvests but a fraction of the ATP available from glucose. Most of the ATP generated in metabolism is provided by the *aerobic* processing of glucose. This process starts with the complete oxidation of glucose derivatives to carbon dioxide. This oxidation begins with pyruvate and takes place in a series of reactions catalyzed by an enormous enzyme cluster called the *pyruvate dehydrogenase complex*. The oxidation ends with the citric acid cycle, a set of eight reactions that forms essentially the center of the complex web of catabolic and biosynthetic transformations known as *metabolism*. The electrons removed in the conversion of pyruvate to carbon dioxide ultimately provide the energy for the synthesis of most of the ATP within a cell.

17.1 The Citric Acid Cycle Harvests High-Energy Electrons

The **citric acid cycle (CAC)**, also known as the **tricarboxylic acid (TCA) cycle** or the **Krebs cycle**, is the final pathway for the oxidation of fuel molecules — carbohydrates, fatty acids, and amino acids. Most fuel molecules enter the cycle as **acetyl CoA** (acetyl coenzyme A).



Acetyl coenzyme A (Acetyl CoA)

Under aerobic conditions, the pyruvate generated from glucose is first oxidatively decarboxylated to form acetyl CoA by a large enzyme

complex called the **pyruvate dehydrogenase complex**. The acetyl CoA then enters the citric acid cycle, where all remaining carbons originally derived from glucose are completely oxidized to CO_2. In eukaryotes, the reactions of the pyruvate dehydrogenase complex and the citric acid cycle take place in the matrix of the mitochondria (**Figure 17.1**), in contrast with those of glycolysis, which take place in the cytoplasm.

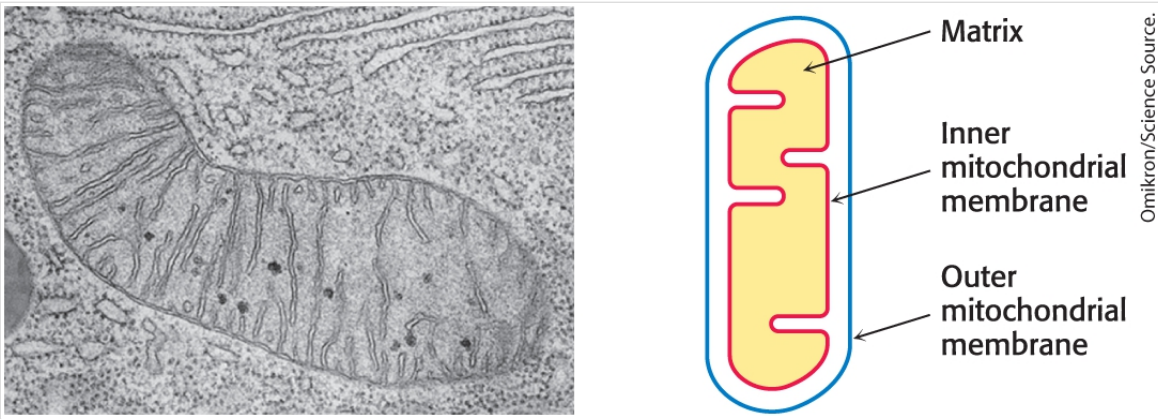


FIGURE 17.1 Mitochondria have distinct compartments defined by two membranes. The double membrane of a single mitochondrion is evident in this electron micrograph. The numerous invaginations of the inner mitochondrial membrane are called *cristae*. The oxidative decarboxylation of pyruvate and the sequence of reactions in the citric acid cycle take place within the matrix.

What is the function of the citric acid cycle in transforming fuel molecules into ATP? Recall that fuel molecules are carbon compounds that are capable of being oxidized — that is, of losing electrons (Section 15.3). The citric acid cycle includes a series of oxidation–reduction reactions that result in the oxidation of an acetyl group to two molecules of carbon dioxide. This oxidation generates high-energy electrons that will be used to power the synthesis of ATP. The catabolic function of the citric acid cycle is the harvesting of high-energy electrons from carbon fuels.

The citric acid cycle is also the central metabolic hub of the cell, providing a link that connects both catabolic and anabolic pathways. It is the gateway to the aerobic metabolism of any molecule that can be transformed into an acetyl group or a component of the citric acid cycle. The cycle is also an important source of precursors for the building blocks of many other molecules such as amino acids, nucleotide bases, and porphyrin (the organic component of heme). The citric acid cycle component, oxaloacetate, is also an important precursor to glucose (Section 16.4).

The overall pattern of the citric acid cycle is shown in **Figure 17.2**. A four-carbon compound (oxaloacetate) condenses with a two-carbon acetyl unit to yield a six-carbon tricarboxylic acid. The six-carbon compound releases CO_2 twice in two successive oxidative decarboxylations that yield high-energy electrons. What remains is a four-carbon compound that is further processed to regenerate oxaloacetate, which can initiate another round of the cycle. Two carbon atoms enter the cycle as an acetyl unit, and two carbon atoms leave the cycle in the form of two molecules of CO_2.

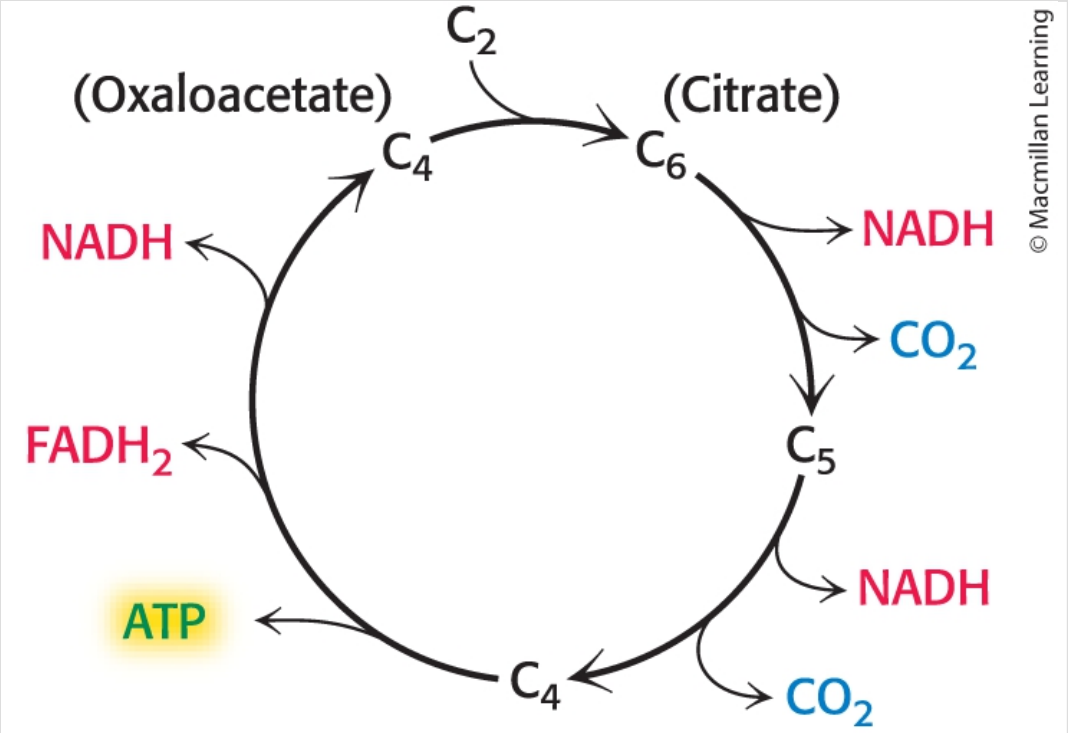


FIGURE 17.2 An overview of the citric acid cycle reveals the flow of carbon atoms and the major products of the cycle. A two-carbon group (C_2) combines with a four-carbon molecule (C_4, oxaloacetate) to form a six-carbon molecule (C_6, citrate). Two carbons are lost as CO_2 in the cycle, ending with the regeneration of oxaloacetate for another round. As the result, each round of the citric acid cycle oxidizes two-carbon units, producing two molecules of CO_2, one molecule of ATP, and high-energy electrons in the form of NADH and $FADH_2$.

Note that the citric acid cycle itself neither generates much ATP nor includes oxygen as a reactant (Figure 17.3). Instead, the citric acid cycle removes electrons from acetyl CoA and uses these electrons to reduce NAD^+ and FAD to form NADH and $FADH_2$. Three hydride ions (hence, six electrons) are transferred to three molecules of nicotinamide adenine dinucleotide (NAD^+), and one pair of hydrogen atoms (hence,

two electrons) is transferred to one molecule of flavin adenine dinucleotide (FAD) each time an acetyl CoA is processed by the cycle. Electrons released in the reoxidation of NADH and $FADH_2$ flow through a series of membrane proteins (referred to as the *electron-transport chain*) to generate a proton gradient across the inner mitochondrial membrane. These protons then flow through ATP synthase to generate ATP from ADP and inorganic phosphate. These electron carriers yield nine molecules of ATP when they are oxidized by O_2 through the process of oxidative phosphorylation (Chapter 18).

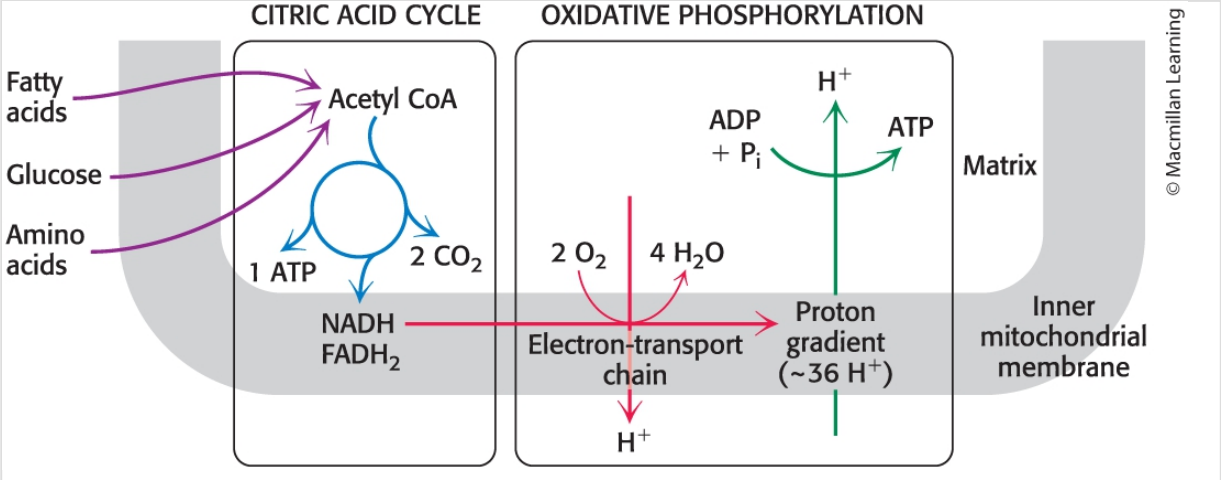


FIGURE 17.3 Cellular respiration removes high-energy electrons from carbon fuel molecules to generate ATP. The citric acid cycle constitutes the first stage in cellular respiration, the removal of high-energy electrons from carbon fuels in the form of NADH and $FADH_2$ (blue pathway). These electrons reduce O_2 to generate a proton gradient (red pathway), which is used to synthesize ATP (green pathway). The reduction of O_2 and the synthesis of ATP constitute oxidative phosphorylation.

The citric acid cycle, in conjunction with oxidative phosphorylation, provides the bulk of energy used by aerobic cells — in human beings, greater than 90%. It is highly efficient because the oxidation of a limited number of citric acid cycle molecules can generate large amounts of

NADH and $FADH_2$. Note in Figure 17.2 that the four-carbon molecule, oxaloacetate, that initiates the first step in the citric acid cycle is regenerated at the end of one passage through the cycle. Thus, one molecule of oxaloacetate is capable of participating in the oxidation of many acetyl groups.

17.2 The Pyruvate Dehydrogenase Complex Links Glycolysis to the Citric Acid Cycle

Carbohydrates, most notably glucose, are processed by glycolysis into pyruvate (Chapter 16). Under anaerobic conditions, the pyruvate is converted into lactate or ethanol, depending on the organism. Under aerobic conditions, the pyruvate is transported into mitochondria by a specific carrier protein embedded in the mitochondrial membrane. In the mitochondrial matrix, pyruvate is oxidatively decarboxylated by the pyruvate dehydrogenase complex — a highly integrated unit of three distinct enzymes — to form acetyl CoA.

$$\text{Pyruvate} + \text{CoA} + \text{NAD}^+ \rightarrow \text{acetyl CoA} + \text{CO}_2 + \text{NADH} + \text{H}^+$$

This irreversible reaction is the link between glycolysis and the citric acid cycle (**Figure 17.4**). Note that the pyruvate dehydrogenase complex produces CO_2 and captures high-transfer-potential electrons in the form of NADH. Thus, the pyruvate dehydrogenase reaction has many of the key features of the reactions of the citric acid cycle itself.

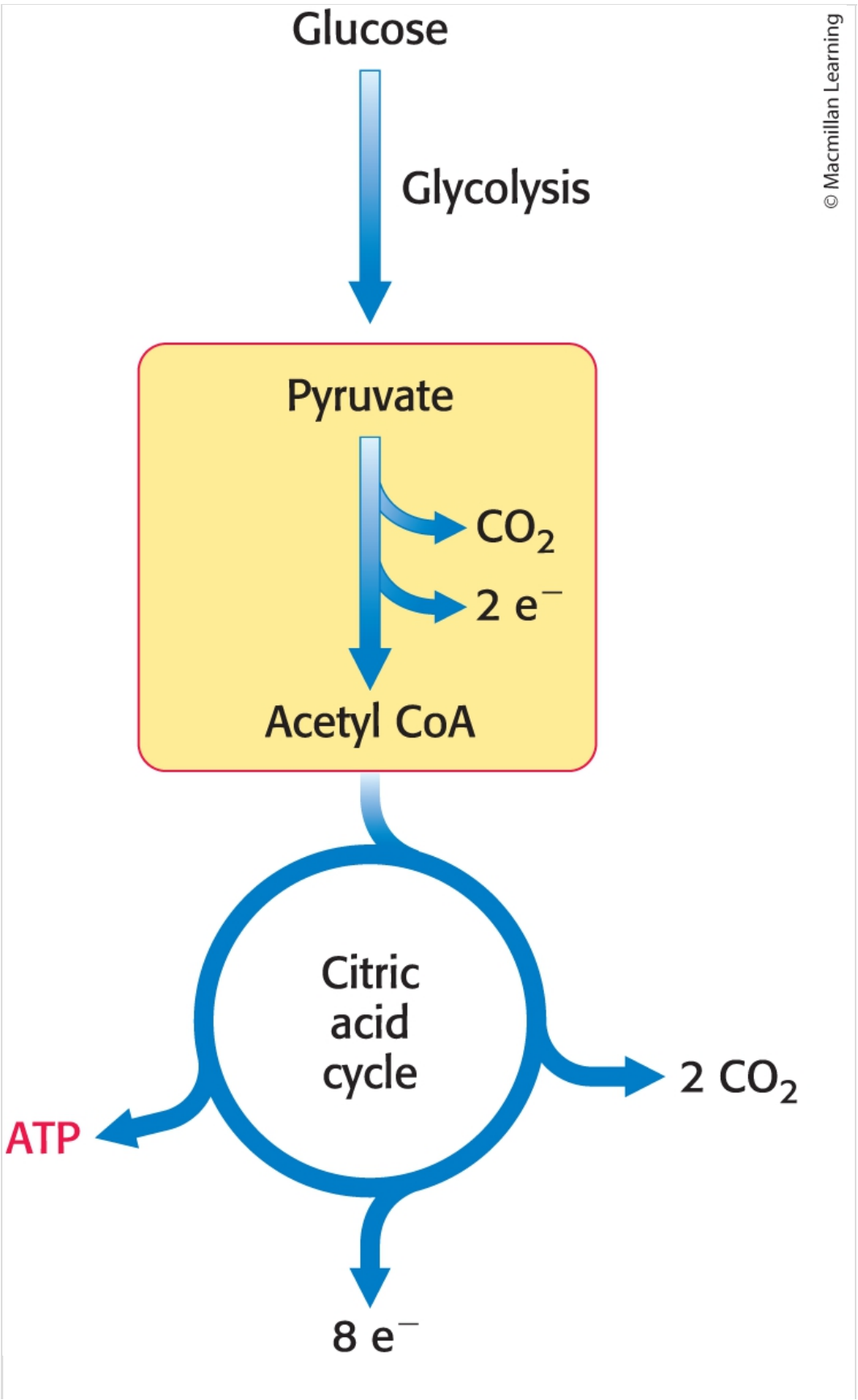

Glucose
Glycolysis
Pyruvate
CO_2
2 e^-
Acetyl CoA
Citric acid cycle
2 CO_2
ATP
8 e^-
© Macmillan Learning

FIGURE 17.4 The pyruvate dehydro-genase complex connects glycolysis and the citric acid cycle. Pyruvate produced by glycolysis is converted into acetyl CoA, the fuel of the citric acid cycle.



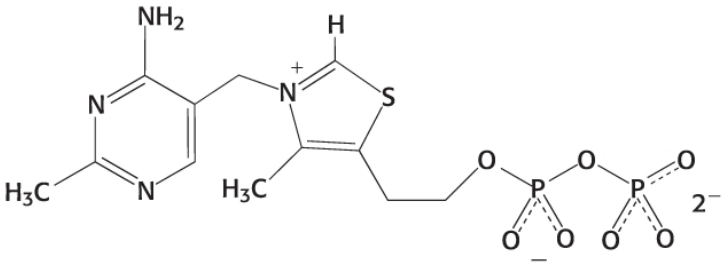
The pyruvate dehydrogenase complex, the components of which are detailed in **Table 17.1**, is another example of the organization of enzymes into supramolecular structures (Section 16.3). Pyruvate dehydrogenase complex is a member of a family of homologous complexes that include the citric acid cycle enzyme α-ketoglutarate dehydrogenase complex (Section 17.3). These complexes are giant, larger than ribosomes, with molecular masses ranging from 4 million to 10 million Da. As we will see, their elaborate structures allow groups to travel from one active site to another, connected by tethers to the core of the structure.

TABLE 17.1 Pyruvate dehydrogenase complex of *E. coli*

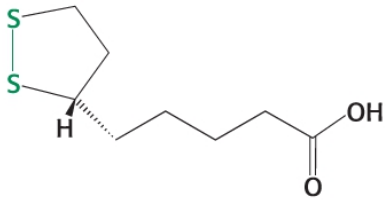
Enzyme	Abbreviation	Prosthetic group	Reaction catalyzed
Pyruvate dehydrogenase component	E_1	TPP	Oxidative decarboxylation of pyruvate
Dihydrolipoyl transacetylase	E_2	Lipoamide	Transfer of acetyl group to CoA
Dihydrolipoyl dehydrogenase	E_3	FAD	Regeneration of the oxidized form of lipoamide

Mechanism: The synthesis of acetyl coenzyme A from pyruvate requires three enzymes and five coenzymes

The mechanism of the pyruvate dehydrogenase reaction is wonderfully complex, more so than is suggested by its simple stoichiometry. The reaction requires the participation of the three enzymes of the pyruvate dehydrogenase complex and five coenzymes. The coenzymes thiamine pyrophosphate (TPP), lipoic acid, and FAD serve as catalytic cofactors, and CoA and NAD^+ are stoichiometric cofactors, cofactors that function as substrates.

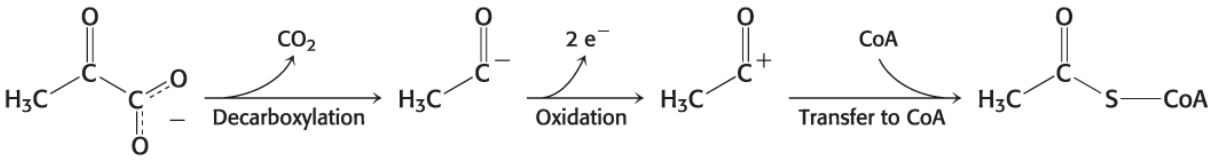


Thiamine pyrophosphate (TPP)



Lipoic acid

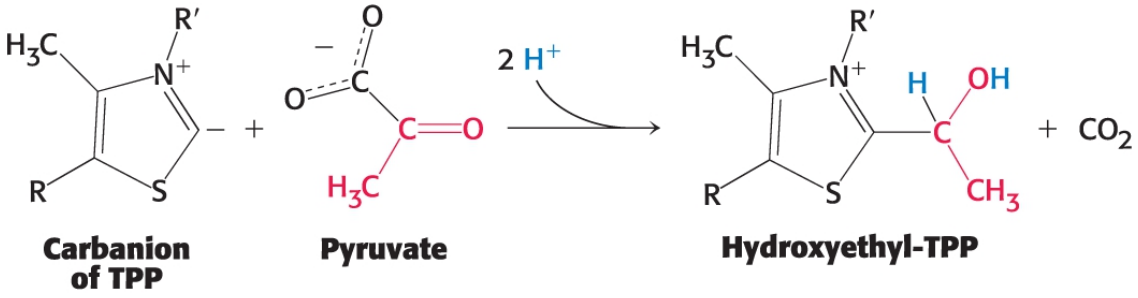
The conversion of pyruvate into acetyl CoA consists of decarboxylation, oxidation, and transfer of the resultant acetyl group to CoA. A fourth step is required to regenerate the active enzyme.



Pyruvate **Acetyl CoA**

These steps must be coupled to preserve the free energy derived from the decarboxylation step to drive the formation of NADH and acetyl CoA. Let us look into each step in more detail:

1. *Decarboxylation*. Pyruvate combines with TPP and is then decarboxylated to yield hydroxyethyl-TPP.



This reaction, the rate-limiting step in acetyl CoA synthesis, is catalyzed by the pyruvate dehydrogenase component (E_1) of the multienzyme complex. TPP is the prosthetic group of the pyruvate dehydrogenase component (**Figure 17.5**).

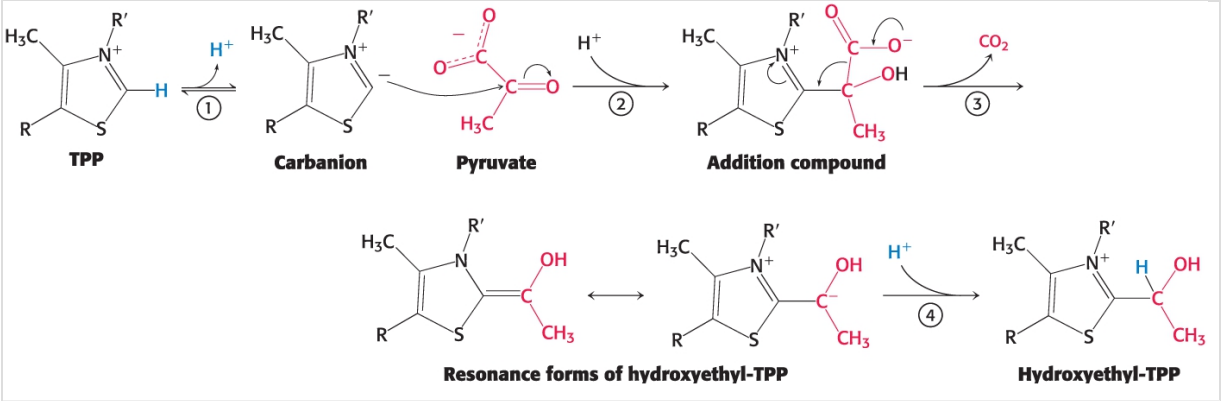
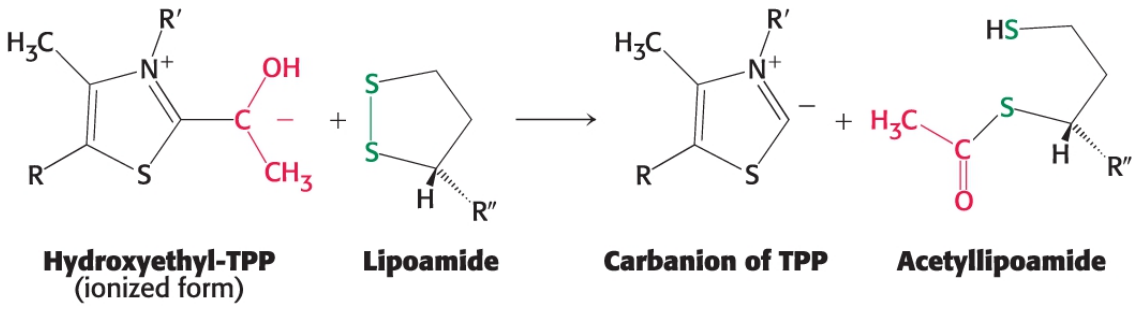


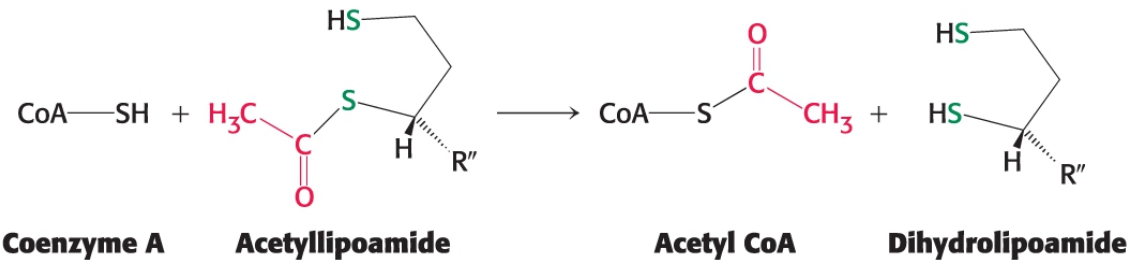
FIGURE 17.5 The mechanism of the E_1 decarboxylation reaction uses a critical thiamine-derived prosthetic group. E_1 is the pyruvate dehydrogenase component of the pyruvate dehydrogenase complex. A key feature of the prosthetic group, TPP, is that the carbon atom between the nitrogen and sulfur atoms in the thiazole ring is much more acidic than most $=C-$ groups, with a pK_a value near 10. (1) This carbon center ionizes to form a *carbanion.* (2) The carbanion readily adds to the carbonyl group of pyruvate. (3) This addition is followed by the decarboxylation of pyruvate. The positively charged ring of TPP acts as an electron sink that stabilizes the negative charge that is transferred to the ring as part of the decarboxylation. (4) Protonation yields hydroxyethyl-TPP.

2. *Oxidation*. The hydroxyethyl group attached to TPP is oxidized to form an acetyl group while being simultaneously transferred to lipoamide, a derivative of lipoic acid that is linked to the side chain of a lysine residue by an amide linkage. Note that this transfer results in the formation of an energy-rich thioester bond.



The oxidant in this reaction is the disulfide group of lipoamide, which is reduced to its disulfhydryl form. This reaction, also catalyzed by the pyruvate dehydrogenase component E_1, yields acetyllipoamide.

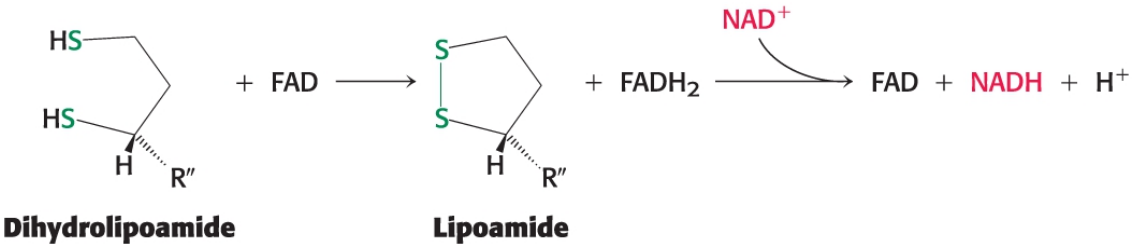
3. *Formation of acetyl CoA*. The acetyl group is transferred from acetyllipoamide to CoA to form acetyl CoA.



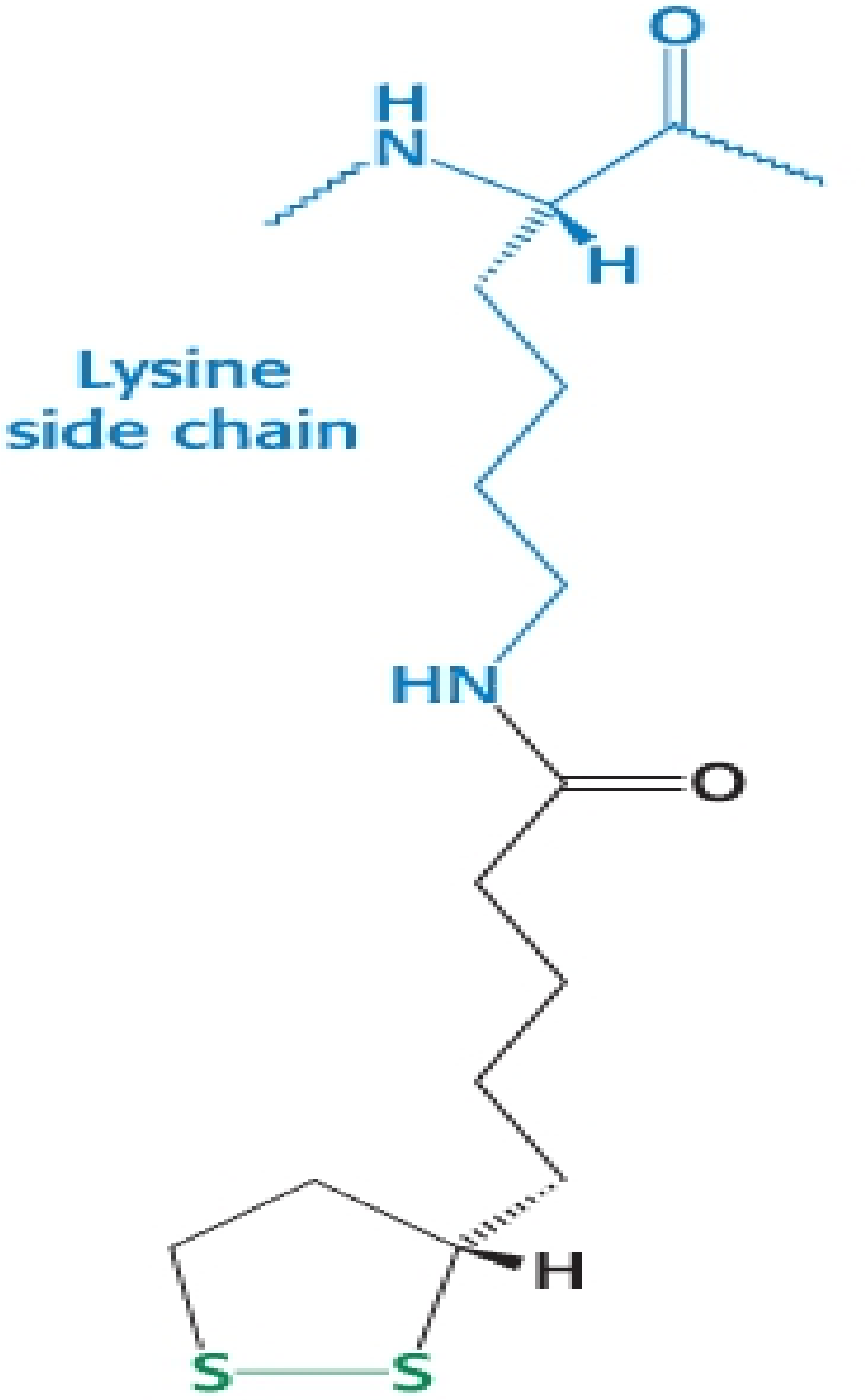
Dihydrolipoyl transacetylase (E_2) catalyzes this reaction. The energy-rich thioester bond is preserved as the acetyl group is transferred to CoA. Recall that CoA serves as a carrier of many activated acyl groups, of which acetyl is the simplest (Section 15.4). Acetyl CoA, the fuel for the citric acid cycle, has now been generated from pyruvate.

4. *Regeneration of oxidized lipoamide*. The pyruvate dehydrogenase complex cannot complete another catalytic cycle until the dihydrolipoamide is oxidized to lipoamide. In the fourth step,

the oxidized form of lipoamide is regenerated by dihydrolipoyl dehydrogenase (E_3). Two electrons are transferred to an FAD prosthetic group of the enzyme and then to NAD^+.



This electron transfer from FAD to NAD^+ is unusual because the common role for FAD is to receive electrons from NADH. The electron-transfer potential of FAD is increased by its chemical environment within the enzyme, enabling it to transfer electrons to NAD^+. Proteins tightly associated with FAD or flavin mononucleotide (FMN) are called **flavoproteins**.



Reactive disulfide bond

Lipoamide

Flexible linkages allow lipoamide to move between different active sites

The structures and precise composition of the component enzymes of the pyruvate dehydrogenase complex vary among species. However, there are common features.

The core of the complex is formed by 60 molecules of the transacetylase component E_2 (**Figure 17.6**). Transacetylase consists of 20 catalytic trimers assembled to form a hollow cube. Each of the three subunits forming a trimer has three major domains (**Figure 17.7**). At the amino terminus is a small domain that contains a bound flexible lipoamide cofactor attached to a lysine residue. This domain is homologous to biotin-binding domains such as that of pyruvate carboxylase (Figure 16.29). The lipoamide domain is followed by a small domain that interacts with E_3 within the complex. A larger transacetylase domain completes an E_2 subunit.

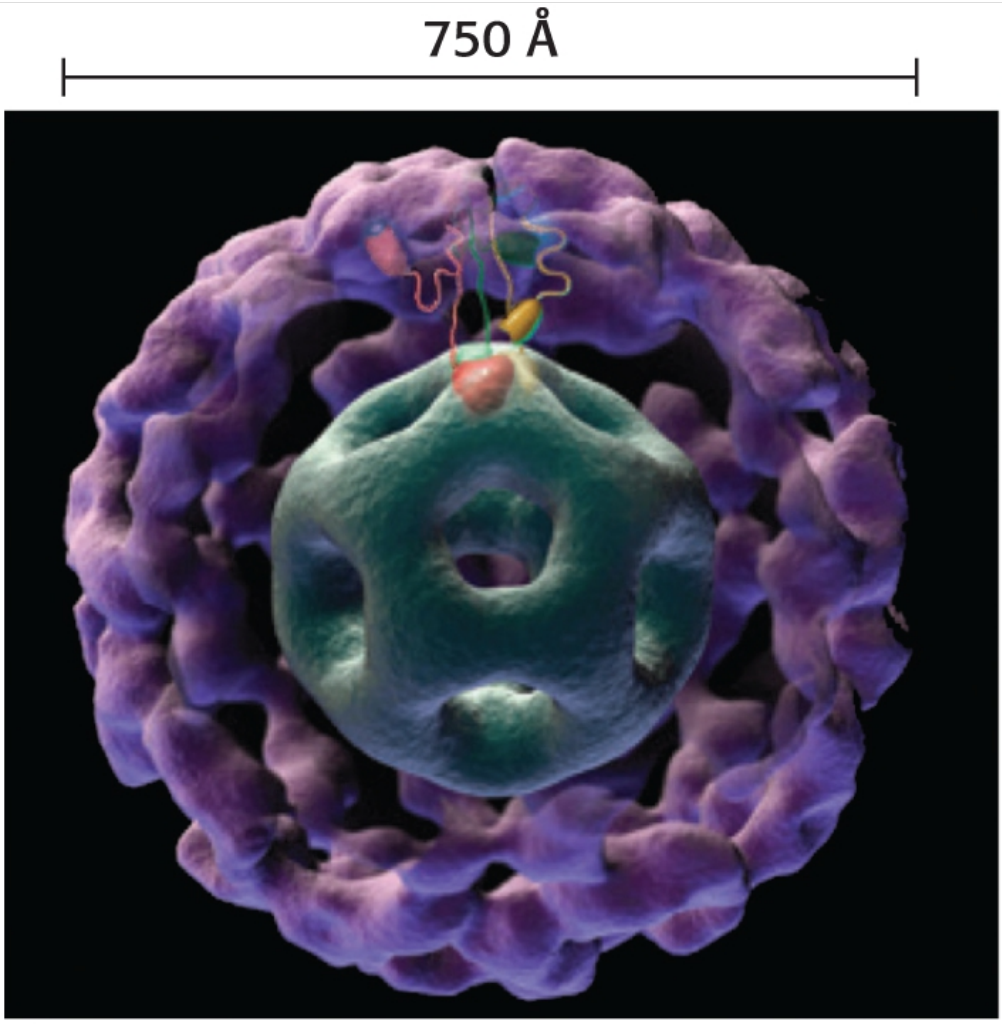


FIGURE 17.6 The structure of the pyruvate dehydrogenase complex from bacteria reveals a massive protein complex. The image of the complex from *B. stearothermophilus*, which was derived from cryo-electron microscopic data (Section 4.5), shows an inner core consisting of the E_2 enzyme. The shell surrounding the core consists of E_1 and E_3 enzymes, although only the E_1 enzymes are shown in this structure. Two of the 60 lipoamide arms are shown (red and yellow).

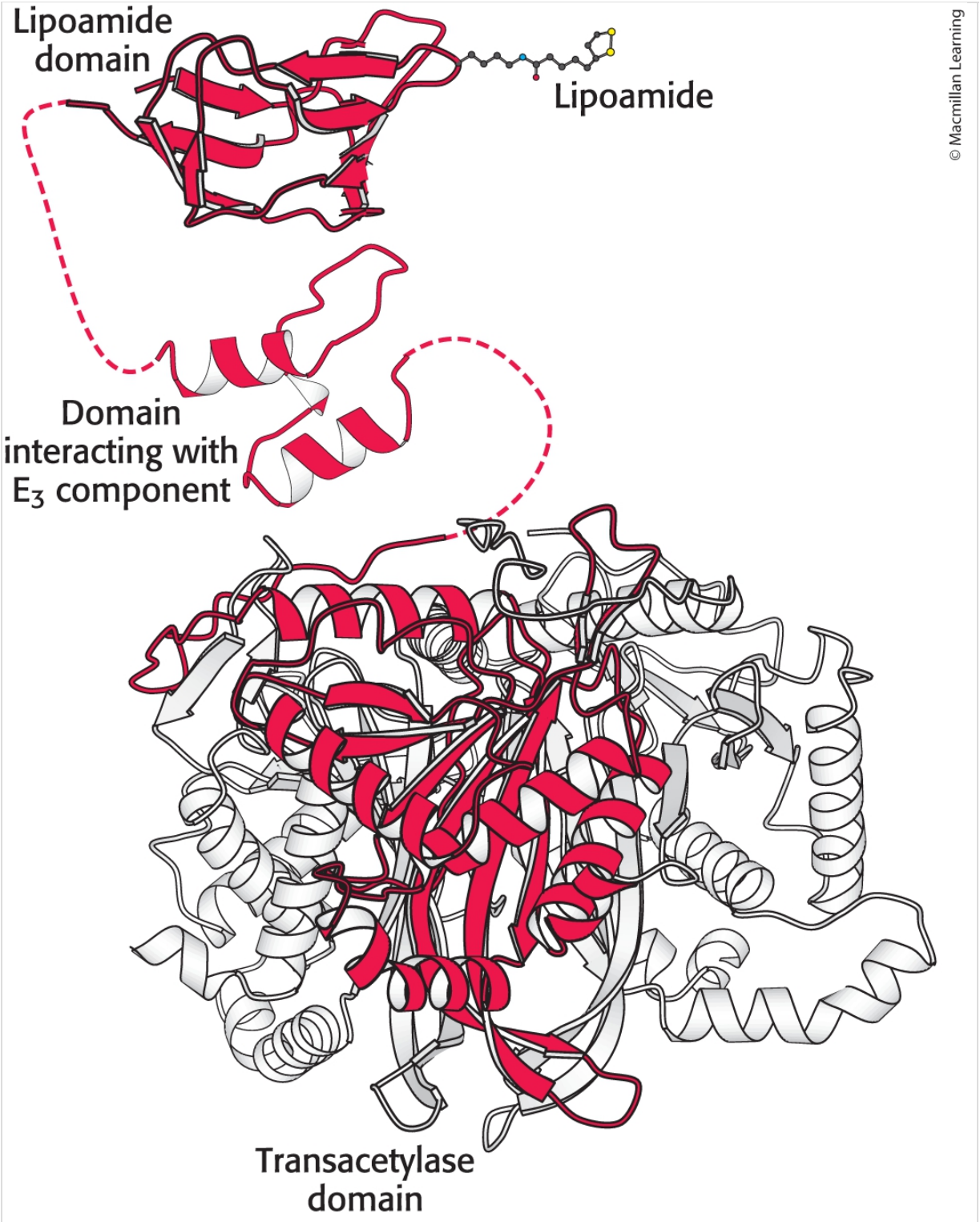


FIGURE 17.7 The transacetylase (E_2) core is made up of three distinct domains. The figure shows one subunit of the transacetylase trimer. *Notice* that each subunit consists of three domains: a lipoamide-binding domain, a small domain that interacts with E_3, and a

large transacetylase catalytic domain. The catalytic domains interact with one another to form the catalytic trimer. Transacetylase domains of three identical subunits are shown, with one depicted in red and the others in white in the ribbon representation.

Surrounding the core transacetylase is a shell composed of ~ 45 copies of the E_1 and ~ 10 copies of E_3 enzymes. In mammals, E_1 is an $\alpha_2\beta_2$ tetramer, and E_3 is an $\alpha\beta$ dimer, and this core contains another protein, E_3-binding protein (E_3-BP), which facilitates the interaction between E_2 and E_3. If E_3-BP is missing, the complex has greatly reduced activity. The gap between the outer shell and the transacetylase core allows the lipoamide arms to visit the various active sites (Figure 17.6).

How do the three distinct active sites work in concert? The key is the long, flexible lipoamide arm of the E_2 subunit, which carries substrate from active site to active site (**Figure 17.8**):

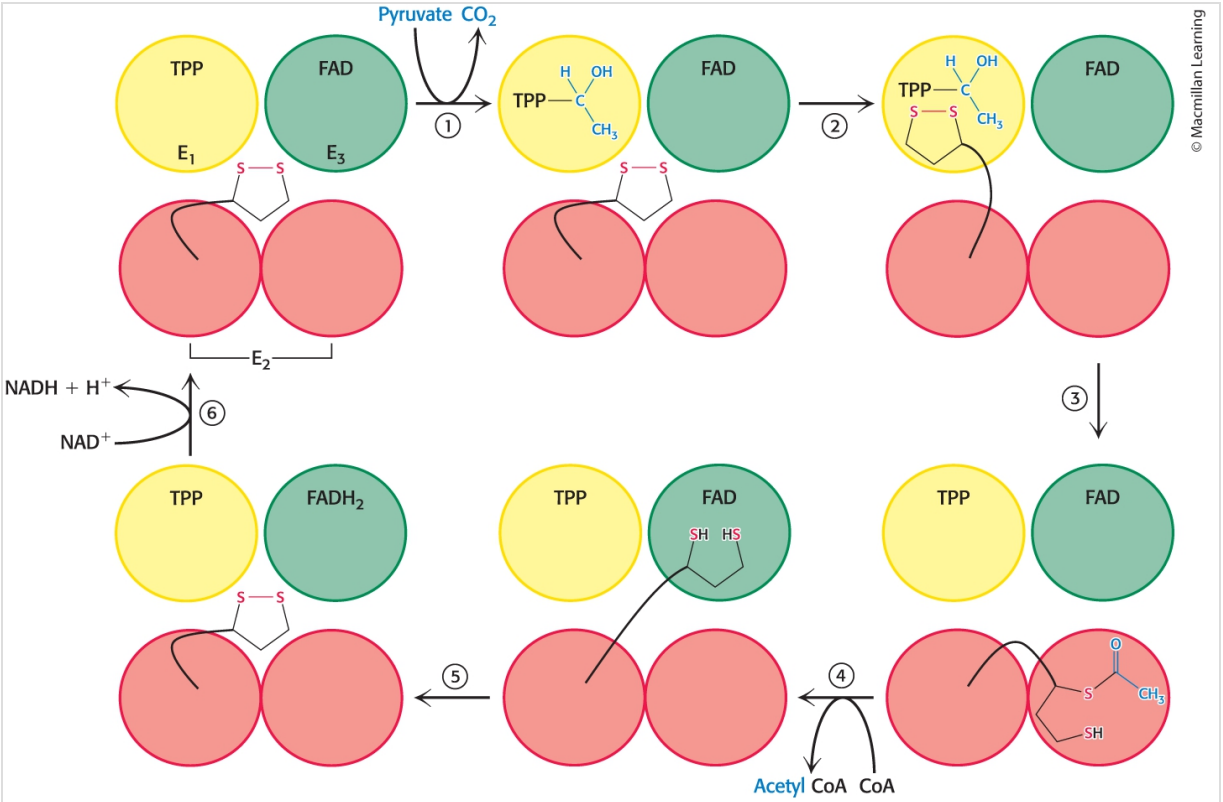


FIGURE 17.8 Three enzymes cooperate in the full reactions of the pyruvate dehydrogenase complex. At the top left, the enzyme (represented by a yellow, a green, and two red spheres) is unmodified and ready for a catalytic cycle. (1) Pyruvate is decarboxylated to form hydroxyethyl-TPP. (2) The lipoamide arm of E_2 moves into the active site of E_1. (3) E_1 catalyzes the transfer of the two-carbon group to the lipoamide group to form the acetyl–lipoamide complex. (4) E_2 catalyzes the transfer of the acetyl moiety to CoA to form the product acetyl CoA. The dihydrolipoamide arm then swings to the active site of E_3. E_3 catalyzes (5) the oxidation of the dihydrolipoamide and (6) the transfer of the protons and electrons to NAD^+ to complete the reaction cycle.

1. Pyruvate is decarboxylated at the active site of E_1, forming the hydroxyethyl-TPP intermediate, and CO_2 leaves as the first product. This active site lies deep within the E_1 complex,

connected to the enzyme surface by a 20-Å-long hydrophobic channel.

2. E_2 inserts the lipoamide arm of the lipoamide domain into the deep channel in E_1 leading to the active site.

3. E_1 catalyzes the transfer of the acetyl group to the lipoamide. The acetylated arm then leaves E_1 and enters the E_2 cube to visit the active site of E_2, located deep in the cube at the subunit interface.

4. The acetyl moiety is then transferred to CoA, and the second product, acetyl CoA, leaves the cube. The reduced lipoamide arm then swings to the active site of the E_3 flavoprotein.

5. At the E_3 active site, the lipoamide is oxidized by coenzyme FAD. The reactivated lipoamide is ready to begin another reaction cycle.

6. The final product, NADH, is produced with the reoxidation of $FADH_2$ to FAD.

The structural integration of three kinds of enzymes and the long, flexible lipoamide arm make the coordinated catalysis of a complex reaction possible. The proximity of one enzyme to another increases the overall reaction rate and minimizes side reactions. All the intermediates in the oxidative decarboxylation of pyruvate remain bound to the complex throughout the reaction sequence and are readily transferred as the flexible arm of E_2 calls on each active site in turn.

Self-Check Question



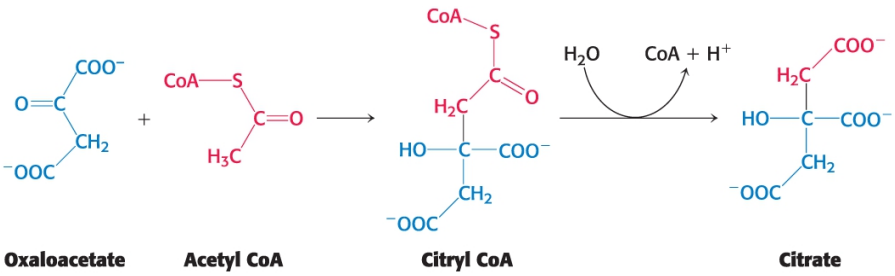
A key product of pyruvate dehydrogenase complex reaction, acetyl CoA, is released after the fourth step. What is the purpose of the remaining steps?

17.3 The Citric Acid Cycle Oxidizes Two-Carbon Units

The conversion of pyruvate into acetyl CoA by the pyruvate dehydrogenase complex is the link between glycolysis and cellular respiration because acetyl CoA is the fuel for the citric acid cycle. Indeed, under aerobic conditions, all fuels are ultimately metabolized to acetyl CoA or components of the citric acid cycle.

Citrate synthase forms citrate from oxaloacetate and the acetyl group from acetyl coenzyme A

The citric acid cycle begins with the addition of a four-carbon unit, oxaloacetate, and a two-carbon unit, the acetyl group of acetyl CoA. Oxaloacetate reacts with acetyl CoA and H_2O to yield citrate and CoA.



This reaction, which is an aldol addition followed by a hydrolysis, is catalyzed by citrate synthase. Oxaloacetate first combines with acetyl CoA to form citryl CoA, a molecule that is energy rich because it contains the thioester bond that originated in acetyl CoA. The hydrolysis of citryl CoA thioester to citrate and CoA drives the overall reaction far in the direction of the synthesis of citrate. In essence, the hydrolysis of the thioester powers the synthesis of a new molecule from two precursors.

Mechanism: The mechanism of citrate synthase prevents undesirable reactions

Because the condensation of acetyl CoA and oxaloacetate initiates the citric acid cycle, it is very important that side reactions, notably the hydrolysis of acetyl CoA to acetate and CoA, be

minimized. Let us briefly consider how citrate synthase prevents the wasteful hydrolysis of acetyl CoA.

Mammalian citrate synthase is a dimer of identical 49-kDa subunits. Each active site is located in a cleft between the large and the small domains of a subunit, adjacent to the subunit interface. X-ray crystallographic studies of citrate synthase and its complexes with several substrates and inhibitors have revealed that the enzyme undergoes large conformational changes in the course of catalysis. Citrate synthase exhibits sequential, ordered kinetics: oxaloacetate binds first, followed by acetyl CoA.

The reason for the ordered binding is that oxaloacetate induces a major structural rearrangement leading to the creation of a binding site for acetyl CoA. The binding of oxaloacetate converts the open form of the enzyme into a more closed form (Figure 17.9). In each subunit, the small domain rotates 19 degrees relative to the large domain. Movements as large as 15 Å are produced by the rotation of α helices elicited by quite small shifts of side chains around bound oxaloacetate. These structural changes create a binding site for acetyl CoA.

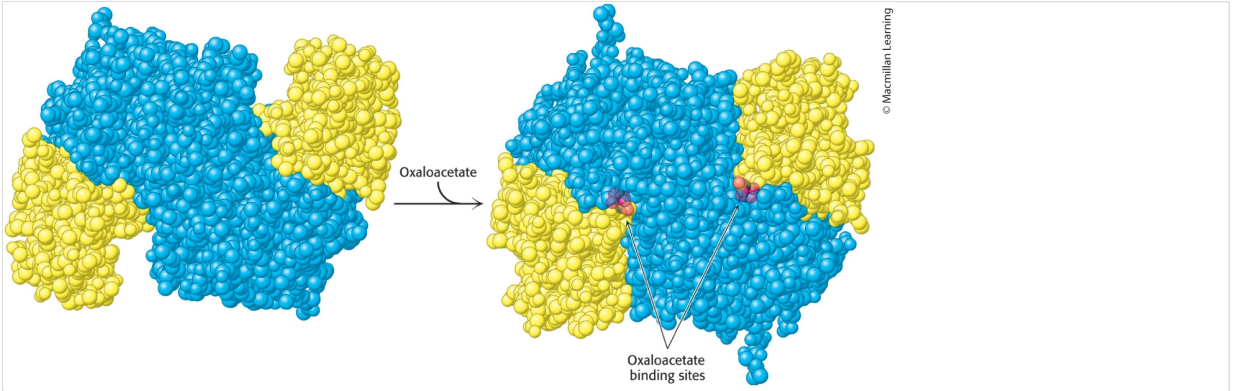


FIGURE 17.9 The ordered binding of substrates by citrate synthase is explained by conformational changes upon binding oxaloacetate. The small domain of each subunit of the homodimer is shown in yellow; the large domains are shown in blue. (Left) The open form of enzyme alone is shown. (Right) The closed form of the oxaloacetate-enzyme complex reveals significant structural changes upon oxaloacetate binding that create a binding site with high affinity for acetyl CoA, the second substrate to bind.

[Drawn from 5CSC.pdb and 4CTS.pdb.]

INTERACT with this model in Achieve

Citrate synthase catalyzes the condensation reaction by bringing the substrates into close proximity, orienting them, and polarizing certain bonds (Figure 17.10). The donation and removal of protons transforms acetyl CoA into an enol intermediate. The enol attacks oxaloacetate to form a carbon–carbon double bond linking acetyl CoA and oxaloacetate. The newly formed citryl CoA induces additional structural changes in the enzyme, causing the active site to become completely enclosed. The enzyme cleaves the citryl CoA thioester by hydrolysis.

CoA leaves the enzyme, followed by citrate, and the enzyme returns to the initial open conformation.

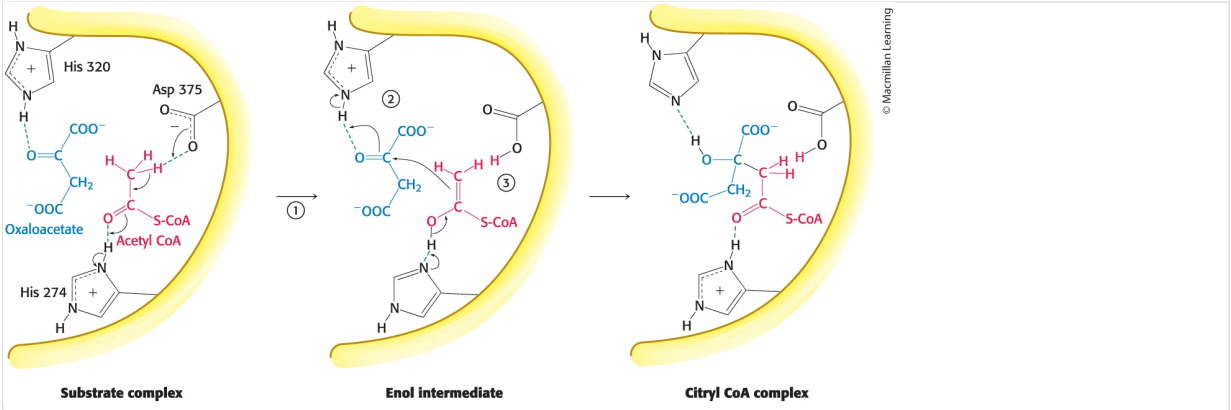
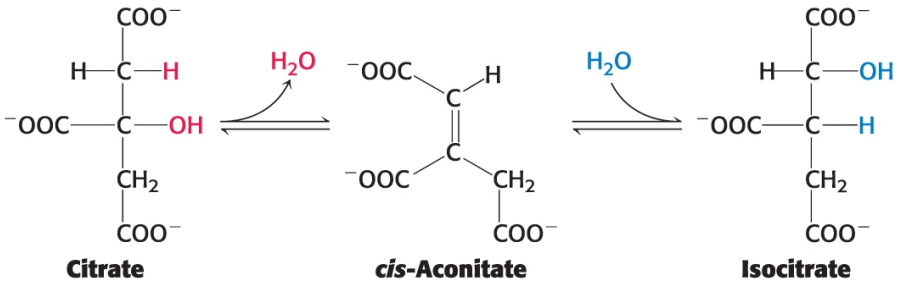


FIGURE 17.10 The first part of the citrate synthase mechanism forms citryl CoA. (1) In the substrate complex (left), His 274 donates a proton to the carbonyl oxygen of acetyl CoA to promote the removal of a methyl proton by Asp 375 to form the enol intermediate (center). (2) Oxaloacetate is activated by the transfer of a proton from His 320 to its carbonyl carbon atom. (3) Simultaneously, the enol of acetyl CoA attacks the carbonyl carbon of oxaloacetate to form a carbon–carbon bond linking acetyl CoA and oxaloacetate. His 274 is reprotonated, and citryl CoA is formed. His 274 participates again as a proton donor to hydrolyze the thioester (not shown), yielding citrate and CoA.

We can now understand how the wasteful hydrolysis of acetyl CoA is prevented. Citrate synthase is well suited to hydrolyze *citryl* CoA but not *acetyl* CoA. How is this discrimination accomplished? First, acetyl CoA does not bind to the enzyme until oxaloacetate is bound and ready for condensation. Second, the catalytic residues crucial for the hydrolysis of the thioester linkage are not appropriately positioned until citryl CoA is formed. As with hexokinase and triose phosphate isomerase (Section 16.2), induced fit prevents an undesirable side reaction.

Citrate is isomerized into isocitrate

The hydroxyl group is not properly located in the citrate molecule for the oxidative decarboxylations that follow. Thus, citrate is isomerized into isocitrate to enable the six-carbon unit to undergo oxidative decarboxylation. The isomerization of citrate is accomplished by a dehydration step followed by a hydration step. The result is an interchange of an H and an OH. The enzyme catalyzing both steps is called *aconitase* because *cis*-aconitate is an intermediate.



Aconitase is an iron–sulfur protein, or nonheme iron protein, in that it contains iron that is not bonded to heme. Rather, its four iron atoms are complexed to four inorganic sulfides and three cysteine sulfur atoms, leaving one iron atom available to bind citrate through one of its COO^- groups and an OH group (Figure 17.11). This Fe–S cluster participates in dehydrating and rehydrating the bound substrate.

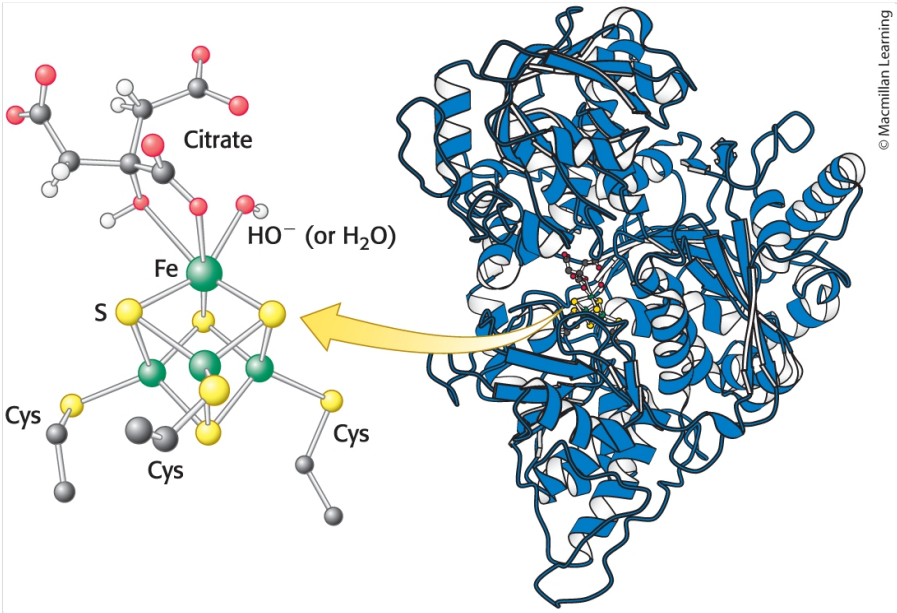


FIGURE 17.11 Citrate binds directly to the iron–sulfur complex of aconitase. A 4Fe–4S iron–sulfur cluster is a component of the active site of aconitase. Notice that one of the iron atoms of the cluster binds to a COO^- group and an OH group of citrate.

[Drawn from 1C96.pdb.]

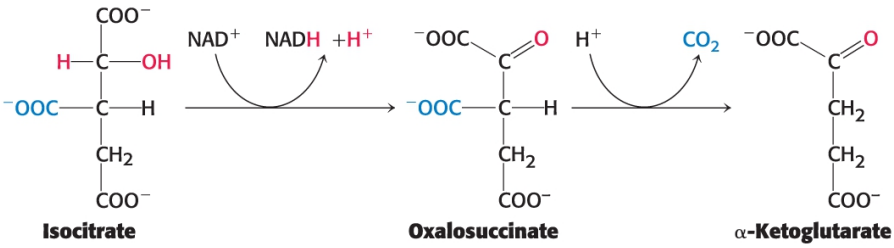
INTERACT with this model in Achieve

Isocitrate is oxidized and decarboxylated to alpha-ketoglutarate

We come now to the first of four oxidation–reduction reactions in the citric acid cycle. The oxidative decarboxylation of isocitrate is catalyzed by isocitrate dehydrogenase.

$$\text{Isocitrate} + \text{NAD}^+ \rightarrow \alpha\text{–ketoglutarate} + \text{CO}_2 + \text{NADH}$$

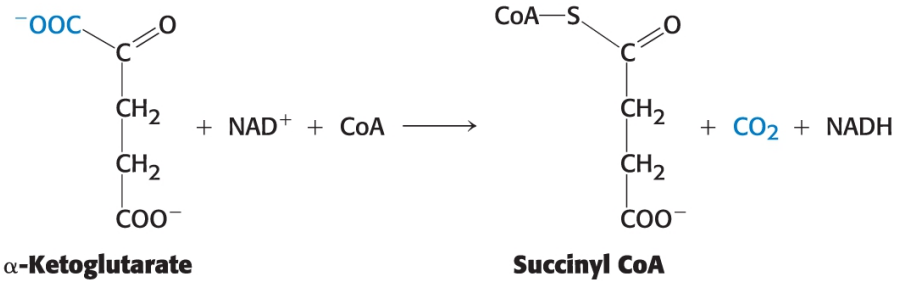
The intermediate in this reaction is oxalosuccinate, an unstable β-ketoacid. While bound to the enzyme, it loses CO_2 to form α-ketoglutarate.



This oxidation generates the first high-transfer-potential electron carrier, NADH, in the cycle.

Succinyl coenzyme A is formed by the oxidative decarboxylation of alpha-ketoglutarate

The conversion of isocitrate into α-ketoglutarate is followed by a second oxidative decarboxylation reaction, the formation of succinyl CoA from α-ketoglutarate.



This reaction is catalyzed by the **α-ketoglutarate dehydrogenase complex**, an organized assembly of three kinds of enzymes that is homologous to the pyruvate dehydrogenase complex. In fact, the E_3 component is identical in both enzymes. The oxidative decarboxylation of α-ketoglutarate closely resembles that of pyruvate (Section 17.2), also an α-ketoacid.

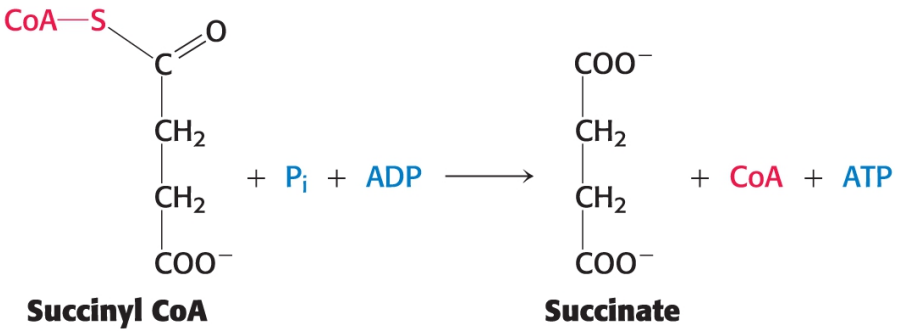
$$\text{Pyruvate} + \text{CoA} + \text{NAD}^+ \xrightarrow{\text{Pyruvate dehydrogenase complex}} \text{acetyl CoA} + \text{CO}_2 + \text{NADH} + \text{H}^+$$

$$\alpha\text{–Ketoglutarate} + \text{CoA} + \text{NAD}^+ \xrightarrow{\alpha\text{–Ketoglutarate dehydrogenase complex}} \text{succinyl CoA} + \text{CO}_2 + \text{NADH}$$

Both reactions include the decarboxylation of an α-ketoacid and the subsequent formation of a thioester linkage with CoA that has a high transfer potential. The reaction mechanisms are entirely analogous.

A compound with high phosphoryl-transfer potential is generated from succinyl coenzyme A

Succinyl CoA is an energy-rich thioester compound. The $\Delta G^{\circ\prime}$ for the hydrolysis of succinyl CoA is about $-33.5\ \text{kJ mol}^{-1}(-8.0\ \text{kcal mol}^{-1})$, which is comparable to that of ATP $(-30.5\ \text{kJ mol}^{-1}$, or $-7.3\ \text{kcal mol}^{-1})$. In the citrate synthase reaction, the cleavage of the thioester bond powers the synthesis of the six-carbon citrate from the four-carbon oxaloacetate and the two-carbon fragment. The cleavage of the thioester bond of succinyl CoA is coupled to the phosphorylation of a purine nucleoside diphosphate, usually ADP. This reaction, which is readily reversible, is catalyzed by succinyl CoA synthetase.



This reaction is the only step in the citric acid cycle that directly yields a compound with high phosphoryl-transfer potential. In mammals, there are two isozymic forms of the enzyme, one specific for ADP and one for GDP. In tissues that perform large amounts of cellular respiration, such as skeletal and heart muscle, the ADP-requiring isozyme predominates. In tissues that perform many anabolic reactions, such as the liver, the GDP-requiring enzyme is common. The GDP-requiring enzyme is believed to work in reverse of the direction observed in the TCA cycle; that is, GTP is used to power the synthesis of succinyl CoA, which is a precursor for heme synthesis (Section 25.4). The specificity and nucleoside used varies also by species. For example, the enzyme in *E. coli* can use either GDP or ADP as the phosphoryl-group acceptor.

Note that the enzyme **nucleoside diphosphokinase**, which catalyzes the following reaction,

$$\mathrm{XTP} + \mathrm{YDP} \rightleftharpoons \mathrm{XDP} + \mathrm{YTP}$$

allows the γ phosphoryl group to be readily transferred from any nucleotide triphosphate (XTP) to any other nucleotide diphosphate (YDP); for example, from GTP to form ATP from ADP. This reaction thereby allows the adjustment of the concentration of GTP or ATP to meet the cell's need and keeps the concentrations of all the various nucleoside triphosphates in the cell near equilibrium with one another.

Mechanism: Succinyl coenzyme A synthetase transforms types of biochemical energy

The mechanism of this reaction is a clear example of an energy transformation: energy inherent in the thioester molecule is transformed into phosphoryl-group-transfer potential (**Figure 17.12**). First, coenzyme A is displaced by orthophosphate (step 1), which generates another energy-rich compound, succinyl phosphate. A histidine residue plays a key role as a moving arm that detaches the phosphoryl group (step 2), then swings over to a bound ADP (step 3) and transfers the group to form ATP (step 4). The participation of high-energy compounds in all the steps is attested to by the fact that the reaction is readily reversible:
$\Delta G^{\circ\prime} = -3.4\ \mathrm{kJ\ mol^{-1}} (-0.8\ \mathrm{kcal\ mol^{-1}})$. The formation of ATP at the expense of succinyl CoA is an example of substrate-level phosphorylation (Section 16.2).

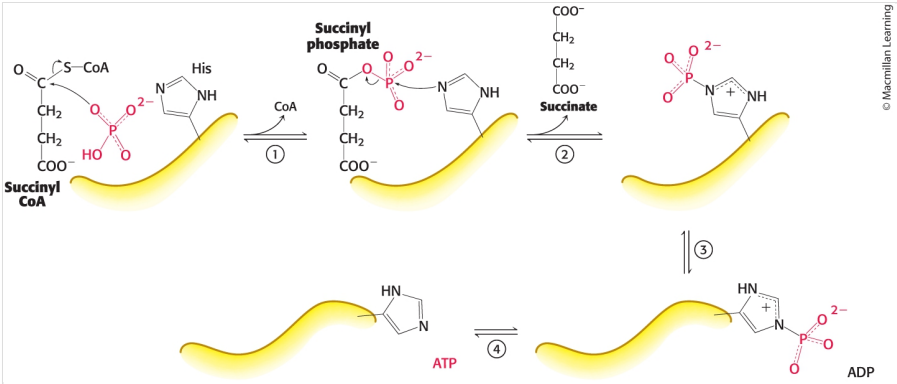
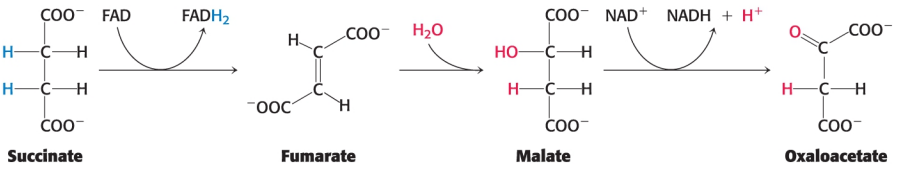


FIGURE 17.12 The mechanism of succinyl CoA synthetase allows the formation of a phosphoanhydride through a phosphorylated enzyme intermediate. (1) Orthophosphate displaces coenzyme A, which generates another energy-rich compound, succinyl phosphate. (2) A histidine residue removes the phosphoryl group with the concomitant generation of succinate and phosphohistidine. (3) The phosphohistidine residue then swings over to a bound ADP, and (4) the phosphoryl group is transferred to form ATP.

Oxaloacetate is regenerated by the oxidation of succinate

Reactions of four-carbon compounds constitute the final stage of the citric acid cycle: the regeneration of oxaloacetate.



The reactions constitute a metabolic motif that we will see again in fatty acid synthesis and degradation as well as in the degradation of some amino acids. A methylene group (CH_2) is converted into a carbonyl group $C{=}O$ in three steps: an oxidation, a hydration, and a second oxidation reaction. Oxaloacetate is thereby regenerated for another round of the cycle, and more energy is extracted in the form of $FADH_2$ and NADH.

Succinate is oxidized to fumarate by succinate dehydrogenase. The hydrogen acceptor is FAD rather than NAD^+, which is used in the other three oxidation reactions in the cycle. FAD is the electron acceptor in this reaction because the free-energy change is insufficient to reduce

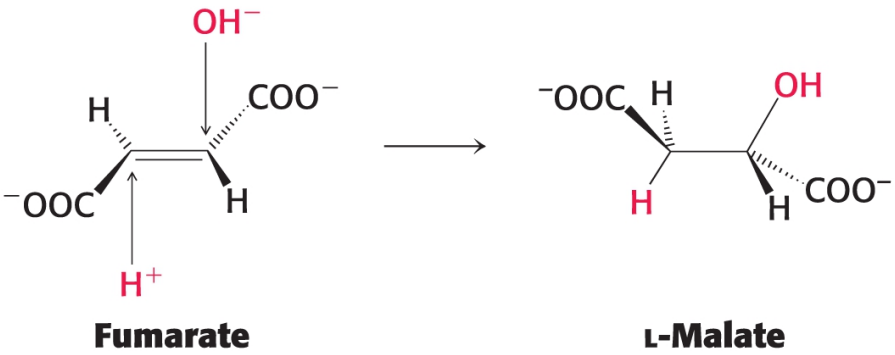
NAD^+. FAD is nearly always the electron acceptor in oxidations that remove two hydrogen atoms from a substrate. In succinate dehydrogenase, the isoalloxazine ring of FAD is covalently attached to a histidine side chain of the enzyme (denoted E-FAD).

$$\text{E-FAD} + \text{succinate} \rightleftharpoons \text{E-FADH}_2 + \text{fumarate}$$

Succinate dehydrogenase, like aconitase, is an iron–sulfur protein. Indeed, succinate dehydrogenase contains three different kinds of iron–sulfur clusters: 2Fe–2S (two iron atoms bonded to two inorganic sulfides), 3Fe–4S, and 4Fe–4S. Succinate dehydrogenase differs from other enzymes in the citric acid cycle because it is embedded in the inner mitochondrial membrane. In fact, succinate dehydrogenase is directly associated with the electron-transport chain, the link between the citric acid cycle and ATP formation.

$FADH_2$ produced by the oxidation of succinate does not dissociate from the enzyme, in contrast with NADH produced in other oxidation–reduction reactions. Rather, two electrons are transferred from $FADH_2$ directly to iron–sulfur clusters of the enzyme, which in turn passes the electrons to coenzyme Q. Coenzyme Q, an important member of the electron-transport chain, passes electrons ultimately to the final acceptor, molecular oxygen, as we shall see in Chapter 18.

The next step is the hydration of fumarate to form L-malate. Fumarase catalyzes a stereospecific trans addition of H^+ and OH^-. The OH^- group adds to only one side of the double bond of fumarate; hence, only the L isomer of malate is formed.



Fumarate **L-Malate**

Finally, malate is oxidized to form oxaloacetate. This reaction is catalyzed by malate dehydrogenase, and NAD^+ is again the hydrogen acceptor.

$$\text{Malate} + \text{NAD}^+ \rightleftharpoons \text{oxaloacetate} + \text{NADH} + \text{H}^+$$

The standard free energy for this reaction, unlike that for the other steps in the citric acid cycle, is significantly positive ($\Delta G^{\circ\prime} = +29.7\ \text{kJ mol}^{-1}$, or $+7.1\ \text{kcal mol}^{-1}$). The oxidation of malate is driven by the use of the products — oxaloacetate by citrate synthase and NADH by the electron-transport chain.

Self-Check Question



Fluoroacetate is a toxic molecule that enters the citric acid cycle (CAC) due to its similarity to an acetyl group, but ultimately it inhibits the CAC. When fluoroacetate is added to mitochondria, fluorocitrate builds up. What step of the CAC is inhibited by fluoroacetate?

The citric acid cycle produces high-transfer-potential electrons, ATP, and CO_2

The net reaction of the citric acid cycle is

$$\text{Acetyl CoA} + 3\ \text{NAD}^+ + \text{FAD} + \text{ADP} + \text{P}_\text{i} + 2\ \text{H}_2\text{O} \rightarrow 2\ \text{CO}_2 + 3\ \text{NADH} + \text{FADH}_2 + \text{ATP} + 2\text{H}^+ + \text{CoA}$$

Let us recapitulate the reactions that give this stoichiometry (Figure 17.13 and Table 17.2) and summarize.

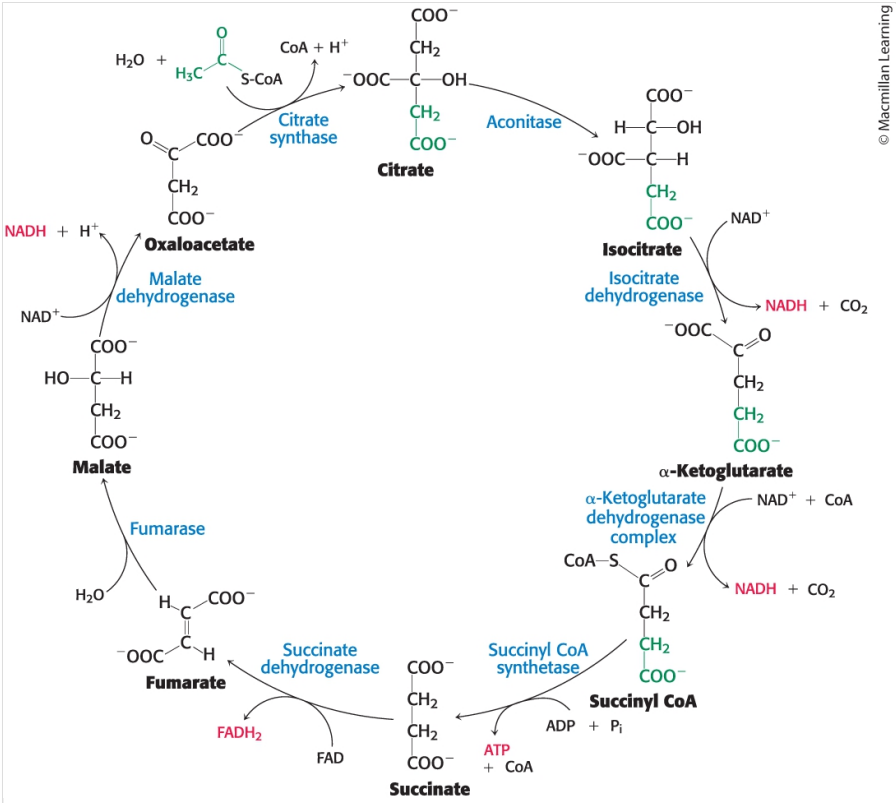


FIGURE 17.13 Eight enzyme-catalyzed reactions make up the full citric acid cycle. Notice that since succinate is a symmetric molecule, the identity of the carbons from the acetyl unit is lost.

TABLE 17.2 Citric acid cycle

Step	Reaction	Enzyme	Prosthetic group	Type *	ΔG°′ kJ mol^{-1}	ΔG°′ kcal mol^{-1}
1	Acetyl CoA + oxaloacetate + H_2O → citrate + CoA + H^+	Citrate synthase		a	−31.4	−7.5
2a	Citrate ⇌ *cis*-aconitate + H_2O	Aconitase	Fe–S	b	+8.4	+2.0

2b	*cis*-Aconitate + H_2O ⇌ isocitrate	Aconitase	Fe–S	c	−2.1	−0.5
3	Isocitrate + NAD^- ⇌ α-ketoglutarate + CO_2 + NADH	Isocitrate dehydrogenase		d+e	−8.4	−2.0
4	α-Ketoglutarate + NAD^+ + CoA ⇌ succinyl CoA + CO_2 + NADH	α-Ketoglutarate dehydrogenase complex	Lipoic acid, FAD, TPP	d+e	−30.1	−7.2

TABLE 17.2 Citric acid cycle

					ΔG°′	
Step	**Reaction**	**Enzyme**	**Prosthetic group**	**Type***	**kJ mol^{-1}**	**kcal mol^{-1}**
5	Succinyl CoA + P_i + ADP ⇌ succinate + ATP + CoA	Succinyl CoA synthetase		f	−3.3	−0.8
6	Succinate + FAD (enzyme-bound) ⇌ fumarate + $FADH_2$ (enzyme-bound)	Succinate dehydrogenase	FAD, Fe–S	e	0	0
7	Fumarate + H_2O ⇌ L-malate	Fumarase		c	−3.8	−0.9
8	L-Malate + NAD^+ ⇌ oxaloacetate + NADH + H^+	Malate dehydrogenase		e	+29.7	+7.1

*Reaction type: (a) condensation; (b) dehydration; (c) hydration; (d) decarboxylation; (e) oxidation; (f) substrate-level phosphorylation.

- Two carbon atoms enter the cycle in the condensation of an acetyl unit (from acetyl CoA) with oxaloacetate. Two carbon atoms leave the cycle in the form of CO_2 in the successive decarboxylations catalyzed by isocitrate dehydrogenase and α-ketoglutarate dehydrogenase.

- Four pairs of hydrogen atoms leave the cycle in four oxidation reactions. Two NAD^+ molecules are reduced in the oxidative decarboxylations of isocitrate and α-ketoglutarate, one FAD molecule is reduced in the oxidation of succinate, and one NAD^+ molecule is reduced in the oxidation of malate. Recall also that one NAD^+ molecule is reduced in the oxidative decarboxylation of pyruvate to form acetyl CoA.
- One compound with high phosphoryl-transfer potential, usually ATP, is generated from the cleavage of the thioester linkage in succinyl CoA.
- Two water molecules are consumed: one in the synthesis of citrate by the hydrolysis of citryl CoA and the other in the hydration of fumarate.

Isotope-labeling studies have revealed that the two carbon atoms that enter each cycle are not the ones that leave. The two carbon atoms that enter the cycle as the acetyl group are retained during the initial two decarboxylation reactions (Figure 17.13) and then remain incorporated in the four-carbon acids of the cycle. Note that succinate is a symmetric molecule. Consequently, the two carbon atoms that enter the cycle can occupy any of the carbon positions in the subsequent metabolism of the four-carbon acids. The two carbons that enter the cycle as the acetyl group will be released as CO_2 in later rounds of the cycle.

Various techniques, such as fluorescence recovery after photobleaching (FRAP, Section 12.5) and tandem mass spectroscopy analysis (Section 4.3), have established that there is a physical association of all of the enzymes of the citric acid cycle into a supramolecular complex. Recall that this close arrangement of enzymes allows for substrate channeling (Chapter 16), which enhances the efficiency of the citric acid cycle because a reaction product can pass directly from one active site to the next through connecting channels.

As will be considered in Chapter 18, the electron-transport chain oxidizes the NADH and $FADH_2$ formed in the citric acid cycle. The transfer of electrons from these carriers to O_2, the final electron acceptor, leads to the generation of a proton gradient across the inner mitochondrial membrane. This proton-motive force then powers the generation of ATP; the net stoichiometry is about 2.5 ATP per NADH, and 1.5 ATP per $FADH_2$. Consequently, nine high-transfer-potential phosphoryl groups are generated when the electron-transport chain oxidizes 3 NADH molecules and $1\ FADH_2$ molecule, and one ATP is directly formed in one round of the citric acid cycle. Thus, one acetyl unit generates approximately 10 molecules of ATP. In dramatic contrast, the anaerobic glycolysis of an entire glucose molecule generates only 2 molecules of ATP (and 2 molecules of lactate).

Recall that molecular oxygen does not participate directly in the citric acid cycle. However, the cycle operates only under aerobic conditions because NAD^+ and FAD can be regenerated in the mitochondrion only by the transfer of electrons to molecular oxygen. In contrast, glycolysis can proceed under anaerobic conditions because NAD^+ is regenerated in the conversion of pyruvate into lactate. Glycolysis has both an aerobic and an anaerobic mode, whereas the citric acid cycle is strictly aerobic.

Self-Check Question



The nucleoside trisphosphate produced directly in the citric acid cycle is sometimes GTP. Explain why a GTP molecule, or another nucleoside triphosphate, is energetically equivalent to an ATP molecule in metabolism.

17.4 Entry to the Citric Acid Cycle and Metabolism Through It Are Controlled

The citric acid cycle is the final common pathway for the aerobic oxidation of fuel molecules. Moreover, as we will see shortly (Section 17.5) and repeatedly elsewhere in our study of biochemistry, the cycle is an important source of building blocks for a host of important biomolecules. As befits its role as the metabolic hub of the cell, entry into the cycle and the rate of the cycle itself are controlled at several stages.

The pyruvate dehydrogenase complex is regulated allosterically and by reversible phosphorylation

As stated earlier, glucose can be formed from pyruvate. However, the formation of acetyl CoA from pyruvate is an irreversible step in animals and thus they are unable to convert acetyl CoA back into glucose. The oxidative decarboxylation of pyruvate to acetyl CoA commits the carbon atoms of glucose to one of two principal fates: oxidation to CO_2 by the citric acid cycle, with the concomitant generation of energy, or incorporation into lipids (**Figure 17.14**).

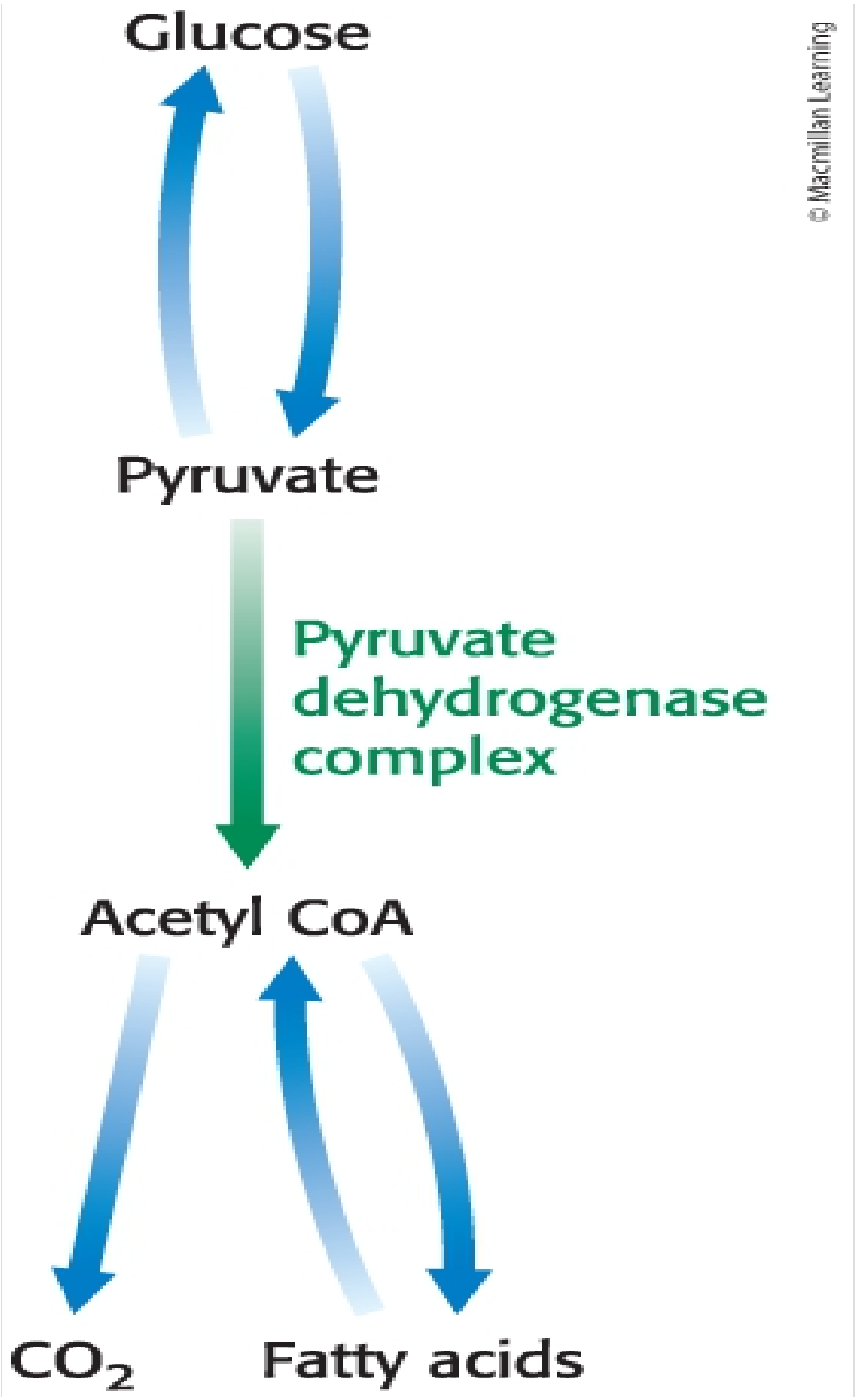

Glucose
Pyruvate
Pyruvate dehydrogenase complex
Acetyl CoA
CO_2
Fatty acids
© Macmillan Learning

FIGURE 17.14 The synthesis of acetyl CoA by the pyruvate dehydrogenase complex is a key irreversible step in glucose metabolism.

EXPLORE this pathway further in the Metabolic Map in Achieve

As expected of an enzyme at a critical branch point in metabolism, the activity of the pyruvate dehydrogenase complex is tightly regulated. High concentrations of reaction products inhibit the reaction: acetyl CoA inhibits the transacetylase component (E_2) by binding directly, whereas NADH inhibits the dihydrolipoyl dehydrogenase (E_3). High concentrations of NADH and acetyl CoA inform the enzyme that the energy needs of the cell have been met or that fatty acids are being degraded to produce acetyl CoA and NADH. In either case, there is no need to metabolize pyruvate to acetyl CoA. This inhibition has the effect of conserving glucose, because most pyruvate is derived from glucose by glycolysis (Section 16.2).

The key means of regulation of the complex in eukaryotes is reversible covalent modification (**Figure 17.15**). Phosphorylation of the pyruvate dehydrogenase component (E_1) by one of four tissue-specific isozymes of pyruvate dehydrogenase kinase (PDK) switches off the activity of the complex. Deactivation is then reversed by one of two isozymes of pyruvate dehydrogenase phosphatase (PDP). In mammals, both the kinase and phosphatase are associated with the E_2-E_3-BP core complex, and the activities of both are regulated and subject to tissue-specific hormonal control.

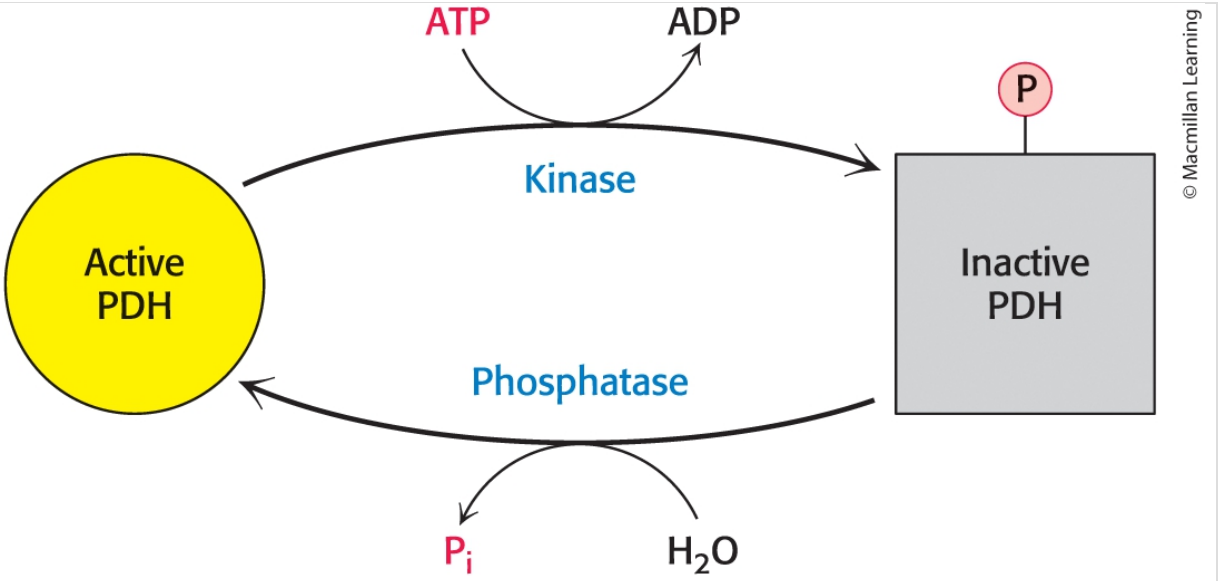


FIGURE 17.15 The activity of the pyruvate dehydrogenase complex is regulated by reversible phosphorylation. A specific kinase phosphorylates and inactivates pyruvate dehydrogenase (PDH), and a phosphatase activates the dehydrogenase by removing the phosphoryl group. The kinase and the phosphatase also are highly regulated enzymes.

To see how this regulation works in biological conditions, consider muscle that is becoming active after a period of rest (Figure 17.16). At rest, the muscle will not have significant energy demands. Consequently, the $NADH/NAD^+$, acetyl CoA/CoA, and ATP/ADP ratios will be high. These high ratios promote phosphorylation and inactivation of the complex by activating PDK. In other words, high concentrations of immediate products of the reaction (acetyl CoA and NADH) and a final product of the pathway (ATP) inhibit the activity. Thus, pyruvate dehydrogenase is switched off when the energy charge is high.

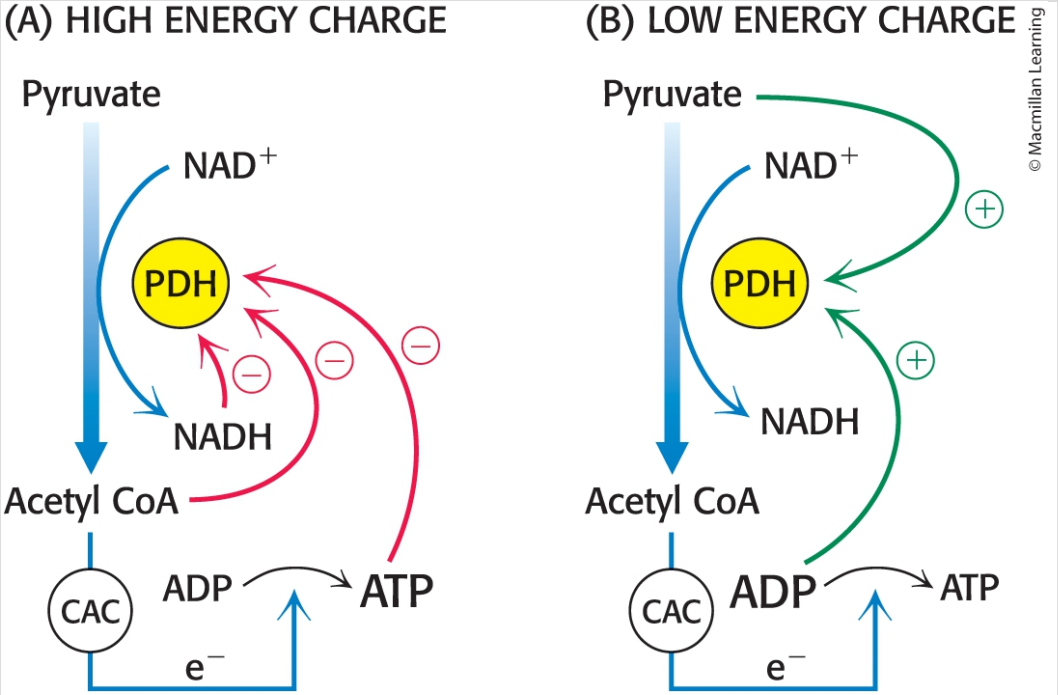


FIGURE 17.16 The pyruvate dehydrogenase complex responds to changes in the energy charge of the cell. (A) The complex (PDH) is inhibited by its immediate products, NADH and acetyl CoA, as well as by the ultimate product of the citric acid cycle (CAC) and oxidative phosphorylation, ATP. (B) PDH is activated by pyruvate and ADP, which inhibit the kinase that phosphorylates PDH.

As exercise begins, the concentrations of ADP and pyruvate will increase as muscle contraction consumes ATP and glucose is converted into pyruvate to meet the energy demands. Both ADP and pyruvate activate the dehydrogenase by inhibiting the kinase. Moreover, the phosphatase is stimulated by Ca^{2+}, the same signal that initiates muscle contraction. A rise in the cytoplasmic Ca^{2+} concentration increases the mitochondrial Ca^{2+} concentration. The rise in mitochondrial Ca^{2+} activates the phosphatase, enhancing pyruvate dehydrogenase activity.

In some tissues, the phosphatase is also controlled by hormones. For example, in liver tissue, epinephrine binds to the α-adrenergic receptor to initiate the phosphatidylinositol pathway (Section 14.2), causing an increase in Ca^{2+} concentration that activates the phosphatase. In tissues capable of fatty acid synthesis, such as liver and adipose tissue, insulin — the hormone that signifies the fed state — stimulates the phosphatase, increasing the conversion of pyruvate into acetyl CoA. Acetyl CoA is the precursor for fatty acid synthesis (Section 22.5). In these tissues, the pyruvate dehydrogenase complex is activated to funnel glucose to pyruvate and then to acetyl CoA and ultimately to fatty acids. In people with a pyruvate dehydrogenase phosphatase deficiency, pyruvate dehydrogenase is always phosphorylated and thus inactive. Consequently, glucose is processed to lactate rather than acetyl CoA, resulting in lactic acidosis. Lactic acidosis causes many tissues to malfunction, including the central nervous system.

Diabetic neuropathy may be due to inhibition of the pyruvate dehydrogenase complex



Diabetic neuropathy — a numbness, tingling, or pain in the hands, arm, fingers, toes, feet, and legs — is a common complication of both type 1 and type 2 diabetes, affecting approximately 50% of patients. There is no cure for the condition, and treatment relies on painkillers. Recent research in mice and tissue culture suggests that overproduction of lactic acid by cells in the dorsal root ganglion, a

part of the nervous system responsible for pain perception, may be a significant contributor.

Lactate, which is produced by some cells of the nervous system, is a common fuel for neurons, which import and convert it to pyruvate for use in cellular respiration. However, it appears that hyperglycemia (high glucose concentration), the defining feature of diabetes, increases pyruvate dehydrogenase kinase activity in the cells of the dorsal root ganglion, leading to inhibition of the pyruvate dehydrogenase complex. Glycolytically produced pyruvate is then processed to lactate. The overabundance of lactate leads to an increase in acid-sensing nociceptors (pain receptors), a type of G-protein-coupled receptor (Section 14.2), resulting in diabetic neuropathy. In experimental systems, three approaches — pharmacological inhibition of either pyruvate dehydrogenase kinase or lactic acid dehydrogenase, or genetic elimination of the kinase gene — greatly reduce, but do not eliminate, diabetic neuropathy. Thus, the search for good therapeutics shows promise but must continue.

The citric acid cycle is regulated at several points

The rate of the citric acid cycle is precisely adjusted to meet an animal cell's needs for ATP (**Figure 17.17**). Two allosteric enzymes primarily regulate the rate of cycling: isocitrate dehydrogenase and α-ketoglutarate dehydrogenase, the first two enzymes in the cycle to generate high-energy electrons.

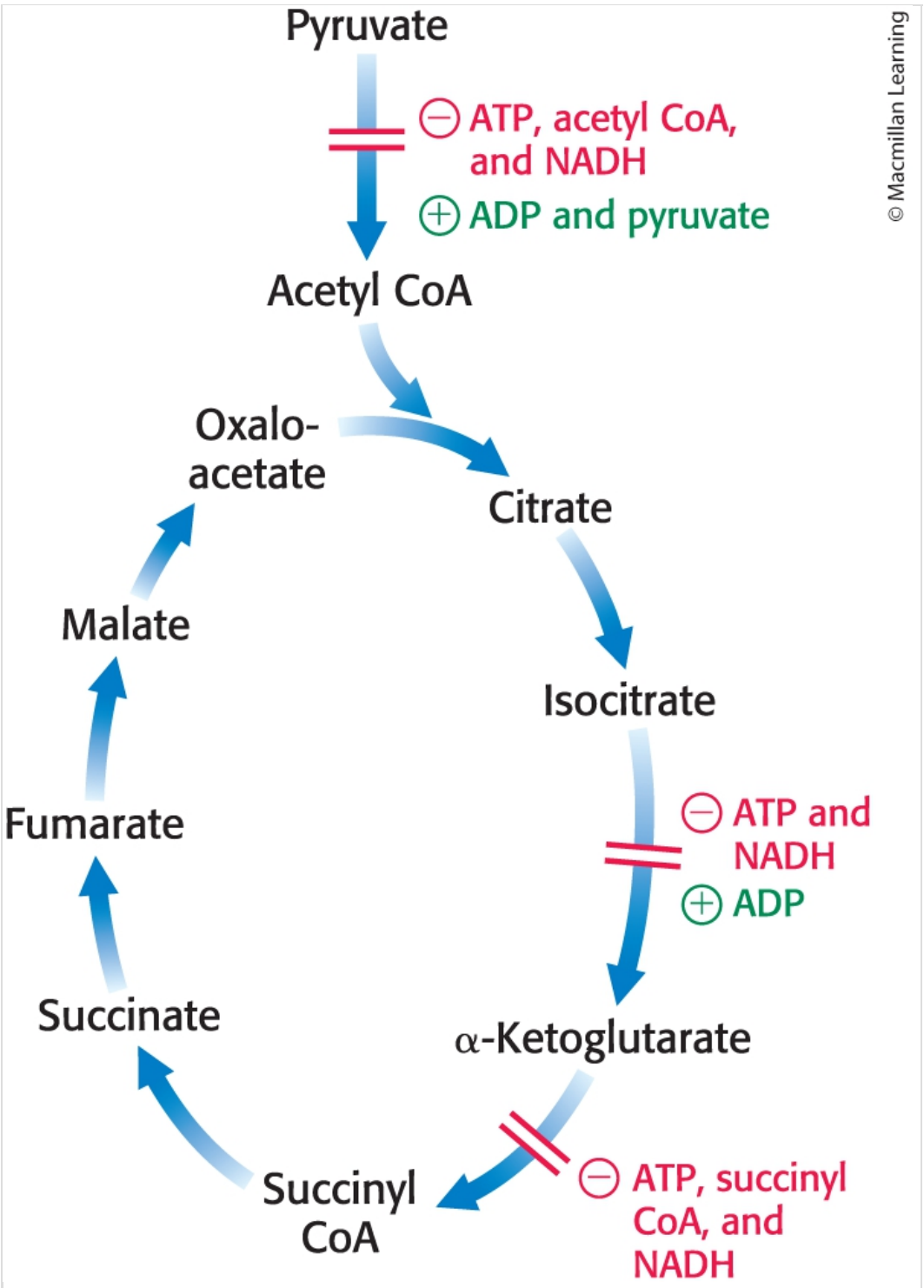


FIGURE 17.17 The citric acid cycle is regulated primarily by the concentrations of ATP and NADH. The key control points are the enzymes isocitrate dehydrogenase and α-ketoglutarate dehydrogenase.

1. *Isocitrate dehydrogenase is allosterically stimulated by ADP, which enhances the enzyme's affinity for substrates.* The binding of isocitrate, NAD^+, Mg^{2+}, and ADP are all mutually synergistic, whereas ATP is inhibitory. The reaction product NADH also inhibits isocitrate dehydrogenase by directly displacing NAD^+. It is important to note that several steps in the cycle require NAD^+ or FAD, which are abundant only when the energy charge is low.

2. The α-*ketoglutarate dehydrogenase complex catalyzes the rate-limiting step.* Some aspects of this enzyme complex's regulation are like those of the pyruvate dehydrogenase complex, as might be expected from the homology of the two enzymes. α-Ketoglutarate dehydrogenase is inhibited by succinyl CoA and NADH, the products of the reaction that it catalyzes. In addition, α-ketoglutarate dehydrogenase is inhibited by ATP, so that the rate of the citric acid cycle is reduced when cellular ATP is abundant. *α*-Ketoglutarate dehydrogenase deficiency is observed in a number of neurological disorders, including Alzheimer's disease.

In many bacteria, the synthesis of citrate from oxaloacetate and acetyl CoA carbon units is another important control point. In these organisms, ATP is an allosteric inhibitor of citrate synthase, causing an increase in the apparent value of K_M for acetyl CoA. The result is that as the level of ATP increases, less citrate synthase is bound to acetyl CoA and so less citrate is formed.

The use of isocitrate dehydrogenase and α-ketoglutarate dehydrogenase as points of regulation in human metabolism integrates the citric acid cycle with other pathways and highlights the central role of the citric acid cycle in metabolism. For instance, the inhibition of isocitrate dehydrogenase leads to a buildup of citrate, because the interconversion of isocitrate and citrate is readily reversible under intracellular conditions. Citrate can be transported to the cytoplasm, where it signals phosphofructokinase to halt glycolysis (Section 16.3) and where it can serve as a source of acetyl CoA for fatty acid synthesis (Section 22.5). The α-ketoglutarate that accumulates when α-ketoglutarate dehydrogenase is inhibited can be used as a precursor for several amino acids and the purine bases (Chapters 25 and 26). Finally, as we will explore in Chapter 24, defects in the citric acid cycle and related enzymes can lead to the formation of cancer.

Self-Check Question



The citric acid cycle is part of aerobic respiration, but no O_2 is required for the cycle. Explain this apparent paradox.

17.5 The Citric Acid Cycle Is a Source of Biosynthetic Precursors

Thus far, discussion has focused on the citric acid cycle as the major degradative pathway for the generation of ATP. As a major metabolic hub of the cell, the citric acid cycle also integrates many of the cell's other metabolic pathways, including those of carbohydrates, fats, amino acids, and porphyrins. This integration is aided by the fact that the cytoplasmic and mitochondrial pools of citric acid cycle components are shared, allowing the use of citric acid intermediates for biosyntheses taking place throughout the cell (**Figure 17.18**). For example, most of the carbon atoms in porphyrins come from succinyl CoA in a pathway that occurs both in the cytoplasm and mitochondria; fats are synthesized in the cytoplasm from mitochondrial citrate; and many of the amino acids, used throughout the cell, are derived from α-ketoglutarate and oxaloacetate. The details of these biosynthetic processes will be considered in subsequent chapters.

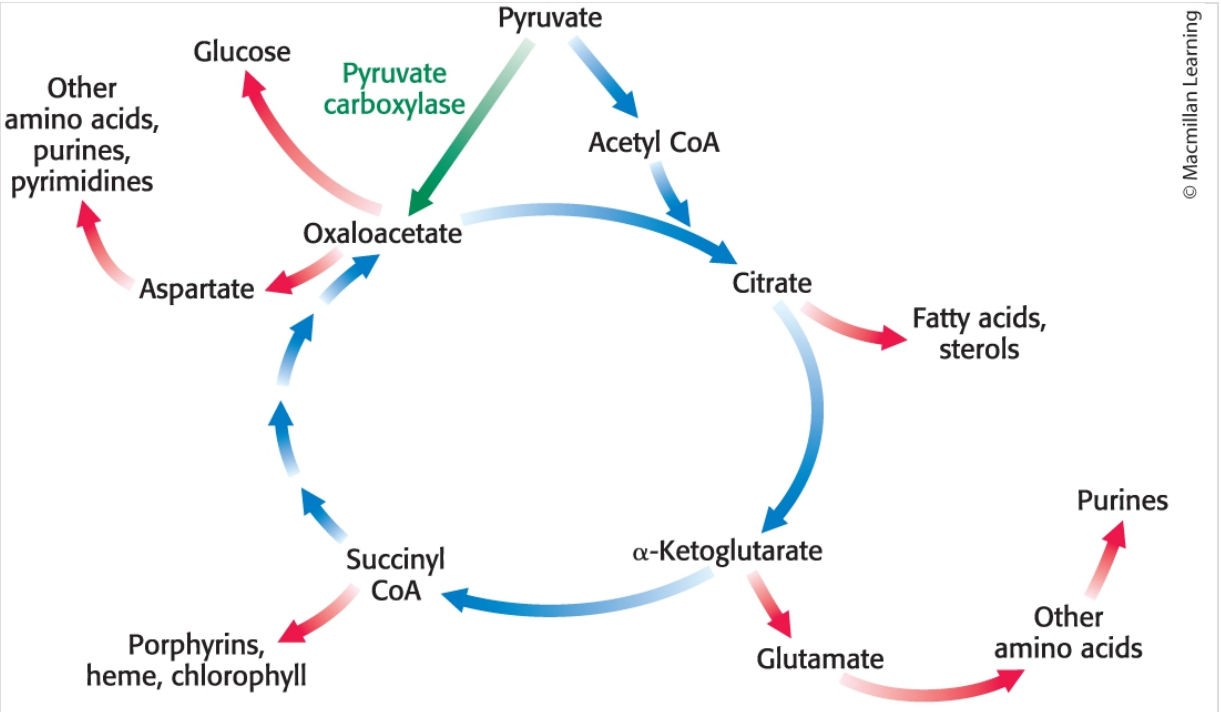


FIGURE 17.18 The citric acid cycle plays an important role in biosynthesis. Intermediates are drawn off for biosyntheses (shown by red arrows) when the energy needs of the cell are met. Intermediates are replenished by a variety of anaplerotic reactions, the most important of which is the formation of oxaloacetate from pyruvate by pyruvate carboxylase.

EXPLORE this pathway further in the Metabolic Map in Achieve

The citric acid cycle must be capable of being rapidly replenished

An important consideration is that citric acid cycle intermediates must be replenished if any are drawn off for biosyntheses. Suppose that much oxaloacetate is converted into amino acids for protein synthesis and, subsequently, the energy needs of the cell rise. The citric acid cycle will operate to a reduced extent unless new oxaloacetate is formed, because acetyl CoA cannot enter the cycle

unless it condenses with oxaloacetate. Even though oxaloacetate is recycled, a minimal level must be maintained to allow the cycle to function.

How is oxaloacetate replenished? Mammals lack the enzymes for the net conversion of acetyl CoA into oxaloacetate or any other citric acid cycle intermediate, so no matter how much acetyl CoA enters the cycle, there is never any *net* increase in the number of oxaloacetate molecules. Rather, oxaloacetate is formed by the carboxylation of pyruvate, in a reaction catalyzed by the biotin-dependent enzyme pyruvate carboxylase (Figure 17.18).

$$\text{Pyruvate} + CO_2 + \text{ATP} + H_2O \rightarrow \text{oxaloacetate} + \text{ADP} + P_i + 2H^+$$

Recall that this enzyme plays a crucial role in gluconeogenesis (Section 16.4). It is active only in the presence of acetyl CoA, which signifies the need for more oxaloacetate. If the energy charge is high, oxaloacetate is converted into glucose. If the energy charge is low, oxaloacetate replenishes the citric acid cycle. The synthesis of oxaloacetate by the carboxylation of pyruvate is an example of an **anaplerotic reaction** (*anaplerotic* is of Greek origin, meaning to "fill up"), a reaction that leads to the net synthesis, or replenishment, of pathway components. Note that because the citric acid cycle is a cycle, it can be replenished by the generation of any of the intermediates. For example, aspartate can be deaminated to also generate oxaloacetate. Glutamine is an especially important source of citric acid cycle intermediates in rapidly growing cells, including cancer cells. Glutamine is converted into glutamate and then into α-ketoglutarate (Section 23.5).

The disruption of pyruvate metabolism is the cause of beriberi and poisoning by mercury and arsenic



A neurologic and cardiovascular disorder known as **beriberi** is caused by a dietary deficiency of thiamine (also called *vitamin* B_1). The disease is prevalent in areas of the world where rice is the major food staple, because white rice has a rather low content of thiamine. This deficiency is partly overcome if the whole rice grain is soaked in water before milling, because some of the thiamine in the husk then leaches into the rice kernel. The problem is worsened if the rice is polished to remove the outer layer (that is, converted from brown to white rice), because only the outer layer contains significant amounts of thiamine. A common form of beriberi called *wet beriberi* is characterized by swelling in the abdomen and legs due to cardiac abnormalities.

Another form of beriberi, called *Wernicke's encephalopathy*, is also occasionally seen in alcoholics who are severely malnourished and thus thiamine deficient. The disease is characterized by neurologic and cardiac symptoms. Damage to the peripheral nervous system is expressed as pain in the limbs, weakness of the musculature, and distorted skin sensation. The heart may be enlarged and the cardiac output inadequate.

Which biochemical processes might be affected by a deficiency of thiamine? Thiamine is the precursor of the cofactor thiamine pyrophosphate (TPP). This cofactor is the prosthetic group of three important enzymes: pyruvate dehydrogenase, α-ketoglutarate

dehydrogenase, and transketolase. (Transketolase functions in the pentose phosphate pathway, which will be considered in Chapter 20.) The common feature of enzymatic reactions using TPP is the transfer of an activated aldehyde unit.

In patients with beriberi, the levels of pyruvate and α-ketoglutarate in the blood are higher than normal, and the increase in the level of pyruvate in the blood is especially pronounced after the ingestion of glucose. A related finding is that the activities of the pyruvate and α-ketoglutarate dehydrogenase complexes are abnormally low. The low transketolase activity of red blood cells in beriberi is an easily measured and reliable diagnostic indicator of the disease.

Why does TPP deficiency lead primarily to cardiac and neurological disorders? Heart tissue is highly sensitive to metabolic disruptions, as its need for ATP is never-ending and it has no appreciable stores of energy. The nervous system relies essentially on glucose as its only fuel. The product of glycolysis, pyruvate, can enter the citric acid cycle only through the pyruvate dehydrogenase complex. With that enzyme deactivated, the nervous system has no source of fuel. In contrast, most other tissues can use fats as a source of fuel for the citric acid cycle.

Symptoms similar to those of beriberi appear in organisms exposed to mercury or arsenite (AsO_3^{3-}). Both materials have a high affinity for neighboring (vicinal) sulfhydryls, such as those in the reduced dihydrolipoyl groups of the E_3 component of the pyruvate dehydrogenase complex (**Figure 17.19**). The binding of mercury or arsenite to the dihydrolipoyl groups inhibits the complex and leads to central nervous system pathologies. The proverbial phrase “mad as a hatter” refers to the strange behavior of poisoned hatmakers who used mercury nitrate, which is absorbed through the skin, to soften and shape animal furs. Similar symptoms afflicted the early

photographers, who used vaporized mercury to create daguerreotypes.

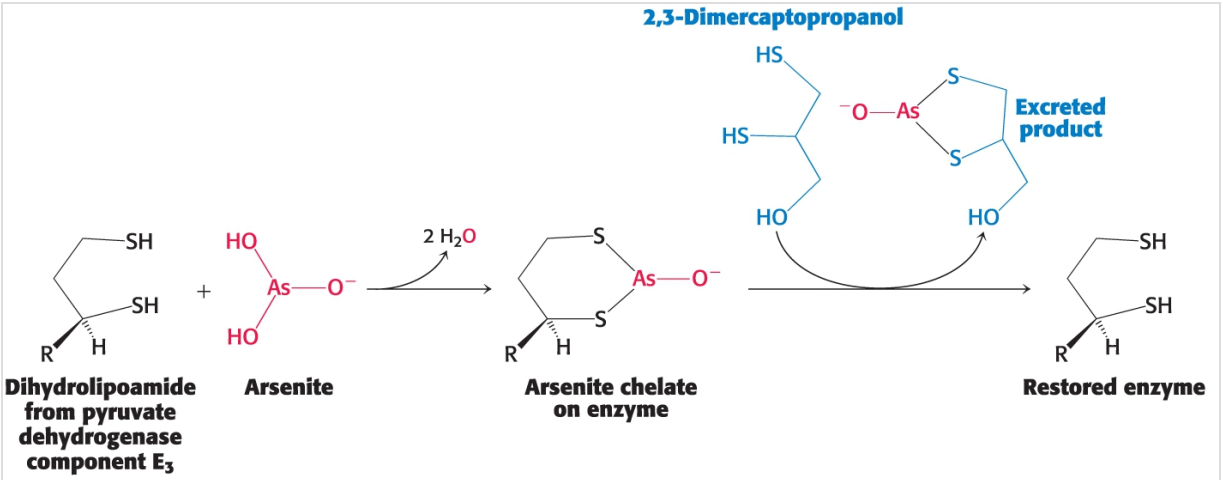


FIGURE 17.19 Arsenite inhibits the pyruvate dehydrogenase complex by inactivating the dihydrolipoamide component of the transacetylase. Some sulfhydryl reagents, such as 2,3-dimercaptoethanol, relieve the inhibition by forming a complex with the arsenite that can be excreted.

Treatment for these poisons is the administration of sulfhydryl reagents with adjacent sulfhydryl groups to compete with the dihydrolipoyl residues for binding with the metal ion. The reagent–metal complex is then excreted in the urine. Indeed, 2,3-dimercaptopropanol (Figure 17.19) was developed after World War I as an antidote to an arsenic-based chemical weapon.

The citric acid cycle likely evolved from preexisting pathways

How did the citric acid cycle come into being? Although definitive answers are elusive, informed speculation is possible. We can hypothesize how evolution might work at the level of biochemical pathways.

The citric acid cycle was most likely assembled from preexisting reaction pathways. As noted earlier, many of the intermediates formed in the citric acid cycle are used in metabolic pathways for amino acids and porphyrins. Thus, compounds such as pyruvate, α-ketoglutarate, and oxaloacetate were likely present early in evolution for biosynthetic purposes. The oxidative decarboxylation of these α-ketoacids is quite favorable thermodynamically and can be used to drive the synthesis of both acyl CoA derivatives and NADH. These reactions almost certainly formed the core of processes that preceded the citric acid cycle evolutionarily. Interestingly, α-ketoglutarate and oxaloacetate can be interconverted by transamination of the respective amino acids by aspartate aminotransferase, another key biosynthetic enzyme. Thus, cycles comprising smaller numbers of intermediates used for a variety of biochemical purposes could have existed before the present form evolved.

17.6 The Glyoxylate Cycle Enables Plants and Bacteria to Grow on Acetate

Acetyl CoA that enters the citric acid cycle has but one fate: oxidation to CO_2 and H_2O. The citric acid cycle cannot convert acetyl CoA into glucose. Although oxaloacetate, a key precursor to glucose, is formed in the citric acid cycle, the two decarboxylations that take place before the regeneration of oxaloacetate preclude the *net* conversion of acetyl CoA into glucose.

However, in plants and in some microorganisms, there is a metabolic pathway that allows the conversion of acetyl CoA generated from fat stores into glucose. This reaction sequence, called the **glyoxylate cycle**, is similar to the citric acid cycle in some ways but different in that it bypasses the two decarboxylation steps of the cycle. Another important difference is that two molecules of acetyl CoA enter per turn of the glyoxylate cycle, compared with one in the citric acid cycle.

The glyoxylate cycle (**Figure 17.20**), like the citric acid cycle, begins with the condensation of acetyl CoA and oxaloacetate to form citrate, which is then isomerized to isocitrate. Instead of being decarboxylated, as in the citric acid cycle, isocitrate is cleaved by isocitrate lyase into succinate and glyoxylate. The ensuing steps regenerate oxaloacetate from glyoxylate. First, acetyl CoA condenses with glyoxylate to form malate in a reaction catalyzed by malate synthase, and then malate is oxidized to oxaloacetate, as in the citric acid cycle. The sum of these reactions is

$$2\ \text{Acetyl CoA} + \text{NAD}^+ + 2\ \text{H}_2\text{O} \rightarrow \text{succinate} + 2\ \text{CoA} + \text{NADH} + 2\ \text{H}^+$$

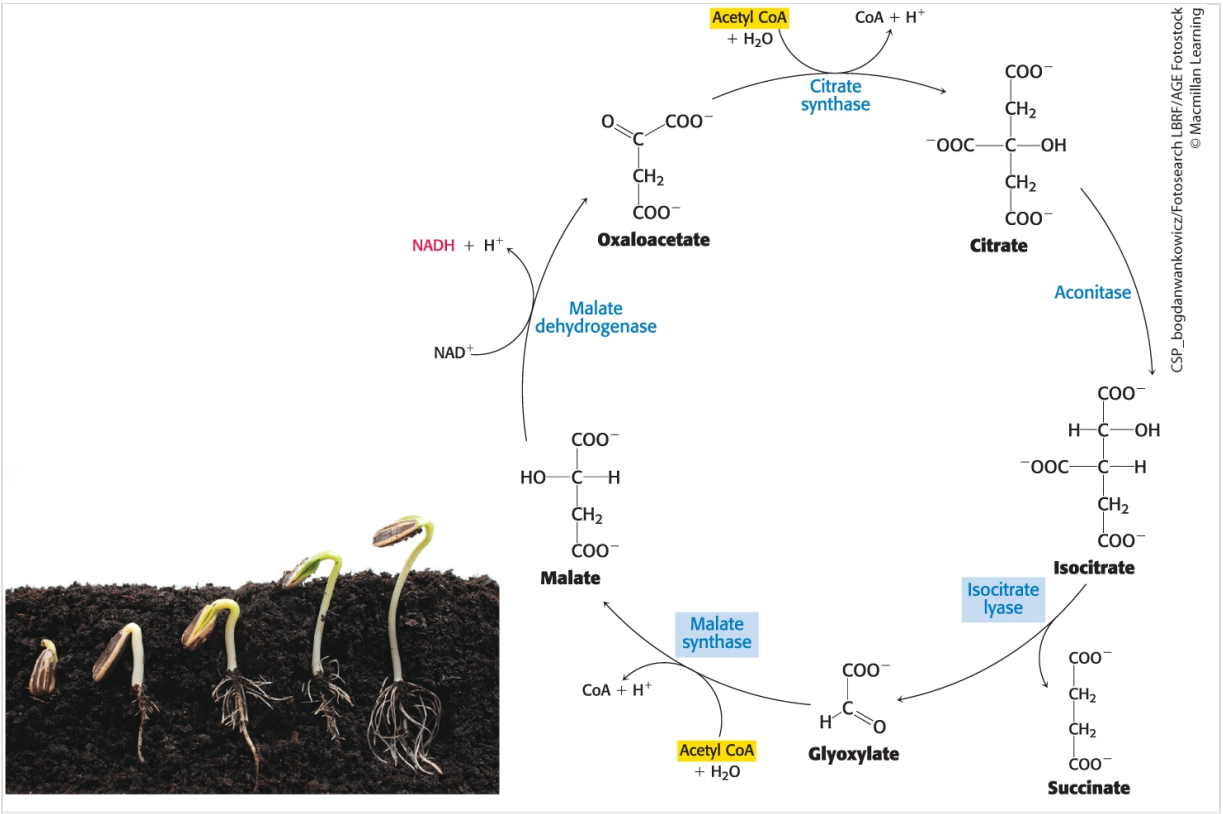


FIGURE 17.20 The glyoxylate cycle allows plants to use acetyl groups for biosynthesis. Plant seeds germinate using acetyl groups derived from stored triacylglycerides. The cycle bypasses the decarboxylation steps of the citric acid cycle and incorporates two acetyl groups per cycle. The reactions of this cycle are the same as those of the citric acid cycle except for the ones catalyzed by isocitrate lyase and malate synthase, which are boxed in blue.

The glyoxylate cycle is especially prominent in oil-rich seeds, such as those from sunflowers, cucumbers, and castor beans, where it takes place in organelles called **glyoxysomes**. Succinate, released midcycle, can be converted into carbohydrates by a combination of the citric acid cycle and gluconeogenesis. The carbohydrates power

seedling growth until the cell can begin photosynthesis. Thus, organisms with the glyoxylate cycle gain metabolic versatility because they can use acetyl CoA as a precursor of glucose and other biomolecules.



ZUMAPRESS.com/Keystone Pictures USA/AGE Fotostock

HANS KREBS The groundbreaking work of Hans Krebs, a German-born scientist of Jewish ancestry, resulted in his co-discoveries of the urea cycle (Chapter 23), the citric acid cycle (later named for him), and the glyoxylate cycle. Despite his tremendous successes, Krebs also experienced significant setbacks in his career. Foremost, following his work identifying the urea cycle as the first cyclic pathway in human metabolism, his life was upended when he was dismissed

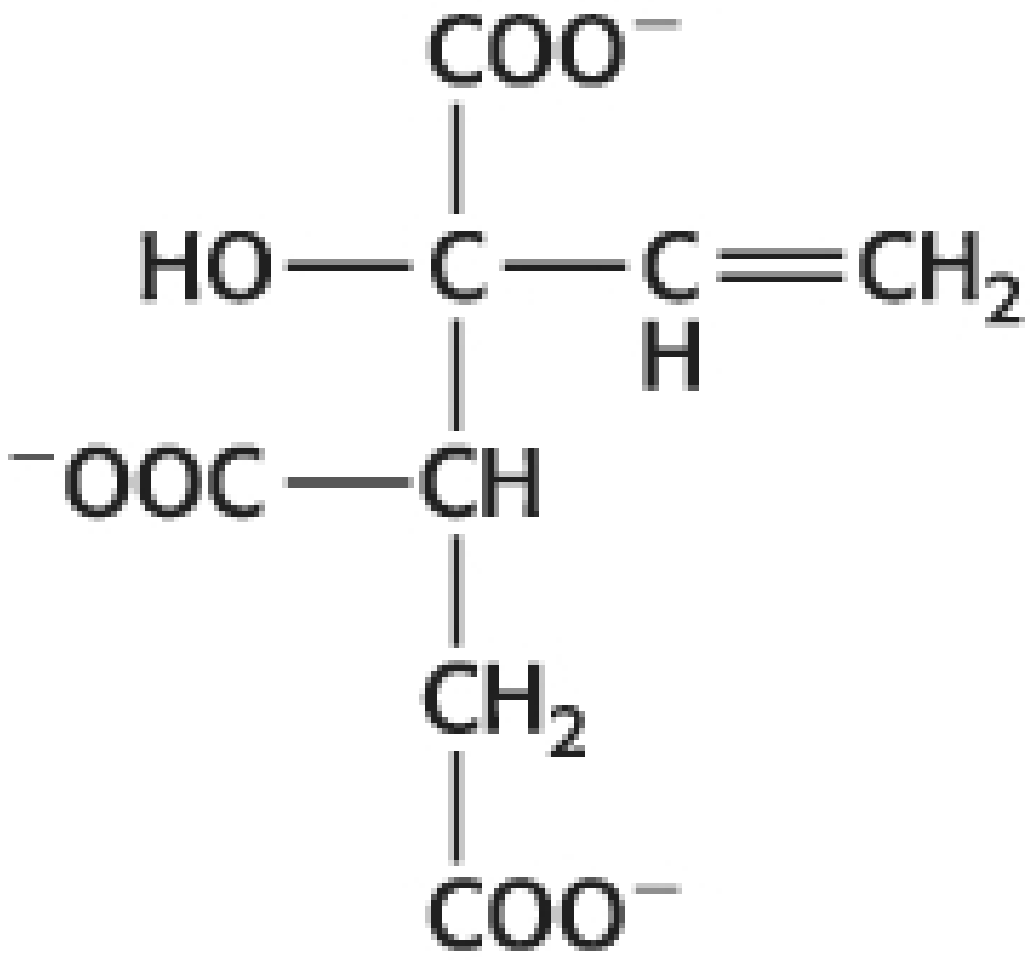
from his position by the Nazi Party in 1933. Then, after moving to the University of Cambridge, UK, his paper announcing the elucidation of the citric acid cycle was famously rejected from the journal *Nature*, in 1937. For the rest of his life he proudly showed the rejection letter to younger scientists to encourage them to persevere in the face of adversity. Finally, experiments in 1941 appeared to discredit his work on the citric acid cycle (see problem 18 at the end of the chapter). This issue plagued him until it was finally resolved by another investigator in 1948. In 1953 Krebs received the Nobel Prize in Physiology or Medicine for his work in determining the pathways of central metabolism.

Blocking the glyoxylate cycle may lead to new treatments for tuberculosis



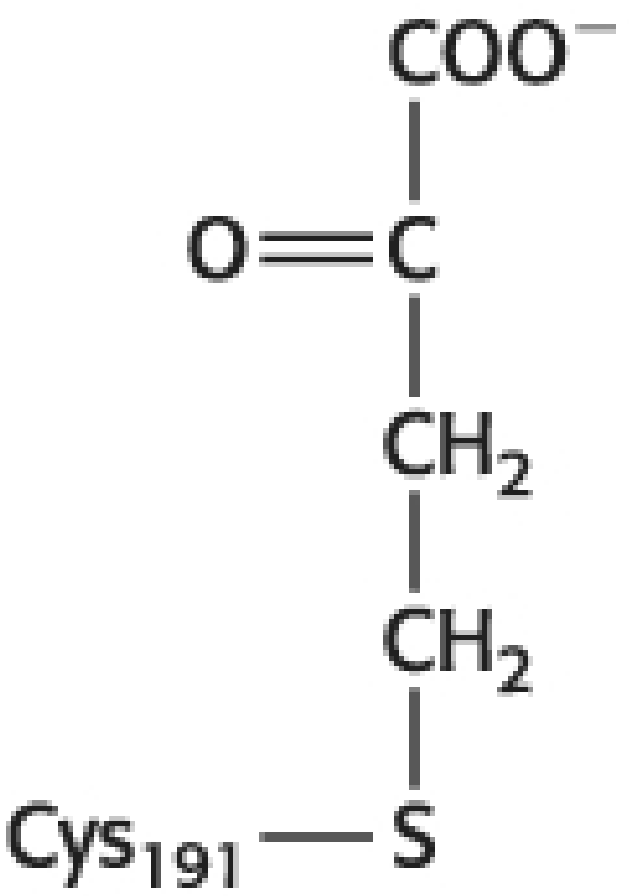
Tuberculosis (TB) is one of the leading causes of death throughout the world. In 2020, according to the World Health Organization, 10 million people contracted TB, including 1.1 million children, and 1.5 million people died from the disease. The bacterium responsible, *Mycobacterium tuberculosis*, is transmitted by people with active lung infections by coughing and sneezing. A common treatment for tuberculosis is the antibiotic rifampicin, an inhibitor of bacterial RNA synthesis (Chapter 31). However, strains of *M. tuberculosis* are developing resistance to rifampicin, so new treatments are urgently needed.

Some exciting new research suggests a possible treatment that relies on the bacterium's dependence on the glyoxylate cycle to convert fats to glucose, especially when in a latent (not actively dividing) state in the lungs. A suicide inhibitor or mechanism-based inhibitor (Section 5.6) for isocitrate lyase, 2-vinyl-isocitrate, has been synthesized that may halt the bacterium's metabolism.



2-Vinyl-isocitrate

During catalysis, a reactive thiolate is formed on $^{Cys}_{191}$ in the active site. When the lyase reacts with the inhibitor, succinate is released as in the normal reaction, but a thioether-linked homopyruvoyl moiety is covalently linked to $^{Cys}_{191}$, inhibiting the enzyme.



Homopyruvoyl-modified isocitrate lyase

This development may be an important opening into TB therapy because the active site $^{Cys}{}_{191}$ is conserved in all strains of *M. tuberculosis*, which reduces the likelihood of the development of resistance to the treatment. Although this research is quite new, it will be interesting to see if this ultimately leads to an effective medication for TB.

Chapter 17 Summary

17.1 The Citric Acid Cycle Harvests High-Energy Electrons

- The citric acid cycle is the final common pathway for the oxidation of fuel molecules and also serves as a source of building blocks for biosyntheses.
- Most fuel molecules enter the cycle as acetyl CoA.

17.2 The Pyruvate Dehydrogenase Complex Links Glycolysis to the Citric Acid Cycle

- The link between glycolysis and the citric acid cycle is the oxidative decarboxylation of pyruvate to form acetyl CoA by a massive three-enzyme complex.
- In eukaryotes, this reaction and those of the cycle take place inside mitochondria, in contrast with glycolysis, which takes place in the cytoplasm.

17.3 The Citric Acid Cycle Oxidizes Two-Carbon Units

- The cycle starts with the condensation of oxaloacetate and the acetyl unit of acetyl CoA to produce citrate (the citrate synthase reaction).
- Two carbon atoms from acetyl CoA leave the cycle as CO_2 in two successive decarboxylations catalyzed by isocitrate dehydrogenase and α-ketoglutarate dehydrogenase, resulting in the formation of succinyl CoA.
- The thioester bond of succinyl CoA is cleaved by orthophosphate to yield succinate, and a nucleoside trisphosphate is concomitantly generated.
- Succinate is oxidized to fumarate, which is then hydrated to form malate. Finally, malate is oxidized to regenerate a

molecule of oxaloacetate for the next round of the cycle.
- In the four oxidation–reduction reactions in the cycle, three pairs of electrons are transferred to NAD^+ and one pair to FAD.

  These reduced electron carriers are subsequently oxidized by the electron-transport chain to generate approximately nine additional molecules of ATP.
- A total of 10 molecules of ATP are generated for each two-carbon fragment that is completely oxidized to H_2O and CO_2.

17.4 Entry to the Citric Acid Cycle and Metabolism Through It Are Controlled

- The citric acid cycle operates only under aerobic conditions because it requires a supply of NAD^+ and FAD, which are

  regenerated in oxidative phosphorylation. Consequently, the rate of the citric acid cycle depends on the need for ATP.
- The irreversible formation of acetyl CoA from pyruvate is an important regulatory point: the activity of the pyruvate dehydrogenase complex is stringently regulated by reversible phosphorylation.
- In eukaryotes, two enzymes in the citric acid cycle are also important for regulation: isocitrate dehydrogenase and α-ketoglutarate dehydrogenase. Energy-rich molecules decrease the activities of these regulatory enzymes.
- These mechanisms complement each other in reducing the rate of formation of acetyl CoA when the energy charge of the cell is high and when biosynthetic intermediates are abundant.

17.5 The Citric Acid Cycle Is a Source of Biosynthetic Precursors

- When the cell has adequate energy available, the citric acid cycle can provide a source of building blocks for a host of important biomolecules, such as nucleotide bases, proteins, and heme groups. This use depletes the cycle of intermediates.

- When the cycle again needs to metabolize fuel, anaplerotic reactions replenish the cycle intermediates.

17.6 The Glyoxylate Cycle Enables Plants and Bacteria to Grow on Acetate

- The glyoxylate cycle enables plants and bacteria to subsist on acetate because it bypasses the two decarboxylation steps of the citric acid cycle.
- The glyoxylate cycle is especially prominent in oil-rich seeds where it takes place in glyoxysomes. The succinate produced can be converted into carbohydrates by a combination of the citric acid cycle and gluconeogenesis.

Key Terms

citric acid (tricarboxylic acid, TCA; Krebs) cycle (CAC)
acetyl CoA
pyruvate dehydrogenase complex
flavoprotein
iron–sulfur protein (nonheme iron protein)
α-ketoglutarate dehydrogenase complex
nucleoside diphosphokinase
anaplerotic reaction
beriberi
glyoxylate cycle
glyoxysome

Problems

1. Write the reaction that links glycolysis and the citric acid cycle. What is the enzyme that catalyzes the reaction? 1

2. Which of the following catalytic cofactors are required by the pyruvate dehydrogenase complex?

a. NAD^+, lipoic acid, thiamine pyrophosphate

b. NAD^+, biotin, thiamine pyrophosphate

c. NAD^+, FAD, lipoic acid

d. FAD, lipoic acid, thiamine pyrophosphate

3. The pyruvate dehydrogenase complex is mechanistically and structurally similar to which of the following?

a. Isocitrate dehydrogenase
b. α-Ketoglutarate dehydrogenase
c. Glyceraldehyde 3-phosphate dehydrogenase
d. Fumarase

4. What coenzymes are required by the pyruvate dehydrogenase complex? What are their roles? 1

5. Distinguish between catalytic coenzymes and stoichiometric coenzymes in the pyruvate dehydrogenase complex.

6. What is the $\Delta G^{\circ\prime}$ for the complete oxidation of the acetyl unit of acetyl CoA by the citric acid cycle?

7. Patients with pyruvate dehydrogenase deficiency show high levels of lactic acid in the blood. However, in some cases,

treatment with dichloroacetate (DCA), which inhibits the kinase associated with the pyruvate dehydrogenase complex, lowers lactic acid levels. 2

a. How does DCA act to stimulate pyruvate dehydrogenase activity?
b. What does this suggest about pyruvate dehydrogenase activity in patients who respond to DCA?

8.

a. Predict the effect of a mutation that enhances the activity of the kinase associated with the pyruvate dehydrogenase complex. 2
b. Predict the effect of a mutation that reduces the activity of the phosphatase associated with the pyruvate dehydrogenase complex.

9. Match each term with its description.

1. Acetyl CoA
2. Citric acid cycle
3. Pyruvate dehydrogenase complex
4. Thiamine pyrophosphate
5. Lipoic acid

1. Catalyzes the link between glycolysis and the citric acid cycle
2. Coenzyme required by transacetylase
3. Final product of pyruvate dehydrogenase
4. Catalyzes the formation of acetyl CoA
5. Regenerates active transacetylase
6. Fuel for the citric acid cycle

6. Pyruvate dehydrogenase
7. Acetyllipoamide
8. Dihydrolipoyl transacetylase
9. Dihydrolipoyl dehydrogenase
10. Beriberi

7. Coenzyme required by pyruvate dehydrogenase
8. Catalyzes the oxidative decarboxylation of pyruvate
9. Due to a deficiency of thiamine
10. Central metabolic hub

---

10. Match each enzyme with its description.

1. Pyruvate dehydrogenase complex
2. Citrate synthase
3. Aconitase
4. Isocitrate dehydrogenase
5. α-Ketoglutarate dehydrogenase
6. Succinyl CoA synthetase
7. Succinate dehydrogenase
8. Fumarase

1. Catalyzes the formation of isocitrate
2. Synthesizes succinyl CoA
3. Generates malate
4. Generates ATP
5. Converts pyruvate into acetyl CoA
6. Converts pyruvate into oxaloacetate
7. Condenses oxaloacetate and acetyl CoA
8. Catalyzes the formation of oxaloacetate

9. Malate dehydrogenase	9. Synthesizes fumarate
10. Pyruvate carboxylase	10. Catalyzes the formation of α-ketoglutarate

---

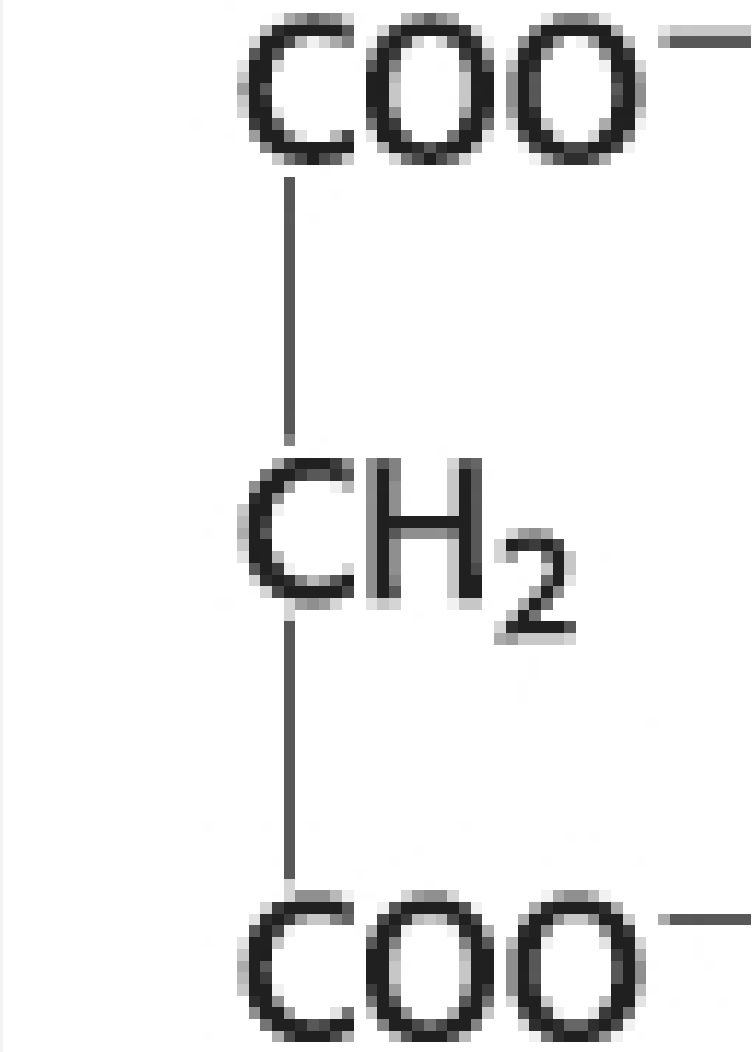
11. How is succinate dehydrogenase unique compared with the other enzymes in the citric acid cycle?

12. The oxidation of malate by NAD^+ to form oxaloacetate is a highly endergonic reaction under standard conditions [$\Delta G^{\circ\prime} = 29\ kJ\ mol^{-1}\ (7\ kcal\ mol^{-1})$]. The reaction proceeds readily under physiological conditions. 4

a. Explain why the reaction proceeds as written under physiological conditions.
b. Assuming an $[NAD^+]/[NADH]$ ratio of 8 and a pH of 7, what is the lowest [malate]/[oxaloacetate] ratio at which oxaloacetate can be formed from malate?

13. It is possible, with the use of the reactions and enzymes considered in this chapter, to convert pyruvate into α-ketoglutarate without depleting any of the citric acid cycle components. Write a balanced reaction scheme for this conversion, showing cofactors and identifying the required enzymes. 6

14. Malonate is a competitive inhibitor of succinate dehydrogenase. How will the concentrations of citric acid cycle intermediates change immediately after the addition of malonate? Why is malonate not a substrate for succinate dehydrogenase?



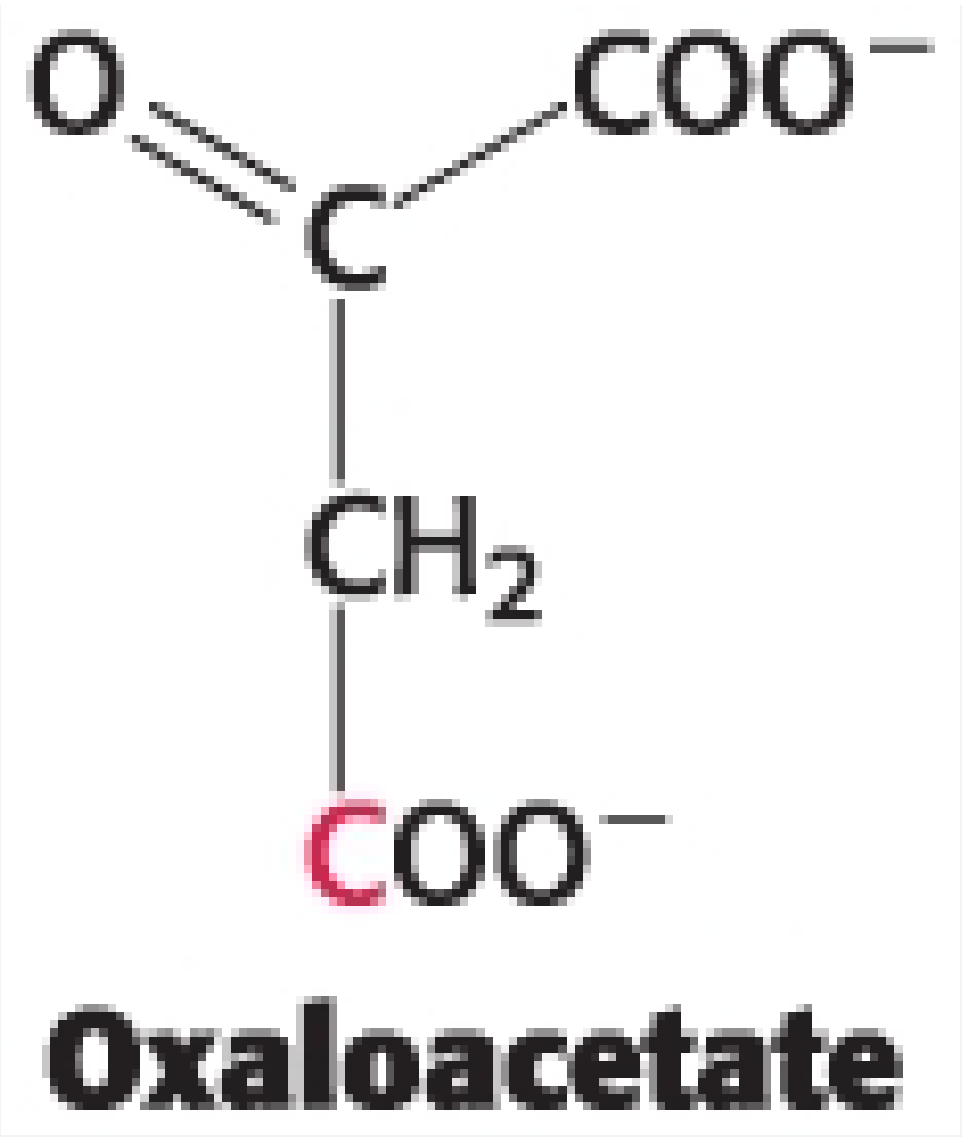
Malonate

15. What is the chief benefit of being able to perform the glyoxylate cycle? 7

16. Fats are usually metabolized into acetyl CoA and then further processed through the citric acid cycle. In Chapter 16, we saw that glucose can be synthesized from oxaloacetate, a citric acid cycle intermediate. Why, then, after a long bout of exercise depletes our carbohydrate stores, do we need to replenish those stores by eating carbohydrates? Why do we not simply replace them by converting fats into carbohydrates?

17. As we will see (Chapter 22), fatty acid breakdown generates a large amount of acetyl CoA. What will be the effect of fatty acid breakdown on pyruvate dehydrogenase complex activity? On glycolysis? 2

18. In experiments carried out in 1941 to investigate the citric acid cycle, oxaloacetate labeled with ^{14}C in the carboxyl carbon atom farthest from the keto group was introduced to an active preparation of mitochondria.



Analysis of the α-ketoglutarate formed showed that none of the radioactive label had been lost. Decarboxylation of α-ketoglutarate then yielded succinate devoid of radioactivity. All the label was in the released CO_2.

a. Why were the early investigators of the citric acid cycle surprised that *all* the label emerged in the CO_2? (*Note: you should answer this question first before reading any further.*)
b. The interpretation of these experiments was that citrate (or any other symmetric compound) cannot be an intermediate in the formation of α-ketoglutarate, because of the asymmetric fate of the label, thus appearing to disprove Hans Krebs's assertions about the cycle. This view seemed compelling until Alexander Ogston incisively pointed out in 1948 that "it is possible that an asymmetric enzyme which attacks a symmetrical compound can distinguish between its identical groups." For simplicity, consider a molecule in which two hydrogen atoms, a group X and a different group Y, are bonded to a tetrahedral carbon atom as a model for citrate. Explain how a symmetric molecule can react with an enzyme in an asymmetric way.

19. As will become clearer in Chapter 18, the activity of the citric acid cycle can be monitored by measuring the amount of O_2 consumed. The greater the rate of O_2 consumption, the faster the rate of the cycle. Hans Krebs used this assay to investigate the cycle in 1937. He used as his experimental system minced pigeon-breast muscle, which is rich in mitochondria. In one set of experiments, Krebs measured the O_2 consumption in the presence of carbohydrate only and in the presence of carbohydrate and citrate. The results are shown in the following table. 5

Effect of citrate on oxygen consumption by minced pigeon-breast muscle

	Micromoles of oxygen consumed	
Time (min)	**Carbohydrate only**	**Carbohydrate plus 3 µmol of citrate**
10	26	28
60	43	62
90	46	77
150	49	85

a. How much O_2 would be absorbed if the added citrate were completely oxidized to H_2O and CO_2?
b. On the basis of your answer to part (a), what do the results given in the table suggest?

20. The bacterium *Mycobacterium tuberculosis*, the cause of tuberculosis, can invade the lungs and persist in a latent state for years. During this time, the bacteria reside in granulomas — nodular scars containing bacteria and host-cell debris in the center and surrounded by immune cells. The granulomas are lipid-rich, oxygen-poor environments. How these bacteria manage to persist is something of a mystery. The results of research suggest that the glyoxylate cycle is required for the persistence. The following data show the amount of bacteria, presented as colony-forming units (cfu), in mice lungs in the weeks after an infection. 7



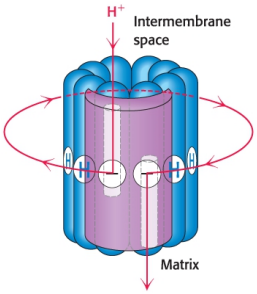
In graph A, the black circles represent the results for wild-type bacteria and the red circles represent the results for bacteria from which the gene for isocitrate lyase was deleted.

a. What is the effect of the absence of isocitrate lyase?

The techniques described in Chapter 9 were used to reinsert the gene encoding isocitrate lyase into bacteria from which it had previously been deleted. In graph B, black circles represent bacteria into which the gene was reinserted and red circles represent bacteria in which the gene was still missing.

b. Do these results support those obtained in part (a)?
c. What is the purpose of the experiment in part (b)?
d. Why do these bacteria perish in the absence of the glyoxylate cycle?

Chapter 18
Oxidative Phosphorylation





Melvyn Longhurst/Corbis Documentary/Getty Images
© Macmillan Learning

Waterwheels capture and convert the kinetic energy of water by rotating a wheel which spins a central axis, or rotor. While humans have used waterwheels for millennia to mill grains and accomplish many other tasks, nature beat humans in the race to develop a rotational motor by at least 1.5 billion years, prior to the divergence of eukaryotes and prokaryotes. Remarkably, ATP synthase, the final complex of the mitochondrial respiratory machinery, uses the flow of protons across a membrane to spin a protein wheel and rotor to generate ATP. This enzyme is the world's smallest rotary motor.

Outline

18.1 Cellular Respiration Drives ATP Formation by Transferring Electrons to Molecular Oxygen
18.2 Oxidative Phosphorylation Depends on Electron Transfer

18.3 The Respiratory Chain Consists of Four Complexes: Three Proton Pumps and a Physical Link to the Citric Acid Cycle
18.4 A Proton Gradient Powers the Synthesis of ATP
18.5 Many Shuttles Allow Movement Across Mitochondrial Membranes
18.6 The Regulation of Cellular Respiration Is Governed Primarily by the Need for ATP
18.7 Proton Gradients Generated by Respiratory Chains Drive Many Biochemical Processes

---

Learning Goals



By the end of this chapter, you should be able to:

1. Describe the key components of the electron-transport chain and how they are arranged.
2. Explain the benefits of having the electron-transport chain located in a membrane.
3. Describe how the proton-motive force is converted into ATP.
4. Identify the ultimate determinant of the rate of cellular respiration.

The amount of ATP that human beings require to go about their lives is staggering: a sedentary person of 70 kg (154 lbs) requires about 8400 kJ (2000 kcal) for a day's worth of activity. To provide this much energy requires 83 kg of ATP. However, human beings possess only about 250 g of ATP at any given moment.

The disparity between the amount of ATP that we have and the amount that we require is compensated by recycling ADP back to ATP. Each ATP molecule is recycled approximately 300 times per day. This recycling takes place primarily through oxidative

phosphorylation. The process of oxidative phosphorylation finally completes the capture of chemical energy from glucose and its derivatives that originated with glycolysis.

18.1 Cellular Respiration Drives ATP Formation by Transferring Electrons to Molecular Oxygen

We begin our study of **oxidative phosphorylation** by examining the oxidation–reduction reactions that allow the flow of electrons from NADH and $FADH_2$ to oxygen. The electron flow takes place in four large protein complexes that are embedded in the inner mitochondrial membrane, together called the **respiratory chain** or the **electron-transport chain**.

$$NADH + {}^1/_2O_2 + H^+ \rightarrow H_2O + NAD^+$$
$$\Delta G^{\circ\prime} = -220.1\ \text{kJ mol}^{-1} (-52.6\ \text{kcal mol}^{-1})$$

The overall reaction is exergonic. Importantly, three of the complexes of the electron-transport chain use the energy released by the electron flow to pump protons out of the mitochondrial matrix. In essence, energy is transformed. The resulting unequal distribution of protons generates a pH gradient and a transmembrane electrical potential that creates a **proton-motive force**. ATP is synthesized when protons flow back to the mitochondrial matrix through an enzyme complex.

$$ADP + P_i + H^+ \rightarrow ATP + H_2O$$
$$\Delta G^{\circ\prime} = +30.5\ \text{kJ mol}^{-1} (+7.3\ \text{kcal mol}^{-1})$$

Thus, the oxidation of fuels and the phosphorylation of ADP are coupled by a proton gradient across the inner mitochondrial membrane (**Figure**

18.1). Collectively, the generation of high-transfer-potential electrons by the citric acid cycle, their flow through the respiratory chain, and the accompanying synthesis of ATP is called **respiration** or **cellular respiration**.

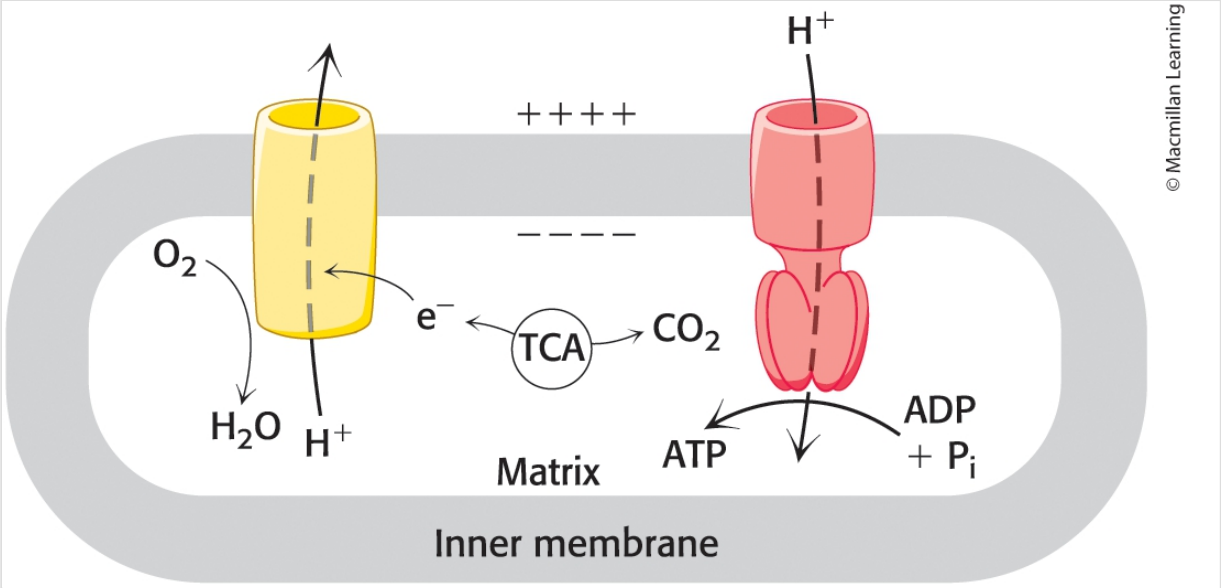


FIGURE 18.1 Oxidative phosphorylation is fundamentally the combination of two processes. Oxidation and ATP synthesis are coupled by transmembrane proton fluxes. Electrons from NADH and $FADH_2$, formed in the TCA cycle, flow through the electron-transport chain to reduce oxygen to water (yellow cylinder). Some components of the chain pump protons from the mitochondrial matrix to the intermembrane space. The protons return to the matrix by flowing through another protein complex, ATP synthase (red structure), powering the synthesis of ATP.

Eukaryotic oxidative phosphorylation takes place in mitochondria

Recall that a biochemical role of the citric acid cycle, which takes place in the mitochondrial matrix, is the generation of high-energy electrons. It is fitting, therefore, that oxidative phosphorylation, which will utilize

the energy of these electrons to create ATP, also takes place in mitochondria.

Electron microscopic studies revealed that mitochondria have two membranes: an *outer membrane* and an extensive, highly folded *inner membrane.* Hence, there are two compartments in mitochondria: (1) the **intermembrane space (IM space)** between the outer and the inner membranes and (2) the **matrix**, which is bounded by the inner membrane (**Figure 18.2**). The mitochondrial matrix is the site of most of the reactions of the citric acid cycle and fatty acid oxidation, whereas oxidative phosphorylation takes place in the inner mitochondrial membrane.

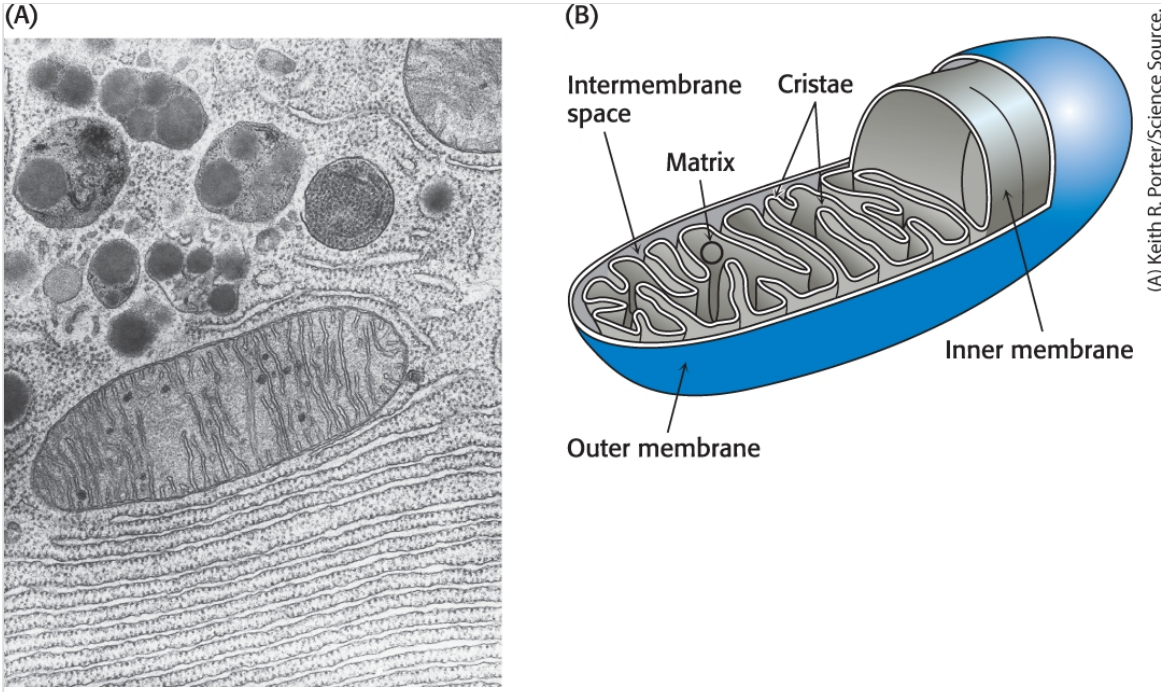


FIGURE 18.2 Mitochondria are bound by a double membrane, which creates two distinct internal compartments. (A) An electron micrograph and (B) a diagram of a mitochondrion. Mitochondria are oval-shaped organelles, typically ~2 μm in length and 0.5 μm in diameter, or approximately the size of a bacterium.

The inner membrane is folded into a series of internal ridges and tube-like structures collectively called *cristae*. The increase in surface area of the inner mitochondrial membrane provided by the cristae creates more sites for oxidative phosphorylation than would be the case with a simple, unfolded membrane. Humans contain an estimated $14{,}000\ m^2$ of inner mitochondrial membrane, which is the approximate equivalent of three football fields in the United States.

The outer membrane is quite permeable to most small molecules and ions because it contains mitochondrial porin, a 30- to 35-kDa pore-forming protein also known as VDAC, for voltage-dependent anion channel. VDAC, the most prevalent protein in the outer mitochondrial membrane, plays a role in the regulated flux of metabolites — usually anionic species such as phosphate, chloride, organic anions, and the adenine nucleotides — across the outer membrane. In contrast, the inner membrane is impermeable to nearly all ions and polar molecules. A large family of transporters shuttles metabolites such as ATP, pyruvate, and citrate across the inner mitochondrial membrane. The two faces of this membrane will be referred to as the *matrix side* and the *cytoplasmic side* (the latter because it is freely accessible to most small molecules in the cytoplasm). They are also called the *N* and *P* sides, respectively, because the membrane potential is negative on the matrix side and positive on the cytoplasmic side (Figure 18.1).

In bacteria, the electron-driven proton pumps and ATP-synthesizing complexes are located in the cytoplasmic membrane, the inner of two membranes. In many bacteria, the outer membrane, like that of mitochondria, is permeable to most small metabolites because of the presence of porins.

Mitochondria are the result of an endosymbiotic event

Mitochondria are semiautonomous organelles that live in an endosymbiotic relationship with the host cell. These organelles contain their own DNA, which encodes a variety of different proteins and RNAs. The genomes of mitochondria range broadly in size across species. Human mitochondrial DNA comprises 16,569 bp and encodes 13 respiratory-chain proteins as well as the small and large ribosomal RNAs and enough tRNAs to translate all codons. However, mitochondria also contain many proteins encoded by nuclear DNA. Cells that contain mitochondria depend on these organelles for oxidative phosphorylation, and the mitochondria in turn depend on the cell for their very existence. How did this intimate symbiotic relationship come to exist?

It is now well established that an endosymbiotic event occurred in the evolution of eukaryotic organisms in which a free-living organism capable of oxidative phosphorylation was engulfed by another cell. Formerly a hypothesis famously championed by biologist Lynn Margulis, this explanation of the origins of both mitochondria and chloroplasts is now widely accepted as the *endosymbiotic theory*. The shape, size, double-membrane, and circular DNA (with exceptions) all resemble characteristics of some gram-negative bacteria; however, it is the evidence from DNA sequences that is conclusive. Thanks to the rapid accumulation of sequence data for mitochondrial and bacterial genomes, speculation on the origin of the first mitochondrion with some authority is now possible. The most mitochondrial-like bacterial genome is that of *Rickettsia prowazekii,* the cause of louse-borne typhus. The genome for this organism is more than 1 million base pairs in size and contains 834 protein-encoding genes. Sequence data suggest that all extant mitochondria are derived from an ancestor of *R. prowazekii* as the result of a single endosymbiotic event.



Nancy R. Schiff/Getty Images

LYNN MARGULIS The concept of an endosymbiotic origin for mitochondria and chloroplasts, first proposed over a century ago, was quite controversial for decades. In 1967, Professor Lynn Margulis (then Lynn Sagan) published a 50-page paper, “On the Origin of Mitosing Cells,” with an extensive analysis of the characteristics of different groups of unicellular organisms and possible endosymbiotic events. She and others continued to collect evidence to support the claims in the paper, but the scientific community remained skeptical of the endosymbiosis hypothesis for many

years. Eventually, many lines of evidence came together to support the conclusion that chloroplasts and mitochondria each arose from independent endosymbiotic events more than 1 billion years ago. Margulis received the National Medal of Science in 1999 and has been described as a “vindicated heretic.”

The evidence that modern mitochondria result from a single event comes from examination of the most bacteria-like mitochondrial genome, that of the protozoan *Reclinomonas americana.* Its genome contains 97 genes, of which 62 specify proteins. The genes encoding these proteins include all of the protein-coding genes found in all of the sequenced mitochondrial genomes. Yet, this genome encodes less than 2% of the protein-coding genes in the bacterium *E. coli.* In other words, a small fraction of bacterial genes — 2% — is found in all examined mitochondria.

How is it possible that all mitochondria have the same 2% of the bacterial genome? It seems unlikely that mitochondrial genomes resulting from several endosymbiotic events could have been independently reduced to the same set of genes found in *R. americana.* What was the fate of the mitochondrial genes no longer harbored by the mitochondria? The reduced genomes of the mitochondria are the result of endosymbiotic gene transfer, in which the mitochondrial genes became part of the nuclear genome. Thus, the original bacterial cell lost DNA, making it incapable of independent living, and the host cell became dependent on the ATP generated by its tenant.

Self-Check Question



Name the cellular compartments and membranes, in order, that a molecule passes through when traveling from the cytosol into the center of a mitochondrion. Additionally, what are the ridges and tube-like structures in a mitochondrion called, and what membrane are they made from?

18.2 Oxidative Phosphorylation Depends on Electron Transfer

In Chapter 17, the generation of NADH and $FADH_2$ by the oxidation of acetyl CoA was identified as an important function of the citric acid cycle. In oxidative phosphorylation, electrons from NADH and $FADH_2$ are used to reduce molecular oxygen to water. The highly exergonic reduction is accomplished by a number of electron-transfer reactions, which take place in a set of membrane proteins known as the electron-transport chain.

The electron-transfer potential of an electron is measured as redox potential

In oxidative phosphorylation, the *electron*-transfer potential of NADH or $FADH_2$ is converted into the *phosphoryl*-transfer potential of ATP. To better understand this conversion, we need quantitative expressions for these forms of free energy. The measure of phosphoryl-transfer potential is already familiar to us: it is given by $\Delta G^{\circ\prime}$ for the hydrolysis of the activated phosphoryl compound. The corresponding expression for the electron-transfer potential is E'_0, the **reduction potential** (also called the **redox potential** or **oxidation–reduction potential**).

Consider a substance that can exist in an oxidized form X and a reduced form X^-. Such a pair is called a *redox couple* and is designated $X : X^-$. The reduction potential of this couple can be determined by measuring the electromotive force generated by an apparatus called a *sample half-cell* connected to a *standard reference half-cell* (**Figure 18.3**). The sample half-cell consists of an electrode immersed in a solution of 1 M oxidant (X) and 1 M reductant (X^-). The standard reference half-cell consists of an electrode immersed in a $1\ M\ H^+$ solution that is in equilibrium with H_2 gas at 1 atm of pressure. The electrodes are connected to a voltmeter, and an agar bridge allows ions to move from one half-cell to the other, establishing electrical continuity between the half-cells. Electrons then flow from one half-cell to the other through the wire connecting the two half-cells to the voltmeter. If the reaction proceeds in the direction

$$X^- + H^+ \rightarrow X + {}^1/_2\ H_2$$

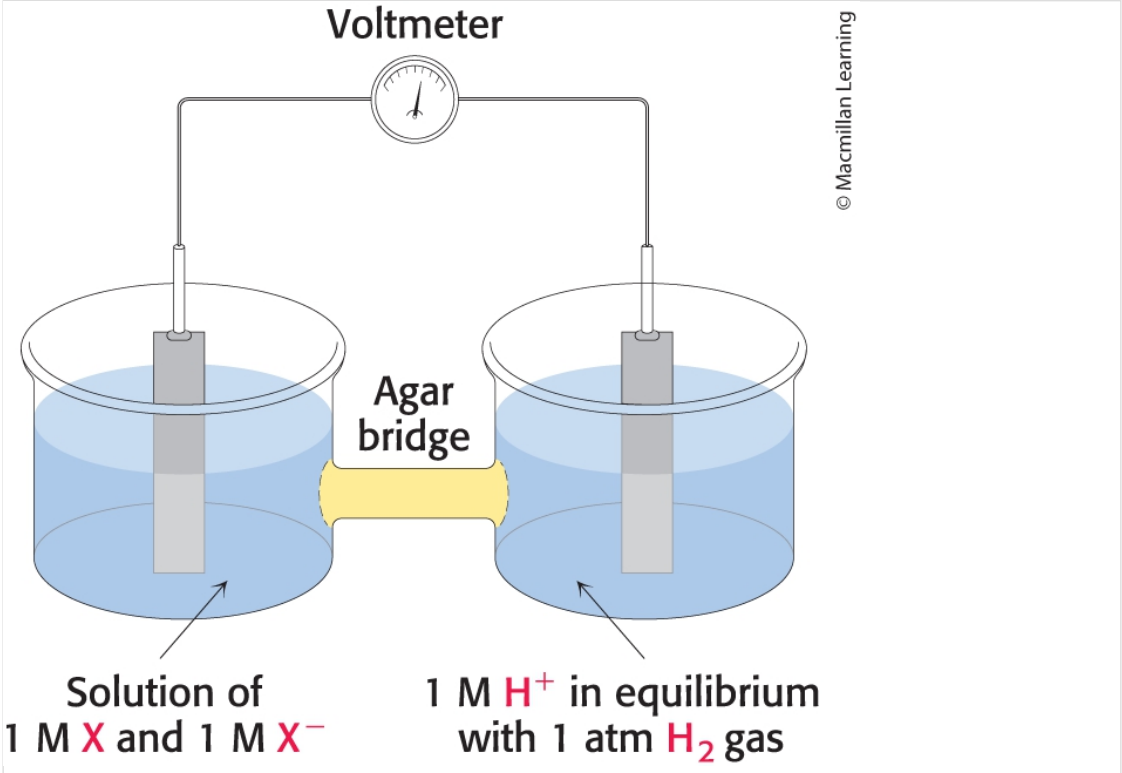


FIGURE 18.3 Redox potential can be precisely measured. In the apparatus for the measurement of the standard oxidation–reduction potential of a redox couple, electrons flow through the wire connecting the cells, whereas ions flow through the agar bridge.

the reactions in the half-cells (referred to as *half-reactions* or *couples*) must be

$$X^- \rightarrow X + e^- \qquad H^+ + e^- \rightarrow \tfrac{1}{2} H_2$$

Thus, electrons flow from the sample half-cell to the standard reference half-cell, and the sample-cell electrode is taken to be negative with respect to the standard-cell electrode. The reduction potential of the $X : X^-$ couple is the observed voltage at the start of the experiment (when X, X^-, and H^+ are 1 M with 1 atm of H_2). The reduction potential of the $H^+ : H_2$ couple is defined to be 0 volts. In oxidation–reduction reactions, the donor of electrons, in this case X^-, is called the *reductant* or *reducing agent*, whereas the acceptor of electrons, H^+ here, is called the *oxidant* or *oxidizing agent*.

The meaning of the reduction potential is now evident. A negative reduction potential means that the oxidized form of a substance has lower affinity for electrons than does H_2, as in the preceding example. A positive reduction potential means that the oxidized form of a substance has higher

affinity for electrons than does H_2. These comparisons refer to standard conditions — namely, 1 M oxidant, 1 M reductant, $1\ M\ H^+$, and 1 atm H_2. Thus, a strong reducing agent (such as NADH) is poised to donate electrons and has a negative reduction potential, whereas a strong oxidizing agent (such as O_2) is ready to accept electrons and has a positive reduction potential.

The reduction potentials of many biologically important redox couples are known (**Table 18.1**). Table 18.1 is like those presented in chemistry textbooks, except that a hydrogen ion concentration of $10^{-7}\ M$ (pH 7) instead of 1 M (pH 0) is the standard state adopted by biochemists. This difference is denoted by the prime in E'_0. Recall that the prime in $\Delta G^{\circ\prime}$ denotes a standard free-energy change at pH 7.

TABLE 18.1 Standard reduction potentials of some reactions

Oxidant	Reductant	*n*	E'_0 (V)
Succinate + CO_2	α-Ketoglutarate	2	−0.67
Acetate	Acetaldehyde	2	−0.60
Ferredoxin (oxidized)	Ferredoxin (reduced)	1	−0.43
$2\ H^+$	H_2	2	−0.42
NAD^+	$NADH + H^+$	2	−0.32
$NADP^+$	$NADPH + H^+$	2	−0.32
Lipoate (oxidized)	Lipoate (reduced)	2	−0.29
Glutathione (oxidized)	Glutathione (reduced)	2	−0.23
FAD	$FADH_2$	2	−0.22
Acetaldehyde	Ethanol	2	−0.20
Pyruvate	Lactate	2	−0.19

TABLE 18.1 Standard reduction potentials of some reactions

$2\ H^+$	H_2	2	0.00[1]
Fumarate	Succinate	2	−0.03
Cytochrome *b* $(+3)$	Cytochrome *b* $(+2)$	1	+0.07
Dehydroascorbate	Ascorbate	2	+0.08
Ubiquinone (oxidized)	Ubiquinone (reduced)	2	+0.10
Cytochrome *c* $(+3)$	Cytochrome *c* $(+2)$	1	+0.22
Fe $(+3)$	Fe $(+2)$	1	+0.77
$\frac{1}{2}\ O_2 + 2\ H^+$	H_2O	2	+0.82

Note: E'_0 is the standard oxidation–reduction potential (pH 7, 25°C), and *n* is the number of electrons transferred. E'_0 refers to the partial reaction written as $\text{Oxidant} + e^- \rightarrow \text{reductant}$.

[1] Standard oxidation − reduction potential at $pH = 0$. Compare with $E'_0 = -0.42$ at $pH = 7$.

The standard free-energy change $\Delta G^{\circ\prime}$ is related to the change in reduction potential $\Delta E'_0$ by

$$\Delta G^{\circ\prime} = -nF\Delta E'_0 \tag{1}$$

in which *n* is the number of electrons transferred, *F* is a proportionality constant called the *Faraday constant* ($96.48\ \text{kJ mol}^{-1}\text{V}^{-1}$ or $23.06\ \text{kcal mol}^{-1}\text{V}^{-1}$), $\Delta E'_0$ is in volts, and $\Delta G^{\circ\prime}$ is in kilojoules or kilocalories per mole.

The free-energy change of an oxidation–reduction reaction can be readily calculated from the reduction potentials of the reactants.

Example

Calculating the Standard Free Energy of a Reaction from Reduction Potentials

Problem:

Calculate $\Delta G^{\circ\prime}$ for the reduction of pyruvate by NADH, catalyzed by lactate dehydrogenase. Recall that this reaction maintains redox balance in lactic acid fermentation (see Figure 16.11).

$$\text{Pyruvate} + \text{NADH} + \text{H}^+ \rightleftharpoons \text{lactate} + \text{NAD}^+ \tag{A}$$

Getting Started:

From Table 18.1 we see that the reduction potential of the NAD^+ : NADH couple, or half-reaction, is $-0.32\ \text{V}$, whereas that of the pyruvate:lactate couple is $-0.19\ \text{V}$. By convention, reduction potentials (as in Table 18.1) refer to partial reactions written as reductions: $\text{oxidant} + \text{e}^- \rightarrow \text{reductant}$. Hence,

$$\text{Pyruvate} + 2\ \text{H}^+ + 2\ \text{e}^- \rightarrow \text{lactate} \quad E'_0 = -0.19\ \text{V} \tag{B}$$

$$\text{NAD}^+ + \text{H}^+ + 2\ \text{e}^- \rightarrow \text{NADH} \quad E'_0 = -0.32\ \text{V} \tag{C}$$

To obtain reaction A from reactions B and C, we need to reverse the direction of reaction C so that NADH appears on the left side of the arrow. In doing so, the sign of E'_0 must be changed.

$$\text{Pyruvate} + 2\ \text{H}^+ + 2\ \text{e}^- \rightarrow \text{lactate} \quad E'_0 = -0.19\ \text{V} \tag{B}$$

$$\text{NADH} \rightarrow \text{NAD}^+ + \text{H}^+ + 2\text{e}^- \quad E'_0 = +0.32\ \text{V} \tag{D}$$

Finally, recall that the Faraday constant is $96.48\ \text{kJ mol}^{-1}\ \text{K}^{-1}$.

Calculate:

Let's begin by calculating $\Delta G^{\circ\prime}$ for reaction B using equation 1 and substituting in the value of the Faraday constant and $n = 2$ since two electrons are exchanged.

$$\begin{aligned}\Delta G^{\circ\prime} &= -2 \times 96.48\ \text{kJ mol}^{-1}\,\text{V}^{-1} \times -0.19\ \text{V} \\ &= +36.7\ \text{kJ mol}^{-1}\end{aligned}$$

Likewise, for reaction D,

$$\begin{aligned}\Delta G^{\circ\prime} &= -2 \times 96.48\ \text{kJ mol}^{-1}\,\text{V}^{-1} \times +0.32\ \text{V} \\ &= -61.7\ \text{kJ mol}^{-1}\end{aligned}$$

Thus, the free energy for reaction A is given by

$$\begin{aligned}\Delta G^{\circ\prime} &= \Delta G^{\circ\prime}\,(\text{for reaction B}) + \Delta G^{\circ\prime}\,(\text{for reaction D}) \\ &= +36.7\ \text{kJ mol}^{-1} - 61.7\ \text{kJ mol}^{-1} \\ &= -25.0\ \text{kJ mol}^{-1}\ \text{or}\ -6.0\ \text{kcal mol}^{-1}\end{aligned}$$

Reflect:

What does $\Delta G^{\circ\prime}$ tell us? We can see from this result that under standard conditions the reaction is exergonic, releasing 25.0 kJ per mole. Thus, the reduction of pyruvate to lactate by NADH is spontaneous because electrons are more attracted to pyruvate than NAD^+. Note that all of this information was deduced entirely from the known reduction potentials.

Electron flow from NADH to molecular oxygen powers the formation of a proton gradient

Let's now consider the driving force of oxidative phosphorylation, which is the electron-transfer potential of NADH or $FADH_2$ relative to that of O_2. How much energy is released by the reduction of

O_2 with NADH? Let us calculate $\Delta G^{\circ\prime}$ for this reaction. The pertinent half-reactions are

$$\tfrac{1}{2}\,O_2 + 2\,H^+ + 2e^- \rightarrow H_2O \quad E'_0 = +0.82\ V$$
$$NAD^+ + H^+ + 2e^- \rightarrow NADH \quad E'_0 = -0.32\ V$$

The combination of the two half-reactions, as it proceeds in the electron-transport chain, yields

$$\tfrac{1}{2}O_2 + NADH + H^+ \rightarrow H_2O + NAD^+$$

The standard free energy for this reaction is then given by

$$\begin{aligned}\Delta G^{\circ\prime} &= (-2 \times 96.48\ kJ\ mol^{-1}V^{-1} \times +0.82\ V) \\ &\quad + (-2 \times 96.48\ kJ\ mol^{-1}V^{-1} \times +0.32\ V) \\ &= -158.2\ kJ\ mol^{-1} + (-61.9)\ kJ\ mol^{-1} \\ &= -220.1\ kJ\ mol^{-1}\ or\ -52.6\ kcal\ mol^{-1}\end{aligned}$$

This release of free energy is substantial. Recall that $\Delta G^{\circ\prime}$ for the synthesis of ATP is $30.5\ kJ\ mol^{-1}$ $(7.3\ kcal\ mol^{-1})$. The released energy is initially used to generate a proton gradient that is then used for the synthesis of ATP and the transport of metabolites across the mitochondrial membrane.

How can the energy associated with a proton gradient be quantified? Recall from Section 13.1 that the free-energy change for a species moving from one side of a membrane where it is at concentration c_1 to the other side where it is at a concentration c_2 is given by

$$\Delta G = RT\ \ln\left(c_2 / c_1\right) + ZF\Delta V \qquad (2)$$

in which Z is the electrical charge of the transported species, and ΔV is the potential in volts across the membrane. Under typical conditions for the inner mitochondrial membrane, the pH outside is 1.4 units lower than inside [corresponding to $\ln\left(c_2/c_1\right)$ of 3.2], and the membrane potential is 0.14 V, the outside being positive. Finally, recall that the gas constant, R, is

$-8.315 \times 10^{-3}\ \text{kJ mol}^{-1}\ \text{K}^{-1}$. Because $Z = +1$ for protons, from equation 2 we see that the free-energy change is
$(8.32 \times 10^{-3}\ \text{kJ mol}^{-1}\ \text{K}^{-1} \times 310\ \text{K} \times 3.2) + (+1 \times 96.48\ \text{kJ mol}^{-1}\ \text{V}^{-1} \times 0.14\ \text{V}) = 21.8\ \text{kJ mol}^{-1}$
or $5.2\ \text{kcal mol}^{-1}$. Thus, each proton that is transported out of the matrix to the cytoplasmic side corresponds to $21.8\ \text{kJ mol}^{-1}$ of free energy.

Self-Check Question



Identify the oxidant and the reductant in the following reaction: $\text{Pyruvate} + \text{NADH} + \text{H}^+ \rightleftharpoons \text{lactate} + \text{NAD}^+$

18.3 The Respiratory Chain Consists of Four Complexes: Three Proton Pumps and a Physical Link to the Citric Acid Cycle

Electrons are transferred from NADH to O_2 through a chain of three large protein complexes called *NADH-Q oxidoreductase, Q-cytochrome* c *oxidoreductase,* and *cytochrome* c *oxidase* (**Figure 18.4** and **Table 18.2**). Electron flow within these transmembrane complexes is highly exergonic and powers the transport of protons across the inner mitochondrial membrane. A fourth large protein complex, called *succinate-Q reductase,* contains the succinate dehydrogenase that generates $FADH_2$ in the citric acid cycle. Electrons from this $FADH_2$ enter the electron-transport chain at Q-cytochrome *c* oxidoreductase. Succinate-Q reductase, in contrast with the other complexes, does not pump protons. NADH-Q oxidoreductase, succinate-Q reductase, Q-cytochrome *c* oxidoreductase, and cytochrome *c* oxidase are also called *Complex I, II, III,* and *IV,* respectively. Complexes I, III, and IV appear to be associated in a supramolecular complex which facilitates the rapid transfer of substrate and prevents the release of reaction intermediates, as will be discussed further at the end of this section.

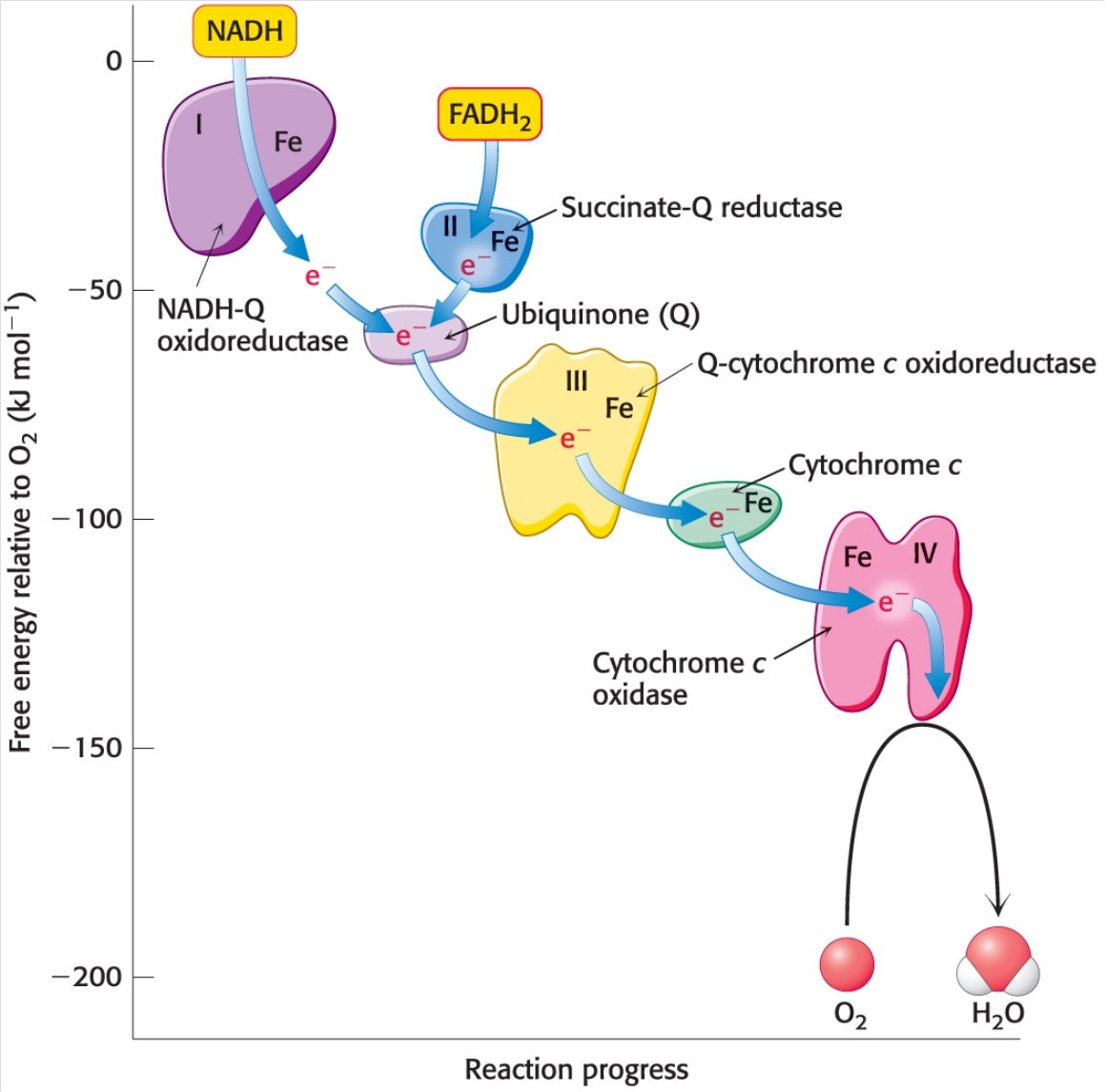


FIGURE 18.4 Components of the electron-transport chain allow the flow of electrons to molecular oxygen. Electrons flow down an energy gradient from NADH or $FADH_2$ to O_2. Th flow is catalyzed by four protein complexes, and the energy released is used to generate a proto gradient.

[Information from D. Sadava et al., *Life*, 8th ed. (Sinauer, 2008), p. 150.]

TABLE 18.2 Components of the mitochondrial electron-transport chain

			Oxidant or reductant		
Enzyme complex	**Mass (kDa)**	**Prosthetic group**	**Matrix side**	**Membrane core**	**Intermembrane side**
NADH-Q oxidoreductase	> 900	FMN	NADH	Q	
		Fe–S			
Succinate-Q reductase	140	FAD	Succinate	Q	
		Fe–S			
Q-cytochrome *c* oxidoreductase	250	Heme b_H		Q	Cytochrome *c*
		Heme b_L			
		Heme c_1			
		Fe–S			
Cytochrome *c* oxidase	160	Heme *a*			Cytochrome *c*
		Heme a_3			
		Cu_A and Cu_B			

Information from: J. W. DePierre and L. Ernster, *Annu. Rev. Biochem.* 46:215, 1977; Y. Hatefi, *Annu. Rev. Biochem.* 54:1015, 1985; and J. E. Walker, *Q. Rev. Biophys.* 25:253, 1992.

Two electron carriers ferry the electrons from one complex to the next. The first is **coenzyme Q** (or **Q**, for short), which is also known as *ubiquinone* because it is a ubiquitous quinone in biological systems. Coenzyme Q is a hydrophobic quinone that diffuses rapidly within the inner mitochondrial membrane. Electrons are carried from NADH-Q oxidoreductase to Q-cytochrome *c* oxidoreductase, the third complex of the chain, by the reduced form of Q. Electrons from the $FADH_2$ generated by the citric acid cycle are transferred first to ubiquinone and then to the Q-cytochrome *c* oxidoreductase complex.

Coenzyme Q is a quinone derivative with a long tail consisting of five-carbon isoprene units that account for its hydrophobic nature. The number of isoprene units in the tail depends on the species. The most common mammalian form contains 10 isoprene units (coenzyme Q_{10}). For simplicity, the subscript will be omitted from this abbreviation because all varieties function in an identical manner.

Quinones can exist in several oxidation states. In the fully oxidized state (Q), coenzyme Q has two keto groups (**Figure 18.5**). The addition of one electron and one proton results in the semiquinone form $(QH\cdot)$. The semiquinone can lose a proton to form a semiquinone radical anion $(Q\cdot^-)$. The addition of a second electron and proton to the semiquinone generates ubiquinol (QH_2), the fully reduced form of coenzyme Q, which holds its protons more tightly. Thus, for quinones, electron-transfer reactions are coupled to proton binding and release, a property that is key to transmembrane proton transport. Because ubiquinone is soluble in the membrane, a pool of Q and QH_2 — called the *Q pool* — is thought to exist in the inner mitochondrial membrane, although recent research suggests that the Q pool is confined to the protein complexes of the electron-transport chain.

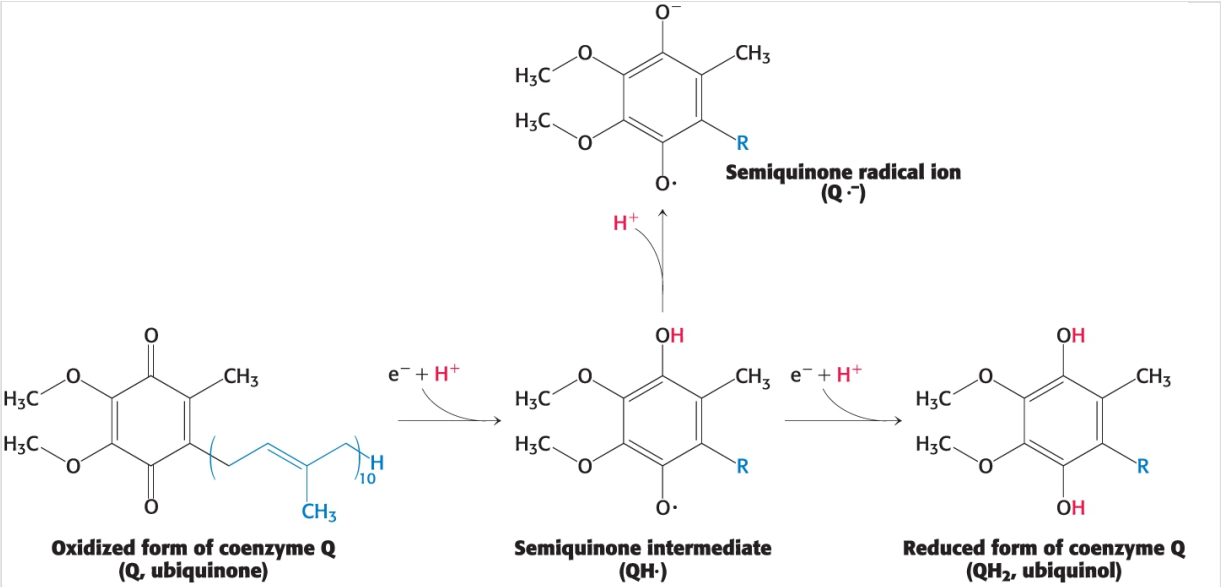


FIGURE 18.5 Quinones can have three different oxidation states, two of which are stable. The reduction of ubiquinone (Q) to ubiquinol (QH_2) proceeds through a semiquinone intermediate $(QH\cdot)$. The R group indicates the same isoprenoid units shown in the image on the left.

In contrast with Q, the second special electron carrier is a protein called a *cytochrome*. ***Cytochromes*** are electron-transferring proteins that contain a heme prosthetic group. **Cytochrome *c***, a small soluble protein that is loosely associated with the inner mitochondrial membrane, shuttles electrons from Q-cytochrome *c* oxidoreductase to cytochrome *c* oxidase, the final component in the chain and the one that catalyzes the reduction of O_2. Cytochrome *c* is present in all organisms having mitochondrial respiratory chains, evolving more than 1.5 billion years ago, before the divergence of plants and animals. Its structure and function have been conserved throughout this period, as evidenced by the fact that the cytochrome c of any eukaryotic species reacts in vitro with the cytochrome c oxidase of any other species. For example, wheat-germ cytochrome *c* reacts with human cytochrome *c* oxidase. Even bacterial cytochromes closely resemble cytochrome *c* from tuna-heart

mitochondria (Figure 18.6). This evidence attests to an efficient evolutionary solution to electron transfer bestowed by the structural and functional characteristics of cytochrome *c*.

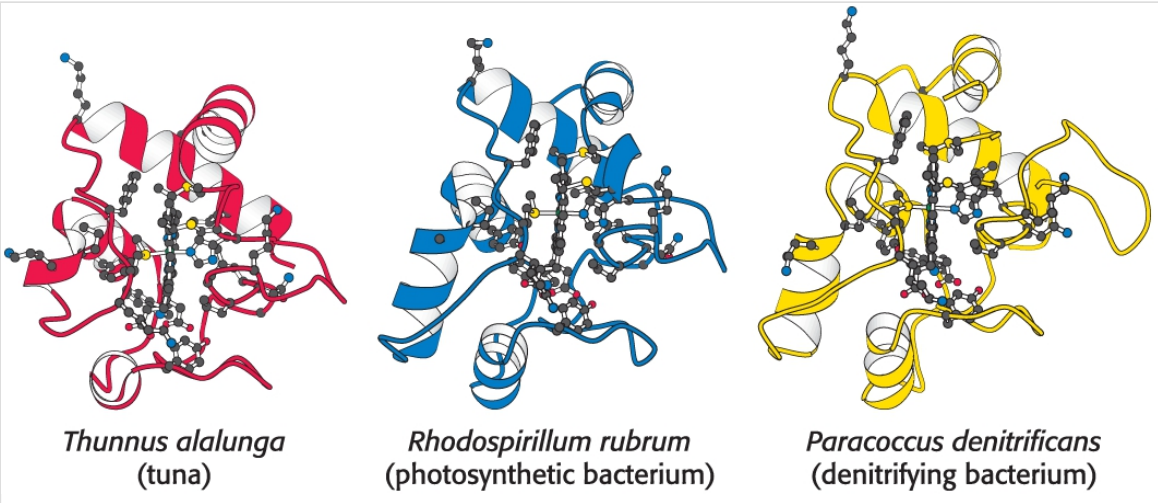


FIGURE 18.6 The three-dimensional structure of cytochrome *c* is remarkably conserved amo distantly related species. The side chains are shown for 21 conserved amino acids as well as th centrally located planar heme.

[Drawn from 3CYT.pdb, 3C2C.pdb, and 155C.pdb.]

INTERACT with these models in Achieve

Iron–sulfur clusters are common components of the electron-transport chain

Iron–sulfur clusters in **iron–sulfur proteins** (also called **nonheme iron proteins**) play a critical role in a wide range of reduction reactions in biological systems. Several types of Fe–S clusters are known (**Figure 18.7**). In the simplest kind, a single iron ion is tetrahedrally coordinated to the sulfhydryl groups of four cysteine residues of the protein (Figure 18.7A). A second kind, denoted by 2Fe–2S, contains two iron ions, two inorganic sulfides, and usually four cysteine residues (Figure 18.7B). A

third type, designated 4Fe–4S, contains four iron ions, four inorganic sulfides, and four cysteine residues (Figure 18.7C). NADH-Q oxidoreductase contains both 2Fe–2S and 4Fe–4S clusters. Iron ions in these Fe–S complexes cycle between Fe^{2+} (reduced) and Fe^{3+} (oxidized) states. Unlike quinones and flavins, iron–sulfur clusters generally undergo oxidation–reduction reactions without releasing or binding protons.

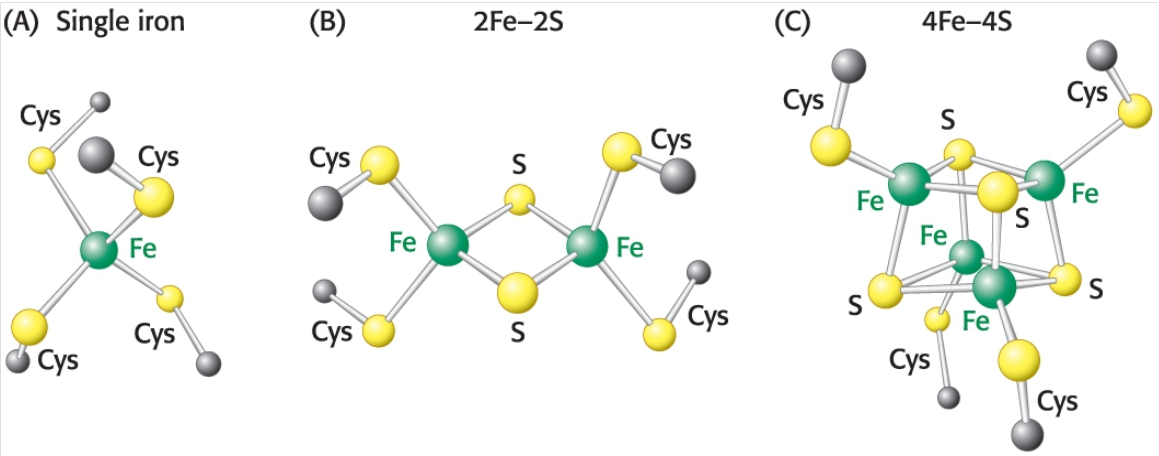


FIGURE 18.7 Three different types of iron–sulfur clusters are commonly found in biological systems. Each of these clusters can undergo oxidation–reduction reactions. (A) A single iron ion bound by four cysteine residues. (B) 2Fe–2S cluster with iron ions bridged by sulfide ions. (C) 4Fe–4S cluster.

The importance of Fe–S clusters is illustrated by the loss of function of the protein frataxin. Frataxin is a small (14.2-kDa) mitochondrial protein that is crucial for the synthesis of Fe–S clusters. Mutations in frataxin causes Friedreich's ataxia, a disease of varying severity that affects the central and peripheral nervous system as well as the heart and skeletal system. Severe cases lead to death in young adult life. The most common mutation is trinucleotide expansion (Section 28.4) in the gene for frataxin.

Self-Check Question



Explain why the structure of coenzyme Q makes it an effective mobile electron carrier in the electron-transport chain.

The high-potential energy electrons of NADH enter the respiratory chain at NADH-Q oxidoreductase

The electrons of NADH enter the chain at **NADH-Q oxidoreductase** (also called **Complex I**), an enormous enzyme $(>900\ \text{kDa})$ consisting of approximately 45 polypeptide chains organized into 14 core subunits that are found in all species with respiratory chains. This proton pump, like that of the other two in the respiratory chain, is encoded by genes residing in both the mitochondria and the nucleus. NADH-Q oxidoreductase is L-shaped, with a horizontal arm lying in the membrane and a vertical arm that projects into the matrix.

The reaction catalyzed by this enzyme appears to be

$$\text{NADH} + \text{Q} + 5\ \text{H}^+_{\text{matrix}} \rightarrow \text{NAD}^+ + \text{QH}_2 + 4\ \text{H}^+_{\text{intermembrane space}}$$

The initial step is the binding of NADH and the transfer of its two high-potential electrons to the flavin mononucleotide (FMN) prosthetic group, yielding the reduced form, FMNH_2 (**Figure 18.8**). The electron acceptor of FMN, the isoalloxazine ring, is identical with that of FAD.

Electrons are then transferred from $FMNH_2$ to a series of iron–sulfur clusters, the second type of prosthetic group in NADH-Q oxidoreductase.

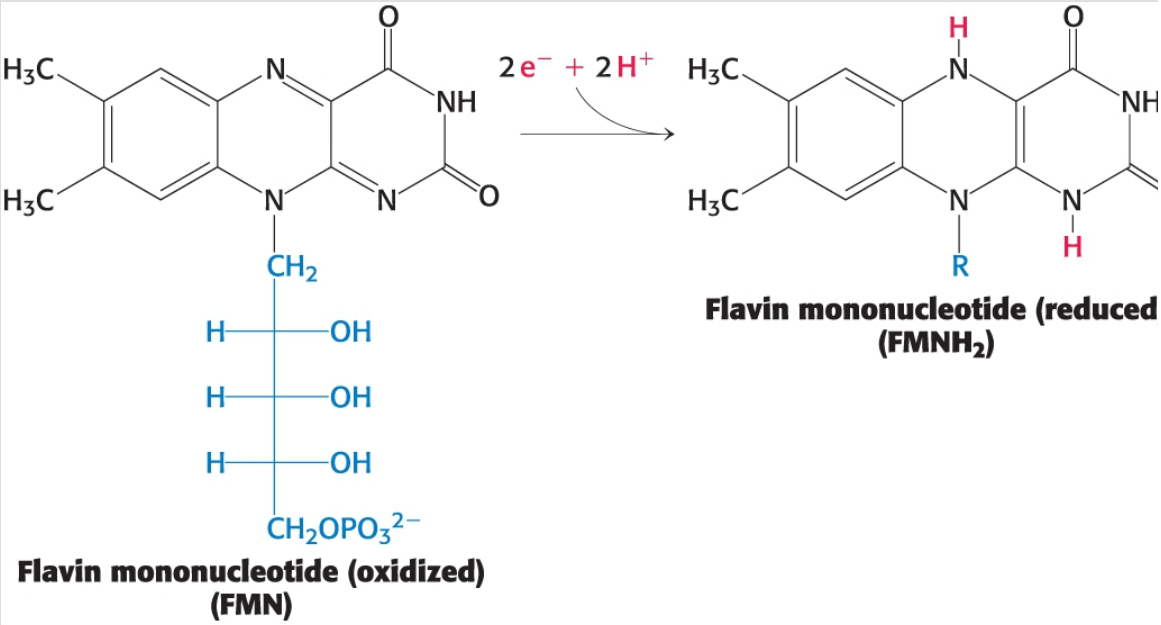


FIGURE 18.8 Flavins have two oxidation states. The states are exchanged by the binding or lo
of two electrons and two protons.

Recent structural studies have suggested how Complex I acts as a proton pump. What are the structural elements required for proton-pumping? The membrane-embedded part of the complex has four proton half-channels consisting, in part, of vertical helices. One set of half-channels is exposed to the matrix and the other to the intermembrane space (Figure 18.9). The vertical helices are linked on the matrix side by a long horizontal helix (HL) that connects the matrix half-channels, while the intermembrane space half-channels are joined by a series of β-hairpin-helix connecting elements (βH). An enclosed Q chamber, the site where Q accepts electrons from NADH, exists near the junction of the hydrophilic portion and the membrane-embedded portion. Finally, a

hydrophilic funnel connects the Q chamber to a water-lined channel (into which the half channels open) that extends the entire length of the membrane-embedded portion.

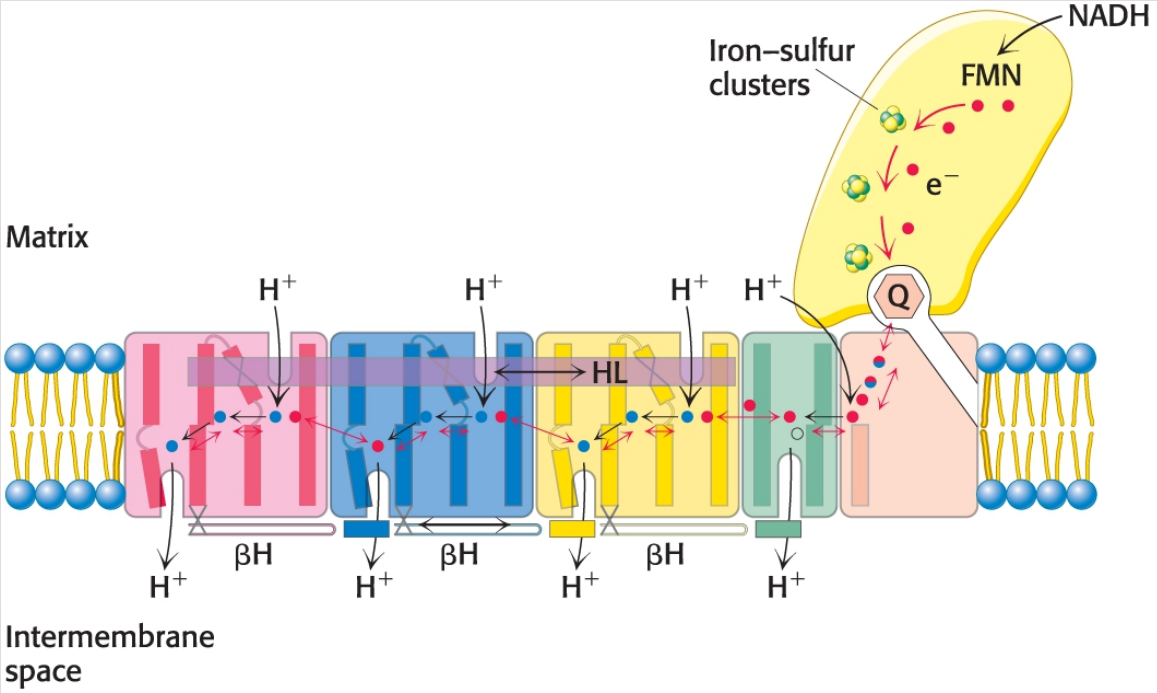
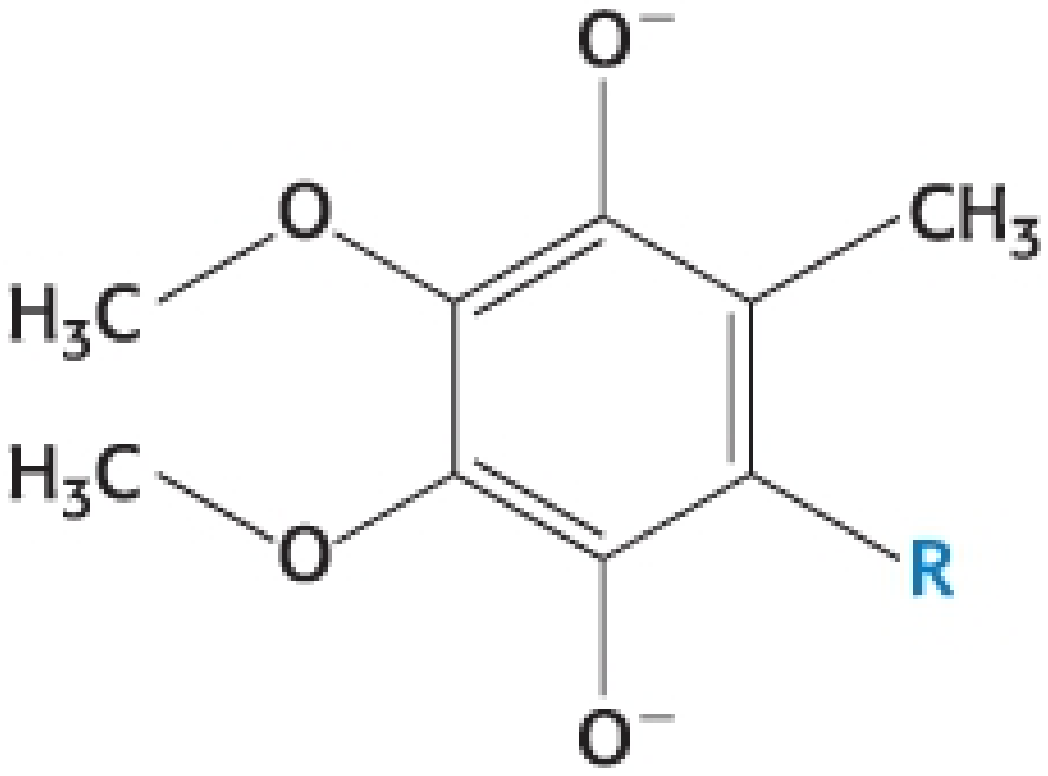


FIGURE 18.9 Electron transfer through NADH-Q oxidoreductase is coupled to proton transfer reactions. Electrons flow in Complex I from NADH through FMN and a series of iron–sulfur clusters to ubiquinone (Q), forming Q^{2-}. The charges on Q^{2-} are electrostatically transmitted to hydrophilic amino acid residues — shown as red (glutamate) and blue (lysine or histidine) balls — that power the movement of HL and βH components. This movement change the conformation of the transmembrane helices and results in the transport of four protons out of the mitochondrial matrix.

[Information from R. Baradaran et al., *Nature* 494:443–448, 2013.]

How do these structural elements cooperate to pump protons out of the matrix? When Q accepts two electrons from NADH, generating Q^{2-}, the negative charges on Q^{2-} interact electrostatically with negatively charged amino acid residues in the membrane-embedded arm, causing

conformational changes in the long horizontal helix and the βH elements. These changes in turn alter the structures of the connected vertical helices that change the pK_a of amino acids, allowing protons from the matrix to first bind to the amino acids, then dissociate into the water-lined channel, and finally enter the intermembrane space. Thus, the flow of two electrons from NADH to coenzyme Q through NADH-Q oxidoreductase leads to the pumping of four hydrogen ions out of the matrix of the mitochondrion. Q^{2-} subsequently takes up two protons from the matrix as it is reduced to QH_2. The removal of these protons from the matrix contributes to the formation of the proton-motive force. The QH_2 subsequently leaves the enzyme for the Q pool, allowing another reaction cycle to occur.



Reduced ubiquinone
(Q^{2-})



It is important to note that the citric acid cycle and the pyruvate dehydrogenase complex are not the only sources of mitochondrial NADH. As we will see in Chapter 22, fatty acid degradation, which also takes place in mitochondria, is another crucial source of NADH for the electron-transport chain. Moreover, electrons from NADH generated in the cytoplasm can be transported into mitochondria for use by the electron-transport chain, as we will see in Section 18.5.

Ubiquinol is the entry point for electrons from $FADH_2$ of flavoproteins

Recall that $FADH_2$ is formed in the citric acid cycle, in the oxidation of succinate to fumarate by succinate dehydrogenase (Section 17.3). Succinate dehydrogenase is part of **succinate-Q reductase (Complex II)**, an integral membrane protein complex of the inner mitochondrial membrane. $FADH_2$ does not actually leave the complex, however. Rather, its electrons are transferred to Fe–S centers and then finally to Q to form QH_2, which then is ready to transfer electrons further down the electron-transport chain. Importantly, succinate-Q reductase, in contrast with NADH-Q oxidoreductase, does not pump protons from one side of the membrane to the other. Consequently, less ATP is formed from the oxidation of $FADH_2$ than from NADH.

Electrons flow from ubiquinol to cytochrome *c* through Q-cytochrome *c* oxidoreductase

What is the fate of ubiquinol generated by Complexes I and II? The electrons from QH_2 are passed on to cytochrome *c* (Cyt *c*) by the second of the three proton pumps in the respiratory chain, **Q-cytochrome *c* oxidoreductase** (also known as **Complex III** and as **cytochrome *c* reductase**). The flow of a pair of electrons through this complex leads to the effective net transport of $2\ H^+$ to the intermembrane space, half the yield obtained with NADH-Q reductase because of a smaller thermodynamic driving force.

$$QH_2 + 2\ \text{Cyt}\ c_{ox} + 2\ H^+_{\text{matrix}} \rightarrow Q + 2\ \text{Cyt}\ c_{red} + 4\ H^+_{\text{intermembrane space}}$$

Q-cytochrome *c* oxidoreductase itself contains two types of cytochromes, named *b* and c_1 (**Figure 18.10**). The heme prosthetic group in cytochromes *b*, c_1, and *c* is iron-protoporphyrin IX, the same heme present in myoglobin and hemoglobin (Section 3.2). The iron ion of a cytochrome, in contrast to hemoglobin and myoglobin, alternates between a reduced ferrous $(+2)$ state and an oxidized ferric $(+3)$ state during electron transport. The two cytochrome subunits of Q-cytochrome *c* oxidoreductase contain a total of three hemes: two hemes within cytochrome *b*, termed heme b_L (L for low affinity) and heme b_H (H for high affinity), and one heme within cytochrome c_1. These identical hemes have different electron affinities because they are in different polypeptide environments. For example, heme b_L, which is located in a cluster of helices near the intermembrane face of the membrane, has lower affinity for an electron than does heme b_H, which is near the matrix side.

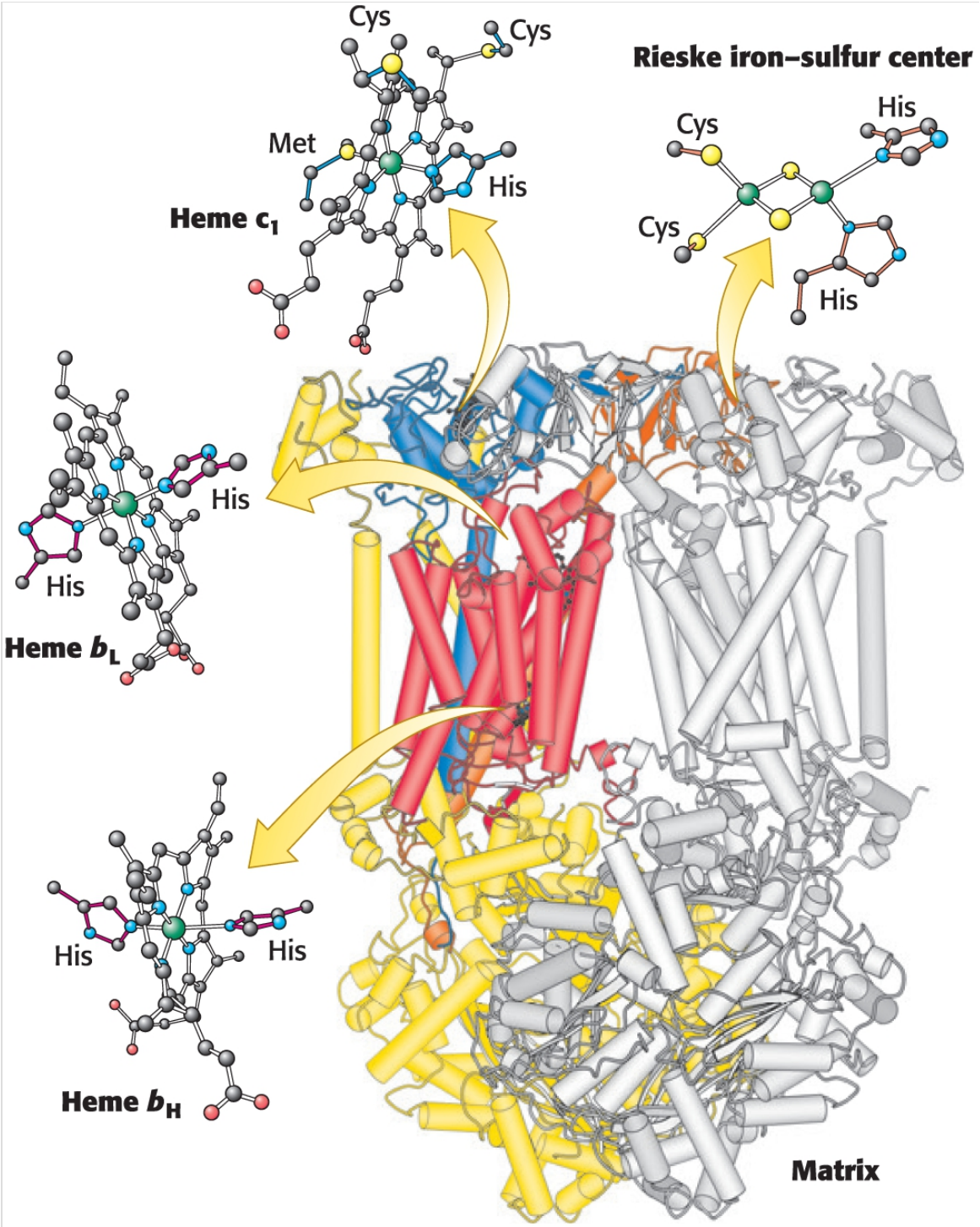


FIGURE 18.10 Q-cytochrome c oxidoreductase is a homodimer, with each monomer consistin of 11 distinct polypeptide chains. Although both monomers are identical, key parts are shown color in only one monomer for ease of viewing. *Notice* that the major prosthetic groups — three hemes and a 2Fe–2S cluster — are located either near the edge of the complex bordering the intermembrane space (top) or in the region embedded in the membrane (α helices represented by tubes). They are well-positioned to mediate the electron-transfer reactions between quinone in the membrane and cytochrome *c* in the intermembrane space.

[Drawn from 1BCC.pdb.]

INTERACT with this model in Achieve

In addition to the hemes, the enzyme contains an iron–sulfur protein with a 2Fe–2S center. This center, termed the *Rieske center*, is unusual in that one of the iron ions is coordinated by two histidine residues rather than two cysteine residues. This coordination stabilizes the center in its reduced form, raising its reduction potential so that it can readily accept electrons from QH_2.

The Q cycle funnels electrons from a two-electron carrier to a one-electron carrier while pumping protons

QH_2 passes two electrons to Q-cytochrome *c* oxidoreductase, but the acceptor of electrons in this complex, cytochrome *c*, can accept only one electron. How does the switch from the two-electron carrier ubiquinol to the one-electron carrier cytochrome *c* take place without the release of dangerous radicals? The mechanism for the coupling of electron transfer from QH_2 to cytochrome *c* to transmembrane proton transport is known as the **Q cycle** (**Figure 18.11**). Two QH_2 molecules bind to the complex consecutively, each giving up two electrons and two H^+. These protons are released to the intermembrane space.

Additionally, one molecule of oxidized Q binds and it is this molecule, along with two molecules of cytochrome c, that accept the four electrons. The Q cycle occurs in two halves:

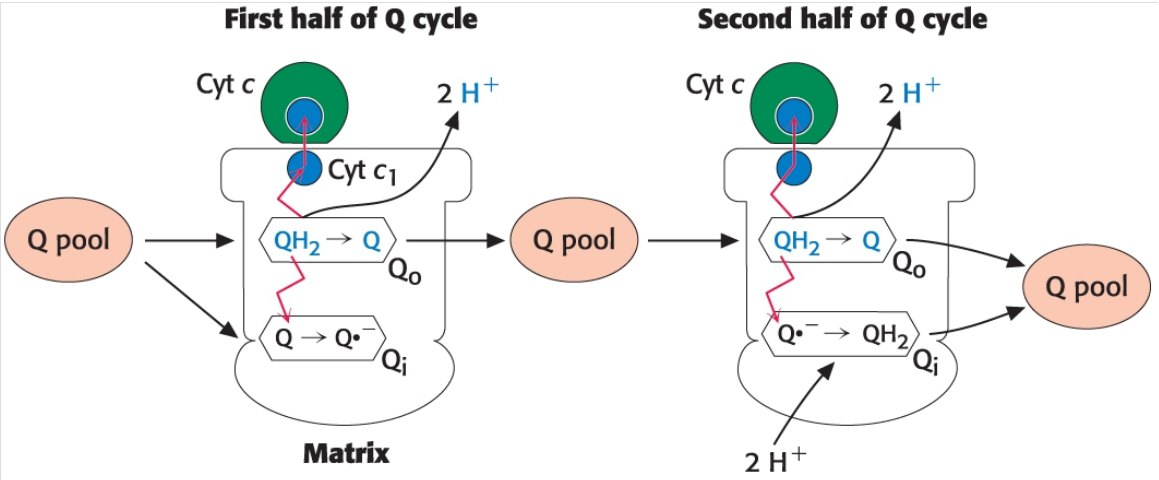


FIGURE 18.11 The Q cycle allows the safe transfer of electrons from QH_2 to cytochrome *c*. The Q cycle takes place in Complex III, which is represented in outline form. In the first half of th cycle, two molecules of Q bind, one oxidized (Q) and the other reduced (QH_2). Two electrons of the bound QH_2 are transferred, one to cytochrome *c* and the other to the bound Q in the second binding site to form the semiquinone radical anion $Q\cdot^-$. The newly formed Q dissociates and enters the Q pool. In the second half of the cycle, a second QH_2 also gives up electrons to Complex III, one to a second molecule of cytochrome *c* and the other to reduce $Q\cdot^-$ to QH_2. This second electron transfer results in the uptake of two protons from the matrix. The path of electron transfer is shown in red.

1. In the first half of the cycle, two molecules of Q from the Q pool — one reduced (QH_2) and one oxidized (Q) — first bind to two distinct sites called Q_o and Q_i, respectively. The QH_2 bound to Q_o passes its two electrons through the complex to different destinations. One electron flows first to the Rieske 2Fe–2S cluster, then to cytochrome c_1, and finally to the first molecule of oxidized cytochrome *c*, converting it into its reduced form. The reduced cytochrome *c* molecule is free to diffuse away from the enzyme to continue down the respiratory chain. The second electron passes through two heme groups of cytochrome *b* to the oxidized Q molecule bound at

the Q_i site, reducing it to a dangerous semiquinone radical anion $(Q\cdot^-)$ which is held tightly within the complex to prevent its release. The now fully oxidized Q leaves the Q_o site and reenters the Q pool.

2. In the second half of the cycle, a second molecule of QH_2 binds to the Q_o site and reacts in the same way as the first. One of the electrons is transferred to cytochrome *c*, which becomes reduced and leaves, while the second electron is transferred to the semiquinone radical anion still bound in the Q_i binding site from the first half of the cycle. On the addition of the second electron, the radical accepts two protons from the matrix and forms QH_2, which then rejoins the Q pool along with the second oxidized Q molecule from the Q_o site. The removal of these two protons from the matrix contributes to the formation of the proton gradient.

Thus, with each full cycle, two reduced QH_2 and one oxidized Q enter the complex and two oxidized Q and one QH_2 leave. The two electrons that are extracted from the Q pool each cycle pass to two molecules of cytochrome *c*, without releasing a radical to solution. Finally, four protons are released into the intermembrane space, and two protons are removed from the mitochondrial matrix. The overall reaction is:

$$2\ QH_2 + Q + 2\ \text{Cyt}\ c_{ox} + 2\ H^+_{\text{matrix}} \rightarrow 2\ Q + QH_2 + 2\ \text{Cyt}\ \ c_{red} + 4\ H^+_{\text{intermembrane space}}$$

The problem of how to funnel electrons safely and efficiently from a two-electron carrier (QH_2) to a one-electron carrier (cytochrome *c*) is solved by the Q cycle. The cytochrome *b* component of the reductase is in essence a recycling device that enables both electrons of QH_2 to be used effectively.

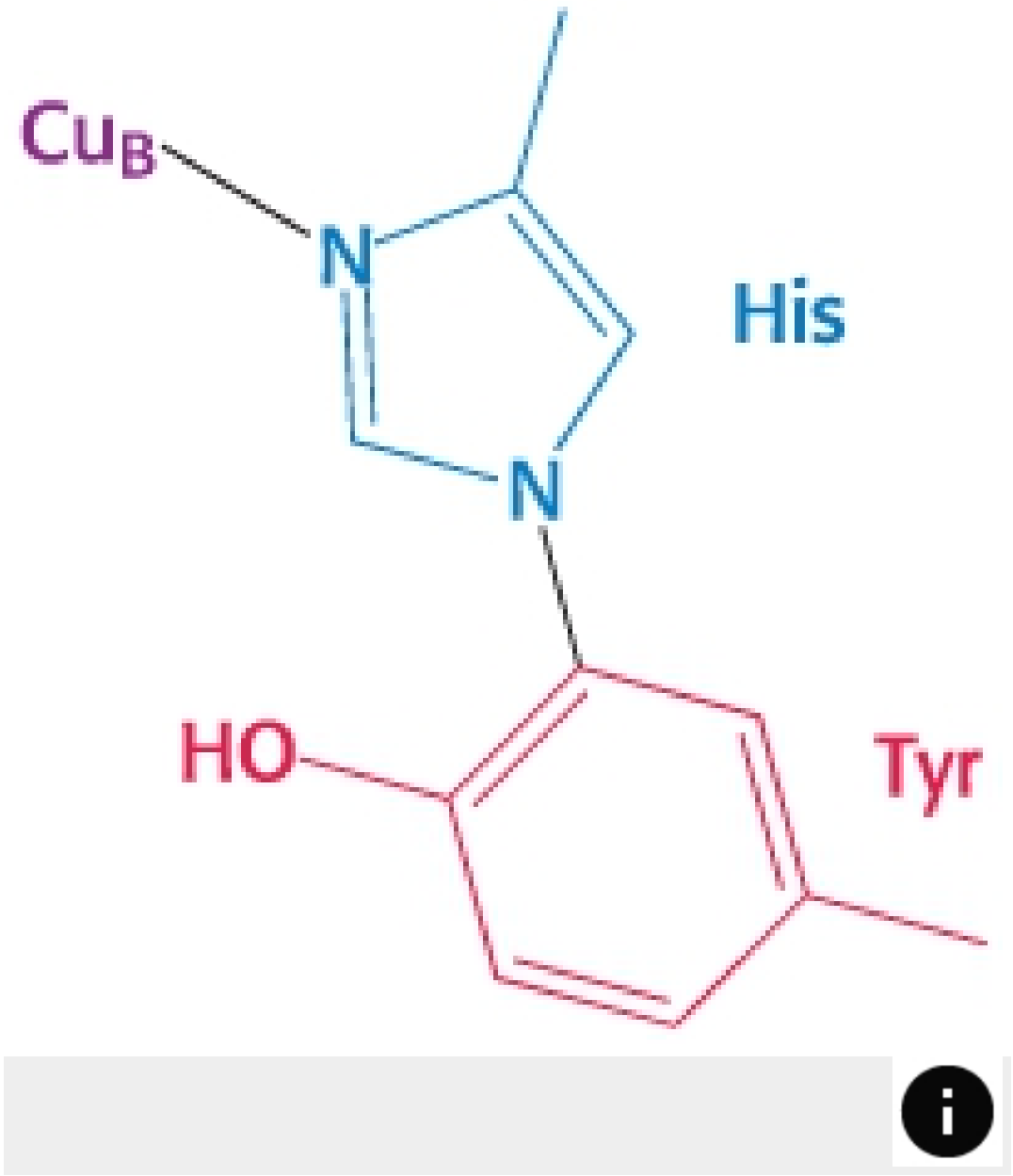
Cytochrome *c* oxidase catalyzes the reduction of molecular oxygen to water

The last of the three proton-pumping assemblies of the respiratory chain is **cytochrome c oxidase (Complex IV)**. Cytochrome *c* oxidase catalyzes the transfer of electrons from the reduced form of cytochrome *c* to molecular oxygen, the final acceptor.

$$4\ \text{Cyt}\ c_{\text{red}} + 8\ \text{H}^+_{\text{matrix}} + \text{O}_2 \rightarrow 4\ \text{Cyt}\ c_{\text{ox}} + 2\ \text{H}_2\text{O} + 4\ \text{H}^+_{\text{intermembrane space}}$$

The requirement of oxygen for this reaction is what makes "aerobic" organisms aerobic. To obtain oxygen for this reaction is the primary reason that human beings must breathe. Four electrons are funneled to O_2 to completely reduce it to H_2O, and, concomitantly, protons are pumped from the matrix into the intermembrane space.

This reaction is quite thermodynamically favorable. From the reduction potentials in Table 18.1, the standard free-energy change for this reaction is calculated to be $\Delta G^{\circ\prime} = -231.8\ \text{kJ mol}^{-1}\ (-55.4\ \text{kcal mol}^{-1})$. As much of this free energy as possible must be captured in the form of a proton gradient for subsequent use in ATP synthesis.



Our understanding of mammalian cytochrome *c* oxidase is reasonably well understood at the structural level because of extensive studies of bovine cytochrome *c* oxidase (Figure 18.12). It consists of 13 subunits, three of which are encoded by the mitochondrion's own genome. Cytochrome *c* oxidase contains two heme A groups and three copper ions, arranged as two copper centers, designated *A* and *B*. One center, Cu_A/Cu_A, contains two copper ions linked by two bridging cysteine

residues. This center initially accepts electrons from reduced cytochrome *c*. The remaining copper ion, Cu_B, is bonded to three histidine residues, one of which is modified by covalent linkage to a tyrosine residue. The copper centers alternate between the reduced Cu^+ (cuprous) form and the oxidized Cu^{2+} (cupric) form as they accept and donate electrons.

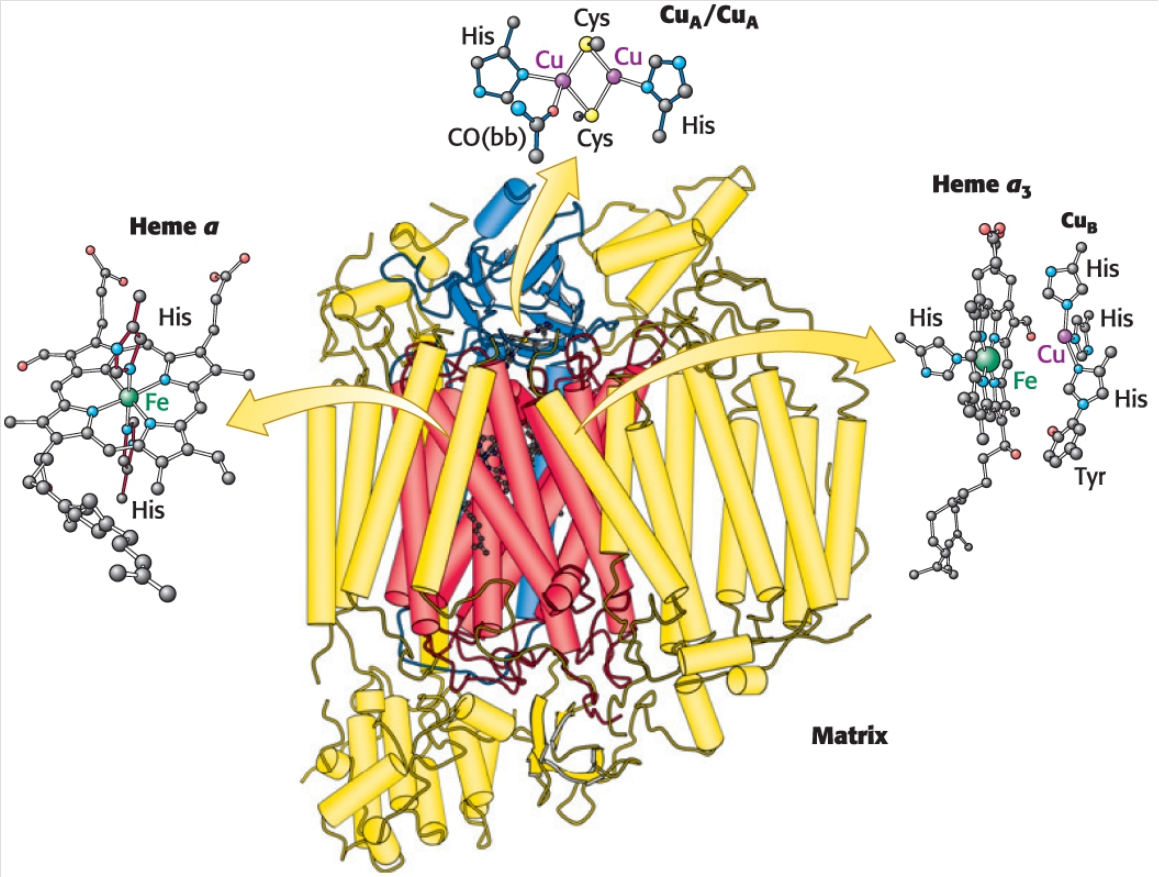
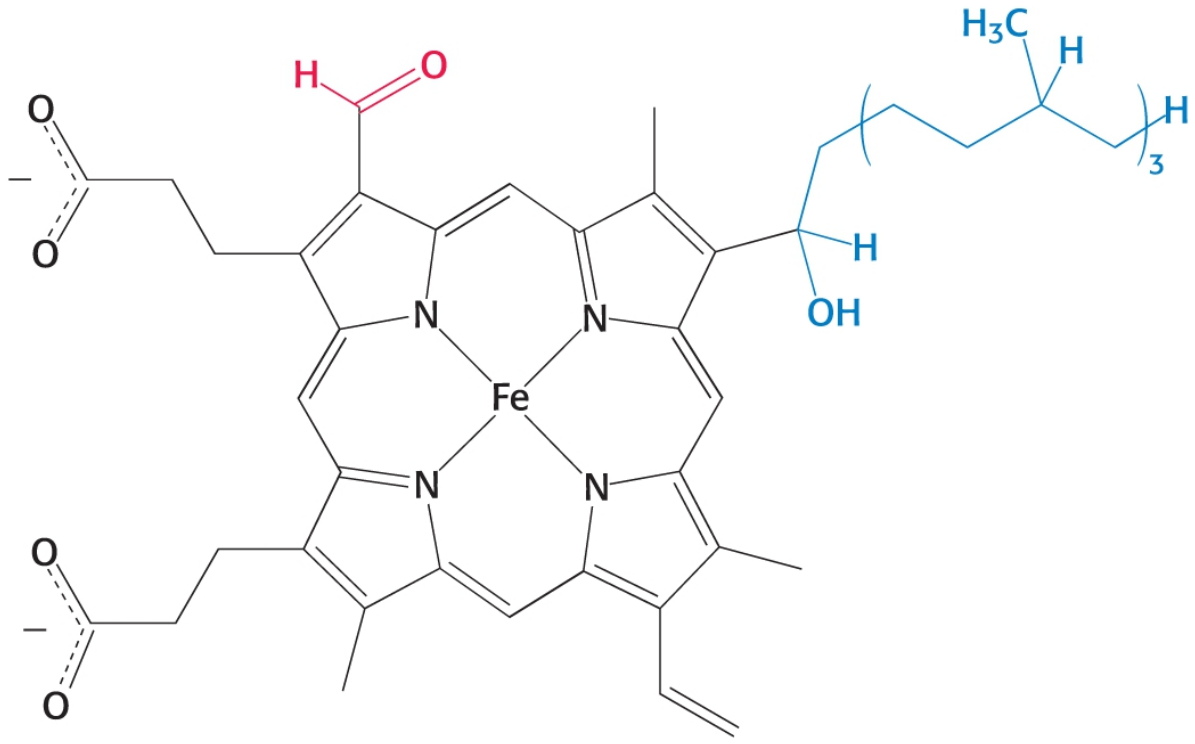


FIGURE 18.12 The structure of bovine cytochrome *c* oxidase reveals 13 polypeptide chains ar numerous electron carriers. Notice that most of the complex, as well as two major prosthetic groups (heme *a* and heme $a_3 - Cu_B$) are embedded in the membrane (α helices are represented by vertical cylinders). Heme $a_3 - Cu_B$ is the site of the reduction of oxygen to water. The Cu_A/Cu_A prosthetic group is positioned near the intermembrane space to bette accept electrons from cytochrome *c*. CO(bb) is a carbonyl group of the peptide backbone. [Drawn from 2OCC.pdb.]

INTERACT with this model in Achieve

In cytochrome *c* oxidase, there are two heme A molecules, called *heme* a and *heme* a_3, which differ from the heme in cytochrome *c* and c_1 in three ways: (1) a formyl group replaces a methyl group, (2) a C_{17} hydrocarbon chain replaces one of the vinyl groups, and (3) the heme is not covalently attached to the protein.



Heme A

Heme *a* and heme a_3 have distinct redox potentials because they are located in different environments within cytochrome *c* oxidase. An electron flows from cytochrome *c* to Cu_A/Cu_A, to heme *a*, to heme a_3,

to Cu_B, and finally to O_2. Heme a_3 and Cu_B are directly adjacent. Together, heme a_3 and Cu_B form the active center at which O_2 is reduced to H_2O.

Four molecules of cytochrome *c* bind consecutively to the enzyme and transfer an electron to reduce one molecule of O_2 to H_2O (**Figure 18.13**):

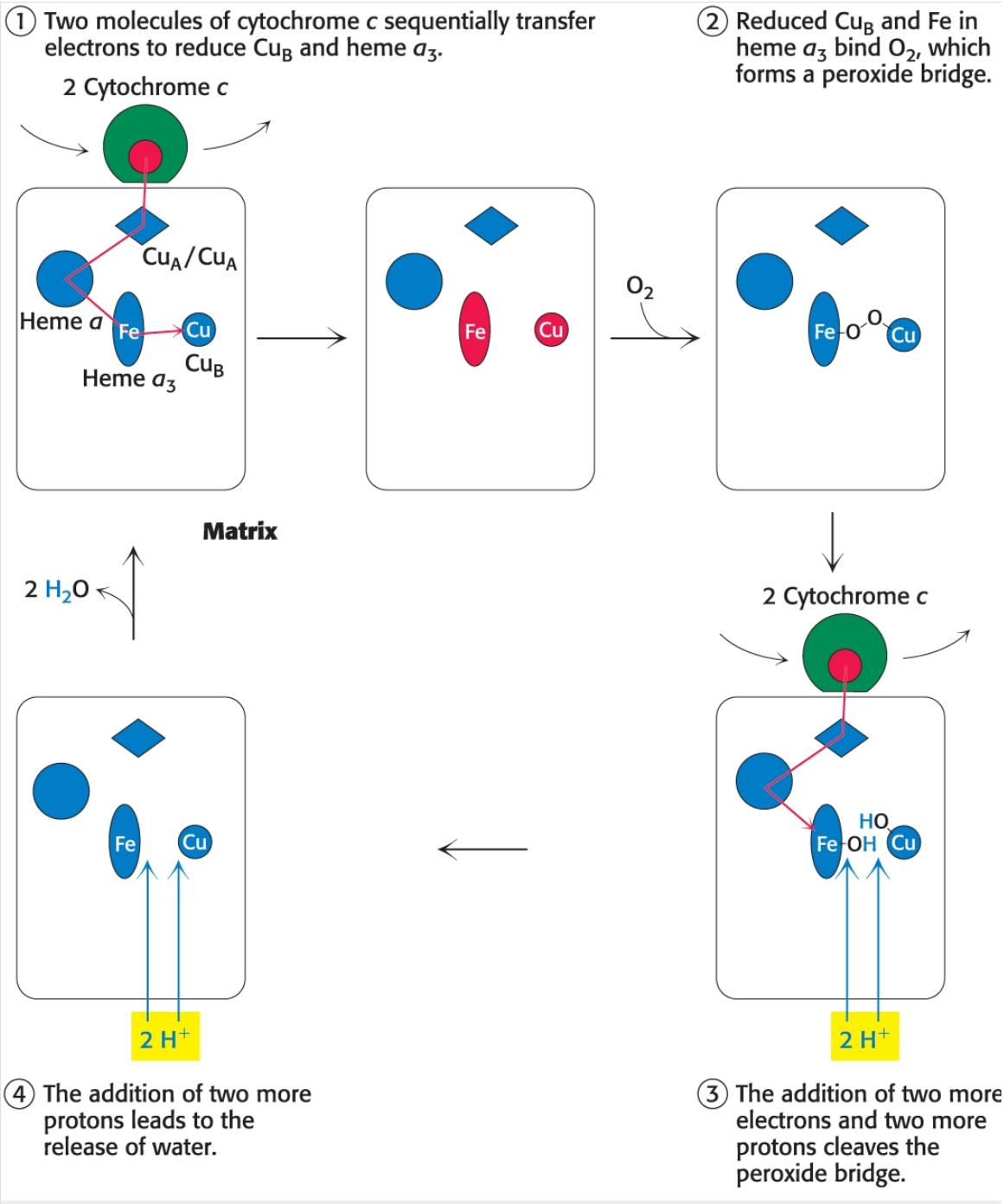


FIGURE 18.13 The mechanism of cytochrome *c* oxidase prevents early oxygen release. The cycle begins and ends with all prosthetic groups in their oxidized forms (shown in blue). Reduce forms are in red. Four cytochrome *c* molecules donate four electrons, allowing the binding and cleavage of an O_2 molecule and the import of four H^+ from the matrix to form two molecules of H_2O, which are released from the enzyme to regenerate the initial state.

1. Electrons from two molecules of reduced cytochrome *c* flow down an electron-transfer pathway within cytochrome *c* oxidase, one stopping at Cu_B and the other at heme a_3. With both centers in the reduced state, they together can now bind an oxygen molecule.
2. As molecular oxygen binds, it abstracts an electron from each of the nearby ions in the active center to form a peroxide (O_2^{2-}) bridge between them (**Figure 18.14**).

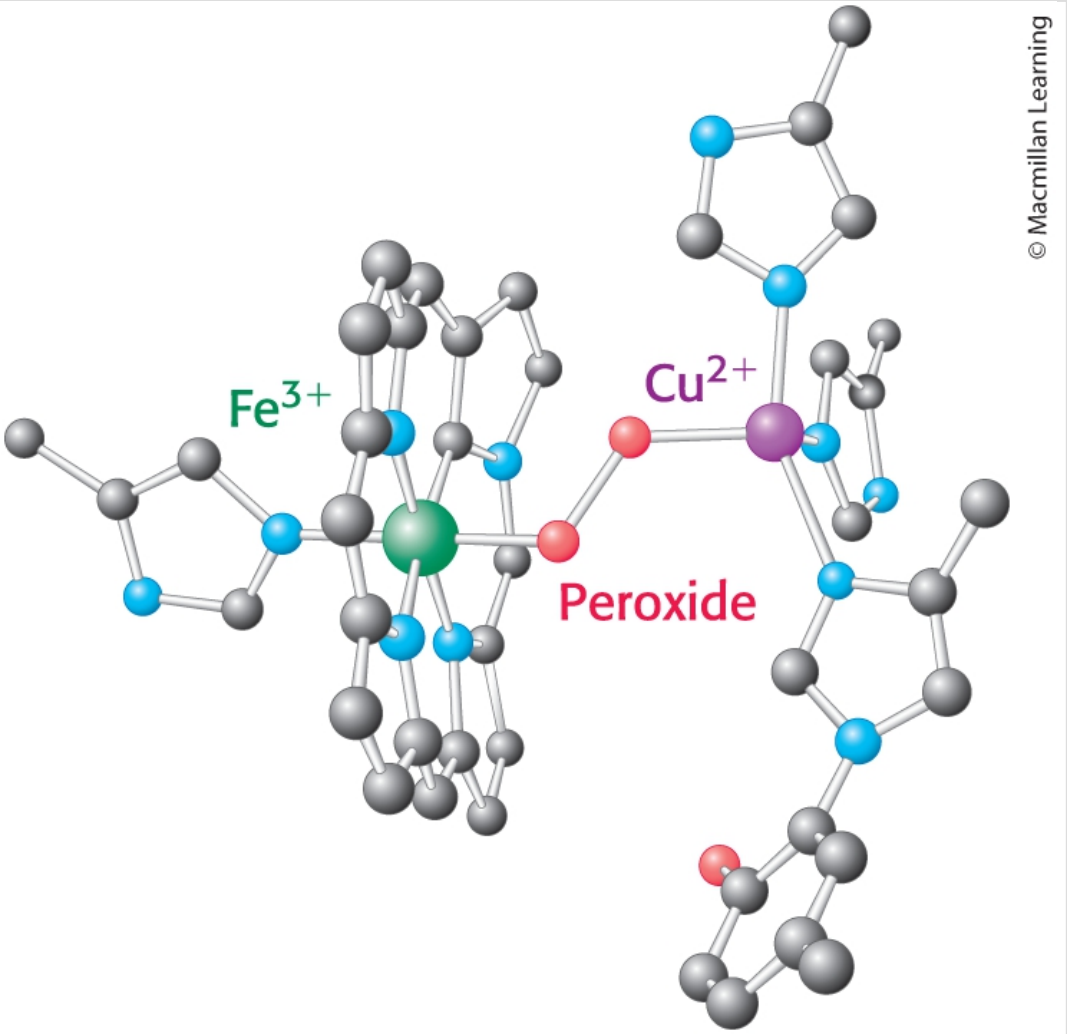


FIGURE 18.14 Two metals form a peroxide bridge in cytochrome *c* oxidase. The oxygen bound to heme a_3 is reduced to peroxide by the presence of Cu_B.

3. Two more molecules of cytochrome *c* bind and release electrons that travel to the active center. The addition of an electron as well as H^+ to each oxygen atom reduces the two ion–oxygen groups to $Cu_B^{2+}—OH$ and $Fe^{3+}—OH$.

4. Reaction with two more H^+ ions allows the release of two molecules of H_2O and resets the enzyme to its initial, fully oxidized form.

$$4\ \text{Cyt}\ c_{red} + 4\ H^+_{matrix} + O_2 \rightarrow 4\ \text{Cyt}\ c_{ox} + 2\ H_2O$$

The four protons in the reaction shown in Step 4 come exclusively from the matrix. Thus, the consumption of these four protons contributes directly to the proton gradient. Recall that each proton contributes $21.8\ \text{kJ mol}^{-1}\ (5.2\ \text{kcal mol}^{-1})$ to the free energy associated with the proton gradient; so these four protons contribute $87.2\ \text{kJ mol}^{-1}\ (20.8\ \text{kcal mol}^{-1})$, an amount substantially less than the free energy available from the reduction of oxygen to water. What is the fate of this missing energy? Remarkably, cytochrome c oxidase uses this energy to pump four additional protons from the matrix into the intermembrane space in the course of each reaction cycle for a total of eight protons removed from the matrix (**Figure 18.15**). The details of how these protons are transported through the protein are still under study. However, two effects contribute to the mechanism. First, charge neutrality tends to be maintained in the interior of proteins. Thus, the addition of an electron to a site inside a protein tends to favor the binding of H^+ to a nearby site. Second, conformational changes take place, particularly around the heme a_3-Cu_B center, in the course of the reaction cycle. Presumably, in one conformation, protons may enter the protein exclusively from the matrix side, whereas, in another, they may exit exclusively to the intermembrane space. Thus, the overall process catalyzed by cytochrome *c* oxidase is

$$4\ \text{Cyt}\ c_{red} + 8\ H^+_{matrix} + O_2 \rightarrow 4\ \text{Cyt}\ c_{ox} + 2\ H_2O + 4\ H^+_{\text{intermembrane space}}$$

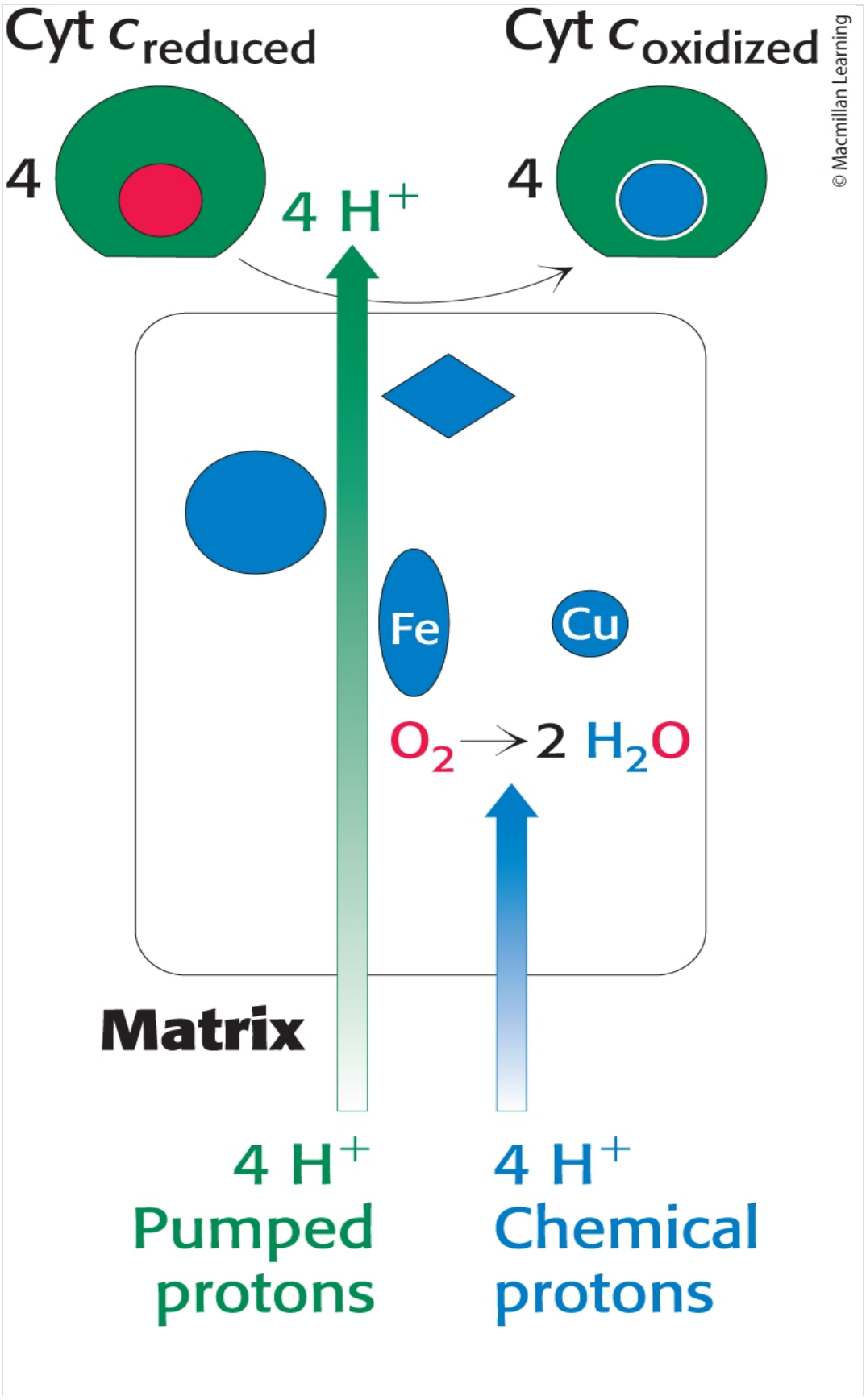

Cyt $c_{reduced}$
Cyt $c_{oxidized}$
4
4
4 H^+
Fe
Cu
$O_2 \rightarrow 2\ H_2O$
Matrix
4 H^+
Pumped protons
4 H^+
Chemical protons
© Macmillan Learning

FIGURE 18.15 Proton transport by cytochrome *c* oxidase has two components. Four protons are taken up from the matrix side to reduce one molecule of O_2 to two molecules of H_2O. These protons are called *chemical protons* because they participate in a clearly defined reaction with O_2. Four additional *pumped protons* are transported out of the matrix and released into the intermembrane space in the course of the reaction.



[Figure 18.16](#) summarizes the flow of electrons from NADH and $FADH_2$ through the respiratory chain. This series of exergonic reactions is coupled to the pumping of protons from the matrix. As we will see shortly, the energy inherent in the proton gradient will be used to synthesize ATP.

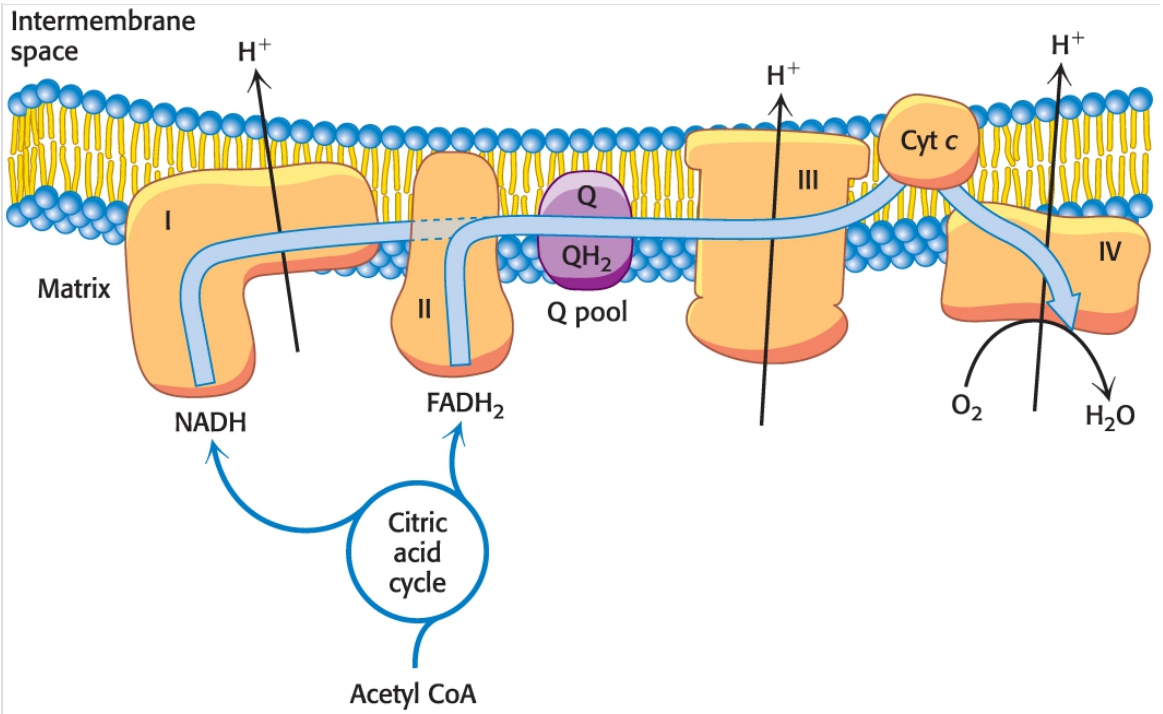


FIGURE 18.16 Electrons flow via two pathways through the electron-transport chain. High-energy electrons in the form of either NADH or $FADH_2$ are generated by the citric acid cycle. These electrons flow through the respiratory chain, which powers proton pumping and results i the reduction of O_2.

EXPLORE this pathway further in the Metabolic Map in Achieve

Most of the electron-transport chain is organized into a larger complex called the respirasome

The portrayal of the electron-transport chain in Figure 18.16 shows the individual components as isolated units. Although fine for illustrative purposes, this depiction is too simplistic. Recent research has established that three of the components of the electron-transport chain are arranged into a massive complex called the **respirasome**. The human respirasome consists of two copies of Complex I, Complex III, and Complex IV (**Figure 18.17**). The respirasome forms a circular structure with two copies each of Complex I and Complex IV surrounding two copies of Complex III. Although not experimentally established, the structure allows for Complex II to associate in a gap between Complexes I and IV. The structure of the respirasome was solved using the technique of cryo-electron microscopy (cryo-EM) (Section 4.5). The respirasome provides yet another example of multienzyme pathways that are organized into large complexes to enhance efficiency.

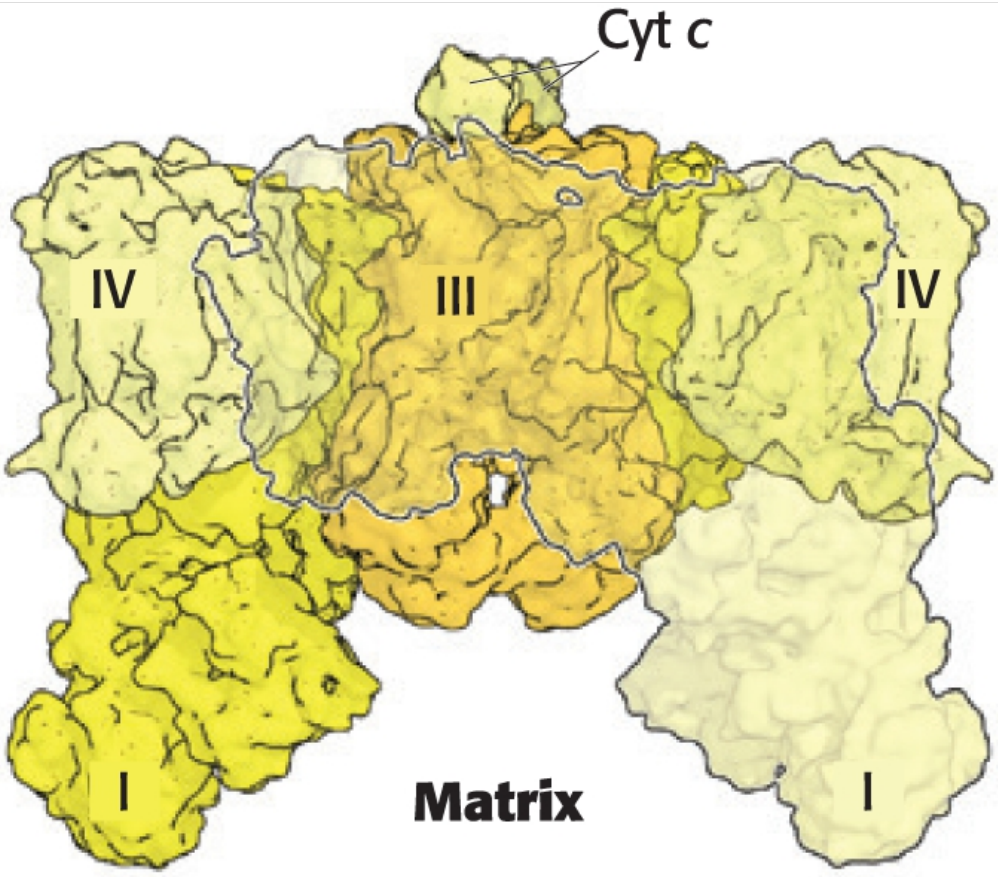
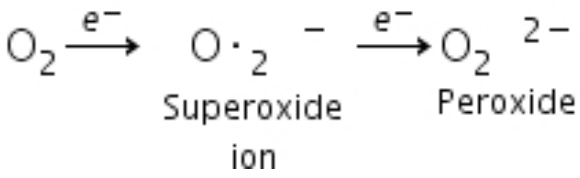


FIGURE 18.17 Three complexes of the ETC associate to form the respirasome. The structure of the electron-transport-chain supercomplex (or respirasome) has been determined by cryo-electron microscopy.

Toxic derivatives of molecular oxygen such as superoxide radicals are scavenged by protective enzymes

As discussed earlier, molecular oxygen is an ideal terminal electron acceptor, because its high affinity for electrons provides a large thermodynamic driving force. However, danger lurks in the reduction of

O_2. The transfer of four electrons leads to safe products (two molecules of H_2O), but partial reduction generates hazardous compounds. In particular, the transfer of a single electron to O_2 forms a superoxide ion, whereas the transfer of two electrons yields peroxide.



Both compounds are potentially destructive. The strategy for the safe reduction of O_2 is clear: the catalyst avoids releasing partly reduced intermediates. Cytochrome *c* oxidase meets this crucial criterion by holding O_2 tightly between Fe and Cu ions.

Although cytochrome *c* oxidase and other proteins that reduce O_2 are remarkably successful in not releasing intermediates, small amounts of superoxide anion and hydrogen peroxide are unavoidably formed. Superoxide, hydrogen peroxide, and species that can be generated from them such as the hydroxyl radical $(OH\cdot)$ are collectively referred to as *reactive oxygen species* or *ROS*. Oxidative damage caused by ROS has been implicated in the aging process as well as in a growing list of diseases (Table 18.3).

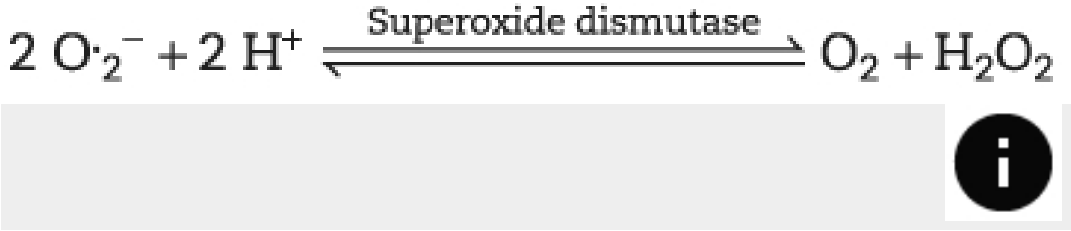
TABLE 18.3 Pathological conditions that may entail free-radical injury

Atherogenesis
Emphysema; bronchitis
Parkinson's disease

Duchenne muscular dystrophy
Cervical cancer
Alcoholic liver disease
Diabetes
Acute renal failure
Down syndrome
Retrolental fibroplasia
Cerebrovascular disorders
Ischemia; reperfusion injury

Information from M. Lieberman and A. D. Marks, *Basic Medical Biochemistry: A Clinical Approach,* 4th ed. (Lippincott, Williams & Wilkins, 2012), p. 437.

What are the cellular defense strategies against oxidative damage by ROS? Chief among them is the enzyme superoxide dismutase. This enzyme scavenges superoxide radicals by catalyzing the conversion of two of these radicals into hydrogen peroxide and molecular oxygen.



Eukaryotes contain two forms of this enzyme, a manganese-containing version located in mitochondria and a copper-and-zinc-dependent cytoplasmic form. These enzymes perform the dismutation reaction by a similar mechanism (Figure 18.18). The oxidized form of the enzyme is

reduced by superoxide to form oxygen. The reduced form of the enzyme, formed in this reaction, then reacts with a second superoxide ion to form peroxide, which takes up two protons along the reaction path to yield hydrogen peroxide.

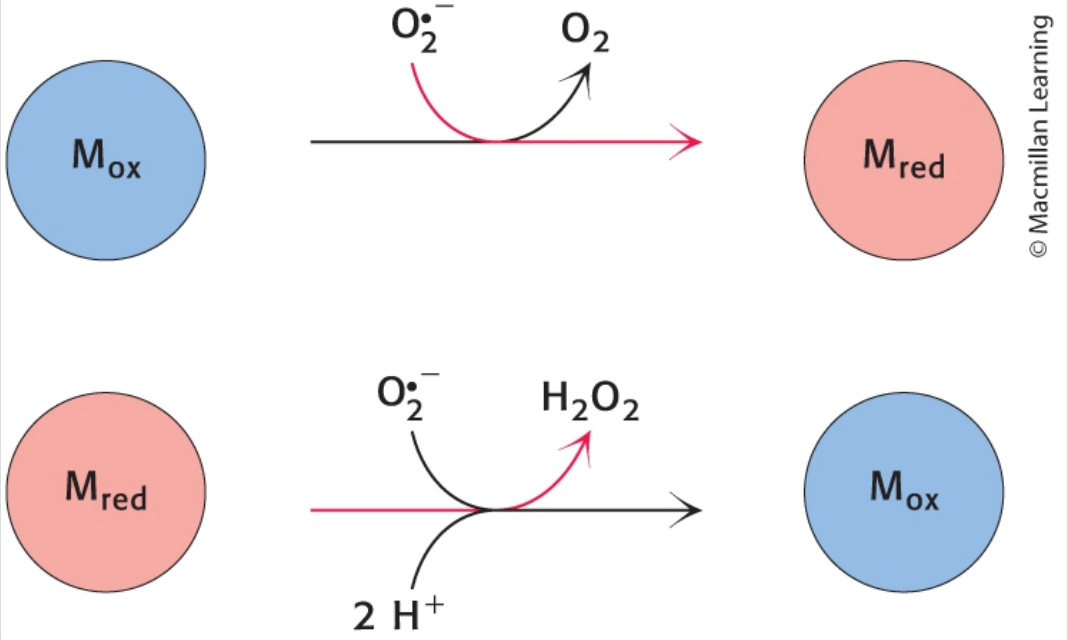


FIGURE 18.18 The superoxide dismutase mechanism has two phases. The oxidized form of superoxide dismutase (M_{ox}) reacts with one superoxide ion to form O_2 and generate the reduced form of the enzyme (M_{red}). The reduced form then reacts with a second superoxide and two protons to form hydrogen peroxide and regenerate the oxidized form of the enzyme.

The hydrogen peroxide formed by superoxide dismutase and by other processes is scavenged by *catalase*, a ubiquitous heme protein that catalyzes the dismutation of hydrogen peroxide into water and molecular oxygen.

$$2H_2O_2 \xrightleftharpoons{\text{Catalase}} O_2 + 2\ H_2O$$

Superoxide dismutase and catalase are remarkably efficient, performing their reactions at or near the diffusion-limited rate (Section 5.4). Glutathione peroxidase also plays a role in scavenging H_2O_2 (Section 20.5). Other cellular defenses against oxidative damage include the antioxidant vitamins, vitamins E and C. Because it is lipophilic, vitamin E is especially useful in protecting membranes from lipid peroxidation.

 A long-term benefit of exercise may be to increase the amount of superoxide dismutase in the cell. The elevated aerobic metabolism during exercise causes more ROS to be generated. In response, the cell synthesizes more protective enzymes. The net effect is one of protection, because the increase in superoxide dismutase more effectively protects the cell during periods of rest.

Despite the fact that reactive oxygen species are known hazards, recent evidence suggests that, under certain circumstances, the controlled generation of these molecules may be an important component of signal-transduction pathways. For instance, growth factors have been shown to increase ROS levels as part of their signaling pathway, which in turn regulate channels and transcription factors. ROS have been implicated in the control of cell differentiation, the immune response, and autophagy, as well as other metabolic activities. The dual role of ROS is an excellent example of the wondrous complexity of biochemistry of living systems: even potentially harmful substances can be harnessed to play useful roles.

Self-Check Question



Which electron-transport chain complex is not a member of the respirasome? Which one contains an enzyme of the citric acid cycle? Finally, which one uses FAD as a coenzyme?

Electrons can be transferred between groups that are not in contact

How are electrons transferred between electron-carrying groups of the respiratory chain? This question is intriguing because these groups are frequently buried in the interior of a protein in fixed positions and are therefore not directly in contact with one another. Electrons can move through space, even through a vacuum. However, the rate of electron transfer through space falls off rapidly as the electron donor and electron acceptor move apart from each other, decreasing by a factor of 10 for each increase in separation of 0.8 Å.

The protein environment provides more-efficient pathways for electron conduction: typically, the rate of electron transfer decreases by a factor of 10 every 1.7 Å (**Figure 18.19**). For groups in contact, electron-transfer reactions can be quite fast, with rates of approximately $10^{13}\ s^{-1}$. Within proteins in the electron-transport chain, electron-carrying groups are typically separated by 15 Å beyond their van der Waals contact distance. For such separations, we expect electron-transfer rates of approximately $10^{4}\ s^{-1}$ (i.e., electron transfer in less than 1 ms), assuming that all other factors are optimal. Without the mediation of the protein, an electron transfer over this distance would take approximately 1 day.

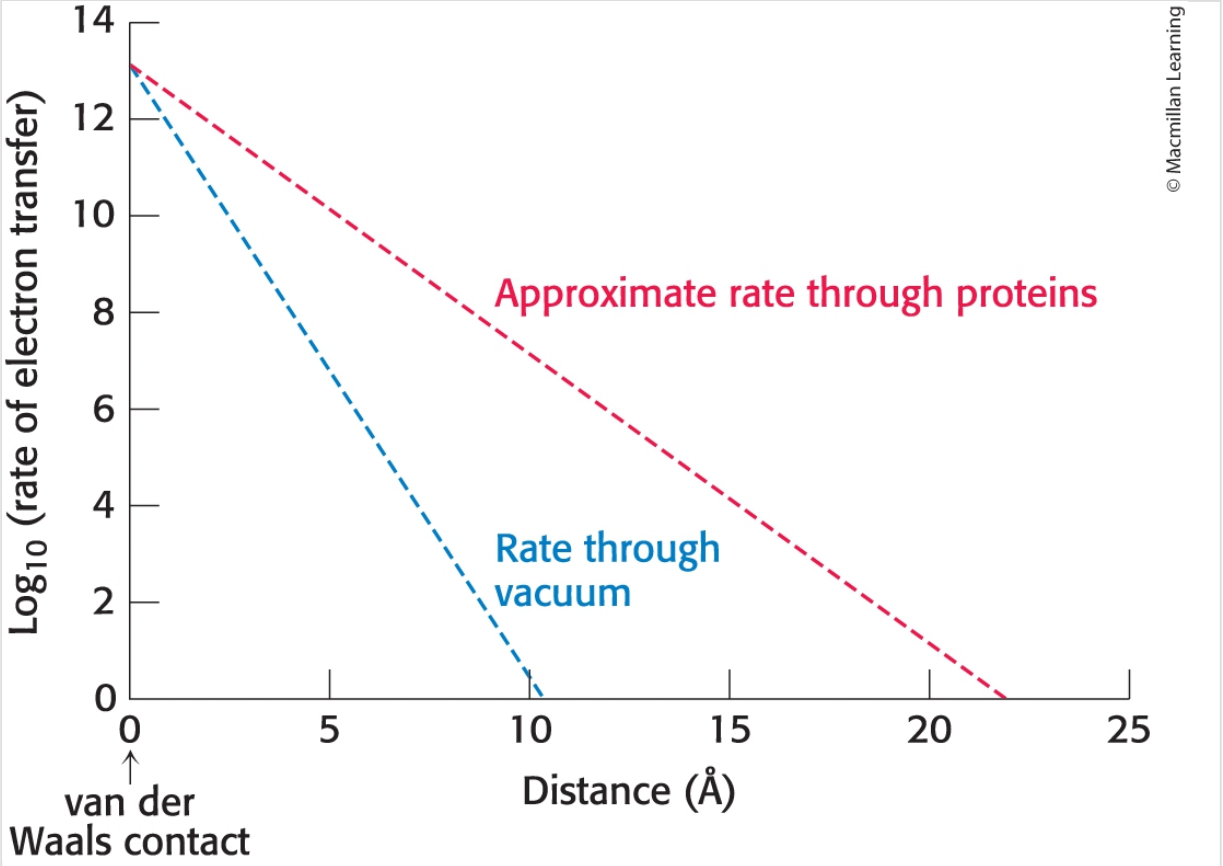


FIGURE 18.19 Proteins dramatically improve the rate of electron transfer between atoms at a distance. The rate of electron transfer decreases as the electron donor and the electron acceptor move apart. In a vacuum, the rate decreases by a factor of 10 for every increase of 0.8 Å. In proteins, the rate decreases more gradually, by a factor of 10 for every increase of 1.7 Å; however, this rate is only approximate because variations in the structure of the intervening protein medium can affect it.

The case is more complicated when electrons must be transferred between two distinct proteins, such as when cytochrome *c* accepts electrons from Complex III or passes them on to Complex IV. A series of hydrophobic interactions bring the heme groups of cytochrome *c* and c_1 to within 4.5 Å of each other, with the iron atoms separated by 17.4 Å. This distance could allow cytochrome *c* reduction at a rate of $8.3 \times 10^6\ s^{-1}$.

18.4 A Proton Gradient Powers the Synthesis of ATP

Thus far, we have considered the flow of electrons from NADH to O_2, an *exergonic* process.

$$NADH + \tfrac{1}{2}O_2 + H^+ \rightleftharpoons H_2O + NAD^+$$
$$\Delta G^{\circ\prime} = -220.1 \text{ kJ mol}^{-1} \ (-52.6 \text{ kcal mol}^{-1})$$

Next, we consider how this process is coupled to the synthesis of ATP, an *endergonic* process.

$$ADP + P_i + H^+ \rightleftharpoons ATP + H_2O$$
$$\Delta G^{\circ\prime} = +30.5 \text{ kJ mol}^{-1} \ (+7.3 \text{ kcal mol}^{-1})$$

A molecular assembly in the inner mitochondrial membrane carries out the synthesis of ATP. This enzyme complex was originally called the *mitochondrial ATPase* or F_1F_0 *ATPase* because it was discovered through its catalysis of the reverse reaction, the hydrolysis of ATP. **ATP synthase**, its preferred name, emphasizes its actual role in the mitochondrion. It is also called **Complex V**.

How is the oxidation of NADH coupled to the phosphorylation of ADP? Electron transfer was first suggested to lead to the formation of a covalent high-energy intermediate that serves as a compound having a high phosphoryl-transfer potential, analogous to the generation of ATP by the formation of 1,3-bisphosphoglycerate in glycolysis (Section 16.2). An alternative proposal was that electron transfer aids the formation of an activated protein conformation, which then drives ATP synthesis.

However, the search for such intermediates for several decades proved fruitless.

The chemiosmotic hypothesis suggested that ATP formation is powered by a proton gradient

In 1961, Peter Mitchell suggested a radically different mechanism called the *chemiosmotic hypothesis*. He proposed that electron transport and ATP synthesis are coupled by a proton gradient across the inner mitochondrial membrane. In his model, the transfer of electrons through the respiratory chain leads to the pumping of protons from the matrix to the intermembrane space. The H^+ concentration becomes lower in the matrix, and an electric field with the matrix side negative is generated (Figure 18.20). Protons then flow back into the matrix to equalize the distribution. Mitchell's idea was that this flow of protons drives the synthesis of ATP by ATP synthase.

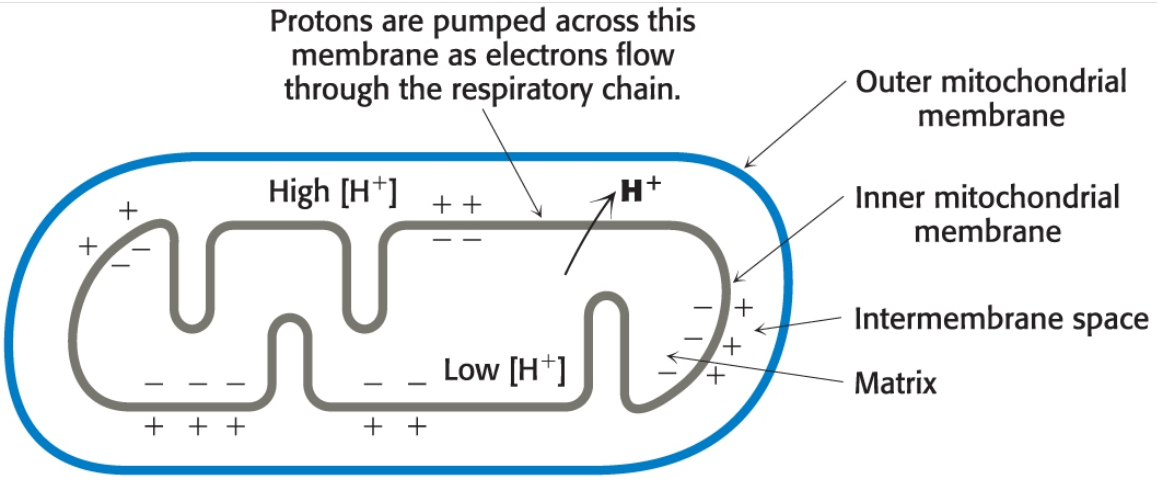


FIGURE 18.20 The chemiosmotic hypothesis states that electron-driven proton transport and ATP synthesis are coupled. Electron transfer through the respiratory chain leads to the pumping of protons from the matrix to the intermembrane space. The pH gradient and membrane potential constitute a proton-motive force that is used to drive ATP synthesis.

As noted earlier, the energy-rich unequal distribution of protons across a membrane is called the *proton-motive force*. The proton-motive force is composed of two components: a chemical gradient and a charge gradient. The chemical gradient for protons can be represented as a pH gradient. The charge gradient is created by the positive charge on the unequally distributed protons forming the chemical gradient. Mitchell proposed that both components power the synthesis of ATP.

$$\text{Proton-motive force } (\Delta p) = \text{chemical gradient } (\Delta p\text{H}) + \text{charge gradient } (\Delta\psi)$$

Mitchell's highly innovative hypothesis is now supported by a wealth of evidence. Indeed, electron transport does generate a proton gradient across the inner mitochondrial membrane. The pH outside is 1.4 units lower than inside, and the membrane potential is 0.14 V, the outside being positive. As we calculated in Section 18.2, this membrane potential corresponds to a free energy of 21.8 kJ (5.2 kcal) per mole of protons.

An artificial system was created to elegantly demonstrate the basic principle of the chemiosmotic hypothesis. The role of the respiratory chain was played by bacteriorhodopsin, a membrane protein from halobacteria that pumps protons when illuminated (Chapter 19). Synthetic vesicles containing bacteriorhodopsin and mitochondrial ATP synthase purified from beef heart were created (**Figure 18.21**). When the vesicles were exposed to light, ATP was formed. This key experiment clearly showed that the respiratory chain and ATP synthase are biochemically separate systems, linked only by a proton-motive force.

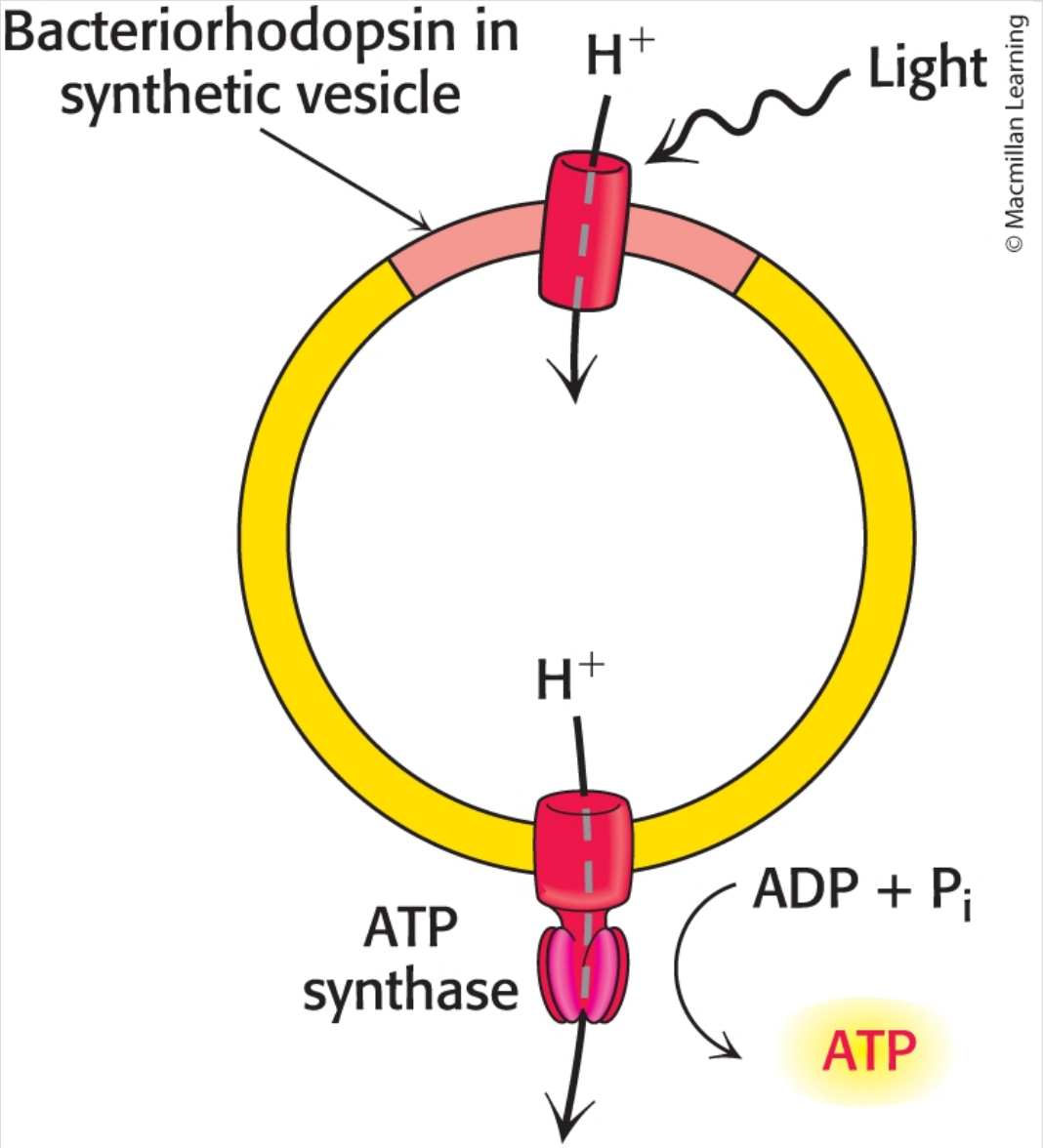


FIGURE 18.21 The chemiosmotic hypothesis is supported by experiments using bacterial proton pumps. ATP is synthesized when reconstituted membrane vesicles containing bacteriorhodopsin (a light-driven proton pump) and ATP synthase are exposed to light.

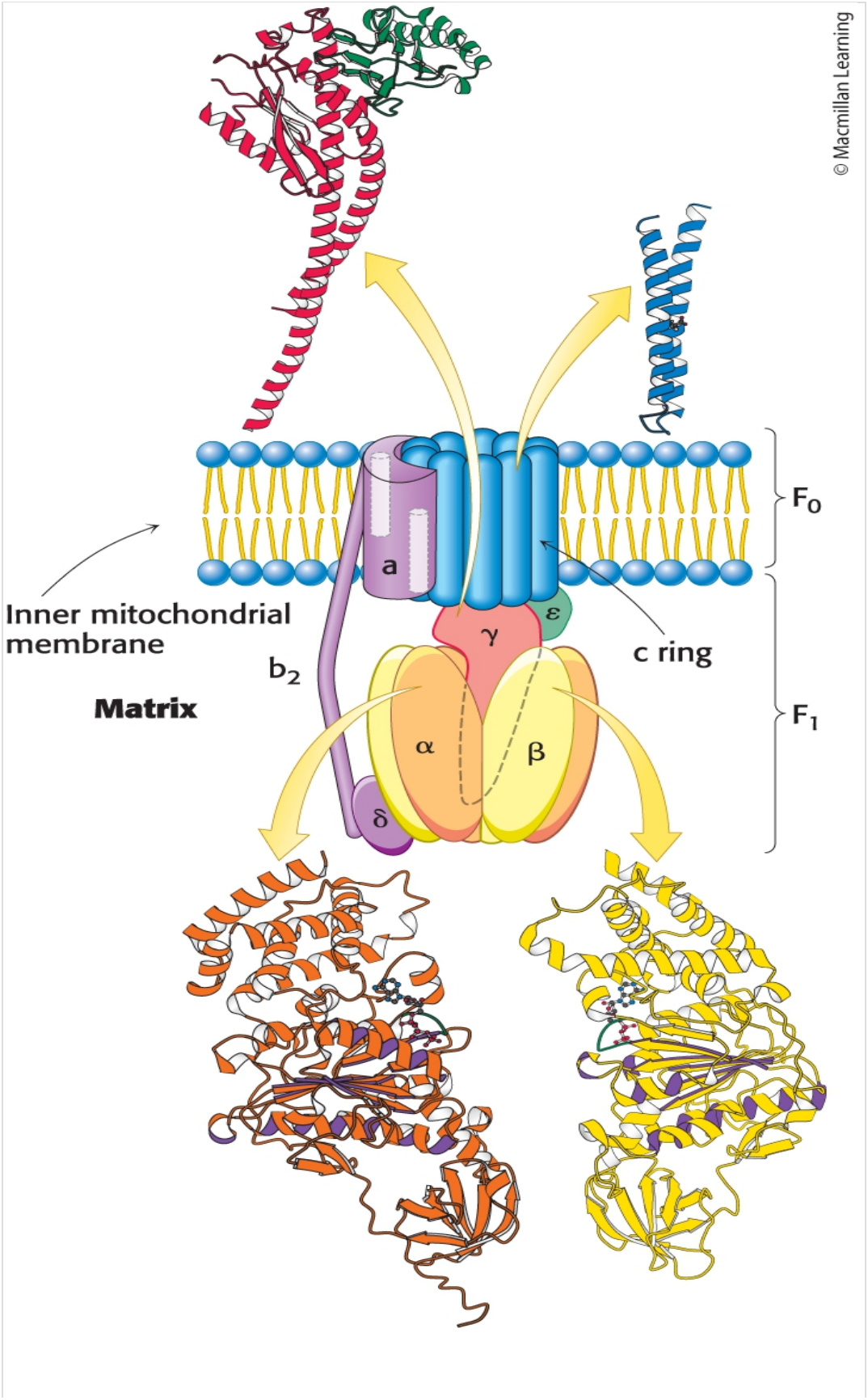
Some have argued that, along with the elucidation of the structure of DNA, the discovery that ATP synthesis is powered by a proton gradient is one of the two major advances in biology in the twentieth century.

Mitchell's initial postulation of the chemiosmotic theory was not warmly received by all: some scientists thought of Mitchell as a "court jester," whose work was of no consequence. In Chapter 19 we will discuss how collaboration with another scientist changed this perception. Eventually, Peter Mitchell was awarded the Nobel Prize in Chemistry for his contributions to understanding oxidative phosphorylation.

ATP synthase is composed of a proton-conducting unit and a catalytic unit

Two parts of the puzzle of how NADH oxidation is coupled to ATP synthesis are now evident: (1) electron transport generates a proton-motive force, and (2) ATP synthesis by ATP synthase can be powered by a proton-motive force. How is the proton-motive force converted into the high phosphoryl-transfer potential of ATP?

Biochemical, electron microscopic, and crystallographic studies of ATP synthase have revealed many details of its structure (**Figure 18.22**). It is a large, complex enzyme resembling a ball on a stick. Much of the "stick" part, called the F_0 subunit, is embedded in the inner mitochondrial membrane. The 85-Å-diameter ball, called the F_1 subunit, protrudes into the mitochondrial matrix. The F_1 subunit contains the catalytic activity of the synthase. In fact, isolated F_1 subunits display ATPase activity.



© Macmillan Learning

FIGURE 18.22 The structure of ATP synthase reveals a complex molecular rotational motor. A schematic structure is shown along with representations of the components for which structures have been determined to high resolution. The P-loop NTPase domains of the α and β subunits are indicated by purple shading. Notice that part of the enzyme complex is embedded in the inner mitochondrial membrane, whereas the remainder resides in the matrix.

[Drawn from 1E79.pdb and 1C0V.pdb.]

INTERACT with this model in Achieve

The F_1 subunit consists of five types of polypeptide chains (α_3, β_3, γ, δ, and ε) with the indicated stoichiometry. The α and β subunits, which make up the bulk of the F_1, are arranged alternately in a hexameric ring; they are homologous to one another and are members of the P-loop NTPase family (Section 9.4). Both bind nucleotides but only the β subunits are catalytically active. Just below the α and β subunits is a central stalk consisting of the γ and ε proteins. The γ subunit includes a long helical coiled coil that extends into the center of the $\alpha_3\beta_3$ hexamer. The γ subunit breaks the symmetry of the $\alpha_3\beta_3$ hexamer: each of the β subunits is distinct by virtue of its interaction with a different, asymmetrical, face of γ. Distinguishing the three β subunits is crucial for understanding the mechanism of ATP synthesis.

The F_0 subunit is a hydrophobic segment that spans the inner mitochondrial membrane. F_0 contains the proton channel of the complex. This channel consists of a ring comprising from 8 to 14 **c** subunits that are embedded in the membrane. A single **a** subunit binds to the outside of the ring. The F_0 and F_1 subunits are connected in two ways: by the central γε stalk and by an exterior column. The exterior column consists of one **a** subunit, two **b** subunits, and the δ subunit.

ATP synthases interact with one another to form dimers, which then associate to form large oligomers of dimers (Figure 18.23). This association stabilizes the individual enzymes to the rotational forces required for catalysis, which we will examine shortly, and facilitates the curvature of the inner mitochondrial membrane. The formation of the cristae allows the proton pumps of the electron-transport chain to localize the proton gradient in the vicinity of the synthases, which are located at the tips of the cristae, thereby enhancing the efficiency of ATP synthesis (Figure 18.24).

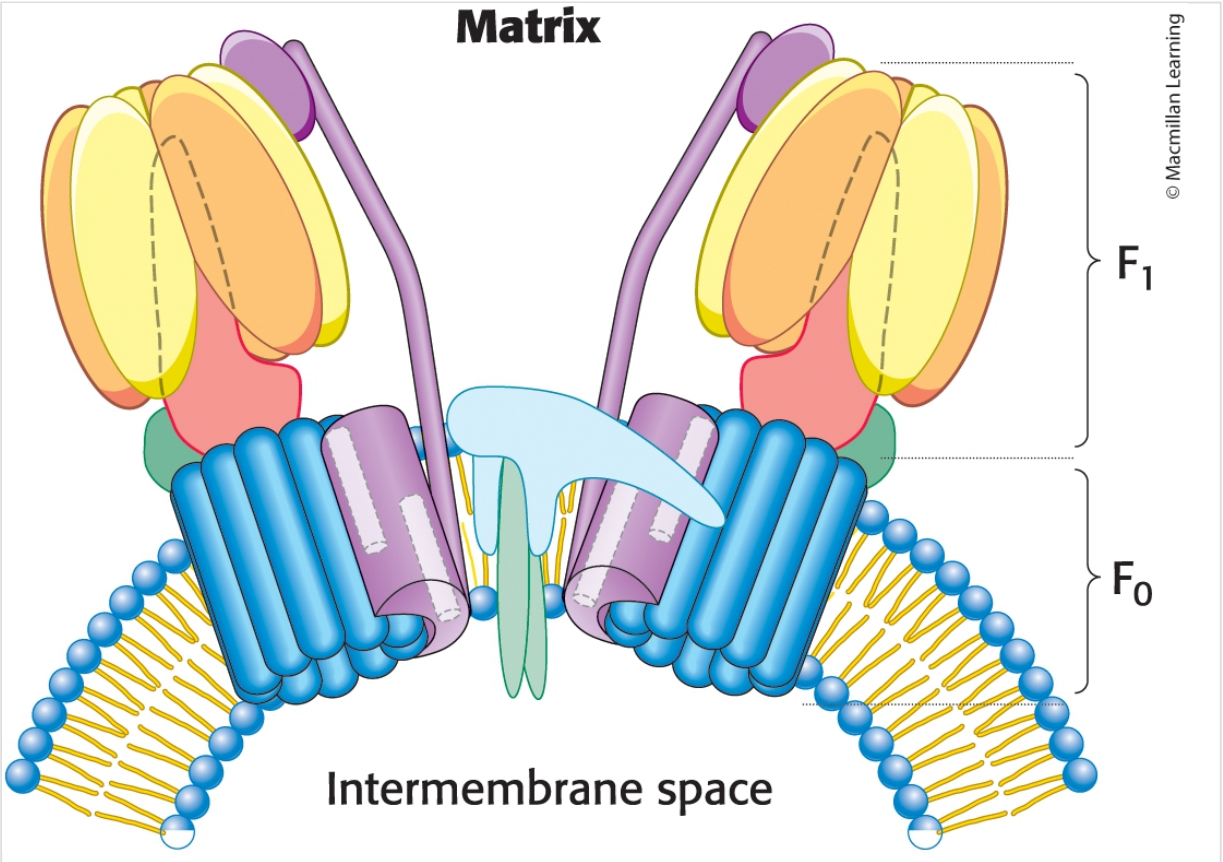


FIGURE 18.23 Mitochondrial ATP synthase forms homodimers. A schematic representation of a dimer of mitochondria ATP synthase is shown embedded in the inner mitochondrial membrane. The dimer, joined by an assortment of proteins, assists in bending the inner mitochondria membrane. The structure of the dimer was determined by cryo-electron microscopy.

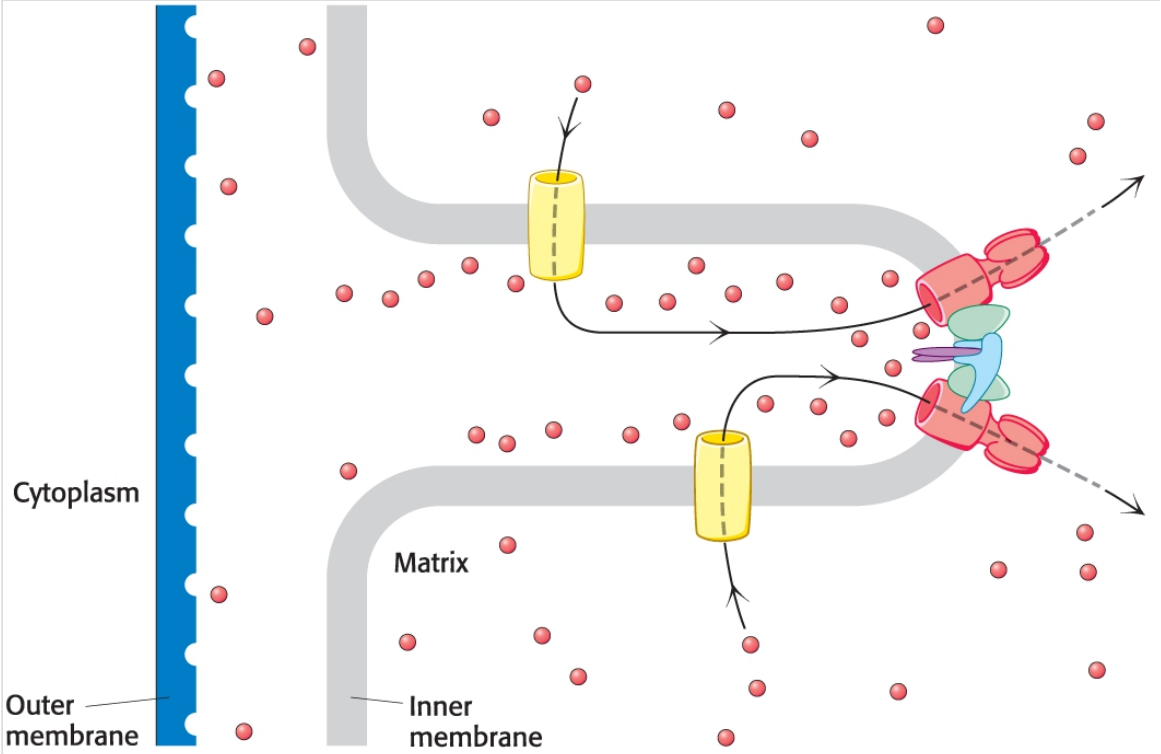


FIGURE 18.24 ATP synthase assists in the formation of cristae. Oligomers of ATP synthase dimers facilitate cristae formation, creating an area where the protons (shown as red balls) are concentrated and have ready access to the F_o portion of the ATP synthase. The electron-transport chain is represented by the yellow cylinders embedded in the inner mitochondrial membrane.

[Information from K. M. Davies et al., *Proc. Natl. Acad. Sci. U.S.A.* 108:14121–14126, 2011.]

Proton flow through ATP synthase leads to the release of tightly bound ATP via the binding-change mechanism

ATP synthase catalyzes the formation of ATP from ADP and orthophosphate.

$$ADP^{3-} + HPO_4^{2-} + H^+ \rightleftharpoons ATP^{4-} + H_2O$$

The actual substrates are ADP and ATP complexed with Mg^{2+}, as in all known phosphoryl-transfer reactions with these nucleotides. A terminal oxygen atom of ADP attacks the phosphorus atom of P_i to form a pentacovalent intermediate, which then dissociates into ATP and H_2O (Figure 18.25).

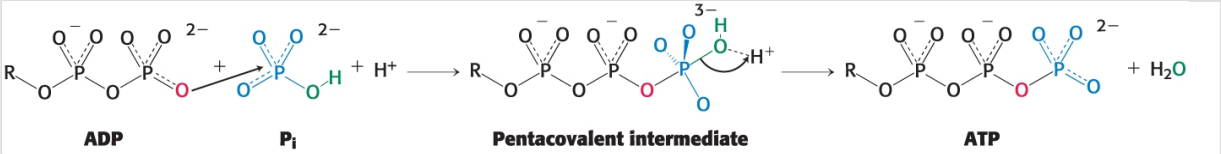


FIGURE 18.25 ATP-synthesis is catalyzed by ATP synthase. One of the oxygen atoms of ADP attacks the phosphorus atom of P_i to form a pentacovalent intermediate, which then forms ATP and releases a molecule of H_2O.

How does the flow of protons drive the synthesis of ATP? Isotopic-exchange experiments unexpectedly revealed that enzyme-bound ATP forms readily in the absence of a proton-motive force. When ADP and P_i were added to ATP synthase in $H_2{}^{18}O$, ^{18}O became incorporated into P_i through the synthesis of ATP and its subsequent hydrolysis (Figure 18.26). The rate of incorporation of ^{18}O into P_i showed that about equal amounts of bound ATP and ADP are in equilibrium at the catalytic site, even in the absence of a proton gradient. However, ATP does not leave the catalytic site unless protons flow through the enzyme. Thus, the role of the proton gradient is not to form ATP but to release it from the synthase.

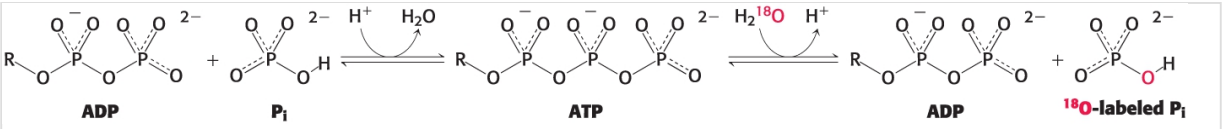


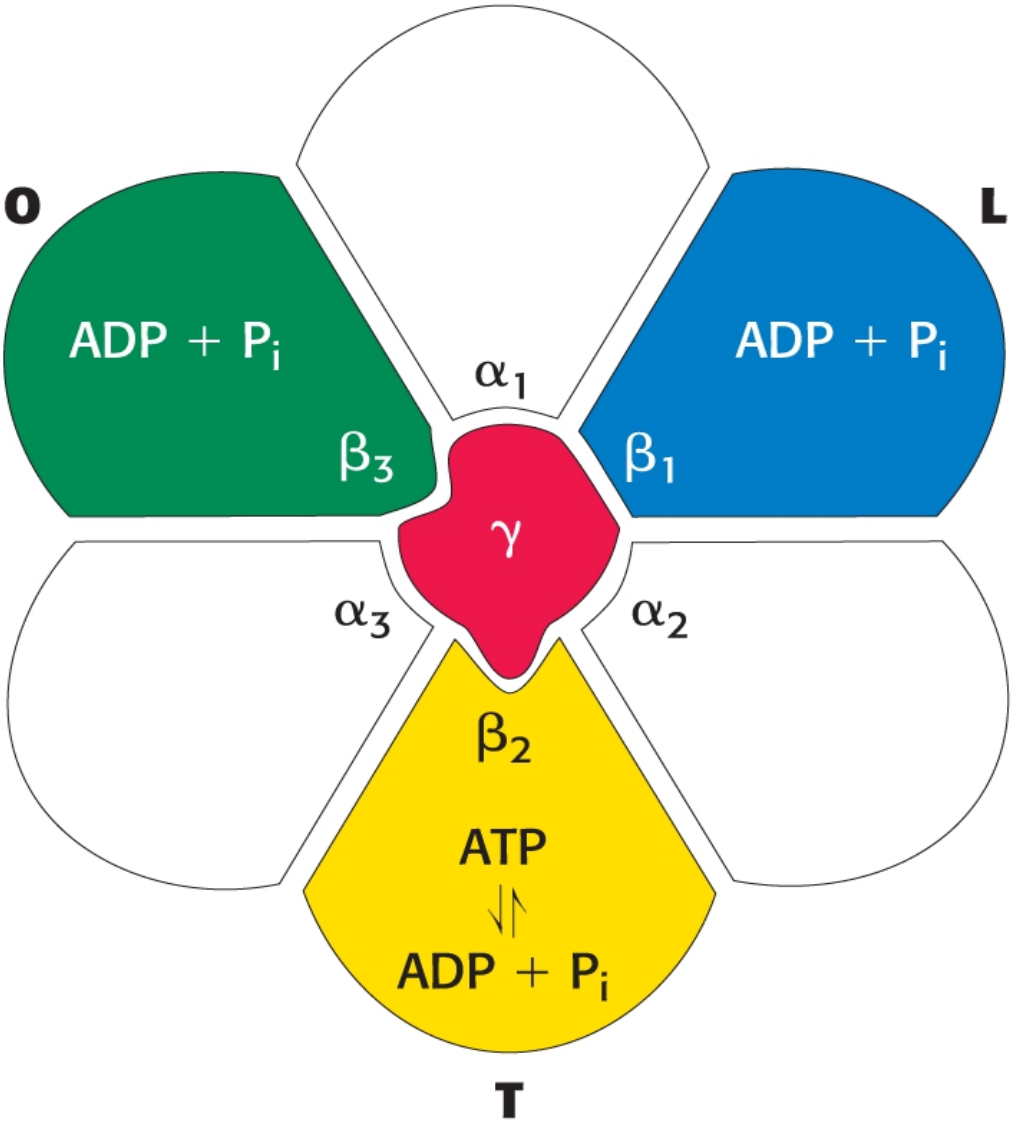
FIGURE 18.26 ATP forms without a proton-motive force but is not released. The results of isotopic-exchange experiments indicate that enzyme-bound ATP is formed from ADP and P_i in the absence of a proton-motive force.

The fact that three β subunits are components of the F_1 moiety of the ATPase means that there are three active sites on the enzyme, each performing one of three different functions at any instant. The proton-motive force causes the three active sites to sequentially change functions as protons flow through the membrane-embedded component of the enzyme. Indeed, we can think of the enzyme as consisting of a moving part and a stationary part: (1) the moving unit, or *rotor,* consists of the **c** ring and the γε stalk; and (2) the stationary unit, or *stator,* is composed of the remainder of the molecule.

How do the three active sites of ATP synthase respond to the flow of protons? A number of experimental observations suggested what is known as the *binding-change mechanism* for proton-driven ATP synthesis. This proposal states that a β subunit can perform each of three sequential steps in the synthesis of ATP by changing conformation. These steps are (1) ADP and P_i binding, (2) ATP synthesis, and (3) ATP release. As already noted, interactions with the γ subunit make the three β subunits structurally distinct (Figure 18.27). At any given moment, one β subunit will be in the L, or loose, conformation. This conformation binds ADP and P_i. A second subunit will be in the T, or tight, conformation. This conformation binds ATP with great affinity, so much so that it will convert bound ADP and P_i into ATP. Both the T and L conformations are sufficiently constrained that they cannot release bound nucleotides. The final subunit will be in the O, or open,

form. This form has a more open conformation and can bind or release adenine nucleotides.

(A)



© Macmillan Learning

(B)

β subunit 1	L → T → O → L → T → O...
β subunit 2	O → L → T → O → L → T...
β subunit 3	T → O → L → T → O → L...

FIGURE 18.27 ATP synthase nucleotide-binding sites cycle through distinct conformational states. (A) The γ subunit passes through the center of the $\alpha_3\beta_3$ hexamer and makes the nucleotide-binding sites in the β subunits distinct from one another. The β subunits are colored to distinguish them from one another, whereas the conformational states are denoted "O," "L," and "T." (B) The progressive and simultaneous alteration of the conformational states of all three β subunits of ATP synthase shows that each subunit cycles through the three different states in the same order but at different times as the γ subunit rotates.

The rotation of the γ subunit drives the interconversion of these three forms (**Figure 18.28**). Consider a single subunit, like the one shown in yellow in Figure 18.28, which is initially in the T form in which bound ADP and P_i are transiently combining to form ATP. Suppose that the γ subunit is rotated by 120 degrees in a counterclockwise direction (as viewed from the top). This rotation converts the T-form site into an O-form site with the nucleotide bound as ATP. Concomitantly, the L-form site is converted into a T-form site, enabling the transformation of an additional ADP and P_i into ATP. The ATP in the O-form site can now depart from the enzyme to be replaced by ADP and P_i. An additional 120-degree rotation converts this O-form site into an L-form site, trapping these substrates. Each subunit progresses from the T to the O to the L form with no two subunits ever present in the same conformational form. This mechanism suggests that ATP can be synthesized and released by driving the rotation of the γ subunit in the appropriate direction.

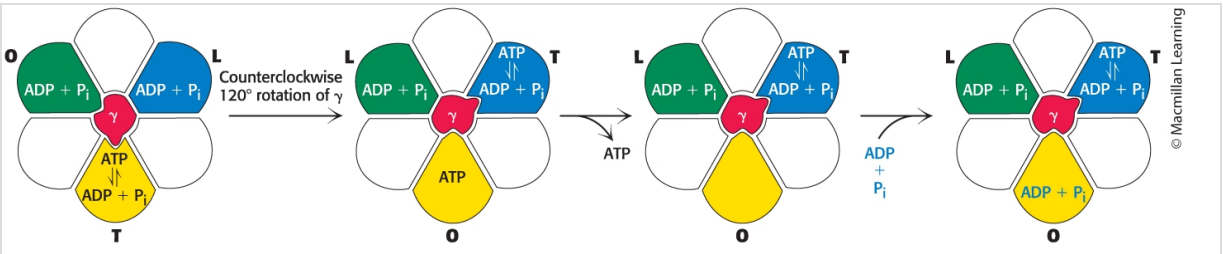


FIGURE 18.28 The binding-change mechanism involves the cycling of all three β subunits through three conformations. The rotation of the γ subunit interconverts the three β subunits.

The subunit in the T (tight) form interconverts ADP and P_i and ATP but does not allow ATP to be released. When the γ subunit is rotated by 120 degrees in a counterclockwise direction, the T-form subunit is converted into the O form, allowing ATP release. ADP and P_i can then bind to the O-form subunit. An additional 120-degree rotation (not shown) traps these substrates in an L-form subunit.



Rotational catalysis is the world's smallest molecular motor

Is it possible to observe the proposed rotation directly? Elegant experiments, using single-molecule techniques (Section 5.5), have demonstrated the rotation through the use of a simple experimental system consisting solely of cloned $\alpha_3\beta_3\gamma$ subunits (**Figure 18.29**). The β subunits were engineered to contain amino-terminal polyhistidine tags, which have a high affinity for nickel ions. This property of the tags allowed the $\alpha_3\beta_3$ assembly to be immobilized on a glass surface that had been coated with nickel ions. The γ subunit was linked to a fluorescently labeled actin filament to provide a long segment that could be observed under a fluorescence microscope. Remarkably, the addition of ATP caused the actin filament to rotate unidirectionally in a counterclockwise direction, confirming visually that the γ subunit was rotating, driven by the hydrolysis of *ATP.* Thus, the catalytic activity of an individual molecule could be observed. The counterclockwise rotation is consistent with the predicted mechanism for hydrolysis because the molecule was viewed from below relative to the view shown in Figure 18.29.

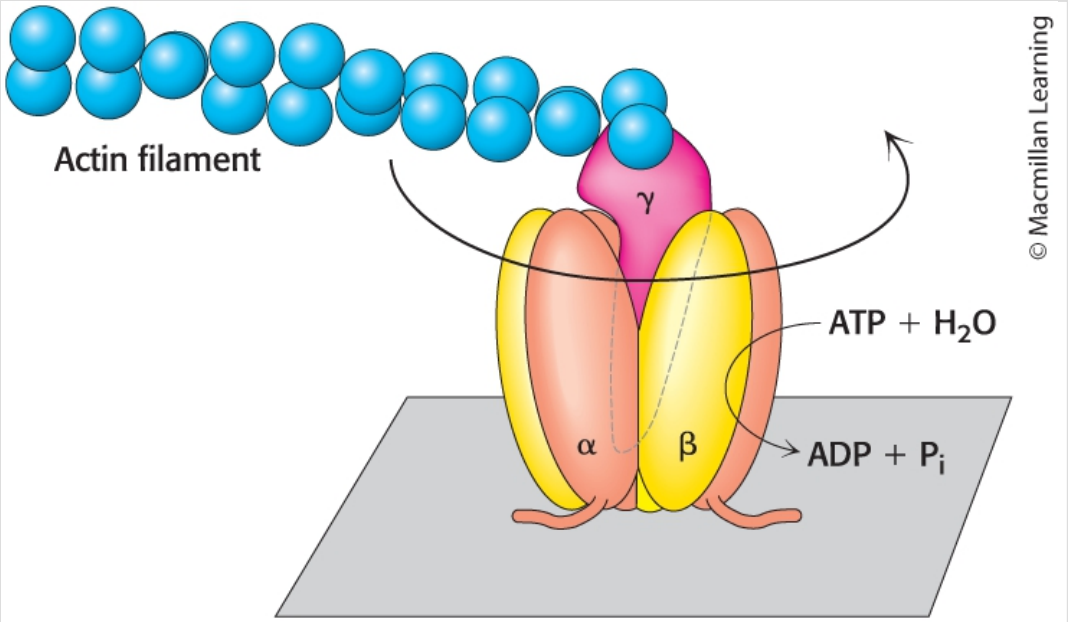


FIGURE 18.29 The ATP-driven rotation in ATP synthase has been directly observed. The $\alpha_3\beta_3$ hexamer of ATP synthase is fixed to a surface, with the γ subunit projecting upward and linked to a fluorescently labeled actin filament. The addition and subsequent hydrolysis of ATP result in the counterclockwise rotation of the γ subunit, which can be directly seen under a fluorescence microscope.

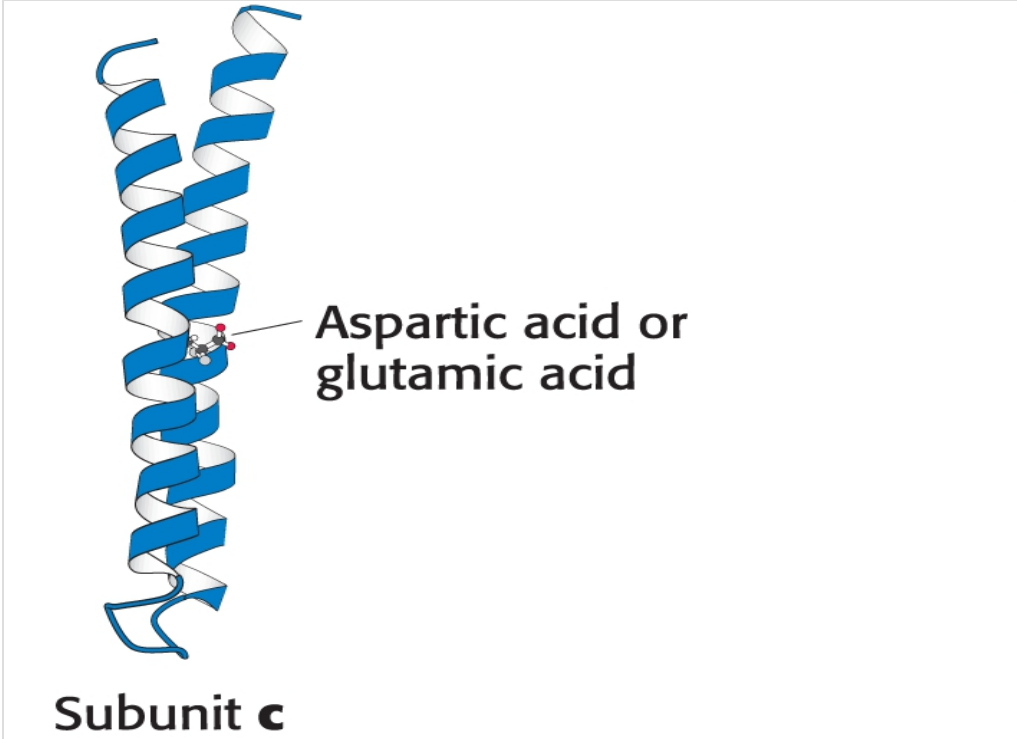
More-detailed analysis in the presence of lower concentrations of ATP revealed that the γ subunit rotates in 120-degree increments. Each increment corresponds to the hydrolysis of a single ATP molecule. In addition, from the results obtained by varying the length of the actin filament and measuring the rate of rotation, the enzyme appears to operate near 100% efficiency; that is, essentially all of the energy released by ATP hydrolysis is converted into rotational motion.

Self-Check Question

Recall our study of enzymes in previous chapters: Why do isolated F_1 subunits of ATP synthase catalyze ATP hydrolysis?

Proton flow around the c ring powers ATP synthesis

The direct observation of rotary motion of the γ subunit is strong evidence for the rotational mechanism for ATP synthesis. The last remaining question is: How does proton flow through F_0 drive the rotation of the γ subunit? The mechanism depends on the structures of the **a** and **c** subunits of F_0 (**Figure 18.30**). The stationary **a** subunit directly abuts the membrane-spanning ring formed by 8 to 14 **c** subunits. The **a** subunit includes two hydrophilic half-channels that do not span the membrane (Figure 18.30). Thus, protons can pass into either of these channels, but they cannot move completely across the membrane. The **a** subunit is positioned such that each half-channel directly interacts with one **c** subunit.



© Macmillan Learning

FIGURE 18.30 Components of the proton-conducting unit of ATP synthase include two half channels and a critical charged residue. The **c** subunit consists of two α helices that span the membrane. In *E. coli*, an aspartic or glutamic acid residue in one of the helices lies on the center of the membrane. The structure of the **a** subunit has not yet been directly observed, but it appears to include two half-channels that allow protons to enter and pass partway but not completely through the membrane.



The structure of the **c** subunit was determined both by NMR methods and by x-ray crystallography. Each polypeptide chain forms a pair of α helices that span the membrane. A glutamic acid (or aspartic acid) residue is found in the middle of one of the helices. If the glutamate is charged (unprotonated), the **c** subunit will not move into the membrane. The key to proton movement across the membrane is that, in a proton-rich environment, such as the intermembrane space, a proton will enter a channel and bind the glutamate residue, while the glutamic acid in a proton-poor environment of the other half-channel will release a proton (Figure 18.31). The **c** subunit with the bound proton then moves into the membrane as the ring rotates by one **c** subunit. This rotation brings the newly deprotonated **c** subunit from the matrix half-channel to the proton-rich intermembrane space half-channel, where it can bind a proton. The movement of protons through the half-channels from the high proton concentration of the intermembrane space to the low proton concentration of the matrix powers the rotation of the **c** ring. The **a** unit remains stationary as the **c** ring rotates. Each proton that enters the intermembrane space half-channel of the **a** unit moves through the membrane by riding around on the rotating **c** ring to exit through the matrix half-channel into the proton-poor environment of the matrix (Figure 18.32).

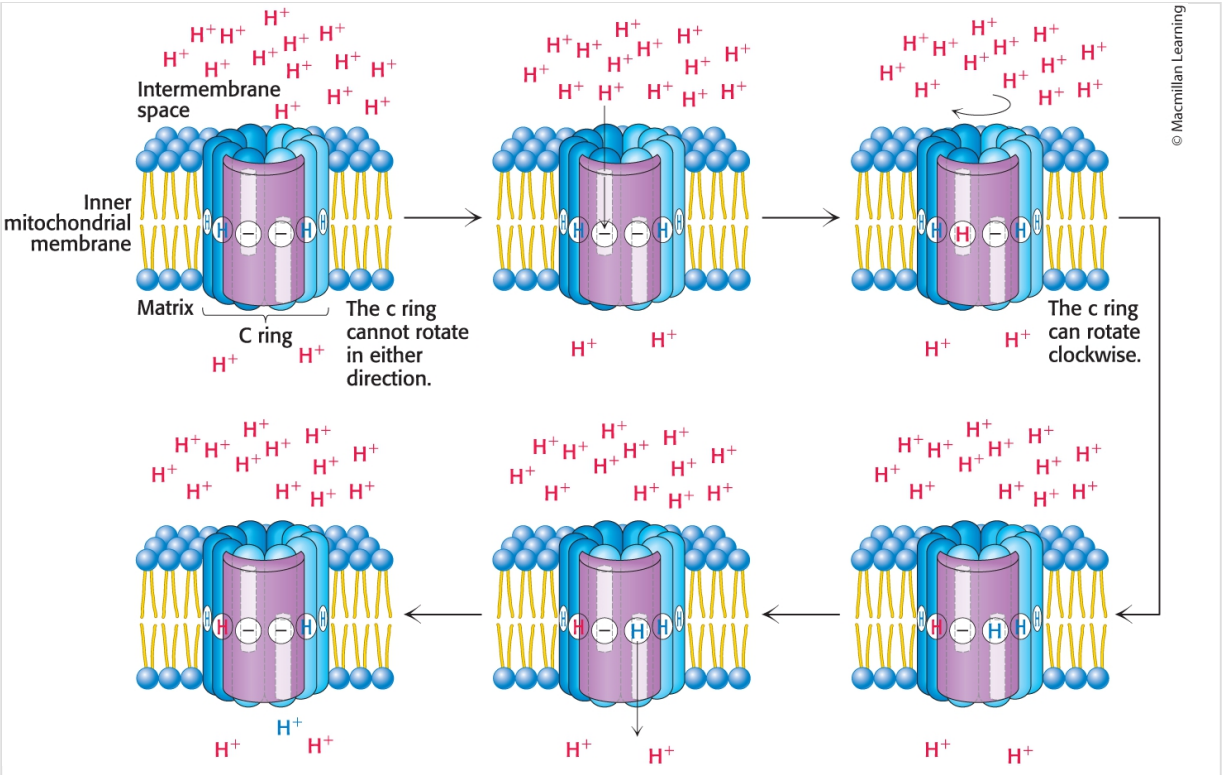


FIGURE 18.31 Proton motion across the membrane drives rotation of the c ring. A proton enters from the intermembrane space into the cytoplasmic half-channel to neutralize the charge on an aspartate or glutamate residue in a **c** subunit. With this charge neutralized, the **c** ring can rotate clockwise by one **c** subunit, moving an aspartic or glutamic acid residue out of the membrane into the matrix half-channel. This proton can move into the matrix, resetting the system to its initial state.

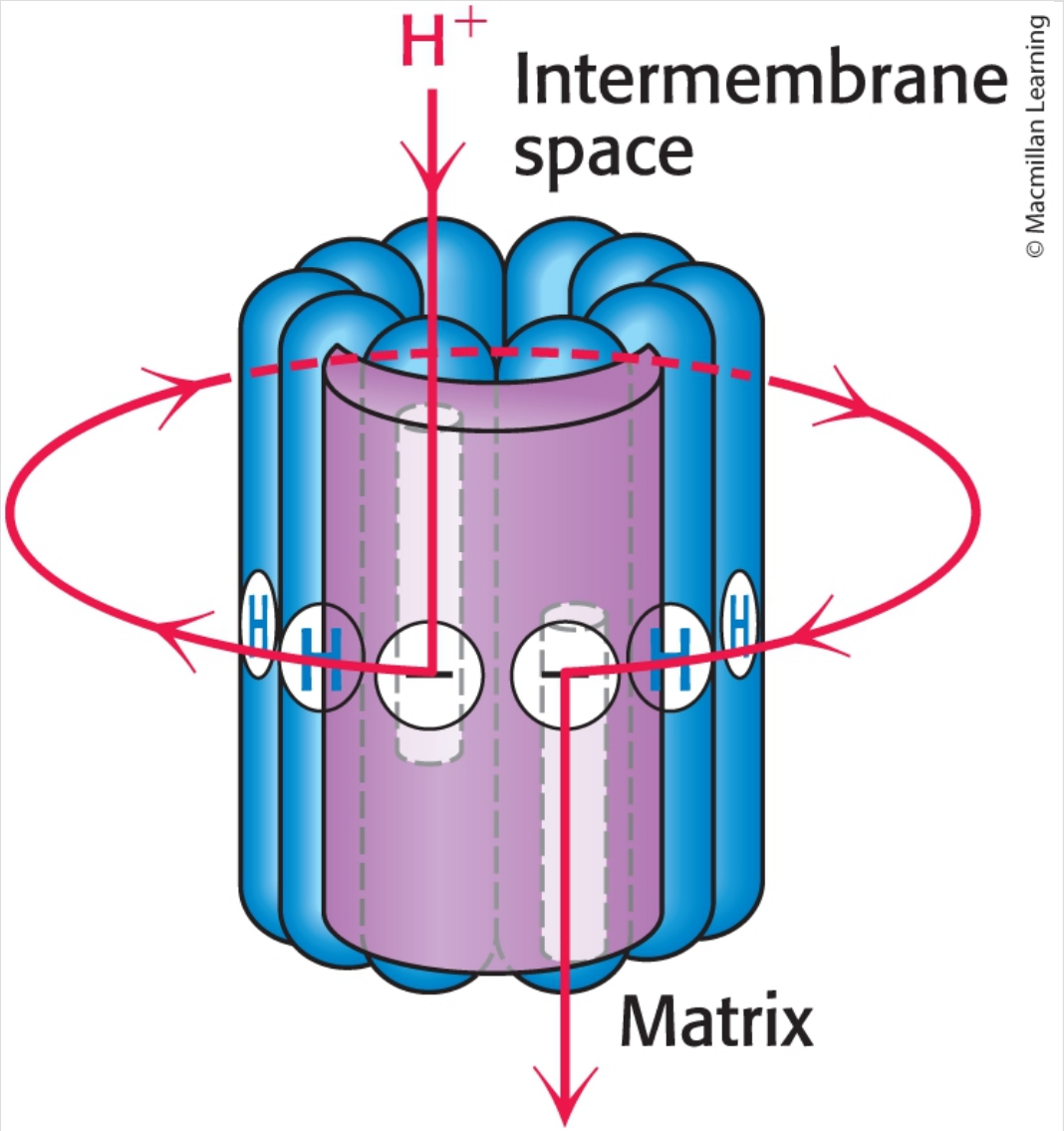


FIGURE 18.32 Protons must travel around the c ring to cross the membrane. Each proton enters the cytoplasmic half-channel, follows a complete rotation of the **c** ring, and exits through the other half-channel into the matrix.

How does the rotation of the **c** ring lead to the synthesis of ATP? The **c** ring is tightly linked to the γ and ε subunits. Thus, as the **c** ring turns, the γ and ε subunits are turned inside the $\alpha_3\beta_3$ hexamer unit of F_1. The rotation of the γ subunit in turn promotes the synthesis of ATP through

the binding-change mechanism. The exterior column formed by the two **b** chains and the δ subunit prevents the $\alpha_3\beta_3$ hexamer from rotating along with the **c** ring. Recall that the dimerization and subsequent oligomerization of the synthase in the cristae also stabilizes the enzyme to rotational forces.

As stated earlier, the number of **c** subunits in the **c** ring appears to range between 8 and 14. This number is significant because it determines the number of protons that must be transported to generate a molecule of ATP. Each 360-degree rotation of the γ subunit leads to the synthesis and release of three molecules of ATP. Thus, if there are 10 **c** subunits in the ring (as was observed in a crystal structure of yeast mitochondrial ATP synthase), each ATP generated requires the transport of $10/3 = 3.33$ protons. Recent evidence shows that the **c** rings of all vertebrates are composed of 8 subunits, making vertebrate ATP synthase the most efficient ATP synthase known, with the transport of only 2.7 protons required for ATP synthesis. For simplicity in calculations, we will assume a rounded average of these two numbers — 3 protons — must flow into the matrix for each ATP formed, but we must keep in mind that the true value may differ. As we will see, the electrons from NADH pump enough protons to generate 2.5 molecules of ATP, whereas those from $FADH_2$ yield 1.5 molecules of ATP.

Let us return for a moment to the example with which we began this chapter. If a resting human being requires 85 kg of ATP per day for bodily functions, then 3.3×10^{25} protons must flow through the ATP synthase per day, or 3.9×10^{20} protons per second. **Figure 18.33** summarizes the process of oxidative phosphorylation.

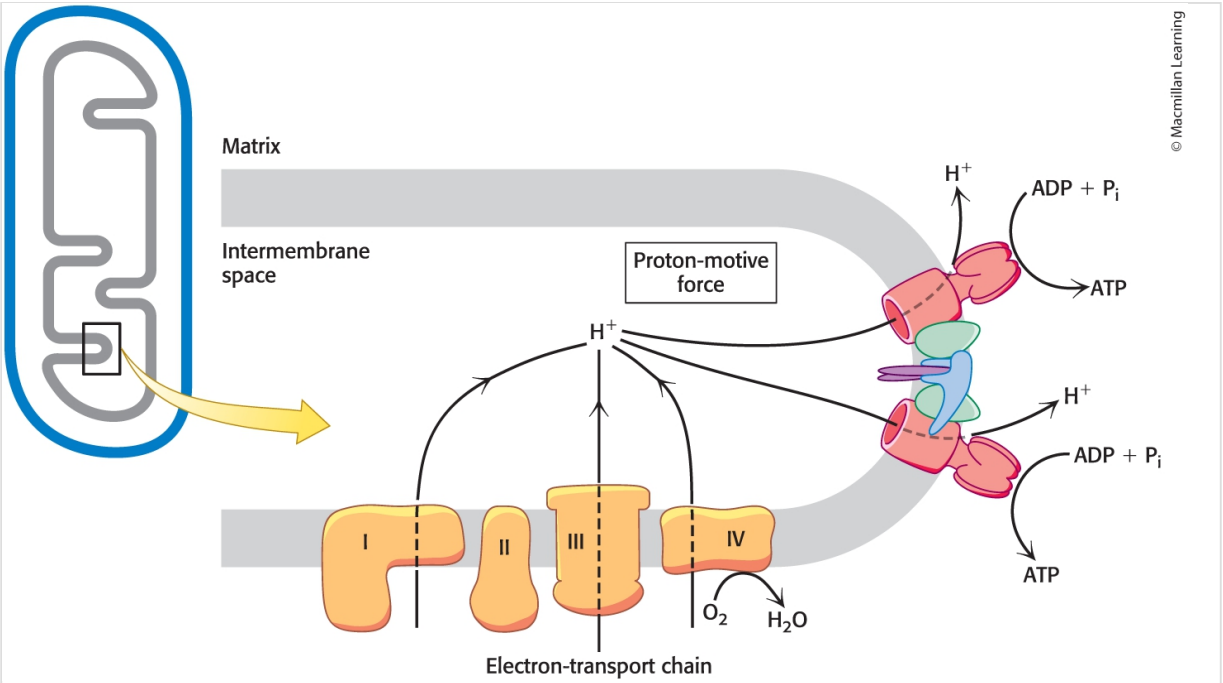


FIGURE 18.33 An overview of oxidative phosphorylation shows the spatial relationship of the components. The electron-transport chain generates a proton gradient by pumping protons into the cristae, which is used to synthesize ATP by ATP synthase concentrated on the ends of the cristae.

ATP synthase and G proteins have several common features

The α and β subunits of ATP synthase are members of the P-loop NTPase family of proteins. In Section 14.2, we learned that the signaling properties of other members of this family, the G proteins, depend on their ability to bind nucleoside triphosphates and diphosphates with great tenacity. They do not exchange nucleotides unless they are stimulated to do so by interaction with other proteins. The binding-change mechanism of ATP synthase is a variation on this theme. The P-loop regions of the β subunits will bind either ADP or ATP (or release

ATP), depending on which of three different faces of the γ subunit they interact with. The conformational changes take place in an orderly way, driven by the rotation of the γ subunit.

Self-Check Question



How many ATP are generated for each 360-degree rotation of the γ subunit of ATP synthase? Recall that the number of **c** subunits in the **c** ring varies across species. How many protons are required to form one ATP if the ring has 14 **c** subunits?

18.5 Many Shuttles Allow Movement Across Mitochondrial Membranes

The inner mitochondrial membrane must be impermeable to most molecules, yet much exchange has to take place between the cytoplasm and the mitochondria. This exchange is mediated by an array of membrane-spanning transporter proteins.

Electrons from cytoplasmic NADH enter mitochondria by shuttles

One function of the respiratory chain is to regenerate NAD^+ for use in glycolysis. NADH generated by the citric acid cycle and fatty acid oxidation is already in the mitochondrial matrix, but how is cytoplasmic NADH reoxidized to NAD^+ under aerobic conditions? NADH cannot simply pass into mitochondria for oxidation by the respiratory chain, because the inner mitochondrial membrane is impermeable to NADH and NAD^+. The solution is that *electrons from NADH,* rather than NADH itself, are carried across the mitochondrial membrane. One of several means of introducing electrons from NADH into the electron-transport chain is the **glycerol 3-phosphate shuttle** (**Figure 18.34**):

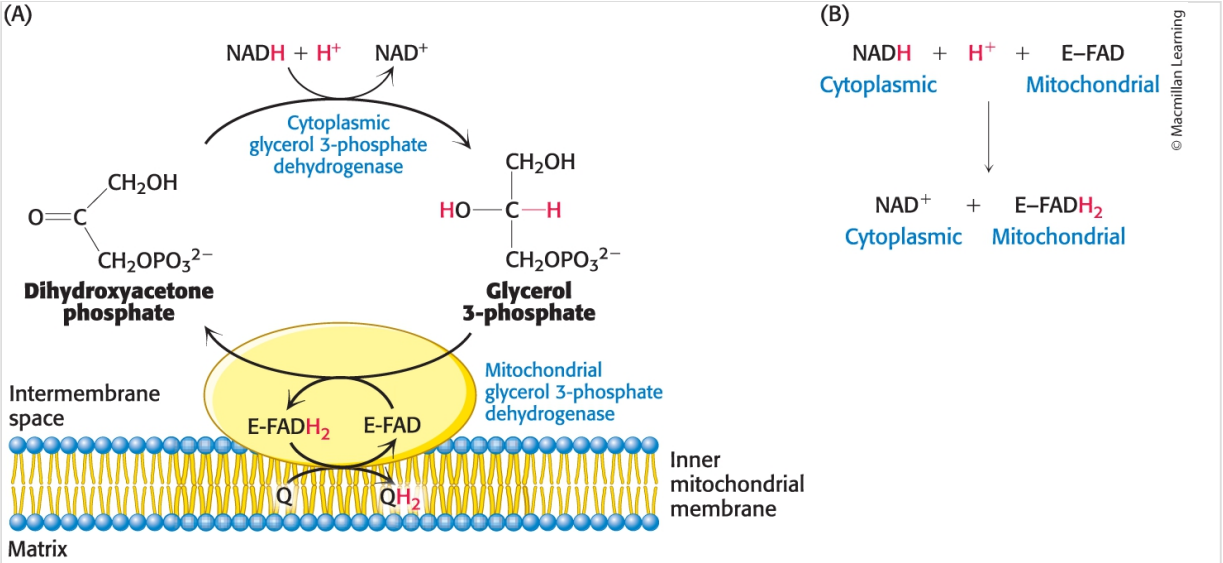


FIGURE 18.34 The glycerol 3-phosphate shuttle allows for rapid rates of oxidative phosphorylation at the cost of energetic efficiency. Electrons from NADH can enter the mitochondrial electron-transport chain by being used to reduce dihydroxyacetone phosphate to glycerol 3-phosphate. Glycerol 3-phosphate is reoxidized by electron transfer to an FAD prosthetic group in a membrane-bound glycerol 3-phosphate dehydrogenase. Subsequent electron transfer to Q to form QH_2 allows these electrons to enter the electron-transport chain.

- First, a pair of electrons is transferred from NADH to dihydroxyacetone phosphate, a glycolytic intermediate, to form glycerol 3-phosphate by cytosolic glycerol 3-phosphate dehydrogenase.
- Next, glycerol 3-phosphate moves into the mitochondrion where it is reoxidized to dihydroxyacetone phosphate on the outer surface of the inner mitochondrial membrane by a membrane-bound isozyme of glycerol 3-phosphate dehydrogenase. The reaction passes the electron pair to an FAD prosthetic group in this enzyme to form $FADH_2$, and regenerates dihydroxyacetone phosphate.
- Finally, the reduced flavin transfers its electrons to a molecule of Q, which then enters the respiratory chain as QH_2, and thus

ultimately delivers the electrons to Complex III.

When cytoplasmic NADH transported by the glycerol 3-phosphate shuttle is oxidized by the respiratory chain, 1.5 rather than 2.5 molecules of ATP are formed. The yield is lower because FAD rather than NAD^+ is the electron acceptor in mitochondrial glycerol 3-phosphate dehydrogenase. The use of FAD enables electrons from cytoplasmic NADH to be transported into mitochondria against an NADH concentration gradient. The price of this transport is one molecule of ATP per two electrons. This glycerol 3-phosphate shuttle is especially prominent in muscle, enabling it to sustain a very high rate of oxidative phosphorylation.

In the heart and liver, electrons from cytoplasmic NADH are brought into mitochondria by the **malate–aspartate shuttle**, which is mediated by two membrane carriers and four enzymes (**Figure 18.35**). Electrons are transferred from NADH in the cytoplasm to oxaloacetate, forming malate, which traverses the inner mitochondrial membrane in exchange for α-ketoglutarate and is then reoxidized by NAD^+ in the matrix to form NADH in a reaction catalyzed by the citric acid cycle enzyme malate dehydrogenase. The resulting oxaloacetate does not readily cross the inner mitochondrial membrane, and so a transamination reaction (Section 23.3) is needed to form aspartate, which can be transported to the cytoplasmic side in exchange for glutamate. Glutamate donates an amino group to oxaloacetate, forming aspartate and α-ketoglutarate. In the cytoplasm, aspartate is then deaminated to form oxaloacetate, and the cycle is restarted.

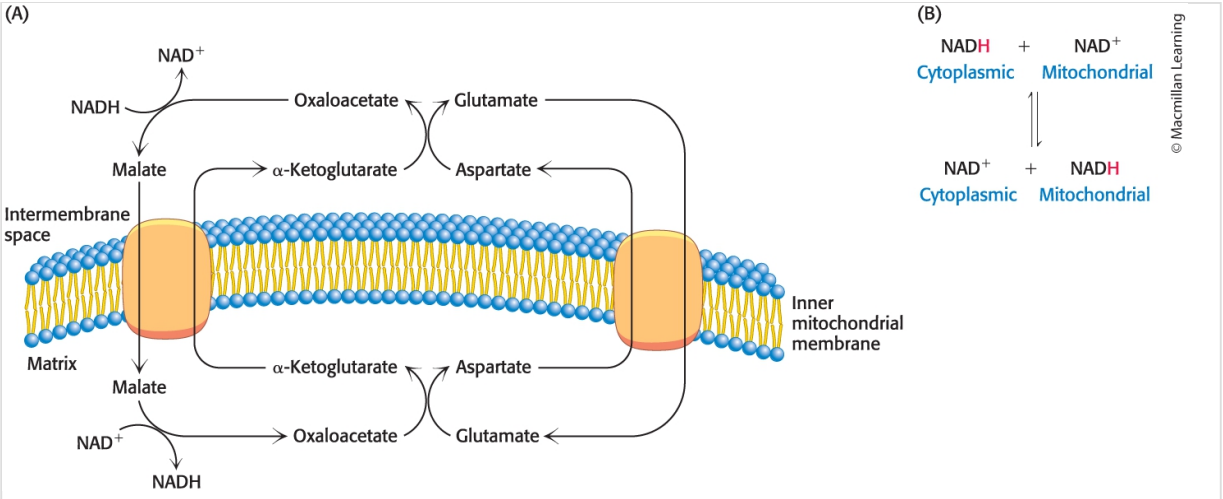


FIGURE 18.35 The malate–aspartate shuttle preserves all the chemical potential energy of cytoplasmically generated NADH. NADH produced in the matrix as a result of the shuttle is free to enter the ETC at Complex I.

The entry of ADP into mitochondria is coupled to the exit of ATP by ATP-ADP translocase

The major function of oxidative phosphorylation is to generate ATP from ADP. ATP and ADP do not diffuse freely across the inner mitochondrial membrane. How are these highly charged molecules moved across the inner membrane into the cytoplasm? A specific transport protein, **ATP-ADP translocase** (also called **adenine nucleotide translocase** or **ANT**), enables these molecules to traverse this permeability barrier. Most important, the flows of ATP and ADP are coupled. ADP enters the mitochondrial matrix only if ATP exits, and vice versa. This process is carried out by the translocase, an antiporter:

$$ADP^{3-}_{cytoplasm} + ATP^{4-}_{matrix} \rightarrow ADP^{3-}_{matrix} + ATP^{4-}_{cytoplasm}$$

ANT is highly abundant, constituting about 15% of the protein in the inner mitochondrial membrane. The abundance is a manifestation of the fact that human beings exchange the equivalent of their weight in ATP each day.

The 30-kDa translocase contains a single nucleotide-binding site that alternately faces the matrix and the cytoplasmic sides of the membrane (Figure 18.36). ATP and ADP bind to ANT without Mg^{2+}, and ATP has one more negative charge than that of ADP. Thus, in an actively respiring mitochondrion with a positive membrane potential, ATP transport out of the mitochondrial matrix is favored, but the additional negative charge moving out dissipates some of the proton-motive force.

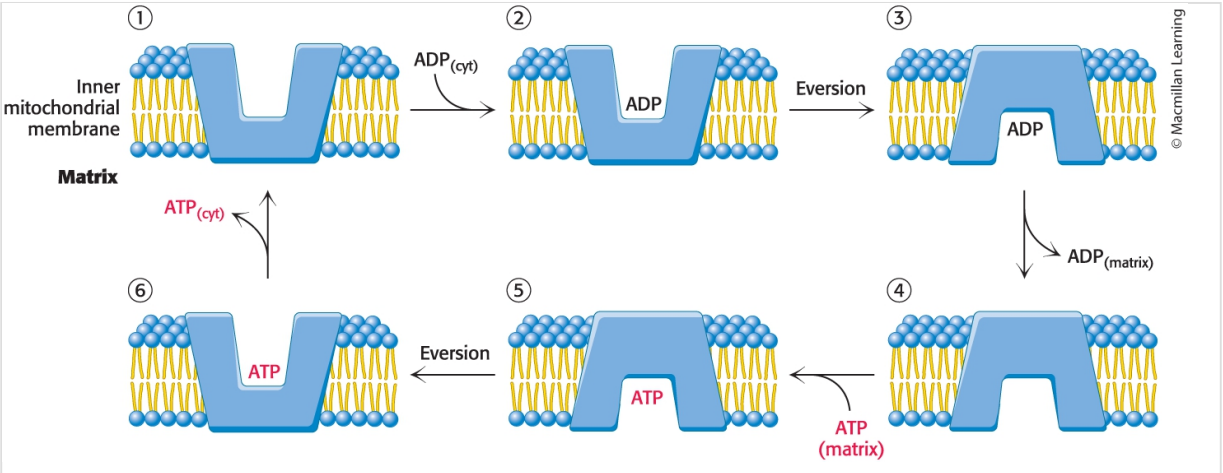


FIGURE 18.36 The ATP-ADP translocase catalyzes the exchange of entry of ADP and ATP. The binding of ADP from the cytoplasm (1) favors eversion of the transporter (2) to release ADP into the matrix (3). Subsequent binding of ATP from the matrix to the everted form (4) favors eversion back to the original conformation (5), releasing ATP into the cytoplasm (6).

A second transporter called the *phosphate carrier* (**Figure 18.37**) works in concert with ANT. By mediating the electroneutral exchange (antiport) of $H_2PO_4^-$ for OH^-, phosphate carrier allows one OH^- to move into the IM space, which is thermodynamically favorable because it is equivalent to a proton moving in the opposite direction. The combined action of these two transporters leads to the exchange of cytoplasmic ADP and P_i for matrix ATP at the expense of about one quarter of the proton-motive force. These two transporters, which provide ATP synthase with its substrates, are associated with the synthase to form a large complex called the *ATP synthasome.* The inhibition of ANT leads to the subsequent inhibition of cellular respiration as well, as we will see in the next section.

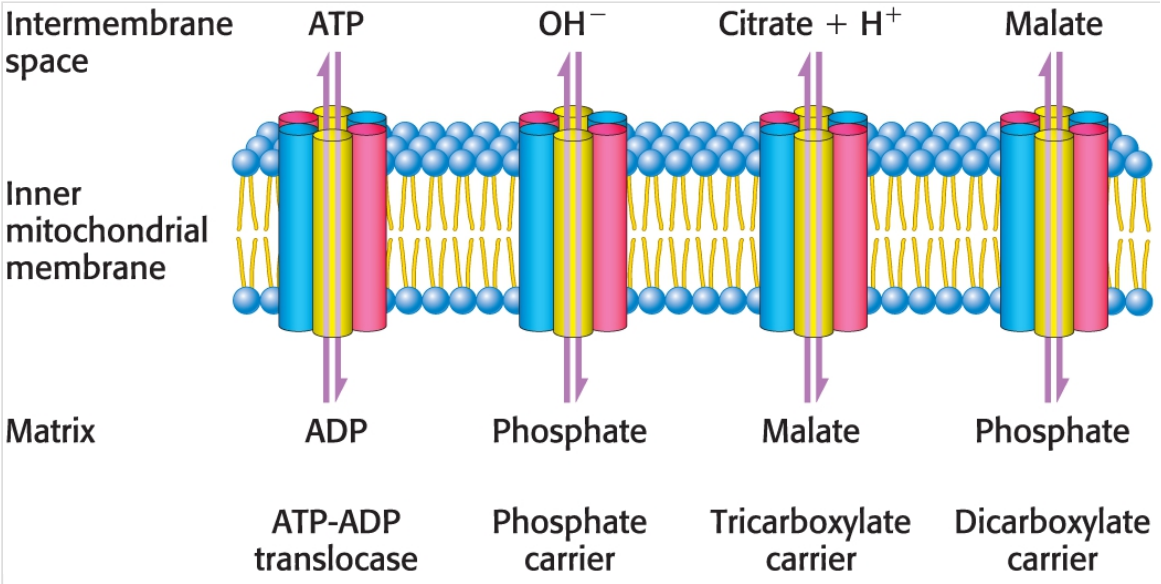


FIGURE 18.37 Multiple structurally homologous mitochondrial transporters carry specific metabolites across the inner mitochondrial membrane.

ANT and phosphate carrier are just two of many structurally homologous mitochondrial transporters for ions and charged metabolites present in the inner mitochondrial membrane (Figure

18.37). The dicarboxylate carrier enables malate, succinate, and fumarate to be exported from the mitochondrial matrix in exchange for P_i. The tricarboxylate carrier exchanges citrate and H^+ for malate. In all, more than 40 such carriers are encoded in the human genome.

Self-Check Question



Recall what thermodynamically drives the action of the ATP-ADP translocase (ANT). Why must this enzyme use Mg^{2+}-free forms of ATP and ADP?

18.6 The Regulation of Cellular Respiration Is Governed Primarily by the Need for ATP

Because ATP is the end product of cellular respiration, the ATP needs of the cell are the ultimate determinant of the rate of respiratory pathways and their components.

The complete oxidation of glucose yields about 30 molecules of ATP

We can now estimate how many molecules of ATP are formed when glucose is completely oxidized to CO_2. The number of ATP molecules formed in glycolysis and the citric acid cycle is unequivocally known because it is determined by the stoichiometries of chemical reactions. In contrast, the ATP yield of oxidative phosphorylation is less certain because the stoichiometries of proton pumping, ATP synthesis, and metabolite-transport processes need not be an integer or even have fixed values.

Recall from Section 18.3 that the best current estimates for the number of protons pumped out of the matrix per electron pair by Complexes I, III, and IV are four, two, and four, respectively. The synthesis of a molecule of ATP is driven by the flow of about three protons through ATP synthase. An additional proton is consumed in transporting ATP from the matrix to the cytoplasm. Hence, about 2.5 molecules of cytoplasmic ATP are generated as a result of the flow of a pair of electrons from NADH to O_2. For electrons that enter at Complex III, such as those from the oxidation of succinate or cytoplasmic NADH

transferred by the glycerol-phosphate shuttle, the yield is about 1.5 molecules of ATP per electron pair.

Hence, as tallied in Table 18.4, about 30 molecules of ATP are formed when glucose is completely oxidized to CO_2. Most of the ATP, 26 of 30 molecules formed, is generated by oxidative phosphorylation, while two of the remaining four are made in the citric acid cycle, which is oxygen-dependent (aerobic). Recall that the anaerobic metabolism of glucose yields only two molecules of ATP. One of the effects of endurance exercise, a practice that calls for much ATP for an extended period of time, is to increase the number of mitochondria and blood vessels in muscle and thus increase the extent of ATP generation by oxidative phosphorylation.

TABLE 18.4 ATP yield from the complete oxidation of glucose

Reaction sequence	ATP yield per glucose molecule
Glycolysis: Conversion of glucose into pyruvate (in the cytoplasm)	
Phosphorylation of glucose	−1
Phosphorylation of fructose 6-phosphate	−1
Dephosphorylation of 2 molecules of 1,3-BPG	+2
Dephosphorylation of 2 molecules of phosphoenolpyruvate	+2
2 molecules of NADH are formed in the oxidation of 2 molecules of glyceraldehyde 3-phosphate	
Conversion of pyruvate into acetyl CoA (inside mitochondria)	

2 molecules of NADH are formed	
Citric acid cycle (inside mitochondria)	
2 molecules of adenosine triphosphate are formed from 2 molecules of succinyl CoA	+2
6 molecules of NADH are formed in the oxidation of 2 molecules each of isocitrate, α-ketoglutarate, and malate	
2 molecules of $FADH_2$ are formed in the oxidation of 2 molecules of succinate	
Oxidative phosphorylation (inside mitochondria)	
2 molecules of NADH formed in glycolysis; each yields 1.5 molecules of ATP (assuming transport of NADH by the glycerol 3-phosphate shuttle)	+3
2 molecules of NADH formed in the oxidative decarboxylation of pyruvate; each yields 2.5 molecules of ATP	+5
2 molecules of $FADH_2$ formed in the citric acid cycle; each yields 1.5 molecules of ATP	+3
6 molecules of NADH formed in the citric acid cycle; each yields 2.5 molecules of ATP	+15
Net Yield per Molecule of Glucose	+30

Information on the ATP yield of oxidative phosphorylation is from values given in P. C. Hinkle, M. A. Kumar, A. Resetar, and D. L. Harris, *Biochemistry* 30:3576, 1991.
Note: The current value of 30 molecules of ATP per molecule of glucose supersedes the earlier value of 36 molecules of ATP. The stoichiometries of proton pumping, ATP synthesis, and metabolite transport should be regarded as estimates. About 2 more molecules of ATP are formed per molecule of glucose oxidized when the malate–aspartate shuttle rather than the glycerol 3-phosphate shuttle is used.

The rate of oxidative phosphorylation is determined by the need for ATP

How is the rate of the electron transport through the chain controlled? Under most physiological conditions, electron transport is tightly coupled to phosphorylation. Electrons do not usually flow through the electron-transport chain to O_2 unless ADP is simultaneously phosphorylated to ATP. When ADP concentration rises, as would be the case in active muscle, the rate of oxidative phosphorylation increases to meet the ATP needs of the muscle. The regulation of the rate of oxidative phosphorylation by the ADP level is called *respiratory control* or *acceptor control*.

The need for ATP likewise affects the rate of the citric acid cycle. At low concentrations of ADP, as in a resting muscle, NADH and $FADH_2$ are not consumed by the electron-transport chain. The citric acid cycle slows because there is less NAD^+ and FAD to feed the cycle. As the ADP level rises and oxidative phosphorylation speeds up, NADH and $FADH_2$ are oxidized, and the citric acid cycle becomes more active. The coordination of the components of cellular respiration, as shown in **Figure 18.38**, makes such regulation possible.

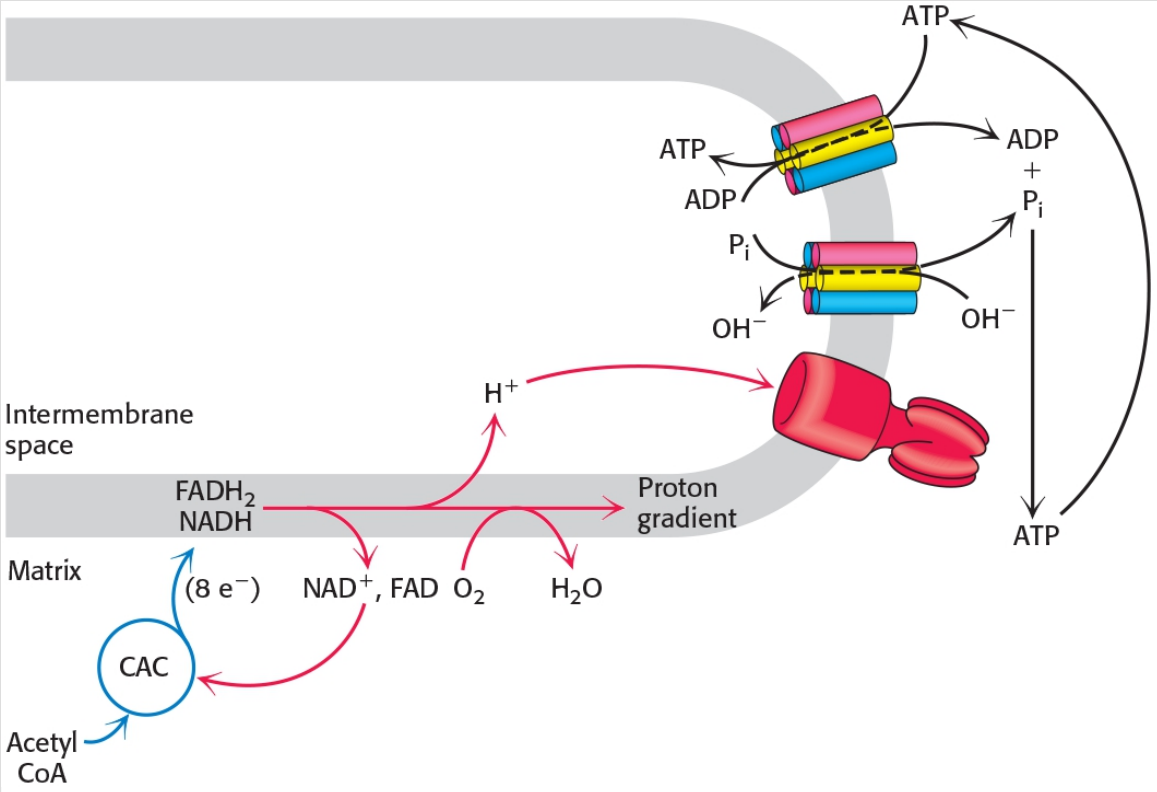


FIGURE 18.38 ATP synthase depends upon the rest of the ATP synthesome, as well as the ETC and CAC. The citric acid cycle (CAC) generates high-energy electrons by oxidizing acetyl CoA. Th electrons are used to reduce oxygen to water and in the process develop a proton gradient. The proton gradient powers the synthesis of ATP, which requires the coordination of ATP synthase, the ATP-ADP translocase, and the phosphate carrier.

ATP synthase can be regulated

Mitochondria contain an evolutionarily conserved protein, *inhibitory factor 1* (IF1), that specifically inhibits the potential hydrolytic activity of the F_0F_1 ATP synthase. What is the function of IF1? Consider a circumstance where tissues may be deprived of oxygen (ischemia), as might happen during a stroke or heart attack. Without oxygen as the electron acceptor, the electron-transport chain will be unable to

generate the proton-motive force. The ATP in the mitochondria would be hydrolyzed by the synthase, working in reverse. The role of IF1 is to prevent the wasteful hydrolysis of ATP by inhibiting the hydrolytic activity of the synthase.

How is this inhibition regulated? IF1 dimerizes when the pH in the matrix decreases due to the dissipation of the proton-motive force. IF1 dimers then bind tightly to ATP synthase dimers, preventing the β subunits from changing conformation and thus halting any action of ATP synthase until the pH of the matrix is returned to normal. IF1 is also overexpressed in many types of cancer. This overexpression plays a role in the induction of the Warburg effect, the switch from oxidative phosphorylation to aerobic glycolysis as the principal means for ATP synthesis (Section 16.3).

Regulated uncoupling leads to the generation of heat

Some organisms possess the ability to uncouple oxidative phosphorylation from ATP synthesis to generate heat. Such uncoupling is a means to maintain body temperature in hibernating animals, in some newborn animals (including human beings), and in many adult mammals, especially those adapted to cold. The skunk cabbage uses an analogous mechanism to heat its floral spikes in early spring, increasing the evaporation of odoriferous molecules that attract insects to fertilize its flowers. In animals, the uncoupling is in brown adipose tissue, which is specialized tissue for the process called *nonshivering thermogenesis,* or the ability to generate heat without using the rapid, unconscious contraction of skeletal muscles (shivering). In contrast, white adipose tissue, which constitutes the bulk of adipose tissue, plays no role in thermogenesis directly but serves as an insulating layer, an energy source, and an endocrine gland (Chapters 24 and 27).

Brown adipose tissue is very rich in mitochondria. The tissue appears brown from the combination of the greenish-colored cytochromes in the numerous mitochondria and the red hemoglobin present in the extensive blood supply, which helps to carry the heat through the body. The inner mitochondrial membrane of these mitochondria contains a large amount of **uncoupling protein (UCP-1)**, also called *thermogenin,* a dimer of 33-kDa subunits that resembles ANT. UCP-1 transports protons from the intermembrane space to the matrix with the assistance of fatty acids.

In essence, UCP-1 generates heat by short-circuiting the mitochondrial proton battery. The energy of the proton gradient, normally captured as ATP, is released as heat as the protons flow through UCP-1 to the mitochondrial matrix. This dissipative proton pathway is activated when the core body temperature begins to fall. In response to a temperature drop, α-adrenergic hormones stimulate the release of free fatty acids from triacylglycerols stored in cytoplasmic lipid granules (**Figure 18.39**). Long-chain fatty acids bind to the cytoplasmic face of UCP-1, and the carboxyl group binds a proton. This causes a structural change in UCP-1 so that the protonated carboxyl now faces the proton-poor environment of the matrix, and the proton is released. Proton release resets UCP-1 to the initial state.

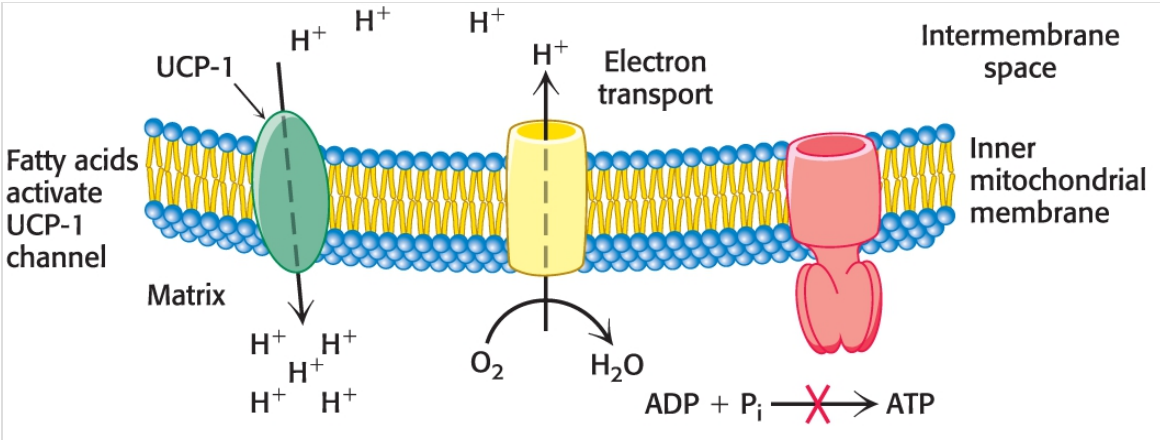
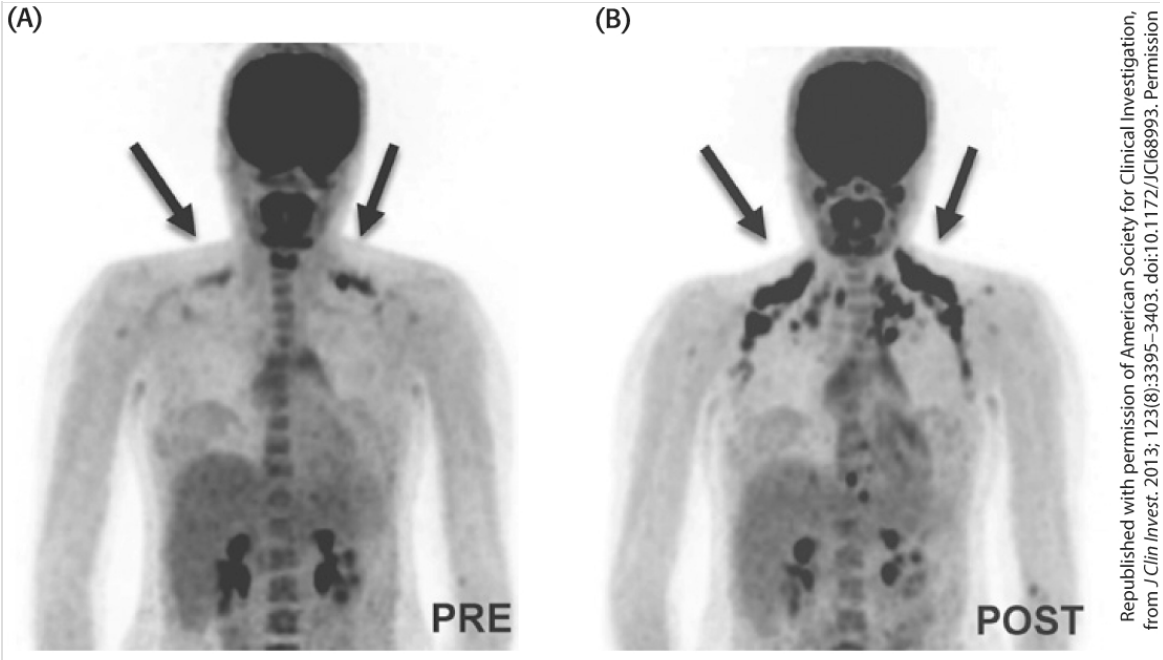


FIGURE 18.39 UCP-1 generates heat by transporting protons without the synthesis of ATP.

In addition to UCP-1, two other uncoupling proteins have been identified: UCP-2, which is found in a wide variety of tissues, and UCP-3, which is localized to skeletal muscle and brown fat. Both proteins share greater than 50% identity with UCP-1. This family of uncoupling proteins may play a role in energy homeostasis, and the genes for UCP-2 and UCP-3 map to regions of the human and mouse chromosomes that have been linked to obesity, supporting the notion that they function as a means of regulating body weight. Until recently, adult humans were believed to lack brown fat tissue. However, new studies have established that adults have brown adipose tissue in the neck and upper chest regions that is activated by cold (Figure 18.40). Obesity, which is predominantly caused by the swelling of intracellular lipid droplets in white adipose tissue, also leads to a decrease in brown adipose tissue.



Republished with permission of American Society for Clinical Investigation, from *J Clin Invest.* 2013; 123(8):3395–3403. doi:10.1172/JCI68993. Permission

FIGURE 18.40 Brown adipose tissue is revealed on en adipose tissue is revealed on exposure t cold. The results of PET–CT scanning show the uptake and distribution of ^{18}F-

fluorodeoxyglucose (^{18}F-FDG) in adipose tissue. The patterns of ^{18}F-FDG uptake in the same subject are dramatically different under thermoneutral conditions (A) and after exposure cold (B).

Reintroduction of UCP-1 into pigs may be economically valuable

We can witness the effects of a lack of nonshivering thermogenesis by examining pig behavior. The ancestors of pigs are believed to have lost the gene for UCP-1 ~20 million years ago when they inhabited tropical and subtropical environments where they could survive without nonshivering thermogenesis. As the range of pigs expanded, however, the lack of UCP-1 (and hence, the absence of functional brown fat) became a liability to which pigs have adapted with distinctive behavioral traits. Among mammals, pigs have unusually large litters, and they are the only ungulates (hoofed mammals) that build nests for birth; piglets generate heat by huddling with their littermates in an insulated nest and shivering.

The deficiency of UCP-1 has important implications for pig farming. Even with the use of heat lamps, which account for 35% of the energy cost of raising pigs, piglet mortality may be as high as 20% because of hypothermia. Furthermore, because of their lack of UCP-1, pigs accumulate fat in white adipose tissue as a thermal insulator, meaning there is less lean meat available.

Recently, researchers have inserted the gene for UCP-1 into pig embryos. The resulting pigs are cheaper to raise due to the decrease in energy costs and provide more high-quality lean meat. The gene for

UCP-1 was inserted into the pig embryos using the CRISPR technique described in Chapter 9. We see here another example of the expanding reach of biochemistry into areas of the economy beyond just the biomedical arena.

Oxidative phosphorylation can be inhibited at many stages

Many potent and lethal poisons exert their effect by inhibiting oxidative phosphorylation at one of a number of different locations (**Figure 18.41**).

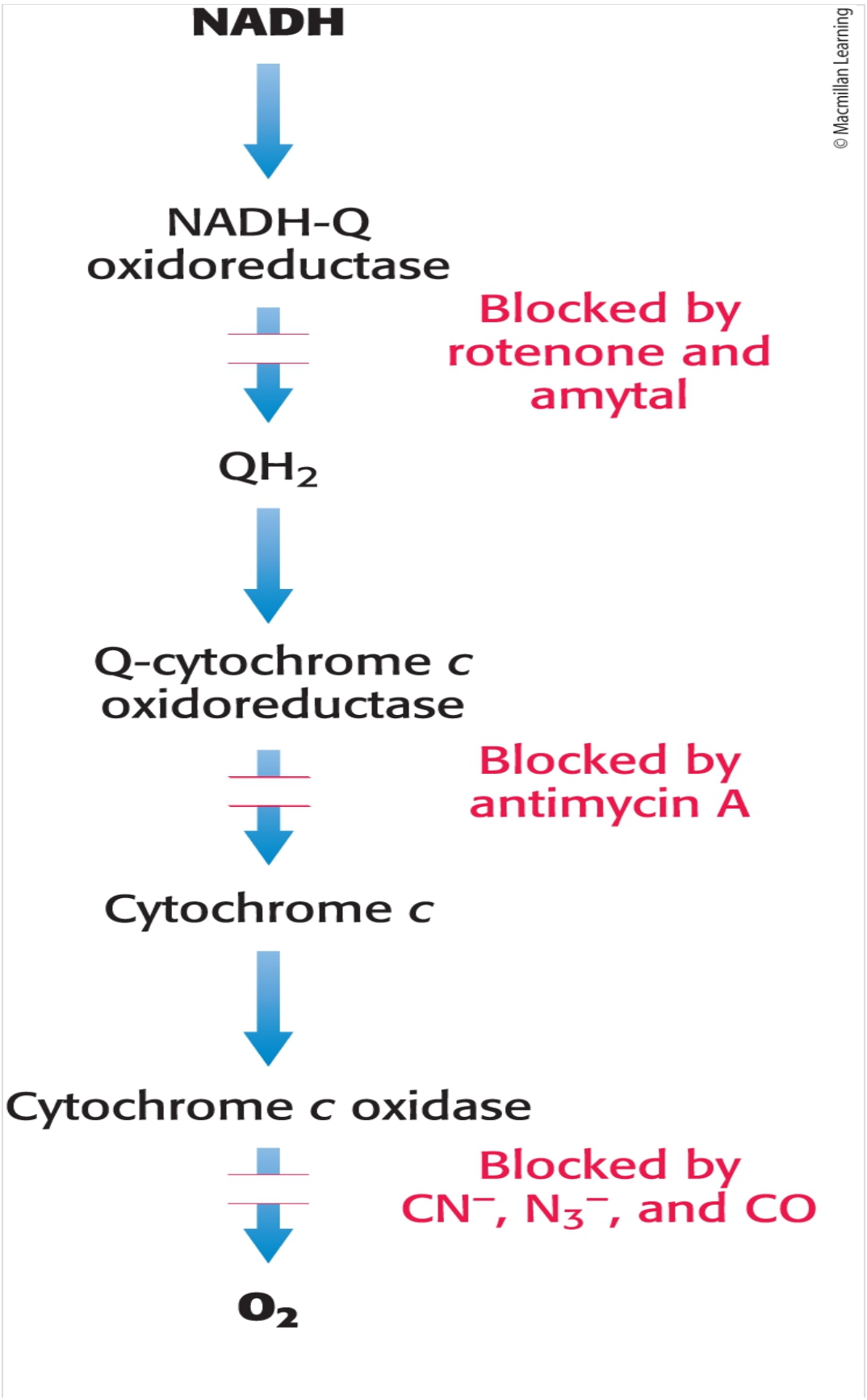

NADH
NADH-Q oxidoreductase
Blocked by rotenone and amytal
QH_2
Q-cytochrome *c* oxidoreductase
Blocked by antimycin A
Cytochrome *c*
Cytochrome *c* oxidase
Blocked by CN^-, N_3^-, and CO
O_2
© Macmillan Learning

FIGURE 18.41 Inhibitors of electron transport block the process at a variety of sites.



Inhibition of the electron-transport chain

Rotenone, which is used as a fish and insect poison, and amytal, a barbiturate sedative, block electron transfer in NADH-Q oxidoreductase and thereby prevent the use of NADH as a substrate. In the presence of rotenone and amytal, electron flow resulting from the oxidation of succinate is unimpaired, because these electrons enter through QH_2, beyond the block. As an electron-transport-chain inhibitor, rotenone may play a role, along with genetic susceptibility, in the development of Parkinson's disease.

Other drugs block the chain at different points. For example, Antimycin *A* interferes with electron flow from cytochrome b_H in Q-cytochrome *c* oxidoreductase. Furthermore, electron flow in cytochrome *c* oxidase can be blocked by cyanide (CN^-), azide (N_3^-), and carbon monoxide (CO). Cyanide and azide react with the ferric form of heme a_3, whereas carbon monoxide inhibits the ferrous form. Inhibition of the electron-transport chain also inhibits ATP synthesis because the proton-motive force can no longer be generated.

Inhibition of ATP synthase

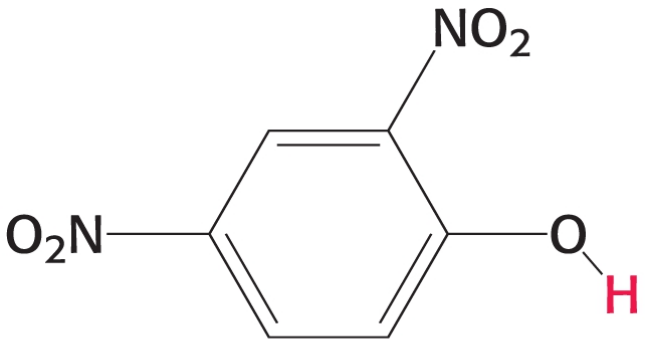
Oligomycin, an antibiotic used as an antifungal agent, and dicyclohexylcarbodiimide (DCC) prevent the influx of protons through ATP synthase by binding to the carboxylate group of the **c** subunits required for proton binding. Modification of only one **c** subunit by DCC is sufficient to inhibit the rotation of the entire **c** ring and hence ATP

synthesis. If actively respiring mitochondria are exposed to an inhibitor of ATP synthase, the electron-transport chain ceases to operate. This observation clearly illustrates that electron transport and ATP synthesis are normally tightly coupled.

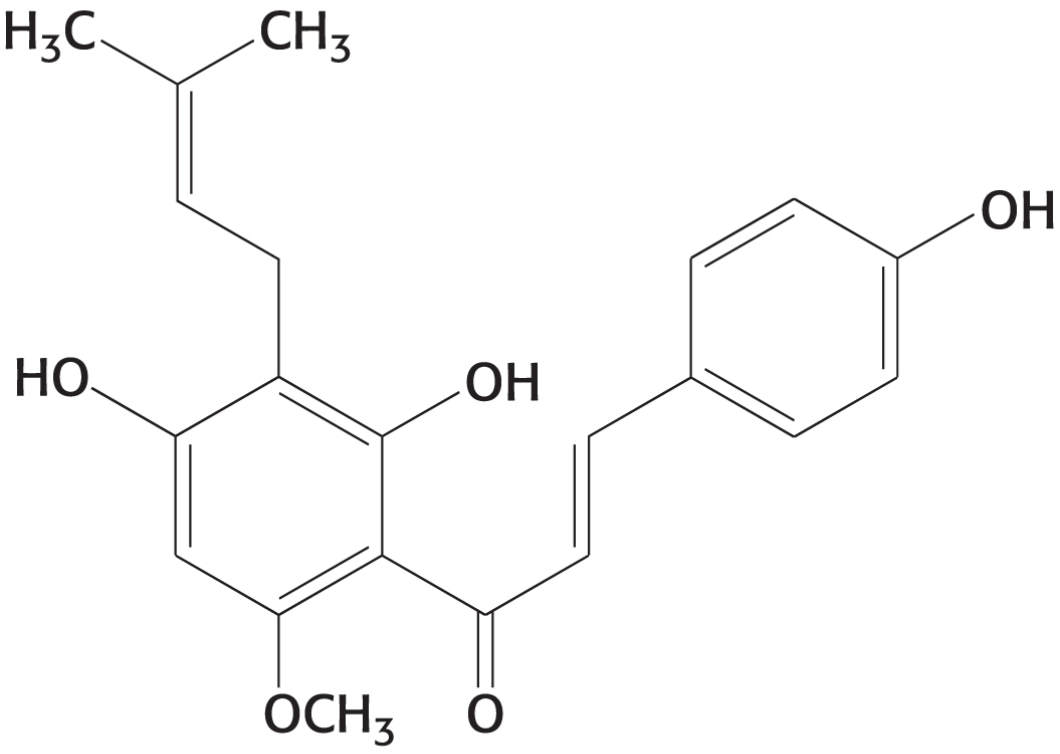
Uncoupling electron transport from ATP synthesis

The tight coupling of electron transport and phosphorylation in mitochondria can be uncoupled *pathologically*, in an unregulated way, by small molecules instead of *beneficially*, in a regulated way, by uncoupling proteins. Certain acidic aromatic compounds, including 2,4-dinitrophenol (DNP), carry protons across the inner mitochondrial membrane, down their concentration gradient. In the presence of these uncouplers, electron transport from NADH to O_2 proceeds in a normal fashion, but ATP is not formed by mitochondrial ATP synthase, because the proton-motive force across the inner mitochondrial membrane is continuously dissipated. This loss of respiratory control leads to increased oxygen consumption and oxidation of NADH. Indeed, in the accidental or intentional ingestion of uncouplers, large amounts of metabolic fuels are consumed, but no energy is captured as ATP. Rather, energy is released as heat.

DNP is the active ingredient in some herbicides and fungicides. There are reports that Soviet soldiers were given DNP to keep them warm during the long Russian winters. Remarkably, some people consume DNP today as a weight-loss drug, despite the fact that the FDA banned its use in 1938, calling it “extremely dangerous and not fit for human consumption.” Its use can lead to death by hyperthermia, with body temperatures reaching in excess of 43°C prior to death.



2,4-Dinitrophenol (DNP)



Xanthohumol

Drugs are being sought that would function as mild uncouplers, uncouplers not as potentially lethal as DNP, for use in treatment of obesity and related pathologies. Xanthohumol, a prenylated chalcone found in hops and beer, shows promise in this regard. Xanthohumol also scavenges free radicals and is used for treatment of certain types of cancers.

Inhibition of ATP export

ANT is specifically inhibited by very low concentrations of atractyloside (a plant glycoside) or bongkrekic acid (an antibiotic from a mold). Atractyloside binds to the translocase when its nucleotide site faces the intermembrane space, whereas bongkrekic acid binds when this site faces the mitochondrial matrix. Oxidative phosphorylation stops soon after either inhibitor is added, demonstrating the essentiality of ANT for maintaining adequate amounts of ADP to accept the energy associated with the proton-motive force.

The effects of various inhibitors can now be reliably measured using Seahorse XF technology (Agilent Technologies), which now allows the measurement of the rate of aerobic respiration and lactic acid fermentation simultaneously in real time in cultured cells. The extent of aerobic respiration is determined by measuring the oxygen consumption rate, while the rate of glycolysis correlates with the extracellular acidification rate. This method is now widely used in both industry and academia in drug discovery, cancer research, and many other areas.

New mitochondrial diseases are constantly being discovered



The number of diseases that can be attributed to mitochondrial mutations is steadily growing in step with our growing understanding of the biochemistry and genetics of mitochondria. Mitochondrial diseases are estimated to affect from 10 to 15 per 100,000 people, roughly equivalent to the prevalence of the muscular dystrophies. Some of these mutations impair the use of NADH, whereas others block electron transfer to Q. Mutations in Complex I are the most frequent cause of mitochondrial diseases; indeed, the first mitochondrial disease to be understood was Leber hereditary optic neuropathy (LHON), a form of blindness that strikes in midlife as a result of mutations in Complex I. The accumulation of mutations in mitochondrial genes in a span of several decades may contribute to aging, degenerative disorders, and cancer.

Mitochondrial disease is primarily inherited maternally, because a human egg harbors several hundred thousand molecules of mitochondrial DNA, whereas a sperm contributes only a few hundred. Thus, the paternal contribution has little effect on the mitochondrial genotype. Because the maternally inherited mitochondria are present in large numbers but not all of the mitochondria may be affected, the pathologies of mitochondrial mutants can be quite complex. Even within a single family carrying an identical mutation, chance variations in the percentage of mitochondria with the mutation lead to large variations in the nature and severity of the symptoms of the pathological condition as well as the time of onset. As the percentage of defective mitochondria increases, energy-generating capacity diminishes until, at some threshold, the cell can no longer function properly. Defects in cellular respiration are doubly dangerous: not only does energy transduction decrease, but also the likelihood that reactive

oxygen species will be generated increases. Organs that are highly dependent on oxidative phosphorylation, such as the nervous system, the retina, and the heart, are most vulnerable to mutations in mitochondrial DNA.

Self-Check Question



4,6-Dinitro-o-cresol (DNOC) was used as a pesticide until it was banned because it causes a dramatic rise in body temperature, profuse sweating, rapid breathing, and a decrease in body fat. When tested, it affected isolated mitochondria. What do you expect is its effect on oxygen consumption by isolated mitochondria, and why?

Mitochondria play a key role in apoptosis

In the course of development or in cases of significant cell damage, individual cells within multicellular organisms undergo a form of programmed cell death called **apoptosis**, with mitochondria acting as control centers regulating this process. Although the details continue to be established, the outer membrane of damaged mitochondria becomes highly permeable, a process referred to as *mitochondrial outer membrane permeabilization* (MOMP). This permeabilization is instigated by a family of proteins (Bcl family) that were initially discovered because of their role in cancer.

One of the most potent activators of apoptosis, cytochrome *c,* exits the mitochondria and interacts with apoptotic peptidase-activating factor 1 (APAF-1), which leads to the formation of a protein complex called the *apoptosome*. The apoptosome recruits and activates a proteolytic enzyme called *caspase 9,* a member of the cysteine protease family (Section 6.2) that in turn activates a cascade of other caspases. Each caspase type

destroys a particular target, such as the proteins that maintain cell structure. Another target is a protein that inhibits an enzyme that destroys DNA (an enzyme called caspase-activated DNAse or CAD), freeing CAD to cleave the genetic material. This cascade of proteolytic enzymes has been called “death by a thousand tiny cuts.”

Self-Check Question



The most common metabolic sign of mitochondrial disorders is lactic acidosis. Why?

18.7 Proton Gradients Generated by Respiratory Chains Drive Many Biochemical Processes

The main concept presented in this chapter is that mitochondrial electron transfer and ATP synthesis are linked by a transmembrane proton gradient. ATP synthesis in bacteria and chloroplasts also is driven by proton gradients. Here we will briefly consider how these gradients can be used in additional ways, sometimes with startling effects. As a case in point, in many bacteria, the proton gradient is responsible for providing the power for a simple but important aspect of these organisms: how they move.

Proton flow through a rotary motor allows bacteria to swim

In one second, a motile bacterium can move 25 μm, or about 10 body lengths. A human being sprinting at a proportional rate would complete the 100-meter dash in slightly more than 5 s. Bacteria such as *Escherichia coli* and *Salmonella typhimurium* swim at such speed by rotating flagella that lie on their surfaces (**Figure 18.42**). When the flagella rotate in a counterclockwise direction (viewed from outside a bacterium), the separate flagella form a bundle that very efficiently propels the bacterium through solution. The motors that power this impressive motion are strikingly different from the eukaryotic motors that we explored in Section 6.5. In the bacterial motor, an element spins around a central axis rather than moving along a polymeric track. Early experiments by Julius Adler demonstrated

that ATP is *not* required for flagellar motion. Rather, the necessary free energy is derived from the proton gradient that exists across the plasma membrane, established by the electron-transport chains of these organisms that pump protons into the periplasm.

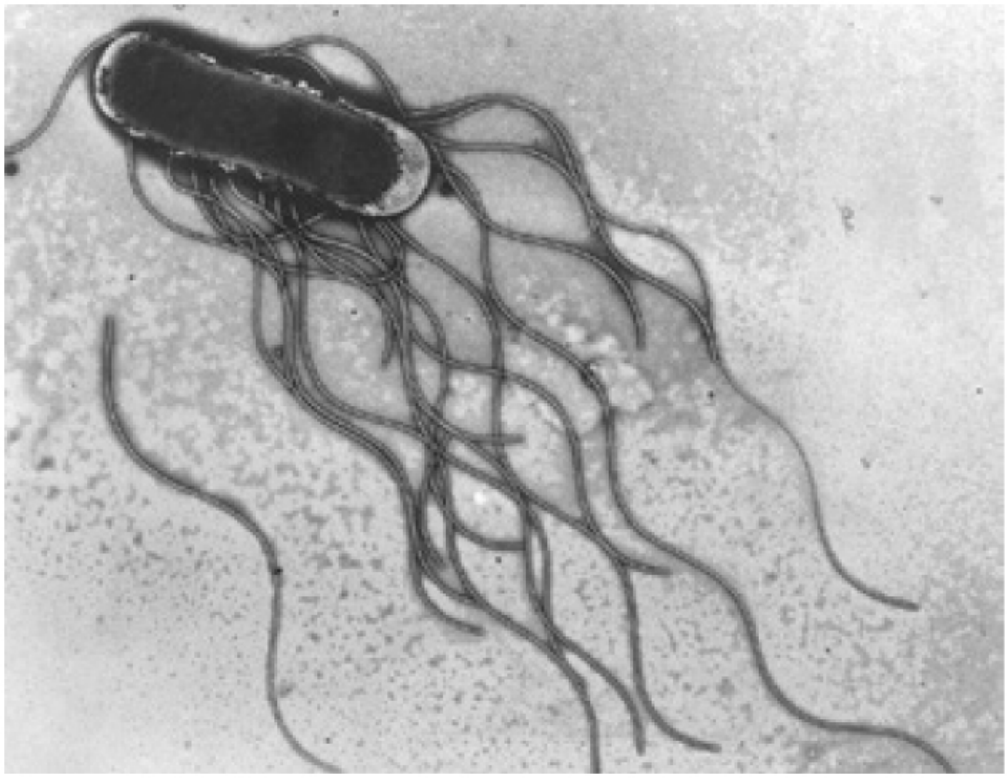


FIGURE 18.42 Bacterial flagella allow bacteria to swim rapidly. An electron micrograph of *Salmonella typhimurium* shows flagella directed backwards, where they can form a bundle under appropriate circumstances. Bacterial flagella are polymers approximately 15 nm in diameter and as much as 15 µm in length, composed of subunits of a protein called flagellin. These subunits associate into a left-handed helical structure with a hollow core. At its base, each flagellum has a rotary motor.

Although the flagellar motor is quite complex, five components particularly crucial to motor function have been identified through genetic studies (Figure 18.43). MotA and MotB are membrane proteins, each with cytoplasmic and periplasmic domains, respectively. Approximately 11 MotA–MotB pairs form a ring around

the base of the flagellum. The proteins FliG, FliM, and FliN are part of a disc-like structure called the MS (membrane and supramembrane) ring, with approximately 30 FliG subunits coming together to form the ring. The MotA–MotB pair and FliG combine to create a proton channel that drives the rotation of the flagellum similar to the proton-driven rotary motion of ATP synthase. In fact, such a mechanism was first proposed by Howard Berg to explain flagellar rotation before the rotary mechanism of ATP synthase was elucidated. Each MotA–MotB pair is conjectured to form a structure that has two half-channels (**Figure 18.44A**); FliG serves as the rotating proton carrier. In this scenario, a proton from the periplasmic space passes into the outer half-channel and is transferred to an FliG subunit. The MS ring rotates, rotating the flagellum with it and allowing the proton to pass into the inner half-channel and into the cell (**Figure 18.44B**). Ongoing structural and mutagenesis studies are testing and refining this hypothesis.

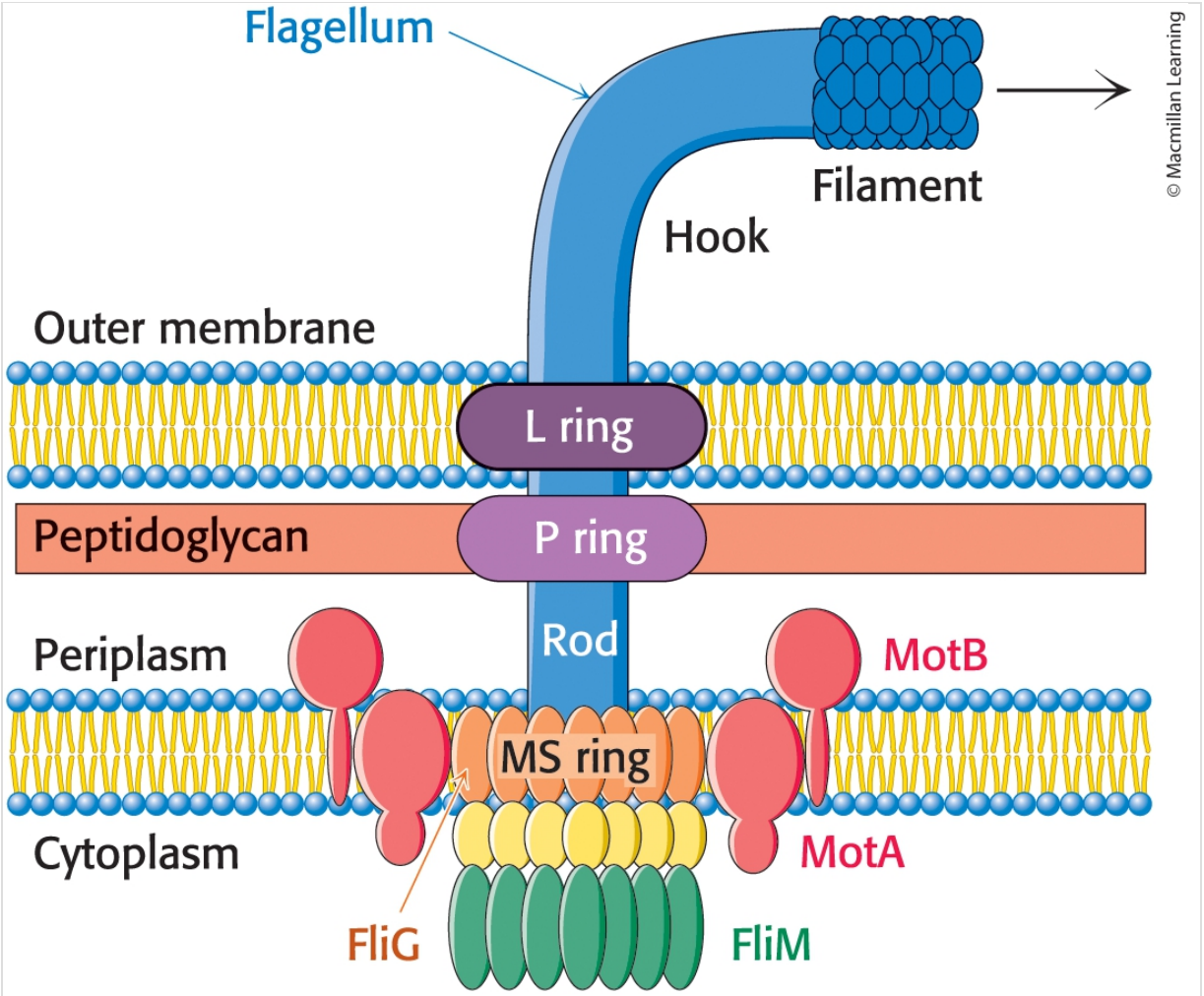


FIGURE 18.43 The flagellar motor is a complex structure containing as many as 40 distinct types of proteins. A schematic view of the flagellar motor is shown with the approximate positions of the proteins MotA and MotB (red), FliG (orange), FliN (yellow), and FliM (green).

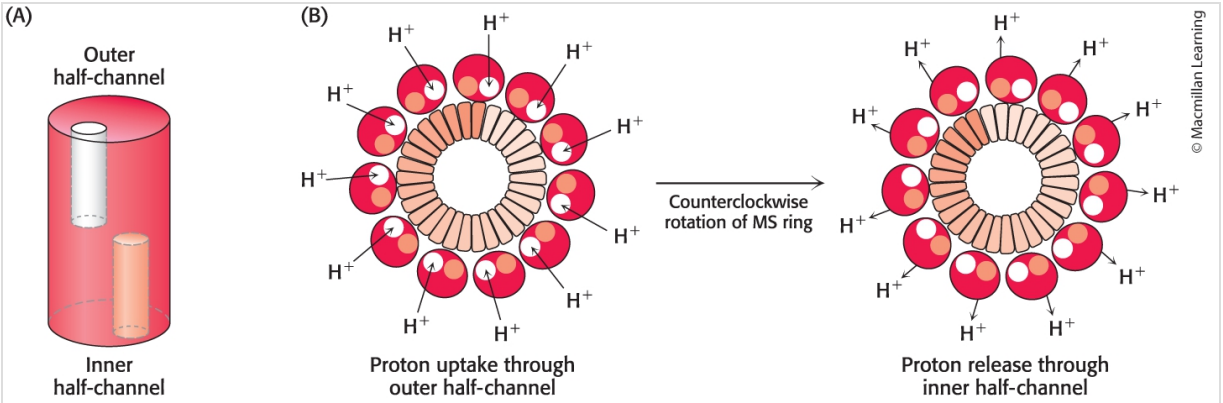


FIGURE 18.44 Rotation of the flagellum involves proton half-channels like ATP synthase. (A) MotA–MotB may form a structure having two half-channels. (B) One model for the mechanism of coupling rotation to a proton gradient requires protons to be taken up into the outer half-channel and transferred to the MS ring. The MS ring rotates in a counterclockwise direction, and the protons are released into the inner half-channel. The flagellum is linked to the MS ring and so the flagellum rotates as well.

Power transmission by proton gradients is a central motif of bioenergetics

Proton gradients power a variety of energy-requiring processes, some of which we have explored already, such as the rotation of bacterial flagella, the generation of heat by nonshivering thermogenesis, the active transport of calcium ions by mitochondria, the entry of some amino acids and sugars into bacteria, and the transfer of electrons from $NADP^+$ to NADPH. It's clear that proton gradients are a central, interconvertible currency of free energy in biological systems (**Figure 18.45**). Peter Mitchell, who established the chemiosmotic hypothesis (Section 18.4), noted that the proton-motive force is a marvelously simple and effective

store of free energy because it requires only a thin, closed lipid membrane between two aqueous phases.

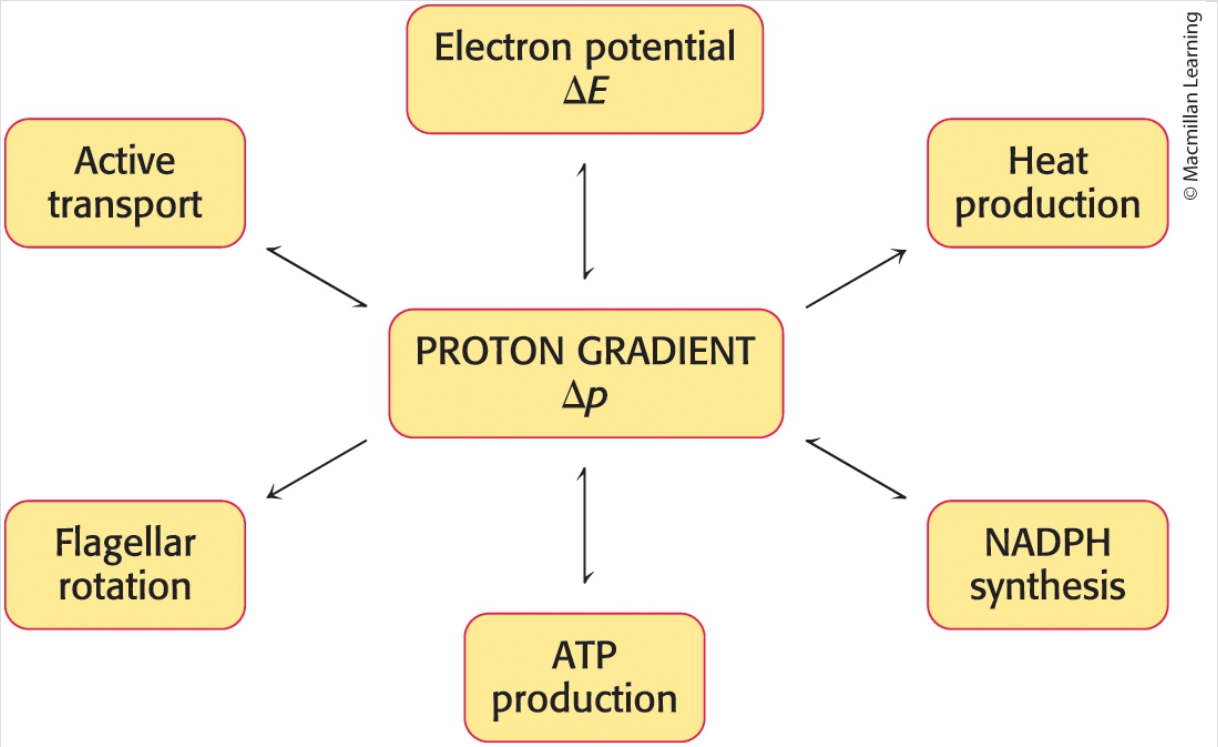


FIGURE 18.45 The proton gradient is an interconvertible form of free energy.

Self-Check Question

When bacteria such as *E. coli* are starved to a sufficient extent, they become nonmotile. However, when such bacteria are placed in an acidic solution, they resume swimming. Explain.

Chapter 18 Summary

18.1 Cellular Respiration Drives ATP Formation by Transferring Electrons to Molecular Oxygen

- Mitochondria generate most of the ATP required by aerobic cells through a combination of the reactions of the citric acid cycle and oxidative phosphorylation.
- Mitochondria are descendants of a free-living bacterium that established a symbiotic relationship with another cell.

18.2 Oxidative Phosphorylation Depends on Electron Transfer

- In oxidative phosphorylation, the synthesis of ATP is coupled to the flow of electrons from NADH or $FADH_2$ to O_2 by a proton gradient across the inner mitochondrial membrane.
- Electron flow through three asymmetrically oriented transmembrane complexes results in the pumping of protons out of the mitochondrial matrix and the generation of a membrane potential. ATP is synthesized when protons flow back to the matrix through ATP synthase.

18.3 The Respiratory Chain Consists of Four Complexes: Three Proton Pumps and a Physical Link to the Citric Acid Cycle

- The respiratory assembly of the inner mitochondrial membrane has numerous different electron carriers. Electrons from NADH are transferred to NADH-Q oxidoreductase (Complex I), the first of four complexes with the electrons emerging on QH_2, the reduced form of ubiquinone (Q).
- The citric acid cycle enzyme succinate dehydrogenase is a component of the succinate-Q reductase complex (Complex II), which donates electrons from $FADH_2$ to Q to form QH_2.

Regardless of the source, QH_2 transfers its electrons to Q-cytochrome *c* oxidoreductase (Complex III) which reduces cytochrome *c,* a water-soluble peripheral membrane protein.
- Cytochrome *c* transfers electrons to cytochrome *c* oxidase (Complex IV). A heme iron ion and a copper ion in this oxidase transfer electrons to O_2, the ultimate acceptor, to form H_2O. Complexes I, III, and IV are organized into a large molecular structure called the respirasome.

18.4 A Proton Gradient Powers the Synthesis of ATP

- The flow of electrons through Complexes I, III, and IV leads to the transfer of protons from the matrix to the IM space, generating a proton-motive force consisting of a pH gradient and a membrane potential.
- ATP synthesis is driven by the flow of protons back to the matrix through ATP synthase, an enzyme complex that is a molecular motor made of two operational units: a rotating component and a stationary component.
- The rotation of ATP synthase's γ subunit induces structural changes in the β subunit that result in the synthesis and release of ATP from the enzyme.

18.5 Many Shuttles Allow Movement Across Mitochondrial Membranes

- The electrons of cytoplasmic NADH are transferred into mitochondria by the glycerol phosphate shuttle to form $FADH_2$ from FAD, or by the malate–aspartate shuttle to form mitochondrial NADH.
- The exchange of ADP and ATP between the matrix and IM space is mediated by two transporters, ANT and phosphate carrier, driven by membrane potential.

18.6 The Regulation of Cellular Respiration Is Governed Primarily by the Need for ATP

- Approximately 30 molecules of ATP are generated when a molecule of glucose is completely oxidized to CO_2 and H_2O.
- Electron transport is normally tightly coupled to phosphorylation. NADH and $FADH_2$ are oxidized only if ADP is simultaneously phosphorylated to ATP.
- Proteins and small molecules can inhibit oxidative phosphorylation at many different points, or can uncouple electron transport from ATP synthesis, with dramatic effects on human physiology.

18.7 Proton Gradients Generated by Respiratory Chains Drive Many Biochemical Processes

- A proton gradient across the plasma membrane, rather than ATP hydrolysis, powers the rotational flagellar motor of motile bacteria in a manner analogous to the way ATP synthase functions.
- Proton gradients drive diverse physiological processes because the mechanism is fundamentally simple and can be used in many ways by proteins.

Key Terms

oxidative phosphorylation
electron-transport chain (respiratory chain)
proton-motive force
cellular respiration (respiration)
intermembrane space (IM space)
matrix

reduction potential (redox or oxidation–reduction potential)
coenzyme Q (Q, ubiquinone)
cytochrome *c*
iron–sulfur proteins (nonheme iron proteins)
NADH-Q oxidoreductase (Complex I)
succinate-Q reductase (Complex II)
Q-cytochrome *c* oxidoreductase (Complex III)
Q cycle
cytochrome *c* oxidase (Complex IV)
respirasome
ATP synthase (Complex V)
glycerol 3-phosphate shuttle
malate–aspartate shuttle
ATP-ADP translocase (adenine nucleotide translocase, ANT)
uncoupling protein (UCP-1)
apoptosis

Problems

1. Which of the following electron-transport chain complexes is also a member of the citric acid cycle and not a component of the respirasome? 1

a. Complex I
b. Complex II
c. Complex III
d. Complex IV

2. The final electron acceptor for the electron-transport chain is which of the following? 1

a. O_2
b. Coenzyme Q
c. CO_2
d. NAD^+

3. Electrons are passed on to cytochrome *c* using which of the following? 1

a. The Cori cycle
b. The Q cycle
c. The glucose-alanine cycle
d. The Krebs cycle

4. Which of the following statements about the proton-motive force is not true? 2, 3

a. It requires an intact membrane.
b. It consists of an unequal distribution of protons.
c. It is used to synthesize ATP.
d. It is powered by the hydrolysis of ATP.

5. The standard oxidation–reduction potential (E'_0) for the reduction of O_2 to H_2O is given as 0.82 V in Table 18.1. However, the value given in textbooks of chemistry is 1.23 V. Account for this difference.

6. Why are electrons carried by $FADH_2$ not as energy rich as those carried by NADH? What is the consequence of this difference? Calculate the energy released by the reduction of O_2 with $FADH_2$.

7. Compare the $\Delta G^{\circ\prime}$ values for the oxidation of succinate by NAD^+ and by FAD. Use the data given in Table 18.1 to find the E'_0 of the $NAD^+ - NADH$ and fumarate-succinate couples, and assume that E'_0 for the $FAD - FADH_2$ redox couple is nearly 0.05 V. Why is FAD rather than NAD^+ the electron acceptor in the reaction catalyzed by succinate dehydrogenase?

8. Place the following components of the electron-transport chain in their proper order: 1

a. Cytochrome *c*
b. Q-cytochrome *c* oxidoreductase
c. NADH-Q reductase
d. Cytochrome *c* oxidase
e. Ubiquinone

9. Match each term below with its alternative name. 1

1. Complex I	1. Q-cytochrome *c* oxidoreductase
2. Complex II	2. Coenzyme Q
3. Complex III	3. Succinate-Q reductase
4. Complex IV	4. NADH-Q oxidoreductase
5. Ubiquinone	5. Cytochrome *c* oxidase

---

10. Rotenone inhibits electron flow through NADH-Q oxidoreductase. Antimycin A blocks electron flow between cytochromes *b* and c_1. Cyanide blocks electron flow through cytochrome *c* oxidase to O_2. Predict the relative oxidation–reduction state of each of the following respiratory-chain

components in mitochondria that are treated with each of the inhibitors: 1

a. NAD^+
b. NADH-Q oxidoreductase
c. Coenzyme Q
d. Cytochrome c_1
e. Cytochrome *c*
f. Cytochrome *a*

11. What is the yield of ATP when each of the following substrates is completely oxidized to CO_2 by a mammalian cell homogenate? Assume that glycolysis, the citric acid cycle, and oxidative phosphorylation are fully active.

a. Pyruvate
b. Lactate
c. Fructose 1,6-bisphosphate
d. Phosphoenolpyruvate
e. Galactose
f. Dihydroxyacetone phosphate

12. What is the effect of each of the following inhibitors on electron-transport and ATP formation by the respiratory chain? 1, 3

a. Azide
b. Atractyloside
c. Rotenone
d. DNP
e. Carbon monoxide
f. Antimycin A

13. Arsenate (AsO_4^{3-}) closely resembles phosphate in structure and reactivity. However, arsenate esters are unstable and are spontaneously hydrolyzed. If arsenate is added to actively respiring mitochondria, what would be the effect on ATP synthesis? On the rate of the electron-transport chain? Briefly explain.

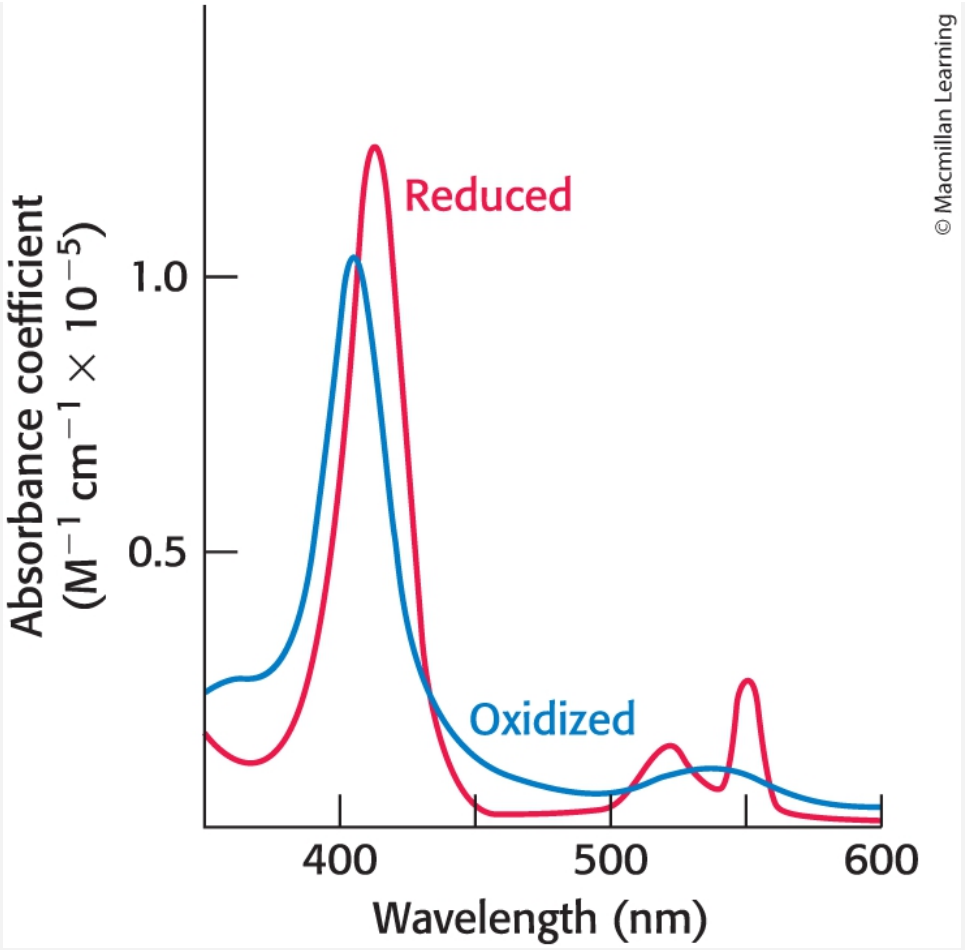
14. Oxidative phosphorylation in mitochondria is often monitored by measuring oxygen consumption. When oxidative phosphorylation is proceeding rapidly, the mitochondria will rapidly consume oxygen. If there is little oxidative phosphorylation, only small amounts of oxygen will be used. You are given a suspension of isolated mitochondria and directed to add the following compounds in the order from *a* to *h*. With the addition of each compound, all of the previously added compounds remain present. Predict the effect of each addition on oxygen consumption by the isolated mitochondria.
1, 2, 3, 4

a. Glucose
b. $ADP + P_i$
c. Citrate
d. Oligomycin
e. Succinate
f. Dinitrophenol
g. Rotenone
h. Cyanide

15. The number of molecules of inorganic phosphate incorporated into organic form per atom of oxygen consumed, termed the *P:O ratio,* was frequently used as an index of oxidative phosphorylation.

a. What are the relationships among the P:O ratio to the ratio of the number of protons translocated per electron pair $(H^+/2e^-)$ and the ratio of the number of protons needed to synthesize ATP and transport it to the cytoplasm (P/H^+)?
b. What are the P:O ratios for electrons donated by matrix NADH and by succinate?

16. The precise site of action of a respiratory-chain inhibitor can be revealed by the *crossover technique*. Britton Chance devised elegant spectroscopic methods for determining the proportions of the oxidized and reduced forms of each carrier. This determination is feasible because the forms have distinctive absorption spectra, as illustrated in the graph for cytochrome *c*.

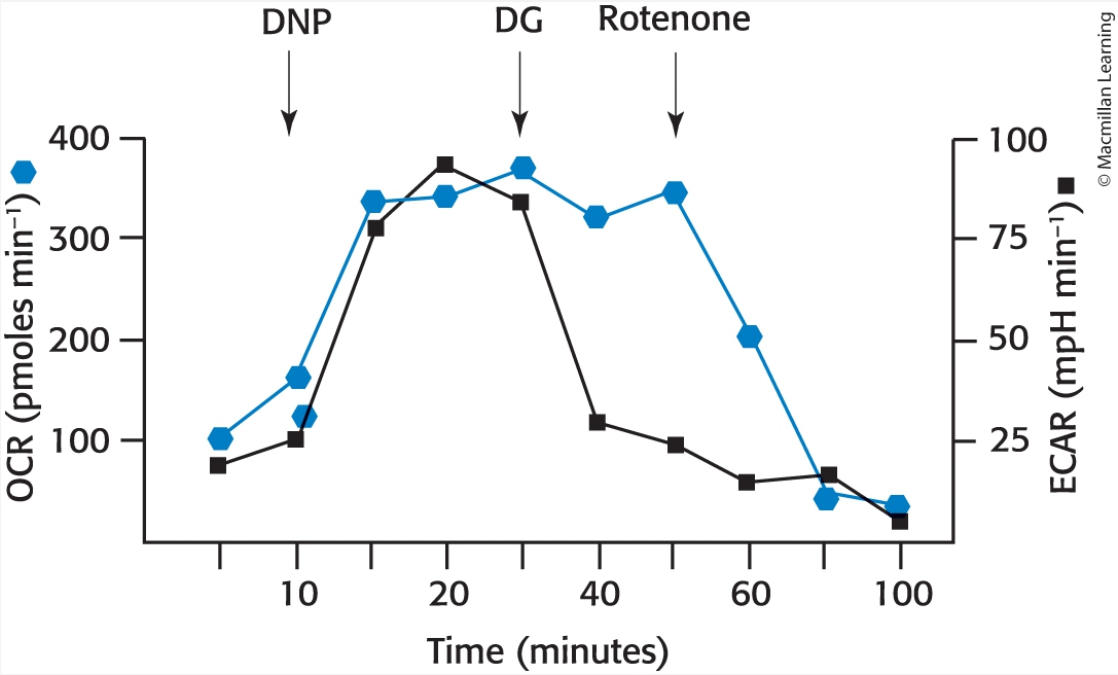


Suppose you are given a new inhibitor and find that its addition to respiring mitochondria causes the carriers between NADH and QH_2 to become more reduced and those between cytochrome *c* and O_2 to become more oxidized. Where does your inhibitor act? 1, 2

17. Years ago, uncouplers were suggested to make wonderful diet drugs. Explain why this idea was proposed and why it was rejected. Why might the producers of antiperspirants be supportive of the idea? 3, 4

18. Give an example of the use of the proton-motive force in ways other than for the synthesis of ATP.

19. XF technology (Seahorse Bioscience) now allows the measurement of the rate of aerobic respiration and lactic acid fermentation simultaneously in real time in cultured cells. The extent of aerobic respiration is determined by measuring the oxygen consumption rate (OCR, measured in picomoles of oxygen consumed per minute), while the rate of glycolysis correlates with the extracellular acidification rate (ECAR-milli pH per minute, or the changes in pH that occur over time). The next graph shows the results of an experiment using the new technology.



Dinitrophenol (DNP), the glycolysis inhibitor 2-deoxyglucose (DG), and rotenone were added sequentially to cell cultures. **1, 2**

a. What is the effect on OCR and ECAR of adding DNP to the cell culture? Explain these results.
b. Explain the effect of the addition of 2-deoxyglucose.
c. Explain how 2-deoxyglucose acts as an inhibitor of glycolysis?
d. Explain the effect of the addition of rotenone.

20. A mutation in a mitochondrial gene encoding a component of ATP synthase has been identified. People who have this mutation suffer from muscle weakness, ataxia (a loss of coordination), and retinitis pigmentosa (retinal degeneration). A tissue biopsy was performed on each of three patients having this mutation, and submitochondrial particles were isolated that were capable of succinate-sustained ATP synthesis. First, the activity of the ATP synthase was measured on the addition of succinate and the following results were obtained. 3, 4

ATP synthase activity (nmol of ATP formed $min^{-1} mg^{-1}$)	
Controls	3.0
Patient 1	0.25
Patient 2	0.11
Patient 3	0.17

a. What was the purpose of the addition of succinate?

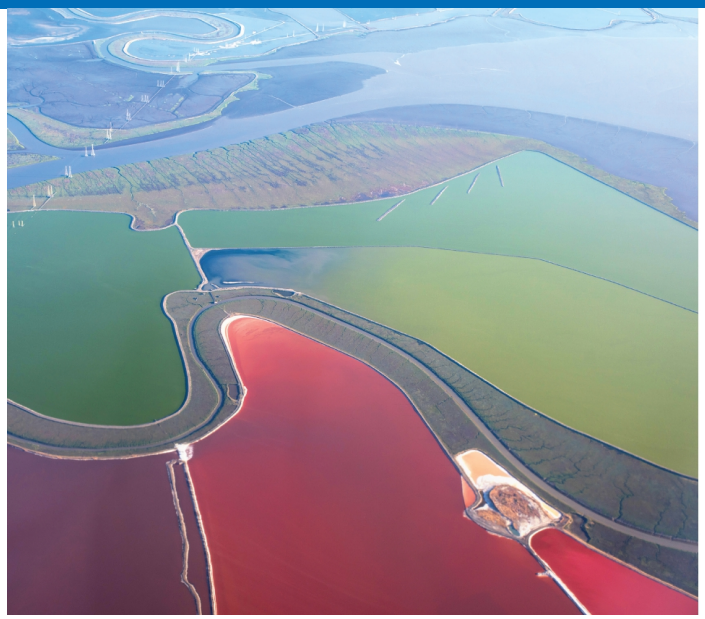
b. What is the effect of the mutation on succinate-coupled ATP synthesis?

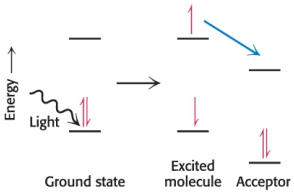
Next, the ATPase activity of the enzyme was measured by incubating the submitochondrial particles with ATP in the absence of succinate.

	ATP hydrolysis (nmol of ATP hydrolyzed $min^{-1} mg^{-1}$)
Controls	33
Patient 1	30
Patient 2	25
Patient 3	31

c. Why was succinate omitted from the reaction?
d. What is the effect of the mutation on ATP hydrolysis?
e. What do these results, in conjunction with those obtained in the first experiment, tell you about the nature of the mutation?

CHAPTER 19
Phototrophy and the Light Reactions of Photosynthesis





flowertiare/Deposit Photos
© Macmillan Learning

Phototrophic halobacteria are visible from the air in salt ponds near the San Francisco Bay. Although nonphotosynthetic, these reddish-purple archaea have the ability to produce additional ATP with energy from sunlight using an evolutionary relative of rhodopsin, a light-activated protein found in your eyes. Photosynthetic green algae are also visible in nearby ponds, which, in contrast, use sunlight exclusively for metabolic energy needs and can produce sugar from carbon dioxide. Both organisms accomplish phototrophy, the key to which is the ability of electrons to absorb visible light and then transfer from one molecule to another using the process of photoinduced charge separation diagrammed above.

Outline

19.1 Phototrophy Converts Light Energy into Chemical Energy
19.2 In Eukaryotes, Photosynthesis Takes Place in Chloroplasts
19.3 Light Absorption by Chlorophyll Molecules Induces Electron Transfer
19.4 Two Photosystems Generate a Proton Gradient and Reducing Power in Cyanobacteria and Photosynthetic Eukaryotes
19.5 A Proton Gradient across the Thylakoid Membrane Drives ATP Synthesis
19.6 Accessory Pigments Funnel Energy into Reaction Centers
19.7 The Ability to Convert Light into Chemical Energy Is Ancient

---

Learning Goals



By the end of this chapter, you should be able to:

1. Describe phototrophy and the light reactions.
2. Identify the key products of the light reactions.
3. Explain how redox balance is maintained during the light reactions.
4. Explain how ATP is synthesized in chloroplasts.
5. Describe the function of the light-harvesting complex.

Every year, Earth is bathed in photons with a total energy content of approximately 10^{24} kJ. By comparison, a major hurricane has one billionth that amount of energy. The source of the energy is, of course, the electromagnetic radiation from the sun. On our planet, there are organisms capable of collecting a fraction, approximately 2%, of this solar energy, and converting it into chemical energy. Green plants are the most obvious of these organisms, although 60%

of this conversion is carried out by algae, bacteria, and archaea. Although only a small amount of the incident energy is captured, it powers almost all life on Earth. This transformation is perhaps the most important of all of the energy transformations that we will see in our study of biochemistry; without it, the vast majority of life as we know it on our planet simply could not exist.

19.1 Phototrophy Converts Light Energy into Chemical Energy

The metabolisms of living organisms can be subdivided into two pairs of fundamental groups based upon how they capture energy and obtain carbon. The process of converting electromagnetic radiation into chemical energy is called *phototrophy*, and, as noted in Chapter 15, organisms which utilize this mechanism to capture energy are called **phototrophs** (literally, "light-feeders").

An example of a phototroph is the archaeon *Halobacterium salinarum* that grows in extremely salty water such as that found in the Dead Sea, the Great Salt Lake, or in evaporation ponds used to isolate salt, as shown at the start of this chapter. When grown under low oxygen conditions, this organism generates additional ATP by using just two membrane proteins (**Figure 19.1**), relatives of which we have already encountered in other contexts. The first is ATP synthase, which utilizes a proton gradient to produce ATP (Section 18.4). The second is **bacteriorhodopsin**, which we discussed briefly in Section 12.4.

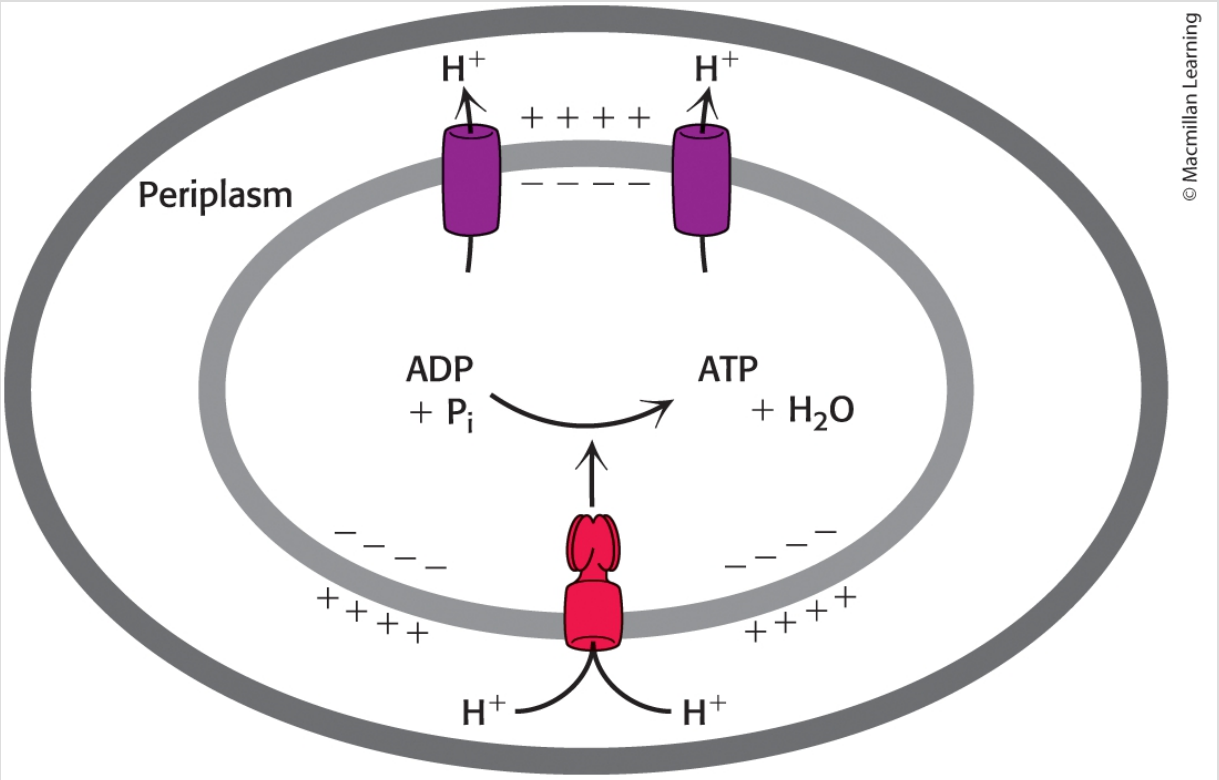


FIGURE 19.1 Phototrophy can be accomplished by the cooperation of just two proteins. The archaeon *Halobacterium salinarum* accomplishes phototrophy by expressing the light-absorbing protein bacteriorhodopsin in its inner cell membrane. Bacteriorhodopsin (purple structures) uses the energy from sunlight to transport protons across the membrane and into the periplasm. These protons return through ATP synthase (red structure) to make ATP.

Bacteriorhodopsin is similar to the 7-transmembrane helix protein rhodopsin involved in vision (Section 14.6). Like rhodopsin, bacteriorhodopsin includes bound 11-*cis* retinal, absorbing sunlight efficiently and producing all-trans retinal. Unlike rhodopsin, bacteriorhodopsin does not signal through other proteins but acts as a proton pump, transporting one proton — for each photon absorbed — from the cytoplasm to the periplasm, the space between the cell membrane and the cell wall.

Many phototrophic organisms use captured light energy, along with electrons harvested from a donor molecule, to convert carbon dioxide into carbohydrate in a complex process known as **photosynthesis**. The most common form of photosynthesis on Earth today, used by all plants, algae, and many bacteria, is called *oxygenic photosynthesis* and is the primary subject of this chapter. Oxygenic photosynthesis is so named because water is the electron donor and oxygen is produced as a waste product.

$$CO_2 + H_2O \xrightarrow{\text{Light}} (CH_2O) + O_2$$

In accordance with how the term is most commonly used, we will simply use the term "photosynthesis" to refer to oxygenic photosynthesis and will explicitly refer to alternative types as *anoxygenic photosynthesis* when they arise. In the above reaction, CH_2O represents carbohydrate, primarily sucrose and starch. Photosynthetic carbohydrate synthesis constantly regenerates organic molecules from carbon dioxide. These can then be used as energy sources for **chemotrophs**, like humans, which derive energy from chemicals as opposed to sunlight.

Photosynthetic organisms are also **autotrophs** ("self-feeders") because they obtain carbon primarily from carbon dioxide, rather than from organic molecules. Autotrophs can synthesize chemical fuels such as glucose from carbon dioxide and water. Photosynthetic organisms capture and store energy from sunlight and then later utilize this energy from the synthesized glucose through the glycolytic pathway and aerobic metabolism. In contrast to autotrophs, organisms that obtain carbon primarily from organic chemicals are called **heterotrophs**, which ultimately depend on autotrophs for these molecules. Thus, the carbohydrates produced

by photosynthetic organisms provide not only energy to run much of the biological world, but also the carbon molecules used by many organisms to make a wide array of biomolecules.

Photosynthesis comprises light reactions and dark reactions

Photosynthesis is composed of two parts: the light reactions and the dark reactions. In the **light reactions**, light energy is captured as chemical energy through the formation of ATP and electrons are extracted to provide reducing power for biosynthetic reactions. The products of the light reactions are then used in the so-called *dark reactions* to drive the reduction of CO_2 and its conversion into glucose and other sugars. The dark reactions are also called the *Calvin–Benson cycle* or *light-independent reactions* and will be discussed in Chapter 20.

The same biochemical principles govern both respiration and photosynthesis

As we will see soon, the light reactions of photosynthesis closely resemble the events of oxidative phosphorylation, whereas the dark reactions accomplish the reversal of cellular respiration. In Chapters 17 and 18, we learned that cellular respiration is the oxidation of glucose to CO_2 with the reduction of O_2 to water, a process that generates ATP.

$$C_6H_{12}O_6 + 6\,O_2 \xrightarrow{\text{Cellular respiration}} 6\,CO_2 + 6\,H_2O + \text{energy}$$

In photosynthesis, this process must be reversed — reducing CO_2 and oxidizing H_2O to synthesize glucose.

$$\text{Energy} + 6\,H_2O + 6\,CO_2 \xrightarrow{\text{Photosynthesis}} C_6H_{12}O_6 + 6\,O_2$$

Although the processes of respiration and photosynthesis are chemically opposite each other, the biochemical principles governing the two processes are nearly identical. The key to both processes is the generation of high-energy electrons.

- *During respiration, the citric acid cycle oxidizes carbon fuels to CO_2 to generate high-energy electrons*. The flow of these high-energy electrons down an electron-transport chain generates a proton-motive force. This proton-motive force is then transduced by ATP synthase to form ATP.

- *During photosynthesis, energy from light boosts electrons from a low-energy state to a high-energy state*. In the high-energy, unstable state, these electrons can be passed to nearby molecules. These electrons are then used to (1) produce reducing power in the form of NADPH and (2) generate a proton-motive force across a membrane, which subsequently drives the synthesis of ATP (**Figure 19.2**).

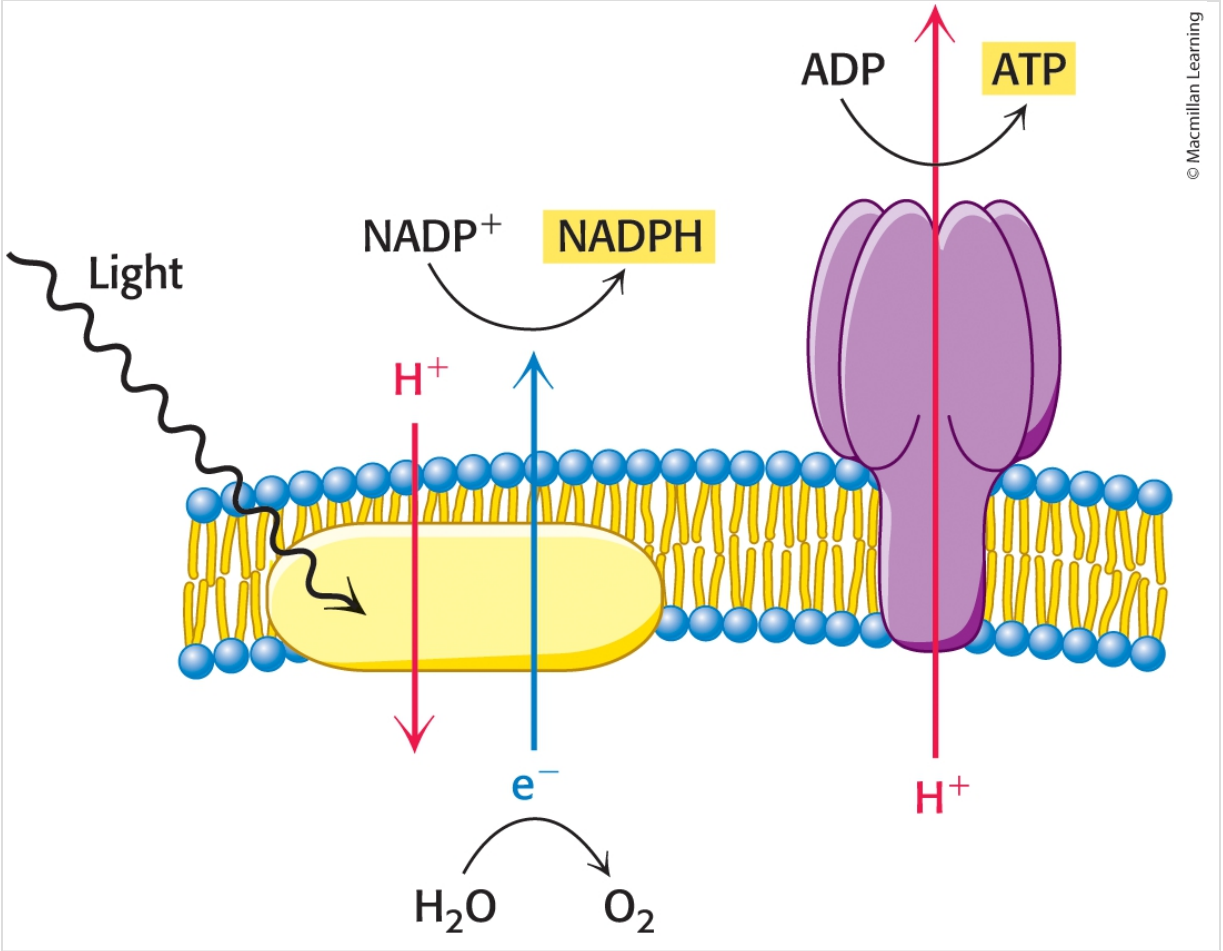


FIGURE 19.2 The light reactions of oxygenic photosynthesis generate both ATP and reducing power. Light is absorbed and the energy is used to drive electrons from water to generate NADPH, which can be used later for reduction reactions, and to drive protons across a membrane. In the same fashion as shown for the halobacterium in Figure 19.1, these protons return through ATP synthase (purple structure) to make ATP.

Self-Check Question

Photosynthesis is a complex metabolic process that is the sum of which two of the following four metabolic schemes for carbon and energy capture: chemotrophy,

Two kinds of light reactions take place in the green plants

Photosynthesis in green plants is mediated by two kinds of light reactions, which take place in two distinct transmembrane protein complexes, called *photosystems*. **Photosystem I** generates reducing power in the form of NADPH but, in the process, becomes electron deficient. **Photosystem II** oxidizes water and transfers the electrons to replenish the electrons lost by photosystem I. A side product of these reactions is O_2. Electron flow from photosystem II to photosystem I generates the transmembrane proton gradient, augmented by the protons released by the oxidation of water, that drives the synthesis of ATP. In keeping with the similarity of their principles of operation, in eukaryotes both respiration and photosynthesis take place in double-membrane organelles: mitochondria for cellular respiration and chloroplasts for photosynthesis.

19.2 In Eukaryotes, Photosynthesis Takes Place in Chloroplasts

In eukaryotes, photosynthesis takes place in specialized organelles called **chloroplasts**, typically $5\ \mu m$ long. Like a mitochondrion, a chloroplast has an outer membrane and an inner membrane, with an intervening intermembrane space (**Figure 19.3**). The inner membrane surrounds a space called the **stroma**, which is the site of the dark reactions of photosynthesis (Chapter 20). In the stroma are membranous structures called **thylakoids**, which are flattened sacs, or discs. The thylakoid sacs are stacked to form a **granum**. Different grana are linked by regions of thylakoid membrane called *stroma lamellae*. The thylakoid membranes separate the thylakoid space from the stroma space. Thus, chloroplasts have three different membranes (*outer, inner*, and *thylakoid membranes*) and three separate spaces (*intermembrane, stroma,* and *thylakoid lumen*). In a developing chloroplast, thylakoids arise from budding of the inner membrane, and so they are analogous to the mitochondrial cristae. Like the mitochondrial cristae, they are the site of coupled oxidation–reduction reactions of the light reactions that generate the proton-motive force.

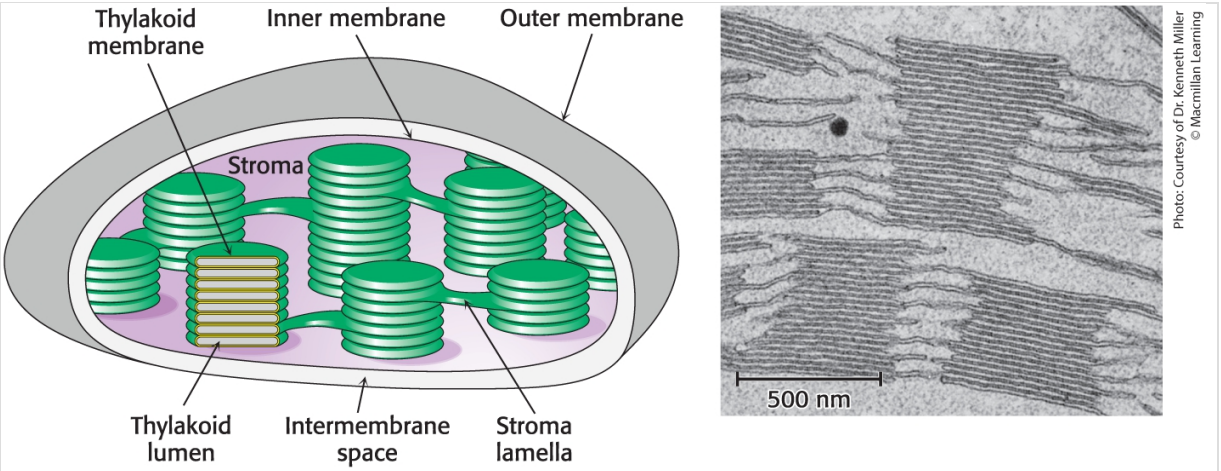


FIGURE 19.3 The anatomy of a chloroplast reveals complex membrane-enclosed structures. Plant-leaf cells contain between 1 and 100 chloroplasts, depending on the species, cell type, and growth conditions. At far right, an electron micrograph of a chloroplast from a spinach leaf shows thylakoid membranes packed together to form grana.

The primary events of photosynthesis take place in thylakoid membranes

The thylakoid membranes contain the energy-transforming machinery: light-harvesting proteins, reaction centers, electron-transport chains, and ATP synthase. These membranes contain nearly equal amounts of lipids and proteins. The lipid composition is highly distinctive: about 75% of the total lipids are galactolipids and 10% are sulfolipids, whereas only 10% are phospholipids. The thylakoid membrane and the inner membrane, like the inner mitochondrial membrane, are impermeable to most molecules and ions. The outer membrane of a chloroplast, like that of a mitochondrion, is highly permeable to small molecules and ions. The stroma contains the soluble enzymes that utilize the NADPH and ATP synthesized by the thylakoids to convert CO_2 into sugar.

Chloroplasts arose from an endosymbiotic event

Chloroplasts contain their own DNA and the machinery for replicating and expressing it. However, chloroplasts are not independent from the rest of the cell; they also contain many proteins encoded by nuclear DNA. How did the intriguing relationship between the cell and its chloroplasts develop? It is now widely accepted that, in a manner analogous to the evolution of mitochondria (Section 18.1), chloroplasts are also the result of endosymbiotic events in which a photosynthetic microorganism was engulfed by a eukaryotic host. Evidence suggests that chloroplasts in both higher plants and green algae are derived from a single endosymbiotic event, when an ancestor of a modern-day cyanobacterium was engulfed (**Figure 19.4**), whereas those in red and brown algae are derived from at least one additional event.



Elif Bayraktar/Shutterstock

FIGURE 19.4 Cyanobacteria are the prokaryotic photosynthesizers that are the most similar to plant chloroplasts. A colony of the photosynthetic filamentous cyanobacterium *Anabaena* is shown at 500× magnification. Ancestors of these bacteria are thought to have evolved into present-day chloroplasts of plants.

The chloroplast genome is smaller than that of a cyanobacterium, but the two genomes have key features in common. Both are circular and have a single start site for DNA replication, and the genes of both are arranged in operons — sequences of functionally related genes under common control. In the course of evolution, many of the genes of the chloroplast ancestor were transferred to the plant cell's nucleus or, in some cases, lost entirely, thus establishing a fully dependent relationship.

Self-Check Question



Explain the relationship between the following terms: thylakoid, stroma, chloroplast, and endosymbiosis.

19.3 Light Absorption by Chlorophyll Molecules Induces Electron Transfer

The trapping of light energy is the key to phototrophy, and therefore also photosynthesis. The first event is the absorption of light by a photoreceptor molecule. The principal photoreceptors in the chloroplasts of most green plants are collectively chlorophylls, and of particular importance among these is the pigment molecule **chlorophyll *a***, a substituted tetrapyrrole (**Figure 19.5**). The four nitrogen atoms of the pyrroles are coordinated to a magnesium ion. Unlike a porphyrin such as heme, chlorophyll *a* has a reduced pyrrole ring and an additional 5-carbon ring fused to one of the pyrrole rings. Another distinctive feature of chlorophyll *a* is the presence of *phytol,* a highly hydrophobic 20-carbon alcohol, esterified to an acid side chain.

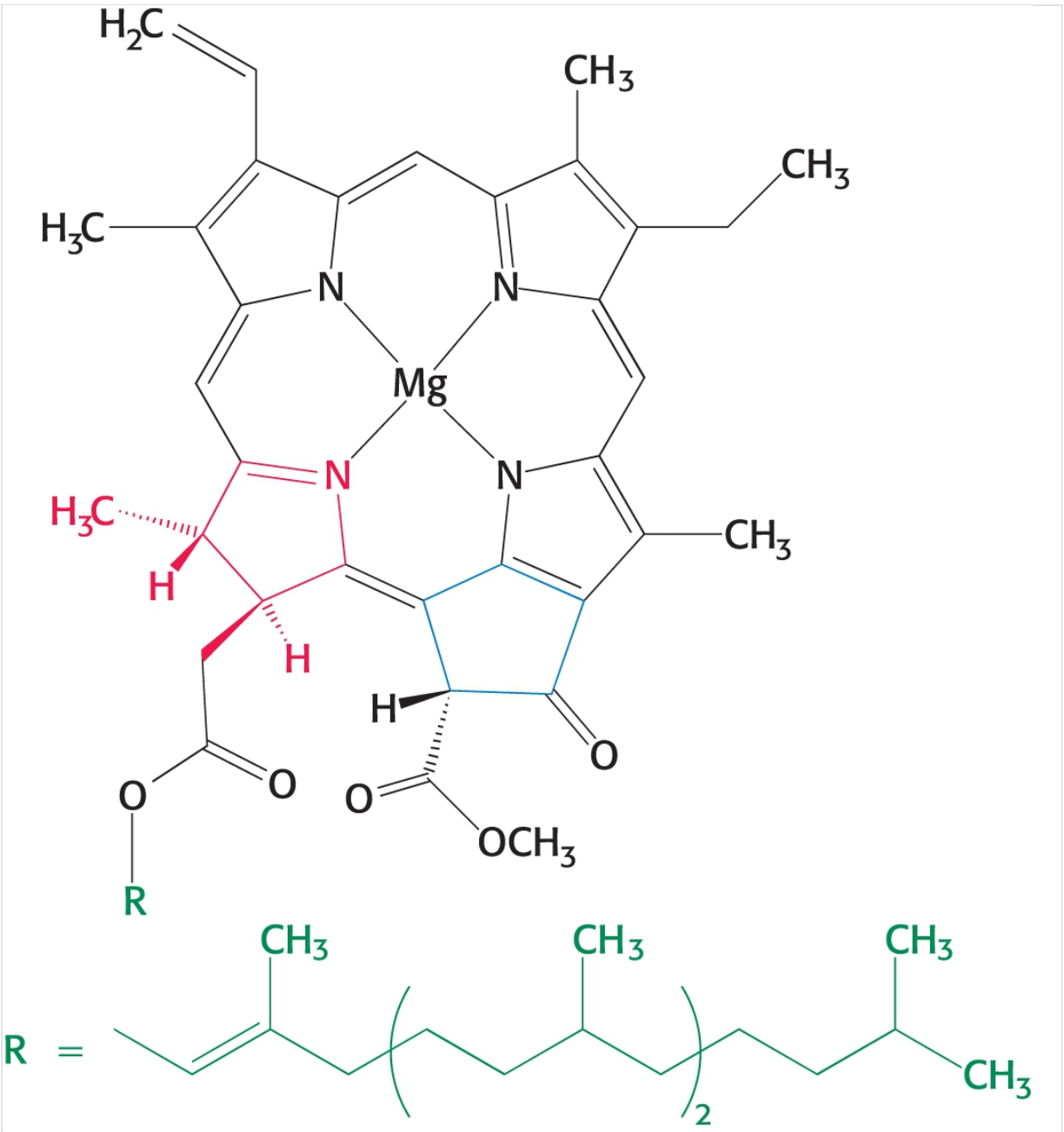


FIGURE 19.5 Chlorophyll *a* is structurally similar to heme. Like heme, chlorophyll *a* is a cyclic tetrapyrrole. One of the pyrrole rings (shown in red) is reduced, and an additional five-carbon ring (shown in blue) is fused to another pyrrole ring. A phytol chain (shown in green) is connected by an ester linkage. Magnesium ion binds at the center of the structure.

Chlorophylls are very effective photoreceptors because they contain networks of conjugated double bonds — alternating single and double bonds. Such compounds are called conjugated polyenes. In polyenes, the electrons are not localized to a particular atomic nucleus. Upon the absorption of light energy, the electron transitions from a low-energy molecular orbital to a higher-energy orbital.

Chlorophylls have very strong absorption bands in the visible region of the spectrum, where the solar output reaching Earth is maximal (**Figure 19.6**). Chlorophyll *a*'s peak molar extinction coefficient (ε), a measure of a compound's ability to absorb light, is greater than $10^5\ M^{-1}\ cm^{-1}$, among the highest observed for organic compounds.

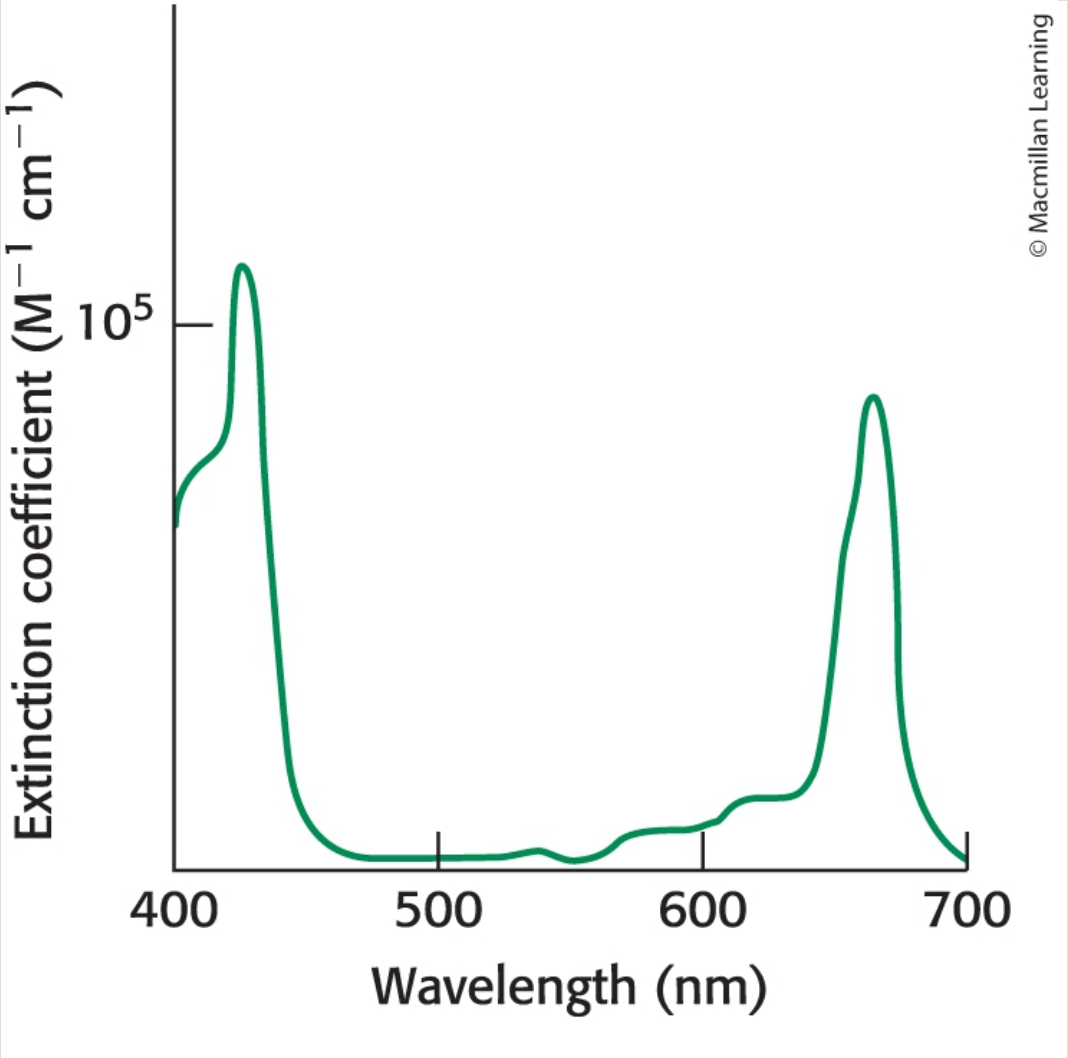


FIGURE 19.6 Chlorophyll *a* has a distinct absorbance spectrum in the visible range. Chlorophyll *a* absorbs visible light efficiently, as judged by the extinction coefficient near $10^5\ M^{-1}\ cm^{-1}$.

Transferring electrons allows energy to be captured instead of lost as heat

What happens when light is absorbed by a pigment molecule? The energy from the light excites an electron from its ground energy level to an excited energy level (Figure 19.7).

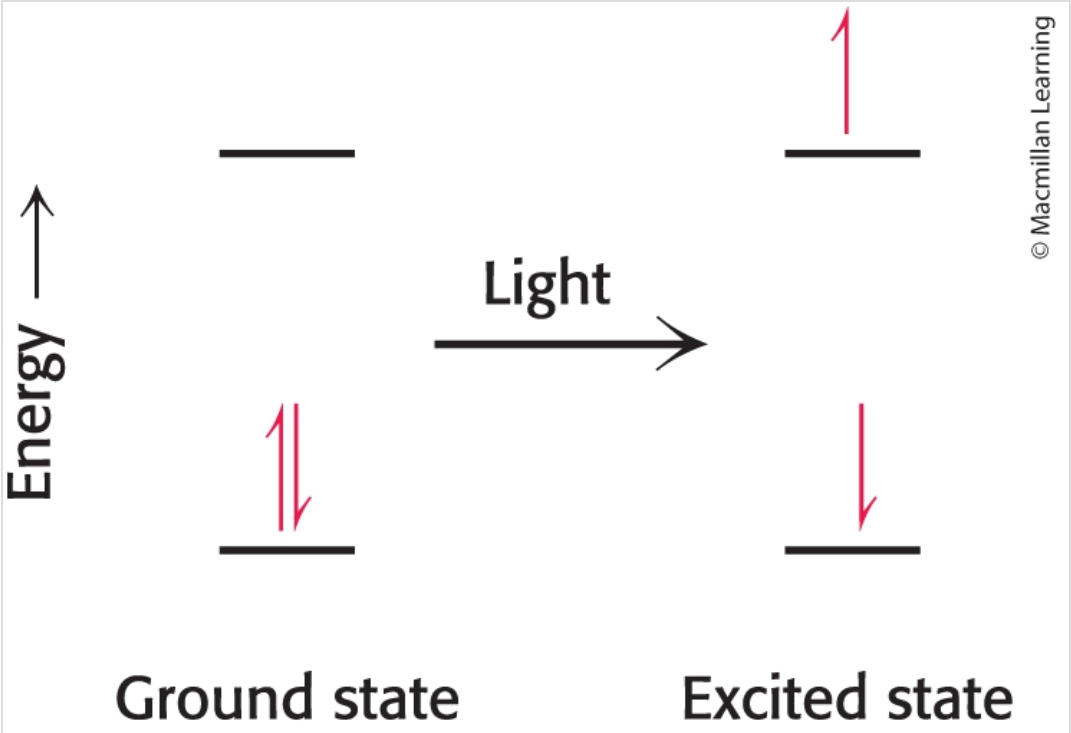


FIGURE 19.7 The absorption of light leads to the excitation of an electron from its ground state to a higher energy level.

This high-energy electron can have one of several fates. For the vast majority of compounds that absorb light, the electron simply returns to the ground state and the absorbed energy is converted into heat; however, the energy can also be emitted as light (fluorescence or phosphorescence) or transferred to another nearby electron (resonance energy transfer). However, one remaining possibility is the key to phototrophy: if a suitable electron acceptor is nearby, as is the case for chlorophylls in photosynthetic systems, the excited electron can move from the initial molecule to the acceptor (Figure 19.8). A positive charge forms on the initial molecule, owing to the loss of an electron, and a negative charge forms on the acceptor, owing to the gain of an electron. Hence, this process is referred to as **photoinduced charge separation**.

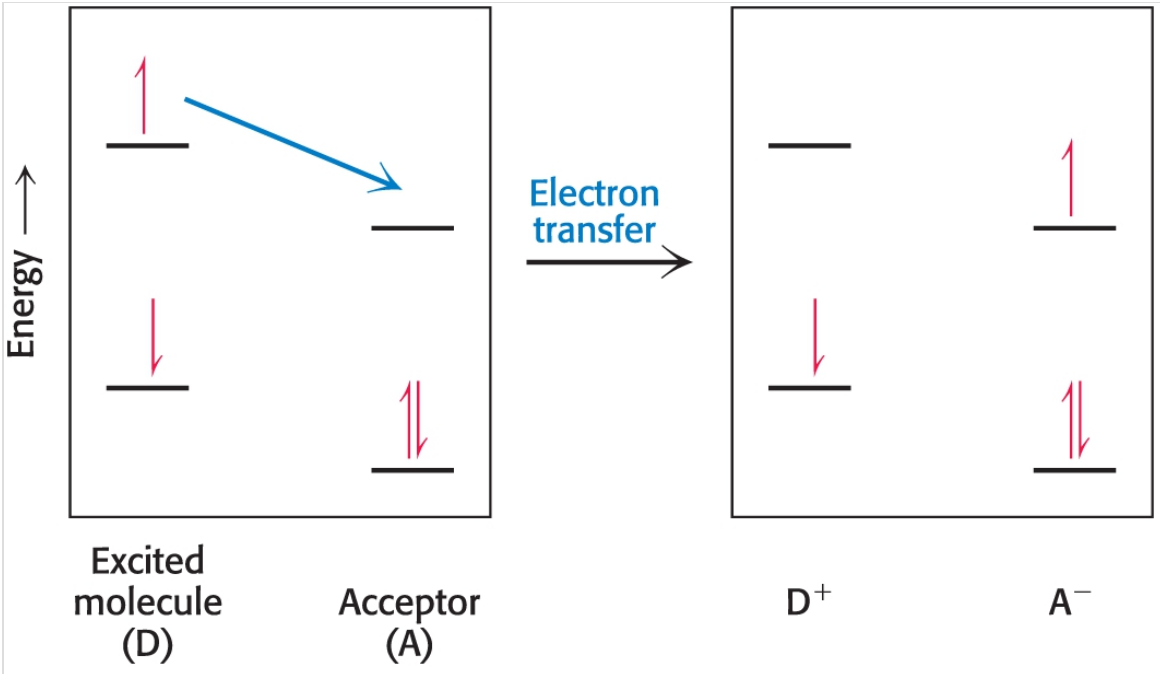


FIGURE 19.8 The key to photosynthesis is photoinduced charge separation. If a suitable electron acceptor is nearby, an electron that has been moved to a high energy level by light absorption can move from the excited molecule to the acceptor.

In chloroplasts, the arrangement of the photosynthetic apparatus maximizes photoinduced charge separation and minimizes an unproductive return of the electron to its ground state. The electron, extracted from its initial site by the absorption of light, now has reducing power: it can reduce other molecules to store the energy originally obtained from light in chemical forms.

A "special pair" of chlorophylls initiate charge separation

The specific site at which photoinduced charge separation occurs is called the **reaction center**. The structure of the reaction center from anoxygenic photosynthetic bacteria — such as the nonsulfur purple bacterium *Rhodopseudomonas viridis* — was the first one determined. This reaction center consists of four polypeptides, abbreviated L, M, H, and C (**Figure 19.9**). Sequence comparisons and subsequent structural studies have confirmed that this bacterial reaction center is homologous to the more complex cyanobacterial and plant systems. Thus, many of our observations of the purple bacterial system also apply these other systems.

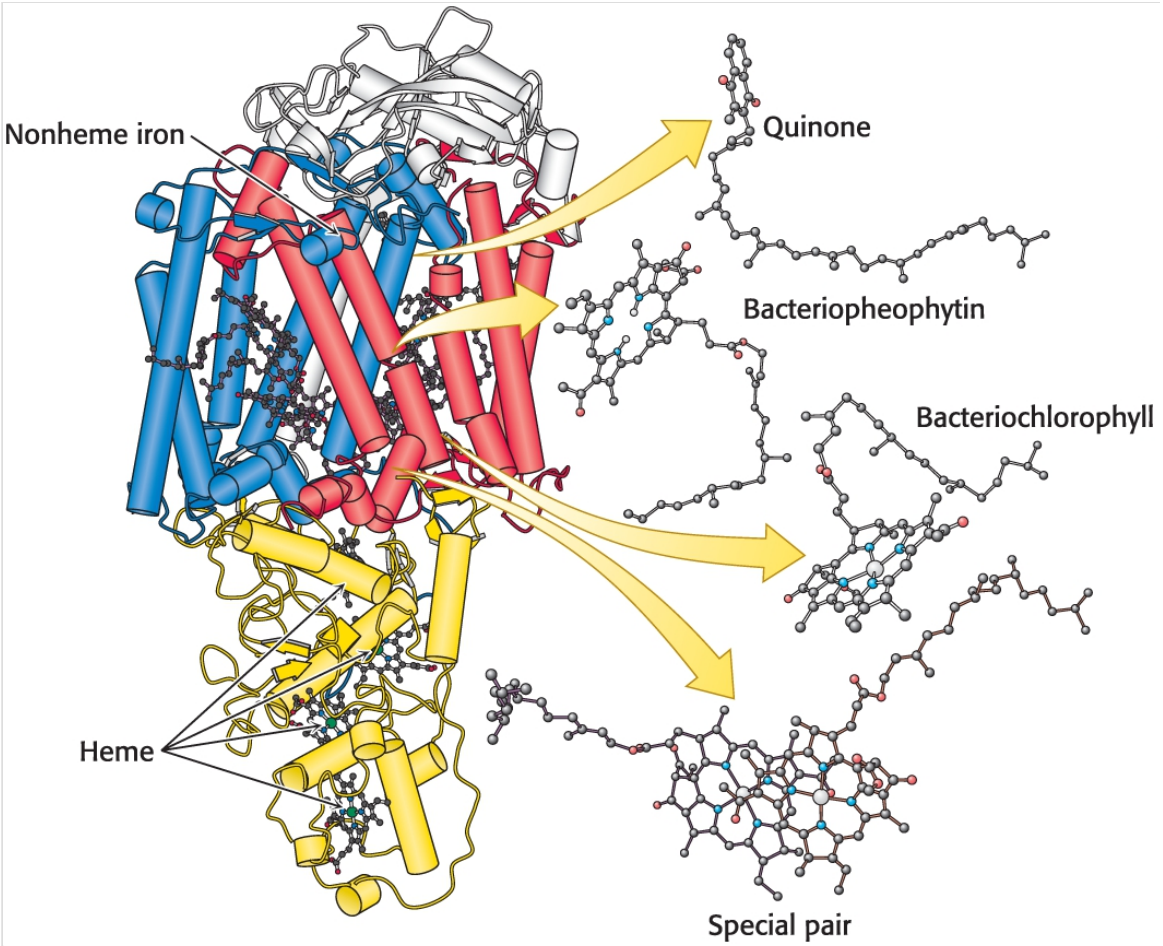


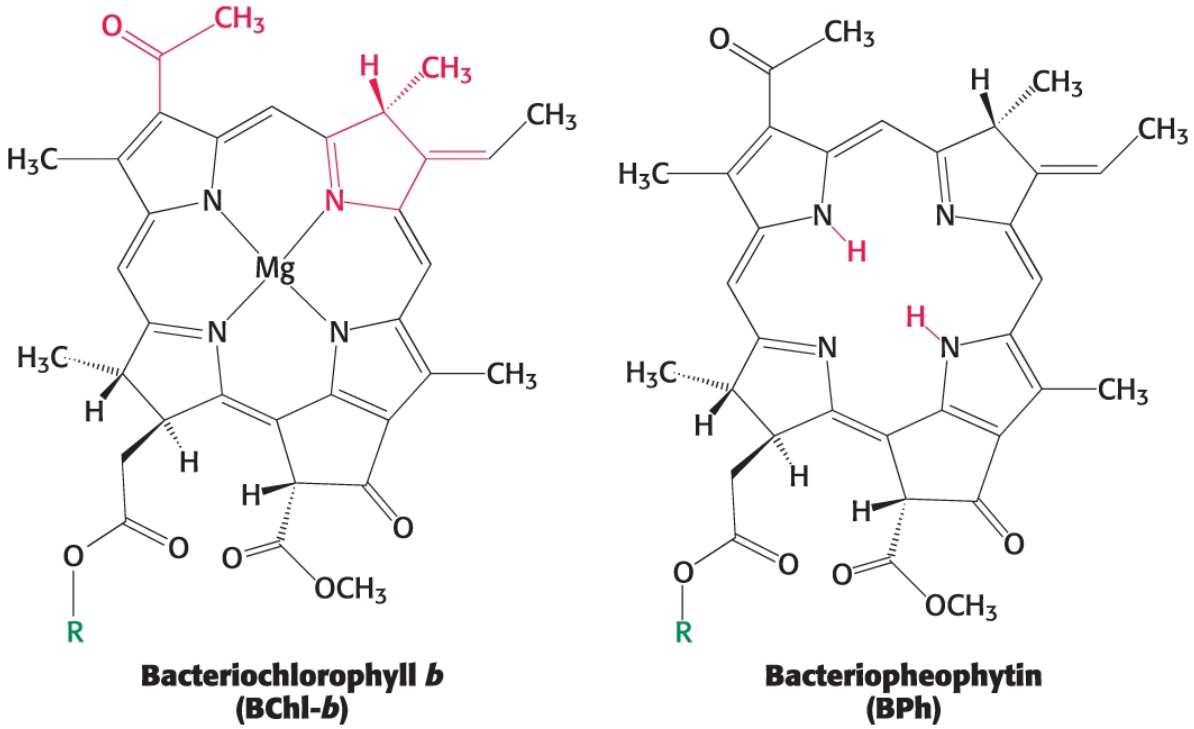
FIGURE 19.9 The photosynthetic reaction center in a nonsulfur purple bacterium is a large complex with many electron-carrying groups and one special pair. The core of the reaction center from *Rhodopseudomonas viridis* consists of two similar chains: L (shown in red) and M (blue). An H chain (white) and a cytochrome subunit (yellow) complete the structure. Notice tha the L and M subunits are composed largely of α helices that span the membrane. Also notice tha a chain of electron-carrying prosthetic groups, beginning with a special pair of bacteriochlorophylls and ending at a bound quinone, runs through the structure from bottom t top in this view.

[Drawn from 1PRC.pdb.]

INTERACT with this model in Achieve

The L and M subunits form the structural and functional core of the purple bacterial photosynthetic reaction center. Each of these

homologous subunits contains five transmembrane helices, in contrast with the H subunit, which has just one. The H subunit lies on the cytoplasmic side of the cell membrane, and the cytochrome subunit lies on the exterior face of the cell membrane, called the *periplasmic side* because it faces the periplasm — the space between the cell membrane and the cell wall. Four bacteriochlorophyll *b* (BChl-*b*) molecules, two bacteriopheophytin *b* (BPh) molecules, two quinones (Q_A and Q_B), and a ferrous ion are associated with the L and M subunits.



Bacteriochlorophylls are photoreceptors similar to chlorophylls, except for the reduction of an additional pyrrole ring and other minor differences that shift their absorption maxima to the near infrared, to wavelengths as long as 1000 nm. *Bacteriopheophytin* is the term for a bacteriochlorophyll that has two protons instead of a magnesium ion at its center.

The reaction begins with light absorption by a pair of BChl-*b* molecules that lie near the periplasmic side of the membrane in the L–M dimer.

The pair of BChl-*b* molecules is called the **special pair** because of its fundamental role in photosynthesis. The special pair absorbs light maximally at 960 nm and, for this reason, is often called P960 (*P* stands for pigment). After absorbing light, the excited special pair ejects an electron, which is transferred through another BChl-*b* to the bacteriopheophytin in the L chain (Figure 19.10, steps 1 and 2). This initial charge separation yields a positive charge on the special pair $(P960^{+})$ and a negative charge on BPh (BPh^{-}). The electron ejection and transfer take place in less than 10 picoseconds $(10^{-12}\ s)$, again illustrating the incredibly short timeframes of molecular interactions at the biochemical timescale.

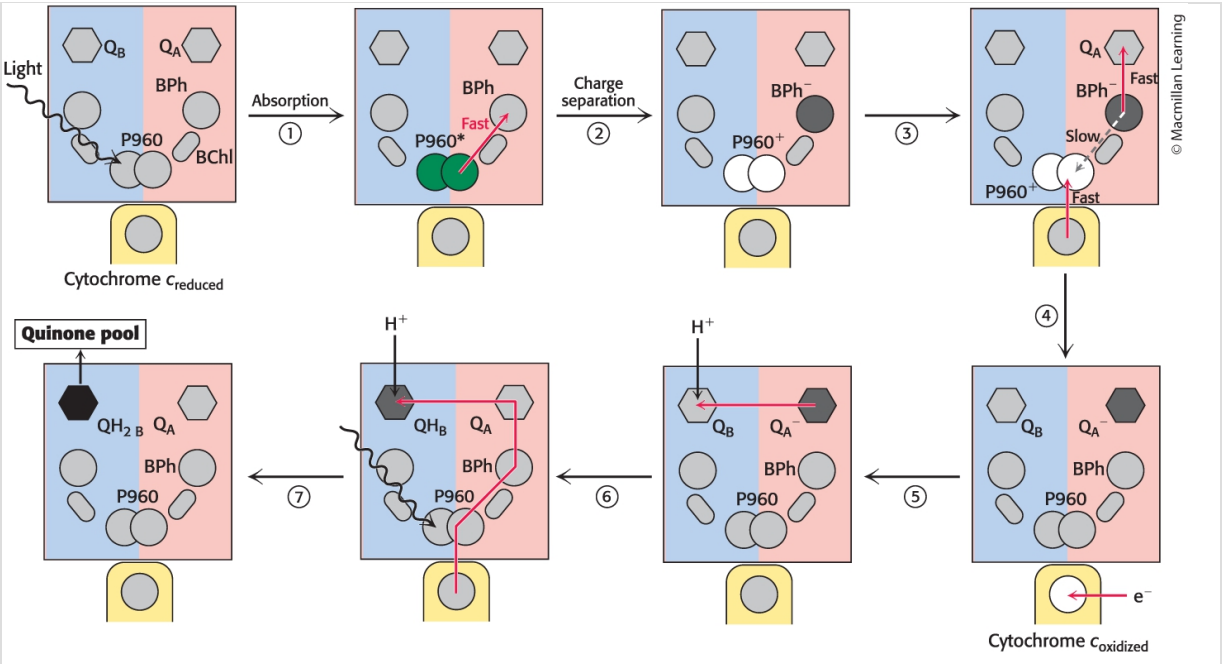


FIGURE 19.10 In the reaction center of nonsulfur purple bacteria, electrons flow from the special pair to a quinone. The absorption of light by the special pair (P960) results in the rapid transfer of an electron from this site to a bacteriopheophytin (BPh), creating a photoinduced charge separation (steps 1 and 2). (The asterisk on P960 stands for excited state.) The possible return of the electron from the pheophytin to the oxidized special pair is suppressed by the "hole" in the special pair being refilled with an electron from the cytochrome subunit and the electron from the pheophytin being transferred to a quinone (Q_A) that is farther away from the special pair (steps 3 and 4). Q_A passes the electron to Q_B. The reduction of a quinone (Q_B) on

the cytoplasmic side of the membrane results in the uptake of two protons from the cytoplasm (steps 5 and 6). The reduced quinone can move into the quinone pool in the membrane (step 7).



A proton gradient across the membrane is established

A nearby electron acceptor, a tightly bound quinone (Q_A), quickly grabs the electron away from BPh^- before the electron has a chance to fall back to the P960 special pair. From Q_A, the electron moves to a more loosely associated quinone, Q_B. The absorption of a second photon and the movement of a second electron from the special pair through the bacteriopheophytin to the quinones completes the two-electron reduction of Q_B from Q to QH_2. Because the Q_B-binding site lies near the cytoplasmic side of the membrane, two protons are taken up from the cytoplasm, contributing to the development of a proton gradient across the cell membrane (Figure 19.10, steps 5, 6, and 7).

In their high-energy states, $P960^+$ and BPh^- could undergo charge recombination; that is, the electron on BPh^- could move back to neutralize the positive charge on the special pair. Its return to the special pair would waste a valuable high-energy electron and simply convert the absorbed light energy into heat. How is charge recombination prevented? Two factors in the structure of the reaction center work together to suppress charge recombination nearly completely (Figure 19.10, steps 3 and 4). First, the next electron acceptor (Q_A) is less than 10 Å away from BPh^-, and so the electron is rapidly transferred farther away from the special pair. Second, one of the hemes of the cytochrome subunit is less than 10 Å away from the

special pair, and so the positive charge on P960 is neutralized by the transfer of an electron from the reduced cytochrome.

Cyclic electron flow reduces the cytochrome of the reaction center

The cytochrome subunit of the reaction center must regain an electron to complete the cycle. It does so by taking back two electrons from reduced quinone (QH_2). QH_2 first enters the Q pool in the membrane where it is reoxidized to Q by complex bc_1, which is homologous to Complex III of the respiratory electron-transport chain. Complex bc_1 transfers the electrons from QH_2 to cytochrome c_2, a water-soluble protein in the periplasm, and in the process pumps protons into the periplasmic space. The electrons now on cytochrome c_2 flow to the cytochrome subunit of the reaction center. The flow of electrons is thus cyclic in these bacteria, and oxygen is not evolved (**Figure 19.11**). The proton gradient generated in the course of this cycle drives the synthesis of ATP through the action of ATP synthase.

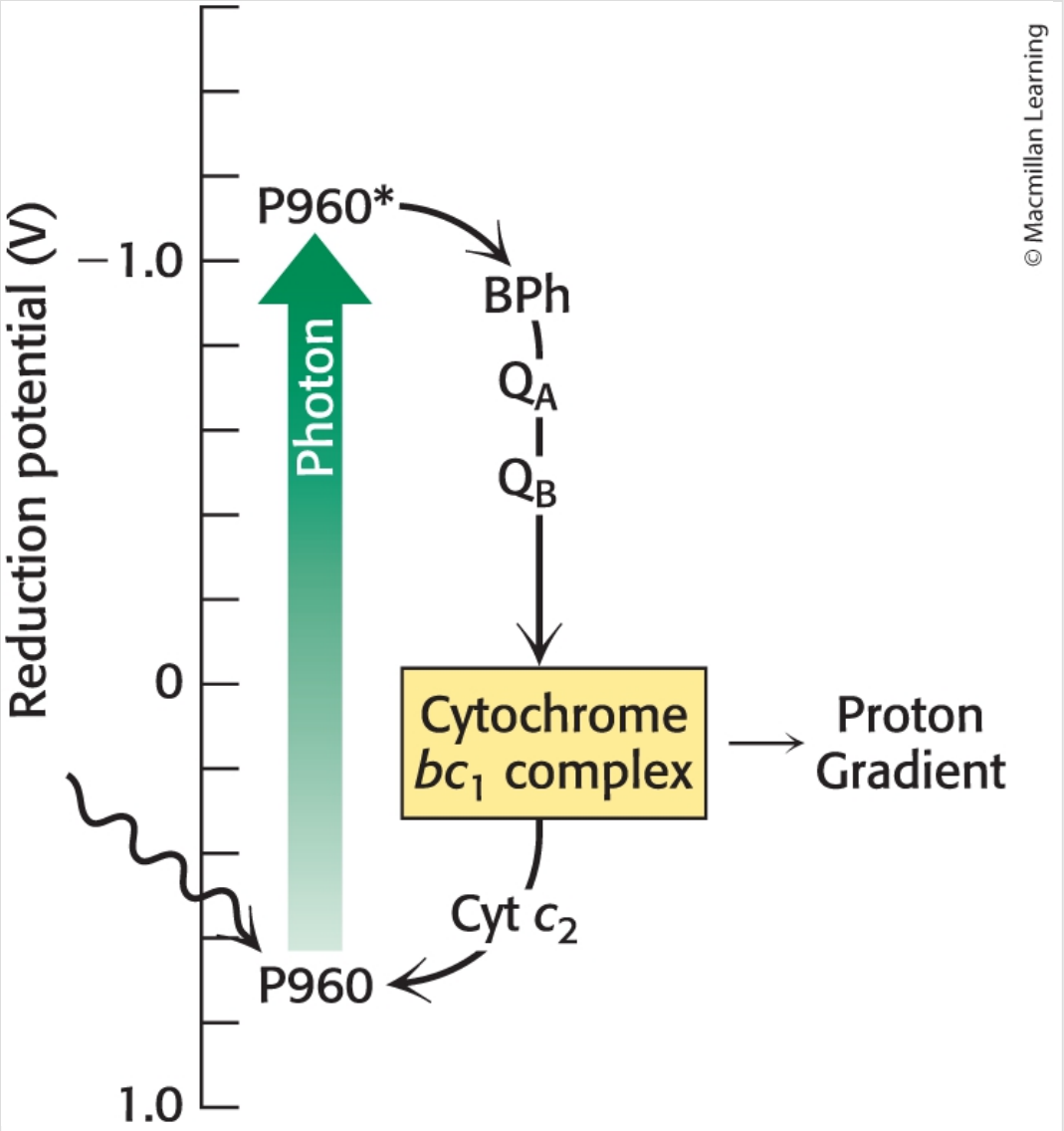


FIGURE 19.11 Cyclic electron flow in the bacterial reaction center allows the generation of ATP but not reducing power. Excited electrons from the P960 reaction center flow through bacteriopheophytin (BPh), a pair of quinone molecules (Q_A and Q_B), cytochrome bc_1 complex, and finally through cytochrome c_2 to the reaction center. The cytochrome bc_1 complex pumps protons as a result of electron flow, which powers the formation of ATP.

Self-Check Question



What is meant by a “special pair” in the context of photosynthesis, and what important role does it play?

19.4 Two Photosystems Generate a Proton Gradient and Reducing Power in Cyanobacteria and Photosynthetic Eukaryotes

Photosynthesis is more complicated in eukaryotes and cyanobacteria than in the purple photosynthetic bacteria discussed in the previous section. In these other organisms including all green plants, photosynthesis depends on the interplay of two kinds of membrane-bound, light-sensitive complexes — photosystem I (PS I) and photosystem II (PS II), as shown in **Figure 19.12**. Note that photosystem I is so named because it was discovered first, but it is actually photosystem II that acts first in the sequence of events that take place during photosynthesis.

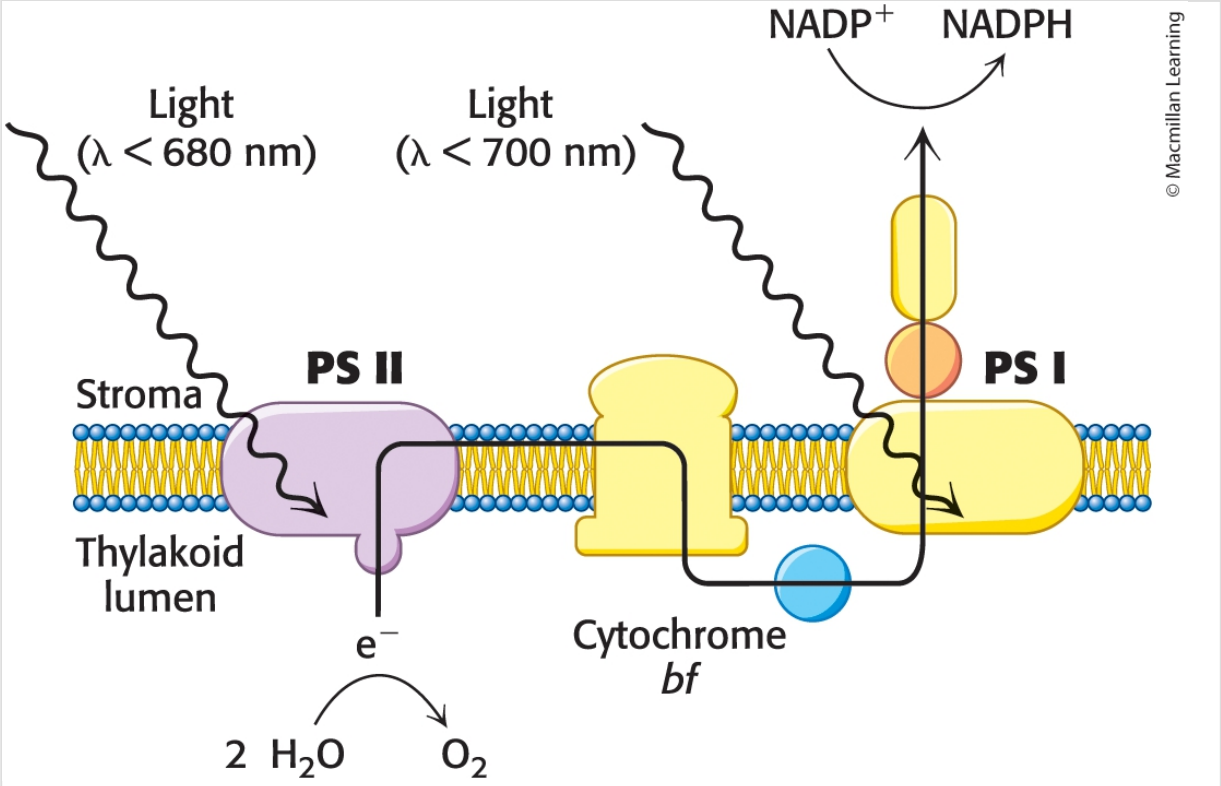


FIGURE 19.12 In green plants, electrons can flow through two photosystems. The absorption of photons by two distinct photosystems (PS II and PS I) is required for complete electron flow from water to $NADP^+$.

There are similarities in photosynthesis between green plants and purple photosynthetic bacteria. Both require light to energize reaction centers consisting of special pairs, and both transfer electrons by using electron-transport chains. However, in plants, electron flow can be cyclic, but it progresses linearly from photosystem II to photosystem I under most circumstances.

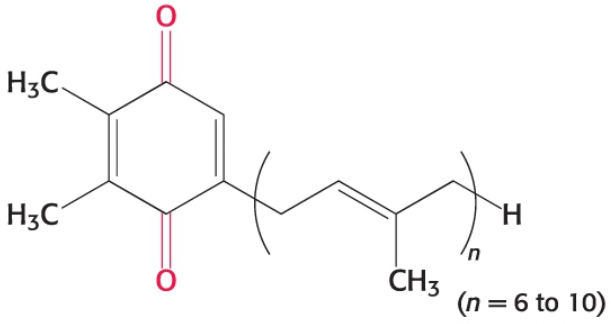
Photosystem II transfers electrons from water to plastoquinone and generates a

proton gradient

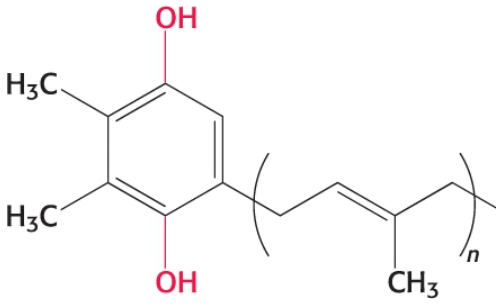
Photosystem II, an enormous transmembrane assembly of more than 20 subunits, catalyzes the light-driven transfer of electrons from water to plastoquinone. This electron acceptor closely resembles ubiquinone, a component of the mitochondrial electron-transport chain. Plastoquinone cycles between an oxidized form (Q) and a reduced form (QH_2, plastoquinol). The overall reaction catalyzed by photosystem II is

$$2\,Q + 2\,H_2O \xrightarrow{\text{Light}} O_2 + 2\,QH_2$$

The electrons in QH_2 are at a higher redox potential than those in H_2O. Recall that, in oxidative phosphorylation, electrons flow downhill from ubiquinol to an acceptor, O_2, which is at a *lower* potential. In contrast, photosystem II drives the reaction in a thermodynamically uphill direction by using the energy of light.



Plastoquinone
(oxidized form, Q)



Plastoquinol
(reduced form, QH_2)

Photosystem II is comparable to the purple bacterial reaction center

This light-driven transfer of elections is similar to the transfer reactions catalyzed by the purple bacterial system in that a quinone is converted from its oxidized into its reduced form. The core of photosystem II is reasonably similar to the purple bacterial reaction center (Figure 19.13). The core of the photosystem is formed by D1 and D2, a pair of similar 32-kDa subunits spanning the thylakoid membrane that are homologous to the L and M chains of the bacterial reaction center. Unlike the purple bacterial system, photosystem II contains a large number of additional subunits that bind more than 30 chlorophyll molecules altogether and increase the efficiency with which light energy is absorbed and transferred to the reaction center.

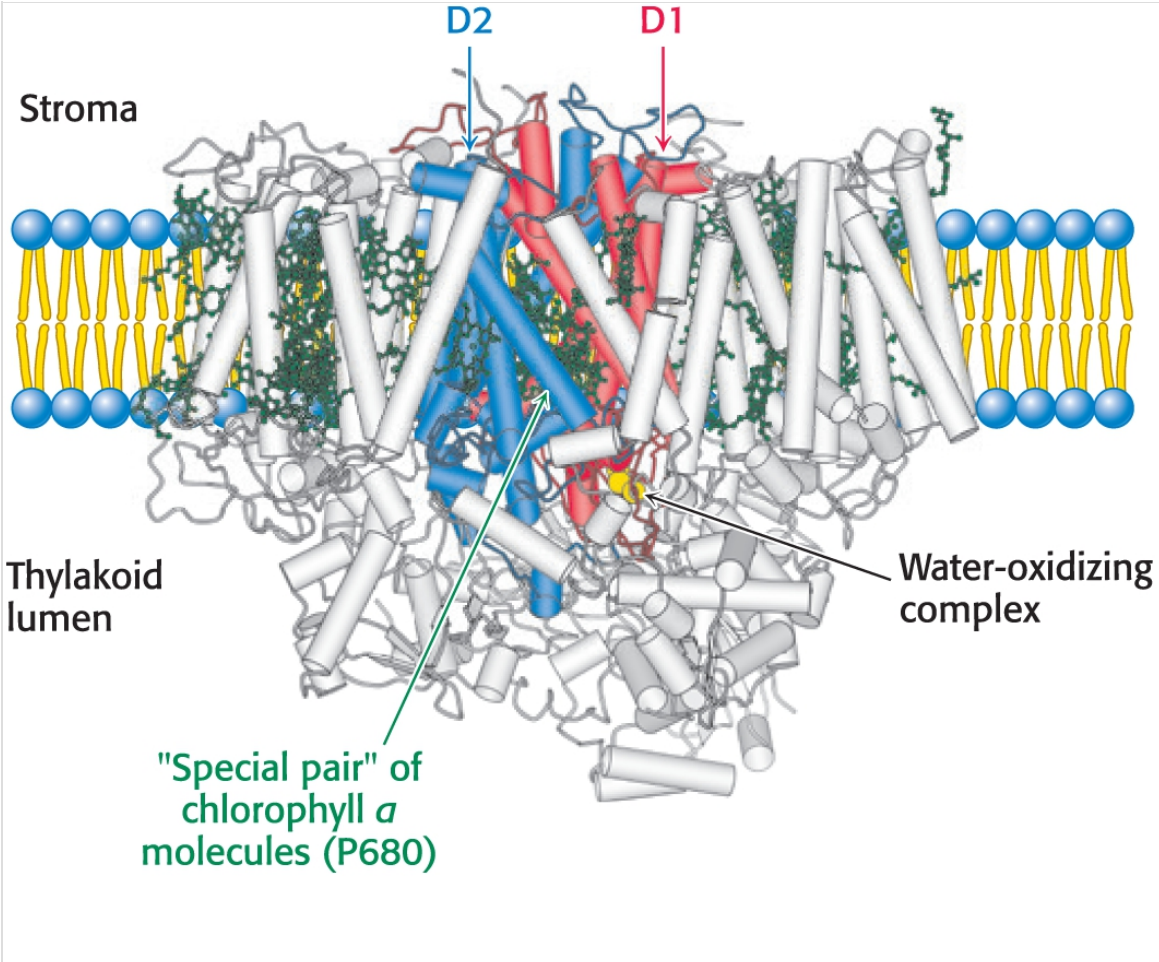


FIGURE 19.13 Photosystem II is a large membrane protein complex with many chlorophyll molecules, one special pair, and the water-oxidizing complex. The D_1 and D_2 subunits and the numerous bound chlorophyll molecules (green) are shown. Notice that the special pair and the water-oxidizing complex lie toward the thylakoid-lumen side of the membrane.

[Drawn from 1S5L.pdb.]

INTERACT with this model in Achieve

The electron flow in the thylakoid membrane is analogous to that in the bacterial membrane. The photochemistry of photosystem II begins with excitation of a special pair of chlorophyll molecules that are bound by the D1 and D2 subunits (Figure 19.14). Because the chlorophyll *a* molecules of the special pair absorb light at 680 nm, the special pair is often called *P680*. On excitation, P680 rapidly transfers an electron to a nearby pheophytin. From there, the electron is transferred first to a tightly bound plastoquinone at site Q_A and then to a mobile plastoquinone at site Q_B. With the arrival of a second electron and the uptake of two protons, the mobile plastoquinone is reduced to QH_2. At this point, the energy of two photons has been safely and efficiently stored in the reducing potential of QH_2.

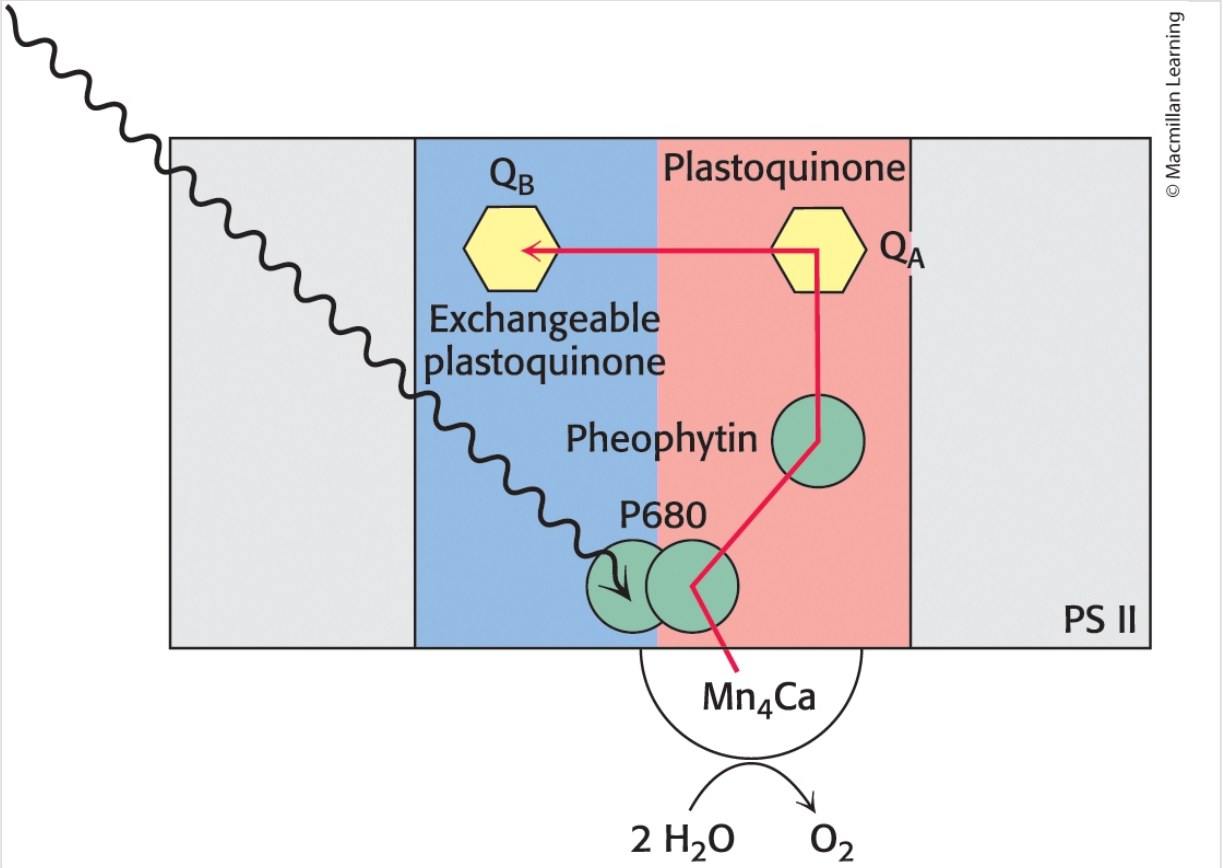


FIGURE 19.14 In photosystem II, electrons flow from manganese atoms to plastoquinone. Light absorption induces electron transfer from P680 down an electron-transfer pathway to an exchangeable plastoquinone. The positive charge on P680 is neutralized by electron flow from water molecules bound at the manganese center. Gray represents the rest of the photosystem beyond the reaction center core.

However, the source of elections is different from that of the bacterial reaction center. The major difference between the bacterial system and photosystem II is the source of the electrons that are used to neutralize the positive charge formed on the special pair. $P680^+$, a very strong oxidant, extracts electrons from water molecules bound at the **water-oxidizing complex (WOC)**, also called the **manganese center**. The core of this complex includes four manganese ions, one calcium ion, five oxide (O^{2-}) ions, and four water molecules (**Figure 19.15**). Manganese

is well suited for a role in this process because of its ability to exist in multiple oxidation states and to form strong bonds with oxygen-containing species.

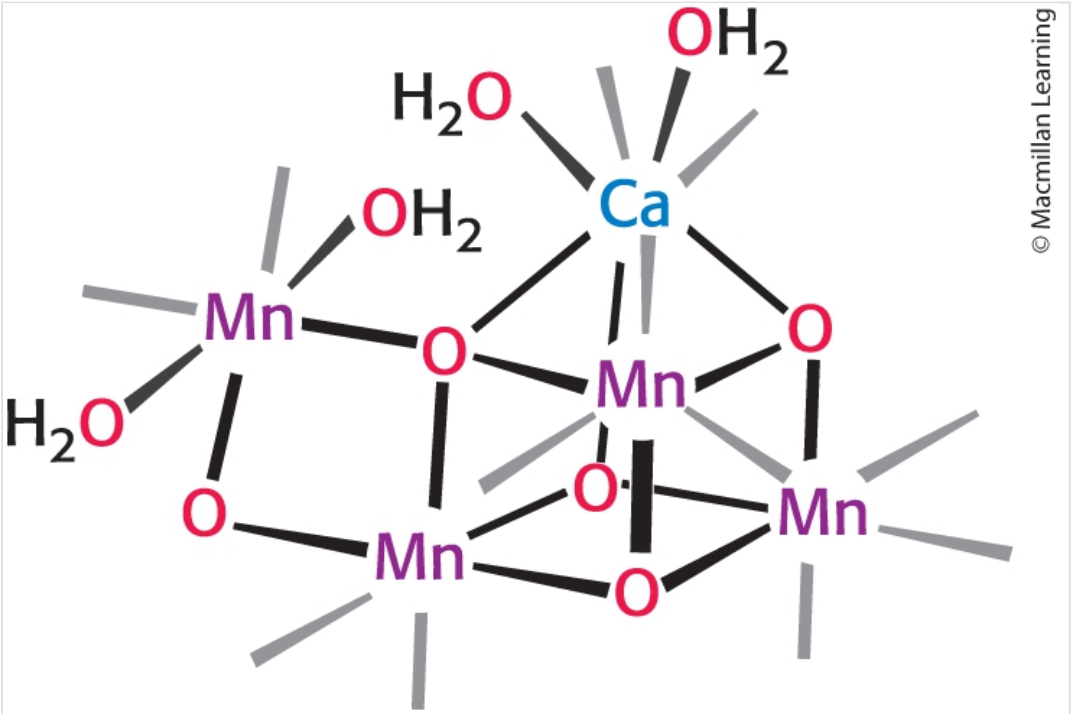


FIGURE 19.15 The core of the water-oxidizing complex includes four manganese ions and one calcium ion. The center is oxidized, one electron at a time, until two H_2O molecules are oxidized to form a molecule of O_2, which is then released from the complex.

Each time the absorption of a photon powers the removal of an electron to form $P680^+$, the positively charged special pair extracts an electron from a tyrosine residue that lies between P680 and the WOC to form a tyrosine radical. The tyrosine radical then removes an electron from the manganese center. Repeats of this process produce a center that is capable of carrying out the remarkable water oxidation reaction that generates oxygen.

The ability to control light pulses in the laboratory provides a powerful probe of the oxygen-generation process (Figure 19.16). Starting with chloroplasts that have remained in the dark for some time, an initial short flash of light produces very little oxygen. Application of a second flash produces the same result. However, with a third flash, a substantial amount of oxygen is produced. Additional flashes reveal that large amounts of oxygen are produced with every fourth flash thereafter.

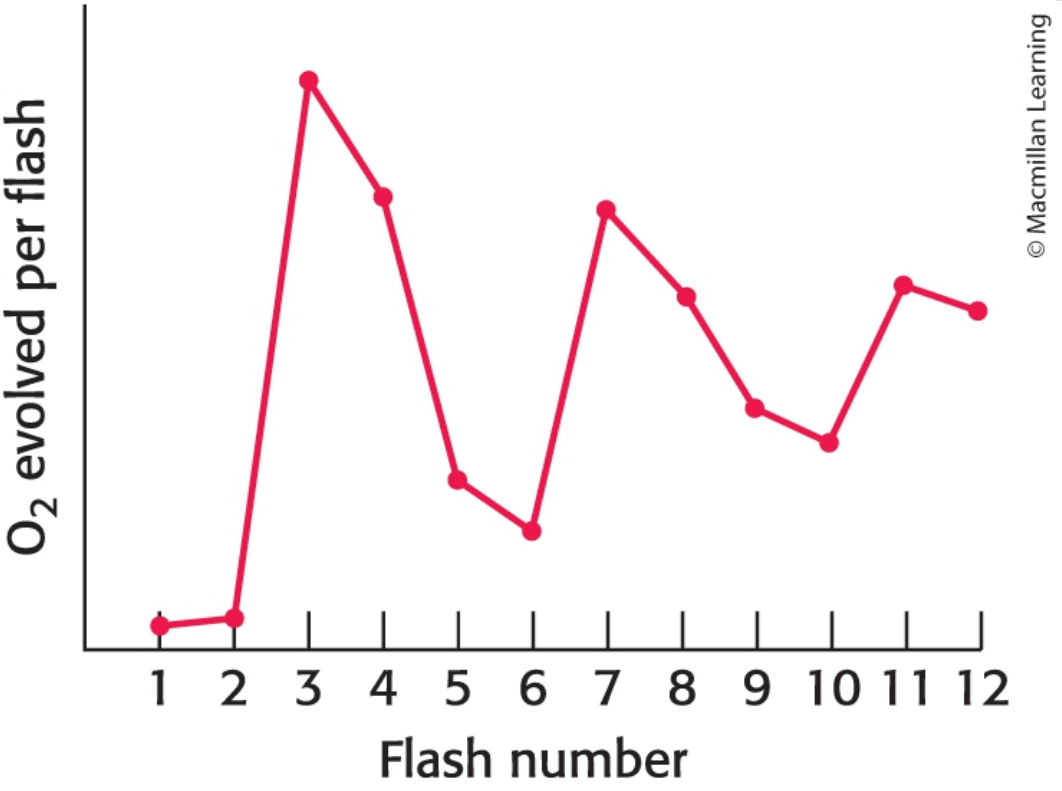


FIGURE 19.16 Four photons are required to generate one oxygen molecule after the first cycle. When dark-adapted chloroplasts are exposed to a brief flash of light, one electron passes through photosystem II. Monitoring the O_2 released after each flash reveals that O_2 is released after the 3rd, 7th, and 11th flashes.

Scientists have combined these observations with the results from other experiments to propose a mechanism for the oxygen-generating process (Figure 19.17). The formation of the oxygen–oxygen bond is proposed to involve an attack of a hydroxide ion bound to the calcium ion on a highly electrophilic oxo group bound to a manganese ion. The formation of the oxygen–oxygen bond requires the release of four electrons. An essential feature of the manganese center is its ability to develop and maintain a sufficiently oxidized state to take up these four electrons. The rates for the steps in this cycle have also been measured, revealing that the process that generates the oxygen powering so much of the life on our planet takes place in less than two milliseconds.

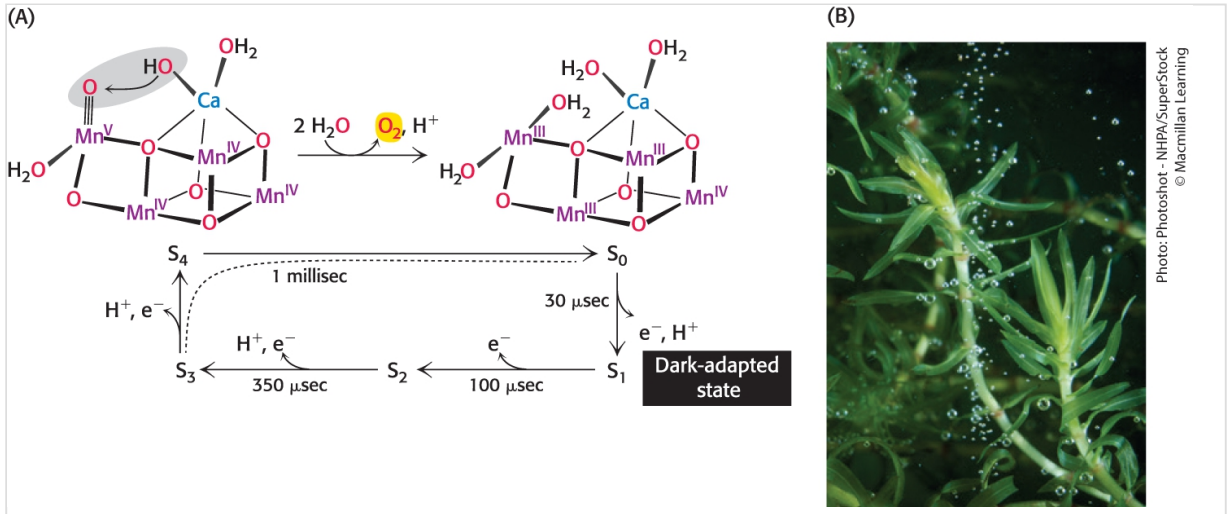


FIGURE 19.17 The model for the water-oxidizing complex explains the light-flash experiments. (A) The absorption of each photon by the reaction center generates a tyrosine radical that extracts one electron at a time from the manganese ions. The structures are designated S_0 to S_4, indicating the number of electrons removed. The model additionally explains why the first O_2 release occurs after three flashes: the dark-adapted chloroplasts start in the S_1 state — that is, the one-electron reduced state. (B) Evolution of oxygen is evident by the generation of bubbles in the aquatic plant *Elodea*.

In summary, all oxygenic phototrophs — the most common type of photosynthetic organism — use the same inorganic core and protein components for capturing the energy of sunlight. A single solution to the biochemical problem of extracting electrons from water evolved billions of years ago, and has been conserved for use under a wide variety of phylogenetic and ecological circumstances.

Similar to those of the purple bacterial reaction center, the reactions of photosystem II establish a proton gradient. Photosystem II spans the thylakoid membrane such that the site of quinone reduction is on the side of the stroma, whereas WOC lies in the thylakoid lumen. Thus, the two protons that are taken up with the reduction of Q to QH_2 come from the stroma, and the four protons that are liberated in the course of water oxidation are released into the lumen. This distribution of protons generates a proton gradient across the thylakoid membrane characterized by an excess of protons in the thylakoid lumen compared with the stroma (**Figure 19.18**).

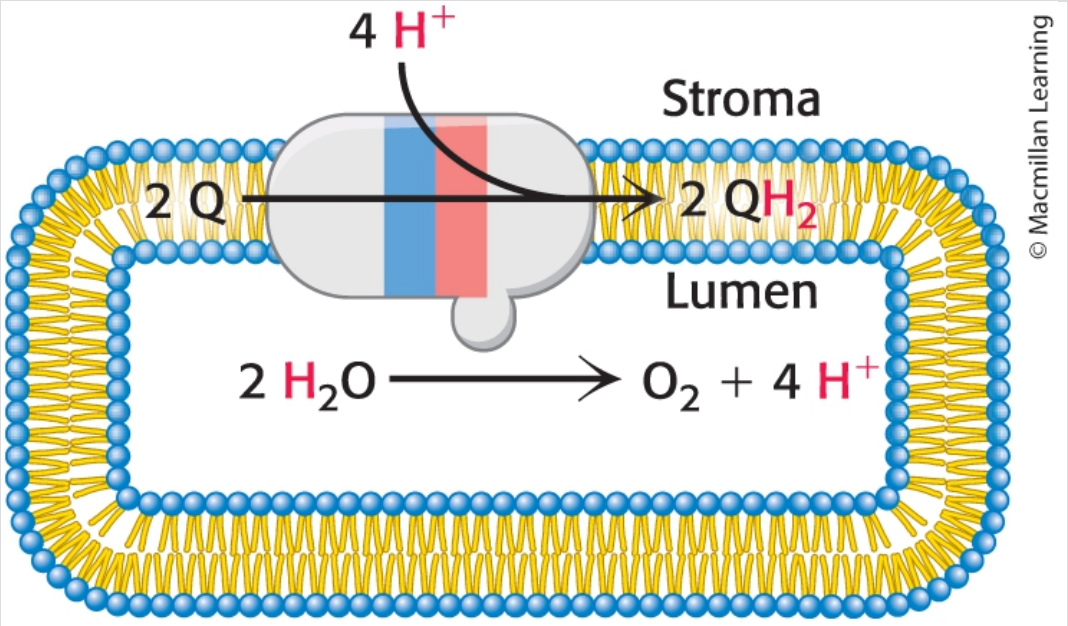


FIGURE 19.18 Photosystem II releases protons into the thylakoid lumen and takes them up from the stroma. The result is a pH gradient across the thylakoid membrane with an excess of protons (low pH) inside.

Cytochrome *bf* links photosystem II to photosystem I

Electrons flow from photosystem II to photosystem I through the **cytochrome *bf*** complex. This complex catalyzes the transfer of electrons from plastoquinol (QH_2) to plastocyanin (Pc), a small, soluble copper protein in the thylakoid lumen.

$$QH_2 + 2\ Pc(Cu^{2+}) \rightarrow Q + 2\ Pc(Cu^{+}) + 2\ H^{+}_{\text{thylakoid lumen}}$$

The two protons from plastoquinol are released into the thylakoid lumen. This reaction is reminiscent of that catalyzed by Complex III in oxidative phosphorylation, and most components of the cytochrome *bf* complex are homologous to those of Complex III.

This complex catalyzes the reaction by proceeding through the Q cycle (Figure 18.11). In the first half of the Q cycle, plastoquinol (QH_2) is oxidized to plastoquinone (Q), one electron at a time. The electrons from plastoquinol flow through the cytochrome *bf* complex to convert oxidized plastocyanin (Pc) into its reduced form (**Figure 19.19**).

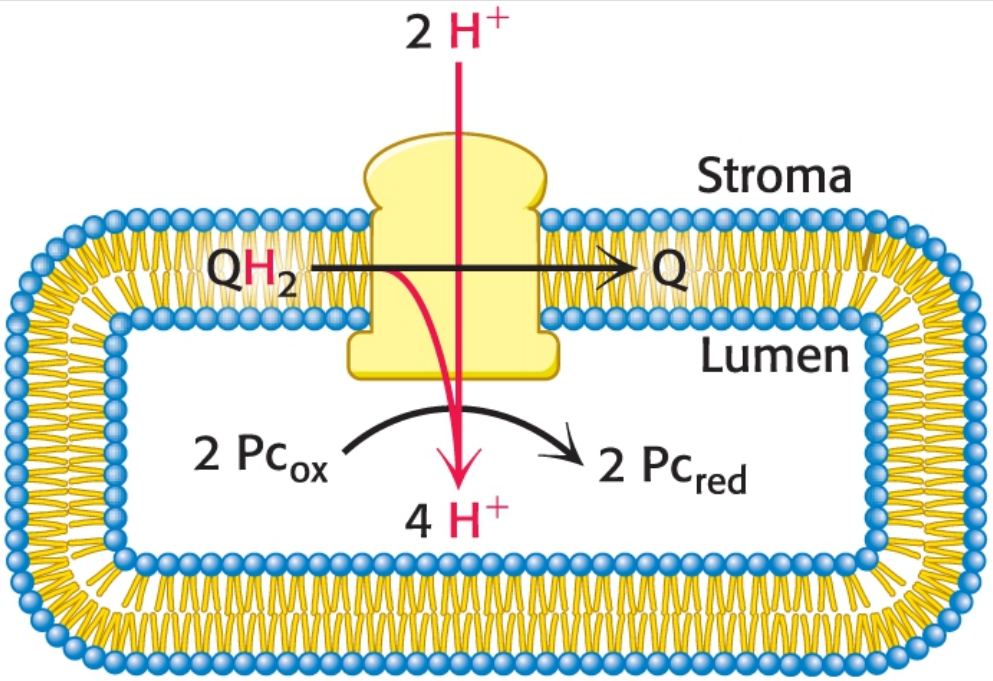


FIGURE 19.19 Electron flow through cytochrome *bf* contributes to the proton gradient. The cytochrome *bf* complex oxidizes QH_2 to Q through the Q cycle. Four protons are released into the thylakoid lumen in each cycle.

In the second half of the Q cycle, cytochrome *bf* reduces a molecule of plastoquinone from the Q pool to plastoquinol, taking up two protons from one side of the membrane, and then reoxidizes plastoquinol to release these protons on the other side. The enzyme is oriented so that protons are released into the thylakoid lumen and taken up from the stroma, contributing further to the proton gradient across the thylakoid membrane (Figure 19.19).

Photosystem I uses light energy to generate reduced ferredoxin, a powerful reductant

The final stage of the light reactions is catalyzed by photosystem I, a transmembrane complex consisting of about 15 polypeptide chains and multiple associated proteins and cofactors (Figure 19.20). The core of this system is a pair of similar subunits — psaA and psaB — which bind 80 chlorophyll molecules as well as other redox factors. These subunits are quite a bit larger than the core subunits of photosystem II and the purple bacterial reaction center. Nonetheless, they appear to be homologous; the terminal 40% of each subunit is similar to a corresponding subunit of photosystem II.

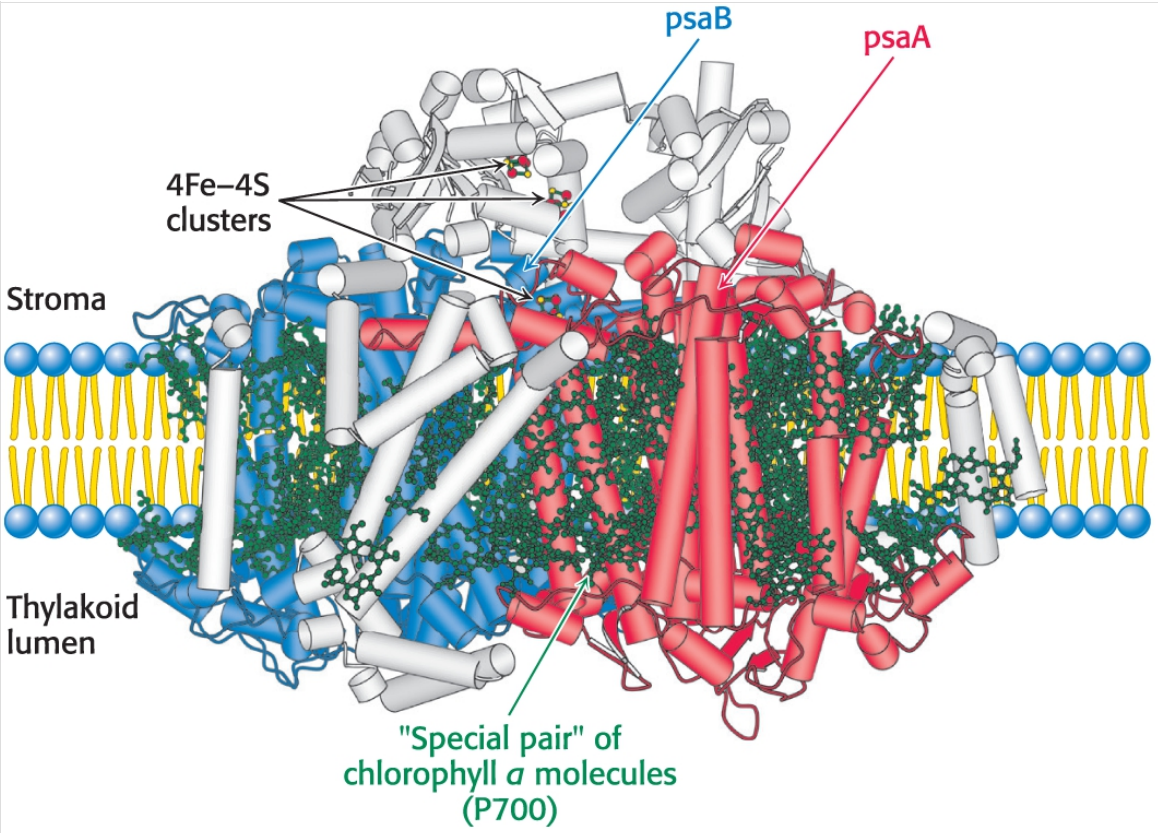


FIGURE 19.20 Photosystem I is a protein complex with numerous chlorophyll molecules and one special pair. Notice the numerous bound chlorophyll molecules, shown in green, including the special pair, as well as the iron–sulfur clusters that facilitate electron transfer from the stroma.

[Drawn from 1JB0.pdb.]



A special pair of chlorophyll *a* molecules lies at the center of photosystem I, where they absorb light maximally at 700 nm. This center, called *P700*, initiates photoinduced charge separation (Figure 19.21). The electron travels from P700 down a pathway through chlorophyll at site A_0 and quinone at site A_1 to a set of 4Fe–4S clusters.

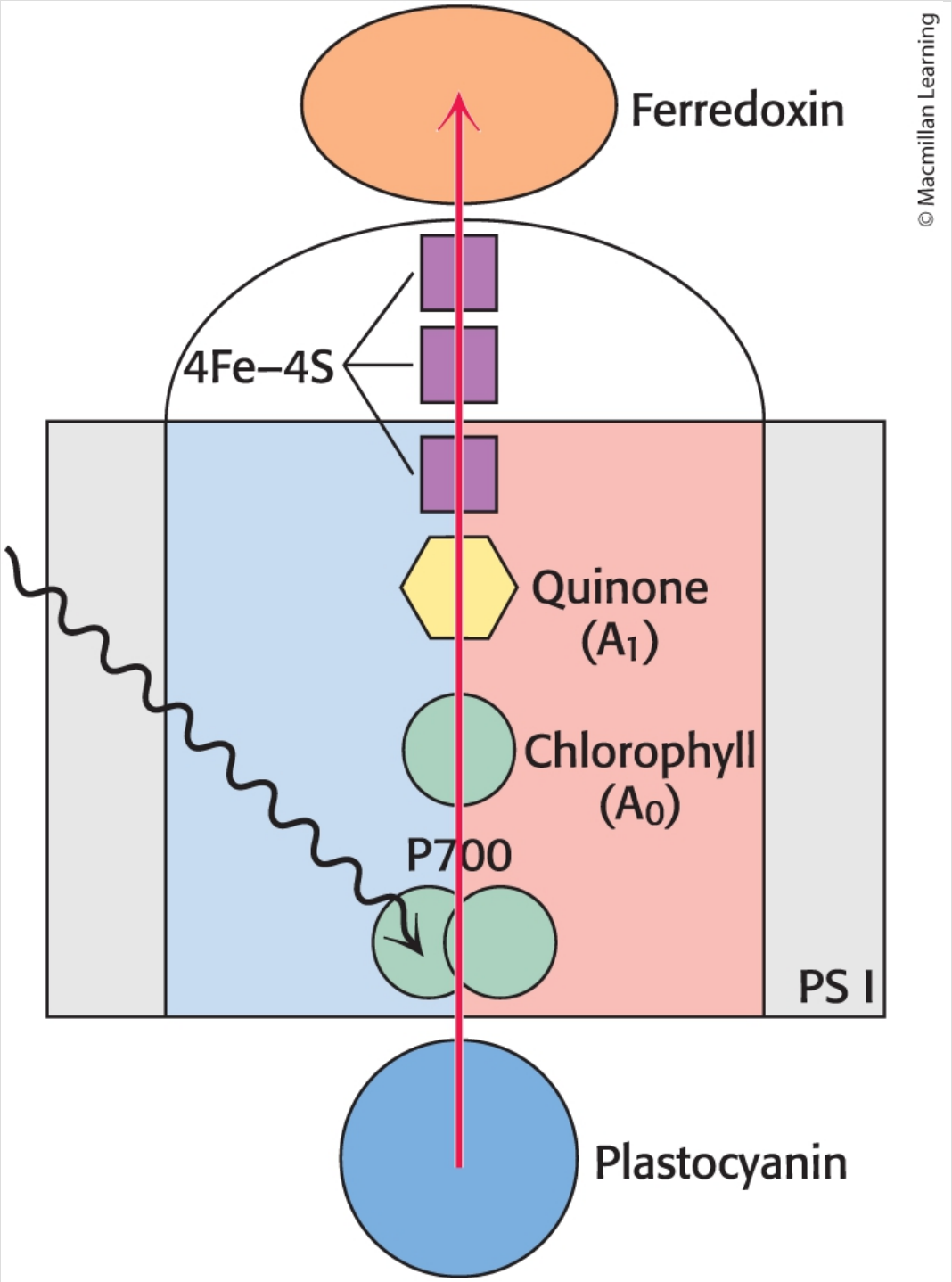


FIGURE 19.21 In photosystem I, electrons flow to ferredoxin. Light absorption induces electron transfer from P700 down an electron-transfer pathway that includes a chlorophyll molecule, a quinone molecule, and three 4Fe–4S clusters to reach ferredoxin. The positive charge left on P700 is neutralized by electron transfer from reduced plastocyanin. Gray represents the rest of the photosystem beyond the reaction center core.

The next step is the transfer of the electron to ferredoxin (Fd), a soluble protein containing a 2Fe–2S cluster coordinated to four cysteine residues (Figure 19.22). Ferredoxin transfers electrons to $NADP^+$. Meanwhile, $P700^+$ captures an electron from reduced plastocyanin provided by photosystem II to return to P700 so that P700 can be excited again. Thus, the overall reaction catalyzed by photosystem I is a simple one-electron oxidation–reduction reaction.

$$Pc(Cu^+) + Fd_{ox} \xrightarrow{\text{Light}} Pc(Cu^{2+}) + Fd_{red}$$

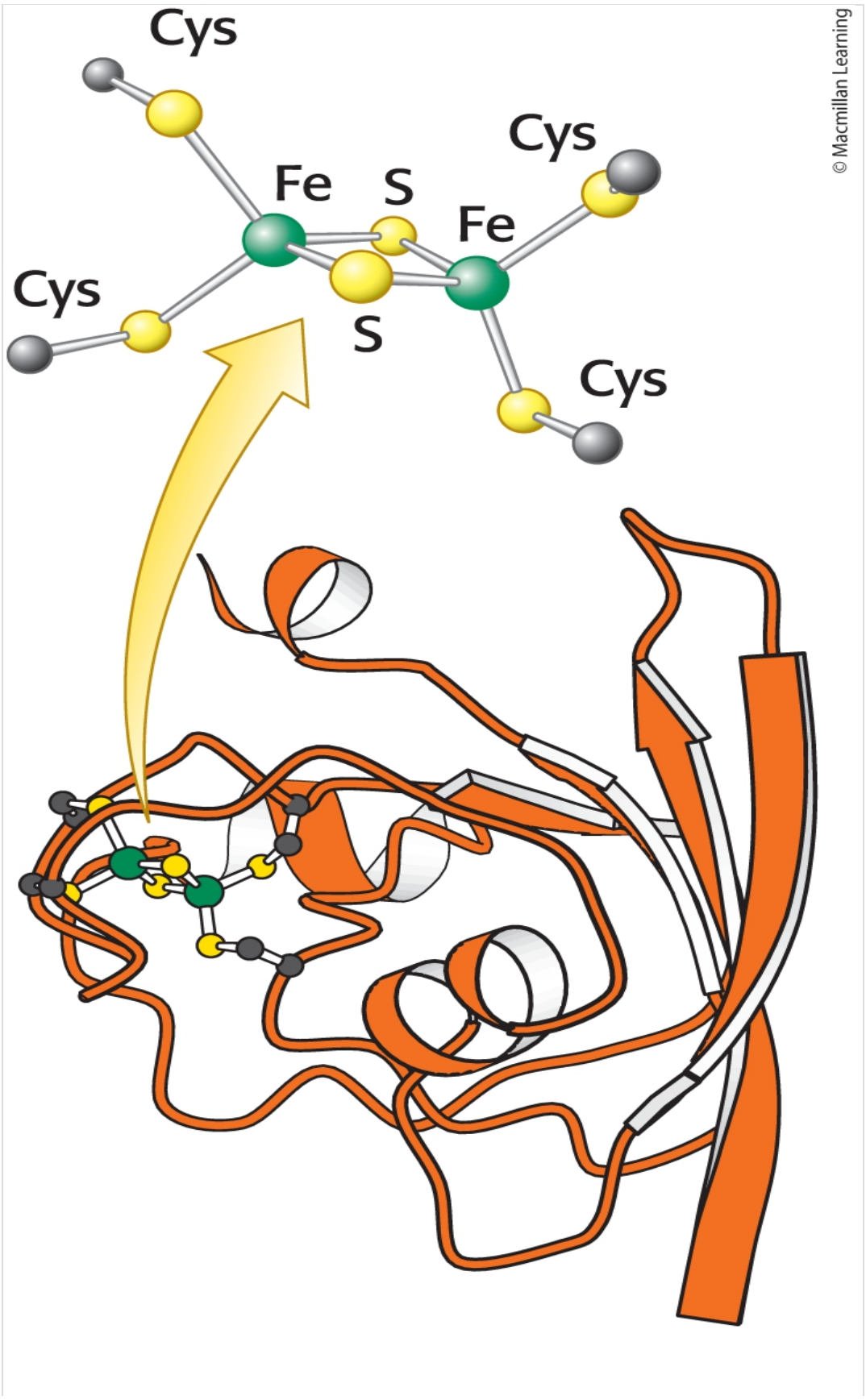

Cys
Cys
Fe
S
Fe
Cys
S
Cys
© Macmillan Learning

FIGURE 19.22 Ferredoxin is an electron-carrying, iron-sulfur protein. In plants, ferredoxin contains a 2Fe–2S cluster. This protein accepts electrons from photosystem I and carries them to ferredoxin–$NADP^+$ reductase.

[Drawn from 1FXA.pdb.]

INTERACT with this model in Achieve

Given that the reduction potentials for plastocyanin and ferredoxin are $+0.37\ V$ and $-0.45\ V$, respectively, the standard free energy for this reaction is $+79.1\ kJ\ mol^{-1}\ (+18.9\ kcal\ mol^{-1})$. This uphill reaction is driven by the absorption of a 700-nm photon, which has an energy of $171\ kJ\ mol^{-1}\ (40.9\ kcal\ mol^{-1})$.

Ferredoxin–$NADP^+$ reductase converts $NADP^+$ into NADPH

The reduced ferredoxin generated by photosystem I is a strong reductant that is used as an electron source for a variety of reactions, most notably the fixation of N_2 into NH_3 (Section 25.1). However, ferredoxin is not useful for driving many reactions, in part because ferredoxin carries only one available electron. In contrast, NADPH, a two-electron reductant, is a widely used electron donor in biosynthetic processes, including the reactions of the Calvin–Benson cycle (Chapter 20).

How is reduced ferredoxin used to drive the reduction of $NADP^+$ to NADPH? This reaction is catalyzed by *ferredoxin–$NADP^+$ reductase,* a flavoprotein with an FAD prosthetic group (**Figure 19.23A**). The bound

FAD moiety accepts two electrons and two protons from two molecules of reduced ferredoxin to form $FADH_2$ (Figure 19.23B). The enzyme then transfers a hydride ion (H^-) to $NADP^+$ to form NADPH. This reaction takes place on the stromal side of the membrane. Hence, the uptake of a proton in the reduction of $NADP^+$ further contributes to the generation of the proton gradient across the thylakoid membrane.

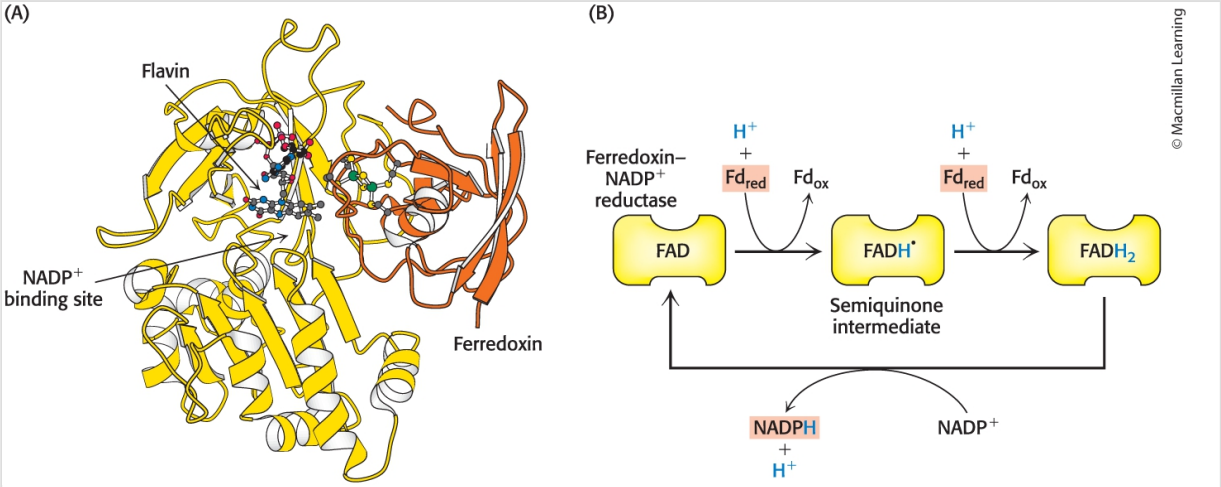


FIGURE 19.23 Ferredoxin–$NADP^+$ reductase transfers electrons from the protein ferredoxin to $NADP^+$. (A) The structure of ferredoxin–$NADP^+$ reductase is shown. This enzyme accepts electrons, one at a time, from ferredoxin (shown in orange). (B) Ferredoxin–$NADP^+$ reductase first accepts two electrons, generated by photosystem I, and two protons from the lumen to form two molecules of reduced ferredoxin (Fd). Reduced ferredoxin is then used to form $FADH_2$, which then transfers two electrons and a proton to $NADP^+$ to form NADPH in the stroma.

[Drawn from 1EWY.pdb.]

INTERACT with this model in Achieve

The cooperation between photosystem I and photosystem II creates a flow of electrons from H_2O to $NADP^+$. The pathway of electron flow is called the **Z scheme of photosynthesis** because the redox diagram from P680 to P700* looks like a letter Z on its side (Figure 19.24).

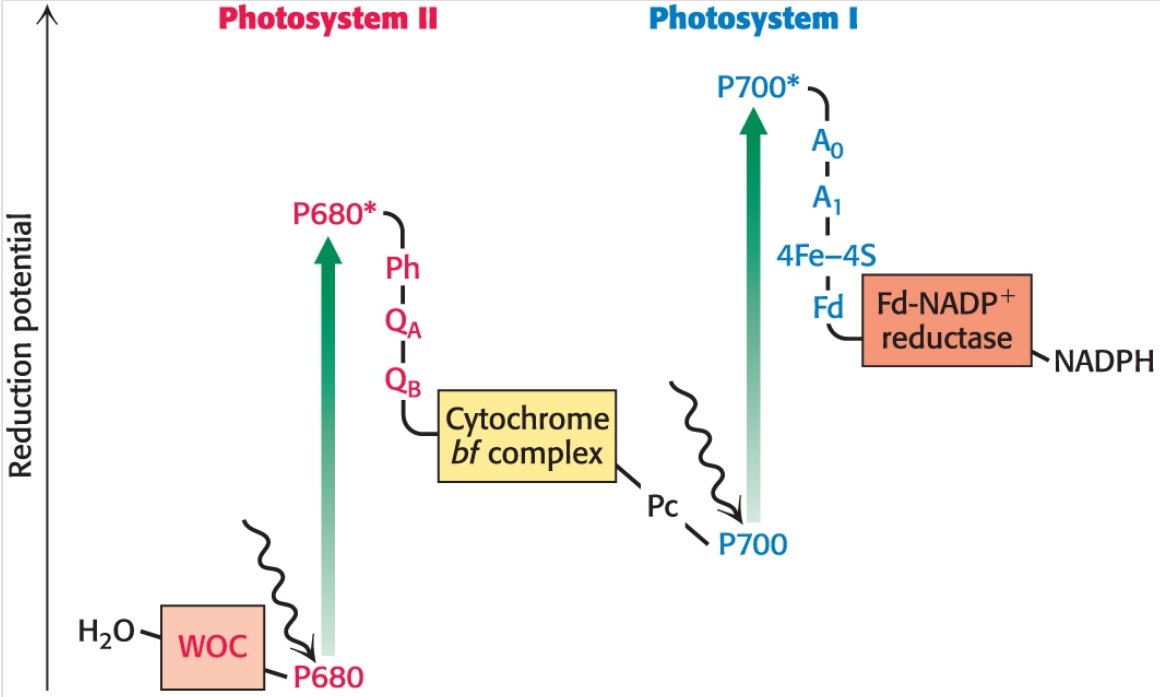


FIGURE 19.24 The "Z" scheme of photosynthesis is the linear path of electrons from H_2O to $NADP^+$. This endergonic reaction is made possible by the absorption of light by photosystem II (P680) and photosystem I (P700). Abbreviations: Ph, pheophytin; Q_A and Q_B, plastoquinone-binding proteins; Pc, plastocyanin; A_0 and A_1, acceptors of electrons from P700*; Fd, ferredoxin; WOC, water-oxidizing complex.

Self-Check Question

PS I creates a powerful reductant, while PS II creates a powerful oxidant. Identify each and describe their roles.

19.5 A Proton Gradient across the Thylakoid Membrane Drives ATP Synthesis

In 1966, André Jagendorf showed that chloroplasts synthesize ATP in the dark when an artificial pH gradient is imposed across the thylakoid membrane. He soaked chloroplasts in a pH 4.0 buffer and then rapidly mixed them with a pH 8.0 buffer containing ADP and P_i. While the pH of the thylakoid lumen remained at 4.0, the pH of the stroma suddenly increased to 8.0, resulting in a burst of ATP synthesis that accompanied the disappearance of the pH gradient. This incisive experiment was one of the first to unequivocally support the hypothesis put forth by Peter Mitchell that ATP synthesis is driven by proton-motive force (Section 18.4).

Top: AP Images; bottom: Photo courtesy School of Integrative Plant Science, Cornell University

PETER MITCHELL AND ANDRÉ JAGENDORF The chemiosmotic hypothesis proposed by Peter Mitchell (shown at top) was initially poorly received by other scientists. But this changed dramatically when André Jagendorf (shown below Mitchell) demonstrated that chloroplasts can synthesize ATP in the dark if a pH gradient is created. Jagendorf credits a third scientist, Geoffrey Hind, for helping him make the connection. Jagendorf said, "I had heard Peter Mitchell talk about chemiosmosis…. His words went into one of my ears and out the other, leaving me feeling annoyed [that the conference organizers] had allowed such a ridiculous and incomprehensible speaker in. But Geoffrey [Hind] read *Nature*. He read Mitchell's paper and came to me. At this point I began to communicate with Peter [and] later that summer I did the experiment …" Jagendorf's results only made sense through the lens of Mitchell's chemiosmotic hypothesis, which eventually won Mitchell the Nobel Prize in Chemistry. Their mutually beneficial relationship illustrates the importance of open communication and collaboration in science.

The principles of ATP synthesis in chloroplasts are nearly identical to those in mitochondria. ATP formation is driven by a proton-motive force in both photophosphorylation and oxidative phosphorylation. We have seen how light induces electron transfer through photosystems II and I and the cytochrome *bf* complex. At various stages in this process, protons are released into the thylakoid lumen or taken up from the stroma, generating a proton gradient.

As discussed in Section 18.4, energy inherent in the proton gradient, called the *proton-motive force* (Δp), is described as the sum of two components: a charge gradient and a chemical gradient. The gradient is maintained because the thylakoid membrane is essentially impermeable to protons. The thylakoid lumen becomes markedly acidic, with the pH approaching 4.0, whereas the stroma reaches a pH around 8.0. The light-induced transmembrane proton gradient is about 3.5 pH units. In chloroplasts, nearly all of Δp arises from the pH gradient, whereas in mitochondria, the contribution from the membrane potential is larger. The reason for this difference is that the thylakoid membrane is quite permeable to Cl^- and Mg^{2+}. The light-induced transfer of H^+ into the thylakoid space is accompanied by the transfer of either Cl^- in the same direction or Mg^{2+} ($1\ Mg^{2+}$ per $2\ H^+$)

in the opposite direction. Consequently, electrical neutrality is maintained and no membrane potential is generated. The influx of Mg^{2+} into the stroma plays a role in the regulation of the Calvin–Benson cycle (Section 20.2). A pH gradient of 3.5 units across the thylakoid membrane corresponds to a proton-motive force of 0.20 V or a ΔG of $-20.0\ kJ\ mol^{-1}$ $(-4.8\ kcal\ mol^{-1})$.

The ATP synthase of chloroplasts closely resembles those of mitochondria and prokaryotes

The proton-motive force generated by the light reactions is converted into ATP by the **ATP synthase of chloroplasts**, also called the CF_1-CF_0 **complex** (C stands for chloroplast; F for factor). CF_0 conducts protons across the thylakoid membrane, whereas CF_1 catalyzes the formation of ATP from ADP and P_i. The CF_1-CF_0 complex closely resembles the F_1-F_0 ATP synthase of mitochondria (Section 18.4). Remarkably, the β subunits of ATP synthase in corn chloroplasts are more than 60% identical in amino acid sequence with those of human ATP synthase, despite the passage of approximately 1 billion years since the separation of the plant and animal kingdoms.

Note that the membrane orientation of CF_1-CF_0 is reversed compared with that of the mitochondrial ATP synthase (**Figure 19.25**). However, the functional orientation of the two synthases is identical: protons flow from the lumen through the enzyme to either the thylakoid stroma or the mitochondrial matrix, where ATP is synthesized. Because CF_1 is on the stromal surface of the thylakoid membrane, the newly synthesized ATP is released directly into the stromal space. Likewise, NADPH formed by photosystem I is released into the stromal space. Thus, ATP and NADPH, the products of the light reactions of photosynthesis, are

appropriately positioned for the subsequent dark reactions in which CO_2 is converted into carbohydrate (Section 20.1).

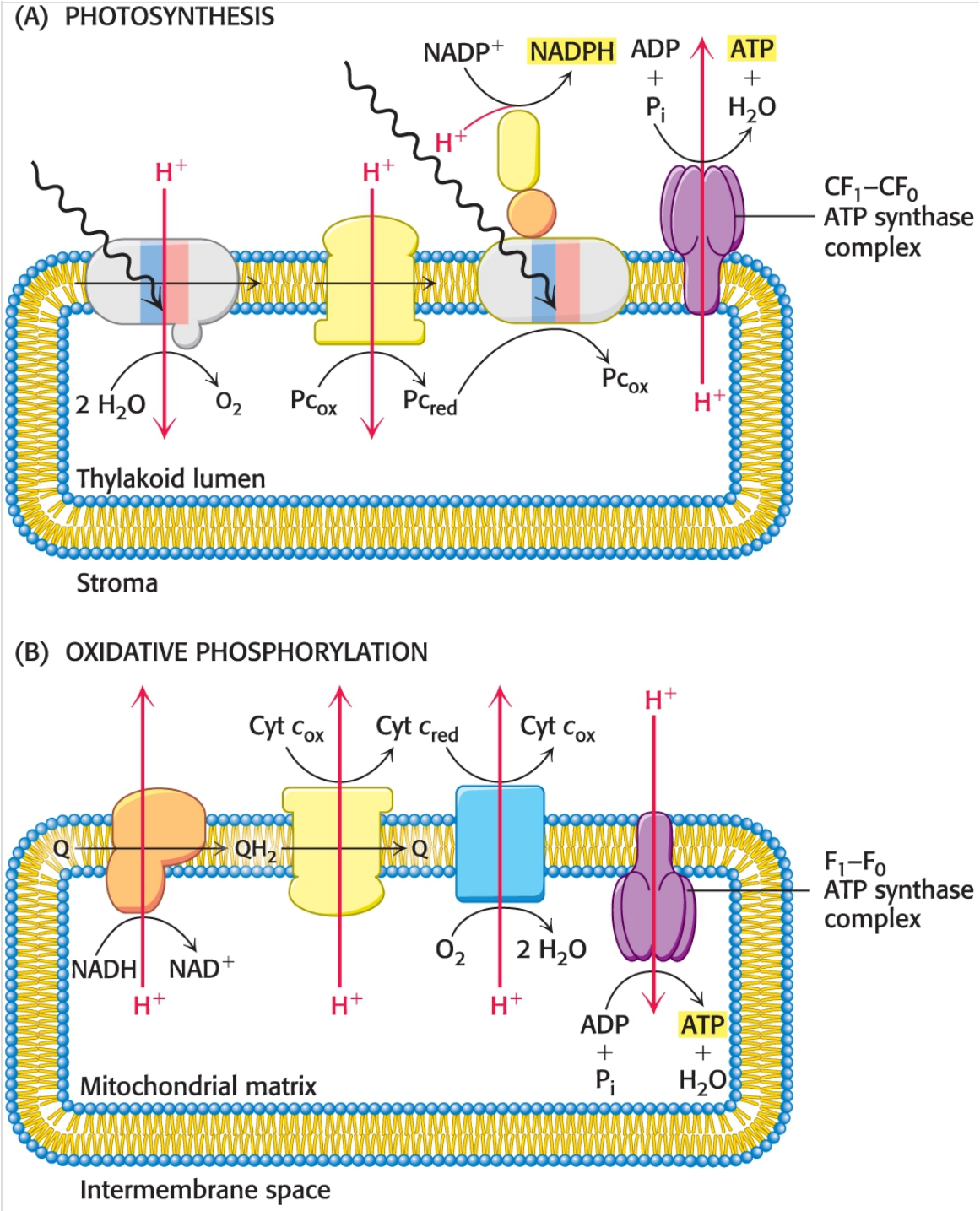
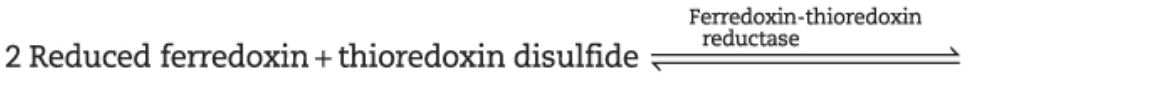


FIGURE 19.25 Photosynthesis and oxidative phosphorylation have a similar layout but differ a number of ways. (A) The light-induced electron transfer in photosynthesis drives protons into the thylakoid lumen. The excess protons flow out of the lumen through ATP synthase to genera

ATP in the stroma. (B) In oxidative phosphorylation, electron flow down the electron-transport chain pumps protons out of the mitochondrial matrix. Excess protons from the intermembrane space flow into the matrix through ATP synthase to generate ATP in the matrix.

The activity of chloroplast ATP synthase is regulated

The activity of the ATP synthase is sensitive to the redox conditions in the chloroplast. For maximal activity, a specific disulfide bond in the γ subunit must be reduced to two cysteines. The reductant is reduced thioredoxin, which is formed from ferredoxin generated in photosystem I, by ferredoxin–thioredoxin reductase, an iron–sulfur containing enzyme.



Conformational changes in the ε subunit also contribute to synthase regulation. The ε subunit appears to exist in two conformations. One conformation inhibits ATP hydrolysis by the synthase, while the other, which is generated by an increase in the proton-motive force, allows ATP synthesis and facilitates the reduction of the disulfide bond in the γ subunit. Thus, synthase activity is maximal when biosynthetic reducing power and a proton gradient are available. We will see in Chapter 20 that redox regulation is also important in photosynthetic carbon metabolism.

Cyclic electron flow through photosystem I leads to the production of ATP instead of NADPH

On occasion, when the ratio of NADPH to $NADP^+$ is very high, as might be the case if there was another source of electrons to form NADPH (Section 20.3), $NADP^+$ may be unavailable to accept electrons from reduced ferredoxin. In these circumstances, specific large protein complexes allow cyclic electron flow that powers ATP synthesis. Excited electrons from P700, the reaction center of photosystem I, generate reduced ferredoxin. The electron in reduced ferredoxin is transferred to the cytochrome *bf* complex rather than to $NADP^+$. This electron then flows back through the cytochrome *bf* complex to reduce plastocyanin, which can then be reoxidized by $P700^+$ to complete a cycle. The net outcome of this cyclic flow of electrons is the pumping of protons by the cytochrome *bf* complex. The resulting proton gradient then drives the synthesis of ATP. In this process, called **cyclic photophosphorylation**, ATP is generated without the concomitant formation of NADPH (**Figure 19.26**), reminiscent of the cyclic phototrophic scheme of the nonsulfur purple bacteria (Section 19.3). Note that because photosystem II does not participate in cyclic photophosphorylation, O_2 is not formed from H_2O.

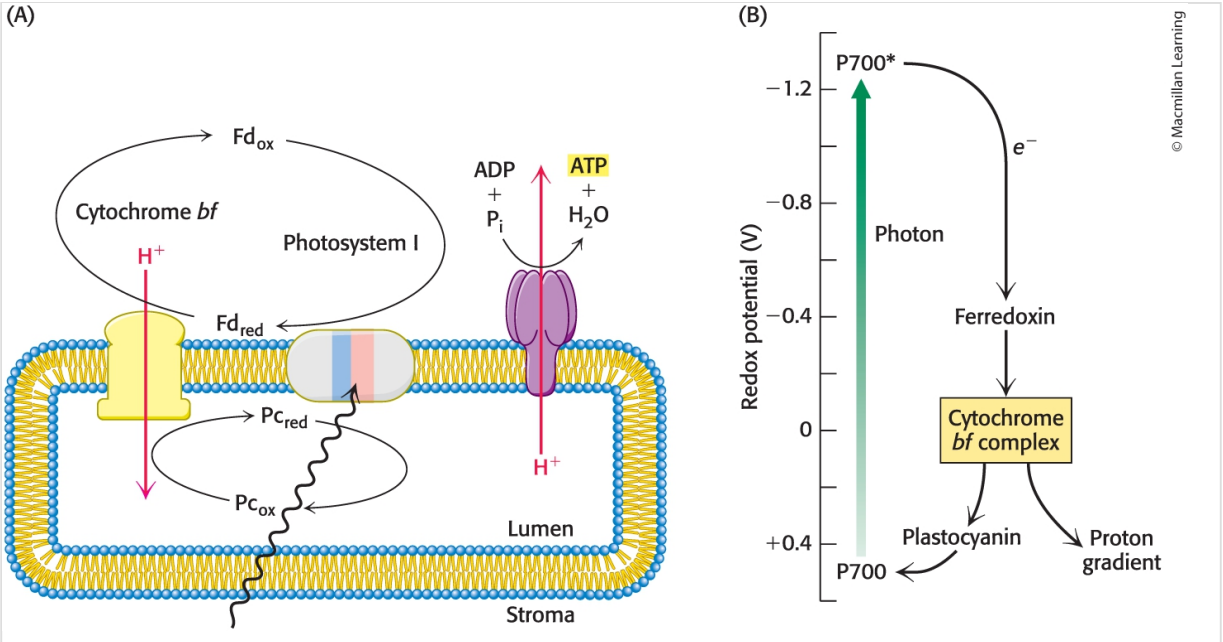


FIGURE 19.26 Cyclic photophosphorylation allows ATP production without a need for an electron source. (A) In this pathway, electrons from reduced ferredoxin are transferred to cytochrome *bf* rather than to ferredoxin–$NADP^+$ reductase, and thus can be reused indefinitely without the need for an external electron source. The flow of electrons through cytochrome *bf* pumps protons into the thylakoid lumen. These protons flow through ATP synthase to generate ATP. Neither NADPH nor O_2 is generated by this pathway. Abbreviations: Fd, ferredoxin; Pc, plastocyanin. (B) A scheme showing the energetic basis for cyclic photophosphorylation.

The absorption of eight photons yields one O_2, two NADPH, and three ATP molecules

We can now estimate the overall stoichiometry for the light reactions. The absorption of four photons by photosystem II generates one molecule of O_2 and releases four protons into the thylakoid lumen. The two molecules of plastoquinol are oxidized by the Q cycle of the cytochrome *bf* complex to release eight protons into the lumen. Finally,

the electrons from four molecules of reduced plastocyanin are driven to ferredoxin by the absorption of four additional photons. The four molecules of reduced ferredoxin generate two molecules of NADPH. Thus, the overall reaction is

$$2\ H_2O + 2\ NADP^+ + 10\ H^+_{stroma} \rightarrow O_2 + 2\ NADPH + 12\ H^+_{lumen}$$

The 12 protons released in the lumen can then flow through ATP synthase. Let's assume that 12 protons must pass through CF_0 to complete one full rotation of CF_1. A single rotation generates three molecules of ATP. Given the ratio of 3 ATP for 12 protons, the overall reaction is

$$2\ H_2O + 2\ NADP^+ + 10\ H^+_{stroma} \longrightarrow O_2 + 2\ NADPH + 12\ H^+_{lumen}$$

$$\frac{3\ ADP^{3-} + 3\ P_i^{2+} + 3\ H^+ + 12\ H^+_{lumen} \longrightarrow 3\ ATP^{4-} + 3\ H_2O + 12H^+_{stroma}}{2\ NADP^+ + 3\ ADP^{3-} + 3\ P_i^{2-} + H^+ \longrightarrow O_2 + 2\ NADPH + 3\ ATP^{4-} + H_2O}$$

Thus, eight photons are required to yield three molecules of ATP (2.7 photons/ATP).

Cyclic photophosphorylation is a somewhat more productive way to synthesize ATP than noncyclic photophosphorylation (the Z scheme shown in Figure 19.24). The absorption of four photons by photosystem I leads to the release of eight protons into the lumen by the cytochrome *bf* system. These protons flow through ATP synthase to yield two molecules of ATP. Thus, each two absorbed photons yield one molecule of ATP. No NADPH is produced.

Self-Check Question

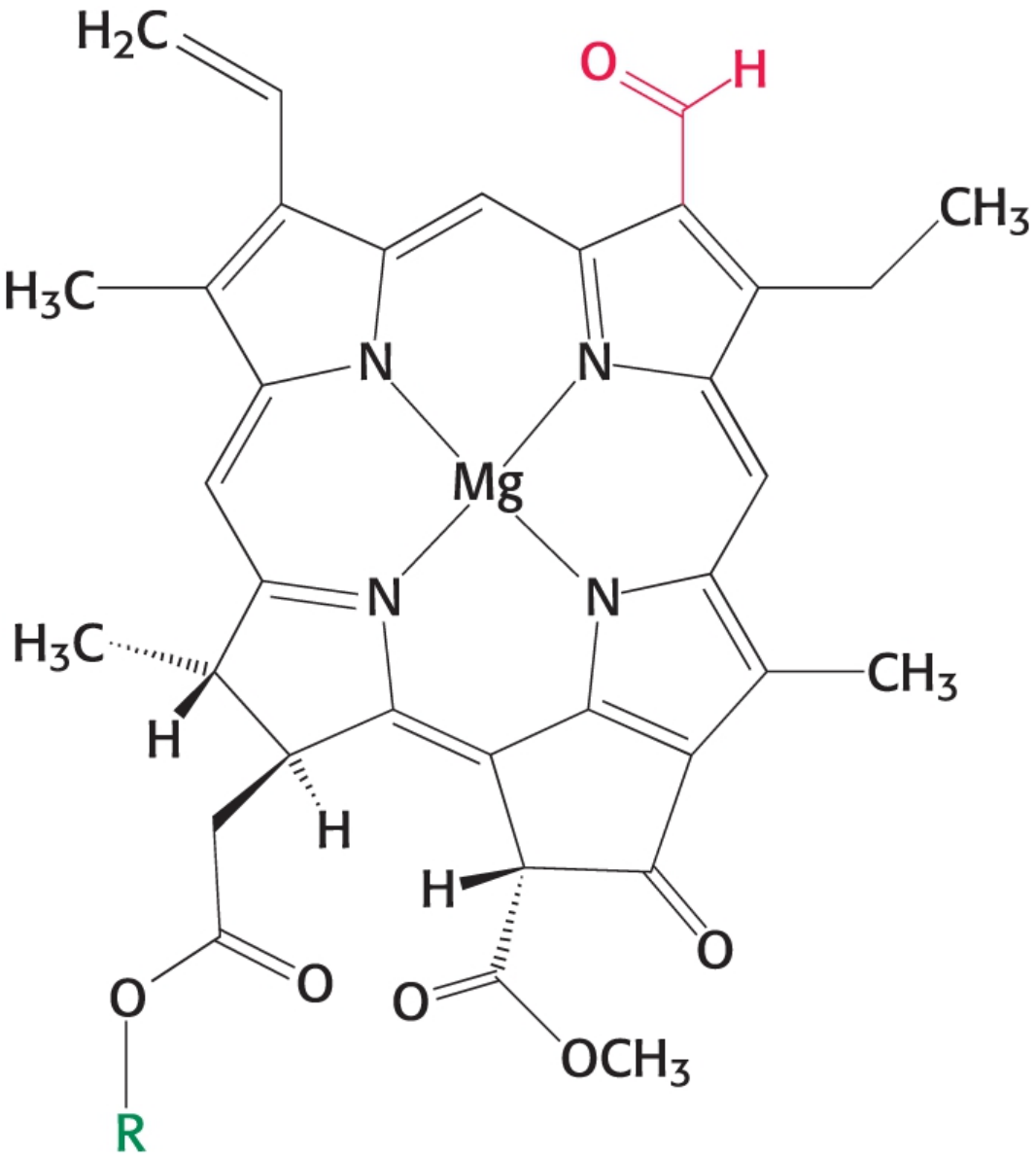


The relative proportions of the components of the proton-motive force that drive ATP synthesis in chloroplasts are different from those in mitochondria. What are these two components, and which dominates in chloroplasts? Given the similarities between the synthases in both organelles, explain the basis of this difference.

19.6 Accessory Pigments Funnel Energy into Reaction Centers

A light-harvesting system that relied only on the chlorophyll *a* molecules of the special pair would be rather inefficient for two reasons. First, chlorophyll *a* molecules absorb light only at specific wavelengths (Figure 19.6). A large gap is present in the middle of the visible region between approximately 450 and 650 nm. This gap falls right at the peak of the solar spectrum, and so failure to collect this light would constitute a considerable lost opportunity. Second, even on a cloudless day, many photons that can be absorbed by chlorophyll *a* pass through the chloroplast without being absorbed, because the density of chlorophyll *a* molecules in a reaction center is not very great.

Helping to solve these problems are accessory pigments, both additional chlorophylls, such as chlorophyll *b*, and other classes of molecules, such as carotenoids. Accessory pigments are closely associated with reaction centers, where they absorb light and funnel the energy to the reaction center for conversion into chemical forms. Thus, accessory pigments prevent the reaction center from sitting idle.



Chlorophyll *b*

Chlorophyll *b* and carotenoids are important accessory pigments that funnel energy to the reaction center. Chlorophyll *b* differs from chlorophyll *a* in having a formyl group in place of a methyl group. This small difference shifts its two major absorption peaks toward the center

of the visible region. In particular, chlorophyll *b* efficiently absorbs light with wavelengths between 450 and 500 nm (Figure 19.27).

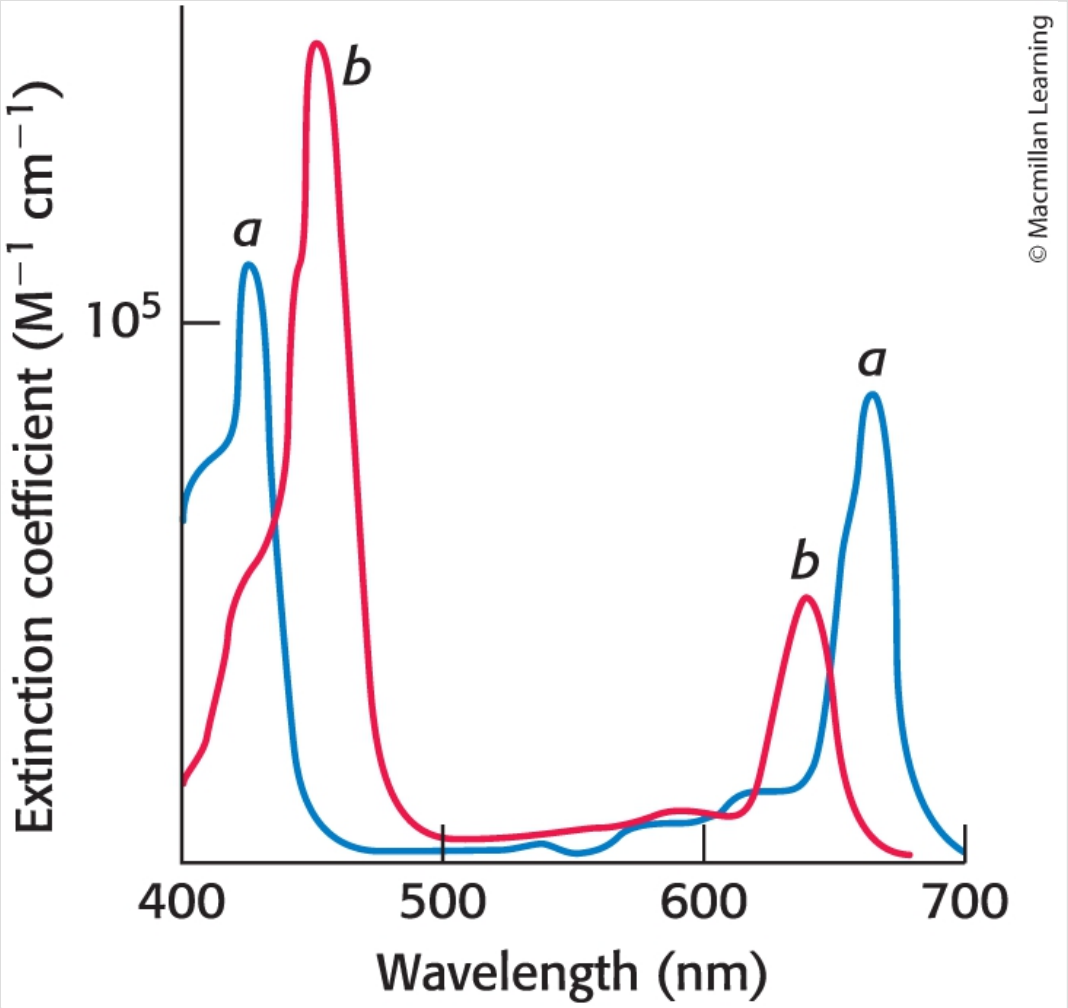
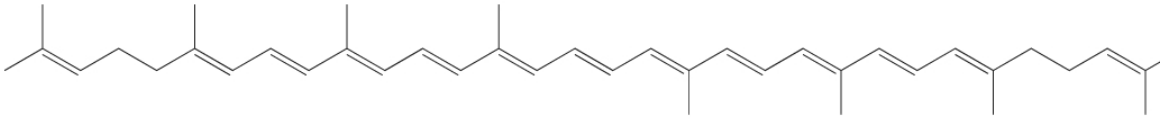


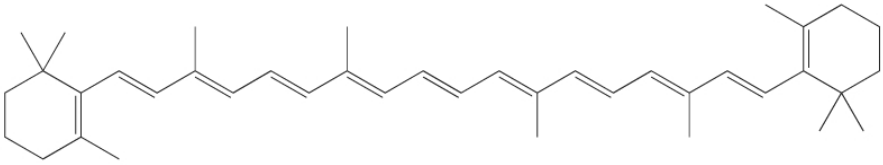
FIGURE 19.27 Chlorophylls *a* and *b* absorb light maximally at different wavelengths. Shown are the absorption spectra of chlorophylls *a* and *b*.

Carotenoids are extended polyenes that absorb light between 400 and 500 nm. The carotenoids are responsible for most of the yellow and red colors of fruits and flowers, and they provide the brilliance of fall, when the chlorophyll molecules degrade first, revealing the carotenoids. Tomatoes are especially rich in the carotenoid lycopene, which accounts

for their red color, whereas carrots and pumpkins have abundant amounts of the carotenoid β-carotene, accounting for their orange color.



Lycopene



β-Carotene

Resonance energy transfer allows energy to move from the site of initial absorbance to the reaction center

How is energy funneled from accessory pigments to a reaction center? As discussed at the beginning of the chapter, the absorption of a photon does not always lead to electron excitation and transfer. More commonly, excitation energy is transferred from one molecule to a nearby molecule through electromagnetic interactions through space (**Figure 19.28**). The rate of this process, called *resonance energy transfer,* depends strongly on the distance between the energy-donor and the energy-acceptor molecules; an increase in the distance between the donor and the acceptor by a factor of 2 typically results in a decrease in the energy-transfer rate by a factor of $2^6 = 64$. For reasons of energy conservation, energy transfer must be from a donor in the excited state to an acceptor of equal or lower energy. The excited state of the special

pair of chlorophyll molecules is lower in energy than that of single chlorophyll molecules, allowing reaction centers to trap the energy transferred from other molecules.

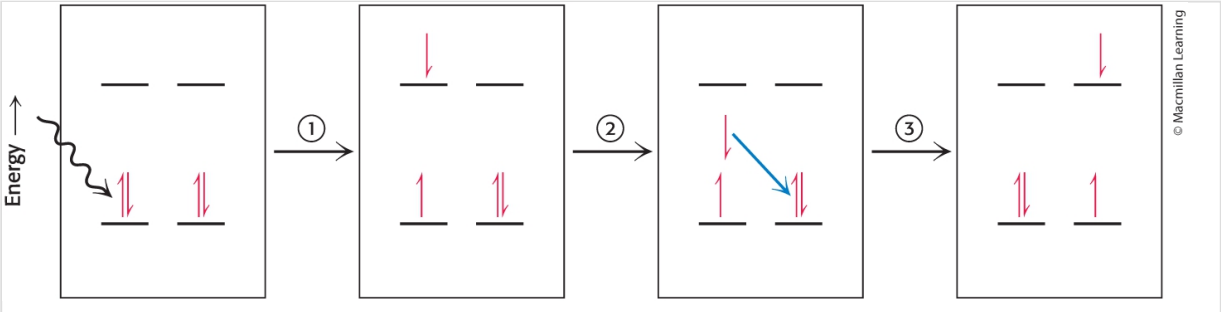


FIGURE 19.28 Resonance energy transfer allows electrons to transfer energy over a distance. (1) An electron can accept energy from electromagnetic radiation of appropriate wavelength and jump to a higher energy state. (2) When the excited electron falls back to its lower energy state, the absorbed energy is released. (3) The released energy can be absorbed by an electron in a nearby molecule, and this electron jumps to a high energy state.

What is the structural relationship between the accessory pigment and the reaction center? The accessory pigments are arranged in numerous **light-harvesting complexes** that completely surround the reaction center (**Figure 19.29**). The 26-kDa subunit of light-harvesting complex II (LHC-II) is the most abundant membrane protein in chloroplasts. This subunit binds seven chlorophyll *a* molecules, six chlorophyll *b* molecules, and two carotenoid molecules. Similar light-harvesting assemblies exist in many photosynthetic bacteria.

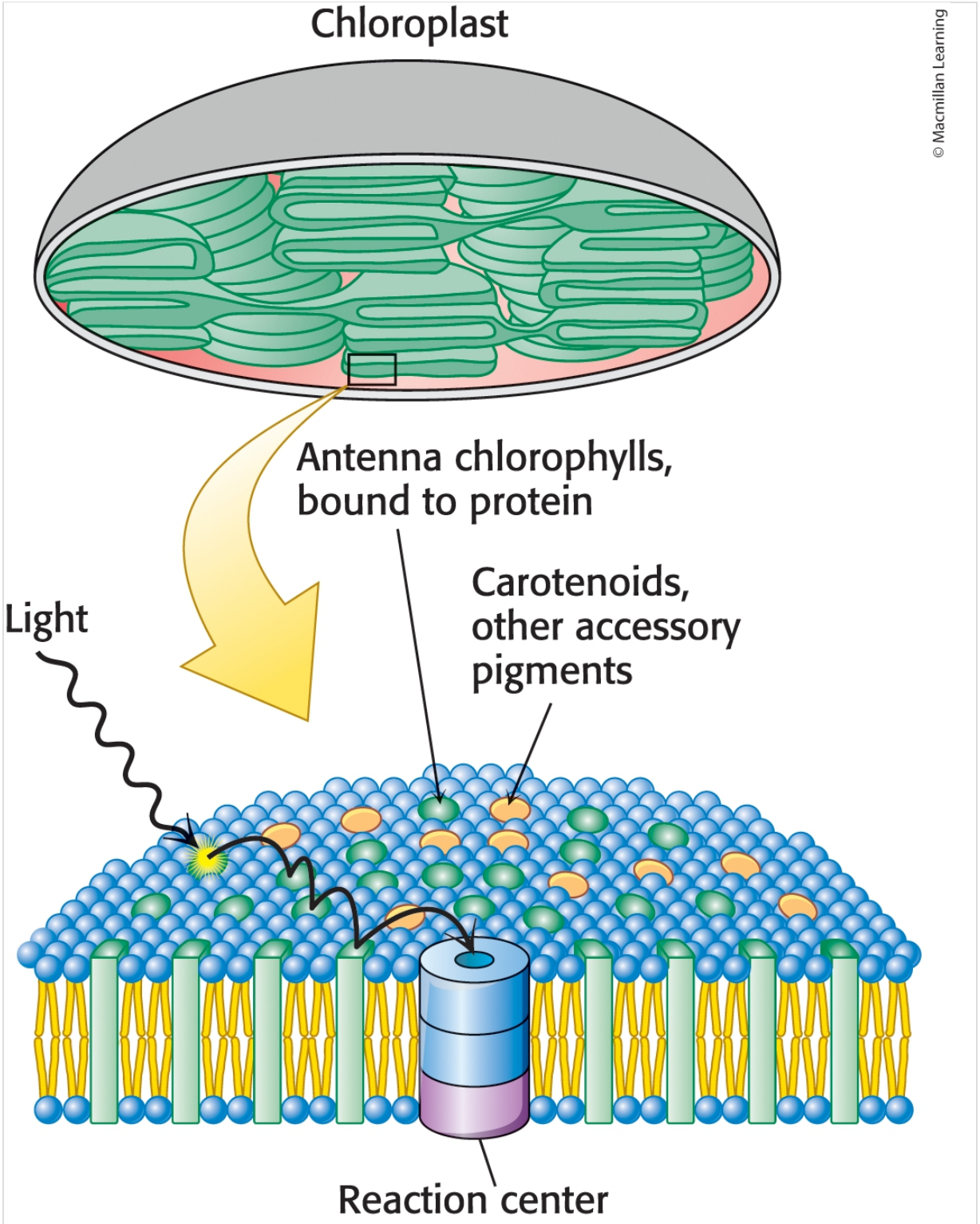


FIGURE 19.29 Energy is transferred from accessory pigments to reaction centers. Light energy absorbed by accessory chlorophyll molecules or other pigments can be transferred to reaction centers by resonance energy transfer (black arrows), where it drives photoinduced charge separation.

[Source: D. L. Nelson and M. M. Cox, *Lehninger Principles of Biochemistry*, 5th ed. (W. H. Freeman and Company, 2008), Fig. 19.52.]

Accessory pigments also protect plants from reactive oxygen

In addition to their role in transferring energy to reaction centers, the carotenoids and other accessory pigments serve a safeguarding function. Carotenoids suppress harmful photochemical reactions, particularly those including oxygen, that can be induced by bright sunlight. The reactive oxygen species would otherwise damage the cell and eventually the entire plant. To protect against bright sunlight, plants use a mechanism called **nonphotochemical quenching (NPQ)**. When NPQ is operating, photons are directed away from the light-harvesting complex, and the energy of the photons is released as heat. This protection may be especially important in the fall when the primary pigment chlorophyll is being degraded and thus not able to absorb light energy. Plants lacking carotenoids are quickly killed on exposure to light and oxygen.

Increasing the efficiency of photosynthesis will increase crop yields

NPQ is a means by which plants protect themselves from damaging reactive oxygen species that are generated by intense sunlight — essentially a botanical sunscreen. Understanding NPQ, a complex process consisting of several components, is an active area of research. It is established that NPQ requires a proton gradient across the

thylakoid membrane and, in higher photosynthetic organisms such as plants, a particular protein, photosystem II subunit S (PsbS). PsbS, in the presence of a pH gradient, acts in seconds to help to initiate NPQ by interacting with protein components of the light-harvesting complex. This interaction redirects the energy absorbed by the light-harvesting complex from the reaction centers so that the energy is lost as heat. Although quick to be activated, NPQ is slow to turn off, depressing photosynthetic yields to be as much as 30% in some crops. This slow turn off is a target for biochemists hoping to increase the efficiency of photosynthesis and, consequently, crop yield.

Why is it necessary to boost photosynthesis? Traditional plant breeding has greatly increased crop yield over the past century. Additionally, modern farming practices and tools such as fertilizers, pesticides, and irrigation have contributed to increased yield. However, studies suggest that the ability to increase crop yields by traditional means may have reached its limits. And yet, the Food and Agricultural Organization of the United Nations estimates that in 30 years, the world's population will be about 10 billion, an increase of more than 2 billion from the current 7.8 billion. To feed all of these people, agricultural production will need to increase by 50% in the developed world and 400% in the developing world.

To tackle the problem of not enough food, biochemists are trying to increase the efficiency of photosynthesis by reducing the time required to turn off NPQ. Using techniques described in Chapter 9, genes were introduced into the model organism — the tobacco plant — that increased the speed of NPQ shutdown. The result was a 15% increase in plant size. Similar results have now been observed in rice, and the next steps are to modify other crops such as wheat and cowpea — important sources of protein in sub-Saharan Africa.

The components of photosynthesis are highly organized

The intricacy of photosynthesis, seen already in the elaborate interplay of complex components, extends even to the placement of the components in the thylakoid membranes. Thylakoid membranes of most plants are differentiated into stacked and unstacked regions (**Figure 19.30**). Stacking increases the amount of thylakoid membrane in a given chloroplast volume. Both regions surround a common internal thylakoid space, but only unstacked regions make direct contact with the chloroplast stroma.

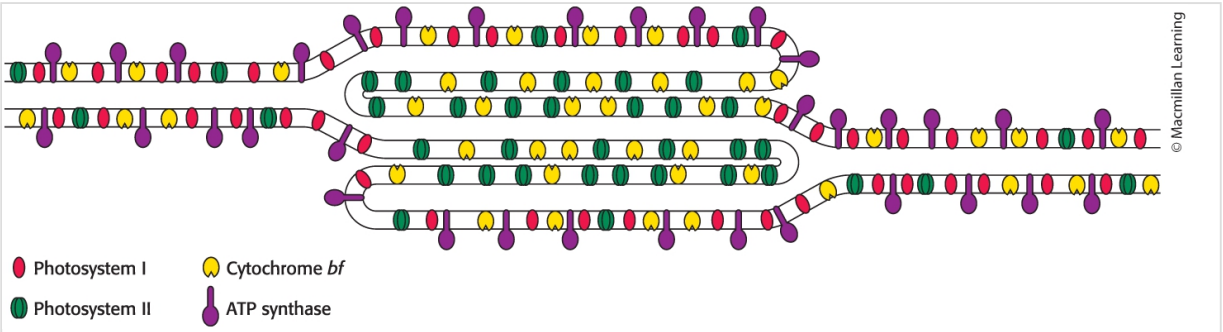


FIGURE 19.30 Photosynthetic assemblies are differentially distributed in the stacked and unstacked regions of thylakoid membranes.

[Information from Dr. Jan M. Anderson and Dr. Bertil Andersson.]

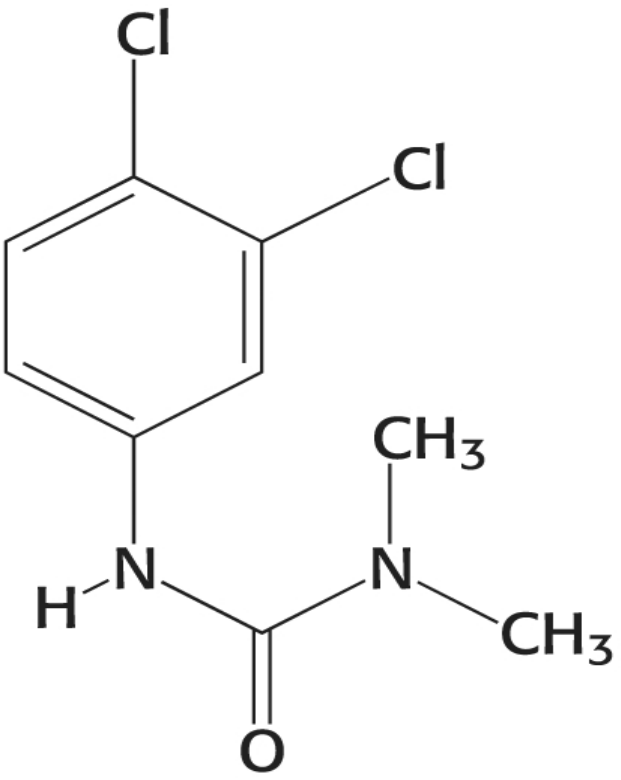
Stacked and unstacked regions differ in the nature of their photosynthetic assemblies (Figure 19.30). Photosystem I and ATP synthase are located almost exclusively in unstacked regions, whereas photosystem II is present mostly in stacked regions. The cytochrome *bf* complex is found in both regions. A common internal thylakoid space enables protons liberated by photosystem II in stacked membranes to be used by ATP synthase molecules that are located far away in unstacked membranes. Plastoquinone and plastocyanin are the mobile

carriers of electrons between assemblies located in different regions of the thylakoid membrane.

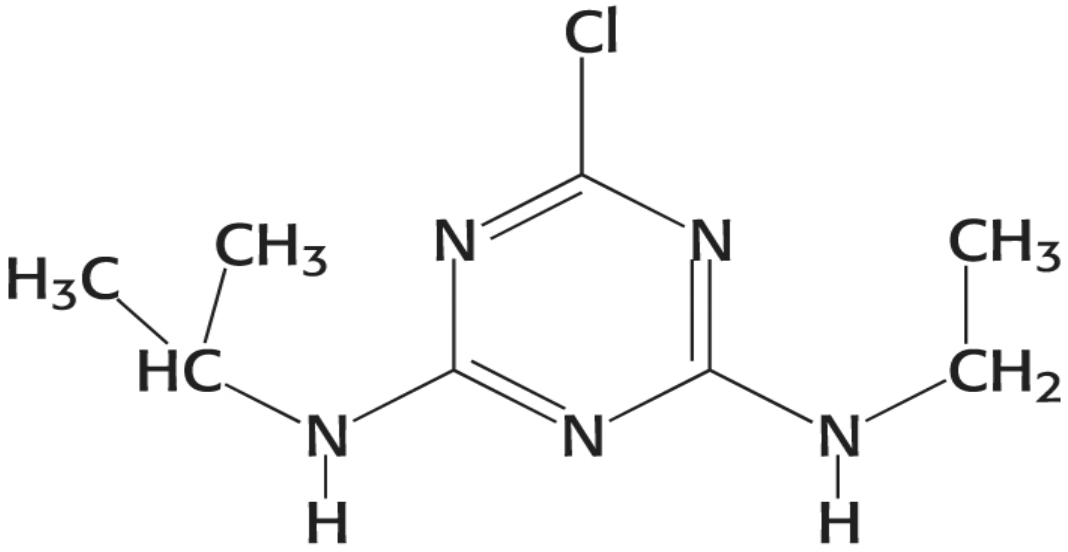
What is the functional significance of the structural variety in the thylakoid membrane system? The positioning of photosystem I in the unstacked membranes gives it direct access to the stroma for the reduction of $NADP^+$. ATP synthase is also located in the unstacked region, which provides the space needed for its large CF_1 globule and gives it access to ADP. In contrast, the tight quarters of the stacked region pose no problem for photosystem II, which interacts with a small polar electron donor (H_2O) and a highly lipid-soluble electron carrier (plastoquinone).

Many herbicides inhibit the light reactions of photosynthesis

Many commercial herbicides kill weeds by interfering with the action of photosystem II or photosystem I. Inhibitors of PS II block electron flow, whereas inhibitors of PS I divert electrons from its terminal part. PS II inhibitors include urea derivatives such as *diuron* and triazine derivatives such as *atrazine*. These chemicals bind to the Q_B site of the D1 subunit of photosystem II and block the formation of plastoquinol (QH_2). PS I inhibitors include Paraquat $(1,1'-dimethyl-4-4'-bipyridinium)$, a dication, which can accept electrons from photosystem I to become a radical. This radical reacts with O_2 to produce reactive oxygen species such as superoxide (O_2^-) and hydroxyl radical (OH•). Such reactive oxygen species react with many biomolecules, including double bonds in membrane lipids, damaging the membrane.



Diuron



Atrazine

19.7 The Ability to Convert Light into Chemical Energy Is Ancient

The ability to convert light energy into chemical energy is a tremendous evolutionary advantage. Geological evidence suggests that oxygenic photosynthesis became important approximately 2 billion years ago. Anoxygenic photosynthetic systems arose much earlier in the 3.5-billion-year history of life on Earth (Table 19.1).

TABLE 19.1 Major groups of photosynthetic prokaryotes

Bacteria	Photosynthetic electron donor	O_2 use
Green sulfur	H_2, H_2S, S	Anoxygenic
Green nonsulfur	Variety of amino acids and organic acids	Anoxygenic
Purple sulfur	H_2, H_2S, S	Anoxygenic
Purple nonsulfur	Usually organic molecules	Anoxygenic
Cyanobacteria	H_2O	Oxygenic

As we discussed at various points in this chapter, the photosynthetic reaction center of the nonsulfur purple bacterium *Rhodopseudomonas viridis* has many features common to oxygenic photosynthetic systems and clearly predates them. Green sulfur bacteria such as *Chlorobium thiosulfatophilum* carry out a reaction that also seems to have appeared before oxygenic photosynthesis and is even more similar to oxygenic photosynthesis than the photosystem of *R. viridis*. Reduced sulfur

species such as H_2S are electron donors in the overall photosynthetic reaction

$$CO_2 + 2\ H_2S \xrightarrow{\text{Light}} (CH_2O) + 2\ S + H_2O$$

Nonetheless, photosynthesis did not evolve immediately at the origin of life. No photosynthetic organisms have been discovered in the domain Archaea, implying that photosynthesis evolved in the domain Bacteria after archaea and bacteria diverged from a common ancestor. All domains of life do have electron-transport chains in common, however. As we have seen, components such as the ubiquinone–cytochrome *c* oxidoreductase (Section 18.3) and cytochrome *bf* family (Section 19.4) are present in both respiratory and photosynthetic electron-transport chains. These components were the foundations on which light-energy-capturing systems evolved.

Artificial photosynthetic systems may provide clean, renewable energy

As we have learned, oxygenic photosynthetic organisms use sunlight to oxidize H_2O, producing O_2 and protons used to power ATP synthesis and generate NADPH. Research is currently underway to try to mimic this process in order to provide clean energy. The idea is that photovoltaic cells could use light energy to oxidize water, producing O_2 as well as H_2. Hydrogen gas is a fuel that, upon reaction with oxygen, releases energy and only water as a waste product. Recent work suggests that semiconductors composed of organic–inorganic material show great promise in this application.

Photovoltaic cells are now being paired with microorganisms to generate a variety of biomolecules, including fuels, in a clean,

renewable fashion. One example of such a hybrid-biological-inorganic (HBI) system is shown in **Figure 19.31**). Sunlight is converted into an electrical current by the photovoltaic cell. The current flows to the anode, where water is oxidized and the resulting electrons are taken up by the cathode. Bacteria, such as *Cupriavidus necator* (also used in bioremediation because of its ability to degrade chlorinated hydrocarbons) live in direct contact with the cathode. The bacteria use the electrons generated by the oxidation of water to reduce CO_2 to industrially important biomolecules. The efficiency of such HBI systems for converting sunlight into chemical energy is nearly 10%, with the potential for improvement, surpassing the efficiency of natural photosynthesis, which has an efficiency of 2%.

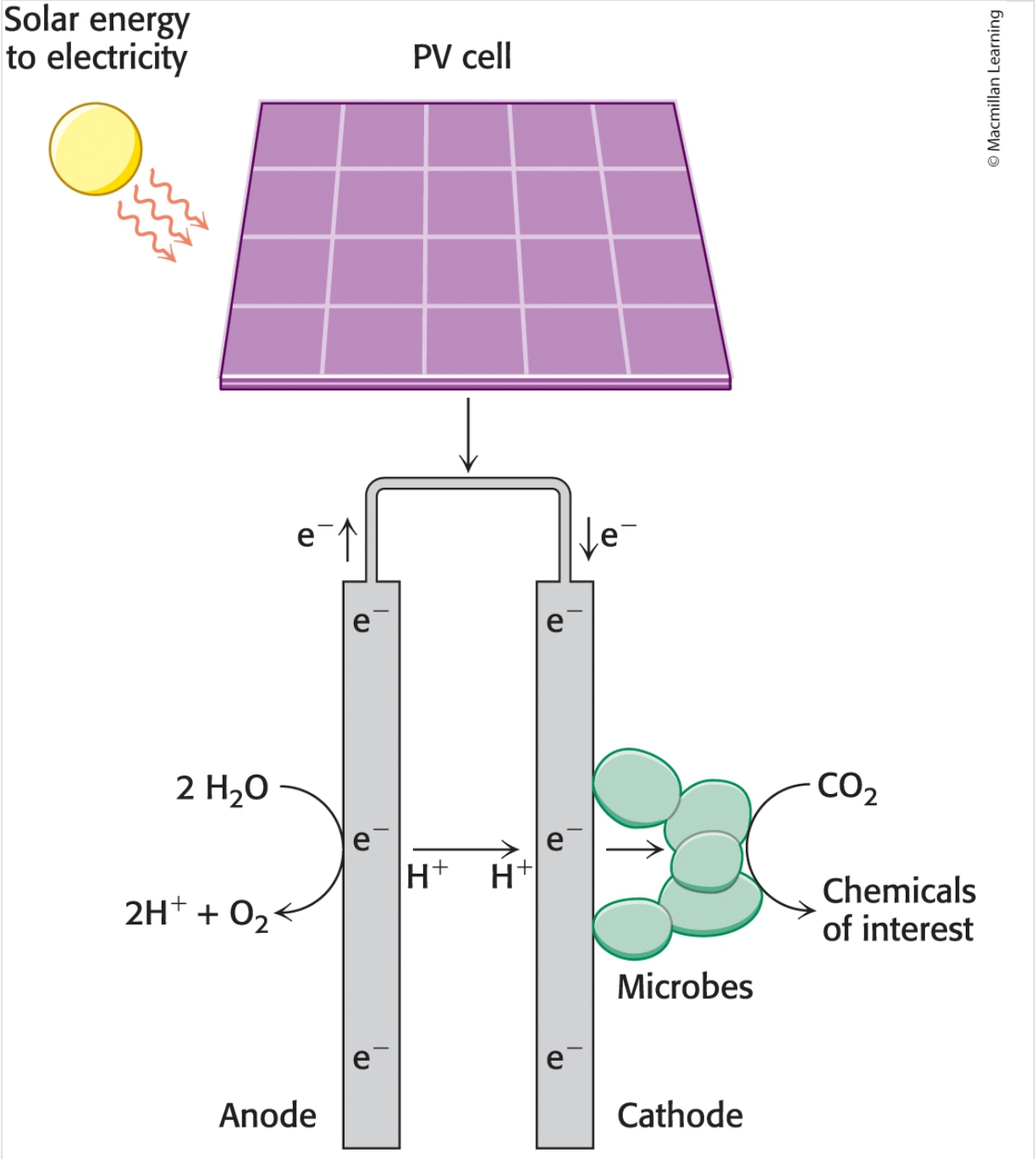


FIGURE 19.31 Photovoltaic cells can drive artificial photosynthesis. After a PV cell absorbs light, the resulting current flows to the anode to oxidize water, with the electrons then taken up by the cathode. Bacteria in contact with the cathode use the electrons to reduce CO_2 to biomolecules.

Photosensitive proteins are transforming other fields

Phototrophic organisms use a range of light-sensitive proteins in addition to those discussed thus far. Scientists have taken advantage of these proteins to develop new research tools and even therapies. A key example is channelrhodopsin first characterized from green algae, where it plays a role in light sensing. Channelrhodopsin is homologous to bacteriorhodopsin but functions as an ion channel rather than a proton pump. Thus, exposure of cells with channelrhodopsin present in their cell membranes to light results in ion channel opening and the flow of ions down any gradients.

Scientists have expressed channelrhodopsin in neurons, making these neurons sensitive to light. The firing of these neurons can then be controlled by applying short flashes of light to initiate action potentials (Figure 19.32) for cells in culture but also in engineered experimental animals. These methods, termed *optogenetics*, facilitate exploration of the mechanisms of nervous system function with unprecedented precision, again demonstrating the power of biochemical discoveries to transform other fields.

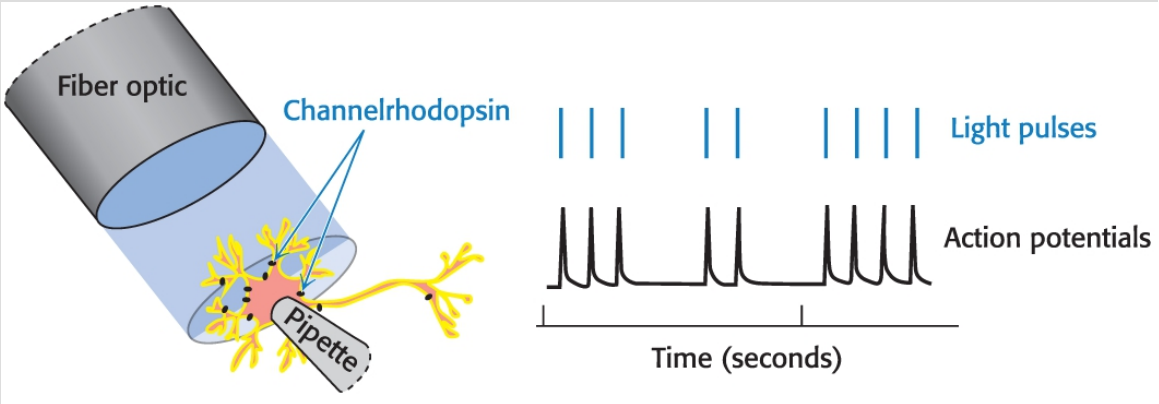


FIGURE 19.32 Optogenetics allows neurons to be controlled using light. Neurons engineered t
express the light-sensitive ion channel channelrhodopsin in their cell membrane respond to

pulses of light. Light causes channelrhodopsin to open and allow the flow of ions across the membrane. This flow of ions triggers neuron action potentials, which can be detected with a small pipette in a setup known as a patch clamp.



Chapter 19 Summary

19.1 Phototrophy Converts Light Energy into Chemical Energy

- The process of living organisms capturing light energy as chemical energy is called phototrophy.
- Photosynthesis is the combination of phototrophy with the reduction of carbon dioxide to form carbohydrate.

19.2 In Eukaryotes, Photosynthesis Takes Place in Chloroplasts

- The proteins that participate in the light reactions of photosynthesis are located in the thylakoid membranes of chloroplasts.
- The light reactions result in (1) the creation of reducing power for the production of NADPH, (2) the generation of a transmembrane proton gradient for the formation of ATP, and (3) the production of O_2.

19.3 Light Absorption by Chlorophyll Molecules Induces Electron Transfer

- An electron excited to a high-energy state by the absorption of a photon can move to nearby electron acceptors. In photosynthesis, an excited electron leaves a pair of associated chlorophyll molecules — the special pair — that are located in reaction centers.
- In the reaction center of a purple bacterium, the electron moves from the special pair containing bacteriochlorophyll to a bacteriopheophytin to quinones.
- The reduction of quinones leads to the generation of a proton gradient, which drives ATP synthesis in a manner analogous to that of oxidative phosphorylation.

19.4 Two Photosystems Generate a Proton Gradient and Reducing Power in Cyanobacteria and Photosynthetic Eukaryotes

- Photosynthesis in green plants, algae, and cyanobacteria is mediated by two linked photosystems. In photosystem II (PS II), the excitation of a special pair of chlorophyll molecules called P680 leads to electron transfer to plastoquinone. The electrons are replenished by the extraction of electrons from a water molecule at the manganese-containing water-oxidizing complex, generating O_2.
- The plastoquinol produced by PS II is reoxidized by the cytochrome *bf* complex. The electrons are transferred to plastocyanin, and then photosystem I (PS I).
- In PS I, the excitation of special pair P700 releases electrons that flow to ferredoxin, a powerful reductant. Ferredoxin–$NADP^+$ reductase, a flavoprotein, then catalyzes the formation of NADPH.
- A proton gradient is generated as electrons pass through PS II, through the cytochrome *bf* complex, and through ferredoxin–$NADP^+$ reductase.

19.5 A Proton Gradient across the Thylakoid Membrane Drives ATP Synthesis

- The proton gradient across the thylakoid membrane creates a proton-motive force that is used by the $CF_0 - CF_1$ ATP synthase of chloroplasts synthase to form ATP.
- If the NADPH:$NADP^+$ ratio is high, electrons transferred to ferredoxin by PS I can reenter the cytochrome *bf* complex during cyclic photophosphorylation, which leads to the generation of a proton gradient by the cytochrome *bf* complex without the formation of NADPH or O_2.

19.6 Accessory Pigments Funnel Energy into Reaction Centers

- Light-harvesting complexes that surround the reaction centers contain additional chlorophyll and carotenoid molecules that absorb light in the center of the visible spectrum.
- These accessory pigments increase the efficiency of light capture by absorbing light and transferring the energy to reaction centers through resonance energy transfer.

19.7 The Ability to Convert Light into Chemical Energy Is Ancient

- The photosystems have structural features in common that suggest a mutual evolutionary origin.
- Similarities in organization and molecular structure to those of oxidative phosphorylation suggest that the photosynthetic apparatus evolved from an early energy-transduction system.

Key Terms

phototroph
bacteriorhodopsin
photosynthesis
chemotroph
autotroph
heterotroph
light reactions
photosystem I (PS I)
photosystem II (PS II)
chloroplast
stroma
thylakoid
granum
chlorophyll *a*

photoinduced charge separation
reaction center
special pair
water-oxidizing complex (WOC) (manganese center)
cytochrome *bf*
Z scheme of photosynthesis
ATP synthase of chloroplasts ($CF_1 - CF_0$ complex)
cyclic photophosphorylation
carotenoid
light-harvesting complex
nonphotochemical quenching (NPQ)

Problems

1. Under normal circumstances, photosystem I donates electrons to:

a. Photosystem II
b. ATP synthase
c. P700
d. $NADP^+$

2. The water-oxidizing complex provides electrons to:

a. P680
b. P450
c. P700
d. Cytochrome *c*

3. Cyclic photophosphorylation allows the generation of _____ without the synthesis of _____.

a. ATP, NADPH
b. NADPH, ATP
c. ATP, NADH
d. ATP, O_2

4. Which description of resonance energy transfer is true?

a. Results in separation of charge
b. Directly powers ATP synthesis
c. Allows energy flux in the light-harvesting complex
d. Does not exist

5. Human beings do not capture energy by photosynthesis, yet this process is critical to our survival. Explain.

6. What is the overall reaction for the light reactions of photosynthesis? 1

7. Indicate whether each of the following applies to photosystem I or photosystem II: 1

a. Generates NADPH
b. Establishes a proton gradient
c. Oxidizes water
d. Produces O_2
e. Uses reduced ferredoxin to generate a biosynthetic reductant

8. Photosynthesis can be measured by measuring the rate of oxygen production. When plants are exposed to light of wavelength 680 nm, more oxygen is evolved than if the plants are exposed to light of 700 nm. If plants are illuminated by a combination of light of 680 nm and 700 nm, the oxygen production exceeds that of either wavelength alone. Explain both results. 1

9. What is the advantage of having an extensive set of thylakoid membranes in the chloroplasts? 1, 2

10. Explain how light-harvesting complexes enhance the efficiency of photosynthesis. 5

11. What is the ultimate electron acceptor in oxygenic photosynthesis? The ultimate electron donor? What powers the electron flow between the donor and the acceptor? 3

12. What are the various sources of protons that contribute to the generation of a proton gradient in chloroplasts? 4

13. Calculate the $\Delta E'_0$ and $\Delta G^{\circ\prime}$ for the reduction of $NADP^+$ by ferredoxin. Use data given in Table 18.1.

14. It can be argued that, if life were to exist elsewhere in the universe, it would require some process like photosynthesis. If a starship were to land on a distant planet and find no measurable oxygen in the atmosphere, could the crew conclude that photosynthesis is not taking place? 1

15. Dichlorophenyldimethylurea (DCMU), a herbicide, interferes with photophosphorylation and O_2 evolution. However, it does not block O_2 evolution in the presence of an artificial electron acceptor such as ferricyanide. Propose a site for the inhibitory action of DCMU.

16. Predict the effect of the herbicide dichlorophenyldimethylurea (DCMU) on a plant's ability to perform cyclic photophosphorylation.

17. Consider the relation between the energy of a photon and its wavelength.

a. Some bacteria are able to harvest 1000-nm light. What is the energy (in kilojoules or kilocalories) of a mole (also called an *einstein*) of 1000-nm photons?
b. What is the maximum increase in redox potential that can be induced by a 1000-nm photon?
c. What is the minimum number of 1000-nm photons needed to form ATP from ADP and P_i? Assume a ΔG of $50\ kJ\ mol^{-1}\ (12\ kcal\ mol^{-1})$ for the phosphorylation reaction.

18. What structural features of mitochondria corresponds to the thylakoid membranes and the stroma? 1, 2, 3, 4

19. Compare and contrast oxidative phosphorylation and photosynthesis. 1, 2, 3, 4

CHAPTER 20

The Calvin–Benson Cycle and the Pentose Phosphate Pathway

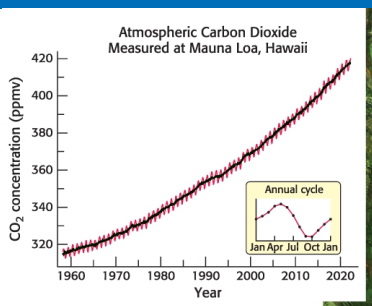




Photo: Travelpix Ltd/Photographer's Choice RF/Getty Images
© Macmillan Learning

Atmospheric carbon dioxide measurements at Mauna Loa, Hawaii, show the increase in atmospheric carbon dioxide concentration since 1960 in units of parts per million by volume (ppmv). The sawtooth appearance of the curve is the result of annual cycles resulting from seasonal variation in CO_2 fixation by the Calvin–Benson cycle in terrestrial plants (graph inset). Much of this fixation takes place in rain forests, which account for approximately 50% of terrestrial fixation.

[Data from http://www.esrl.noaa.gov/gmd/ccgg/trends]

OUTLINE

20.1 The Calvin–Benson Cycle Synthesizes Hexoses from Carbon Dioxide and Water
20.2 The Activity of the Calvin–Benson Cycle Depends on Environmental Conditions
20.3 The Pentose Phosphate Pathway Generates NADPH and Synthesizes Pentoses
20.4 The Metabolism of Glucose 6-Phosphate by the Pentose Phosphate Pathway Is Coordinated with Glycolysis
20.5 Glucose 6-Phosphate Dehydrogenase Plays a Key Role in Protection Against Reactive Oxygen Species

Learning Goals



By the end of this chapter, you should be able to:

1. Explain the function of the Calvin–Benson cycle.
2. Describe how the light reactions and the Calvin–Benson cycle are coordinated.
3. Identify the two stages of the pentose phosphate pathway and explain how the pathway is coordinated with glycolysis and gluconeogenesis.
4. Identify the regulation of the oxidative phase of the pentose phosphate pathway, including the key enzyme and its importance in health and disease.

Photosynthesis proceeds in two parts. The light reactions, discussed in Chapter 19, transform light energy into ATP and biosynthetic reducing power, NADPH. The dark reactions use the ATP and NADPH produced by the light reactions to reduce carbon atoms from their fully oxidized state as carbon dioxide to a more reduced state as a hexose. The dark reactions are called the **Calvin–Benson cycle**, after Melvin Calvin and Andrew Benson, two of the biochemists who helped elucidated the pathway, or sometimes simply the Calvin cycle.

This chapter also examines the pentose phosphate pathway that allows glucose to be oxidized to generate NADPH. The pentose phosphate pathway and Calvin–Benson cycle have several enzymes and intermediates in common. The Calvin–Benson cycle uses NADPH to reduce carbon dioxide to generate hexoses, whereas the pentose phosphate pathway oxidizes glucose to carbon dioxide to generate NADPH.

20.1 The Calvin–Benson Cycle Synthesizes Hexoses from Carbon Dioxide and Water

As we learned in Chapter 16, glucose can be formed from noncarbohydrate precursors, such as lactate and amino acids, by gluconeogenesis. The energy powering gluconeogenesis ultimately comes from previous catabolism of carbon fuels. In contrast, photosynthetic organisms can use the Calvin–Benson cycle to synthesize glucose from carbon dioxide gas and water, by using sunlight as an energy source. The Calvin–Benson cycle introduces into life all the carbon atoms that will be used as fuel and as the carbon backbones of biomolecules. Photosynthetic organisms are autotrophs as they can convert sunlight into chemical energy, which they subsequently use to power their biosynthetic processes.

The Calvin–Benson cycle was elucidated through studies that depended on the availability of radioactive ^{14}C through cyclotrons at the University of California, Berkeley, starting just after World War II. Unicellular algae were exposed to $^{14}CO_2$ for short periods of time, and the radioactive compounds were separated, identified, and quantified.



Arthur Nonomura, Ph. D.

ANDREW BENSON After completing his PhD in carbohydrate chemistry from Caltech, Andrew Benson moved to the University of California, Berkeley, where he was exposed to research in photosynthesis. Using radioisotopes of carbon including ^{14}C, he worked as part of a team with Melvin Calvin on the pathway of CO_2 fixation. He was the first to identify ribulose 1,5-bisphosphate as the key component that captures CO_2, among other discoveries.

The elucidation of this pathway represents a good example of how a team of scientists from different backgrounds can solve important problems. Unfortunately, it also revealed the challenges of such collaborations. Calvin dismissed Benson in 1954, shortly after the pathway was elucidated. Calvin was awarded the Nobel Prize by himself in 1961 and barely mentioned Benson in his Nobel lecture. After leaving Berkeley, Dr. Benson went on to have an impressive career working on plant lipids

and a range of topics in marine biology, primarily at the Scripps Institution for Oceanography, where he also served as an important scientific leader.

These studies revealed that the Calvin–Benson cycle comprises three stages (**Figure 20.1**):

1. The fixation of CO_2 to ribulose 1,5-bisphosphate to form two molecules of 3-phosphoglycerate;
2. The reduction of 3-phosphoglycerate to form hexose sugars; and
3. The regeneration of ribulose 1,5-bisphosphate so that more CO_2 can be fixed.

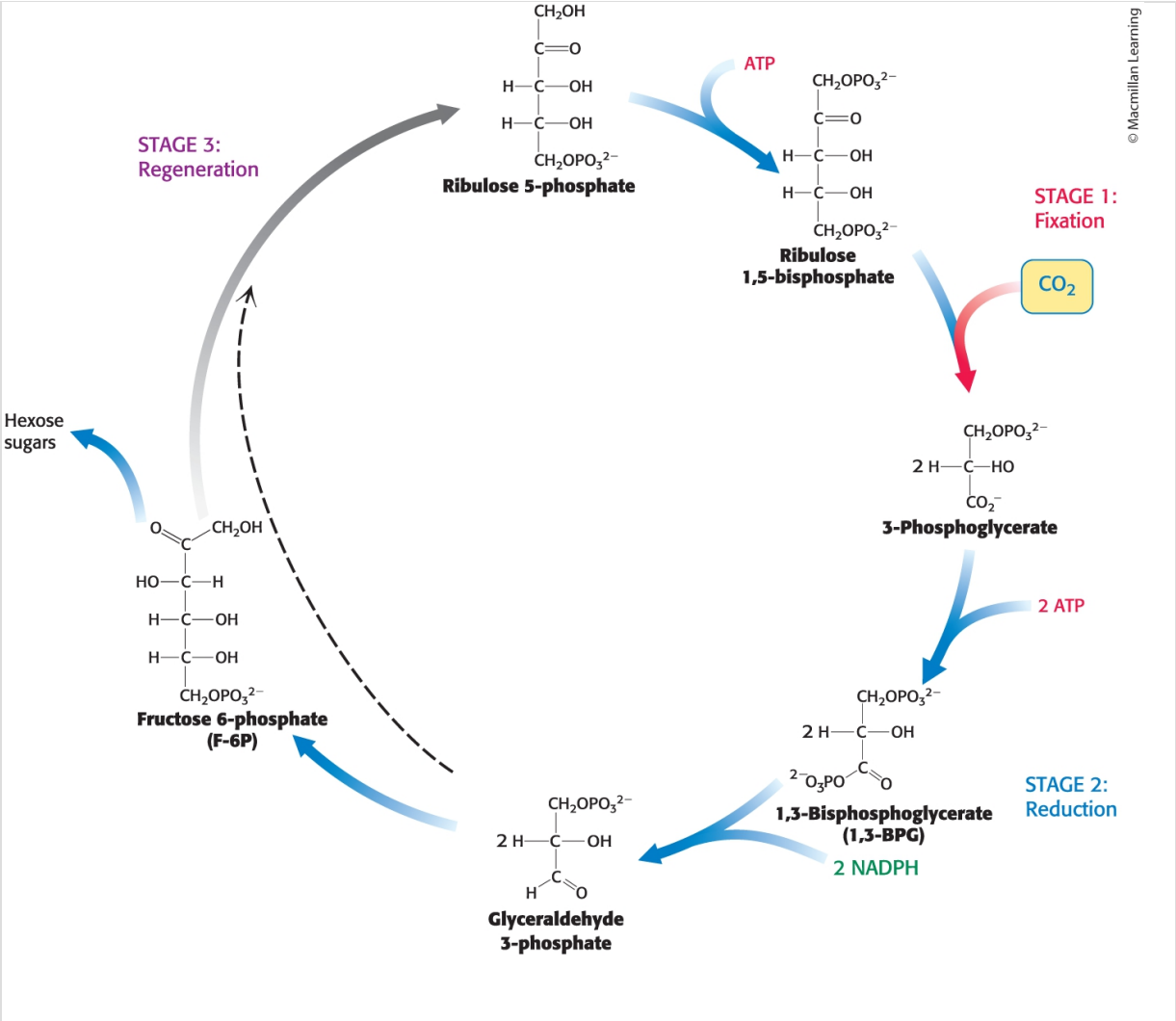
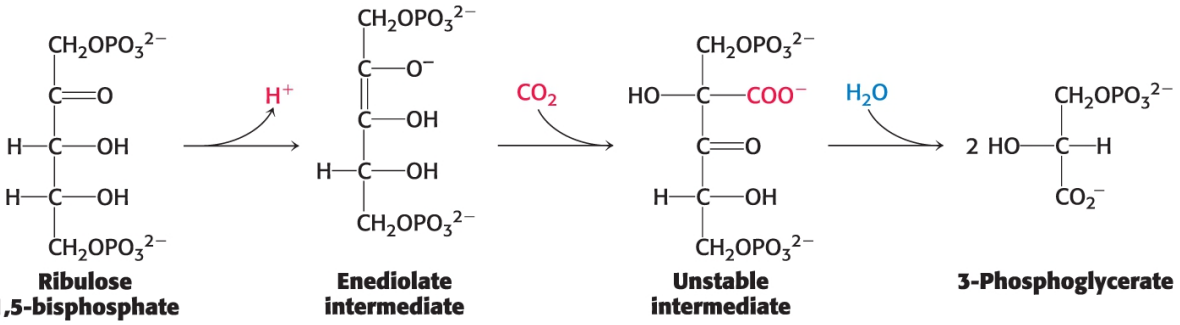


FIGURE 20.1 The Calvin–Benson cycle consists of three stages. Stage 1 is the fixation of carbon by the carboxylation of ribulose 1,5-bisphosphate. Stage 2 is the reduction of the fixed carbon to begin the synthesis of hexose. Stage 3 is the regeneration of the starting compound ribulose 1,5-bisphosphate.

This set of reactions takes place in the stroma of chloroplasts — the photosynthetic organelles (Figure 19.3).

Stage 1: Carbon dioxide reacts with ribulose 1,5-bisphosphate to form two molecules of 3-phosphoglycerate

The first step in the Calvin–Benson cycle is the fixation of CO_2. This begins with the conversion of ribulose 1,5-bisphosphate into a highly reactive enediolate intermediate. The CO_2 molecule condenses with the enediolate intermediate to form an unstable six-carbon compound, which is rapidly hydrolyzed to two molecules of 3-phosphoglycerate.



This highly exergonic reaction $[\Delta G^{\circ\prime} = -51.9\ \text{kJ mol}^{-1}\ (-12.4\ \text{kcal mol}^{-1})]$ is catalyzed by **ribulose 1,5-bisphosphate carboxylase/oxygenase** (often called *Rubisco* or *RuBisCo*), an enzyme located on the stromal surface of the thylakoid membranes of chloroplasts. This important reaction is the rate-limiting step in hexose synthesis.

In plants and green algae, Rubisco consists of eight large (L, 55-kDa) subunits and eight small (S, 15-kDa) ones (**Figure 20.2**). Each L chain contains a catalytic site and a regulatory site. The S chains enhance the catalytic activity of the L chains. This enzyme is abundant in chloroplasts, accounting for approximately 30% of the total leaf protein in some plants. In fact, Rubisco is the most abundant enzyme and perhaps the most abundant protein in the entire biosphere. Large amounts are present because Rubisco is a relatively slow enzyme; its maximal catalytic rate is only $3\ \text{s}^{-1}$.

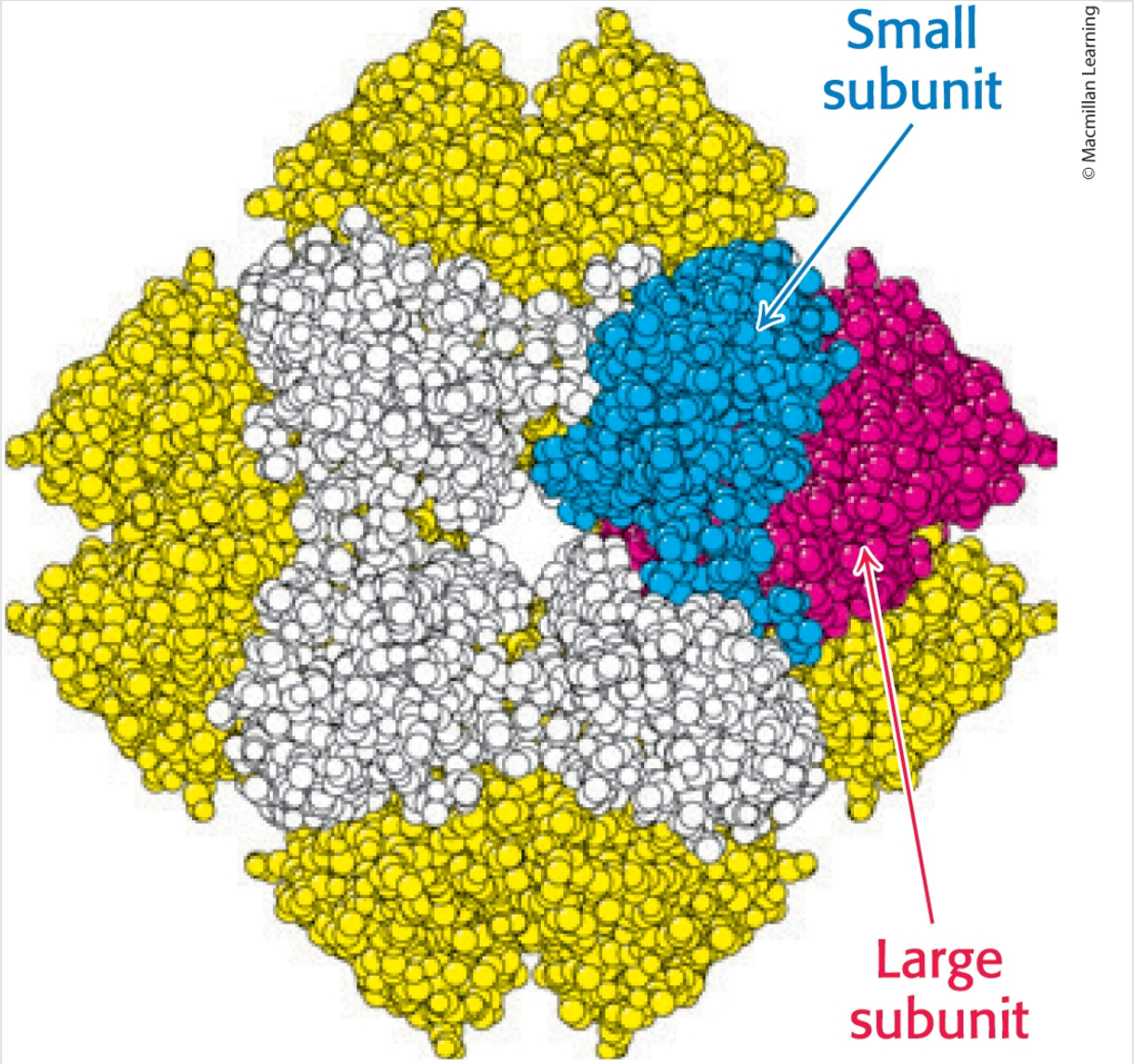


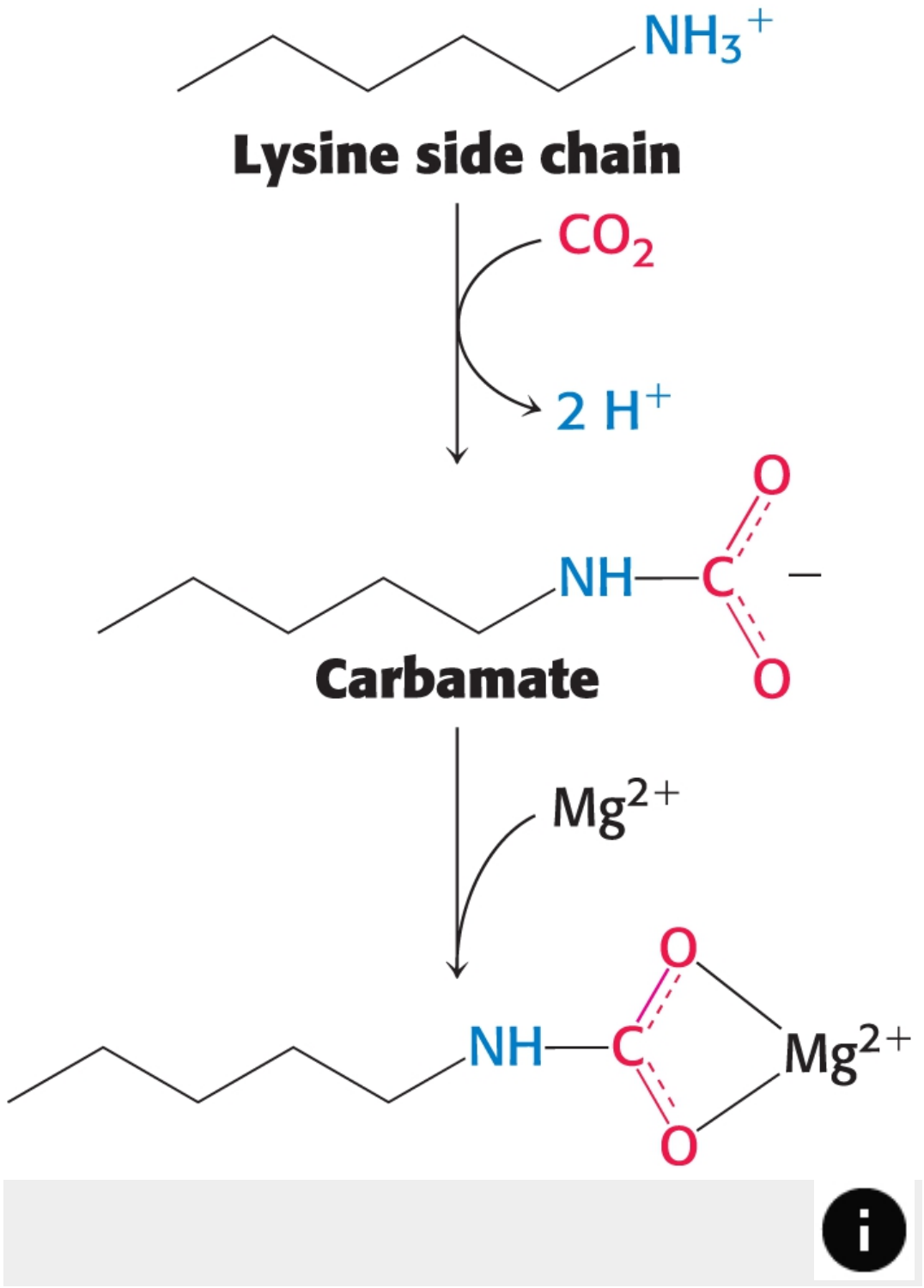
FIGURE 20.2 The enzyme ribulose 1,5-bisphosphate carboxylase/oxygenase (Rubisco) comprises 16 subunits. There are eight small subunits, one shown in blue and the others in white, and eight large subunits (partially obscured by the small units), one shown in red and the others in yellow. The active sites lie in the large subunits.

[Drawn from 1RXO.pdb.]

INTERACT with this model in Achieve

Rubisco activity depends on magnesium and carbamate

Rubisco requires a bound divalent metal ion for activity, usually magnesium ion. Like the zinc ion in the active site of carbonic anhydrase (Section 6.3), this metal ion serves to activate a bound substrate molecule by stabilizing a negative charge. Interestingly, a CO_2 molecule other than the substrate is required to complete the assembly of the Mg^{2+}-binding site in Rubisco. This CO_2 molecule adds to the uncharged ε-amino group of lysine 201 to form a carbamate. This negatively charged carbamate then binds the Mg^{2+} ion.



The metal center plays a key role in binding ribulose 1,5-bisphosphate and activating it so that it reacts with CO_2 (Figure 20.3). Ribulose 1,5-

bisphosphate binds to Mg^{2+} through its keto group and an adjacent hydroxyl group. This complex is readily deprotonated to form an enediolate intermediate. This reactive species, analogous to the zinc-hydroxide species in carbonic anhydrase, reacts with CO_2, forming the new carbon–carbon bond. The resulting 2-carboxy-3-keto-D-arabinitol 1,5-bisphosphate is coordinated to the Mg^{2+} ion through three groups, including the newly formed carboxylate. A molecule of H_2O is then added to this β-ketoacid to form an intermediate that cleaves to form two molecules of 3-phosphoglycerate (Figure 20.4).

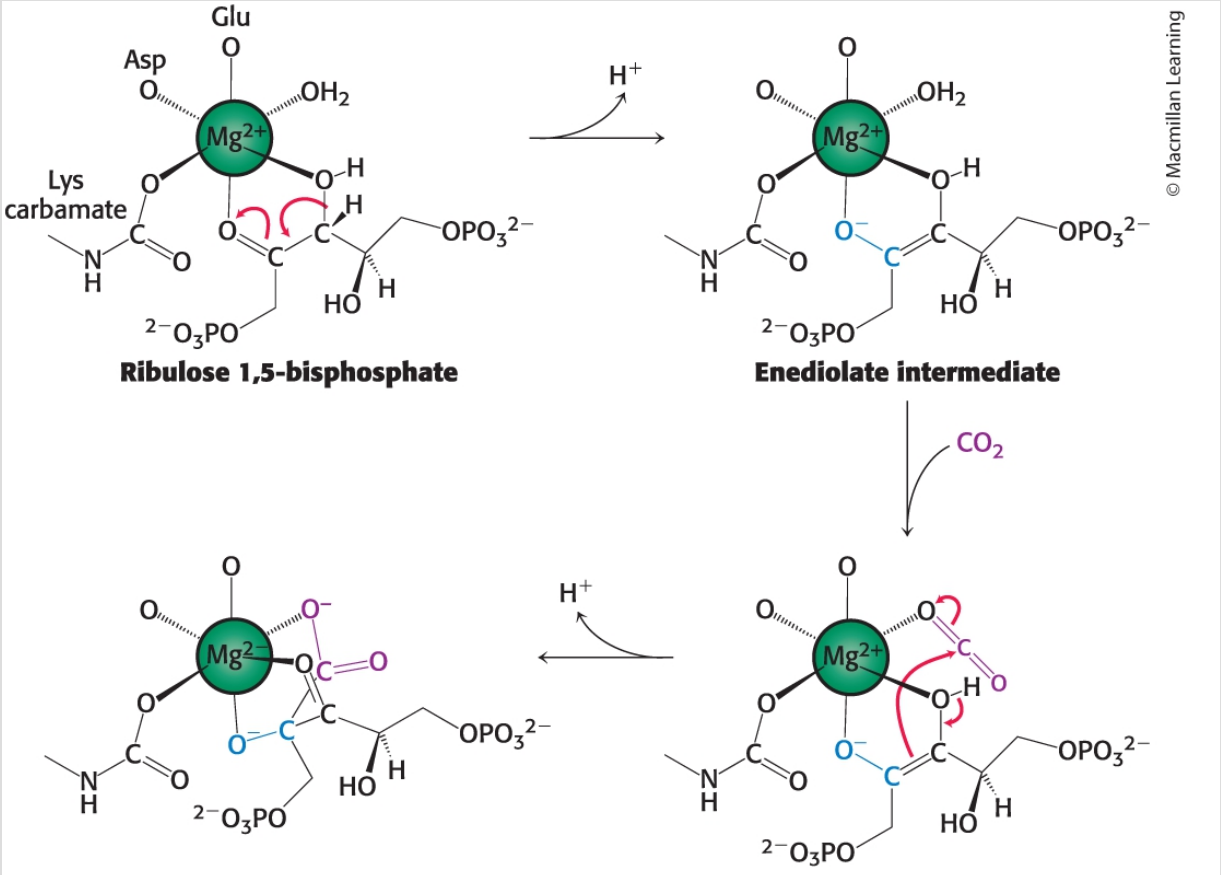


FIGURE 20.3 Magnesium-coordinated ribulose 1,5-bisphosphate facilitates CO_2 fixation.

Ribulose 1,5-bisphosphate binds to a magnesium ion that is linked to Rubisco through a glutamate residue, an aspartate residue, and the lysine carbamate. The coordinated ribulose 1,5-bisphosphate gives up a proton to form a reactive enediolate species that reacts with CO_2 to form a new carbon–carbon bond.

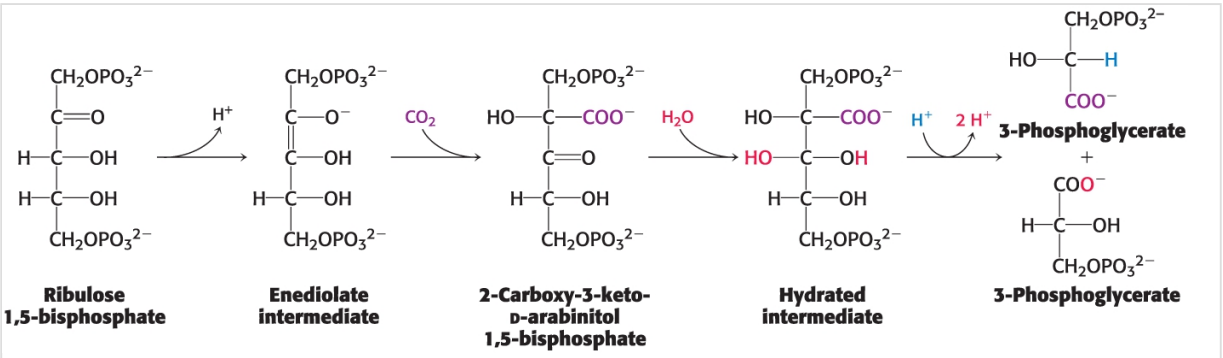


FIGURE 20.4 In stage 1 of the Calvin–Benson cycle, 3-phosphoglycerate is formed. The pathway for the conversion of ribulose 1,5-bisphosphate and CO_2 into two molecules of 3-phosphoglycerate is shown. Although the free species are shown, these steps take place on the magnesium ion.

Rubisco also catalyzes a wasteful oxygenase reaction

The reactive enediolate intermediate generated on the Mg^{2+} ion sometimes reacts with O_2 instead of CO_2; thus, Rubisco also catalyzes a deleterious oxygenase reaction, yielding the products phosphoglycolate and 3-phosphoglycerate (Figure 20.5). The rate of the carboxylase reaction is four times that of the oxygenase reaction under normal atmospheric conditions at 25°C; the stromal concentration of CO_2 is then 10 μM and that of O_2 is 250 μM. The oxygenase reaction, like the carboxylase reaction, requires that lysine 201 be in the carbamate form.

Because this carbamate forms only in the presence of CO_2, Rubisco is prevented from catalyzing the oxygenase reaction exclusively when CO_2 is absent.

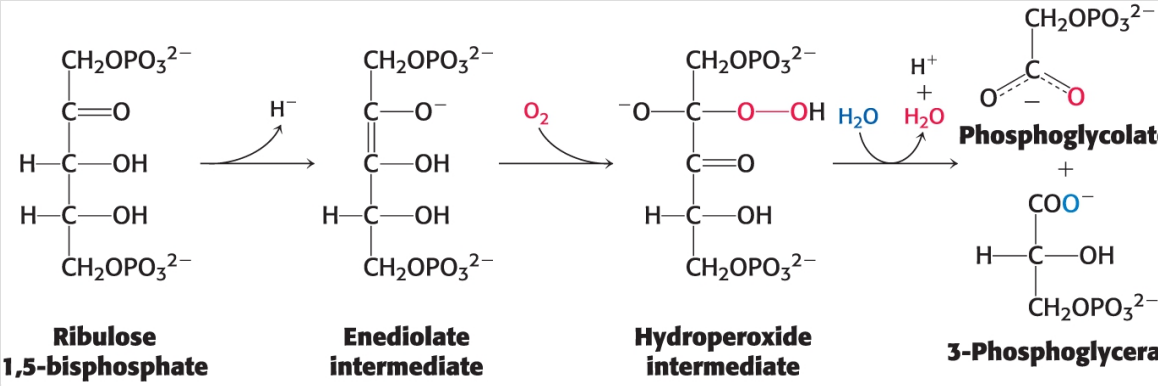


FIGURE 20.5 The enediolate on Rubisco can react with oxygen in a wasteful side reaction. The reactive enediolate intermediate on Rubisco also reacts with molecular oxygen to form a hydroperoxide intermediate, which then proceeds to form one molecule of 3-phosphoglycerate and one molecule of phosphoglycolate.

Phosphoglycolate is not a versatile metabolite. A salvage pathway recovers part of its carbon skeleton (Figure 20.6). A specific phosphatase converts phosphoglycolate into glycolate, which enters peroxisomes (Figure 20.7). Glycolate is then oxidized to glyoxylate by glycolate oxidase, an enzyme with a flavin mononucleotide prosthetic group. The H_2O_2 produced in this reaction is cleaved by catalase to H_2O and O_2. Transamination of glyoxylate then yields glycine, which then enters the mitochondria.

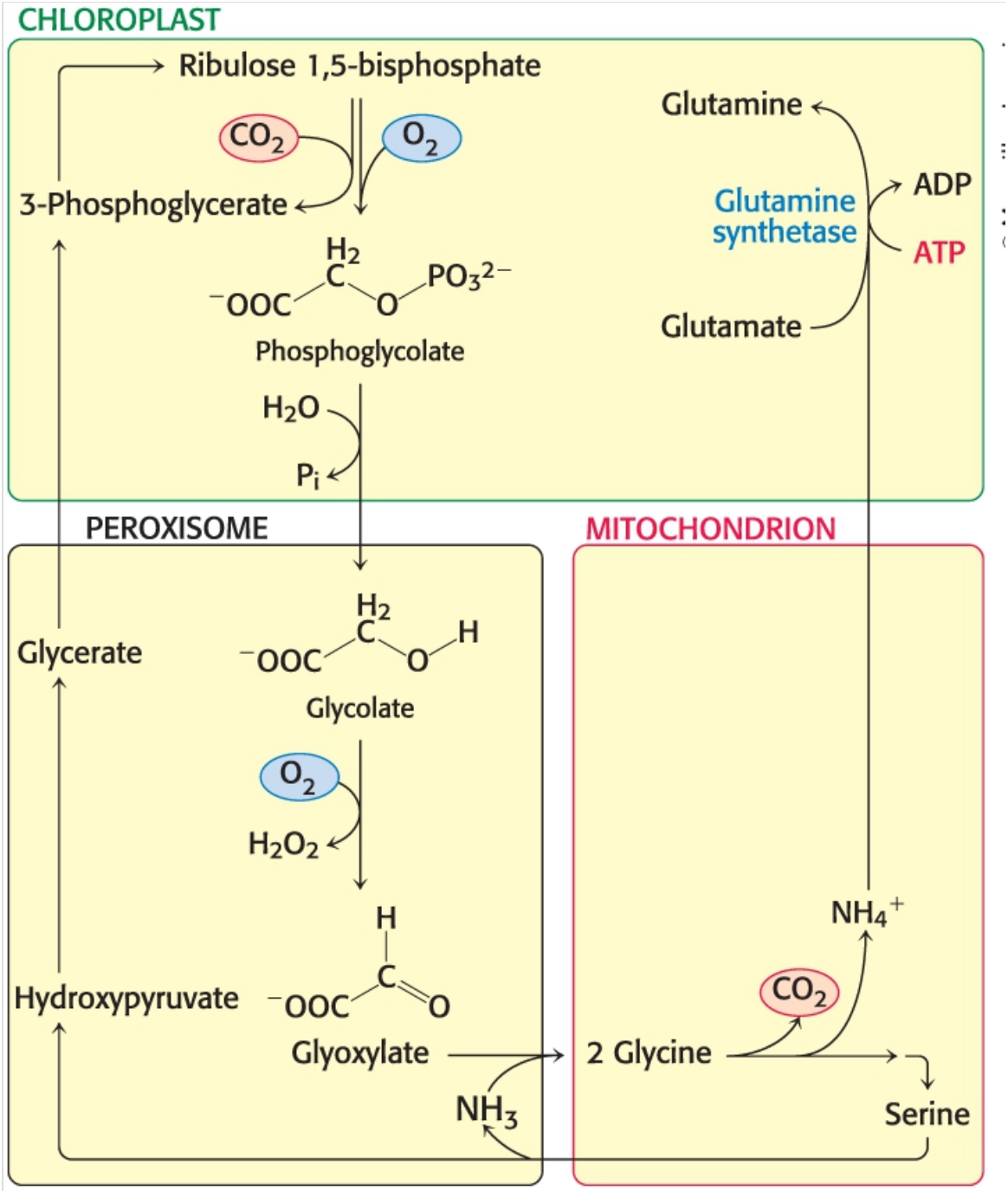
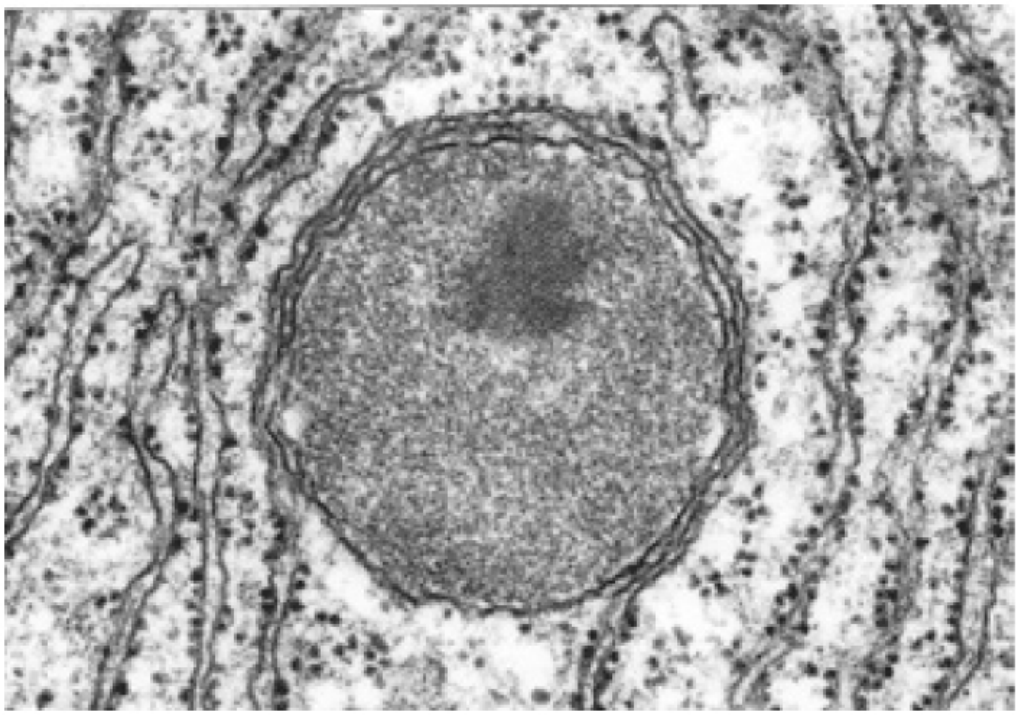


FIGURE 20.6 Photorespiration consumes O_2 and produces CO_2. Phosphoglycolate is forme as a product of the oxygenase reaction in chloroplasts. After dephosphorylation, glycolate is transported into peroxisomes, where it is converted into glyoxylate and then glycine. In mitochondria, two glycines are converted into serine, after losing a carbon as CO_2 and ammonium ion. The serine is converted back into 3-phosphoglycerate, and the ammonium ion salvaged in chloroplasts.



Don W. Fawcett/Science Source

FIGURE 20.7 Peroxisomes are organelles defined by a single membrane. An electron micrograph of a peroxisome is shown. The peroxisomes are surrounded by rough endoplasmic reticulum.

Two glycine molecules can unite to form serine with the release of CO_2 and ammonium ion (NH_4^+). The ammonium ion, used in the synthesis of nitrogen-containing compounds, is salvaged by a glutamine synthetase reaction. Serine reenters the peroxisome, where it donates its ammonia to glyoxylate and is subsequently converted back into 3-phosphoglycerate.

This salvage pathway serves to recycle three of the four carbon atoms of two molecules of glycolate. However, one carbon atom is lost as CO_2. This process is called **photorespiration** because O_2 is consumed and

CO_2 is released. Photorespiration is wasteful because organic carbon is converted into CO_2 without the production of ATP, NADPH, or another energy-rich metabolite. Although evolutionary processes have presumably enhanced the preference of Rubisco for carboxylation — for instance, the Rubisco of higher plants is eight times more specific for carboxylation than that of photosynthetic bacteria — photorespiration still accounts for the loss of up to 25% of the carbon fixed.

Self-Check Question

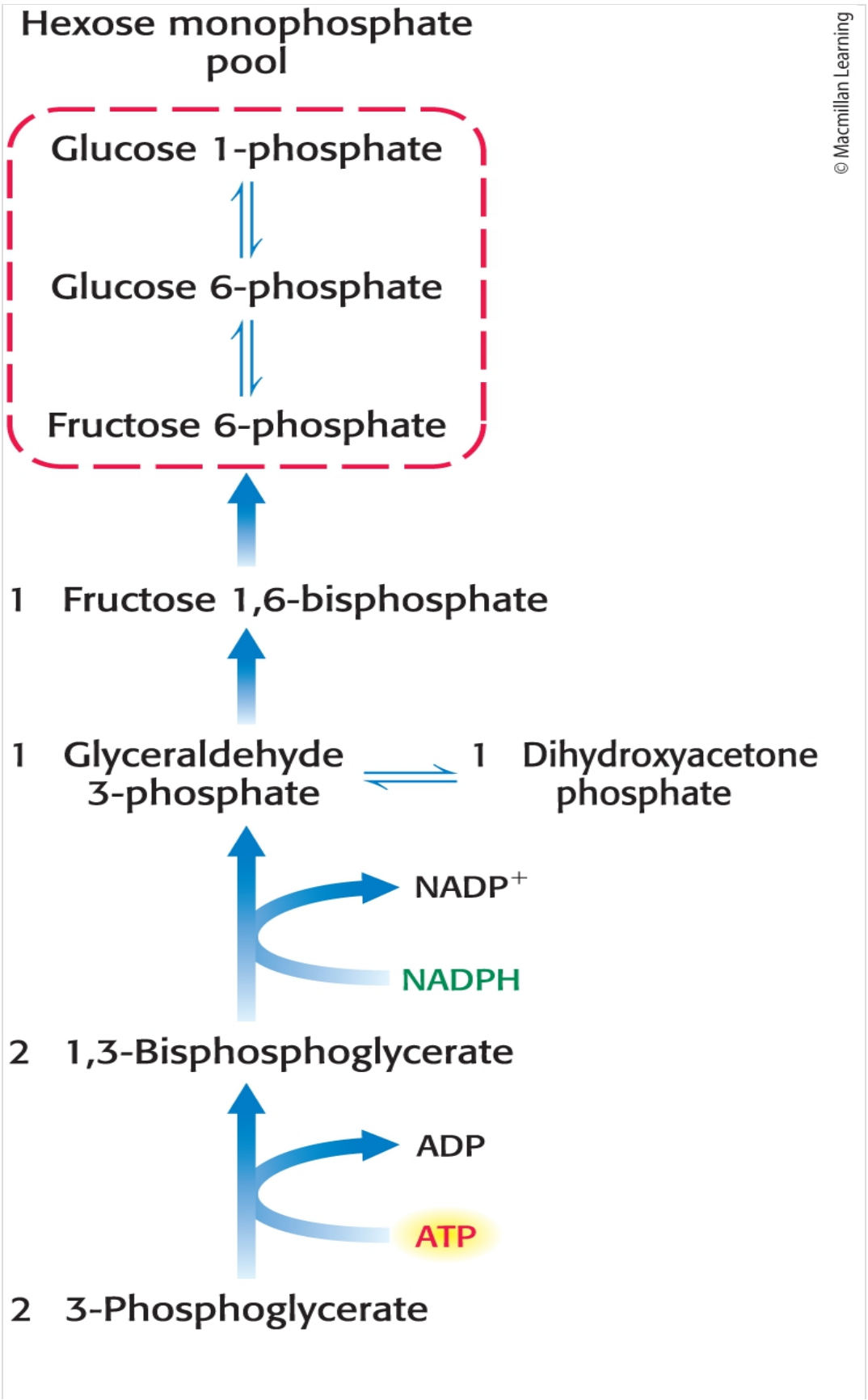


Suppose ribulose 1,5-bisphosphate reacts with pure $^{14}CO_2$ in the absence of oxygen. One half of the 3-phosphoglycerate is labeled with ^{14}C. Why?

Stage 2: Hexose phosphates are made from phosphoglycerate

The 3-phosphoglycerate product of Rubisco is used to synthesize 6-carbon sugars. First, 3-phosphoglycerate is converted into fructose 6-phosphate, which is readily converted to glucose 6-phosphate and then to glucose 1-phosphate. The mixture of the three phosphorylated hexoses is called the hexose monophosphate pool. The steps in this conversion (Figure 20.8) are like those of the gluconeogenic pathway, except that glyceraldehyde 3-phosphate dehydrogenase in chloroplasts — which generates glyceraldehyde 3-phosphate (GAP) — is specific for NADPH rather than NADH. These reactions and that catalyzed by Rubisco bring CO_2 to the level of a hexose, converting CO_2 into a

chemical fuel at the expense of NADPH and ATP generated from the light reactions.

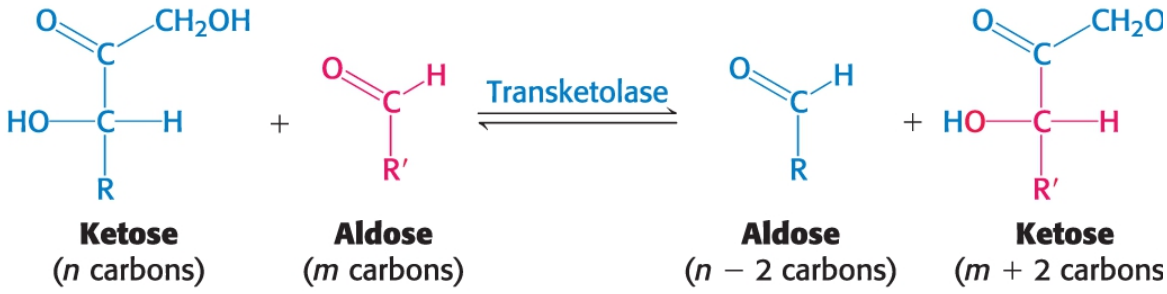


© Macmillan Learning

FIGURE 20.8 In stage 2 of the Calvin–Benson cycle, hexose phosphate is formed. 3-Phosphoglycerate is converted into fructose 6-phosphate in a pathway parallel to that of gluconeogenesis.

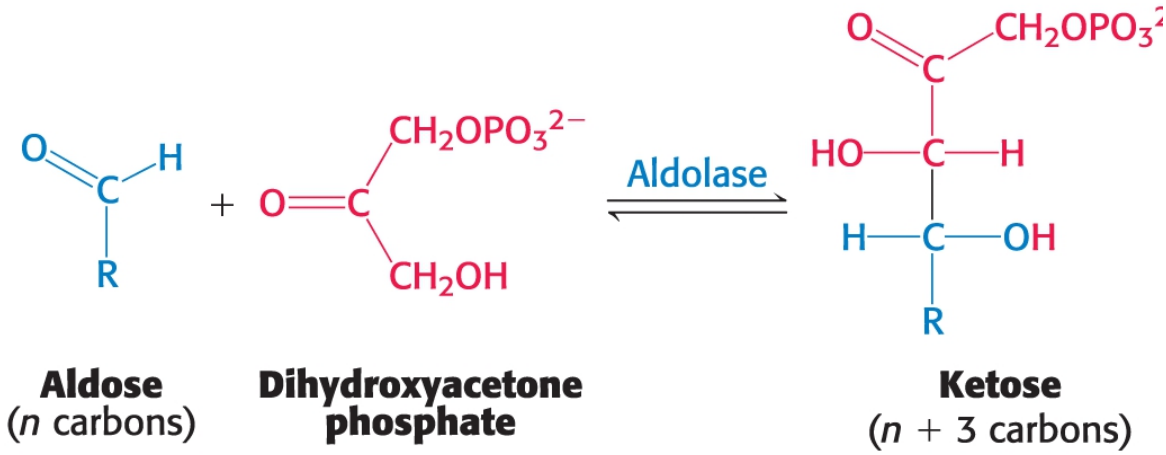
Stage 3: Ribulose 1,5-bisphosphate is regenerated

The third phase of the Calvin–Benson cycle is the regeneration of ribulose 1,5-bisphosphate, the acceptor of CO_2 in the first step. The problem is to construct a five-carbon sugar from six-carbon and three-carbon sugars. A transketolase and an aldolase play the major role in the rearrangement of the carbon atoms. The transketolase, which we will see again in the pentose phosphate pathway, requires the coenzyme thiamine pyrophosphate (TPP) to transfer a two-carbon unit $(CO—CH_2OH)$ from a ketose to an aldose.



The **transketolase** converts fructose 6-phosphate and glyceraldehyde 3-phosphate into erythrose 4-phosphate and xylulose 5-phosphate.

Aldolase, which we have already encountered in glycolysis, catalyzes an aldol condensation between dihydroxyacetone phosphate (DHAP) and an aldehyde. This enzyme is highly specific for dihydroxyacetone phosphate, but it accepts a wide variety of aldehydes.



Aldolase generates sedoheptulose 1,7-bisphosphate from erythrose 4-phosphate and dihydroxyacetone phosphate. A phosphatase removes a phosphate from sedoheptulose 1,7-bisphosphophosphate to form sedoheptulose 7-phosphate. Transketolase again enters the action to combine sedoheptulose 7-phosphate with another molecule of glyceraldehyde 3-phosphate to form the five-carbon sugar ribose 5-phosphate as well as a second molecule of xylulose 5-phosphate (Figure 20.9).

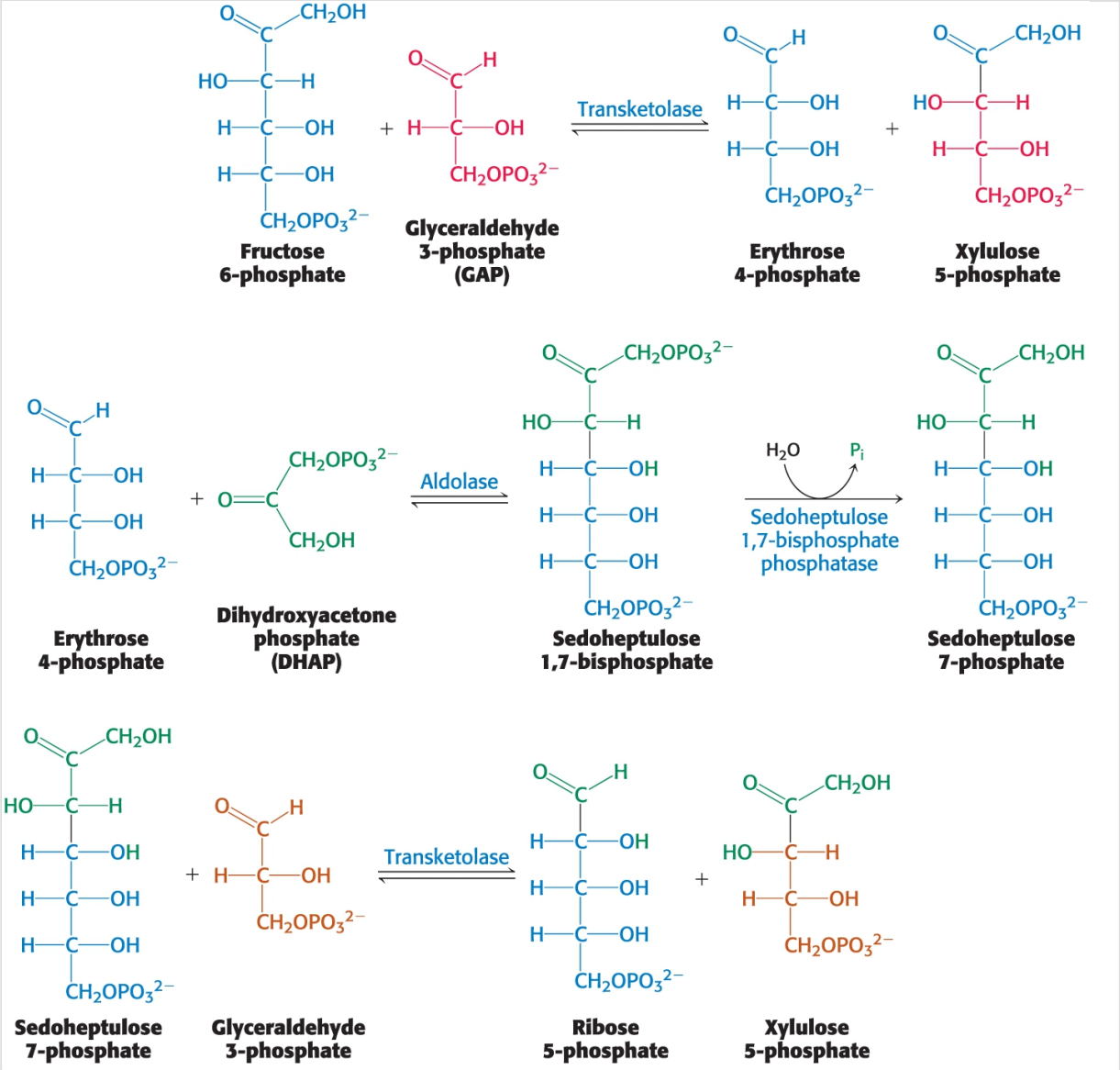


FIGURE 20.9 Five-carbon sugars are formed from six-carbon and three-carbon sugars. First, transketolase converts a six-carbon sugar and a three-carbon sugar into a four-carbon sugar and a five-carbon sugar. Then, aldolase combines the four-carbon product and a three-carbon sugar to form a seven-carbon sugar. Finally, this seven-carbon sugar reacts with another three-carbon sugar to form two additional five-carbon sugars.

Finally, ribose 5-phosphate is converted into ribulose 5-phosphate by phosphopentose isomerase, whereas the two molecules of xylulose 5-

phosphate are converted into ribulose 5-phosphate by phosphopentose epimerase. Ribulose 5-phosphate is converted into ribulose 1,5-bisphosphate through the action of phosphoribulokinase (Figure 20.10).

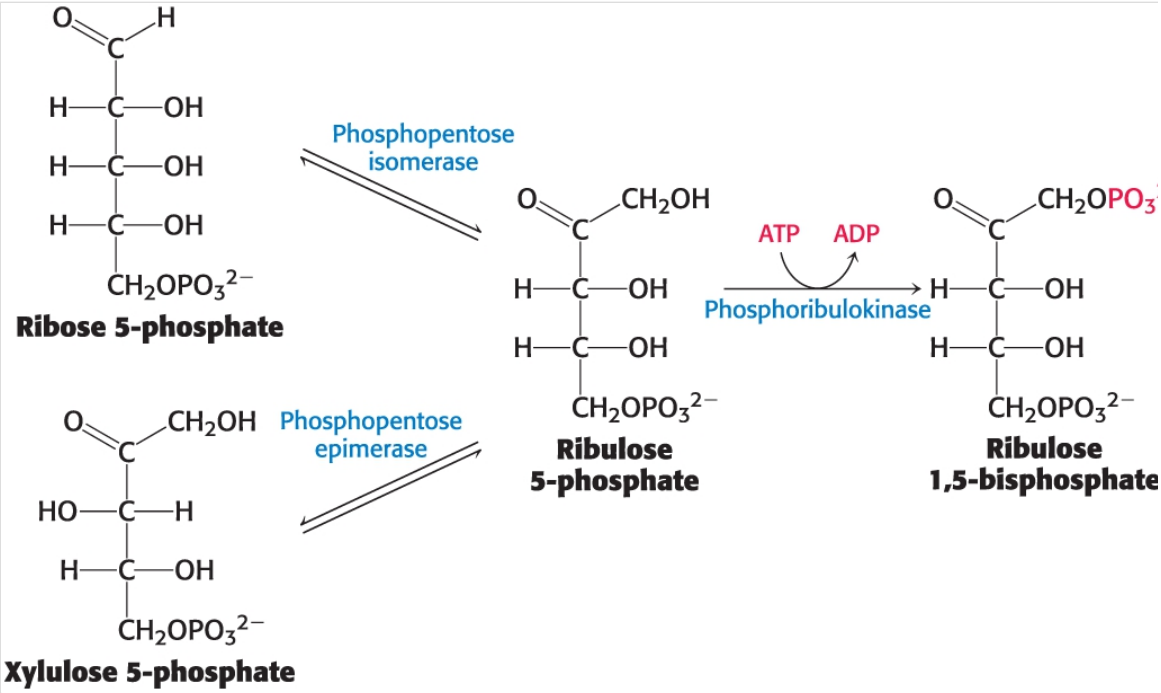


FIGURE 20.10 In stage 3 of the Calvin–Benson cycle, ribulose 1,5-bisphosphate is regenerated
Both ribose 5-phosphate and xylulose 5-phosphate are converted into ribulose 5-phosphate, which is then phosphorylated to complete the regeneration of ribulose 1,5-bisphosphate.

The sum of these reactions shown in Figures 20.9 and 20.10 is:

Fructose 6–phosphate + 2 glyceraldehyde 3–phosphate + dihydroxyacetone phosphate + 3 ATP → 3 ribulose 1,5–bisphosphate + 3 ADP

Figure 20.11 presents the required reactions with the proper stoichiometry to convert three molecules of CO_2 into one molecule of DHAP. However, two molecules of DHAP are required for the synthesis of a member of the hexose monophosphate pool. Consequently, the cycle as presented must take place twice to yield a hexose monophosphate. The outcome of the Calvin–Benson cycle is the generation of a hexose and the regeneration of the starting compound, ribulose 1,5-bisphosphate. In essence, ribulose 1,5-bisphosphate acts catalytically, similarly to oxaloacetate in the citric acid cycle.

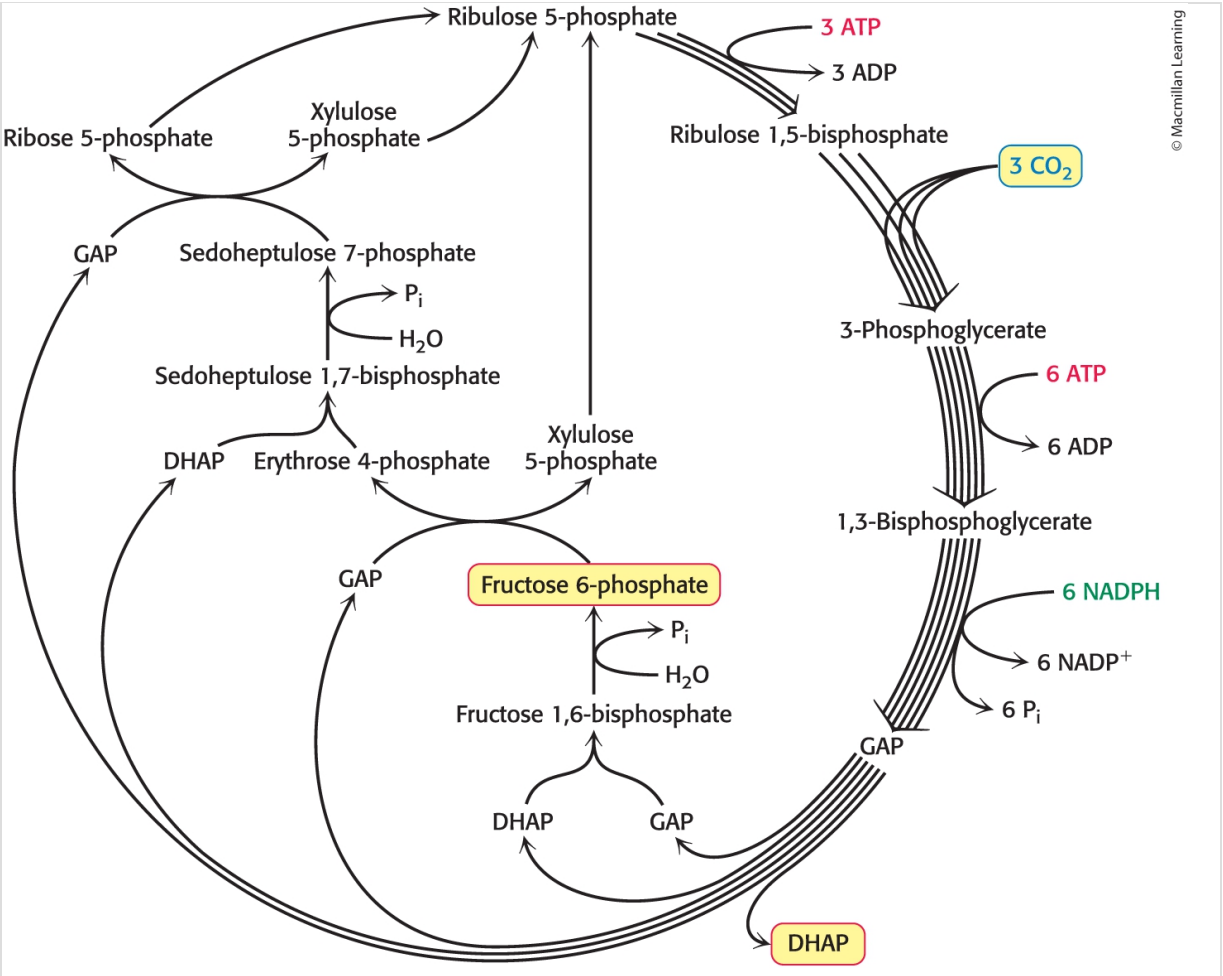


FIGURE 20.11 The full Calvin–Benson cycle process for converting three molecules of CO_2 to dihydroxyacetone phosphate is complex. The cycle is not as simple as presented in Figure 20.1; rather, it entails many reactions that lead ultimately to the synthesis of glucose and the regeneration of ribulose 1,5-bisphosphate.

[Information from J. R. Bowyer and R. C. Leegood. "Photosynthesis," in *Plant Biochemistry*, P. M. Dey and J. B. Harborne, Eds. (Academic Press, 1997), p. 85.]

18 ATP and 12 NADPH molecules are used to bring six carbon dioxides to the level of a hexose

What is the energy expenditure for synthesizing a hexose?

- Six rounds of the Calvin–Benson cycle are required, because one carbon atom is reduced in each round.
- 12 molecules of ATP are expended in phosphorylating 12 molecules of 3-phosphoglycerate to 1,3-bisphosphoglycerate.
- 12 molecules of NADPH are consumed in reducing 12 molecules of 1,3-bisphosphoglycerate to glyceraldehyde 3-phosphate.
- An additional six molecules of ATP are spent in regenerating ribulose 1,5-bisphosphate.

We can now write a balanced equation for the net reaction of the Calvin–Benson cycle:

$$6\,CO_2 + 18\,ATP + 12\,NADPH + 12\,H_2O \rightarrow$$
$$C_6H_{12}O_6 + 18\,ADP + 18\,P_i + 12\,NADP^+ + 6\,H^+$$

Thus, three molecules of ATP and two molecules of NADPH are consumed in incorporating a single CO_2 molecule into a hexose such as glucose or fructose.

Starch and sucrose are the major carbohydrate stores in plants

What are the fates of the members of the hexose monophosphate pool? These molecules are used in a variety of ways, but there are two primary roles. Plants contain two major storage forms of sugar: starch and sucrose. **Starch**, like its animal counterpart glycogen, is a polymer of glucose residues, but it is less branched than glycogen because it contains a smaller proportion of α-1,6-glycosidic linkages. Another difference is that ADP-glucose, not UDP-glucose, is the activated precursor. Starch is synthesized and stored in chloroplasts.

In contrast, **sucrose** (common table sugar), a disaccharide, is synthesized in the cytoplasm. Plants lack the ability to transport hexose phosphates across the chloroplast membrane, but they are able to transport triose phosphates from chloroplasts to the cytoplasm. Triose phosphate intermediates such as glyceraldehyde 3-phosphate cross into the cytoplasm in exchange for phosphate through the action of an abundant triose phosphate-phosphate antiporter. Fructose 6-phosphate formed from triose phosphates joins the glucose unit of UDP-glucose to form sucrose 6(F)-phosphate (**Figure 20.12**). The hydrolysis of the phosphate ester by sucrose phosphatase yields sucrose, a readily transportable and mobilizable sugar that is stored in many plant cells, such as those in sugar beets and sugarcane.

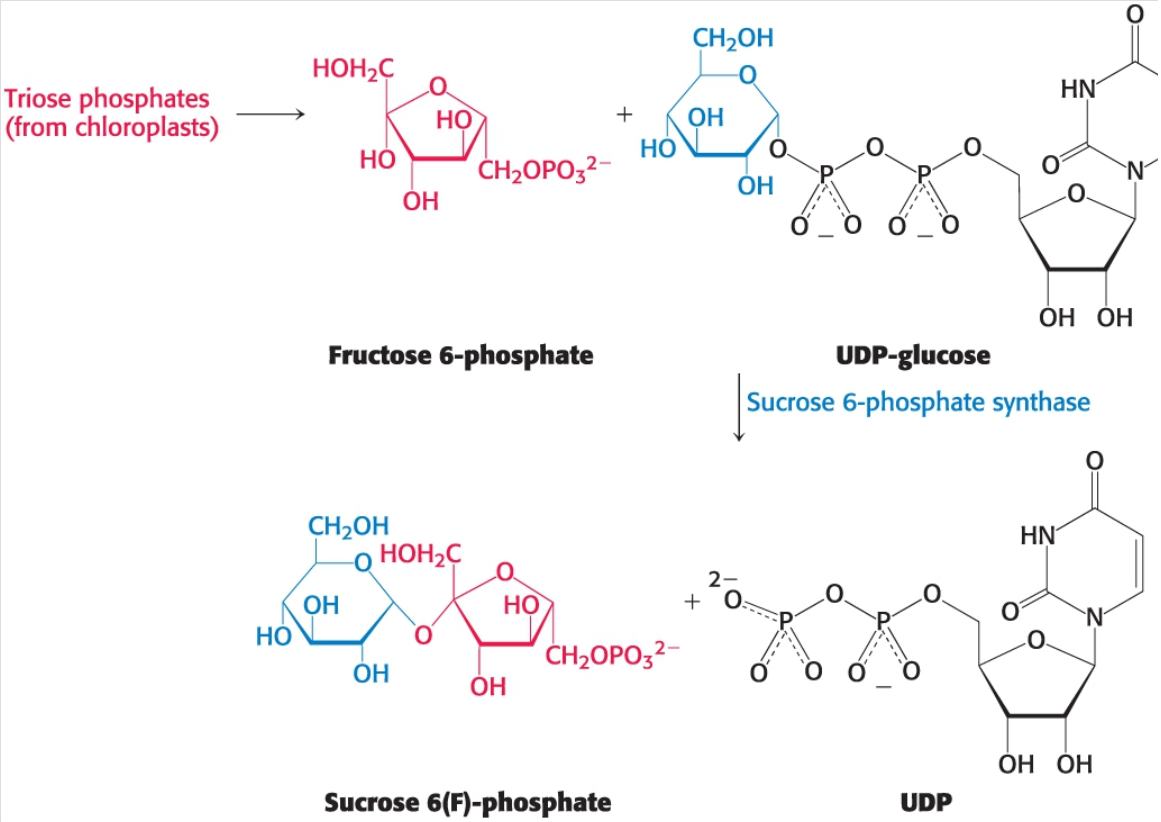


FIGURE 20.12 Carbohydrates are stored as sucrose. Sucrose 6-phosphate is formed by the reaction between fructose 6-phosphate and the activated intermediate uridine diphosphate glucose (UDP-glucose). Sucrose phosphatase subsequently generates free sucrose (not shown).

Self-Check Question

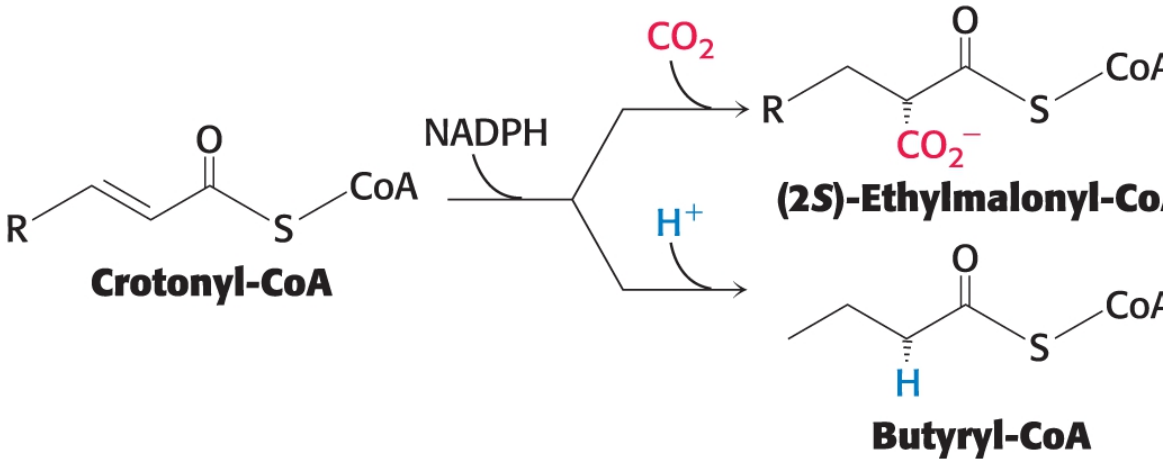
What role does magnesium play in the dark reactions of photosynthesis? Explain the role that this same element plays in the light reactions.

Inspired by the Calvin–Benson cycle, scientists are developing new methods for fixing carbon dioxide

Carbon dioxide is a potential plentiful carbon source for the production of organic compounds. Applying the knowledge of biochemical pathways from a wide range of organisms, scientists have conceptually developed and, in some cases, implemented cycles that fix carbon dioxide into organic compounds. One such cycle referred to as the CETCH cycle — for crotonyl–coenzyme A (CoA)/ethylmalonyl-CoA/hydroxybutyryl-CoA — catalyzes the conversion of 2 molecules of CO_2 to 1 molecule of glyoxylate, $^{-}O_2C-CHO$, C-CHO. This cycle involves 12 steps and 15 enzymes. The balanced chemical reaction is

$$2\,CO_2 + 4\,NADPH + 2\,FADH2 + 4\,ATP + 2\,O_2 + 3\,H^+ \rightarrow$$
$$^{-}O_2C-CHO + 4\,NADP^+ + 2\,FAD + 4\,ADP + 2\,P_i + 5\,H_2O$$

Carbon fixation occurs via the reaction catalyzed by enoyl-CoA carboxylases/reductases.



These enzymes are several times more efficient at fixing CO_2 than is Rubisco and do not react with oxygen.

This reaction scheme has been harnessed in an artificial photosynthesis system in microdroplets containing thylakoids to generate ATP and NADPH in response to light (Figure 20.13). With the addition of one additional step to the CETCH cycle, this process allows CO_2 to be converted to glycolate, a versatile organic building block, in a light-driven process. This is an example of synthetic biology, where engineering principles are used to develop potentially useful devices.

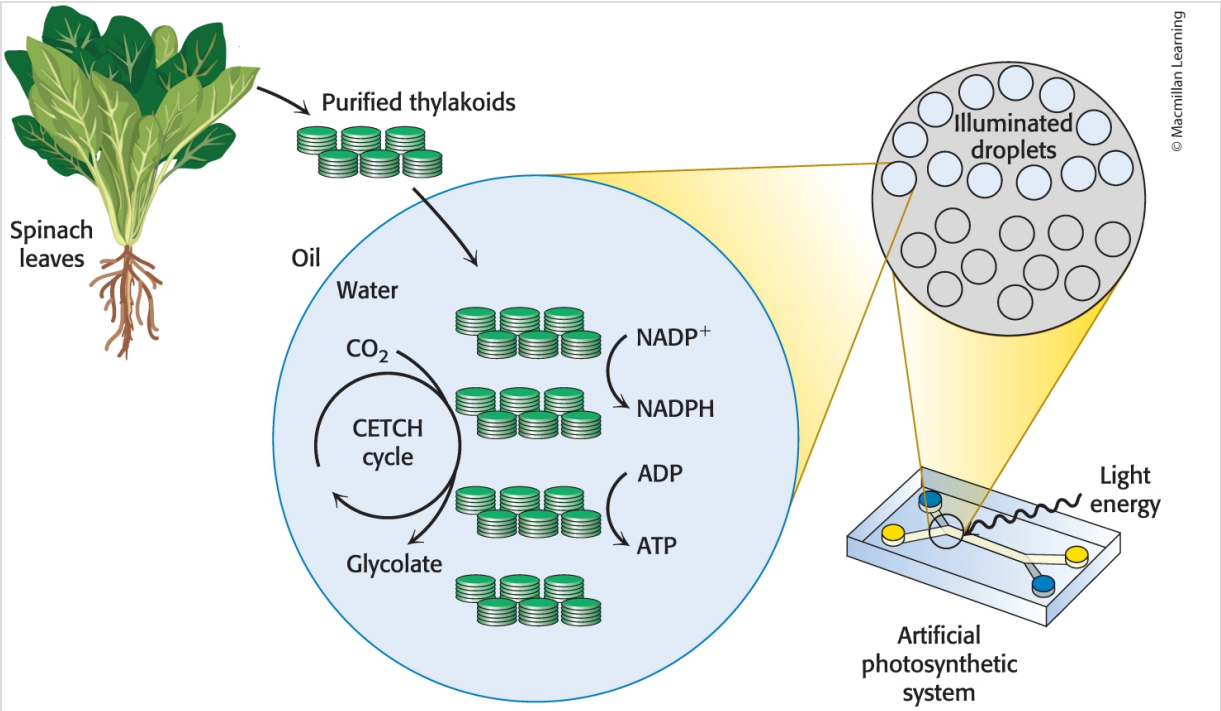


FIGURE 20.13 Scientists have engineered artificial photosynthesis using alternative CO_2 fixation pathways. A synthetic photosynthetic system is shown using purified thylakoids to drive the light reactions and a designed CO_2 fixation system for the dark reactions.

[From N. J. Gaut and K. P. Adamala, "Toward Artificial Photosynthesis," *Science* 368:587–588, 2020.]



20.2 The Activity of the Calvin–Benson Cycle Depends on Environmental Conditions

Light levels, temperature, and availability of CO_2 in different environments are crucial factors for effective carbon fixation and avoidance of processes damaging to plants. How are the light reactions linked to the dark reactions to regulate fixing CO_2 into biomolecules? The principal means of regulation is alteration of the stromal environment by the light reactions. The light reactions lead to an increase in stromal pH (a decrease in the H^+ concentration), as well as an increase in the stromal concentrations of Mg^{2+}, NADPH, and reduced ferredoxin — changes that contribute to the activation of certain Calvin–Benson cycle enzymes, located in the stroma (Figure 20.14).

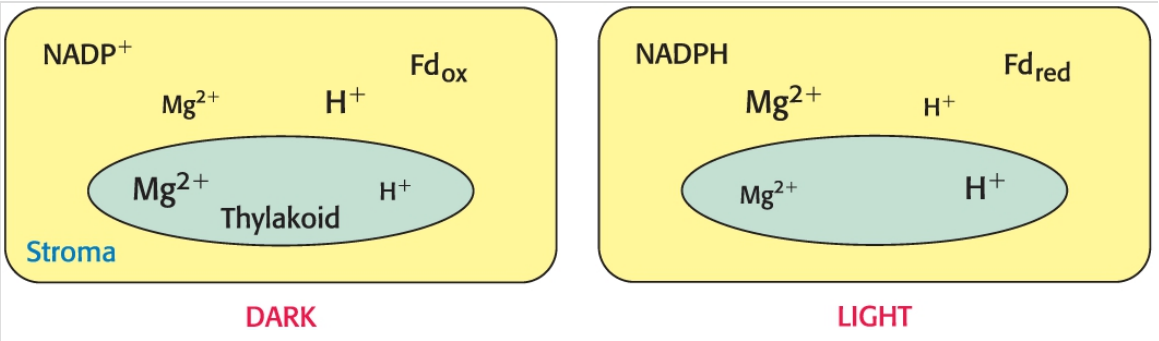


FIGURE 20.14 Light regulates the Calvin–Benson cycle. The light reactions of photosynthesis transfer electrons out of the thylakoid lumen into the stroma and transfer protons from the stroma into the thylakoid lumen. As a consequence of these processes, the concentrations of NADPH, reduced ferredoxin (Fd), and Mg^{2+} in the stroma are higher in the light than in the dark. The stromal pH is also increased (the concentration of H^+ is lowered) in the light as a result of proton pumping from the stroma to the thylakoid lumen. Each of these concentration changes helps couple the Calvin–Benson cycle reactions to the light reactions.

Rubisco is activated by light-driven changes in proton and magnesium ion concentrations

As stated earlier, the rate-limiting step in the Calvin–Benson cycle is the carboxylation of ribulose 1,5-bisphosphate to form two molecules of 3-phosphoglycerate. The activity of Rubisco increases markedly on illumination because light facilitates the carbamate formation necessary for enzyme activity (Figure 20.3). In the stroma, the pH increases from 7 to 8, and the level of Mg^{2+} rises. Both effects are consequences of the light-driven pumping of protons into the thylakoid space. Mg^{2+} ions from the thylakoid space are released into the stroma to compensate for the influx of protons. Carbamate formation is favored at alkaline pH. CO_2 adds to a deprotonated form of lysine 201 of Rubisco, and Mg^{2+} ion binds to the carbamate to generate the active form of the enzyme. Thus, light leads not only to the generation of ATP and NADPH, but also to regulatory signals that stimulate CO_2 fixation.

Thioredoxin plays a key role in regulating the Calvin–Benson cycle

As we saw in Chapter 19, light-driven reactions lead to electron transfer from water to ferredoxin and, eventually, to NADPH in photosystem I. The presence of reduced ferredoxin and NADPH are good signals that conditions are right for biosynthesis. One way in which this information is conveyed to biosynthetic enzymes is by thioredoxin, a 12-kDa protein

containing neighboring cysteine residues that cycle between a reduced sulfhydryl and an oxidized disulfide form (Figure 20.15).

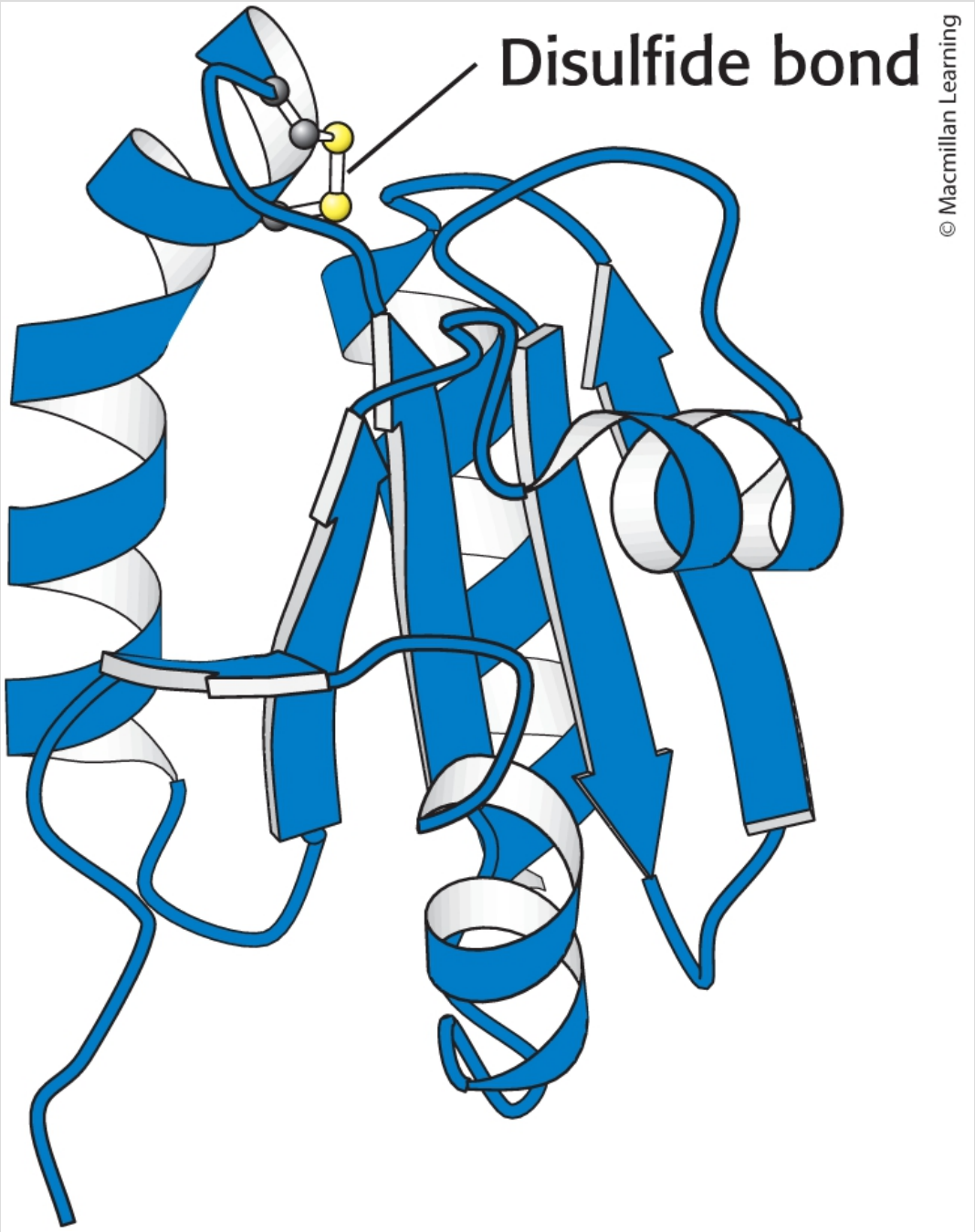


FIGURE 20.15 Thioredoxin has a redox-active disulfide bond. The oxidized form of thioredoxin contains a disulfide bond. When thioredoxin is reduced by reduced ferredoxin, the disulfide bond is converted into two free sulfhydryl groups. Reduced thioredoxin can cleave disulfide bonds in enzymes, activating certain Calvin–Benson cycle enzymes and inactivating some degradative enzymes.

[Drawn from 1F9M.pdb.]

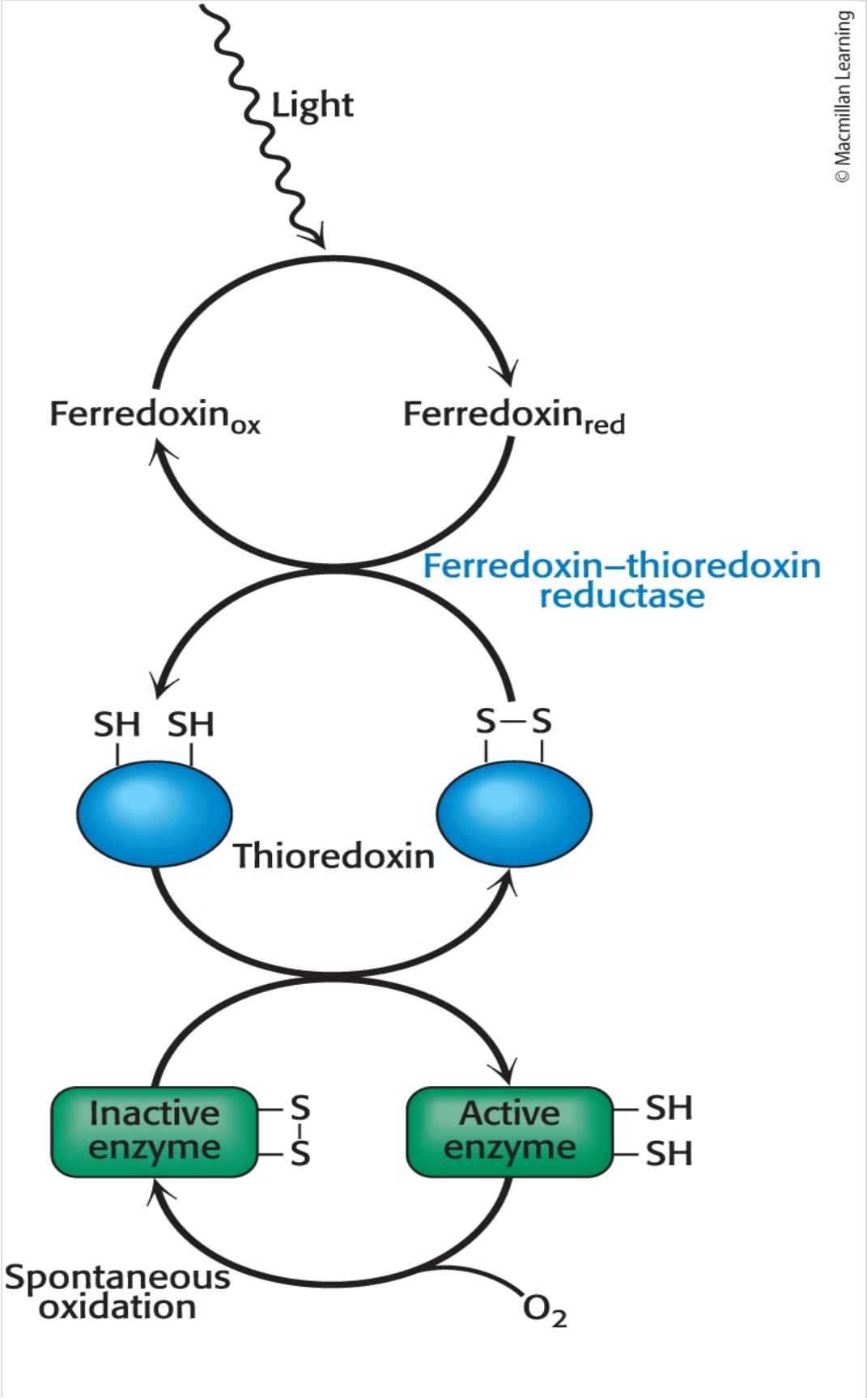
INTERACT with this model in Achieve

The reduced form of thioredoxin activates many biosynthetic enzymes, including the chloroplast ATP synthase, by reducing disulfide bridges that control their activity. Reduced thioredoxin also inhibits several degradative enzymes by the same means (Table 20.1).

TABLE 20.1 Enzymes regulated by thioredoxin

Enzyme	Pathway
Rubisco	Carbon fixation in the Calvin–Benson cycle
Fructose 1,6-bisphosphatase	Gluconeogenesis
Glyceraldehyde 3-phosphate dehydrogenase	Calvin–Benson cycle, gluconeogenesis, glycolysis
Sedoheptulose 1,7-bisphosphatase	Calvin–Benson cycle
Glucose 6-phosphate dehydrogenase	Pentose phosphate pathway
Phenylalanine ammonia lyase	Lignin synthesis
Phosphoribulokinase	Calvin–Benson cycle
$NADP^+$-malate dehydrogenase	C_4 pathway
CF_1–CF_0 ATP synthase	The light reactions

In chloroplasts, oxidized thioredoxin is reduced by ferredoxin in a reaction catalyzed by ferredoxin–thioredoxin reductase. Thus, the activities of the light and dark reactions of photosynthesis are coordinated through electron transfer from reduced ferredoxin to thioredoxin and then to component enzymes containing regulatory disulfide bonds (**Figure 20.16**).



© Macmillan Learning

FIGURE 20.16 Thioredoxin can activate enzymes by reducing them. Reduced thioredoxin activates certain Calvin–Benson cycle enzymes by cleaving regulatory disulfide bonds.



NADPH is a signal molecule that activates two biosynthetic enzymes, phosphoribulokinase and glyceraldehyde 3-phosphate dehydrogenase. In the dark, these enzymes are inhibited by association with an 8.5-kDa protein called CP12, an intrinsically disordered protein. NADPH disrupts this association by promoting the formation of two disulfide bonds in CP12, leading to the release of the active enzymes.

The C_4 pathway of tropical plants and grasses accelerates photosynthesis by concentrating carbon dioxide

The oxygenase activity of Rubisco presents a biochemical challenge to tropical plants because the oxygenase activity increases more rapidly with temperature than does the carboxylase activity. How, then, do plants that grow in hot climates, such as sugarcane, prevent very high rates of wasteful photorespiration? Their solution to this problem is to achieve a high local concentration of CO_2 at the site of the Calvin–Benson cycle in their photosynthetic cells. The essence of this process is that four-carbon (C_4) compounds such as oxaloacetate and malate carry CO_2 from mesophyll cells, which are in contact with air, to bundle-sheath cells, which are the major sites of photosynthesis (Figure 20.17). The decarboxylation of the four-carbon compound in a bundle-sheath cell maintains a high concentration of CO_2 at the site of the Calvin–Benson cycle. The three-carbon product returns to the mesophyll cell

for another round of carboxylation. This metabolic pathway is called the C_4 pathway or the Hatch–Slack pathway.

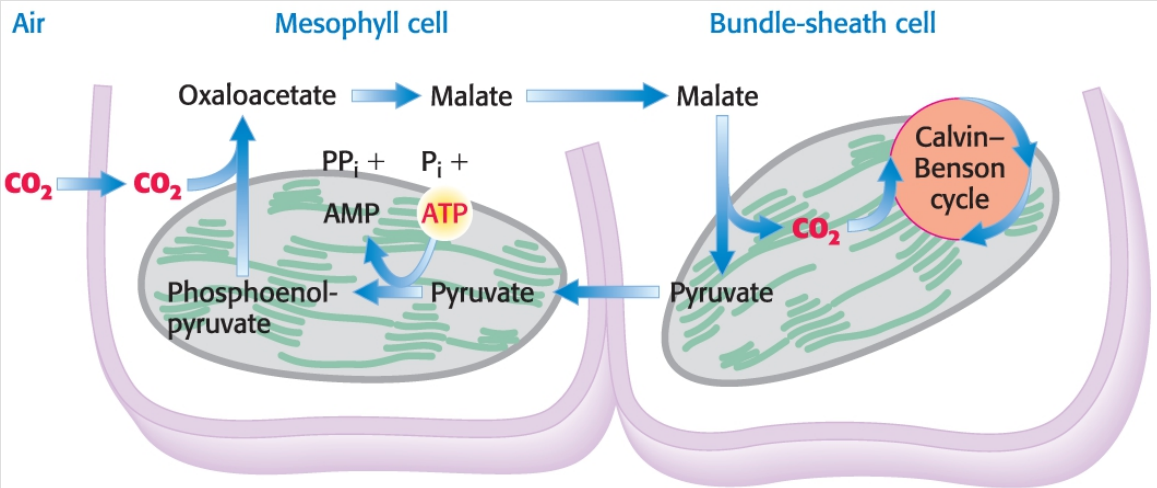


FIGURE 20.17 The C_4 pathway can concentrate CO_2. Carbon dioxide is concentrated in bundle-sheath cells by the expenditure of ATP in mesophyll cells.

In addition to tropical plants, grasses and sedges in temperate climates employ the C_4 pathway. In fact, they are the most common users of the pathway. Corn or maize, domesticated by selective breeding from the Mexican grass teosinte about 9,000 years ago, is a C_4 plant of tremendous economic and agricultural importance, accounting for approximately 20% of human nutrition worldwide.

The C_4 pathway for the transport of CO_2 starts in a mesophyll cell, with the condensation of CO_2 in the form of bicarbonate and phosphoenolpyruvate to form *oxaloacetate* in a reaction catalyzed by phosphoenolpyruvate carboxylase. Oxaloacetate is converted into malate by an $NADP^+$-linked malate dehydrogenase. Malate enters the bundle-sheath cell and is oxidatively decarboxylated within the

chloroplasts by an $NADP^+$-linked malate dehydrogenase. The released CO_2 enters the Calvin–Benson cycle in the usual way by condensing with ribulose 1,5-bisphosphate. Pyruvate formed in this decarboxylation reaction returns to the mesophyll cell. Finally, phosphoenolpyruvate is formed from pyruvate by pyruvate-P_i dikinase.

The net reaction of this C_4 pathway is

$$CO_2 \text{ (in mesophyll cell)} + ATP + 2\ H_2O \rightarrow$$
$$CO_2 \text{ (in bundle-sheath cell)} + AMP + 2\ P_i + 2\ H^+$$

Since the products are AMP and two equivalents of inorganic phosphate, the energetic equivalent of two ATP molecules is consumed in transporting CO_2 to the chloroplasts of the bundle-sheath cells. Note that six molecules of CO_2 are required to synthesize glucose so the C_4 pathway requires an extra 12 ATP when compared to the C_3 pathway. In essence, this process is active transport: the pumping of CO_2 into the bundle-sheath cell is driven by the hydrolysis of one molecule of ATP to one molecule of AMP and two molecules of orthophosphate. The CO_2 concentration can be 20 times as great in the bundle-sheath cells as in the mesophyll cells. Interestingly, phosphoenolpyruvate carboxylase has a higher affinity for CO_2 (as bicarbonate) than does Rubisco. C_4 plants use this affinity difference to their advantage. The high CO_2 affinity of phosphoenolpyruvate carboxylase means Rubisco can be adequately supplied with CO_2, while the stomata — the openings in the leaves that allow gas exchange (**Figure 20.18**) — do not have to open as completely in the heat of the tropical day, thereby preventing water loss.



Power and Syred/Science Source

FIGURE 20.18 Stomata can open to facilitate gas exchange. A scanning electron micrograph shows a closed stoma and an open stoma.

When the C_4 pathway and the Calvin–Benson cycle operate together, the net reaction is

$$6\,CO_2 + 30\,ATP + 12\,NADPH + 24\,H_2O \rightarrow$$
$$C_6H_{12}O_6 + 30\,ADP + 30\,P_i + 12\,NADP^+ + 18\,H^+$$

Note that 30 molecules of ATP are consumed per hexose molecule formed when the C_4 pathway delivers CO_2 to the Calvin–Benson cycle, in contrast with 18 molecules of ATP per hexose molecule in the absence of the C_4 pathway. The high concentration of CO_2 in the bundle-sheath cells of C_4 plants — which is the result of the expenditure of the additional 12 molecules of ATP — is critical for their rapid

photosynthetic rate, because CO_2 is limiting when light is abundant. A high CO_2 concentration also minimizes the energy loss caused by photorespiration.

Tropical plants with a C_4 pathway do little photorespiration because the high concentration of CO_2 in their bundle-sheath cells accelerates the carboxylase reaction relative to the oxygenase reaction. This effect is especially important at higher temperatures. The geographic distribution of plants having this pathway (C_4 plants) and those lacking it (C_3 plants) can now be understood in molecular terms. C_4 plants have the advantage in a hot environment and under high illumination, which accounts for their prevalence in the tropics. C_3 plants, which consume only 18 molecules of ATP per hexose molecule formed in the absence of photorespiration (compared with 30 molecules of ATP for C_4 plants), are more efficient at temperatures lower than about 28°C, and so they predominate in temperate environments (Figure 20.19). Although C_4 plants comprise only 3% of all flowering plants, they account for 25% of all terrestrial carbon fixation because of their minimization of photorespiration.

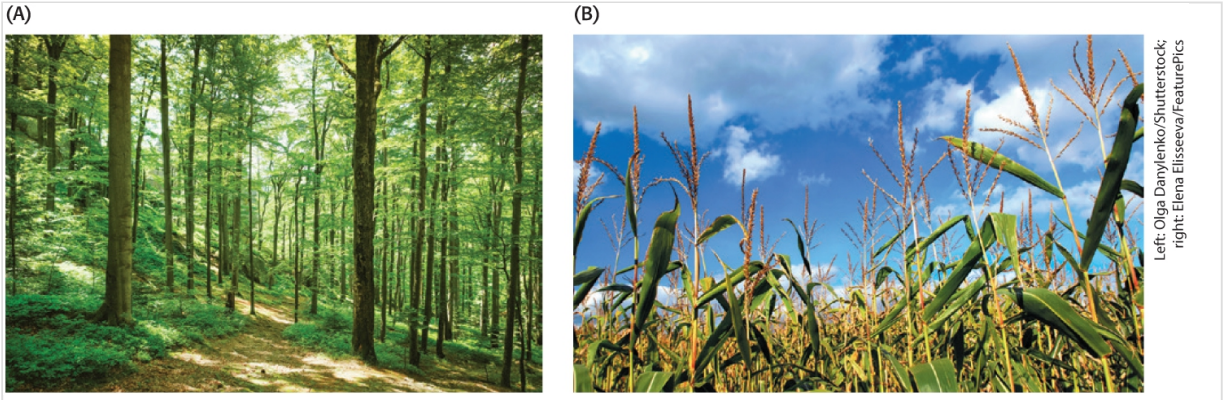


FIGURE 20.19 Both C_3 and C_4 plants are important. (A) C_3 plants, such as trees, account for approximately 95% of plant species. (B) Corn is a C_4 plant of tremendous agricultural importance.

Crassulacean acid metabolism permits growth in arid ecosystems

Many plants, including some that grow in hot, dry climates, keep the stomata of their leaves closed in the heat of the day to prevent water loss (see Figure 20.18). As a consequence, CO_2 cannot be absorbed during the daylight hours, when it is needed for glucose synthesis. Rather, CO_2 enters the leaf when the stomata open at the cooler temperatures of night.

To store the CO_2 until it can be used during the day, such plants make use of an adaptation called **crassulacean acid metabolism (CAM)**, named after the genus *Crassulacea* (the succulents). Carbon dioxide is fixed by the C_4 pathway into malate, which is stored in vacuoles. During the day, malate is decarboxylated and the CO_2 becomes available to the Calvin–Benson cycle. In contrast with C_4 plants, CAM plants separate CO_2 accumulation from CO_2 utilization temporally rather than spatially.

Although CAM plants do prevent water loss, the use of malate as the sole source of CO_2 comes at a metabolic cost. Because malate storage is limited, CAM plants cannot generate CO_2 as rapidly as it can be imported by C_3 and C_4 plants. Consequently, the growth rate of CAM plants is slower than that of C_3 and C_4 plants. The saguaro cactus, a CAM plant that can live up to 200 years and reach a height of 60 feet, can take 15 years to grow to only 1 foot in height (**Figure 20.20**).



yenwen/Getty Images

FIGURE 20.20 Crassulacean acid metabolism facilitates growth in arid climates. Because of crassulacean acid metabolism, plants such as cacti are well suited to life in the desert.

20.3 The Pentose Phosphate Pathway Generates NADPH and Synthesizes Pentoses

While photosynthetic organisms can use the light reactions for generation of some NADPH, the **pentose phosphate pathway** meets the NADPH needs of nonphotosynthetic organisms and of the non-photosynthetic tissues in plants. The pentose phosphate pathway occurs in the cytoplasm of all organisms and is a crucial source of NADPH for use in reductive biosynthesis (Table 20.2) as well as for protection against oxidative stress. It consists of two phases (Figure 20.21):

1. *The oxidative generation of NADPH*. In the oxidative phase, NADPH is generated when glucose 6-phosphate is oxidized to ribulose 5-phosphate.

$$\text{Glucose 6-phosphate} + 2\ \text{NADP}^+ + \text{H}_2\text{O} \rightarrow$$
$$\text{ribulose 5-phosphate} + 2\ \text{NADPH} + 2\ \text{H}^+ + \text{CO}_2$$

2. *The nonoxidative interconversion of sugars.* In the nonoxidative phase, the pathway catalyzes the interconversion of three-, four-, five-, six-, and seven-carbon sugars in a series of nonoxidative reactions. Excess five-carbon sugars may be converted into intermediates of the glycolytic pathway. These interconversions rely on the same reactions that lead to the regeneration of ribulose 1,5-bisphosphate in the Calvin–Benson cycle.

TABLE 20.2 Pathways requiring NADPH

Reductive biosynthesis
Fatty acid biosynthesis
Cholesterol biosynthesis
Neurotransmitter biosynthesis

Nucleotide biosynthesis
Protection from oxidative stress
Reduction of oxidized glutathione
Cytochrome P450 monooxygenases

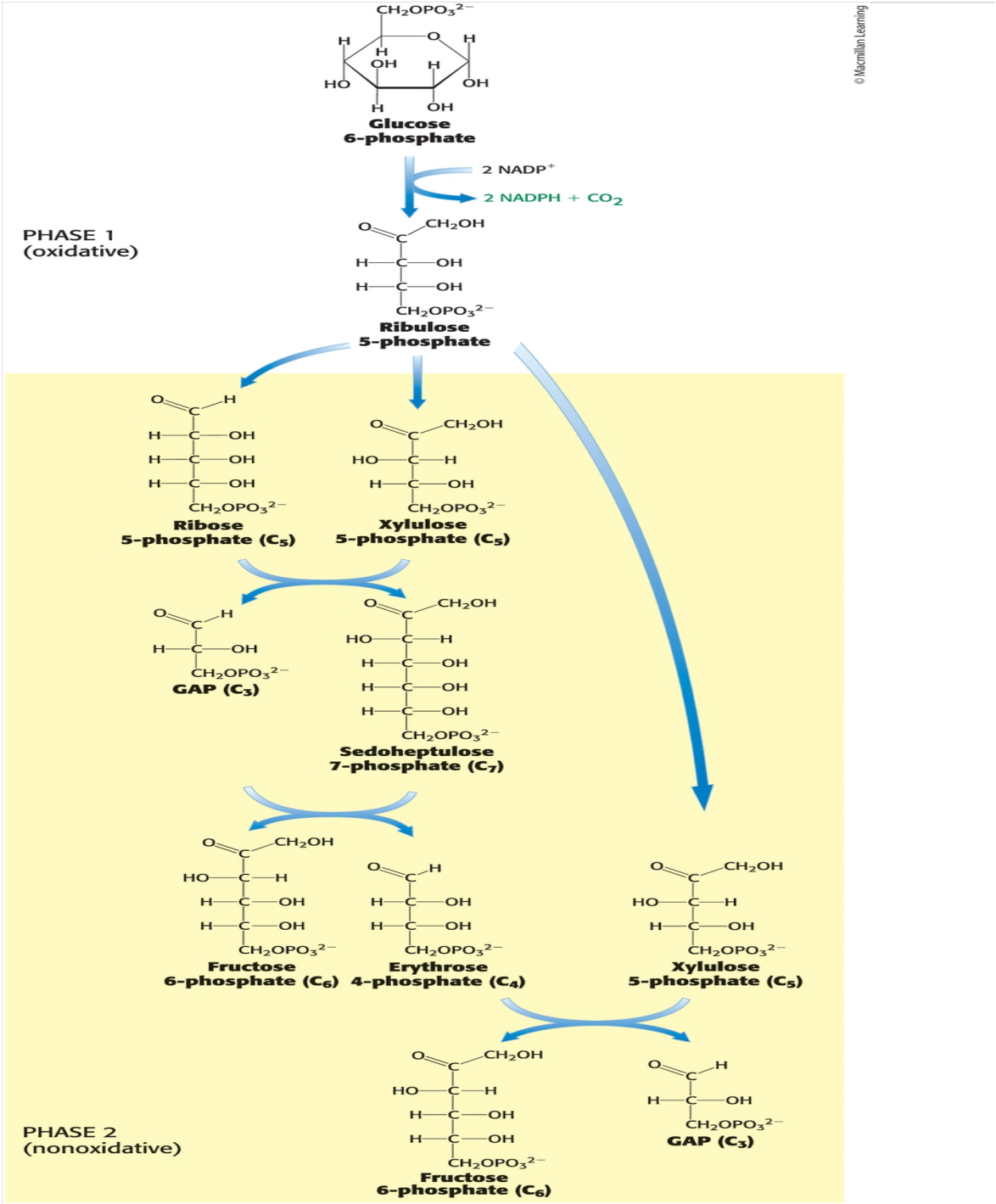


FIGURE 20.21 The pentose phosphate pathway consists of an oxidative and a nonoxidative phase. The oxidative phase generates NADPH, and the nonoxidative phase interconverts phosphorylated sugars.

EXPLORE this pathway further in the Metabolic Map in Achieve

Two molecules of NADPH are generated in the conversion of glucose 6-phosphate into ribulose 5-phosphate

The oxidative phase of the pentose phosphate pathway starts with the dehydrogenation of glucose 6-phosphate at carbon 1, a reaction catalyzed by glucose 6-phosphate dehydrogenase (Figure 20.22). This enzyme is highly specific for $NADP^+$; the K_M for NAD^+ is about a thousand times as great as that for $NADP^+$.

The product is 6-phosphoglucono-δ-lactone, which is an intramolecular ester between the C-1 carboxyl group and the C-5 hydroxyl group. The next step is the hydrolysis of 6-phosphoglucono-δ-lactone by a specific lactonase to give 6-phosphogluconate. This six-carbon sugar acid is then oxidatively decarboxylated by 6-phosphogluconate dehydrogenase to yield ribulose 5-phosphate. $NADP^+$ is again the electron acceptor.

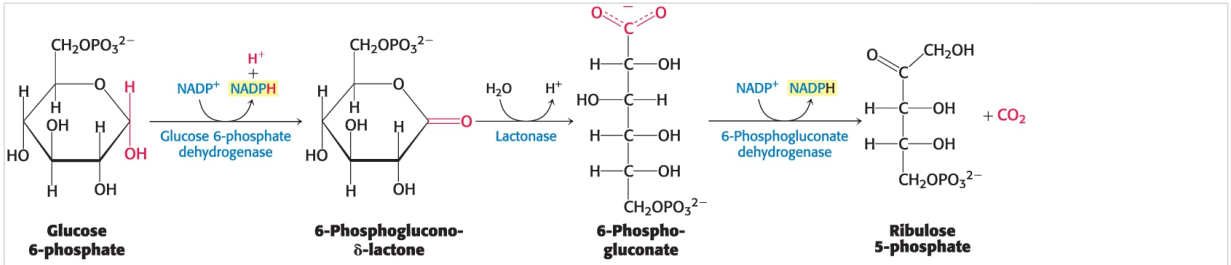
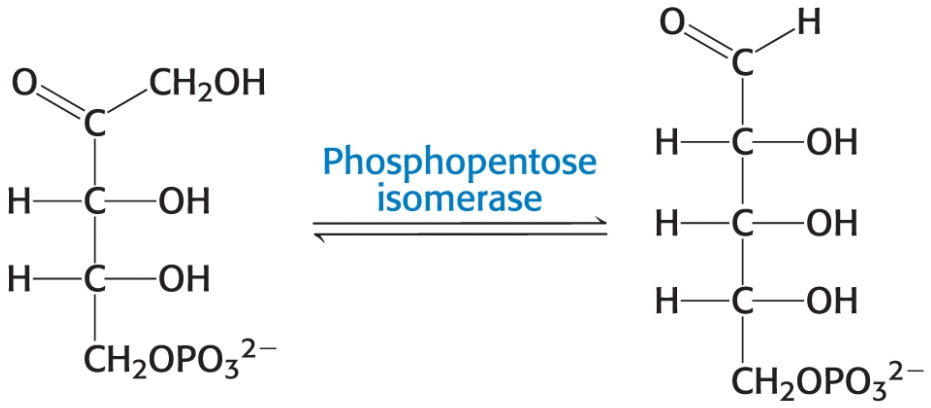


FIGURE 20.22 The oxidative phase of the pentose phosphate pathway yields two molecules of NADPH. Glucose 6-phosphate is oxidized to 6-phosphoglucono-δ-lactone to generate one molecule of NADPH. The lactone product is hydrolyzed to 6-phosphogluconate, which is oxidatively decarboxylated to ribulose 5-phosphate with the generation of a second molecule of NADPH.

EXPLORE this pathway further in the Metabolic Map in Achieve

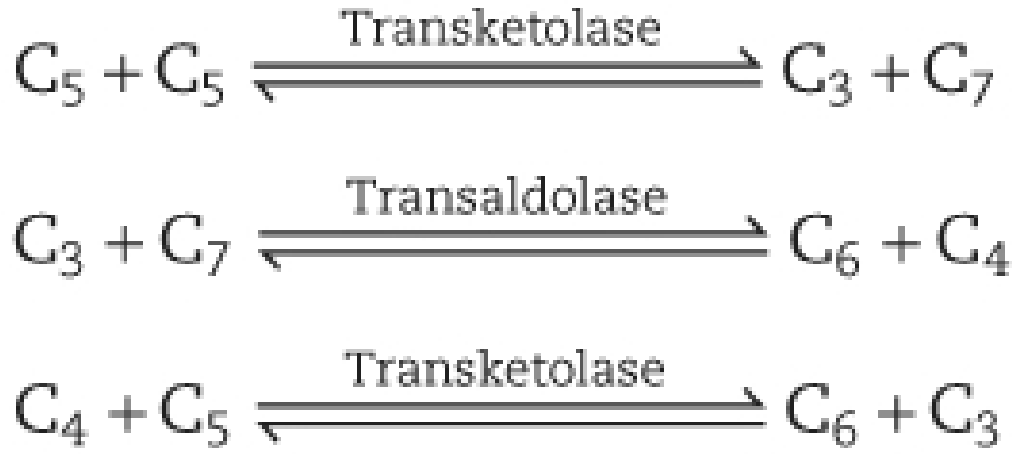
The pentose phosphate pathway and glycolysis are linked by transketolase and transaldolase

The preceding reactions yield two molecules of NADPH and one molecule of ribulose 5-phosphate for each molecule of glucose 6-phosphate oxidized. The ribulose 5-phosphate is subsequently isomerized to ribose 5-phosphate by phosphopentose isomerase.



Ribulose 5-phosphate **Ribose 5-phosphate**

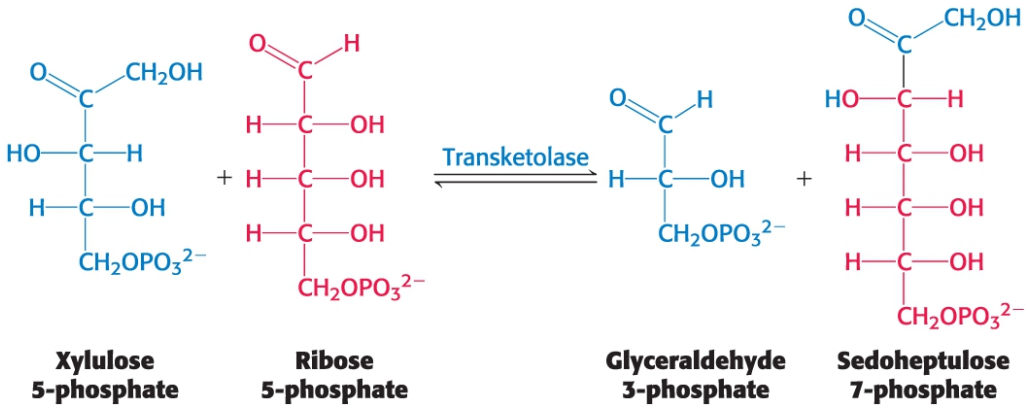
Ribose 5-phosphate and its derivatives are components of RNA and DNA, as well as of ATP, NADH, FAD, and coenzyme A. Although ribose 5-phosphate is a precursor to many biomolecules, many cells need NADPH for reductive biosyntheses much more than they need ribose 5-phosphate for incorporation into nucleotides. For instance, adipose tissue, the liver, and mammary glands require large amounts of NADPH for fatty acid synthesis. In these cases, ribose 5-phosphate is converted into the glycolytic intermediates glyceraldehyde 3-phosphate and fructose 6-phosphate by transketolase and transaldolase. These enzymes create a reversible link between the pentose phosphate pathway and glycolysis by catalyzing three successive reactions:



The net result of these reactions is the formation of two hexoses and one triose from three pentoses:



The first of the three reactions linking the pentose phosphate pathway and glycolysis is the formation of glyceraldehyde 3-phosphate and sedoheptulose 7-phosphate from two pentoses.

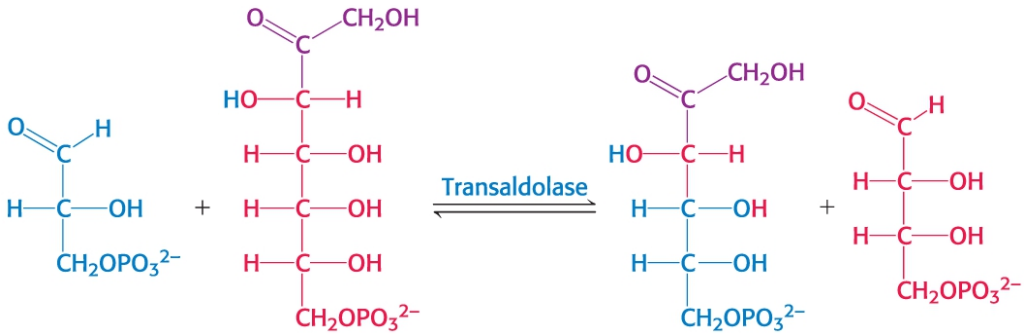


The donor of the two-carbon unit in this reaction is xylulose 5-phosphate, an epimer of ribulose 5-phosphate. A ketose is a substrate of transketolase only if its hydroxyl group at C-3 has the configuration of xylulose rather than ribulose. Ribulose 5-phosphate is converted into the appropriate epimer for the transketolase reaction by phosphopentose epimerase in the reverse reaction of that which takes place in the Calvin–Benson cycle.



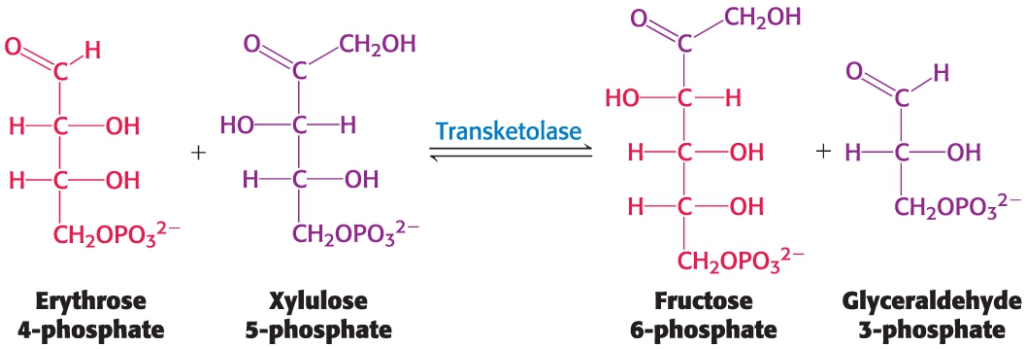
Ribulose 5-phosphate **Xylulose 5-phosphate**

Glyceraldehyde 3-phosphate and sedoheptulose 7-phosphate generated by the transketolase then react to form fructose 6-phosphate and erythrose 4-phosphate. This synthesis of a four-carbon sugar and a six-carbon sugar is catalyzed by transaldolase.



Glyceraldehyde 3-phosphate **Sedoheptulose 7-phosphate** **Fructose 6-phosphate** **Erythrose 4-phosphate**

In the third reaction, transketolase catalyzes the synthesis of fructose 6-phosphate and glyceraldehyde 3-phosphate from erythrose 4-phosphate and xylulose 5-phosphate.



The sum of these reactions is

$$2\ \text{Xylulose 5-phosphate} + \text{ribose 5-phosphate} \rightleftharpoons 2\ \text{fructose 6-phosphate} + \text{glyceraldehyde 3-phosphate}$$

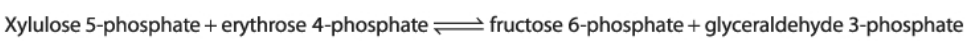
Xylulose 5-phosphate can be formed from ribose 5-phosphate by the sequential action of phosphopentose isomerase and phosphopentose epimerase, and so the net reaction starting from ribose 5-phosphate is

$$3\ \text{Ribose 5-phosphate} \rightleftharpoons 2\ \text{fructose 6-phosphate} + \text{glyceraldehyde 3-phosphate}$$

Thus, excess ribose 5-phosphate formed by the pentose phosphate pathway can be completely converted into glycolytic intermediates. Moreover, any ribose ingested in the diet can be processed into glycolytic intermediates by this pathway. The carbon skeletons of sugars can be extensively rearranged to meet physiological needs (Table 20.3).

TABLE 20.3 Pentose phosphate pathway

Reaction	Enzyme
Oxidative phase	

$\text{Glucose 6-phosphate} + NADP^+ \rightarrow \text{6-phosphoglucono-}\delta\text{-lactone} + NADPH + H^+$	Glucose 6-phosphate dehydrogenase
$\text{6-Phosphoglucono-}\delta\text{-lactone} + H_2O \rightarrow \text{6-phosphogluconate} + H^+$	Lactonase
$\text{6-Phosphogluconate} + NADP^+ \rightarrow \text{ribulose 5-phosphate} + CO_2 + NADPH + H^+$	6-Phosphogluconate dehydrogenase
Nonoxidative phase	
	Phosphopentose isomerase
	Phosphopentose epimerase
	Transketolase
	Transaldolase
	Transketolase

Transketolase and transaldolase stabilize carbanionic intermediates by different mechanisms

The reactions catalyzed by transketolase and transaldolase are distinct, yet similar in many ways. One difference is that transketolase transfers a two-carbon unit, whereas transaldolase transfers a three-carbon unit. Each of these units is transiently attached to the enzyme in the course of the reaction, and thus, these enzymes are examples of double displacement reactions.

Transketolase reaction

Transketolase contains a tightly bound thiamine pyrophosphate as its prosthetic group. The enzyme transfers a two-carbon glycoaldehyde from a ketose donor to an aldose acceptor. The site of the addition of the two-carbon unit is the thiazole ring of thiamine pyrophosphate (TPP).

Transketolase is homologous to the E_1 subunit of the pyruvate dehydrogenase complex, and the reaction mechanism is similar (**Figure 20.23**), proceeding as follows:

1. The C-2 carbon atom of bound TPP readily ionizes to give a carbanion.
2. The negatively charged carbon atom of this reactive intermediate attacks the carbonyl group of the ketose substrate.
3. The resulting addition compound releases the aldose product to yield an activated glycoaldehyde unit.
4. The positively charged nitrogen atom in the thiazole ring acts as an electron sink in the development of this activated intermediate. The carbonyl group of a suitable aldose acceptor then condenses with the activated glycoaldehyde unit to form a new ketose.
5. The ketose is then released from the enzyme.

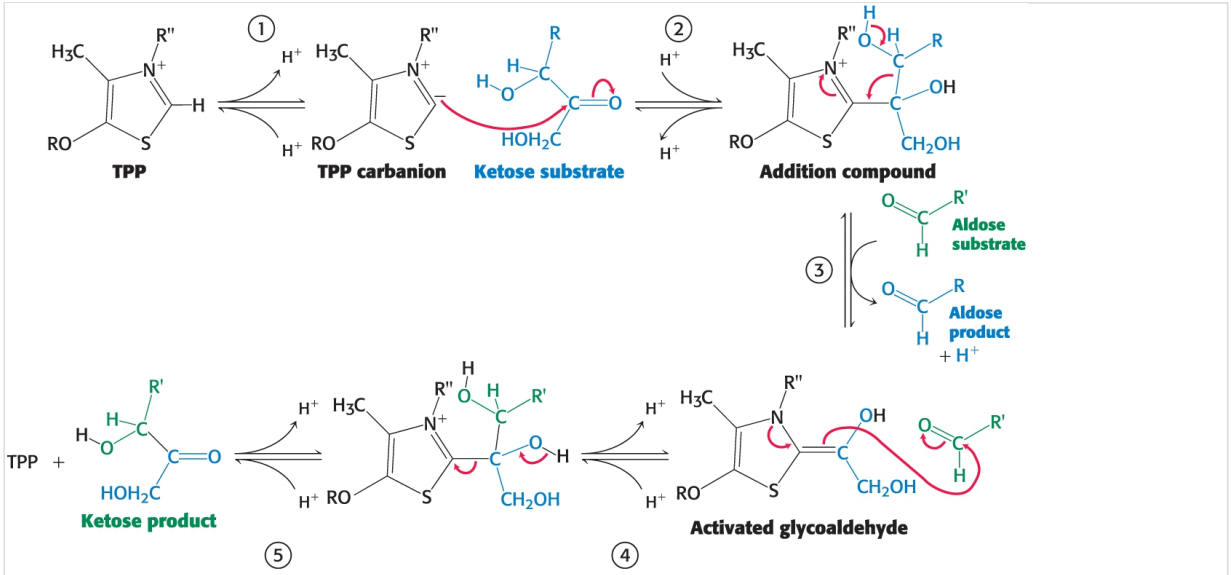


FIGURE 20.23 The transketolase reaction takes place on thiamine pyrophosphate. (1) Thiamine pyrophosphate (TPP) ionizes to form a carbanion. (2) The carbanion of TPP attacks the ketose substrate. (3) Cleavage of a carbon–carbon bond frees the aldose product and leaves a two-carbon fragment joined to TPP. (4) This activated glycoaldehyde intermediate attacks the aldose substrate to form a new carbon–carbon bond. (5) The ketose product is released, freeing the TPP for the next reaction cycle.

Transaldolase reaction

Transaldolase transfers a three-carbon dihydroxyacetone unit from a ketose donor to an aldose acceptor. Transaldolase, in contrast to transketolase, does not contain a prosthetic group. Rather, a Schiff base is formed between the carbonyl group of the ketose substrate and the ε-amino group of a lysine residue at the active site of the enzyme (Figure 20.24). This kind of covalent enzyme–substrate intermediate is like that formed in fructose 1,6-bisphosphate aldolase in the glycolytic pathway and, indeed, the enzymes are homologous. The reaction proceeds as follows:

1. The first step is the formation of the Schiff base.
2. The Schiff base becomes protonated and the bond between C-3 and C-4 is split.
3. Upon reprotonation, the aldose product is released, leaving a three-carbon fragment bound to the enzyme. The negative charge on the Schiff-base carbanion moiety is stabilized by resonance (Figure 20.24). The positively charged nitrogen atom of the protonated Schiff base acts as an electron sink.

4. The Schiff-base adduct is stable until a suitable aldose becomes bound.

5. The dihydroxyacetone moiety then reacts with the carbonyl group of the aldose. Protonation allows the formation of a new carbon–carbon bond.

6. Subsequent deprotonation occurs.

7. Following deprotonation, hydrolysis of the Schiff base releases the ketose product.

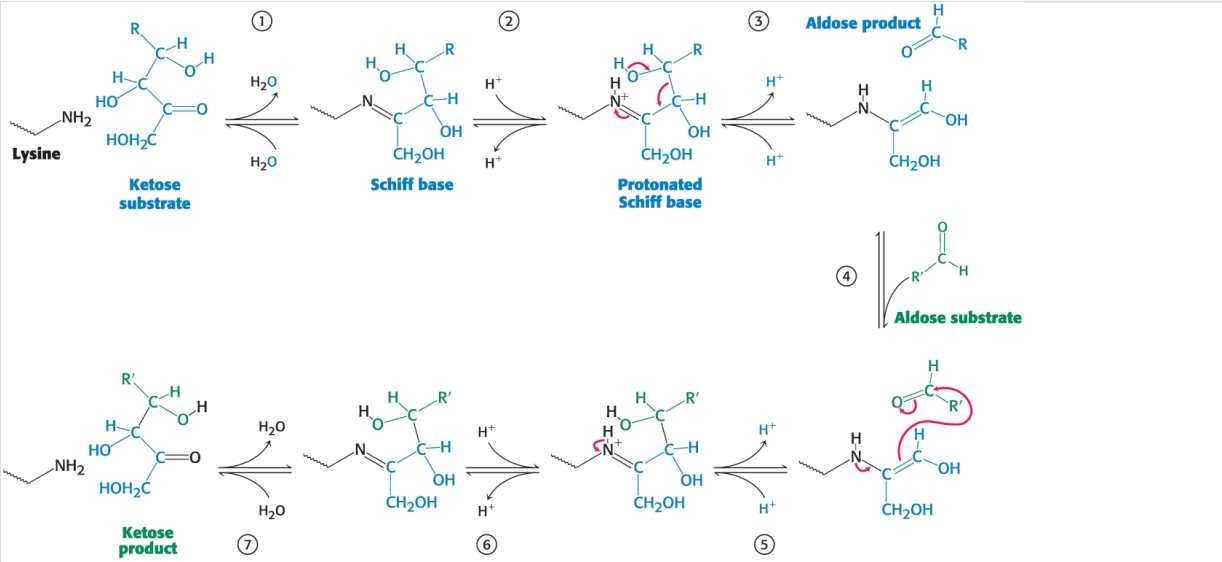


FIGURE 20.24 The transaldolase reaction involves a Schiff base intermediate. (1) The reaction begins with the formation of a Schiff base between a lysine residue in transaldolase and the ketose substrate. (2) Protonation of the Schiff base occurs. (3) Deprotonation leads to the release of the aldose product, leaving a three-carbon fragment attached to the lysine residue. (4) This intermediate adds to the aldose substrate. (5) Protonation occurs, forming a new carbon–carbon bond. (6) Subsequent deprotonation and (7) hydrolysis of the Schiff base releases the ketose product from the lysine side chain, completing the reaction cycle.

The nitrogen atom of the protonated Schiff base plays the same role in transaldolase as the thiazole-ring nitrogen atom does in transketolase. In each enzyme, a group within an intermediate reacts like a carbanion in attacking a carbonyl group to form a new carbon–carbon bond. In each case, the charge on the carbanion is stabilized by resonance (Figure 20.25).

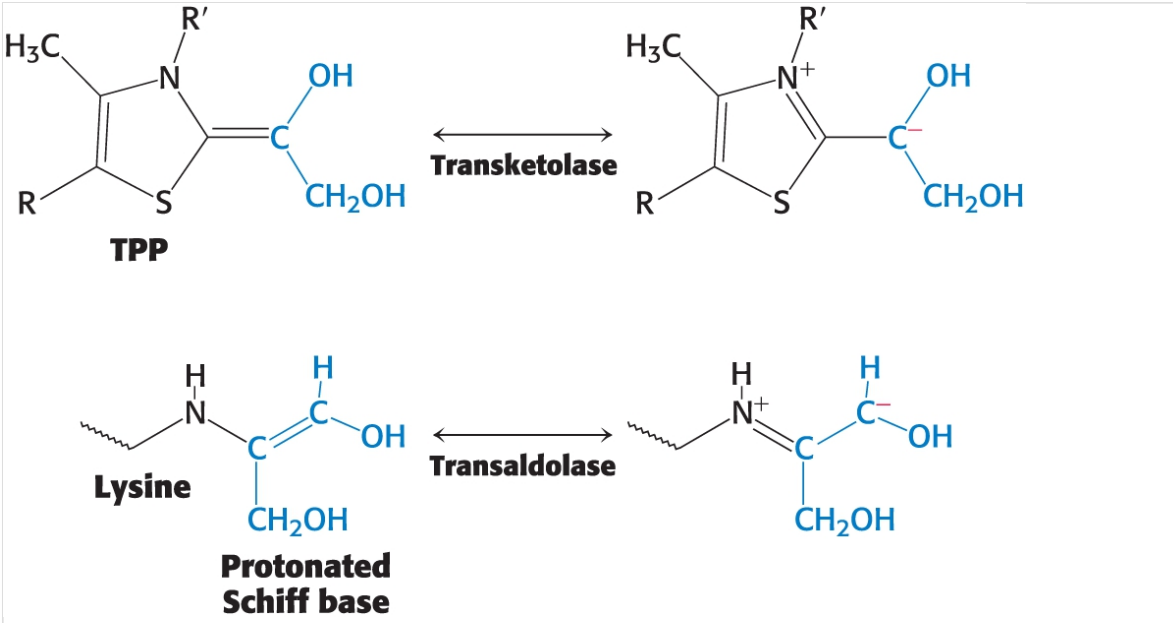


FIGURE 20.25 For transketolase and transaldolase, a carbanion intermediate is stabilized by resonance. In transketolase, TPP stabilizes this intermediate; in transaldolase, a protonated Schiff base plays this role.

20.4 The Metabolism of Glucose 6-Phosphate by the Pentose Phosphate Pathway Is Coordinated with Glycolysis

Glucose 6-phosphate is metabolized by both the glycolytic pathway and the pentose phosphate pathway. How is the processing of this important metabolite partitioned between these two metabolic routes? The cytoplasmic concentration of $NADP^+$ plays a key role in determining the fate of glucose 6-phosphate.

The rate of the oxidative phase of the pentose phosphate pathway is controlled by the level of $NADP^+$

The first reaction in the oxidative branch of the pentose phosphate pathway — the dehydrogenation of glucose 6-phosphate — is essentially irreversible. In fact, this reaction is rate limiting under physiological conditions and serves as the control site for the oxidative branch of the pathway. The most important regulatory factor is the level of $NADP^+$. Low levels of $NADP^+$ limit the dehydrogenation of glucose 6-phosphate because it is needed as the electron acceptor. The effect of low levels of $NADP^+$ is intensified by the fact that NADPH competes with $NADP^+$ in binding to the

enzyme. The ratio of $NADP^+$ to NADPH in the cytoplasm of a liver cell from a well-fed rat is about 0.014.

The marked effect of the $NADP^+$ level on the rate of the oxidative phase ensures that NADPH is not generated unless the supply needed for reductive biosyntheses or protection against oxidative stress is low. The nonoxidative phase of the pentose phosphate pathway is controlled primarily by the availability of substrates.

The flow of glucose 6-phosphate depends on the need for NADPH, ribose 5-phosphate, and ATP

We can grasp the intricate interplay between glycolysis and the pentose phosphate pathway by examining the metabolism of glucose 6-phosphate in four different metabolic situations (**Figure 20.26**).

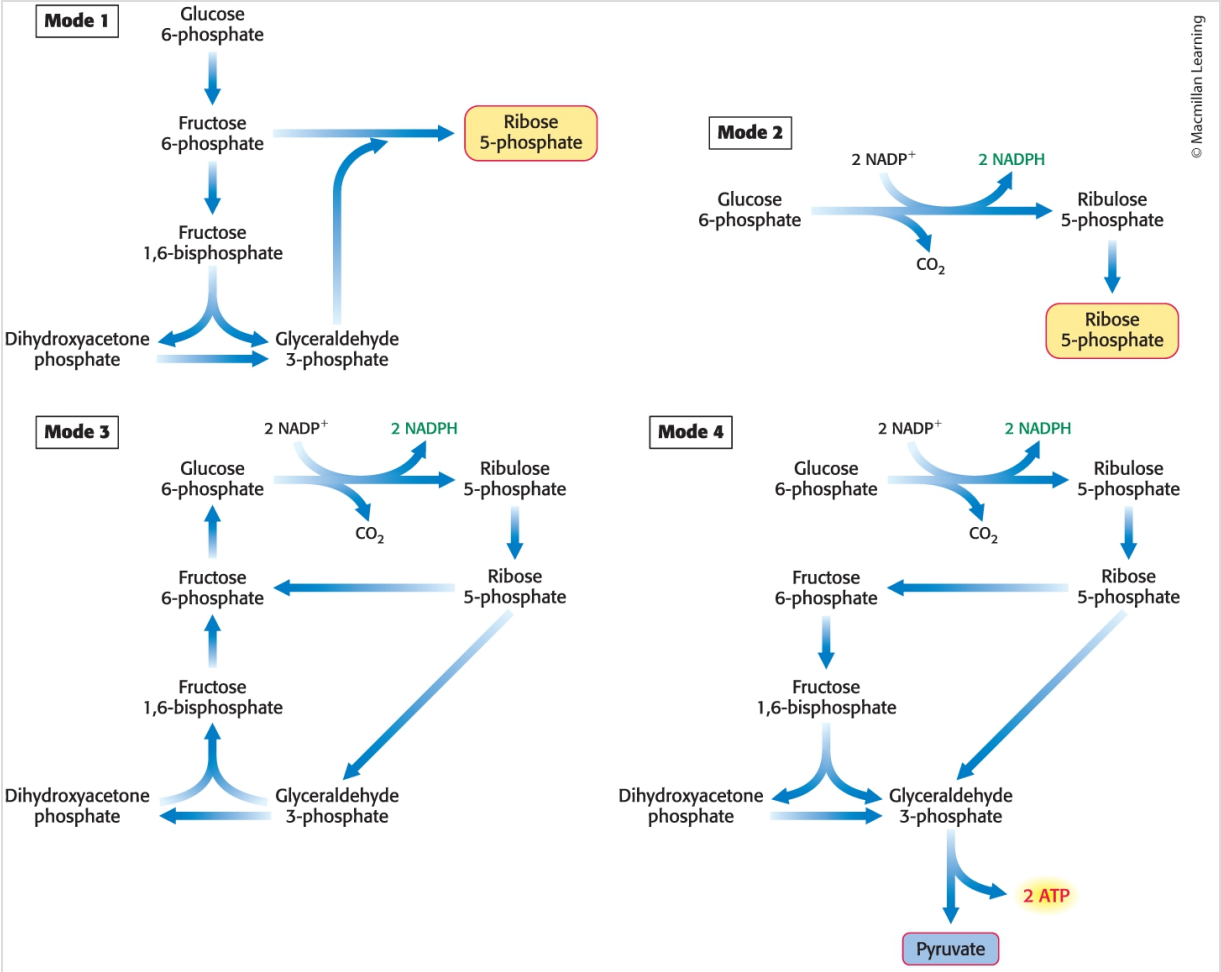


FIGURE 20.26 The pentose phosphate pathway can operate in four modes. Major products are shown in color.

EXPLORE this pathway further in the Metabolic Map in Achieve

Mode 1

Much more ribose 5-phosphate than NADPH is required. For example, rapidly dividing cells need ribose 5-phosphate for the synthesis of nucleotide precursors of DNA. Most of the glucose 6-phosphate is converted into fructose 6-phosphate and glyceraldehyde 3-

phosphate by the glycolytic pathway. Transaldolase and transketolase then convert two molecules of fructose 6-phosphate and one molecule of glyceraldehyde 3-phosphate into three molecules of ribose 5-phosphate by a reversal of the reactions described earlier. The stoichiometry of mode 1 is

$$5\ \text{Glucose 6–phosphate} + \text{ATP} \rightarrow 6\ \text{ribose 5–phosphate} + \text{ADP} + H^+$$

Mode 2

The needs for NADPH and for ribose 5-phosphate are balanced. Under these conditions, glucose 6-phosphate is processed to one molecule of ribulose 5-phosphate while generating two molecules of NADPH. Ribulose 5-phosphate is then converted into ribose 5-phosphate. The stoichiometry of mode 2 is

$$\text{Glucose 6–phosphate} + 2\ NADP^+ + H_2O \rightarrow$$
$$\text{ribose 5–phosphate} + 2\ NADPH + 2\ H^+ + CO_2$$

Mode 3

Much more NADPH than ribose 5-phosphate is required. For example, adipose tissue requires a high level of NADPH for the synthesis of fatty acids (**Table 20.4**). In this case, glucose 6-phosphate is completely oxidized to CO_2.

TABLE 20.4 Tissues with active pentose phosphate pathways

Tissue	Function
Adrenal gland	Steroid synthesis
Liver	Fatty acid and cholesterol synthesis
Testes	Steroid synthesis
Adipose tissue	Fatty acid synthesis
Ovary	Steroid synthesis
Mammary gland	Fatty acid synthesis
Red blood cells	Maintenance of reduced glutathione

Three groups of reactions are active in this situation. First, the oxidative phase of the pentose phosphate pathway forms two molecules of NADPH and one molecule of ribulose 5-phosphate. Then, ribulose 5-phosphate is converted into fructose 6-phosphate and glyceraldehyde 3-phosphate by transketolase and transaldolase. Finally, glucose 6-phosphate is resynthesized from fructose 6-phosphate and glyceraldehyde 3-phosphate by the gluconeogenic pathway. The stoichiometries of these three sets of reactions are

$$6\ \text{Glucose 6–phosphate} + 12\ NADP^+ + 6\ H_2O \rightarrow$$
$$6\ \text{Ribose 5–phosphate} + 12\ NADPH + 12\ H^+ + 6\ CO_2$$
$$6\ \text{Ribose 5–phosphate} \rightarrow$$
$$4\ \text{Fructose 6–phosphate} + 2\ \text{glyceraldehyde 3–phosphate}$$
$$4\ \text{Fructose 6–phosphate} + 2\ \text{glyceraldehyde 3–phosphate} + H_2O \rightarrow$$
$$5\text{–Glucose 6–phosphate} + P_i$$

The sum of the mode 3 reactions is

$$\text{Glucose 6–phosphate} + 12\ NADP^+ + 7\ H_2O \rightarrow 6\ CO_2 + 12\ NADPH + 12\ H^+ + P_i$$

Thus, the equivalent of glucose 6-phosphate can be completely oxidized to CO_2 with the concomitant generation of NADPH. In essence, ribose 5-phosphate produced by the pentose phosphate pathway is recycled into glucose 6-phosphate by transketolase, transaldolase, and some of the enzymes of the gluconeogenic pathway.

Mode 4

Both NADPH and ATP are required. Alternatively, ribulose 5-phosphate formed from glucose 6-phosphate can be converted into pyruvate. Fructose 6-phosphate and glyceraldehyde 3-phosphate derived from ribose 5-phosphate enter the glycolytic pathway rather than reverting to glucose 6-phosphate. In this mode, ATP and NADPH are concomitantly generated, and five of the six carbons of glucose 6-phosphate emerge in pyruvate.

$$3\ \text{Glucose 6–phosphate} + 6\ NADP^+ + 5\ NAD^+ + 5\ P_i + 8\ ADP \rightarrow$$
$$5\ \text{pyruvate} + 3\ CO_2 + 6\ NADPH + 5\ NADH + 8\ ATP + 2\ H_2O + 8\ H^+$$

Pyruvate formed by these reactions can be oxidized to generate more ATP, or it can be used as a building block in a variety of biosyntheses.

The pentose phosphate pathway is required for rapid cell growth

Rapidly dividing cells, such as cancer cells, require ribose 5-phosphate for nucleic acid synthesis and NADPH for fatty acid synthesis, which in turn is required to form membrane lipids. Recall that rapidly dividing cells switch to aerobic glycolysis to meet their ATP needs. Glucose 6-phosphate and glycolytic intermediates are then used to generate NADPH and ribose 5-phosphate using the nonoxidative phase of the pentose phosphate pathway.

The diversion of glycolytic intermediates into the nonoxidative phase is facilitated by the expression of the gene for a pyruvate kinase isozyme, PKM. PKM has a low catalytic activity, creating a bottleneck in the glycolytic pathway. Glycolytic intermediates accumulate and are then used by the pentose phosphate pathway to synthesize NADPH and ribose 5-phosphate. The shunting of phosphorylated intermediates into the nonoxidative phase of the pentose phosphate pathway is further enabled by the inhibition of triose phosphate isomerase by phosphoenolpyruvate, the substrate of PKM.

The Calvin–Benson cycle and the pentose phosphate pathway are essentially mirror images of one another

The complexities of the Calvin–Benson cycle and the pentose phosphate pathway are easier to comprehend if we consider them as functional mirror images of each other. The Calvin–Benson cycle begins with the fixation of CO_2 and proceeds to use NADPH in the synthesis of glucose. The pentose phosphate pathway begins with the oxidation of a glucose-derived carbon atom to CO_2 and concomitantly generates NADPH. The regeneration phase of the Calvin–Benson cycle converts C_6 and C_3 molecules back into the starting material — the C_5 molecule ribulose 1,5-bisphosphate. The pentose phosphate pathway converts a C_5 molecule, ribulose 5-phosphate, into C_6 and C_3 intermediates of the glycolytic pathway. Not surprisingly, in photosynthetic organisms, many enzymes are common to the two pathways. We see here the economy of evolution: the use of identical enzymes for similar reactions with different ends.

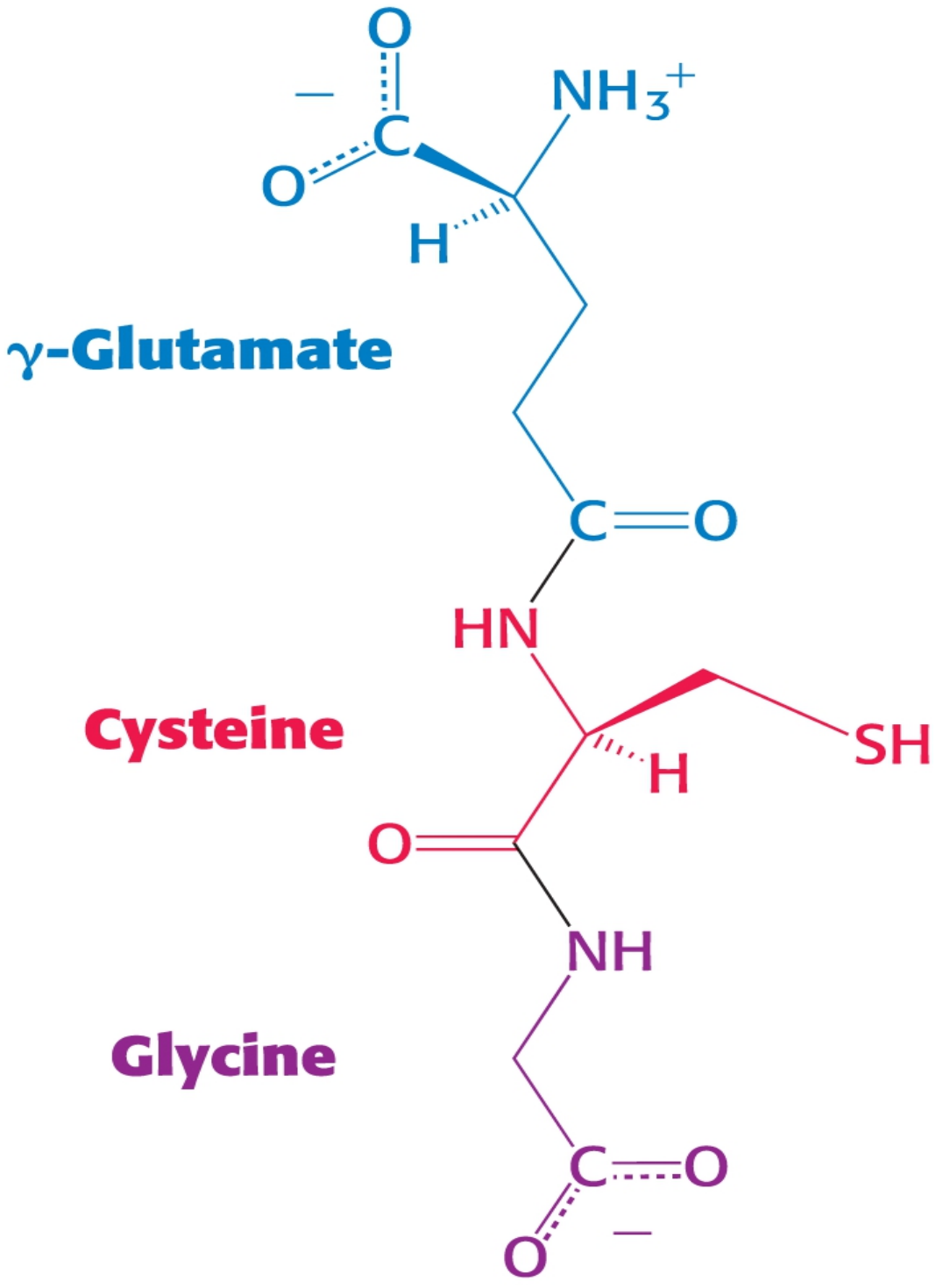
Self-Check Question



Name a reaction in the pentose phosphate pathway that involves erythrose 4-phosphate, and name the associated enzyme. Which reaction in the Calvin–Benson cycle involves erythrose 4-phosphate and the same enzyme?

20.5 Glucose 6-Phosphate Dehydrogenase Plays a Key Role in Protection Against Reactive Oxygen Species

The NADPH generated by the pentose phosphate pathway plays a vital role in protecting the cells from reactive oxygen species (ROS). Reactive oxygen species generated in oxidative metabolism inflict damage on all classes of macromolecules and can ultimately lead to cell death. Indeed, ROS are implicated in a number of human diseases, such as diabetes. Reduced **glutathione** (GSH), a tripeptide with a free sulfhydryl group, combats oxidative stress by reducing ROS to harmless forms. Its task accomplished, the glutathione is now in the oxidized form (GSSG) and must be reduced to regenerate GSH. The reducing power is supplied by the NADPH generated by glucose 6-phosphate dehydrogenase in the pentose phosphate pathway. Indeed, cells with reduced levels of glucose 6-phosphate dehydrogenase are especially sensitive to oxidative stress.

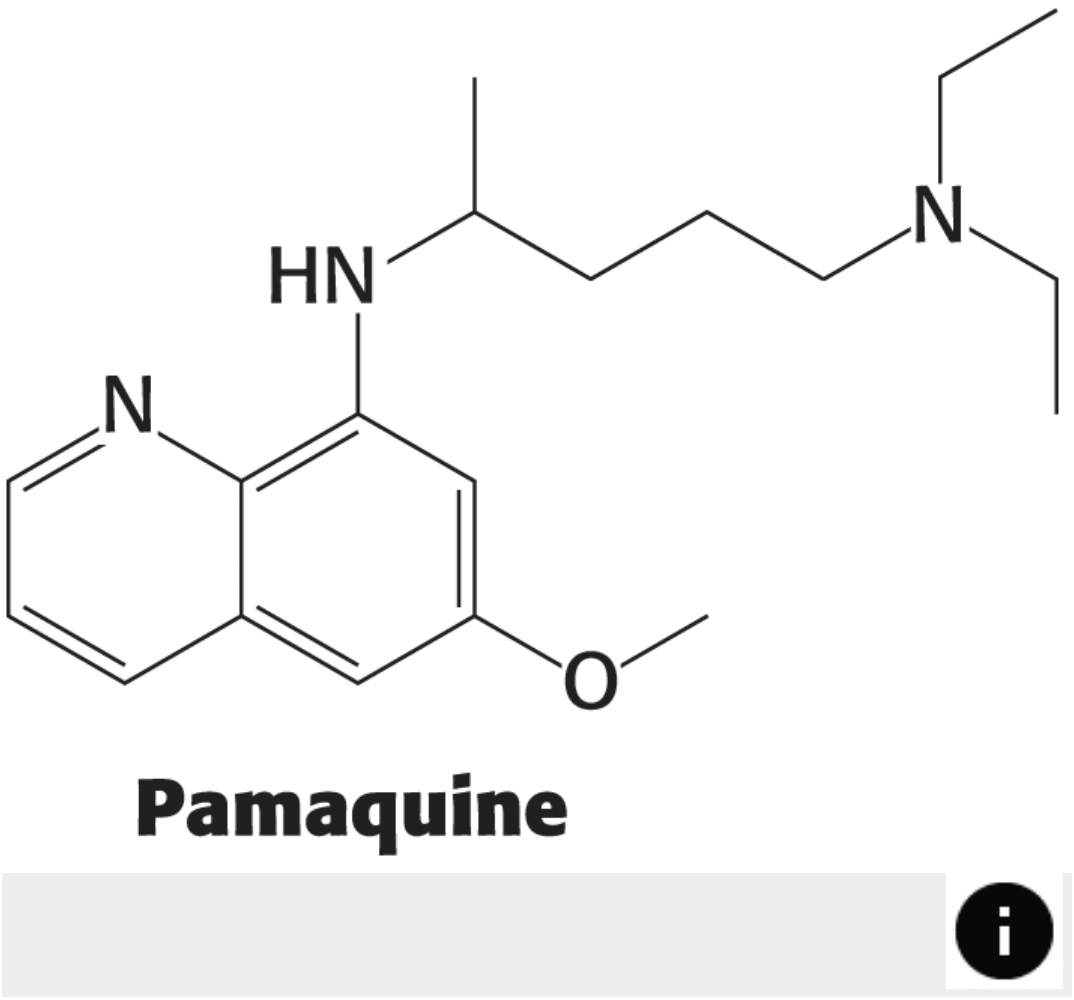


Glutathione (reduced)
(γ-Glutamylcysteinylglycine)

Glucose 6-phosphate dehydrogenase deficiency causes a drug-induced hemolytic anemia



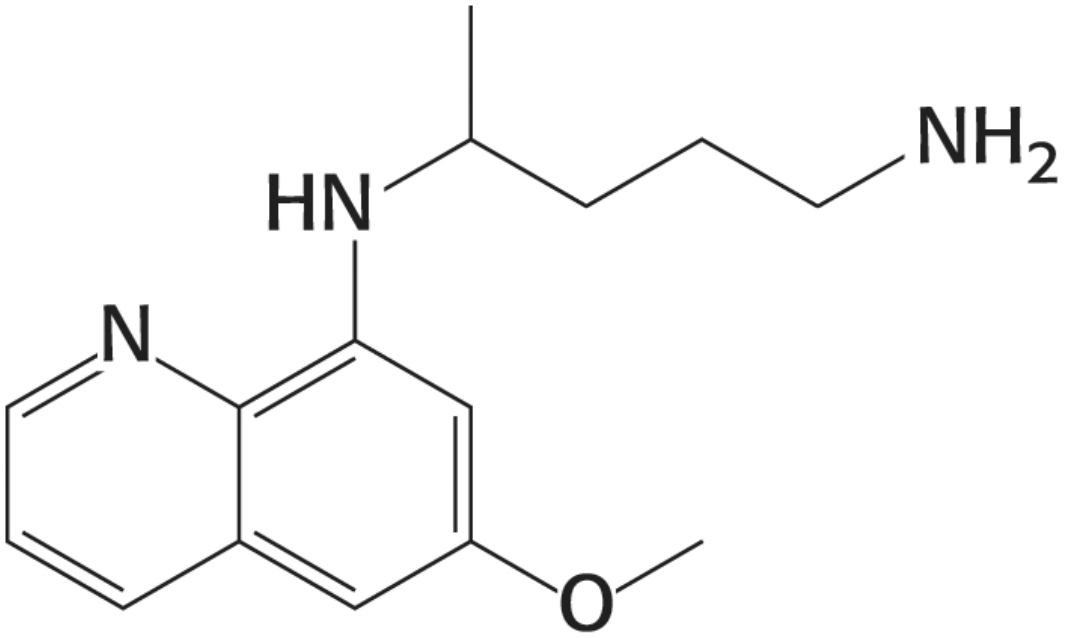
The importance of the pentose phosphate pathway is highlighted by some people's atypical responses to certain drugs. For instance, pamaquine, the first synthetic antimalarial drug introduced in 1926, was associated with the appearance of severe and mysterious ailments. Most patients tolerated the drug well, but a few developed severe symptoms within a few days after therapy was started. Their urine turned black, jaundice developed, and the hemoglobin content of the blood dropped sharply. In some cases, massive destruction of red blood cells caused death.



This drug-induced hemolytic anemia was shown 30 years later to be caused by a deficiency of glucose 6-phosphate dehydrogenase, the enzyme catalyzing the first step in the oxidative branch of the pentose phosphate pathway. The result is a dearth of NADPH in all cells, but this deficiency is most acute in red blood cells because they lack mitochondria and have no alternative means of generating reducing power. This defect, which is inherited on the X chromosome, is the most common condition that results from an enzyme malfunction, affecting hundreds of millions of people.

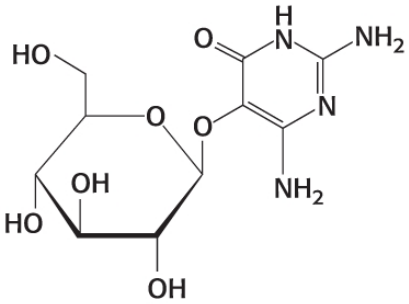
Pamaquine sensitivity is not simply a historical oddity about malaria treatment many decades ago. Primaquine, an antimalarial closely related to pamaquine, is widely used in malaria-prone regions of the world. Vicine, a pyrimidine glycoside of fava beans (**Figure 20.27**), can

also induce hemolysis. People deficient in glucose 6-phosphate dehydrogenase suffer hemolysis from eating fava beans or inhaling the pollen of the fava flowers, a response called favism.



Primaquine





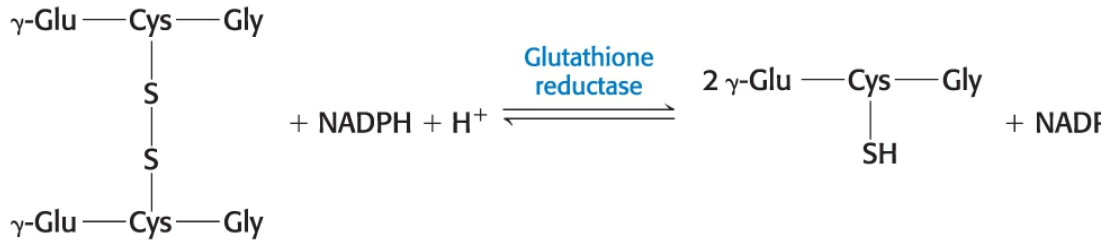
Vicine

FIGURE 20.27 Fava beans produce a pyrimidine glycoside. The Mediterranean plant *Vicia fabia* the source of fava beans that contain the pyrimidine glycoside vicine.

How can we explain hemolysis caused by pamaquine, primaquine, and vicine biochemically? These chemicals are oxidative agents that generate peroxides, reactive oxygen species that can damage membranes as well as other biomolecules. Peroxides are usually eliminated by the enzyme glutathione peroxidase, which uses reduced glutathione as a reducing agent.

$$2\ GSH + ROOH \xrightarrow{\text{Glutathione peroxidase}} GSSG + H_2O + ROH$$

The major role of NADPH in red blood cells is to reduce the disulfide form of glutathione to the sulfhydryl form. The enzyme that catalyzes the regeneration of reduced glutathione is glutathione reductase.



Oxidized glutathione (GSSG) **Reduced glutathione (GSH)**

Red blood cells with a lowered level of reduced glutathione are more susceptible to hemolysis. In the absence of glucose 6-phosphate dehydrogenase, peroxides continue to damage membranes because no

NADPH is being produced to restore reduced glutathione. Thus, the answer to our question is that glucose 6-phosphate dehydrogenase is required to maintain reduced glutathione levels to protect against oxidative stress. In the absence of oxidative stress, however, the deficiency is quite benign. The sensitivity to oxidative agents of people having this dehydrogenase deficiency also clearly demonstrates that atypical reactions to drugs may have a genetic basis.

Reduced glutathione is also essential for maintaining the normal structure of red blood cells by maintaining the structure of hemoglobin. The reduced form of glutathione serves as a sulfhydryl buffer that keeps the residues of hemoglobin in the reduced sulfhydryl form. Without adequate levels of reduced glutathione, the hemoglobin sulfhydryl groups can no longer be maintained in the reduced form. Hemoglobin molecules then cross-link with one another to form aggregates called *Heinz bodies* on cell membranes (**Figure 20.28**). Membranes damaged by Heinz bodies and reactive oxygen species become deformed, and the cell is likely to undergo lysis.

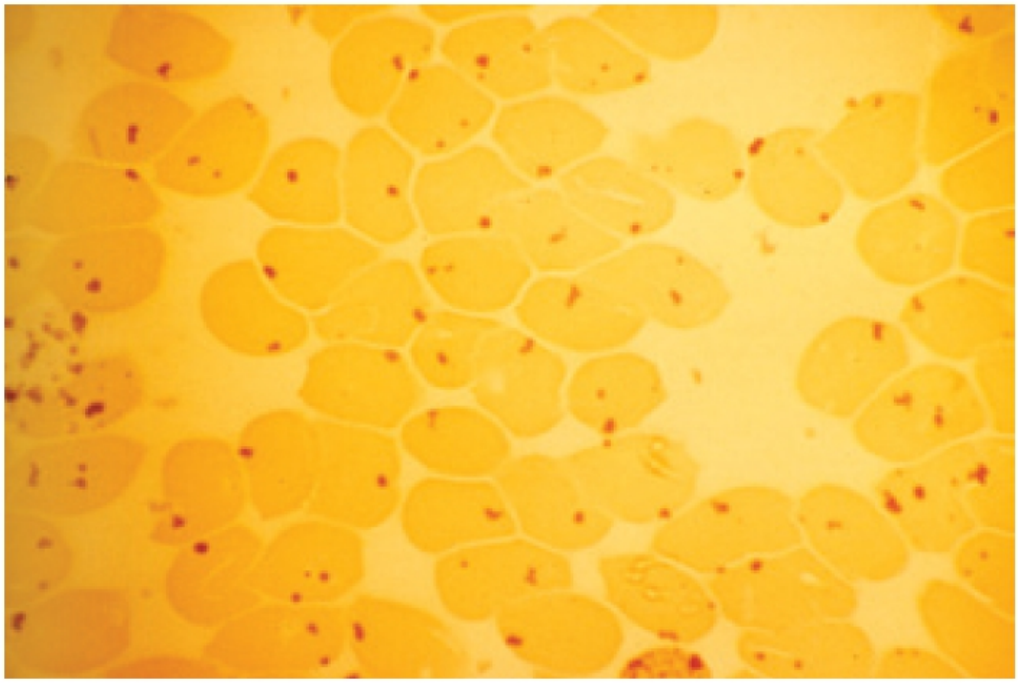


FIGURE 20.28 Heinz bodies are made of denatured hemoglobin. The light micrograph shows red blood cells obtained from a person deficient in glucose 6-

phosphate dehydrogenase. The dark particles, called Heinz bodies, inside the cells are clumps of denatured hemoglobin that adhere to the plasma membrane and stain with basic dyes. Red blood cells in such people are highly susceptible to oxidative damage.

A deficiency of glucose 6-phosphate dehydrogenase can be protective against malaria

The incidence of the most common form of glucose 6-phosphate dehydrogenase deficiency, characterized by a 10-fold reduction in enzymatic activity in red blood cells, is 11% among Americans of African heritage compared to less than 1% in Americans of European descent. This high frequency suggests that the deficiency may be advantageous under certain environmental conditions found in Africa but not Europe. Indeed, glucose 6-phosphate dehydrogenase deficiency protects against the deadliest form of malaria, which is prevalent in Africa's subtropical regions. The parasites causing this disease require NADPH for growth. Moreover, infection by the parasites induces oxidative stress in infected human cells. Because the pentose phosphate pathway is compromised, the cells and parasite die from oxidative damage. Thus, glucose 6-phosphate dehydrogenase deficiency is a mechanism of protection against malaria, which accounts for its high frequency in malaria-prone regions of the world. We see here once again the interplay of heredity and environment in the effect of drugs and diet on physiology.

The ability of glucose 6-phosphate dehydrogenase deficiency to protect against malaria does, however, create a public health conundrum. Primaquine is a commonly used and effective antimalarial drug. However, indiscriminate use of primaquine causes hemolysis in individuals deficient in glucose 6-phosphate dehydrogenase. Scientists

are actively pursuing alternative ways of addressing malaria, and the first antimalarial vaccine was approved in late 2021.

Chapter 20 Summary

20.1 The Calvin–Benson Cycle Synthesizes Hexoses from Carbon Dioxide and Water

- The dark phase of photosynthesis, called the Calvin–Benson cycle, starts with the reaction of CO_2 and ribulose 1,5-bisphosphate to form two molecules of 3-phosphoglycerate, in a reaction catalyzed by Rubisco.
- The steps in the conversion of 3-phosphoglycerate into fructose 6-phosphate and glucose 6-phosphate are like those of gluconeogenesis, except that glyceraldehyde 3-phosphate dehydrogenase in chloroplasts is specific for NADPH rather than NADH.
- Ribulose 1,5-bisphosphate is regenerated from fructose 6-phosphate, glyceraldehyde 3-phosphate (GAP), and dihydroxyacetone phosphate by a complex series of reactions.
- Three molecules of ATP and two molecules of NADPH are consumed for each molecule of CO_2 converted into a hexose.
- Rubisco also catalyzes a competing oxygenase reaction, which produces phosphoglycolate and 3-phosphoglycerate. The process of photorespiration recycles phosphoglycolate, which leads to the release of CO_2 and further consumption of O_2.

20.2 The Activity of the Calvin–Benson Cycle Depends on Environmental Conditions

- Reduced thioredoxin formed by the light-driven transfer of electrons from ferredoxin activates enzymes of the Calvin–Benson cycle by reducing disulfide bridges.
- The light-induced increase in pH and Mg^{2+} levels of the stroma are important in stimulating the carboxylation of ribulose 1,5-

bisphosphate by Rubisco.
- Photorespiration is minimized in tropical plants and grasses, which have an accessory pathway — the C_4 pathway — for concentrating CO_2 at the site of the Calvin–Benson cycle.
- Some plants use crassulacean acid metabolism (CAM) to prevent dehydration. In CAM plants, the C_4 pathway is active during the night; during the day, gas exchange is eliminated and CO_2 is generated from malate stored in vacuoles.

20.3 The Pentose Phosphate Pathway Generates NADPH and Synthesizes Pentoses

- The pentose phosphate pathway consists of two phases: an oxidative phase that generates NADPH and ribulose 5-phosphate in the cytoplasm, and a nonoxidative phase.
- In the nonoxidative phase, ribose 5-phosphate is converted into GAP and fructose 6-phosphate by transketolase and transaldolase. These two enzymes create a reversible link between the pentose phosphate pathway and glycolysis.
- When NADPH needs are paramount, fructose 6-phosphate and GAP from the nonoxidative phase are used to synthesize glucose 6-phosphate for metabolism in the oxidative phase, generating 12 molecules of NADPH for each molecule of glucose 6-phosphate that is completely oxidized to CO_2.

20.4 The Metabolism of Glucose 6-Phosphate by the Pentose Phosphate Pathway Is Coordinated with Glycolysis

- Only the nonoxidative branch of the pathway is significantly active when much more ribose 5-phosphate than NADPH must be synthesized.
- Under these conditions, fructose 6-phosphate and GAP are converted into ribose 5-phosphate without the formation of NADPH. Alternatively, ribose 5-phosphate formed by the

oxidative branch can be converted into pyruvate through fructose 6-phosphate and GAP. In this mode, ATP and NADPH are generated.
- The interplay of the glycolytic and pentose phosphate pathways enables the levels of NADPH, ATP, and building blocks such as ribose 5-phosphate and pyruvate to be continuously adjusted to meet cellular needs.

20.5 Glucose 6-Phosphate Dehydrogenase Plays a Key Role in Protection Against Reactive Oxygen Species

- NADPH generated by glucose 6-phosphate dehydrogenase maintains the appropriate levels of reduced glutathione required to combat oxidative stress, and it ensures the proper reducing environment in the cell.
- Cells with diminished glucose 6-phosphate dehydrogenase activity are especially sensitive to oxidative stress.

Key Terms

Calvin–Benson cycle
ribulose 1,5-bisphosphate carboxylase/oxygenase (Rubisco)
peroxisome
photorespiration
transketolase
aldolase
starch
sucrose
synthetic biology
C_4 pathway (Hatch–Slack pathway)
crassulacean acid metabolism (CAM)
pentose phosphate pathway

glucose 6-phosphate dehydrogenase
glutathione

Problems

1. In chloroplasts, glyceraldehyde 3-phosphate dehydrogenase uses NADPH as a cofactor in the synthesis of glucose. In cytoplasmic gluconeogenesis, however, the isozyme of this dehydrogenase uses NADH. Why is it advantageous for the enzyme in the chloroplast to use NADPH? 1

a. NADPH is harmful to chloroplasts when levels become too high.
b. NADPH is abundant in chloroplasts, because it is generated by the light reactions.
c. The presence of NADH increases the rate of wasteful photorespiration.

2. Arrange the steps to outline the Calvin–Benson cycle (first stage to last stage) 1

a. Conversion of 3-phosphoglycerate into hexose
b. Regeneration of ribulose 1,5-bisphosphate
c. Fixation of CO_2 with ribulose 1,5-bisphosphate
d. Formation of 3-phosphoglycerate

3. Match each characteristic to either the Calvin–Benson cycle or the Krebs cycle. 1

a. Matrix
b. Requires high-energy electrons from NADPH
c. Regenerates ribose 1,5-bisphosphate

d. Regenerates oxaloacetate
e. Releases CO_2
f. Stroma
g. Carbon chemistry for photosynthesis
h. Fixes CO_2
i. Harvests high-energy electrons to form NADH
j. Carbon chemistry for cellular respiration

4. What statement best describes photorespiration? 1

a. Plants transform light energy into ATP.
b. Plants consume NADPH to reduce carbon atoms.
c. Plants consume O_2 and release CO_2.
d. Plants oxidize glucose to generate NADPH.

5. Rubisco catalyzes both a carboxylase reaction and a wasteful oxygenase reaction. Use the kinetic parameters for the two reactions in the table to determine the specificity constant, k_{cat}/K_M, for each substrate in units of $M^{-1}s^{-1}$. 1

Substrate	$k_{cat}(s^{-1})$	$K_M(mM)$
CO_2	3	10
O_2	2	500

6. Which of the following stromal changes occur in response to light that regulate the Calvin–Benson cycle? 2

a. Increased pH
b. Increased levels of Mg^{2+}

c. Decreased levels of carbamate
d. Decreased concentration of NADPH
e. Increased amounts of the reduced form of ferredoxin

7. Rubisco requires a molecule of CO_2 covalently bound to lysine 201 for catalytic activity. The carboxylation of Rubisco is favored by high pH and high Mg^{2+} concentration in the stroma. Why does it make physiological sense for these conditions to favor Rubisco carboxylation? 2

a. They are present when the light reactions occur.
b. They are the normal environment in the stroma.
c. They are present in the dark, when Calvin–Benson cycle reactions occur.
d. They concentrate CO_2 and prevent photorespiration.

8. The enzyme ribose 5-phosphate isomerase catalyzes the conversion between ribose 5-phosphate (R5P) and ribulose 5-phosphate (Ru5P) through an enediolate intermediate. In the Calvin–Benson cycle, Ru5P is used to replenish ribulose 1,5-bisphosphate, a substrate for Rubisco.

For the conversion of R5P to Ru5P, if $G^{\circ\prime} = 0.460\ \text{kJ/mol}$ and $\Delta G = 3.80\ \text{kJ/mol}$, what is the ratio of Ru5P to R5P at 298 K? Which of the statements is true?

a. This reaction is favorable, and it is likely regulated.
b. This reaction is not favorable, and it is likely regulated.
c. This reaction is favorable, and it is not likely regulated.
d. This reaction is not favorable, and it is not likely regulated.

9. Which phrases describe the light reactions of photosynthesis, which describe the Calvin–Benson cycle, and which describe both? 2

a. Capture light energy using chlorophyll
b. Use CO_2
c. Require water
d. Take place in the chloroplasts of plants
e. Generate oxygen gas
f. Synthesize ATP and NADPH
g. Produce sugars
h. Need ribulose 1,5-bisphosphate

10. The Calvin–Benson cycle must repeat six times in order for a cell to have enough material to construct a complete glucose molecule. A variety of molecules are used and produced during this process. Sort the molecules into three categories: molecules brought in and used in six turns of the Calvin–Benson cycle, molecules produced during six turns of the Calvin–Benson cycle that leave the cycle, and molecules used and regenerated within the Calvin–Benson cycle during six turns. 1

a. 18 ATP
b. 18 ADP
c. 6 Ribulose 1,5-bisphosphate
d. 12 NADPH
e. $12\ NADP^+ + 12\ H^+$
f. $6\ CO_2$
g. 2 glyceraldehyde 3-phosphate
h. 10 glyceraldehyde 3-phosphate

11. Fill in the blanks: Insulin _____ glucose uptake and oxidation. Entry of glucose into cells is accompanied by its

phosphorylation to form glucose 6-phosphate (G6P). Not only is G6P able to be processed glycolytically to generate ATP, but it can also be shunted into the pentose phosphate pathway (PPP) to generate _____ and _____. An abundance of G6P, as would be present upon insulin signaling, would likely _____ the flux of G6P into the PPP. 3

12. The net equation for the oxidative reactions of the pentose phosphate pathway is

$$\text{Glucose 6-phosphate} + 2\ NADP^+ + H_2O \rightarrow$$
$$\text{ribulose 5-phosphate} + 2\ NADPH + CO_2 + 2\ H^+$$

Select true statements about the pentose phosphate pathway. 3

a. Glucose is a precursor of the pentose phosphate pathway.
b. The pentose phosphate pathway contributes to nucleotide synthesis.
c. Carbon atoms from the pentose sugar products may enter the glycolytic pathway.
d. Glucose 6-phosphate is reduced to ribulose 5-phosphate in this series of reactions.

13. Consider a cell that requires much more ribose 5-phosphate than NADPH. The cell needs ribose 5-phosphate but has a relatively high concentration of NADPH and a low concentration of $NADP^+$. These conditions may occur in rapidly dividing cells. Choose the statements that describe the fate of glucose 6-phosphate, glycolytic intermediates, and pentose phosphate pathway intermediates in this cell. 3

a. Conversion of glycolytic intermediates to ribose 5-phosphate requires transketolase and transaldolase.
b. Most of the glucose 6-phosphate enters the glycolytic pathway and is converted to fructose 6-phosphate and glyceraldehyde 3-phosphate.
c. The oxidative pentose phosphate pathway reaction catalyzed by glucose 6-phosphate dehydrogenase is slowed down.
d. Three molecules of glyceraldehyde 3-phosphate and two molecules of fructose 6-phosphate are used to generate five molecules of ribose 5-phosphate.
e. Under the given conditions, all triose phosphates are converted to pyruvate by the glycolytic pathway.
f. Most of the glucose 6-phosphate enters the pentose phosphate pathway.

14. Radioactive-labeling experiments can yield estimates of the amount of glucose 6-phosphate metabolized by the pentose phosphate pathway (PPP) and the amount metabolized aerobically by the combined action of glycolysis, the pyruvate dehydrogenase complex, and the citric acid cycle. A researcher has a tissue sample and two radioactively labeled glucose samples, one labeled with ^{14}C at C-1 and the other labeled with ^{14}C at C-6. To determine the relative activity of aerobic glucose metabolism compared with glucose metabolism by the PPP, the research should compare the radioactivity of which product? What is the rationale for the experiment? 3

a. Aerobic glucose metabolism decarboxylates C-1 and C-6, whereas the PPP only decarboxylates C-1.
b. Glucose 6-phosphate is only metabolized by the PPP.
c. Aerobic glucose metabolism in oxidative, whereas the PPP is completely nonoxidative.

d. Aerobic glucose metabolism reduces NAD^+, whereas the PPP reduces $NADP^+$.
e. In the PPP, C-1 of glucose 6-phosphate becomes C-1 of ribose 5-phosphate.

15. Which molecule controls the rate of the pentose phosphate pathway? 3

a. $NADP^+/NADPH$
b. Ribose 5-phosphate
c. ADP/ATP
d. Glucose
e. $NAD^+/NADH$

16. Think about which reaction is influenced by the molecule in Question 15. Choose the enzyme that catalyzes the reaction.

a. Glucose 6-phosphate dehydrogenase
b. Transketolase
c. Transaldolase
d. Lactonase
e. Phosphopentose isomerase
f. Phosphopentose epimerase

17. Provide an example of pathogen resistance provided by the loss of the activity of an enzyme (name the pathogen and the enzyme). Provide an example of another genetic modification associated with resistance to this pathogen. 4

18. Why might a diet that includes fava beans pose a risk for some individuals? 4

19. What is the stoichiometry of the synthesis of

a. ribose 5-phosphate from glucose 6-phosphate without the concomitant generation of NADPH, and
b. NADPH from glucose 6-phosphate without concomitant formation of pentose sugars? 3

20. Why is the C_4 pathway valuable for tropical plants? 1

21. Which of the following is not a component of the pentose phosphate pathway? 3

a. NADPH
b. CO_2
c. Ribose 5-phosphate
d. Phosphoenolpyruvate
e. Erythrose 4-phosphate

Chapter 21
Glycogen Metabolism





Left: DE AGOSTINI PICTURE LIBRARY/De Agostini/Getty Images; right: WESTOCK PRODUCTIONS/Shutterstock

The brain requires glucose at all times, while muscles require extra glucose during bouts of exercise. Glycogen, a molecule used to store glucose, is used by the liver to keep the brain fed between meals, including while you sleep. The same molecule is used by muscles to power intense exercise.

Outline

21.1 Glycogen Metabolism Is the Regulated Release and Storage of Glucose in Multiple Tissues
21.2 Glycogen Breakdown Requires the Interplay of Several Enzymes
21.3 Phosphorylase Is Regulated by Allosteric Interactions and Controlled by Reversible Phosphorylation
21.4 Glucagon and Epinephrine Signal the Need for Glycogen Breakdown
21.5 Glycogen Synthesis Requires Several Enzymes and Uridine Diphosphate Glucose

21.6 Glycogen Breakdown and Synthesis Are Reciprocally Controlled by Hormones

---

Learning Goals



By the end of this chapter, you should be able to:

1. List and describe the steps of glycogen breakdown and identify the enzymes required.
2. Explain the regulation of glycogen breakdown.
3. Describe the steps of glycogen synthesis and identify the enzymes required.
4. Describe how glycogen degradation and synthesis are coordinated and regulated.
5. Compare the different roles of glycogen metabolism in liver and muscle.

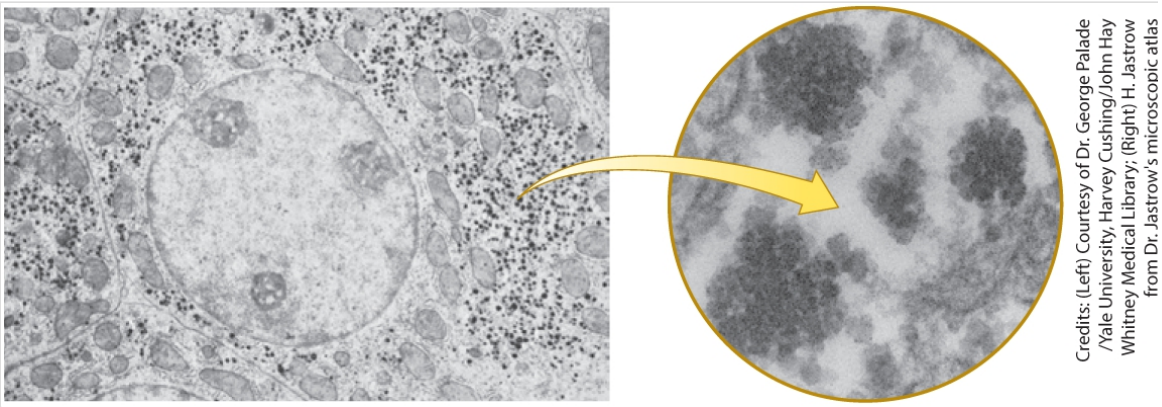
Glucose is an important fuel and a key precursor for the biosynthesis of many molecules. However, glucose itself cannot be stored, because high concentrations of glucose disrupt the osmotic balance of the cell, which would cause cell damage or death. Instead, glucose is stored as glycogen, a significantly less osmotically active and highly branched polymer that can be rapidly broken down to yield glucose molecules when energy is needed. Glycogen is present in bacteria, archaea, protists, and animals, while plants store glucose primarily as starch, a similar, but less-branched polymer.

Glycogen is not as reduced as fatty acids are and consequently is not as energy-rich, so why isn't all excess fuel stored as fatty acids rather than as glycogen? In animals, the controlled release of glucose from glycogen maintains blood-glucose concentration between meals, including during sleep. The circulating blood keeps the brain

supplied with glucose, which is virtually the only fuel it uses, except during prolonged starvation (Chapter 24). Moreover, the readily mobilized glucose from glycogen is a good source of energy for sudden, strenuous activity as, unlike fatty acids, it can be metabolized in the absence of oxygen and can thus supply energy for anaerobic activity (Section 16.2).

21.1 Glycogen Metabolism Is the Regulated Release and Storage of Glucose in Multiple Tissues

In humans, most tissues have some glycogen, although the two major sites of glycogen storage are the liver and skeletal muscle. The concentration of glycogen is higher in the liver than in muscle (10% versus 2% by weight), but more glycogen is stored in skeletal muscle overall because of muscle's much greater mass. Glycogen is present in the cytoplasm, with the molecule appearing as granules consisting of multiple glycogen molecules (Figure 21.1). An individual glycogen molecule has approximately 12 layers of glucose molecules and can be as large as 40 nm, containing approximately 55,000 glucose residues and a single protein, called *glycogenin*, at the core (Figure 21.2).



Credits: (Left) Courtesy of Dr. George Palade /Yale University, Harvey Cushing/John Hay Whitney Medical Library; (Right) H. Jastrow from Dr. Jastrow's microscopic atlas

FIGURE 21.1 Liver and muscle tissue are the primary storage sites for glycogen. An electron micrograph of a liver cell reveals a high density of glycogen granules (the dark spots) in the cytoplasm.

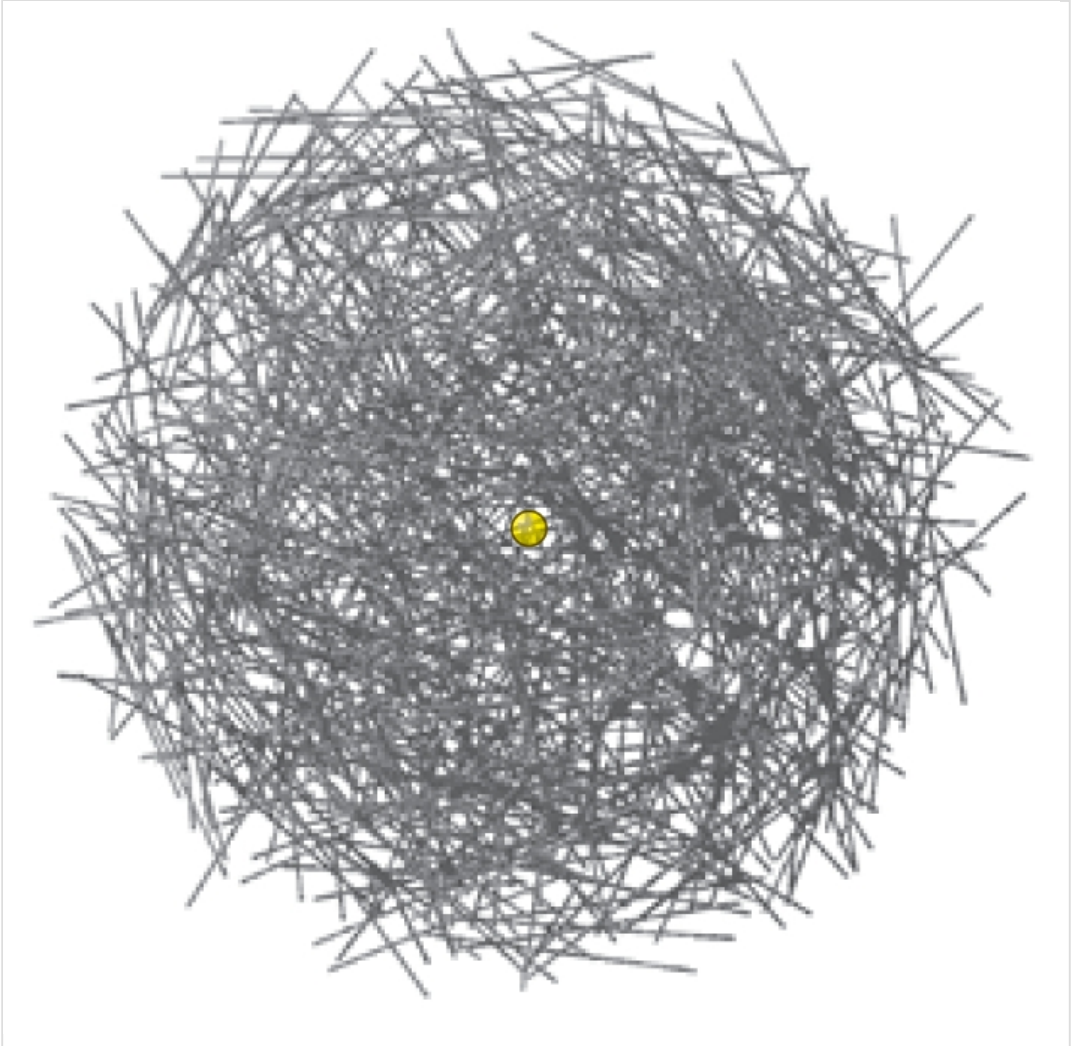


FIGURE 21.2 Glycogen is a complex homopolymer of glucose with a protein core. At the core of the glycogen molecule is the protein glycogenin (yellow). Each line represents glucose molecules joined by α-1,4-glycosidic linkages. The nonreducing ends of the glycogen molecule form the surface of the glycogen granule, where degradation takes place.

[Information from R. Melendez et al., *Biophys. J.* 77:1327–1332, 1999.]

Recall that most of the glucose residues in glycogen are linked by α-1,4-glycosidic bonds (**Figure 21.3**); but branches at about every 12 residues are created by α-1,6-glycosidic bonds. α-Glycosidic linkages form open helical polymers, whereas β linkages produce nearly straight strands that form structural fibrils, as in cellulose (Figure 11.14).

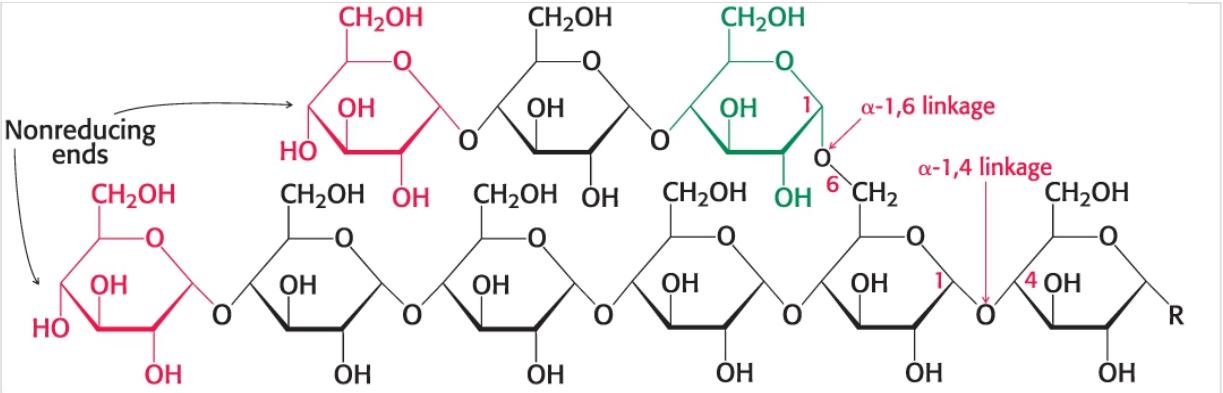


FIGURE 21.3 The fundamental structure of glycogen is a linear polymer with occasional branches. In this structure of two outer branches of a glycogen molecule, the residues at the nonreducing ends are shown in red and the residue that starts a branch is shown in green. The rest of the glycogen molecule is represented by R.

Glycogen degradation and synthesis are relatively simple biochemical processes. Glycogen degradation consists of three steps, ultimately producing glucose 6-phosphate for further metabolism. Glucose 6-phosphate has three possible fates (Figure 21.4): (1) it can be metabolized by glycolysis, (2) in the liver it can be converted into free glucose for release into the bloodstream, or (3) it can be processed by the pentose phosphate pathway to yield NADPH and ribose derivatives. Glycogen synthesis also requires several steps; it takes place when glucose is abundant and glycogen is depleted.

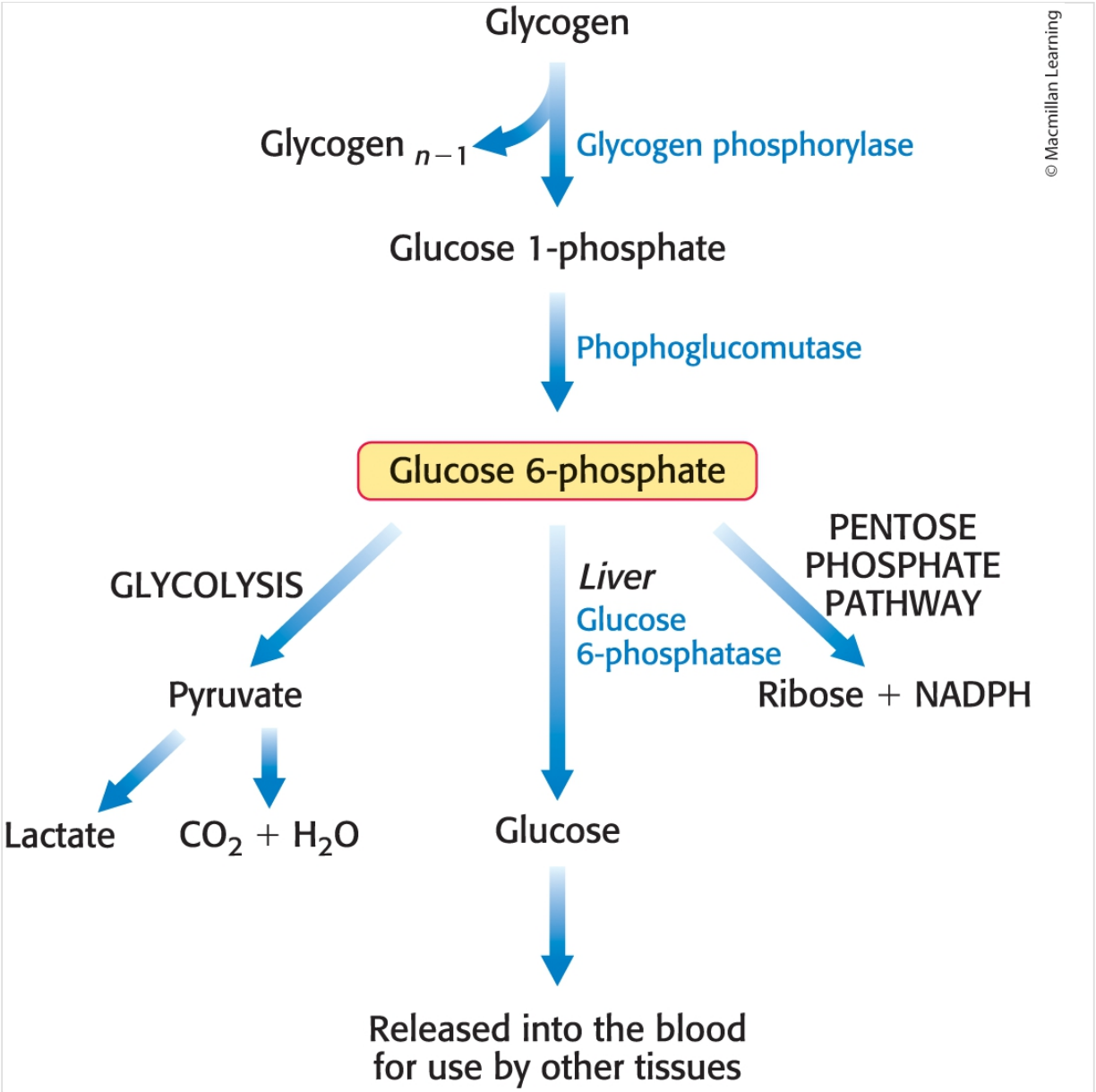


FIGURE 21.4 Glucose 6-phosphate can have many metabolic fates. Glucose 6-phosphate derived from glycogen can be (1) used as a fuel for anaerobic or aerobic metabolism as in, for instance, muscle; (2) converted into free glucose in the liver and subsequently released into the blood; or (3) processed by the pentose phosphate pathway to generate NADPH and ribose in a variety of tissues.

The regulation of glycogen degradation and synthesis is complex, in part because all of the enzymes involved in glycogen metabolism and its regulation are associated with the glycogen particle. Several enzymes taking part in glycogen metabolism allosterically respond to metabolites that signal the energy needs of the cell. Through these allosteric responses, enzyme activity is adjusted to meet the needs of the individual cell. In contrast, hormones may initiate signal cascades that lead to the reversible phosphorylation of enzymes, which alters their catalytic rates in tissue-specific manners to meet the needs of the whole organism.

21.2 Glycogen Breakdown Requires the Interplay of Several Enzymes

The efficient breakdown of glycogen to provide glucose 6-phosphate for further metabolism requires four enzyme activities: one to degrade glycogen, two to remodel glycogen so that it can remain a substrate for degradation, and one to convert the product of glycogen breakdown into a form suitable for further metabolism. We will examine each of these activities in turn.

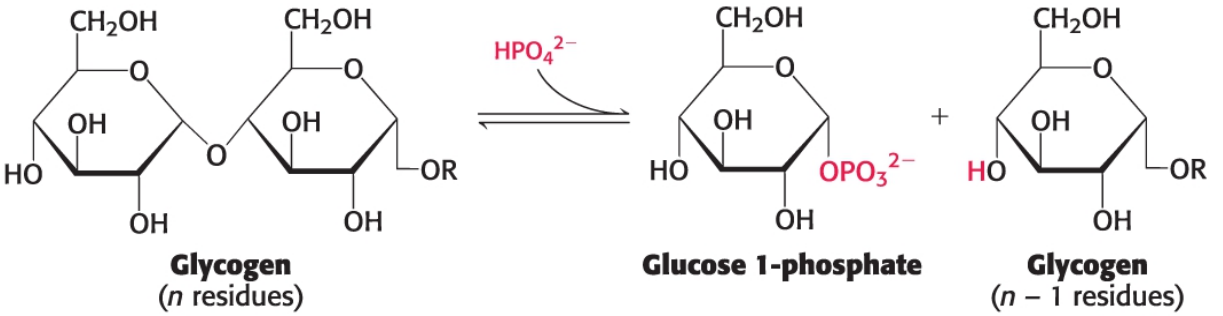
Phosphorylase catalyzes the phosphorolytic cleavage of glycogen to release glucose 1-phosphate

The key enzyme in glycogen breakdown, **glycogen phosphorylase** (often just called **phosphorylase**), cleaves its substrate by the addition of orthophosphate (P_i) to yield glucose 1-phosphate. The cleavage of a bond by the addition of orthophosphate is referred to as **phosphorolysis**.

$$\underset{(n \text{ residues})}{\text{Glycogen} + P_i} \rightleftharpoons \text{glucose 1-phosphate} + \underset{(n-1 \text{ residues})}{\text{glycogen}}$$

Phosphorylase catalyzes the sequential removal of glucosyl residues from the nonreducing ends of the glycogen molecule (the ends with a free OH group on carbon 4). Orthophosphate splits the glycosidic linkage between C-1 of the terminal residue and C-4 of the adjacent one. Specifically, it cleaves the bond between the C-1 carbon atom

and the glycosidic oxygen atom, and the α configuration at C-1 is retained.



Glucose 1-phosphate released from glycogen can be readily converted into glucose 6-phosphate, an important metabolic intermediate, by the enzyme phosphoglucomutase.

The reaction catalyzed by phosphorylase is readily reversible in vitro. At pH 6.8, the equilibrium ratio of orthophosphate to glucose 1-phosphate is 3.6. The value of $\Delta G^{\circ\prime}$ for this reaction is small because a glycosidic bond is replaced by a phosphoryl ester bond that has a nearly equal transfer potential. However, phosphorolysis proceeds far in the direction of glycogen breakdown in vivo because the $[P_i]/[\text{glucose 1-phosphate}]$ ratio is usually greater than 100, substantially favoring phosphorolysis. We see here an example of how the cell can alter the free-energy change to favor a reaction's occurrence by altering the ratio of substrate and product.

The phosphorolytic cleavage of glycogen is energetically advantageous because the released sugar is already phosphorylated. In contrast, a hydrolytic cleavage would yield glucose, which would then have to be phosphorylated at the expense of a molecule of ATP

to enter the glycolytic pathway. An additional advantage of phosphorolytic cleavage for muscle cells is that no transporters exist for glucose 1-phosphate, which is negatively charged under physiological conditions, and so it cannot be transported or diffuse out of the cell.

Mechanism: Pyridoxal phosphate participates in the phosphorolytic cleavage of glycogen

The special challenge faced by phosphorylase is to cleave glycogen phosphorolytically rather than hydrolytically to save the ATP required to phosphorylate free glucose. Thus, water must be excluded from the active site. Phosphorylase is a dimer of two identical 97-kDa subunits, each compactly folded into an amino-terminal domain containing a glycogen-binding site and a carboxyl-terminal domain (**Figure 21.5**). The catalytic site in each subunit is located in a deep crevice formed by residues from both domains. Substrates bind synergistically, causing the crevice to narrow, thereby excluding water.

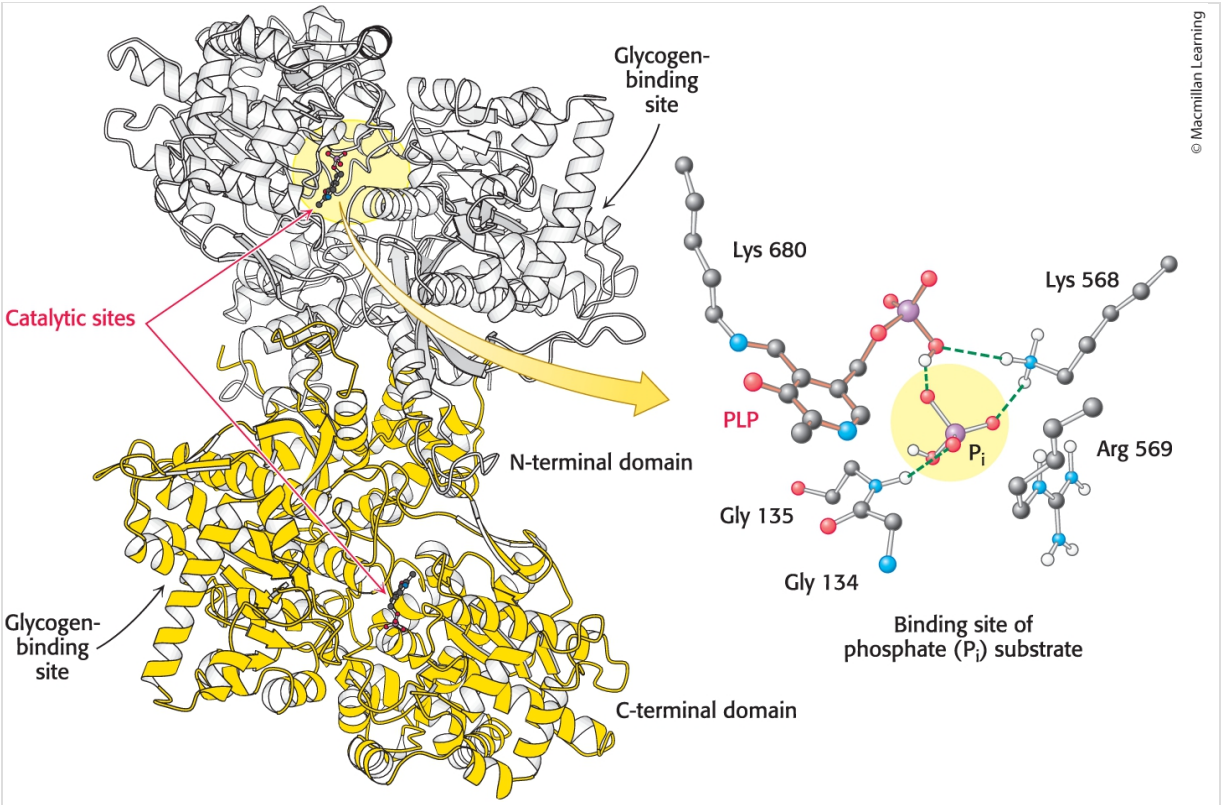


FIGURE 21.5 Glycogen phosphorylase forms a homodimer with a pyridoxal phosphate (PLP) group in each active site. One subunit is shown in white and the other in yellow. Each catalytic site includes a PLP group linked to lysine 680 of the enzyme. The binding site for the phosphate (P_i) substrate is shown. Notice that the catalytic site lies between the C-terminal domain and the glycogen-binding site. A narrow crevice, which binds four or five glucose units of glycogen, connects the two sites. The separation of the sites allows the catalytic site to phosphorolyze several glucose units before the enzyme must rebind the glycogen substrate.

[Drawn from 1NOI.pdb.]

INTERACT with this model in Achieve

What is the mechanistic basis of the phosphorolytic cleavage of glycogen? Several clues suggest a mechanism. First, both the glycogen substrate and the glucose 1-phosphate product have an α configuration at C-1. A direct attack by phosphate on C-1 of a sugar

would invert the configuration at this carbon atom because the reaction would proceed through a pentacovalent transition state. The observation that the glucose 1-phosphate formed has an α rather than a β configuration suggests that an even number of steps (most simply, two) is required. A likely explanation for these results is that a carbocation intermediate is formed from the glucose residue.

A second clue to the catalytic mechanism of phosphorylase is its requirement for the coenzyme **pyridoxal phosphate (PLP)**, a derivative of pyridoxine (vitamin B_6, Section 15.4). The aldehyde group of this coenzyme forms a Schiff-base linkage with a specific lysine side chain of the enzyme (**Figure 21.6**). Structural studies indicate that the reacting orthophosphate group takes a position between the $5'$-phosphate group of PLP and the glycogen substrate (**Figure 21.7**). The $5'$-phosphate group of PLP acts in tandem with orthophosphate by serving as a proton donor and then as a proton acceptor (i.e., as a general acid–base catalyst). Orthophosphate (in the HPO_4^{2-} form) donates a proton to the oxygen atom attached to carbon 4 of the departing glycogen chain and simultaneously acquires a proton from PLP. The carbocation intermediate formed in this step is then attacked by orthophosphate to form α-glucose 1-phosphate, with the concomitant return of a proton to pyridoxal phosphate.

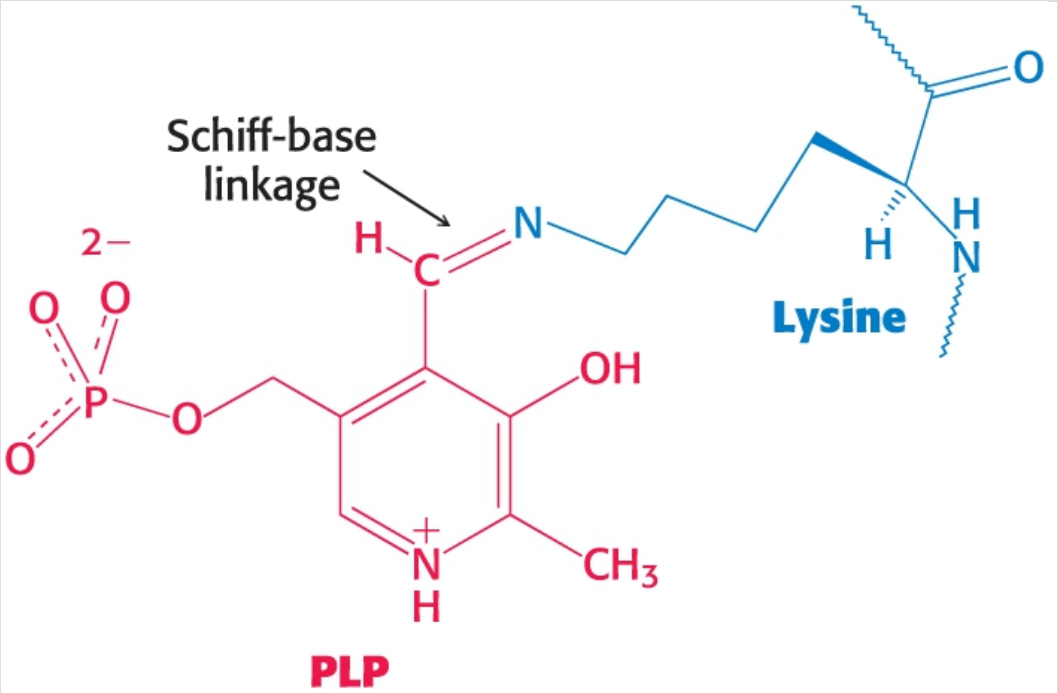


FIGURE 21.6 PLP forms a Schiff-base linkage with lysine. A pyridoxal phosphate (PLP) group (red) forms a Schiff base with a lysine residue (blue) at the active site of phosphorylase, where it functions as a general acid–base catalyst.

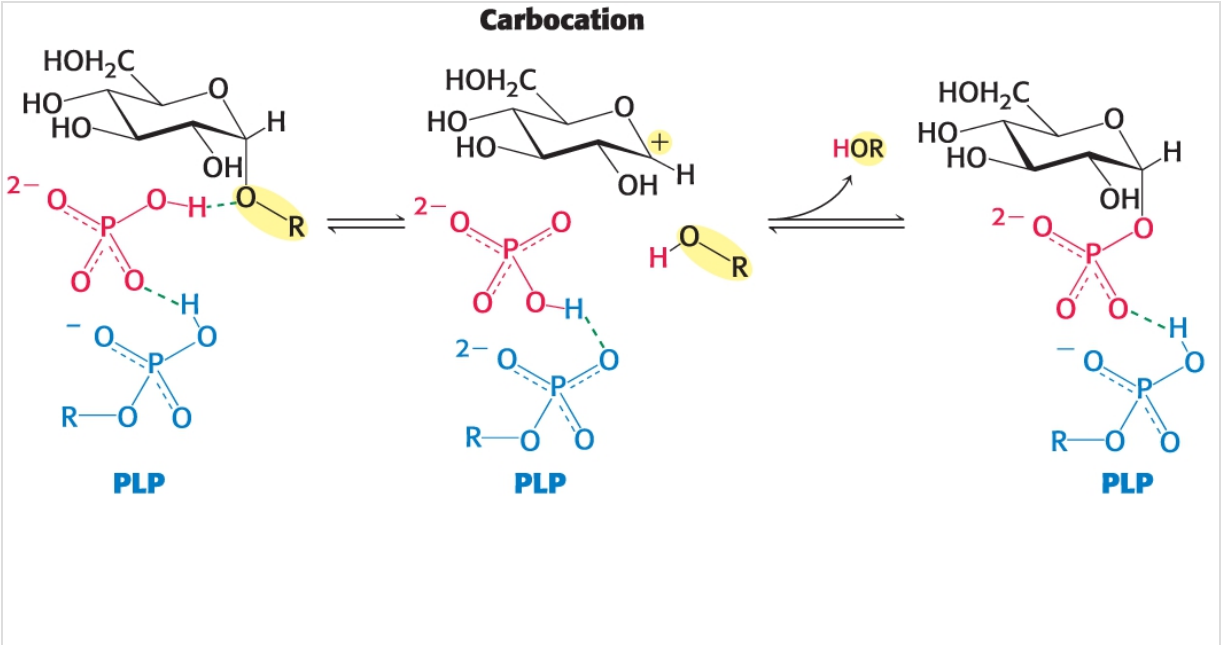


FIGURE 21.7 The mechanism of phosphorylase involves PLP and the formation of a carbocation. A bound HPO_4^{2-} group (red) favors the cleavage of the glycosidic bond by donating a proton to the C-4 oxygen of the departing glycosyl group (black).



The glycogen-binding site is 30 Å away from the catalytic site (Figure 21.5), but it is connected to the catalytic site by a narrow crevice able to accommodate four or five glucose units. The large separation between the binding site and the catalytic site enables the enzyme to phosphorolyze many residues without having to dissociate and reassociate after each catalytic cycle. An enzyme that can catalyze many reactions without having to dissociate and reassociate after each catalytic step is said to be *processive* — a property of enzymes that synthesize and degrade large polymers. We will see such enzymes again when we consider DNA and RNA synthesis.

Debranching enzyme also is needed for the breakdown of glycogen

Glycogen phosphorylase acting alone degrades glycogen to a limited extent. The enzyme can break α-1,4-glycosidic bonds on glycogen branches but soon encounters an obstacle. The α-1,6-glycosidic bonds at the branch points are not susceptible to cleavage by phosphorylase. Indeed, phosphorylase stops cleaving α-1,4 linkages when it reaches a terminal residue four residues away from a branch point. Because about 1 in 12 residues is branched, cleavage by the phosphorylase alone would come to a halt after the release of eight glucose molecules per branch.

How can the remainder of the glycogen molecule be mobilized for use as a fuel? Two additional enzyme activities are necessary to remodel glycogen for continued degradation by the phosphorylase (Figure 21.8).

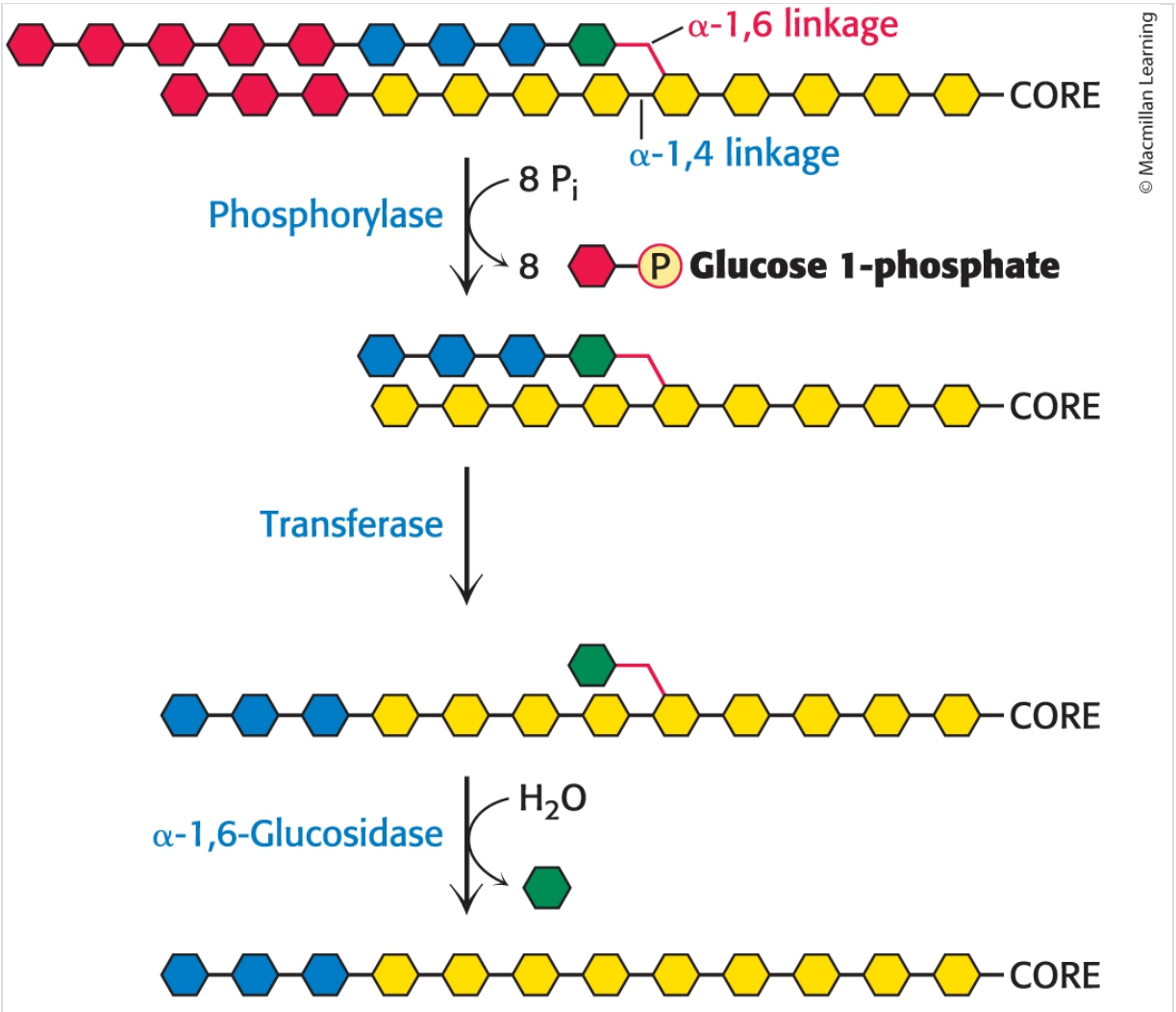
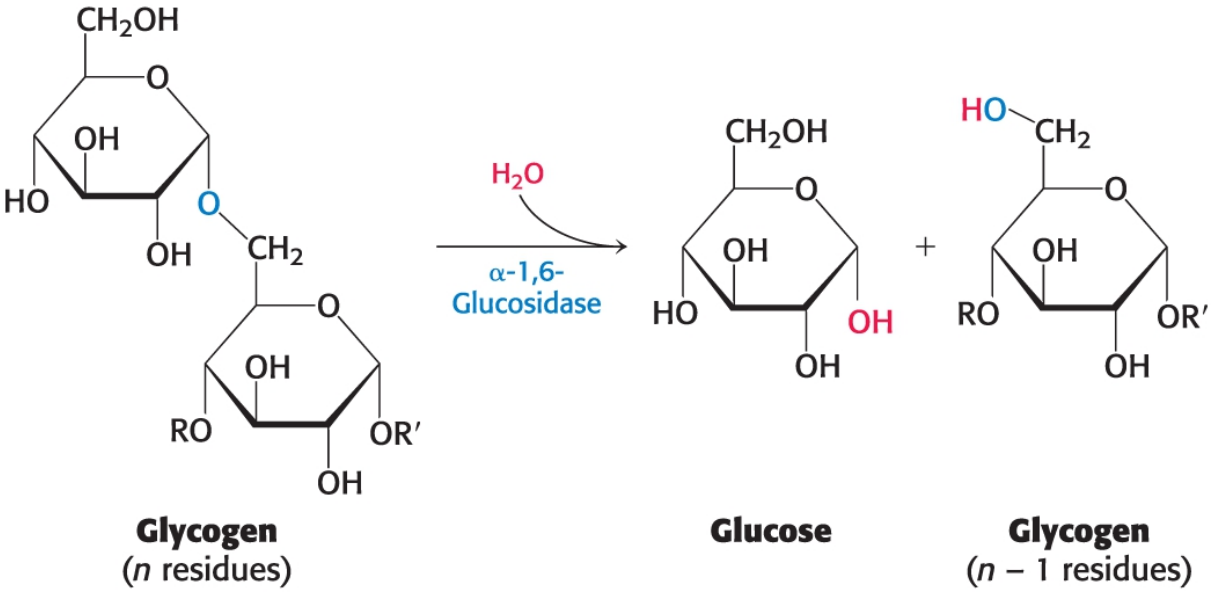


FIGURE 21.8 Glycogen remodeling requires three distinct catalytic activities. First, α-1,4-glycosidic bonds on each branch are cleaved by phosphorylase, leaving four residues along each branch. The transferase shifts a block of three glucosyl residues from one outer branch to the other. In this reaction, the α-1,4-glycosidic link between the blue and the green residues is broken and a new α-1,4 link between the blue and the yellow residues is formed. The green residue is then removed by α-1,6-glucosidase, leaving a linear chain with all α-1,4 linkages, suitable for further cleavage by phosphorylase.

A transferase shifts a block of three glucosyl residues from one outer branch to another, thus exposing a single glucose residue joined by an α-1,6-glycosidic linkage. The α-1,6-glucosidase activity then hydrolyzes the α-1,6-glycosidic bond.



In eukaryotes, the transferase and the α-1,6-glucosidase activities are present in a single 160-kDa protein, called *debranching enzyme*, providing yet another example of a bifunctional enzyme. A free glucose molecule is released and then phosphorylated by the glycolytic enzyme hexokinase, if the glucose is to be processed by glycolysis or the pentose phosphate pathway. Thus, the transferase and α-1,6-glucosidase activities of debranching enzyme convert the

branched structure into a linear one, which paves the way for further cleavage by phosphorylase.

Phosphoglucomutase converts glucose 1-phosphate into glucose 6-phosphate

Glucose 1-phosphate formed in the phosphorolytic cleavage of glycogen must be converted into glucose 6-phosphate to enter the metabolic mainstream. This shift of a phosphoryl group is catalyzed by phosphoglucomutase. Recall that this enzyme is also used in galactose metabolism (Section 16.2). To cause this shift, the enzyme exchanges a phosphoryl group with the substrate (**Figure 21.9**). The key to this mechanism is that the catalytic site of an active mutase molecule already contains a phosphorylated serine residue. This phosphoryl group is transferred from the serine residue to the C-6 hydroxyl group of glucose 1-phosphate to form glucose 1,6-bisphosphate. To regenerate the phosphoserine and complete the mechanism, the C-1 phosphoryl group of the bisphosphate intermediate is then shuttled to the same serine residue, resulting in the formation of glucose 6-phosphate and the regeneration of the phosphoenzyme.

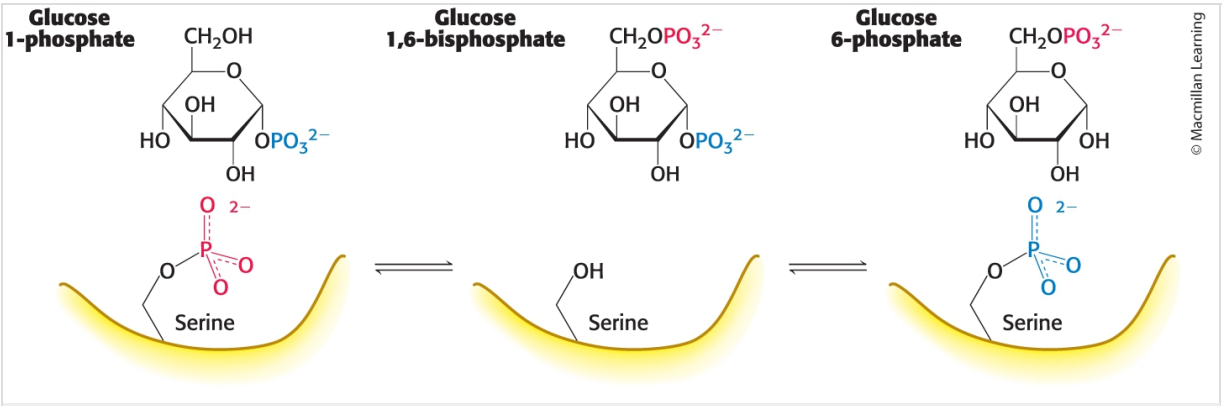


FIGURE 21.9 Phosphoglucomutase transfers a phosphoryl group to the substrate. A different phosphoryl group is transferred back to restore the enzyme to its initial state.

Self-Check Question



The complete oxidation of glucose 6-phosphate derived from free glucose yields 30 molecules ATP, whereas glucose 6-phosphate derived from glycogen yields 31 molecules of ATP. How can you account for this difference?

The liver contains glucose 6-phosphatase, a hydrolytic enzyme absent from muscle

A major function of the liver is to maintain a nearly constant concentration of glucose in the blood to keep the brain, red blood cells, and other tissues adequately supplied. The liver achieves this by releasing glucose into the blood between meals and during muscular activity through the action of glucose 6-phosphatase, the last enzyme in gluconeogenesis (Section 16.4). This enzyme hydrolytically cleaves the phosphoester linkage to form orthophosphate and free glucose, which can then exit the liver by the action of GLUT transporters (Section 16.1). Recall that glucose 6-phosphatase is located on the lumenal side of the smooth endoplasmic reticulum membrane, and so glucose 6-phosphate is transported into the endoplasmic reticulum while glucose and orthophosphate are then shuttled back into the cytoplasm (Section 16.4).

$$\text{Glucose 6-phosphate} + H_2O \rightarrow \text{glucose} + P_i$$

Glucose 6-phosphatase is absent from most other tissues. Muscle tissues retain glucose 6-phosphate for the generation of ATP. In contrast, glucose is not a major fuel for the liver.

Self-Check Question



What four enzymes are required for the liver to release glucose into the blood when an animal is asleep and fasting?

21.3 Phosphorylase Is Regulated by Allosteric Interactions and Controlled by Reversible Phosphorylation

Glycogen degradation is precisely controlled by multiple interlocking mechanisms, with the enzyme glycogen phosphorylase playing a central role. Phosphorylase is regulated by several allosteric effectors that signal the energy state of the cell, as well as controlled by reversible phosphorylation, which is responsive to hormones such as insulin, epinephrine, and glucagon. We will examine the differences in the control of two isozymic forms of glycogen phosphorylase: one specific to liver and one specific to skeletal muscle. These differences are because the liver maintains glucose homeostasis of the organism as a whole, whereas the muscle uses glucose to produce energy for itself.

Liver phosphorylase produces glucose for use by other tissues

The dimeric phosphorylase exists in two interconvertible forms: a usually *active* phosphorylated *a* form and a usually *inactive* unphosphorylated *b* form (**Figure 21.10**). Each of these two forms exists in equilibrium between an active relaxed (R) state and a much less active tense (T) state, but the equilibrium for phosphorylase *a* favors the active R state, whereas the equilibrium for phosphorylase *b* favors the less-active T state (**Figure 21.11**).

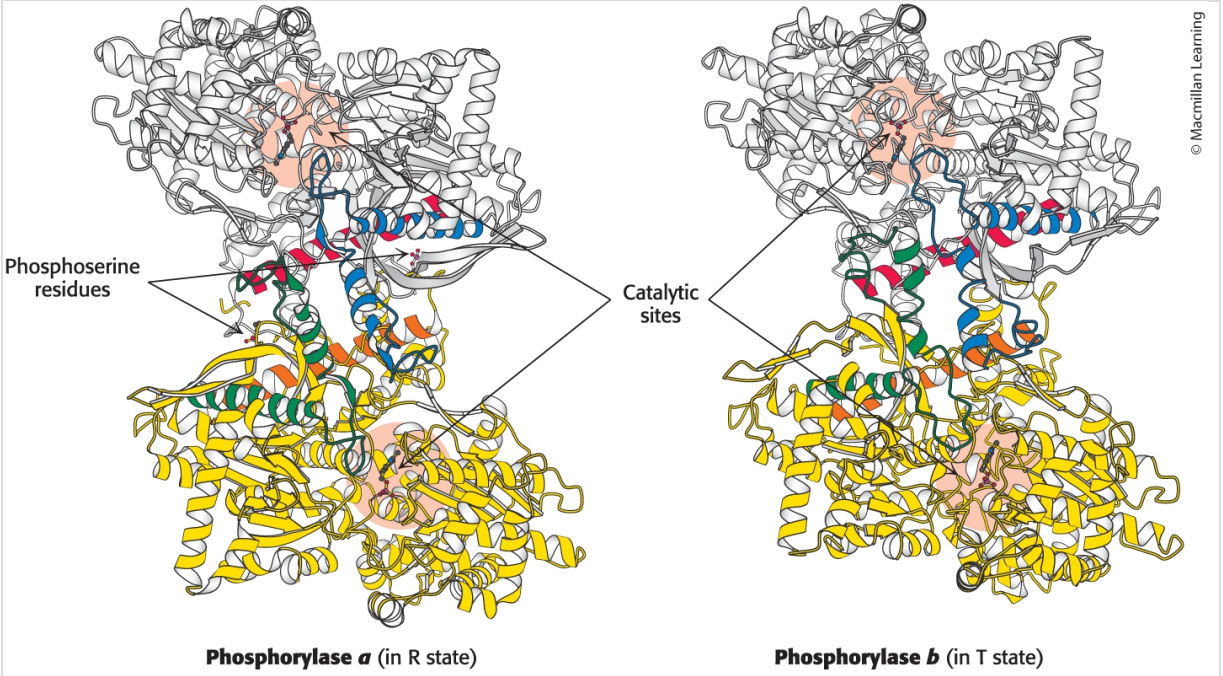


FIGURE 21.10 Phosphorylase exists in two distinct quaternary states. Phosphorylase *a* is phosphorylated on serine 14 of each subunit. This modification favors the structure of the more-active R state. One subunit is shown in white, with helices and loops important for regulation shown in blue and red. The other subunit is shown in yellow, with the regulatory structures shown in orange and green. Phosphorylase *b* is not phosphorylated and exists predominantly in the T state. Notice that the catalytic sites are partly occluded in the T state.

[Drawn from 1GPA.pdb and 1NOJ.pdb.]

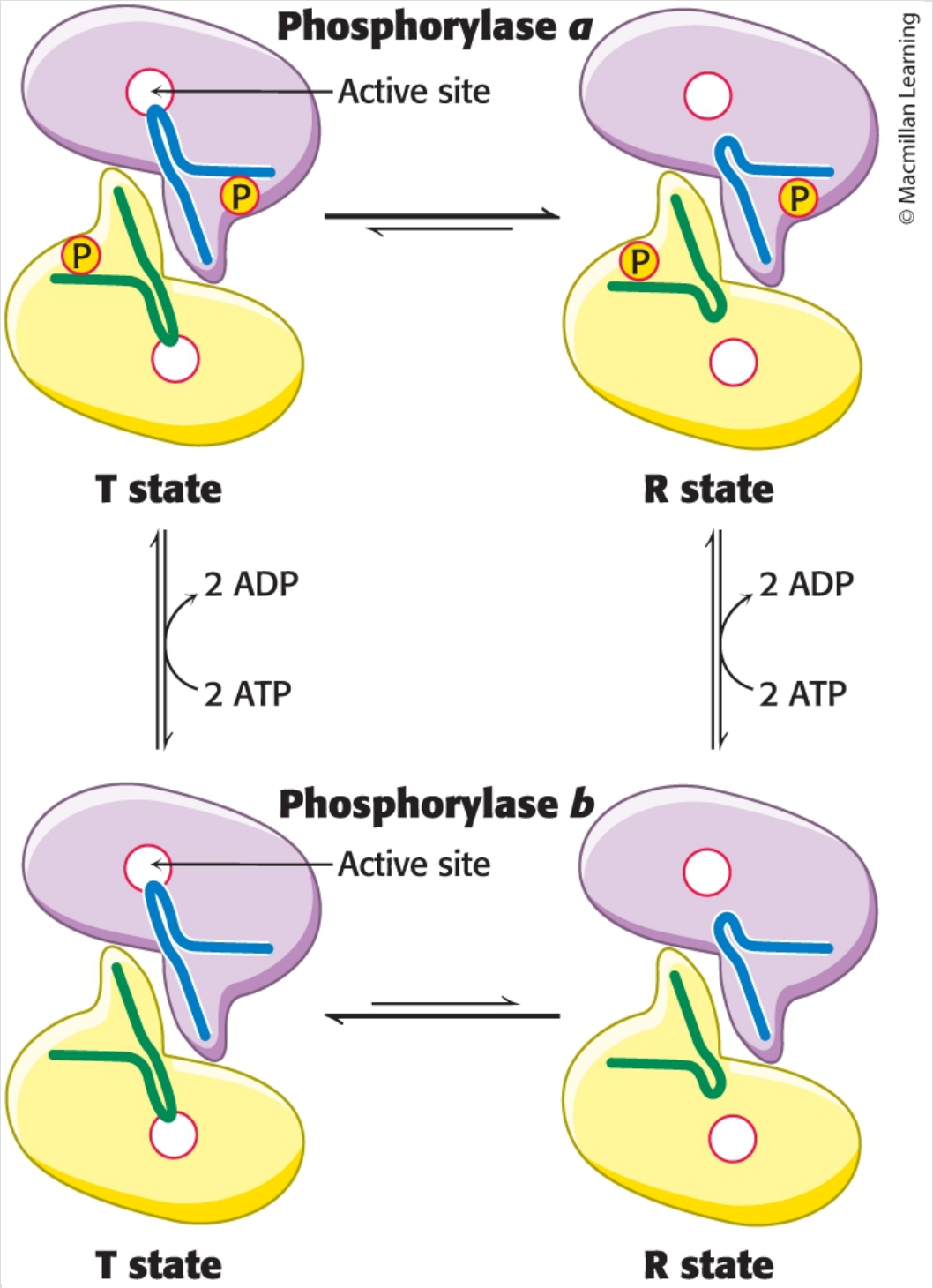


FIGURE 21.11 Phosphorylase is regulated by phosphorylation. Both phosphorylase *b* and phosphorylase *a* exist as equilibria between an active R state and a less-active T state. Phosphorylase *b* is usually inactive because the equilibrium favors the T state. Phosphorylase *a* is usually active because the equilibrium favors the R state. Regulatory structures are shown in blue and green.

The role of glycogen degradation in the liver is to form glucose for export to other tissues when the blood-glucose concentration is low. Consequently, we can think of the default state of liver phosphorylase as being the *a* form: glucose is to be generated unless the enzyme is signaled otherwise. The liver phosphorylase *a* form thus exhibits the most responsive R ↔ T transition (Figure 21.12). The binding of glucose to the active site shifts the *a* form from the active R state to the less-active T state. In essence, the enzyme reverts to the low-activity T state only when it detects the presence of sufficient glucose. If glucose is present in the diet, there is no need to degrade glycogen.

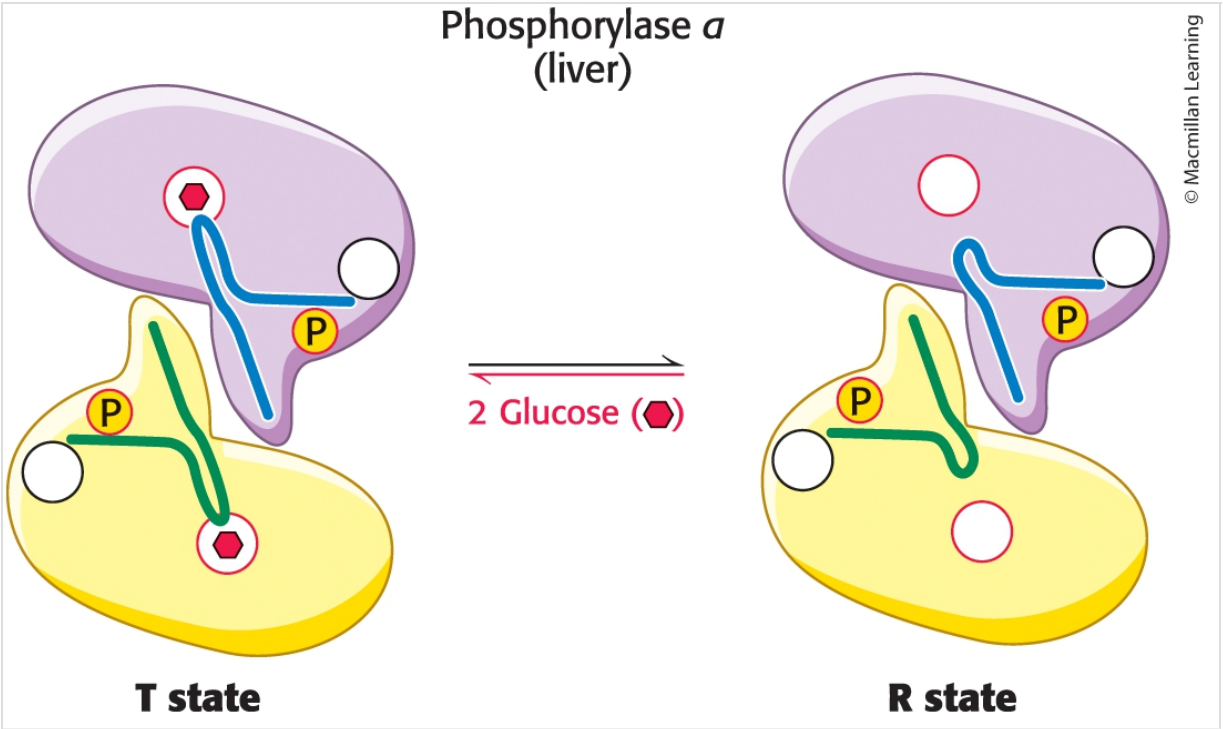


FIGURE 21.12 Liver phosphorylase is allosterically inhibited by glucose. The binding of glucose to phosphorylase *a* shifts the equilibrium to the T state and inactivates the enzyme. Thus, glycogen is not mobilized when glucose is already abundant.

Muscle phosphorylase is regulated by changes in AMP and ATP concentrations

In contrast to the liver isozyme, the default state of muscle phosphorylase is the *b* form, owing to the fact that, for muscle, phosphorylase must be primarily active only during muscle contraction. Muscle phosphorylase *b* is activated by the presence of high concentrations of AMP, which binds to a nucleotide-binding site and stabilizes the conformation of phosphorylase *b* in the active R state (**Figure 21.13**). Thus, when a muscle contracts and ATP is converted into AMP by the sequential action of myosin (Section 6.4) and adenylate kinase (Section 16.3), the phosphorylase is signaled to degrade glycogen. ATP acts as a negative allosteric effector by competing with AMP. Thus, the transition of phosphorylase *b* between the active R state and the less-active T state is controlled by the concentrations of these metabolites in muscle cells. If ATP is unavailable, glucose 6-phosphate may bind at the ATP-binding site and stabilize the less-active state of phosphorylase *b*, an example of feedback inhibition. In resting muscle, phosphorylase *b* is inactive because of the inhibitory effects of ATP and glucose 6-phosphate. In contrast, phosphorylase *a* is fully active, regardless of the concentration of AMP, ATP, and glucose 6-phosphate.

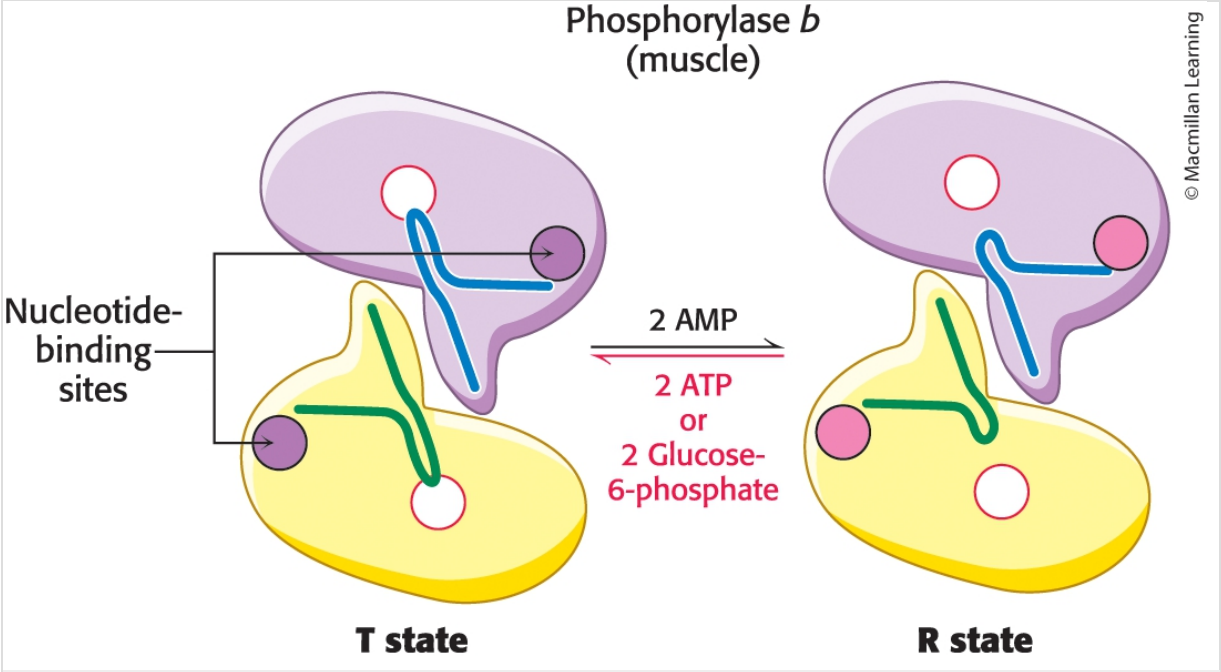


FIGURE 21.13 Muscle phosphorylase is allosterically regulated by ATP, AMP, and glucose 6-phosphate. A low energy charge, represented by high concentrations of AMP, favors the transition to the R state. ATP and glucose 6-phosphate stabilize the T state.

Unlike the enzyme in muscle, the liver phosphorylase is insensitive to regulation by AMP because the liver does not undergo the dramatic changes in the concentrations of AMP and ATP seen in a contracting muscle. We see here a clear example of the use of isozymes to establish the tissue-specific biochemical properties of the liver and muscle. In human beings, liver phosphorylase and muscle phosphorylase are approximately 90% identical in amino acid sequence, yet the 10% difference results in subtle but important shifts in the regulation of the two enzymes.

Self-Check Question



Crystals of phosphorylase *a* grown in the presence of glucose shatter when a substrate such as glucose 1-phosphate is added. Why?

Biochemical characteristics of muscle fiber types differ

Not only do the biochemical needs of liver and muscle differ with respect to glycogen metabolism, but the biochemical needs of different muscle fiber types also vary. Skeletal muscle consists of three different fiber types: type I, or slow-twitch muscle; type IIb (also called type IIx), or fast-twitch fibers; and type IIa fibers that have properties intermediate between the other two fiber types.

- *Type I (slow-twitch) fibers rely predominantly on cellular respiration to derive energy.* These fibers are powered by fatty acid degradation and are rich in mitochondria, the site of fatty acid degradation and the citric acid cycle. As we will see in Chapter 22, fatty acids are an excellent energy storage form, but generating ATP from fatty acids is slower than from glycogen. Glycogen is not an important fuel for type I fibers, and consequently the amount of glycogen phosphorylase is low. Type I fibers power endurance activities.

- *Type IIb (fast-twitch) fibers use glycogen as their main fuel.* Consequently, the glycogen and glycogen phosphorylase are abundant. These fibers are also rich in glycolytic enzymes

needed to process glucose quickly in the absence of oxygen and poor in mitochondria. Type IIb fibers power burst activities such as sprinting and weight lifting.

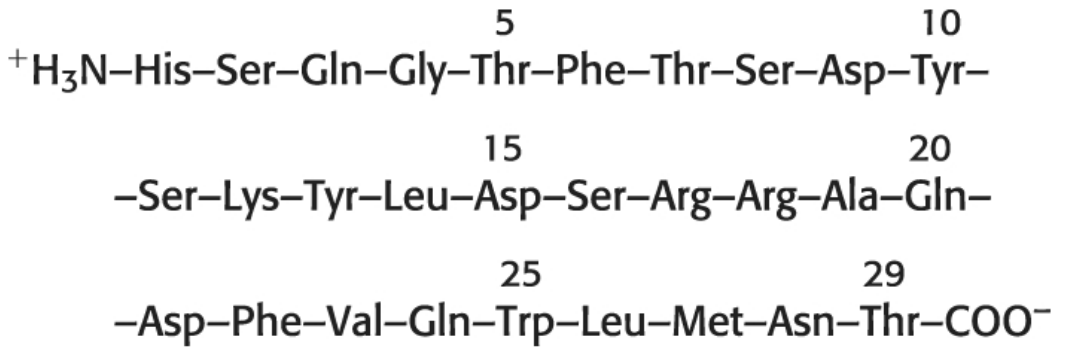
No amount of training can interconvert type I fibers and type IIb fibers. However, there is some evidence that type IIa fibers are "trainable"; that is, endurance training enhances the oxidative capacity of type IIa fibers, while burst activity training enhances the glycolytic capacity. Table 21.1 shows the biochemical profile of the fiber types.

TABLE 21.1 Biochemical characteristics of muscle fiber types

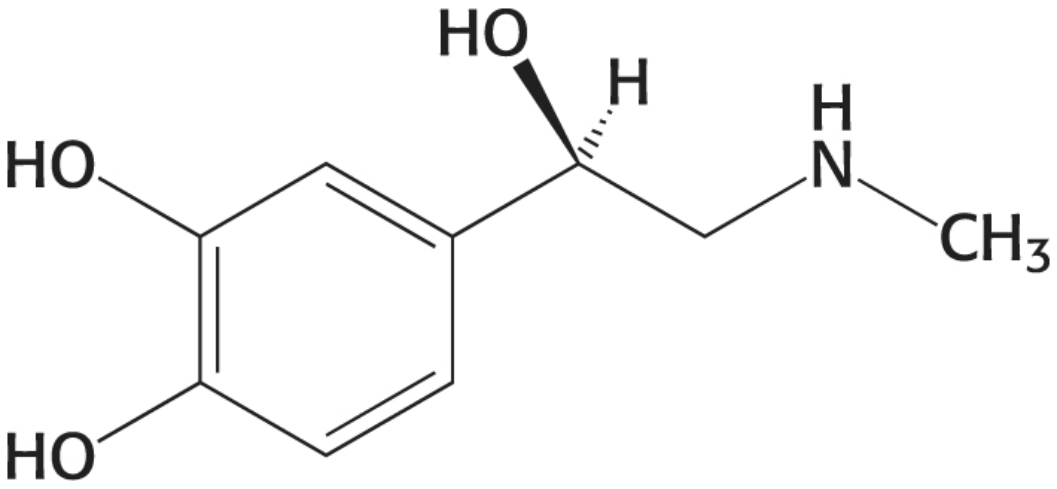
Characteristic	Type I	Type IIa	Type IIb
Fatigue resistance	High	Intermediate	Low
Mitochondrial density	High	Intermediate	Low
Metabolic type	Oxidative	Oxidative/glycolytic	Glycolytic
Myoglobin content	High	Intermediate	Low
Glycogen content	Low	Intermediate	High
Triacylglycerol content	High	Intermediate	Low
Glycogen phosphorylase activity	Low	Intermediate	High
Phosphofructokinase activity	Low	Intermediate	High
Citrate synthase activity	High	Intermediate	Low

Phosphorylation promotes the conversion of phosphorylase *b* to phosphorylase *a*

In both liver and muscle, hormones initiate the conversion of phosphorylase *b* into phosphorylase *a* by the phosphorylation of a single serine residue (serine 14) in each subunit. Low blood concentration of glucose leads to the secretion of the peptide hormone **glucagon** from the α cells of the pancreas, which results in phosphorylation of the enzyme, converting it to the phosphorylase *a* form in liver. The hormone **epinephrine (adrenaline)**, a catecholamine derived from tyrosine, also induces this conversion when it binds to receptors in muscle and liver.



Glucagon



Epinephrine

Emotions like the excitement of exercise or fear will cause release of epinephrine from the adrenal medulla into the blood. Epinephrine binds to receptors in muscle (and in liver), again inducing the phosphorylation of phosphorylase *b* to phosphorylase *a*. The regulatory enzyme **phosphorylase kinase** catalyzes this covalent modification in response to either hormone.

Comparison of the structures of phosphorylase *a* in the R state and phosphorylase *b* in the T state reveals that subtle structural changes at the subunit interfaces are transmitted to the active sites (Figure 21.10). The transition from the T state (the prevalent state of phosphorylase *b*) to the R state (the prevalent state of phosphorylase *a*) entails a 10-degree rotation around the twofold axis of the dimer. Most important, this transition is associated with structural changes in α helices that move a loop out of the active site of each subunit. Thus, the T state is less active because the catalytic site is partly blocked. In contrast, in the R state, the catalytic site is more accessible, and a binding site for orthophosphate is well organized.

Phosphorylase kinase is activated by phosphorylation and calcium ions

Phosphorylase kinase converts phosphorylase *b* into the *a* form by attaching a phosphoryl group. The subunit composition of phosphorylase kinase in skeletal muscle is $(\alpha\beta\gamma\delta)_4$, and the mass of this very large protein is 1300 kDa. The enzyme consists of two $(\alpha\beta\gamma\delta)_2$ lobes that are joined by a β_4 bridge that is the core of the enzyme and serves as a scaffold for the other subunits (**Figure 21.14**). The γ subunit contains the active site, while all of the remaining subunits ($\approx 90\%$ by mass) play regulatory roles. The δ subunit is the Ca^{2+} binding protein calmodulin, a calcium sensor that stimulates many enzymes in eukaryotes (Section 14.2).

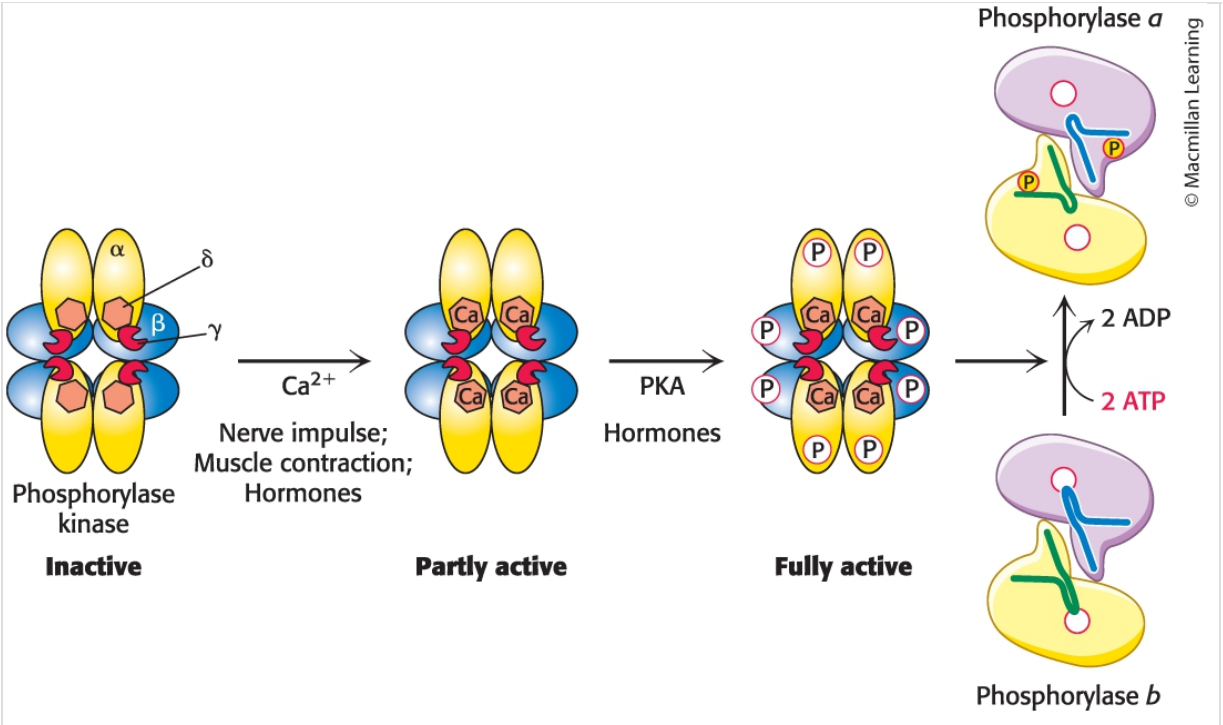


FIGURE 21.14 Phosphorylase kinase is activated by calcium ions and hormonally controlled phosphorylation. Phosphorylase kinase, an $(\alpha\beta\gamma\delta)_4$ assembly, is partly

activated by Ca^{2+} binding to the δ subunits. Activation is maximal when the β and α subunits are phosphorylated in response to hormonal signals. When active, the enzyme converts phosphorylase *b* into phosphorylase *a*.



Activation of phosphorylase kinase is initiated when Ca^{2+} binds to the δ subunit. This mode of activation of the kinase is especially noteworthy in muscle, where muscle contraction is triggered by the release of Ca^{2+} from the sarcoplasmic reticulum (Figure 21.14). Maximal activation is achieved with the phosphorylation of the β and α subunits of the Ca^{2+}-bound kinase. The α and β subunits of the calcium-bound enzyme are targets of protein kinase A. The β subunit is phosphorylated first, followed by the phosphorylation of the α subunit. The stimulation of phosphorylase kinase is one step in a signal-transduction cascade initiated by signal molecules such as glucagon and epinephrine.

21.4 Glucagon and Epinephrine Signal the Need for Glycogen Breakdown

Protein kinase A (PKA) activates phosphorylase kinase, which in turn activates glycogen phosphorylase. But what activates PKA? What is the signal that ultimately triggers an increase in glycogen breakdown?

G proteins transmit the signal for the initiation of glycogen breakdown

Let's now explore in greater depth the signaling mechanisms of the two hormones that trigger glycogen breakdown: glucagon and epinephrine. Their activities are tissue-dependent. The liver is highly responsive to glucagon, which is released in response to low glucose concentrations in the blood. Physiologically, glucagon signifies the fasted state (**Figure 21.15**) and stimulates the liver to release glucose into the blood. In contrast, because muscle plays no regulatory role in maintaining glucose concentrations and cannot release glucose into the blood, muscle is insensitive to glucagon. Instead, muscular activity or its anticipation leads to the release of epinephrine, which markedly stimulates glycogen breakdown in muscle and, to a lesser extent, in the liver. The breakdown of liver glycogen in response to epinephrine is meant to provide adequate glucose to the muscles for the expected increase in muscle contraction following the initiation of the "fight-or-flight" response.

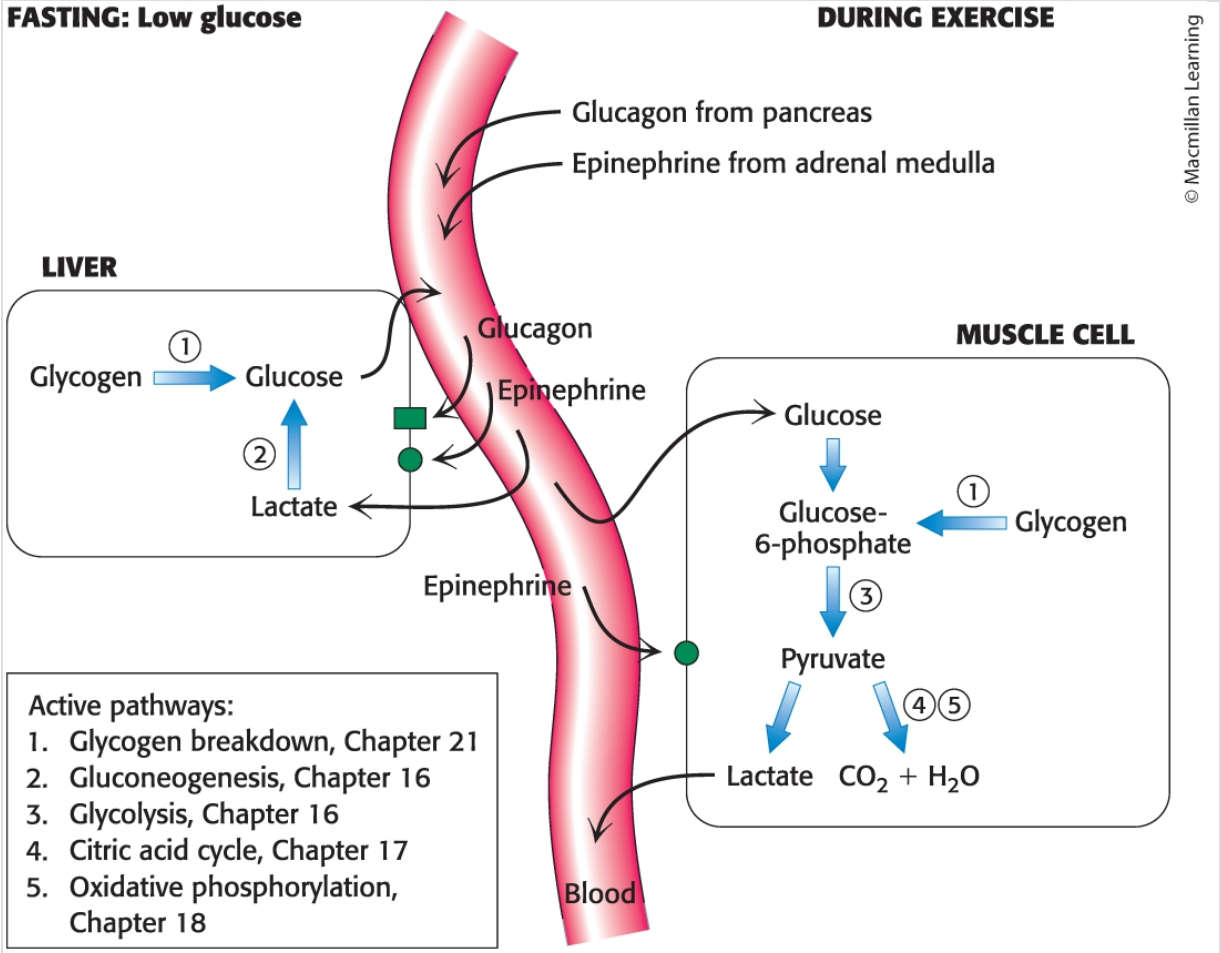


FIGURE 21.15 Glycogen breakdown is controlled by the combined effects of multiple hormones in a tissue-specific manner. Glucagon stimulates liver-glycogen breakdown when blood glucose is low. Epinephrine enhances glycogen breakdown in muscle and the liver to provide fuel for muscle contraction.

EXPLORE this pathway further in the Metabolic Map in Achieve

How do glucagon and epinephrine trigger the breakdown of glycogen? They initiate a cyclic AMP signal-transduction cascade (**Figure 21.16**):

1. The signal molecules glucagon and epinephrine bind to specific seven-transmembrane (7TM) receptors in the plasma

membranes of target cells (Section 14.2). Epinephrine binds to the β-adrenergic receptor in muscle, whereas glucagon binds to the glucagon receptor in the liver. These binding events activate the G_s protein: a specific external signal has been transmitted into the cell through structural changes, first in the receptor and then in the G protein.

2. The GTP-bound subunit of G_s activates the transmembrane protein adenylate cyclase. This enzyme catalyzes the formation of the second messenger cyclic AMP (cAMP) from ATP.

3. The elevated cytoplasmic concentration of cAMP activates PKA (Section 7.3). The binding of cAMP to inhibitory regulatory subunits of PKA triggers their dissociation from the catalytic subunits. The free catalytic subunits are now active.

4. PKA phosphorylates phosphorylase kinase, first on the β subunit and then on the α subunit, which activates glycogen phosphorylase.

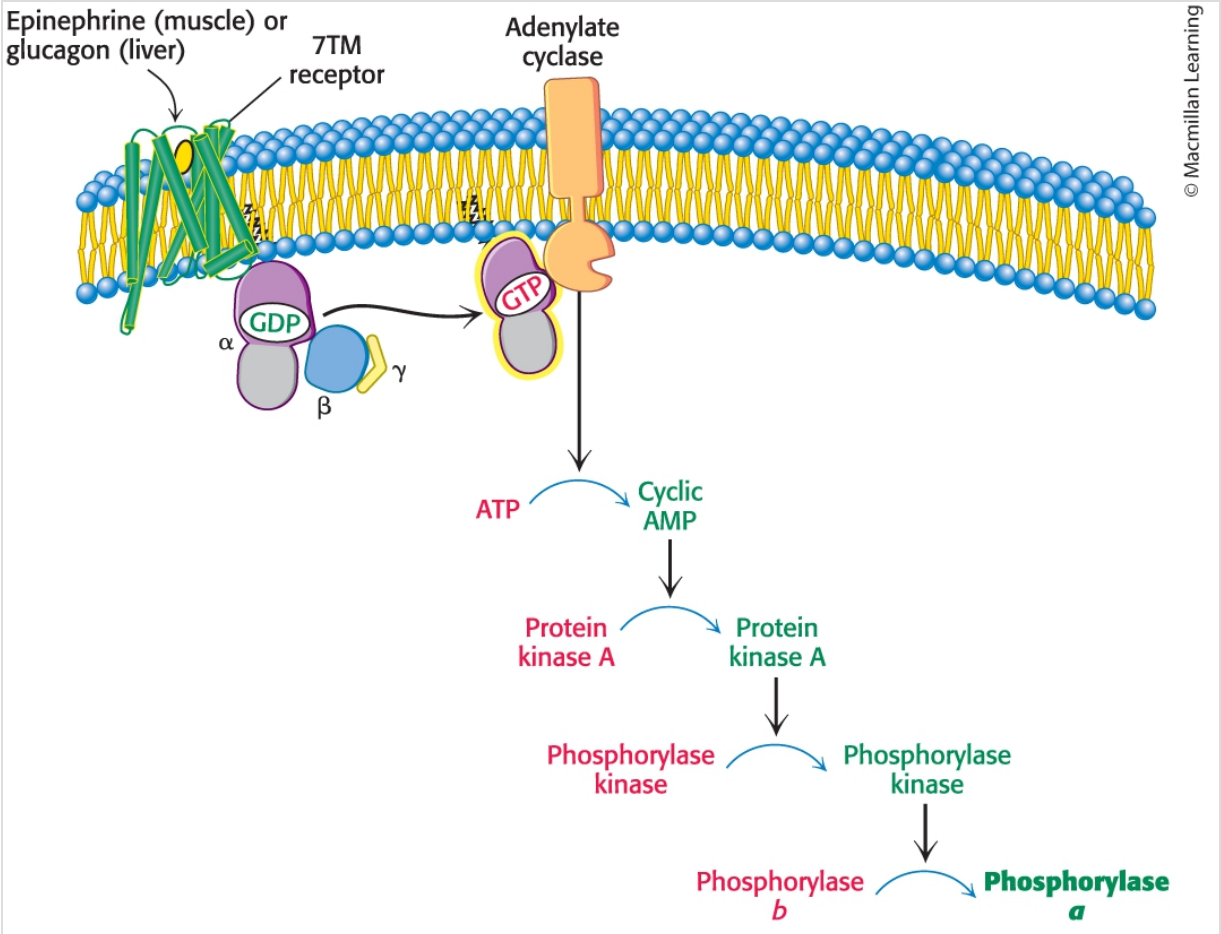


FIGURE 21.16 Glycogen degradation is stimulated by hormone binding to 7TM receptors. Hormone binding to 7TM receptors in the appropriate cells (liver or muscle) initiates a G-protein-dependent signal-transduction pathway that results in the phosphorylation and activation of glycogen phosphorylase. The inactive forms of the enzymes are shown in red and the active forms in green.

The signal-transduction processes in the liver are more complex than those in muscle. Epinephrine can also elicit glycogen degradation in the liver. However, in addition to binding to the β-adrenergic receptor, it binds to the 7TMα-adrenergic receptor, which then initiates the *phosphoinositide cascade* (Section 14.2) that induces the release of Ca^{2+} from endoplasmic reticulum stores. Recall that

the δ subunit of phosphorylase kinase is the Ca^{2+} sensor calmodulin. The binding of Ca^{2+} to calmodulin leads to a partial activation of phosphorylase kinase. Stimulation by both glucagon and epinephrine leads to maximal mobilization of liver glycogen.

The cyclic AMP cascade highly amplifies the effects of hormones, resulting in a high-gain system. Gain is the ratio of the output signal to the input signal. In the case of glycogen metabolism, the binding of a small number of hormone molecules to cell-surface receptors leads to the release of a very large number of glucose units. Indeed, much of the stored glycogen would be mobilized within seconds were it not for a counterregulatory system.

Glycogen breakdown must be rapidly turned off when necessary

It is crucial that the high-gain system of glycogen breakdown be terminated quickly to prevent the wasteful depletion of glycogen after energy needs have been met and to prevent dangerously high blood-glucose concentrations. When glucose needs have been satisfied, phosphorylase kinase and glycogen phosphorylase are dephosphorylated and inactivated. Simultaneously, glycogen synthesis is activated.

The signal-transduction pathway leading to the activation of glycogen phosphorylase is shut down automatically when secretion of the initiating hormone ceases. The inherent GTPase activity of the G protein converts the bound GTP into inactive GDP, and phosphodiesterases that are always present in the cell convert cyclic AMP into AMP. **Protein phosphatase 1 (PP1)** removes the

phosphoryl groups from phosphorylase kinase, thereby inactivating the enzyme. Finally, PP1 also removes the phosphoryl group from glycogen phosphorylase, converting the enzyme into the usually inactive *b* form.

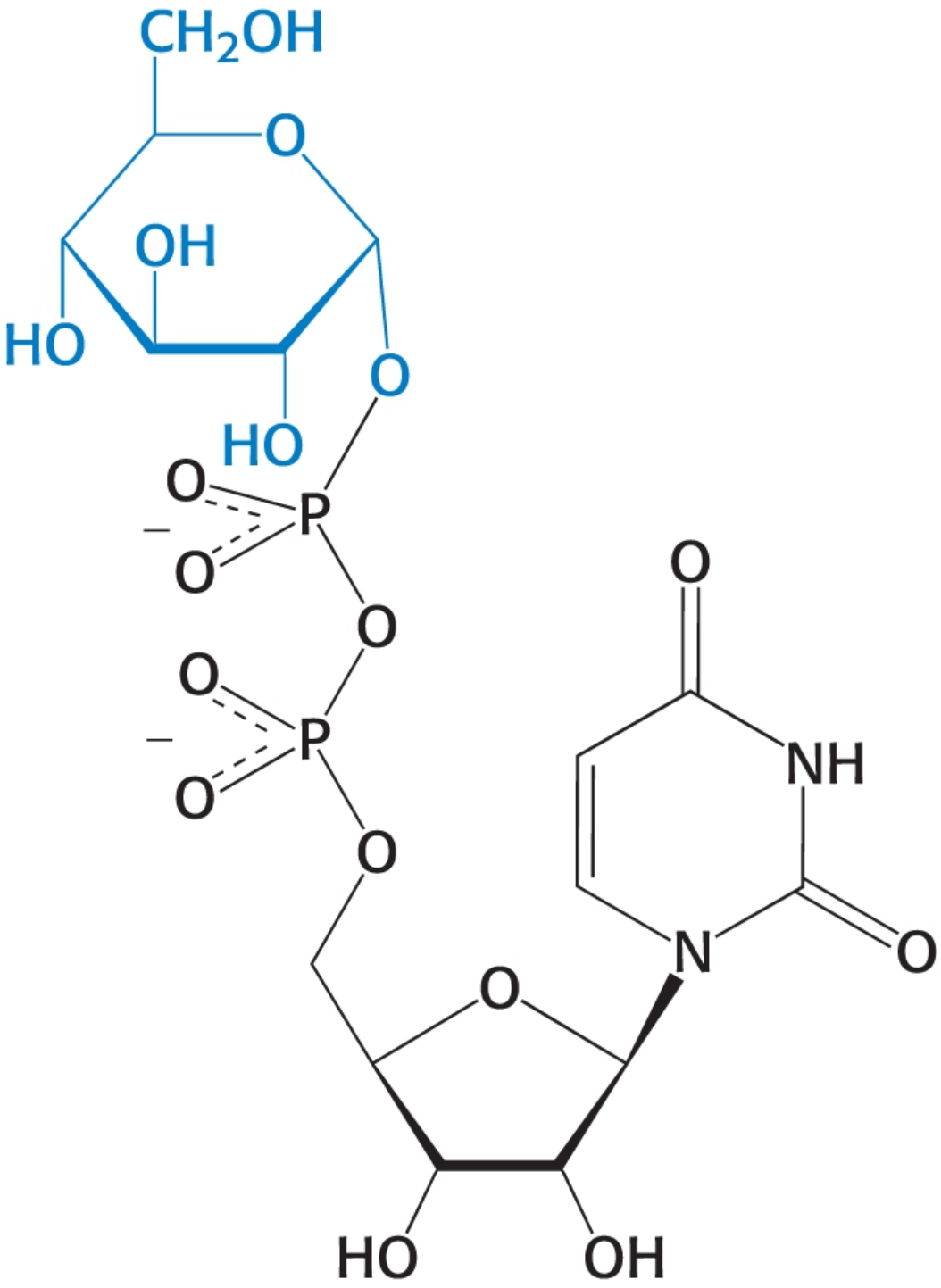
21.5 Glycogen Synthesis Requires Several Enzymes and Uridine Diphosphate Glucose

As we saw with glycolysis and gluconeogenesis (Chapter 16), related degradative and biosynthetic pathways rarely operate by precisely the same reactions in the forward and reverse directions. Glycogen metabolism provided the first known example of this important principle: separate pathways afford much greater flexibility, both in energetics and in control.

Glycogen is synthesized by a pathway that utilizes **uridine diphosphate glucose (UDP-glucose)** as the activated glucose donor.

$$\text{Synthesis: Glycogen}_n + \text{UDP–glucose} \rightarrow \text{glycogen}_{n+1} + \text{UDP}$$

$$\text{Degradation: Glycogen}_{n+1} + P_i \rightarrow \text{glycogen}_n + \text{glucose 1–phosphate}$$

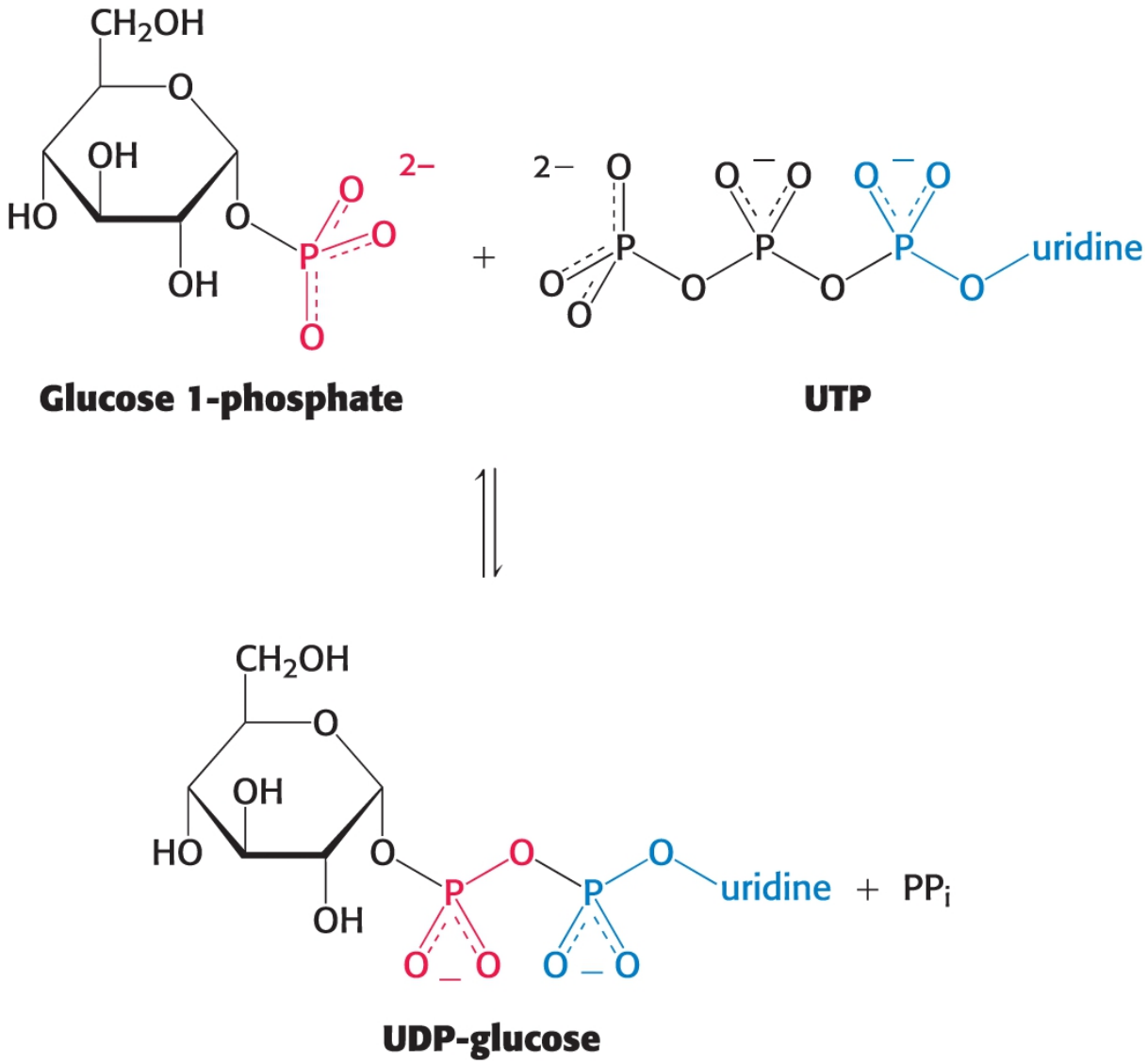


Uridine diphosphate glucose (UDP-glucose)

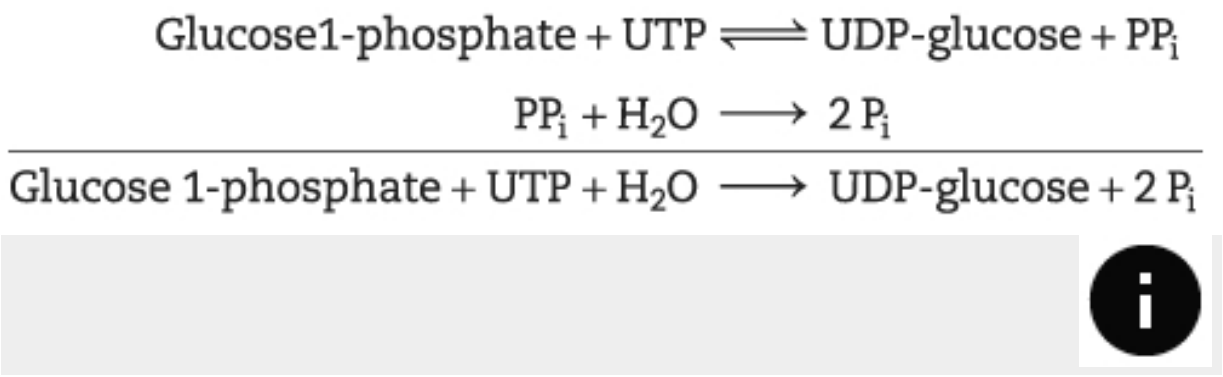
UDP-glucose is an activated form of glucose

UDP-glucose, the glucose donor in the biosynthesis of glycogen, is called an *activated* form of glucose, just as ATP and acetyl CoA are activated forms of orthophosphate and acetate, respectively. The C-1 carbon atom of the glucosyl unit of UDP-glucose is activated because its hydroxyl group is esterified to the diphosphate moiety of UDP.

UDP-glucose is synthesized from glucose 1-phosphate and uridine triphosphate (UTP) in a reaction catalyzed by UDP-glucose pyrophosphorylase. This reaction liberates the outer two phosphoryl residues of UTP as pyrophosphate.



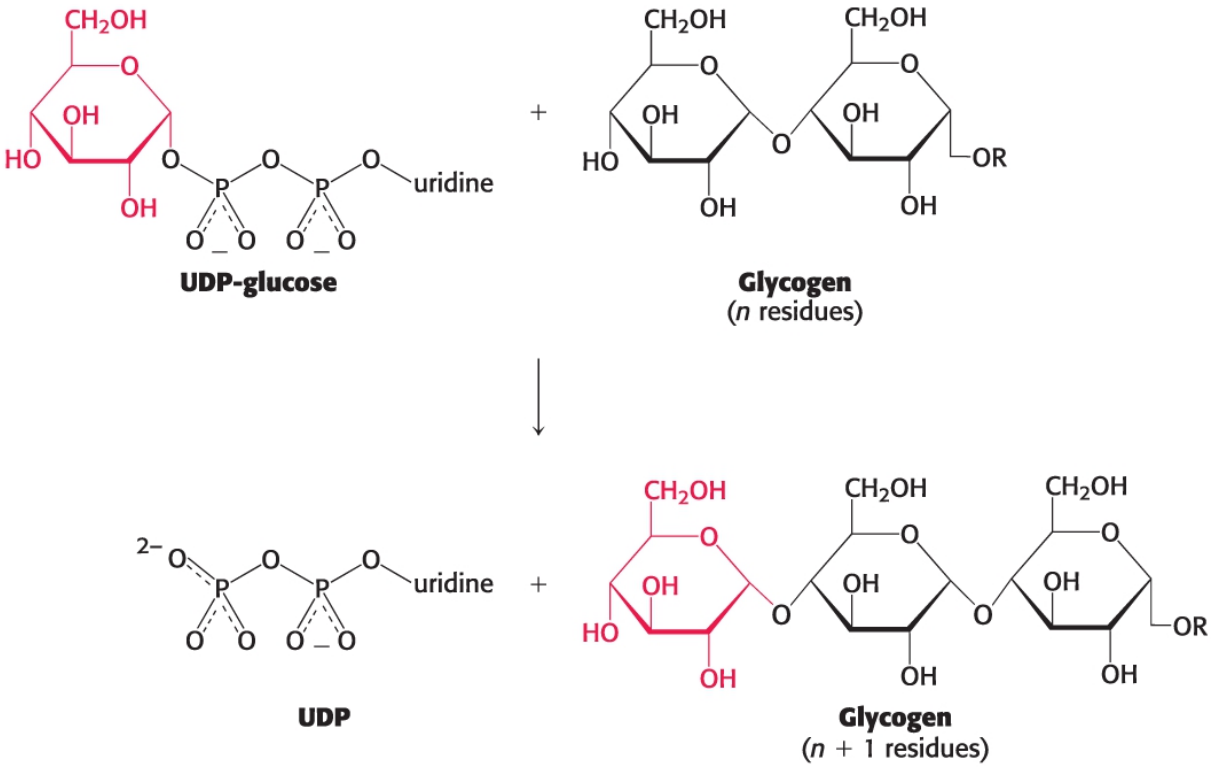
This reaction is readily reversible. However, pyrophosphate is rapidly hydrolyzed in vivo to orthophosphate by an inorganic pyrophosphatase, keeping the concentration of pyrophosphate consistently low. Thus, the essentially irreversible hydrolysis of pyrophosphate drives the synthesis of UDP-glucose because the concentration of one of the products is kept near zero, making ΔG large and negative.



The synthesis of UDP-glucose exemplifies another recurring theme in biochemistry: many biosynthetic reactions are driven by the hydrolysis of pyrophosphate.

Glycogen synthase catalyzes the transfer of glucose from UDP-glucose to growing chains

The key regulatory enzyme in glycogen synthesis is **glycogen synthase**, which adds new glucosyl units to the nonreducing terminal residues of glycogen. Humans have two isozymes of glycogen synthase: one is specific to the liver, while the other is expressed in muscle and other tissues. The activated glucosyl unit of UDP-glucose is transferred to the hydroxyl group at C-4 of a terminal residue to form an α-1,4-glycosidic linkage. UDP is displaced by the terminal hydroxyl group of the growing glycogen molecule.



Glycogen synthase can add glucosyl residues only to a polysaccharide chain already containing at least four residues. Thus, glycogen synthesis requires a primer. This priming function is carried out by **glycogenin**, a Mn^{2+}-requiring glycosyltransferase composed of two identical 37-kDa subunits. Each subunit of glycogenin catalyzes the formation of α-1,4-glucose polymers on the other subunit (*inter*molecular autoglycosylation), or within the same subunit (*intra*molecular autoglycosylation). UDP-glucose is used to processively add glucosyl units to the phenolic hydroxyl group of a specific tyrosine residue in each glycogenin subunit. This proceeds until the chains reach 10 to 20 glucosyl units in length, at which point glycogen synthase takes over to extend the glycogen molecules attached to each subunit. Thus, every glycogen molecule has a glycogenin monomer covalently attached at its core (Figure 21.2).

A branching enzyme forms α-1,6 linkages

Glycogen synthase catalyzes only the synthesis of α-1,4 linkages; another enzyme is required to form the α-1,6 linkages that make glycogen a branched polymer. Branching takes place after a number of glucosyl residues are joined in α-1,4 linkages by glycogen synthase (Figure 21.17).

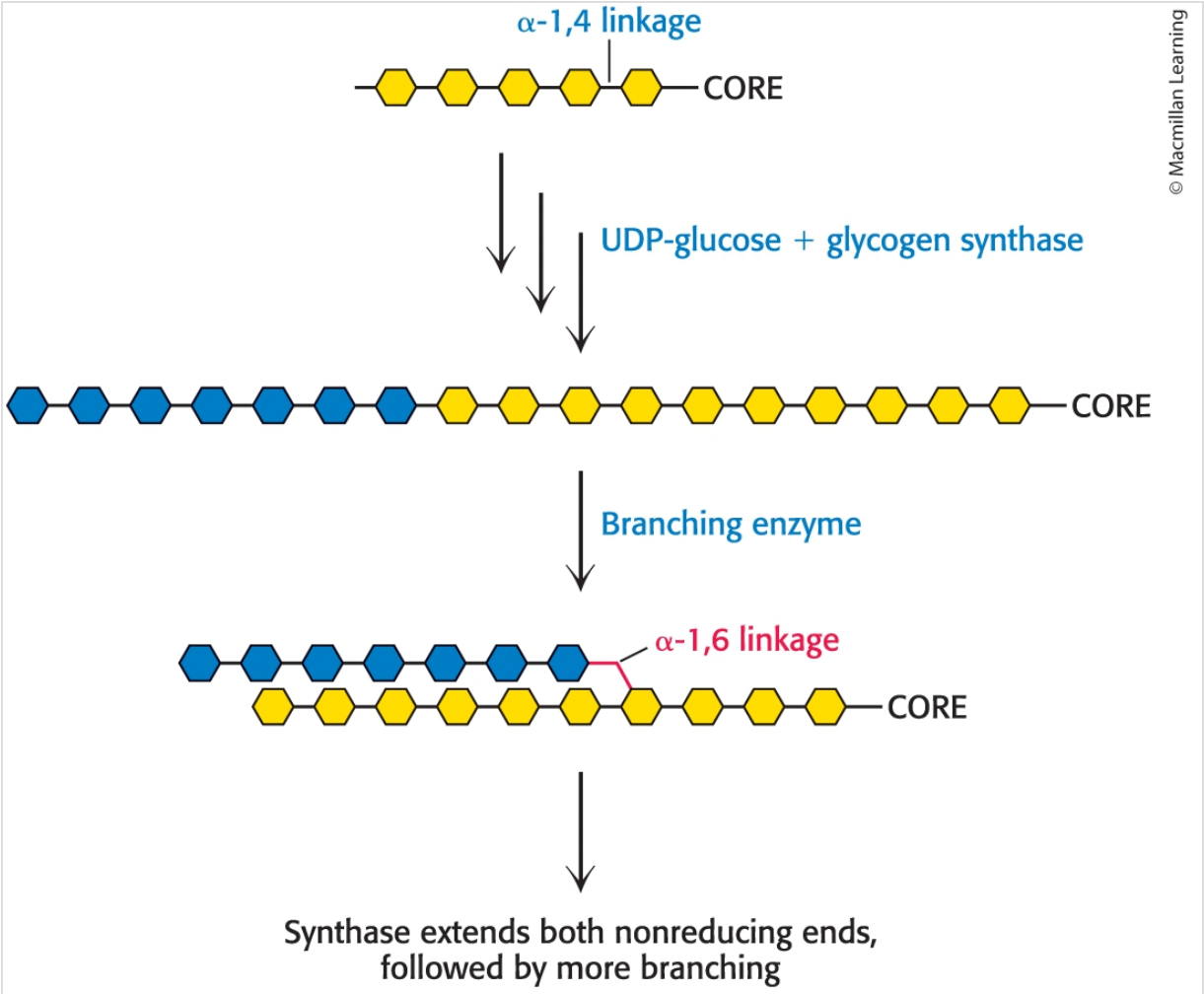


FIGURE 21.17 Branching enzyme removes approximately seven residues from the nonreducing end and reattaches them with an α-1,6 linkage.

A branch is created by the breaking of an α-1,4 link and the formation of an α-1,6 link, transferring a block of residues, typically seven, to a more interior site. The branching enzyme catalyzing this reaction requires that the block of residues must include the nonreducing terminus, and must come from a chain at least 11 residues long. In addition, the new branch point must be at least four residues away from a preexisting one.

Branching is important because it increases the solubility of glycogen. Furthermore, branching creates a large number of terminal residues, the sites of action of glycogen phosphorylase and synthase (**Figure 21.18**). Thus, branching increases the rate of glycogen synthesis and degradation.

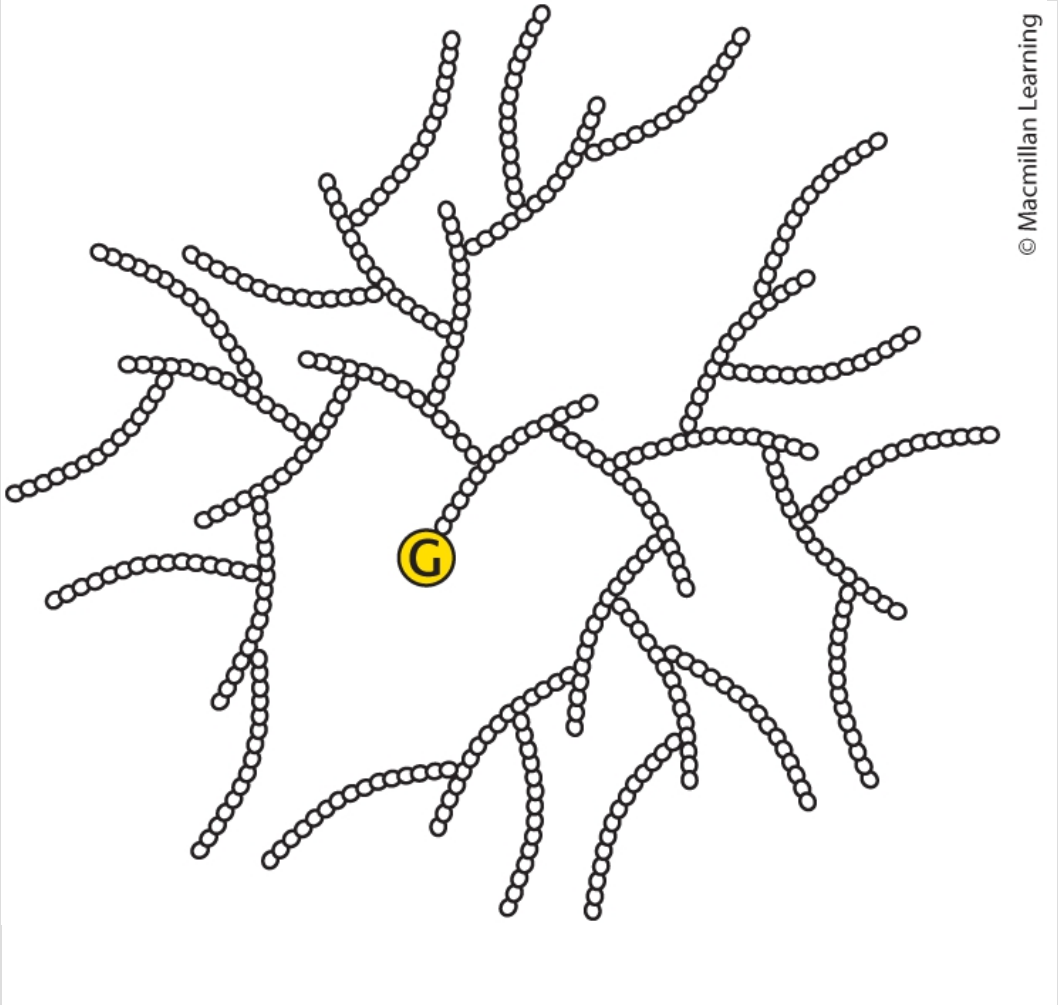


FIGURE 21.18 A cross section of a glycogen molecule reveals the basic branching structure. The component labeled G is glycogenin. Note that this is a cross section of the three-dimensional structure illustrated in Figure 21.2.

Glycogen synthase is the key regulatory enzyme in glycogen synthesis

Glycogen synthase, like phosphorylase, exists in two forms: an active nonphosphorylated *a* form and a usually inactive phosphorylated *b* form. Again, like the phosphorylase, the interconversion of the two forms is controlled extracellularly by the action of hormones; however, note that phosphorylation has opposite effects on the enzymatic activities of glycogen synthase and glycogen phosphorylase.

Glycogen synthase is phosphorylated at multiple sites by several protein kinases — notably, **glycogen synthase kinase**, which is under the control of insulin, and PKA. The function of the multiple phosphorylation sites is still under investigation. In contrast, the key means of automatically regulating glycogen synthase activity is by allosteric regulation of the phosphorylated form of the enzyme, glycogen synthase *b*. Glucose 6-phosphate is a powerful activator of the enzyme, stabilizing the R state of the enzyme relative to the T state and providing automatic activation of the enzyme when the concentrations of glucose-phosphates are high within a given cell.

Glycogen is an efficient storage form of glucose

What is the cost of converting glucose 6-phosphate into glycogen and back into glucose 6-phosphate? The pertinent reactions have already been described except for reaction 5 below, which is the regeneration of UTP. ATP phosphorylates UDP in a reaction catalyzed by nucleoside diphosphokinase.

$$\text{Glucose 6-phosphate} \rightarrow \text{glucose 1-phosphate} \quad \textbf{(1)}$$

$$\text{Glucose 1-phosphate} + \text{UTP} \rightarrow \text{UDP-glucose} + PP_i \quad \textbf{(2)}$$

$$PP_i + H_2O \rightarrow 2\ P_i \quad \textbf{(3)}$$

$$\text{UDP-glucose} + \text{glycogen}_n \rightarrow \text{glycogen}_{n+1} + \text{UDP} \quad \textbf{(4)}$$

$$\text{UDP} + \text{ATP} \rightarrow \text{UTP} + \text{ADP} \quad \textbf{(5)}$$

Sum: $\text{Glucose 6-phosphate} + \text{ATP} + \text{glycogen}_n + H_2O \rightarrow \text{glycogen}_{n+1} + \text{ADP} + 2\ P_i$

Thus, one molecule of ATP is hydrolyzed to incorporate glucose 6-phosphate into glycogen. The energy yield from the breakdown of glycogen is highly efficient. About 90% of the residues are phosphorolytically cleaved to glucose 1-phosphate, which is converted at no cost into glucose 6-phosphate. The other residues are branch residues, which are hydrolytically cleaved. One molecule of ATP is then used to phosphorylate each of these glucose molecules to glucose 6-phosphate. The complete oxidation of glucose 6-phosphate yields about 31 molecules of ATP, and storage consumes slightly more than one molecule of ATP per molecule of glucose 6-phosphate; so the overall efficiency of storage is nearly 97%.

21.6 Glycogen Breakdown and Synthesis Are Reciprocally Controlled by Hormones

An important control mechanism prevents glycogen from being synthesized at the same time as it is being broken down. The same glucagon- and epinephrine-triggered cAMP cascades that initiate glycogen breakdown in the liver and muscle, respectively, also shut off glycogen synthesis. Glucagon and epinephrine control both glycogen breakdown and glycogen synthesis through PKA (**Figure 21.19**). Recall that PKA adds a phosphoryl group to phosphorylase kinase, activating that enzyme and initiating glycogen breakdown. Both glycogen synthase kinase and PKA add phosphoryl groups to glycogen synthase, but this phosphorylation leads to a *decrease* in enzymatic activity. In this way, glycogen breakdown and synthesis are reciprocally regulated. How is the enzymatic activity reversed so that glycogen breakdown halts and glycogen synthesis begins?

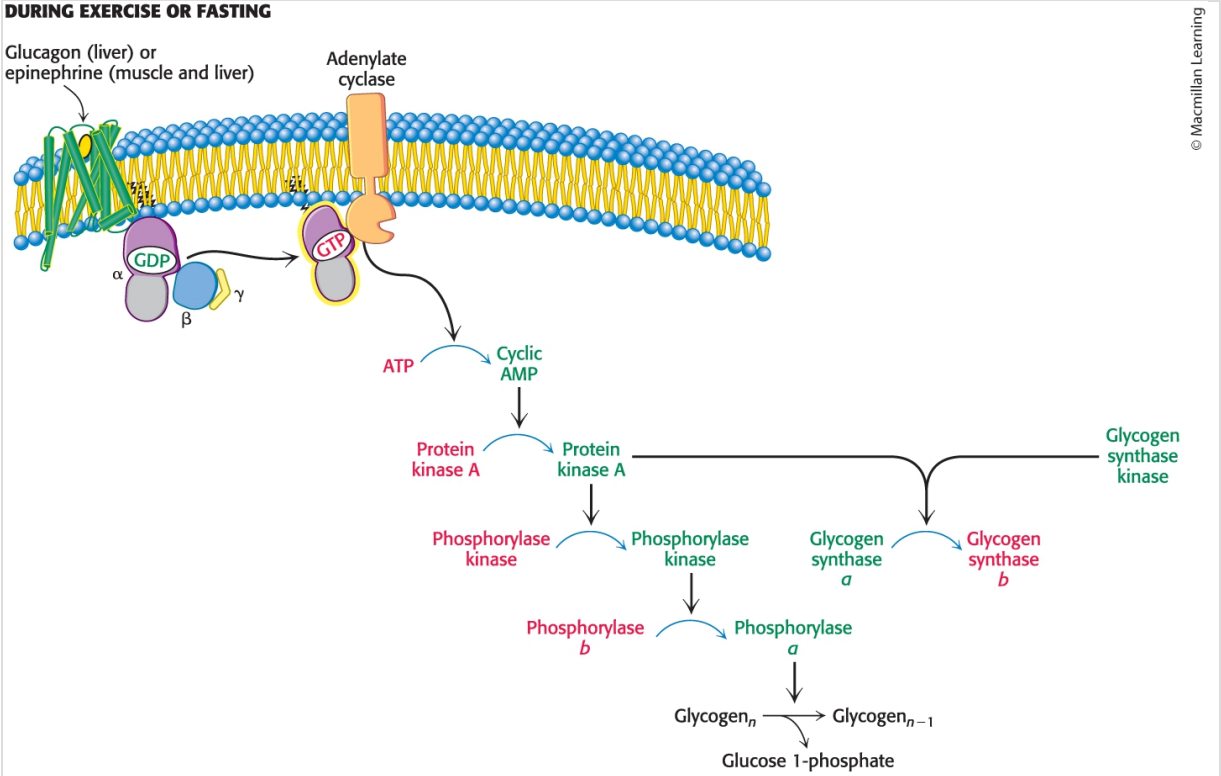


FIGURE 21.19 Glycogen metabolism is regulated in part by hormone-triggered cyclic AMP cascades. The sequence of reactions leading to the activation of protein kinase A ultimately activates glycogen degradation. At the same time, protein kinase A along with glycogen synthase kinase inactivates glycogen synthase, shutting down glycogen synthesis. The inactive forms of the enzymes are shown in red and the active forms in green.

EXPLORE this pathway further in the Metabolic Map in Achieve

Protein phosphatase 1 reverses the effects of kinases on glycogen metabolism

After a bout of exercise, muscle must shift from a glycogen-degrading mode to one of glycogen replenishment. A first step in this metabolic task is to shut down the phosphorylated proteins that stimulate glycogen breakdown. This task is accomplished by protein

phosphatases that catalyze the hydrolysis of phosphorylated serine and threonine residues in proteins.

Protein phosphatase 1 (PP1) plays key roles in regulating glycogen metabolism (Figure 21.20). PP1 decreases the rate of glycogen breakdown by reversing the effects of the phosphorylation cascade: it inactivates phosphorylase *a* and phosphorylase kinase by dephosphorylating them. PP1 also removes phosphoryl groups from glycogen synthase *b* to convert it into the more active glycogen synthase *a* form. Thus, PP1 accelerates glycogen synthesis; it is yet another molecular device for coordinating carbohydrate storage.

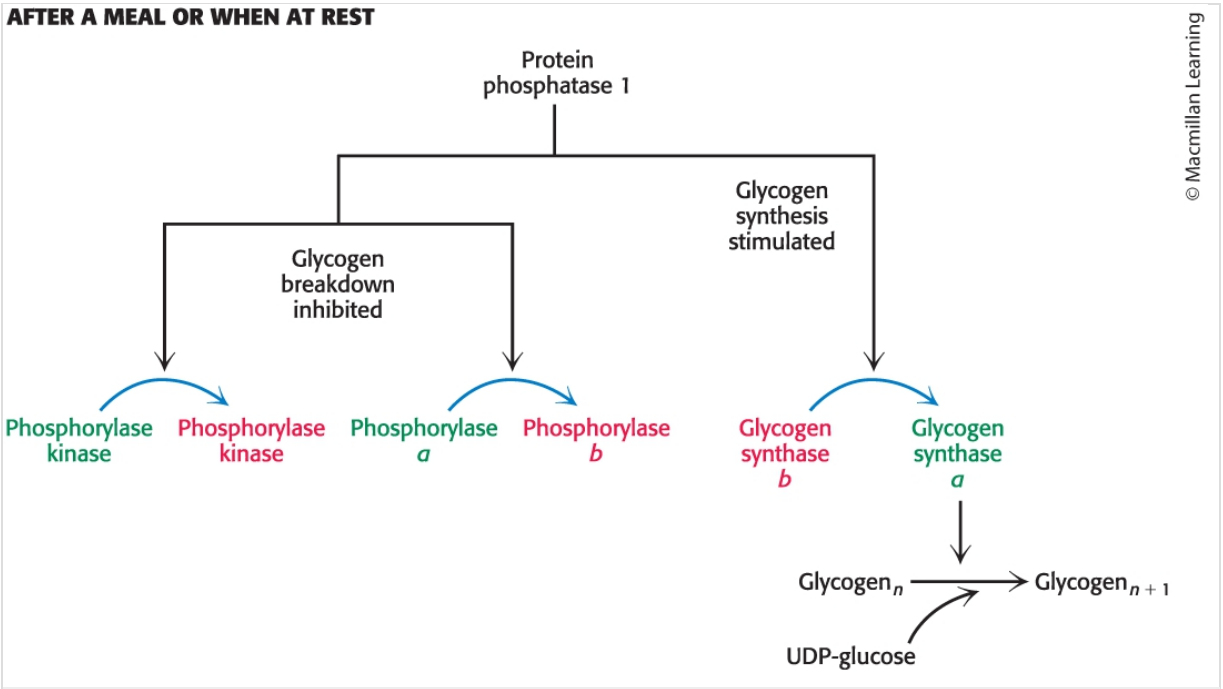


FIGURE 21.20 Glycogen synthesis is regulated by protein phosphatase 1 (PP1). PP1 stimulates glycogen synthesis while inhibiting glycogen breakdown. The inactive forms of the enzymes are shown in red and the active forms in green.

The catalytic subunit of PP1 is a 37-kDa single-domain protein that is usually bound to one of a family of regulatory subunits with masses of approximately 120 kDa. In skeletal muscle and heart, the most prevalent regulatory subunit is G_M, whereas in the liver, the most prevalent subunit is G_L. These regulatory subunits have modular structures with domains that participate in interactions with glycogen, with the catalytic subunit, and with target enzymes. Thus, these regulatory subunits act as scaffolds, bringing together the phosphatase and its substrates on the glycogen particle.

What prevents the phosphatase activity of PP1 from always inhibiting glycogen degradation? When glycogen degradation is called for, glucagon or epinephrine initiates the cAMP cascade that activates PKA (**Figure 21.21**), which reduces the activity of PP1 by two mechanisms. First, in muscle, G_M is phosphorylated in the domain responsible for binding the catalytic subunit. The catalytic subunit is released from glycogen and from its substrates, and its phosphatase activity is greatly reduced. Second, almost all tissues contain small proteins (Inhibitor in Figure 21.21) that, when phosphorylated, bind to the catalytic subunit of PP1 and inhibit it. Thus, when glycogen degradation is switched on by cAMP, the accompanying phosphorylation of these inhibitors keeps phosphorylase in its active *a* form and glycogen synthase in its inactive *b* form.

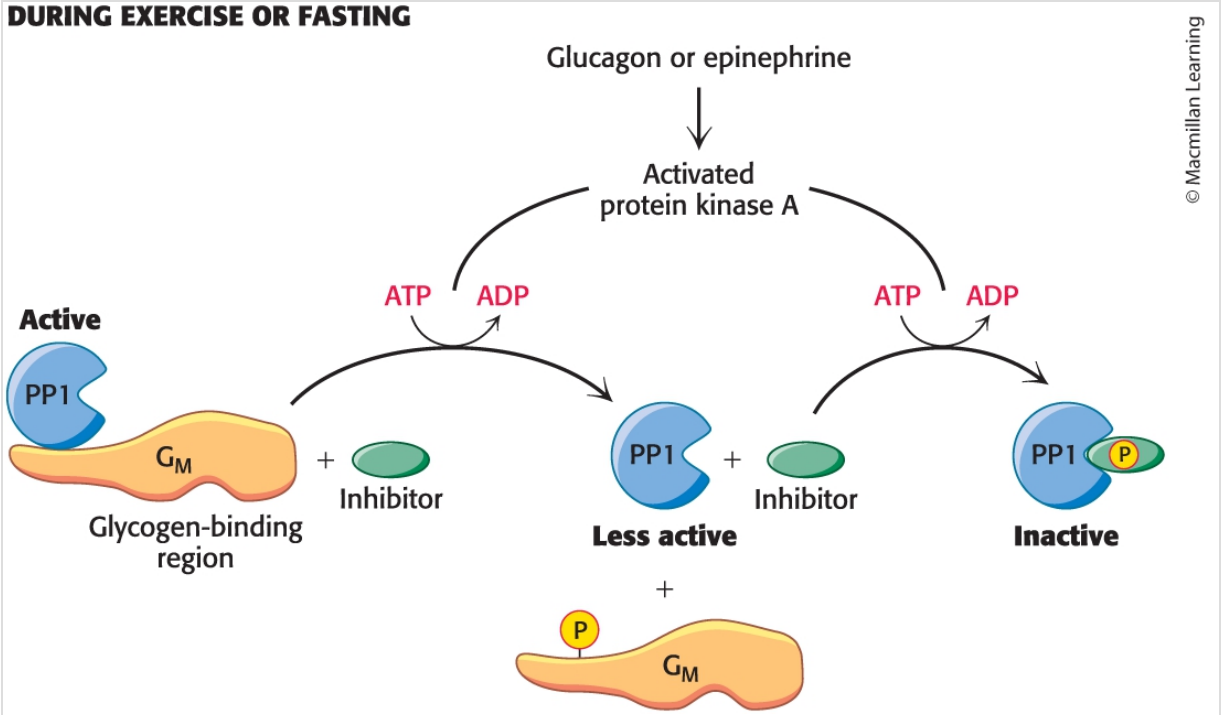
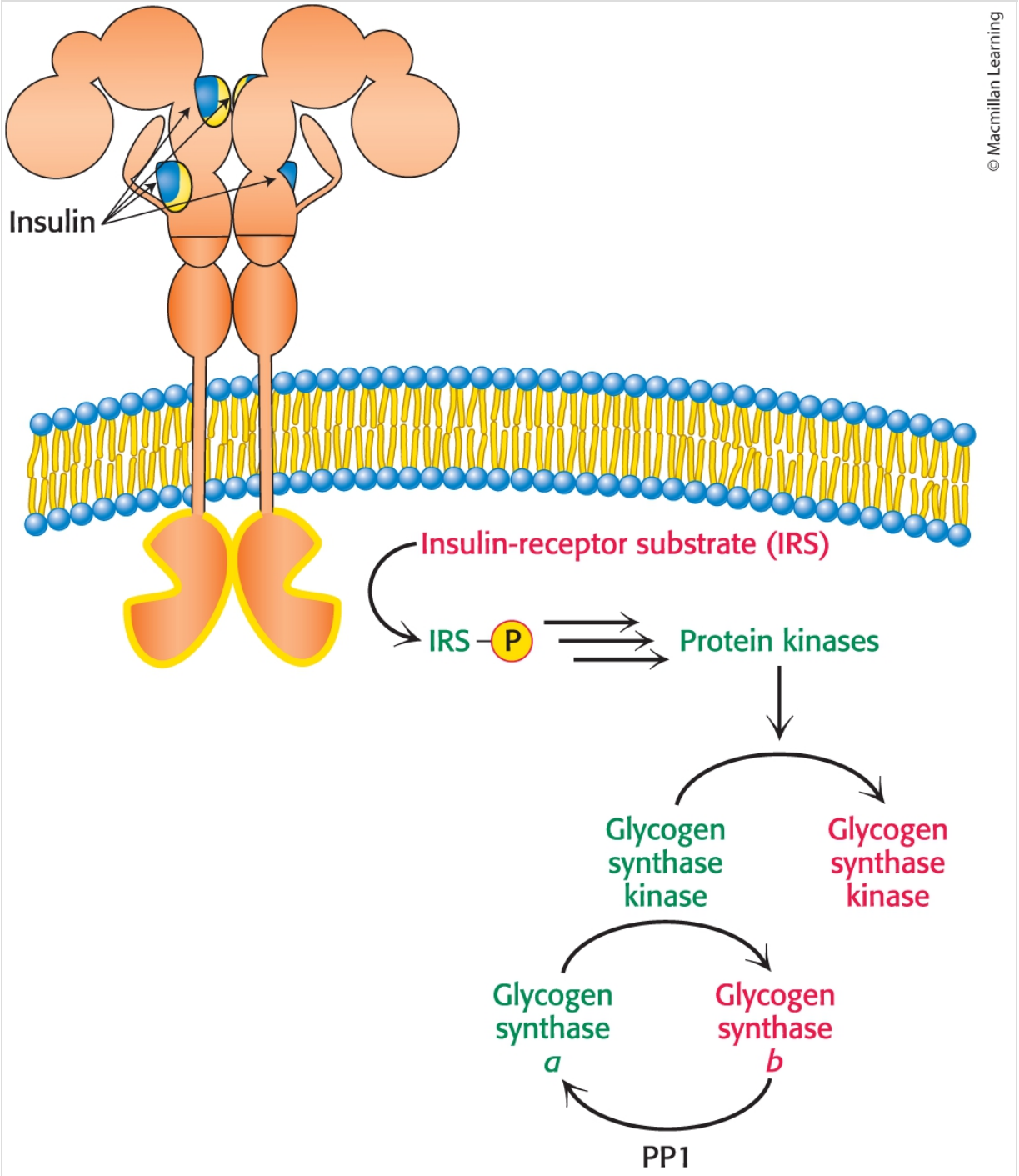


FIGURE 21.21 PP1 is regulated by hormonally controlled cascades. Protein phosphatase 1 (PP1) regulation in muscle takes place in two steps. First, phosphorylation of G_M by protein kinase A dissociates the catalytic subunit from its substrates in the glycogen particle and reduces its activity. Then, phosphorylation of the inhibitor subunit by protein kinase A and its subsequent binding by the phosphatase completely inactivates the catalytic subunit of PP1.

Interestingly, recent research suggests that glycogen phosphorylase is also regulated by acetylation (Section 7.3). Acetylation not only inhibits the enzyme, but also enhances dephosphorylation by promoting the interaction with PP1. Acetylation is stimulated by glucose and insulin, but inhibited by glucagon. It is fascinating that glycogen phosphorylase, one of the first allosteric enzymes identified and one of the most studied enzymes, is still revealing secrets.

Insulin stimulates glycogen synthesis by inactivating glycogen synthase kinase

After exercise, people often consume carbohydrate-rich foods to restock their glycogen stores. How is glycogen synthesis stimulated? When blood-glucose concentration is high, insulin stimulates the synthesis of glycogen by inactivating glycogen synthase kinase, one of the enzymes that maintains glycogen synthase in its phosphorylated, inactive state (**Figure 21.22**). The first step in the action of insulin is its binding to its receptor, a tyrosine kinase receptor in the plasma membrane which, once activated, phosphorylates insulin-receptor substrates (Section 14.3). These phosphorylated proteins then trigger signal-transduction pathways that eventually lead to the activation of protein kinases that phosphorylate and inactivate glycogen synthase kinase. The inactive kinase can no longer maintain glycogen synthase in its phosphorylated, inactive state. Additionally, PP1 dephosphorylates glycogen synthase, activating it, and restoring glycogen reserves. Finally, recall that insulin also increases the amount of glucose in the cell by increasing the number of glucose transporters in the membrane (Section 16.1). The net effect of insulin is thus the replenishment of glycogen stores.



© Macmillan Learning

FIGURE 21.22 Insulin inactivates glycogen synthase kinase. Insulin triggers a cascade that leads to the phosphorylation and inactivation of glycogen synthase kinase and prevents the phosphorylation of glycogen synthase. Protein phosphatase 1 (PP1) removes the phosphates from glycogen synthase, thereby activating the enzyme and allowing glycogen synthesis. The inactive forms of the enzymes are shown in red and the active forms in green.

Glycogen metabolism in the liver regulates the blood-glucose concentration

After a meal rich in carbohydrates, blood-glucose concentration rises, and glycogen synthesis is stepped up in the liver. Although insulin is the primary signal for glycogen synthesis, another is the concentration of glucose in the blood, which normally ranges from about 4.4–6.7 mM. The liver senses the concentration of glucose in the blood and takes up or releases glucose accordingly. Experiments performed in rodents established that the amount of liver phosphorylase *a* decreases rapidly when glucose is infused (**Figure 21.23**). After a lag period, the amount of glycogen synthase *a* increases, which results in glycogen synthesis. How does phosphorylase perform its function as the glucose sensor in liver cells, facilitating the switch from degradation to synthesis?

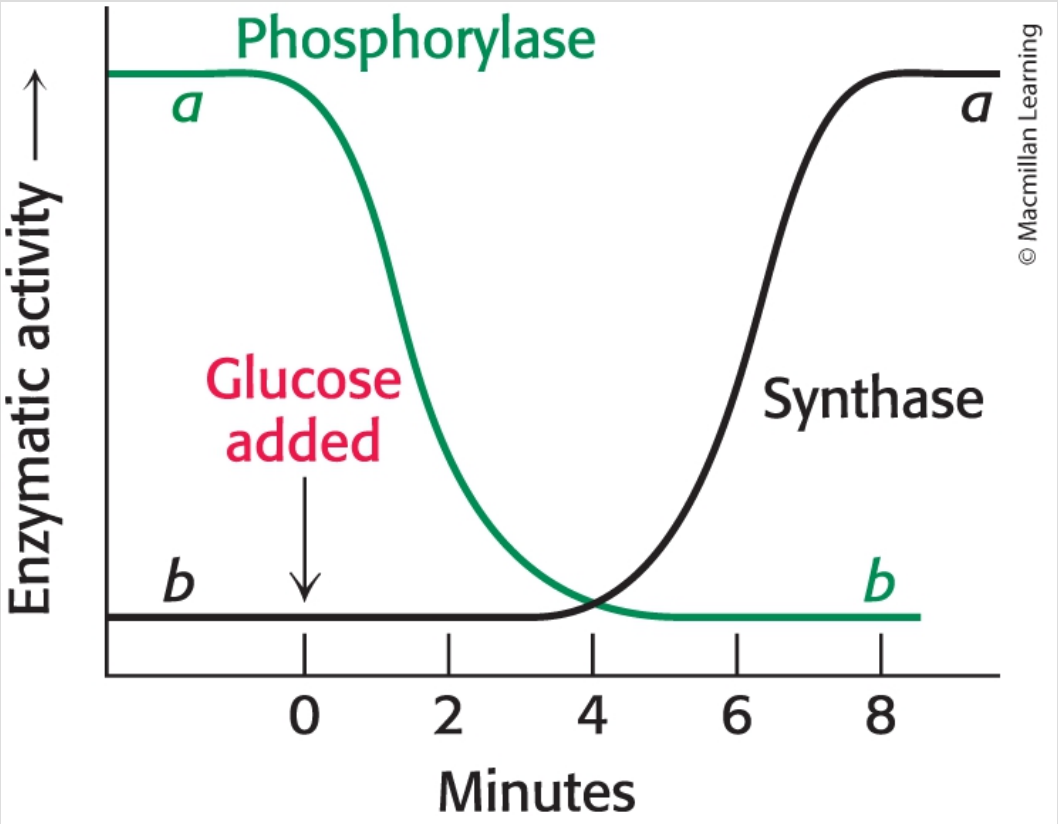


FIGURE 21.23 Blood glucose regulates liver-glycogen metabolism. The infusion of glucose into the bloodstream leads to the inactivation of phosphorylase, followed by the activation of glycogen synthase, in the liver.

[Data from W. Stalmans, H. De Wulf, L. Hue, and H.-G. Hers, *Eur. J. Biochem.* 41:117–134, 1974.]

Phosphorylase *a* and PP1 are localized to the glycogen particle by interactions with the G_L subunit of PP1. The binding of glucose to phosphorylase *a* shifts its allosteric equilibrium from the active R form to the inactive T form (Figure 21.12). This conformational change renders the phosphoryl group on serine 14 a substrate for PP1. PP1 binds tightly to phosphorylase *a* only when the phosphorylase is in the R state, but PP1 is inactive when bound. When glucose induces the transition to the T form, PP1 and the phosphorylase dissociate from each other and the glycogen particle,

and PP1 becomes active, converting phosphorylase *a* to the *b* form (Figure 21.11). Recall that the R ↔ T transition of muscle phosphorylase *a* is unaffected by glucose and is thus unaffected by the rise in blood-glucose concentration (Section 21.3).

How does glucose binding to glycogen phosphorylase stimulate glycogen synthesis? As mentioned above, the conversion of *a* into *b* is accompanied by the release of PP1, which is then free to activate glycogen synthase (**Figure 21.24**). The removal of the phosphoryl group of inactive glycogen synthase *b* converts it into the active *a* form. What accounts for the lag between termination of glycogen degradation and the beginnings of glycogen synthesis (Figure 21.23)? There are about 10 phosphorylase *a* molecules per molecule of PP1. Consequently, the activity of glycogen synthase begins to increase only after most of phosphorylase *a* is converted into *b*. The lag between the decrease in glycogen degradation and the increase in glycogen synthesis prevents the two pathways from operating simultaneously. This remarkable glucose-sensing system depends on three key elements: (1) communication within phosphorylase between the allosteric site for glucose and the serine phosphate, (2) the use of PP1 to inactivate phosphorylase and activate glycogen synthase, and (3) the binding of PP1 to phosphorylase *a* to prevent the premature activation of glycogen synthase.

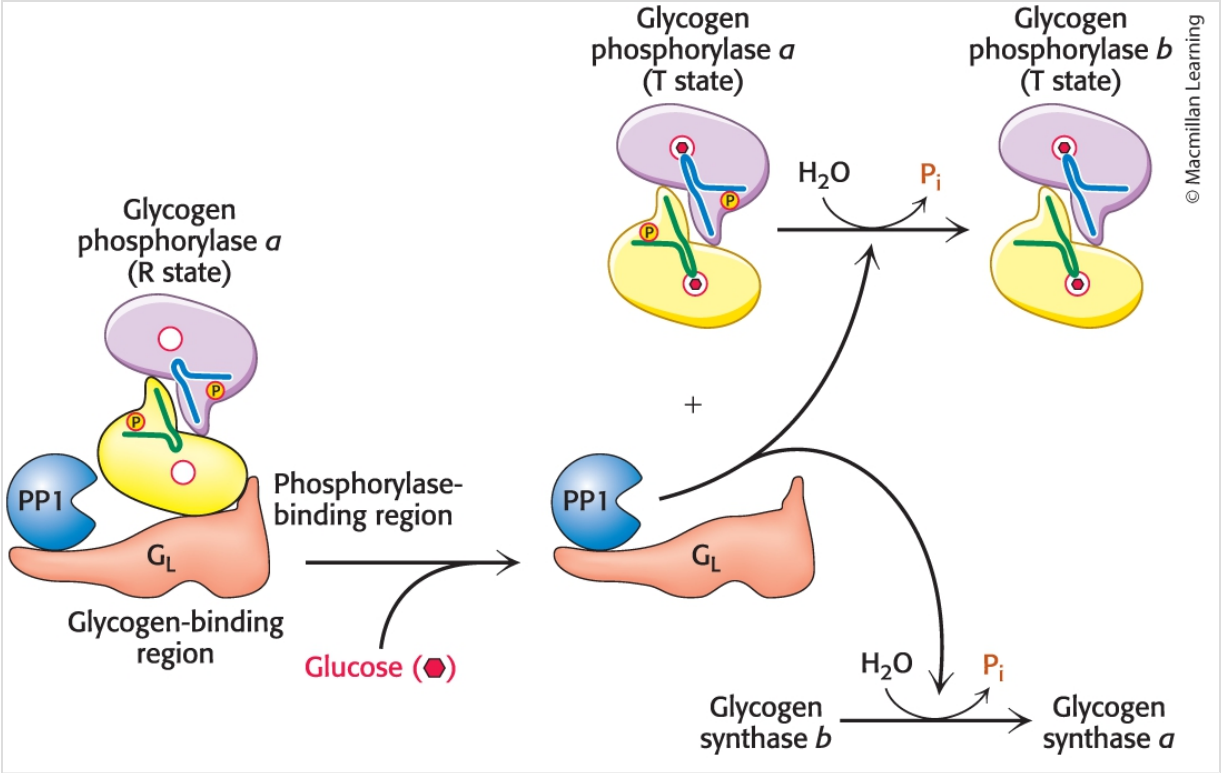


FIGURE 21.24 Glucose regulates liver-glycogen metabolism. After a carbohydrate-rich meal, glucose binds to and inhibits glycogen phosphorylase *a* in the liver, facilitating the formation of the T state of phosphorylase *a*. The T state of phosphorylase *a* does not bind protein phosphate 1 (PP1), leading to the dissociation of PP1 from glycogen phosphorylase *a*. The free PP1 is no longer inhibited and dephosphorylates glycogen phosphorylase *a* and glycogen synthase *b*, leading to the inactivation of glycogen breakdown and the activation of glycogen synthesis.

Efforts are underway to develop drugs that disrupt the interaction of liver phosphorylase with the G_L subunit as a treatment for type 2 diabetes, a disease characterized by excess blood glucose (Section 24.3). One experimental drug binds at a unique site on the enzyme that, synergistically with glucose, stabilizes the T state of phosphorylase and thereby enhances the transition to glycogen synthesis, as described earlier. Hence, disrupting the association of

phosphorylase with the G_L would render it a substrate for PP1. Glycogen degradation would decrease and glucose release into the blood would be inhibited.

Self-Check Question



What pathway, in addition to the cAMP-induced signal-transduction pathway, is used in the liver to maximize glycogen breakdown?

Biochemists have uncovered the biochemical basis of multiple glycogen-storage diseases



In 1929, Edgar von Gierke described the first glycogen-storage disease, which subsequently bore his name. Patients with von Gierke disease have a distended abdomen, caused by a massive enlargement of the liver, and pronounced hypoglycemia (low blood glucose) between meals. Furthermore, the blood-glucose concentration does not rise on administration of epinephrine and glucagon. In 1952, Gerty and Carl Cori discovered the mechanism for this disease: the liver lacks glucose 6-phosphatase (Figure 21.4). This finding was the first demonstration of an inherited deficiency of a liver enzyme.

The absence of glucose 6-phosphatase in the liver causes hypoglycemia because glucose cannot be formed from glucose 6-phosphate, which cannot cross the plasma membrane to leave the liver. Thus, the glycogen in the liver of a patient with von Gierke disease is normal in structure but is present in abnormally large amounts. The presence of excess glucose 6-phosphate also triggers an increase in glycolysis in the liver, leading to high concentrations of lactate and pyruvate in the blood. This disease can also be produced by a mutation in the gene that encodes the glucose 6-phosphate transporter. Recall that glucose 6-phosphate must be transported into the lumen of the endoplasmic reticulum to be hydrolyzed by phosphatase (Section 16.4). Mutations in the other three essential proteins of this system can likewise lead to von Gierke disease.

Seven other glycogen-storage diseases have been characterized (**Table 21.2**). In Pompe disease (type II), lysosomes become engorged with glycogen because they lack α-1,4-glucosidase, a hydrolytic enzyme confined to these organelles (**Figure 21.25**). There are several subtypes of glycogen-storage disease III, affecting either muscle or liver. Regardless of subtype, the outer branches of the glycogen are very short. Patients with type III lack the debranching enzyme (α-1,6-glucosidase), and so only the outermost branches of glycogen can be effectively utilized. Thus, only a small fraction of this abnormal glycogen is functionally active as an accessible store of glucose.

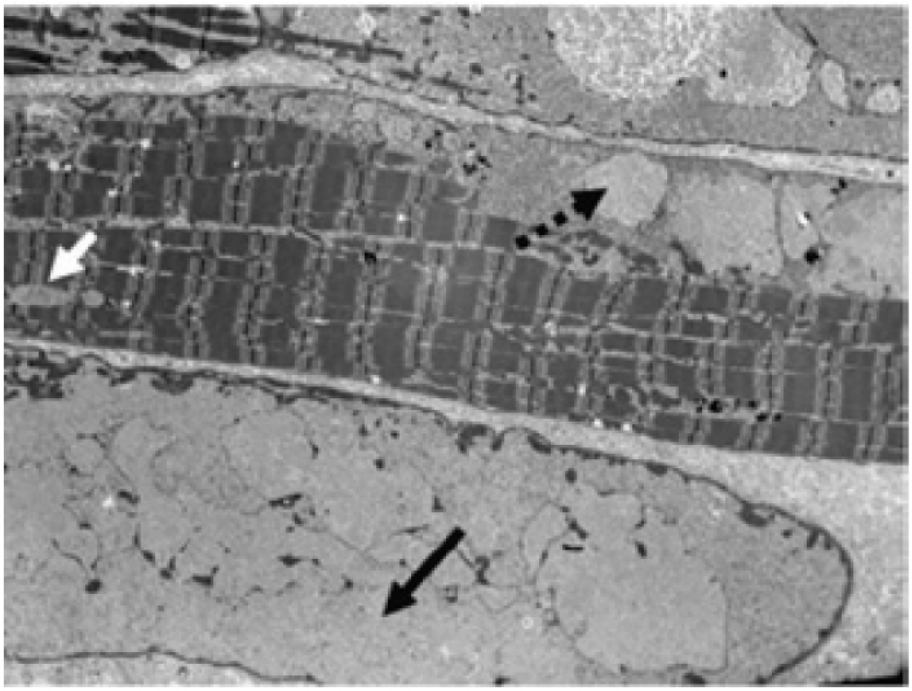
TABLE 21.2 Glycogen-storage diseases

Type	Defective enzyme	Organ affected	Glycogen in the affected organ	Clinical features

I von Gierke	Glucose 6-phosphatase or transport system	Liver and kidney	Increased amount; normal structure	Massive enlargement of the liver; failure to thrive; severe hypoglycemia, ketosis, hyperuricemia, hyperlipemia
II Pompe	α-1,4-glucosidase (lysosomal)	All organs	Massive increase in amount; normal structure	Cardiorespiratory failure causes death, usually before age 2
III Cori	α-1,6-glucosidase (debranching enzyme)	Muscle and liver	Increased amount; short outer branches	Like type I, but milder course
IV Andersen	Branching enzyme $(\alpha-1,4 \rightarrow \alpha-1,6)$	Liver and spleen	Normal amount; very long outer branches	Progressive cirrhosis of the liver; liver failure causes death, usually before age 2
V McArdle	Phosphorylase	Muscle	Moderately increased amount; normal structure	Limited ability to perform strenuous exercise because of painful muscle cramps; otherwise patient is normal and well developed
VI Hers	Phosphorylase	Liver	Increased amount	Like type I, but milder course
VII	Phosphofructokinase	Muscle	Increased amount;	Like type V

			normal structure	
VIII	Phosphorylase kinase	Liver	Increased amount; normal structure	Mild liver enlargement; mild hypoglycemia

Note: Types I through VII are inherited as autosomal recessives. Type VIII is sex-linked.



Credit: Reproduced with permission of the author, from Thurberg, B.L., et al., Characterization of pre- and post-treatment pathology after enzyme replacement for pompe disease. *Lab. Invest*, 2006 Dec: 86(12):1208–20.

FIGURE 21.25 An electron micrograph of a muscle cell from a patient with Pompe disease reveals enlarged lysosomes. Glycogen-engorged lysosomes are seen throughout the cell, including in the myofibrils (white arrow) and at the cell periphery (dashed black arrow). As the disease progresses, lysosomes may rupture, releasing large amounts of glycogen into the cytoplasm. Such accumulations of cytoplasmic glycogen are called *glycogen lakes* (solid black arrow).

A defect in glycogen metabolism confined to muscle is found in McArdle disease (type V) when muscle phosphorylase activity is

absent, limiting the capacity to perform strenuous exercise. Despite this limitation, patients with McArdle disease are otherwise normal and well developed, illustrating that effective utilization of muscle glycogen is not essential for life. We will examine McArdle disease further in Chapter 24.

Chapter 21 Summary

21.1 Glycogen Metabolism Is the Regulated Release and Storage of Glucose in Multiple Tissues

- Glycogen, a readily mobilized fuel store, is a branched polymer of glucose residues with α-1,4-glycosidic linkages and branches approximately every 12th residue created by an α-1,6-glycosidic bond.
- Glycogen is present to some extent in nearly all tissues but found in large amounts in muscle cells and in liver cells, where it is stored in the cytoplasm in the form of hydrated granules.

21.2 Glycogen Breakdown Requires the Interplay of Several Enzymes

- Most of the glycogen molecule is degraded to glucose 1-phosphate by the action of glycogen phosphorylase, which uses orthophosphate to split the α-1,4-glycosidic linkages; glucose 1-phosphate can then be reversibly converted into glucose 6-phosphate.
- Branch points are degraded by the combined actions of an oligosaccharide transferase and an α-1,6-glucosidase, both part of the bifunctional enzyme called *debranching enzyme*.

21.3 Phosphorylase Is Regulated by Allosteric Interactions and Controlled by Reversible Phosphorylation

- Phosphorylase *b*, which is usually inactive, is converted into active phosphorylase *a* by the phosphorylation of a single serine residue by phosphorylase kinase.

- In the liver, phosphorylase *a* liberates glucose for export to other organs, such as skeletal muscle and the brain; phosphorylase *a* is inhibited by the presence of glucose.
- In muscle, phosphorylase *b* can be activated by the binding of AMP to generate glucose for use inside the cells as a fuel for contractile activity. The effect of AMP is counteracted by ATP and glucose 6-phosphate.

21.4 Glucagon and Epinephrine Signal the Need for Glycogen Breakdown

- Epinephrine and glucagon stimulate glycogen breakdown through specific 7TM receptors.
- Muscle is responsive to epinephrine, whereas the liver is responsive to both epinephrine and glucagon.
- Both signal molecules initiate a kinase cascade that leads to the activation of phosphorylase kinase, which in turn converts glycogen phosphorylase *b* to the phosphorylated *a* form.

21.5 Glycogen Synthesis Requires Several Enzymes and Uridine Diphosphate Glucose

- The pathway for glycogen synthesis differs from that for glycogen breakdown: Glycogen synthase catalyzes the transfer of glucose from UDP-glucose to the C-4 hydroxyl group of a terminal residue in the growing glycogen molecule.
- Synthesis is primed by glycogenin, an autoglycosylating protein that contains a covalently attached oligosaccharide unit on a specific tyrosine residue.
- Branching enzyme converts some of the α-1,4 linkages into α-1,6 linkages, thus increasing the number of ends and allowing glycogen to be made and degraded more rapidly.

21.6 Glycogen Breakdown and Synthesis Are Reciprocally Controlled by Hormones

- Glycogen synthesis and degradation are coordinated by several amplifying reaction cascades: epinephrine and glucagon stimulate glycogen breakdown and inhibit its synthesis by increasing the cytoplasmic concentration of cyclic AMP, which activates PKA.
- PKA activates glycogen breakdown by attaching a phosphate to phosphorylase kinase, and it inhibits glycogen synthesis by phosphorylating glycogen synthase. Glycogen synthase kinase also inhibits synthesis by phosphorylating the synthase.
- The glycogen-mobilizing actions of PKA are reversed by PP1, which is regulated by several hormones: epinephrine inhibits PP1, while insulin triggers a cascade that phosphorylates and inactivates glycogen synthase kinase. Hence, glycogen synthesis is decreased by epinephrine and increased by insulin.

Key Terms

glycogen phosphorylase
phosphorolysis
pyridoxal phosphate (PLP)
glucagon
epinephrine (adrenaline)
phosphorylase kinase
protein phosphatase 1 (PP1)
uridine diphosphate glucose (UDP-glucose)
glycogen synthase
glycogenin
glycogen synthase kinase

Problems

1. What are the three steps in glycogen degradation, and what enzymes are required? 1

2. Which molecule is the immediate product of glycogen phosphorylase? 1

a. Glucose 6-phosphate
b. Glucose 1-phosphate
c. Fructose 1-phosphate
d. Glucose 1,6-bisphosphate

3. Which of the following is a substrate for glycogen synthase? 3

a. UTP-glucose
b. Glucose 1-phosphate
c. CDP-glucose
d. UDP-glucose

4. α-Amylose is an unbranched glucose polymer. Why would this polymer not be as effective a storage form of glucose as glycogen?

5. Compare the allosteric regulation of phosphorylase in the liver and in muscle, and explain the significance of the difference. 2, 5

6. Why is water excluded from the active site of phosphorylase? Predict the effect of a mutation that allows water molecules to enter. 1

7. Outline the signal-transduction cascade for glycogen degradation in muscle. 2

8. There must be a way to shut down glycogen breakdown quickly to prevent the wasteful depletion of glycogen after energy needs have been met. What mechanisms are employed to turn off glycogen breakdown?

9. Phosphorylation has opposite effects on glycogen synthesis and breakdown. What is the advantage of its having opposing effects? 4

10. What enzymes are required for the synthesis of a glycogen particle starting from glucose 6-phosphate? 3

11. The following reaction accounts for the synthesis of UDP-glucose. This reaction is readily reversible. How is it made irreversible in vivo?

$$\text{Glucose 1-phosphate} + \text{UTP} \rightleftharpoons \text{UDP-glucose} + \text{PP}_i$$

12. Why does activation of the phosphorylated *b* form of glycogen synthase by high concentrations of glucose 6-phosphate make good biochemical sense? 4

13. Write a balanced equation showing the effect of simultaneous activation of glycogen phosphorylase and glycogen synthase. Include the reactions catalyzed by phosphoglucomutase and UDP-glucose pyrophosphorylase. 4

14. How does insulin stimulate glycogen synthesis? 4

15. Write a balanced equation for the formation of glycogen from galactose. 3

16. In exercising muscle, glycogen degradation supplies the muscle with glucose 6-phosphate. In order to stimulate muscle

glycogen degradation, protein phosphatase 1 (PP1) must be inhibited. Four of the five following events are involved in the inactivation of PP1 in exercising muscle. Which are they? 2, 4

a. PKA phosphorylates an inhibitor of PP1.
b. Phosphorylated PP1 inhibitor binds to PP1, facilitating glycogen degradation by phosphorylase *a*.
c. PKA phosphorylates G_M in the $G_M - PP1$ complex, resulting in its dissociation.
d. Epinephrine initiates a cAMP signal-transduction cascade that utilizes PKA.
e. Insulin initiates a protein kinase cascade that utilizes glycogen synthase kinase.

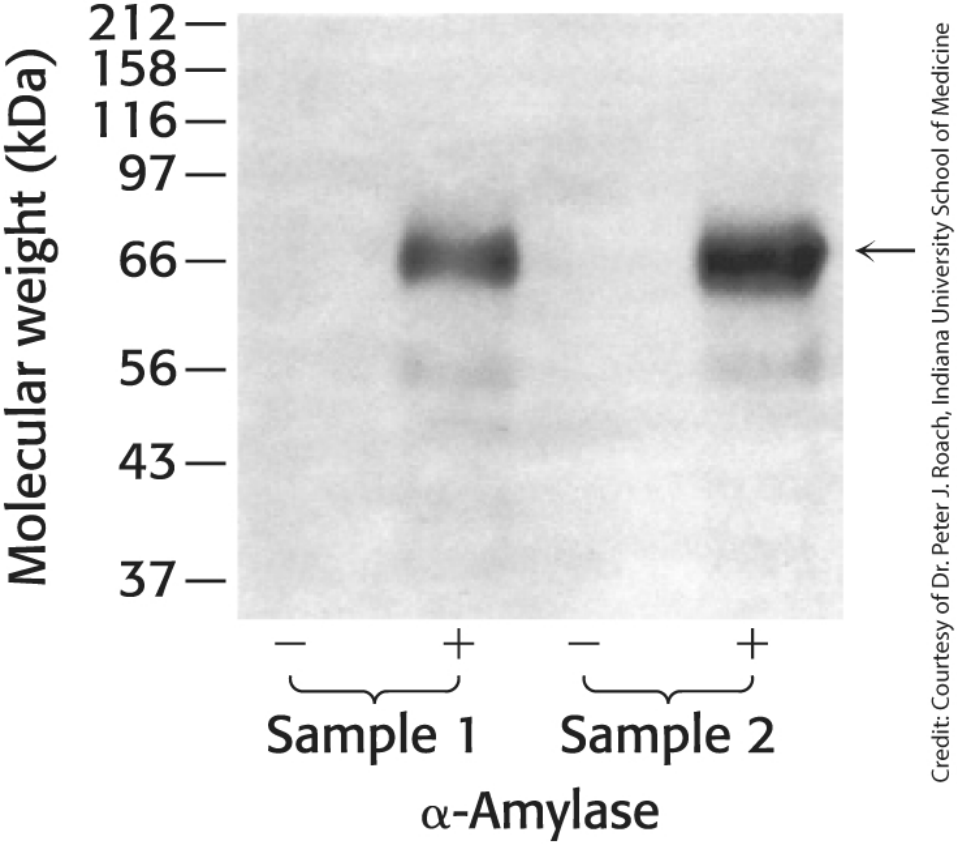
17. Suggest another mutation in glucose metabolism that causes symptoms similar to those of von Gierke disease.

18. Experiments were performed in which serine (S)14 of glycogen phosphorylase was replaced by glutamate (E). The V_{max} of the mutant enzyme was then compared with the wild-type phosphorylase in both the *a* and the *b* form.

V_{max} μmoles of glucose $1-PO_4$ released min^{-1} mg^{-1}	
Wild-type phosphorylase *b*	25 ± 0.4
Wild-type phosphorylase *a*	100 ± 5
S to E mutant	60 ± 3

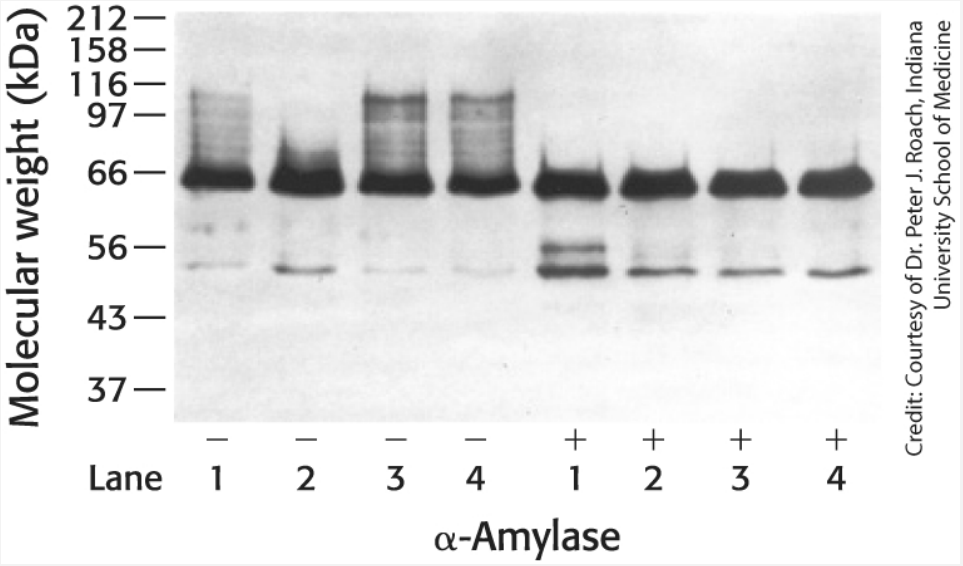
a. Explain the results obtained with the mutant.
b. Predict the effect of substituting aspartic acid for the serine.

19. The liver is a major storage site for glycogen. Purified from two samples of human liver, glycogen was either treated or not treated with α-amylase and subsequently analyzed by SDS-PAGE and western blotting with the use of antibodies to glycogenin (see Chapter 4 to review these techniques). The results are presented below.



a. Why are no proteins visible in the lanes without amylase treatment?
b. What is the effect of treating the samples with α-amylase? Explain the results.
c. List other proteins that you might expect to be associated with glycogen. Why are other proteins not visible?

20. The gene for glycogenin was transfected into a cell line that normally stores only small amounts of glycogen. The cells were then manipulated according to the following protocol, and glycogen was isolated and analyzed by SDS-PAGE and western blotting by using an antibody to glycogenin with and without α-amylase treatment. The results are presented below.

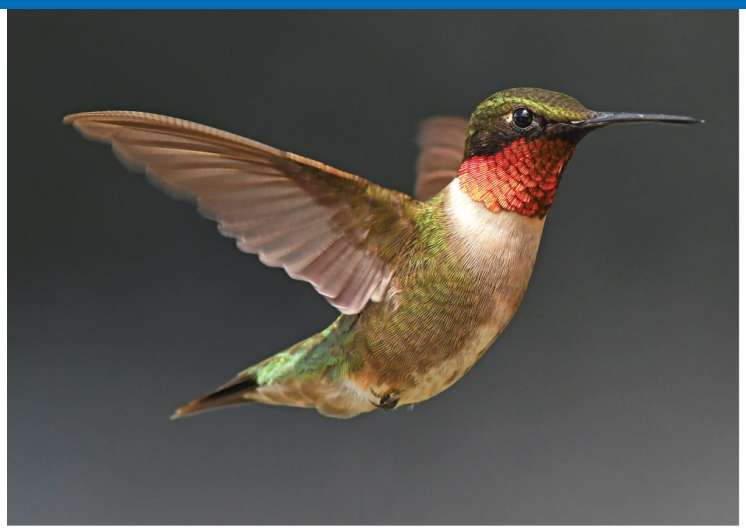


The protocol: Cells cultured in growth medium and 25 mM glucose (lane 1) were switched to medium containing no glucose for 24 hours (lane 2). Glucose-starved cells were refed with medium containing 25 mM glucose for 1 hour (lane 3) or 3

hours (lane 4). Samples (12 μg of protein) were either treated or not treated with α-amylase, as indicated, before being loaded on the gel. 3

a. Why did the western analysis produce a “smear” — that is, the high-molecular-weight staining in lane $1(-)$?
b. What is the significance of the decrease in high-molecular-weight staining in lane $2(-)$?
c. What is the significance of the difference between lanes $2(-)$ and $3(-)$?
d. Suggest a plausible reason why there is essentially no difference between lanes $3(-)$ and $4(-)$.
e. Why are the bands at 66 kDa the same in the lanes treated with amylase, despite the fact that the cells were treated differently?

Chapter 22
Fatty Acid and Triacylglycerol Metabolism



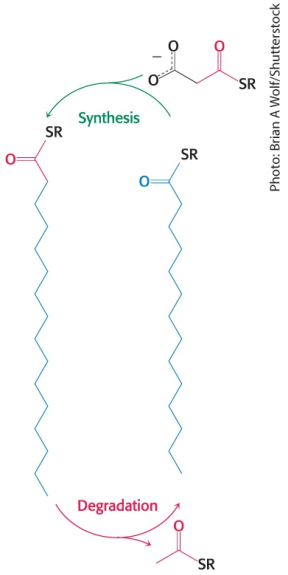


Photo: Brian A Wolf/Shutterstock

Like mammals, birds such as the ruby-throated hummingbird store energy for later use in the most weight-efficient way using fats. This bird beats its wings approximately 50 times per second nonstop to fly across the Gulf of Mexico using the energy stored in its tiny body as fat. Shown at right, the processes of fatty acid synthesis (preparation for energy storage) and fatty acid degradation (preparation for energy use) are, in many ways, the reverse of each other.

Outline

22.1 Triacylglycerols Are Highly Concentrated Energy Stores
22.2 The Use of Fatty Acids as Fuel Requires Three Stages of Processing

22.3 Unsaturated and Odd-Chain Fatty Acids Require Additional Steps for Degradation
22.4 Ketone Bodies Are a Fuel Source Derived from Fats
22.5 Fatty Acids Are Synthesized by Fatty Acid Synthase
22.6 The Elongation and Unsaturation of Fatty Acids Are Accomplished by Accessory Enzyme Systems
22.7 Acetyl CoA Carboxylase Plays a Key Role in Controlling Fatty Acid Metabolism

Learning Goals



By the end of this chapter, you should be able to:

1. Identify the repeated steps of fatty acid degradation.
2. Describe ketone bodies and their role in metabolism.
3. Explain how fatty acids are synthesized.
4. Explain how fatty acid metabolism is regulated.

We turn now from the metabolism of carbohydrates to that of fatty acids, which have four major physiological roles:

1. *Fatty acids are fuel molecules.* Fatty acids are mobilized from storage in fat tissue and oxidized to meet the energy needs of a cell or organism. During rest or moderate exercise, such as walking, fatty acids are our primary source of energy.

2. *Fatty acids are building blocks of phospholipids and glycolipids.* These amphipathic molecules are important components of biological membranes, as discussed in Chapter 12.

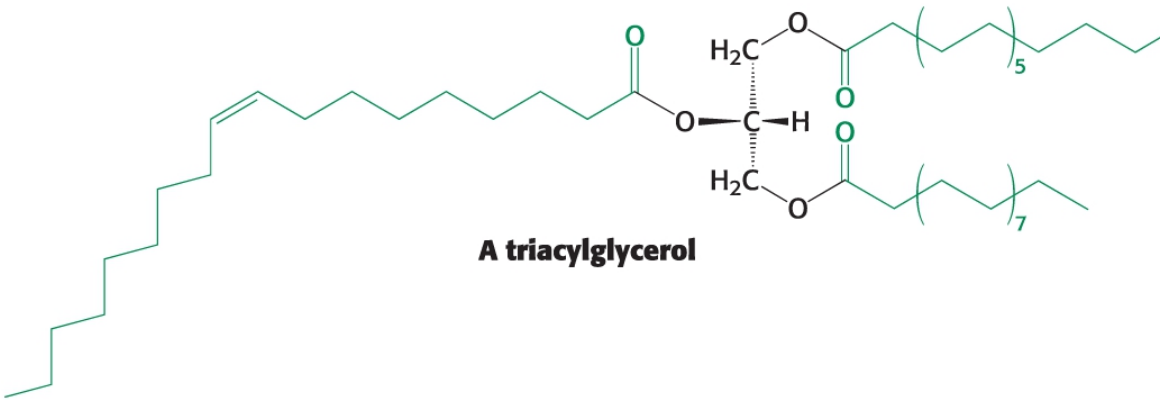
3. *Many proteins are modified by the covalent attachment of fatty acids.* The attached fatty acids target proteins to membrane locations (Section 12.4).

4. *Fatty acid derivatives serve as hormones and intracellular messengers.*

In this chapter, we focus on the degradation and synthesis of fatty acids.

22.1 Triacylglycerols Are Highly Concentrated Energy Stores

Fatty acids are stored as **triacylglycerols** (also called **neutral fats** or **triglycerides**), which are uncharged esters of fatty acids with glycerol.



Triacylglycerols are stored mainly in adipose tissue, composed of cells called *adipocytes* (**Figure 22.1**). Triacylglycerols are highly concentrated stores of metabolic energy because they are reduced and anhydrous (containing no water). The yield from the complete oxidation of fatty acids is about $38\ kJ\ g^{-1}\ (9\ kcal\ g^{-1})$, in contrast with about $17\ kJ\ g^{-1}\ (4\ kcal\ g^{-1})$ for carbohydrates and proteins. The basis of this large difference in caloric yield is that fatty acids are much more reduced than carbohydrates or proteins. Furthermore, triacylglycerols are nonpolar, and so they are stored in a nearly anhydrous form, whereas much more polar carbohydrates are more highly hydrated. In fact, 1 g of dry glycogen binds about 2 g of water. Consequently, a gram of nearly anhydrous fat stores 6.75 times as much energy as a gram of

hydrated glycogen, which is likely the reason that triacylglycerols rather than glycogen were selected in evolution as the major energy reservoir.



Biophoto Associates/Science Source

FIGURE 22.1 An electron micrograph of an adipocyte reveals an enormous intracellular lipid droplet. A small band of cytoplasm surrounds the large deposit of triacylglycerols.

Consider a typical 70-kg man, who has fuel reserves of 420,000 kJ (100,000 kcal) in triacylglycerols, 100,000 kJ (24,000 kcal) in protein (mostly in muscle), 2500 kJ (600 kcal) in glycogen, and 170 kJ (40 kcal) in glucose. Triacylglycerols constitute about 11 kg of his total body weight. If this amount of energy were stored in glycogen, his total body weight would be 64 kg greater. The glycogen and glucose stores provide enough energy to sustain physiological function for about 24 hours, whereas the triacylglycerol stores allow survival for several weeks.

In mammals, the major site of triacylglycerol accumulation is the cytoplasm of adipocytes (fat cells). This fuel-rich, white adipose tissue is located throughout the body, notably under the skin (subcutaneous fat) and surrounding the internal organs (visceral fat). Triacylglycerols coalesce to form a large globule, called a *lipid droplet*, which may occupy most of the cell volume (Figure 22.1). The lipid droplet is surrounded by a monolayer of phospholipids and numerous proteins required for triacylglycerol metabolism. Originally believed to be inert-lipid deposits, lipid droplets are now understood to be dynamic organelles essential for the regulation of lipid metabolism. Adipose cells are specialized for the synthesis and storage of triacylglycerols and for their mobilization into fuel molecules, which are transported in the blood to other tissues. Muscle also stores triacylglycerols for its own energy needs. Indeed, triacylglycerols are evident as the "marbling" of expensive cuts of beef.

It's generally well known that many mammals like mice and bears hibernate over the long winter months. Although their metabolism slows during hibernation, the energy needs of the animal must still be met, primarily by fat metabolism. However, the utility of triacylglycerols as an energy source is perhaps most dramatically illustrated by the abilities of migratory birds like the ruby-throated hummingbird featured on the first page of the chapter, which can fly great distances without eating. Another example is the American golden plover, which flies from Alaska to the southern tip of South America; a large segment of the flight (3800 km, or 2400 miles) is over open ocean, where the birds

cannot feed. Fatty acids provide the energy source for these prodigious feats.

Dietary lipids are digested by pancreatic lipases

Most lipids are ingested in the form of triacylglycerols and must be degraded to fatty acids for absorption across the intestinal epithelium. Intestinal enzymes called **lipases**, secreted by the pancreas, degrade triacylglycerols to free fatty acids and monoacylglycerol (Figure 22.2). Lipids present a special problem because, unlike carbohydrates and proteins, these molecules are not soluble in water. They exit the stomach as an emulsion — particles with a triacylglycerol core surrounded by cholesterol and cholesterol esters.

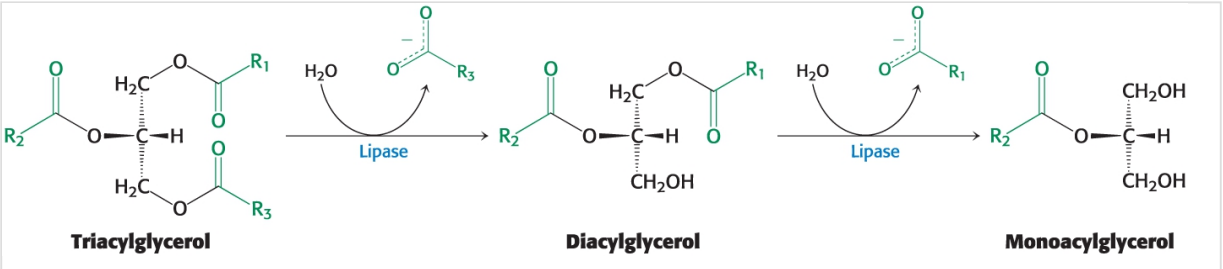
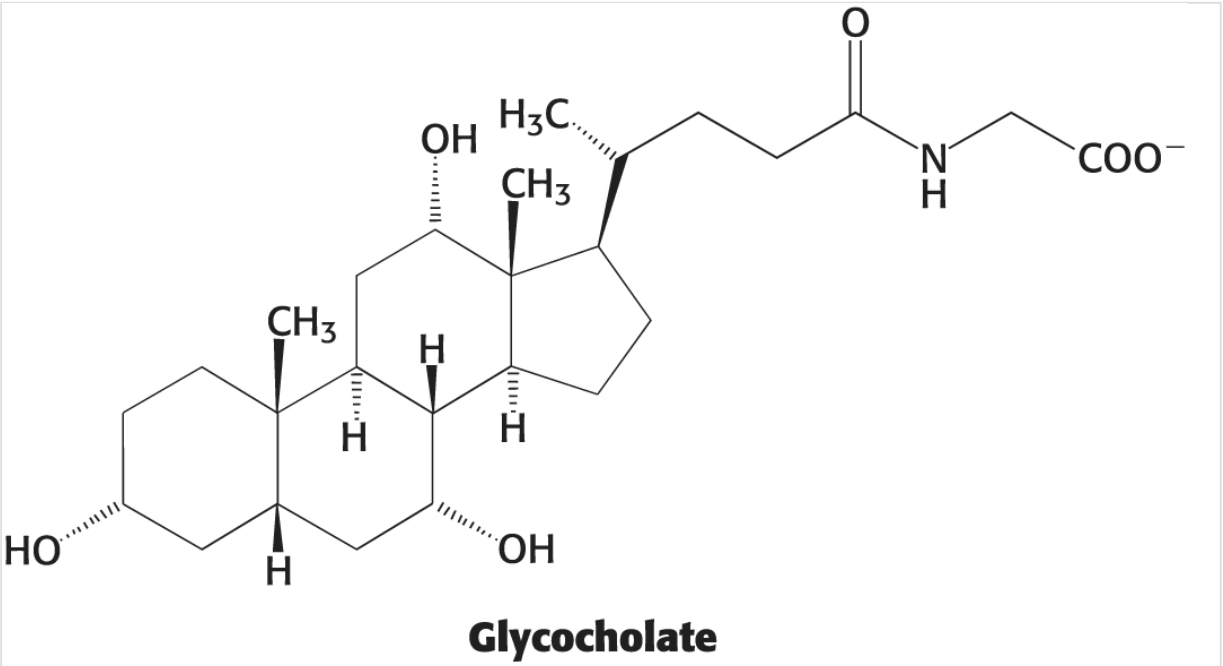


FIGURE 22.2 Pancreatic lipases convert triacylglycerols into fatty acids and monoacylglycerol for absorption into the intestine.

How are the lipids made accessible to the lipases, which are in aqueous solution? First, the particles are coated with bile acids (Figure 22.3), amphipathic molecules synthesized from cholesterol in the liver and secreted from the gallbladder. The ester bonds of each lipid are oriented toward the surface of the bile salt-coated particle, rendering the bond more accessible to digestion by lipases in aqueous solution. However, in this form, the particles are still not substrates for digestion. The protein

colipase (another pancreatic secretory product) must bind the lipase to the particle to permit lipid degradation. If the production of bile salts is inadequate due to liver disease, large amounts of fats (as much as $30\ g\ day^{-1}$) are excreted in the feces. This condition is referred to as *steatorrhea,* after stearic acid, a common fatty acid.



Glycocholate

FIGURE 22.3 Bile acids, such as glycocholate, facilitate lipid digestion in the intestine.

Dietary lipids are transported in chylomicrons

The final digestion products of intestinal lipases, free fatty acids and monoacylglycerol, are carried in micelles to the plasma membrane of intestinal epithelial cells where they are transported inside by membrane proteins such as fatty-acid transport proteins (FATPs)

(**Figure 22.4**). Once inside the cell, fatty-acid binding proteins (FABPs) ferry them to the cytosolic face of the smooth endoplasmic reticulum (SER), where triacylglycerols are resynthesized. After transport into the lumen of the SER, newly synthesized triacylglycerols associate with specific proteins, phospholipids, and cholesterol to form lipoprotein transport particles called **chylomicrons**. Chylomicrons are stable particles approximately 2000 Å (200 nm) in diameter that are composed of 98% triacylglycerols, with the proteins, phospholipids, and cholesterol on the surface (Figure 22.4).

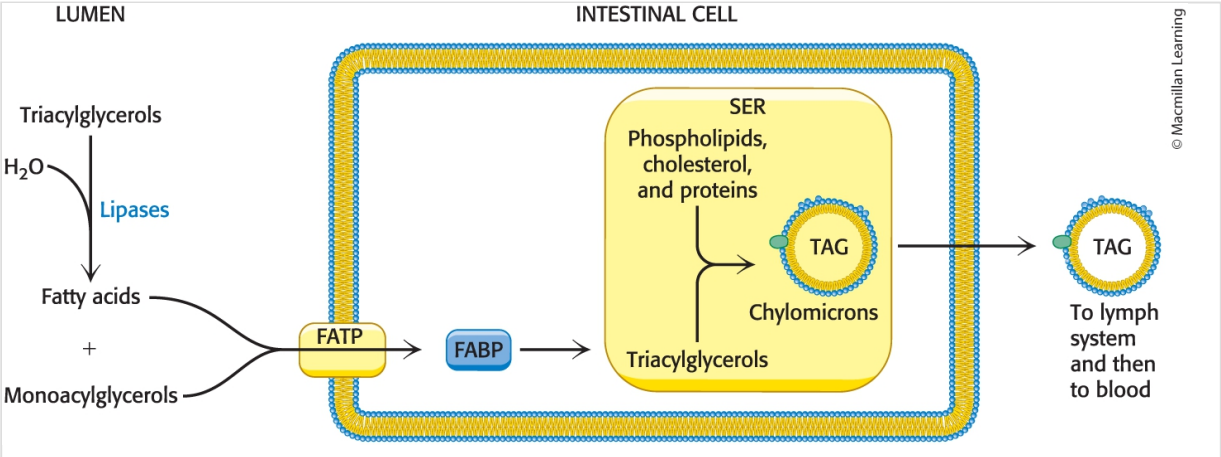
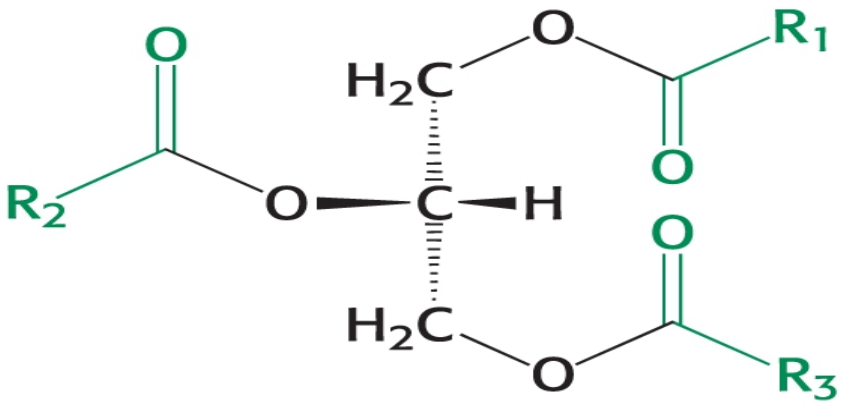
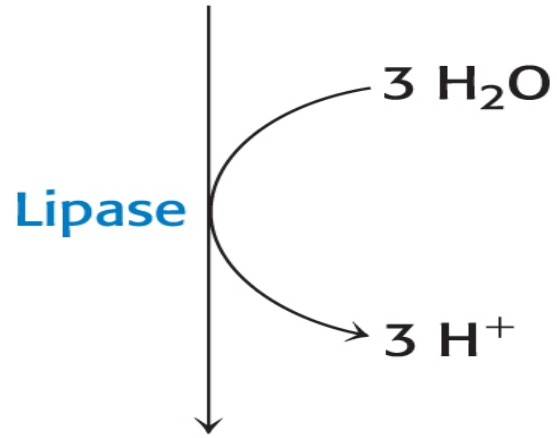


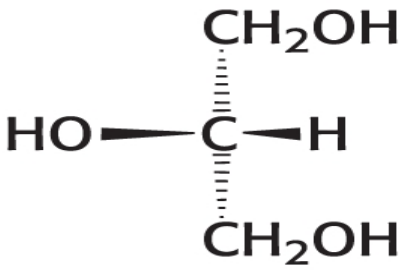
FIGURE 22.4 Fat absorption and transport is a complex process involving multiple proteins. Free fatty acids and monoacylglycerols are absorbed by intestinal epithelial cells through the action of protein transporters. Triacylglycerols are resynthesized in the cytosol and then transported into the smooth endoplasmic reticulum (SER) where they are packaged with other lipids and proteins to form chylomicrons. Finally, chylomicrons are released into the lymph system and then the blood to transport dietary triacylglycerols to various tissues.

Chylomicrons, which also transport fat-soluble vitamins and cholesterol, are next released into the lymph system and then into the blood. These particles bind to membrane-bound lipases, primarily at adipose tissue and muscle, where the triacylglycerols are once again degraded into free fatty acids and monoacylglycerols for transport into the tissue. The triacylglycerols are then resynthesized inside the cell and stored. In the muscle, they can be oxidized to provide energy.



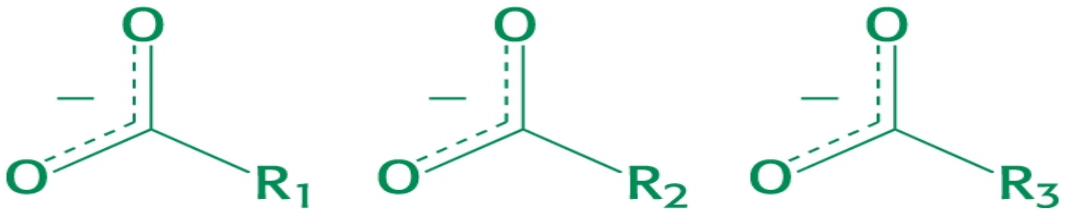
Triacylglycerol





Glycerol

+



Fatty acids

Self-Check Question



Assuming you start in the intestinal lumen with a dietary triacylglyceride that will go directly to storage, how many times will this molecule be hydrolyzed and resynthesized before it is finally stored in an adipocyte?

22.2 The Use of Fatty Acids as Fuel Requires Three Stages of Processing

Tissues throughout the body gain access to the lipid energy reserves stored in adipose tissue through three stages of processing.

1. *Mobilization.* Lipids must first be mobilized. In this process, triacylglycerols are degraded to fatty acids and glycerol, which are released from the adipose tissue and transported to the energy-requiring tissues.

2. *Activation and transport.* In the energy-requiring tissues, the fatty acids must be activated and transported into mitochondria for degradation.

3. *Breakdown into acetyl CoA.* Third, the fatty acids are broken down in a step-by-step fashion into acetyl CoA, which is then processed in the citric acid cycle.

Mobilization: Triacylglycerols are hydrolyzed by hormone-stimulated lipases

Consider someone who has just awakened from a night's sleep and begins a bout of exercise. Glycogen stores will be low, but lipids are readily available. How are these lipid stores mobilized?

Before fats can be used as fuels, the triacylglycerol storage form must be hydrolyzed to yield isolated fatty acids. This reaction is catalyzed by hormonally controlled lipases. Under the physiological conditions facing an early-morning runner, glucagon and epinephrine will be present. In adipose tissue, these hormones trigger 7TM receptors that

activate adenylate cyclase (Section 14.2). The increased level of cyclic AMP then stimulates protein kinase A, which phosphorylates two key proteins: perilipin, a fat-droplet-associated protein, and hormone-sensitive lipase (**Figure 22.5**). The phosphorylation of perilipin has two crucial effects. First, it restructures the fat droplet so the triacylglycerols are more accessible to the mobilization. Second, the phosphorylation of perilipin triggers the release of a coactivator for adipose triglyceride lipase (ATGL). Once bound to the coactivator, ATGL initiates the mobilization of triacylglycerols by releasing a fatty acid from triacylglycerol, forming diacylglycerol. Diacylglycerol is converted into a free fatty acid and monoacylglycerol by the hormone-sensitive lipase. Finally, a monoacylglycerol lipase completes the mobilization of fatty acids with the production of a free fatty acid and glycerol. Thus, epinephrine and glucagon induce lipolysis. Although their role in muscle is not as firmly established, these hormones probably also regulate the use of triacylglycerol stores in that tissue.

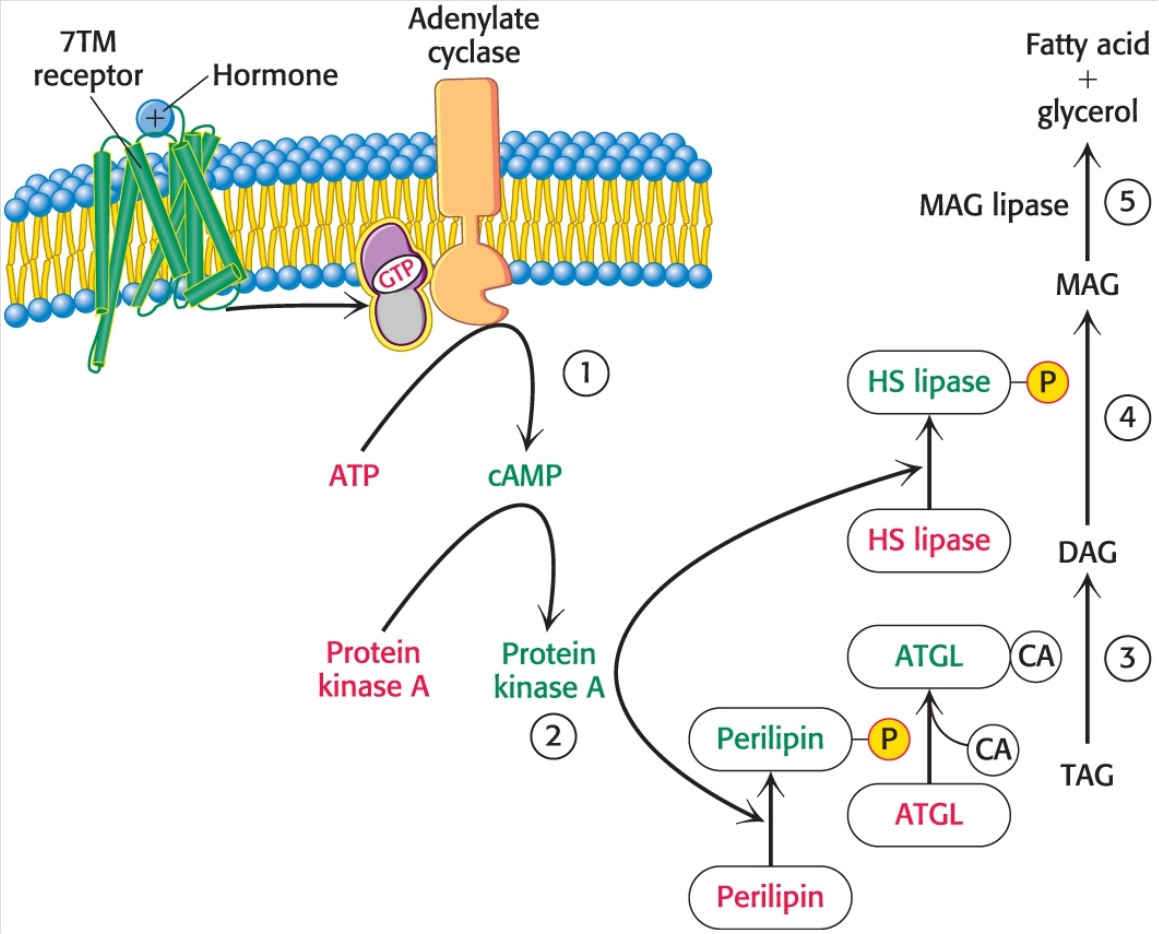


FIGURE 22.5 Triacylglycerols in adipose tissue are converted into free fatty acids in response to hormonal signals. (1) The hormones activate protein kinase A through the cAMP cascade. (2) Protein kinase A phosphorylates perilipin, resulting in the restructuring of the lipid droplet and release of the coactivator of ATGL, thereby activating ATGL. (3) ATGL converts triacylglycerol int diacylglycerol. (4) Hormone-sensitive lipase releases a fatty acid from diacylglycerol, generating monoacylglycerol. (5) Monoacylglycerol lipase completes the mobilization process. Abbreviations: 7TM, seven transmembrane receptor; ATGL, adipose triglyceride lipase; CA, coactivator; HS lipase, hormone-sensitive lipase; MAG lipase, monoacylglycerol lipase; DAG, diacylglycerol; TAG, triacylglycerol.

Although adipocytes are the primary site of triacylglycerol metabolism, the liver plays a crucial role in lipid metabolism, as we will examine in more detail in Chapters 24 and 27. Hepatocytes are the most common type of liver cells, and these cells function in all aspects of lipid

metabolism, including import, synthesis, storage, and secretion of lipids. These processes are responsive to diet and energy needs of the liver and other tissues. Recent research suggests that the epinephrine/cAMP pathway also regulates lipolysis from lipid droplets in cultured hepatocytes. Interestingly, this signaling pathway is disrupted by ethanol, and this disruption may play a role in the development of fatty liver, a risk factor for obesity and diabetes (Section 24.3).

Mobilization continues: Free fatty acids and glycerol are released into the blood

Fatty acids are not soluble in aqueous solutions. In order to reach tissues that require fatty acids, the released fatty acids bind to the blood protein albumin, which has seven binding sites for fatty acids of varying affinity, and delivers them to tissues in need of fuel.

Glycerol formed by lipolysis is absorbed by the liver and phosphorylated. It is then oxidized to dihydroxyacetone phosphate, which is isomerized to glyceraldehyde 3-phosphate. This molecule is an intermediate in both the glycolytic and the gluconeogenic pathways. Hence, glycerol can be converted into pyruvate or glucose in the liver, which contains the appropriate enzymes (**Figure 22.6**).

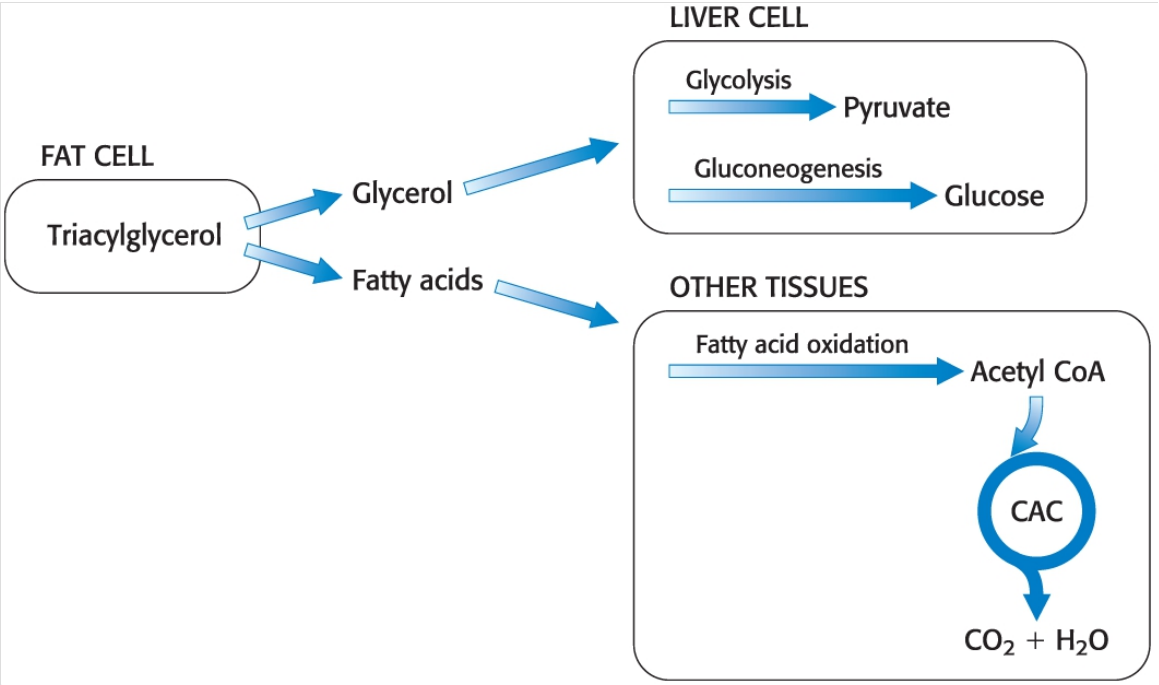
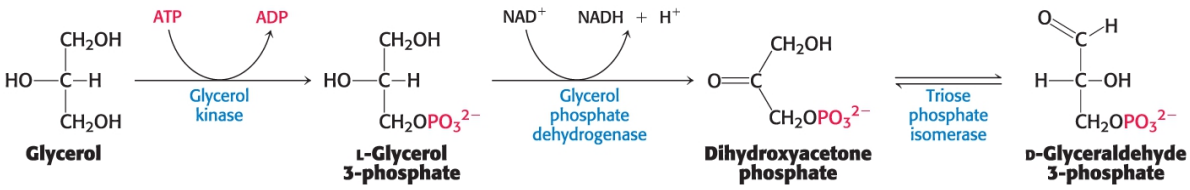


FIGURE 22.6 Lipolysis generates fatty acids and glycerol. The fatty acids are used as fuel by many tissues. The liver processes glycerol by either the glycolytic or the gluconeogenic pathway depending on its metabolic circumstances. Abbreviation: CAC, citric acid cycle.

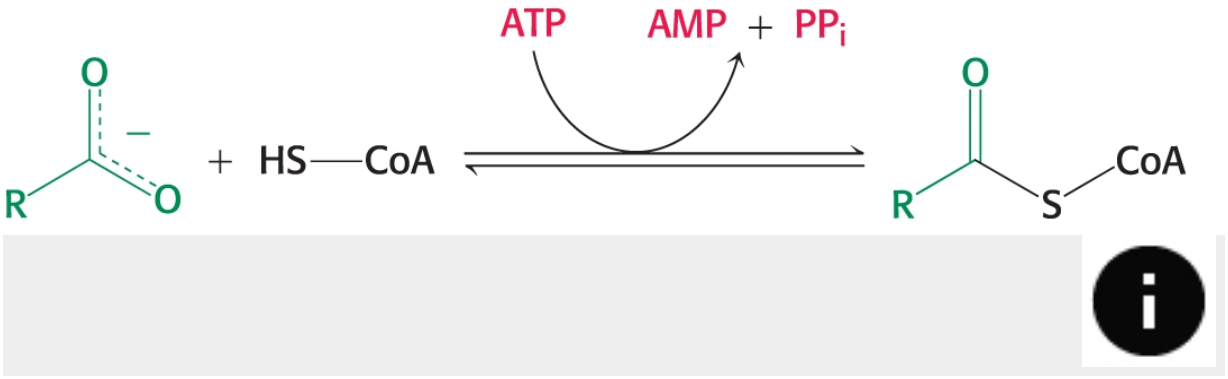
The reverse process can take place by the reduction of dihydroxyacetone phosphate to glycerol 3-phosphate. Hydrolysis by a phosphatase then gives glycerol. Thus, glycerol and glycolytic intermediates are readily interconvertible.



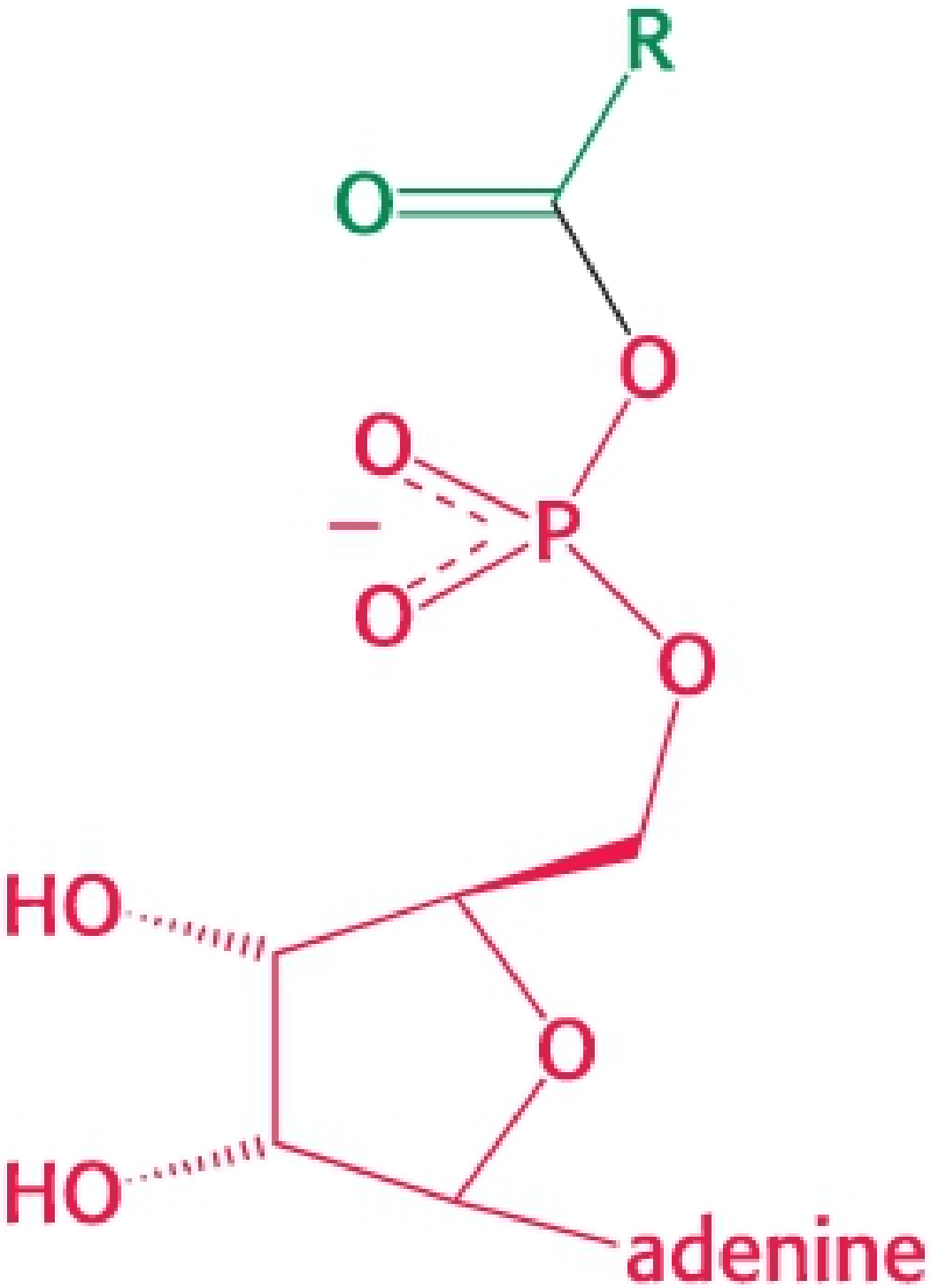
Activation: Fatty acids are linked to coenzyme A before they are oxidized

Fatty acids separate from the albumin in the blood stream and diffuse across the cell membrane with the assistance of fatty-acid transport proteins, the same proteins that facilitate their uptake into intestinal cells (Figure 22.4). Within the cell, fatty acids are transported while bound to fatty-acid binding proteins.

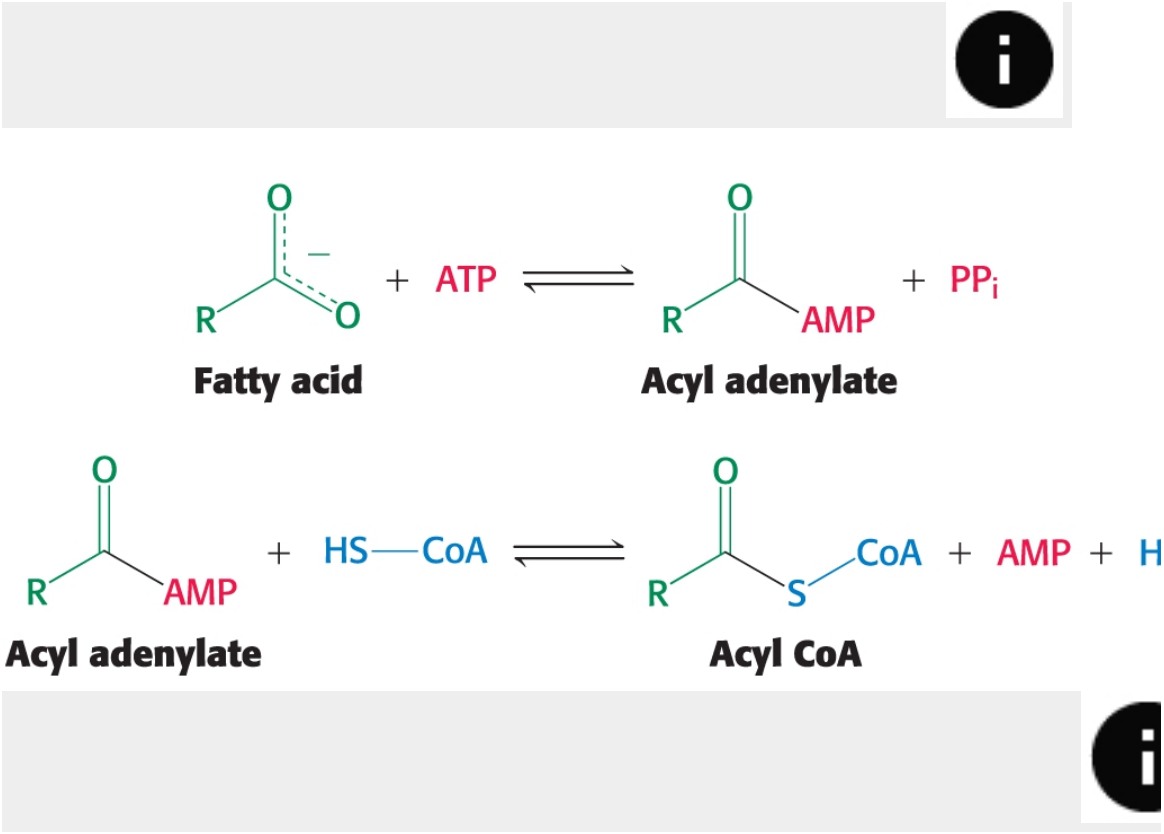
Fatty acid oxidation occurs in the mitochondrial matrix, but in order to enter the mitochondria, the fatty acids are first activated through the formation of a thioester linkage to coenzyme A. ATP drives the formation of the thioester linkage between the carboxyl group of a fatty acid and the sulfhydryl group of coenzyme A. This activation reaction takes place on the outer mitochondrial membrane, where it is catalyzed by acyl CoA synthetase.



Acyl CoA synthetase accomplishes the activation of a fatty acid in two steps. First, the fatty acid reacts with ATP to form an **acyl adenylate**. In this mixed anhydride, the carboxyl group of a fatty acid is bonded to the phosphoryl group of AMP. The other two phosphoryl groups of the ATP substrate are released as pyrophosphate. In the second step, the sulfhydryl group of coenzyme A attacks the acyl adenylate, which is tightly bound to the enzyme, to form acyl CoA and AMP.



Acyl adenylate



These partial reactions are freely reversible. In fact, the equilibrium constant for the sum of these reactions is close to 1. One high-transfer-potential compound is cleaved (between PP_i and AMP), and one high-transfer-potential compound is formed (the thioester acyl CoA). How is the overall reaction driven forward? The answer is that pyrophosphate is rapidly hydrolyzed by a pyrophosphatase. The complete reaction is

$$RCOO^- + CoA + ATP + H_2O \rightarrow RCO{-}CoA + AMP + 2\ P_i + 2\ H^+$$

This reaction is quite favorable because the equivalent of two molecules of ATP is hydrolyzed, whereas only one high-transfer-potential compound is formed. We see here another example of a recurring theme in biochemistry: many biosynthetic reactions are made irreversible by the hydrolysis of inorganic pyrophosphate.

Another motif recurs in this activation reaction. The enzyme-bound acyl adenylate intermediate is not unique to the synthesis of acyl CoA. Acyl adenylates are frequently formed when carboxyl groups are activated in biochemical reactions. Amino acids are activated for protein synthesis by a similar mechanism (Section 30.2), although the enzymes that catalyze this process are not homologous to acyl CoA synthetase. Thus, activation by adenylation recurs in part because of convergent evolution.

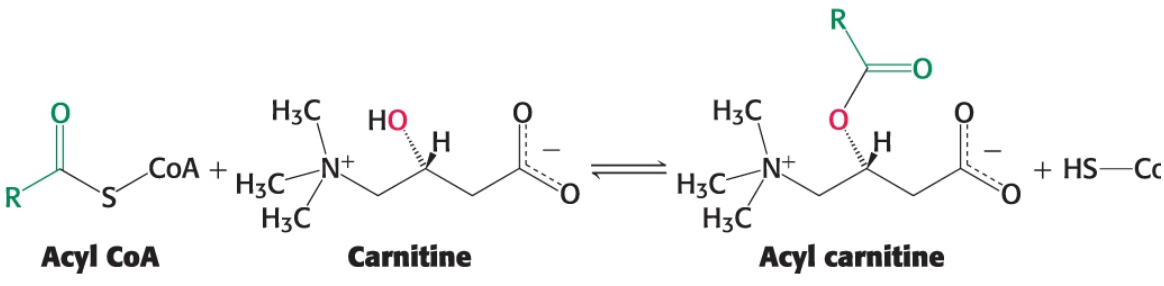
Self-Check Question



Suppose that a promoter mutation leads to the overproduction of protein kinase A in adipose cells. How might fatty acid metabolism be altered by this mutation?

Transport: Carnitine carries long-chain activated fatty acids into the mitochondrial matrix

Fatty acids are activated on the outer mitochondrial membrane, whereas they are oxidized in the mitochondrial matrix. A special transport mechanism is needed to carry activated long-chain fatty acids across the inner mitochondrial membrane. These fatty acids must be conjugated to **carnitine**, an alcohol with both a positive and a negative charge (a zwitterion). The acyl group is transferred from the sulfur atom of coenzyme A to the hydroxyl group of carnitine to form acyl carnitine. This reaction is catalyzed by carnitine acyltransferase I (CATI), which is bound to the outer mitochondrial membrane.



Acyl carnitine is then shuttled across the inner mitochondrial membrane by a translocase (Figure 22.7). The acyl group is transferred back to coenzyme A on the matrix side of the membrane. This reaction, which is catalyzed by carnitine acyltransferase II (CATII), is simply the reverse of the reaction that takes place in the cytoplasm. The reaction is thermodynamically feasible because of the zwitterionic nature of carnitine. The *O*-acyl link in carnitine has a high group-transfer potential, apparently because, being zwitterions, carnitine and its esters are solvated differently from most other alcohols and their esters. Finally, the translocase returns carnitine to the cytoplasmic side in exchange for an incoming acyl carnitine.

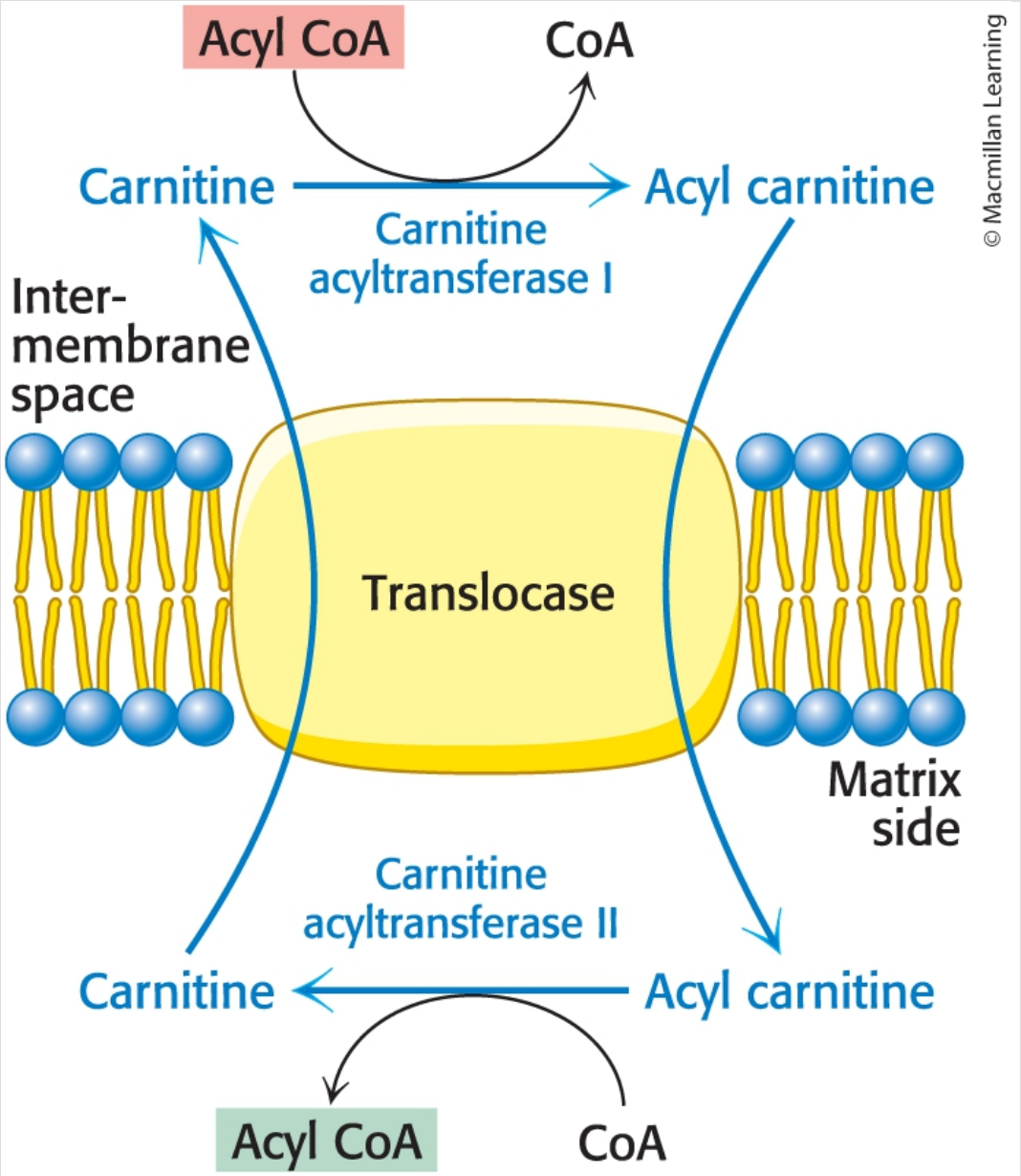


FIGURE 22.7 Acyl carnitine translocase mediates the entry of acyl carnitine into the mitochondrial matrix. Carnitine returns to the cytoplasmic side of the inner mitochondrial membrane in exchange for acyl carnitine.

A number of diseases have been traced to a deficiency of carnitine, the transferase, or the translocase. Inability to synthesize

carnitine may be a contributing factor to the development of autism in some people. The symptoms of carnitine deficiency range from mild muscle cramping to severe weakness and even death. In general, muscle, kidney, and heart are the tissues primarily impaired. Muscle weakness during prolonged exercise is a symptom of a deficiency of carnitine acyltransferases because muscle relies on fatty acids as a long-term source of energy. Medium-chain $(C_8 - C_{10})$ fatty acids are oxidized normally in these patients because these fatty acids can enter the mitochondria, to some degree, in the absence of carnitine. These diseases illustrate that the impaired flow of a metabolite from one compartment of a cell to another can lead to a pathological condition.

Breakdown: Acetyl CoA, NADH, and $FADH_2$ are generated in each round of fatty acid oxidation

A saturated acyl CoA is degraded by a recurring sequence of four reactions: oxidation by flavin adenine dinucleotide (FAD), hydration, oxidation by NAD^+, and thiolysis by coenzyme A (**Figure 22.8**). The fatty acid chain is shortened by two carbon atoms as a result of these reactions, and $FADH_2$, NADH, and acetyl CoA are generated. Because oxidation takes place at the β carbon atom, this series of reactions is called the **β-oxidation pathway**. The four reactions of each round of β-oxidation are described below and summarized in **Table 22.1**.

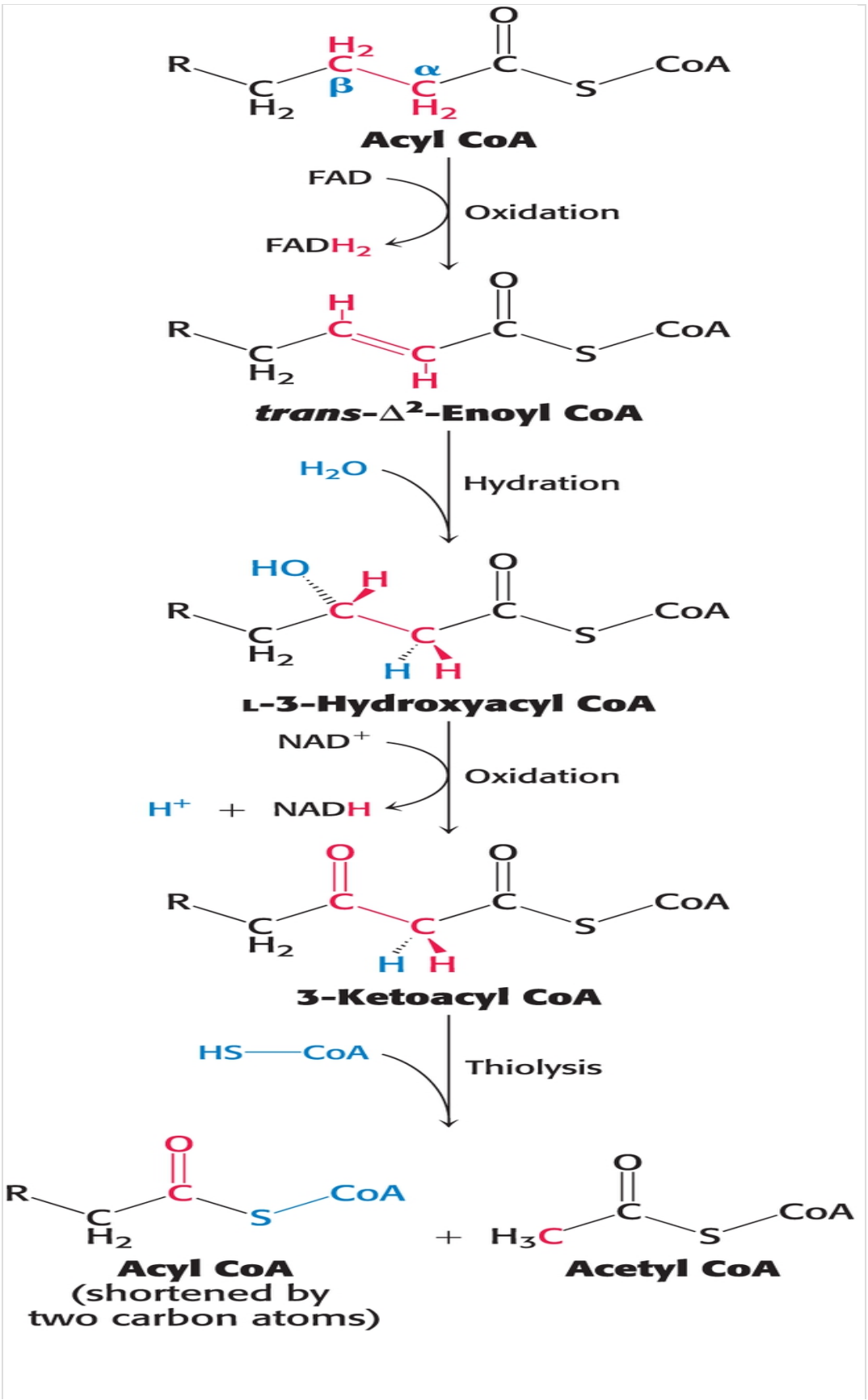

Acyl CoA
FAD
FADH2
Oxidation
trans-Δ2-Enoyl CoA
H2O
Hydration
L-3-Hydroxyacyl CoA
NAD+
H+ + NADH
Oxidation
3-Ketoacyl CoA
HS—CoA
Thiolysis
Acyl CoA
(shortened by
two carbon atoms)
Acetyl CoA

FIGURE 22.8 The reaction sequence for the degradation of fatty acids has four sequential steps. Fatty acids are degraded by the repetition of a four-reaction sequence called *β-oxidation*, consisting of oxidation, hydration, oxidation, and thiolysis.

EXPLORE this pathway further in the Metabolic Map in Achieve

TABLE 22.1 Principal reactions in fatty acid oxidation

Step	Reaction	Enzyme
Activation	$\text{Fatty acid} + \text{CoA} + \text{ATP} \rightleftharpoons \text{acyl CoA} + \text{AMP} + \text{PP}_i$	Acyl CoA synthetase (also called fatty acid thiokinase and fatty acid:CoA ligase)*
Transport	$\text{Carnitine} + \text{acyl CoA} \rightleftharpoons \text{acyl carnitine} + \text{CoA}$	Carnitine acyltransferase (also called carnitine palmitoyl transferase)
1st Oxidation	$\text{Acyl CoA} + \text{E}-\text{FAD} \rightarrow \textit{trans}-\Delta^2-\text{enoyl CoA} + \text{E}-\text{FADH}_2$	Acyl CoA dehydrogenases (several isozymes having different chain-length specificity)
Hydration	$\textit{trans}\text{-}\Delta^2\text{-Enoyl CoA} + \text{H}_2\text{O} \rightleftharpoons \text{L-3-Hydroxyacyl CoA}$	Enoyl CoA hydratase (also called crotonase

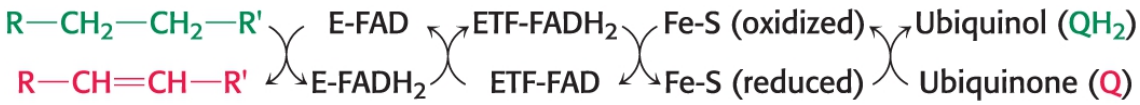
		or 3-hydroxyacyl CoA hydrolyase)
2nd Oxidation	L-3-Hydroxyacyl CoA + NAD^+ ⇌ 3-ketoacyl CoA + NADH + H^+	L-3-Hydroxyacyl CoA dehydrogenase
Cleavage	3-Ketoacyl CoA + CoA ⇌ acetyl CoA + acyl CoA (shortened by C_2)	β-Ketothiolase (also called thiolase)

*An AMP-forming ligase.

1. *Oxidation of acyl CoA, generating* $FADH_2$. This reaction is catalyzed by acyl CoA dehydrogenase to give an enoyl CoA with a trans double bond between C-2 and C-3.

$$\text{Acyl CoA} + \text{E}-\text{FAD} \rightarrow \textit{trans}-\Delta^2-\text{enoyl CoA} + \text{E}-\text{FADH}_2$$

As in the dehydrogenation of succinate in the citric acid cycle, FAD rather than NAD^+ is the electron acceptor because the ΔG for this reaction is insufficient to drive the reduction of NAD^+. Electrons from the $FADH_2$ prosthetic group of the reduced acyl CoA dehydrogenase are transferred to a second flavoprotein called *electron-transferring flavoprotein* (ETF). In turn, ETF donates electrons to ETF: ubiquinone reductase, an iron–sulfur protein. Ubiquinone is thereby reduced to ubiquinol, which delivers its high-potential electrons to the second proton-pumping site of the respiratory chain (Section 18.3). Consequently, 1.5 molecules of ATP are generated per molecule of $FADH_2$ formed in this dehydrogenation step, as in the oxidation of succinate to fumarate.



2. *Hydration of enyol CoA*. The next step is the hydration of the double bond between C-2 and C-3 by enoyl CoA hydratase.

$$\textit{trans}\text{-}\Delta^2\text{-Enoyl CoA} + H_2O \rightleftharpoons \text{L-3-hydroxyacyl CoA}$$

The hydration of enoyl CoA is stereospecific. Only the L isomer of 3-hydroxyacyl CoA is formed when the *trans*-Δ^2 double bond is hydrated. The enzyme also hydrates a *cis*-Δ^2 double bond, but the product then is the D isomer. We shall return to this point shortly in considering how unsaturated fatty acids are oxidized. The hydration of enoyl CoA is a prelude to the next reaction.

3. *Second oxidation, generating NADH*. This reaction converts the hydroxyl group at C-3 into a keto group and generates NADH. This oxidation is catalyzed by L-3-hydroxyacyl CoA dehydrogenase, which is specific for the L isomer of the hydroxyacyl substrate.

$$\text{L-3-Hydroxyacyl CoA} + NAD^+ \rightleftharpoons \text{3-ketoacyl CoA} + NADH + H^+$$

The preceding reactions have oxidized the methylene group at C-3 to a keto group, setting up the final step.

4. *Cleavage, generating a shortened acyl CoA and acetyl CoA*. The final step is the cleavage of 3-ketoacyl CoA by the thiol group of a second molecule of coenzyme A, which yields acetyl CoA and an acyl CoA shortened by two carbon atoms. This thiolytic cleavage is catalyzed by β-ketothiolase.

$$\underset{(n \text{ carbons})}{\text{3-Ketoacyl CoA}} + \text{CoA} \rightleftharpoons \text{acetyl CoA} + \underset{(n-2 \text{ carbons})}{\text{acyl CoA}}$$

The shortened acyl CoA then undergoes another cycle of oxidation, starting with the reaction catalyzed by acyl CoA dehydrogenase (**Figure 22.9**). Fatty acid chains containing from 12 to 18 carbon atoms are oxidized by the long-chain acyl CoA dehydrogenase. The medium-chain acyl CoA dehydrogenase oxidizes fatty acid chains having from 4 to 14 carbons, whereas the short-chain acyl CoA dehydrogenase acts only on 4- and 6-carbon fatty acid chains. In contrast, β-ketothiolase, hydroxyacyl dehydrogenase, and enoyl CoA hydratase act on fatty acid molecules of almost any length.

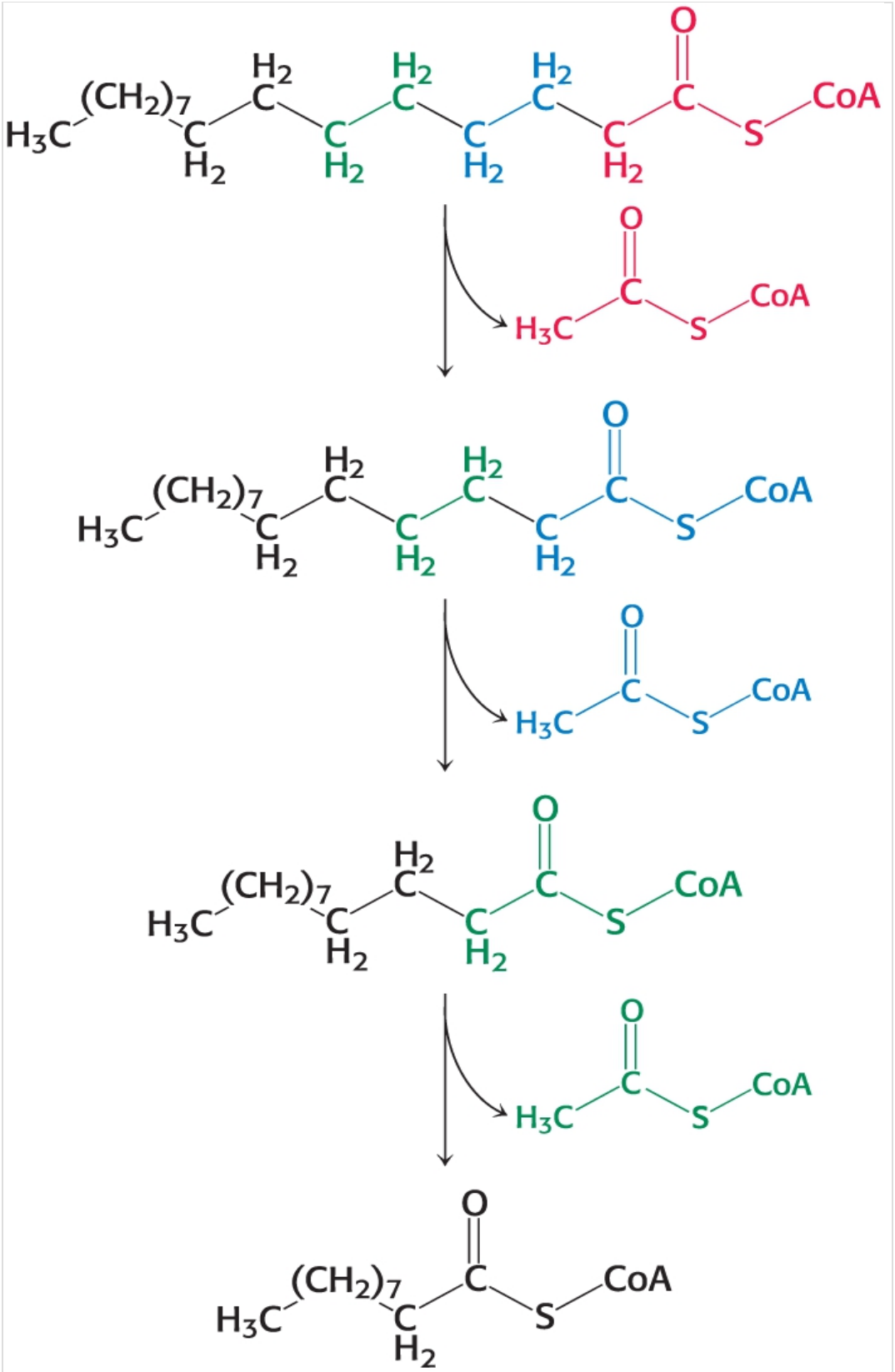

O
H2
H2
H2
(CH2)7
H3C
C
C
C
C
C
S
CoA
H2
H2
H2
O
C
H3C
S
CoA
O
H2
H2
(CH2)7
H3C
C
C
C
S
CoA
H2
H2
H2
O
C
H3C
S
CoA
O
H2
(CH2)7
H3C
C
C
S
CoA
H2
H2
O
C
H3C
S
CoA
O
(CH2)7
H3C
C
C
S
CoA
H2

FIGURE 22.9 Each round of fatty acid degradation removes two carbons. The first three rounds in the degradation of palmitate are shown. Notice that two-carbon units are sequentially removed from the carboxyl end of the fatty acid.



The complete oxidation of palmitate yields 106 molecules of ATP

We can now calculate the energy yield derived from the oxidation of a fatty acid. In each reaction cycle, an acyl CoA is shortened by two carbon atoms, and one molecule each of $FADH_2$, NADH, and acetyl CoA are formed.

$$C_n\text{–acyl CoA} + FAD + NAD^+ + H_2O + CoA \rightarrow$$

$$C_{n-2}\text{–acyl CoA} + FADH_2 + NADH + \text{acetyl CoA} + H^+$$

The degradation of palmitoyl CoA (C_{16}-acyl CoA) requires seven reaction cycles. In the seventh cycle, the C_4-ketoacyl CoA is thiolyzed to two molecules of acetyl CoA. Hence, the stoichiometry of the oxidation of palmitoyl CoA is

$$\text{Palmitoyl CoA} + 7\ FAD + 7\ NAD^+ + 7\ CoA + 7\ H_2O \rightarrow$$

$$8\ \text{acetyl CoA} + 7\ FADH_2 + 7\ NADH + 7\ H^+$$

Approximately 2.5 molecules of ATP are generated when the respiratory chain oxidizes each of these NADH molecules, whereas 1.5 molecules of ATP are formed for each $FADH_2$ because their electrons enter the chain at the level of ubiquinol. Recall that the oxidation of acetyl CoA by the citric acid cycle yields 10 molecules of ATP. Hence, the number of ATP molecules formed in the oxidation of palmitoyl CoA is 10.5 from the seven $FADH_2$, 17.5 from the seven NADH, and 80 from the eight acetyl CoA molecules, which gives a total of 108. The equivalent of 2 molecules of ATP is consumed in the activation of palmitate, in which ATP is split into AMP and 2 molecules of orthophosphate. Thus, the complete oxidation of a molecule of palmitate yields 106 molecules of ATP.

Self-Check Question



Explain why people with a hereditary deficiency of carnitine acyltransferase II have muscle weakness. Why are the symptoms more severe during fasting?

22.3 Unsaturated and Odd-Chain Fatty Acids Require Additional Steps for Degradation

The β-oxidation pathway accomplishes the complete degradation of saturated fatty acids having an even number of carbon atoms. Most fatty acids have such structures because of their mode of synthesis (to be addressed later in this chapter). However, not all fatty acids are so simple. The oxidation of fatty acids containing double bonds requires additional steps, as does the oxidation of fatty acids containing an odd number of carbon atoms.

An isomerase and a reductase are required for the oxidation of unsaturated fatty acids

The oxidation of unsaturated fatty acids presents some difficulties, yet many such fatty acids are available in the diet. Most of the reactions are the same as those for saturated fatty acids. In fact, only two additional enzymes — an isomerase and a reductase — are needed to degrade a wide range of unsaturated fatty acids.

Consider the oxidation of palmitoleate (**Figure 22.10**). This C_{16} unsaturated fatty acid, which has one double bond between C-9 and C-10, is activated and transported across the inner mitochondrial membrane in the same way as saturated fatty acids are. Palmitoleoyl CoA then undergoes three cycles of degradation, which are carried out by the same enzymes as those in the oxidation of saturated fatty acids. However, the *cis*-Δ^3-enoyl CoA formed in the third round is not a substrate for acyl CoA dehydrogenase. The presence of a double bond

between C-3 and C-4 prevents the formation of another double bond between C-2 and C-3. This impasse is resolved by a new reaction that shifts the position and configuration of the *cis*-Δ^3 double bond. *cis*-Δ^3-Enoyl CoA isomerase converts this double bond into a trans-Δ^2 double bond (Figure 22.10). The double bond is now between C-2 and C-3. The subsequent reactions are those of the saturated fatty acid oxidation pathway, in which the *trans*-Δ^2-enoyl CoA is a regular substrate.

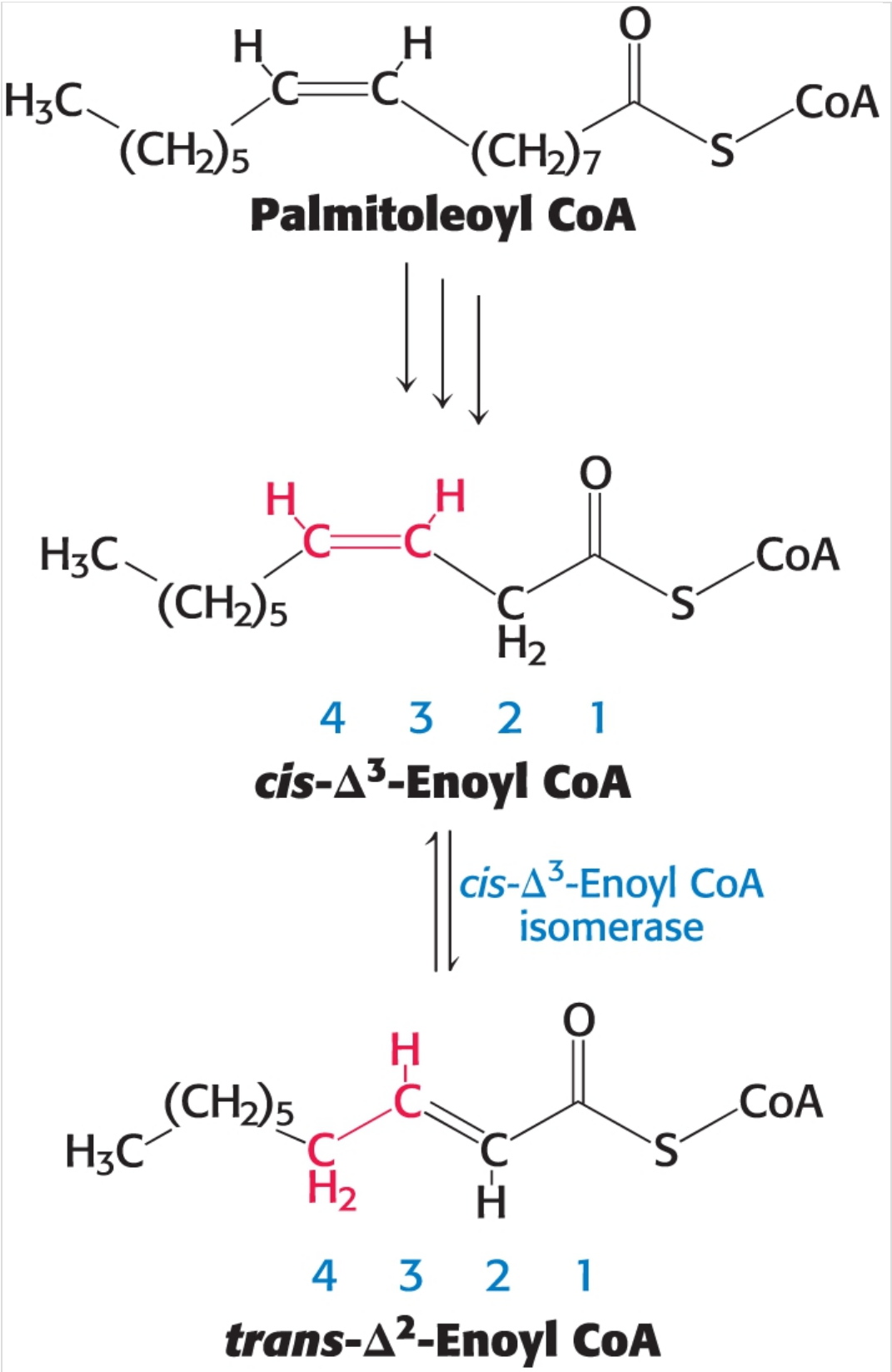

Palmitoleoyl CoA
4 3 2 1
cis-Δ3-Enoyl CoA
cis-Δ3-Enoyl CoA isomerase
4 3 2 1
trans-Δ2-Enoyl CoA

FIGURE 22.10 The degradation of a monounsaturated fatty acid involves an additional enzymatic step. *Cis*-Δ^3-Enoyl CoA isomerase allows continued β-oxidation of fatty acids with a single double bond.



Human beings require polyunsaturated fatty acids (Section 22.6), which have multiple double bonds, as important precursors for signal molecules. Excess polyunsaturated fatty acids are degraded by β-oxidation. However, another problem arises with the oxidation of polyunsaturated fatty acids. Consider linoleate, a C_{18} polyunsaturated fatty acid with *cis*-Δ^9 and *cis*-Δ^{12} double bonds (**Figure 22.11**). The *cis*-Δ^3 double bond (between carbons 3 and 4) formed after three rounds of β-oxidation is converted into a *trans*-Δ^2 double bond (between carbons 2 and 3) by the aforementioned isomerase. The acyl CoA produced by another round of β-oxidation contains a *cis*-Δ^4 double bond. Dehydrogenation of this species by acyl CoA dehydrogenase yields a 2,4-dienoyl intermediate (double bond between carbons 2 and 3 and carbons 4 and 5), which is not a substrate for the next enzyme in the β-oxidation pathway. This impasse is circumvented by 2,4-dienoyl CoA reductase, an enzyme that uses NADPH to reduce the 2,4-dienoyl intermediate to *trans*-Δ^3-enoyl CoA. *cis*-Δ^3-Enoyl CoA isomerase then converts *trans*-Δ^3-enoyl CoA into the *trans*-Δ^2 form, a customary intermediate in the β-oxidation pathway (Figure 22.11). These catalytic strategies are elegant and economical. Only two extra enzymes are needed for the oxidation of *any* polyunsaturated fatty acid. Odd-numbered double bonds are handled by the isomerase, and even-numbered ones by the reductase and the isomerase.

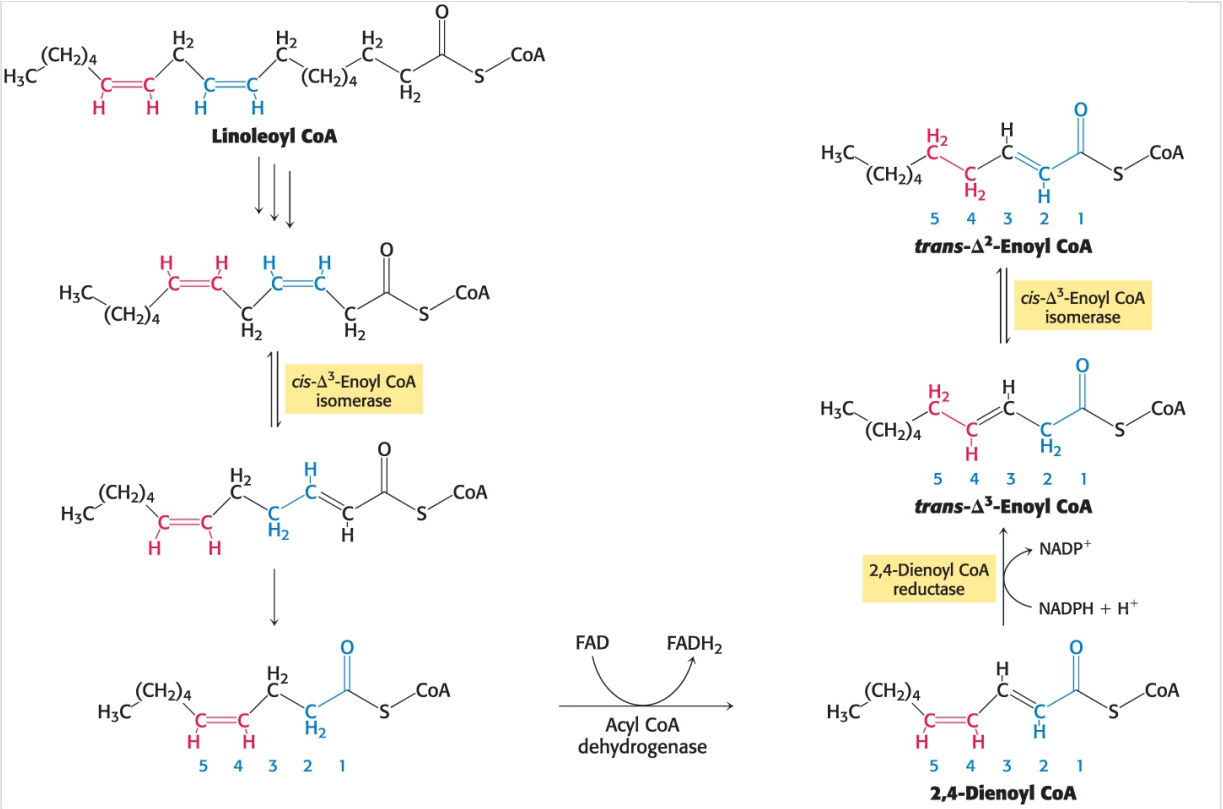


FIGURE 22.11 Multiple additional enzymes are necessary to oxidize polyunsaturated fatty acids. The oxidation of linoleoyl CoA is shown. The complete oxidation of the diunsaturated fatty acid linoleate is facilitated by the activity of enoyl CoA isomerase and 2,4-dienoyl CoA reductase. Eventually, the action of *cis*-Δ^3-enoyl CoA isomerase shifts the double bond to the Δ^2 position, making the molecule identical to an intermediate of saturated fatty acid degradation.

Odd-chain fatty acids yield propionyl CoA in the final thiolysis step

Fatty acids having an odd number of carbon atoms are minor species. They are oxidized in the same way as fatty acids having an even number, except that propionyl CoA and acetyl CoA, rather than two molecules of acetyl CoA, are produced in the final round of degradation. The

activated three-carbon unit in propionyl CoA enters the citric acid cycle after it has been converted into succinyl CoA (Figure 22.12). Interestingly, this is the only product of fatty acid catabolism that can serve as a gluconeogenic substrate. Succinyl CoA can be converted into oxaloacetate to provide carbon for glucose biosynthesis, a unique benefit of odd-numbered fatty acids.

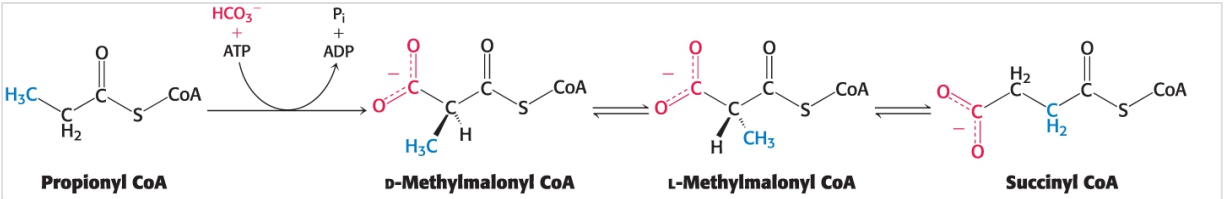


FIGURE 22.12 The final product of odd-numbered fatty acid degradation is converted into a CAC intermediate. Propionyl CoA, generated from fatty acids with an odd number of carbons as well as some amino acids, is converted into the citric acid cycle intermediate succinyl CoA, which can be a substrate for gluconeogenesis.

The pathway from propionyl CoA to succinyl CoA is especially interesting because it entails a rearrangement that requires vitamin B_{12} (also known as cobalamin). Propionyl CoA is carboxylated at the expense of the hydrolysis of a molecule of ATP to yield the D isomer of methylmalonyl CoA (Figure 22.12). This carboxylation reaction is catalyzed by propionyl CoA carboxylase, a biotin enzyme that has a catalytic mechanism like that of the homologous enzyme pyruvate carboxylase (Section 16.4). The D isomer of methylmalonyl CoA is racemized to the L isomer, the substrate for a mutase that converts it into succinyl CoA by an intramolecular rearrangement. The $-CO-S-CoA$ group migrates from C-2 to a methyl group in exchange for a hydrogen atom. This very unusual isomerization is catalyzed by methylmalonyl CoA mutase, which contains a derivative of cobalamin as its coenzyme.

Vitamin B_{12} contains a corrin ring and a cobalt atom

Cobalamin enzymes, which are present in most organisms, catalyze three types of reactions: (1) intramolecular rearrangements; (2) methylations, as in the synthesis of methionine (Section 25.2); and (3) the reduction of ribonucleotides to deoxyribonucleotides (Section 26.3). In mammals, only two reactions are known to require coenzyme B_{12}. The conversion of L-methylmalonyl CoA into succinyl CoA is one, and the formation of methionine by the methylation of homocysteine is the other (Section 25.2). The latter reaction is especially important because methionine is required for the generation of coenzymes that participate in the synthesis of purines and thymine, which are needed for nucleic acid synthesis. Interestingly, vitamin B_{12} is a molecule that is made only by prokaryotic organisms; all animals obtain coenzyme B_{12} either from diet or absorption from gut microorganisms, and plants and algae obtain it via their symbiosis with prokaryotes.

The core of cobalamin consists of a corrin ring with a central cobalt atom (**Figure 22.13**). The corrin ring, like a porphyrin, has four pyrrole units. Two of them are directly bonded to each other, whereas the others are joined by methine bridges, as in porphyrins. The corrin ring is more reduced than that of porphyrins, and the substituents are different. A cobalt atom is bonded to the four pyrrole nitrogens. The fifth substituent linked to the cobalt atom is a derivative of dimethylbenzimidazole that contains ribose 3-phosphate and aminoisopropanol. One of the nitrogen atoms of dimethylbenzimidazole is linked to the cobalt atom. In coenzyme B_{12}, the sixth substituent linked to the cobalt atom is a $5'$-deoxyadenosyl unit or a methyl group. This position can also be occupied by a cyano group. Cyanocobalamin is the form of the coenzyme administered to treat B_{12} deficiency. In all of these compounds, the cobalt is in the $+3$ oxidation state. Our knowledge of vitamin B_{12}, and countless other molecules

including pepsin, penicillin, and insulin, was made possible by the pioneering work of Prof. Dorothy Hodgkin, sometimes called the "Queen of Crystallography" for the numerous advances she made over a six-decade career.

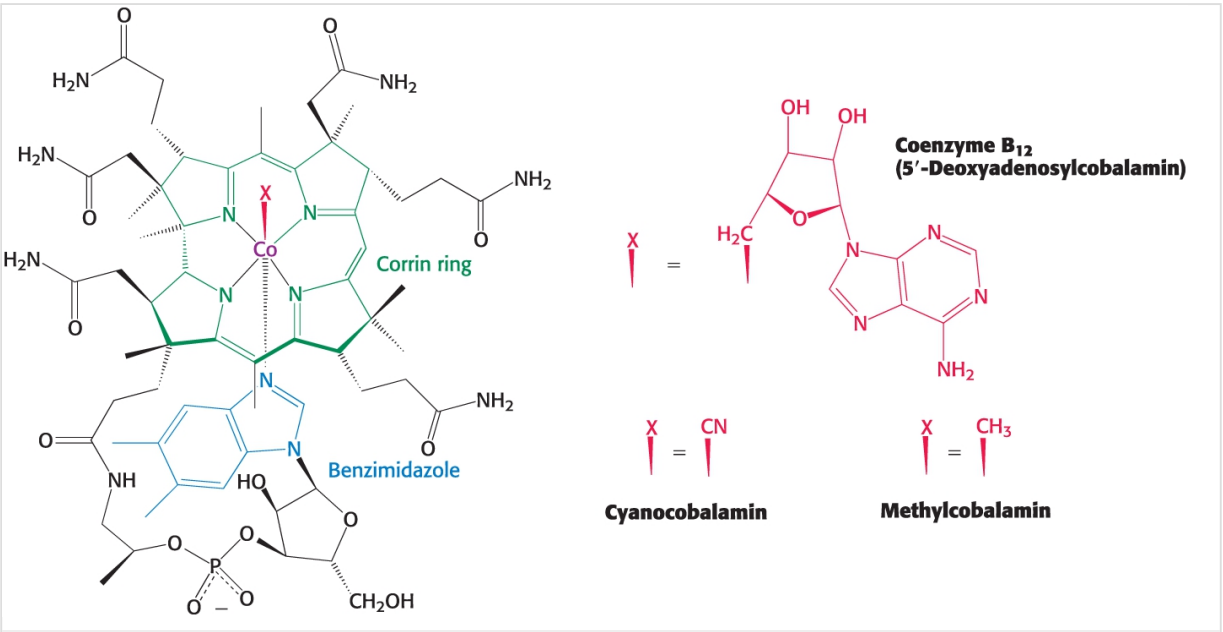


FIGURE 22.13 Coenzyme B_{12} (cobalamin) is a class of molecules with a complex structure.

Forms of coenzyme B_{12} vary depending on the component designated X in the left-hand structure. 5′-Deoxyadenosylcobalamin is the form of the coenzyme in methylmalonyl mutase. Substitution of methyl and cyano groups for X creates methylcobalamin and cyanocobalamin, respectively.



Harold Clements/Hulton Archive/Getty Images

DOROTHY HODGKIN As a teenager in England in the mid-1920s, Dorothy Hodgkin petitioned her grammar school to be educated in chemistry along with her male peers. During her PhD training she published the first data from hydrated protein crystals in 1934, and then captured the first images of insulin in her own lab in 1935. She went on to determine the structure of penicillin, which paved the way for its mass production. In 1956, she determined the structure of vitamin B_{12}, by far the most complex structure ever solved, an accomplishment that Nobel laureate Sir Lawrence Bragg likened to "breaking the sound barrier." Dr. Hodgkin was nominated for a Nobel Prize 32 times in either Physics or Chemistry before finally winning in Chemistry in 1964. Five years later, she solved the structure of insulin, after 34 years of work. She accomplished this, and much more, all while suffering from rheumatoid arthritis since the age of 28. Despite her arthritis dramatically affecting her hands later in life, she worked until age 84 and died in 1994. One of her former students,

Margaret Thatcher, famously hung a picture of Prof. Hodgkin in her office while serving as Prime Minister of the UK.

Mechanism: Methylmalonyl CoA mutase catalyzes a rearrangement to form succinyl CoA

The rearrangement reactions catalyzed by coenzyme B_{12} are exchanges of two groups attached to adjacent carbon atoms of the substrate (Figure 22.14).



FIGURE 22.14 Cobalamin enzymes catalyze specific rearrangement reactions. A group on one carbon is exchanged with a proton on an adjacent carbon. The R group can be an amino group, a hydroxyl group, or a substituted carbon.

A hydrogen atom migrates from one carbon atom to the next, and an R group (such as the $-CO-S-CoA$ group of methylmalonyl CoA) concomitantly moves in the reverse direction. The first step in these intramolecular rearrangements is the cleavage of the carbon–cobalt bond of $5'$-deoxyadenosylcobalamin to generate the Co^{2+} form of the coenzyme and a $5'$-deoxyadenosyl radical, $-CH_2\cdot$ (Figure 22.15). In this homolytic cleavage reaction, one electron of the Co–C bond stays

with Co (reducing it from the $^{+3}$ to the $^{+2}$ oxidation state), whereas the other electron stays with the carbon atom, generating a free radical. In contrast, nearly all other cleavage reactions in biological systems are heterolytic: an electron *pair* is transferred to one of the two atoms that were bonded together.

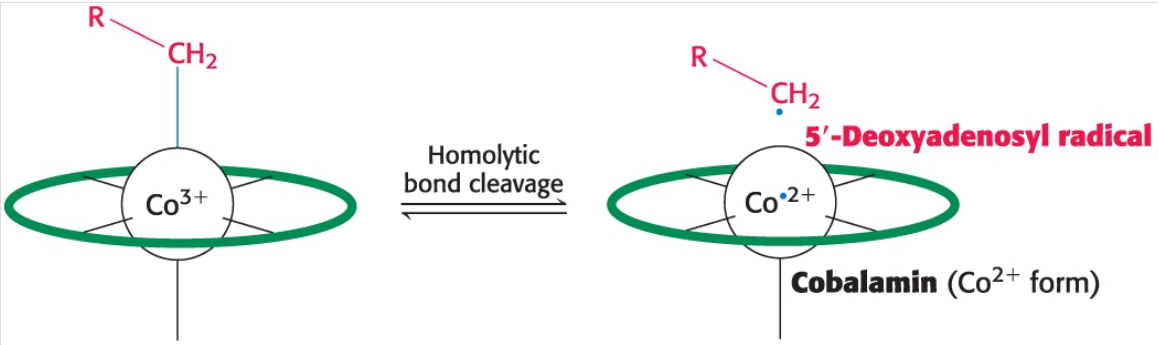


FIGURE 22.15 Cobalamin enzymes accomplish homolytic bond cleavage to form a radical. Th methylmalonyl CoA mutase reaction begins with the homolytic cleavage of the bond joining Co^{3+} of coenzyme B_{12} to a carbon atom of the ribose of the adenosine moiety of the enzym The cleavage generates a $5'$-deoxyadenosyl radical and leads to the reduction of Co^{3+} to Co^{2+}. The letter R represents the $5'$-deoxyadenosyl component of the coenzyme, and the green oval represents the remainder of the coenzyme.

What is the role of this very unusual $-CH_2\cdot$ radical? This highly reactive species abstracts a hydrogen atom from the substrate to form $5'$-deoxyadenosine and a substrate radical (Figure 22.16). This substrate radical spontaneously rearranges: the carbonyl CoA group migrates to the position formerly occupied by H on the neighboring carbon atom to produce a different radical. This product radical abstracts a hydrogen atom from the methyl group of $5'$-deoxyadenosine to complete the rearrangement and return the deoxyadenosyl unit to the radical form.

The role of coenzyme B_{12} in such intramolecular migrations is to serve as a source of free radicals for the abstraction of hydrogen atoms.

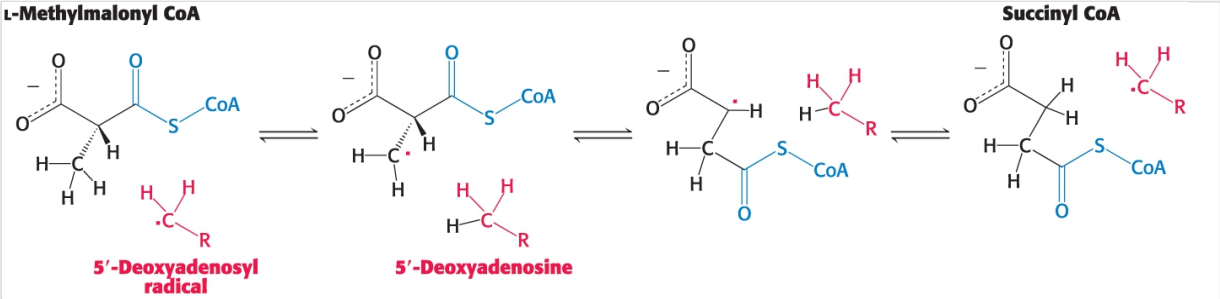


FIGURE 22.16 Succinyl CoA is formed from methylmalonyl CoA by a rearrangement reaction. A free radical abstracts a hydrogen atom in the rearrangement of methylmalonyl CoA to succinyl CoA.

An essential property of coenzyme B_{12} is the weakness of its cobalt–carbon bond, which is readily cleaved to generate a radical. To facilitate the cleavage of this bond, enzymes such as methylmalonyl CoA mutase displace the benzimidazole group from the cobalamin and bind to the cobalt atom through a histidine residue (Figure 22.17). The steric crowding around the cobalt–carbon bond within the corrin ring system contributes to the bond weakness.

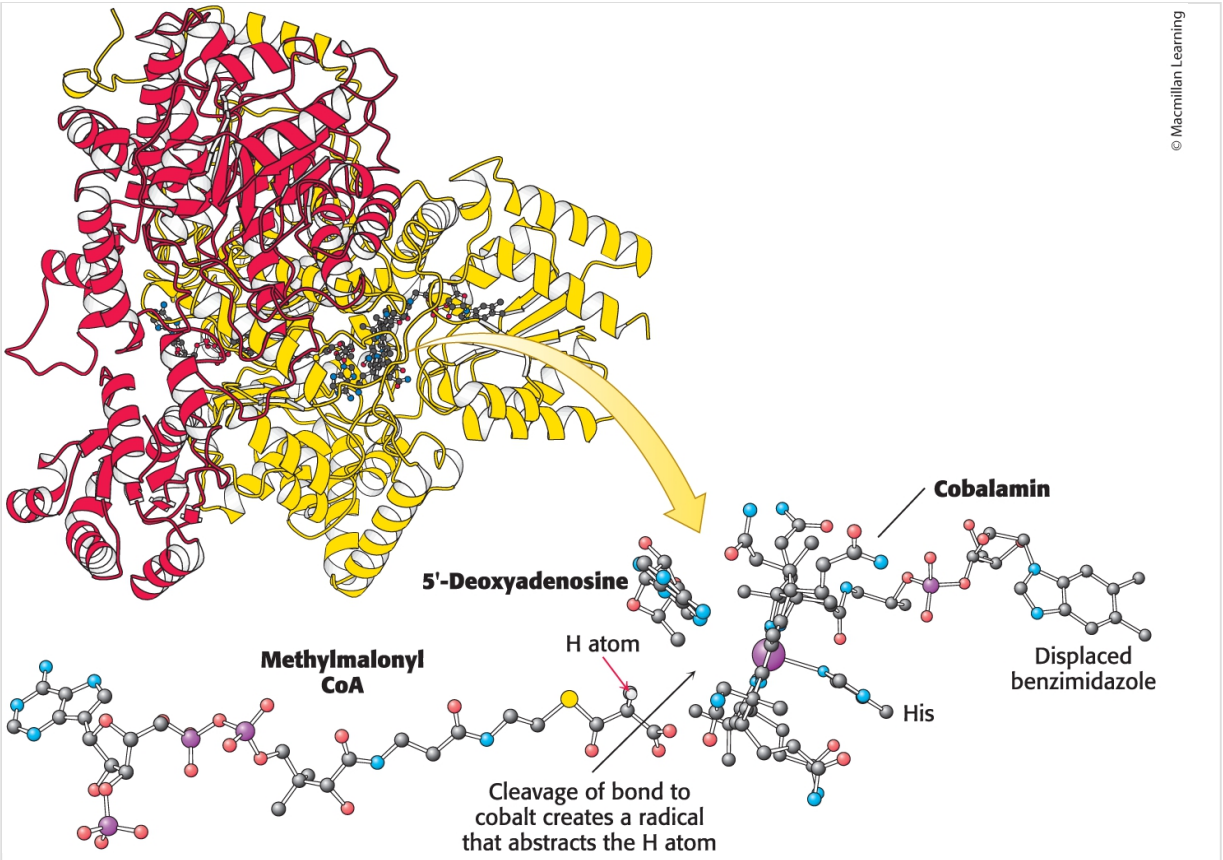


FIGURE 22.17 The active site of methylmalonyl CoA mutase reveals how radical formation is accomplished. Notice that a histidine residue from the enzyme binds to cobalt in place of benzimidazole. This arrangement of substrate and coenzyme in the active site facilitates the cleavage of the cobalt–carbon bond and the subsequent abstraction of a hydrogen atom from the substrate.

[Drawn from 4REQ.pdb.]

INTERACT with this model in Achieve

Fatty acids are also oxidized in peroxisomes

Although most fatty acid oxidation takes place in mitochondria, oxidation of long-chain and branched fatty acids takes place in cellular

organelles called **peroxisomes**. These organelles are small membrane-bounded compartments that are present in the cells of most eukaryotes. Fatty acid oxidation in these organelles, which halts at octanoyl CoA, serves to shorten very long chains (C_{26}) to make them better substrates of β-oxidation in mitochondria. Peroxisomal oxidation differs from β-oxidation in the initial dehydrogenation reaction (**Figure 22.18**). In peroxisomes, acyl CoA dehydrogenase — a flavoprotein — transfers electrons from the substrate to FAD and then to O_2 to yield H_2O_2. In mitochondrial β-oxidation, the high-energy electrons would be captured as $FADH_2$ for use in the electron-transport chain. Because H_2O_2 is produced instead of $FADH_2$, peroxisomes contain high concentrations of the enzyme catalase to degrade H_2O_2 into water and O_2. Subsequent steps are identical with those of their mitochondrial counterparts, although they are carried out by different isoforms of the enzymes.

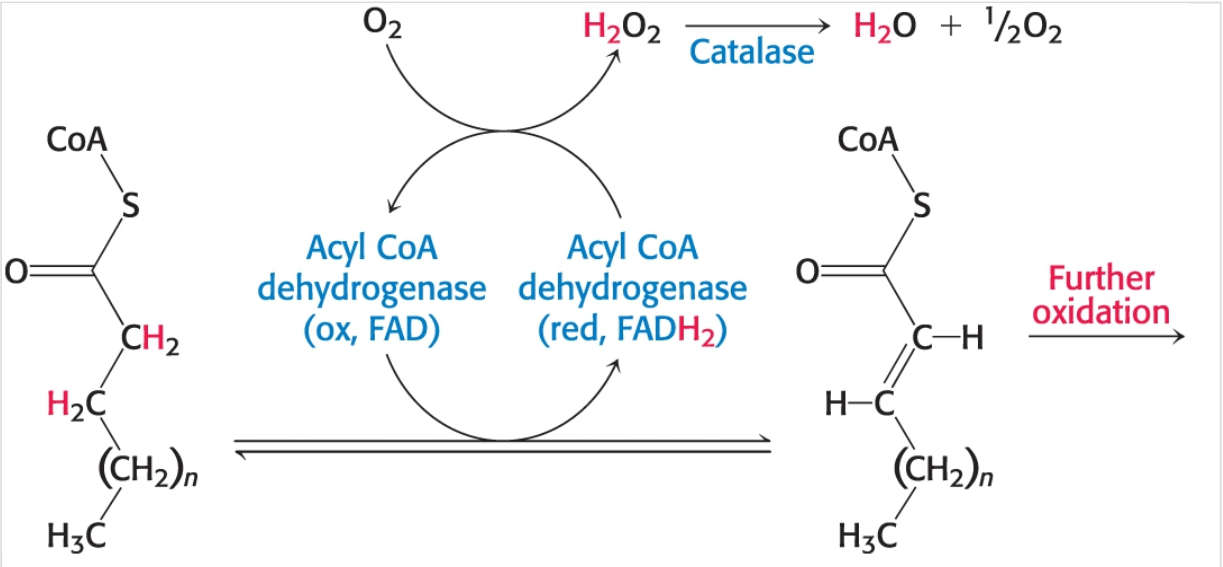


FIGURE 22.18 Initiation of peroxisomal fatty acid degradation requires a flavoprotein. The first dehydrogenation in the degradation of fatty acids in peroxisomes requires a flavoprotein dehydrogenase that transfers electrons from its $FADH_2$ moiety to O_2 to yield H_2O_2.

 Peroxisomes do not function in patients with Zellweger syndrome. Liver, kidney, and muscle abnormalities usually lead to death by age 6 years. The syndrome is caused by a defect in the import of enzymes into the peroxisomes. Here we see a pathological condition resulting from an inappropriate cellular distribution of enzymes.

Some fatty acids contribute to the development of pathological conditions



As we will see shortly (Section 22.5), certain polyunsaturated fatty acids are essential for life, serving as precursors to various signal molecules. Vegetable oils, used commonly in food preparation, are rich in polyunsaturated fatty acids. However, polyunsaturated fatty acids are unstable and are readily oxidized. This tendency to become rancid reduces their shelf life and renders them undesirable for cooking. To circumvent this problem, polyunsaturated fatty acids are sometimes hydrogenated, converting them to saturated and monounsaturated fats. However, the conditions of hydrogenation also cause an undesirable isomerization of some cis-double bonds, resulting in the unwanted production of trans unsaturated fatty acids (popularly known as “trans fats”), a variety of fat that is rare in nature.

Epidemiological evidence suggests that consumption of large amounts of saturated fatty acids and trans fat promotes obesity, type 2 diabetes, and atherosclerosis. The mechanism by which these fats exert these effects is under active investigation. Some evidence suggests that they slow β-oxidation directly, while other evidence suggests that they promote an inflammatory response and may mute the action of insulin and other hormones.

22.4 Ketone Bodies Are a Fuel Source Derived from Fats

The acetyl CoA formed in fatty acid oxidation enters the citric acid cycle only if fat and carbohydrate degradation are appropriately balanced. Acetyl CoA must combine with oxaloacetate to gain entry to the citric acid cycle. The availability of oxaloacetate, however, depends on an adequate supply of carbohydrate. Recall that oxaloacetate is normally formed from pyruvate, the product of glucose degradation in glycolysis, by pyruvate carboxylase (Section 16.4). If carbohydrate is unavailable or improperly utilized, the concentration of oxaloacetate is lowered and acetyl CoA cannot enter the citric acid cycle.

In fasting or diabetes, oxaloacetate is consumed to form glucose by the gluconeogenic pathway (Section 16.4) and hence is unavailable for condensation with acetyl CoA. Under these conditions, acetyl CoA is diverted to the formation of acetoacetate and D-3-hydroxybutyrate. Acetoacetate, D-3-hydroxybutyrate, and acetone are often referred to as **ketone bodies**. Abnormally high levels of ketone bodies are present in the blood of untreated diabetics.

Acetoacetate is formed from acetyl CoA in three steps (**Figure 22.19**). Two molecules of acetyl CoA condense to form acetoacetyl CoA. This reaction, which is catalyzed by thiolase, is the reverse of the thiolysis step in the oxidation of fatty acids. Acetoacetyl CoA then reacts with acetyl CoA and water to give 3-hydroxy-3-methylglutaryl CoA (HMG-CoA) and CoA. This condensation resembles the one catalyzed by citrate synthase (Section 17.3). This reaction, which has a favorable equilibrium owing to the hydrolysis of a thioester linkage, compensates for the unfavorable equilibrium in the formation of acetoacetyl CoA. 3-Hydroxy-3-methylglutaryl CoA is then cleaved to acetyl CoA and acetoacetate. The sum of these reactions is

$$2\ \text{Acetyl CoA} + H_2O \rightarrow \text{acetoacetate} + 2\ \text{CoA} + H^+$$

D-3-Hydroxybutyrate is formed by the reduction of acetoacetate in the mitochondrial matrix by D-3-hydroxybutyrate dehydrogenase. The ratio of hydroxybutyrate to acetoacetate depends on the $NADH/NAD^+$ ratio inside mitochondria.

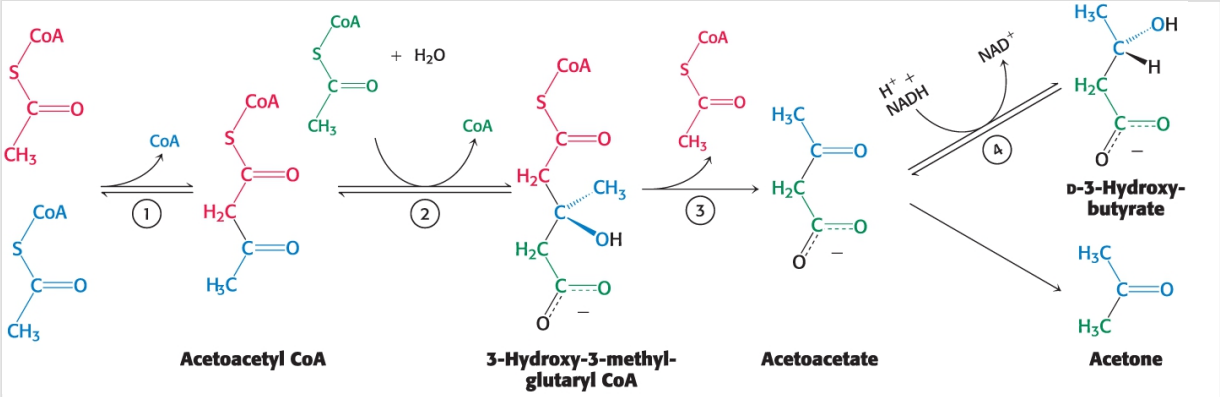


FIGURE 22.19 Ketone bodies are formed from acetyl CoA primarily in the liver. Three molecules are known as ketone bodies: acetoacetate, D-3-hydroxybutyrate, and acetone. Liver enzymes catalyzing the ketone body formation reactions are (1) 3-ketothiolase, (2) hydroxymethylglutaryl CoA synthase, (3) hydroxymethylglutaryl CoA cleavage enzyme, and (4) D-3-hydroxybutyrate dehydrogenase. Acetoacetate spontaneously decarboxylates to form acetone.

Because it is a β-ketoacid, acetoacetate also undergoes a slow, spontaneous decarboxylation to acetone. The odor of acetone may be detected in the breath of a person who has a high level of acetoacetate in the blood. Under starvation conditions, some of the acetone may be captured to synthesize small amounts of glucose.

Ketone bodies are a major fuel in some tissues

The liver is the major site of the production of acetoacetate and 3-hydroxybutyrate. These molecules are carried from the liver mitochondria into the blood by transport proteins and are conveyed to other tissues such as heart and kidney (**Figure 22.20**). Acetoacetate and 3-hydroxybutyrate are normal fuels of respiration and are quantitatively important as sources of energy. Indeed, heart muscle and the renal cortex use acetoacetate in preference to glucose. In contrast, glucose is the major fuel for the brain and red blood cells in well-nourished people on a balanced diet. However, the brain adapts to the utilization of acetoacetate during starvation and diabetes. In prolonged starvation, 75% of the fuel needs of the brain are met by ketone bodies (Section 24.5).

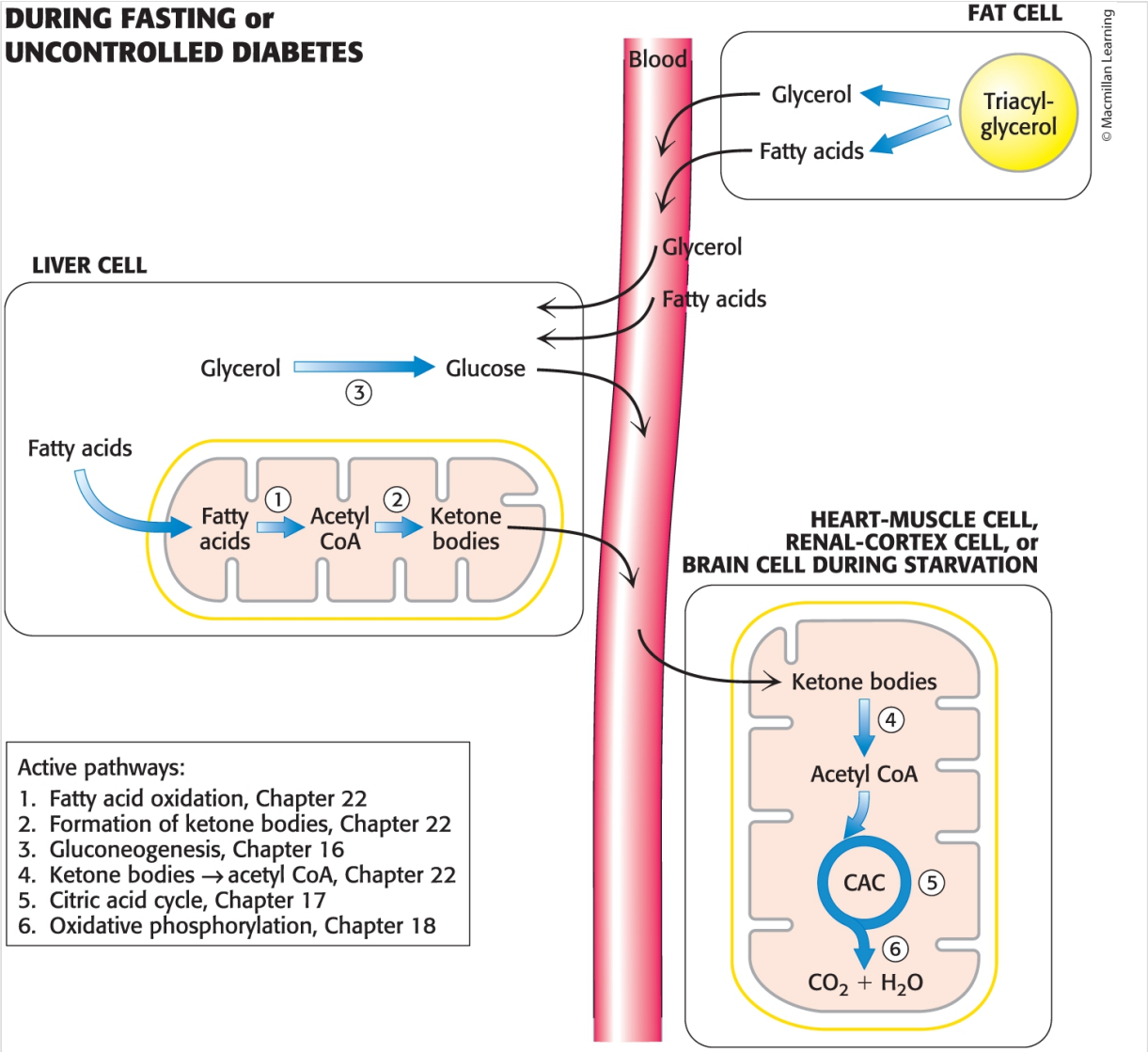


FIGURE 22.20 Pathway Integration: The liver supplies ketone bodies to the peripheral tissues. During fasting or in untreated diabetics, the liver converts fatty acids into ketone bodies, which are a fuel source for a number of tissues. Ketone-body production is especially important during starvation, when ketone bodies are the predominant fuel.

Acetoacetate is converted into acetyl CoA in two steps. First, acetoacetate is activated by the transfer of CoA from succinyl CoA in a reaction catalyzed by a specific CoA transferase. Second, acetoacetyl

CoA is cleaved by thiolase to yield two molecules of acetyl CoA, which can then enter the citric acid cycle (Figure 22.21).

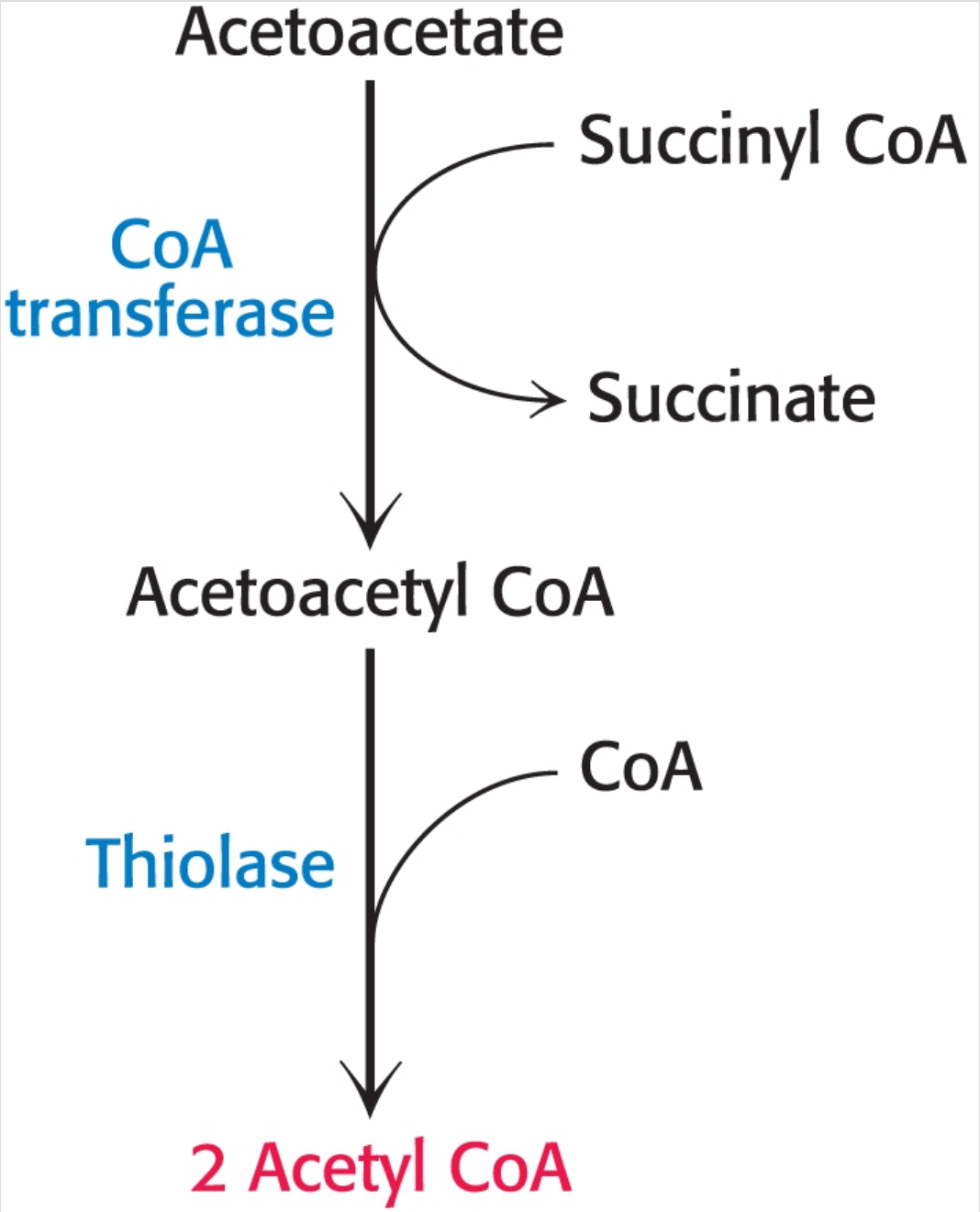
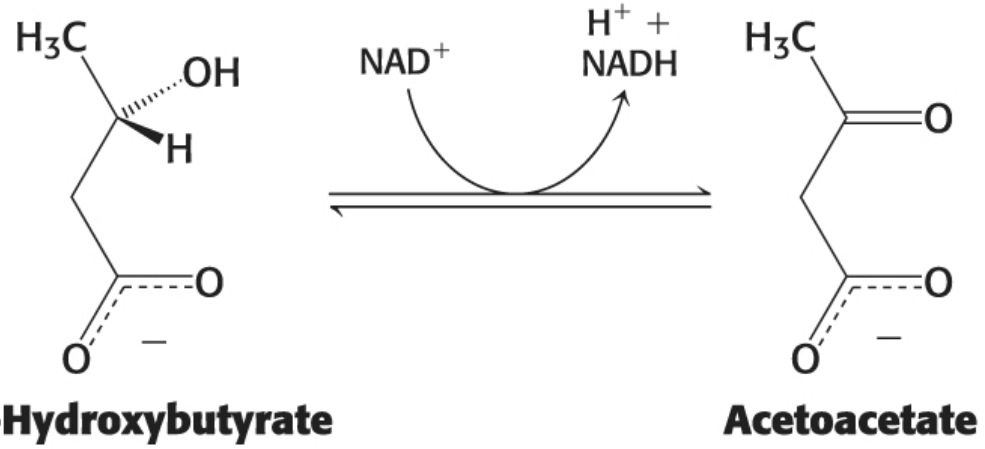


FIGURE 22.21 Acetoacetate can be used as a fuel to drive ATP formation.
Acetoacetate can be converted into two molecules of acetyl CoA, which then enter the citric acid cycle.

The liver has acetoacetate available to supply to other organs because it lacks this particular CoA transferase. 3-Hydroxybutyrate requires an additional step to yield acetyl CoA. It is first oxidized to produce acetoacetate, which is processed as described up to this point, and NADH for use in oxidative phosphorylation.



Ketone bodies can be regarded as a water-soluble, transportable form of acetyl units. Fatty acids are released by adipose tissue and converted into acetyl units by the liver, which then exports them as acetoacetate. As might be expected, both acetoacetate and 3-hydroxybutyrate also have regulatory roles. A high concentration of each in the blood signifies an abundance of acetyl units and leads to a decrease in the rate of lipolysis in adipose tissue. Although the liver produces ketone bodies for other tissues to use, it also gains energy in the process of synthesizing and releasing ketone bodies, because the production of acetyl CoA from fatty acids by β-oxidation produces both NADH and $FADH_2$ for ATP production by oxidative phosphorylation.

Interestingly, diets that promote ketone-body formation, called *ketogenic diets*, are frequently used as a therapeutic option for children with drug-resistant epilepsy. Ketogenic diets are rich in fats and low in carbohydrates, with adequate amounts of protein. In essence, the body is forced into starvation mode, where fats and ketone bodies become the main fuel source (Section 24.5). Remarkably, recent research in mice suggests that ketogenic diets alter the intestinal flora — the microbiome — and it is this alteration in the microbiome that is responsible for the therapeutic effects of the diet. The altered microbiome in some fashion regulates the levels of certain neurotransmitters, thereby reducing seizures.

Recent research in mice has also established that ketogenic diets extend lifespan, improve memory, and maintain long-term health. It will be interesting to learn if these effects apply to human beings, although gathering such data from humans is much more difficult than experiments with mice.

Diabetic ketoacidosis is a dangerous pathological condition caused by excessive ketone body formation

A high concentration of ketone bodies in the blood, the result of certain pathological conditions, can be life threatening. The most common of these conditions is diabetic ketoacidosis in patients with insulin-dependent diabetes. These patients are unable to produce insulin, which would normally be released after meals, signaling tissues to take up glucose and curtailing fatty acid mobilization by adipose tissue. The absence of insulin has two major biochemical consequences (**Figure**

22.22). First, the liver cannot absorb glucose and consequently cannot provide oxaloacetate to process fatty acid-derived acetyl CoA. Second, adipose cells continue to release fatty acids into the bloodstream; these fatty acids are then taken up by the liver and converted into ketone bodies. The liver thus produces large amounts of ketone bodies, which are acids, resulting in severe acidosis. The decrease in pH impairs tissue function, most importantly in the central nervous system.

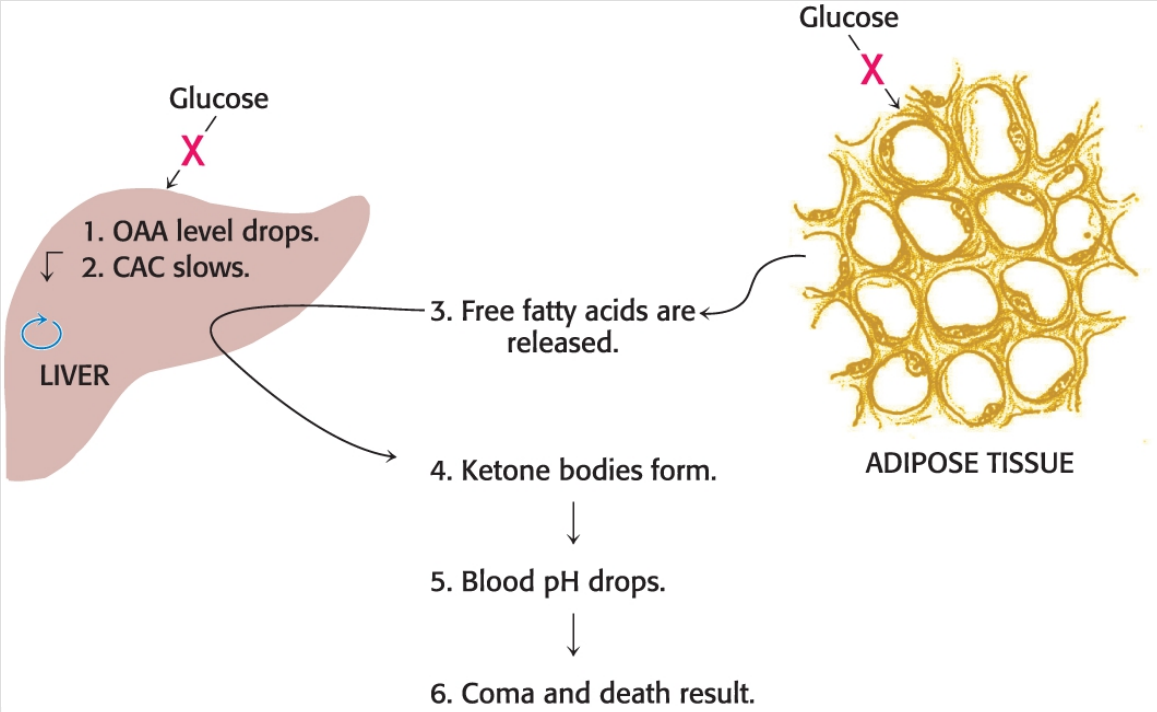


FIGURE 22.22 Diabetic ketosis results when insulin signaling is impaired. In the impairment of insulin signaling, fats are released from adipose tissue, and glucose cannot be absorbed by the liver or adipose tissue. The liver degrades the fatty acids by β-oxidation but cannot process the acetyl CoA, because of a lack of glucose-derived oxaloacetate (OAA). Excess ketone bodies are formed and released into the blood.

Self-Check Question

Calculate the number of molecules of ATP generated by the liver in the conversion of palmitate, a C_{16} fatty acid, into acetoacetate.

Animals cannot convert fatty acids into glucose

A typical human being has far greater fat stores than glycogen stores. However, glycogen is necessary to fuel very active muscle, as well as the brain, which normally uses only glucose as a fuel. When glycogen stores are low, why can't the body make use of fat stores and convert fatty acids into glucose? Because animals are unable to accomplish the net synthesis of glucose from fatty acids. Specifically, acetyl CoA cannot be converted into gluconeogenic substrates — pyruvate or oxaloacetate — in animals.

Recall that the reaction that generates acetyl CoA from pyruvate, catalyzed by the pyruvate dehydrogenase complex, is irreversible (Section 17.2). Additionally, when the two carbon atoms of the acetyl group of acetyl CoA enter the citric acid cycle, two carbon atoms also leave the cycle in the two decarboxylation reactions catalyzed by isocitrate dehydrogenase and α-ketoglutarate dehydrogenase (Section 17.3). Consequently, oxaloacetate is regenerated, but it is not formed de novo when the acetyl unit of acetyl CoA is oxidized by the citric acid cycle. In essence, two carbon atoms enter the cycle as an acetyl group, but two carbons leave the cycle as CO_2 before oxaloacetate is generated. As a result, no net synthesis of oxaloacetate is possible, and thus humans have no way of using the carbon in an acetyl group to synthesize glucose.

Also recall that, in contrast, plants and many microorganisms have the glyoxylate cycle; they have two additional enzymes that enable them to

convert the carbon atoms of acetyl CoA into oxaloacetate (Section 17.6). In conclusion, although a tremendous amount of human metabolism consists of reactions that are interconnected such that the carbon from one molecule can be used to make most anything else, this inability to convert acetyl groups into glucose can be viewed as the central disconnect in animal metabolism. We will explore the consequences of this inability more in Chapter 24.

22.5 Fatty Acids Are Synthesized by Fatty Acid Synthase

Fatty acids are synthesized by a complex of enzymes that together are called **fatty acid synthase**. Because eating most typical diets meets our physiological needs for fats and lipids, adult human beings have little need for de novo fatty acid synthesis. However, many tissues, such as liver and adipose tissue, are capable of synthesizing fatty acids, and this synthesis is required under certain physiological conditions. For instance, fatty acid synthesis is necessary during embryonic development and during lactation in mammary glands. Inappropriate fatty acid synthesis in the liver from excess caloric consumption or alcohol contributes to liver failure.

Acetyl CoA, the end product of fatty acid degradation, is the precursor for virtually all fatty acids. The biochemical challenge is to link the two carbon units together and reduce the carbons to produce palmitate, a C_{16} fatty acid. Palmitate then serves as a precursor for the variety of other fatty acids.

Fatty acid degradation and synthesis mirror each other in their chemical reactions

Fatty acid degradation and synthesis each consist of four steps that are the reverse of each other in their basic chemistry (**Figure 22.23**). As we have already seen, degradation is an oxidative process that converts a fatty acid into a set of activated acetyl units. Fatty acid synthesis is essentially the reverse of this process. The process starts with the individual units to be assembled — in this case, with an activated acyl group (most simply, an acetyl unit) and a malonyl unit (Figure 22.23). The malonyl unit condenses with the acetyl unit to form a four-carbon

fragment. To produce the required hydrocarbon chain, the carbonyl group is reduced to a methylene group in three steps: a reduction, a dehydration, and another reduction, exactly the opposite of degradation. The product of the reduction is butyryl CoA. Another activated malonyl group condenses with the butyryl unit, and the process is repeated until a C_{16} or shorter fatty acid is synthesized.

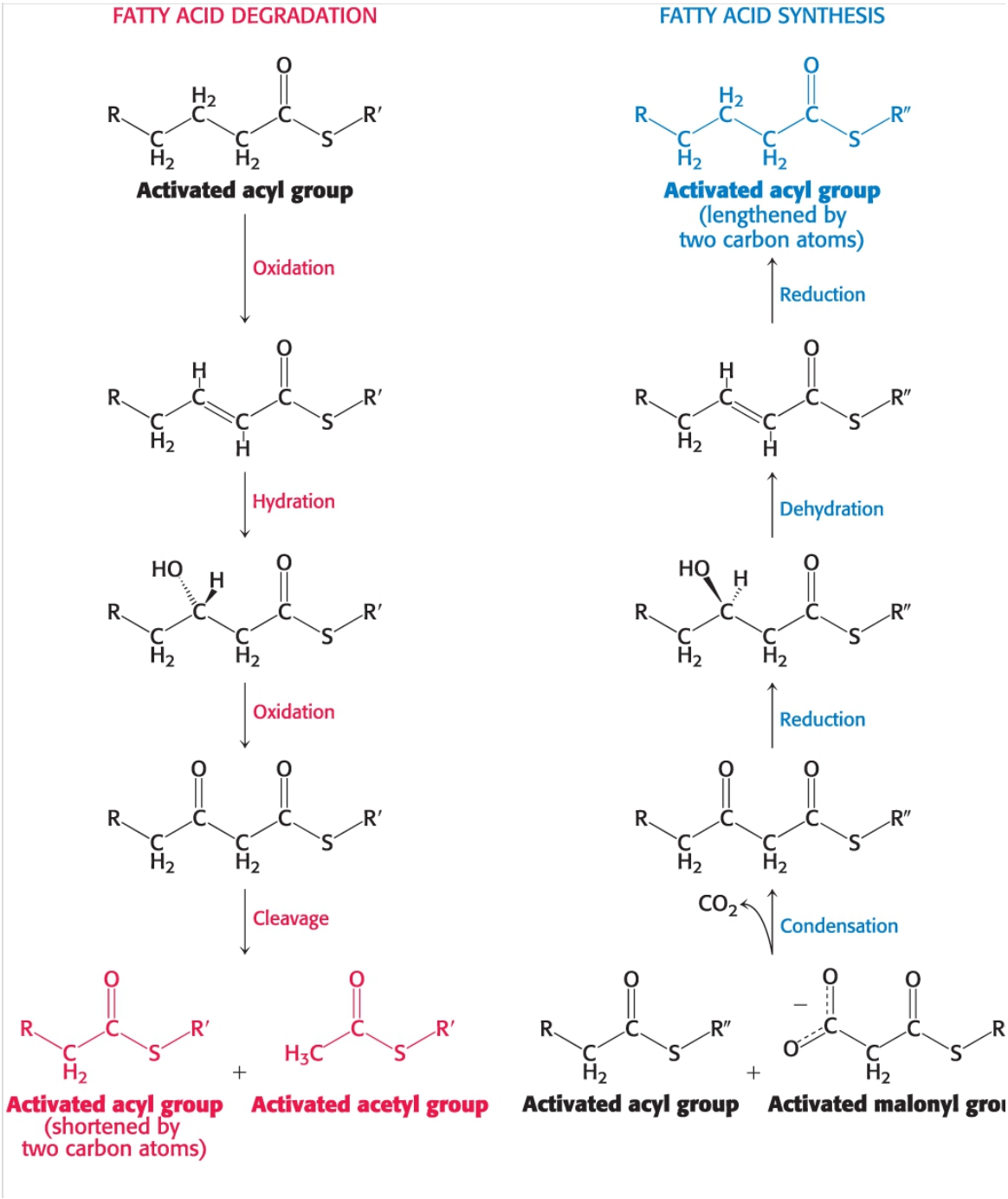


FIGURE 22.23 The steps in fatty acid degradation and synthesis are chemically similar. The tw
processes are in many ways mirror images of each other.

EXPLORE this pathway further in the Metabolic Map in Achieve



Fatty acids are synthesized and degraded by different pathways

Although fatty acid synthesis is the reversal of the degradative pathway in regard to basic chemical reactions, the synthetic and degradative pathways are different mechanistically, again exemplifying the principle that synthetic and degradative pathways are almost always distinct. Some important differences between the pathways are as follows:

1. Synthesis takes place in the cytoplasm, in contrast with degradation, which takes place primarily in the mitochondrial matrix.

2. Intermediates in fatty acid synthesis are covalently linked to the sulfhydryl groups of an **acyl carrier protein (ACP)**, whereas intermediates in fatty acid breakdown are covalently attached to the sulfhydryl group of coenzyme A.

3. The enzymes of fatty acid synthesis in higher organisms are joined in a single polypeptide chain called fatty acid synthase. In contrast, the degradative enzymes are not linked covalently.

4. The growing fatty acid chain is elongated by the sequential addition of two-carbon units derived from acetyl CoA. The activated donor of

two-carbon units in the elongation step is malonyl ACP. The elongation reaction is driven by the release of CO_2.

5. The reductant in fatty acid synthesis is NADPH, whereas the oxidants in fatty acid degradation are NAD^+ and FAD.

6. The isomeric form of the hydroxyacyl intermediate in degradation is L, while the D form is used in synthesis.

The formation of malonyl CoA is the committed step in fatty acid synthesis

Fatty acid synthesis starts with the carboxylation of acetyl CoA to **malonyl CoA**. This irreversible reaction is the committed step in fatty acid synthesis.

The synthesis of malonyl CoA is catalyzed by the cytosolic isozyme of a critical regulatory enzyme, **acetyl CoA carboxylase (ACC)**. ACC contains a biotin prosthetic group, with the carboxyl group of biotin covalently attached to the ε amino group of a lysine residue, as in pyruvate carboxylase (Figure 16.28) and propionyl CoA carboxylase (Section 22.3). As with these other enzymes, a carboxybiotin intermediate is formed at the expense of the hydrolysis of a molecule of ATP. The activated CO_2 group in this intermediate is then transferred to acetyl CoA to form malonyl CoA.

$$\text{Biotin-enzyme} + \text{ATP} + HCO_3^- \rightleftharpoons CO_2\text{-biotin-enzyme} + \text{ADP} + P_i$$

$$CO_2\text{-biotin-enzyme} + \text{acetyl CoA} \longrightarrow \text{malonyl CoA} + \text{biotin-enzyme}$$

ACC has two isozymes — ACC1, the cytosolic form, and ACC2, which is located in the mitochondria. We will discuss the regulatory roles of these proteins in Section 22.7.

Intermediates in fatty acid synthesis are attached to an acyl carrier protein

The intermediates in fatty acid synthesis are linked to an acyl carrier protein. Specifically, they are linked to the sulfhydryl terminus of a phosphopantetheine group. In the degradation of fatty acids, this unit is present as part of coenzyme A, whereas, in their synthesis, it is attached to a serine residue of the acyl carrier protein (Figure 22.24). Thus, ACP — a single polypeptide chain of 77 residues — can be regarded as a giant prosthetic group, a "macro CoA."

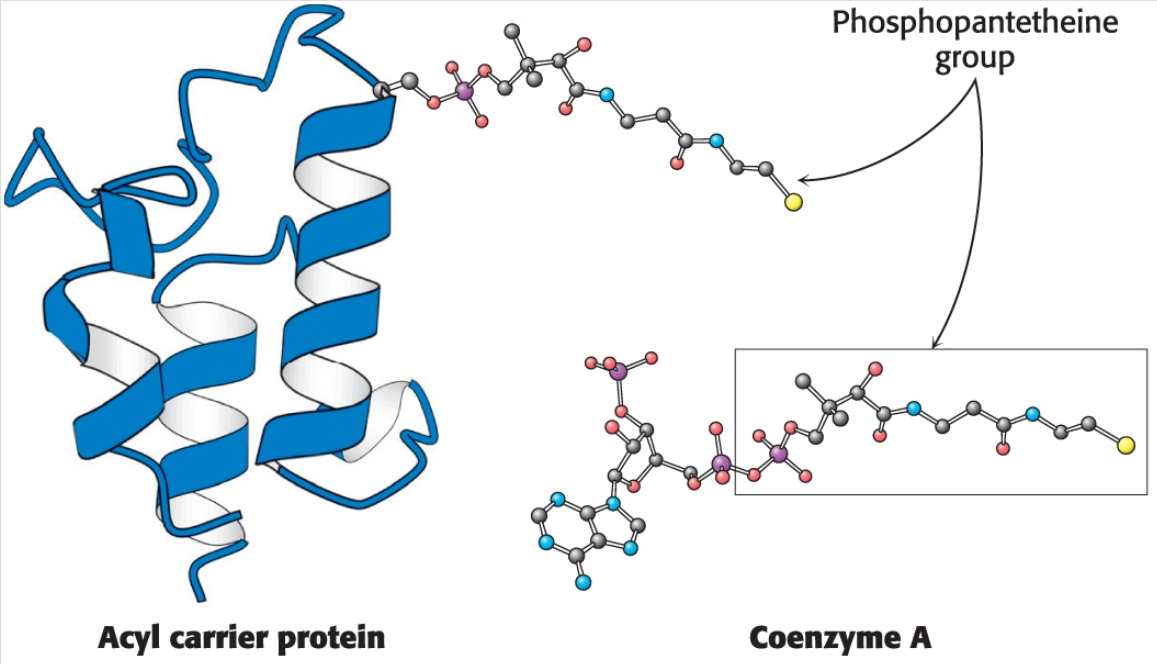


FIGURE 22.24 Both acyl carrier protein and coenzyme A include phosphopantetheine as their reactive units.

[Drawn from 1ACP.pdb.]

Fatty acid synthesis consists of a series of condensation, reduction, dehydration, and reduction reactions

The enzyme system that catalyzes the synthesis of saturated long-chain fatty acids from acetyl CoA, malonyl CoA, and NADPH is called *fatty acid synthase*. The synthase is actually a complex of distinct enzymes. The fatty acid synthase complex in bacteria is readily dissociated into individual enzymes when the cells are broken apart. The availability of these isolated enzymes has helped biochemists elucidate the steps in fatty acid synthesis (Table 22.2). In fact, the reactions leading to fatty acid synthesis in higher organisms are very much like those of bacteria.

TABLE 22.2 Principal reactions in fatty acid synthesis in bacteria

Step	Reaction	Enzyme
1	$\text{Acetyl CoA} + HCO_3^- + \text{ATP} \rightarrow \text{malonyl CoA} + \text{ADP} + P_i + H^+$	Acetyl CoA carboxylase
2	$\text{Acetyl CoA} + \text{ACP} \rightleftharpoons \text{acetyl ACP} + \text{Co A}$	Acetyl transacylase
3	$\text{Malonyl CoA} + \text{ACP} \rightleftharpoons \text{malonyl ACP} + \text{CoA}$	Malonyl transacylase
4	$\text{Acetyl ACP} + \text{malonyl ACP} \rightarrow \text{acetoacetyl ACP} + \text{ACP} + CO_2$	β-Ketoacyl synthase

5	$\text{Acetoacetyl ACP} + \text{NADPH} + \text{H}^+ \rightleftharpoons \text{D-3-hydroxybutyryl ACP} + \text{NADP}^+$	β-Ketoacyl reductase
6	$\text{D-3-Hydroxybutyryl ACP} \rightleftharpoons \text{crotonyl ACP} + \text{H}_2\text{O}$	3-Hydroxyacyl dehydratase
7	$\text{Crotonyl ACP} + \text{NADPH} + \text{H}^+ \rightarrow \text{butyryl ACP} + \text{NADP}^+$	Enoyl reductase

The elongation phase of fatty acid synthesis starts with the formation of acetyl ACP and malonyl ACP. Acetyl transacylase and malonyl transacylase catalyze these reactions.

$$\text{Acetyl CoA} + \text{ACP} \rightleftharpoons \text{acetyl ACP} + \text{CoA}$$

$$\text{Malonyl CoA} + \text{ACP} \rightleftharpoons \text{malonyl ACP} + \text{CoA}$$

Malonyl transacylase is highly specific, whereas acetyl transacylase can transfer acyl groups other than the acetyl unit, though at a much slower rate. The synthesis of fatty acids with an odd number of carbon atoms starts with propionyl ACP, which is formed from propionyl CoA by acetyl transacylase.

Acetyl ACP and malonyl ACP react to form acetoacetyl ACP (**Figure 22.25**). The β-ketoacyl synthase, also called the condensing enzyme, catalyzes this condensation reaction.

$$\text{Acetyl ACP} + \text{malonyl ACP} \rightarrow \text{acetoacetyl ACP} + \text{ACP} + \text{CO}_2$$

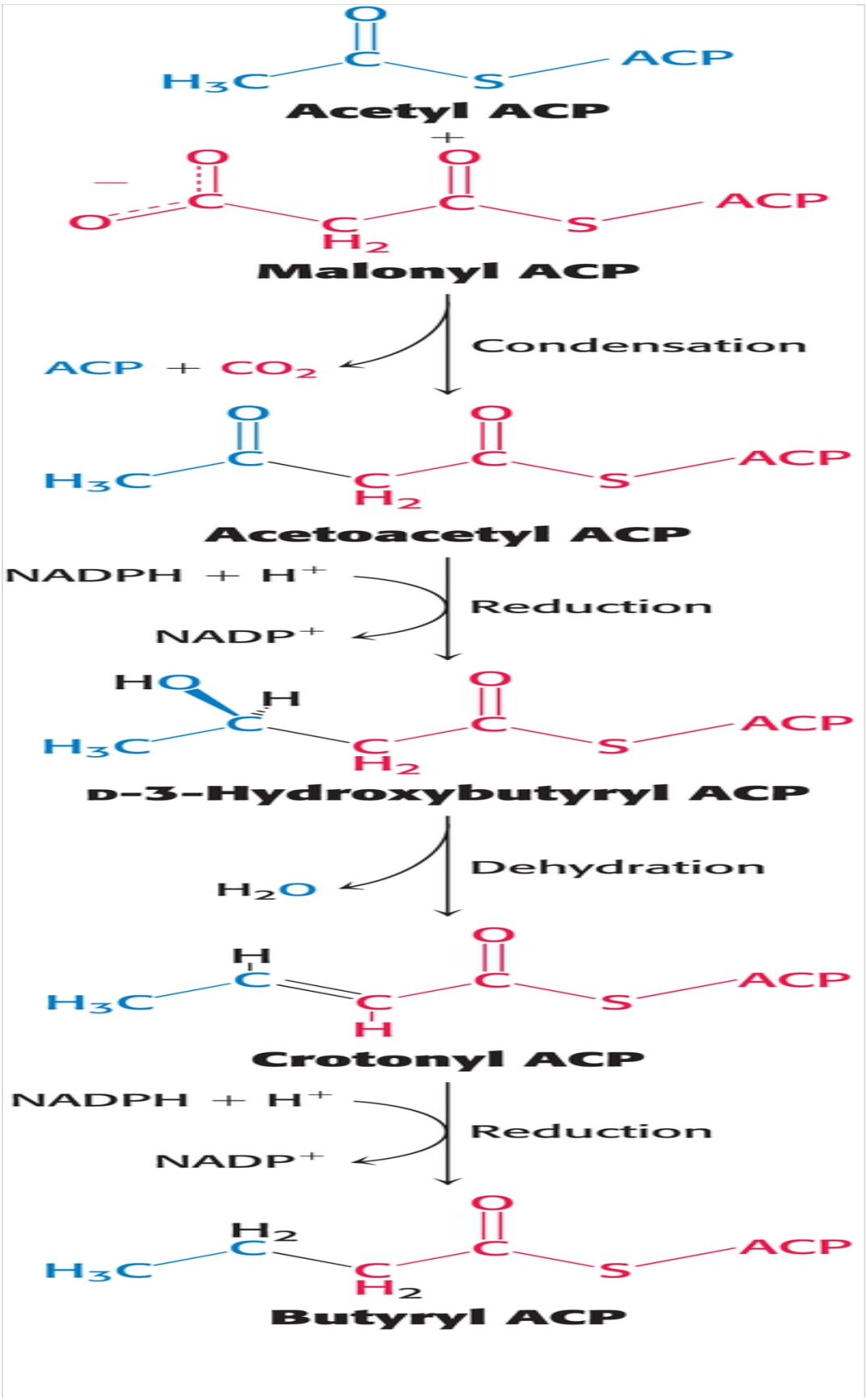

Acetyl ACP
Malonyl ACP
Condensation
ACP + CO2
Acetoacetyl ACP
NADPH + H+
NADP+
Reduction
D–3–Hydroxybutyryl ACP
Dehydration
H2O
Crotonyl ACP
NADPH + H+
NADP+
Reduction
Butyryl ACP

FIGURE 22.25 Like β-oxidation, saturated fatty acid synthesis consists of four steps. Saturated fatty acid synthesis begins with the condensation of malonyl ACP and acetyl ACP to form acetoacetyl ACP. Acetoacetyl ACP is then reduced, dehydrated, and reduced again to form butyryl ACP. Another cycle begins with the condensation of butyryl ACP and malonyl ACP. The sequence of reactions is repeated until the final product palmitate is formed.



In the condensation reaction, a four-carbon unit is formed from a two-carbon unit and a three-carbon unit, and CO_2 is released. Why is the four-carbon unit not formed from two 2-carbon units — say, two molecules of acetyl ACP? The answer is that the equilibrium for the synthesis of acetoacetyl ACP from two molecules of acetyl ACP is highly unfavorable. In contrast, the equilibrium is favorable if malonyl ACP is a reactant because its decarboxylation contributes a substantial release of free energy. In effect, ATP drives the condensation reaction, though ATP does not directly participate in the condensation reaction. Instead, ATP is used to carboxylate acetyl CoA to malonyl CoA. The free energy thus stored in malonyl CoA is released in the decarboxylation accompanying the formation of acetoacetyl ACP. Although HCO_3^- is required for fatty acid synthesis, its carbon atom does not appear in the product because it is released in the subsequent decarboxylation. Rather, all the carbon atoms of fatty acids containing an even number of carbon atoms are derived only from acetyl CoA.

The next three steps in fatty acid synthesis reduce the keto group at C-3 to a methylene group (Figure 22.25). First, acetoacetyl ACP is reduced to D-3-hydroxybutyryl ACP by β-ketoacyl reductase. This reaction differs from the corresponding one in fatty acid degradation in two respects: (1) the D rather than the L isomer is formed; and (2) NADPH is the reducing agent, whereas NAD^+ is the oxidizing agent in β-oxidation. This difference exemplifies the general principle that NADPH is typically consumed in biosynthetic reactions, whereas NADH is typically generated in energy-yielding reactions. Then, D-3-

hydroxybutyryl ACP is dehydrated to form crotonyl ACP, which is a *trans*-Δ^2-enoyl ACP by 3-hydroxyacyl dehydratase. The final step in the cycle reduces crotonyl ACP to butyryl ACP. NADPH is again the reductant, whereas FAD is the oxidant in the corresponding reaction in β-oxidation. The bacterial enzyme that catalyzes this step, enoyl reductase, can be inhibited by triclosan, a broad-spectrum antibacterial agent that is added to a variety of products such as toothpaste, soaps, and skin creams. These last three reactions — a reduction, a dehydration, and a second reduction — convert acetoacetyl ACP into butyryl ACP, which completes the first elongation cycle.

In the second round of fatty acid synthesis, butyryl ACP condenses with malonyl ACP to form a C_6-β-ketoacyl ACP. This reaction is like the one in the first round, in which acetyl ACP condenses with malonyl ACP to form a C_4-β-ketoacyl ACP. Reduction, dehydration, and a second reduction convert the C_6-β-ketoacyl ACP into a C_6-acyl ACP, which is ready for a third round of elongation. The elongation cycles continue until C_{16}-acyl ACP is formed. This intermediate is a good substrate for a thioesterase that hydrolyzes C_{16}-acyl ACP to yield palmitate and ACP. The thioesterase acts as a ruler to determine fatty acid chain length. The synthesis of longer-chain fatty acids is discussed in Section 22.6.

Self-Check Question

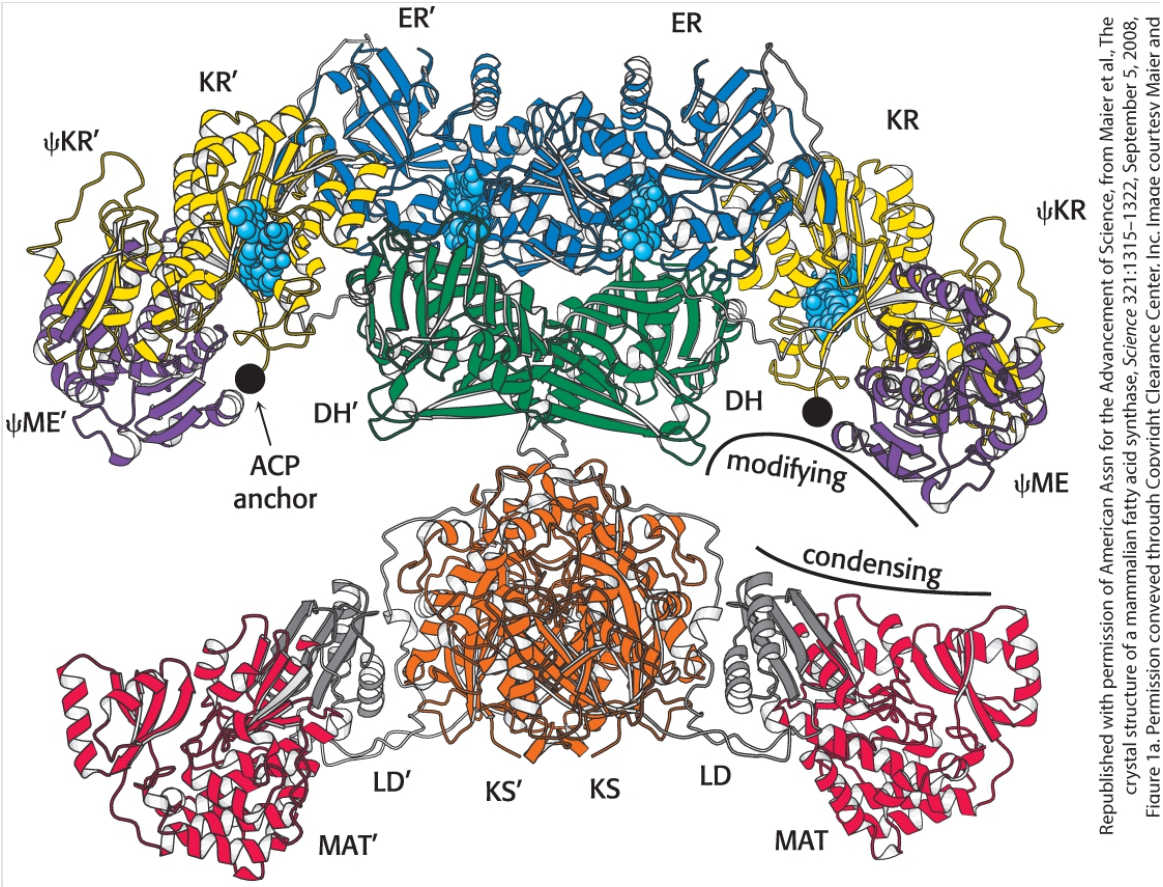


Although HCO_3^- is required for fatty acid synthesis, its carbon atom does not appear in the product. Explain how this omission is possible.

Fatty acids are synthesized by a multifunctional enzyme complex in animals

Although the basic biochemical reactions in fatty acid synthesis are very similar in *E. coli* and eukaryotes, the structure of the synthase varies considerably. The component enzymes of animal fatty acid synthases, in contrast with those of *E. coli* and plants, are linked in a large polypeptide chain.

The structure of a large part of the mammalian fatty acid synthase has been determined, with the acyl carrier protein and thioesterase remaining to be resolved. The enzyme is a dimer of identical 270-kd subunits. Each chain contains all of the active sites required for activity, as well as an acyl carrier protein tethered to the complex (**Figure 22.26**). Despite the fact that each chain possesses all of the enzymes required for fatty acid synthesis, the monomers are not active. A dimer is required.



Republished with permission of American Assn for the Advancement of Science, from Maier et al., The crystal structure of a mammalian fatty acid synthase, *Science* 321:1315–1322, September 5, 2008, Figure 1a. Permission conveyed through Copyright Clearance Center. Inc. Image courtesy Maier and

FIGURE 22.26 Mammalian fatty acid synthase is a large, dimeric, multidomain protein complex. The complex is a dimer of two multidomain monomers and can be described as consisting of two main parts: the body of the lower part is the β-ketosynthase (KS), while the malonylacetyl transferase (MAT) domains comprise the legs. These structures are joined by a linker domain (LD). The lower part is connected at the waist to the upper part, which consists of dehydratase (DH) and enoyl reductase (ER), which together comprise the upper body. The ketoreductase (KR) domains form the arms. The noncatalytic domains are ψKR and ψME Bound $NADP^+$ cofactors are shown as blue spheres and the attachment site for the acyl carrier protein, and thioesterase is shown as a black sphere. The domains of the second chain are indicated by the abbreviation followed by a prime.

The two component chains interact such that the enzyme activities are partitioned into two distinct compartments, a lower body and an upper body, joined by a waist. The lower body contains the β-ketosynthase, while the legs comprise the malonylacetyl transferase domains which

are joined to the body by a linker domain. The body and the legs catalyze the condensing reactions. The upper body contains dehydratase and enoyl reductase, and the arms contain the ketoreductase domains. The upper body and the arms catalyze the modification reactions, the reduction and dehydration activities that result in the saturated fatty acid product. Interestingly, the mammalian fatty acid synthase has one active site — malonyl/acetyl transacylase — that adds both acetyl CoA and malonyl CoA. In contrast, most other fatty acid synthases have two separate enzyme activities — one for acetyl CoA and one for malonyl CoA. The enzyme also contains noncatalytic domains, designated by symbol ψ. The ψKR resembles the ketoreductase domain, and the ψME domain is homologous to methyltransferase enzymes. Both the ψKR and ψME domains play a role in maintaining enzyme structure.

Let us consider one catalytic cycle of the fatty acid synthase complex (**Figure 22.27**). An elongation cycle begins after malonyl/acetyl transacylase (MAT) moves an acetyl unit from coenzyme A to the acyl carrier protein (ACP). β-Ketosynthase (β-KS) accepts the acetyl unit, which forms a thioester with a cysteine residue at the β-KS active site. The vacant ACP is reloaded by MAT, this time with a malonyl moiety. Malonyl ACP visits the active site of β-KS where the condensation of the two 2-carbon fragments takes place on the ACP with the concomitant release of CO_2. The selecting and condensing process concludes with the β-ketoacyl product attached to the ACP.

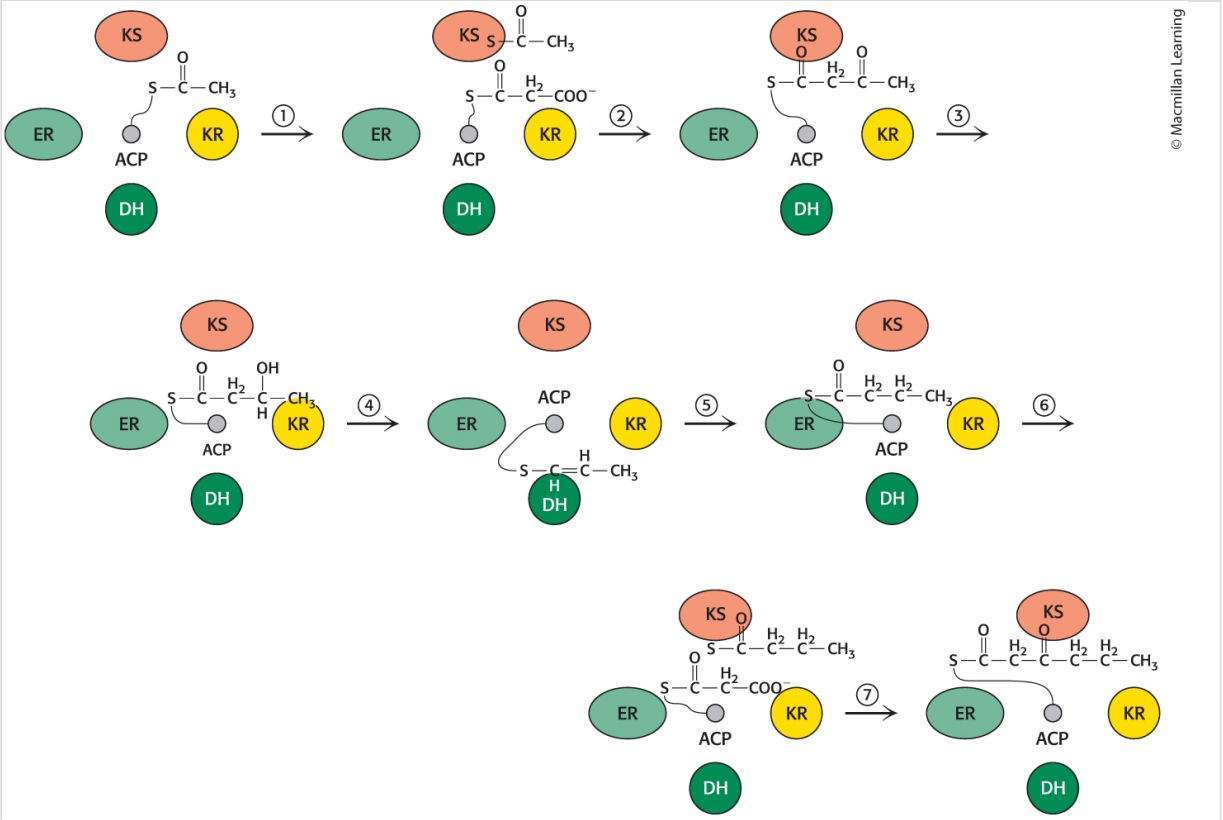


FIGURE 22.27 One catalytic cycle of mammalian fatty acid synthase consists of seven steps. The cycle begins after MAT (not shown) attaches an acetyl unit to ACP. (1) ACP delivers the acetyl unit to KS, and MAT then attaches a malonyl unit to ACP. (2) ACP visits KS again, which condenses the acetyl and malonyl units to form the β-ketoacyl product, attached to the ACP. (3) ACP delivers the β-ketoacyl product to the KR enzyme, which reduces the keto group to an alcohol. (4) The β-hydroxyl product then visits DH, which introduces a double bond with the loss of water. (5) The enoyl product is delivered to the ER enzyme, where the double bond is reduced. (6) ACP hands the reduced product to KS and is recharged with malonyl CoA by MAT. (7) KS condenses the two molecules on ACP, which is now ready to begin another cycle. See Figure 22.26 for abbreviations.

The loaded ACP then sequentially visits the active sites of the modification compartment of the enzyme. Here, the β-keto group of the substrate is reduced to — OH, dehydrated, and finally reduced to yield the saturated acyl product, still attached to the ACP. With the completion of the modification process, the reduced product is transferred to the β-KS while the ACP accepts another malonyl unit. Condensation takes place and is followed by another modification cycle.

The process is repeated until the thioesterase releases the final C_{16} palmitic acid product.

Many eukaryotic multienzyme complexes are multifunctional proteins in which different enzymes are linked covalently. Multifunctional enzymes such as fatty acid synthase seem likely to have arisen in eukaryotic evolution by fusion of the individual genes of evolutionary ancestors.

The synthesis of palmitate requires 8 molecules of acetyl CoA, 14 molecules of NADPH, and 7 molecules of ATP

The stoichiometry of the synthesis of palmitate is

$$\text{Acetyl CoA} + 7\ \text{malonyl CoA} + 14\ \text{NADPH} + 20\ H^+ \rightarrow$$

$$\text{palmitate} + 7\ CO_2 + 14\ NADP^+ + 8\ \text{CoA} + 6\ H_2O$$

The equation for the synthesis of the malonyl CoA used in the preceding reaction is

$$7\ \text{Acetyl CoA} + 7\ CO_2 + 7\ \text{ATP} \rightarrow 7\ \text{malonyl CoA} + 7\ \text{ADP} + 7\ P_i + 14\ H^+$$

Hence, the overall stoichiometry for the synthesis of palmitate is

$$8\ \text{Acetyl CoA} + 7\ \text{ATP} + 14\ \text{NADPH} + 6\ H^+ \rightarrow$$

$$\text{palmitate} + 14\ NADP^+ + 8\ CoA + 6\ H_2O + 7\ ADP + 7\ P_i$$

Citrate carries acetyl groups from mitochondria to the cytoplasm for fatty acid synthesis

Fatty acids are synthesized in the cytoplasm, whereas acetyl CoA is formed from pyruvate in mitochondria. Hence, acetyl CoA must be transferred from mitochondria to the cytoplasm for fatty acid synthesis. Mitochondria, however, are not readily permeable to acetyl CoA. Recall that carnitine carries only long-chain fatty acids. How is this obstacle overcome?

The barrier to acetyl CoA is bypassed by citrate, which carries acetyl groups across the inner mitochondrial membrane. As you will recall from Chapter 17, citrate is formed in the mitochondrial matrix by the condensation of acetyl CoA with oxaloacetate (**Figure 22.28**). When present at high levels, citrate is transported to the cytoplasm, where it is cleaved by ATP-citrate lyase.

$$\text{Citrate} + ATP + CoA + H_2O \rightarrow \text{acetyl CoA} + ADP + P_i + \text{oxaloacetate}$$

This reaction occurs in three steps: (1) The formation of a phospho-enzyme with the donation of a phosphoryl group from ATP; (2) binding of citrate and CoA followed by the formation of citroyl CoA and release of the phosphate; and (3) cleavage of citroyl CoA to yield acetyl CoA and oxaloacetate. As we will see shortly (Section 22.6), citrate stimulates acetyl CoA carboxylase, the enzyme that regulates fatty acid metabolism. Recall also, the presence of citrate in the cytoplasm

inhibits phosphofructokinase, the enzyme that controls the glycolytic pathway.

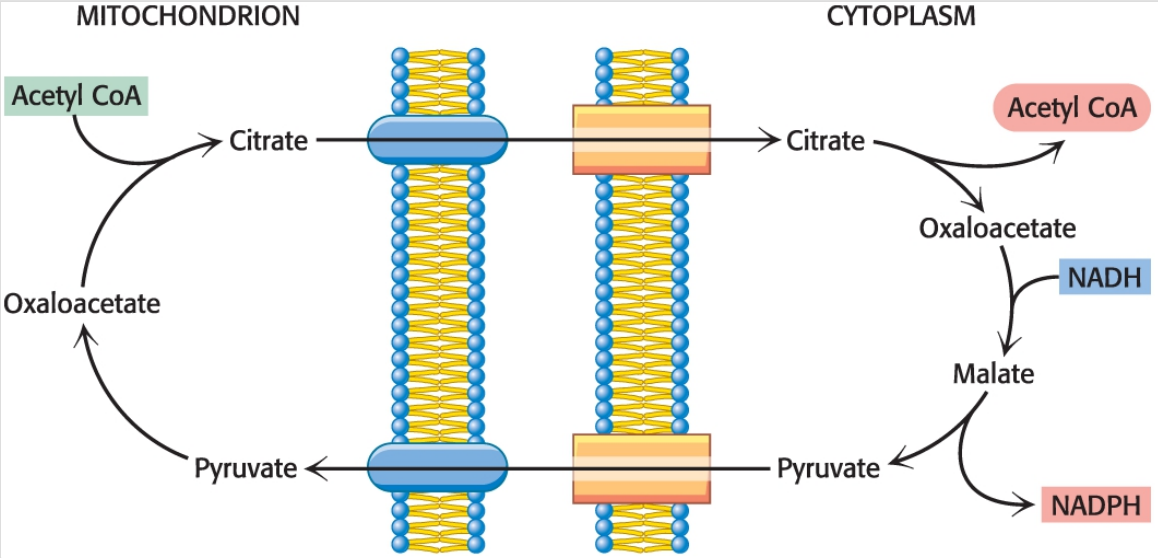


FIGURE 22.28 Acetyl CoA can be transferred from the mitochondrial matrix to the cytoplasm. Acetyl CoA is transferred from mitochondria to the cytoplasm, and the reducing potential of NADH is concomitantly converted into that of NADPH by this series of reactions.

ATP-citrate lyase is stimulated by insulin, which initiates a signal transduction pathway that ultimately results in the phosphorylation and activation of the lyase by protein kinase B (also called Akt).

Several sources supply NADPH for fatty acid synthesis

Oxaloacetate formed in the transfer of acetyl groups to the cytoplasm must now be returned to the mitochondria. The inner mitochondrial membrane is impermeable to oxaloacetate. Hence, a series of bypass reactions are needed. These reactions also generate much of the

NADPH needed for fatty acid synthesis. First, oxaloacetate is reduced to malate by NADH. This reaction is catalyzed by a malate dehydrogenase in the cytoplasm.

$$\text{Oxaloacetate} + \text{NADH} + \text{H}^+ \rightleftharpoons \text{malate} + \text{NAD}^+$$

Second, malate is oxidatively decarboxylated by $^{\text{NADP}^+}$-linked malate enzyme (also called *malic enzyme*).

$$\text{Malate} + \text{NADP}^+ \rightarrow \text{pyruvate} + \text{CO}_2 + \text{NADPH}$$

The pyruvate formed in this reaction readily enters mitochondria, where it is carboxylated to oxaloacetate by pyruvate carboxylase.

$$\text{Pyruvate} + \text{CO}_2 + \text{ATP} + \text{H}_2\text{O} \rightarrow \text{oxaloacetate} + \text{ADP} + \text{P}_i + 2\text{H}^+$$

The sum of these three reactions is

$$\text{NADP}^+ + \text{NADH} + \text{ATP} + \text{H}_2\text{O} \rightarrow \text{NADPH} + \text{NAD}^+ + \text{ADP} + \text{P}_i + \text{H}^+$$

Thus, one molecule of NADPH is generated for each molecule of acetyl CoA that is transferred from mitochondria to the cytoplasm. Hence, eight molecules of NADPH are formed when eight molecules of acetyl CoA are transferred to the cytoplasm for the synthesis of palmitate. The additional six molecules of NADPH required for this process come from the pentose phosphate pathway (Section 20.3).

The accumulation of the precursors for fatty acid synthesis is a wonderful example of the coordinated use of multiple pathways. The

citric acid cycle, transport of oxaloacetate from the mitochondria, and pentose phosphate pathway provide the carbon atoms and reducing power, whereas glycolysis and oxidative phosphorylation provide the ATP to meet the needs for fatty acid synthesis (Figure 22.29).

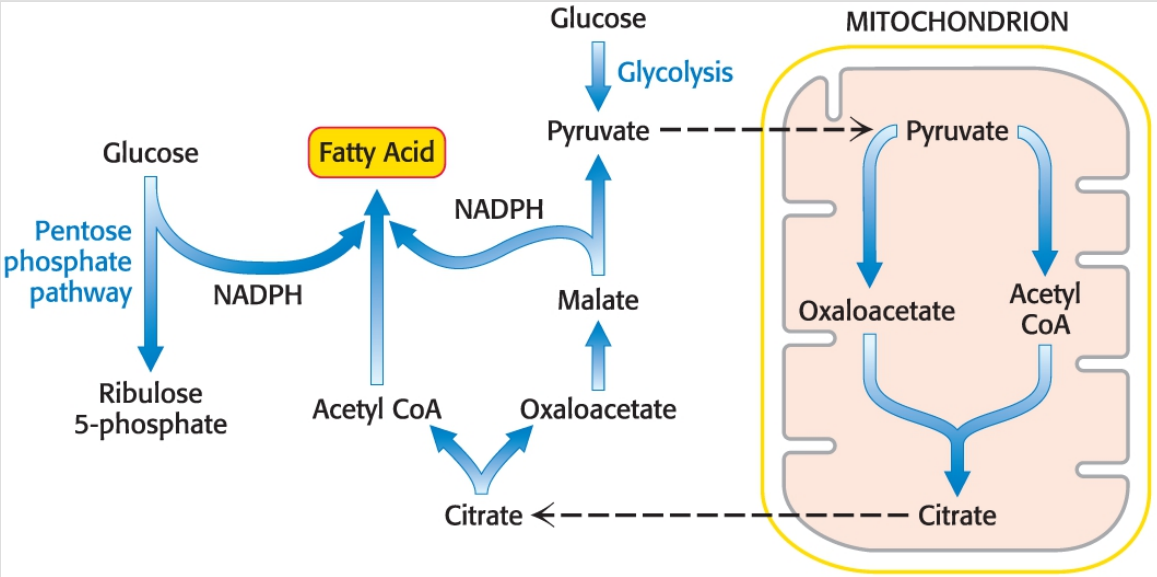


FIGURE 22.29 Pathway Integration: Fatty acid synthesis requires the cooperation of various pathways in different cellular compartments. The combination of glycolysis, the citric acid cycle, and the pentose phosphate pathway can be used to efficiently convert glucose into fatty acids.

EXPLORE this pathway further in the Metabolic Map in Achieve

Fatty acid metabolism is altered in tumor cells

We have previously seen that cancer cells alter glucose metabolism to meet the needs of rapid cell growth. Cancer cells must also increase fatty acid synthesis for use as signal molecules, as well as for incorporation into membrane phospholipids for the construction of new cell membranes in rapidly dividing cells. Many of the enzymes of fatty acid synthesis are overexpressed in most human cancers, and this expression is correlated with tumor malignancy. Recall that normal cells do little de novo fatty acid synthesis, relying instead on dietary intake to meet their fatty needs.

The dependence of de novo fatty acid synthesis provides possible therapeutic targets to inhibit cancer cell growth. Inhibition of β-ketoacyl ACP synthase — the enzyme that catalyzes the condensation step of fatty acid synthesis — does indeed inhibit phospholipid synthesis and subsequent cell growth in some cancers, apparently by inducing apoptosis. However, another startling observation was made: mice treated with inhibitors of the β-ketoacyl ACP synthase showed remarkable weight loss because they ate less. Thus, fatty acid synthase inhibitors are exciting candidates both as antitumor and as anti-obesity drugs.

ACC is also being investigated as a possible target for inhibiting cancer cell growth. Inhibition of the carboxylase in prostate and breast cancer cell lines induces apoptosis in the cancer cells, and yet is without effect in normal cells. Understanding the alteration of fatty acid metabolism in cancer cells is a developing area of research that holds promise of generating new cancer therapies.

Triacylglycerols may become an important renewable energy source

Work is underway to develop efficient means of generating triacylglycerols for use as renewable biodiesel fuel. Briefly, CO_2, CO,

and H_2 (collectively called *syngas* because they can be used to make synthetic natural gas) are captured from municipal waste or generated from other waste sources and fed to anaerobic acetogenic bacteria. Acetogenic bacteria contain a complex pathway, called the *Wood-Ljungdahl pathway*, that can synthesize acetate from syngas. In this pathway, CO_2 and CO are reduced to a methyl group which then reacts with CO and coenzyme A to form acetyl CoA. The acetate can be harvested from the bacteria, then used as a carbon source for oleaginous yeast, which can synthesize and accumulate triacylglycerols to 20% to 70% of their cell mass, depending on culture conditions. Using large fermenters and complex algorithms to control bacterial and yeast growth, triacylglycerols can be synthesized in sufficient quantities for biodiesel and other renewable products.

22.6 The Elongation and Unsaturation of Fatty Acids Are Accomplished by Accessory Enzyme Systems

The major product of the fatty acid synthase is palmitate. In eukaryotes, longer fatty acids are formed by elongation reactions catalyzed by enzymes on the cytoplasmic face of the endoplasmic reticulum membrane. These reactions add two-carbon units sequentially to the carboxyl ends of both saturated and unsaturated fatty acyl CoA substrates. Malonyl CoA is the two-carbon donor in the elongation of fatty acyl CoAs. Again, condensation is driven by the decarboxylation of malonyl CoA.

Membrane-bound enzymes generate unsaturated fatty acids

Endoplasmic reticulum enzymes also introduce double bonds into long-chain acyl CoAs. For example, in the conversion of stearoyl CoA into oleoyl CoA, a *cis*-Δ^9 double bond is inserted by an oxidase that employs molecular oxygen and NADH (or NADPH).

$$\text{Stearoyl CoA} + \text{NADH} + \text{H}^+ + \text{O}_2 \rightarrow \text{oleoyl CoA} + \text{NAD}^+ + 2\ \text{H}_2\text{O}$$

This reaction is catalyzed by a complex of three membrane-bound proteins: NADH-cytochrome b_5 reductase, cytochrome b_5, and stearoyl CoA desaturase (**Figure 22.30**). First, electrons are transferred from

NADH to the FAD moiety of NADH-cytochrome b_5 reductase. The heme iron atom of cytochrome b_5 is then reduced to the Fe^{2+} state. The nonheme iron atom of the desaturase is subsequently converted into the Fe^{2+} state, which enables it to interact with O_2 and the saturated fatty acyl CoA substrate. A double bond is formed and two molecules of H_2O are released. Two electrons come from NADH and two from the single bond of the fatty acyl substrate.

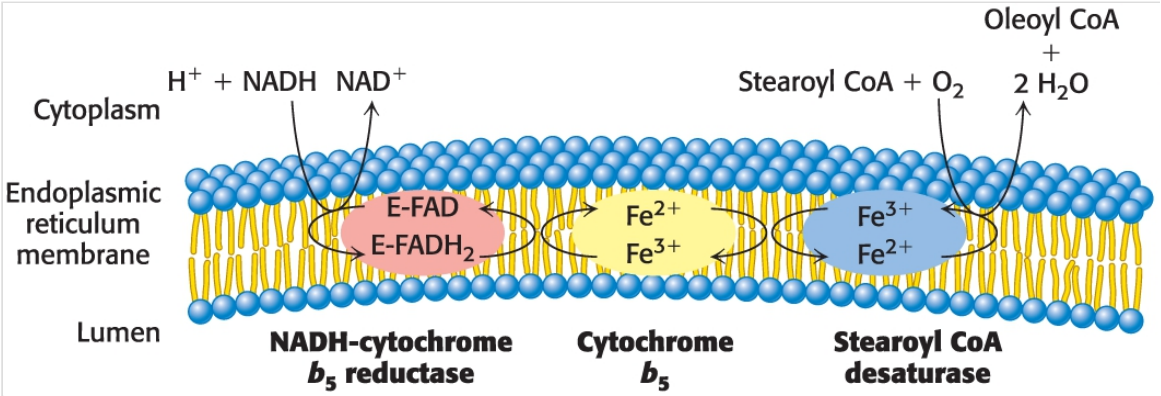


FIGURE 22.30 Fatty acids are desaturated by an electron-transport chain in the ER membran

A variety of unsaturated fatty acids can be formed from oleate by a combination of elongation and desaturation reactions. For example, oleate can be elongated to a 20:1 *cis*-Δ^{11} fatty acid. Alternatively, a second double bond can be inserted to yield an 18:2 *cis*-Δ^{6}, Δ^{9} fatty acid. Similarly, palmitate (16:0) can be oxidized to palmitoleate (16:1 *cis*-Δ^{9}), which can then be elongated to *cis*-vaccenate (18:1 *cis*-Δ^{11}).

Unsaturated fatty acids in mammals are derived from either palmitoleate (16:1 *cis*-Δ^{9}), oleate (18:1 *cis*-Δ^{9}), linoleate (18:2 *cis*-

Δ^{9}, Δ^{12}), or linolenate (18:3 *cis*-$\Delta^{9}, \Delta^{12}, \Delta^{15}$). However, mammals lack the enzymes to introduce double bonds at carbon atoms beyond C-9 in the fatty acid chain. Because mammals cannot synthesize linoleate and linolenate, these are essential fatty acids in human metabolism. The term *essential* means that they must be supplied in the diet because they are required by an organism and cannot be synthesized by the organism itself. It should be noted that this terminology has no relationship to the term *essential oil*, which has no specific chemical definition. Linoleate and linolenate furnished by the diet are the starting points for the synthesis of a variety of other unsaturated fatty acids.

Eicosanoid hormones are derived from polyunsaturated fatty acids

A 20:4 fatty acid derived from linoleate called *arachidonate* (20:4 *cis*-$\Delta^{5}, \Delta^{8}, \Delta^{11}, \Delta^{14}$) is the major precursor of several classes of signal molecules: prostaglandins, prostacyclins, thromboxanes, and leukotrienes (**Figure 22.31**).

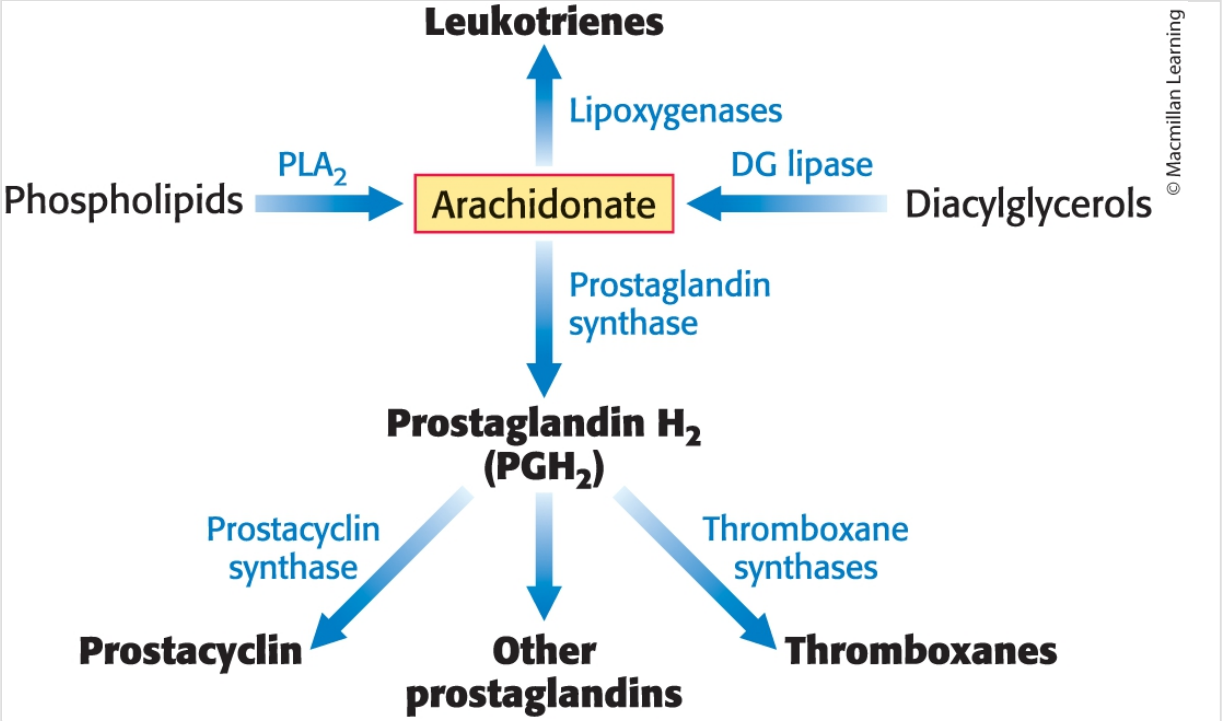


FIGURE 22.31 Several eicosanoid hormones are produced from arachidonate by distinct enzymatic pathways. Prostaglandin synthase catalyzes the first step in a pathway leading eventually to all prostaglandins, prostacyclins, and thromboxanes. Lipoxygenase catalyzes the initial step in a separate pathway leading to leukotrienes.

A **prostaglandin** is a 20-carbon fatty acid containing a 5-carbon ring (**Figure 22.32**). This basic compound is modified by reductases and isomerases to yield nine major classes of prostaglandins, designated PGA through PGI; a subscript denotes the number of carbon–carbon double bonds outside the ring. Prostaglandins with two double bonds, such as PGE_2, are derived from arachidonate; the other two double bonds of this precursor are lost in forming a 5-membered ring. Prostacyclin and thromboxanes are related compounds that arise from a nascent prostaglandin. They are generated by prostacyclin synthase and thromboxane synthase, respectively. Alternatively, arachidonate can be converted into leukotrienes by the action of lipoxygenase. Leukotrienes, first found in leukocytes, contain three conjugated double bonds —

hence the name. Prostaglandins, prostacyclin, thromboxanes, and leukotrienes are called **eicosanoids** (from the Greek *eikosi*, "twenty") because they contain 20 carbon atoms.

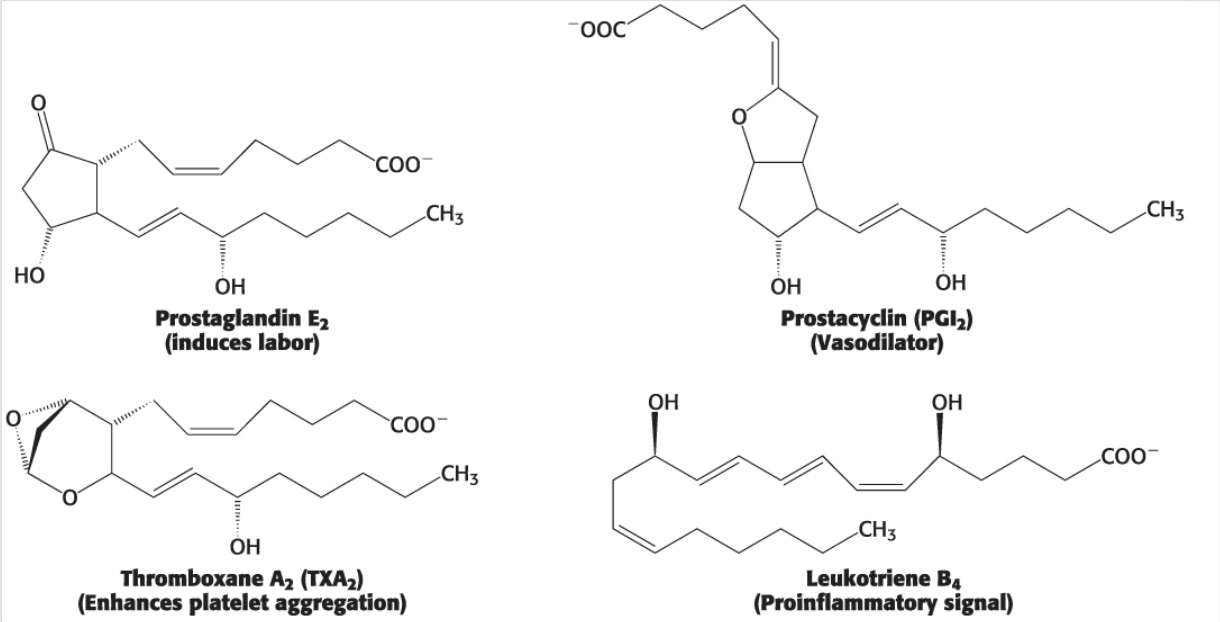


FIGURE 22.32 Eicosanoids have diverse functions but similar 20-carbon structures.

Prostaglandins and other eicosanoids are local hormones because they are short-lived. They alter the activities both of the cells in which they are synthesized and of adjoining cells by binding to 7TM receptors. Their effects may vary from one cell type to another, in contrast with the more-uniform actions of global hormones such as insulin and glucagon. Prostaglandins stimulate inflammation, regulate blood flow to particular organs, control ion transport across membranes, modulate synaptic transmission, and induce sleep.

Recall that aspirin (acetylsalicylate) blocks access to the active site of the enzyme that converts arachidonate into prostaglandin H_2

(Section 12.4). Because arachidonate is the precursor of other prostaglandins, prostacyclin, and thromboxanes, blocking this step interferes with many signaling pathways. Aspirin's ability to obstruct these pathways accounts for its wide-ranging effects on inflammation, fever, pain, and blood clotting.

22.7 Acetyl CoA Carboxylase Plays a Key Role in Controlling Fatty Acid Metabolism

Fatty acid metabolism is stringently controlled so that synthesis and degradation are highly responsive to physiological needs. Fatty acid synthesis is maximal when carbohydrates and energy are plentiful and when fatty acids are scarce. Both ACC1 and ACC2 play essential roles in regulating fatty acid synthesis and degradation. Recall that this enzyme catalyzes the committed step in fatty acid synthesis: the production of malonyl CoA (the activated two-carbon donor). This important enzyme is subject to both local and hormonal regulation. We will examine each of these levels of regulation in turn.

Acetyl CoA carboxylase is regulated by conditions in the cell

ACC1 responds to changes in the cytosol; it is switched off by phosphorylation and activated by dephosphorylation (**Figure 22.33**). **AMP-activated protein kinase (AMPK)** converts the carboxylase into an inactive form by modifying three serine residues. AMPK is essentially a cellular fuel gauge; it is activated by AMP and inhibited by ATP.

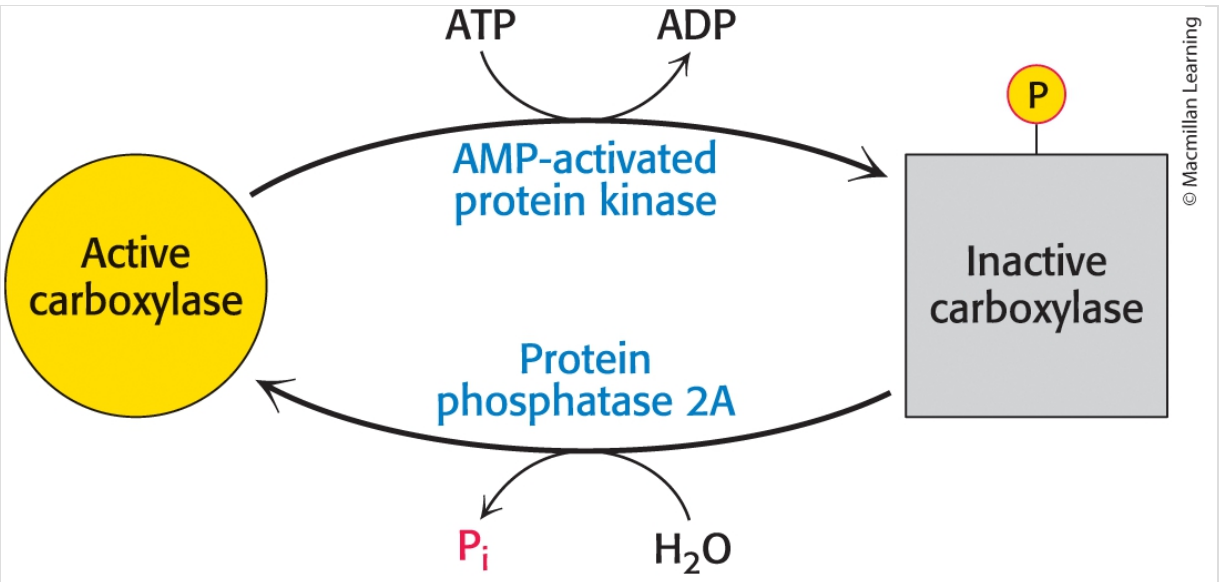
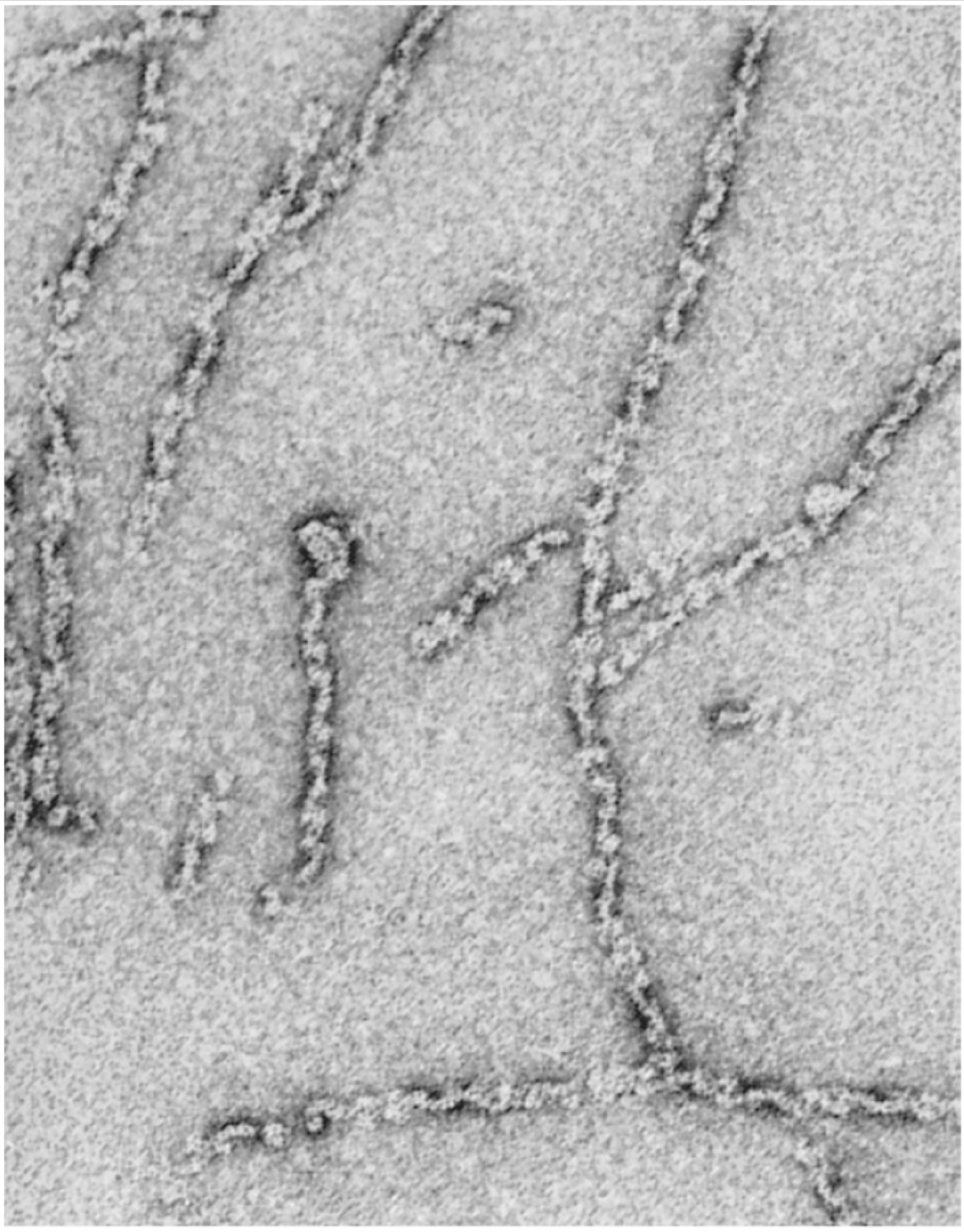


FIGURE 22.33 Acetyl CoA carboxylase is inhibited by phosphorylation by AMPK.

The carboxylase is also allosterically stimulated by citrate. The level of citrate is high when both acetyl CoA and ATP are abundant, signifying that raw materials and energy are available for fatty acid synthesis. Citrate acts in an unusual way on inactive ACC1, which exists as isolated inactive dimers. Citrate facilitates the polymerization of the inactive dimers into active filaments (Figure 22.34).



Courtesy of Dr. M. Daniel Lane.

FIGURE 22.34 Filaments of acetyl CoA carboxylase are enzymatically active. The electron micrograph shows the enzymatically active filamentous form of acetyl CoA carboxylase from chicken liver. The inactive form is a dimer of 265-kDa subunits.

However, polymerization by citrate alone requires supraphysiological concentrations. In the cell, citrate-induced polymerization is facilitated by the protein MIG12, which greatly reduces the amount of citrate required. Polymerization can partly reverse the inhibition produced by phosphorylation (**Figure 22.35**). The stimulatory effect of citrate on the carboxylase is counteracted by palmitoyl CoA, which is abundant when there is an excess of fatty acids. Palmitoyl CoA causes the filaments to disassemble into the inactive subunits. Palmitoyl CoA also inhibits the translocase that transports citrate from mitochondria to the cytoplasm, as well as glucose 6-phosphate dehydrogenase, which generates NADPH in the pentose phosphate pathway.

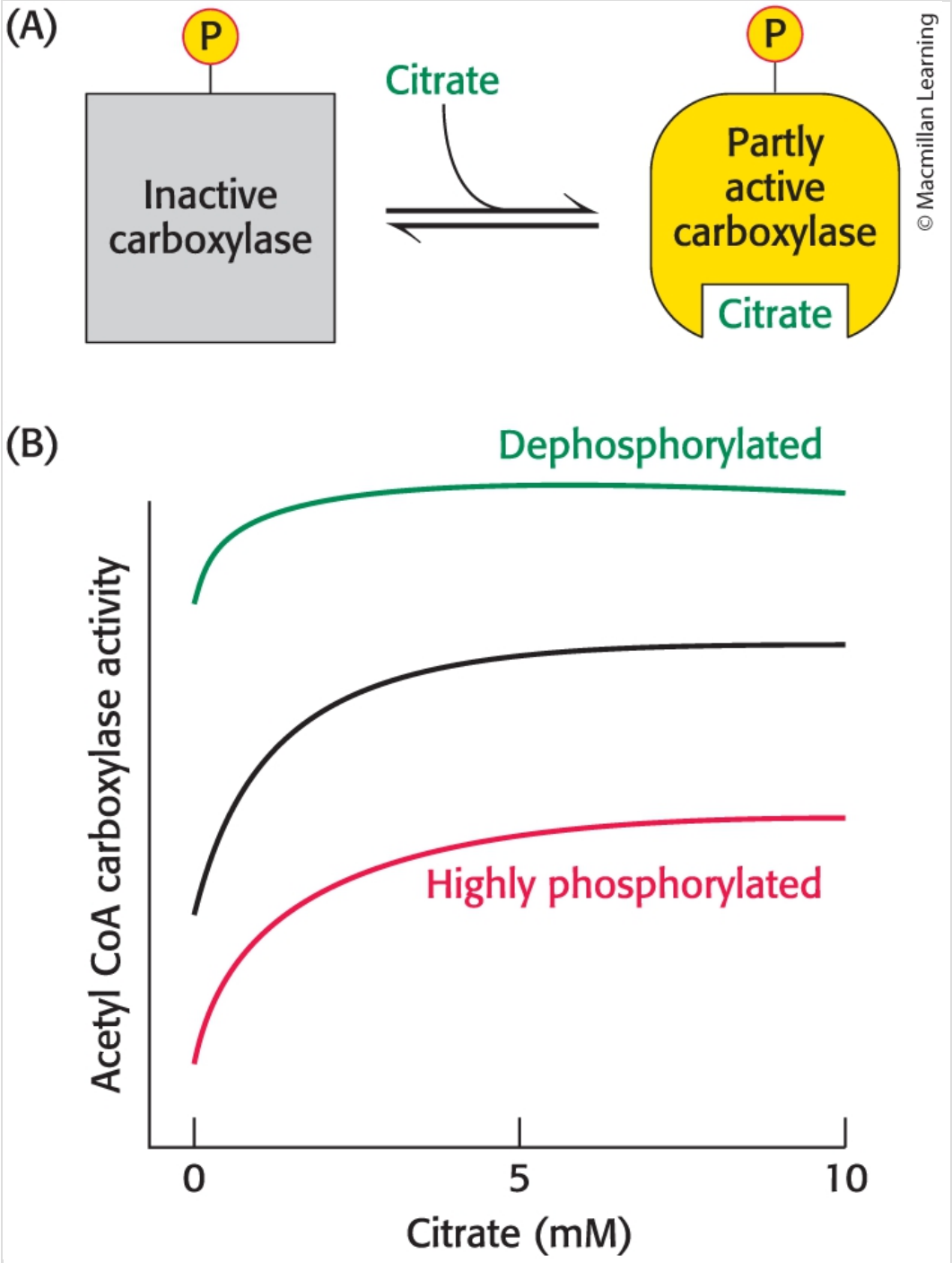


FIGURE 22.35 The catalytic activity of acetyl CoA carboxylase depends upon the concentration of citrate. (A) Citrate can partly activate the phosphorylated carboxylase. (B) The dephosphorylated form of the carboxylase is highly active even when citrate is absent. Citrate partly overcomes the inhibition produced by phosphorylation.

[Information from G. M. Mabrouk, I. M. Helmy, K. G. Thampy, and S. J. Wakil. *J. Biol. Chem.* 265:6330–6338, 1990.]

The isozyme ACC2, located in the mitochondria, plays a role in the regulation of fatty acid degradation. Malonyl CoA, the product of the carboxylase reaction, is present at a high level when fuel molecules are abundant. Malonyl CoA inhibits CATI, preventing the entry of fatty acyl CoAs into the mitochondrial matrix in times of plenty. Malonyl CoA is an especially effective inhibitor of CATI in heart and muscle, tissues that have little fatty acid synthesis capacity of their own. In these tissues, ACC2 may be a purely regulatory enzyme. ACC2 is also phosphorylated and inhibited by AMPK. The reduction in the amount of mitochondrial malonyl CoA following the inhibition of AMPK allows fatty acid transport into the mitochondria for β-oxidation. Thus, AMPK inhibits fatty acid synthesis while stimulating fatty acid oxidation. Activators of AMPK are being investigated to treat nonalcoholic fatty liver disease (NAFLD), a condition due to overnutrition where fats accumulate in the liver. Untreated NAFLD is often a precursor to type 2 diabetes (Section 24.3).

Acetyl CoA carboxylase is controlled by a variety of hormones

ACC is controlled by the hormones glucagon, epinephrine, and insulin, which denote the overall energy status of the organism. Insulin stimulates fatty acid synthesis by activating the carboxylase, whereas glucagon and epinephrine have the reverse effect.

Regulation by glucagon and epinephrine

Consider, again, a person who has just awakened from a night's sleep and begins a bout of exercise. As mentioned, glycogen stores will be low, but lipids are readily available for mobilization.

As stated earlier, the hormones glucagon and epinephrine, present under conditions of fasting and exercise, will stimulate the mobilization of fatty acids from triacylglycerols in fat cells, which will be released into the blood, and probably from muscle cells, where they will be used immediately as fuel. These same hormones will inhibit fatty acid synthesis by inhibiting ACC. Although the exact mechanism by which these hormones exert their effects is not known, the net result is to augment the inhibition by the AMPK. This result makes sound physiological sense: when the energy level of the cell is low, as signified by a high concentration of AMP, and the energy level of the organism is low, as signaled by glucagon, fats should not be synthesized. Epinephrine, which signals the need for immediate energy, enhances this effect. Hence, these catabolic hormones switch off fatty acid synthesis by keeping the carboxylase in the inactive phosphorylated state.

Regulation by insulin

Now consider the situation after the exercise has ended and the runner has had a meal. In this case, the hormone insulin inhibits the mobilization of fatty acids and stimulates their accumulation as triacylglycerols by muscle and adipose tissue. Insulin also stimulates fatty acid synthesis by activating ACC. Insulin activates the carboxylase by enhancing the phosphorylation and inactivation of AMPK by protein kinase B. Insulin also promotes the activity of a protein phosphatase that dephosphorylates and activates ACC. Thus, the signal molecules glucagon, epinephrine, and insulin act in

concert on triacylglycerol metabolism and acetyl CoA carboxylase to carefully regulate the utilization and storage of fatty acids.

Response to diet

Long-term control is mediated by changes in the rates of synthesis and degradation of the enzymes participating in fatty acid synthesis. Animals that have fasted and are then fed high-carbohydrate, low-fat diets show marked increases in their amounts of ACC and fatty acid synthase within a few days. This type of regulation is known as *adaptive control*. This regulation, which is mediated both by insulin and by glucose, is at the level of gene transcription.

Self-Check Question



Consider citrate's role as a regulator of fatty acid metabolism and recall another regulatory connection we saw in Chapter 16 but could not fully explain at that point: citrate is an inhibitor of phosphofructokinase. Explain now why this is appropriate.

AMP-activated protein kinase is a key regulator of metabolism

As we have already seen, AMPK inhibits fatty acid synthesis while simultaneously stimulating fatty acid oxidation. However, this ubiquitous trimeric enzyme (αβγ), which exists in several isozymic

forms, regulates a number of other metabolic processes. As in fatty acid metabolism, AMPK in general activates ATP-generating pathways and inhibits pathways that require ATP. Thus, AMPK stimulates glucose uptake and mitochondria biogenesis, while inhibiting cholesterol synthesis and protein synthesis. In some immune cells AMPK moderates the inflammatory response. AMPK also helps initiate nonshivering thermogenesis in brown adipose tissue (Section 18.6). Finally, its importance to growth is illustrated by the observation that its absence is lethal in mouse embryogenesis, suggesting that AMPK is crucial for early development. Interestingly, the isozymic forms of this key enzyme are themselves regulated by phosphorylation by a number of kinases. Understanding the intricacies of this enzyme will surely keep biochemists engaged for years to come.

Chapter 22 Summary

22.1 Triacylglycerols Are Highly Concentrated Energy Stores

- Fatty acids are physiologically important as (1) fuel molecules, (2) components of phospholipids and glycolipids, (3) hydrophobic modifiers of proteins, and (4) hormones and intracellular messengers.
- Fatty acids are stored as triacylglycerols in lipid droplets within adipocytes of adipose tissue.
- Dietary triacylglycerols are coated with bile acids, rendering them more easily digested by pancreatic lipases. The digestion products are transported inside intestinal cells where triacylglycerols are resynthesized. New triacylglycerols are packaged into chylomicrons which are released into the lymph system and then the blood for transport.

22.2 The Use of Fatty Acids as Fuel Requires Three Stages of Processing

- Triacylglycerols can be mobilized by the action of hormonally controlled lipases. Glucagon and epinephrine stimulate triacylglycerol breakdown, while insulin inhibits it.
- Fatty acids are activated to acyl CoAs, transported across the inner mitochondrial membrane while bound to carnitine, and degraded in the mitochondrial matrix by a recurring sequence of four reactions: oxidation by FAD, hydration, oxidation by NAD^+, and thiolysis by coenzyme A.
- The $FADH_2$ and NADH formed in the oxidation steps transfer their electrons to O_2 by means of the ETC, whereas the acetyl CoA formed in the thiolysis step normally enters the citric acid cycle.

22.3 Unsaturated and Odd-Chain Fatty Acids Require Additional Steps for Degradation

- Fatty acids that contain double bonds or odd numbers of carbon atoms require ancillary steps to be degraded.
- An isomerase and a reductase are required for the oxidation of unsaturated fatty acids, whereas propionyl CoA derived from chains with odd numbers of carbon atoms requires a vitamin B_{12}-dependent enzyme to be converted into succinyl CoA.

22.4 Ketone Bodies Are a Fuel Source Derived from Fats

- Ketone bodies are an important fuel source for some tissues. The primary ketone bodies — acetoacetate and β-hydroxybutyrate — are formed in the liver by condensation of acetyl CoA units.
- Mammals are unable to convert fatty acids into glucose because they lack a pathway for the net production of oxaloacetate, pyruvate, and other gluconeogenic intermediates from acetyl CoA.

22.5 Fatty Acids Are Synthesized by Fatty Acid Synthase

- Fatty acids are synthesized in the cytoplasm by fatty acid synthase. Synthesis starts with the carboxylation of acetyl CoA to malonyl CoA, the committed step. This ATP-driven reaction is catalyzed by acetyl CoA carboxylase (ACC), a biotin enzyme.
- The intermediates in fatty acid synthesis are linked to an acyl carrier protein (ACP). Acetyl ACP and malonyl ACP condense to form acetoacetyl ACP, with the release of CO_2. NADPH is used as a reductant in subsequent reactions which mirror the reverse of β-oxidation. Additional two-carbon units from malonyl ACP are added, typically ending at palmitoyl ACP, which is hydrolyzed to palmitate.

- A reaction cycle based on the formation and cleavage of citrate carries acetyl groups from mitochondria to the cytoplasm, while the NADPH needed for synthesis is generated in the transfer of reducing equivalents from mitochondria.

22.6 The Elongation and Unsaturation of Fatty Acids Are Accomplished by Accessory Enzyme Systems

- Fatty acids are elongated and desaturated by enzyme systems in the ER membrane. Desaturation requires NADH and O_2 and is carried out by a complex consisting of a flavoprotein, a cytochrome, and a nonheme iron protein.
- Mammals lack the enzymes to introduce double bonds distal to C-9, and so they require linoleate and linolenate in their diets.
- Arachidonate is the precursor of several classes of signal molecules — prostaglandins, prostacyclins, thromboxanes, and leukotrienes — that act as messengers and local hormones because of their transience and are called *eicosanoids* because they contain 20 carbon atoms.
- Aspirin (acetylsalicylate), an anti-inflammatory and antithrombotic drug, irreversibly blocks the synthesis of some of these eicosanoids.

22.7 Acetyl CoA Carboxylase Plays a Key Role in Controlling Fatty Acid Metabolism

- Fatty acid synthesis and degradation are reciprocally regulated so that both are not simultaneously active. Acetyl CoA carboxylase (ACC), the essential control site, is phosphorylated and inactivated by AMPK. The phosphorylation is reversed by a protein phosphatase.
- Citrate, which signals an abundance of building blocks and energy, partly reverses the inhibition by phosphorylation. Carboxylase activity is stimulated by insulin and inhibited by glucagon and epinephrine.

- In times of plenty, fatty acyl CoAs do not enter the mitochondrial matrix, because malonyl CoA inhibits carnitine acyltransferase I.

Key Terms

triacylglycerol (neutral fat, triglyceride)
lipase
chylomicron
acyl adenylate
carnitine
β-oxidation pathway
vitamin B_{12} (cobalamin)
peroxisomes
ketone bodies
fatty acid synthase
acyl carrier protein (ACP)
malonyl CoA
acetyl CoA carboxylase (ACC)
prostaglandin
eicosanoid
AMP-activated protein kinase (AMPK)

Problems

1. Write a balanced equation for the conversion of glycerol into pyruvate. Which enzymes are required in addition to those of the glycolytic pathway?

2. Place the following list of reactions or relevant locations in the β-oxidation of fatty acids in the proper order. 1

a. Reaction with carnitine
b. Fatty acid in the cytoplasm
c. Activation of fatty acid by joining to CoA
d. Hydration
e. NAD^+-linked oxidation
f. Thiolysis
g. Acyl CoA in mitochondrion
h. FAD-linked oxidation

3. We have encountered reactions similar to the oxidation, hydration, and oxidation reactions of fatty acid degradation earlier in our study of biochemistry. What other pathway employs this set of reactions? 1

4. Compare the ATP yields from palmitic acid and palmitoleic acid. 1

5. Stearic acid is a C_{18} fatty acid component of chocolate. Suppose you had a depressing day and decided to settle matters by gorging on chocolate. How much ATP would you derive from the complete oxidation of stearic acid to CO_2? 1

6. Write a balanced equation for the conversion of stearate into acetoacetate. 2

7. The β-oxidation pathway degrades activated fatty acids (acyl CoA) to acetyl CoA, which then enters the citric acid cycle. Additional enzymes are required to oxidize unsaturated, odd–chain, long–chain, and branched fatty acids. Which of the following statements is/are true?

a. Even–chain saturated fatty acids are oxidized to acetyl CoA in the β–oxidation pathway.
b. Complete catabolism of the three–carbon remnant of a 15–carbon fatty acid requires some citric acid cycle enzymes.
c. Enoyl–CoA isomerase, an enzyme that converts cis double bonds to trans double bonds in fatty acid metabolism, bypasses a step that reduces Q, resulting in a higher ATP yield.
d. The final round of β–oxidation for a 13–carbon saturated fatty acid yields acetyl CoA and propionyl–CoA, a three–carbon fragment.
e. A 14–carbon monounsaturated fatty acid with cis configuration yields more ATP than a 14–carbon saturated fatty acid.
f. Trans double bonds in unsaturated fatty acids are not well recognized by β–oxidation enzymes.

8. Which of the following statements regarding the body's inability to convert fat to carbohydrates is/are true?

a. The acetyl CoA that is produced from the oxidation of fatty acids enters the citric acid cycle but does not lead to a net gain of oxaloacetate.
b. The decarboxylation steps of the citric acid cycle prevent the net synthesis of glucose precursors from acetyl CoA in animal tissues.
c. Metabolism of odd-chain fatty acids yields propionyl CoA, which is converted to succinyl CoA and can enter the citric acid cycle.
d. Acetyl CoA that is produced from the oxidation of fatty acids and enters the citric acid cycle is used in the *de novo* synthesis of pyruvate.

e. Acetoacetate is a normal, major energy source for the brain, heart muscle, and renal cortex.

9. What is the committed step in fatty acid synthesis, and which enzyme catalyzes the step? 3

10. Compare and contrast fatty acid oxidation and synthesis with respect to

a. site of the process
b. acyl carrier
c. reductants and oxidants
d. stereochemistry of the intermediates
e. direction of synthesis or degradation
f. organization of the enzyme system

11. Lauric acid is a 12-carbon fatty acid with no double bonds. The sodium salt of lauric acid (sodium laurate) is a common detergent used in a variety of products, including laundry detergent, shampoo, and toothpaste. How many molecules of ATP and NADPH are required to synthesize lauric acid? 3

12. Arrange the following steps in fatty acid synthesis in their proper order. 3

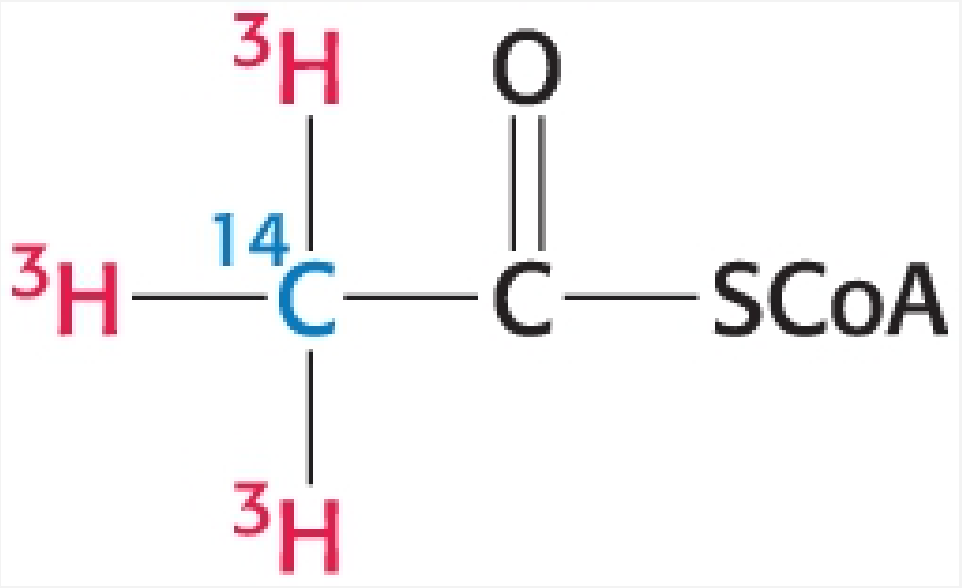
a. Dehydration
b. Condensation
c. Release of a C_{16} fatty acid
d. Reduction of a carbonyl group
e. Formation of malonyl ACP

13. True or False? If false, explain. 3

a. Biotin is required for fatty acid synthase activity.
b. The condensation reaction in fatty acid synthesis is powered by the decarboxylation of malonyl CoA.

c. Fatty acid synthesis does not depend on ATP.
d. Palmitate is the end product of fatty acid synthase.
e. All of the enzyme activities required for fatty acid synthesis in mammals are contained in a single polypeptide chain.
f. Fatty acid synthase in mammals is active as a monomer.
g. The fatty acid arachidonate is a precursor for signal molecules.
h. Acetyl CoA carboxylase is inhibited by citrate.

14. Suppose that you had an in vitro fatty acid–synthesizing system with all of the enzymes and cofactors required for fatty acid synthesis except for acetyl CoA. To this system, you added acetyl CoA that contained radioactive hydrogen $(^3H, \text{tritium})$ and carbon $14(^{14}C)$, as shown here.



The ratio of $^{3}H/^{14}C$ is 3. What would the $^{3}H/^{14}C$ ratio be after the synthesis of palmitic acid (C_{16}) with the use of the radioactive acetyl CoA? 3

15. The serine residues in acetyl CoA carboxylase that are the target of the AMP-activated protein kinase are mutated to alanine. What is a likely consequence of this mutation? 4

16. For each of the following unsaturated fatty acids, indicate whether the biosynthetic precursor in animals is palmitoleate, oleate, linoleate, or linolenate.

a. 18:1 $cis-\Delta^{11}$

b. 18:3 $cis-\Delta^{6}, \Delta^{9}, \Delta^{12}$

c. 20:2 $cis-\Delta^{11},\Delta^{14}$

d. 20:3 $cis-\Delta^{5},\Delta^{8},\Delta^{11}$

e. 22:1 $cis-\Delta^{13}$

f. 22:6 $cis-\Delta^{4}, \Delta^{7}, \Delta^{10}, \Delta^{13}, \Delta^{16}, \Delta^{19}$

17. Figure 22.35 shows the response of acetyl CoA carboxylase to varying amounts of citrate. Explain this effect in light of the allosteric effects that citrate has on the enzyme. Predict the effects of increasing concentrations of palmitoyl CoA. 4

18. Classify each event involved in the regulation of fatty acid metabolism as an outcome of hormonal regulation by insulin or by glucagon and epinephrine:

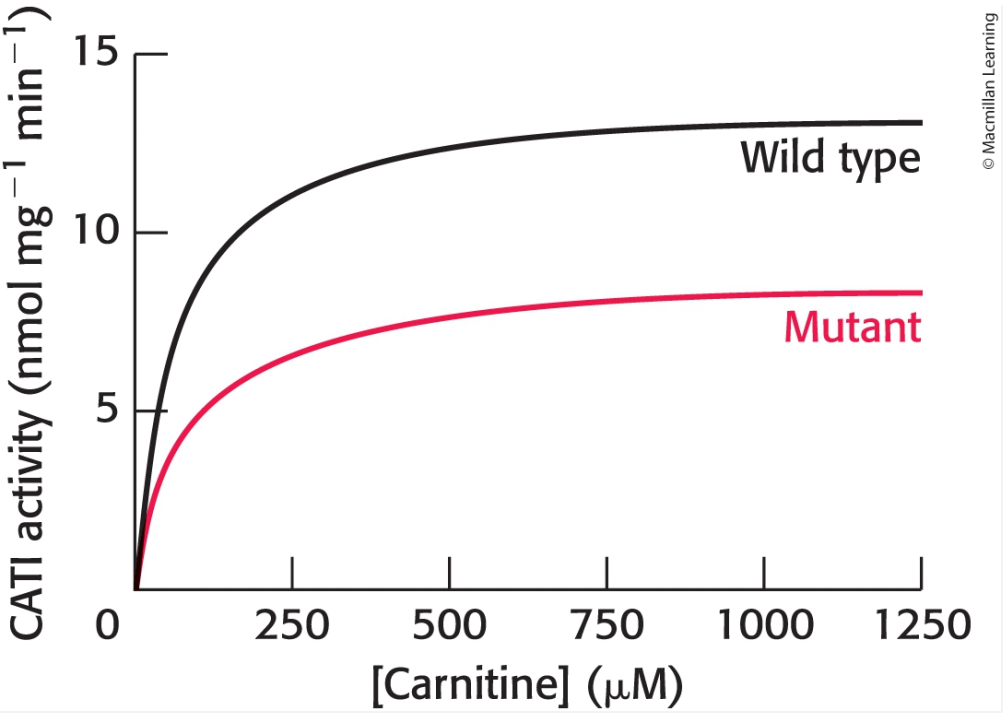
a. Stimulates fatty acid synthesis
b. Activates acetyl CoA carboxylase
c. Inhibits fatty acid synthesis

d. Inhibits acetyl CoA carboxylase
e. Stimulates protein phosphatase activity
f. Increases activity of AMPK

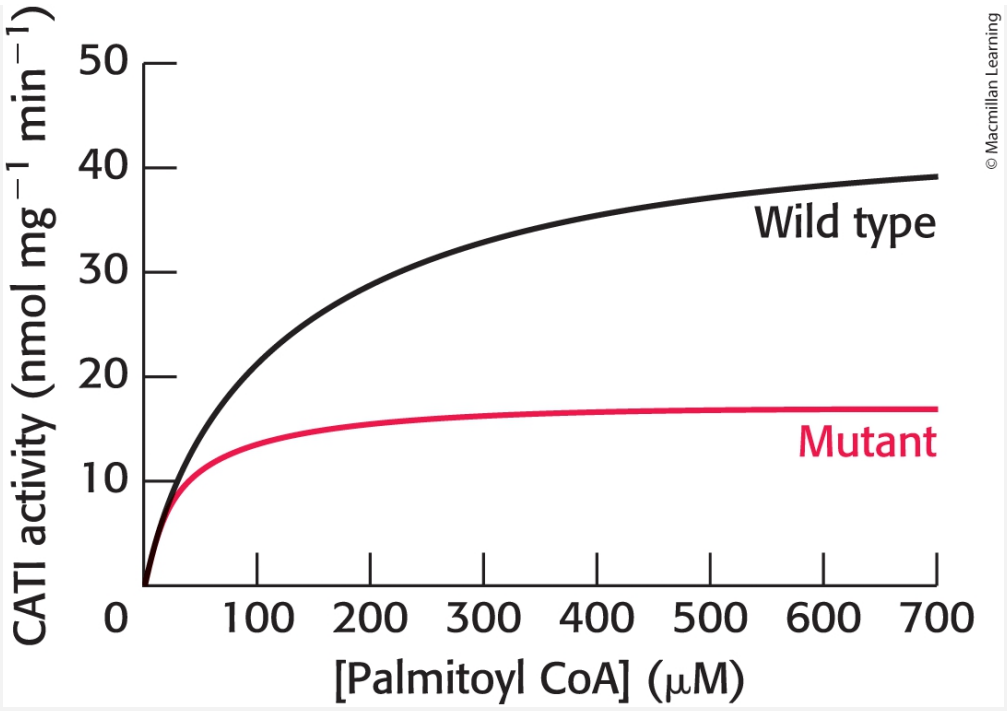
19. What are the three reactions that allow the conversion of cytoplasmic NADH into NADPH? What enzymes are required? Show the sum of the three reactions. 3

20. Carnitine acyltransferase I (CATI) catalyzes the conversion of long-chain acyl CoA into acyl carnitine, a prerequisite for transport into mitochondria and subsequent degradation. A mutant enzyme was constructed with a single amino acid change at position 3 of glutamic acid for alanine. Graphs A through C show data from studies that were performed to identify the effect of the mutation. 1

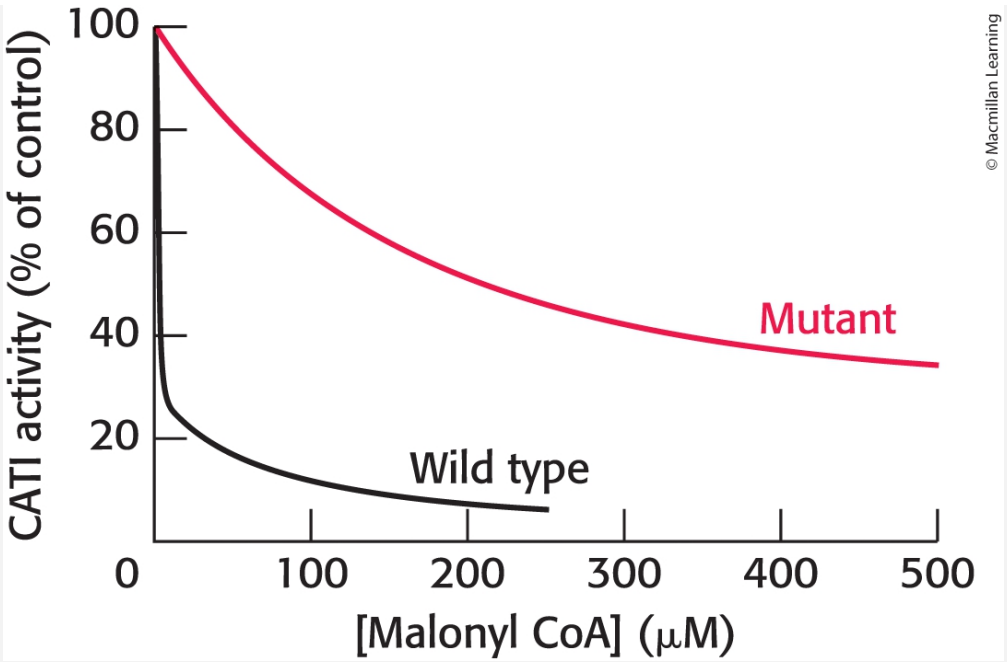
a. What is the effect of the mutation on enzyme activity when the concentration of carnitine is varied? (Results are shown below.) What are the K_M and V_{max} values for the wild-type and mutant enzymes?



b. What is the effect when the experiment is repeated with varying concentrations of palmitoyl CoA? What are the K_M and V_{max} values for the wild-type and mutant enzymes?



c. The next graph shows the inhibitory effect of malonyl CoA on the wild-type and mutant enzymes. Which enzyme is more sensitive to malonyl CoA inhibition?

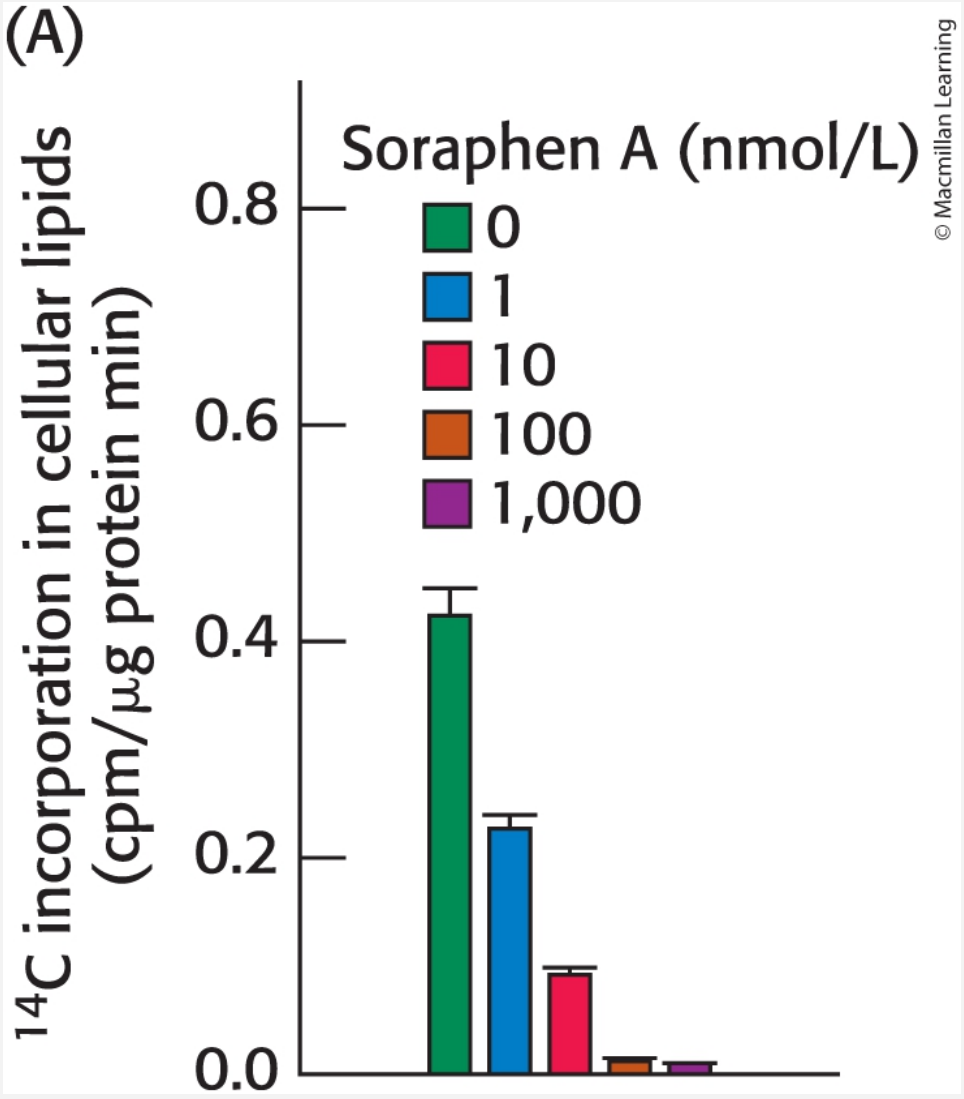


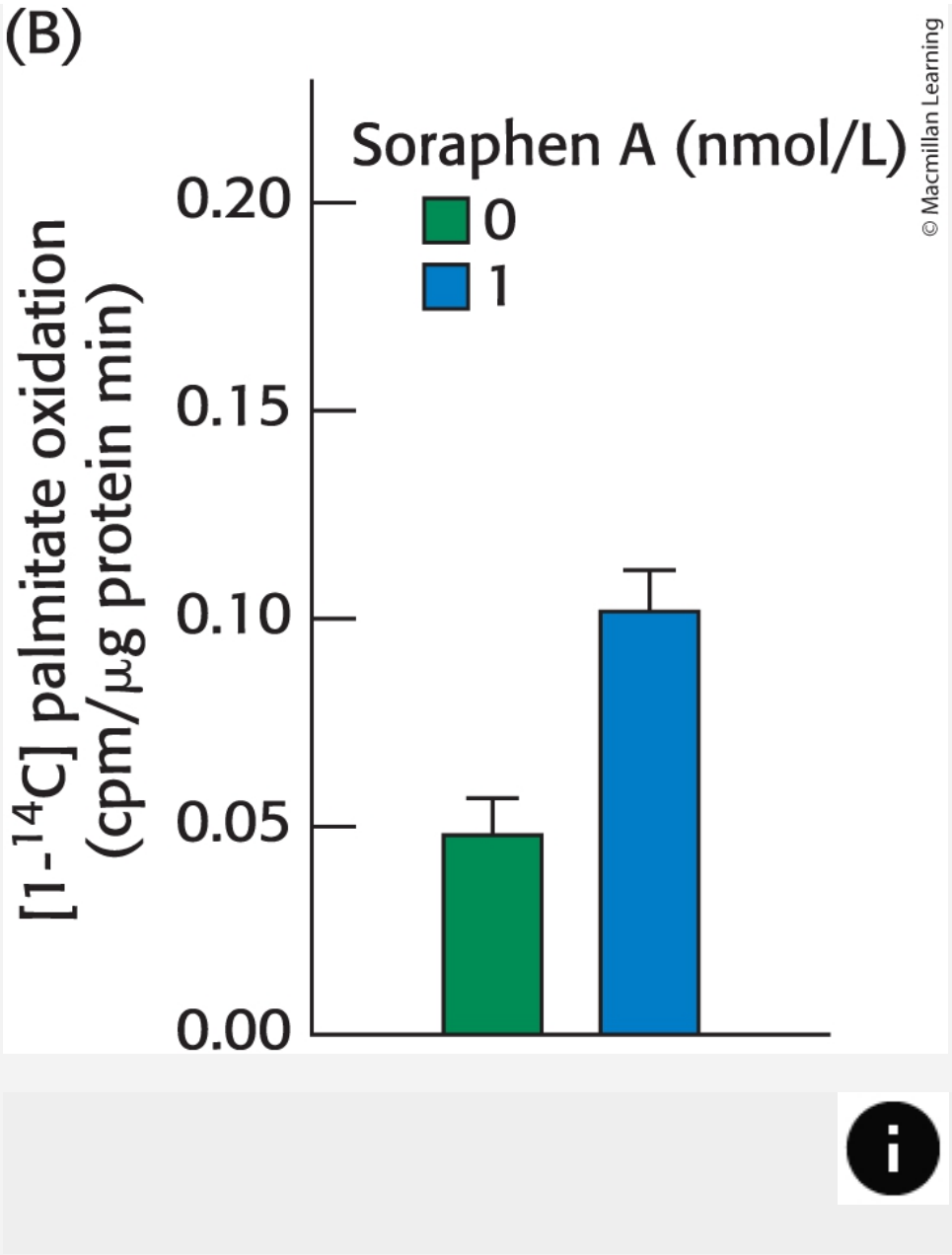
d. Suppose that the concentration of palmitoyl CoA = 100 μM, that of carnitine = 100 μM, and that of malonyl CoA = 10 μM. Under these conditions, what is the most prominent effect of the mutation on the properties of the enzyme?
e. What can you conclude about the role of glutamate 3 in CATI function?

21. Soraphen A is a natural antifungal agent isolated from a myxobacterium. Soraphen A is also a potent inhibitor of acetyl CoA carboxylase, the regulatory enzyme that initiates fatty acid synthesis. As discussed in Section 22.5, cancer cells must produce a large amount of fatty acids to generate phospholipids for membrane synthesis. Thus, acetyl CoA carboxylase might be a target for anticancer drugs. Below are

the results of experiments testing this hypothesis on a cancer line. 4

Figure A shows the effect of various amounts of soraphen A on fatty acid synthesis as measured by the incorporation of radioactive acetate (^{14}C) into fatty acids.





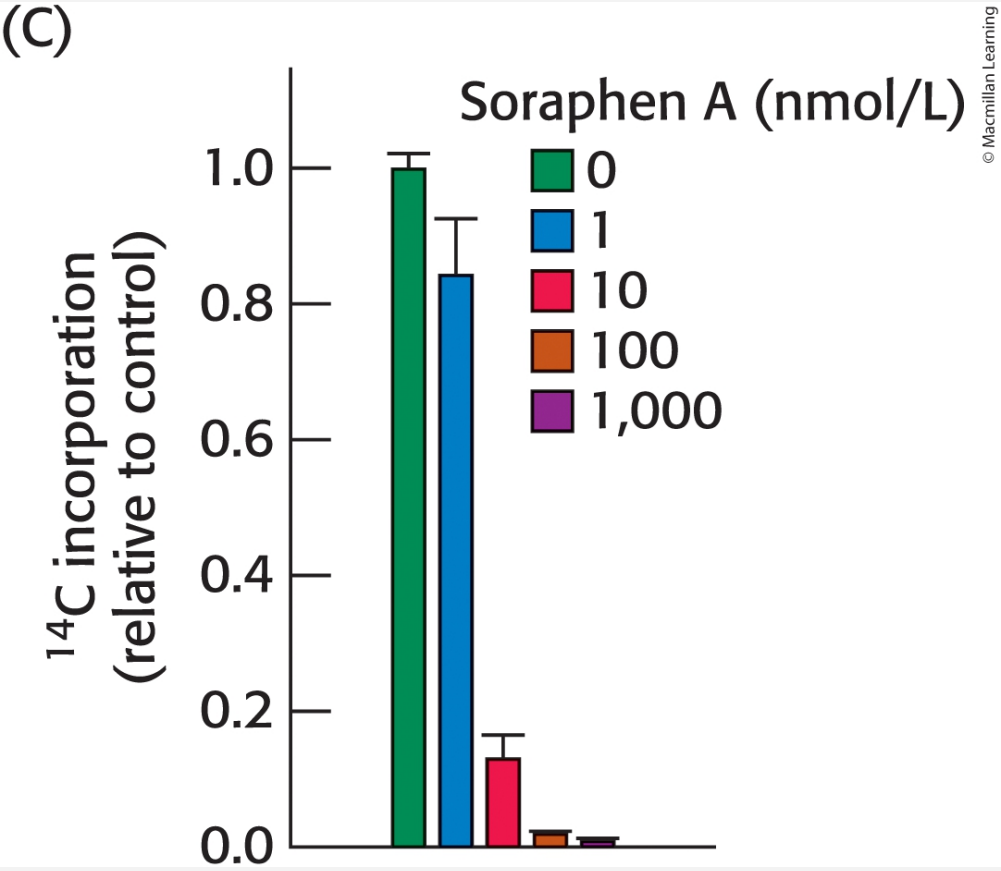
a. How did soraphen A alter fatty acid synthesis? How was synthesis affected by increasing concentrations of soraphen A?

Figure B shows the results obtained when fatty acid oxidation was measured, as the release of radioactive

CO_2 from added radioactive (^{14}C) palmitate, in the presence of soraphen A.

b. How did soraphen A alter fatty acid oxidation?
c. Explain the results obtained in B in light of the fact that soraphen A inhibits acetyl CoA carboxylase.

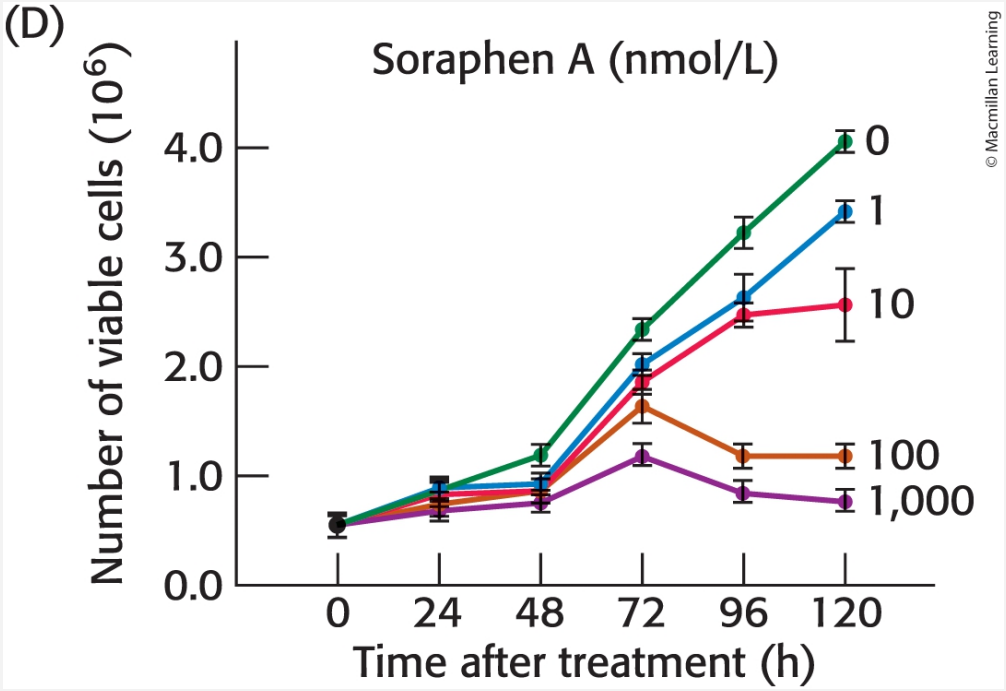
More experiments were undertaken to assess whether carboxylase inhibition did indeed prevent phospholipid synthesis. Again, cells were grown in the presence of radioactive acetate, phospholipids were subsequently isolated, and the amount of ^{14}C incorporated into the phospholipid was determined. The effect of soraphen A on phospholipid synthesis is shown in Figure C.



d. Did the inhibition of carboxylase by the drug alter phospholipid synthesis?
e. How might phospholipid synthesis affect cell viability?

Finally, as shown in Figure D, experiments were performed to determine if the drug inhibits cancer growth in vitro by determining the number of cancer cells surviving upon exposure to soraphen A.

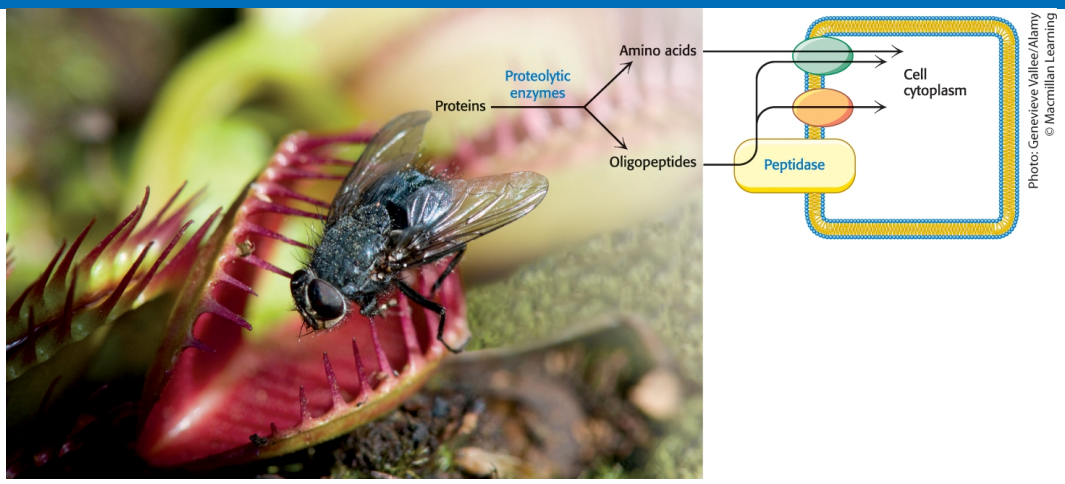
f. How did soraphen A affect cancer cell viability?



[Data from: Beckers, A., Organe, S., Timmermans, L., Scheys, K., Peeters, A., Brusselmans, K., Verhoeven, G., and Swinnen, J. V., Chemical inhibition of acetyl-CoA carboxylase induces growth arrest and cytotoxicity selectively in cancer cells, *Cancer Res.* 67:8180–8187, 2007.]



Chapter 23
Protein Turnover and Amino Acid Catabolism



Nitrogen is a critical component of countless biomolecules. Some plants have adapted to live in nitrogen-depleted soil by capturing and digesting insects. The biochemical mechanisms used by such plants to degrade proteins into amino acids mirror those used by animals and highlight the important role of nitrogen in biochemical biosynthesis.

Outline

23.1 Proteins Are Degraded to Amino Acids
23.2 Protein Turnover Is Tightly Regulated
23.3 The First Step in Amino Acid Degradation Is the Removal of Nitrogen

23.4 Ammonium Ions Are Converted into Urea in Most Terrestrial Vertebrates
23.5 Carbon Atoms of Degraded Amino Acids Emerge as Major Metabolic Intermediates
23.6 Inborn Errors of Metabolism Can Disrupt Amino Acid Degradation

Learning Goals



By the end of this chapter, you should be able to:

1. Explain the importance of the regulation of protein turnover.
2. Identify the primary role of ubiquitin and describe the enzymes required for ubiquitination.
3. Explain the function of the proteasome.
4. Describe the fate of nitrogen that is removed when amino acids are used as fuels.
5. Explain how the carbon skeletons of the amino acids are metabolized after nitrogen removal.
6. Identify metabolic errors in amino acid degradation.

Our study of metabolism has, up to this point, focused on carbohydrates and lipids that contain only carbon, oxygen, and hydrogen. We now turn to the subject of nitrogen metabolism, focusing first on catabolic pathways involving proteins and amino acids. In animals, the digestion of dietary proteins in the intestine and the degradation of proteins within the cell provide a steady supply of amino acids for the biosynthesis of new proteins and nucleotide bases. Cellular proteins are also constantly degraded in response to changing metabolic demands or due to misfolding or damage. Excess amino acids can neither be stored nor excreted; instead, they must be used as metabolic fuel. In this chapter we will

also consider several genetic errors of amino acid degradation. The study of amino acid metabolism is especially rewarding because it is rich in connections between basic biochemistry and clinical medicine.

23.1 Proteins Are Degraded to Amino Acids

Dietary protein is a vital source of amino acids. Especially important dietary proteins are those containing the essential amino acids — amino acids that cannot be synthesized and must be acquired in the diet (Table 23.1). Proteins ingested in the diet are digested into amino acids or small peptides that can be absorbed by the intestine and transported in the blood. Another crucial source of amino acids is the degradation of cellular proteins.

TABLE 23.1 Essential amino acids in human beings

Histidine	Phenylalanine
Isoleucine	Threonine
Leucine	Tryptophan
Lysine	Valine
Methionine	

The digestion of dietary proteins begins in the stomach and is completed in the intestine

Protein digestion begins in the stomach, where the acidic environment denatures proteins into random coils. Denatured proteins are more accessible as substrates for proteolysis than are native proteins. The primary proteolytic enzyme of the stomach is pepsin, a nonspecific protease that, remarkably, is maximally active at pH 2. Thus, pepsin can function in the highly acidic environment of the stomach that disables other proteins.

The partly digested proteins then move from the acidic environment of the stomach to the beginning of the small intestine, called the *duodenum*. The low pH of the food as well as the polypeptide products of pepsin digestion stimulate the release of hormones that promote the secretion from the pancreas of sodium bicarbonate ($NaHCO_3$), which neutralizes the pH of the food, and a variety of pancreatic proteolytic enzymes. Recall that these enzymes are secreted as inactive zymogens that are then converted into active enzymes (Sections 6.1 and 7.4). The battery of enzymes displays a wide array of specificity, and so the substrates are degraded into free amino acids as well as di- and tripeptides (**Figure 23.1**). Digestion is further enhanced by proteolytic enzymes, such as aminopeptidase N, that are located in the plasma membrane of the intestinal cells. Aminopeptidases digest proteins from the amino-terminal end, and the resulting free amino acids — as well as di- and tripeptides — are transported into the intestinal cells.

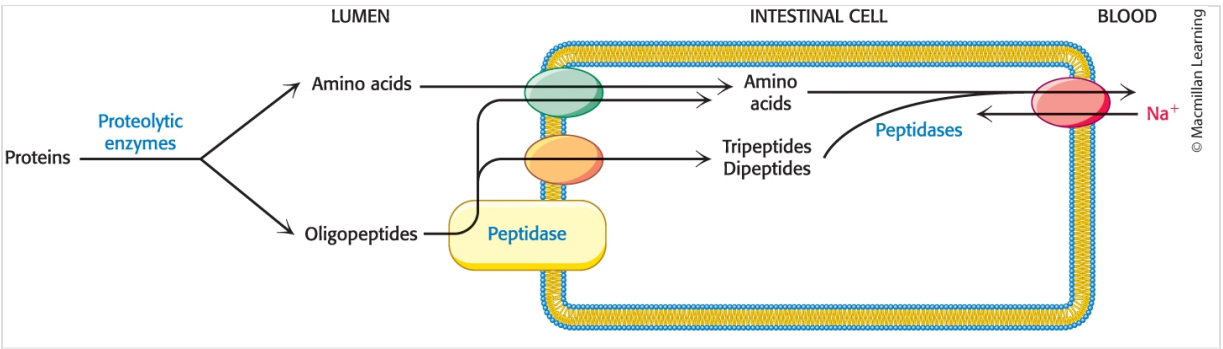


FIGURE 23.1 The products of protein digestion are absorbed by the small intestine. Protein digestion is primarily a result of the activity of enzymes secreted by the pancreas. Aminopeptidases associated with the intestinal epithelium further digest proteins. The amino acids and di- and tripeptides are absorbed into the intestinal cells by specific transporters (green and orange ovals). Free amino acids are then released into the blood by transporters (red oval) for use by other tissues.

At least seven different transporters exist, each specific to a different group of amino acids. A number of inherited disorders result from mutations in these transporters. For example, Hartnup disease, a rare disorder characterized by rashes, ataxia (lack of muscle control), delayed mental development, and diarrhea, results from a defect in the transporter for tryptophan and other nonpolar amino acids. The absorbed amino acids are subsequently released into the blood by a number of Na^+–amino acid antiporters for use by other tissues (Figure 23.1).

Cellular proteins are degraded at different rates

Protein turnover — the degradation and resynthesis of proteins — takes place constantly in cells. Although some proteins are very

stable, many proteins are short lived, particularly those that participate in metabolic regulation. These proteins can be quickly degraded to activate or shut down a signaling pathway. In addition, cells must eliminate damaged proteins. A significant proportion of newly synthesized protein molecules are defective because of errors in translation or misfolding. Even proteins that are normal when first synthesized may undergo oxidative damage or be altered in other ways with the passage of time. These proteins must be removed before they accumulate and aggregate. Indeed, a number of pathological conditions, such as certain forms of Parkinson's disease and Huntington's disease, are associated with protein aggregation.

The half-lives of proteins range over several orders of magnitude. Ornithine decarboxylase, at approximately 11 minutes, has one of the shortest half-lives of any mammalian protein. This enzyme participates in the synthesis of polyamines, which are cellular cations essential for growth and differentiation. The life of hemoglobin, however, is limited only by the life of the red blood cell, and the lens protein crystallin is limited by the life of the organism.

Self-Check Question



Where are dietary amino acids absorbed, and what is the primary fate of both dietary and cellular derived amino acids?

23.2 Protein Turnover Is Tightly Regulated

How can a cell distinguish proteins that should be degraded? **Ubiquitin**, a small, 76-amino-acid protein, is so named because it is ubiquitously present in all eukaryotic cells. Ubiquitin serves many functional roles, but its primary role is to serve as a tag that marks proteins for destruction (**Figure 23.2**). Ubiquitin, in this role then, is the cellular equivalent of the "black spot" of Robert Louis Stevenson's *Treasure Island* — the signal for death.

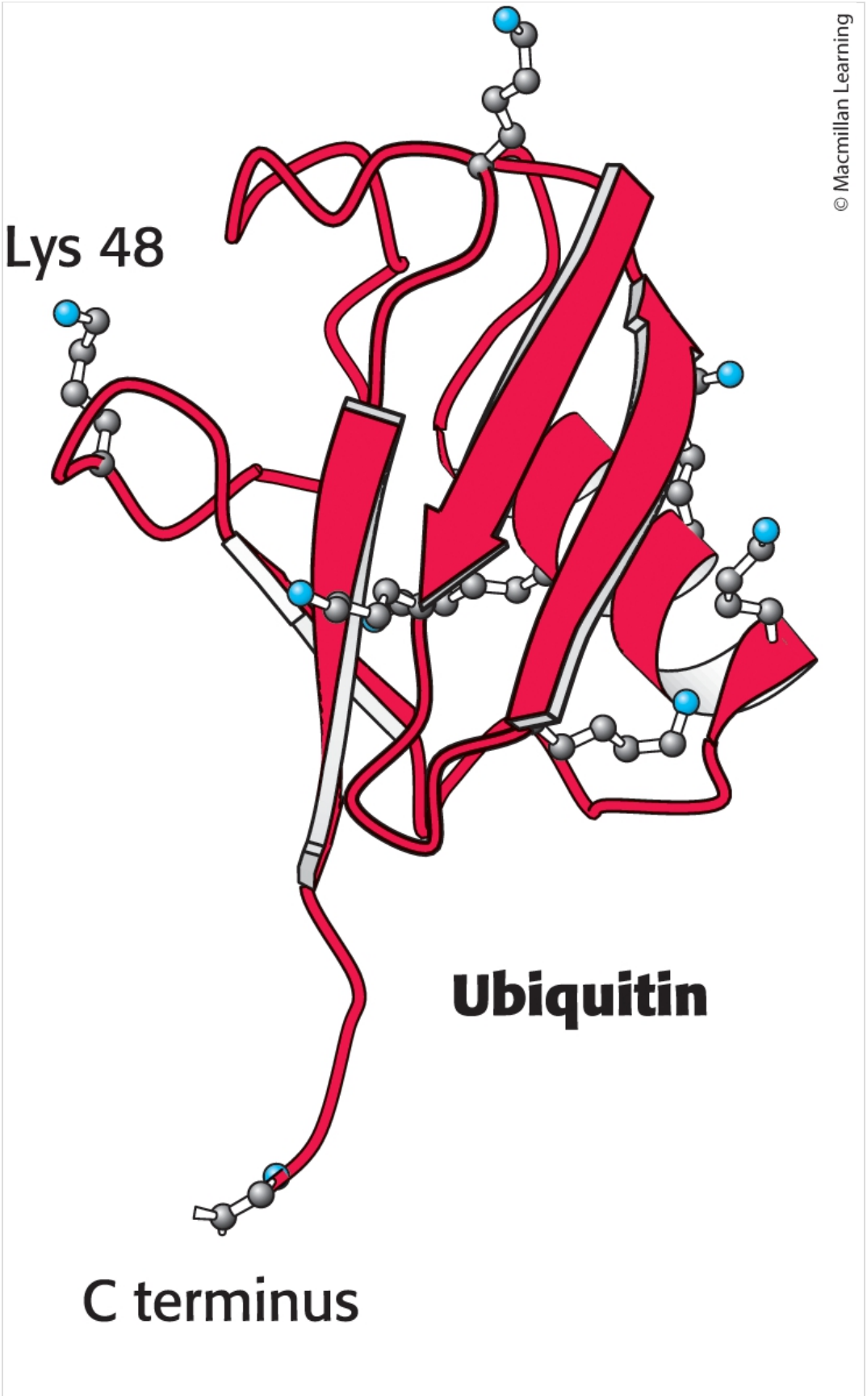

Lys 48
Ubiquitin
C terminus
© Macmillan Learning

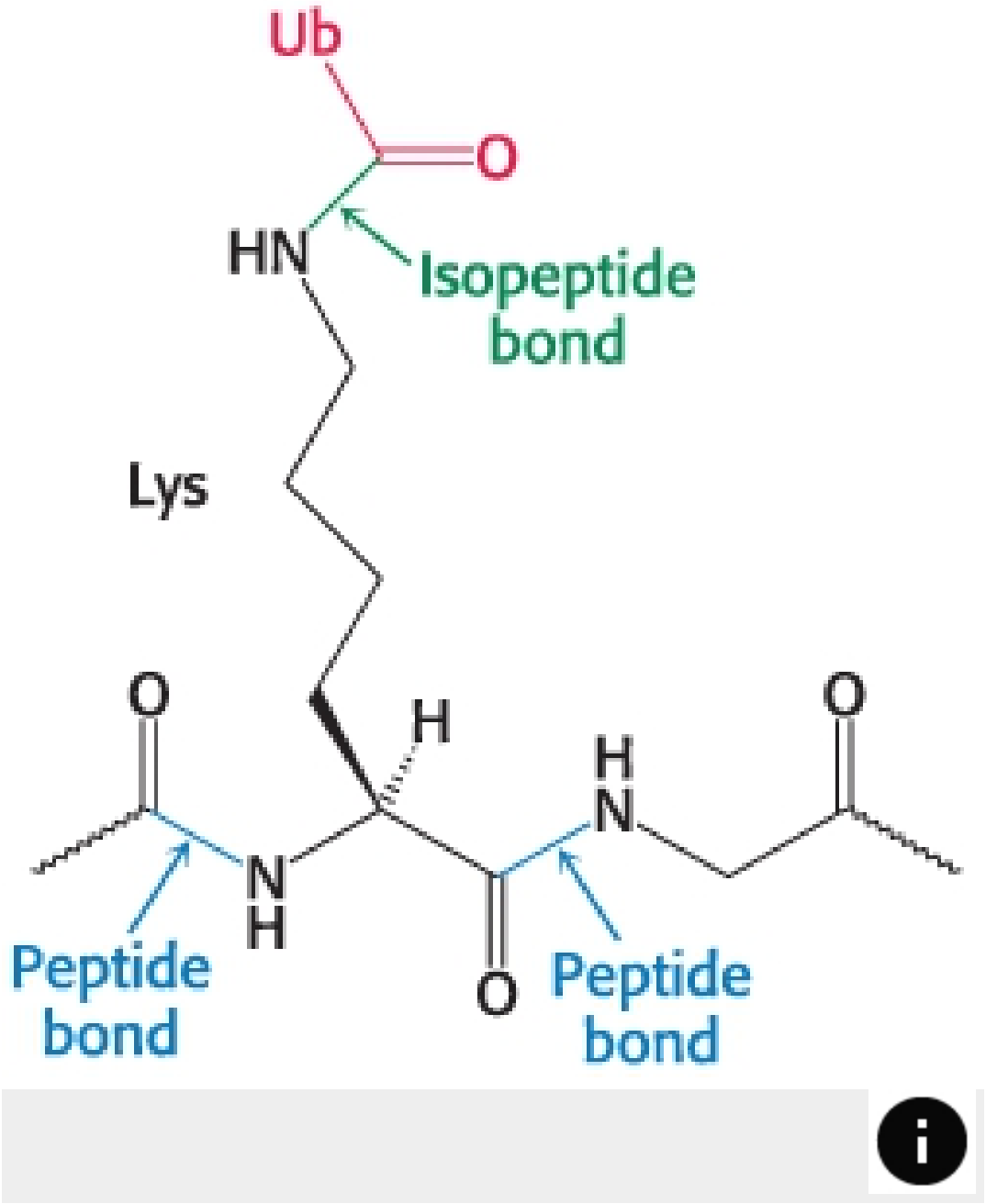
FIGURE 23.2 Ubiquitin is a small, compact protein with seven lysines. Notice that ubiquitin has an extended carboxyl terminus, which is activated and linked to proteins targeted for destruction. Lysine residues, including lysine 48, the major site for linking additional ubiquitin molecules, are shown as ball-and-stick models.

[Drawn from 1UBI.pdb.]

INTERACT with this model in Achieve

Ubiquitin tags proteins for destruction

Ubiquitin is highly conserved in eukaryotes: yeast and human ubiquitin differ at only 3 of 76 residues. A protein destined to be degraded will be covalently modified by the attachment of ubiquitin — by its carboxyl-terminal glycine residue — to the ε-amino groups of one or more lysine residues on the target protein. The energy for the formation of these *iso*peptide bonds (*iso* because ε- rather than α-amino groups are targeted) comes from ATP hydrolysis.



Three enzymes participate in the attachment of ubiquitin to a protein (**Figure 23.3**):

- *Ubiquitin-activating enzyme* (E1). First, the C-terminal carboxylate group of ubiquitin becomes linked to a sulfhydryl group of E1 by a thioester bond. This ATP-driven reaction is reminiscent of fatty acid activation (Section 22.2). In this reaction, an acyl adenylate is

formed at the C-terminal carboxylate of ubiquitin with the release of pyrophosphate, and the ubiquitin is subsequently transferred to a sulfhydryl group of a key cysteine residue in E1.

- *Ubiquitin-conjugating enzyme* (E2). The activated ubiquitin is then shuttled to a sulfhydryl group of E2, a reaction catalyzed by E2 itself.

- *Ubiquitin–protein ligase* (E3). Finally, E3 catalyzes the transfer of ubiquitin from E2 to an ε-amino group on the target protein. E3 does this by bringing E2 and the target protein together. In some cases, the ubiquitin is passed to a cysteine residue of E3 first, whereas in other cases it is transferred directly from the E2 to the target protein.

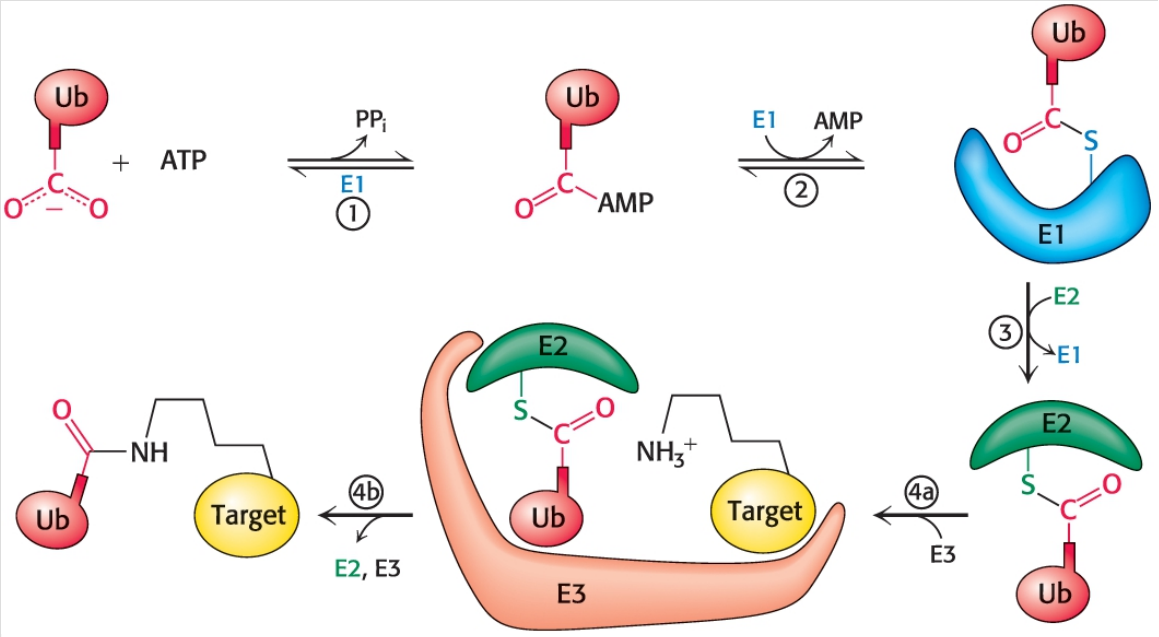
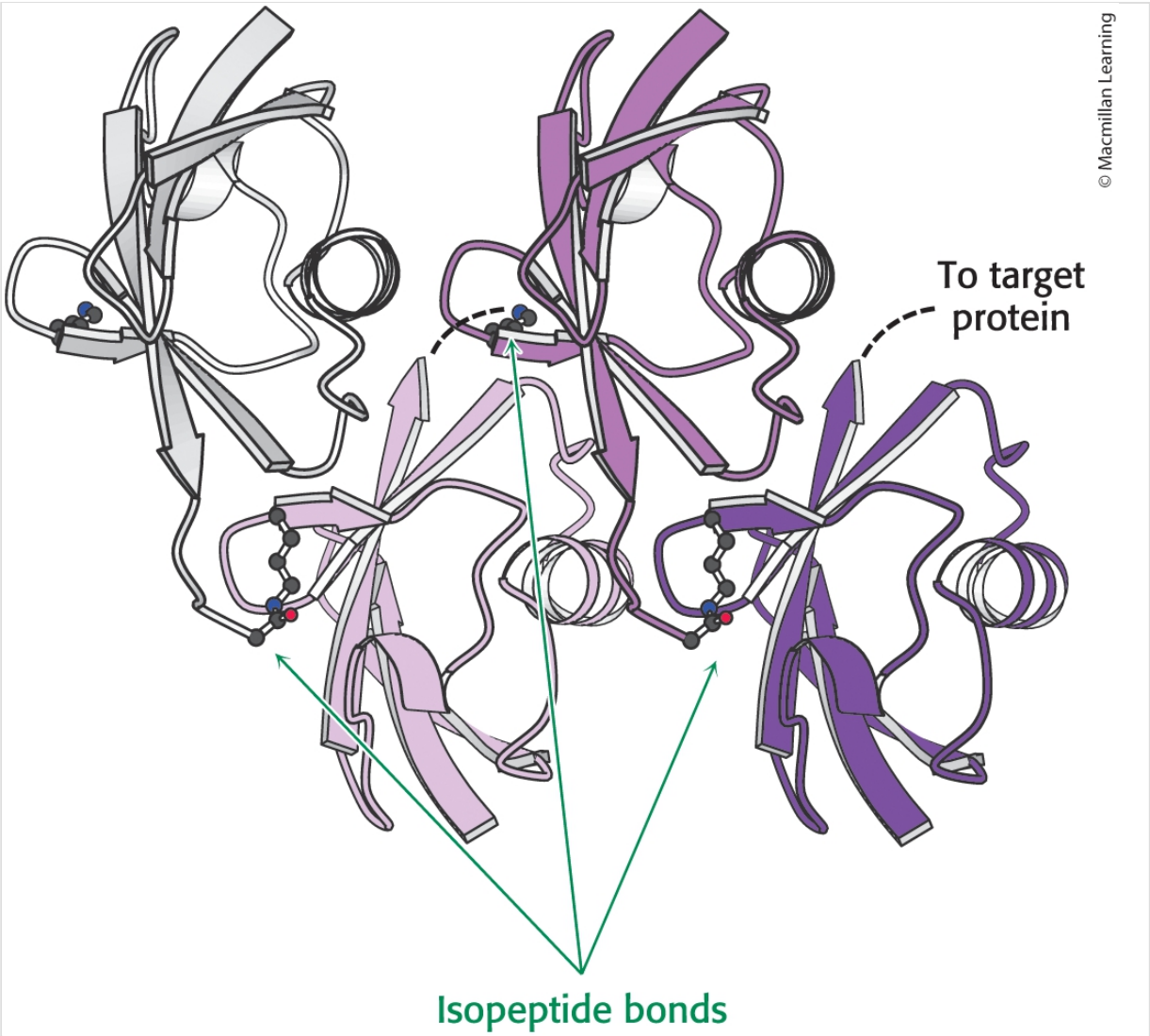


FIGURE 23.3 Ubiquitin conjugation requires three enzymes. The ubiquitin-activating enzyme E adenylates ubiquitin (Ub) (1) and transfers the ubiquitin to one of its own cysteine residues (2). Ubiquitin is then transferred to a cysteine residue in the ubiquitin-conjugating enzyme E2 by th E2 enzyme (3). Finally, the ubiquitin–protein ligase E3 transfers the ubiquitin to a lysine residue on the target protein (4a and 4b).

The ubiquitination reaction can be processive: E3 can remain bound to the target protein and generate a chain of ubiquitin molecules by linking the ε-amino group of a lysine residue of one ubiquitin molecule to the terminal carboxylate of another. Alternatively, in some cases E3 will dissociate after the first ubiquitin addition, and a chain can be extended by another E2/E3 pair. Importantly, ubiquitin can be added onto any of the seven lysines or the N-terminus of the previous ubiquitin, forming chains with different linkages, lengths, and degrees of branching. Some of the linkages signal for proteasomal degradation, while others do not; although the outcome may be context-dependent in different cells. For example, a chain of four or more ubiquitin molecules linked via lysine 48 of ubiquitin has long been known to be an especially effective signal for protein degradation (**Figure 23.4**).



© Macmillan Learning

FIGURE 23.4 In a tetraubiquitin chain, four ubiquitin molecules are linked by isopeptide bonds. Notice that each isopeptide bond is formed by the linkage of the carboxylate group at the end of the extended C terminus with the ε-amino group of a lysine residue, in this case lysine 48. Dashed lines indicate the positions of the extended C-termini that were not observed in the crystal structure. This unit is the primary signal for degradation when linked to a target protein.

[Drawn from 1TBE.pdb.]

INTERACT with this model in Achieve

What determines whether a protein becomes ubiquitinated? A specific sequence of amino acids, termed a **degron**, indicates that a protein should be degraded. One such signal appears to be quite simple: the half-life of a cytoplasmic protein is determined to a large extent by its amino-terminal residue (Table 23.2). This dependency is referred to as the *N-end rule* or the *N-degron*. A yeast protein with methionine at its N terminus typically has a half-life of more than 20 hours, whereas one with arginine at this position has a half-life of about 2 minutes. A highly destabilizing N-terminal residue such as arginine or leucine favors rapid ubiquitination, whereas a stabilizing residue such as methionine or proline does not.

TABLE 23.2 Dependence of the half-lives of cytoplasmic yeast proteins on the identity of their amino-terminal residues

Highly stabilizing residues ($t_{1/2} > 20$ hours)			
Ala	Cys	Gly	Met
Pro	Ser	Thr	Val
Intrinsically destabilizing residues ($t_{1/2} = 2$ to 30 minutes)			
Arg	His	Ile	Leu
Lys	Phe	Trp	Tyr
Destabilizing residues after chemical modification ($t_{1/2} = 3$ to 30 minutes)			
Asn	Asp	Gln	Glu

Data from J. W. Tobias, T. E. Schrader, G. Rocap, and A. Varshavsky, *Science* 254(5036):1374–1377, 1991.

Why is the N-end rule only *apparently* simple? Sometimes the N-degron is exposed only after the protein is proteolytically cleaved. Such degrons are called *pre-N-degrons* or *pro-N-degrons*, in analogy to proenzymes (Section 7.4), because the protein must be cleaved to expose the signal. In other cases, the destabilizing amino acid is added to the protein after the protein is synthesized. Other modifications, notably N-terminal acetylation, can also activate a degron. Additional degrons thought to identify proteins for degradation include cyclin destruction boxes, which are amino acid sequences that mark cell-cycle proteins for destruction, and PEST sequences, which are rich in the amino acids proline (P, single-letter abbreviation), glutamic acid (E), serine (S), and threonine (T).

E3 enzymes are the readers of N-terminal residues. Although most eukaryotes have only one or a small number of distinct E1 enzymes, all eukaryotes have many distinct E2 enzymes and even more E3 enzymes. For example, in baker's yeast there is only one E1 but 10-12 E2 enzymes and 60-100 E3 enzymes. Indeed, the E3 family is one of the largest gene families in human beings, with over 600 predicted E3 ligases in the human genome. The diversity of target proteins that must be tagged for destruction requires a large number of E3 proteins as readers.



Three examples demonstrate the importance of E3 proteins to normal cell function. First, proteins that are not degraded because of a defective E3 may accumulate, causing a disease of protein aggregation such as juvenile or early-onset Parkinson's disease. Second, a defect in another member of the E3 family causes Angelman syndrome, a severe neurological disorder characterized by an unusually happy disposition, cognitive disability, absence of speech, uncoordinated movement, and hyperactivity. Fascinatingly, if the same ligase is overexpressed, the result is autism. Third, inappropriate protein turnover also can lead to cancer. For example, human papillomavirus (HPV) encodes a protein

that activates a specific E3 enzyme. The enzyme ubiquitinates the tumor suppressor p53 and other proteins that control DNA repair, which are then destroyed. The activation of this E3 enzyme is observed in more than 90% of cervical carcinomas. Thus, the inappropriate marking of key regulatory proteins for destruction can trigger further events, leading to tumor formation.

As noted above, the role of ubiquitin is much broader than merely marking proteins for destruction. Ubiquitination also regulates proteins involved in DNA repair, chromatin remodeling, innate immunity, membrane trafficking, and autophagy, among other biochemical processes.

The proteasome digests the ubiquitin-tagged proteins

If ubiquitin is the mark of death, what is the executioner? A large protease complex called the **proteasome** (more precisely, the *26S proteasome*) digests the ubiquitinated proteins. This ATP-driven multisubunit protease spares ubiquitin, which is then recycled. The 26S proteasome is a complex of two components: a 20S catalytic unit and a 19S regulatory unit.

The 20S unit is composed of 28 subunits, encoded by 14 genes, arranged into 4 heteroheptameric rings stacked to form a structure resembling a barrel (**Figure 23.5**). The outer two rings of the barrel are made up of α-type subunits and the inner two rings of β-type subunits. The 20S catalytic core is a sealed barrel. Access to its interior is controlled by a 19S regulatory unit, itself a 700-kDa complex made up of 19 subunits. Two such 19S complexes bind to the 20S proteasome core, one at each end, to form the complete 26S proteasome (**Figure 23.6**).

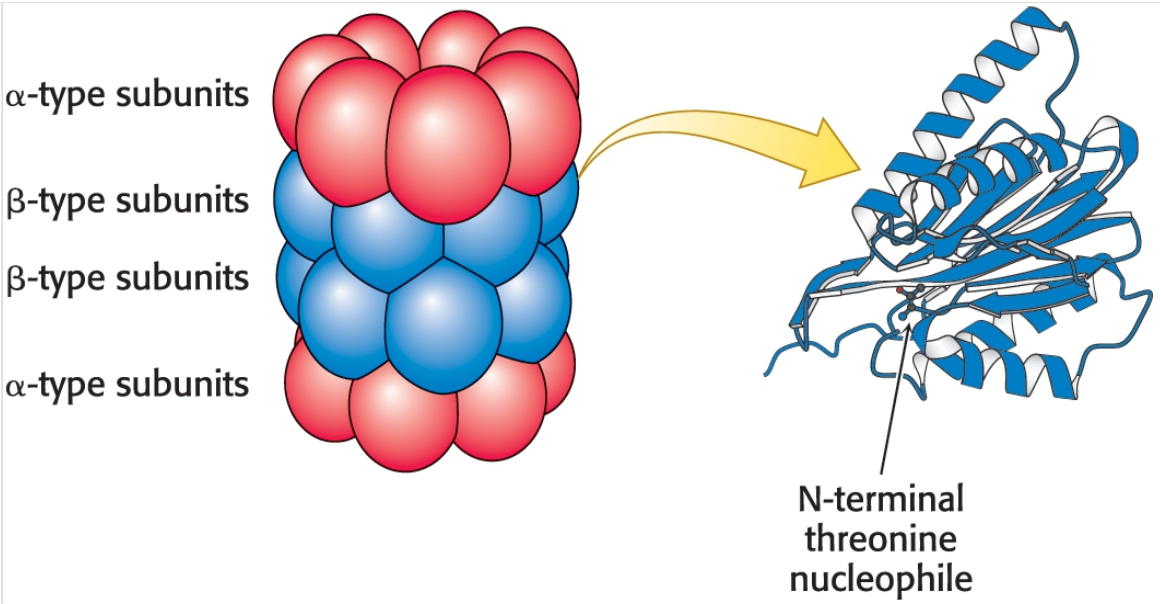


FIGURE 23.5 The 20S proteasome is barrel-shaped and made up of 28 homologous subunits. The subunits (α-type, red; β-type, blue) are arranged in four rings of 7 subunits each. Some of th β-type subunits (right) include protease active sites at their amino termini.

[Subunit drawn from 1RYP.pdb.]

INTERACT with this model in Achieve

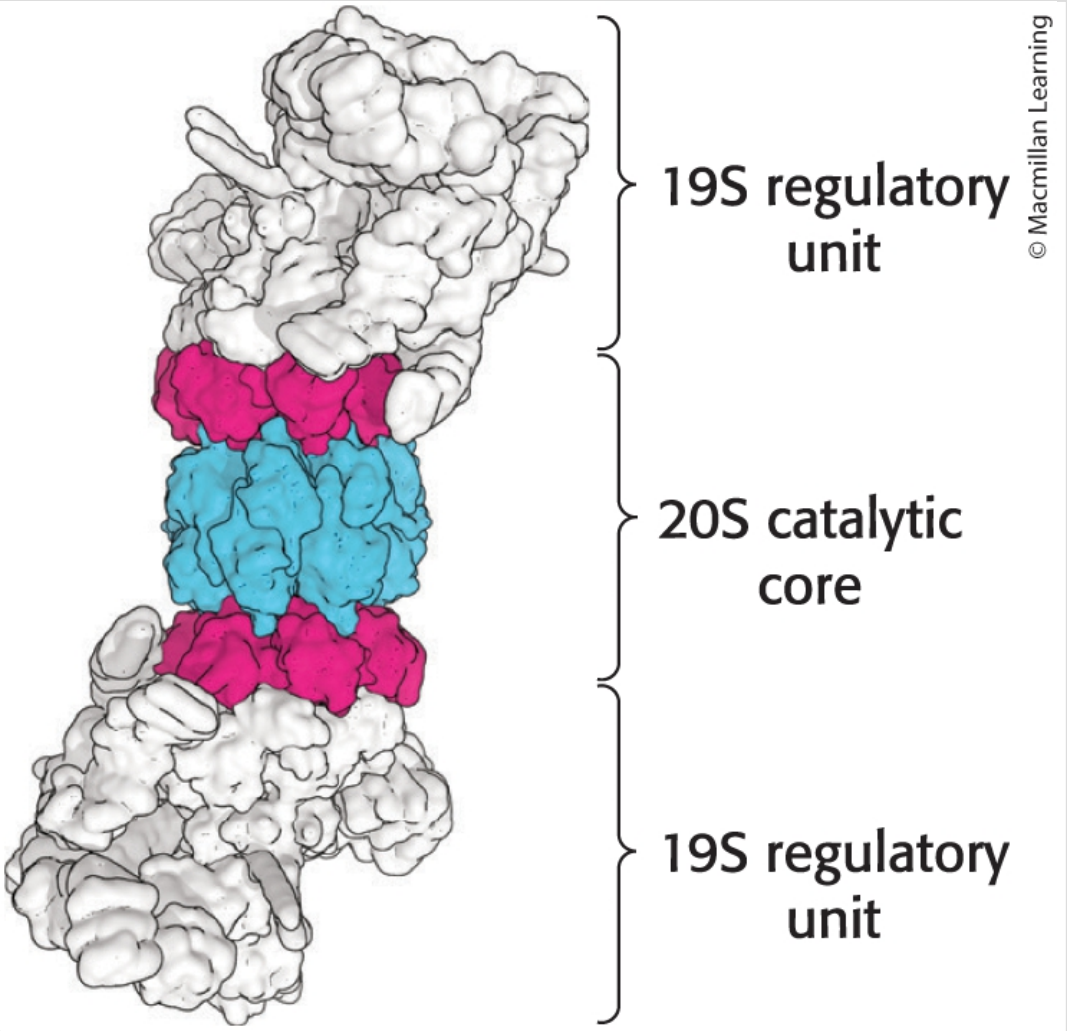


FIGURE 23.6 The 26S proteasome consists of one 20S and two 19S subunits. The 19S are regulatory and each attached at either end of the 20S catalytic unit.

The 19S regulatory unit has three functions. First, components of the 19S unit are ubiquitin receptors that bind specifically to polyubiquitin chains, thereby ensuring that only ubiquitinated proteins are degraded. Second, the doomed protein is unfolded and directed into the catalytic core. Finally, an isopeptidase in the 19S unit cleaves off intact ubiquitin molecules from the proteins so that they can be reused. Key components of the 19S complex are six ATPases of a type called the

AAA + class (ATPases associated with various cellular activities). ATP hydrolysis assists the 19S complex to unfold the substrate and induce conformational changes in the 20S catalytic core (called *gate opening*) so that the substrate can be passed into the center of the complex. Alternative ways to enter the 20S barrel have also been discovered. In some cases, partially unfolded proteins can themselves induce gate opening without the 19S, and there are alternative proteasome caps that also allow the degradation of unstructured proteins.

The proteolytic active sites are sequestered in the interior of the 20S barrel to protect potential substrates until they are directed into the barrel. There are three types of active sites in the β subunits, each with a different specificity, but all employ an N-terminal threonine. The hydroxyl group of the threonine residue is converted into a nucleophile that attacks the carbonyl groups of peptide bonds to form acyl-enzyme intermediates. Substrates are degraded in a processive manner without the release of degradation intermediates, until the substrate is digested to peptides ranging in length from seven to nine residues. These peptide products are released from the proteasome and further degraded by other cellular proteases to yield individual amino acids. Thus, the ubiquitination pathway and the proteasome cooperate to degrade unwanted proteins. **Figure 23.7** presents an overview of the fates of amino acids following proteasomal digestion. A separate process called *autophagy* serves as a second mechanism for protein turnover, although the details of that system are beyond the scope of this chapter.

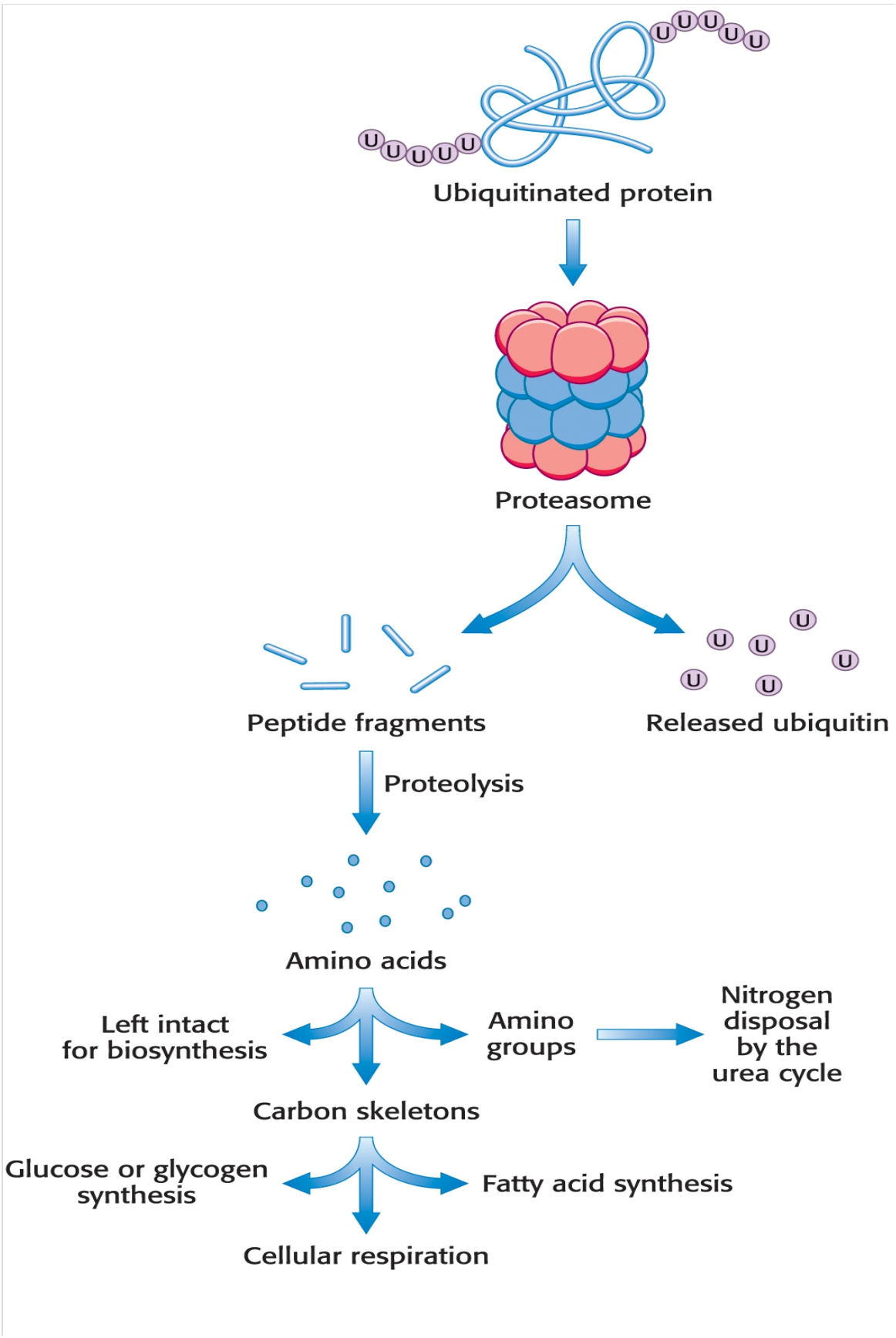

U
Ubiquitinated protein
Proteasome
Peptide fragments
Released ubiquitin
Proteolysis
Amino acids
Left intact for biosynthesis
Amino groups
Nitrogen disposal by the urea cycle
Carbon skeletons
Glucose or glycogen synthesis
Fatty acid synthesis
Cellular respiration

FIGURE 23.7 The proteasome and other proteases generate free amino acids. Ubiquitinated proteins are processed to peptide fragments. Ubiquitin is removed and recycled prior to protein degradation. The peptide fragments are further digested to yield free amino acids, which can be used for biosynthetic reactions, most notably protein synthesis. Alternatively, the amino group can be removed and processed to urea (Figure 23.15) and the carbon skeleton can be used to synthesize carbohydrate or fats or used directly as a fuel for cellular respiration (Section 23.5).



The ubiquitin pathway and the proteasome have prokaryotic counterparts

Both the ubiquitin pathway and the proteasome appear to be present in all eukaryotes. Homologs of the proteasome are also found in some prokaryotes. The proteasomes of some archaea are quite similar in overall structure to their eukaryotic counterparts and similarly have 28 subunits (**Figure 23.8**). In the archaeal proteasome, however, all α outer-ring subunits and all β inner-ring subunits are identical; in eukaryotes, each α or β subunit is one of seven different isoforms. This specialization provides distinct substrate specificity.

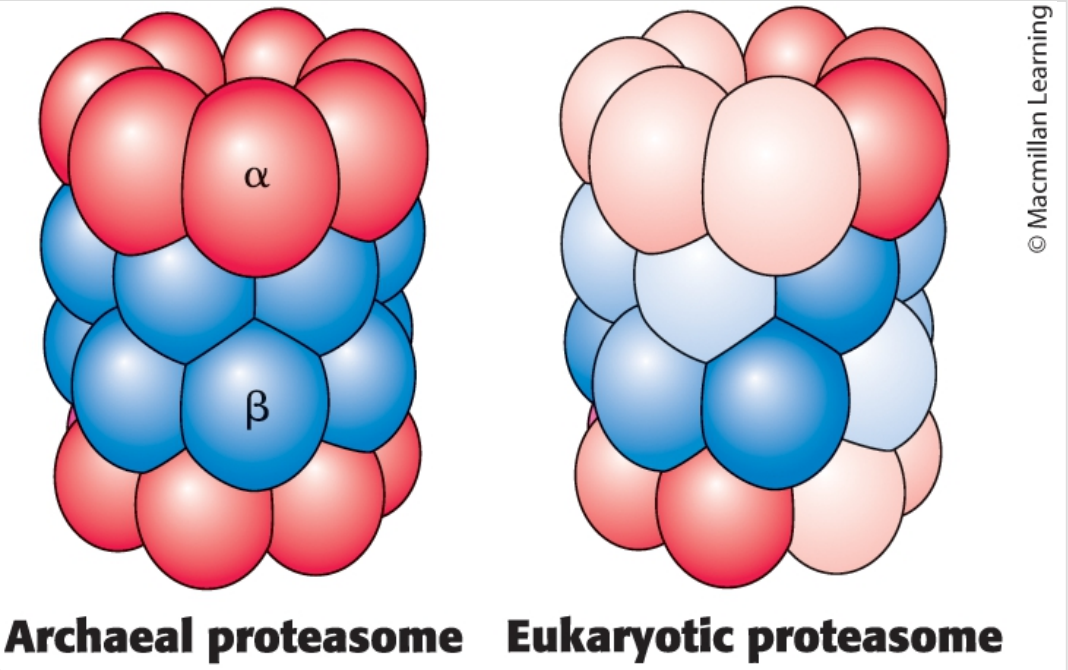


FIGURE 23.8 Proteasomes have become more complex in eukaryotes. The archaeal proteasome consists of 14 identical α subunits and 14 identical β subunits. In the eukaryotic proteasome, gene duplication and specialization has led to 7 distinct subunits of each type. The overall architecture of the proteasome is conserved.

Protein degradation can be used to regulate biological function

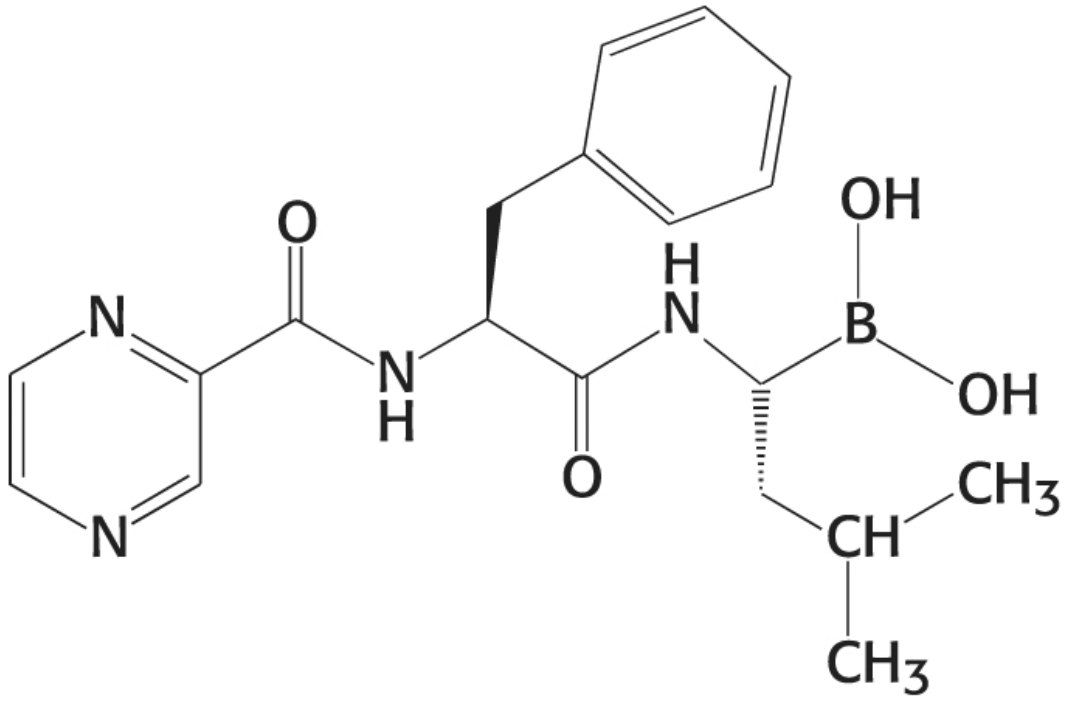
A number of physiological processes are controlled at least in part by protein degradation through the ubiquitin–proteasome pathway (Table 23.3). In each case, the proteins being degraded are regulatory proteins.

TABLE 23.3 Processes regulated by protein degradation

Gene transcription

Cell-cycle progression
Organ formation
Circadian rhythms
Inflammatory response
Tumor suppression
Cholesterol metabolism
Antigen processing

Consider, for example, control of the inflammatory response. A transcription factor, NF-κB (NF for nuclear factor), initiates the expression of a number of the genes that take part in this response. This factor is itself activated by the degradation of an attached inhibitory protein, I-κB (I for inhibitor). In response to inflammatory signals that bind to membrane-bound receptors, I-κB is phosphorylated at two serine residues, creating an E3 binding site. The binding of E3 leads to the ubiquitination and degradation of I-κB, unleashing NF-κB. The liberated transcription factor migrates from the cytoplasm to the nucleus to stimulate the transcription of the target genes. The NF-κB–I-κB system illustrates the interplay of several key regulatory motifs: receptor-mediated signal transduction, phosphorylation, compartmentalization, controlled and specific degradation, and selective gene expression. The importance of the ubiquitin–proteasome system for the regulation of gene expression is highlighted by the use of bortezomib (Velcade), a potent inhibitor of the proteasome, as a therapy for multiple myeloma. Bortezomib is a dipeptidyl boronic acid inhibitor of the proteasome.



Bortezomib
(a dipeptidyl boronic acid)

Degrons are also used as regulatory mechanisms for protein expression. For example, degradation signals are commonly located in protein regions that also facilitate protein–protein interactions. Why might the coexistence of these two functions in the same region be useful? Exposure of such a region to solvent, and therefore to the binding of E3 enzyme, suggests that a component of a multiprotein complex has failed to form properly or that one component has been synthesized in excess. This exposure leads to rapid degradation and the restoration of appropriate stoichiometries.

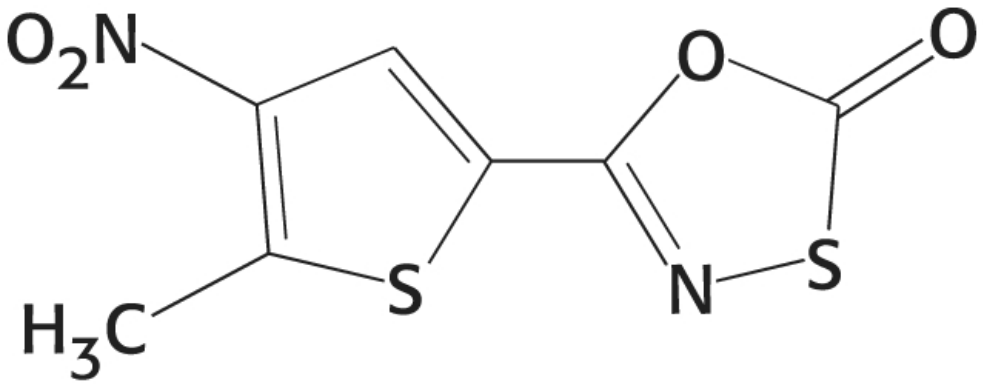


Keith Weller/Johns Hopkins Medicine

CECILE PICKART The observation that some protein degradation processes required ATP hydrolysis suggested that a novel enzymatic system was at work. Several research teams set to work to characterize this system, one of which included Dr. Cecile Pickart. Dr. Pickart had completed her PhD at Brandeis University, working with a leading enzymologist. As a postdoctoral fellow, she worked with Dr. Irwin Rose at Fox Chase Cancer, where she helped characterize the ubiquitin-based protein degradation system. She was so sure-footed that several of her colleagues agreed with the statement by another that she "described the enzymes to the world as though she had obtained the answer sheet." Later, as an independent researcher at SUNY-Buffalo and then Johns Hopkins, she focused completely on various aspects of ubiquitin biochemistry. She was an outstanding mentor to students, both in her own laboratory and throughout the university, helping students through challenges in their research, with deep insights and attention to even seemingly minor details. It was fitting that Dr. Rose and two colleagues shared the Nobel Prize in 2004 based, in

part, on her research. The field of biochemistry lost a great scientist with her untimely death in 2006 at the age of 51.

The evolutionary studies of proteasomes described previously have also yielded potential clinical benefits. The bacterial pathogen *Mycobacterium tuberculosis*, the cause of tuberculosis, harbors a proteasome that is very similar to the human counterpart. Nevertheless, recent work has shown that it is possible to exploit the differences between the human and the bacterial proteasomes to develop specific inhibitors of the *M. tuberculosis* complex. Oxathiazol-2-one compounds such as HT1171 are suicide inhibitors (Section 5.6) of the proteolytic activity of the *M. tuberculosis* proteasome, but have no effect on the proteasomes of the human host. This is especially exciting because these drugs kill the nonreplicating form of *M. tuberculosis*, and thus may not require the prolonged treatment required with conventional drugs, thereby reducing the likelihood of drug resistance due to interruption of the treatment regime.



HT1171
5-(2-methyl-3-nitrothiophen-2-yl)-1,3,4-oxathiazol-2-one

Self-Check Question



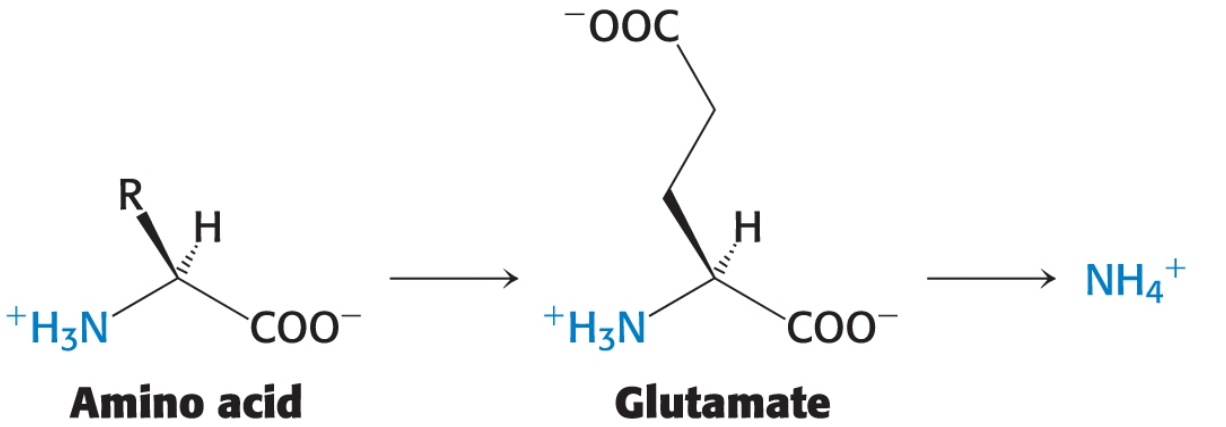
Degrons are often found in parts of proteins that facilitate protein complex formation. Explain why this might be useful.

23.3 The First Step in Amino Acid Degradation Is the Removal of Nitrogen

What is the fate of amino acids released on protein digestion or turnover? The first call is for their use as building blocks for biosynthetic reactions. However, any amino acids not needed as building blocks are degraded to compounds able to enter the metabolic mainstream. The amino group is first removed, and then the remaining carbon skeleton is metabolized to a glycolytic intermediate, to one of several citric acid cycle intermediates, or to acetyl CoA. The major site of amino acid degradation in mammals is the liver, although muscles also readily degrade the branched-chain amino acids (Leu, Ile, and Val). The fate of the α-amino group will be considered first, followed by that of the carbon skeleton (Section 23.5).

Alpha-amino groups are converted into ammonium ions by the oxidative deamination of glutamate in the liver

The α-amino group of many amino acids is transferred to α-ketoglutarate to form glutamate, which is then oxidatively deaminated in the liver to yield ammonium ion (NH_4^+).



[Aminotransferases] (also called **transaminases**) catalyze the transfer of an α-amino group from an α-amino acid to an α-ketoacid.



Aminotransferases generally funnel α-amino groups from a variety of amino acids to α-ketoglutarate for conversion into NH_4^+. Aspartate aminotransferase, one of the most important of these enzymes, catalyzes the transfer of the amino group of aspartate to α-ketoglutarate.

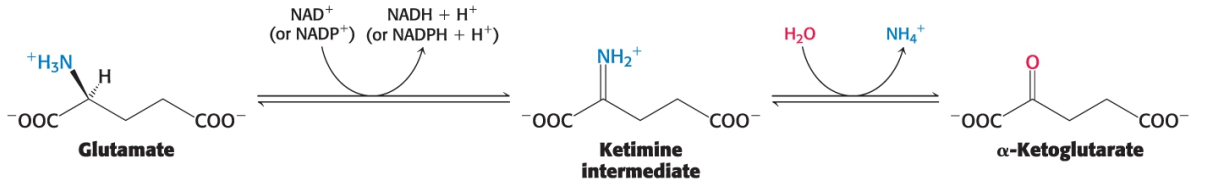
$$\text{Aspartate} + \alpha\text{-ketoglutarate} \rightleftharpoons \text{oxaloacetate} + \text{glutamate}$$

Alanine aminotransferase catalyzes the transfer of the amino group of alanine to α-ketoglutarate.

$$\text{Alanine} + \alpha\text{-ketoglutarate} \rightleftharpoons \text{pyruvate} + \text{glutamate}$$

Transamination reactions are reversible and can thus be used to synthesize amino acids from α-ketoacids, as we shall see in Section 25.2

The nitrogen atom in glutamate is converted into free ammonium ion by oxidative deamination, a reaction catalyzed by **glutamate dehydrogenase**. This enzyme is unusual in being able to utilize either NAD^+ or $NADP^+$, at least in some species. The reaction proceeds by dehydrogenation of the $C-N$ bond, followed by hydrolysis of the resulting ketimine.



This reaction equilibrium constant is close to 1 in the liver, so the direction of the reaction is determined by the concentrations of reactants and products. Normally, the reaction is driven forward by the rapid removal of ammonium ion. Ammonium ions are toxic, and particularly detrimental to the brain, so ammonium is formed only in large amounts in the liver, where it is immediately eliminated by its conversion to urea. Thus, glutamate dehydrogenase is essentially a liver-specific enzyme. To further prevent the release of free ammonium, glutamate dehydrogenase is located in mitochondria along with some of the other enzymes required for the production of urea.

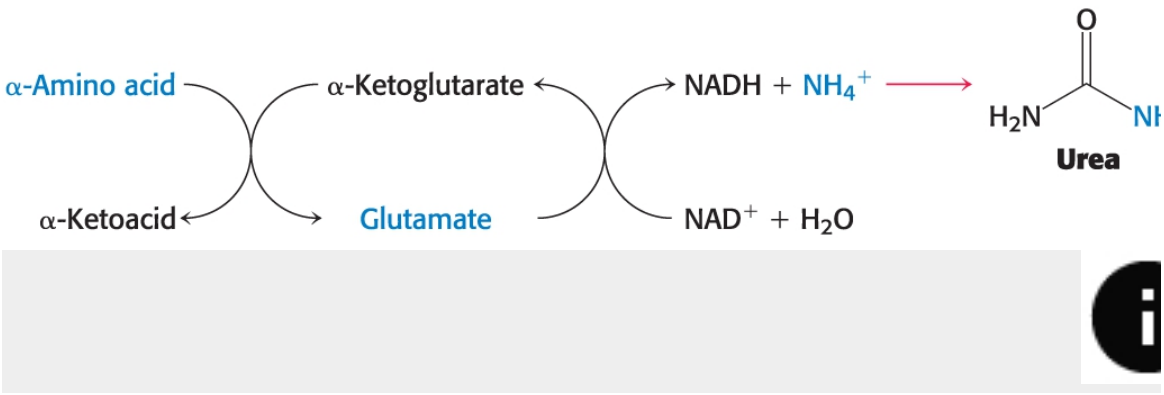
In mammals, but not in other organisms, glutamate dehydrogenase is allosterically inhibited by GTP and stimulated by ADP. These nucleotides exert their regulatory effects in a unique manner: an

abortive complex, a set of molecules bound to the enzyme that cannot move forward toward the final products, is formed when a product is replaced by substrate in the active site before the reaction is complete. For instance, the enzyme bound to glutamate and NAD(P)H is an abortive complex. GTP facilitates the formation of such complexes while ADP destabilizes them.

The sum of the reactions catalyzed by aminotransferases and glutamate dehydrogenase is

$$\alpha\text{-Amino acid} + \underset{(\text{or } NADP^+)}{NAD^+} + H_2O \rightleftharpoons \alpha\text{-ketoacid} + NH_4^+ + \underset{(\text{or } NADPH)}{NADH} + H^+$$

In most terrestrial vertebrates, NH_4^+ is converted into urea, which is excreted.

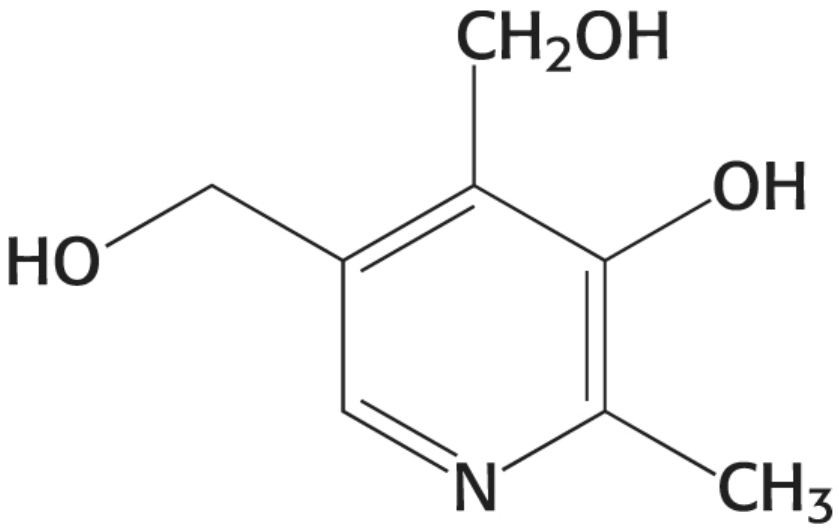


Self-Check Question

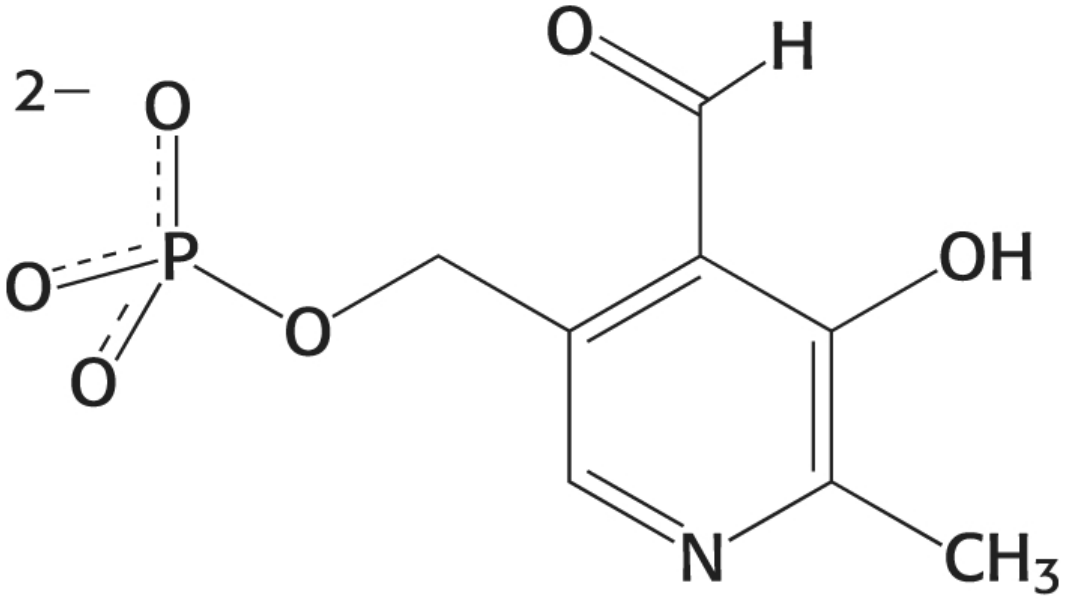
How do aminotransferases and glutamate dehydrogenase cooperate in the metabolism of the amino group of amino acids?

Mechanism: Pyridoxal phosphate forms Schiff-base intermediates in aminotransferases

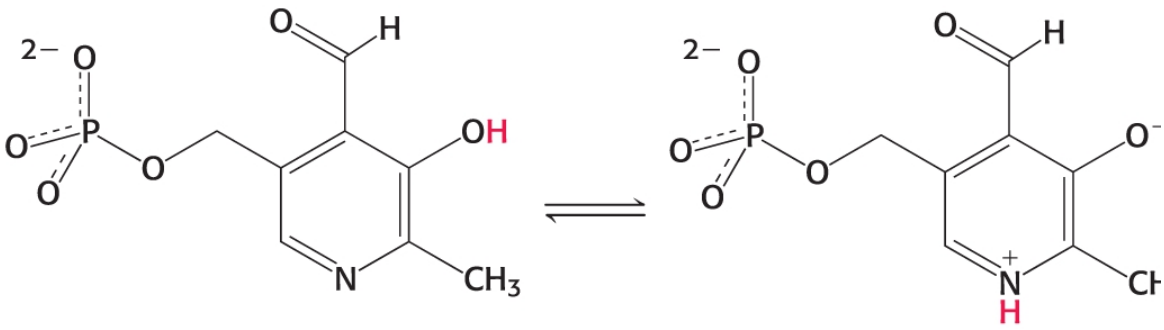
All aminotransferases contain the prosthetic group **pyridoxal phosphate (PLP)**, which is derived from pyridoxine (vitamin B_6). Pyridoxal phosphate includes a slightly basic pyridine ring to which a slightly acidic OH group is attached. Thus, pyridoxal phosphate derivatives can form a stable tautomeric form in which the pyridine nitrogen atom is protonated (hence, positively charged), while the OH group loses a proton and hence is negatively charged, forming a phenolate.



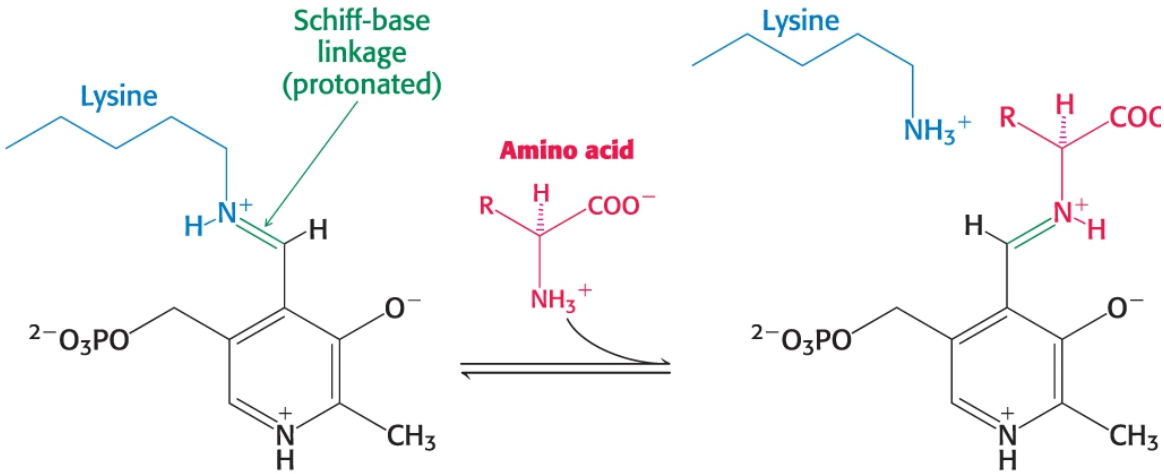
Pyridoxine
(vitamin B_6)



Pyridoxal phosphate
(PLP)



The most important functional group on PLP is the aldehyde. This group forms covalent Schiff-base intermediates with amino acid substrates. Indeed, even in the absence of substrate, the aldehyde group of PLP usually forms a Schiff-base linkage with the ε-amino group of a specific lysine residue at the enzyme's active site. A new Schiff-base linkage is formed on addition of an amino acid substrate.



The α-amino group of the amino acid substrate displaces the ε-amino group of the active-site lysine residue. In other words, an *internal* aldimine becomes an *external* aldimine. The amino acid–PLP Schiff base that is formed remains tightly bound to the enzyme by multiple noncovalent interactions. The Schiff-base linkage often accepts a proton at the nitrogen of the pyridine ring, with the positive charge stabilized by interaction with the negatively charged phenolate group of PLP.

The Schiff base between the amino acid substrate and PLP, the external aldimine, loses a proton from the α-carbon atom of the amino acid to form a quinonoid intermediate (**Figure 23.9**). Reprotonation of this intermediate at the aldehyde carbon atom yields a ketimine, which is then hydrolyzed to an α-ketoacid and pyridoxamine phosphate (PMP). These steps constitute half of the transamination reaction.

$$\text{Amino acid}_1 + \text{E-PLP} \rightleftharpoons \alpha\text{-ketoacid}_1 + \text{E-PMP}$$

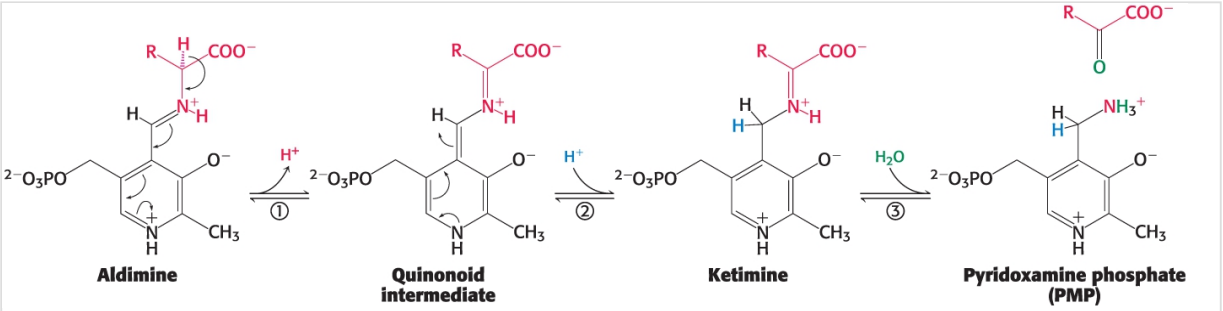
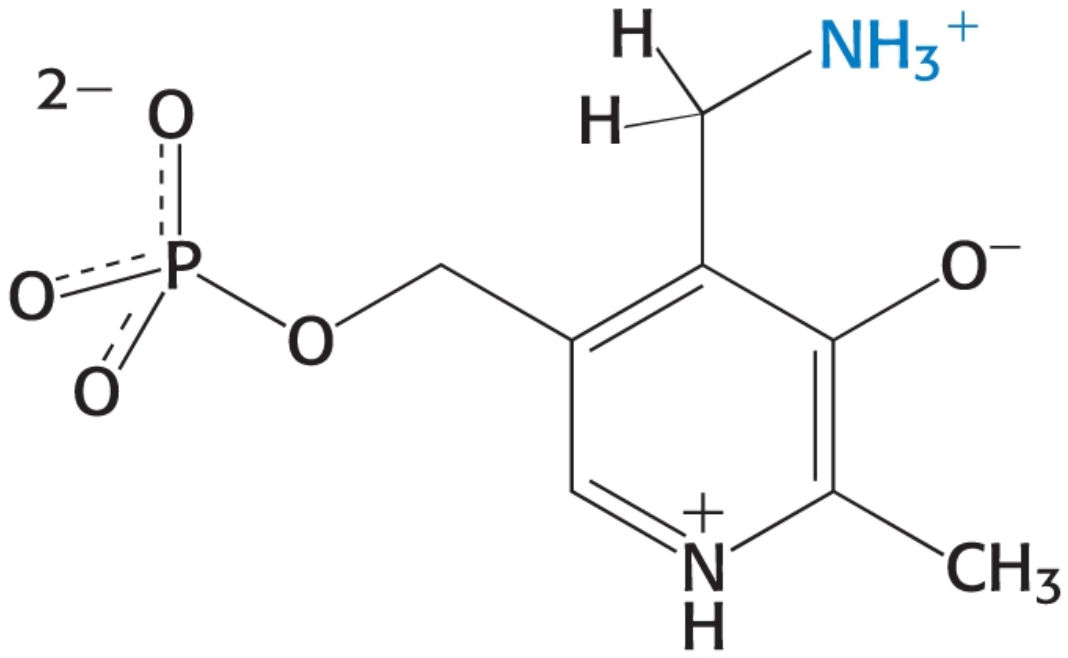


FIGURE 23.9 Transaminations proceed through three steps to form PMP. (1) The external aldimine loses a proton to form a quinonoid intermediate. (2) Reprotonation of this intermediate at the aldehyde carbon atom yields a ketimine. (3) This intermediate is hydrolyzed to generate the α-ketoacid product and pyridoxamine phosphate.



Pyridoxamine phosphate (PMP)

The second half takes place by the reverse of the preceding pathway. A second α-ketoacid reacts with the enzyme–pyridoxamine phosphate complex (E-PMP) to yield a second amino acid and regenerate the enzyme–pyridoxal phosphate complex (E-PLP).

$$\alpha\text{-Ketoacid}_2 + \text{E-PMP} \rightleftharpoons \text{amino acid}_2 + \text{E-PLP}$$

The sum of these partial reactions is

$$\text{Amino acid}_1 + \alpha\text{-ketoacid}_2 \rightleftharpoons \text{amino acid}_2 + \alpha\text{-ketoacid}_1$$

Aspartate aminotransferase is an archetypal pyridoxal-dependent transaminase

The mitochondrial enzyme aspartate aminotransferase provides an especially well-studied example of PLP as a coenzyme for transamination reactions. X-ray crystallographic studies have provided detailed views of how PLP and substrates are bound, confirming much of the proposed catalytic mechanism. Each of the identical 45-kDa subunits of this dimer consists of a large domain and a small one (**Figure 23.10**). PLP is bound to the large domain, in a pocket near the domain interface. In the absence of substrate, the aldehyde group of PLP is in a Schiff-base linkage with lysine 258, as expected. Adjacent to the coenzyme's binding site is a conserved arginine residue that interacts with the α-carboxylate group of the amino acid substrate, helping to orient the substrate appropriately in the active site. A base is necessary to remove a proton from the α-carbon group of the amino acid and to transfer it to the aldehyde carbon atom of PLP (Figure 23.9, steps 1 and 2). The lysine amino group that was initially in Schiff-base linkage with PLP appears to serve as the proton donor and acceptor.

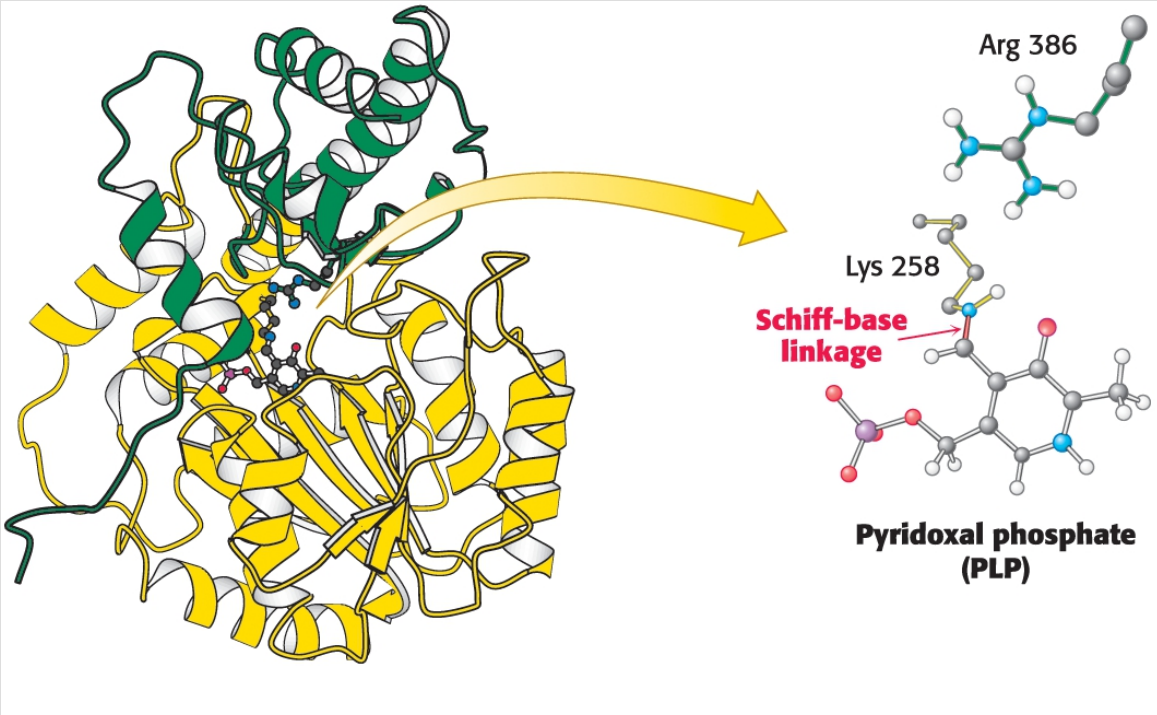


FIGURE 23.10 The active site of aspartate aminotransferase reveals PLP bound to a lysine through a Schiff-base linkage. Aspartate aminotransferase, a prototypical PLP-dependent enzyme, includes pyridoxal phosphate attached to the enzyme by a Schiff-base linkage with lysine 258. An arginine residue in the active site helps orient substrates by binding to their α-carboxylate groups. Only one of the enzyme's two subunits is shown.

[Drawn from 1AAW.pdb.]

INTERACT with this model in Achieve

Blood levels of aminotransferases serve a diagnostic function

The presence of alanine and aspartate aminotransferase in the blood is an indication of liver damage. Liver damage can occur for a number of reasons, including viral hepatitis, long-term excessive alcohol consumption, and reaction to drugs such as acetaminophen (Section 32.3). Under these conditions, liver cell membranes are damaged, and some cellular proteins — including the aminotransferases — leak into the blood. Normal blood values for alanine and aspartate aminotransferase activity are 5–30 units/l and 40–125 units/l, respectively. Depending on the extent of liver damage, the values will reach 200–300 units/l.

Pyridoxal phosphate enzymes catalyze a wide array of reactions

Transamination is just one of a wide range of amino acid transformations that are catalyzed by PLP enzymes. The other reactions catalyzed by PLP enzymes at the α-carbon atom of amino acids are decarboxylations, deaminations, racemizations, and aldol cleavages (Figure 23.11). In addition, PLP enzymes catalyze elimination and replacement reactions at the β-carbon atom (e.g., tryptophan synthetase in the synthesis of tryptophan) and the γ-carbon atom (e.g., cystathionine β-synthase in the synthesis of cysteine) of amino acid substrates. Three common features of PLP catalysis underlie these diverse reactions.

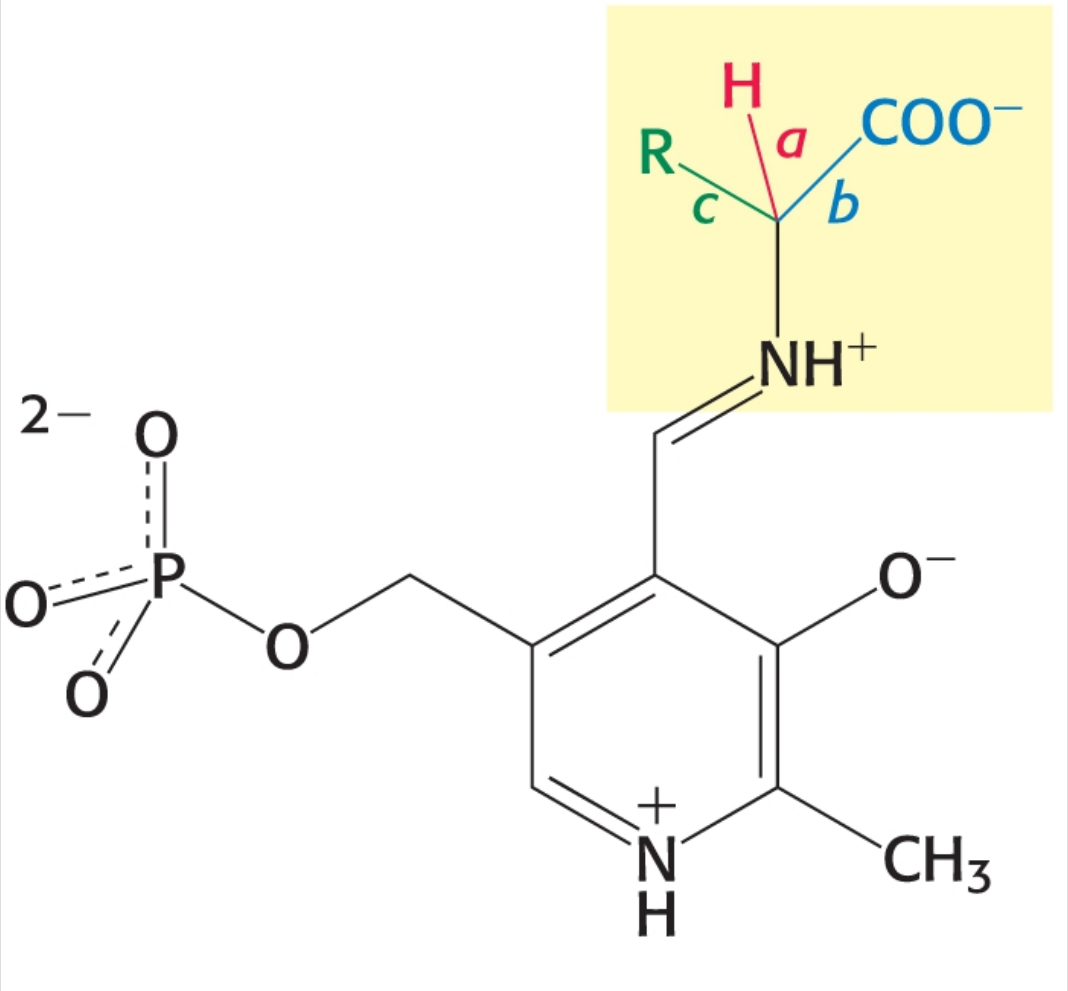


FIGURE 23.11 PLP enzymes labilize one of three bonds at the α-carbon atom of an amino acid substrate. For example, bond *a* is labilized by aminotransferases, bond *b* by decarboxylases, and bond *c* by aldolases (such as threonine aldolases). PLP enzymes also catalyze reactions at the β- and γ-carbon atoms of amino acids.

1. A Schiff base is formed by the amino acid substrate (the amine component) and PLP (the carbonyl component).
2. The protonated form of PLP acts as an electron sink to stabilize catalytic intermediates that are negatively charged. Electrons from these intermediates are attracted to the positive charge on the ring nitrogen atom.
3. The product Schiff base is cleaved at the completion of the reaction.

How does an enzyme selectively break a particular one of three bonds at the α-carbon atom of an amino acid substrate? An important principle is that the bond being broken must be perpendicular to the π bonds of the electron sink (Figure 23.12).

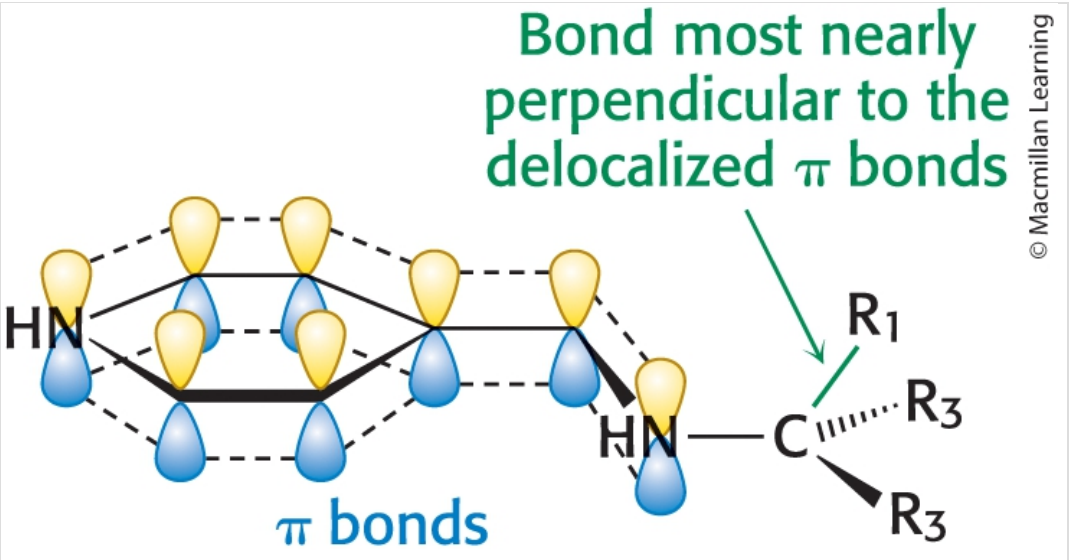


FIGURE 23.12 Stereoelectronic effects determine specific bond cleavage. The orientation about the $N-C_{\alpha}$ bond determines the most favored reaction

catalyzed by a pyridoxal phosphate enzyme. The bond that is most nearly perpendicular to the plane of delocalized π bonds (represented by dashed lines) of the pyridoxal phosphate electron sink is most easily cleaved.



An aminotransferase, for example, binds the amino acid substrate so that the $C_\alpha - H$ bond is perpendicular to the PLP ring (**Figure 23.13**). In serine hydroxymethyltransferase, the enzyme that converts serine into glycine, the $N - C_\alpha$ bond is rotated so that the $C_\alpha - C_\beta$ bond is most nearly perpendicular to the plane of the PLP ring, favoring its cleavage. This means of choosing one of several possible catalytic outcomes is called *stereoelectronic control*.

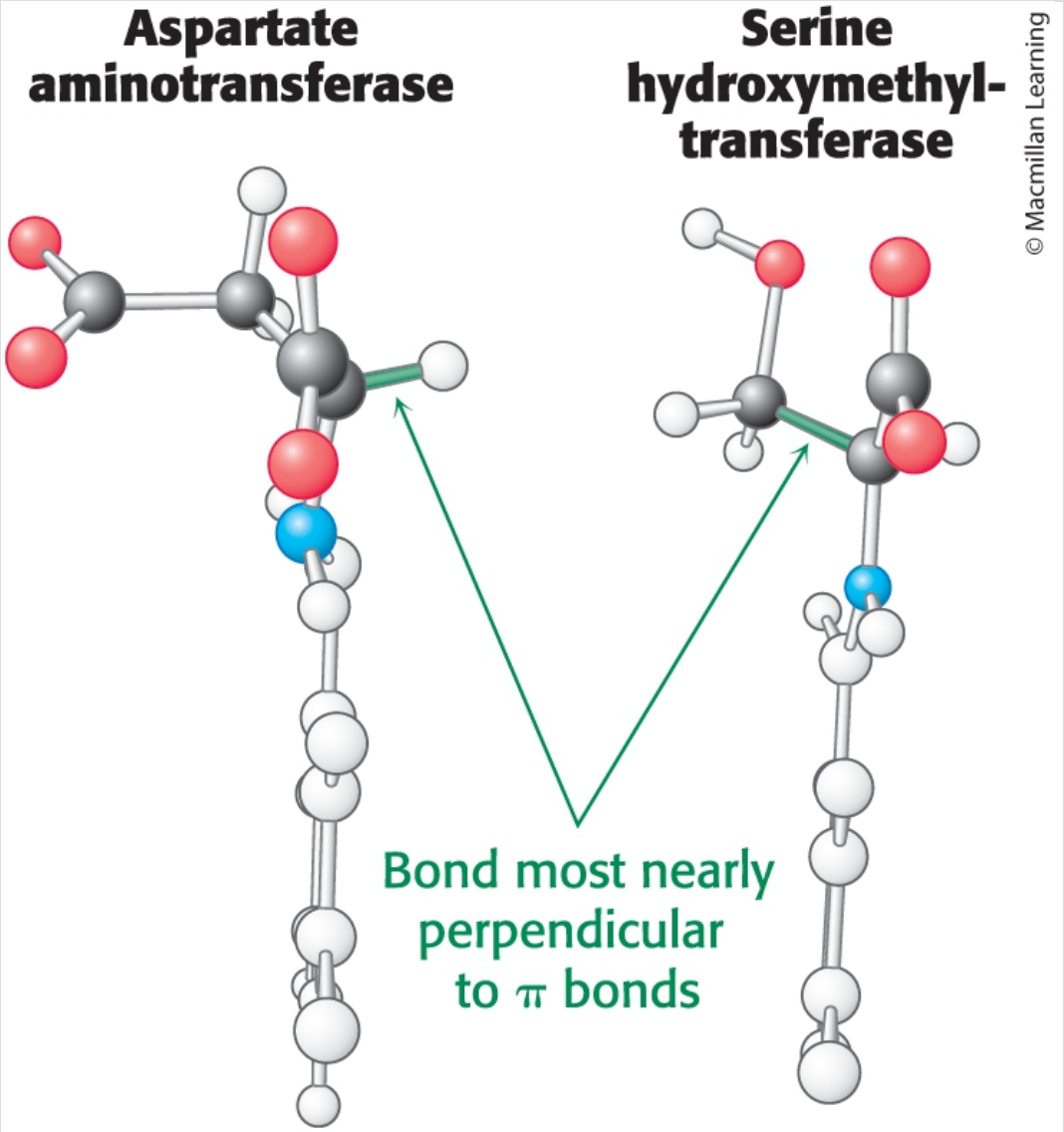


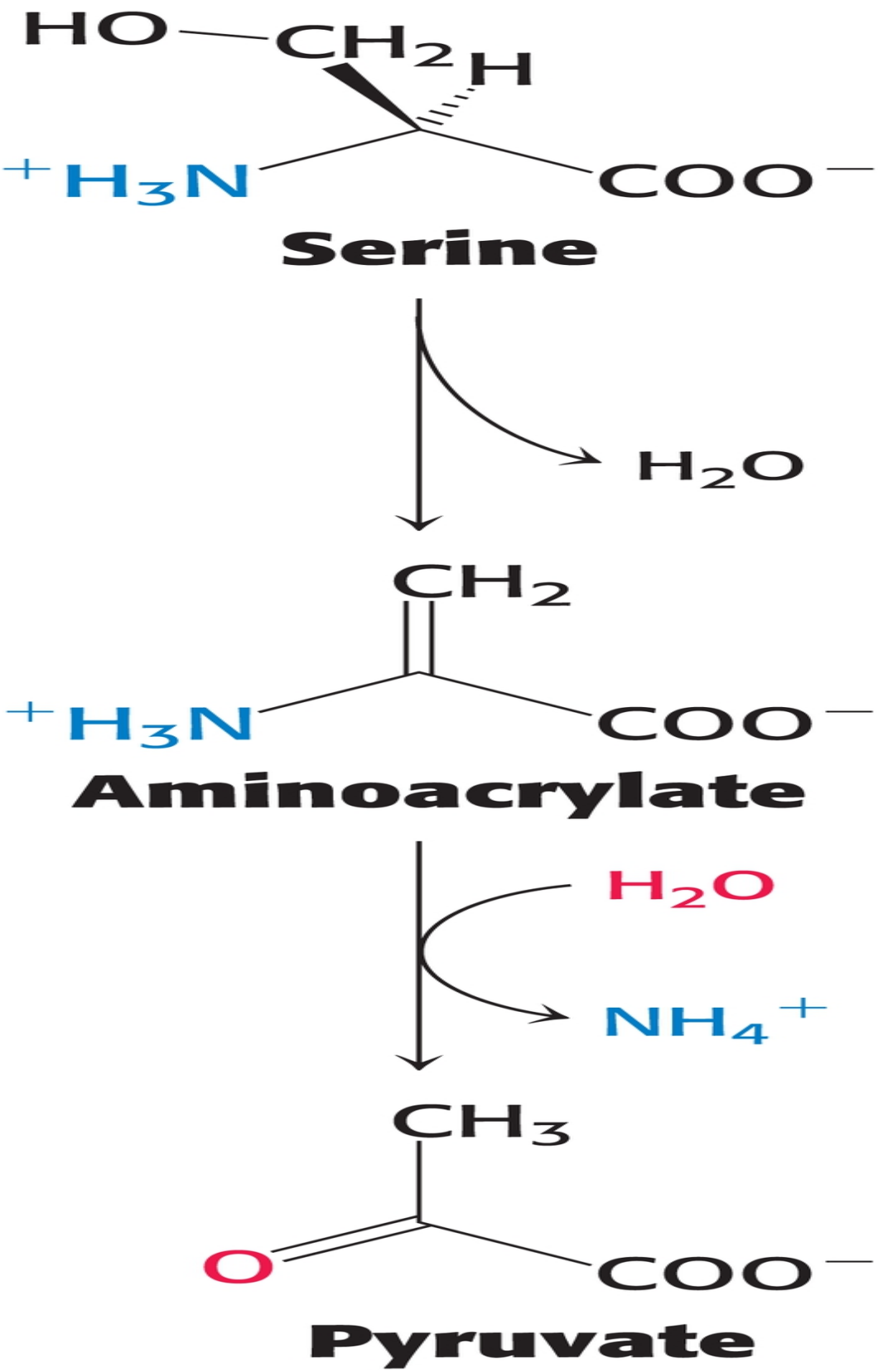
FIGURE 23.13 Bond orientation in the active site determines bond cleavage in different PLP enzymes. In aspartate aminotransferase, the $C_\alpha - H$ bond is most nearly perpendicular to the π-bond system and is cleaved. In serine hydroxymethyltransferase, a small rotation about the $N - C_\alpha$ bond places the $C_\alpha - C_\beta$ bond perpendicular to the π system, favoring its cleavage.

Serine and threonine can be directly deaminated

The α-amino groups of serine and threonine can be directly converted into NH_4^+ without first being transferred to α-ketoglutarate. These direct deaminations are catalyzed by serine dehydratase and threonine dehydratase, in which PLP is the prosthetic group.

$$\text{Serine} \rightarrow \text{pyruvate} + NH_4^+$$

$$\text{Threonine} \rightarrow \alpha\text{-ketobutyrate} + NH_4^+$$


HO
CH2
H
+H3N
COO−
Serine
H2O
CH2
+H3N
COO−
Aminoacrylate
H2O
NH4+
CH3
O
COO−
Pyruvate



These enzymes are called *dehydratases* because dehydration precedes deamination. Serine loses a hydrogen ion from its α-carbon atom and a hydroxide ion group from its β-carbon atom to yield aminoacrylate. This unstable compound reacts with H_2O to give pyruvate and NH_4^+. Thus, the presence of a hydroxyl group attached to the β-carbon atom in each of these amino acids permits the direct deamination.

Peripheral tissues transport nitrogen to the liver

Although most amino acid degradation takes place in the liver, other tissues can degrade amino acids. For instance, muscle uses branched-chain amino acids as a source of fuel during prolonged exercise and fasting. How is the nitrogen processed in these other tissues? As in the liver, the first step is the removal of the nitrogen from the amino acid. However, muscle lacks the enzymes of the urea cycle, and so the nitrogen must be released in a nontoxic form that can be absorbed by the liver and converted into urea.

Nitrogen is transported from muscle to the liver in two principal transport forms: alanine and glutamine. To form alanine, first, glutamate is formed by transamination reactions, but the nitrogen is then transferred to pyruvate. Alanine is then released into the blood (**Figure 23.14**). The liver takes up the alanine and, by transamination, converts it back into pyruvate that can be used for gluconeogenesis; the amino group eventually appears as urea. This transport is referred to as the **glucose–alanine cycle**. It is reminiscent of the Cori cycle discussed earlier (Figure 16.36). However, in contrast with the Cori cycle, pyruvate is not reduced to lactate by NADH, and thus more high-energy electrons

are conserved for oxidative phosphorylation in the muscle by using alanine.

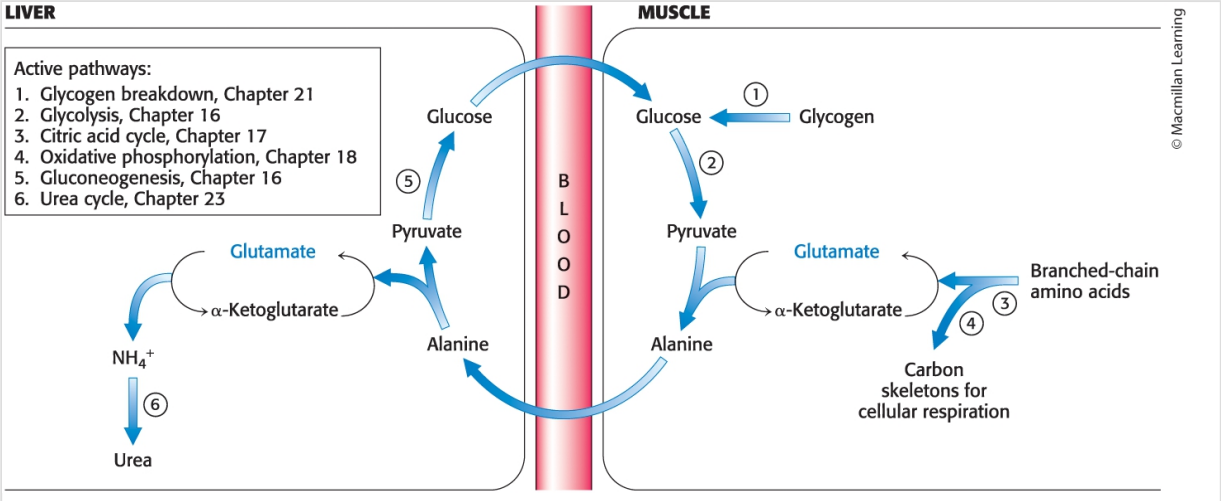


FIGURE 23.14 PATHWAY INTEGRATION: The glucose–alanine cycle allows muscle cells to use amino acids as fuel. During prolonged exercise and fasting, muscle uses branched-chain amino acids as fuel. The nitrogen removed is transferred (through glutamate) to alanine, which is released into the blood stream. In the liver, alanine is taken up and converted into pyruvate for the subsequent synthesis of glucose.

EXPLORE this pathway further in the Metabolic Map in Achieve

Glutamine is also a key transport form of nitrogen. Glutamine synthetase catalyzes the synthesis of glutamine from glutamate and NH_4^+ in an ATP-dependent reaction:

$$NH_4^+ + \text{glutamate} + ATP \xrightarrow{\text{Glutamine synthetase}} \text{glutamine} + ADP + P_i$$

The nitrogens of glutamine can be eliminated by incorporation into urea in the liver.

Self-Check Question



What amino acids can be deaminated directly to produce ammonium without the use of glutamate dehydrogenase, and what structural feature makes this possible?

23.4 Ammonium Ions Are Converted into Urea in Most Terrestrial Vertebrates

Some of the NH_4^+ formed in the breakdown of amino acids is consumed in the biosynthesis of nitrogen compounds. What happens to the rest of it? In most terrestrial vertebrates, the excess NH_4^+ is converted into urea and then excreted. Such organisms are referred to as *ureotelic*.

In terrestrial vertebrates, urea is synthesized by the **urea cycle** (**Figure 23.15**). One of the nitrogen atoms of urea is transferred from an amino acid, aspartate. The other nitrogen atom is derived directly from free NH_4^+, and the carbon atom comes from HCO_3^- (derived by the hydration of CO_2 through the action of carbonic anhydrase).

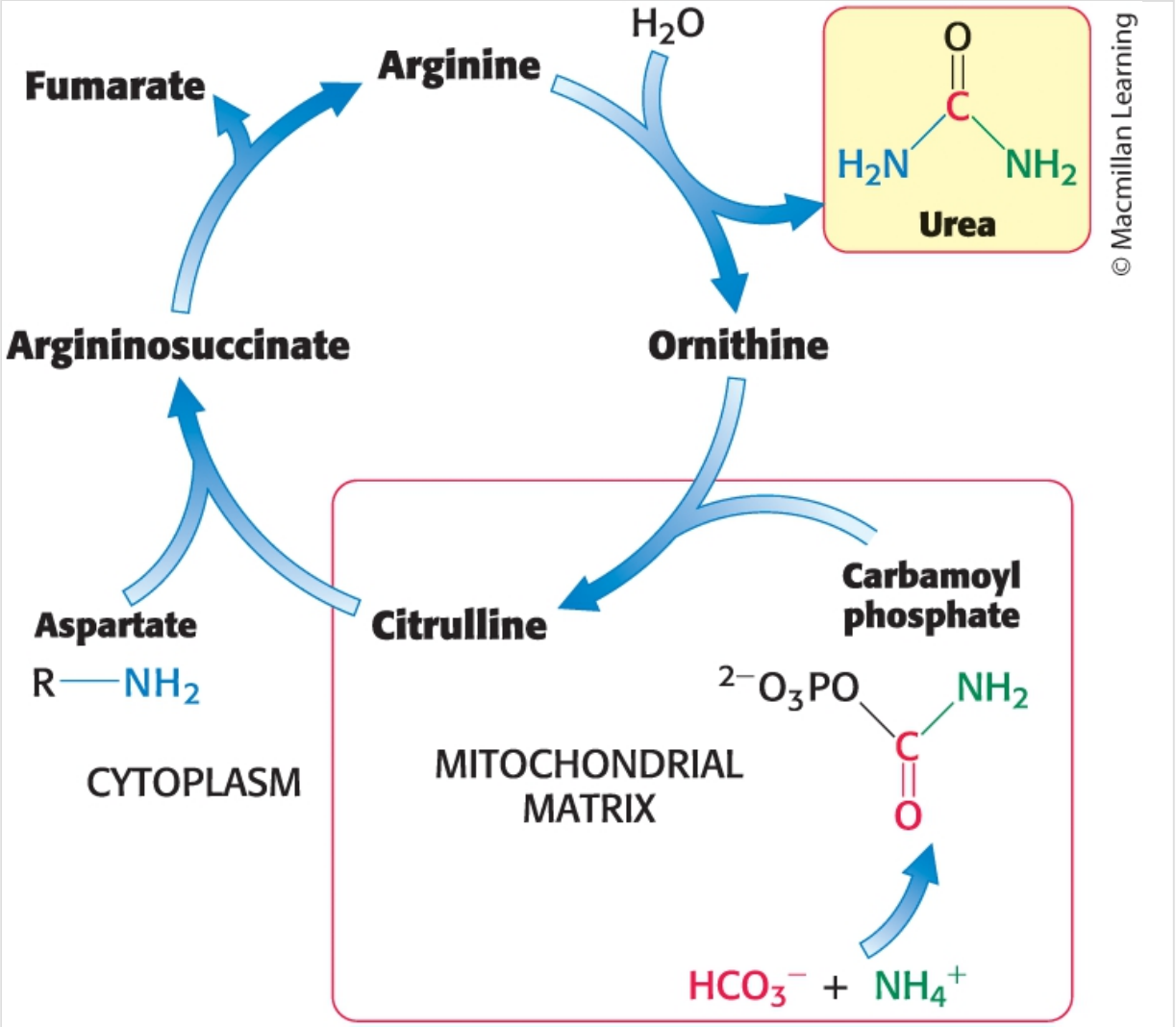


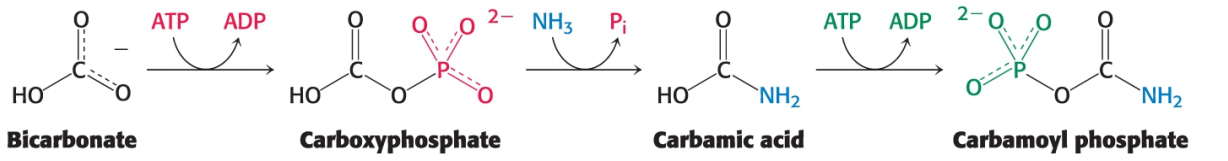
FIGURE 23.15 The urea cycle eliminates both nitrogen and carbon waste products. Two nitrogen atoms enter the cycle and leave as urea. Carbon dioxide is simultaneously eliminated as it is hydrated to bicarbonate, which then enters the cycle.

EXPLORE this pathway further in the Metabolic Map in Achieve

The urea cycle begins with the formation of carbamoyl phosphate

The urea cycle begins with the coupling of free NH_3 with HCO_3^- to form carbamoyl phosphate; this is the committed reaction of the urea cycle, which is catalyzed by **carbamoyl phosphate synthetase I**. In mammals, two distinct isozymes of carbamoyl phosphate synthetase are present. Carbamoyl phosphate synthetase I generates carbamoyl phosphate for both the urea cycle and the first step in pyrimidine biosynthesis (Section 26.1). Carbamoyl phosphate synthetase II is active in other steps of pyrimidine biosynthesis.

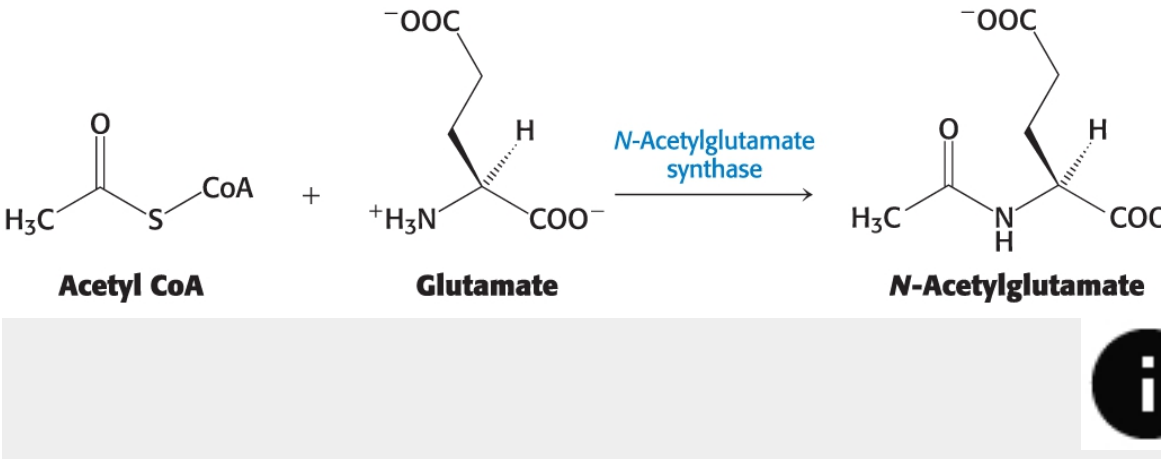
Carbamoyl phosphate is a simple molecule, but its synthesis is complex, requiring three steps.



Note that NH_3, because it is a base, normally exists as NH_4^+ in aqueous solution. However, carbamoyl phosphate synthetase I uses only NH_3 as a substrate. The reaction begins with the phosphorylation of HCO_3^- to form carboxyphosphate, which then reacts with NH_3 to form carbamic acid. Finally, a second molecule of ATP phosphorylates carbamic acid to form carbamoyl phosphate. The structure and mechanism of the enzyme that catalyzes these reactions will be presented in Chapter 26. The consumption of two molecules of ATP makes this synthesis of carbamoyl phosphate essentially irreversible.

Carbamoyl phosphate synthetase I is the key regulatory enzyme for urea synthesis

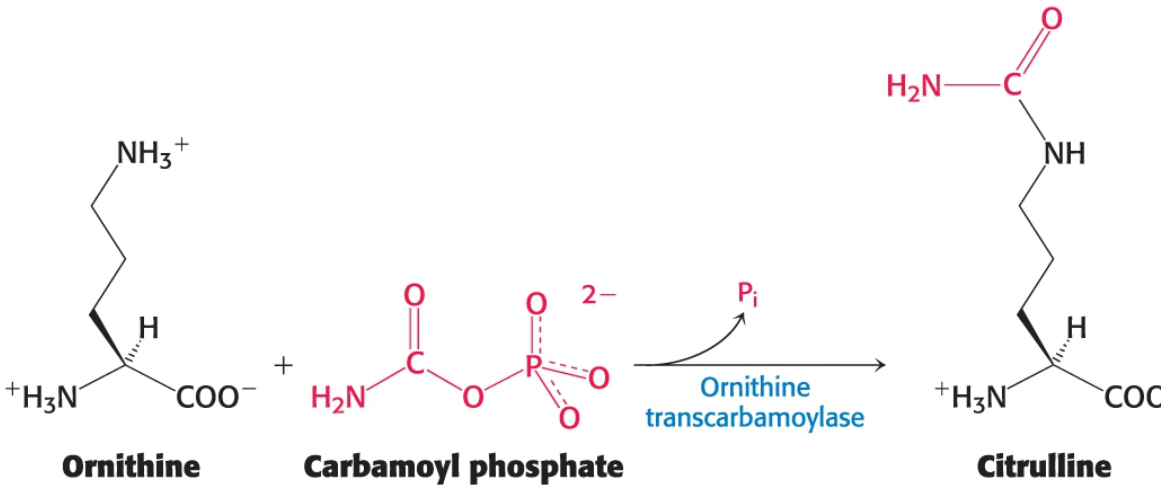
Carbamoyl phosphate synthetase I is regulated both allosterically and by covalent modification so that it is maximally active when amino acids are being metabolized for fuel use. The allosteric regulator *N*-acetylglutamate is required for synthetase activity. This molecule is synthesized by *N*-acetylglutamate synthase.



N-acetylglutamate synthase is itself activated by arginine, an intermediate in the urea cycle. Thus, *N*-acetylglutamate is synthesized when amino acids, as represented by arginine and glutamate, are readily available, and carbamoyl phosphate synthetase I is then activated to process the generated ammonia. When ammonia is not being generated, the synthetase is inhibited by acetylation. A rise in the concentration of mitochondrial NAD^+, indicative of an energy-poor state, stimulates a deacetylase that removes the acetyl group, activating the synthetase and readying the enzyme for processing ammonia from protein degradation. Biochemists have not yet determined how synthetase acetylation is controlled, serving again as a reminder that many discoveries are yet to be made in biochemistry.

Carbamoyl phosphate reacts with ornithine to begin the urea cycle

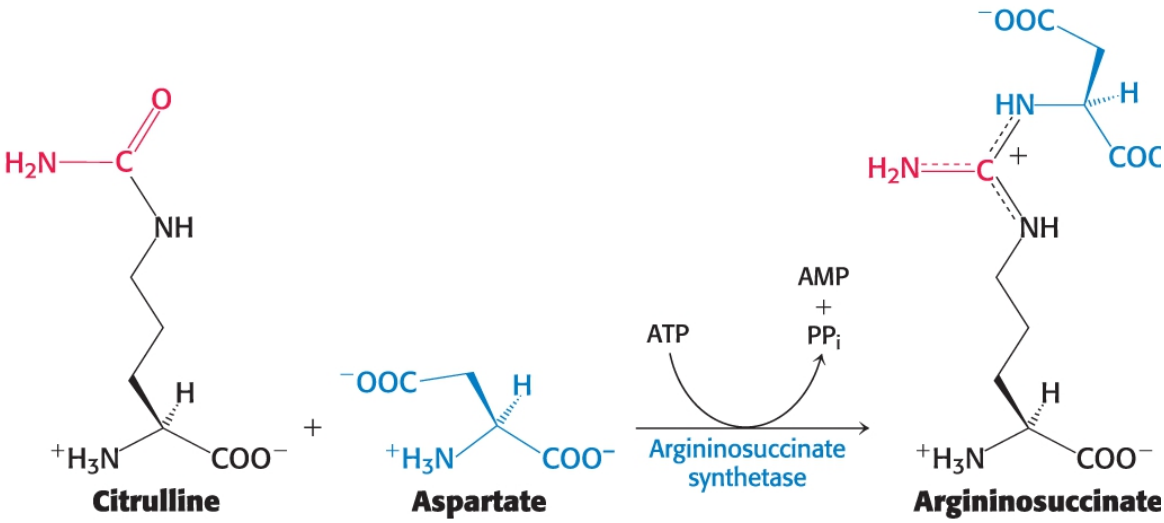
The carbamoyl group of carbamoyl phosphate has a high transfer potential because of its anhydride linkage. The carbamoyl group is transferred to ornithine to form citrulline, in a reaction catalyzed by ornithine transcarbamoylase.



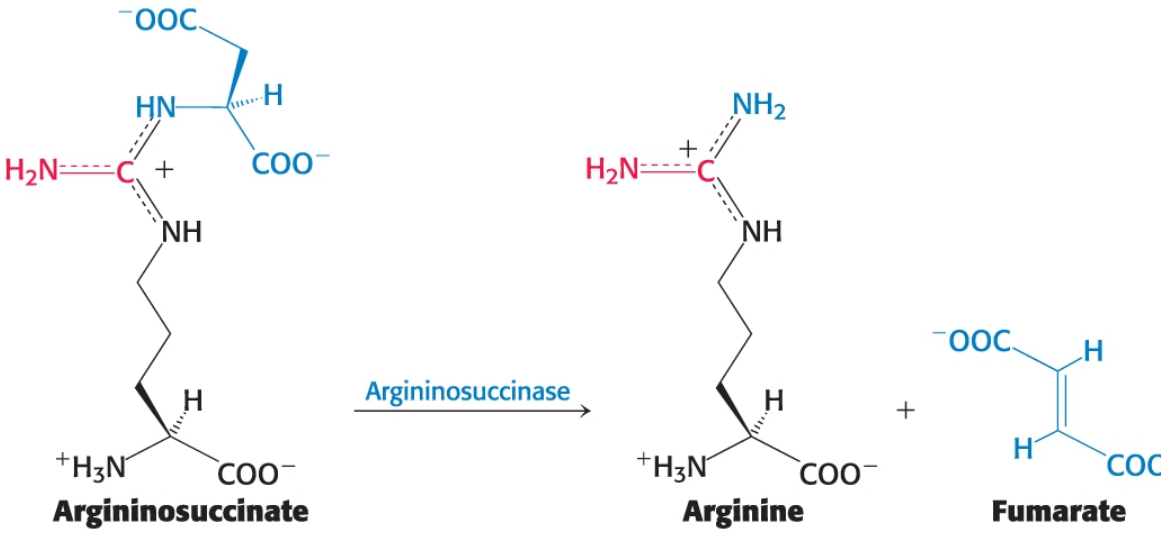
Ornithine and citrulline are amino acids, but they are not proteogenic, meaning they are not used as building blocks of proteins. The formation of NH_4^+ by glutamate dehydrogenase, its incorporation into carbamoyl phosphate as NH_3, and the subsequent synthesis of citrulline take place in the mitochondrial matrix. In contrast, the next three reactions of the urea cycle, which lead to the formation of urea, take place in the cytoplasm.

Citrulline is transported to the cytoplasm, where it condenses with aspartate, the donor of the second amino group of urea. This synthesis of argininosuccinate, catalyzed by argininosuccinate synthetase, is

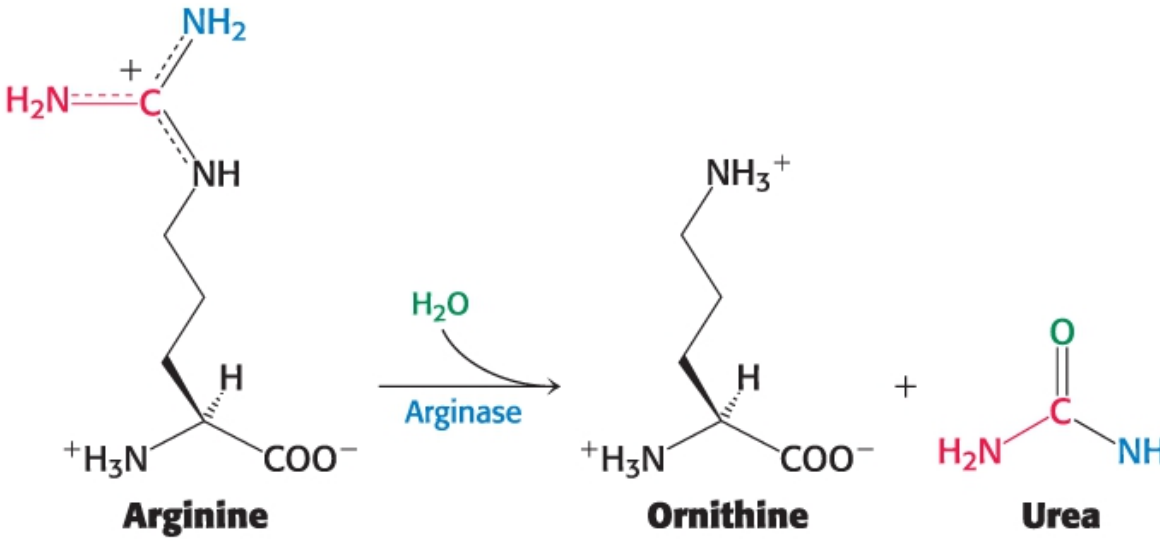
driven by the cleavage of ATP into AMP and pyrophosphate and by the subsequent hydrolysis of pyrophosphate.



Argininosuccinase (also called *argininosuccinate lyase*) cleaves argininosuccinate into arginine and fumarate. Thus, the carbon skeleton of aspartate is preserved in the form of fumarate.



Finally, arginine is hydrolyzed to generate urea and ornithine in a reaction catalyzed by arginase. Ornithine is then transported back into the mitochondrion to begin another cycle, and the urea is excreted. Indeed, human beings excrete about 10 kg (22 pounds) of urea per year.



The urea cycle is linked to gluconeogenesis

The stoichiometry of urea synthesis is

$$CO_2 + NH_4^+ + 3ATP + aspartate + 2H_2O \rightarrow urea + 2ADP + 2P_i + AMP + PP_i + fumarate$$

Pyrophosphate is rapidly hydrolyzed, and so the equivalent of four molecules of ATP are consumed in these reactions to synthesize one

molecule of urea. The synthesis of fumarate by the urea cycle is important because it is a precursor for glucose synthesis (Figure 23.16). Fumarate is hydrated to malate, which is in turn oxidized to oxaloacetate, producing one NADH that can be used to generate 2.5 ATP molecules; thus, the actual energetic cost of urea synthesis is not as great as it may appear. Oxaloacetate can be converted into glucose by gluconeogenesis or transaminated to aspartate for another round of urea synthesis.

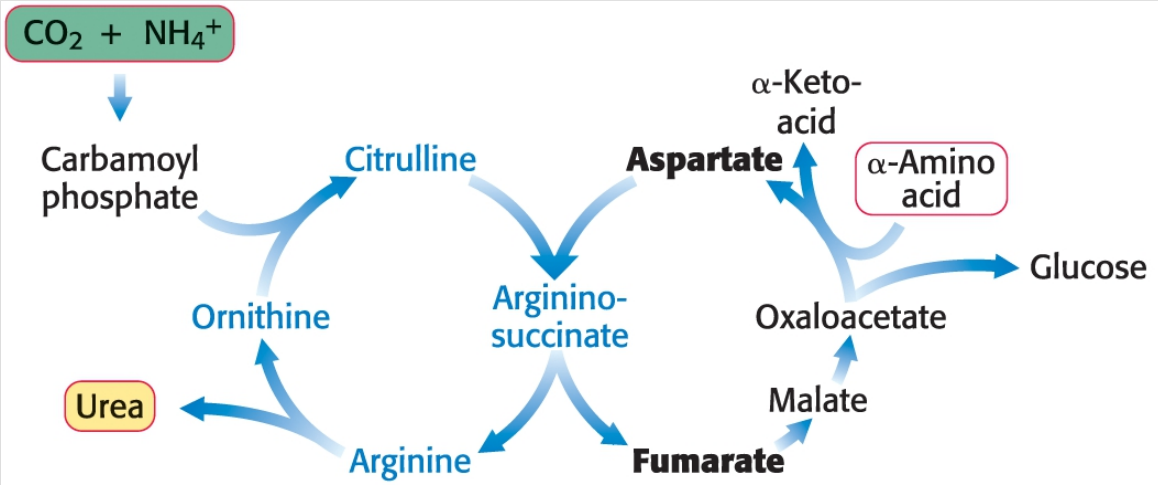


FIGURE 23.16 Nitrogen metabolism is integrated with other pathways. The urea cycle, gluconeogenesis, and the transamination of oxaloacetate are linked by fumarate and aspartate

Inherited defects of the urea cycle cause hyperammonemia and can lead to brain damage

Genetic disorders of the urea cycle that block carbamoyl phosphate synthesis or of any of the four steps of the urea cycle have devastating consequences. The synthesis of urea in the liver is the major route for the removal of NH_4^+; thus, any defect in the urea cycle leads to an elevated level of NH_4^+ in the blood (a condition called *hyperammonemia*). Urea cycle disorders occur with a prevalence of about 1 in 15,000, with some cases becoming evident a day or two after birth, when the afflicted infant becomes lethargic and vomits periodically. Coma and irreversible brain damage may soon follow.

Why are high levels of NH_4^+ toxic? Biochemists do not yet know for certain, but recent work suggests that NH_4^+ may inappropriately activate a sodium-potassium-chloride cotransporter. This activation disrupts the osmotic balance of the nerve cell, causing swelling that damages the cell and results in neurological disorders. Other studies have found that ammonium disrupts neurotransmitter systems, which is reasonable since many neurotransmitters either are amino acids or are derived from amino acids. Additionally, ammonium has been found to impact energy metabolism, levels of oxidative stress, nitric oxide synthesis, and signal-transduction pathways. Due to these many impacts, the effects of ammonium on the brain are probably complex.

Ingenious strategies for coping with deficiencies in urea synthesis have been devised on the basis of a thorough understanding of the underlying biochemistry. Consider, for example, argininosuccinase deficiency. This disorder can be partly bypassed by providing a surplus of arginine in the diet and restricting the total protein intake. In the liver, arginine is split into urea and ornithine, which then reacts with carbamoyl phosphate to form citrulline (**Figure 23.17**). This urea-cycle intermediate condenses with aspartate to yield argininosuccinate, which is then excreted. Note that two nitrogen atoms — one from carbamoyl phosphate and the other from aspartate — are eliminated from the body per molecule of arginine provided in the diet. In essence,

argininosuccinate substitutes for urea in carrying nitrogen out of the body.

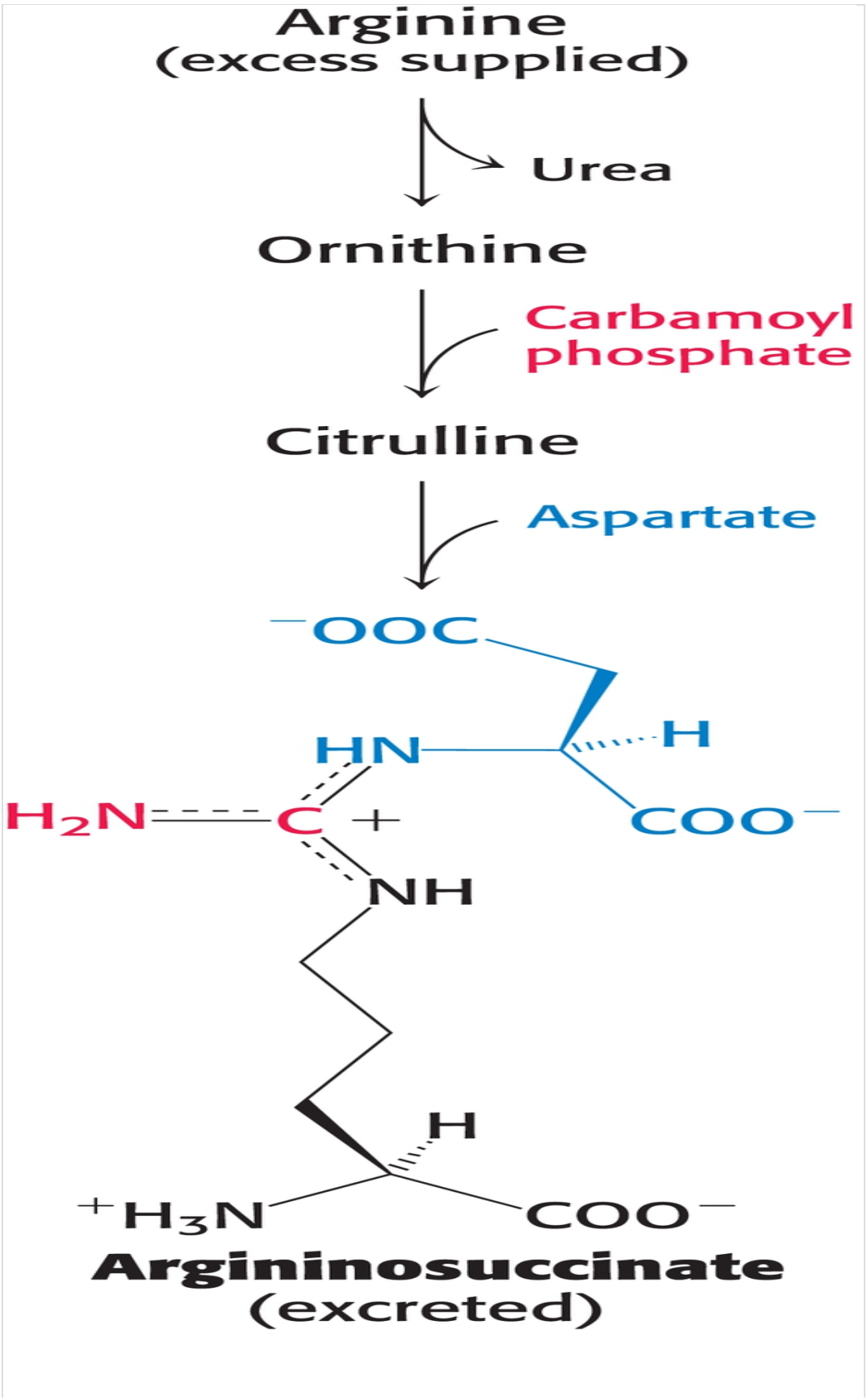

Arginine
(excess supplied)
Urea
Ornithine
Carbamoyl
phosphate
Citrulline
Aspartate
⁻OOC
HN
H
H₂N
C
+
COO⁻
NH
H
⁺H₃N
COO⁻
Argininosuccinate
(excreted)

FIGURE 23.17 Argininosuccinase deficiency can be managed by supplementing the diet with arginine. Nitrogen is excreted in the form of argininosuccinate in the absence of functional argininosuccinase.



The treatment of carbamoyl phosphate synthetase deficiency or ornithine transcarbamoylase deficiency illustrates a different strategy for circumventing a metabolic block. Citrulline and argininosuccinate cannot be used to dispose of nitrogen atoms because their formation is impaired. Under these conditions, excess nitrogen accumulates in glycine and glutamine. The challenge then is to rid the body of the nitrogen accumulating in these two amino acids. That goal is accomplished by supplementing a protein-restricted diet with large amounts of benzoate and phenylacetate. Benzoate is activated to benzoyl CoA, which reacts with glycine to form hippurate, which is excreted (Figure 23.18). Likewise, phenylacetate is activated to phenylacetyl CoA, which reacts with glutamine to form phenylacetylglutamine, which is also excreted. These conjugates substitute for urea in the disposal of nitrogen. Thus, latent biochemical pathways can be activated to partly bypass a genetic defect.

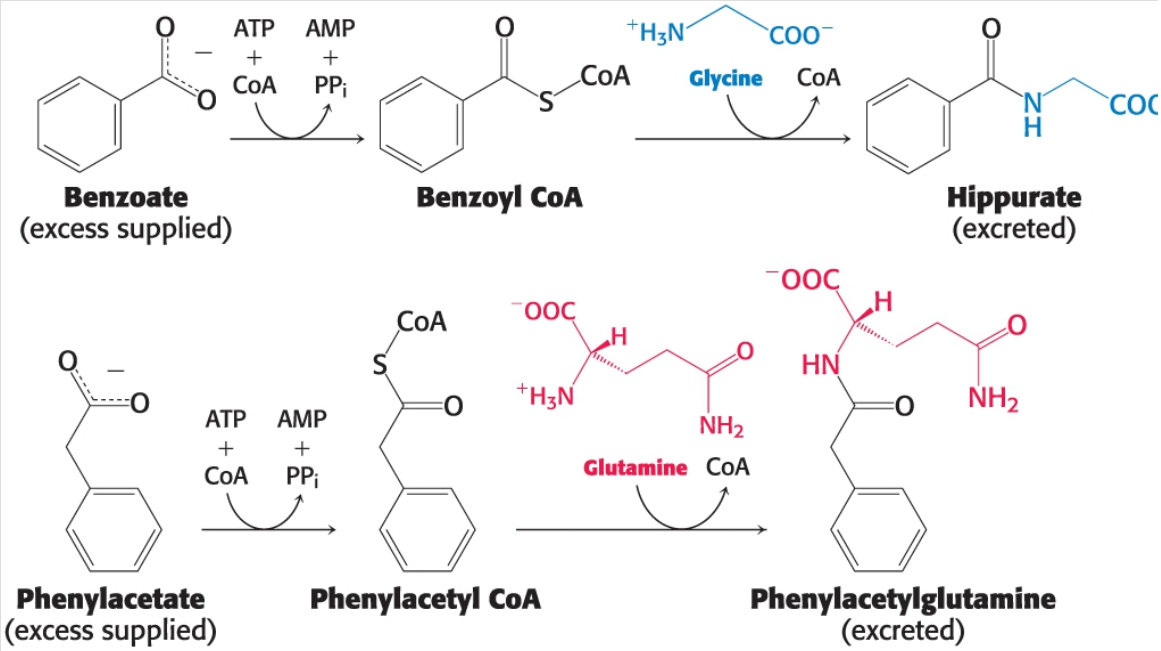
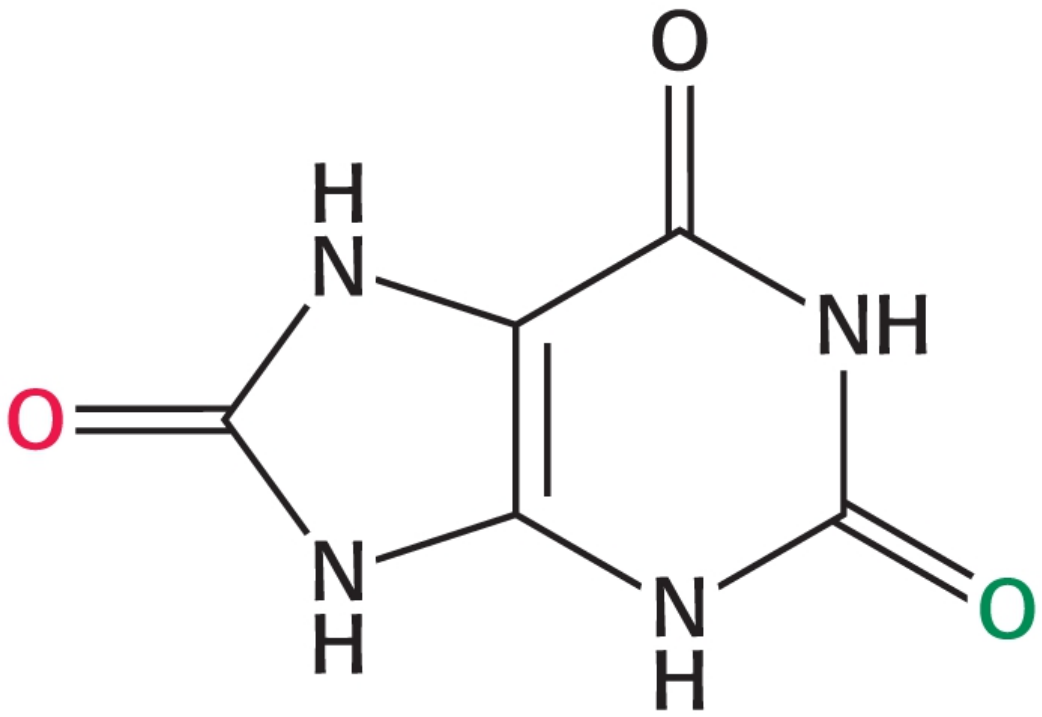


FIGURE 23.18 Both carbamoyl phosphate synthetase and ornithine transcarbamoylase deficiencies can be treated the same way. By supplementing the diet with benzoate and phenylacetate, excess nitrogen can be excreted in the form of hippurate and phenylacetylglutamine.

Urea is not the only means of disposing of excess nitrogen

As stated earlier, most terrestrial vertebrates are *ureotelic*; they excrete excess nitrogen as urea. However, urea is not the only excretable form of nitrogen. *Ammonotelic* organisms, such as aquatic vertebrates and invertebrates, release nitrogen as NH_4^+ and rely on the aqueous environment to dilute this toxic substance. Interestingly, lungfish, which are normally ammonotelic, become ureotelic in time of drought, when they live out of the water.

While both ureotelic and ammonotelic organisms require water (to varying degrees) for nitrogen excretion, *uricotelic* organisms, such as birds and reptiles, secrete nitrogen in an almost-solid slurry, as the purine uric acid. Besides requiring very little water, the secretion of uric acid also has the advantage of removing four atoms of nitrogen per molecule. The pathway for nitrogen excretion observed in different organisms developed over the course of evolution, depending on the habitat of each organism.



Uric acid

Self-Check Question

What are the immediate biochemical sources for the two nitrogen atoms in urea?

23.5 Carbon Atoms of Degraded Amino Acids Emerge as Major Metabolic Intermediates

We now turn to the fates of the carbon skeletons of amino acids after the removal of the α-amino group. The strategy of amino acid degradation is to transform the carbon skeletons into major metabolic intermediates that can be converted into glucose or oxidized by the citric acid cycle. The conversion pathways range from extremely simple to quite complex. In fact, some amino acids can be degraded by alternate pathways. For instance, threonine can be metabolized to succinyl CoA or pyruvate. In all cases, however, the carbon skeletons of the diverse set of 20 fundamental amino acids are funneled into only seven molecules: pyruvate, acetyl CoA, acetoacetyl CoA, α-ketoglutarate, succinyl CoA, fumarate, and oxaloacetate. We see here an example of the remarkable economy of metabolic conversions.

Amino acids that are degraded to acetyl CoA or acetoacetyl CoA are termed **ketogenic amino acids** because they can give rise to ketone bodies or fatty acids. Amino acids that are degraded to pyruvate, α-ketoglutarate, succinyl CoA, fumarate, or oxaloacetate are termed **glucogenic amino acids**, because they can be used to produce glucose. For example, oxaloacetate, generated from pyruvate and other citric acid cycle intermediates, can be converted into phosphoenolpyruvate and then into glucose (Section 16.4). Recall from Chapters 17 and 22 that mammals lack a pathway for the net synthesis of glucose from acetyl CoA or acetoacetyl CoA; thus, any amino acid that produces only these molecules cannot be used to produce glucose.

Of the basic set of 20 amino acids, only leucine and lysine are solely ketogenic (**Figure 23.19**). Isoleucine, phenylalanine, tryptophan, and

tyrosine are both ketogenic and glucogenic. Some of their carbon atoms emerge in acetyl CoA or acetoacetyl CoA, whereas others appear in potential precursors of glucose. The other 14 amino acids are classed as solely glucogenic. We will identify the degradation pathways by the entry point into metabolism.

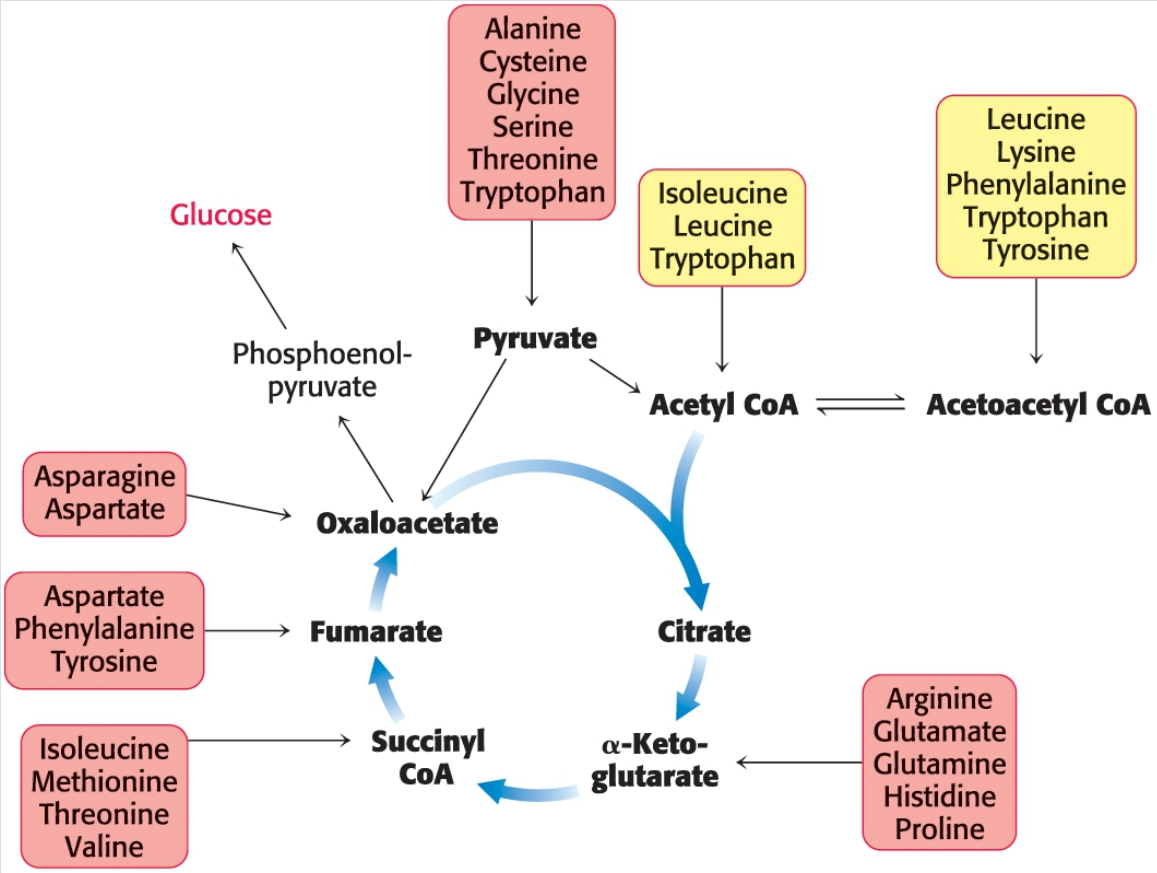


FIGURE 23.19 The carbon skeletons of all 20 proteogenic amino acids enter central metabolism as just seven different molecules. Glucogenic amino acids are shaded red, and ketogenic amino acids are shaded yellow. Several amino acids are both glucogenic and ketogenic.

Pyruvate is an entry point into metabolism for a number of amino acids

Pyruvate is the entry point of the three-carbon amino acids — alanine, serine, and cysteine — into the metabolic mainstream (Figure 23.20). The transamination of alanine directly yields pyruvate.

$$\text{Alanine} + \alpha\text{-ketoglutarate} \rightleftharpoons \text{pyruvate} + \text{glutamat}$$

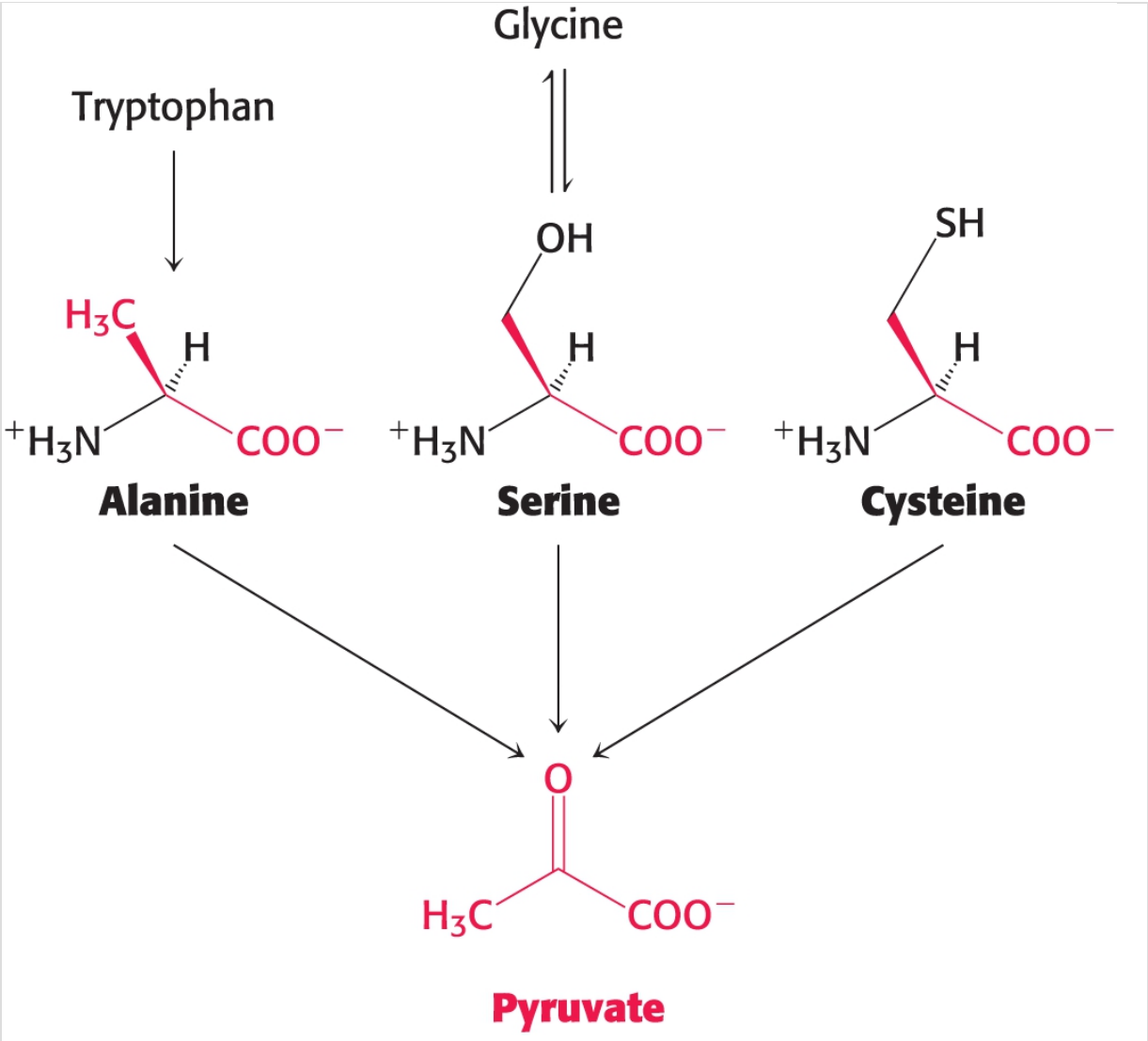


FIGURE 23.20 Pyruvate is the metabolic entry point for the carbon skeletons from three-carbon amino acids. Pyruvate is the point of entry for alanine, serine, cysteine, and glycine. Note

that alanine is eventually produced in the degradation of tryptophan, and that carbon skeleton can then be used to form pyruvate.



As mentioned earlier in the chapter, glutamate is then oxidatively deaminated in the liver, yielding NH_4^+ and regenerating α-ketoglutarate. The sum of these reactions is

$$\text{Alanine} + \text{NAD(P)}^+ + H_2O \rightleftharpoons \text{pyruvate} + NH_4^+ + \text{NAD(P)H} + H$$

Another simple reaction in the degradation of amino acids is the deamination of serine to pyruvate by serine dehydratase (Section 23.3).

$$\text{Serine} \rightarrow \text{pyruvate} + NH_4^+$$

Cysteine can be converted into pyruvate by several pathways, with its sulfur atom emerging in H_2S, SCN^-, or SO_3^{2-}.

The carbon atoms of three other amino acids can be converted into pyruvate. Glycine can be converted into serine by the enzymatic addition of a hydroxymethyl group, or it can be cleaved to give CO_2, NH_4^+, and an activated one-carbon unit. Threonine can give rise to pyruvate through the intermediate 2-amino-3-ketobutyrate. Three carbon atoms of tryptophan can emerge in alanine, which can be converted into pyruvate.

Oxaloacetate is an entry point into metabolism for aspartate and asparagine

Aspartate and asparagine are converted into oxaloacetate, a citric acid cycle intermediate. Aspartate, a four-carbon amino acid, is directly transaminated to oxaloacetate.

$$\text{Aspartate} + \alpha\text{-ketoglutarate} \rightleftharpoons \text{oxaloacetate} + \text{glutamat}$$

Asparagine is hydrolyzed by asparaginase to NH_4^+ and aspartate, which is then transaminated.

Recall that aspartate can also be converted into fumarate by the urea cycle (Figure 23.16). Fumarate is a point of entry for half the carbon atoms of tyrosine and phenylalanine, as will be discussed shortly.

Alpha-ketoglutarate is an entry point into metabolism for amino acids with five-carbon chains

The carbon skeletons of several amino acids with five-carbon chains enter the citric acid cycle as α-ketoglutarate. These amino acids are first converted into glutamate, which is then oxidatively deaminated by glutamate dehydrogenase to yield α-ketoglutarate (**Figure 23.21**).

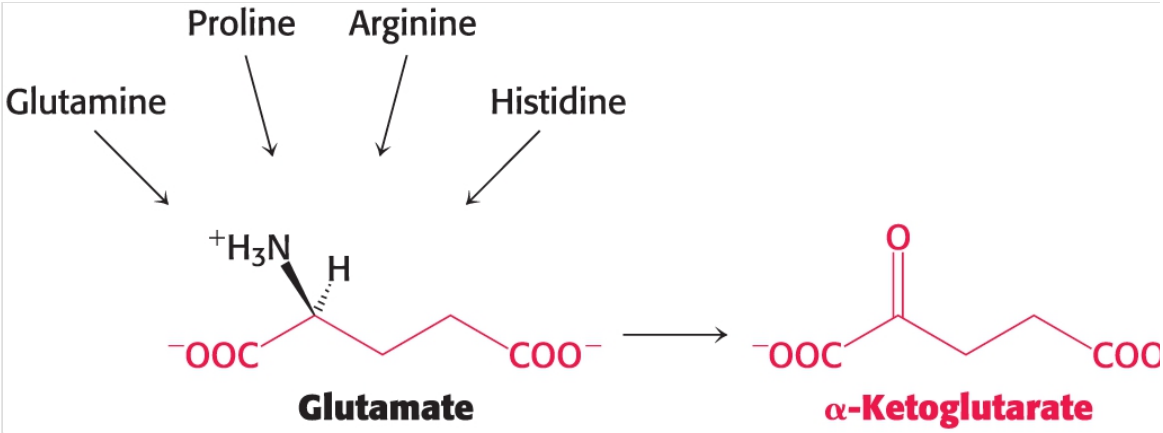


FIGURE 23.21 Four amino acids produce carbon skeletons that enter central metabolism as α-ketoglutarate. These amino acids with five-carbon chains are first converted into glutamate.

Histidine is converted into 4-imidazolone 5-propionate (Figure 23.22). The amide bond in the ring of this intermediate is hydrolyzed to the *N*-formimino derivative of glutamate, which is then converted into glutamate by the transfer of its formimino group to tetrahydrofolate, a carrier of activated one-carbon units (Section 25.2).

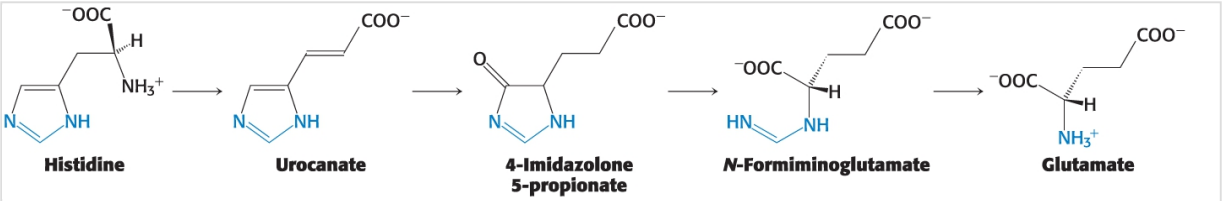


FIGURE 23.22 Histidine is converted to glutamate in four steps. The glutamate produced here is then deaminated to form α-ketoglutarate.

Glutamine is hydrolyzed to glutamate and NH_4^+ by glutaminase. Proline and arginine are each converted into glutamate γ-semialdehyde,

which is then oxidized to glutamate (Figure 23.23).

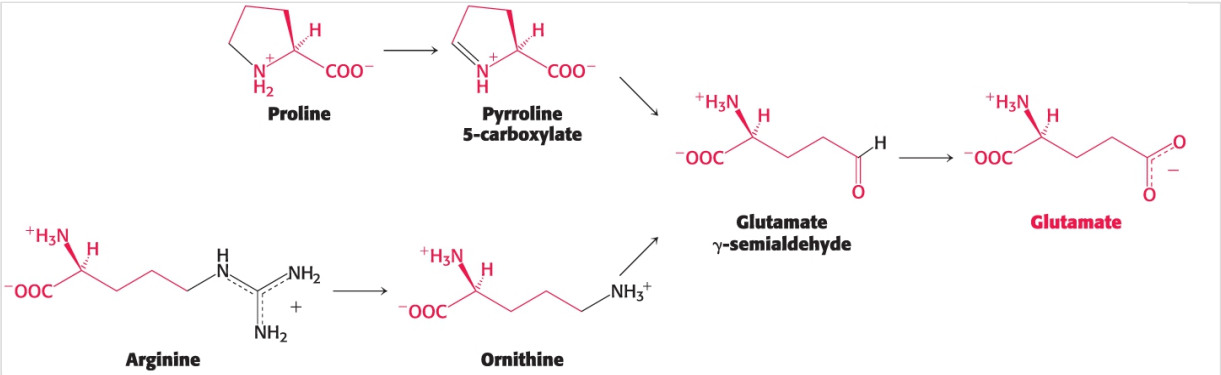


FIGURE 23.23 The degradation pathways for proline and arginine converge on a common intermediate. As with histidine and glutamine, the glutamate produced is deaminated to form α-ketoglutarate.

Succinyl coenzyme A is a point of entry for several amino acids

Succinyl CoA is a point of entry for some of the carbon atoms of methionine, isoleucine, threonine, and valine. Propionyl CoA and then methylmalonyl CoA are intermediates in the breakdown of these four amino acids (Figure 23.24). This pathway from propionyl CoA to succinyl CoA is also used in the oxidation of fatty acids that have an odd number of carbon atoms. The mechanism for the interconversion of propionyl CoA and methylmalonyl CoA was presented in Section 22.3.

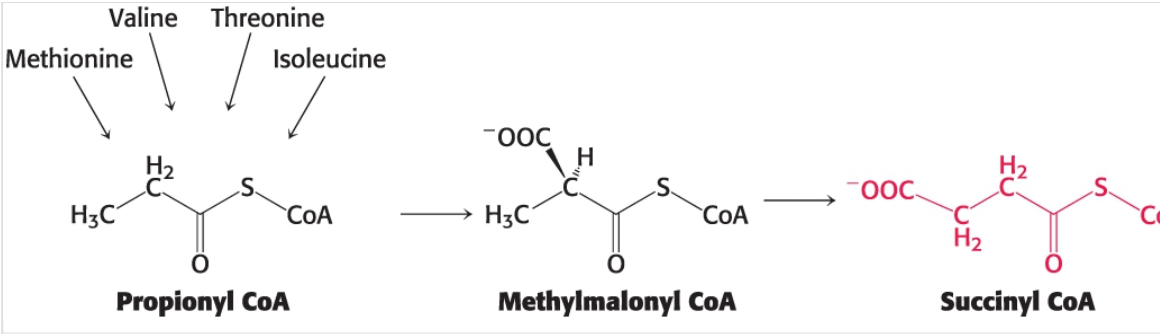


FIGURE 23.24 Succinyl CoA is formed from methionine, isoleucine, threonine, and valine.
Propionyl CoA is a common intermediate in all four pathways.

Methionine degradation requires the formation of a key methyl donor, *S*-adenosylmethionine

Methionine is converted into succinyl CoA in nine steps (**Figure 23.25**). The first step is the adenylation of methionine to form *S*-adenosylmethionine (SAM), a common methyl donor in the cell (Section 25.2). Loss of the methyl and adenosyl groups yields homocysteine, which is eventually processed to α-ketobutyrate. This α-ketoacid is oxidatively decarboxylated by the α-ketoacid dehydrogenase complex to propionyl CoA, which is processed to succinyl CoA, as described in Section 22.3.

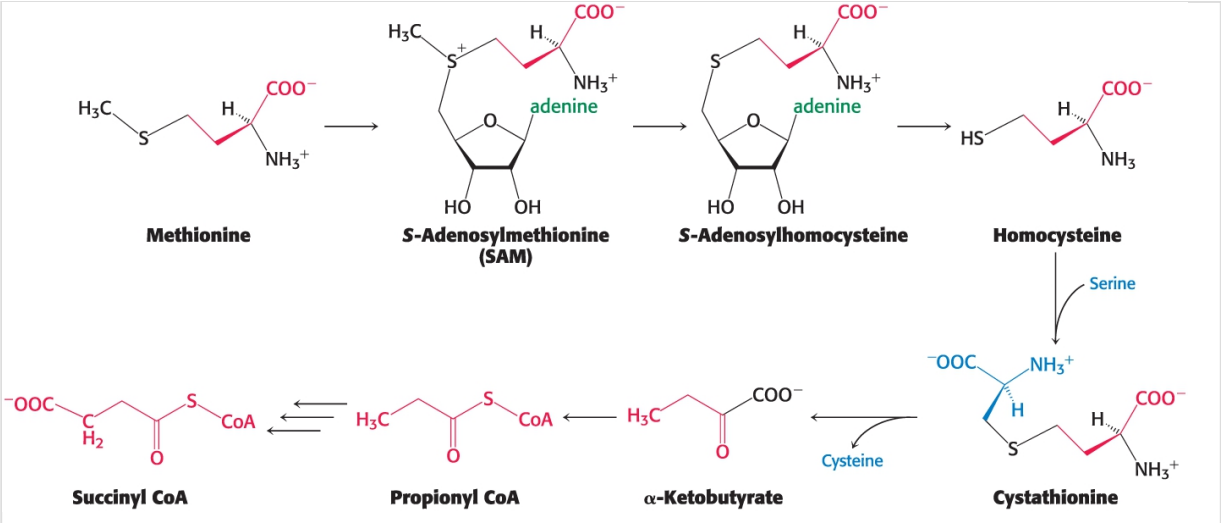
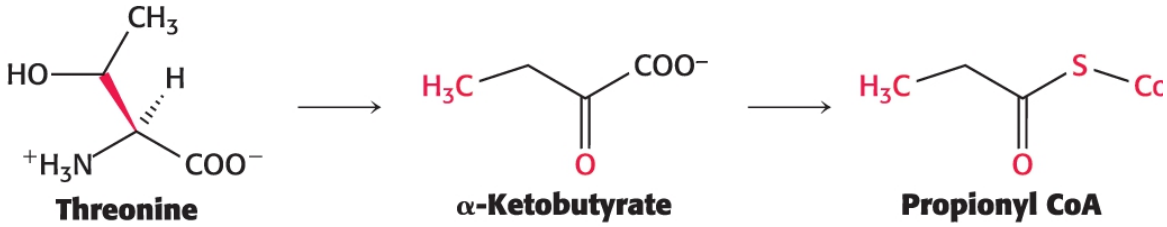


FIGURE 23.25 Methionine catabolism proceeds through the formation of SAM. The pathway for the conversion of methionine into succinyl CoA forms *S*-adenosylmethionine (SAM), an important methyl donor.

Threonine deaminase initiates the degradation of threonine

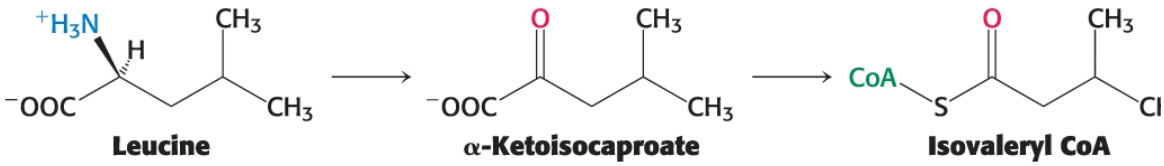
Threonine can be degraded by a number of pathways. One requires the enzyme threonine deaminase, also known as threonine dehydratase. This pyridoxal-dependent enzyme converts threonine into α-ketobutyrate.



α-Ketobutyrate then forms propionyl CoA, which is subsequently metabolized to succinyl CoA, as shown in Figure 23.24.

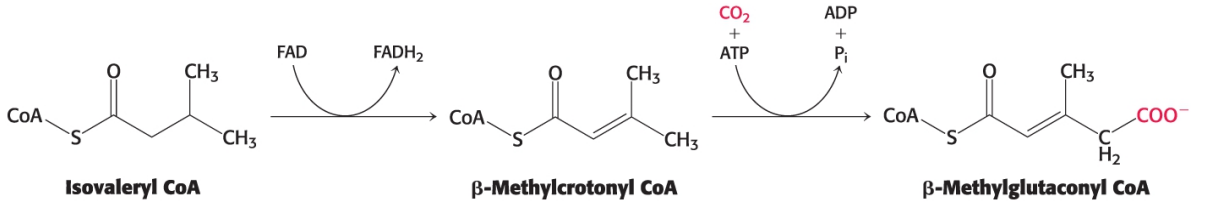
The branched-chain amino acids yield acetyl CoA, acetoacetate, or propionyl CoA

The branched-chain amino acids are degraded by reactions that we have already encountered in the citric acid cycle and fatty acid oxidation. Leucine is transaminated to the corresponding α-ketoacid, called α-*ketoisocaproate*, which is oxidatively decarboxylated to isovaleryl CoA by the branched-chain α-ketoacid dehydrogenase complex.

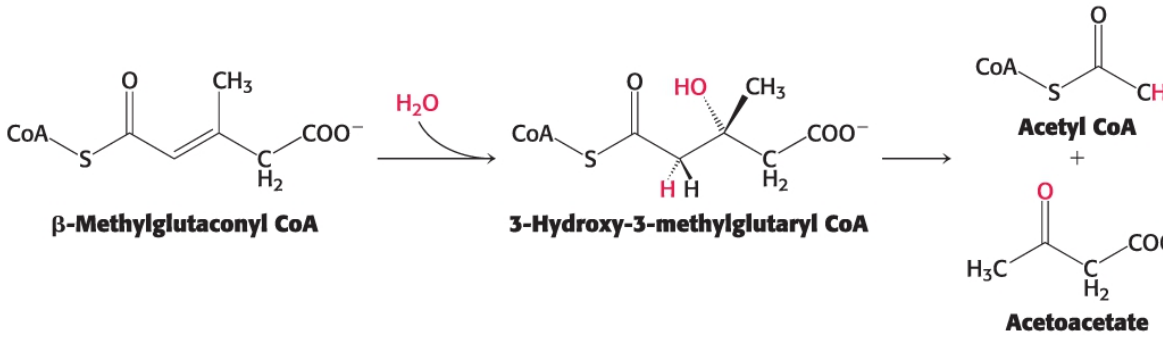


The α-ketoacids of valine and isoleucine, the other two branched-chain aliphatic amino acids, also are substrates (as is α-ketobutyrate derived from methionine). The oxidative decarboxylation of these α-ketoacids is analogous to that of pyruvate to acetyl CoA and of α-ketoglutarate to succinyl CoA. The branched-chain α-ketoacid dehydrogenase, a multienzyme complex, is a homolog of pyruvate dehydrogenase complex (Section 17.2) and α-ketoglutarate dehydrogenase complex (Section 17.3). Indeed, the E3 components of these enzymes, which regenerate the oxidized form of lipoamide, are identical.

The isovaleryl CoA derived from leucine is dehydrogenated to yield β-methylcrotonyl CoA. This oxidation is catalyzed by isovaleryl CoA dehydrogenase, with FAD as the hydrogen acceptor, as in the analogous reaction in fatty acid oxidation that is catalyzed by acyl CoA dehydrogenase. β-Methylglutaconyl CoA is then formed by the carboxylation of β-methylcrotonyl CoA at the expense of the hydrolysis of a molecule of ATP. As might be expected, the carboxylation mechanism of β-methylcrotonyl CoA carboxylase is analogous to that of pyruvate carboxylase and acetyl CoA carboxylase.



β-Methylglutaconyl CoA is then hydrated to form 3-hydroxy-3-methylglutaryl CoA, which is cleaved into acetyl CoA and acetoacetate. This reaction has already been discussed in regard to the formation of ketone bodies from fatty acids (Section 22.4).

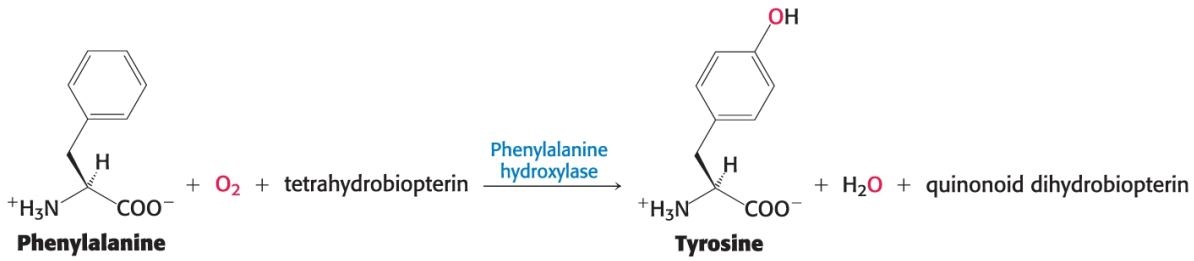


The degradative pathways of valine and isoleucine resemble that of leucine. After transamination and oxidative decarboxylation to yield a CoA derivative, the subsequent reactions are like those of fatty acid oxidation. Isoleucine yields acetyl CoA and propionyl CoA, whereas valine yields CO_2 and propionyl CoA. The degradation of leucine, valine, and isoleucine validate a point made in Chapter 15: the number of reactions in metabolism is large, but the number of *kinds* of reactions is relatively small. The degradation of leucine, valine, and isoleucine provides a striking illustration of the underlying simplicity and elegance of metabolism.

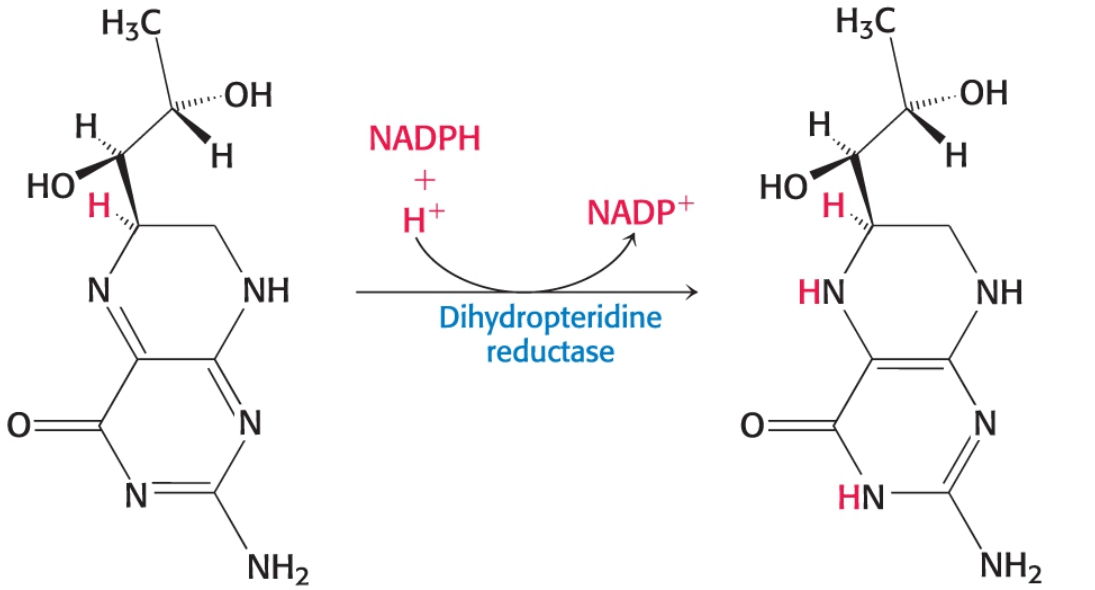
Oxygenases are required for the degradation of aromatic amino acids

The degradation pathways of the aromatic amino acids, which yield the common intermediates acetoacetate, fumarate, and pyruvate, are not as straightforward as that of the amino acids previously discussed. For the aromatic amino acids, molecular oxygen is used to break the aromatic ring.

The degradation of phenylalanine begins with its hydroxylation to tyrosine, a reaction catalyzed by phenylalanine hydroxylase. This enzyme is called a *monooxygenase* (or *mixed-function oxygenase*) because *one* atom of O_2 appears in the product and the other atom in H_2O.



The reductant here is tetrahydrobiopterin, an electron carrier that has not been previously discussed and is derived from the cofactor biopterin, which human beings synthesize de novo. The quinonoid form of dihydrobiopterin is produced in the hydroxylation of phenylalanine. It is reduced back to tetrahydrobiopterin by NADPH in a reaction catalyzed by dihydropteridine reductase.



The sum of the reactions catalyzed by phenylalanine hydroxylase and dihydropteridine reductase is

$$\text{Phenylalanine} + O_2 + \text{NADPH} + H^+ \rightarrow \text{tyrosine} + \text{NADP}^+ + H_2O$$

Note that these reactions can also be used to synthesize tyrosine from phenylalanine.

The next step in the degradation of phenylalanine and tyrosine is the transamination of tyrosine to *p*-hydroxyphenylpyruvate (Figure 23.26). This α-ketoacid then reacts with O_2 to form homogentisate. The enzyme catalyzing this complex reaction, *p*-hydroxyphenylpyruvate hydroxylase, is called a *dioxygenase* because both atoms of O_2 become incorporated into the product, one on the ring and one in the carboxyl group. The aromatic ring of homogentisate is then cleaved by O_2, which yields 4-maleylacetoacetate. This reaction is catalyzed by homogentisate oxidase, another dioxygenase. 4-Maleylacetoacetate is then isomerized to 4-fumarylacetoacetate by an enzyme that uses glutathione as a cofactor. Finally, 4-fumarylacetoacetate is hydrolyzed to fumarate and acetoacetate.

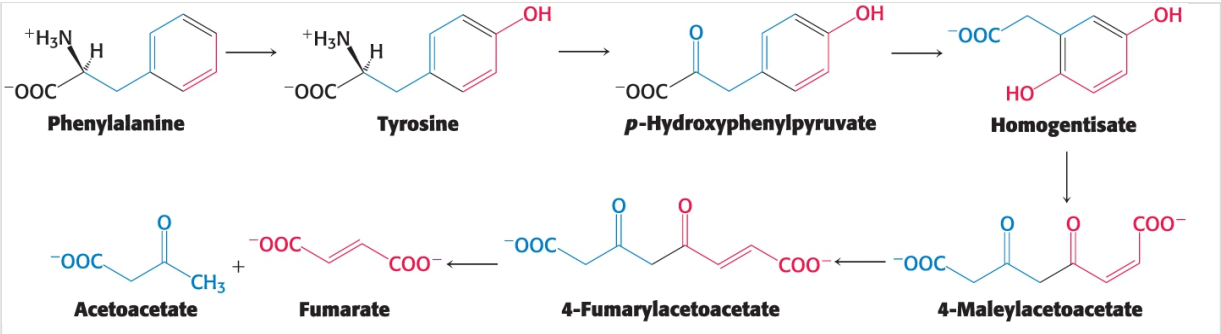


FIGURE 23.26 Phenylalanine and tyrosine degradation produce both acetoacetate and fumarate. This process requires both dioxygenases and monooxygenases.

Tryptophan degradation requires several oxygenases (Figure 23.27). Tryptophan 2,3-dioxygenase cleaves the pyrrole ring, and kynurenine 3-monooxygenase hydroxylates the remaining benzene ring, a reaction similar to the hydroxylation of phenylalanine to form tyrosine. Alanine is removed and the 3-hydroxyanthranilate is cleaved by another

dioxygenase and subsequently processed to acetoacetate. Note that nearly all cleavages of aromatic rings in biological systems are catalyzed by dioxygenases. The active sites of these enzymes contain iron that is not part of heme or an iron–sulfur cluster.

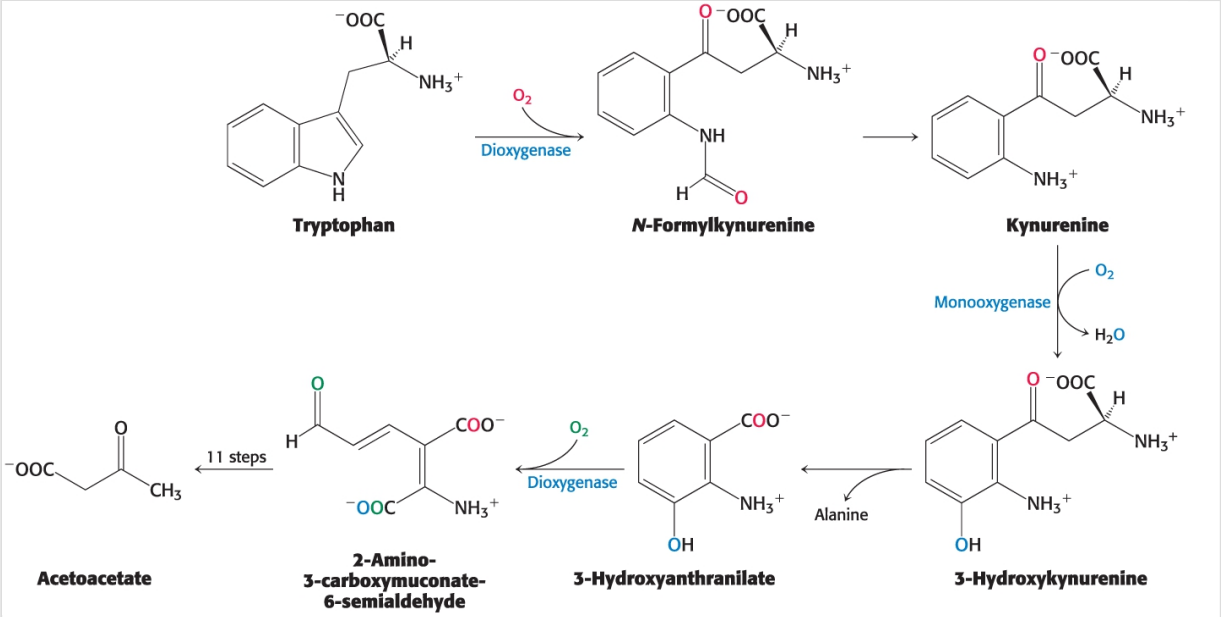


FIGURE 23.27 Tryptophan degradation requires multiple oxygenases and numerous steps.
Note that both alanine and acetoacetate are ultimately formed.

Protein metabolism helps to power the flight of migratory birds

Earlier we learned that fats are the primary fuel for migratory birds that fly great distances without feeding (Section 22.1). Proteins are also degraded to contribute fuel for these impressive feats of endurance. Why would proteins be degraded? There are several likely reasons. First, since the birds are not feeding, proteins involved with digestion and transport of nutrients from the gut are not needed and thus can be

degraded. Second, gluconeogenesis is required to provide glucose for the central nervous system, and the glucogenic amino acids will meet this need. Moreover, some amino acid carbon skeletons can replenish citric acid cycle intermediates to facilitate fat metabolism. Third, the reduction in body mass resulting from protein degradation will reduce the energy cost of flight. There is one final benefit. In addition to not feeding during flight, the migratory birds cannot hydrate, yet they still require water. While the catabolism of fats yields little water — $0.029\ g\ H_2O\ kJ^{-1}$ — protein provides fivefold more water than fats — $0.155\ g\ H_2O\ kJ^{-1}$ — and may be a vital source of water for migratory flights.

Example

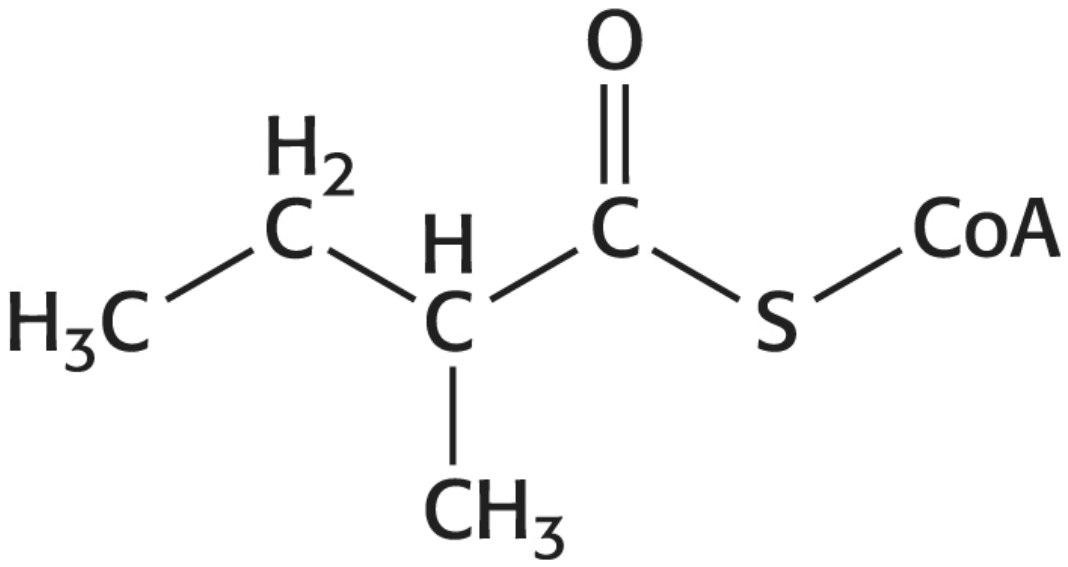
Determining Metabolic Products of Amino Acid Degradation

Problem:

Isoleucine is said to be both a ketogenic and glucogenic amino acid. Starting from 2-methylbutyryl CoA, a degradation intermediate of isoleucine, show that it is both ketogenic and glucogenic.

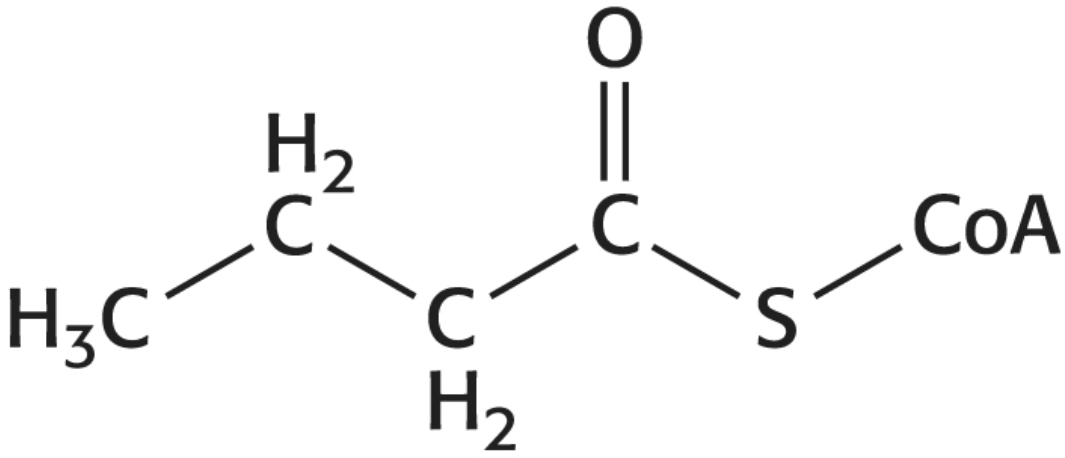
Getting Started:

Let's begin by thinking about the structure of 2-methylbutyryl CoA. We have seen similar molecules before. What general type of biochemical does this look like?



2-Methylbutyryl CoA

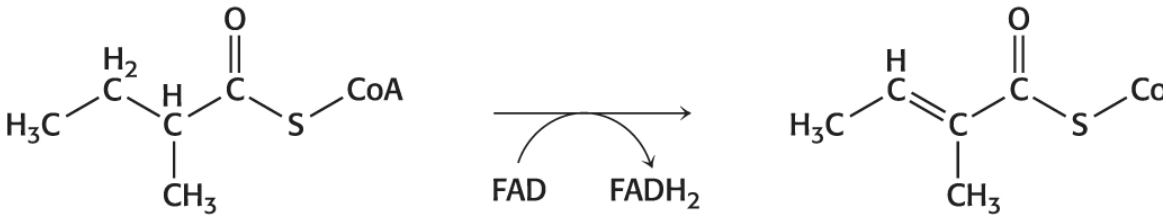
It looks like a fatty acyl CoA, except that there is a methyl group where a hydrogen would be in a fatty acyl CoA. To see this more clearly, let's look at the molecule with the substitution of a hydrogen for the methyl group, butyryl CoA.



Butyryl CoA

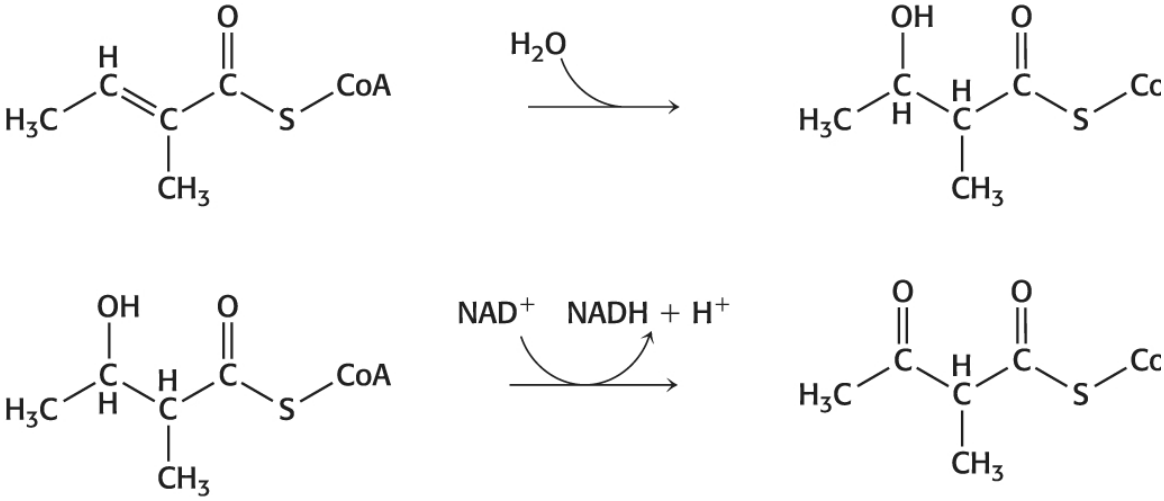
Analyze:

Thinking back to Chapter 22, how would you degrade butyryl CoA? β-Oxidation would be the way to go. So, let's apply β-oxidation to 2-methylbutyryl CoA. Recall that the first step in the β-oxidation is the introduction of a double bond at the β-carbon, accompanied with reduction of FAD. Recall that we saw the reaction in the conversion of succinate into fumarate in the citric acid cycle as well as in β-oxidation.

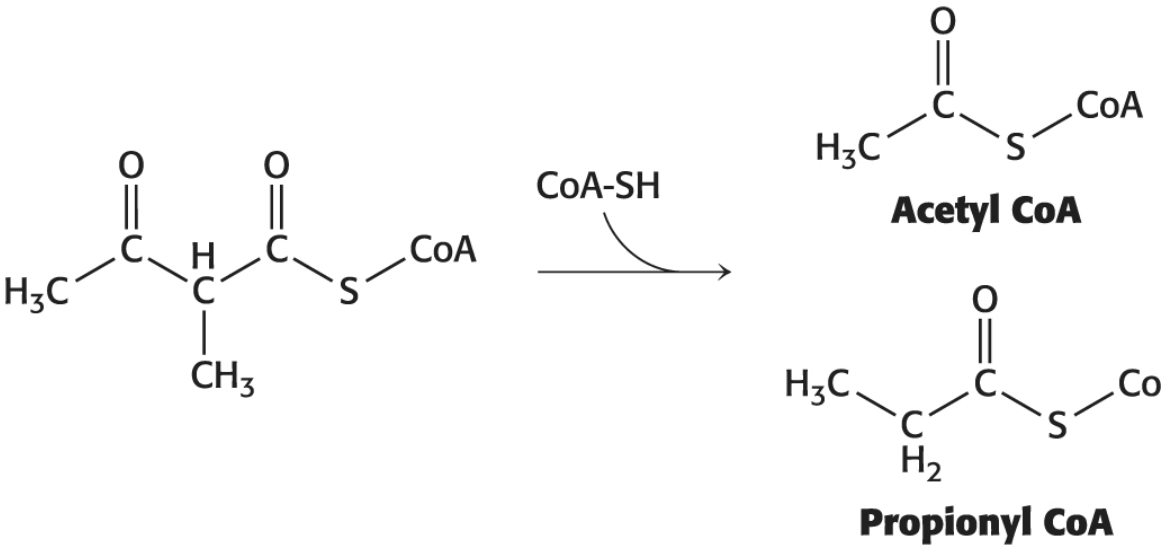


2-Methylbutyryl CoA

Next, recall that the next two reactions of β-oxidation are a hydration followed by an oxidation, with the concomitant reduction of NAD^+.



Finally, the last reaction is thiolysis by addition of CoA.



Thiolysis yields acetyl CoA and propionyl CoA.

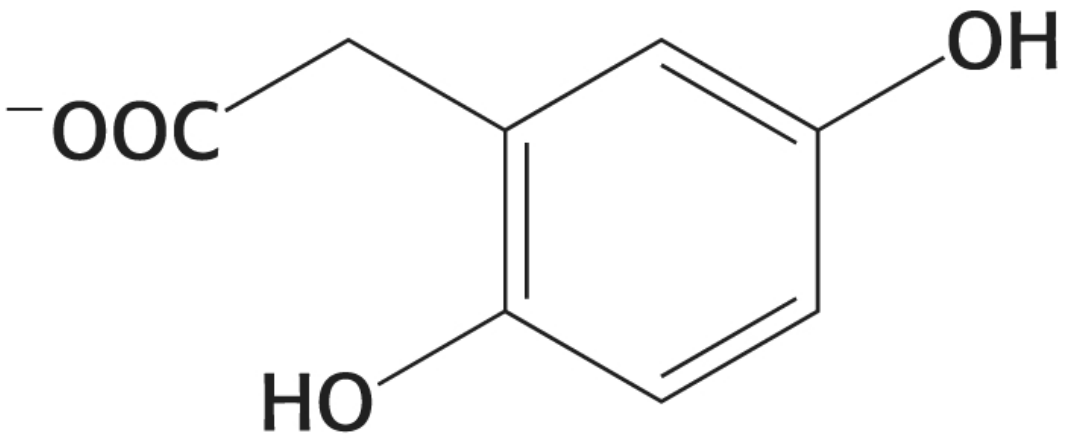
Reflect:

Acetyl CoA can be used for ketone body production, accounting for the fact that isoleucine is a ketogenic amino acid. What is the metabolic fate of propionyl CoA? As we saw in Section 22.3, propionyl CoA is converted into the citric acid intermediate succinyl CoA, which can be metabolized to oxaloacetate, a gluconeogenic substrate (Section 16.4). So we have shown that isoleucine is, in fact, both a ketogenic and a glucogenic amino acid.

23.6 Inborn Errors of Metabolism Can Disrupt Amino Acid Degradation



Many unusual biochemical products are produced or overproduced in a disease state, and can be detected in the urine. Additionally, errors in amino acid metabolism provided some of the first examples of biochemical defects linked to pathological conditions. For instance, *alkaptonuria*, an inherited metabolic disorder caused by the absence of homogentisate oxidase, was described in 1902. Homogentisate, a normal intermediate in the degradation of phenylalanine and tyrosine (Figure 23.26), accumulates in alkaptonuria because its degradation is blocked. Homogentisate is excreted in the urine, which turns dark on standing as homogentisate is oxidized and polymerizes into a dark pigment. Urine has been used as a marker for disease for centuries (**Figure 23.28**).



Homogentisate

Air

Highly colored polymer



Ulrich Pinder. Epiphanie Medicorum. Speculum videndi urinas hominum. Clavis aperiendi portas pulsuum. Berillus discernendi causas & differentias febrium. Nuremberg: 1506. Rosenwald Collection. Rare Book and Special Collections Division, Library of Congress (128.2).

FIGURE 23.28 Urine has long been used to diagnose diseases due to the excretion of unusual biochemical products. This fourteenth-century hand-colored woodcut from Germany depicts a wheel that classifies urine samples according to their color and consistency. In the middle of the wheel, a doctor inspects a patient's urine by sight, smell, and taste. The vials on the wheel aided physicians in diagnosing diseases.

Branched-chain ketoaciduria is a serious disorder of branched-chain amino acid degradation

Although alkaptonuria is a relatively harmless condition, such is not the case with other errors in amino acid metabolism. In branched-chain ketoaciduria, most commonly called *maple syrup urine disease*, the oxidative decarboxylation of α-ketoacids derived from valine, isoleucine, and leucine is blocked because the branched-chain dehydrogenase is missing or defective. Hence, the levels of these α-ketoacids and the branched-chain amino acids that give rise to them are markedly elevated in both blood and urine. The urine of patients has the odor of maple syrup, hence the common name of the disease. The disease usually leads to cognitive and physical disabilities unless the patient is placed on a diet low in valine, isoleucine, and leucine early in life. Thankfully, the disease can be readily detected in newborns by screening urine samples with 2,4-dinitrophenylhydrazine, which reacts with α-ketoacids to form 2,4-dinitrophenylhydrazone derivatives. A definitive diagnosis can be made by mass spectrometry. **Table 23.4** lists some other diseases of amino acid metabolism.

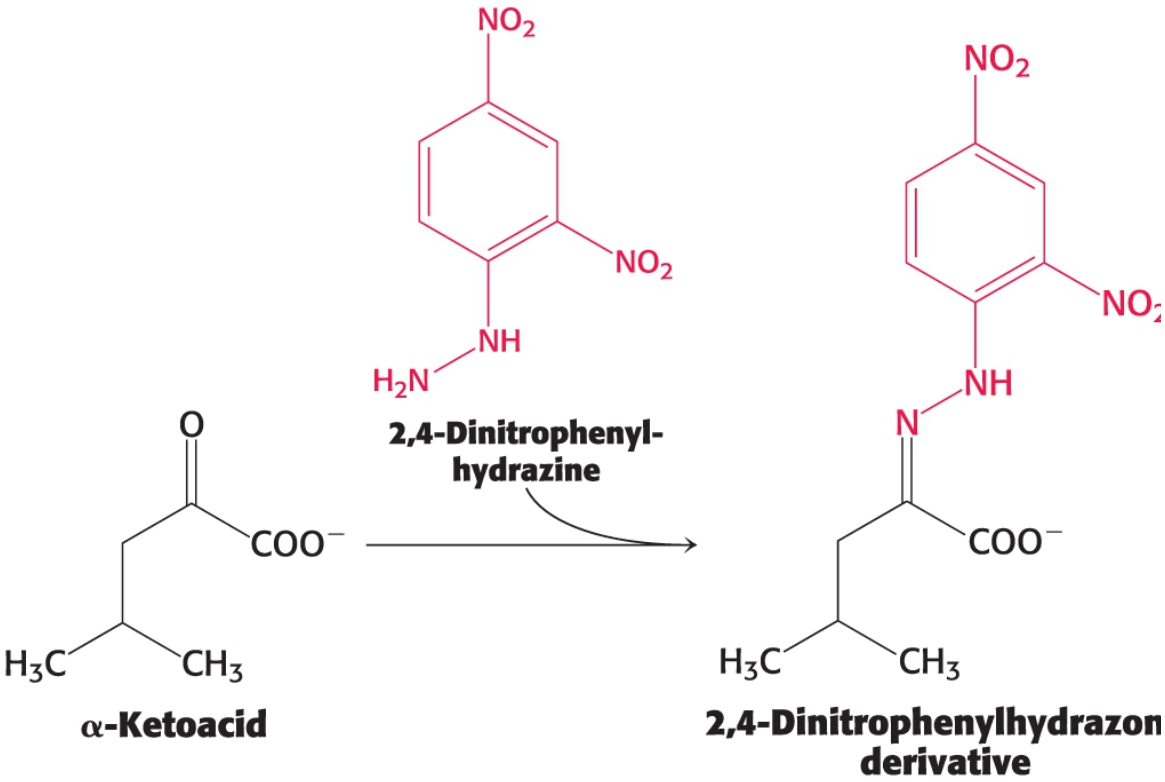


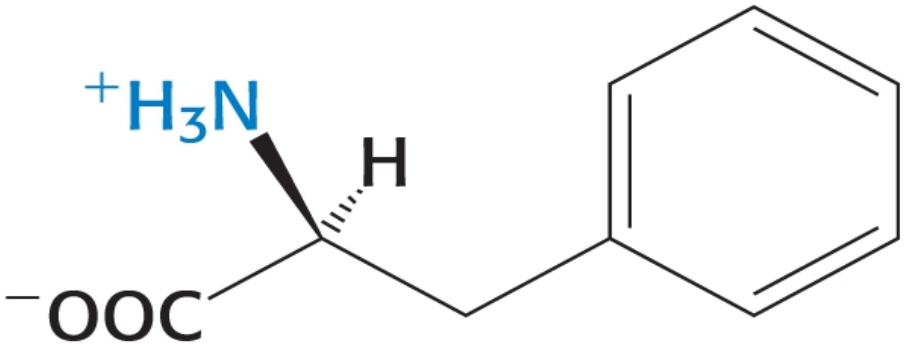
TABLE 23.4 Inborn errors of amino acid metabolism

Disease	Enzyme deficiency	Symptoms
Citrullinemia	Arginosuccinate lyase	Lethargy, seizures, reduced muscle tension
Tyrosinemia	Various enzymes of tyrosine degradation	Weakness, liver damage, cognitive disability
Albinism	Tyrosinase	Absence of pigmentation
Homocystinuria	Cystathionine β-synthase	Scoliosis, muscle weakness, cognitive disability, thin blond hair

Hyperlysine mia	α-Aminoadipic semialdehyde dehydrogenase	Seizures, cognitive disability, lack of muscle tone, ataxia

Phenylketonuria is one of the most common metabolic disorders

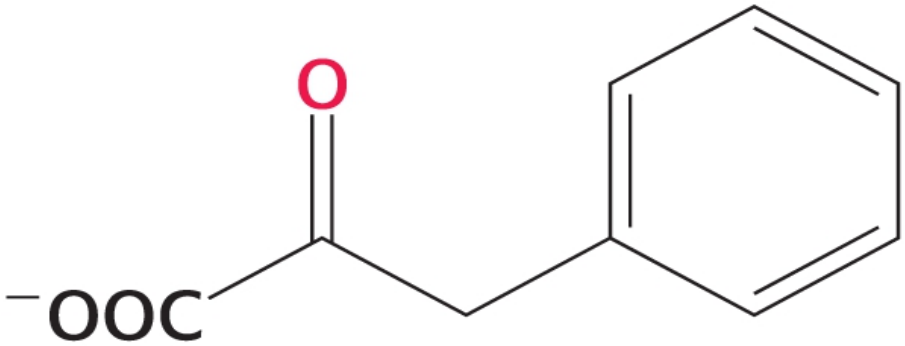
Perhaps the best known of the diseases of amino acid metabolism is **phenylketonuria**, which occurs with a prevalence of 1 in 10,000 births. Phenylketonuria is caused by an absence or deficiency of phenylalanine hydroxylase or, more rarely, of its tetrahydrobiopterin cofactor. Phenylalanine accumulates in all body fluids because it cannot be converted into tyrosine. Normally, three-quarters of phenylalanine molecules are converted into tyrosine, and the other quarter become incorporated into proteins. Because the major outflow pathway is blocked in phenylketonuria, the blood level of phenylalanine is typically at least 20-fold as high as in unaffected people. Minor fates of phenylalanine in people who process phenylalanine normally, such as the formation of phenylpyruvate which is a phenyl ketone, become major products which are then excreted in the urine. Indeed, the initial description of phenylketonuria in 1934 was made by observing the reaction of phenylpyruvate in the urine of phenylketonurics with $FeCl_3$, which turns the urine olive green.



Phenylalanine

α-Ketoacid

α-Amino acid



Phenylpyruvate

Untreated phenylketonuria results almost inexorably in severe cognitive disabilities. Babies with phenylketonuria do not show symptoms at birth but are severely affected by the disease by age 1 if untreated, and if they remain untreated, life expectancy is between 20 and 30 years. The therapy for phenylketonuria is a low-phenylalanine diet supplemented with tyrosine, because tyrosine is normally synthesized from phenylalanine. The aim is to provide just enough phenylalanine to meet the needs for growth and replacement. Proteins that have a low content of phenylalanine, such as casein from milk, are hydrolyzed and phenylalanine is removed by adsorption.

Early diagnosis of phenylketonuria is essential and has been accomplished by mass screening programs of all babies born in the United States and Canada. The phenylalanine level in the blood is the preferred diagnostic criterion because it is more sensitive and reliable than the $FeCl_3$ test. Prenatal diagnosis of phenylketonuria with DNA probes has become feasible because the gene has been cloned and the exact locations of many mutations have been discovered in the protein.

The biochemical basis of the cognitive disabilities is not firmly established, but one hypothesis suggests that the lack of hydroxylase reduces the amount of tyrosine, an important precursor to neurotransmitters such as dopamine. Moreover, high concentrations of phenylalanine prevent amino acid transport of any tyrosine present as well as tryptophan, a precursor to the neurotransmitter serotonin, into the brain. Because all three of the amino acids are transported by the same carrier, phenylalanine will saturate the carrier, preventing access to tyrosine and tryptophan. Lack of these amino acids will impair protein synthesis in the brain. Finally, high blood levels of phenylalanine result in higher levels of phenylalanine in the brain, and evidence suggests this elevated concentration inhibits glycolysis at

pyruvate kinase, disrupts myelination of nerve fibers, and reduces the synthesis of several neurotransmitters.

Self-Check Question



The end products of tryptophan degradation are acetyl CoA and acetoacetyl CoA, yet tryptophan is a gluconeogenic amino acid in animals. Explain.

Chapter 23 Summary

23.1 Proteins Are Degraded to Amino Acids

- Dietary protein is digested in the intestine, producing amino acids that are transported throughout the body.
- Cellular proteins are degraded at widely variable rates, ranging from minutes to the life of the organism. The turnover of cellular proteins is a regulated process requiring complex enzyme systems.

23.2 Protein Turnover Is Tightly Regulated

- Proteins to be degraded by the proteasome are conjugated with ubiquitin, a small conserved protein. The ubiquitin-conjugating system is composed of three distinct enzymes.
- The proteasome is a large, barrel-shaped complex that digests ubiquitinated proteins at the expense of ATP. The resulting amino acids provide a source of precursors for protein, nucleotide bases, and other nitrogenous compounds.

23.3 The First Step in Amino Acid Degradation Is the Removal of Nitrogen

- Surplus amino acids are used as building blocks and as metabolic fuel. The first step in their degradation is the removal of their α-amino groups by transamination to yield α-ketoacids. Transamination is catalyzed by aminotransferases that all use pyridoxal phosphate as a coenzyme.
- The α-amino group funnels into α-ketoglutarate to form glutamate, which is then oxidatively deaminated in the liver by glutamate dehydrogenase to yield NH_4^+ and α-ketoglutarate.

23.4 Ammonium Ions Are Converted into Urea in Most Terrestrial Vertebrates

- The first step in the synthesis of urea is the formation of carbamoyl phosphate, which is synthesized from HCO_3^-, NH_3, and two molecules of ATP by carbamoyl phosphate synthetase I.
- A second reaction in the mitochondria produces citrulline, which leaves the mitochondrion and condenses with aspartate, which provides the second nitrogen of what will become urea. Two subsequent reactions in the cytosol produce urea and regenerate the intermediates of the cycle.

23.5 Carbon Atoms of Degraded Amino Acids Emerge as Major Metabolic Intermediates

- The carbon atoms of degraded amino acids are converted into pyruvate, acetyl CoA, acetoacetate, or an intermediate of the citric acid cycle.
- Most amino acids are solely glucogenic, two are solely ketogenic, and a few are both ketogenic and glucogenic.
- Carbon skeletons of glucogenic amino acids enter major metabolic pathways as pyruvate, oxaloacetate, α-ketoglutarate, or succinyl CoA. Ketogenic amino acids produce acetoacetate or acetyl CoA.
- The rings of aromatic amino acids are degraded by oxygenases. Phenylalanine hydroxylase, a monooxygenase, uses tetrahydrobiopterin as the reductant. One of the oxygen atoms of O_2 emerges in tyrosine and the other in water.
- Subsequent steps in the degradation of these aromatic amino acids are catalyzed by dioxygenases, which catalyze the insertion of both atoms of O_2 into organic products.

23.6 Inborn Errors of Metabolism Can Disrupt Amino Acid Degradation

- Errors in amino acid metabolism were sources of some of the first insights into the correlation between pathology and biochemistry.
- Phenylketonuria, the best known of the many hereditary errors of amino acid metabolism, results from the accumulation of high levels of phenylalanine in the body fluids. This accumulation leads to cognitive disabilities unless the patient is placed on low-phenylalanine diets immediately after birth.

Key Terms

ubiquitin
degron
proteasome
aminotransferases (transaminases)
glutamate dehydrogenase
pyridoxal phosphate (PLP)
glucose–alanine cycle
urea cycle
carbamoyl phosphate synthetase I
ketogenic amino acid
glucogenic amino acid
phenylketonuria

Problems

1. What are the steps required to attach ubiquitin to a target protein? 1, 2

2. Protein hydrolysis is an exergonic process, yet the 26S proteasome is dependent on ATP hydrolysis for activity. 1, 3

a. Explain why ATP hydrolysis is required by the 26S proteasome.
b. Small peptides can be hydrolyzed without the expenditure of ATP. How does this information concur with your answer to part (a)?

3. Aminotransferases require which of the following cofactors?

a. $NAD^+ / NADP^+$
b. Pyridoxal phosphate
c. Thiamine pyrophosphate
d. Biopterin

4. Which of the following compounds readily accepts amino groups from amino acids?

a. Glutamine
b. Isocitrate
c. Malate
d. α-Ketoglutarate

5. The immediate donors of the nitrogen atoms of urea are:

a. Aspartate and glutamate
b. Glutamate and carbamoyl phosphate
c. Aspartate and carbamoyl phosphate
d. Glutamine and aspartate

6. Which compound of the urea cycle is synthesized in the mitochondria and transported into the cytoplasm?

a. Ornithine

b. Citrulline
c. Argininosuccinate
d. Arginine

7. Name the α-ketoacid that is formed by the transamination of each of the following amino acids: 4, 5

a. Alanine
b. Aspartate
c. Glutamate
d. Leucine
e. Phenylalanine
f. Tyrosine

8.

a. Write a balanced equation for the conversion of aspartate into glucose through the intermediate oxaloacetate. Which coenzymes participate in this transformation?
b. Write a balanced equation for the conversion of aspartate into oxaloacetate through the intermediate fumarate.

9. What amino acids yield citric acid cycle components and glycolysis intermediates when deaminated? 4, 5

10. Match the property on the left with the biochemical on the right. 4

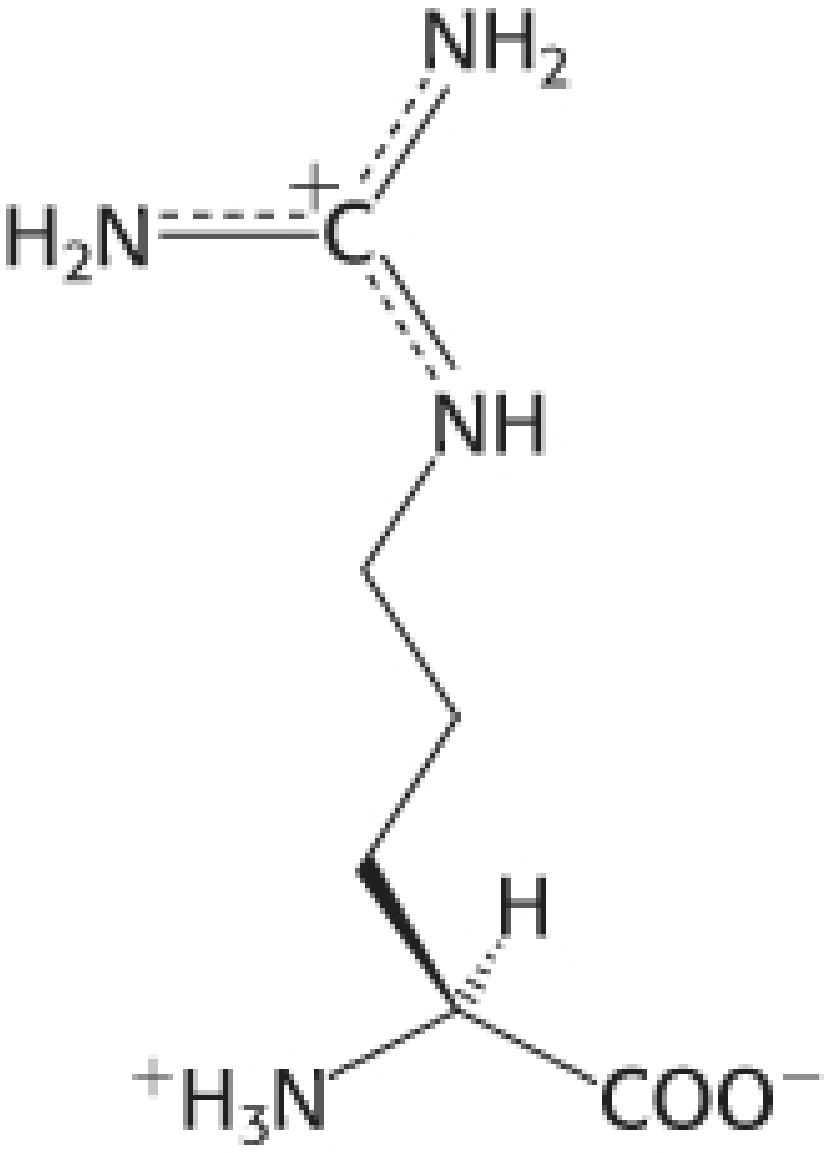
1. Formed from NH_4^+	1. Aspartate
2. Hydrolyzed to yield urea	2. Urea
3. A second source of nitrogen	3. Ornithine

4. Reacts with aspartate	4. Carbamoyl phosphate
5. Cleavage yields fumarate	5. Arginine
6. Accepts the first nitrogen	6. Citrulline
7. Final product	7. Argininosuccinate

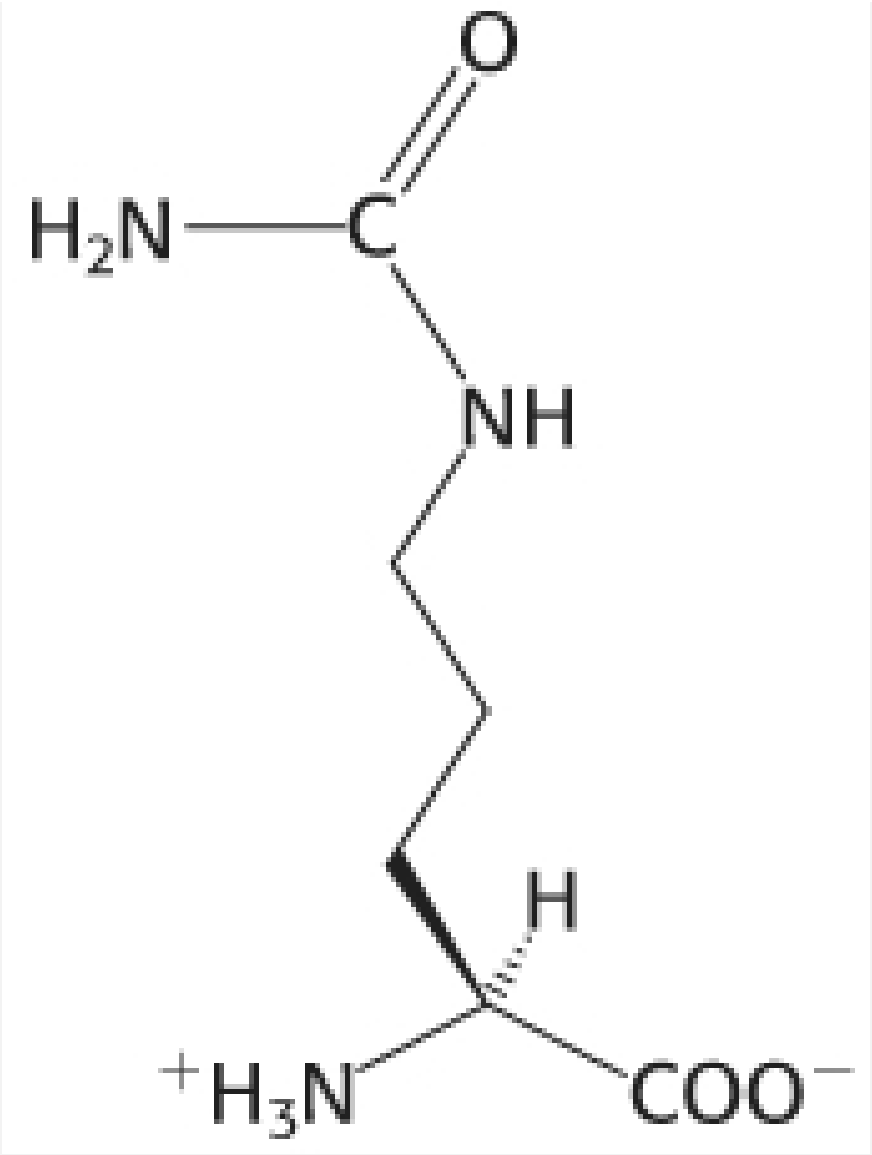
---

11. Identify structures A–D, and place them in the order that they appear in the urea cycle. 4

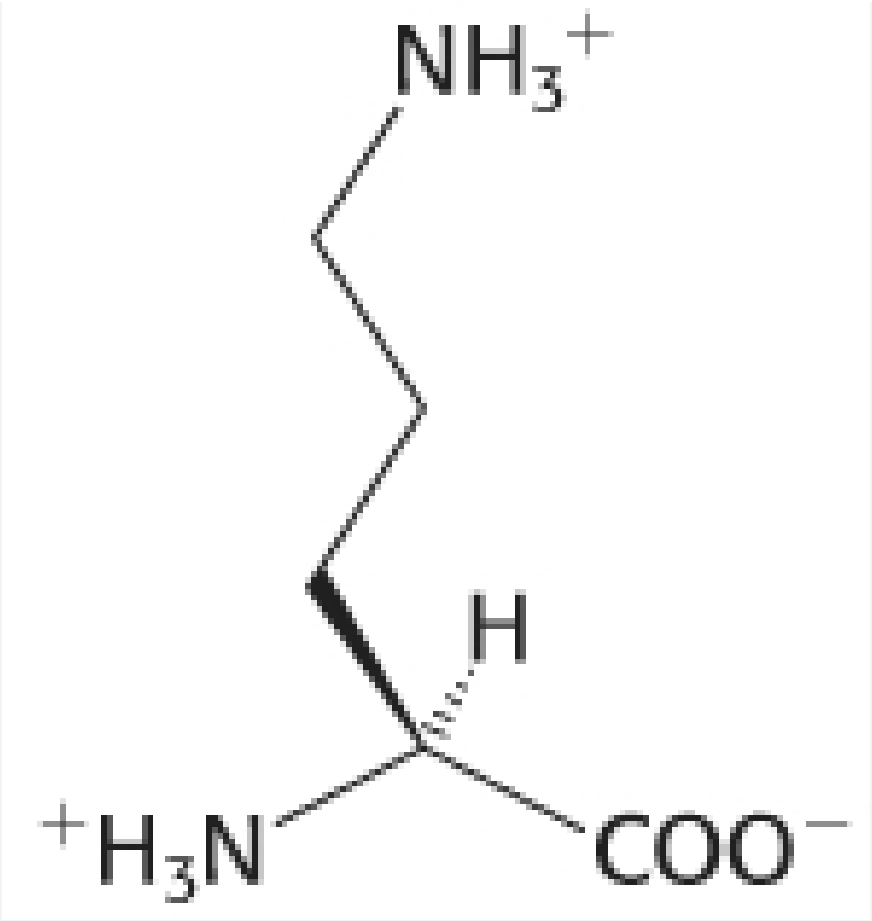
A.



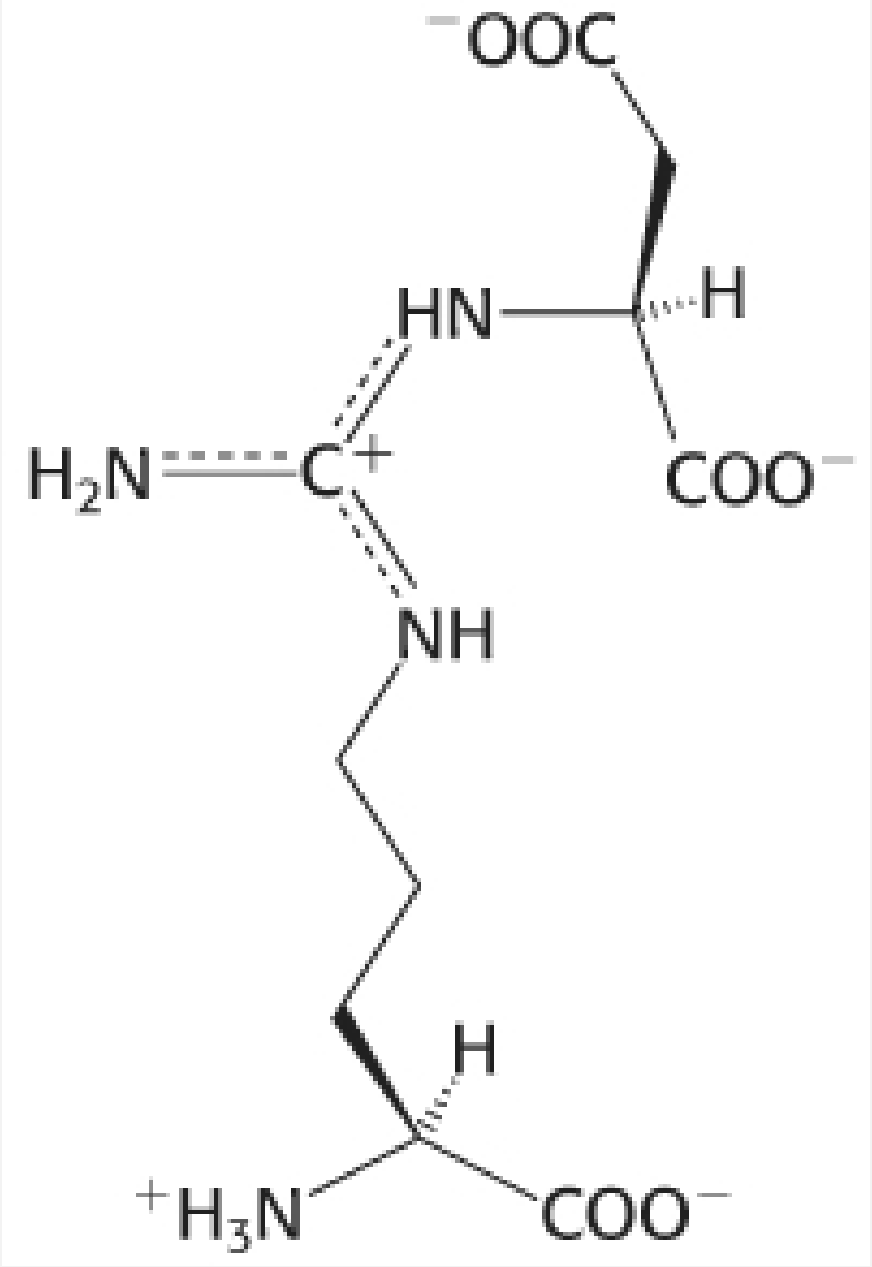
B.



C.



D.



12. Four high-transfer-potential phosphoryl groups are consumed in the synthesis of urea according to the stoichiometry given in Section 23.4. In this reaction, aspartate is

converted into fumarate. Suppose that fumarate is converted into oxaloacetate. What is the resulting stoichiometry of urea synthesis? How many high-transfer-potential phosphoryl groups are spent?

13. A friend bets you a million dollars that you can't prove that the urea cycle is linked to the citric acid cycle and other metabolic pathways. Can you prove it?

14. Why should phenylketonurics avoid using aspartame, an artificial sweetener? (Hint: Aspartame is L-aspartyl-L-phenylalanine methyl ester.) 6

15. What is meant by the terms *ketogenic amino acids* and *glucogenic amino acids*? 5

16. Pyruvate dehydrogenase complex and α-ketoglutarate dehydrogenase complex are huge enzymes consisting of three discrete enzymatic activities. Which amino acids require a related enzyme complex, and what is the name of the enzyme?

17. The carbon skeletons of the 20 common amino acids can be degraded into a limited number of end products. What are the end products, and in what metabolic pathway are they commonly found? 5

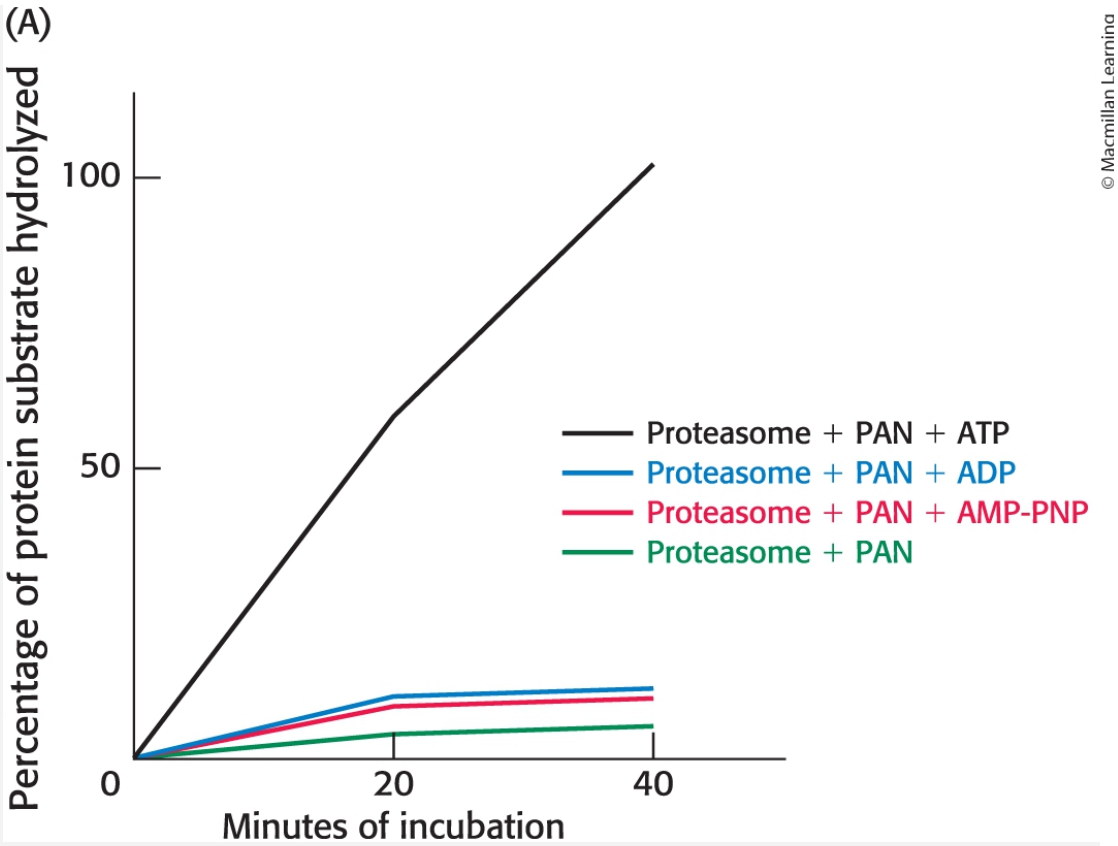
18. In Chapter 5, we learned that there are two types of bisubstrate reactions, sequential and double-displacement. Which type characterizes the action of aminotransferases? Explain your answer.

19. Within a few days after a fast begins, nitrogen excretion accelerates to a higher-than-normal level. After a few weeks, the rate of nitrogen excretion falls to a lower level and continues at this low rate. However, after the fat stores have been depleted, nitrogen excretion rises to a high level. 4, 5

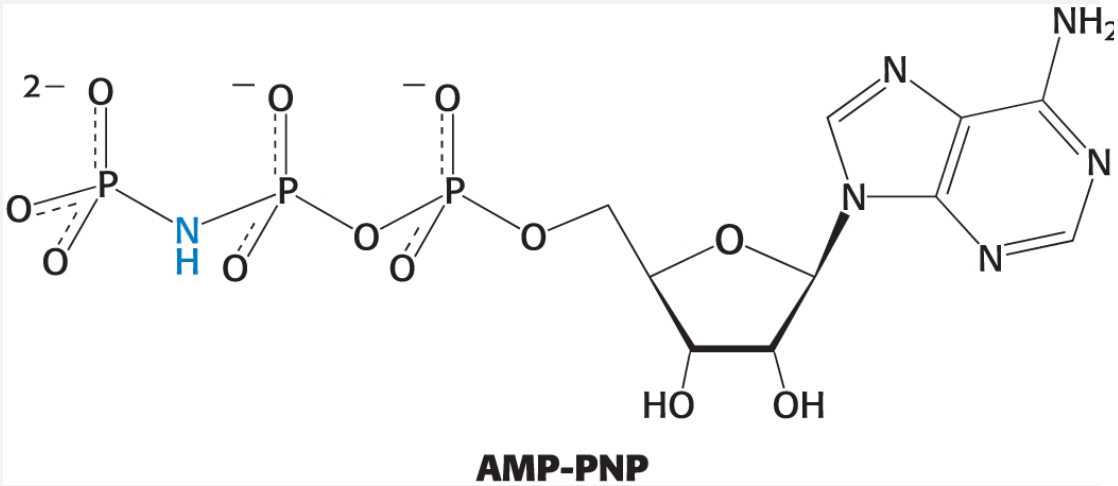
a. What events trigger the initial surge of nitrogen excretion?
b. Why does nitrogen excretion fall after several weeks of fasting?
c. Explain the increase in nitrogen excretion when the lipid stores have been depleted.

20. In eukaryotes, the 20S proteasome component in conjunction with the 19S component degrades ubiquitinated proteins with the hydrolysis of a molecule of ATP. Archaea lack ubiquitin and the 26S proteasome but do contain a 20S proteasome. Some archaea also contain an ATPase that is homologous to the ATPases of the eukaryotic 19S component. This archaeal ATPase activity was isolated as a 650-kDa complex (called PAN) from the archaeon *Thermoplasma*, and experiments were performed to determine if PAN could enhance the activity of the 20S proteasome from *Thermoplasma* as well as other 20S proteasomes.

Protein degradation was measured as a function of time and in the presence of various combinations of components. Graph A shows the results. 1, 2, 3



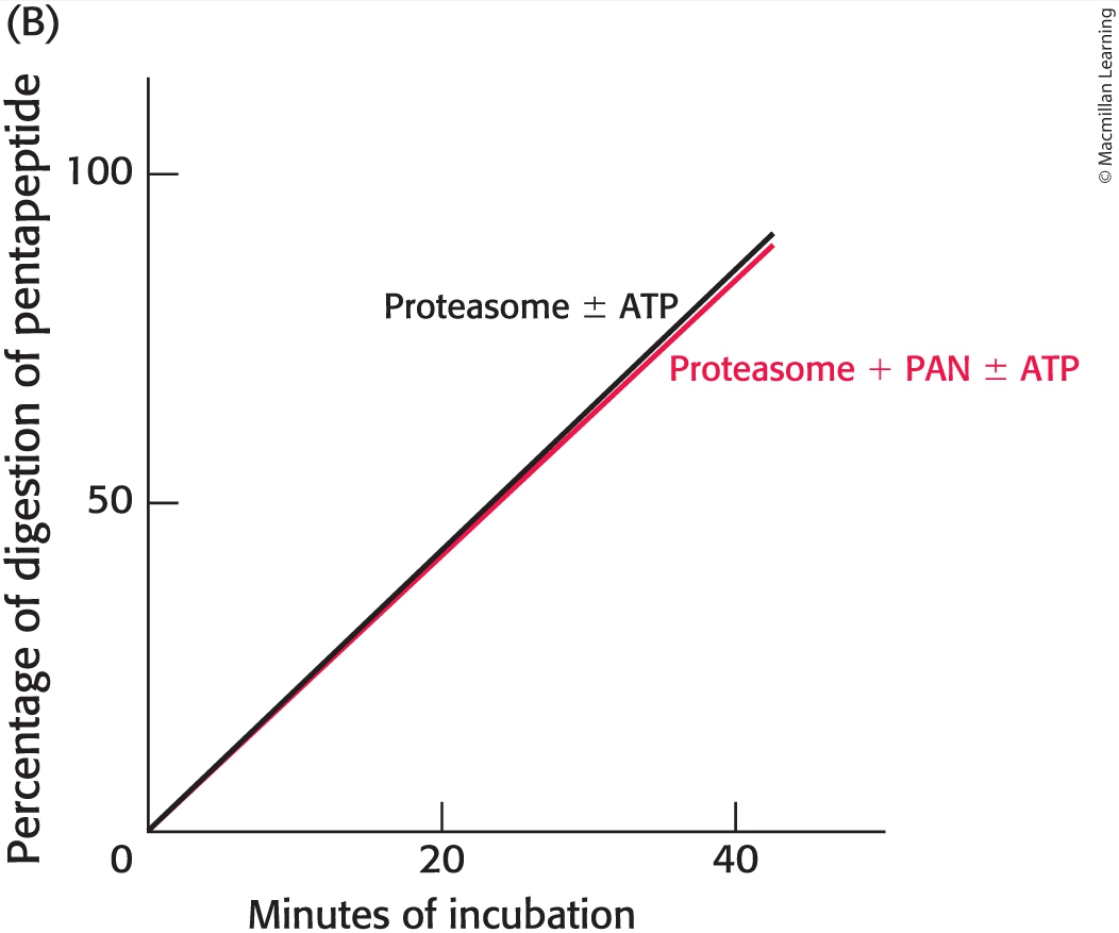
© Macmillan Learning



AMP-PNP

a. What is the effect of PAN on archaeal proteasome activity in the absence of nucleotides?
b. Which nucleotide stimulates protein digestion?
c. What evidence suggests that ATP hydrolysis, and not just the presence of ATP, is required for digestion?

A similar experiment was performed with a small peptide as a substrate for the proteasome instead of a protein. The results obtained are shown in graph B.



d. How do the requirements for peptide digestion differ from those of protein digestion?
e. Suggest some reasons for the difference.

The ability of PAN from the archaeon *Thermoplasma* to support protein degradation by the 20S proteasomes from the archaeon

Methanosarcina and rabbit muscle was then examined.

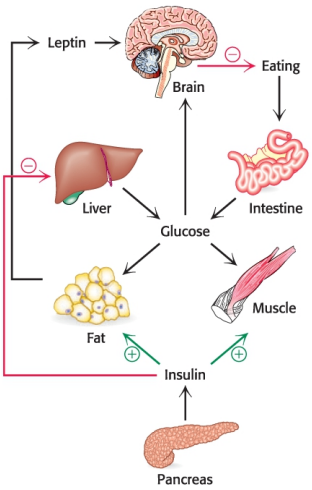
Percentage of digestion of protein substrate (Source of the 20S proteasome)

Additions	Thermoplasma	Methanosarcina	Rabbit muscle
None	11	10	10
PAN	8	8	8
PAN + ATP	100	40	30
PAN + ADP	12	9	10

[Data from P. Zwickl, D. Ng, K. M. Woo, H.-P. Klenk, and A. L. Goldberg, An archaebacterial ATPase, homologous to ATPase in the eukaryotic 26S proteasome, activates protein breakdown by 20S proteasomes, *J. Biol. Chem.* 274(37):26008–26014, 1999.]

f. Can the *Thermoplasma* PAN augment protein digestion by the proteasomes from other organisms?
g. What is the significance of the stimulation of rabbit muscle proteasome by *Thermoplasma* PAN?

Chapter 24
Integration of Energy Metabolism





Debbie Eckert/Alamy
© Macmillan Learning

The maintenance of blood-glucose levels requires the integration of many elaborate metabolic pathways. Disorders affecting the principal organs, hormones, and pathways involved can lead to disease. Type 1 diabetes, for example, results from the dysfunction of specific pancreatic cells that normally release the hormone insulin after meals. Fundraising events support research for better treatments for the approximately 9 million people worldwide who are affected by type 1 diabetes.

Outline

24.1 Caloric Homeostasis Is a Means of Regulating Body Weight
24.2 The Fasted–Fed Cycle Is a Response to Eating and Sleeping Behaviors
24.3 Diabetes Is a Common Metabolic Disease Often Resulting from Obesity

24.4 Exercise Beneficially Alters the Biochemistry of Cells
24.5 Starvation Induces Protein Wasting and Ketone Body Formation
24.6 Ethanol Alters Energy Metabolism in the Liver

Learning Goals



By the end of this chapter, you should be able to:

1. Describe caloric homeostasis and its biochemical importance.
2. Explain the role of the neurotransmitters and hormones in maintaining caloric homeostasis.
3. Differentiate between type 1 and type 2 diabetes, and explain how each develops.
4. Explain how different forms of exercise alter cellular biochemistry.
5. Contrast the biochemical responses to the nightly fasted–fed cycle with those of prolonged starvation.
6. Explain how ethanol alters metabolism in the liver.

So far we have examined metabolism one pathway at a time and have seen how energy is extracted from fuels and used to power biosynthetic reactions. In Chapters 25 through 31, we will extend our study of biosynthetic reactions to the synthesis of nucleic acids, diverse lipids, and proteins. First, however, in this chapter we will take a step back to examine large-scale biochemical interactions that constitute the physiology of the organism and the regulation of energy at the organismal level. We will examine how various biochemical pathways and tissues interact with one another in both resting metabolism and in a variety of states of metabolic perturbation, namely: obesity, fasting, diabetes, intense exercise, starvation, and excessive alcohol consumption.

24.1 Caloric Homeostasis Is a Means of Regulating Body Weight

In this section we will address an apparently simple but actually quite complex question: at the biochemical level, how does an organism know when to eat and when to refrain from eating? The ability to maintain adequate, but not excessive, energy stores is called **caloric homeostasis** or **energy homeostasis**. By now in our study of biochemistry, we are well aware of the fact that carbohydrates, lipids, and the carbon skeletons of amino acids are sources of energy (**Figure 24.1**). We consume these energy sources as foods and capture free energy by re-forming ATP, which we use to power our lives. As illustrated in Figure 24.1, to do this requires an incredible amount of coordination among numerous metabolic pathways that we have explored in Chapters 16 through 23.

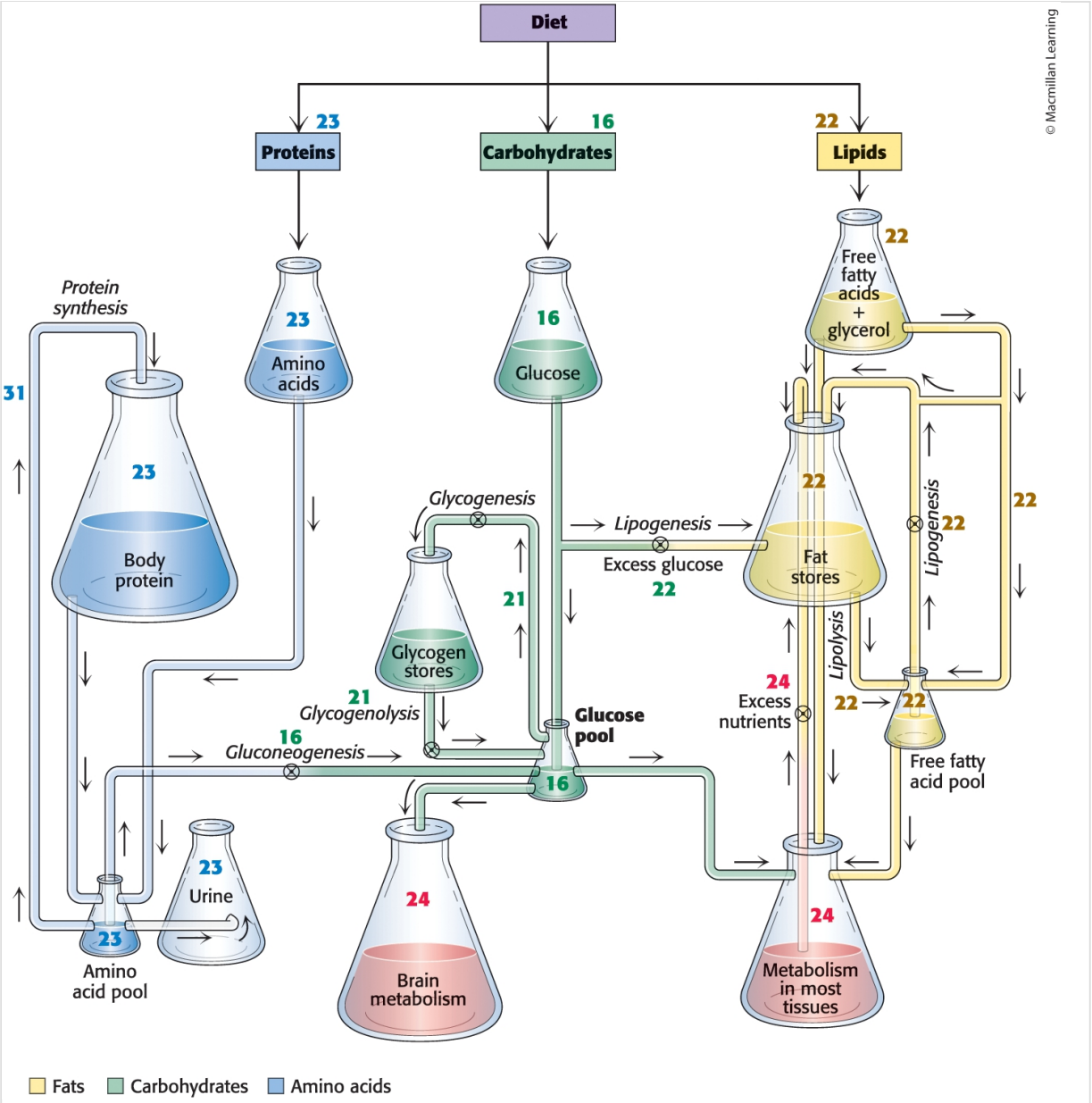


FIGURE 24.1 Maintaining homeostasis requires complex metabolic regulation that coordinates the use of nutrient pools. The numbers indicate the chapters in which the topics are discussed.

[Information from D. U. Silverthorn, *Human Physiology: An Integrated Approach,* 3rd ed. (Pearson, 2004), Fig. 22-2.]

However, despite this mechanistic complexity, like all energy transformations our energy consumption and expenditure are governed

by the laws of thermodynamics. Recall that the First Law of Thermodynamics states that energy can neither be created nor destroyed. Translated into the practical terms of our diets:

$$\text{Energy consumed} = \text{energy expended} + \text{energy stored}$$

This simple equation has severe physiological and health implications: according to the First Law of Thermodynamics, if we consume more energy than we expend, we will eventually become overweight or obese. Regardless of the original source, any excess energy molecules are ultimately converted to triacylglycerols which are stored in adipocytes. The number of adipocytes becomes fixed in adults, and so obesity results in engorged adipocytes. Indeed, the cells may increase as much as 1000-fold in size. Obesity is generally defined as a body mass index (BMI) of more than $30\ \text{kg m}^{-2}$, whereas overweight is defined as a BMI of more than $25\ \text{kg m}^{-2}$.

Obesity is a worldwide problem that is now considered a pandemic, with the number of people considered obese having tripled since 1975 and totaling 650 million people. Obesity is identified as a risk factor in a host of pathological conditions, including diabetes mellitus, hypertension, and cardiovascular disease (Table 24.1). We will consider the biochemical basis of pathologies caused by obesity later in the chapter.

TABLE 24.1 Health consequences of obesity

Coronary heart disease
Type 2 diabetes
Cancers (endometrial, breast, colon, and others)

Hypertension (high blood pressure)
Dyslipidemia (disruption of lipid metabolism)
Stroke
Liver and gallbladder disease
Sleep apnea and respiratory problems
Osteoarthritis (degeneration of joint cartilage/bone)
Gynecological problems (abnormal menses, infertility)
Male infertility problems

Information from Centers for Disease Control and Prevention website (www.cdc.gov).

Before we undertake a biochemical analysis of the results of overconsumption, let us consider why the obesity pandemic is occurring in the first place. There are several overlapping explanations. The first is a commonly held view that our bodies are programmed to rapidly store excess calories in times of plenty, an evolutionary adaptation to the scarcity of food. Consequently, we store calories as if a fast might begin tomorrow, regardless of whether it actually does. We are also no longer subject to predation, which once would have applied selective pressure to maintain low body fats so that our ancestors could more easily flee from an attack.

Another factor is that calorie-dense, highly palatable foods — rich in sugar and fats — are now more readily accessible, stimulating the same reward pathways in the brain that are triggered by drugs such as cocaine. Such reward pathways can be strong enough to override appetite-suppressing signals. These foods, along with other environmental factors such as pollution, can also affect our intestinal

microbiome — the bacteria and other microbes that inhabit our guts — that play a significant role in how we process our food.

Finally, although genetics cannot explain the obesity pandemic affecting vast amounts of the entire human *population*, it is evident that *individuals* respond differently to obesity-inducing environmental conditions, and that this difference has a large genetic component. Various studies have indicated the heritability of fat mass to be between 30% and 70%, making it extra difficult for some people to lose weight.

Regardless of why we may have a propensity to gain weight, this predisposition can be counteracted behaviorally — by eating less and exercising more. It also appears that it is easier to prevent weight gain than it is to lose weight. Clearly, caloric homeostasis is a complicated biological phenomenon that will engage biomedical research scientists for some time to come.

The brain plays a key role in caloric homeostasis

As disturbing as the obesity pandemic is, an equally intriguing observation is that many people are able to maintain an approximately constant weight throughout adult life, despite consuming literally tons of food over a lifetime. Although willpower, exercise, and a bathroom scale often play a role in this homeostasis, some favorable biochemical signaling must also be behind this remarkable physiological feat. What makes this balance of energy input and output possible? As one might imagine, the answer is complicated, entailing many biochemical signals as well as a host of behavioral factors. We will focus on a few key biochemical signals and divide our discussion into two parts: short-term signals that are active during a meal, and long-term signals that report on the overall energy status of the body. These signals originate in the gastrointestinal tract, the β cells of the pancreas, and fat cells. The

primary target of these signals is the brain, in particular a group of neurons in a region of the hypothalamus called the *arcuate nucleus*.

Short-term signals from the gastrointestinal tract induce feelings of satiety

Short-term signals relay feelings of satiety (fullness) from the gut to various regions of the brain and thus reduce the urge to eat during what is known as the *postprandial period*, or the time right after a meal (Figure 24.2).

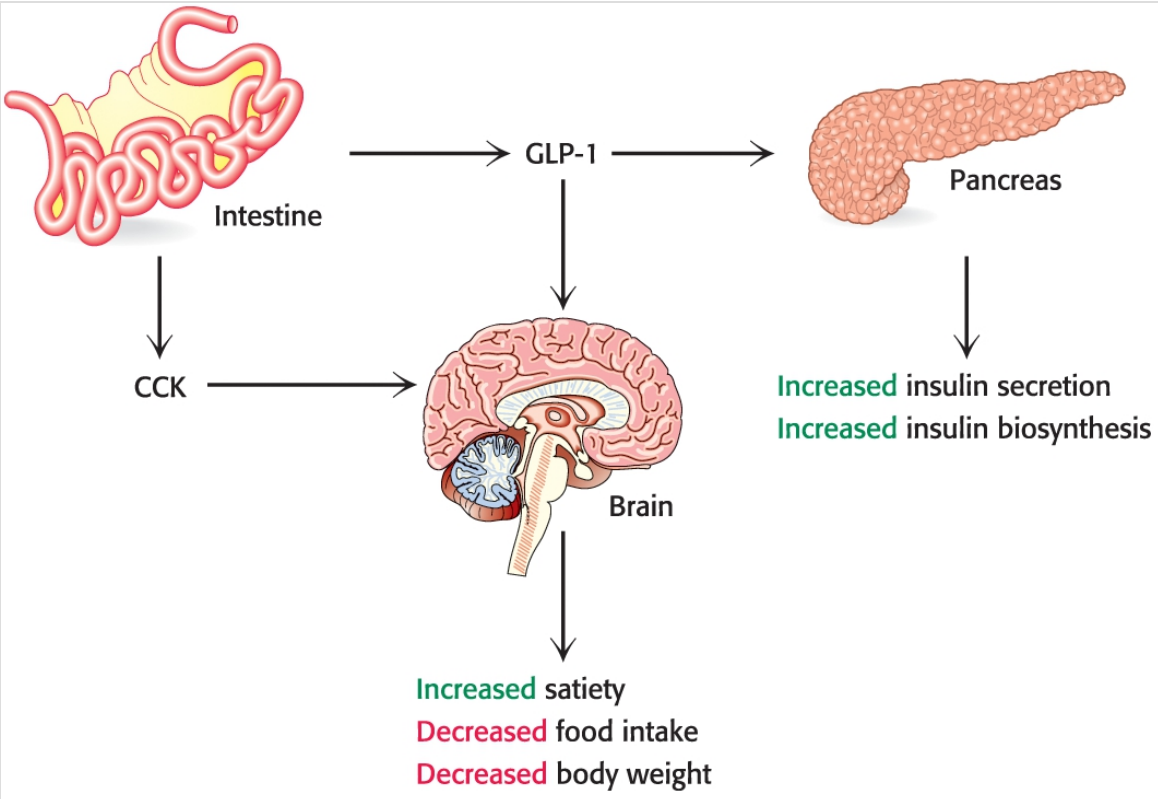


FIGURE 24.2 Signal molecules originating from the gut induce feelings of satiety in the brain. Cholecystokinin (CCK) is secreted by specialized cells of the small intestine in response to a mea and activates satiation pathways in the brain. Glucagon-like peptide 1 (GLP-1), secreted by L cel in the intestine, also activates satiation pathways in the brain and potentiates insulin action in the pancreas.

[Information from S. C. Wood, *Cell Metab*. 9:489–498, 2009, Fig. 1.]

The best-studied short-term signals are cholecystokinin (CCK) and glucagon-like peptide 1 (GLP-1). Both are small peptide hormones secreted into the blood by cells in the upper part of the small intestine as postprandial satiation signals. Both bind to their respective G-protein-coupled receptors (Section 14.2) in peripheral neurons, relaying signals to the brain that generate feelings of satiety. CCK and GLP-1 also play important roles in digestion; CCK stimulates the secretion of pancreatic enzymes and bile salts from the gallbladder, while GLP-1 enhances glucose-induced insulin secretion and inhibits glucagon secretion. Recall that **insulin** causes glucose to be removed from the blood and stimulates the synthesis of glycogen and lipids, while **glucagon** has effects opposite those of insulin.

Although we have examined only two short-term signals, many others are believed to exist (**Table 24.2**). Most of the short-term signals thus far identified are appetite suppressants. However, another small peptide hormone called *ghrelin* — secreted by the stomach — acts on regions of the hypothalamus to stimulate appetite through its G-protein-coupled receptor. Ghrelin secretion increases before a meal and decreases afterward.

TABLE 24.2 Gastrointestinal peptides that regulate food intake

Appetite-suppressing signals
Cholecystokinin
Glucagon-like peptide 1
Glucagon-like peptide 2

Amylin
Somatostatin
Bombesin
Enterostatin
Apolipoprotein A-IV
Gastric inhibitory peptide
Appetite-enhancing peptide
Ghrelin

Information from M. H. Stipanuk, ed., *Biochemical, Physiological, Molecular Aspects of Human Nutrition*, 2nd ed. (Saunders/Elsevier, 2006), p. 627, Box 22-1.

Leptin and insulin regulate long-term control over caloric homeostasis

Two key signal molecules regulate energy homeostasis over the time scale of hours or days: **leptin**, which is secreted by the adipocytes, and insulin, which is secreted by the pancreatic β cells. Leptin communicates the status of the triacylglycerol stores, whereas insulin communicates the status of glucose in the blood — in other words, carbohydrate availability. We will consider leptin first.

Adipose tissue was formerly considered an inert storage form of triacylglycerols. However, later work showed that adipose tissue is an active endocrine tissue, secreting signal molecules called *adipokines*, such as leptin, that regulate a host of physiological processes. Leptin is

secreted by adipocytes in direct proportion to the amount of fat present: the more fat in a body, the more leptin is secreted. Leptin binding to its receptor throughout the body increases the sensitivity of muscle and the liver to insulin, stimulates β oxidation of fatty acids, and decreases triacylglycerol synthesis.

Let us consider the effects of leptin in the brain. Leptin binds to its receptor, thereby activating a signal-transduction pathway. The leptin receptor is found in various regions of the brain, but particularly in the arcuate nucleus of the hypothalamus. There, one population of neurons expresses appetite-stimulating (orexigenic) peptides, called neuropeptide Y (NPY) and agouti-related peptide (AgRP). Leptin inhibits the production and release of NPY and AgRP, thus repressing the desire to eat (**Figure 24.3**).

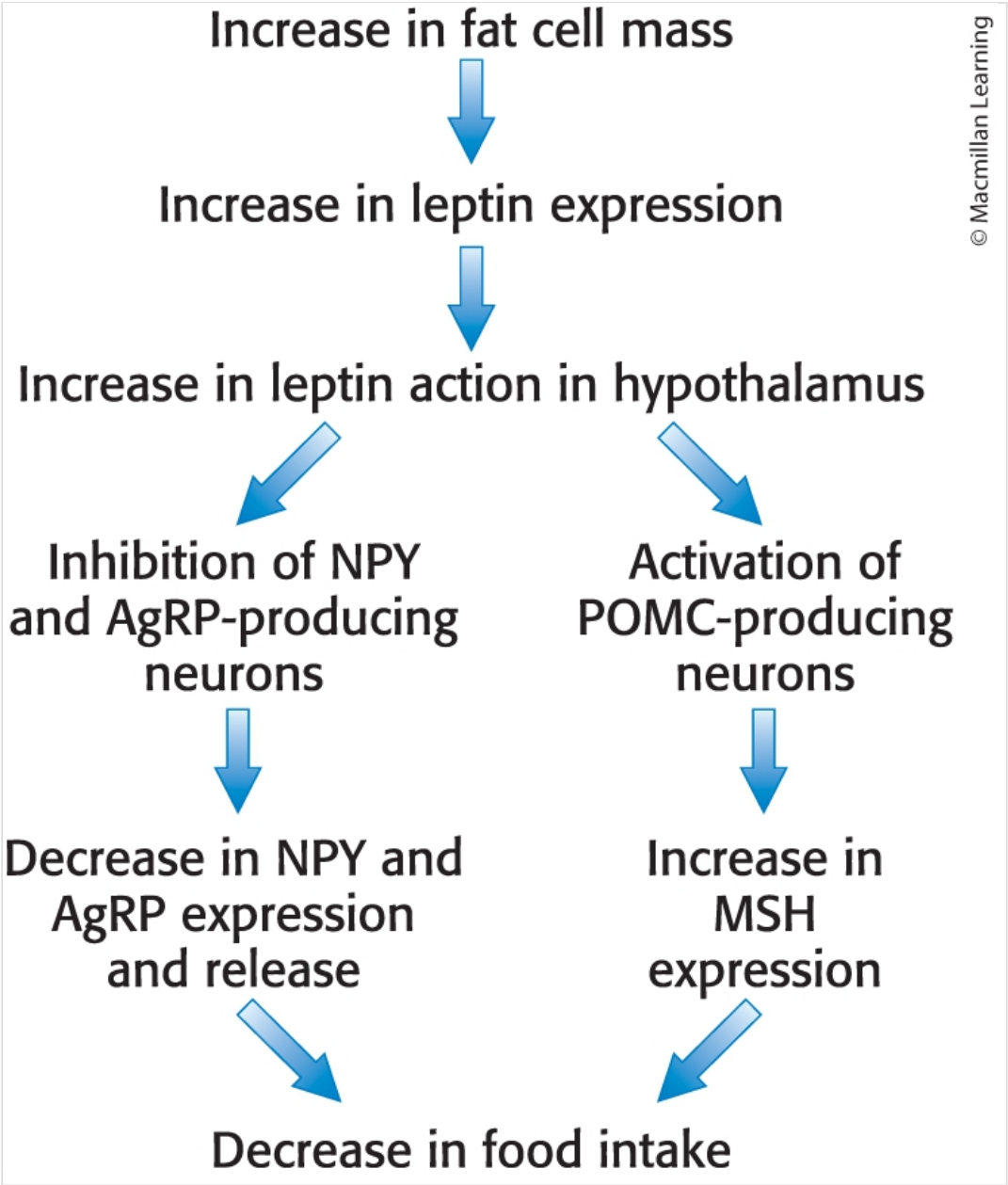


FIGURE 24.3 Leptin suppresses appetite by affecting the brain. Leptin is an adipokine secreted by adipose tissue in direct relation to fat mass. When fat mass increases, leptin inhibits NPY and AgRP secretion while stimulating the release of appetite-suppressing hormone MSH.

[Information from M. H. Stipanuk, *Biochemical, Physiological, & Molecular Aspects of Human Nutrition*, 2nd ed. (Saunders/Elsevier, 2006), Fig. 22-2.]

The second population of neurons containing leptin receptors expresses a large precursor polypeptide, proopiomelanocortin (POMC). Leptin binding to its receptor on POMC neurons causes POMC to be proteolytically processed to yield a variety of signal molecules, one of which is melanocyte-stimulating hormone (MSH). MSH, originally discovered as a stimulator of melanocytes (cells that synthesize the pigment melanin), activates appetite-suppressing (anorexigenic) neurons and thus inhibits food consumption. AgRP also inhibits MSH activity by acting as an antagonist, binding to the MSH receptor but failing to activate the receptor (Figure 24.3). Thus, the net effect of leptin binding to its receptor is the initiation of a complex signal-transduction pathway that ultimately curtails food intake. Insulin receptors are also present in the hypothalamus, although the mechanism of insulin action in the brain is less clear than that of leptin. Insulin appears to inhibit NPY/AgRP-producing neurons, thus inhibiting food consumption.

Self-Check Question



Name two short-term signals that are appetite-suppressing (anorexigenic) and one that is appetite-stimulating (orexigenic).

Leptin is one of several hormones secreted by adipose tissue

Leptin was the first adipokine discovered because of the dramatic effects of its absence. Researchers discovered a strain of mice called ob/ob mice, which completely lack leptin and, as a result, are extremely obese. These mice display hyperphagia (overeating), hyperlipidemia (accumulation of triacylglycerols in muscle and liver), and an

insensitivity to insulin. Since the discovery of leptin, other adipokines have been detected. For instance, adiponectin is another signal molecule produced by the adipocytes; but, unlike leptin, secretion of adiponectin increases in proportion to decreases in fat mass.

A key function of adiponectin appears to be increasing the sensitivity of the organism to insulin. Both leptin and adiponectin exert their effects through the key regulatory enzyme, AMP-activated protein kinase (AMPK) (**Figure 24.4**). Recall that this enzyme is active when AMP levels are elevated and ATP levels are diminished, and this activation leads to a decrease in anabolism and an increase in catabolism, most notably an increase in fatty acid oxidation (Section 22.7). In insulin-resistant obese animals, leptin levels increase while those of adiponectin decrease.

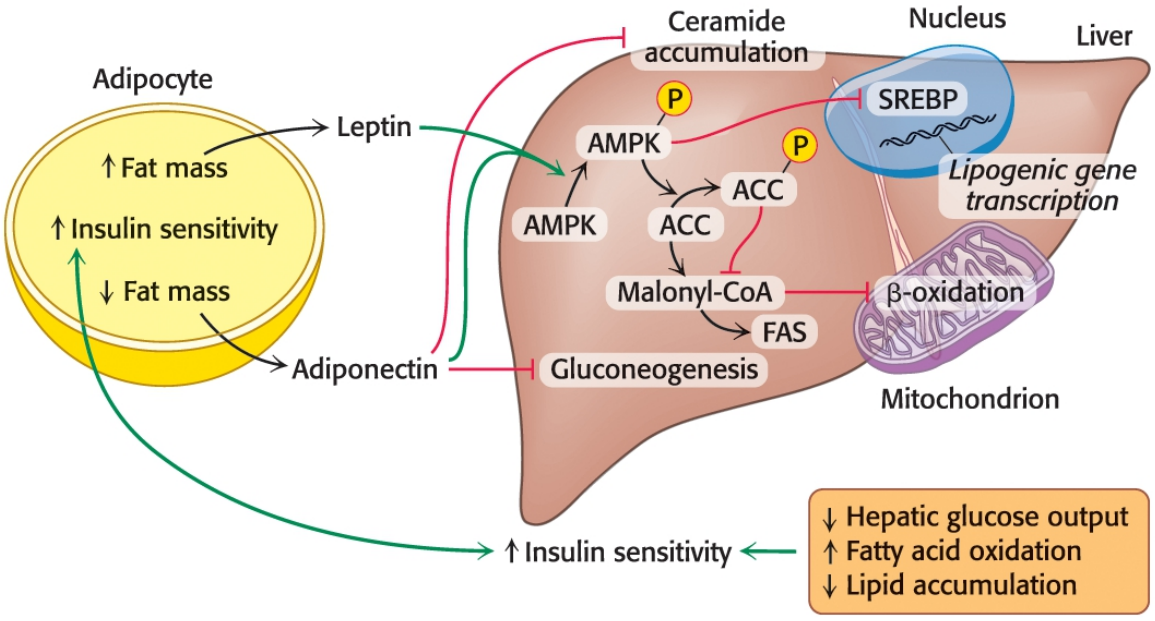


FIGURE 24.4 Adipokines help to maintain systemic lipid and glucose homeostasis. Both leptin and adiponectin act to prevent lipid accumulation in the liver and stimulate fatty acid oxidation by activating AMPK, which decreases the expression of lipogenic transcription factors such as SREBP and inactivates acetyl CoA carboxylase 1 (ACC). Inactivating ACC reduces the concentration of malonyl CoA, which normally inhibits oxidation and stimulates lipogenesis. Adiponectin also inhibits gluconeogenesis and reduces ceramide accumulation, which would otherwise further reduce insulin action. The combined action of leptin and adiponectin on the liver results in decreased glucose output, decreased lipid accumulation, and increased fatty acid oxidation in the liver, all of which enhance insulin sensitivity for the liver and other tissues.

Adipocytes produce two additional hormones, RBP4 (originally discovered as a retinol binding protein) and resistin, that promote insulin resistance. Although it is unclear why adipocytes secrete hormones that facilitate insulin resistance, a pathological condition, we can speculate on the reason. These signal molecules may help to fine-tune the actions of leptin and adiponectin or perhaps to act as "brakes" on the action of leptin and adiponectin to prevent hypoglycemia in the fasted state. Some evidence indicates that enlarged adipocytes that result from obesity may secrete higher levels of insulin-antagonizing hormones and thus contribute to insulin resistance. Resistin has recently been implicated as a causal factor in the increased incidence of cardiovascular disease associated with obesity.

Leptin resistance may be a contributing factor to obesity

If leptin is produced in proportion to body-fat mass and leptin inhibits eating, why do people become obese? Obese people, in most cases, have both functioning leptin receptors and a high blood concentration of leptin. The failure to respond to the anorexigenic effects of leptin is called *leptin resistance*. What is the basis of leptin resistance?

As for most questions in the exciting area of energy homeostasis, the answer is not well worked out, but recent evidence suggests that a group of proteins called *suppressors of cytokine signaling* (SOCS) may take part. These proteins fine-tune some hormonal systems by inhibiting receptor action. SOCS proteins inhibit receptor signaling by a number of means. Consider, for example, the effect of SOCS proteins on the insulin

receptor. Recall that insulin stimulates the autophosphorylation of tyrosine residues on the insulin receptor, which in turn phosphorylates IRS-1, initiating the insulin-signaling pathway (**Figure 24.5A**). SOCS proteins bind to phosphorylated tyrosine residues on receptors or other members of the signal-transduction pathway, thereby disrupting signal flow and thus altering the cell's biochemical activity (**Figure 24.5B**). In other cases, the binding of SOCS proteins to components of the signal-transduction pathway may also enhance proteolytic degradation of these components by the proteasome (Section 23.2).

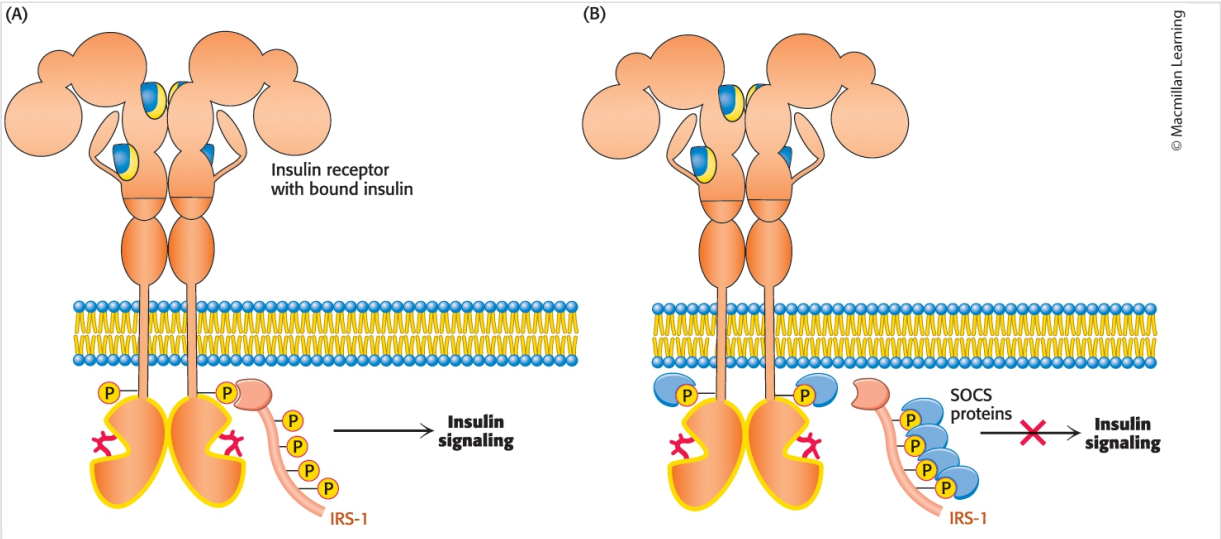


FIGURE 24.5 Suppressors of cytokine signaling (SOCS) regulate insulin receptor function. (A) Insulin binding results in phosphorylation of the receptor and subsequent phosphorylation of IRS-1. These processes initiate the insulin-signaling pathway. (B) SOCS proteins disrupt interactions of components of the insulin-signaling pathway by binding phosphorylated proteins and thereby inhibiting the pathway. The binding of a signal component by SOCS results in proteasomal degradation in some cases. (IRS-1, insulin-receptor substrate 1; SOCS, suppressor of cytokine signaling.)

Evidence in support of a role for SOCS in leptin resistance comes from mice that have had SOCS selectively deleted from POMC-expressing neurons. These mice display an enhanced sensitivity to leptin and are resistant to weight gain even when fed a high-fat diet. The reason why

the activity of SOCS proteins increases, leading to leptin resistance, remains to be determined. Alternatively, leptin resistance can arise by means unrelated to SOCS. For example, to have systemic effects, leptin must enter the brain. Mutations in proteins that transport leptin into the brain or in the brain leptin receptors could also result in leptin resistance.

24.2 The Fasted–Fed Cycle Is a Response to Eating and Sleeping Behaviors

Next, let's examine the natural cycles of human metabolism in a resting and nonpathological state. We begin with a physiological condition called the **fasted–fed cycle**, which we all experience in the hours after an evening meal and through the night's fast. This nightly fasted–fed cycle has three stages: the well-fed (postprandial) state after a meal, the early fasting (postabsorptive) state during the night, and the refed state after breakfast. A major goal of the many biochemical alterations in this period is to maintain **glucose homeostasis** — that is, a constant blood-glucose concentration. Maintaining glucose homeostasis is crucial because glucose is normally the only fuel source for the brain. The two primary signals regulating the fasted–fed cycle are insulin and glucagon.

The postprandial state follows a meal

After we consume and digest a meal, glucose and amino acids are transported from the intestine to the blood. The dietary lipids are packaged into chylomicrons and transported to the blood by the lymphatic system. This fed condition leads to the secretion of insulin, which signals the postprandial state. Insulin stimulates glycogen synthesis in both muscle and the liver, suppresses gluconeogenesis by the liver, and stimulates protein synthesis. Insulin also accelerates glycolysis in the liver, which in turn increases the synthesis of fatty acids.

The liver helps to limit the amount of glucose in the blood during times of plenty by storing it as glycogen, so as to be able to release glucose in

times of scarcity. How is the excess blood glucose present after a meal removed? The liver is able to trap large quantities of glucose because it possesses an isozyme of hexokinase called *glucokinase* that converts glucose into glucose 6-phosphate, which cannot be transported out of the cell. Recall that glucokinase has a high K_M value and is thus highly active only when blood-glucose concentration is high (Section 16.3). Furthermore, glucokinase is not inhibited by glucose 6-phosphate as hexokinase is. Consequently, the liver forms glucose 6-phosphate more rapidly as the blood-glucose concentration rises. The increase in glucose 6-phosphate, which activates glycogen synthase, coupled with the effects of insulin leads to a buildup of glycogen stores.

The hormonal effects on glycogen synthesis and storage are reinforced by a direct action of glucose itself. Phosphorylase *a* is a glucose sensor in addition to being the enzyme that cleaves glycogen. When the glucose level is high, the binding of glucose to phosphorylase *a* renders the enzyme susceptible to the action of a phosphatase that converts it into phosphorylase *b*, which does not readily degrade glycogen (Figure 21.24). Thus, glucose allosterically shifts the glycogen system from a degradative to a synthetic mode.

The high insulin level in the fed state also promotes the entry of glucose into muscle and adipose tissue. Insulin stimulates the synthesis of glycogen by muscle as well as by the liver. The entry of glucose into adipose tissue provides glycerol 3-phosphate for the synthesis of triacylglycerols. The action of insulin also extends to amino acid and protein metabolism. Insulin promotes the uptake of branched-chain amino acids (valine, leucine, and isoleucine) by muscle. Indeed, insulin has a general stimulating effect on protein synthesis, which favors a building up of muscle protein. In addition, it inhibits the intracellular degradation of proteins.

The postabsorptive state occurs at the beginning of a fast

The blood-glucose concentration begins to drop several hours after a meal, leading to a decrease in insulin secretion and a rise in glucagon secretion by the α cells of the pancreas. This period is called the *fasted state* or *postabsorptive state* because it immediately follows the absorption of glucose from the blood that resulted from the previous meal. The regulation of glucagon secretion is poorly understood, but when glucose is abundant, β cells inhibit glucagon secretion. When glucose concentration falls, the inhibition is relieved, and glucagon is secreted by the α cells of the pancreas. Just as insulin signals the fed state, glucagon signals the fasted state, serving to mobilize glycogen stores when there is no dietary intake of glucose.

The main target organ of glucagon is the liver. Glucagon stimulates glycogen breakdown and inhibits glycogen synthesis by triggering the cyclic AMP cascade; this leads to the phosphorylation and activation of phosphorylase and the inhibition of glycogen synthase (Section 21.6). Glucagon also inhibits fatty acid synthesis by diminishing the production of pyruvate and by maintaining the inactive phosphorylated state of acetyl CoA carboxylase. In addition, glucagon stimulates the gluconeogenic state in the liver and blocks glycolysis by decreasing in the amount of fructose 2,6-bisphosphate (F-2,6-BP), which normally stimulates glycolysis and inhibits gluconeogenesis (Section 16.5). Hence, the decrease in F-2,6-BP results in a decrease in glycolytic activity and an increase in gluconeogenesis because of the opposing effects of F-2,6-BP on phosphofructokinase and fructose-1,6-bisphosphatase (Section 16.5; **Figure 24.6**).

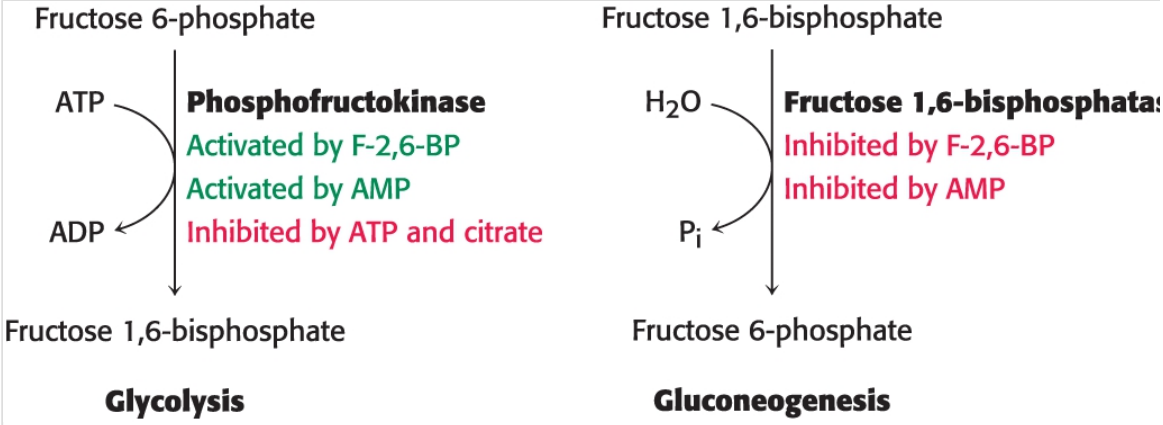


FIGURE 24.6 Glycolysis and gluconeogenesis are reciprocally regulated. Phosphofructokinase is the key enzyme in the regulation of glycolysis, whereas fructose 1,6-bisphosphatase is the principal enzyme controlling the rate of gluconeogenesis. Note the reciprocal relationship between the pathways and the signal molecules.

EXPLORE these pathways further in the Metabolic Map in Achieve

All known actions of glucagon are mediated by protein kinases that are activated by cyclic AMP. The activation of the cyclic AMP cascade results in a higher level of phosphorylase *a* activity and a lower level of glycogen synthase *a* activity. Glucagon's effect on this cascade is reinforced by the low concentration of glucose in the blood. The diminished binding of glucose to phosphorylase *a* makes the enzyme less susceptible to the hydrolytic action of the phosphatase. Instead, the phosphatase remains bound to phosphorylase *a*, and so the synthase stays in the inactive phosphorylated form. Consequently, there is a rapid mobilization of glycogen.

The large amount of glucose formed by the hydrolysis of glucose 6-phosphate derived from glycogen is then released from the liver into the blood. The entry of glucose into muscle and adipose tissue decreases in response to a low insulin level. The diminished utilization of glucose by muscle and adipose tissue also contributes to the maintenance of the blood-glucose concentration. The net result of these actions of glucagon

is to markedly increase the release of glucose by the liver. Both muscle and the liver use fatty acids as fuel when the blood-glucose concentration drops, saving the glucose for use by the brain and red blood cells. Thus, the blood-glucose concentration is kept at or above 4.4 mM by three major factors: (1) the mobilization of glycogen and the release of glucose by the liver, (2) the release of fatty acids by adipose tissue, and (3) the shift in the fuel used by muscle from glucose to fatty acids.

What is the result of the depletion of the liver's glycogen stores? Gluconeogenesis from lactate and alanine continues, but this process merely replaces glucose that had already been converted into lactate and alanine by tissues such as muscle and red blood cells. Moreover, the brain oxidizes glucose completely to CO_2 and H_2O. Thus, for the net synthesis of glucose to take place, another source of carbon is required. Glycerol released from adipose tissue on lipolysis provides some of the carbon atoms, with the remaining carbon atoms coming from the hydrolysis of muscle proteins.

The refed state occurs at the end of a long fast

What are the biochemical responses to a large breakfast? Fat is processed exactly as it is processed in the normal fed state. However, that is not the case for glucose. The difference between the refed state and other postprandial states is the length of the fast. In the case of the first morning meal or any other meal after a long fast, the liver does not initially absorb glucose from the blood, but instead leaves it for the other tissues. Moreover, the liver remains in a gluconeogenic mode. Now, however, the newly synthesized glucose is used to replenish the liver's glycogen stores. As the blood-glucose concentration continues to rise, the liver completes the replenishment of its glycogen stores and begins to process the remaining excess glucose for fatty acid synthesis.

Self-Check Question



What are the three primary sources of glucose 6-phosphate in liver cells?

24.3 Diabetes Is a Common Metabolic Disease Often Resulting from Obesity



Having considered the regulation of body weight and glucose homeostasis, we now examine the biochemical results when regulation fails because of behavior, genetics, or a combination of the two. The most common result of such a failure is obesity. Humans maintain about a day's worth of glycogen and, after these stores have been replenished, excess carbohydrates are converted into fatty acids and then into triacylglycerols. Amino acids are not stored at all, and so excess amino acids are also ultimately converted into triacylglycerols. Thus, regardless of the type of food consumed, excess consumption results in increased fat stores.

We begin our consideration of the effects of disruptions in caloric homeostasis by looking at diabetes mellitus, a complex disease characterized by grossly abnormal fuel usage and named for the excessive urination that is a classic symptom (*diabetes*, from Greek, means "to pass through"). Glucose is overproduced by the liver and underutilized by other organs. As a result, glucose accumulates in the blood and is excreted in the urine when its concentration exceeds the reabsorptive capacity of the renal tubules (*mellitus*, from Latin, means "sweetened with honey"). Water accompanies the excreted glucose, and so an untreated diabetic in the acute phase of the disease is hungry and thirsty. *Mellitus* distinguishes this disease from diabetes *insipidus*, which is caused by impaired renal reabsorption of water. While diabetes insipidus is relatively rare, the incidence of diabetes mellitus is about 6% of the world population, hence it is usually referred to simply as *diabetes*.

Type 1 diabetes is caused by the destruction of the insulin-secreting β cells in the pancreas, usually due to an autoimmune disorder and beginning before age 20. Type 1 diabetes is also referred to as *insulin-dependent diabetes*, meaning that the affected person requires the administration of insulin to live. Most diabetics, in contrast, have a normal or even higher level of insulin in their blood, but they are poorly responsive to the hormone, a characteristic called **insulin resistance**. This form of the disease, known as **type 2 diabetes**, typically arises later in life than does the insulin-dependent form. Although there is a significant genetic component, obesity is a significant predisposing factor for the development of insulin resistance and type 2 diabetes.

In our discussion of diabetes in this chapter, we will consider type 2 first, which accounts for approximately 90% of the diabetes cases throughout the world and is the most common metabolic disease in the world. In the United States, where 10% of the population is affected, it is the leading cause of blindness, kidney failure, and amputation.

Self-Check Question



People who consume little fat but excess carbohydrates can still become obese. How is this result possible?

Insulin initiates a complex signal-transduction pathway in muscle

What is the biochemical basis of insulin resistance? How does insulin resistance lead to failure of the pancreatic β cells that results in type 2 diabetes? How does obesity contribute to this progression? To answer these questions and begin to unravel the mysteries of metabolic

disorders, let us reexamine the mechanism of action of insulin in muscle, the largest tissue target of insulin. Indeed, muscle uses about 85% of the glucose ingested during a meal.

In a normal cell, insulin binds to its receptor, which then autophosphorylates on tyrosine residues, with each subunit of the receptor phosphorylating its partner. Phosphorylation of the receptor generates binding sites for insulin-receptor substrates (IRSs), such as IRS-1 (**Figure 24.7**). Subsequent phosphorylation of IRS-1 by the tyrosine kinase activity of the insulin receptor engages the insulin-signaling pathway (1). Phosphorylated IRS-1 binds to phosphoinositide 3-kinase (PI3K) and activates it. PI3K catalyzes the conversion of phosphatidylinositol 4,5-bisphosphate (PIP_2) into phosphatidylinositol 3,4,5-trisphosphate (PIP_3), a second messenger (2). PIP_3 activates the phosphatidylinositol-dependent protein kinase (PDK) (3), which in turn activates several other kinases, most notably Akt (4), also known as protein kinase B (PKB).

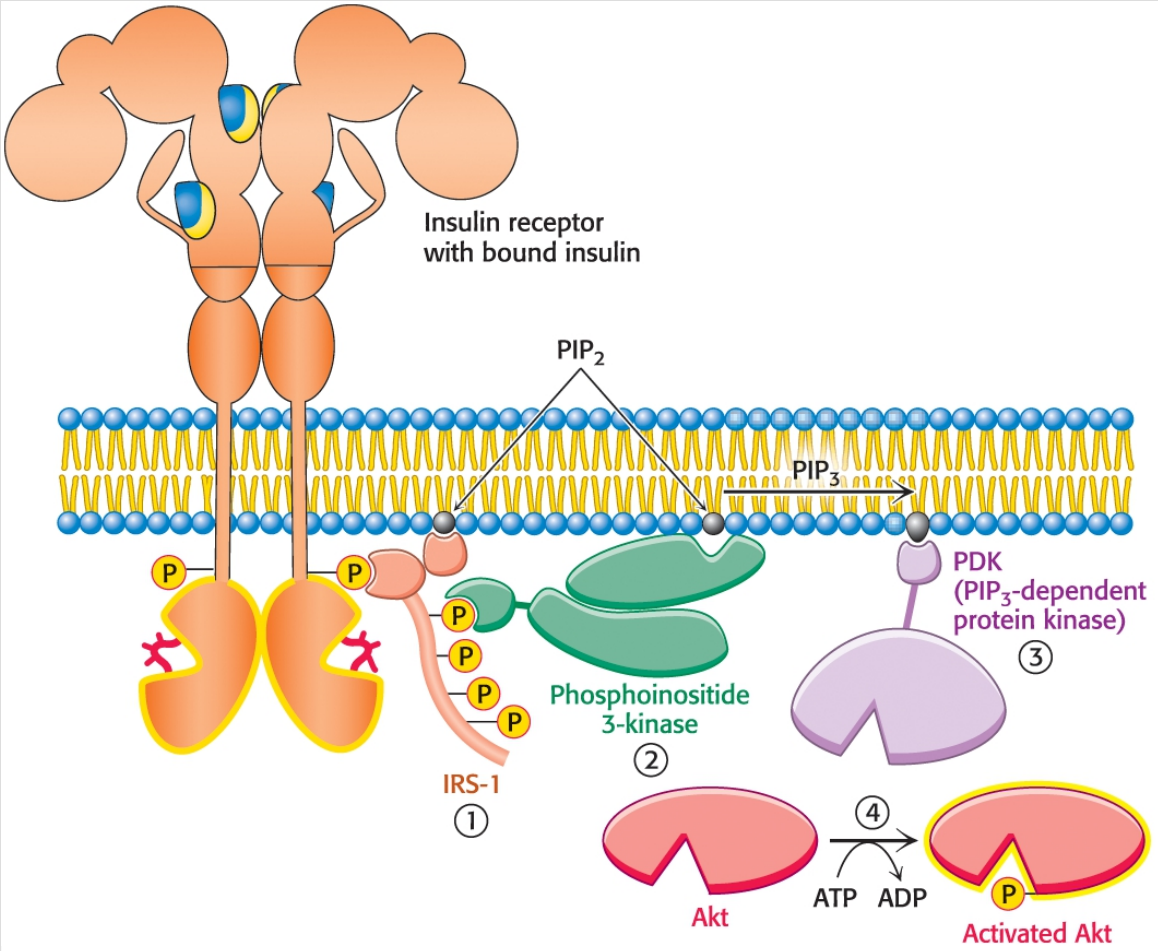


FIGURE 24.7 Insulin signaling activates Akt using the second messenger PIP_3. The binding o insulin results in the cross-phosphorylation and activation of the insulin receptor. Phosphorylated sites on the receptor act as binding sites for insulin-receptor substrates such as IRS-1 (1). The lipid kinase phosphoinositide 3-kinase binds to phosphorylated sites on IRS-1 through its regulatory domain and then converts PIP_2 into PIP_3 (2). Binding to PIP_3 activates PIP_3-dependent protein kinase (3), which phosphorylates and activates kinases such as Akt (4). Activated Akt can then diffuse throughout the cell and continue the signal-transduction pathway.

Akt facilitates the translocation of the glucose transporter (GLUT4)-containing vesicles to the cell membrane, which leads to a more robust absorption of glucose from the blood. Moreover, Akt phosphorylates

and inhibits glycogen synthase kinase (GSK3). Recall that GSK3 inhibits glycogen synthase (Section 21.6). Thus, insulin leads to the absorption of glucose from the blood, activation of glycogen synthase, and enhanced glycogen synthesis.

Like all signal pathways, the insulin-signaling cascade must be capable of being turned off. In addition to the breakdown of insulin itself, three different processes notably contribute to the down-regulation of insulin signaling. First, phosphatases deactivate the insulin receptor and destroy a key second messenger. PTP1B (protein tyrosine phosphatase 1B) removes phosphoryl groups from the receptor, thus inactivating it. The second messenger PIP_3 is inactivated by the phosphatase PTEN (phosphatase and tensin homolog), which dephosphorylates it, forming PIP_2, which is not a second messenger.

Second, the IRS protein can be inactivated by phosphorylation on serine residues by specific Ser/Thr kinases. These kinases are activated by stress signals and may play a role in the development of insulin resistance. Finally, SOCS proteins, the regulatory proteins discussed earlier, interact with the insulin receptor and IRS-1 and apparently facilitate their proteolytic degradation by the proteasome complex.

Metabolic syndrome often precedes type 2 diabetes

With our knowledge of the key components of energy homeostasis, let us begin our investigation of the biochemical basis of insulin resistance and type 2 diabetes. A cluster of pathologies — including insulin resistance, hyperglycemia, and dyslipidemia (characterized by high blood levels of triacylglycerols, cholesterol, and low-density lipoproteins) — often develop together. This clustering, called **metabolic syndrome**, is thought to be a predecessor of type 2 diabetes.

A consequence of obesity is that the amount of triacylglycerols consumed exceeds the adipose tissue's storage capacity. As a result, other tissues begin to accumulate fat, most notably muscle (myosteatosis), and the liver, a condition called *hepatic steatosis* (Figure 24.8). This accumulation results in insulin resistance and ultimately in pancreatic failure. We will focus on muscle and the pancreatic β cells.

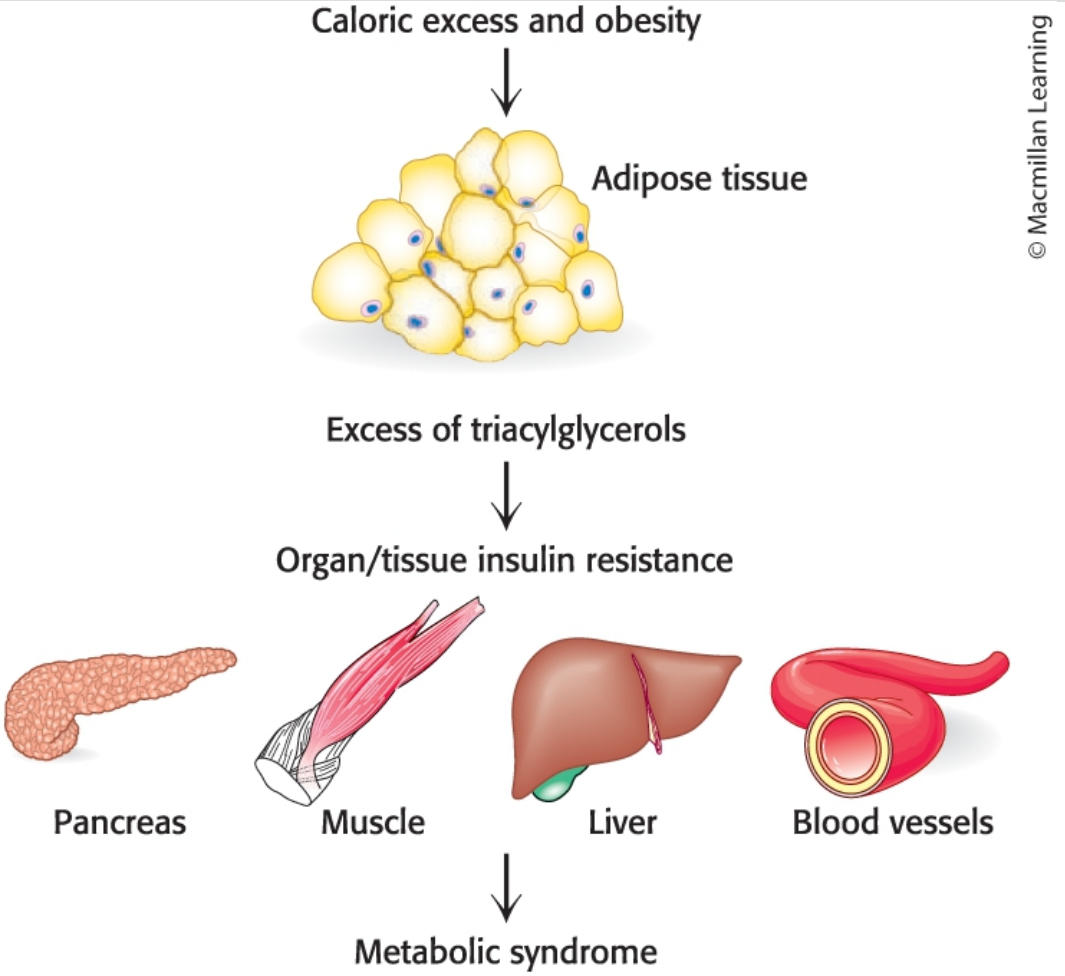


FIGURE 24.8 The storage capacity of fat tissue can be exceeded in obesity. In caloric excess, the storage capacity of adipocytes can be exceeded with deleterious results. The excess fat accumulates in other tissues, resulting in biochemical malfunction of the tissues. When the pancreas, muscle, liver, and cells lining the blood vessels are affected, metabolic syndrome, a condition that often precedes type 2 diabetes, may result.

[Information from S. Fröjdö, H. Vidal, and L. Pirola, *Biochim. Biophys. Acta* 1792:83–92, 2009, Fig. 1.]

Self-Check Question



What would be the effect of a mutation in the gene for PTP1B (protein tyrosine phosphatase 1B) that inactivated the enzyme in a person who has type 2 diabetes?

Excess fatty acids in muscle modify metabolism

Myosteatosis and insulin resistance do not always develop with obesity; however, the pathology begins when more fats are present than can be processed by muscle. Although the rate of β oxidation increases in response to the high concentration of fats, the mitochondria are not capable of processing all of the fatty acids by β oxidation; fatty acids accumulate in the mitochondria and eventually spill over into the cytoplasm. The unprocessed fatty acids are reincorporated into triacylglycerols, resulting in the accumulation of fat in the cytoplasm.

In the cytoplasm, levels of diacylglycerol and ceramide (a component of sphingolipids) also increase. Diacylglycerol is a second messenger that activates protein kinase C (PKC) (Section 14.2). When active, PKC and other Ser/Thr protein kinases are capable of phosphorylating IRS and reducing the ability of IRS to propagate the insulin signal. Saturated and trans unsaturated fatty acids may also activate kinases that block the insulin signal. Ceramide or its metabolites inhibit glucose uptake and glycogen synthesis, apparently by inhibiting PDK and Akt (Section 14.3).

The result is a diet-induced insulin resistance that can, but does not always, develop over time in obese individuals (Figure 24.9).

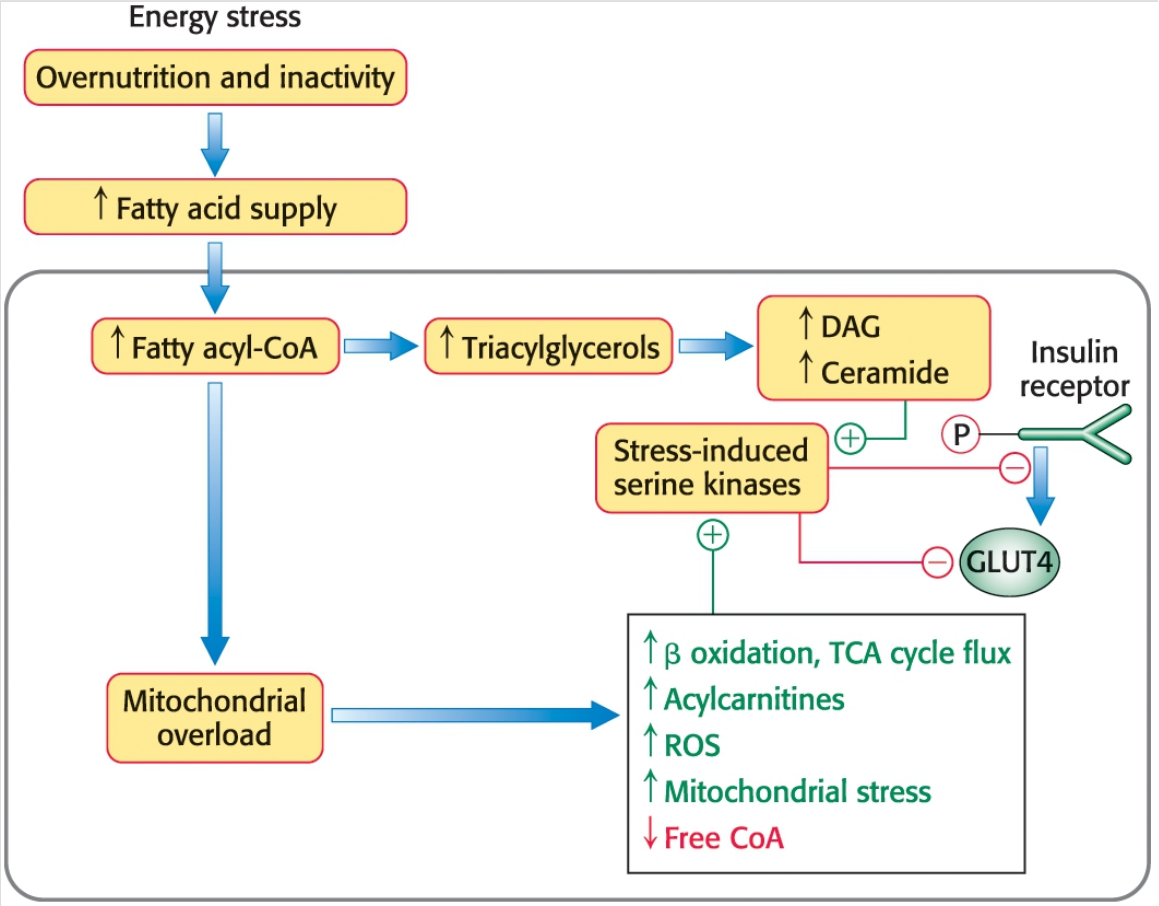


FIGURE 24.9 Excess fat can disrupt signal-transduction pathways and lead to insulin insensitivity. Excess fat accumulation in peripheral tissues, most notably muscle, can disrupt some signal-transduction pathways and inappropriately activate others. In particular, diacylglycerols and ceramide activate stress-induced pathways that interfere with insulin signaling, resulting in insulin resistance. (Abbreviations: DAG, diacylglycerol; GLUT4, glucose transporter 4; TCA, tricarboxylic acid cycle; ROS, reactive oxygen species.)

Insulin resistance in muscle facilitates pancreatic failure

What is the effect of overnutrition on the pancreas? This question is important because a primary function of the pancreas is to respond to the presence of glucose in the blood by secreting insulin. Indeed, the β cell is an insulin factory. The mRNA that encodes proinsulin, the precursor to insulin, constitutes 20% of the total mRNA in the pancreas, and proinsulin itself constitutes 50% of the total protein synthesized in the pancreas.

Glucose enters the pancreatic β cells through the glucose transporter GLUT2. Recall that GLUT2 will allow rapid glucose transport only when blood glucose is plentiful, ensuring that insulin is secreted only when glucose is abundant, such as after a meal (Section 16.1). Likewise, pancreatic glucokinase, with its relatively high K_M value, traps large amounts of glucose within the cell only when blood-glucose concentrations are high. These two proteins, in concert, act as a pancreatic glucose sensor.

The β cell metabolizes glucose to CO_2 and H_2O through cellular respiration, generating ATP. The resulting increase in the ATP/ADP ratio closes an ATP-sensitive K^+ channel that, when open, allows potassium to flow out of the cell (**Figure 24.10**). The resulting alteration in the cellular ionic environment opens a voltage-sensitive Ca^{2+} channel, and the resulting influx of Ca^{2+} causes insulin-containing secretory vesicles to fuse with the cell membrane and release insulin into the blood. Thus, the increase in ATP resulting from the metabolism of glucose has been translated by the membrane proteins into a physiological response — the secretion of insulin and the subsequent removal of glucose from the blood.

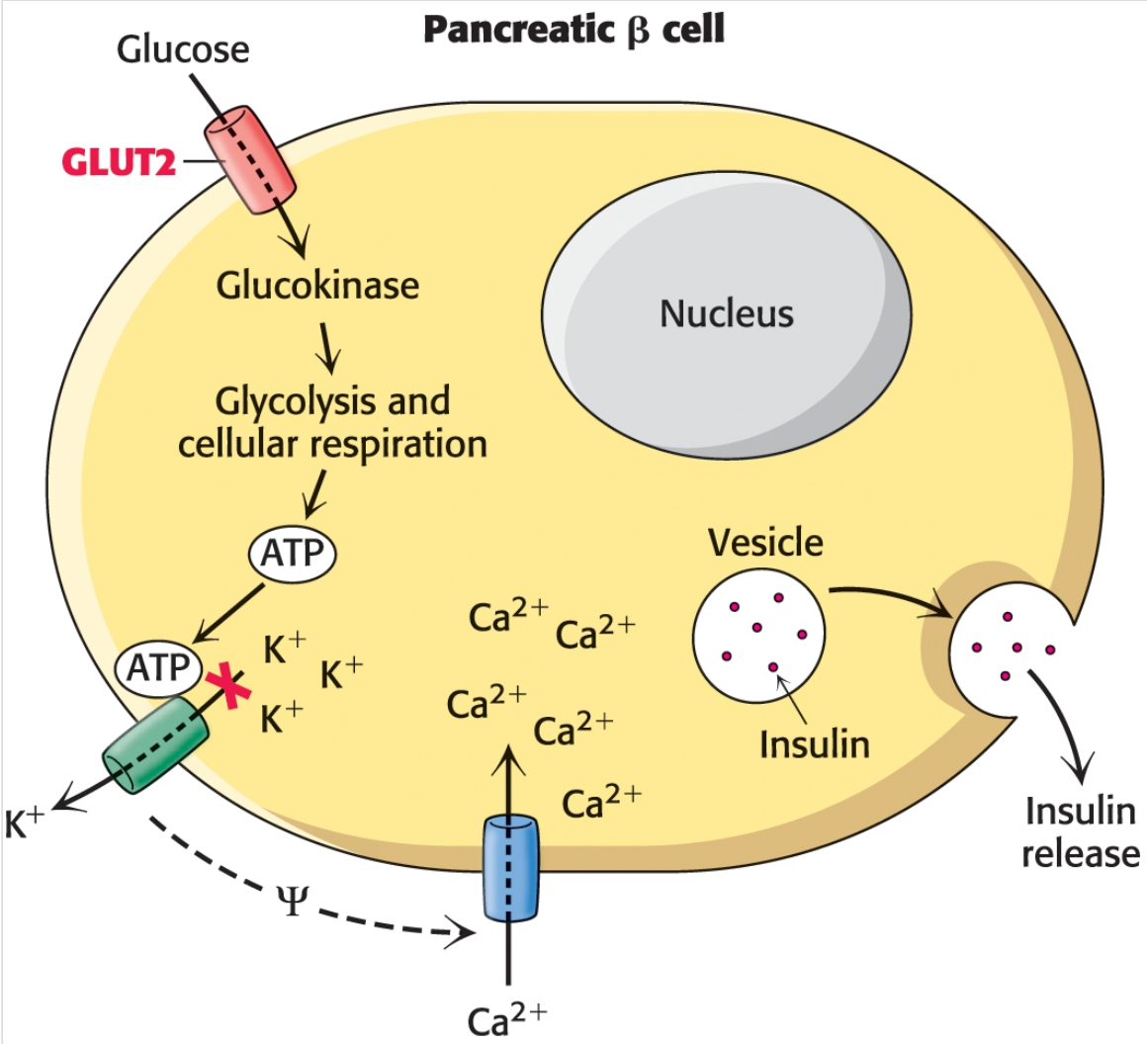


FIGURE 24.10 Insulin release by the pancreas is regulated by blood-glucose concentration, using ATP as a second messenger. The metabolism of glucose by glycolysis and cellular respiration increases the concentration of ATP, which causes an ATP-sensitive potassium chann to close. The closure of this channel alters the charge across the membrane (ψ) and causes a calcium channel to open. The influx of calcium causes insulin-containing granules to fuse with the plasma membrane, releasing insulin into the blood.

What aspect of β cell function ultimately fails, causing the transition from insulin resistance to full-fledged type 2 diabetes? Under normal circumstances, proinsulin synthesized by β cells folds into its three-dimensional structure in the endoplasmic reticulum, is processed to

insulin, and is subsequently packaged into vesicles for secretion. As insulin resistance develops in the muscle, the β cells respond by synthesizing yet more insulin in a futile attempt to drive insulin action. The ability of the endoplasmic reticulum to process all of the proinsulin and insulin becomes compromised, a condition known as **endoplasmic reticulum (ER) stress**, and unfolded or misfolded proteins accumulate.

ER stress initiates a signal pathway called the **unfolded protein response (UPR)**, a pathway intended to save the cell. UPR consists of several steps. First, general protein synthesis is inhibited so as to prevent more proteins from entering the ER. Second, chaperone synthesis is stimulated. Recall that chaperones are proteins that assist the folding of other proteins (Section 2.7). Third, misfolded proteins are removed from the ER and are subsequently delivered to the proteasome for destruction. Finally, if the described response fails to alleviate the ER stress, programmed cell death is triggered, which ultimately leads to β cell death and full-fledged type 2 diabetes.

What are the treatments for type 2 diabetes? Most are behavioral in nature. Type 2 diabetics are advised to count calories, making sure that energy intake does not exceed energy output; to consume a diet rich in vegetables, fruits, and grains; and to get plenty of aerobic exercise. Note that these guidelines are the same as those for healthy living, even for those not suffering from type 2 diabetes. Monitoring of blood-glucose concentration is important (normal is 3.6 to 6.1 mM) and for patients who are not able to maintain proper glucose levels with behavioral modifications, drug treatments are required. The administration of insulin may be necessary upon β cell failure, and/or treatment with metformin (Glucophage), which activates AMPK, may be effective. Recall that AMPK promotes the oxidation of fats while inhibiting fat synthesis and storage. It also stimulates glucose uptake and storage by muscle while inhibiting gluconeogenesis in the liver.

Self-Check Question



What is the relationship between fatty acid oxidation and insulin resistance in the muscle?

Metabolic alterations in type 1 diabetes result from insulin insufficiency and glucagon excess

We now turn to the more-straightforward type 1 diabetes. Recall that in type 1 diabetes, insulin production is usually insufficient because of autoimmune destruction of the pancreatic β cells. Consequently, the glucagon/insulin ratio is always higher than normal. In essence, the diabetic person is in biochemical fasting mode (Section 24.2) despite a high concentration of blood glucose. Because insulin is deficient, the entry of glucose into adipose and muscle cells is impaired, and the liver becomes stuck in a gluconeogenic and ketogenic state. Essentially, the cells' response to a lack of insulin amplifies the amount of glucose in the blood. The high glucagon/insulin ratio in diabetes also promotes glycogen breakdown. Hence, as with type 2 diabetes, an excessive amount of glucose is produced by the liver, released into the blood, and excreted in the urine.

Because carbohydrate utilization is impaired, a lack of insulin leads to the uncontrolled breakdown of lipids and proteins, resulting in the ketogenic state. Large amounts of acetyl CoA are then produced by β oxidation. However, much of the acetyl CoA cannot enter the citric acid cycle because there is insufficient oxaloacetate for the condensation step. Recall that mammals can synthesize oxaloacetate from pyruvate, a

product of glycolysis, but not from acetyl CoA; instead, they generate ketone bodies (Section 22.4). A striking feature of diabetes is the shift in fuel usage from carbohydrates to fats; glucose, more abundant than ever, is unable to be used. In high concentrations, ketone bodies overwhelm the kidney's capacity to maintain acid–base balance. The untreated diabetic can go into a coma because of a lowered blood-pH level and dehydration. Interestingly, diabetic ketosis is rarely a problem in type 2 diabetes because, in most cases, insulin signaling is still active enough to prevent excessive lipolysis in liver and adipose tissue.

What is the treatment for type 1 diabetes? As noted earlier, the regular administration of insulin is required for survival. Likewise, blood-glucose concentration must be monitored. Although the behaviors recommended for type 2 diabetes — watching calories, exercising, and eating a healthy diet — do not treat type 1 diabetes, they are beneficial to managing it and to maintaining a healthy lifestyle.

Self-Check Question



Insulin-dependent diabetes is often accompanied by hypertriglyceridemia, which is an excess blood level of triacylglycerols. Suggest a biochemical explanation.

24.4 Exercise Beneficially Alters the Biochemistry of Cells

Thus far, we have been considering metabolism in the context of excess calorie consumption, as in obesity. We now look at the physiological response when there is an extreme caloric need, as occurs during exercise.

Fuel choice during exercise is determined by the intensity and duration of activity

Skeletal muscle accounts for $\approx 40\%$ of total body mass and $\approx 35\%$ of resting metabolic activity. Moreover, skeletal muscle is the largest target tissue for insulin. Given its biochemical prominence, increased muscle activity — exercise — coupled with a healthy diet is one of the most effective treatments for diabetes as well as a host of other pathological conditions. These include coronary disease, hypertension, depression, age-related muscle wasting (sarcopenia), and a variety of cancers. With regard to type 2 diabetes, exercise increases insulin sensitivity and is in fact more effective than pharmacological interventions. What is the basis of this beneficial effect? To answer this question, we must first consider what energy sources muscles use during exercise.

The fuels used in anaerobic exercises — sprinting, for example — differ from those used in aerobic exercises — such as distance running. The selection of fuels during these different forms of exercise illustrates many important facets of energy transduction and metabolic integration. ATP directly powers myosin, the protein immediately responsible for converting chemical energy into movement (Section 6.4). However, the amount of ATP in muscle is small. Hence, the power

output and, in turn, the velocity of running depend on the rate of ATP production from other fuels.

As shown in **Table 24.3**, creatine phosphate (phosphocreatine) can swiftly transfer its high-potential phosphoryl group to ADP to generate ATP. However, the amount of creatine phosphate, like that of ATP itself, is limited. Creatine phosphate and ATP can power intense muscle contraction for 5 to 6 s. Maximum speed in a sprint can thus be maintained for only 5 to 6 s (Figure 15.6). Thus, the winner in a 100-meter sprint is the runner who both achieves the highest initial velocity and then slows down the least.

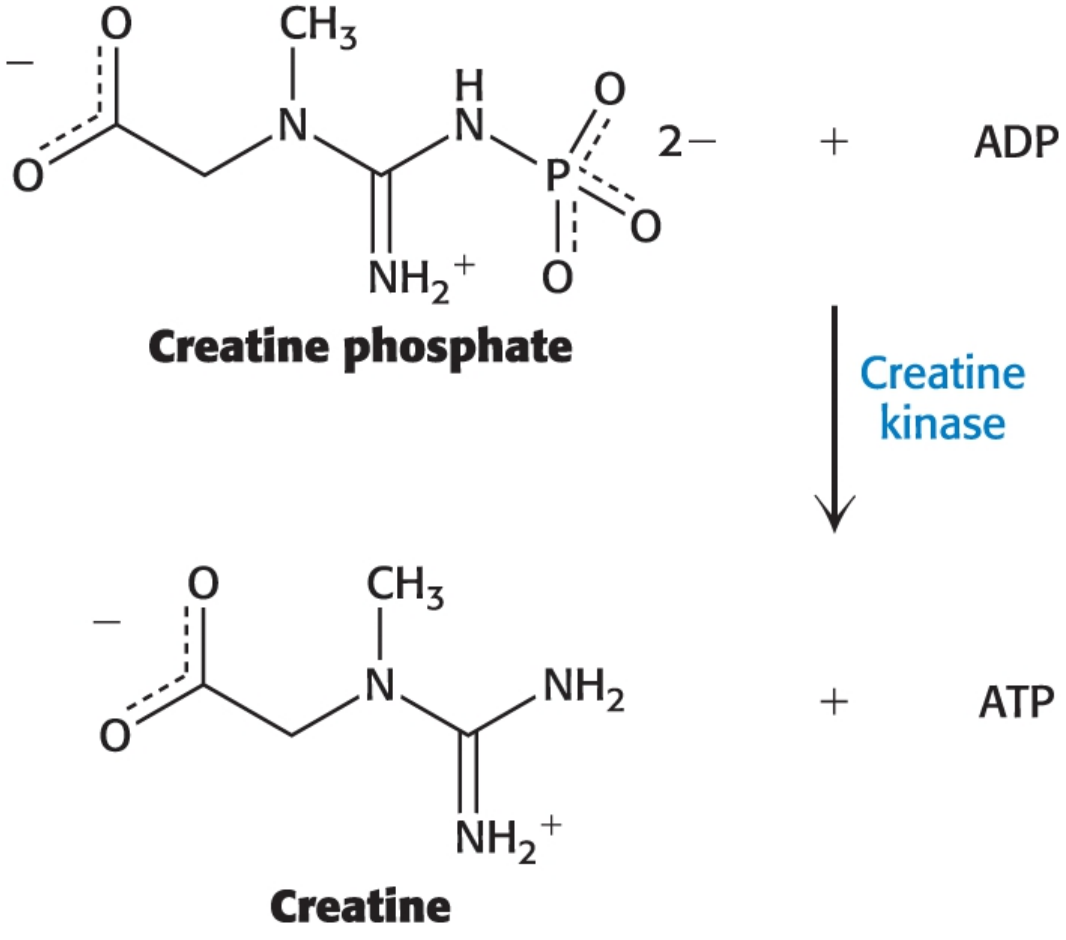


TABLE 24.3 Fuel sources for muscle contraction

Fuel source	Maximal rate of ATP production ($mmol\ s^{-1}$)	Total $\sim P$ available (mmol)
Muscle ATP		223
Creatine phosphate	73.3	446
Conversion of muscle glycogen into lactate	39.1	6700
Conversion of muscle glycogen into CO_2	16.7	84,000
Conversion of liver glycogen into CO_2	6.2	19,000
Conversion of adipose-tissue fatty acids into CO_2	6.7	4,000,000

Note: Fuels stored are estimated for a 70-kg person having a muscle mass of 28 kg.
Data from E. Hultman and R. C. Harris, in *Principles of Exercise Biochemistry,* edited by J. R. Poortmans (Karger, 2004), pp. 78–119.

Sprinting

A 100-meter sprint is powered by stored ATP, creatine phosphate, and the anaerobic glycolysis of muscle glycogen. During a ~ 10-second sprint, the concentration of ATP in muscle drops from 5.2 to 3.7 mM, and that of creatine phosphate decreases from 9.1 to 2.6 mM. Anaerobic glycolysis provides fuel to make up for the loss of ATP and creatine phosphate. The conversion of muscle glycogen into lactate can generate a good deal more ATP, but the rate is slower than that of phosphoryl-

group transfer from creatine phosphate. Because of anaerobic glycolysis, the blood-lactate concentration is increased from 1.6 to 8.3 mM. The release of H^+ from the intensely active muscle concomitantly lowers the blood pH from 7.42 to 7.24. Sprinting is powered by fast-twitch muscle fiber (type IIb) specialized for anaerobic glycolysis. One of the effects of high-intensity training is to increase the amount of lactate transporters in the membranes of slow-twitch fibers (type I), which remove lactate from the blood and slow the fall in blood pH. Nonetheless, the pace of a 100-meter sprint cannot be sustained in a 1000-meter run $(\sim 132\ s)$ for two reasons. First, creatine phosphate is consumed within a few seconds. Second, the lactate produced contributes to acidosis. Thus, alternative fuel sources are needed.

Middle-distance running

Let's examine the fuel use of a middle-distance runner. The complete oxidation of muscle glycogen to CO_2 by aerobic respiration substantially increases the energy available to power the 1000-meter run, but this aerobic process is a good deal slower than anaerobic glycolysis. Because ATP is produced more slowly by oxidative phosphorylation than by glycolysis (Table 24.3), the runner's pace is necessarily slower than in a 100-meter sprint. The championship velocity for the 1000-meter run is about $7.6\ m\ s^{-1}$, compared with approximately $10.4\ m\ s^{-1}$ for the 100-meter event (**Figure 24.11**).

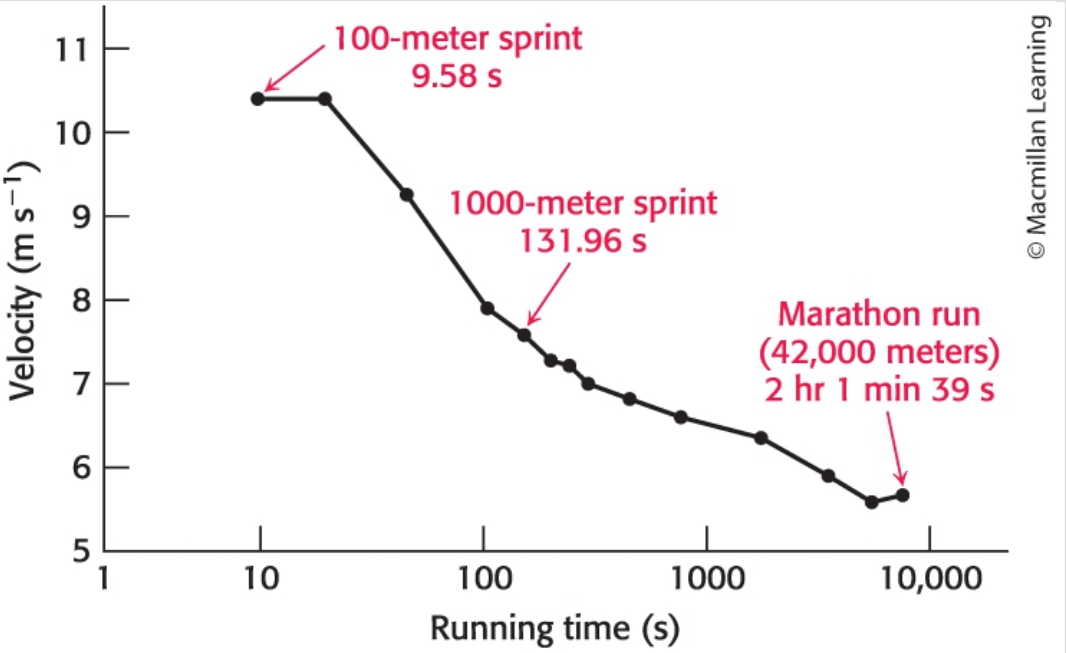


FIGURE 24.11 Running velocity decreases dramatically as a function of the duration of the race. The values shown are world track records.

[Data from trackandfieldnews.com.]

Long-distance running

Running a marathon (26.2 miles or 42,000 meters) requires a different selection of fuels and is characterized by cooperation (depending on the capabilities of the runner) between muscle, liver, and adipose tissue. Liver glycogen complements muscle glycogen as an energy store that can be tapped. Elite marathoners can use the aerobic combustion of glucose to power the entire race, provided they consume fuels during the race. However, for most of us, the total body glycogen stores (103 mol of ATP at best) are insufficient to provide the 150 mol of ATP needed for this grueling event. Much larger quantities of ATP can be obtained by the oxidation of fatty acids derived from the breakdown of fat in adipose tissue, but the maximal rate of ATP generation is slower

yet than that of glycogen oxidation and is more than 10-fold slower than that with creatine phosphate. Thus, ATP is generated much more slowly from high-capacity stores than from limited ones, accounting for the different velocities of anaerobic and aerobic events. Fats are rapidly consumed in activities such as distance running, explaining why extended aerobic exercise is beneficial for people who are insulin resistant.

Is it possible to determine the contribution of each fuel as a function of exercise intensity? The percentage contribution of each fuel can be measured with the use of a respirometer, which measures the **respiratory quotient (RQ)**, the ratio of CO_2 produced to O_2 consumed. Consider the complete combustion of glucose:

$$\underset{\text{Glucose}}{C_6H_{12}O_6} + 6\,O_2 \rightarrow 6\,CO_2 + 6\,H_2O$$

The RQ for glucose is 1. Now consider the oxidation of a typical fatty acid, palmitate:

$$\underset{\text{Palmitate}}{C_{16}H_{32}O_2} + 23\,O_2 \rightarrow 16\,CO_2 + 16\,H_2O$$

The RQ for palmitate oxidation is 0.7. Thus, as aerobic exercise intensity increases, the RQ will rise from 0.7 (only fats are used as fuel) to 1.0 (only glucose is used as fuel). Between these values, a mixture of fuels is used (**Figure 24.12**).

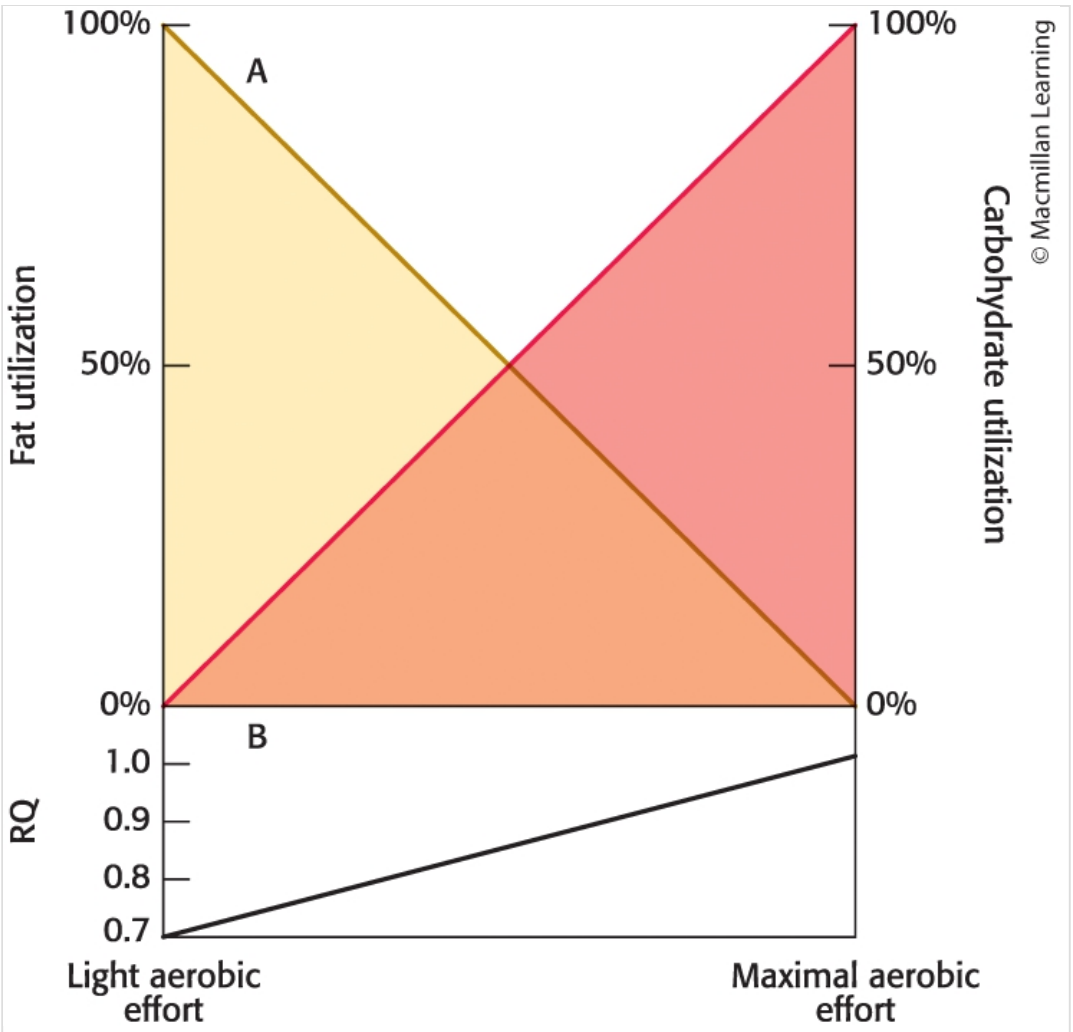


FIGURE 24.12 An idealized representation of fuel use and RQ illustrates major changes as a function of aerobic exercise intensity. (A) With increased exercise intensity, the use of fats as fuels falls as the utilization of carbohydrates increases. (B) The respiratory quotient (RQ) measures the alteration in fuel use.

What is the optimal mix of fuels for use during a marathon? As suggested above, this is a complex question that varies with the athlete and level of training. Studies have shown that, when muscle glycogen has been depleted, the power output of the muscle falls to approximately 50% of maximum. Power output decreases despite the fact that ample supplies of fat are available, suggesting that fats can

supply only about 50% of maximal aerobic effort. Indeed, depletion of glycogen stores during a race is referred to as “bonking” or “hitting the wall,” with the result that the athlete must greatly reduce the pace.

How is an optimal mix of these fuels achieved? A low blood-sugar level leads to a high glucagon/insulin ratio, which in turn mobilizes fatty acids from adipose tissue. Fatty acids readily enter muscle, where they are degraded by β oxidation to acetyl CoA and then to CO_2. The elevated acetyl CoA level decreases the activity of the pyruvate dehydrogenase complex to block the conversion of pyruvate into acetyl CoA. Hence, fatty acid oxidation decreases the funneling of glucose into the citric acid cycle and oxidative phosphorylation. Glucose is spared so that just enough remains available at the end of the marathon to increase the pace as the finish line draws near. The simultaneous use of both fuels gives a higher mean velocity than would be attained if glycogen were totally consumed before the start of fatty acid oxidation. It is important to bear in mind that fuel use is only one of many factors that determine running ability.

The perplexing symptoms of McArdle disease result from the distinct ways skeletal muscle produces ATP



In Section 21.6 we discussed several glycogen storage diseases. We can now explain the complex symptoms of McArdle disease (Type V glycogen storage disease), a rare condition affecting approximately 1 in 100,000 people. Affected individuals experience painful muscle fatigue and have burgundy-colored urine following an attempt at vigorous exercise. The coloration is due to rhabdomyolysis (rapid breakdown of

skeletal muscle), which results in myoglobinuria (myoglobin in the blood and urine) as damaged tissue leaks myoglobin into the blood, which is passed to the urine. Two additional observations are interesting: resting and moderate exercise do not induce the symptoms, and vigorous exercise causes an increase in blood pH, rather than the usually observed decrease in pH. What is the biochemical basis for these symptoms?

As discussed in the previous section, during vigorous exercise, skeletal muscle contractions are powered by glycogen mobilization by glycogen phosphorylase. Patients with McArdle disease lack functional muscle glycogen phosphorylase, leading to the inability to rapidly mobilize glucose from glycogen. In an unaffected individual, intracellular and blood pH fall as lactic acid is produced during anaerobic glycolysis (Section 16.2). Because McArdle patients cannot mobilize glucose, lactic acid will not be produced and there will be no fall in pH; rather, it rises. To explain this, recall again that an immediate source of ATP in skeletal muscle is the phosphorylation of ATP at the expense of creatine phosphate (Section 15.2). In a futile attempt to power exercise, skeletal muscles of an affected individual rapidly synthesize ATP at the expense of creatine phosphate. However, the guanidinium group of creatine is a base, leading to an increase in pH.

Finally, why don't affected individuals experience symptoms at rest or when performing leisurely exercise? As was discussed previously in this chapter, under these conditions, skeletal muscle derives most of its energy from fatty acid oxidation rather than from glycogen mobilization.

Mitochondrial biogenesis is stimulated by muscular activity

Hopefully it is now apparent that muscles must utilize a variety of fuel sources for optimal activity. Now let's consider what biochemical changes exercise induces to optimize athletic performance.

When muscle is stimulated to contract during exercise by receiving nerve impulses from motor neurons, calcium is released from the sarcoplasmic reticulum (**Figure 24.13**). Calcium induces muscle contraction, but recall that calcium is also a potent second messenger and frequently works in association with the calcium-binding protein calmodulin (Section 14.1). In its capacity as a second messenger, calcium stimulates various calcium-dependent enzymes, such as calmodulin-dependent protein kinase. The calcium-dependent enzymes, as well as AMPK, subsequently activate particular transcription-factor complexes.

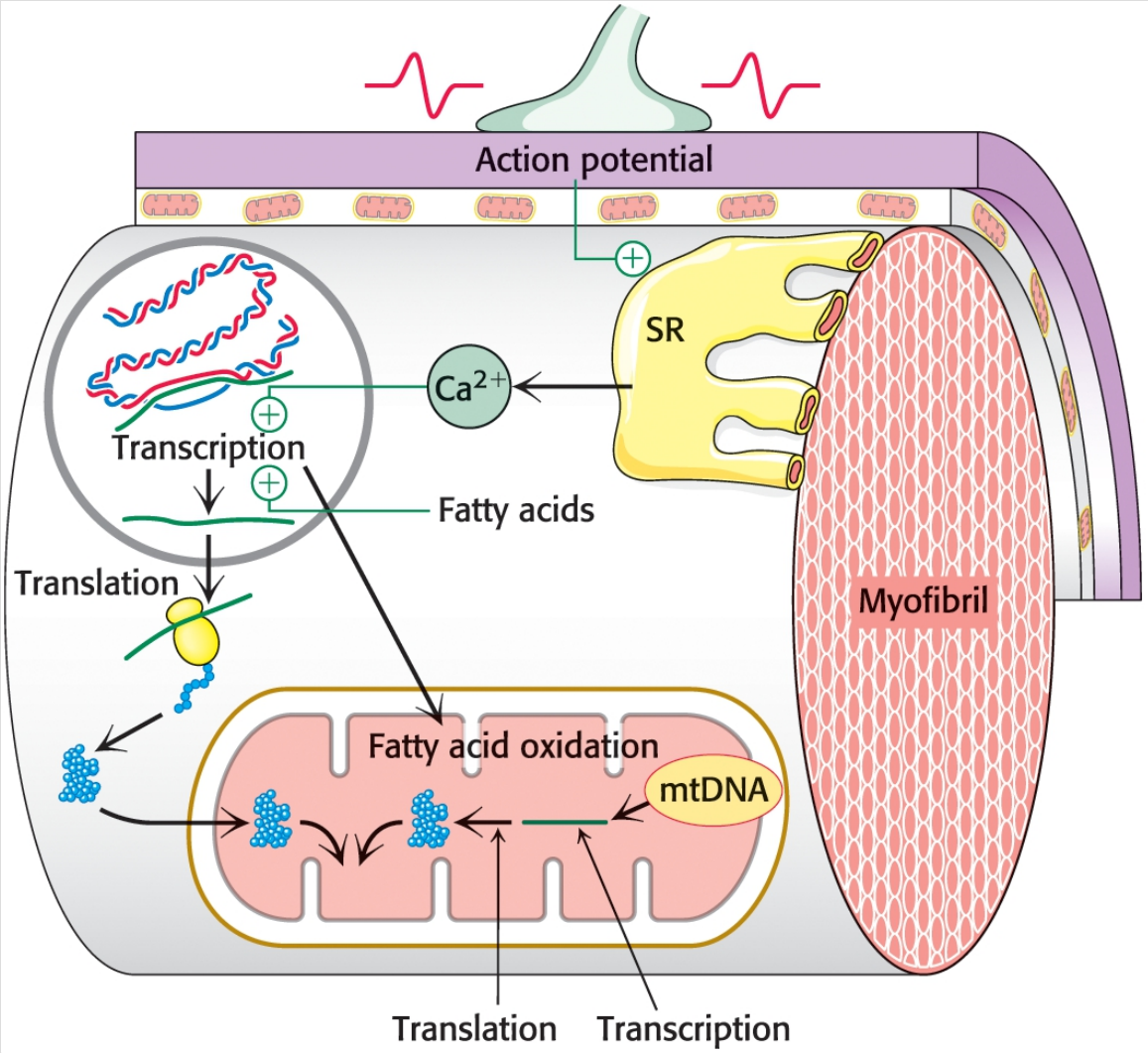


FIGURE 24.13 Exercise results in mitochondrial biogenesis and enhanced fat metabolism. An action potential causes Ca^{2+} release from the sarcoplasmic reticulum (SR), the muscle-cell equivalent of the endoplasmic reticulum. The Ca^{2+}, in addition to instigating muscle contraction, activates nuclear transcription factors that stimulate the expression of specific genes. The products of these genes, in conjunction with the products of mitochondrial genes, a responsible for mitochondrial biogenesis. Fatty acids activate a different set of genes that increase the fatty acid oxidation capability of mitochondria.

[Information from D. A. Hood, *J Appl. Physiol.* 90:1137–1157, 2001, Fig. 2.]

Two patterns of gene expression, in particular, change in response to regular exercise (Figure 24.13). Regular exercise enhances the production of proteins required for fatty acid metabolism, such as the enzymes of β oxidation. Interestingly, fatty acids themselves function as signal molecules to activate the transcription of enzymes involved in fatty acid metabolism. Additionally, another set of transcription factors activated by the calcium signal cascade initiates a signal pathway that increases mitochondrial biogenesis. In concert, the increase in fatty acid oxidizing capability and additional mitochondria allow for the efficient metabolism of fatty acids. Because an excess of fatty acids results in insulin resistance (Section 24.3), efficient metabolism of fatty acids results in an increase in insulin sensitivity. Indeed, muscles of well-trained athletes may contain high concentrations of triacylglycerols yet still maintain exquisite sensitivity to insulin. These alterations of muscle biochemistry are some of the molecular manifestations of the training effects of exercise.

Exercise alters muscle and whole-body metabolism

In addition to the changes to mitochondrial biogenesis and fatty acid metabolism in muscle tissue, exercise has additional biochemical effects on muscle and other tissues. These effects also vary depending on the type and duration/frequency of the exercise. Here we will give a brief overview of the molecular adaptations to exercise, and then we will compare the effects of endurance and resistance training on muscle and whole-body biochemistry.

Regardless of the type of exercise, the timing of the metabolic response, in general, is the same (**Figure 24.14**). The first response to exercise is an alteration in the patterns of gene expression: a variety of transcription factors are activated, and all of these transcription factors stimulate genes encoding proteins that facilitate exercise similar to the

changes described above. In addition to those changes, recall that hypoxia (low oxygen) activates the hypoxia inducible factor (HIF-1), which stimulates the genes encoding glycolytic enzymes, glucose transporters, and angiogenesis-stimulating factors (Section 16.3). Remarkably, as shown in Figure 24.14, even a single bout of exercise can stimulate gene expression several-fold, with levels returning to normal in 24 hours. However, it takes repeated bouts of exercise to accumulate enough mRNA to enhance the synthesis of proteins responding to exercise. In addition to the proteins mentioned above, other examples of such proteins include muscle contractile and structural proteins, and the oxygen-binding proteins hemoglobin and myoglobin (Chapter 3). When these and other proteins accumulate to a sufficient extent, the physiological effects of exercise become apparent. You can run longer and faster, or you can do more repetitions with heavier weights.

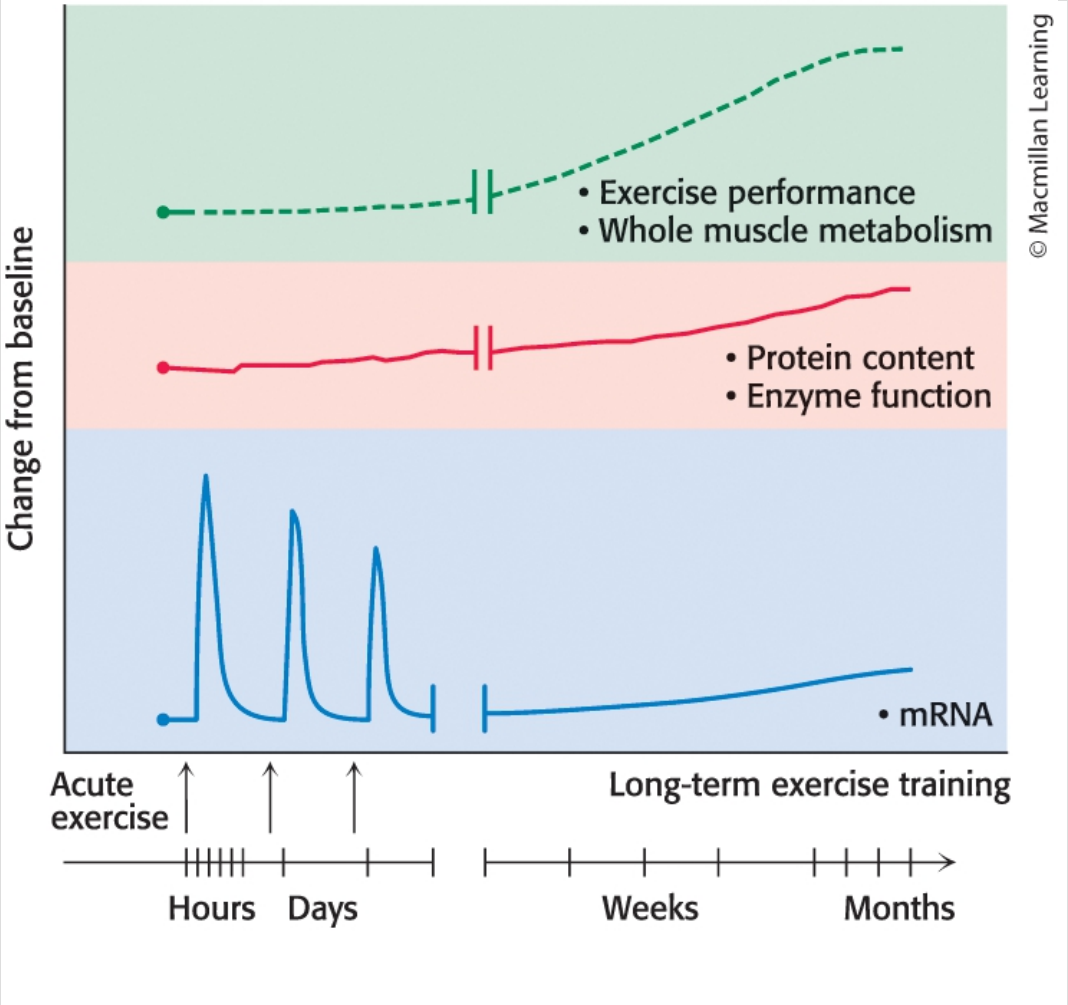


FIGURE 24.14 Biochemical adaptations to exercise vary over a range of time scales. Changes as a function of duration of exercise are shown for mRNA synthesis (bottom), protein synthesis (middle), and exercise performance (top).

[From B. Egan and J. R. Zierath, Exercise metabolism and the molecular regulation of skeletal muscle adaptation, *Cell Metab*. 17:162–184, 2013, Fig. 1.]



Table 24.4 shows some of the molecular adaptations and health benefits accruing from endurance and resistance training. For most of us, some combination of the two will result in maximal health benefits. The American Medical Association and the American College of Sports Medicine launched a global initiative several years ago called *Exercise is Medicine*. As Table 24.4 illustrates, and as we have learned throughout our study of biochemistry, this is indeed the case: exercise *is* medicine.

TABLE 24.4 Biochemical adaptations and health benefits of aerobic and resistance training

	Aerobic (endurance) training	Resistance (strength) training
Biochemical response in skeletal muscle tissue		
Muscle growth (hypertrophy)	↔	↑↑↑
Anaerobic capacity	↑	↑↑
Muscle protein synthesis	↔↑	↑↑↑
Mitochondria protein synthesis	↑↑	↔↑
Lactate tolerance	↑↑	↔↑

Mitochondria density and oxidative capacity	↑↑↑	↔↑
Endurance capacity	↑↑↑	↔↑
Whole-body and metabolic health		
Bone mineral density	↑↑	↑↑
Percent body fat	↓↓	↓
Lean body mass	↔	↑↑
Insulin sensitivity	↑↑	↑↑
Inflammatory markers	↓↓	↓
Resting heart rate	↓↓	↔
Blood pressure at rest	↔↓	↔
Cardiovascular risk	↓↓↓	↓
Basal metabolic rate	↑	↑↑

↑ Values increase; ↓ values decrease; ↔ no change; ↔↑ or ↔↓ little or no change.
Information from B. Egan and J. R. Zierath, Exercise metabolism and the molecular regulation of skeletal muscle adaptation, *Cell Metab*. 17:162–184, 2013, Table 1.

Example

Measuring the Impact of a Single Athletic Activity on Caloric Homeostasis

Problem:

Estimate how long a person has to jog to offset the calories obtained from eating just 10 macadamia nuts, each with a mass of about 2 g.

Getting Started:

Let's make some assumptions about both the energy captured and energy used. First, because a macadamia nut consists mainly of fats ($\sim 37\ \mathrm{kJ\ g^{-1}}$, $\sim 9\ \mathrm{kcal\ g^{-1}}$), we can assume that each nut provides approximately 75 kJ, or 18 kcal. Second, let's assume that jogging has an incremental power consumption of 400 W.

Solve:

The ingestion of 10 nuts results in an intake of about 753 kJ (180 kcal). A watt (W) is equal to 1 joule (J) per second (0.239 calorie per second), so running with a typical power consumption rate of 400 W requires 0.4 kJ per second, or $0.4\ \mathrm{kJ\ s^{-1}}$ ($0.0956\ \mathrm{kcal\ s^{-1}}$). Dividing the total energy captured, 753 kJ, by the rate of energy use, $0.4\ \mathrm{kJ\ s^{-1}}$, gives us 1883 s, the time one would need to run.

Reflect:

So, a person would have to run just over 31 minutes to expend the calories provided by just 10 small nuts! This calculation illustrates why it can be very difficult to offset increased eating with exercise alone and why caloric homeostasis is primarily maintained by hormonal controls on appetite.

24.5 Starvation Induces Protein Wasting and Ketone Body Formation

What happens when the human body becomes deprived of energy sources? This condition, known as starvation, is a circumstance affecting nearly a billion people worldwide. Typically, a well-nourished 70-kg person has fuel reserves totaling about 670,000 kJ (161,000 kcal; Table 24.5). The energy need for a 24-hour period ranges from about 6700 kJ (1600 kcal) to 25,000 kJ (6000 kcal), of course depending on the extent of activity, as we have just examined. Thus, stored fuels suffice to meet caloric needs during starvation for 1 to 3 months. However, the carbohydrate reserves are exhausted in only a day.

TABLE 24.5 Typical fuel reserves in a 70-kg person

	Available energy in kilojoules (kcal)					
Organ	**Glucose or glycogen**		**Triacylglycerols**		**Mobilizable proteins**	
Blood	250	(60)	20	(45)	0	(0)
Liver	1700	(400)	2000	(450)	1700	(400)
Brain	30	(8)	0	(0)	0	(0)
Muscle	5000	(1200)	2000	(450)	100,000	(24,000)

Adipose tissue	330	(80)	560,000	(135,000)	170	(40)

Data from G. F. Cahill, Jr., *Clin. Endocrinol. Metab.* 5:398, 1976.

The first priority during starvation is the maintenance of blood-glucose concentration

Even under starvation conditions, the blood-glucose concentration must be maintained above 2.2 mM. The first priority of metabolism in starvation is to provide sufficient glucose to the brain and other tissues (such as red blood cells) that are absolutely dependent on this fuel. However, precursors of glucose are not abundant. Most energy is stored in the fatty acyl moieties of triacylglycerols. Moreover, recall that fatty acids cannot be converted into glucose, because acetyl CoA resulting from fatty acid breakdown cannot be transformed into pyruvate (Section 22.4). The glycerol moiety of triacylglycerol can be converted into glucose, but only a limited amount is available. The only other potential source of glucose is the carbon skeletons of amino acids derived from the breakdown of proteins. However, proteins are not stored, and so any breakdown will necessitate a loss of function. Thus, the second priority of metabolism in starvation is to preserve protein, which is accomplished by shifting the fuel being used from glucose to fatty acids and ketone bodies (**Figure 24.15**).

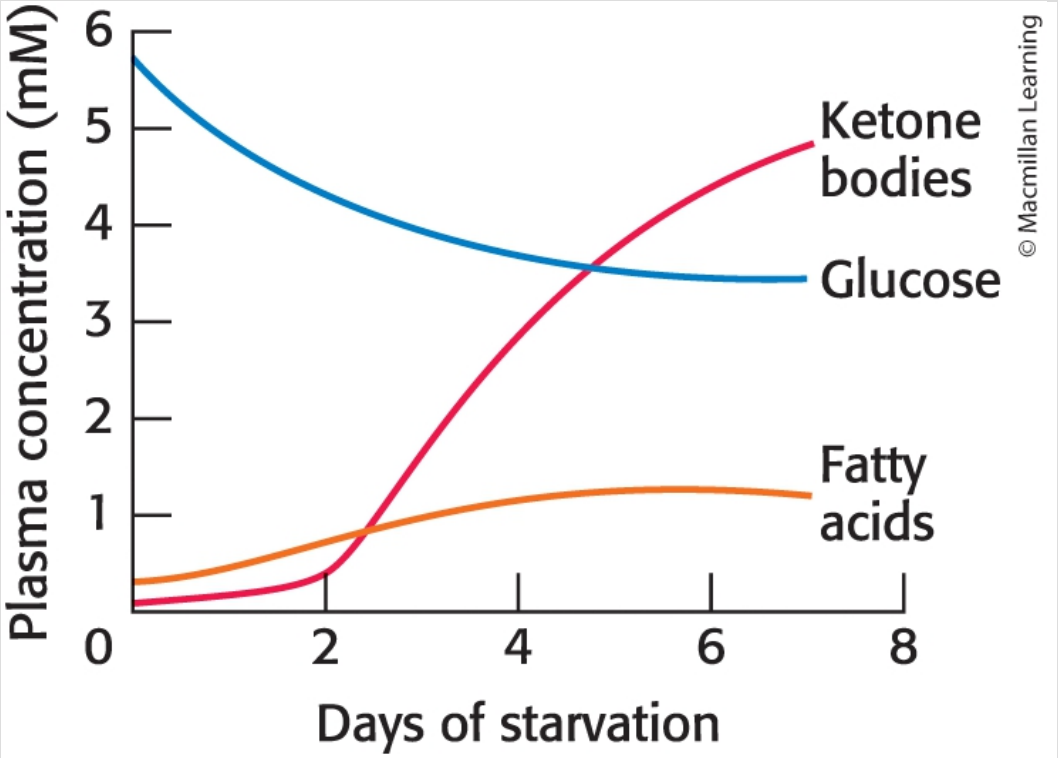


FIGURE 24.15 The blood concentrations of fatty acids and ketone bodies increase in starvation, while glucose decreases.

The metabolic changes on the first day of starvation are like those after an overnight fast. The low blood-sugar level leads to decreased insulin secretion and increased glucagon secretion. The dominant metabolic processes are the mobilization of triacylglycerols in adipose tissue and gluconeogenesis by the liver. The liver obtains energy for its own needs by oxidizing fatty acids released from adipose tissue. The concentrations of acetyl CoA and citrate consequently increase, which switches off glycolysis. The uptake of glucose by muscle is markedly diminished because of the low insulin level, whereas fatty acids enter freely. Consequently, muscle uses almost no glucose and relies nearly exclusively on fatty acids for fuel. The β oxidation of fatty acids by muscle halts the

conversion of pyruvate into acetyl CoA, because acetyl CoA stimulates the phosphorylation of the pyruvate dehydrogenase complex, which renders it inactive (Section 17.4). Hence, any available pyruvate, lactate, and alanine are exported to the liver for conversion into glucose. Glycerol derived from the cleavage of triacylglycerols is another raw material for the synthesis of glucose by the liver.

Proteolysis provides a major source of carbon skeletons for gluconeogenesis. During starvation, degraded proteins are not replenished and instead serve as carbon sources for glucose synthesis. Initial sources of protein are those that turn over rapidly, such as proteins of the intestinal epithelium and the secretions of the pancreas. Proteolysis of muscle protein can provide large amounts of amino acids for gluconeogenesis. However, survival for most animals depends on being able to move rapidly, which requires a large muscle mass, and so muscle protein loss must be minimized.

Self-Check Question



The hormone glucagon signifies the fasted state, yet it inhibits glycolysis in the liver. How do we benefit from this inhibition of an energy-production pathway?

Metabolic adaptations in prolonged starvation minimize protein degradation

How is the loss of muscle and other proteins curtailed? After about 3 days of starvation, the liver forms large amounts of the ketone

bodies, acetoacetate, and D-3-hydroxybutyrate (Section 22.4). Their synthesis from acetyl CoA increases markedly because the citric acid cycle is unable to oxidize all the acetyl units generated by fatty acid degradation. Gluconeogenesis depletes the supply of oxaloacetate, which is essential for the entry of acetyl CoA into the citric acid cycle. Consequently, the liver produces large quantities of ketone bodies, which are released into the blood. At this time, the brain begins to consume significant amounts of acetoacetate in place of glucose. After 3 days of starvation, about a quarter of the brain's energy needs are met by ketone bodies (**Table 24.6**). The heart also uses ketone bodies as fuel.

TABLE 24.6 Fuel metabolism during starvation

	Amount formed or consumed in 24 hours (grams)	
Fuel exchanges and consumption	**3rd day**	**40th day**
Fuel use by the brain		
Glucose	100	40
Ketone bodies	50	100
All other use of glucose	50	40
Fuel mobilization		
Adipose-tissue lipolysis	180	180
Muscle-protein degradation	75	20

Fuel output of the liver		
Glucose	150	80
Ketone bodies	150	150

After several weeks of starvation, ketone bodies become the major fuel of the brain. Acetoacetate is activated by the transfer of CoA from succinyl CoA to give acetoacetyl CoA (Section 22.4). Cleavage by thiolase then yields two molecules of acetyl CoA, which enter the citric acid cycle. In essence, ketone bodies are equivalents of fatty acids that are an accessible fuel source for the brain. Only 40 g of glucose is then needed per day for the brain, compared with about 120 g in the first day of starvation (**Figure 24.16A**). The effective conversion of fatty acids into ketone bodies by the liver and their use by the brain markedly diminishes the need for glucose. Hence, less muscle is degraded than in the first days of starvation. The breakdown of 20 g of muscle daily compared with 75 g early in starvation is most important for survival. How are the amino acids released by muscle processed? The amino acids are transported to the liver where nitrogen is removed as urea, gluconeogenic amino acids are metabolized into glucose, and ketogenic amino acids are used as fuel for the liver or processed to ketone bodies.

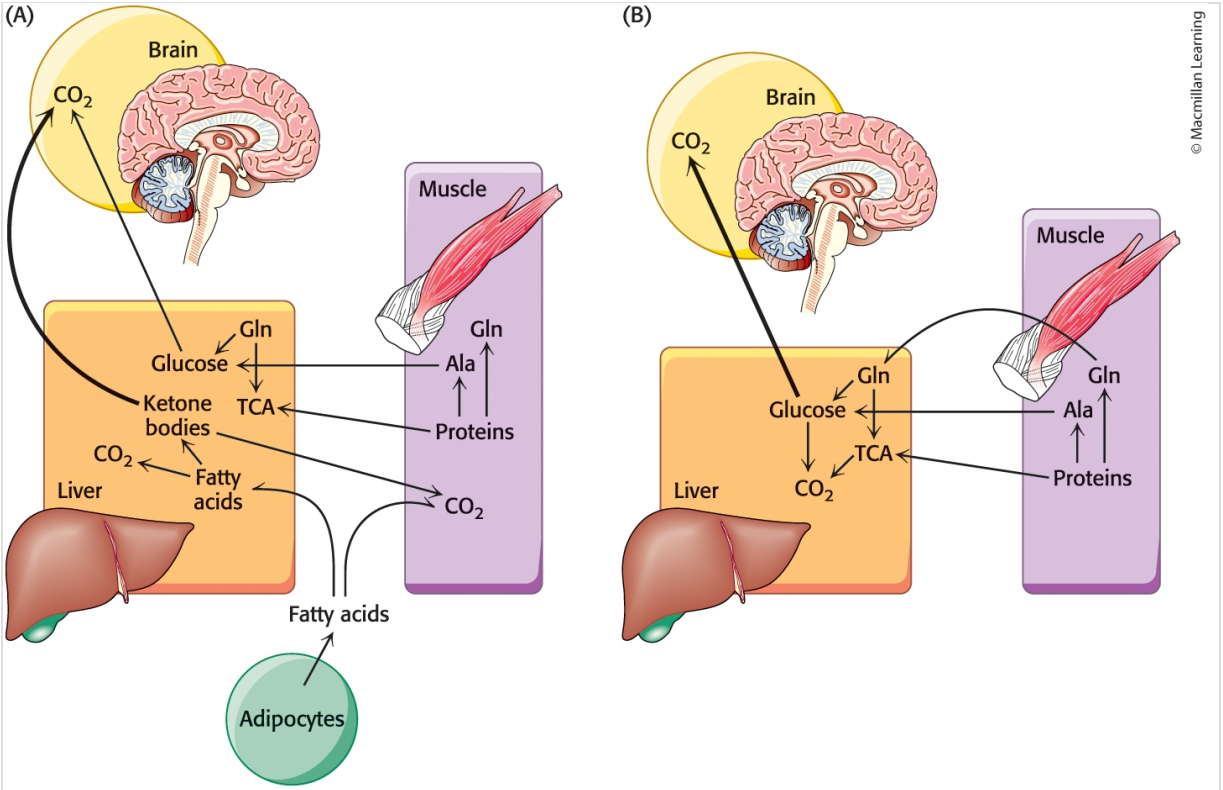


FIGURE 24.16 Fuel use during prolonged starvation changes after fat mass is depleted. A simplified depiction of the relation of adipose tissue, liver, muscle, and brain is shown. (A) Fat mass is adequate. (B) Fat mass is depleted. Only the amino acids alanine and glutamine are shown since they are also important for nitrogen transport.

What happens after depletion of the triacylglycerol stores? The ketone body contribution disappears, and the only source of fuel that remains is protein (Figure 24.16B). Protein degradation accelerates, and a loss of heart, liver, or kidney function inevitably causes death. A person's survival time is mainly determined by the size of the triacylglycerol depot. Examinations of people who have starved themselves to death as a political protest show that lean individuals succumb after about 70 days, whereas obese individuals can survive for 6 or 7 months.

Self-Check Question



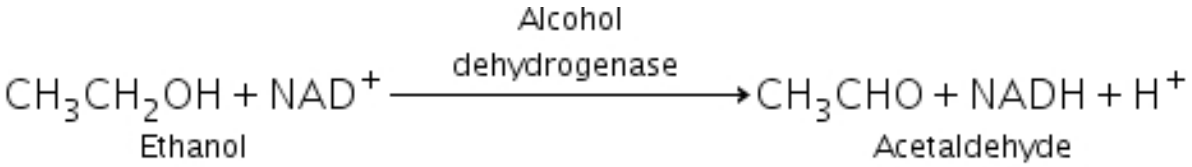
What tissue provides the largest energy supply in a well-nourished human being? What other tissues also store large amounts of energy and in what form?

24.6 Ethanol Alters Energy Metabolism in the Liver

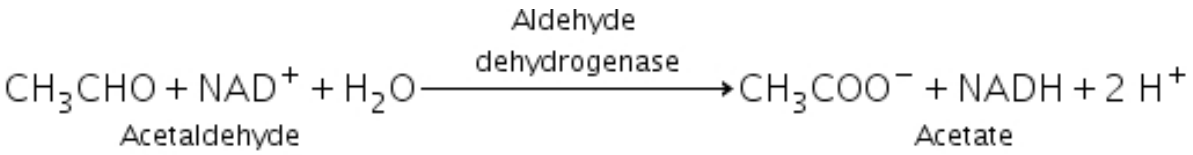
Ethanol has been a part of the human diet for centuries, partly because of its intoxicating effects and partly because alcoholic beverages provided a safe means of hydration when uncontaminated water was scarce. However, its consumption in excess can result in a number of health problems, most notably liver damage. What is the biochemical basis of these health problems?

Ethanol metabolism leads to an excess of NADH

Ethanol cannot be excreted and must be metabolized, primarily by the liver. This metabolism is accomplished by two pathways. The first pathway comprises two steps. The first step, catalyzed by the enzyme *alcohol dehydrogenase,* takes place in the cytoplasm:



The second step, catalyzed by *aldehyde dehydrogenase*, takes place in mitochondria:



Note that ethanol consumption leads to an accumulation of NADH. This high concentration of NADH inhibits gluconeogenesis by preventing the oxidation of lactate to pyruvate. In fact, the high concentration of NADH will cause the reverse reaction to predominate, and lactate will accumulate. The consequences may be hypoglycemia and lactic acidosis.

The overabundance of NADH also inhibits fatty acid oxidation. An important metabolic purpose of fatty acid oxidation is to generate NADH for ATP generation by oxidative phosphorylation, but an alcohol consumer's NADH needs are met by ethanol metabolism. In fact, the excess NADH signals that conditions are right for fatty acid synthesis. Hence, triacylglycerols accumulate in the liver, leading to a condition known as "fatty liver" that is exacerbated in obese persons.

The second pathway for ethanol metabolism uses cytochrome P450 enzymes. This means of ethanol metabolism is also called the *microsomal ethanol-oxidizing system* (MEOS). This cytochrome P450-dependent pathway (Section 27.4) generates acetaldehyde and subsequently acetate while oxidizing biosynthetic reducing power, NADPH, to $NADP^+$. Because it uses oxygen, this pathway generates free radicals that damage tissues. Moreover, because the system consumes NADPH, the antioxidant glutathione cannot be regenerated (Section 20.5), exacerbating the oxidative stress.

Ethanol metabolites cause liver damage

What are the effects of the other metabolites of ethanol? Liver mitochondria can convert acetate into acetyl CoA in a reaction requiring ATP. The enzyme is the acyl CoA synthetase that normally activates short-chain fatty acids.

$$\text{Acetate} + \text{coenzyme A} + \text{ATP} \rightarrow \text{acetyl CoA} + \text{AMP} + PP_i$$

$$PP_i \rightarrow 2\ P_i$$

However, further processing of the acetyl CoA by the citric acid cycle is blocked, because NADH inhibits two important citric acid cycle regulatory enzymes — isocitrate dehydrogenase and α-ketoglutarate dehydrogenase.

The accumulation of acetyl CoA has several consequences. First, ketone bodies will form and be released into the blood, aggravating the acidic condition already resulting from the high lactate concentration. The processing of the acetate in the liver becomes inefficient, leading to a buildup of acetaldehyde. This very reactive compound forms covalent bonds with many important functional groups in proteins, impairing protein function. If ethanol is consistently consumed at high levels, the acetaldehyde can significantly damage the liver, eventually leading to cell death.

Ethanol also alters gene transcription, further exacerbating liver damage. Ethanol in some fashion stimulates the synthesis of sterol regulatory-element binding proteins (SREBPs) (Section 27.3), a family of transcription factors that upregulates the genes that promote fatty acid synthesis. At the same time, acetaldehyde derived from ethanol inactivates another transcription factor, PPARα (peroxisome proliferator-activated receptor), which normally stimulates the genes

involved in fatty acid oxidation. The biochemical effects of ethanol consumption can be quite rapid. For instance, fat accumulates in the liver within a few days of moderate alcohol consumption.

Liver damage from excessive ethanol consumption occurs in three stages. The first stage is the aforementioned development of fatty liver. In the second stage — alcoholic hepatitis — groups of cells die and inflammation results. This stage can itself be fatal. In stage three — cirrhosis — fibrous structure and scar tissue are produced around the dead cells. Cirrhosis impairs many of the liver's biochemical functions. The cirrhotic liver is unable to convert ammonia into urea, and blood levels of ammonia rise. Ammonia is toxic to the nervous system and can cause coma and death. Cirrhosis of the liver arises in about 25% of alcoholics, and about 75% of all cases of liver cirrhosis are the result of alcoholism. Viral hepatitis is a nonalcoholic cause of liver cirrhosis.

Excess ethanol consumption disrupts vitamin metabolism

The adverse effects of ethanol are not limited to the metabolism of ethanol itself. Vitamin A (retinol) is converted into retinoic acid, an important signal molecule for growth and development in vertebrates, by the same dehydrogenases that metabolize ethanol. Consequently, this activation does not take place in the presence of ethanol, which acts as a competitive inhibitor. Moreover, the P450 enzymes induced by ethanol inactivate retinoic acid. These disruptions in the retinoic acid signaling pathway are believed to be responsible, at least in part, for fetal alcohol syndrome as well as the development of a variety of cancers.

The disruption of vitamin A metabolism is a direct result of the biochemical changes induced by excess ethanol consumption. Other disruptions in metabolism result from another common characteristic

of alcoholics — malnutrition. Alcoholics will frequently drink instead of eating. A dramatic neurological disorder, referred to as *Wernicke–Korsakoff syndrome*, results from insufficient intake of the vitamin thiamine. Symptoms include mental confusion, unsteady gait, and lack of fine motor skills.

The symptoms of Wernicke–Korsakoff syndrome are similar to those of beriberi (Section 17.5) because both conditions result from a lack of thiamine. Thiamine is converted into the coenzyme thiamine pyrophosphate, a key constituent of the pyruvate dehydrogenase complex. Recall that this complex links glycolysis with the citric acid cycle. Disruptions in the pyruvate dehydrogenase complex are most evident as neuromuscular disorders because the nervous system is normally dependent on glucose for energy generation.

Alcoholic scurvy is occasionally observed because of an insufficient ingestion of ascorbate (vitamin C). Ascorbate is required for the formation of stable collagen fibers. The symptoms of scurvy include skin lesions and blood-vessel fragility. Most notable are bleeding gums, the loss of teeth, and periodontal infections. Gums are especially sensitive to a lack of ascorbate because the collagen in gums turns over rapidly.

What is the biochemical basis for scurvy? Ascorbate is required for the synth-esis of 4-hydroxyproline, an amino acid necessary for collagen stability. To form this unusual amino acid, proline residues on the amino side of glycine residues in nascent collagen chains become hydroxylated. One oxygen atom from O_2 becomes attached to C-4 of proline, while the other oxygen atom is taken up by α-ketoglutarate, which is converted into succinate (**Figure 24.17**).

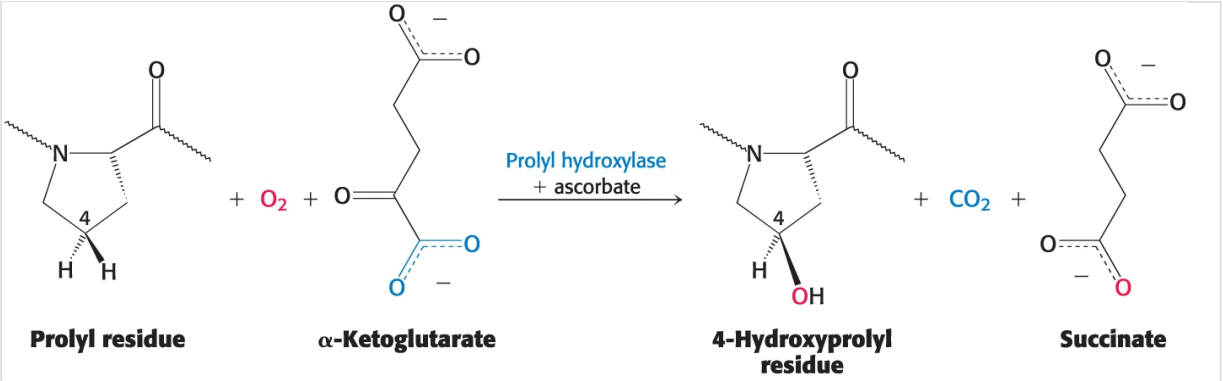


FIGURE 24.17 Formation of 4-hydroxyproline requires ascorbate. Proline is hydroxylated at C-4 by the action of prolyl hydroxylase, an enzyme that activates molecular oxygen.

This reaction is catalyzed by prolyl hydroxylase, a dioxygenase (Section 23.5), which requires an Fe^{2+} ion to activate O_2. The enzyme also converts α-ketoglutarate into succinate without hydroxylating proline. In this partial reaction, an oxidized iron complex is formed, which inactivates the enzyme. How is the active enzyme regenerated? Ascorbate comes to the rescue by reducing the ferric ion of the inactivated enzyme. In the recovery process, ascorbate is oxidized to dehydroascorbic acid (**Figure 24.18**). Thus, ascorbate serves here as a specific antioxidant.

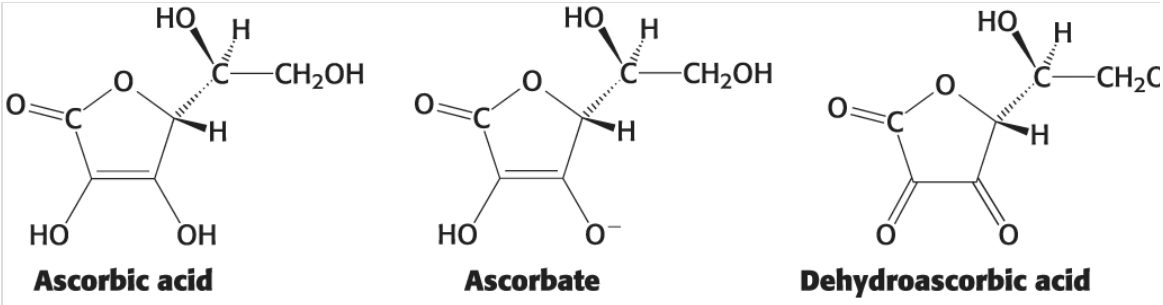


FIGURE 24.18 Ascorbate is the ionized form of vitamin C, and dehydroascorbic acid is the oxidized form of ascorbate.

Why does impaired hydroxylation have such devastating consequences? Collagen synthesized in the absence of ascorbate is less stable than the normal protein. Hydroxyproline stabilizes the collagen triple helix by forming interstrand hydrogen bonds. The abnormal fibers formed by insufficiently hydroxylated collagen account for the symptoms of scurvy. In the next section, we will see that prolyl hydroxylase also plays a critical role in the development of some cancers.

Self-Check Question



What are the two primary means of processing ethanol?

Ethanol and defects in central energy metabolism contribute to the development of cancer



In addition to the numerous detrimental effects outlined above, ethanol is also a well-known carcinogen, although the mechanisms and tissues affected are too numerous to list, and many remain poorly established. There are many other connections between biochemical defects in the enzymes of central metabolism and cancer, some of which are exacerbated by ethanol consumption. For example, mutations that alter

the activity of succinate dehydrogenase, fumarase, or pyruvate dehydrogenase kinase all enhance aerobic glycolysis (Section 16.3). Recall that in aerobic glycolysis, cancer cells preferentially metabolize glucose to lactate even in the presence of oxygen. Defects in these enzymes share a common biochemical link: the transcription factor HIF-1 and its regulation by prolyl hydroxylase.

Normally, HIF-1 upregulates the enzymes and transporters that enhance glycolysis only when oxygen concentration falls, a condition called *hypoxia*. Under aerobic conditions, HIF-1 is hydroxylated by prolyl hydroxylase and is subsequently destroyed by the proteasome (Section 23.2). The degradation of HIF-1 prevents the stimulation of glycolysis. As noted previously (Figure 24.17), prolyl hydroxylase requires α-ketoglutarate, ascorbate, and oxygen for activity. Thus, when ascorbate is unavailable — due to excessive alcohol consumption or when oxygen concentration falls — prolyl hydroxylase is inactive, HIF-1 is not hydroxylated and not degraded, and the synthesis of proteins required for glycolysis is stimulated. As a result, the rate of glycolysis is increased.

Recent research suggests that defects in the enzymes of the citric acid cycle may significantly affect the regulation of prolyl hydroxylase. When either succinate dehydrogenase or fumarase is defective, succinate and fumarate accumulate in the mitochondria and spill over into the cytoplasm. Both succinate and fumarate are competitive inhibitors of prolyl hydroxylase. The inhibition of prolyl hydroxylase results in the stabilization of HIF-1, since HIF-1 is no longer hydroxylated. Lactate, the end product of glycolysis, also appears to inhibit prolyl hydroxylase by interfering with the action of ascorbate. These multiple factors reducing prolyl hydroxylase activity are likely exacerbated by the effects of ethanol consumption described previously.

In addition to increasing the amount of the proteins required for glycolysis, HIF-1 also stimulates the production of pyruvate dehydrogenase kinase (PDK). The kinase inhibits the pyruvate

dehydrogenase complex, preventing the conversion of pyruvate into acetyl CoA. The pyruvate remains in the cytoplasm, further increasing the rate of aerobic glycolysis. Moreover, mutations in PDK that lead to enhanced activity contribute to increased aerobic glycolysis and the subsequent development of cancer. By enhancing glycolysis and increasing the concentration of lactate, the mutations in PDK result in the inhibition of prolyl hydroxylase and the stabilization of HIF-1.

One additional and particularly fascinating example of the manipulation of cellular control by cancer cells comes from recent findings on the mitochondrial enzyme acetyl CoA acetyltransferase. Under normal circumstances, this enzyme synthesizes ketone bodies; however, in certain cancers, acetyl CoA acetyltransferase is phosphorylated, causing it to form active tetramers. Interestingly, the enzyme then acts as a protein acetyltransferase, adding acetyl groups to pyruvate dehydrogenase and pyruvate dehydrogenase phosphatase. The acetylation inhibits the two enzymes and facilitates the metabolic switch from oxidative phosphorylation to aerobic glycolysis, thereby enhancing the Warburg effect (Section 16.3). In essence, the enzyme is hijacked from its normal role in ketone body formation to further cancer growth.

These observations linking central metabolic enzymes to cancer suggest that cancer is also a metabolic disease, not simply a disease of mutant growth factors and cell cycle control proteins. This realization opens the door to new thinking about cancer treatments. Indeed, preliminary experiments suggest that if cancer cells undergoing aerobic glycolysis are forced by pharmacological manipulation to use oxidative phosphorylation, the cancer cells lose their malignant properties. It seems that even in metabolic pathways as well known as the citric acid cycle, which has been studied for the better part of a century, there are still secrets to be revealed by future biochemists.

Chapter 24 Summary

24.1 Caloric Homeostasis Is a Means of Regulating Body Weight

- Maintaining near-constant body weight throughout adult life is accomplished by caloric homeostasis. When energy intake is greater than expenditure, weight gain results, which may lead to obesity. Obesity is at pandemic levels and is implicated as a contributing factor in a host of pathological conditions.
- Various signal molecules act on the brain to control appetite, including short-term signals like CCK and GLP-1, which relay satiety signals to the brain, and signals like leptin and insulin, which regulate appetite over longer periods.
- Leptin is secreted by adipose tissue in proportion to mass and reduces hunger by binding to receptors in the brain. Obesity can develop even with normal amounts of leptin and leptin receptor, suggesting that such individuals are leptin-resistant. Suppressors of cytokine signaling may inhibit leptin signaling, leading to leptin resistance and obesity.

24.2 The Fasted–Fed Cycle Is a Response to Eating and Sleeping Behaviors

- Insulin signals the fed state; it stimulates the formation of glycogen and triacylglycerols. In contrast, glucagon signals a low blood-glucose concentration, i.e., the fasted state; it stimulates glycogen breakdown and gluconeogenesis by the liver, and triacylglycerol hydrolysis by adipose tissue.
- After a meal, the rise in the blood-glucose concentration leads to increased insulin and decreased glucagon secretions, leading to glycogen synthesis in muscle and the liver.
- When the blood-glucose concentration falls, glucose is formed by glycogen degradation and gluconeogenesis, and fatty acids

are released by the hydrolysis of triacylglycerols.
- As a fast continues, the liver and muscle increasingly use fatty acids to meet their own energy needs so that glucose is conserved for use by the brain and the red blood cells.

24.3 Diabetes Is a Common Metabolic Disease Often Resulting from Obesity

- Diabetes is the most common metabolic disease in the world, with type 2 being far more common than type 1.
- Type 1 diabetes results when insulin is absent due to destruction of the pancreatic β cells. The body is still responsive to insulin, which is used to treat the disease.
- Type 2 diabetes is characterized by insulin resistance, in which tissues do not respond normally to insulin. Obesity is a significant predisposing factor for type 2 diabetes.
- Excess fats accumulate in the muscle tissue of an obese individual. These fats are processed to second messengers that activate signal-transduction pathways, which inhibit insulin signaling, leading to insulin resistance.
- Insulin resistance ultimately leads to pancreatic β-cell failure. Increased insulin production to compensate for resistance results in endoplasmic reticulum stress and subsequent activation of apoptotic pathways that lead to β cell death.
- Lack of insulin signaling leads to elevated blood-glucose levels, the mobilization of triacylglycerols, and excessive ketone body formation. Accelerated ketone body formation can lead to acidosis, coma, and death in untreated diabetics.

24.4 Exercise Beneficially Alters the Biochemistry of Cells

- Exercise is a useful treatment for insulin resistance and type 2 diabetes. Muscle activity stimulates mitochondrial biogenesis in a calcium-dependent manner. The increase in the number of

mitochondria facilitates fatty acid oxidation in the muscle, resulting in increased insulin sensitivity.
- Fuel choice in exercise is determined by the intensity and duration of the bout of exercise. Sprinting is powered by stored ATP, creatine phosphate, and anaerobic glycolysis, while running a marathon requires the oxidation of both muscle glycogen and fatty acids derived from adipose tissue.

24.5 Starvation Induces Protein Wasting and Ketone Body Formation

- The metabolic adaptations during starvation serve to prioritize blood glucose yet minimize protein degradation.
- Ketone bodies are formed by the liver from fatty acids within a few days after the onset of starvation and, after several weeks, they become the major fuel of the brain. The diminished need for glucose decreases the rate of muscle breakdown, prolonging survival.

24.6 Ethanol Alters Energy Metabolism in the Liver

- The oxidation of ethanol results in an unregulated overproduction of NADH, which has several consequences. A rise in the blood concentration of lactic acid and ketone bodies causes acidosis. The liver is damaged because the excess NADH causes excessive fat formation as well as the generation of acetaldehyde, a reactive molecule.
- Alterations in the activity of several transcription factors due to ethanol consumption also contribute to liver pathology. Severe liver damage can result with prolonged ethanol use.
- Ethanol disrupts vitamin absorption and is carcinogenic. Numerous defects in central metabolism lead to cancer by a variety of unexpected mechanisms, indicating that in many cases cancer can be viewed as a metabolic disease.

Key Terms

caloric homeostasis (energy homeostasis)
insulin
glucagon
leptin
fasted–fed cycle
glucose homeostasis
type 1 diabetes
insulin resistance
type 2 diabetes
metabolic syndrome
endoplasmic reticulum (ER) stress
unfolded protein response (UPR)
respiratory quotient (RQ)

Problems

1. Pick one answer for each question: Under normal circumstances, what is the most commonly used fuel by the brain? Which becomes a substantial source of energy for the brain after a week of fasting?

a. Glycerol
b. Glucose
c. Fatty acids
d. Ketone bodies

2. Which of the following pathways is not stimulated by epinephrine?

a. Glycogen degradation
b. Mobilization of fatty acids from adipose tissue
c. Glycogen synthesis
d. Glycolysis in muscle

3. As disturbing as the obesity pandemic is, an equally intriguing, almost amazing observation is that many people are able to maintain an approximately constant weight throughout adult life. A few simple calculations of a simplified situation illustrate how remarkable this feat is. Consider a 120-pound woman whose weight does not change significantly between the ages of 25 and 65. Let's say that the woman requires 8400 kJ $(2000\ \text{kcal})\ \text{per day}^{-1}$. For simplicity's sake, let us assume the woman's diet consists predominantly of fatty acids derived from lipids. The energy density of fatty acids is $38\ \text{kJ}\ (9\ \text{kcal})\ \text{g}^{-1}$. How much food has she consumed over the 40 years in question? 1

4. Suppose that our test subject from problem 3 gained 55 pounds between the ages of 25 and 65 (a common occurrence), and that her weight at 65 years of age is 175 pounds. Calculate how many excess calories she consumed per day to gain the 55 pounds over 40 years. Assume that our test subject is 5 feet, 6 inches tall. What is her BMI? Would she be considered obese at 175 pounds? 1

5. Adipose tissue was once only considered a storage site for fat. Why is this view no longer considered correct?

6. What are the two key hormones responsible for long-term maintenance of caloric homeostasis? 2

7. What two biochemical roles does CCK play? GLP-1? 2

8. Match the characteristic (a–i) with the appropriate hormone (1–6). 2

1. Secreted by adipose tissue	1. leptin
2. Stimulates liver gluconeogenesis	2. adiponectin
3. GPCR pathway	3. GLP-1
4. Satiety signal	4. CCK
5. Enhances insulin secretion	5. insulin
6. Secreted by the pancreas during a fast	6. glucagon
7. Secreted after a meal by the pancreas	
8. Stimulates glycogen synthesis	
9. Missing in type 1 diabetes	

---

9. Differentiate between type 1 and type 2 diabetes. 3

10. The typical human adult uses about 160 g of glucose per day, 120 g of which is used by the brain. The available reserve of glucose ($\sim 20\ g$ of circulating glucose and $\sim 190\ g$ of glycogen) is adequate for about one day. After the reserve has been depleted during starvation, what other sources can be used to produce glucose?

a. Glycerol from triacylglycerols
b. Glucogenic amino acids from muscle protein

c. Pyruvate by carboxylation to form oxaloacetate
d. Fatty acids from triacylglycerols
e. Ketogenic amino acids from muscle protein

11. The rate of energy expenditure of a typical 70-kg person at rest is about 70 watts (W), like that of a light bulb.

a. Express this rate in kilojoules per second and in kilocalories per second.
b. How many electrons flow through the mitochondrial electron-transport chain per second under these conditions?
c. Estimate the corresponding rate of ATP production.
d. The total ATP content of the body is about 50 g. Estimate how often an ATP molecule turns over in a person at rest.

12. Recall that the respiratory quotient (RQ) is defined as the volume of CO_2 released divided by the volume of O_2 consumed.

a. Calculate the RQ values for the complete oxidation of glucose and of tripalmitoylglycerol.
b. What do RQ measurements reveal about the contributions of different energy sources during intense exercise? (Assume that protein degradation is negligible.) 4

13. Ingesting large amounts of glucose immediately before a marathon might seem to be a good way of increasing the fuel stores. However, experienced runners do not ingest glucose before a race. What is the biochemical reason for their avoidance of this potential fuel? (Hint: consider the effect of glucose ingestion on the level of insulin.) 2, 4

14. The most common form of malnutrition in children in the world, kwashiorkor, is caused by a diet having ample calories but little protein. The high levels of carbohydrate result in high levels of insulin. 5

a. What is the effect of high levels of insulin on lipid utilization? On protein metabolism?
b. Children suffering from kwashiorkor often have large distended bellies caused by water from the blood leaking into extracellular spaces. Suggest a biochemical basis for this condition.

15. How is the metabolism of the liver coordinated with that of skeletal muscle during strenuous exercise? What is the advantage of converting pyruvate into lactate in skeletal muscle? 4

16. What is the major fuel for resting muscle? What is the major fuel for muscle under strenuous work conditions? 4

17.

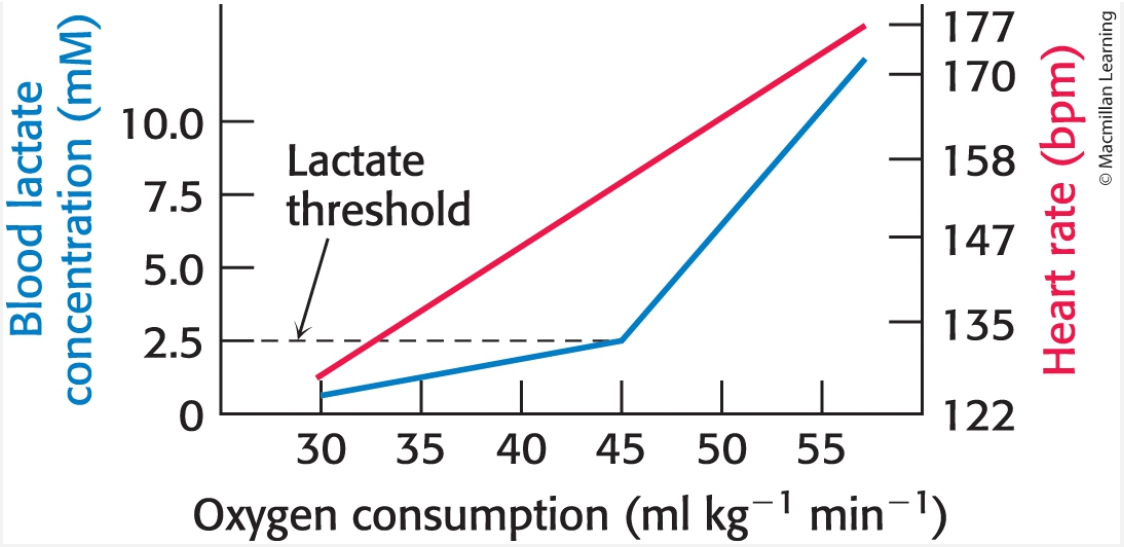
a. After light exercise, the oxygen consumed in recovery is approximately equal to the oxygen deficit, which is the amount of additional oxygen that would have been consumed had oxygen consumption reached steady state immediately. How is the oxygen consumed in recovery used?
b. The oxygen consumed after strenuous exercise stops is significantly greater than the oxygen deficit and is termed *excess post-exercise oxygen consumption* (EPOC). Why is so much more oxygen required after intense exercise? 4

18. Alcohol consumption on an empty stomach results in some interesting biochemical as well as embarrassing behavioral alterations. We will ignore the latter. Gluconeogenesis falls; there are increases in intracellular ratios of lactate to pyruvate, of glycerol 3-phosphate to dihydroxyacetone phosphate, of glutamate to α-ketoglutarate, and of D-3-hydroxybutyrate to acetoacetate. Hypoglycemia develops rapidly. Blood pH also falls. Alcohol consumption by a well-fed individual does not lead to hypoglycemia or alteration in blood pH. 6

a. Why does ethanol consumption result in the altered ratios?
b. Why does hypoglycemia and blood acidosis result in the hungry individual?
c. Why does a well-fed person not experience hypoglycemia?

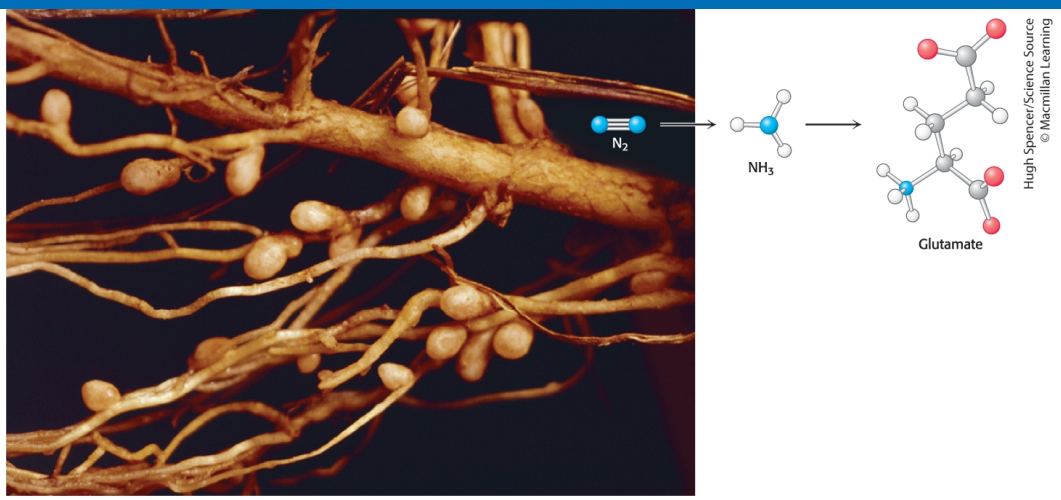
19. Recall that pyruvate carboxylase is the enzyme that catalyzes the most important anaplerotic reaction, which restores CAC intermediates by converting pyruvate into oxaloacetate (Section 17.5). Pyruvate carboxylase deficiency is a fatal disorder. Patients with pyruvate carboxylase deficiency sometimes display some or all of the following symptoms: lactic acidosis, hyperammonemia (excess NH_4^+ in the blood), hypoglycemia, and demyelination of the regions of the brain due to insufficient lipid synthesis. Provide a possible biochemical rationale for each of these symptoms.

20. The graph shows the relation between blood-lactate levels, oxygen consumption, and heart rate during exercise of increasing intensity. The values for oxygen consumption and heart rate are indicators of the degree of exertion. 4



a. Why is some lactate produced even when exercise is moderate?
b. Biochemically, what is taking place when the lactate concentration begins to rise rapidly, a point called the lactate threshold?
c. Endurance athletes will sometimes measure blood-lactate levels during training so that they know their lactate threshold. Then, during events, they will race just at or below their lactate threshold until the late stages of the race. Biochemically, why is this practice wise?
d. Training can increase the lactate threshold. Explain.

CHAPTER 25
Biosynthesis of Amino Acids



While nitrogen, as N_2 gas, makes up the majority of Earth's atmosphere, most organisms cannot directly access it for use in amino acids. They rely on nitrogen-fixing microorganisms, such as bacteria that live in nodules on the roots of yellow clover, to convert N_2 to ammonia (NH_3). Ammonia can then be used to synthesize, first, glutamate, and then other amino acids.

OUTLINE

25.1 Nitrogen Fixation: Microorganisms Use ATP and a Powerful Reductant to Reduce Atmospheric Nitrogen to Ammonia
25.2 Amino Acids Are Made from Intermediates of the Citric Acid Cycle and Other Major Pathways
25.3 Feedback Inhibition Regulates Amino Acid Biosynthesis

25.4 Amino Acids Are Precursors of Many Biomolecules

Learning Goals



By the end of this chapter, you should be able to:

1. Explain the centrality of nitrogen fixation to life and describe how atmospheric nitrogen is converted into biologically useful forms of nitrogen.
2. Identify the sources of carbon atoms for amino acid synthesis.
3. Describe the role of feedback inhibition in controlling amino acid synthesis.
4. Identify important biomolecules that are derived from amino acids.

The assembly of biological macromolecules, including proteins and nucleic acids, requires the generation of appropriate starting materials. In this chapter, we will consider the biosynthesis of amino acids — the building blocks of proteins and the nitrogen source for many other important molecules, including nucleotides, neurotransmitters, and prosthetic groups such as porphyrins.

Amino acid biosynthesis is intimately connected with nutrition because many higher organisms, including human beings, have lost the ability to synthesize some amino acids and must therefore obtain adequate quantities of these essential amino acids in their diets. Furthermore, because some amino acid biosynthetic enzymes are absent in mammals but present in plants and microorganisms, they are useful targets for herbicides and antibiotics.

25.1 Nitrogen Fixation: Microorganisms Use ATP and a Powerful Reductant to Reduce Atmospheric Nitrogen to Ammonia

One of the most challenging biochemical problems organisms face is obtaining nitrogen in a usable form. The nitrogen in amino acids, purines, pyrimidines, and other biomolecules ultimately comes from atmospheric nitrogen, N_2. The extremely strong $N \equiv N$ bond, which has a bond energy of $940\ kJ\ mol^{-1}\ (225\ kcal\ mol^{-1})$, is highly resistant to chemical attack. Indeed, Antoine Lavoisier named nitrogen gas "azote," from Greek words meaning "without life," because it is so unreactive. Nevertheless, the conversion of nitrogen and hydrogen to form ammonia is thermodynamically favorable; the reaction is difficult kinetically because of the activation energy required to form intermediates along the reaction pathway.

Although higher organisms are unable to fix nitrogen, this conversion is carried out by some bacteria and archaea. The biosynthetic process starts with the reduction of N_2 to NH_3 (ammonia), a process called **nitrogen fixation**. For example, symbiotic *Rhizobium* bacteria invade the roots of leguminous plants and form root nodules in which they fix nitrogen, supplying both the bacteria and the plants. The importance of nitrogen fixation by diazotrophic (nitrogen-fixing) microorganisms to the metabolism of all higher eukaryotes cannot be overstated: the amount of N_2 fixed by these species has been estimated to be 10^{11} kilograms per year, about 60% of Earth's newly fixed nitrogen. Lightning and ultraviolet radiation fix another 15%; the other 25% is fixed by

industrial processes. The industrial process for nitrogen fixation devised by Fritz Haber in 1910 is still being used in fertilizer factories.

$$N_2 + 3H_2 \rightleftharpoons 2NH_3$$

The fixation of N_2 is typically carried out by mixing it with H_2 gas over an iron catalyst at about 500°C and a pressure of 300 atmospheres.

Biological nitrogen fixation is catalyzed by the nitrogenase complex

To meet the kinetic challenge, the biological process of nitrogen fixation requires a complex enzyme with multiple redox centers. The **nitrogenase complex**, which carries out this fundamental transformation, consists of two proteins: a *reductase* (also called the iron protein or Fe protein), which provides electrons with high reducing power, and *nitrogenase* (also called the molybdenum–iron protein or MoFe protein), which uses these electrons to reduce N_2 to NH_3. The transfer of electrons from the reductase to the nitrogenase component is coupled to the hydrolysis of ATP by the reductase (**Figure 25.1**).

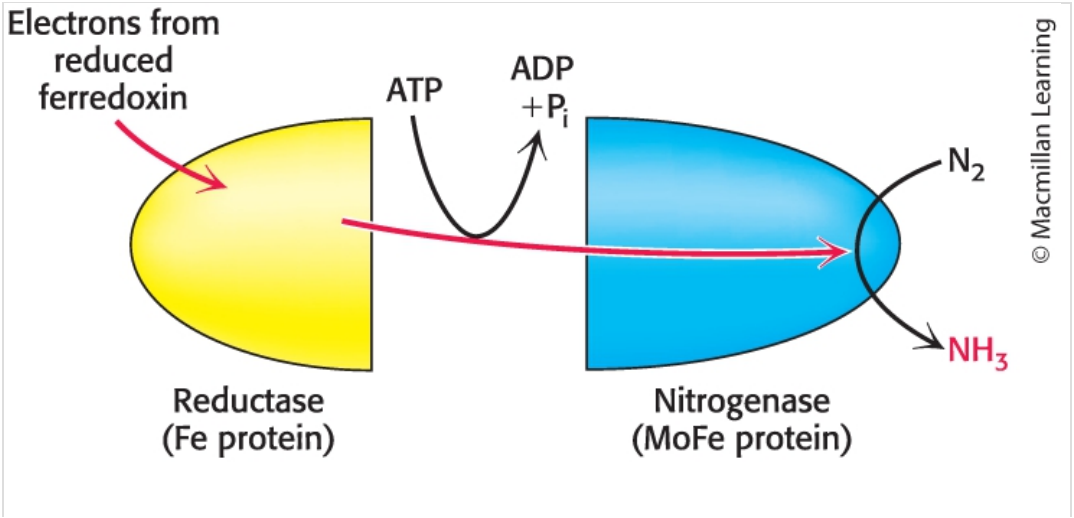


FIGURE 25.1 The nitrogenase complex fixes nitrogen to ammonia. Electrons flow from ferredoxin to the reductase (iron protein, or Fe protein) to nitrogenase (molybdenum–iron protein, or MoFe protein) to reduce nitrogen to ammonia. ATP hydrolysis within the reductase drives conformational changes necessary for the efficient transfer of electrons.



In principle, the reduction of N_2 to NH_3 is a six-electron process.

$$N_2 + 6\,e^- + 6\,H^+ \rightarrow 2\,NH_3$$

However, the biological reaction always generates at least 1 mol of H_2 in addition to 2 mol of NH_3 for each mol of $N \equiv N$. Hence, an input of two additional electrons is required.

$$N_2 + 8\,e^- + 8\,H^+ \rightarrow 2\,NH_3 + H_2$$

In most nitrogen-fixing microorganisms, the eight high-potential electrons come from reduced ferredoxin, generated by oxidative processes. Two molecules of ATP are hydrolyzed for each electron transferred. Thus, at least 16 molecules of ATP are hydrolyzed for each molecule of N_2 reduced.

$$N_2 + 8\,e^- + 8\,H^+ + 16\,ATP + 16\,H_2O \rightarrow 2\,NH_3 + H_2 + 16\,ADP + 16\,P_i$$

Recall that O_2 is required for oxidative phosphorylation to generate the ATP necessary for nitrogen fixation. However, the nitrogenase complex

is exquisitely sensitive to inactivation by O_2. To allow ATP synthesis and nitrogenase to function simultaneously, leguminous plants maintain a very low concentration of free O_2 in their root nodules, the location of the nitrogenase. This is accomplished by binding O_2 to leghemoglobin, a homolog of hemoglobin (Figure 10.13).

The iron–molybdenum cofactor of nitrogenase binds and reduces atmospheric nitrogen

Both the reductase and the nitrogenase components of the complex are iron–sulfur proteins, in which iron is bonded to the sulfur atom of a cysteine residue and to inorganic sulfide. Recall that iron–sulfur clusters act as electron carriers (Section 18.3). The reductase is a dimer of identical 30-kDa subunits bridged by a 4Fe–4S cluster (**Figure 25.2**).

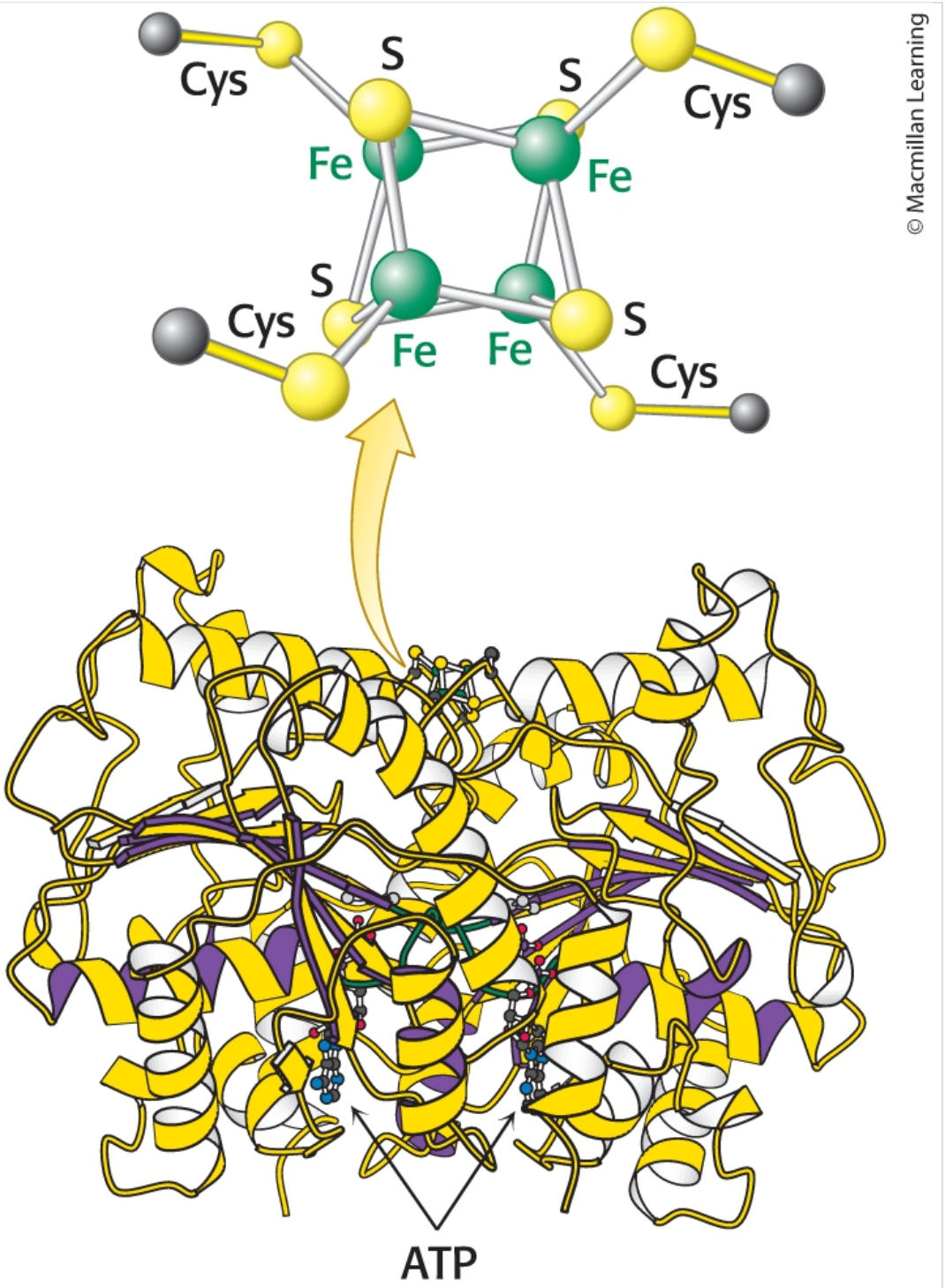


FIGURE 25.2 The Fe protein, or reductase, transfers elections of high reducing power. This protein is a dimer composed of two polypeptide chains linked by a 4Fe–4S cluster. Each monomer is a member of the P-loop NTPase family and contains an ATP-binding site.

[Drawn from 1N2C.pdb.]

INTERACT with this model in Achieve

The role of the reductase is to transfer electrons from a suitable donor, such as reduced ferredoxin, to the nitrogenase component. The 4Fe–4S cluster carries the electrons, one at a time, to nitrogenase. The binding and hydrolysis of ATP triggers a conformational change that moves the reductase closer to the nitrogenase component, whence it is able to transfer its electron to the center of nitrogen reduction.

The nitrogenase component is an $\alpha_2\beta_2$ tetramer (240-kDa), in which the α and β subunits are homologous to each other and structurally quite similar (**Figure 25.3**). The nitrogenase requires the FeMo cofactor, which consists of $[Fe_4\text{-}S_3]$ and $[Mo\text{-}Fe_3\text{-}S_3]$ subclusters joined by three disulfide bonds. A carbon atom (the interstitial carbon), donated by S-adenosylmethionine (Section 23.5), sits between the iron atoms of the FeMo cofactor. The FeMo cofactor is also coordinated to a homocitrate moiety and to the α subunit through one histidine residue and one cysteinate residue.

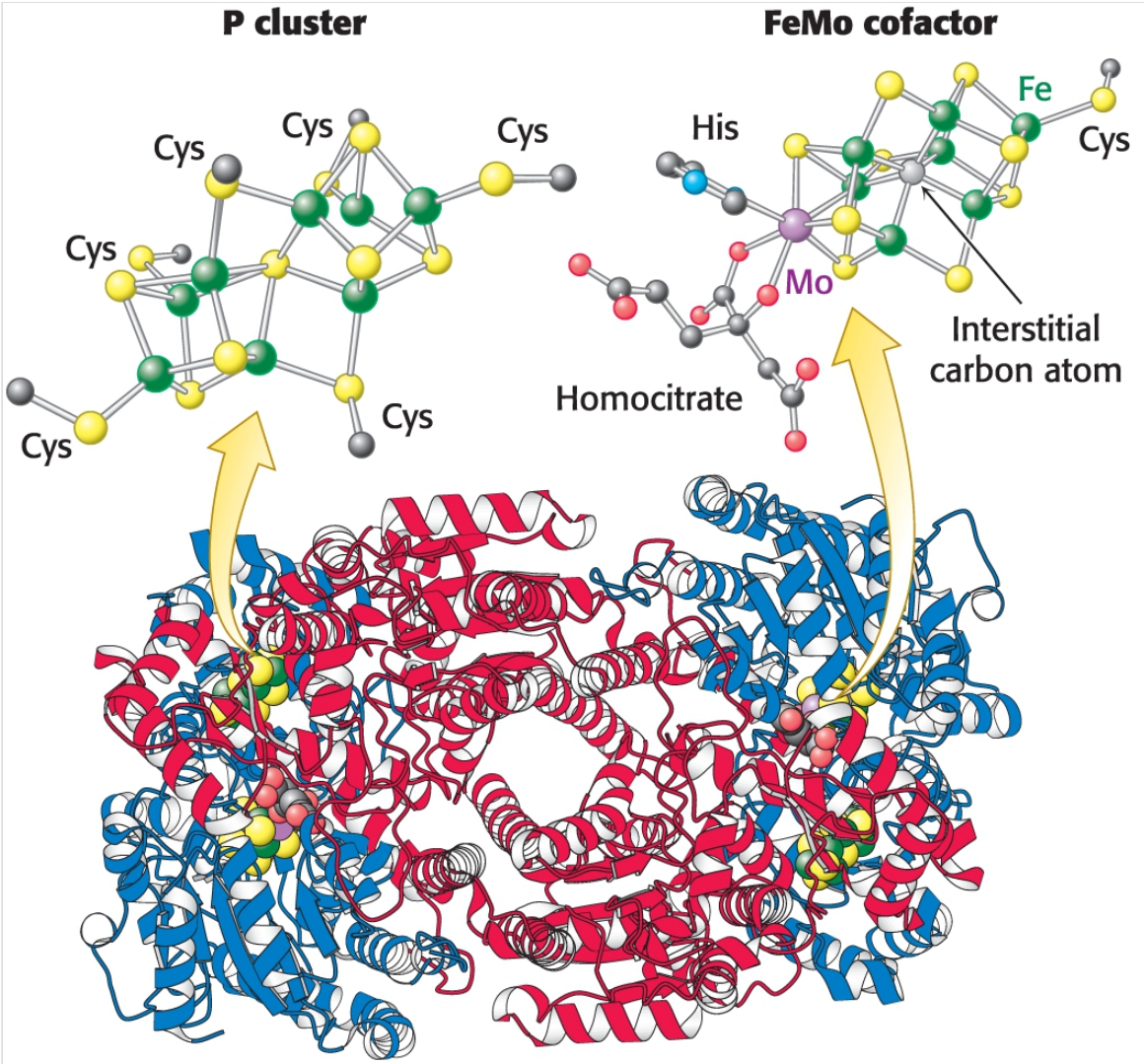


FIGURE 25.3 The MoFe protein, or nitrogenase, catalyzes the reduction of N_2 to NH_3. This protein is a heterotetramer composed of two α subunits (red) and two β subunits (blue). The complex contains two copies each of two types of clusters: P clusters and FeMo cofactors. Each cluster contains eight iron atoms (green) and seven sulfides linked to the protein by six cysteine residues. Each FeMo cofactor contains one molybdenum atom, seven iron atoms, nine sulfides, the interstitial carbon atom, and a homocitrate, and is linked to the protein by one cysteinate residue and one histidine residue.

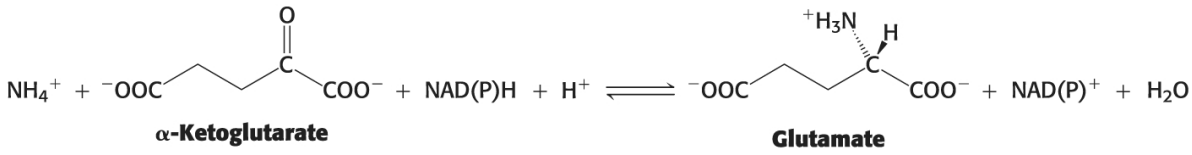
[Drawn from 1M1N.pdb.]

Electrons from the reductase enter at the *P clusters*, which are located at the α–β interface. The role of the P clusters is to store electrons until they can be used productively to reduce nitrogen at the FeMo cofactor. The FeMo cofactor is the site of nitrogen fixation. One face of the FeMo cofactor is likely to be the site of nitrogen reduction. The electron-transfer reactions from the P cluster take place in concert with the binding of hydrogen ions to nitrogen as it is reduced. The mechanism of this remarkable reaction remains an active focus of biochemical research.

Ammonium ion is assimilated into an amino acid through glutamate and glutamine

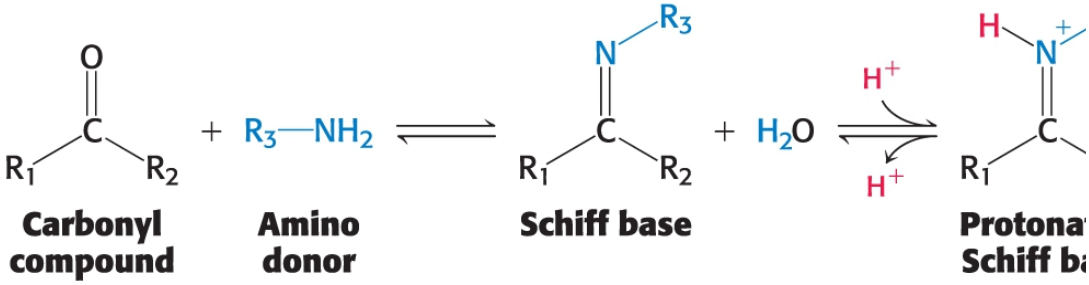
The NH_3 generated by the nitrogenase complex is a base, and becomes NH_4^+ in aqueous solutions. The next step in the assimilation of nitrogen into biomolecules is the entry of NH_4^+ into amino acids. The amino acids glutamate and glutamine play pivotal roles in this regard, acting as nitrogen donors for most amino acids. The α-amino group of most amino acids comes from the α-amino group of glutamate by transamination (Section 23.3). Glutamine, the other major nitrogen donor, contributes its side-chain nitrogen atom in the biosynthesis of a wide range of important compounds, including the amino acids tryptophan and histidine.

Glutamate is synthesized from NH_4^+ and α-ketoglutarate, a citric acid cycle intermediate, by the action of glutamate dehydrogenase. We have already encountered this enzyme in the degradation of amino acids (Section 23.3). Recall that NAD^+ is the oxidant in catabolism, whereas NADPH is the reductant in biosyntheses. Glutamate dehydrogenase is unusual in that it does not discriminate between NADH and NADPH, at least in some species.

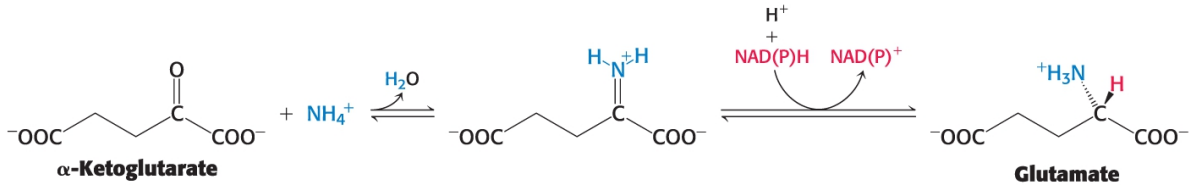


The reaction proceeds in two steps:

1. A Schiff base forms between ammonium ion and α-ketoglutarate. The formation of a Schiff base between an amine and a carbonyl compound is a key reaction that takes place at many stages of amino acid biosynthesis and degradation. Schiff bases are easily protonated.



2. The protonated Schiff base is reduced by the transfer of a hydride ion from NAD(P)H to form glutamate.



The reaction catalyzed by glutamate dehydrogenase is crucial because it establishes the stereochemistry of the α-carbon atom (*S* absolute configuration) in glutamate. The enzyme binds the α-ketoglutarate substrate in such a way that hydride transferred from NAD(P)H is added to form the L isomer of glutamate (Figure 25.4). As we shall see, this stereochemistry is established for other amino acids by transamination reactions that rely on pyridoxal phosphate. Establishing the correct stereochemistry is one of the fundamental challenges of nitrogen incorporation into biomolecules.

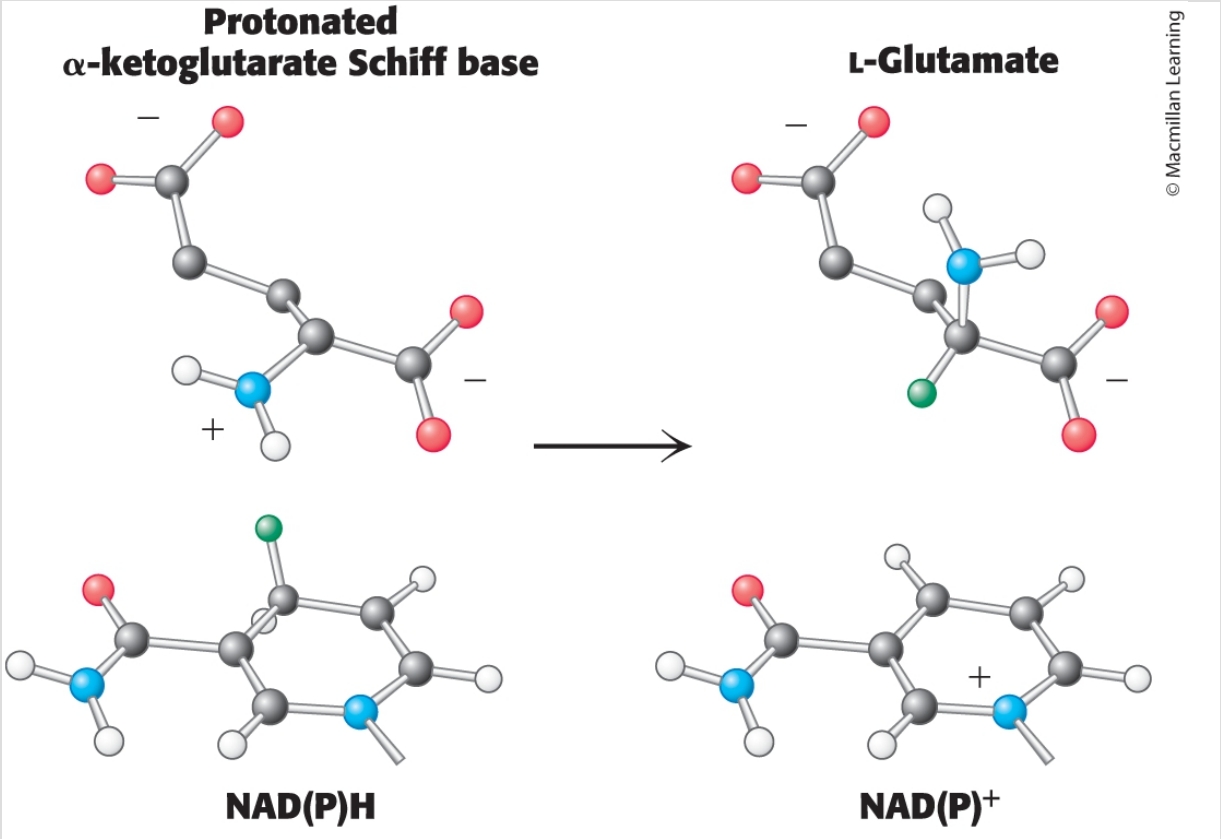
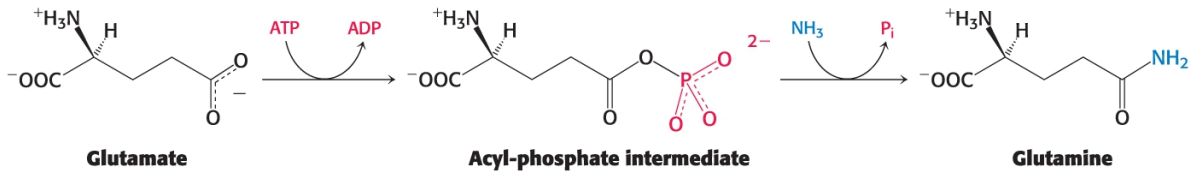


FIGURE 25.4 Glutamate chirality is established by hydride transfer to the Schiff base. In the active site of glutamate dehydrogenase, hydride transfer (green) from NAD(P)H to a specific face of the achiral protonated Schiff base of α-ketoglutarate establishes the L configuration of glutamate.

A second ammonium ion is incorporated into glutamate to form glutamine by the action of glutamine synthetase. This amidation is driven by the hydrolysis of ATP. ATP participates directly in the reaction by phosphorylating the side chain of glutamate to form an acyl-phosphate intermediate, which then reacts with ammonia to form glutamine.



NH_4^+ initially binds to the enzyme, but upon formation of the acyl-phosphate intermediate, ammonium ion is deprotonated as a high-affinity ammonia-binding site is formed. A specific site for ammonia binding is required to prevent attack by water from hydrolyzing the intermediate and wasting a molecule of ATP. As we shall soon see, the regulation of glutamine synthetase plays a critical role in controlling nitrogen metabolism (Section 25.3).

Glutamate dehydrogenase and glutamine synthetase are present in all organisms. Many organisms also contain an evolutionarily unrelated enzyme, glutamate synthase, which catalyzes the reductive amination of α-ketoglutarate to glutamate. Glutamine is the nitrogen donor.

$$\alpha\text{-Ketoglutarate} + \text{glutamine} + \text{NADPH} + \text{H}^+ \rightleftharpoons 2\ \text{glutamate} + \text{NADP}^+$$

The side-chain amide of glutamine is hydrolyzed to generate ammonia within the enzyme, a recurring theme throughout nitrogen metabolism. When NH_4^+ is limiting, most of the glutamate is made by the sequential action of glutamine synthetase and glutamate synthase. The sum of these reactions is

$$NH_4^+ + \alpha\text{-ketoglutarate} + NADPH + ATP \rightarrow \text{glutamate} + NADP^+ + ADP + P_i \quad \textbf{(1)}$$

Note that this stoichiometry differs from that of the glutamate dehydrogenase reaction in that ATP is hydrolyzed. Why do organisms sometimes use this more expensive pathway? The answer is that the value of K_M of glutamate dehydrogenase for NH_4^+ is high $(\sim 1\ mM)$, and so this enzyme is not saturated when NH_4^+ is limiting. In contrast, glutamine synthetase has very low K_M for NH_4^+. Thus, ATP hydrolysis is required to capture ammonia when it is scarce.

Self-Check Question



Write out the balanced reactions for glutamine synthetase and glutamate synthase. Show that the sum of these two reactions matches equation 1.

25.2 Amino Acids Are Made from Intermediates of the Citric Acid Cycle and Other Major Pathways

Thus far, we have considered the conversion of N_2 into NH_4^+ and the assimilation of NH_4^+ into glutamate and glutamine. We turn now to the biosynthesis of the other amino acids, the majority of which obtain their nitrogen from glutamate or glutamine. The pathways for the biosynthesis of amino acids are diverse. However, they have an important common feature: their carbon skeletons come from intermediates of glycolysis, the pentose phosphate pathway, or the citric acid cycle. On the basis of these starting materials, amino acids can be grouped into six biosynthetic families (Figure 25.5).

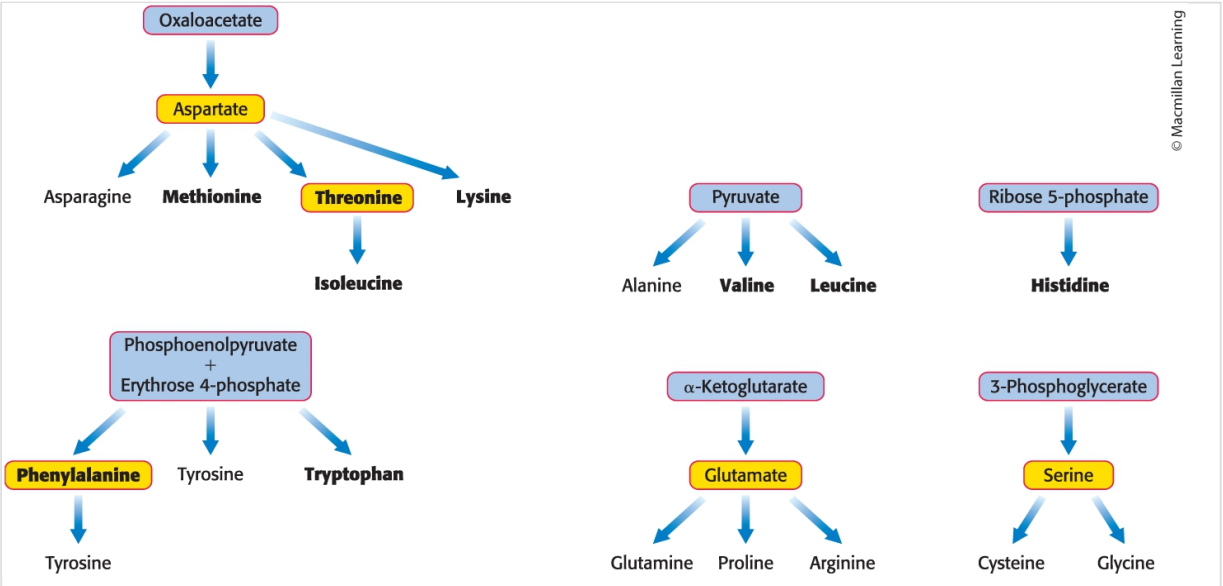


FIGURE 25.5 Amino acids can be sorted into biosynthetic families. Major metabolic precursors are shaded blue. Amino acids that give rise to other amino acids are shaded yellow. Essential amino acids for humans are in boldface type.

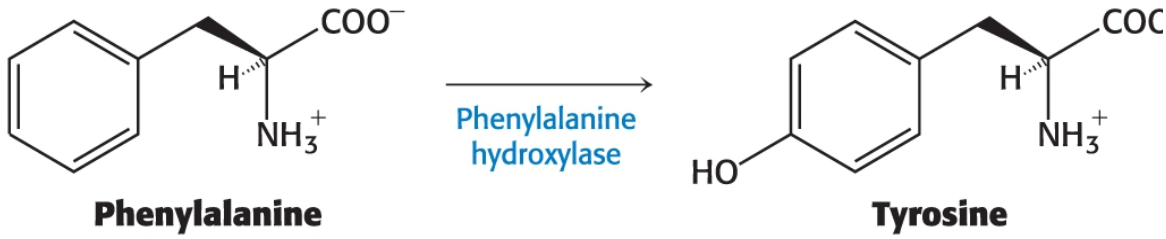
Human beings can synthesize some amino acids but must obtain others from their diet

Most microorganisms, such as *E. coli*, can synthesize the entire set of 20 amino acids, whereas human beings cannot make 9 of them. The amino acids that must be supplied in the diet are called **essential amino acids**, whereas the others, which can be synthesized if dietary content is insufficient, are termed **nonessential amino acids** (Table 25.1).

TABLE 25.1 Basic set of 20 amino acids

Nonessential	Essential
Alanine	Histidine
Arginine	Isoleucine
Asparagine	Leucine
Aspartate	Lysine
Cysteine	Methionine
Glutamate	Phenylalanine
Glutamine	Threonine
Glycine	Tryptophan
Proline	Valine
Serine	

These designations refer to the needs of an organism under a particular set of conditions. For example, enough arginine is synthesized by the urea cycle to meet the needs of an adult, but perhaps not those of a growing child. Likewise, tyrosine is sometimes designated as an essential amino acid, but is not if phenylalanine is present in adequate amounts. In mammals, tyrosine can be synthesized from phenylalanine in one step.



Phenylalanine **Tyrosine**

A deficiency of even one amino acid results in a negative nitrogen balance. In this state, more protein is degraded than is synthesized, and so more nitrogen is excreted than is ingested.

The nonessential amino acids are synthesized by quite simple reactions, whereas the pathways for the formation of the essential amino acids are quite complex. For example, the nonessential amino acids alanine and aspartate are synthesized in a single step from pyruvate and oxaloacetate, respectively. In contrast, the pathways for the essential amino acids require from 5 to 16 steps (**Figure 25.6**). The sole exception to this pattern is arginine, inasmuch as the synthesis of this nonessential amino acid de novo requires 10 steps. Typically, however, it is made in only 3 steps from ornithine as part of the urea cycle. Tyrosine, classified as a nonessential amino acid because it can be synthesized in 1 step from phenylalanine, requires 10 steps to be

synthesized from scratch and is essential if phenylalanine is not abundant.

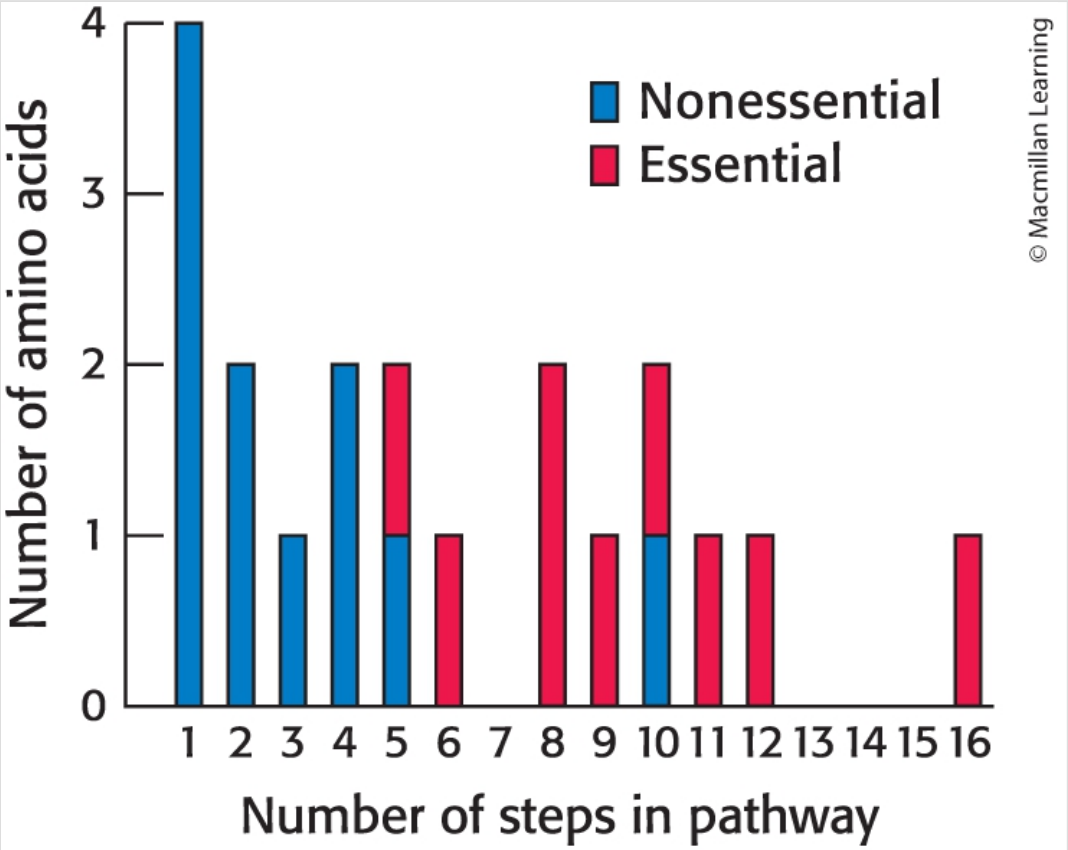


FIGURE 25.6 Essential and nonessential amino acids can be distinguished by the required number of biosynthetic steps. Some amino acids are nonessential to human beings because they can be biosynthesized in a small number of steps. Those amino acids requiring a large number of steps for their synthesis are essential in the diet because some of the enzymes for these steps have been lost in the course of evolution.

Aspartate, alanine, and glutamate are formed by the addition of an amino group to

an alpha-ketoacid

Let us begin with the biosynthesis of nonessential amino acids. Three α-ketoacids — α-ketoglutarate, oxaloacetate, and pyruvate — can be converted into amino acids in one step through the addition of an amino group. We have seen that α-ketoglutarate can be converted into glutamate by reductive amination (Section 23.3). The amino group from glutamate can be transferred to other α-ketoacids by transamination reactions. Thus, aspartate and alanine can be made from the addition of an amino group to oxaloacetate and pyruvate, respectively.

$$\text{Oxaloacetate} + \text{glutamate} \rightleftharpoons \text{aspartate} + \alpha\text{-ketoglutarat}$$

$$\text{Pyruvate} + \text{glutamate} \rightleftharpoons \text{alanine} + \alpha\text{-ketoglutarate}$$

These reactions are carried out by pyridoxal phosphate-dependent aminotransferases. Transamination reactions are required for the synthesis of most amino acids.

In Section 23.3, we considered the mechanism of aminotransferases as applied to the metabolism of amino acids. Let us review the aminotransferase mechanism as it operates in the biosynthesis of amino acids. The reaction pathway begins with **pyridoxal phosphate (PLP)** in a Schiff-base linkage with lysine at the aminotransferase active site, forming an internal aldimine (**Figure 25.7**).

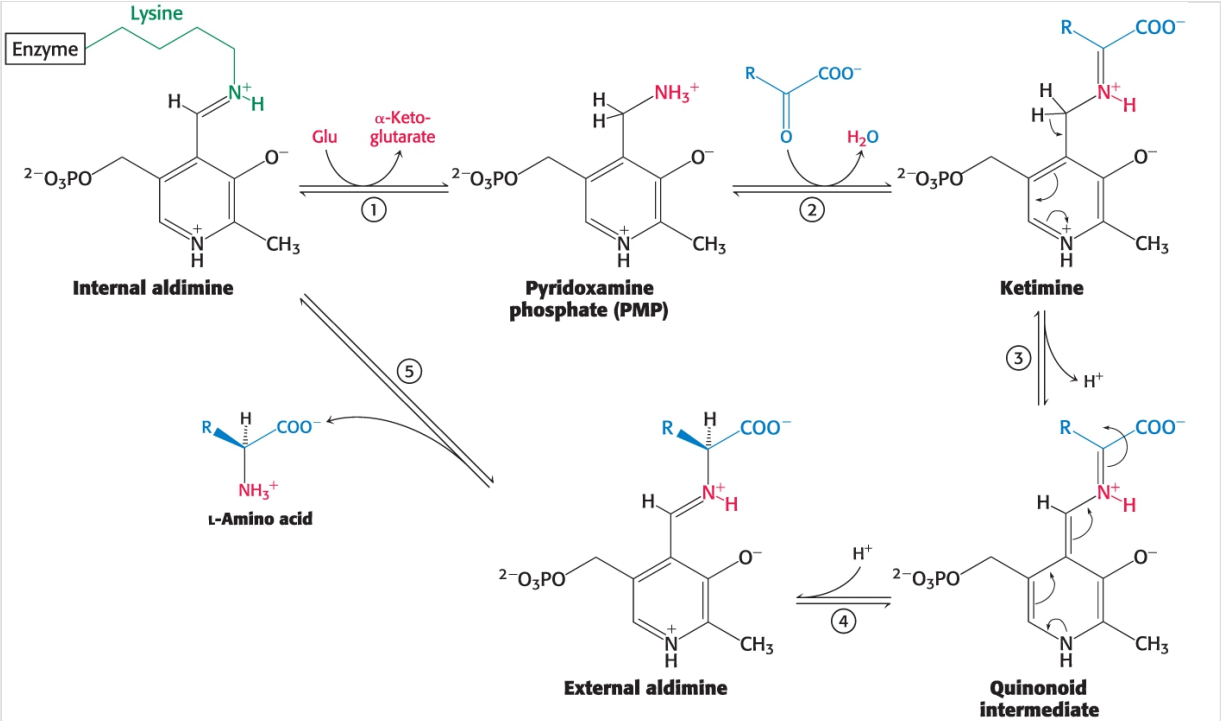


FIGURE 25.7 Transamination is a critical step in the biosynthesis of most amino acids. (1) Within an aminotransferase, the internal aldimine is converted into pyridoxamine phosphate (PMP) by reaction with glutamate in a multistep process not shown. (2) PMP then reacts with an α-ketoacid to generate a ketimine. (3) This intermediate is converted into a quinonoid intermediate (4), which in turn yields an external aldimine. (5) The aldimine is cleaved to release the newly formed amino acid to complete the cycle.

1. An amino group is transferred from glutamate to form pyridoxamine phosphate (PMP), the actual amino donor, in a multistep process.

2. PMP then reacts with an incoming α-ketoacid to form a ketimine.

3. Proton loss forms a quinonoid intermediate.

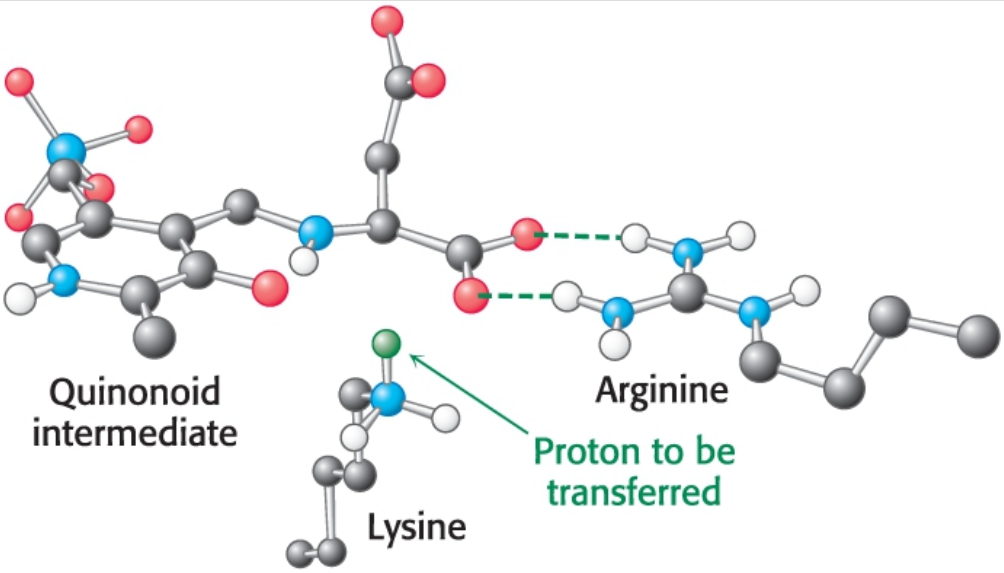
4. Proton addition at a different site forms an external aldimine.

5. The newly formed amino acid is released with the concomitant re-formation of the internal aldimine.

A common step determines the chirality of all amino acids

Aspartate aminotransferase is the prototype of a large family of PLP-dependent enzymes. Comparisons of amino acid sequences as well as several three-dimensional structures reveal that almost all aminotransferases having roles in amino acid biosynthesis are related to aspartate aminotransferase by divergent evolution. An examination of the aligned amino acid sequences reveals that two residues are completely conserved. These residues are the lysine residue that forms the Schiff base with the PLP cofactor (lysine 258 in aspartate aminotransferase) and an arginine residue that interacts with the α-carboxylate group of the ketoacid (Figure 23.10).

An essential step in the transamination reaction is the protonation of the quinonoid intermediate to form the external aldimine. The chirality of the amino acid formed is determined by the direction from which this proton is added to the quinonoid intermediate (**Figure 25.8**). The interaction between the conserved arginine residue and the α-carboxylate group helps orient the substrate so that the lysine residue transfers a proton to the bottom face of the quinonoid intermediate, generating an aldimine with an L configuration at the C_α center.



© Macmillan Learning

FIGURE 25.8 Proton addition during transamination establishes amino acid stereochemistry. In an aminotransferase active site, the addition of a proton from the lysine residue to the bottom face of the quinonoid intermediate determines the L configuration of the amino acid product. The conserved arginine residue interacts with the α-carboxylate group and helps establish the appropriate geometry of the quinonoid intermediate.



© Macmillan Learning

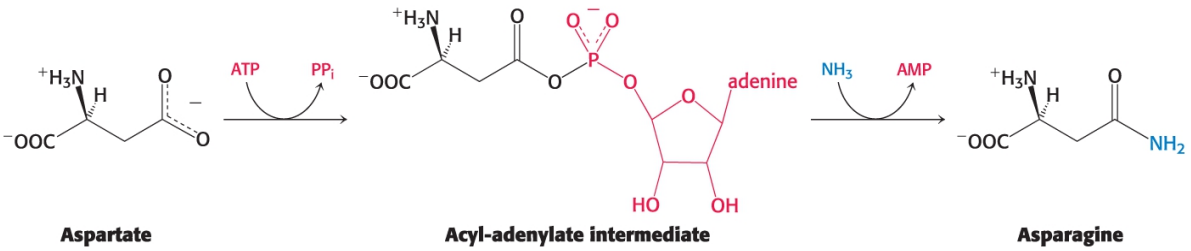
BEVERLY GUIRARD A key contributor to the isolation and characterization of different forms of vitamin B_6, including pyridoxal phosphate, was Dr. Beverly Guirard. Dr. Guirard grew up in St. Martinville, Louisiana, received her BS and MS degrees from Southwestern Louisiana Institute and Louisiana State University, respectively, and went on to receive her PhD from the University of Texas, Austin, in 1945. She identified acetate and several forms of vitamin B_6 working under the supervision of Professors Roger Williams and Esmond Snell. After completing her doctorate, she worked with Professor Fritz Lipmann. During this time, she made a key contribution to the elucidation of the structure of coenzyme A, research for which Dr. Lipmann would share the Nobel Prize. In 1951, she moved back to the University of Texas, where she continued her work with Dr. Snell until her retirement in 1990. She was an accomplished scientist on her own, characterizing several pyridoxal-dependent enzymes, and she played an important role in furthering significant research from many graduate students and postdoctoral fellows over many decades.

The formation of asparagine from aspartate requires an adenylated intermediate

The formation of asparagine from aspartate is chemically analogous to the formation of glutamine from glutamate. Both transformations are amidation reactions, and both are driven by the hydrolysis of ATP. The actual reactions are different, however. In bacteria, the reaction for asparagine synthesis is

$$\text{Aspartate} + NH_4^+ + ATP \longrightarrow \text{asparagine} + AMP + PP_i + H^+$$

Thus, the products of ATP hydrolysis are AMP and PP_i rather than ADP and P_i. Aspartate is activated by adenylation rather than by phosphorylation.



We have encountered this mode of activation in fatty acid degradation and will see it again in lipid and protein synthesis.

In mammals, the nitrogen donor for asparagine is glutamine rather than ammonia as in bacteria. Ammonia is generated by hydrolysis of the side chain of glutamine and directly transferred to activated aspartate, bound in the active site. An advantage is that the cell is not

directly exposed to NH_4^+, which is toxic at high levels to human beings and other mammals. The use of glutamine hydrolysis as a mechanism for generating ammonia for use within the same enzyme is a motif common throughout biosynthetic pathways.

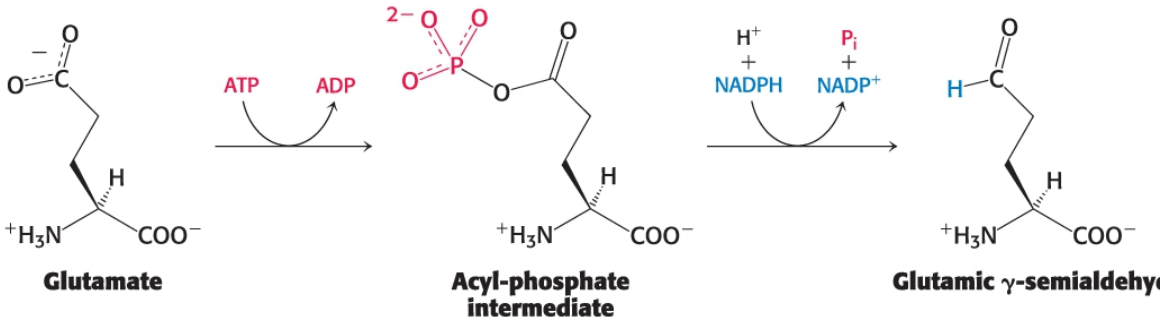
Self-Check Question



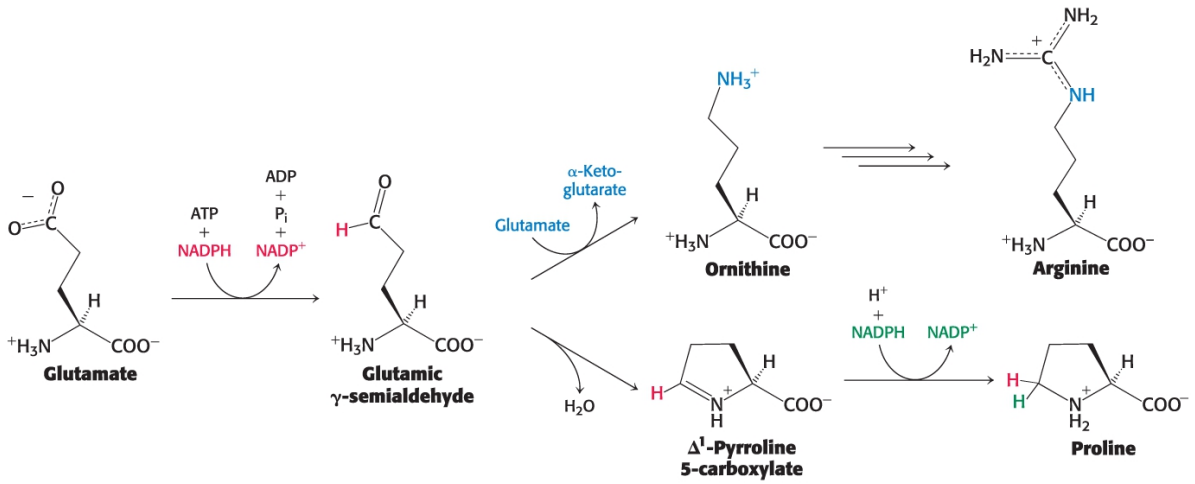
Consider the conversion of glutamate to glutamine and aspartate to asparagine in humans. Name two ways in which these reactions are similar, and two ways in which they differ.

Glutamate is the precursor of glutamine, proline, and arginine

The synthesis of glutamate by the reductive amination of α-ketoglutarate has already been discussed, as has the conversion of glutamate into glutamine (Section 25.1). Glutamate is the precursor of two other nonessential amino acids: proline and arginine. First, the γ-carboxyl group of glutamate reacts with ATP to form an acyl phosphate. This mixed anhydride is then reduced by NADPH to an aldehyde.

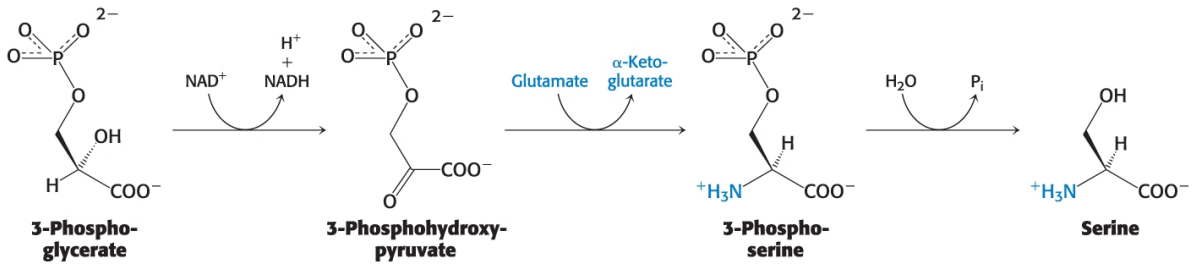


Glutamic γ-semialdehyde cyclizes with a loss of H_2O in a nonenzymatic process to give Δ^1-pyrroline 5-carboxylate, which is reduced by NADPH to proline. Alternatively, the semialdehyde can be transaminated to ornithine, which is converted in several steps into arginine in the urea cycle (Figure 23.16).

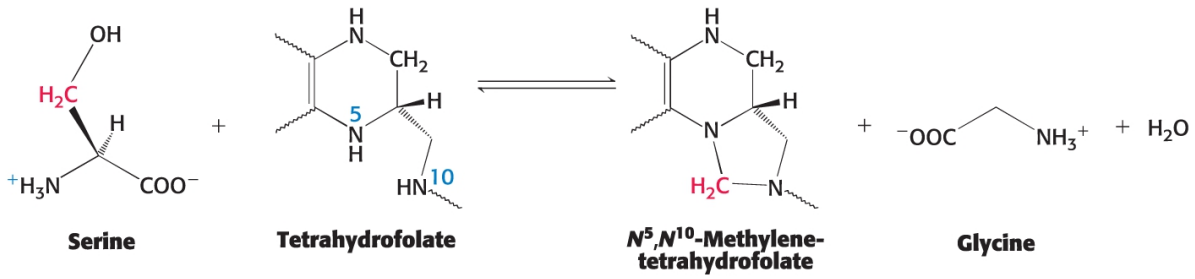


3-Phosphoglycerate is the precursor of serine, cysteine, and glycine

Serine is synthesized from 3-phosphoglycerate, an intermediate in glycolysis. The first step is an oxidation to 3-phosphohydroxypyruvate. This α-ketoacid is transaminated to 3-phosphoserine, which is then hydrolyzed to serine.



Serine is the precursor of *cysteine* and *glycine*. As we shall see, the conversion of serine into cysteine requires the substitution of a sulfur atom derived from methionine for the side-chain oxygen atom. In the formation of glycine, the side-chain methylene group of serine is transferred to tetrahydrofolate, a carrier of one-carbon units that will be discussed shortly.



This interconversion is catalyzed by serine hydroxymethyltransferase, a PLP enzyme that is homologous to aspartate aminotransferase. The formation of the Schiff base of serine renders the bond between its α- and β-carbon atoms susceptible to cleavage, enabling the transfer of the β-carbon to tetrahydrofolate and producing the Schiff base of glycine.

Tetrahydrofolate carries activated one-carbon units at several oxidation levels

Tetrahydrofolate is a highly versatile carrier of activated one-carbon units. This cofactor consists of three groups: a substituted pteridine, *p*-aminobenzoate, and a chain of one or more glutamate residues (Figure 25.9). Mammals can synthesize the pteridine ring, but they are unable to conjugate it to the other two units. They obtain tetrahydrofolate from their diets or from microorganisms in their intestinal tracts.

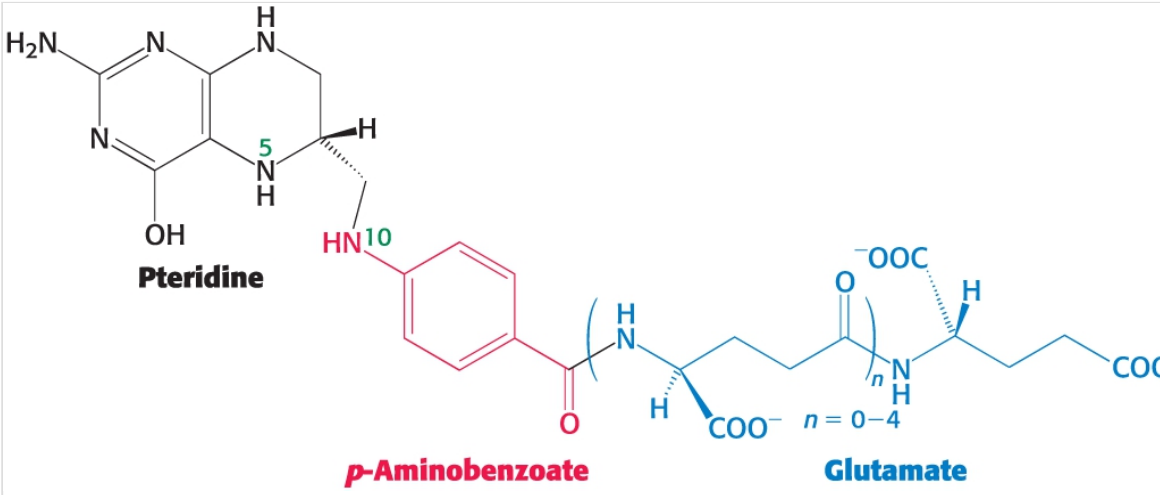


FIGURE 25.9 Tetrahydrofolate is an important carrier of activated one-carbon units. This cofactor includes three components: a pteridine ring, *p*-aminobenzoate, and one or more glutamate residues.

The one-carbon group carried by tetrahydrofolate is bonded to its N-5 or N-10 nitrogen atom (denoted as N^5 and N^{10}) or to both. This unit can exist in three oxidation states (Table 25.2). The most-reduced form carries a *methyl* group, whereas the intermediate form carries a *methylene* group. More-oxidized forms carry a *formyl*, *formimino*, or

methenyl group. The fully oxidized one-carbon unit, CO_2, is carried by biotin rather than by tetrahydrofolate.

TABLE 25.2 One-carbon groups carried by tetrahydrofolate

	Group	
Oxidation state	**Formula**	**Name**
Most reduced (= methanol)	$-CH_3$	Methyl
Intermediate (= formaldehyde)	$-CH_2-$	Methylene
Most oxidized (= formic acid)	$-CHO$ $-CHNH$ $-CH=$	Formyl Formimino Methenyl

The one-carbon units carried by tetrahydrofolate are interconvertible (Figure 25.10). N^5,N^{10}-*Methylene*tetrahydrofolate can be reduced to N^5-*methyl*tetrahydrofolate or oxidized to N^5,N^{10}-*methenyl*tetrahydrofolate. N^5,N^{10}-Methenyltetrahydrofolate can be converted into N^5-*formimino*tetrahydrofolate or N^{10}-*formyl*tetrahydrofolate, both of which are at the same oxidation level. N^{10}-Formyltetrahydrofolate can also be synthesized from tetrahydrofolate, formate, and ATP. N^5-Formyltetrahydrofolate can be reversibly isomerized to N^{10}-formyltetrahydrofolate, or it can be converted into N^5,N^{10}-methenyltetrahydrofolate.

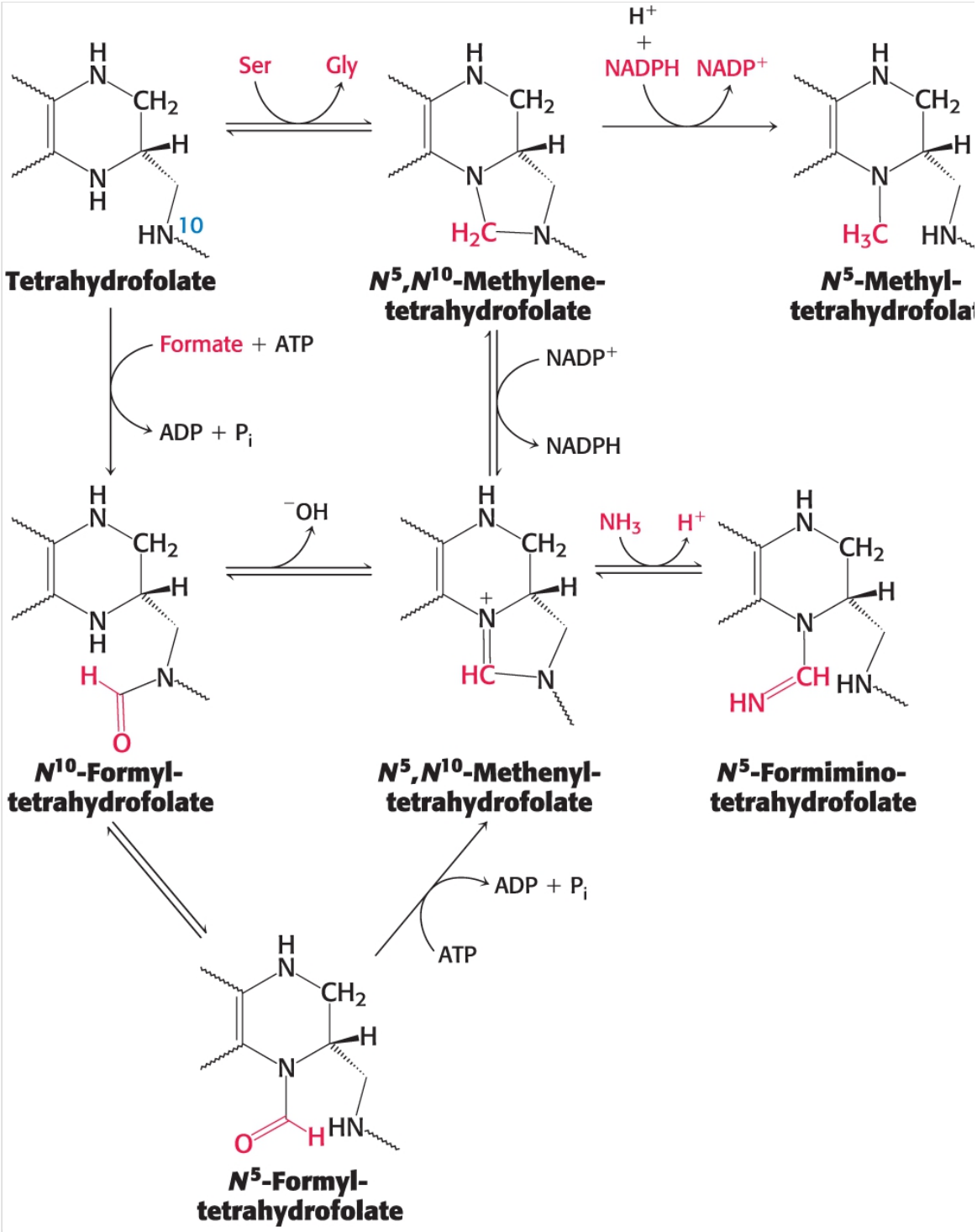


FIGURE 25.10 The one-carbon units attached to tetrahydrofolate are interconvertible.

These tetrahydrofolate derivatives serve as donors of one-carbon units in a variety of biosyntheses. Methionine is regenerated from homocysteine by transfer of the methyl group of N^5-methyltetrahydrofolate, as will be discussed shortly. We shall see in Chapter 26 that some of the carbon atoms of purines are acquired from derivatives of N^{10}-formyltetrahydrofolate. The methyl group of thymine, a pyrimidine, comes from N^5,N^{10}-methylenetetrahydrofolate. This tetrahydrofolate derivative can also donate a one-carbon unit in an alternative synthesis of glycine that starts with CO_2 and NH_4^+, a reaction catalyzed by glycine synthase (called the *glycine cleavage enzyme* when it operates in the reverse direction).

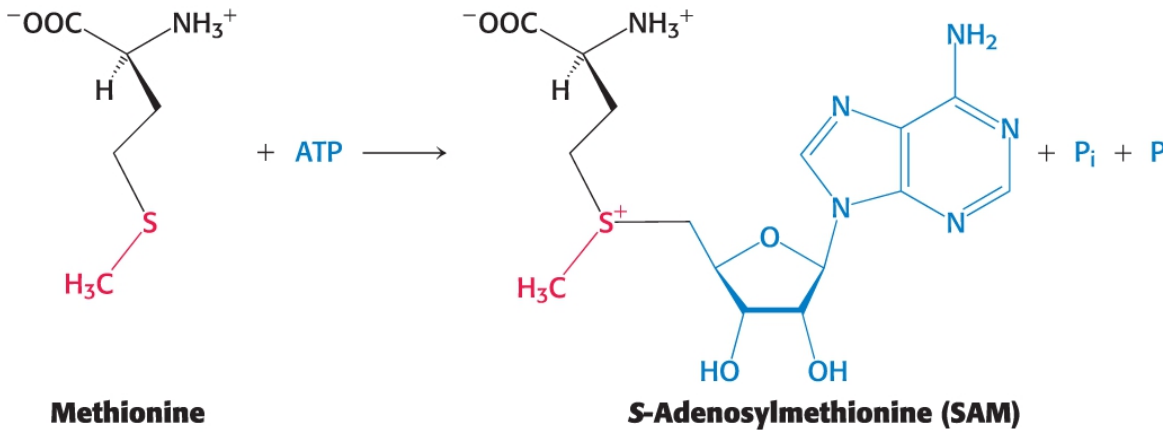
$$CO_2 + NH_4^+ + N^5,N^{10}\text{-methylenetetrahydrofolate} + NADH \rightleftharpoons \text{glycine} + \text{tetrahydrofolate} + NAD^+$$

Thus, one-carbon units at each of the three oxidation levels are utilized in biosyntheses.

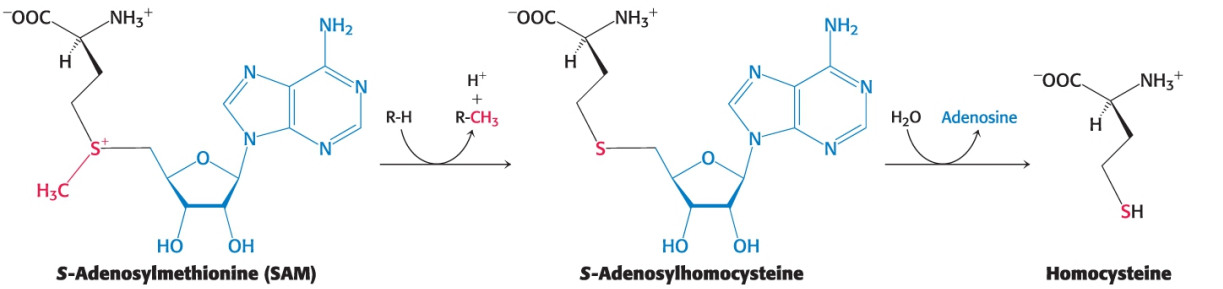
Furthermore, tetrahydrofolate serves as an acceptor of one-carbon units in degradative reactions. The major source of one-carbon units is the facile conversion of serine into glycine by serine hydroxymethyltransferase, which yields N^5, N^{10}-methylenetetrahydrofolate. Serine can be derived from 3-phosphoglycerate, and so this pathway enables one-carbon units to be formed de novo from carbohydrates.

S-Adenosylmethionine is the major donor of methyl groups

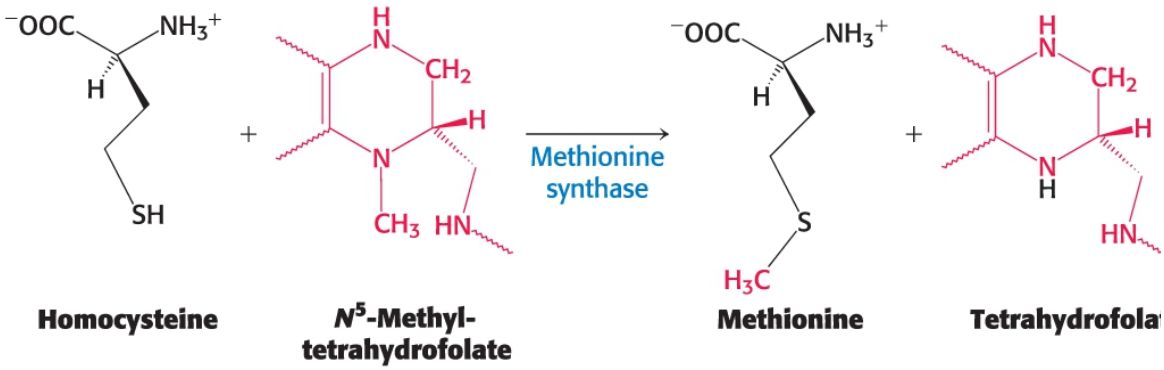
Tetrahydrofolate can carry a methyl group on its N-5 atom, but its transfer potential is not sufficiently high for most biosynthetic methylations. Rather, the activated methyl donor is usually **S-adenosylmethionine (SAM)**, which is synthesized by the transfer of an adenosyl group from ATP to the sulfur atom of methionine.



The methyl group of the methionine unit is activated by the positive charge on the adjacent sulfur atom, which makes the molecule much more reactive than N^5-methyltetrahydrofolate. The synthesis of *S*-adenosylmethionine is unusual in that the triphosphate group of ATP is split into pyrophosphate and orthophosphate; the pyrophosphate is subsequently hydrolyzed to two molecules of P_i. *S*-Adenosylhomocysteine is formed when the methyl group of *S*-adenosylmethionine is transferred to an acceptor. *S*-Adenosylhomocysteine is then hydrolyzed to homocysteine and adenosine.



Methionine can be regenerated by the transfer of a methyl group to homocysteine from N^5-methyltetrahydrofolate, a reaction catalyzed by methionine synthase.



The coenzyme that mediates this transfer of a methyl group is methylcobalamin, derived from vitamin B_{12}. In fact, this reaction and the rearrangement of L-methylmalonyl CoA to succinyl CoA (Section 22.3), catalyzed by a homologous enzyme, are the only two B_{12}-dependent reactions known to take place in mammals. Another enzyme that converts homocysteine into methionine without vitamin B_{12} is also present in many organisms.

These reactions constitute the **activated methyl cycle** (**Figure 25.11**). Methyl groups enter the cycle in the conversion of homocysteine into methionine and are then made highly reactive by the addition of an adenosyl group, which makes the sulfur atoms positively charged and the methyl groups much more electrophilic. The high transfer potential of the *S*-methyl group enables it to be transferred to a wide variety of acceptors. Among the acceptors modified by *S*-adenosylmethionine are specific bases in bacterial DNA. For instance, the methylation of DNA protects bacterial DNA from cleavage by restriction enzymes (Section 6.4). Methylation is also important for the synthesis of phospholipids (Section 27.1).

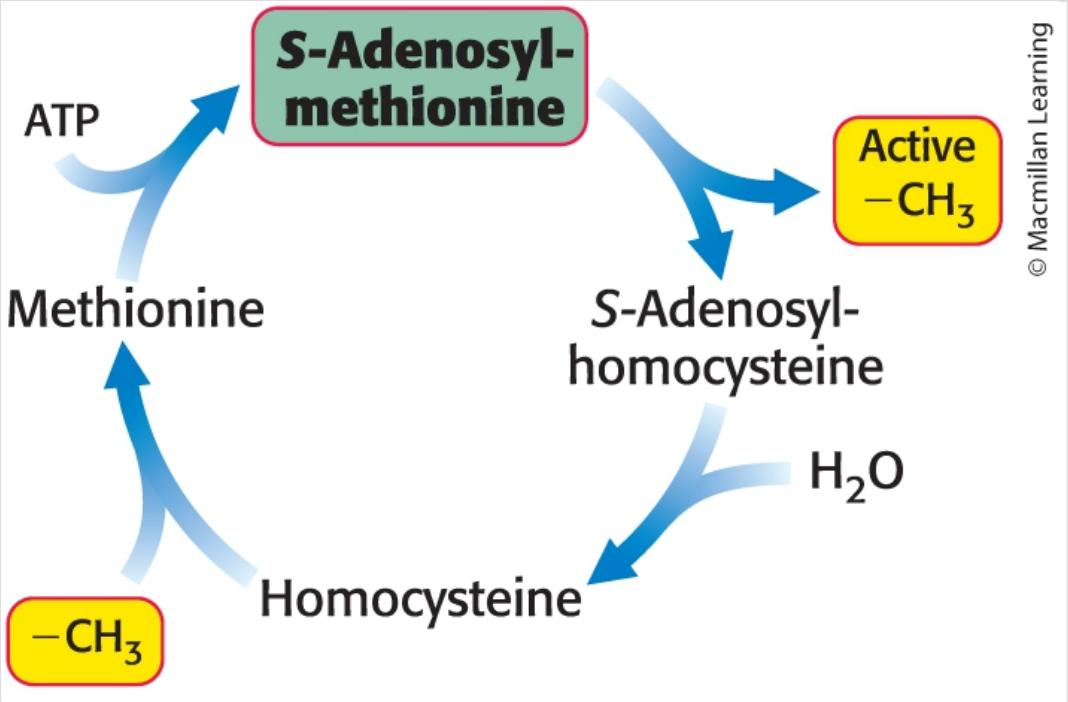


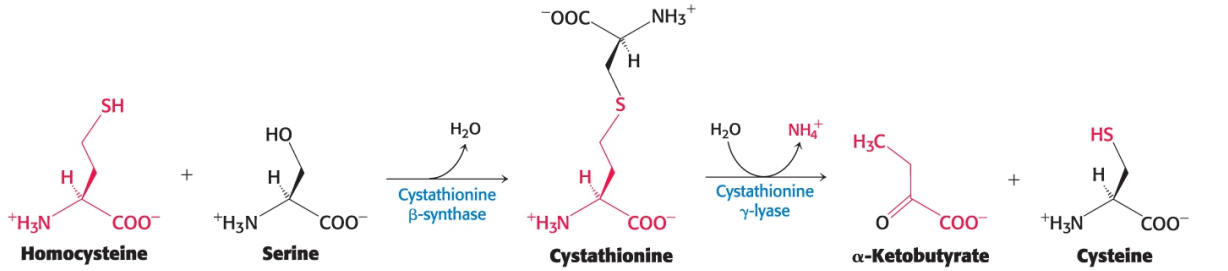
FIGURE 25.11 The activated methyl cycle enables regeneration of methionine. The methyl group of methionine is activated by the formation of *S*-adenosylmethionine.

Self-Check Question

Which derivative of folate is a reactant in the conversion of **(a)** glycine into serine? **(b)** homocysteine into methionine?

Cysteine is synthesized from serine and homocysteine

In addition to being a precursor of methionine in the activated methyl cycle, homocysteine is an intermediate in the synthesis of cysteine. Serine and homocysteine condense to form cystathionine. This reaction is catalyzed by cystathionine β-synthase. Cystathionine is then deaminated and cleaved to cysteine and α-ketobutyrate by cystathionine γ-lyase or cystathionase.



Both of these enzymes utilize PLP and are homologous to aspartate aminotransferase. The net reaction is

$$\text{Homocysteine} + \text{serine} \rightleftharpoons \text{cysteine} + \alpha\text{-ketobutyrate} + NH_4$$

Note that the sulfur atom of cysteine is derived from homocysteine, whereas the carbon skeleton comes from serine.

High homocysteine levels correlate with vascular disease



People with elevated serum levels of homocysteine (homocysteinemia) or the disulfide-linked dimer homocystine (homocystinuria) have an unusually high risk for coronary heart disease and arteriosclerosis. The most common genetic cause of high homocysteine levels is a mutation within the gene encoding cystathionine β-synthase. High levels of homocysteine appear to damage cells lining blood vessels and to increase the growth of vascular smooth muscle. The amino acid raises oxidative stress as well and has also been implicated in the development of type 2 diabetes.

The molecular basis of homocysteine's action has not been clearly identified, but it may result from stimulation of the inflammatory response. Vitamin treatments are sometimes effective in reducing homocysteine levels in some people. Treatment with vitamins maximizes the activity of the two major metabolic pathways processing homocysteine. Pyridoxal phosphate, a vitamin B_6 derivative, is necessary for the activity of cystathionine β-synthase, which converts homocysteine into cystathionine; tetrahydrofolate, as well as vitamin B_{12}, supports the methylation of homocysteine to methionine.

Shikimate and chorismate are intermediates in the biosynthesis of aromatic amino acids

We turn now to the biosynthesis of essential amino acids. These amino acids are synthesized by plants and microorganisms, and those in the human diet are ultimately derived primarily from plants. The essential amino acids are formed by much more complex routes than are the nonessential amino acids. The pathways for the synthesis of aromatic amino acids in bacteria have been selected for discussion here because they are well understood and exemplify recurring mechanistic motifs.

Phenylalanine, tyrosine, and tryptophan are synthesized by a common pathway in *E. coli* (**Figure 25.12**). The initial step is the condensation of phosphoenolpyruvate (a glycolytic intermediate) with erythrose 4-phosphate (a pentose phosphate pathway intermediate). The resulting seven-carbon open-chain sugar is oxidized, loses its phosphoryl group, and cyclizes to 3-dehydroquinate. Dehydration then yields 3-dehydroshikimate, which is reduced by NADPH to shikimate. The phosphorylation of shikimate by ATP gives shikimate 3-phosphate, which condenses with a second molecule of phosphoenolpyruvate. The resulting 5-enolpyruvyl intermediate loses its phosphoryl group, yielding chorismate, the common precursor of all three aromatic amino acids.

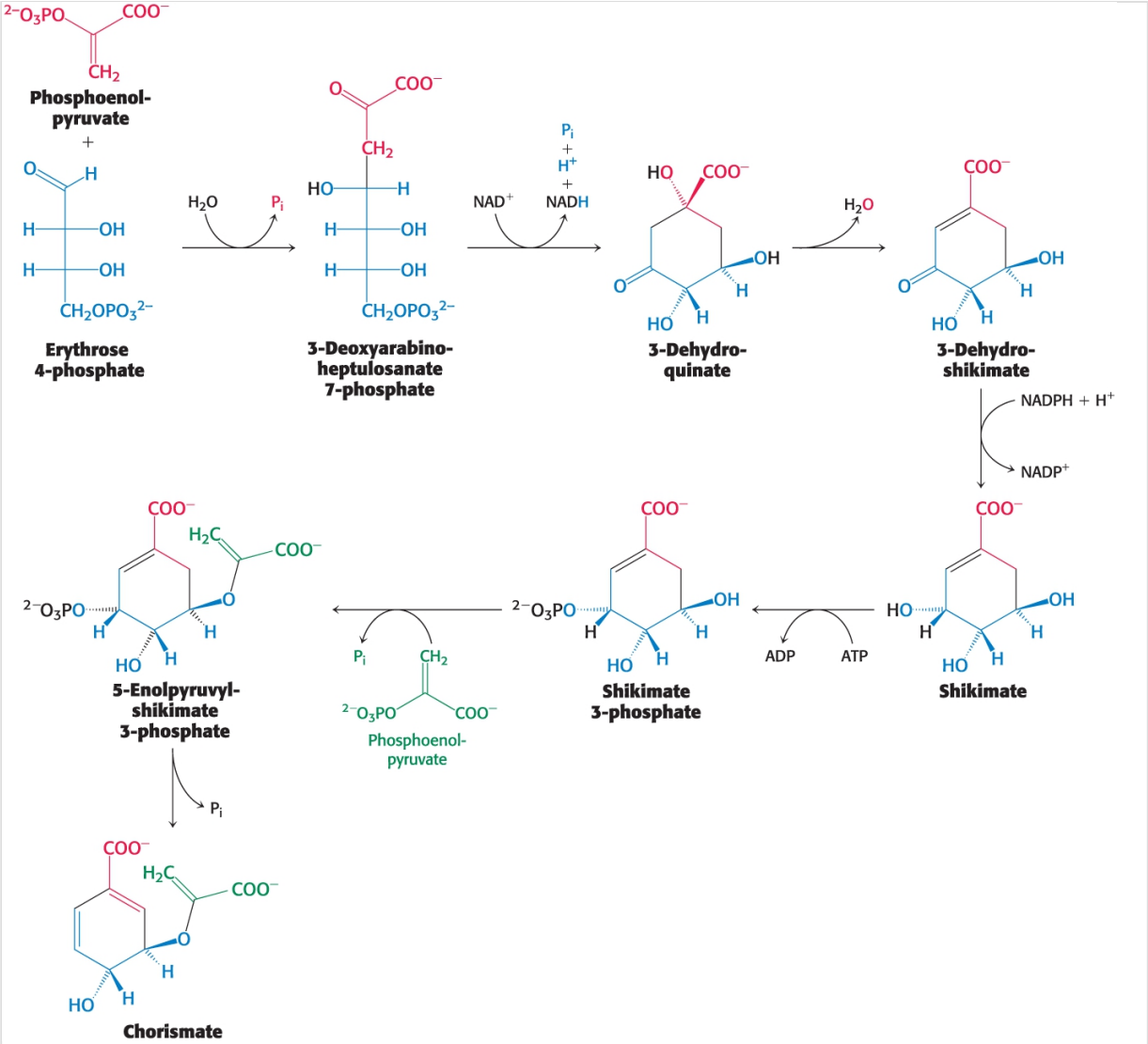
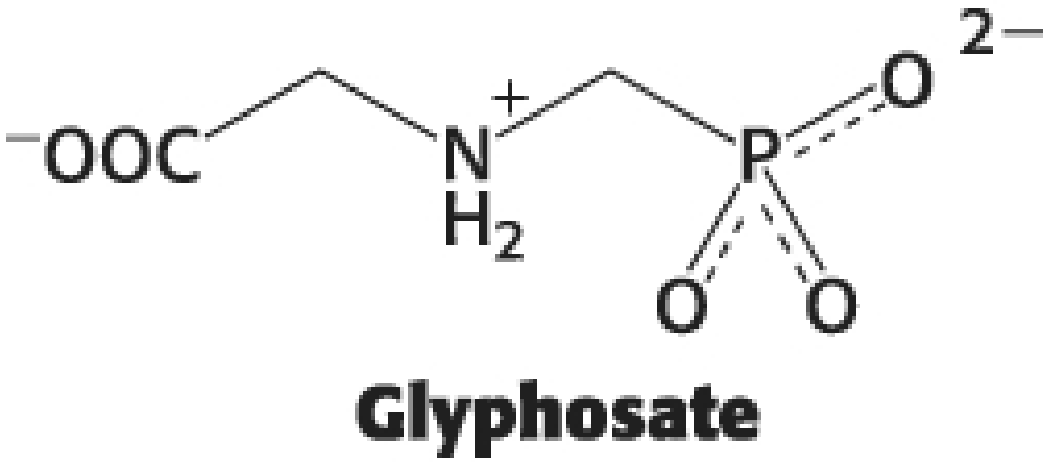


FIGURE 25.12 Chorismate is formed from phosphoenolpyruvate and erythrose 4-phosphate. Chorismate is an intermediate in the biosynthesis of phenylalanine, tyrosine, and tryptophan.

The importance of this pathway is revealed by the effectiveness of glyphosate, a broad-spectrum herbicide. This compound is an uncompetitive inhibitor of the enzyme that produces 5-enolpyruvylshikimate 3-phosphate. It blocks aromatic amino acid biosynthesis in plants but is fairly nontoxic in animals because they lack the enzyme. Recently, there have been claims that glyphosate may

cause cancer, although most scientific evidence does not support the claims.



The pathway bifurcates at chorismate. Let us first follow the *prephenate branch* (**Figure 25.13**). The enzyme chorismate mutase converts chorismate into prephenate, the immediate precursor of the aromatic ring of phenylalanine and tyrosine. This fascinating conversion is a rare example of an electrocyclic reaction in biochemistry, mechanistically similar to the well-known Diels–Alder reaction in organic chemistry. Dehydration and decarboxylation yield phenylpyruvate. Alternatively, prephenate can be oxidatively decarboxylated to *p*-hydroxyphenylpyruvate. These α-ketoacids are then transaminated to form phenylalanine and tyrosine.

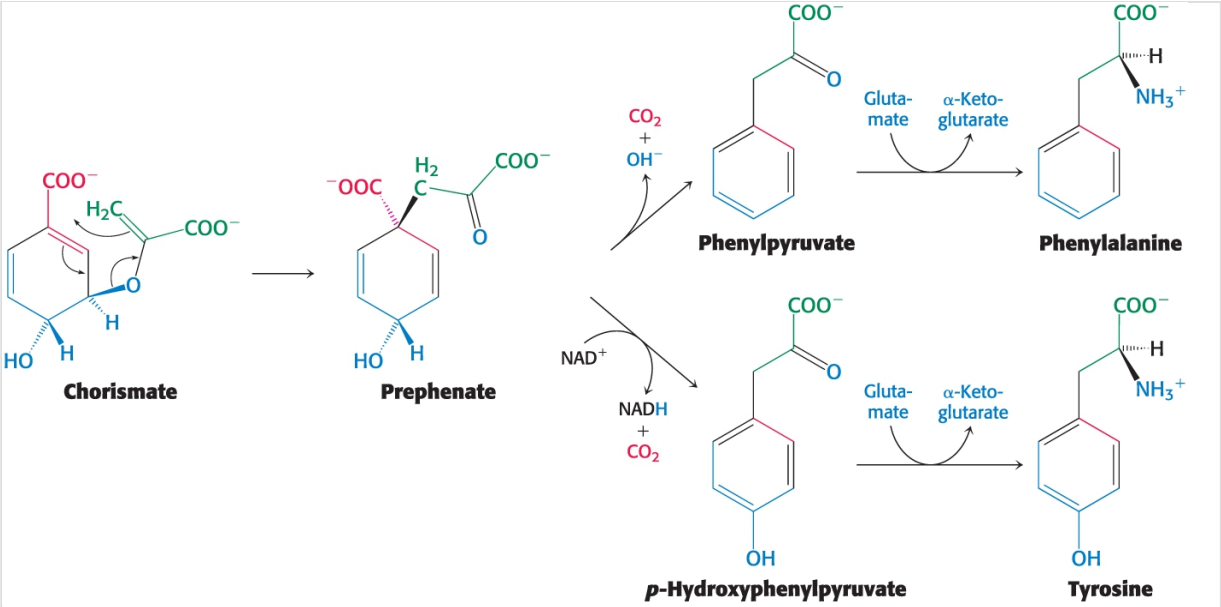


FIGURE 25.13 Phenylalanine and tyrosine are formed in the prephenate branch. Chorismate can be converted into prephenate, which is subsequently converted into phenylalanine and tyrosine.

The *anthranilate branch* leads to the synthesis of tryptophan (Figure 25.14).

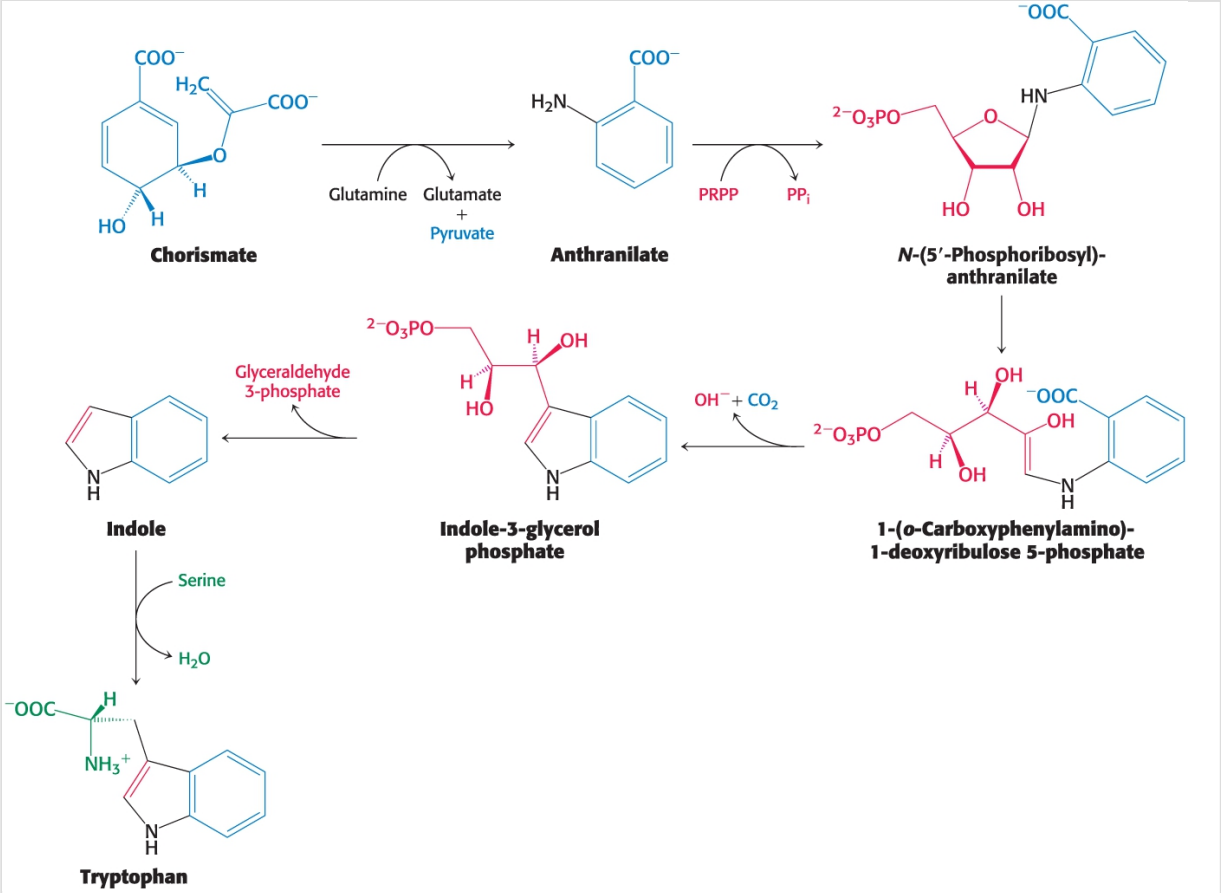
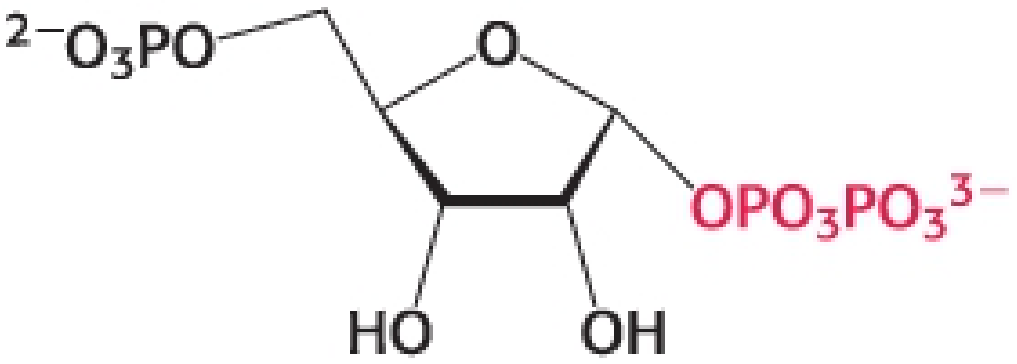


FIGURE 25.14 Tryptophan is formed in the anthranilate branch. Chorismate can be converted into anthranilate, which is subsequently converted into tryptophan.

Chorismate acquires an amino group derived from the hydrolysis of the side chain of glutamine and releases pyruvate to form anthranilate. Anthranilate then condenses with 5-phosphoribosyl-1-pyrophosphate (PRPP), an activated form of ribose phosphate.

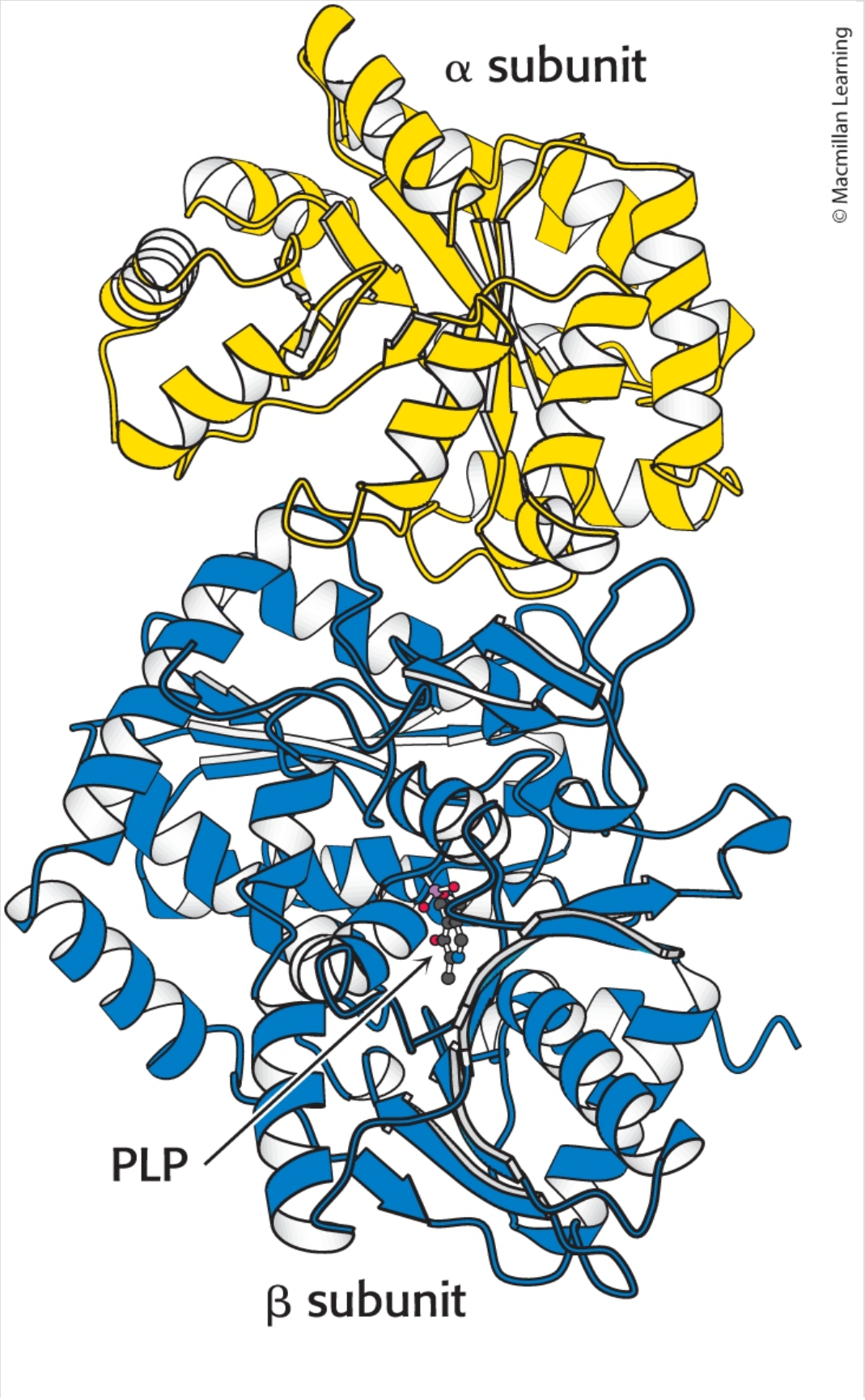


5-Phosphoribosyl-1-pyrophosphate (PRPP)

PRPP is also an important intermediate in the synthesis of histidine, pyrimidine nucleotides, and purine nucleotides (Sections 26.1 and 26.2). The C-1 atom of ribose 5-phosphate becomes bonded to the nitrogen atom of anthranilate in a reaction that is driven by the release and hydrolysis of pyrophosphate. The ribose moiety of phosphoribosylanthranilate undergoes rearrangement to yield 1-(*o*-carboxyphenylamino)-1-deoxyribulose 5-phosphate. This intermediate is dehydrated and then decarboxylated to indole-3-glycerol phosphate. Tryptophan synthase completes the synthesis of tryptophan with the removal of the side chain of indole-3-glycerol phosphate, yielding glyceraldehyde 3-phosphate, and its replacement with the carbon skeleton of serine.

Tryptophan synthase illustrates substrate channeling in enzymatic catalysis

The *E. coli* enzyme tryptophan synthase, an $\alpha_2\beta_2$ tetramer, can be dissociated into two α subunits and a β_2 dimer (**Figure 25.15**).



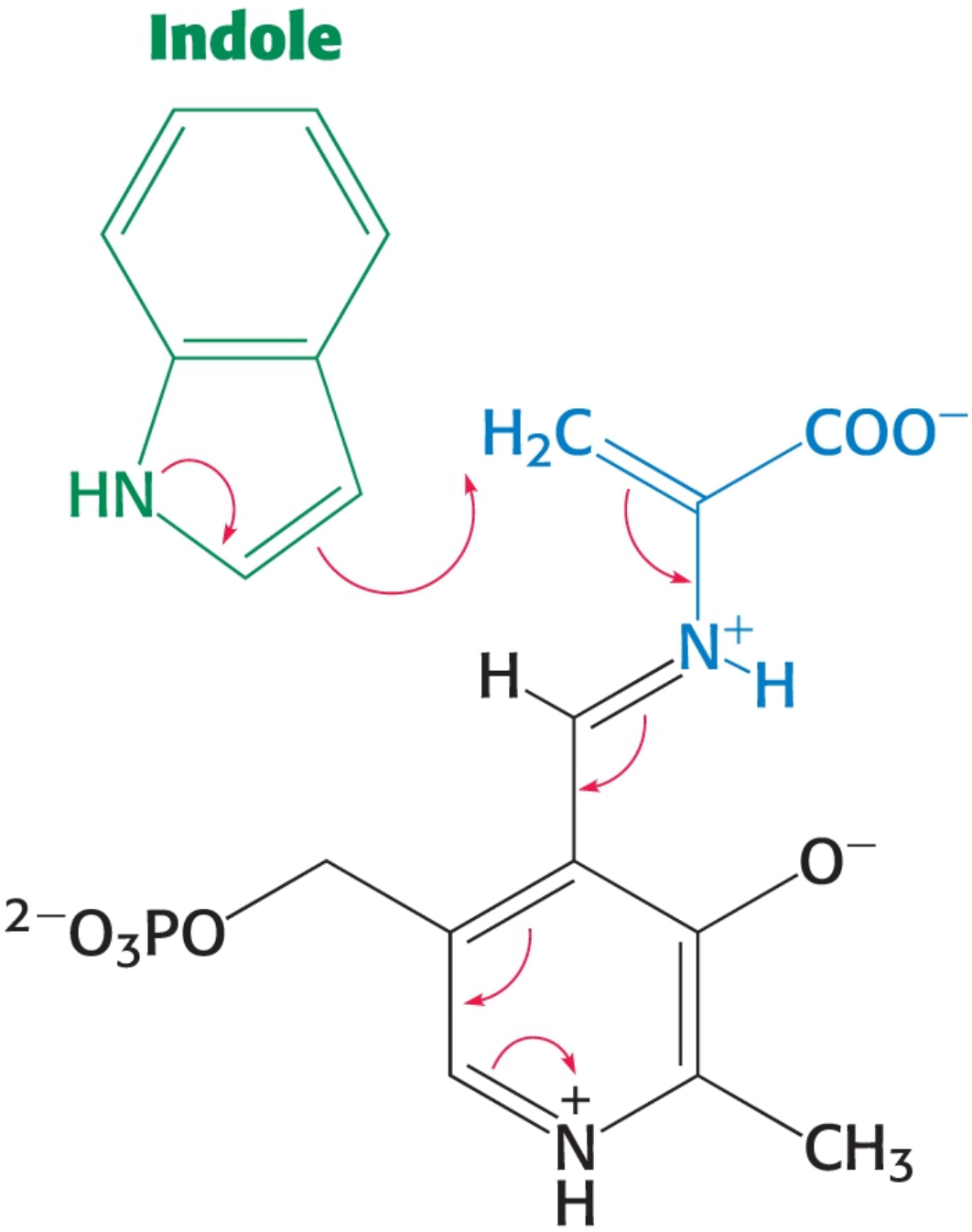
© Macmillan Learning

FIGURE 25.15 Tryptophan synthase contains two remotely positioned catalytic domains. The complex is formed by one α subunit (yellow) and one β subunit (blue). Pyridoxal phosphate (PLP) is bound deeply inside the β subunit, a considerable distance from the α subunit.

[Drawn from 1BKS.pdb.]

INTERACT with this model in Achieve

The α subunit catalyzes the formation of indole from indole-3-glycerol phosphate, whereas each β subunit has a PLP-containing active site that catalyzes the condensation of indole and serine to form tryptophan. Serine forms a Schiff base with this PLP, which is then dehydrated to give the Schiff base of aminoacrylate. This reactive intermediate is attacked by indole to give tryptophan.



Schiff base of aminoacrylate
(derived from serine)

The synthesis of tryptophan poses a challenge. Indole, a hydrophobic molecule, readily traverses membranes and would be lost from the cell if it were allowed to diffuse away from the enzyme. This problem is solved in an ingenious way. A 25-Å-long channel connects the active site of the α subunit with that of the adjacent β subunit in the $\alpha_2\beta_2$ tetramer (**Figure 25.16**). Thus, indole can diffuse from one active site to the other without being released into bulk solvent. Isotope-labeling experiments showed that indole formed by the α subunit does not leave the enzyme when serine is present. Furthermore, the two partial reactions are coordinated. Indole is not formed by the α subunit until the highly reactive aminoacrylate is ready and waiting in the β subunit.

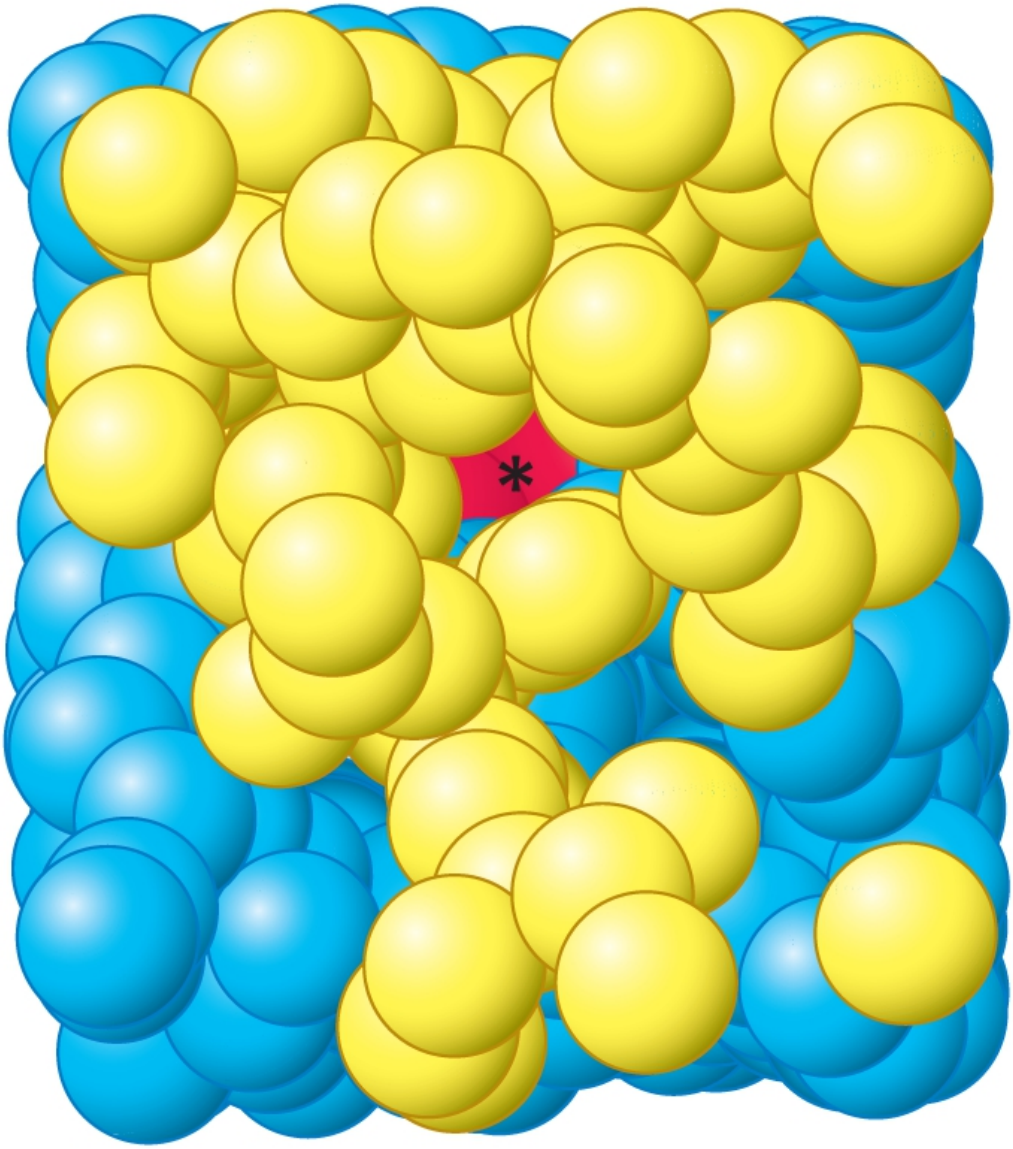


FIGURE 25.16 Tryptophan synthase uses substrate channeling to prevent loss of the indole intermediate. A 25-Å tunnel runs from the active site of the α subunit of tryptophan synthase (yellow) to the PLP cofactor (red) in the active site of the β subunit (blue). The asterisk indicates the center of the tunnel.

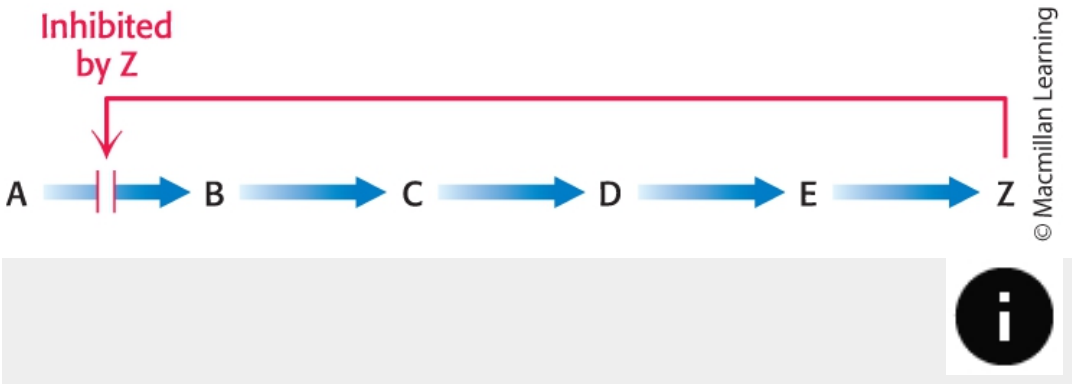
We see here a clear-cut example of **substrate channeling** in catalysis by a multienzyme complex. Channeling substantially increases the catalytic rate. Furthermore, a deleterious side reaction — in this case,

the potential loss of an intermediate — is prevented. We shall encounter other examples of substrate channeling in Chapter 26.

25.3 Feedback Inhibition Regulates Amino Acid Biosynthesis

The rate of synthesis of amino acids depends mainly on the *amounts* of the biosynthetic enzymes and on their *activities*. We now consider the control of enzymatic activity. The regulation of enzyme synthesis in eukaryotes will be discussed in Chapter 31.

In a biosynthetic pathway, the first irreversible reaction is usually an important regulatory site. As we have seen in Section 7.1, this reaction is referred to as the *committed step*. The final product of the pathway (*Z*) often inhibits the enzyme that catalyzes the committed step $(A \rightarrow B)$.



This kind of control is essential for the conservation of building blocks and metabolic energy. Consider the biosynthesis of serine (Section 25.2). The committed step in this pathway is the oxidation of 3-phosphoglycerate, catalyzed by the enzyme 3-phosphoglycerate dehydrogenase. The *E. coli* enzyme is a tetramer of four identical subunits, each comprising a catalytic domain and a serine-binding regulatory domain (**Figure 25.17**). The binding of serine to a regulatory site reduces the value of V_{max} for the enzyme; an enzyme bound to four molecules of serine is essentially inactive. Thus, if serine is abundant in

the cell, the enzyme activity is inhibited, and so 3-phosphoglycerate, a key building block that can be used for other processes, is not wasted.

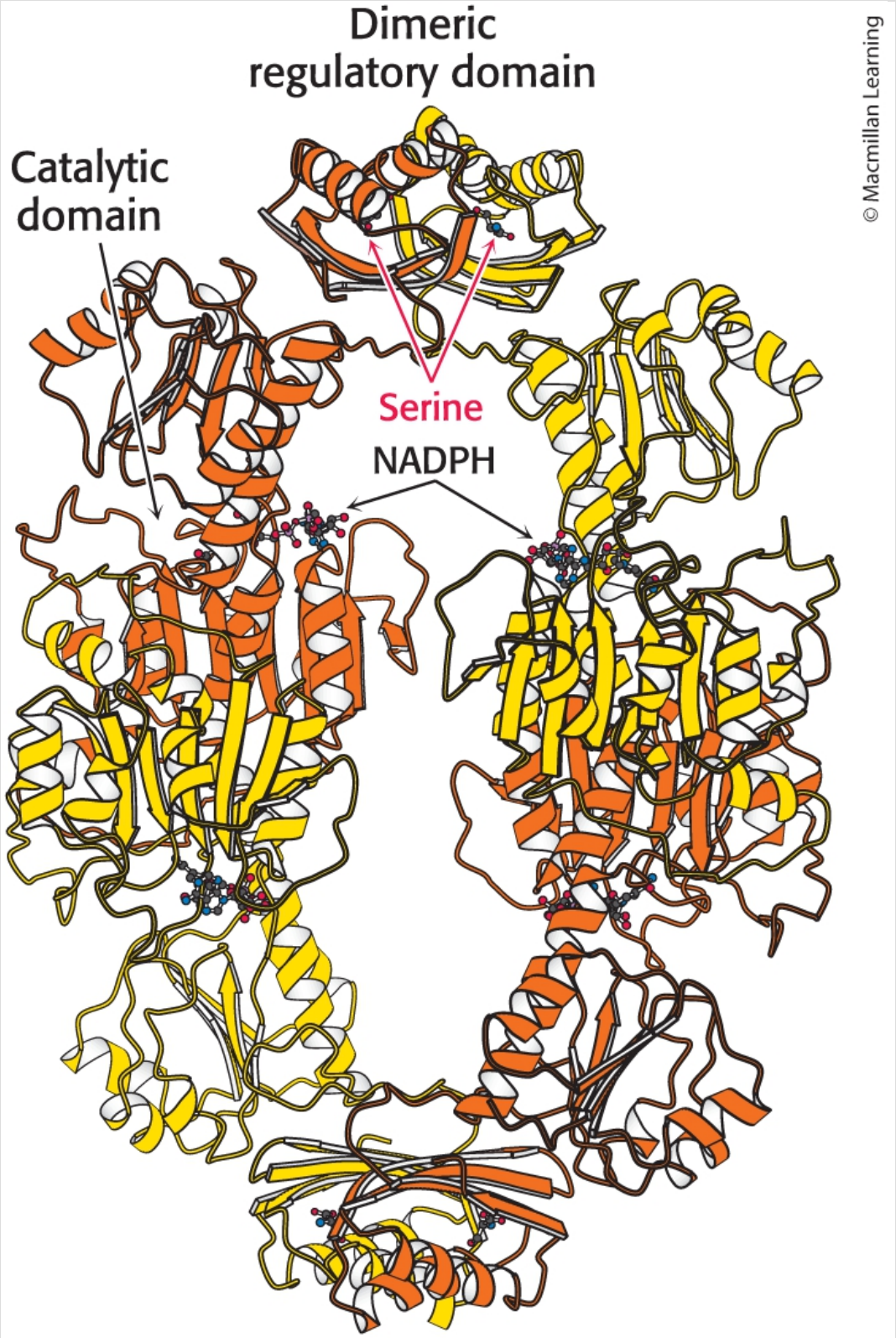


FIGURE 25.17 3-Phosphoglycerate dehydrogenase is a homotetramer. This enzyme, which catalyzes the committed step in the serine biosynthetic pathway, is inhibited

by serine. There are two serine-binding dimeric regulatory domains — one at the top and the other at the bottom of the structure.

[Drawn from 1PSD.pdb.]



Branched pathways require sophisticated regulation

The regulation of branched pathways is more complicated because the concentration of two products must be taken into account. In fact, several intricate feedback mechanisms have been found in branched biosynthetic pathways.

Feedback inhibition and activation

Two pathways with a common initial step may each be inhibited by its own product and activated by the product of the other pathway. Consider, for example, the biosynthesis of the branched chain amino acids valine, leucine, and isoleucine. A common intermediate, hydroxyethyl thiamine pyrophosphate (hydroxyethyl-TPP; Section 17.2), initiates the pathways leading to all three of these amino acids. Hydroxyethyl-TPP reacts with α-ketobutyrate in the initial step for the synthesis of isoleucine. Alternatively, hydroxyethyl-TPP reacts with pyruvate in the committed step for the pathways leading to valine and leucine. Thus, the relative concentrations of α-ketobutyrate and pyruvate determine how much isoleucine is produced compared with valine and leucine.

Threonine deaminase, the PLP enzyme that catalyzes the formation of α-ketobutyrate, is allosterically inhibited by isoleucine (**Figure 25.18**). This enzyme is also allosterically activated by valine. Thus, this enzyme is inhibited by the end product of the pathway that it initiates and is

activated by the end product of a competitive pathway. This mechanism balances the amounts of different amino acids that are synthesized.

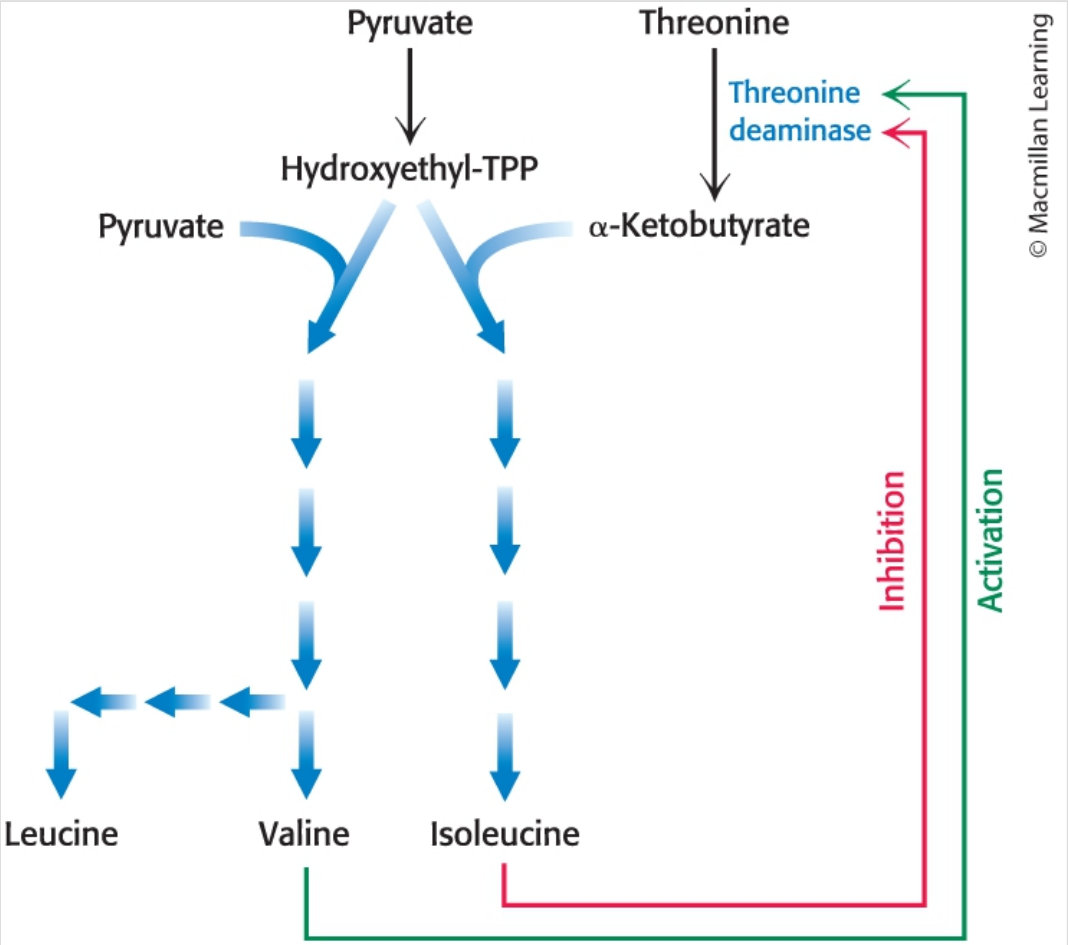


FIGURE 25.18 Threonine deaminase is regulated by feedback inhibition and activation. Threonine is converted into α-ketobutyrate in the committed step, leading to the synthesis of isoleucine. The enzyme that catalyzes this step, threonine deaminase, is inhibited by isoleucine and activated by valine, the product of a parallel pathway.

The regulatory domain in threonine deaminase is very similar in structure to the regulatory domain in 3-phosphoglycerate dehydrogenase (Figure 25.19). In the latter enzyme, regulatory domains of two subunits interact to form a dimeric serine-binding regulatory

unit, and so the tetrameric enzyme contains two such regulatory units. Each unit is capable of binding two serine molecules. In threonine deaminase, the two regulatory domains are fused into a single unit with two differentiated amino acid-binding sites, one for isoleucine and the other for valine. Sequence analysis shows that similar regulatory domains are present in other amino acid biosynthetic enzymes. The similarities suggest that feedback-inhibition processes may have evolved by the linkage of specific regulatory domains to the catalytic domains of biosynthetic enzymes.

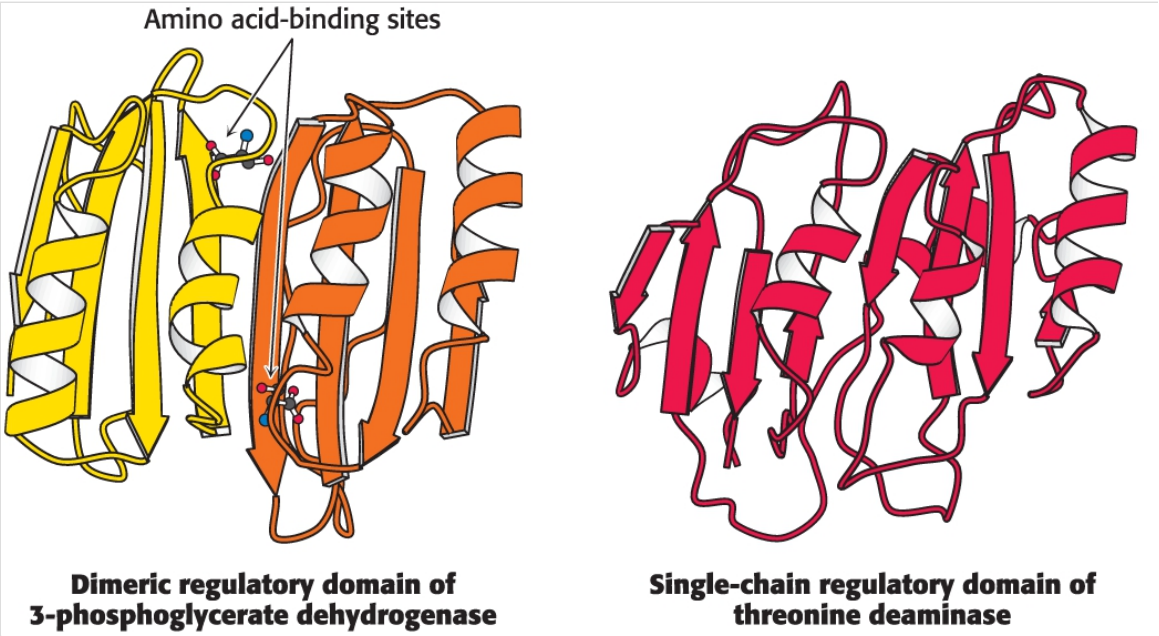
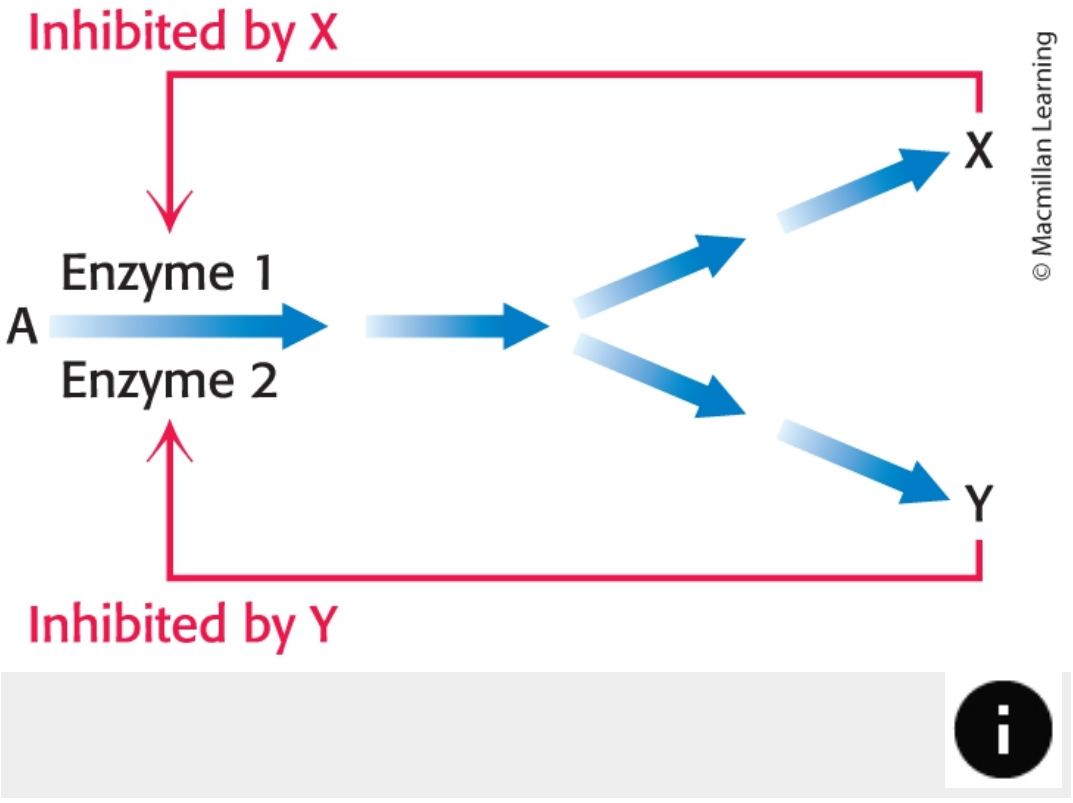


FIGURE 25.19 The regulatory domains of 3-phosphoglycerate dehydrogenase and threonine deaminase are related structurally. The regulatory domain of 3-phosphoglycerate dehydrogenase is comprised of two subunits, while the corresponding domain of threonine deaminase is comprised of a single chain. Both overall structures have four α helices and eight β strands in similar locations. Sequence analyses have revealed this amino acid-binding regulatory domain to be present in other enzymes as well.

[Drawn from 1PSD.pdb and 1TDJ.pdb.]

Enzyme multiplicity

In a process known as **enzyme multiplicity**, the committed step can be catalyzed by two or more isozymes, enzymes with essentially identical catalytic mechanisms but different regulatory properties (Section 7.2). For example, the phosphorylation of aspartate is the committed step in the biosynthesis of threonine, methionine, and lysine. Three distinct aspartokinases, which evolved by gene duplication, catalyze this reaction in *E. coli* (**Figure 25.20**). The catalytic domains of these enzymes show approximately 30% sequence identity. Although the mechanisms of catalysis are the same, their activities are regulated differently: one enzyme is not subject to feedback inhibition, another is inhibited by threonine, and the third is inhibited by lysine.



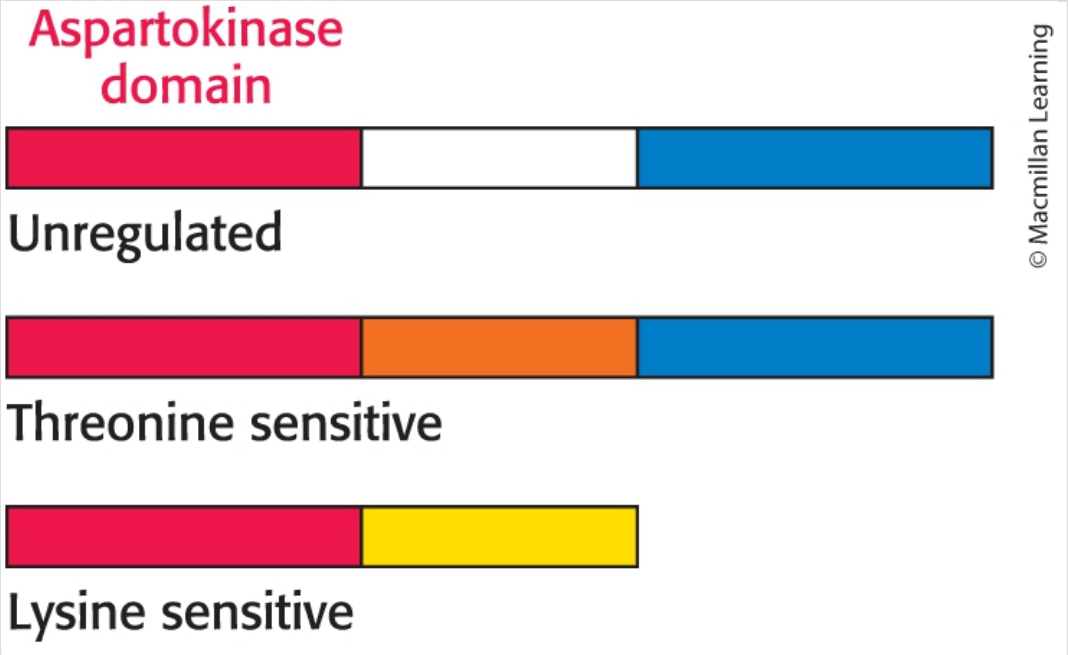


FIGURE 25.20 The three aspartokinases from *E. coli* have different regulatory domains. Each catalyzes the committed step in the biosynthesis of a different amino acid: (top) methionine, (middle) threonine, and (bottom) lysine. They have a catalytic domain in common (red) but differ in their regulatory domains (yellow and orange). The blue domain represents another enzyme (homoserine dehydrogenase) involved in aspartate metabolism. Thus, the top two aspartokinases are bifunctional enzymes.

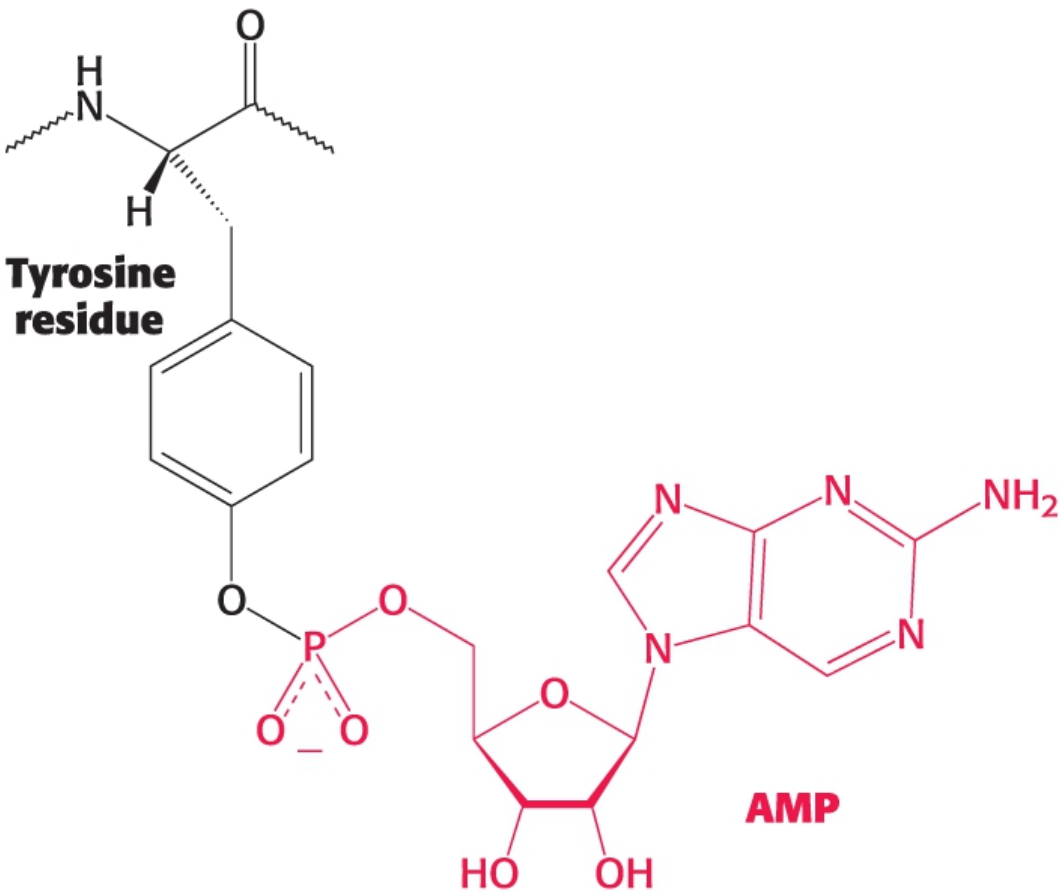
Cumulative feedback inhibition

A common step is partly inhibited by multiple final products, each acting independently. The regulation of glutamine synthetase in *E. coli* is a striking example of **cumulative feedback inhibition**. Recall that glutamine is synthesized from glutamate, NH_4^+, and ATP. Glutamine synthetase consists of 12 identical 50-kDa subunits arranged in two hexagonal rings that face each other. This enzyme regulates the flow of nitrogen and hence plays a key role in controlling bacterial metabolism. The amide group of glutamine is a source of nitrogen in the

biosyntheses of a variety of compounds, such as tryptophan, histidine, carbamoyl phosphate, glucosamine 6-phosphate, cytidine triphosphate, and adenosine monophosphate. Glutamine synthetase is cumulatively inhibited by each of these final products of glutamine metabolism, as well as by alanine and glycine. In cumulative inhibition, each inhibitor can reduce the activity of the enzyme, even when other inhibitors are bound at saturating levels. The enzymatic activity of glutamine synthetase is switched off almost completely when all final products are bound to the enzyme.

The sensitivity of glutamine synthetase to allosteric regulation is altered by covalent modification

The activity of glutamine synthetase is also controlled by reversible covalent modification — the attachment of an AMP unit by a phosphodiester linkage to the hydroxyl group of a specific tyrosine residue in each subunit. This adenylylated enzyme is less active and more susceptible to cumulative feedback inhibition than is the deadenylylated form. The covalently attached AMP unit is removed from the adenylylated enzyme by phosphorolysis.



Tyrosine residue modified by adenylylation

The adenylylation and phosphorolysis reactions are catalyzed by the same enzyme, adenylyl transferase. This enzyme is composed of two homologous halves, one half catalyzing the adenylylation reaction and the other half the phosphorolytic deadenylylation reaction. What determines whether an AMP unit is added or removed? The specificity of adenylyl transferase is controlled by a regulatory protein P_{II}, a trimeric protein that can exist in two forms, unmodified (P_{II}) or covalently bound to UMP (P_{II}-UMP). The complex of P_{II} and adenylyl transferase catalyzes the attachment of an AMP unit to glutamine synthetase, which reduces its activity. Conversely, the complex of P_{II}-

UMP and adenylyl transferase removes AMP from the adenylylated enzyme (Figure 25.21).

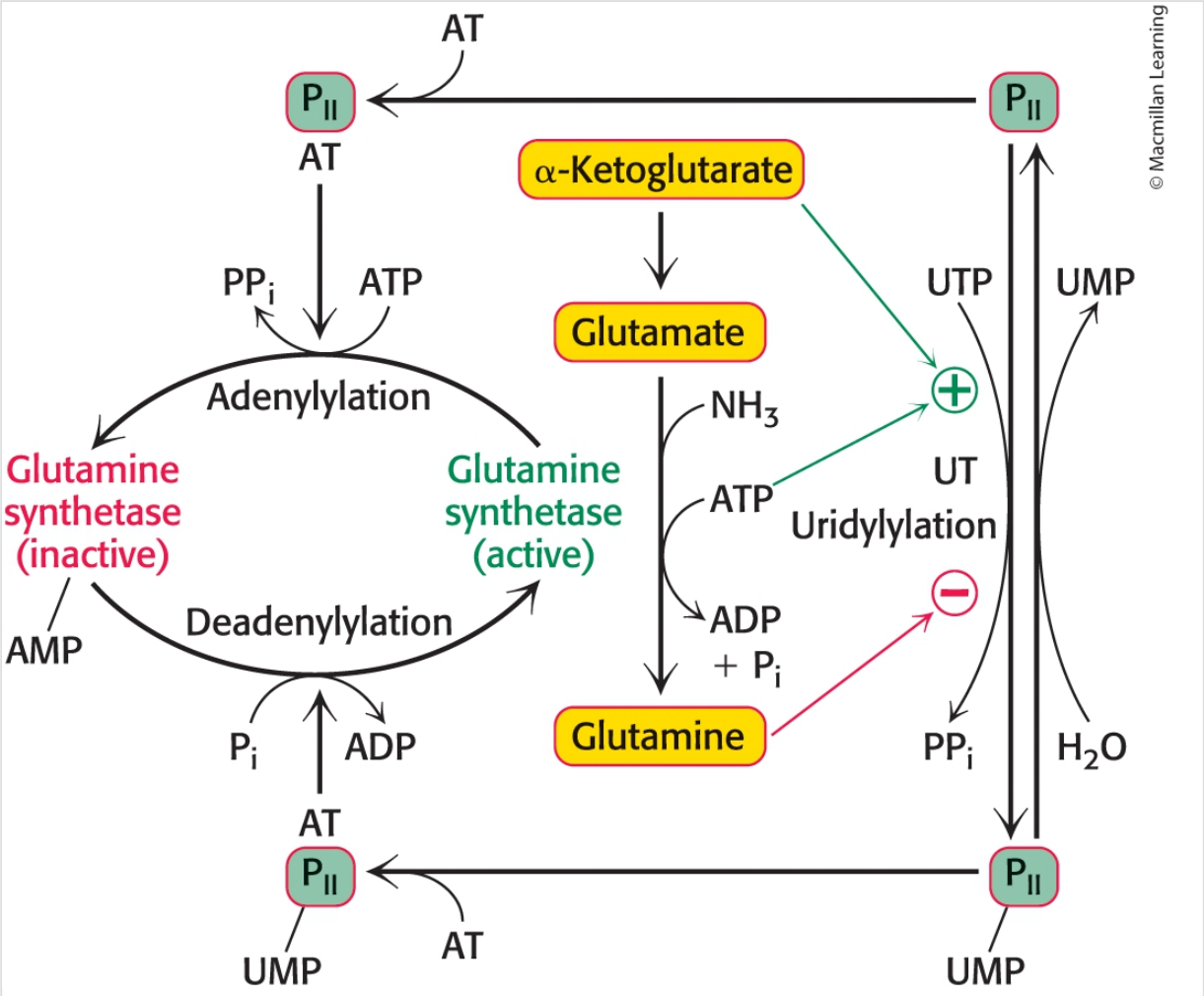


FIGURE 25.21 Glutamine synthetase is regulated by covalent modification. Adenylyl transferase (AT), in association with the regulatory protein P_{II}, adenylylates and inactivates the synthetase. When associated with P_{II} bound to UMP, AT deadenylylates the synthetase, thereby activating the enzyme. Uridylyl transferase (UT), the enzyme that modifies P_{II}, is allosterically regulated by α-ketoglutarate, ATP, and glutamine.

[Information from D. L. Nelson and M. M. Cox, Lehninger Principles of Biochemistry, 7th ed. (W. H. Freeman and Company, 2013), Fig. 22.9.]

This scheme of regulation immediately raises the question, how is the modification of P_{II} controlled? P_{II} is converted into P_{II}-UMP by the attachment of uridine monophosphate to a specific tyrosine residue (Figure 25.21). This reaction, which is catalyzed by uridylyl transferase, is stimulated by ATP and α-ketoglutarate, whereas it is inhibited by glutamine. In turn, the UMP units on P_{II} are removed by hydrolysis, a reaction promoted by glutamine and inhibited by α-ketoglutarate. These opposing catalytic activities are present on a single polypeptide chain and are controlled so that the enzyme does not simultaneously catalyze uridylylation and hydrolysis. In essence, if glutamine is present, the covalent modification system favors adenylylation and inactivation of glutamine synthetase. If glutamine is absent, as indicated by the presence of its precursors α-ketoglutarate and ATP, the control system results in the deadenylylation and activation of the synthetase.

The integration of nitrogen metabolism in a cell requires that a large number of input signals be detected and processed. In addition, the regulatory protein P_{II} also participates in regulating the transcription of genes for glutamine synthetase and other enzymes taking part in nitrogen metabolism. The evolution of covalent regulation superimposed on feedback inhibition provided many more regulatory sites and made possible a finer tuning of the flow of nitrogen in the cell. We have previously seen such a dual regulatory format in the regulation of glycogen metabolism (Section 21.6).

25.4 Amino Acids Are Precursors of Many Biomolecules

In addition to being the building blocks of proteins and peptides, amino acids serve as precursors of many kinds of small molecules that have important and diverse biological roles. Let us briefly survey some of the biomolecules that are derived from amino acids (**Figure 25.22**).

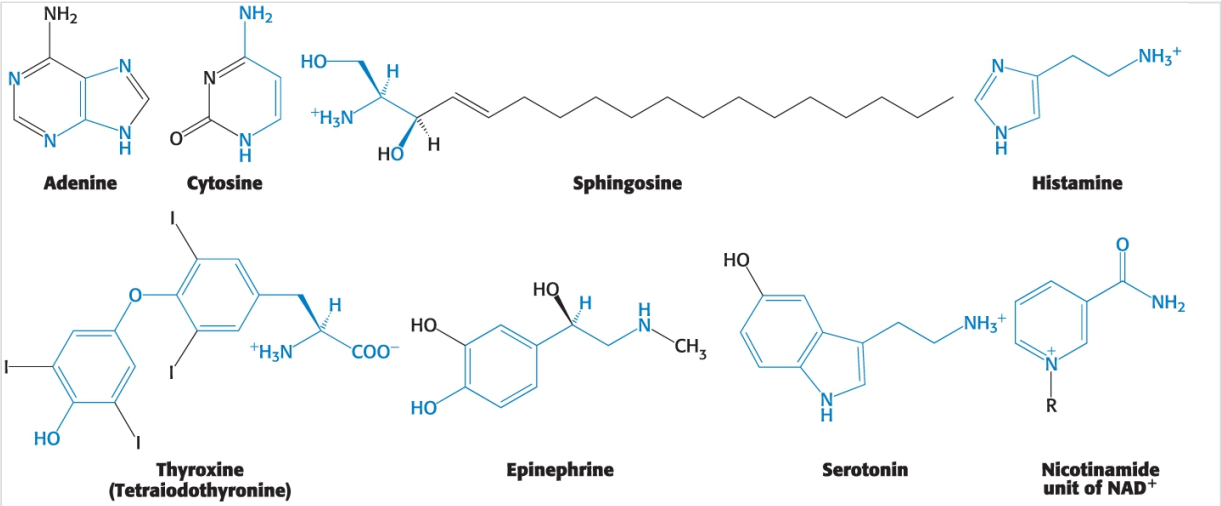


FIGURE 25.22 A diverse array of biomolecules are derived from amino acids. The atoms contributed by amino acids are shown in blue.

Purines and pyrimidines are derived largely from amino acids. The biosynthesis of these precursors of DNA, RNA, and numerous coenzymes will be discussed in detail in Chapter 26. The reactive terminus of sphingosine, an intermediate in the synthesis of sphingolipids (Section 12.2), comes from serine. Histamine, a potent vasodilator, is derived from histidine by decarboxylation. Tyrosine is a precursor of thyroxine (tetraiodothyronine, a hormone that modulates

metabolism), epinephrine (Section 14.2), and melanin (a complex polymeric molecule responsible for skin pigmentation). The neurotransmitter serotonin (5-hydroxytryptamine) and the nicotinamide ring of NAD^+ are synthesized from tryptophan. Let us now consider in more detail three particularly important biochemicals derived from amino acids.

Glutathione, a gamma-glutamyl peptide, serves as a sulfhydryl buffer and an antioxidant

Glutathione, a tripeptide containing a sulfhydryl group, is a highly distinctive amino acid derivative with several important roles (**Figure 25.23**).

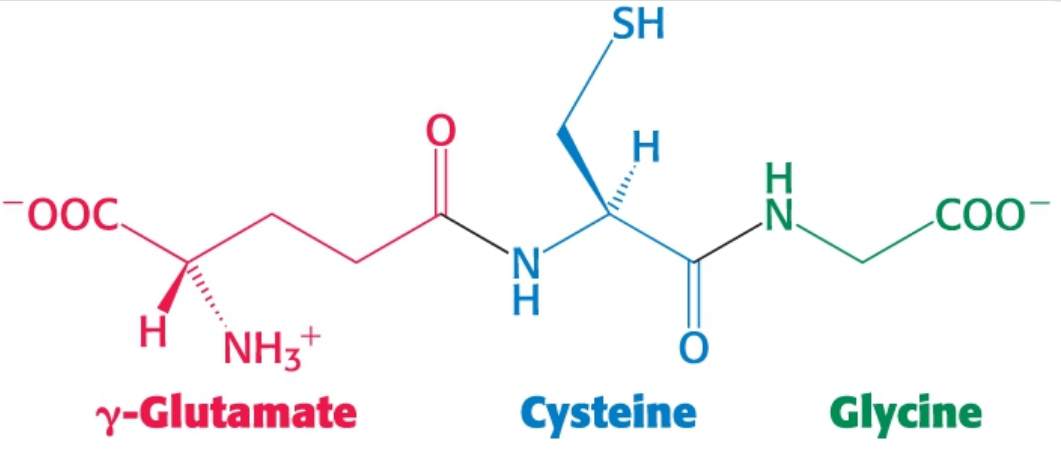


FIGURE 25.23 Glutathione is an important sulfhydryl buffer and antioxidant. This tripeptide consists of a cysteine residue flanked by a glycine residue and a glutamate residue that is linked to cysteine by an isopeptide bond between glutamate's side-chain carboxylate group and cysteine's amino group.

For example, glutathione, present at high levels $(\sim 5\ \text{mM})$ in animal cells, protects red blood cells from oxidative damage by serving as a sulfhydryl buffer (Section 20.5). It cycles between a reduced thiol form (GSH) and an oxidized form (GSSG) in which two tripeptides are linked by a disulfide bond.

$$2\,\text{GSH} + \text{RO—OH} \rightleftharpoons \text{GSSG} + \text{H}_2\text{O} + \text{ROH}$$

GSSG is reduced to GSH by glutathione reductase, a flavoprotein that uses NADPH as the electron source. The ratio of GSH to GSSG in most cells is greater than 500. Glutathione plays a key role in detoxification by reacting with hydrogen peroxide and organic peroxides, the harmful by-products of aerobic life (Section 20.5).

Glutathione peroxidase, the enzyme catalyzing the reaction of GSH with peroxides, is remarkable in having a modified amino acid containing a selenium (Se) atom (**Figure 25.24**). Specifically, its active site contains the selenium analog of cysteine, in which selenium has replaced sulfur.



FIGURE 25.24 Glutathione peroxidase contains a selenocysteine residue in its active site.

[Drawn from 1GP1.pdb.]

INTERACT with this model in Achieve

The selenolate $(E-Se^-)$ form of this residue reduces the peroxide substrate to an alcohol and is in turn oxidized to selenenic acid (E-SeOH). Glutathione then comes into action by forming a selenosulfide adduct (E-Se-S-G). A second molecule of glutathione then regenerates the active form of the enzyme by attacking the selenosulfide to form oxidized glutathione (Figure 25.25).

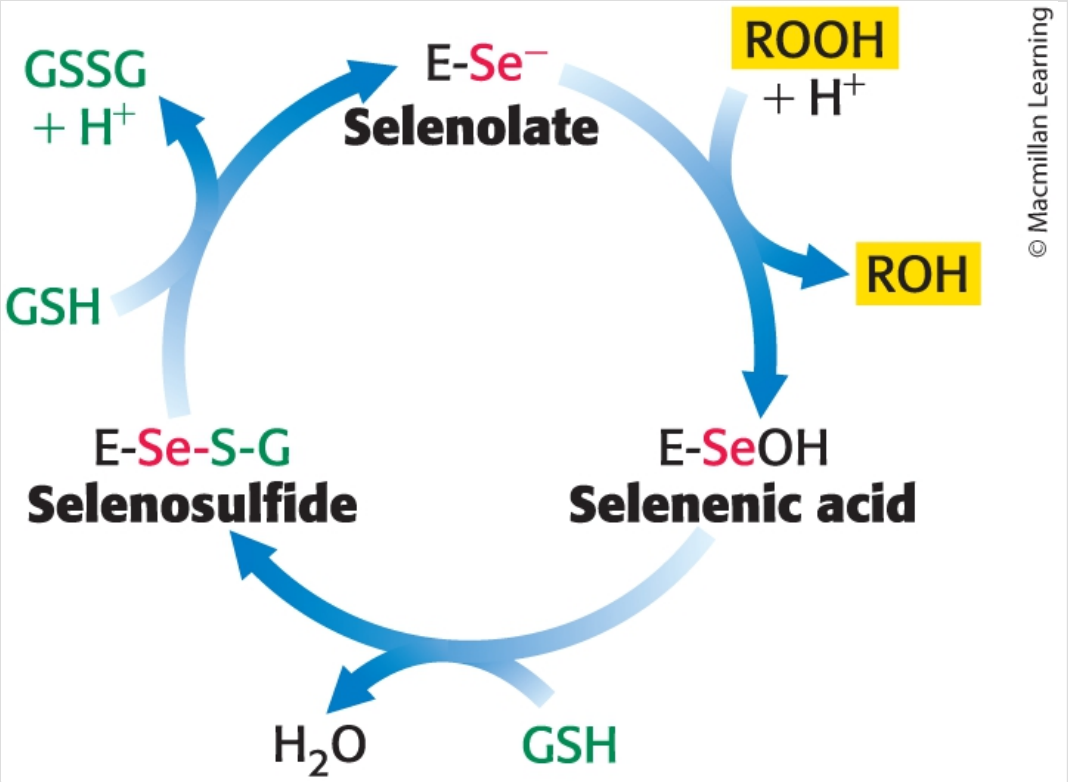


FIGURE 25.25 Glutathione peroxidase uses two molecules of glutathione to regenerate the selenolate active site after peroxide cleavage.

[Information from O. Epp, R. Ladenstein, and A. Wendel. *Eur. J. Biochem.* 133:51–69, 1983.]

Nitric oxide, a short-lived signal molecule, is formed from arginine

Nitric oxide (NO) is an important messenger in many vertebrate signal-transduction processes, identified first as a relaxing factor in the cardiovascular system. It is now known to have a variety of roles not only in the cardiovascular system, but also in the immune and nervous systems (Table 25.3)

TABLE 25.3 Some functions of nitric oxide

Reduces blood pressure by relaxing vascular muscle
Increases blood flow to the kidney
Acts as a neurotransmitter to increase cerebral blood flow
Dilates pulmonary vessels
Mediates erectile function
Controls peristalsis of the gastrointestinal tract
Regulates inflammation

NO has also been shown to stimulate mitochondrial biogenesis. This free-radical gas is produced endogenously from arginine in a complex reaction that is catalyzed by nitric oxide synthase. NADPH and O_2 are required for the synthesis of nitric oxide (**Figure 25.26**). Nitric oxide acts by binding to and activating soluble guanylate cyclase, an important enzyme in signal transduction. Soluble guanylate cyclase is homologous to adenylate cyclase (Section 14.2) but includes a heme-containing domain that binds NO.

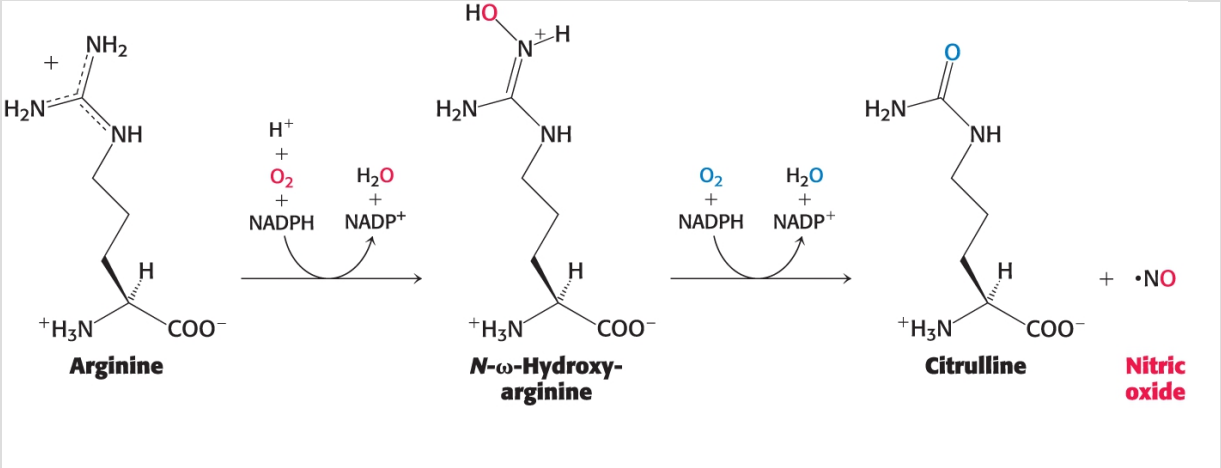


FIGURE 25.26 Nitric oxide is generated by the oxidation of arginine.



Amino acids are precursors for a number of neurotransmitters

Catecholamines, signal molecules with a variety of biological roles, are derived from tyrosine (**Figure 25.27**). Norepinephrine and dopamine are neurotransmitters, and epinephrine is familiar to us for the regulation of fuel use, stimulating glycogen breakdown and lipid mobilization (Section 14.2). In general, the catecholamines are associated with stress and play a role in the "fight or flight" response.

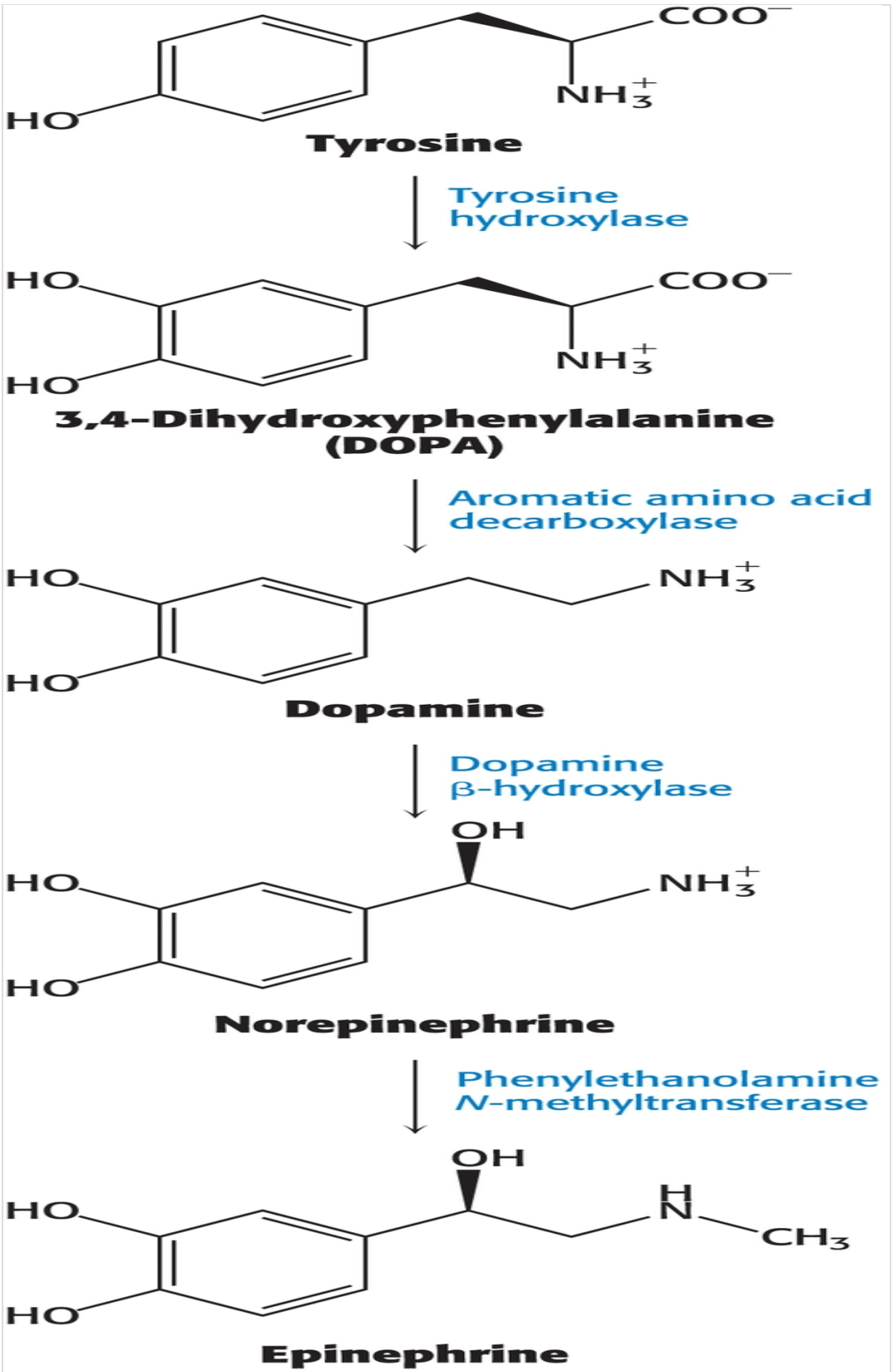

COO⁻
NH3+
HO
Tyrosine
Tyrosine hydroxylase
HO
HO
COO⁻
NH3+
3,4-Dihydroxyphenylalanine (DOPA)
Aromatic amino acid decarboxylase
HO
HO
NH3+
Dopamine
Dopamine β-hydroxylase
OH
HO
HO
NH3+
Norepinephrine
Phenylethanolamine N-methyltransferase
OH
HO
HO
H
N
CH3
Epinephrine

FIGURE 25.27 Tyrosine is a precursor for the catecholamines. The catecholamines — dopamine, norepinephrine, and epinephrine — function as stress-signal molecules.



Tryptophan is a precursor for two neurotransmitters (Figure 25.28A). Serotonin functions in several ways. Most notably, serotonin regulates moods and may be involved in alleviating depression. Serotonin is also found in the gastrointestinal tract, where it regulates intestinal contraction, and platelets, where it facilitates vasoconstriction. Serotonin can be metabolized to another hormone, melatonin, which functions to maintain our natural sleep-wake cycle (Figure 25.28B).

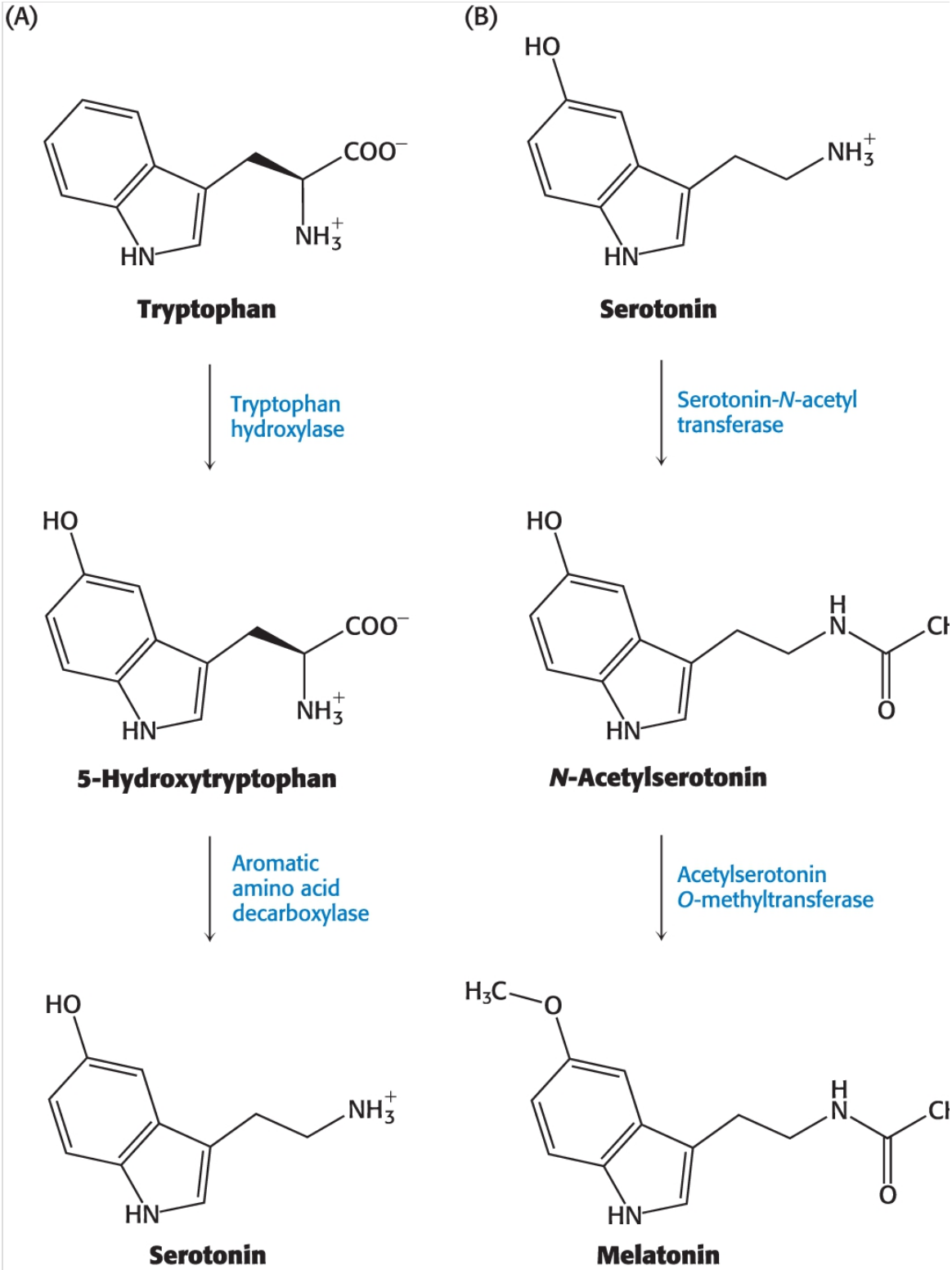


FIGURE 25.28 The neurotransmitters serotonin and melatonin are synthesized from tryptophan. (A) Serotonin is synthesized from tryptophan in two enzymatic steps. (B) Melatonin, in turn, is generated from serotonin in two additional steps.

Porphyrins are synthesized from glycine and succinyl coenzyme A

The participation of an amino acid in the biosynthesis of the porphyrin rings of hemes and chlorophylls was first revealed by isotope-labeling experiments carried out by David Shemin and his colleagues. In 1945, they showed that the nitrogen atoms of heme were labeled after the feeding of $[^{15}N]$ glycine to human subjects, whereas the ingestion of $[^{15}N]$ glutamate resulted in very little labeling.

Experiments using ^{14}C, which had just become available, revealed that 8 of the carbon atoms of heme in nucleated duck erythrocytes are derived from the α-carbon atom of glycine and none from the carboxyl carbon atom. Subsequent studies demonstrated that the other 26 carbon atoms of heme can arise from acetate. Moreover, the ^{14}C in methyl-labeled acetate emerged in 24 of these carbon atoms, whereas the ^{14}C in carboxyl-labeled acetate appeared only in the other 2 (**Figure 25.29**).

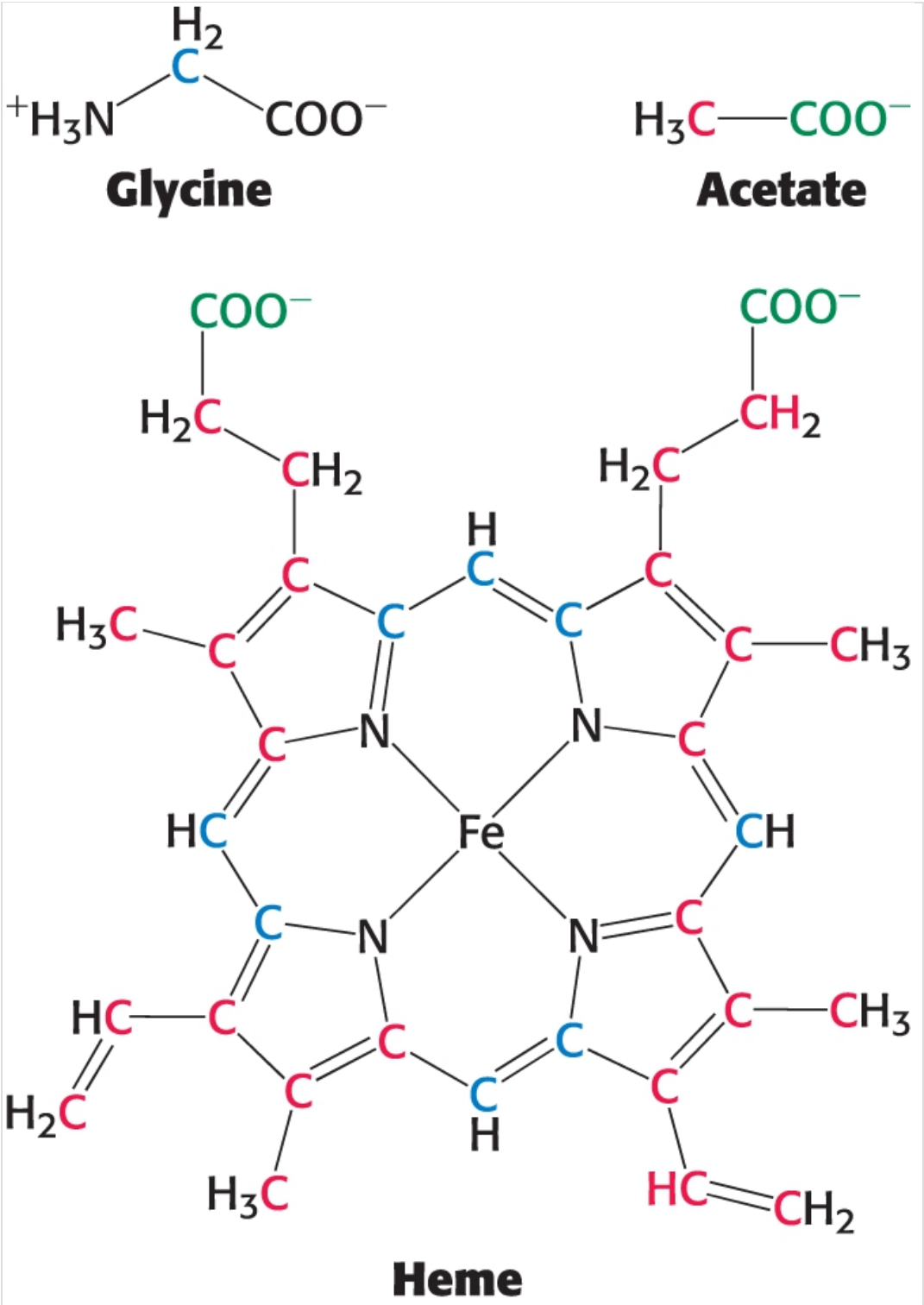
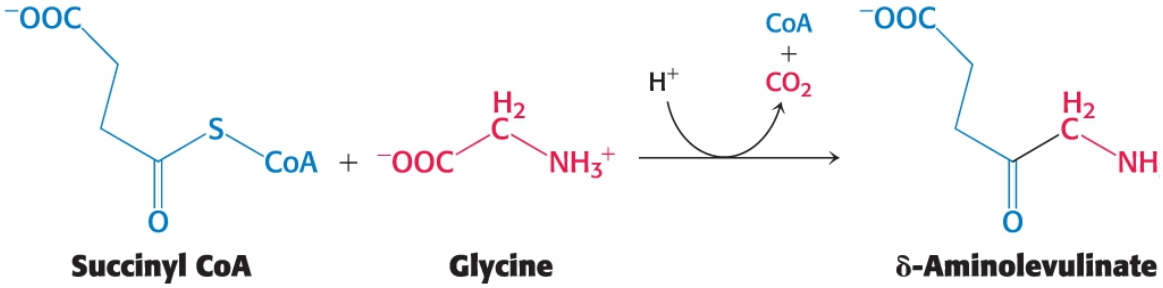


FIGURE 25.29 The origins of atoms in heme were revealed by isotope-labeling studies. The final structure of heme contains 8 carbons from the a-carbon of glycine (blue), 24 carbons from the methyl group of acetate (red), and two carbons from the carboxyl group of acetate (green).

This highly distinctive labeling pattern suggested that acetate is converted to succinyl-CoA through enzymes from the citric acid cycle (Section 17.3) and that a heme precursor is formed by the condensation of glycine with succinyl-CoA. Indeed, the first step in the biosynthesis of porphyrins in mammals is the condensation of glycine and succinyl CoA to form δ-aminolevulinate.



This reaction is catalyzed by δ-aminolevulinate synthase, a PLP enzyme present in mitochondria. Consistent with the labeling studies described earlier, the carbon atom from the carboxyl group of glycine is lost as carbon dioxide, while the α-carbon remains in δ-aminolevulinate.

The reactions required for heme synthesis take place in both the mitochondria and the cytoplasm (**Figure 25.30**), revealing another example of intercompartmental cooperation (Figure 16.30). δ-Aminolevulinate is generated in the mitochondria and is then transported into the cytoplasm, where two molecules of δ-aminolevulinate condense to form porphobilinogen, the next intermediate. Four molecules of porphobilinogen then condense head to tail to form a linear tetrapyrrole in a reaction catalyzed by

porphobilinogen deaminase. The enzyme-bound linear tetrapyrrole then cyclizes to form uroporphyrinogen III, which has an asymmetric arrangement of side chains. This reaction requires a cosynthase. In the presence of synthase alone, uroporphyrinogen I, the nonphysiological symmetric isomer, is produced. Uroporphyrinogen III is also a key intermediate in the synthesis of vitamin B_{12} by bacteria and that of chlorophyll by bacteria and plants.

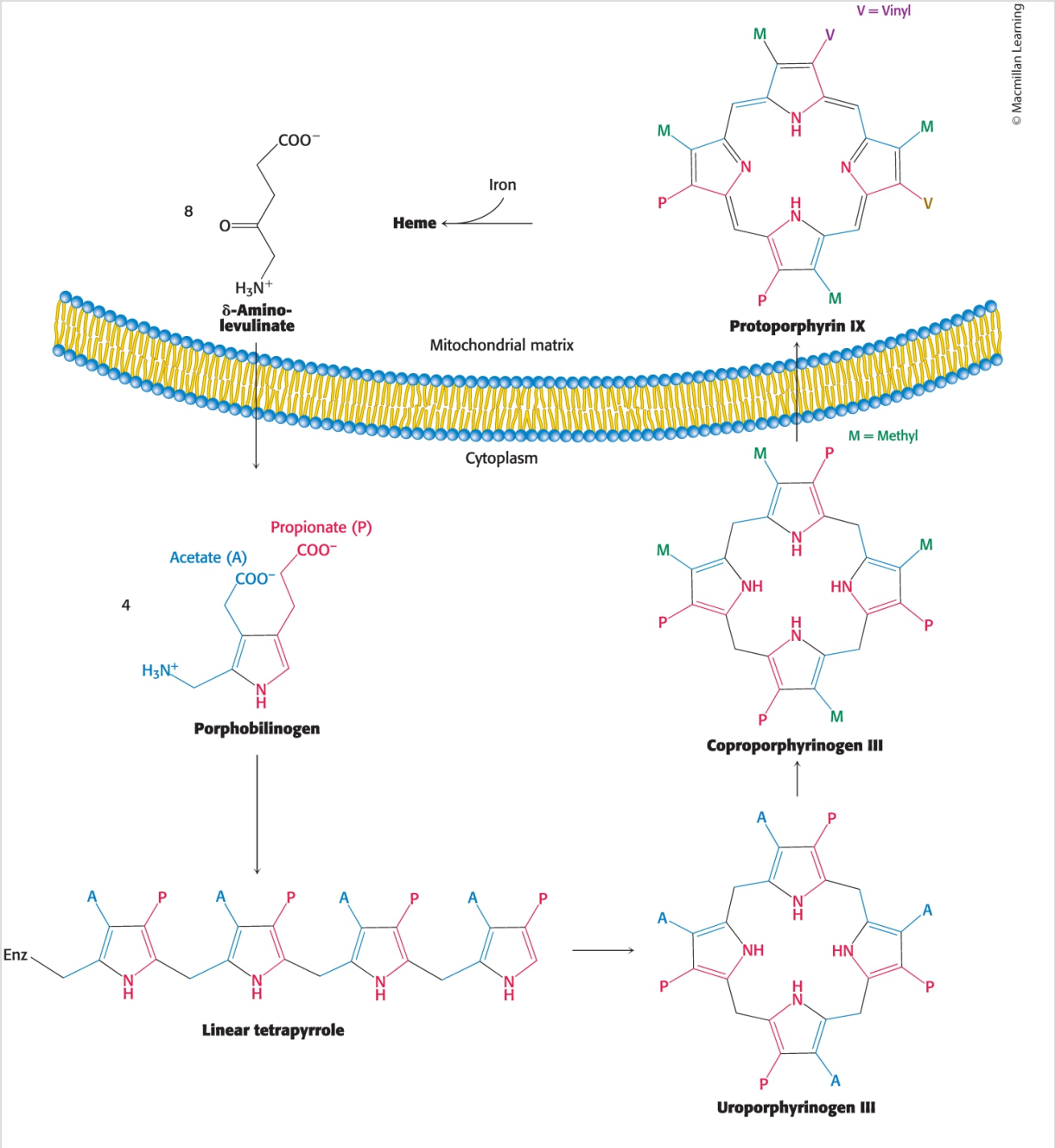


FIGURE 25.30 Heme is synthesized from eight molecules of δ-aminolevulinate. The biosynthetic pathway involves intercompartmental cooperation between the cytoplasm and the mitochondrial matrix.



The porphyrin skeleton is now formed. Subsequent reactions alter the side chains and the degree of saturation of the porphyrin ring (Figure 25.30). Coproporphyrinogen III is formed by the decarboxylation of the acetate side chains and then transported into the mitochondria. There, the desaturation of the porphyrin ring and the conversion of two of the propionate side chains into vinyl groups yield protoporphyrin IX. The chelation of iron finally gives heme, the prosthetic group of proteins such as myoglobin, hemoglobin, catalase, peroxidase, and cytochrome *c*. The insertion of the ferrous form of iron is catalyzed by ferrochelatase. Iron is transported in the plasma by transferrin, a protein that binds two ferric ions, and is stored in tissues inside molecules of ferritin (Section 31.6).

Studies with ^{15}N-labeled glycine revealed that the normal human erythrocyte has a life span of about 120 days. The first step in the degradation of the heme group is the cleavage of its α-methine bridge to form the green pigment biliverdin, a linear tetrapyrrole (**Figure 25.31**). This reaction is catalyzed by heme oxygenase. The central methine bridge of biliverdin is then reduced by biliverdin reductase to form bilirubin, an orange-yellow pigment. The changing color of a bruise is a highly graphic indicator of these degradative reactions.

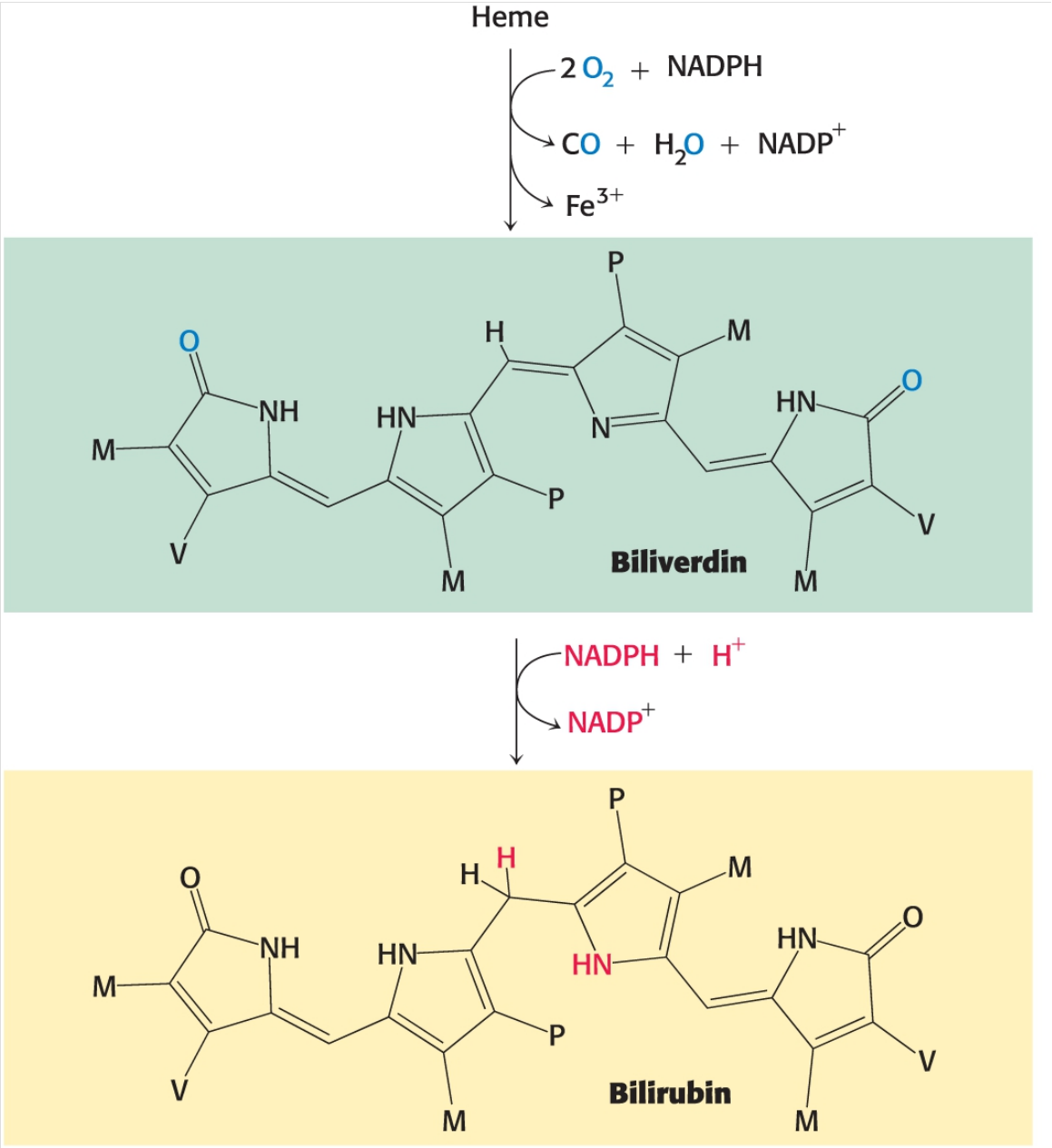


FIGURE 25.31 Heme is degraded into biliverdin and bilirubin. These products are the pigment responsible for the color of bruises. Abbreviations: M, methyl; V, vinyl.

Self-Check Question



The synthesis of δ-aminolevulinate takes place in the mitochondrial matrix, whereas the formation of porphobilinogen takes place in the cytoplasm. Propose a reason for the mitochondrial location of the first step in heme synthesis.

Porphyrins accumulate in some inherited disorders of porphyrin metabolism



Porphyrias are inherited or acquired disorders caused by a deficiency of enzymes in the heme biosynthetic pathway. Porphyrin is synthesized in both the erythroblasts and the liver, and either one may be the site of a disorder. Congenital erythropoietic porphyria, for example, prematurely destroys erythrocytes. This disease results from insufficient cosynthase. In this porphyria, the synthesis of the required amount of uroporphyrinogen III is accompanied by the formation of very large quantities of uroporphyrinogen I, the useless symmetric isomer. Uroporphyrin I, coproporphyrin I, and other symmetric derivatives also accumulate. The urine of patients having this disease is red because of the excretion of large amounts of uroporphyrin I. Their teeth exhibit a strong red fluorescence under ultraviolet light because of the deposition of porphyrins. Furthermore, their skin is usually very sensitive to light because photoexcited porphyrins are quite reactive.

Acute intermittent porphyria is the most prevalent of the porphyrias affecting the liver. This porphyria is characterized by the overproduction of porphobilinogen and δ-aminolevulinate, which

results in severe abdominal pain and neurological dysfunction. The "madness" of George III, king of England during the American Revolution, may have been due to this porphyria.

Chapter 25 Summary

25.1 Nitrogen Fixation: Microorganisms Use ATP and a Powerful Reductant to Reduce Atmospheric Nitrogen to Ammonia

- Nitrogen fixation is the process by which N_2 is reduced to NH_3.
- Using ATP and reduced ferredoxin, microorganisms use the nitrogenase complex to catalyze nitrogen fixation.
- Higher organisms use the fixed nitrogen in the form of NH_4^+ to synthesize amino acids, nucleotides, and other nitrogen-containing biomolecules.
- The major points of entry of NH_4^+ into metabolism are glutamine or glutamate.

25.2 Amino Acids Are Made from Intermediates of the Citric Acid Cycle and Other Major Pathways

- Human beings can synthesize 11 of the basic set of 20 amino acids. These amino acids are called *nonessential*.
- The *essential* amino acids must be supplied in the diet.
- The pathways for the synthesis of nonessential amino acids are quite simple, while those of the essential amino acids tend to contain greater than 5 catalytic steps.
- A transamination reaction takes place in the synthesis of most amino acids. At this step, the chirality of the amino acid is established.
- Alanine, aspartate, and glutamate are synthesized in one step by the addition of an amino group to pyruvate, oxaloacetate, and α-ketoglutarate, respectively.
- Glutamine is synthesized from NH_4^+ and glutamate, and asparagine is synthesized similarly in bacteria. In mammals,

the nitrogen donor for asparagine is glutamine.
- Proline and arginine are derived from glutamate.
- Serine, formed from 3-phosphoglycerate, is the precursor of glycine and cysteine.
- Tyrosine is synthesized by the hydroxylation of phenylalanine, an essential amino acid.
- In many of these pathways, tetrahydrofolate serves as an important carrier of one-carbon units, while *S*-adenosylmethionine acts as a donor of methyl groups.

25.3 Feedback Inhibition Regulates Amino Acid Biosynthesis

- Most of the pathways of amino acid biosynthesis are regulated by feedback inhibition in which the committed step is allosterically inhibited by the final product.
- The regulation of branched pathways requires extensive interaction among the branches that includes both negative and positive regulation.
- The regulation of glutamine synthetase in *E. coli* is a striking demonstration of cumulative feedback inhibition and of control by a cascade of reversible covalent modifications.

25.4 Amino Acids Are Precursors of Many Biomolecules

- Amino acids are precursors of a variety of biomolecules.
- Glutathione (γ-Glu-Cys-Gly) serves as a sulfhydryl buffer and detoxifying agent.
- Nitric oxide, a short-lived messenger, is formed from arginine.
- Porphyrins, the iron-binding groups in heme, are synthesized from glycine and succinyl CoA.

Key Terms

nitrogen fixation
nitrogenase complex
essential amino acids
nonessential amino acids
pyridoxal phosphate (PLP)
tetrahydrofolate
S-adenosylmethionine (SAM)
activated methyl cycle
substrate channeling
enzyme multiplicity
cumulative feedback inhibition
glutathione
nitric oxide (NO)
porphyrias

Problems

1. Identify the two components of the nitrogenase complex and describe their specific tasks. 1

2. Which of the following statements about nitrogen fixation are correct? 1

a. Atmospheric nitrogen is reduced to the biologically useful form NH_3 (or NH_4^+).
b. Nitrogen fixation in nature and in the lab requires a metal cofactor or catalyst.

c. Nitrogen fixation is energetically neutral, using a negligible amount of ATP.
d. The enzyme nitrogenase, which takes part in nitrogen fixation, is inactivated by oxygen.
e. Ammonium from the atmosphere is fixed to more usable forms of nitrogen, such as nitrate (NO_3^-).
f. The availability of fixed nitrogen limits biological productivity.

3. The first step in the incorporation of NH_4^+ into amino acids is catalyzed by glutamate dehydrogenase, in which an α-keto acid is converted to glutamate by transamination. 1

a. Draw the structure of the α-keto acid precursor to glutamate.
b. Besides glutamate, what are the other products of this reaction?

4. The entry of nitrogen into the biosphere is not an energetically cheap process. How many molecules of ATP must be hydrolyzed per N_2 molecule fixed? 1

5. The nitrogenase complex consists of two protein components: the reductase and the nitrogenase. What is the function of each of these proteins? 1

6. What are the seven precursors of the 20 amino acids? 2

7. Write a balanced equation for the synthesis of alanine from glucose. 2

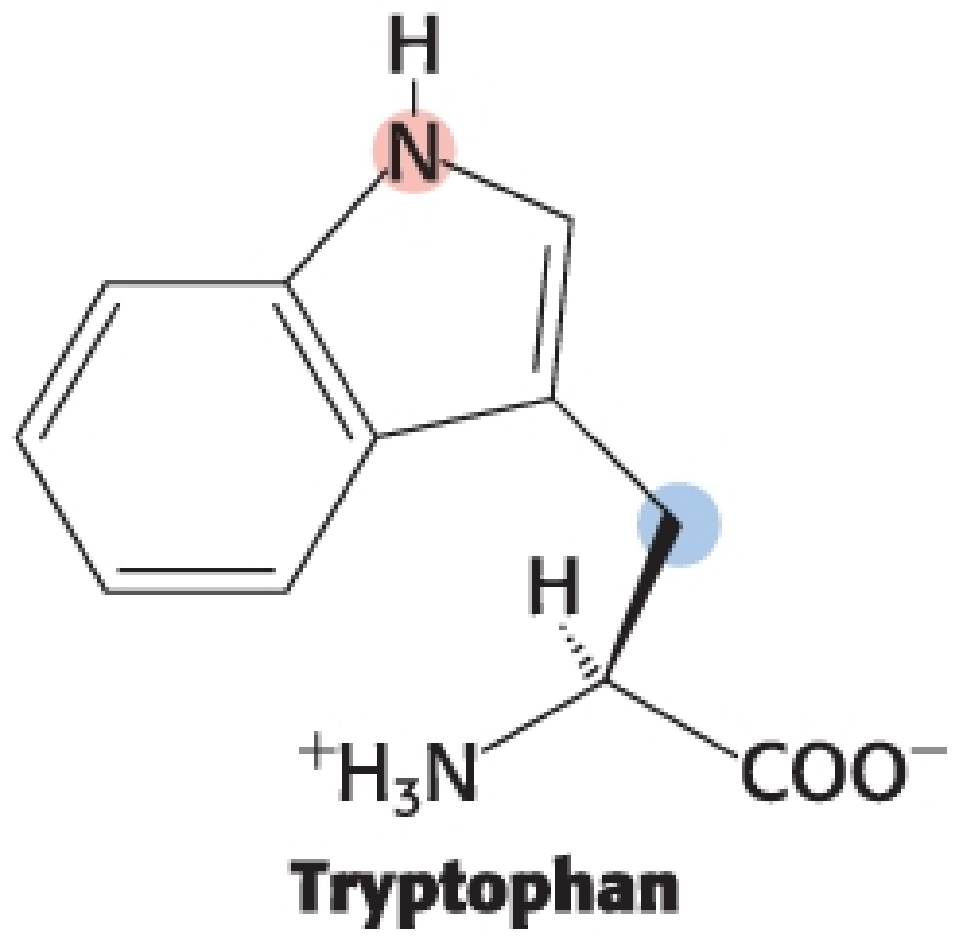
8. Which of the 20 amino acids can be synthesized directly from a common metabolic intermediate by a transamination reaction? 2

9. Which amino acids are formed from the glycolysis intermediate 3-phosphoglycerate? 2

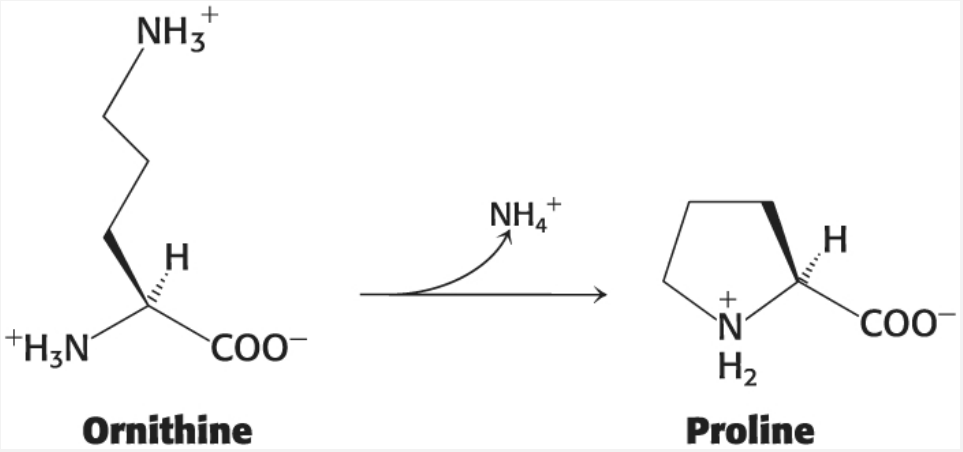
10. Which of the following molecules is the most direct source for the sulfur atom in the sulfur-containing amino acids in human beings? 2

a. Biotin
b. Homocysteine
c. Glutathione
d. Tetrahydrofolate
e. Coenzyme A

11. The atoms from tryptophan shaded below are derived from two other amino acids. Name them. 2

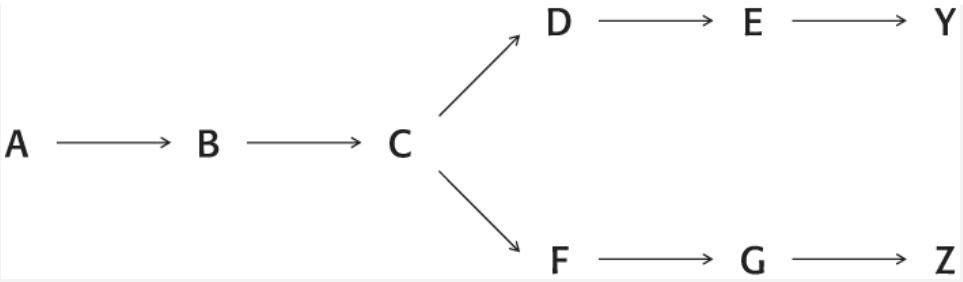


12. Certain species of bacteria possess an enzyme, ornithine cyclodeaminase, that can catalyze the conversion of L-ornithine into L-proline in a single catalytic cycle.



The enzyme lysine cyclodeaminase has also been identified. Predict the product of the reaction catalyzed by lysine cyclodeaminase.

13. For the following example of a branched pathway, propose a feedback inhibition scheme that would result in the production of equal amounts of Y and Z. 3



14. Consider the branched pathway in problem 13. The first common step $(A \rightarrow B)$ is partly inhibited by both of the final products, each acting independently of the other. Suppose that a high level of Y alone decreased the rate of the $A \rightarrow B$ step from 100 to $60\ s^{-1}$ and that a high level of Z alone decreased the rate from 100 to $40\ s^{-1}$. What would the rate be in the presence of high levels of both Y and Z? 3

15. What are the intermediates in the flow of nitrogen from N_2 to heme? 4

16. David Shemin and coworkers used acetate-labeling experiments to conclude that succinyl-CoA is a key intermediate in the biosynthesis of heme. Identify the intermediates in the conversion of acetate into succinyl-CoA. 4

17. Which of the following statements about heme are correct? 4

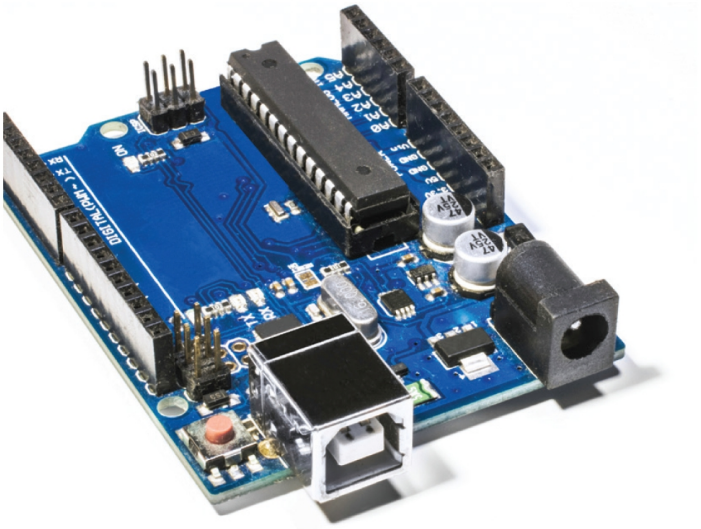
a. Phenylalanine is a precursor to heme.
b. Heme is found in trypsin.

c. Heme is found in cytochrome *c*.
d. Heme contains a magnesium ion.
e. Succinyl-CoA is a precursor to heme.
f. Heme contains an iron ion.

18. In this chapter, we considered three different cofactors/cosubstrates that act as carriers of one-carbon units. Name them.

19. Individuals with an inactivating mutation in phenylalanine hydroxylase require an additional amino acid in their diet which is not an essential amino acid in the ordinary human diet. Which one?

CHAPTER 26
Nucleotide Biosynthesis



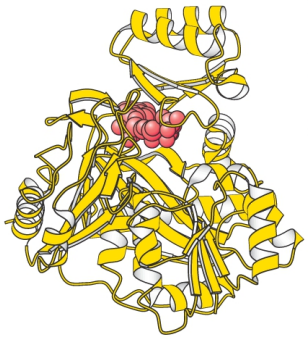


Photo: Sergey Privalov/Shutterstock
© Macmillan Learning

An Arduino board is a versatile electronics component that can be modified to perform a variety of functions. The ability to be adjusted allows this component to participate in many related processes. Similarly, the ATP grasp domain depicted at right is found in many enzymes that participate in nucleotide biosynthesis; evolutionary modifications have allowed enzymes containing such domains to catalyze a range of related reactions.

OUTLINE

26.1 Nucleotides Can Be Synthesized by de Novo or Salvage Pathways
26.2 The Pyrimidine Ring Is Assembled from CO_2, Ammonia, and Aspartate

26.3 Purine Bases Can Be Synthesized from Glycine, Aspartate, and Other Components
26.4 Deoxyribonucleotides Are Synthesized by the Reduction of Ribonucleotides
26.5 Key Steps in Nucleotide Biosynthesis Are Regulated by Feedback Inhibition
26.6 Disruptions in Nucleotide Metabolism Can Cause Pathological Conditions

Learning Goals



By the end of this chapter, you should be able to:

1. Describe how pyrimidine nucleotides are synthesized.
2. Describe the pathway for purine nucleotide synthesis.
3. Explain how deoxyribonucleotides are formed.
4. Name the regulatory steps in nucleotide synthesis.
5. Identify the pathological conditions resulting from impaired nucleotide synthesis.

In this chapter, we describe the biosynthesis of nucleotides, continuing along the path begun in Chapter 25, which described the incorporation of nitrogen into amino acids from inorganic sources such as nitrogen gas. The amino acids glycine and aspartate are the scaffolds on which the ring systems present in nucleotides are assembled. Furthermore, aspartate and the side chain of glutamine serve as sources of NH_2 groups in the formation of nucleotides.

Nucleotide biosynthetic pathways are tremendously important as intervention points for therapeutic agents. Many of the most widely

used drugs in the treatment of cancer block steps in nucleotide biosynthesis, particularly steps in the synthesis of DNA precursors.

26.1 Nucleotides Can Be Synthesized by de Novo or Salvage Pathways

Nucleotides are key biomolecules required for a variety of life processes.

- Nucleotides are the activated precursors of nucleic acids, necessary for the replication of the genome and the transcription of the genetic information into RNA.
- An adenine nucleotide, ATP, is the universal currency of energy.
- A guanine nucleotide, GTP, also serves as an energy source for a more select group of biological processes.
- Nucleotide derivatives such as UDP-glucose participate in biosynthetic processes.
- Nucleotides such as cyclic AMP and cyclic GMP are essential components of signal-transduction pathways.
- ATP acts as the donor of phosphoryl groups transferred by protein kinases in a variety of signaling pathways.

The pathways for the biosynthesis of nucleotides fall into two classes: *de novo* pathways and *salvage* pathways (**Figure 26.1**). In **de novo pathways**, the nucleobases are assembled from scratch; meaning, from simpler compounds. The framework for a pyrimidine base is assembled first and then attached to ribose. In contrast, the framework for a purine base is synthesized piece by

piece directly onto a ribose-based structure. These de novo pathways each comprise a small number of elementary reactions that are repeated with variations to generate different nucleotides, as might be expected for pathways that appeared very early in evolution. In **salvage pathways**, preformed bases are recovered and reconnected to a ribose unit.

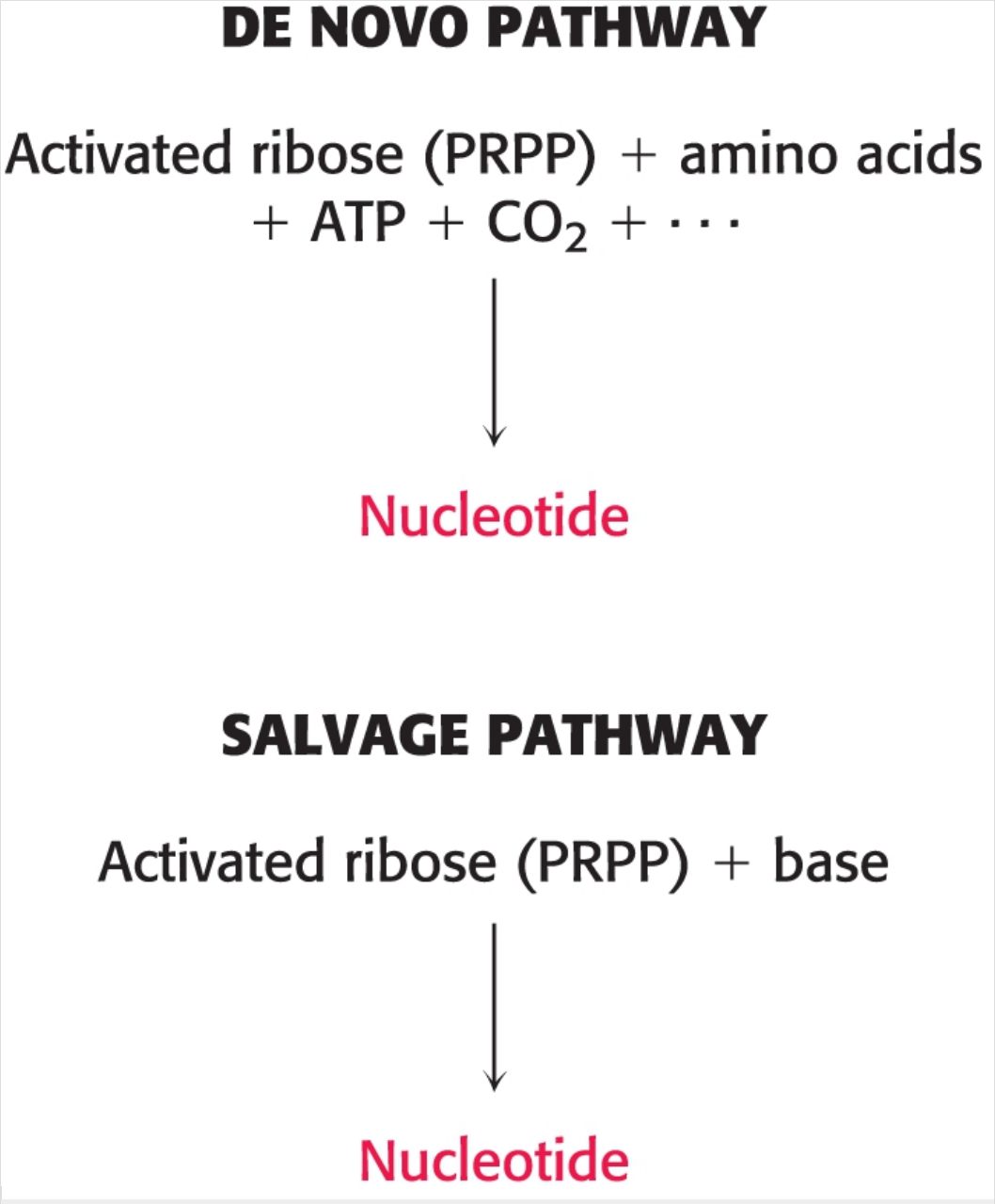


FIGURE 26.1 Nucleotides can be synthesized by de novo and salvage pathways. In de novo synthesis, the base itself is synthesized from simpler

starting materials, including amino acids. ATP hydrolysis is required for de novo synthesis. In a salvage pathway, a base is reattached to a ribose, activated in the form of 5-phosphoribosyl-1-pyrophosphate (PRPP).



De novo pathways lead to the synthesis of *ribo*nucleotides. However, DNA is built from *deoxyribo*nucleotides. Consistent with the notion that RNA preceded DNA in the course of evolution, all deoxyribonucleotides are synthesized from the corresponding ribonucleotides. The deoxyribose sugar is generated by the reduction of ribose within a fully formed nucleotide. Furthermore, the methyl group that distinguishes the thymine of DNA from the uracil of RNA is added at the last step in the pathway.

Recall from Chapter 8 that a *nucleoside* is a purine or pyrimidine base linked to a sugar and that a *nucleotide* is a phosphate ester of a nucleoside. The names of the major bases of RNA and DNA, and of their nucleoside and nucleotide derivatives, are given in **Table 26.1**.

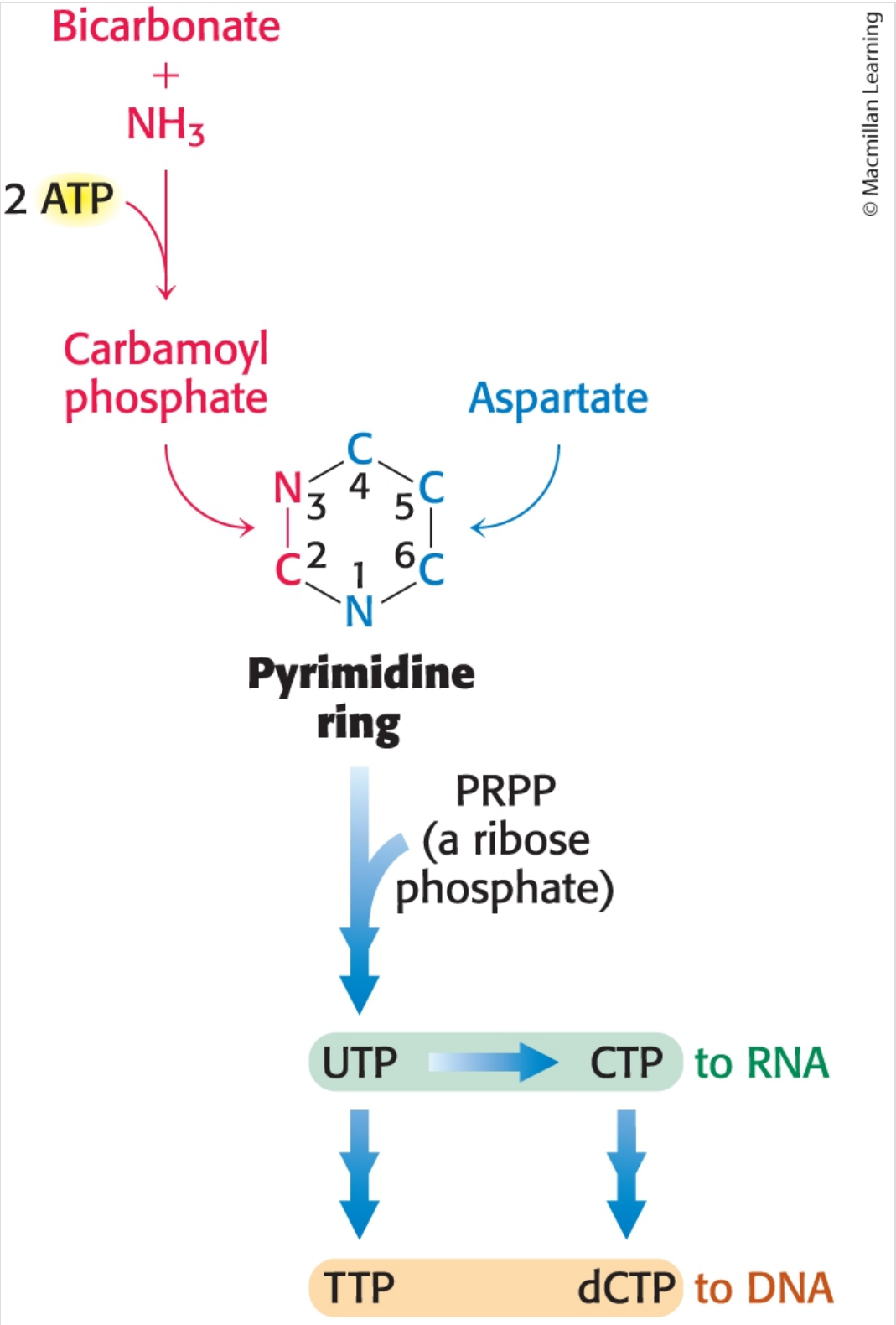
TABLE 26.1 Nomenclature of bases, nucleosides, and nucleotides

RNA		
Base	**Ribonucleoside**	**Ribonucleotide** (5′-monophosphate)
Adenine (A)	Adenosine	Adenylate (AMP)
Guanine (G)	Guanosine	Guanylate (GMP)

Uracil (U)	Uridine	Uridylate (UMP)
Cytosine (C)	Cytidine	Cytidylate (CMP)
DNA		
Base	**Deoxyribonucleoside**	**Deoxyribonucleotide (5′−monophosphate)**
Adenine (A)	Deoxyadenosine	Deoxyadenylate (dAMP)
Guanine (G)	Deoxyguanosine	Deoxyguanylate (dGMP)
Thymine (T)	Thymidine	Thymidylate (TMP)
Cytosine (C)	Deoxycytidine	Deoxycytidylate (dCMP)

26.2 The Pyrimidine Ring Is Assembled from CO_2, Ammonia, and Aspartate

In de novo synthesis of pyrimidines, the ring is synthesized first and then attached to a ribose phosphate to form a pyrimidine nucleotide (Figure 26.2). Pyrimidine rings are assembled from bicarbonate, aspartate, and ammonia. Although an ammonia molecule already present in solution can be used, the ammonia is usually produced from the hydrolysis of the side chain of glutamine.



© Macmillan Learning

FIGURE 26.2 Pyrimidine nucleotides can be synthesized de novo. The C-2 and N-3 atoms in the pyrimidine ring come from carbamoyl phosphate, whereas the other atoms of the ring come from aspartate.

Bicarbonate and other oxygenated carbon compounds are activated by phosphorylation

The first step in de novo pyrimidine biosynthesis is the synthesis of carbamoyl phosphate from bicarbonate and ammonia in a multistep process, requiring the cleavage of two molecules of ATP. This reaction is catalyzed by carbamoyl phosphate synthetase II (CPS II). Recall that carbamoyl phosphate synthetase I facilitates ammonia incorporation into urea (Section 23.4). Carbamoyl phosphate synthetase II is a dimer composed of a small subunit that hydrolyzes glutamine to form NH_3 and a large subunit that completes the synthesis of carbamoyl phosphate. Analysis of the structure of the large subunit reveals two homologous domains, each of which catalyzes an ATP-dependent step (**Figure 26.3**).

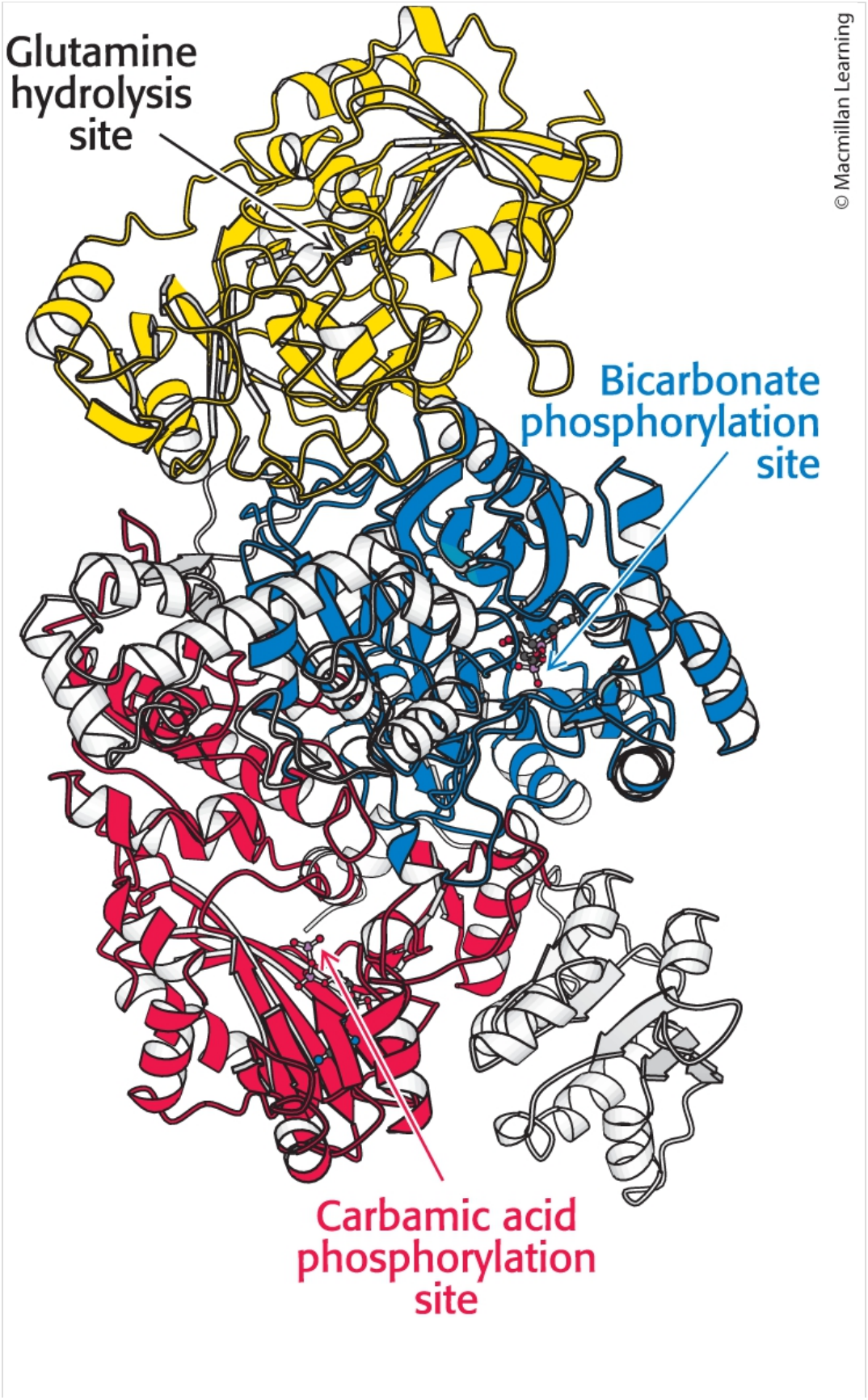
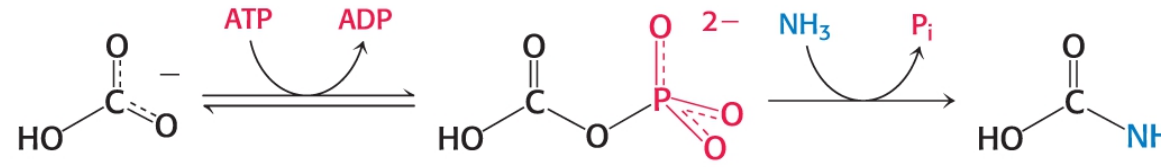

Glutamine hydrolysis site
Bicarbonate phosphorylation site
Carbamic acid phosphorylation site
© Macmillan Learning

FIGURE 26.3 Carbamoyl phosphate synthetase II includes sites for three reactions. This enzyme consists of two chains. The smaller chain (yellow) contains a site for glutamine hydrolysis to generate ammonia. The larger chain includes two ATP-grasp domains (blue and red). In one ATP-grasp domain (blue), bicarbonate is phosphorylated to carboxyphosphate, which then reacts with ammonia to generate carbamic acid. In the other ATP-grasp domain, the carbamic acid is phosphorylated to produce carbamoyl phosphate.

[Drawn from 1JDB.pdb.]

INTERACT with this model in Achieve

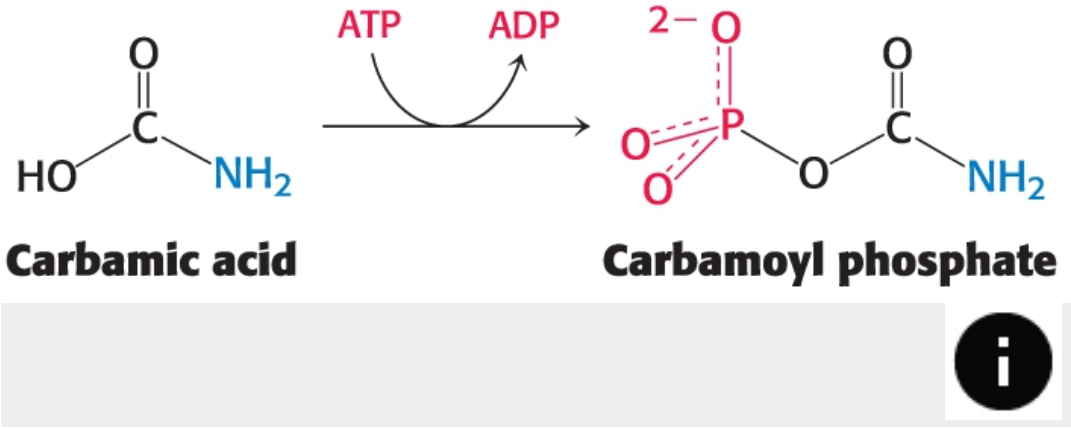
In the first step, bicarbonate is phosphorylated by ATP to form carboxyphosphate and ADP. Ammonia then reacts with carboxyphosphate to form carbamic acid and inorganic phosphate.



The active site for this reaction lies in a domain formed by the amino-terminal third of CPS. This domain forms a structure called an **ATP-grasp fold**, which surrounds ATP and holds it in an orientation suitable for nucleophilic attack at the γ phosphoryl group. Proteins containing ATP-grasp folds catalyze the formation of carbon–nitrogen bonds through acyl-phosphate intermediates. Such ATP-grasp folds are widely used in nucleotide biosynthesis.

In the second step catalyzed by carbamoyl phosphate synthetase II, carbamic acid is phosphorylated by another molecule of ATP to form

carbamoyl phosphate.



This reaction takes place in a second ATP-grasp domain within the enzyme. The active sites leading to carbamic acid formation and carbamoyl phosphate formation are very similar, revealing that this enzyme evolved by a gene duplication event. Indeed, duplication of a gene encoding an ATP-grasp domain followed by specialization was central to the evolution of nucleotide biosynthetic processes, as we shall see.

The side chain of glutamine can be hydrolyzed to generate ammonia

Glutamine is the primary source of ammonia for carbamoyl phosphate synthetase II. The small subunit of the enzyme hydrolyzes glutamine to form ammonia and glutamate. The active site of the glutamine-hydrolyzing component contains a catalytic dyad comprising a cysteine and a histidine residue. Such a catalytic dyad, reminiscent of the active site of cysteine proteases (Figure 6.16A), is conserved in a family of amidotransferases, including CTP synthetase and GMP synthetase.

Carbamoyl phosphate synthetase II contains three different active sites (Figure 26.3), separated from one another by a total of 80 Å.

Intermediates generated at one site move to the next without leaving the enzyme by means of substrate channeling, which is similar to the process described for tryptophan synthetase (**Figure 26.4**; also Figure 25.16). The ammonia generated in the glutamine-hydrolysis active site travels 45 Å through a channel within the enzyme to reach the site at which carboxyphosphate has been generated. The carbamic acid generated at this site then diffuses an additional 35 Å through an extension of the channel to reach the site at which carbamoyl phosphate is generated. This channeling serves two roles: (1) intermediates generated at one active site are captured with no loss caused by diffusion; and (2) labile intermediates, such as carboxyphosphate and carbamic acid (which decompose in less than 1 s at pH 7), are protected from hydrolysis. We will see additional examples of substrate channeling later in this chapter.

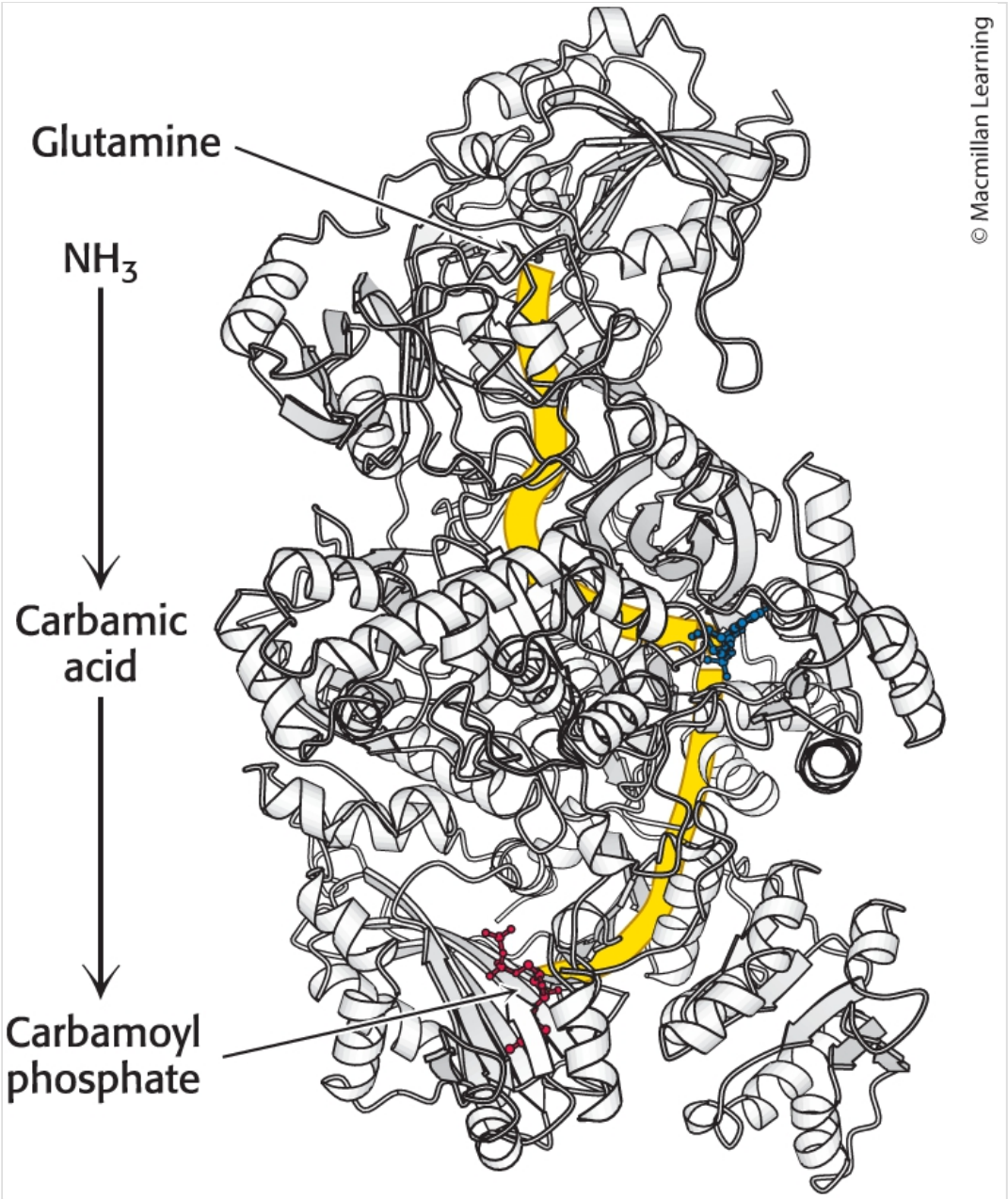


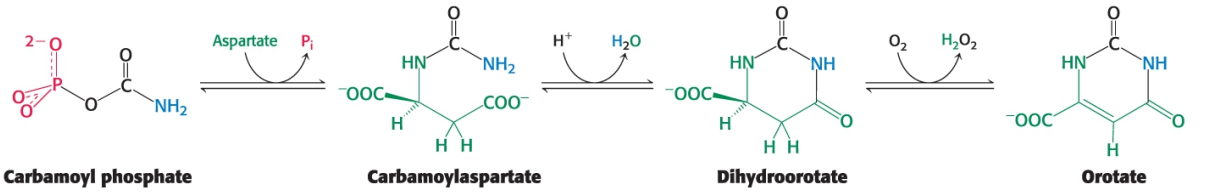
FIGURE 26.4 The three active sites of carbamoyl phosphate synthetase II are linked by a channel through which intermediates pass. The channel is shown in yellow. Glutamine enters one active site, and carbamoyl phosphate, which includes the nitrogen atom from the glutamine side chain, leaves another 80 Å away.

[Drawn from 1JDB.pdb.]

INTERACT with this model in Achieve

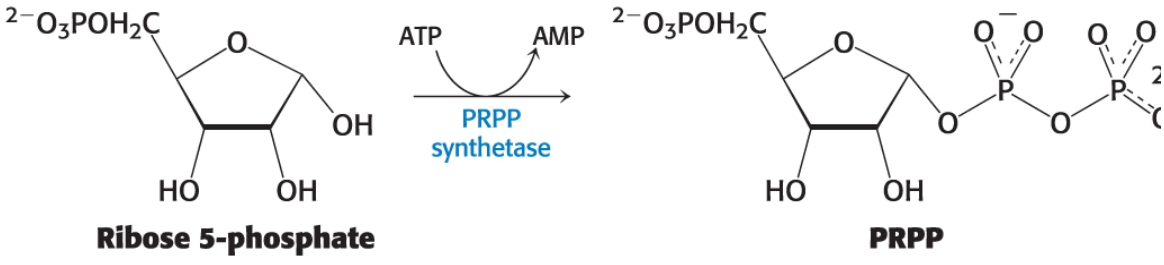
The pyrimidine ring is completed and coupled to ribose

Carbamoyl phosphate reacts with aspartate to form carbamoylaspartate in a reaction catalyzed by aspartate transcarbamoylase. Carbamoylaspartate then cyclizes to form dihydroorotate, which is then oxidized to form orotate.

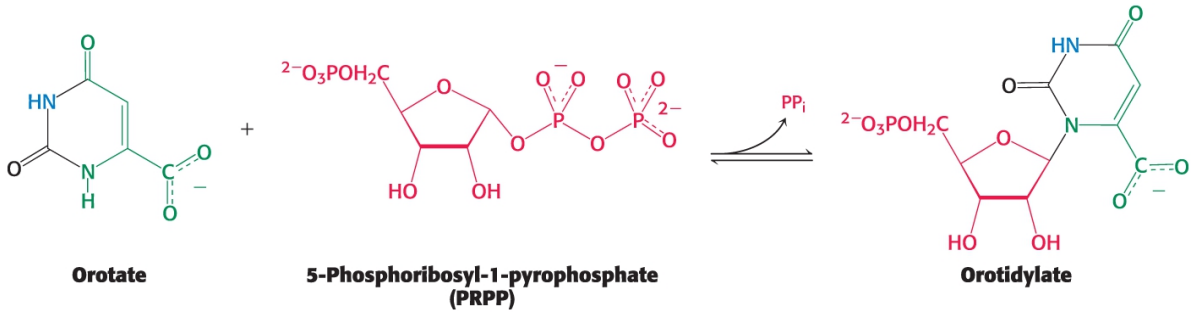


In mammals, the enzymes that form orotate are part of a single large polypeptide chain called CAD, for carbamoyl phosphate synthase, aspartate transcarbamoylase and dihydroorotase.

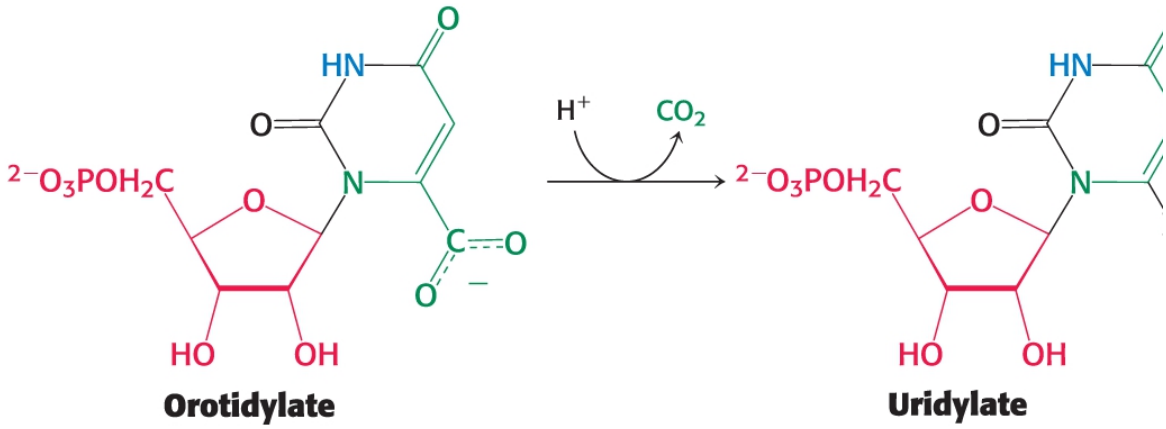
At this stage, orotate couples to ribose, in the form of [5-phosphoribosyl-1-pyrophosphate (PRPP)](), a form of ribose activated to accept nucleobases. 5-Phosphoribosyl-1-pyrophosphate synthetase synthesizes PRPP by adding a pyrophosphate from ATP to ribose-5-phosphate, which is formed by the pentose phosphate pathway.



Orotate reacts with PRPP to form **orotidylate**, a pyrimidine nucleotide. This reaction is driven by the hydrolysis of pyrophosphate. The enzyme that catalyzes this addition, orotate phosphoribosyltransferase, is homologous to a number of other phosphoribosyltransferases that add different groups to PRPP to form the other nucleotides.



Orotidylate is then decarboxylated to form uridylate (UMP), a major pyrimidine nucleotide that is a precursor to RNA. This reaction is catalyzed by orotidylate decarboxylase, also called orotidine 5′-phosphate decarboxylase.



Orotidylate decarboxylase is one of the most proficient enzymes known. In its absence, decarboxylation is extremely slow and is estimated to take place once every 78 million years; with the enzyme present, it takes place approximately once per second, a rate enhancement of 10^{17}-fold.

The phosphoribosyltransferase and decarboxylase activities are located on the same polypeptide chain, providing another example of a bifunctional enzyme. The bifunctional enzyme is called *uridine monophosphate synthetase*.

Self-Check Question



Identify the sources of the atoms that form the pyrimidine ring.

Nucleotide mono-, di-, and triphosphates are interconvertible

How is the other major pyrimidine ribonucleotide, cytidine, formed? It is synthesized from the uracil base of UMP, but the synthesis can take place only after UMP has been converted into UTP. Recall that the diphosphates and triphosphates are the active forms of nucleotides in biosynthesis and energy conversions. Nucleoside monophosphates are converted into nucleoside triphosphates in stages. First, nucleoside monophosphates are converted into diphosphates by specific nucleoside monophosphate kinases that utilize ATP as the phosphoryl-group donor. For example, UMP is phosphorylated to UDP by UMP kinase.

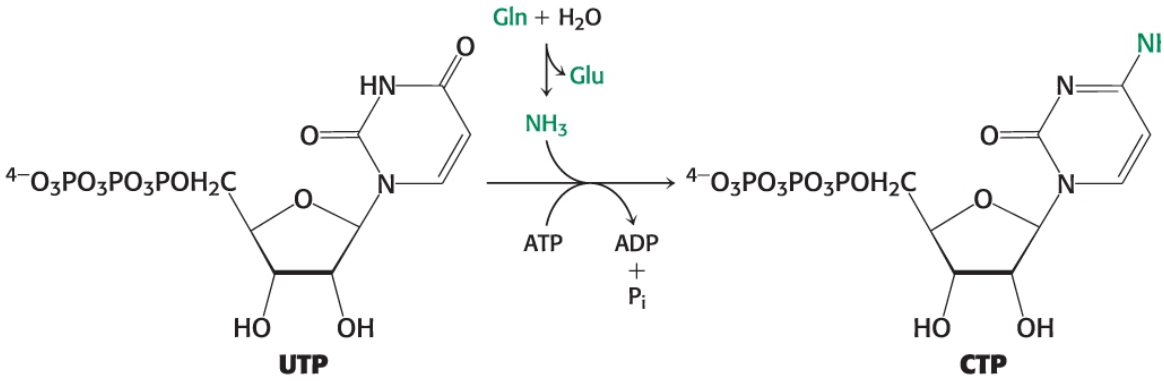
$$UMP + ATP \rightleftharpoons UDP + ADP$$

Nucleoside diphosphates and triphosphates are interconverted by nucleoside diphosphate kinase, an enzyme that has broad specificity, in contrast with the monophosphate kinases. X and Y represent any of several ribonucleosides or even deoxyribonucleosides:

$$XDP + YTP \rightleftharpoons XTP + YDP$$

CTP is formed by amination of UTP

After uridine triphosphate has been formed, it can be transformed into cytidine triphosphate by the replacement of a carbonyl group by an amino group, a reaction catalyzed by cytidine triphosphate synthetase.



Like the synthesis of carbamoyl phosphate, this reaction requires ATP and uses glutamine as the source of the amino group. The reaction proceeds through an analogous mechanism in which the O-4 atom is

phosphorylated to form a reactive intermediate, and then the phosphate is displaced by ammonia, freed from glutamine by hydrolysis. CTP can then be used in many biochemical processes, including lipid and RNA synthesis.

Salvage pathways recycle pyrimidine bases

In adding to production by de novo pathways, pyrimidine bases can also be recovered from the breakdown products of DNA and RNA through salvage pathways, as noted earlier. In these pathways, a preformed base is reincorporated into a nucleotide. We will consider the salvage pathway for the pyrimidine base thymine. Thymine is found in DNA and base-pairs with adenine in the DNA double helix. Thymine released from degraded DNA is salvaged in two steps. First, thymine is converted into the nucleoside thymidine by thymidine phosphorylase.

$$\text{Thymine} + \text{deoxyribose-1-phosphate} \rightleftharpoons \text{thymidine} + \text{I}$$

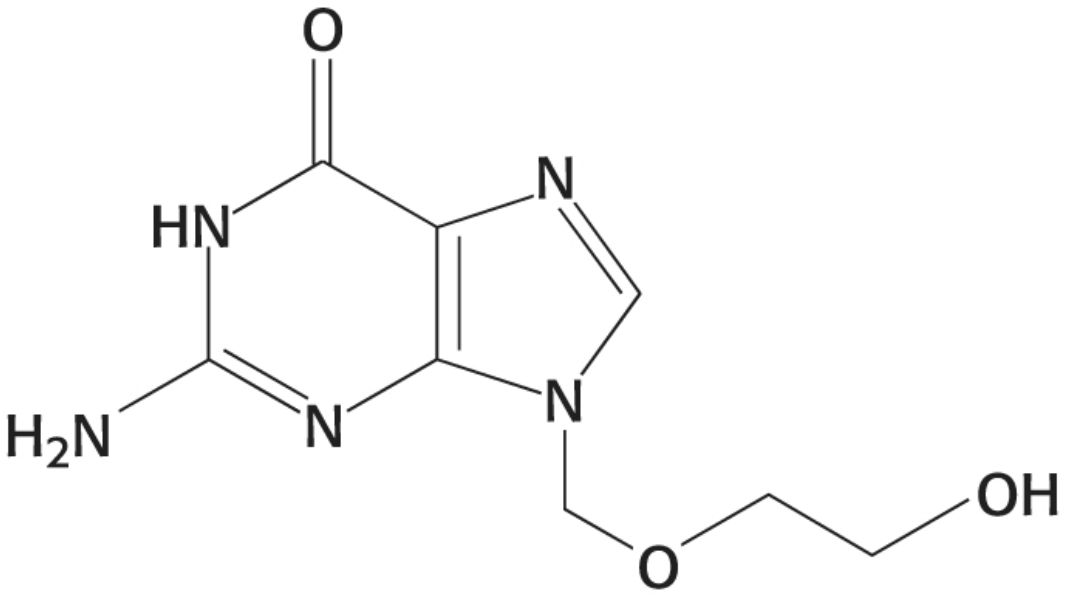
Thymidine is then converted into a nucleotide by thymidine kinase.

$$\text{Thymidine} + \text{ATP} \rightleftharpoons \text{TMP} + \text{ADP}$$



Viral thymidine kinase differs from the mammalian enzyme and thus provides a therapeutic target. For instance, herpes simplex infections are treated with acyclovir (acycloguanosine), which viral thymidine kinase converts into acyclovir monophosphate by adding a phosphate to the hydroxyl group of acyclovir. Viral thymidine kinase binds acyclovir more than 200 times as tightly as cellular thymidine kinase, accounting for its effect on infected cells only. Acyclovir monophosphate is phosphorylated by cellular enzymes to yield acyclovir triphosphate, which competes with dGTP for DNA polymerase.

Once incorporated into viral DNA, acyclovir triphosphate acts as a chain terminator since it lacks a $3'$-hydroxyl required for chain extension. As we will see shortly, thymidine kinase also plays a role in the de novo synthesis of thymidylate.



Acyclovir

26.3 Purine Bases Can Be Synthesized from Glycine, Aspartate, and Other Components

Like pyrimidine nucleotides, purine nucleotides can be synthesized de novo or by salvage pathways. When synthesized de novo, purine synthesis begins with simple starting materials such as amino acids and bicarbonate (**Figure 26.5**). Unlike the bases of pyrimidines, the purine bases are assembled already attached to the ribose ring. Alternatively, purine bases released by the hydrolytic degradation of nucleic acids and nucleotides can be salvaged and recycled. Purine salvage pathways are especially noted for the energy that they save and the remarkable effects of their absence.

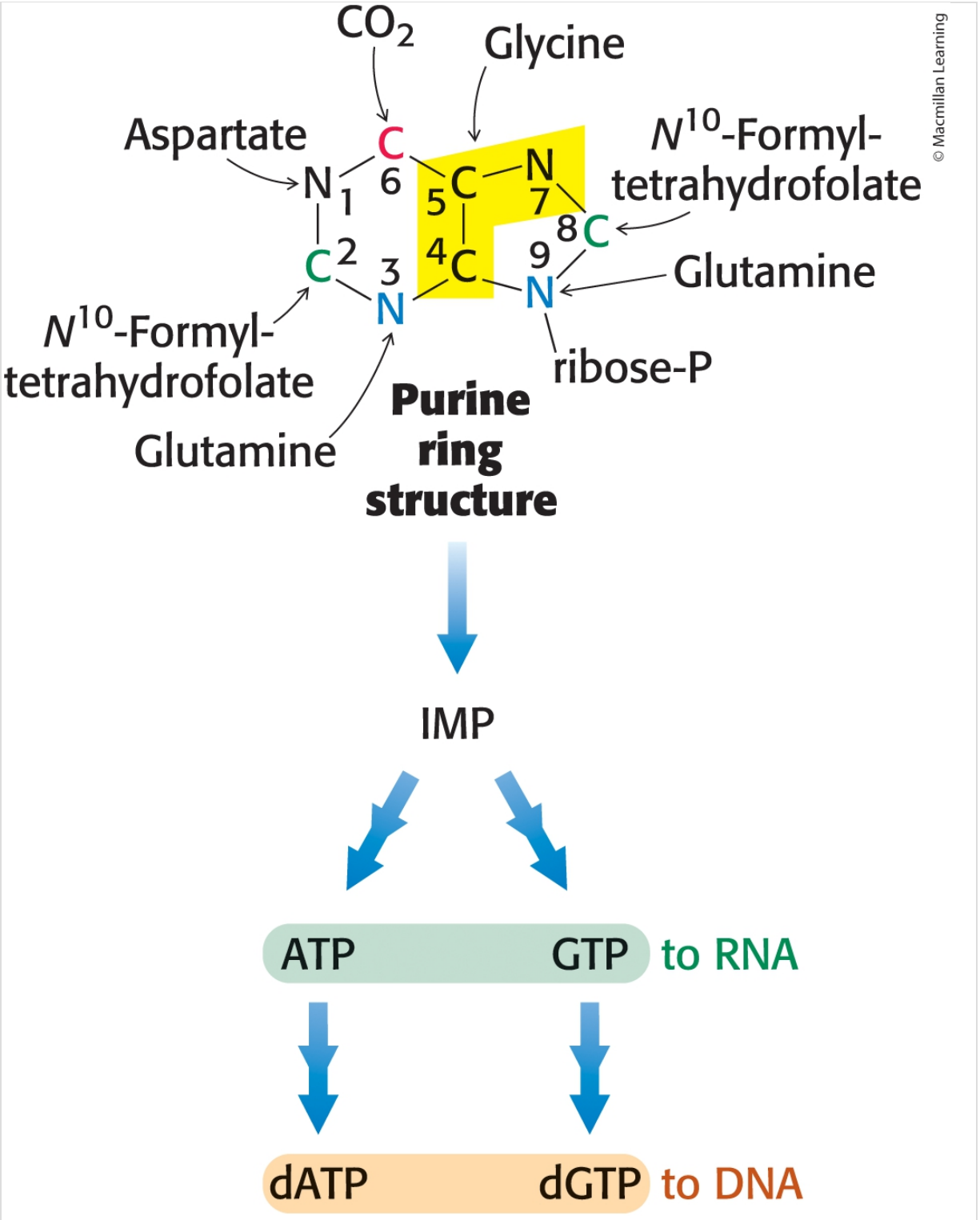
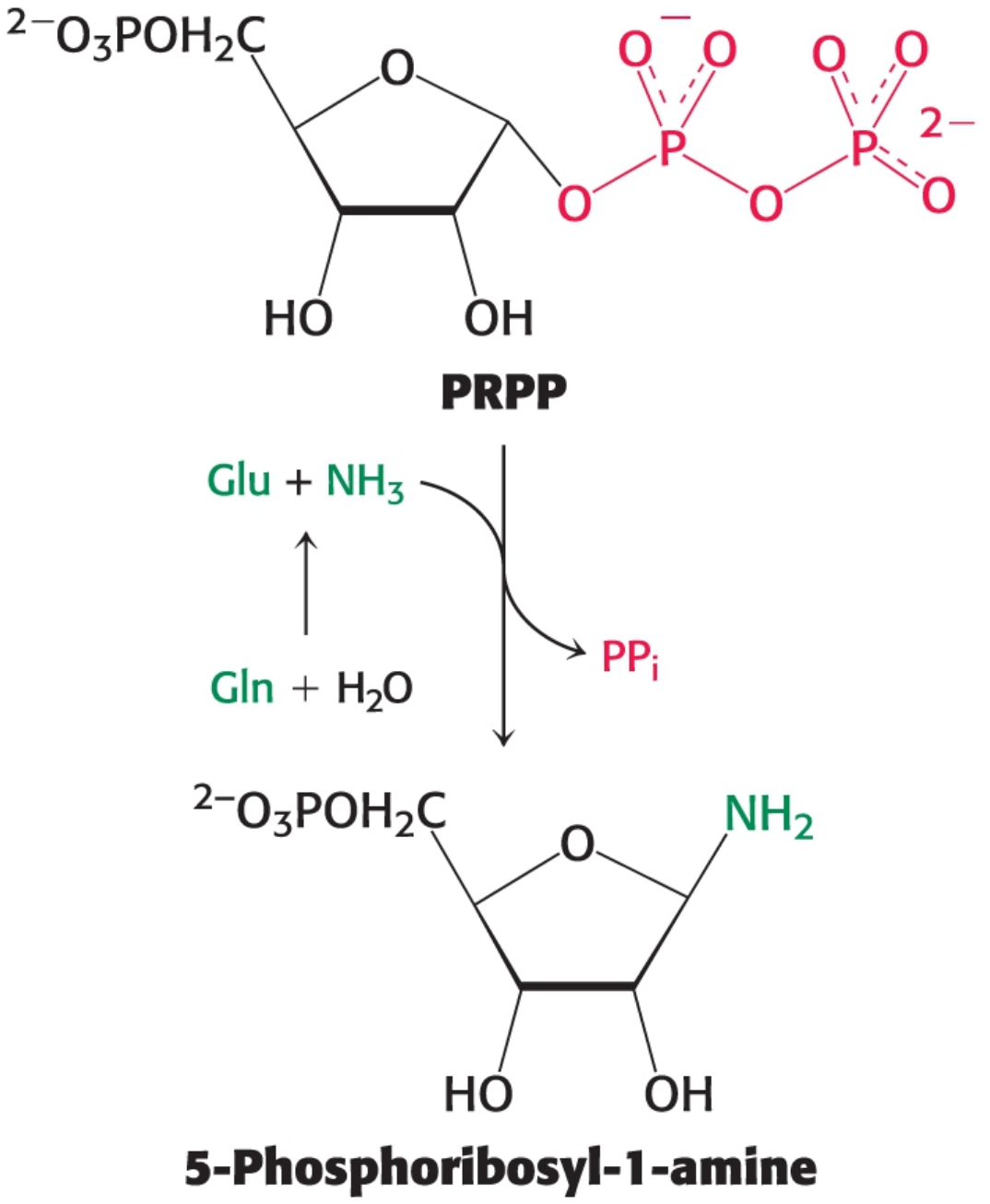


FIGURE 26.5 Purine nucleotides can be synthesized de novo. The origins of the atoms in the purine ring are indicated.

The purine ring system is assembled on ribose phosphate

De novo purine biosynthesis, like pyrimidine biosynthesis, requires PRPP. However, for purines, PRPP provides the foundation on which the bases are constructed. This process is started by the introduction of a nitrogen atom onto the ribose structure. This process, catalyzed by glutamine phosphoribosyl amidotransferase, is the displacement of pyrophosphate by ammonia. This reaction, the committed step in purine biosynthesis, produces 5-phosphoribosyl-1-amine, with the amine in the β configuration.

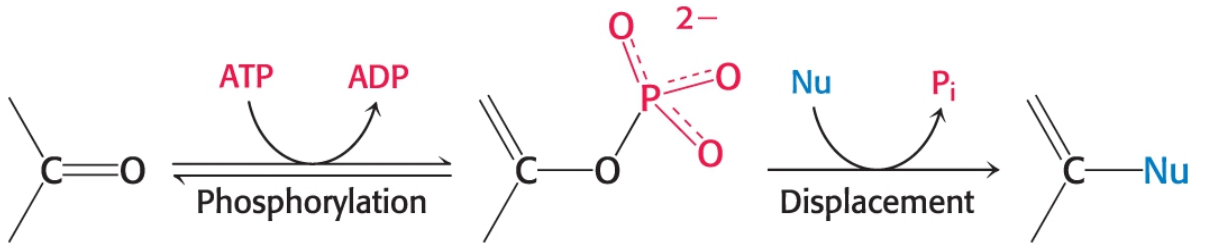


Glutamine phosphoribosyl amidotransferase comprises two domains: the first is homologous to the phosphoribosyltransferases in purine salvage pathways, whereas the second produces ammonia from glutamine by hydrolysis. To prevent wasteful hydrolysis of either

substrate, the amidotransferase assumes the active configuration only on binding of both PRPP and glutamine. As is the case with carbamoyl phosphate synthetase II, the ammonia generated at the glutamine-hydrolysis active site passes through a channel to reach PRPP without being released into solution.

The purine ring is assembled by successive steps of activation by phosphorylation followed by displacement

Nine additional steps are required to assemble the purine ring. Remarkably, the first six steps are analogous reactions. Most of these steps are catalyzed by enzymes with ATP-grasp domains that are homologous to those in carbamoyl phosphate synthetase. Each step consists of the activation of a carbon-bound oxygen atom (typically a carbonyl oxygen atom) by phosphorylation, followed by the displacement of the phosphoryl group by ammonia or an amine group acting as a nucleophile (Nu). The hydrolysis of ATP provides the thermodynamic driving force to favor synthesis over degradation.



De novo purine biosynthesis proceeds as shown in Figure 26.6. Table 26.2 lists the enzymes that catalyze each step of the reaction.

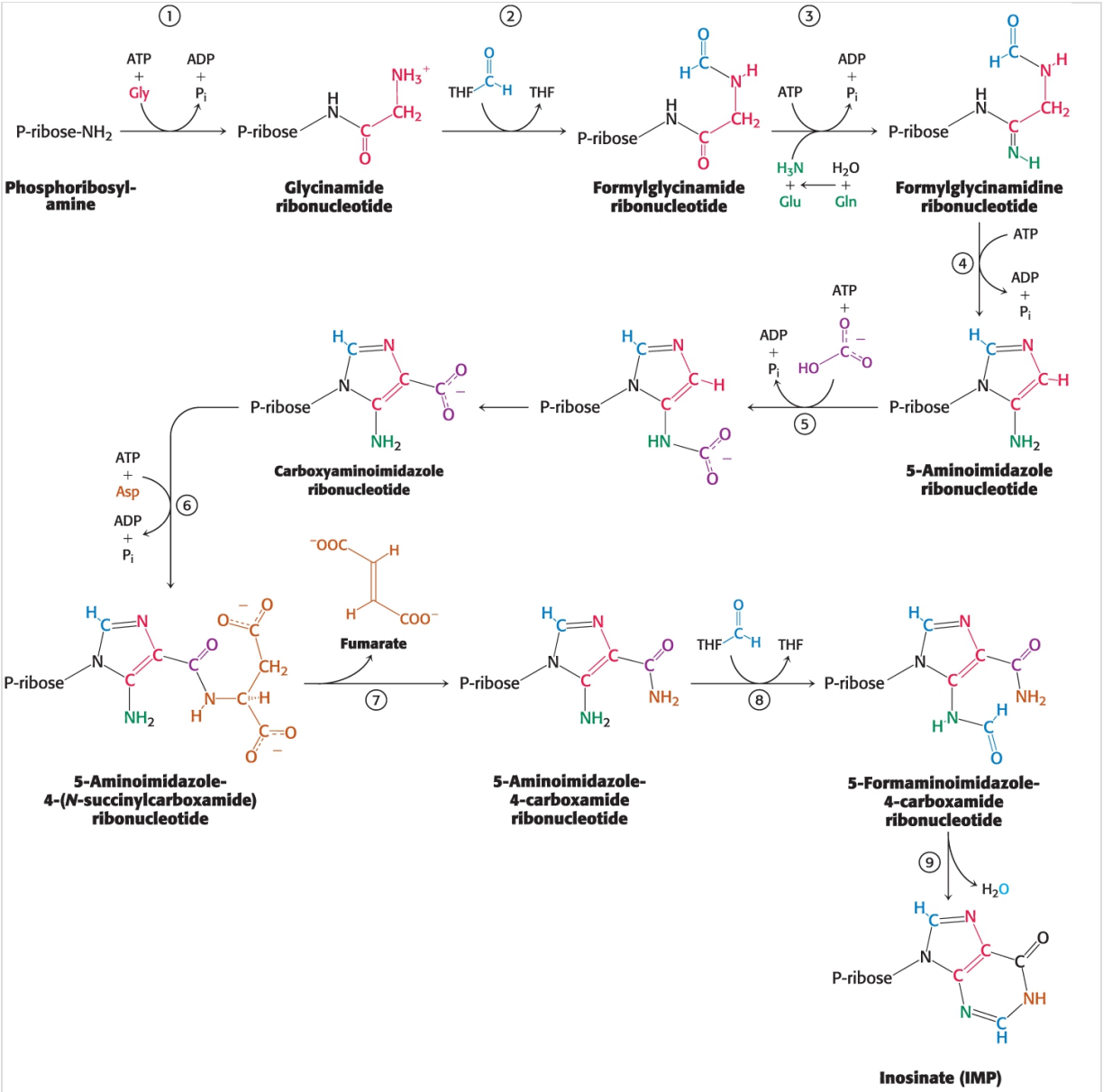


FIGURE 26.6 The de novo purine biosynthesis pathway involves nine steps. (1) Glycine is coupled to the amino group of phosphoribosylamine. (2) N^{10}-Formyltetrahydrofolate (THF) transfers a formyl group to the amino group of the glycine residue. (3) The inner amide group is phosphorylated and converted into an amidine by the addition of ammonia derived from glutamine. (4) An intramolecular coupling reaction forms the five-membered imidazole ring. (5) Bicarbonate adds first to the exocyclic amino group and then to a carbon atom of the imidazole ring. (6) The imidazole carboxylate is phosphorylated, and the phosphate is displaced by the amino group of aspartate. (7) Fumarate is released. (8) A second formyl group is donated from N^{10}-formyltetrahydrofolate (THF). (9) Cyclization completes the synthesis of inosinate, a purine nucleotide.



TABLE 26.2 The enzymes of de novo purine synthesis

Step	Enzyme
1	Glycinamide ribonucleotide (GAR) synthetase
2	GAR transformylase
3	Formylglycinamidine synthase
4	Aminoimidazole ribonucleotide synthetase
5	Carboxyaminoimidazole ribonucleotide synthetase
6	Succinylaminoimidazole carboxamide ribonucleotide synthetase
7	Adenylosuccinate lyase
8	Aminoimidazole carboxamide ribonucleotide transformylase
9	Inosine monophosphate cyclohydrolase

1. The carboxylate group of a glycine residue is activated by phosphorylation and then coupled to the amino group of phosphoribosylamine. A new amide bond is formed, and the amino group of glycine is free to act as a nucleophile in the next step.

2. N^{10}-formyltetrahydrofolate donates a formyl moiety to this amino group to form formylglycinamide ribonucleotide.

3. The inner carbonyl group is activated by phosphorylation and then converted into an amidine by the addition of ammonia derived from glutamine.

4. The product of this reaction, formylglycinamidine ribonucleotide, cyclizes to form the five-membered imidazole ring found in purines. Although this cyclization is likely to be favorable thermodynamically, a molecule of ATP is consumed to ensure irreversibility. The familiar pattern is repeated: a phosphoryl group from the ATP molecule activates the carbonyl group and is displaced by the nitrogen atom attached to the ribose molecule. Cyclization is thus an intramolecular reaction in which the nucleophile and phosphate-activated carbon atom are present within the same molecule. In higher eukaryotes, the enzymes catalyzing steps 1, 2, and 4 (Table 26.2) are components of a single polypeptide chain.

5. Bicarbonate is activated by phosphorylation and then attacked by the exocyclic amino group. The product of the reaction in step 5 rearranges to transfer the carboxylate group to the imidazole ring. Interestingly, mammals do not require ATP for this step; bicarbonate apparently attaches directly to the exocyclic amino group and is then transferred to the imidazole ring.

6. The imidazole carboxylate group is phosphorylated again and the phosphate group is displaced by the amino group of aspartate. Once again, in higher eukaryotes, the enzymes catalyzing steps 5 and 6 (Table 26.2) share a single polypeptide chain.

7. Fumarate, an intermediate in the citric acid cycle, is eliminated, leaving the nitrogen atom from aspartate joined to the imidazole ring. The use of aspartate as an amino-group donor and the concomitant release of fumarate are reminiscent of the conversion

of citrulline into arginine in the urea cycle, and these steps are catalyzed by homologous enzymes in the two pathways (Section 23.4).

8. A formyl group from N^{10}-formyltetrahydrofolate is added to this nitrogen atom to form a final 5-formaminoimidazole-4-carboxamide ribonucleotide.
9. 5-Formaminoimidazole-4-carboxamide ribonucleotide cyclizes with the loss of water to form inosine monophosphate (inosinate).

This pathway completes the formation of the purine ring system.

Self-Check Question



Identify the sources of the atoms that form the purine ring.

AMP and GMP are formed from IMP

A few steps convert inosinate into either AMP or GMP (**Figure 26.7**). Adenylate is synthesized from inosinate by the substitution of an amino group for the carbonyl oxygen atom at C-6. Again, the addition of aspartate followed by the elimination of fumarate contributes the amino group. GTP, rather than ATP, is the phosphoryl-group donor in the synthesis of the adenylosuccinate intermediate from inosinate and aspartate. In accord with the use of GTP, the enzyme that promotes this conversion, adenylosuccinate synthetase, is structurally related to the G-protein family and does not contain an ATP-grasp domain.

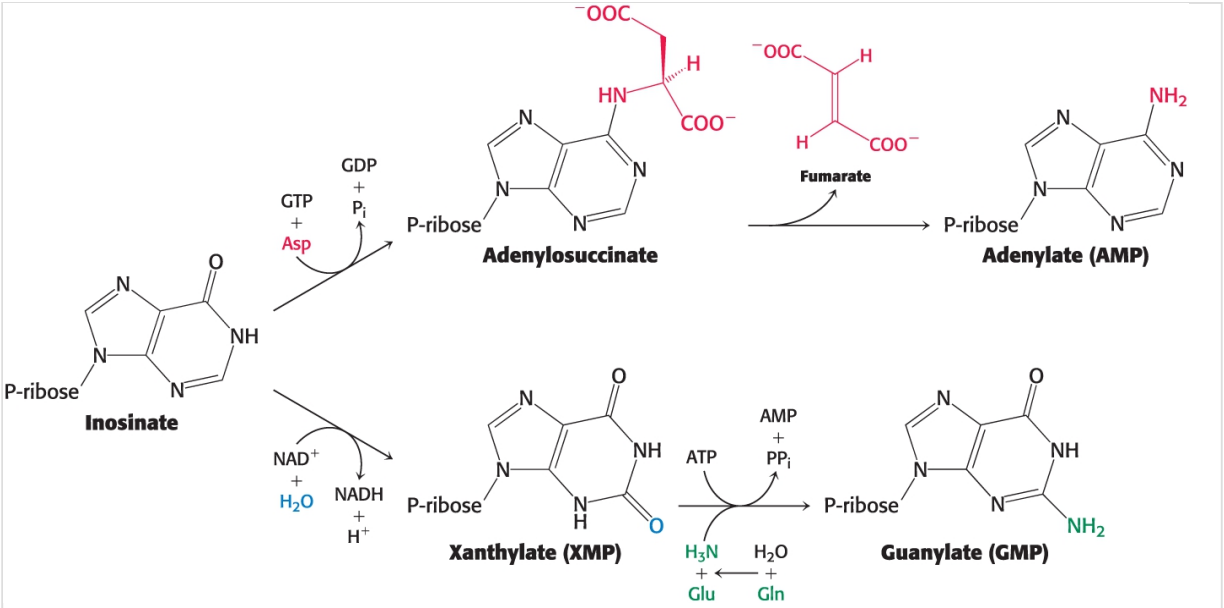


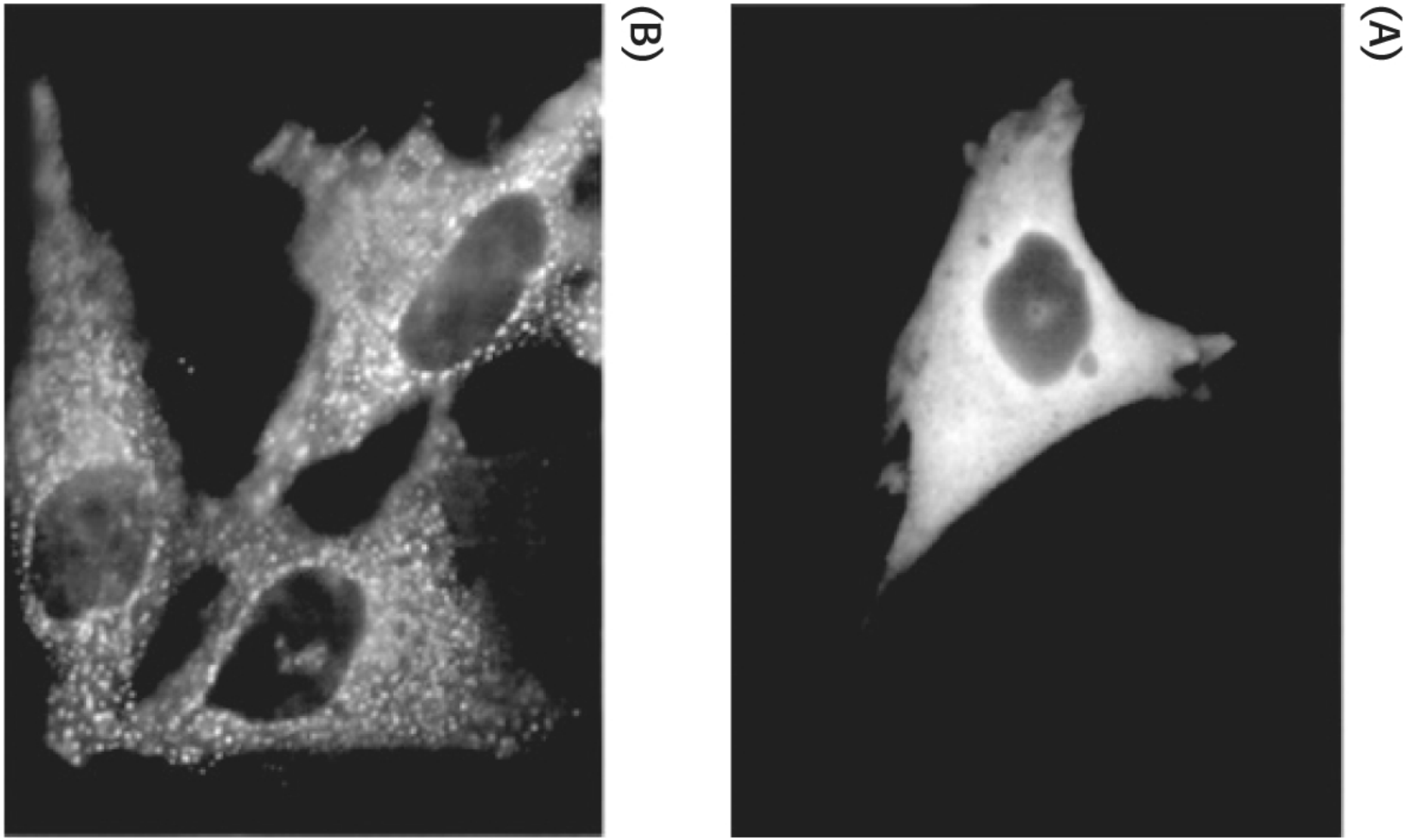
FIGURE 26.7 Inosinate can be converted to AMP and GMP. AMP is formed by the addition of aspartate followed by the release of fumarate. GMP is generated by the addition of water, dehydrogenation by NAD^+, and the replacement of the carbonyl oxygen atom by $-NH_2$ derived by the hydrolysis of glutamine.

Guanylate is synthesized by the oxidation of inosinate to xanthylate (XMP), followed by the incorporation of an amino group at C-2. NAD^+ is the hydrogen acceptor in the oxidation of inosinate, and xanthylate is activated by the transfer of an AMP group (rather than a phosphoryl group) from ATP to the oxygen atom in the newly formed carbonyl group. Ammonia, generated by the hydrolysis of glutamine, then displaces the AMP group to form guanylate, in a reaction catalyzed by GMP synthetase. Note that the synthesis of adenylate requires GTP, whereas the synthesis of guanylate requires ATP. This reciprocal use of nucleotides by the pathways creates an important regulatory opportunity.

Enzymes of the purine biosynthesis pathway associate with one another

Many of the intermediates in the de novo purine biosynthesis pathway degrade rapidly in water, suggesting that the product of one active site might be channeled directly to the next enzyme along the pathway in a manner similar to that described for carbamoyl phosphate synthetase II. In some bacteria, enzymes catalyzing consecutive steps in the purine biosynthetic pathway are fused into single polypeptide chains, likely promoting such channeling.

A more intricate process occurs in human cells. In the presence of sufficient levels of purines, the enzymes of the purine biosynthetic pathway do not appear to be associated with one another. However, when grown under conditions with low concentrations of purines, granules termed **purinosomes** form (**Figure 26.8**). The core of the purinosome comprises the enzymes catalyzing the first six steps of the pathway, with the remaining enzymes more loosely associated. The reversible formation of these large assemblies provides a powerful mode of regulation of purine biosynthesis. The assembly and disassembly of the purinosome is controlled by phosphorylation, enabling the linkage of these processes to the cell cycle and to other events through signal transduction pathways. Thus, the biosynthesis of purines, so central to DNA replication but also to other processes, can be regulated in response to a range of signals other than the concentrations of purines present.



Republished with permission of AAAS, from An, S., Kumar, R., Sheets, E. D., and Benkovic, S. J. 2. Reversible compartmentalization of de novo purine biosynthetic complexes in living cells. *Science* 320: 103–106, 2008; permission conveyed through Copyright Clearance Center, Ltd.

FIGURE 26.8 Purinosomes form when purine synthesis is required. A gene construct encoding a fusion protein consisting of formylglycinamidine synthase and GFP was transfected into and expressed in Hela cells, a human cell line. (A) In the presence of purines (the absence of purine synthesis), the GFP was seen as a diffuse stain throughout the cytoplasm. (B) When the cells were shifted to a purine-free medium, purinosomes formed, seen as cytoplasmic granules, and purine synthesis occurred.



Salvage pathways economize intracellular resource consumption

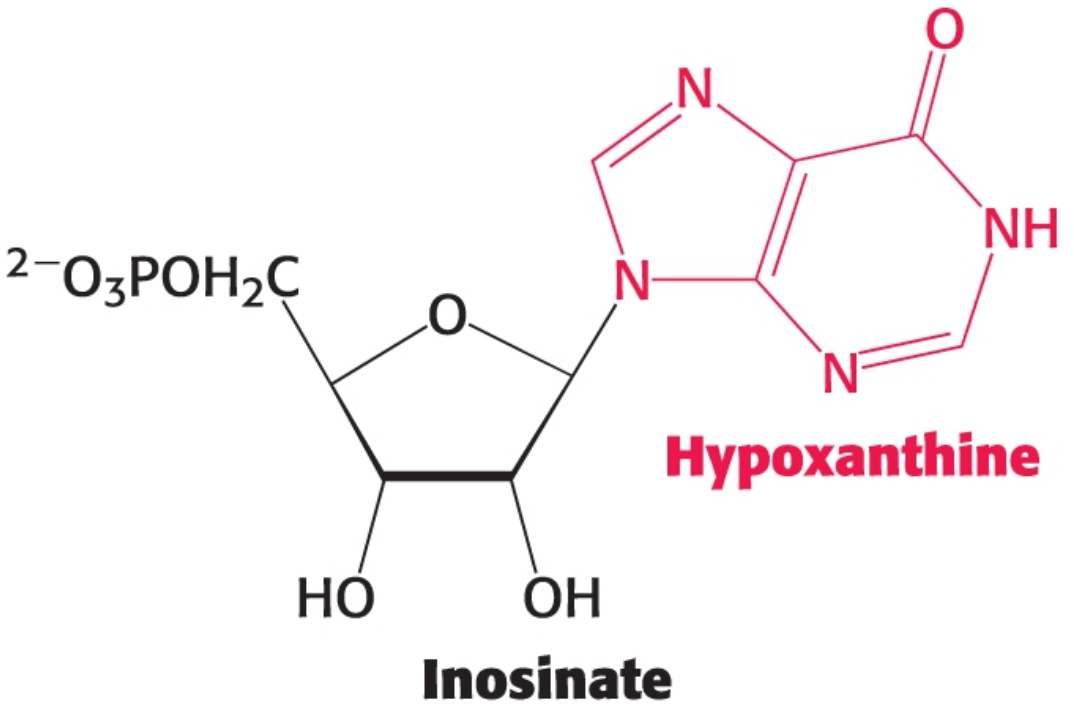
As we have seen, the de novo synthesis of purines requires a substantial investment of ATP as well as starting materials that play roles in many other pathways. Purine salvage pathways provide a more economical means of generating purines. Free purine bases, derived from the turnover of nucleotides or from the diet, can be attached to PRPP to form purine nucleoside monophosphates, in a reaction analogous to the formation of orotidylate. Two salvage enzymes with different specificities recover purine bases. Adenine phosphoribosyltransferase catalyzes the formation of adenylate (AMP):

$$\text{Adenine} + \text{PRPP} \rightarrow \text{adenylate} + PP_i$$

whereas hypoxanthine-guanine phosphoribosyltransferase (HGPRT) catalyzes the formation of guanylate (GMP) as well as inosinate (inosine monophosphate, IMP), a precursor of guanylate and adenylate.

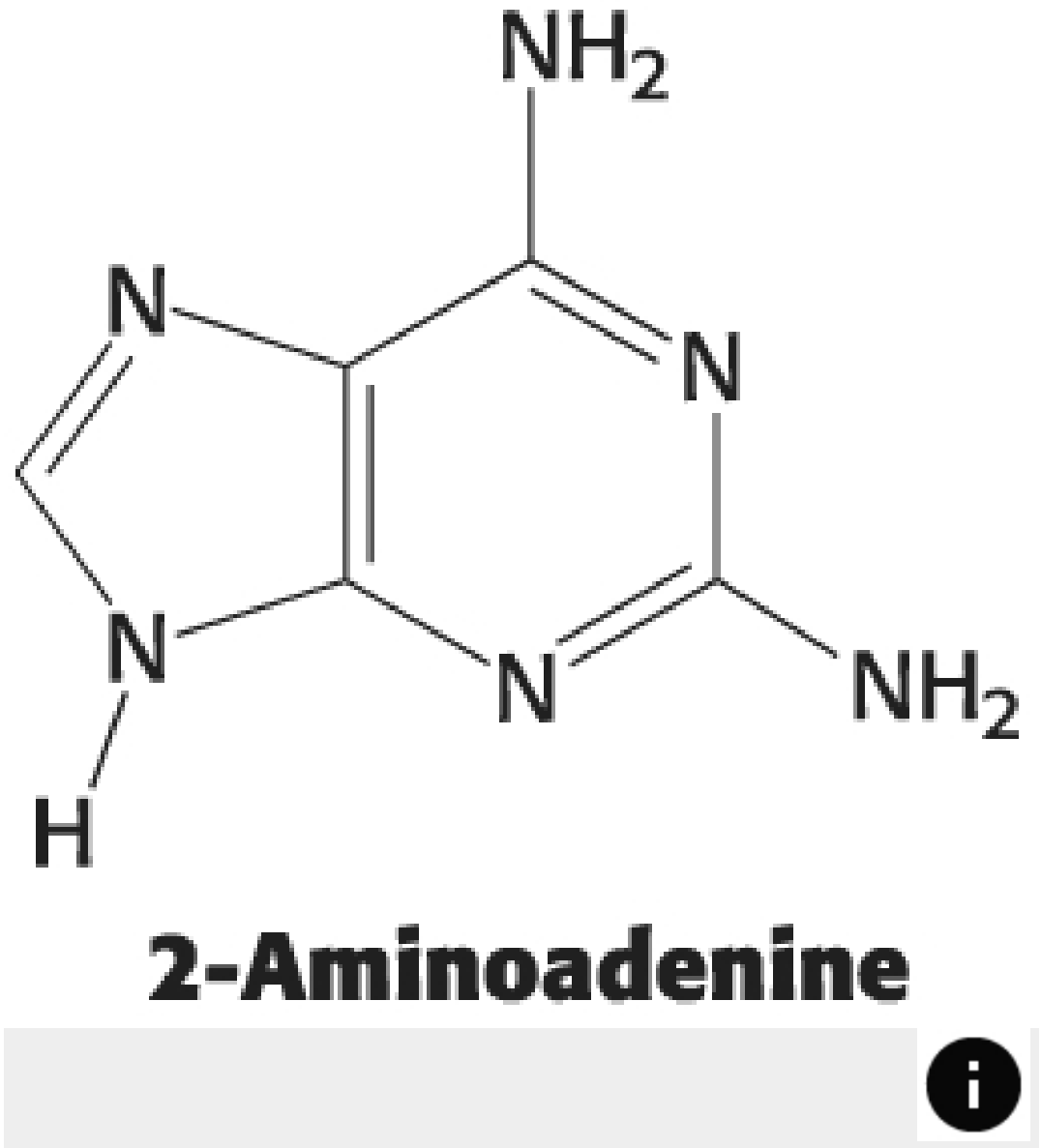
$$\text{Guanine} + \text{PRPP} \rightarrow \text{guanylate} + PP_i$$

$$\text{Hypoxanthine} + \text{PRPP} \rightarrow \text{inosinate} + PP_i$$



An alternative to adenine is used by some viruses

When we first encountered the DNA double helix, you may have noticed that G–C base pairs are held together by three hydrogen bonds, whereas A–T base pairs have only two. However, if one of the hydrogens on adenine were replaced with an amino group, then this alternative could form three hydrogen bonds with T.



2-Aminoadenine

The genomes of certain bacterial viruses contain this nucleobase, termed *2-aminoadenine*, in place of adenine. Nucleotides containing this base are biosynthesized by a pathway that is analogous to that for the conversion of inosinate to adenylate (Figure 26.7) but differs in important details (**Figure 26.9**). The pathway begins with deoxyguanylate. In a first step, aspartate replaces the carbonyl oxygen in a process coupled to the hydrolysis of ATP in reaction catalyzed by the enzyme PurZ. Fumarate is then released to form deoxy 2-aminoadenylate in a subsequent step catalyzed by adenylosuccinate

lyase, the same enzyme that catalyzes the removal to fumarate to form adenylate.

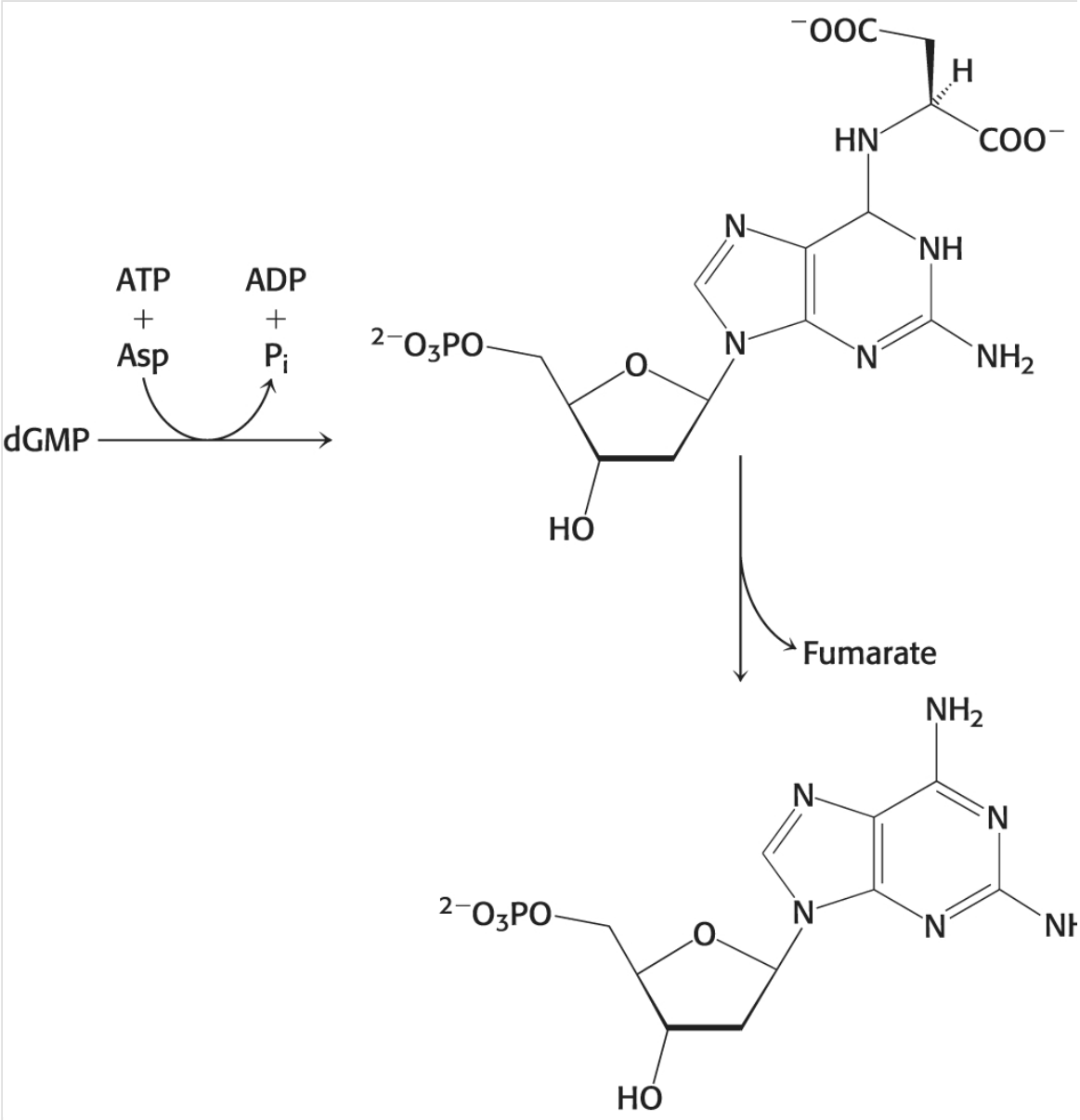


FIGURE 26.9 The nucleotide containing 2-aminoadenine is synthesized from deoxyguanylate
PurZ catalyzes the ATP-coupled replacement of the carbonyl oxygen on dGMP with aspartate. In the second step, catalyzed by adenylosuccinate lyase, fumarate is released, yielding the 2-aminoadenine-containing deoxyribonucleotide.

The identification of the gene encoding PurZ in other viral genomes indicates the likely presence of this pathway, without the need for characterizing the base composition of purified viral DNA. Upon the discovery of this bioinformatic approach, the number of bacterial viruses with evidence of 2-aminoadenine in their genomes increased from less than five to more than 50. As anticipated, DNA containing this base is more thermally stable, consistent with the formation of the additional hydrogen bonds. More important, the unusual base protects the viral genomes from bacterial endonucleases.

26.4 Deoxyribonucleotides Are Synthesized by the Reduction of Ribonucleotides

We turn now to the synthesis of deoxyribonucleotides. These precursors of DNA are formed by the reduction of ribonucleotides; specifically, the $2'$-hydroxyl group on the ribose moiety is replaced by a hydrogen atom. The substrates are ribonucleoside diphosphates, and the ultimate reductant is NADPH. The enzyme **ribonucleotide reductase** is responsible for the reduction reaction for all four ribonucleotides.

The ribonucleotide reductases of different organisms are a remarkably diverse set of enzymes. Yet detailed studies have revealed that they have a common reaction mechanism, and their three-dimensional structural features indicate that these enzymes are homologous.

Ribonucleotide reduction occurs via a radical mechanism

The active sites of ribonucleotide reductases include three conserved cysteine residues and a glutamate residue, all four of which participate in the reduction of ribose to deoxyribose. In the synthesis of a deoxyribonucleotide, the OH bonded to $C-2'$ of the ribose ring is replaced by H, with retention of the configuration at the $C-2'$ carbon atom (**Figure 26.10**).

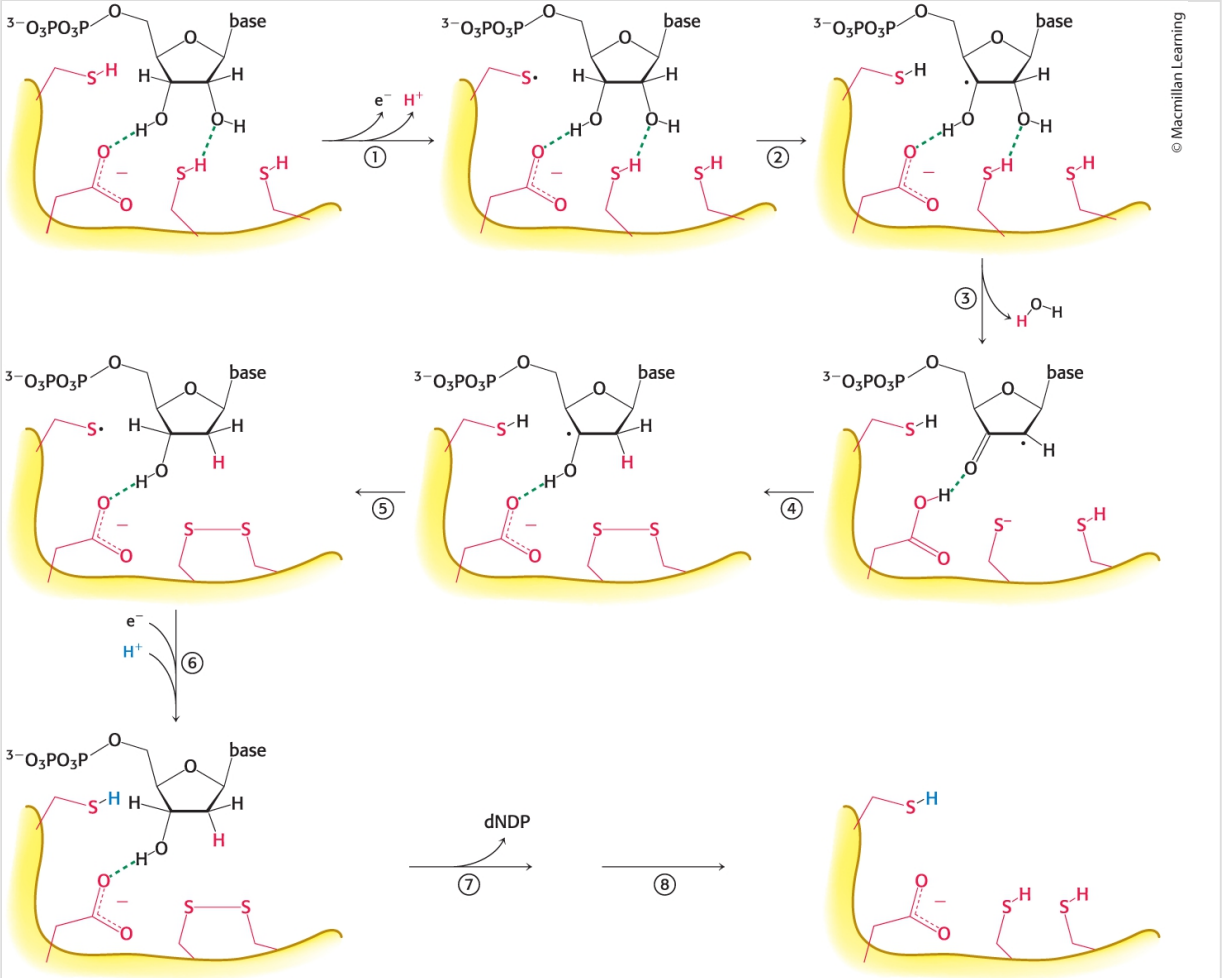


FIGURE 26.10 Ribonucleotide reductase uses a radical mechanism to produce deoxyribonucleotides. (1) An electron is transferred from a cysteine residue on R1 to a tyrosine radical on R2, generating a highly reactive cysteine thiyl radical. (2) This radical abstracts a hydrogen atom from $C-3'$ of the ribose unit. (3) The radical at $C-3'$ releases OH^- from the $C-2'$ carbon atom. Combined with a proton from a second cysteine residue, the OH^- is eliminated as water. (4) A hydride ion is transferred from a third cysteine residue, with the concomitant formation of a disulfide bond. (5) The $C-3'$ radical recaptures the originally abstracted hydrogen atom. (6) An electron is transferred from R2 to reduce the thiyl radical, which also accepts a proton. (7) The deoxyribonucleotide leaves R1. (8) The disulfide formed in the active site is reduced to begin another cycle.

1. The reaction begins with the transfer of an electron from a cysteine residue in the active site of ribonucleotide reductase to an electron acceptor on a second subunit of the enzyme. The loss of an electron generates a highly reactive cysteine thiyl radical.

2. This radical then abstracts a hydrogen atom from $C-3'$ of the ribose unit, generating a radical at that carbon atom.

3. The radical at $C-3'$ promotes the release of the OH^- from the $C-2'$ carbon atom. Protonated by a second cysteine residue, the departing OH^- leaves as a water molecule.

4. A hydride ion (a proton with two electrons) is then transferred from a third cysteine residue to complete the reduction of the position, form a disulfide bond, and regenerate the radical at the $C-3'$ carbon.

5. This $C-3'$ radical recaptures the same hydrogen atom originally abstracted by the first cysteine residue, and the deoxyribonucleotide is free to leave the enzyme.

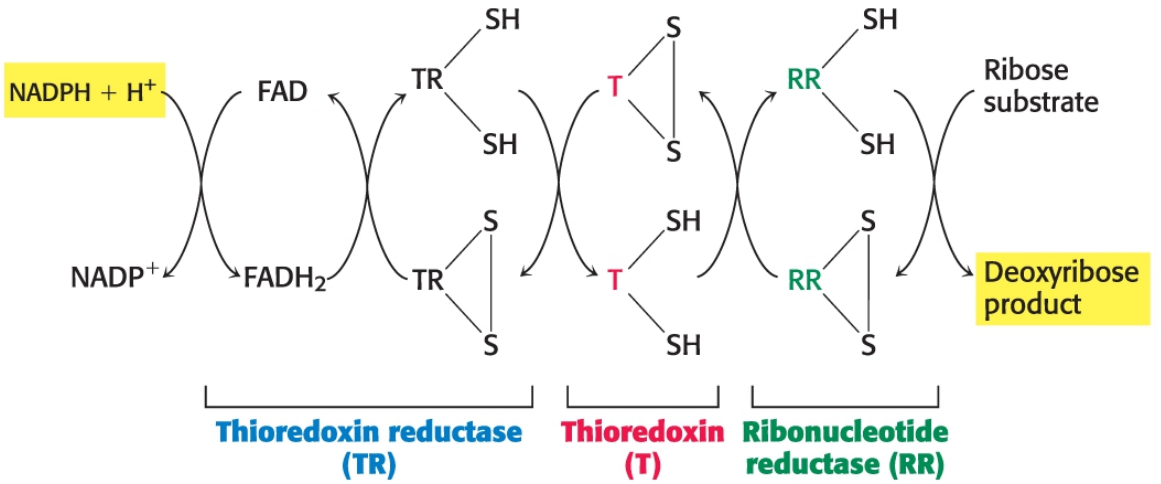
6. An electron from the second subunit of ribonucleotide reductase is transferred to reduce the thiyl radical.

7. The newly synthesized deoxyribonucleotide exits the active site.

8. The disulfide bond generated in the enzyme's active site is reduced to regenerate the active enzyme.

The electrons for this reduction come from NADPH, but not directly. One carrier of reducing power linking NADPH with the reductase is thioredoxin, a 12-kDa protein with two exposed cysteine residues near each other. These sulfhydryls are oxidized to a disulfide in the reaction catalyzed by ribonucleotide reductase itself. In turn, reduced thioredoxin is regenerated by electron flow from NADPH. This reaction is catalyzed by thioredoxin reductase, a flavoprotein. Electrons flow

from NADPH to bound FAD of the reductase, to the disulfide of oxidized thioredoxin, and then to ribonucleotide reductase, and finally to the ribose unit.



Stable radicals are present in ribonucleotide reductases

The most well-studied ribonucleotide reductase is that from *E. coli* grown under aerobic conditions. This enzyme consists of two subunits: R1 (an 87-kDa dimer) and R2 (a 43-kDa dimer). The R1 subunit contains the active site as well as two allosteric control sites (Section 26.5). Each R2 chain contains a tyrosyl radical with an unpaired electron delocalized onto its aromatic ring, generated by a nearby iron center consisting of two ferric (Fe^{3+}) ions bridged by an oxide (O^{2-}) ion (**Figure 26.11**). This very unusual free radical is remarkably stable, with a half-life of 4 days at 4°C. By contrast, free tyrosine radicals in solution have microsecond lifetimes.

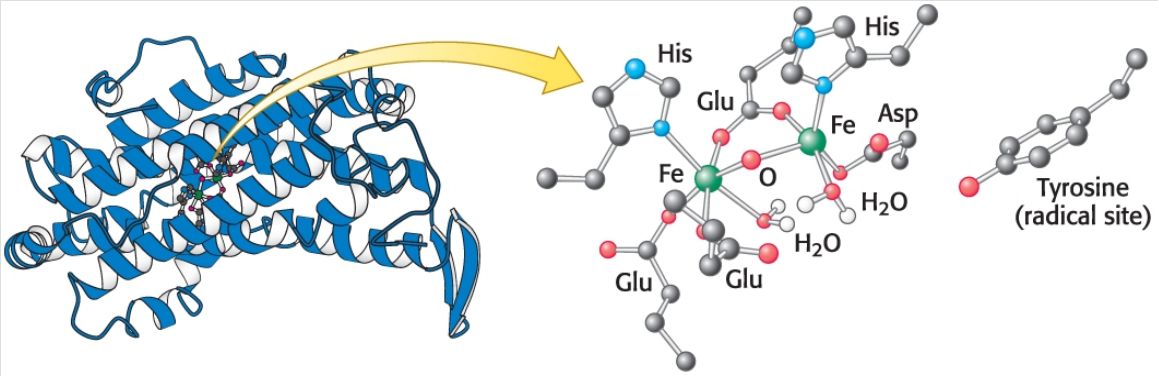


FIGURE 26.11 The ribonucleotide reductase R2 subunit contains a stable free radical on a tyrosine residue. This radical is generated by the reaction of oxygen (not shown) at a nearby sit containing two iron atoms. Two R2 subunits come together to form a dimer.

[Drawn from 1RIB.pdb.]

INTERACT with this model in Achieve

The ribonucleotide reductases from many other organisms, including human beings, are similar to the *E. coli* enzyme, in that they contain the tyrosine radical and the iron center. However, ribonucleotide reductases that do not contain tyrosyl radicals have been characterized in other prokaryotes. Instead, these enzymes contain distinct stable radicals that are generated by other processes. For example, in one class of reductases, the coenzyme adenosylcobalamin (from vitamin B_{12}) is the radical source (Section 22.3). Despite differences in the stable radical employed, the active sites of these enzymes are similar to that of the *E. coli* ribonucleotide reductase, and they appear to act by the same mechanism, based on the exceptional reactivity of cysteine radicals. Thus, these enzymes have a common ancestor but evolved a range of mechanisms for generating stable radical species that function well under different growth conditions. The primordial ribonucleotide reductases appear to have been inactivated by oxygen, whereas the one found in *E. coli* makes use of oxygen to generate the initial tyrosyl radical. Note that the reduction of ribonucleotides to

deoxyribonucleotides is a difficult reaction, likely to require a sophisticated catalyst. The existence of a common protein enzyme framework for this process strongly suggests that proteins joined the RNA world before the evolution of DNA as a stable storage form for genetic information.



Justin Knight

JOANNE STUBBE Trained in chemistry at the University of California, Berkeley, JoAnne Stubbe developed a deep interest in biochemistry and enzyme reaction mechanisms. Dr. Stubbe began her independent career on the faculty of Williams College, teaching and performing research with undergraduate student coworkers. As her interest and accomplishments in research grew, she took a leave of absence to work with a leading enzymologist at Brandeis University. She did not return to Williams but moved to more research-intensive departments, eventually ending up in the Chemistry Department at the Massachusetts Institute of Technology. There, with PhD students and postdoctoral fellows, she elucidated the mechanisms of several important biochemical processes, more notably the radical-based mechanism for ribonucleotide reductases. Her accomplishments have been recognized by important

honors, including the National Medal of Science and the Priestley Medal from the American Chemical Society.

Thymidylate is formed by the methylation of deoxyuridylate

Uracil, produced by the pyrimidine synthesis pathway, is not a component of DNA. Rather, DNA contains *thymine*, a methylated analog of uracil. Another step is required to generate thymidylate from uracil. **Thymidylate synthase** catalyzes this finishing touch: deoxyuridylate (dUMP) is methylated to thymidylate (TMP).

The methyl group becomes attached to the C-5 atom within the aromatic ring of dUMP, but this carbon atom is not a good nucleophile and cannot itself attack the appropriate group on the methyl donor. Thymidylate synthase promotes methylation by adding a thiolate from a cysteine side chain to this ring to generate a nucleophilic species that can attack the methylene group of N^5,N^{10}-methylenetetrahydrofolate (**Figure 26.12**). This methylene group, in turn, is activated by distortions imposed by the enzyme that favor opening the five-membered ring. The attack of the activated dUMP on the methylene group forms the new carbon–carbon bond. The intermediate formed is then converted into product. First a hydride ion is transferred from the tetrahydrofolate ring to transform the methylene group into a methyl group, and then a proton is abstracted from the carbon atom bearing the methyl group to eliminate the cysteine and regenerate the aromatic ring. The tetrahydrofolate derivative loses both its methylene group and a hydride ion and, hence, is oxidized to dihydrofolate.

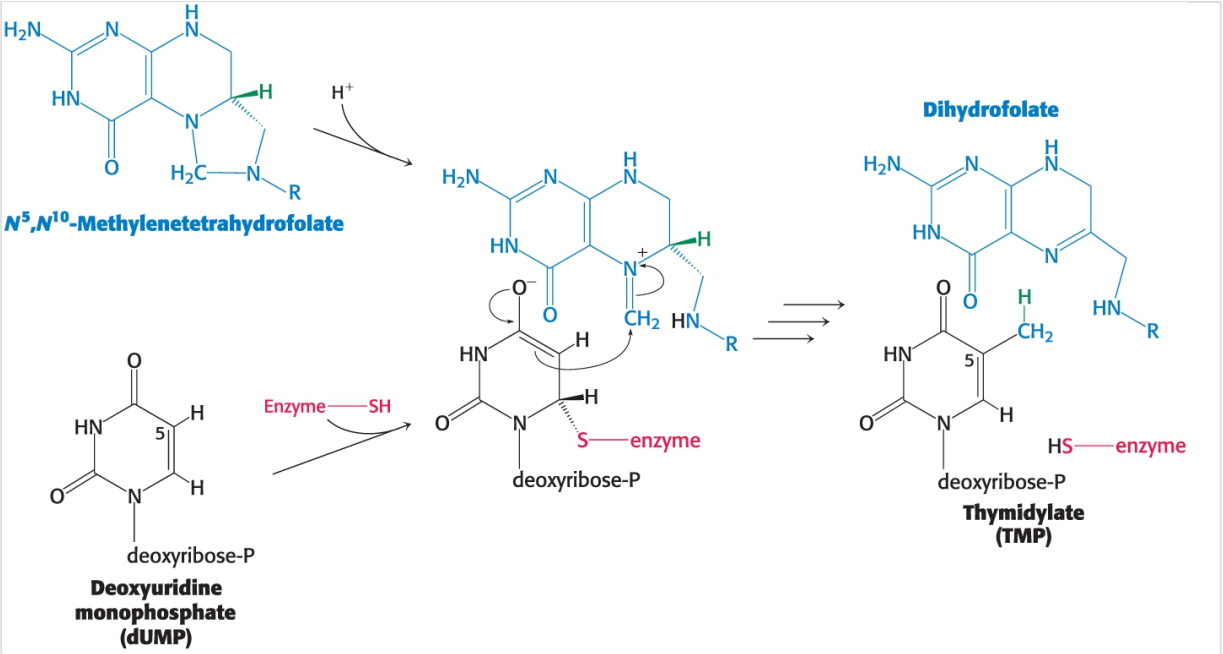
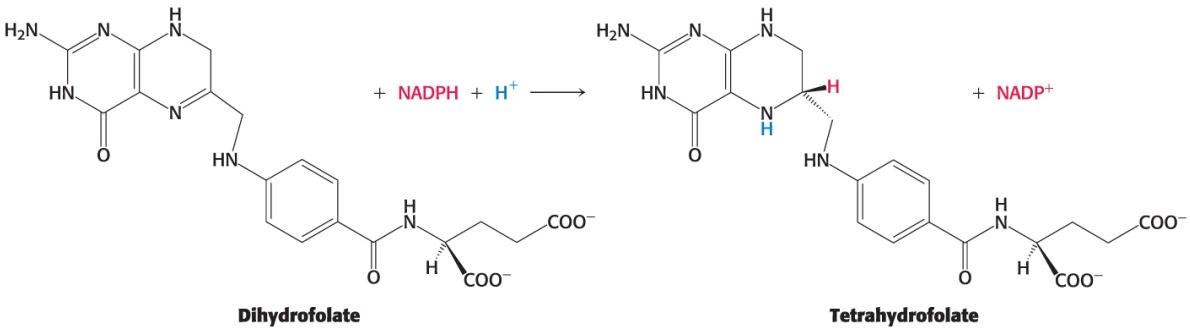


FIGURE 26.12 Thymidylate synthase catalyzes the addition of a methyl group to dUMP to form TMP. The methyl group is derived from N^5,N^{10}-methylenetetrahydrofolate. The addition of a thiolate from the enzyme activates dUMP. Opening the five-membered ring of the THF derivative prepares the methylene group for nucleophilic attack by the activated dUMP. The reaction is completed by the transfer of a hydride ion to form dihydrofolate.

For the synthesis of more thymidylate, tetrahydrofolate must be regenerated. This is achieved by [dihydrofolate reductase] with the use of NADPH as the reductant.



A hydride ion is directly transferred from the nicotinamide ring of NADPH to the pteridine ring of dihydrofolate. The bound dihydrofolate and NADPH are held in close proximity to facilitate the hydride transfer.

Self-Check Question

Describe the path for the synthesis of TTP from UTP.

Several valuable anticancer drugs block the synthesis of thymidylate

Rapidly dividing cells require an abundant supply of thymidylate for the synthesis of DNA. The vulnerability of these cells to the inhibition of TMP synthesis has been exploited in the treatment of cancer. Thymidylate synthase and dihydrofolate reductase are choice targets of chemotherapy (Figure 26.13).

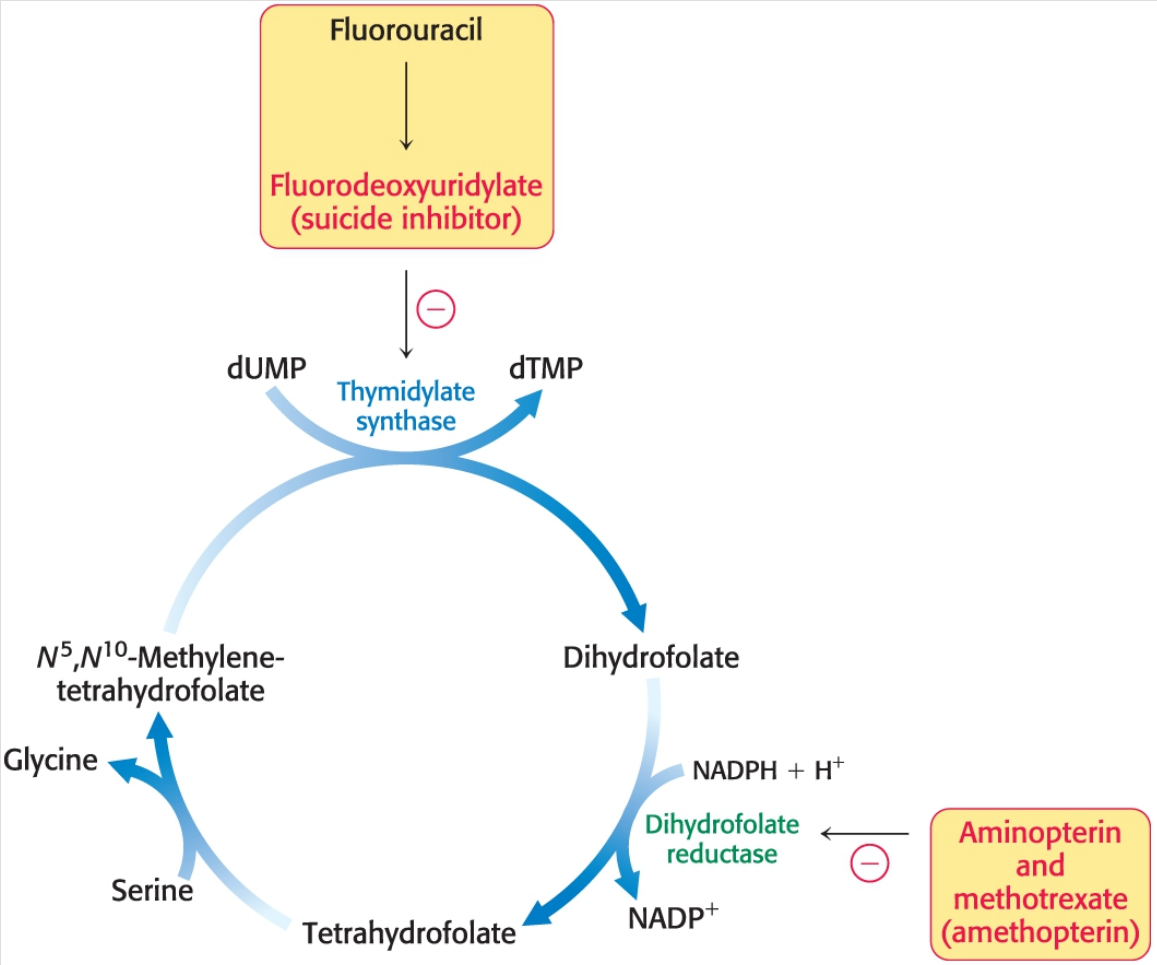


FIGURE 26.13 Enzymes crucial for nucleotide synthesis are anticancer drug targets.
Thymidylate synthase and dihydrofolate reductase are choice targets in cancer chemotherapy because the generation of large quantities of precursors for DNA synthesis is required for rapidly dividing cancer cells.

Fluorouracil, an anticancer drug, is converted in vivo into fluorodeoxyuridylate (F-dUMP). This analog of dUMP irreversibly inhibits thymidylate synthase after acting as a normal substrate through part of the catalytic cycle. Recall that the formation of TMP requires the removal of a proton (H^+) from C-5 of the bound nucleotide (Figure 26.12). However, the enzyme cannot abstract F^+ from F-dUMP, and so

catalysis is blocked at the stage of the covalent complex formed by F-dUMP, methylenetetrahydrofolate, and the sulfhydryl group of the enzyme (Figure 26.14). We see here an example of suicide inhibition, in which an enzyme converts a substrate into a reactive inhibitor that halts the enzyme's catalytic activity.

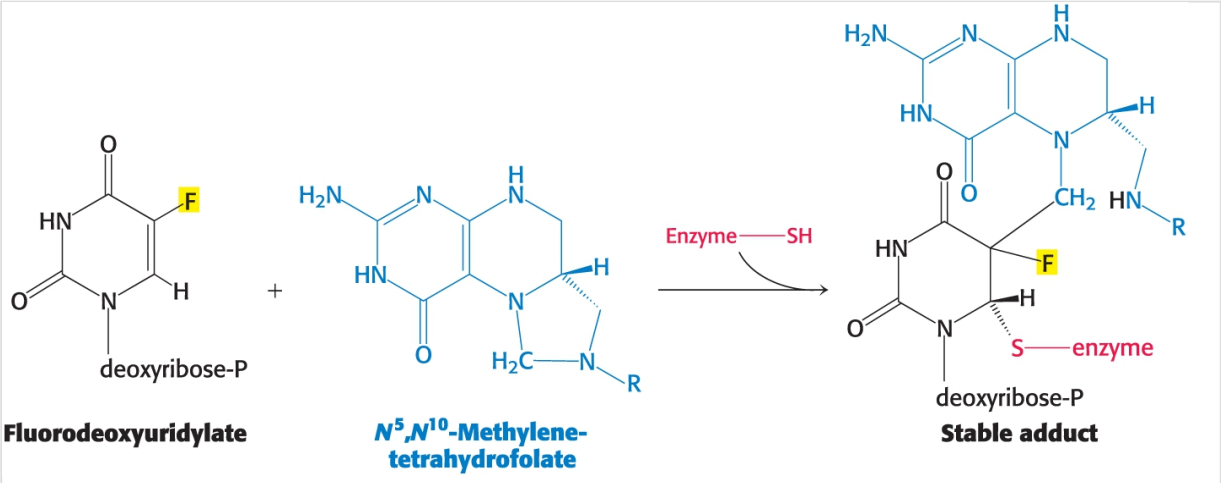
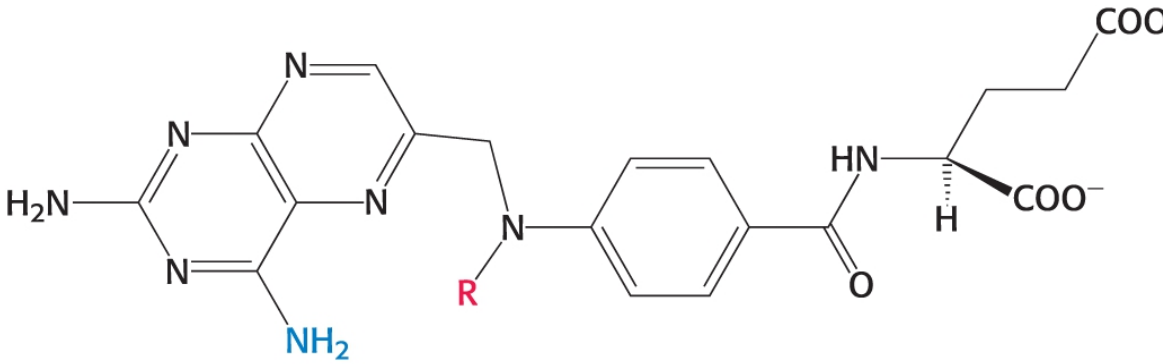


FIGURE 26.14 Fluoruracil acts by suicide inhibition. Fluorodeoxyuridylate (generated from fluorouracil) forms an adduct with tetrahydrofolate that traps thymidylate synthase in a form that cannot proceed down the reaction pathway.

The synthesis of TMP can also be blocked by inhibiting the regeneration of tetrahydrofolate. Analogs of dihydrofolate, such as aminopterin and methotrexate (amethopterin), are potent competitive inhibitors ($K_i < 1$ nM) of dihydrofolate reductase.

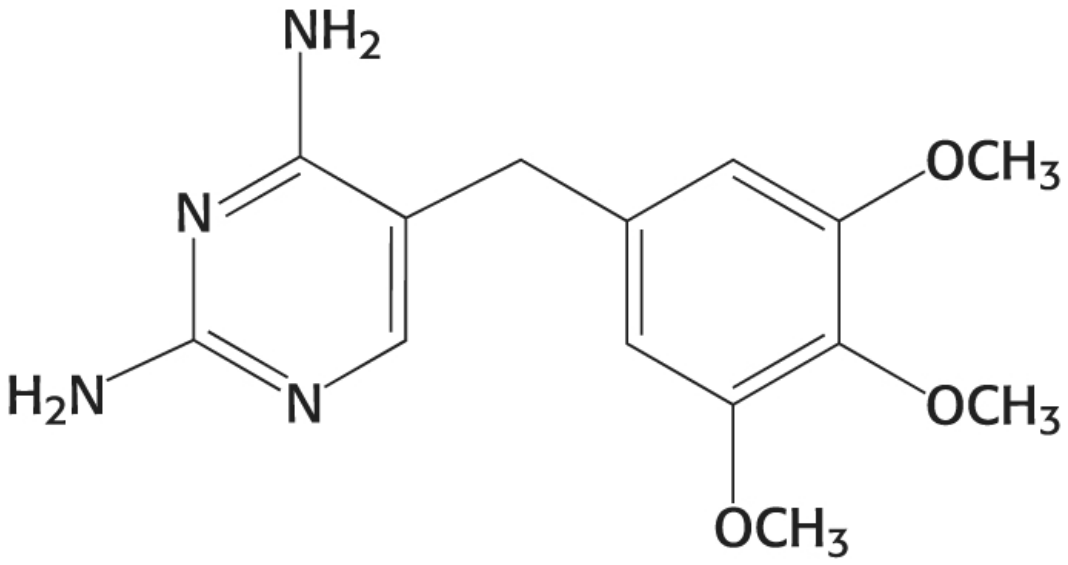


Aminopterin (R = H) or methotrexate (R = CH_3)

Methotrexate is a valuable drug in the treatment of many rapidly growing tumors, such as those in acute leukemia and choriocarcinoma, a cancer derived from placental cells. However, methotrexate kills rapidly replicating cells whether they are malignant or not. Stem cells in bone marrow, epithelial cells of the intestinal tract, and hair follicles are vulnerable to the action of this folate antagonist, accounting for its toxic side effects, which include weakening of the immune system, nausea, and hair loss.

Folate analogs such as trimethoprim have potent antibacterial and antiprotozoal activity. Trimethoprim binds 10^5-fold less tightly to

mammalian dihydrofolate reductase than it does to reductases of susceptible microorganisms. Small differences in the active-site clefts of these enzymes account for the highly selective antimicrobial action. The combination of trimethoprim and sulfamethoxazole (an inhibitor of folate synthesis) is widely used to treat infections such as bronchitis, traveler's diarrhea, and urinary tract infections.



Trimethoprim

26.5 Key Steps in Nucleotide Biosynthesis Are Regulated by Feedback Inhibition

Nucleotide biosynthesis is regulated by feedback inhibition in a manner similar to the regulation of amino acid biosynthesis. These regulatory pathways ensure that the various nucleotides are produced in the required quantities.

Pyrimidine biosynthesis is regulated by aspartate transcarbamoylase

Aspartate transcarbamoylase (ATCase), one of the key enzymes for the regulation of pyrimidine biosynthesis in bacteria, was described in detail in Chapter 7. Recall that ATCase is inhibited by CTP, the final product of pyrimidine biosynthesis, and stimulated by ATP.



The synthesis of purine nucleotides is controlled by feedback inhibition at several

sites

The regulatory scheme for purine nucleotides is more complex than that for pyrimidine nucleotides (Figure 26.15).

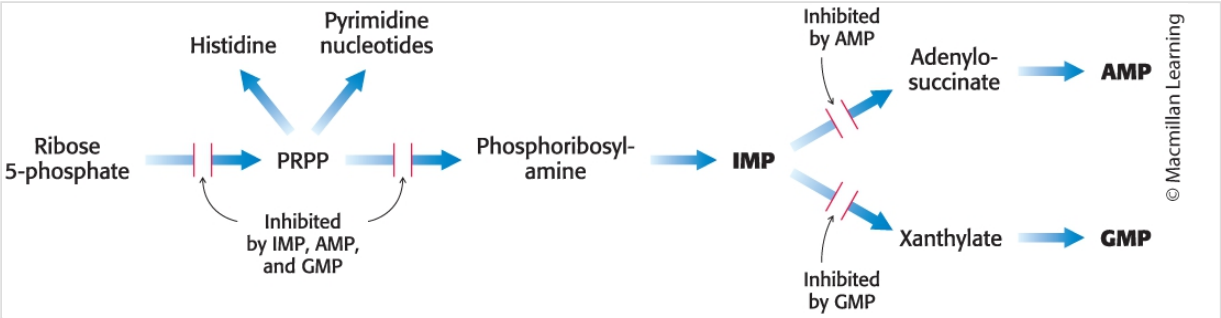


FIGURE 26.15 Purine biosynthesis is regulated at many steps. Feedback inhibition controls both the overall rate of purine biosynthesis and the balance between AMP and GMP production.

1. The committed step in purine nucleotide biosynthesis is the conversion of PRPP into phosphoribosylamine by glutamine phosphoribosyl amidotransferase. This important enzyme is feedback-inhibited by many purine ribonucleotides. It is noteworthy that AMP and GMP, the final products of the pathway, synergistically inhibit the amidotransferase.

2. Inosinate is the branch point in the synthesis of AMP and GMP. The reactions leading away from inosinate are sites of feedback inhibition. AMP inhibits the conversion of inosinate into adenylosuccinate, its immediate precursor. Similarly, GMP inhibits the conversion of inosinate into xanthylate, its immediate precursor.

3. As already noted, GTP is a substrate in the synthesis of AMP, whereas ATP is a substrate in the synthesis of GMP (Figure 26.7). This reciprocal substrate relation tends to balance the synthesis of adenine and guanine ribonucleotides.

Note that the synthesis of PRPP by PRPP synthetase is highly regulated even though it is not the committed step in purine synthesis. Mutations have been identified in PRPP synthetase that result in a loss of allosteric response to nucleotides without any effect on catalytic activity of the enzyme. A consequence of this mutation is an overabundance of purine nucleotides that can result in gout, a pathological condition discussed in Section 26.5.

Self-Check Question



Which enzyme catalyzes the committed step in the synthesis of pyrimidines? Which enzyme catalyzes the committed step in the synthesis of purines?

The synthesis of deoxyribonucleotides is controlled by the regulation of ribonucleotide reductase

The reduction of ribonucleotides to deoxyribonucleotides is precisely controlled by allosteric interactions. Each polypeptide of the R1 subunit of the aerobic *E. coli* ribonucleotide reductase contains two allosteric sites (**Figure 26.16**). One of them controls the overall activity of the enzyme, and the other regulates substrate specificity. The overall catalytic activity of ribonucleotide reductase is diminished by the binding of dATP, which signals an abundance of deoxyribonucleotides. The binding of ATP reverses this feedback inhibition.

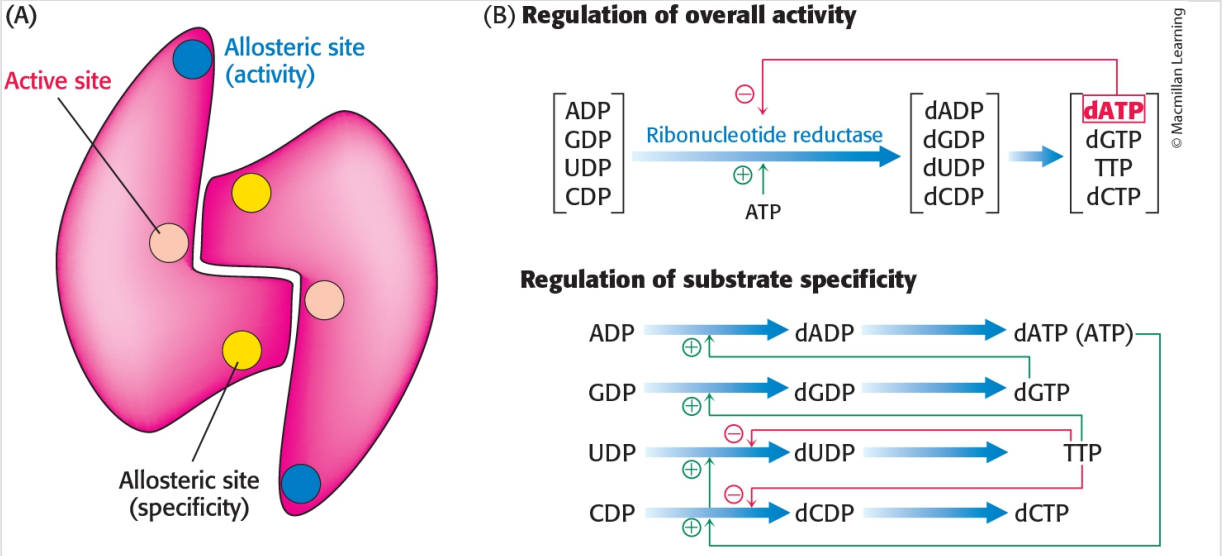


FIGURE 26.16 Ribonucleotide reductase is highly regulated to balance the pool of deoxyribonucleotides. (A) Each subunit in the R1 dimer contains two allosteric sites in addition to the active site. One site regulates the overall activity, and the other site regulates substrate specificity. (B) The patterns of regulation with regard to different nucleoside diphosphates are demonstrated by ribonucleotide reductase.

The binding of dATP or ATP to the substrate-specificity control site enhances the reduction of UDP and CDP, the pyrimidine nucleotides. The binding of thymidine triphosphate (TTP) promotes the reduction of GDP and inhibits the further reduction of pyrimidine ribonucleotides. The subsequent increase in the level of dGTP stimulates the reduction of ATP to dATP. This complex pattern of regulation supplies the appropriate balance of the four deoxyribonucleotides needed for the synthesis of DNA.

26.6 Disruptions in Nucleotide Metabolism Can Cause Pathological Conditions

The nucleotides of a cell undergo continual turnover. This turnover facilitates the proper balance between ribo- and deoxyribonucleotides as well as the removal of damaged bases (Figure 26.17). This turnover begins with the hydrolytic conversion of nucleotides to nucleosides by nucleotidases. The sugars and bases are separated from one another by nucleoside phosphorylases in a reversible process. The free bases are then either reused to form nucleotides by salvage pathways or degraded to products that are excreted.

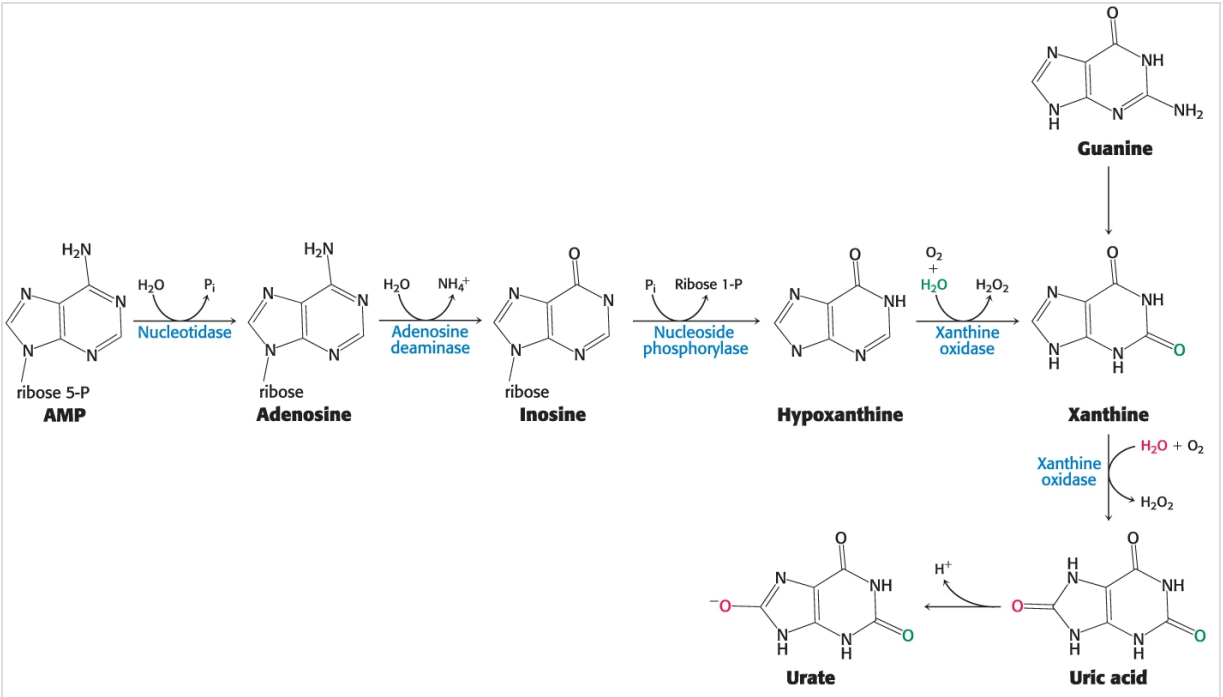


FIGURE 26.17 Purines are catabolized for excretion. Purine bases are converted first into xanthine and then into urate. Xanthine oxidase catalyzes two steps in this process.

The loss of adenosine deaminase activity results in severe combined immunodeficiency



Adenosine is not a substrate for nucleoside phosphorylases in eukaryotes, so that adenosine turnover requires an additional step compared to the turnover of guanosine. In the extra step, adenosine is deaminated by adenosine deaminase to form inosine (Figure 26.17).

A deficiency in adenosine deaminase activity is associated with some forms of **severe combined immunodeficiency (SCID)**, an immunological disorder. Persons with the disorder have acute recurring infections, often leading to death at an early age. SCID is characterized by a loss of T cells, which are crucial to the immune response. A lack of adenosine deaminase results in an accumulation of 50 to 100 times the normal level of dATP, which is toxic to many cells through a variety of mechanisms. Adenosine deaminase deficiency is one of the first conditions to be treated by gene therapy, and recent progress is encouraging.

Gout is induced by high serum levels of urate



Inosine generated by adenosine deaminase is subsequently metabolized by nucleoside phosphorylase to hypoxanthine, which is oxidized by xanthine oxidase — a molybdenum- and iron-containing flavoprotein — to xanthine, and then to uric acid. Uric acid loses a proton at physiological pH to form urate which, in human beings, is the final product of purine degradation and is excreted in the urine.

High serum levels of urate induce the painful joint disease **gout** as the sodium salt of urate crystallizes in the fluid and lining of the joints. The small joint at the base of the big toe is a common site for sodium urate buildup, although the salt also accumulates at other joints. Painful inflammation results when cells of the immune system engulf the sodium urate crystals. The kidneys, too, may be damaged by the deposition of urate crystals. Gout is a common medical problem, affecting 1% of the population of Western countries.

Administration of allopurinol, an analog of hypoxanthine, is one treatment for gout. The mechanism of action of allopurinol is interesting: it acts first as a substrate and then as an inhibitor of xanthine oxidase. The oxidase hydroxylates allopurinol to alloxanthine (oxipurinol), which then remains tightly bound to the active site. The binding of alloxanthine keeps the molybdenum atom of xanthine oxidase in the $^{+4}$ oxidation state instead of it returning to the $^{+6}$ oxidation state as in a normal catalytic cycle, another example of suicide inhibition. The synthesis of urate from hypoxanthine and xanthine decreases soon after the administration

of allopurinol. The serum concentrations of hypoxanthine and xanthine rise, and that of urate drops.



Allopurinol

The average serum level of urate in human beings is close to the solubility limit and is higher than levels found in other primates.

What is the selective advantage of a urate level so high that it teeters on the brink of gout in many people? It turns out that urate has a markedly beneficial action. Urate is a highly effective scavenger of reactive oxygen species. Indeed, urate is about as effective as ascorbate (vitamin C) as an antioxidant. The increased level of urate in human beings may protect against reactive oxygen species that are implicated in a host of pathological conditions.

Lesch–Nyhan syndrome is a dramatic consequence of mutations in a salvage-pathway enzyme



Mutations in genes that encode nucleotide biosynthetic enzymes can reduce levels of needed nucleotides and can lead to an accumulation of intermediates. A nearly total absence of hypoxanthine-guanine phosphoribosyltransferase (HGPRT) has unexpected and devastating consequences. The most striking expression of this inborn error of metabolism, called **Lesch–Nyhan syndrome**, is compulsive, self-destructive behavior. At age 2 or 3, children with this disease begin to bite their fingers and lips and will chew them off if unrestrained. These children also behave aggressively toward others and often show cognitive disabilities and spasticity. Elevated levels of urate in the serum lead to the formation of kidney stones early in life, followed by the symptoms of gout years later. The disease is inherited as a sex-linked recessive disorder.

What is the connection between the absence of HGPRT activity and the behavioral characteristics of Lesch–Nyhan syndrome? The

answer has not been established, but several explanations may contribute. The brain has limited capacity for de novo purine synthesis. Consequently, lack of HGPRT results in a deficiency of purine nucleotides. ATP and ADP, formed from inosinate, are important in the brain as signal molecules. These nucleotides bind to and activate G-protein coupled receptors, which require guanine nucleotides to function. Finally, a cofactor required for dopamine biosynthesis is biosynthesized from GTP. Thus, the lack of HGPRT may result in an imbalance of key neurotransmitters and the pathways they stimulate. Lesch–Nyhan syndrome demonstrates that the salvage pathway for the synthesis of IMP and GMP is not of minor importance. Moreover, Lesch–Nyhan syndrome reveals that abnormal behavior such as self-mutilation and extreme hostility can be caused by the absence of a single enzyme. Psychiatry will no doubt benefit from the unraveling of the molecular basis of such disorders.

Chapter 26 Summary

26.1 Nucleotides Can Be Synthesized by de Novo or Salvage Pathways

- Nucleotide biosynthesis can be divided into either de novo pathways or salvage pathways.
- In de novo pathways, the nucleobases are synthesized from simpler compounds.
- In salvage pathways, pre-formed bases are recovered and reconnected to a ribose unit.

26.2 The Pyrimidine Ring Is Assembled from CO_2, Ammonia, and Aspartate

- In de novo synthesis, pyrimidine rings are first assembled, then attached to a ribose phosphate.
- 5-Phosphoribosyl-1-pyrophosphate is the donor of the ribose phosphate moiety.
- The synthesis of the pyrimidine ring starts with the formation of carbamoylaspartate from carbamoyl phosphate and aspartate, catalyzed by aspartate transcarbamoylase.
- Dehydration, cyclization, and oxidation yield orotate, which reacts with PRPP to give orotidylate, which serves as the precursor to the pyrimidine nucleotides.
- Nucleotide mono-, di-, and triphosphates are interconvertible by the action of nucleoside monophosphate kinases and nucleoside diphosphate kinase.

26.3 Purine Bases Can Be Synthesized from Glycine, Aspartate, and Other Components

- In the de novo pathway, the purine ring is assembled on ribose phosphate from glutamine, glycine, aspartate, N^{10}-formyltetrahydrofolate, and CO_2.
- The committed step in the de novo synthesis of purine nucleotides is the formation of 5-phosphoribosylamine from PRPP and glutamine.
- The purine ring is assembled over nine synthetic steps, predominantly using the activation of a carbon-bound oxygen atom by phosphorylation and subsequent displacement of an amino group.
- AMP and GMP are formed from IMP.

26.4 Deoxyribonucleotides Are Synthesized by the Reduction of Ribonucleotides

- Deoxyribonucleotides, the precursors of DNA, are formed by the reduction of ribonucleoside diphosphates.
- These reactions are catalyzed by ribonucleotide reductases through a radical mechanism.
- TMP is formed by the methylation of dUMP by thymidylate synthase. This reaction oxidizes N^5,N^{10}-methylenetetrahydrofolate to dihydrofolate, which is regenerated by dihydrofolate reductase.
- Thymidylate synthase and dihydrofolate reductase are targets of various anticancer drugs.

26.5 Key Steps in Nucleotide Biosynthesis Are Regulated by Feedback Inhibition

- Pyrimidine biosynthesis is regulated by the feedback inhibition of aspartate transcarbamoylase.
- Regulation of purine biosynthesis is more complex and includes the feedback inhibition of glutamine-PRPP amidotransferase by

purine nucleotides.
- The synthesis of deoxyribonucleotides is controlled by the regulation of ribonucleotide reductase at two allosteric sites: one controls overall enzyme activity, and another regulates substrate specificity.

26.6 Disruptions in Nucleotide Metabolism Can Cause Pathological Conditions

- Severe combined immunodeficiency results from the absence of adenosine deaminase, an enzyme in the purine degradation pathway.
- Purines are degraded to urate in human beings. Gout, a disease that affects joints and leads to arthritis, is associated with an excessive accumulation of urate.
- Lesch–Nyhan syndrome, a genetic disease characterized by self-mutilation, cognitive disabilities, and gout, is caused by the absence of hypoxanthine-guanine phosphoribosyltransferase. This enzyme is essential for the synthesis of purine nucleotides by the salvage pathway.

Key Terms

de novo pathway
salvage pathway
ATP-grasp fold
5-phosphoribosyl-1-pyrophosphate (PRPP)
orotidylate
purinosome
ribonucleotide reductase
thymidylate synthase
dihydrofolate reductase
severe combined immunodeficiency (SCID)

gout
Lesch–Nyhan syndrome

Problems

1. Differentiate between the de novo synthesis of nucleotides and salvage-pathway synthesis. 1

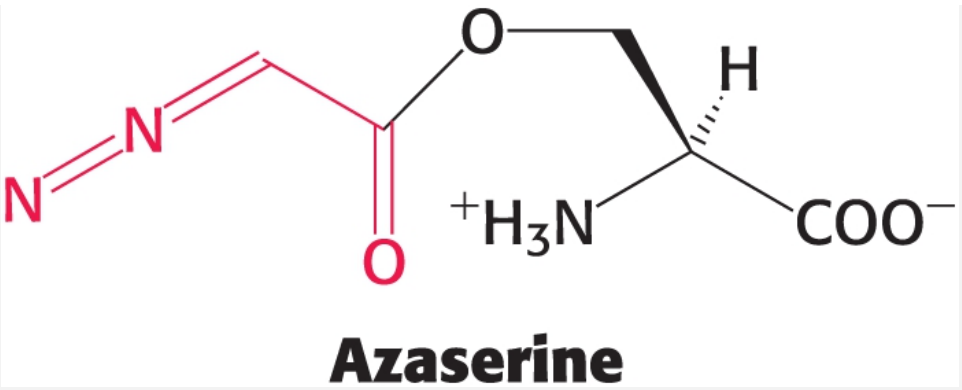
2. How many molecules of ATP are required to synthesize one molecule of CTP from scratch? 1

3. Write a balanced equation for the synthesis of orotate from glutamine, CO_2, and aspartate. 1

4. What is the activated reactant in the biosynthesis of each of the following compounds?

a. Phosphoribosylamine
b. Carbamoylaspartate
c. Orotidylate (from orotate)
d. Phosphoribosylanthranilate

5. Amidotransferases are inhibited by the antibiotic azaserine (*O*-diazoacetyl-L-serine), which is an analog of glutamine. 2



Azaserine

Which intermediates in purine biosynthesis would accumulate in cells treated with azaserine?

6. What intermediate in purine synthesis will accumulate if a strain of bacteria is lacking each of the following biochemicals? 2

a. Aspartate
b. Tetrahydrofolate
c. Glycine
d. Glutamine

7. What major biosynthetic reactions utilize PRPP?

8. Purine biosynthesis is allowed to take place in the presence of $[^{15}N]$ aspartate, and the newly synthesized GTP and ATP are isolated. What positions are labeled in the two nucleotides? 2

9. Write a balanced equation for the synthesis of TMP from dUMP that is coupled to the conversion of serine into glycine. 3

10. Arrange the steps to outline the mechanism by which ribonucleotide reductase converts a ribonucleotide to a deoxyribonucleotide. 3

a. $C-2'$ of the substrate releases an OH^-.
b. The tyrosyl radical on R2 accepts an electron from a cysteine on R1.
c. $C-2'$ accepts a hydride ion from a cysteine residue.
d. A hydrogen atom binds to $C-3'$ of the substrate.
e. The cysteine radical abstracts a hydrogen atom from $C-3'$ of the substrate, forming a radical.

11. Which of the following molecules are substrates of the ribonucleotide reductase reaction? Which are products? 3

a. ADP
b. CDP
c. dADP
d. dCTP

12. Both side-chain oxygen atoms of aspartate 27 at the active site of dihydrofolate reductase form hydrogen bonds with the pteridine ring of folates. The importance of this interaction was assessed by studying two mutants at this position, Asn 27 and Ser 27. The dissociation constant of methotrexate was 0.07 nM for the wild type, 1.9 nM for the Asn 27 mutant, and 210 nM for the Ser 27 mutant, at 25°C. Calculate the standard free energy of the binding of methotrexate by these three proteins. What is the decrease in binding energy resulting from each mutation? 3

13. Which nucleoside triphosphate regulates aspartate transcarbamoylase (ATCase) by feedback inhibition? Which one acts as an allosteric activator of ATCase? 4

14. Which of the following statements correctly describe the regulatory steps of purine synthesis? 4

a. The committed step in purine synthesis is the conversion of PRPP into phosphoribosylamine.
b. Inosinate is the branch point in the synthesis of inhibitors AMP and GMP.
c. The final reaction in purine synthesis, the generation of either AMP or IMP, is the rate-limiting step.
d. AMP is a feedback inhibitor, regulating the conversion of inosinate into xanthylate, its immediate precursor.
e. ATP is not required for the synthesis of GMP.

15. Which two nucleoside triphosphates bind to the allosteric site of the ribonucleotide reductase R1 subunit that controls overall enzyme activity? 4

16. Identify the correct statements about Lesch–Nyhan syndrome. 5

a. This deficiency does not allow purine nucleotide production via the salvage pathway.
b. This syndrome is caused by a deficiency in PRPP.
c. Some symptoms of Lesch–Nyhan syndrome include involuntary movements and self-mutilation.
d. Gout causes Lesch–Nyhan syndrome.

17. In humans, the multifunctional enzyme uridine 5′-monophosphate (UMP) synthase has orotate phosphoribosyltransferase and orotidylate decarboxylase activity. Both enzymatic functions are impaired in patients

with orotic aciduria. Which substance is present in high levels in the urine of these patients? 5

a. Carbamate
b. Carbamoyl phosphate
c. Uridylate (UMP)
d. Orotate
e. Orotidylate

18. Suppose that a person is found who is deficient in an enzyme required for IMP synthesis. How might this person be treated? 5

19. Mutant cells unable to synthesize nucleotides by salvage pathways are very useful tools in molecular and cell biology. Suppose that cell A lacks thymidine kinase, the enzyme catalyzing the phosphorylation of thymidine to thymidylate, and that cell B lacks hypoxanthine-guanine phosphoribosyl transferase.

a. Cell A and cell B do not proliferate in a HAT medium containing hypoxanthine, aminopterin or amethopterin (methotrexate), and thymine. However, cell C, formed by the fusion of cells A and B, grows in this medium. Why?
b. Suppose that you want to introduce foreign genes into cell A. Devise a simple means of distinguishing between cells that have taken up foreign DNA and those that have not.

CHAPTER 27
Biosynthesis of Membrane Lipids and Steroids

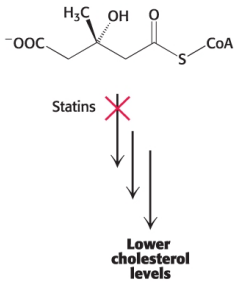




Photo: Kumar Sriskandan/Alamy

Enzymes in biosynthetic pathways involving lipids are important drug targets. For example, statins block the committed step in the biosynthesis of cholesterol, thus helping to control cardiovascular disease.

OUTLINE

27.1 Phosphatidate Is a Common Intermediate in the Synthesis of Phospholipids and Triacylglycerols
27.2 Cholesterol Is Synthesized from Acetyl Coenzyme A in Three Stages
27.3 The Regulation of Cholesterol Biosynthesis Takes Place at Several Levels

27.4 Important Biochemicals Are Synthesized from Cholesterol and Isoprene

---

Learning Goals



By the end of this chapter, you should be able to:

1. Describe the relationship between triacylglycerol synthesis and phospholipid synthesis.
2. Describe the three stages of cholesterol biosynthesis.
3. Identify the regulatory processes controlling cholesterol synthesis.
4. Describe some important molecules synthesized from cholesterol precursors and from cholesterol.

Living cells must replenish their cell membranes and enlarge them when growing and dividing. Furthermore, even seemingly minor variations in lipid structure are associated with participation in different functions, including intracellular and intercellular signaling. Thus, the pathways by which lipids are made and interconverted are of considerable interest.

This chapter examines the biosynthesis of three important components of biological membranes — phospholipids, sphingolipids, and cholesterol. Triacylglycerols also are considered here because the pathway for their synthesis overlaps that of phospholipids. Cholesterol is of interest both as a membrane component and as a precursor of potent signaling molecules, such as the steroid hormones estradiol, testosterone, progesterone, and cortisol. Knowledge of these biosynthetic pathways, particularly that

for cholesterol, has been of great importance for drug development and understanding the mechanisms of drug action.

27.1 Phosphatidate Is a Common Intermediate in the Synthesis of Phospholipids and Triacylglycerols

Lipid synthesis requires the coordinated action of gluconeogenesis and fatty acid metabolism (Figure 27.1). The common step in the synthesis of both phospholipids for membranes and triacylglycerols for energy storage is the formation of **phosphatidate** (diacylglycerol 3-phosphate). In mammalian cells, phosphatidate is synthesized in the endoplasmic reticulum and the outer mitochondrial membrane.

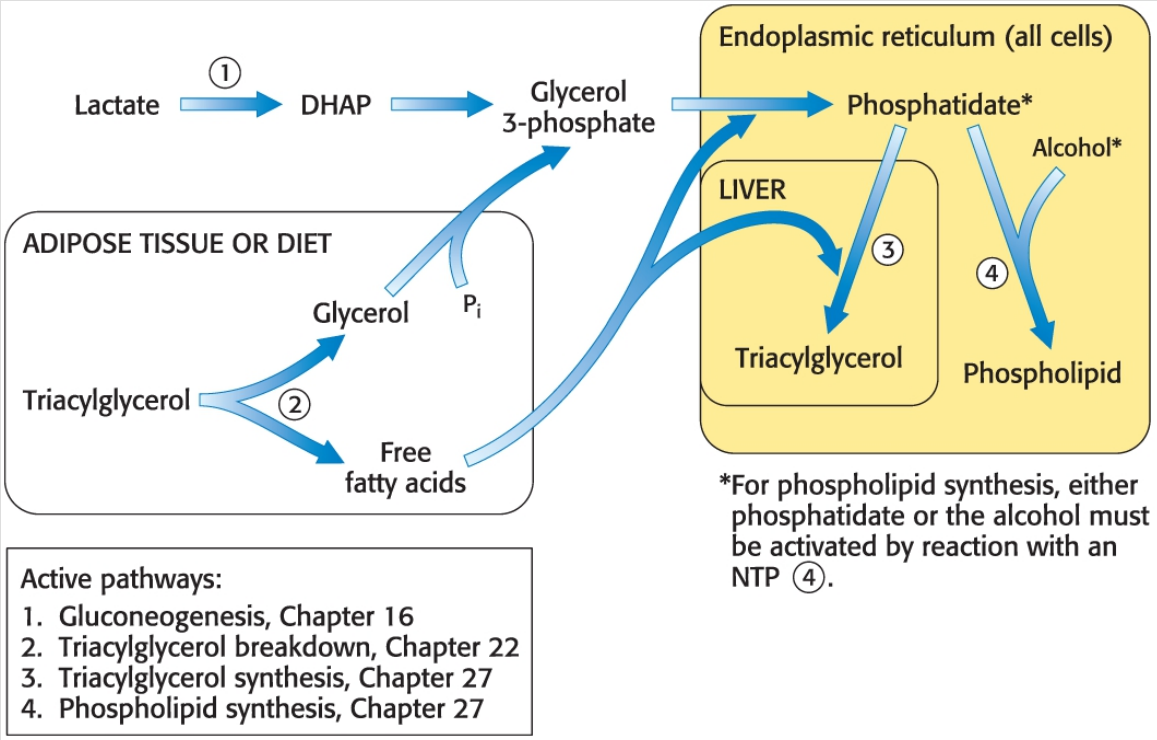
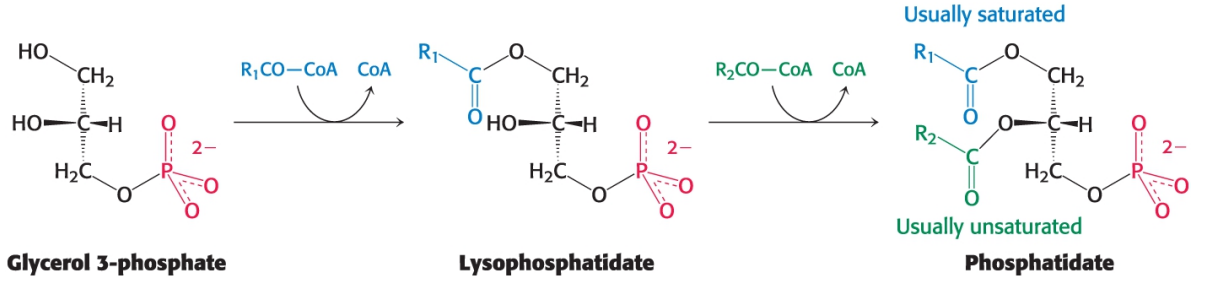


FIGURE 27.1 Phosphatidate is a key intermediate in lipid biosynthesis. Phosphatidate, synthesized from dihydroxyacetone phosphate (DHAP) produced in gluconeogenesis and fatty acids, can be further processed to produce triacylglycerol or phospholipids. Phospholipids and other membrane lipids are continuously produced in all cells.

EXPLORE this pathway further in the Metabolic Map in Achieve

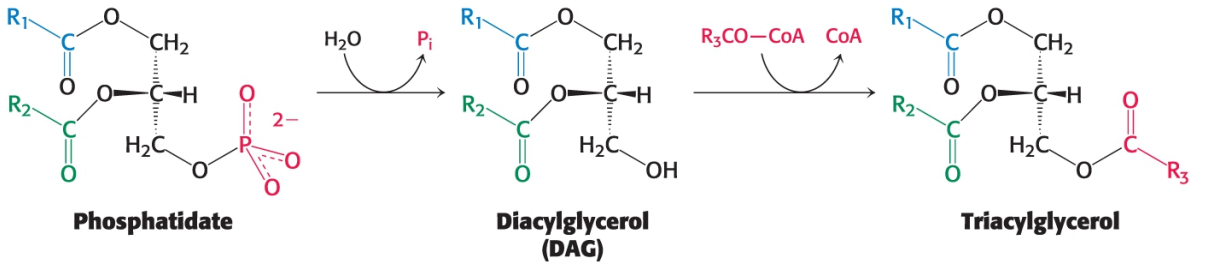
The pathway for the biosynthesis of phosphatidate begins with glycerol 3-phosphate, which is formed primarily by the reduction of dihydroxyacetone phosphate (DHAP) synthesized by the gluconeogenic pathway, and to a lesser extent by the phosphorylation of glycerol. The addition of two fatty acids to glycerol-3-phosphate yields phosphatidate. First, acyl coenzyme A contributes a fatty acid chain to form lysophosphatidate, and then a second acyl CoA contributes a fatty acid chain to yield phosphatidate.



These acylations are catalyzed by glycerol phosphate acyltransferase. In most phosphatidates, the fatty acid chain attached to the C-1 atom is saturated, whereas the one attached to the C-2 atom is unsaturated. Phosphatidate can also be synthesized from diacylglycerol (DAG), in what is essentially a salvage pathway, by the action of diacylglycerol kinase:

Diacylglycerol + ATP → phosphatidate + ADP

The phospholipid and triacylglycerol pathways diverge at phosphatidate. In the synthesis of triacylglycerols, a key enzyme in the regulation of lipid synthesis, phosphatidic acid phosphatase, hydrolyzes phosphatidate to give a diacylglycerol. This intermediate is acylated to a **triacylglycerol** through the addition of a third fatty acid chain in a reaction that is catalyzed by diglyceride acyltransferase. Both enzymes are associated in a triacylglycerol synthetase complex that is bound to the endoplasmic reticulum membrane.



The liver is the primary site of triacylglycerol synthesis. From the liver, the triacylglycerols are transported to the muscles for energy conversion or to the adipose cells for storage.

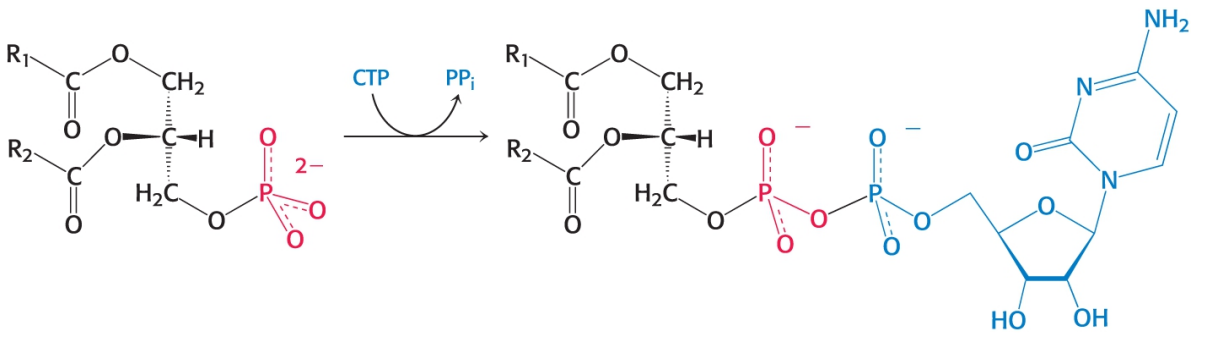
Self-Check Question

You find two samples labeled “Pure phosphatidic acid” but discover that the two samples have slightly different properties including different molecular weights. Explain.

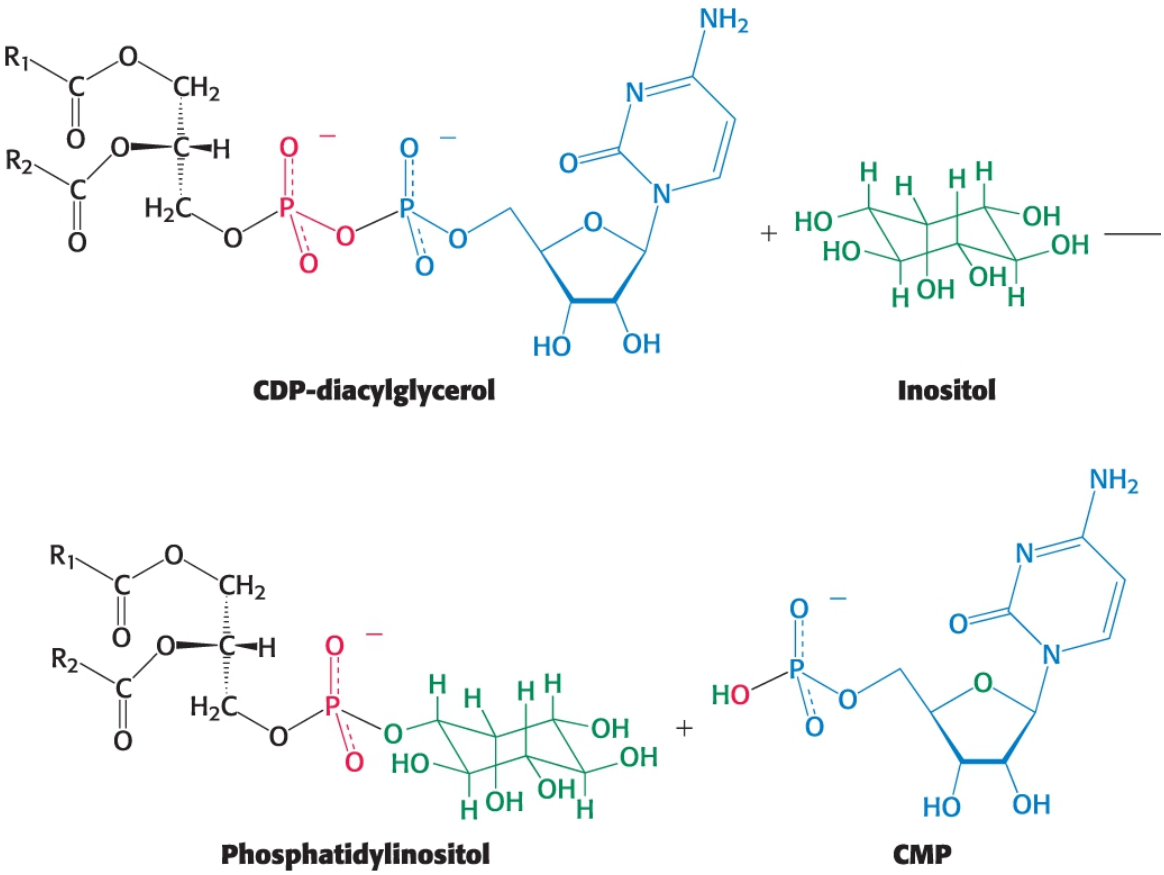
The synthesis of phospholipids requires an activated intermediate

Membrane-lipid synthesis continues in the endoplasmic reticulum and in the Golgi apparatus. Phospholipid synthesis requires the combination of a diacylglycerol with an alcohol. As in most anabolic reactions, one of the components must be activated. In this case, either the diacylglycerol or the alcohol may be activated, depending on the source of the reactants.

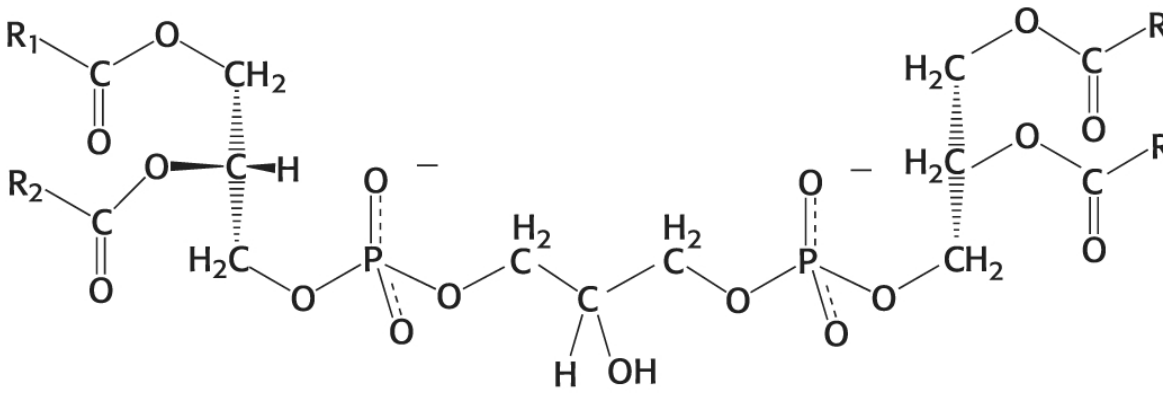
The synthesis of some phospholipids begins with the reaction of phosphatidate with cytidine triphosphate (CTP) to form the activated diacylglycerol, **cytidine diphosphodiacylglycerol (CDP-diacylglycerol)**. This reaction, like those of many biosyntheses, is driven forward by the hydrolysis of pyrophosphate.



The activated phosphatidyl unit then reacts with the hydroxyl group of an alcohol to form a phosphodiester linkage. If the alcohol is inositol, the products are phosphatidylinositol and cytidine monophosphate (CMP).



Subsequent phosphorylations catalyzed by specific kinases lead to the synthesis of phosphatidylinositol 4,5-bisphosphate, the precursor of two intracellular messengers — diacylglycerol and inositol 1,4,5-trisphosphate. If the alcohol is phosphatidylglycerol, the products are diphosphatidylglycerol (cardiolipin) and CMP. In eukaryotes, cardiolipin is synthesized in the mitochondria and is located exclusively in inner mitochondrial membranes.



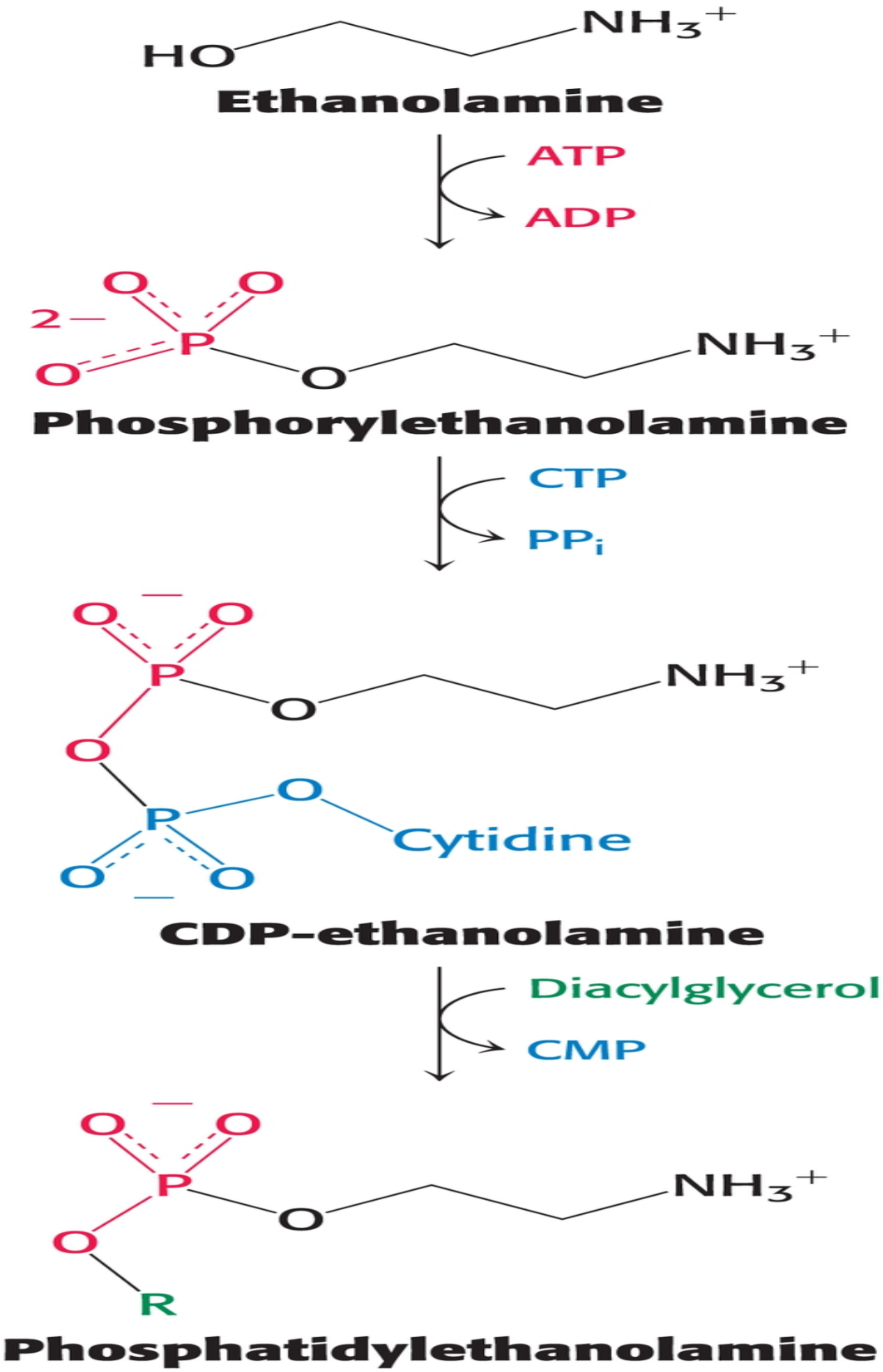
Diphosphatidylglycerol (Cardiolipin)

Cardiolipin is abundant in the inner membrane of mitochondria and plays an important role in the organization of the protein components participating in oxidative phosphorylation. Scientists have also discovered that cardiolipin facilitates the proper folding of α-synuclein in nerve cells. Misfolding of α-synuclein causes the formation of aggregates that are toxic. These α-synuclein deposits are believed to play a role in the development of Parkinson's disease.

The fatty acid components of phospholipids may vary, and thus cardiolipin, as well as most other phospholipids, represents a class of molecules rather than a single species. As a result, a single mammalian cell may contain thousands of distinct phospholipids. Phosphatidylinositol is unusual in that it has a nearly fixed fatty acid composition. Stearic acid usually occupies the C-1 position and arachidonic acid the C-2 position.

Some phospholipids are synthesized from an activated alcohol

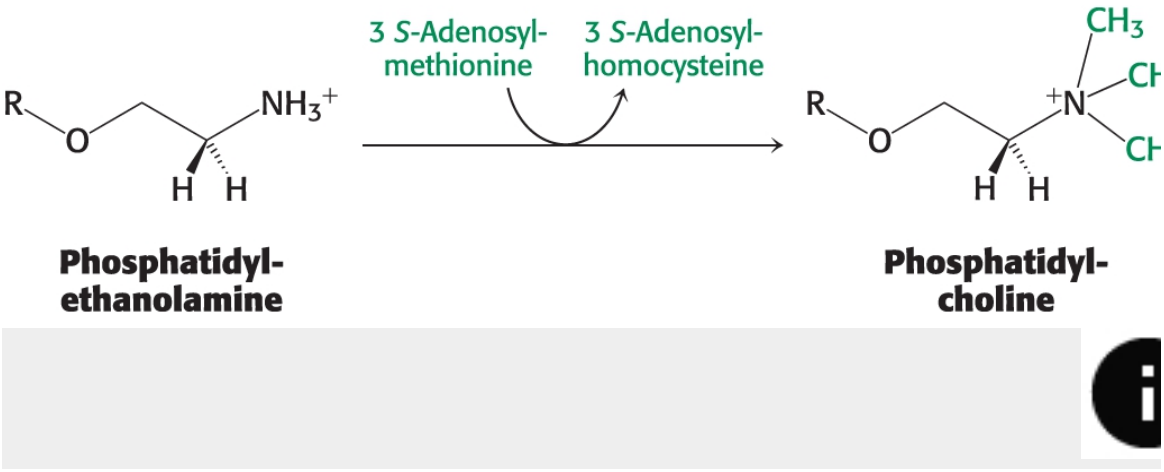
Phosphatidylethanolamine, the major phospholipid of the inner leaflet of cell membranes, is synthesized from the alcohol ethanolamine. To activate the alcohol, ethanolamine is phosphorylated by ATP to form the precursor, phosphorylethanolamine. This precursor then reacts with CTP to form the activated alcohol, CDP-ethanolamine. The phosphorylethanolamine unit of CDP-ethanolamine is transferred to a diacylglycerol to form phosphatidylethanolamine.


HO
NH3+
Ethanolamine
ATP
ADP
2−
O
P
NH3+
Phosphorylethanolamine
CTP
PPi
Cytidine
CDP–ethanolamine
Diacylglycerol
CMP
R
Phosphatidylethanolamine

Phosphatidylcholine is an abundant phospholipid

The most common phospholipid in mammals is phosphatidylcholine, comprising approximately 50% of the membrane mass. Dietary choline is activated in a series of reactions analogous to those in the activation of ethanolamine. CTP-phosphocholine cytidylyltransferase (CCT) catalyzes the formation of CDP-choline, the rate-limiting step in phosphatidylcholine synthesis. CCT is termed an *amphitropic enzyme* — a class of enzymes whose regulator ligand is the membrane itself. A portion of the enzyme, normally associated with the membrane, is sensitive to a decrease in phosphatidylcholine concentration as an alteration in the physical properties of the membrane. When this occurs, another portion of the enzyme inserts into the membrane, leading to enzyme activation. Indeed, the k_{cat}/K_M value increases by three orders of magnitude upon activation, contributing to the restoration of phosphatidylcholine levels.

The liver also possesses an enzyme, phosphatidylethanolamine methyltransferase, which synthesizes phosphatidylcholine from phosphatidylethanolamine when dietary choline is insufficient, a testament to the importance of this vital phospholipid. The amino group of this phosphatidylethanolamine is methylated three times to form phosphatidylcholine. *S*-adenosylmethionine is the methyl donor.



Thus, phosphatidylcholine can be produced by two distinct pathways in mammals, ensuring that this phospholipid can be synthesized even if the components for one pathway are in limited supply.

Base-exchange reactions can generate phospholipids

Phosphatidylserine makes up 10% of the phospholipids in mammals. This phospholipid is synthesized in a base-exchange reaction of serine with phosphatidylcholine or phosphatidylethanolamine. In the reaction, serine replaces choline or ethanolamine.

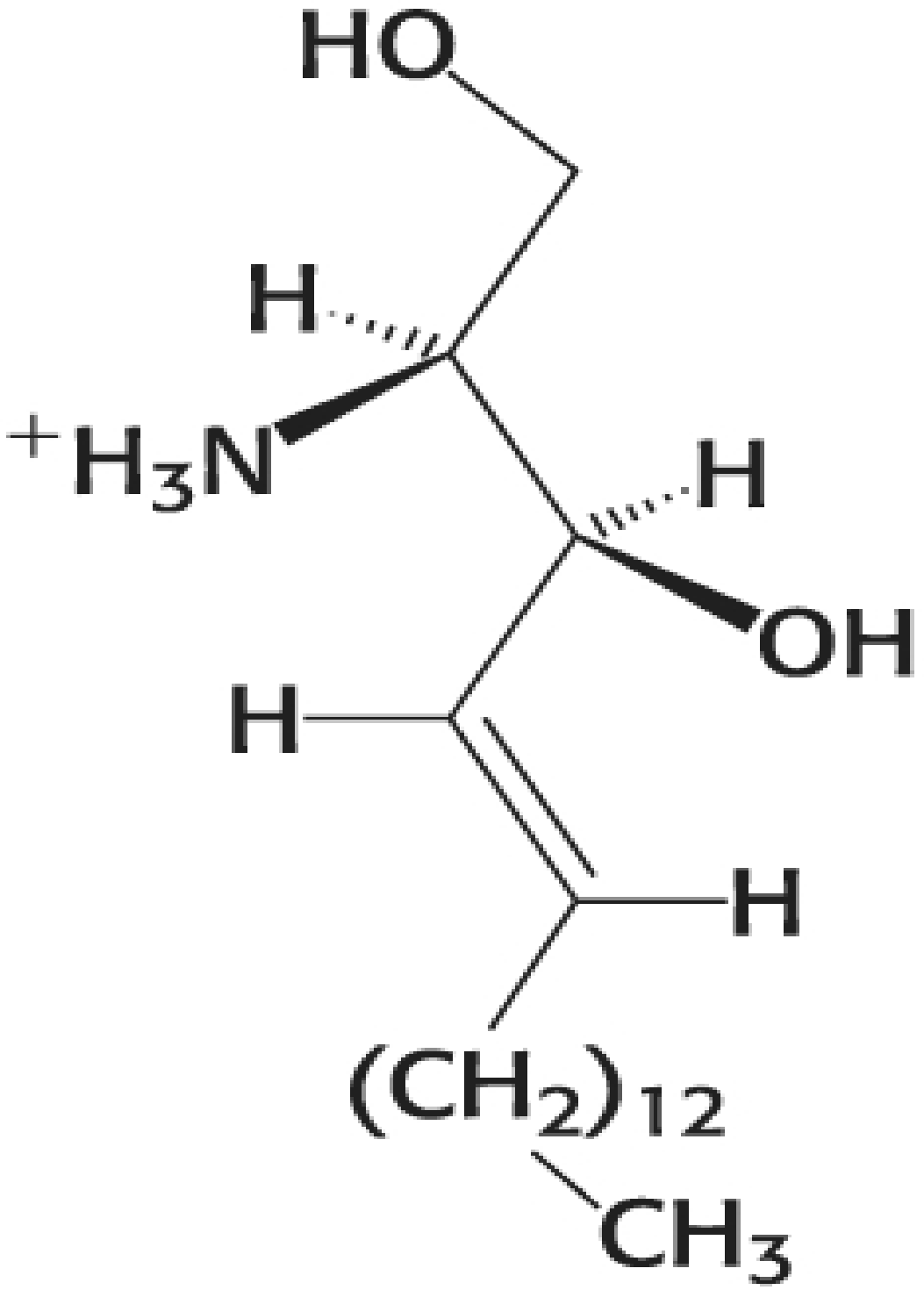
Phosphatidylcholine + serine → choline + phosphatidylserine
Phosphatidylethanolamine + serine → ethanolamine + phosphatidylserine

Phosphatidylserine is normally located in the inner leaflet of the plasma membrane bilayer but is moved to the outer leaflet in apoptosis. There, it serves to attract phagocytes to consume the cell remnants after apoptosis is complete. Phosphatidylserine is translocated from one side of the membrane to the other by an ATP-binding cassette translocase.

Note that a cytidine nucleotide plays the same role in the synthesis of these phosphoglycerides as a uridine nucleotide does in the formation of glycogen (Section 21.4). In all of these biosyntheses, an activated intermediate (UDP-glucose, CDP-diacylglycerol, or CDP-alcohol) is formed from a phosphorylated substrate (glucose 1-phosphate, phosphatidate, or a phosphorylalcohol) and a nucleoside triphosphate (UTP or CTP). The activated intermediate then reacts with a hydroxyl group (the terminus of glycogen, an alcohol, or a diacylglycerol).

Sphingolipids are synthesized from ceramide

We now turn from glycerol-based phospholipids to another class of membrane lipid — the **sphingolipids**. These lipids are found in the plasma membranes of all eukaryotic cells, although the concentration is highest in the cells of the central nervous system. The backbone of a sphingolipid is sphingosine rather than glycerol.



Sphingosine

Palmitoyl CoA and serine condense to form 3-ketosphinganine. The serine–palmitoyl transferase catalyzing this reaction is the rate-limiting step in the pathway and requires pyridoxal phosphate; this reveals again the dominant role of this cofactor in transformations that include amino acids. Ketosphinganine is then reduced to dihydrosphingosine before conversion into **ceramide**, a lipid consisting of a fatty acid chain attached to the amino group of a sphingosine backbone (**Figure 27.2**).

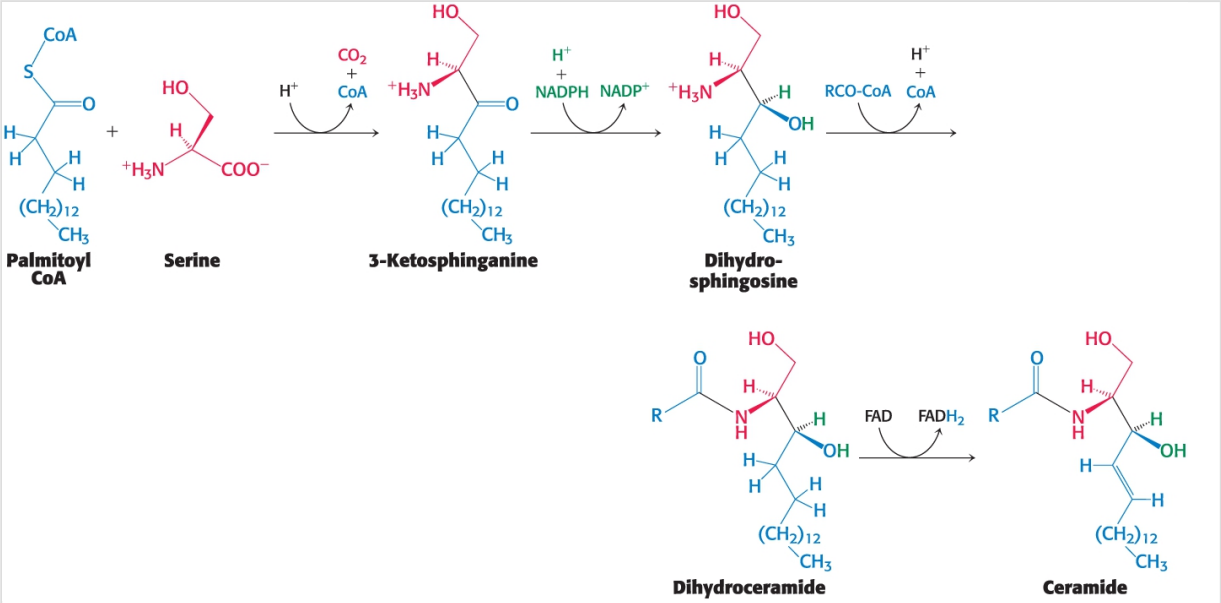


FIGURE 27.2 Biosynthesis of ceramide involves four steps. Palmitoyl CoA and serine combine to initiate the synthesis of ceramide. The product is further elaborated with the incorporation of an additional fatty acid chain and the introduction of a carbon–carbon double bond.

In all sphingolipids, the amino group of ceramide is acylated. The terminal hydroxyl group also is substituted. In sphingomyelin, a component of the myelin sheath covering many nerve fibers, the substituent is phosphorylcholine, which comes from

phosphatidylcholine. In a cerebroside, the substituent is glucose or galactose. UDP-glucose or UDP-galactose is the sugar donor.

Gangliosides are the most complex sphingolipids. In a ganglioside, an oligosaccharide chain is linked to the terminal hydroxyl group of ceramide by a glucose residue (Figure 27.3). This oligosaccharide chain contains at least one acidic sugar, either *N*-acetylneuraminate or *N*-glycolylneuraminate. These acidic sugars are called *sialic acids*. Their nine-carbon backbones are synthesized from phosphoenolpyruvate (a three-carbon unit) and *N*-acetylmannosamine 6-phosphate (a six-carbon unit).

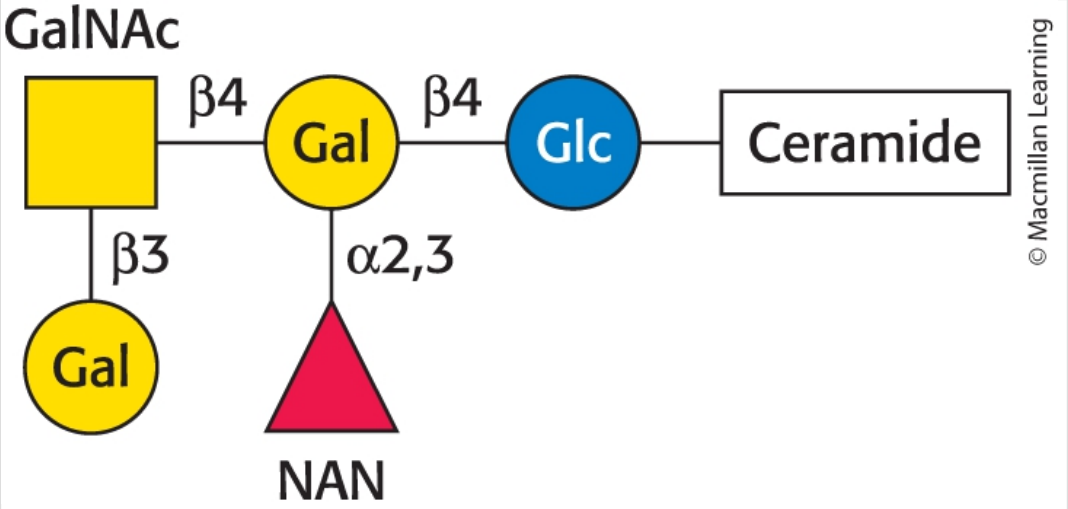


FIGURE 27.3 The ganglioside G_{M1} consists of five monosaccharides linked to ceramide. These sugars include one glucose (Glc) molecule, two galactose (Gal) molecules, one *N*-acetylgalactosamine (GalNAc) molecule, and one *N*-acetylneuraminate (NAN) molecule.

Gangliosides are synthesized by the ordered, step-by-step addition of sugar residues to ceramide (Figure 27.4). The synthesis of these complex lipids requires the activated sugars UDP-glucose, UDP-galactose, and UDP-*N*-acetylgalactosamine, as well as the CMP

derivative of *N*-acetylneuraminate. CMP-*N*-acetylneuraminate is synthesized from CTP and *N*-acetylneuraminate. The sugar composition of the resulting ganglioside is determined by the specificity of the glycosyltransferases in the cell. Almost 200 different gangliosides have been characterized.

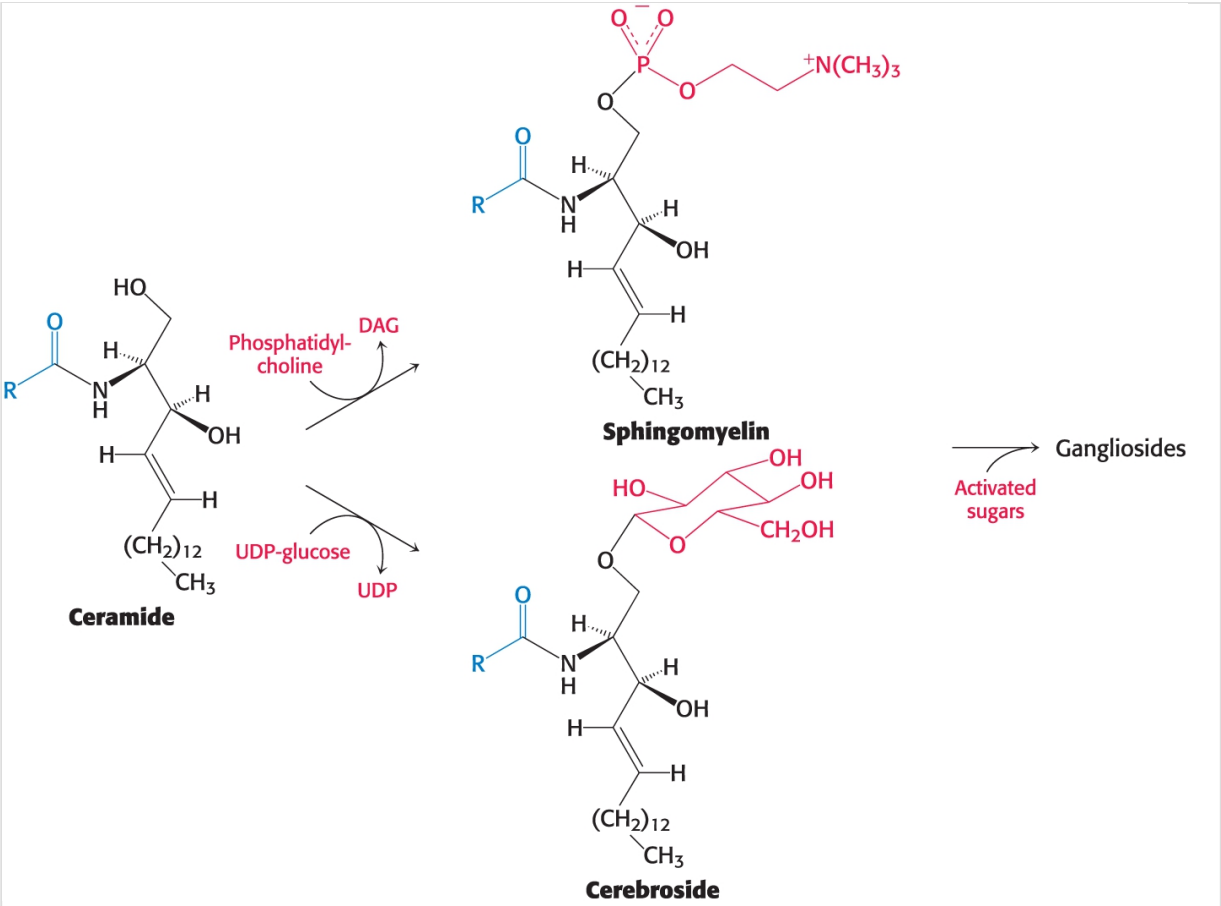


FIGURE 27.4 Ceramide can be converted into sphingomyelin, cerebroside, and gangliosides.

Tay–Sachs disease results from the disruption of lipid metabolism

Tay–Sachs disease is caused by a failure of lipid degradation: an inability to degrade gangliosides. Gangliosides are found in highest concentration in the nervous system, particularly in gray matter, where they constitute 6% of the lipids. Gangliosides are normally degraded inside lysosomes by the sequential removal of their terminal sugars, but in Tay–Sachs disease this degradation does not take place. As a consequence, neurons become significantly swollen with lipid-filled lysosomes (Figure 27.5). An affected infant displays weakness and limited psychomotor skills before 1 year of age and usually dies before age 3.

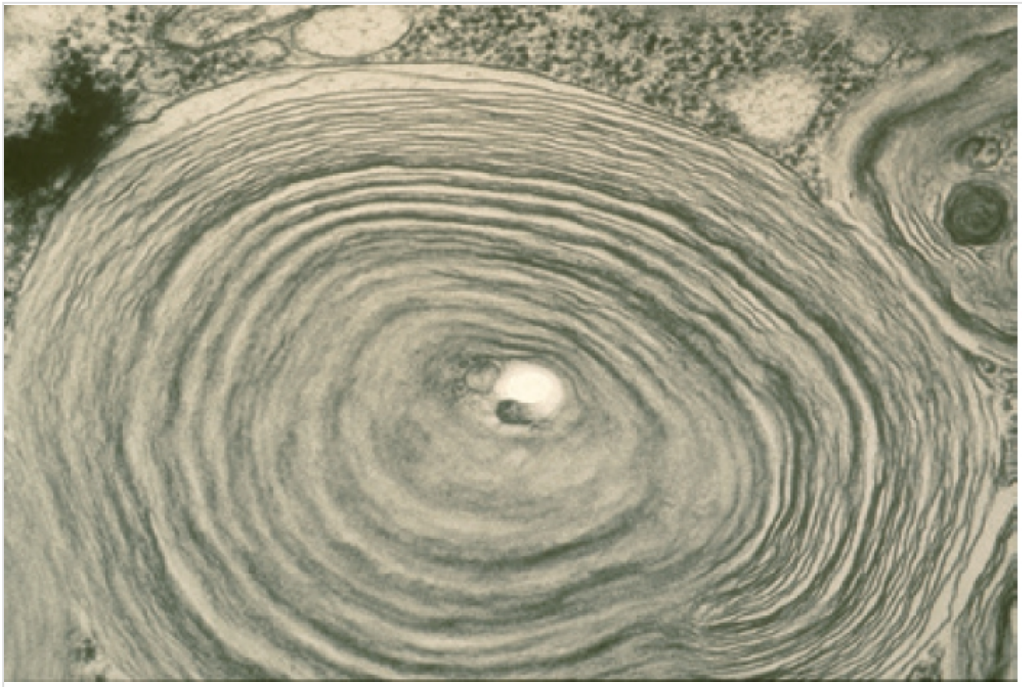
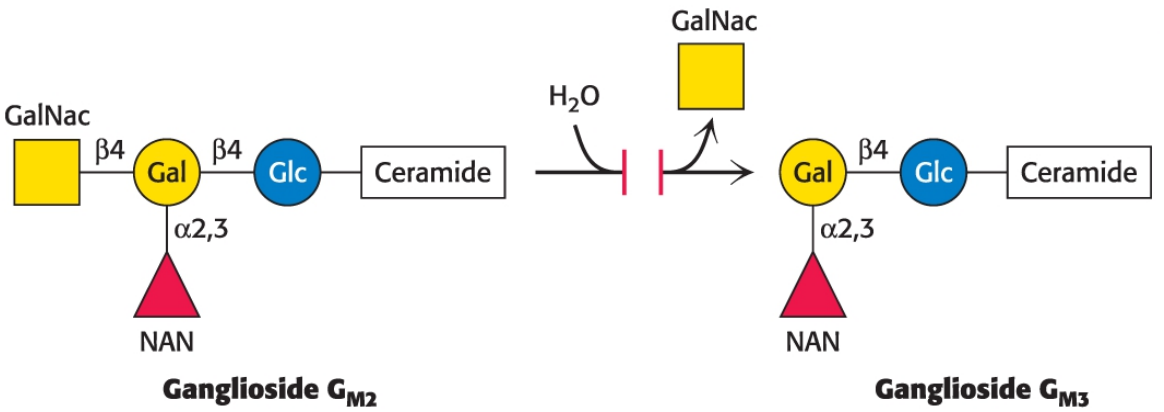


Photo Credit: Science Photo Library/Science Source

FIGURE 27.5 Lysosome sometimes will fill up with lipids. An electron micrograph shows a lysosome engorged with lipids. Such lysosomes are sometimes described as being “onion-skin” like because the layers of undigested lipids resemble a sliced onion.

The ganglioside content of the brain of an infant with Tay–Sachs disease is greatly elevated. The concentration of ganglioside G_{M2} is many times higher than normal because its terminal *N*-acetylgalactosamine residue is removed very slowly or not at all. The missing or deficient enzyme is a specific β-*N*-acetylhexosaminidase.



Carriers of Tay–Sachs can be identified by genetic testing. Moreover, Tay–Sachs disease can be diagnosed in the course of fetal development. Cells obtained from either the villi of the placenta (chorionic villus sampling) or from the amniotic fluid (amniocentesis) are tested for the presence of the defective gene. Tay–Sachs disease was especially prominent among Ashkenazi Jews (descendants of Jews from central and eastern Europe). Genetic testing programs, initiated in the early 1970s upon the development of a simple blood test to identify carriers, have dramatically reduced the incidence of the disease in this population.

Phosphatidic acid phosphatase is a key regulatory enzyme in lipid metabolism

The enzyme phosphatidic acid phosphatase (PAP), working in concert with diacylglycerol kinase, plays a key role in the regulation of lipid synthesis. PAP, also called *lipin 1* in mammals, controls the extent to which triacylglycerols are synthesized relative to phospholipids and regulates the type of phospholipid synthesized (Figure 27.6). For instance, when PAP activity is high, phosphatidate is dephosphorylated and diacylglycerol is produced, which can react with the appropriate activated alcohols to yield phosphatidylethanolamine, phosphatidylserine, or phosphatidylcholine. Diacylglycerol can also be converted into triacylglycerols. Evidence suggests that the formation of triacylglycerols may act as a fatty acid buffer. This buffering helps to regulate the levels of diacylglycerol and sphingolipids, which serve signaling functions.

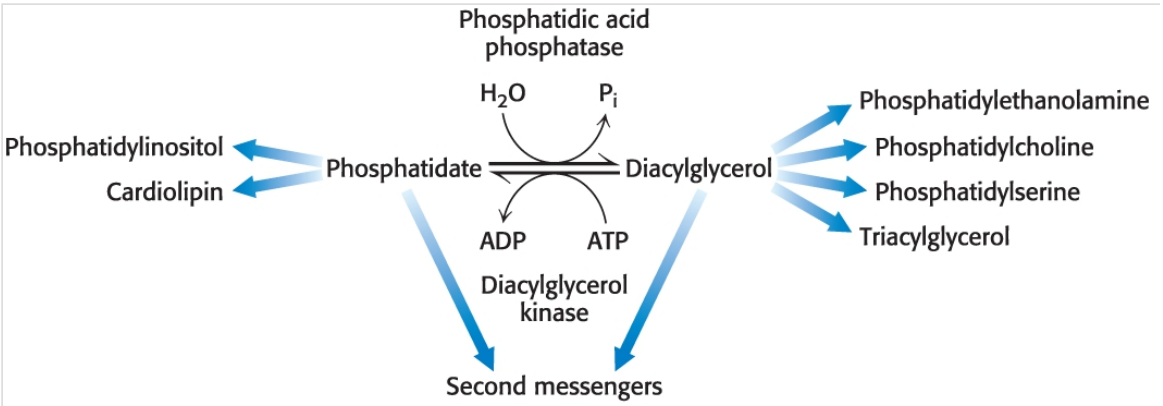


FIGURE 27.6 Phosphatidic acid phosphatase is a key regulatory enzyme in lipid synthesis. When active, PAP generates diacylglycerol (DAG), which can react with activated alcohols to for phospholipids or with fatty acyl CoA to form triacylglycerols. When PAP is inactive, phosphatidate is converted into CMP-DAG for the synthesis of different phospholipids. PAP also controls the amount of DAG and phosphatidate, both of which function as second messengers.

EXPLORE this pathway further in the Metabolic Map in Achieve

When PAP activity is lower, phosphatidate is used as a precursor for different phospholipids, such as phosphatidylinositol and cardiolipin. Moreover, phosphatidate is a signal molecule itself. Phosphatidate regulates the growth of endoplasmic reticulum and nuclear membranes and acts as a cofactor that stimulates the expression of genes in phospholipid synthesis.

27.2 Cholesterol Is Synthesized from Acetyl Coenzyme A in Three Stages

We now turn our attention to the synthesis of the fundamental lipid **cholesterol**. This steroid modulates the fluidity of animal cell membranes and is the precursor of steroid hormones such as progesterone, testosterone, estradiol, and cortisol. All 27 carbon atoms of cholesterol are derived from acetyl CoA in a three-stage synthetic process (**Figure 27.7**). The first stage takes place in the cytoplasm, and the next two in the endoplasmic reticulum.

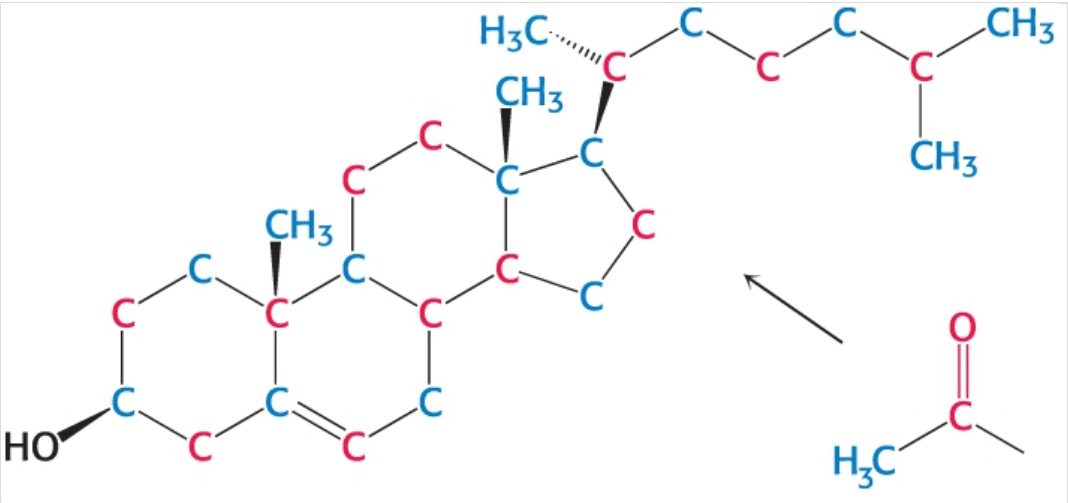


FIGURE 27.7 Isotope-labeling experiments have revealed the source of carbon atoms in cholesterol synthesized from acetate. In this depiction, the source of carbons from acetate's methyl group are shown in blue; carbons from acetate's carboxylate group are shown in red.

Stage 1: The synthesis of mevalonate initiates the synthesis of cholesterol

The first stage in the synthesis of cholesterol is the formation of isopentenyl pyrophosphate from acetyl CoA. This set of reactions starts with the formation of 3-hydroxy-3-methylglutaryl CoA (HMG CoA) from acetyl CoA and acetoacetyl CoA. This intermediate is reduced to **mevalonate** for the synthesis of cholesterol (**Figure 27.8**). Recall that, alternatively, 3-hydroxy-3-methylglutaryl CoA may be generated in the mitochondria and processed to form ketone bodies, which are subsequently secreted to provide fuel for other tissues, notably the brain under starvation conditions.

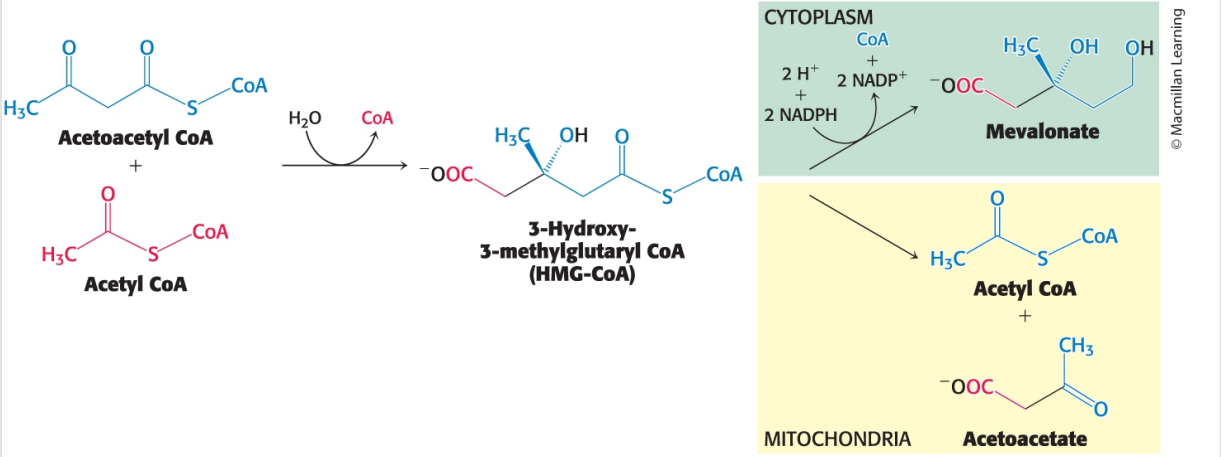
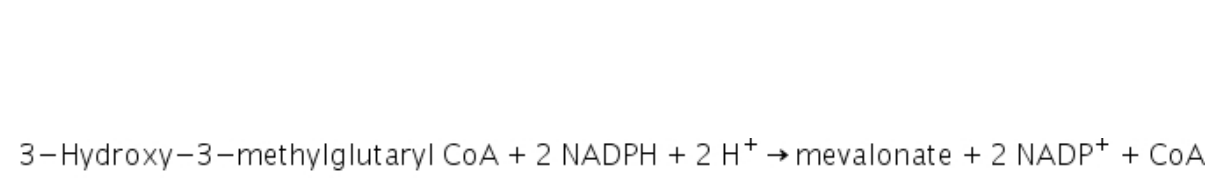


FIGURE 27.8 3-Hydroxy-3-methylglutaryl CoA has different fates. In the cytoplasm, HMG-CoA is converted into mevalonate. In mitochondria, it is converted into acetyl CoA and acetoacetate.

The synthesis of mevalonate is the committed step in cholesterol formation. The enzyme catalyzing this irreversible step, **3-hydroxy-3-methylglutaryl CoA reductase (HMG-CoA reductase)**, is an important control site in cholesterol biosynthesis, as will be discussed shortly.



HMG-CoA reductase is an integral membrane protein in the endoplasmic reticulum.

Mevalonate is converted into 3-isopentenyl pyrophosphate in three consecutive reactions requiring ATP (**Figure 27.9**).

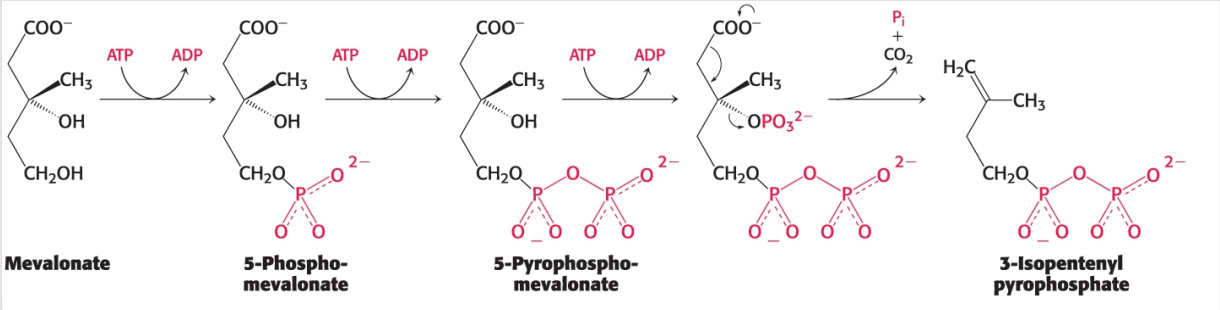
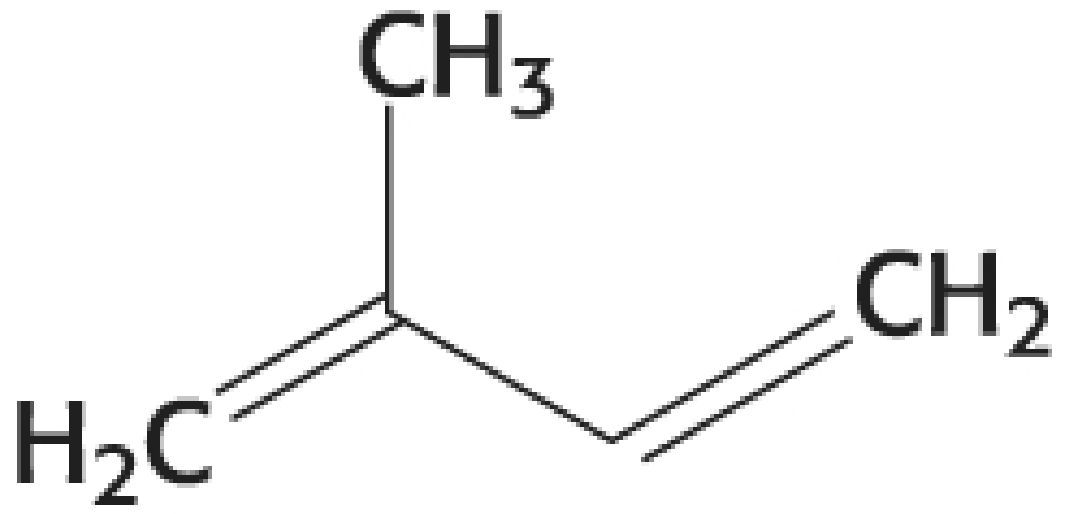


FIGURE 27.9 Mevalonate is converted into isopentenyl pyrophosphate. This activated intermediate is formed from mevalonate in three steps requiring ATP, followed by a decarboxylation.

In the last step, the release of CO_2 yields isopentenyl pyrophosphate, an activated isoprene unit that is a key building block for many important biomolecules throughout the kingdoms of life.



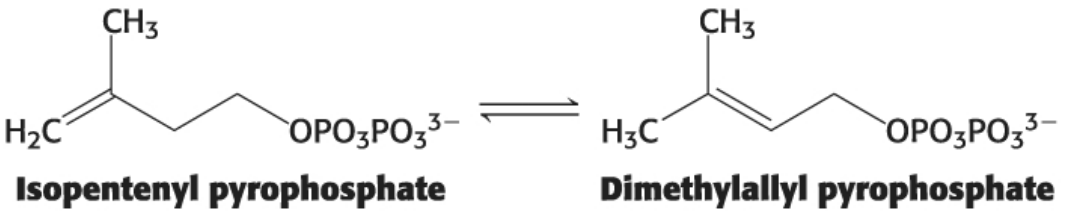
Isoprene

Stage 2: Squalene (C_{30}) is synthesized from six molecules of isopentenyl pyrophosphate (C_5)

Squalene is synthesized from isopentenyl pyrophosphate by the reaction sequence

$$C_5 \rightarrow C_{10} \rightarrow C_{15} \rightarrow C_{30}$$

This stage in the synthesis of cholesterol starts with the isomerization of isopentenyl pyrophosphate to dimethylallyl pyrophosphate.



These two isomeric C_5 units (one of each type) condense to form a C_{10} compound: isopentenyl pyrophosphate attacks an allylic carbocation formed from dimethylallyl pyrophosphate to yield geranyl pyrophosphate (Figure 27.10). The same kind of reaction takes place again: geranyl pyrophosphate is converted into an allylic carbonium ion, which is attacked by isopentenyl pyrophosphate. The resulting C_{15} compound is called farnesyl pyrophosphate. The same enzyme, geranyl transferase, catalyzes each of these condensations.

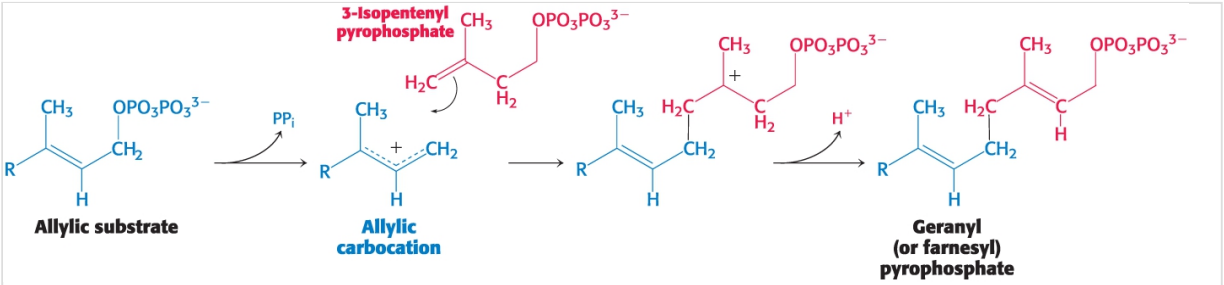
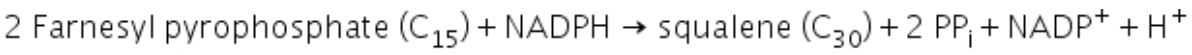


FIGURE 27.10 Condensation reactions build carbon–carbon bonds that eventually form the cholesterol skeleton. The isomeric C_5 units dimethylallyl pyrophosphate and isopentenyl pyrophosphate join to form geranyl pyrophosphate. The same mechanism is used to add an additional isopentenyl pyrophosphate to form farnesyl pyrophosphate.

The last step in the synthesis of squalene is a reductive tail-to-tail condensation of two molecules of farnesyl pyrophosphate catalyzed by the endoplasmic reticulum enzyme squalene synthase.



The reactions leading from C_5 units to squalene, a C_{30} isoprenoid, are summarized in **Figure 27.11**.

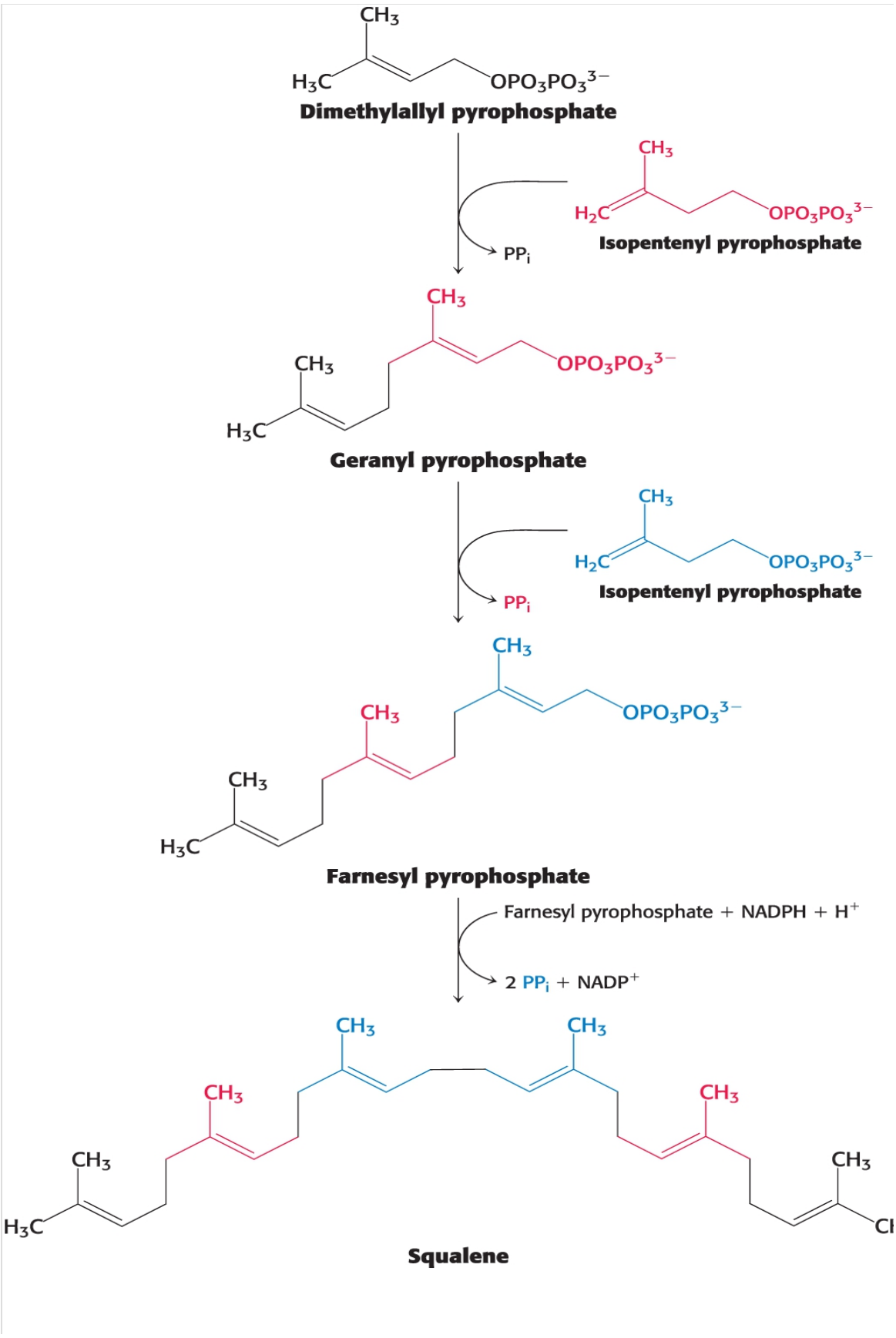

CH3
H3C
OPO3PO3 3−
Dimethylallyl pyrophosphate
CH3
H2C
OPO3PO3 3−
Isopentenyl pyrophosphate
PPi
CH3
CH3
H3C
OPO3PO3 3−
Geranyl pyrophosphate
CH3
H2C
OPO3PO3 3−
Isopentenyl pyrophosphate
PPi
CH3
CH3
CH3
H3C
OPO3PO3 3−
Farnesyl pyrophosphate
Farnesyl pyrophosphate + NADPH + H+
2 PPi + NADP+
CH3
CH3
CH3
CH3
CH3
H3C
CH3
Squalene

FIGURE 27.11 Two molecules of farnesyl pyrophosphate are linked to form squalene. One molecule of dimethylallyl pyrophosphate and two molecules of isopentenyl pyrophosphate condense to form farnesyl pyrophosphate. The tail-to-tail coupling of two molecules of farnesyl pyrophosphate yields squalene.

Stage 3: Squalene cyclizes to form cholesterol

The final stage of cholesterol biosynthesis starts with the cyclization of squalene (Figure 27.12). Squalene is first activated by conversion into squalene epoxide (2,3-oxidosqualene) in a reaction that uses O_2 and NADPH. Squalene epoxide is then cyclized to lanosterol by oxidosqualene cyclase. The enzyme holds squalene epoxide in an appropriate conformation and initiates the reaction by protonating the epoxide oxygen. The carbocation formed spontaneously rearranges to produce lanosterol.

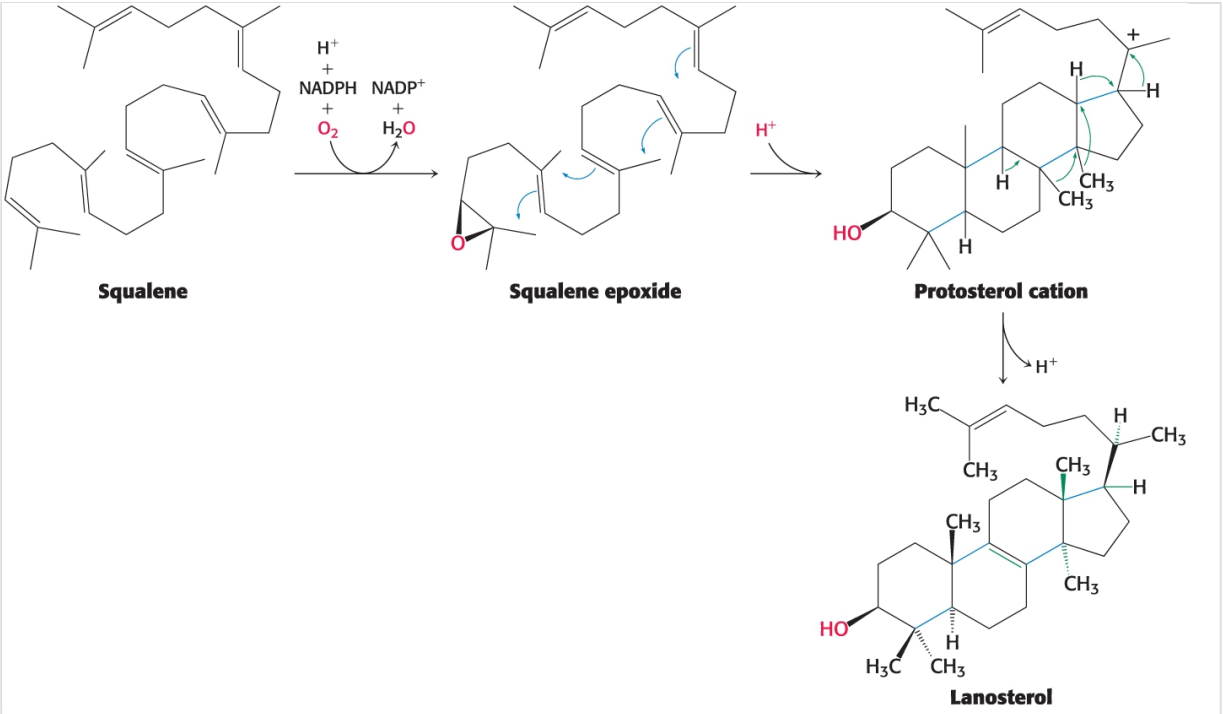
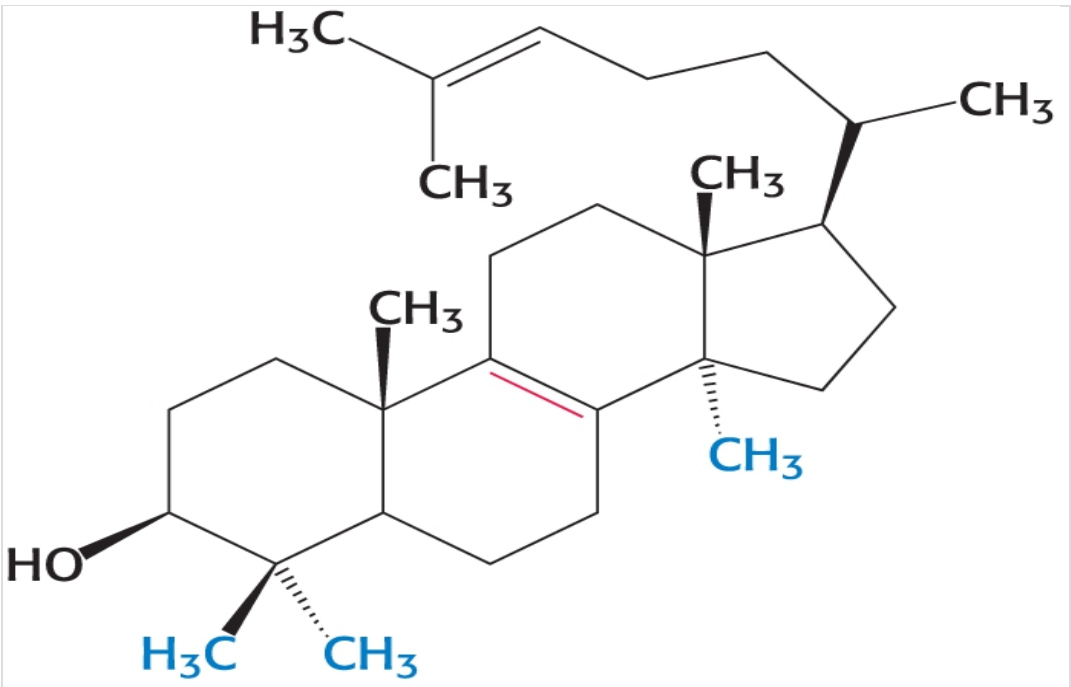
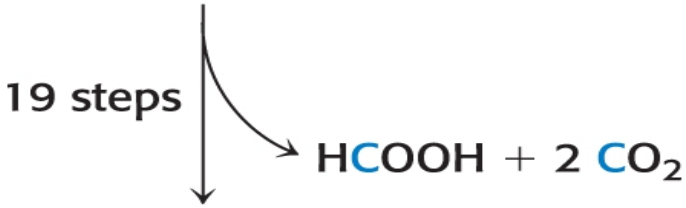


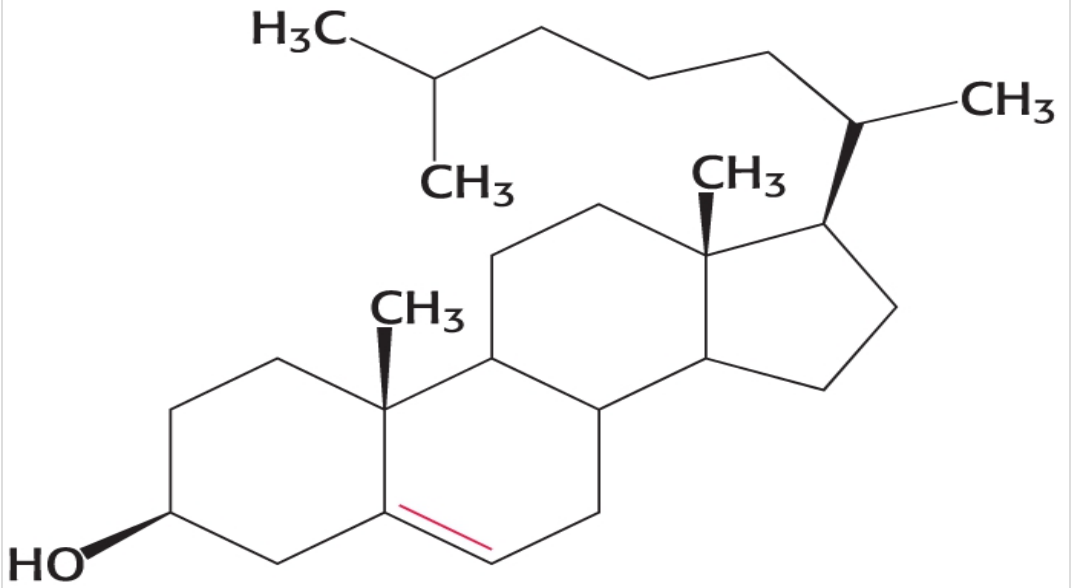
FIGURE 27.12 Squalene cyclization leads to the steroid skeleton in the form of lanosterol. The formation of the steroid nucleus from squalene begins with the formation of squalene epoxide. This intermediate is protonated to form a carbocation that cyclizes to form a tetracyclic structure, which rearranges to form lanosterol.

This is a remarkable chemical transformation, forming the four rings that are characteristic of steroids through four new carbon–carbon bonds. In addition, six new chiral centers are generated. In contrast to this remarkably efficient step, the conversion of lanosterol to cholesterol — which involves the removal of three methyl groups, the reduction of a double bond, and the migration of a different double bond — requires 19 steps and 9 different enzymes (Figure 27.13).



Lanosterol





Cholesterol

FIGURE 27.13 Cholesterol is formed from lanosterol. This complex transformation involves 19 steps and 9 different enzymes.



Self-Check Question



The biosynthesis of cholesterol requires 20 steps and 10 different enzymes. Which enzyme is responsible for the formation of the five-membered ring in the cholesterol structure?

27.3 The Regulation of Cholesterol Biosynthesis Takes Place at Several Levels

Cholesterol can be obtained from the diet or cells can synthesize it de novo, using one of the most highly regulated metabolic pathways known. Biosynthetic rates may vary several hundred-fold, depending on how much cholesterol is consumed in the diet. An adult on a low-cholesterol diet typically synthesizes about 800 mg of cholesterol per day. The liver is the major site of cholesterol synthesis in mammals, although the intestine also forms significant amounts.

The rate of cholesterol formation by the liver and intestine is highly responsive to the cellular level of cholesterol. This feedback regulation is mediated primarily by changes in the amount and activity of 3-hydroxy-3-methylglutaryl CoA reductase. As described earlier, this enzyme catalyzes the formation of mevalonate, the committed step in cholesterol biosynthesis. HMG CoA reductase is controlled in multiple ways:

1. *The rate of synthesis of reductase mRNA is controlled by a transcription factor called SREBP.* **Sterol regulatory element binding protein (SREBP)** is a member of a family of transcription factors that regulate the proteins required for lipid synthesis. SREBP binds to a short DNA sequence called the sterol regulatory element (SRE) on the $5'$ side of the reductase gene when cholesterol levels are low, enhancing transcription of the gene. In its inactive state, SREBP resides in the endoplasmic reticulum membrane, where it is associated with the SREBP cleavage activating protein (SCAP), an integral membrane protein. SCAP is the cholesterol sensor.

When cholesterol levels fall, SCAP escorts SREBP in small membrane vesicles to the Golgi complex, where it is released from the membrane by two specific proteolytic cleavages (Figure 27.14). The first cleavage frees a fragment of SREBP from SCAP, whereas the second cleavage releases the regulatory domain from the membrane. The released protein migrates to the nucleus and binds the SRE of the HMG-CoA reductase gene, as well as several other genes in the cholesterol biosynthetic pathway, to enhance transcription. When cholesterol levels rise, the proteolytic release of the SREBP is blocked, and the SREBP in the nucleus is rapidly degraded by proteasomes located in the nucleus. These two events halt the transcription of genes of the cholesterol biosynthetic pathways.

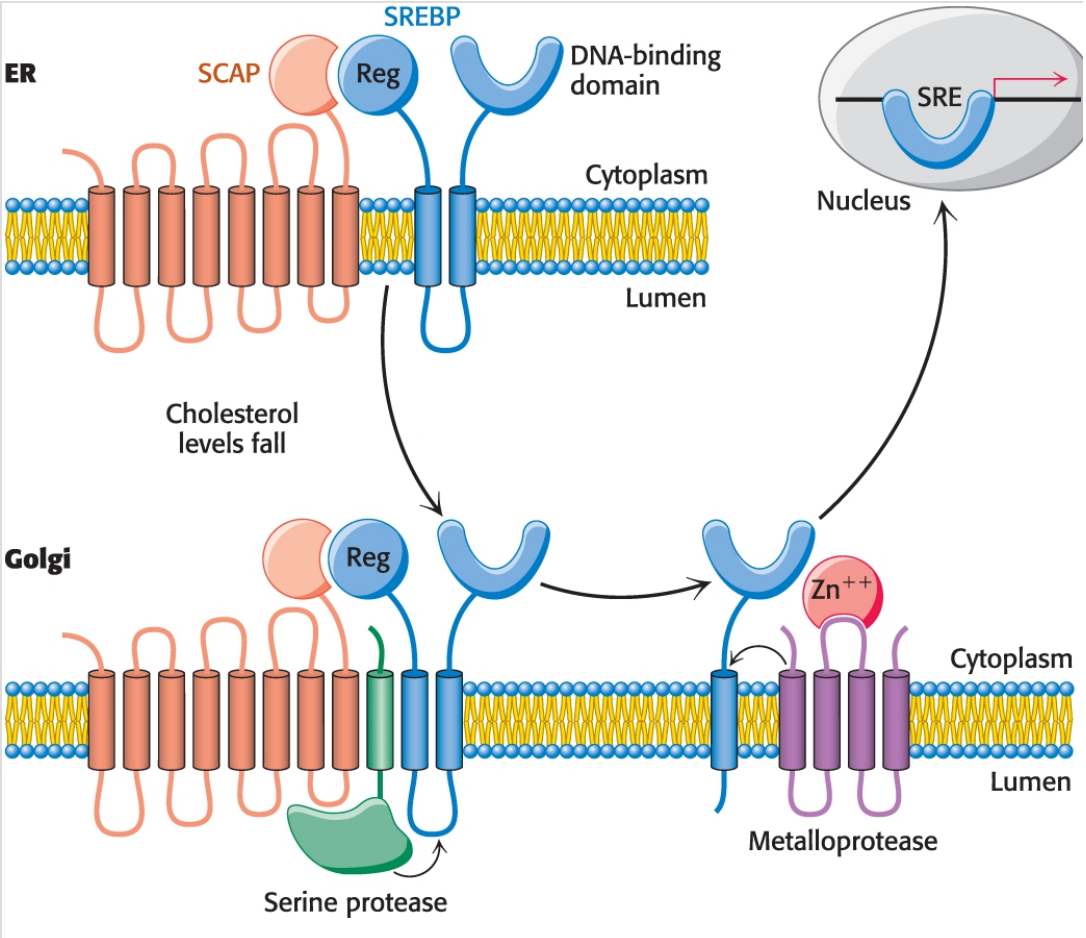


FIGURE 27.14 SREBP regulates gene expression in response to cholesterol levels. Stero regulatory element binding protein (SREBP) resides in the endoplasmic reticulum (ER),

where it is bound to SCAP by its regulatory (Reg) domain. When cholesterol levels fall, SCAP and SREBP move to the Golgi complex, where SREBP undergoes successive proteolytic cleavages by a serine protease and a metalloprotease. The released DNA-binding domain moves to the nucleus to alter gene expression.

[Information from an illustration provided by Dr. Michael Brown and Dr. Joseph Goldstein.]

What is the molecular mechanism that retains SCAP–SREBP in the ER when cholesterol is present but allows movement to the Golgi complex when cholesterol concentration is low? When cholesterol is low, SCAP binds to vesicular proteins that facilitate the transport of SCAP–SREBP to the Golgi apparatus. When cholesterol is present, SCAP binds cholesterol, which causes a structural change in SCAP so that it binds to another endoplasmic reticulum protein called Insig (insulin-induced gene) (Figure 27.15). Insig is the anchor that retains SCAP and thus SREBP in the endoplasmic reticulum in the presence of cholesterol. The interactions between SCAP and Insig can also be forged when Insig binds 25-hydroxycholesterol, a metabolite of cholesterol. Thus, two distinct steroid–protein interactions prevent the inappropriate movement of SCAP–SREBP to the Golgi complex.

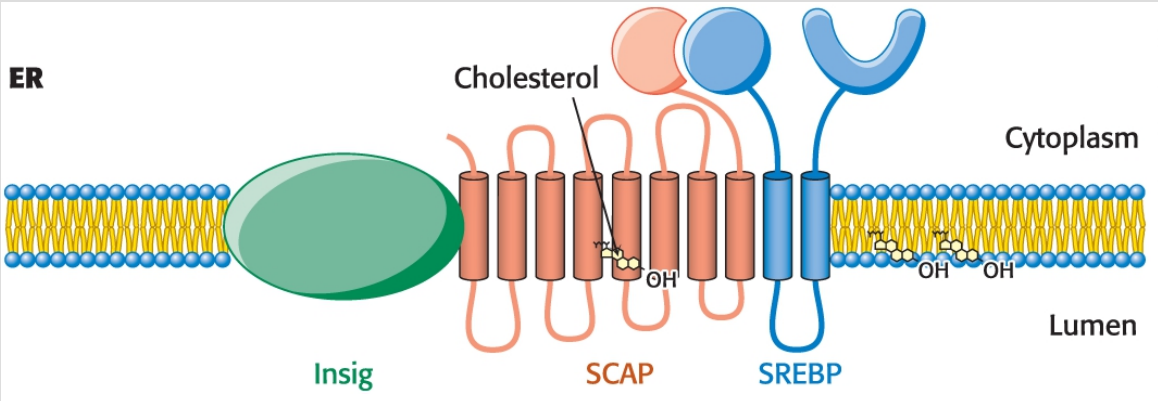


FIGURE 27.15 Insig regulates SCAP–SREBP movement. In the presence of cholesterol, Insig interacts with SCAP–SREBP and prevents the activation of SREBP. Cholesterol binding to SCAP 25-hydroxycholesterol binding to Insig facilitates the interaction of Insig and SCAP, retaining SCAP–SREBP in the endoplasmic reticulum.

2. *The rate of translation of reductase mRNA is inhibited by nonsterol metabolites derived from mevalonate.* This results in an 80% reduction in the rate of reductase protein production.

3. *The degradation of the reductase is stringently controlled.* The enzyme is bipartite: its cytoplasmic domain carries out catalysis, and its membrane domain senses signals that lead to its degradation. The membrane domain may undergo structural changes in response to increasing concentrations of sterols such as lanosterol and 25-hydroxycholesterol. Under these conditions, the reductase appears to bind to a subset of Insigs that are also associated with the ubiquitinating enzymes (Figure 27.16). The reductase is polyubiquitinated and subsequently extracted from the membrane in a process that requires geranylgeraniol. The extracted reductase is then degraded by the proteasome. The combined regulation at the levels of transcription, translation, and degradation can alter the amount of enzyme in the cell more than 200-fold.

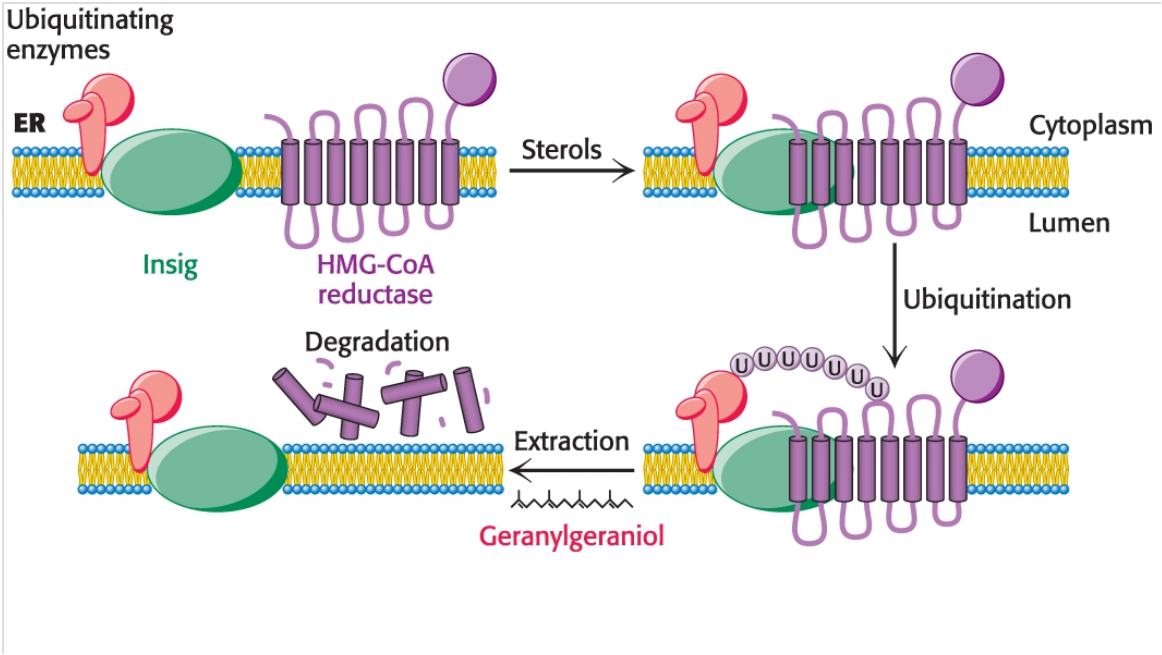


FIGURE 27.16 Insig facilitates the degradation of HMG-CoA reductase. In the presence of sterols, a subclass of Insig associated with ubiquitinating enzymes binds HMG-CoA reductase. This interaction results in the ubiquitination of the enzyme. This modification and the presence of geranylgeraniol results in extraction of the enzyme from the membrane and degradation by the proteasome.



4. *Phosphorylation decreases the activity of the reductase.* This enzyme, like acetyl CoA carboxylase, which catalyzes the committed step in fatty acid synthesis, is switched off by an AMP-activated protein kinase. Thus, cholesterol synthesis ceases when the ATP level is low.

Lipoproteins transport cholesterol and triacylglycerols throughout the organism

Cholesterol and triacylglycerols are transported in body fluids in the form of **lipoprotein particles**, which are important for a number of reasons. First, lipoprotein particles are the means by which triacylglycerols are delivered to tissues, from the intestine or liver, for use as fuel or for storage. Second, the fatty acid constituents of the triacylglycerol components of the lipoprotein particles are incorporated into phospholipids for membrane synthesis. Likewise, cholesterol is a vital component of membranes and is a precursor to the powerful signal molecules — the steroid hormones. Finally, cells are not able to degrade the steroid nucleus. Consequently, the cholesterol must be used biochemically or excreted by the liver. Excess cholesterol plays a role in the development of atherosclerosis. Lipoprotein particles function in cholesterol homeostasis, transporting the molecule from sites of synthesis to sites of use, and finally to the liver for excretion.

Each lipoprotein particle consists of a core of hydrophobic lipids surrounded by a shell of more-polar lipids and proteins. The protein

components of these macromolecular aggregates, called apoproteins, have two roles: they solubilize hydrophobic lipids and contain cell-targeting signals. Apolipoproteins are synthesized and secreted by the liver and the intestine.

Lipoprotein particles are classified according to increasing density (Table 27.1). Lipoprotein particles can shift between classes as they release or pick up cargo, thereby changing their density.

TABLE 27.1 Properties of plasma lipoproteins

					Composition (%)				
Plasma lipoproteins	**Density ($g\ ml^{-1}$)**	**Diameter (nm)**	**Apolipoprotein**	**Physiological role**	**TAG**	**CE**	**C**	**PL**	**P**
Chylomicron	< 0.95	75–1200	B-48, C, E	Dietary fat transport	86	3	1	8	2
Very low-density lipoprotein	0.95–1.006	30–80	B-100, C, E	Endogenous fat transport	52	14	7	18	8
Intermediate-density lipoprotein	1.006–1.019	15–35	B-100, E	LDL precursor	38	30	8	23	11
Low-density lipoprotein	1.019–1.063	18–25	B-100	Cholesterol transport	10	38	8	22	21
High-density	1.063–1.21	7.5–20	A	Reverse cholesterol transport	5–10	14–21	3–7	19–29	33–5

lipoprotein

Abbreviations: TAG, triacylglycerol; CE, cholesteryl ester; C, free cholesterol; PL, phospholipid; P, protein.

Chylomicrons

Triacylglycerols, cholesterol, and other lipids obtained from the diet are carried away from the intestine in the form of large chylomicrons. These particles have a very low density because triacylglycerols constitute about 90% of their content. Apolipoprotein B-48 (apo B-48), a large protein (240 kDa), forms an amphipathic spherical shell around the fat globule; the external face of this shell is hydrophilic.

The triacylglycerols in chylomicrons are released through hydrolysis by lipoprotein lipases. These enzymes are located on the lining of blood vessels in muscle and other tissues that use fatty acids as fuels or in the synthesis of lipids. The liver then takes up the cholesterol-rich residues, known as *chylomicron remnants.*

Very low-density lipoprotein

Lipoprotein particles are also crucial for the transport of lipids from the liver, which is a major site of triacylglycerol and cholesterol synthesis, to other tissues in the body (**Figure 27.17**). Triacylglycerols and cholesterol in excess of the liver's own needs are exported into the blood in the form of very low-density lipoproteins (VLDL). These particles are stabilized by two apolipoproteins — apo B-100 (513 kDa) and apo E (34 kDa).

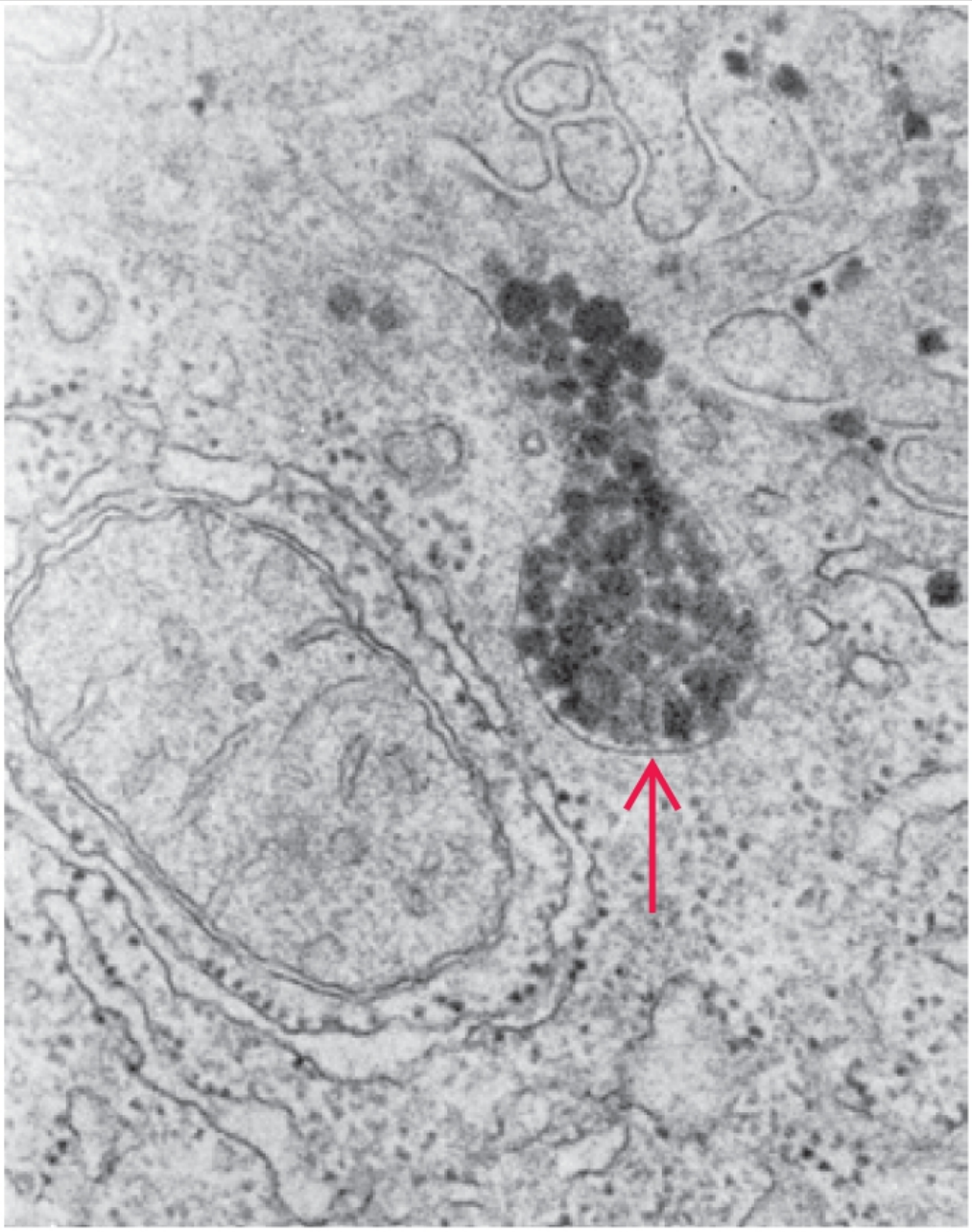


Photo Credit: Courtesy of Dr. George Palade/Yale University, Harvey Cushing/John Hay Whitney Medical Library.

FIGURE 27.17 The liver is the major site of cholesterol synthesis. An electron micrograph shows a part of a liver cell actively engaged in the synthesis and secretion of very low-density lipoprotein (VLDL). The arrow points to a vesicle that is releasing its content of VLDL particles.

Intermediate-density lipoprotein

Triacylglycerols in very low-density lipoproteins, as in chylomicrons, are hydrolyzed by lipases on capillary surfaces, with the released fatty acids being taken up by the muscle and other tissues. The resulting remnants, which are rich in cholesteryl esters, are intermediate-density lipoproteins (IDL). These particles have two fates. Half of them are taken up by the liver for processing, and half are converted into low-density lipoprotein by the removal of more triacylglycerol by tissue lipases that absorb the released fatty acids.

Low-density lipoprotein

The major carrier of cholesterol in blood is **low-density lipoprotein (LDL)** (**Figure 27.18**). It contains a core of some 1500 cholesterol molecules esterified to fatty acids. The most common fatty acid chain in these esters is linoleate, a polyunsaturated fatty acid. A shell of phospholipids and unesterified cholesterol molecules surrounds this highly hydrophobic core. The shell also contains a single copy of apo B-100, which is recognized by target cells. In addition to transporting cholesterol to peripheral tissues, LDL regulates de novo cholesterol synthesis at these sites.

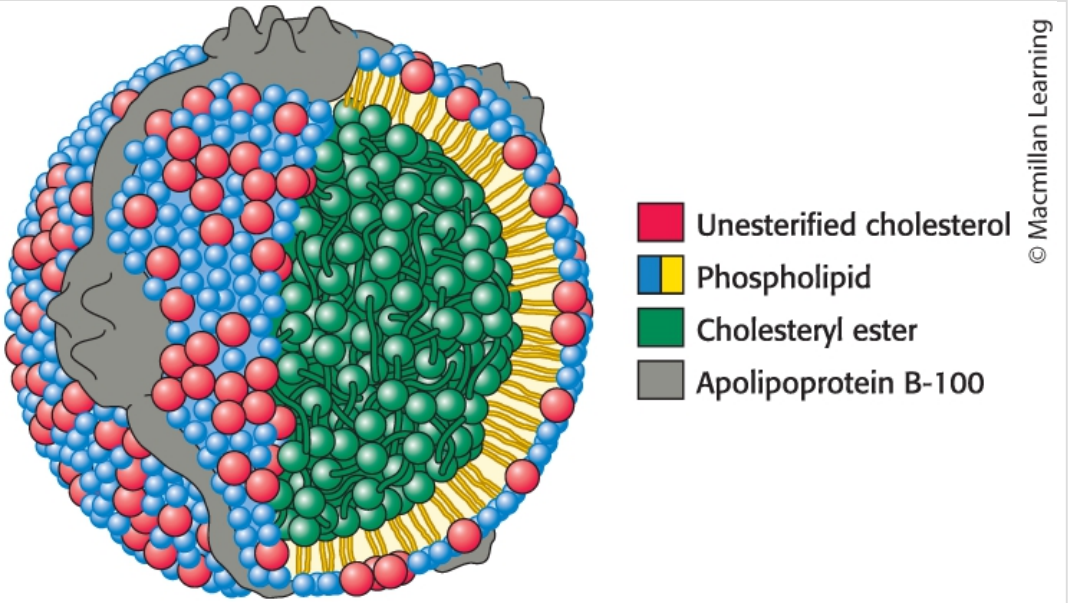


FIGURE 27.18 LDL consists of a core of cholesterol esters surrounded by a single molecule of apolipoprotein B-100. A low-density lipoprotein (LDL) particle is approximately 22 nm (220 Å) in diameter.

High-density lipoprotein

A different purpose is served by **high-density lipoprotein (HDL)**, which picks up cholesterol released into the plasma from dying cells and from membranes undergoing turnover and delivers the cholesterol to the liver for excretion. An acyltransferase in HDL esterifies these cholesterols, which are then returned by HDL to the liver.

Low-density lipoproteins play a central role in cholesterol metabolism

Cholesterol metabolism must be precisely regulated to prevent atherosclerosis. The mode of control in the liver, the primary site of cholesterol synthesis, has already been considered: dietary cholesterol reduces the activity and amount of 3-hydroxy-3-methylglutaryl CoA reductase, the enzyme catalyzing the committed step. In general, cells outside the liver and intestine obtain cholesterol from the plasma rather than synthesizing it de novo. Specifically, their primary source of cholesterol is the low-density lipoprotein. The process of LDL uptake, called **receptor-mediated endocytosis**, serves as a paradigm for the uptake of many molecules (**Figure 27.19**).

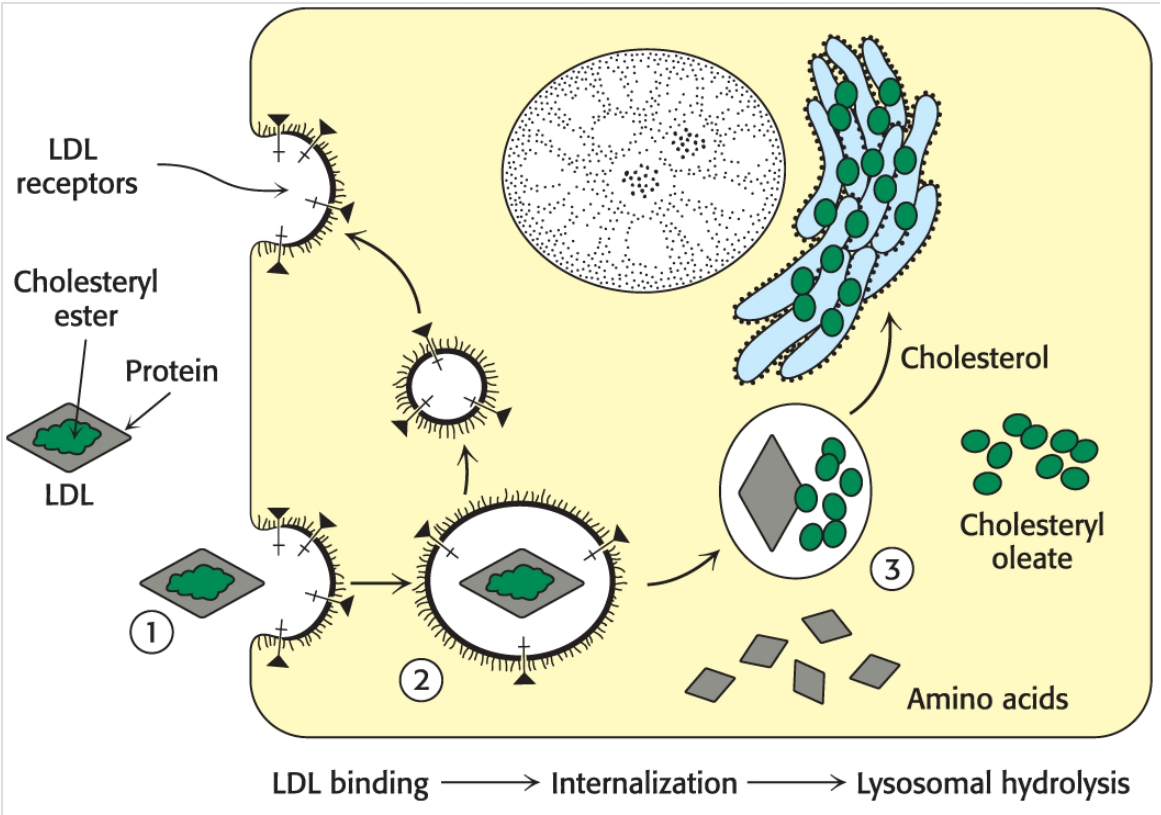


FIGURE 27.19 LDL enters cells through receptor-mediated endocytosis. (1) LDL binds to a specific receptor, the LDL receptor. (2) This complex invaginates to form an endosome. (3) After separation from its receptor, the LDL-containing vesicle fuses with a lysosome, leading to the degradation of the LDL and the release of the cholesterol.

Endocytosis begins when apolipoprotein B-100 on the surface of an LDL particle binds to a specific receptor protein on the plasma membrane of nonhepatic cells. The receptors for LDL are localized in specific regions called *coated pits*, which contain a protein called *clathrin*. The receptor–LDL complex is then internalized by endocytosis; that is, the plasma membrane in the vicinity of the complex invaginates and then fuses to form an endocytic vesicle called an *endosome*. The endosome is acidified by an ATP-dependent proton pump homologous to the Na^+/K^+ ATPase, which causes the receptor to release its cargo. Some of the receptor is returned to the cell membrane in a recycling vesicle, while a portion is degraded along with its cargo. The round-trip time for a receptor is about 10 minutes; in its lifetime of about a day, each receptor may bring hundreds of LDL particles into the cell.

The vesicles containing LDL, and in some cases the receptor, subsequently fuse with *lysosomes*, acidic vesicles that carry a wide array of degradative enzymes. The protein component of LDL is hydrolyzed to free amino acids, while the cholesteryl esters in LDL are hydrolyzed by a lysosomal acid lipase. The released unesterified cholesterol can then be used for membrane biosynthesis. Alternatively, it can be reesterified for storage inside the cell. In fact, free cholesterol activates acyl CoA:cholesterol acyltransferase (ACAT), the enzyme catalyzing this reaction.

Reesterified cholesterol contains mainly oleate and palmitoleate, which are monounsaturated fatty acids, in contrast with the cholesteryl esters in LDL, which are rich in linoleate, a polyunsaturated fatty acid (Table 12.1). It is imperative that the cholesterol be reesterified, because high concentrations of unesterified cholesterol disrupt the integrity of cell membranes.

The synthesis of the LDL receptor is itself subject to feedback regulation. Studies of cultured fibroblasts show that, when cholesterol is abundant inside the cell, new LDL receptors are not synthesized, and so the uptake of additional cholesterol from plasma LDL is blocked. The gene for the LDL receptor, like that for the reductase, is regulated by SREBP, which binds to a sterol regulatory element that controls the rate of mRNA synthesis.

The absence of the LDL receptor leads to hypercholesterolemia and atherosclerosis



The pioneering studies of familial hypercholesterolemia by Michael Brown and Joseph Goldstein revealed the physiological importance of the LDL receptor. The total concentration of cholesterol and LDL in the blood plasma is markedly elevated in this genetic disorder, which results from a mutation at a single autosomal locus. The cholesterol level in the plasma of homozygotes is typically $680\ \mathrm{mg\ dl^{-1}}$, compared with $300\ \mathrm{mg\ dl^{-1}}$ in heterozygotes (clinical assay results are often expressed in milligrams per deciliter, which is equal to milligrams per 100 milliliters). A value of $< 200\ \mathrm{mg\ dl^{-1}}$ is regarded as desirable, but many people have higher levels. In familial hypercholesterolemia, cholesterol is deposited in various tissues because of the high concentration of LDL cholesterol in the plasma. LDL accumulates under the endothelial cells lining the blood vessels, and nodules of cholesterol called *xanthomas* are prominent in skin and tendons.

Of particular concern is the oxidation of the excess LDL to form oxidized LDL (oxLDL), which can instigate the inflammatory response by the immune system, a response that has been implicated in the

development of cardiovascular disease. The oxLDL is taken up by immune system cells called macrophages, which become engorged to form foam cells. These foam cells become trapped in the walls of the blood vessels and contribute to the formation of atherosclerotic plaques that cause arterial narrowing and lead to heart attacks (Figure 27.20). In fact, most people who are homozygous for the hypercholesterolemia allele die of coronary artery disease in childhood. The disease in heterozygotes (1 in 500 people) has a milder and more variable clinical course.

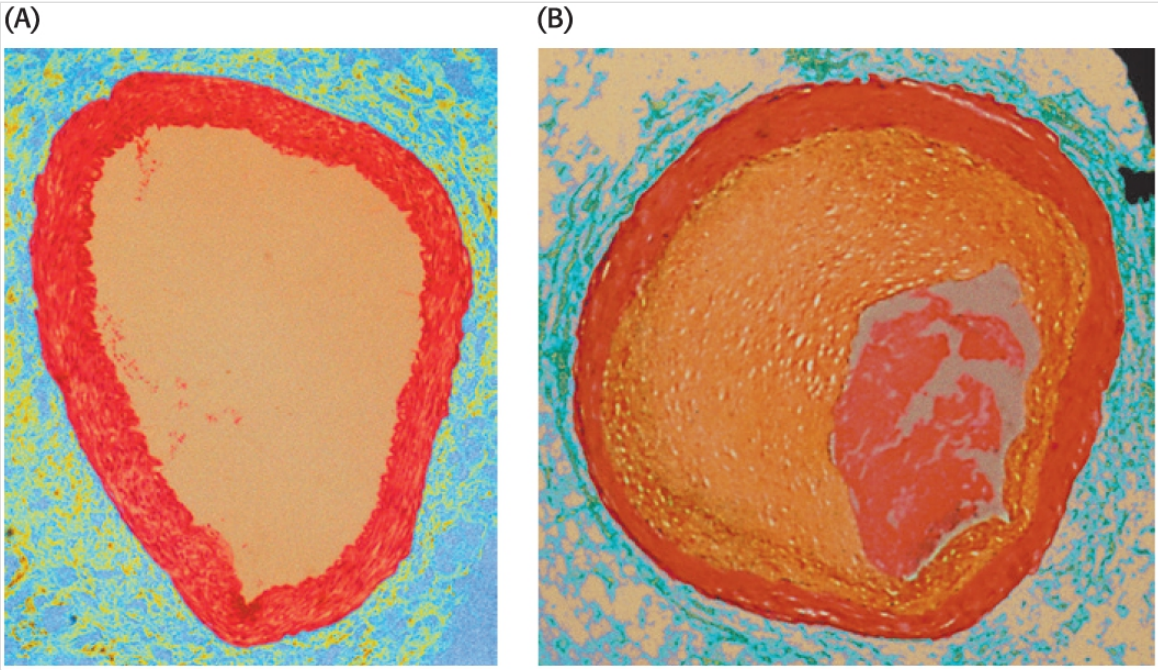


FIGURE 27.20 Arterial plaques are one of the effects of excess cholesterol. Cross sections of (A a normal artery and (B) an artery blocked by a cholesterol-rich plaque are shown.

The molecular defect in most cases of familial hypercholesterolemia is an absence or deficiency of functional receptors for LDL. Receptor mutations that disrupt each of the stages in the endocytotic pathway have been identified. Homozygotes have almost no functional receptors for LDL, whereas heterozygotes have about half the normal number.

The entry of LDL into liver and other cells is impaired, leading to an increased level of LDL in the blood plasma. Furthermore, less IDL enters liver cells because IDL entry, too, is mediated by the LDL receptor. Consequently, IDL stays in the blood longer in familial hypercholesterolemia, and more of it is converted into LDL than in normal people. All deleterious consequences of an absence or deficiency of the LDL receptor can be attributed to the ensuing elevated level of LDL cholesterol in the blood.

Mutations in the LDL receptor prevent LDL release and result in receptor destruction



One class of mutations that results in familial hypercholesterolemia generates receptors that are reluctant to give up the LDL cargo. Let us explore why this is by examining the makeup of the receptor. The human LDL receptor is a 160-kDa glycoprotein with a complicated modular structure (**Figure 27.21**). The receptor exists in two interconvertible states: an extended or open state, capable of binding LDL, and a closed state that results in release of the LDL in the endosome. The receptor maintains the open state while in the plasma membrane, on binding LDL, and throughout its journey to the endosome. The conversion from the open state into the closed state takes place on exposure to the acidic environment of the endosome.

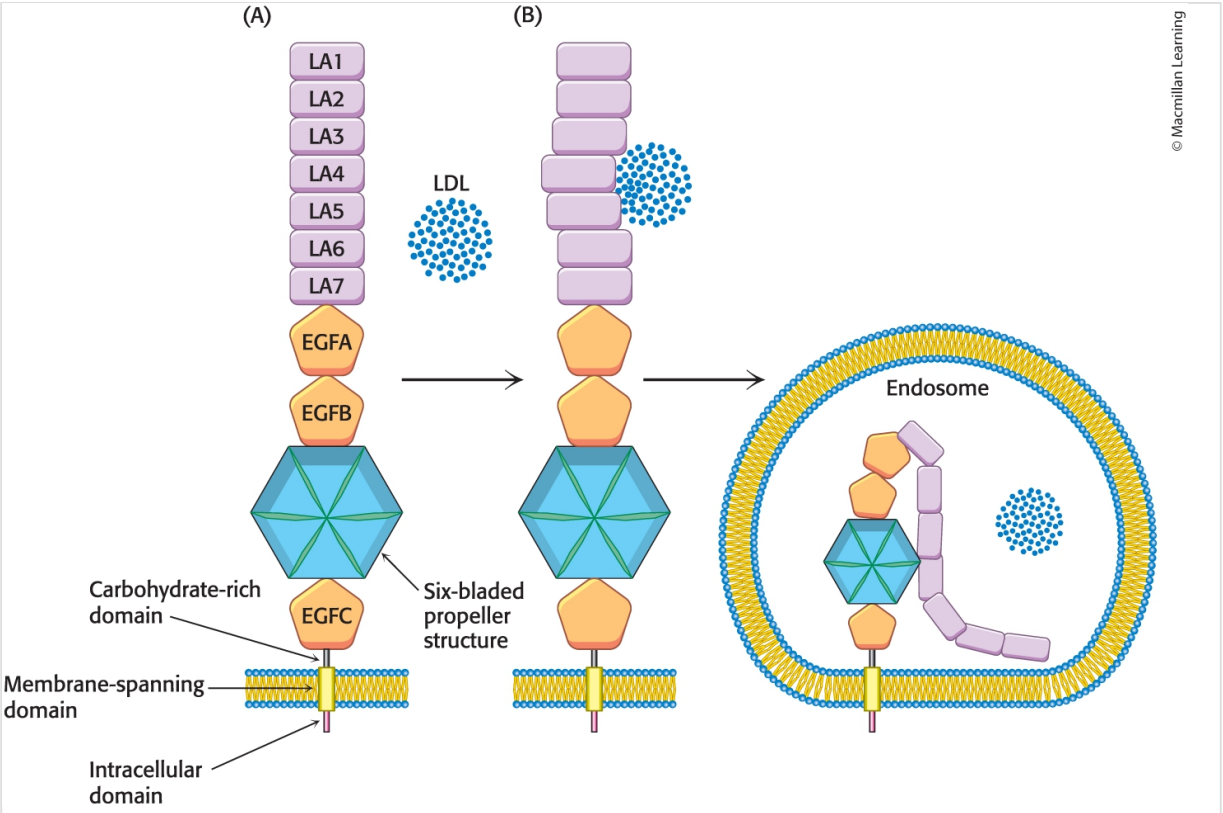


FIGURE 27.21 The LDL receptor releases LDL in the endosome. (A) A schematic representation of the domain structure of the LDL receptor. (B) In the endosome, the receptor converts from the open structure into the closed structure, resulting in the release of the LDL into the endosome.

The importance of this process is highlighted by the fact that more than half of the point mutations that result in familial hypercholesterolemia are due to disruptions in the interconversion between the open state and the closed state. These mutations result in a failure to release the LDL cargo and loss of the receptor by degradation.

Cycling of the LDL receptor is regulated

PCSK9 (proprotein convertase subtilisin/kexin type) is a protease, secreted by the liver, that plays a crucial role in the regulation of cycling

of the LDL receptor. However, despite the fact that PCSK9 is a protease, enzymatic activity of the protein is not required for cycling regulation. PCSK9 in the blood binds to the LDL receptor and locks it in the open conformation even under the acidic conditions of the endosome. Failure to adopt the closed conformation prevents the receptor from returning to the plasma membrane, and it is degraded in the lysosome along with its cargo.

 Individuals having a mutation that reduces the amount of PCSK9 in the blood have greatly reduced levels of LDL in the blood and display an almost 90% reduction in the rate of cardiovascular disease. Presumably, reduced levels of PCSK9 allow more receptor cycling and more efficient removal of LDL from the blood. Several monoclonal antibodies to PCSK9 have been approved for treatment for high LDL levels, but their use has been limited by their high cost.

HDL appears to protect against atherosclerosis

Although the events that result in atherosclerosis take place rapidly in familial hypercholesterolemia, a similar sequence of events takes place in people who develop atherosclerosis over decades. In particular, the formation of foam cells and plaques are especially hazardous occurrences. HDL and its role in returning cholesterol to the liver appear to be important in mitigating these life-threatening circumstances.

HDL has a number of antiatherogenic properties, including the inhibition of LDL oxidation. However, HDL's best-characterized property is the removal of cholesterol from cells, especially macrophages. Earlier, we noted that HDL retrieves cholesterol from other tissues in the body to return the cholesterol to the liver for

excretion as bile or in the feces. This transport, called *reverse cholesterol transport*, is especially important in regard to macrophages. Indeed, when the transport fails, macrophages become foam cells and facilitate the formation of plaques. Macrophages that collect cholesterol from LDL normally transport the cholesterol to HDL particles. The more HDL, the more readily this transport takes place and the less likely that the macrophages will develop into foam cells. Presumably, this robust reverse cholesterol transport accounts for the observation that higher HDL levels confer protection against atherosclerosis.

Until recently, high levels of HDL-bound cholesterol ("good cholesterol") relative to LDL-bound cholesterol ("bad cholesterol") were believed to protect against cardiovascular disease. This belief was based on epidemiological studies. However, a number of recent clinical trials revealed that increased levels of HDL-bound cholesterol may have little protective effect. These studies do not discount the protective effects of HDL alone, but they illustrate the danger of equating free HDL and cholesterol-bound HDL.

Self-Check Question



List three differences between low-density lipoprotein and high-density lipoprotein.

The clinical management of cholesterol levels can be understood at the biochemical level



Homozygous familial hypercholesterolemia can be treated only by a liver transplant. A more generally applicable therapy is available for heterozygotes and others with high levels of cholesterol. The goal is to reduce the amount of cholesterol in the blood by stimulating the synthesis of more than the customary number of LDL receptors. We have already observed that the production of LDL receptors is controlled by the cell's need for cholesterol. The therapeutic strategy is to deprive the cell of ready sources of cholesterol. When cholesterol is required, the amount of mRNA for the LDL receptor rises, and more receptors are found on the cell surface. This state can be induced by a two-pronged approach. First, the reabsorption of **bile salts** — cholesterol derivatives that promote the absorption of dietary cholesterol and dietary fats — from the intestine is inhibited. Second, de novo synthesis of cholesterol is blocked.

The reabsorption of bile is impeded by oral administration of positively charged polymers, such as cholestyramine, that bind negatively charged bile salts and are not themselves absorbed. Cholesterol synthesis can be effectively blocked by a class of compounds called *statins*. A well-known example of such a compound is lovastatin, which is also called mevacor (**Figure 27.22**). Statins are potent competitive inhibitors $(K_i = 1\ \text{nM})$ of HMG-CoA reductase, the essential control point in the biosynthetic pathway. Plasma cholesterol levels decrease by 50% in many patients given both lovastatin and inhibitors of bile-salt reabsorption. Lovastatin and other inhibitors of HMG-CoA reductase are widely used to lower the plasma-cholesterol level in people who have atherosclerosis, which is the leading cause of death in industrialized societies.

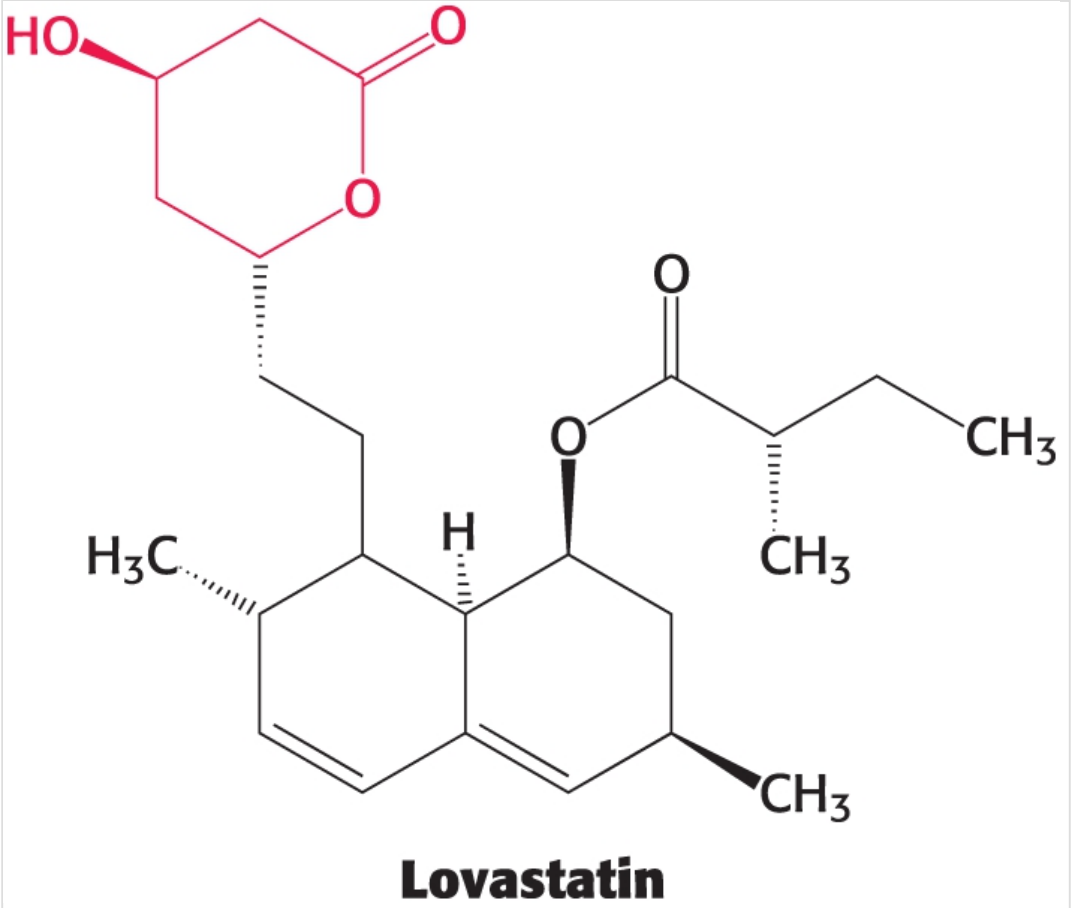


FIGURE 27.22 The statin lovastatin is a competitive inhibitor of HMG-CoA reductase. The part of the structure that resembles the 3-hydroxy-3-methylglutaryl moiety is shown in red.

27.4 Important Biochemicals Are Synthesized from Cholesterol and Isoprene

Cholesterol is the precursor of several other important classes of compounds. Bile salts, the major constituent of bile, are synthesized in the liver, stored and concentrated in the gallbladder, and then released into the small intestine. Bile salts are highly effective at solubilizing dietary lipids because they contain both polar and nonpolar regions. Solubilization increases the effective surface area of lipids with two consequences: (1) more surface area is exposed to the digestive action of lipases and (2) lipids are more readily absorbed by the intestine. Bile salts are also the major breakdown products of cholesterol. The bile salts glycocholate, the primary bile salt, and taurocholate are shown in Figure 27.23.

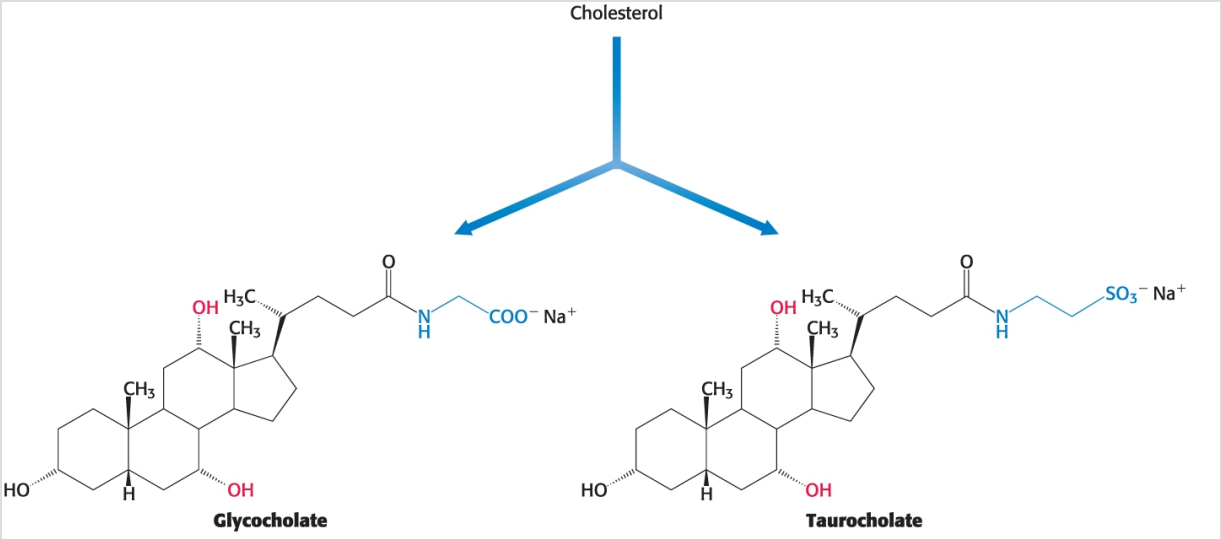


FIGURE 27.23 Bile salts are synthesized from cholesterol. The OH groups in red are added to cholesterol, as are the groups shown in blue. These polar groups make bile salt effective in detergents.

Cholesterol is also the precursor of the five major classes of steroid hormones — progestogens, glucocorticoids, mineralocorticoids, androgens, and estrogens (Figure 27.24). These hormones are powerful signal molecules that regulate a host of organismal functions.

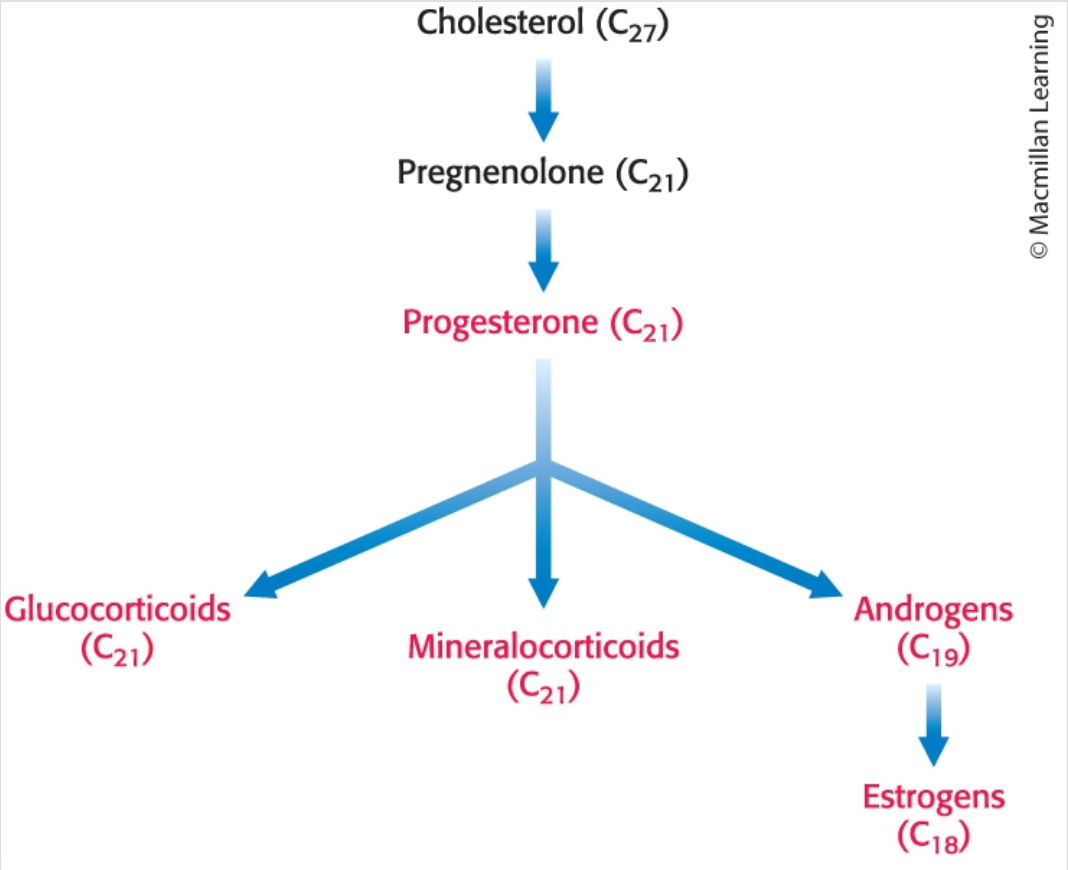


FIGURE 27.24 Different classes of steroid hormones are derived from cholesterol.

- Progesterone, a progestogen, prepares the lining of the uterus for the implantation of an ovum. Progesterone is also essential for the

maintenance of pregnancy by preventing premature uterine contractions.

- Glucocorticoids (such as cortisol) promote gluconeogenesis and glycogen synthesis, enhance the degradation of fat and protein, and inhibit the inflammatory response. They enable animals to respond to stress; indeed, the absence of glucocorticoids can be fatal.
- Mineralocorticoids (primarily aldosterone) act on the distal tubules of the kidney to increase the reabsorption of Na^+ and the excretion of K^+ and H^+, which leads to an increase in blood volume and blood pressure.
- Androgens (such as testosterone) are responsible for the development of male secondary sex characteristics.
- Estrogens (such as estradiol) are required for the development of female secondary sex characteristics. Estrogens, along with progesterone, also participate in the ovarian cycle.

These steroids are described using a common numbering and lettering system (Figure 27.25). The carbons are numbered 1–27 and the rings are denoted by the letters A–D.

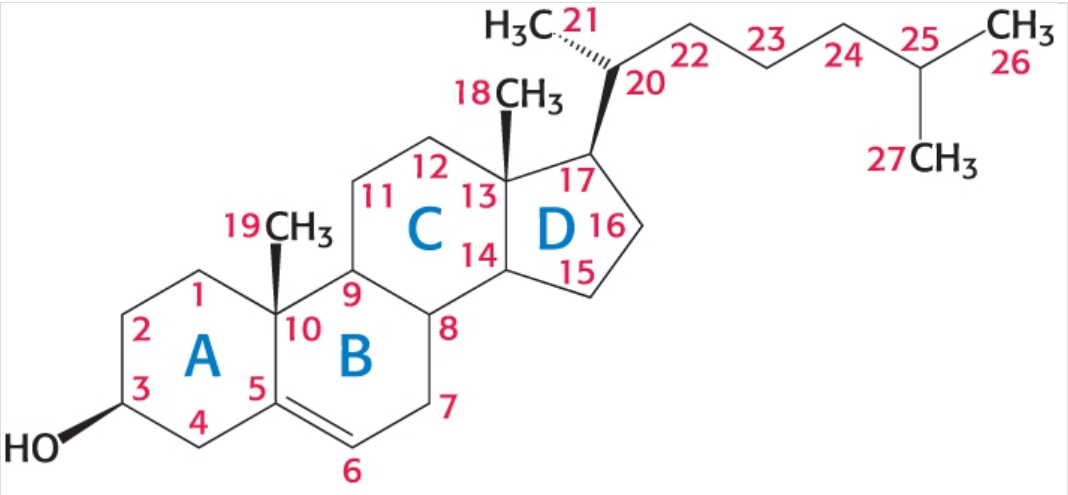


FIGURE 27.25 A common numbering system is used for cholesterol and other steroids. The numbering scheme for the carbon atoms and the naming system for

rings are shown.



The major sites of synthesis of these classes of hormones are the corpus luteum, for progestogens; the testes, for androgens; the ovaries, for estrogens; and the adrenal cortex, for glucocorticoids and mineralocorticoids.

Steroid hormones bind to and activate receptor molecules that serve as transcription factors to regulate gene expression. Despite their relatively similar structures, these compounds are able to have greatly differing physiological effects because the structural variations among them allow each class to be recognized by specific receptor molecules.

Steroids are hydroxylated by cytochrome P450 monooxygenases that use NADPH and O_2

The addition of oxygen atoms plays an important role in the synthesis of cholesterol from squalene and in the conversion of cholesterol into steroid hormones. These oxidation reactions require O_2 but, also, the reducing agent NADPH. One oxygen atom of the O_2 molecule goes into the substrate, while the other is reduced to water. The enzymes catalyzing these reactions are called *monooxygenases* (or *mixed-function oxygenases*). The general form of the most common type of reaction catalyzed by these enzymes is

$$RH + O_2 + NADPH + H^+ \rightarrow ROH + H_2O + NADP^+$$

In the synthesis of steroid hormones and bile salts, these reactions are catalyzed by members of the cytochrome P450 family, a family of heme-containing enzymes that absorb light maximally at 450 nm when complexed in vitro with exogenous carbon monoxide. Oxygen is activated through its binding to the iron atom in the heme group.

The catalytic mechanism for P450 enzymes is shown in **Figure 27.26**. NADPH transfers its high-potential electrons to a flavoprotein, which transfers them, one at a time, to adrenodoxin, a nonheme iron protein. Adrenodoxin transfers one electron to reduce the ferric (Fe^{3+}) form of P450 to the ferrous (Fe^{2+}) form. Without the addition of this electron, P450 will not bind oxygen. Recall that only the ferrous form (Fe^{2+}) of myoglobin and hemoglobin binds oxygen. The binding of O_2 to the heme is followed by the acceptance of a second electron from adrenodoxin. This second electron leads to cleavage of the $O—O$ bond. One of the oxygen atoms is then protonated and released as water. The remaining oxygen atom forms a highly reactive ferryl $(Fe^{4+})Fe{=}O$ intermediate with an additional electron removed from the porphyrin ring of the heme group. This intermediate removes a hydrogen atom from the substrate RH to form R•. This transient free radical captures the OH group from the iron atom to form ROH, the hydroxylated product, returning the iron atom to the ferric state.

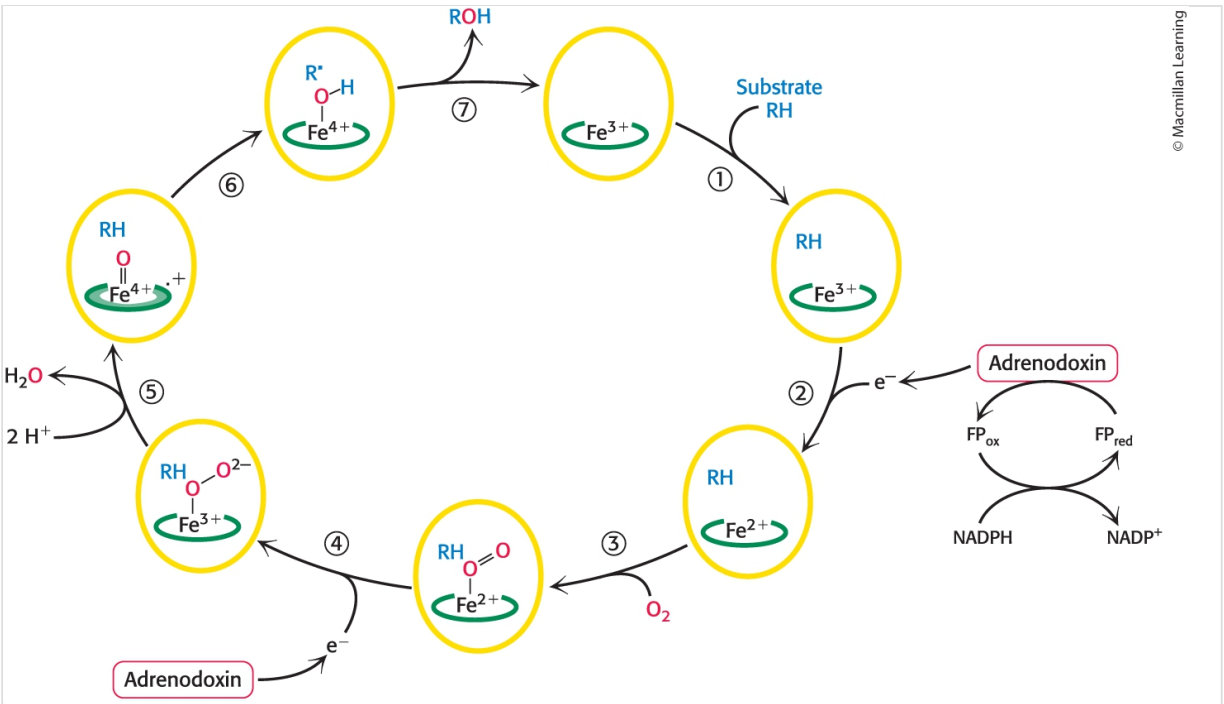


FIGURE 27.26 The reaction mechanism for cytochrome P450 enzymes reveals how oxygen is inserted into R-H bonds. (1) Substrate binds to the enzyme. (2) Adrenodoxin donates an electron, reducing the heme iron. (3) Oxygen binds to Fe^{2+}. (4) Adrenodoxin donates a second electron. (5) The bond between the oxygen atoms is cleaved, a molecule of water is released, and an intermediate with an $Fe^{4+}=O$ group and one electron removed from the porphyrin ring (indicated by shaded ring) is formed. (6) The $Fe^{4+}=O$ intermediate abstracts a hydrogen atom from the substrate to form a substrate radical. (7) The $Fe^{4+}-OH$ intermediate combines with the radical through the oxygen atom to form the hydroxylated product and return the iron to the Fe^{3+} state, ready for another reaction cycle.

Cytochrome P450s are widespread and perform many functions

The human genome encodes 57 members of the cytochrome P450 family, many of which have relatively broad substrate preferences. In addition to their roles in lipid and other biosynthetic pathways, members of the cytochrome P450 family are also important in the metabolism of foreign substances (xenobiotic compounds) including most drugs. For example, the hydroxylation of phenobarbital, a barbiturate, increases its solubility and facilitates its excretion. The duration of action of many drugs depends on their rate of metabolism by cytochrome P450 enzymes.

Some compounds are not active as drugs until they are modified by cytochrome P450 enzymes. These are referred to as *prodrugs*. For example, the anticoagulant clopidogrel (Plavix®) is inactive until it is oxidized by a cytochrome P450 family named cytochrome P450 2C19 (**Figure 27.27**). This requirement is particularly important because the genes encoding this enzyme are variable in the population, with more than 20% of human beings having variants that lead to reduced activity. Clopidogrel does not function well in these individuals. In some settings, a simple genetic is used prior to prescribing clopidogrel, and alternative drugs are used if clopidogrel activation is likely to be inefficient. The appreciation and use of the roles of genomic variations on drug action, a field referred to as *pharmacogenomics*, is of increasing importance.

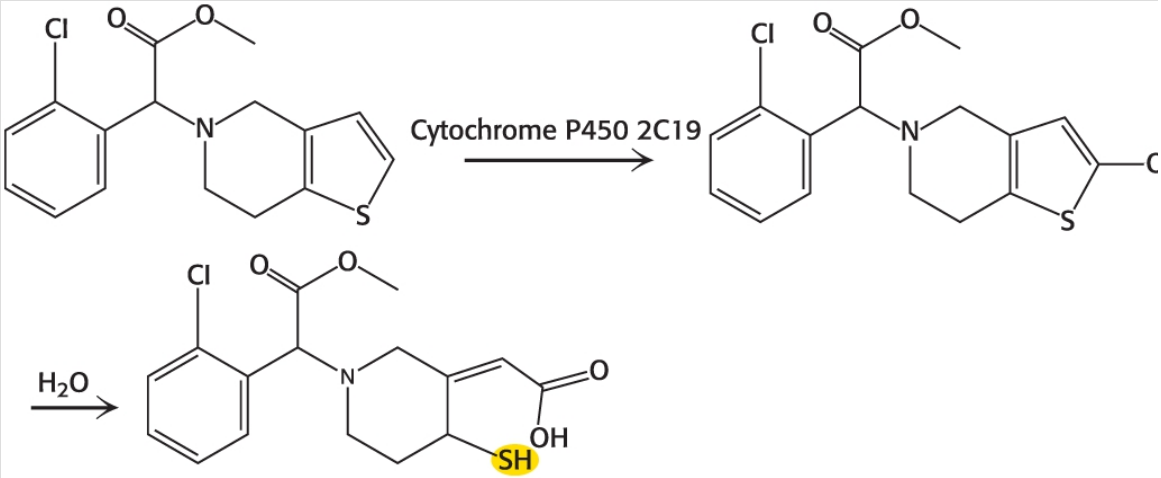


FIGURE 27.27 Cytochrome P450 2C19 converts the prodrug clopidogrel to an active form. The substance taken as clopidogrel is not active. The molecule is hydroxylated by cytochrome P450 2C19, and the product spontaneously hydrolyzes to produce a compound with a reactive thiol group (yellow).

Despite its general protective role in the removal of foreign chemicals, the action of the cytochrome P450 system can also do harm. Some of the most powerful carcinogens are generated from harmless compounds by the cytochrome P450 system in vivo in the process of metabolic activation. In plants, the cytochrome P450 system plays a role in the synthesis of toxic compounds as well as the pigments of flowers.



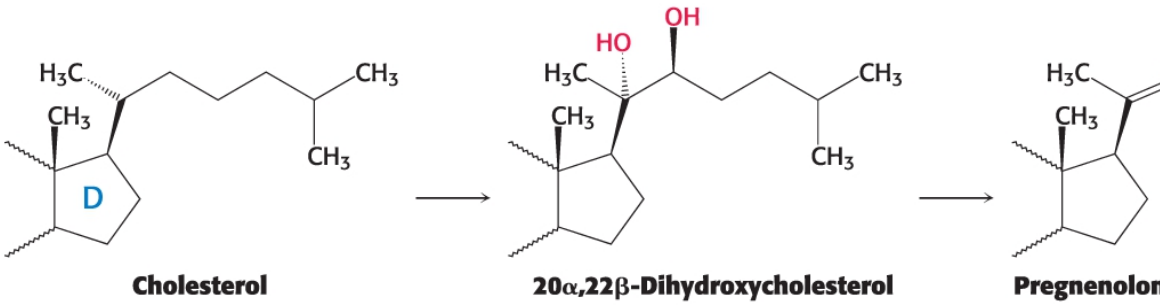
Keith Weller/Johns Hopkins Medicine

NAMANDJÉ BUMPUS After developing an interest in science from tinkering with chemistry sets as a child, Namandjé Bumpus (shown seated in the photo above) now pursues research at the interface between chemistry and medicine. After majoring in biology and becoming the first person in her family to graduate from college in 2003, she went on to earn a PhD in pharmacology that focused on a member of the cytochrome P450 family, a group of enzymes that has remained a primary interest throughout her career. She has also pursued research on the metabolism of drugs used for the treatment of HIV infections, including the importance of variations in genes for drug-metabolizing genes in determining individual responses to drugs. In 2020, Dr. Bumpus was appointed director of the Department of Pharmacology and Molecular Sciences at Johns Hopkins University School of Medicine, becoming the first Black woman to chair a department in the 128-year history of this prestigious

institution. She has received numerous awards including, appropriately enough, the John J. Abel Award in Pharmacology, named for the biochemist and pharmacologist who, in 1893, founded the department she now leads. In 2022, she was named Chief Scientist of the U.S. Food and Drug Administration (FDA).

Pregnenolone is a precursor of many other steroids

Steroid hormones contain 21 or fewer carbon atoms, whereas cholesterol contains 27. Thus, the first stage in the synthesis of steroid hormones is the removal of a six-carbon unit from the side chain of cholesterol to form the steroid pregnenolone. The side chain of cholesterol is hydroxylated at C-20 and at C-22, and then a third time resulting in cleavage of the bond between these atoms. Each of these steps is catalyzed by cytochrome $P450_{scc}$ (for side-chain cleavage), also known as desmolase and cytochrome P450 11A1.



Progesterone and corticosteroids

Progesterone is synthesized from pregnenolone in two steps. The 3-hydroxyl group of pregnenolone is oxidized to a 3-keto group, and the Δ^5 double bond is isomerized to a Δ^4 double bond (Figure 27.28).

Cortisol, the major glucocorticoid, is synthesized from progesterone by hydroxylations at C-11, C-17, and C-21; C-17 must be hydroxylated before C-21 is hydroxylated, whereas C-11 can be hydroxylated at any stage.

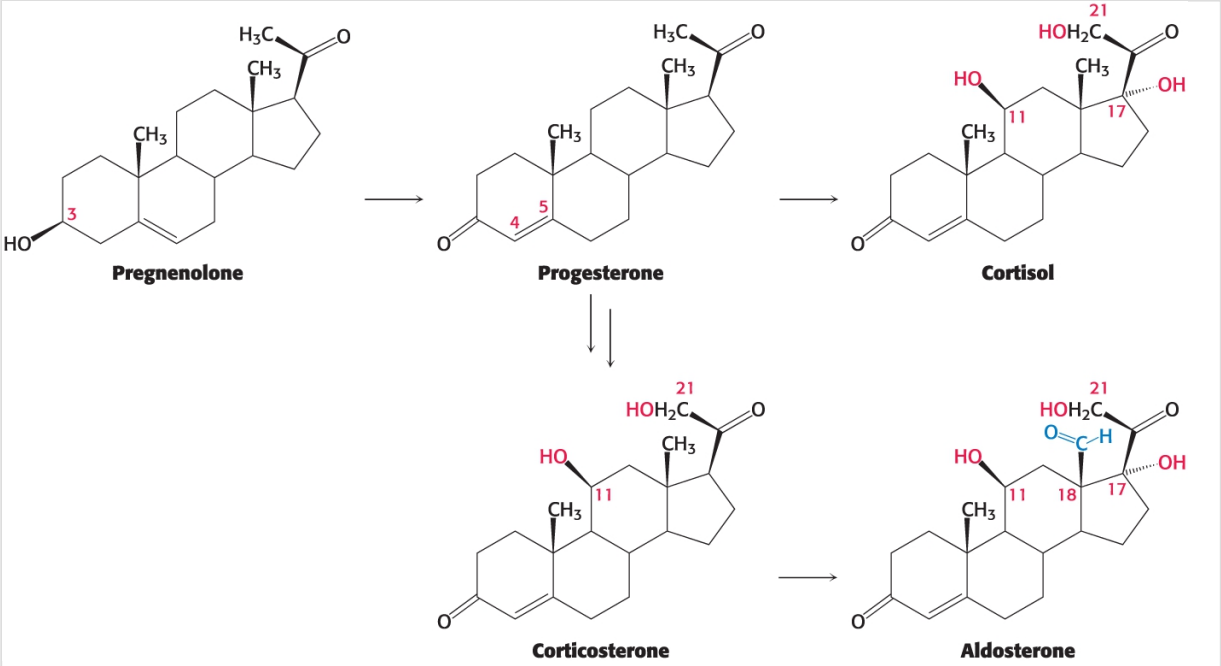


FIGURE 27.28 Pregnenolone is converted into progesterone, cortisol, and aldosterone.

The enzymes catalyzing these hydroxylations are highly specific. The initial step in the synthesis of aldosterone, the major mineralocorticoid, is the hydroxylation of progesterone at C-21. The resulting deoxycorticosterone is hydroxylated at C-11. The oxidation of the C-18 angular methyl group to an aldehyde then yields aldosterone.

Androgens and estrogens

Androgens and estrogens also are synthesized from pregnenolone through the intermediate progesterone. Androgens contain 19 carbon

atoms. The synthesis of androgens starts with the hydroxylation of progesterone at C-17 (Figure 27.29). The side chain consisting of C-20 and C-21 is then cleaved to yield androstenedione, an androgen. Testosterone, another androgen, is formed by the reduction of the 17-keto group of androstenedione.

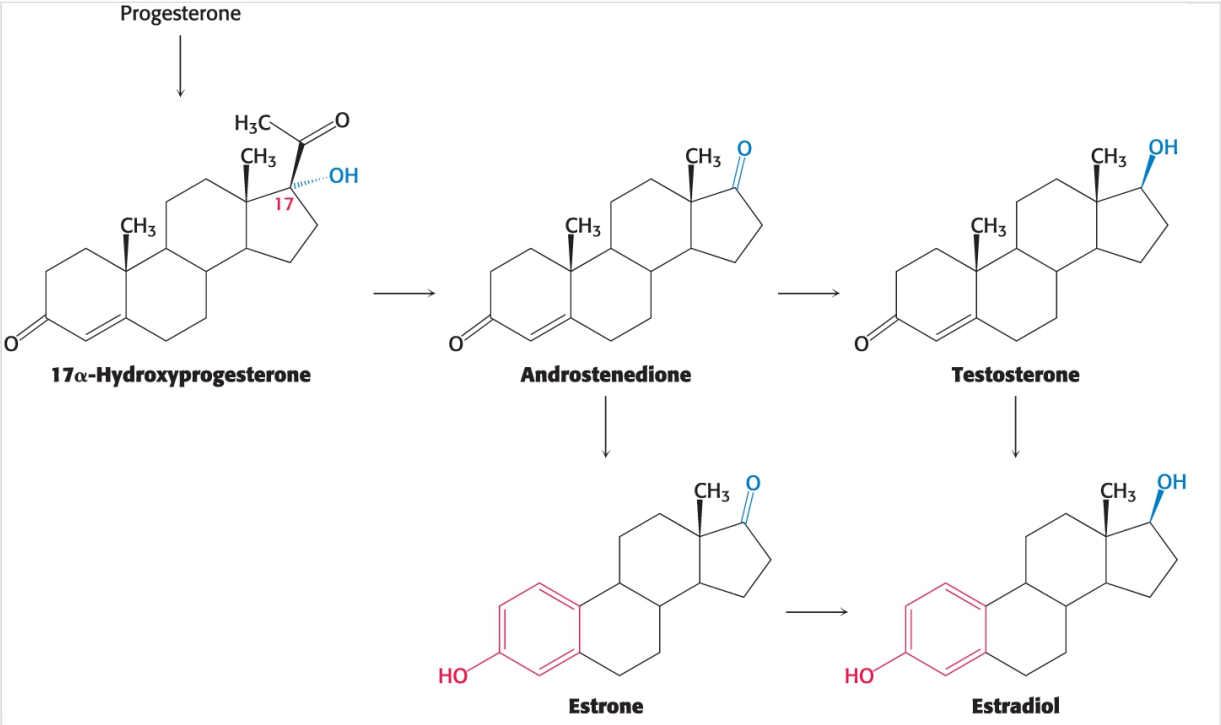
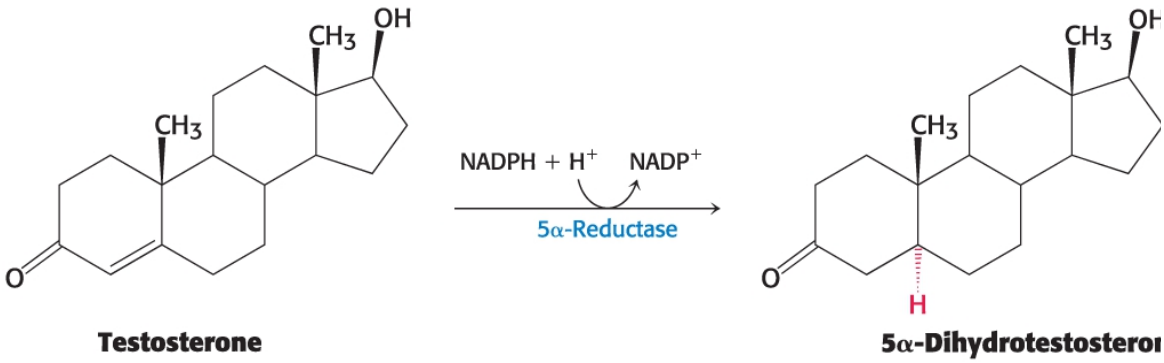


FIGURE 27.29 Progesterone is converted into testosterone and estradiol.

Testosterone is reduced by 5α-reductase to yield dihydrotestosterone, a potent androgen that instigates the development and differentiation of the male phenotype.



Testosterone **5α-Dihydrotestosteron**

Estrogens, the steroid hormones we introduced in Chapter 2, are synthesized from androgens by the loss of the C-19 angular methyl group and the formation of an aromatic A ring. Estrone, an estrogen, is derived from androstenedione, whereas estradiol, the biologically most potent estrogen, is formed from testosterone. Estradiol can also be formed from estrone. The formation of the aromatic A ring is catalyzed by the cytochrome P450 enzyme aromatase.

Because breast and ovarian cancers frequently depend on estrogens for growth, aromatase inhibitors are often used as a treatment for these cancers. Anastrozole (Arimidex) is a competitive inhibitor of the enzyme, whereas exemestane (Aromasin) is a suicide inhibitor that covalently modifies and inactivates the enzyme (**Figure 27.30**). The development of these drugs again reveals how the understanding of biosynthetic pathways can yield important medical and other applications.

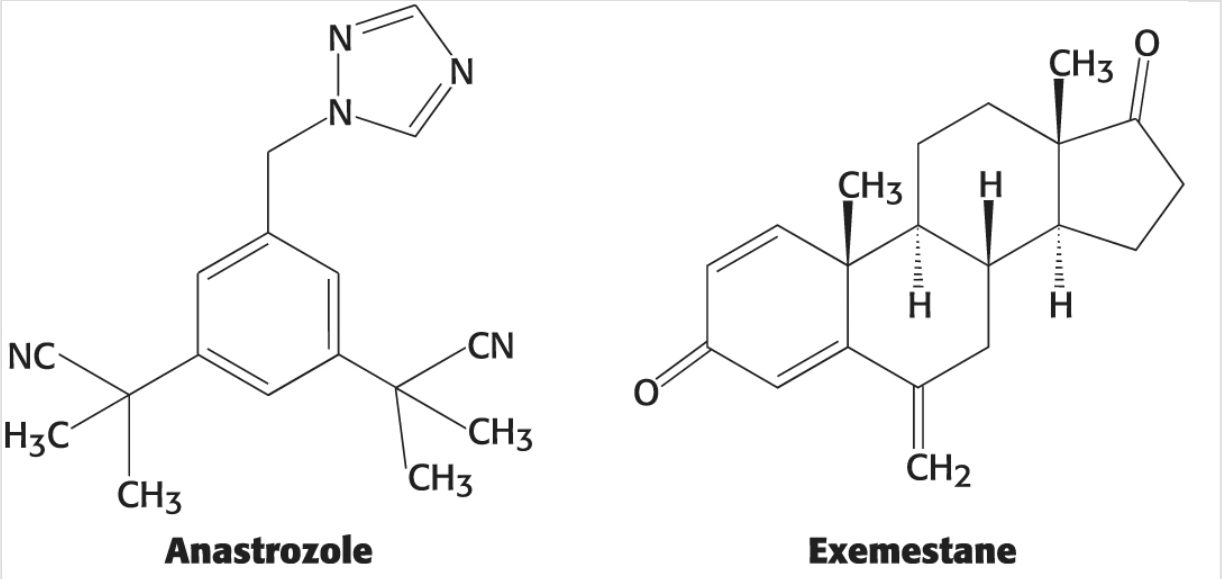


FIGURE 27.30 Drugs such as these for breast cancer can be developed based on knowledge of biosynthetic pathways.

Vitamin D is derived from cholesterol by the ring-splitting activity of light

Cholesterol is also the precursor of vitamin D, which plays an essential role in the control of calcium and phosphorus metabolism. 7-Dehydrocholesterol (provitamin D_3) is photolyzed by the ultraviolet light of sunlight to previtamin D_3, which spontaneously isomerizes to vitamin D_3 (Figure 27.31). Vitamin D_3 (cholecalciferol) is converted into the hormone calcitriol (1,25-dihydroxycholecalciferol), the active form of vitamin D, by hydroxylation reactions in the liver and kidneys. Although not a steroid hormone, vitamin D acts in an analogous fashion. It binds to receptors, homologous to the steroid receptors, to

form complexes that function as transcription factors, regulating gene expression.

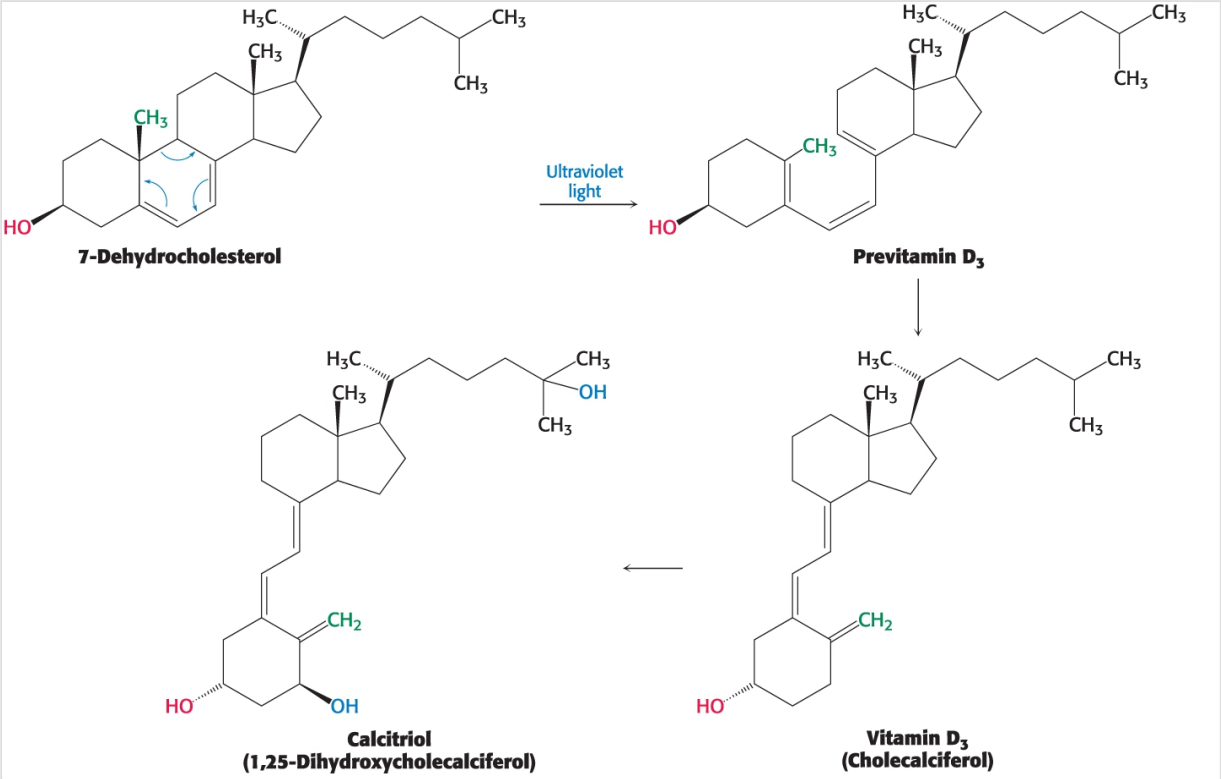


FIGURE 27.31 Vitamin D is synthesized from 7-dehydrocholesterol in a process initiated by absorption of ultraviolet light. The pathway for the conversion of 7-dehydrocholesterol into vitamin D_3 and then into calcitriol (vitamin D) is shown.

Self-Check Question

Label the carbon atoms from 1 to 27 in calcitriol using the numbering scheme from Figure 27.25.

 Vitamin D deficiency in childhood produces rickets, a disease characterized by inadequate calcification of cartilage and bone. Rickets was so common in 17th-century England that it was called the "children's disease of the English." In the typically overcast weather of England, the 7-dehydrocholesterol in the skin of these children was not sufficiently photolyzed to previtamin D_3. Furthermore, their diet provided little vitamin D, because most naturally occurring foods have a low content of this vitamin. Fish-liver oils are a notable exception. Cod-liver oil, abhorred by generations of children because of its unpleasant taste, was used in the past as a rich source of vitamin D. Today, the most reliable dietary sources of vitamin D are fortified foods. Milk, for example, is fortified to a level of 400 international units per quart (10 μg per quart). The recommended daily intake of vitamin D is 200 international units until age 50, after which it increases with age as the skin becomes less able to manufacture previtamin D_3 in response to sunlight; this is a striking reminder that vitamin D is needed by adults as well as by children.

Five-carbon units are joined to form a wide variety of biomolecules

We have seen that a remarkable array of compounds are formed from isopentenyl pyrophosphate, the basic five-carbon building block. The first step, the synthesis of squalene (C_{30}) from isopentenyl pyrophosphate (C_5), exemplifies a fundamental mechanism for the assembly of carbon skeletons of biomolecules. We will end this chapter by looking at a few more biologically important compounds produced from C_5 units.

The fragrances of many plants arise from volatile C_{10} and C_{15} compounds, which are called *terpenes*. For example, myrcene $(C_{10}H_{16})$ from bay leaves, hops, and cannabis, among other plants, consists of two isoprene units, as does limonene $(C_{10}H_{15})$ from lemon oil (**Figure 27.32**). Zingiberene $(C_{15}H_{24})$, from the oil of ginger, is made up of three isoprene units. Some terpenes, such as geraniol from geraniums and menthol from peppermint oil, are alcohols, and others, such as citronellal, are aldehydes. Natural rubber is a linear polymer of *cis*-isoprene units.

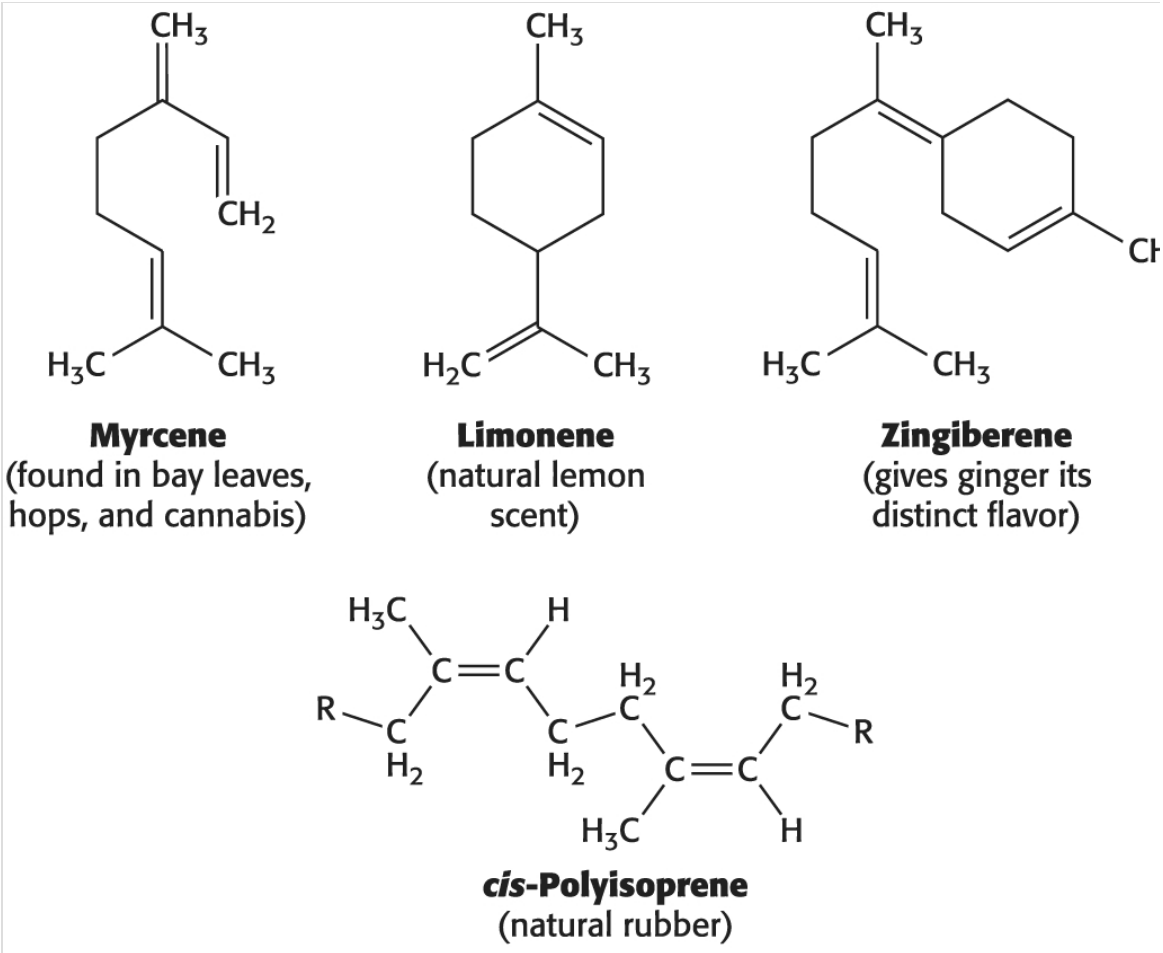


FIGURE 27.32 Some terpenes are familiar from everyday life.

We have already encountered several molecules that contain isoprenoid side chains. The C_{30} hydrocarbon side chain of vitamin K, a key molecule in clotting, is built from six C_5 units. Coenzyme Q_{10} in the mitochondrial respiratory chain has a side chain made up of 10 isoprene units. Yet another example is the phytol side chain of chlorophyll, which is formed from four isoprene units.

Isoprenoids can delight by their color as well as by their fragrance. The color of tomatoes and carrots comes from *carotenoids*, specifically from lycopene and β-carotene, respectively. These compounds absorb light because they contain extended networks of single and double bonds — that is, they are *polyenes*. Their C_{40} carbon skeletons are built by the successive addition of C_5 units to form geranylgeranyl pyrophosphate, a C_{20} intermediate, which then condenses tail-to-tail with another molecule of geranylgeranyl pyrophosphate. This biosynthetic pathway is like that of squalene, except that C_{20} rather than C_{15} units are assembled and condensed.

$$C_5 \rightarrow C_{10} \rightarrow C_{15} \rightarrow C_{30} \qquad \text{(Squalene)}$$

$$C_5 \rightarrow C_{10} \rightarrow C_{15} \rightarrow C_{20} \rightarrow C_{40} \qquad \text{(Phytoene)}$$

Phytoene, the C_{40} condensation product, is dehydrogenated to yield lycopene. Cyclization of both ends of lycopene gives β-carotene (**Figure 27.33**). Carotenoids serve as light-harvesting molecules in photosynthetic assemblies and also play a role in protecting bacteria from the deleterious effects of light. Carotenoids are also essential for

vision. β-Carotene is the precursor of retinal, the chromophore in visual pigments.

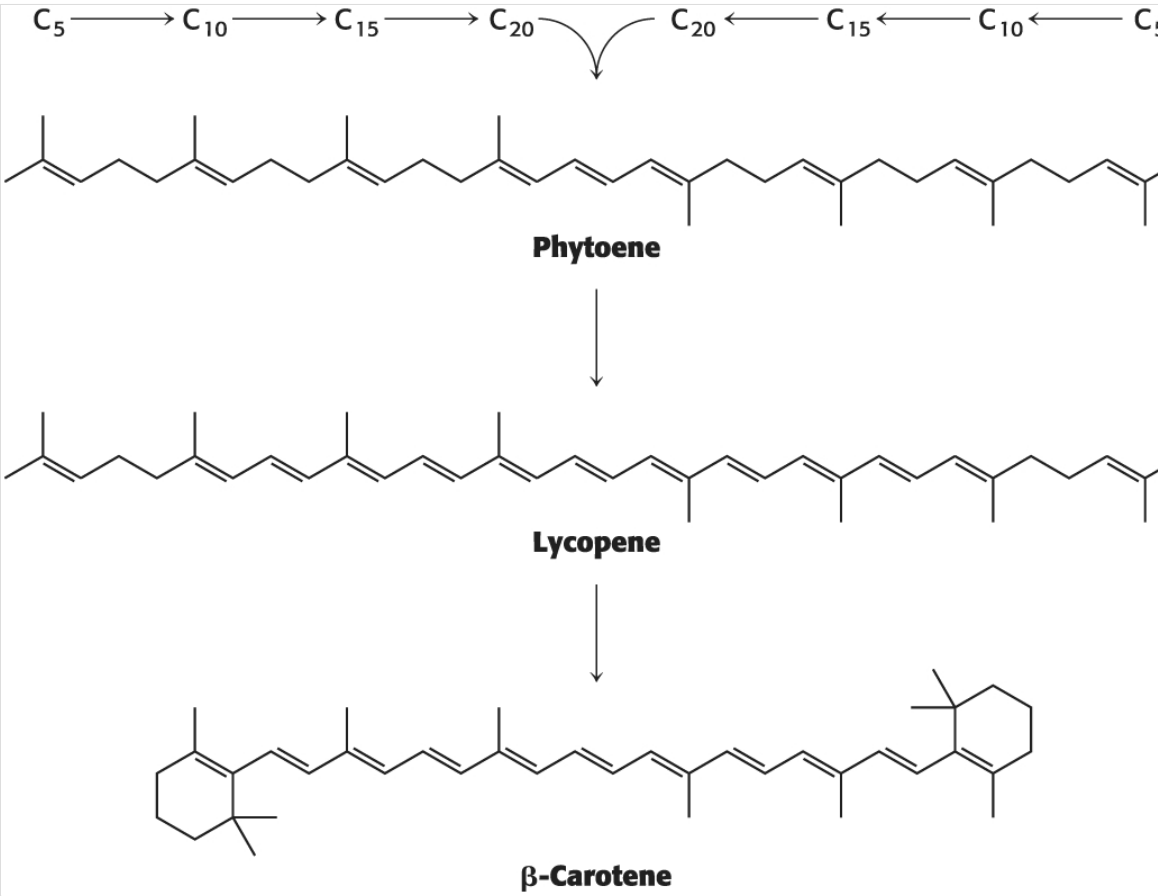
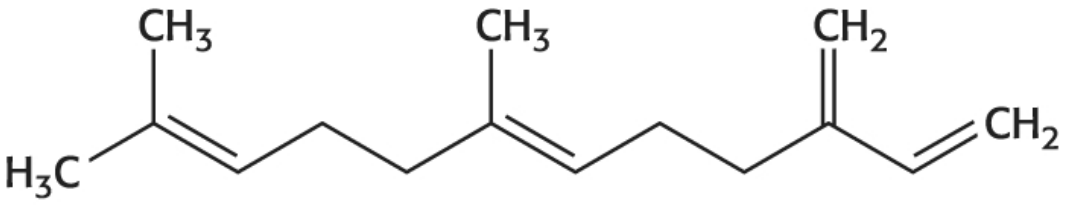


FIGURE 27.33 Two carotenoids responsible for the color of tomatoes and carrots are large isotrenes. Lycopenes give ripe tomatoes their red color, and **b**-carotene gives carrots their orange hue.

Some isoprenoids have industrial applications

Farnesene is an isoprenoid that has potential to meet a wide variety of practical needs (Table 27.2).



Farnesene

TABLE 27.2 Uses of farnesene and its derivatives

As a high-energy density biofuel
As sealants and adhesives
As solvents and lubricants
To make automobile tires that yield improved gas mileage and wet road grip
As a component of cosmetics
To make flavors and fragrances

However, to meet these potential uses in an economical manner, large amounts of farnesene are produced in modified baker's yeast, with genes for four enzymes that were not native to yeast introduced. These genes enable the yeast to ferment sugar cane syrup to farnesene, and

then to secrete the farnesene. The secreted farnesene is 93% pure, and distillation enhances the purity to 98%. This process can be scaled up to industrial levels, thus generating a versatile, renewable biomolecule with a variety of applications.

Chapter 27 Summary

27.1 Phosphatidate Is a Common Intermediate in the Synthesis of Phospholipids and Triacylglycerols

- Phosphatidate is formed by successive acylations of glycerol 3-phosphate by acyl CoA.
- Hydrolysis of the phosphoryl group from phosphatidate followed by acylation yields triacylglycerol.
- CDP-diacylglycerol is formed from phosphatidate and CTP. The activated phosphatidyl unit is then transferred to the hydroxyl group of a polar alcohol to form a phospholipid.
- In mammals, phosphatidylethanolamine is formed by CDP-ethanolamine and diacylglycerol. Phosphatidylethanolamine is methylated by *S*-adenosylmethionine to form phosphatidylcholine. Phosphatidylcholine can also be synthesized by a pathway that utilizes dietary choline.
- Sphingolipids are synthesized from ceramide, which is formed by the acylation of sphingosine.

27.2 Cholesterol Is Synthesized from Acetyl Coenzyme A in Three Stages

- Cholesterol is a steroid component of animal cell membranes and is also a precursor of steroid hormones.
- The committed step in its synthesis is the formation of mevalonate from 3-hydroxy-3-methylglutaryl CoA. Mevalonate is converted into farnesyl pyrophosphate, which condenses with itself to form squalene.
- Squalene cyclizes to lanosterol, which is modified to form cholesterol.

27.3 The Regulation of Cholesterol Biosynthesis Takes Place at Several Levels

- In the liver, cholesterol synthesis is regulated by changes in the amount and activity of 3-hydroxy-3-methylglutaryl CoA reductase. Transcription of the gene, translation of the mRNA, degradation of the enzyme, and enzyme activity are stringently controlled.
- Triacylglycerols exported by the intestine are carried by chylomicrons and then hydrolyzed by lipases lining the capillaries of target tissues. Cholesterol and other lipids in excess of those needed by the liver are exported in the form of very low-density lipoprotein.
- After delivering its content of triacylglycerols to adipose tissue and other peripheral tissue, very-low density lipoprotein is converted into intermediate-density lipoprotein (IDL) and then into low-density lipoprotein (LDL). IDL and LDL carry cholesteryl esters, primarily cholesteryl linoleate.
- Liver and peripheral tissue cells take up LDL by receptor-mediated endocytosis. The LDL receptor, a protein spanning the plasma membrane of the target cell, binds LDL and mediates its entry into the cell.
- Absence of the LDL receptor in the homozygous form of familial hypercholesterolemia leads to a markedly elevated plasma level of LDL cholesterol and the deposition of cholesterol on blood-vessel walls.
- High-density lipoproteins transport cholesterol from the peripheral tissues to the liver.

27.4 Important Biochemicals Are Synthesized from Cholesterol and Isoprene

- Hydroxylations by cytochrome P450 monooxygenases that use NADPH and O_2 play an important role in the synthesis of

steroid hormones and bile salts from cholesterol.

- Five major classes of steroid hormones are derived from cholesterol: progestogens, glucocorticoids, mineralocorticoids, androgens, and estrogens.
- Cytochrome P450 enzymes participate in the detoxification of drugs and other foreign substances.
- Pregnenolone is an essential intermediate in the synthesis of steroids.
- Estrogens are synthesized from androgens by the loss of an angular methyl group and the formation of an aromatic A ring.
- Vitamin D, which is important in the control of calcium and phosphorus metabolism, is formed from a derivative of cholesterol by the action of light.
- A remarkable array of biomolecules in addition to cholesterol and its derivatives are synthesized from isopentenyl pyrophosphate, the basic five-carbon building block.

Key Terms

phosphatidate
triacylglycerol
cytidine diphosphodiacylglycerol (CDP-diacylglycerol)
sphingolipid
ceramide
cholesterol
mevalonate
3-hydroxy-3-methylglutaryl CoA reductase (HMG-CoA reductase)
squalene
sterol regulatory element binding protein (SREBP)
lipoprotein particles
low-density lipoprotein (LDL)
high-density lipoprotein (HDL)

receptor-mediated endocytosis
bile salt

Problems

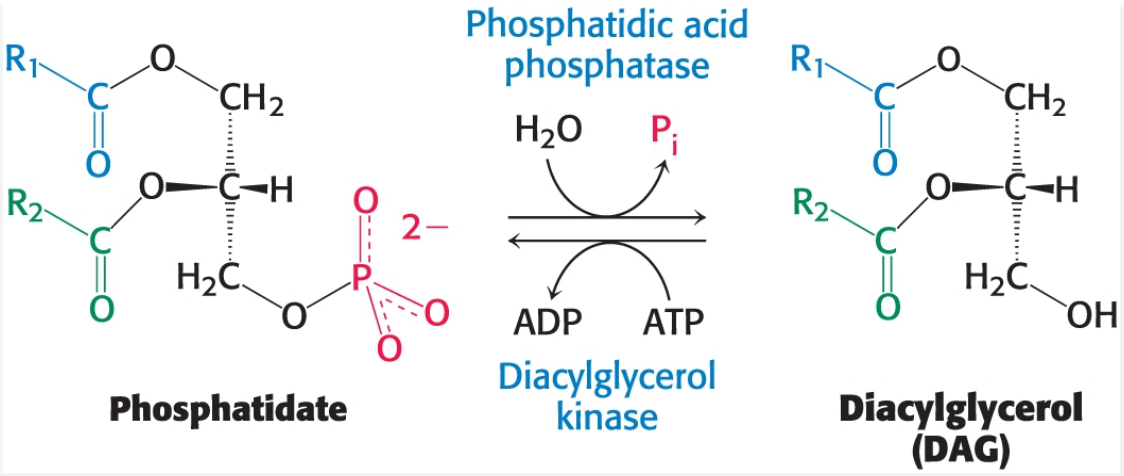
1. How many high-phosphoryl-transfer-potential molecules are required to synthesize phosphatidylethanolamine from ethanolamine and diacylglycerol? Assume that the ethanolamine is the activated component. 1

2. What is the activated reactant in each of the following biosyntheses? 1

a. Phosphatidylinositol from inositol
b. Phosphatidylethanolamine from ethanolamine
c. Ceramide from sphingosine
d. Sphingomyelin from ceramide
e. Cerebroside from ceramide
f. Ganglioside G_{M1} from ganglioside G_{M2}
g. Farnesyl pyrophosphate from geranyl pyrophosphate

3. Write a balanced equation for the synthesis of a triacylglycerol, starting from glycerol and fatty acids. 1

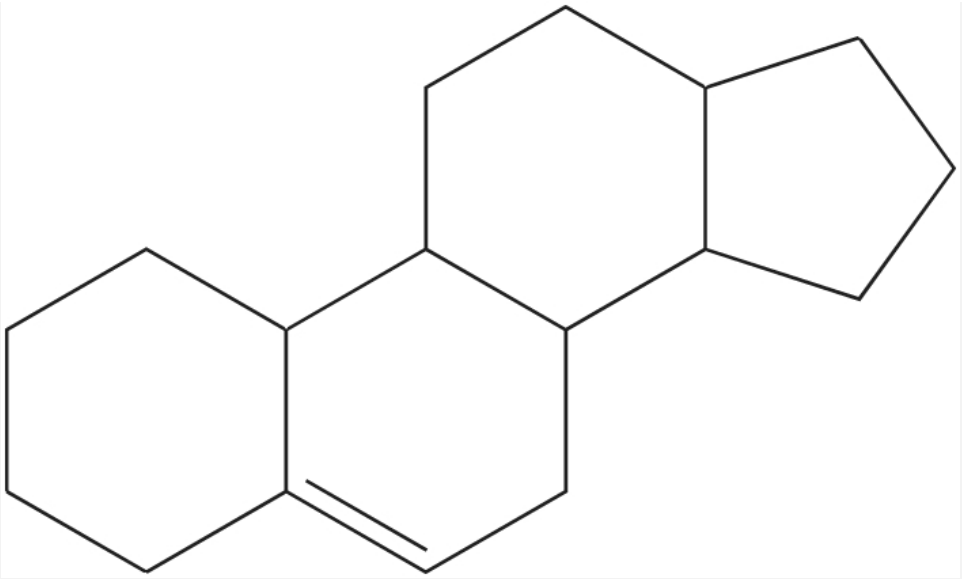
4. Phosphatidic acid phosphatase (PAP) converts phosphatidate to diacylglycerol (DAG). Diacylglycerol kinase converts DAG to phosphatidate.



Consider the effect of an inactivating mutation in the gene encoding PAP on triacylglycerol and phospholipid synthesis. Classify each lipid based on whether its concentration will increase or decrease when the PAP carries this mutation.

a. Phospholipids generated from DAG and activated head groups
b. Triacylglycerols
c. Phospholipids generated from CDP-DAG and a polar head group
d. Phosphatidate
e. Phosphatidylinositol
f. Phosphatidylethanolamine

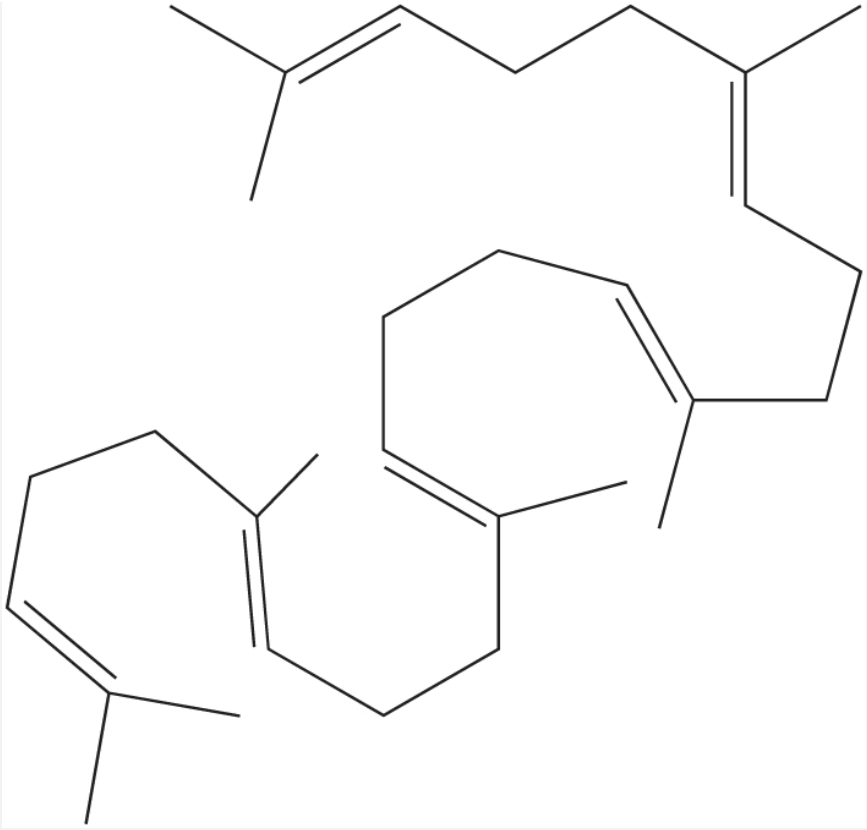
5. Below is the characteristic fused-ring core structure of a steroid. Add atoms as necessary to show the entire structure of cholesterol. 2



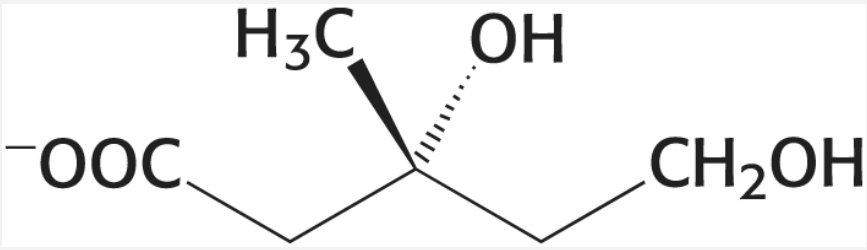
6. What are the three stages required for the synthesis of cholesterol? 2

7. Arrange the molecules in the order they appear in cholesterol synthesis. Note that there may be intermediate steps between these molecules. 2

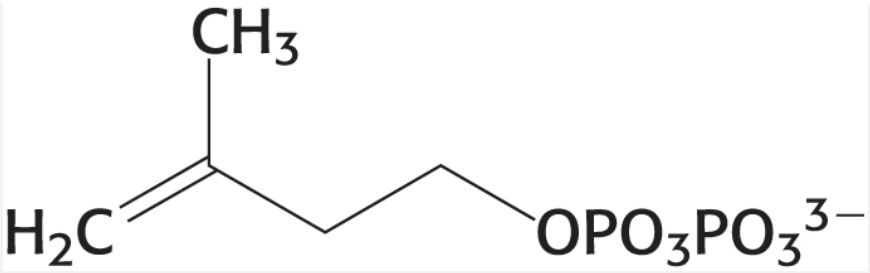
a.



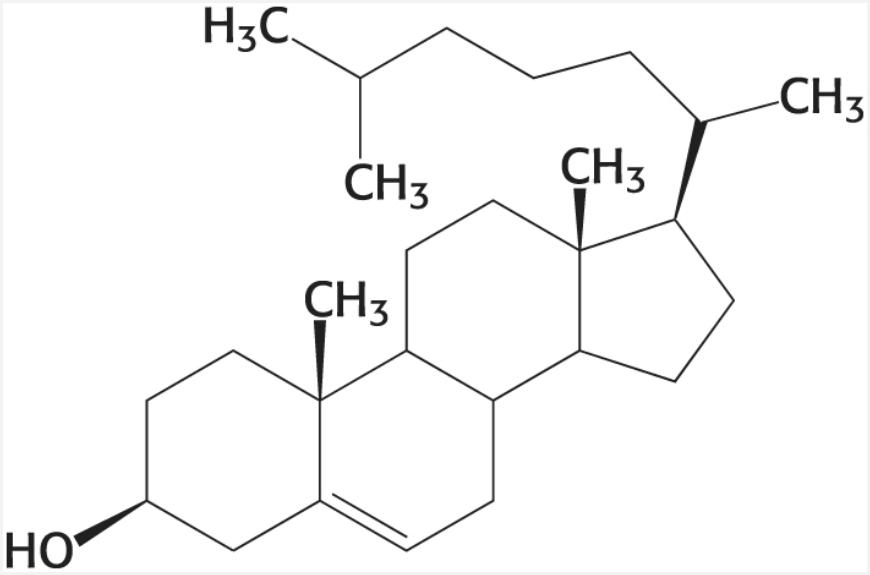
b.



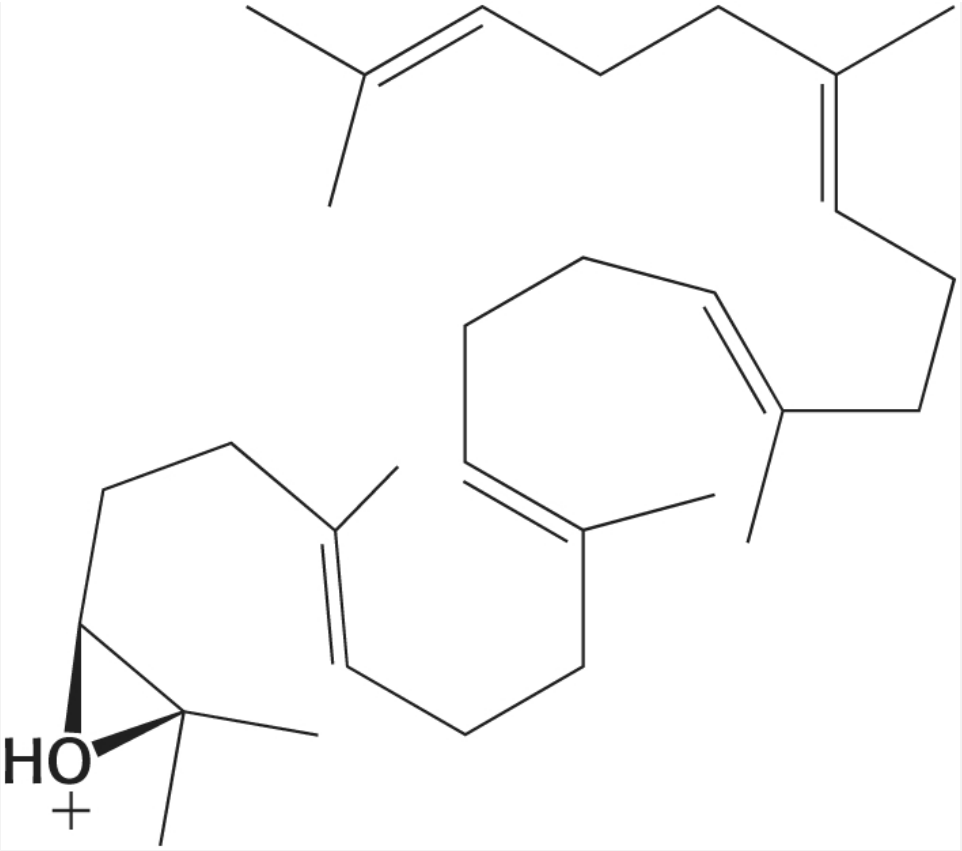
c.



d.



8. A key intermediate in the cyclization of squalene epoxide (in which the epoxide oxygen atom has been protonated) is shown below. Draw arrows indicating the movement of electrons to form the protosterol cation.



9. Arrange the following intermediates in the biosynthesis of cholesterol into their correct order: 2

a. Geranyl pyrophosphate
b. Lanosterol
c. Acetyl CoA
d. Mevalonate
e. Cholesterol
f. Squalene epoxide
g. HMG-CoA
h. Isopentenyl pyrophosphate
i. Farnesyl pyrophosphate

j. Squalene

10. Identify the atoms in mevalonate and isopentenyl pyrophosphate that will be labeled from acetyl CoA labeled with ^{14}C in the carbonyl carbon. 2

11. Outline the mechanisms of the regulation of cholesterol biosynthesis. 3

12. The synthesis of cholesterol is a process that involves over 30 different steps. Which step is the rate-determining step of cholesterol synthesis? 3

13. What are statins? What is their pharmacological function? 3

14. Describe the process of receptor-mediated endocytosis by using LDL as an example. 3

15.

a. Which lipoprotein is the least dense?
b. Which lipoprotein is the most soluble? (Hint: Use Table 27.1 for this question.) 3

16. Match each description to either low-density lipoproteins (LDL) or high-density lipoproteins (HDL): 3

a. Are known as the “bad” cholesterol
b. Have levels that increase with regular exercise
c. Help to remove cholesterol from arteries
d. Can invade artery walls and trigger an inflammatory response

17. At a biochemical level, vitamin D functions like a steroid hormone. Therefore, it is sometimes referred to as an honorary

steroid. Why is vitamin D not an actual steroid? 4

18. Match the steroid or steroid class with its respective function 4

1. Bile salts	1. Regulation of electrolytes (e.g., Na^+, K^+)
2. Androgens	2. Development of female secondary sex characteristics
3. Glucocorticoids	3. Solubilizing dietary lipids
4. Mineralocorticoids	4. Development of male secondary sex characteristics
5. Estrogens	5. Regulation of blood glucose

---

19. 3-Hydroxy-3-methylglutaryl CoA is on the pathway for cholesterol biosynthesis. It is also a component of another pathway. Name the pathway. What determines which pathway 3-hydroxy-3-methylglutaryl CoA follows?

Chapter 28
DNA Replication, Repair, and Recombination



Lou Linwei/Alamy
© Macmillan Learning

Faithful copying is essential to the storage of genetic information. With the precision of a careful artisan copying an exemplar, a DNA polymerase (above) copies DNA strands, preserving the precise sequence of bases with very few errors.

Outline

28.1 DNA Replication Proceeds by the Polymerization of Deoxyribonucleoside Triphosphates Along a Template
28.2 DNA Unwinding and Supercoiling Are Controlled by Topoisomerases
28.3 DNA Replication Is Highly Coordinated
28.4 Many Types of DNA Damage Can Be Repaired

28.5 DNA Recombination Plays Important Roles in Replication, Repair, and Other Processes

---

Learning Goals



By the end of this chapter, you should be able to:

1. Describe the reactions catalyzed by DNA polymerase, DNA primase, and DNA ligase and the roles of the template, the primer, and Okazaki fragments.
2. Discuss the reaction catalyzed by helicases and key aspects of their mechanisms.
3. Define topoisomers of circular DNA molecules and explain the relationship between twist and writhe in determining the linking number.
4. Describe how different activities of DNA replication are coordinated to faithfully copy and maintain the genome of an organism.
5. Compare and contrast prokaryotic and eukaryotic replication.
6. Define telomeres and describe how they are synthesized.
7. Discuss types of DNA damage and how such lesions can be repaired.
8. Discuss the mechanism of DNA recombination and its role in a variety of biological processes.

Perhaps the most exciting aspect of Watson and Crick's deduction of the structure of DNA was their realization "that the specific pairing we have postulated immediately suggests a possible copying mechanism for the genetic material." A double helix separated into two single strands can be replicated because each strand serves as a template on which its complementary sequence can be assembled. To preserve the information encoded in DNA through many cell divisions, copying of the genetic information must be extremely faithful. Although DNA is remarkably robust, ultraviolet light and a range of chemical species can damage DNA, introducing changes in the sequence (mutations) or lesions that can block further DNA

replication. All organisms contain DNA-repair systems that detect DNA damage and act to preserve the original sequence.

28.1 DNA Replication Proceeds by the Polymerization of Deoxyribonucleoside Triphosphates Along a Template

To preserve the information encoded in DNA through many cell divisions, the base sequences of newly synthesized DNA must faithfully match the sequences of parent DNA. To replicate the human genome without mistakes, an error rate of less than 1 bp per 6×10^9 bp must be achieved. Such remarkable precision is achieved through a multilayered system of accurate DNA synthesis (which has an error rate of 1 per 10^3 - 10^4 bases inserted), proofreading during DNA synthesis (which reduces that error rate to approximately 1 per 10^6 - 10^7 bp), and postreplication mismatch repair (which reduces the error rate to approximately 1 per 10^9 - 10^{10} bp).

To achieve faithful replication, each strand within the parent double helix acts as a **template** for the synthesis of a new DNA strand with a complementary sequence, as discussed in Section 8.3. The building blocks for the synthesis of the new strands are deoxyribonucleoside triphosphates. They are added, one at a time, to the $3'$ end of an existing strand of DNA.

Although this reaction is in principle quite simple, it is significantly complicated by specific features of the DNA double helix. First, the two strands of the double helix run in opposite directions. Because DNA strand synthesis always proceeds in the $5'$-to-$3'$ direction, the DNA

replication process must have specific mechanisms to accommodate the oppositely directed strands. Second, the two strands of the double helix interact with one another in such a way that the bases, key templates for replication, are on the inside of the helix. Thus, the two strands must be separated from each other to generate appropriate templates. Finally, the two strands of the double helix wrap around each other. Thus, strand separation also entails the unwinding of the double helix. This unwinding creates supercoils that must themselves be resolved as replication continues. We begin by considering the chemistry that underlies the formation of the phosphodiester backbone of newly synthesized DNA.

DNA polymerases require a template and a primer

Polynucleotide chains are catalyzed by enzymes called **DNA polymerases**. Each incoming nucleoside triphosphate first forms an appropriate base pair with a base in the template. Only then does the DNA polymerase link the incoming base with the predecessor in the chain. Thus, DNA polymerases are template-directed enzymes.

DNA polymerases cannot start synthesis from scratch by adding nucleotides to a single-stranded DNA template — they can only add nucleotides to an existing hydroxyl group at the $3'$ end of a polynucleotide chain. This free hydroxyl group is presented by a **primer** — an initial polynucleotide chain that is already base-paired to the template. The polymerase catalyzes the nucleophilic attack by the $3'$-hydroxyl-group terminus of the polynucleotide chain on the α-phosphoryl group of the nucleoside triphosphate to be added (Figure 8.24). Primers are made by RNA polymerases, which, in contrast to DNA polymerases, can initiate RNA synthesis from scratch (as we shall see in Chapter 29).

DNA polymerases have common structural features

The three-dimensional structures of a number of DNA polymerase enzymes are known. The first such structure was elucidated by Thomas Steitz and coworkers, who determined the structure of the Klenow fragment of DNA polymerase I from *E. coli* (**Figure 28.1**). This fragment comprises two main parts of the full enzyme, including the polymerase unit. This unit approximates the shape of a right hand with domains that are referred to as the fingers, the palm, and the thumb. In addition to the polymerase unit, the Klenow fragment includes a domain with $3' \rightarrow 5'$ **exonuclease** activity that participates in proofreading and correcting the polynucleotide product.

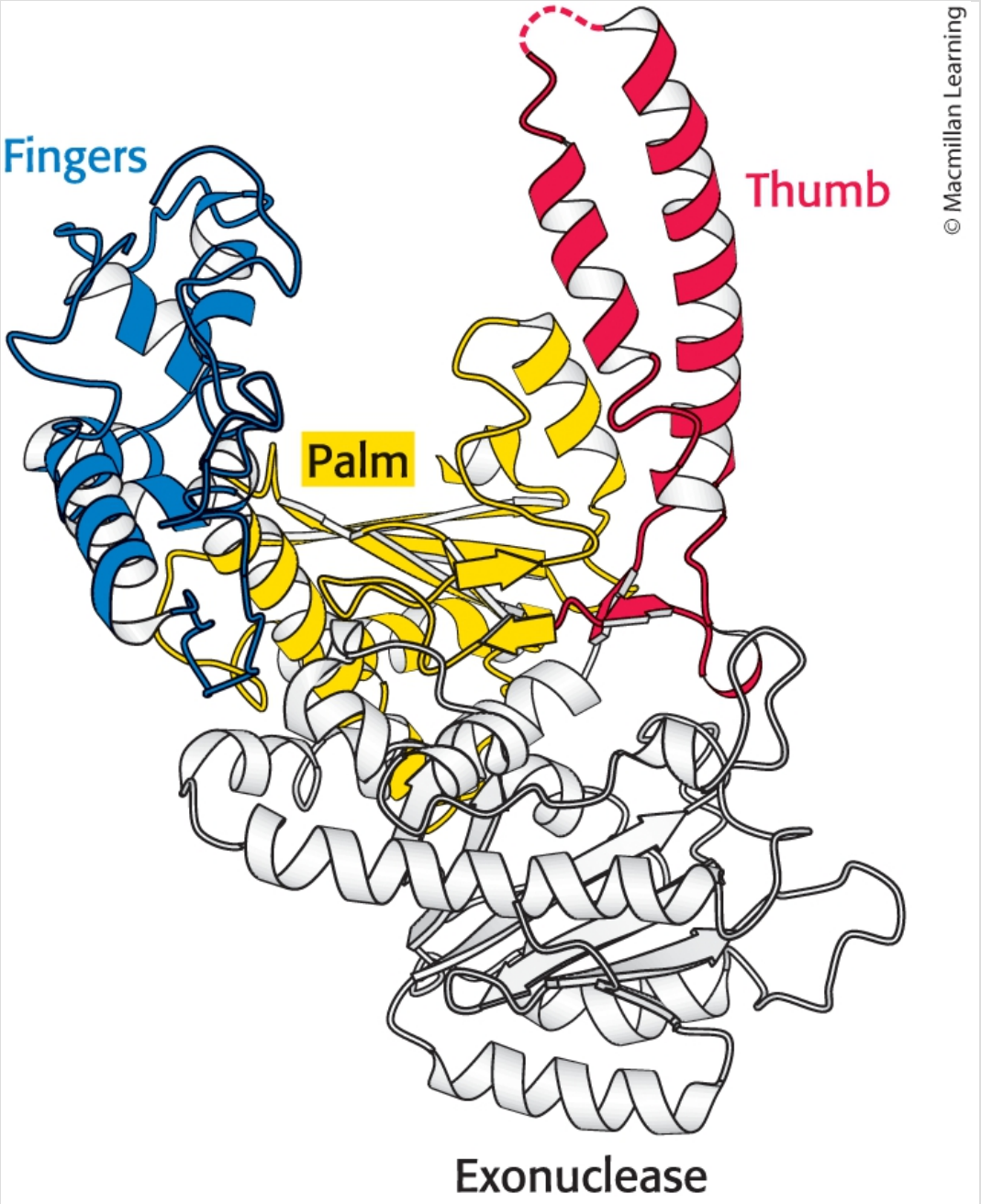


FIGURE 28.1 The structure of the *E.coli* DNA polymerase I Klenow fragment resembles a hand. This was the first DNA polymerase structure to be determined; like the structures of other DNA polymerases determined later, it resembles a right hand with fingers (blue), palm (yellow), and thumb (red). The Klenow fragment also includes an exonuclease domain that removes incorrect nucleotide bases.

[Drawn from 1DPI.pdb.]

INTERACT with this model in Achieve

DNA polymerases are remarkably similar in overall shape, although they differ substantially in detail. At least five structural classes have been identified; some of them are clearly homologous, whereas others appear to be the products of convergent evolution. In all cases, the finger and thumb domains wrap around DNA and hold it across the enzyme's active site, which comprises residues primarily from the palm domain. Furthermore, all DNA polymerases use similar strategies to catalyze the polymerase reaction, making use of a mechanism in which three metal ions take part.

Bound metal ions participate in the polymerase reaction

Like all enzymes with nucleoside triphosphate substrates, DNA polymerases require metal ions for activity. Examination of the structures of DNA polymerases with bound substrates and substrate analogs initially revealed the presence of two metal ions in the active site, but recent data supports a three-metal-ion model. One metal ion binds both the deoxyribonucleoside triphosphate (dNTP) and the $3'$-hydroxyl group of the primer, while the other two interact only with the dNTP (**Figure 28.2**). Two of the three metal ions are bridged by the carboxylate groups of two aspartate residues in the palm domain of the polymerase. These side chains hold the metal ions in the proper positions and orientations. The metal ion bound to the primer activates the $3'$-hydroxyl group of the primer, facilitating its attack on the α-phosphoryl group of the dNTP substrate in the active site. The three metal ions together help stabilize the negative charge that accumulates on the pentacoordinate transition state. The two metal ions initially

bound to the dNTP stabilize the negative charge on the pyrophosphate product.

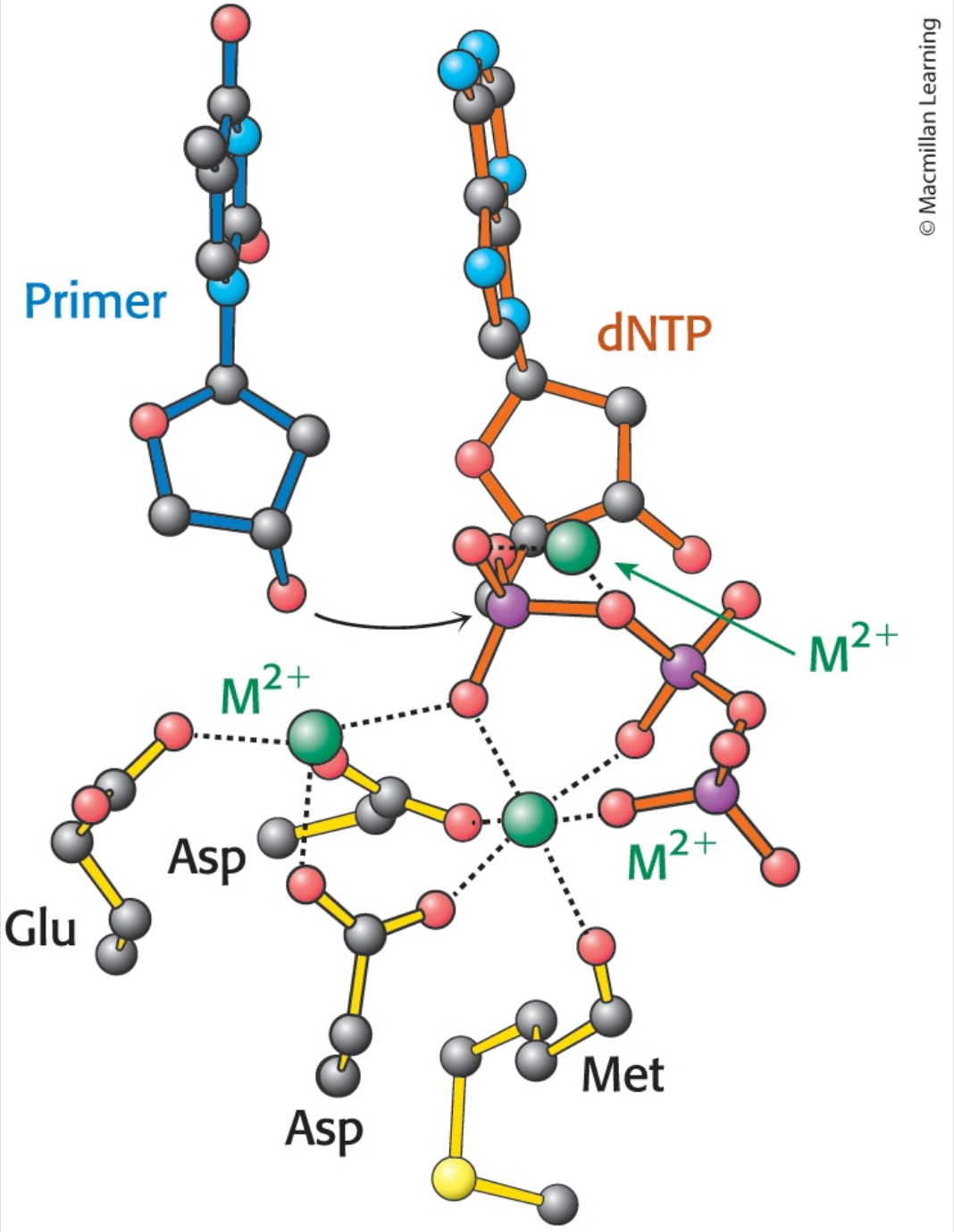


FIGURE 28.2 Three metal ions (typically, Mg^{2+}) participate in the DNA polymerase reaction. One metal ion coordinates the $3'$-hydroxyl group of the

primer, whereas the other two metal ions interact only with the dNTP. The phosphoryl group of the nucleoside triphosphate bridges all three metal ions. Two of the three metal ions are also bridged by the carboxylate groups of two aspartate residues in the polymerase. The hydroxyl group of the primer attacks the phosphoryl group to form a new $O-P$ bond.



Self-Check Question



Provide a chemical explanation of why DNA synthesis proceeds in a $5'$-to-$3'$ direction.

The specificity of replication is dictated by complementarity of shape between bases

Since DNA must be replicated with high fidelity, each base added to the growing chain should, with high probability, be the Watson–Crick complement of the base in the corresponding position in the template strand. The binding of the dNTP containing the proper base is favored by the formation of a base pair with its partner on the template strand. Although hydrogen bonding contributes to the formation of this base pair, overall shape complementarity is crucial. Studies show that a nucleotide with a base that is very similar in shape to adenine but lacks the ability to form base-pairing hydrogen bonds can still direct the incorporation of thymidine, both in vitro and in vivo (Figure 28.3).

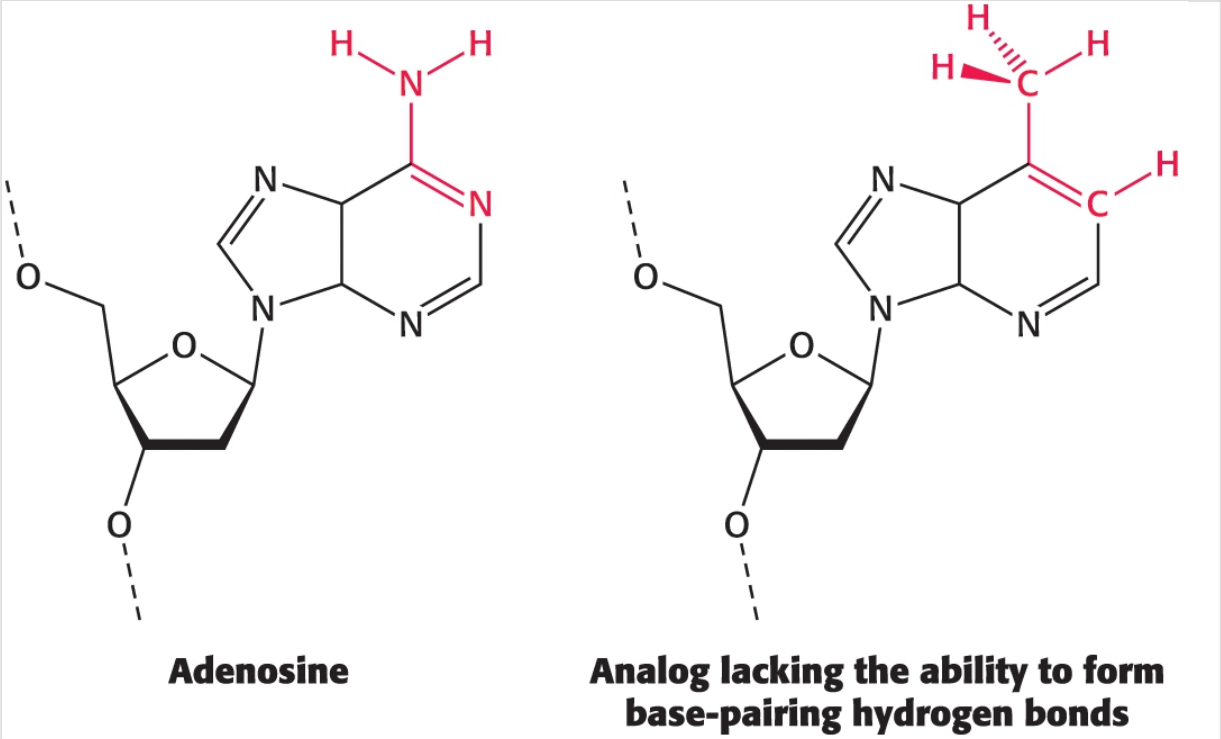


FIGURE 28.3 Base analogs that have the same shape as normal bases can participate in DNA replication. The base analog on the right has the same shape as adenosine, but groups that form hydrogen bonds between base pairs have been replaced by groups not capable of hydrogen bonding (shown in red). Nonetheless, studies reveal that when this analog is incorporated into the template strand, it directs the insertion of thymidine in DNA replication.

An examination of the crystal structures of various DNA polymerases reveals why shape complementarity is so important. First, residues of the enzyme form hydrogen bonds with the minor-groove side of the base pair in the active site (Figure 28.4). In the minor groove, hydrogen-bond acceptors are present in the same positions for all Watson–Crick base pairs. These interactions act as a "ruler" that measures whether a properly spaced base pair has formed in the active site.

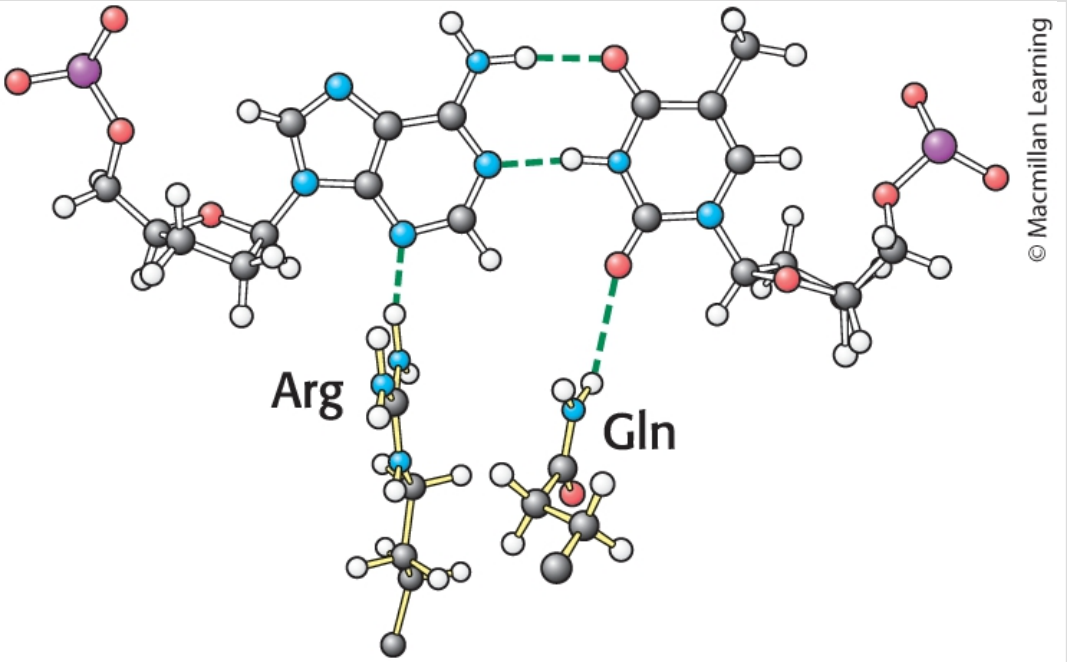


FIGURE 28.4 Minor-groove interactions promote the specificity of DNA replication. DNA polymerases donate two hydrogen bonds to base pairs in the minor groove. Hydrogen-bond acceptors are present in these two positions for all Watson–Crick base pairs, including the A–T base pair shown.

Second, the binding of a dNTP in the active site of a DNA polymerase triggers a conformational change: the finger domain rotates to form a tight pocket into which only a properly shaped base pair will readily fit (Figure 28.5). Many of the residues lining this pocket are important to ensure the efficiency and fidelity of DNA synthesis. For example, mutation of a conserved tyrosine residue that forms part of the pocket results in a polymerase that is approximately 40 times more error prone as the parent polymerase.

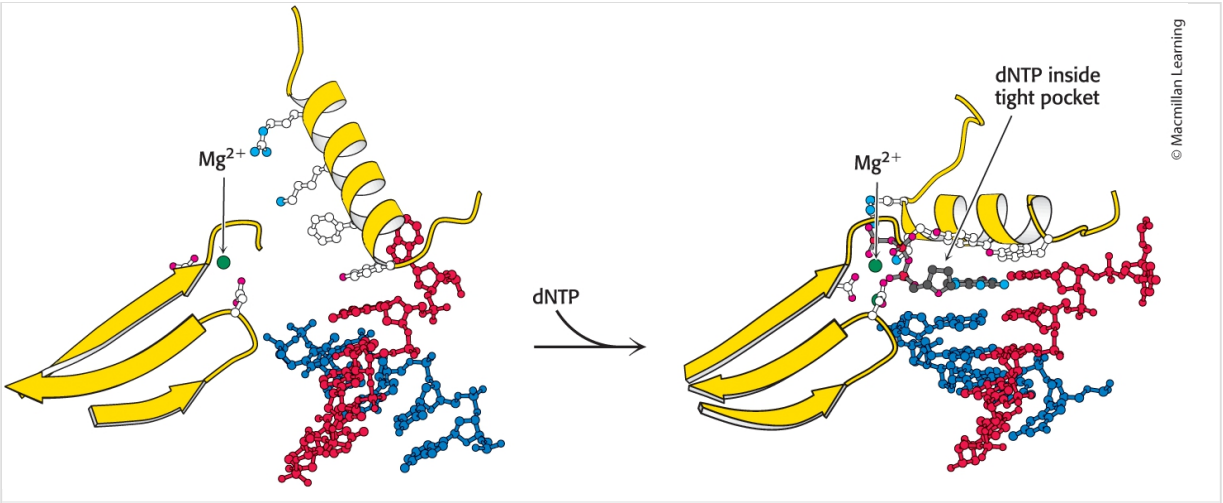


FIGURE 28.5 Shape selectivity promotes the specificity of DNA replication. The binding of a deoxyribonucleoside triphosphate (dNTP) to DNA polymerase induces a conformational change, generating a tight pocket for the base pair consisting of the dNTP and its partner on the template strand. Such a conformational change is possible only when the dNTP corresponds to the Watson–Crick partner of the template base. Only one of the three coordinating metal ions at the active site is shown.

[Drawn from 2BDP.pdb and 1T7P.pdb.]

INTERACT with these models in Achieve

An RNA primer enables DNA synthesis to begin

As discussed above, DNA polymerases require a primer with a free $3'$ end to initiate DNA synthesis. How is this primer formed? An important clue came from the observation that RNA synthesis is essential for the initiation of DNA synthesis. In fact, RNA primes the synthesis of DNA. An RNA polymerase called **primase** synthesizes a short stretch of RNA (about five nucleotides) that is complementary to the template DNA strands (Figure 28.6). Primase, like other RNA polymerases, can initiate

synthesis without a primer. After DNA synthesis has been initiated, the short stretch of RNA is removed by hydrolysis and replaced by DNA.

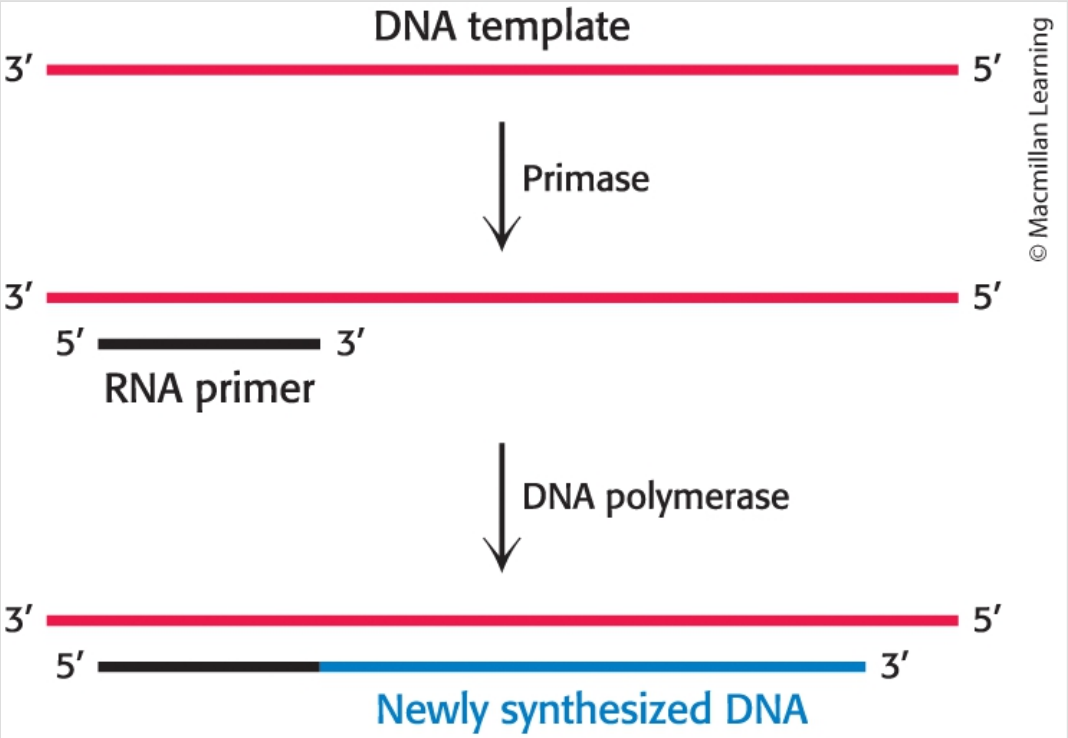


FIGURE 28.6 DNA polymerases require a primer. DNA replication is primed by a short stretch of RNA that is synthesized by primase, an RNA polymerase. The RNA primer is removed at a later stage of replication.

Self-Check Question

DNA replication does not take place in the absence of the ribonucleotides ATP, CTP, GTP, and UTP. Propose an explanation.

One strand of DNA is made continuously, whereas the other strand is synthesized in fragments

Both strands of parental DNA serve as templates for the synthesis of new DNA. The site of DNA synthesis is called the **replication fork** because the complex formed by the newly synthesized daughter helices arising from the parental duplex resembles a two-pronged fork. Recall that the two template strands are antiparallel; that is, they run in opposite directions. Since all known DNA polymerases synthesize DNA only in the $5' \rightarrow 3'$ direction, the two daughter strands must be synthesized in opposite directions: one away from the fork, and one toward the fork. How exactly does this work?

An answer to this question was provided by Reiji Okazaki and his wife Tsuneko Okazaki, who found that a significant proportion of newly synthesized DNA exists as small fragments. These units of about a thousand nucleotides (called **Okazaki fragments**) are present briefly in the vicinity of the replication fork (**Figure 28.7**). As replication proceeds, these fragments become covalently joined, forming a continuous daughter strand. The other new strand is synthesized continuously. The strand formed from Okazaki fragments is termed the **lagging strand**, whereas the one synthesized without interruption is the **leading strand**.

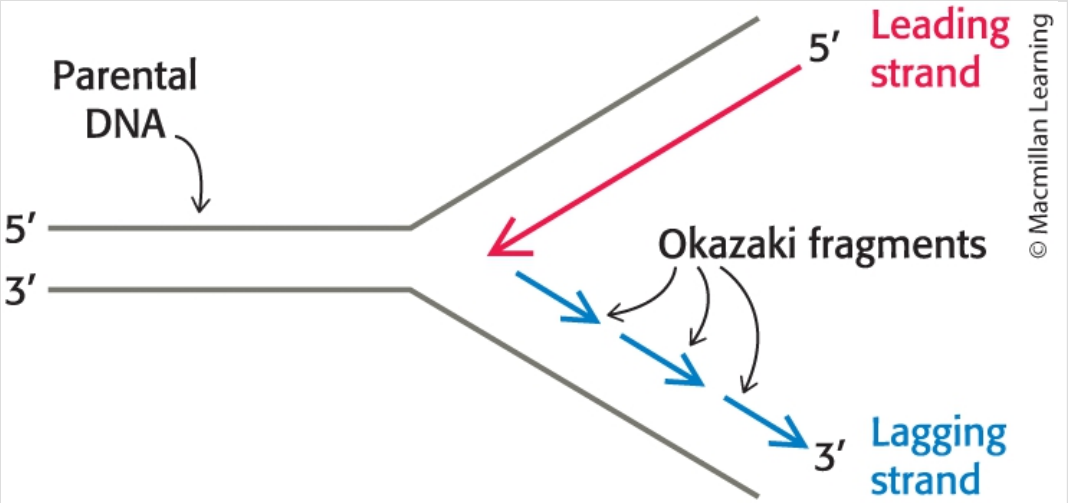


FIGURE 28.7 The lagging strand is made in short pieces called Okazaki fragments.

At a replication fork, both strands are synthesized in the $5' \rightarrow 3'$ direction, but only the leading strand is synthesized continuously



Tsuneko Okazaki, University Professor, Nagoya University

TSUNEKO AND REIJI OKAZAKI Growing up in Japan during World War II, Tsuneko and Reiji Okazaki persevered in their studies despite wartime hardships. Tsuneko's father wanted her to pursue medicine, but she was more interested in biology and became a researcher at a time when it was a very rare career path for women. Tsuneko met and married Reiji while they were both at Nagoya University, and in the early 1960s they briefly worked at Stanford University in the lab of Arthur Kornberg, who had recently extracted DNA polymerase activity from *E.coli*. Back at Nagoya University, they continued to investigate how DNA polymerase could be replicating antiparallel strands of DNA in only one direction, eventually leading to their discovery of the

short-lived DNA fragments that now carry their name. In 1975 Reiji died of leukemia, a consequence of his exposure to intense radiation in Hiroshima as a teenager. Dr. Tsuneko Okazaki continued in research while also raising two children, and she went on to have a distinguished academic career.

DNA ligase seals breaks in double-stranded DNA

The joining of Okazaki fragments requires an enzyme that can connect the ends of two DNA chains. The existence of circular DNA molecules also points to the existence of such an enzyme. In 1967, scientists in several laboratories simultaneously discovered **DNA ligase**, the enzyme that catalyzes the formation of a phosphodiester linkage between the $3'$-hydroxyl group at the end of one DNA chain and the $5'$-phosphoryl group at the end of the other (**Figure 28.8**). An energy source is required to drive this thermodynamically uphill reaction. In eukaryotes and archaea, ATP is the energy source. In bacteria, NAD^+ typically plays this role.

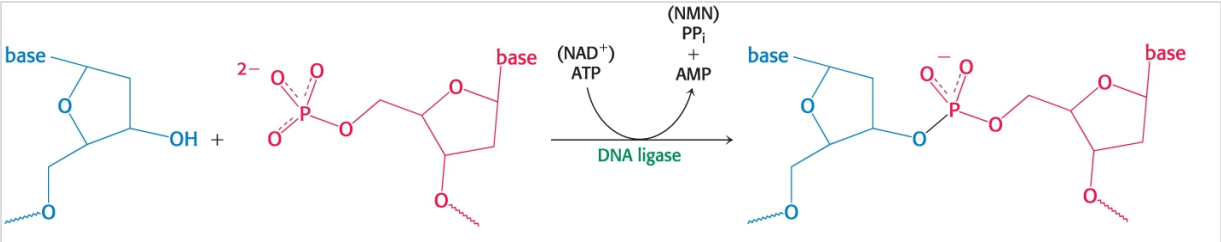


FIGURE 28.8 DNA ligase catalyzes the joining of two DNA strands. In this reaction, one DNA strand with a free $3'$-hydroxyl group is joined to another with a free $5'$-phosphoryl group. In eukaryotes and archaea, ATP is cleaved to AMP and PP_i to drive this reaction. In bacteria, NAD^+ is cleaved to AMP and nicotinamide mononucleotide (NMN).

DNA ligase cannot link two single-stranded DNA molecules or circularize single-stranded DNA. Rather, ligase seals breaks in double-stranded DNA molecules. The enzyme from *E. coli* ordinarily forms a phosphodiester bridge only if there are at least a few bases of single-stranded DNA on the end of a double-stranded fragment that can come together with those on another fragment to form base pairs. Ligase encoded by T4 bacteriophage can link two blunt-ended double-helical fragments, a capability that is exploited in recombinant DNA technology.

The separation of DNA strands requires specific helicases and ATP hydrolysis

For a double-stranded DNA molecule to replicate, the two strands of the double helix must be separated from each other, at least locally. This separation allows each strand to act as a template on which a new polynucleotide chain can be assembled. Specific enzymes, termed **helicases**, harness the energy of ATP hydrolysis to power strand separation.

While helicases are a large and diverse family of enzymes taking part in many biological processes, the helicases in DNA replication are typically oligomers containing six subunits that form a ring structure. The structure of one such helicase, that from bacteriophage T7, has been a source of considerable insight into the helicase mechanism (**Figure 28.9**).

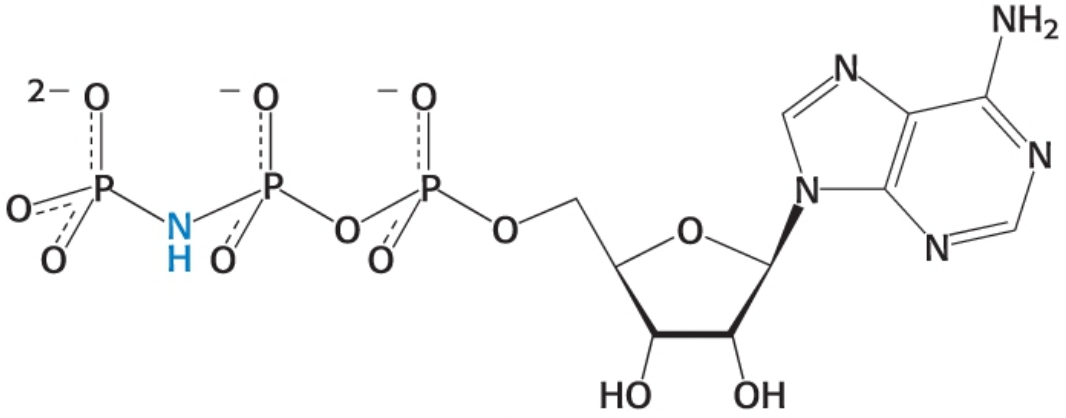


FIGURE 28.9 Helicases are hexamers. The structure of the hexameric helicase from bacteriophage T7 is shown. The loops that participate in DNA binding are highlighted by a yellow oval in one of the subunits. Each subunit interacts closely with its neighbors, and the DNA-binding loops line the hole in the center of the structure.

[Drawn from 1E0K.pdb.]

Each of the subunits within this hexameric structure has two loops that extend toward the center of the ring structure and interact with DNA. Each subunit interacts closely with its two neighbors within the ring structure. Closer examination of this structure reveals that the ring deviates significantly from sixfold symmetry, a deviation that is even

more apparent when helicase is crystallized in the presence of the nonhydrolyzable ATP analog AMP-PNP.



AMP-PNP

The AMP-PNP binds to only four of the six subunits within the ring (**Figure 28.10**). Furthermore, the four nucleotide binding sites are not identical but fall into two classes. One class appears to be well positioned to bind ATP but not catalyze its hydrolysis, whereas the other class is more well-suited to catalyze the hydrolysis but not release the hydrolysis products. The classes are analogous to myosin's two different conformations — one for binding ATP and one for hydrolyzing it (Section 6.4). Finally, the six subunits fall into three classes with regard to their orientation within the overall ring structure, with differences in rotation around an axis in the plane of the ring of approximately 30°. These differences in orientation affect the positions of the two DNA-binding loops in each subunit.

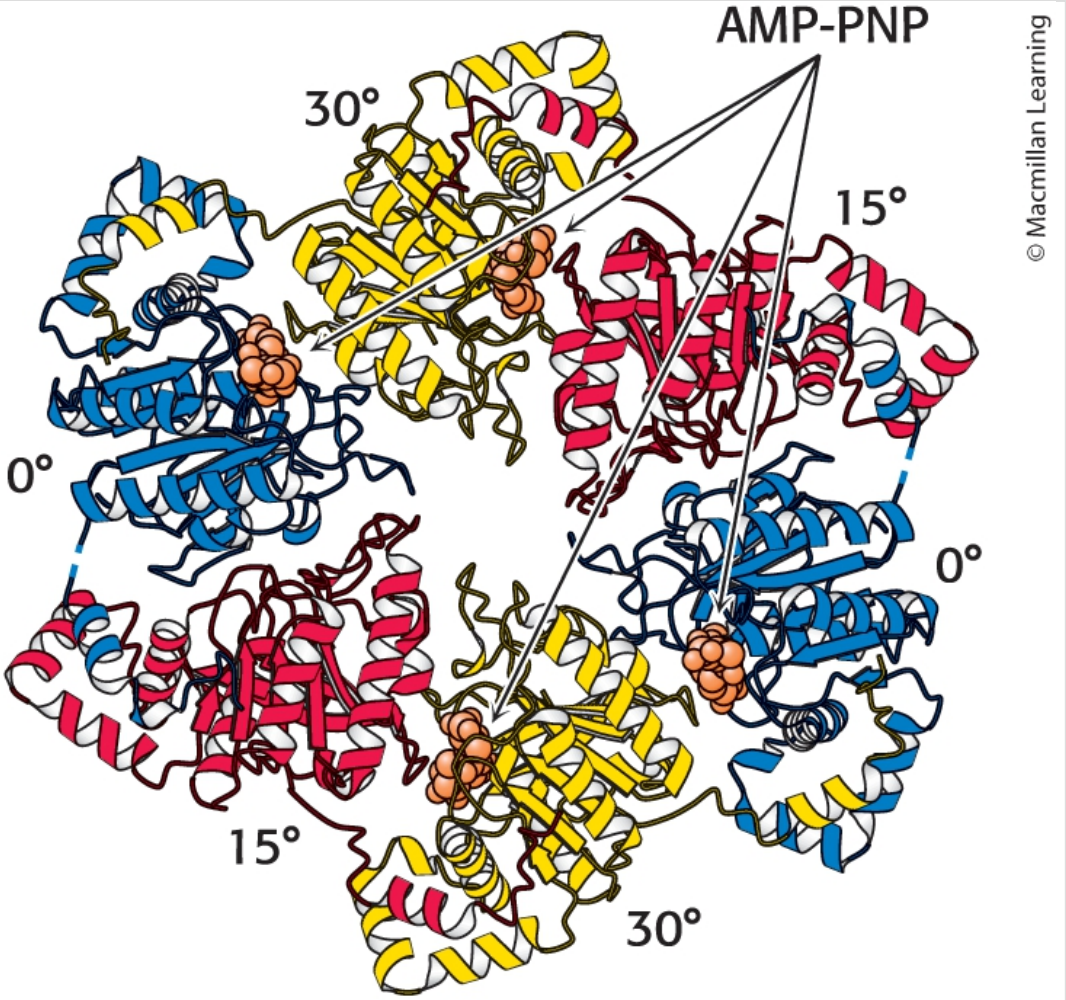


FIGURE 28.10 Helicases have intrinsic asymmetry. The structure of the T7 helicase complexed with the ATP analog AMP-PNP is shown. The three classes of helicase subunits are shown in blue, red, and yellow. The rotation relative to the plane of the hexamer is shown for each subunit. Notice that only four of the subunits, those shown in blue and yellow, bind AMP-PNP.

[Drawn from 1E0K.pdb.]

These observations are consistent with the following mechanism for the helicase (Figure 28.11):

1. Only a single strand of DNA can fit through the center on the ring. This single strand binds to loops on two adjacent subunits, one of

which has bound ATP and the other of which has bound $ADP + P_i$.

2. The binding of ATP to the domains that initially had no bound nucleotides causes a conformational change within the entire hexamer, leading to the release of $ADP + P_i$ from two subunits and the binding of the single-stranded DNA by one of the domains that just bound ATP. This conformational change pulls the DNA through the center of the hexamer.

3. The protein acts as a wedge, forcing the two strands of the double helix apart.

4. This cycle then repeats itself, moving two bases along the DNA strand with each cycle.

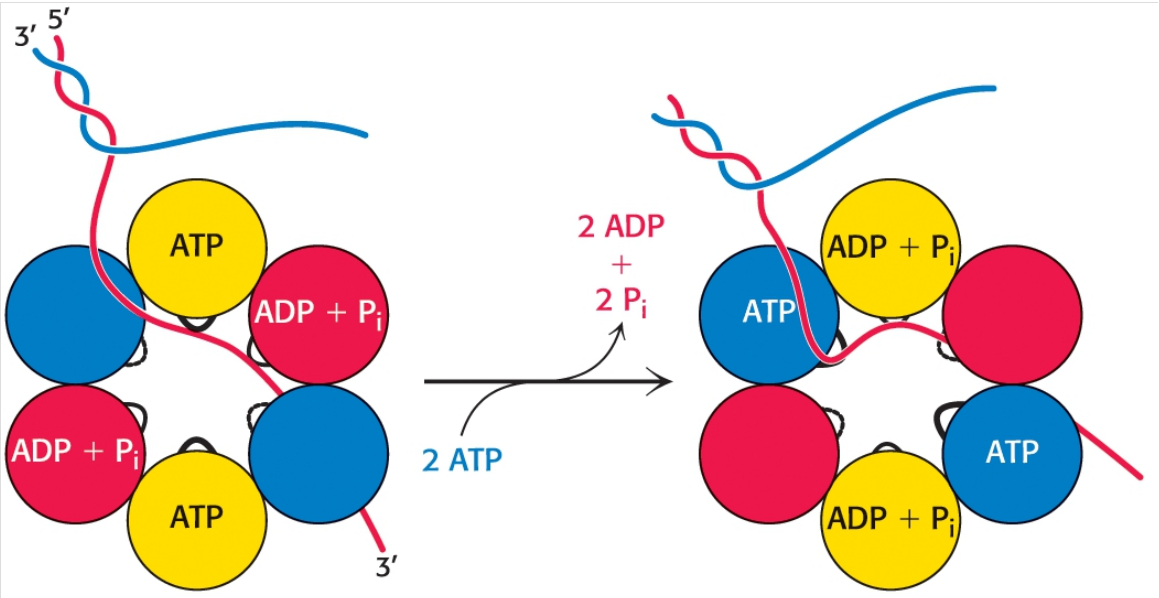


FIGURE 28.11 Helicases unwind DNA. One of the strands of the double helix passes through the hole in the center of the helicase, bound to the loops of two adjacent subunits. Two of the subunits do not contain bound nucleotides. On the binding of ATP to these two subunits and the release of $ADP + P_i$ from two other subunits, the helicase hexamer undergoes a conformational change, pulling the DNA through the helicase. The helicase acts as a wedge to force separation of the two strands of DNA.



28.2 DNA Unwinding and Supercoiling Are Controlled by Topoisomerases

As a helicase moves along unwinding DNA, the DNA in front of the helicase will become overwound in the absence of other changes. DNA double helices that are torsionally stressed tend to fold up on themselves to form tertiary structures created by **supercoiling**. Supercoiling is most readily understood by considering circular DNA molecules, but it also applies to linear DNA molecules constrained to be in loops by other means. In fact, most DNA molecules inside cells are subject to supercoiling. We will first consider the supercoiling of DNA in quantitative terms and then turn to topoisomerases, enzymes that can directly alter DNA winding and supercoiling.

Consider a linear 260-bp DNA duplex in the B-DNA form (**Figure 28.12A**). Because the number of base pairs per turn in an unstressed DNA molecule averages 10.4, this linear DNA molecule has 25 (260/10.4) turns. The ends of this helix can be joined to produce what is called a *relaxed* circular DNA (**Figure 28.12B**). A different circular DNA can be formed by unwinding the linear duplex by two turns before joining its ends (**Figure 28.12C**). What is the structural consequence of unwinding before ligation? Two limiting conformations are possible. The DNA can fold into a structure containing 23 turns of B helix and an unwound loop (**Figure 28.12D**). Alternatively, the double helix can undergo supercoiling, in which it folds up to cross itself. In this example, a supercoiled structure with 25 turns of B helix and 2 turns of right-handed (termed *negative*) supercoils can be formed (**Figure 28.12E**). Unwinding will cause supercoiling in circular DNA molecules, whether covalently closed or constrained in closed configurations by other means.

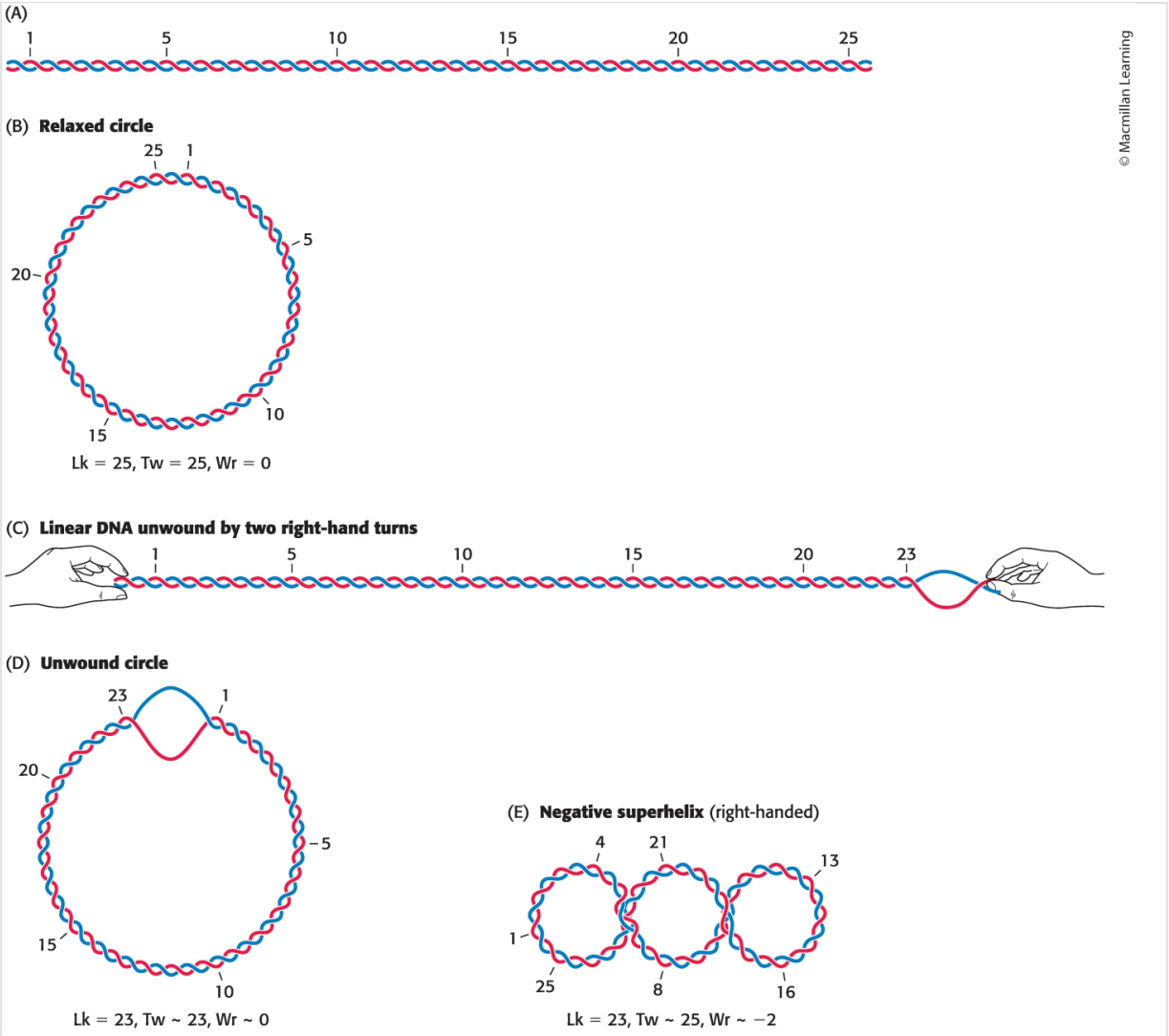
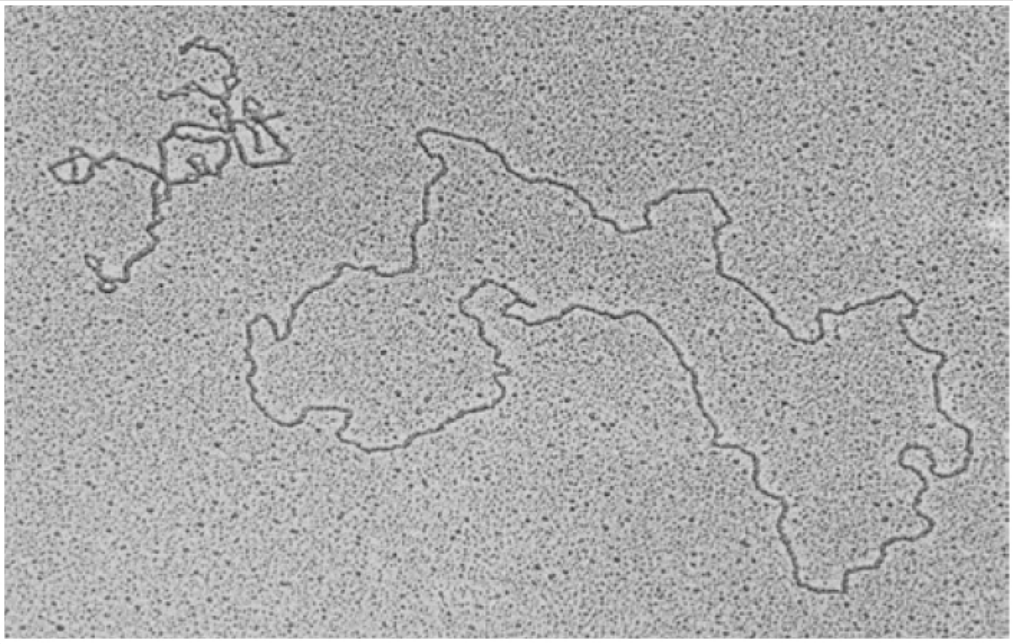


FIGURE 28.12 The linking number (Lk), twist (Tw), and writhe (Wr) of circular DNA are related.

[Information from W. Saenger, *Principles of Nucleic Acid Structure* (Springer Verlag, 1984), p. 452.]

Supercoiling markedly alters the overall form of DNA, because it makes the DNA more compact than a relaxed DNA molecule of the same length. Hence, supercoiled DNA moves faster than relaxed DNA when analyzed by centrifugation or electrophoresis (Figure 28.13).



Courtesy of Dr. Jack Griffith

FIGURE 28.13 Supercoiling condenses DNA topoisomers. An electron micrograph showing negatively supercoiled and relaxed DNA.

The linking number, a topological property, determines the degree of supercoiling

Our understanding of the conformation of DNA is enriched by concepts drawn from topology, a branch of mathematics dealing with structural properties that are unchanged by deformations such as stretching and bending. A key topological property of a circular DNA molecule is its **linking number (Lk)**, which is equal to the number of times that a strand of DNA winds in the right-handed direction around the helix axis when the axis lies in a plane, as shown in Figure 28.12A. For the relaxed DNA shown in Figure 28.12B, $Lk = 25$. For the partly unwound molecule shown in part D and the supercoiled one shown in part E, $Lk = 23$ because the linear duplex was unwound two complete turns before closure. Molecules differing only in linking number are topological isomers, or **topoisomers**, of one another. Topoisomers of DNA can be interconverted only by cutting one or both DNA strands and then rejoining them.

The unwound DNA and supercoiled DNA shown in Figure 28.12D and E are topologically identical but geometrically different. They have the same value of Lk but differ in two measurements: twist and writhe. Although the rigorous definitions of twist and writhe are complex, **twist (Tw)** is a measure of the helical winding of the DNA strands around each other, whereas **writhe (Wr)** is a measure of the coiling of the axis of the double helix — that is, supercoiling. A right-handed coil is assigned a negative number (negative supercoiling), and a left-handed coil is assigned a positive number (positive supercoiling).

Is there a relation between Tw and Wr? Indeed, there is. Topology tells us that the sum of Tw and Wr is equal to Lk:

$$Lk = Tw + Wr$$

In Figure 28.12, the partly unwound circular DNA has $Tw \sim 23$, meaning the helix has 23 turns, and $Wr \sim 0$, meaning the helix has not crossed itself to create a supercoil. The supercoiled DNA, however, has $Tw \sim 25$ and $Wr \sim -2$. These forms can be interconverted without cleaving the DNA chain because they have the same value of Lk — namely, 23.

Topoisomerases prepare the double helix for unwinding

Most naturally occurring DNA molecules are negatively supercoiled. What is the basis for this? As already stated, negative supercoiling arises from the unwinding or underwinding of the DNA. In essence, negative supercoiling prepares DNA for processes requiring separation of the DNA strands, such as replication. Positive supercoiling condenses DNA as effectively, but it makes strand separation more difficult.

The action of the helicase at the replication fork causes the DNA ahead of the fork to be overwound with positive supercoils, making unwinding difficult. Therefore, negative supercoils must be continuously introduced to relax the DNA as the double helix unwinds. Specific enzymes called **topoisomerases** that introduce or eliminate supercoils were discovered by James Wang and Martin Gellert. Type I topoisomerases catalyze the relaxation of supercoiled DNA, a thermodynamically favorable process, while Type II topoisomerases use free energy from ATP hydrolysis to add negative supercoils to DNA. Both type I and type II topoisomerases play important roles in DNA replication as well as in transcription and recombination.

Topoisomerases alter the linking number of DNA by catalyzing a three-step process: (1) the cleavage of one or both strands of DNA, (2) the passage of a segment of DNA through this break, and (3) the resealing of the DNA break. Type I topoisomerases cleave just one strand of DNA, whereas type II enzymes cleave both strands. The two types of enzymes have several common features, including the use of key tyrosine residues to form covalent links to the polynucleotide backbone that is transiently broken.

Type I topoisomerases relax supercoiled structures

The three-dimensional structures determined for several type I topoisomerases reveal many features of the reaction mechanism (**Figure 28.14**). For example, human type I topoisomerase comprises four domains, which are arranged around a central cavity having a diameter of 20 Å, just the correct size to accommodate a double-stranded DNA molecule. This cavity also includes a tyrosine residue (Tyr 723), which acts as a nucleophile to cleave the DNA backbone in the course of catalysis.

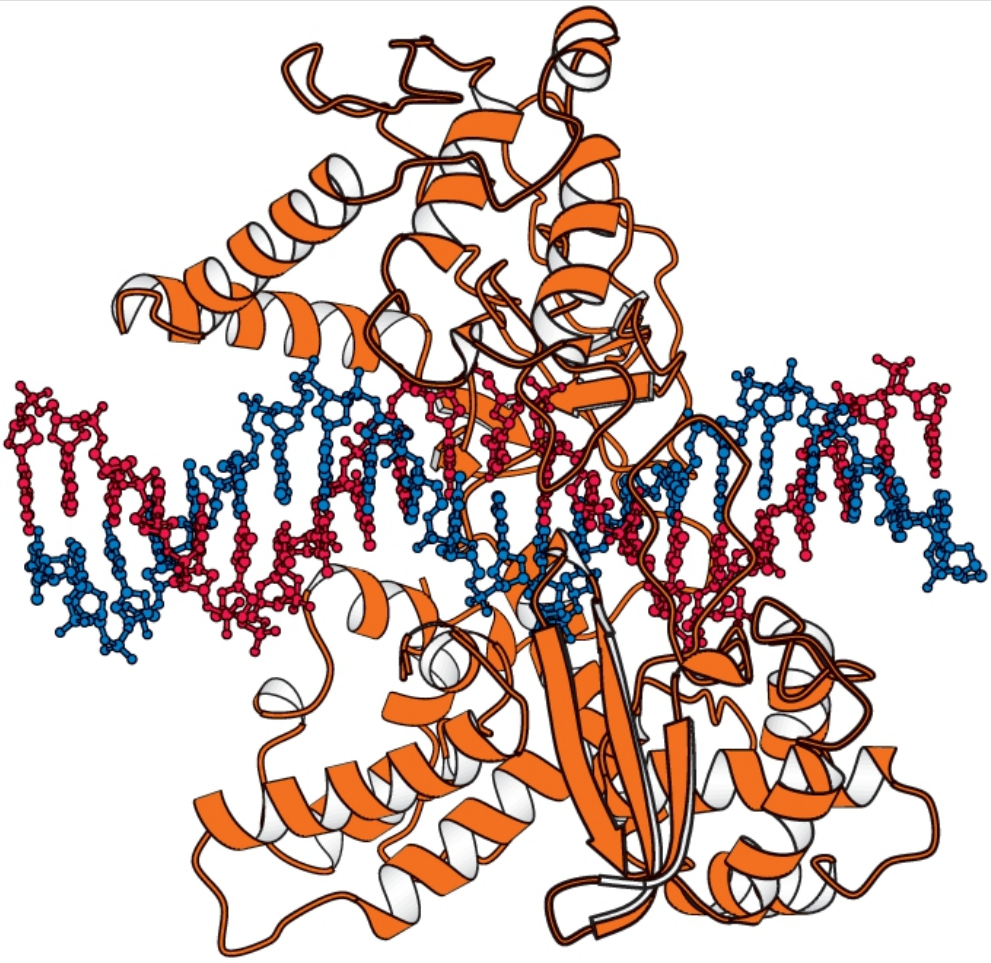


FIGURE 28.14 Topoisomerase I binds to DNA. The structure of a complex between a fragment of human topoisomerase I and DNA is shown. The DNA occupies a central cavity within the enzyme.

[Drawn from 1EJ9.pdb.]

INTERACT with this model in Achieve

From analyses of topoisomerases and the results of other studies, the relaxation of negatively supercoiled DNA molecules is known to proceed in the following manner (Figure 28.15):

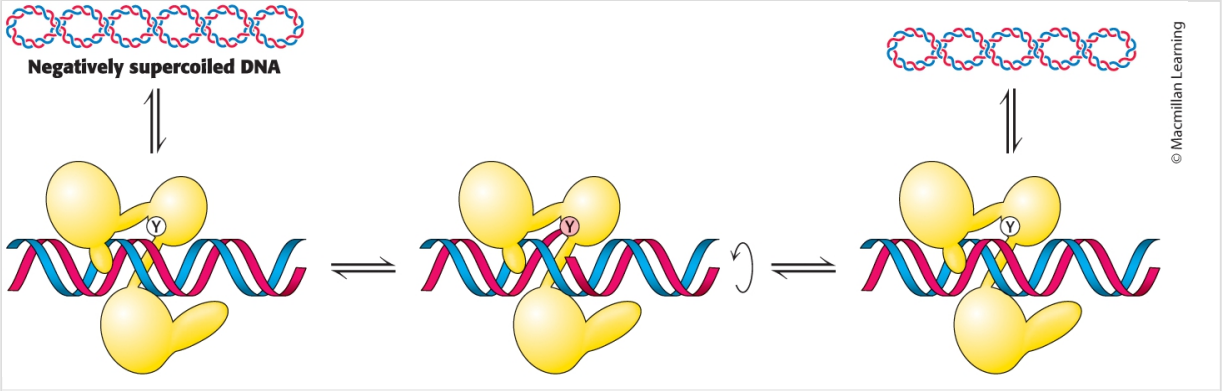
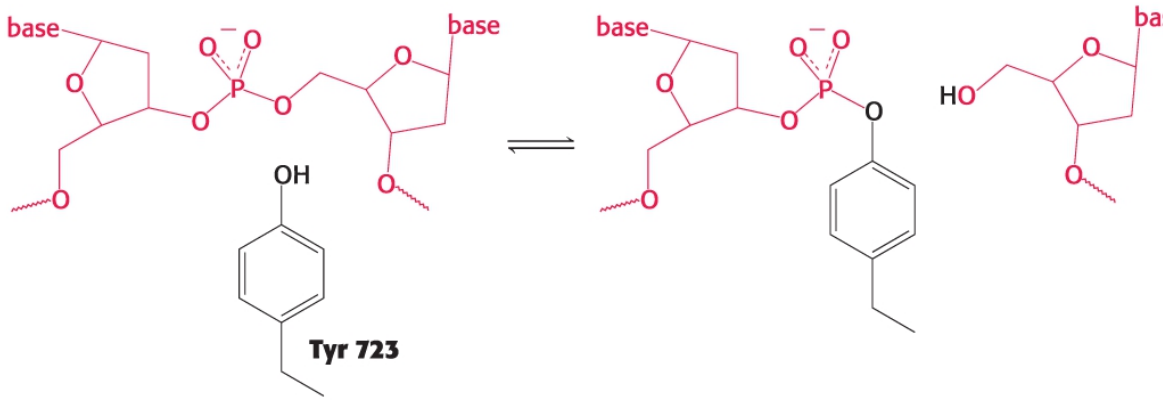


FIGURE 28.15 Topoisomerase I relaxes supercoiled DNA. On binding to DNA, topoisomerase I cleaves one strand of the DNA by means of a tyrosine (Y) residue attacking a phosphoryl group. When the strand has been cleaved, it rotates in a controlled manner around the other strand. The reaction is completed by re-ligation of the cleaved strand. This process results in partial or complete relaxation of a supercoiled plasmid.

1. First, the DNA molecule binds inside the cavity of the topoisomerase. The hydroxyl group of tyrosine 723 attacks a phosphoryl group on one strand of the DNA backbone to form a phosphodiester linkage between the enzyme and the DNA, cleaving the DNA and releasing a free 5′-hydroxyl group.



2. With the backbone of one strand cleaved, the DNA can now rotate around the remaining strand, its movement driven by the release of energy stored because of the supercoiling. The rotation of the DNA unwinds the supercoils. The enzyme controls the rotation so that the unwinding is not rapid.

3. The free hydroxyl group of the DNA attacks the phosphotyrosine residue to reseal the backbone and release tyrosine. The DNA is then free to dissociate from the enzyme. Thus, reversible cleavage of one strand of supercoiled DNA allows controlled rotation to partly relax the supercoils.

Type II topoisomerases introduce negative supercoils through coupling to ATP hydrolysis

Supercoiling requires an input of energy because a supercoiled molecule, in contrast to its relaxed counterpart, is torsionally stressed. The introduction of an additional supercoil into a 3000-bp plasmid typically requires about $30\ \text{kJ mol}^{-1}$ ($7\ \text{kcal mol}^{-1}$).

Supercoiling is catalyzed by type II topoisomerases. These elegant molecular machines couple the binding and hydrolysis of ATP to the directed passage of one DNA double helix through another, temporarily cleaved DNA double helix. These enzymes have several mechanistic features in common with the type I topoisomerases.

Topoisomerase II molecules are dimeric with a large internal cavity (**Figure 28.16**). The large cavity has gates at both the top and the bottom that are crucial to topoisomerase action:

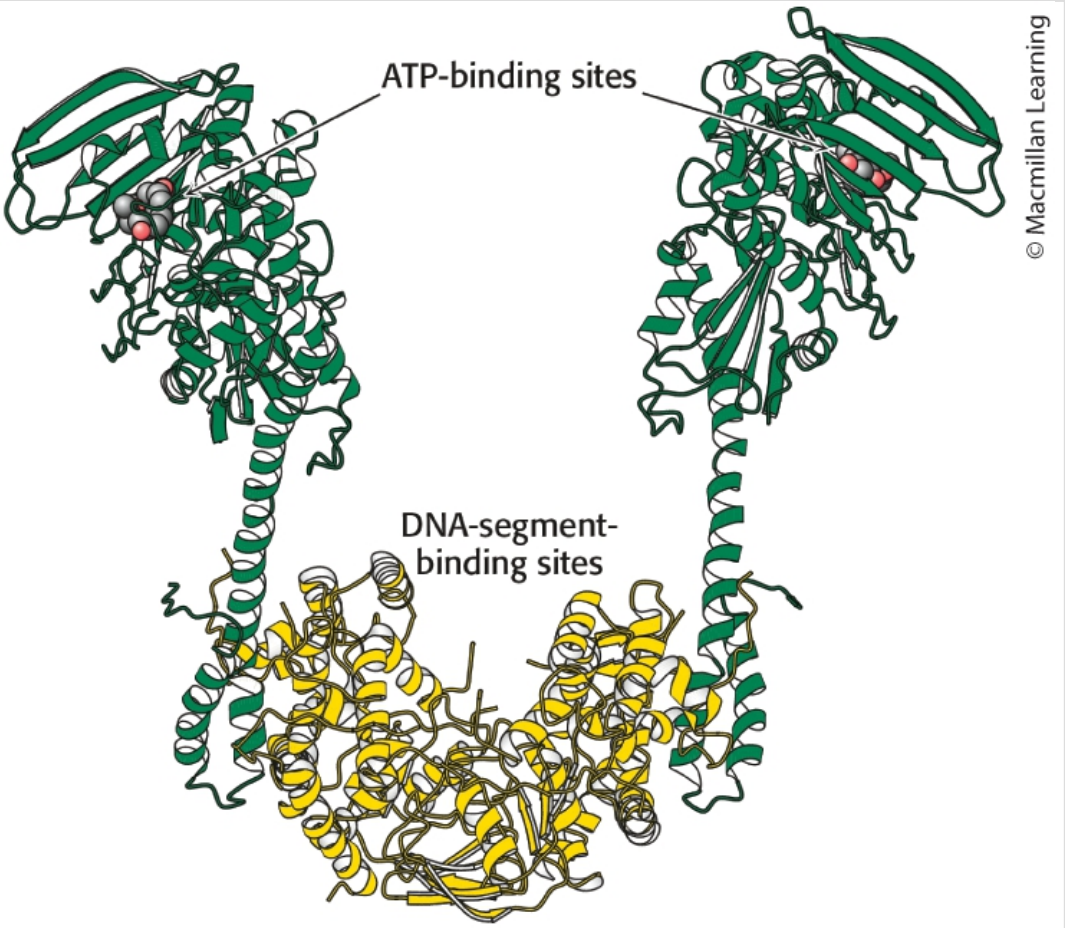


FIGURE 28.16 Topoisomerase II is a dimer. The structure of a typical topoisomerase II, this one from the archaeon *Sulfolobus shibatae*, is shown. Each half of the enzyme has one domain (shown in yellow) that contains a region for binding a DNA double helix and another domain (shown in green) that contains ATP-binding sites.

[Drawn from 2ZBK.pdb.]

INTERACT with this model in Achieve

1. The reaction begins with the binding of one double helix (hereafter referred to as the *G*, for gate, segment) to the enzyme (Figure 28.17). Each strand is positioned next to a tyrosine residue, one from each monomer, capable of forming a covalent linkage with the DNA backbone.

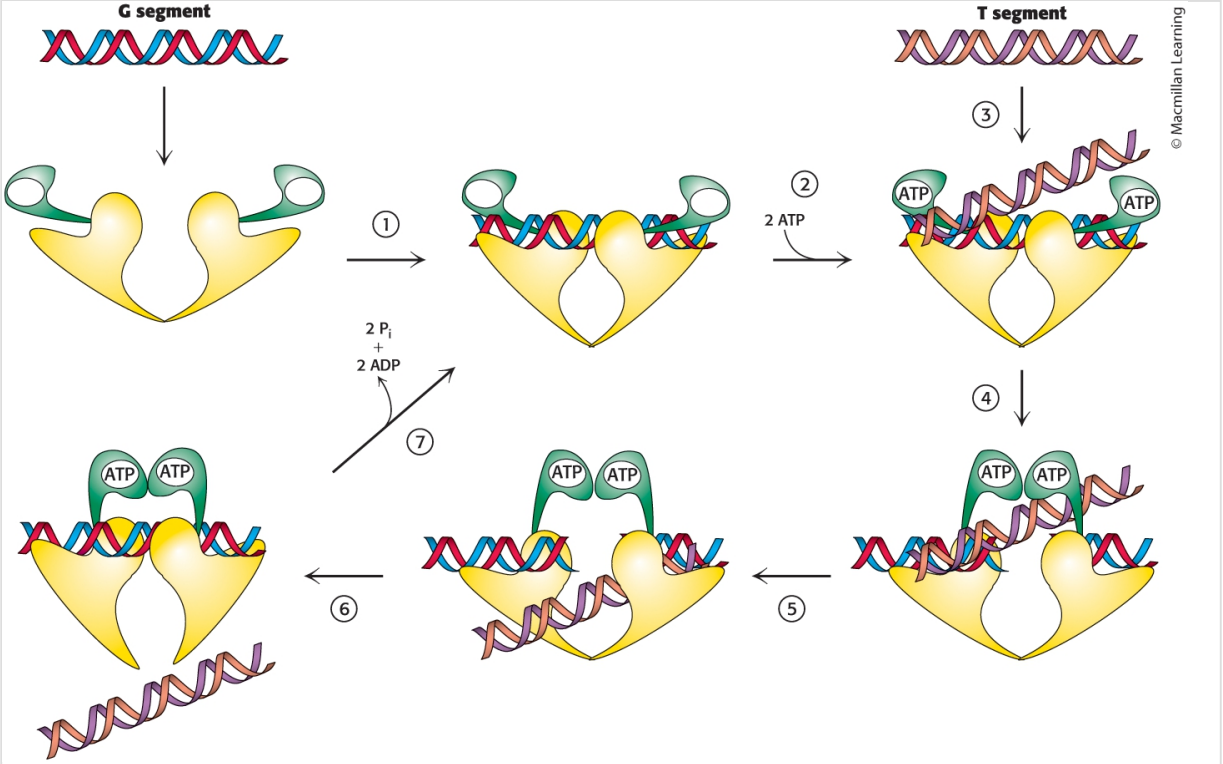


FIGURE 28.17 Topoisomerase II uses ATP hydrolysis to introduce negative supercoils into DNA. Topoisomerase II first binds one DNA duplex termed the G (for gate) segment (1). The binding of ATP to the two N-terminal domains brings these two domains together (2). This conformational change leads to the cleavage of both strands of the G segment and the binding of an additional DNA duplex, the T segment (3). This T segment then moves through the break in the G segment and out the bottom of the enzyme (4 through 6). The hydrolysis of ATP resets the enzyme with the G segment still bound (7). The orientation of the entering T segment results in the introduction of negative supercoils.

2. Each monomer of the enzyme has a domain that binds ATP, eventually leading to a conformational change that strongly favors the coming together of the two domains.

3. This complex then loosely binds a second DNA double helix (hereafter referred to as the *T*, for transported, segment). As the ATP-binding domains come closer together, they trap the bound T segment.

4. This conformational change also forces the separation and cleavage of the two strands of the G segment. Each strand is linked to the enzyme by a tyrosine–phosphodiester bond. Unlike the type I enzymes, the type II topoisomerases hold the DNA tightly so that it cannot rotate.

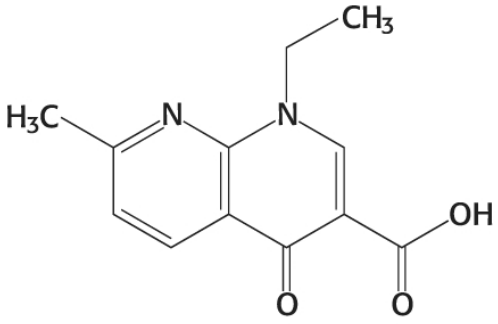
5. The T segment then passes through the cleaved G segment and into the large central cavity.

6. The ligation of the G segment leads to the release of the T segment through the gate at the bottom of the enzyme.

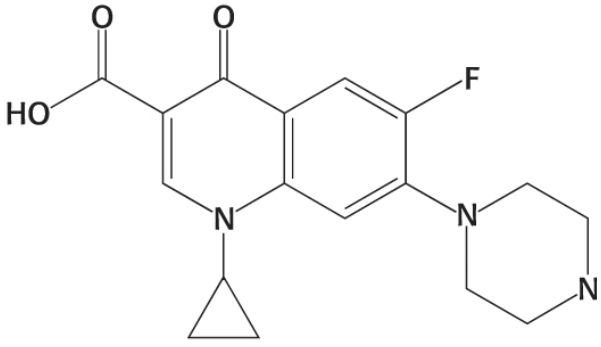
7. The hydrolysis of ATP and the release of ADP and orthophosphate allow the ATP-binding domains to separate, preparing the enzyme to bind another T segment. The overall process leads to a decrease in the linking number by two.



The bacterial topoisomerase II (often called DNA gyrase) is the target of several antibiotics that inhibit the prokaryotic enzyme much more than the eukaryotic one. Novobiocin blocks the binding of ATP to gyrase. Nalidixic acid and ciprofloxacin, in contrast, interfere with the breakage and rejoining of DNA chains. These two gyrase inhibitors are widely used to treat urinary tract and other infections including those due to *Bacillus anthracis* (anthrax). Camptothecin, an antitumor agent, inhibits human topoisomerase I by stabilizing the form of the enzyme covalently linked to DNA.



Nalidixic acid



Ciprofloxacin



28.3 DNA Replication Is Highly Coordinated

DNA replication must be very rapid, given the sizes of the genomes and the rates of cell division. The *E. coli* genome contains 4.6 million base pairs and is copied in less than 40 minutes. Thus, 2000 bases are incorporated per second. Enzyme activities must be highly coordinated to replicate entire genomes precisely and rapidly.

We begin our consideration of the coordination of DNA replication by looking at *E. coli*, which has been extensively studied. For this organism with a relatively small genome, replication begins at a single site and continues around the circular chromosome. The coordination of eukaryotic DNA replication is much more complex because there are many initiation sites throughout the genome and an additional enzyme is needed to replicate the ends of linear chromosomes.

DNA replication requires highly processive polymerases

Replicative polymerases are characterized by their very high catalytic potency, fidelity, and processivity. **Processivity** refers to the ability of an enzyme to catalyze many consecutive reactions without releasing its substrate. These polymerases are assemblies of many subunits that have evolved to grasp their templates and not let go until many nucleotides have been added.

The source of the processivity was revealed by the determination of the three-dimensional structure of the β_2 subunit of the *E. coli* replicative polymerase called DNA polymerase III (**Figure 28.18**). This unit, which has the form of a star-shaped ring, keeps the polymerase associated

with the DNA double helix. A 35 Å-diameter hole in its center can readily accommodate a duplex DNA molecule (around 20 Å in diameter) and leaves enough space between the DNA and the protein to allow rapid sliding during replication. A polymerization rate of 1000 nucleotides per second requires that 100 turns of duplex DNA (a length of 3400 Å, or 0.34 μm) slide through the central hole of β_2 per second. Thus, β_2 plays a key role in replication by serving as a **sliding DNA clamp**.

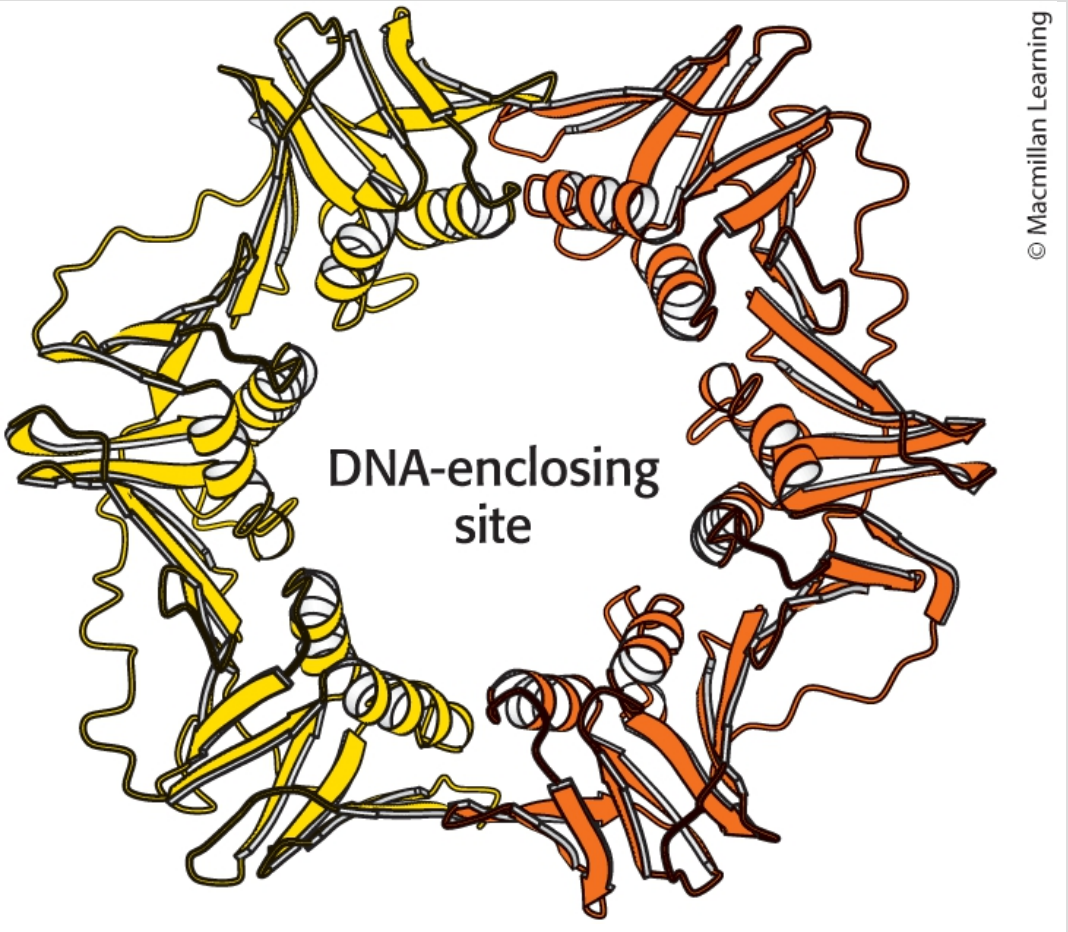


FIGURE 28.18 The sliding clamp subunit of DNA polymerase III is a dimer. The β subunit of DNA polymerase III forms a ring that surrounds the DNA duplex. The DNA template slides through the central cavity. Clasping the DNA molecule in the ring, the polymerase enzyme is able to move without falling off the DNA substrate.

[Drawn from 2POL.pdb.]

INTERACT with this model in Achieve

How does DNA become entrapped inside the sliding clamp? Replicative polymerases also include assemblies of subunits that function as clamp loaders by grasping the sliding clamp and, using the energy of ATP binding, pulling apart one of the interfaces between the two subunits of the sliding clamp. DNA can move through the gap, inserting itself through the central hole. ATP hydrolysis then releases the clamp, which closes around the DNA.

The leading and lagging strands are synthesized in a coordinated fashion

Replicative polymerases such as DNA polymerase III synthesize the leading and lagging strands simultaneously at the replication fork (Figure 28.19). Let's first look at how DNA polymerase III begins the synthesis of the leading strand starting from the RNA primer formed by primase. While the duplex DNA ahead of the polymerase is unwound by a hexameric helicase called DnaB, copies of single-stranded-binding protein (SSB) bind to the unwound strands, keeping the strands separated so that both strands can serve as templates. The leading strand is synthesized continuously by polymerase III, as topoisomerase II concurrently introduces right-handed (negative) supercoils to avert a topological crisis.

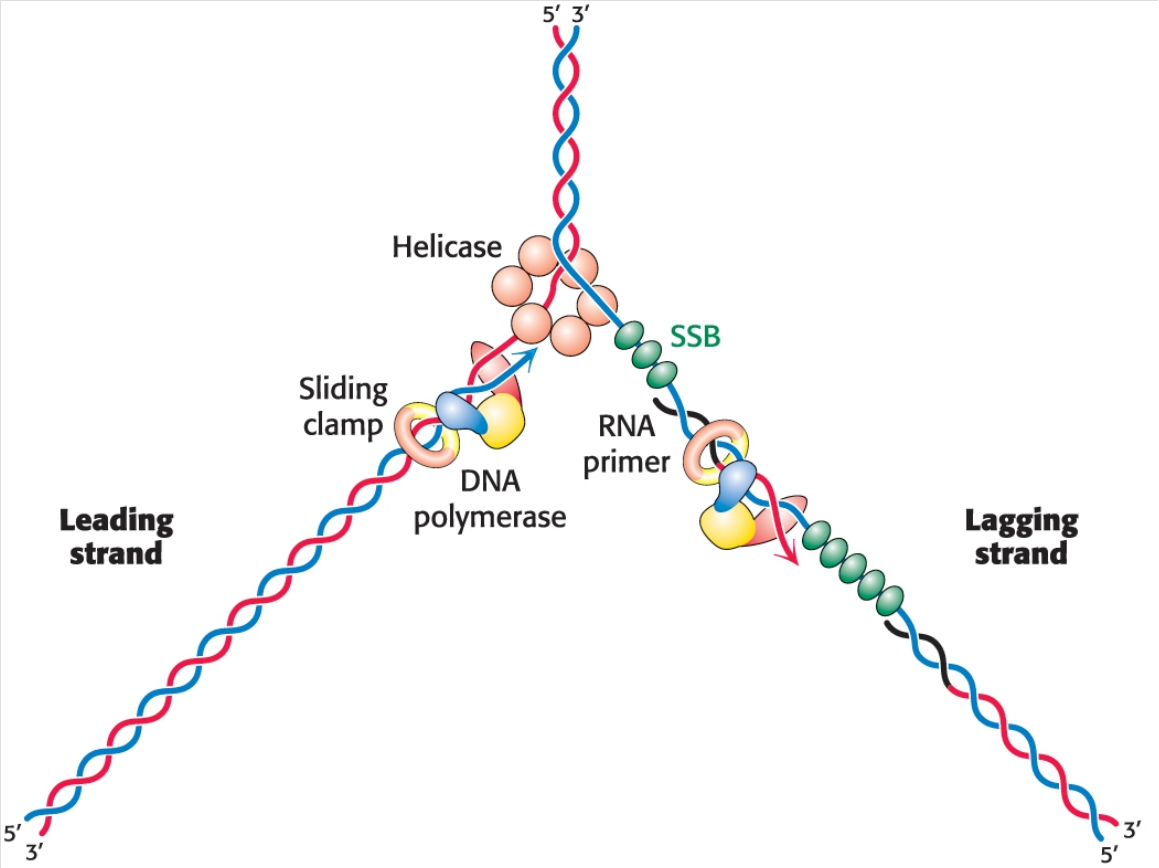


FIGURE 28.19 DNA synthesis at the replication fork is highly coordinated. A schematic view of the arrangement of DNA polymerase III and associated enzymes and proteins involved in the replication of DNA is shown. The helicase separates the two strands of the parent double helix, allowing DNA polymerases to use each strand as a template for DNA synthesis. Abbreviation: SS single-stranded-binding protein.

As mentioned earlier, the lagging strand is synthesized in fragments, so its synthesis is necessarily more complex. Yet the synthesis of the lagging strand is coordinated to be simultaneous with the synthesis of the leading strand. How is this coordination accomplished?

Examination of the subunit composition of the DNA polymerase III holoenzyme reveals an elegant solution for synthesis of the lagging strand (Figure 28.20). The holoenzyme includes two copies of the

polymerase core enzyme, which consists of the DNA polymerase itself (the α subunit); the ε subunit, a 3′-to-5′ proofreading exonuclease; another subunit called θ; and two copies of the dimeric β-subunit sliding clamp. The core enzymes are linked to a central structure having the subunit composition $\gamma\tau_2\delta\delta'\chi\phi$. The $\gamma\tau_2\delta\delta'$ complex serves as the clamp loader, and the χ and ϕ subunits interact with the single-stranded-DNA–binding protein; meanwhile, the entire apparatus interacts with the hexameric helicase DnaB. Eukaryotic replicative polymerases have similar, albeit slightly more complicated, subunit compositions and structures.

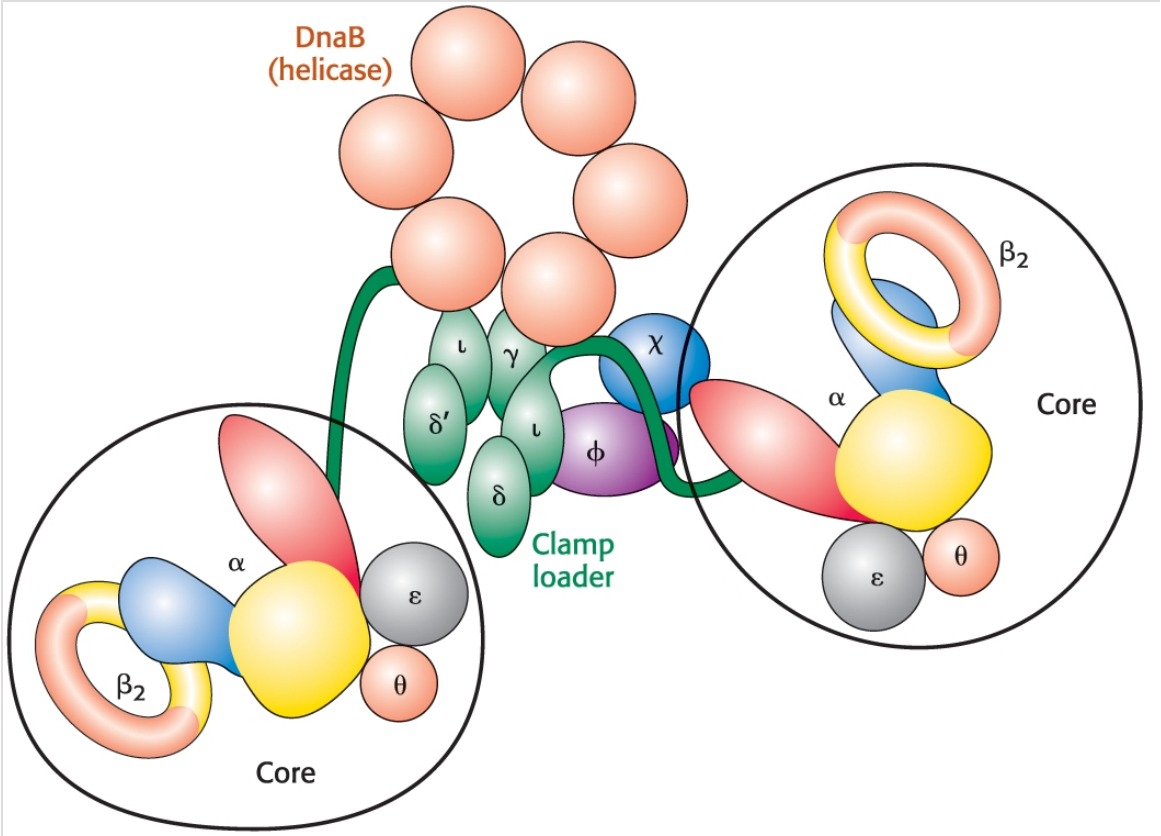


FIGURE 28.20 The DNA polymerase holoenzyme consists of multiple subunits. Each holoenzyme consists of two copies of the polymerase core enzyme, which comprises the α, ε, a θ subunits and two copies of the β subunit, linked to a central structure. The central structure includes the clamp-loader complex and the hexameric helicase DnaB.

The lagging-strand template is looped out so that it passes through the polymerase site in one subunit of a dimeric DNA polymerase III in the same direction as that of the leading-strand template in the other subunit. DNA polymerase III lets go of the lagging-strand template after adding about 1000 nucleotides by releasing the sliding clamp. A new loop is then formed, a sliding clamp is added, and primase again synthesizes a short stretch of RNA primer to initiate the formation of another Okazaki fragment. This mode of replication has been termed the **trombone model** because the size of the loop lengthens and shortens like the slide on a trombone (**Figure 28.21**).

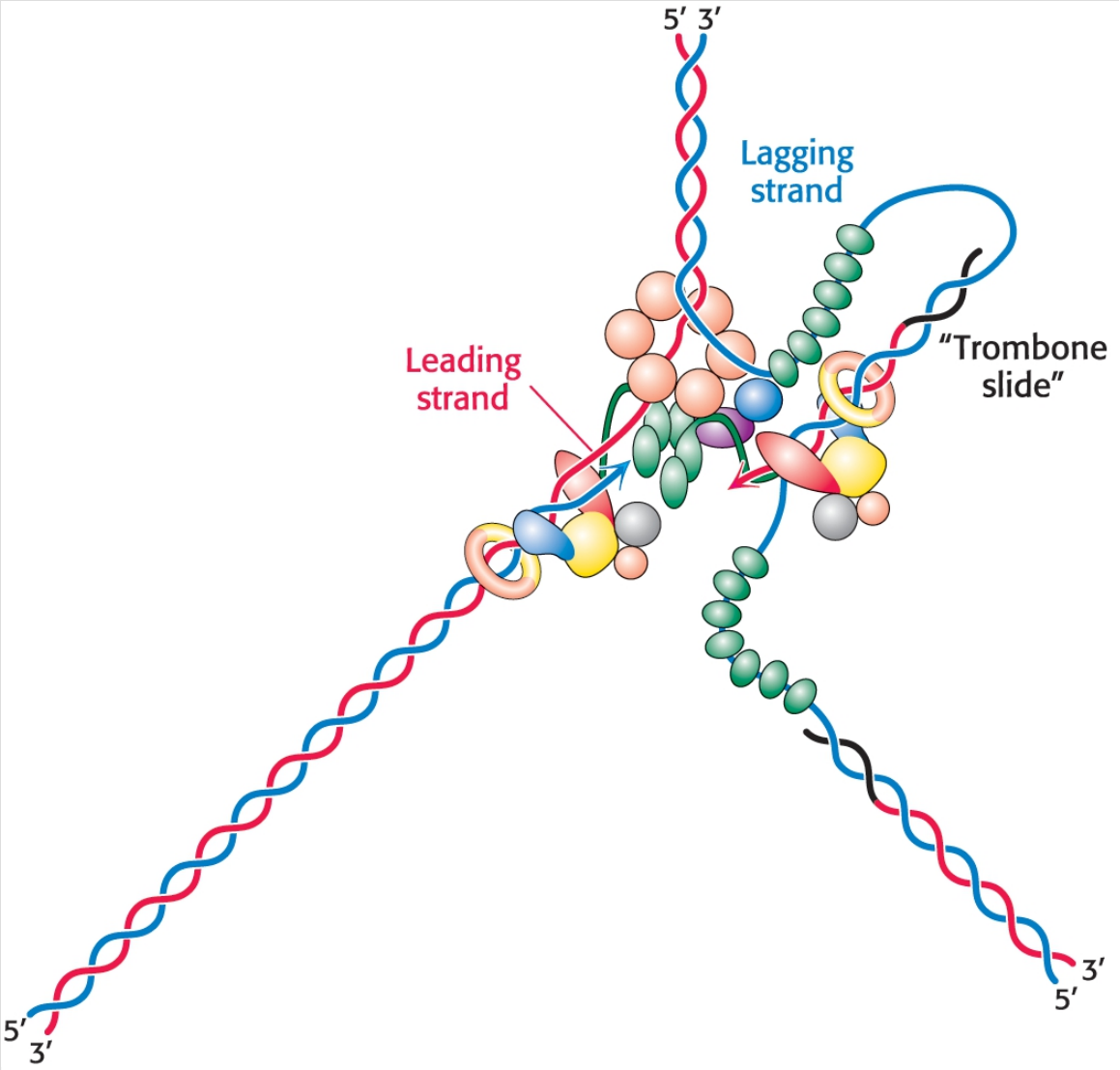


FIGURE 28.21 The trombone model describes the coordination of DNA synthesis at the replication fork. The replication of the leading and lagging strands is coordinated by the loopin out of the lagging strand to form a structure that acts somewhat as a trombone slide, growing a the replication fork moves forward. When the polymerase on the lagging strand reaches a regio that has been replicated, the sliding clamp is released and a new loop is formed.

The gaps between fragments of the nascent lagging strand are filled by DNA polymerase I. This essential enzyme also uses its $5' \rightarrow 3'$ exonuclease activity to remove the RNA primer lying ahead of the

polymerase site. The primer cannot be erased by DNA polymerase III because the enzyme lacks $5' \rightarrow 3'$ editing capability. Finally, DNA ligase connects the fragments.

DNA replication in *E. coli* begins at a unique site

In *E. coli*, DNA replication starts at a unique site within the entire 4.6×10^6 bp genome. This **origin of replication**, called the *oriC locus*, is a 245-bp region that has several unusual features (**Figure 28.22**). The *oriC* locus contains five copies of a sequence that is the preferred binding site for the origin-recognition protein DnaA. In addition, the *oriC* locus contains a tandem array of 13-bp sequences that are rich in AT base pairs.

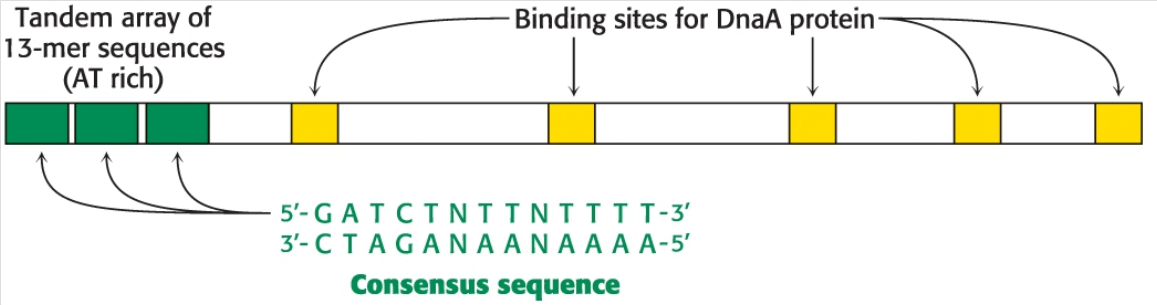


FIGURE 28.22 The *E. coli* chromosome has a single origin of replication. The *oriC* locus has a length of 245 bp and contains a tandem array of three nearly identical 13-nucleotide sequences (green) and five binding sites (yellow) for the DnaA protein.

Several steps are required to prepare for the start of replication:

1. *DnaA proteins bind to the* oriC. DnaA proteins are related to the hexameric helicases. Each DnaA monomer comprises an ATPase domain linked to a DNA-binding domain at its C-terminus. DnaA molecules are able to bind to each other through their ATPase domains; a group of bound DnaA molecules will break apart on the binding and hydrolysis of ATP. The DnaA proteins bind to the five high-affinity sites in *oriC* and then come together with other DnaA molecules bound to lower-affinity sites to form an oligomer, possibly a cyclic hexamer. The DNA is wrapped around the outside of the DnaA hexamer (**Figure 28.23**).

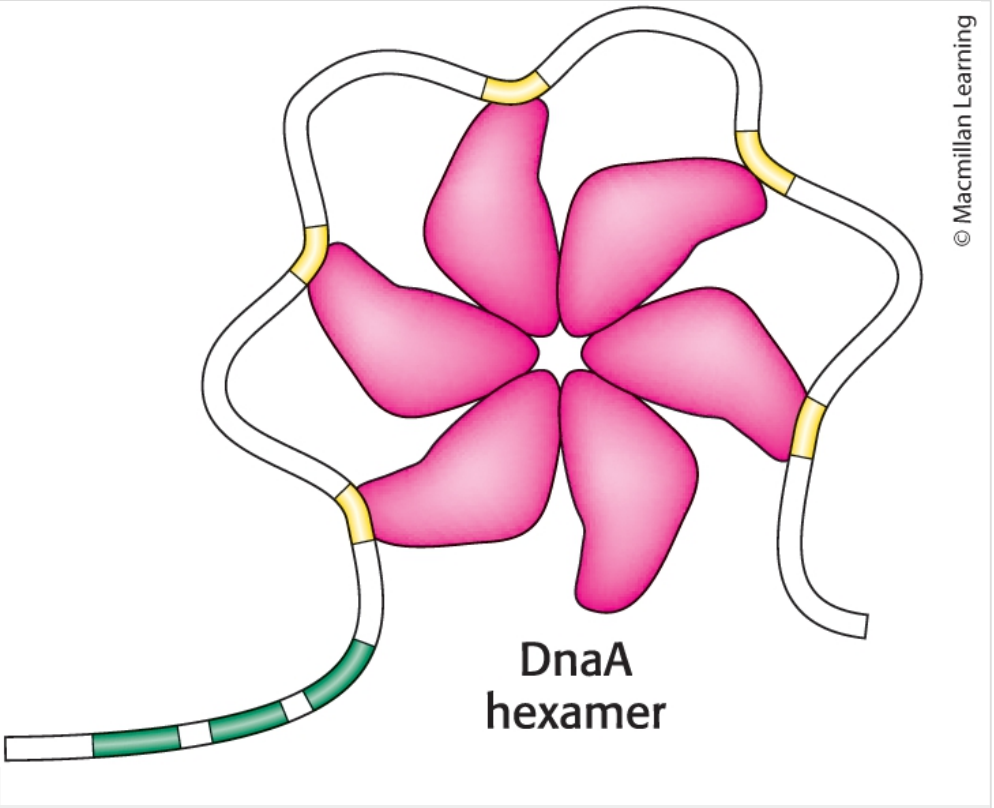


FIGURE 28.23 The assembly of DnaA proteins initiates DNA replication. Monomers of DnaA bind to their binding sites (shown in yellow) in *oriC* and come together to form a complex structure, possibly the cyclic hexamer shown here. This structure marks the origin of replication and favors DNA strand separation in the AT-rich sites (green).

2. *Single DNA strands are exposed in the prepriming complex*. With DNA wrapped around a DnaA hexamer, additional proteins are brought into play. The hexameric helicase DnaB is loaded around the DNA with the help of the helicase loader protein DnaC. Then, local regions of *oriC*, including the AT regions, are unwound and trapped by the single-stranded-DNA–binding protein. The result of this process is the creation of a structure called the *prepriming complex*, which makes single-stranded DNA accessible to other proteins (Figure 28.24). Significantly, the primase, DnaG, is now able to insert the RNA primer.

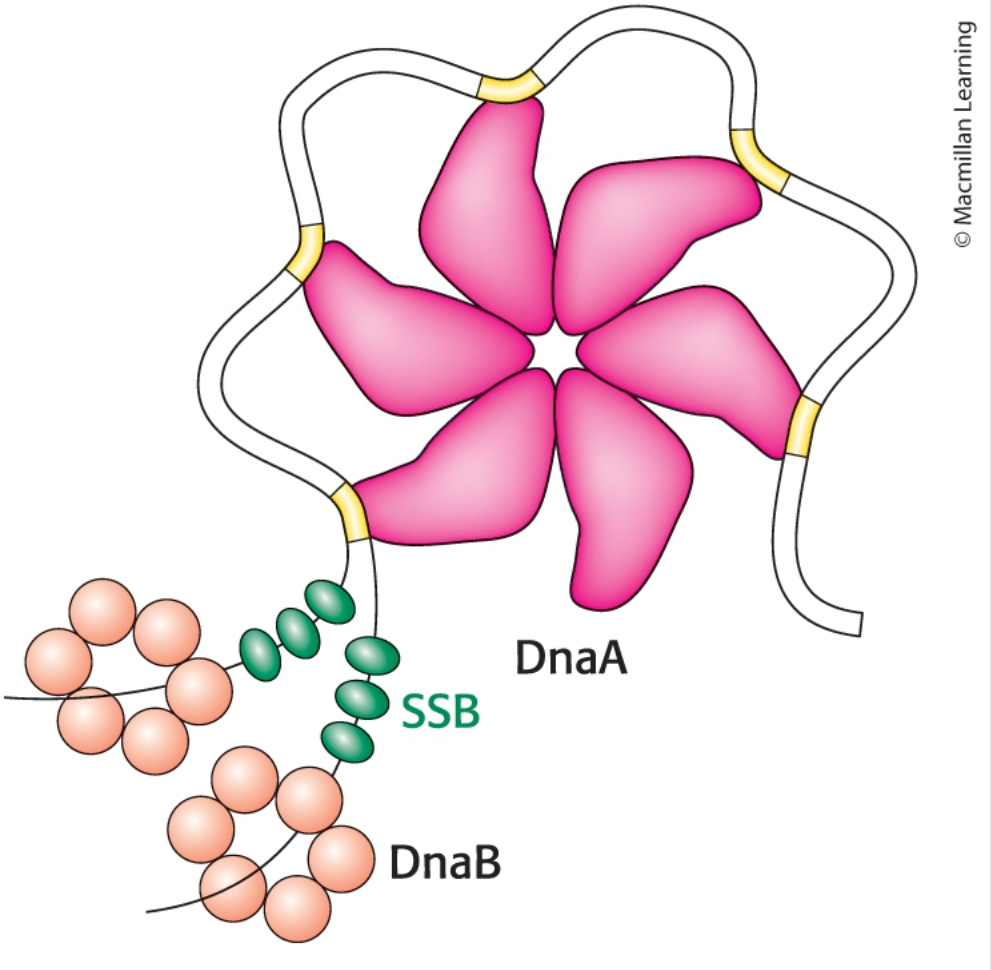


FIGURE 28.24 The prepriming complex prepares the template strands for DNA synthesis. The AT-rich regions are unwound and trapped by the single-stranded-binding protein (SSB). The hexameric DNA helicase DnaB is loaded on each strand. At this stage, the complex is ready for the synthesis of the RNA primers and assembly of the DNA polymerase III holoenzyme.

3. *The polymerase holoenzyme assembles*. The DNA polymerase III holoenzyme assembles on the prepriming complex, initiated by interactions between DnaB and the sliding-clamp subunit of DNA polymerase III. These interactions also trigger ATP hydrolysis within the DnaA proteins, causing them to break up. The breakup of the DnaA assembly prevents additional rounds of replication from beginning at the *oriC*, signaling the end of the preparatory phase.

Once initiated, DNA replication continues around the circular chromosome. To efficiently terminate replication, the *E. coli* chromosome includes specific termination sites (or *Ter* sites) that act as binding sites for a protein called *termination utilization substance*, or *Tus* (**Figure 28.25**). The complexes that form when Tus binds to the Ter sites are not symmetrical, and this asymmetry is central for its function: when a replication fork, led by the helicase DnaB, reaches a Ter–Tus complex from one direction, it can move past it, but when it reaches it from the opposite direction, the Ter–Tus complex effectively blocks the replication fork. The positions and orientations of the Ter sites within the *E. coli* genome facilitate efficient termination when one cycle of termination is complete.

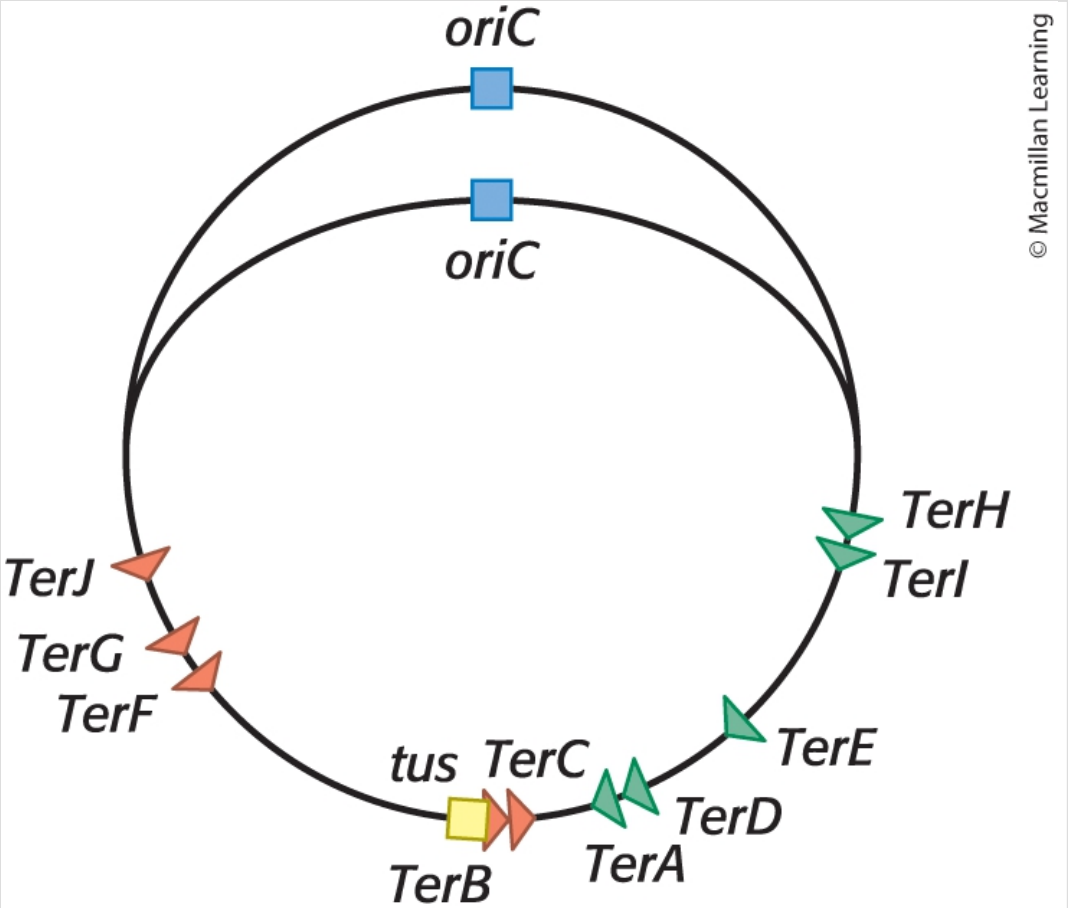


FIGURE 28.25 Replication termination in *E. coli* occurs at Ter sites. The *E. coli* genome includes 10 Ter sites that bind the termination utilization substance (Tus) protein. The Ter–Tus complexes block incoming replication forks in a unidirectional manner (indicated by the orientation of the triangles representing the Ter sites), facilitating termination of replication after a single cycle.

DNA replication in eukaryotes is initiated at multiple sites

Replication in eukaryotes is mechanistically similar to replication in prokaryotes but is more challenging for a number of reasons. One of them is sheer size: *E. coli* must replicate 4.6 million base pairs, whereas

a human diploid cell must replicate more than 6 billion base pairs. Second, the genetic information for *E. coli* is contained on one chromosome, whereas, in human beings, 23 pairs of chromosomes must be replicated. Finally, whereas the *E. coli* chromosome is circular, human chromosomes are linear. Unless countermeasures are taken, linear chromosomes are subject to shortening with each round of replication.

The first two challenges are met by the use of multiple origins of replication. In human beings, replication requires about 30,000 origins of replication, with each chromosome containing several hundred. Each origin of replication is the starting site for a replication unit, or *replicon*. DNA replication can be monitored by single-molecule methods, revealing bidirectional synthesis from different sites (Figure 28.26). In contrast with *E. coli*, the origins of replication in human beings do not have sharply defined sequences. Instead, more broadly defined AT-rich sequences are the sites around which the origin of replication complexes (ORCs) are assembled.



FIGURE 28.26 Eukaryotic chromosomes have multiple origins of replication. The image shows a single molecule of DNA containing two origins of replication. The origins were identified by labeling newly replicated DNA in human cells first with one thymine analog (iodo-deoxyuridine, IdU) and then another (chloro-deoxyuridine, CldU). DNA molecules from these cells were then extended on a microscope slide and labeled with antibodies to IdU (green) and CldU (red) to visualize the DNA. This method allows the detection of replication origins as well as determination of the rate of DNA synthesis.

[Data from: Conti et al., Replication fork velocities at adjacent replication origins are coordinately modified during DNA replication in human cell, *Molecular Biology of the Cell* 18:3059–3067, 2007.]

Initiation of replication in eukaryotes proceeds as follows:

1. *The ORC is assembled.* In human beings, the ORC is composed of six different proteins, each homologous to DnaA in *E. coli.* These proteins come together to form a hexameric structure analogous to the assembly formed by DnaA.

2. *Licensing factors expose single strands of DNA.* After the ORC has been assembled, additional proteins are recruited, including Cdc6, a homolog of the ORC subunits, and Cdt1. These proteins, in turn, recruit a hexameric helicase with six distinct subunits called Mcm2-7. These proteins, including the helicase, are sometimes called *licensing factors* because they permit the formation of the initiation complex. After the initiation complex has formed, Mcm2-7 separates the parental DNA strands, and the single strands are stabilized by the binding of replication protein A, a single-stranded-DNA–binding protein.

3. *Two distinct polymerases are needed to copy a eukaryotic replicon.* An initiator polymerase called *polymerase* α begins replication but is soon replaced by a more processive enzyme. This process is called *polymerase switching* because one polymerase has replaced another. This second enzyme, *DNA polymerase* δ, is the principal replicative polymerase in eukaryotes (**Table 28.1**).

TABLE 28.1 Some types of DNA polymerases

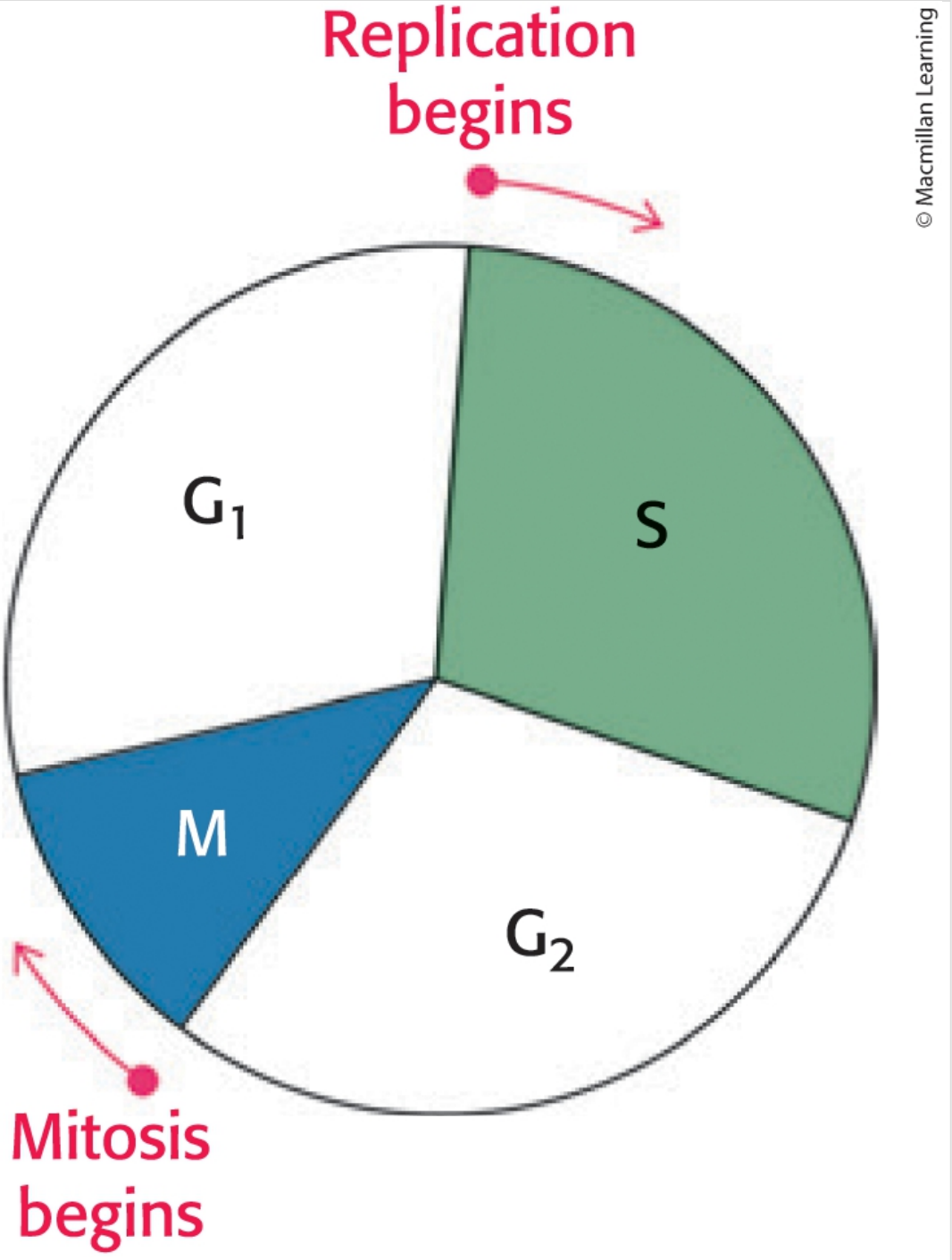
Name	Function
Prokaryotic Polymerases	
DNA polymerase I	Removes primer and fills in gaps on lagging strand
DNA polymerase II (error-prone	DNA repair

polymerase)	
DNA polymerase III	Primary enzyme of DNA synthesis
Eukaryotic Polymerases	
DNA polymerase α	Initiator polymerase
Primase subunit	Synthesizes the RNA primer
DNA polymerase unit	Adds stretch of about 20 nucleotides to the primer
DNA polymerase β (error-prone polymerase)	DNA repair
DNA polymerase δ	Primary enzyme of DNA synthesis

Once initiated, replication proceeds with the binding of DNA polymerase α. This enzyme includes a primase subunit, used to synthesize the RNA primer, as well as an active DNA polymerase. After this polymerase has added a stretch of about 20 deoxynucleotides to the primer, another replication protein, called *replication factor C* (RFC), displaces DNA polymerase α. Replication factor C attracts a sliding clamp called *proliferating cell nuclear antigen* (PCNA), which is homologous to the β_2 subunit of *E. coli* DNA polymerase III. The binding of PCNA to DNA polymerase δ renders the enzyme highly processive and suitable for long stretches of replication. Replication continues in both directions from the origin of replication until adjacent replicons meet and fuse. At this stage the RNA primers are removed and the DNA fragments are ligated by DNA ligase.

The eukaryotic cell cycle ensures coordination of DNA replication and cell division

The use of multiple origins of replication requires mechanisms for ensuring that each sequence is replicated once and only once. Thus, the processes of DNA synthesis and cell division are coordinated in the eukaryotic **cell cycle** so that the replication of all DNA sequences (which occurs during S phase) is complete before the cell progresses into the next phase of the cycle (**Figure 28.27**). This coordination requires several so-called *checkpoints* that control the progression along the cycle. Checkpoints are managed by a family of small proteins termed *cyclins*, which are synthesized and degraded by proteasomal digestion in the course of the cell cycle. Cyclins act by binding to specific cyclin-dependent protein kinases and activating them. One such kinase, cyclin-dependent kinase 2 (cdk2), binds to assemblies at origins of replication and regulates replication through a number of interlocking mechanisms.



© Macmillan Learning

FIGURE 28.27 Eukaryotic DNA replication and cell division are highly coordinated. Mitosis (M) takes place only after DNA synthesis (S). Two gap phases (G_1 and G_2) separate the two processes.

The complexity of the eukaryotic genome includes the three-dimensional organization of chromosomes in specific compartments within the nucleus, a concept referred to as the *3D genome*. This level of organization is related to the fact that certain sections of the genome are replicated at distinct times during the S phase of the cell cycle. Moreover, regions of the genome that are replicated early in S phase also tend to be more highly expressed.

Telomeres are protective structures at the ends of linear chromosomes

Recall that whereas the genomes of essentially all prokaryotes are circular, the chromosomes of human beings and other eukaryotes are linear. The free ends of linear DNA molecules introduce several complications that must be resolved by special enzymes. In particular, complete replication of DNA ends is difficult because polymerases act only in the $5' \rightarrow 3'$ direction. Thus, without some kind of intervention, the lagging strand would have an incomplete $5'$ end after the removal of the RNA primer, and each round of replication would further shorten the chromosome.

The first clue to how this problem is resolved came from sequence analyses of the ends of chromosomes, called **telomeres** (from the Greek *telos*, "an end"). Telomeric DNA contains hundreds of tandem repeats of a six-nucleotide sequence. One of the strands is G rich at the $3'$ end, and it is slightly longer than the other strand. In human beings, the repeating G-rich sequence is AGGGTT.

Extensive investigation of the structure adopted by telomeres suggests that they may form large duplex loops (**Figure 28.28**). The single-stranded region at the very end of the structure has been proposed to

loop back to form a DNA duplex with another part of the repeated sequence, displacing a part of the original telomeric duplex. This loop-like structure is formed and stabilized by specific telomere-binding proteins. Such structures would nicely mask and protect the end of the chromosome.



FIGURE 28.28 Telomeres may form duplex loops. A single-stranded segment of the G-rich strar extends from the end of the telomere. In one model for telomeres, this single-stranded region invades the duplex to form a large duplex loop.

Telomeres are replicated by telomerase, a specialized polymerase that carries its own RNA template

How are these repeated sequences generated? An enzyme, termed **telomerase**, that executes this function has been purified and characterized. When a primer ending in GGTT is added to human telomerase in the presence of dNTPs, the sequences GGTTAGGGTT and GGTTAGGGTTAGGGTT, as well as longer products, are generated. Elizabeth Blackburn and Carol Greider (Chapter 1) discovered that the enzyme adding the repeats contains an RNA molecule that serves as the template for the elongation of the G-rich strand (**Figure 28.29**). Thus, telomerase carries the information necessary to generate the repeated telomeric sequences. Subsequently, a protein component of telomerases also was identified. This component is related to reverse

transcriptases, enzymes first discovered in retroviruses that copy RNA into DNA (Section 8.4). Thus, telomerase is a specialized reverse transcriptase that carries its own template.

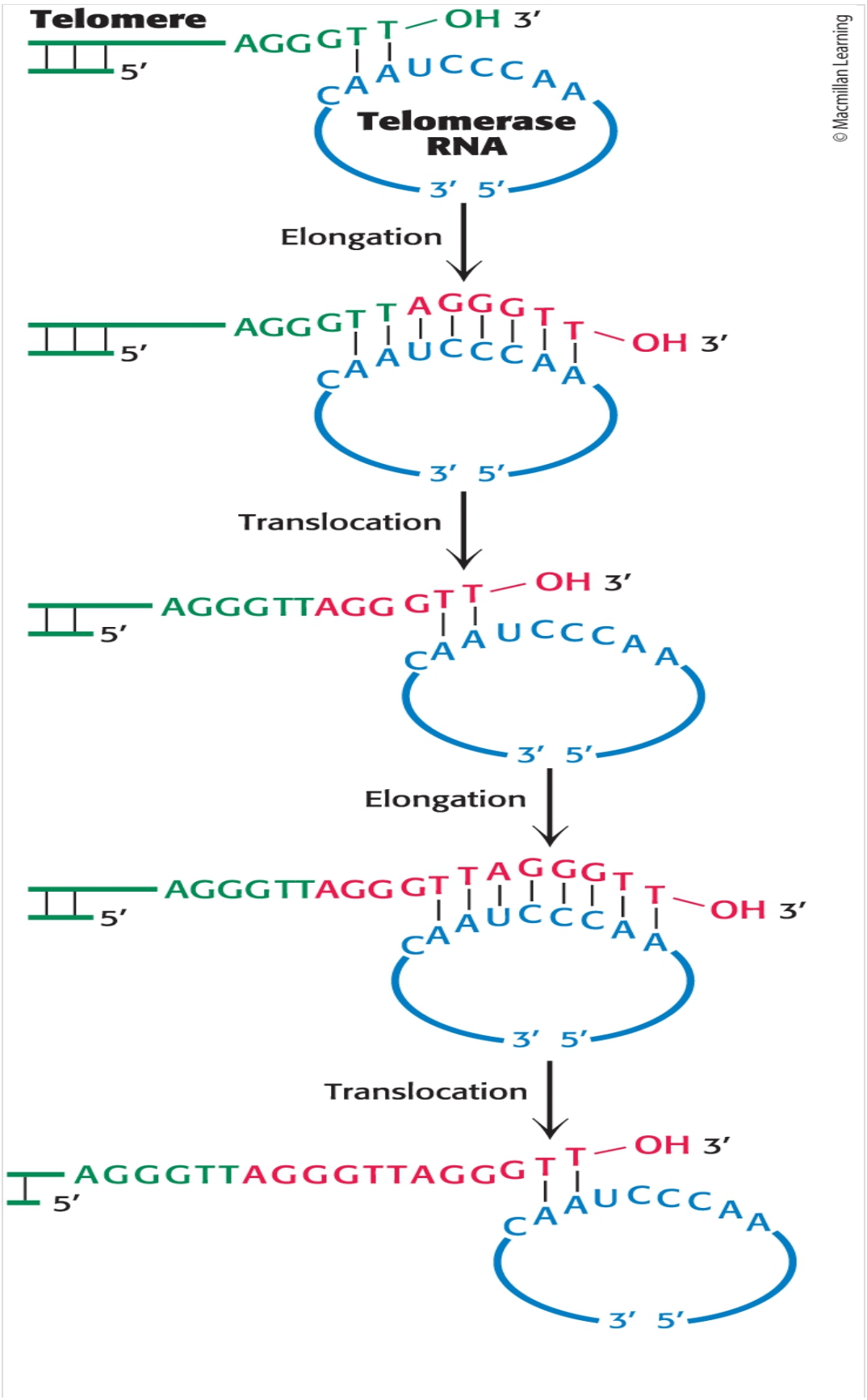

Telomere
AGGGTT
OH 3′
5′
CAAUCCCAA
Telomerase RNA
3′ 5′
Elongation
AGGGTTAGGGTT
Translocation
AGGGTTAGGGTTAGGGTT
© Macmillan Learning

FIGURE 28.29 Telomerase uses its RNA template to synthesize the G-rich strand of telomeres. The RNA template of telomerase is shown in blue and the nucleotides added to the G-rich strand of the primer are shown in red.

[Information from E. H. Blackburn, *Nature* 350:569–573, 1991.]



Telomerase is generally expressed at high levels only in rapidly growing cells, including cancer cells. Thus, telomerase is a potential target for anticancer therapy. A variety of approaches for blocking telomerase expression or blocking its activity are under investigation for cancer treatment and prevention.

Self-Check Question



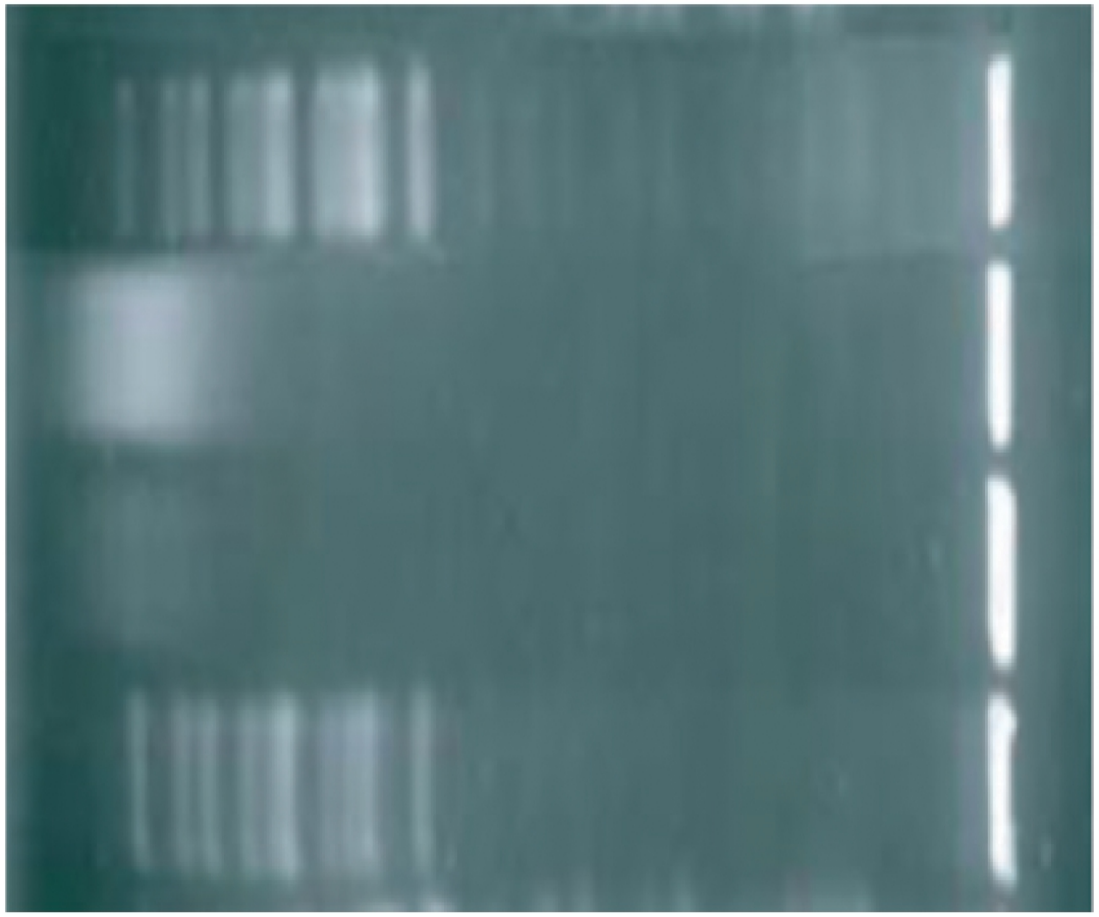
Telomerase is not active in most human cells. Some cancer biologists have suggested that activation of the telomerase gene would be a requirement for a cell to become cancerous. Explain why this might be the case.

28.4 Many Types of DNA Damage Can Be Repaired

We have examined how even very large and complex genomes can, in principle, be replicated with considerable fidelity. However, DNA does become damaged, both in the course of replication and through other processes. Although DNA is remarkably robust, ultraviolet light as well as a range of chemical species can damage DNA, introducing changes in the DNA sequence (mutations) or lesions that can block further DNA replication. DNA damage can also take more complex forms such as the chemical modification of bases, chemical cross-links between the two strands of the double helix, or breaks in one or both of the phosphodiester backbones. The results may be cell death or cell transformation, changes in the DNA sequence that can be inherited by future generations, or blockage of the DNA replication process itself. While a variety of DNA-repair systems have evolved that can recognize DNA damage and, in many cases, restore the DNA molecule to its undamaged form, mutations in genes that encode components of DNA-repair systems are key factors in the development of cancer.

The bacterium *Deinococcus radiodurans* illustrates the extraordinary power of DNA-repair systems. This bacterium was discovered in 1956 when scientists were studying the use of high doses of gamma radiation to sterilize canned meat. In some cases, the meat still spoiled due to the growth of a bacterial species that withstood doses of gamma radiation more than 1000 times larger than those that would kill a human being. Each *D. radiodurans* cell contains between 4 and 10 copies of its genome. Even when these bacterial chromosomes are broken into many fragments by the ionizing radiation, they can reassemble and recombine to regenerate the intact genome with essentially no loss of information (**Figure 28.30**). These cells can also survive extreme desiccation — that is, drying out — much better than other organisms.

This ability is believed to be the selective advantage that favored the evolution of this and related species.



Reprinted with permission of Macmillan Publishers Ltd, from Zahradka, K., Slade, D., Bailone, A. et al. Reassembly of shattered chromosomes in Deinococcus radiodurans. Nature 443, 569–573 (2006); permission conveyed through Copyright Clearance Cener, Inc.

FIGURE 28.30 The bacterium *Deinococcus radiodurans* repairs DNA damage quickly. After irradiation with gamma rays, the fragmented genome of this bacterium is repaired and reassembled within 3 hours. To aid analysis, the genomic DNA samples were digested with a restriction enzyme that cuts at only a few sites within the genome. C = control



Before we discuss various DNA-repair systems, let's begin with some of the sources of DNA damage.

Errors can arise in DNA replication

Errors introduced in the replication process are the simplest source of damage in the double helix. With the addition of each base, there is the possibility that an incorrect base might be incorporated, forming a non-Watson–Crick base pair. These non-Watson–Crick base pairs can locally distort the DNA double helix. Furthermore, such mismatches can be mutagenic; that is, they can result in permanent changes in the DNA sequence. When a double helix containing a non-Watson–Crick base pair is replicated, the two daughter double helices will have different sequences, because the mismatched base is very likely to pair with its Watson–Crick partner. Errors other than mismatches include insertions, deletions, and breaks in one or both strands. Furthermore, replicative polymerases can stall or even fall off a damaged template entirely, causing replication of the genome to halt before it is complete.

A variety of mechanisms have evolved to deal with such interruptions, including specialized DNA polymerases that can replicate DNA across many lesions. A drawback is that such polymerases are substantially more error-prone than are normal replicative polymerases. Nonetheless, these translesion or error-prone polymerases allow the completion of a draft sequence of the genome that can be at least partly repaired by DNA-repair processes. DNA recombination (Section 28.5)

provides an additional mechanism for salvaging interruptions in DNA replication.

DNA can be damaged by oxidizing agents, alkylating agents, and light

A variety of chemical and physical agents, called **mutagens**, can alter specific bases within DNA after replication is complete. Let's look in depth at some of these mutagens.

Reactive oxygen species

For example, hydroxyl radical reacts with guanine to form 8-oxoguanine. 8-Oxoguanine is mutagenic because it often pairs with adenine rather than cytosine in DNA replication. Its pairing partner differs from that of guanine because it uses a different edge of the base to form base pairs (**Figure 28.31**).

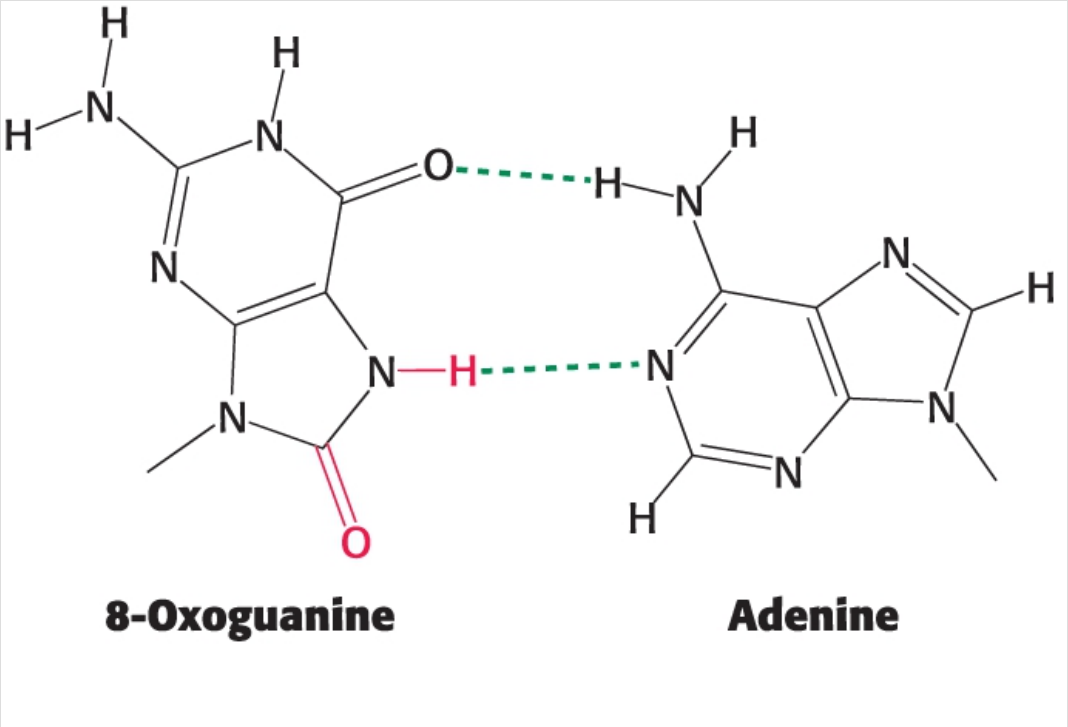


FIGURE 28.31 Damaged DNA bases can form base pairs. When guanine is oxidized to 8-oxoguanine, the damaged base can form a base pair with adenine through an edge of the base that does not normally participate in base-pair formation.

Deaminating agents

Deamination is another potentially deleterious process. For example, nitrous acid will deaminate adenine to form hypoxanthine (Figure 28.32). This process is mutagenic because hypoxanthine pairs with cytosine rather than thymine. Guanine and cytosine can also be deaminated to yield bases that pair differently from the parent base.

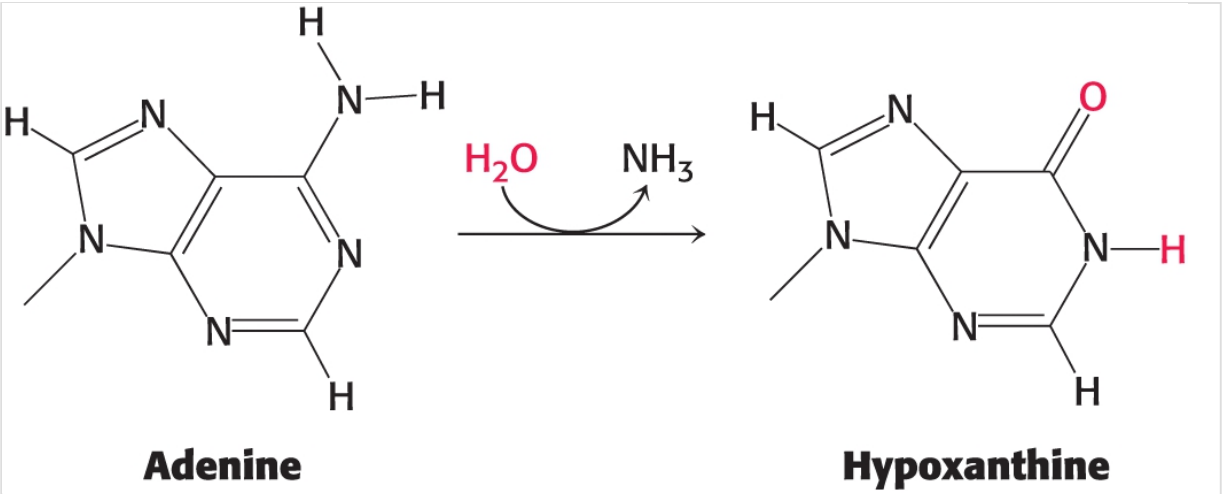
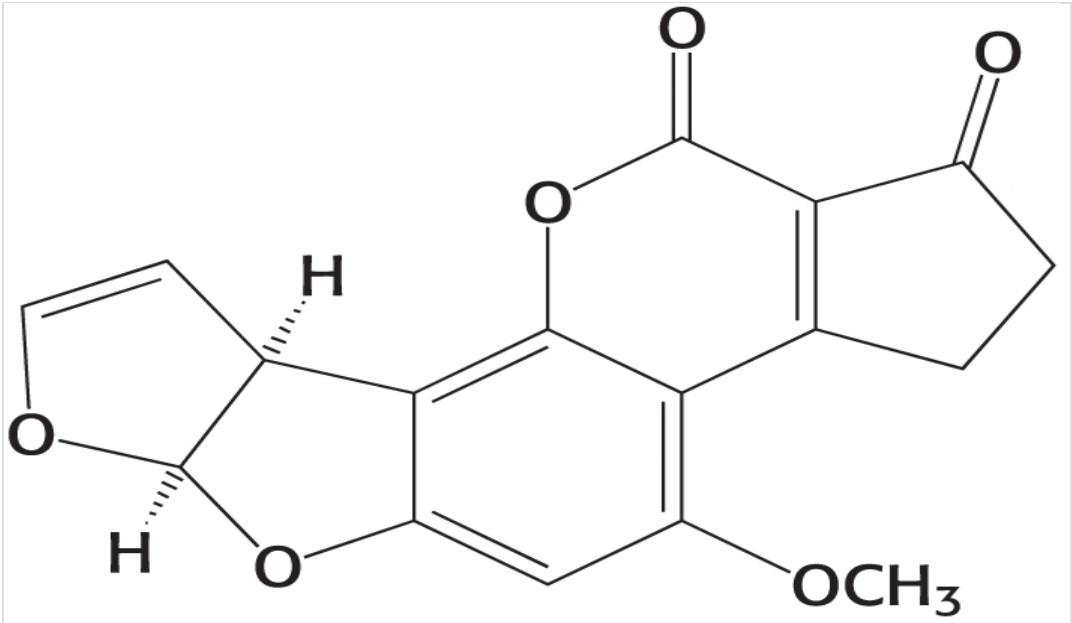


FIGURE 28.32 Adenine can be deaminated to form hypoxanthine. Hypoxanthine forms base pairs with cytosine in a manner similar to that of guanine, and so the deamination reaction can result in mutation.

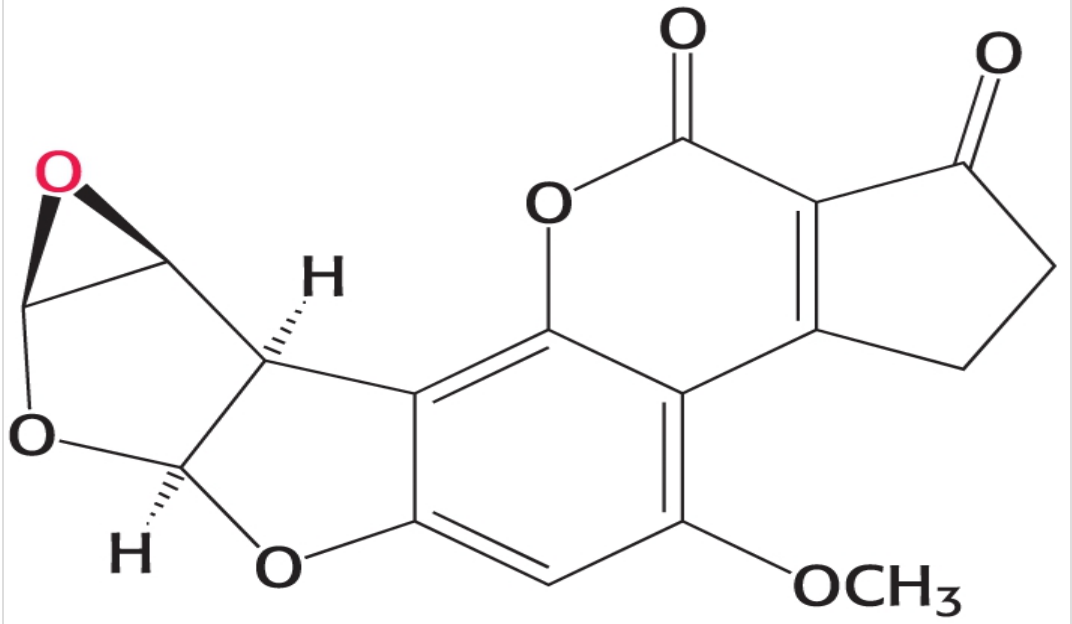
Alkylating agents

In addition to oxidation and deamination, nucleotide bases are subject to alkylation, in which electrophilic centers are attacked by nucleophiles such as N-7 of guanine and adenine to form alkylated adducts. Some compounds are converted into highly active electrophiles through the action of enzymes that normally play a role in detoxification. A striking example is aflatoxin B_1, a compound produced by molds that grow on peanuts and other foods. A cytochrome P450 enzyme (Section 26.4) converts this compound into a highly reactive epoxide (**Figure 28.33**). This agent reacts with the N-7 atom of guanosine to form a mutagenic adduct that frequently leads to a G–C-to-T–A transversion.



Aflatoxin B_1

Cytochrome P450



Active DNA-modifying agent

FIGURE 28.33 Aflatoxin can be activated into a mutagen. Aflatoxin is activated by cytochrome P450 to form a highly reactive species that modifies bases such as guanine in DNA, leading to mutations.



UV light and other cross-linking agents

The ultraviolet component of sunlight is a ubiquitous DNA-damaging agent. Its major effect is to covalently link adjacent pyrimidine residues along a DNA strand (Figure 28.34). Such a pyrimidine dimer cannot fit into a double helix, and so replication and gene expression are blocked until the lesion is removed. A thymine dimer is an example of an *intra*strand cross-link because both participating bases are in the same strand of the double helix. In contrast, *inter*strand cross-links between bases on opposite strands disrupt replication because they prevent strand separation. Interstrand cross-links can be introduced by various agents, including compounds called *psoralens* (Figure 28.35) that are produced by a number of plants, including the common fig. When consumed in high doses and combined with exposure to UV light, psoralens can be mutagenic; but in lower doses, the combination of psoralens and UV light is an approved treatment method for a variety of skin conditions such as psoriasis and eczema.

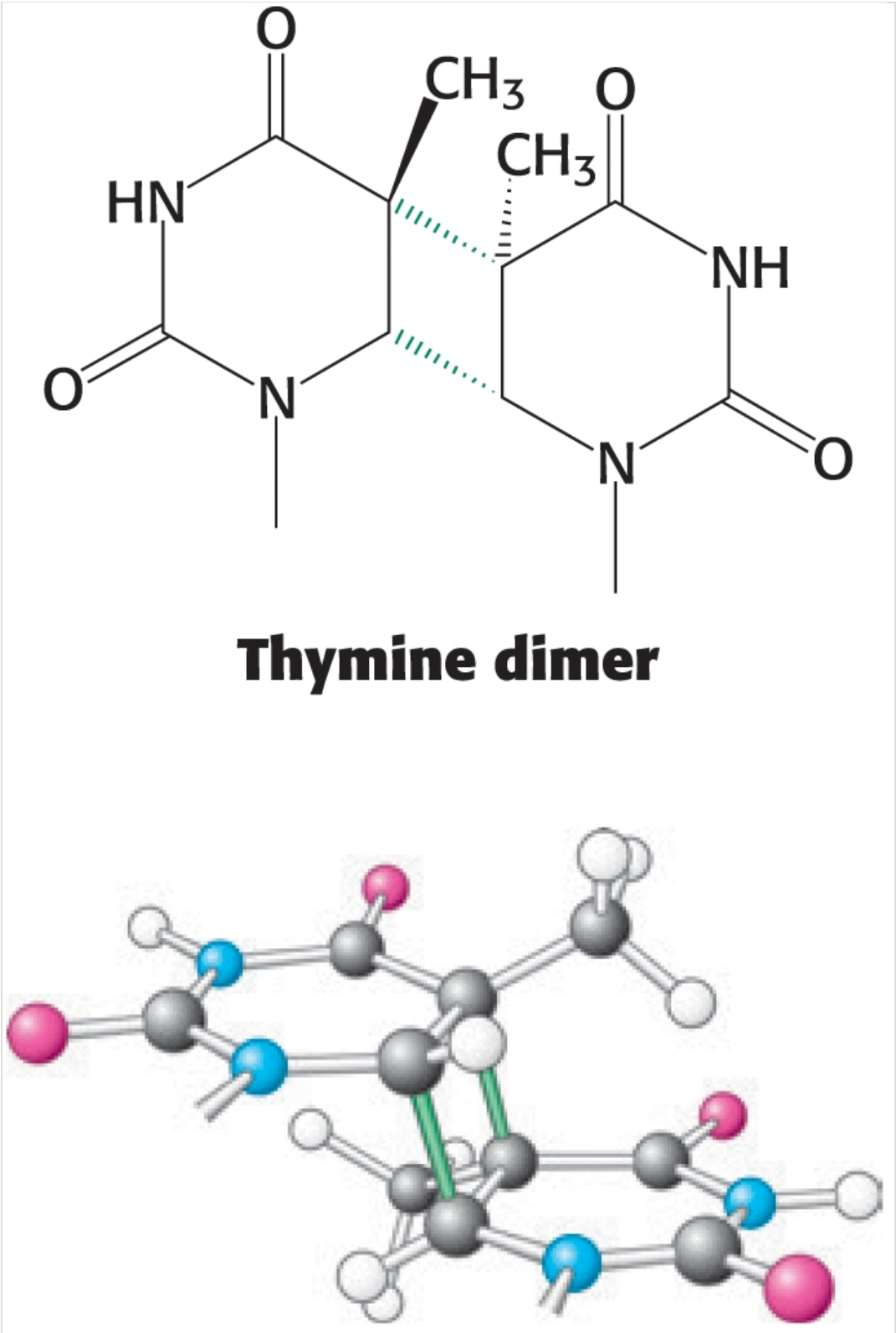


FIGURE 28.34 Ultraviolet light induces cross-links between adjacent pyrimidines along one strand of DNA.

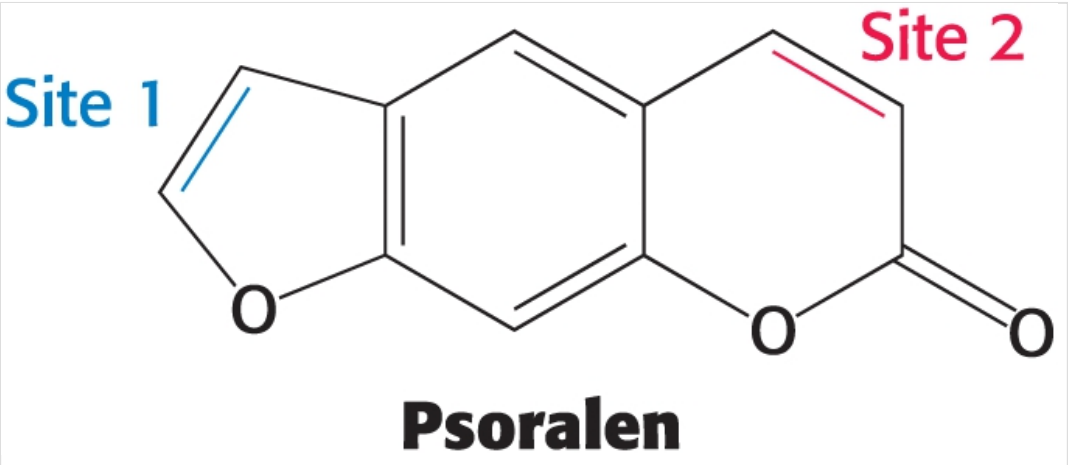


FIGURE 28.35 Psoralen is a cross-linking agent. The compound psoralen and its derivatives can form interstrand cross-links through two reactive sites that can form adducts with nucleotide bases.

High-energy electromagnetic radiation such as x-rays

X-rays can damage DNA by producing high concentrations of reactive species in solution. X-ray exposure can induce several types of DNA damage, including single- and double-stranded breaks in DNA. This ability to induce such DNA damage led Hermann Muller to discover the mutagenic effects of x-rays in *Drosophila* in 1927. This discovery contributed to the development of *Drosophila* as one of the premier organisms for genetic studies.

DNA damage can be detected and repaired by a variety of systems

To protect the genetic message, a wide range of DNA-repair systems are present in most organisms. Many systems repair DNA by using sequence information from the uncompromised strand. Such single-strand replication systems follow a similar mechanistic outline:

1. Recognize the offending base(s).
2. Remove the offending base(s).
3. Repair the resulting gap with a DNA polymerase and DNA ligase.

We will briefly consider examples of several repair pathways. Although many of these examples are taken from *E. coli*, corresponding repair systems are present in most other organisms, including human beings.

Proofreading and repair by DNA polymerases

The replicative DNA polymerases themselves are able to correct many DNA mismatches produced in the course of replication. For example, the ε subunit of *E. coli* DNA polymerase III functions as a $3'$-to-$5'$ exonuclease. This domain removes mismatched nucleotides from the $3'$ end of DNA by hydrolysis. How does the enzyme sense whether a newly added base is correct? As a new strand of DNA is synthesized, it is, in a sense, proofread (**Figure 28.36**). If an incorrect base is inserted, then DNA synthesis slows down, owing to the difficulty of threading a non-Watson–Crick base pair into the polymerase. In addition, the mismatched base is weakly bound and therefore able to fluctuate in position. The delay from the slowdown allows time for these fluctuations to take the newly synthesized strand out of the polymerase active site and into the exonuclease active site. There, the DNA is

degraded, one nucleotide at a time, until it moves back into the polymerase active site and synthesis continues.

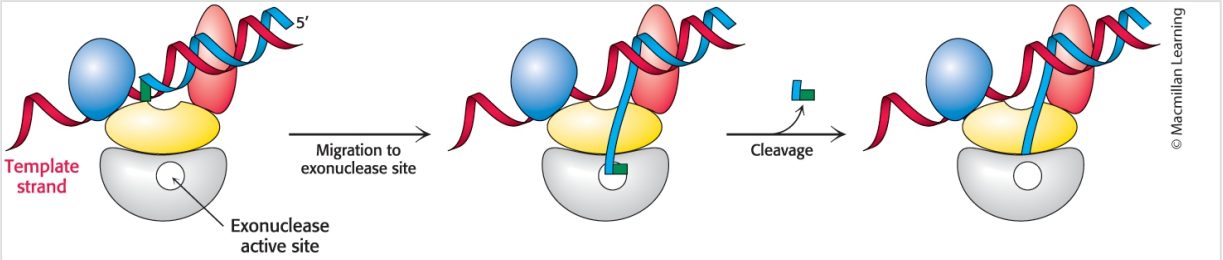


FIGURE 28.36 DNA polymerases have proofreading activities. The growing polynucleotide chain occasionally leaves the polymerase site and migrates to the active site of the exonuclease. There, one or more nucleotides are excised from the newly synthesized chain, removing potentially incorrect bases.

Mismatch repair

A second mechanism is present in essentially all cells to correct errors made in replication that are not corrected by proofreading (Figure 28.37). **Mismatch repair** is achieved by systems of at least two proteins, one for detecting the mismatch and the other for recruiting a restriction endonuclease that cleaves the newly synthesized DNA strand close to the lesion to facilitate repair. In *E. coli*, these proteins are MutS and MutL, and the endonuclease is MutH.

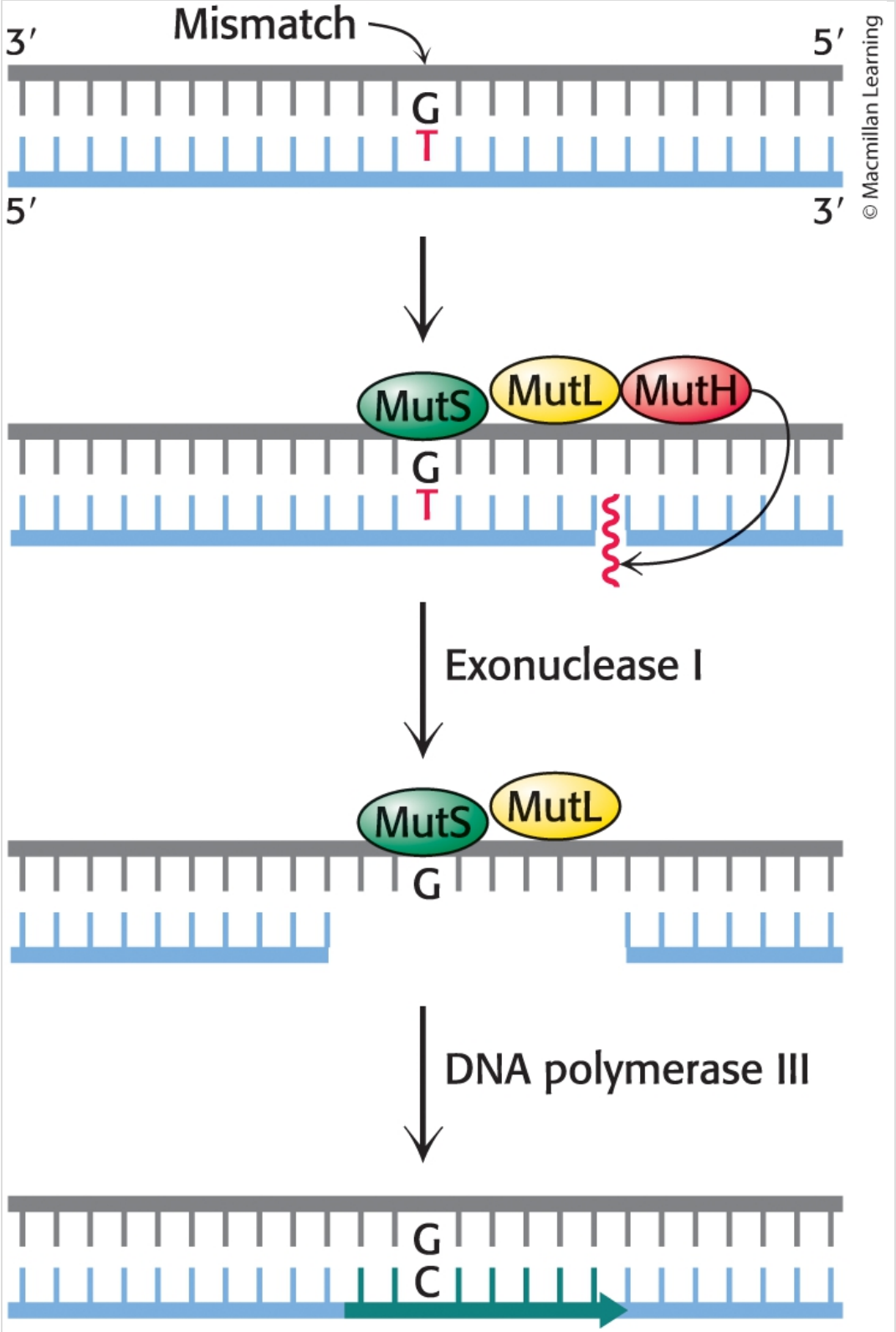


FIGURE 28.37 DNA mismatch repair in *E. coli* involves multiple proteins. First, a G–T mismatch is recognized by the MutS–MutL complex, and then MutH cleaves the

backbone in the vicinity of the mismatch. Subsequently, a segment of the DNA strand containing the erroneous T is removed by exonuclease I and synthesized anew by DNA polymerase III.

[Information from R. F. Service, *Science* 263:1559–1560, 1994.]

Direct repair

Another mechanism of DNA repair is **direct repair**, one example of which is the photochemical cleavage of pyrimidine dimers. Nearly all cells contain a photoreactivating enzyme called *DNA photolyase*. The *E. coli* enzyme, a 35-kDa protein that contains bound N^5, N^{10}-methenyltetrahydrofolate and flavin adenine dinucleotide (FAD) cofactors, binds to the distorted region of DNA. The enzyme uses light energy — specifically, the absorption of a photon by the N^5, N^{10}-methenyltetrahydrofolate coenzyme — to form an excited state that cleaves the dimer into its component bases.

Base-excision repair

Erroneous bases may also be removed. The excision of modified bases such as 3-methyladenine by the *E. coli* enzyme AlkA is an example of **base-excision repair**. The binding of this enzyme to damaged DNA flips the affected base out of the DNA double helix and into the active site of the enzyme (**Figure 28.38**). The enzyme then acts as a glycosylase, cleaving the glycosidic bond to release the damaged base. At this stage, the DNA backbone is intact, but a base is missing. This hole is called an *AP site* because it is apurinic (devoid of A or G) or apyrimidinic (devoid of C or T). An AP endonuclease recognizes this defect and nicks the backbone adjacent to the missing base. Then, deoxyribose

phosphodiesterase excises the residual deoxyribose phosphate unit, and DNA polymerase I inserts an undamaged nucleotide, as dictated by the base on the undamaged complementary strand. Finally, the repaired strand is sealed by DNA ligase.

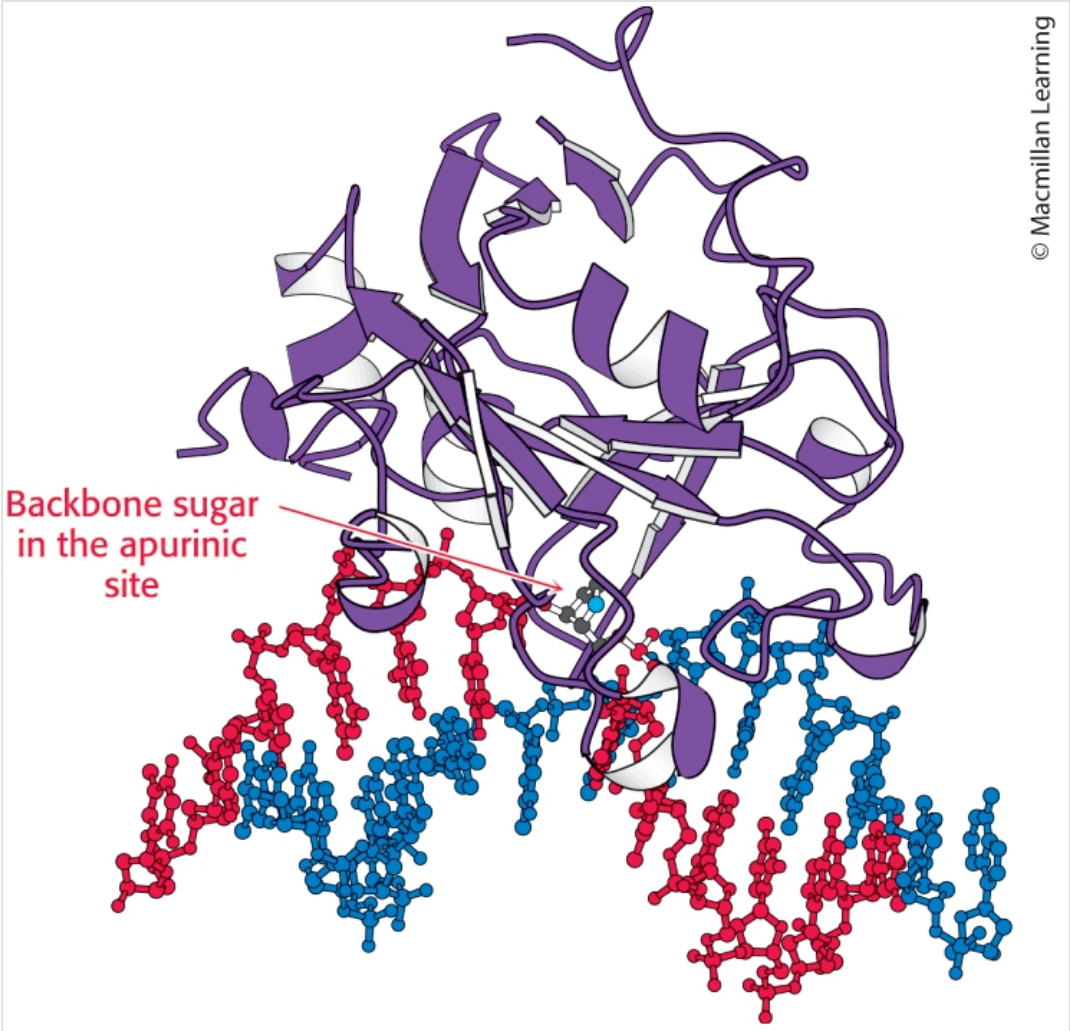


FIGURE 28.38 Base-excision repair enzymes remove damaged bases. A complex between the DNA-repair enzyme AlkA and an analog of a DNA molecule missing a purine base (an apurinic site) is shown. The backbone sugar in the apurinic site is flipped out of the double helix into the active site of the enzyme.

[Drawn from 1BNK.pdb.]

INTERACT with this model in Achieve

Nucleotide-excision repair

Sometimes, more than just the erroneous base is excised; the entire nucleotide may be removed. One of the best-understood examples of **nucleotide-excision repair** is utilized for the excision of a pyrimidine dimer. Three enzymatic activities are essential for this repair process in *E. coli* (**Figure 28.39**). First, an enzyme complex consisting of the proteins encoded by the *uvrABC* genes detects the distortion produced by the DNA damage. The UvrABC enzyme cuts the damaged DNA strand at two sites, 8 nucleotides away from the damaged site on the $5'$ side and 4 nucleotides away on the $3'$ side, and the 12-residue oligonucleotide excised by this highly specific *excinuclease* (from the Latin *exci*, "to cut out") then diffuses away. Second, DNA polymerase I enters the gap to carry out repair synthesis. The $3'$ end of the nicked strand is the primer, and the intact complementary strand is the template. Third, the $3'$ end of the newly synthesized stretch of DNA and the original part of the DNA chain are joined by DNA ligase.

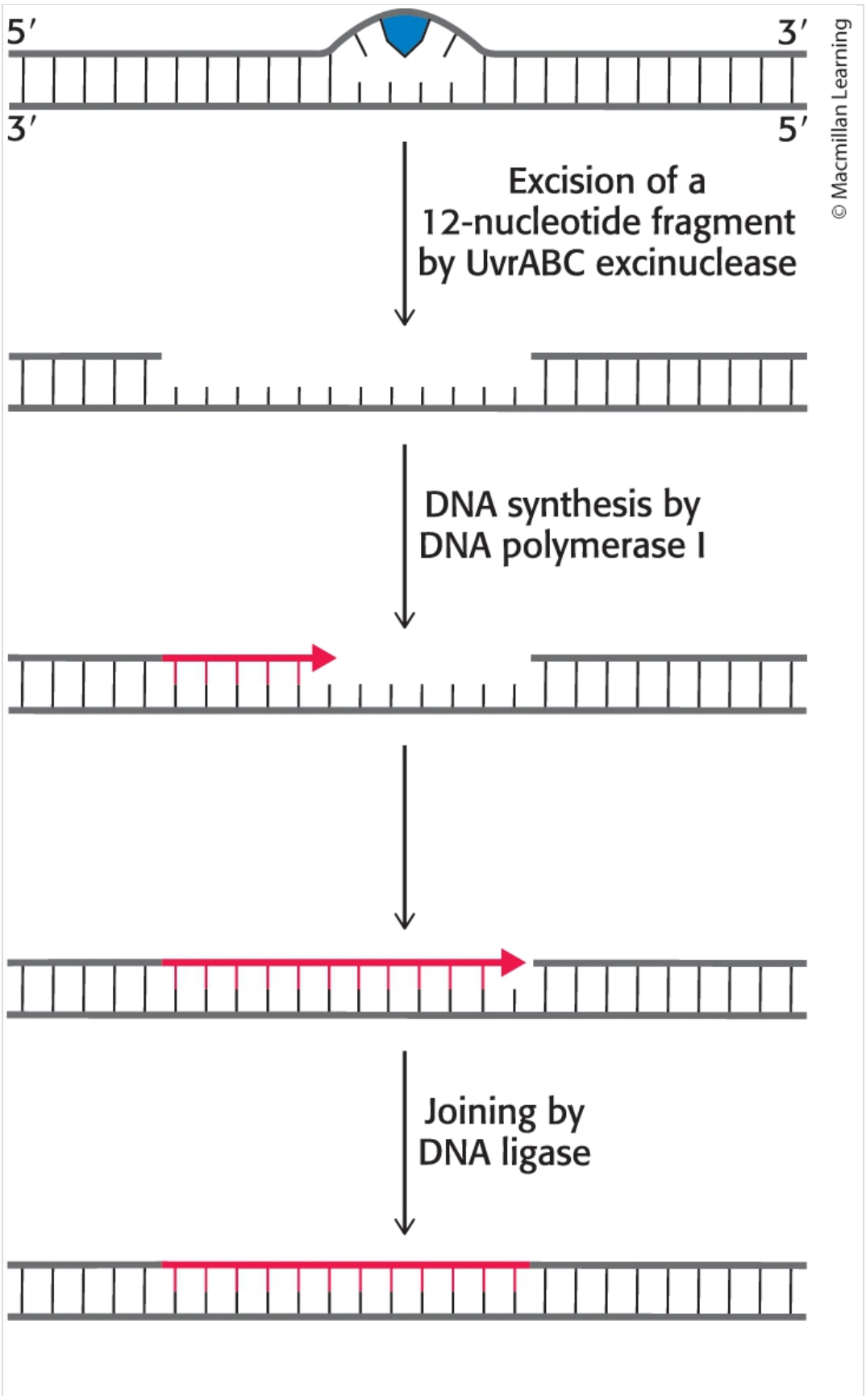

5′
3′
3′
5′
Excision of a
12-nucleotide fragment
by UvrABC excinuclease
DNA synthesis by
DNA polymerase I
Joining by
DNA ligase
© Macmillan Learning

FIGURE 28.39 Nucleotide-excision repair involves the removal of a section of damaged DNA. Repair of a region of DNA containing a thymine dimer by the sequential action of a specific excinuclease, a DNA polymerase, and a DNA ligase. The thymine dimer is shown in blue and the new region of DNA is in red.

[Information from P. C. Hanawalt, *Endeavour* 31:83, 1982.]

Repair of breaks in both strands

While DNA ligase can seal simple breaks in one strand of the DNA backbone, alternative mechanisms are required to repair breaks on both strands that are close enough together that they would otherwise separate the DNA into two double helices. Several distinct mechanisms are able to repair such damage.

One mechanism, **non-homologous end joining (NHEJ)**, does not depend on other DNA molecules in the cell (see Section 9.4). In NHEJ, the free double-stranded ends are bound by a heterodimer of two proteins, Ku70 and Ku80. These proteins stabilize the ends and mark them for subsequent manipulations. Through mechanisms that are not yet well-understood, the Ku70/80 heterodimers act as handles used by other proteins to draw the two double-stranded ends close together so that enzymes can seal the break. Alternative mechanisms of double-stranded-break repair can operate if an intact stretch of double-stranded DNA with an identical or very similar sequence is present in the cell. These repair processes use homologous recombination, presented in Section 28.5.

As noted in Section 9.4, researchers can now take advantage of double-stranded-break repair mechanisms for executing targeted changes in eukaryotic genomes, using techniques such as CRISPR. Specific engineered nucleases are used to introduce double-stranded

breaks in particular locations within the genome. The DNA-repair machinery in the targeted cells will then repair the break, through either NHEJ to disrupt the gene or homologous recombination-based repair with added double-stranded DNA fragments to introduce more elaborate modifications. For example, mutations associated with human diseases can be specifically introduced into the genomes of model organisms such as mice or zebrafish to examine the consequences.

Self-Check Question



Summarize the various ways in which the sequence of DNA is verified or corrected. Why are there so many pathways?

The presence of thymine instead of uracil in DNA permits the repair of deaminated cytosine

The presence in DNA of thymine rather than uracil, as in RNA, was an enigma for many years. Both bases pair with adenine; the only difference between them is a methyl group in thymine in place of the C-5 hydrogen in uracil. Why is a methylated base employed in DNA and not in RNA? The existence of an active repair system to correct the deamination of cytosine provides a convincing solution to this puzzle.

Cytosine in DNA spontaneously deaminates at a perceptible rate to form uracil. The deamination of cytosine is potentially mutagenic because uracil pairs with adenine, and so one of the daughter strands will contain a U–A base pair rather than the original C–G base pair. This

mutation is prevented by a repair system that recognizes uracil to be foreign to DNA (**Figure 28.40**). The repair enzyme, uracil DNA glycosylase, which is homologous to AlkA, hydrolyzes the glycosidic bond between the uracil and deoxyribose moieties but does not attack thymine-containing nucleotides. The AP site generated is repaired to reinsert cytosine.

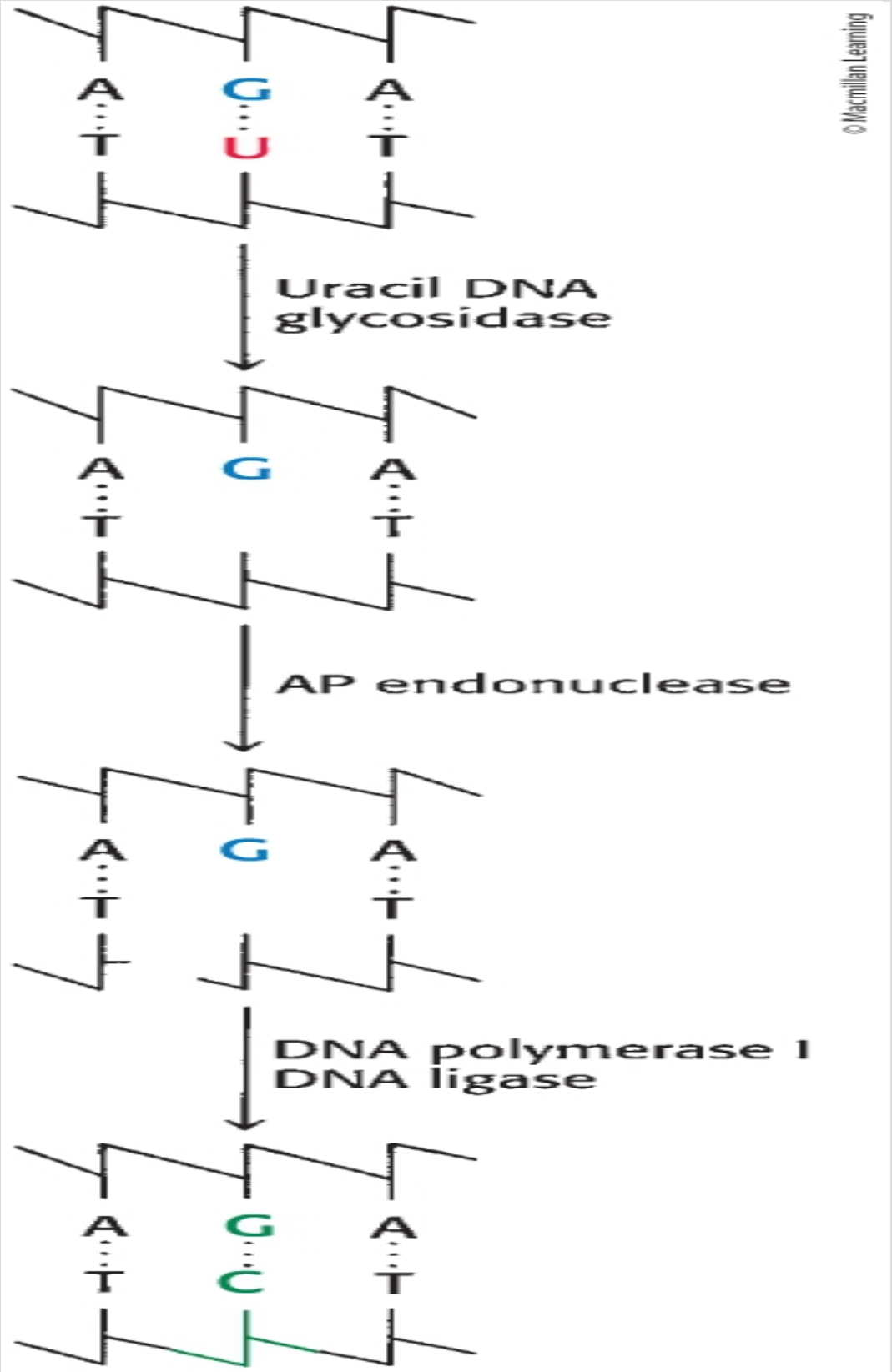


FIGURE 28.40 Uridine bases in DNA are excised and replaced by cytidine.

Thus, we can conclude that the methyl group on thymine acts like a tag that distinguishes thymine from deaminated cytosine. If uracil instead of thymine were used in DNA, correctly placed uracil would be indistinguishable from uracil formed by deamination of cytosine. The defect would persist unnoticed, and so a C–G base pair would necessarily be mutated to U–A in one of the daughter DNA molecules. This mutation is prevented by a DNA-repair system that searches for uracil and leaves thymine alone. In summary, the use of thymine instead of uracil in DNA enhances the fidelity of the genetic message.

Some genetic diseases are caused by the expansion of repeats of three nucleotides



Some genetic diseases are caused by the presence of DNA sequences that are inherently prone to errors during replication and repair. A particularly important class of such diseases is characterized by the presence of long tandem arrays of multiple copies of a particular sequence of three nucleotides, called **trinucleotide repeats**. An example is Huntington's disease, an autosomal dominant neurological disorder with a variable age of onset. The mutated gene in this disease expresses a protein in the brain called *huntingtin*, which contains a stretch of consecutive glutamine residues encoded by a tandem array of CAG sequences within the gene. In unaffected persons, this array is between 6 and 31 repeats, whereas in those with the disease, the array is between 36 and 82 repeats or longer. Moreover, the array tends to become longer from one generation to the next. The consequence is a

phenomenon called *anticipation* in which the children of an affected parent tend to show symptoms of the disease at an earlier age than did the parent.

The tendency of trinucleotide repeats to expand over time is explained by the formation of alternative structures in the course of DNA replication or repair. For example, part of the repeat can loop out without disrupting base-pairing outside this region. Then, in replication, DNA polymerase extends this strand through the remainder of the repeat, leading to an increase in the number of copies of the trinucleotide sequence (**Figure 28.41**).

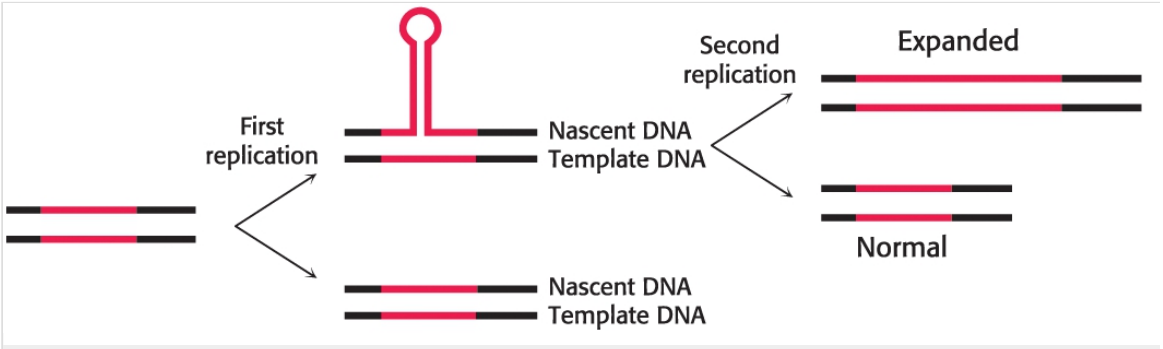


FIGURE 28.41 Trinucleotide repeats can form structures that lead to their expansion during DNA replication. In this example, a hairpin structure forms that results in the expansion of the trinucleotide repeat segment (red) in one of the daughter strands after two rounds of replicatio

How do these long stretches of repeated amino acids cause disease? For huntingtin, it appears that the polyglutamine stretches become increasingly prone to aggregate as their length increases; the additional consequences of such aggregation are still under investigation.

Many cancers are initiated by the defective repair of DNA

As described in Chapter 14, cancers are caused by mutations in genes associated with growth control. Defects in DNA-repair systems increase the overall frequency of mutations and, hence, the likelihood of cancer-causing mutations. Indeed, the synergy between studies of mutations that predispose people to cancer and studies of DNA repair in model organisms has been tremendous in revealing the biochemistry of DNA-repair pathways.

Genes for DNA-repair proteins are often **tumor-suppressor genes**; that is, they suppress tumor development when at least one copy of the gene is free of a deleterious mutation. When both copies of a gene are mutated, however, tumors develop at rates greater than those for the population at large. People who inherit defects in a single tumor-suppressor allele do not necessarily develop cancer but are susceptible to developing the disease because only the one remaining normal copy of the gene must develop a new defect to further the development of cancer. **Table 28.2** lists selected proteins involved in DNA-repair processes that, when mutated, can contribute to certain diseases, including cancers.

TABLE 28.2 Examples of diseases caused by mutations in repair proteins

Disease	Selected Proteins	Affected Repair Pathway
Xeroderma pigmentosum (skin)	XPA, XPB, XPC	Nucleotide-excision repair
Lynch syndrome (colorectal cancer)	MSH2, MLH1	Mismatch repair
Breast and ovarian cancer	BRCA1 and	Double-strand break repair

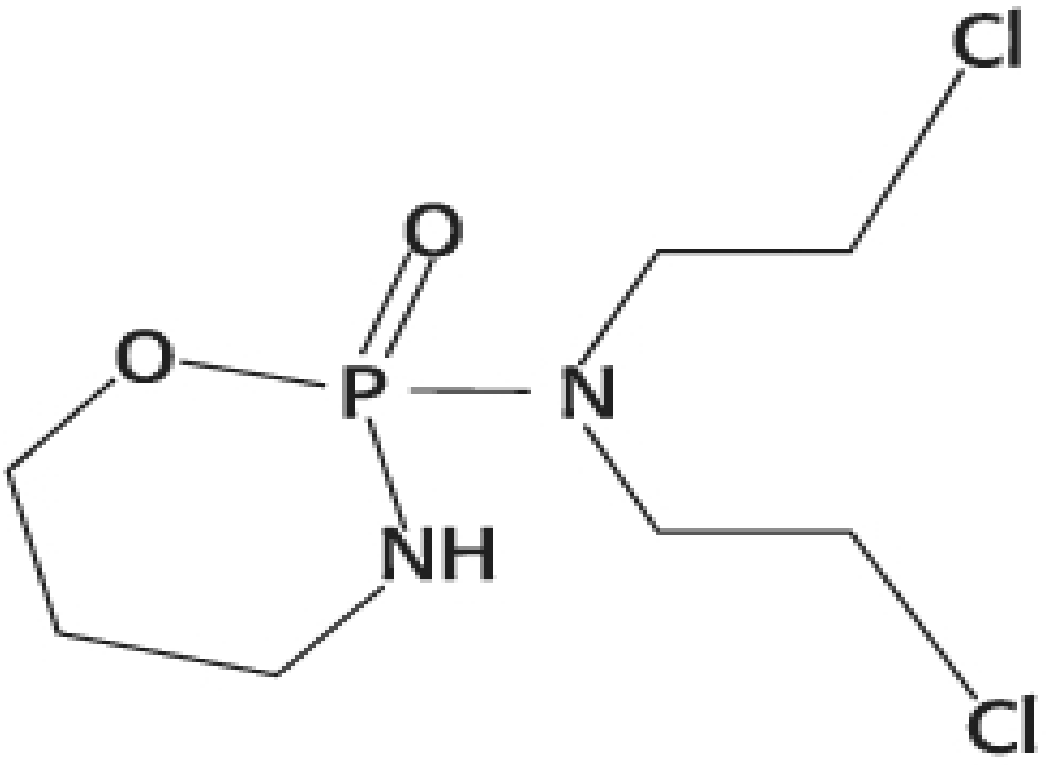
	BRCA2	
Renal and lung cancer	OGG1	Base-excision repair

- *Xeroderma pigmentosum.* In the rare human skin disease xeroderma pigmentosum, the skin of an affected person is extremely sensitive to sunlight or ultraviolet light. Studies of xeroderma pigmentosum patients have revealed that mutations occur in genes for a number of proteins that are components of the human nucleotide-excision-repair pathway, including homologs of the UvrABC subunits. Severe changes in the skin start in infancy and worsen with time, usually resulting in the development of skin cancers at several sites. Many patients die before age 30 from metastases of these malignant skin tumors.

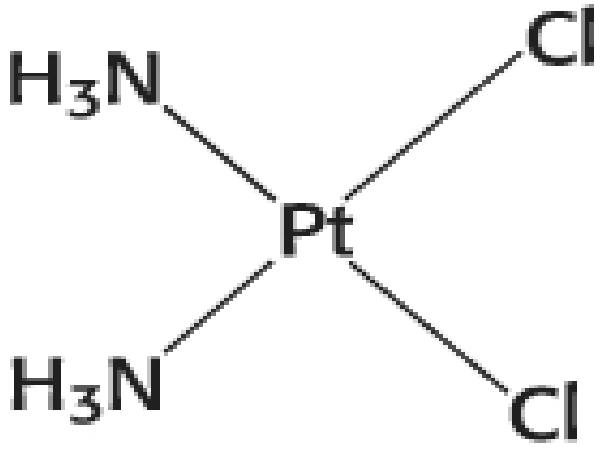
- *Hereditary nonpolyposis colorectal cancer.* As many as 1 in 200 people develop hereditary nonpolyposis colorectal cancer (HNPCC, or Lynch syndrome) resulting from defective DNA mismatch repair. Mutations in two genes, called *hMSH2* and *hMLH1*, account for most cases. The striking finding is that these genes encode the human counterparts of MutS and MutL of *E. coli.* Mutations in *hMSH2* and *hMLH1* likely allow other mutations to accumulate throughout the genome; in time, genes important in controlling cell proliferation become altered, resulting in the onset of cancer.

- *Cancers caused by mutations to* p53. Not all tumor-suppressor genes are specific to particular types of cancer. For example, the *p53* gene is mutated in more than half of all tumors. This gene codes for a protein that helps control the fate of damaged cells, p53. First, the p53 protein plays a central role in sensing DNA damage, especially double-stranded breaks. Then, after sensing damage, the protein either promotes a DNA-repair pathway or activates the apoptosis pathway, leading to cell death. Most mutations in the *p53* gene are sporadic; that is, they occur in somatic cells rather than being inherited, but the mutation can also be inherited. People who

inherit a deleterious mutation in one copy of the *p53* gene have a high probability of developing several types of cancer.



Cyclophosphamide



Cisplatin

Cancer cells often have two characteristics that make them especially vulnerable to agents that damage DNA molecules. First, they divide frequently, and so their DNA replication pathways are more active than they are in most cells. Second, as already noted, cancer cells often have defects in DNA-repair pathways. Several agents widely used in cancer chemotherapy, including cyclophosphamide and cisplatin, act by damaging DNA. Cancer cells are less able to avoid the effect of the induced damage than are normal cells, providing a therapeutic window for specifically killing cancer cells.

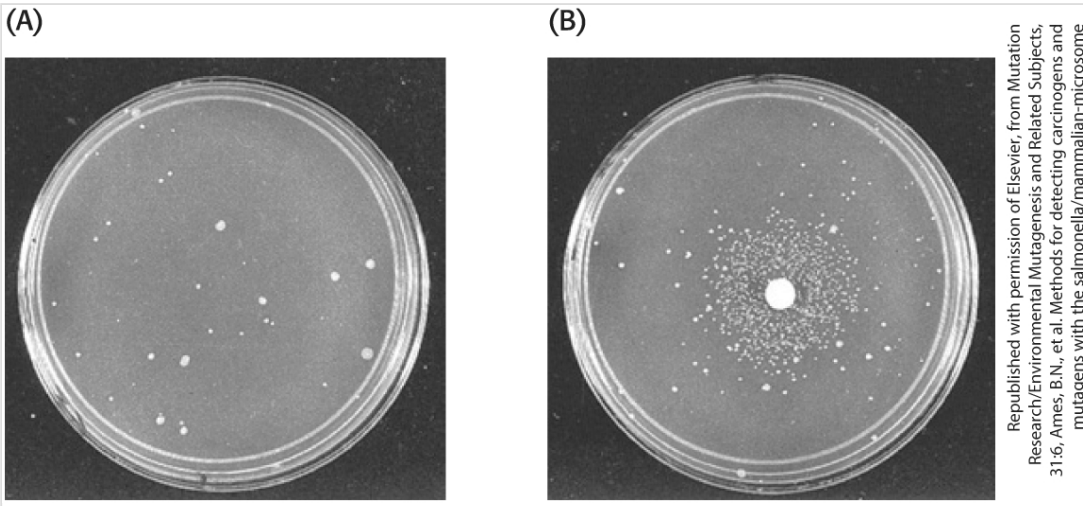
Many potential carcinogens can be detected by their mutagenic action on bacteria

Many human cancers are caused by exposure to chemicals that are mutagens; therefore, it is important to identify such compounds and to ascertain their potency so that exposure to them can be minimized. Bruce Ames devised a simple and sensitive test, called the **Ames test**, for detecting chemical mutagens.

1. A thin layer of agar containing about 10^9 bacteria of a specially constructed tester strain of *Salmonella* is placed on an agar plate. These bacteria are unable to grow in the absence of histidine, because a mutation is present in one of the genes for the biosynthesis of this amino acid.

2. A chemical mutagen is added to the center of the plate, resulting in many new mutations. A small proportion of these mutations reverse the original mutation, allowing the bacteria to synthesize histidine.

3. These so-called *revertants* multiply in the absence of an external source of histidine and appear as discrete colonies after the plate has been incubated at 37°C for 2 days (Figure 28.42). For example, 0.5 μg of 2-aminoanthracene gives 11,000 revertant colonies, compared with only 30 spontaneous revertants in its absence.



Republished with permission of Elsevier, from Mutation Research/Environmental Mutagenesis and Related Subjects, 31:6, Ames, B.N., et al. Methods for detecting carcinogens and mutagens with the salmonella/mammalian-microsome

FIGURE 28.42 The Ames test determines the mutagenicity of various compounds. Two results are shown: (A) an agar plate containing about 10^9 *Salmonella* bacteria that cannot synthesize histidine, and (B) an agar plate containing a filter-paper disc with a mutagen, which produces a large number of revertants that can synthesize histidine. After 2 days, the revertants appear as rings of colonies around the disc. The small number of visible colonies in plate A are spontaneous revertants.

4. A series of concentrations of the chemical mutagen that caused the reversion can be readily tested to generate a dose-response curve.

Different tester strains of *Salmonella* used in the Ames test are sensitive to different kinds of mutations. For example, some of the tester strains are responsive to base-pair substitutions, whereas others detect deletions or additions of base pairs (frameshifts). These specially

designed strains are particularly sensitive to mutations because the genes of their excision-repair systems have been deleted. In addition, potential mutagens enter the tester strains easily because the lipopolysaccharide barrier that normally coats the surface of *Salmonella* is incomplete in these strains. A key feature of this detection system is the inclusion of a mammalian liver homogenate, which promotes the conversion of some potential carcinogens into their active forms. Bacteria lack the enzymes required for this conversion.

The *Salmonella* test is extensively used to help evaluate the mutagenic and carcinogenic risks of a large number of chemicals. This rapid and inexpensive bacterial assay for mutagenicity complements epidemiological surveys and animal tests that are necessarily slower, more laborious, and far more expensive. The *Salmonella* test for mutagenicity is an outgrowth of studies of gene–protein relations in bacteria. It is a striking example of how fundamental research in molecular biology can lead directly to important advances in public health.

28.5 DNA Recombination Plays Important Roles in Replication, Repair, and Other Processes

Most processes associated with DNA replication function to copy the genetic message as faithfully as possible. However, several biochemical processes require **genetic recombination**, the exchange of genetic material between two DNA molecules that results in the reassortment of DNA sequences present on two different double helices (**Figure 28.43**).



FIGURE 28.43 Recombined DNA molecules have segments from both parent molecules.

Recombination is essential in the following processes:

1. When replication stalls, recombination processes can reset the replication machinery so that replication can continue.

2. Some double-stranded breaks in DNA are repaired by recombination.

3. In meiosis, the limited exchange of genetic material between paired chromosomes provides a simple mechanism for generating genetic diversity in a population.

4. Recombination plays a crucial role in generating molecular diversity for antibodies and some other molecules in the immune system.

5. Some viruses employ recombination pathways to integrate their genetic material into the DNA of a host cell.

6. Recombination is used to manipulate genes in, for example, the generation of gene knockout mice and other targeted genome modifications (Section 9.4).

Recombination is most efficient between DNA sequences that are homologous. In homologous recombination, parent DNA duplexes align at regions of sequence similarity, and new DNA molecules are formed by the breakage and joining of homologous segments.

RecA can initiate recombination by promoting strand invasion

In many recombination pathways, a DNA molecule with a free end recombines with a DNA molecule having no free ends available for interaction. DNA molecules with free ends are the common result of double-stranded DNA breaks, but they may also be generated in DNA replication if the replication complex stalls. Double-stranded breaks are among the most potentially devastating types of DNA damage. With both strands of the double helix broken in a local region, neither strand is intact to act as a template for future DNA synthesis. Repairing such lesions relies on DNA recombination.

This type of recombination has been studied extensively in *E. coli*, but it also takes place in other organisms through the action of proteins homologous to those of *E. coli*. Often dozens of proteins participate in the complete recombination process. However, the

key protein is RecA, the homolog of which is Rad51 in human cells. To accomplish the exchange, the single-stranded DNA first displaces one of the strands of the double helix (Figure 28.44). The resulting three-stranded structure is called a *displacement loop* or *D-loop*, and the process is often referred to as *strand invasion*. Because a free $3'$ end is now base-paired to a contiguous strand of DNA, the $3'$ end can act as a primer to initiate new DNA synthesis.

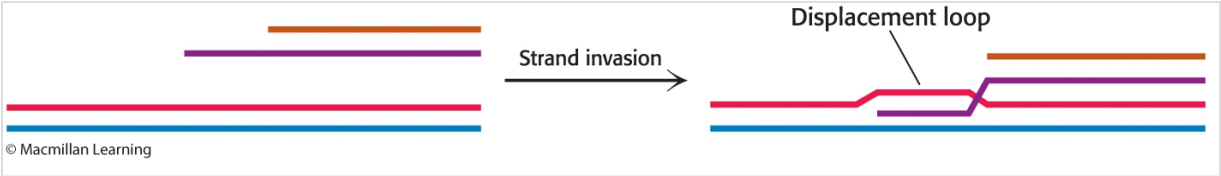


FIGURE 28.44 Strand invasion can initiate recombination. This process is promoted by proteins such as RecA.

Strand invasion can initiate many processes, including the repair of double-stranded breaks and the reinitiation of replication after the replication apparatus has come off its template. In the repair of a break, the recombination partner is an intact DNA molecule with an overlapping sequence.

Some recombination reactions proceed through Holliday-junction intermediates

In recombination pathways for meiosis and some other processes, intermediates form that are composed of four polynucleotide chains in a cross-like structure. Intermediates with these cross-like

structures are referred to as **Holliday junctions**, after Robin Holliday, who proposed their role in recombination in 1964. Such intermediates have been characterized by a wide range of techniques, including x-ray crystallography.

Specific enzymes, termed **recombinases**, bind to these structures and resolve them into separated DNA duplexes. The Cre recombinase from bacteriophage P1 has been extensively studied. The mechanism begins with the recombinase binding to the DNA substrates (**Figure 28.45**).

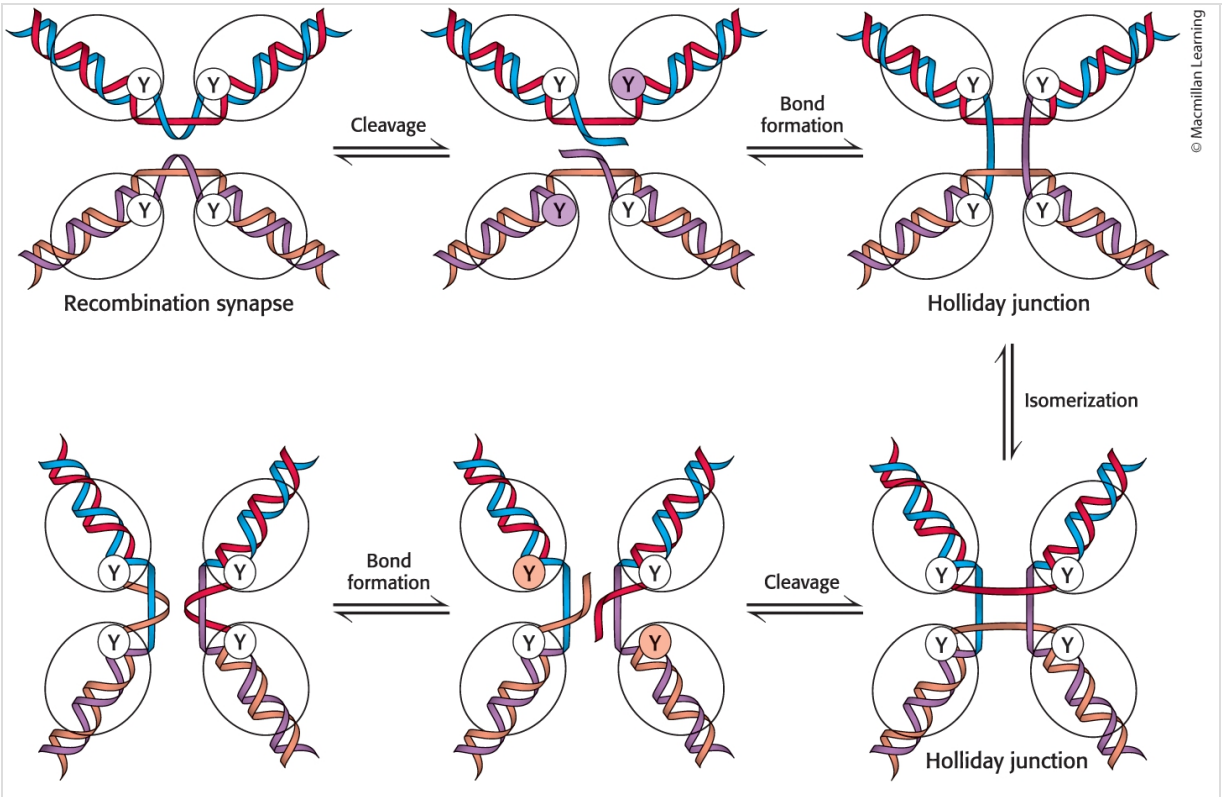


FIGURE 28.45 Holliday junctions are formed and resolved by recombinases. Recombination begins as two DNA molecules and four recombinases come together to form a recombination synapse. One strand from each duplex is cleaved by transesterification with the 3′ end of each of the cleaved strands linked to a tyrosine residue on the recombinase enzyme. New phosphodiester bonds are formed when a 5′ end of the other cleaved strand in the complex attacks these tyrosine–DNA adducts. After isomerization, these steps are repeated to form the recombined products.

1. Four molecules of the enzyme and two DNA molecules come together to form a **recombination synapse**. The reaction begins with the cleavage of one strand from each duplex via transesterification reactions with the $3'$-phosphoryl groups becoming linked to specific tyrosine residues in the recombinase while the $5'$-hydroxyl group of each cleaved strand remains free.

2. The free $5'$ ends invade the other duplex and participate in transesterification reactions to form new phosphodiester bonds and free the tyrosine residues. These reactions result in the formation of a Holliday junction.

3. This junction can then isomerize to form a structure in which the polynucleotide chains in the center of the structure are reoriented.

4. From this junction, the processes of strand cleavage and phosphodiester-bond formation repeat. The result is a synapse containing the two recombined duplexes. Dissociation of this complex generates the final recombined products.

Cre catalyzes the formation of Holliday junctions as well as their resolution. In contrast, other proteins bind to Holliday junctions that have already been formed by other processes and resolve them into separate duplexes. In many cases, these proteins also promote the process of branch migration whereby a Holliday junction is moved along the two component double helices. Branch migration

can affect which segments of DNA are exchanged in a recombination process.

While most recombination events are between homologous sequences, recombination can also occur between different, non-homologous chromosomes. Nonhomologous recombination during cell division leads to genetic translocations, where parts of some chromosomes are moved to or exchanged with other chromosomes. Chromosomal translocations can be harmless or can result in diseases, depending on the chromosomes involved and the genes that are modified or disrupted. The formation of the *bcr-abl* gene, which leads to chronic myelogenous leukemia, was discussed in Section 14.5. During CRISPR manipulations of genomes, gene insertions occur primarily via homologous recombination, but, more rarely, sequences can also be inserted into non-homologous positions.

Chapter 28 Summary

28.1 DNA Replication Proceeds by the Polymerization of Deoxyribonucleoside Triphosphates Along a Template

- DNA polymerases are template-directed enzymes that catalyze the formation of phosphodiester bonds.
- DNA polymerases require a primer with a free $3'$-hydroxyl group to initiate strand synthesis.
- DNA polymerases always synthesize a DNA strand in the $5'$-to-$3'$ direction.
- For both daughter strands to be synthesized simultaneously, one strand is made continuously while the other is synthesized in fragments, called *Okazaki fragments*.

28.2 DNA Unwinding and Supercoiling Are Controlled by Topoisomerases

- A key topological property of DNA is its linking number, which is the number of times one strand of DNA winds around the other in the right-hand direction.
- Molecules differing in linking number can be interconverted only by cutting one or both DNA strands; these reactions are catalyzed by topoisomerases.
- Supercoiled DNA can be relaxed by either topoisomerase I, which acts by transiently cleaving one strand of DNA in a double helix, or by topoisomerase II, which transiently cleaves both strands simultaneously.

28.3 DNA Replication Is Highly Coordinated

- The DNA polymerase holoenzyme comprises two DNA polymerase enzymes (one to act on each template strand) and other subunits.
- As a replicative polymerase moves along a DNA template, the leading strand is copied smoothly while the lagging strand forms loops.
- DNA replication is initiated at the origin of replication, a single site within the *E. coli* genome, where a set of specific proteins assembles the enzymes needed for DNA synthesis.
- The initiation of replication in eukaryotes is more complex than in prokaryotes; DNA synthesis is initiated at thousands of sites throughout the genome.
- Telomerase synthesizes specialized structures called telomeres at the ends of linear chromosomes.

28.4 Many Types of DNA Damage Can Be Repaired

- Different types of DNA damage include mismatched bases incorporated during DNA replication, individual bases damaged by oxidation or alkylation after replication, cross-linked bases, and single- or double-stranded breaks in the DNA backbone.
- Several different repair systems detect and repair DNA damage: the exonuclease activity of the DNA polymerase excises mismatches bases; specific enzymes reverse some DNA lesions such as thymine dimers; still other DNA-repair pathways act through the excision of single damaged bases or short segments of nucleotides.
- Double-stranded breaks in DNA can be repaired by homologous or non-homologous end-joining processes.
- Defects in DNA-repair components are associated with susceptibility to many different types of cancer.

28.5 DNA Recombination Plays Important Roles in Replication, Repair, and Other Processes

- Genetic recombination is important in some types of DNA repair.
- Some recombination pathways are initiated by strand invasion, where a single strand at the end of a DNA double helix forms base pairs with one strand of DNA in another double helix and displaces the other strand.
- In other recombination pathways a Holliday junction (a cross-like structure of four DNA strands) is formed.
- Recombinases promote recombination reactions through the introduction of specific DNA breaks and the formation and resolution of Holliday-junction intermediates.

Key Terms

template
DNA polymerases
primer
exonuclease
primase
replication fork
Okazaki fragments
lagging strand
leading strand
DNA ligase
helicase
supercoiling
linking number (Lk)
topoisomers
twist (Tw)
writhe (Wr)
topoisomerase
processivity

sliding DNA clamp
trombone model
origin of replication
origin of replication complex (ORC)
cell cycle
telomere
telomerase
mutagen
mismatch repair
direct repair
base-excision repair
nucleotide-excision repair
non-homologous end joining (NHEJ)
trinucleotide repeats
tumor-suppressor gene
Ames test
genetic recombination
Holliday junction
recombinases
recombination synapse

Problems

1. A nucleotide pairing between A (adenine) and T (thymine) in the original DNA strand is miscopied during DNA replication. On one strand of DNA, A correctly pairs with T. However, on the other strand, T pairs with G (guanine) instead of A. This mistake is not corrected, and the double strand with the mistake is incorporated into a new cell during cell division. The double strand with the G–T mistake is later replicated without additional mistakes. What nucleotide pairs will be

found in the two new double strands at the site of the G–T mistake? 4

Original DNA sequence	Mistake during replication
A–T	A–T G–T

2. The oxidation of guanine bases in the context of triplet repeats such as CAGCAGCAG can lead to the expansion of the repeat. Explain. 4

3. DNA polymerase I, DNA ligase, and topoisomerase I use an activated intermediate to catalyze the formation of phosphodiester bonds with the release of a leaving group. Match the activated intermediate and the leaving group to each enzyme. 1

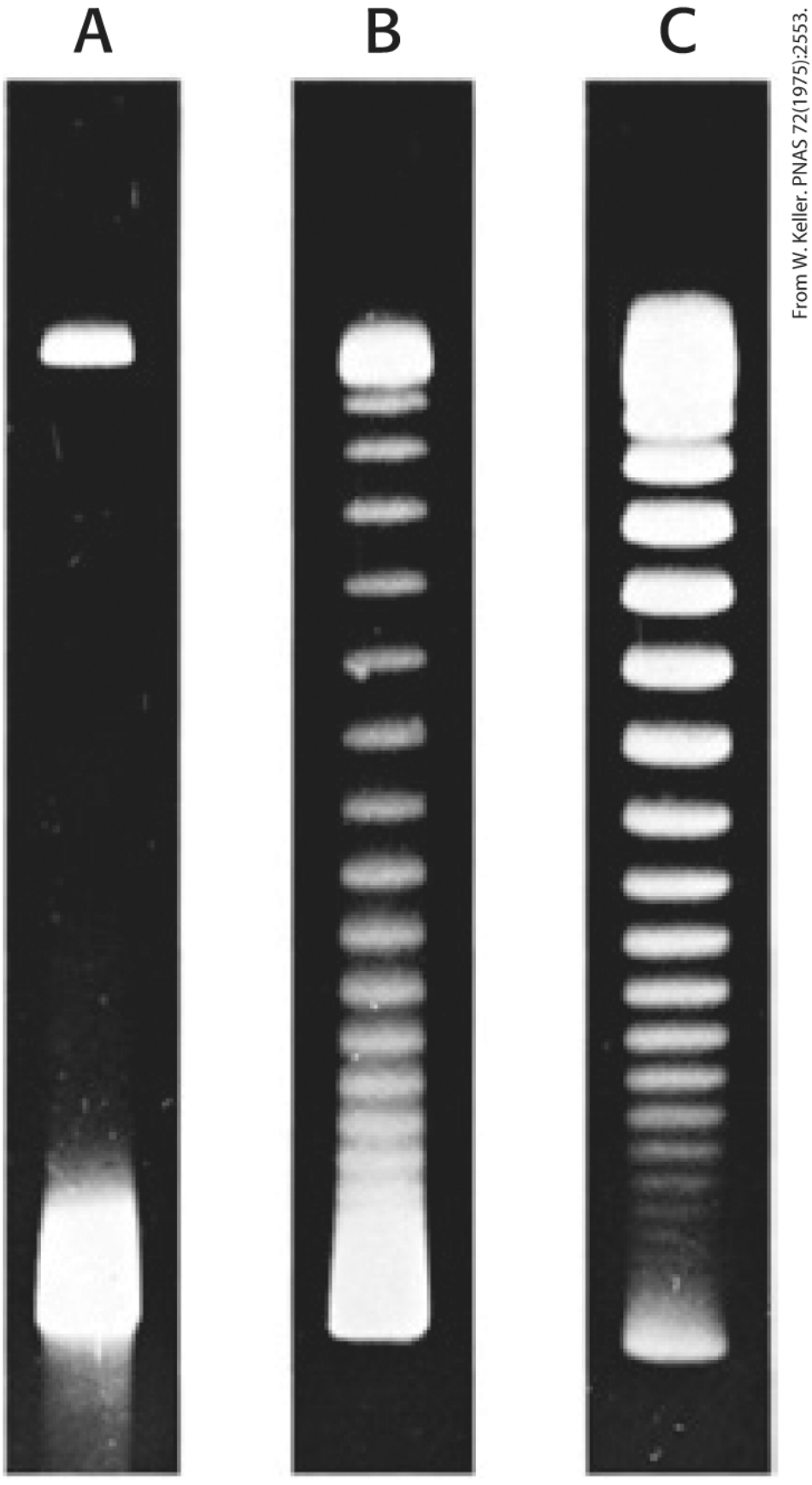
1. DNA polymerase I
2. DNA ligase
3. DNA topoisomerase I

1. Tyrosine
2. AMP
3. DNA-adenylate
4. dNTPs
5. Pyrophosphate
6. DNA-tyrosyl

4. Draw a replication fork. Label the template strands and identify their $5'$ and $3'$ ends. Draw in and add labels for the leading strand, lagging strand, RNA primer(s), and Okazaki fragments. Add $5'$ and $3'$ labels to the daughter strands. Then place the following proteins on your diagram: SSBs, helicase (DnaB), DNA topoisomerase II (gyrase), primase. 1

5. Under standard conditions, the free energy of ATP hydrolysis is about $-30\ \mathrm{kJ\ mol^{-1}}$. Assuming that the energy required to break an average base pair within double-stranded DNA is $10\ \mathrm{kJ\ mol^{-1}}$, estimate the maximum number of base pairs that could be broken per ATP hydrolyzed by a helicase operating under standard conditions. 2

6. Circular DNA from SV40 virus was isolated and subjected to gel electrophoresis. The results are shown in lane A (the control) of the adjoining gel patterns shown below. 3



From W. Keller. PNAS 72(1975):2553.

a. Why does the DNA separate in agarose gel electrophoresis? How does the DNA in each band differ?
b. The DNA was then incubated with topoisomerase I for 5 minutes and again analyzed by gel electrophoresis, with the results shown in lane B. What types of DNA do the various bands represent?
c. Another sample of DNA was incubated with topoisomerase I for 30 minutes and again analyzed as shown in lane C. What is the significance of the fact that more of the DNA is in slower-moving forms?

7. Answer the following questions about supercoiling and linking number (Lk). 3

a. What is Lk for a relaxed, closed-circular DNA with 4784 base pairs?
b. What is Lk for a negatively supercoiled 4784 bp DNA if it is underwound by 4 complete turns?
c. How does Lk change when there is a break in one strand?
d. What is Lk for a negatively supercoiled 4784 bp DNA after treatment with one molecule of topoisomerase II (DNA gyrase) and adequate ATP?

8. Which of the sequences below represents newly synthesized DNA that can be repaired by the proofreading activity of DNA polymerases? For the segments shown, the top strand represents the template strand; the bottom strand represents the newly synthesized strand. 4

a. $3'-GATCAGAATG-5'$
$5'-CTAGGCTTAC-3'$

b. $3'-GATCAGAATG-5'$
$5'-TTAGTCTTAC-3'$

c. $3'-GATCAGAATG-5'$
$5'-CTAGTCTTAT-3'$

d. $3'-GATCAGAATG-5'$
$5'-CTAGTCTTAC-3'$

9. What of the following strategies do cells use to ensure that newly replicated DNA does not contain errors? Select all that apply. 4

a. Enzymes repair mistakes in the new DNA double helix after the new double helix separates from the original double helix.
b. As DNA polymerase synthesizes new DNA, the DNA polymerase finds and corrects misplaced nucleotides.
c. Enzymes proofread the DNA after the DNA has been replicated and replace any mismatched nucleotides.
d. DNA polymerase replaces the newly replicated DNA on any chromosomes on which there are mistakes.
e. Enzymes remove and resynthesize any misshapen sequences in the DNA prior to replication.

10. Place the following steps of prokaryotic DNA replication in order, starting with the bacterium initiating DNA replication, and ending with DNA replication being terminated. 5

a. The bacterium initiates DNA replication.
b. DNA replaces RNA and lagging strands are joined.
c. Tus protein stops replication forks from crossing each other and ends synthesis.
d. The upstream region melts, and helicase binds and unwinds DNA.
e. RNA primers are added to provide a $3'$ end for elongation.
f. DNA replication is terminated.
g. $5'$-to-$3'$ synthesis of the leading strand and short lagging strand is carried out by DNA polymerase.
h. The DnaA protein binds to the single origin of replication.

11. Place the following steps of eukaryotic DNA replication in order, starting from when a germ cell enters gap 1 (G_1) phase and ending with the termination of one cell cycle. 5

a. The cell enters G_1.
b. Each genomic origin of replication assembles a pre-replication complex.
c. RNA primers are added to provide a $3'$ end for elongation.
d. Active telomerase can extend the lost telomere region.
e. One round of the cell cycle terminates.
f. $5'$-to-$3'$ synthesis of the leading and lagging strands is carried out by DNA polymerase.
g. The initiation complex creates an active replication fork as helicase unwinds DNA.
h. RNA is replaced with DNA, and lagging strands are joined.

12. Place the events in which telomerase maintains chromosomal ends during replication in order. 6

a. Additional nucleotides are added to the $3'$ end of the parental DNA strand.
b. Telomerase moves along the newly elongated DNA strand toward its $3'$ end.
c. Nucleotides that are complementary to the RNA component of telomerase are added to the $3'$ end of the DNA overhang.
d. Telomerase is removed from the DNA strand entirely, making way for a DNA polymerase.
e. The RNA component of telomerase binds to a complementary sequence on the $3'$ overhang of the parental DNA strand.
f. DNA polymerase adds bases complementary to the elongated overhang created by telomerase.

13. In contrast to prokaryotes, which have circular chromosomes, eukaryotes have linear chromosomes. A potential problem arises because DNA polymerase cannot replicate the $5'$ ends of linear chromosomes. As a result, the lagging strands of eukaryotic chromosomes shorten with repeated rounds of replication.

Telomerase, an enzyme implicated in aging and cell lifespan, helps overcome this problem. Telomerase adds more deoxynucleotides to the end of the chromosome, lengthening it. This DNA sequence, or telomere, prevents the loss of essential DNA from the ends of chromosomes.

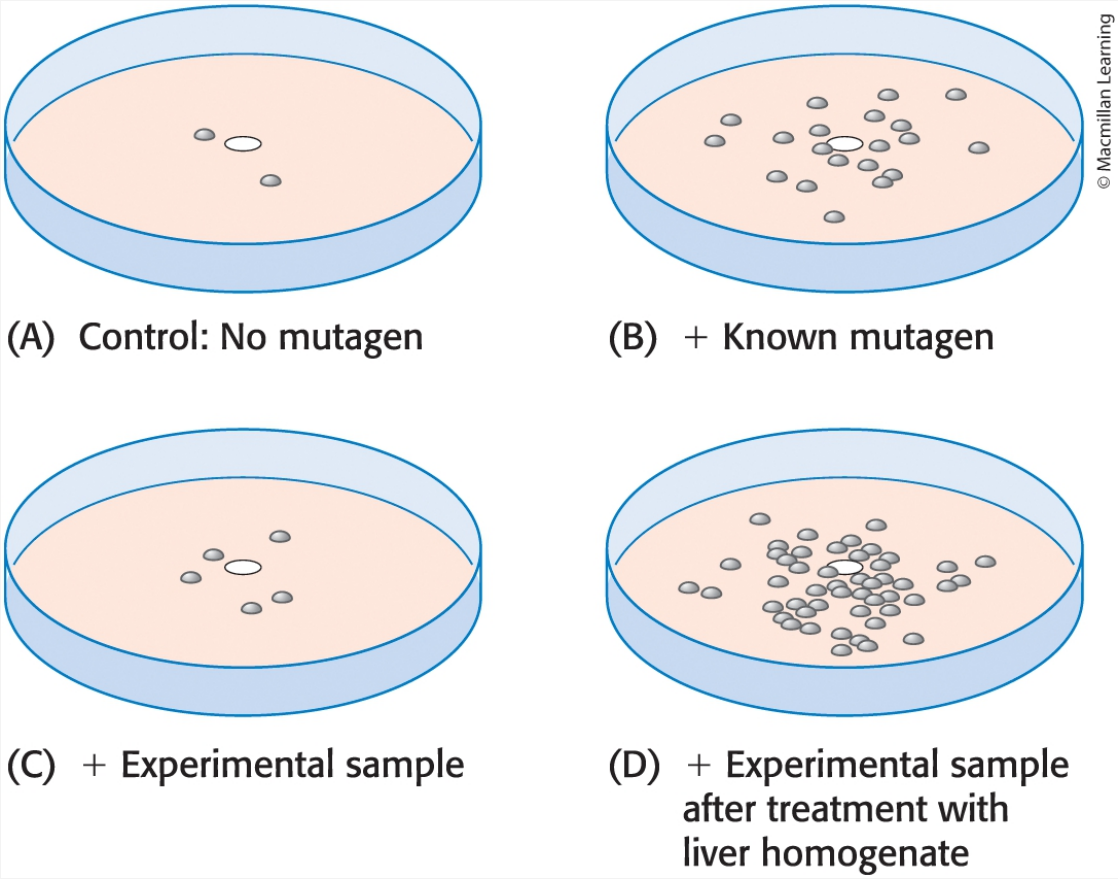
Which of the following statements accurately describe telomeres and the actions of telomerase? Select all that apply. 6

a. Telomerase contains a G-rich template sequence that adds a C-rich DNA sequence to the lagging strand of the chromosome.
b. Inappropriate activation of telomerase can result in cellular immortality, one of the cellular changes implicated in the development of cancer.
c. A telomere forms a loop with a section of the complementary DNA strand, protecting the chromosome from degradation by endonucleases.
d. Telomerase activity is turned off in most human cells, causing the telomeres to gradually shorten as the individual ages.
e. Telomerase consists of an RNA template and a protein component that adds complementary nucleotides to the 3′ end of DNA.

14. The following illustration shows four agar plates used for the Ames test. A piece of filter paper (white circle in the center of each plate) was soaked in one of four preparations and then placed on an agar plate. The four preparations contained (A) purified water (control), (B) a known mutagen, (C) a chemical whose mutagenicity is under investigation, and (D) the same chemical after treatment with liver homogenate. The number of revertants, visible as colonies on the plates, was determined in each case. 7

a. What was the purpose of the control plate, which was exposed only to water?
b. Why was it wise to use a known mutagen in the experimental system?

c. How would you interpret the results obtained with the experimental compound?
d. What liver components would you think are responsible for the effects observed in preparation D?



15. Classify each statement on the right as describing DNA replication in prokaryotes, eukaryotes, both, or neither. 5

1. DNA replication in prokaryotes
2. DNA replication in eukaryotes
3. Both
4. Neither

1. Several origins of replication per chromosome
2. Bidirectional replication
3. Several types of DNA polymerases
4. Occurs during M phase of cell cycle
5. One origin of replication per chromosome

---

16. Determine whether each phrase on the right describes recombination that enables replication with a single-stranded gap, a double-stranded break, or both. Each phrase may only be used once. 8

1. Single-stranded gap
2. Double-stranded break
3. Both

1. Produces two DNA segments with no breaks
2. Occurs between arms of a replication fork
3. A free $3'$ end invades another DNA segment
4. Occurs between homologous DNA segments

5. Involves removal of the $5'$ end(s) of the broken DNA

6. Involves a gap in one strand of a DNA segment

---

17. DNA that contains a gap in a single strand can be replicated through recombination. Place the steps in order from when replication stops to when replication continues. 8

a. The replication fork encounters a single-stranded gap.
b. The crossed-over strands are resolved; a gap remains in one duplicated strand.
c. Replication continues as the lesion is bypassed.
d. The $3'$ end of the unwound DNA is displaced.
e. The displaced $3'$ end is a primer for DNA polymerase, and replication continues in the crossed-over strands.
f. The displaced DNA aligns itself with the complementary bases on the other arm of the replication fork.
g. A helicase unwinds the newly synthesized DNA at the break.

18. Match each key term to its appropriate definition:**3**

1. Positive supercoiling	1. The coiling, or looping, of the double helix around its axis
2. Twist	2. Results from the partial unwinding (right-handed, or underwinding) of the double helix; represents the topology of DNA in vivo; and permits easier strand separation

3. Writhe	3. The winding of two DNA strands around each other
4. Negative supercoiling	4. Permits DNA to maintain a relatively stable conformation when the helix is slightly underwound or overwound
5. Supercoiling	5. Results from the overwinding of the DNA and double helix

---

19. The end-replication problem (telomere problem) exists in eukaryotic chromosomes and is characterized by the chromosomes shortening with each round of DNA replication. Select the statements that best explain why the end-replication problem exists in eukaryotic chromosomes. 6

a. DNA ligase links the $5'$-OH group of one fragment to the $3'$ phosphate group of an adjacent fragment.

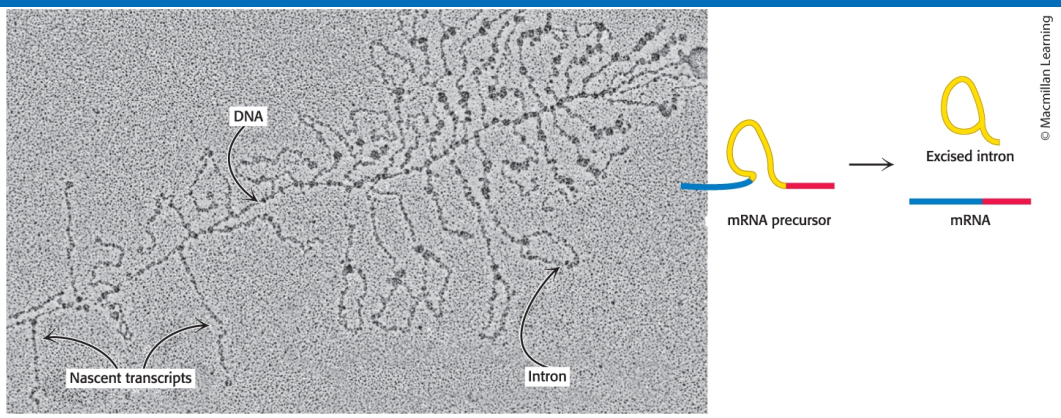
b. DNA polymerase synthesizes DNA from the $5'$ end to the $3'$ end.

c. The lagging strand is synthesized from the $3'$ end to the $5'$ end.

d. DNA polymerase requires a primer for DNA synthesis.

e. The RNA primer is removed in a $3'$-to-$5'$ direction.

CHAPTER 29
RNA Functions, Biosynthesis, and Processing



RNA synthesis is a key step in the expression of genetic information. This electron micrograph shows a DNA template from a fruit fly in the genus *Drosophila* (the center "stem") being actively transcribed into RNAs (the "branches"). In eukaryotic organisms such as fruit flies, the initial RNA transcript often contains sections that do not encode protein sequence (introns). These sections are removed by splicing; proteins associated with RNA splicing can be seen as dark blobs on the mRNA transcripts in the image on the left.

Data from *Does the pachytene checkpoint, a feature of meiosis, filter out mistakes in double-strand DNA break repair and as a side-effect strongly promote adaptive speciation?* Foe, Victoria E, Integrative Organismal Biology, 10 Apr 2022, Vol. 4, Issue 1 Oxford University Press, Open Access article distributed under the terms of the Creative Commons Attribution License (https://creativecommons.org/licenses/by/4.0/)

OUTLINE

29.1 RNA Molecules Play Different Roles, Primarily in Gene Expression

29.2 RNA Polymerases Catalyze Transcription
29.3 Transcription Is Highly Regulated
29.4 Some RNA Transcription Products Are Processed
29.5 The Discovery of Catalytic RNA Revealed a Unique Splicing Mechanism

Learning Goals



By the end of this chapter, you should be able to:

1. Discuss the primary function of RNA polymerases, the reaction they catalyze, and the chemical mechanism of that reaction.
2. Describe transcription, including the processes of initiation, elongation, and termination.
3. Compare the roles of eukaryotic RNA polymerases I, II, and III in producing ribosomal, transfer, and messenger RNAs.
4. Recognize the significance of transcription factors and enhancers in the regulation of transcription in eukaryotes.
5. Describe the process of RNA splicing, including the roles of the spliceosome and self-splicing RNA molecules.
6. Understand some of the differences between transcription in bacteria and in eukaryotes.

DNA stores genetic information in a stable form that can be readily replicated. The expression of this genetic information requires its flow from DNA to RNA and, usually, to protein, as was introduced in Chapter 8. This chapter examines transcription, which, you will recall, is the process of synthesizing an RNA transcript from a DNA template, transferring the sequence information within the DNA to the new RNA molecule. We begin with a brief discussion of the diverse types of RNA molecules; then we will turn to RNA polymerases, the large and complex enzymes that carry out the

synthetic process. This will lead into a discussion of transcription in bacteria and focus on the three stages of transcription: promoter binding and initiation, elongation of the nascent RNA transcript, and termination. We then examine transcription in eukaryotes, focusing on the distinctions between bacterial and eukaryotic transcription.

29.1 RNA Molecules Play Different Roles, Primarily in Gene Expression

While the function of some RNAs has been known for some time, other classes of RNAs have only recently been discovered. The investigation of some of these RNA molecules has been one of the most productive areas of biochemical research in recent years.

RNAs play key roles in protein biosynthesis

As we will explore in Chapter 30, the long-known ribosomal and transfer RNA molecules, along with messenger RNAs, are central to protein synthesis. Ribosomal RNAs are critical components of ribosomes (the sites of protein synthesis), and transfer RNAs play a role in delivering amino acids (the building blocks of proteins) to the ribosome. Messenger RNAs carry the information that ribosomes use for the production of specific protein sequences.

Some RNAs can guide modifications of themselves or other RNAs

In eukaryotes, one of the most striking examples of RNA modification is the splicing of mRNA precursors, a process that is catalyzed by large complexes composed of both proteins and small nuclear RNAs. These small nuclear RNAs play a crucial role in guiding the splicing of messenger RNAs.

Remarkably, some RNA molecules can splice themselves in the absence of other proteins and RNAs. This landmark discovery of self-splicing introns, which we will discuss later in this chapter, revealed that RNA molecules can serve as catalysts, which greatly influenced our view of molecular evolution. Many other types of RNAs, such as small regulatory RNAs and long noncoding RNAs, have been discovered more recently, and while their functions are still under active investigation, our understanding is rapidly expanding.

Some viruses have RNA genomes

While DNA is the genetic material in most organisms, some viruses have genomes made of RNA (Section 8.4). RNA viruses are responsible for several diseases, such as influenza, polio, mumps, Ebola, the common cold, and — of particular note — COVID-19. The coronavirus SARS-CoV-2, which causes COVID-19, belongs to a family of coronaviruses that have an unusually large, single-stranded RNA genome. Coronaviruses cause a variety of diseases in mammals and birds that have a wide range of symptoms, including respiratory distress in humans that can potentially be lethal.

RNA viruses vary in their genome organization. They have either single- or double-stranded RNA molecules arranged in single or multiple fragments. Inside their hosts, RNA viruses replicate their genomes with a virus-encoded RNA polymerase that uses RNA as a template. In some viruses, a complementary RNA molecule is made from the single-stranded viral RNA genome, while in other viruses, a double-stranded DNA copy is made that can integrate itself into the host's genome. Viral RNA polymerases do not have the same proofreading ability of other polymerases, which leads to high mutation rates of RNA viruses.

Messenger RNA vaccines provide protection against diseases

Messenger RNA (mRNA) vaccines take advantage of the fact that cells can be tricked into making proteins they don't usually make, even those from other organisms such as viruses. Unlike other vaccines that use parts of a weakened or inactivated pathogen to trigger an immune response, mRNA vaccines — including those available for the SARS-CoV-2 virus — use sections of pathogenic (usually viral) mRNA that have been generated in the laboratory. When human cells are injected with this mRNA, they will produce the corresponding protein from this set of instructions. This "foreign" protein will be presented on the surface of the cells, trigger an immune response, and provide some level of protection if and when the actual pathogen invades. Even though research on mRNA vaccines had been going on for many years, the COVID-19 pandemic accelerated the development, approval, and distribution of mRNA vaccines to the public.

Self-Check Question

Compare the biological roles of RNA and DNA. What aspects of the structure and chemistry of RNA make it so versatile?

29.2 RNA Polymerases Catalyze Transcription

Transcription, the synthesis of RNA molecules from a DNA template, is catalyzed by large enzymes called **RNA polymerases**. The basic biochemistry of RNA synthesis is shared by all organisms, a commonality that has been beautifully illustrated by the three-dimensional structures of representative RNA polymerases from prokaryotes and eukaryotes (**Figure 29.1**). Despite substantial differences in size and number of polypeptide subunits, the overall structures of these enzymes are quite similar, revealing a common evolutionary origin.

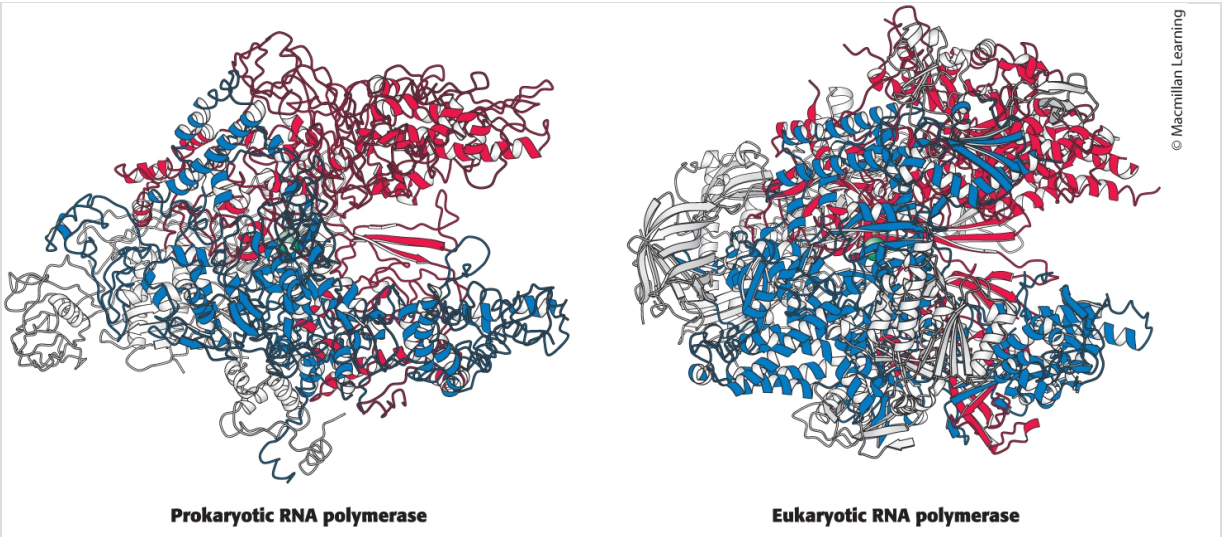


FIGURE 29.1 RNA polymerase structures in prokaryotes and eukaryotes resemble each other. In these three-dimensional models of RNA polymerases from a prokaryote (*Thermus aquaticus*) and a eukaryote (*Saccharomyces cerevisiae*), the two largest subunits for each structure are shown in dark red and dark blue. Both structures contain a central metal ion (green) in their active sites, near a large cleft on the right. The similarity of these structures reveals that these enzymes have the same evolutionary origin and have many mechanistic features in common.

[Drawn from 1I6V.pdb and 1I6H.pdb.]

INTERACT with these models in Achieve

RNA polymerases are very large, complex enzymes. For example, the core of the RNA polymerase of *E. coli* consists of five kinds of subunits with the composition $\alpha_2\beta\beta'\omega$ (Table 29.1). A typical eukaryotic RNA polymerase is larger and more complex, having 12 subunits and a total molecular mass of more than 500 kDa. Despite this complexity, the detailed structures of RNA polymerases have been determined by x-ray crystallography in work pioneered by Roger Kornberg and Seth Darst. The structures of many additional RNA polymerase complexes have been determined by cryo-electron microscopy.

TABLE 29.1 Subunits of RNA polymerase from *E. coli*

Subunit	Gene	Number	Mass (kDa)
α	*rpoA*	2	37
β	*rpoB*	1	151
β'	*rpoC*	1	155
ω	*rpoZ*	1	10
σ^{70}	*rpoD*	1	70

RNA synthesis comprises three stages: initiation, elongation, and termination

RNA synthesis, like all biological polymerization reactions, takes place in three stages: *initiation*, *elongation*, and *termination*. RNA polymerases perform multiple functions in this process:

1. They search DNA for initiation sites, also called *promoter sites* or simply **promoters**. For instance, *E. coli* DNA has about 2000 promoters in its 4.6×10^6 bp genome.

2. They unwind a short stretch of double-helical DNA to produce single-stranded DNA templates from which the sequence of bases can be easily read out.

3. They select the correct ribonucleoside triphosphate and catalyze the formation of a phosphodiester bond. This process is repeated many times as the enzyme moves along the DNA template. RNA polymerase is completely processive — a transcript is synthesized from start to end by a single RNA polymerase molecule.

4. They detect termination signals that specify where a transcript ends.

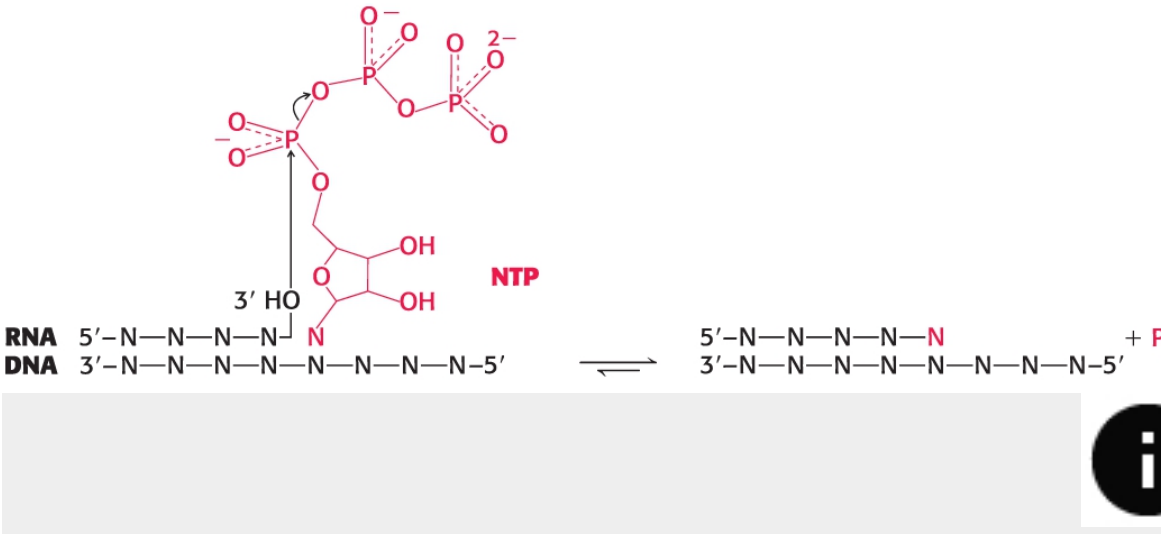
5. Their activity is regulated by activator and repressor proteins that interact with the promoter and modulate the ability of the RNA polymerase to initiate transcription. Gene expression is controlled substantially at the level of transcription, as will be discussed in detail in Chapter 31.

The chemistry of RNA synthesis is identical for all forms of RNA, including messenger RNAs, transfer RNAs, ribosomal RNAs, and small regulatory RNAs, so the basic steps just outlined apply to all forms. Their synthetic processes differ mainly in regulation, the specific RNA polymerase that creates them, and their posttranscriptional processing.

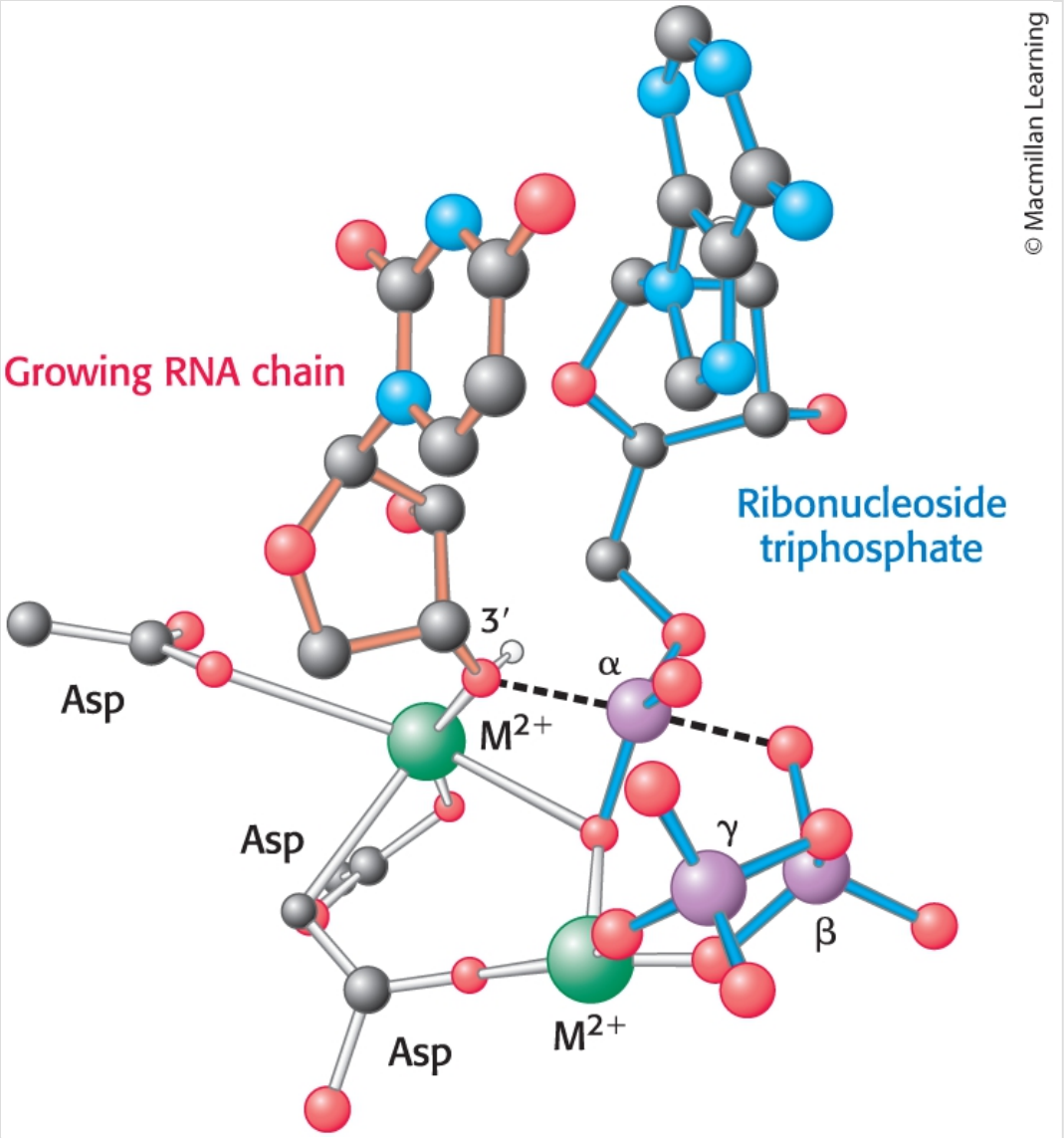
RNA polymerases catalyze the formation of a phosphodiester bond

The fundamental reaction of RNA synthesis, like that of DNA synthesis, is the formation of a phosphodiester bond. The 3′-hydroxyl group of the

last nucleotide in the chain makes a nucleophilic attack on the α-phosphoryl group of the incoming nucleoside triphosphate, releasing a pyrophosphate.



The catalytic sites of all RNA polymerases include two metal ions, normally magnesium ions (**Figure 29.2**). One ion remains tightly bound to the enzyme, whereas the other ion comes in with the nucleoside triphosphate and leaves with the pyrophosphate. Three conserved aspartate residues participate in binding these metal ions. Given the recent appreciation of the role of a third metal ion in the active site of DNA polymerases (see Section 28.1), it will be interesting to see if RNA polymerases show similarities to that model.



© Macmillan Learning

FIGURE 29.2 The RNA polymerase active site contains metal ions. In this model of the transition state for phosphodiester-bond formation in the active site of RNA polymerase, the 3′-hydroxyl group of the growing RNA chain attacks the α-phosphoryl group of the incoming nucleoside triphosphate, resulting in the release of pyrophosphate. This transition state is structurally similar to that in the active site of DNA polymerase (see Figure 28.2).

The polymerization reactions that are catalyzed by both prokaryotic and eukaryotic RNA polymerases take place within a complex in DNA termed a **transcription bubble** (**Figure 29.3**). This complex consists of double-stranded DNA that has been locally unwound in a region of approximately 17 base pairs. The edges of the bases that normally take part in Watson–Crick base pairs are exposed in the unwound region. We will begin with a detailed examination of the elongation process, including the role of the DNA template read by RNA polymerase and the reactions catalyzed by the polymerase, before returning to the more complex processes of initiation and termination.

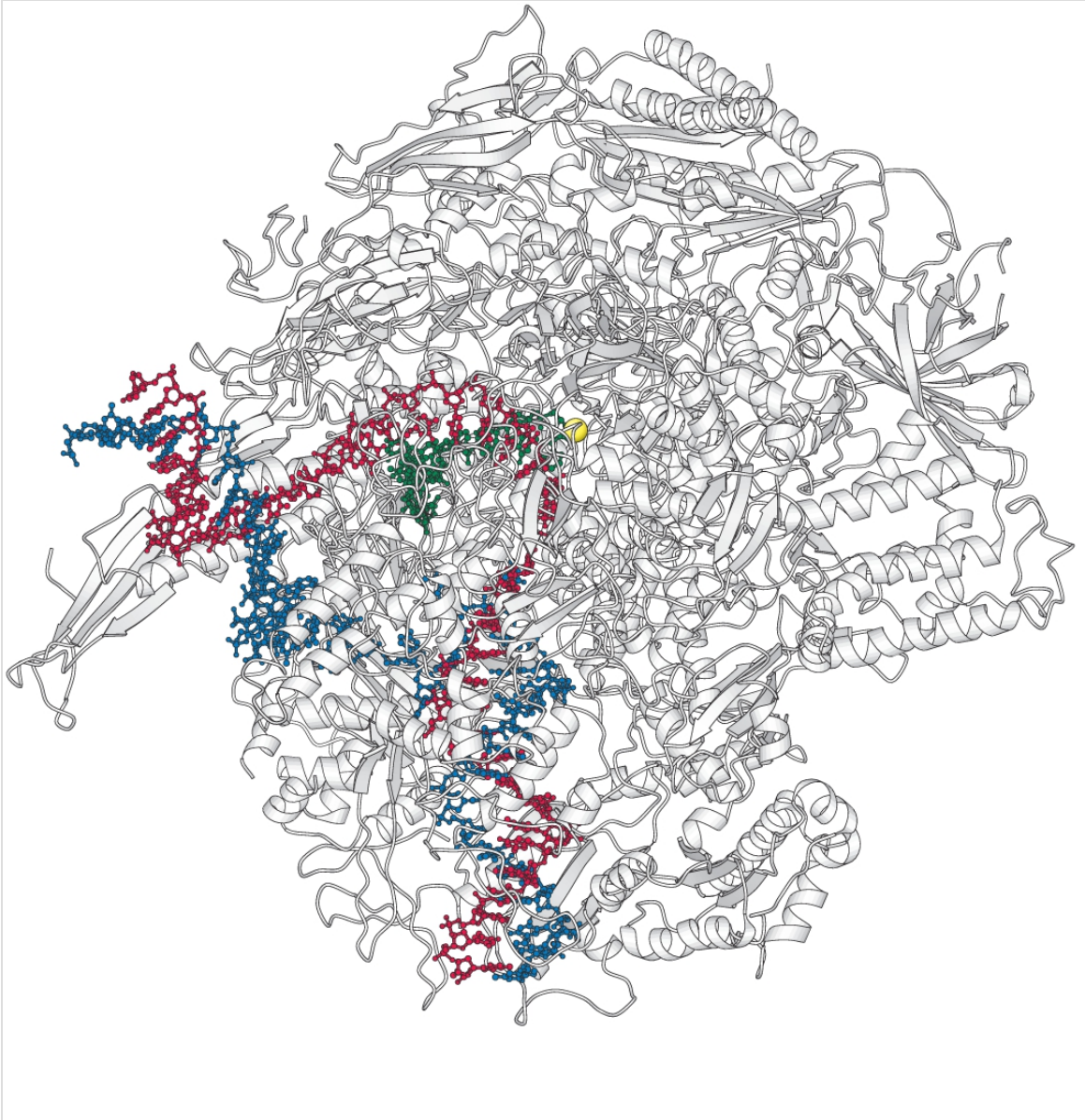


FIGURE 29.3 RNA polymerase separates a region of the double helix to form the transcription bubble. The red (template) and blue (nontemplate) strands of DNA are shown along with the RN molecule being synthesized (shown in green). The position of the active site magnesium is indicated (yellow sphere). The DNA enters from the left and exits at the bottom.

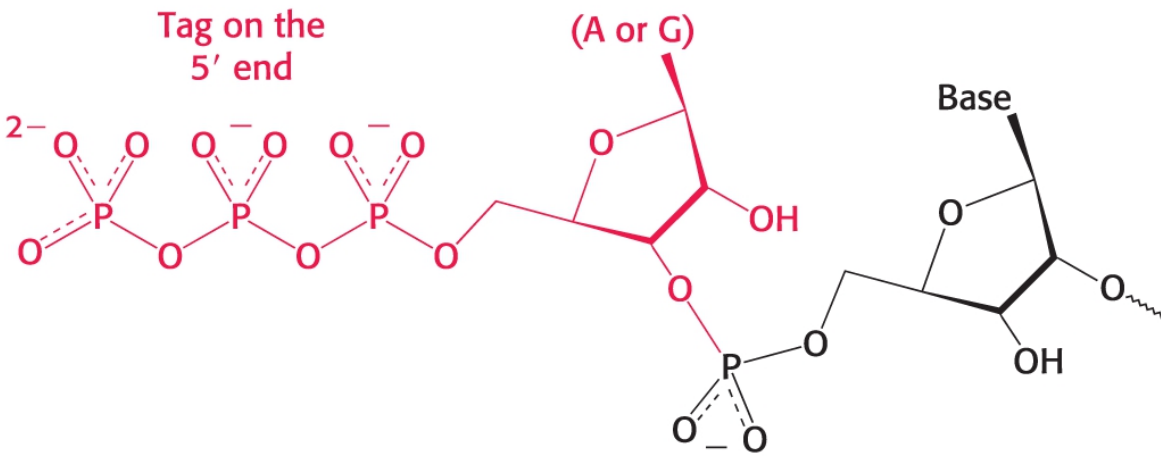
RNA chains are formed de novo and grow in the 5′-to-3′ direction

Let us begin our examination of transcription by considering the DNA template. The first nucleotide (the start site) of a DNA sequence to be transcribed is denoted as $+1$ and the second one as $+2$; the nucleotide preceding the start site is denoted as -1. These designations refer to the coding strand of DNA. Recall that the sequence of the *template strand* of DNA is the complement of that of the RNA transcript (Figure 29.4). In contrast, the *coding strand* of DNA has the same sequence as that of the RNA transcript except for thymine (T) in place of uracil (U). The coding strand is also known as the *sense* $(+)$ *strand*, and the template strand as the *antisense* $(-)$ *strand*.



FIGURE 29.4 The RNA transcript is complementary to the template, or antisense $(-)$, strand

In contrast with DNA synthesis, RNA synthesis can start de novo, without the requirement for a primer. Most newly synthesized RNA chains carry a highly distinctive tag on the 5′ end: the first base at that end is either pppG or pppA.



The presence of the triphosphate moiety confirms that RNA synthesis starts at the 5′ end.

The dinucleotide shown above is synthesized by RNA polymerase as part of the complex process of initiation, which will be discussed later in the chapter. After initiation takes place, RNA polymerase elongates the nucleic acid chain as follows (Figure 29.5).

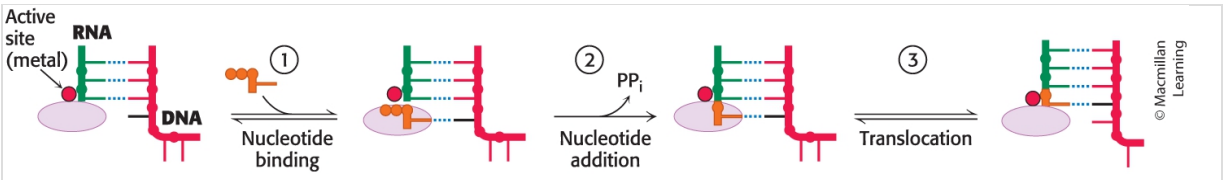


FIGURE 29.5 The elongation mechanism involves a series of steps. A ribonucleoside triphosphate binds adjacent to the growing RNA chain and forms a Watson–Crick base pair with a base on the DNA template strand (1). The 3′-hydroxyl group at the end of the RNA chain attacks

the newly bound nucleotide and forms a new phosphodiester bond, releasing pyrophosphate (2). After nucleotide addition, the RNA–DNA hybrid can translocate through the RNA polymerase (3), bringing a new DNA base into position to base-pair with an incoming nucleoside triphosphate.

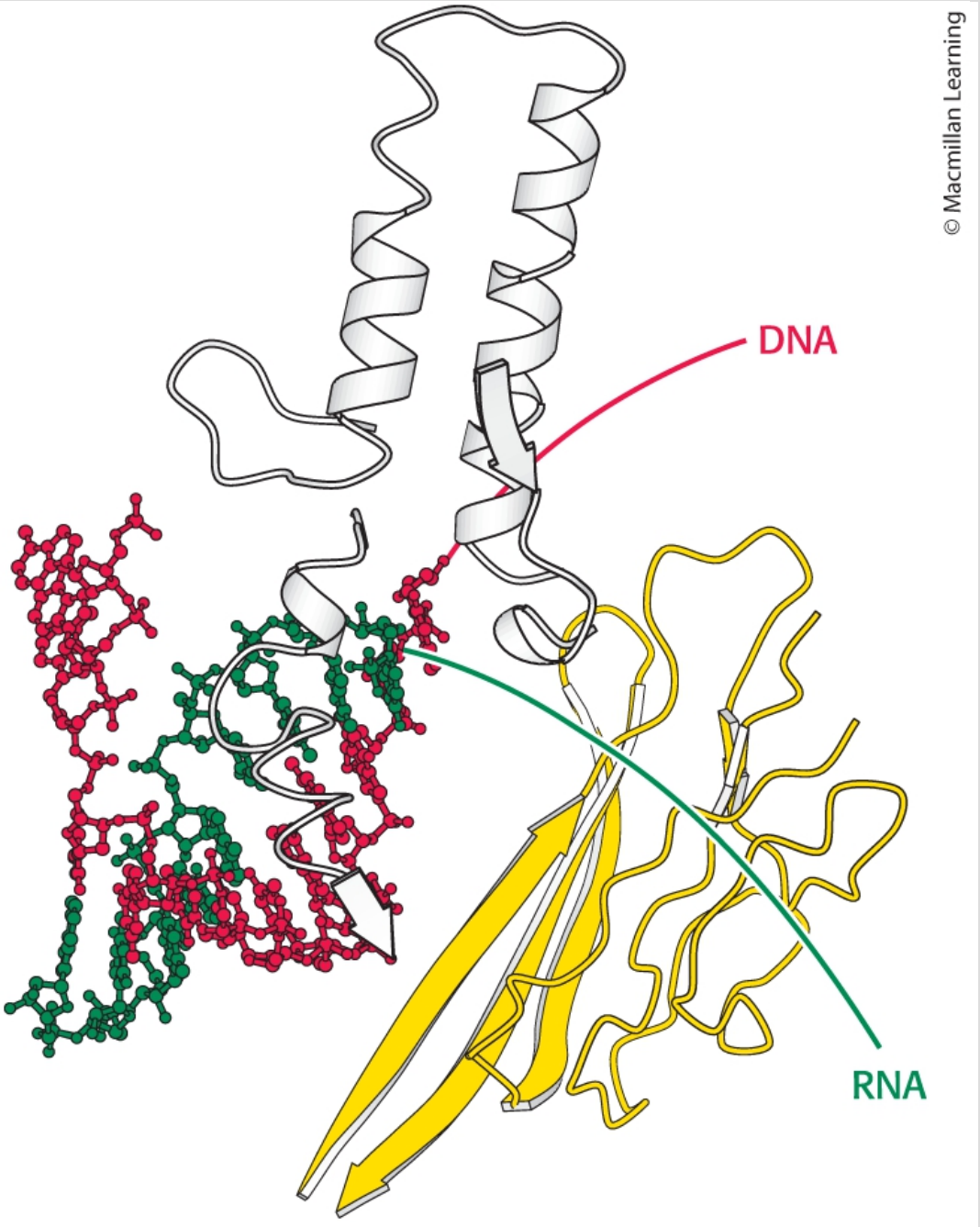


1. A ribonucleoside triphosphate binds in the active site of the RNA polymerase directly adjacent to the growing RNA chain, and it forms a Watson–Crick base pair with the template strand.

2. The $3'$-hydroxyl group of the growing RNA chain, which is oriented and activated by the tightly bound metal ion, attacks the α-phosphoryl group to form a new phosphodiester bond, displacing pyrophosphate.

3. Next, the RNA–DNA hybrid must move relative to the polymerase to bring the $3'$ end of the newly added nucleotide into proper position for the next nucleotide to be added. This translocation step does not include breaking any bonds between base pairs and is reversible; but, once it has taken place, the addition of the next nucleotide, favored by the triphosphate cleavage and pyrophosphate release and cleavage, drives the polymerization reaction forward.

The lengths of the RNA–DNA hybrid and of the unwound region of DNA stay rather constant as RNA polymerase moves along the DNA template. The length of the RNA–DNA hybrid is determined by a structure within the enzyme that forces the RNA–DNA hybrid to separate, allowing the RNA chain to exit from the enzyme and the DNA chain to rejoin its DNA partner (**Figure 29.6**).



© Macmillan Learning

FIGURE 29.6 A structure within RNA polymerase forces the separation of the RNA–DNA hybrid. Notice that the DNA strand exits in one direction and the RNA product exits in another.

[Drawn from 1I6H.pdb.]

INTERACT with this model in Achieve

RNA polymerases backtrack and correct errors

The RNA–DNA hybrid can also move in the direction opposite that of elongation (Figure 29.7). This backtracking is energetically less favorable than moving forward because it breaks the bonds between a base pair. However, backtracking is very important for *proofreading*. The incorporation of an incorrect nucleotide introduces a non-Watson–Crick base pair. In this case, breaking the bonds between this base pair and backtracking is energetically less costly.

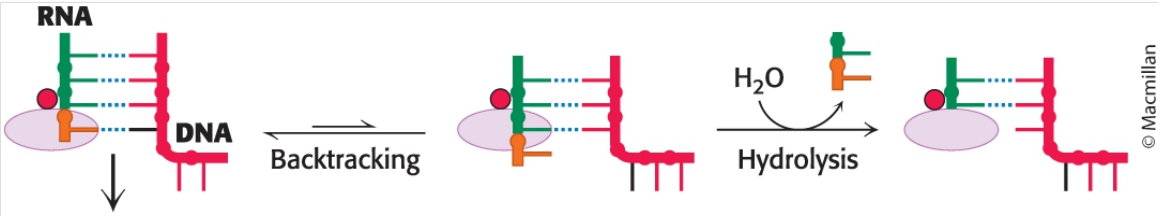


FIGURE 29.7 The RNA–DNA hybrid can occasionally backtrack within the RNA polymerase. In the backtracked position, hydrolysis can take place, producing a configuration equivalent to tha after translocation. Backtracking is more likely if a mismatched base is added, facilitating proofreading.

After the polymerase has backtracked, the phosphodiester bond one base pair before the one that has just formed is adjacent to the metal ion in the active site. In this position, a hydrolysis reaction in which a water molecule attacks the phosphate can result in the cleavage of the

phosphodiester bond and the release of a dinucleotide that includes the incorrect nucleotide.

Studies of single molecules of RNA polymerase have confirmed that the enzymes pause and backtrack to correct errors. Furthermore, these proofreading activities are often enhanced by accessory proteins.

The final error rate of the order of one mistake per 10^4 or 10^5 nucleotides is higher than that for DNA replication, including all error-correcting mechanisms. The lower fidelity of RNA synthesis can be tolerated because mistakes are not transmitted to progeny. For most genes, many RNA transcripts are synthesized; a few defective transcripts are unlikely to be harmful.

Self-Check Question



List some ways in which RNA polymerases are similar to DNA polymerases, and how they are different.

RNA polymerase binds to promoter sites on the DNA template in bacteria to initiate transcription

While the elongation process is common to all organisms, the processes of initiation and termination differ substantially in bacteria and eukaryotes. We begin with a discussion of these processes in bacteria, starting with initiation of transcription.

The bacterial RNA polymerase discussed earlier with the composition $\alpha_2\beta\beta'\omega$ is referred to as the *core enzyme*. The inclusion of an additional subunit (σ) produces the *holoenzyme* with composition $\alpha_2\beta\beta'\omega\sigma$. The **σ subunit** helps find the promoters, sites on DNA where transcription begins. At these sites, the σ subunit participates in the initiation of RNA synthesis and then dissociates from the rest of the enzyme.

Sequences upstream of the promoter site are important in determining where transcription begins. A striking pattern is evident when the sequences of bacterial promoters are compared: Two common motifs are present on the upstream side of the transcription start site. They are known as the -10 *sequence* and the -35 *sequence* because they are centered at about 10 and 35 nucleotides upstream of the start site. The region containing these sequences is called the *core promoter*. The -10 and -35 sequences are each 6 bp long. Their **consensus sequences**, deduced from analyses of many promoters (**Figure 29.8**), are:



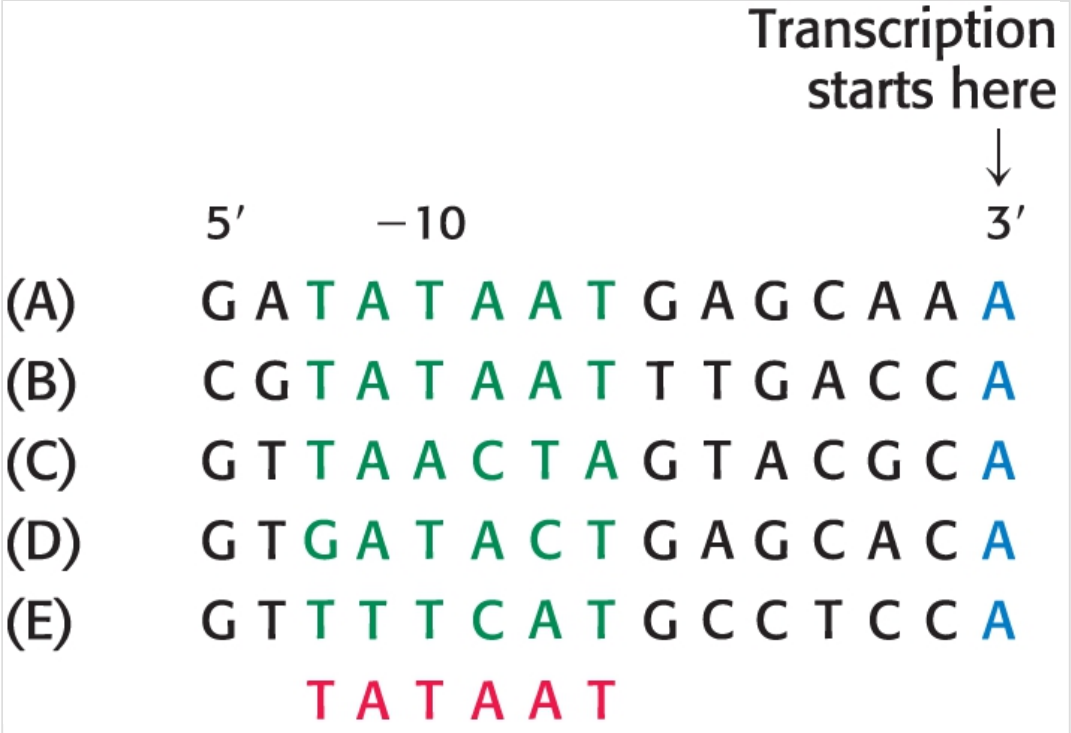


FIGURE 29.8 Bacterial promoters contain conserved sequences. A comparison of five sequences from prokaryotic promoters reveals a recurring sequence of TATAAT centered on position -10. The -10 consensus sequence (in red) was deduced from a large number of promoter sequences. The sequences are from the (A) *uvrD*, (B) *uncI*, and (C) *trp* operons of *E. coli*, from (D) λ phage, and from (E) ϕX174 phage.

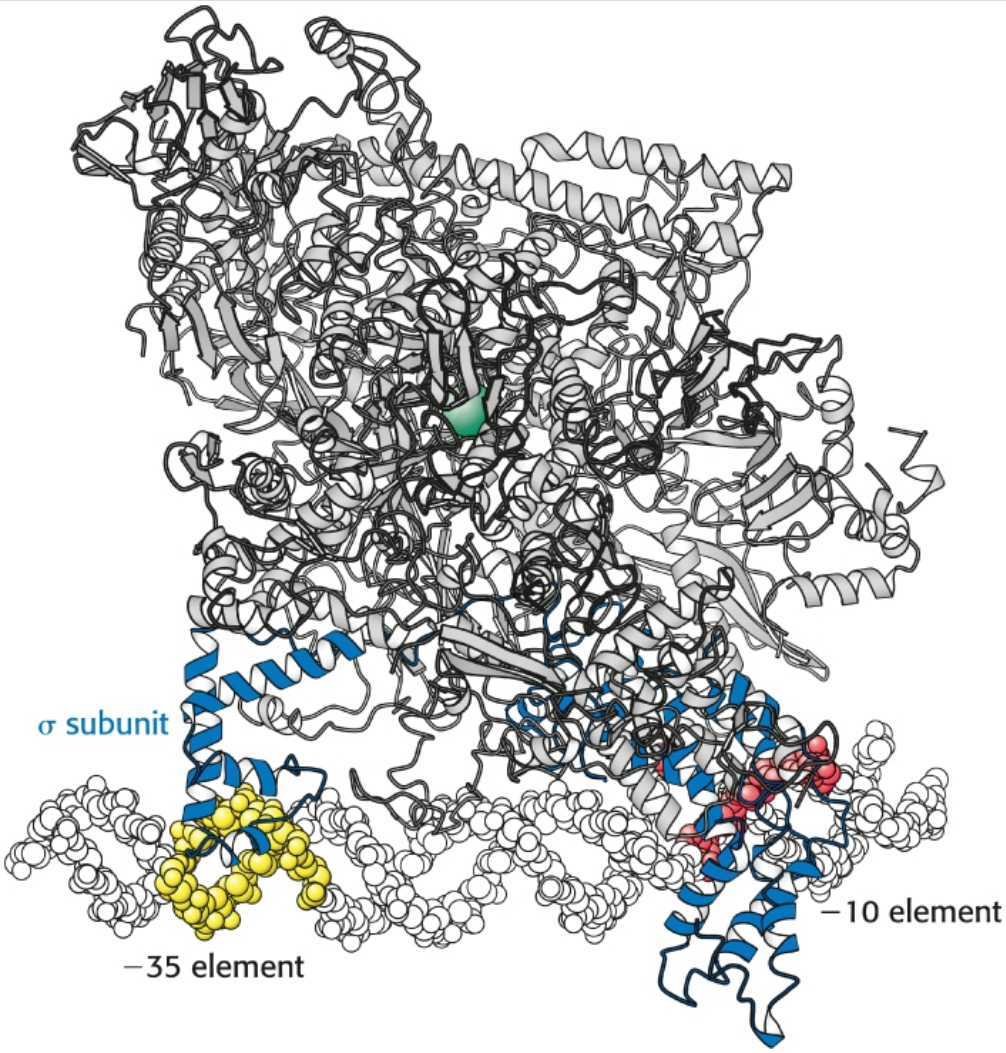
Promoters differ markedly in their efficacy. Some genes are transcribed frequently — as often as every 2 seconds in *E. coli*. The promoters for these genes are referred to as *strong promoters*. In contrast, other genes are transcribed much less frequently, about once in 10 minutes; the promoters for these genes are *weak promoters*. The -10 and -35 regions of most strong promoters have sequences that correspond closely to the consensus sequences, whereas weak promoters tend to have multiple substitutions at these sites. Indeed, mutation of a single base in either the -10 sequence or the -35 sequence can diminish promoter activity.

The distance between these conserved sequences also is important; a separation of 17 nucleotides is optimal. Thus, the efficiency or strength of a promoter sequence serves to regulate transcription. Regulatory proteins that bind to specific sequences near promoter sites and interact with RNA polymerase (Chapter 31) also markedly influence the frequency of transcription of many genes.

Outside the core promoter in a subset of highly expressed genes is the *upstream element* (also called the UP element). This sequence is present from 40 to 60 nucleotides upstream of the transcription start site. The UP element is bound by the α subunit of RNA polymerase and serves to increase the efficiency of transcription by creating an additional interaction site for the polymerase.

Sigma subunits of RNA polymerase in bacteria recognize promoter sites

To initiate transcription, the $\alpha_2\beta\beta'\omega$ core of RNA polymerase must bind the promoter. However, it is the σ subunit that makes this binding possible by enabling RNA polymerase to recognize promoter sites. In the presence of the σ subunit, the RNA polymerase binds weakly to the DNA and slides along the double helix until it dissociates or encounters a promoter. The σ subunit recognizes the promoter through several interactions with the nucleotide bases of the promoter DNA. The structure of a bacterial RNA polymerase holoenzyme bound to a promoter site shows the σ subunit interacting with DNA at the -10 and -35 regions essential to promoter recognition (**Figure 29.9**). Therefore, the σ subunit is responsible for the specific binding of the RNA polymerase to a promoter site on the template DNA. The σ subunit is generally released when the nascent RNA chain reaches 9 or 10 nucleotides in length. After its release, it can associate with another core enzyme and assist in a new round of initiation.



© Macmillan Learning

FIGURE 29.9 *E. coli* RNA polymerase holoenzyme complex binds to conserved promoter sequences. The σ subunit (blue) of the bacterial RNA polymerase holoenzyme makes sequence-specific contacts with the -10 (red) and -35 (yellow) promoter elements. The active site of the polymerase is revealed by a bound metal ion (purple).

[Drawn from 1L9Z.pdb].

INTERACT with this model in Achieve

The template double helix must be unwound for transcription to take place

Although the bacterial RNA polymerase can search for promoter sites when bound to double-helical DNA, a segment of the DNA double helix must be unwound before synthesis can begin. The transition from the closed promoter complex (in which DNA is double helical) to the open promoter complex (in which a DNA segment is unwound) is an essential event in both bacterial and eukaryotic transcription. In bacteria it is the RNA polymerase itself that accomplishes this (Figure 29.10), while in eukaryotes additional proteins are required to unwind the DNA template.

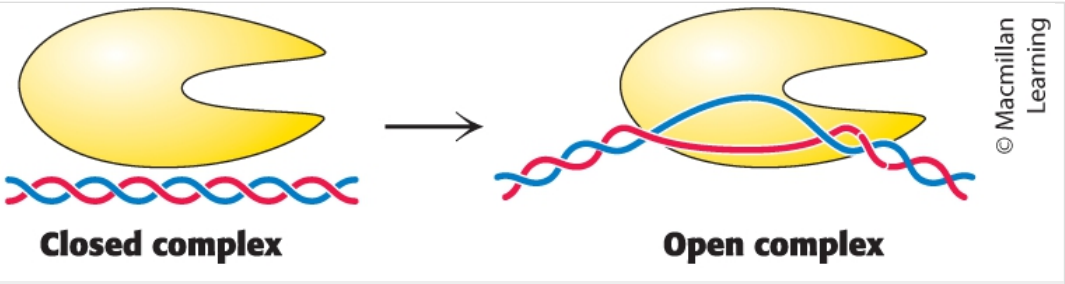


FIGURE 29.10 *E. coli* RNA polymerase binds to a promoter sequence. The transition from the closed promoter complex to the open promoter complex requires the unwinding of approximately 17 base pairs of DNA.

We know that, in bacteria, the free energy necessary to break the bonds between approximately 17 base pairs in the double helix is derived from additional interactions between the template and the bacterial RNA polymerase. These interactions become possible when the DNA distorts to wrap around the RNA polymerase; they also occur between the single-stranded DNA regions and other parts of the enzyme. These interactions stabilize the open promoter complex and help pull the template strand into the active site. The -35 element remains in a double-helical state, whereas the -10 element is unwound. The stage is

now set for the formation of the first phosphodiester bond of the new RNA chain.

Elongation takes place at transcription bubbles that move along the DNA template

The elongation phase of RNA synthesis begins with the formation of the first phosphodiester bond, after which repeated cycles of nucleotide addition can take place. However, until about 10 nucleotides have been added, RNA polymerase sometimes releases the short RNA, which dissociates from the DNA and gets degraded. Once RNA polymerase passes this point, the enzyme stays bound to its template until a termination signal is reached.

The region containing the unwound DNA template and nascent RNA corresponds to the transcription bubble (**Figure 29.11**). The newly synthesized RNA forms a hybrid helix with the template DNA strand. This RNA–DNA helix is about 8 bp long, which corresponds to nearly one turn of a double helix. The $3'$-hydroxyl group of the RNA in this hybrid helix is positioned so that it can attack the α-phosphorus atom of an incoming ribonucleoside triphosphate. The core bacterial RNA polymerase also contains a binding site for the coding strand of DNA.

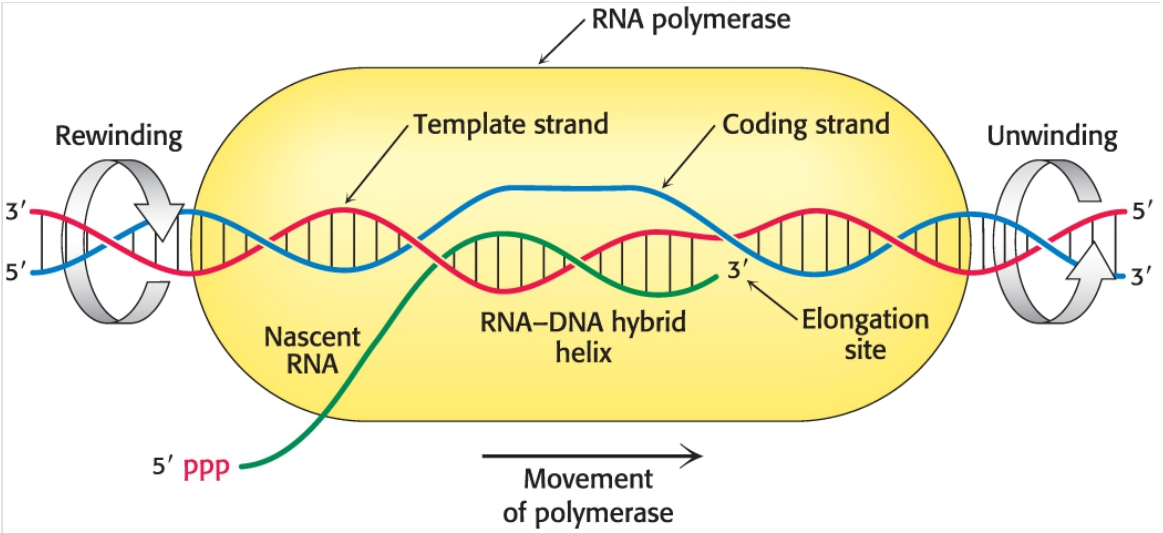


FIGURE 29.11 The transcription bubble moves with the RNA polymerase during elongation. I this schematic representation of a transcription bubble in the elongation of an RNA transcript, duplex DNA is unwound at the forward end of RNA polymerase and rewound at its rear end. The RNA–DNA hybrid rotates during elongation.

As in the initiation phase, about 17 bp of DNA are unwound throughout the elongation phase. The transcription bubble moves a distance of 170 Å (17 nm) in a second, which corresponds to a rate of elongation of about 50 nucleotides per second. Although rapid, it is much slower than the rate of DNA synthesis, which is 800 nucleotides per second.

Sequences within the newly transcribed RNA signal termination

How does the RNA polymerase know where to stop transcription? In the termination phase of transcription, the formation of phosphodiester bonds ceases, the RNA–DNA hybrid dissociates, the unwound region of DNA rewinds, and RNA polymerase releases the DNA. This process is as precisely controlled as initiation. So what determines where

transcription is terminated? In both eukaryotes and bacteria, the transcribed regions of DNA templates contain so-called *intrinsic* termination signals.

In bacteria, the simplest intrinsic termination signal is a palindromic GC-rich region followed by an AT-rich region. The RNA transcript of this DNA palindrome is self-complementary (**Figure 29.12**). Hence, its bases can pair to form a hairpin structure with a stem and loop, a structure favored by its high content of G and C residues. Guanine–cytosine base pairs are more stable than adenine–thymine pairs, primarily because of the preferred base-stacking interactions in G–C base pairs (Section 1.3). This stable hairpin is followed by a sequence of four or more uracil residues, which also are crucial for termination. The RNA transcript ends within or just after them.

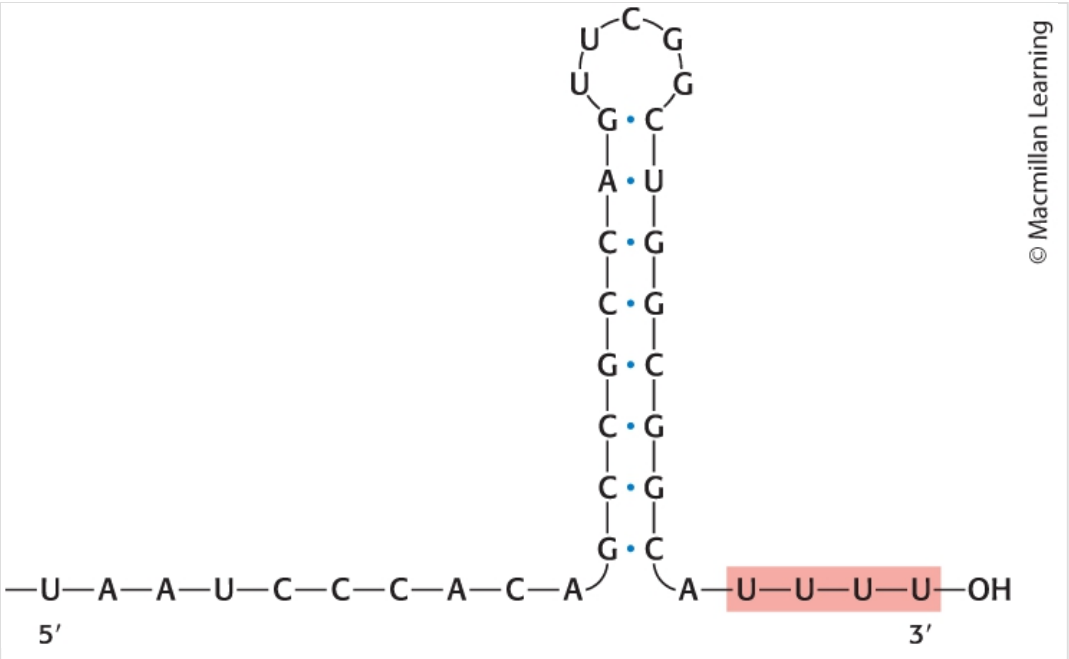


FIGURE 29.12 Some genes contain intrinsic termination signals. A typical intrinsic termination signal found at the 3′ end of an mRNA transcript consists of a series of bases that form a stable stem-loop structure followed by a string of U residues.

How does this combination hairpin–oligo(U) structure terminate transcription? First, RNA polymerase likely pauses immediately after it has synthesized a stretch of RNA that folds into a hairpin. Furthermore, the RNA–DNA hybrid helix produced after the hairpin is unstable because its rU–dA base pairs are the weakest of the four kinds. Hence, the pause in transcription caused by the hairpin permits the weakly bound nascent RNA to dissociate from the DNA template and then from the enzyme. The solitary DNA template strand rejoins its partner to re-form the DNA duplex, and the transcription bubble closes.

In bacteria, the rho protein helps to terminate the transcription of some genes

Bacterial RNA polymerase needs no help to terminate transcription at the intrinsic sites described above. At other sites, however, termination requires the participation of an additional factor. This discovery was prompted by the observation that some RNA molecules synthesized in vitro by RNA polymerase acting alone are longer than those made in vivo. The missing factor, a protein that caused the correct termination, was isolated and named **rho (ρ)**.

Additional information about the action of ρ was obtained by adding this termination factor to an incubation mixture at various times after the initiation of RNA synthesis (**Figure 29.13**). RNAs with sedimentation coefficients of 10S, 13S, and 17S were obtained when ρ was added at initiation, a few seconds after initiation, and 2 minutes after initiation, respectively. If no ρ was added, transcription yielded a 23S RNA product. It is evident that the template contains at least three termination sites that respond to ρ (yielding 10S, 13S, and 17S RNA) and one termination site that does not (yielding 23S RNA). Thus, specific termination at a site producing 23S RNA can take place in the absence of ρ. However, ρ detects additional termination signals that are not recognized by RNA polymerase alone.

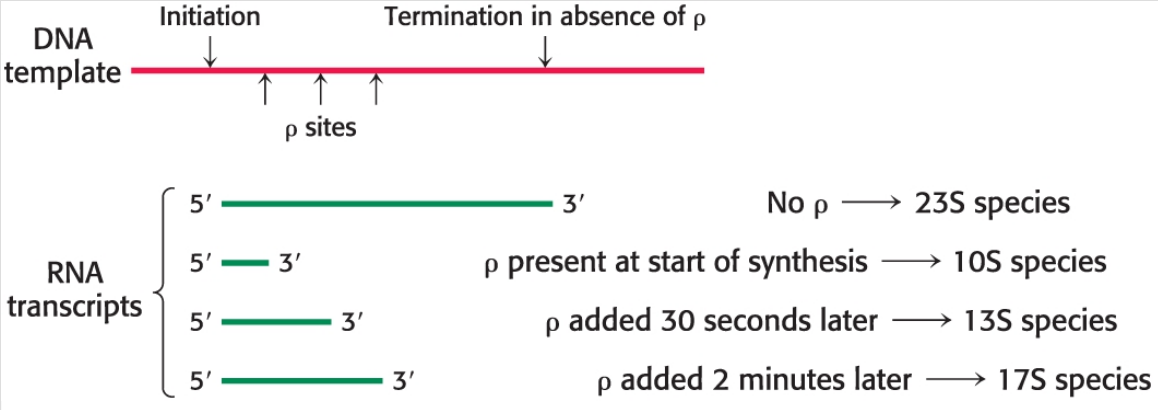


FIGURE 29.13 ρ protein promotes the termination of transcription. The DNA template shown here contains three ρ-dependent termination sites and one site that does not require the actior of the ρ protein.

The ρ protein promotes about 20% of termination events in bacteria, but exactly how it selects its target termination signals is not clear. Unlike the hairpin–oligo(U) sequence of intrinsic termination sites, the identification of conserved patterns in ρ-dependent terminators has proven more difficult.

How does ρ promote the termination of RNA synthesis? A key clue is the finding that ρ is hexameric and hydrolyzes ATP in the presence of single-stranded RNA but not in the presence of DNA or duplex RNA. Thus ρ is a helicase, homologous to the hexameric helicases that we encountered in our discussion of DNA replication (Section 28.1). The role of ρ in the termination of transcription in bacteria is as follows (**Figure 29.14**):

- The ρ protein is brought into action by sequences located in the nascent RNA that are rich in cytosine and poor in guanine.
- A stretch of nucleotides is bound in such a way that the RNA passes through the center of the structure.

- The helicase activity of ρ enables the protein to pull the nascent RNA while pursuing RNA polymerase.
- When ρ catches RNA polymerase at the transcription bubble, it breaks the RNA–DNA hybrid by functioning as an RNA–DNA helicase.

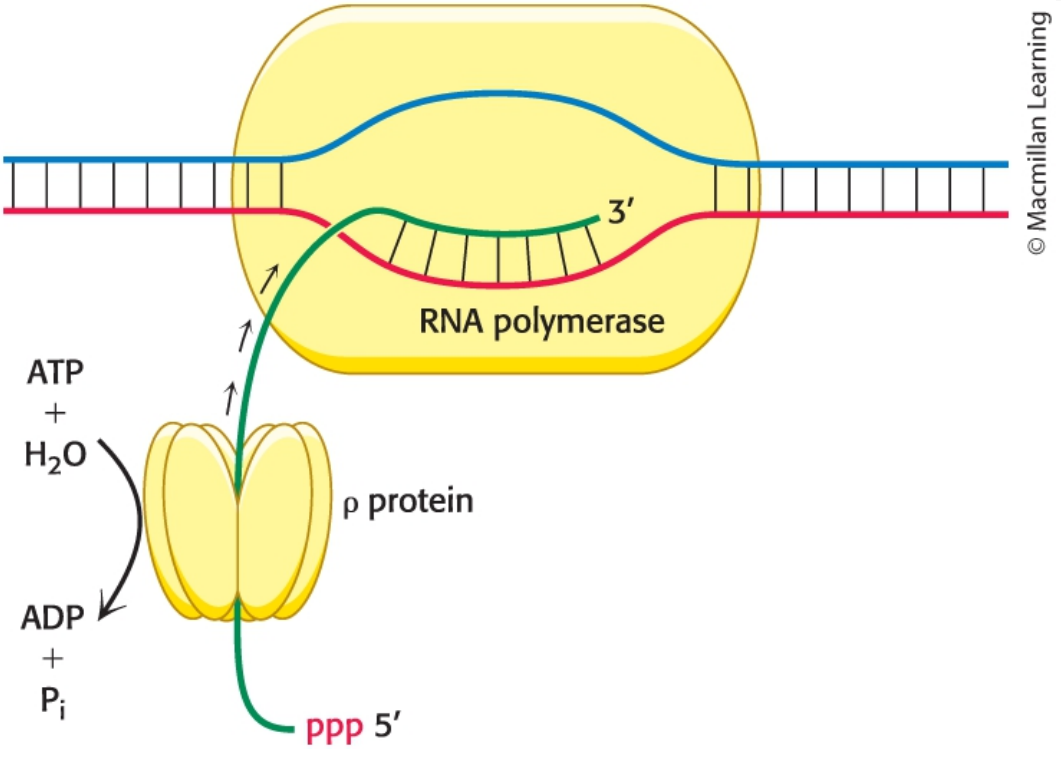


FIGURE 29.14 ρ protein is an ATP-dependent helicase. ρ promotes the termination of transcription by binding the nascent RNA chain and pulling it away from the RNA polymerase and the DNA template. The small arrows represent the movement of ρ protein along the transcript.

Proteins in addition to ρ may promote termination. For example, the NusA protein enables RNA polymerase in *E. coli* to recognize a characteristic class of termination sites. A common feature of transcription termination, whether it relies on a protein or not, is that

the functioning signals lie in newly synthesized RNA rather than in the DNA template.

29.3 Transcription Is Highly Regulated

As we will see in Chapter 31, the level at which different genes are transcribed is highly regulated. Regulated gene expression is critical for the development of multicellular organisms, the differentiation of various cell types, and the response of bacteria to changes in their environment. Here, we will discuss a few examples of how transcription can be controlled.

Alternative sigma subunits in bacteria control transcription in response to changes in conditions

As noted above, the σ factor allows for the specific binding of the bacterial RNA polymerase to a promoter site on the template DNA. *E. coli* has seven distinct σ factors for recognizing several types of promoter sequences in *E. coli* DNA. The type that recognizes the consensus sequences described earlier is called σ^{70} because it has a mass of 70 kDa. A different σ factor comes into play when the temperature is raised abruptly. *E. coli* responds by synthesizing σ^{32}, which recognizes the promoters of so-called *heat-shock genes*. These promoters exhibit -10 sequences that are somewhat different from the -10 sequence for standard promoters (**Figure 29.15**). The increased transcription of heat-shock genes leads to the coordinated synthesis of a series of protective proteins. Other σ factors respond to environmental conditions, such as nitrogen starvation. These findings demonstrate

that σ plays the key role in determining when and where RNA polymerase initiates transcription.

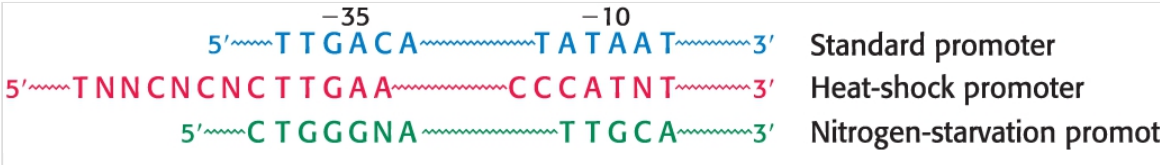


FIGURE 29.15 Alternative promoters vary in their consensus sequences at conserved sites. A comparison is shown of the consensus sequences of standard, heat-shock, and nitrogen-starvation promoters of *E. coli.* These promoters are recognized by σ^{70}, σ^{32}, and σ^{54}, respectively.

Some other bacteria contain a much larger number of σ factors. For example, the genome of the soil bacterium *Streptomyces coelicolor* encodes more than 60 σ factors recognized on the basis of their amino acid sequences. This repertoire allows these cells to adjust their gene-expression programs to the wide range of conditions, with regard to nutrients and competing organisms, that they may experience.

Some messenger RNAs directly sense metabolite concentrations

As we shall explore in Chapter 31, the expression of many genes is controlled in response to the concentrations of metabolites and signaling molecules within cells. One set of control mechanisms found in both prokaryotes and eukaryotes depends on the remarkable ability of some mRNA molecules to form secondary structures that are capable of directly binding small molecules. These structures are termed **riboswitches**.

Consider a riboswitch that controls the synthesis of genes that participate in the biosynthesis of riboflavin in the bacterium *Bacillus subtilis* (Figure 29.16). When flavin mononucleotide (FMN), a key intermediate in riboflavin biosynthesis, is present at high concentration, it binds to the RNA transcript. Binding of FMN to the transcript induces a hairpin structure that favors premature termination. By trapping the RNA transcript in this termination-favoring conformation, FMN prevents the production of functional full-length mRNA. However, when FMN is present at low concentration, it does not readily bind to the mRNA. Without FMN bound, the transcript adopts an alternative conformation without the terminator hairpin, allowing the production of the full-length mRNA. The occurrence of riboswitches serves as a vivid illustration of how RNAs are capable of forming elaborate, functional structures, though in the absence of specific information we tend to depict them as simple lines.

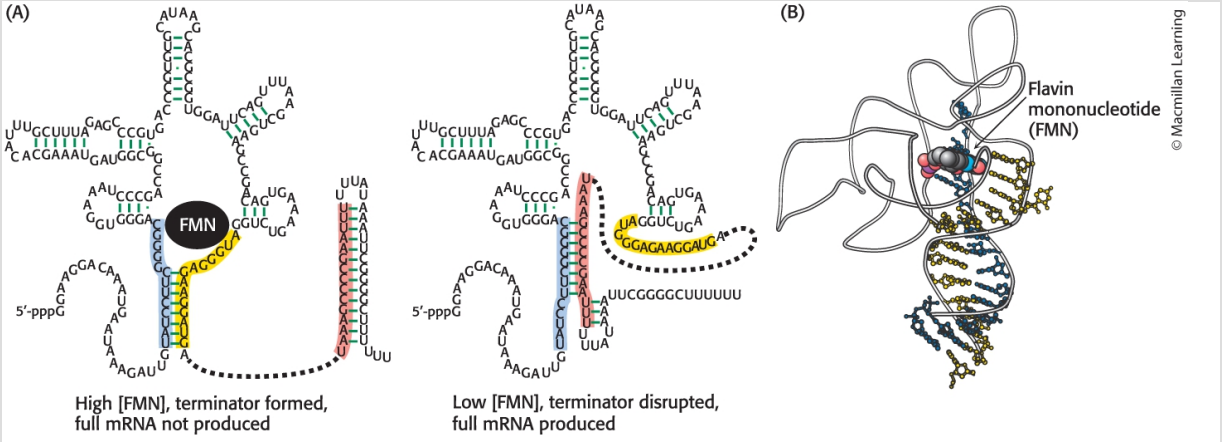


FIGURE 29.16 Riboswitches use metabolite concentrations to regulate transcription. (A) The 5′ end of an mRNA that encodes proteins engaged in the production of flavin mononucleotide (FMN) folds to form a structure that is stabilized by binding FMN. This structure includes a terminator that leads to premature termination of the mRNA. At lower concentrations of FMN, an alternative structure that lacks the terminator is formed, leading to the production of full-length mRNA. (B) In the three-dimensional structure of a related FMN-binding riboswitch bound to FMN, the blue and yellow stretches correspond to regions highlighted in the same colors in part A. The yellow strand contacts the bound FMN, stabilizing the structure.

[Drawn from 3F2Q.pdb].

INTERACT with this model in Achieve

Control of transcription in eukaryotes is highly complex

We turn now to transcription in eukaryotes, a much more complex process than in bacteria. Eukaryotic cells have a remarkable ability to regulate precisely the time at which each gene is transcribed and how much RNA is produced. This ability led to the evolution of multicellular eukaryotes with distinct tissues. That is, multicellular eukaryotes use differential transcriptional regulation to create different cell types.

Gene expression is influenced by three important characteristics unique to eukaryotes: the nuclear membrane, complex transcriptional regulation, and RNA processing.

1. *The nuclear membrane allows transcription and translation to take place in different cellular compartments.* Transcription takes place in the membrane-bound nucleus, whereas translation takes place outside the nucleus in the cytoplasm. In bacteria, the two processes are closely coupled (**Figure 29.17**). Indeed, the translation of bacterial mRNA begins while the transcript is still being synthesized. The spatial and temporal separation of transcription and translation enables eukaryotes to regulate gene expression in much more intricate ways, contributing to the richness of eukaryotic form and function.

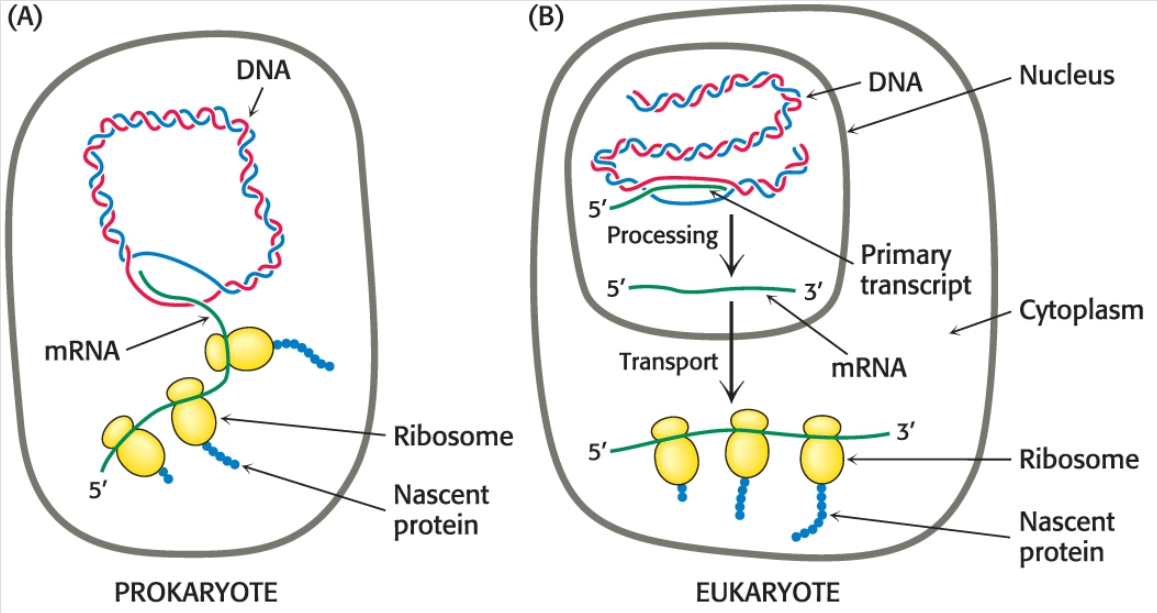


FIGURE 29.17 Transcription and translation are closely coupled in prokaryotes, whereas they are spatially and temporally separate in eukaryotes. (A) In prokaryotes, the primary transcript serves as mRNA and is used immediately as the template for protein synthesis. (B) In eukaryote mRNA precursors are processed and spliced in the nucleus before being transported to the cytoplasm for translation into protein.

[Information from J. Darnell, H. Lodish, and D. Baltimore. *Molecular Cell Biology*, 2nd ed. (Scientific American Book 1990), p. 230.]

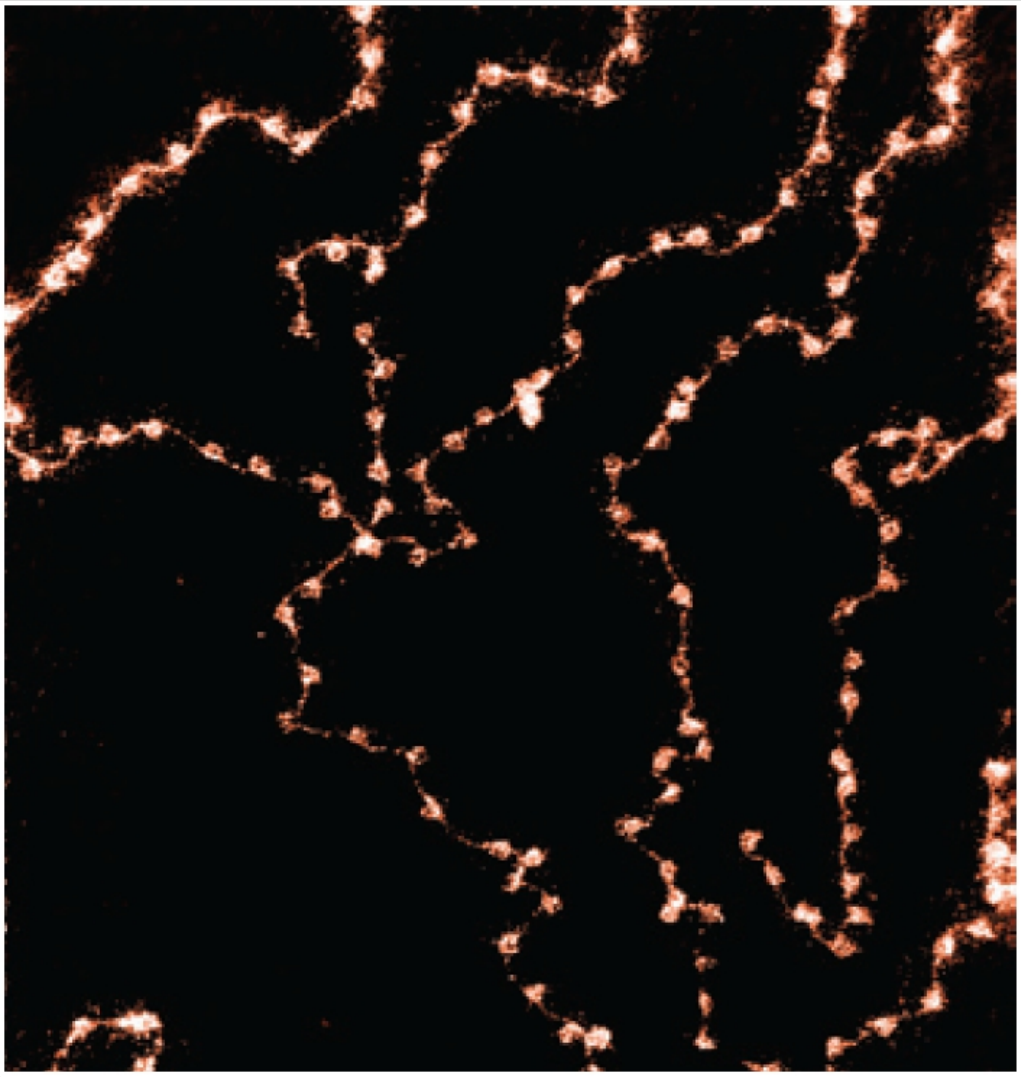
2. *A variety of types of promoter elements enables complex transcriptional regulation*. Like bacteria, eukaryotes rely on conserved sequences in DNA to regulate the initiation of transcription. But bacteria have only three promoter elements (the -10, -35, and UP elements), whereas eukaryotes use a variety of types of promoter elements, each identified by its own conserved sequence. Not all possible types will be present together in the same promoter. In eukaryotes, elements that regulate transcription can be found upstream or downstream of the start site and sometimes at distances much farther from the start site than in prokaryotes. For example, enhancer elements located on DNA far from the start site increase the promoter activity of specific genes.

3. *The degree of RNA processing is much greater in eukaryotes than in bacteria*. Although both bacteria and eukaryotes modify RNA, eukaryotes very extensively process nascent RNA destined to become mRNA. This processing includes modifications to both ends and, most significantly, splicing out segments of the primary transcript. RNA processing is described in Section 29.4.

Eukaryotic DNA is organized into chromatin

Whereas bacterial genomic DNA is relatively accessible to the proteins involved in transcription, eukaryotic DNA is packaged into **chromatin**, a complex formed between the DNA and a particular set of proteins. Chromatin compacts and organizes eukaryotic DNA, and its presence has dramatic consequences for gene regulation. Although the principles for the construction of chromatin are relatively simple, the chromatin structure for a complete genome is quite complicated. Importantly, in any given eukaryotic cell, some genes and their associated regulatory regions are relatively accessible for transcription and regulation, whereas other genes are tightly packaged, less accessible, and therefore inactive. Eukaryotic gene regulation frequently requires the manipulation of chromatin structure.

Chromatin viewed with the electron microscope has the appearance of beads on a string (**Figure 29.18**). Partial digestion of chromatin with DNase exposes these particles, which consist of fragments of DNA (the "string") wrapped around octamers of proteins called *histones* (the "beads"). The complex formed by a histone octamer and a 145-bp DNA fragment is called the **nucleosome** (**Figure 29.19**).



Don. W. Fawcett/Science Source.

FIGURE 29.18 Eukaryotic chromatin structure resembles beads on a string. In this electron micrograph of chromatin, the “beads” correspond to DNA complexed with specific proteins into nucleosomes. Each bead has a diameter of approximately 100 Å.

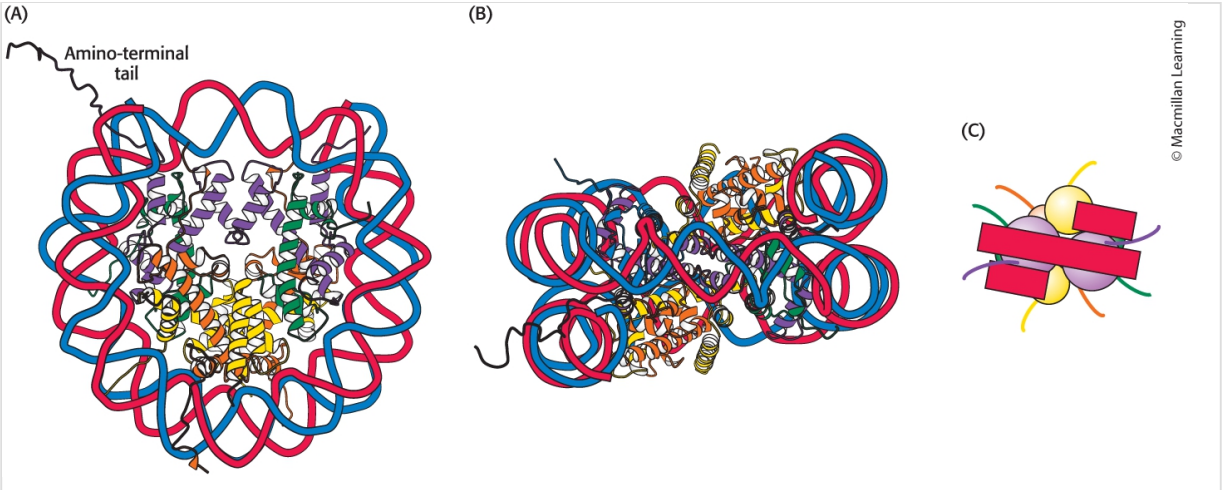


FIGURE 29.19 The structure of the nucleosome consists of eight histone proteins surrounded by DNA. (A) A view showing the DNA wrapping around the histone core. (B) A 90-degree rotation of the view in part A. The DNA forms a left-handed superhelix as it wraps around the core. (C) A schematic view.

[Drawn from 1AOI.pdb.]

The overall structure of the nucleosome was revealed through electron microscopic and x-ray crystallographic studies pioneered by Aaron Klug and his colleagues. More recently, the three-dimensional structures of reconstituted nucleosomes have been determined to higher resolution by x-ray diffraction methods. The histone octamer is a complex of four different types of histones (H2A, H2B, H3, and H4) that are homologous and similar in structure.

The eight histones in the core are arranged into a $(H3)_2(H4)_2$ tetramer and a pair of H2A–H2B dimers. The tetramer and dimers come together to form a left-handed superhelical ramp around which the DNA wraps. In addition, each histone has an amino-terminal tail that extends out from the core structure. These tails are flexible and contain many lysine and arginine residues. As we shall see in Chapter 31, covalent modifications of these tails play an essential role in regulating gene expression.

Three types of RNA polymerase synthesize RNA in eukaryotic cells

In bacteria, RNA is synthesized by a single kind of polymerase. In contrast, the nucleus of a typical eukaryotic cell contains three types of RNA polymerase differing in template specificity and location in the nucleus (Table 29.2). The three polymerases are named for the order in which they were discovered, which has no bearing on the relative importance of their function. We will discuss them in an order that reflects their similarities in localization, function, and regulation. We will emphasize RNA polymerase II, since it transcribes all of the protein-coding genes and has therefore been the focus of much research investigating transcriptional mechanisms.

TABLE 29.2 Eukaryotic RNA polymerases

Type	Location	Cellular transcripts	Effects of α-amanitin
I	Nucleolus	18S, 5.8S, and 28S rRNA	Insensitive
II	Nucleoplasm	mRNA precursors and snRNA	Strongly inhibited
III	Nucleoplasm	tRNA and 5S rRNA	Inhibited by high concentrations

RNA polymerase I is located in specialized structures within the nucleus called nucleoli, where it transcribes the tandem array of genes for 18S, 5.8S, and 28S rRNA. The other rRNA molecule (5S rRNA) and all the tRNA molecules are synthesized by *RNA polymerase III*, which is located in the nucleoplasm rather than in nucleoli. *RNA polymerase II*, which

also is located in the nucleoplasm, synthesizes the precursors of mRNA as well as several small RNA molecules, such as those of the splicing apparatus and many of the precursors to small regulatory RNAs. All three of the polymerases are large proteins, containing from 8 to 14 subunits and having total molecular masses greater than 500 kDa (or 0.5 MDa), and it is likely that they evolved from a single enzyme that was present in a common ancestor of eukaryotes, bacteria, and archaea. In fact, many components of the eukaryotic transcriptional machinery evolved from those in a common ancestor.

Although all eukaryotic RNA polymerases are homologous to one another and to prokaryotic RNA polymerases, RNA polymerase II contains a unique **carboxyl-terminal domain** (CTD) on the 220-kDa subunit; this domain is unusual because it contains multiple repeats of a YSPTSPS consensus sequence. The activity of RNA polymerase II is regulated by phosphorylation, mainly on the serine residues of the CTD.

The different polymerases were originally distinguished through their variable responses to the toxin α-amanitin, a cyclic octapeptide that contains several modified amino acids and is produced by a genus of poisonous mushroom (**Figure 29.20**). α-Amanitin binds very tightly ($K_d = 10$ nM) to RNA polymerase II and thereby blocks the elongation phase of RNA synthesis. Higher concentrations of α-amanitin (1 μM) inhibit RNA polymerase III, whereas RNA polymerase I is insensitive to this toxin. This pattern of sensitivity is highly conserved throughout the animal and plant kingdoms.



Tisha Razumovsky/Shutterstock

α-Amanitin

FIGURE 29.20 α-Amanitin is produced by poisonous mushrooms in the genus *Amanita*. Pictured is *Amanita phalloides*, also called the *death cap* or the *destroying angel*.

Finally, eukaryotic polymerases differ from each other in the promoters to which they bind. Eukaryotic genes, like prokaryotic genes, require promoters for transcription initiation. Like prokaryotic promoters, eukaryotic promoters consist of conserved sequences that attract the polymerase to the start site. However, eukaryotic promoters differ distinctly in sequence and position, depending on the type of RNA polymerase that binds to them (**Figure 29.21**).

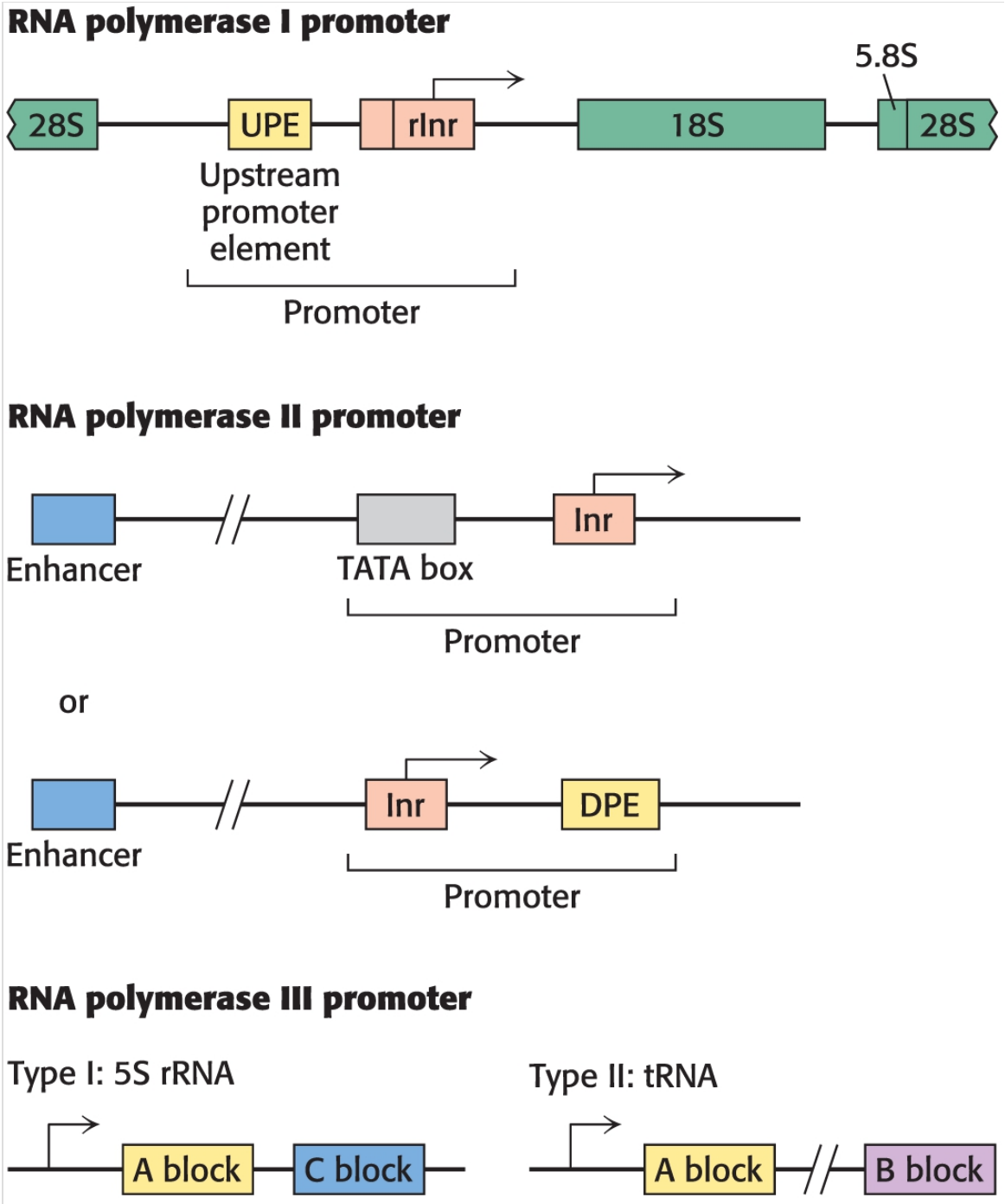


FIGURE 29.21 Eukaryotic promoters share common elements. Each eukaryotic RNA polymera recognizes a set of promoter elements — sequences in DNA that promote transcription. The RN polymerase I promoter consists of a ribosomal initiator (rInr) and an upstream promoter eleme (UPE). The RNA polymerase II promoter likewise includes an initiator element (Inr) and may als include either a TATA box or a downstream promoter element (DPE). Separate from the promot region, enhancer elements bind specific transcription factors. RNA polymerase III promoters consist of conserved sequences that lie within the transcribed genes.



- *The promoter sequences for RNA polymerase I are located in stretches of DNA separating the ribosomal DNA (rDNA) it transcribes.* These rRNA genes are arranged in several hundred tandem repeats, each containing a copy of each of three rRNA genes. At the transcriptional start site lies a TATA-like sequence called the *ribosomal initiator element* (rInr). Farther upstream, 150 to 200 bp from the start site, is the *upstream promoter element* (UPE). Both elements aid transcription by binding proteins that recruit RNA polymerase I.

- *Promoters for RNA polymerase II, like prokaryotic promoters, include a set of consensus sequences that define the start site and recruit the polymerase.* However, the promoter can contain any combination of a number of possible consensus sequences. Unique to eukaryotes, they also include enhancer elements that can be more than 1 kb from the start site.

- *Promoters for RNA polymerase III are within the transcribed sequence, downstream of the start site*. This is contrast to promoters for RNA polymerase I and II, which are *upstream* of the transcription start site. There are two types of intergenic promoters for RNA polymerase III. Type I promoters, found in the 5S rRNA gene, contain two short, conserved sequences, the A block and the C block. Type II promoters, found in tRNA genes, consist of two 11-bp sequences, the A block and the B block, situated about 15 bp from either end of the gene.

Three common elements can be found in the RNA polymerase II promoter region

RNA polymerase II transcribes all of the protein-coding genes in eukaryotic cells. Promoters for RNA polymerase II, like those for bacterial polymerases, are generally located upstream of the start site for transcription. Because these sequences are on the *same* molecule of DNA as the genes being transcribed, they are called *cis-acting elements*.

1. The most commonly recognized cis-acting element for genes transcribed by RNA polymerase II is called the **TATA box** on the basis of its consensus sequence (**Figure 29.22**). The TATA box is usually found between positions -30 and -100. Note that the eukaryotic TATA box closely resembles the prokaryotic -10 sequence (TATAAT) but is farther from the start site. The mutation of a single base in the TATA box markedly impairs promoter activity. Thus, the precise sequence, not just a high content of AT pairs, is essential.



FIGURE 29.22 The sequence of the TATA box is highly conserved.
Comparisons of the sequences of more than 100 eukaryotic promoters led to the consensus sequence shown. The subscripts denote the frequency (%) of the base at that position.

2. The TATA box is often paired with an *initiator element* (Inr), a sequence found at the transcriptional start site, between positions -3 and $+5$. This sequence defines the start site because the other

promoter elements are at variable distances from that site. Its presence increases transcriptional activity.

3. A third element, the *downstream core promoter element* (DPE), is commonly found in conjunction with the Inr in transcripts that lack the TATA box. In contrast with the TATA box, the DPE is found downstream of the start site, between positions $+28$ and $+32$.

Regulatory cis-acting elements are recognized by different mechanisms

Additional regulatory sequences are located between -40 and -150. Many promoters contain a *CAAT box*, and some contain a *GC box* (**Figure 29.23**). Constitutive genes (genes that are continuously expressed rather than regulated) tend to have GC boxes in their promoters. The positions of these upstream sequences vary from one promoter to another, in contrast with the quite constant location of the -35 region in prokaryotes. Another difference is that the CAAT box and the GC box can be effective when present on the template (antisense) strand, unlike the -35 region, which must be present on the coding (sense) strand.

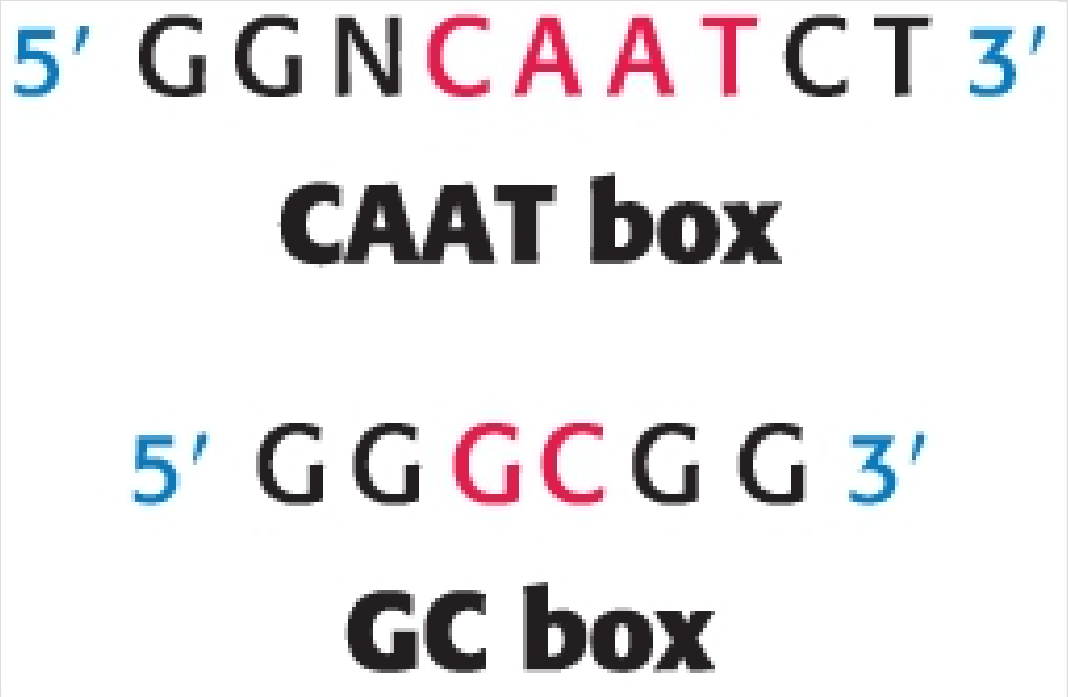


FIGURE 29.23 The sequences of the CAAT box and GC box are also highly conserved. Consensus sequences are shown for the CAAT and GC boxes of eukaryotic promoters for mRNA precursors.

These differences between prokaryotes and eukaryotes correspond to fundamentally different mechanisms for the recognition of cis-acting elements. The -10 and -35 sequences in prokaryotic promoters are binding sites for RNA polymerase and its associated σ factor. In contrast, the TATA, CAAT, and GC boxes and other cis-acting elements in eukaryotic promoters are recognized by proteins other than RNA polymerase itself.

The TFIID protein complex initiates the assembly of the active transcription complex in eukaryotes

Cis-acting elements constitute only part of the puzzle of eukaryotic gene expression. **Transcription factors** that bind to these elements also are required. For example, RNA polymerase II is guided to the start site by a set of transcription factors known collectively as *TFII* (*TF* stands for transcription factor, and *II* refers to RNA polymerase II). Individual TFII factors are called TFIIA, TFIIB, and so on.

In TATA-box promoters, the key initial event is the recognition of the TATA box by the TATA-box-binding protein (TBP), a 30-kDa component of the 700-kDa TFIID complex. In TATA-less promoters, other proteins in the TFIID complex bind the core promoter elements; however, because less is known about these interactions, we will consider only the TATA-box–TBP binding interaction. TBP binds 10^5 times as tightly to the TATA box as to nonconsensus sequences; the dissociation constant of the TBP–TATA-box complex is approximately 1 nM.

The TATA box of DNA binds to the concave surface of TBP, inducing large conformational changes in the bound DNA (**Figure 29.24**). The double helix is substantially unwound to widen its minor groove, enabling it to make extensive contact with the antiparallel β strands on the concave side of TBP. Hydrophobic interactions are prominent at this interface. Four phenylalanine residues, for example, are intercalated between base pairs of the TATA box. The flexibility of AT-rich sequences is generally exploited here in bending the DNA. Immediately outside the TATA box, classical B-DNA resumes. The TBP–TATA-box complex is distinctly asymmetric, a property that is crucial for specifying a unique start site and ensuring that transcription proceeds unidirectionally.

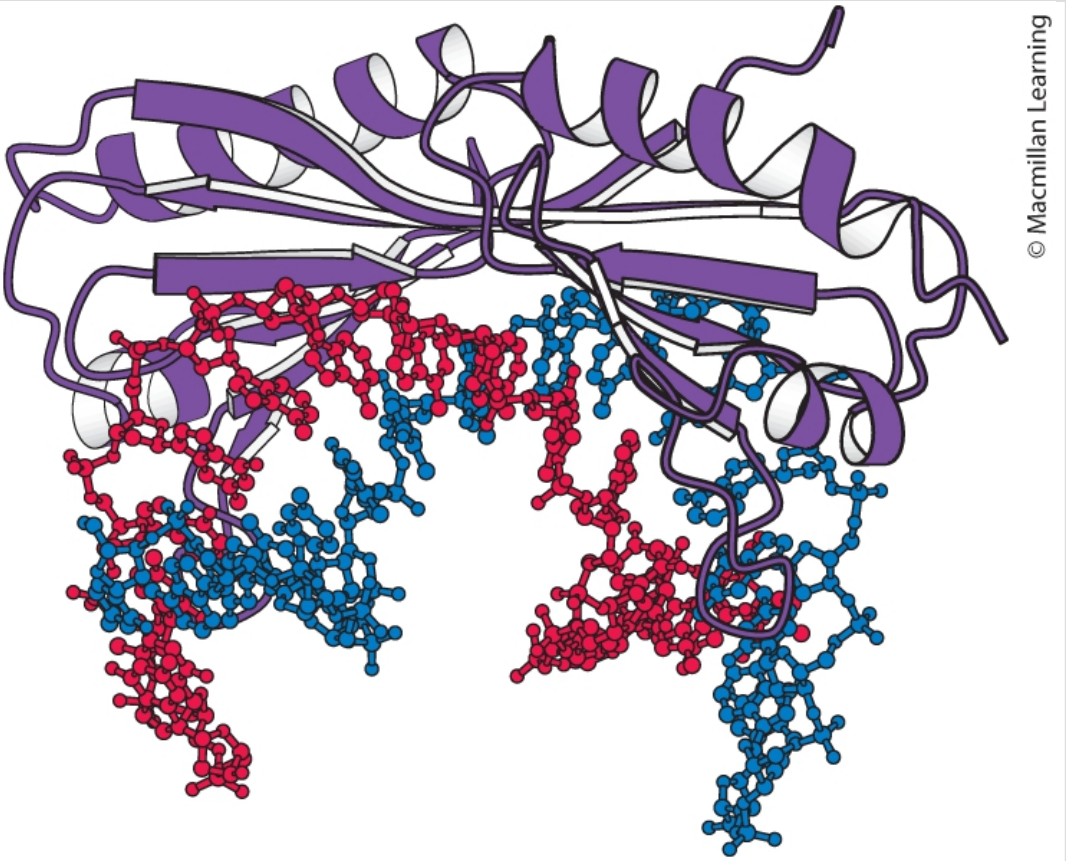


FIGURE 29.24 The TATA-box-binding protein binds to DNA. TBP is a saddle-shaped protein consisting of two similar domains. The saddle-like structure of the protein sits atop a DNA fragment, which is significantly unwound and bent.

[Drawn from 1CDW.pdb.]

INTERACT with this model in Achieve

TBP bound to the TATA box is the heart of the initiation complex (Figure 29.25). The surface of the TBP saddle provides docking sites for the binding of other components, with additional transcription factors assembling on this nucleus in a defined sequence. TFIIA is recruited, followed by TFIIB; then TFIIF, RNA polymerase II, TFIIE, and TFIIH join the other factors to form a complex called the *pre-initiation complex* (PIC).

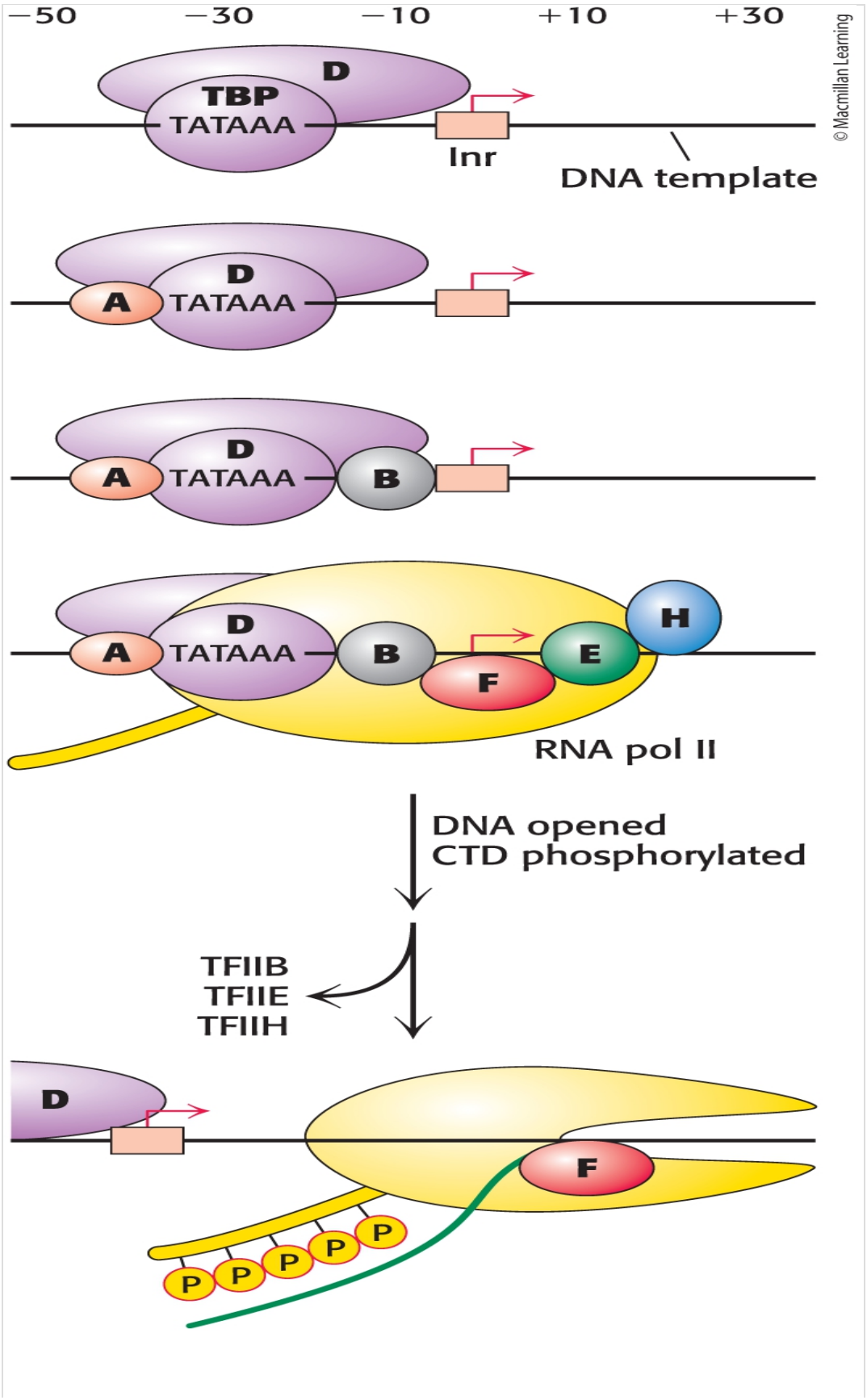

−50
−30
−10
+10
+30
D
TBP
TATAAA
Inr
DNA template
D
A
TATAAA
D
A
TATAAA
B
D
A
TATAAA
B
F
E
H
RNA pol II
DNA opened
CTD phosphorylated
TFIIB
TFIIE
TFIIH
D
F
P
P
P
P
P
P
© Macmillan Learning

FIGURE 29.25 General transcription factors are essential in initiating transcription by RNA polymerase II. The step-by-step assembly of these general transcription factors begins with the binding of TFIID (purple) to the TATA box. [The TATA-box-binding protein (TBP), a component of TFIID, recognizes the TATA box.] After assembly, TFIIH opens the DNA double helix and phosphorylates the carboxyl-terminal domain (CTD), allowing the polymerase to leave the promoter and begin transcription. The red arrow marks the transcription start site.



These additional transcription factors play specific roles in this complex. As we saw above, TFIID recognizes core promoter elements and is central to the assembly process. While TFIIA is not essential for the assembly or function of the PIC in vitro, it may aid in the binding of TFIID to the DNA. TFIIB is a DNA-binding protein that recognizes specific cis-acting promoter elements called *B recognition elements*, which are often found near the TATA box. TFIIF aids in the recruitment of polymerase II, while TFIIE brings TFIIH to the complex. TFIIH is a multisubunit complex with helicase and protein kinase activities, both of which are critical in the initiation of transcription. The helicase activity unwinds the DNA template, and the kinase activity phosphorylates specific amino acids in the CTD of polymerase II.

During the formation of the PIC, the carboxyl-terminal domain (CTD) is unphosphorylated and plays a role in transcription regulation through its binding to an enhancer-associated complex called *mediator* (Section 31.4). Phosphorylation of the CTD by TFIIH marks the transition from initiation to elongation. The phosphorylated CTD stabilizes transcription elongation by RNA polymerase II and recruits RNA-processing enzymes that act during the course of elongation. The importance of the carboxyl-terminal domain is highlighted by the finding that yeast cells containing mutant polymerase II with fewer than 10 repeats in the CTD are not viable.

The PIC described above initiates transcription at a low (basal) frequency, and the transcription factors associated with it are referred

to as *basal* or *general* transcription factors. Additional transcription factors that bind to other sites are required to achieve a high rate of mRNA synthesis. Their role is to selectively stimulate *specific* genes. In summary, transcription factors and other proteins that bind to regulatory sites on DNA can be regarded as passwords that cooperatively open multiple locks, giving RNA polymerase access to specific genes.

Self-Check Question



The function of the σ subunit of *E. coli* RNA polymerase is analogous to the function of general transcription factors in eukaryotes. Briefly describe their common function.

Enhancer sequences can stimulate transcription at start sites thousands of bases away

The activities of many promoters in higher eukaryotes are greatly increased by another type of cis-acting element called an **enhancer**.

- Enhancer sequences have no promoter activity of their own yet can exert their stimulatory actions over distances of several thousand base pairs.
- Enhancers can be upstream, downstream, or even in the middle of a transcribed gene.
- Enhancers are effective when present on either the coding or noncoding DNA strand.

- A particular enhancer is effective only in certain cells; for example, the immunoglobulin enhancer functions in B lymphocytes but not elsewhere.

 Cancer can result if the relation between genes and enhancers is disrupted. In Burkitt lymphoma and B-cell leukemia, a chromosomal translocation brings the proto-oncogene *myc* (a transcription factor itself) under the control of a powerful immunoglobulin enhancer. The consequent dysregulation of the *myc* gene is hypothesized to play a role in the progression of the cancer.

The discovery of promoters and enhancers has allowed us to gain a better understanding of how genes are selectively expressed in eukaryotic cells. The regulation of eukaryotic gene transcription, discussed in Chapter 31, is the fundamental means of controlling gene expression.

29.4 Some RNA Transcription Products Are Processed

Virtually all the initial products of eukaryotic transcription are further processed, and even some prokaryotic transcripts are modified. As we will see next, the particular processing steps and the factors taking part vary according to the type of RNA precursor and the type of RNA polymerase that produced it.

Precursors of transfer and ribosomal RNA are cleaved and chemically modified after transcription

In bacteria, messenger RNA molecules undergo little or no modification after synthesis by RNA polymerase. Indeed, many mRNA molecules are translated while they are being transcribed. In contrast, transfer RNA (tRNA) and ribosomal RNA (rRNA) molecules are generated by modifications of nascent RNA chains.

- *The transcript can be cleaved at specific sites along its sequence.* For example, in *E. coli*, the three rRNAs and a tRNA are excised from a single primary RNA transcript that also contains spacer regions (**Figure 29.26**). Other transcripts contain arrays of several kinds of tRNA or several copies of the same tRNA. The nucleases that cleave and trim these precursors of rRNA and tRNA are highly precise. *Ribonuclease P* (RNase P), for example, generates the correct $5'$ terminus of all tRNA molecules in *E. coli.* Sidney Altman and his coworkers showed that this interesting enzyme contains a catalytically active RNA molecule. *Ribonuclease III* (Rnase III) excises 5S, 16S, and 23S rRNA precursors from the primary

transcript by cleaving double-helical hairpin regions at specific sites.

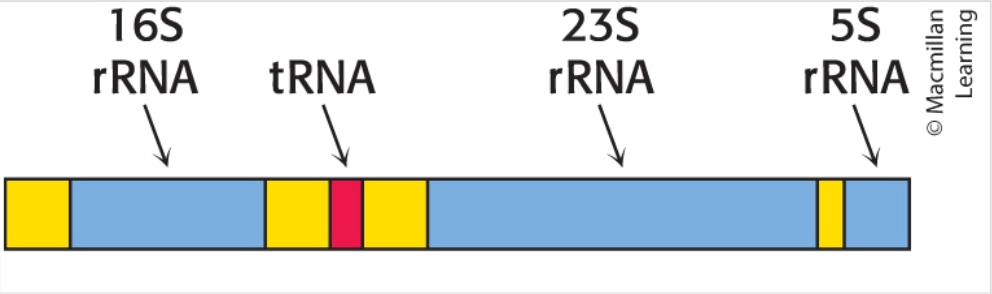
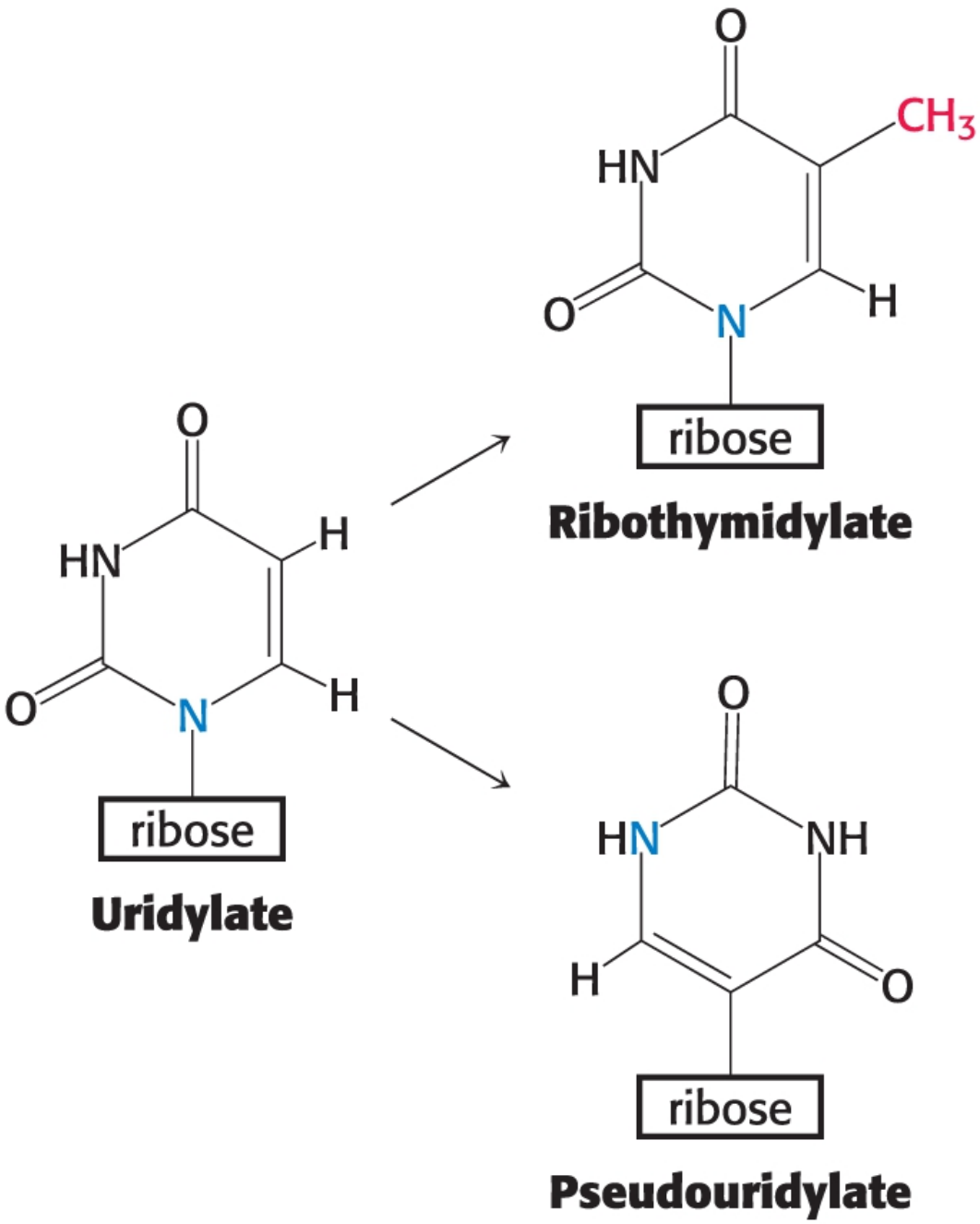


FIGURE 29.26 Cleavage of a primary RNA transcript in *E. coli* produces 5S, 16S, and 23S rRNA molecules and a tRNA molecule. Spacer regions are shown in yellow.

- *Nucleotides can be added to the termini of some RNA chains.* For example, CCA, a terminal sequence required for the function of all tRNAs, is added to the $3'$ ends of tRNA molecules for which this terminal sequence is not encoded in the DNA. The enzyme that catalyzes the addition of CCA is atypical for an RNA polymerase in that it does not use a DNA template.

- *Bases and ribose units of RNAs can be modified.* For example, some bases of rRNA are methylated. Furthermore, all tRNA molecules contain unusual bases formed by the enzymatic modification of a standard ribonucleotide in a tRNA precursor. For example, uridylate residues are modified after transcription to form ribothymidylate and pseudouridylate. These modifications generate diversity, allowing greater structural and functional versatility.


O
HN
CH3
O
N
H
ribose
Ribothymidylate
O
HN
H
O
N
H
ribose
Uridylate
O
HN
NH
H
O
ribose
Pseudouridylate

RNA polymerase I produces three ribosomal RNAs

Several RNA molecules are key components of ribosomes. In eukaryotes, RNA polymerase I transcription produces a single precursor (45S in mammals) that encodes three RNA components of the ribosome: the 18S rRNA, the 28S rRNA, and the 5.8S rRNA (Figure 29.27).

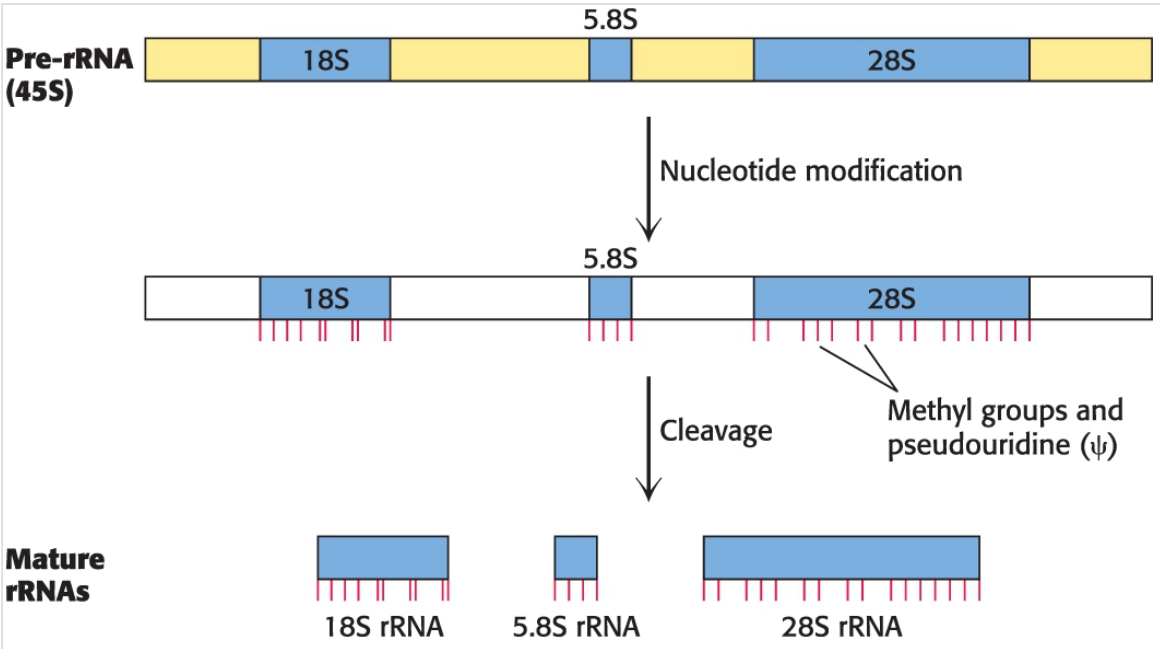


FIGURE 29.27 The processing of eukaryotic pre-rRNA produces mature rRNAs. The mammalia pre-rRNA transcript contains the RNA sequences destined to become the 18S, 5.8S, and 28S rRNAs of the small and large ribosomal subunits. First, nucleotides are modified: small nucleola ribonucleoproteins methylate specific nucleoside groups and convert selected uridines into pseudouridines (indicated by red lines). Next, the pre-rRNA is cleaved and packaged to form mature ribosomes, in a highly regulated process in which more than 200 proteins take part.

The 18S rRNA is the RNA component of the small ribosomal subunit (40S), and the 28S and 5.8S rRNAs are two RNA components of the large ribosomal subunit (60S). The other RNA component of the large

ribosomal subunit, the 5S rRNA, is transcribed by RNA polymerase III as a separate transcript. Processing of the precursor proceeds as follows:

- First, the nucleotides of the pre-rRNA sequences destined for the ribosome undergo extensive modification, on both ribose and base components, directed by many **small nucleolar ribonucleoproteins (snoRNPs)**, each of which consists of one snoRNA and several proteins.
- The pre-rRNA is then assembled with ribosomal proteins, as guided by processing factors, to form a large ribonucleoprotein. For instance, the small-subunit (SSU) processome is required for 18S rRNA synthesis and can be visualized in electron micrographs as a terminal knob at the $5'$ ends of the nascent rRNAs (**Figure 29.28**).

Reprinted by permission from Macmillan Publishers Ltd, from Dragon, F., Gallagher, J., Compagnone-Post, P. et al. A large nucleolar U3 ribonucleoprotein required for 18S ribosomal RNA biogenesis. Nature 417, 967–970 (2002); permission conveyed through Copyright Clearance Center, ltd.

FIGURE 29.28 Electron microscopy gives a window into rRNA transcription and processing in eukaryotes. The assemblies of transcribed rRNA into precursor ribosomes resemble fir trees: the trunk is the rDNA, and each branch is a pre-rRNA transcript. Transcription starts at the top of the tree, where the shortest transcripts can be seen, and progresses down the rDNA to the end of the gene. The terminal knobs visible at the end of some pre-rRNA transcripts likely correspond to the SSU processome, a large ribonucleoprotein required for processing the pre-rRNA.



- Finally, rRNA cleavage (sometimes coupled with additional processing steps) releases the mature rRNAs assembled with ribosomal proteins as ribosomes. Like those of RNA polymerase I transcription itself, most of these processing steps take place in the cell's nucleolus.

RNA polymerase III produces transfer RNAs

Eukaryotic tRNA transcripts are among the most processed of all RNA polymerase III transcripts. Like those of prokaryotic tRNAs, the $5'$ leader is cleaved by RNase P, the $3'$ trailer is removed, and CCA is added by the CCA-adding enzyme (Figure 29.29). Eukaryotic tRNAs are also heavily modified on base and ribose moieties; these modifications are important for function. In contrast with prokaryotic tRNAs, many eukaryotic pre-tRNAs are also spliced by an endonuclease and a ligase to remove an intron.

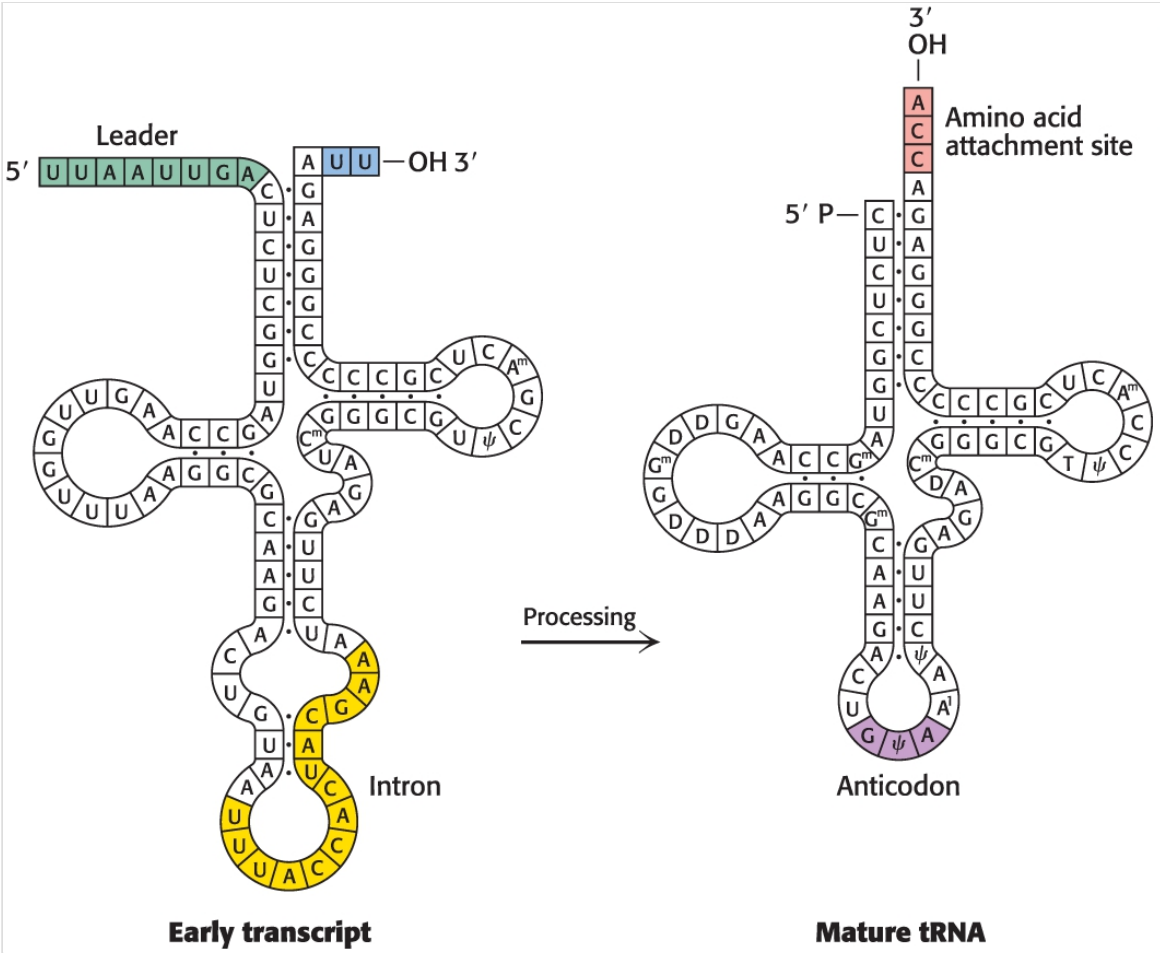


FIGURE 29.29 Transfer RNA precursors are processed. The conversion of a yeast tRNA precurso into a mature tRNA requires the removal of a 14-nucleotide intron (yellow), the cleavage of a 5′ leader (green), and the removal of UU and the attachment of CCA at the 3′ end (red). In additio several bases are modified.

The product of RNA polymerase II, the pre-mRNA transcript, acquires a 5′ cap and a 3′

poly(A) tail

Perhaps the most extensively studied transcription product is the product of RNA polymerase II: most of this RNA will be processed to mRNA. The immediate product of RNA polymerase II is sometimes referred to as precursor-to-messenger RNA, or **pre-mRNA**. Most pre-mRNA molecules are spliced to remove the introns, which we will discuss in greater detail below. In addition, both the $5'$ and the $3'$ ends are modified, and both modifications are retained as the pre-mRNA is converted into mRNA.

As in prokaryotes, eukaryotic transcription usually begins with A or G. However, the $5'$ triphosphate end of the nascent RNA chain is immediately modified:

- First, a phosphoryl group is released by hydrolysis.
- The diphosphate $5'$ end then attacks the α-phosphorus atom of GTP to form a very unusual $5'-5'$ triphosphate linkage. This distinctive terminus is called a **$5'$ cap** (**Figure 29.30**).

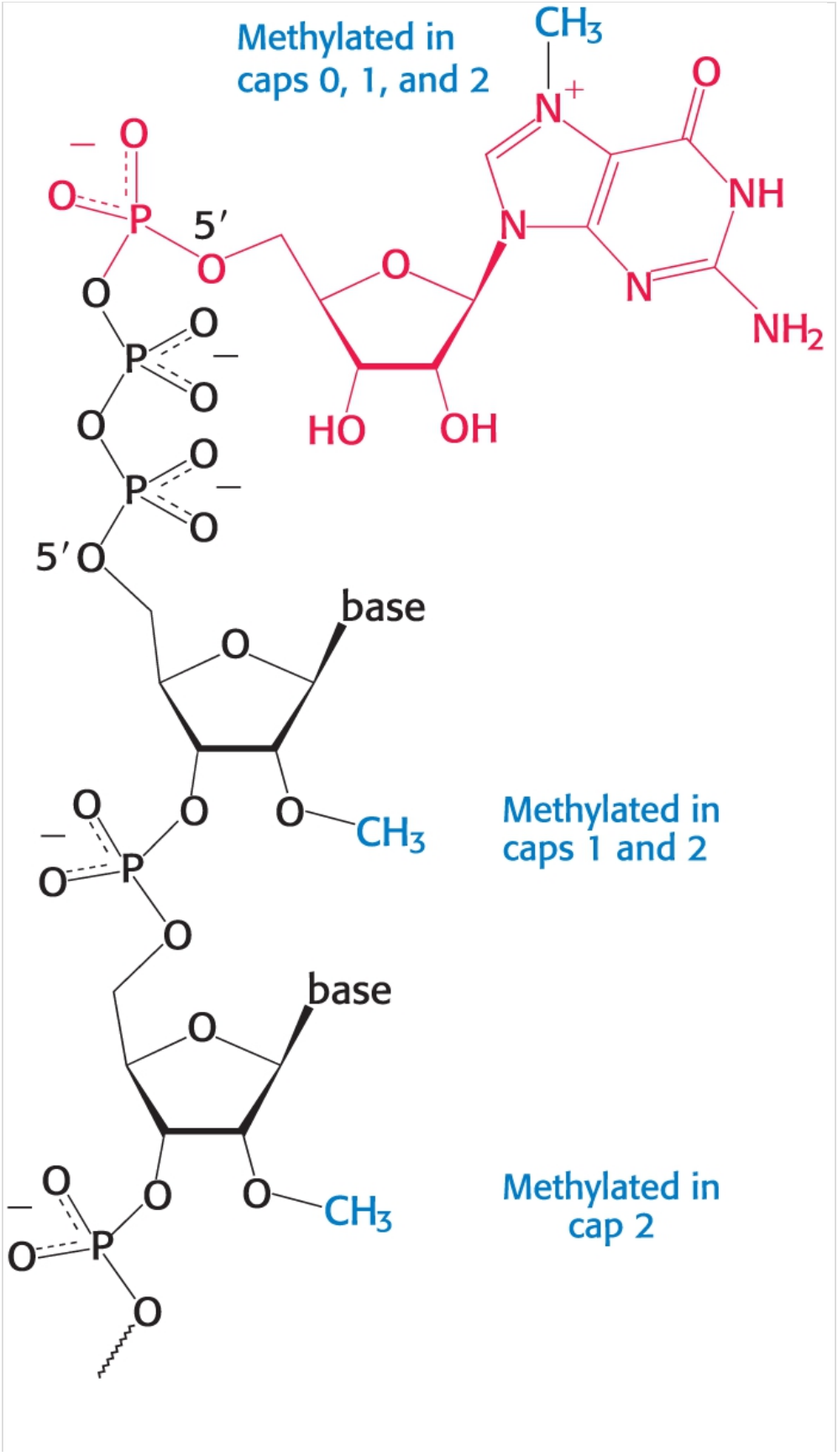

Methylated in caps 0, 1, and 2
CH3
N+
O
NH
N
N
NH2
O
5′
O
HO
OH
5′ O
base
O
O
CH3
Methylated in caps 1 and 2
base
O
O
CH3
Methylated in cap 2

FIGURE 29.30 The 5′ ends of eukaryotic mRNAs are capped. Caps at the 5′ end of eukaryotic mRNA include 7-methylguanylate (red) attached by a triphosphate linkage to the ribose at the 5′ end. None of the riboses are methylated in cap 0, one is methylated in cap 1, and both are methylated in cap 2.

- The N-7 nitrogen of the terminal guanine is then methylated by *S*-adenosylmethionine to form cap 0. The adjacent riboses may be methylated to form cap 1 or cap 2.

Caps contribute to the stability of mRNAs by protecting their 5′ ends from phosphatases and nucleases. In addition, caps enhance the translation of mRNA by eukaryotic protein-synthesizing systems. Transfer RNA and ribosomal RNA molecules, in contrast with messenger RNAs and with small RNAs that participate in splicing, do not have caps.

As mentioned earlier, pre-mRNA is also modified at the 3′ end. Most eukaryotic mRNAs contain a string of adenine nucleotides — a **poly(A) tail** — at that end. This poly(A) tail is added *after* transcription has ended, since the DNA template does not encode this sequence. Indeed, the nucleotide preceding poly(A) is not the last nucleotide to be transcribed. Some primary transcripts contain hundreds of nucleotides beyond the 3′ end of the mature mRNA.

How is the 3′ end of the pre-mRNA given its final form? Eukaryotic primary transcripts are cleaved by a specific endonuclease that recognizes the sequence AAUAAA (**Figure 29.31**). Cleavage does not take

place if this sequence or a segment of some 20 nucleotides on its 3′ side is deleted. The presence of internal AAUAAA sequences in some mature mRNAs indicates that AAUAAA is only part of the cleavage signal; its context also is important. After cleavage of the pre-RNA by the endonuclease, a *poly(A) polymerase* adds about 250 adenylate residues to the 3′ end of the transcript; ATP is the donor in this reaction.

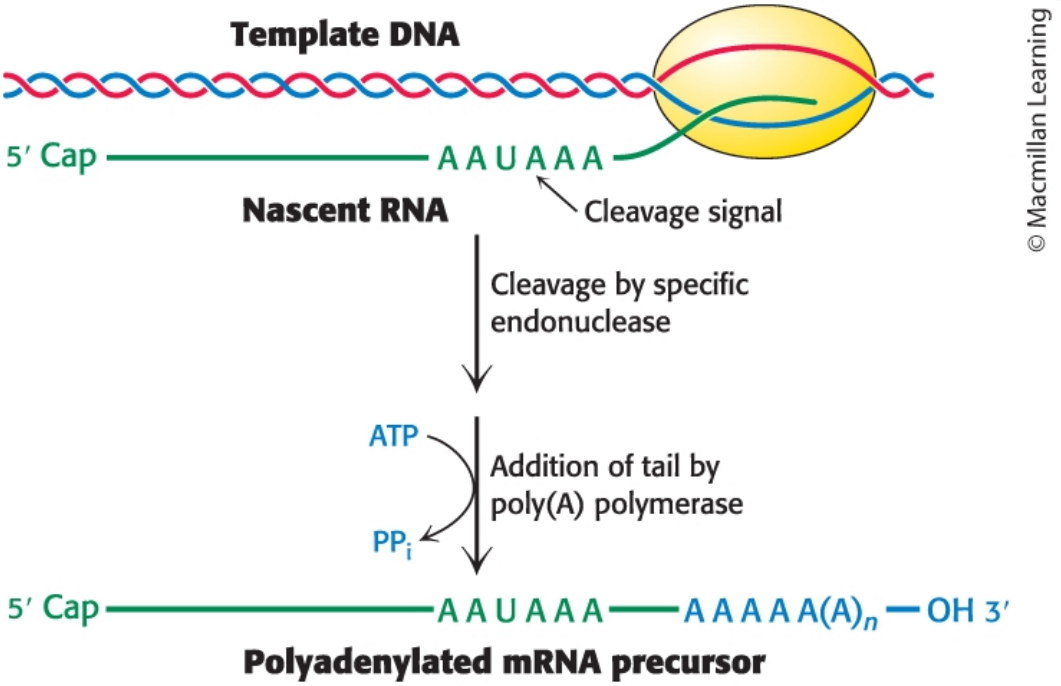


FIGURE 29.31 Primary transcripts in eukaryotes are polyadenylated. A specific endonuclease cleaves the RNA downstream of AAUAAA. Poly(A) polymerase then adds about 250 adenylate residues.

The role of the poly(A) tail is still not firmly established despite much effort. However, evidence is accumulating that it enhances translation efficiency and the stability of mRNA. Blocking the synthesis of the poly(A) tail by exposure to 3′-deoxyadenosine (cordycepin) does not interfere with the synthesis of the primary transcript. Messenger RNA

without a poly(A) tail can be transported out of the nucleus. However, an mRNA molecule without a poly(A) tail is usually much less effective as a template for protein synthesis than one with a poly(A) tail. Indeed, some mRNAs are stored in an unadenylated form and receive the poly(A) tail only when translation is imminent. The half-life of an mRNA molecule may be determined in part by the rate of degradation of its poly(A) tail.

Sequences at the ends of introns specify splice sites in mRNA precursors

Most genes in higher eukaryotes are composed of exons and introns (Section 8.7). The introns must be excised and the exons linked to form the final mRNA in a process called **RNA splicing**. This splicing must be exquisitely sensitive; splicing just one nucleotide upstream or downstream of the intended site would create a one-nucleotide shift, which would alter the reading frame on the $3'$ side of the splice to give an entirely different amino acid sequence, likely including a premature stop codon. Thus, the correct splice site must be clearly marked.

Does a particular sequence denote the splice site? The sequences of thousands of intron–exon junctions within RNA transcripts are known. In eukaryotes from yeast to mammals, these sequences have a common structural motif: the intron begins with GU and ends with AG. The consensus sequence at the $5'$ splice in vertebrates is AGGUAAGU, where the GU is invariant (**Figure 29.32**). At the $3'$ end of an intron, the consensus sequence is a stretch of 10 pyrimidines (U or C; termed the *polypyrimidine tract*), followed by any base, then by C, and ending with the invariant AG. Introns also have an important internal site located between 20 and 50 nucleotides upstream of the $3'$ splice site; it is called

the *branch site* for reasons that will be evident shortly. In yeast, the branch-site sequence is nearly always UACUAAC, whereas in mammals a variety of sequences are found.

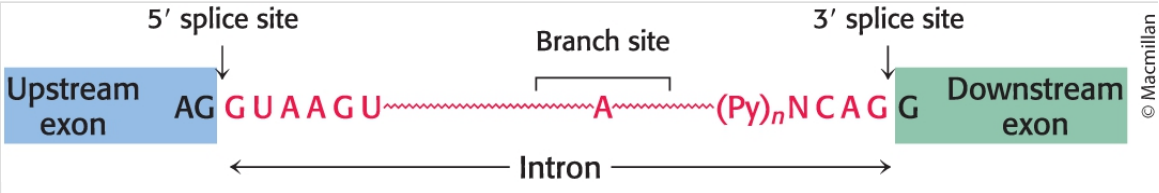


FIGURE 29.32 Splice sites are identified by conserved sequences. Consensus sequences for th 5′ splice site and the 3′ splice site are shown. Py stands for pyrimidine.

The 5′ and 3′ splice sites and the branch site are essential for determining where splicing takes place. Mutations in each of these three critical regions lead to aberrant splicing. Introns vary in length from 50 to 10,000 nucleotides, and so the splicing machinery may have to find the 3′ site several thousand nucleotides away. Specific sequences near the splice sites (in both the introns and the exons) play an important role in splicing regulation, particularly in designating splice sites when there are many alternatives. Researchers are currently attempting to determine the factors that contribute to splice-site selection for individual mRNAs. Despite our knowledge of splice-site sequences, predicting pre-mRNAs and their protein products from genomic DNA sequence information remains a challenge.

Splicing consists of two sequential transesterification reactions

The splicing of nascent mRNA molecules is a complicated process. It requires the cooperation of several small RNAs and proteins that form a large complex called a **spliceosome**. However, the chemistry of the splicing process is simple. Splicing begins with the cleavage of the phosphodiester bond between the upstream exon (exon 1) and the $5'$ end of the intron (**Figure 29.33**). The attacking group in this reaction is the $2'\text{–OH}$ group of an adenylate residue in the branch site. A $2'\text{–}5'$ phosphodiester bond is formed between this A residue and the $5'$ terminal phosphate of the intron in a transesterification reaction.



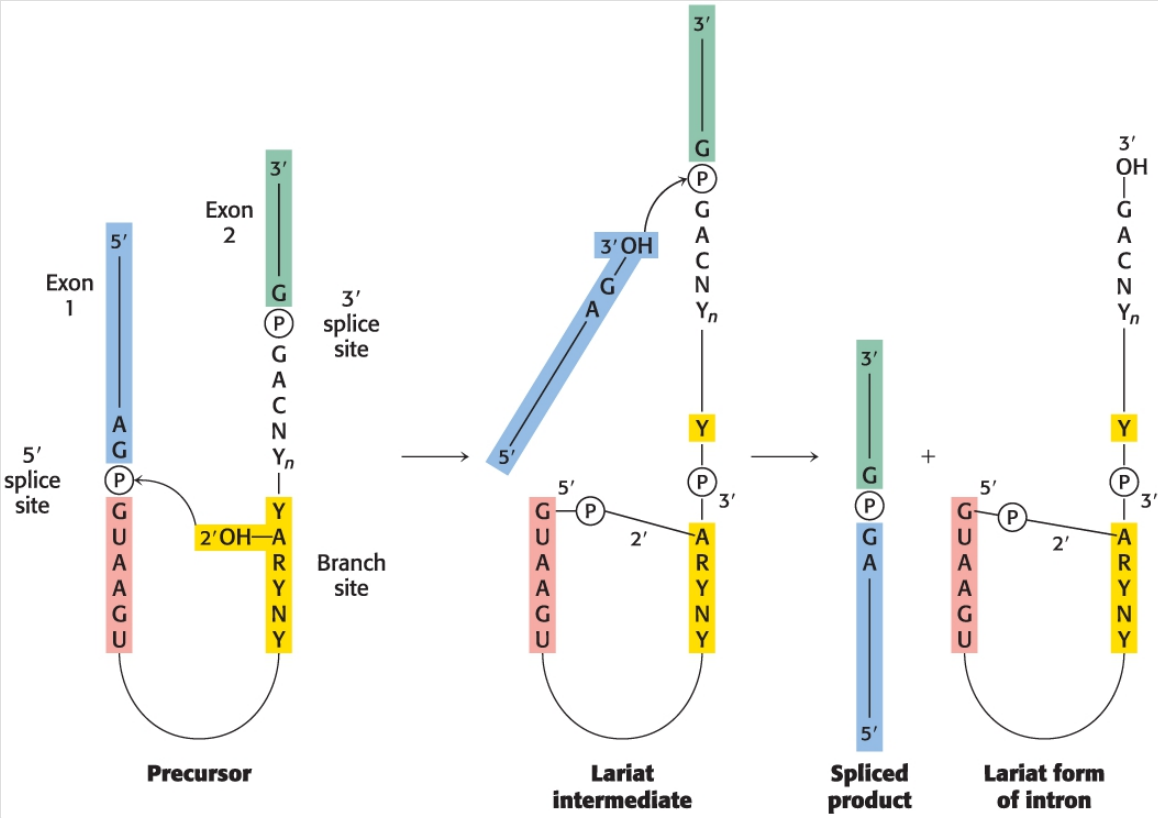


FIGURE 29.33 The splicing mechanism for mRNA precursors involves a lariat intermediate. Th upstream $(5')$ exon is shown in blue, the downstream $(3')$ exon in green, and the branch site i yellow. Y stands for a pyrimidine nucleotide, R for a purine nucleotide, and N for any nucleotide The $5'$ splice site is attacked by the $2'-OH$ group of the branch-site adenosine residue. The $3'$ splice site is attacked by the newly formed $3'-OH$ group of the upstream exon. The exons are joined, and the intron is released in the form of a lariat.

[Information from P. A. Sharp, *Cell* 42:397–408, 1985.]

Note that this adenylate residue is also joined to two other nucleotides by normal $3'-5'$ phosphodiester bonds (Figure 29.34). Hence, a branch is generated at this site, and a lariat (loop) intermediate is formed.

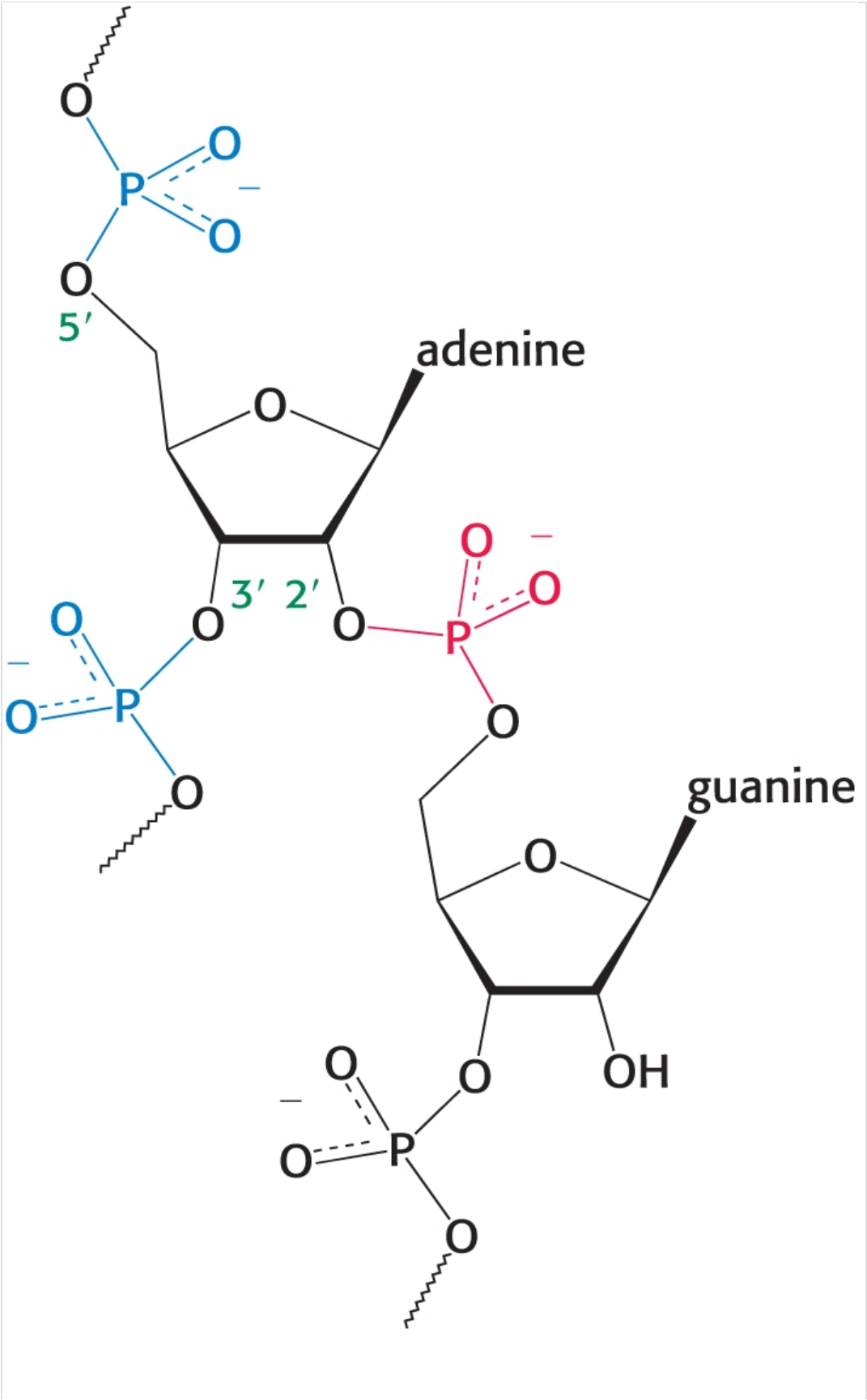

adenine
guanine
5′
3′
2′
OH

FIGURE 29.34 The splicing branch point has a unique structure. The structure of the branch point in the lariat intermediate in which the adenylate residue is joined to three nucleotides by phosphodiester bonds. The new $2'$-to-$5'$ linkage is shown in red, and the usual $3'$-to-$5'$ linkages are shown in blue.



The $3'-OH$ terminus of exon 1 then attacks the phosphodiester bond between the intron and exon 2. In another transesterification reaction, exons 1 and 2 become joined, and the intron is released in lariat form. Splicing is thus accomplished by two transesterification reactions rather than by hydrolysis followed by ligation.

Both transesterification reactions are promoted by the pair of bound magnesium ions, in reactions reminiscent of those for DNA and RNA polymerases. The first reaction generates a free $3'-OH$ group at the $3'$ end of exon 1, and the second reaction links this group to the $5'$-phosphate of exon 2. The number of phosphodiester bonds stays the same during these steps, which is crucial because it allows the splicing reaction itself to proceed without an energy source such as ATP or GTP.

Small nuclear RNAs in spliceosomes catalyze the splicing of mRNA precursors

The nucleus contains many types of small RNA molecules with fewer than 300 nucleotides, referred to as **small nuclear RNAs (snRNAs)**. A few of them — designated U1, U2, U4, U5, and U6 — are essential for splicing mRNA precursors. The secondary structures of these RNAs are highly conserved in organisms ranging from yeast to human beings.

snRNA molecules are associated with specific proteins to form complexes termed **small nuclear ribonucleoproteins (snRNPs)**; investigators often speak of them as "snurps" (**Table 29.3**). SnRNPs and their role in RNA splicing were discovered by Joan Steitz and Michael Lerner in 1980. One major piece of evidence suggesting a role for snRNPs in splicing was the base complementarity between portions of the U1 snRNA and the splice sites found in the unprocessed mRNAs.

TABLE 29.3 Roles of small nuclear ribonucleoproteins (snRNPs) in the splicing of mRNA precursors

snRNP	Size of snRNA (nucleotides)	Role
U1	165	Binds the 5′ splice site
U2	185	Binds the branch site
U5	116	Binds the 5′ splice site and then the 3′ splice site
U4	145	Masks the catalytic activity of U6
U6	106	Catalyzes splicing

SnRNPs associate with hundreds of other proteins (called *splicing factors*) and the mRNA precursors to form the large (60S) spliceosomes. The large and dynamic nature of the spliceosome made the determination of the detailed three-dimensional structure a great challenge. However, with the maturation of cryo-electron microscopy (Section 4.5), the structures of spliceosomes from several species in a number of different stages of their function have been determined (**Figure 29.35**). These structures have added to our understanding of the splicing process (**Figure 29.36**).



FIGURE 29.35 The spliceosome consists of proteins and RNAs. This three-dimensional structur displays one form of the spliceosome from a yeast determined by high-resolution cryo-electron microscopy. The key RNA components U2, U5, and U6 are shown in red, yellow, and blue, respectively.

[Drawn from 3JB9.pdb.]

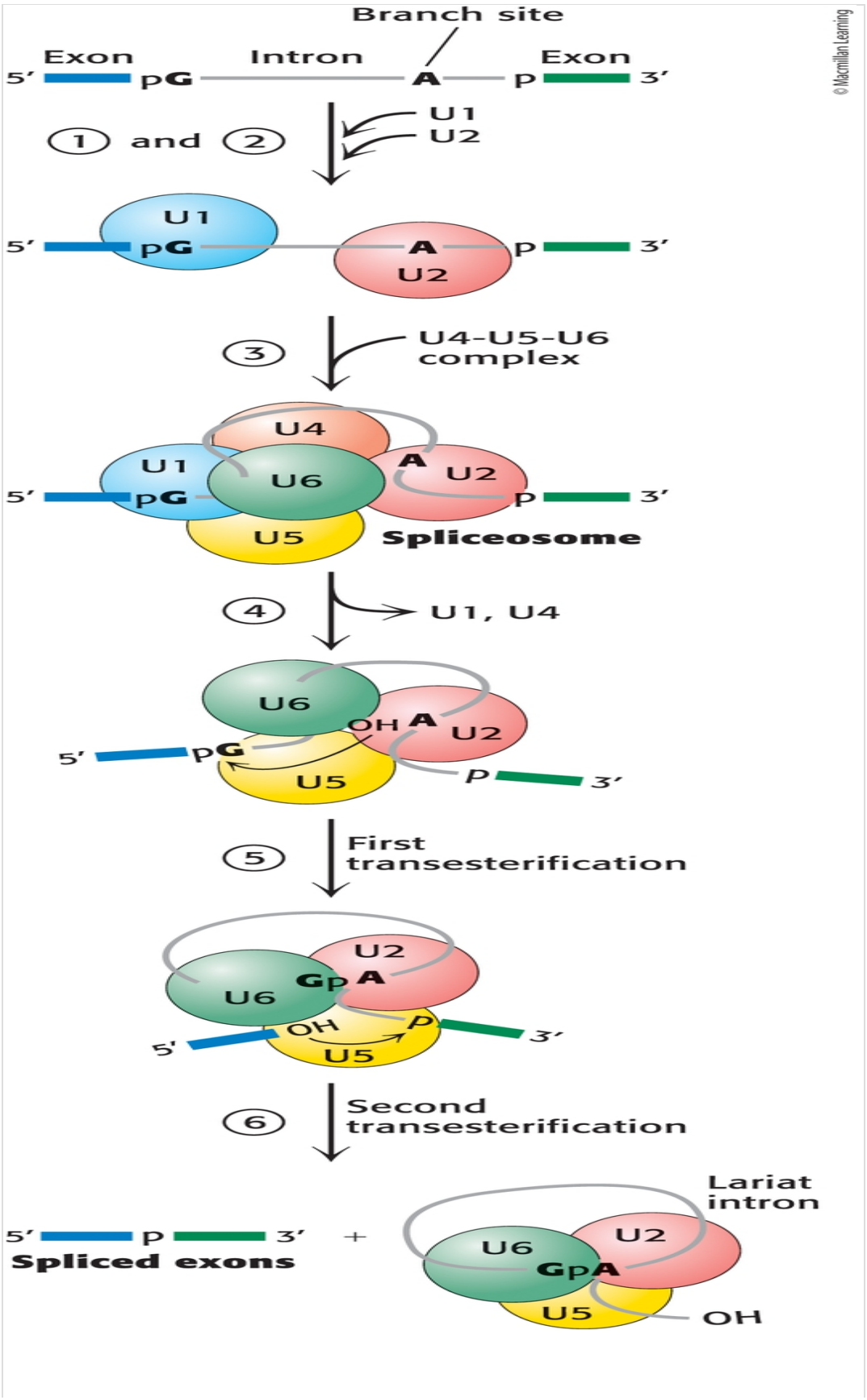
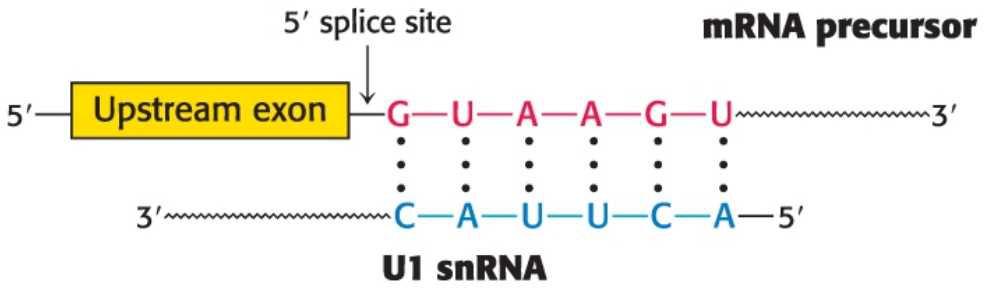

Branch site
Exon
Intron
Exon
5′
pG
A
p
3′
1 and 2
U1
U2
U1
pG
A
U2
3
U4–U5–U6
complex
U4
U1
U6
A
U2
U5
Spliceosome
4
U1, U4
U6
OH
A
U2
pG
U5
p
3′
5
First
transesterification
U2
Gp
A
U6
OH
p
3′
U5
6
Second
transesterification
Lariat
intron
Spliced exons
U6
U2
GpA
U5
OH
© Macmillan Learning

FIGURE 29.36 The spliceosome promotes the splicing of some genes. (1) U1 binds the 5′ splice site and (2) U2 binds to the branch point. (3) A preformed U4-U5-U6 complex then joins the assembly to form the complete spliceosome. (4) The U6 snRNA re-folds and binds the 5′ splice site, displacing U1. Extensive interactions between U6 and U2 displace U4. (5) Then, in the first transesterification step, the branch-site adenosine attacks the 5′ splice site, making a lariat intermediate. (6) U5 holds the two exons in close proximity, and the second transesterification takes place, with the 5′ splice-site hydroxyl group attacking the 3′ splice site. These reactions result in the mature spliced mRNA and a lariat form of the intron bound by U2, U5, and U6.

[Information from T. Villa, J. A. Pleiss, and C. Guthrie, *Cell* 109:149–152, 2002.]

1. Splicing begins with the recognition of the 5′ splice site by the U1 snRNP. U1 snRNA contains a highly conserved six-nucleotide sequence, not covered by protein in the snRNP, that base-pairs to the 5′ splice site of the pre-mRNA. This binding initiates spliceosome assembly on the pre-mRNA molecule.



2. U2 snRNP then binds the branch site in the intron by base-pairing between a highly conserved sequence in U2 snRNA and the pre-mRNA. U2 snRNP binding requires ATP hydrolysis.

3. A preassembled U4-U5-U6 tri-snRNP joins this complex of U1, U2, and the mRNA precursor to form the spliceosome. This association also requires ATP hydrolysis. Experiments with a reagent that cross-links neighboring pyrimidines in base-paired regions revealed that in this assembly U5 interacts with exon sequences in the $5'$ splice site and subsequently with the $3'$ exon.

4. Next, U6 disengages from U4 and undergoes an intramolecular rearrangement that permits base-pairing with U2 as well as interaction with the $5'$ end of the intron, displacing U1 and U4 from the spliceosome. U4 serves as an inhibitor that masks U6 until the specific splice sites are aligned. The catalytic center includes two bound magnesium ions bound primarily by phosphate groups from the U6 RNA (**Figure 29.37**).

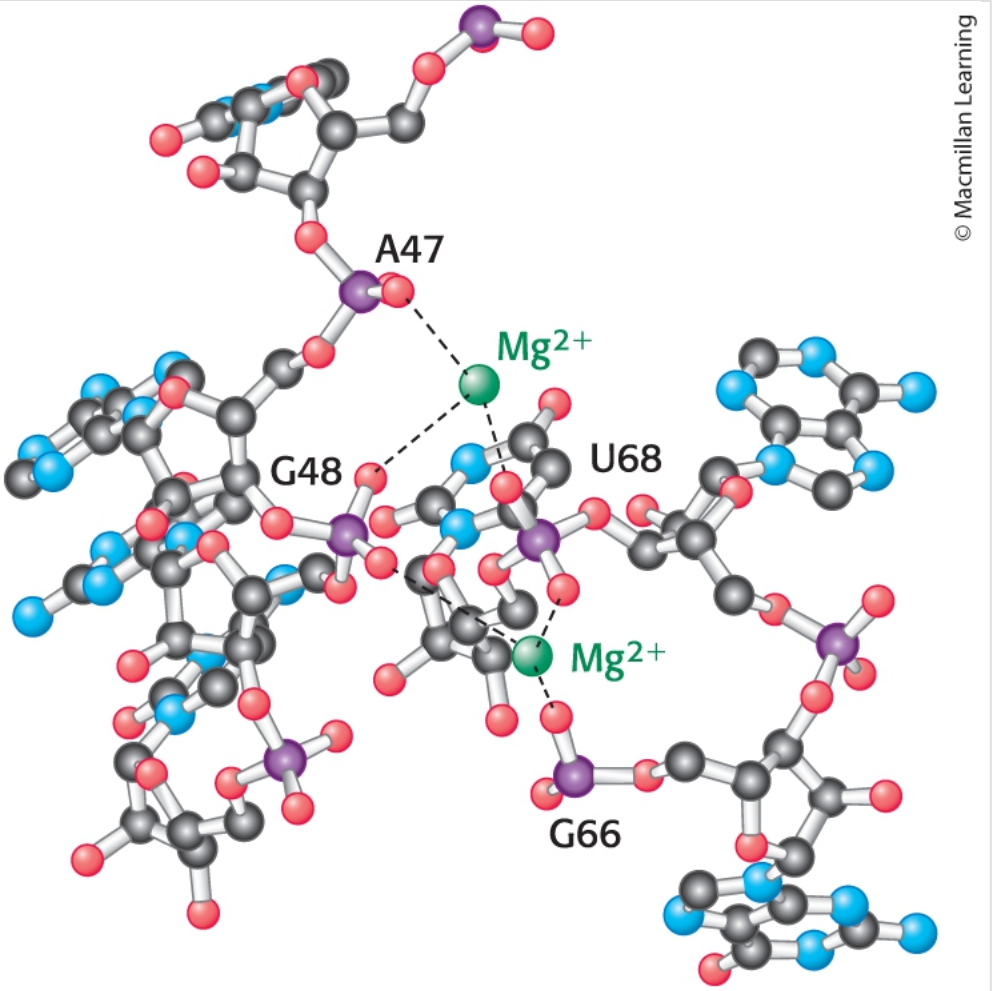


FIGURE 29.37 The spliceosome's catalytic center includes two key magnesium ions. These ions bind to the U6 RNA and promote the two transesterification reactions that are central to RNA splicing.

5. These rearrangements result in the first transesterification reaction, cleaving the 5′ exon and generating the lariat intermediate.

6. Further rearrangements of RNA in the spliceosome facilitate the second transesterification. In these rearrangements, U5 aligns the

free $5'$ exon with the $3'$ exon such that the $3'$-hydroxyl group of the $5'$ exon is positioned to make a nucleophilic attack on the $3'$ splice site to generate the spliced product. U2, U5, and U6 bound to the excised lariat intron are released, completing the splicing reaction.

Many of the steps in the splicing process require ATP hydrolysis. How is the free energy associated with ATP hydrolysis used to power splicing? To achieve the well-ordered rearrangements necessary for splicing, ATP-powered RNA helicases must unwind RNA helices and allow alternative base-pairing arrangements to form. Thus, two features of the splicing process are noteworthy. First, RNA molecules play key roles in directing the alignment of splice sites and in carrying out catalysis. Second, ATP-powered helicases unwind RNA duplex intermediates that facilitate catalysis and induce the release of snRNPs from the mRNA.

Mutations that affect pre-mRNA splicing cause disease



Mutations in either the pre-mRNA (cis-acting) or the splicing factors (trans-acting) can cause defective pre-mRNA splicing that manifests in disease. In fact, mutations affecting splicing have been estimated to cause at least 15% of all genetic diseases. We will look at two examples here.

First, we will consider the possible effects of cis-acting mutations on hemoglobin function. Mutations in the pre-mRNA cause some forms of thalassemia, a group of hereditary anemias characterized by the defective synthesis of hemoglobin (Section 3.3). Cis-acting mutations that cause aberrant splicing can occur at the $5'$ or $3'$ splice sites in

either of the two introns of the hemoglobin β chain or in its exons. Typically, mutations in the 5′ splice site alter that site such that the splicing machinery cannot recognize it, forcing the machinery to find another 5′ splice site in the intron and introducing the potential for a premature stop codon. The defective mRNA is normally degraded rather than translated. Alternatively, mutations in the intron itself may create a new 5′ splice site; in this case, either one of the two splice sites may be recognized (Figure 29.38). Consequently, some normal protein can be made, and so the disease is less severe.

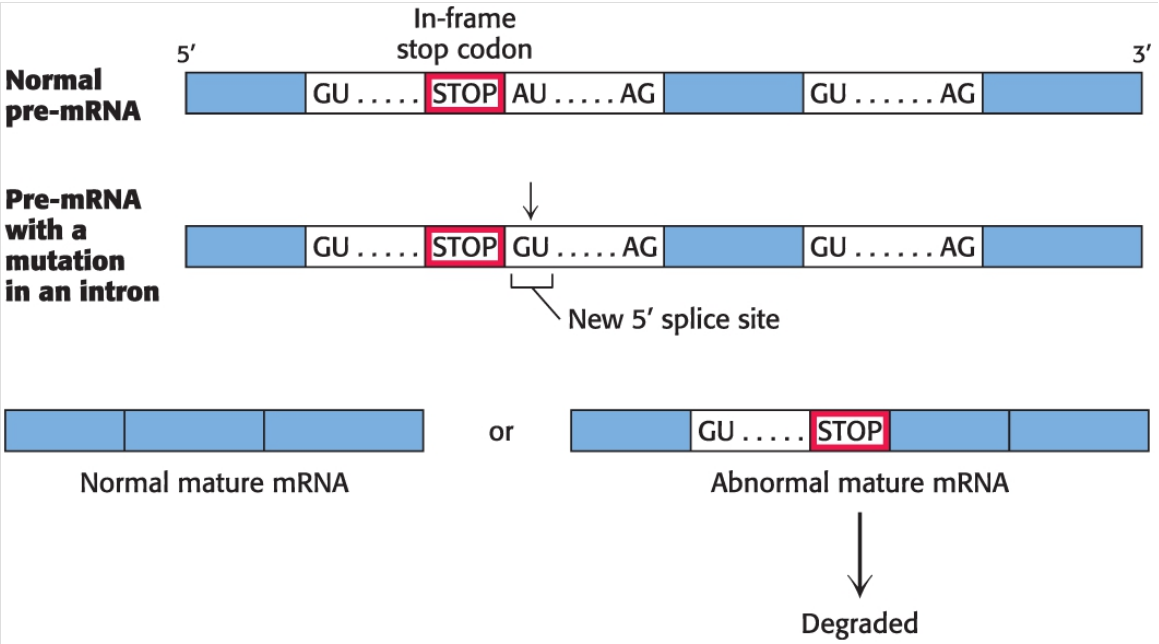


FIGURE 29.38 Mutations in splice sites can cause diseases such as thalassemia. An A-to-G mutation within the first intron of the gene for the human hemoglobin β chain creates a new 5′ splice site (GU). Both 5′ splice sites are recognized by the U1 snRNP; thus, splicing may sometimes create a normal mature mRNA and an abnormal mature mRNA that contains intron sequences. The normal mature mRNA is translated into a hemoglobin β chain. Because it includes intron sequences, the abnormal mature mRNA now has a premature stop codon and is degraded.

Second, we will consider the possible effects of trans-acting mutations on eyesight. Disease-causing mutations may also appear in splicing factors. Retinitis pigmentosa is a disease of acquired blindness, first described in 1857, with an incidence of 1/3500. About 5% of the autosomal dominant form of retinitis pigmentosa is likely due to mutations in the hPrp8 protein, a pre-mRNA splicing factor that is a component of the U4-U5-U6 tri-snRNP. How a mutation in a splicing factor that is present in all cells causes disease only in the retina is not clear; nevertheless, retinitis pigmentosa is a good example of how mutations that disrupt spliceosome function can cause disease.

Most human pre-mRNAs can be spliced in alternative ways to yield different proteins

As a result of **alternative splicing**, different combinations of exons from the same gene may be spliced into a mature RNA, producing distinct forms of a protein for specific tissues, developmental stages, or signaling pathways. What controls which splicing sites are selected? The selection is determined by the binding of trans-acting splicing factors to cis-acting sequences in the pre-mRNA. Most alternative splicing leads to changes in the coding sequence, resulting in proteins with different functions.

Alternative splicing provides a powerful mechanism for generating protein diversity. It expands the versatility of genomic sequences through combinatorial control. Consider a gene with five positions at which splicing can take place. With the assumption that these

alternative splicing pathways can be regulated independently, a total of $2^5 = 32$ different mRNAs can be generated.

Sequencing of the human genome has revealed that most pre-mRNAs are alternatively spliced, leading to a much greater number of proteins than would be predicted from the number of genes. An example of alternative splicing leading to the expression of two different proteins, each in a different tissue, is provided by the gene encoding both calcitonin and calcitonin-gene-related peptide (CGRP; Figure 29.39). In the thyroid gland, the inclusion of exon 4 in one splicing pathway produces calcitonin, a peptide hormone that regulates calcium and phosphorus metabolism. In neuronal cells, the exclusion of exon 4 in another splicing pathway produces CGRP, a peptide hormone that acts as a vasodilator. A single pre-mRNA thus yields two very different peptide hormones, depending on cell type.

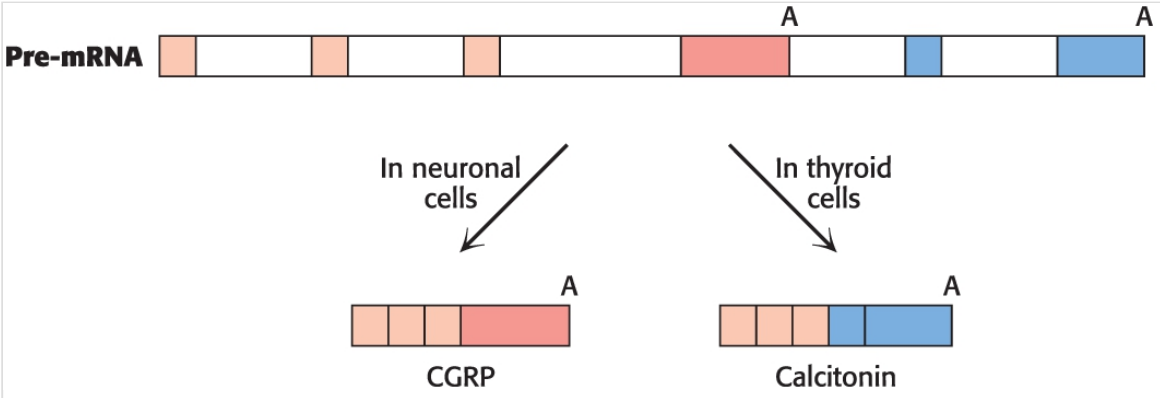


FIGURE 29.39 Alternative splicing produces different mRNAs. In human beings, two very different hormones are produced from a single calcitonin/CGRP pre-mRNA. Alternative splicing produces the mature mRNA for either calcitonin or CGRP (calcitonin-gene-related protein), depending on the cell type in which the gene is expressed. Each alternative transcript incorporates one of two alternative polyadenylation signals (A) present in the pre-mRNA.

In the above example, only two proteins result from alternative splicing; however, in other cases, many more can be produced. An extreme

example is the *Drosophila* pre-mRNA that encodes DSCAM, a neuronal protein affecting axon connectivity. Alternative splicing of this pre-mRNA has the potential to produce 38,016 different combinations of exons, a greater number than the total number of genes in the *Drosophila* genome. However, only a fraction of these potential mRNAs appear to be produced, owing to regulatory mechanisms that are not yet well understood.

Several human diseases that can be attributed to defects in alternative splicing are listed in **Table 29.4**. Further understanding of alternative splicing and the mechanisms of splice-site selection will be crucial to understanding how the proteome represented by the human genome is expressed.

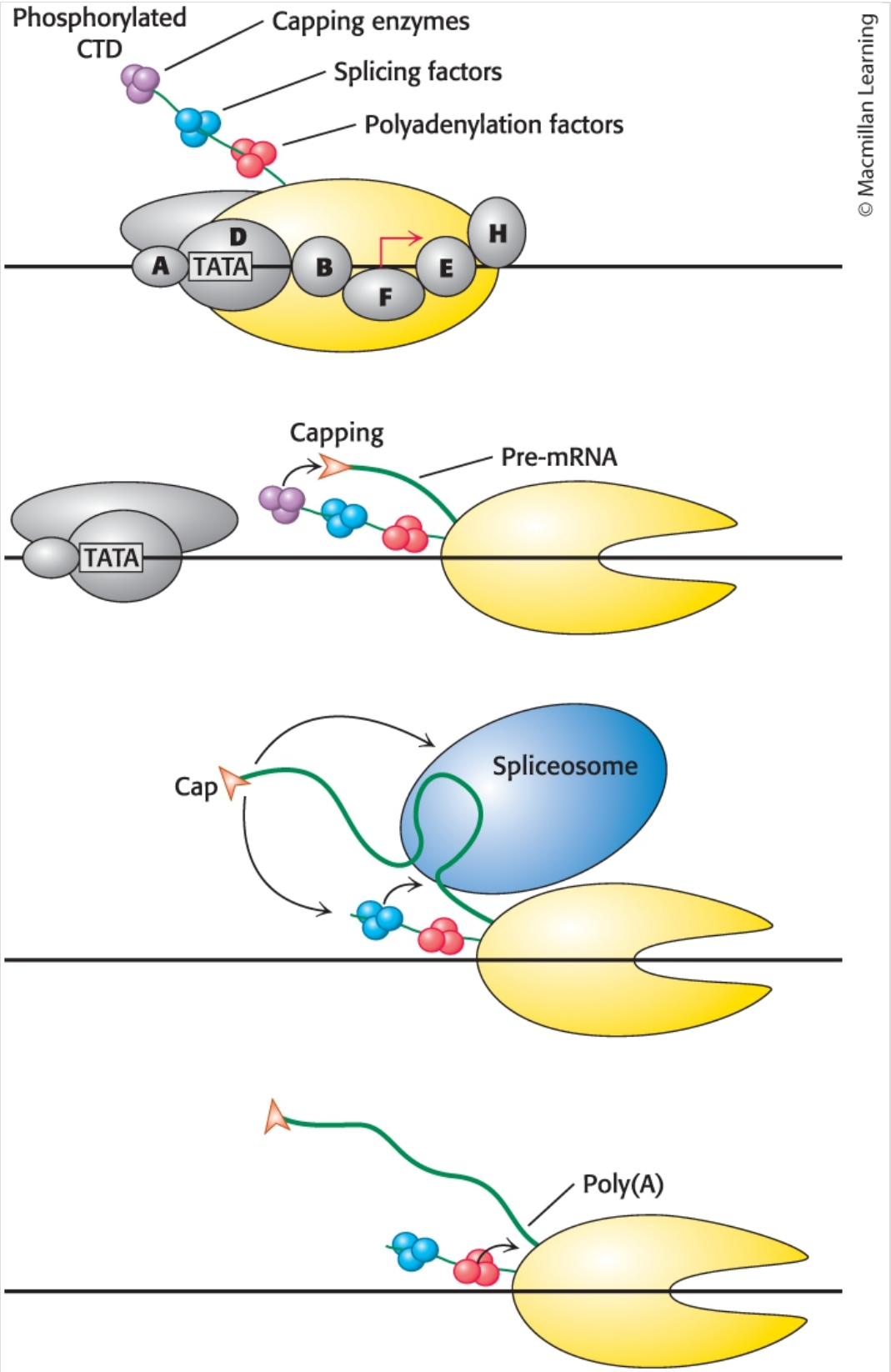
TABLE 29.4 Selected human disorders attributed to defects in alternative splicing

Disorder	Gene or its product
Acute intermittent porphyria	Porphobilinogen deaminase
Breast and ovarian cancer	*BRCA1*
Cystic fibrosis	*CFTR*
Frontotemporal dementia	T protein
Hemophilia A	Factor VIII
HGPRT deficiency (Lesch–Nyhan syndrome)	Hypoxanthine-guanine phosphoribosyltransferase
Leigh encephalomyelopathy	Pyruvate dehydrogenase E1 α

Severe combined immunodeficiency	Adenosine deaminase
Spinal muscle atrophy	*SMN1* or *SMN2*

Transcription and mRNA processing are coupled

Although we have described the transcription and processing of mRNAs as separate events in gene expression, experimental evidence suggests that the two steps are coordinated by the carboxyl-terminal domain of RNA polymerase II. We have seen that the CTD consists of a unique repeated seven-amino-acid sequence, YSPTSPS. Either S_2, S_5, or both may be phosphorylated in the various repeats. The phosphorylation state of the CTD is controlled by a number of kinases and phosphatases and leads the CTD to bind many of the proteins having roles in RNA transcription and processing. The CTD contributes to efficient transcription by recruiting certain proteins to the pre-mRNA (**Figure 29.40**). These proteins include:



© Macmillan Learning

FIGURE 29.40 The CTD couples transcription to pre-mRNA processing. The transcription factor TFIIH phosphorylates the carboxyl-terminal domain (CTD) of RNA polymerase II, signaling the transition from transcription initiation to elongation. The phosphorylated CTD binds factors required for pre-mRNA capping, splicing, and polyadenylation. These proteins are brought in close proximity to their sites of action on the nascent pre-mRNA as it is transcribed during elongation.

[Information from P. A. Sharp, *Trends in Biochemical Sciences* 30:279–281, 2005.]



1. Capping enzymes, which methylate the $5'$ guanine on the pre-mRNA immediately after transcription begins
2. Components of the splicing machinery, which initiate the excision of each intron as it is synthesized
3. An endonuclease that cleaves the transcript at the poly(A) addition site, creating a free $3'-OH$ group that is the target for $3'$ adenylation

These events take place sequentially, directed by the phosphorylation state of the CTD.

Small regulatory RNAs are cleaved from larger precursors

Cleavage plays a role in the processing of small single-stranded RNAs (approximately 20–23 nucleotides) called **microRNAs**. MicroRNAs play key roles in gene regulation in eukaryotes, as we shall see in Chapter 31. They are generated from initial transcripts produced by RNA polymerase II and, in some cases, RNA polymerase III. These transcripts fold into hairpin structures that are cleaved by specific nucleases at various stages (**Figure 29.41**). The final single-stranded

RNAs are bound by regulatory proteins, where the RNAs help target the regulation of specific genes.

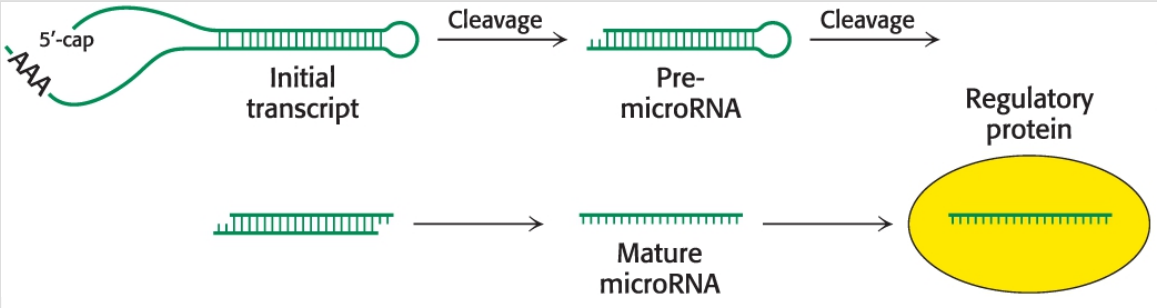


FIGURE 29.41 Small regulatory RNAs are involved in gene regulation. The initial transcription product is first cleaved to a small double-stranded RNA called a pre-microRNA. One of the strands of the pre-microRNA, the mature microRNA, is then bound by a regulatory protein.

RNA editing can lead to specific changes in mRNA

Remarkably, the amino acid sequence information encoded by some mRNAs is altered after transcription. This phenomenon is referred to as **RNA editing**, a posttranscriptional change in the nucleotide sequence of RNA that is caused by processes other than RNA splicing. RNA editing is prominent in some systems; next, we will consider three examples.

RNA editing is key to the process of lipid transport by apolipoprotein B (apo B). Apo B plays an important role in the transport of triacylglycerols and cholesterol by forming an amphipathic spherical shell around the lipids carried in lipoprotein particles (Section 27.3). Apo B exists in two forms, a 512-kDa *apo B-100* and a 240-kDa *apo B-48*. The larger form, synthesized by the liver, participates in the transport of lipids synthesized in the cell. The smaller form, synthesized by the

small intestine, carries dietary fat in the form of chylomicrons. Apo B-48 contains the 2152 N-terminal residues of the 4536-residue apo B-100. This truncated molecule can form lipoprotein particles but cannot bind to the low-density-lipoprotein receptor on cell surfaces.

What is the relationship between these two forms of apo B? Experiments revealed that a totally unexpected mechanism for generating diversity is at work: the changing of the nucleotide sequence of mRNA *after* its synthesis (**Figure 29.42**). A specific cytidine residue of mRNA is deaminated to uridine, which changes the codon at residue 2153 from CAA (Gln) to UAA (stop). The deaminase that catalyzes this reaction is present in the small intestine, but not in the liver, and is expressed only at certain developmental stages.

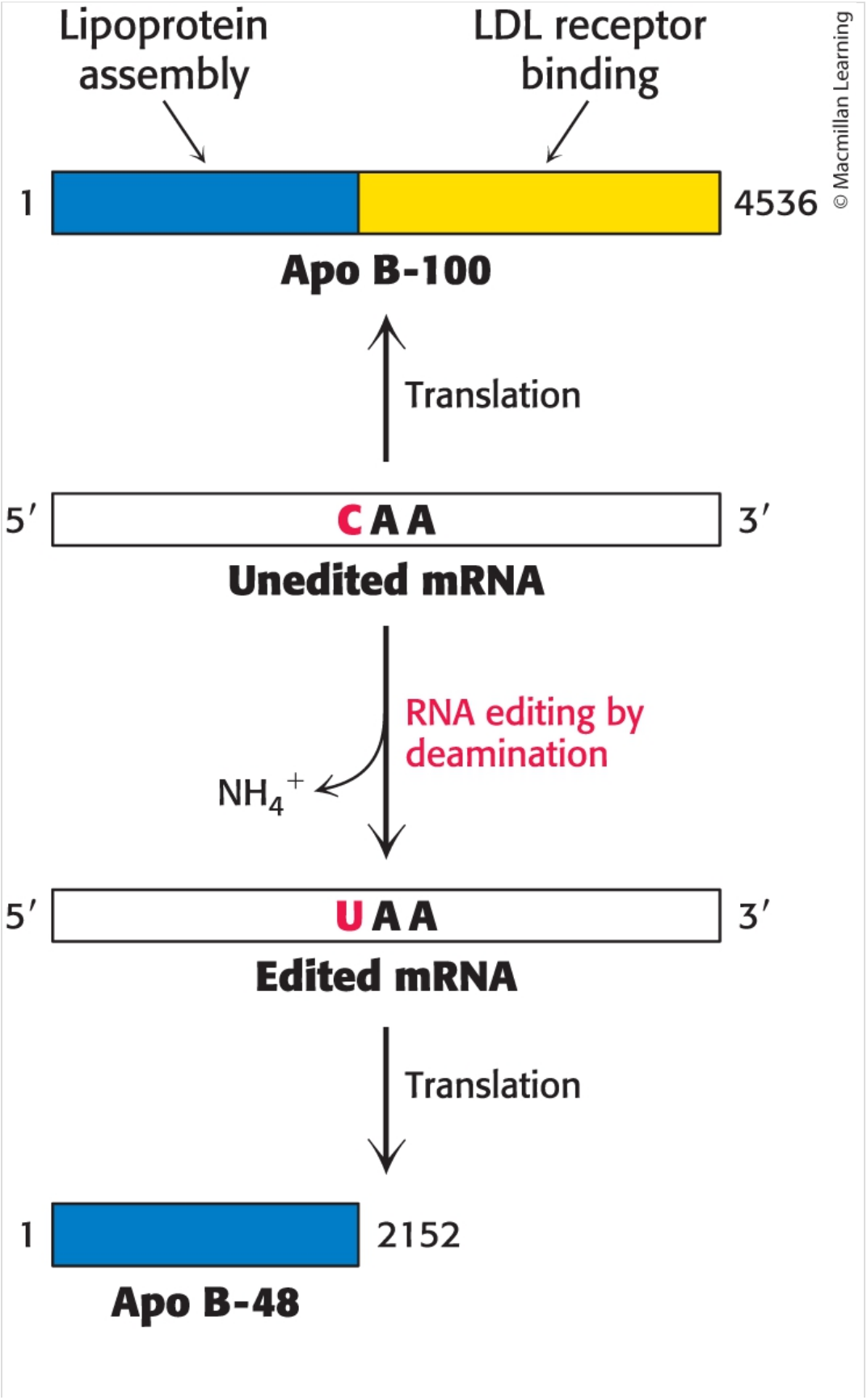

Lipoprotein assembly
LDL receptor binding
1
4536
Apo B-100
Translation
5′
CAA
3′
Unedited mRNA
RNA editing by deamination
NH_4^+
5′
UAA
3′
Edited mRNA
Translation
1
2152
Apo B-48
© Macmillan Learning

FIGURE 29.42 RNA editing alters the coding sequence of mRNAs. Enzyme-catalyzed deamination of a specific cytidine residue in the mRNA for apolipoprotein B-100 changes a codon for glutamine (CAA) to a stop codon (UAA). Apolipoprotein B-48, a truncated version of the protein lacking the LDL receptor-binding domain, is generated by this posttranscriptional change in the mRNA sequence.

[Information from P. Hodges and J. Scott, *Trends in Biochemical Sciences* 17:77, 1992.]



RNA editing also plays a role in the regulation of postsynaptic receptors. Glutamate opens cation-specific channels in the vertebrate central nervous system by binding to receptors in postsynaptic membranes. RNA editing changes a single glutamine codon (CAG) in the mRNA for the glutamate receptor to the codon for arginine (CGG). The substitution of Arg for Gln in the receptor prevents Ca^{2+}, but not Na^{+}, from flowing through the channel.

In trypanosomes (parasitic protozoans), a different kind of RNA editing markedly changes several mitochondrial mRNAs. Nearly half the uridine residues in these mRNAs are inserted by RNA editing. A guide RNA molecule identifies the sequences to be modified, and a poly(U) tail on the guide RNA donates uridine residues to the mRNAs undergoing editing.

DNA sequences evidently do not always faithfully represent the sequence of encoded proteins; crucial functional changes to mRNA can take place. RNA editing is likely much more common than was formerly thought. The chemical reactivity of nucleotide bases — including the susceptibility to deamination that necessitates complex DNA-repair mechanisms — has been harnessed as an engine for generating molecular diversity at the RNA and, hence, protein levels.

29.5 The Discovery of Catalytic RNA Revealed a Unique Splicing Mechanism

RNAs form a surprisingly versatile class of molecules. As we have seen, splicing is catalyzed largely by RNA molecules, with proteins playing a secondary role. RNA is also a key component of ribonuclease P, which catalyzes the maturation of tRNA by endonucleolytic cleavage of nucleotides from the $5'$ end of the precursor molecule. Finally, as we shall see in Chapter 30, the RNA component of ribosomes is the catalyst that carries out protein synthesis.

Some RNAs can promote their own splicing

The versatility of RNA first became clear from observations of the processing of ribosomal RNA in a single-cell eukaryote, a ciliated protozoan in the genus *Tetrahymena*. In *Tetrahymena*, a 414-nucleotide intron is removed from a 6.4-kb precursor to yield the mature 26S rRNA molecule.

In an elegant series of studies of this splicing reaction, Thomas Cech and his coworkers established that, in the absence of protein, the RNA spliced itself to precisely excise the intron. Indeed, the RNA alone is catalytic and, under certain conditions, is thus a **ribozyme**. More than 1500 similar introns have since been found in species as widely dispersed as bacteria and eukaryotes, though not in vertebrates. Collectively, they are referred to as group I **self-splicing introns**.



Glenn Asakawa, University of Colorado Boulder

THOMAS CECH Fascinated by the structure of chromosomes, Thomas Cech pursued this topic as a graduate student and postdoctoral fellow. He then accompanied his wife, Dr. Carol Cech, to the University of Colorado in Boulder (UCB), where they had both been offered faculty positions. They had met in chemistry class while they were undergraduate students at Grinnell College. At UCB, Dr. Cech set out to purify enzymes involved in the splicing of a particular RNA molecule, but he and his

coworkers soon discovered that the RNA molecule spliced itself. This fundamental discovery of RNA catalysis, which changed our view of both modern biochemistry and our evolutionary past, was recognized with the Nobel Prize in Chemistry in 1989. Dr. Cech has remained at UCB, teaching with infectious enthusiasm throughout his career. He also served as an investigator (and president from 2000 to 2009) of the Howard Hughes Medical Institute (HHMI), a leading private funder of biomedical research.

The self-splicing reaction in the group I intron requires an added guanosine nucleotide (**Figure 29.43**). Nucleotides were originally included in the reaction mixture because it was thought that ATP or GTP might be needed as an energy source. Instead, the nucleotides were found to be necessary as cofactors. The required cofactor proved to be a guanosine unit, in the form of guanosine, GMP, GDP, or GTP. G (denoting any one of these species) serves not as an energy source but as an attacking group that becomes transiently incorporated into the RNA. G binds to the RNA and then attacks the $5'$ splice site to form a phosphodiester bond with the $5'$ end of the intron. This transesterification reaction generates a $3'-OH$ group at the end of the upstream exon. This $3'-OH$ group then attacks the $3'$ splice site in a second transesterification reaction that joins the two exons and leads to the release of the 414-nucleotide intron.

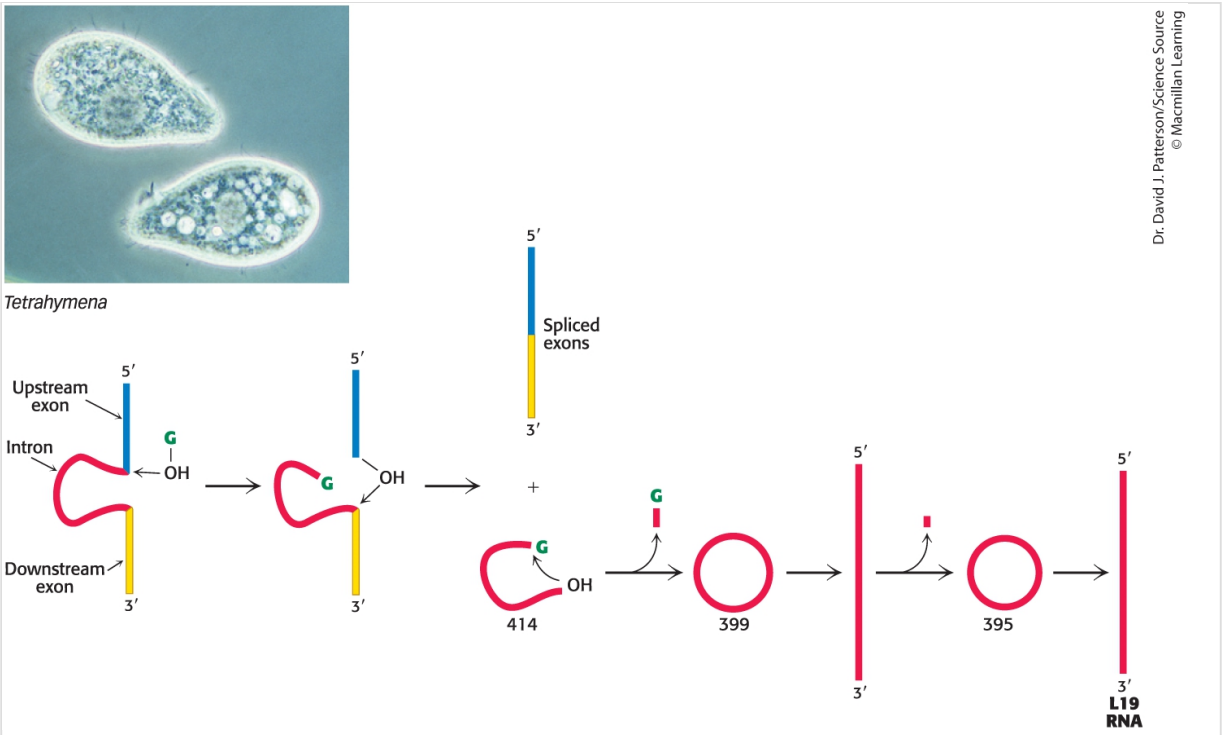
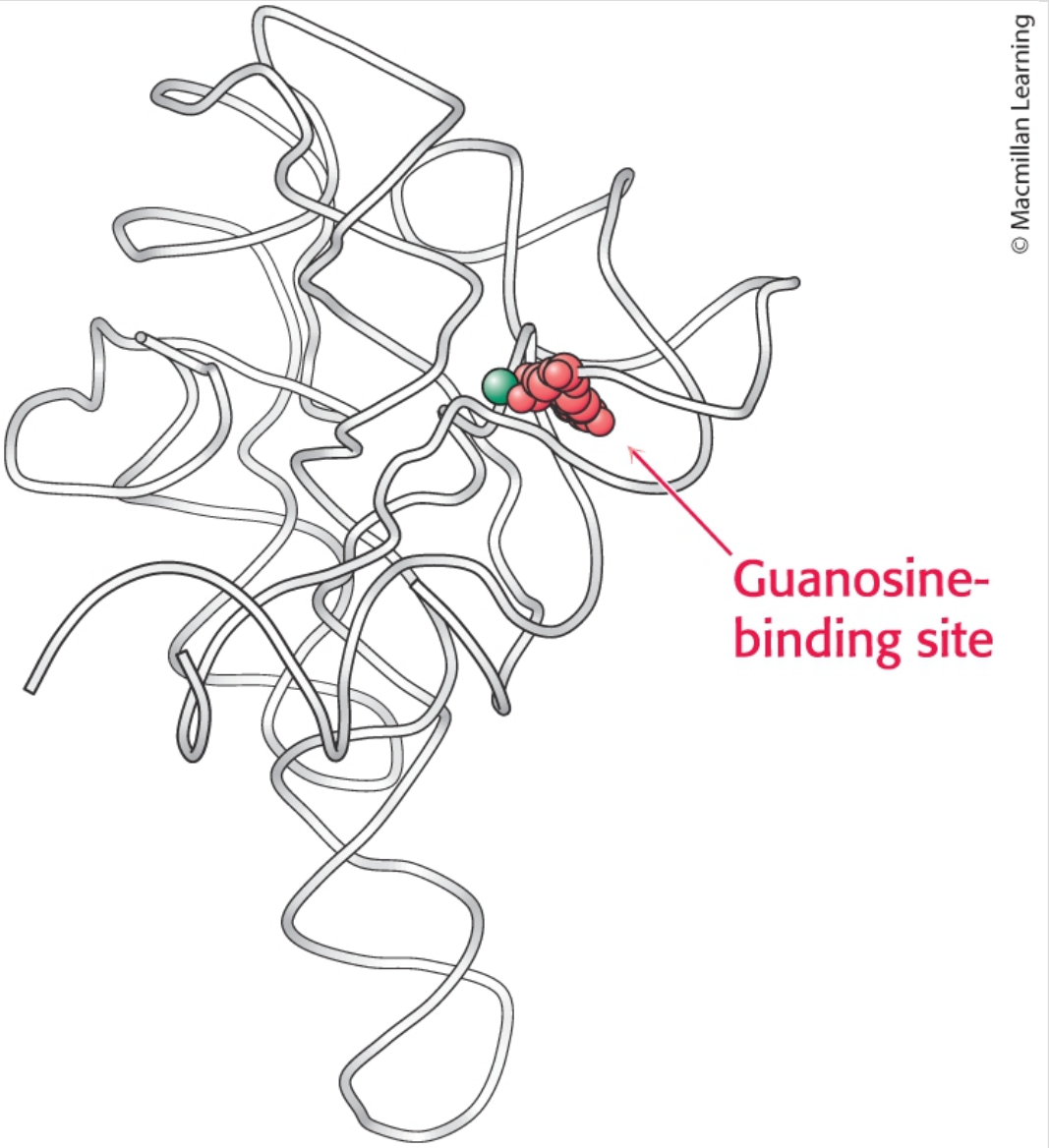


FIGURE 29.43 Some introns are capable of self-splicing. A ribosomal RNA precursor representative of the group I introns, from the protozoan *Tetrahymena*, splices itself in the presence of a guanosine cofactor (G, shown in green). A 414-nucleotide intron (red) is released in the first splicing reaction. This intron then splices itself twice again to produce a linear RNA that has lost a total of 19 nucleotides. This L19 RNA is catalytically active.

[Information from T. Cech, RNA as an enzyme. Copyright © 1986 by Scientific American, Inc. All rights reserved.]

Self-splicing depends on the structural integrity of the RNA precursor. Much of the group I intron is needed for self-splicing. This molecule, like many RNAs, has a folded structure formed by many double-helical stems and loops (Figure 29.44), with a well-defined pocket for binding the guanosine. Examination of the three-dimensional structure of a catalytically active group I intron determined by x-ray crystallography reveals the coordination of magnesium ions in the active site analogous to that observed in protein enzymes such as DNA polymerase.



© Macmillan Learning

FIGURE 29.44 Self-splicing introns have a complex structure. The structure of a large fragment of the self-splicing intron from *Tetrahymena* reveals a complex folding pattern of helices and loops. The guanosine binding site is highlighted in red.

[Drawn from 1GRZ.pdb].

INTERACT with this model in Achieve

Analysis of the base sequence of the rRNA precursor suggested that the splice sites are aligned with the catalytic residues by base-pairing

between the *internal guide sequence* (IGS) in the intron and the $5'$ and $3'$ exons (**Figure 29.45**). The IGS first brings together the guanosine cofactor and the $5'$ splice site so that the $3'-OH$ group of G can make a nucleophilic attack on the phosphorus atom at this splice site. The IGS then holds the downstream exon in position for attack by the newly formed $3'-OH$ group of the upstream exon. A phosphodiester bond is formed between the two exons, and the intron is released as a linear molecule. Like catalysis by protein enzymes, self-catalysis of bond formation and breakage in this rRNA precursor is highly specific.

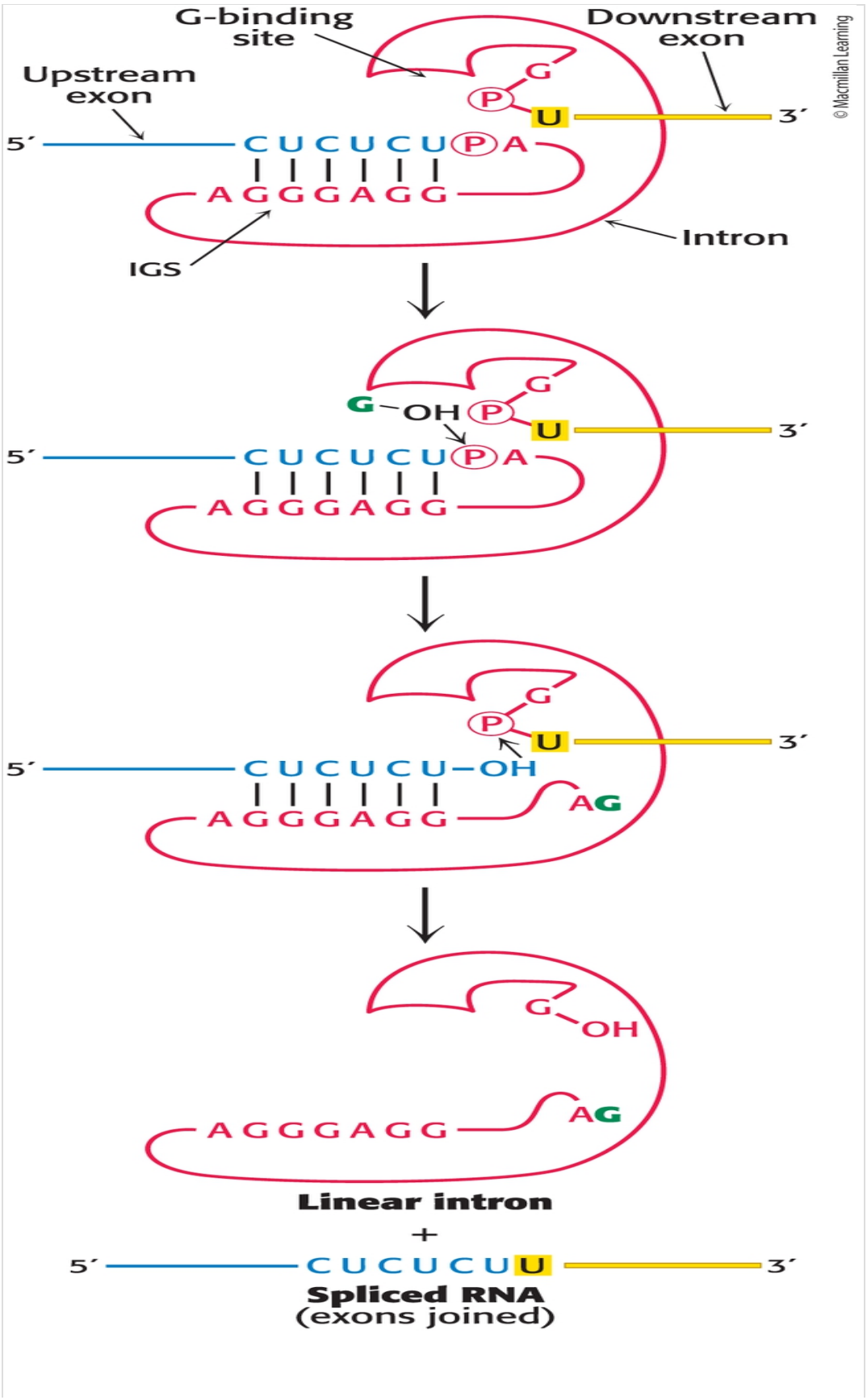

G-binding site
Downstream exon
Upstream exon
G
P
U
3′
5′
C U C U C U P A
A G G G A G G
Intron
IGS
G
OH
P
U
3′
5′
C U C U C U P A
A G G G A G G
G
P
U
3′
5′
C U C U C U–OH
A G G G A G G
AG
G
OH
AG
A G G G A G G
Linear intron
+
5′
C U C U C U U
3′
Spliced RNA
(exons joined)
© Macmillan Learning

FIGURE 29.45 The catalytic mechanism of the group I self-splicing intron includes a series of transesterification reactions.

[Information from T. Cech, RNA as an enzyme. Copyright © 1986 by Scientific American, Inc. All rights reserved.]



The finding of enzymatic activity in the self-splicing intron and in the RNA component of RNase P has opened new areas of inquiry and changed the way in which we think about molecular evolution. As mentioned in an earlier chapter, the discovery that RNA can be a catalyst as well as an information carrier suggests that an RNA world may have existed early in the evolution of life, before the appearance of DNA and protein.

Messenger RNA precursors in the mitochondria of yeast and fungi also undergo self-splicing, as do some RNA precursors in the chloroplasts of unicellular organisms such as *Chlamydomonas*. Self-splicing reactions can be classified according to the nature of the unit that attacks the upstream splice site. Group I self-splicing is mediated by a guanosine cofactor, as in *Tetrahymena*. The attacking moiety in group II splicing is the $2'-OH$ group of a specific adenylate of the intron (**Figure 29.46**).

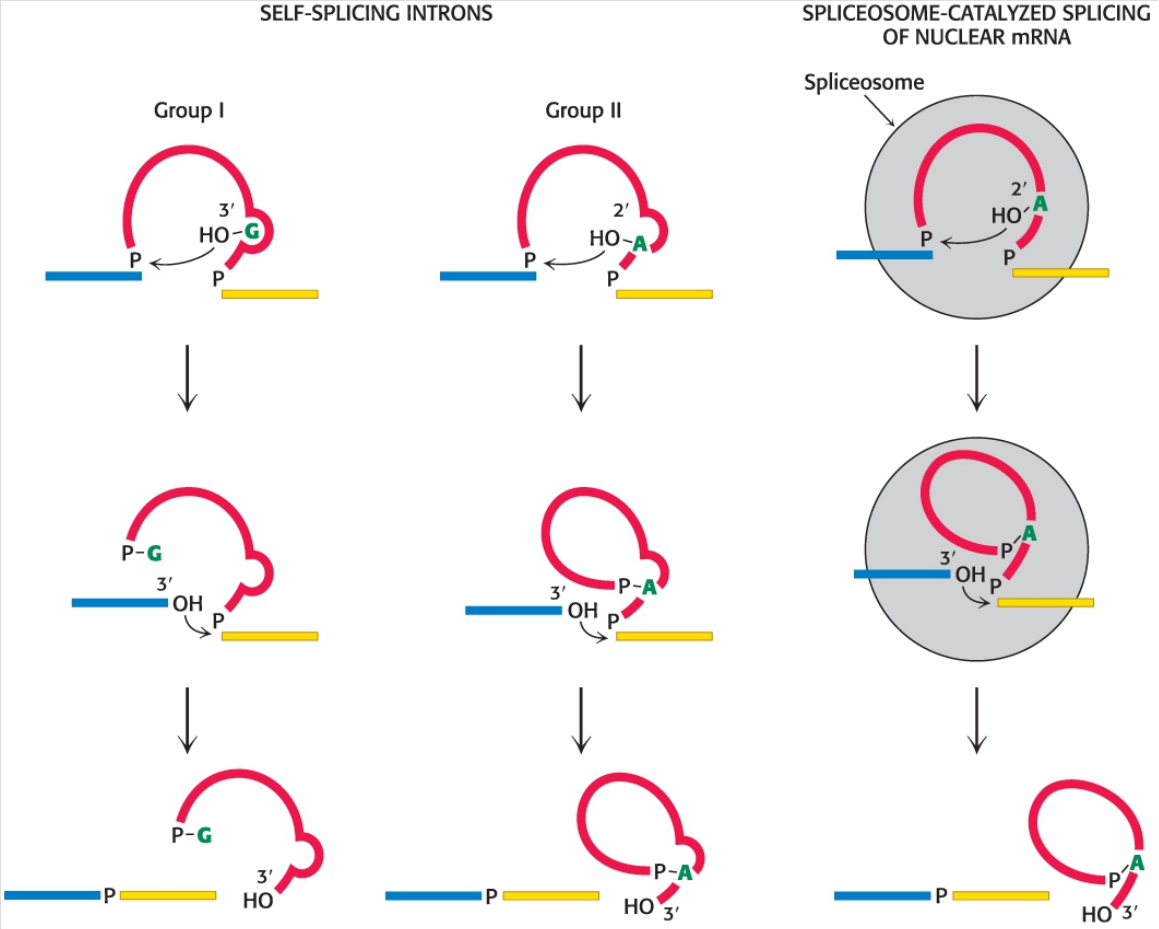


FIGURE 29.46 In self-splicing mechanisms, the catalytic site is formed by the intron itself. The exons being joined are shown in blue and yellow, and the attacking unit is shown in green. The catalytic site is formed by the intron itself (red) in group I and group II splicing. In contrast, the splicing of nuclear mRNA precursors is catalyzed by snRNAs and their associated proteins in the spliceosome.

[Information from P. A. Sharp, *Science* 235:766–771, 1987.]

Group I and group II self-splicing resembles spliceosome-catalyzed splicing in two respects. First, in the initial step, a ribose hydroxyl group attacks the $5'$ splice site. The newly formed $3'\text{–OH}$ terminus of the upstream exon then attacks the $3'$ splice site to form a phosphodiester bond with the downstream exon. Second, both reactions are

transesterifications in which the phosphate moieties at each splice site are retained in the products. The number of phosphodiester bonds stays constant.

Group II splicing is like the spliceosome-catalyzed splicing of mRNA precursors in several additional ways. First, the attack at the $5'$ splice site is carried out by a part of the intron itself (the $2'-OH$ group of adenosine) rather than by an external cofactor (G). Second, the intron is released in the form of a lariat. Third, in some instances, the group II intron is transcribed in pieces that assemble through hydrogen bonding to the catalytic intron, in a manner analogous to the assembly of the snRNAs in the spliceosome.

The similarities in mechanism have led to the suggestion that the spliceosome-catalyzed splicing of mRNA precursors evolved from RNA-catalyzed self-splicing. Group II splicing may well be an intermediate between group I splicing and the splicing in the nuclei of higher eukaryotes. A major step in this transition was the transfer of catalytic power from the intron itself to other molecules. The formation of spliceosomes gave genes a new freedom because introns were no longer constrained to provide the catalytic center for splicing. Another advantage of external catalysts for splicing is that they can be more readily regulated.

However, it is important to note that similarities do not establish ancestry. The similarities between group II introns and mRNA splicing may be a result of convergent evolution. Perhaps there are only a limited number of ways to carry out efficient, specific intron excision. The determination of whether these similarities stem from ancestry or from chemistry will require expanding our understanding of RNA biochemistry.

Self-Check Question



Compare and contrast the three different splicing mechanisms that have been identified.

RNA enzymes can promote many reactions, including RNA polymerization

In this chapter, we have discussed the role of many different RNA molecules, including those that promote reactions such as splicing. In Chapter 30, we will discuss the key roles that RNAs play in protein biosynthesis, and we will see that ribosomal RNAs have a significant role in the catalysis of peptide bonds.

While the ribosomal RNAs have a role in the polymerization of amino acids into proteins, some RNAs are also capable of catalyzing the polymerization of other RNA molecules or even themselves. In vitro experiments have identified the possibility of self-ligating ribozymes: RNA molecules capable of joining other, short RNAs to their own end. The ability of RNAs to direct the synthesis of other catalytic molecules gives us a glimpse into how, in a primordial RNA world, ribozymes may have accelerated chemical reactions critical for life.

Chapter 29 Summary

29.1 RNA Molecules Play Different Roles, Primarily in Gene Expression

- RNA molecules are integral to many different cellular functions; for example, protein biosynthesis.
- Some RNAs can direct their own modification.

29.2 RNA Polymerases Catalyze Transcription

- RNA polymerases synthesize all cellular RNA molecules according to instructions given by DNA templates.
- The direction of RNA synthesis is $5' \rightarrow 3'$, as in DNA synthesis.

  RNA polymerases, unlike DNA polymerases, do not need a primer.
- RNA polymerase in *E. coli* is a multisubunit enzyme. The subunit composition of the $\sim 500\text{-kDa}$ holoenzyme is $\alpha_2\beta\beta'\omega\sigma$ and that of the core enzyme is $\alpha_2\beta\beta'\omega$.
- Transcription is initiated at promoter sites.
- The σ subunit enables the holoenzyme to recognize promoter sites. The σ subunit usually dissociates from the holoenzyme after the initiation of the new chain.
- Elongation takes place at transcription bubbles that move along the DNA template at a rate of about 50 nucleotides per second.
- The nascent RNA chain contains stop signals that end transcription. One stop signal is an RNA hairpin, which is followed by several U residues. A different stop signal is read by the *rho* protein, an ATPase.
- In *E. coli,* precursors of transfer RNA and ribosomal RNA are cleaved and chemically modified after transcription, whereas

messenger RNA is used unchanged as a template for protein synthesis.

29.3 Transcription Is Highly Regulated

- Bacteria use alternate σ factors to adjust the transcription levels of various genes in response to external stimuli.
- Some genes are regulated by riboswitches, structures that form in RNA transcripts and bind specific metabolites.
- Eukaryotic DNA is tightly bound to basic proteins called histones; the combination is called chromatin. DNA wraps around an octamer of core histones to form a nucleosome.
- There are three types of eukaryotic RNA polymerases in the nucleus, where transcription takes place: RNA polymerase I makes ribosomal RNA precursors, II makes messenger RNA precursors, and III makes transfer RNA precursors.
- Eukaryotic promoters are composed of several different elements. The activity of many promoters is greatly increased by enhancer sequences that have no promoter activity of their own.

29.4 Some RNA Transcription Products Are Processed

- The $5'$ ends of mRNA precursors become capped and methylated during transcription.
- A $3'$ poly(A) tail is added to most mRNA precursors after the nascent chain has been cleaved by an endonuclease.
- The splicing of mRNA precursors is carried out by spliceosomes, which consist of small nuclear ribonucleoproteins. Splice sites in mRNA precursors are specified by sequences at ends of introns and by branch sites near the $3'$ ends of introns.

- RNA editing alters the nucleotide sequence of some mRNAs, such as the one for apolipoprotein B.

29.5 The Discovery of Catalytic RNA Revealed a Unique Splicing Mechanism

- Some RNA molecules undergo self-splicing in the absence of protein.
- Spliceosome-catalyzed splicing may have evolved from self-splicing.
- The discovery of catalytic RNA has opened new vistas in our exploration of early stages of molecular evolution and the origins of life.

Key Terms

transcription
RNA polymerase
promoter
transcription bubble
sigma (σ) subunit
consensus sequence
rho (ρ) protein
riboswitch
chromatin
nucleosome
carboxyl-terminal domain (CTD)
TATA box
transcription factor
enhancer
small nucleolar ribonucleoprotein (snoRNP)
pre-mRNA

5′ cap

poly(A) tail
RNA splicing
spliceosome
small nuclear RNA (snRNA)
small nuclear ribonucleoprotein (snRNP)
alternative splicing
microRNA
RNA editing
ribozyme
self-splicing introns

Problems

1. Why is RNA synthesis not as carefully monitored for errors as is DNA synthesis? 1, 2

2. What are the functions of RNA polymerases? Select all that apply. 1, 3

a. Polymerization of polypeptides from RNA transcripts
b. Elongation of ribosomal RNA (rRNA)
c. Initiation of transcription at promoter sites
d. Elongation of messenger RNA (mRNA) transcripts
e. Initiation of translation from RNA transcripts

3. The overall structures of RNA polymerase and DNA polymerase are very different, yet their active sites show considerable similarities. What do the similarities suggest about the evolutionary relationship between these two important enzymes? 1

4. The sequence of part of an mRNA transcript is

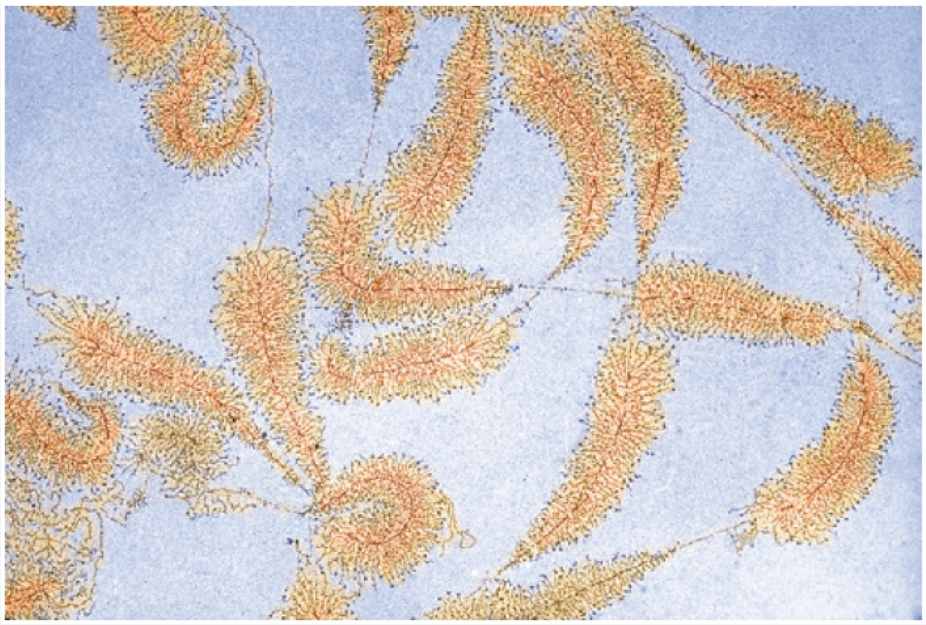
$$5'-\text{AUGGGGAACAGCAAGAGUGGGGCCCUGUCCAAGGAG}-3'$$

What is the sequence of the DNA coding strand? Of the DNA template strand? 1

5. Sigma protein by itself does not bind to promoter sites. Predict the effect of a mutation enabling σ to bind to the -10 region in the absence of other subunits of RNA polymerase. 2

6. The molecular weight of an amino acid is approximately 110 Da, and *E. coli* RNA polymerase has a transcription rate of approximately 5050 nucleotides per second. What is the minimum length of time required by *E.coli* polymerase for the synthesis of an mRNA encoding a 100-kDa protein? Round your answer to the nearest whole number. 1

7. The autoradiograph below depicts several bacterial genes undergoing transcription. Identify the DNA. What are the strands of increasing length? Where is the beginning of transcription? The end of transcription? What can you conclude about the number of enzymes participating in RNA synthesis on a given gene? 2



8. Fill in the blanks to complete the statements about the capping process: Capping occurs at the **(a)** _____ end of the mRNA. The nucleoside that is added is **(b)** _____. The nucleoside is connected to the mRNA through a **(c)** _____ linkage. The added nucleoside is modified by methylation at **(d)** _____ atom. The mRNA is further modified by methylation of ribose residues at the **(e)** _____ -hydroxyl position. 3

9. Suppose that RNA polymerase was transcribing a eukaryotic gene with several introns all contained within the coding region. In what order would the RNA polymerase encounter the elements in the DNA sequence of the gene, from earliest to latest? 2

a. Splice donor site
b. 3′ untranslated region (UTR)
c. Transcription start site
d. Translation start codon

e. 5′ untranslated region (UTR)

f. Translation termination codon

10. For the three genes shown below, transcription occurs from right to left for gene *A* and gene *B*, whereas transcription occurs from left to right for gene *C*. Identify which strand (top or bottom) is the template strand for each gene. 1



11. Which would you expect to have more types of **σ** factors: a free–living prokaryote in a fluctuating environment, or a prokaryote in a relatively stable environment with adequate nutrients? Why? 2

12. The three different eukaryotic RNA polymerases perform different functions and can be distinguished experimentally by their sensitivity to the toxin α–amanitin. Match the appropriate function and α–amanitin sensitivity to each RNA polymerase. Each function and sensitivity will be used only once. 3

Type of polymerase	Function and sensitivity
1. RNA polymerase I	1. Inhibited by high concentrations of α-amanitin

2. RNA polymerase II	2. Not inhibited by α-amanitin
	3. Synthesizes pre-ribosomal RNA
3. RNA polymerase III	4. Synthesizes primarily tRNA and small RNAs
	5. Synthesizes mostly pre-messenger RNA
	6. Inhibited by low concentrations of α-amanitin

---

13. Fill in the blanks to complete the statements about ribosomal RNA processing in eukaryotes: RNA polymerase I generates the **(a)** _____ kb rRNA transcript, which has a sedimentation coefficient of **(b)** _____. The RNA transcript is processed in a series of steps to yield three smaller rRNA molecules: **(c)** _____. The **(d)** _____ rRNA assembles with the **€** _____ rRNA, the **(f)** _____ rRNA, and proteins into **(g)** _____ ribosomal subunits. The 5S rRNA genes are transcribed by **(h)** _____. The 18S rRNA is associated with **(i)** _____ ribosomal subunits. 3

14. Which of the following statements regarding promoters is correct? Select all that apply. 1, 4, 6

a. In prokaryotes, the promoter is recognized by general transcription factors, which recruit the RNA polymerase holoenzyme.
b. In both prokaryotes and eukaryotes, the promoter is located in the 5′ direction, upstream from the transcription start site.
c. In eukaryotes, the promoter attracts the small and large ribosomal subunits with the help of initiation factors.

d. In prokaryotes, the promoter contains a -35 and -10 region upstream of the transcription start site.
e. In eukaryotes, the promoter recruits the preinitiation complex, which includes the TATA–binding protein.

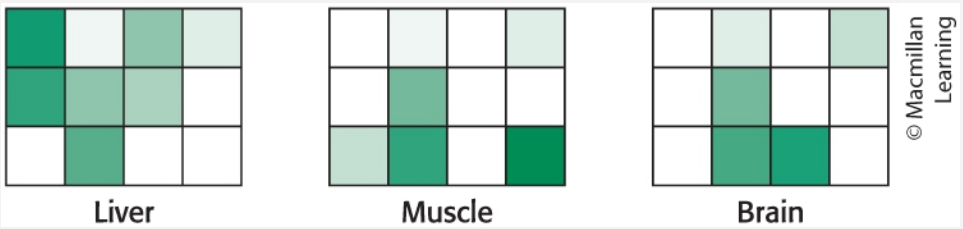
15. Match each RNA type with its appropriate function. Each function will be used only once. 3

Type of RNA	Function
1. small nuclear RNA (snRNA)	1. Helps to regulate the expression of specific genes
2. ribosomal RNA (rRNA)	2. Carries genetic information to ribosomes for protein synthesis
3. transfer RNA (tRNA)	3. Combines with proteins to form ribosomes
4. messenger RNA (mRNA)	4. Brings amino acids to sites of mRNA during protein synthesis
5. microRNA (miRNA)	5. Involved in the splicing process when mRNA is formed

16. A gene contains eight sites where alternative splicing is possible. Assuming that the splicing pattern at each site is independent of that at all other sites, how many splicing products are possible? 5

17. What processes considered in this chapter make the proteome more complex than the genome? What processes might further enhance this complexity? 5

18. Nuclei were isolated from brain, liver, and muscle. The nuclei were then incubated with $\alpha-[^{32}P]$ UTP under conditions that allow RNA synthesis, except that an inhibitor of RNA initiation was present. The radioactive RNA was isolated and annealed to various DNA sequences that had been attached to a gene chip. In the adjoining graphs, the intensity of the shading indicates roughly how much mRNA was attached to each DNA sequence. 4

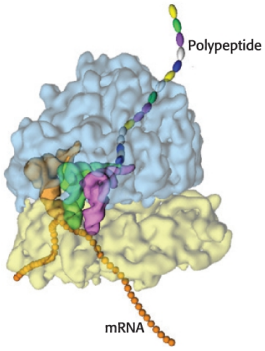


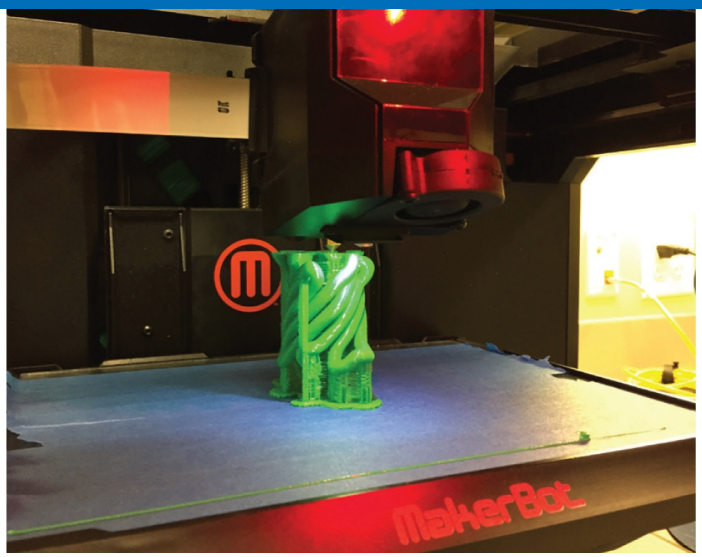
a. Why does the intensity of hybridization differ between genes?
b. What is the significance of the fact that some of the RNA molecules display different hybridization patterns in different tissues?
c. Some genes are expressed in all three tissues. What is the nature of these genes?
d. Suggest a reason why an initiation inhibitor was included in the reaction mixture.

19. Eukaryotic messenger RNA can undergo postsynthetic processing after transcription and before translation. One of the processing steps is splicing, where portions of the RNA are removed and the remaining RNA are joined together. Classify the statements regarding mRNA splicing as true or false. 5

a. Splicing occurs while the mRNA is attached to the nucleosome.
b. One mRNA can sometimes code for more than one protein by splicing at alternative sites.
c. Splicing occurs while the mRNA is still in the nucleus.
d. In splicing, intron sequences are removed from the mRNA in the form of lariats (loops) and are degraded.
e. Splicing of mRNA does not involve any proteins.

Chapter 30
Protein Biosynthesis





© Jess Petree
© Macmillan Learning

The ribosome, shown above, is a cellular machine that is not unlike a 3D printer. The ribosome follows specific instructions in mRNA to create a polypeptide from amino acids. Each amino acid is connected to a transfer tRNA molecule and brought to the ribosome, one at a time, to be joined to the growing polypeptide chain. Once complete, the polypeptide chain detaches from the ribosome and adopts a three-dimensional structure.

Outline

30.1 Protein Biosynthesis Requires the Translation of Nucleotide Sequences into Amino Acid Sequences
30.2 Aminoacyl-tRNA Synthetases Establish the Genetic Code
30.3 The Ribosome Is the Site of Protein Biosynthesis

30.4 Ribosomes Bound to the Endoplasmic Reticulum Manufacture Secretory and Membrane Proteins
30.5 A Variety of Antibiotics and Toxins Inhibit Protein Biosynthesis

Learning Goals



By the end of this chapter, you should be able to:

1. Explain how nucleic acid information is translated into amino acid sequence and define the role of aminoacyl tRNA synthetases in this process.
2. Define the role of ribosomes in protein biosynthesis.
3. Compare and contrast bacterial and eukaryotic protein biosynthesis.
4. Describe the pathway for the biosynthesis of secretory and membrane proteins.
5. Describe how certain chemicals can inhibit protein biosynthesis.

Einstein is reported to have said, “The more I learn, the more I realize how much I don’t know.” He might as well have been talking about ribosomes, enormous molecular complexes containing several large RNA molecules and dozens of proteins. What makes ribosomes so fascinating? Ribosomes are responsible for protein biosynthesis, and since proteins play most of the functional roles in cells, ribosomes are therefore critical to cell survival. Any errors in this process can have detrimental effects on cells by interfering with normal cellular functions. In addition, toxins and antibiotics that bind to the ribosome and prevent its ability to make proteins can cause cell death. As we will see in this chapter, protein biosynthesis depends not just on the ribosome, but also on many additional nucleic acid and protein factors. There is still much to discover about this intricate process, and “ribosomology” is certain to keep biochemists busy for years to come.

30.1 Protein Biosynthesis Requires the Translation of Nucleotide Sequences into Amino Acid Sequences

In this chapter we discuss the mechanism of protein biosynthesis, a process called **translation** because the 4-letter alphabet of nucleic acids is translated into the entirely different 20-letter alphabet of proteins. Because of this conversion of one alphabet into another, translation is a conceptually more complex process than either replication or transcription, both of which take place within the framework of a common base-pairing language. The basics of protein biosynthesis are the same across all kingdoms of life — evidence that the protein-biosynthesis system arose very early in evolution. An mRNA is translated, or decoded, in the $5'$-to-$3'$ direction one codon at a time, and the corresponding protein is synthesized in the amino-to-carboxyl direction by the sequential addition of amino acids to the carboxyl end of the growing peptide chain (**Figure 30.1**). Amino acids are delivered to the ribosome attached to specific tRNAs. Once the tRNA has delivered its amino acid, it is released from the ribosome and can be linked to another amino acid, and the cycle of peptide chain elongation continues. For each amino acid there is at least one kind of tRNA, and specific enzymes link amino acids to their corresponding tRNAs. This linking is essential to the accurate translation of the language of nucleic acids to that of proteins and thus to the accuracy of the genetic code.

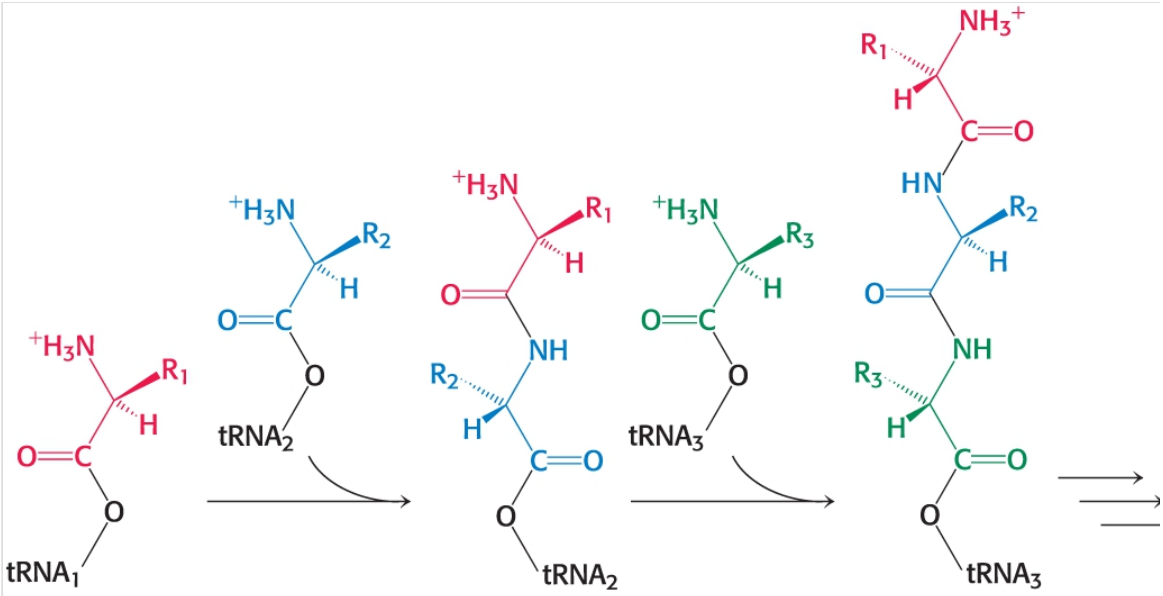


FIGURE 30.1 Polypeptides are synthesized by the successive addition of amino acids to the carboxyl terminus.

The biosynthesis of long proteins requires a low error frequency

The process of transcribing DNA into mRNA is analogous to copying, word for word, a page of a book. There is no change of alphabet or vocabulary, so the likelihood of a change in meaning is small. In contrast, translating the base sequence of an mRNA molecule into a sequence of amino acids is analogous to translating the page of a book into another language. Translation is a complex process, entailing many steps and dozens of molecules, and a potential for error exists at each step. The complexity of translation creates a conflict between two requirements: the process must be accurate yet fast enough to meet a cell's needs. In *E. coli*, translation can take place at a rate of 20 amino acids per second, a truly impressive speed considering the complexity of the process.

How accurate must protein biosynthesis be? Let us consider error rates. The probability of forming a protein with no errors depends on the number of amino acid residues and on the frequency (ε) of insertion of a wrong amino acid. As Table 30.1 shows, an error frequency of 10^{-2} is intolerable, even for quite small proteins $(\sim 100 \text{ residues})$. An ε value of 10^{-3} usually leads to the error-free synthesis of an average-sized 300-residue protein $(\sim 33 \text{ kDa})$ but not of a large 1000-residue protein $(\sim 110 \text{ kDa})$; the error frequency must not exceed approximately 10^{-4} to produce the larger proteins effectively. While lower error frequencies are conceivable, they will not dramatically increase the percentage of proteins with accurate sequences, except for really large proteins $(> 1000 \text{ residues})$. In addition, such lower error rates are likely to be possible only by a reduction in the rate of protein biosynthesis because additional time for proofreading is required. In fact, the observed values of ε are close to 10^{-4}, allowing for the accurate production of proteins consisting of as many as 1000 amino acids while maintaining a remarkably rapid rate for protein biosynthesis.

TABLE 30.1 Accuracy of protein synthesis

Frequency of inserting an incorrect amino acid	Probability of synthesizing an error-free protein		
	Number of amino acid residues		
	100	300	1000
10^{-2}	0.366	0.049	0.000
10^{-3}	0.905	0.741	0.368

10^{-4}	0.990	0.970	0.905
10^{-5}	0.999	0.997	0.990

Note: The probability p of forming a protein with no errors depends on n, the number of amino acids, and ε the frequency of insertion of a wrong amino acid: $p = (1 - \epsilon)^n$.

Transfer RNA (tRNA) molecules have a common design

The fidelity of protein biosynthesis requires accurate recognition of three-base **codons** on mRNA (Section 8.5). An amino acid cannot itself recognize a codon. Consequently, an amino acid is attached to a specific tRNA molecule that recognizes the codon by Watson–Crick base-pairing. **Transfer RNA** serves as the adapter molecule: not only does the tRNA contain an **anticodon** that binds to a specific codon, but it also brings with it an amino acid for incorporation into the polypeptide chain.

Thousands of tRNA sequences are known. All tRNA molecules must be able to interact in nearly the same way with the ribosomes, mRNAs, and protein factors that participate in translation. So, it's not surprising that tRNA molecules have many shared structural features and underlying commonalities in their sequences:

- Each tRNA is a single chain containing between 73 and 93 ribonucleotides.
- Each tRNA sequence can be arranged in a cloverleaf pattern in which about half the residues are base-paired (**Figure 30.2**).

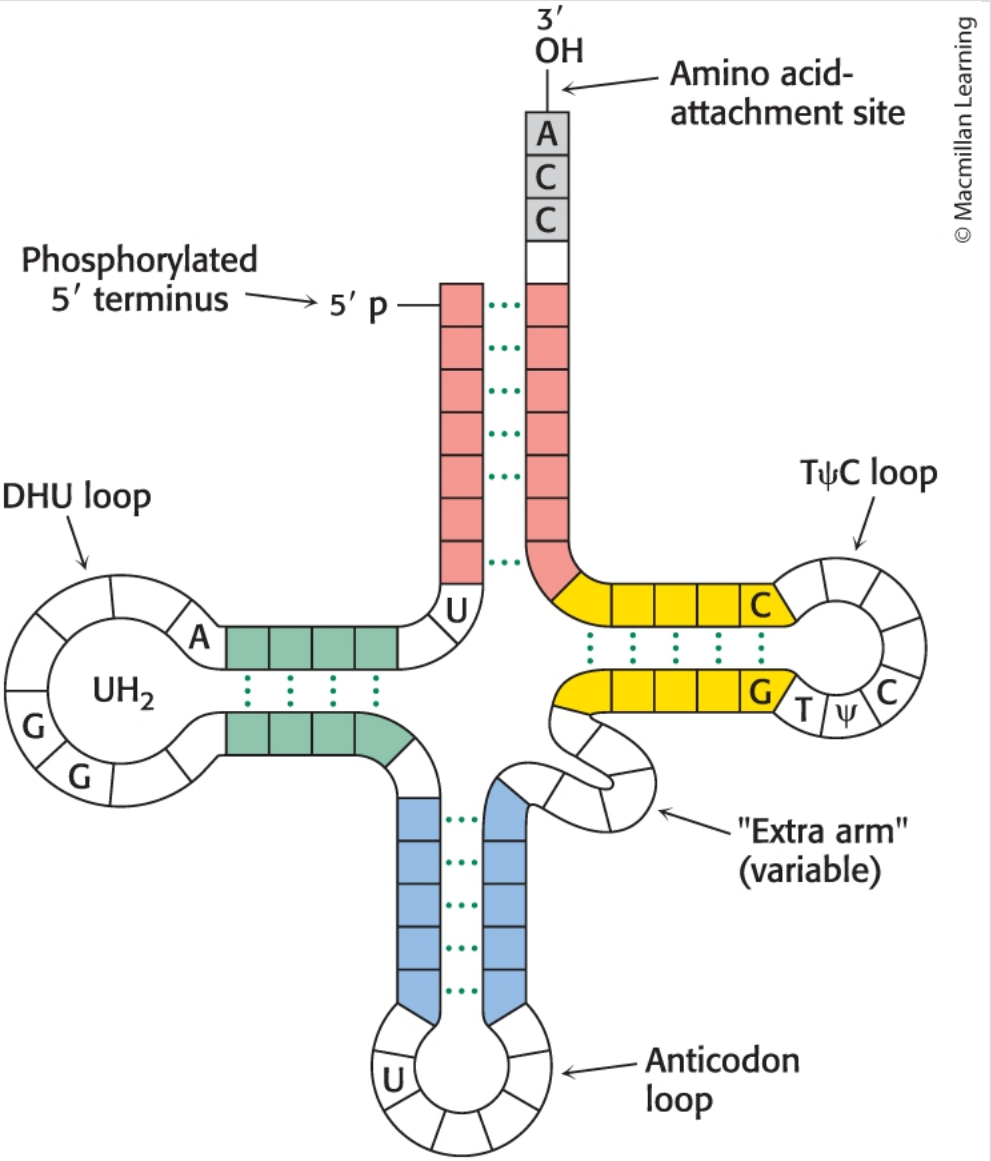


FIGURE 30.2 The secondary structure of all transfer RNAs resembles a cloverleaf. Comparison of the base sequences of many tRNAs reveals a number of conserved features.

- The molecule is L-shaped (Figure 30.3).

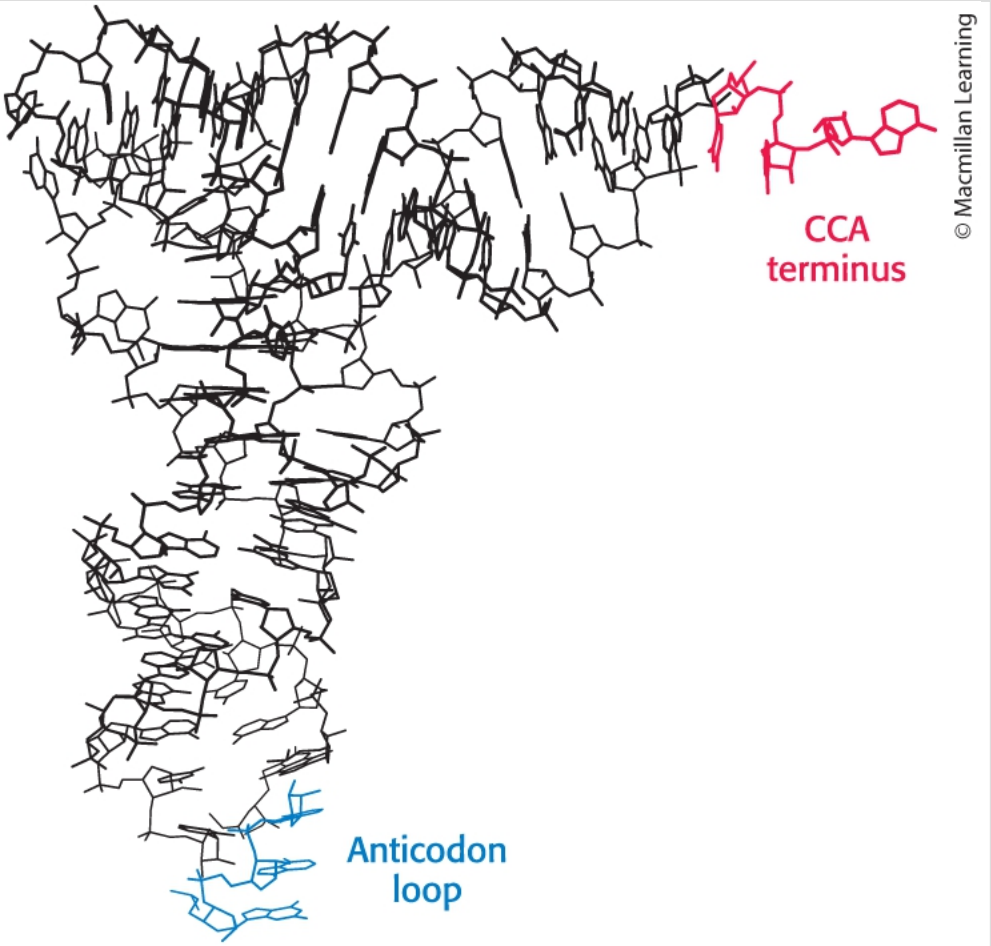


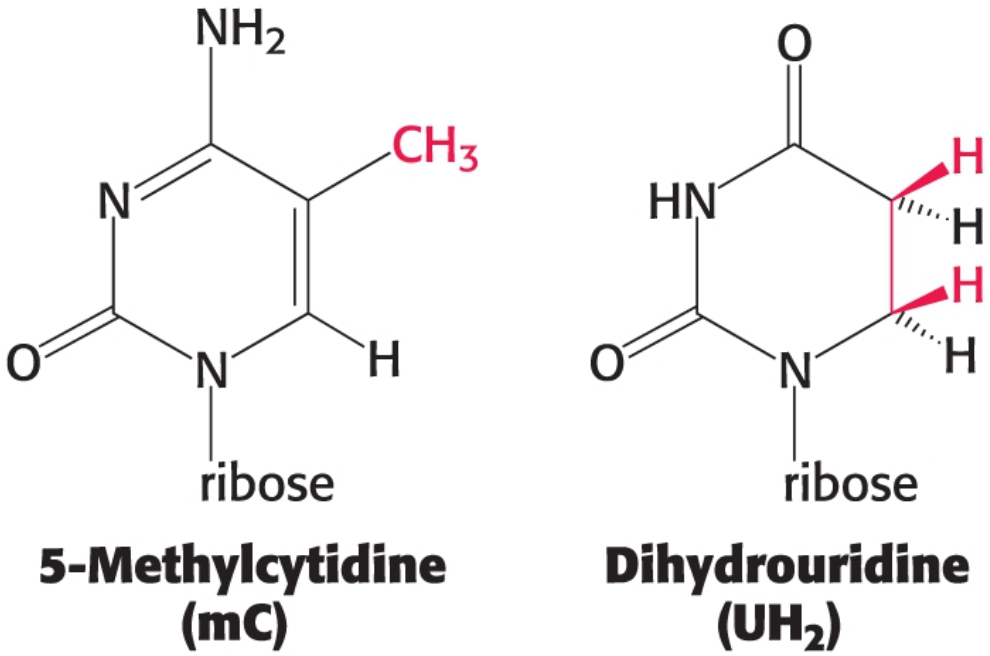
FIGURE 30.3 Transfer RNAs have an L-shaped tertiary structure. The L-shaped structure is revealed by this skeletal model of yeast phenylalanyl-tRNA. The CCA region is at the end of one arm, and the anticodon loop is at the end of the other.

[Drawn from 1EHZ.pdb.]

INTERACT with this model in Achieve

- They contain many unusual bases, typically between 7 and 15 per molecule. Some of these bases are methylated or dimethylated derivatives of A, U, C, and G formed by enzymatic modification of a precursor tRNA. Two examples of such modified bases are 5-

methylcytidine (mC) and dihydrouridine (UH_2). Methylation imparts a hydrophobic character to some regions of tRNAs, which may be important for their interaction with synthetases and ribosomal proteins. Some methylations also prevent bases from forming proper base pairs, allowing them to interact with other bases. Other modifications alter codon recognition, as will be described shortly.



- About half the nucleotides in tRNAs are base-paired to form double helices. The four helical regions are arranged to form two apparently continuous segments of double helix. These segments are like A-form DNA, as expected for an RNA helix (Section 4.2). One helix contains the 5′ and 3′ ends and runs horizontally in the model shown in **Figure 30.4**; it forms one arm of the L. The other helix, which contains the anticodon and runs vertically in Figure 30.4, forms the other arm of the L.

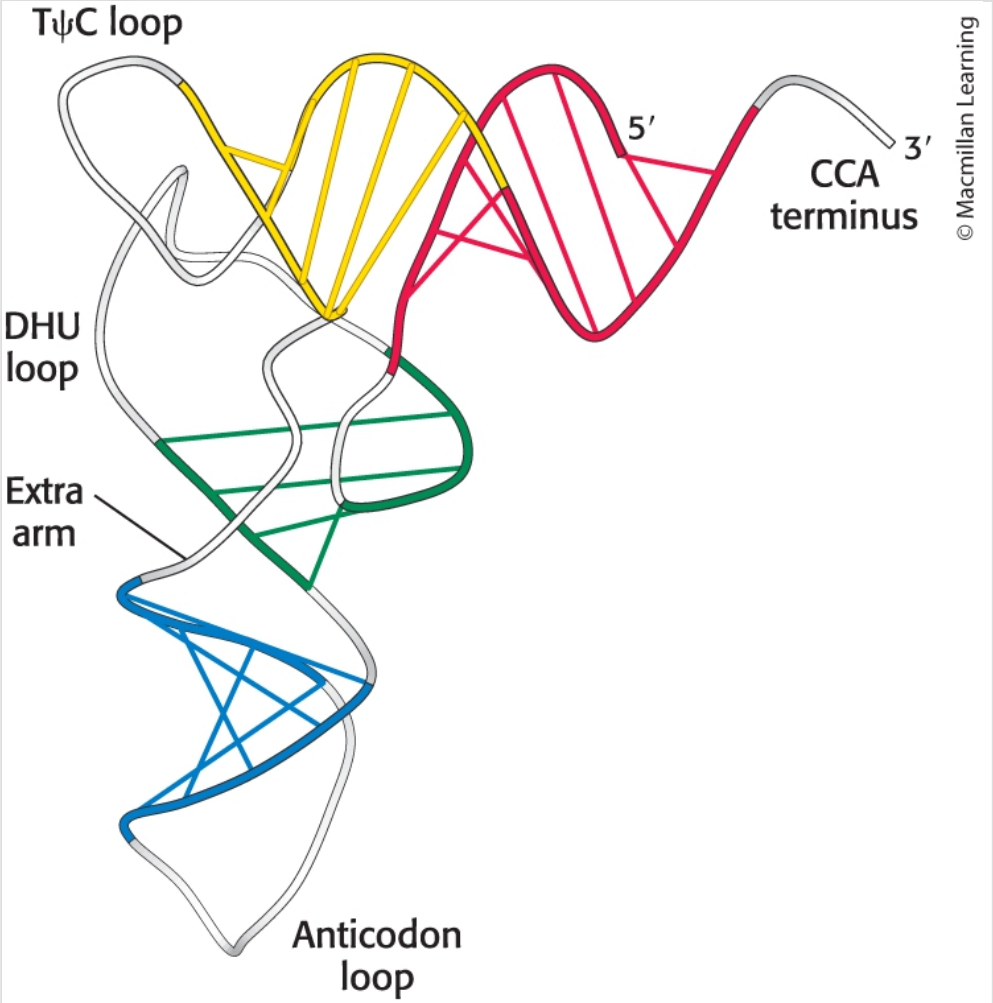


FIGURE 30.4 The four double-stranded regions of a tRNA stack to form an L-shaped structure.

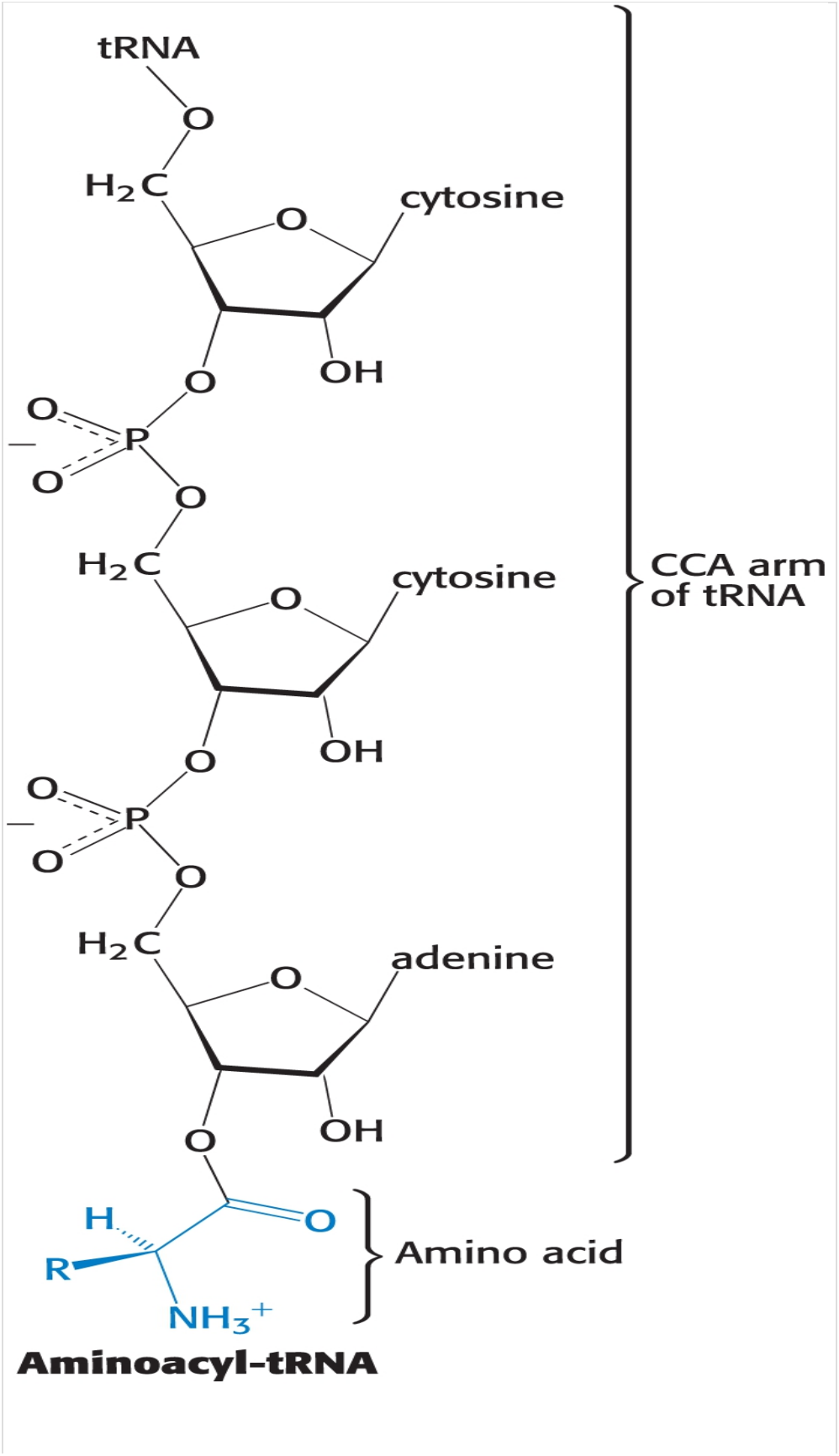
[Drawn from 1EHZ.pdb.]

INTERACT with this model in Achieve

Five groups of bases are not base-paired in this way: the 3′ CCA terminal region, which is part of a region called the *acceptor stem*; the TψC *loop*, which is named for its ribothymidine-pseudouracil-cytosine; the "*extra arm*," which contains a variable number of

residues; the *DHU loop*, which contains several dihydrouracil residues; and the *anticodon loop*. Most of the bases in the nonhelical regions participate in hydrogen-bonding interactions, even if the interactions are not like those in Watson–Crick base pairs. Although they are structurally similar overall, the structural diversity generated by this combination of helices and loops containing modified bases ensures that the tRNAs can be uniquely distinguished.

- The $5'$ end of a tRNA is phosphorylated. The $5'$ terminal residue is usually pG.
- An activated amino acid is attached to a hydroxyl group of the adenosine residue in the amino-acid-attachment site, located at the end of the $3'$ CCA component of the acceptor stem (**Figure 30.5**).



Aminoacyl-tRNA

FIGURE 30.5 Ester linkages couple amino acids to tRNAs. While a linkage to the $3'$-hydroxyl group is shown here, these bonds can be to either the $2'$- or the $3'$-hydroxyl group of the $3'$-adenosine residue on the tRNA.



- The anticodon loop, which is present in a loop near the center of the sequence, is at the other end of the L, making the three bases that constitute the anticodon accessible for interaction with a codon.

Thus, the architecture of the tRNA molecule is well suited to its role as adaptor: the anticodon is available to interact with an appropriate codon on mRNA, while the end that is linked to an amino acid is well positioned to participate in peptide-bond formation.

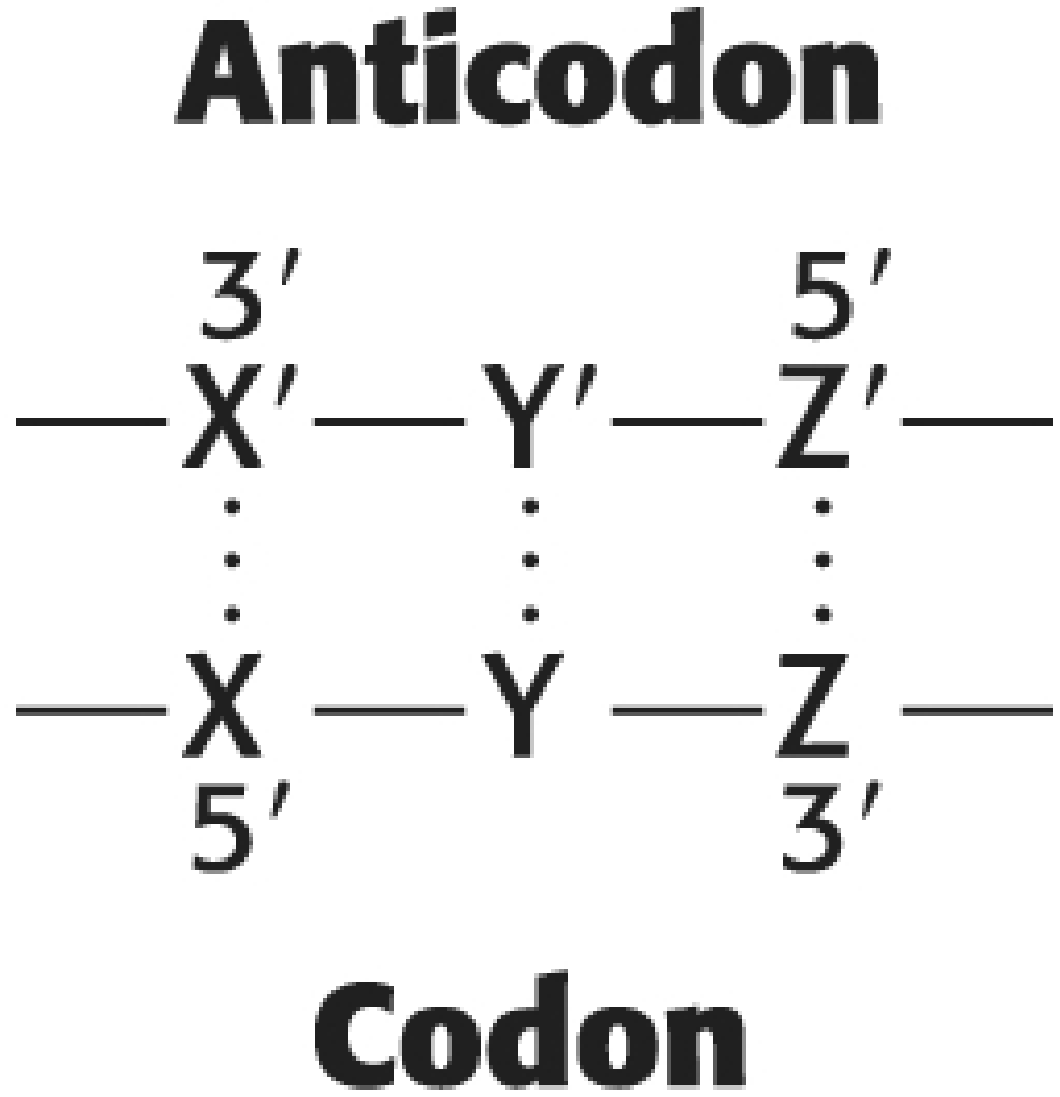
Self-Check Question



What features are common to all tRNA molecules?

Some transfer RNA molecules recognize more than one codon because of wobble in base-pairing

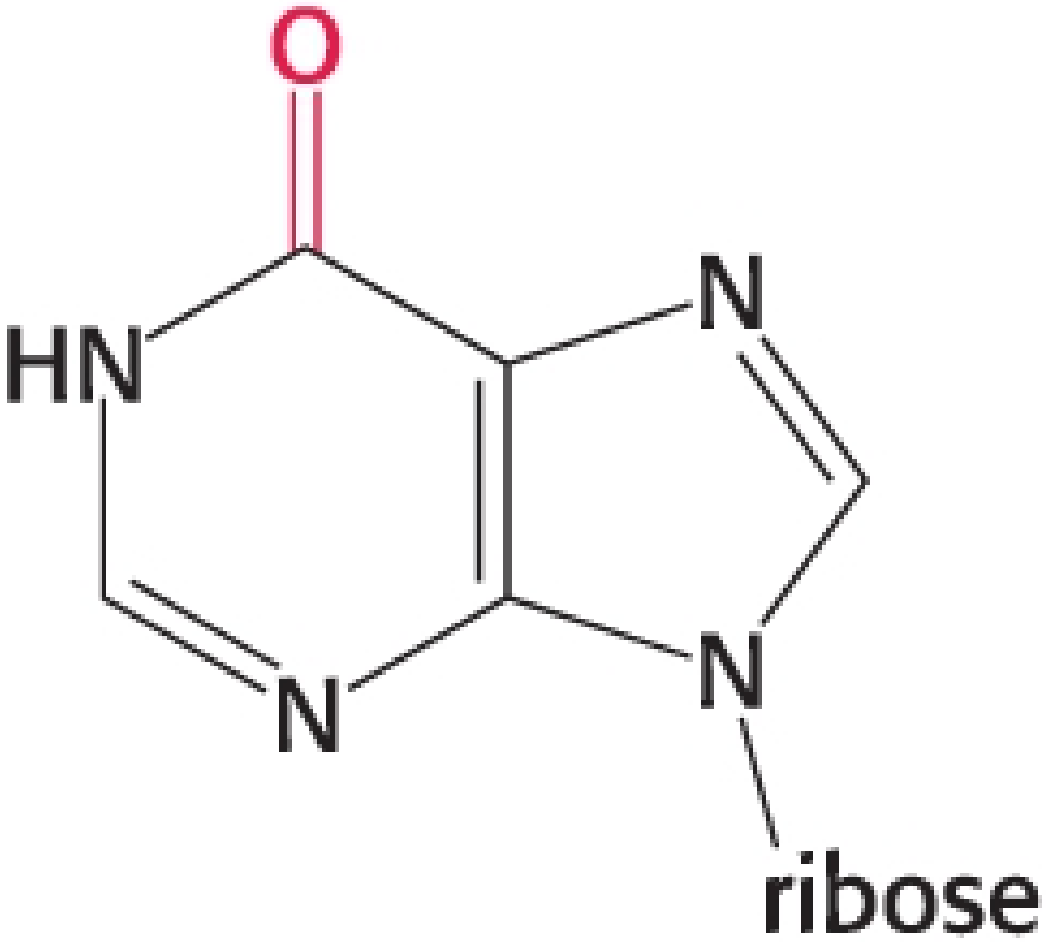
What are the rules that govern the recognition of a codon by the anticodon of a tRNA? A simple hypothesis is that each of the bases of the codon forms a Watson–Crick base pair with a complementary base on the anticodon of the tRNA. The codon and anticodon would then be lined up in an antiparallel fashion, where the prime denotes the complementary base in the anticodon. Thus X and X' would be either A and U (or U and A) or G and C (or C and G). According to this model, a particular anticodon can recognize only *one* codon.



Experiments show, however, that some tRNA molecules can recognize more than one codon. For example, the yeast alanyl-tRNA binds to *three* codons: GCU, GCC, and GCA. The first two bases of these codons are the same, whereas the third is different. Could it be that recognition of the third base of a codon is sometimes less discriminating than recognition of the other two? The redundancy, or degeneracy, of the genetic code indicates that it might be so. XYU and XYC always encode the same amino acid; XYA and XYG usually do. These data suggest that the steric

criteria might be less stringent for pairing of the third base than for the other two. In other words, there is some steric freedom ("wobble") in the pairing of the third base of the codon.

The **wobble hypothesis** is now firmly established (**Table 30.2**). The anticodons of tRNAs of known sequence bind to the codons predicted by this hypothesis; for example, the anticodon of yeast alanyl-tRNA is IGC (*I* is the purine base inosine). This tRNA recognizes the codons GCU, GCC, and GCA. Recall that, by convention, nucleotide sequences are written in the $5' \rightarrow 3'$ direction unless otherwise noted. Hence, I (the $5'$ base of this anticodon) pairs with U, C, or A (the $3'$ base of the codon), as predicted.



Inosine

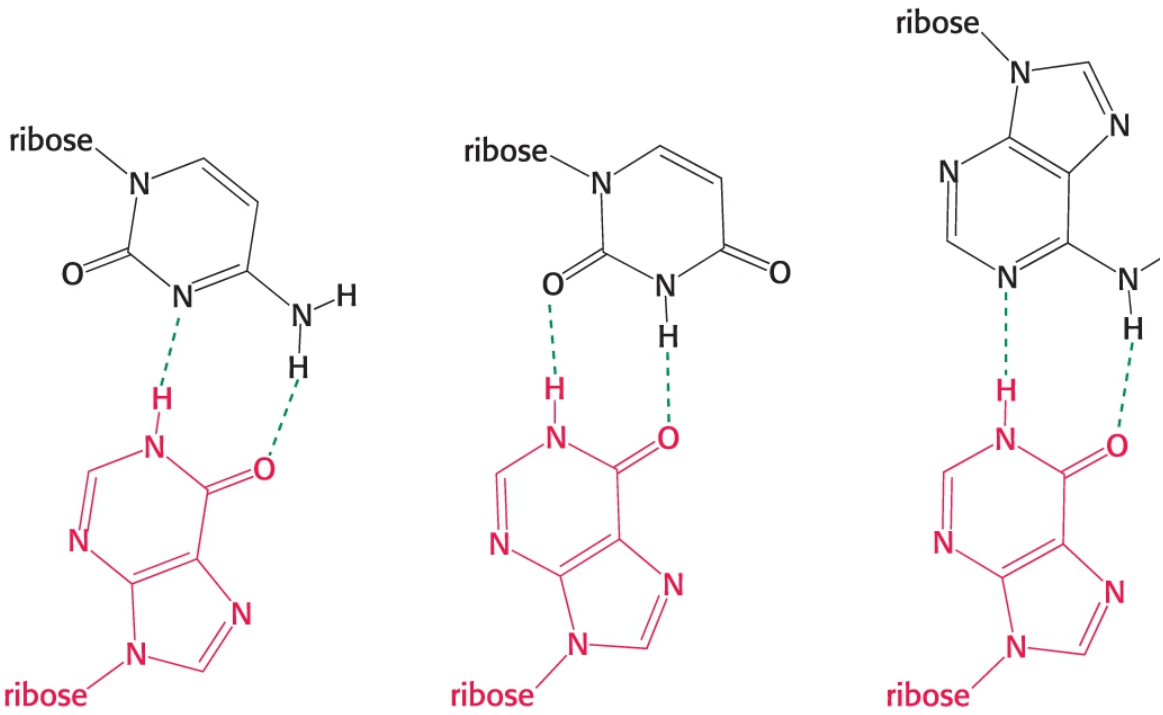


TABLE 30.2 Allowed pairings at the third base of the codon according to the wobble hypothesis

First base of anticodon	Third base of codon
C	G
A	U
U	A or G
G	U or C
I	U, C, or A

Two generalizations concerning the codon–anticodon interaction can be made:

1. *Codons that differ in either of their first two bases must be recognized by different tRNAs.* The first two bases of a codon pair in the standard way, and recognition is precise. For example, both UUA and CUA encode leucine but are read by different tRNAs.

2. *Part of the degeneracy of the genetic code arises from imprecision (wobble) in the pairing of the third base of the codon with the first base of the anticodon.* The first base of an anticodon determines whether a particular tRNA molecule reads one, two, or three kinds of codons: C or A (one codon), U or G (two codons), or I (three codons).

We see here a strong reason for the frequent appearance of inosine, one of the unusual nucleosides, in anticodons: inosine maximizes the number of codons that can be read by a particular tRNA molecule. The inosine bases in tRNA are formed by the deamination of adenosine after the synthesis of the primary transcript.

Why is wobble tolerated in the third position of the codon but not in the first two? This question is answered by considering the interaction of the tRNA with the ribosome. As we will soon examine in greater detail, **ribosomes** are huge RNA–protein complexes consisting of two subunits. One of these subunits has three universally conserved bases in its RNA molecule that form hydrogen bonds only with correctly formed base pairs in the codon–anticodon duplex (**Figure 30.6**). These interactions ensure that Watson–Crick base pairs are present in the first two positions of the codon–anticodon duplex, but not the third position, so more varied base pairs are tolerated. Thus, the ribosome plays an active role in decoding the codon–anticodon interactions.

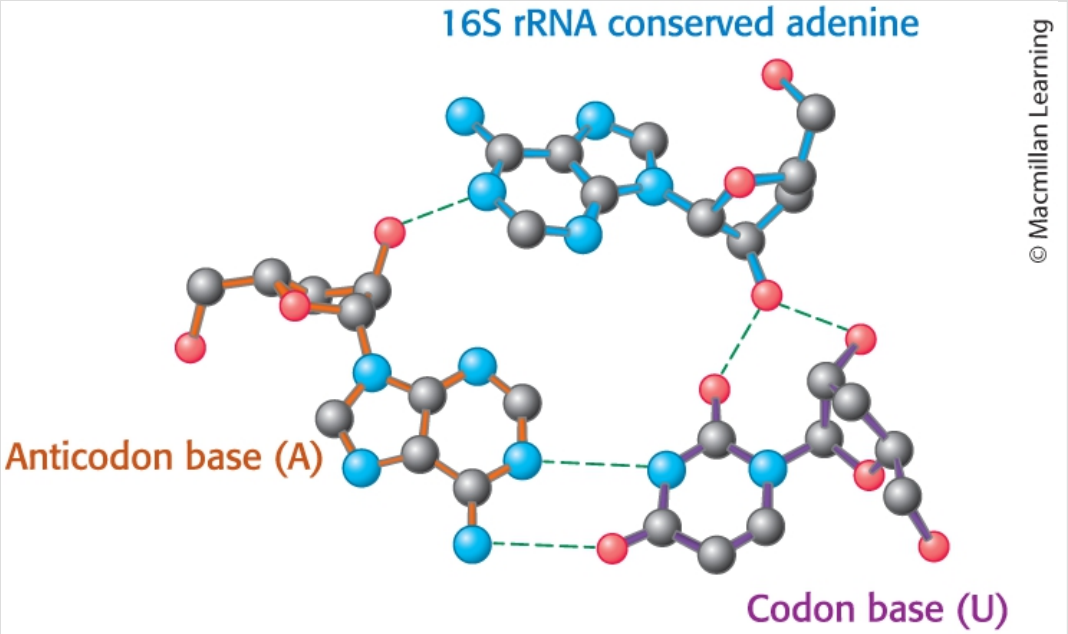


FIGURE 30.6 16S rRNA monitors base-pairing between the codon and the anticodon. One of three universally conserved bases in 16S rRNA (an adenine) forms hydrogen bonds with the bases in both the codon and the anticodon only if the codon and anticodon are correctly paired. Only one anticodon base (adenine) and one codon base (uracil) are shown. Hydrogen atoms are omitted for clarity.

[Information from J. M. Ogle and V. Ramakrishnan, *Annu. Rev. Biochem*. 74:129–177, 2005, Fig. 2a.]

Self-Check Question

Explain how it is possible that some tRNA molecules recognize more than one codon.

30.2 Aminoacyl-tRNA Synthetases Establish the Genetic Code

Before codon and anticodon meet, the amino acids required for protein biosynthesis must first be attached to specific tRNA molecules, linkages that are crucial for two reasons:

- *The attachment of a given amino acid to a particular tRNA establishes the genetic code.* When an amino acid has been linked to a tRNA, it will be incorporated into a growing polypeptide chain at a position dictated by the anticodon of the tRNA.

- *Because the formation of a peptide bond between free amino acids is not thermodynamically favorable, the amino acid must first be activated for protein biosynthesis to proceed.* The activated intermediates in protein biosynthesis are amino acid esters, in which the carboxyl group of an amino acid is linked to either the $2'$- or the $3'$-hydroxyl group of the ribose unit at the $3'$ end of tRNA. An amino acid ester of tRNA is called an **aminoacyl-tRNA** or sometimes a *charged tRNA* (Figure 30.6). For a specific amino acid attached to its cognate tRNA — for instance, threonine — the charged tRNA is designated $\mathrm{Thr{-}tRNA}^{\mathrm{Thr}}$.

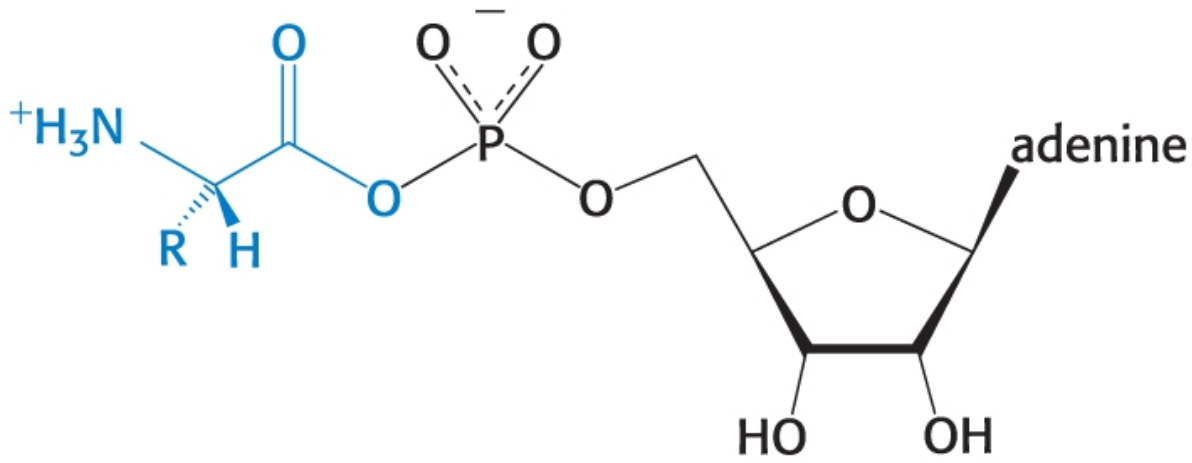
Amino acids are first activated by adenylation

The activation reaction is catalyzed by specific **aminoacyl-tRNA synthetases**. These enzymes activate an amino acid and then link it to

its corresponding tRNA in a two-step reaction. The first step is the formation of an aminoacyl adenylate from an amino acid and ATP.

$$\text{Amino acid} + \text{ATP} \rightleftharpoons \text{aminoacyl-AMP} + \text{PP}_\text{i}$$

This activated species is a mixed anhydride in which the carboxyl group of the amino acid is linked to the phosphoryl group of AMP; hence, it is also known as *aminoacyl-AMP*.



Aminoacyl-AMP

The next step is the transfer of the aminoacyl group of aminoacyl-AMP to a particular tRNA molecule to form aminoacyl-tRNA.

$$\text{Aminoacyl-AMP} + \text{tRNA} \rightleftharpoons \text{aminoacyl-tRNA} + \text{AMP}$$

The sum of these activation and transfer steps is

$$\text{Amino acid} + \text{ATP} + \text{tRNA} \rightleftharpoons \text{aminoacyl-tRNA} + \text{AMP} + \text{PP}_\text{i}$$

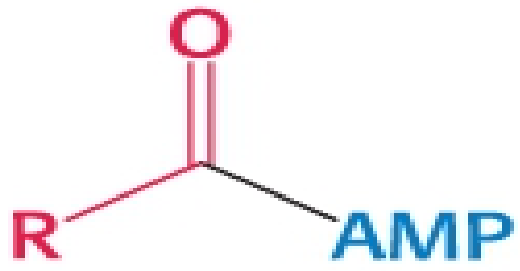
The $\Delta G^{\circ\prime}$ of this reaction is close to 0, because the free energy of hydrolysis of the ester bond of aminoacyl-tRNA is similar to that for the hydrolysis of ATP to AMP and PP_i. As we have seen many times, the reaction is driven by the hydrolysis of pyrophosphate. The sum of these three reactions is highly exergonic:

$$\text{Amino acid} + \text{ATP} + \text{tRNA} + H_2O \rightarrow \text{aminoacyl}-\text{tRNA} + \text{AMP} + 2P_i$$

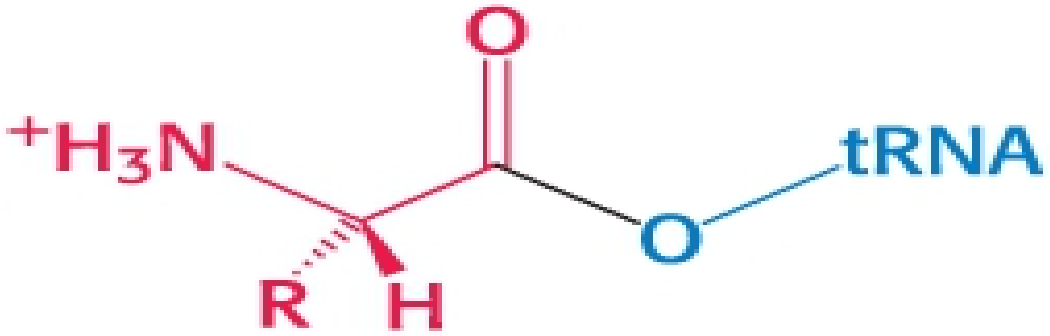
There are two key points to note about this reaction:

- *The equivalent of two molecules of ATP is consumed in the synthesis of each aminoacyl-tRNA*. One of them is consumed in forming the ester linkage of aminoacyl-tRNA, whereas the other is consumed in driving the reaction forward.

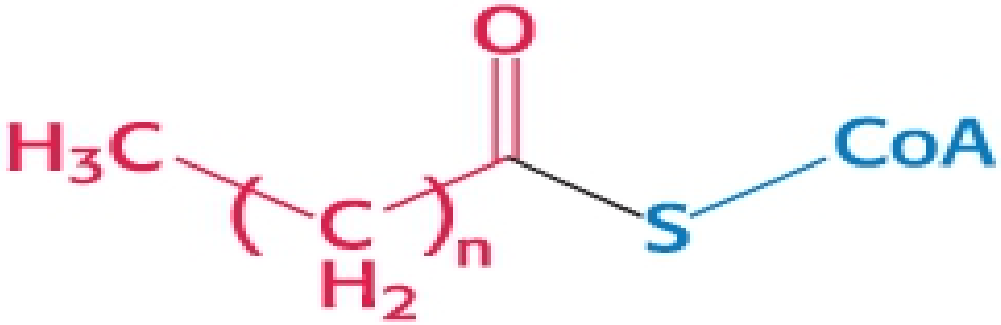
- *The aminoacyl-AMP intermediate does not dissociate from the synthetase*. Rather, it is tightly bound to the active site of the enzyme by noncovalent interactions. This means that the activation and transfer steps for a particular amino acid are catalyzed by the same aminoacyl-tRNA synthetase.



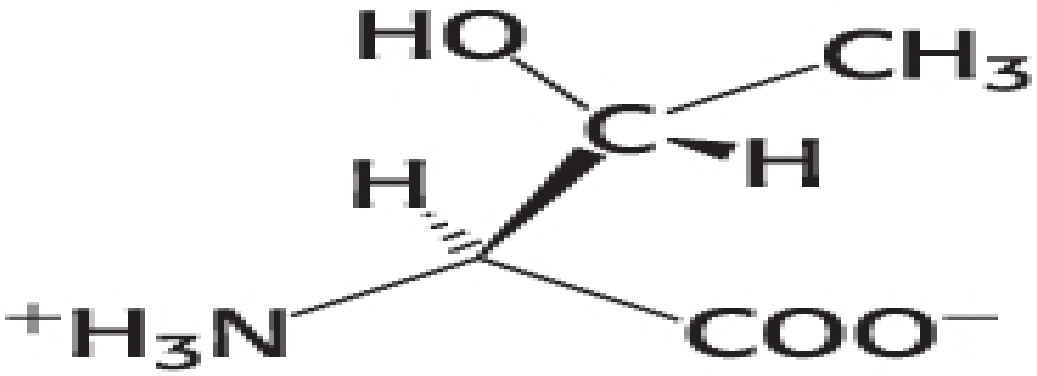
Acyl adenylate intermediate



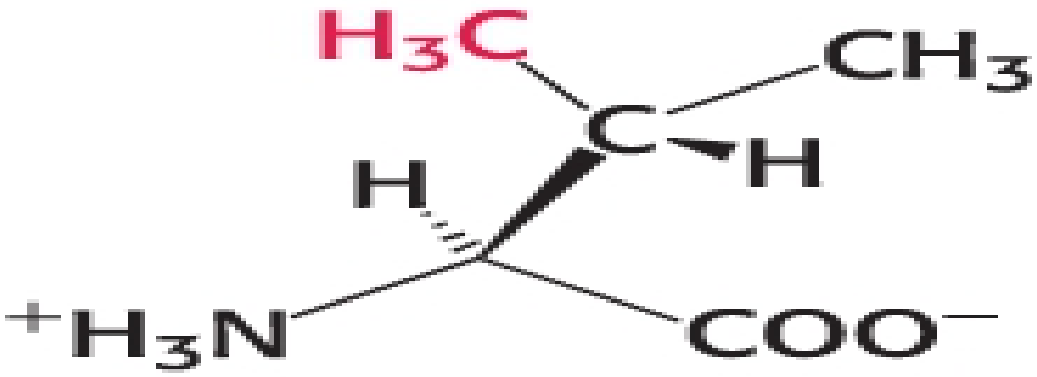
Aminoacyl-tRNA



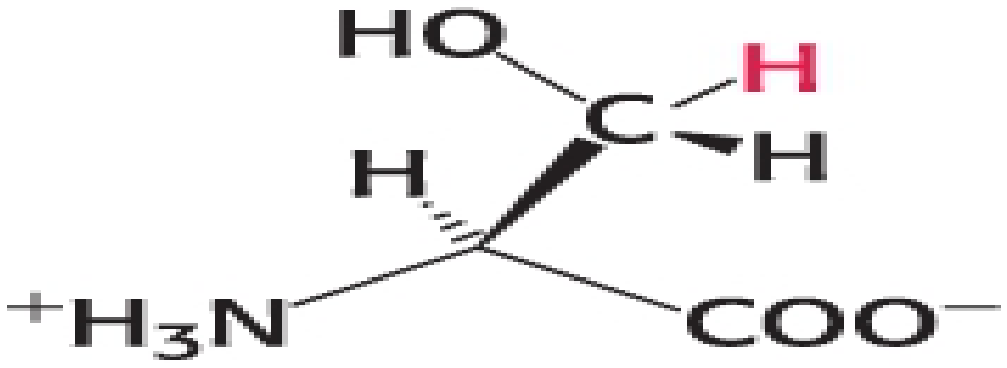
Fatty acyl CoA



Threonine



Valine



Serine

We have already encountered an acyl adenylate intermediate in fatty acid activation (Section 22.2). The major difference between these reactions is that the acceptor of the acyl group is CoA in fatty acid activation and tRNA in amino acid activation. The energetics of these biosyntheses are very similar: both are made irreversible by the hydrolysis of pyrophosphate.

Aminoacyl-tRNA synthetases have highly discriminating amino acid activation sites

Each aminoacyl-tRNA synthetase is highly specific for a given amino acid. Indeed, a synthetase will link an incorrect amino acid to a tRNA only once in 10^4 or 10^5 reactions. How is this level of specificity achieved? Each aminoacyl-tRNA synthetase takes advantage of the properties of its amino acid substrate. Consider the challenge faced by threonyl-tRNA synthetase. Threonine is especially similar to two other amino acids: valine and serine. Valine has almost exactly the same shape as that of threonine, except that valine has a methyl group in place of a hydroxyl group. Serine has a hydroxyl group, as does threonine, but lacks the methyl group. How can the threonyl-tRNA synthetase avoid coupling these incorrect amino acids to threonyl-tRNA (abbreviated $tRNA^{Thr}$)?

The structure of the amino acid-binding site of threonyl-tRNA synthetase reveals how valine is avoided (**Figure 30.7**). The synthetase contains a zinc ion bound to the enzyme by two histidine residues and one cysteine residue, with the remaining coordination sites available for substrate binding. The use of a zinc ion appears to be unique to threonyl-tRNA synthetase; other aminoacyl-tRNA synthetases have different strategies for recognizing their cognate amino acids.

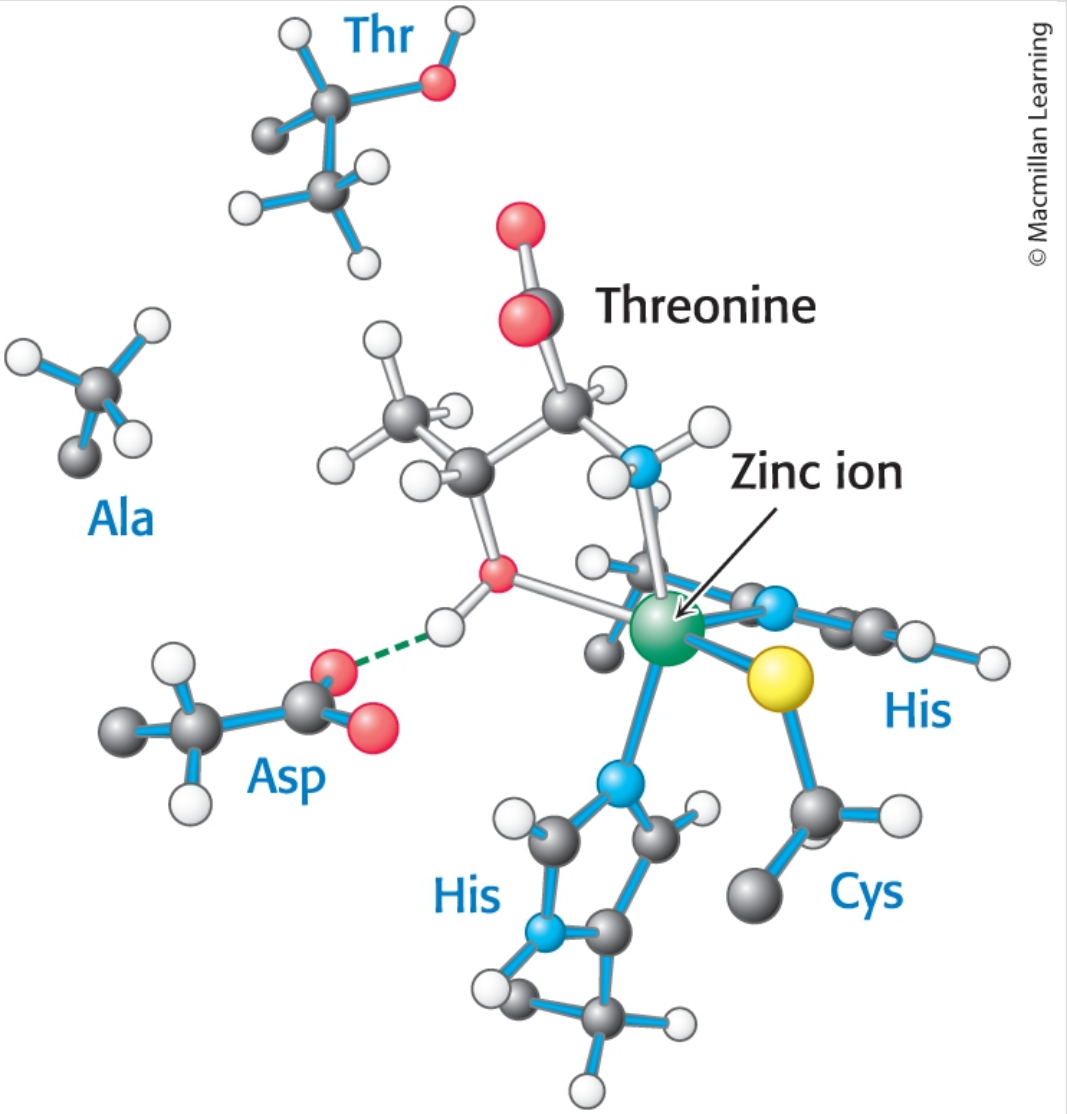


FIGURE 30.7 The amino acid-binding site of threonyl-tRNA synthetase contains a zinc ion. This zinc ion (green ball) binds to the amino and hydroxyl groups of threonine (white). Selected amino acids from the synthetase are shown in blue.

Threonine binds to the zinc ion through its amino group and its side-chain hydroxyl group. The side-chain hydroxyl group is further recognized by an aspartate residue that hydrogen-bonds to it. The methyl group present in valine in place of this hydroxyl group cannot participate in these interactions; it is excluded from this active site and,

hence, does not become adenylated and transferred to $tRNA^{Thr}$. The carboxylate group of the correctly positioned threonine is available to attack the α-phosphoryl group of ATP to form the aminoacyl adenylate.

The zinc site is less able to discriminate against serine because this amino acid does have a hydroxyl group that can bind to the zinc ion. Indeed, with only this mechanism available, threonyl-tRNA synthetase does mistakenly couple serine to $tRNA^{Thr}$ at a rate 10^{-2} to 10^{-3} times that for threonine. This error rate is likely to lead to many translation errors, so how is a higher level of specificity achieved?

Proofreading by aminoacyl-tRNA synthetases increases the fidelity of protein biosynthesis

Threonyl-tRNA synthetase can be incubated with $tRNA^{Thr}$ that has been covalently linked with serine ($Ser-tRNA^{Thr}$); the tRNA has been "mischarged." The reaction is immediate: a rapid hydrolysis of the aminoacyl-tRNA forms serine and free tRNA. In contrast, incubation with correctly charged $Thr-tRNA^{Thr}$ results in no reaction. Thus, threonyl-tRNA synthetase contains an additional functional site that hydrolyzes $Ser-tRNA^{Thr}$ but not $Thr-tRNA^{Thr}$. This editing site provides an opportunity for the synthetase to correct its mistakes and improve its fidelity to less than one mistake in 10^4.

The results of structural and mutagenesis studies revealed that the editing site for threonyl-tRNA synthase is more than 20 Å from the activation site (**Figure 30.8**). This editing site readily accepts and cleaves

$Ser-tRNA^{Thr}$ but does not cleave $Thr-tRNA^{Thr}$. The discrimination of serine from threonine is easy because threonine contains an extra methyl group; a site that conforms to the structure of serine will sterically exclude threonine. The structure of the complex between threonyl-tRNA synthetase and its substrate reveals that the aminoacylated CCA can swing out of the activation site and into the editing site (**Figure 30.9**). Thus, the aminoacyl-tRNA can be edited without dissociating from the synthetase. This proofreading depends on the conformational flexibility of a short stretch of polynucleotide sequence.

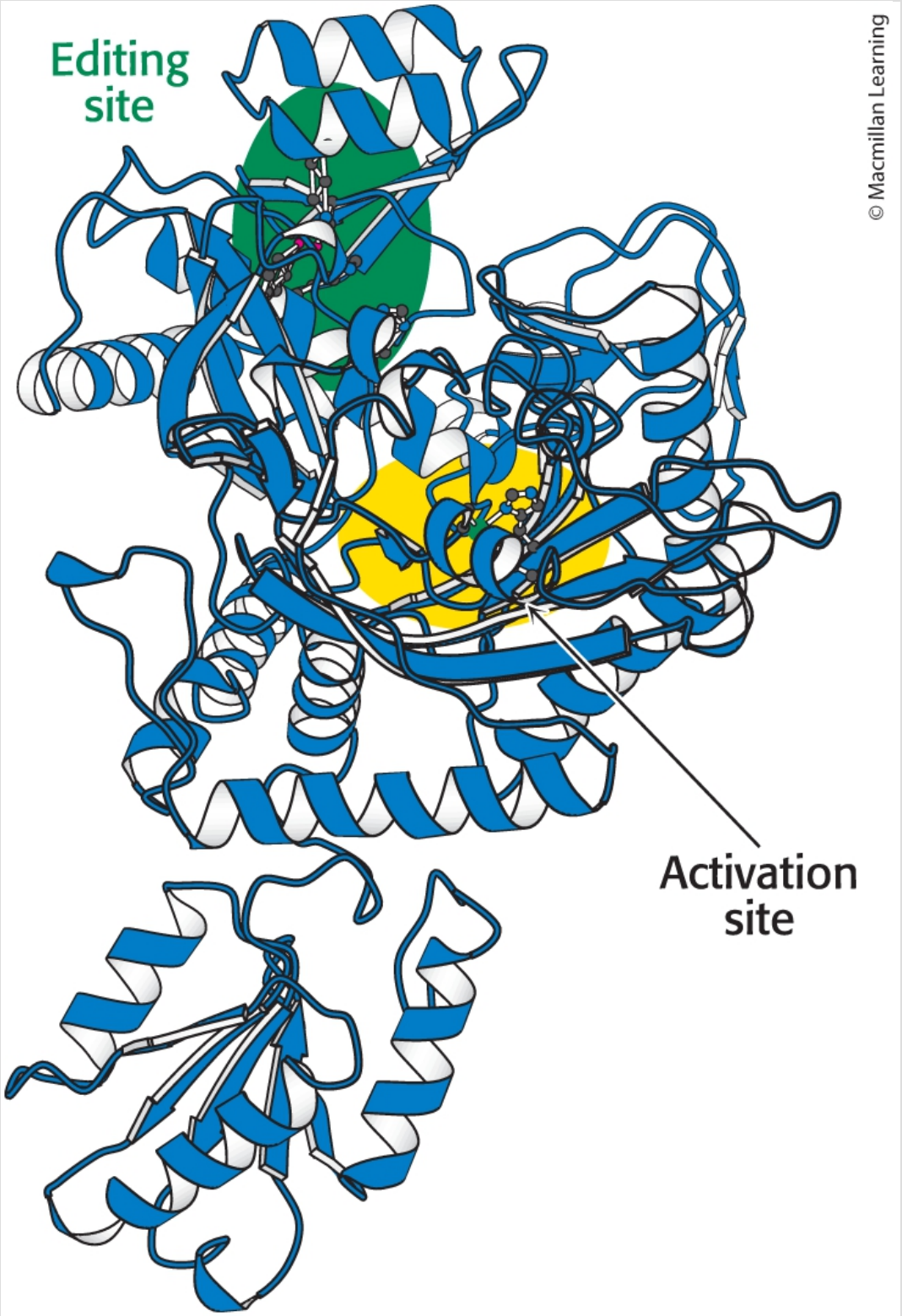


FIGURE 30.8 Threonyl-tRNA synthetase also contains an editing site. Mutagenesis studies revealed the position of the editing site (shown in green) in threonyl-tRNA

synthetase. The activation site is shown in yellow. Only one subunit of the dimeric enzyme is shown here and in subsequent illustrations.

[Drawn from 1QF6.pdb.]

INTERACT with this model in Achieve

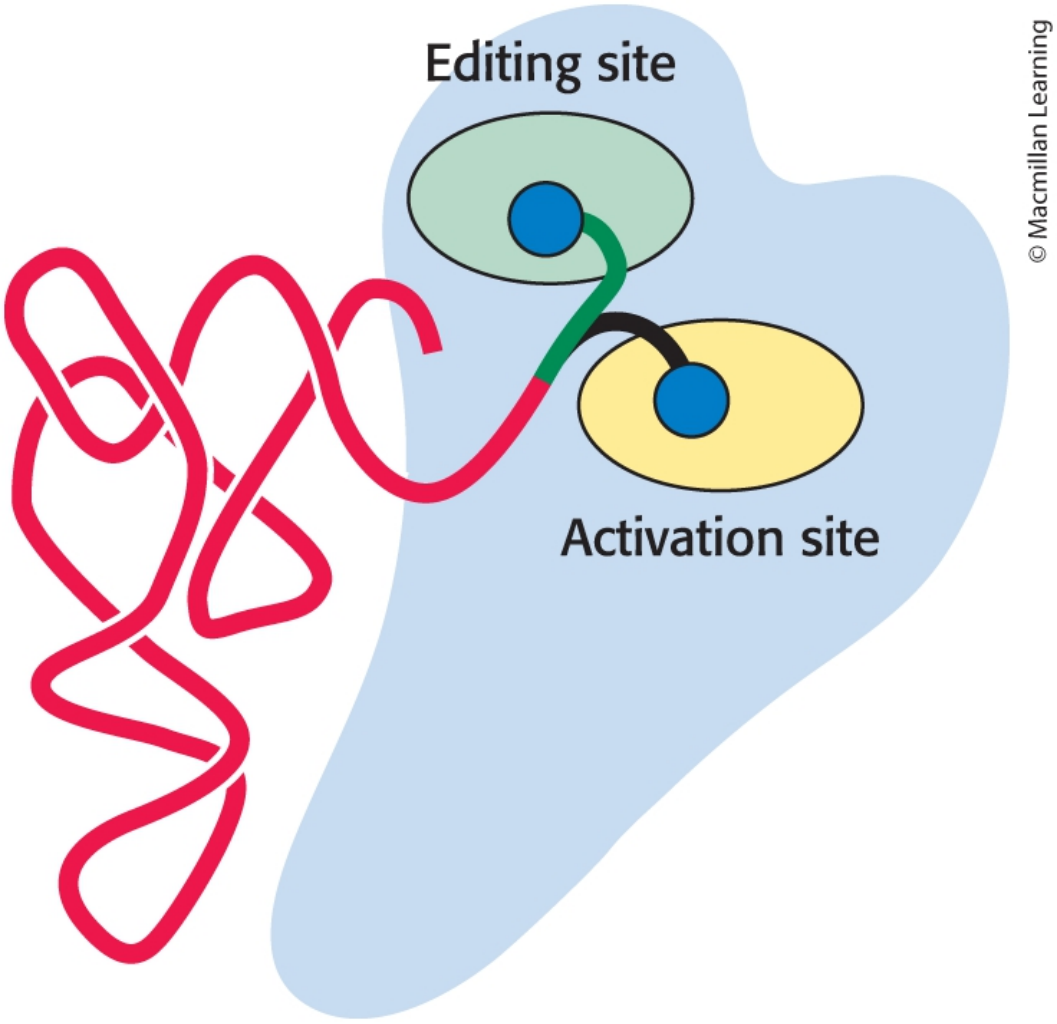


FIGURE 30.9 Amino acids move between the activation site and the editing site of an aminoacyl-tRNA synthetase. The flexible CCA arm of an aminoacyl-tRNA can swing the attached amino acid from the activation site (yellow) to the editing site (green). If the amino acid fits well into the editing site, the amino acid is removed by hydrolysis. Only one amino acid is attached to the tRNA at a time, and this amino acid can only occupy either the editing site or the activation site.

Most aminoacyl-tRNA synthetases contain editing sites in addition to activation sites. Together, these complementary sites ensure very high fidelity. In general, the acylation site rejects amino acids that are *larger* than the correct one because there is insufficient room for them, whereas the hydrolytic site cleaves activated species that are *smaller* than the correct one.

A few synthetases achieve high accuracy without editing. For example, tyrosyl-tRNA synthetase has no difficulty discriminating between tyrosine and phenylalanine; the hydroxyl group on the tyrosine ring enables tyrosine to bind to the enzyme 10^4 times as strongly as phenylalanine. In conclusion, proofreading has evolved only when fidelity must be enhanced beyond what can be obtained through an initial binding interaction.

Kinetic proofreading increases the fidelity of protein biosynthesis

As noted above, the integrity and validity of the genetic code depends on the fidelity with which tRNAs are linked to their cognate amino acids. The free energy difference of binding an incorrect versus a correct substrate is often too small to explain the accuracy of protein biosynthesis. So how is it possible? Aminoacyl-tRNA synthetases prevent many mistakes by introducing an irreversible step that facilitates their removal. This mechanism, called *kinetic proofreading*, locks in the equilibrium favoring the correct product, then selectively removes incorrect products to increase specificity further (**Figure**

30.10). For aminoacyl-tRNA synthetases, this results in additional hydrolysis of ATP, but it increases specificity.

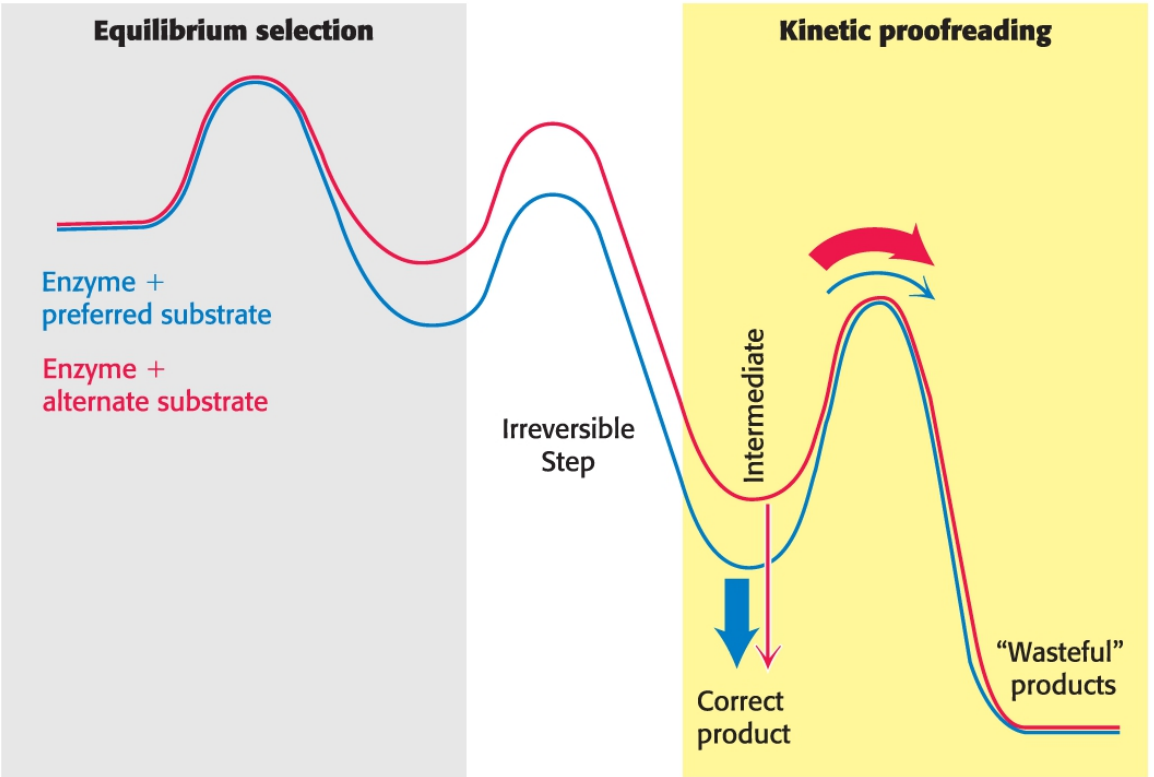


FIGURE 30.10 Kinetic proofreading can increase reaction specificity. Consider a substrate that binds to an enzyme more tightly (curve shown in blue) than an alternate substrate (curve shown in red). The preferred substrate is selected by the binding equilibrium to the enzyme. This selected equilibrium can be locked in place by an irreversible step to produce an intermediate that can either go on to the final product or undergo a side reaction to produce wasteful products. This side reaction is likely to be faster for the alternate substrate, resulting in an increased ratio of the preferred-to-alternate products. For aminoacyl-tRNA synthetases, the intermediate is an aminoacyl adenylate and the wasteful products are free amino acids and AM

Kinetic proofreading benefits other processes as well: aminoacyl-tRNA synthetases use it to discriminate between cognate and noncognate amino acids as well as tRNAs, and ribosomes use it during codon–anticodon recognition, thereby further adding to the integrity of the genetic code. Kinetic proofreading is employed by many additional

molecular processes (including DNA replication) to ensure the faithful selection of substrates.

Synthetases recognize various features of transfer RNA molecules

How do synthetases choose their tRNA partners? This enormously important step is the point at which the actual "translation" takes place: when the correlation between the amino acid and the nucleic acid worlds is made. In a sense, aminoacyl-tRNA synthetases are the only molecules in biology that "know" the genetic code. Their precise recognition of tRNAs is as important for high-fidelity protein biosynthesis as is the accurate selection of amino acids, and this recognition is sometimes referred to as the "second genetic code." In general, tRNA recognition by the synthetase is different for each synthetase and tRNA pair:

- *Some synthetases recognize their tRNA partners primarily on the basis of their anticodons*. The most direct evidence comes from crystallographic studies of complexes formed between synthetases and their cognate tRNAs. Consider, for example, the structure of the complex between threonyl-tRNA synthetase and $tRNA^{Thr}$ (**Figure 30.11**). As expected, the CCA arm extends into the zinc-containing activation site, where it is well-positioned to accept threonine from threonyl adenylate. The enzyme interacts extensively not only with the acceptor stem of the tRNA, but also with the anticodon loop. The interactions with the anticodon loop are particularly revealing. Each base within the sequence $5'-CGU-3'$ of the anticodon participates in hydrogen bonds with the enzyme; those with the second two bases (G and U) appear to be more important because the synthetase interacts just as efficiently with the anticodons GGU and UGU.

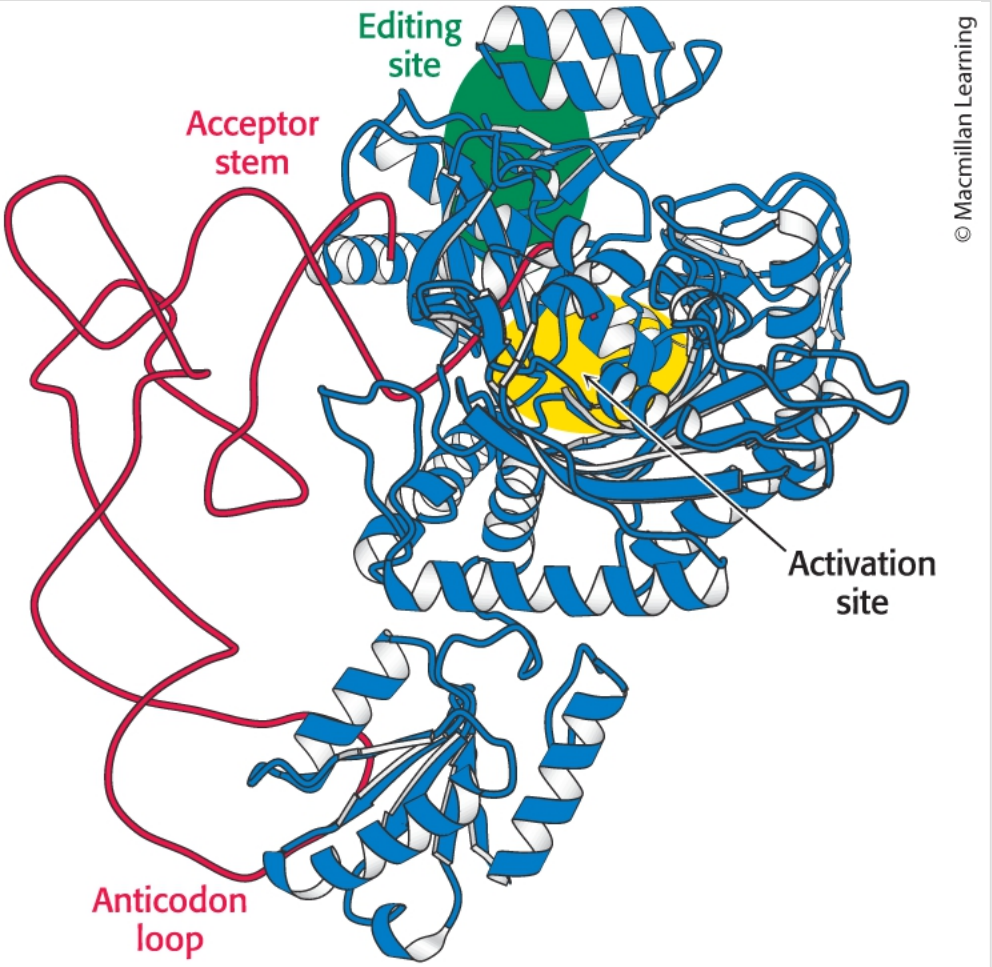


FIGURE 30.11 Aminoacyl-tRNA synthetases bind to both the acceptor stem and the anticodon loop of a tRNA. This structure shows the complex between threonyl-tRNA synthetase (blue) and $tRNA^{Thr}$ (red).

[Drawn from 1QF6.pdb.]

INTERACT with this model in Achieve

- *Synthetases may also recognize other aspects of tRNA structure that vary among different tRNAs.* Although interactions between the enzyme and the anticodon are often crucial for correct recognition, Figure 30.12 shows that many aspects of tRNA molecules are recognized

by synthetases. Note that many of the recognition sites are loops rich in unusual bases that can provide structural identifiers.

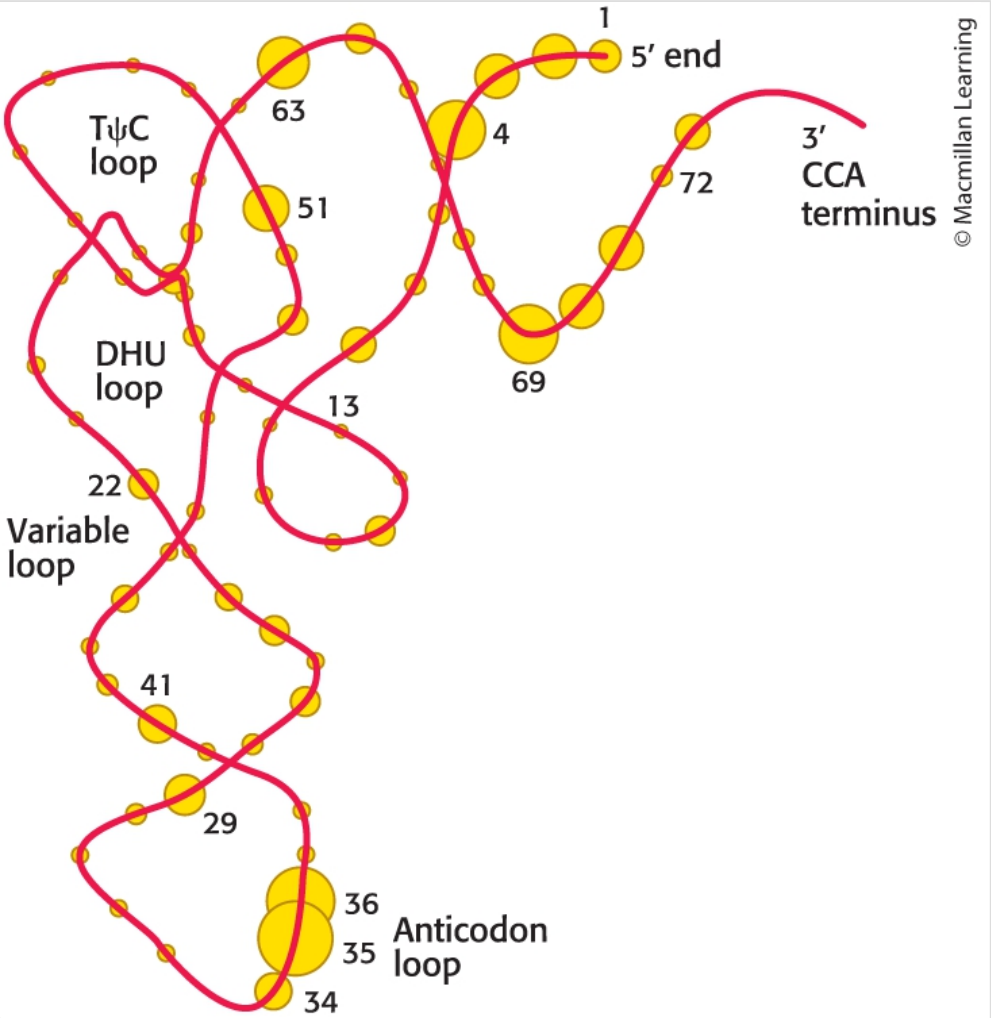


FIGURE 30.12 tRNAs have multiple recognition sites for aminoacyl-tRNA synthetases. Circles represent nucleotides, and the sizes of the circles are proportional to the frequency with which they are used as recognition sites by aminoacyl-tRNA synthetases. The numbers indicate the positions of the nucleotides in the base sequence, beginning from the 5′ end of the tRNA molecule.

[Information from M. Ibba and D. Söll, *Annu. Rev. Biochem*. 69:617–650, 1981, p. 636.]

Aminoacyl-tRNA synthetases are divided into two classes

The diverse sizes, subunit composition, and sequences of aminoacyl-tRNA synthetases were bewildering for many years. Could it be that essentially all synthetases evolved independently? The determination of the three-dimensional structures of several synthetases followed by more refined sequence comparisons revealed that different synthetases are, in fact, related.

Specifically, synthetases fall into two classes, termed *class I* and *class II*, each of which includes enzymes specific for 10 of the 20 amino acids (**Table 30.3**). Intriguingly, synthetases from the two classes bind to different faces of the tRNA molecule (**Figure 30.13**). The CCA arm of tRNA adopts different conformations to accommodate these interactions; the arm is in the helical conformation observed for free tRNA (Figures 30.3 and 30.4) for class II enzymes and in a hairpin conformation for class I enzymes. These two classes also differ in other ways:

TABLE 30.3 Classification and subunit structure of aminoacyl-tRNA synthetases in *E. coli*

Class I	Class II
Arg (α)	Ala (α_4)
Cys (α)	Asn (α_2)
Gln (α)	Asp (α_2)
Glu (α)	Gly ($\alpha_2\beta_2$)
Ile (α)	His (α_2)

Leu (α)	Lys (α2)
Met (α)	Phe (α2β2)
Trp (α2)	Ser (α2)
Tyr (α2)	Pro (α2)
Val (α)	Thr (α2)

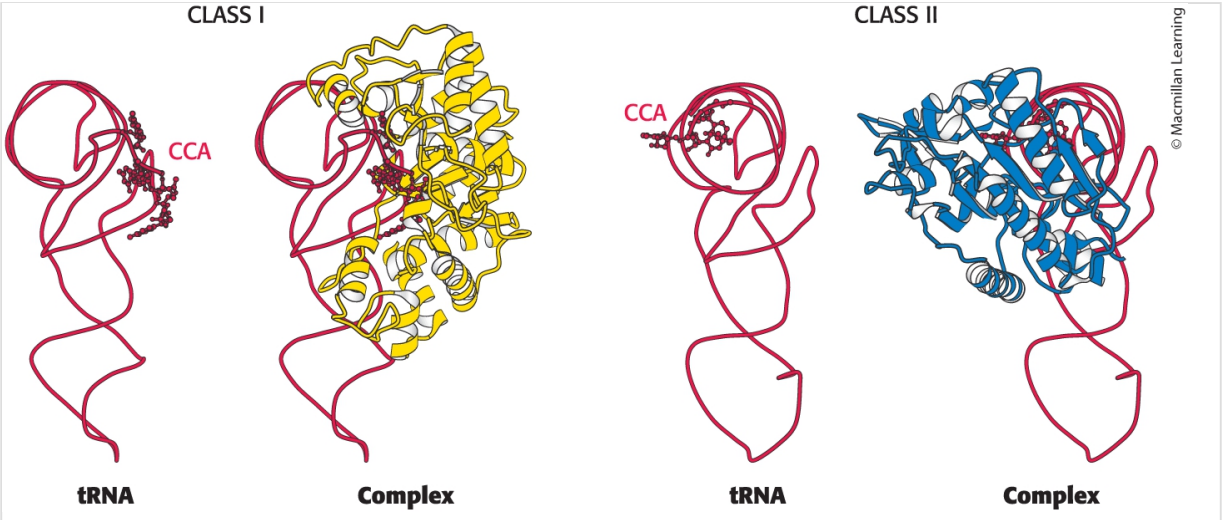


FIGURE 30.13 Class I and class II aminoacyl-tRNA synthetases recognize different faces of the tRNA molecule. The CCA arm of tRNA adopts different conformations in complexes with the two classes of synthetase. Note that the CCA arm of the tRNA is turned toward the viewer (as compared to Figures 30.3 and 30.4). Only the CCA-binding domains of the aminoacyl-tRNA synthetases are shown.

[Drawn from 1EUY.pdb and 1QF6.pdb.]

INTERACT with these models in Achieve

- Class I enzymes acylate the $2'$-hydroxyl group of the terminal adenosine of tRNA, whereas class II enzymes (except the enzyme

for $tRNA^{Phe}$) acylate the $3'$-hydroxyl group.

- The two classes bind ATP in different conformations.
- Most class I enzymes are monomeric, whereas most class II enzymes are dimeric.

Why did two distinct classes of aminoacyl-tRNA synthetases evolve? The observation that the two classes bind to distinct faces of tRNA suggests a possibility. Recognition sites on both faces of tRNA may have been required to allow the recognition of 20 different tRNAs.

30.3 The Ribosome Is the Site of Protein Biosynthesis

We turn now to ribosomes, the molecular machines that coordinate the interplay of aminoacyl-tRNAs, mRNA, and proteins that leads to protein biosynthesis. We will focus our discussion first on ribosomes and protein biosynthesis in bacteria, then discuss the differences observed in eukaryotes.

The 20,000 ribosomes in a bacterial cell constitute nearly a quarter of its mass. An *E. coli* ribosome is a ribonucleoprotein assembly with a mass of about 2300 kDa, a diameter of approximately 250 Å, and a sedimentation coefficient (Section 4.1) of 70S.

A 70S ribosome can dissociate into a **large subunit (50S)** and a **small subunit (30S)**, each of which can be further split into their constituent proteins and RNAs. The 30S subunit contains 21 different proteins (referred to as S1 through S21) and a 16S RNA molecule. The 50S subunit contains 34 different proteins (L1 through L34) and two RNA molecules, a 23S and a 5S species. A 70S ribosome contains one copy of each RNA molecule, two copies each of the L7 and L12 proteins, and one copy of each of the other proteins. The L7 protein is identical to L12 except that its amino terminus is acetylated (Section 7.3).

Both the 30S and the 50S subunits can be reconstituted in vitro from their constituent proteins and RNA. This reconstitution is an outstanding example of the principle that supramolecular complexes can form spontaneously from their macromolecular constituents.

The structures of both the 30S and the 50S subunits as well as the complete 70S ribosome have been determined (**Figure 30.14**). The features of these structures are in remarkable agreement with

interpretations of less-direct experimental analyses of the structure and function of the ribosome. These structures provide an invaluable framework for examining the mechanism of protein biosynthesis.

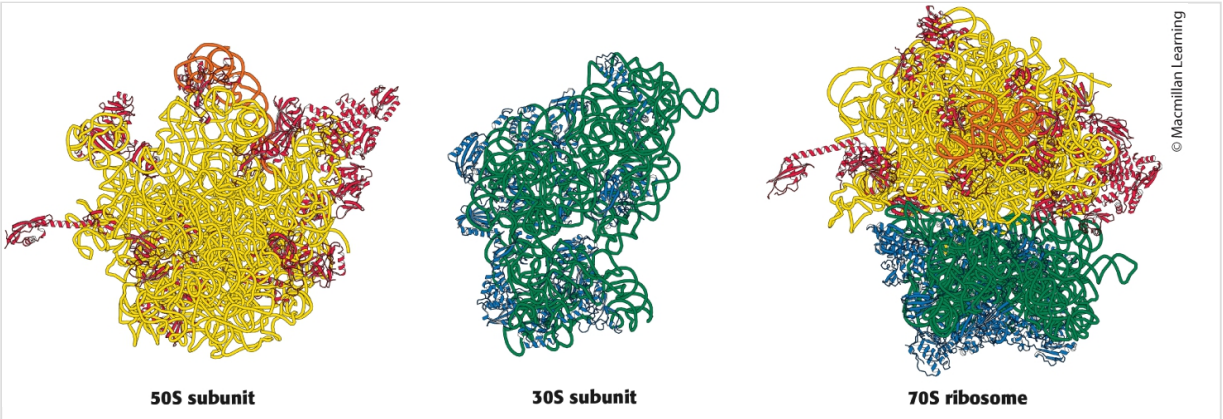


FIGURE 30.14 The ribosome consists of a large subunit and a small subunit. These detailed models of a bacterial ribosome are based on high-resolution x-ray crystallographic data of the 70S ribosome and the 30S and 50S subunits. (Left) View of the part of the 50S subunit that interacts with the 30S subunit. (Center) View of the part of the 30S subunit that interacts with the 50S subunit. (Right) View of the 70S ribosome (note that this view is rotated with respect to the other two views). 23S rRNA is shown in yellow, 5S rRNA in orange, 16S rRNA in green, proteins of the 50S subunit in red, and proteins of the 30S subunit in blue. The interface between the 50S and the 30S subunits consists primarily of RNA.

[Drawn from 1GIX.pdb and 1GIY.pdb.]

Ribosomal RNAs (5S, 16S, and 23S rRNA) play central roles in protein biosynthesis

The prefix *ribo* in the name *ribosome* is apt because RNA constitutes nearly two-thirds of the mass of these large molecular assemblies. The three RNAs present — 5S, 16S, and 23S — are critical for ribosomal architecture and function. They are formed by the cleavage of primary 30S transcripts and further processing. These molecules fold into structures that allow them to form internal base pairs. Their base-pairing patterns were deduced by comparing the nucleotide sequences

of many species to detect conserved sequences as well as conserved base pairings. For instance, the 16S RNA of one species may have a G–C base pair, whereas another may have an A–U base pair, but the location of the base pair is the same in both molecules. Chemical modification and digestion experiments supported the structures deduced from sequence comparisons (Figure 30.15). The striking finding is that across all species, ribosomal RNAs (rRNAs) are folded into defined structures that have many short intramolecular duplex regions.

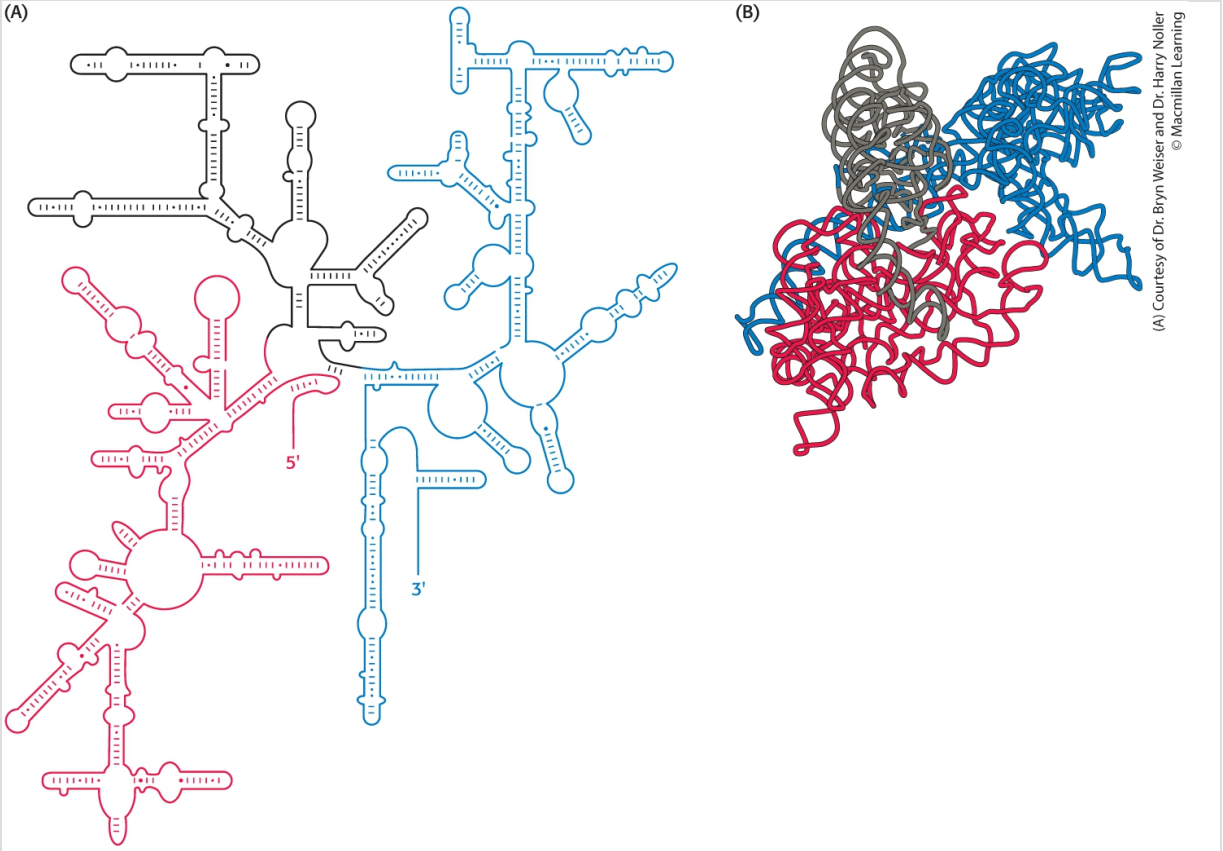


FIGURE 30.15 Ribosomal RNAs form intramolecular base pairs. (A) The secondary structure of 16S rRNA deduced from sequence comparison and the results of chemical studies. Dashes represent standard Watson–Crick base pairs, and dots represent non-Watson–Crick base pairs. (B) The tertiary structure of 16S rRNA determined by x-ray crystallography.

[(B) drawn from 1FJG.pdb.]

INTERACT with this model in Achieve

For many years, ribosomal proteins were presumed to orchestrate protein biosynthesis and ribosomal RNAs were presumed to serve primarily as structural scaffolding. The current view is almost the reverse. The discovery of catalytic RNA (Section 29.5) made biochemists receptive to the possibility that RNA plays a much more active role in ribosomal function. In fact, bacterial ribosomes can be stripped of most of their protein components in vitro and still retain their ability to catalyze peptide-bond formation. In addition, the detailed structures show that the key sites in the ribosome, such as those that catalyze the formation of the peptide bond and those that interact with mRNA and tRNA, are composed almost entirely of rRNA. Contributions from the proteins are minor. The almost inescapable conclusion is that the ribosome initially consisted only of RNA and that the proteins were added later to fine-tune its functional properties. This conclusion has the pleasing consequence of dodging a "chicken and egg" question: How can complex proteins be synthesized if complex proteins are required for protein biosynthesis?

Ribosomes have three transfer RNA-binding sites that bridge the 30S and 50S subunits

Three tRNA-binding sites in ribosomes are arranged to allow the formation of peptide bonds between amino acids encoded by the codons on mRNA (**Figure 30.16**). The mRNA fragment being translated at a given moment is bound within the 30S subunit. Each of the tRNA molecules is in contact with both the 30S subunit and the 50S subunit. At the 30S end, two of the three tRNA molecules are bound to the mRNA through anticodon–codon base pairs. These binding sites are called the

A site (for aminoacyl) and the P site (for peptidyl). The third tRNA molecule is bound to an adjacent site called the E site (for exit).

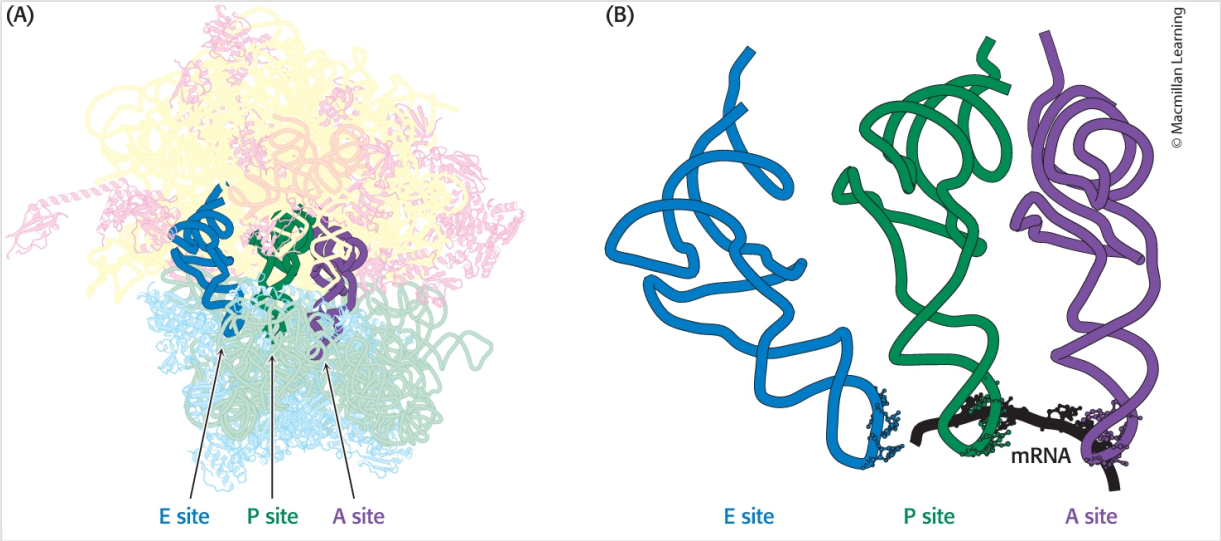


FIGURE 30.16 The ribosome has three binding sites for transfer RNAs. (A) The three tRNA binding sites on the 70S ribosome are called the A (for aminoacyl), P (for peptidyl), and E (for exit) sites. Each tRNA molecule contacts both the 30S and the 50S subunit. (B) The tRNA molecules in sites A and P are base-paired with mRNA.

[(B) Drawn from 1JGP.pdb.]

INTERACT with this model in Achieve

The other end of each tRNA molecule, the end without the anticodon, interacts with the 50S subunit. The acceptor stems of the tRNA molecules occupying the A site and the P site converge at a site where a peptide bond is formed. A tunnel connects this site to the back of the ribosome, through which the polypeptide chain passes during synthesis (Figure 30.17).

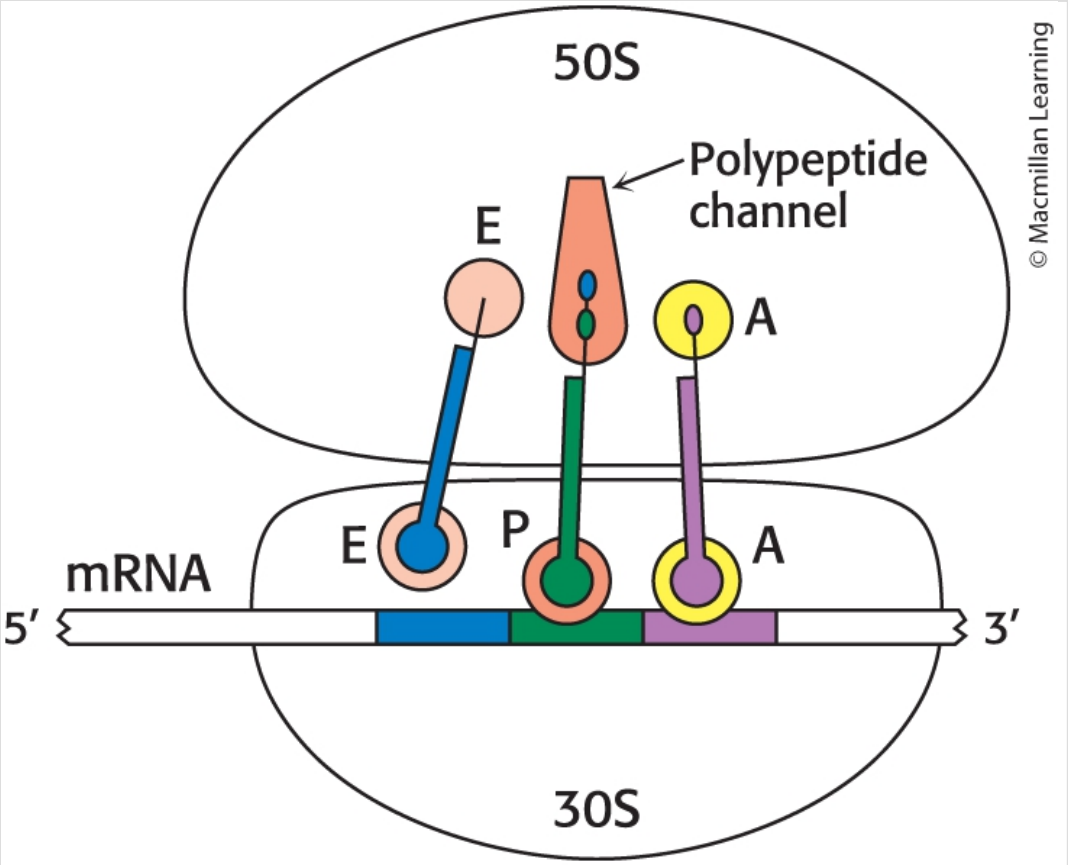


FIGURE 30.17 The key components of the translation machinery interact on an active ribosome. This schematic representation shows the relationship between the ribosomal subunits, tRNAs, and mRNA.

The start signal is usually AUG preceded by several bases that pair with 16S rRNA

How does protein biosynthesis start? The simplest possibility would be for the first three nucleotides of each mRNA to serve as the first codon; no special start signal would then be needed. However, experiments show that translation in bacteria does not begin immediately at the 5′

terminus of mRNA. Indeed, the first translated codon is nearly always more than 25 nucleotides away from the $5'$ end. Furthermore, in bacteria, many mRNA molecules encode two or more polypeptide chains. For example, a single mRNA molecule about 7000 nucleotides long specifies five enzymes in the biosynthetic pathway for tryptophan in *E. coli.* Each of these five proteins has its own start and stop signals on the mRNA. In fact, all known mRNA molecules contain signals that define the beginning and end of each encoded polypeptide chain.

A clue to the mechanism of initiation was the finding that nearly half the amino-terminal residues of proteins in *E. coli* are methionine. In fact, the initiating codon in mRNA is AUG (methionine) or, less frequently, GUG (valine) or, rarely, UUG (leucine). What additional signals are necessary to specify a translation start site? The first step toward answering this question was the isolation of initiator regions from a number of mRNAs. This isolation was accomplished by using ribonuclease to digest mRNA–ribosome complexes (formed under conditions in which protein biosynthesis could begin but elongation could not take place). As expected, each initiator region usually displays an AUG codon (**Figure 30.18**). In addition, each initiator region contains a purine-rich sequence centered about 10 nucleotides on the $5'$ side of the initiator codon.

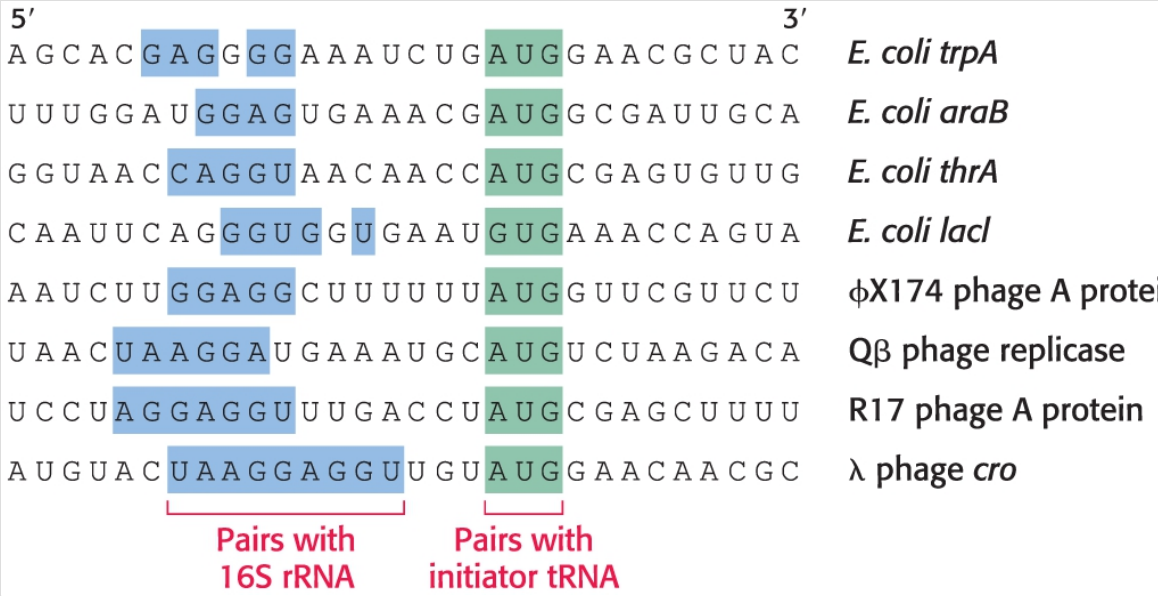


FIGURE 30.18 Initiator regions in mRNA determine where protein biosynthesis starts. This sequence alignment of mRNA initiation sites in some bacterial and viral mRNA molecules revea some recurring features. The purine-rich sequence on the 5′ side of the initiator codon pairs wi a conserved sequence on the 16S rRNA. The first downstream AUG, GUG (less frequent), or UUG (rare) codon acts as the initiator codon for protein biosynthesis.

The role of this purine-rich region, called the **Shine–Dalgarno sequence** (after John Shine and Lynn Dalgarno, who first described the sequence), became evident when the sequence of 16S rRNA was determined. The 3′ end of this rRNA component of the 30S subunit contains a sequence of several bases that is complementary to the Shine–Dalgarno sequence in the mRNA. Mutagenesis of the CCUCC sequence near the 3′ end of 16S rRNA to ACACA markedly interferes with the recognition of start sites in mRNA. This result and other evidence show that the initiator region of mRNA binds very near the 3′ end of the 16S rRNA. The number of base pairs linking mRNA and 16S rRNA ranges from three to nine. This interaction between the 5′ end of

the mRNA and the $3'$ end of the 16S rRNA positions the initiator codon of the mRNA in the P site of the ribosome, ready for recognition by the anticodon of an initiator tRNA molecule.

Bacterial protein biosynthesis is initiated by *N*-formylmethionyl-transfer RNA

As stated earlier, methionine is the first amino acid in many *E. coli* proteins. However, the methionine residue found at the amino-terminal end of *E. coli* proteins is usually modified. In fact, protein biosynthesis in bacteria starts with the modified amino acid *N*-formylmethionine (fMet). A distinct tRNA brings *N*-formylmethionine to the ribosome to initiate protein biosynthesis. This tRNA, called *initiator tRNA* (abbreviated as $tRNA^{fMet}$), differs from the tRNA that inserts methionine in internal positions (abbreviated as $tRNA^{Met}$). The superscript "fMet" indicates that methionine attached to the initiator tRNA can be formylated, whereas it cannot be formylated when attached to $tRNA^{Met}$. Although virtually all proteins synthesized in *E. coli* begin with *N*-formylmethionine, in approximately one-half of the proteins, *N*-formylmethionine is removed when the nascent, or growing, chain is 10 amino acids long.

Methionine is linked to these two kinds of tRNAs by the same aminoacyl-tRNA synthetase. A specific enzyme then formylates the amino group of the methionine molecule that is attached to $tRNA^{fMet}$ (Figure 30.19). The activated formyl donor in this reaction is N^{10}-formyltetrahydrofolate, a folate derivative that carries activated one-

carbon units (Section 25.2). Free methionine and methionyl-$tRNA^{Met}$ are not substrates for this transformylase.

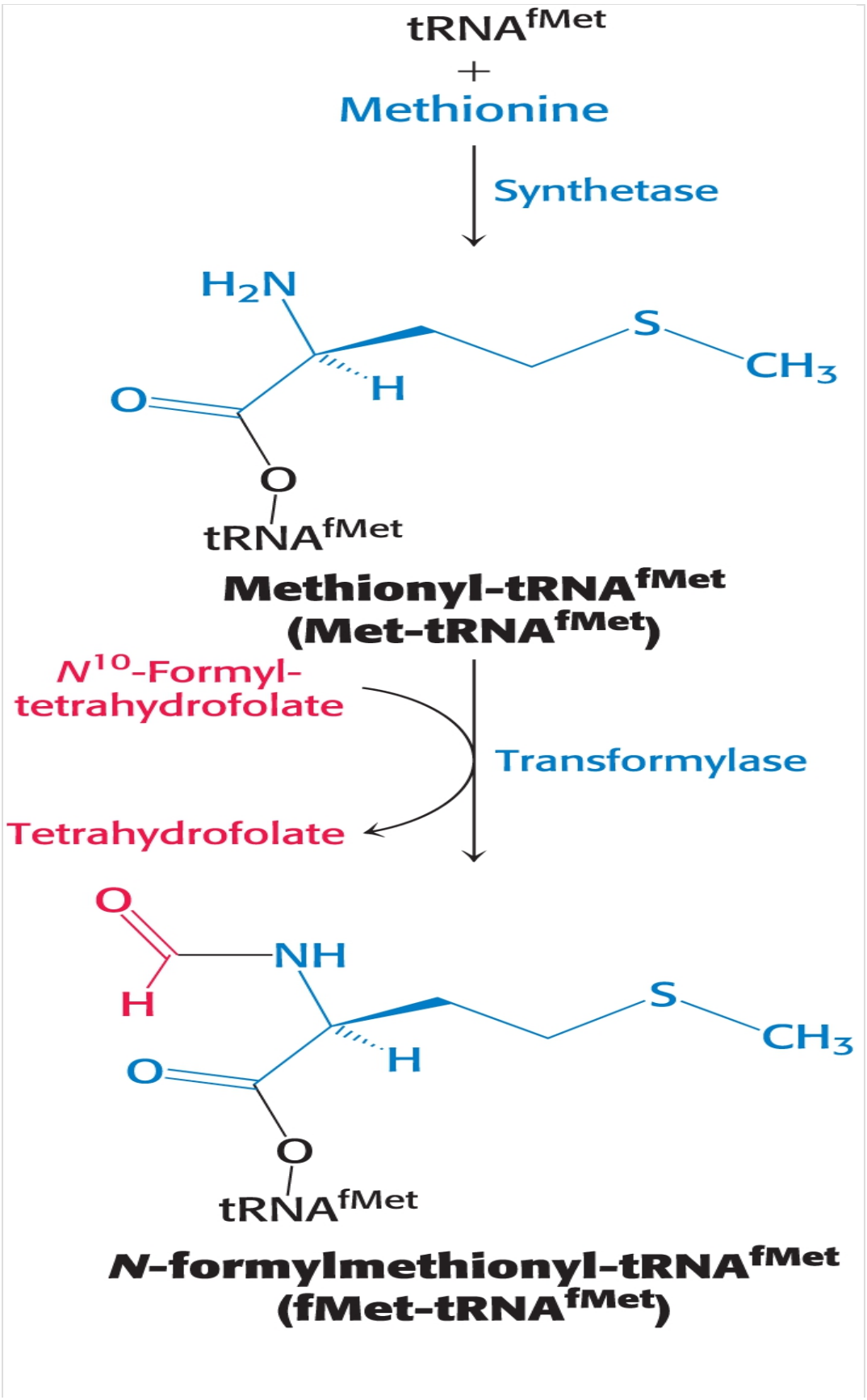

tRNA^fMet
+
Methionine
Synthetase
H2N
S
CH3
H
O
O
tRNA^fMet
Methionyl-tRNA^fMet
(Met-tRNA^fMet)
N10-Formyl-
tetrahydrofolate
Transformylase
Tetrahydrofolate
O
NH
H
S
CH3
H
O
O
tRNA^fMet
N-formylmethionyl-tRNA^fMet
(fMet-tRNA^fMet)

FIGURE 30.19 Methionyl-tRNA is formylated to create a modified amino acid. Initiator tRNA ($tRNA^{fMet}$) is first charged with methionine, and then a formyl group is transferred to the methionyl-$tRNA^{fMet}$ from N^{10}-formyltetrahydrofolate.



N-Formylmethionyl-$tRNA^{fMet}$ is placed in the P site of the ribosome in the formation of the 70S initiation complex

Messenger RNA and *N*-formylmethionyl-$tRNA^{fMet}$ must be brought to the ribosome for protein biosynthesis to begin. How is this task accomplished? Three protein **initiation factors** (IF1, IF2, and IF3) are essential. The 30S ribosomal subunit first forms a complex with IF1 and IF3 (**Figure 30.20**). The binding of these factors to the 30S subunit prevents it from prematurely joining the 50S subunit to form a dead-end 70S complex, devoid of mRNA and $fMet-tRNA^{fMet}$. IF1 binds near the A site and directs the $fMet-tRNA^{fMet}$ to the P site. IF2, a member of the G-protein family, binds GTP, and the concomitant conformational change enables IF2 to associate with $fMet-tRNA^{fMet}$. The IF2–GTP–initiator-tRNA complex binds with mRNA (correctly positioned by the interaction of the Shine–Dalgarno sequence with the 16S rRNA) and the 30S subunit to form the 30S initiation complex. Structural changes then lead to the ejection of IF1 and IF3. IF2 stimulates the association of the 50S subunit to the complex. The GTP bound to IF2 is hydrolyzed upon arrival of the 50S subunit, releasing IF2. The result is a 70S initiation complex. The

formation of the 70S initiation complex is the rate-limiting step in protein biosynthesis.

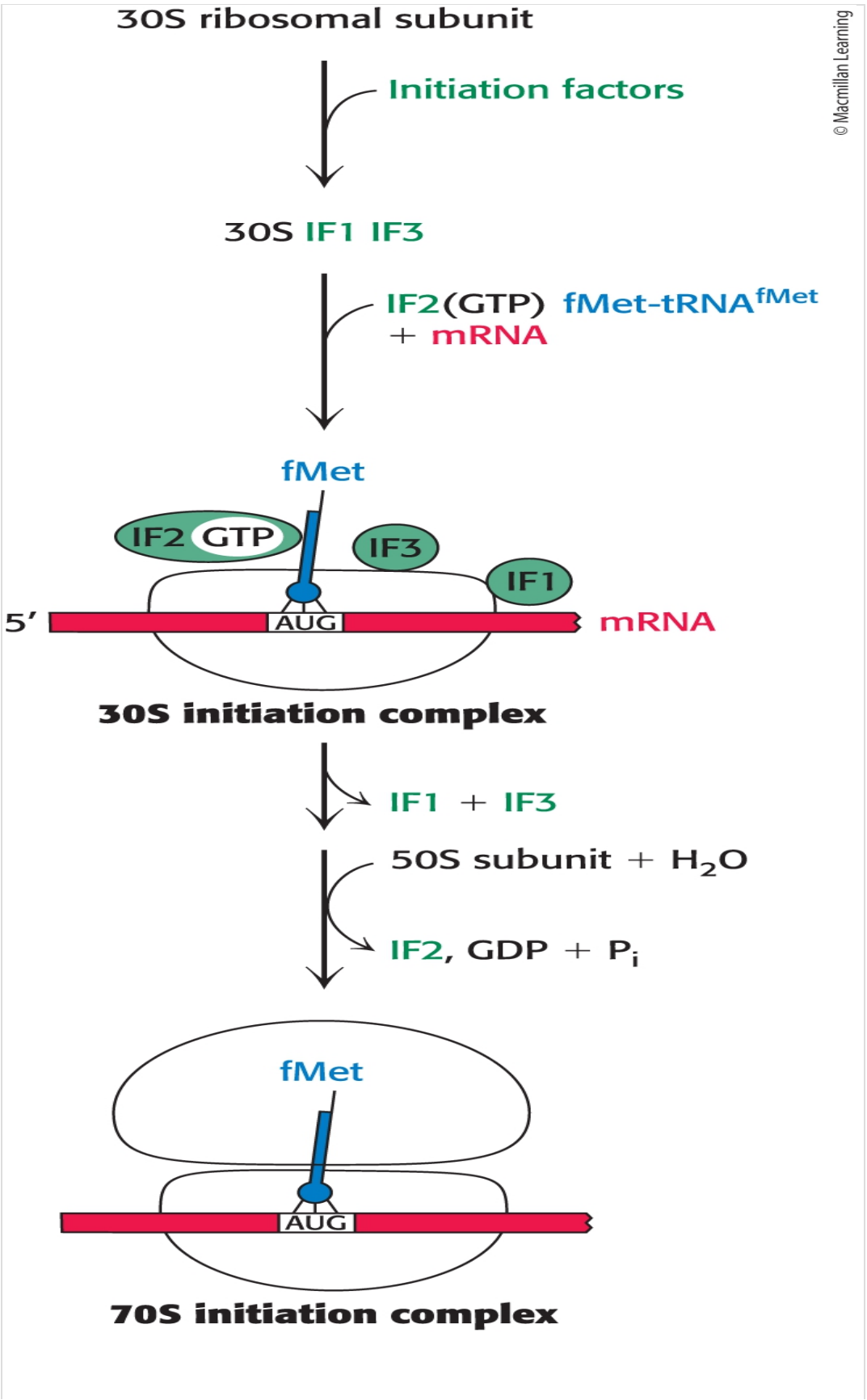

30S ribosomal subunit
Initiation factors
30S IF1 IF3
IF2(GTP) fMet-tRNA^fMet
+ mRNA
fMet
IF2 GTP
IF3
IF1
5'
AUG
mRNA
30S initiation complex
IF1 + IF3
50S subunit + H2O
IF2, GDP + Pi
fMet
AUG
70S initiation complex
© Macmillan Learning

FIGURE 30.20 Prokaryotic initiation factors aid the assembly of initiation complexes. These factors first aid assembly of the 30S initiation complex, and then of the 70S initiation complex. IF1 interacts with the 30S near the A site and prevents any tRNAs from binding there. IF3 also binds to the 30S and prevents the 50S from prematurely interacting with the 30S. IF2 delivers the initiator tRNA (or *N*-formylmethionyl-$tRNA^{fMet}$) to the P site as a ternary complex with GTP.

When the 70S initiation complex has been formed, the ribosome is ready for the elongation phase of protein biosynthesis. The $fMet-tRNA^{fMet}$ molecule occupies the P site on the ribosome, positioned so that its anticodon pairs with the initiating codon on mRNA. The other two sites for tRNA molecules, the A site and the E site, are empty. This interaction establishes what is termed the *reading frame* for the translation of the entire mRNA (Section 8.6). After the initiator codon has been located, groups of three nonoverlapping nucleotides are decoded by the ribosome to create the polypeptide chain.

Elongation factors deliver aminoacyl-tRNAs to the ribosome

At this point, $fMet-tRNA^{fMet}$ occupies the P site, and the A site is vacant. The particular aminoacyl-tRNA inserted into the empty A site depends on the mRNA codon in the A site. However, the appropriate aminoacyl-tRNA does not simply leave the synthetase and diffuse to the A site. Rather, it is delivered to the A site in association with a 43-kDa protein called **elongation factor Tu (EF-Tu)**, another member of the G-protein family. EF-Tu, the most abundant bacterial protein, binds aminoacyl-tRNA only in its GTP form (**Figure 30.21**).

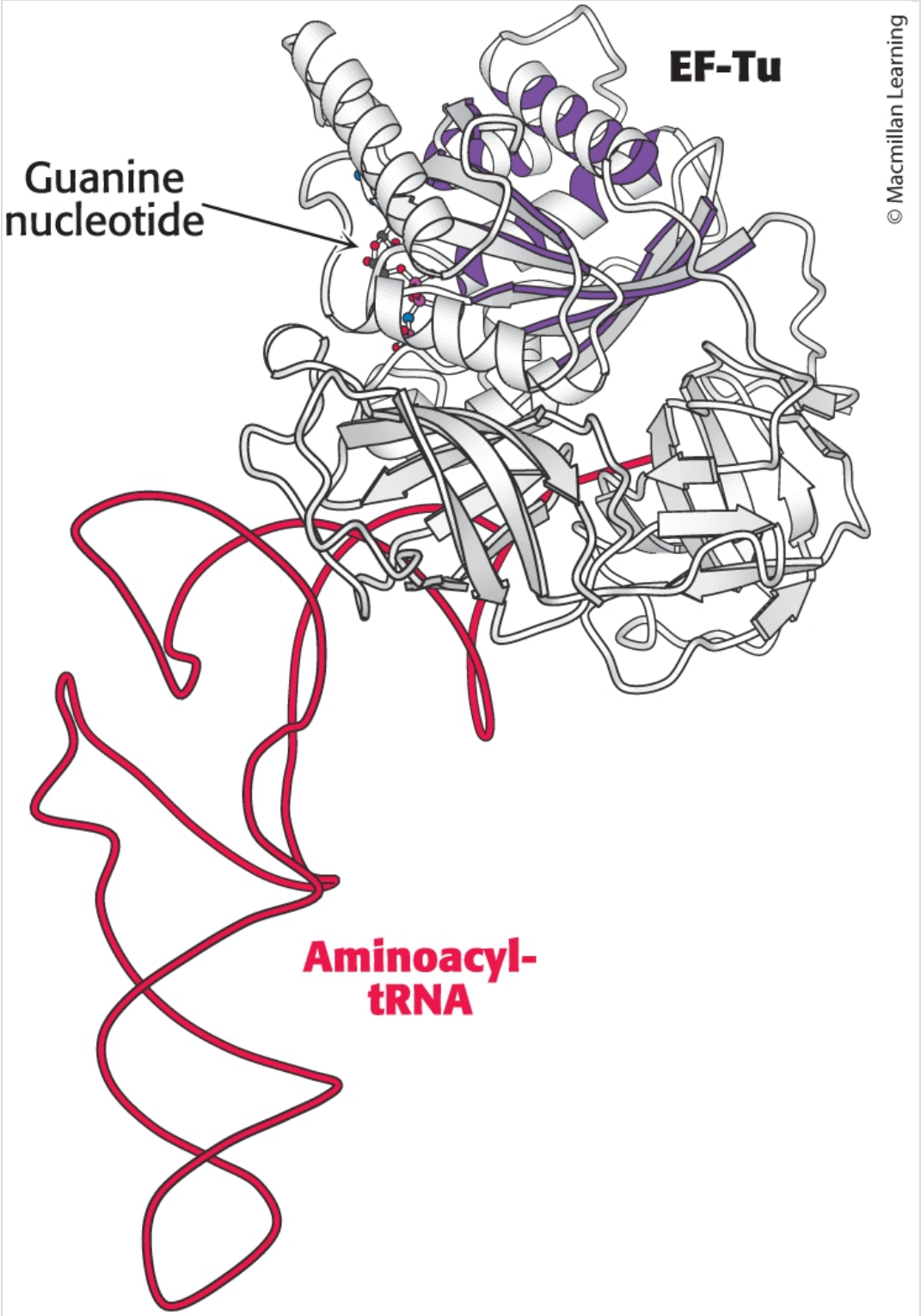


FIGURE 30.21 The structure of elongation factor Tu (EF-Tu) and an aminoacyl-tRNA resembles those of other G proteins. The P-loop NTPase domain (purple shading) at the amino-terminal end of EF-Tu is also found in other G proteins.

[Drawn from 1B23.pdb.]

INTERACT with this model in Achieve

The binding of EF-Tu to aminoacyl-tRNA serves two functions. First, EF-Tu protects the delicate ester linkage in aminoacyl-tRNA from hydrolysis. Second, EF-Tu contributes to the accuracy of protein biosynthesis because GTP hydrolysis and expulsion of the EF-Tu-GDP complex from the ribosome occurs only if the pairing between the anticodon and the codon is correct. EF-Tu interacts with the 16S rRNA, which monitors the accuracy of the base pairing at positions 1 and 2 of the codon (Figure 30.6).

Correct codon recognition induces structural changes in the 30S subunit that move the EF-Tu to a highly conserved site in the 23S rRNA in the 50S subunit called the sarcin-ricin loop (SRL). The interaction with the SRL of the 50S subunit activates the GTPase activity of EF-Tu, releasing EF-Tu-GDP from the ribosome. These same structural changes also rotate the aminoacyl-tRNA in the A site so that the amino acid is brought into proximity with the aminoacyl-tRNA in the P site on the 50S subunit, a process called *accommodation*. Accommodation aligns the amino acids for peptide-bond formation.

Released EF-Tu is then reset to its GTP form by a second elongation factor, **elongation factor Ts** (**Figure 30.22**). EF-Ts induces the dissociation of GDP. GTP binds to EF-Tu, and EF-Ts concomitantly departs. It is noteworthy that EF-Tu does not interact with $\mathrm{fMet-tRNA^{fMet}}$. Hence, this initiator tRNA is not delivered to the A site. In contrast, $\mathrm{Met-tRNA^{Met}}$, like all other aminoacyl-tRNAs, does bind to EF-Tu. These findings account for the fact that internal AUG codons are not read by the initiator tRNA. Conversely, IF2 recognizes $\mathrm{fMet-tRNA^{fMet}}$ but no other tRNA.

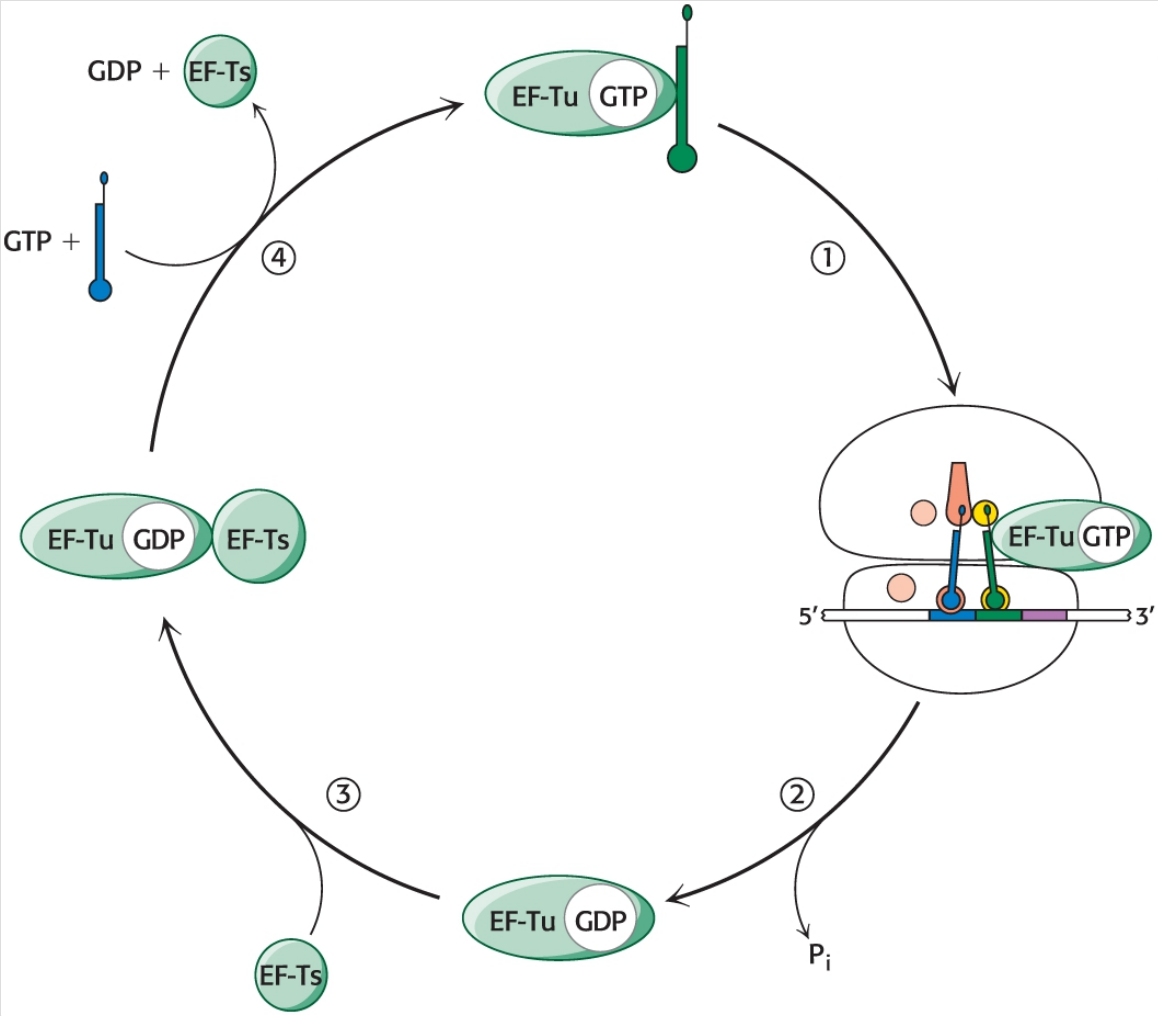


FIGURE 30.22 The GTPase EF-Tu binds aminoacyl-tRNA only in its GTP form. (1) EF-Tu-GTP binds aminoacyl-tRNA and delivers it to the A site on the ribosome. (2) Correct codon recognitic stimulates the GTPase activity of EF-Tu, which leaves it in its GDP form. (3) EF-Ts binds to EF-Tu-GDP. (4) EF-Ts induces release of GDP. EF-Ts departs as another GTP and aminoacyl-tRNA bind t EF-Tu-GTP, and the complex is ready for another delivery to the ribosome.

This GTP–GDP cycle of EF-Tu is reminiscent of those of the heterotrimeric G proteins in signal transduction (Section 14.2) and the Ras proteins in growth control (Section 14.4). This similarity is due to their shared evolutionary heritage, seen in the homology of the amino-terminal domain of EF-Tu to the P-loop NTPase domains in the other G

proteins. In all these related enzymes, the change in conformation between the GTP and the GDP forms leads to a change in interaction partners. A further similarity is the requirement that an additional protein catalyzes the exchange of GTP for GDP; EF-Ts catalyzes the exchange for EF-Tu, just as an activated receptor does for a heterotrimeric G protein.

Peptidyl transferase catalyzes peptide-bond formation

With both the P site and the A site occupied by aminoacyl-tRNA, the stage is set for the formation of a peptide bond: the *N*-formylmethionine molecule linked to the initiator tRNA will be transferred to the amino group of the amino acid in the A site. The formation of the peptide bond, one of the most important reactions in life, is a thermodynamically spontaneous reaction catalyzed by a site on the 23S rRNA of the 50S subunit called the **peptidyl transferase center**. This catalytic center is located deep in the 50S subunit near the tunnel that allows the nascent peptide to leave the ribosome.

The ribosome, which enhances the rate of peptide-bond synthesis by a factor of 10^7 over the uncatalyzed reaction $(\sim 10^{-4}\,M^{-1}\,s^{-1})$, derives much of its catalytic power from catalysis by proximity and orientation. The ribosome positions and orients the two substrates so that they are situated to take advantage of the inherent reactivity of an amine group (on the aminoacyl-tRNA in the A site) with an ester (on the initiator tRNA in the P site). The amino group of the aminoacyl-tRNA in the A site, in its unprotonated state, makes a nucleophilic attack on the ester linkage between the initiator tRNA and the *N*-formylmethionine molecule in the P site (**Figure 30.23A**). The nature of the transition state that follows the attack is not established, and several models are plausible. One model proposes roles for the $2'$ OH of the adenosine of

the tRNA in the P site and a molecule of water at the peptidyl transferase center. The nucleophilic attack of the α-amino group generates an eight-membered transition state in which three protons are shuttled about in a concerted manner. The proton of the attacking amino group hydrogen bonds to the $2'$ oxygen of ribose of the tRNA. The hydrogen of $2'$ OH in turn interacts with the oxygen of the water molecule at the center, which then donates a proton to the carbonyl oxygen. Collapse of the transition state with the formation of the peptide bond allows protonation of the $3'$ OH of the now-empty tRNA in the P site (Figure 30.23B). The stage is now set for translocation and formation of the next peptide bond.

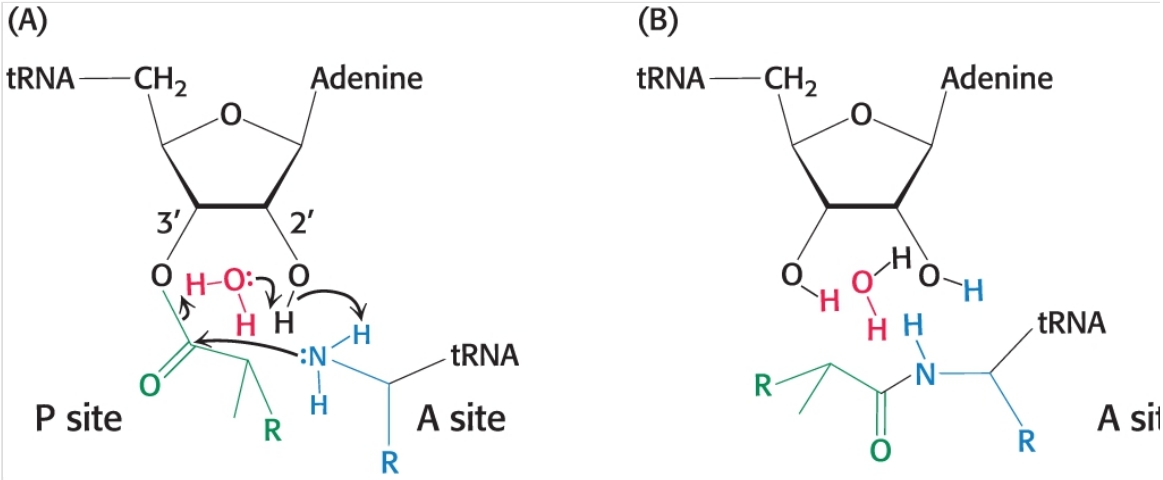


FIGURE 30.23 Peptide-bond formation links amino acids. (A) The amino group of the aminoacyl-tRNA in the A site attacks the carbonyl group of the ester linkage of the peptidyl-tRN in the P site. An eight-membered transition state is formed with the addition of a molecule of water. Notice that not all atoms are shown, and some bond lengths are exaggerated for clarity. (B) This transition state collapses to form the peptide bond and release the deacylated tRNA.

Self-Check Question



Why is the ribosome considered to be a ribozyme?

GTP hydrolysis-driven translocation of tRNAs and mRNA follows peptide-bond formation

With the formation of the peptide bond, the peptide chain is now attached to the tRNA whose anticodon is in the A site on the 30S subunit. The two ribosomal subunits rotate with respect to one another. This structural change places the acceptor end of the same tRNA and its peptide in the P site of the large subunit while its anticodon end is still in the A site (Figure 30.24). However, protein biosynthesis cannot continue unless the next codon is presented in the A site and the site is open for the next aminoacyl-tRNA to be delivered. This requires the translocation of the mRNA and the tRNAs within the ribosome.

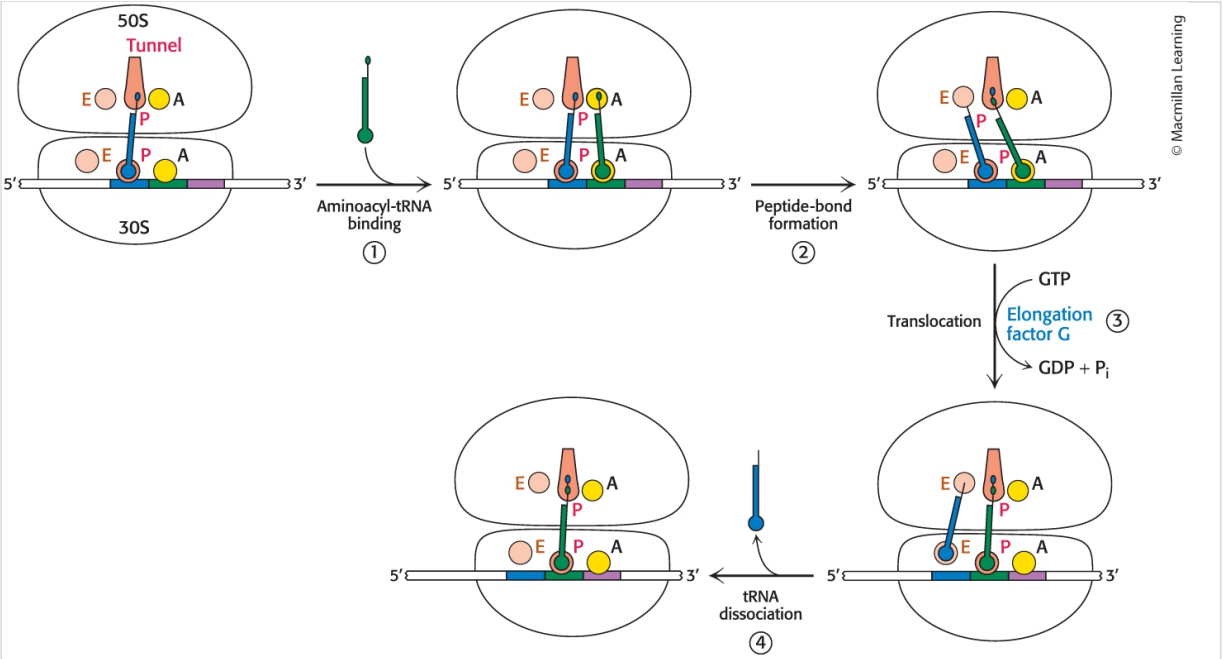


FIGURE 30.24 Protein biosynthesis is a cyclical process. The cycle begins with peptidyl-tRNA in the P site. (1) An aminoacyl-tRNA binds in the A site. (2) With both sites occupied, a new peptide bond is formed. (3) The tRNAs and the mRNA are translocated through the action of elongation factor G, which moves the deacylated tRNA to the E site. (4) Once there, the tRNA is free to dissociate to complete the cycle.

Elongation factor G (**EF-G**, also called **translocase**) catalyzes the movement of mRNA, at the expense of GTP hydrolysis, by a distance of three nucleotides. Now, the next codon is positioned in the A site for interaction with the incoming aminoacyl-tRNA-EF-Tu-GTP complex. Simultaneously, the anticodon end of the peptidyl-tRNA moves out of the A site into the P site on the 30S subunit and the anticodon end of the deacylated tRNA moves out of the P site into the E site. This deacylated tRNA is subsequently released from the ribosome. The movement of the peptidyl-tRNA into the P site shifts the mRNA by one codon, exposing the next codon to be translated in the A site.

The three-dimensional structure of the ribosome undergoes significant change during translocation, and evidence suggests that translocation

may result from properties of the ribosome itself. However, EF-G accelerates the process. A possible mechanism for accelerating the translocation process is shown in **Figure 30.25**. First, EF-G in the GTP form binds to the ribosome near the A site, interacting with the 23S rRNA of the 50S subunit. The binding of EF-G to the ribosome stimulates the GTPase activity of EF-G. On GTP hydrolysis, EF-G undergoes a conformational change that displaces the peptidyl-tRNA in the A site to the P site, which carries the mRNA and the deacylated tRNA with it. The dissociation of EF-G leaves the ribosome ready to accept the next aminoacyl-tRNA into the A site. This cycle of elongation is repeated, with mRNA translation taking place in the $5' \rightarrow 3'$ direction. As new aminoacyl-tRNAs move into the A site, the polypeptide is elongated until a termination codon is met. Note that the peptide chain remains in the P site on the 50S subunit throughout this cycle, growing into the exit tunnel.

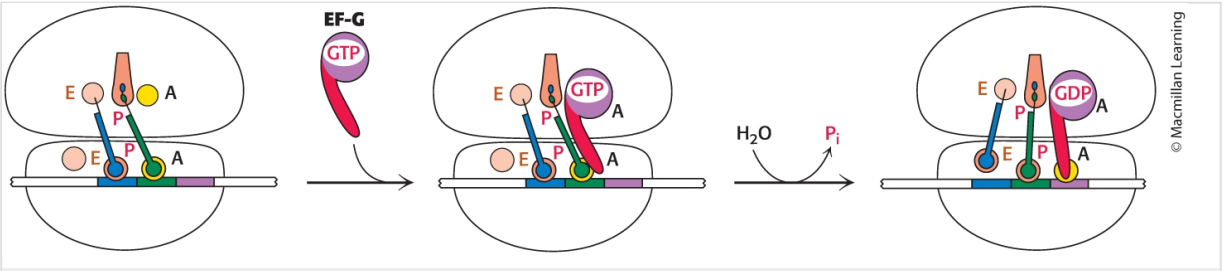


FIGURE 30.25 Translocation repositions tRNAs and mRNA with respect to the ribosome. In the GTP form, EF-G binds to the A site on the 50S subunit. This binding stimulates GTP hydrolysis, inducing a conformational change in EF-G that forces the tRNAs and mRNA to move through the ribosome by a distance corresponding to one codon.

The direction of translation has important consequences. Recall that transcription is also in the $5' \rightarrow 3'$ direction (Section 29.2). If the direction of translation were opposite that of transcription, only fully synthesized mRNA could be translated. Since the directions of synthesis

are the same, translation can occur while an mRNA is being synthesized.

Self-Check Question



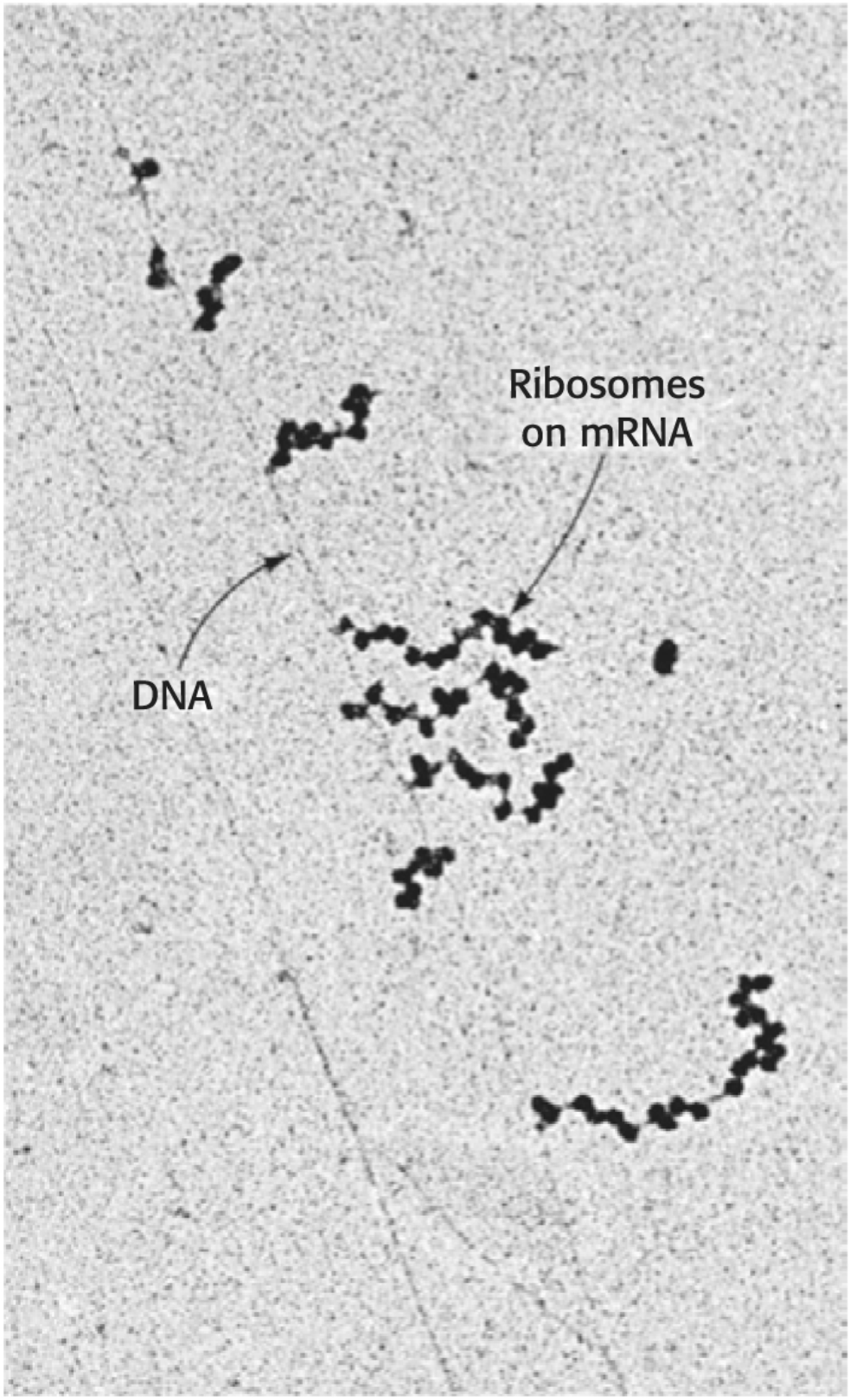
Summarize the role of G proteins and GTP hydrolysis in translation initiation and elongation in bacteria.

In bacteria, transcription and translation are coupled in space and time

In bacteria, almost no time is lost between transcription and translation. The $5'$ end of mRNA interacts with ribosomes very soon after it is made, well before the $3'$ end of the mRNA molecule is finished. Recent experiments with *E. coli* using cryo-electron microscopy (Section 4.5) have established the existence of an expressome, a transcribing and translating complex consisting of RNA polymerase and the 70S ribosome. The interaction of the polymerase with the ribosome occurs at the carboxyl-terminal domain of the polymerase.

Many ribosomes can be translating an mRNA molecule simultaneously. A group of ribosomes bound to an mRNA molecule is called a *polyribosome* or a **polysome** (**Figure 30.26**). Recent work shows that the ribosomes are arranged so as to protect the mRNA and to facilitate easy exchange of the substrates and products with the cytoplasm. The ribosomes in the polysome are in a helical array around the mRNA with

the tRNA binding sites and peptide exit tunnel exposed to the cytoplasm.



Republished with permission of AAAS, from Visualization of Bacterial Genes in Action, O. L. Miller, Jr., B. A. Hamkalo, and C. A. Thomas, Jr. *Science* 169(1970): 392; permission conveyed through Copyright Clearance Center, Inc.

FIGURE 30.26 In prokaryotes, polysomes can simultaneously translate one mRNA. Transcription of a segment of DNA from *E. coli* generates mRNA molecules that are

immediately translated by multiple ribosomes (polysomes).

Protein biosynthesis is terminated by release factors that read stop codons

The final phase of translation is termination. How does the synthesis of a polypeptide chain come to an end when a stop codon is encountered? No tRNAs with anticodons complementary to the stop codons — UAA, UGA, or UAG — exist in normal cells. Instead, these stop codons are recognized by proteins called **release factors (RFs)**. One of these release factors, RF1, recognizes UAA or UAG. A second factor, RF2, recognizes UAA or UGA. A third factor, RF3, another GTPase, catalyzes the removal of RF1 or RF2 from the ribosome upon release of the newly synthesized protein.

RF1 and RF2 are compact proteins that resemble a tRNA molecule. When bound to the ribosome, the proteins unfold to bridge the gap between the stop codon on the mRNA and the peptidyl transferase center on the 50S subunit (**Figure 30.27**). The RF interacts with the peptidyl transferase center using a loop containing a highly conserved glycine-glycine-glutamine (GGQ) sequence, with the glutamine methylated on the amide nitrogen atom of the R group. This modified glutamine (assisted by the peptidyl transferase) is crucial in promoting a water-molecule attack on the ester linkage between the tRNA and the polypeptide chain, freeing the polypeptide chain.

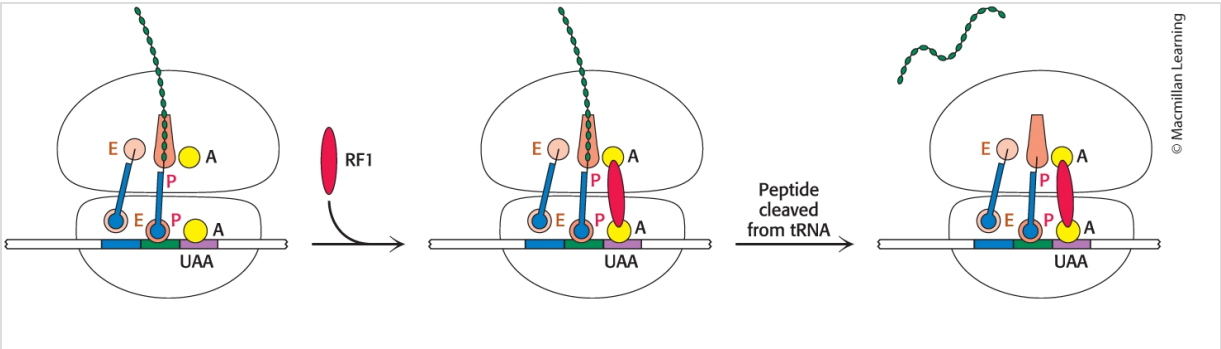
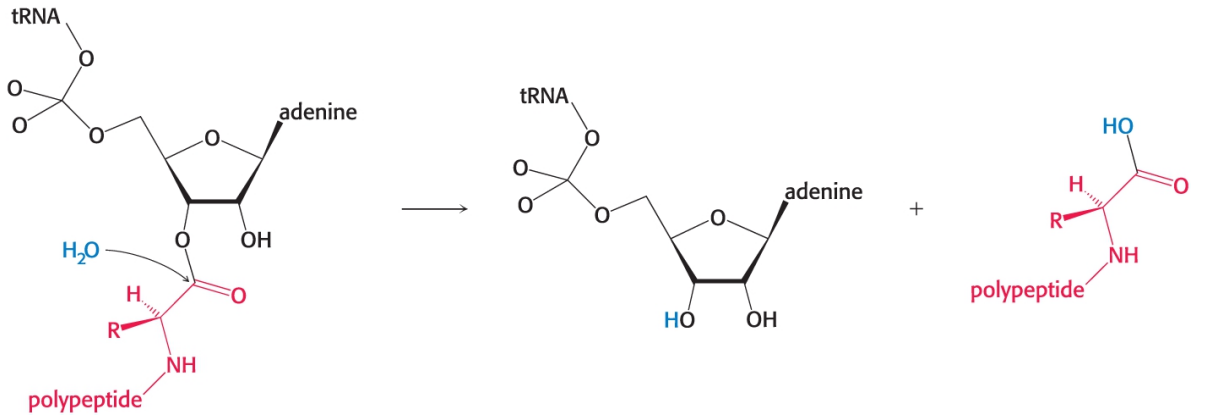


FIGURE 30.27 Release factors facilitate the termination of protein biosynthesis. A release factor recognizes a stop codon in the A site and stimulates the release of the completed protein from the tRNA in the P site.



Next, the detached polypeptide leaves the ribosome. Transfer RNA and mRNA remain briefly attached to the 70S ribosome until the entire complex is dissociated through the hydrolysis of GTP in response to the binding of EF-G and another factor, called the *ribosome release factor* (RRF).

Eukaryotic protein biosynthesis differs from bacterial protein biosynthesis primarily in translation initiation

The basic plan of protein biosynthesis in eukaryotes and archaea is similar to that in bacteria. The major structural and mechanistic themes

recur in all domains of life. However, eukaryotic protein biosynthesis entails more protein components than does bacterial protein biosynthesis, and some steps are more intricate. Some noteworthy similarities and differences include:

- *Eukaryotic ribosomes are larger than those of bacteria*. They consist of a 60S large subunit and a 40S small subunit, which come together to form an 80S particle having a mass of 4200 kDa, compared with 2300 kDa for the bacterial 70S ribosome. The 40S subunit contains an 18S rRNA that is homologous to the bacterial 16S rRNA. The 60S subunit contains three RNAs: the 5S rRNA, which is homologous to the bacterial 5S rRNA; the 28S rRNA, which is homologous to the bacterial 23S molecule; and the 5.8S rRNA, which is homologous to the $5'$ end of the 23S rRNA of bacteria.

- *In eukaryotes, the initiating amino acid is methionine rather than N-formylmethionine*. However, as in bacteria, a special tRNA participates in initiation. This aminoacyl-tRNA is called $\mathrm{Met-tRNAi^{Met}}$ ("i" stands for *initiation*).

- *In eukaryotes, the initiating codon in eukaryotes is almost always AUG (sometimes it is CUG), while in bacteria it can infrequently be GUG or UUG in addition to AUG.* Eukaryotes, in contrast with bacteria, do not have a Shine–Dalgarno sequence on the $5'$ side to distinguish initiator AUGs from internal ones. Instead, the AUG nearest the $5'$ end of mRNA is usually selected as the start site. Eukaryotes use many more initiation factors than do bacteria, and the interplay of these factors is much more complex. The prefix *eIF* denotes a eukaryotic initiation factor.

Initiation begins with the formation of a ternary complex consisting of the 40S ribosome and $\mathrm{Met-tRNAi^{Met}}$ in association with eIF-2. This

complex is called the *43S preinitiation complex* (PIC). The PIC binds to the $5'$ end of mRNA and begins searching for an AUG codon by moving step-by-step in the $3'$ direction. Meanwhile, initiation factor eIF-4E binds to the $5'$ cap of the mRNA (Section 29.3) and facilitates binding of the PIC to the mRNA (**Figure 30.28**). This scanning process is catalyzed by helicases that move along the mRNA powered by ATP hydrolysis. When the anticodon of $\text{Met}-\text{tRNAi}^{\text{Met}}$ finds and pairs with the AUG codon of mRNA, it signals that the target has been found. In almost all cases, eukaryotic mRNA has only one start site and hence is the template for only a single protein. In contrast, a bacterial mRNA can have multiple start sites and can serve as a template for the synthesis of several proteins.

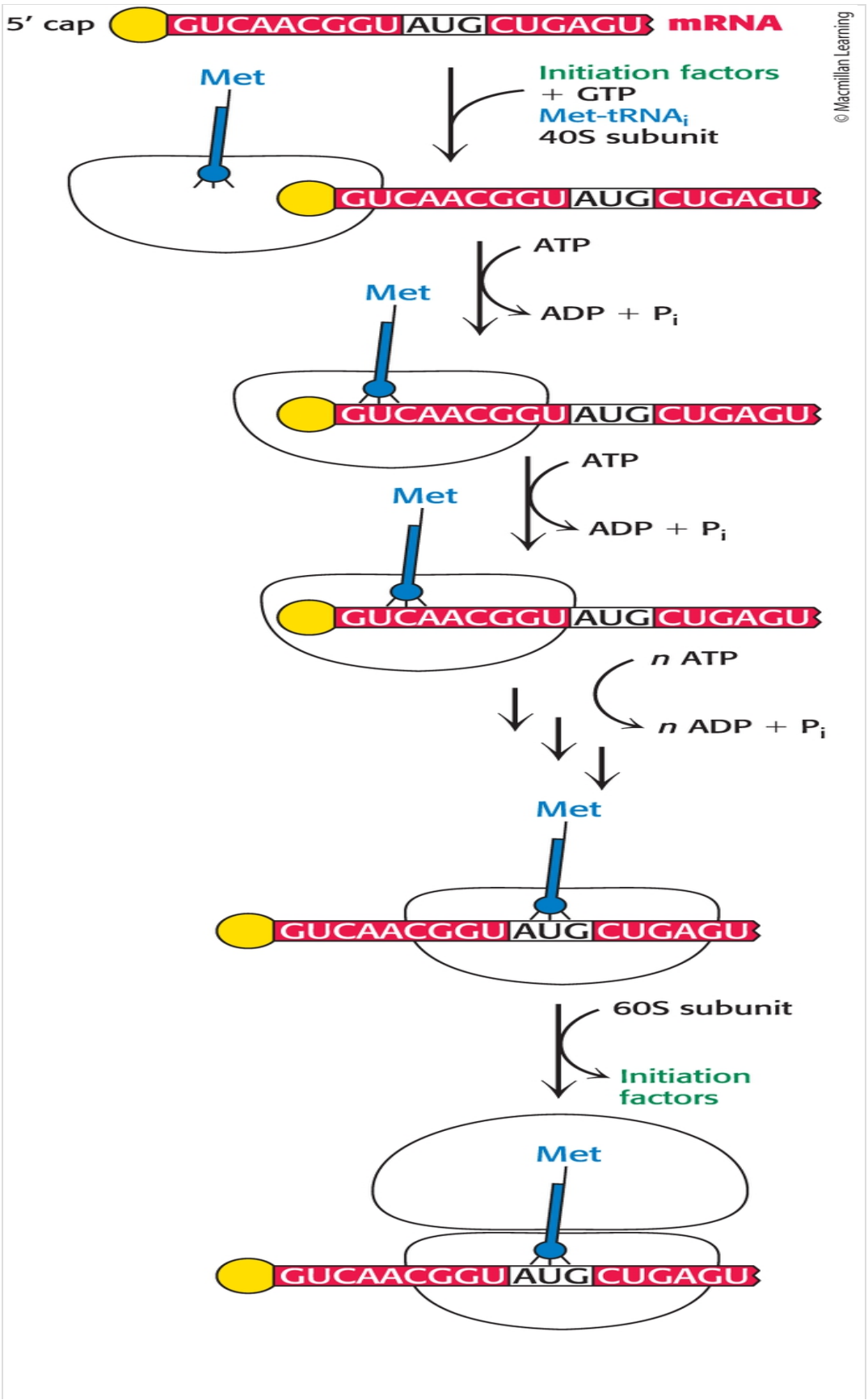

5′ cap
GUCAACGGU AUG CUGAGU
mRNA
Met
Initiation factors
+ GTP
Met-tRNA$_i$
40S subunit
GUCAACGGU AUG CUGAGU
ATP
ADP + P$_i$
Met
GUCAACGGU AUG CUGAGU
ATP
ADP + P$_i$
Met
GUCAACGGU AUG CUGAGU
n ATP
n ADP + P$_i$
Met
GUCAACGGU AUG CUGAGU
60S subunit
Initiation
factors
Met
GUCAACGGU AUG CUGAGU
© Macmillan Learning

FIGURE 30.28 Translation initiation differs in eukaryotes as compared with prokaryotes. In eukaryotes, translation initiation starts with the assembly of a complex on the $5'$ cap that includes the 40S subunit and $\text{Met}-\text{tRNAi}^{\text{Met}}$. Driven by ATP hydrolysis, this complex scans the mRNA until the first AUG is reached. The 60S subunit is then added to form the 80S initiation complex.



The difference in initiation mechanism between bacteria and eukaryotes is, in part, a consequence of the difference in RNA processing. The $5'$ end of mRNA is readily available to ribosomes immediately after transcription in bacteria. In contrast, in eukaryotes, pre-mRNA must be processed and transported to the cytoplasm before translation is initiated. The $5'$ cap provides an easily recognizable starting point. In addition, the complexity of eukaryotic translation initiation provides another mechanism for regulation of gene expression that we shall explore further in Chapter 31.

Although most eukaryotic mRNA molecules rely on the $5'$ cap to initiate protein biosynthesis, recent work has established that some mRNA molecules can recruit ribosomes for initiation without the use of a $5'$ cap and cap-binding proteins. In these mRNAs, highly structured RNA sequences called *internal ribosome entry sites* (IRES) facilitate 40S ribosome binding to the mRNA. IRES were first discovered in the genomes of RNA viruses and have since been found in other viruses, as well as in a subset of cellular mRNA that appears to take part in development and stress responses (such as to a viral infection). The molecular mechanism by which IRES function to initiate protein biosynthesis remains to be determined.

- *Eukaryotic mRNAs adopt a unique structure.* Soon after the PIC binds the mRNA, eIF-4G links eIF-4E to a protein associated with the

poly(A) tail, called *the poly(A)-binding protein 1* (PABP1; **Figure 30.29**). Cap and tail are thus brought together to form a circle of mRNA. One benefit of circularization of eukaryotic mRNAs is that it may prevent translation of mRNA molecules that have lost their poly(A) tails (Section 29.3).

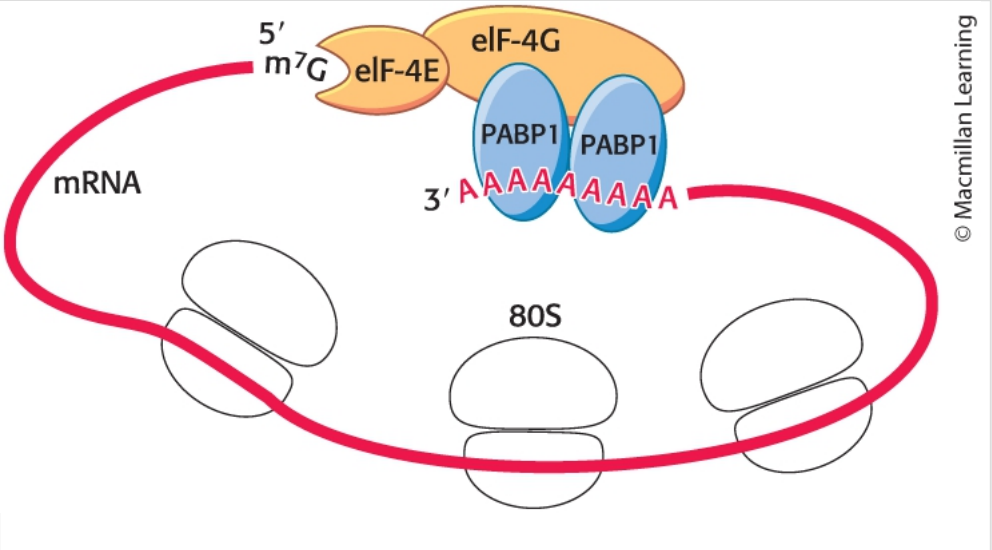


FIGURE 30.29 Protein interactions circularize eukaryotic mRNA. Eukaryotic IFs bound to the 5′ cap and PABP1 bound to the 3′ poly(A) tail come together to create a circular mRNA. This circularization may regulate translation of certain mRNAs.

[Information from H. Lodish et al., *Molecular Cell Biology*, 5th ed. (W. H. Freeman and Company, 2004), Fig. 4.31.]

- *Bacterial elongation and release factors have structural and functional counterparts in eukaryotes.* Eukaryotic elongation factors EF1α and EF1βγ are the counterparts of bacterial EF-Tu and EF-Ts. The GTP form of EF1α delivers aminoacyl-tRNA to the A site of the ribosome, and EF1βγ catalyzes the exchange of GTP for bound GDP. Eukaryotic EF2 mediates GTP-driven translocation in much the same way as does bacterial EF-G. Termination in eukaryotes is

carried out by a single release factor, eRF1, compared with two in bacteria. Release factor eIF-3 accelerates the activity of eRF-1.

- *The components of the translation machinery in higher eukaryotes are organized into large complexes associated with the cytoskeleton*. This association is believed to facilitate the efficiency of protein biosynthesis. Recall that organization of elaborate biochemical processes into physical complexes is a recurring theme in biochemistry (for example, the ATP synthasome in Section 18.5 and purine biosynthesis in Section 26.2).

Ribosomes selectively control gene expression

Ribosomes were once thought to all be the same, regardless of cell type or physiological state. Recent evidence suggests otherwise and points to a more significant role for ribosomes in the regulation of gene expression.

First, the composition of ribosomes has been shown to change in a cell-specific manner. For instance, mutations in certain ribosomal proteins result in Diamond-Blackfan anemia, which is characterized by bone marrow failure in blood stem-cell differentiation. Although protein biosynthesis is impaired in the blood stem cells, protein biosynthesis in other tissues is apparently normal. If mutations in ribosomal proteins lead to loss of ribosomal function in a tissue-specific manner, might changes to ribosomal protein amounts or posttranslational modifications also regulate ribosomal function in a tissue-specific manner? This question remains to be answered.

Second, nonribosomal proteins can also control ribosome activity. One example is FMRP (fragile X mental retardation protein), which is essential for human cognitive development and also for reproductive

function in women. FMRP, an RNA-binding protein, binds to the 80S ribosome to inhibit the translation of specific mRNAs. Mutations in FMRP result in cognitive disabilities, ovarian failure, and other pathologies. In another startling example, an isozyme of the glycolytic enzyme pyruvate kinase, pyruvate kinase M (Section 16.3), binds to the ribosome to control the translation of proteins destined for the endoplasmic reticulum.

How else might ribosomes regulate translation? Ribosome concentration, which varies 3- to 10-fold among different tissues, may play a role. For instance, a low ribosome concentration might discriminate against certain mRNAs that do not initiate well. This might be the case if mRNA has a complex three-dimensional structure in the $5'$ untranslated region, the part of the mRNA upstream of the initiator codon. Indeed, an insufficient ribosome concentration that results in the impaired translation of a specific subset of mRNA is hypothesized to cause some cases of Diamond-Blackfan anemia. What determines ribosome concentration in different cell types remains unknown.



Dan Porges/Archive Photos/Getty Images

ADA YONATH Jerusalem-born Ada Yonath and her family experienced poverty and grief, but her parents always supported her desire for understanding the world. In 1970, after completing her postdoctoral work in the United States, Dr. Yonath returned to Israel and set up the country's first biological x-ray crystallography lab at the Weizmann Institute. Fascinated by genetic code translation, she began structural studies on ribosomes but, like many others, failed to arrive at a solution, owing to the ribosomes' complexity and marked instability. She continued only a few years later, after she read about how the ribosomes of hibernating polar bears are arranged in an ordered fashion within their cells, indicating to her the natural tendency to maintain stability. This inspired her to pursue the crystallization of ribosomes from bacteria that live under pressure. Then she confronted another problem: extreme damage to the ribosomal crystals by the x-rays used to visualize them, which prevented structure determination. Her novel solution — taking measurements of frozen crystals of ribosomes at sub-zero temperatures, called *cryo-crystallography* — became popular immediately and has allowed the determination of more than

100,000 structures of various biological materials. Dr. Yonath was awarded the Nobel Prize in Chemistry with Drs. Venkatraman Ramakrishnan and Thomas Steitz in 2009.

Scientists have manipulated protein biosynthesis pathways to incorporate unnatural amino acids in preselected positions

Knowledge of how aminoacyl-tRNA synthetases charge tRNAs with amino acids, and how the ribosome decodes the information in mRNA, has allowed biochemists to synthesize modified proteins with unnatural amino acids (amino acids that are not normally found in nature). These unnatural amino acids can be incorporated at specific positions within the polypeptide chain. Examples of unnatural amino acids include those that have been modified to contain a fluorescent moiety (Figure 30.30), heavy atoms, or other reactive groups, providing the protein that contains them with new and useful chemical and biological properties.

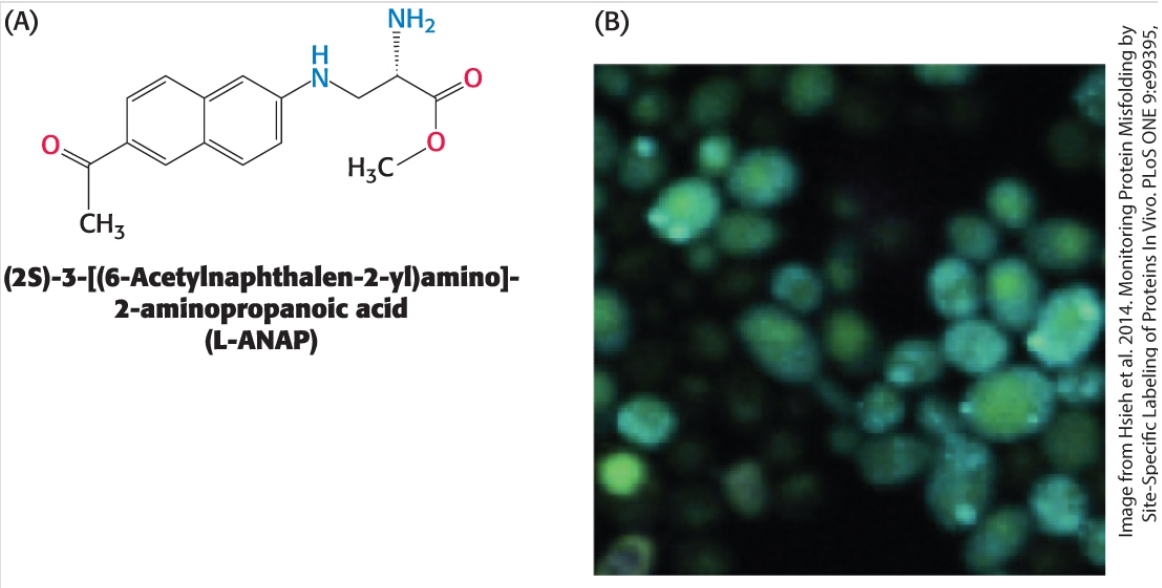


FIGURE 30.30 Unnatural amino acids can be incorporated into proteins. Unnatural amino acid give proteins novel characteristics that are useful for experimental studies. (A) The structure of

ANAP ((2S)-3-[(6-Acetylnaphthalen-2-yl)amino]-2-aminopropanoic acid), a fluorescent unnatura
amino acid, is shown. (B) Fluorescent proteins are easy to visualize and thus localize, as seen in
this image of yeast cells that express a protein containing L-ANAP.



How are unnatural amino acids introduced into proteins? There are multiple strategies to accomplish this, but in all cases the three key players involved are a tRNA, the unnatural amino acid itself, and the aminoacyl-tRNA synthetase that charges the particular tRNA with the unnatural amino acid. In addition to these players, it is often necessary to usurp one of the three termination codons to introduce the unnatural amino acid into the polypeptide chain (since all other mRNA codons are already set to code for the 20 natural amino acids). Recall that termination codons are not recognized by any cellular tRNAs. To introduce an unnatural amino acid into a protein, the tRNA is engineered to recognize a termination codon, and the aminoacyl-tRNA synthetase is engineered to charge that tRNA with the unnatural amino acid. All of these components can be introduced into a living cell for in vivo protein production. More recent research focuses on creating unnatural proteins in vitro.

Modifying proteins through the incorporation of unnatural amino acids is likely less disruptive to overall protein function than posttranslational modification or labeling. These “designer” proteins can be used in experimental studies of protein folding, localization, and many other characteristics, both in vitro and in vivo. Consider, for example, a synthetic protein with fluorescent unnatural amino acids incorporated near its surface: the exact in vivo sub-cellular localization of this protein can be easily determined via fluorescent microscopy. If the functions of this protein are largely undetermined, knowing where it is located, and what other factors it colocalizes with, might give some insights into what its functions might be.

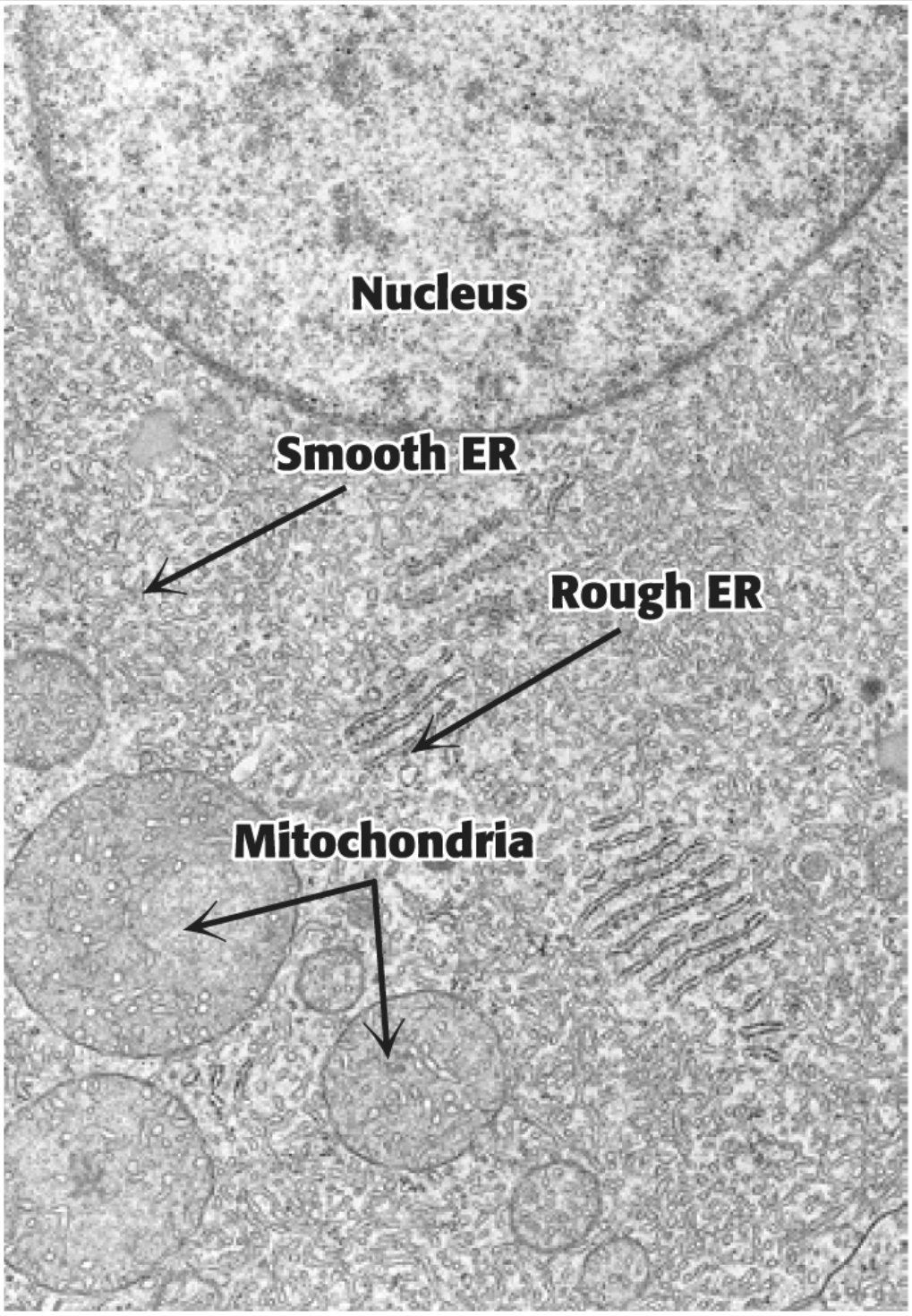
30.4 Ribosomes Bound to the Endoplasmic Reticulum Manufacture Secretory and Membrane Proteins

Not all newly synthesized proteins are destined to function in the cytoplasm. Eukaryotic cells can direct proteins to internal sites such as mitochondria, the nucleus, and the endoplasmic reticulum, a process called *protein targeting* or *protein sorting*. How is this sorting accomplished? There are two general mechanisms by which sorting takes place. In one mechanism, the protein is synthesized in the cytoplasm, and then the completed protein is delivered to its intracellular location posttranslationally. Proteins destined for the nucleus, chloroplasts, mitochondria, and peroxisomes are delivered by this general process. The other mechanism, termed the *secretory pathway*, directs proteins into the endoplasmic reticulum (ER), the extensive membrane system that comprises about half the total membrane of a cell. This mechanism delivers the proteins to the ER cotranslationally — that is, while the protein is being synthesized. Approximately 30% of all proteins are sorted by the secretory pathway, including secreted proteins, residents of the ER, the Golgi complex, lysosomes, and integral membrane proteins of these organelles as well as integral plasma membrane proteins. We will focus our attention on the secretory pathway only.

Protein biosynthesis begins on ribosomes that are free in the cytoplasm

In eukaryotic cells, a ribosome remains free in the cytoplasm unless it is directed to the ER. The region of the ER that ribosomes bind to is called the *rough ER* because of its studded appearance in contrast with the

smooth ER, which is devoid of ribosomes (**Figure 30.31**). The synthesis of proteins sorted by the secretory pathway begins on free ribosomes that soon associate with the ER. Free ribosomes that are synthesizing proteins for use in the cell are apparently identical with those attached to the ER, so ribosomes synthesizing proteins destined to enter the ER need to bind to the ER. How is this accomplished?



Don W. Fawcett/Science Source.

FIGURE 30.31 Ribosomes are bound to the endoplasmic reticulum. In this electron micrograph, ribosomes appear as small black dots binding to the cytoplasmic side of the endoplasmic reticulum to give a rough appearance. In contrast, the smooth endoplasmic reticulum is devoid of ribosomes.

Signal sequences mark proteins for translocation across the endoplasmic reticulum membrane

The synthesis of proteins destined to leave the cell or become embedded in the plasma membrane begins on a free ribosome. However, shortly after synthesis begins, the process is halted until the ribosome is directed to the cytoplasmic side of the ER. When the ribosome docks with the ER membrane, protein biosynthesis begins again. As the newly forming peptide chain exits the ribosome, it is transported — while being translated — through the membrane into the lumen of the ER. The translocation consists of four components:

1. *The signal sequence*. The **signal sequence** is a sequence of 9 to 12 hydrophobic amino acid residues, sometimes containing positively charged amino acids (**Figure 30.32**). This sequence, which adopts an α-helical structure, is usually near the amino terminus of the nascent polypeptide chain. The presence of the signal sequence identifies the nascent peptide as one that must cross the ER membrane. Some signal sequences are maintained in the mature protein, whereas others are cleaved by a **signal peptidase** on the lumenal side of the ER membrane.

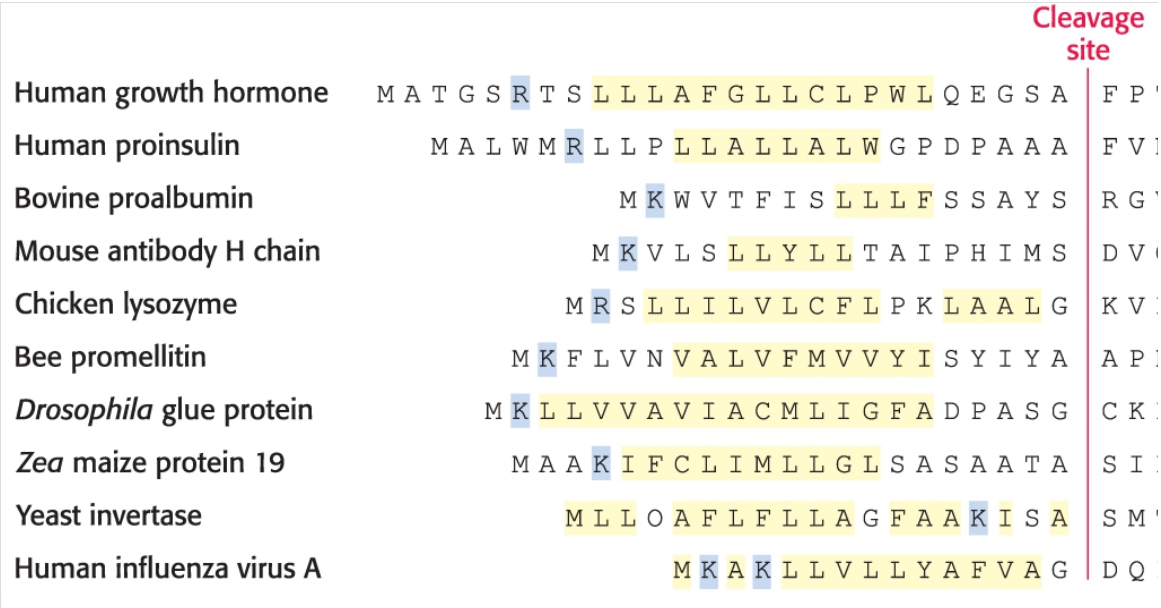


FIGURE 30.32 The signal sequences of eukaryotic secretory and plasma membrane proteins contain hydrophobic residues. This alignment of the amino-terminal signal sequences of some eukaryotic secretory and plasma membrane proteins highlights the hydrophobic core (yellow), which is preceded by basic residues (blue) and followed by a cleavage site (red) for signal peptidase.

2. *The signal-recognition particle*. The **signal-recognition particle (SRP)** recognizes the signal sequence and binds the sequence and the ribosome as soon as the signal sequence exits the ribosome. SRP then shepherds the ribosome and its nascent polypeptide chain to the ER membrane. SRP is a ribonucleoprotein consisting of a 7S RNA and six different proteins (**Figure 30.33**). One protein, SRP54, is a GTPase that is crucial for SRP function. SRP samples all ribosomes until it locates one exhibiting a signal sequence. After SRP binds to the signal sequence, interactions between the ribosome and the SRP block the elongation-factor-binding site, thereby halting protein biosynthesis.

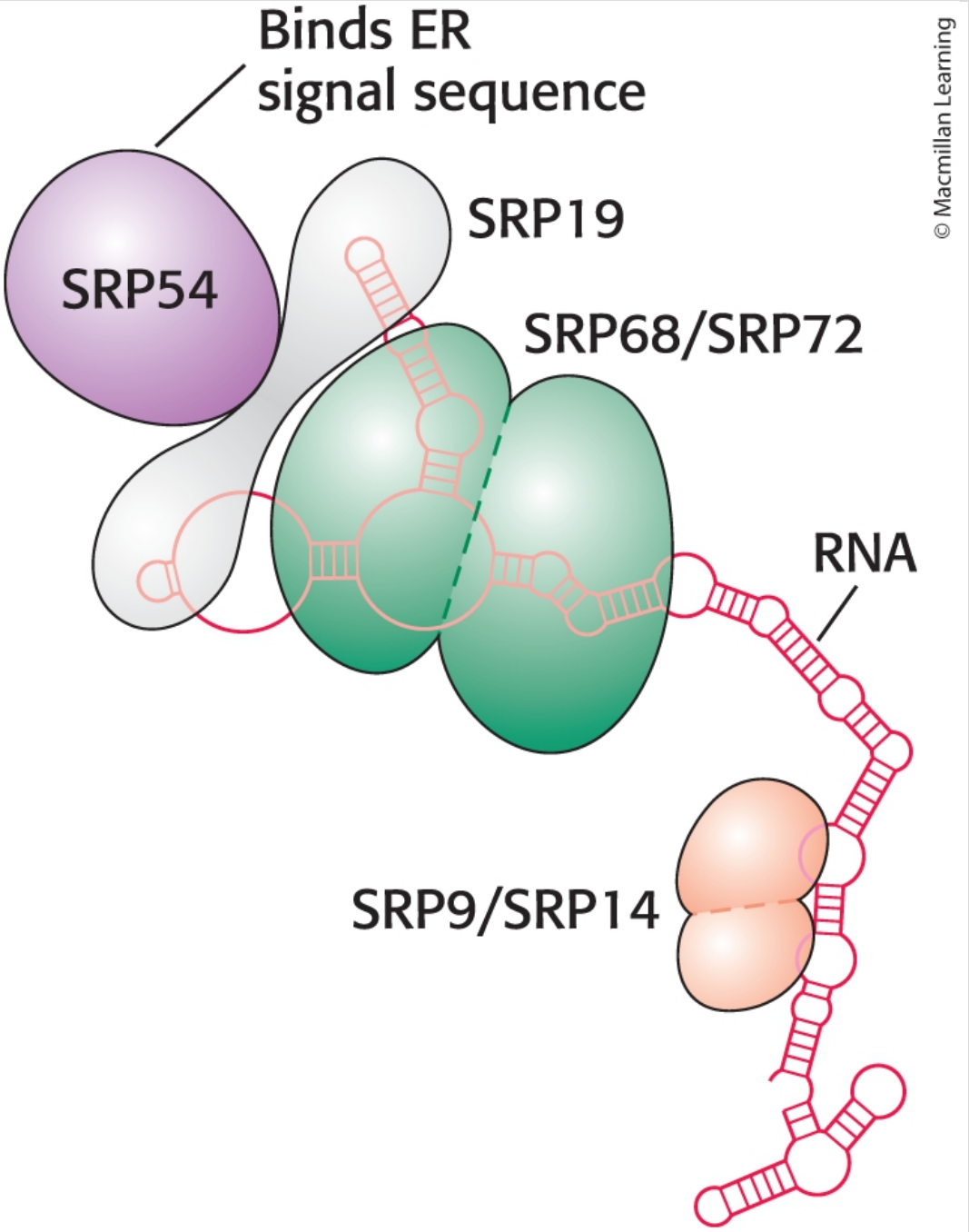


FIGURE 30.33 The signal-recognition particle (SRP) consists of six proteins and one 300-nucleotide RNA. The RNA has a complex structure with many double-helical stretches punctuated by single-stranded regions, shown as circles.

[Information from H. Lodish et al., *Molecular Cell Biology*, 5th ed. (W. H. Freeman and Company, 2004). Data from K. Strub et al., *Mol. Cell Biol*. 11:3949–3959, 1991, and S. High and B. Dobberstein, *J. Cell Biol*. 113:229–233, 1991.]

3. *The SRP receptor*. The SRP–ribosome complex diffuses to the ER, where SRP binds the **SRP receptor (SR)**, an integral membrane protein consisting of two subunits, SRα and SRβ. SRα is, like SRP54, a GTPase.

4. *The translocon*. The SRP–SR complex delivers the ribosome to the translocation machinery, called the **translocon**, a multisubunit assembly of integral and peripheral membrane proteins. The translocon is a protein-conducting channel that opens when the translocon and ribosome bind to each other. Protein biosynthesis resumes with the growing polypeptide chain passing through the translocon channel into the lumen of the ER.

The interactions of the components of the translocation machinery are shown in **Figure 30.34**. Both the SRP54 and the SRα subunits of SR must bind GTP to facilitate the formation of the SRP–SR complex. For the SRP–SR complex to then deliver the ribosome to the translocon, the two GTP molecules — one in SRP and the other in SR — are aligned in what is essentially an active site shared by the two proteins. The formation of the alignment is catalyzed by the 7S RNA of the SRP. After the ribosome has been passed along to the translocon, the GTPs are hydrolyzed, SRP and SR dissociate, and SRP is free to search for another signal sequence to begin the cycle again. Thus, SRP acts catalytically. The signal peptidase, which is associated with the translocon in the lumen of the ER, removes the signal sequence from most proteins.

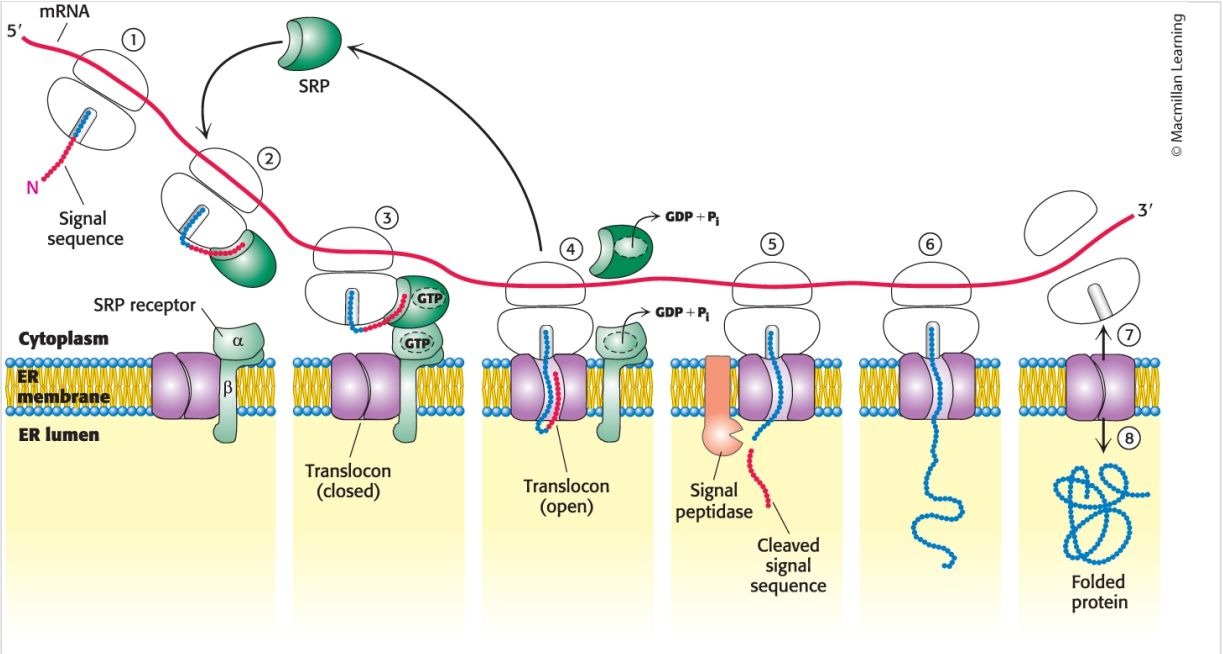


FIGURE 30.34 The SRP targeting cycle delivers nascent proteins containing a signal sequence to the ER. (1) Protein biosynthesis begins on free ribosomes. (2) After the signal sequence has exited the ribosome, it is bound by the SRP, and protein biosynthesis halts. (3) The SRP–ribosome complex docks with the SRP receptor in the ER membrane. (4) The SRP and the SRP receptor simultaneously hydrolyze bound GTPs. Protein biosynthesis resumes and the SRP is free to bind another signal sequence. (5) The signal peptidase may remove the signal sequence as it enters the lumen of the ER. (6) Protein biosynthesis continues as the protein is synthesized directly into the ER. (7) On completion of protein biosynthesis, the ribosome is released. (8) The protein tunnel in the translocon closes.

[Information from H. Lodish et al., *Molecular Cell Biology*, 5th ed. (W. H. Freeman and Company, 2004), Fig. 16.6.]

Transport vesicles carry cargo proteins to their final destinations

As the proteins are synthesized, they fold into their three-dimensional structures in the lumen of the ER. Some proteins are modified by the attachment of N-linked carbohydrates (Section 11.3). Finally, the proteins must be sorted and transported to their final destinations.

Regardless of the destination, the principles of transport are the same. Transport is mediated by **transport vesicles** that bud off the ER (**Figure 30.35**). Transport vesicles from the ER carry their cargo (the proteins) to the Golgi complex, where the vesicles fuse and deposit the cargo inside the complex. There the cargo proteins are further modified — for instance, by the attachment of O-linked carbohydrates. From the Golgi complex, transport vesicles carry the cargo proteins to their final destinations, as shown in Figure 30.35.

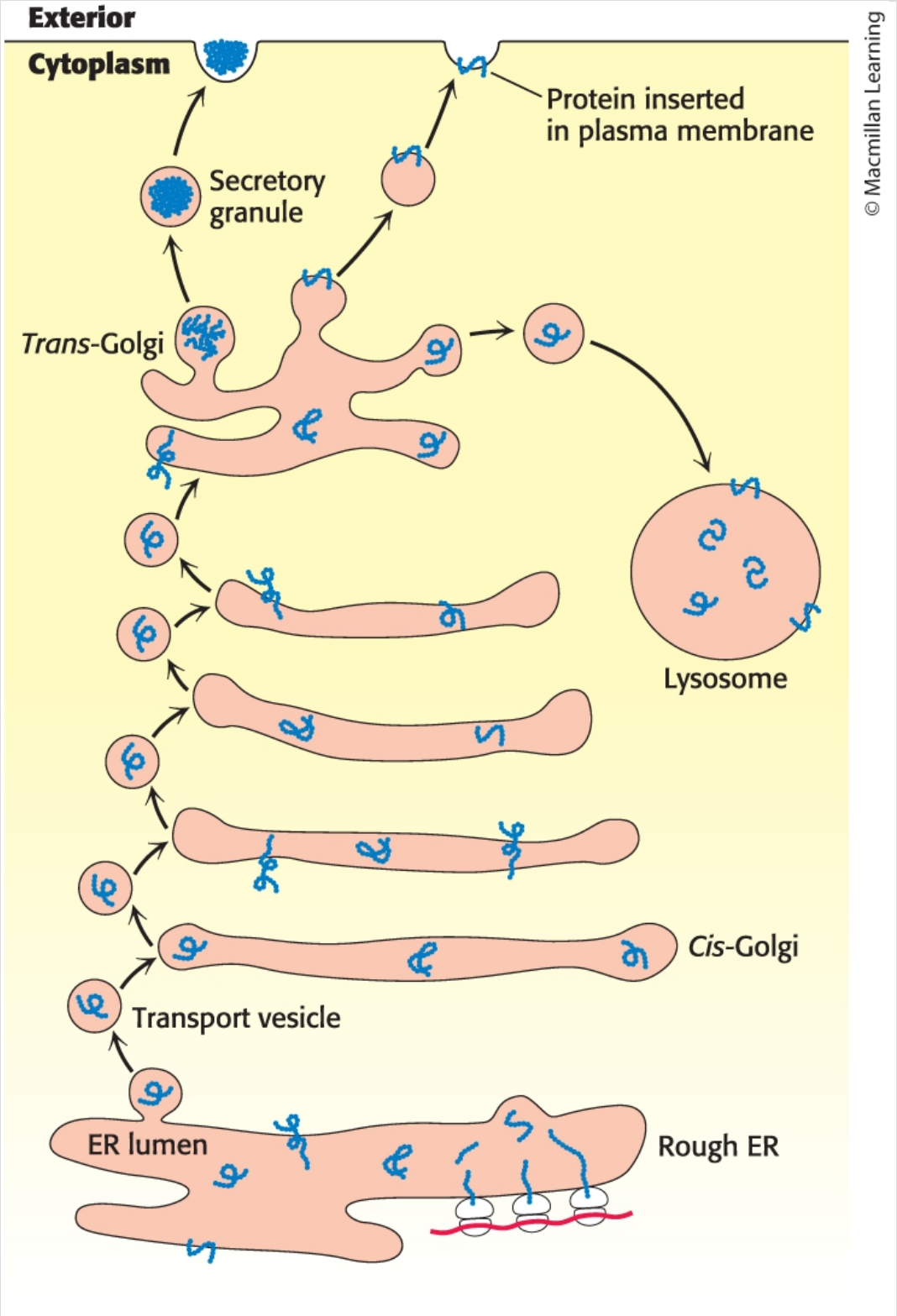


FIGURE 30.35 Protein-sorting pathways deliver proteins to their final destinations. Newly synthesized proteins in the lumen of the ER are collected into membrane buds. These buds pinch off to form transport vesicles. The transport vesicles carry

the cargo proteins to the Golgi complex, where the cargo proteins are modified. Transport vesicles then carry the cargo to the final destination as directed by the v-SNARE and t-SNARE proteins.

How does a protein end up at the correct destination? A newly synthesized protein will float inside the ER lumen until it binds to an integral membrane protein called a *cargo receptor*. This binding sequesters the cargo protein into a small region of the membrane that can subsequently form a membrane bud. The bud will carry the protein to a specific destination — plasma membrane, lysosome, or cell exterior. The key to ensuring that the protein reaches the proper destination is that the protein must bind to a receptor in the ER region associated with the protein's destination. To ensure the proper match of protein with ER region, cargo receptors recognize various characteristics of the cargo protein, such as a particular amino acid sequence or an added carbohydrate.

The formation of buds is facilitated by the binding of coat proteins to the cytoplasmic side of the bud. The coat proteins associate with one another to pinch off the vesicle. After the transport vesicle has formed and is released, the coat proteins are shed to reveal another integral protein, called **v-SNARE** ("v" for vesicle) (Section 12.6). The binding of v-SNARE to a particular **t-SNARE** ("t" for target) in the target membrane leads to the fusion of the transport vesicle to the target membrane, and the cargo is delivered. Thus, the assignment of identical v-SNARE proteins to the same region of the ER membrane causes an ER region to be associated with a particular destination.

Self-Check Question

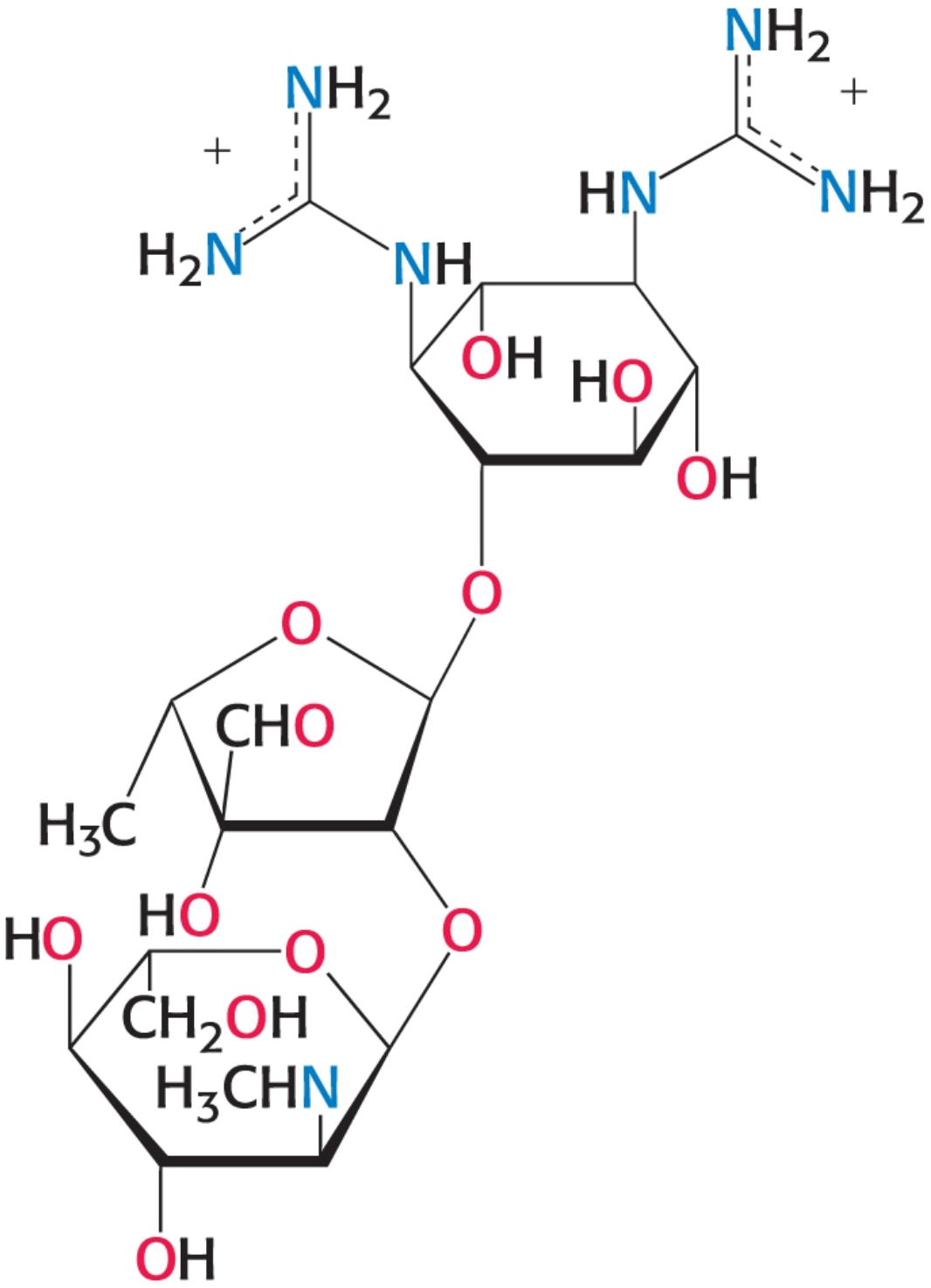
What is the role of the signal-recognition particle in protein translocation?

30.5 A Variety of Antibiotics and Toxins Inhibit Protein Biosynthesis

Many chemicals that inhibit various aspects of protein biosynthesis have been identified. These chemicals are powerful experimental tools and clinically useful drugs.

Some antibiotics inhibit protein biosynthesis

The differences between eukaryotic and bacterial ribosomes can be exploited for the development of antibiotics (Table 30.4). For example, the antibiotic streptomycin, a highly basic trisaccharide, interferes with the binding of fMet-$tRNA^{fMet}$ to ribosomes in bacteria and thereby prevents the correct initiation of protein biosynthesis. Other aminoglycoside antibiotics such as neomycin, kanamycin, and gentamycin interfere with the interaction between tRNA and the 16S rRNA of the 30S subunit of bacterial ribosomes. Chloramphenicol acts by inhibiting peptidyl transferase activity. Erythromycin binds to the 50S subunit and blocks translocation. Cycloheximide, another antibiotic, blocks translocation in eukaryotic ribosomes, making it a useful laboratory tool for blocking protein biosynthesis in eukaryotic cells.



Streptomycin

TABLE 30.4 Antibiotic inhibitors of protein biosynthesis

Antibiotic	Action
Streptomycin and other aminoglycosides	Inhibit initiation and cause the misreading of mRNA (bacteria)
Tetracycline	Binds to the 30S subunit and inhibits the binding of aminoacyl-tRNAs (bacteria)
Chloramphenicol	Inhibits the peptidyl transferase activity of the 50S ribosomal subunit (bacteria)
Cycloheximide	Inhibits translocation (eukaryotes)
Erythromycin	Binds to the 50S subunit and inhibits translocation (bacteria)
Puromycin	Causes premature chain termination by acting as an analog of aminoacyl-tRNA (bacteria and eukaryotes)

The antibiotic puromycin inhibits protein biosynthesis in both bacteria and eukaryotes by causing nascent polypeptide chains to be released before their synthesis is completed. Puromycin is an analog of the terminal part of aminoacyl-tRNA (**Figure 30.36**) that binds to the A site on the ribosome and blocks the entry of aminoacyl-tRNA. Furthermore, puromycin contains an α-amino group. This amino group, like the one on aminoacyl-tRNA, forms a peptide bond with the carboxyl group of the growing peptide chain. The product, a peptide having a covalently attached puromycin residue at its carboxyl end, dissociates from the ribosome. While no longer used medicinally, puromycin remains an experimental tool for the investigation of protein biosynthesis.

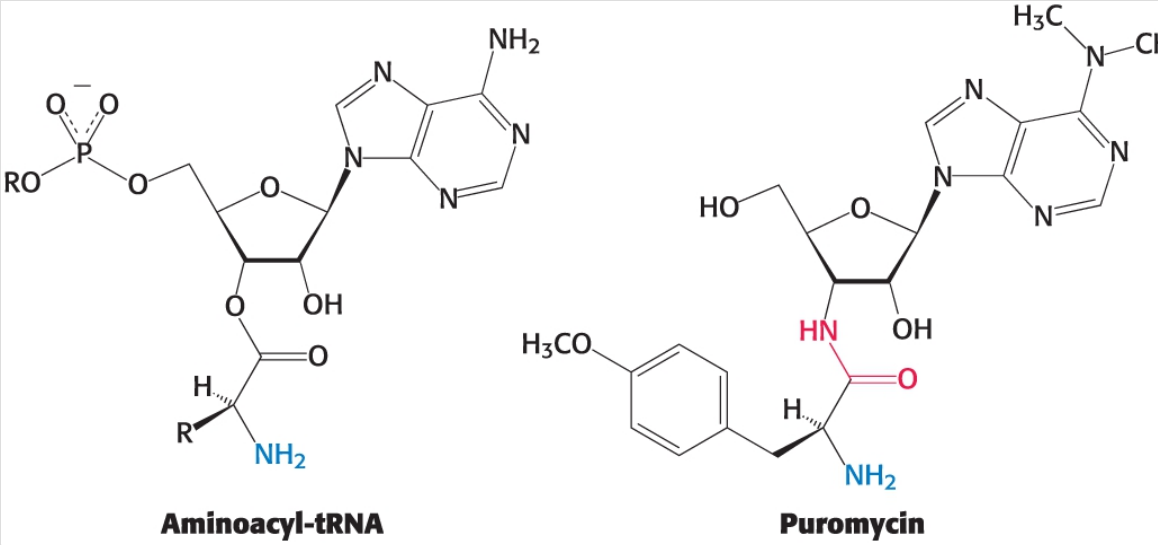


FIGURE 30.36 The antibiotic puromycin resembles the aminoacyl terminus of an aminoacyl-tRNA. The amino group of puromycin joins the carboxyl group of the growing polypeptide chain to form peptidyl-puromycin that dissociates from the ribosome. Peptidyl-puromycin is stable because puromycin has an amide (shown in red) rather than an ester linkage.

Diphtheria toxin blocks protein biosynthesis in eukaryotes by inhibiting translocation

Many antibiotics, harvested from bacteria for medicinal purposes, are inhibitors of bacterial protein biosynthesis. However, some bacteria produce compounds that inhibit eukaryotic protein biosynthesis, leading to diseases such as diphtheria, which was a major cause of childhood death before the advent of effective immunization.

Pathogenic strains of *Corynebacterium diphtheriae*, a bacterium that grows in the upper respiratory tract of an infected person, have a prophage inserted into their genomes that produces the diphtheria

toxin. The toxin consists of a single polypeptide chain that is cleaved into a 21-kDa A fragment and a 40-kDa B fragment shortly after entering the target cell. The role of the B fragment in the intact protein is to bind to the cell, enabling the toxin to enter the cytoplasm of its target cell. The A fragment catalyzes the covalent modification of EF2, the elongation factor catalyzing translocation in eukaryotic protein biosynthesis.

A single A fragment of the toxin in the cytoplasm can kill a cell. Why is it so lethal? EF2 contains diphthamide, an unusual amino acid residue that enhances the fidelity of codon shifting during translocation. Diphthamide is formed by a highly conserved complicated pathway that posttranslationally modifies histidine. The A fragment of the diphtheria toxin catalyzes the transfer of the ADP ribose unit of NAD^+ to the diphthamide ring (**Figure 30.37**). This ADP ribosylation of a single side chain of EF2 blocks EF2's capacity to carry out the translocation of the growing polypeptide chain. Protein biosynthesis ceases, accounting for the remarkable toxicity of diphtheria toxin. A few micrograms of diphtheria toxin are usually lethal in an unimmunized person.

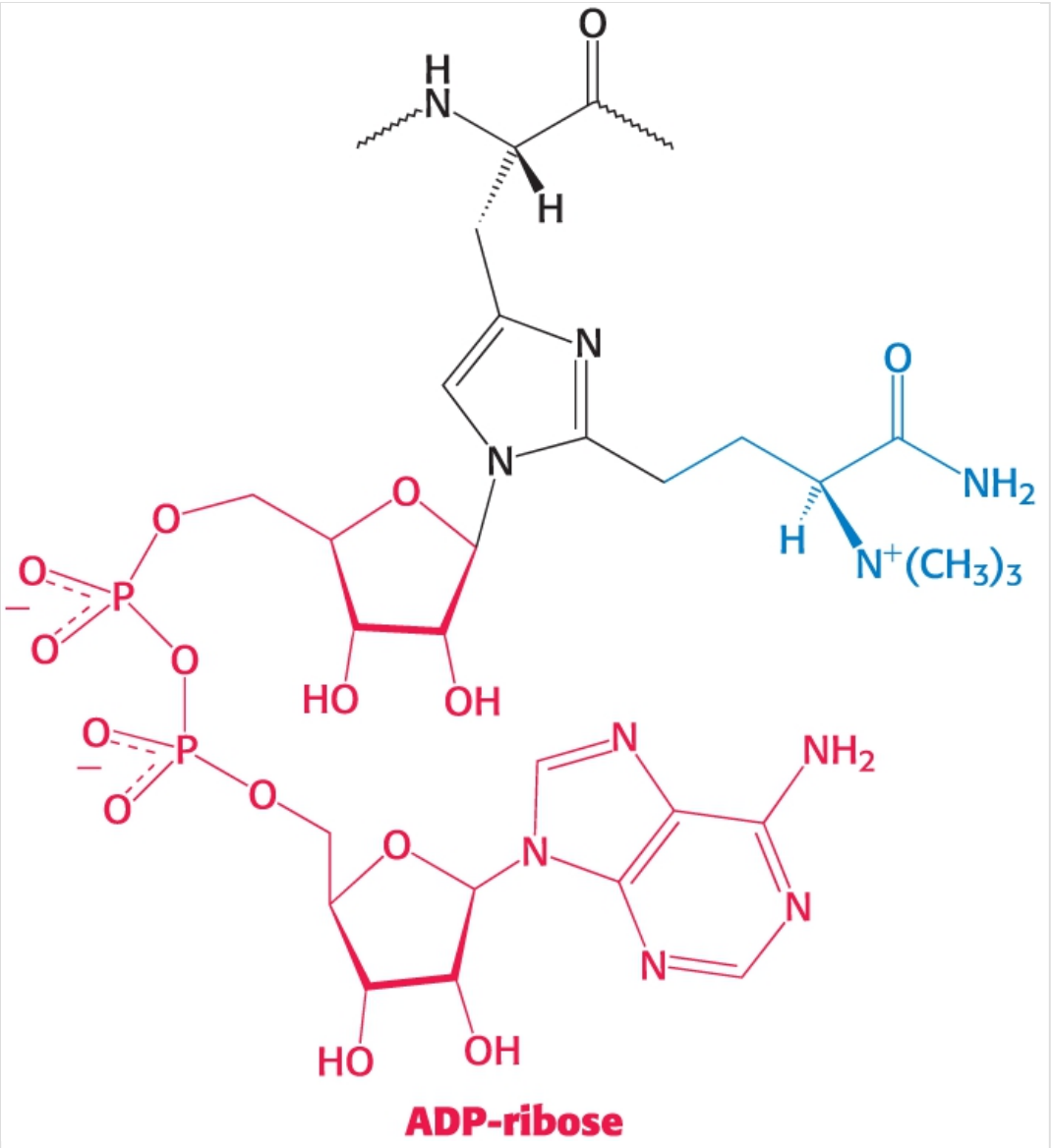


FIGURE 30.37 Diphtheria toxin inhibits protein biosynthesis in eukaryotes.
Diphtheria toxin blocks translocation by catalyzing the transfer of an ADP-ribose unit from NAD^+ to diphthamide, a modified amino acid residue in EF2 (translocase). Diphthamide is formed by the posttranslational modification (blue) of a histidine residue.

Some toxins modify 28S ribosomal RNA

α-Sarcin is a 17kDa ribonuclease secreted by filamentous fungi. It penetrates cells by interacting with membrane lipids and cleaves a specific single phosphodiester linkage in the 28S rRNA of the large ribosomal subunit. This cleavage completely inhibits protein biosynthesis.

Another toxin, ricin, also affects the 28S rRNA in the same region as α-sarcin (the sarcin-ricin loop; Section 30.3) but is a glycoside hydrolase, not a ribonuclease. Ricin is a small protein (65 kDa) found in the seeds of the castor oil plant, *Ricinus communis*. It is indeed a deadly molecule because as little as 500 μg is lethal for an adult human being, and a single molecule can inhibit all protein biosynthesis in a cell, resulting in cell death.

Ricin is a heterodimeric protein composed of a catalytic A chain joined by a single disulfide bond to a B chain. The B chain allows the toxin to bind to the target cell, and this binding leads to an endocytotic uptake of the dimer and the eventual release of the A chain into the cytoplasm. The A chain is an N-glycoside hydrolase that cleaves adenine from a particular adenosine nucleotide on the 28S rRNA that is found in all eukaryotic ribosomes. Removal of the adenine base completely inactivates the ribosome by preventing the binding of elongation factors.

Thus, diphtheria toxin, α-sarcin, and ricin all act by inhibiting protein-synthesis elongation; ricin and α-sarcin do so by covalently modifying rRNA, and diphtheria toxin does so by covalently modifying the elongation factor. Interestingly, attempts are underway to modify α-sarcin for use as an antitumor drug.

Chapter 30 Summary

30.1 Protein Biosynthesis Requires the Translation of Nucleotide Sequences into Amino Acid Sequences

- Protein biosynthesis is called translation because information in a nucleic acid sequence is translated into a different language, the sequence of amino acids in a protein.
- This complex process is mediated by the coordinated interplay of more than a hundred macromolecules, including mRNA, rRNAs, tRNAs, aminoacyl-tRNA synthetases, and protein factors.
- Transfer RNAs are the adaptors that make the link between a nucleic acid and an amino acid.

30.2 Aminoacyl-tRNA Synthetases Establish the Genetic Code

- Each amino acid is activated and linked to a specific tRNA by an aminoacyl-tRNA synthetase. There is at least one specific aminoacyl-tRNA synthetase and at least one specific tRNA for each amino acid.
- By specifically recognizing both amino acids and tRNAs, aminoacyl-tRNA synthetases implement the instructions of the genetic code.
- The codons of mRNA recognize the anticodons of transfer RNAs rather than the amino acids attached to the tRNAs. A codon on mRNA forms base pairs with the anticodon of the tRNA.
- Some tRNAs are recognized by more than one codon because pairing of the third base of a codon is less crucial than that of the other two (the wobble mechanism).

30.3 The Ribosome Is the Site of Protein Biosynthesis

- Protein biosynthesis takes place on ribosomes, which are huge ribonucleoprotein particles consisting of large and small subunits.
- In *E. coli*, the 70S ribosome (2300 kDa) is made up of 30S and 50S subunits.
- The ribosome includes three sites for tRNA binding, called the A (aminoacyl) site, the P (peptidyl) site, and the E (exit) site.
- Protein biosynthesis takes place in three phases: initiation, elongation, and termination.
- In bacteria, mRNA, *N*-formylmethionyl-$tRNA^{fMet}$ and a 30S ribosomal subunit come together with the assistance of initiation factors to form a 30S initiation complex. A 50S ribosomal subunit then joins this complex to form a 70S initiation complex, in which $fMet-tRNA^{fMet}$ occupies the P site of the ribosome.
- During elongation, an EF-Tu-GTP complex delivers the appropriate aminoacyl-tRNA to the ribosome's A site as a ternary complex.
- A peptide bond is formed when the amino group of the aminoacyl-tRNA nucleophilically attacks the ester linkage of the peptidyl-tRNA.
- After peptide-bond formation, the tRNAs and mRNA are translocated for the next cycle to begin. The deacylated tRNA moves to the E site and then leaves the ribosome, and the peptidyl-tRNA moves from the A site into the P site.
- Protein biosynthesis is terminated by release factors, which recognize the termination codons UAA, UGA, and UAG and cause the hydrolysis of the ester bond between the polypeptide and tRNA.
- Eukaryotic ribosomes (80S) consist of a 40S small subunit and a 60S large subunit.
- The initiation of protein biosynthesis is more complex in eukaryotes than in bacteria.

- The regulation of translation in eukaryotes provides a means for regulating gene expression.

30.4 Ribosomes Bound to the Endoplasmic Reticulum Manufacture Secretory and Membrane Proteins

- Proteins contain signals that determine their ultimate destination. The synthesis of all proteins begins on free ribosomes in the cytoplasm.
- In eukaryotes, protein biosynthesis continues in the cytoplasm unless the nascent chain contains a signal sequence that directs the ribosome to the endoplasmic reticulum.
- The signal-recognition particle recognizes signal sequences and brings ribosomes bearing them to the ER. The nascent chain is then translocated across the ER membrane.

30.5 A Variety of Antibiotics and Toxins Inhibit Protein Biosynthesis

- Many clinically important antibiotics function by inhibiting protein biosynthesis.
- All steps of protein biosynthesis are susceptible to inhibition by antibiotics or toxins.

Key Terms

translation
codon
transfer RNA (tRNA)
anticodon
wobble hypothesis
ribosome
aminoacyl-tRNA

aminoacyl-tRNA synthetase
large subunit (50S)
small subunit (30S)
Shine–Dalgarno sequence
initiation factor
elongation factor Tu (EF-Tu)
elongation factor Ts (EF-Ts)
peptidyl transferase center
elongation factor G (EF-G) (translocase)
polysome
release factor (RF)
signal sequence
signal peptidase
signal-recognition particle (SRP)
SRP receptor (SR)
translocon
transport vesicle
v-SNARE
t-SNARE

Problems

1. Which of the following reaction steps are required to form an aminoacyl-tRNA? (Select all that apply.) 1

a. Formation of an aminoacyl adenylate from an amino acid and ATP
b. Transfer of an aminoacyl group to a tRNA molecule
c. Formation of an acyl adenylate from a fatty acid and ATP
d. Attack of the ester linkage of a peptidyl-tRNA by an amino group

2. Ribosomes were isolated from bacteria grown in a “heavy” medium (^{13}C and ^{15}N) and from bacteria grown in a “light” medium (^{12}C and ^{14}N). These 70S ribosomes were then added to an in vitro system engaged in protein synthesis. Several hours later, an aliquot was removed and analyzed by density-gradient centrifugation. How many bands of 70S ribosomes would you expect to see in the density gradient? 2

3. A tRNA with a UGU anticodon is enzymatically conjugated to ^{14}C-labeled cysteine. The cysteine unit is then chemically modified to alanine. The altered aminoacyl-tRNA is added to a protein-synthesizing system containing normal components except for this tRNA. The mRNA added to this mixture contains the following sequence:

$$5'-UUUUGCCAUGUUUGUGCU-3'$$

What is the sequence of the corresponding radiolabeled peptide? 1

4. Match each factor with its associated phase of translation in prokaryotes. Factors can be used more than once. 2

1. Initiation	1. GTP
2. Elongation	2. AUG
3. Termination	3. fMet
	4. RRF

5. IF2

6. Shine–Dalgarno

7. EF-Tu

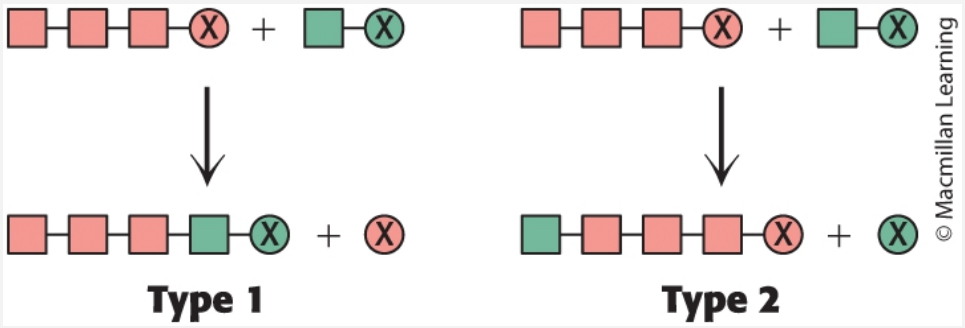
8. Peptidyl transferase

9. UGA

10. Transformylase

---

5. The two basic mechanisms for the elongation of biomolecules are represented in the adjoining illustration. In type 1, the activating group (X) is released from the growing chain. In type 2, the activating group is released from the incoming unit as it is added to the growing chain. Indicate whether each of the following biosyntheses is by means of a type 1 or a type 2 mechanism: 1



a. Glycogen synthesis
b. Fatty acid synthesis

c. $C_5 \rightarrow C_{10} \rightarrow C_{15}$ in cholesterol synthesis
d. DNA synthesis
e. RNA synthesis
f. Protein synthesis

6. What is the smallest number of molecules of ATP and GTP consumed in the synthesis of a 200-residue protein, starting from amino acids? Assume that the hydrolysis of PP_i is equivalent to the hydrolysis of ATP for this calculation. 1, 2

7. Compare and contrast protein biosynthesis by ribosomes with protein synthesis by the solid-phase method (Section 4.4). 1, 2

8. Suppose that you have a protein-synthesis system that is synthesizing a protein designated A. Furthermore, you know that protein A has four trypsin-sensitive sites, equally spaced in the protein, that, on digestion with trypsin, yield the peptides A_1, A_2, A_3, A_4, and A_5. Peptide A_1 is the amino-terminal peptide, and A_5 is the carboxyl-terminal peptide. Finally, you know that your system requires 4 minutes to synthesize a complete protein A. At $t = 0$, you add all 20 amino acids, each carrying a ^{14}C label. 2

a. At $t = 1$ minute, you isolate intact protein A from the system, cleave it with trypsin, and isolate the five peptides. Which peptide is most heavily labeled?
b. At $t = 3$ minutes, what will be the order of the labeling of peptides from greatest to least?
c. What does this experiment tell you about the direction of protein synthesis?

9. Every ribosome has three tRNA binding sites: the A site, the P site, and the E site. For the given sentences, identify whether it refers to the P site, A site, or E site. 2

a. This site binds the tRNA molecule that is attached to the growing peptide chain.
b. This site binds the aminoacyl-tRNA.
c. This site may bind deacylated (uncharged) tRNA.
d. This site binds the peptidyl-tRNA.

10. EF-Tu, a member of the G-protein family, plays a crucial role in the elongation process of translation. Suppose that a slowly hydrolyzable analog of GTP were added to an elongating system. What would be the effect on the rate of protein synthesis? 2

11. List the differences between bacterial and eukaryotic protein biosynthesis. 3

12. Match each label or component with its associated ribosomal subunit. Some labels can be used more than once. 3

1. Prokaryotic large ribosomal subunit	1. 30S subunit
2. Prokaryotic small ribosomal subunit	2. 40S subunit
3. Eukaryotic large ribosomal subunit	3. 50S subunit
4. Eukaryotic small ribosomal subunit	4. 60S subunit

5. 5S rRNA

6. 5.8S rRNA

7. 16S rRNA

8. 18S rRNA

9. 23S rRNA

10. 28S rRNA

---

13. There are several key differences between prokaryotic and eukaryotic ribosomes which have been exploited by some antibiotics to selectively target bacterial ribosomes. Match each antibiotic with the best description of how it inhibits translation. Not all descriptions will be used. 5

1. Streptomycin is an aminoglycoside. It binds to the 16S rRNA, which interferes with the proofreading function of the 30S subunit.

2. Tetracyclines bind to and distort the A site.

3. Puromycin has a structure similar to the 3′ end of an aminoacyl-tRNA. It binds to the A site and reacts with the peptidyl-tRNA to form peptidylpuromycin, which cannot be translocated to the P site and has a weak affinity for the A site.

1. Prevents initiation

2. Causes dissociation of covalently modified polypeptide

3. Prevents binding of aminoacyl-

4. Azithromycin is a macrolide. It binds to the 50S subunit and interferes with the exit of the growing polypeptide chain from the ribosome.

tRNA at the A site

4. Causes misreading of mRNA codons

5. Prevents termination

6. Causes premature termination

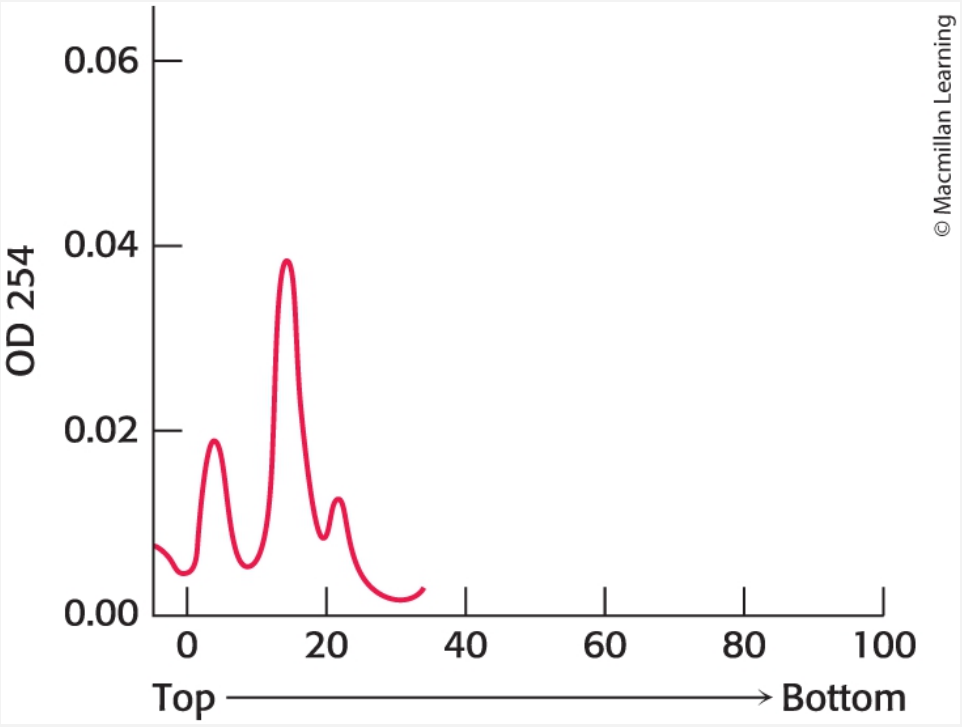
---

14. Fill in the blanks in the following paragraph:

Transcription in prokaryotes begins as promoter sites bind RNA polymerase. Prokaryotic cells have two sites that function as promoters: the **(a)** _____, which has the consensus sequence TTGACA, and the **(b)** _____, which is centered at -10 and has the consensus sequence TATAAT. Transcription starts at position **(c)** _____. Transcription ends when RNA polymerase transcribes a **(d)** _____, which in *E. coli* is a hairpin loop. In translation, ribosomal RNA pairs with the **(e)** _____, a purine-rich region of the mRNA molecule upstream from the start codon. Translation starts as the first tRNA recognizes the start codon, **(f)** _____, on mRNA.

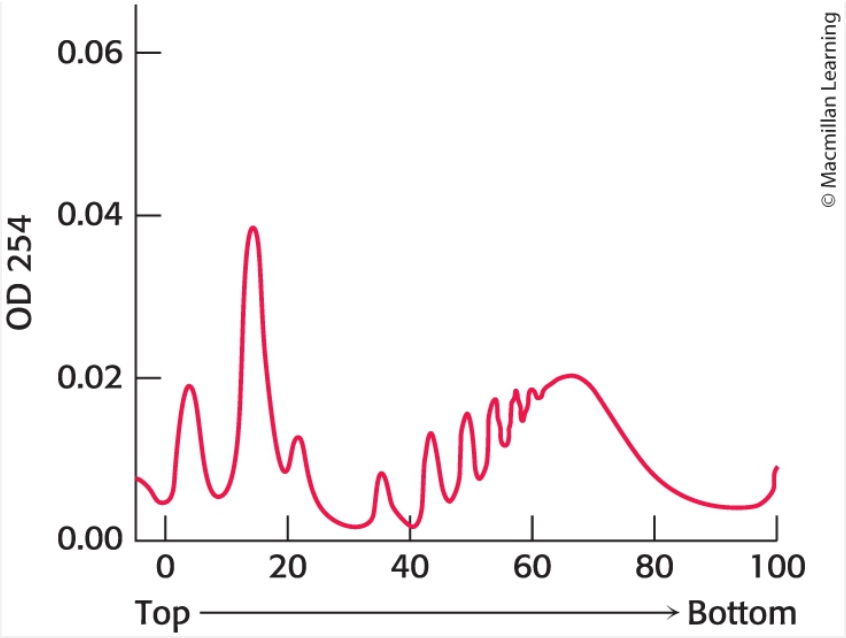
15. The protein-synthesizing machinery was isolated from eukaryotic cells and briefly treated with a low concentration of RNase. The sample was then subjected to sucrose density-gradient centrifugation. The gradient was fractionated, and the

absorbance, or optical density (OD), at 254 nm was recorded for each fraction. The following plot was obtained. 3



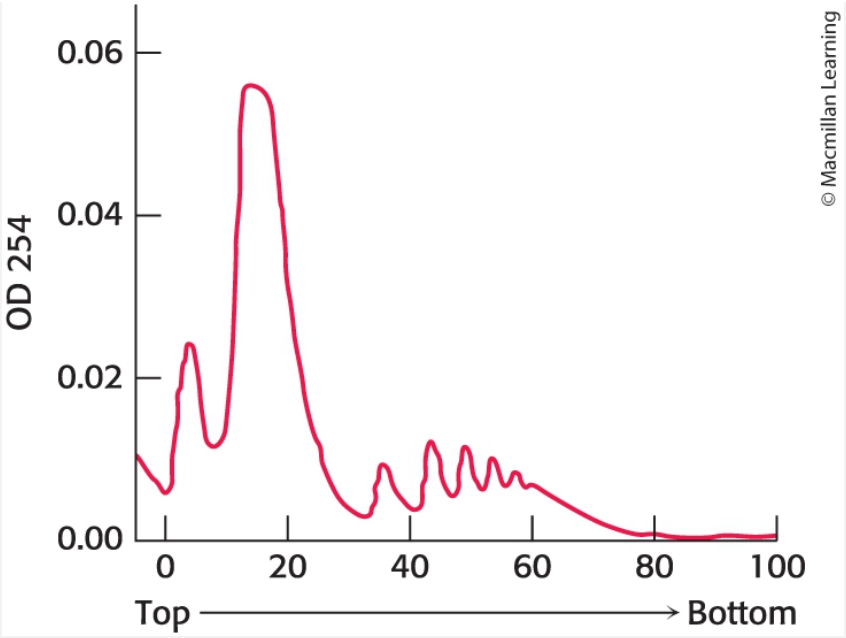
a. What do the three peaks of absorbance represent?

The experiment was repeated except that, this time, the RNase treatment was omitted.



b. Why is the centrifugation pattern now more complex? What does the series of peaks near the bottom of the centrifuge tube represent?

Before the isolation of the protein-synthesizing machinery, the cells were grown in low concentrations of oxygen (hypoxic conditions). Again the experiment was repeated without RNase treatment. The next graph shows the results.



c. What happens to cells grown in hypoxic conditions?

16. Place the following steps of the membrane translocation of eukaryotic secretory proteins in order, starting with the signal peptide exiting the ribosome during translation, and ending with the protein being transported by vesicles out of the ER.
4

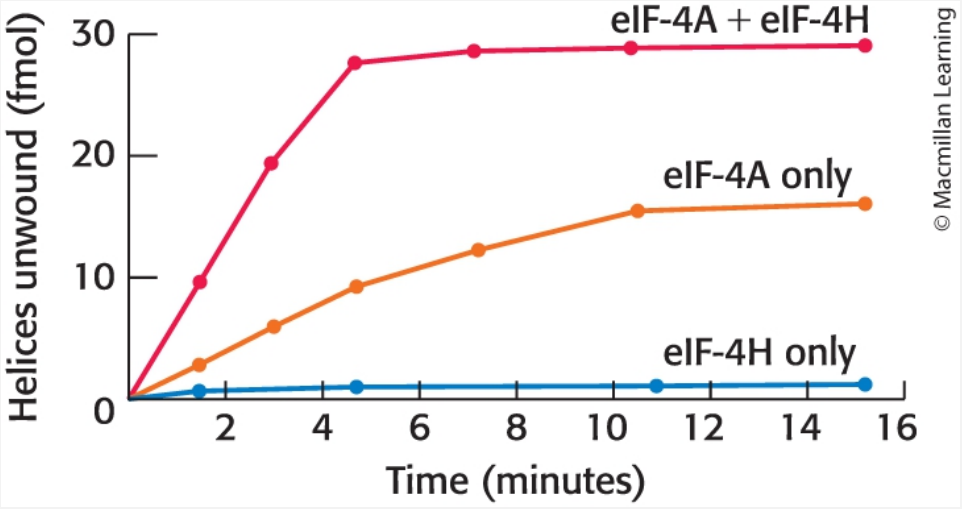
a. The signal peptide exits the ribosome during translation.
b. Signal peptidase removes the signal peptide from the growing polypeptide.
c. Translation resumes.
d. SRP binds to the signal peptide and translation stops.
e. Protein is transported out of the ER.

f. The growing polypeptide crosses the ER membrane through the translocon.
g. The remainder of the polypeptide is moved into the ER lumen.
h. Ribosome docks to a translocon.
i. SRP moves the ribosome to the ER membrane.

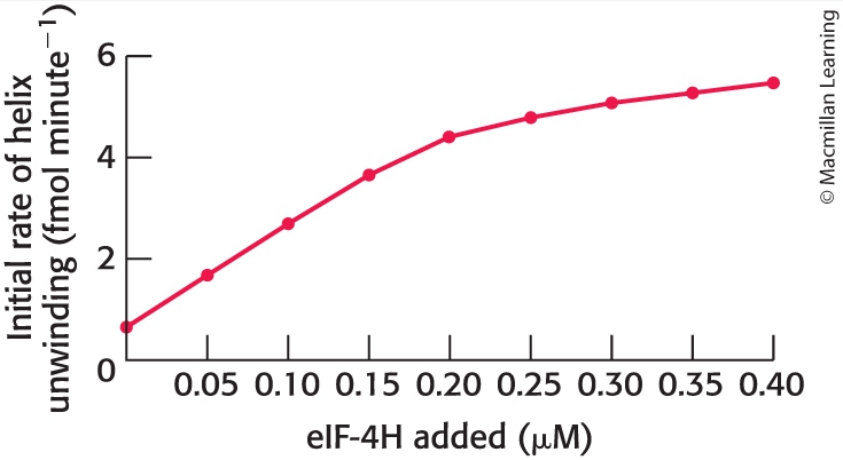
17.

a. What four components are required for the translocation of proteins across the endoplasmic reticulum membrane? 4
b. What is the energy source that powers the cotranslational movement of proteins across the endoplasmic reticulum? 4

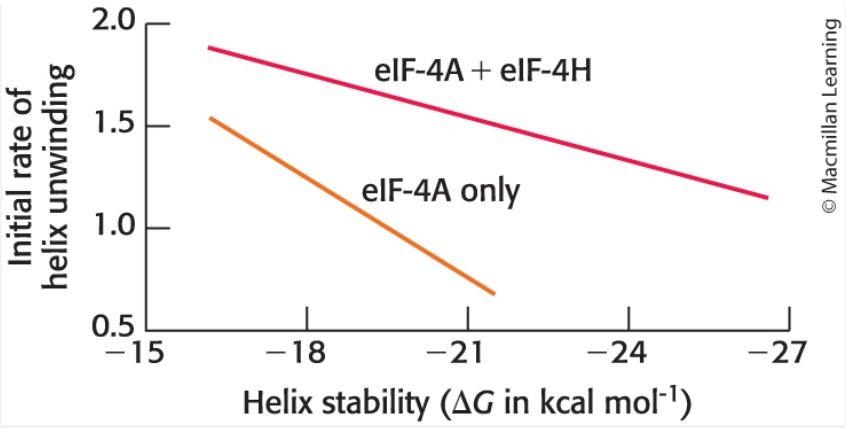
18. The initiation factor eIF-4 displays ATP-dependent RNA helicase activity. Another initiation factor, eIF-4H, has been proposed to assist the action of eIF-4. The graph shows some of the experimental results from an assay that can measure the activity of eIF-4 helicase in the presence of eIF-4H. 3



a. What are the effects on eIF-4 helicase activity in the presence of eIF-4H?
b. Why did measuring the helicase activity of eIF-4H alone serve as an important control?
c. The initial rate of helicase activity of 0.2 μM of eIF-4 was then measured with varying amounts of eIF-4H. What ratio of eIF-4H to eIF-4 yielded optimal activity?



d. Next, the effect of RNA–RNA helix stability on the initial rate of unwinding in the presence and absence of eIF-4H was tested. How does the effect of eIF-4H vary with helix stability?



e. How might eIF-4H affect the helicase activity of eIF-4A?

19. Consider the 5′-to-3′ DNA sequence of three consecutive codons below.

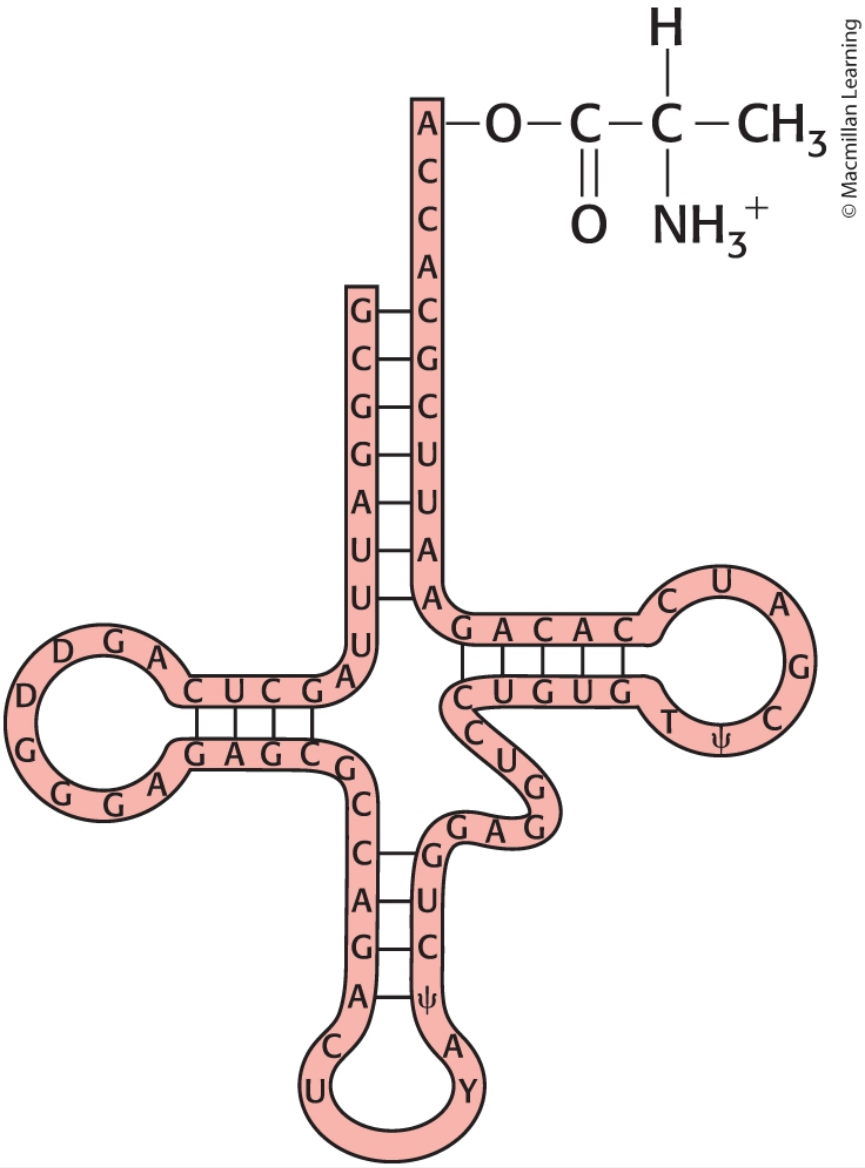
5′–TTAGAGCGC–3′

Determine the following sequences: 1

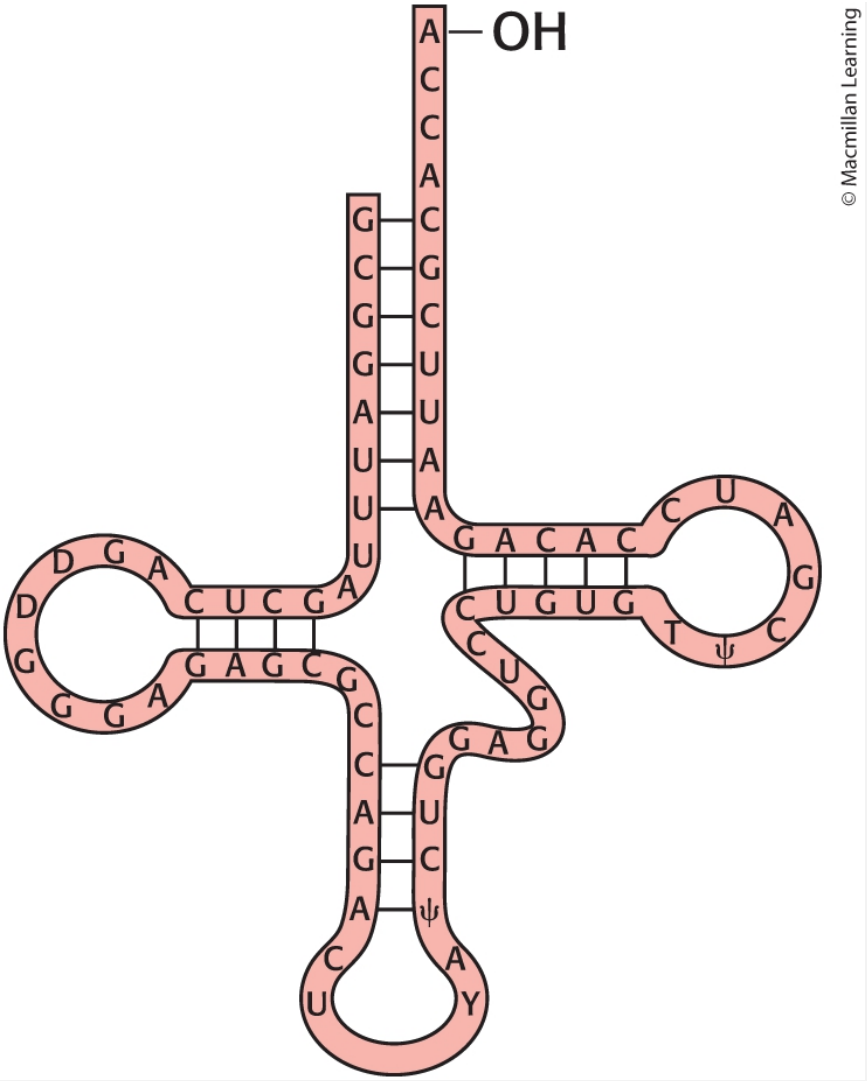
a. The complementary DNA strand (3′ to 5′)
b. The transcribed mRNA
c. The tRNA anticodons
d. The amino acids

20. Consider the following tRNA molecules. **(a)** Which tRNA is the activated version? **(b)** What is the name of the amino acid side chain? 1

A.



B.


A — OH
A C C A C G C U U A A
G C G G A U U U A
G A U C U C G A
D G A D G G A
G A G C G C C A G A
C U G U G C U G G
C U A G T ψ C
G A G G U C ψ A
C U Y
© Macmillan Learning

Chapter 31
Control of Gene Expression





Oxford Scientific/The Image Bank/Getty Images
© Macmillan Learning

Complex biological processes often require coordinated control of the expression of many genes. The maturation of a tadpole into a frog is largely controlled by thyroid hormone. This hormone regulates gene expression by binding to a protein, the thyroid-hormone receptor, as shown at the right. In response to the hormone's binding, this protein binds to specific DNA sites in the genome and modulates the expression of nearby genes.

Outline

31.1 Bacterial DNA-Binding Proteins Bind to Specific Regulatory Sites
31.2 In Bacteria, Genes Are Often Arranged into Clusters Under the Control of a Single Regulatory Sequence

31.3 Regulatory Circuits Can Result in Switching Between Patterns of Gene Expression
31.4 Regulation of Gene Expression Is More Complex in Eukaryotes
31.5 The Control of Gene Expression in Eukaryotes Can Require Chromatin Remodeling
31.6 Gene Expression Can Be Controlled at the Posttranscriptional Level

Learning Goals



By the end of this chapter, you should be able to:

1. Evaluate the control of transcription by bacterial and eukaryotic DNA-binding proteins.
2. Analyze the common structural features of bacterial and eukaryotic DNA-binding proteins that allow them to recognize specific DNA sequences.
3. Understand the roles of the various components in the *E. coli lac* operon.
4. Describe how genetic switches work, using the lytic versus lysogenic path in bacteriophage lambda as an example.
5. Discuss the role of chromatin modifications in controlling eukaryotic gene expression.
6. Contrast the control of gene expression in bacteria and in eukaryotes.
7. Understand examples of mechanisms of posttranscriptional gene regulation.

The development of multicellular organisms; the changes that distinguish normal cells from cancer cells; bacteria responding to changes in their environment — all of these intriguing phenomena have one thing in common: they rely on the regulation of gene expression. A gene is expressed when it is transcribed into RNA and, for most genes, translated into proteins. While some of the thousands of genes that make up a genome are expressed all the time, many other genes are expressed only under some

circumstances. For example, the level of expression of some genes in bacteria may vary more than a thousand-fold in response to the supply of nutrients or to environmental challenges. In this chapter, we will learn about several strategies that allow for the coordinated regulation of gene expression, both in bacteria and eukaryotes.

31.1 Bacterial DNA-Binding Proteins Bind to Specific Regulatory Sites

How do regulatory systems distinguish the genes that need to be activated or repressed from genes that are *constitutive*, or expressed all the time? The DNA sequences of genes themselves do not have any distinguishing features that would allow regulatory systems to recognize them. Instead, gene regulation depends on other sequences in the genome. In bacteria, these regulatory sites are close to the region of the DNA that is transcribed. Regulatory sites are usually binding sites for specific DNA-binding proteins, which can either stimulate or repress gene expression.

Many DNA-binding proteins match the symmetry in their target DNA sequences

Regulatory sites were first identified in *E. coli* through experiments that looked at changes in gene expression in response to nutrient availability. For example, if the usual energy source (the sugar glucose) is not available to the bacterium, but lactose *is* available, the bacterium starts to express a gene encoding **β-galactosidase**, an enzyme that can process lactose for use as a carbon and energy source. The sequence of the regulatory site for this gene is shown in **Figure 31.1**. The nucleotide sequence of this site shows a nearly perfect inverted repeat, indicating that the DNA in this region has an approximate twofold axis of symmetry. Recall that cleavage sites for restriction enzymes such as EcoRV have similar symmetry properties (Section 9.2). Symmetry in such regulatory sites usually corresponds to symmetry in the protein that binds the site. Symmetry matching is a recurring theme in protein–DNA interactions.



FIGURE 31.1 The sequence of the *lac* regulatory site is a nearly perfect inverted repeat. This leads to twofold rotational symmetry in the DNA. Parts of the sequences that are related by this symmetry are shown in the same color.

To understand these protein–DNA interactions in detail, scientists determined the structure of the complex between the regulatory site for the gene encoding β-galactosidase and the DNA-binding unit from the protein that binds to it (Figure 31.2). The protein that recognizes this particular regulatory site is called the *lac repressor*, because it represses the expression of the lactose-processing gene when bound to the regulatory site.

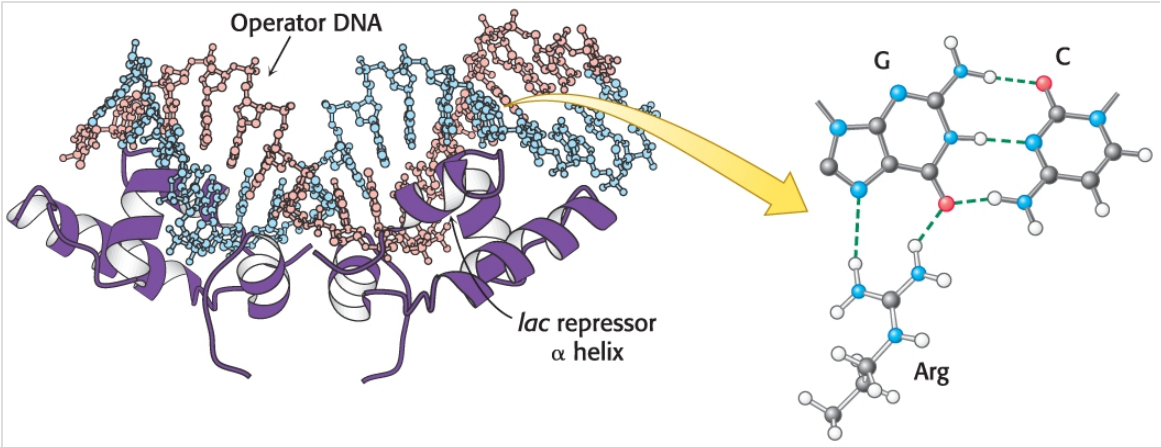


FIGURE 31.2 The *lac* repressor binds to operator DNA. The DNA-binding domain from the *lac* repressor binds to a DNA fragment containing its preferred binding site by inserting an α helix into the major groove of operator DNA. A specific contact forms between an arginine residue of the repressor and a G–C base pair in the binding site.

[Drawn from 1EFA.pdb.]

INTERACT with this model in Achieve

As expected, the DNA-binding unit from the *lac* repressor binds as a dimer, and the twofold axis of symmetry of the dimer matches the symmetry of the DNA. An α helix from each monomer of the protein is inserted into the major groove of the DNA, where amino acid side chains make specific contacts with exposed edges of the base pairs. For example, the side chain of an arginine residue of the protein forms a pair of hydrogen bonds with a guanine residue of the DNA, which would not be possible with any other base. This interaction and similar ones allow the *lac* repressor to bind more tightly to this site than to the wide range of other sites present in the *E. coli* genome.

The helix-turn-helix motif is common to many bacterial DNA-binding proteins

Do other bacterial DNA-binding proteins use similar strategies? The structures of many such proteins have now been determined, and amino acid sequences are known for many more. Strikingly, the DNA-binding surfaces of many, but not all, of these proteins consist of a pair of α helices separated by a tight turn, called a **helix-turn-helix motif** (**Figure 31.3**). In complexes with DNA, the second of these two helices (often called the *recognition helix*) lies in the major groove, where amino acid side chains make contact with the edges of base pairs. In contrast, residues of the first helix participate primarily in contacts with the DNA backbone. Helix-turn-helix motifs are present in many proteins that bind DNA as dimers, and thus two of the units will be present, one in each monomer.

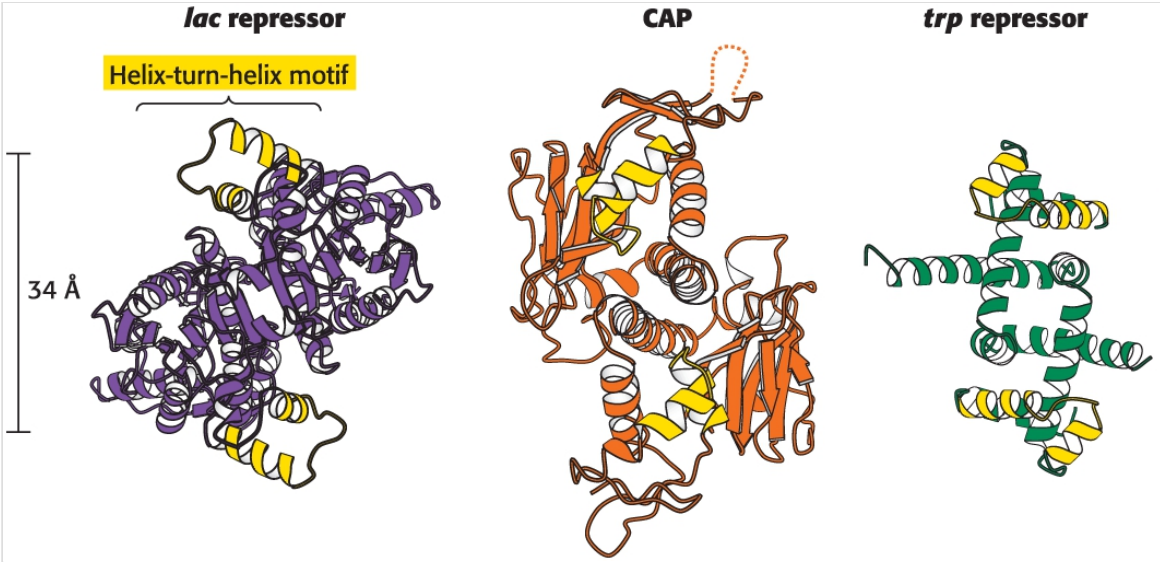


FIGURE 31.3 Sequence-specific DNA-binding proteins interact with DNA through a helix-turn-helix motif. In each case, the helix-turn-helix units (highlighted in yellow) within a protein dime are approximately 34 Å apart, corresponding to one full turn of DNA.

[Drawn from 1EFA.pdb, 1RUN.pdb, and 1TRO.pdb.]

Although the helix-turn-helix motif is the most commonly observed DNA-binding unit in bacteria, not all regulatory proteins bind DNA through such units. The *E. coli* methionine repressor (Figure 31.4), for example, binds DNA through the insertion of a pair of β strands into the major groove. A historically important example for gene regulation in *E. coli*, discussed next, reveals many common principles and elucidates the role of DNA-binding proteins in controlling transcription.

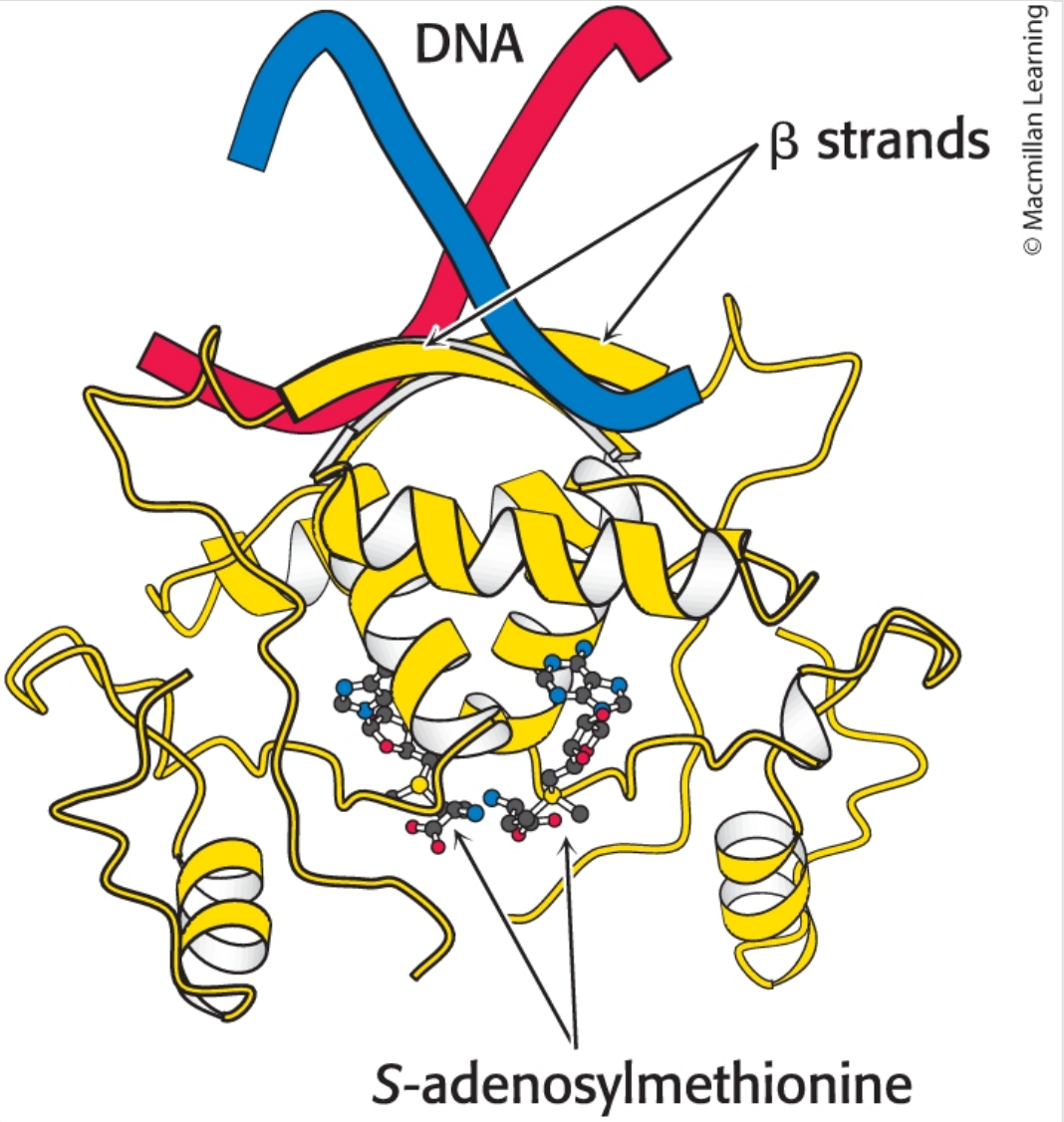


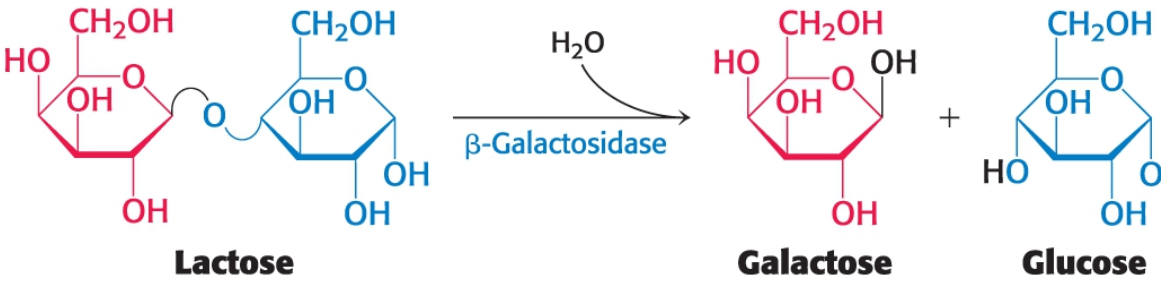
FIGURE 31.4 Some DNA-binding proteins recognize specific DNA sequences through β strands. The methionine repressor complexed with its co-repressor *S*-adenosylmethionine is shown bound to DNA (blue and red ribbon). In this example residues in β strands, rather than in α helices, participate in the crucial interactions between the protein and the DNA.

[Drawn from 1CMA.pdb.]

INTERACT with the models shown in Figure 31.3 and Figure 31.4 in Achieve

31.2 In Bacteria, Genes Are Often Arranged into Clusters Under the Control of a Single Regulatory Sequence

As noted above, bacteria such as *E. coli* usually rely on glucose as their source of carbon and energy, even when other sugars are available. However, when glucose is scarce, *E. coli* can use lactose as their carbon source, even though this disaccharide does not lie on any major metabolic pathways. β-Galactosidase is an essential enzyme in the metabolism of lactose because it hydrolyzes lactose into galactose and glucose. These products are then metabolized by pathways discussed in Chapter 16.



This reaction can be conveniently followed in the laboratory through the use of alternative galactoside substrates, such as X-Gal, that form colored products (**Figure 31.5**).

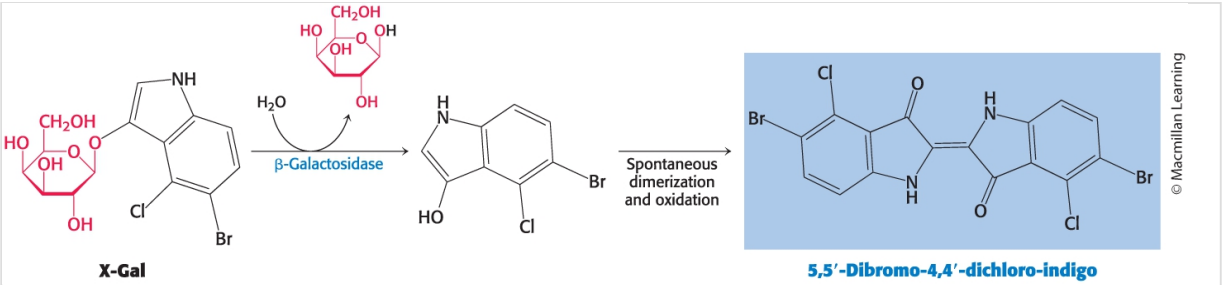


FIGURE 31.5 The β-galactosidase reaction can be monitored using a colored indicator. The galactoside substrate X-Gal produces a colored product when cleaved by β-galactosidase. The appearance of this colored product provides a convenient means for monitoring the amount of the enzyme both in vitro and in vivo.

An *E. coli* cell growing on a carbon source such as glucose or glycerol contains fewer than 10 molecules of β-galactosidase. In contrast, the same cell will contain several thousand molecules of the enzyme when grown on lactose (Figure 31.6). The presence of lactose in the culture medium induces the large increase in the amount of β-galactosidase by up-regulating the gene that codes for it, resulting in the synthesis of new enzyme molecules.

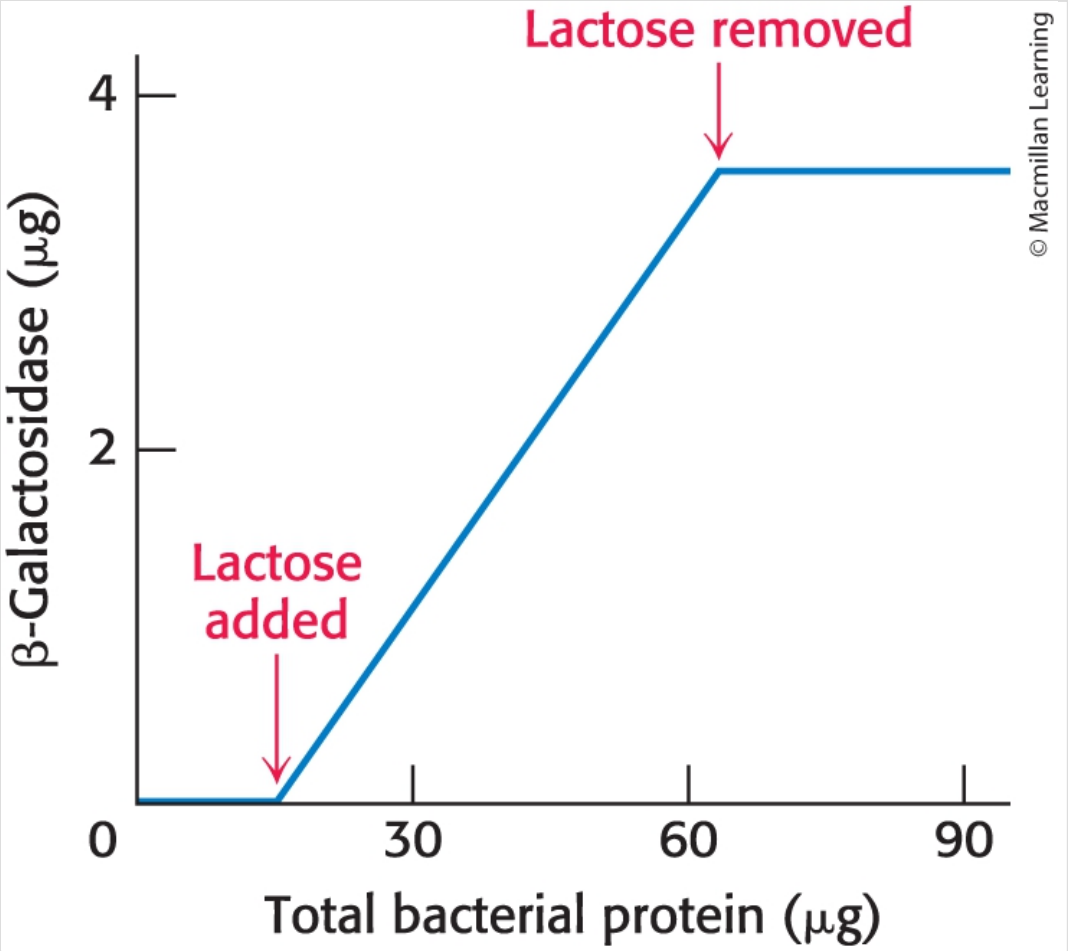


FIGURE 31.6 The production of β-galactosidase can be increased by the addition of lactose. The addition of lactose to an *E. coli* culture causes the production of β-galactosidase to increase from very low amounts to much larger amounts. The increase in the amount of enzyme parallels the increase in the number of cells in the growing culture. β-Galactosidase constitutes 6.6% of the total protein synthesized in the presence of lactose.

A crucial clue to the mechanism of gene regulation was the observation that two other proteins are synthesized in concert with β-galactosidase — namely, galactoside permease and thiogalactoside transacetylase. The permease is required for the transport of lactose across the bacterial cell membrane (Section 13.3). The transacetylase is not essential for lactose metabolism but appears to play a role in the detoxification of

compounds that also may be transported by the permease. Thus, the expression levels of a set of enzymes that all contribute to the adaptation to a given change in the environment are regulated together. Such a coordinated unit of gene expression is called an **operon**.

An operon consists of regulatory elements and protein-encoding genes

The parallel regulation of β-galactosidase, the permease, and the transacetylase suggested that the expression of genes encoding these enzymes is controlled by a common mechanism. François Jacob and Jacques Monod proposed the so-called *operon model* to account for this parallel regulation as well as the results of other genetic experiments. The genetic elements of the model are a regulator gene that encodes a regulatory protein (with its promoter), a regulatory DNA sequence called an **operator site**, and a set of structural genes with a separate promoter (**Figure 31.7**).

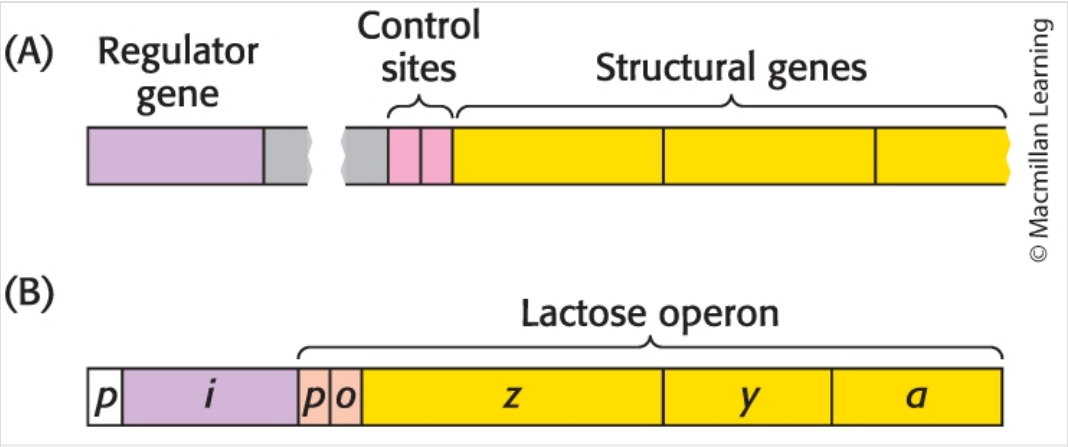


FIGURE 31.7 Operons are clusters of genes under a common control. (A) The general structure of an operon as conceived by Jacob and Monod. In some cases, the regulator gene may be some distance away from the structural genes, as indicated by the break. (B) The structure of the lactose operon. In addition to the promoter, *p*, in the operon, a second promoter is present in front of the regulator gene, *i*, to drive the synthesis of the regulator.

The regulator gene encodes a **repressor** protein that binds to the operator site. The binding of the repressor to the operator prevents transcription of the structural genes. The operator and its associated structural genes constitute the operon. For the *lactose (lac) operon*, the *i* gene encodes the repressor, *o* is the operator site, and the *z*, *y*, and *a* genes are the structural genes for β-galactosidase, the permease, and the transacetylase, respectively. The operon also contains a promoter site (denoted by *p*), which directs the RNA polymerase to the correct transcription initiation site. The *i* gene is under the control of a separate promoter (also denoted *p*). The *z*, *y*, and *a* genes are transcribed to give a single mRNA molecule that encodes all three proteins. An mRNA molecule encoding more than one protein is known as a *polygenic* or *polycistronic* transcript.

The *lac* repressor protein can block transcription

In the absence of lactose, the lactose operon is repressed. How does the *lac* repressor mediate this repression? The *lac* repressor exists as a tetramer of 37-kDa subunits with two pairs of subunits coming together to form the DNA-binding unit previously discussed. In the absence of lactose, the repressor binds very tightly and rapidly to the operator, which is directly downstream of the promoter. When the *lac* repressor is bound to the operator DNA, it prevents transcription of the protein-coding genes because it blocks the progress of RNA polymerase along the DNA template.

How does the *lac* repressor locate the operator site in the *E. coli* chromosome? The *lac* repressor binds 4×10^6 times as strongly to operator DNA as it does to random sites in the genome. This high degree of selectivity allows the repressor to find the operator efficiently even with a large excess of other sites within the *E. coli* genome. The dissociation constant for the repressor–operator complex is approximately $0.1\ \text{pM}\ (10^{-13}\ \text{M})$. The rate constant for association $(\approx 10^{10}\ \text{M}^{-1}\ \text{s}^{-1})$ is strikingly high, indicating that the repressor finds the operator primarily by diffusing along a DNA molecule (a one-dimensional search) rather than encountering it from the aqueous medium (a three-dimensional search). This diffusion has been confirmed by studies that monitored the behavior of fluorescently labeled single molecules of *lac* repressor inside living *E. coli* cells.

Inspection of the complete *E. coli* genome sequence reveals two sites within 500 bp of the primary operator site that approximate the sequence of the operator. When one dimeric DNA-binding unit binds to the operator site, the other DNA-binding unit of the *lac* repressor tetramer can bind to one of these sites with similar sequences. The DNA between the two bound sites forms a loop. No other sites that closely match the sequence of the *lac* operator site are present in the rest of the *E. coli* genome sequence. Therefore, the DNA-binding specificity of the *lac* repressor is sufficient to target two closely related sites within the *E. coli* genome.

The three-dimensional structure of the *lac* repressor has been determined in various forms. Each monomer consists of a small amino-terminal domain that binds DNA and a larger domain that mediates the formation of the dimeric DNA-binding unit and the tetramer (**Figure 31.8**). A pair of the amino-terminal domains come together to form the functional DNA-binding unit. Each monomer has a helix-turn-helix unit that interacts with the major groove of the bound DNA.

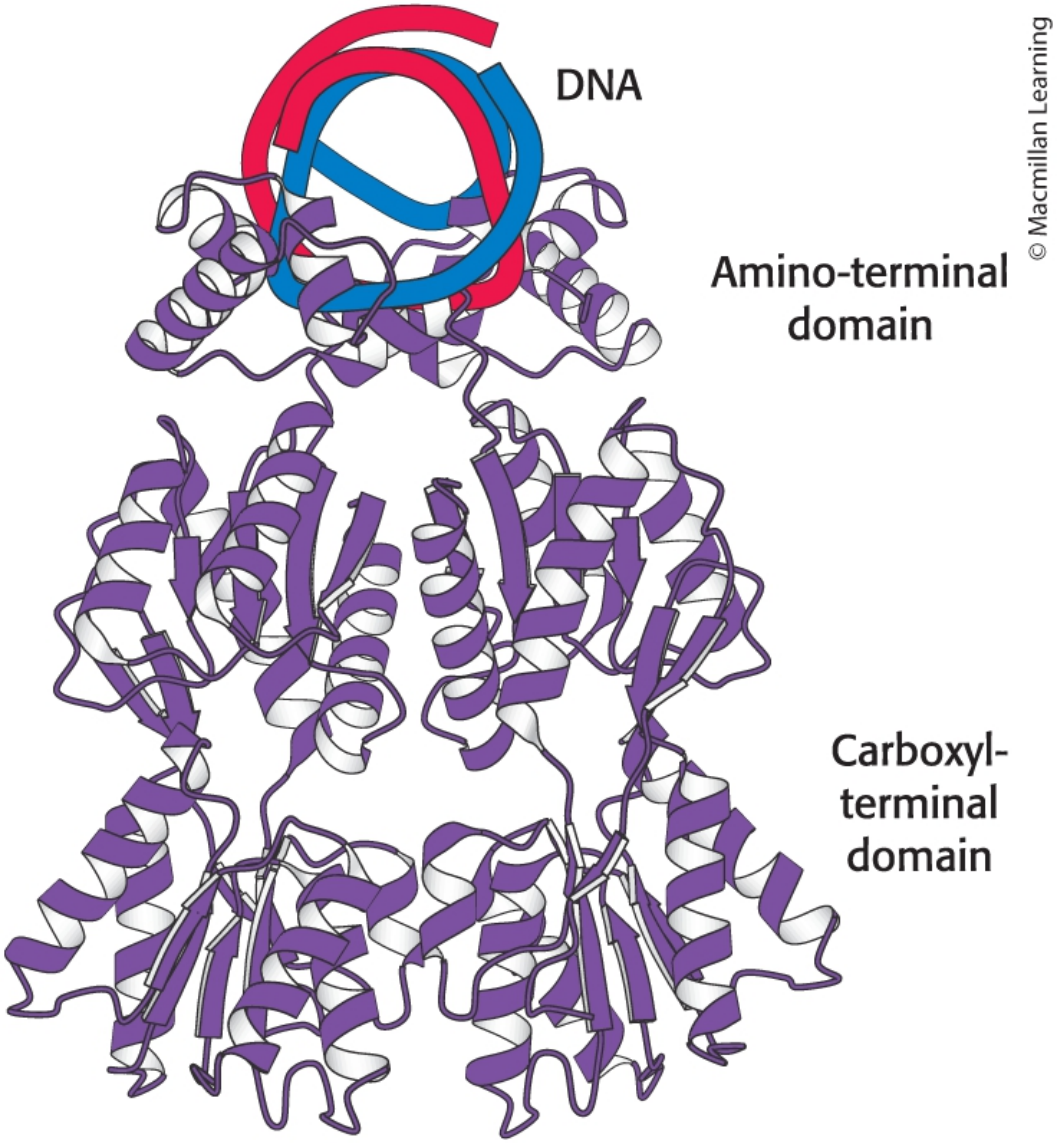
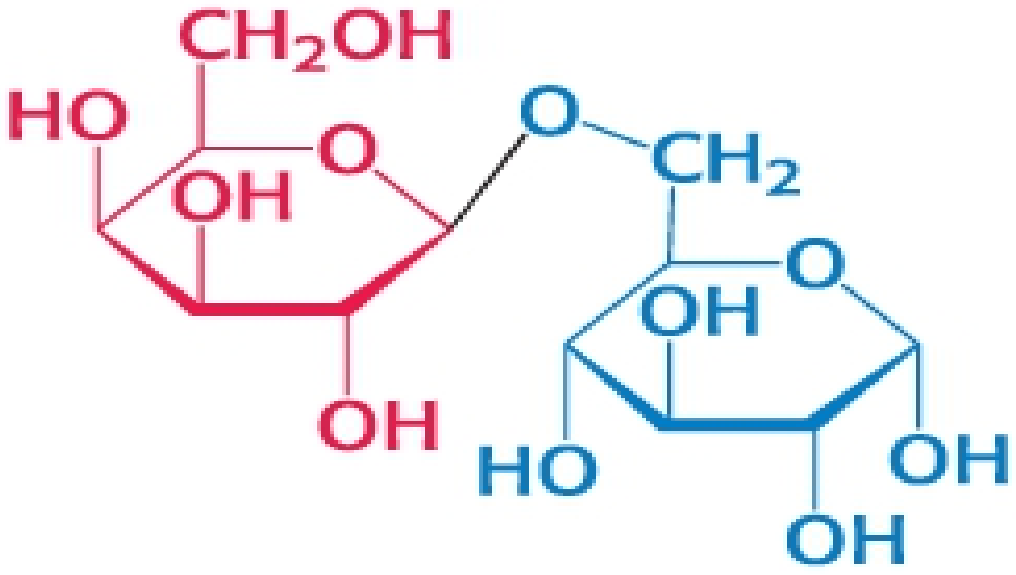


FIGURE 31.8 The *lac* repressor binds to DNA as a dimer. The amino-terminal domain binds to DNA, whereas the carboxyl-terminal domain forms a separate structure. A part of the structure that mediates the formation of *lac* repressor tetramers is not shown.

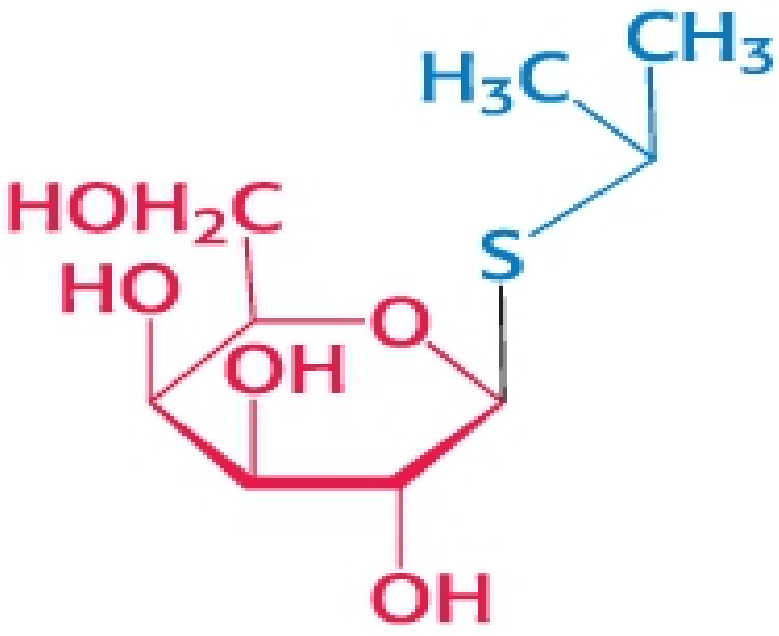
[Drawn from 1EFA.pdb.]

Ligand binding can induce structural changes in regulatory proteins

In the situation just described, glucose is present, lactose is absent, and the *lac* operon is repressed. How does the presence of lactose trigger the relief of this repression and, hence, the expression of the *lac* operon? Interestingly, lactose itself does not have this effect; rather, allolactose, a combination of galactose and glucose with an α-1,6 rather than an α-1,4 linkage, does. Allolactose is thus referred to as the **inducer** of the *lac* operon. Allolactose is a side product of the β-galactosidase reaction and is produced at low levels by the few molecules of β-galactosidase that are present before induction. Some other β-galactosides such as isopropylthiogalactoside (IPTG) are potent inducers of β-galactosidase expression, although they are not substrates of the enzyme. IPTG is useful in the laboratory as a tool for inducing gene expression in engineered bacterial strains.



1,6-Allolactose



Isopropylthiogalactoside (IPTG)

The inducer triggers gene expression by preventing the *lac* repressor from binding the operator. The inducer binds to the *lac* repressor and thereby greatly reduces the repressor's affinity for operator DNA. An inducer molecule binds in the center of the large domain within each monomer. This binding leads to subtle conformational changes that modify the relation between the two small DNA-binding domains (Figure 31.9). These domains can no longer easily contact DNA simultaneously, leading to a dramatic reduction in DNA-binding affinity.

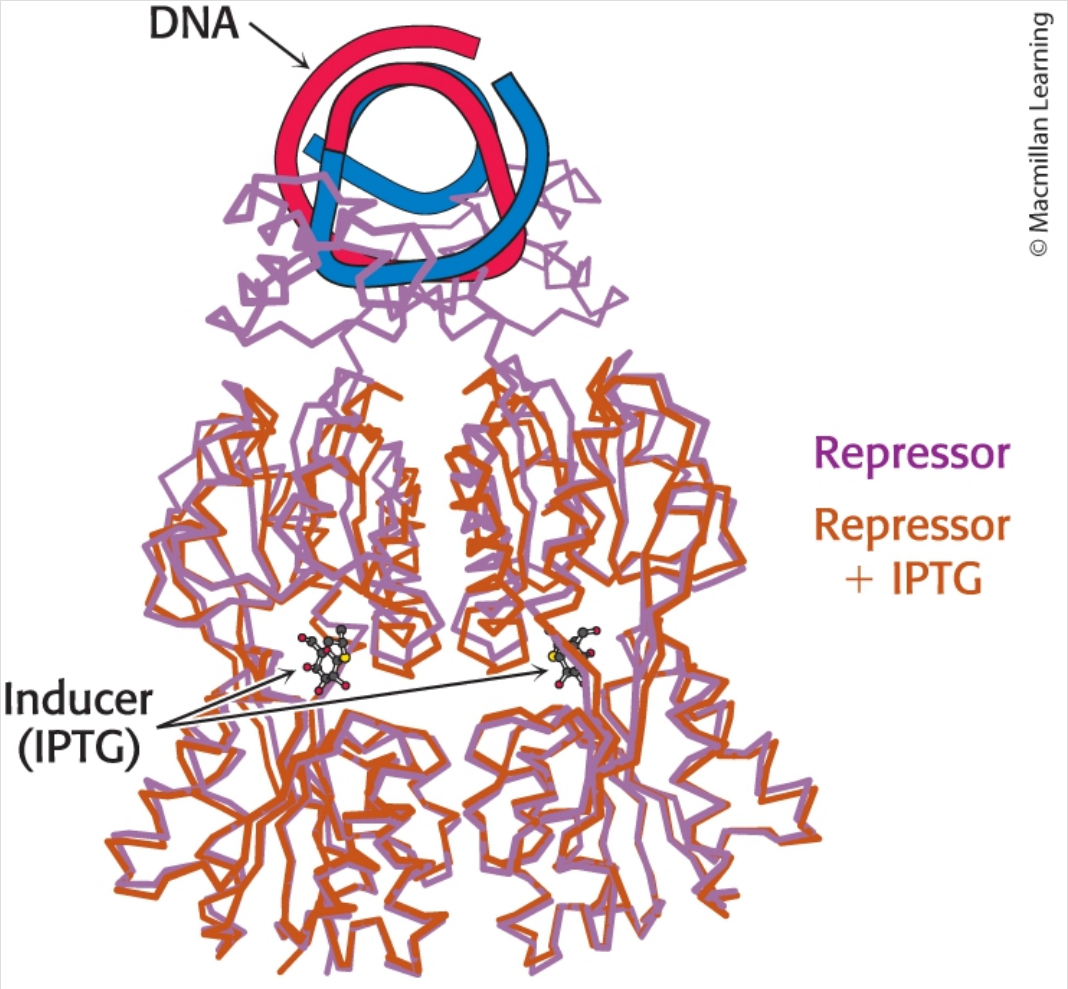


FIGURE 31.9 Binding of IPTG alters the *lac* repressor structure and affects its ability to bind DNA. The structure of the *lac* repressor bound to the inducer isopropylthiogalactoside (IPTG), shown in orange, is superimposed on the structure of the *lac* repressor bound to DNA, shown in purple. The binding of IPTG induces only subtle structural changes, but these are large enough near the interface of the DNA-binding domains that the repressor cannot interact effectively with DNA. The DNA-

binding domains of the *lac* repressor bound to IPTG are not shown, because these regions are not well ordered in the crystals studied.



How does this fit in with the regulation of gene expression in the lactose operon? Let's review the process (**Figure 31.10**). In the absence of inducer, the *lac* repressor is bound to DNA in a manner that blocks RNA polymerase from transcribing the *z*, *y*, and *a* genes. Thus, very little β-galactosidase, permease, or transacetylase is produced. The addition of lactose to the environment leads to the formation of allolactose. This inducer binds to the *lac* repressor, leading to conformational changes and the release of DNA by the *lac* repressor. With the operator site unoccupied, RNA polymerase can then transcribe the other *lac* genes and the bacterium will produce the proteins necessary for the efficient use of lactose.

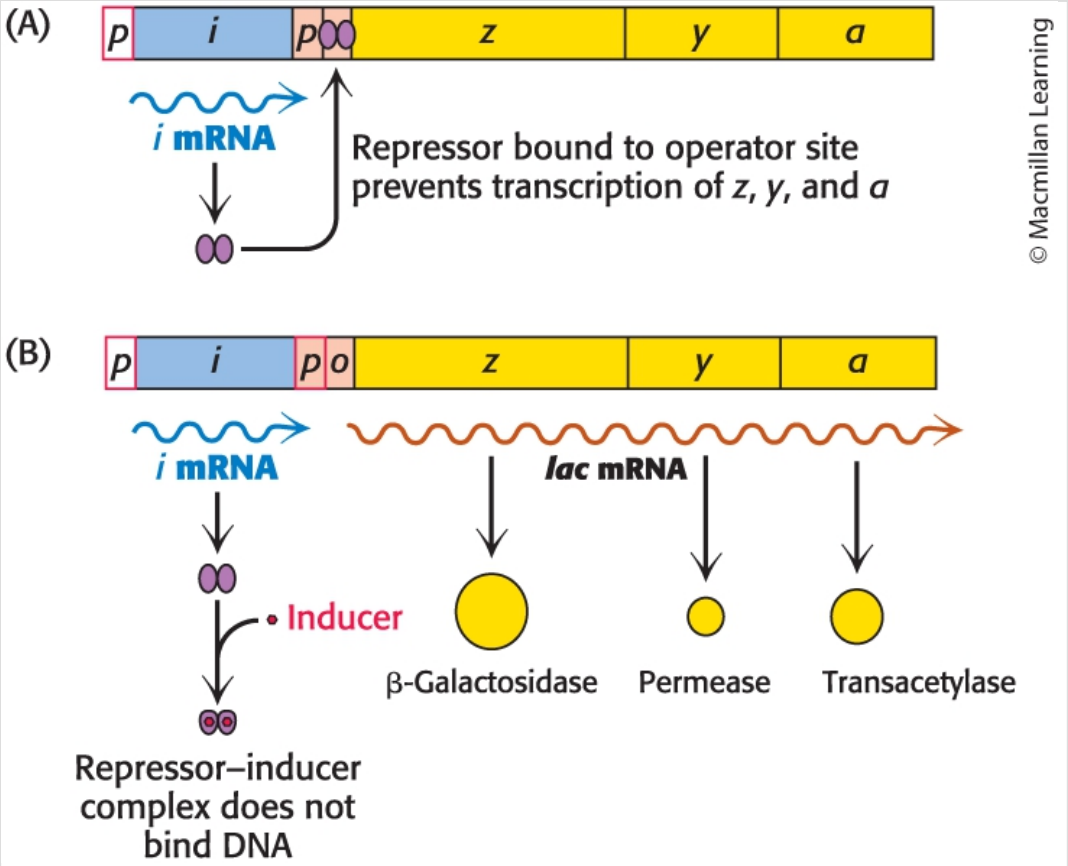


FIGURE 31.10 The *lac* operon can be induced. (A) In the absence of lactose, the *lac* repressor binds DNA and represses transcription from the *lac* operon. (B) Allolactose or another inducer binds to the *lac* repressor, leading to its dissociation from DNA and to the production of *lac* mRNA.

The operon is a common regulatory unit in bacteria

The lac operon is just one well-studied example of an operon in *E. coli*. In fact, there are an estimated 600–700 operons in *E. coli*, all of which contain genes that are connected via a common metabolic function or pathway. Clustering genes in operons provides the clear advantage of a

coordinated regulatory mechanism for enzymes that are functionally related.

Many other gene-regulatory networks are controlled in ways analogous to those of the *lac* operon. For example, genes taking part in purine and, to a lesser degree, pyrimidine biosynthesis are repressed by the *pur* repressor. This dimeric protein is 31% identical in sequence with the *lac* repressor and has a similar three-dimensional structure. However, the behavior of the *pur* repressor is opposite that of the *lac* repressor: whereas the *lac* repressor is released from DNA by binding to a small molecule, the *pur* repressor binds DNA specifically, blocking transcription, only when bound to a small molecule. Such a small molecule is called a **corepressor**. For the *pur* repressor, the corepressor can be either guanine or hypoxanthine.

The dimeric *pur* repressor binds to inverted-repeat DNA sites of the form $5'-$AN**G**C**AA**N**CG**N**TT**N**C**NT$-3'$, in which the bases shown in boldface type are particularly important. Examination of the *E. coli* genome sequence reveals the presence of more than 20 such sites, regulating 19 operons and including more than 25 genes (**Figure 31.11**).

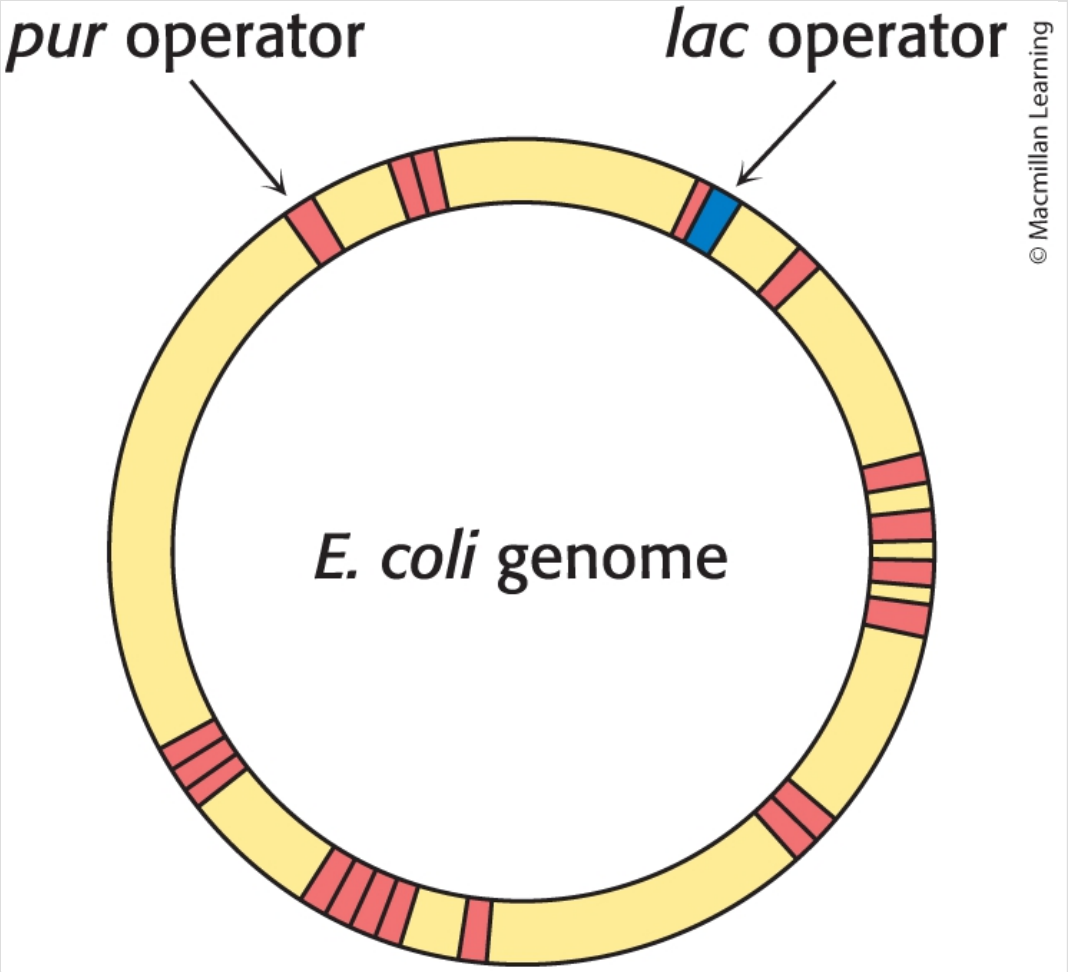


FIGURE 31.11 Operator sites are not distributed evenly across the E. *coli* genome. The *E. coli* genome contains only a single region that closely matches the sequence of the *lac* operator (shown in blue). In contrast, 19 sites match the sequence of the *pur* operator (shown in red). Thus, the *pur* repressor regulates the expression of many more genes than does the *lac* repressor.

Because the DNA-binding sites for these regulatory proteins are short, it is likely that they evolved independently and are not related by divergence from an ancestral regulatory site. Once a ligand-regulated DNA-binding protein is present in a cell, binding sites for the protein may arise by mutation adjacent to additional genes. Binding sites for the *pur* repressor have evolved in the regulatory regions of a wide range of

genes taking part in nucleotide biosynthesis. All such genes can then be regulated in a concerted manner.

The organization of bacterial genes into operons is useful for the analysis of completed genome sequences. Sometimes a gene of unknown function is discovered to be part of an operon containing well-characterized genes. Such associations can provide powerful clues to the biochemical and physiological functions of the uncharacterized gene.

Some DNA-binding proteins stimulate transcription

All the DNA-binding proteins discussed thus far function by inhibiting transcription until some environmental condition, such as the presence of lactose, is met. There are also DNA-binding proteins that stimulate transcription. One particularly well-studied example is a protein in *E. coli* that stimulates the expression of catabolic enzymes.

E. coli grown on glucose, a preferred energy source, have very low levels of catabolic enzymes for metabolizing other sugars. Synthesizing these enzymes when glucose is abundant would be wasteful. In fact, glucose has an inhibitory effect on the genes encoding these enzymes, an effect called **catabolite repression**. How does this work? Glucose achieves this inhibitory effect by lowering the concentration of cyclic AMP in *E. coli*. To understand the consequences of this, let us first consider the role of cAMP in the regulation of transcription.

High concentrations of cAMP stimulate the concerted transcription of many catabolic enzymes by acting through a protein called the **catabolite activator protein (CAP)**, also known as the *cAMP receptor protein* (CRP). When bound to cAMP, CAP stimulates the transcription of

lactose- and arabinose-catabolizing genes. CAP is a sequence-specific DNA-binding protein. Within the *lac* operon, CAP binds to an inverted repeat that is centered near position -61 relative to the start site for transcription (**Figure 31.12**). This site is approximately 70 base pairs from the operator site. As expected from the symmetry of the binding site, CAP functions as a dimer of identical subunits. CAP binding also bends DNA in a manner that favors interactions with RNA polymerase.

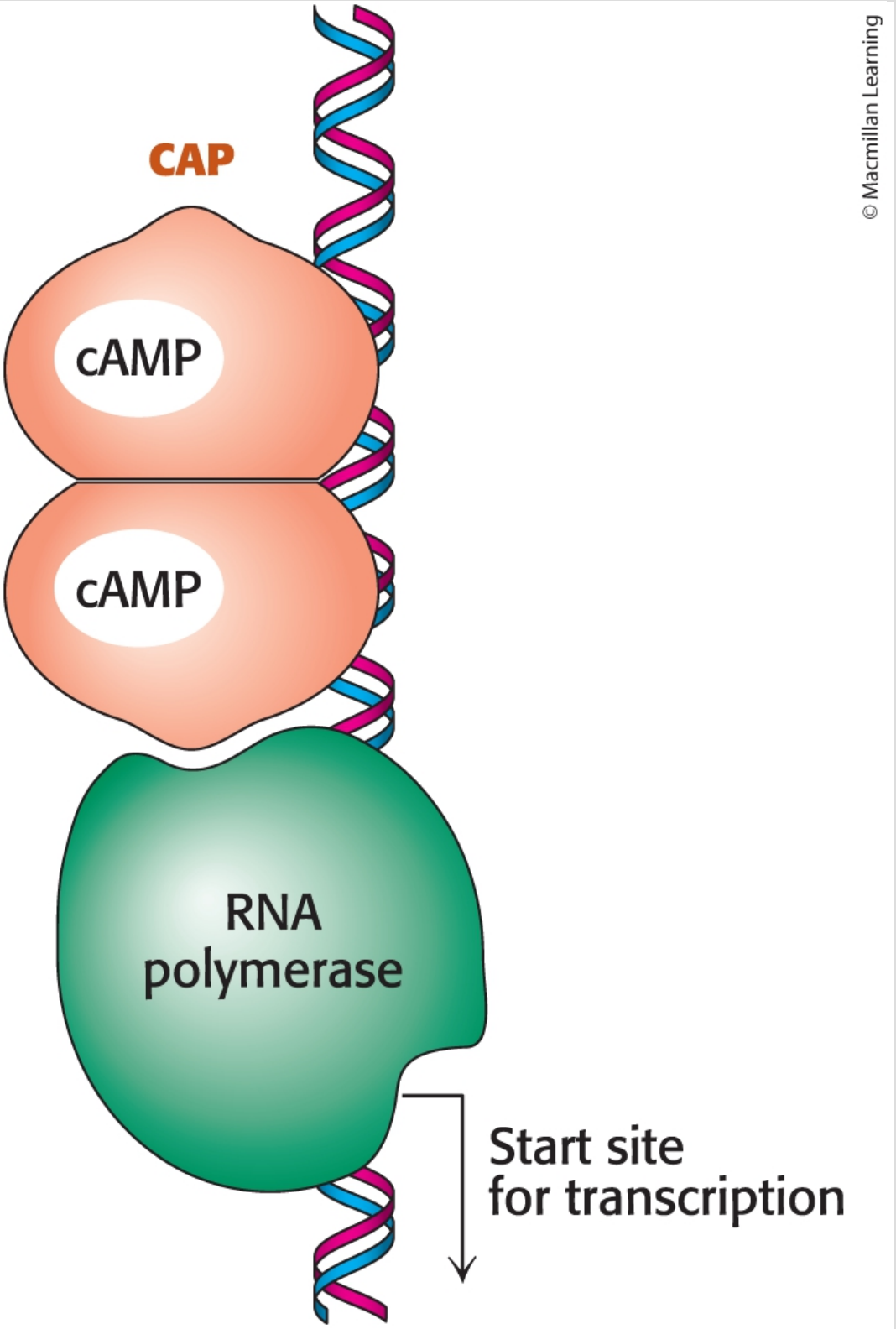


FIGURE 31.12 The catabolite activator protein (CAP) binds to DNA as a dimer. This protein binds to an inverted repeat that is at position −61 relative to the start site

of transcription. The CAP-binding site on DNA is adjacent to the position at which RNA polymerase binds.

The CAP–cAMP complex stimulates the initiation of transcription by approximately a factor of 50. Energetically favorable contacts between CAP and RNA polymerase increase the likelihood that transcription will be initiated at sites to which the CAP–cAMP complex is bound (Figure 31.13). Thus, for the *lac* operon, gene expression is maximal when the binding of allolactose relieves the inhibition by the *lac* repressor and the CAP–cAMP complex stimulates the binding of RNA polymerase.

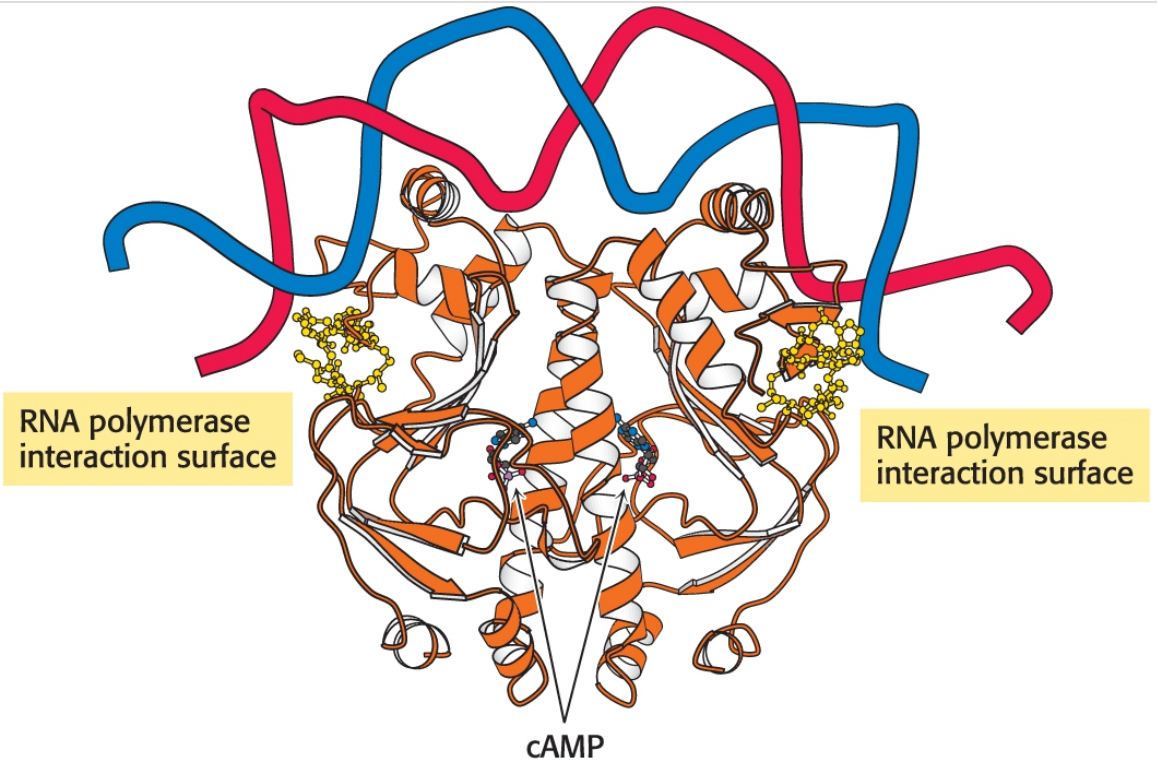


FIGURE 31.13 The CAP dimer binds to DNA and to RNA polymerase. The residues shown in yellow in each CAP monomer have been implicated in direct interactions with RNA polymerase.

[Drawn from 1RUN.pdb.]

The *E. coli* genome contains many CAP-binding sites in positions appropriate for interactions with RNA polymerase. Thus, an increase in the cAMP level inside an *E. coli* bacterium results in the formation of CAP–cAMP complexes that bind to many promoters and stimulate the transcription of genes encoding a variety of catabolic enzymes. Conversely, as noted above, when glucose levels are high, the concentration of cAMP is low. This results in fewer CAP–cAMP complexes and reduced expression of the genes encoding the catabolic enzymes.

Self-Check Question



Under conditions of high glucose and high lactose, *E. coli* will first metabolize glucose before switching to lactose. How do you explain this?

31.3 Regulatory Circuits Can Result in Switching Between Patterns of Gene Expression

The study of viruses that infect bacteria has led to significant advances in our understanding of the processes that control gene expression. Again, sequence-specific DNA-binding proteins play key roles in these processes. Investigations of bacteriophage λ have been particularly revealing.

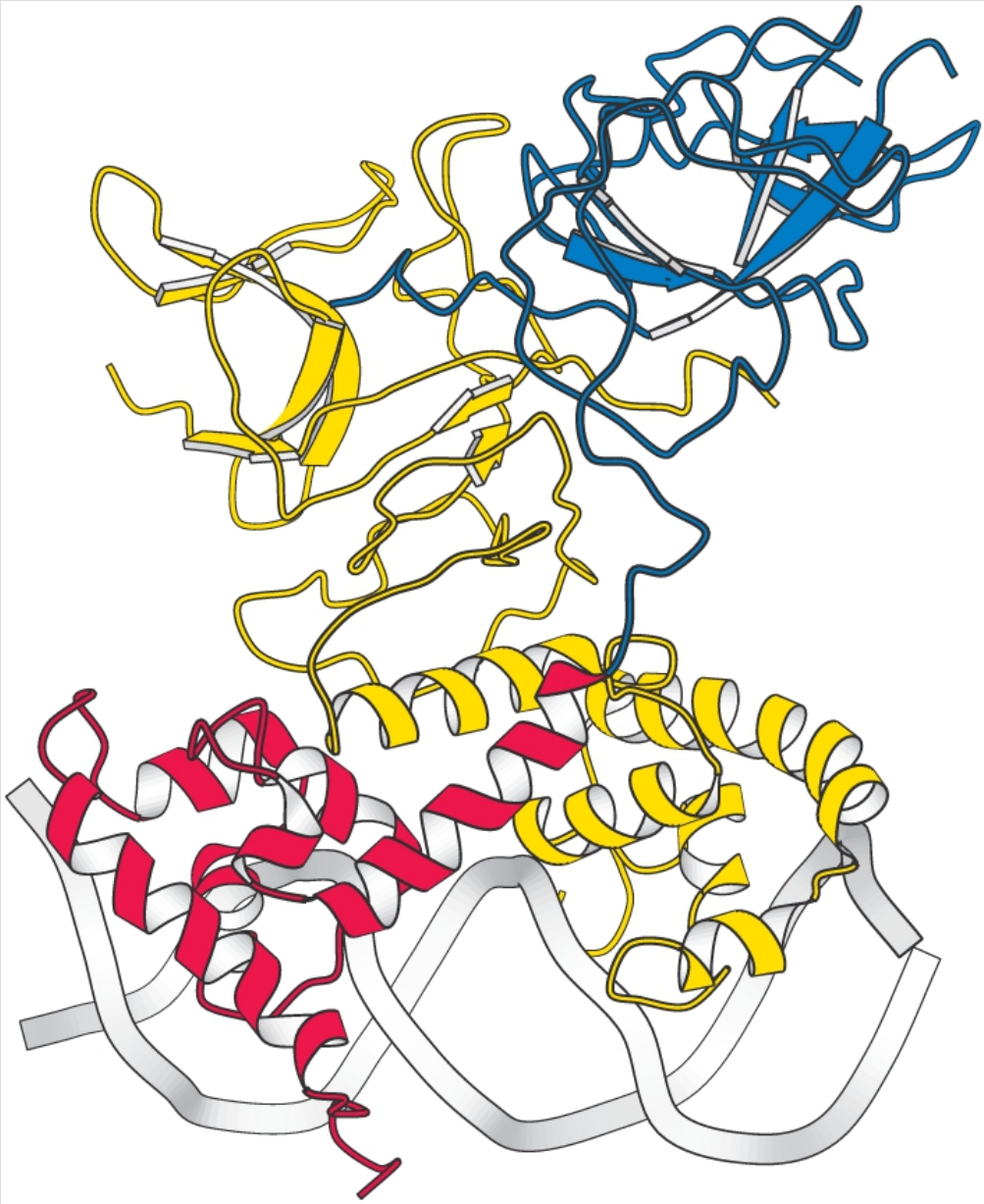
We examined the alternative infection modes of λ phage in Chapter 9. In the lytic pathway, most of the genes in the viral genome are transcribed, initiating the production of many virus particles and leading to the eventual lysis of the bacterial cell with the concomitant release of approximately 100 virus particles. In the lysogenic pathway, the viral genome is incorporated into the bacterial DNA where most of the viral genes remain unexpressed, allowing the viral genome to be carried along as the bacteria replicate. Two key proteins and a set of regulatory sequences in the viral genome are responsible for the switch that determines which of these two pathways is followed.

The λ repressor regulates its own expression

The first protein that we will discuss is the **λ repressor**, sometimes known as the λ cI protein. This protein is key because it blocks, either directly or indirectly, the transcription of almost all genes

encoded by the virus. The one exception is the gene that encodes the λ repressor itself.

The λ repressor consists of an amino-terminal DNA-binding domain and a carboxyl-terminal domain that participates in protein oligomerization (**Figure 31.14**). This protein binds to a number of key sites in the λ phage genome. The sites of greatest interest for our present discussion are in the so-called *right operator* (**Figure 31.15**). This region includes three binding sites for the λ repressor dimer, as well as two promoters within a section of approximately 80 base pairs. One promoter drives the expression of the gene for the λ repressor itself, whereas the other drives the expression of several other viral genes.



© Macmillan Learning

FIGURE 31.14 The λ repressor binds to DNA as a dimer. The amino-terminal domain of one subunit is shown in red and the carboxyl-terminal domain is shown in blue. In the other subunit, both domains are shown in yellow. Notice how α helices on the amino-terminal domains fit into the major groove of the DNA.

[Drawn from 3BDN.pdb.]

INTERACT with the models in Figure 31.13 and Figure 31.14 in



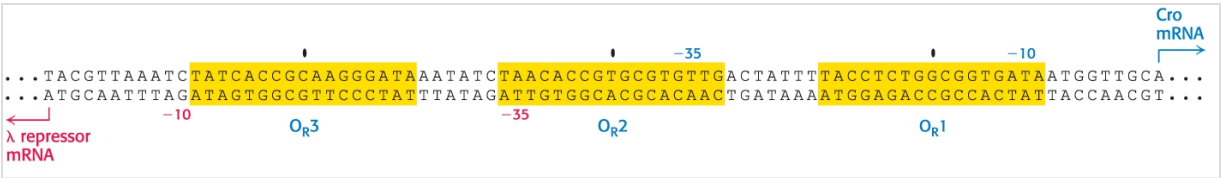
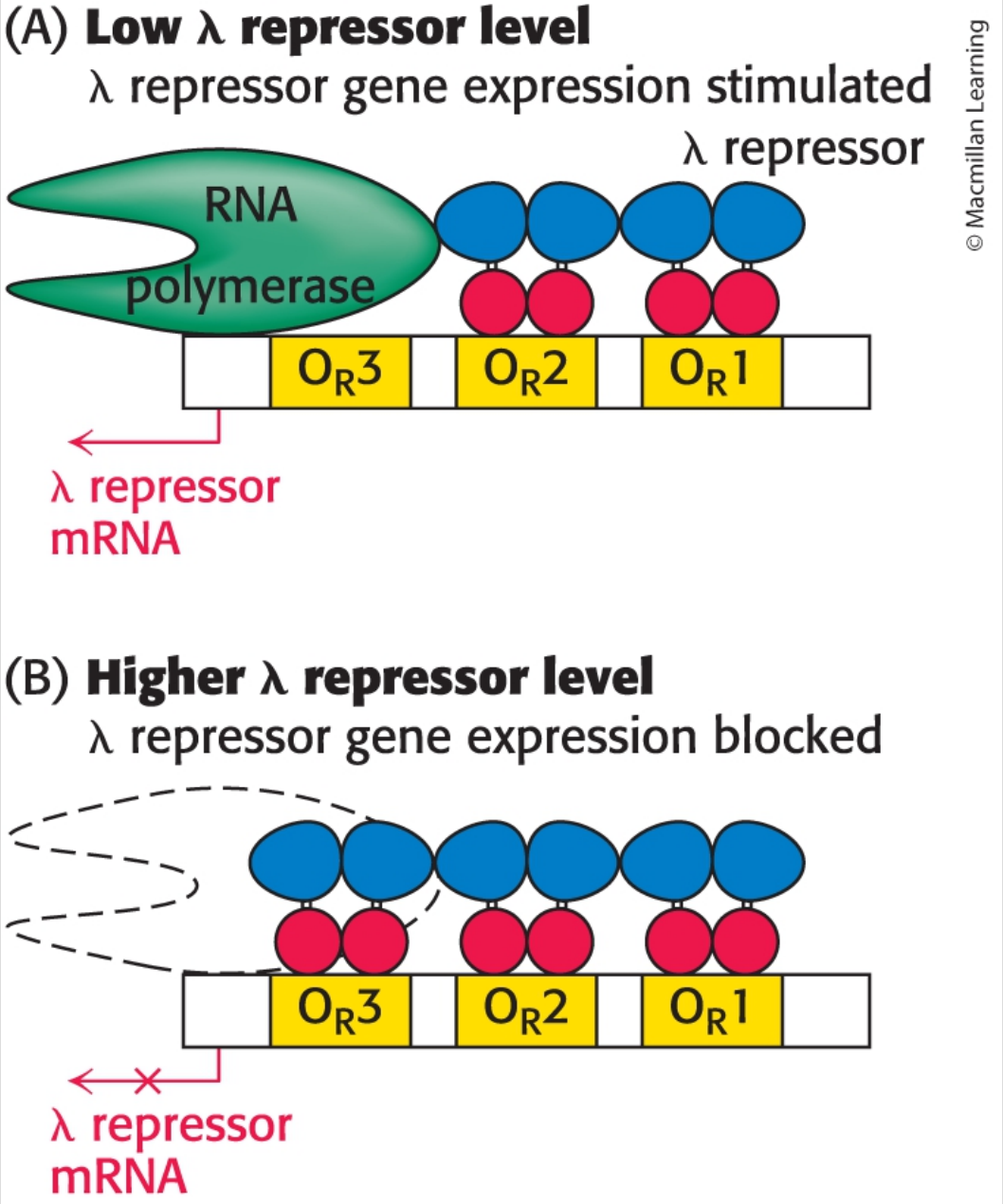


FIGURE 31.15 The sequence of the λ right operator is a binding target for regulatory proteins. The three operator sites (O_R1, O_R2, and O_R3) are shaded yellow with their centers indicated. The start sites for the λ repressor mRNA and the Cro mRNA are indicated, as are the -10 and -35 positions of their respective promoters.

The λ repressor does not have the same affinity for the three sites; it binds the site O_R1 with the highest affinity. In addition, the binding to adjacent sites is cooperative so that, after a λ repressor dimer has bound at O_R1, the likelihood that a protein will bind to the adjacent site O_R2 increases by approximately 25-fold. Thus, when the λ repressor is present in the cell at moderate concentrations, the most likely configuration has the λ repressor bound at O_R1 and O_R2, but not at O_R3. In this configuration, the λ repressor dimer bound at O_R1 blocks access to the promoter on the right side of the operator sites. This represses transcription of the adjacent gene, which encodes a protein termed **Cro** (controller of repressor and others), while the repressor dimer at O_R2 can be in contact with RNA polymerase and stimulate transcription of the promoter that controls the transcription of the gene that encodes the λ repressor itself.

Thus, the λ repressor stimulates its own production. As the concentration of the λ repressor increases further, an additional repressor dimer can bind to the O_R3 site, blocking the other promoter and repressing the production of additional repressor. Thus, the O_R3 site serves to maintain the λ repressor in a narrow, stable concentration range (**Figure 31.16**). The λ repressor also blocks other promoters in the λ phage genome so that the repressor is the only phage protein produced, maintaining the lysogenic state.



© Macmillan Learning

FIGURE 31.16 The λ repressor controls its own synthesis. (A) When λ repressor levels are relatively low, the repressor binds to sites O_R1 and O_R2 and stimulates the transcription of the gene that encodes the λ repressor itself. (B) When λ repressor levels are higher, the repressor also binds to site O_R3, blocking access to its promoter and repressing transcription from this gene.

A circuit based on the λ repressor and Cro forms a genetic switch

What stimulates the switch to the lytic pathway? Changes such as DNA damage initiate the cleavage of the λ repressor at a specific bond between the DNA-binding and oligomerization domains. This process is mediated by the *E. coli* RecA protein (Section 28.5). After this cleavage has taken place, the affinity of the λ repressor for DNA is reduced. After the λ repressor is no longer bound to the O_R1 site, the Cro gene can be transcribed. Cro is a small protein that binds to the same sites as the λ repressor does, but with a different order of affinity for the three sites in the right operator. In particular, Cro has the highest affinity for O_R3. Cro bound at this site blocks the production of new λ repressor. The absence of λ repressor activates the expression of other phage genes, leading to the production of virus particles and the eventual lysis of the host cells.

Thus, this genetic circuit acts as a switch with two stable states: (1) λ repressor high, Cro low, corresponding to the lysogenic state; and (2) Cro high, λ repressor low, corresponding to the lytic state (**Figure 31.17**). Regulatory circuits with two stable states are often referred to as being *bistable*. In these bistable circuits, positive and negative transcriptional control are tightly linked, with different DNA-binding proteins controlling the expression of each other's genes. This is a common motif for controlling gene expression in all systems, from viruses to eukaryotes. In eukaryotes, for example, genetic switches can determine distinct cellular fates, analogous to the lysogenic and lytic infection modes of λ phage.

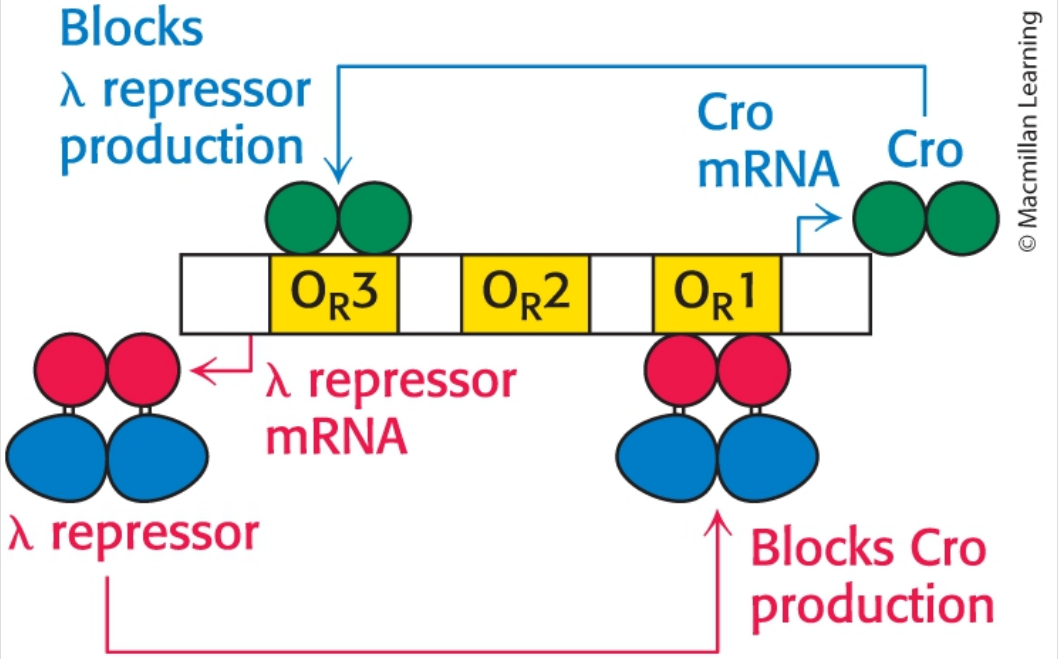


FIGURE 31.17 The λ repressor and Cro form a genetic circuit. The λ repressor blocks the production of Cro by binding most favorably to site O_R1, whereas Cro blocks the production of the λ repressor by binding most favorably to site O_R3. This circuit forms a switch that determines whether the lysogenic or the lytic pathway is followed.

31.4 Regulation of Gene Expression Is More Complex in Eukaryotes

Gene regulation in eukaryotes is significantly more complex than in bacteria in several ways. First, the genomes being regulated are significantly larger. The *E. coli* genome consists of a single, circular chromosome containing 4.6 megabases (Mb). This genome encodes approximately 2000 proteins. In comparison, one of the simplest eukaryotes, *Saccharomyces cerevisiae* (baker's yeast), contains 16 chromosomes ranging in size from 0.2 to 2.2 Mb. The yeast genome totals 12 Mb and encodes approximately 6000 proteins. The genome within a human cell contains 23 pairs of chromosomes ranging in size from 50 to 250 Mb. Approximately 20,000 protein-coding genes are present within the 3000 Mb of human DNA. Second, recall from Section 29.3 that eukaryotic DNA is packaged into chromatin. Third, eukaryotic genes are not generally organized into operons. Instead, genes that encode proteins for steps within a given pathway are often spread widely across the genome. This characteristic requires that other mechanisms function to regulate genes in a coordinated way.

Despite these differences, some aspects of gene regulation in eukaryotes are quite similar to those in bacteria. In particular, proteins that recognize specific DNA sequences are central to many gene-regulatory processes. Eukaryotic transcription factors — DNA-binding proteins similar in many ways to the bacterial proteins that we encountered earlier — can act directly by interacting with the transcriptional machinery, or indirectly by influencing chromatin structure. Key features of eukaryotic promoters, transcription factors, and enhancer sequences that can act far away from transcription start sites were introduced in Section 29.3.

A range of DNA-binding motifs are employed by eukaryotic DNA-binding proteins

The structures of many eukaryotic DNA-binding proteins have been determined and a range of structural motifs have been observed, but we will focus on three that reveal the common features and the diversity of these motifs. The first type of eukaryotic DNA-binding motif that we will consider is the **homeodomain** (**Figure 31.18**). The structure of the homeo-domain and its mode of recognition of DNA are very similar to those of the bacterial helix-turn-helix proteins. In eukaryotes, homeodomain proteins often form heterodimeric structures, sometimes with other homeodomain proteins, that recognize asymmetric DNA sequences.

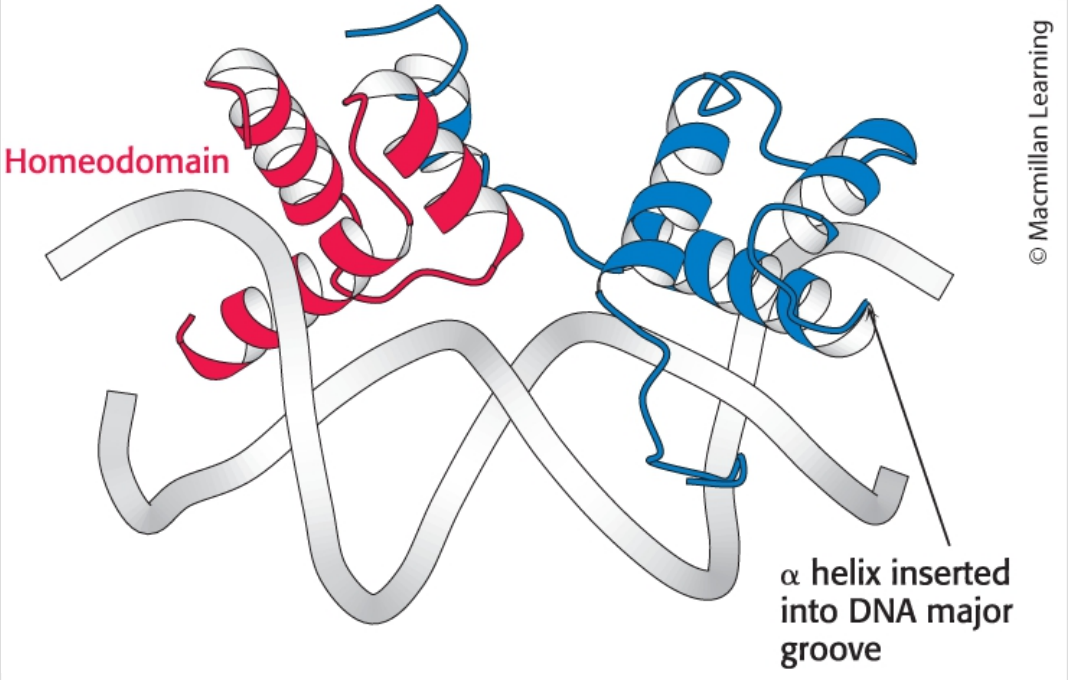


FIGURE 31.18 Two different DNA-binding homeodomains can form a heterodimer. Each homeodomain has a helix-turn-helix motif with one helix inserted into the major groove of DNA.

[Drawn from 1AKH.pdb.]

Another class of eukaryotic DNA-binding motif comprises the **basic-leucine zipper (bZip) proteins** (**Figure 31.19**). This DNA-binding motif consists of a pair of long α helices. The first part of each α helix is a basic region that lies in the major groove of the DNA and makes contacts responsible for DNA-site recognition. The second part of each α helix forms a coiled-coil structure with its partner. When these units are stabilized by appropriately spaced leucine residues, they are referred to as *leucine zippers*.

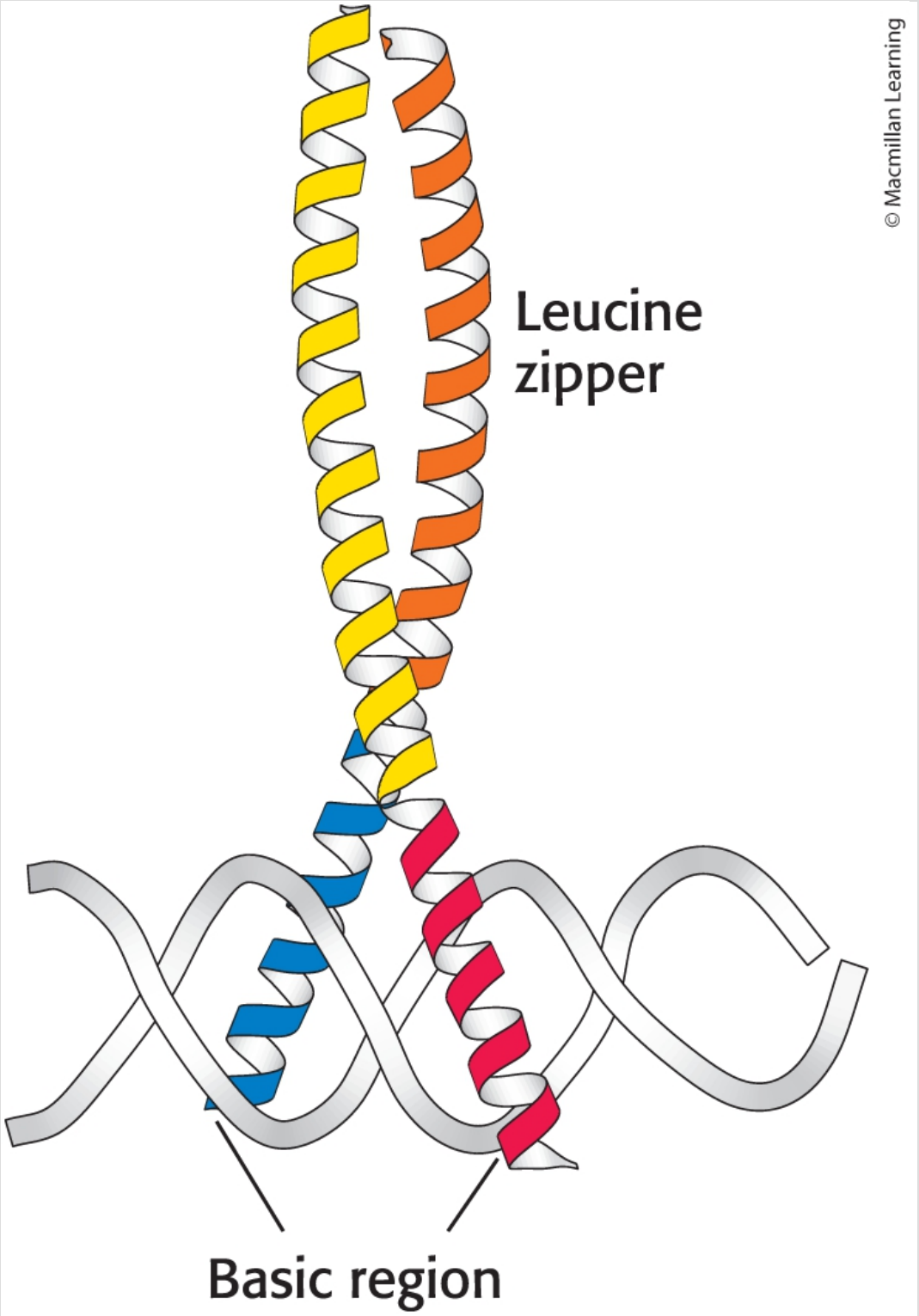


FIGURE 31.19 Two basic-leucine zipper proteins can form a heterodimer. The basic region lies in the major groove of DNA. The leucine zipper stabilizes the protein dimer.

[Drawn from 1FOS.pdb.]

The final class of eukaryotic DNA-binding motifs that we will consider here are the Cys_2His_2 **zinc-finger domains** (**Figure 31.20**). This motif comprises tandem sets of small domains, each of which binds a zinc ion through conserved sets of two cysteine and two histidine residues. These structures, often just called zinc-finger domains, form a string that follows the major groove of DNA. An α helix from each domain makes specific contacts with the edges of base pairs within the groove. Some proteins contain arrays of 10 or more zinc-finger domains, potentially enabling them to contact long stretches of DNA. The human genome encodes several hundred proteins that contain zinc-finger domains of this type. We will encounter another class of zinc-based DNA-binding domain when we consider nuclear hormone receptors in Section 31.5.

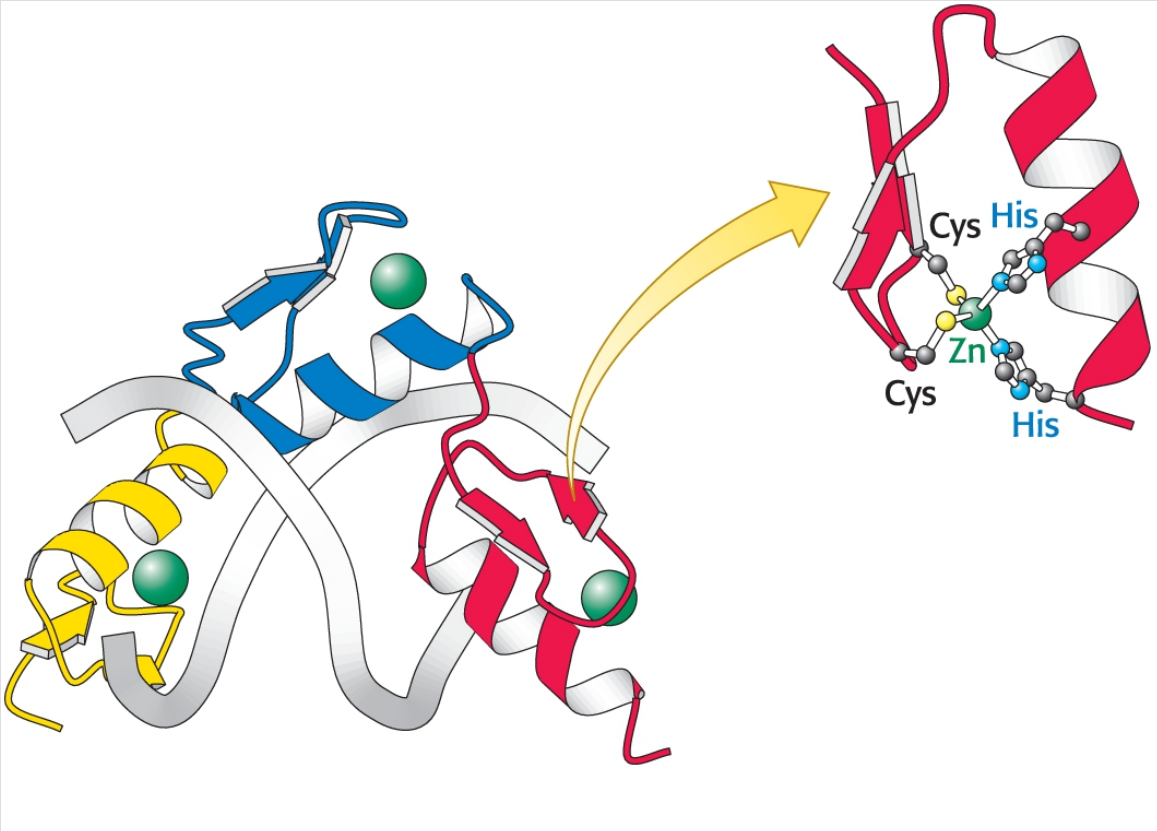


FIGURE 31.20 Zinc-finger domains bind to DNA. A DNA-binding domain comprising three Cys_2His_2 zinc-finger domains (shown in yellow, blue, and red) is shown in a complex with DNA. Each zinc-finger domain is stabilized by a bound zinc ion (shown in green) through interactions with two cysteine residues and two histidine residues. Notice how the protein wrap around the DNA in the major groove.

[Drawn from 1AAY.pdb.]

INTERACT with the models in Figures 31.18–31.20 in Achieve

Self-Check Question

The α helix is the most common element used by both bacterial and eukaryotic DNA-binding motifs. Why is this?

DNA-binding transcription factors are key to gene regulation in eukaryotes, just as they are in bacteria. However, the roles of eukaryotic transcription factors are different in several ways:

- Whereas the DNA-binding sites crucial for the control of gene expression in bacteria are usually quite close to promoters, those in eukaryotes can be farther away from promoters and can exert their action at a distance.
- Most bacterial genes are regulated by single transcription factors, and multiple genes in a pathway are expressed in a coordinated fashion because such genes are often transcribed as part of a polycistronic mRNA. In eukaryotes, the expression of each gene is typically controlled by multiple transcription factors, and the coordinated expression of different genes depends on having similar transcription-factor-binding sites in each gene in the set.

- In bacteria, transcription factors usually interact directly with RNA polymerase. In eukaryotes, while some transcription factors interact directly with RNA polymerase, many others act more indirectly, interacting with other proteins associated with RNA polymerase or modifying chromatin structure.

Eukaryotic transcription factors usually consist of several domains. As discussed above, the **DNA-binding domain** binds to regulatory sequences that can either be adjacent to the promoter or at some distance from it. Most commonly, transcription factors include additional domains that help activate transcription. When a transcription factor is bound to the DNA, its **activation domain** promotes transcription by interacting with RNA polymerase, by interacting with other associated proteins, or by modifying the local structure of chromatin.

Activation domains interact with other proteins

The activation domains of transcription factors generally recruit other proteins that promote transcription. In some cases, these activation domains interact directly with RNA polymerase. In other cases, the activation domains bind to closely associated proteins that bridge the transcription factors and the polymerase.

One example of an important bridge between transcription factors and promoter-bound RNA Polymerase II is **mediator**, a protein complex of 25 to 30 subunits that is conserved from yeast to human beings (**Figure 31.21**). Studies using cryo-electron microscopy are revealing the details of mediator structure and its interactions with RNA polymerase II and transcription factors. These structures provide insights into how mediator facilitates the phosphorylation of the carboxyl-terminal domain of RNA polymerase to promote the transition from transcription initiation to elongation.

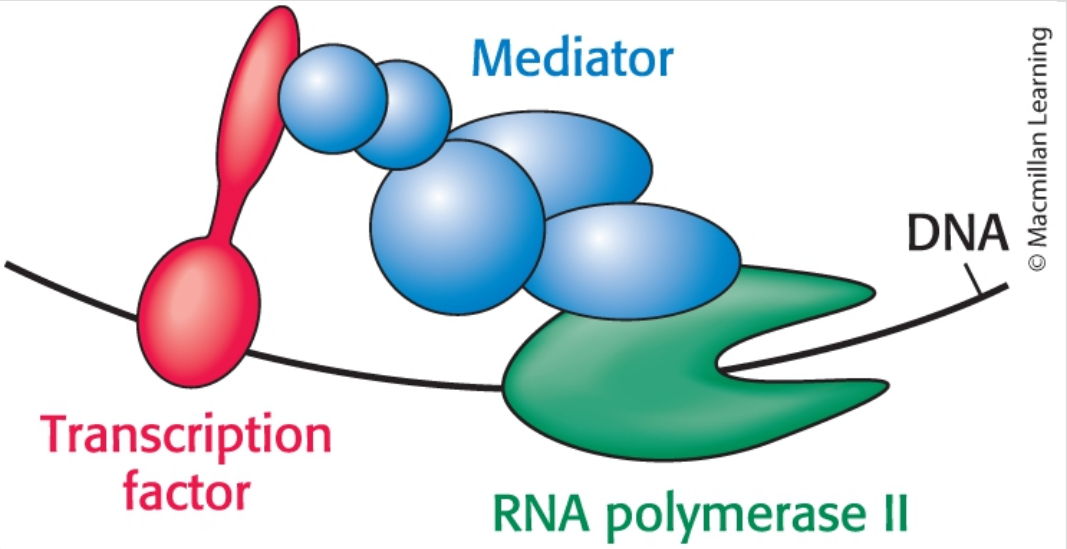


FIGURE 31.21 The mediator complex binds to transcription factors and to RNA polymerase II. Mediator acts as a bridge between transcription factors bearing activation domains and RNA polymerase II. These interactions help recruit and stabilize RNA polymerase II near specific genes that are then transcribed.

Interestingly, despite their critical role in the regulation of transcription, activation domains are quite diverse and share very little sequence similarity. For example, they may be acidic, hydrophobic, glutamine rich, or proline rich. However, they do have certain features in common. First, they are often redundant; that is, a part of the activation domain can be deleted without loss of function. Second, they are modular and can activate transcription when paired with a variety of DNA-binding domains. Third, they can act synergistically: two activation domains acting together create a stronger effect than either of them acting separately.

We have been considering the case in which gene control increases the expression level of a gene. In many cases, the expression of a gene must be decreased by blocking transcription. The agents in such cases are *transcriptional repressors*. In many cases, transcriptional repressors act by altering chromatin structure.

Multiple transcription factors interact with eukaryotic regulatory regions

The pre-initiation complex described in Chapter 29 initiates transcription at a low frequency. Recall that several general transcription factors join with RNA polymerase II to form the pre-initiation complex (PIC). Additional transcription factors must bind to other sites that can be near the promoter or quite distant for a gene to achieve a higher rate of mRNA synthesis. In contrast with the regulators of bacterial transcription, few eukaryotic transcription factors have any effect on their own. Instead, each factor recruits other proteins to build up large complexes that interact with the transcriptional machinery to activate transcription.

A major advantage of this mode of regulation is that a given regulatory protein can have different effects, depending on what other proteins are present in the same cell. This phenomenon, called *combinatorial control*, is crucial to multicellular organisms that have many different cell types. Even in unicellular eukaryotes such as yeast, combinatorial control allows for the generation of distinct cell types.

31.5 The Control of Gene Expression in Eukaryotes Can Require Chromatin Remodeling

Recall from Section 29.3 that to fit inside the nucleus, eukaryotic DNA is compacted into chromatin, a complex of DNA and a special set of proteins. One of the fundamental features of chromatin is the nucleosome, where DNA is wrapped around an octamer of histone proteins H2A, H2B, H3, and H4. In this section we will discuss how chromatin modifications affect gene expression.

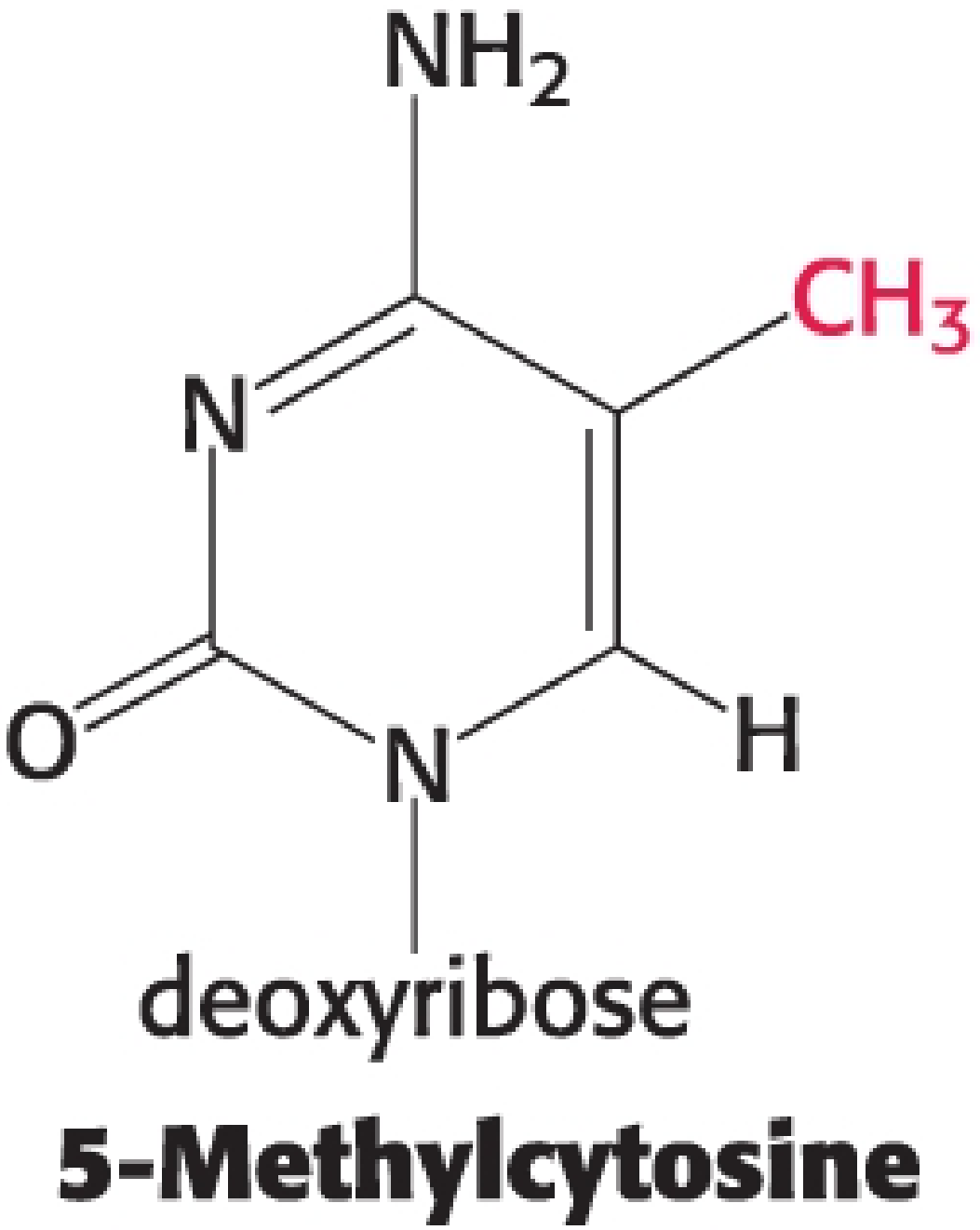
Early studies investigating the effect of nucleases on chromatin suggested a correlation between chromatin structure and gene expression. DNA that is densely packaged into chromatin is less susceptible to cleavage by the nonspecific DNA-cleaving enzyme DNase I. Regions adjacent to genes that are being transcribed are more sensitive to cleavage by DNase I than are other sites in the genome, suggesting that the DNA in these regions is less compacted than it is elsewhere and is thus more accessible to regulatory proteins.

In addition, some sites, called *hypersensitive sites,* are extremely sensitive to DNase I and other nucleases. These sites are usually within 1 kb of the start site of an active gene and correspond to regions that have few nucleosomes or contain nucleosomes in an altered conformation. Hypersensitive sites are cell-type specific and developmentally regulated. For example, globin genes in the precursors of erythroid cells from 20-hour-old chicken embryos are insensitive to DNase I. However, when hemoglobin synthesis begins at 35 hours, regions adjacent to these genes become highly susceptible to digestion. In tissues such as the brain that produce no hemoglobin, the globin genes remain resistant to DNase I throughout development and into adulthood. These

studies and additional lines of evidence suggest that chromatin structure is altered in active genes compared with inactive ones and that one prerequisite for gene expression is a relaxing of the chromatin structure.

Chromatin remodeling and DNA methylation regulate access to DNA-binding sites

If, as mentioned above, the relaxing of chromatin structure allows for gene expression, then it makes sense that the packaging of DNA into nucleosomes will inhibit gene expression. Another mechanism of regulating gene expression is provided by the degree of methylation of DNA, especially at cytosines. Specific methyltransferases methylate carbon 5 of cytosine, converting it into 5-methylcytosine.



About 70% of the $5'-CpG-3'$ sequences (where “p” represents the phosphate residue in the DNA backbone) in mammalian genomes are methylated. This modification is associated with gene silencing because

the methyl group of 5-methylcytosine protrudes into the major groove of DNA where it may interfere with the binding of proteins that stimulate transcription.

The distribution of these methylated CpG sequences in mammalian genomes is not uniform. Many CpG sequences have been converted into TpG through mutation by the deamination of 5-methylcytosine to thymine. In addition, some regions contain primarily *non-methylated* CpG dinucleotides, referred to as **CpG islands**. The promoters of ca. 70% of mammalian genes are associated with CpG islands, making them more accessible by transcription factors. The relative absence of 5-methylcytosines near gene promoters is referred to as *hypomethylation*.

The distribution of methylated CpG sequences may also depend on the cell type. Consider the β-globin gene. In cells that are actively expressing hemoglobin, the region from approximately 1 kb upstream of the start site to approximately 100 bp downstream of the start site is less methylated than the corresponding region in cells that do not express this gene.

These observations suggest that methylation of CpG sequences may block DNA recognition by transcription factors, thus influencing gene expression. Recent evidence suggests that non-methylated CpG sequences are specifically bound by certain transcription factors. These transcription factors may also recruit histone-modifying enzymes that alter the chromatin structure. We will discuss histone modifications in more detail below.

Epigenetic modifications influence gene expression

DNA methylation and histone modification (to be discussed below) are two mechanisms associated with **epigenetics** — modifications to the

genome that affect gene expression but do not alter the DNA sequence. A third mechanism involves RNA-mediated silencing, which we will discuss in Section 31.6. Several human disorders, including Fragile X syndrome, Angelman's syndrome, and various forms of cancer, are thought to be caused by epigenetic modifications and influenced by diet, exercise, age, or exposure to environmental toxins.

Cancer was the first human disease to be linked to epigenetics when it was discovered that cancerous cells had abnormally high levels of methylation as compared to normal cells. Further investigations showed that in cancer cells, many CpG islands become methylated, silencing genes such as tumor-suppressor genes that are critical for the control of cell division and should not be turned off.



PBH Images/Alamy

SARAH STEWART Dr. Sarah Stewart was born in Mexico in 1905 to an American father and a Mexican mother. Her family relocated to the United States in 1911, and she pursued her interests in bacteriology and chemistry, earning a PhD in microbiology in 1939. Dr. Stewart wanted to research the possible link between cancer and viruses at a time when that idea was considered preposterous, even though research as early as 1911 suggested such a link. Unable to obtain funding for her research, she instead pursued a medical degree. In 1949 she was the first woman to ever receive an MD

from Georgetown University School of Medicine, having completed that degree in only two years. She was 43 at the time. Dr. Stewart returned to research, and in 1953 she isolated a small agent from cancerous tissue that is also capable of causing cancer in healthy tissue, thus pioneering the field of viral oncology. Sadly, Dr. Stewart succumbed to the same disease she was investigating; she died of cancer in 1976.

Enhancers stimulate transcription by recruiting activator proteins that alter chromatin structure

Let us now turn to the action of enhancers, which were introduced in Section 29.3. Recall that enhancers are DNA sequences that have no promoter activity of their own but greatly increase transcription, even when they are located several thousand base pairs from the gene being expressed.

Enhancers function by serving as binding sites for specific transcription factors. An enhancer is effective only in the specific cell types in which appropriate regulatory proteins are expressed. In many cases, these DNA-binding proteins influence transcription initiation by altering the local chromatin structure to expose a gene or its regulatory sites rather than by direct interactions with RNA polymerase. This mechanism accounts for the ability of enhancers to act at a distance.

The properties of enhancers are illustrated by studies of the enhancer controlling the gene Islet-1. This gene encodes a homeodomain-containing protein that plays important roles in the developing nervous system. DNA fragments were constructed by connecting the promoter and enhancer regions associated with the Islet-1 gene to a gene expressing green fluorescent protein (GFP; **Figure 31.22**). When this DNA construct was introduced into zebrafish, an organism useful for imaging studies because of its size and transparency, the expression of green fluorescent protein could be visualized by microscopy. The green

fluorescence of GFP was only seen in motor neurons and only during one stage of zebrafish development (**Figure 31.23**), revealing the power of the enhancer in limiting gene expression to particular cells.

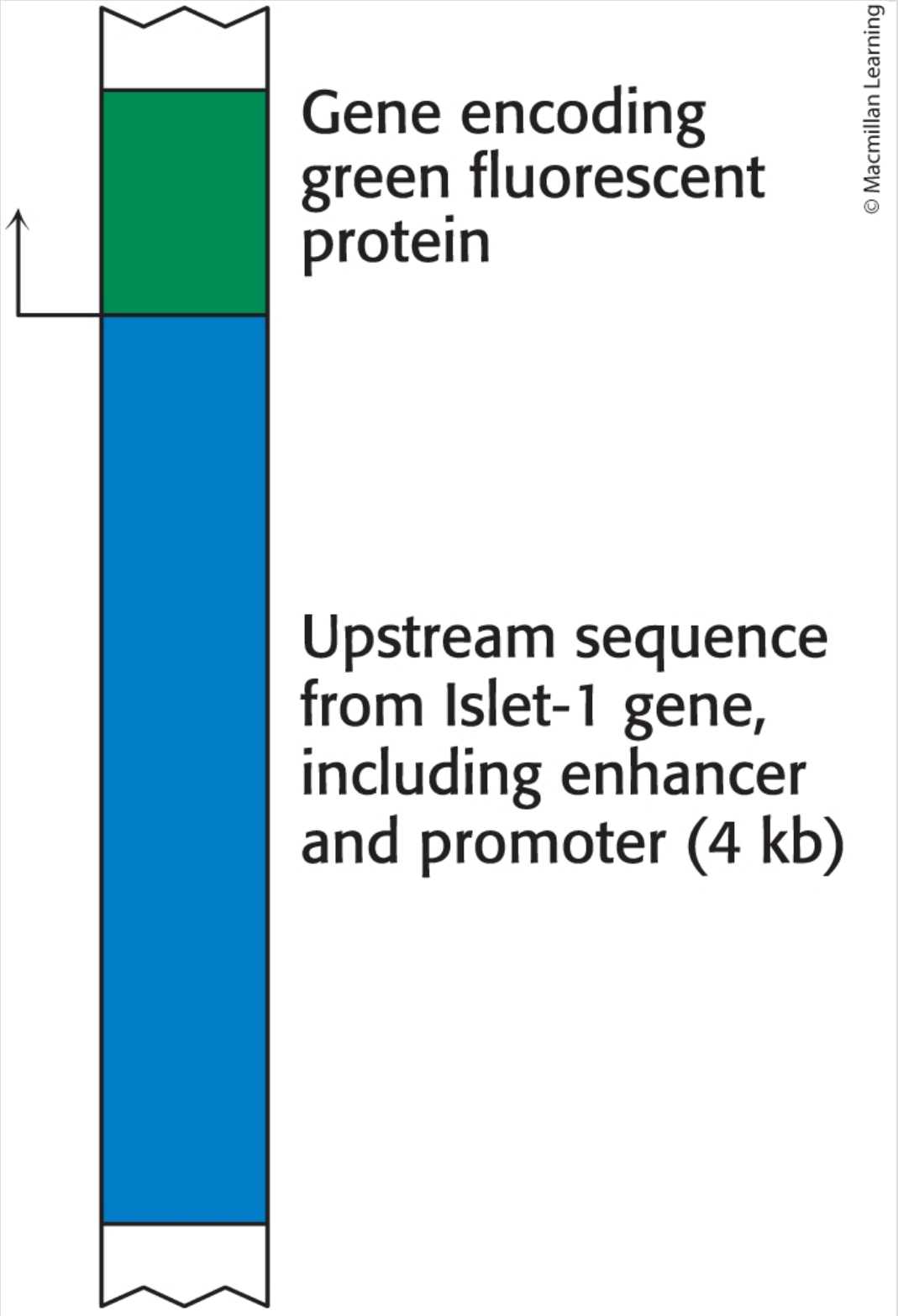
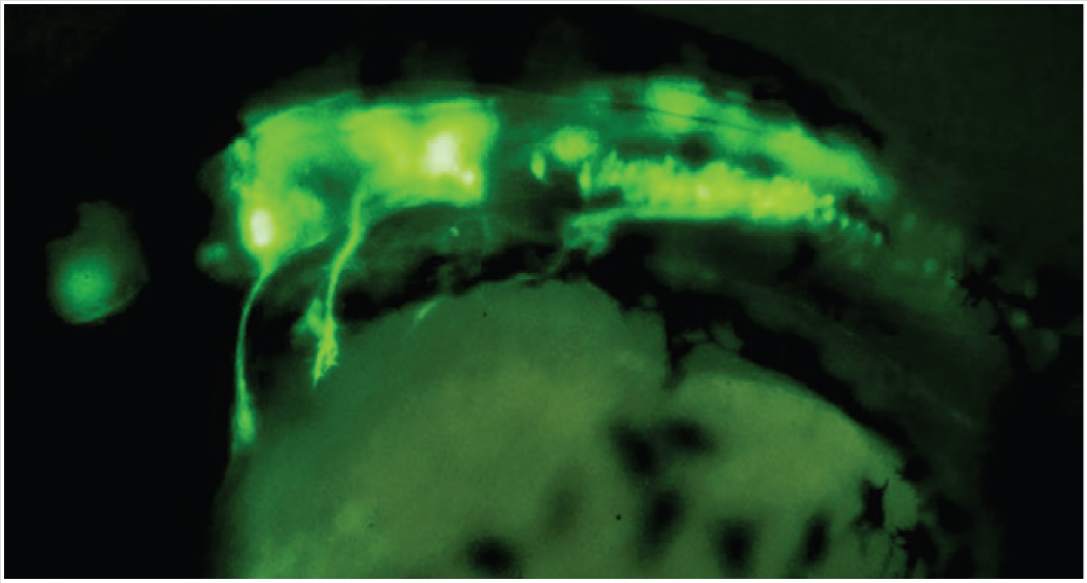


FIGURE 31.22 Enhancer function can be assayed with a reporter construct. A DNA construct that includes a gene encoding green fluorescent protein adjacent to 4 kilobases of the DNA upstream of the start site for the Islet-1 gene. If this construct is

introduced into cells in which Islet-1 is expressed, then the enhancer and promoter should lead to the production of green fluorescent protein.



Republished with permission of Society for Neuroscience, from Higashijima S., Hotta Y., Okamoto H., Visualization of Cranial Motor Neurons in Live Zebrafish. *J. Neurosci.*, January 1, 2000, 20(1):206–218;

FIGURE 31.23 Enhancer function can be demonstrated in vivo. This microscopic image shows developing zebrafish embryo into which the probe for enhancer function (Figure 31.22) has bee introduced. The green fluorescence reveals that green fluorescent protein is expressed only in a subset of cells, shown to be cranial motor neurons.

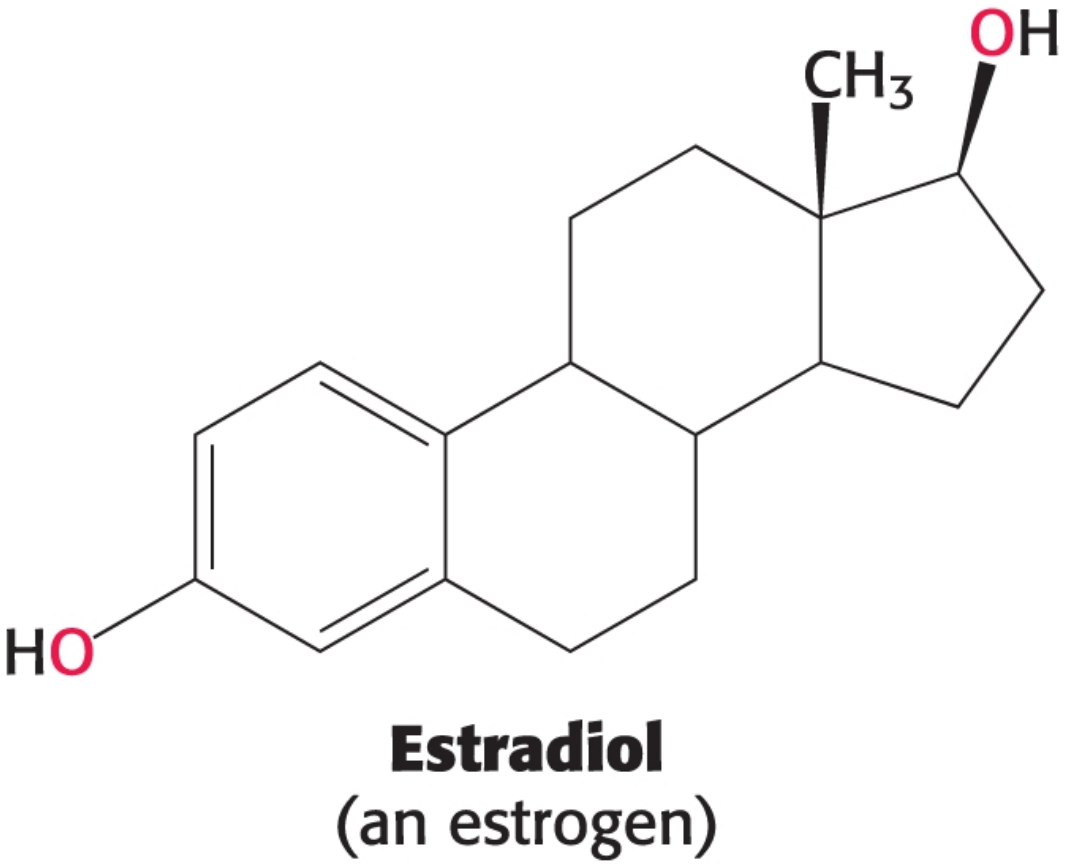
Self-Check Question

Why is eukaryotic DNA compacted into chromatin? How does this impact the activation or repression of gene expression? What must happen to chromatin in order for genes to be transcribed or silenced?

Nuclear hormone receptors are transcription factors that cause changes in chromatin

structure

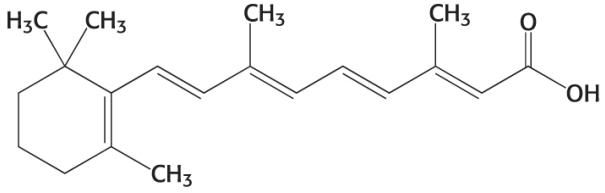
How do transcription factors stimulate changes in chromatin structure and thus influence gene expression? To illustrate this, let's discuss the system that detects and responds to estrogens, cholesterol-derived steroid hormones (Section 27.4). Synthesized and released by the ovaries, estrogens, such as estradiol, are required for the development of female secondary sex characteristics and, along with progesterone, participate in the ovarian cycle.



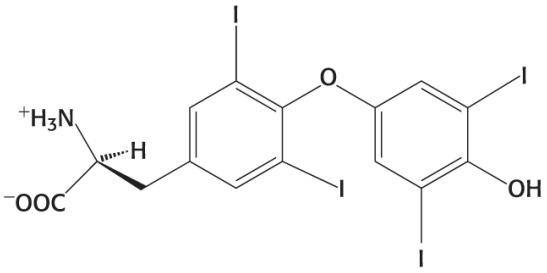
Estradiol
(an estrogen)

Because they are hydrophobic molecules, estrogens easily diffuse across cell membranes. When inside a cell, estrogens bind to highly specific, soluble receptor proteins. Estrogen receptors are members of a large

family of proteins that act as receptors for a wide range of hydrophobic molecules, including other steroid hormones, thyroid hormones, and retinoids.



All-*trans*-retinoic acid
(a retinoid)



Thyroxine
(L-3,5,3′,5′-Tetraiodothyronine)
(a thyroid hormone)

The human genome encodes approximately 50 members of this family of receptors, often referred to as **nuclear hormone receptors**. The genomes of other multicellular eukaryotes encode similar numbers of nuclear hormone receptors, although they are absent in yeast.

All these receptors have a similar mode of action. On binding of the signal molecule (called, generically, a *ligand*), the ligand–receptor complex modifies the expression of specific genes by binding to control elements in the DNA. Estrogen receptors bind to specific DNA sites (referred to as estrogen response elements or EREs) that contain the consensus sequence $5'-AGGTCANNNTGACCT-3'$. As expected from the symmetry of this sequence, an estrogen receptor binds to such sites as a dimer.

A comparison of the amino acid sequences of members of this family reveals two highly conserved domains: a DNA-binding domain and a ligand-binding domain (**Figure 31.24**). The DNA-binding domain lies toward the center of the molecule and consists of a set of zinc-based domains different from the Cys_2His_2 zinc-finger proteins introduced in

Section 31.4. These zinc-based domains bind to specific DNA sequences by virtue of an α helix that lies in the major groove in the specific DNA complexes formed by estrogen receptors.

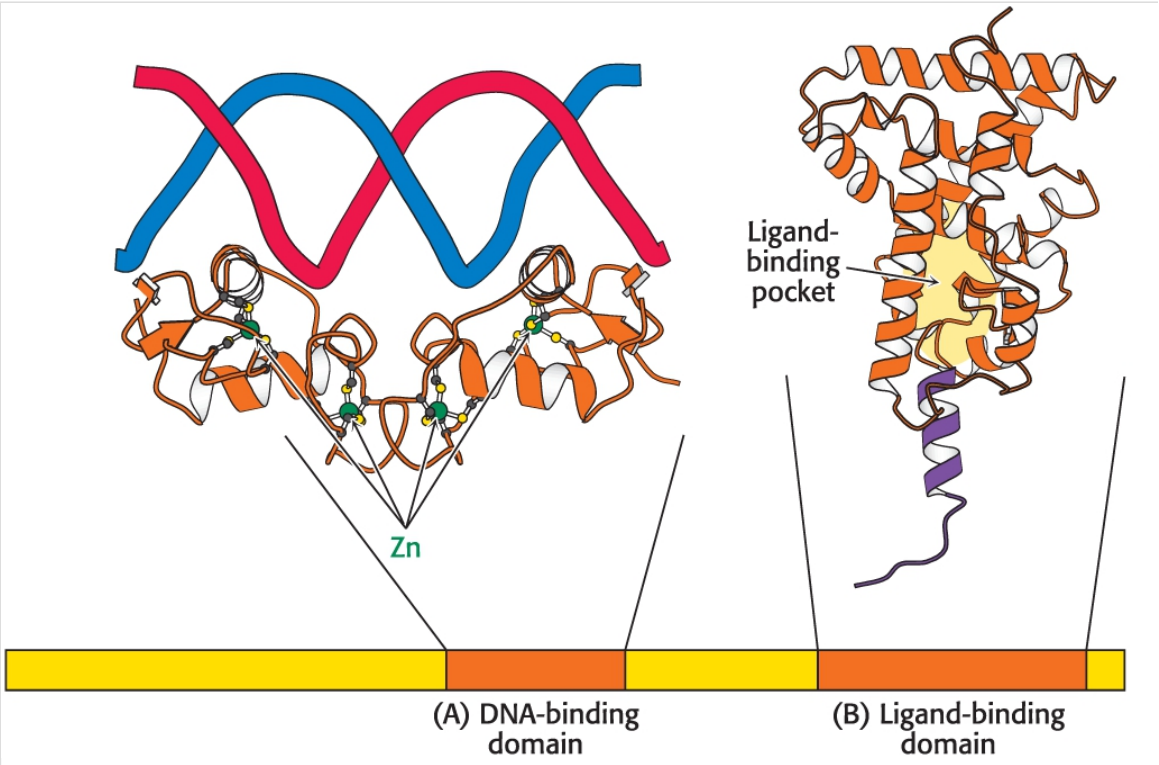


FIGURE 31.24 Nuclear hormone receptors contain two important conserved domains. These domains are: (A) a DNA-binding domain toward the center of the protein sequence, and (B) a ligand-binding domain toward the carboxyl terminus. The structure of a dimer of the DNA-binding domain bound to DNA is shown, as is one monomer of the normally dimeric ligand-binding domain.

[Drawn from 1HCQ.pdb and 1LBD.pdb.]

INTERACT with these models in Achieve

The second highly conserved domain of the nuclear receptor proteins is the ligand-binding site, which lies near the carboxyl terminus. This domain folds into a structure that consists almost entirely of α helices, arranged in three layers. The ligand binds in a hydrophobic pocket that

lies in the center of this array of helices (Figure 31.25). This domain changes conformation when it binds its ligand, estrogen.

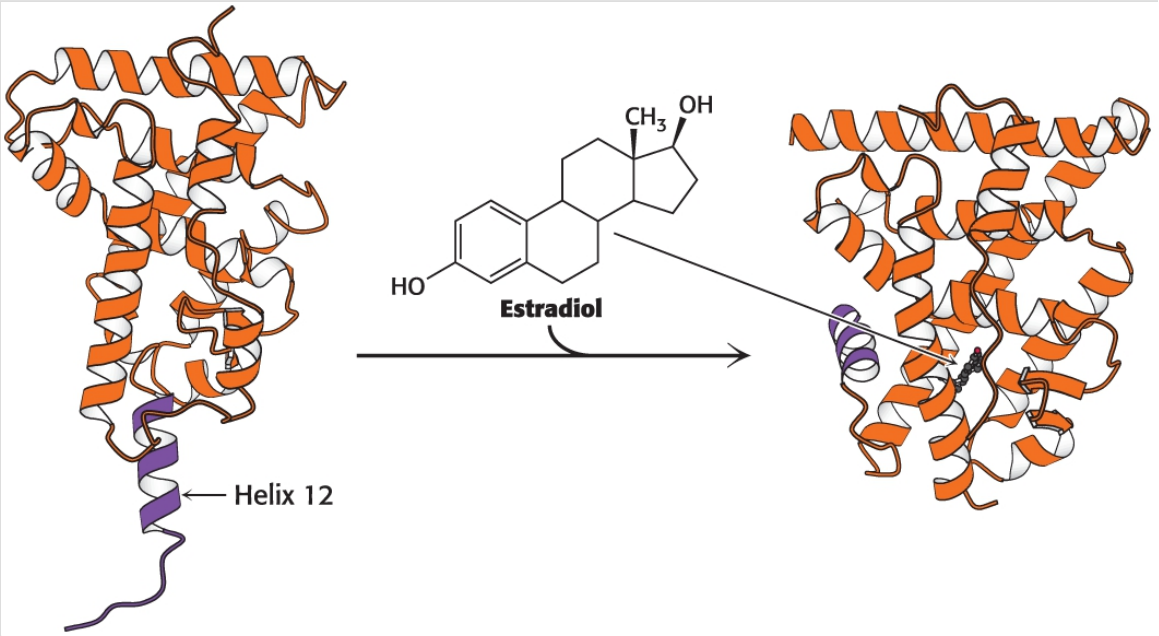


FIGURE 31.25 Nuclear hormone receptors interact with ligands. The ligand lies completely surrounded within a pocket in the ligand-binding domain. Notice that the last α helix, helix 12 (shown in purple), folds into a groove on the side of the structure once the ligand binds.

[Drawn from 1LDB.pdb and 1ERE.pdb.]

INTERACT with this model in Achieve

How does ligand binding lead to changes in gene expression? The simplest model would have the binding of ligand alter the DNA-binding properties of the receptor, much like the *lac* repressor in bacteria. However, experiments with purified nuclear hormone receptors revealed that ligand binding does *not* significantly alter DNA-binding affinity and specificity. The effect must be due to a different mechanism.

Nuclear hormone receptors regulate transcription by recruiting coactivators to the transcription complex

Is it possible that nuclear hormone receptors interact with specific proteins only in the presence of a ligand? Experiments to answer this question led to the identification of several related proteins called **coactivators**, such as SRC-1 (steroid receptor coactivator-1), GRIP-1 (glucocorticoid receptor interacting protein-1), and NcoA-1 (nuclear hormone receptor coactivator-1). These coactivators are referred to as the p160 family because of their size. The binding of ligand to the receptor induces a conformational change that allows the recruitment of a coactivator (**Figure 31.26**). In many cases, these coactivators are enzymes that catalyze reactions that lead to the modification of chromatin structure.

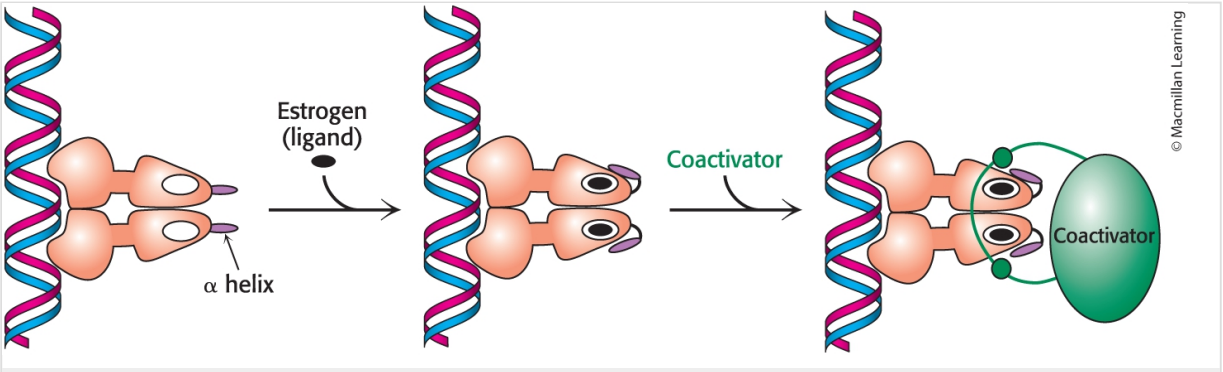
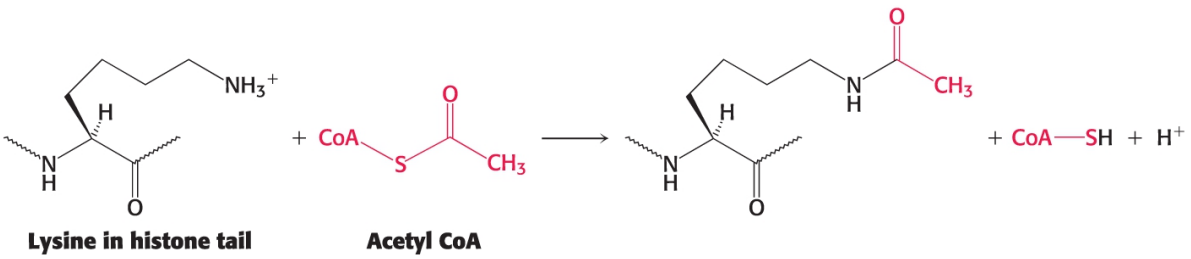


FIGURE 31.26 Nuclear hormone receptors recruit coactivators upon ligand binding. The binding of ligand to a nuclear hormone receptor induces a conformational change in the ligand-binding domain. This change in conformation generates favorable sites for the binding of a coactivator.

Chromatin structure is modulated through covalent modifications of histone tails

We have seen that nuclear receptors respond to signal molecules by recruiting coactivators. So now the question is: how do coactivators modulate transcriptional activity? The answer is that these proteins act to loosen the histone complex from the DNA, exposing additional DNA regions to the transcription machinery.

Much of the effectiveness of coactivators appears to result from their ability to covalently modify the amino-terminal tails of histones as well as regions on other proteins. Some of the p160 coactivators and the proteins that they recruit catalyze the transfer of acetyl groups from acetyl CoA to specific lysine residues in these amino-terminal tails.



Enzymes that catalyze such reactions are called **histone acetyltransferases (HATs)**. The histone tails are readily extended so they can fit into the HAT active site and become acetylated (**Figure 31.27**).

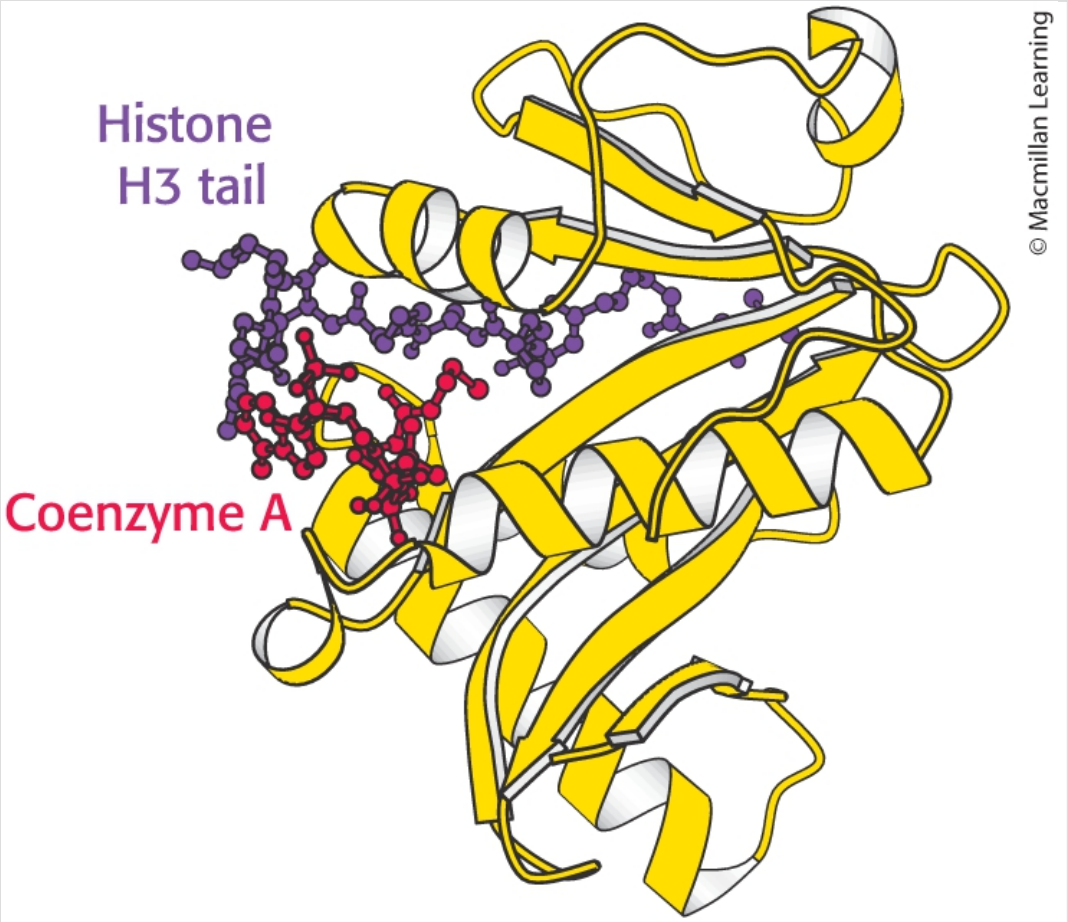


FIGURE 31.27 Histone acetyltransferase modifies histone tails. In this structure, the amino-terminal tail of histone H3 extends into a pocket in the histone acetyltransferase enzyme (yellow). A lysine side chain on the histone tail can accept an acetyl group from acetyl Coenzyme A bound in an adjacent site on the enzyme.

[Drawn from 1QSN.pdb.]

INTERACT with this model in Achieve

What are the consequences of histone acetylation? Lysine bears a positively charged ammonium group at neutral pH. The addition of an acetyl group generates an uncharged amide group. This change dramatically reduces the affinity of the histone tail for DNA and modestly decreases the affinity of the entire histone complex for DNA,

loosening the histone complex from the DNA and relaxing the chromatin structure.

In addition, the acetylated lysine residues interact with a specific acetyllysine-binding domain that is present in many proteins that regulate eukaryotic transcription. This domain, also termed a **bromodomain**, comprises approximately 110 amino acids that form a four-helix bundle containing a peptide-binding site at one end (**Figure 31.28**).



FIGURE 31.28 Bromodomains interact with acetyllysine. In this structure, the four-helix-bundle bromodomain binds an acetylated peptide from histone H4.

[Drawn from 1E6I.pdb.]

INTERACT with this model in Achieve

Bromodomain-containing proteins are components of two large complexes essential for transcription. One is a complex of more than 10 polypeptides that binds to the TATA-box-binding protein (TBP). Recall that TBP is an essential transcription factor for many genes (Section 29.3). Proteins that bind to the TATA-box-binding protein are called **TAFs** (for **TATA-box-binding protein associated factors**), and together with TBP they form TFIID (Section 29.3). In particular, TAF1 contains a pair of bromodomains near its carboxyl terminus. The two domains are oriented such that each can bind one of two acetyllysine residues at positions 5 and 12 in the histone H4 tail. Thus, acetylation of the histone tails provides a mechanism for recruiting other components of the transcriptional machinery.

Bromodomains are also present in some components of large complexes known as **chromatin-remodeling complexes**. These complexes, which also contain domains homologous to those of helicases, use the free energy of ATP hydrolysis to shift the positions of nucleosomes along the DNA and to induce other conformational changes in chromatin (**Figure 31.29**). Histone acetylation can lead to a reorganization of the chromatin structure via these ATP-dependent remodeling complexes, potentially exposing binding sites for other factors. Thus, histone acetylation can activate transcription through a combination of three mechanisms: by reducing the affinity of the histones for DNA, by recruiting other components of the transcriptional machinery, and by initiating the remodeling of the chromatin structure.

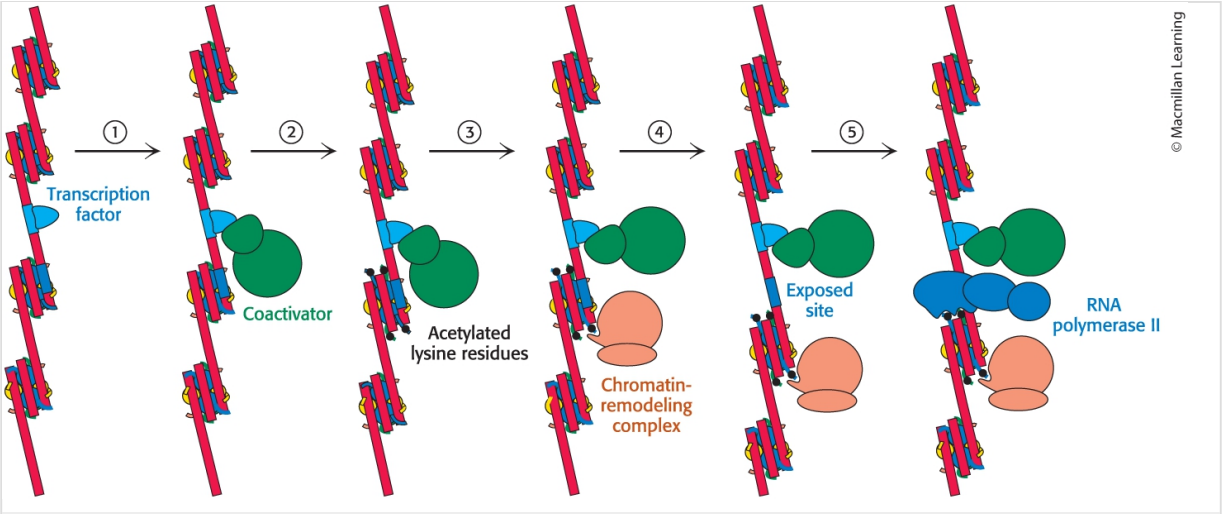


FIGURE 31.29 Gene regulation can involve chromatin remodeling. Eukaryotic gene regulation begins with an activated transcription factor bound to a specific site on DNA. One scheme for the initiation of transcription by RNA polymerase II requires five steps: (1) recruitment of a coactivator, (2) acetylation of lysine residues in the histone tails, (3) binding of a remodeling-engine complex to the acetylated lysine residues, (4) ATP-dependent remodeling of the chromatin structure to expose a binding site for RNA polymerase II or for other factors, and (5) recruitment of RNA polymerase II. Only two subunits are shown for each complex, although the actual complexes are much larger. Other schemes are possible.

Nuclear hormone receptors also include regions that interact with components of the mediator complex. Thus, two mechanisms of gene regulation can work in concert. Modification of histones and chromatin remodeling can open up regions of chromatin into which the transcription complex can be recruited through protein–protein interactions.

Transcriptional repression can be achieved through histone deacetylation and other modifications

Just as in bacteria, some changes in a cell's environment lead to the repression of genes that had been active. The modification of histone tails again plays an important role. However, in repression, a key reaction appears to be the *deacetylation* of acetylated lysine, catalyzed by specific **histone deacetylase** enzymes.

In many ways, the acetylation and deacetylation of lysine residues in histone tails (and, likely, in other proteins) is analogous to the phosphorylation and dephosphorylation of serine, threonine, and tyrosine residues in other stages of signaling processes. Like the addition of phosphoryl groups, the addition of acetyl groups can induce conformational changes and generate novel binding sites. Without a means of removal of these groups, however, these signaling switches will become stuck in one position and lose their effectiveness. Like phosphatases, deacetylases help reset the switches.

Acetylation is not the only modification of histones and other proteins in gene-regulation processes. The methylation of specific lysine and arginine residues also can be important. Some of the more common modifications are shown in Table 31.1.

TABLE 31.1 Selected histone modifications

Modification	Effect
H3 K9 acetylation	Activation
H3 K27 acetylation	Activation

H4 K16 acetylation	Activation
H3 K4 monomethylation	Activation
H3 K9 trimethylation	Repression
H3 K27 trimethylation	Repression
H3 R17 methylation	Activation
H2B S14 phosphorylation	DNA repair
H2B K120 ubiquitination	Activation

The elucidation of the roles of these modifications is a very active area of research. The relation between various histone modifications and their roles in controlling gene expression is sometimes referred to as "the histone code," and important generalizations have been elucidated. For example, trimethylation of lysine 27 on histone H3 (H3 K27) is associated with repression of gene expression. This modification is promoted by a protein complex termed *polycomb repressive complex-2* (PRC-2). PRC-2 both binds to histones containing the trimethylated H3 K27 and catalyzes the addition of methyl groups to other H3 K27 substrates. This allows an initial modification to spread to adjacent histone octamers, facilitating gene repression.

The development and application of methods that allow probing of histone modifications on a genome-wide scale in a range of cell types has provided large data sets that can be examined to test and refine models of transcription regulation via chromatin modifications.

Self-Check Question



Summarize the various aspects of chromatin modifications discussed above and how they affect gene expression.

31.6 Gene Expression Can Be Controlled at the Posttranscriptional Level

The modulation of the rate of transcription initiation is the most common mechanism of gene regulation. However, other stages of transcription also can be targets for regulation. In addition, the process of translation provides other points of intervention for regulating the level of a protein produced in a cell. In Chapter 29, we considered riboswitches that control transcription termination (Section 29.3). Other riboswitches control gene expression by other mechanisms, such as the formation of structures that inhibit translation. Additional mechanisms for posttranscriptional gene regulation have been discovered in both bacteria and eukaryotes, some of which will be described here.

Attenuation regulates transcription in bacteria through the modulation of nascent RNA secondary structure

A different mechanism for regulating transcription in bacteria was discovered by Charles Yanofsky and his colleagues as a result of their studies of the tryptophan operon. This operon encodes five enzymes that convert chorismate into tryptophan. Analysis of the 5′ end of *trp* mRNA revealed the presence of a leader sequence of 162 nucleotides before the initiation codon of the first enzyme.

The next striking observation was that bacteria produced a transcript consisting of only the first 130 nucleotides when the tryptophan level was high, but they produced a 7000-nucleotide *trp* mRNA, including the

entire leader sequence, when tryptophan was scarce. Thus, when tryptophan is plentiful and the biosynthetic enzymes are not needed, transcription is abruptly broken off before any mRNA coding for the enzymes is produced. The site of termination is called the attenuator, and this mode of regulation is called **attenuation**.

Attenuation depends on features at the 5′ end of the mRNA product (**Figure 31.30**). The first part of the leader sequence encodes a 14-amino-acid leader peptide. Following the open reading frame for the peptide is the attenuator, a region of RNA that is capable of forming several alternative structures. Recall that transcription and translation are tightly coupled in bacteria. Thus, the translation of the *trp* mRNA begins soon after the ribosome-binding site has been synthesized.

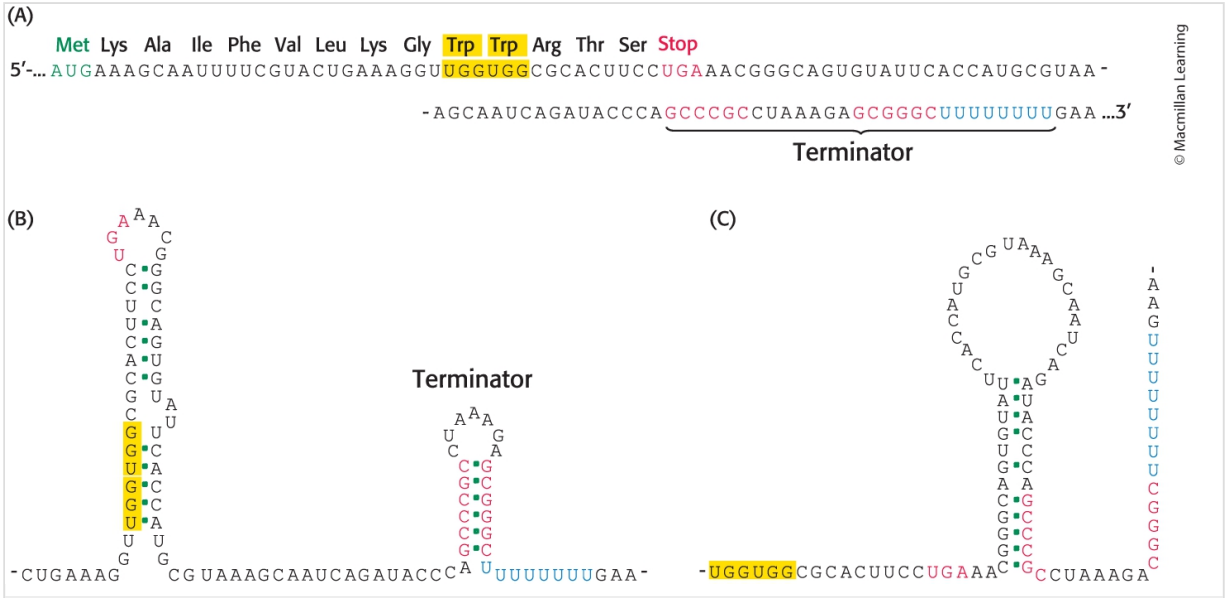


FIGURE 31.30 The leader region of *trp* mRNA includes tryptophan codons. (A) The nucleotide sequence of the 5′ end of *trp* mRNA includes a short open reading frame that encodes a peptide comprising 14 amino acids; the leader encodes two tryptophan residues and has an untranslated attenuator region that includes a region that can form a terminator structure (red and blue). (B and C) The attenuator region can adopt either of two distinct stem-loop structures.

How does the level of tryptophan alter transcription of the *trp* operon? An important clue was the finding that the 14-amino-acid leader peptide includes two adjacent tryptophan residues. A ribosome is able to translate the leader region of the mRNA product only in the presence of adequate concentrations of tryptophan. When enough tryptophan is present, a stem-loop structure forms in the attenuator region, which leads to the release of RNA polymerase from the DNA (Figure 31.31). However, when tryptophan is scarce, transcription is terminated less frequently. Little tryptophanyl-tRNA is present, and so the ribosome stalls at the tandem UGG codons encoding tryptophan. This delay leaves the adjacent region of the mRNA exposed as transcription continues. An alternative RNA structure that does not function as a terminator is formed, and transcription continues into and through the coding regions for the enzymes. Thus, attenuation provides an elegant means of sensing the supply of tryptophan required for protein synthesis.

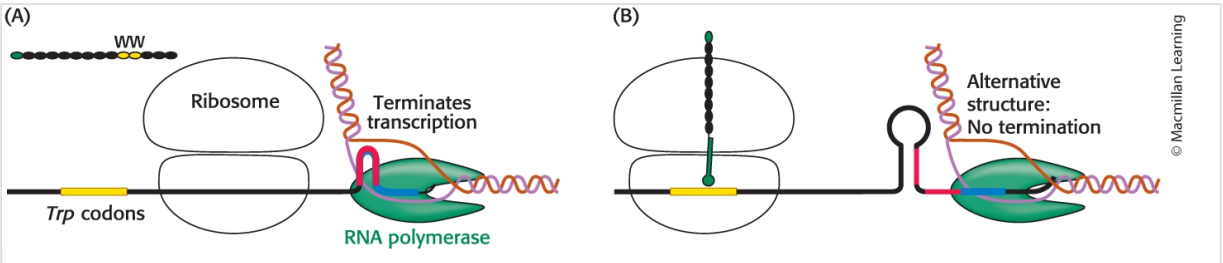


FIGURE 31.31 Attenuation regulates transcription. (A) In the presence of adequate concentrations of tryptophan (and, hence, Trp-tRNA), translation proceeds rapidly and an RNA structure forms that terminates transcription. (B) At low concentrations of tryptophan, translation stalls while awaiting Trp-tRNA, giving time for an alternative RNA structure to form that prevents the formation of the terminator and allows transcription to proceed.

Several other operons for the biosynthesis of amino acids in *E. coli* also are regulated by attenuator sites. The leader peptide of each contains an abundance of the amino acid residues of the type synthesized by the operon (Figure 31.32). For example, the leader peptide for the phenylalanine operon includes 7 phenylalanine residues among 15

residues. The threonine operon encodes enzymes required for the synthesis of both threonine and isoleucine; the leader peptide contains 8 threonine and 4 isoleucine residues in a 16-residue sequence. The leader peptide for the histidine operon includes 7 histidine residues in a row. In each case, low levels of the corresponding charged tRNA cause the ribosome to stall, trapping the nascent mRNA in a state that can form a structure that allows RNA polymerase to read through the attenuator site. Evolution has apparently converged on this strategy repeatedly as a mechanism for controlling amino acid biosynthesis.



FIGURE 31.32 The leader sequences of several operons contain codons for the specific amino acid that they regulate. Shown here are the amino acid sequences and the corresponding mRNA nucleotide sequences of the (A) threonine operon, (B) phenylalanine operon, and (C) histidine operon. In each case, an abundance of one amino acid in the leader peptide sequence leads to attenuation.

This example of posttranscriptional gene regulation that we have been describing comes from bacteria, as opposed to archaea. The transcriptional apparatus present in archaea shares many features with that found in eukaryotes. This commonality is frequently interpreted to suggest that eukaryotes evolved after a cell fusion event in which a bacterial cell was engulfed by an archaeal cell. Nonetheless, the key principles of gene regulation such as the occurrence of operons and the roles of DNA-binding proteins in directly blocking or stimulating RNA polymerase are the same in bacteria and archaea, perhaps because of

similar genome sizes. As we shall see next, eukaryotic cells with larger genomes and, often, many distinct cell types, use quite different strategies.

Eukaryotes use different mechanisms to control gene expression at the posttranscriptional level

Just as in bacteria, gene expression in eukaryotes can be regulated subsequent to transcription. We shall consider two examples. The first is the regulation of genes taking part in iron metabolism through key features in RNA secondary structure, similar in many ways to attenuation in bacteria. The second entails an entirely new mechanism, in which certain small regulatory RNA molecules allow the regulation of gene expression through interaction with a range of target mRNAs. Remarkably, this mechanism, discovered relatively recently, affects the expression of approximately 60% of all human genes.

Genes associated with iron metabolism are translationally regulated in animals

RNA secondary structure plays a role in the regulation of iron metabolism in eukaryotes. Iron is an essential nutrient, required for the synthesis of hemoglobin, cytochromes, and many other proteins. However, excess iron can be quite harmful because, untamed by a suitable protein environment, iron can initiate a range of free-radical reactions that damage proteins, lipids, and nucleic acids.

Animals have evolved sophisticated systems for the accumulation of iron in times of scarcity and for the safe storage of excess iron for later

use. Key proteins include **transferrin**, a transport protein that carries iron in the serum, **transferrin receptor**, a membrane protein that binds iron-loaded transferrin and initiates its entry into cells, and **ferritin**, an impressively efficient iron-storage protein found primarily in the liver and kidneys. Twenty-four ferritin polypeptides form a nearly spherical shell that encloses as many as 2400 iron atoms, a ratio of one iron atom per amino acid (**Figure 31.33**).

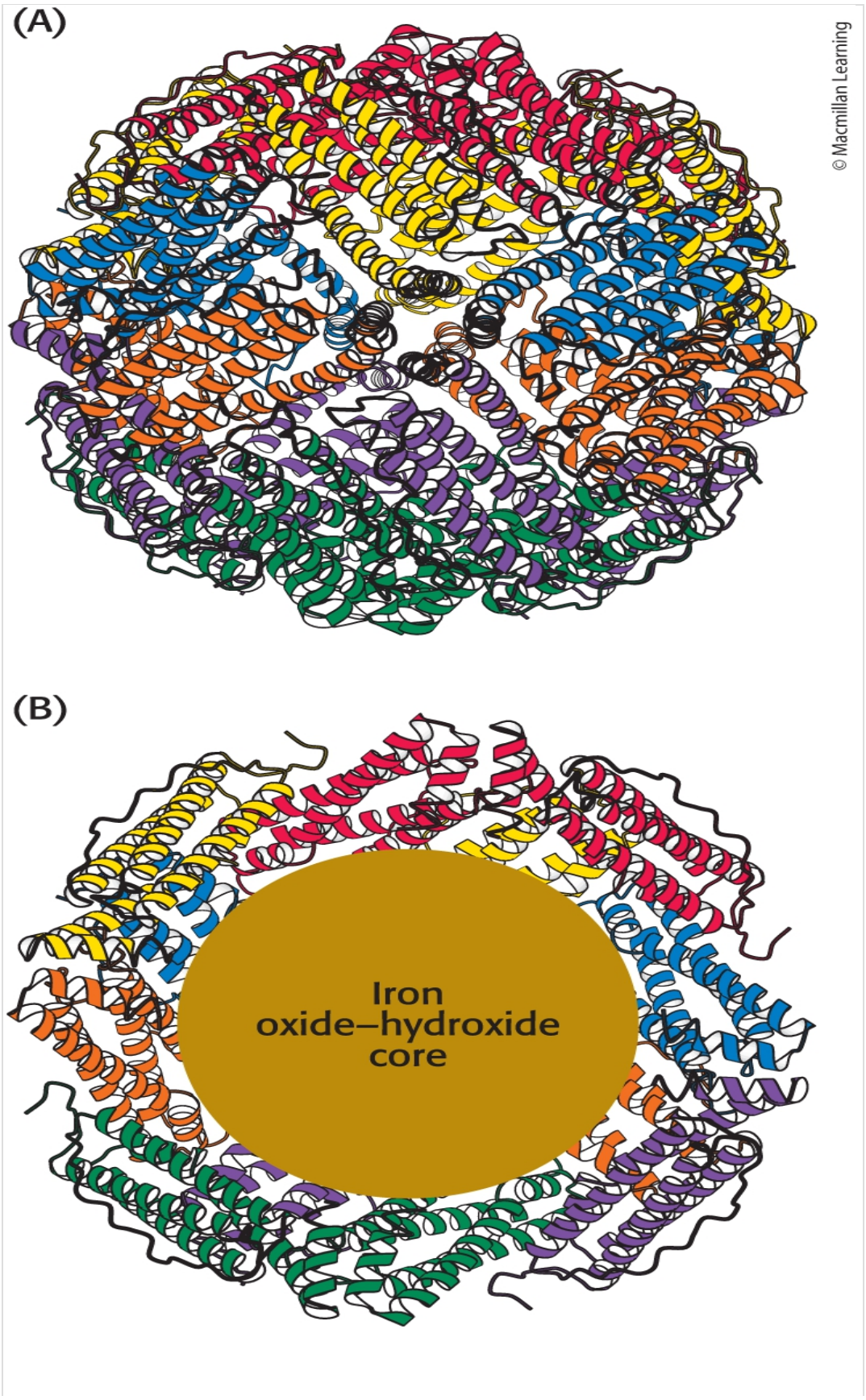

(A)
(B)
Iron
oxide–hydroxide
core
© Macmillan Learning

FIGURE 31.33 The structure of ferritin forms a sphere. (A) Twenty-four ferritin polypeptides form a nearly spherical shell. (B) A cutaway view reveals the core that stores iron as an iron oxide–hydroxide complex.

[Drawn from 1IES.pdb.]



Ferritin and transferrin receptor expression levels are reciprocally related in their responses to changes in iron levels. When iron is scarce, the amount of transferrin receptor increases and little or no new ferritin is synthesized. Interestingly, the extent of mRNA synthesis for these proteins does not change correspondingly. Instead, regulation takes place at the level of translation.

Consider ferritin first. Ferritin mRNA includes a stem-loop structure termed an *iron-response element* (IRE) in its $5'$ untranslated region (**Figure 31.34**). A 90 kDa protein, the IRE-binding protein (IRP), binds to this stem-loop and blocks the initiation of translation at the downstream coding region. When the iron level increases, the IRP binds iron as a 4Fe–4S cluster. The IRP bound to iron cannot bind RNA, because the binding sites for iron and RNA substantially overlap. Thus, in the presence of iron, ferritin mRNA is released from the IRP and translated to produce ferritin, which sequesters the excess iron.

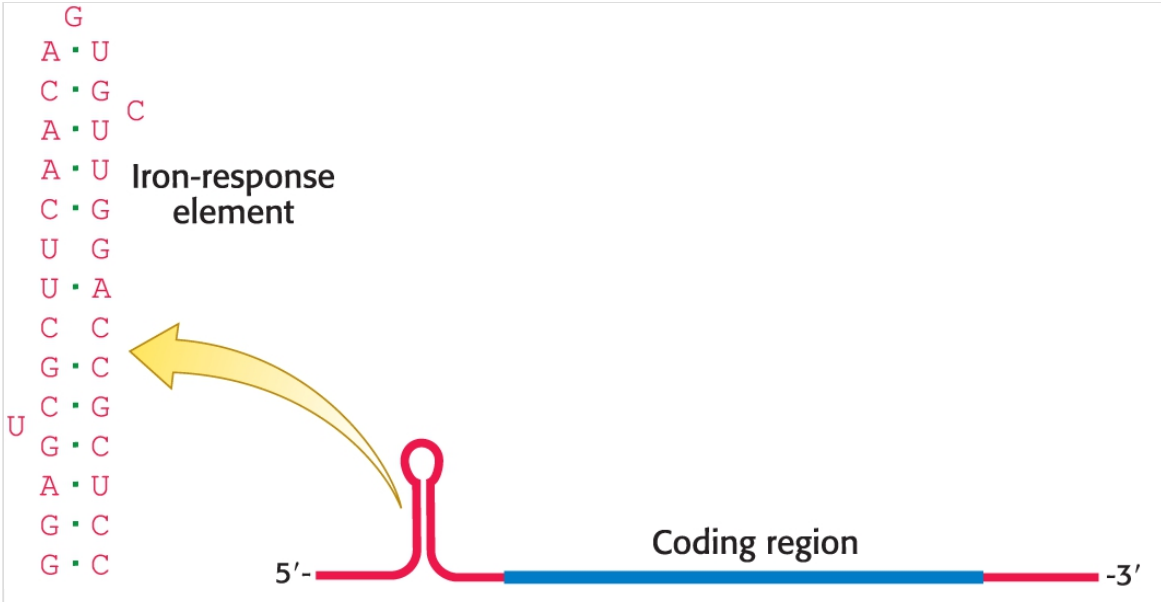


FIGURE 31.34 Ferritin mRNA includes an iron-response element in its 5′ untranslated region

A specific protein binds to the IRE stem-loop structure in the 5′ untranslated region of the mRN and blocks the translation of this mRNA under low-iron conditions.

An examination of the nucleotide sequence of transferrin receptor mRNA reveals the presence of several IRE-like regions. However, these regions are located in the 3′ untranslated region rather than in the 5′ untranslated region (Figure 31.35). Under low-iron conditions, IRP binds to these IREs. However, given the location of these binding sites, the transferrin receptor mRNA can still be translated.

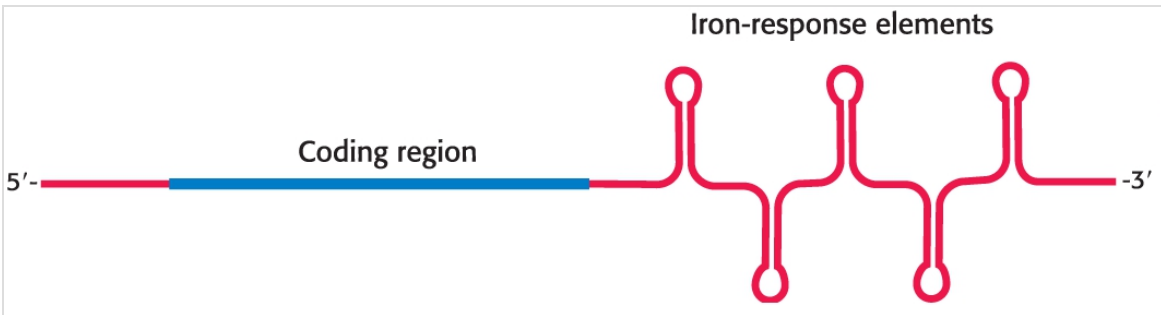


FIGURE 31.35 Transferrin receptor mRNA has a set of iron-response elements (IREs) in its 3′ untranslated region. The binding of the IRE-binding protein to these elements stabilizes the mRNA but does not interfere with translation.

What happens when the iron level increases and the IRP no longer binds transferrin receptor mRNA? Freed from the IRP, transferrin receptor mRNA is rapidly degraded. Thus, an increase in the cellular iron level leads to the destruction of transferrin receptor mRNA and, hence, a reduction in the production of transferrin receptor protein.

The purification of the IRP and the cloning of its cDNA were sources of truly remarkable insight into evolution. The IRP was found to be approximately 30% identical in amino acid sequence with the citric acid cycle enzyme aconitase from mitochondria. Further analysis revealed that the IRP is, in fact, an active aconitase enzyme; it is a cytoplasmic aconitase that had been known for a long time, but its function was not well understood (Figure 31.36). The iron–sulfur center at the active site of the IRP is rather unstable, and loss of the iron triggers significant changes in protein conformation. Thus, this protein can serve as an iron-sensing factor.

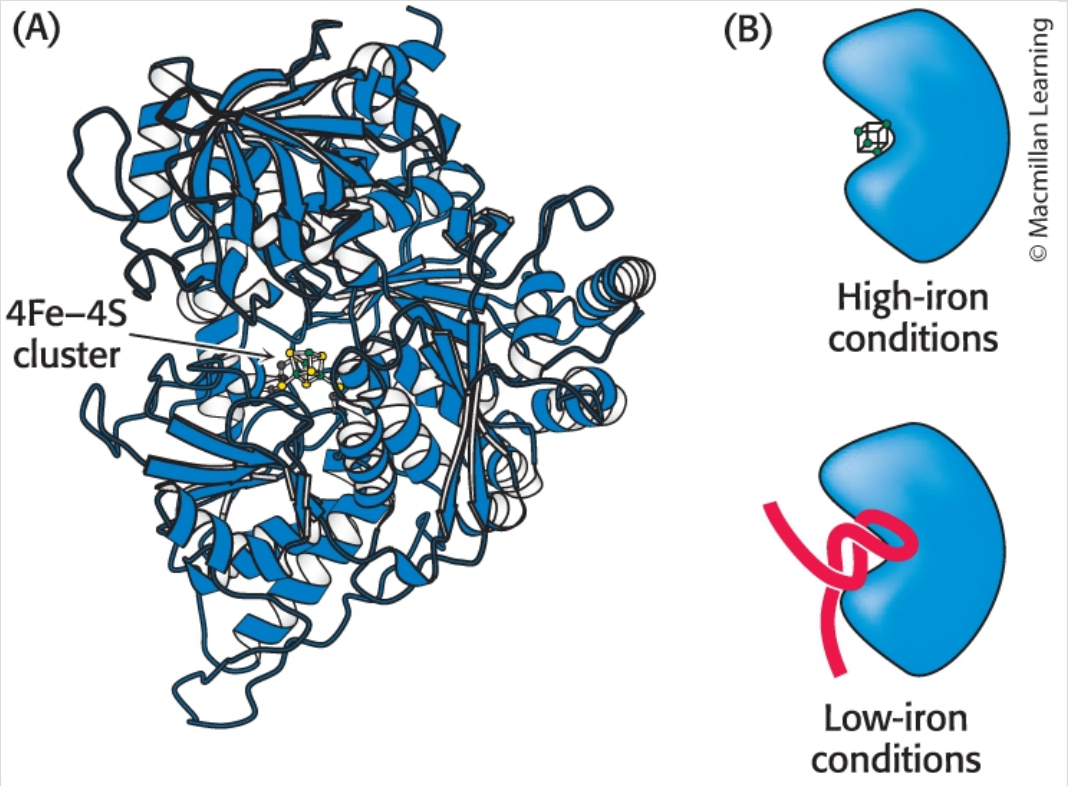


FIGURE 31.36 The IRP is an aconitase. (A) Aconitase contains an unstable 4Fe–4S cluster at its center. (B) Under conditions of low iron, the 4Fe–4S cluster dissociates and appropriate RNA molecules can bind in its place.

[Drawn from 1C96.pdb.]

INTERACT with this model in Achieve

Other mRNAs, including those taking part in heme synthesis, have been found to contain IREs. Thus, genes encoding proteins required for iron metabolism acquired sequences that, when transcribed, provided binding sites for the iron-sensing protein. An environmental signal — the concentration of iron — controls the translation of proteins required for the metabolism of this metal. Thus, mutations in the untranslated region of mRNAs have been selected for beneficial regulation by iron levels.

Small RNAs are involved in posttranscriptional gene regulation in eukaryotes

Other mechanisms of posttranscriptional gene regulation, particularly silencing, involve small regulatory RNAs, most of which were only recently discovered. These small RNAs represent an important class of gene-regulatory molecules.

One prominent mechanism of gene silencing is known as **RNA interference (RNAi)**, in which small RNAs interact with a protein complex and guide it to a target mRNA. Subsequently, the target mRNA will either be degraded or its translation will somehow be inhibited.

How was RNAi discovered? Genetic studies of development in *C. elegans* revealed that a gene called *lin-4* encodes an RNA molecule 61 nucleotides long that can regulate the expression of certain other genes. The 61-nucleotide *lin-4* RNA does not encode a protein, but rather is cleaved into a 22-nucleotide RNA that possesses the regulatory activity. This discovery was the first view of a large class of regulatory RNA molecules known as microRNAs (miRNAs), which were briefly introduced in Section 29.4. The key to the activity of microRNAs and their specificity for particular genes is their ability to form Watson–Crick base-pair-stabilized complexes with the mRNAs of those genes.

MicroRNAs do not function on their own, however. They bind to members of a highly conserved family of proteins called **Argonaute** (**Figure 31.37**). Argonaute–miRNA complexes bind target mRNAs due to sequence complementarity between the miRNA and the mRNA. Thus, the miRNAs serve as guide RNAs that determine the specifi-city of the Argonaute protein, which will cleave the target mRNA through its intrinsic RNase activity (**Figure 31.38**). Argonaute proteins form part of

a larger complex called the *RNA-induced silencing complex* (RISC), which is central to the process of RNAi.

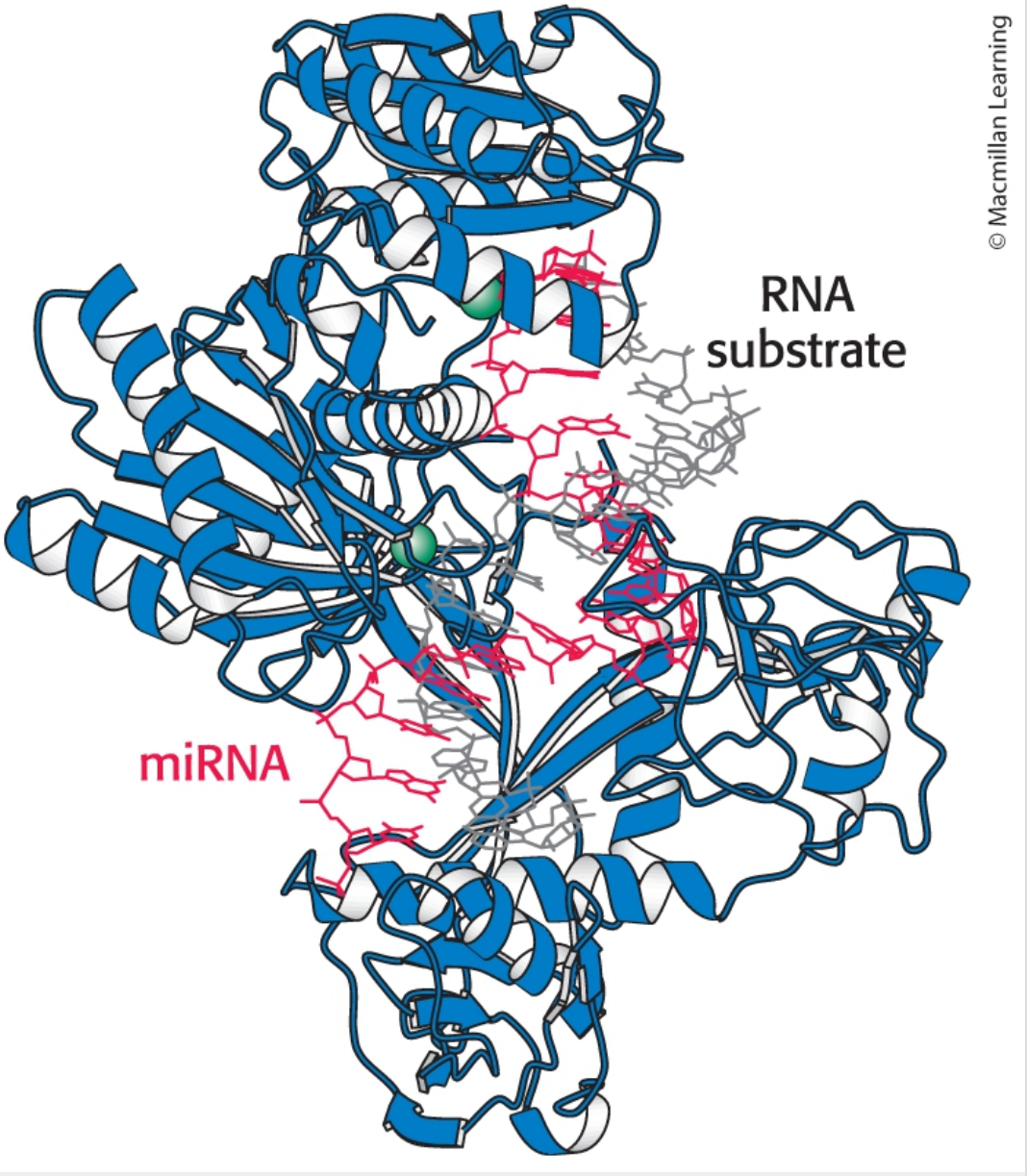


FIGURE 31.37 MicroRNAs bind to the Argonaute complex. The miRNA (shown in red) is bound by the Argonaute protein. The miRNA serves as a guide that binds the RNA substrate (shown in gray) through the formation of a double helix. Two magnesium ions are shown in green.

[Drawn from 3HK2.pdb.]

INTERACT with the above model in Achieve

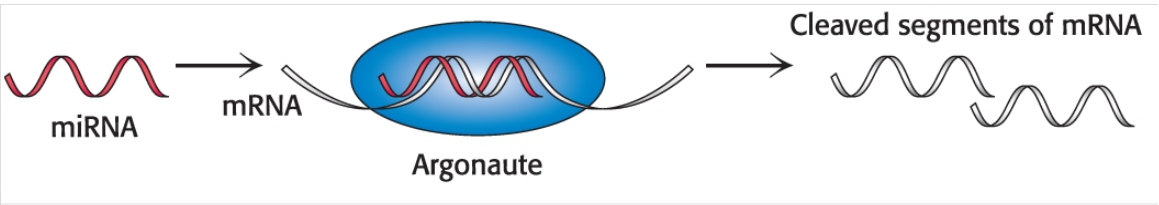


FIGURE 31.38 MicroRNA–Argonaute complexes target specific mRNA molecules for cleavage.

Interestingly, Argonaute proteins can bind to other types of small noncoding RNAs, including small interfering RNAs (siRNAs). Both siRNAs and miRNAs are generated through cleavage by an RNA endonuclease called *Dicer*, but they differ from each other in that they originate from different sources. MicroRNAs are generated from large, genetically encoded, single-stranded pri-microRNA precursors transcribed in the cell, as described in Figure 29.41. These miRNA precursors adopt a stem-loop structure which is cleaved and processed into mature miRNAs by Dicer. In contrast, siRNAs are derived from longer double-stranded extra-cellular RNAs, many of which might be invading viral sequences. It is also possible to produce siRNAs in vitro and introduce them into cells experimentally. This approach provides researchers with the opportunity to examine the phenotypic effects of controlled targeted gene silencing.

The occurrence of gene regulation by small noncoding RNAs was originally thought to be limited to a relatively small number of species. However, subsequent studies have revealed that this mode of gene regulation is nearly ubiquitous in eukaryotes. Indeed, more than 1900 miRNAs encoded by the human genome have been identified. Each miRNA can regulate many different genes because many different target

sequences are present in each mRNA. An estimated 60% of all human genes are regulated by one or more miRNAs.

As one example, consider the human miRNA called miR-206. This miRNA down-regulates the expression of one isoform of the estrogen receptor. In addition, it appears to down-regulate the expression of several different coactivators that interact with the estrogen receptor. Thus, this miRNA can mute the influence of estrogen by blocking the estrogen-initiated signaling pathway at several different steps.

The microRNA pathway has tremendous implications for the evolution of gene-regulatory pathways. Most of the target sites for miRNAs are present in the 3′-untranslated regions of mRNAs. These sequences are

quite free to mutate because they do not encode proteins and are not required to fold into any specific structures. Thus, in the context of a set of expressed miRNAs, mutations in this region of any particular gene could, in principle, increase or decrease the affinity for one or more miRNAs and, hence, alter the regulation of the gene.

Self-Check Question



Gene expression in all systems involves the conversion of information present in a genomic DNA sequence into a functional protein. Give general examples of the control of gene expression at different steps along this pathway.

Chapter 31 Summary

31.1 Bacterial DNA-Binding Proteins Bind to Specific Regulatory Sites

- In bacteria, specific DNA-binding proteins recognize regulatory sites that usually lie adjacent to the genes whose transcription is regulated by these proteins.
- The helix-turn-helix motif is a common DNA-binding motif.

31.2 In Bacteria, Genes Are Often Arranged into Clusters Under the Control of a Single Regulatory Sequence

- In bacteria, many genes are clustered into operons, which consist of control sites (an operator and a promoter) and a set of structural genes.
- Regulator genes encode proteins that interact with the operator and promoter sites in an operon to stimulate or inhibit transcription.
- The treatment of *E. coli* with lactose induces an increase in the production of β-galactosidase and two additional proteins that are encoded in the lactose operon.
- In the absence of lactose, the *lac* repressor protein binds to an operator site on the DNA and blocks transcription.
- The binding of allolactose, a derivative of lactose, to the *lac* repressor induces a conformational change that leads to dissociation from DNA. RNA polymerase can then move through the operator to transcribe the *lac* operon.
- The binding of the cAMP–CAP complex to a specific site in the promoter region of an inducible catabolic operon enhances the binding of RNA polymerase and the initiation of transcription.

31.3 Regulatory Circuits Can Result in Switching Between Patterns of Gene Expression

- Bacteriophage λ can maintain either a lytic or a lysogenic life cycle.
- A key regulatory protein, the λ repressor, regulates its own expression, promoting transcription of the gene that encodes the repressor when repressor levels are low and blocking transcription of the gene when levels are high.
- The Cro protein binds to the same sites as does the λ repressor, but with reversed affinities. When Cro is present at sufficient concentrations, it blocks the transcription of the gene for the λ repressor while allowing the transcription of its own gene.

31.4 Regulation of Gene Expression Is More Complex in Eukaryotes

- In eukaryotes, transcription factors are required to activate the expression of most genes. Transcription factors bind DNA and interact directly or indirectly with RNA polymerases.
- Eukaryotic transcription factors are modular: they consist of separate DNA-binding and activation domains.
- Important classes of DNA-binding domains include the homeodomains, the basic-leucine zipper proteins, and Cys_2His_2 zinc-finger proteins.
- Activation domains interact with RNA polymerases or their associated factors, or with other protein complexes such as mediator.
- Enhancers are DNA elements that can modulate gene expression from more than 1000 bp away from the start site of transcription.

31.5 The Control of Gene Expression in Eukaryotes Can Require Chromatin Remodeling

- Chromatin structure is crucial to the control of gene expression; it is more open and the DNA is less methylated near the

transcription start sites of actively transcribed genes.
- Steroids such as estrogens bind to eukaryotic transcription factors called nuclear hormone receptors. The binding of ligands to the receptors induces a conformational change that allows the recruitment of additional proteins called coactivators.
- Coactivators can catalyze the addition of acetyl groups to lysine residues in the tails of histone proteins. Histone acetylation decreases the affinity of the histones for DNA, making additional genes accessible for transcription.
- In addition, acetylated histones are targets for proteins containing specific binding units called bromodomains. Bromodomains are components of two classes of large complexes that open up sites on chromatin and initiate transcription.

31.6 Gene Expression Can Be Controlled at the Posttranscriptional Level

- In bacteria, many operons important in amino acid biosynthesis are regulated by attenuation, a process that depends on the formation of alternative structures in mRNA.
- In eukaryotes, genes encoding proteins that transport and store iron are regulated at the translational level.
- RNA interference (RNAi) is a common gene-silencing mechanism that involves small noncoding RNAs. These small regulatory RNAs function as guides to identify specific target mRNA molecules for cleavage by nucleases.

Key Terms

β-galactosidase
helix-turn-helix motif
operon

operator site
repressor
inducer
corepressor
catabolite repression
catabolite activator protein (CAP)
λ repressor
Cro
homeodomain
basic-leucine zipper (bZip) protein
Cys_2His_2 zinc-finger domain
DNA-binding domain
activation domain
mediator
CpG island
epigenetics
nuclear hormone receptor
coactivator
histone acetyltransferase (HAT)
bromodomain
TATA-box-binding protein associated factor (TAF)
chromatin-remodeling complex
histone deacetylase
attenuation
transferrin
transferrin receptor
ferritin
RNA interference (RNAi)
Argonaute

Problems

1. Predict the effects of deleting the following regions of DNA:

a. The gene encoding *lac* repressor
b. The *lac* operator
c. The gene encoding CAP 1, 3

2. The *lac* repressor and the *pur* repressor are homologous proteins with very similar three-dimensional structures, yet they have different effects on gene expression. Describe two important ways in which the gene-regulatory properties of these proteins differ. 2

3. Which types of mutation in the *lac* operon stop *E. coli* from using lactose as a carbon source? Select all that apply. 3

a. Operator deletion
b. Promoter deletion
c. Lactose-binding site mutation
d. Repressor DNA-binding site mutation

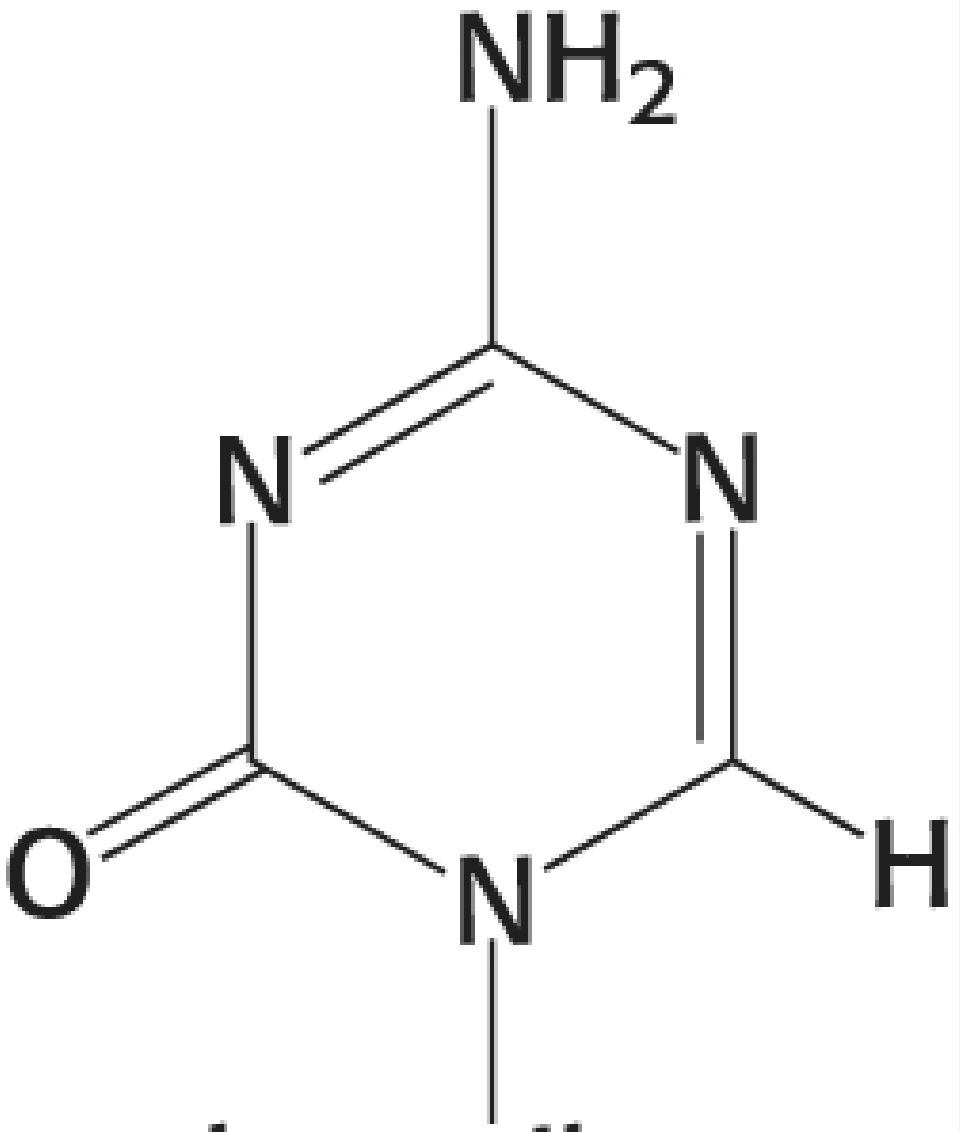
4. Consider a hypothetical mutation in O_R2 that blocks both λ repressor and Cro binding. How would this mutation affect the likelihood of bacteriophage λ entering the lytic phase? 4

5. Place the events of gene regulation by the *lac* operon in order of their occurrence, starting with the introduction of lactose into the environment, and ending with the cell digesting lactose. 3

a. The repressor is inactivated by allolactose.
b. RNA polymerase binds to the promoter region.
c. The repressor is removed from the operator.

d. The cell begins to digest lactose.
e. Lactose is introduced into the environment.
f. Lactose enzyme genes are expressed by the operon.

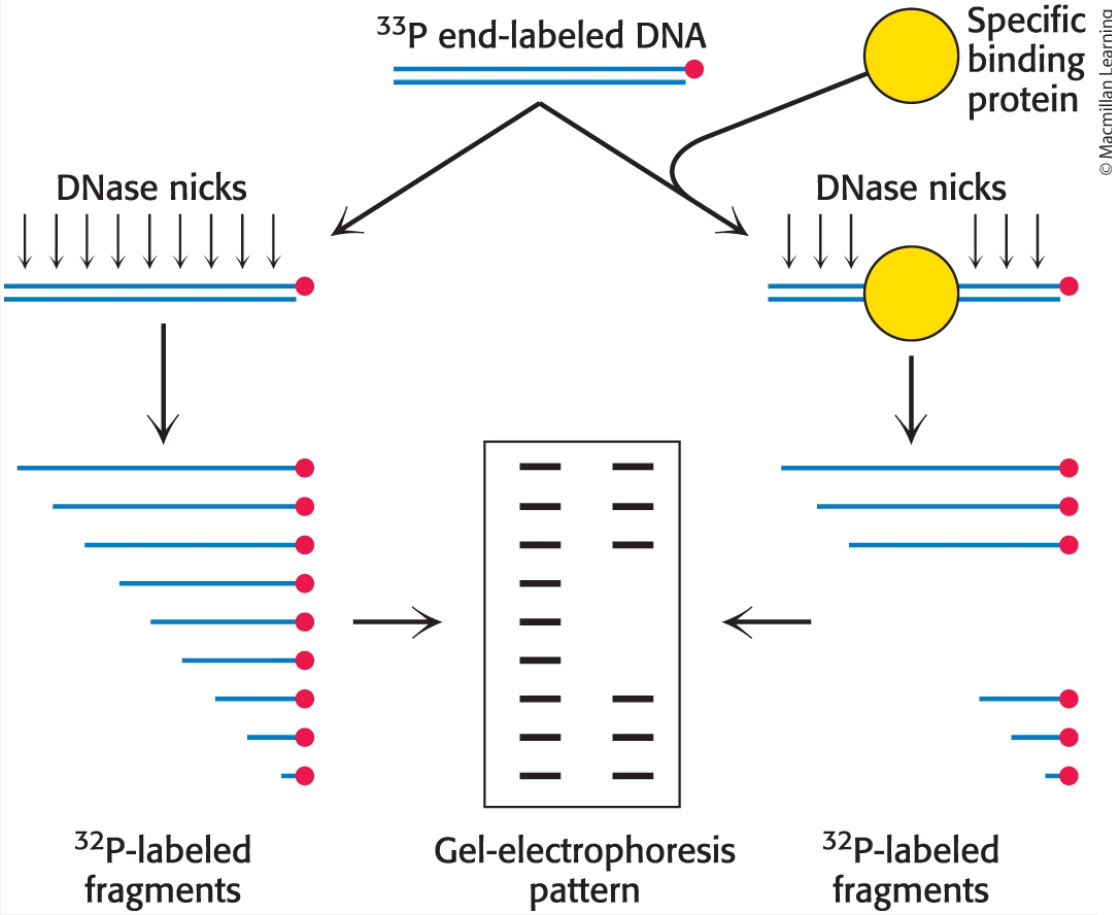
6. Growth of mammalian cells in the presence of 5-azacytidine results in the activation of some normally inactive genes. Propose an explanation.  5



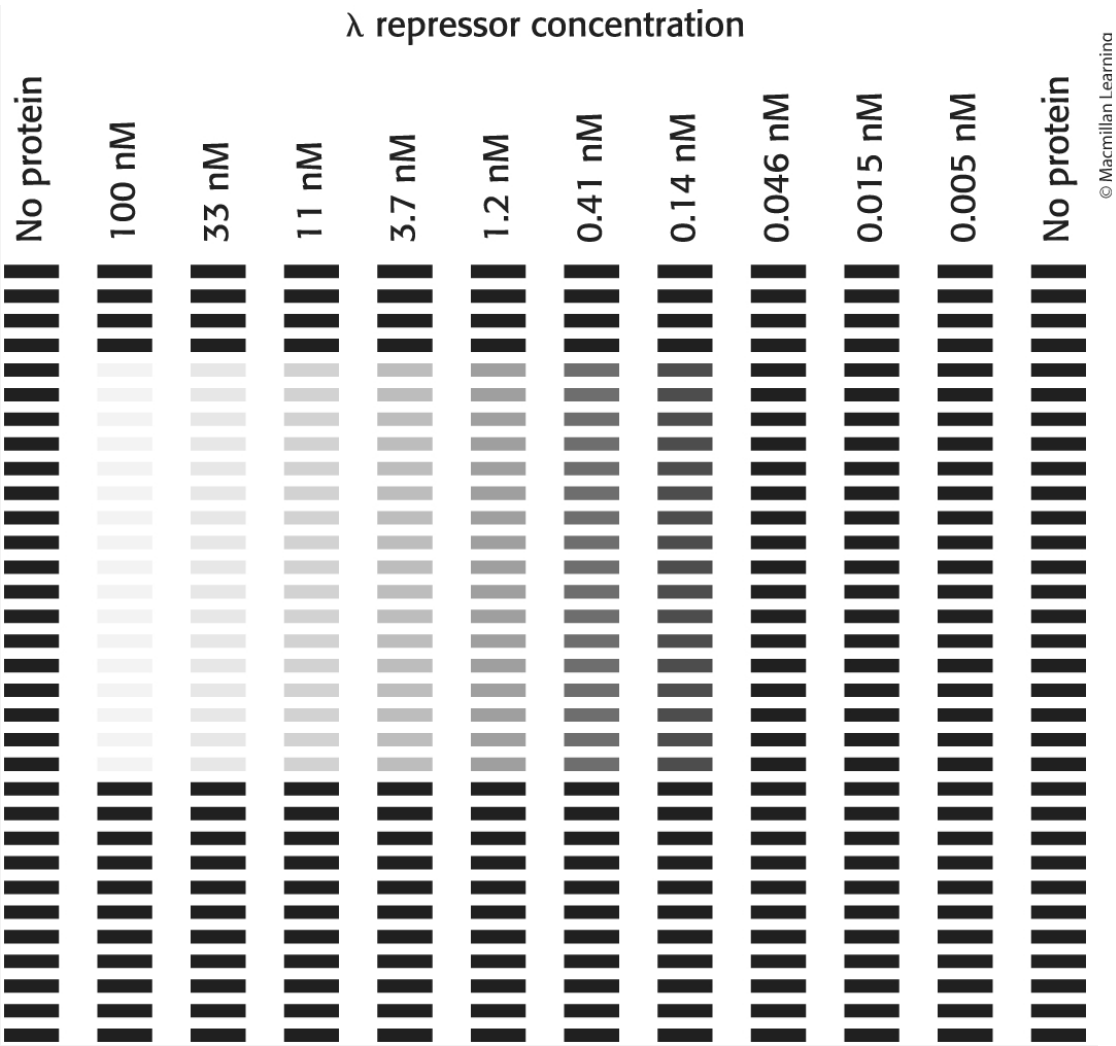
5-Azacytidine

7. What is the effect of an increased Cro concentration on the expression of the gene for the λ repressor? Of an increased concentration of λ repressor on the expression of the Cro gene? Of an increased concentration of λ repressor on the expression of the λ repressor gene? 1, 4

8. A powerful method for examining protein–DNA interactions is called *DNA footprinting*. In this method, a DNA fragment containing a potential binding site is radiolabeled on one end. The labeled DNA is then treated with a DNA-cleaving agent such as DNase I such that each DNA molecule within the population is cut only once. The same cleavage process is carried out in the presence of the DNA-binding protein. The bound protein protects some sites within the DNA from cleavage. The patterns of DNA fragments in the cleaved pool of DNA molecules are then examined by electrophoresis followed by autoradiography.



This method is applied to a DNA fragment containing a single binding site for the λ repressor in the presence of different concentrations of the λ repressor. The results are shown below:



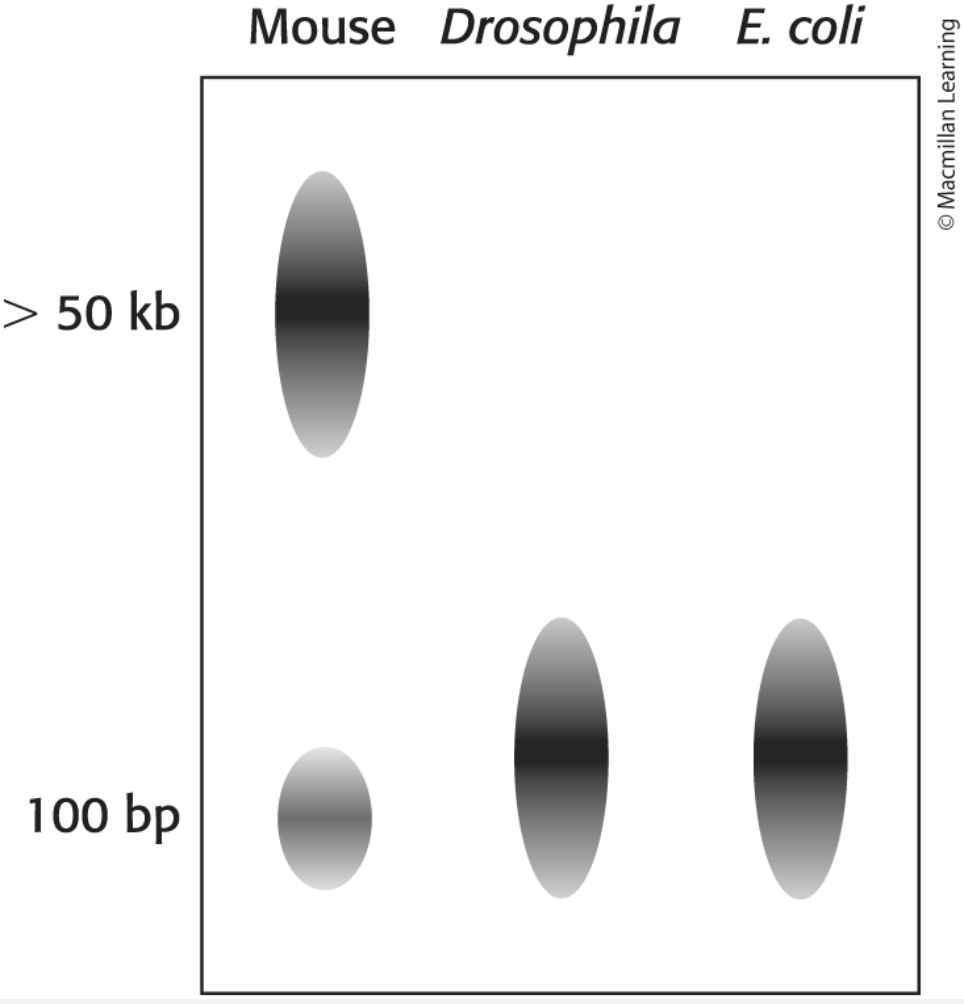
Estimate the dissociation constant for the λ repressor–DNA complex and the standard free energy of binding. 4

9. Which of the following statements about miRNAs and RNA interference are true? 7

a. miRNAs suppress gene expression by interfering with transcription.

b. Small RNAs interfere with gene expression by interacting with mRNA, bringing about mRNA degradation.
c. siRNAs and miRNAs are produced by the Dicer enzyme complex from various precursors.
d. miRNAs are about 45 nucleotides long.

10. The restriction enzyme HpaII is a powerful tool for analyzing DNA methylation. This enzyme cleaves sites of the form $5'-CCGG-3'$ but will not cleave such sites if the DNA is methylated on any of the cytosine residues. Genomic DNA from different organisms is treated with HpaII, and the results are analyzed by gel electrophoresis (see below). Provide an explanation for the observed patterns. 5



11. Which of the following statements are true? (Select all that apply.) 6

a. Chromatin packaging occurs in eukaryotes.
b. The structure of adenine is different in eukaryotic DNA compared with prokaryotic DNA.
c. Eukaryotic DNA contains enhancers.
d. Multiple general transcription factors are found in eukaryotes.
e. Nuclear export of RNA occurs in bacteria.

12. A protein domain that recognizes 5-methylcytosine in the context of double-stranded DNA has been characterized. What role might proteins containing such a domain play in regulating gene expression? Where on a double-stranded DNA molecule would you expect such a domain to bind? 1, 2

13. What is the effect of acetylation of a lysine residue on the charge of a histone protein? Of lysine methylation? 5

14. Place the events in the order necessary for an epigenetic modification to be inherited in the next generation, starting with methylated CpG sites present on one inherited DNA strand, and ending with the epigenetic silencing being passed to the offspring. 5

a. A methyl group is added to the cytosine residue of the DNA sequence.
b. Certain CpG methylation sites are not erased during gametogenesis or embryogenesis.
c. Epigenetic silencing is passed to the offspring.

d. Methylated CpG sites are present on one inherited DNA strand.
e. DNA methyltransferase maintains the methylation pattern on both DNA strands.
f. DNA methyltransferase recognizes and binds CpG sites on DNA.

15. Through recombinant DNA methods, a modified steroid hormone receptor was prepared that consists of an estrogen receptor with its ligand-binding domain replaced by the ligand-binding domain from the progesterone receptor. Predict the expected responsiveness of gene expression for cells treated with estrogen or with progesterone. 1

16. What effect would you expect from the addition of an IRE to the $5'$ end of a gene that is not normally regulated by iron levels? To the $3'$ end? 7

17. The following is the amino acid sequence of a eukaryotic transcription factor that belongs to one of the three structural classes discussed in Section 31.4. Identify the class. 2

HTCDYAGCGKTYTKSSHLKAHLRTHTGEKPYHCDWDGC GWKFARSDELTRHYRKHTGHRPFQCQKCDRAFSRSDHL ALHMKRHF

18. Modifications to chromatin can affect transcriptional activity by changing the accessibility of DNA to the transcription machinery. The given descriptions are examples of various processes that cause remodeling of chromatin. Match each description to the effect it has on transcriptional activity. 5

Chromatin modification description	Effect on transcriptional activity via chromatin

	remodeling
1. Histone methylation occurs at different amino acids. 2. Histone acetyltransferases attach acetyl groups to the N-terminus of histones. 3. Methylated CpG regions are found close to transcription start sites.	1. Activates 2. Inactivates 3. Activates and inactivates

19. Nuclear hormone receptors form a complex with their ligands, other proteins, and DNA control elements in order to regulate the expression of specific genes. Match each nuclear hormone receptor domain to the characteristic(s) with which it is associated. 2

Nuclear hormone receptor domain	Characteristic
1. Activation domain 2. DNA-binding domain 3. Ligand-binding domain	1. Zinc-finger domain 2. Binds coactivators 3. Center of the receptor 4. Carboxyl-terminal end 5. Steroid-binding hydrophobic pocket

20. Classify the following examples of gene expression as positive or negative regulation. 6

a. In the presence of lactose and low glucose, the *lac* operon is expressed 20-fold higher than in the absence of lactose.
b. In the absence of lactose, the *lac* repressor binds to the *lac* operator.
c. Low levels of tryptophan in *E. coli* result in the production of the full-length *trp* mRNA.
d. Elevated iron levels in eukaryotes prevent the IRP from binding to the transferrin receptor mRNA, allowing it to be translated.
e. miRNAs direct the Argonaute nuclease to a target mRNA.

Chapter 32
Principles of Drug Discovery and Development



Many drugs are based on natural products. Paclitaxel (marketed as Taxol) is a molecule isolated from the bark of the Pacific yew tree (*Taxus brevifolia*) that potently inhibits cell division and is used to treat various forms of cancer. Recently, methods have been developed to synthesize paclitaxel without destruction of the Pacific yew, significantly reducing the ecological impact of drug preparation.

Outline

32.1 Drug Discovery Begins with Target Identification and Validation
32.2 Lead Molecules Can Be Discovered in Many Ways
32.3 Compounds Must Meet Stringent Criteria to Be Developed into Drugs
32.4 Biologics are a Growing Family of Drugs

32.5 The Clinical Development of Medicines Proceeds Through Several Phases

---

Learning Goals



By the end of this chapter, you should be able to:

1. Describe the importance of target validation and tractability in the early drug discovery process.
2. List some ways in which lead molecules are identified.
3. Explain the criteria the compounds must meet in order to be developed into drugs.
4. Describe the processes by which the body interacts with drug molecules.
5. Describe how structural information can be used to assist in drug development.
6. Differentiate small molecule drugs and biologics.
7. Distinguish the clinical phases of drug development.

The development of drugs is among the most important interfaces between biochemistry and medicine. In most cases, drugs act by binding to proteins and inhibiting or otherwise modulating their activities. An effective drug is much more than a potent modulator of its target, however. Drugs must be readily administered to patients and must persist within the body long enough to reach their targets. Furthermore, to prevent unwanted physiological effects, drugs must not modulate the properties of biomolecules other than the intended targets. These requirements tremendously limit the number of compounds that have the potential to be clinically useful drugs.

32.1 Drug Discovery Begins with Target Identification and Validation

In this chapter, we will explore the science of **pharmacology**, which encompasses the discovery, chemistry, composition, identification, biological and physiological effects, uses, and manufacture of drugs. The journey from knowledge of a biochemical pathway to a clinically approved medicine is long, laborious, and expensive. This process is typically divided into two phases (Figure 32.1). In the **discovery phase**, molecules with the desired physiological effects are identified and optimized such that they can be introduced into humans; in the **development phase**, clinical trials are conducted with the optimal candidate molecule. Each of these phases is subdivided into stages. At the transition point from one stage to the next, the data are evaluated and a decision is made to approve the investment required to progress into the next stage.

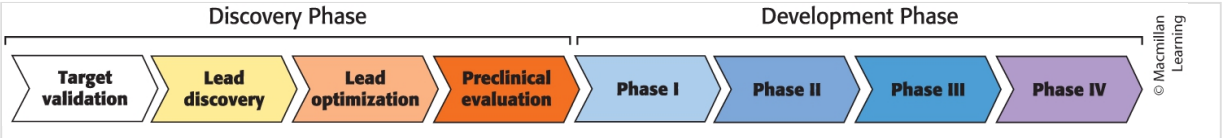


FIGURE 32.1 The journey to an approved drug is divided into a discovery phase and a development phase. Each phase is subdivided into stages. At the end of each stage, the data obtained up to that point are evaluated, and a decision is made on whether to progress to the next step.

Drug targets must be validated and tractable

The initial steps of the discovery phase first require the identification of a **target** — a protein or an oligonucleotide whose activity, when

modulated by a drug, will alter the progression of a human disease process. Throughout the previous chapters in this book, we have encountered a number of types of proteins — enzymes, receptors, and transporters — that serve as targets for a majority of the drugs in clinical use (**Figure 32.2**). Before embarking on the process of developing a drug against a particular target, researchers must first establish confidence that the target exhibits two critical properties.

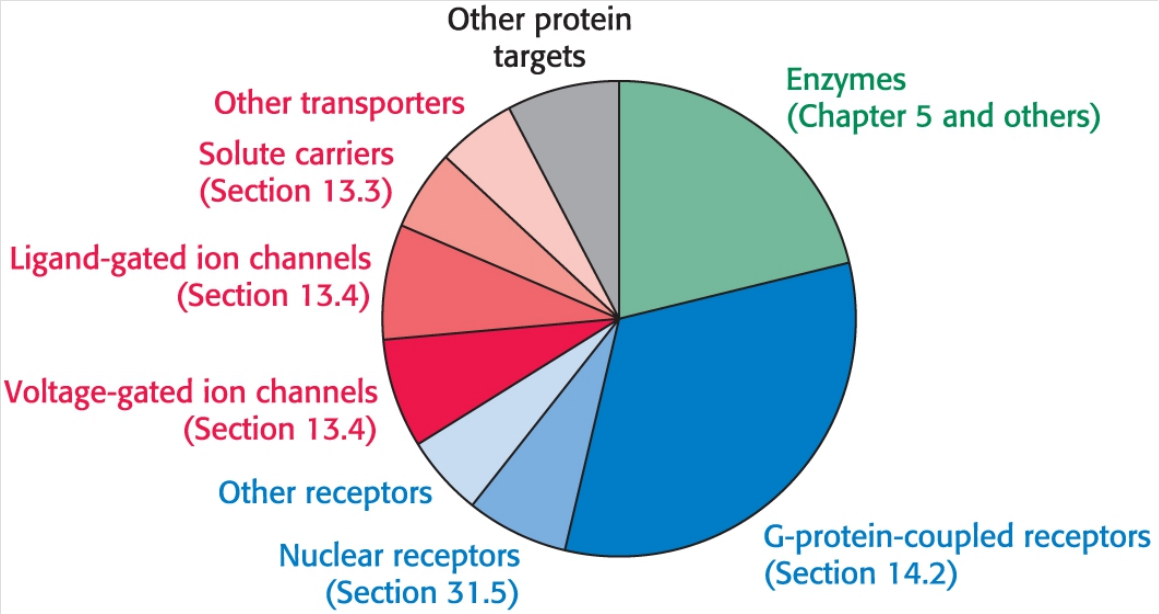


FIGURE 32.2 Drug targets span a variety of protein classes. In this pie chart, currently used drugs that modulate human proteins are sorted by target type: enzymes in green, receptors in blue, transporters in red, and other targets in gray.

[Data from M. Rask-Andersen et al., *Nat. Rev. Drug Discov.* 10:579–590, 2011.]

There should be sufficient evidence that the target plays an important role in disease progression in humans. The process of obtaining this evidence is referred to as **target validation**. Researchers achieve validation of a target from a variety of experiments, such as human genetic analyses, RNA interference, or transgenic or knockout animal models (Section 9.4); they may also conduct studies with *tool compounds* — molecules

that are usable in cellular or animal experiments but not necessarily suitable as drugs for humans.

There should be sufficient evidence that a molecule can be designed to interact with the target in a potent and specific manner. This property is referred to as a drug's **tractability**, or **druggability**. Assessment of target tractability is made significantly easier if the structure of the target, or a closely related protein, is known. A tractable target contains structural features, such as ligand-binding pockets, with which drug-like molecules can interact with a high degree of potency and specificity.

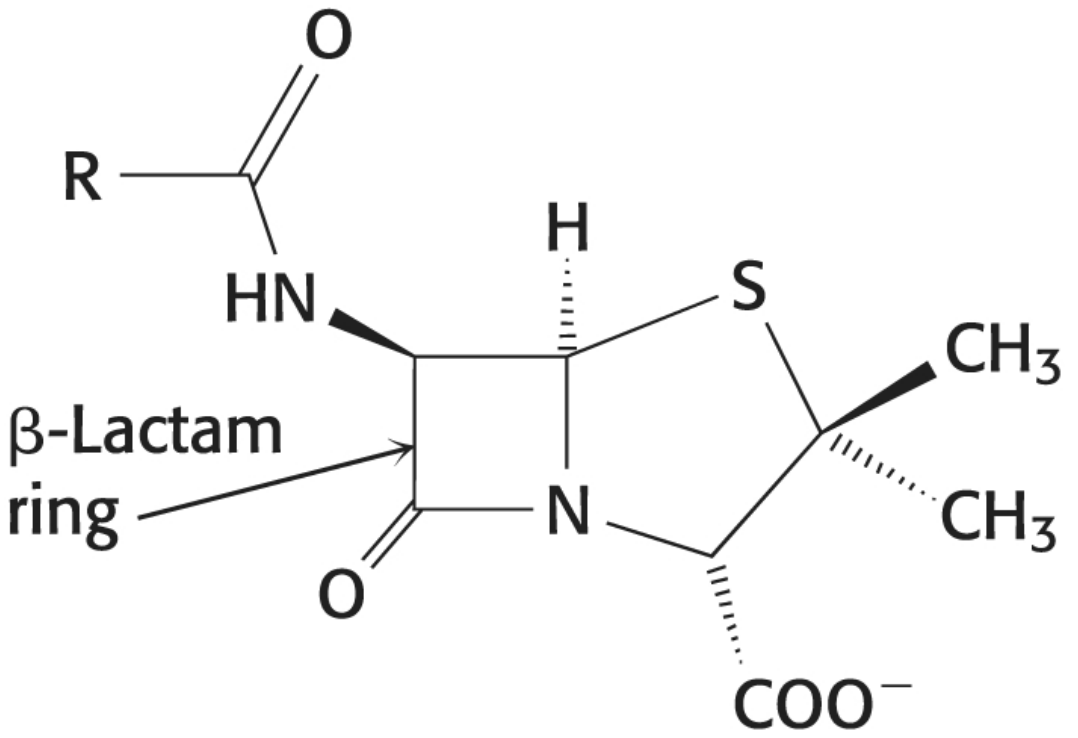
In practice, very few targets are known to be well-validated and highly tractable during the early stages of the discovery phase. As the target proceeds through the further investigation, additional data are obtained that either support or refute initial projections of the target's validation and tractability. One of the primary goals of the pharmaceutical scientist is to design experiments which can provide this information as early as possible. If the data do not lend support for a particular target, it can be abandoned in favor of more attractive targets.

Serendipitous observations can drive drug development



One cannot recount the history of drug discovery without acknowledging the role played by serendipity, or chance observations. Perhaps the most well-known example is Alexander Fleming's observation in 1928 that colonies of the bacterium *Staphylococcus aureus* died when they were adjacent to colonies of the mold *Penicillium notatum*, after spores of the mold had landed accidentally on plates growing the bacteria. Fleming determined that the mold produced a

substance that could kill disease-causing bacteria. This discovery led to a fundamentally new approach to the treatment of bacterial infections. Howard Florey and Ernest Chain developed a powdered form of the substance, termed penicillin, that became a widely used antibiotic in the 1940s. When the structure of penicillin was elucidated in 1945, it was found to contain a four-membered β-lactam ring. This unusual feature is key to the antibacterial function of penicillin, as noted in Section 5.6.



Penicillin

Three steps were crucial to fully capitalize on Fleming's discovery. First, an industrial process was developed for the production of penicillin from *Penicillium* mold on a large scale. Second, penicillin and its derivatives were chemically synthesized. The availability of synthetic penicillin derivatives opened the way for scientists to explore the

relationship between structure and function. Finally, in 1965, Jack Strominger and James Park independently determined that penicillin exerts its antibiotic activity by blocking a critical transpeptidase reaction in bacterial cell-wall biosynthesis (Figure 32.3). Many penicillin derivatives remain widely used today.

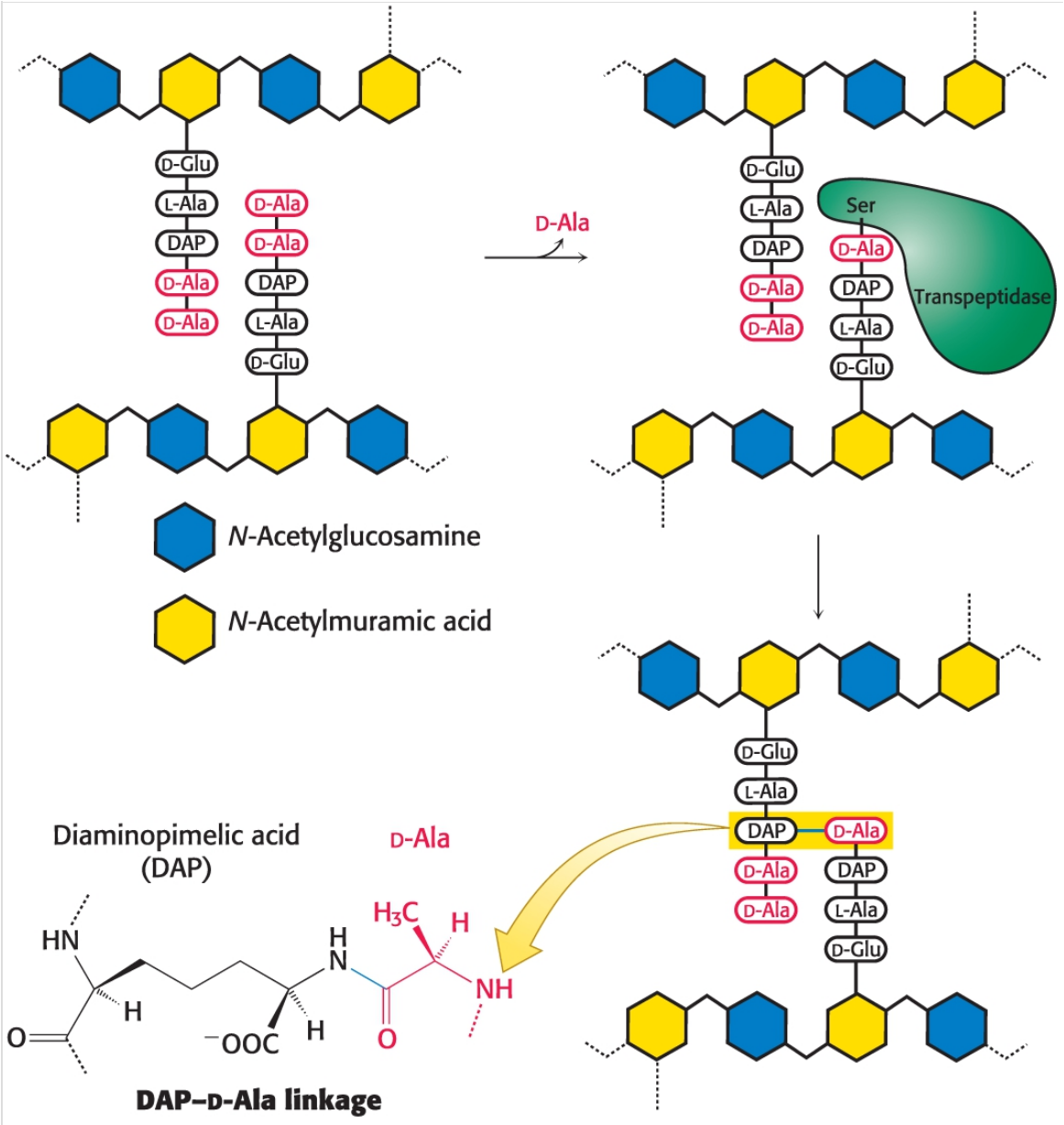


FIGURE 32.3 Penicillin disrupts the biosynthesis of the bacterial cell wall. A transpeptidase enzyme catalyzes the formation of cross-links between peptidoglycan groups. In the case show the transpeptidase catalyzes the linkage of D-alanine at the end of one peptide chain to the amino acid diaminopimelic acid (DAP) on another peptide chain. The diaminopimelic acid linkage (bottom left) is found in Gram-negative bacteria such as *E. coli.* Linkages of glycine-rich

peptides are found in Gram-positive bacteria. Penicillin inhibits the action of the transpeptidase so bacteria exposed to the drug have weak cell walls that are susceptible to lysis.

A more recent example of a drug discovered by serendipity is sildenafil. This compound was developed as an inhibitor of phosphodiesterase 5 (PDE5), an enzyme that catalyzes the hydrolysis of cGMP to GMP (Figure 32.4). The compound was intended as a treatment for hypertension and angina because cGMP plays a central role in the relaxation of smooth-muscle cells in blood vessels (Figure 32.5). The inhibition of PDE5 was expected to increase the concentration of cGMP by blocking the pathway for its degradation. In the course of early clinical trials in Wales, some men reported unusual penile erections, but whether this chance observation by a few men was due to the compound or to other effects was unclear. However, the observation made some biochemical sense because smooth-muscle relaxation due to increased cGMP levels had been previously discovered to play a role in penile erection.

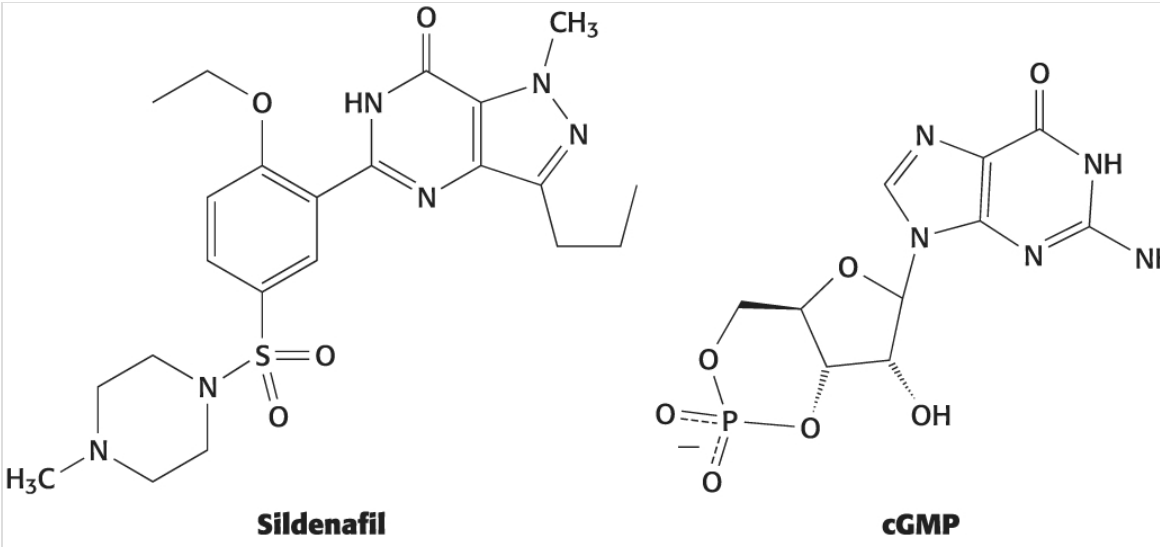


FIGURE 32.4 Sildenafil was designed to resemble cGMP, the substrate of phosphodiesterase 5 (PDE5).

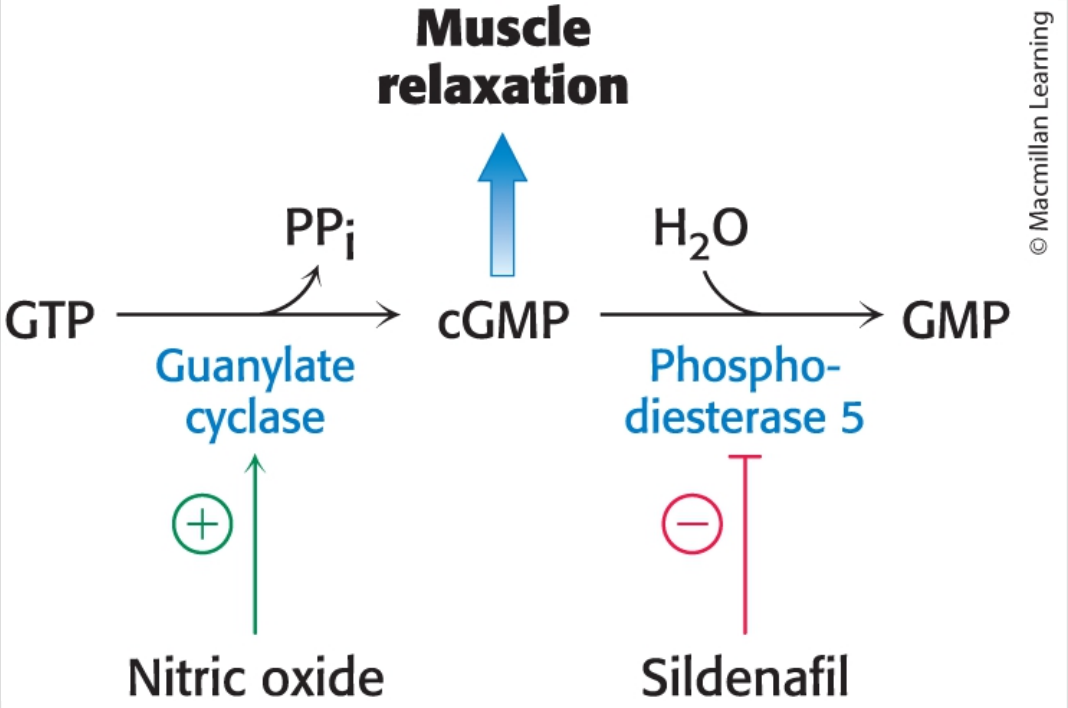


FIGURE 32.5 cGMP stimulates muscle relaxation. Increases in nitric oxide levels stimulate guanylate cyclase, which produces cGMP. PDE5 hydrolyzes cGMP, which lowers the cGMP concentration. The inhibition of PDE5 by sildenafil maintains elevated levels of cGMP.

Subsequent clinical trials directed toward the evaluation of sildenafil for erectile dysfunction were successful. This account testifies to the importance of collecting comprehensive information from clinical-trial participants. In this case, incidental observations led to a new treatment for erectile dysfunction and a multibillion-dollar-per-year drug market.

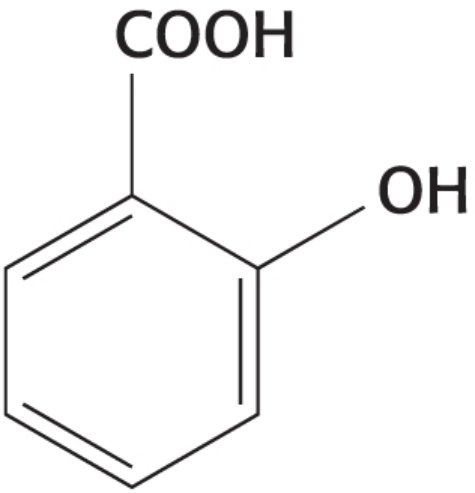
32.2 Lead Molecules Can Be Discovered in Many Ways

Once a target has been selected, molecules which interact with the target and impact its activity must be identified. Initial drug-like molecules, also called **lead molecules** or **leads**, are the starting points for optimization into drug candidates that can be tested in humans. How are lead molecules identified? As we have seen, there are many examples where drugs were discovered by serendipity, or chance observation. Despite these successes, scientists have sought more reliable methods for lead identification. More recently, leads have been discovered by screening collections of natural products or large compound libraries for molecules that have desired biochemical properties. We will examine several examples of each of these pathways to reveal common principles.

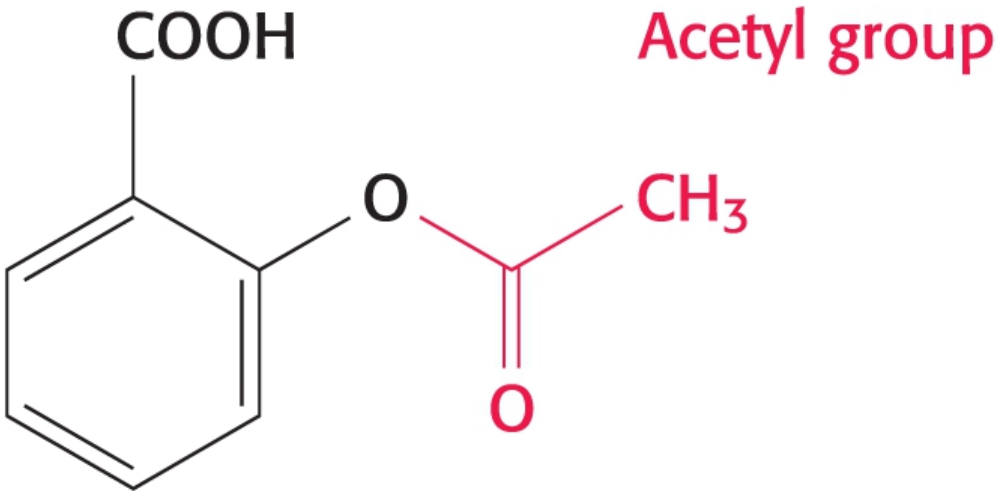
Natural products are a valuable source of lead molecules

No drug is as widely used as aspirin. Observers at least as far back as Hippocrates (~400 B.C.E.) have noted the use of extracts from the bark and leaves of the willow tree for pain relief. In 1829, a mixture called *salicin* was isolated from willow bark, and subsequent analysis identified salicylic acid as the active component. Although it was used to treat pain, salicyclic acid often irritated the stomach. Several investigators attempted to find a means to neutralize salicylic acid. Felix Hoffmann, a chemist working at the German company Bayer, developed a less irritating derivative by treating salicylic acid with a base and acetyl chloride. This derivative, acetylsalicylic acid, was named *aspirin* from “a” for acetyl chloride, “spir” for *Spiraea ulmaria* (meadowsweet, a flowering plant that also contains salicylic acid), and “in” (a common

ending for drugs). Each year, approximately 35,000 tons of aspirin (nearly the weight of the *Titanic*) are taken worldwide.



Salicylic acid



Aspirin (acetylsalicylic acid)

As discussed in Section 12.4, the acetyl group in aspirin is transferred to the side chain of a serine residue that lines the hydrophobic channel from the membrane to the active site of the cyclooxygenase component of prostaglandin H_2 synthase (Figure 12.24). In this position, the acetyl

group blocks access to the active site. Thus, even though aspirin binds in the same pocket on the enzyme as salicylic acid, the acetyl group of aspirin dramatically increases its effectiveness as a drug. This account illustrates the value of screening extracts from plants and other materials that are believed to have medicinal properties for active compounds. The large number of herbal and folk medicines are a treasure trove of new drug leads.

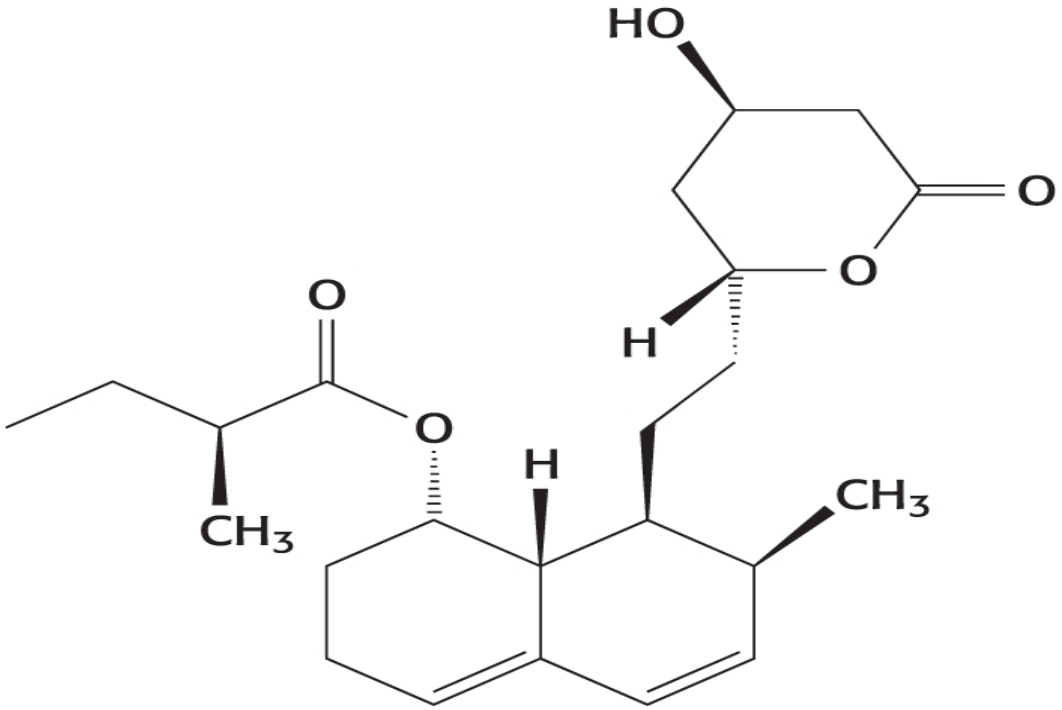
Let us consider another example, which has also had a significant impact on the clinical management of individuals with cardiovascular disease. More than 100 years ago, a fatty, yellowish material was discovered on the arterial walls of patients who had died of vascular disease. The presence of the material was termed *atheroma* from the Greek word for porridge. This material proved to be cholesterol. The Framingham Heart Study, initiated in 1948, documented a correlation between high blood-cholesterol levels and high mortality rates from heart disease. This observation led to the notion that blocking cholesterol synthesis might lower blood-cholesterol levels and, in turn, lower the risk of heart disease.

Initial attempts at blocking cholesterol synthesis focused on targets near the end of the pathway. However, these efforts were abandoned because the accumulation of the insoluble substrate for the inhibited enzyme led to the development of cataracts and other side effects. Investigators eventually identified a more favorable target — namely, the enzyme HMG-CoA reductase (Section 27.2). This enzyme acts on a substrate, HMG-CoA (3-hydroxy-3-methylglutaryl coenzyme A), that does not accumulate, because it is water-soluble and can be utilized by other pathways.

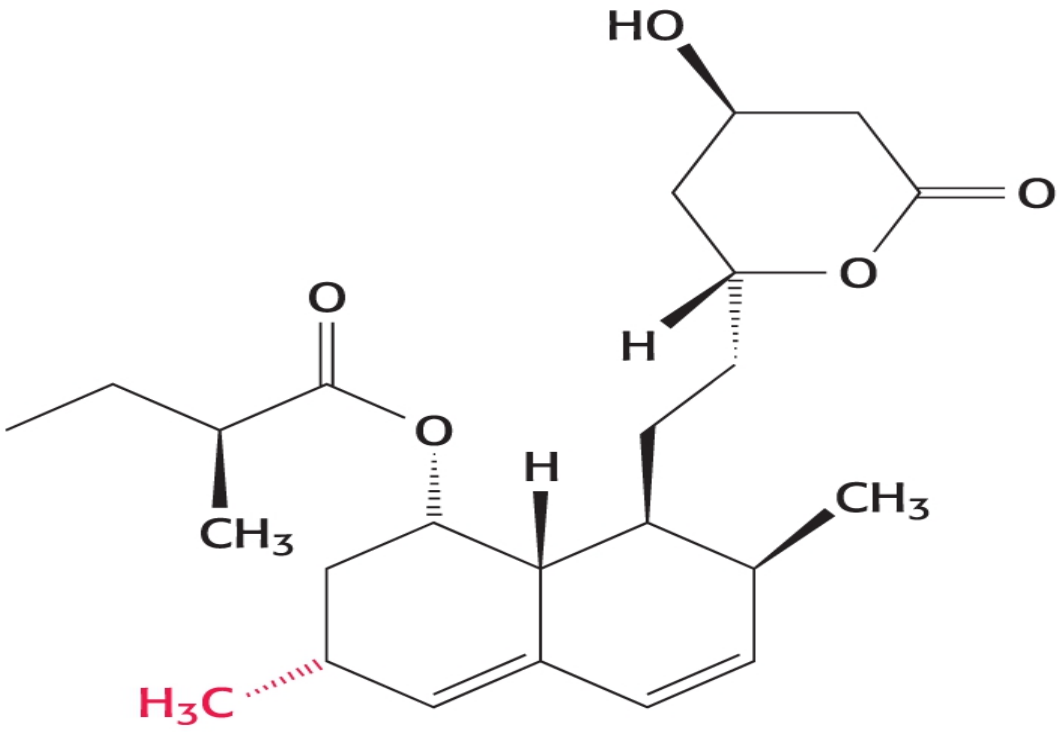


A promising natural product, called *compactin*, was discovered in a screen of compounds from a fermentation broth from *Penicillium citrinum* in a search for antibacterial agents. In some animal studies, compactin was found to inhibit HMG-CoA reductase and to lower serum

cholesterol levels. In 1982, a new HMG-CoA reductase inhibitor was discovered in a fermentation broth from another mold, *Aspergillus terreus*. This compound, now called *lovastatin*, was found to be structurally very similar to compactin, bearing one additional methyl group. After many studies, the Food and Drug Administration (FDA) approved lovastatin for treating high serum cholesterol levels. A structurally related HMG-CoA reductase inhibitor was later shown to cause a statistically significant decrease in deaths due to coronary heart disease, validating the clinical benefits of lowering serum cholesterol levels.



Compactin

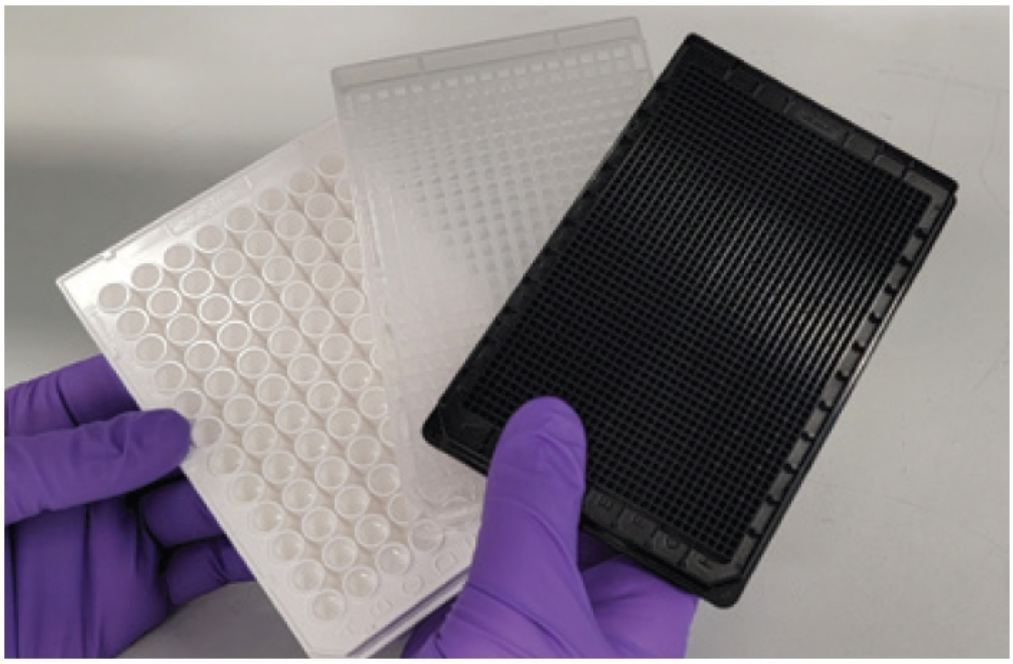


Lovastatin

High-throughput screening expands the opportunity for lead identification

Drug developers can screen large libraries of either natural products or purely synthetic compounds to identify lead molecules with desired activities. Under favorable circumstances, millions of compounds can be tested in this process, termed **high-throughput screening (HTS)**.

The success of a high-throughput screen depends on the development of a robust and sensitive assay. Earlier, we introduced the necessity of a specific assay to assess the progress of a protein purification scheme (Section 4.1). A similar assay is needed to rapidly and sensitively detect molecules that have a desired activity such as the ability to inhibit an enzyme or block an ion channel. Since a high-throughput screen will assess a large number of compounds, screening assays are typically run in very small volumes (usually between 1 and 100 µl) in microtiter plates that contain hundreds, if not thousands, of wells (**Figure 32.6**). Additionally, screening is often conducted using automation equipment to handle the repetitive workload and ensure precise timing.



Gregory J. Gatto, Jr.

FIGURE 32.6 High-throughput screens are conducted in microtiter plates. Shown here are plates that contain 96, 384, and 1536 wells. As the number of wells increases, the maximum volume that each well can hold is reduced.

To achieve the required level of assay sensitivity, methods that rely on fluorescence or luminescence detection are often employed. While numerous methods are available, let us consider one approach to introduce a sensitive detection method into an enzyme assay. Recall the reaction of a protein kinase (Section 7.3), an enzyme which uses ATP to attach phosphoryl groups to the side chains of serine, threonine, or tyrosine residues.

$$\text{Protein-OH} + \text{ATP} \xrightleftharpoons{\text{Protein kinase}} \text{Protein-OPO}_3^{2-} + \text{ADP}$$

Neither the substrates (ATP or the unphosphorylated protein) nor the products (ADP or the phosphorylated protein) of this reaction are inherently fluorescent. However, by including additional enzymes (pyruvate kinase, pyruvate oxidase, and peroxidase) and the necessary substrates in the reaction, the production of ADP by the kinase can be coupled to the generation of the fluorescent dye resorufin (**Figure 32.7**). The successive actions of multiple enzymes to detect a reaction product is referred to as a **coupled assay**. Such assays can be quite effective for use in high-throughput screening. Follow-up assays, also called *secondary assays*, must be run on any hits from a coupled assay screen to ensure that the hits are not blocking the activity of the coupling enzymes, rather than the target kinase.

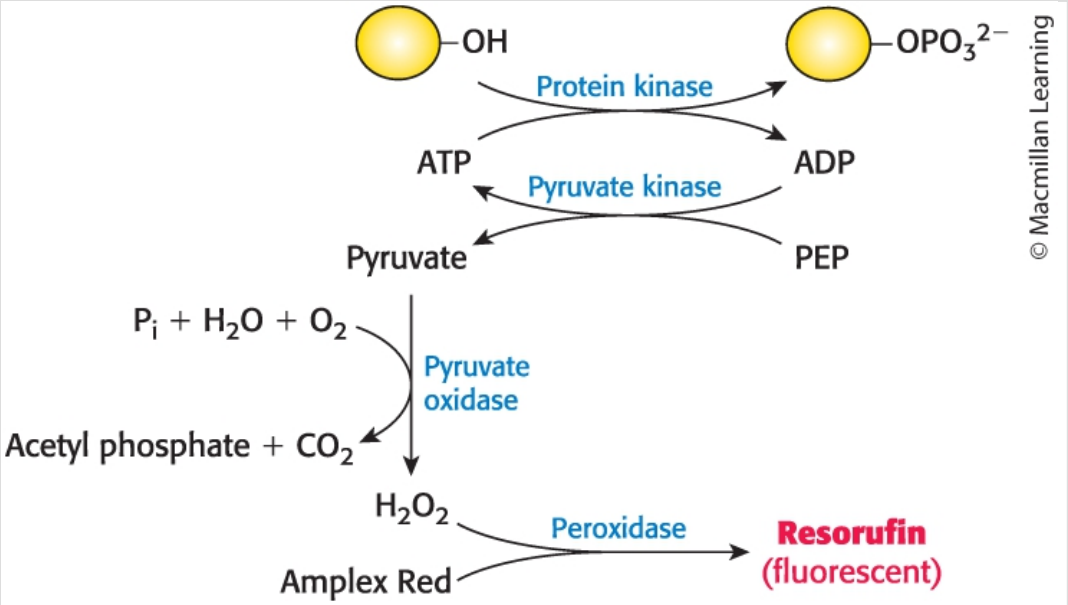


FIGURE 32.7 Coupled assays link the activity of an enzyme to the production of a fluorescent product. In this example, the hydrolysis of ATP to ADP by a protein kinase is linked via the successive action of three enzymes — pyruvate kinase, pyruvate oxidase, and peroxidase — to the production of the fluorescent dye resorufin.

[Information from N. W. Charter et al., *J. Biomol. Screen.* 11:390–399, 2006.]

Self-Check Question

Some compounds in a screening library are themselves fluorescent. Why might they be problematic in a high-throughput screening experiment?

Screening libraries can be prepared using combinatorial chemistry

The final component needed for a high-throughput screen is a diverse chemical library. While compounds in these libraries can be synthesized one at a time for testing, an alternative approach is to synthesize all at once a large number of structurally related compounds that differ from one another at only one or a few positions. This approach is termed **combinatorial chemistry**. Here, compounds are synthesized with the use of the same chemical reactions but a variable set of reactants, enabling the generation of thousands of possible compounds over a few chemical steps.

A key method in combinatorial chemistry is **split-pool synthesis** (**Figure 32.8**). The method depends on solid-phase synthetic methods, first developed for the synthesis of peptides (Section 4.4). Compounds are synthesized on small beads. Beads containing an appropriate starting scaffold are produced and divided (split) into n sets, with n corresponding to the number of building blocks to be used at one site. Reactions adding the reactants at the first site are run, and the beads are isolated by filtration. The n sets of beads are then combined (pooled), mixed, and split again into m sets, with m corresponding to the number of reactants to be used at the second site. Reactions adding these m reactants are run, and the beads are again isolated. The important result is that each bead contains only one compound, even though the entire library of beads contains many. Furthermore, although only $n + m$ reactions were run, $n \times m$ compounds are produced. Suppose that a molecular scaffold is constructed with two reactive sites and that $n = 20$ reactants can be used in the first site and $m = 40$ reactants can be used in the second site. Over two synthetic steps, $20 + 40 = 60$ reactions produce $20 \times 40 = 800$ compounds.

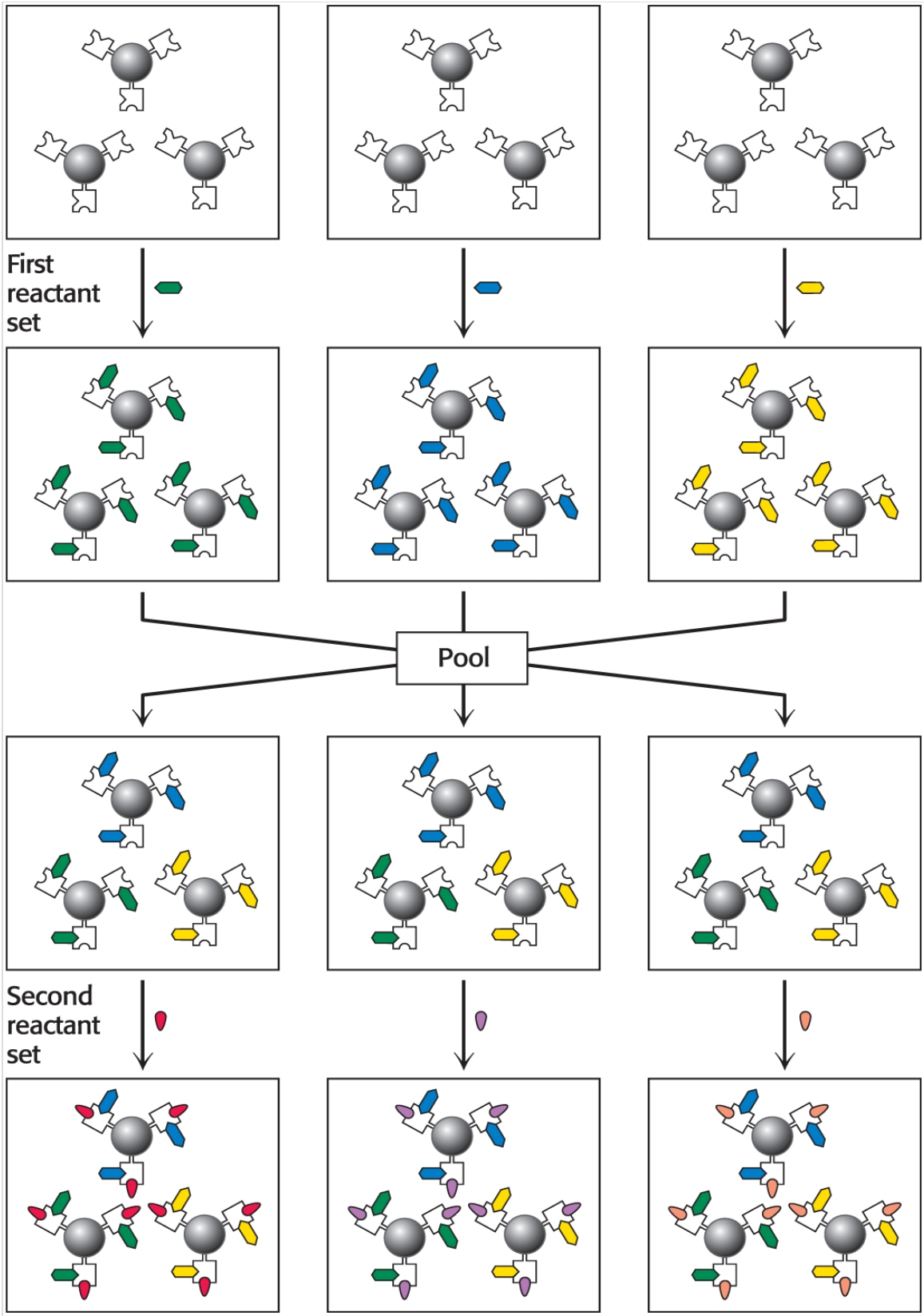
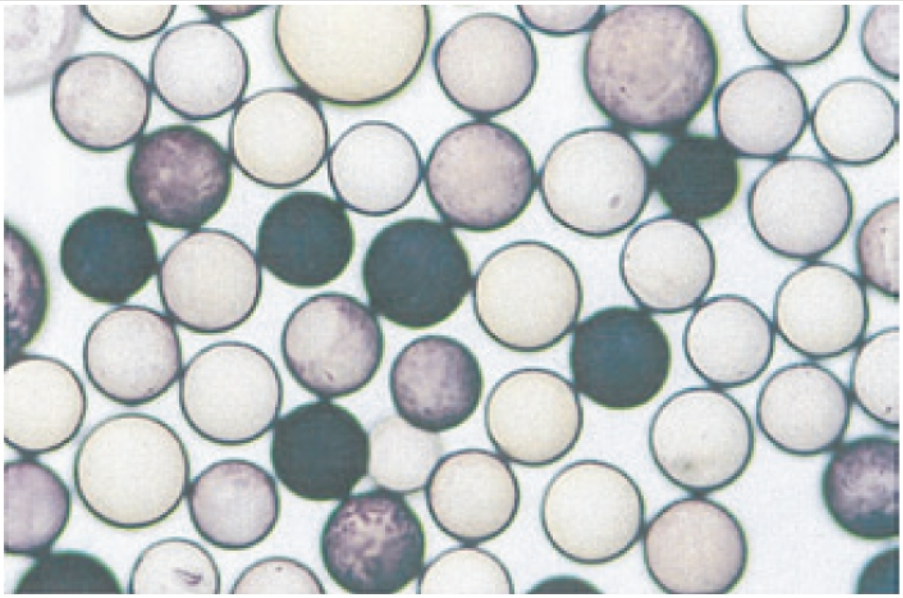

First reactant set
Pool
Second reactant set

FIGURE 32.8 Compound libraries can be generated by split-pool synthesis. Reactions are performed on beads, shown in gray, that have the same initial structural scaffold, shown in white. Each of the reactions with the first set of reactants is performed on a separate set of bead The beads are then pooled, mixed, and split into sets. The second set of reactants is then added Many different compounds will be produced, but all of the compounds on a single bead will be identical.

In some cases, assays can be performed directly with the compounds still attached to the bead to find compounds with desired properties (Figure 32.9). Alternatively, each bead can be isolated and the compound cleaved from the bead to produce free compounds for analysis. After an interesting compound has been identified, analytical methods of various types must be used to identify which of the $n \times m$ compounds are present.



From Figure 3 in Liang et al., "Polyvalent binding to carbohydrates immobilized on an insoluble resin," Proceedings of the National Academy of Sciences, USA, vol. 94, pp. 10554–10559. Copyright 1997 National Academy of Sciences, USA.

FIGURE 32.9 A library of synthesized carbohydrates can be screened using an "on-bead" assay. A small combinatorial library of carbohydrates synthesized on the surface of 130-mm beads is screened for carbohydrates that are bound tightly by a lectin from peanuts. Beads that have such carbohydrates are darkly stained through the action of an enzyme linked to the lectin.

DNA-encoded libraries provide very large compound libraries for lead identification

The "universe" of drug-like compounds is vast. More than an estimated 10^{40} compounds are possible with molecular weights less than 750. So, even with a library of millions of compounds, only a tiny fraction of the chemical possibilities, referred to as **chemical space**, is represented in a particular compound collection.

In an effort to develop libraries that encompass even greater regions of chemical space, scientists have developed **DNA-encoded libraries (DELs)**. In a DEL, compounds are synthesized using split-pool methods directly on a short sequence of DNA. At each synthetic step, a new synthetic oligonucleotide is also ligated to the DNA portion of the molecule. The sequence of this oligonucleotide is unique to the identity of the building block added. Essentially, the synthetic DNA tag acts as a bar code. In this manner, a vast array of compounds can be generated, each with its own uniquely identifying DNA sequence (**Figure 32.10**).

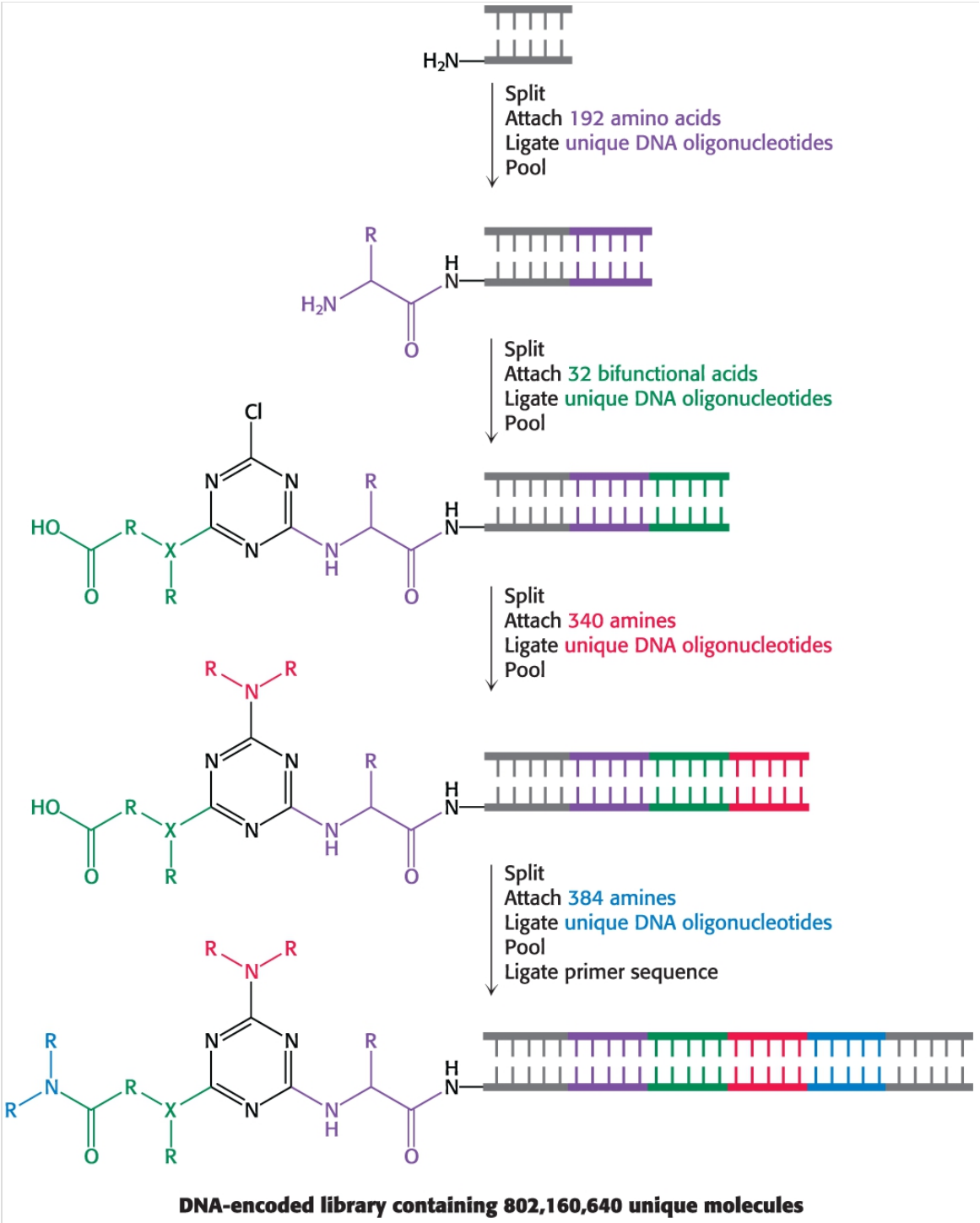


FIGURE 32.10 Diverse DNA-encoded libraries are generated by split pool synthesis. In the construction of a DNA-encoded library (DEL), compounds are synthesized directly on a short strand of double-stranded DNA. At each step, the pool of compounds is split, and different building blocks are added. Before pooling, a short oligonucleotide is ligated to the DNA strand. The sequence of this oligonucleotide is unique to the particular chemical building block that wa added. In this example, after four steps, a library containing over 800 million unique molecules

constructed, each linked to a DNA sequence that specifically encodes the reaction history of tha molecule.

[Information from P. A. Harris et al., *Nature Chem. Biol.* 5:647–654, 2009, Fig. 1.]



How are DELs then screened? In one approach reminiscent of affinity chromatography, the target of interest is attached to a solid resin support, usually through a recombinantly added affinity tag (Section 4.1). The DEL is then passed over the resin; molecules with high affinity for the target will remain bound to the target, while the others pass through unbound. The protein is then denatured, and the bound molecules are eluted. The DNA tags are then amplified by PCR and sequenced using next-generation methods (Section 9.3), revealing the identity of the hits. Since DELs are tested in a single pool, as opposed to individual compounds each dispensed into separate wells in a standard HTS, much larger libraries can be screened over a shorter period of time. The PCR amplification step enables identification of very small amounts of the hit compounds.

A number of follow-up studies must be performed to confirm the hits and explore their properties. For example, once the structures of the positive hits are inferred by DNA sequencing, the compounds must be prepared "off-DNA" to ensure that their affinity to the target was driven solely by the compound, and not influenced by any region of the attached DNA. Furthermore, this screening approach identifies only compounds that *bind* to the target; separate experiments must be conducted to determine if these molecules have *functional impact* on the activity of the target. Despite these challenges, leads have been identified by DEL screening for a number of protein targets, and several of these have been further optimized into highly potent candidates that have entered clinical testing, as we will explore in Section 32.3.

Phenotypic screening provides an alternative to the target-centered approach

Thus far, we have discussed a path to drug discovery that starts with the identification and validation of desired targets. Then, assays specific for these targets are used to screen compound libraries for chemical starting points for further optimization. This approach, called **target-based screening** (Figure 32.11A), is widely applied throughout the pharmaceutical industry. However, target-based screening presents significant challenges that must be overcome: compelling validation evidence for the target must be accumulated; assays specific to the target must be developed; and, as we shall see, compounds must be chemically optimized to be functional in physiological environments.

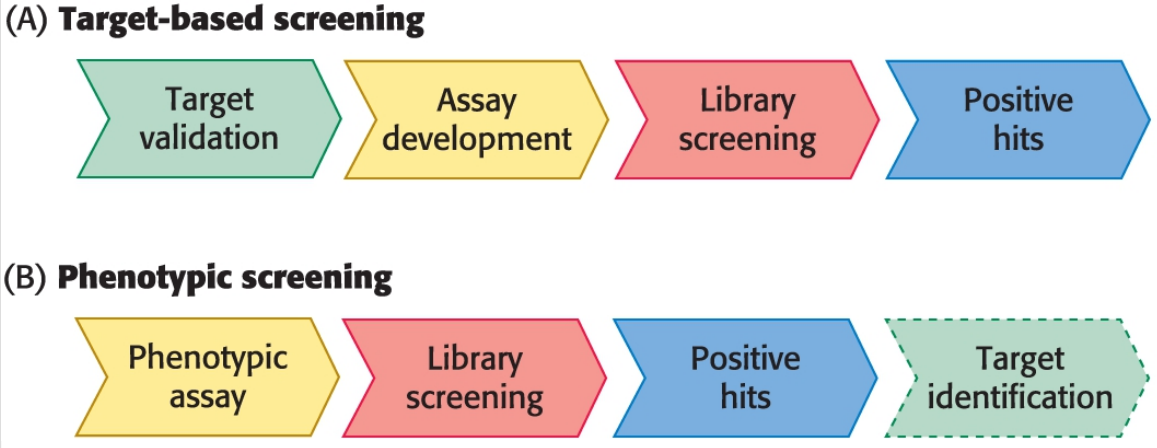


FIGURE 32.11 Target-based screening and phenotypic screening are two paths to early drug discovery. (A) In target-based screening, a molecular target is identified and validated. An assay for this target's activity is used to screen a compound library. Hits can then be tested for their physiological effects and optimized into drug candidates. (B) In phenotypic screening, an assay for a disease-relevant phenotype is developed in a cellular or animal model system. This assay is used to screen a compound library, from which hits can be optimized into drug candidates. These compounds can also be used to identify the molecular target.

Alternatively, leads may be identified by **phenotypic screening** (**Figure 32.11B**). In this approach, libraries of compounds are screened in an assay designed to detect a desired phenotype in a cellular system or animal model. For example, compounds may be tested for their ability to promote cellular survival or enhance resistance to specific toxic stimuli. In phenotypic screening, a biological effect is known before the target is identified. One advantage to this method is that any positive screening hits are already known to have the desired pharmacological effect in a physiological setting.

A significant challenge to phenotypic screening is that the target is not always obvious. As we have seen in our discussions on signal transduction (Chapter 14), a physiological phenotype could be modulated at a wide variety of potential points. Hence, the mode of action of the compound, including the identity of its target or targets, must be identified later. These target identification experiments typically require a substantial amount of effort.

Self-Check Question



Propose an experiment that could enable identification of a target, using the knowledge of a phenotypic screening hit.

32.3 Compounds Must Meet Stringent Criteria to Be Developed into Drugs

In the previous section, we described the process by which leads are identified. During the next stage, **lead optimization**, numerous molecules related to the leads are synthesized to identify those which meet the strict criteria for further development into a **candidate**, a molecule suitable for testing in humans. Many compounds have significant effects when taken into the body, but only a very small fraction of them have the potential to be useful drugs. A foreign compound, not adapted to its role in the cell over the course of evolution, must have a range of special properties to function effectively without causing serious harm. Let us consider some of the challenges faced by drug developers.

Drugs must be potent and selective

Most drugs bind to specific proteins, usually receptors or enzymes, within the body. To be effective, a drug should bind a sufficient number of its target proteins when taken at a dose that can be reasonably administered to patients. One factor in determining drug effectiveness is the strength of the interaction between the drug and its target. Recall from Section 3.1 that a molecule that binds to some target protein is often referred to as a *ligand*. A prototypical ligand-binding curve is shown in **Figure 32.12**. The tendency of a ligand to bind to its target is measured by the dissociation constant, K_d, defined by the expression

$$K_d = [R][L]/[RL]$$

where [R] is the concentration of the free receptor, [L] is the concentration of the free ligand, and [RL] is the concentration of the receptor–ligand complex. The dissociation constant is a measure of the strength of the interaction between the drug candidate and the target; the lower the value, the stronger the interaction. The concentration of free ligand at which one-half of the binding sites are occupied equals the *dissociation constant*, as long as the concentration of binding sites is substantially less than the dissociation constant.

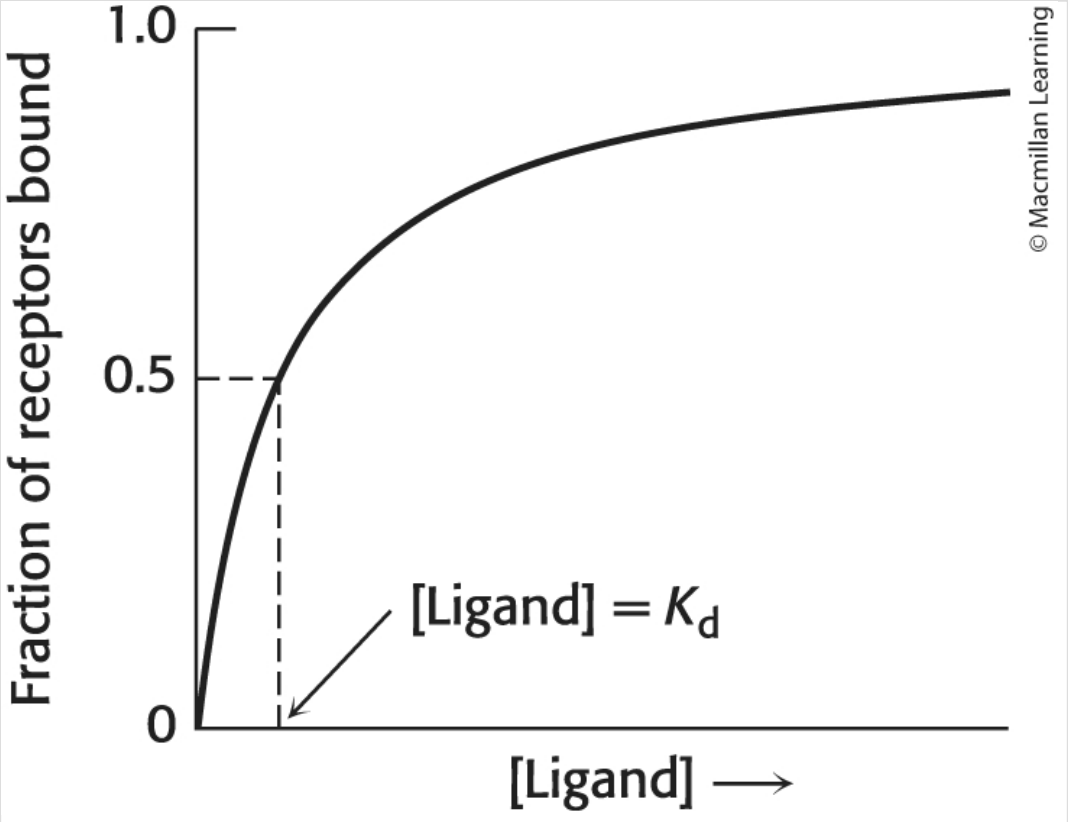


FIGURE 32.12 Simple ligand binding results in a hyperbolic curve. The titration of a receptor, R, with a ligand, L, results in the formation of the complex RL. In uncomplicated cases, the binding reaction follows a simple saturation curve. Half of the receptors are bound to ligand when the ligand concentration equals the dissociation constant, K_d, for the RL complex.

In many cases, biological assays using living cells or tissues (rather than direct enzyme or binding assays) are employed to examine the potency of drug candidates. More potent molecules exert their effects at a lower concentration than less potent ones. For example, the fraction of bacteria killed by a drug might indicate the potency of a potential antibiotic. In these cases, values such as EC_{50} are used. EC_{50}, where EC stands for *effective concentration*, is the concentration of the drug candidate required to elicit 50% of the maximal biological response (**Figure 32.13**). Similarly, EC_{90} is the concentration required to achieve 90% of the maximal response. In the example of an antibiotic, EC_{90} would be the concentration required to kill 90% of bacteria exposed to the drug. For drug candidates that are inhibitors, the corresponding terms IC_{50} and IC_{90}, where IC stands for *inhibitory concentration*, are often used to describe the concentrations of the inhibitor required to reduce a response by 50% or 90%, respectively.

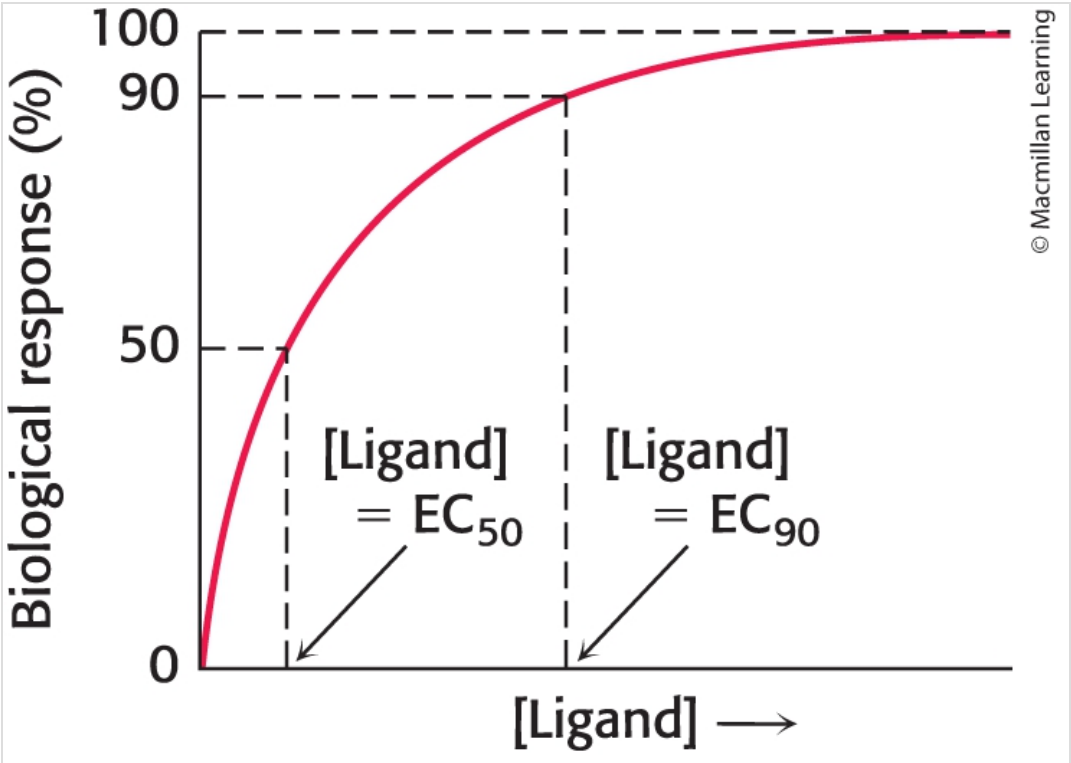


FIGURE 32.13 Effective concentration (EC) describes the amount of compound required to elicit a particular biological response. The EC_{50} value describes the

concentration required to elicit 50% of the maximum response, while the EC_{90} describes that required to elicit 90% of the maximum response.



Values such as the EC_{50} and IC_{50} are measures of the potency of a drug candidate in modulating the activity of the desired biological target. Additionally, to prevent unwanted effects, often called **side effects**, ideal drug candidates should be selective. That is, they should not bind biomolecules other than the target to any significant extent. The degree of selectivity can be described in terms of the ratio of the K_d values for the binding of the drug candidate to any other molecules to the K_d value for the binding to the desired target.

Under physiological conditions, achieving potent and selective binding of a target site by a drug can be quite challenging. Most drug targets also bind ligands normally present in tissues; often, the drug and these ligands will compete for binding sites on the target. We encountered this scenario when we considered competitive inhibitors in Section 5.6. Suppose that the drug target is an enzyme and the drug candidate is competitive with respect to the enzyme's natural substrate. The concentration of the drug candidate necessary to inhibit the enzyme will depend on the physiological concentration of the normal substrate (**Figure 32.14**). Biochemists Yung-Chi Cheng and William Prusoff described the relationship between the IC_{50} of an enzyme inhibitor and its inhibition constant K_i (analogous to the dissociation constant, K_d, of a ligand). For a competitive inhibitor,

$$IC_{50} = K_i(1 + [S]/K_M)$$

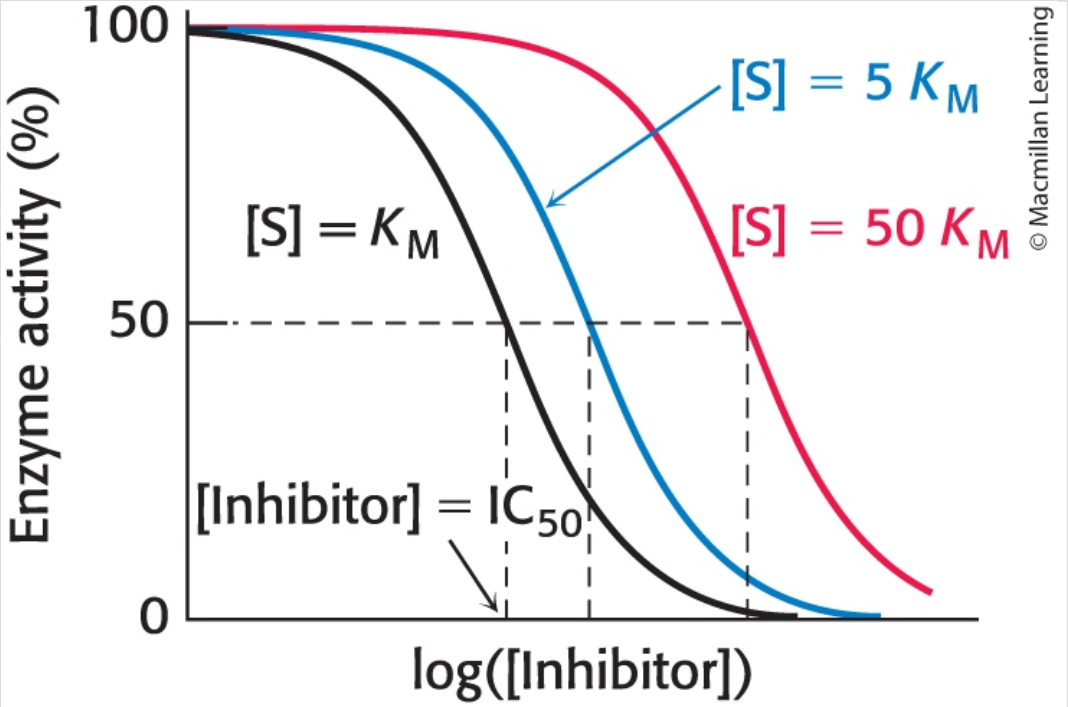


FIGURE 32.14 Inhibitors compete with substrates for enzyme active sites. The measured IC_{50} of a competitive inhibitor to its target enzyme depends on the concentration of substrate present.

This relationship, referred to as the Cheng–Prusoff equation, demonstrates that the IC_{50} of a competitive inhibitor will depend on the concentration and the Michaelis constant (K_M) for the substrate S. The higher the concentration of the natural substrate, the higher the concentration of drug needed to inhibit the enzyme.

Example

Determining the IC_{50} for an Inhibitor

PROBLEM:

The activity of an enzyme was measured in the presence of varying concentrations of Compound A and reported in the table shown. Estimate the IC_{50} for this compound. If Compound A is known to be a competitive inhibitor with respect to the enzyme substrate and the assay was run at a concentration of substrate equal to its K_M, what is the K_i of Compound A?

Compound A (nM)	Percent enzyme activity
0	100
45	90
140	84
410	65
800	51
3700	22
11,200	8
33,100	4

Getting Started:

The IC_{50} is defined as the concentration at which the activity of an enzyme is inhibited by 50%. Reassuringly, the first row of the table confirms that the activity of the enzyme in the absence of Compound A is 100%. Hence, a good first approximation for the IC_{50} would be close to the concentration where the enzyme activity is 50%. From the table, this is about 800 nM.

Calculate:

Since we know that Compound A is competitive with respect to substrate, and the assay was run at a substrate concentration equal to its K_M, we can use the Cheng–Prusoff equation to estimate the K_i:

$$IC_{50} = K_i\left(1 + \frac{[S]}{K_M}\right)$$

$$IC_{50} = K_i\left(1 + \frac{K_M}{K_M}\right) = 2K_i$$

$$K_i = \frac{IC_{50}}{2} = \frac{800\ \text{nM}}{2} = 400\ \text{nM}$$

Reflect:

Pharmacologists describe inhibitor potency in a variety of ways. Note that while IC_{50} values are commonly used, they are dependent upon assay conditions, whereas K_i values are reflective of the intrinsic affinity of the inhibitor for its target. Also, be careful when applying the Cheng–

Prusoff equation! The equation provided in the text is specific for competitive inhibitors with respect to the substrate S. More complicated equations are needed to describe this relationship for other inhibitory modalities.

Drugs must have suitable properties to reach their targets

Thus far, we have focused on the ability of molecules to act on specific target molecules. However, an effective drug also has other requisite characteristics. It must be easily administered and must reach its target at sufficient concentration to be effective. After a drug molecule has entered the body, it is acted upon by several processes — absorption, distribution, metabolism, and excretion — that will determine its effective concentration over time (**Figure 32.15**). A drug's response to these processes is referred to as its **ADME** (pronounced "add-me") **properties**.

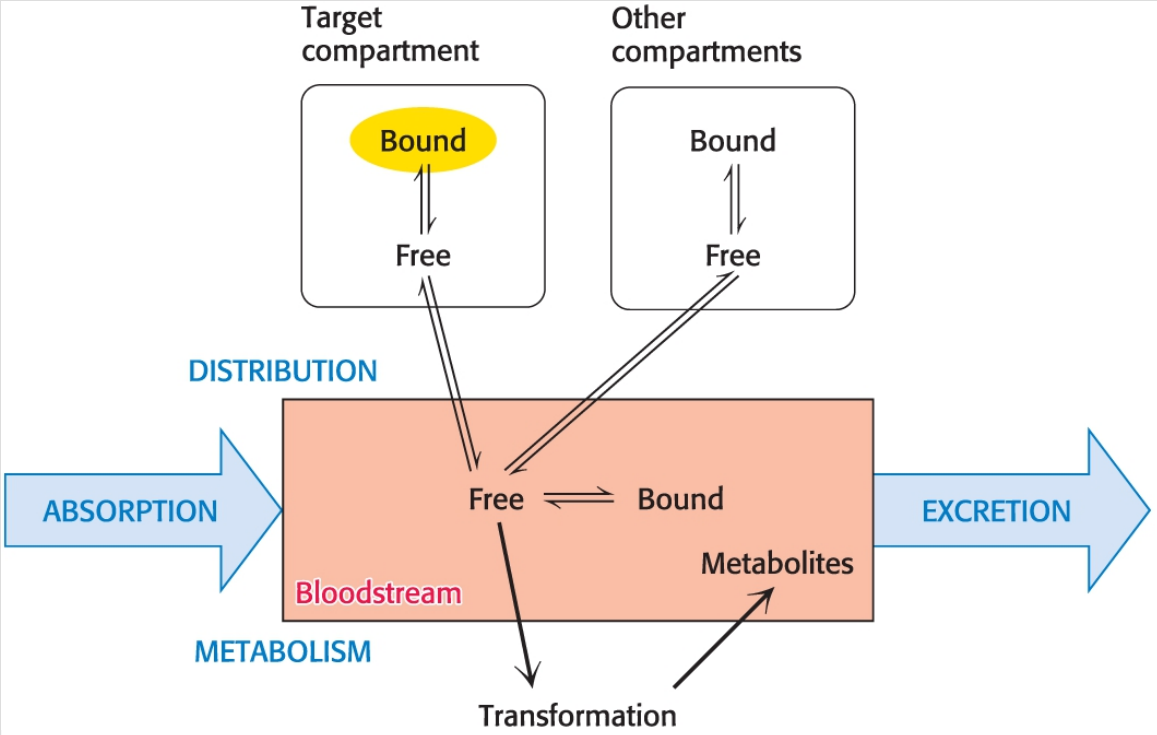


FIGURE 32.15 The pharmacokinetics of a compound in a living organism is described by its absorption, distribution, metabolism, and excretion (ADME) properties. The concentration of compound at its target site (yellow) is affected by the magnitudes and rates of absorption, distribution, metabolism, and excretion.

Administration and absorption

Ideally, a drug can be taken orally as a small tablet. An orally administered active compound must be able to survive the acidic conditions in the gut and then be absorbed through the intestinal epithelium. Thus, the compound must be able to pass through cell membranes at a significant rate. Larger molecules such as proteins cannot be administered orally, because they often cannot survive the acidic conditions in the stomach and, if they do, they are not readily absorbed. Even many small molecules are not absorbed well; they may be too polar and unable to pass through cell membranes easily, for example. The ability to be absorbed is often quantified in terms of the

oral bioavailability. This quantity is defined as the ratio of the peak concentration of a compound given orally to the peak concentration of the same dose injected directly into the bloodstream. Bioavailability can vary considerably from species to species, so results from animal studies may be difficult to apply to human beings. Despite this variability, some useful generalizations have been made. One powerful set consists of Lipinski's rules, developed by the pharmaceutical chemist Christopher A. Lipinski.

Lipinski's rules tell us that poor absorption is likely when

1. The molecular weight is greater than 500 daltons.
2. The number of hydrogen-bond donors is greater than 5.
3. The number of hydrogen-bond acceptors is greater than 10.
4. The partition coefficient [measured as log(*P*)] is greater than 5.

The partition coefficient is a way to measure the tendency of a molecule to enter lipid membranes, which correlates with its ability to dissolve in organic solvents. It is determined by allowing a compound to equilibrate between water and an organic phase, *n*-octanol. The log(*P*) value is defined as $\log_{10}$ of the ratio of the concentration of a compound in *n*-octanol to the concentration of the compound in water:

$$\log(P) = \log\left(\frac{[\text{compound}]_{\text{n-octanol}}}{[\text{compound}]_{\text{water}}}\right)$$

For example, if the concentration of the compound in the *n*-octanol phase is 100 times that in the aqueous phase, then log(*P*) is 2. Although the ability of a drug to partition in organic solvents is ideal, as it implies that the compound can penetrate membranes, a log(*P*) value that is too

high suggests that the molecule may be poorly soluble in an aqueous environment.

Morphine, for example, satisfies all of Lipinski's rules and has moderate bioavailability (Figure 32.16). Still, a drug that violates one or more of these rules may also have satisfactory bioavailability. Nonetheless, these rules, and other similar guidelines that have since been developed, serve as useful principles for evaluating new drug candidates.

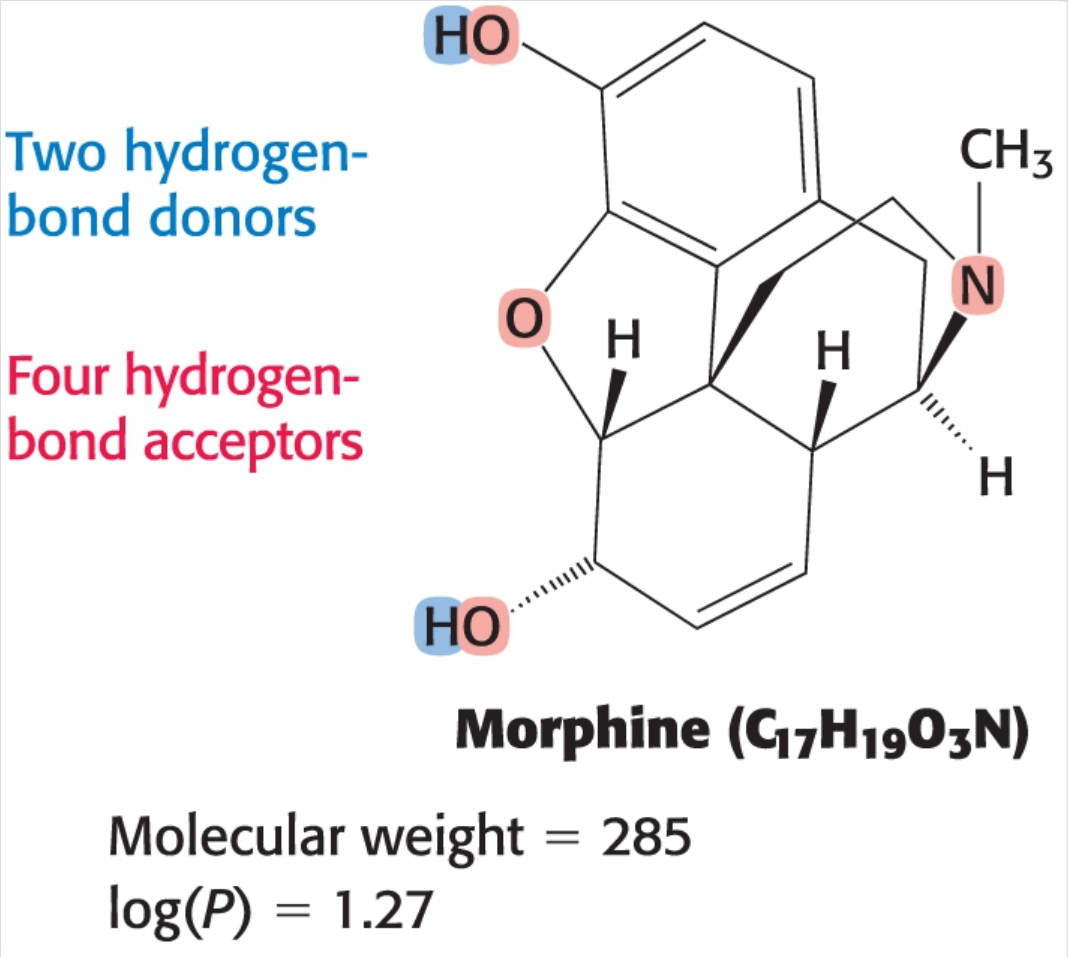


FIGURE 32.16 Lipinski's rules serve as a guide to predict oral bioavailability. Morphine satisfies all of Lipinski's rules and has an oral bioavailability in human beings of 33%.

Distribution

Compounds taken up by intestinal epithelial cells can pass into the bloodstream. However, hydrophobic compounds and many others do not freely dissolve in the bloodstream. These compounds bind to proteins, such as albumin (Figure 32.17), that are abundant in the blood serum. Because albumin is present in the circulation at high concentrations (nearly 0.7 mM) and can bind a wide variety of compounds, it can dramatically affect the free concentration of drug in the bloodstream. Nevertheless, the binding capacity of albumin enables transport of the drug throughout the circulatory system.

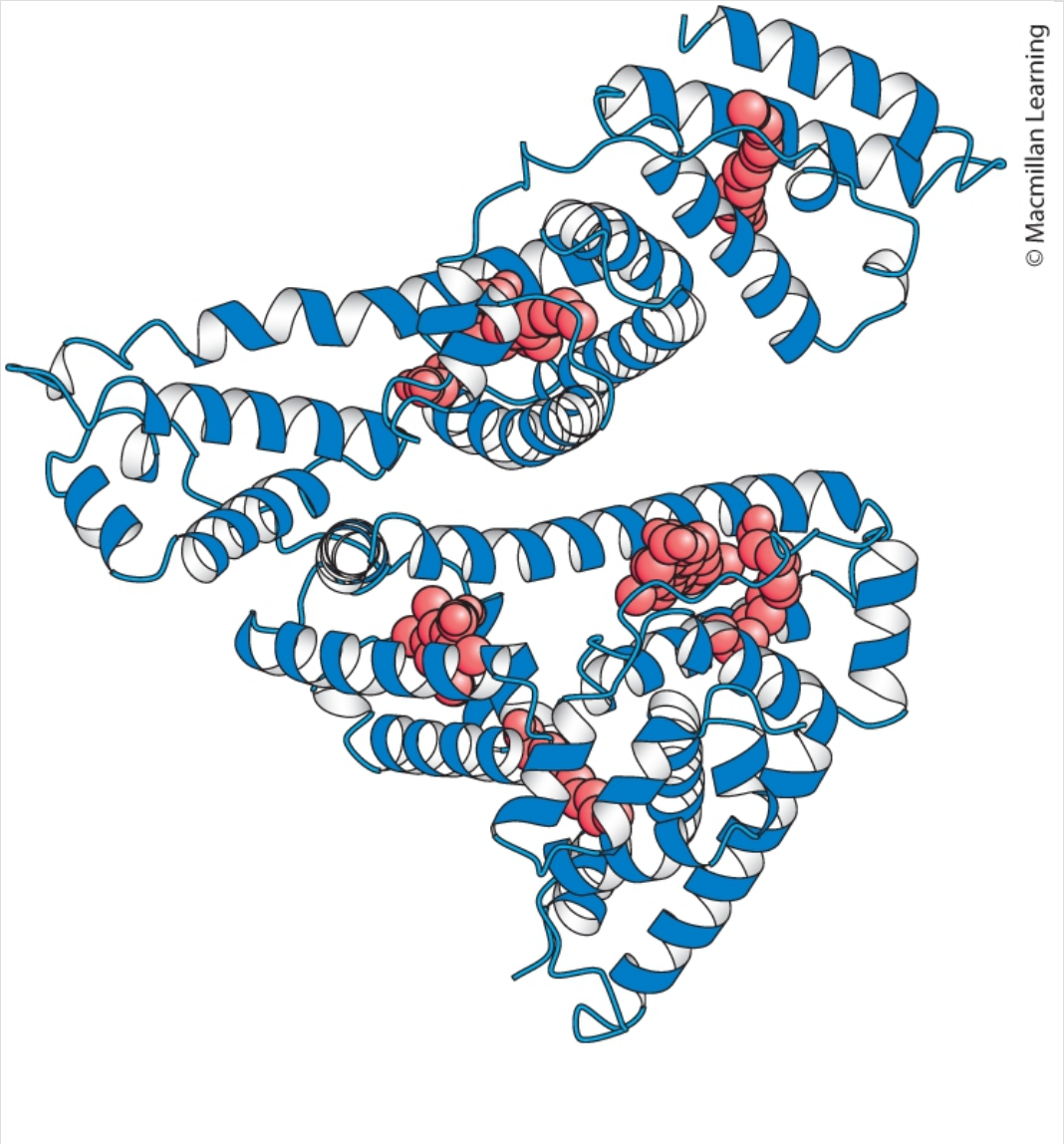
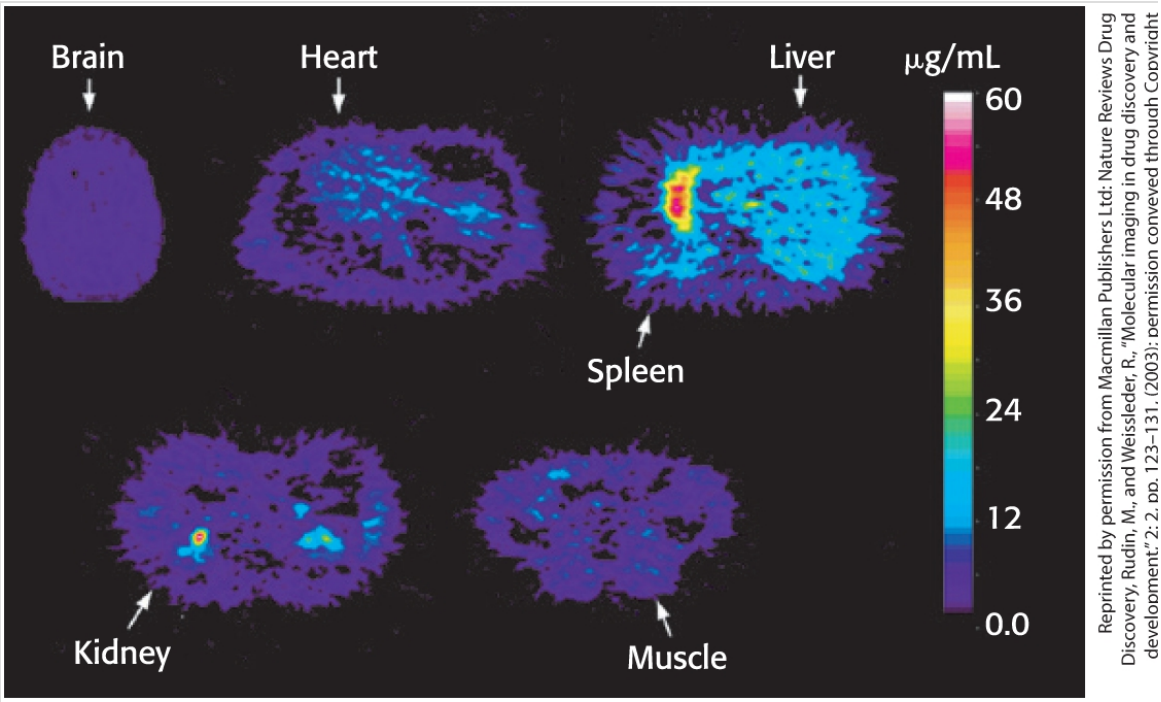

© Macmillan Learning

FIGURE 32.17 Albumin is abundant in the bloodstream and binds hydrophobic compounds. Seven hydrophobic molecules (in red) are shown bound to a single molecule of serum albumin.

[Drawn from 1BKE.pdb.]

When a compound has reached the bloodstream, it is distributed to different fluids and tissues, which are often referred to as *compartments*. Some compounds are highly concentrated in their target compartments, either by binding to the target molecules themselves or by other mechanisms. Other compounds are distributed more widely (Figure 32.18). An effective drug will reach the target compartment in sufficient quantity; the concentration of the compound in the target compartment is reduced whenever the compound is distributed into other compartments.



Reprinted by permission from Macmillan Publishers Ltd: Nature Reviews Drug Discovery, Rudin, M., and Weissleder, R., "Molecular imaging in drug discovery and development," 2: 2, pp. 123–131. (2003); permission conveyed through Copyright

FIGURE 32.18 Once absorbed, compounds distribute to various organs within the body. The distribution of the antifungal agent fluconazole has been monitored through the use of positron emission tomography (PET) scanning. These images were taken of a healthy human volunteer 9

minutes after injection of a dose of $5\ mg\ kg^{-1}$ of fluconazole containing trace amounts of fluconazole labeled with the positron-emitting isotope ^{18}F.



Some target compartments are particularly hard to reach. For example, many compounds are excluded from the central nervous system by the tight junctions between endothelial cells that line blood vessels within the brain and spinal cord, referred to as the *blood-brain barrier*.

Metabolism

A potential drug molecule must evade the body's defenses against foreign compounds, also called **xenobiotics**. Many compounds are released from the body in the urine or stool, often after having been metabolized to aid in excretion. This **drug metabolism** poses a considerable threat to drug effectiveness, because the concentration of the desired compound decreases as it is metabolized. Thus, a rapidly metabolized compound must be administered more frequently or at higher doses.

Drug metabolism takes place primarily in the liver. Because blood flows from the intestine directly to the liver through the portal vein, xenobiotic metabolism often alters drug compounds before they ever reach full circulation. This process, referred to as *first-pass metabolism*, can substantially limit the availability of compounds taken orally.

Two of the most common pathways in xenobiotic metabolism are oxidation, often referred to as **phase I transformations**, and conjugation (which are called **phase II transformations**). Oxidation reactions can aid excretion in at least two ways: by increasing water

solubility, and thus ease of transport, and by introducing functional groups that participate in subsequent metabolic steps. These reactions are often promoted by cytochrome P450 enzymes in the liver (Section 27.4). The human genome encodes more than 50 different P450 isozymes, many of which participate in xenobiotic metabolism. A typical reaction catalyzed by a P450 isozyme is the hydroxylation of ibuprofen (**Figure 32.19**).

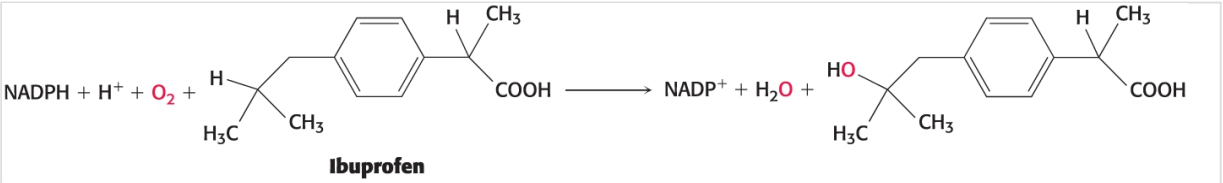


FIGURE 32.19 Cytochrome P450 isozymes catalyze xenobiotic metabolic reactions such as hydroxylation. In this example, one P450 isozyme introduces an oxygen atom derived from molecular oxygen into the anti-inflammatory drug ibuprofen.

Conjugation is the addition of particular groups to the xenobiotic compound. Common groups added are glutathione (Section 20.5), glucuronic acid, and sulfate (**Figure 32.20**). These additions often increase water solubility and promote excretion. Note that an oxidation reaction often precedes conjugation because the oxidation reaction can generate modifications, such as the hydroxyl group, to which groups such as glucuronic acid can be attached.

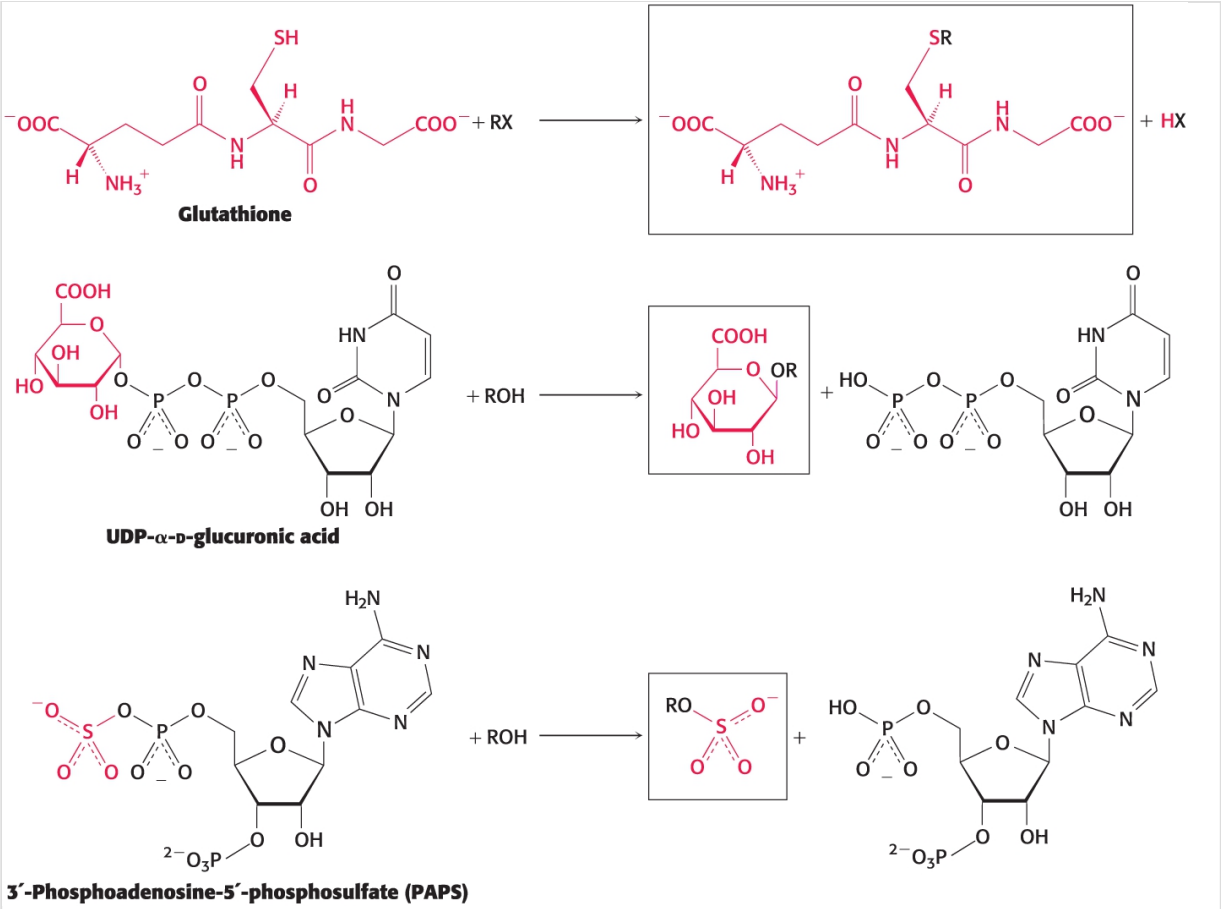
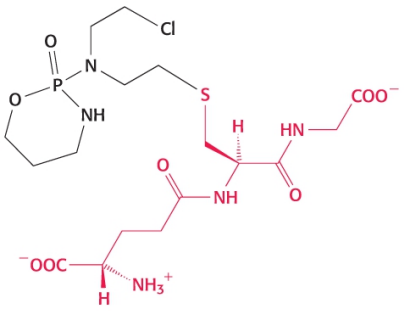
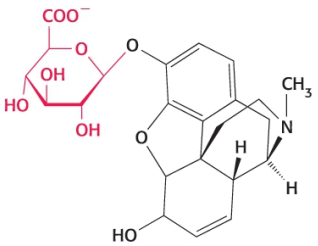


FIGURE 32.20 Compounds that have certain functional groups are often modified by conjugation reactions. Such reactions include the addition of glutathione (top), glucuronic acid (middle), or sulfate (bottom). The conjugated product is shown boxed.

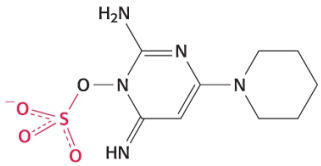
Examples of conjugation include the addition of glutathione to the anticancer drug cyclophosphamide, the addition of glucuronidate to the analgesic morphine, and the addition of a sulfate group to the hair-growth stimulator minoxidil. While the metabolic products of a drug are usually less active than the drug itself, there are notable exceptions. For example, the sulfation of minoxidil produces a compound that is more active in stimulating hair growth than is the unmodified compound.



Cyclophosphamide-glutathione conjugate



Morphine glucuronidate



Minoxidil sulfate

Excretion

After compounds have entered the bloodstream, they can be removed from circulation and excreted from the body by two primary pathways. First, they can be absorbed through the kidneys and excreted in the urine. In this process, the blood passes through networks of fine capillaries, called *glomeruli*, in the kidney that act as filters. Compounds with molecular weights less than approximately 60,000 pass though the glomeruli. Many of the water molecules, glucose molecules, nucleotides, and other low-molecular-weight compounds that pass through the glomeruli are reabsorbed into the bloodstream, either by transporters that have broad specificities or by the passive transfer of hydrophobic molecules through membranes. Drugs and metabolites that pass through the first filtration step and are not reabsorbed are subsequently excreted.

Second, compounds can be actively transported into bile by a process that takes place in the liver. After concentration in the gallbladder, bile flows into the intestine. In the intestine, the drugs and metabolites can be reabsorbed into the bloodstream, further degraded by digestive enzymes, or excreted through the stool. Sometimes, compounds are recycled from the bloodstream into the intestine and back into the bloodstream, a process referred to as *enterohepatic cycling* (**Figure**

32.21). This process can significantly decrease the rate of excretion of some compounds, because they escape from an excretory pathway and reenter the circulation.

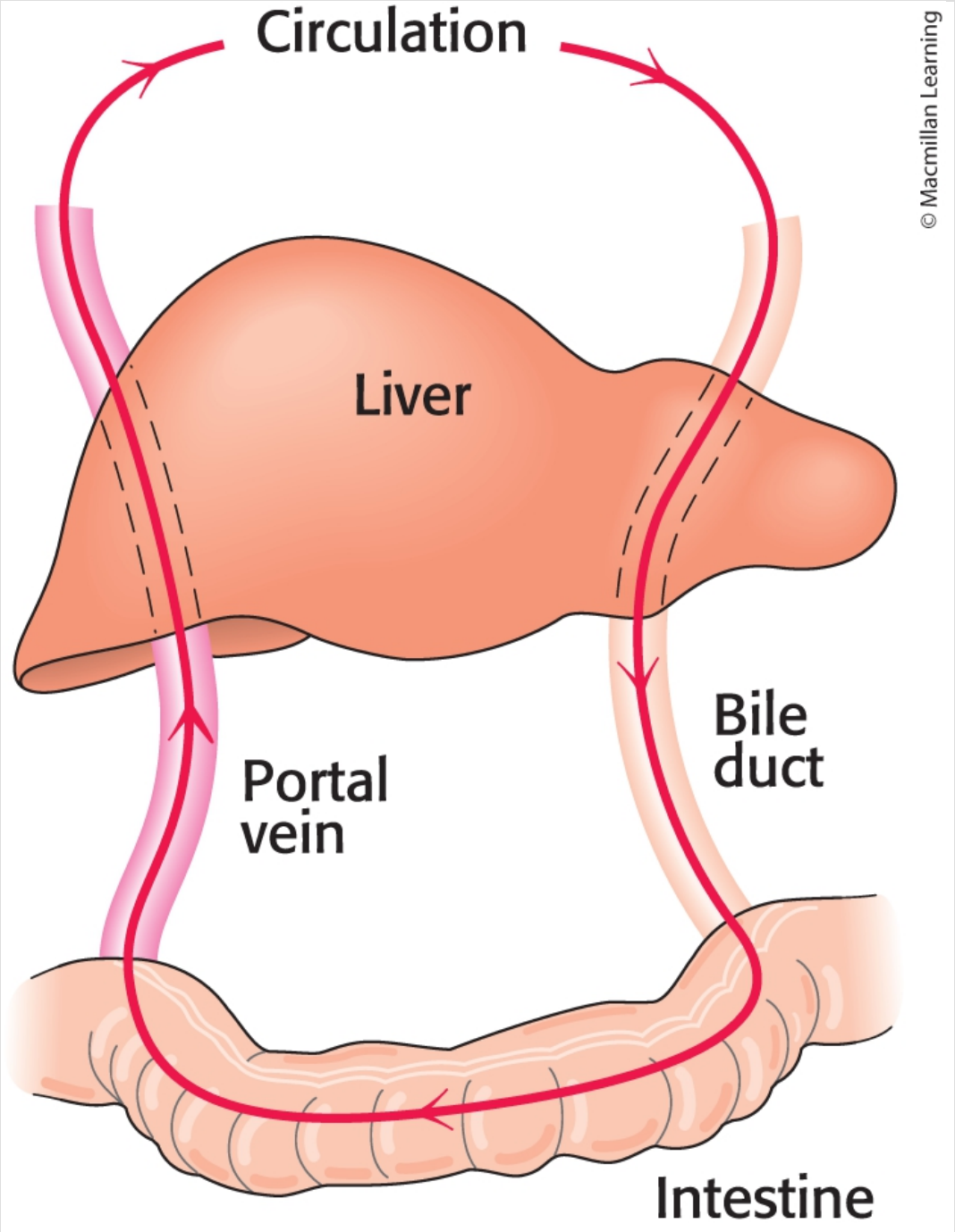


FIGURE 32.21 Drugs can move between the intestine and the circulation via enterohepatic cycling. In this pathway, some drugs can move from the blood

circulation to the liver, into the bile, into the intestine, to the liver, and back into circulation. This cycling decreases the rate of drug excretion.

The kinetics of compound excretion is often complex. In some cases, a fixed percentage of the remaining compound is excreted over a given period of time (Figure 32.22). This pattern of excretion results in exponential loss of the compound from the bloodstream that can be characterized by a half-life $(t_{1/2})$. The half-life is the fixed period of time required to eliminate 50% of the remaining compound. It is a measure of how long an effective concentration of the compound remains in the system after administration. As such, the half-life is a major factor in determining how often a drug must be taken. A drug with a long half-life might need to be taken only once per day, whereas a drug with a short half-life might need to be taken three or four times per day.

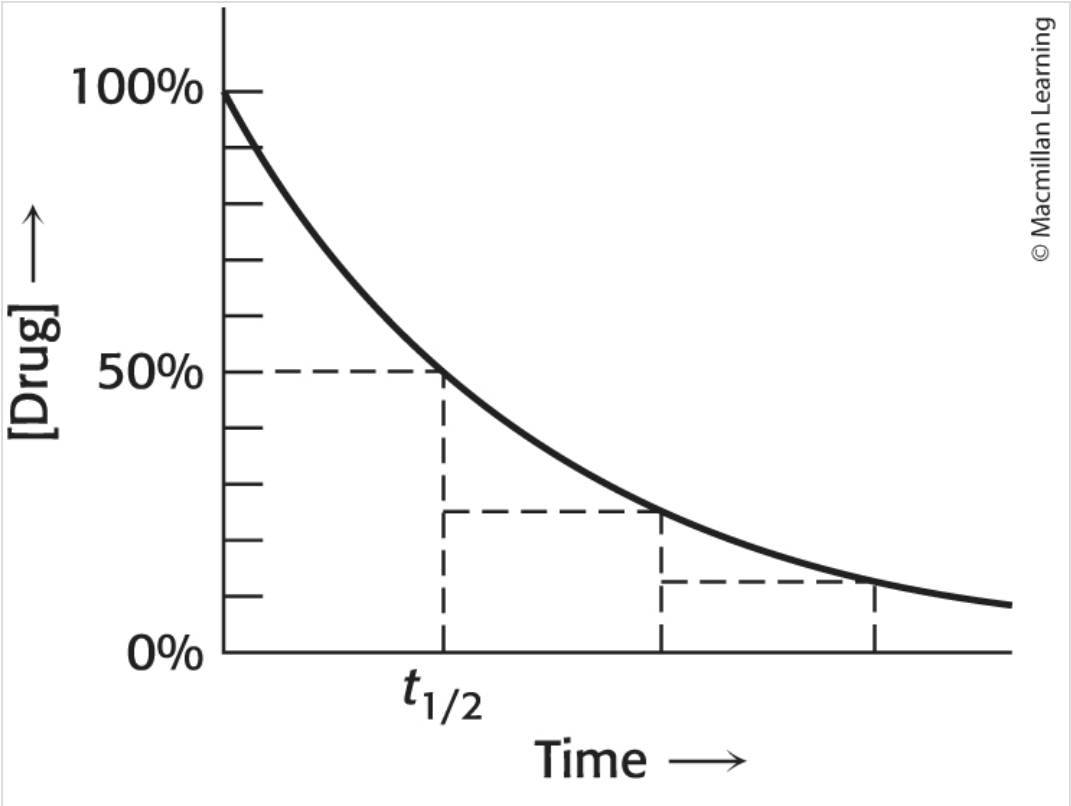


FIGURE 32.22 Drug excretion may be measured by its half-life. The concentration of a drug in the bloodstream decreases to one-half of its value in a period of time, $t_{1/2}$, referred to as its half-life.



Toxicity can limit drug effectiveness

An effective drug must not be so toxic that it seriously harms the person who takes it. A drug may be toxic for any of several reasons. First, it may modulate the target molecule itself too effectively, referred to as **mechanism-based**, or **on-target**, **toxicity**. For example, the presence of too much of the anticoagulant drug coumadin can result in dangerous, uncontrolled bleeding and death.

Second, the compound may modulate the properties of proteins that are distinct from the target molecule itself, referred to as **off-target toxicity**. Compounds that are directed to one member of a family of enzymes or receptors often bind to other family members. For example, an antiviral drug directed against viral proteases may be toxic if it also inhibits proteases that perform critical functions in the body, such as those that regulate blood pressure. A compound may also be toxic if it modulates the activity of a protein unrelated to its intended target. For example, many compounds block ion channels such as the potassium channel hERG (Section 13.4), causing potentially life-threatening disturbances of cardiac rhythm. To prevent cardiac side effects, many compounds are screened for their ability to block such channels.

Finally, even if a compound is not itself toxic, its metabolic by-products may be. Phase I metabolic processes can generate damaging reactive groups in products. An important example is liver toxicity observed with large doses of the common pain reliever acetaminophen (**Figure 32.23**).

A particular cytochrome P450 isozyme oxidizes acetaminophen to *N*-acetyl-*p*-benzoquinone imine, and the resulting compound is conjugated to glutathione. With large doses, however, the liver's supply of glutathione is exhausted, and the liver is no longer able to protect itself from the imine and other metabolites. Initial symptoms of excessive acetaminophen include nausea and vomiting. Within 24 to 48 hours, symptoms of liver failure may appear. Acetaminophen poisoning accounts for about 35% of cases of severe acute liver failure in the United States. A liver transplant is often the only effective treatment.

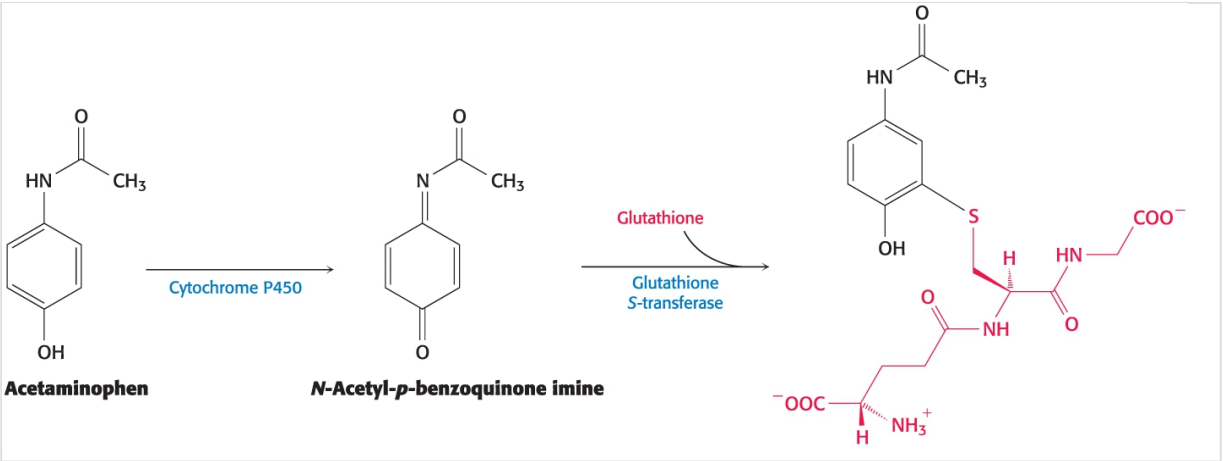


FIGURE 32.23 Acetaminophen metabolism results in its toxicity. A minor metabolic product of acetaminophen is *N*-acetyl-*p*-benzoquinone imine, which is conjugated to glutathione. Large doses of acetaminophen can thus deplete liver glutathione stores.

The toxicity of a drug candidate can be described in terms of the **therapeutic index**. This measure of toxicity is determined through animal tests, usually with mice or rats. The therapeutic index is defined as the ratio of the dose of a compound that is required to kill one-half of the animals (referred to as the LD_{50} for "lethal dose") to a comparable measure of the effective dose, usually the EC_{50}. So, if the therapeutic index is 1000, then lethality is significant only when 1000 times the

effective dose is administered. Analogous indices can provide measures of toxicity less severe than lethality.

Many compounds have favorable properties in vitro, yet they fail when administered to a living organism because of difficulties with ADME and toxicity. Expensive and time-consuming animal studies are required to verify that a drug candidate is not toxic, yet differences between animal species in their response can confound decisions about moving forward with a compound toward human studies. One hope is that, with more understanding of the biochemistry of these processes, scientists can develop computer-based models to replace or augment animal tests. Such models would need to accurately predict the fate of a compound inside a living organism from its molecular structure or other properties that are easily measured in the laboratory without the use of animals.

Lead molecules can be optimized on the basis of three-dimensional structural information about their targets

Many drugs bind to their targets in a manner reminiscent of Emil Fischer's lock-and-key model (Figure 5.8). In principle, we should be able to design a key, given enough knowledge about the shape and chemical composition of the lock. In the idealized case, we could design a small molecule that is complementary in shape and electronic structure to a target protein so that it binds effectively to the targeted site. Yet, despite our ability to determine three-dimensional structures rapidly, the achievement of this goal remains elusive. Designing stable compounds from scratch that have the correct shape and properties to fit precisely into a binding site is difficult because predicting the structure that will best fit into a binding site is difficult. Prediction of binding affinity requires a detailed understanding of the interactions between a compound and its binding partner and of the interactions

between the compound and the solvent when the compound is free in solution.

Nonetheless, **structure-based drug design** has proved to be a powerful tool in drug development. In this approach, the structure of the target complexed with compounds of interest are determined. Chemists can use these structural data to make directed changes to these molecules that are predicted to improve their affinities to the target. The structures of these new molecules can then be determined in complex with the target, and the process can be repeated over several cycles.

 One of the most prominent successes of structure-based drug design has been the development of drugs that inhibit the protease from the human immunodeficiency virus (HIV). In this case, two sets of promising inhibitors that had high potency but poor solubility and bioavailability were discovered. X-ray crystallographic analysis and molecular-modeling findings suggested that a hybrid of these two inhibitor sets might have both high potency and improved bioavailability (**Figure 32.24**). The synthesized hybrid compound did show improvements but required further optimization.

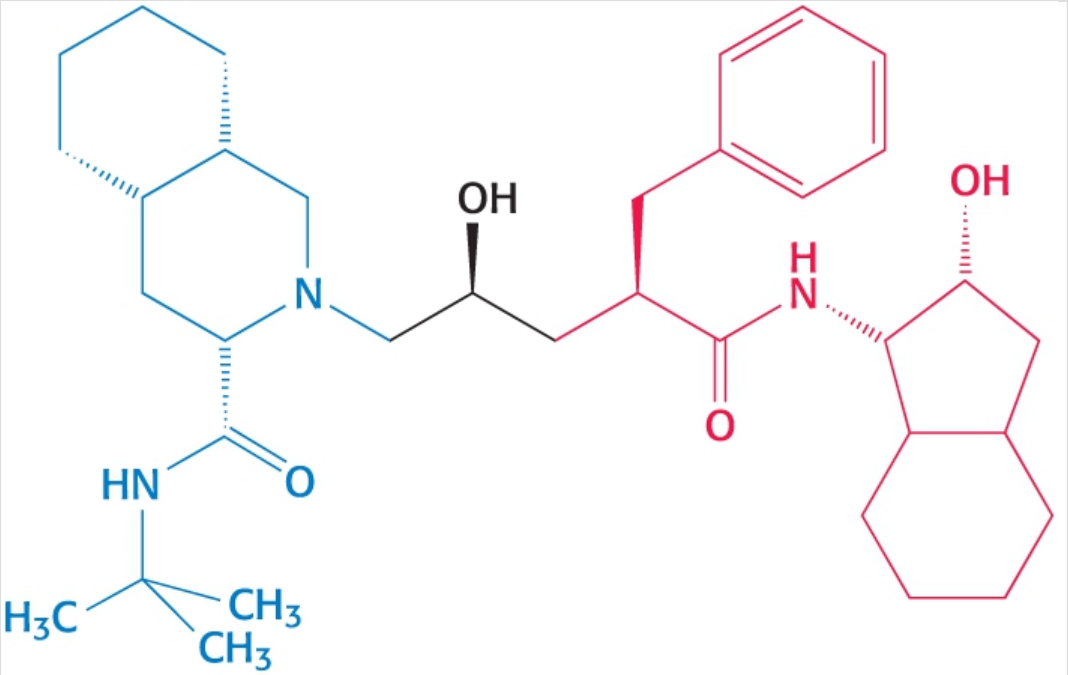


FIGURE 32.24 Structural information led to the initial design of an HIV protease inhibitor. This compound was designed by combining part of one compound with good inhibition activity but poor solubility (shown in red) with part of another compound with better solubility (shown in blue).

Guided by structural data, a series of compounds were prepared and tested for their ability to inhibit the protease (**Figure 32.25**). These data demonstrate a **structure–activity relationship (SAR)**; they provide an opportunity to correlate each compound's structure with its function to guide the design of further molecules. The most active compound showed poor bioavailability, but one of the other compounds (highlighted in yellow in Figure 32.25) showed good bioavailability and acceptable activity. The maximum serum concentration available through oral administration was significantly higher than the levels required to suppress replication of the virus. Ultimately, this molecule became the marketed HIV protease inhibitor indinavir (Section 6.2). This drug, as well as other protease inhibitors developed at about the same time, has been used in combination with other drugs to treat HIV

infection and AIDS with much more encouraging results than had been obtained previously.

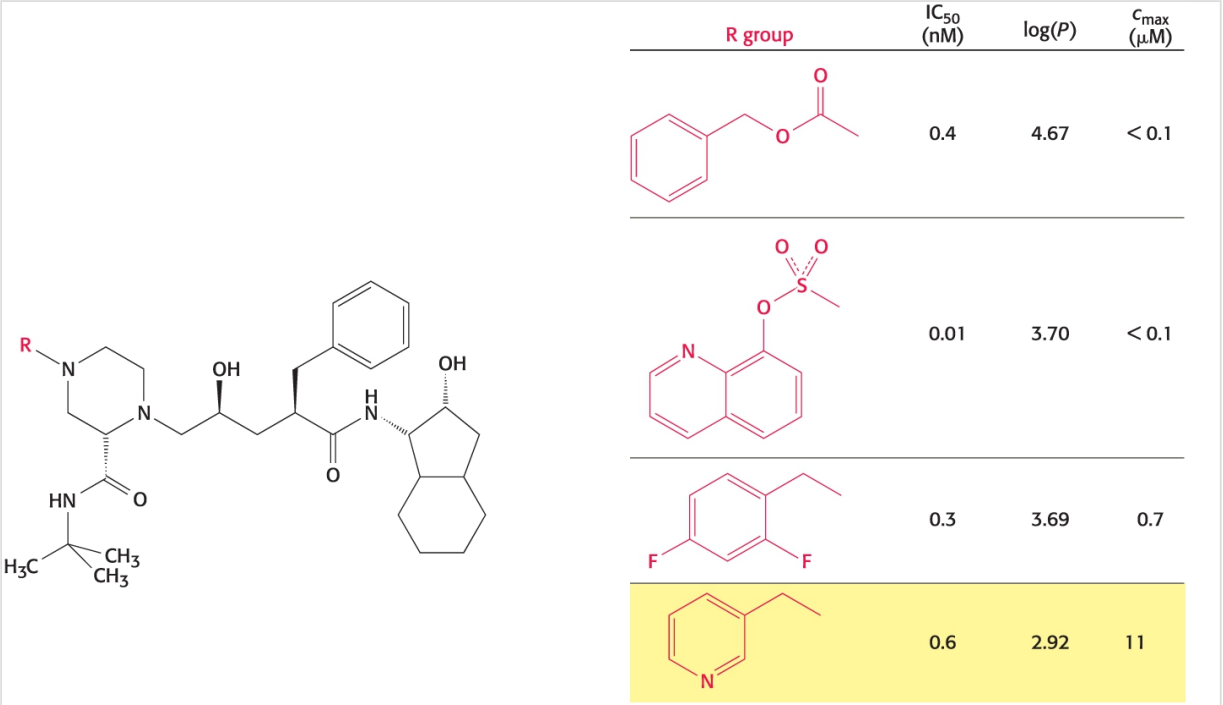


FIGURE 32.25 Optimizing lead molecules requires the balancing of multiple compound properties. Four HIV protease inhibitors were evaluated for characteristics, including the IC_{50}, log(*P*), and C_{max} (the maximal concentration of compound present) measured in the serum of dogs. The compound shown at the bottom (highlighted in yellow) has the weakest inhibitory power (measured by IC_{50}) but by far the best bioavailability (measured by C_{max}). This compound was selected for further development, ultimately leading to the drug indinavir.

The development of indinavir represents an example of the challenges faced by pharmaceutical scientists during the process of lead optimization. Potency is only one of multiple properties that must be optimized during this stage. During the course of a discovery program, thousands of compounds may be synthesized and tested. Improvements in one property may be to the detriment of other properties. The collaboration of many scientists — biochemists, pharmacologists,

chemists, and biologists, just to name a few — is required to attain a molecule suitable for testing in humans.

32.4 Biologics Are a Growing Family of Drugs

In this chapter, we have primarily focused on small molecules as drugs. These molecules are typically less than 500 Da in molecular weight (as described by Lipinski's rules), may be orally bioavailable, and bind to specific structural pockets on their targets. Many small molecule drugs are membrane-permeable, enabling them to access intracellular targets. However, they also exhibit some limitations, including short half-lives and a high susceptibility to off-target toxicity.

Over the past several decades, a new class of therapeutics has emerged. Broadly defined, **biologics** are medicines derived from living cells or through biological processes. With each scientific advancement, the number and different types of biologics have grown significantly (Table 32.1). As this is a highly diverse group of medicines, we will consider some of the more prominent examples here.

TABLE 32.1 Examples of biologics

Recombinant proteins
Monoclonal antibodies
Vaccines
Blood and blood components

Allergenics (molecules that elicit an allergic response)
Cells and tissues

The majority of biologics are recombinant proteins

Earlier, we discussed the first approved biologic: recombinant human insulin produced in *E. coli* (Section 9.2). Approved by the U.S. Food and Drug Administration (FDA) in 1982, this groundbreaking drug enabled the treatment of millions of diabetic patients without the risk of allergic reactions caused by insulins produced by other animal species.

Since the approval of insulin, a number of recombinant proteins have been approved for clinical use. For example, granulocyte colony-stimulating factor (G-CSF) is a 174-amino-acid glycoprotein that stimulates the production of granulocytes in the bone marrow. A recombinant form of G-CSF (filgrastim) was approved by the FDA in 1991 for patients suffering from low neutrophil counts due to HIV infection or some forms of chemotherapy. Similarly, other signaling proteins have been developed as biologics.

Recombinant protein biologics may be chemically modified to improve their pharmacokinetic properties. For example, filgrastim has a short half-life of around 3.5 hours, requiring once- or twice-daily dosing. Through the covalent attachment of a 20-kD polyethylene glycol (PEG) moiety to filgrastim, a process referred to as *pegylation*, its half-life can be extended to 40 hours. A single injection of the pegylated form of filgrastim, pegfilgrastim, exhibits

the same biological effect as 11 daily doses of the nonpegylated protein.

Monoclonal antibodies are highly specific and potent recombinant protein biologics

As we discussed in Section 3.4, antibody-producing cells have evolved remarkable mechanisms for generating a broad range of recognition diversity. Scientists can take advantage of nature's own combinatorial chemistry to generate numerous distinct antibodies that can bind to a specific ligand. In addition, the hybridoma method (Section 4.2) can be used to prepare large quantities of monoclonal antibodies that exhibit high affinities for their targets.

As drugs, monoclonal antibodies have unique advantages over small molecules. For example, they can recognize a broader surface of the target; they are not limited to the smaller pockets typically bound by small molecule drugs. This larger interaction surface enables the development of drugs with very high potency and specificity. Furthermore, the Fc region of monoclonal antibodies (Figure 3.40) binds to an endogenous salvage pathway receptor, the *neonatal Fc receptor* (FcRn), permitting the drug to persist in an active form for a very long half-life, on the order of weeks. Hence, monoclonal antibodies can be dosed much less frequently (e.g., weekly to monthly) than small-molecule drugs (e.g., daily).

There are some limitations to using monoclonal antibodies as drugs. First, as they are proteins, they are unable to withstand the harsh environment of the gastrointestinal tract. Hence, antibodies cannot be dosed orally and are usually administered under the skin (subcutaneously) or directly into blood vessels (intravenously).

Additionally, antibodies do not cross membranes readily, so they generally are usable only against secreted or cell-surface targets. Despite these limitations, however, over 60 monoclonal antibodies are currently in clinical use as therapeutics, with hundreds more in clinical development.

How do monoclonal antibodies exert their therapeutic effects? In many cases, they serve as antagonists, blocking receptors from interacting with their corresponding ligands. This was the case for cetuximab, the chemotherapeutic monoclonal antibody that blocks the epidermal growth factor (EGF) receptor from binding EGF (Section 14.5). Alternatively, some monoclonal antibodies bind specific circulating ligands, preventing them from exerting their cellular effects. In other cases, monoclonal antibodies can be used to target specific cell-surface proteins — such as markers specific for tumor cells — for degradation by the host's own immune system.

Another unique example is the *antibody-drug conjugate* (ADC). In this case, a small molecule drug is conjugated to an antibody specific for a particular cell type. Once the antibody-target complex is internalized by the cell, the linker between the antibody and the drug is cleaved, and the free drug can exert its effects. In this manner, the off-target toxicity of a particular drug can be limited by directing its activity to a small subset of cells within the body.

Monoclonal antibodies represent a rapidly growing and exciting drug class. These versatile molecules have been exploited in numerous creative ways to provide clinical benefit for a variety of diseases besides cancer, including inflammatory, infectious, cardiovascular, and ophthalmologic conditions.



Will & Deni McIntyre/The Chronicle Collection/Getty Images

GERTRUDE ELION At the age of 15, Gertrude Elion was inspired to pursue a career in science and medicine after her grandfather's death from stomach cancer. Her family was bankrupted by the stock market crash in 1929, but she was able to attend Hunter College for free, where she achieved great academic success. At the age of 19, she took jobs as a secretary, a chemistry teacher, and an unpaid laboratory assistant, after which she had saved enough money to enroll in the graduate program at New York University, where she obtained her Master of Science degree in chemistry in 1941. During World War II, with many male chemists serving overseas, Elion was able to secure a research position at

Burroughs Wellcome, where she began a lifelong collaboration with George Hitchings (both scientists are shown above). Together, they eschewed the “trial-and-error” approach to drug discovery, exploiting differences in metabolism between human cells and pathogens to target infectious organisms and tumors. Her work with Hitchings led to the discovery of numerous antibacterial, antiviral, immunosuppressive, and chemotherapeutic medicines, and their efforts were recognized with the Nobel Prize in Physiology or Medicine in 1988.

Self-Check Question



A number of Fc domain mutations have been discovered that enhance the affinity of an antibody for FcRn. What effect would those mutations have on the half-life of a monoclonal antibody drug?

32.5 The Clinical Development of Medicines Proceeds Through Several Phases

In the United States, the FDA requires demonstration that drug candidates be effective and safe before they may be used in human beings on a large scale. This requirement is particularly true for drug candidates that are to be taken by people who are relatively healthy. More side effects are acceptable for drug candidates intended to treat significantly ill patients such as those with serious forms of cancer, where there are clear, unfavorable consequences for not having an effective treatment.

Clinical trials are time-consuming and expensive

Clinical trials test the effectiveness and potential side effects of a candidate drug before it is approved by the FDA for general use. These trials proceed in at least three phases (Figure 32.26). In Phase I, a small number (typically from 10 to 100) of usually healthy volunteers take the drug for an initial assessment of safety. These volunteers are given a range of doses and are monitored for signs of toxicity. The efficacy of the drug candidate is not specifically evaluated.

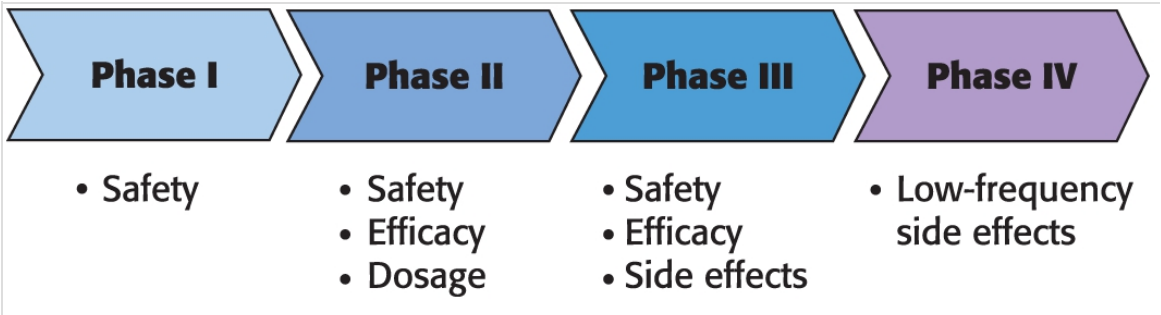


FIGURE 32.26 Clinical trials proceed in phases examining safety and efficacy in increasingly large groups.



In Phase II, the efficacy of the drug candidate is tested in a small number of persons who might benefit from the drug, and further data regarding the drug's safety are obtained. Such trials are often controlled and double-blinded. In a **controlled study**, subjects are divided randomly into two groups. Subjects in the treatment group are given the treatment under investigation. Subjects in the control group are given either a **placebo** — that is, a treatment such as sugar pills known to not have intrinsic value — or the best standard treatment available, if withholding treatment altogether would be unethical. In a **double-blinded study**, neither the subjects nor the researchers know which subjects are in the treatment group and which are in the control group. A double-blinded study prevents bias in the course of the trial. Only when the trial has been completed are the assignments of the subjects into treatment and control groups unsealed and the results for the two groups compared. A variety of doses are often investigated in Phase II trials to determine which doses appear to be free of serious side effects and which doses appear to be effective.

The power of the **placebo effect** — that is, the tendency to perceive improvement in subjects who believe that they are receiving a potentially beneficial treatment — should not be underestimated. In a study of arthroscopic surgical treatment for knee pain, for example, subjects who were led to believe that they had received surgery through the use of videotapes and other means showed the same level of improvement, on average, as subjects who actually received the procedure.

In Phase III, similar studies are performed on a larger and more diverse population. This phase is intended to more firmly establish the efficacy

of the drug candidate and to detect side effects that may develop in a small percentage of the subjects who receive treatment. Thousands of subjects may participate in a typical Phase III study.

Clinical trials can be extremely costly and time-consuming. Hundreds or thousands of patients must be recruited and monitored for the duration of the trial. Many physicians, nurses, clinical pharmacologists, statisticians, and others participate in the design and execution of the trial. Costs can run from tens to hundreds of millions of dollars. Extensive records must be kept, including documentation of any adverse reactions. These data are compiled and submitted to the FDA. Furthermore, many drugs fail to show efficacy in these larger studies where the patient population is more diverse. The full cost of developing a drug is currently estimated to be more than $800 million.

Even after a drug has been approved and is in use, difficulties can arise. Clinical trials that are run after a drug has entered the market, referred to as Phase IV or *postmarketing surveillance* studies, are designed to identify low-frequency side effects that may emerge only after widespread or long-term use. For example, the cyclooxygenase-2 inhibitor rofecoxib was withdrawn from the market after significant cardiac side effects were detected in Phase IV clinical trials. Such events highlight the necessity for doctors and patients to balance beneficial effects against potential risks for any medicine.

The evolution of drug resistance can limit the utility of drugs for infectious agents and cancer

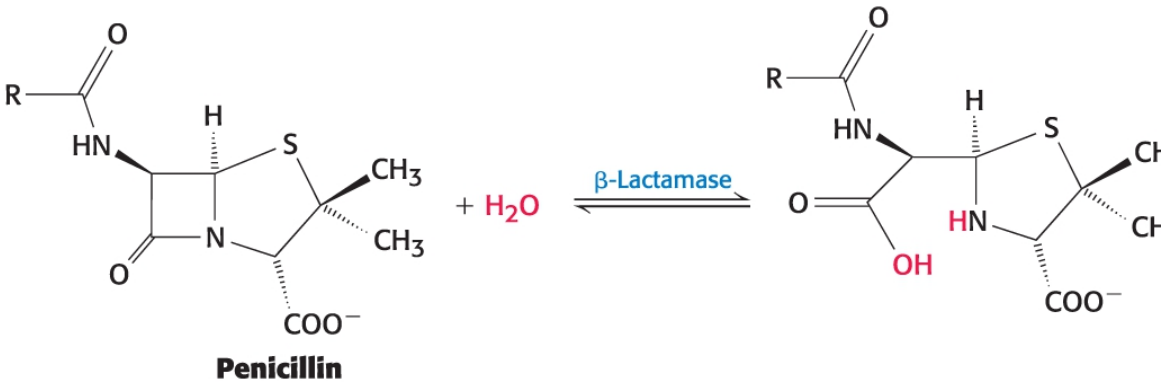
Many drugs are used for long periods of time without any loss of effectiveness. However, in some cases, particularly for the treatment of cancer or infectious diseases, drug treatments that were initially

effective become less so. In other words, the disease becomes resistant to the drug therapy. Why does this resistance develop? Infectious diseases and cancer have a common feature — namely, that an affected person contains many cells (or viruses) that can mutate and reproduce, meeting the two conditions necessary for evolution to take place. Thus, an individual virus, microorganism, or cancer cell may, by chance, have a genetic variation that makes it more suitable for growth and reproduction in the presence of the drug. These microorganisms or cells are more fit than others in their population, and they will tend to take over the population. As the selective pressure due to the drug is continually applied, the population of microorganisms or cancer cells will tend to become more and more resistant to the presence of the drug. Note that resistance can develop by a number of mechanisms.

The HIV protease inhibitors discussed in Section 32.3 provide an important example of the evolution of drug resistance. Retroviruses such as HIV are very well suited to this sort of evolution because reverse transcriptase carries out replication without a proofreading mechanism. In a genome of approximately 9750 bases, each possible single point mutation is estimated to appear in a virus particle more than 1000 times per day in each infected person. At this mutation rate, multiple point mutations occur. While most of these mutations either have no effect or are detrimental to the virus, a few of the mutant virus particles encode proteases that are less susceptible to inhibition by the drug. In the presence of an HIV protease inhibitor, these virus particles will tend to replicate more effectively than does the population at large. With the passage of time, the less susceptible viruses will come to dominate the population and the virus population will become resistant to the drug.

Pathogens may become resistant to antibiotics by completely different mechanisms. Some pathogens contain enzymes that inactivate or degrade specific antibiotics. For example, many bacteria are resistant to β-lactams such as penicillin because they contain β-lactamase enzymes.

These enzymes hydrolyze the β-lactam ring and render the drugs inactive.



Many of these enzymes are encoded in plasmids, small circular pieces of DNA often carried by bacteria (Section 9.2). Many plasmids are readily transferred from one bacterial cell to another, transmitting the capability for antibiotic resistance. Plasmid transfer thus contributes to the spread of antibiotic resistance, a major health-care challenge.

Drug resistance commonly emerges in the course of cancer treatment. Cancer cells are characterized by their ability to grow rapidly without the constraints that apply to normal cells. Many drugs used for cancer chemotherapy inhibit processes that are necessary for this rapid cell growth. However, individual cancer cells may accumulate genetic changes that mitigate the effects of such drugs. These altered cancer cells will tend to grow more rapidly than others and will become dominant within the cancer-cell population. This ability of cancer cells to mutate quickly has been a challenge to one of the major breakthroughs in cancer treatment: the development of inhibitors for proteins specific to cancer cells present in certain leukemias (Section 14.5). For example, tumors become undetectable in patients treated with imatinib, a Bcr-Abl protein kinase inhibitor, but in many patients the tumors recur after a period of years. In many of these cases,

mutations have altered the Bcr-Abl protein so that it is no longer inhibited by the concentrations of imatinib used in therapy.

Finally, cancer patients often take multiple drugs concurrently in the course of chemotherapy, and, in many cases, cancer cells become simultaneously resistant to many or all of them. This multiple-drug resistance can be due to the proliferation of cancer cells that overexpress a number of ABC transporter proteins that pump drugs out of the cell (Section 13.2). Thus, cancer cells can evolve drug resistance by overexpressing normal human proteins or by modifying proteins responsible for the cancer phenotype.

Chapter 32 Summary

32.1 Drug Discovery Begins with Target Identification and Validation

- The process of drug discovery is divided into two phases: the discovery phase, where molecules are optimized for testing in humans, and the development phase, where clinical trials are conducted.
- A drug target is a protein or oligonucleotide whose activity, when modulated by a drug, will alter the progression of a disease process.
- Targets should be validated, in that sufficient evidence suggests that it plays an important role in disease progression.
- Targets should also be tractable, in that sufficient evidence suggests that a molecule can be designed to interact with a target.
- Serendipity has played a significant role in the history of drug discovery.

32.2 Lead Molecules Can Be Discovered in Many Ways

- Lead molecules are starting points for optimization into drug candidates.
- Natural products are often a robust source of lead molecules. For example, the first HMG-CoA reductase inhibitors were derived from compounds isolated from the broths of bacteria and fungi.
- High-throughput screening (HTS), in which up to millions of compounds can be tested for their activity against a target, is a valuable source of lead molecules.
- HTS depends on the construction of a large chemical library. Combinatorial chemistry can be used to prepare large

populations of compounds using only a few synthetic steps.
- In phenotypic screening, compounds are tested for their ability to affect a disease-relevant phenotype. The identity of the targets of hits from such screens are determined in subsequent steps.

32.3 Compounds Must Meet Stringent Criteria to Be Developed into Drugs

- Lead optimization is the process by which leads are modified into drug candidates suitable for testing in humans.
- To be effective, drugs must bind to their targets with high affinity and specificity.
- Most compounds are poorly absorbed and rapidly excreted from the body, or they are modified by metabolic pathways that target foreign compounds. Consequently, a drug's ADME properties, related to its absorption, distribution, metabolism, and excretion, must be optimized.
- A compound may also not be a useful drug because it is toxic; it may either modulate the target molecule too effectively (mechanism-based toxicity) or bind to proteins other than the target (off-target toxicity).
- Structural information on the interaction of a compound and its target can be used to drive further optimization of potency and selectivity.

32.4 Biologics Are a Growing Family of Drugs

- Biologics are a diverse class of drugs that are derived from living cells or through biological processes.
- The majority of biologics are recombinant proteins.
- Monoclonal antibodies represent a large proportion of recombinant protein biologics, as they are capable of a high degree of potency and selectivity.

- Because of their interaction with an endogenous salvage pathway, monoclonal antibodies typically exhibit very long half-lives, allowing them to be dosed weekly or monthly.

32.5 The Clinical Development of Medicines Proceeds Through Several Phases

- Before compounds can be given to human beings as drugs, they must be extensively tested for safety and efficacy.
- Clinical trials are performed in stages: first testing safety, then safety and efficacy in a small population; finally, safety and efficacy in a larger population to detect rarer adverse effects.
- With regard to infectious diseases and cancer, patients often develop resistance to a drug after it has been administered for a period of time because variants of the disease agent that are less susceptible to the drug have a selective advantage over more susceptible variants when the drug is present.

Key Terms

pharmacology
discovery phase
development phase
target
target validation
tractability (druggability)
lead molecules (leads)
high-throughput screening (HTS)
coupled assay
combinatorial chemistry
split-pool synthesis
chemical space
DNA-encoded libraries (DELs)

target-based screening
phenotypic screening
lead optimization
candidate
side effect
ADME properties
oral bioavailability
xenobiotic compounds
drug metabolism
phase I transformation
phase II transformation
mechanism-based (on-target) toxicity
off-target toxicity
therapeutic index
structure-based drug design
structure–activity relationship (SAR)
biologics
controlled study
placebo
double-blinded study
placebo effect

Problems

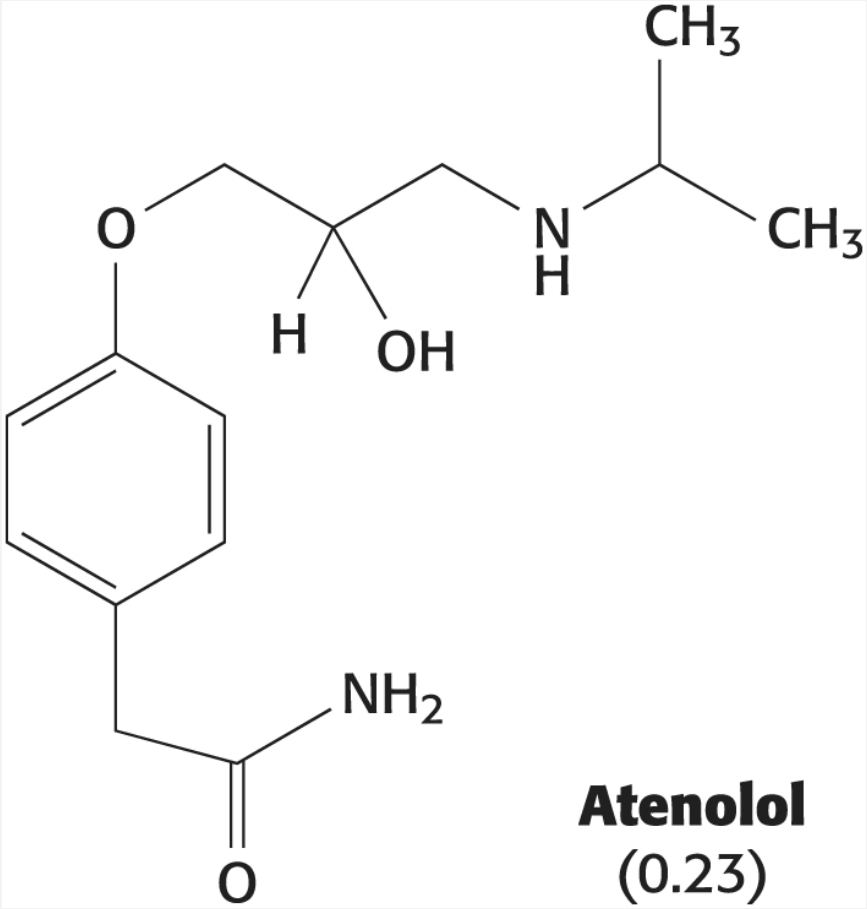
1. Sildenafil induces its physiological effects by increasing the intracellular concentrations of cGMP, leading to muscle relaxation. On the basis of the scheme shown in Figure 32.5, identify another approach for increasing cGMP levels with a small molecule. 1

2. For each of the following drugs, indicate whether the drug discovery was accidental, a result of natural product screening, or the result of targeted design. 2

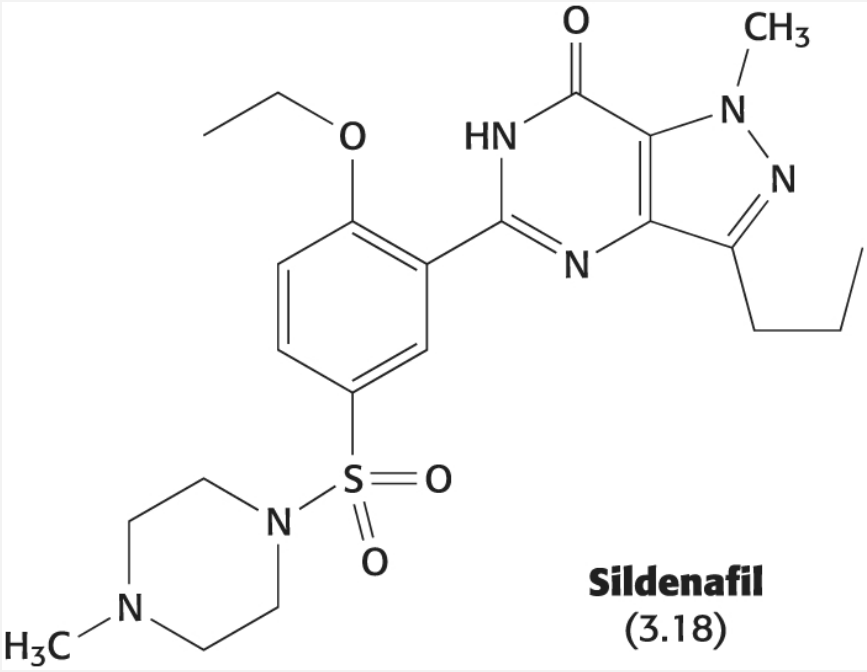
a. Penicillin
b. Lovastatin
c. Sildenafil
d. Aspirin
e. Indinavir

3. Which of the following compounds satisfy all of Lipinski's rules? Note that log(*P*) values are given in parentheses. 3

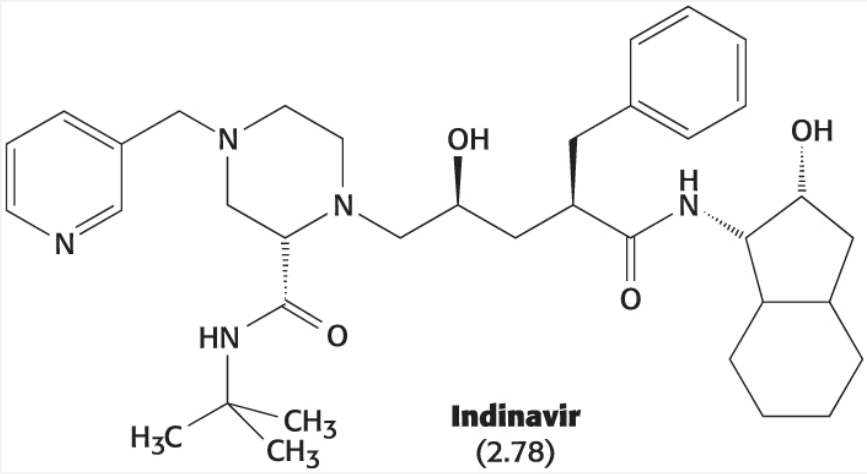
A.



B.


O
CH3
N
HN
N
O
N
S
O
N
O
N
H3C
Sildenafil
(3.18)

C.

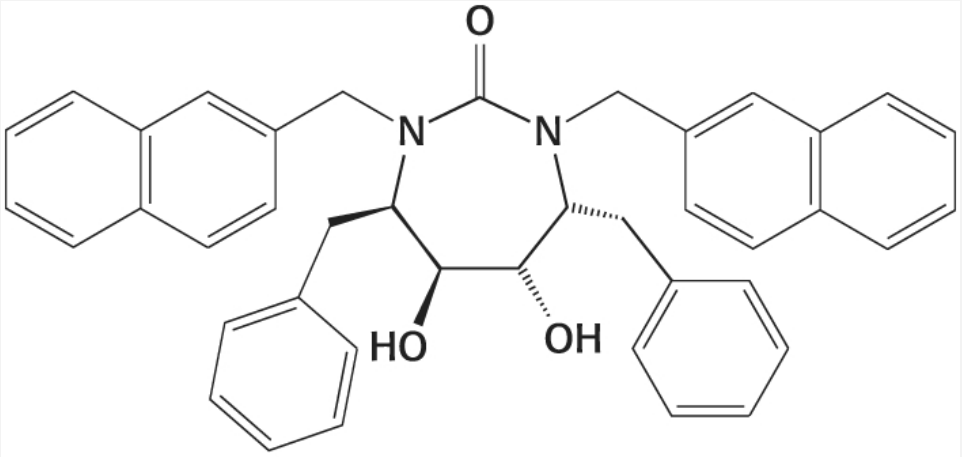

N
OH
OH
N
N
H
N
O
HN
O
H3C
CH3
CH3
Indinavir
(2.78)

4. Name one advantage of a noncompetitive inhibitor as a potential drug compared with a competitive inhibitor. 3

5. Explain why drugs that inhibit P450 enzymes may be particularly dangerous when used in combination with other medications. 4

6. Coumadin can be a very dangerous drug because too much can cause uncontrolled bleeding. Persons taking coumadin must be careful about taking other drugs, particularly those that bind to albumin. Propose a mechanism for this drug–drug interaction.

7. Compound A is one of a series that were designed to be potent inhibitors of HIV protease.



Compound A

Compound A was tested by using two assays: (1) direct inhibition of HIV protease in vitro and (2) inhibition of viral RNA production in HIV-infected cells, a measure of viral replication; results are shown in the following table. The HIV protease activity is measured with a substrate peptide present at a concentration equal to its K_M value.

Compound A (nM)	HIV protease activity (arbitrary units)	Compound A (nM)	Viral RNA production (arbitrary units)
0	11.2	1	4.0
0.2	9.9	2	2.2
0.4	7.4	10	0.9
0.6	5.6	100	0.2
0.8	4.8	0	760
		1.0	740
		2.0	380
		3.0	280
		4.0	180
		5.0	100
		10	30

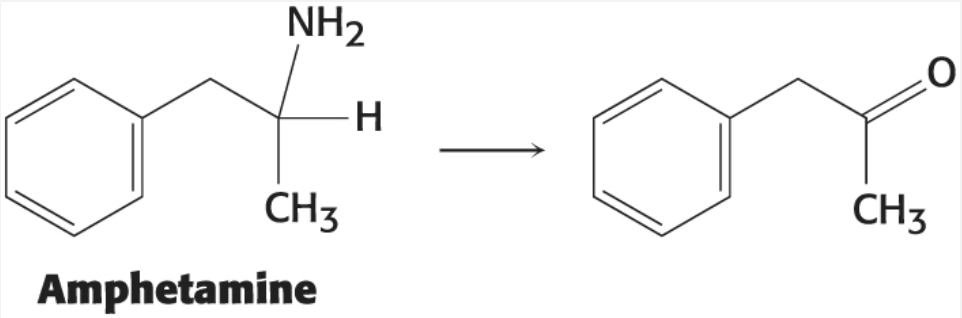
	50	20

a. Estimate the values for the K_I of compound A in the protease-activity assay and for its IC_{50} in the viral-RNA-production assay.
b. Treating rats with the relatively high oral dose of $20\ mg\ kg^{-1}$ results in a maximum concentration of compound A of 0.4 μM. On the basis of this value, do you expect compound A to be effective in preventing HIV replication when taken orally? Explain.

8. Considerable effort has been expended to develop computer programs that can estimate log(*P*) values entirely on the basis of chemical structure. Why would such programs be useful? 3

9. Distinguish between Phase I and Phase II clinical trials in regard to number of persons enrolled, the state of health of the subjects, and the goals of the study. 7

10. The metabolism of amphetamine by cytochrome P450 enzymes results in the conversion shown here. Propose a mechanism, and indicate any additional products.



Amphetamine

11. You are studying a collection of competitive inhibitors of an exciting new enzyme. The K_M value for the natural substrate is 1 μM. One member of your team presents to you a list of IC_{50} values for these compounds using an assay that employs a substrate concentration of 20 μM. A week later, another member of your team tells you about her assay that requires a substrate concentration of only 1 μM. She presents you a list of IC_{50} values for the same set of compounds, which are consistently about 10-fold lower than those previously determined. Explain why this drop in IC_{50} is not at all surprising.

12. What are some advantages of using a monoclonal antibody as a drug, as opposed to using a small molecule? 6

Chemistry Review Appendix

Visualizing Molecular Structures

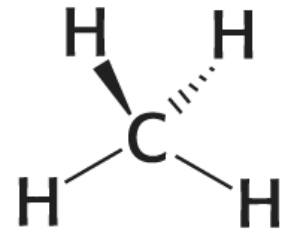
The authors of a biochemistry textbook face the problem of trying to present three-dimensional molecules in the two dimensions available on the printed page. The interplay between the three-dimensional structures of biomolecules and their biological functions are discussed extensively throughout this book. Toward this end, we frequently use representations that, although of necessity are rendered in two dimensions, emphasize the three-dimensional structures of molecules.

Depicting Structural Formulas

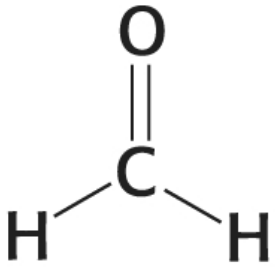
Structural formulas in this book are often shown in two different ways.

Stereochemical Renderings

Most of the chemical formulas in this book are drawn to depict the geometric arrangement of atoms — the stereochemistry — crucial to chemical bonding and reactivity, as accurately as possible. For example, the carbon atom of methane is tetrahedral, with H–C–H angles of 109.5 degrees, whereas the carbon atom in formaldehyde has bond angles of 120 degrees.



Methane

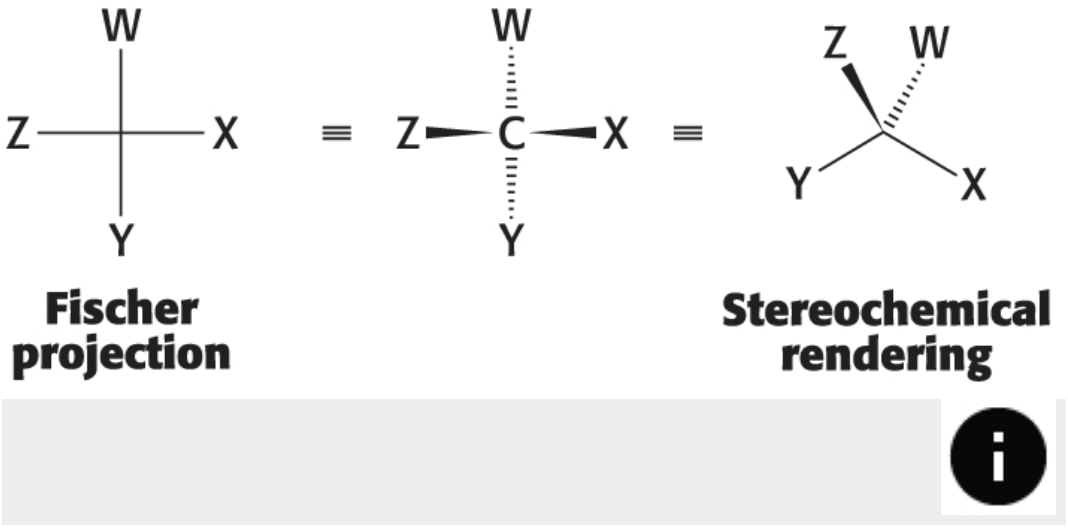


Formaldehyde

To illustrate the correct stereochemistry about tetrahedral carbon atoms, wedges are used to depict the direction of a bond into or out of the plane of the page. A solid wedge with the broad end away from the carbon atom denotes a bond coming toward the viewer out of the plane. A dashed wedge, with its broad end at the carbon atom, represents a bond going away from the viewer behind the plane of the page. The remaining two bonds are depicted as straight lines.

Fischer Projections

Although representative of the actual structure of a compound, stereochemical structures are often difficult to draw quickly. An alternative, less-representative method of depicting structures with tetrahedral carbon centers relies on the use of Fischer projections.



In a Fischer projection, the bonds to the central carbon are represented by horizontal and vertical lines from the substituent atoms to the carbon atom, which is assumed to be at the center of the cross. By convention, the horizontal bonds are assumed to project out of the page toward the viewer, whereas the vertical bonds are assumed to project behind the page away from the viewer.

Depicting Small Molecules

For depicting the molecular architecture of small molecules in more detail, two types of models are often used in this book: space filling and ball-and-stick. These models show structures at the atomic level.

Space-Filling Models

The space-filling models are the most realistic. The size and position of an atom in a space-filling model are determined by its bonding properties and van der Waals contact distance, or the van der Waals radius. The van der Waals radius describes how closely two atoms can

approach each other when they are not linked by a covalent bond. The colors of the model are set by convention.

Carbon, black	Hydrogen, white	Nitrogen, blue
Oxygen, red	Sulfur, yellow	Phosphorus, purple

Space-filling models of several simple molecules are shown in Figure 1.

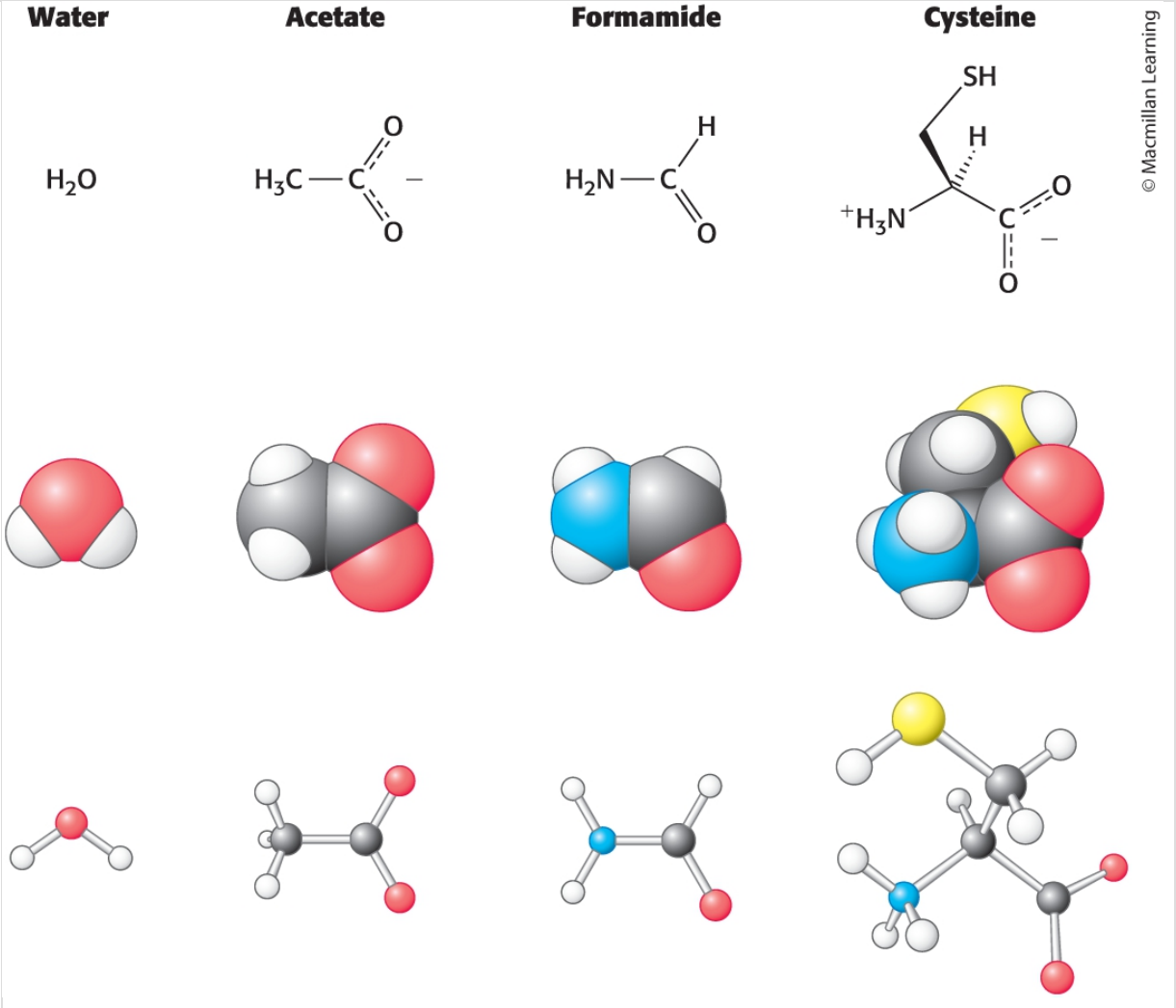


FIGURE 1 Molecules are depicted in various ways. Structural formulas (top), space-filling representations (middle), and ball-and-stick models (bottom) of several molecules are

shown.



Ball-and-Stick Models

Ball-and-stick models are not as realistic as space-filling models, because the atoms are depicted as spheres of radii smaller than their van der Waals radii. However, the bonding arrangement is easier to see because the bonds are explicitly represented as sticks. The taper of a stick helps to depict perspective and indicates which of a pair of bonded atoms is closer to the reader. Thus, a ball-and-stick model reveals a complex structure more clearly than a space-filling model does. Ball-and-stick models of several simple molecules are shown in Figure 1.

Depicting Protein Structures

Many of the powerful techniques for the determination of protein structure discussed in Chapter 4 allow the positions of the thousands of atoms within a protein to be determined. The final results include the x, y, and z coordinates for each atom in the structure. These coordinate files are compiled in the Protein Data Bank (https://www.wwpdb.org), from which they can be readily downloaded. These structures comprise thousands or even tens of thousands of atoms.

The complexity of proteins with thousands of atoms presents a challenge for the depiction of their structure. Several different types

of representations are used to portray proteins, each with its own strengths and weaknesses. The types that you will see most often in this book are space-filling models, ball-and-stick models, backbone models, and ribbon diagrams. Where appropriate, structural features of particular importance or relevance are noted in an illustration's legend.

Space-Filling Models

Space-filling models are the most realistic type of representation. Each atom is shown as a sphere with a size corresponding to the van der Waals contact distance of the atom. Bonds are not shown explicitly but are represented by the intersection of the spheres shown when atoms are closer together than the sum of their van der Waals contact distances. All atoms are shown, including those that make up the backbone and those in the side chains. A space-filling model of lysozyme is depicted in **Figure 2**.

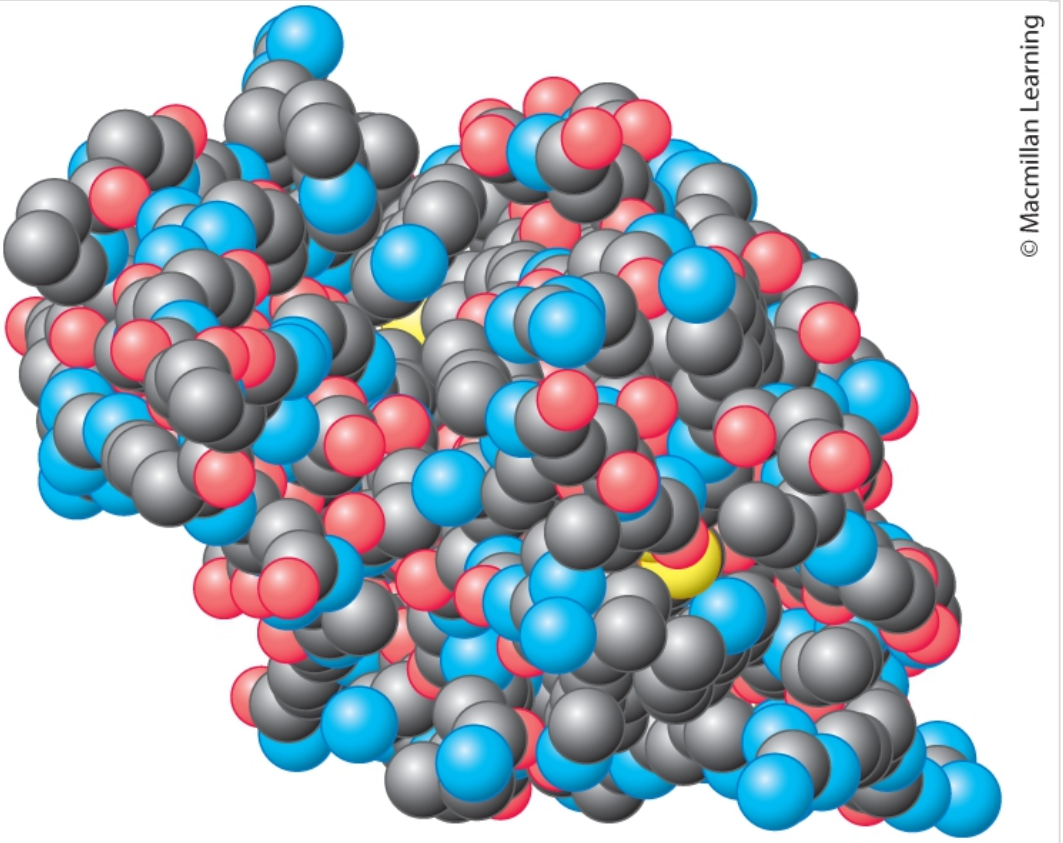


FIGURE 2 A space-filling model shows the atoms tightly packed. Hydrogen atoms are often omitted because their positions are not often readily determined and because excluding them aids visualization of the other atoms. The protein lysozyme is depicted here and in the next four figures.

Space-filling models convey a sense of how little open space there is in a protein's structure, which always has many atoms in van der Waals contact with one another. These models are particularly useful in showing conformational changes in a protein from one set of circumstances to another. A disadvantage of space-filling models is that the secondary and tertiary structures of the protein are difficult to see. Thus, these models are not very effective in distinguishing one protein from another — many space-filling models of proteins look very much alike.

Ball-and-Stick Models

Ball-and-stick models are not as realistic as space-filling models. Realistically portrayed atoms occupy more space, determined by their van der Waals contact distances, than do the atoms depicted in ball-and-stick models. However, the bonding arrangement is easier to see because the bonds are explicitly represented as sticks (Figure 3). A ball-and-stick model reveals a complex structure more clearly than a space-filling model does. Yet, the depiction is so complicated that structural features such as α helices or potential binding sites are difficult to discern.

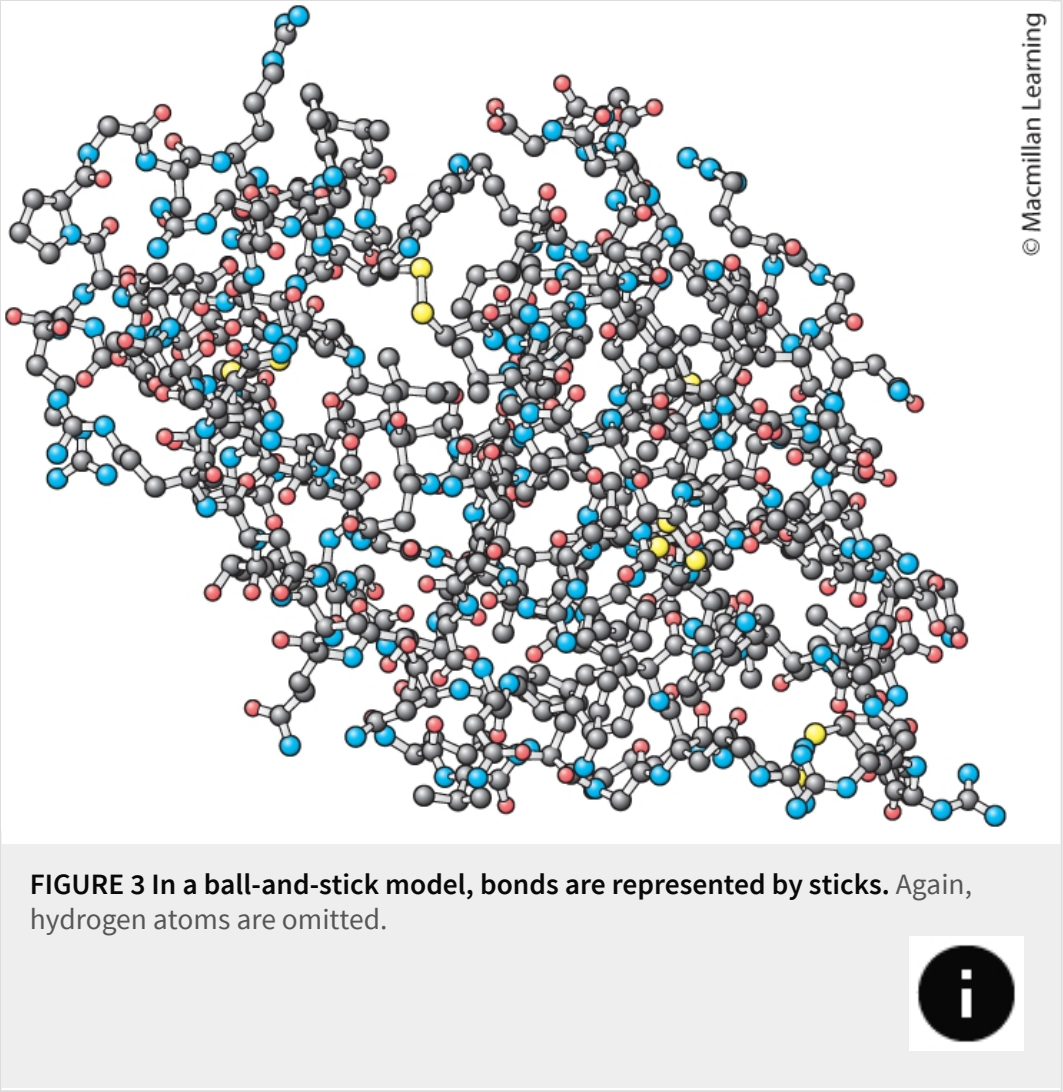


FIGURE 3 In a ball-and-stick model, bonds are represented by sticks. Again, hydrogen atoms are omitted.

Because space-filling and ball-and-stick models depict protein structures at the atomic level, the large number of atoms in a complex structure makes it difficult to distinguish the relevant structural features. Thus, representations that are more schematic — such as backbone models and ribbon diagrams — have been developed for the depiction of macromolecular structures. In these representations, most or all atoms are not shown explicitly.

Backbone Models

Backbone models show only the backbone atoms of a polypeptide chain, or sometimes only the α-carbon atom of each amino acid. Atoms are linked by lines representing bonds; if only α-carbon atoms are depicted, lines connect α-carbon atoms of amino acids that are adjacent in the amino acid sequence (**Figure 4**). While in Figure 4, the α-carbon atoms are shown, elsewhere in this book backbone models show only the lines connecting the α-carbon atom positions; bonds to other carbon atoms are not depicted.

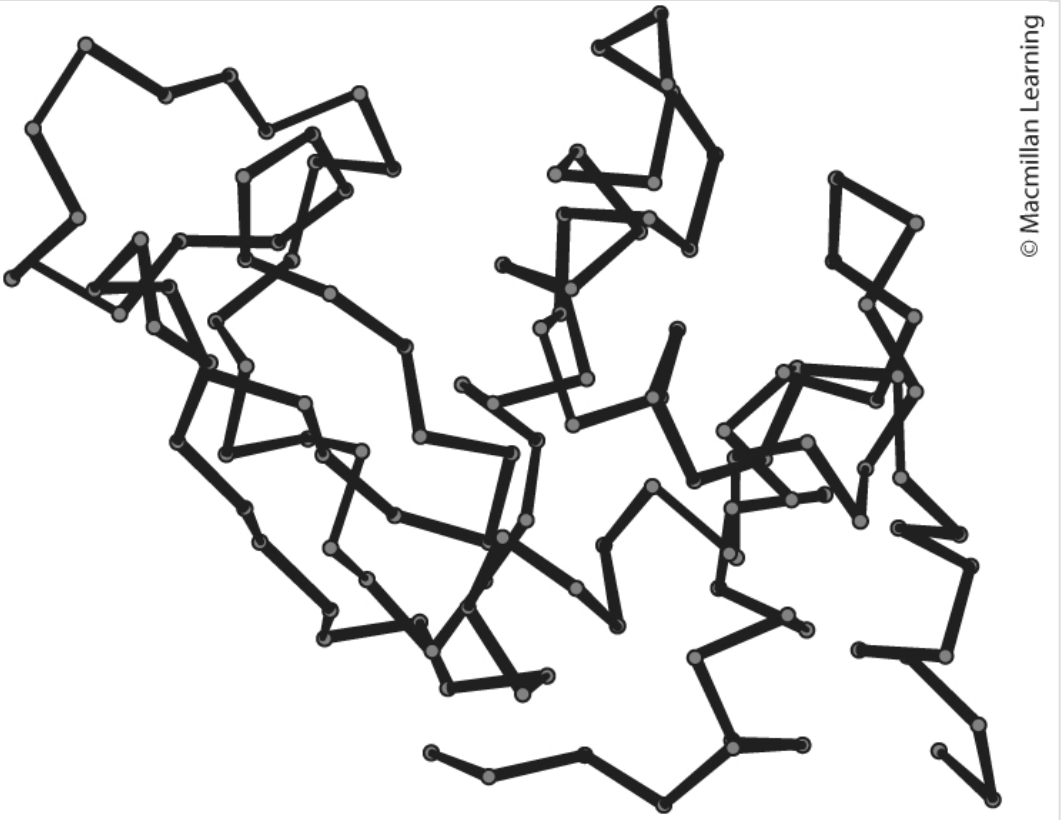


FIGURE 4 In a backbone model, only the backbone polypeptide chain is represented. In this model, the α carbons of the adjacent amino acids are shown in gray and lines relating their positions in black. Many backbone models omit the atoms and include only the lines.

A backbone model shows the overall course of the polypeptide chain much better than a space-filling or ball-and-stick model does. However, secondary structural elements are still difficult to see.

Ribbon Diagrams

Ribbon diagrams are highly schematic and most commonly used to accent a few dramatic aspects of protein structure, such as the α

helix, depicted as a coiled ribbon or a cylinder. The β strand is depicted as a broad arrow, and loops, turns, and random coil structure are all shown with thin tubes. These structural depictions provide the clearest views of the folding patterns of proteins (**Figure 5**). The ribbon diagram allows the course of a polypeptide chain to be traced and readily shows the secondary structural elements. Thus, ribbon diagrams of proteins that are related to one another by evolutionary divergence appear similar (as shown in Figure 10.13), whereas unrelated proteins are clearly distinct.

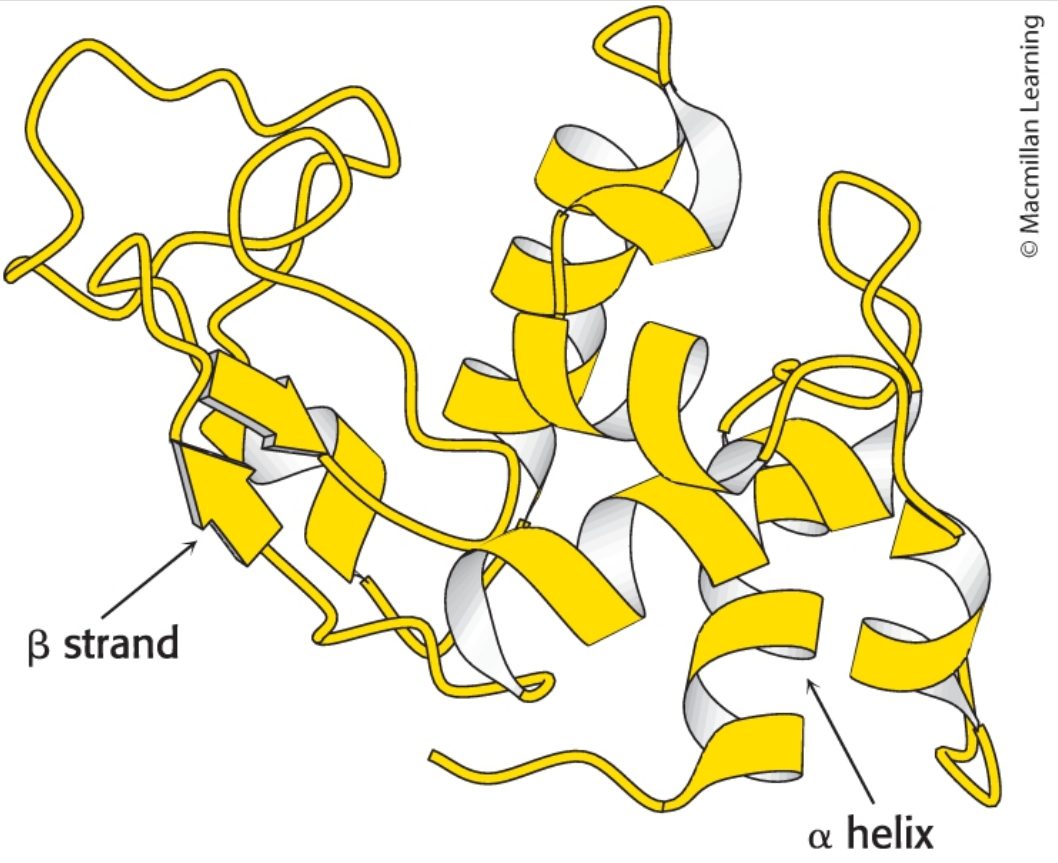


FIGURE 5 In a simple ribbon diagram, the α helices are shown as coiled ribbons and β strands are depicted as arrows. More irregular structures are shown as thin tubes.

In this book, coiled ribbons are generally used to depict α helices. However, for membrane proteins, which are often quite complex, cylinders are used rather than coiled ribbons. This convention also makes membrane proteins with their membrane-spanning α helices easy to recognize (as shown in Figure 12.18).

Bear in mind that the open appearance of ribbon diagrams is deceptive. As noted earlier, protein structures are tightly packed and have little open space. However, the openness of ribbon diagrams makes them particularly useful as frameworks in which to highlight additional aspects of protein structure. Active sites, substrates, bonds, and other structural fragments can be included in ball-and-stick or space-filling form within a ribbon diagram (**Figure 6**).

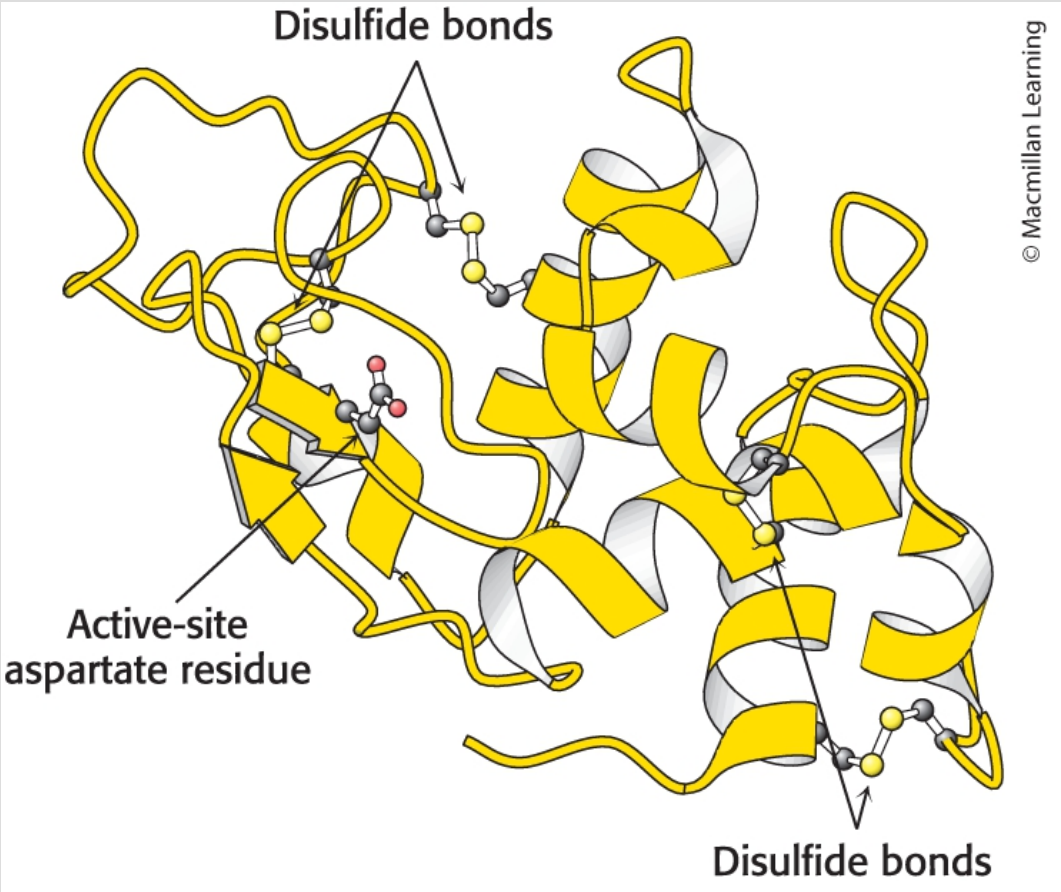


FIGURE 6 An enhanced ribbon diagram may show functionally important areas using ball-and-stick. Four disulfide bonds and a functionally important aspartate

residue of lysozyme are shown in ball-and-stick form.



Functional Groups

Biochemistry depends on many concepts and principles from organic chemistry. The properties of individual atoms are substantially affected by the other atoms to which they are bonded. Functional groups are specific combinations of a small number of atoms that often have properties that are relatively independent of other aspects of the molecules in which they are found. There are many functional groups in organic chemistry, but a relatively small number of these are central to biochemistry:

- *Hydroxyl group,* $-OH$ A hydroxyl group comprises an oxygen atom bonded to a hydrogen atom. The hydroxyl group can both donate and accept hydrogen bonds. The hydroxyl group is both a very weak acid and a very weak base.

- *Amino group,* $-NH_2$ An amino group comprises a nitrogen atom bonded to two hydrogen atoms. The amino group can both donate and accept hydrogen bonds. The amino group often behaves as a base, accepting a hydrogen ion to form an ammonium group, $-NH_3^+$.

- *Carbonyl group,* $\rangle C{=}O$ A carbonyl group comprises a carbon atom double bonded to an oxygen atom. The carbonyl group can act as a hydrogen bond acceptor but not a donor. The carbonyl

group is found in many different classes of compounds, depending on the other groups that are bonded to the carbon atom. The most important carbonyl-containing functional group in biochemistry is the amide, in which the carbonyl carbon is bonded to one carbon and one nitrogen.

It may be beneficial to review the name and structure of some common functional groups so that you can recognize them readily during your study of biochemistry. Figure 7 lists some commonly encountered groups.

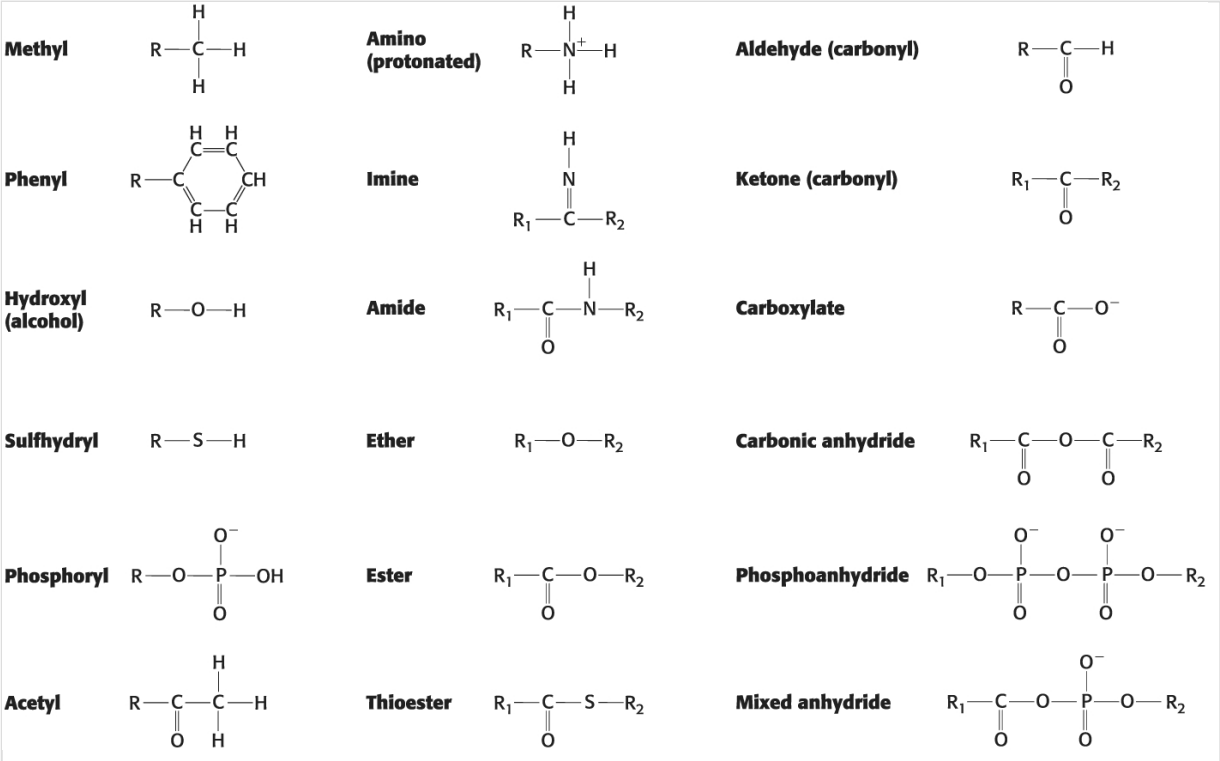
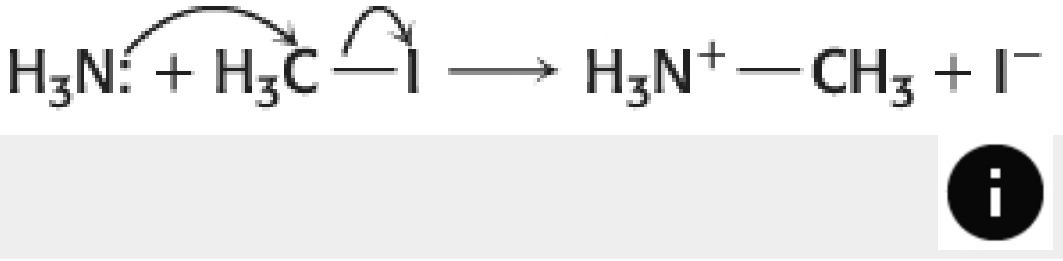


FIGURE 7 Functional groups define many important properties of macromolecules.

Reaction Mechanisms: “Arrow Pushing”

Many aspects of biochemistry depend on chemical reactions in which covalent bonds are broken and formed. These reactions involve the flow of electrons out of bonds and into spaces between atoms in which new bonds are formed. It is often useful to depict such reactions with arrows to represent this electron flow. The process of analyzing reactions in this way is sometimes referred to informally as “arrow pushing” or “electron pushing.”

Consider the reaction between ammonia, NH_3, and methyl iodide, $H_3C—I$. NH_3 has a lone pair of electrons on the nitrogen atom that can participate in bond formation. The iodine atom in $H_3C—I$ can accept electrons to form the relatively stable iodide ion, I^-. The reaction and its mechanism are shown below:



The first arrow depicts the flow of the electron pair from the nitrogen to the space between the nitrogen and the carbon to form the new nitrogen–carbon bond. The second arrow shows the flow of electrons from the carbon–iodine bond to the iodine to form the iodide ion. The initial product of this reaction is methylammonium ion, methylamine in its protonated form. In this reaction, ammonia is the nucleophile, meaning the molecule or group that donates an electron pair during a reaction.

In this book, we encounter many examples of reaction mechanisms, particularly when we discuss the actions of enzymes — the essential

catalysts that facilitate so much of biochemistry.

Answers to Self-Check Questions

Chapter 1

Page 7 TATCGGACCT
Page 14 The enthalpy change (heat released or absorbed by the system) accounts for entropy changes in the surroundings.
Page 20 15.14
Page 26 No

Chapter 2

Page 41 Isoleucine and threonine. Both these atoms feature four unique groups emerging from the first carbon atom in their side chains. These atoms are indicated by an asterisk in Figures 2.6 and 2.7.

Page 46 Proline and glycine. The cyclic side chain of proline linking the nitrogen and α-carbon atoms limits φ to a very narrow range (around -60 degrees). The lack of steric hindrance exhibited by the side chain hydrogen atom of glycine enables this amino acid to access a much greater area of the Ramachandran plot.

Page 50 There are about 3.6 amino acids per turn of an α helix, so residues three or four amino acids apart will appear on the same face. By contrast, adjacent amino acids appear on opposite faces of a β strand, so every other residue will lie on the same face.

Page 53 The amino acids would be hydrophobic in nature. An α helix is especially suited to crossing a membrane because all of the amide hydrogen atoms and carbonyl oxygen atoms of the peptide backbone take part in intrachain hydrogen bonds, thus stabilizing these polar atoms in a hydrophobic environment.

Page 57 If the protein concentration was high upon denaturation, groups from different molecules might interact to form a large, insoluble aggregate.

Chapter 3

Page 72 $50\ \text{nanograms/ml} = 2.3 \times 10^{-9}\ \text{M} = 2.3\ \text{nM}$. The $L_{1/2}$ value would be expected to be in the same range.
Page 72 The dissociation rate is equal to the association rate at equilibrium. $5\ s^{-1}$.

Page 79 b.
Page 80 Since the proximal histidine is not attached to the protein, it is free to move into the plane of the heme when oxygen binds; so, the oxygen affinity is high, similar to that of myoglobin.
Page 88 Total number, 12. Total not counting duplicates, 6; 3 from the light chain and 3 from the heavy chain.
Page 94 The association rate constant is $k_1 = 10^4\ s^{-1}/10^{-3}\ M = 10^7\ M^{-1}s^{-1}$. The dissociation rate constant is $k_{-1} = 50\ s^{-1}$. The dissociation constant is $K_d = 50\ s^{-1}/10^7\ M^{-1}s^{-1} = 5 \times 10^6\ M$.

Chapter 4

Page 107 Note in Figure 4.10 that the relative electrophoretic mobility of proteins is proportional to the *logarithm* of their individual masses. The mass of the protein is 50 kDa.

Page 116 A sandwich ELISA experiment requires both antibodies to be able to simultaneously bind the antigen. If the capture antibody on the plate and the detection antibody both recognize the same epitope, then each antibody will displace the other. Either the antigen will remain bound to the capture antibody and will not be detected, or the antigen will bind to the soluble detection antibody and will be washed away before the detection step.

Page 121 Isoleucine and leucine are isomers and, hence, have identical masses. Peptide sequencing by mass spectrometry as described in this chapter is incapable of distinguishing these two residues. Further analytical techniques are required to differentiate them.

Page 132 Protein crystal formation requires the ordered arrangement of identically positioned molecules. Proteins with flexible linkers can introduce disorder into this arrangement and prevent the formation of suitable crystals.

Chapter 5

Page 144 All three terms apply, but prosthetic group is the most specific.

Page 158 K_M is an intrinsic property of an enzyme because it is independent of the quantity of enzyme measured. In contrast, V_{max} is an extrinsic property because it does depend on the quantity of enzyme observed.

Page 159 The mutation made the enzyme a more efficient catalyst as the catalytic efficiency (k_{cat}/K_M) increased by 50%.

Page 169 Competitive.

Chapter 6

Page 180 Catalysis by approximation (since it brings two substrates together).

Page 189 The same as is shown in Figure 6.8, except that cysteine replaces serine in the active site and no aspartate is present.

Page 193 $10^4\ s^{-1}$. The maximum expected buffer-assisted rate is $10^9\ M^{-1}s^{-1} \times 10^{-6}\ M = 10^3\ s^{-1}$, but the unassisted maximum rate is $10^4\ s^{-1}$.

Page 199 EcoRV binds all sequences with approximately equal affinity but discriminates at the cleavage step.

Page 204 ATP is reversible hydrolyzed in the myosin active site with incorporation of ^{18}O. Some of this ATP is released as ATP rather than $ADP + P_i$ and this ATP will include ^{18}O.

Chapter 7

Page 216 All of the enzyme would be in the R form all of the time. There would be no cooperativity. The kinetics would look like that of a Michaelis–Menten enzyme.

Page 221 The net outcome of the two reactions is the hydrolysis of ATP to ADP and P_i, which has a ΔG of $-50\ \text{kJ mol}^{-1}\ (-12\ \text{kcal mol}^{-1})$ of under cellular conditions.

Page 226 Although quite rare, cases of enteropeptidase deficiency have been reported. The affected person has diarrhea and fails to thrive because digestion is inadequate. In particular, protein digestion is impaired.

Page 232 Antithrombin III is a very slowly hydrolyzed substrate of thrombin. Hence, its interaction with thrombin requires a fully formed active site on the enzyme.

Chapter 8

Page 242 There would be too much charge repulsion from the negative charges on the phosphoryl groups. These charges must be countered by the addition of cations.

Page 248 (a) Hydrogen bonds between base pairs and van der Waals interactions among the bases. The van der Waals interactions come into play because of the hydrophobic effect, which forces the bases to the interior of the helix. (b) One possible explanation is that GC base pairs have three hydrogen bonds compared with two for AT base pairs; the higher content of GC would mean more hydrogen bonds and greater helix stability. Another possibility is that the base stacking interactions are stronger for GC base pairs than for AT base pairs. Careful measurements support the second explanation: the favorable base-stacking energy of GC base pairs largely contributes to the increases in melting temperature.

Page 256 The genetic code is degenerate. Of the 20 amino acids, 18 are specified by more than one codon. Hence, many nucleotide changes (especially in the third base of a codon) do not alter the nature of the encoded amino acid. Mutations leading to an altered amino acid are usually more deleterious than those that do not and hence are subject to more stringent selection.

Chapter 9

Page 266 The presence of the AluI sequence would, on average, be $(1/4)^4$, or $1/256$, because the likelihood of any base being at any position is one-fourth and there are four positions. By the same reasoning, the presence of the NotI sequence would be $(1/4)^8$, or $1/65{,}536$. Thus, the average product of digestion by AluI would be 250 base pairs (0.25 kb) in length, whereas that by NotI would be 66,000 base pairs (66 kb) in length.

Page 270 At high temperatures of hybridization, only very close matches between primer and target would be stable because all (or most) of the bases would need to find partners to stabilize the primer–target helix. As the temperature is lowered, more mismatches would be tolerated; so the amplification is likely to yield genes with less sequence similarity. In regard to the yeast gene, synthesize primers corresponding to the ends of the gene, and then use these primers and human DNA as the target. If nothing is amplified at 54°C, the human gene differs from the yeast gene, but a counterpart may still be present. Repeat the experiment at a lower temperature of hybridization.

Page 278 The average frequency of EcoRI sites in the genome is $(1/4)^6 = 1/4{,}096$, or about once in every 4 kb. Because most human genes are much longer than 4 kb, this would not be a suitable cloning strategy, as most fragments would contain only a small part of a complete gene.

Page 294 Since PAM sequences are required downstream of a particular target site, variants of Cas9 that recognize different PAMs would increase the likelihood that a sgRNA could be designed against a particular target sequence.

Chapter 10

Page 305 Placement of too many gaps in an alignment could artificially increase the number of identities.
Page 309 44% identity.
Page 314 To detect pairs of residues with correlated mutations, there must be variability in these sequences. If the alignment is overrepresented by closely related organisms, there may not be enough changes in their sequences to allow the identification of potential base-pairing patterns.

Chapter 11

Page 330 D-Fructopyranose; the chair conformation of D-fructopyranose; bulky groups in equatorial positions about a ring structure; β-anomer of D-glucopyranose
Page 333 All three are reducing sugars.
Page 337 Maltose, cellulose, starch, amylose, and glycogen; cellulose and chitin.
Page 346 The genome is the least complex; the glycome is likely the most complex.

Chapter 12

Page 358 Phospholipids, glycolipids (which are a subclass of sphingolipids), and cholesterol. Examples of polar head groups include serine, ethanolamine, choline, and inositol.
Page 360 Essentially an “inside-out” membrane. The hydrophilic groups would come together on the interior of the structure, away from the solvent, whereas the hydrocarbon chains would interact with the solvent.
Page 369 In a hydrophobic environment, the formation of intrachain hydrogen bonds stabilizes the amide hydrogen atoms and carbonyl oxygen atoms of the polypeptide chain, and so an α helix forms. In an aqueous environment, these groups are stabilized by interaction with water, and so there is no energetic reason to form an α helix. Thus, the α helix would be more likely to form in a hydrophobic environment.
Page 372 The presence of a cis double bond introduces a kink in the fatty acid chain that prevents tight packing and reduces the number of atoms in van der Waals contact. The kink lowers the melting point compared with that of a saturated fatty acid. Trans fatty acids do not have the kink, and so their melting temperatures are higher, more similar to those of saturated fatty acids. Because trans fatty acids have no structural effect, they are rarely observed.

Chapter 13

Page 390 SERCA, a P-type ATPase, uses a mechanism by which a covalent phosphorylated intermediate (at an aspartate residue) is formed. At steady state, a subset of the SERCA molecules is trapped in the E_2-P state and, as a result, radiolabeled. The MDR protein is an ABC transporter and does not operate through a phosphorylated intermediate. Hence, a radiolabeled band would not be observed for MDR.

Page 392 FCCP effectively creates a pore in the bacterial membrane through which protons can pass rapidly. Protons that are pumped out of the bacteria will pass through this pore preferentially (the "path of least resistance"), rather than participate in H^+/lactose symport.

Page 398 An ion channel must transport ions in either direction at the same rate. The net flow of ions is determined only by the composition of the solutions on either side of the membrane.

Page 407 Cardiac muscle must contract in a highly coordinated manner in order to pump blood effectively. Numerous gap junctions, abundant in connexin proteins, mediate the orderly cell-to-cell propagation of the action potential through the heart during each beat.

Chapter 14

Page 424 In cardiac muscle, increased cAMP levels lead to increased protein kinase A activity, which leads to increased phosphorylation of troponin, resulting in muscle contraction. In smooth muscle, decreased cAMP levels lead to decreased protein kinase A activity, which decreases the level of phosphorylation of myosin light chains, thus decreasing the extent of muscle contraction.
Page 430 No, the substrate preference and the activation loop sequence are quite different.
Page 433 Both Ras and a heterotrimeric G protein are activated by GTP for GDP exchange. Ras is a small monomeric protein, whereas heterotrimeric G proteins are larger and exist as trimers in their inactive states. (Other answers are possible.)
Page 437 One would expect the loss of sensitivity to the odor of one or a small number of compounds detectable by most individuals.
Page 441 Olfaction: odorant molecules; vision: light in the visible range; hearing: pressure waves (vibrations) in the air. Odorant molecules bind to odorant receptors; light absorption results in isomerization of 11-cis-retinal in visual pigments; air vibrations result in relative displacement of stereocilia in hair bundles.

Chapter 15

Page 449 A can still be converted to B despite a positive $\Delta G^{\circ\prime}$ value if the concentrations of A and B are sufficiently imbalanced such that ΔG is negative. Alternatively, the reaction that converts A into B can be coupled to another reaction with a negative $\Delta G^{\circ\prime}$ value by an enzyme such that the overall reaction now has a negative $\Delta G^{\circ\prime}$ value.

Page 459 Statement 3 is the only true statement. Statement 1 is false because energy is required to break covalent bonds and is released upon bond formation with water, and Statement 2 is false because ATP has an intermediate phosphoryl transfer potential.

Page 468 Coenzyme A; $NADP^+$; Vitamins.

Chapter 16

Page 484 The 1-arseno-3-phosphoglycerate that will be formed will be rapidly hydrolyzed so no ATP can be generated by the next reaction of glycolysis by phosphoglycerate kinase. Thus, arsenate eliminates one of the two ATP-synthesizing steps in glycolysis. In fact, all enzymes that use phosphate could use arsenate, severely compromising the energy production of the cell, leading to cell damage. If the arsenate concentration were high enough, death would result.
Page 486 Two molecules of NADH and four molecules of ATP.
Page 488 Two molecules of ATP and zero molecules of NADH.
Page 492 Classic galactosemia is much more detrimental to human health. If a person was galactosemic, it would be better to be lactose intolerant so that less galactose would be absorbed when lactose is consumed in the diet.
Page 499 ATP initially stimulates PFK activity, as would be expected for a substrate, but at higher concentrations, it inhibits the enzyme. Although this effect seems counterintuitive for a substrate, recall that the function of glycolysis in muscle is to generate ATP. Consequently, high concentrations of ATP signal that the ATP needs are met and glycolysis should stop. In addition to being a substrate, ATP is an allosteric inhibitor of PFK, with the allosteric site having a lower affinity for ATP than the active site.
Page 508 The energy needs of a muscle cell vary widely, from rest to intense exercise, so the rapid regulation of phosphofructokinase by ATP and AMP is vital. In other tissues, such as the liver, ATP concentration is less likely to fluctuate and will not be a key regulator of phosphofructokinase, but rather the enzyme, and its counterpart in gluconeogenesis, fructose 1,6-bisphosphatase, are subject to hormonal control through the action of fructose 2,6-bisphosphate instead.

Page 509 Forming lactate allows tissues that are anaerobic, either temporarily, like skeletal muscle, or permanently, like some parts of the skin, to continue to produce ATP without oxygen. The burden of resynthesizing glucose from lactate at the expense of ATP can be borne by other tissues, like the liver, that are replete with oxygen and energy stores. Thus, the Cori cycle allows an important division of labor in the body.

Page 511 Fructose 2,6-bisphosphate, present at high concentration when glucose is abundant, normally slows gluconeogenesis by inhibiting fructose 1,6-bisphosphatase. In this genetic disorder, the phosphatase is active irrespective of the glucose level. Hence, substrate cycling is increased. The level of fructose 1,6-bisphosphate is consequently lower than normal. Less pyruvate is formed, and thus less ATP is generated.

Chapter 17

Page 521 The remaining steps regenerate oxidized lipoamide, which is required to begin the next reaction cycle. Moreover, this regeneration results in the production of high-energy electrons in the form of NADH.

Page 529 The fact that fluorocitrate is formed tells us something about the immediate metabolic fate of fluoroacetate: It must first be converted to fluoroacetyl CoA and enter the citric acid cycle. Fluoroacetyl CoA must react with oxaloacetate to form fluorocitrate, but while citrate is normally converted into isocitrate by the enzyme aconitase, it appears that fluorocitrate is not a substrate for aconitase, and so it accumulates.

Page 531 The enzyme nucleoside diphosphokinase transfers a phosphoryl group from GTP (or any nucleoside triphosphate) to ADP according to the reversible reaction: $\mathrm{GTP + ADP \rightleftharpoons GDP + ATP}$

Page 534 The CAC depends on a steady supply of $\mathrm{NAD^+}$ as an oxidant, generating NADH. $\mathrm{O_2}$ is never directly utilized in the cycle. However, $\mathrm{NAD^+}$ is regenerated via donation of electrons to $\mathrm{O_2}$ by way of the electron transport chain, so eventually a lack of $\mathrm{O_2}$ will cause the cycle to cease due to a lack of $\mathrm{NAD^+}$. The same is true of FAD and $\mathrm{FADH_2}$.

Chapter 18

Page 545 From the cytosol it would pass through the mitochondrial outer membrane, into the intermembrane space (IM space), then through the mitochondrial inner membrane, and finally into the mitochondrial matrix. The infoldings are called cristae, and they are formed by the mitochondrial inner membrane.
Page 549 Pyruvate accepts electrons and is thus the oxidant. NADH gives up electrons and is the reductant.
Page 552 The 10 isoprene units render coenzyme Q soluble in the hydrophobic environment of the inner mitochondrial membrane. The two oxygen atoms can reversibly bind two electrons and two protons as the molecule transitions between the quinone form and quinol form.
Page 561 The answer to all three questions is Succinate-Q reductase (Complex II).
Page 562 Complex I would be reduced, whereas Complexes II, III, and IV would be oxidized. The citric acid cycle would halt because it has no way to oxidize NADH.
Page 567 Recall from the discussion of enzyme-catalyzed reactions that the direction of a reaction is determined by the ΔG difference between substrate and products and that enzymes accelerate the rate of both the forward and the backward reactions. The hydrolysis of ATP is exergonic, and so ATP synthase will enhance the hydrolytic reaction.
Page 570 3 ATP per full rotation; $14 \text{ protons} / 3 \text{ ATP} = 4.7$ protons per ATP if there are 14 **c** subunits.
Page 573 The extra negative charge on ATP relative to that on ADP accounts for ATP's translocation out of the mitochondrial matrix toward the more positively charged side of the inner mitochondrial membrane. Mg^{2+} lessens the charge differences between ATP and

ADP, reducing the impact of charge on the directionality of transport. Additionally, by decreasing the difference between the two ligands, the metal may make ADP more readily compete with ATP for transport to the cytoplasm.

Page 579 DNOC must be an uncoupler, similar to DNP. Recall that uncouplers deplete the proton gradient, allowing the electron-transport chain to operate in the absence of ATP synthesis. In the presence of DNOC, the energy released by the electron-transport chain is released as heat instead of being used to synthesize ATP. Oxygen consumption will increase as more fuel molecules are metabolized to try to make up for the lack of ATP produced by ATP synthase.

Page 579 In the presence of poorly functioning mitochondria, the only means of generating ATP is by anaerobic glycolysis, which will lead to an accumulation of lactic acid in blood.

Page 581 A proton-motive force across the plasma membrane is necessary to drive the flagellar motor. Under conditions of starvation, this proton-motive force is depleted. In acidic solution, the pH difference across the membrane is sufficient to power the motor.

Chapter 19

Page 587 Phototrophy and autotrophy.
Page 589 Chloroplasts are descended from an ancient bacterium that was engulfed and became codependent with another organism, a phenomenon called endosymbiosis. Within chloroplasts are membrane-enclosed compartments called thylakoids. The internal compartment of the thylakoid is called the stroma.
Page 593 The special pair is a specific pair of chlorophyll molecules in the reaction center that absorb light energy and transfer an electron away, creating photoinduced charge separation, the key to photosynthesis.
Page 599 PS I generates reduced ferredoxin, a powerful reductant that reduces $NADP^+$ to NADPH. PS II activates the WOC, a powerful oxidant capable of oxidizing water, generating O_2. The WOC releases the electrons that will ultimately reduce $NADP^+$ and generates protons to form the proton gradient used to drive the synthesis of ATP.
Page 602 The two components are the chemical gradient and the charge gradient. The chemical gradient is nearly entirely responsible for ATP production in chloroplasts because the thylakoid membrane is quite permeable to Cl^- and Mg^{2+}. Thus, as H^+ is pumped into the thylakoid lumen, Mg^{2+} moves out of the lumen while Cl^- move in, dissipating any charge gradient that would otherwise form.

Chapter 20

Page 615 When ribulose 1,5-bisphosphate reacts with CO_2, it forms a six-carbon compound that splits into two molecules of 3-phosphoglycerate. Only one will have ^{14}C.

Page 618 In the dark reactions, magnesium serves to bind ribulose 1,5-bisphosphate and activate it for reaction with CO_2. In the light reactions, magnesium is present in chlorophyll.

Page 634 In the pentose phosphate pathway, erythrose 4-phosphate reacts with xylulose 5-phosphate to produce fructose 6-phosphate and glyceraldehyde 3-phosphate in a reaction catalyzed by transketolase. In the Calvin–Benson cycle, erythrose 4-phosphate reacts with dihydroxyacetone phosphate to form sedoheptulose 1,7-bisphosphate in a reaction catalyzed by aldolase.

Chapter 21

Page 646 Phosphorylase, debranching enzyme, phosphoglucomutase, and glucose 6-phosphatase.

Page 647 Free glucose must be phosphorylated at the expense of one ATP, whereas glucose 6-phosphate derived from glycogen is formed by phosphorolytic cleavage, sparing one molecule of ATP. Thus, the net yield of ATP when glycogen-derived glucose is processed to pyruvate is three molecules of ATP compared with two molecules of ATP from free glucose.

Page 649 Glucose is an allosteric inhibitor of phosphorylase *a*. Hence, crystals grown in its presence are in the T state. The addition of glucose 1-phosphate, a substrate, causes a conformational change in the enzyme toward the R state which is sufficiently large that the crystal shatters.

Page 660 In the liver, glucagon stimulates the cAMP-dependent pathway that activates protein kinase A. Epinephrine binds to a 7TM α-adrenergic receptor in the liver plasma membrane, which activates phospholipase C and the phosphoinositide cascade. This activation causes calcium ions to be released from the endoplasmic reticulum, which bind to calmodulin, and further stimulates phosphorylase kinase and glycogen breakdown.

Chapter 22

Page 668 Two times each. The triacylglycerol will be hydrolyzed in the intestinal lumen, resynthesized in the intestinal cell, hydrolyzed again in the blood, and resynthesized again in the adipocyte.
Page 671 Fat mobilization in adipocytes is activated by phosphorylation. Hence, overproduction of the cAMP-activated kinase will lead to an accelerated breakdown of triacylglycerols and a depletion of fat stores.
Page 674 Fatty acids cannot be transported into mitochondria for oxidation. The muscles cannot use fats as a fuel. Muscles could use glucose derived from glycogen. However, when glycogen stores are depleted, as after a fast, the effect of the deficiency is especially apparent.
Page 683 Eight molecules of acetyl CoA combine to form four molecules of acetoacetate for release into the blood, and so they do not contribute to the energy yield in the liver. However, the $FADH_2$ and $NADH$ generated in the preparation of acetyl CoA can be processed by oxidative phosphorylation to yield ATP.

$$1.5\ ATP/FADH_2 \times 7 = 10.5\ ATP$$
$$2.5\ ATP/NADH \times 7 = 17.5\ ATP$$

The equivalent of 2 ATP were used to form palmitoyl CoA. Thus, 26 ATP were generated for use by the liver.
Page 687 HCO_3^- is attached to acetyl CoA to form malonyl CoA. When malonyl CoA condenses with acetyl CoA to form the four-carbon ketoacyl CoA, the HCO_3^- is lost as CO_2.
Page 696 Phosphofructokinase controls the flux down the glycolytic pathway which generates ATP or building blocks for biosynthesis, depending on the tissue. The presence of citrate in the cytoplasm

means that the cell favors fatty acid synthesis over degradation, indicating that those needs are met, and there is no need to catabolize glucose.

Chapter 23

Page 703 Dietary amino acids are absorbed in the upper part of the small intestine (the duodenum). The primary fate of both dietary and cellular-derived amino acids is as building blocks for cellular proteins and other nitrogen-containing molecules.
Page 707 Exposure of such a region suggests that a component of a multiprotein complex has failed to form properly or that one component has been synthesized in excess. This exposure leads to rapid degradation and the restoration of appropriate stoichiometries.
Page 709 Aminotransferases transfer the α-amino group to α-ketoglutarate to form glutamate. Glutamate is oxidatively deaminated to form an ammonium ion in the liver by glutamate dehydrogenase.
Page 713 Ser and Thr. The presence of a hydroxyl group on the β-carbon.
Page 718 Carbamoyl phosphate and aspartate.
Page 728 As shown in Figure 23.27, alanine, a gluconeogenic amino acid, is released during the metabolism of tryptophan to acetyl CoA and acetoacetyl CoA.

Chapter 24

Page 736 Cholecystokinin (CCK) and glucagon-like peptide 1 (GLP-1) are short-term and anorexigenic. Ghrelin is short-term and orexigenic.
Page 741 Phosphorylation of dietary glucose after it enters the liver; gluconeogenesis; glycogen breakdown.
Page 742 When glycogen stores are filled, the excess carbohydrates are metabolized to acetyl CoA, which is then converted into fats. Human beings cannot convert fats into carbohydrates, but they can certainly convert carbohydrates into fats.
Page 743 Such a mutation would increase the phosphorylation of the insulin receptor and IRS in muscle and would improve insulin sensitivity. Indeed, PTP1B is an attractive therapeutic target for type 2 diabetes.
Page 745 The inability of muscle mitochondria to process all of the fatty acids leads to excessive levels of diacylglycerol (DAG) and ceramide in the muscle cytoplasm. DAG is a second messenger that activates protein kinase C, which phosphorylates IRS, reducing its ability to propagate the insulin signal. Ceramide inhibits Akt.
Page 746 In the absence of insulin, lipid mobilization will take place to an extent that it overwhelms the ability of the liver to convert the lipids into ketone bodies. The excess is re-esterified and released into the blood.
Page 753 A role of the liver is to provide glucose for other tissues. In the liver, glycolysis is used not for energy production but for biosynthetic purposes. Consequently, in the presence of glucagon, liver glycolysis stops so the glucose can be released into the blood.
Page 754 Adipose tissue. Other tissues are the liver and muscle which store glycogen, and the skeletal muscle which technically acts as a storage of energy if necessary in the form of muscle proteins.

Page 757 Ethanol is oxidized to yield acetaldehyde by alcohol dehydrogenase, which is subsequently oxidized to acetate and acetaldehyde. Ethanol is also metabolized to acetaldehyde by the P450 enzymes, with the subsequent depletion of NADPH.

Chapter 25

Page 767 Glutamine synthetase:

$$\text{Glutamate} + \text{ATP} + \text{NH}_3 \rightarrow \text{glutamine} + \text{ADP} + \text{P}_i$$

Glutamate synthase:

$$\alpha\text{–Ketoglutarate} + \text{glutamine} + \text{NADPH} + \text{H}^+ \rightarrow 2\ \text{glutamate} + \text{NADP}^+$$

The sum of these reactions is:

$$\text{NH}_4^{\ +} + 2\ \alpha\text{–ketoglutarate} + \text{NADPH} + \text{ATP} \rightarrow \text{glutamate} + \text{NADP}^+ + \text{ADP} + \text{P}_i$$

Page 771 Both conversions are amidation reactions that require ATP hydrolysis. In the conversion of glutamate to glutamine, the nitrogen donor is ammonia and the side chain carboxylate is activated by phosphorylation. In the conversion of aspartate to asparagine in human beings, the nitrogen donor is glutamine and the side chain carboxylate is activated by adenylation.

Page 775 (a) N^5,N^{10}-Methylenetetrahydrofolate; (b) N^5-methyltetrahydrofolate.

Page 788 Succinyl CoA is formed in the mitochondrial matrix as part of the citric acid cycle.

Chapter 26

Page 795 Aspartate and carbamoyl phosphate.

Page 799 Carbon dioxide, glycine, aspartate, glutamine, and N^{10}-formyltetrahydrofolate.

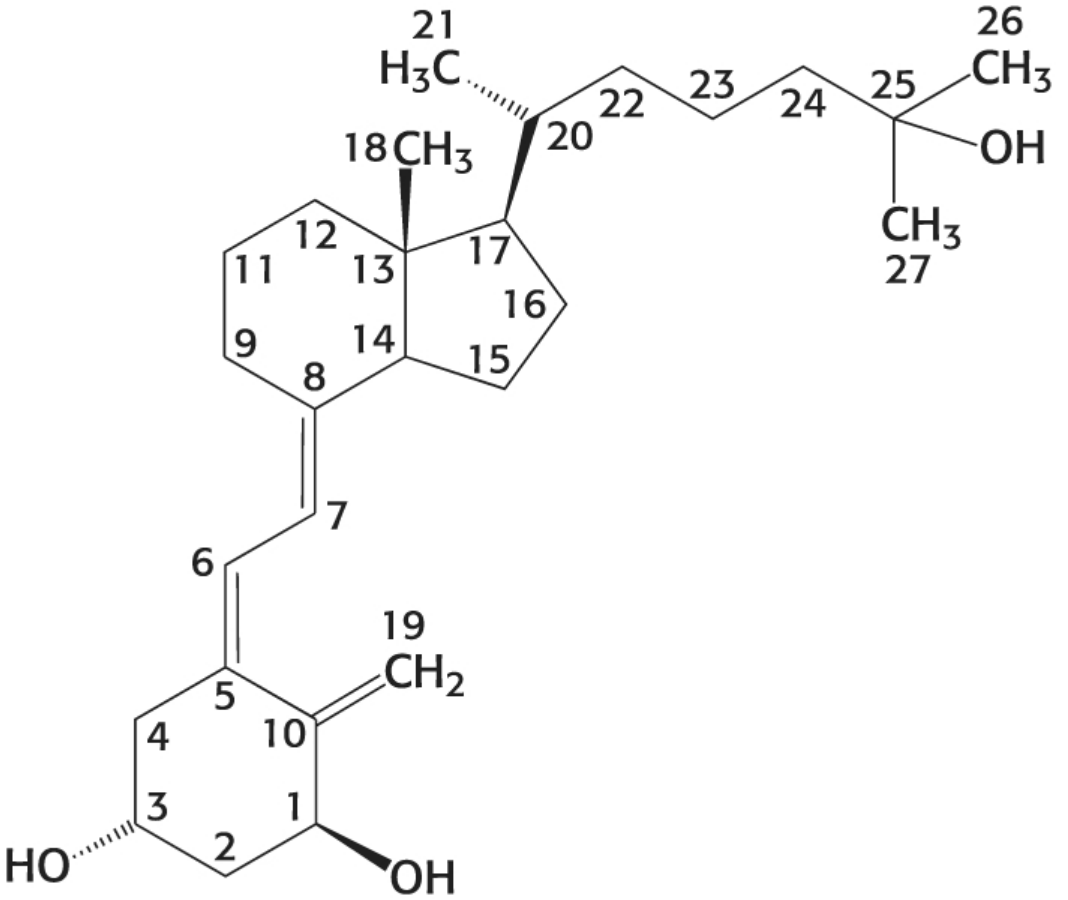
Page 805 UTP is first converted into UDP. Ribonucleotide reductase generates dUDP. DeoxyUDP is converted to dUMP. Thymidylate synthase generates TMP from dUMP. Monophosphate and diphosphate kinases subsequently form TTP.

Page 808 The committed step in pyrimidine biosynthesis is catalyzed by aspartate transcarbamoylase (ATCase). The committed step in purine biosynthesis is catalyzed by glutamine phosphoribosyl amidotransferase.

Chapter 27

Page 816 Phosphatidic acid includes two acyl groups that can vary in structure, leading to molecular weight differences.
Page 825 Oxidosqualene cyclase.
Page 832 Density, protein composition, lipid composition. See Table 27.1.

Page 839



Chapter 28

Page 847 The nucleotides used for DNA synthesis have the triphosphate attached to the $5'$-hydroxyl group with free $3'$-hydroxyl groups. Such nucleotides can be used only for $5'$-to-$3'$ DNA synthesis.

Page 848 DNA replication requires RNA primers. Without appropriate ribonucleotides, such primers cannot be synthesized.

Page 864 A hallmark of most cancer cells is prolific cell division, which requires DNA replication. If the telomerase were not activated, the chromosomes would shorten until they became nonfunctional, leading to cell death.

Page 868 DNA polymerase has proofreading activity, so it will immediately fix any bases that were wrongly incorporated, much like using a backspace key to correct typos. Any errors that are not fixed during replication can be repaired afterwards by mismatch repair. Damaged DNA is fixed via base-excision repair or nucleotide-excision repair. More significant damage, such as double-stranded breaks, can be repaired via recombination pathways. There are so many systems because the integrity of the DNA sequence is critically important, and it must be duplicated with fidelity. Each system provides added levels of accuracy.

Chapter 29

Page 881 RNA is mostly single-stranded, although it can form short duplexed sections, such as hairpins. The sugar in RNA is ribose, which has an extra hydroxyl group on the $2'$ carbon. This extra $2'-OH$ gives RNA its catalytic characteristics.

Page 885 RNA polymerases are similar to DNA polymerases in that they catalyze the formation of a phosphodiester bond in an active site that contains metal ions. Unlike DNA polymerases, RNA polymerases do not require an existing $3'-OH$ for this reaction and can therefore build RNA strands de novo. RNA polymerases have a greater error rate than DNA polymerases.

Page 898 The σ subunit as well as the eukaryotic transcription factors play a significant role in recruiting the RNA polymerase (bacterial or eukaryotic, respectively) to the promoter in order to facilitate the initiation of transcription at the appropriate site(s) and not randomly within the genome.

Page 912 All three reaction mechanisms involve two sequential transesterification reactions. Group I and group II self-splicing introns do not require the spliceosome. In group 1 splicing, the first reaction is an intermolecular nucleophilic attack (the $3'-OH$ group from a G). In group II and spliceosomal splicing, the first reaction is an intramolecular nucleophilic attack by the $2'-OH$ group from an adenylate within the intron.

Chapter 30

Page 920 (i) Each is a single chain. (ii) They contain unusual bases. (iii) Approximately half of the bases are base-paired to form double helices. (iv) The $5'$ end is phosphorylated and is usually pG. (v) The amino acid is attached to the hydroxyl group of the A residue of the CCA sequence at the $3'$ end of the tRNA. (vi) The anticodon is located in a loop near the center of the tRNA sequence. (vii) The molecules are l-shaped.

Page 921 The first two bases in a codon form Watson–Crick base pairs with their corresponding bases in the anticodon. These interactions are checked for fidelity by bases of the 16S rRNA. The interaction of the third base with its corresponding base in the anticodon is not inspected for accuracy, and so some variation is tolerated. This leads to the redundancy of the genetic code.

Page 933 The ribosome is a ribozyme because the peptide bond is catalyzed by rRNA. The peptidyl transferase center in the large subunit consists entirely of rRNA, with no ribosomal proteins near that active site. In addition, a ribosome stripped of its protein components is still able to catalyze peptide bond formation.

Page 935 During translation initiation in bacteria, the IF-2-GTP-initiator-tRNA complex forms part of the 30S initiation complex. Hydrolysis of GTP occurs once the 50S subunit joins this complex and will result in the release of IF2. During translation elongation, the EF-Tu-GTP complex binds the aminoacyl-tRNA and delivers it to the ribosome. Hydrolysis of GTP will release the EF-Tu-GDP complex from the ribosome.

Page 942 The SRP binds to the signal sequence and inhibits further translation. The SRP ushers the inhibited ribosome to the ER, where it interacts with the SRP receptor (SR). The $\mathrm{SRP{-}SR}$ complex binds

the translocon and simultaneously hydrolyzes GTP. On GTP hydrolysis, SRP and SR dissociate from each other and from the ribosome. Protein synthesis resumes, and the nascent protein is channeled through the translocon.

Chapter 31

Page 956 High concentrations of lactose cause the inducer (allolactose) to prevent the repressor from binding to the operator DNA, allowing for transcription of the structural genes in the operon. High concentrations of glucose, however, result in low levels of cAMP, meaning there would be no positive regulation (activation) of the *lac* operon by CAP. Under these conditions, the lack of positive regulation results in little to no expression of the structural genes, despite the negative control (repression) having been removed. In the absence of β-galactosidase, glucose is metabolized first. Once glucose levels have been depleted, cAMP levels are high, and cAMP–CAP complexes stimulate the transcription of the operon.
Page 959 Alpha helices fit into the major groove of DNA and are able to make specific contacts with the bases presented there.
Page 962 Eukaryotic DNA must be compacted and organized into chromatin in order to fit into the nucleus. This compaction makes it difficult for RNA polymerase and other regulatory proteins to gain access to the DNA. Chromatin structure must be relaxed in order for transcription to be activated. Gene expression can also be silenced by chromatin remodeling.
Page 967 The various aspects of chromatin modification include DNA methylation, histone methylation, histone acetylation, and histone deacetylation. DNA methylation, histone methylation, and histone deacetylation typically silence gene expression by making the DNA less accessible to transcription factors. Histone acetylation activates transcription by relaxing the chromatin structure and recruiting transcription factors and other components of the transcriptional machinery.
Page 972 During transcription, regulatory proteins determine the amount of mRNA produced from certain genes. Posttranscriptionally, regulatory mechanisms can affect the stability and translatability of

mRNAs. Once a protein is made, its functionality can be regulated via covalent modifications.

Chapter 32

Page 982 If an enzyme assay used in a high-throughput screen relies on a fluorescence readout, compounds that are themselves fluorescent may interfere with the assay and appear to be hits (i.e., false positives).

Page 986 In a manner reminiscent of affinity chromatography, the compound identified as a phenotypic screening hit could be attached to a solid support, and the extract of the type of cell used in the initial screen could be passed over the resin. Proteins that bind to the resin could be potential targets for the compound. If numerous proteins are identified, then this experiment could be repeated on other screening hits, and one could look for proteins that were common to both.

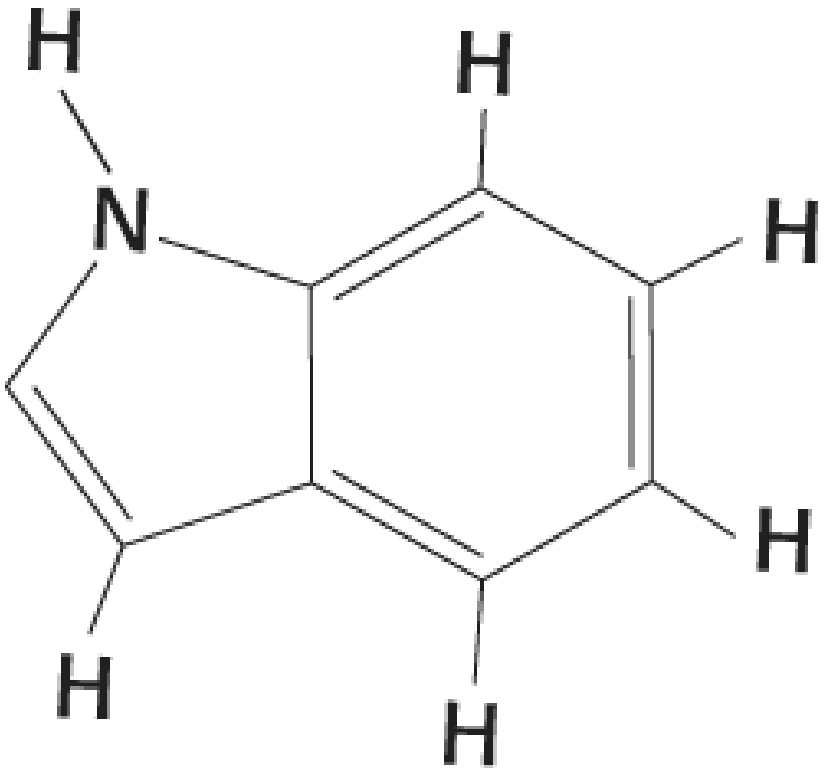
Page 996 A monoclonal antibody with higher affinity for FcRn would be more likely to be salvaged and retained in the body, thus prolonging its half-life.

Answers to Problems

Chapter 1

1. The hydrogen-bond donors are the NH and NH_2 groups. The hydrogen-bond acceptors are the carbonyl oxygen atoms and those ring nitrogen atoms that are not bonded to hydrogen or to deoxyribose.

2.



3. (a) Ionic interactions; (b) van der Waals interactions.

4. a and b.

5. $\Delta S_{system} = -661\ J\ mol^{-1}\ K^{-1} (-158\ kcal\ mol^{-1}\ K^{-1})$

$\Delta S_{surroundings} = +842\ J\ mol^{-1}\ K^{-1} (+201\ cal\ mol^{-1}\ K^{-1})$

6. 0.815

7. 55.6 M

8. 447; 0.00050

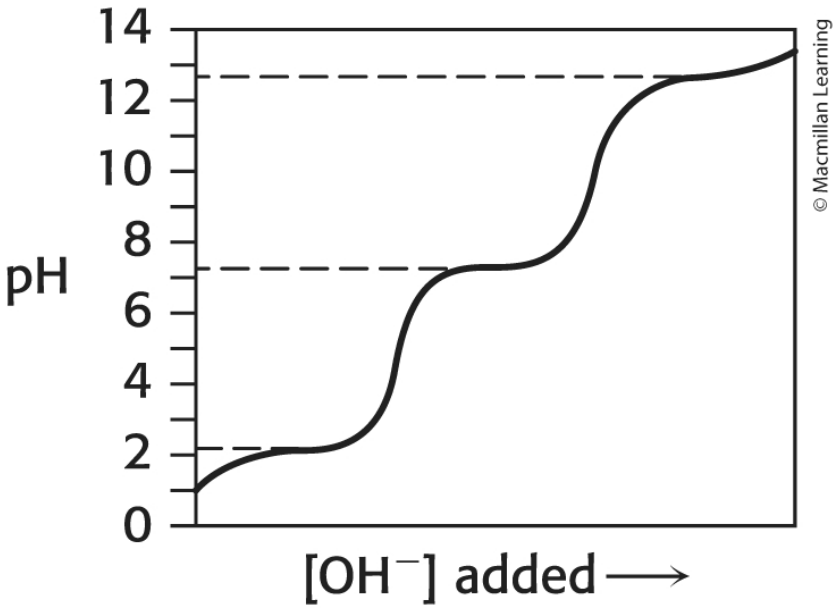
9. 6.0; 5.5

10. 7.8

11. 1.86

12. (a) 0.45; (b) 1.00; (c) 1.62

13.



14. (a) No; (b) Around pH 2.

15. 90 mM acetic acid; 160 mM sodium acetate, 0.18 moles acetic acid; 0.32 moles sodium acetate; 10.81 g acetic acid; 26.25 g sodium acetate.

16. (a) MOPS; (b) MES

17. Buffer, because the sodium ions will shield the electrostatic repulsion between the phosphate groups.

18. $+1.45\ \text{kJ mol}^{-1}\ (+0.35\ \text{kcal mol}^{-1})$; $+57.9\ \text{kJ mol}^{-1} (+13.8\ \text{kcal mol}^{-1})$

19. The hydrophobic effect

20. 100%. No, it would not be a useful clock because it changes too slowly.

21. 7.9%

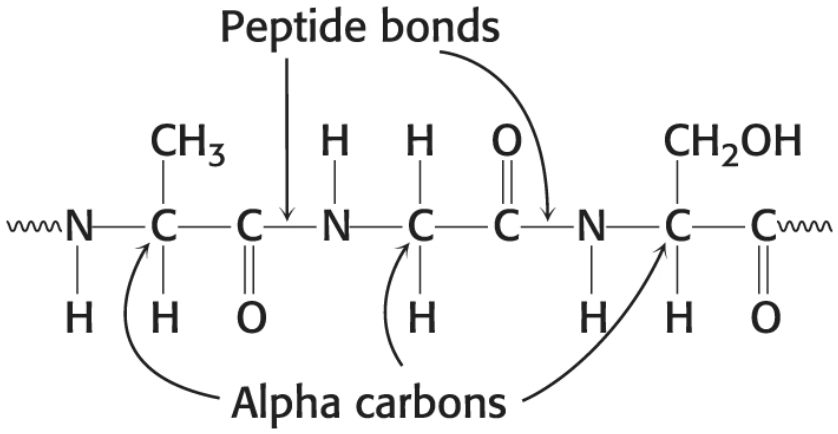
Chapter 2

1. (A) Proline, Pro, P; (B) tyrosine, Tyr, Y; (C) leucine, Leu, L; (D) lysine, Lys, K.

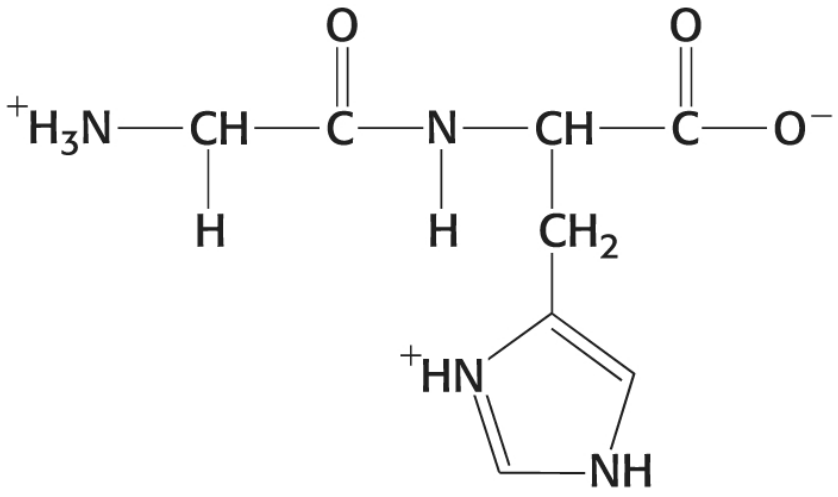
2. (a) D; (b) none; (c) A, C; (d) B.

3. Ser, Glu, Tyr, Thr.

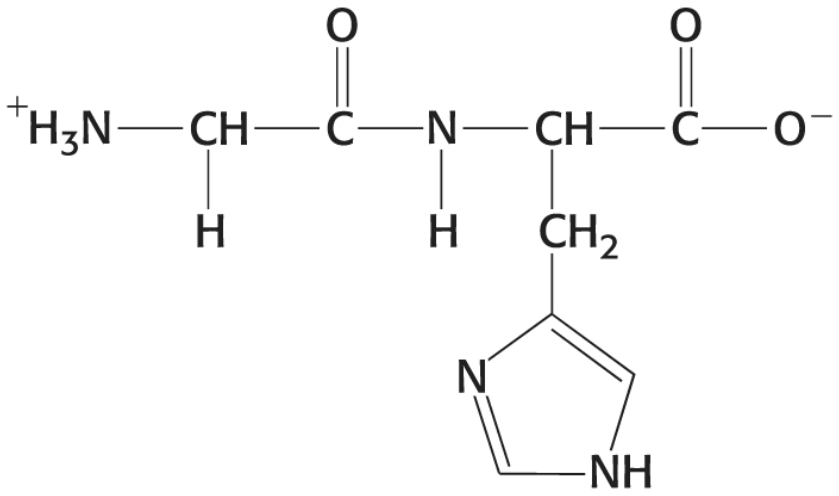
4. (a) Alanine-glycine-serine; (b) alanine; (c) 2.



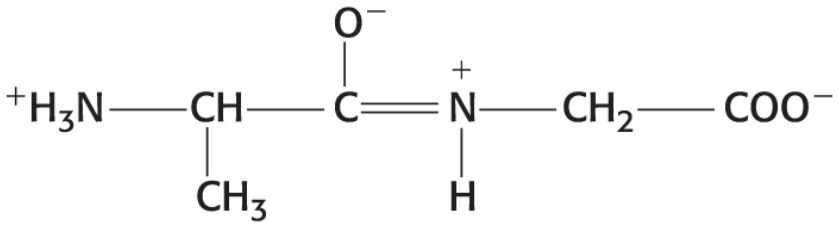
5. At pH 5.5, the net charge is $^{+1}$:



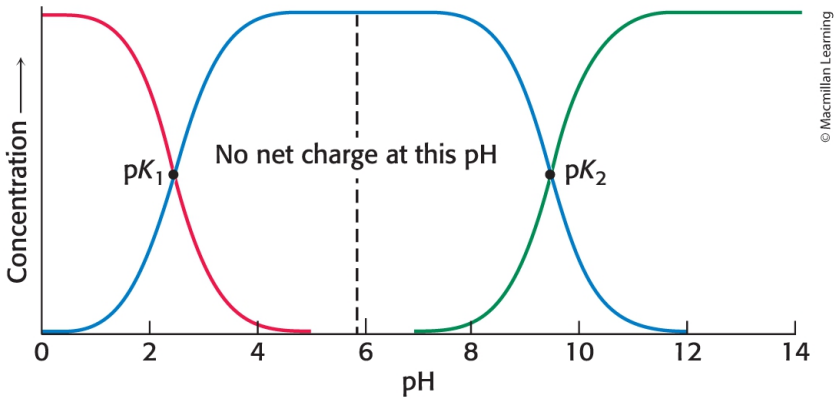
At pH 7.5, the net charge is 0:



6.



7. The solution would have no net charge at the pH in the midpoint of the zwitterionic species curve (blue), effectively at the midpoint between pK_1 and pK_2:



8. (a) pH 1.5; (b) pH 3.0 and pH 4.9

9. (a) Each strand is 35 kDa and hence has about 318 residues (the mean residue mass is 110 daltons). Because the rise per residue in an α helix is 1.5 Å, the length is 477 Å. More precisely, for an α-helical coiled coil, the rise per residue is 1.46 Å; so the length is 464 Å. (b) Eighteen residues in each strand (40 minus 4 divided by 2) are in a β-sheet conformation. Because the rise per residue is 3.5 Å, the length is 63 Å.

10. The methyl group attached to the β-carbon atom of isoleucine sterically interferes with α-helix formation. In leucine, this methyl group is attached to the γ-carbon atom, which is farther from the main chain and hence does not interfere.

11. The native conformation of insulin is not the thermodynamically most stable form, because it contains two separate chains linked by disulfide bonds. Insulin is formed from proinsulin, a single-chain precursor, that is cleaved to form insulin, a 51-residue molecule, after the disulfide bonds have formed.

12. A 12 kDa single-stranded α helix contains about 109 residues:

$$12\ \text{kDa} \times \frac{1000\ \text{Da}}{1\ \text{kDa}} \times \frac{1\ \text{residue}}{110\ \text{Da}} = 109\ \text{residues}$$

A single turn of the helix (each repeating unit) extends about 5.4 Å. There are 3.6 residues per turn. Therefore, the rise per residue is 1.5 Å. The length of the segment is 164 Å

$$109\ \text{residues} \times \frac{1.5\ \text{Å}}{1\ \text{residue}} = 164\ \text{Å}$$

13. (a). This peptide has a large number of aromatic and beta-branched amino acids, which tend to be disfavored in α helices and accommodated well by β sheets.

14. (a) a; (b) a, b, c.

15. (a) All; (b) β sheets; (c) α helices; (d) reverse turn; (e) α helices.

16. Recall that hemoglobin exists as a tetramer while myoglobin is a monomer. Consequently, the hydrophobic residues on the surface of hemoglobin subunits are probably involved in van der Waals interactions with similar regions on the other subunits, and will be shielded from the aqueous environment by this interaction.

17. Using the Henderson–Hasselbalch equation, we find the ratio of alanine-COOH to alanine-COO^- at pH 7 to be 10^{-4}. The ratio of alanine-NH_2 to alanine-NH_3^+, determined in the same fashion, is 10^{-1}. Thus, the ratio of neutral alanine to the zwitterionic species is $10^{-4} \times 10^{-1} = 10^{-5}$.

18. ELVISISLIVINGINLASVEGAS

19. No, Pro—X would have the characteristics of any other peptide bond. The steric hindrance in X—Pro arises because the R group of Pro is bonded to the amino group. Hence, in X—Pro, the proline R group is near the R group of X, which would not be the case in Pro—X.

20. A, c; B, e; C, d; D, a; E, b.

21. Disulfide pairings are not positioned correctly unless weak bonding interactions are present.

Chapter 3

1. $^{1}/_{2}$

2. 1.44×10^{-2} grams; 1.44×10^{-1} grams; 128

3. No, because oxygen binding requires partial electron transfer to oxygen.

4. No. The Bohr effect requires changes in quaternary structure and myoglobin in monomeric.

5. Less tight, because n-hexyl isocyanide is likely too large to easily fit into the oxygen-binding cavity.

6. lowered; raised; raised

7. (a) 1.0, expected for a monomeric protein; (b) 2.8. This suggests substantial cooperativity but is less that 4.0 expected for full cooperativity

8. (a) 61.7%; (b) Her hemoglobin P_{50} increases, promoting oxygen delivery to tissues.

9. The two copper ions move together upon binding oxygen, and this motion could promote cooperativity.

10. (c) because of its negative charge.

11. Uracil is found in RNA, characteristic of potential viral infection.

12. Uracil to avoid the potential innate immune response.

13. Each IgG has two arms and each hemoglobin has two copies of each potential binding site. These could come together to form a large insoluble polymer. This is not possible for myoglobin because it is monomeric.

14. (a) L**L**QATYSA**V**

15. 0.17; 0.67, 0.95, 0.995

16. (a) $R_{free} = R = 1.0 - 0.14 - 0.71 = 0.15 R_{total}$. (b) $\text{Estradiol}_{free} = 1\ \text{nM} - 0.14 R_{total}$. (c) $\text{BPA}_{free} = 1\ \mu\text{M} - 0.71 R_{total}$. (d) Estradiol $K_d = (R_{free} \times \text{Estradiol}_{free})/[R\text{–Estradiol}] = (0.15\ R_{total}) \times (1\ \text{nM} - 0.14\ R_{total})/0.14 R_{total} = (0.15/0.14) \times (1\ \text{nM}$ assuming R_{total} is much less than 1 nM, BPA $K_d = (R_{free} \times \text{BPA}_{free})/[R\text{–BPA}] = (0.15\ R_{total}) \times (1\ \mu\text{M} - 0.71 R_{total})/0.71 R_{total} = (0.15/0.71) \times (1\ \mu\text{M} - 0.71 R_{tota}$.

17. $\text{Rate} = k_1 [L] = 5 \times 10^{-3}\ s^{-1}$ when $[L] = 10\ \mu\text{M}$ so that $k_1 = 5 \times 10^{8}\ M^{-1} s^{-1}$. $k_{-1} = K_d \times k_1 = (20\ \text{nM}) \times (5 \times 10^{8}\ M^{-1} s^{-1}) = 10\ s^{-1}$.

18. 0.5 nM

19. $10^{-6}\,\mathrm{M}$

20. Essentially all (100%) of the irons will be bound to carbon dioxide.

Chapter 4

1. (a), (c), (d)

2.

Purification procedure	Total protein (mg)	Total activity (units)	Specific activity (units mg^{-1})	Purification level	Yield (%)
Crude extract	20,000	4,000,000	200	1	100
$(NH_4)_2SO_4$ precipitation	5000	3,000,000	600	3	75
DEAE-cellulose chromatography	1500	1,000,000	667	3.3	25
Gel-filtration chromatography	500	750,000	1500	7.5	19
Affinity chromatography	45	675,000	15,000	75	17

3. (a) 0.4 mM; (b) 0.02 mM

4. A fluorescence-labeled derivative of a bacterial degradation product (e.g., a formylmethionyl peptide) would bind to cells containing the receptor of interest.

5. (a) Trypsin cleaves after arginine (R) and lysine (K), generating AVGWR, VK, and S. Because they differ in size, these products could be separated by molecular exclusion chromatography. (b) Chymotrypsin, which cleaves after large aliphatic or aromatic R groups, generates two peptides of equal size (AVGW) and (RVKS). Separation based on size would not be effective. The peptide RVKS has two positive charges (R and K), whereas the other peptide is neutral. Therefore, the two products could be separated by ion-exchange chromatography.

6. (a) Ion exchange chromatography will remove Proteins A and D, which have a substantially lower isoelectric point; then gel filtration chromatography will remove Protein C, which has a lower molecular weight. (b) If Protein B carries a His tag, a single affinity chromatography step with an immobilized nickel(II) column may be sufficient to isolate the desired protein from the others.

7. Mass spectrometry is highly sensitive and capable of detecting the mass difference between a protein and its deuterated counterpart. Fragmentation techniques can be used to identify the amino acids that retained the isotope label. Alternatively, NMR spectroscopy can be used to detect the isotopically labeled atoms because the deuteron and the proton have very different nuclear-spin properties.

8. (c), (e), (b), (a), (d).

9. The difference between the predicted and the observed masses for this fragment equals 28.0, exactly the mass shift that would be expected in a formylated peptide. This peptide is likely formylated at its

amino terminus and corresponds to the most N-terminal fragment of the protein.

10. (b)

11. (a) Three fragments; the smallest is Ser-Arg. (b) One “fragment”; this peptide does not contain any chymotrypsin cleavage sites (no Phe, Tyr, Trp, Leu, or Met). The sequence would remain Gly-Ser-Lys-Ala-Gly-Arg-Ser-Arg.

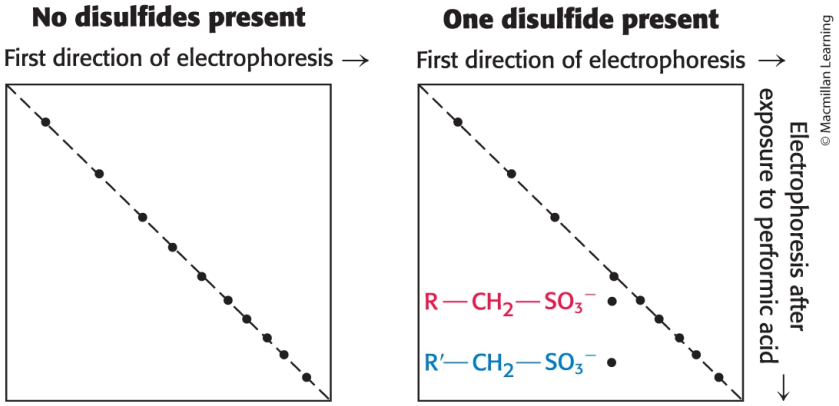
12. (a) d and e; (b) b.

13. TRMKPAMLICWMPD

14. Met-Val-Lys-Tyr-Thr-Trp-Ala-Phe-Gly-Arg

15. (a) (A): Native PAGE; (B): Non-reducing SDS-PAGE; (C) Reducing SDS-PAGE (b) Protein X consists of two 50 kDa polypeptide chains, resulting in a total mass of 100 kDa. According to the nonreducing SDS-PAGE gel, intact protein X has a total molecular weight of 100 kDa. Therefore, the molecular weights of the protein X polypeptide chains must add up to 100 kDa. The only peptides indicated by the reducing SDS-PAGE gel that combine to yield a 100-kDa protein are two 50-kDa chains. (c) Protein Y consists of two 60-kDa chains and one 30-kDa chain, for a total mass of 150 kDa. According to the nonreducing SDS-PAGE gel, the intact protein Y has a total molecular weight of 150 kDa. Therefore, the molecular weights of the protein Y polypeptides must add up to 150 kDa. Although three 50 kDa could make up a 150-kDa polypeptide, the reducing SDS-PAGE method shows bands of 30 kDa and 60 kDa. Therefore, protein Y must include chains of 30 kDa and 60 kDa. The association of two 60-kDa chains and one 30-kDa chain would yield the 150-kDa protein Y.

16. If the protein did not contain any disulfide bonds, then the electrophoretic mobility of the trypsin fragments would be the same before and after performic acid treatment: all the fragments would lie along the diagonal of the paper. If one disulfide bond were present, the disulfide-linked trypsin fragments would run as a single peak in the first direction, and then as two separate peaks after performic acid treatment. The result would be two peaks appearing off the diagonal:



These fragments could then be isolated from the chromatography paper and analyzed by mass spectrometry to determine their amino acid composition and thus identify the cysteines participating

in the disulfide bond.

17. From top to bottom: (d), (e), (f), (a), (c), (b)

18. From low pH to high pH: (d), (e), (f), (c), (b), (a)

Chapter 5

1. A cofactor.

2. d, e, and f.

3. The energy required to reach the transition state (the activation energy) is returned when the transition state proceeds to product.

4. The product is more stable than the substrate in graph A; so ΔG is negative and the reaction is exergonic. In graph B, the product has more energy than the substrate has; ΔG is positive, meaning that the reaction is endergonic.

5. (a) $K = \dfrac{[P]}{[S]} = \dfrac{k_F}{k_R} = \dfrac{10^{-4}}{10^{-6}} = 100$. Using equation 5 in the text, $\Delta G^{\circ\prime} = -11.42\ \text{kJ mol}^{-1}\ (-2.73\ \text{kcal mol}^{-1})$. (b) $k_F = 10^{-2}\ \text{s}^{-1}$ and $k_R = 10^{-4}\ \text{s}^{-1}$. The equilibrium constant and $\Delta G^{\circ\prime}$ values are the same for both the uncatalyzed and catalyzed reactions.

6. There would be no catalytic activity. If the enzyme–substrate complex is more stable than the enzyme–transition-state complex, the transition state would not form and catalysis would not take place.

7. (a) 0; (b) $+28.53$; (c) -22.84; (d) -11.42; (e) $+5.69$.

8.

(a)
$$\Delta G^{\circ\prime} = -RT \ln K'_{eq}$$
$$+1.8 = -(1.98 \times 10^{-3}\ \text{kcal}^{-1}\ \text{K}^{-1}\ \text{mol}^{-1})(298\ \text{K})(\ln[\text{G1P}]/[\text{G6P}])$$
$$-3.05 = \ln [\text{G1P}]/[\text{G6P}]$$
$$+3.05 = \ln [\text{G6P}]/[\text{G1P}]$$
$$K'^{-1}_{eq} = 21 \text{ or } K'_{eq} = 4.8 \times 10^{-2}$$

Because $[\text{G6P}]/[\text{G1P}] = 21$, there is 1 molecule of G1P for every 21 molecules of G6P. Because we started with 0.1 M, the [G1P] is $1/22\ (0.1\ \text{M}) = 0.0045\ \text{M}$ and [G6P] must be 21/22 (0.1 M) or 0.096 M. Consequently, the reaction does not proceed as written to a significant extent. (b) Supply G6P at a high rate and remove G1P at a high rate by other reactions. In other words, make sure that the [G6P]/[G1P] is kept large.

9. $K_{eq} = 19$, $\Delta G = -7.3\ \text{kJ mol}^{-1}\ (-1.77\ \text{kcal mol}^{-1})$

10. No, K_M is not equal to the dissociation constant and thus does not measure affinity because the numerator also contains k_2, the rate constant for the conversion of the enzyme substrate complex into enzyme and product. If, however, k_2 is much smaller than k_{-1}, $K_M \approx K_d$.

11. Competitive inhibition: 2, 3, 9; uncompetitive: 4, 5, 6; noncompetitive: 1, 7, 8.

12. When $[S] = 10\ K_M, V_0 = 0.91\ V_{max}$. When $[S] = 20\ K_M, V_0 = 0.95\ V_{max}$. So, any Michaelis–Menten curves showing that the enzyme actually attains V_{max} are pernicious lies.

13. (a) $31.1\ \mu mol$; (b) $0.05\ \mu mol$; (c) $622\ s^{-1}$, a midrange value for enzymes (Table 8.5).

14. (a) Yes, $K_M = 5.2 \times 10^{-6}\ M$; (b) $V_{max} = 6.8 \times 10^{-10}\ mol\ minute^{-1}$; (c) $337\ s^{-1}$.

15. (a) V_{max} is $8.9\ \mu mol\ minute^{-1}$ K_M is $9.9 \times 10^{-5}\ M$, the same as without inhibitor. (b) Noncompetitive. (c) $2.5 \times 10^{-5}\ M$ (d) $f_{ES} = 0.73$, in the presence or absence of this noncompetitive inhibitor.

16. (a) $V_0 = V_{max} - (V_0/[S])\ K_M$; (b) $Slope = -K_M, y-intercept = V_{max}, x-intercept = V_{max}/K_M$; (c) An Eadie Hofstee plot.

17. Sequential reactions are characterized by the formation of a ternary complex consisting of the enzyme and both substrates. Double-displacement reactions always require the formation of a temporarily substituted enzyme intermediate.

18. (a) K_M is a measure of affinity *only* if k_2 is rate limiting, which is the case here. Therefore, the lower K_M means higher affinity. The mutant enzyme has a higher affinity. (b) $50\ \mu mol\ minute^{-1}$. 10 mM is K_M, and K_M yields $1/2\ V_{max}$. V_{max} is $100\ \mu mol\ minute^{-1}$, and so (c) Enzymes do not alter the equilibrium of the reaction.

19. If the total amount of enzyme $[E]_T$ is increased, V_{max} will increase, because $V_{max} = k_2[E]_T$. But $K_M = (k_{-1} + k_2)/k_1$; that is, it is independent of enzyme concentration. The middle graph describes this situation.

20. Enzyme 2. Despite the fact that enzyme 1 has a higher V_{max} than enzyme 2, enzyme 2 shows greater activity at the concentration of the substrate in the environment because enzyme 2 has a lower K_M for the substrate.

21.

Experimental condition	V_{max}	K_M
(a) Twice as much enzyme is used	Doubles	No change
(b) Half as much enzyme is used	Half as large	No change
(c) A competitive inhibitor is present	No change	Increases
(d) An uncompetitive inhibitor is present	Decreases	Decreases
(e) A pure noncompetitive is present	Decreases	No change

22. The first step will be the rate-limiting step. Enzyme E_B is operating at $\frac{1}{2}\ V_{max}$, and E_C is very close to maximum velocity, whereas the K_M for enzyme E_A is greater than the substrate concentration. E_A would be operating at approximately $10^{-2}\ V_{max}$.

23. At substrate concentrations near the K_M, the enzyme is elastic, meaning that it displays significant catalysis yet is still sensitive to changes in substrate concentration.

24. (a) This piece of information is necessary for determining the correct dosage of succinylcholine to administer. (b) The duration of the paralysis depends on the ability of the serum cholinesterase to clear the drug. If there were one-eighth the amount of enzyme activity, paralysis could last eight times as long. (c) K_M is the concentration needed by the enzyme to reach $1/2\ V_{max}$. Consequently, for a given concentration of substrate, the reaction catalyzed by the enzyme with the lower K_M will have the higher rate. The patient with the higher K_M will clear the drug at a much lower rate.

Chapter 6

1. For the amide substrate, the formation of the acyl-enzyme intermediate is slower than the hydrolysis of the acyl-enzyme intermediate, and so no burst is observed. A burst is observed for ester substrates, because the formation of the acyl-enzyme intermediate is faster, leading to the observed burst.

2. The histidine residue in the substrate can substitute to some extent for the missing histidine residue of the catalytic triad of the mutant enzyme.

3. No. The catalytic triad works as a unit. After this unit has been made ineffective by the mutation of histidine to alanine, the further mutation of serine to alanine should have only a small effect.

4. The substitution corresponds to one of the key differences between trypsin and chymotrypsin, and so trypsin-like specificity (cleavage after lysine and arginine) might be predicted. In fact, additional changes are required to affect this specificity change.

5. Imidazole is apparently small enough to reach the active site of carbonic anhydrase and compensate for the missing histidine. Buffers with large molecular components cannot do so, and the effects of the mutation are more evident.

6. No, because the enzyme would destroy the host DNA before protective methylation could take place.

7. EDTA will bind to Zn^{2+} and remove the ion, which is required for enzyme activity, from the enzyme.

8. (a) The aldehyde reacts with the active-site serine. (b) A hemiacetal is formed.

9. lysine; trypsin; aspartate

10. $k_{cat} = 60{,}000\ s^{-1}$. The reaction is expected to be slower by a factor of 10 because the rate depends on the pK_a of the zinc-bound water.

11. EDTA binds the Mg^{2+} necessary for the enzymatic reaction to proceed.

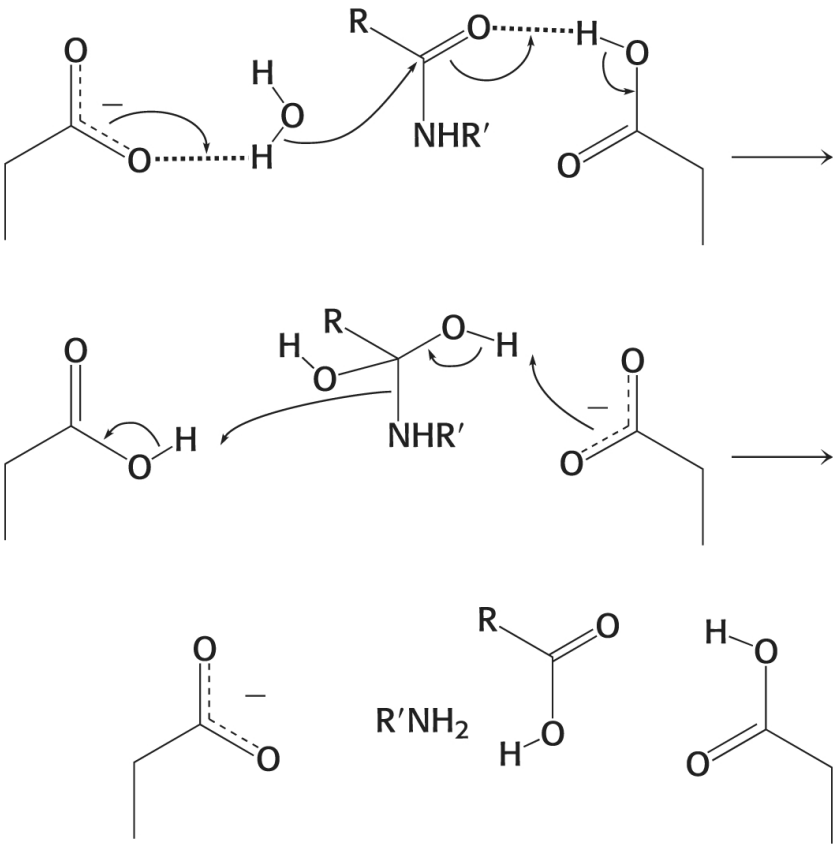
12. If the aspartate is mutated, the protease is inactive and the virus will not be viable.

13. Water substitutes for the hydroxyl group of serine 236 in mediating proton transfer from the attacking water and the γ-phosphoryl group.

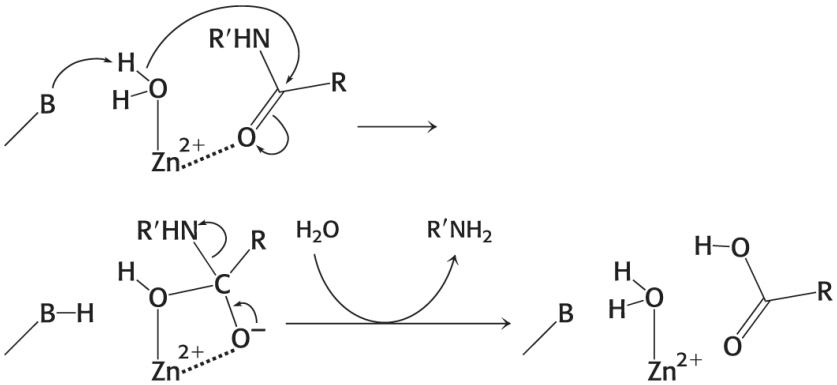
14. For subtilisin, the catalytic power is approximately $30\ s^{-1}/10^{-8}\ s^{-1} = 3 \times 10^9$. For carbonic anhydrase (at pH 7), the catalytic power is approximately $500{,}000\ s^{-1}/0.15\ s^{-1} = 3.3 \times 10^6$. Subtilisin is the more powerful enzyme by this criterion.

15. The triple mutant still catalyzes the reaction by a factor of approximately 1000-fold compared to the uncatalyzed reaction. This could be due to the enzyme binding the substrate and holding it in a conformation that is susceptible to attack by water.

16. (a) Cysteine protease. The same as Figure 6.8 except that cysteine replaces serine and no aspartate is present. (b) Aspartyl protease.



(c) Metalloprotease.



17. From a biological perspective, highly specific enzymes allow control of which reactions occur at appreciable rates. From a chemical perspective, enzymes generally require a tight fit between enzyme and substrate, likely leading to high specificity. An enzyme with high catalytic activity but low specificity would require the ability to bind substrates with substantial parts of the substrate not in close contact with the enzyme.

18. Myosin will bind and hydrolyze ATP but will release the products ADP and P_i very slowly, limiting the overall rate of hydrolysis.

Chapter 7

1. a, b, and d are true.

2. a, c, and d.

3. Homotropic effectors are the substrates of allosteric enzymes. Heterotropic effectors are the regulators of allosteric enzymes. Homotropic effectors account for the sigmoidal nature of the velocity versus substrate concentration curve, whereas heterotropic effectors alter the K_M of the curve. Ultimately, both types of effectors work by altering the T/R ratio.

4. CTP is formed by the addition of an amino group to UTP. Evidence indicates the UTP is also capable of inhibiting ATCase in the presence of CTP.

5. Kinases: (a), (b), (f); Phosphatases: (c), (g); Neither: (d), (h); Both: (e).

6. (b), (d), (f).

7. (a) CTP and UTP; (b) PALA; (c) ATP.

8. (c), (d), (b), (a).

9. (a) Decrease; (b) Decrease; (c) Decrease; (d) The activity of enzyme 1 increases.

10. Replacing methionine with leucine would be a good choice. Leucine is resistant to oxidation and has nearly the same volume and degree of hydrophobicity as methionine has.

11. (b).

12. (a) Enteropeptidase and trypsin; (b) All four zymogens are directly activated by trypsin!

13. (b), (d), (f), (a), (e), (c).

14. The simple sequential model predicts that the fraction of catalytic chains in the R state, f_R, is equal to the fraction containing bound substrate, *Y*. The concerted model, in contrast, predicts that f_R increases more rapidly than *Y* as the substrate concentration is increased. The change in f_R leads to the change in *Y* on addition of substrate, as predicted by the concerted model.

15. (a) e_1, e_4, e_5, and e_7; (b) The product of e_1, B, has two possible fates, conversion to C or B'. Thus, the product is not committed to the synthesis of G. The first enzyme that catalyzes a reaction that commits the pathway to the synthesis of G is enzyme e_4. This enzyme is most likely the allosteric enzyme.

16. (a) When crowded, the control group displays gregarious behavior. (b) Inhibition of PKA appears to prevent gregarious behavior, while inhibition of PKG has no effect on the behavior. (c) The effect of PKG inhibition was investigated to establish that the effect seen with PKA inhibition is specific and not just due to the inhibition of any kinase. (d) PKA plays a role in altering behavior of insects.

17. The binding of PALA switches ATCase from the T to the R state because PALA acts as a substrate analog. PALA disrupts the equilibrium in favor of R. Thus, the limited amount of substrate can more

readily bind the R state, and the ATCase activity initially increases with increasing PALA. Once the inhibitor occupies more and more active sites, the real substrate will be unable to bind the enzyme. When PALA occupies all of the active sites, the catalytic activity falls to zero.

18. (a) 100. If the binding of the substrate is 100 times tighter for the R form, then $c = 1/100$ (recall that tighter binding means a lower dissociation constant). Thus, $\frac{[T_1]}{[R_1]} = c^1 L = \frac{1}{100} L$ and the change in $[R]/[T]$ will 100-fold. Note that the change in the $[R]/[T]$ ratio on binding one substrate molecule must be the same as the ratio of the substrate affinities of the two forms. (b) 10. With four substrates bound, we can use the equation to determine:

$$\frac{[T_4]}{[R_4]} = c^4 L = \left(\frac{1}{100}\right)^4 L = 10^{-8} \cdot 10^7 = \frac{1}{10}$$

Hence, the $[R]/[T]$ ratio in the fully liganded molecule is 10.

Chapter 8

1. Nucleosides: (c), (f); Nucleotides: (a), (e), (g); Both: (b), (d), (h)

2. (a) Guanosine $5'$-diphosphate (GDP); (b) Deoxyuridine; (c) Adenosine

3. T is always equal to A, and so these two nucleotides constitute 40% of the bases. G is always equal to C, and so the remaining 60% must be 30% G and 30% C.

4. (a) TTGATC; (b) GTTCGA; (c) ACGCGT; (d) ATGGTA.

5. DNA: (b), (c), (f); RNA: (a), (d), (e), (g)

6. (a) purine, ribose; (b) pyrimidine, ribose; (c) purine, deoxyribose

7. B-DNA: (b), (f); A-DNA: (a), (c), (i); Z-DNA: (d), (g); All three: (e), (h)

8. (a) Tritiated thymine or tritiated thymidine. (b) dATP, dGTP, dCTP, and TTP labeled with ^{32}P in the innermost (α) phosphorus atom.

9. Molecules in parts *(a)* and *(b)* would not lead to DNA synthesis, because they lack a $3'-OH$ group (a primer). The molecule in part *(d)* has a free $3'-OH$ group at one end of each strand but no template strand beyond. Only the molecule in part *(c)* would lead to DNA synthesis.

10. (a) 50%; (b) 0%

11. The diameter of DNA is 20 Å, and $1\ Å = 0.1\ nm$, so the diameter is 2 nm. Because $1\ \mu m = 10^3\ nm$, the length is $2 \times 10^4\ nm$. Thus, the axial ratio is 1×10^4.

12. There are 2 μm missing in the deletion mutant, or 20,000 Å of DNA. Given a base separation of 3.4 Å in B-DNA, this corresponds to $20000/3.4$, or about 5.88×10^3 base pairs.

13. (a) 2, 4, 8; (b) 1, 6, 10; (c) 3, 5, 7, 9.

14. (a) $5'-UAACGGUACGAU-3'$ (b) Leu-Pro-Ser-Asp-Trp-Met (c) Poly(Leu-Leu-Thr-Tyr)

15. (a) Deoxyribonucleoside triphosphates versus ribonucleoside triphosphates. (b) $5' \rightarrow 3'$ for both. (c) Semiconserved for DNA polymerase I; conserved for RNA polymerase. (d) DNA polymerase I needs a primer, whereas RNA polymerase does not.

16. Three nucleotides encode an amino acid; the code is nonoverlapping; the code has no punctuation; the code exhibits directionality; the code is degenerate.

17. tRNA: (c), (e); mRNA: (a), (d); rRNA: (b)

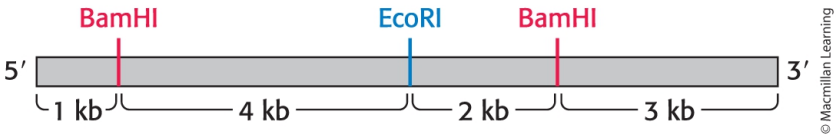
18. Prokaryotic promoters: (a), (d); Eukaryotic promoters: (c), (e); Both: (b)

19. It shows that the genetic code and the biochemical means of interpreting the code are common to even very distantly related life forms. It also testifies to the unity of life: that all life arose from a common ancestor.

20. (a) 3; (b) 6; (c) 2; (d) 5; (e) 7; (f) 1; (g) 4.

Chapter 9

1.



2. A mutation in person B has altered one of the alleles for gene *X*, leaving the other intact. The fact that the mutated allele is smaller suggests that a deletion has occurred in one copy of the gene. The one functioning copy is transcribed and translated and apparently produces enough protein to render the person asymptomatic.

Person C has only the smaller version of the gene. This gene is neither transcribed (negative northern blot) nor translated (negative western blot).

Person D has a normal-size copy of the gene but no corresponding RNA or protein. There may be a mutation in the promoter region of the gene that prevents transcription.

Person E has a normal-size copy of the gene that is transcribed, but no protein is made, which suggests that a mutation prevents translation. There are a number of possible explanations, including a mutation that introduced a premature stop codon in the mRNA.

Person F has a normal amount of protein but still displays the metabolic problem. This finding suggests that the mutation affects the activity of the protein—for instance, a mutation that compromises the active site of enzyme Y.

3. Chongqing: residue 2, L → R, CTG → CGG
Karachi: residue 5, A → P, GCC → CCC
Swan River: residue 6, D → G, GAC → GGC

4. Careful comparison of the sequences reveals that there is a 7-bp region of complementarity at the 3′ ends of these two primers:

$$5'\text{–GGATCGATG}\mathbf{CTCGCGA}\text{–}3'$$
$$3'\text{–}\mathbf{GAGCGCT}\text{GGGCTAGGA–}5'$$

In a PCR experiment, these primers would likely anneal to one another, preventing their interaction with the template DNA. During DNA synthesis by the polymerase, each primer would act as a template

for the other primer, leading to the amplification of a 25-bp sequence corresponding to the overlapped primers.

5. The encoded protein contains four repeats of a specific sequence.

6. (b), (d), (a), (c)

7. EcoRI and HindIII. Cleavage with PstI would disrupt the ampicillin resistance gene in pSAP, while cleavage with EcoRI and SmaI would remove the origin of replication from pSAP. Based on the information given, the other remaining restriction enzymes do not have cleavage sites on the fragment.

8. On the basis of the comparative genome map shown in Figure 9.29, the region of greatest overlap with human chromosome 20 can be found on mouse chromosome 2.

9. The codon(s) for each amino acid can be used to determine the number of possible nucleotide sequences that encode each peptide sequence (Table 8.5):

Ala–Met–Ser–Leu–Pro–Trp:

$$4 \times 1 \times 6 \times 6 \times 4 \times 1 = 576 \text{ total sequences}$$

Gly–Trp–Asp–Met–His–Lys:

$$4 \times 1 \times 2 \times 1 \times 2 \times 2 = 32 \text{ total sequences}$$

Cys–Val–Trp–Asn–Lys–Ile:

$$2 \times 4 \times 1 \times 2 \times 2 \times 3 = 96 \text{ total sequences}$$

Arg–Ser–Met–Leu–Gln–Asn:

$$6 \times 6 \times 1 \times 6 \times 2 \times 2 = 864 \text{ total sequences}$$

The set of DNA sequences encoding the peptide Gly-Trp-Asp-Met-His-Lys would be most ideal for probe design because it encompasses only 32 total oligonucleotides.

10. In this sequence, the GTG codon encodes valine. To change this to an alanine codon, one should use the primer sequence: ATG–CGC–GAA–CTG–G**C**G–AAC–TAA

11. Since the N could be any one of the four bases, the presence of the NGG trinucleotide would occur with a frequency of $\frac{4}{4} \times \frac{1}{4} \times \frac{1}{4}$, or once every 16 bases, on average.

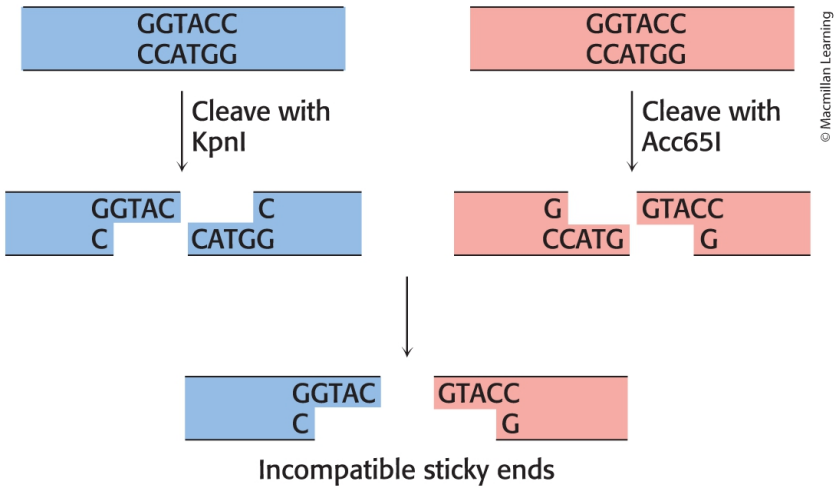
12. (a) In order to confirm the success of a knockdown experiment, one should use a method that can rapidly detect the loss of mRNA transcript. The most convenient method would be qPCR (real-time PCR) to compare the transcript levels in a knockdown study versus a control sample. One could also look for changes in the expressed protein level by western blotting if an appropriate antibody is available. (b) Whole-genome complementary DNA (cDNA) includes fully processed mRNA transcripts that have already had their introns spliced out. Therefore, cDNA represents the best source for an RNAi library because the mature mRNA is what researchers want to target and degrade in order to knock down the gene products.

13. 1: (b); 2: (c); 3: (a)

14. (a) Individual II; (b) Individual IV; (c) Cannot be determined with the current probe.

15. This particular person is heterozygous for this particular mutation: one allele is wild type, whereas the other carries a point mutation at this position. Both alleles are PCR amplified in this experiment, yielding the “dual peak” appearance on the sequencing chromatogram.

16. Although the two enzymes cleave the same recognition site, they each break different bonds within the 6-bp sequence. Cleavage by KpnI yields an overhang on the $3'$ strand, whereas cleavage by Acc65I produces an overhang on the $5'$ strand. These sticky ends do not overlap.



17. The amount of dsDNA doubles with each cycle, so the amount of dsDNA present is equal to 2^x, where x is the number of cycles. Hence, after 1 cycle, there will be 2 molecules of dsDNA; after 3 cycles, 8 molecules of dsDNA; and after 30 cycles, ~1 billion molecules of dsDNA.

18. (c); (d); (e); (g).

19. (a): 2, 8; (b): 1, 6; (c): 3, 7; (d): 4, 5.

20. RNA-seq detects transcripts whether or not a gene is annotated in the genome, while in microarray analysis, researchers quantify expression levels based on binding to an array of oligonucleotides known to represent annotated genes, so transcripts of unannotated genes are not measured. RNA-seq has a wider dynamic range than microarray analysis, meaning it detects changes in high and low expression level genes. Another advantage of RNA-seq is its sensitivity to splice variants among mRNAs produced from the same gene. In fact, microarray analysis cannot identify splice variants unless each variant is represented and distinguishable in the oligonucleotides on the microarray.

Chapter 10

1. Paralogs are homologs that are present within one species and often differ in their detailed biochemical functions. Orthologs are homologs that are present within different species and have very similar or identical functions.

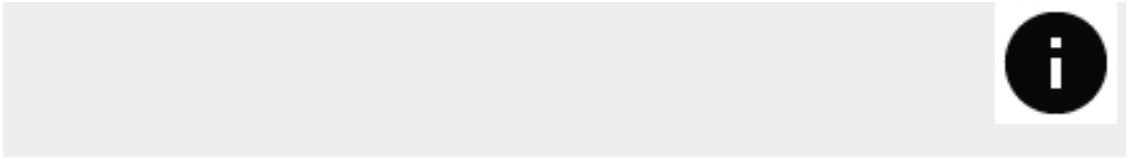
2. Orthologs: (b), (e), (f); Paralogs: (a), (c), (d)

3. There are 27 identities (highlighted in yellow) and two gaps, for a score of 220. The two sequences are approximately 27% identical. For an alignment of 27% identity over almost 100 residues, it is likely these two proteins are evolutionarily related and structurally similar.

```
WYLGKITRMDAEVLLKKPTVRDGHFLVTQCESSPGEF
WYFGKITRRESERLLLNPENPRGTFLVRESETTKGAY

SISVRFGDSVQ-----HFKVLRDQNGKYYLWAVK-FN
CLSVSDFDNAKGLNVKHYKIRKLDSGGFYITSRTQFS

SLNELVAYHRTASVSRTHTILLSDMNV
SSLQQLVAYYSKHADGLCHRLTNV
```



4. Protein shuffling involves randomly rearranging one of the protein sequences and comparing the alignment between the two sequences. Researchers repeat this process multiple times to produce a distribution plot that displays alignment scores of the randomly aligned sequences. If the alignment score for the two sequences is significantly higher than the randomly generated plot, then the sequences are likely significantly homologous.

5. Alignment score of sequences (1) and (2) is $6 \times 10 = 60$. Many answers are possible, depending on the randomly reordered sequence. A possible result is

Shuffled sequence:	(2) LYEGADKAKT
Alignment:	(1) ASNFLDKAGK (2) LYEGADKAKT
Alignment score is $3 \times 10 = 30$	

6. Replacement of cysteine, glycine, and proline never yields a positive score. Each of these residues exhibits features unlike those of its other 19 counterparts: cysteine is the only amino acid capable of forming disulfide bonds, glycine is the only amino acid without a side chain and is highly flexible, and

proline is the only amino acid that is highly constrained through the bonding of its side chain to its amine nitrogen.

7. According to the Blosum-62 matrix, substitution of an aspartate residue with a glutamate residue yields a score of $+2$.

8. (1) $\text{Identity score} = -25$; $\text{Blosum score} = 14$; (2) $\text{Identity score} = 15$; $\text{Blosum score} = 4$.

9. (a) The proteins almost certainly diverged from a common ancestor. (b) The proteins almost certainly diverged from a common ancestor. (c) The proteins may have diverged from a common ancestor, but the sequence alignment may not provide supporting evidence. (d) The proteins may have diverged from a common ancestor, but the sequence alignment is unlikely to provide supporting evidence.

10. There are 4^{40}, or 1.2×10^{24}, different molecules. Each molecule has a mass of 2.2×10^{-20} g, because 1 mol of polymer has a mass of $330 \text{ g mol}^{-1} \times 40$, and there are 6.02×10^{23} molecules per mole. Therefore, 26.4 kg of RNA would be required.

11. #1, Solvin A; #2, Solvin D; #3, Solvin C; #4, Solvin B. Solvin B and Solvin E are most similar, having diverged from each other 100 million years ago.

12. Convergent evolution: (a), (g); Divergent evolution: (d), (e), (f); Both: (b), (c)

13. (a) Divergent evolution; (b) Convergent evolution; (c) Divergent evolution.

14. Protein A is clearly homologous to protein B, given 65% sequence identity, and so A and B are expected to have quite similar three-dimensional structures. Likewise, proteins B and C are clearly homologous, given 55% sequence identity, and so B and C are expected to have quite similar three-dimensional structures. Thus, proteins A and C are likely to have similar three-dimensional structures, even though they are only 15% identical in sequence.

15. After RNA molecules have been selected and reverse transcribed, PCR is performed to introduce additional mutations into these strands. The use of this error-prone, thermostable polymerase in the amplification step would enhance the efficiency of this random mutagenesis.

Chapter 11

1. a, b, and c

2. b, c, d, and e

3. d

4. Three amino acids can be linked by peptide bonds in only six different ways. However, three different monosaccharides can be linked in a plethora of ways. The monosaccharides can be linked in a linear or branched manner, with α or β linkages, with bonds between C-1 and C-3, between C-1 and C-4, between C-1 and C-6, and so forth. In fact, the three monosaccharides can form 12,288 different trisaccharides.

5. (a) 10; (b) 6; (c) 8; (d) 9; (e) 2; (f) 4; (g) 1; (h) 5; (i) 7; (j) 3.

6. (a) aldose-ketose; (b) epimers; (c) aldose-ketose; (d) anomers; (e) aldose-ketose; (f) epimers.

7. b and c

8. Erythrose: tetrose aldose; ribose: pentose aldose; glyceraldehyde: triose aldose; dihydroxyacetone: triose ketose; erythrulose: tetrose ketose; ribulose: pentose ketose; fructose: hexose ketose.

9. The proportion of the α anomer is 0.36, and that of the β anomer is 0.64.

10. (a) Not a reducing sugar; no open-chain forms are possible; (b) D-galactose, D-glucose, D-fructose; (c) D-galactose and sucrose (glucose + fructose).

11. (a) Each glycogen molecule has one reducing end, whereas the number of nonreducing ends is determined by the number of branches, or α-1,6 linkages. (b) Because the number of nonreducing ends greatly exceeds the number of reducing ends in a collection of glycogen molecules, all of the degradation and synthesis of glycogen takes place at the nonreducing ends, thus maximizing the rate of degradation and synthesis.

12. b, c, and e

13. (a) Cellulose; (b) chitin; (c) glycogen; (d) chitin, glycogen, cellulose, and starch; (e) glycogen and starch.

14. Simple glycoproteins are often secreted proteins and thus play a variety of roles. For example, the hormone EPO is a glycoprotein. Usually, the protein component constitutes the bulk of the glycoprotein by mass. In contrast, proteoglycans and mucoproteins are predominantly carbohydrates. Proteoglycans have glycosaminoglycans attached and play structural roles as in cartilage and the extracellular matrix. Mucoproteins often serve as lubricants and have multiple carbohydrates attached through an *N*-acetylgalactosamine moiety.

15. b and c

16. Asparagine, serine, and threonine.

17. A glycoprotein is a protein that is decorated with carbohydrates. A lectin is a protein that specifically recognizes carbohydrates. A lectin can also be a glycoprotein.

18. Each site either is or is not glycosylated, and so there are $2^6 = 64$ possible proteins.

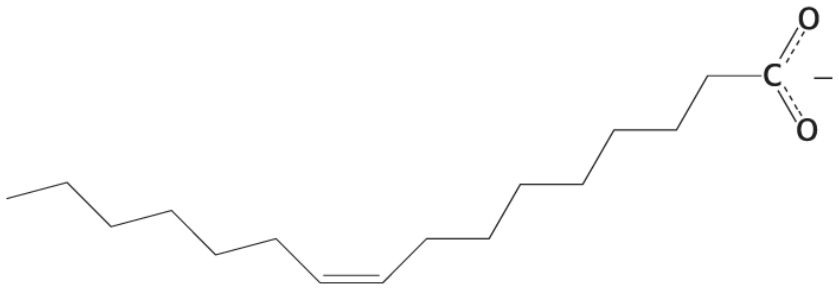
19. If the carbohydrate specificity of the lectin is known, an affinity column with the appropriate carbohydrate attached could be prepared. The protein preparation containing the lectin of interest could be passed over the column. Indeed, the use of this method was how the glucose-binding lectin concanavalin A was purified.

20. (a) Aggrecan is heavily decorated with glycosaminoglycans. If glycosaminoglycans are released into the media, aggrecan must be undergoing degradation. (b) Another enzyme might be present that cleaves glycosaminoglycans from aggrecan without degrading aggrecan. Other experiments not shown established that glycosaminoglycan release is an accurate measure of aggrecan destruction. (c) The control provides a baseline of “background” degradation inherent in the assay. (d) Aggrecan degradation is greatly enhanced. (e) Aggrecan degradation is reduced to the background system. (f) It is an in vitro system in which not all the factors contributing to cartilage stabilization in vivo are present.

Chapter 12

1. This fatty acid contains 18 carbons and two cis double bonds, which are located at carbons 9 and 12. Hence, its designation is $18{:}2(cis, cis, -\Delta^{9,12})$. Its common name is linoleate. Counting from the distal, or ω carbon, the two double bonds are located at positions ω-6 and ω-9.

2.



The common name for this fatty acid is palmitoleate.

3. The C_{16} alkyl chain is attached by an ether linkage. The C-2 carbon atom of glycerol has only an acetyl group attached by an ester linkage instead of a fatty acid, as is the case with most phospholipids.

4. (a) Phospholipids; (b) Sphingolipids, glycolipids, cholesterol; (c) Cholesterol; (d) Sphingomyelin, glycolipids; (e) Glycolipids; (f) Archaeal lipids.

5. 2×10^{-7} cm, 6×10^{-6} cm, and 2×10^{-4} cm.

6. Phospholipids and sphingolipids. Lipid molecules capable of aligning side by side to form a lipid bilayer must be amphipathic as well as have an appropriate geometry. Cholesterol molecules are almost completely hydrophobic and are therefore not capable of forming a lipid bilayer. Fatty acids, triacylglycerols, glycerophospholipids, and sphingomyelins are all amphipathic lipid molecules; however, the geometries of fatty acids and triacylglycerols are not favorable for aligning side by side to form a lipid bilayer.

7. Integral membrane proteins: (a); Peripheral membrane proteins: (b), (d); Lipid-anchored membrane protein: (c).

8. Membrane-spanning α helix: (c); Membrane-spanning β strands: (e); Lipid-anchored membrane protein: (a); Peripheral membrane protein: (b), (d).

9. The protein plotted in part *c* is a transmembrane protein from *C. elegans.* It spans the membrane with four α helices that are prominently displayed as hydrophobic peaks in the hydropathy plot.

Interestingly, the protein plotted in part *a* also is a membrane protein, a porin. This protein is made primarily of β strands, which lack the prominent hydrophobic window of membrane helices. This example shows that, although hydropathy plots are useful, they are not infallible.

10. The protein may contain an α helix that passes through the hydrophobic core of the protein. This helix is likely to feature a stretch of hydrophobic amino acids similar to those observed in transmembrane helices.

11. The radius of this molecule is 3.1×10^{-7} cm, and its diffusion coefficient is $7.4 \times 10^{-9}\ \text{cm}^2\ \text{s}^{-1}$. The average distances traversed are 1.7×10^{-7} cm in 1 μs, 5.4×10^{-6} cm in 1 ms, and 1.7×10^{-4} cm in 1 s.

12. (a) The graph shows that, as temperature increases, the phospholipid bilayer becomes more fluid. T_m is the temperature of the transition from the predominantly less-fluid state to the predominantly more-fluid state. Cholesterol broadens the transition from the less-fluid to the more-fluid state. In essence, cholesterol makes membrane fluidity less sensitive to temperature changes. (b) This effect is important because the presence of cholesterol tends to stabilize membrane fluidity by preventing sharp transitions. Because protein function depends on the proper fluidity of the membrane, cholesterol maintains the proper environment for membrane-protein function.

13. $S = 7.2\ \mu\text{m}$.

14. From lowest melting point to highest: d, c, b, e, a. The fatty acid with the lowest melting point is the one with the highest number of double bonds, α-lineoleic acid (18:3). Palmitoleic acid (16:1) has a higher melting point than α-linoleic acid (18:3) because it only contains one double bond. Oleic acid (18:1) also contains one double bond, but it has a longer fatty acid chain than palmitoleic acid, and subsequently, a higher melting point. Fatty acids without double bonds have the highest melting points, and those that are longer have higher melting points. Thus, palmitic acid (16:0) has a higher melting point than oleic acid (18:1). Stearic acid (18:0) has the highest melting point.

15. Each of the 21 v-SNARE proteins could interact with each of 7 t-SNARE partners. Multiplication gives the total number of different interacting pairs: $7 \times 21 = 147$ different v-SNARE–t-SNARE pairs.

16. The membrane underwent a phase transition from a highly fluid to a nearly frozen state when the temperature was lowered. A carrier can shuttle ions across a membrane only when the bilayer is highly fluid. A channel, in contrast, allows ions to traverse its pore even when the bilayer is quite rigid.

17. (a) H_2O; (b) Indole; (c) H_2O. Permeability is most directly correlated with the solubility in a nonpolar solvent.

18. Hibernators selectively feed on plants that have a high proportion of polyunsaturated fatty acids with lower melting temperature.

19. Saturated phospholipids: c; Unsaturated phospholipids: a, d; Both: b.

20. (a) Prostaglandin H_2 synthase-1 recovers its activity immediately after removal of ibuprofen, suggesting that this inhibitor dissociates rapidly from the enzyme. In contrast, the enzyme remains significantly inhibited 30 minutes after removal of indomethacin, suggesting that this inhibitor dissociates slowly from its active site. (b) Aspirin covalently modifies prostaglandin H_2 synthase-1, indicating that it would dissociate very slowly (if at all). Hence, one would anticipate that very low activity would be evident in all conditions where inhibitor has been added (columns 2, 3, and 4).

Chapter 13

1. In simple diffusion, the substance in question can diffuse down its concentration gradient through the membrane. In facilitated diffusion, the substance is not lipophilic and cannot directly diffuse through the membrane. A channel or carrier is required to facilitate movement down the gradient.

2. Uniporters act as enzymes do; their transport cycles include large conformational changes, and only a few molecules interact with the protein per transport cycle. In contrast, channels, after having opened, provide a pore in the membrane through which many ions may pass. As such, channels mediate transport at a much higher rate than do uniporters.

3. Passive transport: (b), (d); Active transport: (a), (c).

4. For chloride, $z = -1$. At the concentrations given, the equilibrium potential for chloride is $-97\ \text{mV}$.

5. (a) Using $\Delta G = RT \ln (c_2 / c_1) + ZF\Delta V$, where the inside of the cell is side 2 and the outside is side 1, the free energy of sodium transport is:

$$\begin{aligned}\Delta G_{Na} &= (8.315 \times 10^{-3}\ \text{kJ mol}^{-1}\ \text{deg}^{-1}) \times (310\ \text{deg}) \times \ln(17/155) \\ &\quad + (1) \times (96.5\ \text{kJ mol}^{-1}\ \text{V}^{-1}) \times (-0.055\ \text{V}) \\ \Delta G_{Na} &= -11.0\ \text{kJ mol}^{-1}\end{aligned}$$

Because two Na^+ ions are transported for each glucose molecule, the maximum energy available for establishing the glucose gradient is $-22.0\ \text{kJ mol}^{-1}$.

(b) For an uncharged solute like glucose, the minimum energy required to pump glucose against a concentration gradient is given by:

$$\Delta G_{gluc} = RT \ln([\text{glucose}]_{in} / [\text{glucose}]_{out})$$

Rearranging this equation, we obtain:

$$[\text{glucose}]_{in} / [\text{glucose}]_{out} = e^{\frac{\Delta G_{gluc}}{RT}} = e^{\frac{(22.0\ \text{kJ mol}^{-1})}{(8.315 \times 10^{-3}\ \text{kJ mol}^{-1}\ \text{K}^{-1})(310\ \text{K})}} = 5100$$

6. At pH 7.4, $[H^+] = 3.98 \times 10^{-8}\ \text{M}$, and at pH 2.0, $[H^+] = 0.01\ \text{M}$. Using $\Delta G = RT \ln(c_2 / c_1) + ZF\Delta V$:

$$\begin{aligned}\Delta G &= (8.315 \times 10^{-3}\ \text{kJ mol}^{-1}\ \text{deg}^{-1}) \times (310\ \text{deg}) \times \ln\left(\frac{0.01}{3.98 \times 10^{-8}}\right) \\ &\quad + (1) \times (96.5\ \text{kJ mol}^{-1}\text{V}^{-1}) \times (0.070\text{V}) \\ \Delta G &= 38.8\ \text{kJ mol}^{-1}\end{aligned}$$

7. ABC transporters: (b), (f); P-type ATPases: (c), (d); Both: (a), (e).

8. (b), (c), (f), (g).

9. After the addition of ATP and calcium, SERCA will pump Ca^{2+} ions into the vesicle. However, the accumulation of Ca^{2+} ions inside the vesicle will rapidly lead to the formation of an electrical gradient that cannot be overcome by ATP hydrolysis. The addition of calcimycin will allow the pumped Ca^{2+} ions to flow back out of the vesicle, dissipating the charge buildup, and enabling the pump to operate continuously.

10. The three types of carriers are symporters, antiporters, and uniporters. Symporters and antiporters can mediate secondary active transport.

11. Facilitated diffusion: (e), (i); Primary active transport: (b), (g); Secondary active transport: (c), (d), (h); Both primary and secondary active transport: (a), (f).

12. When a potassium ion passes through the channel, it remains hydrated for most of the distance. However, the channel narrows after the ion passes about 22 Å into the membrane, and K^+ must relinquish its hydration shell. This is energetically costly, but it is compensated by the interaction of K^+ with the carbonyl oxygen atoms in the interior of the channel at its narrow point. Since Na^+ is small compared to K^+, it cannot interact optimally with these oxygen atoms, and can thus not adequately compensate for the high energy cost of Na^+ desolvation.

13. A mutation that impairs the ability of the sodium channel to inactivate would prolong the duration of the depolarizing sodium current, thus lengthening the cardiac action potential.

14. Batrachotoxin blocks the transition from the open to the closed state.

15. (a) Only ASIC1a is inhibited by the toxin. (b) Yes; when the toxin was removed, the activity of the acid-sensing channel began to be restored. (c) 0.9 nM.

16. The blockage of ion channels inhibits action potentials, leading to loss of nervous function. Like tetrodotoxin, these toxin molecules are useful for isolating and specifically inhibiting particular ion channels.

17. Ligand-gated ion channels: (c), (e); Voltage-gated ion channels: (a); Both: (b), (d).

18. After repolarization, the ball domains of the ion channels engage the channel pore, rendering them inactive for a short period of time. During this time, the channels cannot be reopened until the ball domains disengage and the channel returns to the “closed” state.

19. (b), (d), (e), (c), (a), (f).

20. Compound A is TEA, Compound B is TTX.

Chapter 14

1. c, d, a, f, g, e, b

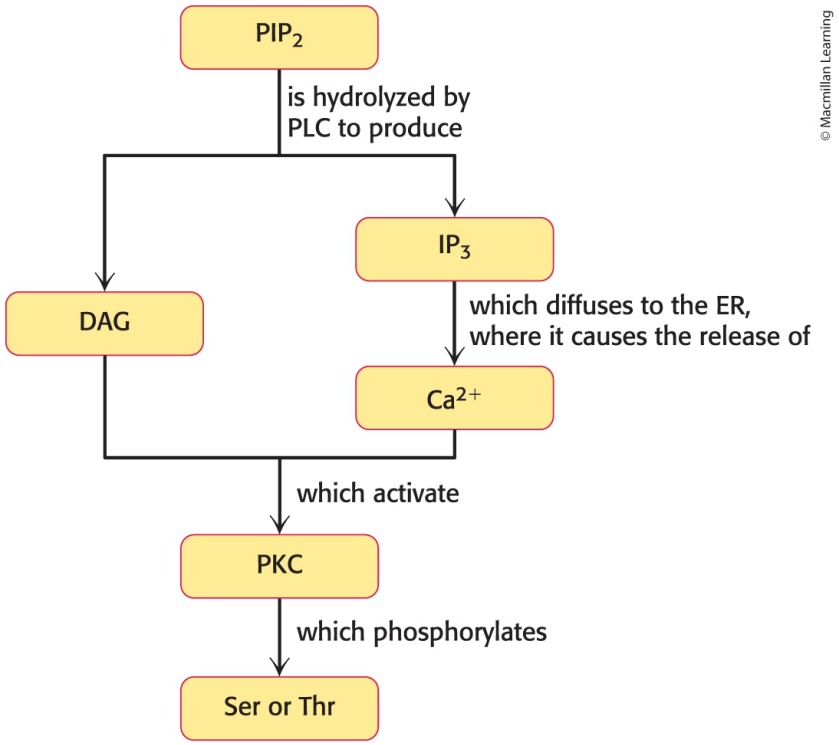
2. c, b, d, a, e, f

3. The rate of cAMP production will be 10^5 per second; in 10 seconds, 10^6 molecules of cAMP will be produced.

4. The mutated α subunit will always be in the GTP (that is, active) form; thus, it would stimulate its signaling pathway.

5. $G_{\alpha s}$ stimulates adenylate cyclase, leading to the generation of cAMP. This signal then leads to glucose mobilization (Chapter 21). If cAMP phosphodiesterase were inhibited, then cAMP levels would remain high even after the termination of the adrenaline signal, and glucose mobilization would continue.

6. (a)



© Macmillan Learning

(b) IP_3, DAG, and Ca^{2+} are considered second messengers.

7. b, c, f

8. G protein-coupled receptors: c, d, g, i

Receptor tyrosine kinases: a, e, f

Both: f

Neither: b

9. Imatinib (Gleevec) is a small molecule that targets the active site of a tyrosine kinase inside the cell; cetuximab (Erbitux) is an antibody that binds to the extracellular domain of the receptor, preventing ligand binding.

10. a, d, e

11. In the reaction catalyzed by adenylate cyclase, the $3'-OH$ group undergoes a nucleophilic attack on the α-phosphorus atom attached to the $5'-OH$ group, leading to displacement of pyrophosphate. The reaction catalyzed by DNA polymerase is similar except that the $3'-OH$ group is on a different nucleotide.

12. $GTP\gamma S$ is not hydrolyzed by the G_α subunit, leading to prolonged activation.

13. (a) Use ATP labeled at the γ (gamma) phosphate; (b) Use ATP labeled at the α (alpha) phosphate.

14. (a) $X \approx 10^{-7}\ M; Y \approx 5 \times 10^{-6}\ M; Z \approx 10^{-3}\ M$. (b) Because much less X is required to fill half of the sites, X displays the highest affinity. (c) The binding affinity almost perfectly matches the ability to stimulate adenylate cyclase, suggesting that the hormone receptor complex leads to the stimulation of adenylate cyclase. (d) Try performing the experiment in the presence of antibodies to $G_{\alpha s}$.

15. The transgenic nematode would avoid the compound. The identity of the ligand is determined by the receptor, whereas the behavioral response is dictated by the neuron in which the receptor is expressed.

16. Only a mixture of compounds $C_5\text{-}COOH$ and $HOOC\text{-}C_7\text{-}COOH$ is predicted to yield this pattern.

17. Sound travels 0.15 m in 428 μs. The human hearing system is capable of sensing time differences of close to a microsecond, and so the difference in arrival times at the two ears is substantial. A system based on G proteins is unlikely to be able to reliably distinguish between signals arriving at the two ears, because G proteins typically respond in milliseconds.

18. (a) 380 (one for each receptor); (b) there are $(380 \times 379)/2! = 72{,}010$ combinations of two receptors; (c) $(380 \times 379 \times 378)/3! = 9{,}073{,}260$ combinations of three receptors.

19. The absorption of light converts 11-*cis*-retinal into all-*trans*-retinal.

Chapter 15

1. Anabolism is the set of biochemical reactions that build new molecules and ultimately new cells and generally use energy. Catabolism is the set of biochemical reactions that break down biomolecules and generally extract energy from fuel sources.

2. Phototrophs derive energy by transforming light into chemical energy. Chemotrophs derive energy from the oxidation of chemicals, either organic such as glucose and fatty acids, or inorganic sources like iron, sulfur, or ammonia.

3. Stage 1 is digestion, where the larger molecules in food are broken into smaller molecules. No ATP is generated. In stage 2, these smaller molecules are converted to key molecules of metabolism. A small amount of ATP is generated in this stage. Stage 3 consists of the complete oxidation of fuel molecules to CO_2 and H_2O. Most of the ATP is produced in stage 3.

4. Cellular movements and the performance of mechanical work; active transport; biosynthetic reactions.

5. Charge repulsion, resonance stabilization, increase in entropy, and stabilization by hydration.

6. Increasing the concentration of ATP or decreasing the concentration of cellular ADP or P_i (by rapid removal by other reactions, for instance) would make the reaction more exergonic. Likewise, altering the Mg^{2+} concentration could raise or lower the ΔG of the reaction (see problem 20).

7. Reactions in parts (a) and (c), to the left; reactions in parts (b) and (d), to the right.

8. (a) $\Delta G^{\circ\prime} = +31.4\ \text{kJ mol}^{-1} (+7.5\ \text{kcal mol}^{-1})$ and $K'_{eq} = 3.06 \times 10^{-6}$; (b) 3.28×10^4.

9. $\Delta G^{\circ\prime} = +7.1\ \text{kJ mol}^{-1} (+1.7\ \text{kcal mol}^{-1})$. The equilibrium ratio is 17.5.

10. (a) $\text{Acetate} + \text{CoA} + H^+$ goes to acetyl $\text{CoA} + H_2O$, $\Delta G^{\circ\prime} = -31.4\ \text{kJ mol}^{-1} (-7.5\ \text{kcal mol}^{-1})$. ATP hydrolysis to AMP and PP_i, $\Delta G^{\circ\prime} = -45.6\ \text{kJ mol}^{-1} (-10.9\ \text{kcal mol}^{-1})$. Overall reaction, $\Delta G^{\circ\prime} = -14.2\ \text{kJ mol}^{-1} (-3.4\ \text{kcal mol}^{-1})$. (b) With pyrophosphate hydrolysis, $\Delta G^{\circ\prime} = -33.4\ \text{kJ mol}^{-1} (-7.98 \text{kcalmol}^{-1})$. Pyrophosphate hydrolysis makes the overall reaction even more exergonic.

11. Arginine phosphate in invertebrate muscle, like creatine phosphate in vertebrate muscle, serves as a reservoir of high-potential phosphoryl groups. Arginine phosphate maintains a high level of ATP in muscular exertion.

12. An ADP unit.

13. (a) The rationale behind creatine supplementation is that it would be converted into creatine phosphate and thus serve as a rapid means of replenishing ATP after muscle contraction. (b) If creatine supplementation is beneficial, it would affect activities that depend on short bursts of activity; any

sustained activity would require ATP generation by fuel metabolism, which, as Figure 15.7 shows, requires more time.

14. Under standard conditions, $\Delta G^{\circ\prime} = -RT \ln [\text{products}]/[\text{reactants}]$. Substituting $+23.8\ \text{kJ mol}^{-1} (+5.7\ \text{kcal mol}^{-1})$q for $\Delta G^{\circ\prime}$ and solving for $[\text{products}]/[\text{reactants}]$ yields 9.9×10^{-5}. In other words, the forward reaction does not take place to a significant extent. Under intracellular conditions, ΔG is $-1.3\ \text{kJ mol}^{-1} (-0.3\ \text{kcal mol}^{-1})$. Using the equation $\Delta G = \Delta G^{\circ\prime} + RT \ln [\text{products}]/[\text{reactants}]$ and solving for $[\text{products}]/[\text{reactants}]$ gives a ratio of 5.96×10^{-5}. Thus, a reaction that is endergonic under standard conditions can be converted into an exergonic reaction by maintaining the [products]/[reactants] ratio below the equilibrium value. This conversion is usually attained by using the products in another coupled reaction as soon as they are formed, thus artificially decreasing their concentration and driving the proceeding reaction forward (Le Chatelier's Principle).

15. Liver: $-45.2\ \text{kJ mol}^{-1} (-10.8\ \text{kcal mol}^{-1})$; muscle: $-48.1\ \text{kJ mol}^{-1} (-11.5\ \text{kcal mol}^{-1})$; brain: $-48.5\ \text{kJ mol}^{-1} (-11.6\ \text{kcal mol}^{-1})$. The ΔG is most negative in brain cells.

16. (a) Ethanol; (b) lactate; (c) succinate; (d) isocitrate; (e) malate.

17. NADH and $FADH_2$ are electron carriers for catabolism; NADPH is the carrier for anabolism.

18. Oxidation–reduction reactions; ligation reactions; isomerization reactions; group-transfer reactions; hydrolytic reactions; cleavage of bonds by means other than hydrolysis or oxidation.

19. Controlling the amount of enzymes; controlling enzyme activity; controlling the availability of substrates.

20. (a) As the Mg^{2+} concentration falls, the ΔG of hydrolysis becomes more negative. Note that pMg is a logarithmic plot, and so each number on the *x*-axis represents a 10-fold change in $[Mg^{2+}]$. (b) Mg^{2+} would bind to the phosphates of ATP and help to mitigate charge repulsion. As the $[Mg^{2+}]$ falls, charge stabilization of ATP would be less, leading to greater charge repulsion and ΔG of hydrolysis becoming more negative.

Chapter 16

1. a and e.

2. b and d.

3. (a) 4; (b) 3; (c) 1; (d) 6; (e) 8; (f) 2; (g) 10; (h) 9; (i) 7; (j) 5.

4. In both cases, the electron donor is glyceraldehyde 3-phosphate. In lactic acid fermentation, the electron acceptor is pyruvate, converting it into lactate. In ethanol fermentation, acetaldehyde is the electron acceptor, forming ethanol.

5. Glucokinase enables the liver to remove glucose from the blood when hexokinase is saturated, ensuring that glucose is captured for later use.

6. The GAP formed is immediately removed by subsequent reactions, resulting in the conversion of DHAP into GAP by the enzyme.

7. Glucose 6-phosphate must have other fates. Indeed, it can be converted into glycogen (Chapter 21) or processed to yield reducing power for biosynthesis (Chapter 20).

8. The conversion of glucose into glucose 6-phosphate by hexokinase; the conversion of fructose 6-phosphate into fructose 1,6-bisphosphate by phosphofructokinase; the formation of pyruvate from phosphoenolpyruvate by pyruvate kinase.

9. GLUT2 transports glucose only when the blood concentration of glucose is high, which is precisely the condition in which the β cells of the pancreas secrete insulin.

10. Without triose isomerase, only one of the two three-carbon molecules generated by aldolase could be used to generate ATP. Only two molecules of ATP would result from the metabolism of each glucose. But two molecules of ATP would still be required to form fructose 1,6-bisphosphate, the substrate for aldolase. The net yield of ATP would be zero, a yield incompatible with life.

11. The equilibrium concentrations of fructose 1,6-bisphosphate, dihydroxyacetone phosphate, and glyceraldehyde 3-phosphate are 7.8×10^{-4} M, 2.2×10^{-4} M, and 2.2×10^{-4} M, respectively.

12. (a) 2, 3, 6, 9; (b) 1, 4, 5, 7, 8.

13. Glucose is an important energy source for both tissues and is essentially the only energy source for the brain. Consequently, these tissues should never release glucose. Glucose release is prevented by the absence of glucose 6-phosphatase.

14. 6 NTP (4 ATP and 2 GTP); 2 NADH.

15. 50 pyruvate, 100 ATP, and 50 NADH.

16. (a) Increased; (b) increased; (c) increased; (d) decreased.

17. b and e.

18. This example illustrates the difference between the *stoichiometric* and the *catalytic* use of a molecule. If cells used NAD^+ stoichiometrically, a new molecule of NAD^+ would be required each time a molecule of lactate was produced. The synthesis of NAD^+ requires ATP. On the other hand, if the NAD^+ that is converted into NADH could be recycled and reused, a small amount of the molecule could regenerate a vast amount of lactate, which is the case in the cell. NAD^+ is regenerated by the oxidation of NADH and reused. NAD^+ is thus used catalytically.

19. Using the Michaelis–Menten equation to solve for [S] when $K_M = 50\ \mu M$ and $V_0 = 0.9V_{max}$ shows that a substrate concentration of 0.45 mM yields 90% of V_{max}. Under normal conditions, the enzyme is essentially working at V_{max}.

20. (a) If both enzymes operated simultaneously, the net result would be simply:

$$ATP + H_2O \rightarrow ADP + P_i$$

The energy of ATP hydrolysis would be released as heat. (b) Not really. For the cycle to generate heat, both enzymes must be functional at the same time in the same cell. (c) The species *B. terrestris* and *B. rufocinctus* might show some futile cycling because both enzymes are active to a substantial degree. (d) No. These results simply suggest that simultaneous activity of phosphofructokinase and fructose 1,6-bisphosphatase is unlikely to be employed to generate heat in the species shown.

Chapter 17

1. The pyruvate dehydrogenase complex catalyzes the following reaction, linking glycolysis and the citric acid cycle:

$$\text{Pyruvate} + \text{CoA} + \text{NAD}^+ \rightarrow \text{acetyl CoA} + \text{NADH} + \text{H}^+ + \text{CO}_2$$

2. a

3. b

4. Thiamine pyrophosphate plays a role in the decarboxylation of pyruvate. Lipoic acid (as lipoamide) transfers the acetyl group. Coenzyme A accepts the acetyl group from lipoic acid to form acetyl CoA. FAD accepts the electrons and hydrogen ions when reduced lipoic acid is oxidized. NAD^+ accepts electrons from FADH_2.

5. Catalytic coenzymes (TPP, lipoic acid, and FAD) are modified but regenerated in each reaction cycle. Thus, they can play a role in the processing of many molecules of pyruvate. Stoichiometric coenzymes (coenzyme A and NAD^+) are used in only one reaction because they are the components of products of the reaction.

6. $-41.0\ \text{kJ mol}^{-1} (-9.8\ \text{kcal mol}^{-1})$

7. (a) DCA inhibits pyruvate dehydrogenase kinase. (b) The fact that inhibiting the kinase results in more dehydrogenase activity suggests that there must be some residual activity that is being inhibited by the kinase.

8. (a) Enhanced kinase activity will result in a decrease in the activity of the PDH complex because phosphorylation by the kinase inhibits the complex. (b) Phosphatase activates the complex by removing a phosphate. If the phosphatase activity is diminished, the activity of the PDH complex also will decrease.

9. (a) 6; (b) 10; (c) 1; (d) 7; (e) 2; (f) 8; (g) 3; (h) 4; (i) 5; (j) 9.

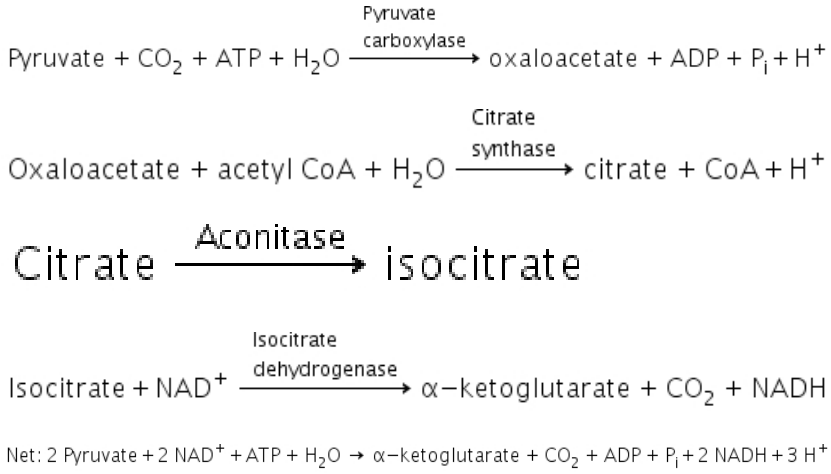
10. (a) 5; (b) 7; (c) 1; (d) 10; (e) 2; (f) 4; (g) 9; (h) 3; (i) 8; (j) 6.

11. Succinate dehydrogenase is the only enzyme in the citric acid cycle that is embedded in the mitochondrial membrane, which makes it associated with the electron-transport chain.

12. (a) The steady-state concentrations of the products are low compared with those of the substrates. (b) The ratio of malate to oxaloacetate must be greater than 1.57×10^4 for oxaloacetate to be formed.

13.

$$\text{Pyruvate} + \text{CoA} + \text{NAD}^+ \xrightarrow[\text{complex}]{\text{Pyruvate dehydrogenase}} \text{acetyl CoA} + \text{CO}_2 + \text{NADH}$$



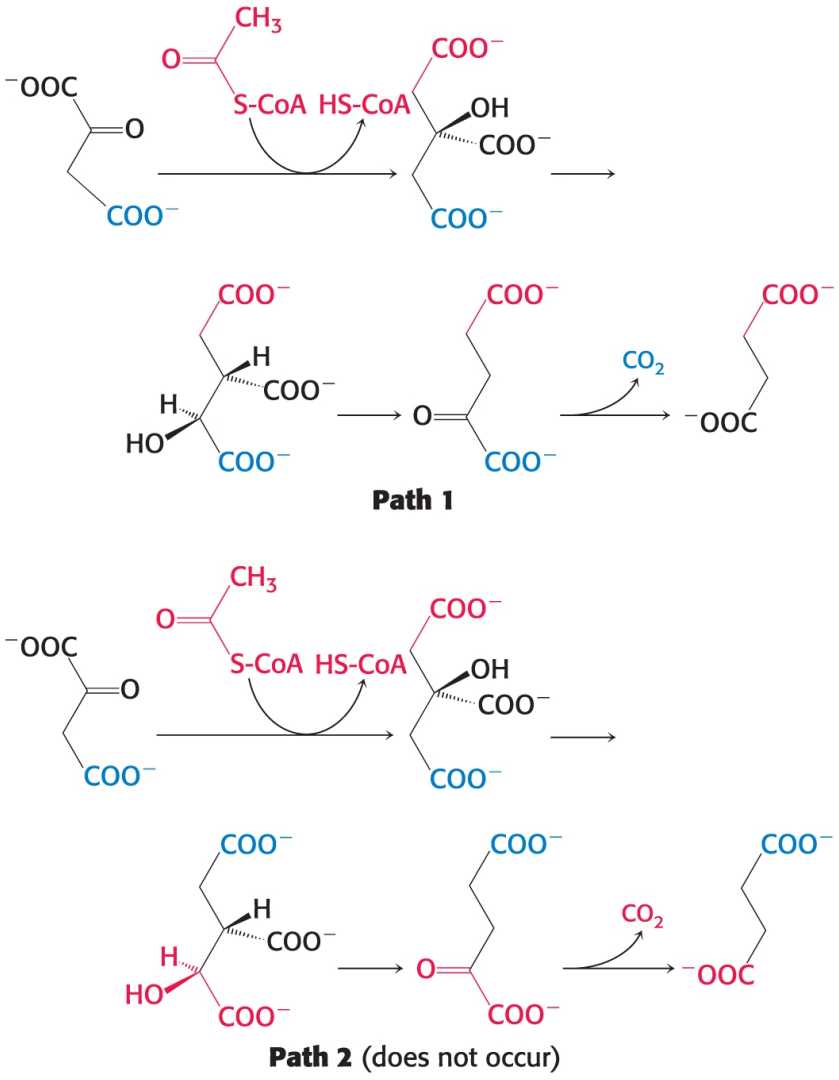
14. Succinate will increase in concentration, followed by α-ketoglutarate and the other intermediates "upstream" of the site of inhibition. Succinate has two methylene groups that are required for the dehydrogenation, whereas malonate has but one.

15. It enables organisms such as plants and bacteria to convert fats, through acetyl CoA, into glucose.

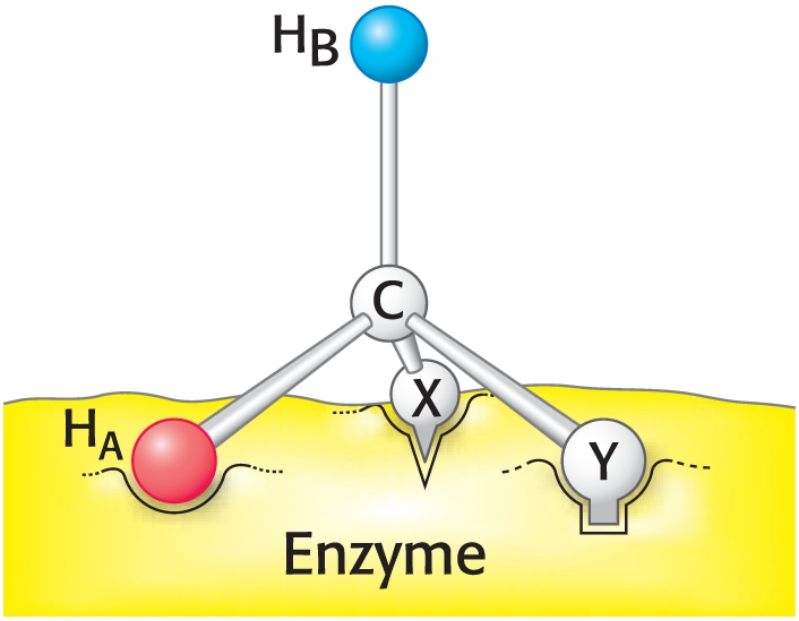
16. We cannot get the net conversion of fats into glucose, because the only means to get the carbon atoms from fats into oxaloacetate, the precursor of glucose, is through the citric acid cycle. However, although two carbon atoms enter the cycle as acetyl CoA, two carbon atoms are lost as CO_2 before oxaloacetate is formed. Thus, although some carbon atoms from fats may end up as carbon atoms in glucose, we cannot obtain a *net* synthesis of glucose from fats.

17. Acetyl CoA will inhibit the complex. Glucose metabolism to pyruvate will be slowed because acetyl CoA is being derived from an alternative source.

18. (a) Citrate is a symmetric molecule. Consequently, the investigators assumed that the two $-CH_2COO^-$ groups in it would react identically. Thus, for every citrate molecule undergoing the reactions shown in path 1, they thought that another citrate molecule would react as shown in path 2. If so, then only *half* the label should have emerged in the CO_2.



(b) Call one hydrogen atom A and the other B. Now suppose that an enzyme binds three groups of this substrate—X, Y, and H—at three complementary sites. The adjoining diagram shows X, Y, and H_A bound to three points on the enzyme. In contrast, X, Y, and H_B cannot be bound to this active site; two of these three groups can be bound, but not all three. Thus, H_A and H_B will have different fates.



© Macmillan Learning

Sterically nonequivalent groups such as H_A and H_B will almost always be distinguished in enzymatic reactions. The essence of the differentiation of these groups is that the enzyme holds the substrate in a specific orientation. Attachment at three points, as depicted in the diagram, is a readily visualized way of achieving a particular orientation of the substrate, but it is not the only means of doing so.

19. (a) The complete oxidation of citrate requires $4.5\ \mu mol$ of O_2 for every micromole of citrate.

$$C_6H_8O_7 + 4.5\ O_2 \rightarrow 6\ CO_2 + 4\ H_2O$$

Thus, 13.5 μmol of O_2 would be consumed by 3 μmol of citrate. (b) Citrate led to the consumption of far more O_2 than can be accounted for simply by the oxidation of citrate itself. Citrate thus facilitated O_2 consumption.

20. (a) The initial infection is unaffected by the absence of isocitrate lyase, but the absence of this enzyme inhibits the latent phase of the infection. (b) Yes. (c) A critic could say that, in the process of deleting the isocitrate lyase gene, some other gene was damaged, and it is the absence of this other gene that prevents latent infection. Reinserting the isocitrate lyase gene into the bacteria from which it had been removed renders the criticism less valid. (d) Isocitrate lyase enables the bacteria to synthesize carbohydrates that are necessary for survival, including carbohydrate components of the cell membrane.

Chapter 18

1. b

2. a

3. b

4. d

5. Biochemists use E_0', the value at pH 7, whereas chemists use E_0, the value in $1\ M\ H^+$. The prime denotes that pH 7 is the standard state.

6. The reduction potential of $FADH_2$ is less than that of NADH (Table 18.1). Consequently, when those electrons are passed along to oxygen, less energy is released. The consequence of the difference is that electron flow from $FADH_2$ to O_2 pumps fewer protons than do the electrons from NADH. The $\Delta G^{\circ\prime}$ for the reduction of oxygen by $FADH_2$ is $-200\ kJ\ mol^{-1}(-48\ kcal\ mol^{-1})$.

7. $\Delta G^{\circ\prime}$ is $+67\ kJ\ mol^{-1}(+16.1\ kcal\ mol^{-1})$ for oxidation by NAD^+ and $-3.8\ kJ\ mol^{-1}(-0.92\ kcal\ mol^{-1})$ for oxidation by FAD. The oxidation of succinate by NAD^+ is not thermodynamically feasible.

8. c, e, b, a, d.

9. (a) 4; (b) 3; (c) 1; (d) 5; (e) 2.

10. Rotenone: NADH, NADH-Q oxidoreductase will be reduced. The remainder will be oxidized. Antimycin A: NADH, NADH-Q oxidoreductase and coenzyme Q will be reduced. The remainder will be oxidized. Cyanide: All will be reduced.

11. (a) 12.5; (b) 14; (c) 32; (d) 13.5; (e) 30; (f) 16.

12. (a) It blocks electron transport and proton pumping at Complex IV. (b) It blocks electron transport and ATP synthesis by inhibiting the exchange of ATP and ADP across the inner mitochondrial membrane. (c) It blocks electron transport and proton pumping at Complex I. (d) It blocks ATP synthesis without inhibiting electron transport by dissipating the proton gradient. (e) It blocks electron transport and proton pumping at Complex IV. (f) It blocks electron transport and proton pumping at Complex III.

13. ATP synthase will from an arsenate (AsO_4^{3-}) anhydride with ADP. Such compounds are unstable and rapidly hydrolyzed. Under these conditions, no ATP synthesis can occur, but the synthase will continue catalyzing the useless reaction. Consequently, the electron-transport system will keep running, most likely at a higher than normal rate. In essence, arsenate is acting as an uncoupler.

14. (a) No effect; mitochondria cannot metabolize glucose. (b) No effect; no fuel is present to power the synthesis of ATP. (c) $[O_2]$ falls because citrate is a fuel and ATP can be formed from ADP and P_i. (d) Oxygen consumption stops because oligomycin inhibits ATP synthesis, which is coupled to the activity

of the electron-transport chain. (e) No effect, for the reasons given in part (*d*). (f) $[O_2]$ falls rapidly because the system is uncoupled and does not require ATP synthesis to lower the proton-motive force. (g) $[O_2]$ falls, though at a lower rate. Rotenone inhibits Complex I, but the presence of succinate will enable electrons to enter at Complex II. (h) Oxygen consumption ceases because Complex IV is inhibited and the entire chain backs up.

15. (a) The $P:O$ ratio is equal to the product of $(H^+/2e^-)$ and (P/H^+). Note that the $P:O$ ratio is identical with the $P:2\ e^-$ ratio. (b) 2.5 and 1.5, respectively.

16. This inhibitor (like antimycin A) blocks the reduction of cytochrome c_1 by QH_2.

17. If oxidative phosphorylation were uncoupled, no ATP could be produced. In a futile attempt to generate ATP, much fuel would be consumed. The danger lies in the dose. Too much uncoupling would lead to tissue damage in highly aerobic organs such as the brain and heart, which would have severe consequences for the organism as a whole. The energy that is normally transformed into ATP would be released as heat. To maintain body temperature, sweating might increase, although the very process of sweating itself depends on ATP.

18. In humans, the proton motive force is also used to drive the export of ATP from the matrix and the import of phosphate into the matrix. In bacteria, it drives flagellar motion.

19. (a) DNP is an uncoupler that prevents the use of the proton-motive force for ATP synthesis. Consequently, the rate of oxygen consumption rises (reflecting the rate of the electron transport chain) in a futile attempt to synthesize ATP. Because mitochondrial ATP synthesis is inhibited, the rate of glycolysis, as measured by ECAR, increases in an attempt meet the cells ATP needs. (b) Because glycolysis is now inhibited, no lactic acid will be produced, and the rate of extracellular acidification will fall. Because DNP is still present, oxygen consumption will still occur at a high rate. (c) A key step in glycolysis is the isomerization of glucose 6-phosphate to fructose 6-phosphate. 2-Deoxyglucose is incapable of undergoing the isomerization. (d) Rotenone inhibits electron flow through Complex I, the electron transport chain is inhibited, and oxygen consumption ceases.

20. (a) Succinate is oxidized by Complex II, and the electrons are used to establish a proton-motive force that powers ATP synthesis. (b) The ability to synthesize ATP is greatly reduced. (c) The goal was to measure ATP hydrolysis. If succinate had been added in the presence of ATP, no reaction would have taken place, because of respiratory control. (d) The mutation has little effect on the ability of the enzyme to catalyze the hydrolysis of ATP. (e) They suggest two things: (1) the mutation did not affect the catalytic site on the enzyme, because ATP synthase is still capable of catalyzing the reverse reaction, and (2) the mutation did not affect the amount of enzyme present, given that the controls and patients had similar amounts of activity.

Chapter 19

1. d

2. a

3. a

4. c

5. The oxygen we require is produced by photosynthesis. Moreover, most of the carbon atoms of which we are made, not just carbohydrates, enter the biosphere through the process of photosynthesis.

6. $2\ NADP^+ + 3\ ADP^{3-} + 3\ P_i^{\ 2-} + H^+ \rightarrow O_2 + 2\ NADPH + 3\ ATP^{4-} + H_2O$

7. (a) PS I; (b) PS II; (c) PS II; (d) PS II; (e) PS I.

8. Photosystem II, in conjunction with the water-oxidizing complex, powers oxygen release. The reaction center of photosystem II absorbs light maximally at 680 nm. Oxygen consumption will be maximal when photosystems I and II are operating cooperatively. Oxygen will be efficiently generated when electrons from photosystem II fill the electron holes in photosystem I, which were generated when the reaction center of photosystem I was illuminated by light of 700 nm.

9. The light reactions take place on thylakoid membranes. Increasing the membrane surface increases the number of ATP- and NADPH-generating sites.

10. These complexes absorb more light than a reaction center alone can absorb by using additional pigments. The light-harvesting complexes funnel light energy to the reaction centers using resonance energy transfer.

11. $NADP^+$ is the acceptor. H_2O is the donor. Light energy.

12. Protons released by the oxidation of water; protons pumped into the lumen by the cytochrome *bf* complex; protons removed from the stroma by the reduction of $NADP^+$ and plastoquinone.

13. $\Delta E_0' = 10.11\ V$, and $\Delta G^{\circ\prime} = -21.3\ kJ\ mol^{-1} (-5.1\ kcal\ mol^{-1})$.

14. Not at all. Chemicals other than water can donate electrons and protons as they do in anoxygenic photosynthesis on Earth today.

15. DCMU inhibits electron transfer in the link between photosystems II and I. O_2 can evolve in the presence of DCMU if an artificial electron acceptor such as ferricyanide can accept electrons from Q.

16. DCMU will have no effect, because it blocks photosystem II, and cyclic photophosphorylation uses photosystem I and the cytochrome *bf* complex.

17. (a) $+120\ kJ\ einstein^{-1} (+28.7\ kcal\ einstein^{-1})$; (b) 1.24 V; (c) One 1000-nm photon has the free-energy content of 2.4 molecules of ATP. A minimum of 0.42 photon is needed to drive the synthesis of a molecule of ATP.

18. The cristae, formed by the inner mitochondrial membrane, and the matrix.

19. In eukaryotes, both processes take place in specialized organelles. Both depend on high-energy electrons to generate ATP. In oxidative phosphorylation, the high-energy electrons originate in fuels and are extracted as reducing power in the form of NADH. In photosynthesis, the high-energy electrons are generated by light and are captured as reducing power in the form of NADPH. Both processes use redox reactions to generate a proton gradient, and the enzymes that convert the proton gradient into ATP are very similar in both processes. In both systems, electron transport takes place in membranes inside organelles.

Chapter 20

1. b.

2. c, d, a, b.

3. Calvin–Benson cycle: b, c, f, g, h. Krebs cycle: a, d, e, i, j.

4. c.

5. For CO_2, $k_{cat}/K_M = 3 \times 10^5\ M^{-1}\ s^{-1}$; for O_2, $k_{cat}/K_M = 4 \times 10^3\ M^{-1}\ s^{-1}$

6. a, c, e.

7. a.

8. $[Ru5P]/[R5P] = 3.8$; d.

9. Light reactions: a, e, f; Calvin–Benson cycle: b, **c**, g, h; Both: d.

10. Brought in and used in six turns of the Calvin–Benson cycle: a, d, f; Produced during six turns of the Calvin–Benson cycle that leave the cycle: b, e, g; Regenerated within the Calvin–Benson cycle during six turns: c, h.

11. Increases; NADPH, ribose; increase.

12. a, b, c.

13. a, b, c.

14. CO_2; a.

15. a.

16. a.

17. Falciparum malaria, glucose 6-phosphate dehydrogenase; sickle-cell anemia.

18. Fava beans can be dangerous for individuals with glucose 6-phosphate deficiency.

19. (a) $5\ \text{Glucose 6–phosphate} + ATP \rightarrow 6\ \text{ribose 5–phosphate} + ADP + H^+$. (b) $\text{Glucose 6–phosphate} + 12\ NADP^+ + 7\ H_2O \rightarrow 6\ CO_2 + 12\ NADPH + 12\ H^+ + P_i$.

20. The C_4 pathway allows the CO_2 concentration to increase at the site of carbon fixation. High concentrations of CO_2 inhibit the oxygenase reaction of Rubisco. This inhibition is important for tropical plants because the oxygenase activity increases more rapidly with temperature than does the carboxylase activity.

21. d.

Chapter 21

1. Step 1 is the release of glucose 1-phosphate from glycogen by glycogen phosphorylase. Step 2 is the formation of glucose 6-phosphate from glucose 1-phosphate, a reaction catalyzed by phosphoglucomutase. Step 3 is the remodeling of the glycogen by the transferase and the α-1,6-glucosidase.

2. b.

3. d.

4. As an unbranched polymer, α-amylose has only one nonreducing end. Therefore, only one glycogen phosphorylase molecule could degrade each α-amylose molecule. Because glycogen is highly branched, there are many nonreducing ends per molecule. Consequently, many phosphorylase molecules can release many glucose molecules per glycogen molecule, providing a rapid source of energy.

5. In muscle, the *b* form of phosphorylase is activated by AMP. In the liver, the *a* form is inhibited by glucose. The difference corresponds to the difference in the metabolic role of glycogen in each tissue. Muscle uses glycogen as a fuel for contraction, whereas the liver uses glycogen to maintain blood-glucose concentration.

6. Water is excluded from the active site to prevent hydrolysis. The entry of water could lead to the formation of glucose rather than glucose 1-phosphate. A site-specific mutagenesis experiment is revealing in this regard. In phosphorylase, Tyr 573 is hydrogen bonded to the $2'-OH$ group of a glucose residue. The ratio of glucose 1-phosphate to glucose product is 9,000:1 for the wild-type enzyme and 500:1 for the Phe 573 mutant. Model building suggests that a water molecule occupies the site normally filled by the phenolic OH group of tyrosine and occasionally attacks the carbocation intermediate to form glucose.

7. Epinephrine binds to its G-protein-coupled receptor. The resulting structural changes activate a G_α protein, which in turn activates adenylate cyclase. Adenylate cyclase synthesizes cAMP, which activates protein kinase A. Protein kinase A partly activates phosphorylase kinase, which phosphorylates and activates glycogen phosphorylase. The calcium released during muscle contraction also activates the phosphorylase kinase, leading to further stimulation of glycogen phosphorylase.

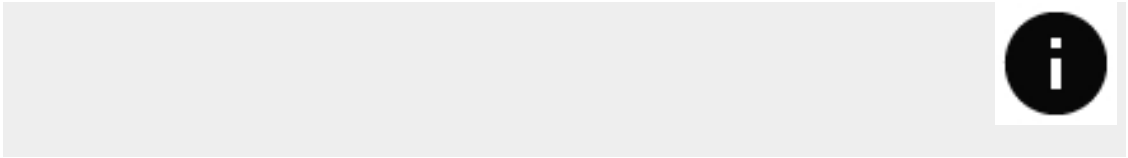
8. First, the signal-transduction pathway is shut down when the initiating hormone is no longer present. Second, the inherent GTPase activity of the G protein converts the bound GTP into inactive GDP. Third, phosphodiesterases convert cyclic AMP into AMP. Fourth, PP1 removes the phosphoryl group from glycogen phosphorylase, converting the enzyme into the usually inactive *b* form.

9. It prevents both from operating simultaneously, which would lead to a useless expenditure of energy.

10. Phosphoglucomutase, UDP-glucose pyrophosphorylase, pyrophosphatase, glycogenin, glycogen synthase, and branching enzyme.

11. The enzyme pyrophosphatase converts the pyrophosphate into two molecules of inorganic phosphate. This conversion renders the overall reaction irreversible.

$$\text{Glucose 1-phosphate} + \text{UTP} \rightleftharpoons \text{UDP-glucose} + PP_i$$
$$PP_i + H_2O \longrightarrow 2\ P_i$$
$$\text{Glucose 1-phosphate} + \text{UTP} + H_2O \longrightarrow \text{UDP-glucose} + 2\ P_i$$



12. The presence of high concentrations of glucose 6-phosphate indicates that glucose is abundant and that it is not being used by glycolysis. Therefore, this valuable resource is saved by incorporation into glycogen.

13. $\text{Glycogen}_n + P_i \rightarrow \text{glycogen}_{n-1} + \text{glucose 6-phosphate}$

$$\text{Glucose 6-phosphate} \rightarrow \text{glucose 1-phosphate}$$

$$\text{UTP} + \text{glucose 1-phosphate} \rightarrow \text{UDP-glucose} + 2\ P_i$$

$$\text{Glycogen}_{n-1} + \text{UDP-glucose} \rightarrow \text{glycogen}_n + \text{UDP}$$

$$\text{Sum: Glycogen}_n + \text{UTP} \rightarrow \text{glycogen}_n + \text{UDP} + P_i$$

14. Insulin binds to its receptor and activates the tyrosine kinase activity of the receptor, which in turn triggers a pathway that activates protein kinases. The kinases phosphorylate and inactivate glycogen synthase kinase. Protein phosphatase 1 then removes the phosphate from glycogen synthase and thereby activates the synthase.

15. $\text{Galactose} + \text{ATP} + \text{UTP} + H_2O + \text{glycogen}_n \longrightarrow \text{glycogen}_{n+1} + \text{ADP} + \text{UDP} + 2\ P_i + H^+$.

16. a, b, c, and d.

17. This disease can also be produced by a mutation in the gene that encodes the glucose 6-phosphate transporter. Recall that glucose 6-phosphate must be transported into the lumen of the endoplasmic reticulum to be hydrolyzed by phosphatase. Mutations in the other three essential proteins of this system can likewise lead to von Gierke disease.

18. (a) Apparently, the glutamate, with its negatively charged R group, can mimic to some extent the presence of a phosphoryl group on serine. That the stimulation is not as great is not surprising in that the carboxyl group is smaller and not as charged as the phosphate. (b) Substitution of aspartate would give some stimulation, but because it is smaller than the glutamate, the stimulation would be smaller.

19. (a) Glycogen was too large to enter the gel and, because analysis was by western blot with the use of an antibody specific to glycogenin, we would not expect to see background proteins. (b) α-Amylase degrades glycogen, releasing the protein glycogenin, which can be visualized by a western blot. (c) Glycogen phosphorylase, glycogen synthase, and protein phosphatase 1. These proteins might be visible if the gel were stained for protein, but a western analysis using only an anti-glycogenin antibody reveals the presence of glycogenin only.

20. (a) The smear was due to molecules of glycogenin with increasingly large amounts of glycogen attached to them. (b) In the absence of glucose in the medium, glycogen is metabolized, resulting in a loss of the high-molecular-weight material. (c) Glycogen could have been resynthesized and added to the glycogenin when the cells were fed glucose again. (d) No difference between lanes 3 and 4 suggests that, by 1 hour, the glycogen molecules had attained maximum size in this cell line. Prolonged incubation does not apparently increase the amount of glycogen. (e) α-Amylase removes essentially all of the glycogen, and so only the glycogenin remains.

Chapter 22

1. $\text{Glycerol} + 2\ NAD^+ + P_i + ADP \rightarrow \text{pyruvate} + ATP + H_2O + 2\ NADH + H^+$

Glycerol kinase and glycerol phosphate dehydrogenase

2. b, c, a, g, h, d, e, f.

3. The citric acid cycle. The reactions that take succinate to oxaloacetate, or the reverse, are similar to those of fatty acid metabolism (Section 17.3).

4. Palmitic acid yields 106 molecules of ATP. Palmitoleic acid has a double bond between carbons C-9 and C-10. When palmitoleic acid is processed in β-oxidation, one of the oxidation steps (to introduce a double bond before the addition of water) will not take place, because a double bond already exists. Thus, $FADH_2$ will not be generated, and palmitoleic acid will yield 1.5 fewer molecules of ATP than palmitic acid, for a total of 104.5 molecules of ATP.

5. To form stearoyl CoA requires the equivalent of 2 molecules of ATP.

$$\text{Stearoyl CoA} + 8\ FAD + 8\ NAD^+ + 8\ CoA + 8\ H_2O \rightarrow$$
$$9\ \text{acetylCoA} + 8\ FADH_2 + 8\ NADH + 8\ H^+$$

9 acetyl CoA at $10\ ATP/\text{acetyl CoA}$	+90 ATP
8 NADH at $2.5\ ATP/NADH$	+20 ATP
$8\ FADH_2$ at $1.5\ ATP/FADH_2$	+12 ATP
Activation fee	−2.0
Total	**122 ATP**

6. $\text{Stearate} + ATP + 13.5\ H_2O + 8\ FAD + 8\ NAD^+ \rightarrow$
$4.5\ \text{acetoacetate} + 14.5\ H^+ + 8\ FADH_2 + 8\ NADH + AMP + 2\ P_i$.

7. a, b, and d.

8. a, b, and c.

9. The formation of malonyl CoA from acetyl CoA by acetyl CoA carboxylase 1.

10. (a) Oxidation in mitochondria; synthesis in the cytoplasm. (b) Coenzyme A in oxidation; acyl carrier protein for synthesis. (c) FAD and NAD^+ in oxidation; NADPH for synthesis. (d) The l isomer of 3-

hydroxyacyl CoA in oxidation; the d isomer in synthesis. (e) From carboxyl to methyl in oxidation; from methyl to carboxyl in synthesis. (f) The enzymes of fatty acid synthesis, but not those of oxidation, are organized in a multienzyme complex.

11. We will need six acetyl CoA units. One acetyl CoA unit will be used directly to become the two carbon atoms farthest from the acid end. The other five units must be converted into malonyl CoA. The synthesis of each malonyl CoA molecule costs 1 molecule of ATP; so 5 molecules of ATP will be required. Each round of elongation requires 2 molecules of NADPH, 1 molecule to reduce the keto group to an alcohol, and 1 molecule to reduce the double bond. As a result, 10 molecules of NADPH will be required. Therefore, 5 molecules of ATP and 10 molecules of NADPH are required to synthesize lauric acid.

12. e, b, d, a, c.

13. (a) False. Biotin is required for acetyl CoA carboxylase activity. (b) True. (c) False. ATP is required to synthesize malonyl CoA. (d) True. (e) True. (f) False. Fatty acid synthase is a dimer. (g) True. (h) False. Acetyl CoA carboxylase is stimulated by citrate, which is cleaved to yield its substrate acetyl CoA.

14. All of the labeled carbon atoms will be retained. Because we need 8 acetyl CoA molecules and only 1 carbon atom is labeled in the acetyl group, we will have 8 labeled carbon atoms. The only acetyl CoA used directly will retain 3 tritium atoms. The 7 acetyl CoA molecules used to make malonyl CoA will lose 1 tritium atom on addition of the CO_2 and another one at the dehydration step. Each of the 7 malonyl CoA molecules will retain 1 tritium atom. Therefore, the total retained tritium is 10 atoms. The ratio of tritium to carbon is 1.25.

15. The mutant enzyme will be persistently active because it cannot be inhibited by phosphorylation. Fatty acid synthesis will be abnormally active. Such a mutation might lead to obesity.

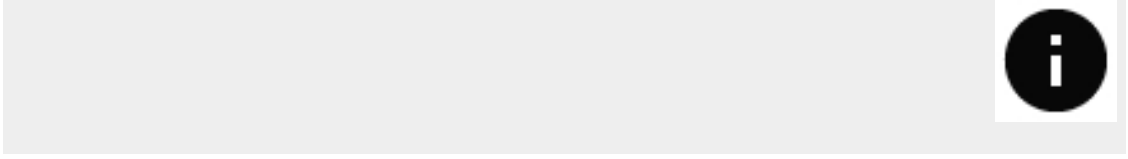
16. (a) Palmitoleate; (b) linoleate; (c) linoleate; (d) oleate; (e) oleate; (f) linolenate.

17. Citrate works by facilitating, in cooperation with the protein MIG12, the formation of active filaments from inactive monomers. In essence, it increases the number of active sites available, or the concentration of enzyme. Consequently, its effect is visible as an increase in the value of V_{max}. Allosteric enzymes that alter their V_{max} values in response to regulators are sometimes called V-class enzymes. The more common type of allosteric enzyme, in which K_M is altered, comprises K-class enzymes. Palmitoyl CoA causes depolymerization and thus inactivation.

18. Regulation by insulin: a, b, e; regulation by glucagon or epinephrine: c, d, f.

19. The first reaction

$$\text{Oxaloacetate} + \text{NADH} + \text{H}^+ \rightleftharpoons \text{malate} + \text{NAD}^+$$



is catalyzed by cytoplasmic malate dehydrogenase. The next reaction is catalyzed by malic enzyme:

$$\text{Malate} + \text{NADP}^+ \rightarrow \text{pyruvate} + \text{CO}_2 + \text{NADPH}$$

Finally, oxaloacetate is regenerated from pyruvate by pyruvate carboxylase.

$$\text{Pyruvate} + \text{CO}_2 + \text{ATP} + \text{H}_2\text{O} \rightarrow \text{oxaloacetate} + \text{ADP} + \text{P}_\text{i} + 2\,\text{H}^+$$

The sum of the reactions is

$$\text{NADP}^+ + \text{NADH} + \text{ATP} + \text{H}_2\text{O} \rightarrow \text{NADPH} + \text{NAD}^+ + \text{ADP} + \text{P}_\text{i} + \text{H}^+$$

20. (a) The V_{max} is decreased and the K_M is increased. $V_{max}(\text{wild type}) = 13\ \text{nmol minute}^{-1}\,\text{mg}^{-1}$; $K_M(\text{wildtype}) = 45\ \mu\text{M}$; $V_{max}(\text{mutant}) = 8.3\ \text{nmol minute}^{-1}\,\text{mg}^{-1}$; $K_M(\text{mutant}) = 74\ \text{mM}$. (b) Both the V_{max} and the K_M are decreased. $V_{max}(\text{wild type}) = 41\ \text{nmol minute}^{-1}\,\text{mg}^{-1}$; $K_M\text{wild type} = 104\ \mu\text{M}$; $23\ \text{nmol minute}^{-1}\,\text{mg}^{-1}$; $K_M(\text{mutant}) = 69\ \mu\text{M}$. (c) The wild type is significantly more sensitive to malonyl CoA. (d) With respect to carnitine, the mutant displays approximately 65% of the activity of the wild type; with respect to palmitoyl CoA, approximately 50% activity. On the other hand, 10 μM of malonyl CoA inhibits approximately 80% of the wild type but has essentially no effect on the mutant enzyme. (e) The glutamate appears to play a more prominent role in regulation by malonyl CoA than in catalysis.

21. (a) Soraphen A inhibits fatty acid synthesis in a dose-dependent manner. (b) Fatty acid oxidation is increased in the presence of soraphen A. (c) Recall that acetyl CoA carboxylase 2 synthesizes malonyl CoA to inhibit the transport of fatty acids into the mitochondria, thereby preventing fatty acid oxidation. Soraphen A apparently inhibits both forms of the carboxylase. (d) Phospholipid synthesis was inhibited in a dose-dependent manner. (e) Phospholipids are required for membrane synthesis. (f) Soraphen A inhibits cell proliferation, especially at higher concentrations.

Chapter 23

1. First, the ubiquitin-activating enzyme (E1) links ubiquitin to a sulfhydryl group on E1 itself. Next, the ubiquitin is transferred to a cysteine residue on the ubiquitin-conjugating enzyme (E2) by E2. The ubiquitin-protein ligase (E3), using the ubiquitinated E2 as a substrate, transfers the ubiquitin to the target protein.

2. (a) The ATPase activity of the 26S proteasome resides in the 19S subunit. The energy of ATP hydrolysis is used to unfold the substrate, which is too large to enter the catalytic barrel. ATP may also be required for translocation of the substrate into the barrel. (b) Substantiates the answer in part (*a*). Because they are small, the peptides do not need to be unfolded. Moreover, small peptides could probably enter all at once and not require translocation.

3. b

4. d

5. c

6. b

7. (a) Pyruvate; (b) oxaloacetate; (c) α-ketoglutarate; (d) α-ketoisocaproate; (e) phenylpyruvate; (f) hydroxyphenylpyruvate.

8. (a) $\text{Aspartate} + \alpha\text{-ketoglutarate} + \text{GTP} + \text{ATP} + 2\ H_2O + \text{NADH} + H^+ \rightarrow \frac{1}{2}\text{glucose} + \text{glutamate} + CO_2 + \text{ADP} + \text{GDP} + NAD^+ + 2\ P_i$.

The required coenzymes are pyridoxal phosphate in the transamination reaction and NAD^+/NADH in the redox reactions. (b) $\text{Aspartate} + CO_2 + NH_4^+ + 3\ \text{ATP} + NAD^+ + 4\ H_2O \rightarrow \text{oxaloacetate} + \text{urea} + 2\ \text{ADP} + 4\ P_i + \text{AMP} + \text{NADH} + H^+$.

9. Aspartate (oxaloacetate), glutamate (α-ketoglutarate), alanine (pyruvate).

10. (a) 4; (b) 5; (c) 1; (d) 6; (e) 7; (f) 3; (g) 2.

11. A, arginine; B, citrulline; C, ornithine; D, argininosuccinate. The order of appearance: C, B, D, A.

12. $CO_2 + NH_4^+ + 3\ \text{ATP} + NAD^+ + \text{aspartate} + 3\ H_2O \rightarrow \text{urea} + 2\ \text{ADP} + 2\ P_i + \text{AMP} + PP_i + \text{NADH} + H^+ + \text{oxaloacetate}$.

Four high-transfer-potential phosphoryl groups are spent. Note, however, that an NADH is generated if fumarate is converted into oxaloacetate. NADH can generate 2.5 ATP in the electron-transport chain. Taking these ATP into account, only 1.5 high-transfer-potential phosphoryl groups are spent.

13. The synthesis of fumarate by the urea cycle is important because it links the urea cycle and the citric acid cycle. Fumarate is hydrated to malate, which, in turn, is oxidized to oxaloacetate. Oxaloacetate has several possible fates: (1) transamination to aspartate, (2) conversion into glucose by

the gluconeogenic pathway, (3) condensation with acetyl CoA to form citrate, or (4) conversion into pyruvate.

14. Aspartame, a dipeptide ester (L-aspartyl-L-phenylalanine methyl ester), is hydrolyzed to L-aspartate and L-phenylalanine. High levels of phenylalanine are harmful in phenylketonurics.

15. The carbon skeletons of ketogenic amino acids can be converted into ketone bodies or fatty acids. Only leucine and lysine are purely ketogenic. Glucogenic amino acids are those with carbon skeletons that can be converted into glucose.

16. The branched-chain amino acids leucine, isoleucine, valine, and threonine. The required enzyme is the branched-chain α-ketoacid dehydrogenase complex.

17. Pyruvate (glycolysis and gluconeogenesis), acetyl CoA (citric acid cycle and fatty acid synthesis), acetoacetyl CoA (ketone-body formation), α-ketoglutarate (citric acid cycle), succinyl CoA (citric acid cycle), fumarate (citric acid cycle), and oxaloacetate (citric acid cycle and gluconeogenesis).

18. Double-displacement. A substituted enzyme intermediate is formed.

19. (a) Depletion of glycogen stores. When they are gone, proteins must be degraded to meet the glucose needs of the brain. The resulting amino acids are deaminated, and the nitrogen atoms are excreted as urea. (b) The brain has adapted to the use of ketone bodies, which are derived from fatty acid catabolism. In other words, the brain is being powered by fatty acid breakdown. (c) When the glycogen and lipid stores are gone, the only available energy source is protein.

20. (a) Virtually no digestion in the absence of nucleotides. (b) Protein digestion is greatly stimulated by the presence of ATP. (c) AMP-PNP, a nonhydrolyzable analog of ATP, is no more effective than ADP. (d) The proteasome requires neither ATP nor PAN to digest small substrates. (e) PAN and ATP hydrolysis may be required to unfold the peptide and translocate it into the proteasome. (f) Although *Thermoplasma* PAN is not as effective with the other proteasomes, it nonetheless results in threefold to fourfold stimulation of digestion. (g) In light of the fact that the archaea and eukarya diverged several billion years ago, the fact that *Thermoplasma* PAN can stimulate the rabbit muscle proteasome suggests homology not only between the proteasomes, but also between PAN and the 19S subunit (most likely the ATPases) of the mammalian 26S proteasome.

Chapter 24

1. Normal circumstances: b; after fasting: d.

2. c.

3. Over the 40 years under consideration, our test subject will have consumed

$$40\ \text{years} \times 365\ \text{days year}^{-1} \times 8400\ \text{KJ (2000 kcal) day}^{-1}$$
$$= 1.2 \times 10^8\ \text{kJ} (2.9 \times 10^7\ \text{kcals})\ \text{in 40 years.}$$

Thus, over the 40-year span, our subject has ingested

$$1.2 \times 108 (2.9 \times 10^7\ \text{kcal}) / 38\ \text{kJ} (9\ \text{kcal g}^{-1})$$
$$= 3.2 \times 10^6\ \text{g} = 3200\ \text{kg of food,}$$

which is equivalent to more than 6 tons of food!

4. $2.55\ \text{pounds} = 25\ \text{kg} = 25{,}000\ \text{g} = \text{total weight gain}$

$$40\ \text{years} \times 365\ \text{days year}^{-1} = 14{,}600\ \text{days}$$
$$25{,}000\ \text{g} / 14{,}600\ \text{days} = 1.7\ \text{g day}^{-1}$$

which is equivalent to an extra pat of butter per day. Her BMI is 26.5, and she would be considered overweight but not obese.

5. Adipose tissue is now known to be an active endocrine organ, secreting signal molecules called adipokines.

6. Leptin and insulin.

7. CCK produces a feeling of satiety and stimulates the secretion of digestive enzymes by the pancreas and the secretion of bile salts by the gallbladder. GLP-1 also produces a feeling of satiety; in addition, it potentiates the glucose-induced secretion of insulin by the β cells of the pancreas.

8. (a) 1, 2; (b) 6; (c) 3, 4; (d) 3, 4; (e) 3; (f) 6; (g) 5; (h) 5; (i) 5.

9. Type 1 diabetes is due to autoimmune destruction of the insulin-producing cells of the pancreas. Type 1 diabetes is also called insulin-dependent diabetes because affected people require insulin to survive. Type 2 diabetes is characterized by insulin resistance. Insulin is produced, but the tissues that should respond to insulin, such as muscle, do not.

10. a, b, and c.

11. (a) A watt is equal to 1 joule (J) per second (0.239 calorie per second). Hence, 70 W is equivalent to $0.07\ kJ\ s^{-1} (0.017\ kcal\ s^{-1})$. (b) A watt is a current of 1 ampere (A) across a potential of 1 volt (V). For simplicity, let us assume that all the electron flow is from NADH to O_2 (a potential drop of 1.14 V). Hence, the current is 61.4 A, which corresponds to 3.86×10^{20} electrons per second $(1A = 1coulomb\ s^{-1} = 6.28 \times 10^{18}\ charge\ s^{-1})$. (c) About 2.5 molecules of ATP are formed per molecule of NADH oxidized (two electrons). Hence, 1 molecule of ATP is formed per 0.8 electron transferred. A flow of $3.86 \times 10^{20}\ electrons$ per second therefore leads to the generation of 4.83×10^{20} molecules of ATP per second, or $0.80\ mmols^{-1}$. (d) The molecular weight of ATP is $507\ g/mol$. The total body content of ATP of 50 g is equal to 0.099 mol. Hence, ATP turns over about once in 125 seconds when the body is at rest.

12. (a) The stoichiometry of the complete oxidation of glucose is

$$C_6H_{12}O_6 + 6\ O_2 \rightarrow 6\ CO_2 + 6\ H_2O$$

and that of tripalmitoylglycerol is

$$C_{51}H_{98}O_2 + 72.5\ O_2 \rightarrow 51\ CO_2 + 49\ H_2O$$

Hence, the RQ values are 1.0 and 0.703, respectively. (b) An RQ value reveals the relative use of carbohydrates and fats as fuels. The RQ of an amateur marathon runner typically decreases from 0.97 to 0.77 in the course of a race. The lowering of the RQ indicates the shift in fuel from carbohydrates to fat.

13. A high blood-glucose level triggers the secretion of insulin, which stimulates removal of glucose from the blood for the synthesis of glycogen and triacylglycerols. A high insulin level would impede the mobilization of fuel reserves during the marathon.

14. (a) Insulin inhibits lipid utilization. Insulin stimulates protein synthesis, but there are no amino acids in the children's diet. Moreover, insulin inhibits protein breakdown. Consequently, muscle proteins cannot be broken down and used for the synthesis of essential proteins. (b) Because proteins cannot be synthesized, blood osmolarity is too low. Consequently, fluid leaves the blood. An especially important protein for maintaining blood osmolarity is albumin.

15. During strenuous exercise, muscle converts glucose into pyruvate through glycolysis. Some of the pyruvate is processed by cellular respiration. However, some of it is converted into lactate and released into the blood. The liver takes up the lactate and converts it into glucose through gluconeogenesis. Muscle may process the carbon skeletons of branched-chain amino acids aerobically. The nitrogens of these amino acids are transferred to pyruvate to form alanine, which is released into the blood and taken up by the liver. After the transamination of the amino group to α-ketoglutarate, the resulting pyruvate is converted into glucose. Finally, muscle glycogen may be mobilized, and the released glucose can be used by muscle. The conversion of pyruvate to lactate allows muscle to function anaerobically. NAD^+ is regenerated when pyruvate is reduced to lactate, and so energy can continue to be extracted from glucose during strenuous exercise. The liver converts the lactate into glucose.

16. Fatty acids and glucose, respectively.

17. (a) The oxygen consumption at the end of exercise is used to replenish ATP and creatine phosphate and to oxidize any lactate produced. (b) After strenuous exercise, oxygen is used in oxidative phosphorylation to resynthesize ATP and creatine phosphate. The liver converts lactate released by the muscle into glucose. Blood must be circulated to return the body temperature to normal, and so the heart cannot return to its resting rate immediately. Hemoglobin must be reoxygenated to replace the oxygen used in exercise. The muscles that power breathing must continue working at the same time as the exercised muscles are returning to resting states. In essence, all the biochemical systems activated in intense exercise need increased oxygen to return to the resting state.

18. (a) The increase in all of the ratios is due to the NADH glut caused by the metabolism of alcohol. (b) The increased amounts of lactate and d-3-hydroxybutyrate are released into the blood, accounting for the acidosis. (c) Drinking on an empty stomach suggests that glycogen stores are low. Because of the NADH glut, gluconeogenesis cannot occur. Consequently, hypoglycemia results. A well-fed drinker will have glucose in the blood from the meal and thus will not experience hypoglycemia.

19. The precise cause of all of the symptoms is not firmly established, but a likely explanation depends on the centrality of oxaloacetate to metabolism. A lack of pyruvate carboxylase would reduce the amount of oxaloacetate. The lack of oxaloacetate would reduce the activity of the citric acid cycle and so ATP would be generated by lactic acid formation. If the concentration of oxaloacetate is low, aspartate cannot be formed and the urea cycle would be compromised. Oxaloacetate is also required to form citrate, which transports acetyl CoA to the cytoplasm for fatty acid synthesis. Finally, oxaloacetate is required for gluconeogenesis.

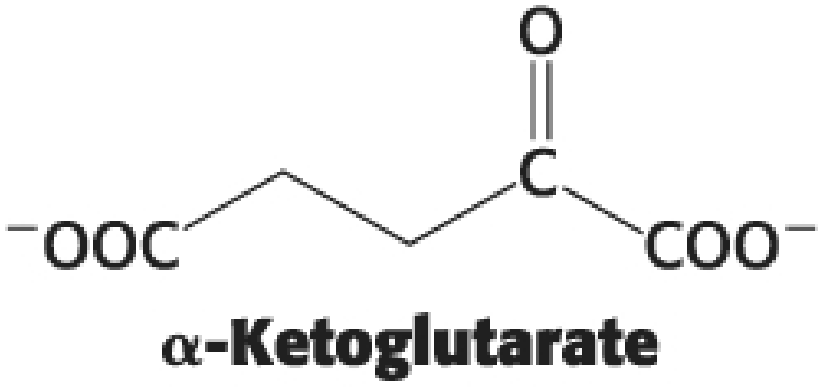
20. (a) Red blood cells always produce lactate, and fast-twitch or type II muscle fibers also produce a large amount of lactate. (b) At that point, the athlete is beginning to move into anaerobic exercise, in which most energy is produced by anaerobic glycolysis. (c) The lactate threshold is essentially the point at which the athlete switches from aerobic exercise, which can be done for extended periods, to anaerobic exercise, essentially sprinting, which can be done for only short periods. The idea is to race at the extreme of his or her aerobic capacity until the finish line is in sight and then to switch to anaerobic. (d) Training increases the number of blood vessels and of muscle mitochondria. Together, they increase the ability to process glucose aerobically. Consequently, a greater effort can be expended before the switch to anaerobic energy production.

Chapter 25

1. The reductase provides electrons with high reducing power, whereas the nitrogenase, which requires ATP hydrolysis, uses the electrons to reduce N_2 to NH_3.

2. a, b, d, f.

3. (a) The α-keto acid precursor to glutamate is α-ketoglutarate:



α-Ketoglutarate

(b) $NAD(P)^+$ and H_2O

4. 16

5. The reductase protein provides electrons with high reducing power. The nitrogenase uses these electrons to reduce N_2 to NH_3.

6. Oxaloacetate, pyruvate, ribose-5-phosphate, phosphoenol-pyruvate, erythrose-4-phosphate, α-ketoglutarate, and 3-phosphoglycerate.

7. $\text{Glucose} + 2\ \text{ADP} + 2\ P_i + 2\ NAD^+ + 2\ \text{glutamate} \rightarrow$
$2\ \text{alanine} + 2\ \alpha\text{-ketoglutrate} + 2\ \text{ATP} + 2\ \text{NADH} + 2\ H_2O + 2\ H^+$

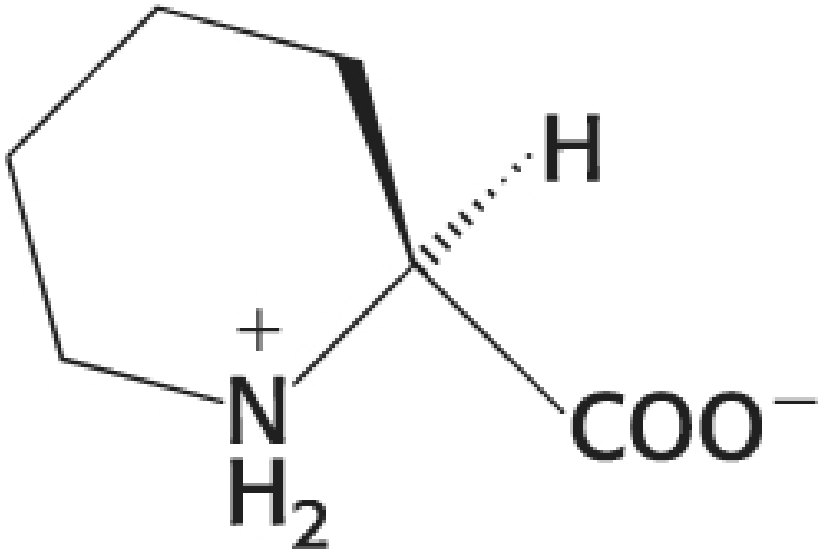
8. Alanine from pyruvate; aspartate from oxaloacetate; glutamate from α-ketoglutarate.

9. Serine, glycine, and cysteine.

10. (b). As an essential amino acid, methionine is not synthesized de novo in human beings, but it can, however, be regenerated via methylation of homocysteine to yield methionine. Homocysteine is also an intermediate in cysteine synthesis. Homocysteine condenses with serine to form cystathionine, which is deaminated and cleaved to yield α-ketobutyrate and cysteine.

11. The nitrogen atom shaded red is derived from glutamine. The carbon atom shaded blue is derived from serine.

12. Lysine cyclodeaminase converts L-lysine into the six-membered ring analog of proline, also referred to as L-homoproline or L-pipecolate:



Pipecolate

13. Y could inhibit the $C \rightarrow D$ step, Z could inhibit the $C \rightarrow F$ step, and C could inhibit $A \rightarrow B$. This scheme is an example of sequential feedback inhibition. Alternatively, Y could inhibit the $C \rightarrow D$ step, Z could inhibit the $C \rightarrow F$ step, and the $A \rightarrow B$ step would be inhibited only in the presence of both Y and Z. This scheme is called concerted feedback inhibition.

14. The rate of the $A \rightarrow B$ step in the presence of high levels of Y and Z would be $24\ s^{-1}(0.6 \times 0.4 \times 100\ s^{-1})$.

15. $N_2 \rightarrow NH_4^+$ → glutamate → serine → glycine → δ-aminolevulinate → porphobilinogen → heme

16. Acetate → acetyl-CoA → citrate → isocitrate → α-ketoglutarate → succinyl-CoA

17. c, e, f.

18. *S*-Adenosylmethionine, tetrahydrofolate, and methylcobalamin.

19. In human beings, tyrosine is synthesized from phenylalanine by phenylalanine hydroxylase. If this enzyme is defective, the biosynthetic route to tyrosine is blocked, and tyrosine must be obtained from the diet. Tyrosine is sometimes said to be “conditionally essential” because its synthesis is dependent on the essential amino acid phenylalanine.

Chapter 26

1. In de novo synthesis, the nucleotides are synthesized from simpler precursor compounds, in essence from scratch. In salvage pathways, preformed bases are recovered and attached to riboses.

2.

The synthesis of carbamoyl phosphate requires 2 ATP	2 ATP
The formation of PRPP from ribose 5-phosphate yields an AMP*	2 ATP
The conversion of UMP to UTP requires 2 ATP	2 ATP
The conversion of UTP to CTP requires 1 ATP	1 ATP
Total	**7 ATP**

*Remember that AMP is the equivalent of 2 ATP because an ATP must be expended to generate ADP, the substrate for ATP synthesis.

3. $\text{Glutamine} + \text{aspartate} + CO_2 + 2\ \text{ATP} + NAD^+ \rightarrow$
$\text{orotate} + 2\ \text{ADP} + 2\ P_i + \text{glutamate} + \text{NADH} + H^+$.

4. (a, c, and d) PRPP; (b) carbamoyl phosphate.

5. PRPP and formylglycinamide ribonucleotide.

6. (a) Carboxyaminoimidazole ribonucleotide; (b) glycinamide ribonucleotide; (c) phosphoribosyl amine; (d) formylglycinamide ribonucleotide.

7. PRPP is the activated intermediate in the synthesis of phosphoribosylamine in the de novo pathway of purine formation; of purine nucleotides from free bases by the salvage pathway; of orotidylate in the formation of pyrimidines; of nicotinate ribonucleotide; and of phosphoribosylanthranilate in the pathway leading to tryptophan.

8. N-1 in both cases, and the amine group linked to C-6 in ATP.

9. $\text{dUMP} + \text{serine} + \text{NADPH} + H^+ \rightarrow \text{TMP} + NADP^+ + \text{glycine}$.

10. b, e, a, c, d.

11. Substrates: a, b; Product: c.

12. The free energies of binding are -57.7 (wild type), -49.8 (Asn 27), and $-38.1\ (\text{Ser27})\ \text{kJ mol}^{-1}$ ($-13.8, -11.9$, and $-9.1\ \text{kcal mol}^{-1}$, respectively). The loss in binding energy is $+7.9\ \text{kJ mol}^{-1} (+1.9\ \text{kcal mol}^{-1})$ and $+19.7\ \text{kJ mol}^{-1} (+4.7\ \text{kcal mol}^{-1})$.

13. CTP is a feedback inhibitor of ATCase, while ATP is an allosteric activator.

14. a and b.

15. ATP and dATP.

16. a and c.

17. d.

18. Inosine or hypoxanthine could be administered.

19. (a) Cell A cannot grow in a HAT medium, because it cannot synthesize TMP either from thymidine or from dUMP. Cell B cannot grow in this medium, because it cannot synthesize purines by either the de novo pathway or the salvage pathway. Cell C can grow in a HAT medium because it contains active thymidine kinase from cell B (enabling it to phosphorylate thymidine to TMP) and hypoxanthine guanine phosphoribosyltransferase from cell A (enabling it to synthesize purines from hypoxanthine by the salvage pathway). (b) Transform cell A with a plasmid containing foreign genes of interest and a functional thymidine kinase gene. The only cells that will grow in a HAT medium are those that have acquired a thymidylate kinase gene; nearly all of these transformed cells will also contain the other genes on the plasmid.

Chapter 27

1. Three. One molecule of ATP to form phosphorylethanolamine and two molecules of ATP to regenerate CTP from CMP.

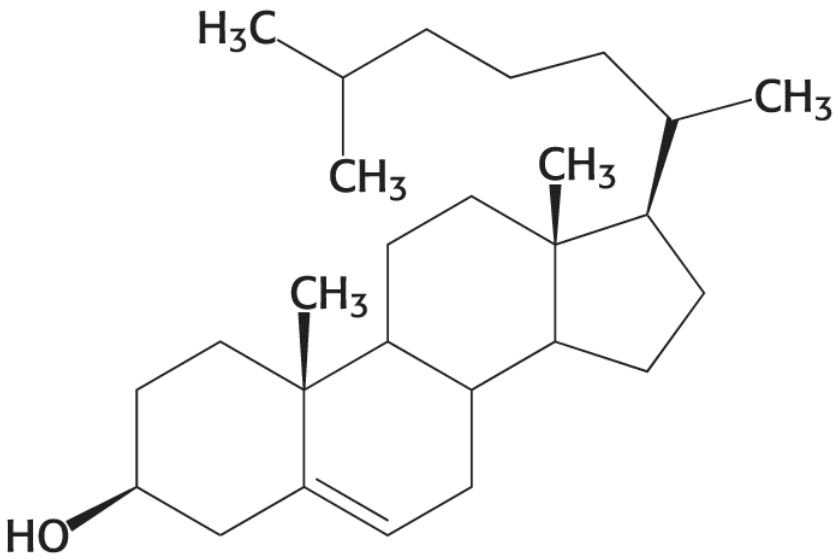
2. (a) CDP-diacylglycerol; (b) CDP-ethanolamine; (c) acyl CoA; (d) phosphatidylcholine; (e) UDP-glucose or UDP-galactose; (f) UDP-galactose; (g) geranyl pyrophosphate.

3. $\text{Glycerol} + 4\,\text{ATP} + 3\,\text{fatty acids} + 4\,H_2O \rightarrow \text{triacylglycerol} + \text{ADP} + 3\,\text{AMP} + 7\,P_i + 4\,H^+$.

4. If PAP activity were to decline due to a mutation, phosphatidate conversion to DAG would decrease. Therefore, the concentration of DAG would decline and the concentration of phosphatidate would be high. Hence, the concentrations of lipids derived from activated phosphatidate will likely increase, and the concentrations of lipids derived from DAG and an activated head group would decrease.

The following would decrease: a, b, f. The following would increase: c, d, e.

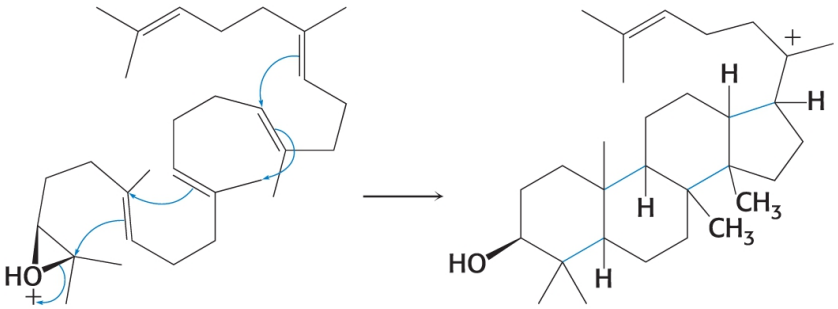
5.



6. (1) The synthesis of activated isoprene units (isopentyl pyrophosphate), (2) the condensation of six of the activated isoprene units to form squalene, and (3) cyclization of the squalene to form cholesterol.

7. b, c, a, d

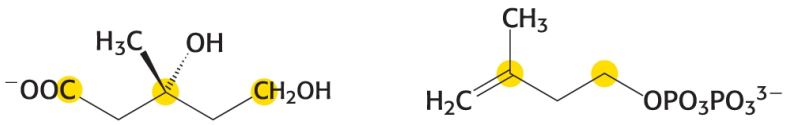
8.



Protosterol cation

9. c, g, d, h, a, i, j, f, b, e

10.



Labeled mevalonate **Labeled isopentenyl pyrophosphate**

11. The amount of reductase and its activity control the regulation of cholesterol biosynthesis. Transcriptional control is mediated by SREBP. Translation of the reductase mRNA also is controlled. The reductase itself may undergo regulated proteolysis. Finally, the activity of the reductase is inhibited by phosphorylation by AMP kinase when ATP levels are low.

12. The conversion of HMG-CoA to mevalonate by HMG-CoA reductase is the rate-determining step.

13. Statins are competitive inhibitors of HMG-CoA reductase. They are used as drugs to inhibit cholesterol synthesis in patients with high levels of cholesterol.

14. The LDL contains apolipoprotein B-100, which binds to an LDL receptor on the cell surface in a region known as a coated pit. On binding, the complex is internalized by endocytosis to form an internal vesicle. The vesicle is separated into two components. One, with the receptor, is transported back to the cell surface and fuses with the membrane, allowing continued use of the receptor. The other vesicle fuses with lysosomes inside the cell. The cholesteryl esters are hydrolyzed, and free cholesterol is made available for cellular use. The LDL protein is hydrolyzed to free amino acids.

15. (a) Lipids are less dense than proteins. Chylomicrons, which have the highest percentage by weight of lipids, are the least dense lipoproteins. (b) In a lipoprotein, the protein components are generally

soluble and the lipid components are not. Lipoproteins with more proteins are more soluble. High-density lipoproteins (HDLs) have more protein than other lipoproteins and are the most soluble.

16. LDL: a and d; HDL: b and c

17. The core structure of a steroid is four fused rings: three cyclohexane rings and one cyclopentane ring. In vitamin D, the B ring is split by ultraviolet light.

18. (a) 3; (b) 4; (c) 5; (d) 1; (e) 2.

19. 3-Hydroxy-3-methylglutaryl CoA is also a precursor for ketone-body synthesis. If fuel is needed elsewhere in the body, as might be the case during a fast, 3-hydroxy-3-methylglutaryl CoA is converted into the ketone body acetoacetate. If energy needs are met, the liver will synthesize cholesterol. Remember also that cholesterol synthesis occurs in the cytoplasm while ketone bodies are synthesized in the mitochondria.

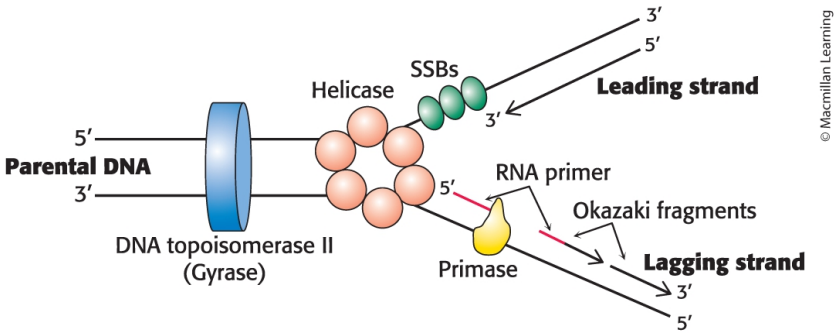
Chapter 28

1. One new strand will have an A–T pair, and the other strand will have a G–C pair.

2. The oxidation of guanine could lead to DNA repair: DNA strand cleavage could allow looping out of the triplet repeat regions and triplet expansion.

3. (a) 4, 5; (b) 3, 2; (c) 6, 1

4.



© Macmillan Learning

5. In principle, it could be used to break three base pairs.

6. (a) Size; the top is relaxed and the bottom is supercoiled DNA. (b) Topoisomers. (c) The DNA is becoming progressively more unwound, or relaxed, and thus slower-moving.

7. (a) $Lk = 460$ (b) $Lk = 456$; (c) Lk is undefined; (d) $Lk = 458$

8. c

9. b, c, e

10. a, h, d, e, g, b, c, f

11. a, b, g, c, f, h, d, e

12. e, c, b, a, d, f

13. b, d, e

14. (a) It was used to determine the number of spontaneous revertants—that is, the background mutation rate. (b) The known mutagen was used to firmly establish that the system was working. A known mutagen's failure to produce revertants would indicate that something was wrong with the

experimental system. (c) The chemical itself has little mutagenic ability but is apparently activated into a mutagen by the liver homogenate. (d) Components of the cytochrome P450 system.

15. (a) 5; (b) 1; (c) 2, 3; (d) 4

16. (a) 6, 4; (b) 1, 5; (c) 3, 4

17. a, g, d, f, e, b, c

18. (a) 5; (b) 3; (c) 1; (d) 2; (e) 4

19. b, d

Chapter 29

1. An error will affect only one molecule of mRNA of many synthesized from a gene. In addition, the errors do not become a permanent part of the genomic information.

2. b, c, d.

3. The active sites are related by convergent evolution.

4. The sequence of the coding ($^{+}$, sense) strand is

$5'-ATGGGGAACAGCAAGAGTGGGGCCCTGTCCAAGGAG-3'$ and the sequence of the template (–, antisense) strand is $3'-TACCCCTTGTCGTTCTCACCCCGGGACAGGTTCCTC-5'$

5. This mutant σ will competitively inhibit the binding of holoenzyme and prevent the specific initiation of RNA chains at promoter sites.

6. A 100-kDa protein contains about 910 residues, which are encoded by 2730 nucleotides. At a maximal transcription rate of 50 nucleotides per second, the mRNA would be synthesized in 55 s.

7. DNA is the single strand that forms the trunk of the tree. Strands of increasing length are RNA molecules; the beginning of transcription is where growing chains are the smallest; the end of transcription is where chain growth stops. Many enzymes are actively transcribing each gene.

8. (a) $5'$; (b) guanosine; (c) triphosphate; (d) a nitrogen; (e) $2'$.

9. c, e, d, a, f, b.

10. Gene A, top; gene B, top; gene C, bottom.

11. The organism in the fluctuating environment, because it is exposed to more extremes.

12. (a) 2, 3; (b) 5, 6; (c) 1, 4

13. (a) 13.7; (b) 45S; (c) 18S, 5.8S, and 28S; (d) 28S; (e) 5.8S; (f) 5S; (g) large (60S); (h) RNA polymerase III; (i) small (40S).

14. b, d, e.

15. (a) 5; (b) 3; (c) 4; (d) 2; (e) 1.

16. There are $2^8 = 256$ possible products.

17. Alternative splicing, RNA editing. Covalent modification of the proteins after synthesis.

18. (a) Different amounts of RNA are present for the various genes. (b) Although all of the tissues have the same genes, the genes are expressed to different extents in different tissues. (c) These genes are called housekeeping genes—genes that most tissues express all the time. They might include genes for glycolysis or citric acid cycle enzymes. (d) The point of the experiment is to determine which genes are

initiated in vivo. The initiation inhibitor is added to prevent initiation at start sites that may have been activated during the isolation of the nuclei.

19. True: b, c, d; False: a, e.

Chapter 30

1. (a) and (b) only.

2. Four bands: light, heavy, a hybrid of light 30S and heavy 50S, and a hybrid of heavy 30S and light 50S.

3. The peptide would be Phe-Cys-His-Val-Ala-Ala. The codons UGC and UGU encode cysteine but, because the cysteine was modified to alanine, alanine is incorporated in place of cysteine.

4. (a) 1, 2, 3, 5, 6, 10; (b) 1, 2, 7, 8; (c) 1, 4, 8, 9.

5. (a, d, and e) Type 2; (b, c, and f) Type 1.

6. Two hundred molecules of ATP are converted into $200\ AMP + 400\ P_i$ to activate the 200 amino acids, which is equivalent to 400 molecules of ATP. One molecule of GTP is required for initiation, and 398 molecules of GTP are needed to form 199 peptide bonds, for a total of 399 molecules of GTP.

7. Proteins are synthesized from the amino to the carboxyl end on ribosomes, whereas they are synthesized in the reverse direction in the solid-phase method. The activated intermediate in ribosomal synthesis is an aminoacyl-tRNA; in the solid-phase method, it is the adduct of the amino acid and dicyclohexylcarbodiimide.

8. (a) A_5. (b) $A_5 > A_4 > A_3 > A_2$. (c) Synthesis is from the amino terminus to the carboxyl terminus.

9. (a) P site; (b) A site; (c) E site; (d) P site.

10. The rate would fall because the elongation step requires that the GTP be hydrolyzed before any further elongation can take place.

11.

	Bacteria	**Eukaryotes**
Ribosome size	70S	80S
Initiation	Shine–Dalgarno is required	First AUG is used
Protein factors	Required	Many more required
Relation to transcription	Translation can start before transcription is completed	Transcription and translation are spatially separated
First amino acid	fMet	Met

12. (a) 3, 5, 9; (b) 1, 7; (c) 4, 5, 6, 10; (d) 2, 8.

13. (a) 4; (b) 3; (c) 2; (d) 6.

14. (a) -35 sequence; (b) Pribnow box; (c) $+1$; (d) terminator sequence; (e) Shine–Dalgarno sequence; (f) AUG.

15. (a) The three peaks represent, from left to right, the 40S ribosomal subunit, the 60S ribosomal subunit, and the 80S ribosome. (b) Not only are ribosomal subunits and the 80S ribosome present, but polysomes of various lengths also are apparent. The individual peaks in the polysome region represent polysomes of discrete length. (c) The treatment significantly inhibited the number of polysomes while increasing the number of free ribosomal subunits. This outcome could be due to inhibited protein-synthesis initiation or inhibited transcription.

16. a, d, i, h, c, f, b, g, e.

17. (a) The signal sequence, signal-recognition particle (SRP), the SRP receptor, and the translocon. (b) The formation of peptide bonds, which in turn are powered by the hydrolysis of the aminoacyl-tRNAs.

18. (a) eIF-4H has two effects: (i) the extent of unwinding is increased; and (ii) the rate of unwinding is increased, as indicated by the increased rise in activity at early reaction times. (b) To firmly establish that the effect of eIF-H4 was not due to any inherent helicase activity. (c) Half-maximal activity was achieved at 0.11 μM of eIF-4H. Therefore, maximal stimulation would be achieved at a ratio of 1:1. (d) eIF-4H enhances the rate of unwinding of all helices, but the effect is greater as the helices increase in stability. (e) The results in graph C suggest that eIF-4H increases the processivity.

19. (a) $3'-AATCTCGCG-5'$; (b) UUAGAGCGC; (c) AAU, CUC, GCG; (d) leucine, glutamic acid, arginine.

20. (a) A; (b) alanine.

Chapter 31

1. (a) and (b) Cells will express β-galactosidase, *lac* permease, and thiogalactoside transacetylase even in the absence of lactose. (c) The levels of catabolic enzymes such as β-galactosidase and arabinose isomerase will remain low even at low levels of glucose.

2. The *lac* repressor does not bind DNA when the repressor is bound to a small molecule (the inducer), whereas the *pur* repressor binds DNA only when the repressor is bound to a small molecule (the corepressor). The *E. coli* genome contains only a single *lac* repressor-binding region, whereas it has many sites for the *pur* repressor.

3. b, c.

4. Bacteriophage λ would be more likely to enter the lytic phase because the cooperative binding of the λ repressor to O_R2 and O_R1, which supports the lysogenic pathway, would be disrupted.

5. e, a, c, b, f, d.

6. 5-Azacytidine cannot be methylated. Some genes, normally repressed by methylation, will be active. 5-Azacytidine is also an inhibitor of DNA methyltransferase, resulting in lower levels of methylation and, hence, lower levels of gene repression.

7. Increased Cro concentration reduces the expression of the λ repressor gene. Increased λ repressor concentration reduces the expression of the Cro gene. At low λ repressor concentrations, increased λ repressor concentration increases the expression of the λ repressor gene. At higher λ repressor concentrations, increased λ repressor concentration decreases the expression of the λ repressor gene.

8. The footprint appears to have approximately 50% of its intensity near 3.7 nM so that the dissociation constant is approximately 3.7 nM, corresponding to a standard free energy of binding of $-48\ \text{kJ/mol}\ (-11\ \text{kcal/mol})$ at $T = 298\text{K}$.

9. b, c.

10. In mouse DNA, most of the HpaII sites are methylated and therefore not cut by the enzyme, resulting in large fragments. Some small fragments are produced from CpG islands that are unmethylated. For *Drosophila* and *E. coli* DNA, there is no methylation, and all sites are cut.

11. a, c, d.

12. Proteins containing these domains will be targeted to methylated DNA in repressed promoter regions. They would likely bind in the major groove, because that is where the methyl group is located.

13. The acetylation of lysine will reduce the charge from $+1$ to 0. The methylation of lysine will not reduce the charge.

14. d, f, a, e, b, c.

15. Gene expression is not expected to respond to the presence of estrogen. However, genes for which expression normally responds to estrogen will respond to the presence of progesterone.

16. The addition of an IRE to the $5'$ end of the mRNA is expected to block translation in the absence of iron. The addition of an IRE to the $3'$ end of the mRNA is not expected to block translation, but it might affect mRNA stability.

17. On the basis of the pattern of cysteine and histidine residues, this region appears to contain three zinc-finger domains.

18. (a) 3; (b) 1; (c) 2.

19. (a) 2; (b) 3, 1; (c) 4, 5.

20. Positive: a, c, d; negative: b, e.

Chapter 32

1. Sildenafil increases cGMP levels by inhibiting the phosphodiesterase-mediated breakdown of cGMP to GMP. Intracellular cGMP levels can also be increased by activating its synthesis. This activation can be achieved with the use of NO donors (such as sodium nitroprusside and nitroglycerin) or compounds that activate guanylate cyclase activity. Drugs that act by the latter mechanism are currently in clinical trials.

2. (a) Accidental; (b) natural product screening; (c) accidental; (d) natural product screening; (e) targeted design.

3. (A) Yes; (B) yes; (C) no $(MW > 600)$.

4. Unlike competitive inhibition, noncompetitive inhibition cannot be overcome with additional substrate. Hence, a drug that acts by a noncompetitive mechanism will be unaffected by changing levels of the physiological substrate.

5. A drug that inhibits a P450 enzyme may dramatically affect the disposition of another drug that is metabolized by that same enzyme. If this inhibited metabolism is not accounted for when dosing, the second drug may reach very high, and sometimes toxic, levels in the blood.

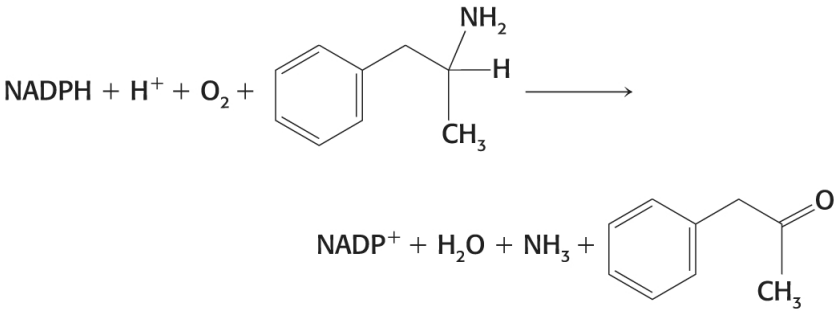
6. The binding of other drugs to albumin could cause extra coumadin to be released. (Albumin is a general carrier for hydrophobic molecules.)

7. (a) $K_I \approx 0.3\ nM$. $IC_{50} \approx 2.0\ nM$. (b) Yes, compound A should be effective when taken orally because 400 nM is much greater than the estimated values of K_I and IC_{50}.

8. The computational prediction of log(P) values on the basis of chemical structure enables a more rapid assessment of drug-like properties of a molecule, and it avoids the need for experimental phase partitioning studies. Many such algorithms are now available to pharmacologists.

9. In Phase I clinical trials, approximately 10 to 100 usually healthy volunteers are typically enrolled in a study designed to assess safety. In contrast, a larger number of subjects are enrolled in a typical Phase II trial. Moreover, these persons may benefit from the drug administered. In a Phase II trial, efficacy, dosage, and safety can be assessed.

10. A reasonable mechanism would be an oxidative deamination following an overall mechanism similar to that in Figure 32.19, with release of ammonia.





11. Recall that for a competitive inhibitor, the IC_{50} will shift depending on the substrate concentration. According to the Cheng–Prusoff equation, for an enzyme with a K_M of 1 μM the IC_{50} of a competitive inhibitor at $[S] = 20\ \mu M$ will be $21 \times K_I$, while at $[S] = K_M$, the IC_{50} will be $2 \cdot K_I$, a 10-fold shift.

12. Because monoclonal antibodies interact with a broader surface on the target, they can achieve greater potency than small molecules, as well as achieve a higher degree of selectivity versus proteins similar to the target. Also, because they are retained in the body via the FcRn receptor-mediated salvage pathway, they can maintain much longer half-lives than small molecules.

Glossary

α carbon
The central carbon of an amino acid, linked to an amino group, a carboxylic acid group, a hydrogen atom, and a side chain.

α helix
A common structural motif in proteins, in which a polypeptide main chain forms the inner part of a right-handed helix, with the side chains extending outward; the helix is stabilized by intrachain hydrogen bonds between amino and carboxyl groups of the main chain.

β pleated sheet (β sheet)
A common structural motif in proteins, in which a number of β strands are associated as stacks of chains, stabilized by interchain hydrogen bonds.

β strand
A polypeptide chain that is almost fully extended rather than being tightly coiled as in the α helix.

3-hydroxy-3-methylglutaryl CoA reductase (HMG-CoA reductase)
A highly regulated enzyme that catalyzes the committed step in cholesterol synthesis, which is the formation of mevalonate from 3-hydroxy-3-methylglutaryl CoA.

5-phosphoribosyl-1-pyrophosphate (PRPP)
A form of ribose activated to accept nucleotide bases.

5′ cap

A structure at the $5'$ end of eukaryotic mRNA that stabilizes the mRNA and enhances its translation. The cap contains a 7-methyl guanylate residue attached by a triphosphate linkage to the sugar at the $5'$ end of the mRNA in a rare $5'$-$5'$ linkage.

ABC transporters

A class of pumps that use the ATP-binding cassette for nucleotide binding and hydrolysis.

acetyl CoA
An activated two-carbon acetyl unit formed by the thioester linkage to coenzyme A.

acetyl CoA carboxylase (ACC)
A regulatory enzyme that catalyzes the ATP-dependent synthesis of malonyl CoA from acetyl CoA and carbon dioxide, the committed step in fatty acid synthesis.

acid-base reaction
A reaction in which hydrogen ions are added to or removed from molecules.

activated carrier
A small molecule carrying activated functional groups that can be donated to another molecule. For instance, ATP carries activated phosphoryl groups and coenzyme A carries activated acyl groups.

activated methyl cycle
A series of reactions in which methyl groups from methionine are converted into a biochemically reactive form through the formation of *S*-adenosylmethionine.

activation domain
The part of eukaryotic transcription factors that interacts with RNA polymerase or other proteins, or modifies chromatin structure.

activation loop
A structure found in protein kinases that changes conformation, often in response to the phosphorylation of specific tyrosine or serine/threonine residues.

active site
A specific region of an enzyme that binds the enzyme's substrate and carries out catalysis.

active transport
The transport of an ion or a molecule against a concentration gradient, where ΔG for the transported species is positive. The process must be coupled to an input of free energy from a source such as ATP, an electrochemical gradient, or light.

acyl adenylate

A mixed anhydride in which the carboxyl group of a molecule is linked to the phosphoryl group of AMP. It serves as a means of activating carboxyl groups, such as the formation of fatty acyl CoA molecules from a free fatty acid and coenzyme A.

acyl carrier protein (ACP)
A polypeptide that is linked to phosphopantetheine and acts as a carrier of the growing fatty acyl chain in fatty acid biosynthesis.

adenosine triphosphate (ATP)
A nucleotide that is the free energy donor in most energy-requiring processes such as motion, active transport, or biosynthesis. Most of catabolism consists of reactions that extract energy from fuels such as carbohydrates and fats and convert it into ATP.

adenylate cyclase
An enzyme that converts ATP to cyclic AMP.

ADME properties
A drug's response to the absorption, distribution, metabolism, and excretion processes within a living organism.

adrenergic receptors
A cell surface receptor that signals in response to the binding of adrenaline.

aerobic glycolysis
The tendency of cancer cells to use glucose at high rates via glycolysis and lactic acid fermentation, even in the presence of molecular oxygen. Also called the *Warburg effect*.

affinity chromatography
A method of separation based on a specific interaction between a protein and a ligand. The ligand is immobilized on inert material, and a protein mixture is passed over the ligand. Only the protein with the specific interaction will bind.

affinity label (reactive substrate analog)
A substrate analog used to map the active site of an enzyme by binding to the active site and forming a covalent bond with a nearby amino acid.

agonists
A molecule that binds to and activates a receptor.

Aldolase
An enzyme that catalyzes an aldol condensation reaction.

allosteric (regulatory) site
A region of an enzyme, distinct from the active site, where a regulatory molecule binds and affects catalytic activity.

allosteric effector
A small molecule that affects the properties of a protein or enzyme by binding to a site distinct from the active site.

allosteric enzyme
An enzyme having multiple active sites and/or distinct regulatory sites that control the flux of biochemicals through a metabolic pathway. The regulation of catalytic activity is by environmental signals, often the final product of the metabolic pathway regulated by the enzyme; its kinetics are more complex than those of single subunit enzymes

alternative splicing
The generation of unique but related mRNA molecules by the differential splicing of the pre-mRNA transcript; increases the encoding potential of the genome.

Ames test
A simple, rapid means of detecting carcinogens by measuring a chemical's ability to induce mutations in *Salmonella* bacteria.

amino acids
An organic compound containing an amino group, a carboxyl group, and a unique functional group that are each bonded to a common carbon atom.

aminoacyl-tRNA
A tRNA molecule that has been covalently linked to the amino acid corresponding to its anticodon sequence.

aminoacyl-tRNA synthetases
An enzyme that activates an amino acid and then links it to transfer RNA. Each aminoacyl-tRNA synthetase is specific for a particular amino acid. It is also known as an *activating enzyme*.

Aminotransferases

A class of enzymes that transfer an α-amino group from an α-amino acid to an α-ketoacid. Also called **transaminases**.

AMP-activated protein kinase (AMPK)
A protein kinase, conserved among eukaryotes, that is activated on binding AMP and inhibited by ATP. It functions as a cellular fuel gauge, inhibiting certain processes by phosphorylating key enzymes when the energy supply is low.

amphibolic pathways
A metabolic pathway consisting of reactions that can be anabolic or catabolic, depending on the energy conditions and biosynthetic needs of the cell.

amphipathic molecules (amphiphilic molecules)
A molecule, such as a membrane lipid, that contains both a hydrophobic and a hydrophilic moiety.

amyloid fibrils (amyloid plaques)
Protein aggregates composed of insoluble fibers rich in β sheets that are found in the brains of patients with certain neurological diseases, including Alzheimer disease and Parkinson disease.

anabolism
The set of metabolic reactions that creates more complex molecules from simpler precursors, frequently requiring energy.

anaplerotic reaction
A reaction that leads to the net synthesis, or replenishment, of pathway components.

anion exchange
A form of ion-exchange chromatography where cationic beads are used to bind negatively charged proteins.

anomer
Isomers that differ at a new asymmetric carbon atom generated by intramolecular hemiacetal or hemiketal formation; that carbon atom is known as the anomeric carbon atom.

antagonists
A molecule that binds to a receptor but does not activate it and, therefore, blocks the effects of activating ligands (agonists).

antibodies (immunoglobulins)
Proteins produced by the immune system that bind specifically to particular foreign molecules and help lead to the sequestration or destruction of viruses, bacteria, or infected cells.

anticoagulant drugs
Medicines that reduce blood clot formation.

anticodon
A nucleotide triplet in tRNA that binds to a specific codon within an mRNA molecule during transcription.

Antigen
A foreign substance that induces an immune response, especially the production of antibodies.

antigenic determinant (epitope)
A specific group or cluster of amino acids on an antigen that is recognized by an antibody.

Antiporters
A secondary transporter that couples the downhill flow of one species to the uphill flow of another in the opposite direction across the membrane.

apoenzyme
An enzyme without its cofactor(s).

apoptosis
A form of programmed cell death specific to multicellular organisms. One pathway of activation involves the release of cytochrome *c* from mitochondria, leading to the activation of caspases.

aptamers
Synthetic single-stranded oligonucleotides that can specifically bind ligands.

aquaporins
A membrane transporter that facilitates the rapid transport of water molecules.

Archaea
One of the two domains of prokaryotic life forms, unicellular organisms that lack a well-defined nucleus. The existence of this second domain of prokaryotes was discovered in 1977. They differ from the other such domain, Bacteria, in several

ways, including the sequences of ribosomal RNA, the composition of cell membranes, and the use of some biochemical pathways.

Argonaute
A family of proteins that, when bound to miRNA, will cleave specific target mRNAs.

assay
Any procedure to measure the activity of a biomolecule, such as an enzyme.

ATP synthase
A molecular assembly of the inner mitochondrial membrane responsible for the respiratory-chain-driven synthesis of ATP. Also called **Complex V**.

ATP synthase of chloroplasts
Molecular assembly of the thylakoid membrane responsible for the photo-induced synthesis of ATP. Also called the CF_1-CF_0 **complex**.

ATP-ADP translocase
A transport protein in the inner mitochondrial membrane that carries ADP into the mitochondria and ATP out in a coupled fashion. Also called **adenine nucleotide translocase** or **ANT**.

ATP-binding cassettes (ABCs)
The nucleotide-binding domains found within ABC transporter proteins.

ATP-grasp fold
A structural motif found in several nucleotide biosynthesis enzymes in which ATP is held in a conformation suitable for nucleophilic attack at the γ phosphoryl group.

ATPase
An enzyme that hydrolyzes ATP to ADP plus inorganic phosphate.

attenuation
A mechanism for regulating gene expression in bacteria that involves the formation of alternative mRNA structures that alter transcription.

autotrophs
An organism that obtains the majority of its carbon for biosynthesis from the reduction of carbon dioxide, as opposed to using organic sources.

Bacteria
One of the two domains of prokaryotic life forms, unicellular organisms that lack a well-defined nucleus. Members of Bacteria differ from members of the other prokaryotic domain, Archaea, in several ways, including the sequences of ribosomal RNA, the composition of cell membranes, and the use of some biochemical pathways.

bacteriophage lambda (λ phage)
A bacterial virus that is frequently used as a cloning vector.

bacteriorhodopsin
An archaeal membrane protein that is evolutionarily related to rhodopsin. Bacteriorhodopsin uses retinal to absorb photons to drive conformational changes that pump protons across the cell membrane for the purpose of ATP generation by ATP synthase.

ball-and-chain model
A model for ion channel inactivation in which a cytoplasmic unit (the ball) at the end of a flexible polypeptide (the chain) occludes the open pore.

base pair
A specific structure that forms in nucleic acids such as DNA involving two nitrogenous bases joined by hydrogen bonds. Units with adenine form base pairs with those with thymine, and units with cytosine form base pairs with those with guanine.

base-excision repair
A means of repairing DNA in which the damaged base is removed and replaced by a base complementary to the undamaged DNA strand.

basic local alignment search tool (BLAST) search
A database query which seeks to identify homologous sequences to a submitted amino acid sequence.

basic-leucine zipper (bZip) proteins
A DNA-binding motif found in eukaryotic transcription factors, consisting of a pair of long α helices.

beriberi
A neurological and cardiovascular disorder caused by a dietary deficiency of thiamine (vitamin B_1).

bifunctional enzyme
An enzyme with two different, often opposing, catalytic activities on one polypeptide chain.

bile salts
A polar derivative of cholesterol that solubilizes dietary lipids, facilitating their digestion and absorption.

binding energy
The free energy released in the formation of the weak interactions between enzyme and substrate, some of which can facilitate the formation of the transition state for catalysis.

binding energy
The free energy released in the formation of the noncovalent interactions between enzyme and substrate that facilitate the formation of the transition state.

biochemical timescale
The timescale over which most chemical interactions and processes take place, measured in picoseconds to microseconds $(10^{-12} - 10^{-6}\ s)$.

biological macromolecules
Large organic molecules, often constructed from smaller building blocks, present within living organisms. Examples include nucleic acids such as DNA or proteins such as hemoglobin.

biologics
Medicines derived from living cells or through biological processes.

Bohr effect
The observation that H^+ and CO_2 promote the release of oxygen from oxyhemoglobin, named for Christian Bohr.

bromodomain
A domain consisting of a four-helix bundle that binds peptides containing acetyllysine. It is also called *acetyllysine-binding domain*.

buffer
A solution that resists change in pH upon the addition of acid or base.

C_4 pathway

A means by which four-carbon compounds, such as oxaloacetate and malate, carry carbon dioxide from mesophyll cells in contact with the air to bundle-sheath cells, which are the major sites of photosynthesis. The pathway accelerates photosynthesis by concentrating carbon dioxide in photosynthetic cells. Also known as the **Hatch–Slack pathway**.

calmodulin (CaM)

A protein present in many cells that binds calcium ions, changes conformation, and binds certain α-helical structures, often to activate enzymes.

caloric homeostasis

The maintenance of an adequate but not excessive amount of body fat; the balancing of caloric input and use. Also called **energy homeostasis**.

Calvin–Benson cycle

A cyclic metabolic pathway in plants, in which carbon dioxide is incorporated into ribulose 1,5-bisphosphate to yield compounds that can be used for the synthesis of hexoses.

candidate

In drug discovery, a molecule that has been optimized for potency, selectivity, pharmacokinetics, and safety such that it can be tested in humans.

carbamoyl phosphate synthetase I

An enzyme that begins the urea cycle by catalyzing the synthesis of carbamoyl phosphate from bicarbonate, ammonium ion, and ATP.

carbon monoxide

A colorless, odorless gas that can bind to heme proteins such as myoglobin and hemoglobin in competition with oxygen.

carbonic anhydrases

An enzyme that hydrates carbon dioxide to form bicarbonate HCO_3^-.

carboxyl-terminal domain

A regulatory domain in RNA polymerase II. Phosphorylation of this domain regulates aspects of transcription and splicing.

carnitine

A zwitterionic alcohol formed from lysine that acts as a carrier of long-chain fatty acids from the cytoplasm to the mitochondrial matrix.

carotenoids
An extended polyene that absorbs light between 400 and 500 nm and serves as an accessory pigment in photosynthesis by funneling the energy to the photosynthetic reaction center.

Carriers
A membrane protein that transports ions or molecules across the membrane without hydrolysis of ATP.

cassette mutagenesis
A method for introducing mutations into a target sequence where a portion of the target gene is removed by restriction digestion, and a synthetic oligonucleotide containing the mutations is ligated in its place.

catabolism
The set of metabolic reactions that breaks complex molecules into simpler ones, typically transforming fuels into cellular energy.

catabolite activator protein (CAP)
The cAMP-response protein. When bound to cyclic AMP, CAP binds to an inverted repeat in the *lac* operon to stimulate transcription.

catabolite repression
The repression by glucose of enzymes required to catabolize sugars other than glucose.

catalysis by approximation
Increases in the rate of a reaction that occur by bringing multiple substrates together along a single binding surface of an enzyme.

catalyst
An agent that enhances the rate of a chemical reaction without being permanently affected itself.

catalytic triad
A constellation of three residues, found in many proteolytic enzymes, in which two of the residues convert the remaining residue, usually a serine or cysteine residue, into a potent nucleophile.

cation exchange
A form of ion-exchange chromatography where anionic beads are used to bind positively charged proteins.

cDNA library
A collection of cDNA molecules inserted into cloning vectors; the library consists of all the mRNA molecules expressed by a particular cell.

cell
The smallest structural and functional unit of an organism, consisting of a collection of biological macromolecules and metabolites surrounded by a membrane.

cell cycle
A sequence of regulated stages that allow a cell to complete cell division. One of these stages involves the replication of the cell's genome.

Cell-mediated immunity
An adaptive immune response mediated by cytotoxic T lymphocytes and not by antibodies.

cellular respiration
The process that includes the generation of high-transfer-potential electrons by the citric acid cycle, their flow through the respiratory chain to reduce oxygen to water, and the accompanying synthesis of ATP. Also called **respiration**.

cellulose
An unbranched homopolysaccharide in plants, composed of glucose residues in β-1,4 linkage; the major structural polysaccharide in plants.

ceramide
A sphingosine with a long-chain acyl group attached to its amino group.

chemical modification reaction
A reaction in which an enzyme or proteins is covalently modified, usually by a relatively reactive reagent.

chemical shift
The frequency of electromagnetic radiation at which an intrinsically magnetic nucleus resonates. This value is dependent upon the local environment of the nucleus.

chemical space
The range of chemical possibilities for compounds within a given range of molecular weights.

chemotrophs
An organism that obtains energy by the oxidation of chemicals. Can be further subclassified as an organochemotroph or a lithotroph if the chemical energy sources are organic, or inorganic, respectively.

chiral
The property of asymmetry in which a structure and its mirror image are not superimposable.

chlorophyll *a*
A substituted tetrapyrrole that is the principal photoreceptor in plants.

chloroplasts
The organelle in plants and algae in which eukaryotic photosynthesis takes place.

cholesterol
A sterol that is an important constituent of eukaryotic membranes and lipoproteins; also a precursor of steroid hormones.

chromatin
A complex of DNA and proteins found in eukaryotes that helps to package the DNA into a more compact structure.

chromatin-remodeling complexes
Large protein complexes that utilize the free energy of ATP hydrolysis to induce changes in chromatin structure.

chromogenic substrate
A substrate that generates a colored product when acted on by an enzyme.

chylomicrons
A lipoprotein particle, composed primarily of triacylglycerol, that transports dietary triacylglycerols from the intestine to other tissues.

citric acid cycle (CAC)
A cyclic series of metabolic reactions that completely oxidize acetyl units to carbon dioxide. Also called **tricarboxylic acid (TCA) cycle**; **Krebs cycle**.

class I MHC proteins
A class of proteins found on the surfaces of many cells that present peptides in a groove for potential recognition by T-cell receptors.

cloning vectors
A class of vector, usually a plasmid, that is designed for the facile insertion and stable replication of DNA inserts.

co-immunoprecipitation
An antibody-based precipitation technique used to identify binding partners to a protein of interest.

coactivators
A protein that enhances transcription by binding to a transcription factor. Coactivators themselves do not bind to DNA.

codon
A nucleotide triplet in mRNA that encodes a particular amino acid.

codons
A nucleotide triplet in mRNA that encodes a particular amino acid.

coenzyme
A cofactor that is a small organic molecule; vitamins are often components or precursors of coenzymes.

coenzyme Q
A mobile electron carrier that is a component of the respiratory chain. It shuttles between the oxidized ubiquinone form and the reduced ubiquinol form through a semiquinone intermediate, accepting electrons from NADH-Q oxidoreductase as well as succinate-Q reductase. Also called **Q** or **ubiquinone**.

cofactor
A small molecule on which the catalytic activity of an enzyme may depend. The cofactor's precise role varies with the cofactor and the enzyme. Cofactors can be subdivided into two groups: (1) small organic molecules called coenzymes and (2) metals.

cohesive (sticky) ends
Complementary strands produced when a restriction enzyme cleaves the DNA target sequence in a staggered fashion.

combinatorial chemistry
A process by which millions of compounds are synthesized in a single process.

committed step
The first irreversible step in a metabolic pathway under physiological conditions; this step is catalyzed by an allosteric enzyme and commits the product to a particular chemical fate.

common ancestor
An individual from which all members of a group have descended.

competitive inhibition
The reduction in the rate of enzyme activity observed when a reversible inhibitor binds only to the free enzyme, not to the substrate-bound enzyme; thus, the enzyme can bind the substrate or the inhibitor, but not both. A type of reversible inhibition, many competitive inhibitors resemble the substrate and compete with it for reversible binding to the enzyme's active site. Relief from inhibition by increasing substrate concentration is a kinetic hallmark of competitive inhibition.

complementary DNA (cDNA)
DNA that is complementary to mRNA. It is synthesized by reverse transcriptase with the use of mRNA as a template.

complementary sequences
Single-stranded DNA sequences that have the potential to form double helices through base pairs. Examples include the sequences CGATTAAT and ATTAATCG.

concerted model
A model for hemoglobin oxygen-binding cooperativity where the hemoglobin tetramers undergo "all-or-none" transitions between the T and R states.

connexon
A hexagonal array of connexin proteins expressed on the surface of one cell, which joins with the corresponding array on a neighboring cell to form a gap junction. Also called a **hemichannel**.

consensus sequence
In the context of protein kinases, a group of related peptide sequences recognized by a specific protein kinase.

consensus sequences
An idealized base sequence that represents common features of a promoter site.

conservative substitution
An amino acid change in which an amino acid is replaced with another that is similar in biochemical properties.

controlled study
A clinical study in which patients are divided into two groups: one group receives the therapeutic to be tested, while the other group receives either a placebo or the current standard treatment available.

controlled termination of replication
A DNA-sequencing technique based on the generation of DNA fragments whose length depends on the last base in the sequence. Also called the **Sanger dideoxy method**.

convergent evolution
The process by which entities (species, populations, proteins, etc.) not derived from a common ancestor independently arrive at similar solutions to a particular problem.

cooperative transition
In protein folding, an "all-or-none" process where conditions that lead to the disruption of any part of a protein structure are likely to unravel the entire protein completely.

corepressor
A small molecule that binds to a repressor and promotes its interaction with an operator to block transcription.

Cori cycle
A cyclic, inter-organ metabolic pathway in which lactate from active muscle is converted into glucose by the liver, which in turn supplies newly synthesized glucose to muscle and other tissues.

coupled assay
The use of multiple enzyme steps to link the activity of an enzyme with the production of easily detectable (i.e. fluorescent) product.

covalent bond
A bond formed by the sharing of a pair of electrons between adjacent atoms; covalent bonds are the strongest bonds between atoms in biochemistry.

covalent catalysis

Catalysis in which the active site contains a reactive group that becomes temporarily covalently modified.

CpG islands
A region of a mammalian genome that contains about four times as many CpG sequences as the rest of the genome.

crassulacean acid metabolism (CAM)
An adaptation by plants living in an arid environment. The C_4 pathway concentrates carbon dioxide at night, and gas exchange with the environment is curtailed during the heat of the day by closure of the stomata.

CRISPR-Cas system
A gene editing system derived from a primitive prokaryotic immune system that uses a single guide RNA to deliver the Cas nuclease to specific sites in the genome, allowing removal and addition of new DNA sequences.

Cro
A small protein in bacteriophage λ that is expressed once the λ repressor no longer binds to the operator. Cro blocks the production of new λ repressor.

cryo-electron microscopy (cryo-EM)
A method for protein structure determination in which a protein solution is frozen very quickly and then exposed to an incident electron beam. This method is particularly suitable for the determination of very large complexes.

cumulative feedback inhibition
A regulatory strategy in which the enzyme catalyzing the committed step common to several pathways is incrementally inhibited by the products of each of the pathways.

cyclic photophosphorylation
In photosynthesis, the generation of ATP without the concomitant formation of NADPH. Electrons cycle from the reaction center of photosystem I to ferredoxin and then back to the reaction center through cytochrome *b6f* and plastoquinone, generating a proton gradient that is used to drive ATP formation.

Cys_2His_2 zinc-finger domains
A conserved sequence-specific DNA-binding domain, found in members of the nuclear hormone-receptor family.

cytidine diphosphodiacylglycerol (CDP-diacylglycerol)
An activated precursor for the synthesis of many phospholipids formed by the reaction of phosphatidate with cytidine triphosphate.

cytochrome *bf*
A cytochrome complex that links photosystem II and photosystem I in green plants; cytochrome *bf* contributes to the proton gradient by oxidizing plastoquinol to plastoquinone.

Cytochrome *c*
A water-soluble, highly conserved cytochrome component of the respiratory chain that accepts electrons from cytochrome *c* reductase and is in turn oxidized by cytochrome *c* oxidoreductase.

cytochrome *c* oxidase
The final complex of the respiratory chain, which transfers electrons from cytochrome *c* to molecular oxygen and concomitantly pumps protons across the inner mitochondrial membrane to generate the proton-motive force. Also called **Complex IV**.

Cytochromes
Heme-containing proteins that often function in oxidation-reduction reactions.

cytoskeleton
The internal scaffolding of cells, made up of actin filaments and other proteins, that enables cells to transport materials intracellularly, change shape, and migrate.

Cytotoxic T lymphocytes (killer T cells)
A class of white blood cells that promote the destruction of cells infected with viruses or perceived as damaged in other ways.

dalton
A unit of mass equal to one atomic mass unit, or very nearly equal to that of a hydrogen atom.

de novo pathways
A biosynthetic pathway in which a molecule is synthesized from simple precursors.

degron

A feature of a protein that targets it for destruction by the ubiquitin-proteasome system. Degrons can be amino acid sequences, structural motifs, or even single residues.

denatured protein
A protein that has been converted into a randomly coiled peptide that lacks its normal activity.

deoxyhemoglobin
The oxygen-carrier protein hemoglobin in its form without bound oxygen.

deoxymyoglobin
The oxygen-storage protein myoglobin in its form without bound oxygen.

deoxyribonucleic acid (DNA)
A nucleic acid, usually found in a double helical structure, that serves as the primary storage point of genetic information in essentially all organisms.

deoxyribonucleic acid (DNA)
A nucleic acid constructed of four different deoxyribonucleotides; contains the genome and exists as a double-stranded helix in all higher organisms.

deoxyribose
A five-carbon monosaccharide $(C_5H_{10}O_4)$ that constitutes the carbohydrate moiety of a deoxynucleotide; the deoxyribose commonly found in deoxynucleotides is 2-deoxyribose.

development phase
The second phase of drug discovery, in which clinical trials are conducted to determine the safety, efficacy, and side effects of a drug in humans.

dialysis
A process of removing small molecules from a mixture of solutes using a semipermeable bag through which only small molecules can diffuse.

dihydrofolate reductase
An enzyme that catalyzes the regeneration of tetrahydrofolate from dihydrofolate formed in the synthesis of thymidylate.

dipolar ion (zwitterion)
An ion carrying both a positive and a negative charge.

direct repair
A means of repairing damaged DNA in which the damaged region is corrected in place. For example, pyrimidine dimers are simply cleaved to restore the original nucleotides.

disaccharide
A carbohydrate consisting of two sugars, usually joined by an *O*-glycosidic linkage.

discovery phase
The first phase of drug discovery, in which molecules with the desired physiological effects are identified and optimized for testing in humans.

distal histidine
The histidine residue in myoglobin and hemoglobin on the opposite side of the heme group from the proximal histidine and, therefore, on the same side as the bound oxygen molecule.

disulfide bond
A covalent bond formed by the oxidation of two sulfhydryl groups; the oxidation of cysteine residues in a polypeptide yields a disulfide bond linking the two residues.

divergent evolution
The process by which entities (species, populations, proteins, etc.) derived from a common ancestor accumulate differences over time, potentially gaining new functions.

DNA ligase
An enzyme that catalyzes the formation of a phosphodiester linkage between the $3'$-hydroxyl group at the end of one DNA strand and the $5'$-phosphoryl group at the end of another strand. DNA ligase takes part in the synthesis, repair, and splicing of DNA.

DNA methylases
An enzyme that adds a methyl group to a DNA substrate.

DNA microarray
A collection of known DNA sequences attached to a specific location on a solid surface, to which fluorescently labeled cDNA is hybridized to reveal the expression level of each gene.

DNA polymerases
Enzymes that catalyze the template-directed, primer-dependent addition of deoxynucleotide units to the $3'$ end of a DNA chain; chain growth is in the $5'$-to-$3'$ direction; such enzymes replicate and repair DNA.

DNA probe
A short stretch of single-stranded DNA that contains a known base sequence.

DNA-binding domain
The part of eukaryotic transcription factors that interacts with regulatory sequences.

DNA-encoded libraries (DELs)
A combinatorial compound library in which molecules are synthesized while covalently attached to a DNA oligonucleotide; the sequence of the oligonucleotide encodes the reaction history for that particular molecule.

domain
An independently folded unit in the tertiary structure of a polypeptide chain, often connected to other similar regions by a flexible polypeptide segment.

double helix
A structure with two strands spiraling around a common axis. Double-stranded DNA forms a double helix.

double-blinded study
A clinical study in which neither the subjects nor the researchers know which subjects are in the treatment group and which are in the control group.

double-displacement (Ping-Pong) reaction
A reaction having multiple substrates in which one or more products are released before all substrates bind the enzyme. The defining feature of these reactions is the formation of a substituted-enzyme intermediate.

drug metabolism
The process by which the body alters drugs to aid in their excretion.

EF hand
A structure found in calcium-binding proteins that consists of two α helices joined by a loop.

eicosanoids
Cell signaling molecules derived from 20-carbon-long polyunsaturated fatty acids, including arachidonic acid.

elasticity
The responsiveness of the velocity of an enzyme to changes in substrate concentration. Diminishes as substrate concentrations increase significantly above the K_M value.

electric dipole (dipole)
A characteristic of a molecule or fragment due to an uneven distribution of electrons so that some regions are partially negatively charged and other regions are partially positively charged.

electrochemical potential
The energetic cost that is required to establish a concentration gradient of a charged species across a membrane. Also called **membrane potential**.

electron-density map
The output from an x-ray crystallographic experiment, which reveals the most electron-dense regions of a crystal, that is, where the atoms are located.

electron-transport chain
Four large protein complexes embedded in the inner mitochondrial membrane in which the oxidation–reduction reactions that allow the flow of electrons from NADH and FADH2 to oxygen take place. Also called **respiratory chain**.

electrophilic
Describing the tendency of a molecule or group to attract or acquire electrons.

electroporation
A method for transfection of foreign DNA in which intense electric field pulses are applied to the host cells, rendering their membranes transiently permeable to large molecules.

electrospray ionization (ESI)
A method of ionizing samples for mass spectrometry in which a solution is passed through an electrically charged nozzle into a chamber of very low pressure.

elongation factor G (EF-G) (translocase)

A member of the G-protein family required for protein synthesis in eukaryotes. By hydrolyzing GTP, EF-G causes the tRNAs and mRNA to move through the ribosome a distance corresponding to one codon.

elongation factor Ts
A protein that binds to the GDP-bound form of EF-Tu and induces the release of GDP, thereby enabling EF-Tu to participate in another elongation step.

elongation factor Tu (EF-Tu)
A member of the G-protein family that delivers aminoacyl-tRNAs to the A site of the ribosome with the concomitant hydrolysis of GTP to GDP.

endoplasmic reticulum (ER)
An extensive system of cytoplasmic membranes that comprises about half the total cell membrane. The region of the ER that binds ribosomes is called the rough ER, and the region that is devoid of ribosomes is called the smooth ER.

endoplasmic reticulum (ER) stress
stress A condition in which the ability of the ER to fold proteins becomes compromised, resulting in protein misfolding and triggering of the unfolded protein response. If unresolved, it can lead to apoptosis.

endosomes
The intracellular vesicles that are formed during receptor-mediated endocytosis.

energy charge
A means of determining and conceptualizing the energy status of the cell; equal to the concentration of ATP plus one-half the concentration of ADP, all divided by the total adenine nucleotide concentration.

enhancer
A DNA sequence that has no promoter activity itself but can greatly enhance the activity of other promoters. Enhancers can exert their stimulatory effect over a distance of several thousand nucleotides.

enthalpy
In thermodynamics, enthalpy is a quantity equivalent to the total heat content of a system.

entropy
In thermodynamics, entropy is a specific measure of the degree of randomness or disorder in a system.

enzymatic cascade
A series of zymogen activations used to achieve a rapid response, such as that observed in blood clotting pathways.

enzyme
A biological macromolecule that acts as a catalyst for a biochemical reaction; although almost all enzymes are composed of protein, some RNA molecules are catalytically active (see **ribozyme**).

enzyme multiplicity
A regulatory strategy in which the committed step common to several pathways is catalyzed by distinct enzymes that have the same catalytic properties but different regulatory properties.

enzyme-linked immunosorbent assay (ELISA)
An immunological-based means of detecting and quantifying proteins.

enzymes
A biological macromolecule that acts as a catalyst for a biochemical reaction; although almost all enzymes are composed of protein, some RNA molecules are catalytically active.

epigenetics
Modifications to the genome that do not alter the DNA sequence but may affect gene expression.

epimers
A pair of molecules, each with more than one asymmetric center, that differ in configuration at only one such center. For example, glucose and galactose are epimers, differing only in the configuration at carbon 4 (C-4).

epinephrine
A hormone released under conditions of stress that increases heart rate, blood circulation, and carbohydrate metabolism.

epinephrine (adrenaline)
A catecholamine released by the adrenal medulla in response to muscle activity or its anticipation that stimulates the breakdown of muscle glycogen. Also called **adrenaline**.

equilibrium potential

The membrane voltage at which the movement of ion down its concentration gradient is balanced by the opposite electrostatic force.

essential amino acids
Amino acids that cannot be synthesized de novo and therefore must be acquired from the diet.

ethanol fermentation
The anaerobic conversion of glucose into ethanol with the concomitant production of ATP.

Eukarya (eukaryotes)
The domain of life that includes all multicellular organisms and as well some single-celled organisms such as yeast. Members of Eukarya are characterized by the presence of a well-defined cell nucleus.

eversion
The process of interconverting conformations typically observed in membrane pumps and secondary transporters.

evolutionary tree
A branching diagram that represents the evolutionary relationships among various species or entities and indicates the time at which different populations diverged.

exon shuffling
During evolution, the rearrangement of exons encoding discrete elements, binding sites, and catalytic sites, all of which can generate novel gene sequences.

exons
Region of pre-mRNA that is retained in mature mRNA.

exonuclease
An enzyme that digests nucleic acids from the ends of the molecules, rather than at an internal site. Exonucleases can be specific for digestion from the $3'$ or $5'$ ends of the nucleic acid.

expression vectors
A class of vector, usually a plasmid, that is designed for the expression of proteins encoded in their DNA inserts.

facilitated diffusion
The transport of an ion or a molecule down a concentration gradient, where ΔG for the transported species is negative. Also called **passive transport**.

facultative anaerobes
An organism that can both utilize molecular oxygen for aerobic metabolism as well as survive and grow in its absence through fermentation pathways.

fasted–fed cycle
A series of metabolic changes, primarily involving the liver, that maintain glucose homeostasis during the changing conditions that follow meals or periods of fasting.

fatty acid synthase
An enzyme system that catalyzes the synthesis of saturated long-chain fatty acids from acetyl CoA, malonyl CoA, and NADPH.

Fatty acids
A carboxylic acid that contains a long hydrocarbon chain. Fatty acids are an important fuel source as well as a key component of membrane lipids.

feedback inhibition
The inhibition of an enzyme by the end product of the pathway.

feedforward stimulation
The activation of an allosteric enzyme in a later stage of a pathway by the product of a reaction that takes place earlier in the reaction pathway. Also called **feedforward activation**.

fermentation
A redox neutral metabolic scheme for the production of ATP from an organic chemical source. Fermentations allow ATP production without the use of oxygen, although they can still occur in its presence.

ferritin
An iron-storage protein found primarily in the liver and kidneys.

fibrous protein
A protein that adopts a long, extended structure with repeated sequences.

flavoproteins

A protein tightly associated with FAD or FMN. Flavoproteins play important roles in many oxidation–reduction reactions.

fluid mosaic model
A model that describes the overall organization of biological membranes as two-dimensional solutions of oriented lipids and globular proteins.

fluorescence microscopy
Visualization of cells and tissues using fluorescence-labeled markers, including antibodies.

fractional saturation
A measure of the fraction of a potential binding site that is occupied with ligand.

free energy (Gibbs free energy)
In thermodynamics, the free energy is a quantity that satisfies the equation $\Delta G = \Delta H_{system} - T\Delta S_{system}$ where ΔH_{system} is the change in enthalpy of the system and ΔS_{system} is the change in entropy of the system.

G protein
A signaling protein that depends on binding guanine (G)-containing nucleotides.

G-protein-coupled receptors (GPCRs)
A member of a large family of cell surface receptors with seven membrane-spanning α helices that signal through G proteins. See also **seven-transmembrane-helix (7TM) receptor**.

gap junction
A channel permeable to ions and small hydrophilic molecules. Gap junctions connect the interiors of contiguous cells. Also called a **cell-to-cell channel**.

gel electrophoresis
A technique for separating biomolecules, such as nucleic acids and proteins, on the basis of charge and size. When placed under an electric field, the biomolecules move through the gel (a cross-linked polymer such as polyacrylamide), with larger molecules moving more slowly than smaller molecules.

gel-filtration chromatography
A method of separation where porous beads are used to differentiate proteins on the basis of size. Small molecules can enter the beads and thus take longer to pass

through the column.

gene disruption (gene knockout)
The removal of a specific gene in the genome, using one of a number of gene editing techniques.

general acid–base catalysis
Catalysis in which a molecule other than water plays the role of a proton donor or acceptor.

genetic code
The relationship between nucleic acid sequence information and protein sequence information.

genetic recombination
The exchange of genetic material between two DNA molecules, resulting in the reassortment of DNA sequences.

genome editing
One of a number of techniques that allow the highly specific modification of the genome.

genomic library
A collection of DNA fragments, inserted into a cloning vector, that represents the entire genome of an organism.

Gibbs free energy of activation
The energy required to form the transition state from the substrate of a reaction when considered from a particular direction. Also called the **activation energy**.

globular protein
A protein that forms a tightly packed structure, usually water soluble and devoid of overall symmetry.

glucagon
A polypeptide hormone that is secreted by the α cells of the pancreas when the blood-glucose level is low, leading to glycogen breakdown in the liver and the release of glucose to the blood.

glucogenic amino acids
An amino acid with a carbon skeleton that can be converted, entirely or in part, into substrates for gluconeogenesis.

gluconeogenesis
The synthesis of glucose from noncarbohydrate precursors, including lactate, glycerol, and amino acids.

glucose 6-phosphate dehydrogenase
An enzyme that initiates the oxidative phase of the pentose phosphate pathway by oxidizing glucose 6-phosphate to 6-phosphoglucono-δ-lactone to generate one molecule of NADPH.

glucose homeostasis
The regulation of glucose concentrations in the blood, primarily by the liver, to maintain adequate levels for the brain and other tissues.

glucose–alanine cycle
A cyclic pathway in which nitrogen and pyruvate are transported from muscle to the liver as alanine.

glutamate dehydrogenase
An enzyme that catalyzes the oxidative deamination of glutamate in the liver, yielding ammonium ion and α-ketoglutarate.

glutathione
A tripeptide playing a role in combating oxidative stress by maintaining the reduced state of the cell. Glutathione cycles between the reduced (GSH) and oxidized (GSSG) state.

glycerol 3-phosphate shuttle
A pathway, prominent in muscle tissue, that transfers electrons from cytoplasmic NADH into the mitochondria.

glycogen
A readily mobilized storage form of glucose in which the glucose monomers are linked by α-1,4-glycosidic linkages and in which there are branches (α-1,6-glycosidic linkages) at about every 12th residue.

glycogen phosphorylase
An allosteric enzyme that catalyzes the phosphorolysis of glycogen to yield glucose 1-phosphate; it is regulated by reversible covalent modification. Commonly referred to simply as **phosphorylase**.

glycogen synthase

An allosteric enzyme that can be reversibly covalently regulated and is responsible for the synthesis of glycogen. It transfers glucose from UDP-glucose to the hydroxyl group at a C-4 terminus of glycogen.

glycogen synthase kinase
An enzyme that phosphorylates glycogen synthase, keeping glycogen synthase in its inactive state.

glycogenin
A protein that bears an oligosaccharide of α-1,4 glucose units and is the primer for glycogen synthase. Glycogenin uses UDP-glucose to catalyze autoglycosylation.

glycolipids
A sugar-containing lipid that is derived from sphingosine; the sugar moiety is attached at the alcohol on sphingosine.

Glycolysis
A sequence of reactions that convert glucose into pyruvate with the concomitant generation of energy.

glycoprotein
A protein that has a specific carbohydrate moiety attached.

glycosaminoglycan
A heteropolysaccharide made of repeating disaccharide units and containing the amino sugar glucosamine or galactosamine.

glycosidic linkage
A covalent linkage between an aldehyde or ketone of a monosaccharide and an oxygen, nitrogen, or sulfur atom of another molecule. The most common glycosidic linkages are *O*-links between the anomeric carbon atom of a sugar and a hydroxyl group of another saccharide.

glycosyltransferases
Any of a number of specific enzymes that catalyze the formation of glycosidic linkages.

glyoxylate cycle
A metabolic pathway found primarily in microorganisms and plants that converts two-carbon acetyl units into succinate for energy production and biosyntheses.

glyoxysomes

An organelle containing enzymes of the glyoxylate pathway; found only in plants and filamentous fungi.

Golgi complex
In the cytoplasm, a stack of membranous sacs that constitute the major sorting center for proteins that reside in cell membranes and the lumen of organelles.

gout
A disease characterized by inflammation of the joints and kidneys due to the precipitation of abnormally high levels of sodium urate, a breakdown product of purines.

Gram staining
A method for staining bacteria using crystal violet that can distinguish between bacteria that possess a single membrane and a thick cell wall (Gram positive), and those that have a double lipid bilayer (Gram negative).

granum
A stack of thylakoid membranes in the chloroplast.

group-specific reagent
A reagent that reacts with specific R groups (side chains) of amino acids.

helicases
An enzyme that catalyzes the ATP-driven unwinding of nucleic acids. DNA helicases are important in DNA replication.

helix-turn-helix motif
The most common type of DNA-binding motif found in bacterial DNA-binding proteins.

heme
The prosthetic group of myoglobin and hemoglobin as well as other proteins; consists of an organic constituent, protoporphyrin IX, and an iron atom.

hemoglobin
A heme-containing oxygen carrier found in the bloodstream.

hemostasis
The process of blood clot formation and dissolution.

Henderson—Hasselbalch equation

The equation relating pH, the pK_a of an acid, and the ratio of the ionized and unionized form of the acid: $pH = pK_a + \log([A^-]/[HA])$.

heterotrophs
An organism that obtains the majority of its carbon for biosynthesis from organic molecules, rather than from carbon dioxide.

heterotropic effects
The effect of nonsubstrate molecules on catalytic activity by acting at sites distinct from the enzyme active site.

high-density lipoprotein (HDL)
A lipoprotein that picks up cholesterol from dying cells and from membranes undergoing turnover, esterifies it, and then transfers the cholesterol esters to the liver and other steroid-synthesizing tissues.

high-performance liquid chromatography (HPLC)
An enhanced column chromatography technique in which the separation materials are more finely divided and thus possess more interaction sites, resulting in greater resolution.

high-throughput screening (HTS)
The testing of a large compound library to identify molecules that bind to or affect the activity of a particular target.

histone acetyltransferases (HATs)
An enzyme that catalyzes the attachment of acetyl groups from acetyl CoA to specific lysine residues in the amino-terminal domains of histones.

histone deacetylase
An enzyme that contributes to transcriptional repression by the deacetylation of acetylated lysine residues in histones.

Holliday junctions
A cross-like structure, formed by four polynucleotide chains, that is a key intermediate in the recombination process.

holoenzyme
A complete and functional enzyme that consists of the protein component forming the main body of the enzyme (the apoenzyme) and any necessary cofactors.

homeodomain
A DNA-binding motif found in eukaryotic transcription factors, similar to bacterial helix-turn-helix motifs.

homodimer
A protein complex containing two identical subunits.

homogenate
The mixture formed when a tissue is treated in such a way that the plasma membranes are disrupted.

homologous recombination
The process by which two DNA molecules with strong sequence similarity exchange segments, allowing the transfer of foreign DNA into a genome.

homologs
Molecules that are related to each other by being derived from a common ancestor.

homotropic effects
The cooperative effect of substrate binding in one active site on the affinity at the comparable active site elsewhere in the enzyme.

horizontal gene transfer
The exchange of genetic material between species that provides a selective advantage to the recipient.

hybridoma
A cell formed from the fusion of immortal myeloma cancer cells with antibody-producing cells from the spleen of an inoculated organism. These cells produce large quantities of a single monoclonal antibody and have very long life spans.

hydrogen bond
A specific type of dipole–dipole interaction in which a hydrogen atom is partially shared by two electronegative atoms such as nitrogen or oxygen. Hydrogen bonds are relatively weak, with energies ranging from 4 to $20\ \mathrm{kJ\ mol^{-1}}$ (from 1 to $5\ \mathrm{kcal\ mol^{-1}}$), but are very important for specificity in biochemical interactions.

hydrogen-bond acceptor

The atom and its lone pair of electrons within a hydrogen bond that is less tightly linked to the hydrogen atom.

hydrogen-bond donor
The group within a hydrogen bond that includes both the hydrogen atom and the atom to which the hydrogen atom is more tightly linked.

hydropathy plot
An analysis of amino acid sequence used to locate potential membrane-spanning alpha helices by identifying highly hydrophobic regions across a defined sequence window.

hydrophobic effect
The tendency of nonpolar molecules to associate with one another in water.

Hypervariable loops (complementarity-determining regions)
Loops found on one end of an antibody structure that differ greatly between antibodies and determine antigen-binding specificity.

identities
The number of matched amino acid residues between two sequences.

Immunoglobulin fold
The three-dimensional structure of domains found in antibodies and other proteins comprising a disulfide-link sandwich structure of two antiparallel beta sheets with loops on the ends.

induced fit
The modification of the shape of an active site in an enzyme, toward a structure complementary to the transition state, after the substrate has been bound.

induced fit
The modification of the shape of an active site in an enzyme that occurs upon substrate binding.

inducer
A small molecule that binds to a repressor and alters its interaction with an operator to activate transcription.

initiation factors
One of a set of proteins that assist in the association of the ribosome, mRNA, and initiator tRNA to initiate the process of protein synthesis.

innate immune system
The first line of defense against invading pathogens that recognizes molecular structures common to pathogens, such as viruses and bacteria, that are not found outside cells in our bodies.

insulin
A hormone secreted by the pancreas that promotes the absorption of glucose from the bloodstream.

insulin resistance
The gradual reduction of the signaling response to insulin, despite adequate or excessive quantities of insulin produced; part of the metabolic syndrome. This often progresses to a near complete loss of insulin responsiveness.

Integral membrane proteins
A protein found in membranes that interacts extensively with the hydrocarbon chains of the membrane lipids and usually spans the membrane.

intermembrane space (IM space)
The compartment bounded by the inner and outer mitochondrial membranes into which protons are pumped by the action of the electron-transport chain.

introns
Region of the primary transcript that is removed in the mature mRNA. Also called the *intervening sequence*.

ion channels
A passive-transport system for ions capable of very high transport rates. Ion channels often display a high degree of specificity for the transported ion.

ion-exchange chromatography
A method of separation that takes advantage of the differences in net charge among proteins.

ionic interaction
An interaction involving one charged group interacting with another charged group. Such interactions are available if the two groups have charges of opposite sign.

iron–sulfur protein

A protein containing clusters of iron and sulfur that plays a role in electron-transfer reactions; iron cycles between the Fe^{2+} and Fe^{3+} state. Also called **nonheme iron protein**.

iron–sulfur proteins
Proteins containing clusters of iron and sulfur that play a role in electron-transfer reactions; iron cycles between the Fe^{2+} and Fe^{3+} state. Also called **nonheme iron proteins**.

isoelectric focusing
A means of separating proteins electrophoretically based on the relative content of acidic and basic residues of the proteins.

isoelectric point
The pH at which the net charge of a protein is zero.

isozymes (isoenzymes)
Enzymes that are encoded by different genes and that catalyze the same reaction, yet display different kinetic parameters and respond to different regulatory molecules.

k_{cat}/K_M (specificity constant)
A single number that directly relates the rate of a reaction to the concentration of the reactant and allows comparison of the efficiency of an enzyme capable of reacting with different substrates. Also called the catalytic efficiency.

ketogenic amino acids
An amino acid with a carbon skeleton that is degraded, entirely or in part, into acetyl CoA or acetoacetyl CoA; only leucine and lysine are solely ketogenic.

ketone bodies
Acetoacetate, b-hydroxybutyrate, and acetone produced when acetyl CoA is diverted from the citric acid cycle to the formation of acetoacetyl CoA in the liver. Ketone bodies act to transport acetyl groups from one tissue to another.

Kinases
An enzyme that catalyzes the attachment or removal of a phosphoryl group to a substrate by using ATP as a phosphoryl donor or ADP as the acceptor.

K_M (Michaelis constant)
The concentration of substrate at which an enzyme is operating at one-half maximum velocity.

lactic acid fermentation
The anaerobic metabolism of glucose to yield lactic acid with the concomitant production of ATP.

lagging strand
A newly synthesized strand of DNA at the replication fork that is initially synthesized as Okazaki fragments. See also *leading strand*.

large subunit (50S)
The large subunit of the bacterial 70S ribosome. The site of peptide-bond synthesis, it contains 34 different proteins, a 5S RNA species, and a 23S RNA species.

lateral diffusion
The ability of lipid and protein molecules to move laterally in the membrane rapidly and spontaneously.

lead molecules (leads)
Initial drug-like molecules that are the starting points for optimization into a drug candidate.

lead optimization
The process by which lead compounds are optimized into molecules suitable for testing in humans.

leading strand
A newly synthesized strand of DNA at the replication fork that is synthesized continuously. See also *lagging strand*.

lectins
A protein with a high affinity for a specific sugar residue; as such, lectins are important probes of carbohydrate containing molecules.

leptin
An adipokine hormone produced by adipose tissue in proportion to mass. Leptin induces feelings of satiety to regulate body mass.

Lesch–Nyhan syndrome
A disease resulting from the loss of a single enzyme in the salvage pathway for purines. It is marked by cognitive disabilities, extreme hostility, and self-mutilation.

ligand-gated channel
An ion channel whose opening is controlled by the presence of specific ligands.

ligands
A molecule or group that binds to a receptor including a metal ion.

light reactions
In chloroplasts, the reactions in which light is used to create reducing potential, to form ATP, and to generate oxygen.

light-harvesting complexes
A complex of light-absorbing pigments and protein that completely surrounds the reaction center of photosynthesis, funneling the energy of absorbed light to the reaction center.

Lineweaver–Burk plot
A plot of $1/V_0$ versus 1/[S] yields a straight line with a *y*-intercept of $1/V_{max}$ and a slope of K_M/V_{max}. Also called a double-reciprocal plot.

linking number (Lk)
The number of times that a strand of DNA winds in the right-handed direction around the helix axis when the axis lies in a plane.

lipases
An enzyme that degrades a triacylglycerol into free fatty acids and monoacylglycerol.

lipid bilayer
A bimolecular sheet formed by amphipathic molecules in which the hydrophobic moieties are on the inside of the sheet and the hydrophilic ones are on the aqueous outside.

lipid rafts
Complexes that are formed by cholesterol and some phospholipids, notably sphingolipids. Lipid rafts may concentrate in specific regions within membranes,

forming structures that are thicker, more stable, and less fluid than the rest of the membrane.

lipids
Water-insoluble biomolecules that are highly soluble in organic solvents such as chloroform.

lipoprotein particles
Clusters of molecules, consisting of a core of hydrophobic lipids surrounded by a shell of polar lipids and specific proteins, that play a role in the transport of cholesterol and triacylglycerols.

liposome (lipid vesicle)
An artificial membrane structure that consists of an aqueous compartment enclosed by a lipid bilayer.

Long QT syndrome (LQTS)
A genetic disorder in which the recovery of the action potential from its peak potential to the resting equilibrium potential is delayed.

loop
A segment of residues where the polypeptide chain reverses direction, usually longer and more elaborate than a reverse turn.

low-density lipoprotein (LDL)
The major carrier of cholesterol in the blood, consisting of a core of esterified cholesterol molecules surrounded by a shell of phospholipids, unesterified cholesterol, and apoprotein B-100. LDL is the primary source of cholesterol for cells other than those in the liver or intestine.

main chain (backbone)
The regularly repeating part of a polypeptide, including the amino group, α-carbon, and carbonyl groups.

Major histocompatibility complex (MHC)
A group of genes that encode proteins found on the surfaces of cells that help the immune system recognize foreign substances.

malate–aspartate shuttle
A reversible shuttle, found in the liver and heart, that transports electrons from cytoplasmic NADH to mitochondrial NAD^+.

malonyl CoA
Carboxylated acetyl CoA, the activated form of acetyl CoA used in fatty acid synthesis.

mass spectrometry
A technique for determining a protein's mass and identity and for sequencing a protein.

matrix
The central compartment of a mitochondrion, bounded by the inner mitochondrial membrane.

matrix-assisted laser desorption/ionization (MALDI)
A method of ionizing samples for mass spectrometry in which laser pulses ionize a sample embedded within a volatile matrix.

mechanism-based (on-target) toxicity
Toxicity caused by actions of a drug against its intended target.

mechanism-based (suicide) inhibitor
An inhibitor that binds to an enzyme as a substrate and initiates the normal catalytic mechanism, but via a subsequent mechanism generates a chemically reactive intermediate that inactivates the enzyme irreversibly through covalent modification.

mediator
A multisubunit complex that acts as a bridge between enhancer-bound activators and promoter-bound RNA polymerase II.

melting temperature
For a DNA double helix, the temperature at which half of the helical structure is lost.

Messenger RNA (mRNA)
A class of RNA molecules that serve as templates for the synthesis of proteins.

metabolic syndrome
A spectrum of metabolic changes that typically precede the development of type 2 diabetes and are often associated with obesity. These include hyperglycemia, dyslipidemia, and insulin resistance.

metabolism

A highly integrated network of chemical pathways that enables a cell to extract energy from the environment and use this energy for biosynthetic purposes. Also called **intermediary metabolism**.

metabolites
Small organic molecules (typically with molecular weight less than 1000 gm/mol) found in biological systems. This term derives from *metabolism,* the chemical processes that occur within living cells.

metal ion catalysis
Catalysis in which a metal acts as an electrophilic catalyst by stabilizing a negative charge on a reaction intermediate, generates a nucleophile by increasing the acidity of nearby molecules, or increases the binding energy of the enzyme–substrate interaction by binding to substrates.

mevalonate
A precursor for the synthesis of cholesterol. Its formation by 3-hydroxy-3-methylglutaryl CoA reductase constitutes the committed step in cholesterol biosynthesis.

micelle
A globular structure, typically formed from free fatty acids that contain only one hydrocarbon chain, in which the polar head groups form the outside surface and the hydrocarbon tails are sequestered inside.

Michaelis–Menten equation
An equation that expresses the initial velocity (V_0) of an enzyme-catalyzed reaction in terms of maximum velocity, V_{max}, substrate concentration, [S], and the Michaelis–Menten constant, K_M. The equation accounts for the hyperbolic kinetics observed when V_0 is plotted as a function of S; the equation is

$$V_0 = V_{max}\frac{[S]}{[S] + K_M}.$$

microbiome
The microorganisms that live on or within a macroscopic organism such as a human being.

microRNAs

A type of noncoding RNAs found in plants, invertebrates, and vertebrates. These ~21-nucleotide-long RNA molecules are excised from longer double-stranded RNAs and play a role in post-transcriptional regulation.

Mismatch repair
A system of DNA repair that consists of at least two proteins, one for detecting the mismatch and the other for recruiting an endonuclease that cleaves the newly synthesized DNA strand near the lesion. An exonuclease can then excise the incorrect base, and a polymerase fills the gap.

mixed noncompetitive inhibition
The reduction in the rate of enzyme activity observed when a reversible inhibitor binds significantly to both the enzyme–substrate complex and to the free enzyme but with different affinities. Mixed noncompetitive inhibitors always decrease the turnover number; however, the effect on the apparent value of K_M depends on the inhibitor's relative affinity for either E or ES. As such, mixed noncompetitive inhibitors can either increase or decrease the apparent K_M for an enzyme.

molecular clock hypothesis
The hypothesis stating that the extent of sequence difference between the same protein from two organisms can be used to infer the amount of time that has passed since these organisms had a common ancestor.

molecular recognition
Specific complex formation between two or more molecules via noncovalent interactions.

monoclonal antibody
An antibody, produced by a cloned hybridoma cell, that binds to only one epitope on a specific antigen.

monosaccharides
A single aldehyde or ketone that has two or more hydroxyl groups; monosaccharides are the simplest carbohydrates and are also called sugars.

motif (supersecondary structure)
Certain combinations of secondary structure present in many proteins, which frequently exhibit similar functions.

mucin

One of a class of glycoproteins, consisting mainly of carbohydrate, in which the protein component is extensively glycosylated to serine or threonine by *N*-acetylgalactosamine. Also called a **mucoprotein**.

multidrug resistance
When observed in tumor cells, the development of resistance to one drug that renders cells less sensitive to a range of other compounds

mutagens
An agent that perturbs the base sequence of DNA and causes a mutation. A mutagen is often a chemical, but it can also be an energy source such as ultraviolet light.

Myelin
A specialized membrane structure that serves as an electrical insulator around certain nerve fibers.

myoglobin
A heme-containing oxygen storage protein found in muscle.

myosins
A class of molecular motor proteins that hydrolyze DNA and use the free energy of hydrolysis to move along actin filaments.

NADH-Q oxidoreductase
A large component of the respiratory chain that transfers electrons from NADH to ubiquinone and, in the process, pumps protons across the inner mitochondrial membrane to generate the proton-motive force. Also called *NADH dehydrogenase* or **Complex I**.

native protein
A protein in its original active and folded form.

nerve impulse
An electrical signal produced by the coordinated flow of ions across the plasma membrane of a neuron. Also called an **action potential**.

neurotransmitters
Small, diffusible molecules that communicate nerve impulses across synapses.

next-generation sequencing (NGS)

A family of techniques that enable the rapid sequencing of short stretches of DNA in a massively parallel fashion (i.e., millions of sequences in a single experiment).

Nitric oxide (NO)
A free radical gas that serves as an important messenger in many vertebrate signal transduction processes, including vascular relaxation and mitochondrial biogenesis.

nitrogen fixation
The reduction of nitrogen gas (N_2) into ammonia (NH_3).

nitrogenase complex
An enzyme complex that catalyzes the reduction of N_2 to ammonia (nitrogen fixation); it is found in certain bacteria and the blue-green algae (cyanobacteria).

nitrogenous bases (bases)
One of the four possible substituents on the backbone of nucleic acids such as DNA. In DNA, these bases are adenine, cytosine, guanine, and thymine.

non-homologous end joining (NHEJ)
A mechanism used to repair double-stranded breaks in DNA. It joins two free double-stranded ends that are not related in sequence.

nonconservative substitution
An amino acid change in which an amino acid is replaced with one that is structurally dissimilar.

nonessential amino acids
Amino acids that can be synthesized by an organism and are thus not a dietary requirement.

nonphotochemical quenching (NPQ)
A process in chloroplasts that, in bright sunlight, directs photons from the reaction center, releasing the energy as heat. NPQ protects against the generation of reactive oxygen species.

nonpolar molecule
A molecule that cannot participate in hydrogen bonding or ionic interactions.

northern blotting

A technique that allows the identification of a specific RNA molecule using a ^{32}P-labeled probe complementary to the RNA molecule of interest.

nuclear hormone receptors
A member of a large family of transcription factors that, on the binding of a signal molecule such as a steroid hormone, modify the expression of specific genes by binding to control elements in the DNA.

nuclear magnetic resonance (NMR) spectroscopy
A method for determining the structure of molecules in solution by measuring the chemical environment of and contacts between intrinsically magnetic nuclei (such as protons) within the sample.

nuclear Overhauser effect
An interaction between nuclei that is proportional to the inverse sixth power of the distance between them. This effect is exploited in NMR spectroscopy to identify pairs of atoms within 5 Å of each other.

nucleophilic
Describing the tendency of a molecule or group to donate electrons or react at relatively electron-poor sites.

nucleoside
A purine or pyrimidine base linked to a sugar.

nucleoside diphosphokinase
An enzyme that exchanges the gamma phosphate between a nucleoside triphosphate and nucleoside diphosphate, allowing the equilibration of pools of energetically equivalent nucleoside trisphosphates in the cell.

nucleosome
A key structure of chromatin that is formed by the wrapping of ca. 145 bp of DNA around an octamer of histone proteins.

nucleotide
A nitrogenous purine or pyrimidine base linked to a sugar, which is in turn linked to one or more phosphoryl groups.

nucleotide-excision repair
A means of repairing DNA in which a stretch of DNA around the site of damage is removed and replaced.

obligate anaerobes
An organism that cannot survive in the presence of oxygen and thus is usually dependent on fermentation as a source of cellular energy.

off-target toxicity
Toxicity caused by actions of a drug against proteins that are distinct from the intended target.

Okazaki fragments
Small fragments of DNA (approximately 1000 nucleotides) that are formed on the lagging strand at the replication fork of DNA synthesis and later joined. Okazaki fragments enable $5'$-to-$3'$ polymerization at the nucleotide level while overall growth is in the $3'$-to-$5'$ direction.

oligopeptides (peptides)
Polypeptide chains made of small numbers of amino acids.

Oligosaccharides
A carbohydrate composed of 2 to 12 monosaccharide units.

oncogenes
A gene that can initiate the development of cancer.

open reading frames (ORFs)
A protein-coding region within a genome.

operator site
A regulatory sequence found in an operon to which regulatory proteins bind.

operon
A grouping of genes in bacteria whose expression is regulated in a coordinated manner because they are transcribed into one mRNA from a single promoter.

oral bioavailability
The ability of an orally administered drug to be absorbed into the bloodstream. It is defined as the ratio of the peak concentration of a compound given orally to the peak concentration of the same dose injected directly into the bloodstream

origin of replication
A particular sequence in a genome at which replication begins.

origin of replication complexes (ORCs)
A complex of six different proteins that promotes initiation of DNA replication in eukaryotes.

orotidylate
A nucleotide precursor to uridylate and cytidylate formed by the reaction of orotate with 5-phosphoribosyl-1-pyrophosphate (PRPP).

Orthologs
Homologs that are present within different species and have very similar or identical functions.

overlap peptides
Peptides generated by a cleavage method that enable the ordering of fragments generated by an orthogonal method.

oxidative phosphorylation
The process in which ATP is formed as a result of the transfer of electrons from NADH or $FADH_2$ to O_2 by a series of electron carriers.

oxyanion hole
A region on certain proteolytic enzymes that stabilizes the oxyanion constituent of the tetrahedral intermediate of the reaction.

oxyhemoglobin
The oxygen-carrier protein hemoglobin in its form with bound oxygen.

oxymyoglobin
The oxygen-storage protein myoglobin in its form with bound oxygen.

P-type ATPases
A class of pumps whose reaction mechanism includes a phosphorylaspartate intermediate.

Paralogs
Homologs that are present within one species and often differ in their detailed biochemical functions.

patch-clamp technique
A method for the measurement of the ion conductance through a small patch of cell membrane, capable of measuring the current through a single ion channel.

pentose phosphate pathway
A metabolic pathway that generates NADPH and five-carbon sugars such as ribose 5-phosphate from glucose 6-phosphate. Also referred to as the *hexose monophosphate shunt* or the *phosphogluconate pathway*.

peptide bond (amide bond)
A covalent linkage formed between the α-carboxyl group of one amino acid and the α-amino group of another.

peptide mass fingerprinting
The use of protein cleavage, followed by chromatographic separation and mass spectrometry to rapidly identify and quantitate proteins present within a sample.

peptidyl transferase center
A region of the large ribosomal subunit that catalyzes peptide-bond formation between the aminoacyl (or peptidyl) tRNA in the P site and the aminoacyl tRNA in the A site.

Peripheral membrane proteins
A protein that is associated with the surface of a membrane by electrostatic and hydrogen-bond interactions.

peroxisomes
A membrane-bound organelle that, in plants, houses enzymes that convert glycolate to glyoxylate as part of photorespiration.

pH
A measure of the concentration of hydrogen ions in solution nd is given by the equation $\mathrm{pH} = -\log [\mathrm{H}^+]$.

pharmacology
The scientific discipline which encompasses the discovery, chemistry, composition, identification, biological and physiological effects, uses, and manufacture of drugs.

phase I transformations
The oxidation reactions of drug metabolism.

phase II transformations
The conjugation reactions of drug metabolism.

phenotypic screening
A lead identification approach to early drug discovery in which compounds are screened for their ability to affect a disease-relevant phenotype of cells or tissues.

phenylketonuria
A disease caused by the inability to convert phenylalanine into tyrosine, which results in excess phenylalanine and its secondary metabolites. If untreated, it causes severe cognitive deficiencies and reduced lifespan.

phosphatase
An enzyme that catalyzes the attachment or removal of a phosphoryl group to a substrate by using inorganic phosphate as a phosphoryl donor or water as the acceptor.

phosphatidate
A precursor to triacylglycerols and to many phospholipids.

phospholipid
An important constituent of membranes that is composed of three components: a backbone (usually glycerol or sphingosine), two fatty acid chains, and a phosphorylated alcohol.

phosphoproteome
The proteins expressed by the genome that have been phosphorylated.

phosphorolysis
The cleavage of a bond by orthophosphate, as in the degradation of glycogen to glucose 1-phosphate.

phosphoryl-transfer potential
A measure of the tendency of a phosphorylated compound to transfer a phosphoryl group to another compound, presented as the $\Delta G^{\circ\prime}$ of hydrolysis of the phosphorylated compound. The more negative the $\Delta G^{\circ\prime}$ of hydrolysis, the greater the phosphoryl-group-transfer potential.

phosphorylase kinase
An enzyme that activates phosphorylase *b* by attaching a phosphoryl group in the regulation of glycogen degradation. This kinase is itself under dual control: it is activated both by phosphorylation and by increases in Ca^{2+} levels.

photoinduced charge separation
The excitation of an electron from its ground state to a higher energy level by light absorption and the subsequent movement of the excited electron from the initial molecule to an acceptor, resulting in a positive charge on the initial molecule and a negative charge on the acceptor molecule.

photorespiration
The conversion of organic carbon into carbon dioxide without the production of energy-rich metabolites, as the result of the oxygenase reaction catalyzed by Rubisco and subsequent steps.

photosynthesis
A metabolic scheme involving both phototropy and autotrophy, in which energy from sunlight is used to drive both the production of ATP and the reduction of carbon dioxide to synthesize carbohydrate. Photosynthesis may be oxygen-forming (oxygenic) or anoxygenic.

Photosystem I
In chloroplasts, a photosynthetic unit that includes a light-harvesting complex, a reaction center, and an electron-transport chain. The system catalyzes the light-driven transfer of electrons from reduced plastoquinone to ferredoxin, which in turn drives the formation of NADPH. PS I requires light of wavelength shorter than 700 nm.

Photosystem II
In chloroplasts, a photosynthetic unit that includes a light-harvesting complex, a reaction center, and an electron-transport chain. The system catalyzes the light-driven transfer of electrons from water to plastoquinone, with the concomitant generation of oxygen. PS II requires light of wavelength shorter than 680 nm.

Phototrophs
An organism that can meet its energy needs by converting light energy into chemical energy.

pK_a value

A measure of the acidity of a group HA and is defined by $pK_a = -\log(K_a)$ where K_a is the equilibrium constant $K_a = [H^+][A^-]/[HA]$.

placebo

A treatment given in controlled clinical trials that is known to not have intrinsic value.

placebo effect
The tendency to perceive improvement in a subject who believes that he or she is receiving a potentially beneficial treatment.

Plasmids
In bacteria, a small circular DNA separate from the bacterial chromosomal DNA that can replicate independently of the chromosomal DNA and often carries genes that confer antibiotic resistance.

pleckstrin homology domain
A protein domain that can bind phosphatidylinositol lipids.

polarity
The property of an object in which one end is different than the other. A strand of DNA has polarity and so, for example, the sequence -AGC- is distinct from -CGA-.

poly(A) tail
A long (as many as 250 nucleotides) polyadenylate segment added post-transcriptionally to the 3′ end of most eukaryotic mRNA.

polyclonal antibodies
Antibodies against a single antigen that are derived from multiple antibody-producing cell populations and thus recognize multiple epitopes on the antigen.

polylinker
A portion of a vector that contains multiple overlapping unique restriction sites. The presence of a polylinker allows for many different cohesive ends to be used for DNA insertion.

polymerase chain reaction (PCR)
A technique used to amplify a target DNA sequence over several orders of magnitude. A PCR cycle consists of three steps—strand separation, hybridization of primers, and DNA synthesis—that are repeated 20 or 30 times.

polymorphisms
An instance of genetic variation found within a population.

polysaccharides

A carbohydrate composed of a large number of covalently linked monosaccharide units; homopolysaccharides are composed of large numbers of one type of sugar, whereas heteropolysaccharides contain more than one type.

polysome
A group of ribosomes bound to an mRNA molecule and simultaneously carrying out translation. It is also called a *polyribosome* or the *primary transcript*.

Porphyrias
Inherited or acquired disorders caused by a deficiency of enzymes in the heme biosynthetic pathway.

posttranslational modification
Alterations in the structure of a protein after it has been synthesized in the cell.

pre-mRNA
The unspliced immediate product of RNA polymerase II in eukaryotes. It is also called the *primary transcript*.

primary messenger
A hormone, neurotransmitter, or other molecule that carries information to a cell or tissue by binding to a receptor, usually on the cell surface.

primary structure
The linear sequence of amino acids in a protein.

primase
A specialized RNA polymerase that synthesizes the RNA primers for DNA synthesis.

primer
In the elongation of polymers, the initial segment of the polymer that is to be extended. In DNA synthesis, elongation depends on the primer.

Processivity
A property of an enzyme that enables it to catalyze multiple rounds of elongation or the digestion of a polymer while the polymer stays bound to the enzyme.

prokaryote
A unicellular organism whose cells lack a well-defined nucleus.

promoter sites

A specific sequence of DNA, usually just upstream of a gene, that specifies the start site and extent of transcription of the associated gene.

promoters
A specific sequence of DNA, usually just upstream of a gene, that specifies the start site and extent of transcription of the associated gene.

prostaglandin
A class of short-lived signal molecules that are 20-carbon fatty acids containing a five-membered ring.

prosthetic group
A coenzyme that is tightly bound or covalently linked to an enzyme such that it does not readily dissociate but instead remains continuously associated with an enzyme.

protease
A class of enzymes that hydrolyze the peptide bonds between amino acids, thus digesting proteins. Also called a *proteolytic enzyme*.

protease inhibitors
A chemical that blocks or reduces the activity of a protease enzyme; some protease inhibitors are important drugs.

Proteases
A class of enzymes that catalyze the hydrolysis of peptide bonds between amino acids, thus digesting proteins.

proteasome
A large barrel-shaped protein complex primarily responsible for protein turnover in eukaryotes. Homologous systems exist in archaea and bacteria.

protein
A member of a class of biological macromolecules built of chains of units called amino acids. There are 20 different possible amino acids.

protein kinases
An enzyme that catalyzes the attachment of a phosphoryl group to a protein substrate by using ATP as a phosphoryl donor.

Protein phosphatase 1 (PP1)

A protein phosphatase stimulated by insulin that inhibits glycogen degradation and stimulates glycogen synthesis.

Protein phosphatases
An enzyme that catalyzes the removal of a phosphoryl group from a protein substrate by hydrolysis.

proteoglycans
A protein containing one or more covalently linked glycosaminoglycan chains. Cartilage proteoglycan contains keratan sulfate and chondroitin chains linked to a polypeptide backbone.

proteome
A term that refers to the proteins expressed by the genome, encompassing the types, functions, and interactions of proteins that yield a functional unit. Unlike the genome, the proteome varies with cell type, developmental state, and environmental conditions.

proto-oncogenes
A normal gene that can be converted to an oncogene by mutation.

proton shuttle
A group that facilitates the transfer of protons into or out of the active site of an enzyme.

proton-motive force
The energy inherent in the proton gradient established during the functioning of the respiratory chain, consisting of a membrane potential as well as a chemical gradient.

proximal histidine
The histidine residue in myoglobin and hemoglobin that is bound to the heme iron atom.

pseudogenes
A formerly functional gene that has accumulated enough mutations that it no longer produces protein.

pseudosubstrate sequence
A peptide sequence that matches the consensus sequence for a particular protein kinase substrate, but lacks the hydroxyl group required for phosphoryl transfer.

Pumps
Membrane proteins that catalyze the active transport of ions against their electrochemical gradients.

pure noncompetitive inhibition
The reduction in the rate of enzyme activity observed when a reversible inhibitor binds equally well to both the enzyme–substrate complex and to the free enzyme. Pure noncompetitive inhibitors decrease the turnover number, but do not alter the K_M, for an enzyme; their effects are not overcome by increased substrate concentration.

purine
A nitrogenous base that includes a pyrimidine ring fused with a five-membered imidazole ring; the purine derivatives adenine and guanine are found in nucleotides and nucleic acids.

purinosomes
A complex formed upon the association of the enzymes of purine synthesis.

pyridoxal phosphate (PLP)
A prosthetic group derived from vitamin B_6 (pyridoxine) that plays a key role in transamination reactions.

pyrimidine
A nitrogenous base that is a six-membered heterocyclic ring containing two nitrogen atoms and four carbon atoms; the pyrimidine derivatives cytosine, uracil, and thymine are found in nucleotides and nucleic acids.

pyrosequencing
A next-generation sequencing method that measures the DNA polymerase-catalyzed addition of a nucleotide by enzymatically converting the pyrophosphate product into light.

pyruvate dehydrogenase complex
A large mitochondrial enzyme complex that catalyzes the oxidative decarboxylation of pyruvate to form acetyl CoA. This irreversible reaction is the link between glycolysis and the citric acid cycle.

Q cycle
A set of reactions in which coenzyme Q cycles between the fully reduced state and the fully oxidized state through one-electron-transfer reactions.

Q-cytochrome c oxidoreductase
A component of the respiratory chain that carries electrons from coenzyme Q to cytochrome *c*, pumping protons out of the mitochondrial matrix to generate the proton-motive force. Also called *cytochrome* c *reductase* or **Complex III**.

quantitative PCR (qPCR)
A polymerase chain reaction technique capable of determining the quantity of individual mRNA transcripts. Also called real-time PCR.

quaternary structure
In proteins containing more than one polypeptide chain, the spatial arrangements of those chains (subunits) and the nature of the contacts between them.

R state
The quaternary structure adopted by oxyhemoglobin, where "R" refers to *relaxed* compared to the T (*tense*) state adopted by deoxyhemoglobin.

Ramachandran plot
A steric contour diagram that depicts allowed ranges of the angles φ and ψ for amino acid residues in polypeptide chains.

reaction center
In a photosynthetic unit, a specialized chlorophyll molecule that collects excitation energy from other chlorophyll molecules and mediates the transformation of light into chemical energy.

receptor-mediated endocytosis
The process of importing specific proteins into a cell by their binding to plasma-membrane receptors and their subsequent endocytosis and inclusion into vesicles.

receptors
A biological macromolecule, usually a cell-surface protein, that binds a molecule such as a hormone and initiates signaling cascades.

recognition sequences
A nucleic acid sequence that acts as a preferred binding, cleavage, or modification site for a DNA binding or modification protein such as a restriction enzyme.

recombinases
Enzymes that resolve Holliday junctions into separate DNA duplexes.

recombination synapse
A structure formed when four molecules of a recombinase and two DNA double helices come together before forming a Holliday junction.

recovery
In ion channels, the process by which an inactivated channel returns to the closed state.

reducing sugars
A sugar that converts into a form with a free aldehyde group that is readily oxidized and can thus reduce another compound.

reduction potential

The electron-transfer potential, expressed symbolically as E'_0. Also called **redox potential** or **oxidation–reduction potential**.

refractory period
The time after an action potential in which a subsequent action potential cannot be induced.

release factors (RFs)
One of a set of proteins that recognize stop codons on mRNA at the A site on the ribosome, which leads to the release of the completed protein from the tRNA in the P site of the ribosome.

replication fork
The site of DNA synthesis where the parental strands are separated and daughter strands complementary to each parent are synthesized.

reporter genes
A gene that encodes an easily detectable marker such as an antibiotic-resistance enzyme or a fluorescent protein. When used in vectors, they enable the rapid identification of clones that have successfully incorporated a DNA fragment.

repressor
A protein that binds to an operator sequence and inhibits the transcription of the structural genes in the operon.

residue
An amino acid unit within a polypeptide chain.

resonance structure
A structure that represents alternative arrangements of single and double bonds within the same structural framework. The true structure is intermediate between these alternative structures and is lower in energy than the individual resonance structures.

respirasome
A supramolecular complex consisting of two copies each of Complexes I, III, and IV of the electron-transport chain.

respiratory quotient (RQ)
A commonly used metabolic index defined as the volume of CO_2 released divided by the volume of O_2 consumed at a defined pressure. RQ is used to estimate the ratio of glucose vs. fatty acids used during rest or exercise.

restriction enzyme (restriction endonuclease)
A prokaryotic enzyme that recognizes specific base sequences in DNA and cleaves, at these specific places, both strands of DNA.

restriction enzymes
A bacterial enzyme that recognizes specific base sequences in double-helical DNA and cleaves, at specific places, both strands of DNA. Also called **restriction endonuclease**.

Restriction-fragment-length polymorphisms (RFLPs)
A polymorphism within restriction sites that changes the sizes of restriction fragments produced by the appropriate restriction enzyme.

restriction-modification systems
A combination of a restriction enzyme and a methylase that allows a host cell to cleave viral or other foreign DNA while not affecting host DNA.

retroviruses
A class of RNA viruses in which genetic information flows from RNA to DNA following the insertion of a copy of the viral RNA genome into the host's DNA.

reverse turn (β turn; hairpin turn)
A short segment of residues where the polypeptide chain reverses direction, often featuring a hydrogen bond between the CO group of residue i and the NH group of $i + 3$.

rho (ρ)
An ATP-dependent bacterial helicase that breaks the RNA–DNA hybrid at the transcription bubble and thereby terminates transcription.

ribonucleic acid (RNA)
A long unbranched polymer consisting of ribonucleotides joined by $3' \rightarrow 5'$ phosphodiester linkages that plays many roles in the cell, including that of catalyst. RNA is similar to DNA in composition except that it contains the base uridine instead of thymine, its sugar component has an extra hydroxyl group, and it is single-stranded.

ribonucleotide reductase
An enzyme that catalyzes the reduction of all four ribonucleotides to deoxyribonucleotides.

ribose
A five-carbon monosaccharide $(C_5H_{10}O_5)$ that constitutes the carbohydrate moiety of ATP, other ribonucleosides and ribonucleotides, and cofactors such as NAD^+ and coenzyme A.

Ribosomal RNA (rRNA)
The RNA components of ribosomes.

ribosomes
A large ribonucleoprotein assembly that catalyzes the formation of peptide bonds; a molecular machine that coordinates protein synthesis.

riboswitches
A structural component of some bacterial mRNA molecules that can bind to specific small molecules and thereby prevent further transcription of the mRNA.

ribozyme
A member of a class of RNA molecules that display enzymatic activity.

ribulose 1,5-bisphosphate carboxylase/oxygenase
An enzyme that catalyzes the reaction of carbon dioxide with ribulose 1,5-bisphosphate to form two molecules of 3-phosphoglycerate.

RNA editing

A process, distinct from RNA splicing, that changes the nucleotide sequence of mRNA after transcription.

RNA interference (RNAi)
The regulation of gene expression post-transcriptionally by small molecules of RNA.

RNA polymerases
A member of a class of enzymes that synthesize RNA molecules complementary to DNA templates.

RNA splicing
The process by which introns are removed and exons are ligated from precursors of RNA to form mature RNA.

RNA-seq
A method for measuring the transcriptome of cells or tissues in which cDNA is generated from the mRNA in the sample and then sequenced by next-generation sequencing techniques.

***S*-adenosylmethionine (SAM)**
An activated methyl donor that consists of an adenosyl group linked to the sulfur atom of methionine.

salvage pathways
A biosynthetic pathway that synthesizes the final product from preformed components.

scissile bond
The bond in a molecule that is cleaved by an enzymatic reaction.

SDS–polyacrylamide gel electrophoresis (SDS-PAGE)
A form of gel electrophoresis in which protein samples are first denatured in the presence of SDS, then run through a polyacrylamide gel and separated by size.

second messengers
An intracellular signaling molecule, such as a calcium ion or cyclic AMP, whose concentration changes in response to the arrival of a primary messenger.

secondary active transport
The coupling of the thermodynamically unfavorable flow of one species of ion or molecule up a concentration gradient to the favorable flow of a different species

down a concentration gradient

secondary structure
In proteins, the spatial arrangement of amino acid residues that are near one another in the linear sequence.

secondary transporter
A transporter that uses the energy of the downhill (exergonic) flow of one ion or molecule to power the uphill (endergonic) flow of another. Also called a **cotransporter**.

selectins
A carbohydrate-binding protein that constrains immune-system cells to the site of injury in an inflammatory response by mediating cell–cell interactions.

selectivity filter
A region of ion-channel proteins that determines the specificity of a particular channel.

self-splicing introns
Introns that are able to remove themselves from precursor RNA and assist in the splicing of exons to form mature RNA.

semiconservative replication
The type of replication observed in the duplication of DNA, in which one of the strands of each daughter molecule is newly synthesized, whereas the other is unchanged from the parental DNA double helix.

sequence alignment
A method in which two sequences are systematically aligned with respect to each other to identify regions of significant overlap.

sequence template
A map of conserved residues that are structurally and functionally important and characteristic of particular families of proteins.

sequential model
A model for hemoglobin oxygen-binding cooperativity where each hemoglobin subunit undergoes a structural change upon oxygen binding.

sequential reaction

A reaction having multiple reactants, in which all substrates bind to the enzyme before any product is released. Thus, in a reaction with two substrates, a ternary complex of the enzyme and both substrates forms.

seven-transmembrane-helix (7TM) receptors
A member of a large family of cell surface receptors with seven membrane-spanning α helices that signal through G proteins. See also **G-protein-coupled receptor (GPCR)**.

severe combined immunodeficiency (SCID)
An immunological disorder characterized by a loss of T cells and severe recurring infections, often leading to death at an early age.

Shine–Dalgarno sequence
In bacterial messenger RNA, a purine-rich region of about 10 nucleotides on the $5'$ side of an initiator codon that pairs with the $3'$ end of 16S RNA in the 30S ribosomal subunit; helps to determine where translation is initiated on an mRNA molecule.

sickle-cell anemia
A blood disease associated with distortion of red blood cells into a crescent shape when deprived of oxygen caused by a single amino acid substitution in one hemoglobin chain.

side chain (R group)
The distinctive variable group bonded to the α-carbon atom of an amino acid.

side effects
Unwanted effects caused by the administration of drugs in humans.

sigmoid
A descriptor for a curve with an "S" shape that indicates something other than a simple binding process.

signal peptidase
An enzyme that cleaves signal sequences in mature proteins on the lumenal side of the endoplasmic reticulum membrane.

signal sequence
A sequence of 9 to 12 hydrophobic amino acid residues that identifies the nascent peptide as one that must cross the endoplasmic reticulum membrane.

signal-recognition particle (SRP)
A ribonucleoprotein complex that recognizes and binds the signal sequence to the ribosome and then shepherds the ribosome and its nascent polypeptide chain to the endoplasmic reticulum membrane.

simple diffusion
The movement of molecules down a concentration gradient.

single guide RNA
The RNA component of the CRISPR-Cas system that directs the nuclease activity of Cas to particular genome sequences.

site-directed mutagenesis
A method for introducing mutations into a target sequence where a primer containing the desired change is used for DNA polymerization.

sliding DNA clamp
The dimeric β2 subunit of DNA polymerase III through which the DNA template slides. By clasping the DNA molecule, it allows the polymerase to move without falling off its substrate.

small nuclear ribonucleoproteins (snRNPs)
Complexes of small nuclear RNA and specific proteins that catalyze the splicing of mRNA precursors.

small nuclear RNAs (snRNAs)
A member of the class of small RNAs confined to the nucleus, some of which play a role in splicing.

small nucleolar ribonucleoproteins (snoRNPs)
A structure, consisting of one small nucleolar RNA and several proteins, that directs the extensive modification of the ribose and base components of nucleotides of pre-rRNA sequences destined for the ribosome.

small subunit (30S)
The small subunit of the bacterial 70S ribosome, containing 21 different proteins and a 16S RNA molecule.

solid-phase method
A method for synthesizing peptides and oligonucleotides in which monomer units are added to a growing chain tethered to a solid support.

Southern blotting
A technique that allows the identification of a specific DNA sequence using a ^{32}P-labeled probe complementary to the DNA sequence of interest.

special pair
In a photosynthetic reaction center, the pair of chlorophyll molecules that collect excitation energy from antenna chlorophyll molecules and then transfer high-energy electrons to other electron acceptors.

specific activity
The ratio of the enzyme activity to the amount of protein within a sample.

sphingolipids
A lipid having sphingosine rather than glycerol as its backbone. This is found in the plasma membranes of all eukaryotic cells and at highest concentrations in the cells of the central nervous system.

Sphingomyelin
Common in brain tissue, a sphingolipid in which the terminal hydroxyl group of ceramide has a phosphorylcholine substituent.

sphingosine
An amino alcohol containing a long, unsaturated hydrocarbon chain that is a component of the phospholipid sphingomyelin and of glycolipids. Sphingosine serves a role analogous to that of glycerol in phospholipids.

spliceosome
An assembly of proteins and small nuclear RNAs that splices, or joins together, primary transcripts to form mature mRNA.

Splicing
The removal of introns and the ligation of exons from precursors of RNA to form mature RNA.

split-pool synthesis
A combinatorial chemistry method where compounds on a solid support are split into individual pools for a reaction step, then pooled and re-split before the next synthetic step.

Squalene

A 30-carbon polyunsaturated hydrocarbon that is the precursor to cholesterol and steroid hormones.

SRP receptor (SR)
An integral membrane protein consisting of two subunits to which a complex consisting of a signal-recognition particle and a ribosome binds.

starch
A homopolysaccharide that is a storage form of glucose in plant chloroplasts. Amylopectin, the branched form of starch, has approximately one α-1,6 linkage per thirty α-1,4 linkages, whereas amylose is unbranched, composed of glucose residues in α-1,4 linkage.

stem-loop
A nucleic acid structure, commonly seen in RNA, created when two complementary sequences within a single strand come together to form a double-helical structure, which constitutes the stem. The two strands of the stem are linked by the loop.

Sterol regulatory element binding protein (SREBP)
A transcription factor that binds to the sterol regulatory element of the HMG-CoA reductase gene, stimulating the gene's transcription. It also stimulates transcription of other genes involved in cholesterol and fatty acid metabolism.

Stochastic
A process is said to be stochastic if the result is randomly determined from among possible outcomes.

stop codons
In most organisms, one of three nucleotide triplets in mRNA that designate the termination of transcription.

stroma
The matrix of the chloroplast; contains thylakoids as well as soluble enzymes and is enclosed by the inner membrane of the chloroplast.

structure-based drug design
A method of drug optimization in which structural information about the target and its interaction with compounds is used to design more potent and selective molecules.

structure–activity relationship (SAR)
The relationship between the structures of compounds and their activity against a particular drug target.

substitution matrix
A scoring system for the replacement of any amino acid with each of the other 19 amino acids.

substrate
A reactant in a chemical reaction. An enzyme catalyzes a single chemical reaction or a set of closely related reactions, and the components of those reactions are called substrates.

substrate channeling
The transfer of the product of one enzyme-catalyzed reaction directly to another enzyme for which the molecule is the substrate, without the release of the molecule to the bulk solvent.

substrate cycle
A pair of thermodynamically irreversible biochemical reactions that simultaneously produce and consume a pair of metabolic intermediates; these paired pathways may amplify metabolic signals and, in some cases, can generate heat for the maintenance of temperature in tissues. Also called a *futile cycle*.

substrate-level phosphorylation
The formation of ATP from ADP in which the phosphate donor is a substrate with a higher phosphoryl-transfer potential than that of ATP.

subunit
An individual polypeptide chain within a protein that contains multiple chains.

succinate-Q reductase
An integral-membrane-protein complex of the inner mitochondrial membrane that transfers electrons from $FADH_2$ formed in the citric acid cycle to coenzyme Q. Also called **Complex II**.

sucrose
A disaccharide of glucose and fructose (commonly known as table sugar) that is readily transportable and stored in many plant cells.

supercoiling

The ability of closed, circular DNA to coil upon itself.

surface complementarity
The property relating two surfaces such that when they meet, hydrogen-bond donors align with hydrogen-bond acceptors, and nonpolar surfaces come together to maximize van der Waals interactions and minimize nonpolar surface area exposed to water.

symporters
A secondary transporter that couples the downhill flow of one species to the uphill flow of another in the same direction across the membrane.

synaptic cleft
The gap between excitable membranes across which a nerve impulse is transmitted.

synthetic biology
An emerging discipline in which engineering principles are used to produce organisms or biochemically based devices that perform desired functions.

T state
The quaternary structure adopted by deoxyhemoglobin, where "T" refers to *tense*, due to structural constraints to stabilize this structure compared to the R (*relaxed*) state adopted by oxyhemoglobin.

t-SNARE
An integral membrane protein found in target membranes. Binding of v-SNAREs to t-SNARES leads to fusion of the vesicle and target membranes and the delivery of the cargo.

tandem mass spectrometry
A method of generating ion fragments within the mass spectrometer, enabling sequencing of peptides.

target
A protein or an oligonucleotide whose activity, when modulated by a drug, will alter the progression of a human disease process.

target validation
The process of accumulating evidence that a proposed drug target plays an important role in disease progression in humans.

target-based screening
A lead identification approach to early drug discovery in which the target is first selected, then screened for chemical starting points.

TATA box
A promoter element that is found in nearly all eukaryotic genes. The TATA box is centered between 30 and 90 residues upstream of the transcription start site and has the consensus sequence $5'-TATAAAA-3'$.

TATA-box-binding protein associated factor (TAF)
One of a group of proteins, many of which contain bromodomains, that bind to the TATA-box-binding protein.

telomerase
A reverse transcriptase that contains its own template; a highly processive enzyme that elongates the $3'$-ending strand of a telomere.

telomeres
Each end of a chromosome. The DNA at the telomere consists of hundreds of repeats of a hexanucleotide sequence characteristic of the organism.

template
In DNA or RNA, a sequence that directs the production of a complementary sequence.

template strand
In DNA or RNA, a sequence that directs the production of a complementary sequence.

tertiary structure
In proteins, the spatial arrangement of amino acid residues that are far from each other in the linear sequence, as well as the pattern of disulfide bonds.

Tetrahydrofolate
A highly versatile carrier of activated one-carbon units.

therapeutic index
A measure of the toxicity of a drug relative to its effective dose.

thylakoids

In chloroplasts, a membranous sac, or vesicle, that contains the energy-transducing machinery of photosynthesis, including light-harvesting proteins, reaction centers, electron-transport chains, and ATP synthase.

Thymidylate synthase
An enzyme that catalyzes the methylation of deoxyuridylate (dUMP) to form thymidylate (TMP).

time-of-flight (TOF) mass analyzer
A method for measuring ions within a mass spectrometer in which ions are passed through an elongated chamber of fixed electrostatic potential. The amount of time needed to traverse the chamber is proportional to the mass-to-charge ratio of the ion.

titration
An experiment in which known amounts of reagent are gradually added to a solution with which the reagent reacts while monitoring the results.

topoisomerases
An enzyme that catalyzes the interconversion of topoisomers of DNA, and that can relax supercoiled DNA.

topoisomers
Molecules of DNA that differ only in their linking number. Topoisomers of DNA can be interconverted only by cutting one or both DNA strands and then rejoining them.

torsion angle
A measure of the rotation about a bond, usually taken to lie between -180 and $+180$ degrees.

tractability (druggability)
The evidence that a molecule can be designed to interact with a drug target in a potent and specific manner.

transcription
DNA-directed synthesis of RNA catalyzed by RNA polymerase.

Transcription activator-like effector nucleases (TALENs)
An artificial restriction endonuclease whose DNA binding domain consists of amino acid repeats, called TALE repeats, that direct the nuclease to specific sites

in the target DNA.

transcription bubble
The site of RNA synthesis or transcription. This site contains RNA polymerase, a locally melted "bubble" of DNA, and hybrid helices consisting of the template strand and the newly synthesized RNA.

Transcription factors
A protein that assists RNA polymerase in the initiation of RNA synthesis. It binds to a specific promoter element.

transcriptome
The pattern and level of expression of all genes in a particular cell or tissue.

transduction
The transmission of information, often with the conversion of one form of information carrier into another.

Transfer RNA
The adaptor molecule in protein synthesis. tRNA contains an amino-acid-recognition site as well as a template-recognition site, or anticodon.

Transfer RNA (tRNA)
The adaptor molecule in protein synthesis; contains an amino-acid-recognition site as well as a template-recognition site, or anticodon.

transferrin
A transport protein that carries iron in the blood serum.

transferrin receptor
A membrane protein that binds iron-loaded transferrin and initiates its entry into cells.

transgenic mice
A mouse harboring a foreign gene that has been introduced into its genome.

transition state
A chemical species that has the highest free energy and the lowest concentration of those on the pathway from a substrate to a product.

transition-state analog

A compound resembling the transition state of a catalyzed reaction; such compounds are usually potent competitive inhibitors of enzyme-catalyzed reactions.

transketolase
An enzyme that transferase a ketone-containing group from one carbohydrate to another.

translation
The process of cellular protein synthesis, so named because the four-letter alphabet of nucleic acids is translated into the different amino acids that make up proteins.

translocon
A multisubunit assembly of integral and peripheral membrane proteins that binds to the ribosome, forming a channel to translocate a nascent protein across the endoplasmic reticulum.

transport vesicles
A small, membrane-enclosed cellular compartment that facilitates the transport of cargo proteins to specific destinations within the cell.

triacylglycerol
A glycerol that has fatty acyl chains esterified to each of its hydroxyl groups; a storage form of fats.

triacylglycerol
A glycerol that has fatty acyl chains esterified to each of its hydroxyl groups; the storage form of fatty acids called *fat* or *oil*, depending on melting point. Also called **neutral fat** or **triglyceride**.

trinucleotide repeats
Many repetitions of a trinucleotide sequence found in a stretch of DNA; these segments of DNA can expand in the course of DNA replication, causing such genetic diseases as Huntington's disease.

trombone model
A model for the stage of the DNA replication process when the lagging strand loops out to form a structure that acts somewhat as a trombone slide does, growing as the replication fork moves forward. When the polymerase on the lagging strand reaches a region that has been replicated, the sliding clamp is released and a new loop is formed.

Tumor-inducing plasmids (Ti plasmids)
A plasmid carried by the soil bacterium *Agrobacterium tumefaciens* that carries instructions to switch its plant host into a tumor growth state; because a small portion of the plasmid is integrated into the host genome, it is an ideal vector for the introduction of foreign DNA into plant species.

tumor-suppressor genes
A gene that, if present in even a single copy, can suppress the development of cancer.

turnover number
The number of substrate molecules converted into product by an enzyme active site in a unit time when the enzyme is fully saturated with substrate; equal to the kinetic constant k_2 (see K_M).

twist (Tw)
A measure of the helical winding of the DNA strands around each other.

two-dimensional electrophoresis
A means of obtaining high-resolution separations of proteins in a mixture, in which the protein mixture is first separated in one dimension by isoelectric focusing and then separated in a second dimension by SDS-PAGE.

Type 1 diabetes
The form of diabetes mellitus caused by inadequate production of insulin, usually due to the destruction of the β cells of the pancreas by an autoimmune disorder. Type 1 diabetes is treated by the regular administration of insulin.

type 2 diabetes
The form of diabetes mellitus caused by inadequate insulin sensitivity, usually due to a combination of genetics and behavioral factors, and most notably obesity. This is commonly preceded by metabolic syndrome.

Ubiquitin
A small protein, ubiquitously found in all cells that is used to mark proteins by covalent addition. Its primary role is to target proteins for degradation by the proteasome; however, numerous other biological functions have now been determined.

ultracentrifugation

The process of using centrifugation at very high velocities to determine the mass, density, shape, and interactions of proteins.

uncompetitive inhibition
Reversible enzyme inhibition distinguished by the fact that the inhibitor binds only to the enzyme–substrate complex and not to the free enzyme. Uncompetitive inhibitors decrease both the turnover number and the apparent value of K_M for an enzyme; their effects are not overcome by increased substrate concentration.

uncoupling protein (UCP-1)
A mitochondrial membrane protein that forms a pathway for the flow of protons into the matrix of the mitochondria, thereby generating heat without synthesizing ATP. Also called *thermogenin*.

unfolded protein response (UPR)
An adaptive cellular stress response involving several pathways and chaperone protein families, triggered by the accumulation of misfolded proteins in the ER lumen.

Uniporters
A secondary transporter that can transport a specific species in either direction governed only by concentrations of that species on either side of the membrane.

urea cycle
A cyclic pathway that converts excess ammonia into urea for secretion; the first metabolic pathway to be discovered.

uridine diphosphate glucose (UDP-glucose)
The activated form of glucose used in the synthesis of glycogen. It is formed from glucose 1-phosphate and UTP.

v-SNARE
An integral membrane protein found in transport vesicles. It binds to a particular t-SNARE.

van der Waals contact distance
The distance at which two molecules or groups have an optimal van der Waals interaction.

van der Waals interaction

A weak interaction due to fluctuating dipoles in one group inducing complementary dipoles on a nearby group with which it interacts favorably. At shorter distances, the van der Waals interaction becomes strongly unfavorable due to repulsive interactions between the electron clouds on the two groups.

vector
A small DNA molecule that can replicate autonomously in an appropriate organism.

virus
An entity that comprises a nucleic acid genome (DNA or RNA) surrounded by a protein coat that can infect specific cells and use the components of these cells to replicate itself.

vitamin B_{12}
A water-soluble vitamin used as a cofactor for two enzymes in human metabolism, among other functions. It is composed of a cobalt atom bound by a derivatized corrin-ring heterocycle. Also called **cobalamin.**

vitamins
An organic molecule that must be consumed in small quantities by a particular organism to allow a number of essential biochemical reactions to proceed.

V_{max} (maximal rate)
The theoretical maximum velocity of an enzyme catalyzed reaction at infinite substrate concentration. The asymptote line defining the upper limit of the hyperbolic relationship of V_0 as a function of substrate concentration, i.e., the Michaelis–Menten equation.

voltage-gated channels
An ion channel whose opening is controlled by changes in the voltage across the membrane.

water-oxidizing complex (WOC)
The site of oxygen generation in photosynthesis in green plants. The complex, which includes four manganese ions, donates electrons to positively charged P680, and then oxidizes two molecules of water to replenish its electrons; it thus forms a single molecule of molecular oxygen and four protons. Also called the **manganese center**.

western blotting
A means of detecting small quantities of a protein of interest in a cell or bodily fluid using a labeled antibody specific for the protein of interest. Also called immunoblotting.

wobble hypothesis
Refers to steric freedom in the pairing of the third base of an mRNA codon with the anticodon of a tRNA molecule, which allows more than one codon to be recognized by a particular tRNA.

writhe (Wr)
A measure of the coiling of the axis of the double helix; in other words, the degree of supercoiling.

x-ray crystallography
A method for determining molecular structure in which the sample (such as a protein) is crystallized. The diffraction of an x-ray beam through the crystal can be recorded and calculated into an electron density map, indicating the atomic positions within the crystal.

xenobiotics
Foreign compounds, including drugs, introduced into a living organism.

Z scheme of photosynthesis
The pathway of electron flow between photosystem I and photosystem II; so called because the redox diagram from P680 to P700 looks like the letter Z.

Zinc-finger nucleases (ZFNs)
An artificial restriction endonuclease formed by fusing the nuclease domain of a restriction enzyme with a specific DNA-binding domain consisting of zinc-fingers.

zymogen (proenzyme)
A catalytically inactive precursor of an enzyme.

α-ketoglutarate dehydrogenase complex
A regulatory citric acid cycle enzyme that catalyzes the oxidative decarboxylation of α-ketoglutarate to yield succinyl CoA. It is structurally and mechanistically similar to the pyruvate dehydrogenase complex.

β-galactosidase

An essential enzyme in lactose metabolism that hydrolyzes lactose into galactose and glucose.

β-oxidation pathway
The primary metabolic pathway for the oxidation and degradation of fatty acids. It is a sequence of oxidation, hydration, and oxidation reactions that converts a methylene group at the C-3 carbon atom of a fatty acyl CoA molecule into a β-keto group, with subsequent cleavage yielding acetyl CoA.

λ repressor
A protein in bacteriophage λ that blocks the transcription of all viral genes.

σ subunit
A component of bacterial RNA polymerase that enables the core RNA polymerase to recognize promoter sites.

Index

Note: Page numbers followed by f, t, and b refer to figures, tables, and boxed material.
Boldface page numbers indicate structural formulas and ribbon diagrams.

A site, ribosomal, 929, 929f, 933, 934, 935
AAA ATPases, 706
Ab initio prediction, 61
ABC transporters
    ATP hydrolysis reaction and, 390
    defined, 388
    domain arrangement of, 388, 388f
    in drug resistance, 999
    eukaryotic, 390
    mechanism, 388–390, 389f
    prokaryotic, 390
    structure of, 388, **389f**
ABO blood groups, 343–344, 343f, 344f
Abortive complex, 709
Absorption
    of dietary proteins, 702, 702f
    drug, 988–989
    light, 439–440, 590, 590f
Acarbose, 334, **334**
Acceptor control. *See* Respiratory control
Acceptor stem, 919, 925, 925f
Accessory pigments in photosynthesis, 602–605, 603f, 604f
Accommodation process, 932
Acetaldehyde, 486f

Acetaminophen, 992–993, 993f, **993f**
Acetate, 822f
Acetoacetate, **681**. *See also* Ketone bodies
from branched chain amino acids, 722–723
conversion into acetyl CoA, 681–682, 681f
formation of, 680, 724f
in gluconeogenesis, 753–754
from phenylalanine, 724, **724**
in respiration, 680–681
from tryptophan, 724, 724f
utilization as fuel, 680–681, 681f
Acetoacetyl CoA, 718
Acetyl ACP, 686–687
Acetyl CoA (acetyl coenzyme A)
acetoacetate conversion into, 681–682, 681f
acetyl-group-transfer potential, **462**
in amino acid degradation, 718, 722–723
cholesterol synthesis and, 821–825
in citric acid cycle, 502, 516, 518–520, 522–524, 524f, 535
defined, 462, 516
in fatty acid metabolism, 532, 670–671, 672–673, 690, 690f, 691
in fatty acid oxidation, 672–673
in fatty acid synthesis, 532
formation from ketone bodies, 679–680
formation of, 488, 520
formation of ketone bodies, 680f
in glyoxylate cycle, 536–537, 537f
oxidation of, 459
pyruvate and, 486f
pyruvate dehydrogenase complex and, 520
structure of, **462**, **516**, **726b**
synthesis of, 518–520
transfer to cytoplasm, 690, 690f
Acetyl CoA acetyltransferase, 758
Acetyl CoA carboxylase, 502

in citrate concentration, 695, 695f
in fatty acid metabolism, 685, 694–696, 694f, 722
filaments of, 695f
regulation of, 694f, 695–696
Acetyl transacylase, 686
Acetylated lysine, **218**
Acetylation
defined, 219t
in gene regulation, 965–966, 967
glycogen phosphorylase and, 658
in metabolism regulation, 218
protein, 219–220
Acetylcholine, 400–402
Acetylcholine receptor, 404
defined, 400
as ligand-gated channel, 400–402
as nonspecific cation channel, 403
structure of, **400**, **401f**
Acetylgalactosamine, **332f**

N-acetylglucosamine phosphotransferase, 345
N-acetylglutamate, 714–715
N-acetylglutamate synthase, 714
N-acetyl-l-phenylalanine p-nitrophenyl ester, 182, 182f
Acetyllysine-binding domain, 966, 966f
N-acetylneuraminate, 819
Acetylsalicylic acid, 141, 980–981, **980**
Achiral molecules, 36
Acid-base reactions, 17–18
Acids. *See also* Amino acids; Fatty acids; Nucleic acids
bile, 667, 667f
protonation/deprotonation of, 19–20
sialic, 819
Aconitase, 524–525, 525f, 971, 971f

Acquired immune deficiency syndrome (AIDS). *See* Human immunodeficiency virus (HIV) infection
Actin/actin filaments, 207f
    myosin and, 204–206, 205f, 206f
    structure of, 310, **311f**
Action potentials, 405
    defined, 392, 400
    integration, 402–404
    ion channels and, 392, 392f
    mechanism, 403–404, 404f
Activated carriers
    defined, 460
    as derived from vitamins, 463–464
    of electrons for fuel oxidation, 460–461
    of electrons for reductive biosynthesis, 461
    in metabolism, 460–463, 463t
    recurring set of, 463
    of two-carbon fragments, 462–463
Activated glycoaldehyde unit, 629
Activated methyl cycle, 775, 775f
Activation domains, 960
Activation energy
    defined, 148
    enzyme decrease of, 148–149, 148f
    product or substrate accumulation, 151
    symbol, 148
Activation loop, 426, 427f
Active membrane transport, 382–383, 384
Active sites
    ATCase, 213–214, **213f**, **214f**
    chymotrypsin, 183f
    concentration of, 156
    as crevice, 150
    defined, 149
    enzyme and substrate interaction, 150–151

mapping with irreversible inhibitors, 169–172
as microenvironments, 150
myosin, 204, 204f
proteases, 188f
residues, 150, 150f, 486f
RNA polymerases, 882, 883f
volume of enzyme, 150
Active transport, 382–383
Acute intermittent porphyria, 788
Acyclovir monophosphate, 797
Acyclovir triphosphate, 797
Acyl adenylate, 670–671
Acyl carnitine, 671–672, 671f
Acyl carrier protein (ACP), 685, 686f, 689, 689f
Acyl CoA, 462
Acyl CoA synthetase, 670–671
Acyl CoA: cholesterol acyltransferase (ACAT), 829
Acyl intermediates, 173
Acyl-enzyme intermediates, 183, 183f, 706
Adaptive control, 696
Adaptive immune system, 86–88
Adaptor proteins, 428
ADC. *See* Antibody-drug conjugate (ADC)
Adenine, 4, 5
deamination of, 865, 865f
methylation of, 200, 200f
resonance structures, **8**
structure of, **4**, **5f**
synthesis of, **783f**
Adenine nucleotide translocase (ANT). *See* ATP-ADP translocase
Adenine phosphoribosyltransferase, 800
Adenosine, **424**
Adenosine 5′-triphosphate. *See* ATP (adenosine triphosphate)
Adenosine deaminase, 809–810

Adenosine diphosphate. *See* ADP (adenosine diphosphate)
Adenosine monophosphate, **332f**
Adenosine nucleotides, 505–506
Adenosine triphosphate. *See* ATP (adenosine triphosphate)

S-adenosylhomocysteine, 774, **775**
S-adenosylmethionine (SAM)
    in activated methyl cycle, 774–775, 775f
    in adenylation of methionine, 721
    in amino acid degradation, 721, 721f
    in amino acid synthesis, 774–775
    in phospholipid synthesis, 818
Adenylate, 799
Adenylate cyclase, 418, 418f, 423–424, 424f
Adenylated intermediates, 770–771
Adenylation
    in amino acid activation, 921–922
    in amino acid synthesis, 782–783, 782f
    in translation, 921–922
Adenylosuccinate synthetase, 800
Adenylyl transferase, 782, 782f
Adipocytes, 666, 666f, 737
Adipokines, 736, 737f
Adiponectin, 736–737, 737f
Adipose cells (fat cells), 666
Adipose tissue
    brown, 575, 576f
    fat in, 748
    glycerol released from, 753
    leptin secretion, 736–737
    triacylglycerols in, 753
    white, 575
Adipose triglyceride lipase (ATGL), 669, 669f
Adler, Julius, 580
ADME properties of drugs, 988–989, 988f

ADP (adenosine diphosphate)
ATP hydrolyzed to, 450–451
formation of, 200
in oxidative phosphorylation, 572–573, 572f, 575f
in random sequential reaction, 160
structure of, **200**, **219**, **450f**
Adrenaline, 221, 412, 414, **414**, 650. *See also* Epinephrine
Adrenergic receptors, 415
Adrenocorticotropic hormone, 63
Advanced glycation end product (AGE), 331, 480, 510
Aequorea victoria, 63, 117
Aerobic exercise, 747
Aerobic glycolysis, 497–498, 531
Affinity chromatography, 104–105, 104f, 110
Affinity labels, 170, 170f
Affinity tags, 112, 170f
Aflatoxin activation, 865, 865f
Aggrecan, 340–341
Agonists, 415, 416f
Agouti-related peptide (AgRP), 736, 736f
Agre, Peter, 1, 27–28, 407
Agrobacterium tumefaciens, 295–296, 295f
Akt. *See* Protein kinase B (PKB)
Alanine
defined, 36
formation of, 769–770
in gluconeogenesis, 509
in muscle contraction, 509
pyruvate formation from, 719, 719f
site-directed mutagenesis and, 187–188, 187f
structure of, **37f**, 38
from tryptophan, 724f
tryptophan in, 719
Alanine aminotransferase, 708

Albinism, 727t
Albumin, **989f**
Alcaptonuria, 726
Alcohol dehydrogenase, 755
Alcoholic fermentation, 472, 486–487
Alcoholic hepatitis, 756
Alcoholic scurvy, 756–757, 757f
Alcohols
    fermentation of, 472, 486–487
    formation from pyruvate, 486–487
    metabolism of, 755–759
    monosaccharides and, 331–332
    phospholipids, synthesis of, 817–818
    toxicity of, 756–757
Aldehyde dehydrogenase, 755
Aldehydes, oxidation of energy, 480–481
Alder, Julius, 580
Aldimine, 710, **710**
Aldol cleavages, 711
Aldolase, 478
    in Calvin–Benson cycle, 616
    in transaldolase reaction, 629–630
Aldoses
    conversion to ketoses, 477
    defined, 325
    structure of, **615**
Aldosterone, 834, 837, **837f**
Alkali cations, properties of, 396t
Alkali digestion, 278
Alkylating agents, 865
Allergenics, 995t
Allolactose, 954, 956
Allopurinol, 810, **810**
Allosteric coefficient (L), 215
Allosteric control, 210–217

Allosteric effector, 81
Allosteric enzymes, 161f
concerted model, 215
control of, 468
defined, 161
homotropic effects on, 215
sequential model, 215
sigmoidal kinetics, 212, 212f
substrate concentration and, 215
threshold effects, 215f, 216
T-to-R equilibrium in, 216–217, 216f, 217f
T-to-R state transition, 215, 216f
Allosteric sites, 211
Alloxanthine, 810
All-*trans*-retinal, 439f
All-*trans*-retinoic acid, **963**
α_1-antiproteinase, 227, 228f
AlphaFold, 61, 62f
α carbon, 35
α chains, 75
α helix, 46–48
formation of, 57–59
hydrogen-bonding scheme, 47f
of membrane proteins, 368–369, 368f, 368t
pitch of, 47
as right-handed, 47, 47f
schematic view of, 48f
screw sense, 47
structure of, **47f**, 58f
α-1,4-glycosidic linkage, 333
α-1,6 linkages, 655, 655f
α-amino acids, 35, 41
α-glucosidase, 473–474
α-glucosidase inhibitors, 334

α-helical coiled coil, 53
α-hemoglobin
    alignment with gap insertion, 304f
    amino acid sequences, 303–305, 303f
α-keratin, 53
α-sarcin, 944
αβ dimers, 75
α-synuclein, 817
Alternative splicing
    defects in, 907t
    defined, 906
    example of, 907f
    pre-mRNA, 906–907
Altman, Sidney, 899
Alu sequences, 284
Alzheimer's disease, 62–63, 63f
Amanita phalloides, 894f
α-amanitin, 894, **894f**
American College of Sports Medicine, 751
American Medical Association, 751
Ames, Bruce, 871
Ames test, 871, 871f
Amide bonds. *See* Peptide bonds
Amines, monosaccharides and, 331–332
Amino acid degradation, 701–728
    acetoacetyl CoA in, 718
    acetyl CoA in, 718, 722–723
    amino acid use through, 701
    aminotransferases in, 708–711
    of aromatic amino acids, 723–724
    of branched-chain amino acids, 708–713, 722–723
    carbon atoms of as metabolic intermediates, 718–726
    digestive enzymes in, 702
    fumarate in, 718, 719f

glucose-alanine cycle in, 713, 713f
glutamate dehydrogenase in, 708–709
a-ketobutyrate in, 720
α-ketoglutarate in, 718, 719, 719f, 720, 720f
liver in, 708–709, 712–713
metabolic products of, 725b–726b
metabolism errors and, 723–728, 727t
overview of, 702–703
oxaloacetate in, 718, 719–720, 719f
oxygenases in, 723–724
propionyl CoA in, 722–723
proteasomes in, 705–707, 706f, 707f
in protein turnover, 703–705
pyridoxal phosphate (PLP) in, 709–710, 711–712
pyruvate in, 712–713, 718, 719, 719f
regulation function of, 707, 707t
Schiff-base intermediates in, 709–711, 711f
serine dehydratase in, 712
starvation and, 754, 754f
succinyl CoA in, 718, 719f, 721, 721f
threonine dehydratase in, 712
transaminases in, 708–713
ubiquitin in, 703–705, 704f
ubiquitination in, 703–705
urea cycle in, 713–718
Amino acid sequences, 33–34
alignment of, 302–309, 303f, 304f
collagen, 53–54, 54f
comparison of, 123–124
determination of, 100
directionality of, 42, 42f
in DNA probe creation, 124
DNA sequences and, 123f
evolution of, 44
evolutionary pathways and, 123

gap insertion, 303, 304f
of hemoglobin, 303–305, 303f
homologous, 308–309
identities, 303
importance of, 43–44
information provided by, 123–124
of insulin, 43, 43f
of myoglobin, 303–305, 303f
porin, 364–365, 364f, 365f
probes generated from, 277, 277f
in protein identification, 123–124
in protein structure determination, 55–64
protein structures and, 43, 43f
recombinant DNA technology and, 123
ribonuclease, 56–57, 56f, 57f
searching for internal repeats, 124, 124f
shuffled, 305, 305f
as signals, 124
statistical comparison of alignment, 305, 305f
substitution in, 305–308, 306f, 307f, 309f
transmembrane helices from, 367–369, 368f
Amino acid side chains
aliphatic, 36
aromatic, 37
charge of, 39–40, 39f, 41f
covalent modifications, 63f
defined, 35
distribution of, 51
hydrocarbon, 36
hydrophilic, 38
hydrophobic, 38
hydroxyl-containing, 38, 38f
ionizable, 40, 40t
sulfhydryl-containing, 39
thiol-containing, 39

types of, 36–40
Amino acid synthesis, 763–788
S-adenosylmethionine in, 774–775
adenylation in, 782–783, 782f
ammonia in, 764–767
aromatic amino acids, 776–779
branched pathways in, 780–782
chorismate in, 776–779, 777f
enzyme multiplicity in, 781
essential amino acids, 768–769, 769f
feedback inhibition/activation in, 780–783, 780f
glutamine synthetase in, 782–783, 782f
human, 768–769
α-ketoglutarate in, 766–767, 769
nitrogen fixation in, 764–767, 764f
nonessential amino acids, 768, 768f
overview of, 763
regulation of, 780–783
regulatory domains in, 780–782, 781f
Schiff bases in, 766, 767f
shikimate in, 776–779
tetrahydrofolate in, 772–774, 773f
threonine deaminase in, 780–781, 780f, 781f
by transamination, 767, 769–770, 769f, 770f
Amino acids. *See also* Proteins
abbreviations for, 40, 41t
activation by adenylation, 921–922
activation sites, 922–923, 923f
aromatic, 38, 723–724, 776–779
basic set of, 768t
biosynthetic families of, 768f
branched-chain, 708–713, 722–723
as building block, 25
carbon skeletons, fates of, 719f

chirality of, 35, 769f, 770
conservation across species, 40–41
D isomer, 35, 35f
defined, 25, 35
dipolar form of, 35
essential, 702, 702t, 768–769, 768f, 768t
glucogenic, 718, 719f
in gluconeogenesis, 499
hydrophilic, 38, 52
hydrophobic, 36–38, 37f, 51f, 52f
hydroxyl groups of, 38–39, 63
“inside out” distribution of, 52f
ionization state of, 36, 36f
ketogenic, 718, 719f
L isomer, 35, 35f
metabolism, 726–728, 727t
negatively charged, 39–40, 39f
nitrogen in, 764
nonessential, 768, 768f, 768t
nonproteinogenic, 126
peptide bonds, 42, 42f
polar, 38–39, 38f
positively charged, 39, 39f
as precursors, 783–788
as precursors for neurotransmitters, 785
protein folding and, 25, 25f
proteinogenic, 126
pyruvate formation from, 719, 719f
reactive, 38, 41, 41f
residue, 42, 51
in secondary structures, 58t
undesirable reactivity in, 41f
unnatural, 938–939, 938f
Amino sugar, 332
Amino-acid signal sequences, 940–941, 940f

Aminoacrylate, Schiff bases of, 779, **779**
Aminoacyl adenylate, **922**
Aminoacyl-AMP, 922
Aminoacyl-tRNA
    defined, 921
    editing of, 923–924, 923f
    elongation factors and, 931–932, 931f
Aminoacyl-tRNA synthetases
    accuracy of, 931
    activation sites of, 922–923, 923f
    amino acid activation sites, 922–923
    binding to acceptor stem and anticodon loop, 925, 925f
    classes of, 926, 926f, 926t
    defined, 921
    editing sites, 923–924, 923f
    evolution of, 926
    genetic code and, 921–926
    proofreading by, 923–925, 924f
    subunit structure, 926, 926t
2-aminoadenine, 801, 801f, **801**
Aminoglycoside antibiotics, 942
δ-aminolevulinate, 786–787, 787f
δ-aminolevulinate synthase, 786–787
Aminopeptidase N, 702
Aminopterin, 806f, 807
Aminotransferases
    in amino acid degradation, 708–711
    blood levels of, 711
    defined, 708
    Schiff-base intermediates formation in, 709–711
Ammonia
    in amino acid degradation, 708–709
    in amino acid synthesis, 764–767
    conversion to urea, 713–718
    formation of, 708–709

in glutamate synthesis, 766–767
in glutamine synthesis, 766–767
in purine synthesis, 800
in pyrimidine synthesis, 793
Ammoniotelic organisms, 718
AMP (adenosine monophosphate)
ATP hydrolyzed to, 450–451
energy charge and, 505–506
phosphofructokinase (PFK), regulation of, 493–494
in purine synthesis, 799–800, 799f
structure of, **450f**
synthesis of, 807–808, 808f
AMP-activated protein kinase (AMPK), 695, 696, 737, 737f, 745
Amphibolic pathways, 448
Amphipathic (amphiphilic) molecules, 358
Amphitropic enzyme, 818
AMP-PNP, 850–851, **850**, **851f**
α-amylase, 335, 473
Amylin, 735t
Amyloid fibrils, 62–63, 62f, 63f
Amyloid plaques, 62, 63f
Amylopectin, 335
Amylose, 335
Amyotrophic lateral sclerosis (ALS), 271, 290
Amytal, 577, 577f
Anabolic reactions, 451–452
Anabolism, 448
Anaerobic exercise, 747
Anaerobic glycolysis, 531
Analytes, 118
Anaplerotic reaction, 535
Anastrozole, 838, **839f**
Anchor residues, 90
Ancient DNA, 318–319
Anderson disease, 661t

Androgens
functions of, 834
pathways for formation of, 838f
synthesis of, 837–838, 838f
Androstenedione, 838, **838f**
Anemia, 21, 83–84, 339
Anfinsen, Christian, 56–57
Angelman syndrome, 705
Angiogenin, 302, **302f**
Animals
fatty acid synthesis in, 687–689
fatty acids and, 683
as models in drug target testing, 993
vision in, 442
Anion exchange, 104
Anomeric carbon atom, 328
Anomers, 326f, 328
Anoxygenic photosynthesis, 586
Antagonists, 424
Anthranilate branch, 778–779
Anthrax, 857
Antibiotics
aminoglycoside, 942
protein synthesis inhibition by, 942–944, 943f, 943t, 944f
resistance to, 998
translocation inhibition by, 943–944, 944f
Antibodies. *See also* Immunoglobulins
in adaptive immune system, 89
amino acid sequence data in making, 124
antibody binding of, 88–89
antigen binding of, 88–89
antigen interaction, 113f
defined, 69, 86
diversity of, 89
generation of, 112–113

monoclonal, 113–114, 113f, 114f, 434, 434f, 995–996, 995t
polyclonal, 113, 113f
primary, 116
secondary, 116
structures of, 87–88
Antibody-drug conjugate (ADC), 996
Antibody-protein interactions, 87–88
Anticancer drugs
in blocking thymidylate synthesis, 805–807, 806f
resistance to, 998–999
targets, 806f
Anticipation, 869
Anticoagulants, 231, 231f
Anticodon loop, 919, 925, 925f
Anticodons
base/base pair, 920–921, 921f
defined, 918
in translation, 919–921, 921f
Antidiuretic hormone, 126, 127f
Antigenic determinants, 113
Antigens
ABO blood group, 343–344, 343f, 344f
antibody interaction, 113, 113f
defined, 86, 112–113
synthetic peptides as, 126
Antimycin A, 577, 577f
Antiporters, 390, 390f
Antisense (-) strand, 884, 884f
Antiserum, 113
Antithrombin III, 232
AP endonuclease, 867
Apoenzyme, 144
Apolipoprotein A-IV, 735t
Apolipoprotein B (apo B), 909, 909f
Apolipoproteins, 827

Apoproteins, 827
Apoptosis, 224, 579
Apoptosome, 579
Apoptotic peptidase-activating factor 1 (APAF-1), 579
Approximation, catalysis by, 180
Aptamers, 320–321
Apyrase, 285
Aquaporins, 407, 408f
Arabidopsis thaliana, 2f, 283
Arachidonate, 693, 693f
Arachidonic acid, 366, 366f
Archaea
    defined, 3, 3f
    membranes of, 358, 358f, 373
    proteasomes of, 707
Archaeal lipid, 359f
Arcuate nucleus, 735
Arginase, 716
Arginine
    argininosuccinase and, 715, 716
    degradation of, 720, 720f
    nitric oxide from, 784–785, 784f
    structure of, 39, **39f**, **40t**
    supplementation of, 717
    synthesis of, 771
Argininosuccinase, 715, 716
Argininosuccinase deficiency, 717, 717f
Argininosuccinate, 715, **715**, 717
Argininosuccinate synthetase, 715
Argonaute complex, 971–972, 971f
Aromatase, 838
Aromatase inhibitors, 838
Aromatic amino acids
    degradation of, 723–724
    side chains, 38

synthesis of, 776–779
Arrestin, 420
Arsenate, 459
Arsenite poisoning, 535–536, 536f
Arthropods, polysaccharides of, 336–337, 337f
Artificial intelligence, 61
Artificial photosynthetic systems, 606–607, 607f, 620, 620f
Ascorbic acid (vitamin C)
deficiency, alcohol related, 756–757, 757f
forms of, 757, 757f
function of, 464t
Asparaginase, 719
Asparagine
conversion into oxaloacetate, 719–720
structure of, **38f**, 39
synthesis of, 770
Aspartate, **160**
conversion into oxaloacetate, 719–720
deamination of, 535
formation of, 769–770
phosphorylation of, 781
structure of, 39, **39f**, **160**
synthesis of, 771
Aspartate aminotransferase, 708, 711, 711f
Aspartate transcarbamoylase. *See* ATCase
Aspartic acid, 39, **40t**
Aspartokinases, 781, 781f
Aspartyl proteases, 188, 188f, **188f**
Aspergillus terreus, 981
Aspirin, 141
discovery and development of, 980–981
effect on prostaglandin H2 synthase-1, 366, 366f
as prostaglandin inhibitor, 694, 981
Assays

"on-bead," 983f
coupled, 982, 982f
defined, 101
enzyme-linked immunosorbent (ELISA), 114–115, 115f
in protein purification, 101
secondary, 982
sensitivity of, 982
ATCase (aspartate transcarbamoylase)
active site of, 213–214, **213f**, **214f**
allosteric interactions in, 212–216
catalytic subunit, 212, 212f, 213f
concerted model, 215
cooperativity, 215
defined, 211
feedback inhibition, 211
impact of CTP vs. ATP, 217f
inhibition by CTP, 807
reaction, 211, 211f
regulatory subunit, 212, 212f
separable subunits, 212
sigmoidal curve, 215, 215f
sigmoidal kinetics, 212, 212f, 215, 215f
structure of, 212–216, **213f**, **214f**
tense and relaxed states, 214f, 215
T-to-R transition, 214f, 215
Atheroma, 981
Atherosclerosis, 679, 827, 830–831, 832
ATP (adenosine triphosphate)
as activated carrier, 460
binding of, 320–321, 320f, 321f
in Calvin–Benson cycle, 618
catabolism generation, 456
in catabolism stages, 458–459, 459f
as cellular energy currency, 221
in citric acid cycle, 517, 526–531, 533, 534–535

defined, 448, 449–450
effect on ATCase kinetics, 216f, 217, 217f
electrostatic repulsion, 453
as energy source, 792
as energy-coupling agent, 452
as energy-rich molecule, 450
entropy increase in, 453
enzymes and, 145
in exercise, 454–455, 455f, 498–499, 747–749, 747t
export, inhibition of, 578
formation of, 448, 601, 601f, 602
free energy and, 449–456
generation by NADH, 461
glucose oxidation and, 573–574
hydration stabilization in, 453
hydrolysis of, 179
as immediate donor of free energy, 456
in insulin release, 744, 745f
ion gradients in, 458–459, 458f
membrane proteins and, 384–390
in mitochondria, 570–571, 572f
in muscle, 747, 749
in muscle contraction, 493, 747–749
in nitrogen fixation, 764–769
in oxidative phosphorylation, 573–574, 574t, 575f
phosphoryl-transfer potential, 453–455, 454f
in random sequential reaction, 160
resonance structures, 453, 453f
structure of, **200**, **219**, 450–451, **450f**
synthesis, 456, 543–545, 543f
ATP formation
1,3-bisphosphoglycerate (1,3-BPG) and, 482–484
citric acid cycle and, 529–531
by cyclic photophosphorylation, 601, 601f, 602
enzyme-bound, 565

fermentation in, 486
from glucose to pyruvate conversion, 484–485
from glycolysis, 485–486
from phosphoryl transfer, 482–484
proton-motive force and, 565–567, 565f
pyruvate in, 485–486
ATP hydrolysis
ABC transporters and, 388
ATP as base to promote, 202, 202f
in DNA replication, 850–851, 850f
in DNA supercoiling, 855–857, 856f
in driving metabolism, 451–452
enzyme use of, 201
as exergonic, 450–451
free energy from, 449–456
γ subunit in, 567
hydrolysis, 201
magnesium ions in, 201–202
myosin and, 200–207
myosin conformational changes, 202f, 203
reversible, within myosin active site, 204, 204f
rotational motion, 567
in transcription, 905
transition state formation for, 202–203
ATP synthase
α subunit of, 564
a subunit of, 564, 567–569, 567f
ATP synthesis and, 565–566, 565f
ATP-driven rotation in, 566, 567f
b subunit of, 564
β subunit of, 564, 566, 567, 600
bind-change mechanism for, 565–567, 566f
c ring of, 567–569, 568f
c subunit of, 566, 567–569

of chloroplasts, 600–601
cristae and, 565f
defined, 562, 563
δ subunit of, 564
dimer of, 564f
discovery, 563
efficiency of, 570f
F_0 subunit of, 564
F_1 subunit of, 564
G proteins and, 569
γ subunit of, 564, 566, 569
γε stalk, 564, 566
inhibition of, 577
in mitochondria, 564f, 570–571
nucleotide-binding sites, 566, 566f
proton flow through, 563, 565–567
proton motion across membrane in, 568f
proton path through membrane in, 568f
proton-conducting unit, 564, 567f
regulation of, 575
rotational catalysis in, 567, 567f
structure of, 564, 564f
ATP synthasome, 572
ATP synthesis
ATP synthase and, 565–566, 565f
in chloroplasts, 599–602
efficiency of, 567
as endergonic process, 562–563
mechanism, 564–567, 565f
oxidative phosphorylation uncoupling from, 575–576, 576f
proton flow around c ring in, 567–569
proton gradient across thylakoid membrane, 599–602
proton gradients in, 562–569
proton motion across membrane in, 567–569

proton path through membrane in, 567–569
uncoupling electron transport from, 577–578
ATP yield, 573–574, 574t
ATP–ADP cycle, 451, 456f
ATP-ADP translocase, 572–573, 572f, 573f, 578
ATPases, 201
AAA, 706
domains of myosin, 201, 201f, 202, 202f
mitochondrial. *See* ATP synthase
Na^+_K^+, 384, 387
P-type, 384–387, 388
SERCA, 384–387, **385f**, 386f
ATP-binding cassettes (ABCs). *See also* ABC transporters
ATP binding with, 388, 388f
defined, 388
distance between, 388
ATP-citrate lyase, 690
ATP-driven pump, 384
ATP-grasp fold, 793–794, 793f
Atractyloside, 578
Atrazine, **605**
Attenuation, 967–969, 968f
Autism, 705
Autophagy, 707
Autotrophs, 586, 611
Avian influenza, 348
Avogadro's number, 15
Axel, Richard, 436
Axial bonds, 329–330, 329f
Azide, 577, 577f

B recognition elements, 897
B. stearothermophilus, 520f
B vitamins. *See* Vitamins

Bacillus amyloliquefaciens, 186
Bacillus anthracis, 857
Bacillus subtilis, 891
Backbones, in polypeptide chains, 42, 42f
Bacteria, 3f. *See also Escherichia coli (E. coli)*
attenuation in, 967–969, 968f
carcinogen action on, 871–872, 871f
cell membranes of, 371, 373
chromosomes, 864, 864f
defined, 3
flagella movement of, 579–580, 579f
gene expression in, 935, 950–951
glyoxylate cycle in, 536–538, 537f
gram staining of, 373, 374f
intrinsic termination signals in, 888
nitrogen fixation in, 764–767
photosynthetic, 606–607, 606t, 607f
proinsulin synthesis by, 279, 279f
promoters in, 886–887, 886f, 887f
reaction centers, 591f, 592–593, 592f, 593f
restriction enzymes in, 194, 265–266
ribosomes, 936–937
RNA polymerases in, 886–887
sigma factors in, 890–892
transcription and translation in, 935, 935f
transcription factors in, 958
transcription in, 886, 935, 935f
translation in, 930, 931f, 935, 935f, 936–937
upstream promoter elements in, 886
Bacterial reaction center, 592f, 593f
cyclic electron flow in, 592–593
defined, 591
electron chain in, 591f
Bacteriochlorophylls, 591, **591**

Bacteriophage λ, 55, 55f, 272, 275–276
Bacteriopheophytins, 591, **591**, 592, 592f, 593f
Bacteriorhodopsin, 364, 364f, 365, 586, 586f
Baculovirus, 290
Ball-and-chain model, 399–400, 400f
Basal transcription factors, 898
Base-exchange reactions, 818
Base-excision repair, 867, 867f
Base-pair substitutions, tests for, 871
Bases/base pairs
    adenine, 5f, **5**
    anticodon, 920–921, 921f
    cytosine, 5f, **5**
    damage to, 864–865
    double helix, 11
    guanine, 5f, **5**
    hydrogen bonds, 5
    minor-groove side of, 848
    mutagenic, 864
    nomenclature of, 792t
    non-Watson–Crick, 864, 866, 885
    rRNA in, 927–928, 928f
    stacking of, 12, 12f
    thymine, 5f, **5**
    in translation, 919
    tRNA, 919
    Watson–Crick, 920–921
Basic-leucine zipper (bZip), 959, 959f
Bayer, 980
B-cell leukemia, 898
Bcr-abl gene, 435, 435f, 874
Benson, Andrew, 610, 611b
Benzaldehyde, **436**
Benzoate, 717

Benzoyl CoA, 717
Berg, Howard, 580
Berg, Jeremy, 28
Beriberi, 535–536, 756
Bertozzi, Carolyn, 347b
β chains, 82f, 83
β oxidation, 748, 753
β pleated sheets, 46, 48–50
    amino acid residues in, 57–59, 58t
    antiparallel, 48, 49f
    defined, 48
    formation of, 57–59
    mixed, structure of, 49f
    parallel, 48, 49f
    protein rich, 50f
    twisted, schematic, 50f
β strands
    defined, 48
    DNA recognition through, 951, 951f
    of membrane proteins, 364–365, 364f
    Ramachandran plot for, 48f
    structure of, 48f, 58f
β turns, 46, 50, 57–59
β-adrenergic receptor, 415, 415f, 416f, 419f
β-carotene, 841, 841f, **841f**
β-galactosidase, 950
β-lactam ring, 172, 172f
β-oxidation pathway, 672–673
Bicarbonate, 793–794
Bifunctional enzyme, 506–507, 506f
Bile, 832, 833
Bile acids, 667, 667f
Bile salts, 833, 833f
Bilirubin, 787, 788f

Biliverdin, 787, 788f
Biliverdin reductase, 787
Bimolecular reactions, 152
Bimolecular sheets, 359–362
Binding
    association and dissociation, 72, 72f
    as fundamental process, 69–72
    immune system and, 84–91
    myoglobin and, 73–75
    oxygen and, 75–84
    partners, concentrations of, 69–70, 70f
    proteins and, 70–72
Binding energy, 151, 180, 199
Binding partners of protein, 116
Binding propensity, 91–95
    dissociation constant for, 91–93, 92f
    kinetic parameters, 94–95
    specificity, 93–94
Binding-change mechanism, 565–567, 566f
Biochemical timescale, 7
Biochemistry
    biological diversity and, 2–4
    biological molecules, properties of, 6–21
    careers in, 27f
    chemistry concepts in, 6–21
    defined, 1
    DNA, form and function of, 4–6
    DNA sequencing, 21–27
    evolution timeline, 3f
    genome sequencing and, 21–22
    genomic revolution and, 21–27
    research in, 27–29, 27f
    unifying concepts, 2–4
Bioenergetics, 580–581, 581f
Bioinformatics, 265

Biological diversity
biochemical unity underlying, 2–4
similarity and, 2f
Biological macromolecules, 2
Biological membranes. *See* Membranes
Biologics, 995–996, 995t
Biomarkers, A1C as, 331
Biomolecules, 840–841
Biopterin, 723
Biotechnology, 264, 265
Biotin, 463t, 501, 501f
Biotin carboxyl carrier protein (BCCP), 502, 502f
Bisphenol A (BPA), 93–94, 93f, **93**
1,3-bisphosphoglycerate (1,3-BPG)
as acyl phosphate, 480–481
ATP formation and, 482–484
in glycolysis, 457–458, 480–481, 483–484
oxidation of energy, 457–458
phosphoryl-transfer potential, 453–454, 454f
structure of, **457**, **458**
2,3-bisphosphoglycerate (2,3-BPG)
allosteric effector, 81
binding of, 80–81, 80f
defined, **80**
in oxygen affinity determination, 80–81, 80f
Bistable circuits, 958
Bisubstrate analog, 213, 213f
Bjorkman, Pamela, 90, 91b
Blackburn, Elizabeth, 863
BLAST (Basic Local Alignment Search Tool) search, 309, 309f
The Blind Watchmaker (Dawkins), 60
Blood clotting, 223
Ca^{2+}, 229
clots, 231–232

enzymatic cascades, 228–229, 228f
extrinsic pathway of, 228
intrinsic pathway of, 228
regulation of, 231–232
zymogen activation in, 228–229, 228f
Blood glucose homeostasis, 334
Blood groups, 343–344, 343f, 344f
Blood sugar, 330. *See also* Glucose homeostasis
Blood-brain barrier, 990
Blood-glucose concentration. *See* Glucose homeostasis
Blosum- 62
alignment of identities only versus, 307f
defined, 306
graphic view of, 306f
myoglobin and leghemoglobin, 308f
Blotting techniques, 265, 266–267, 267f
Boat form, 329–330, 329f
Body mass index (BMI), 733f, 734
Body weight, regulation of, 733–738. *See also* Obesity
Bohr, Christian, 81
Bohr effect, 81–83
Bombardment-mediated transformation, 296
Bombesin, 735t
Bonds
axial, 329–330, 329f
covalent, 5, 7–8
disulfide, 43, 43f
electrostatic interactions, 8
equatorial, 329–330, 329f
glycosidic, 331–332, 332f, 336, 336f, 338
hydrogen. *See* hydrogen bonds
hydrophobic effect and, 10–11, 11f
hydrophobic interactions and, 11
ionic interactions, 8–9, 11f

isopeptide, 703, 704f
noncovalent, 7–11
peptide. *See* peptide bonds
van der Waals interactions, 9–10, 10f, 12, 52, 360
Bortezomib, **707**
Bound receptors, fraction of, 92b–93b
Bovine ribonuclease, **302f**
Brain
glucose in, 740
ketone bodies and, 753–754
leptin effects in, 736, 736f
role in caloric homeostasis, 734–735
Branch points, 902, 903f
Branched-chain amino acids, 708–713, 722–723
Branched-chain ketoaciduria, 727
Branching enzyme, 655, 655f
Branson, Herman, 46, 46b
Brittle bone disease, 54
Bromodomains, 966, **966f**
Bronchitis, 341
Brown, Michael, 830
Brown adipose tissue (BAT), 575, 576f
Brown fat mitochondria, 576
Buchner, Edward, 472
Buchner, Hans, 472
Buck, Linda, 436
Buffers
action, 19f
in deprotonation, 193
pH and, 19–20, 19f
protonation, 19f
Bumpus, Namandjé, 836b
Burkitt lymphoma, 898
Butyryl CoA, **725b**

C_3 plants, 623, 624f
C_4 pathway, 622–623, 622f
C_4 plants, 623, 624f
CAAT box, 896, 896f
Caenorhabditis elegans, 125, 283, 295
Caffeine, **424**
Calcitriol, 464t, 839, 839f, 840
Calcium, 749, 750f
Calcium ion channels, 397, 397f
Calcium ion pump, 384–387, 386f
Calcium ions
    calmodulin activation, 423
    coordination to multiple ligands, 422, 422f
    imaging, 422, 422f
    in phosphorylase activation, 650–651, 650f
    pump structure, 386f
    pumping, 384–387, 386f
    as second messenger, 413–414, 421–422
    in signal transduction, 420–422, 422f
Calmodulin (CaM), 124, 124f
    defined, 420, 423, 651
    in mitochondrial biogenesis, 749
    in signal transduction, 420, 423, 423f
Calmodulin-dependent protein kinases (CaM kinases), 423, 423f
Calnexin, 347
Caloric homeostasis, 733–738
    in body weight regulation, 733–738
    brain role in, 734–735
    defined, 733
    in diabetes, 741–746
    evolution and, 734
    exercise and, 752b
    impact of athletic activity on, 752b
    insulin in, 736

leptin in, 736–737
obesity and, 734
satiation signals in, 735–736, 735f
signaling in, 735–736
suppressors of cytokine signaling (SOCS) in, 737–738, 738f
Calreticulin, 347
Calvin, Melvin, 610, 611b
Calvin–Benson cycle, 610–624
ATP (adenosine triphosphate) in, 618
C_4 pathway and, 622–623, 622f
carbon dioxide in, 611–620, 622–623
defined, 587, 610
environmental factors in, 620–624
five-carbon sugar formation in, 615, 616f
fructose 6-phosphate in, 615, 615f, 616f, 618, 619f
glycine in, 614f, 615
glycolate in, 614f, 615
hexose sugar formation in, 615–618, 616f
illustrated, 612f
light regulation of, 620–621, 620f
magnesium ion and, 612–613, 613f, 621
NADPH in, 610, 618, 622
overview of, 610
oxygenase reaction in, 614–615, 614f
pentose phosphate pathway and, 633–634
3-phosphoglycerate formation in, 611–612, 612f, 613f, 614f, 615, 615f
photorespiration in, 614f, 615
reactions in, 611–620, 617f
regulation of, 620–622
ribulose 1,5-bisphosphate in, 611–612, 613f
rubisco in, 611–615, 612f, 613f, 614f, 621
salvage pathway in, 614–615
stages, 611–612, 612f, 613f, 615–618, 615f

thioredoxin in, 621–622, 621t, **621f**
cAMP. *See* Cyclic AMP (cAMP)
cAMP receptor protein (CRP). *See* Catabolite activator protein (CAP)
Camptothecin, 857
Cancer
adenocarcinomas, 341
aerobic glycolysis in, 497–498
breast, 838, 839f, 870t
colorectal, 870
defective DNA repair in, 869–871, 870t
drug resistance in, 998–999
epigenetics and, 962
ethanol metabolism in, 758–759
fatty acid metabolism in, 691–692
glycolysis in, 497–498
lung, 870t
ovarian, 838, 870t
renal, 870t
signal transduction abnormalities in, 433, 434, 434f, 435f
skin, in xeroderma pigmentosum, 870
treatments for, 870–871
tumor hypoxia in, 498
tumor suppressor genes and, 870
tumor visualization, 497, 498f
Warburg effect in, 497
Cancer therapy, 805–807
Candidates, in drug development, 986. *See also* Drug candidates
Capillary electrophoresis, 268
Captopril, 189
Carbamate
in Calvin–Benson cycle, 613, 614
formation of, 82, **82f**
Carbamate groups, 82
Carbamoyl phosphate

in pyrimidine synthesis, 793
reaction, 714
in urea cycle, 714–716
Carbamoyl phosphate synthetase, deficiency of, 717, 717f
Carbamoyl phosphate synthetase I, 714–715
Carbamoyl phosphate synthetase II
in pyrimidine synthesis, 793, 793f, 794, 794f
structure of, 793, **793f**
Carbanion, 629
Carbanion intermediates, 628–630, 631f
Carbocation, 644f
Carbohydrate–asparagine adduct, **63f**
Carbohydrates, 324–348
disaccharides, 333–334
as fuel, 457f
glucose generation from, 473–474
isomeric forms of, 326f
lectins and, 346–348, 347f
monosaccharide, 325–333
N-linked, 338, 338f
oligosaccharides, 333, 342–343, 343f
O-linked, 338
overview of, 324
polysaccharides, 335, 336f
proteins linkage, 337–346
Carbon, oxidation of, 456–459
Carbon dioxide
binding site, 192, 192f
in Calvin–Benson cycle, 611–612, 622–623
defined, 82
fixation of, 619–620, 620f
hydration acceleration, 190
hydration of, 193, 194f
oxygen release and, 81–83
pH and, 82, 82f

transport from tissue to lungs, 82, 82f
Carbon fuels, free energy of, 456–459, 457f
Carbon monoxide, 74
defined, 82
myoglobin and, 74–75, **75f**
in oxygen transport disruption, 81, 82–83
poisoning, 82–83
Carbonic anhydrases, 141
bound zinc in, 190–191
in carbon dioxide hydration acceleration, 190
catalytic strategies of, 179, 190–194
defined, 190
evolution of, 193
mechanism of, 192, 192f
pH effect on, 190–191, 191f
proton availability and, 192–194
proton shuttle, 193, 194f
regeneration of, 192–194
structure of, **190**
Carbon–nitrogen bond, 181
Carboxamides, 38f, 39
Carboxybiotin, 501f
γ-carboxyglutamate, **63f**, 231, 231f
Carboxyhemoglobin, 83, 83f
Carboxylation of pyruvate, 501–502, 535
Carboxyl-terminal domain (CTD)
in coupling transcription to pre-mRNA, 908, 908f
defined, 894
phosphorylation of, 897, 897f
serine residues of, 894
Carcinogens, tests for, 871–872, 871f
Cardiac muscles, 416, 416f, 419, 419f
Cardiotonic steroids, 387, 387f
Cargo receptor, 942
Carnitine, 671–672, 671f

Carnitine acyltransferase I, 671
Carnitine acyltransferase II, 672
Carotenoids, 602–603, 841, 841f
Carriers, 390
Cartilage, 340–341, 340f
Caspases, 579
Cassette mutagenesis, 281, 281f
Catabolism
    ATP generation by, 456
    defined, 448
    energy from, 456–459
    free energy of, 456–459, 459f
    roles of, 456
    stages of, 459, 459f
Catabolite activator protein (CAP), 955–956, 955f, 956f
Catabolite repression, 955
Catalase, 561
Catalysis
    by approximation, 180
    by ATCase, 211
    Circe effect in, 159
    covalent, 180, 181, 181f, 183f
    efficiency of, 158–159
    enzyme–substrate binding in, 151
    enzyme–substrate complex formation in, 149, 149f
    general acid–base, 180
    maximal rate, 154–155, 156
    metal ion, 180
    specificity constant, 158
    transition state formation and, 148
    velocity of, 158
    zinc activation of water molecule, 191–192, 192f
Catalysts, 142, 181
Catalytic RNA, 909–912
Catalytic strategies, 180

of carbonic anhydrases, 179, 190–194
in chymotrypsin, 181–182, 181f, 182f
of myosins, 179, 200–207
overview of, 179
of restriction endonucleases, 179, 194–200
of serine proteases, 179, 183–185
Catalytic triads
defined, 183
in elastase, 186–187
in hydrolytic enzymes, 184f, 186–187, 186f
serine in, 183–185, 183f
site-directed mutagenesis and, 187–188, 187f
of subtilisin, 186–187, 187f
in trypsin, 186–187, 186f
Cataracts, 491, 491f
Catecholamines, 785, 785f
Cation exchange, 104
cDNA library, 279
CDP-ethanolamine, 818, **818**
Cech, Carol, 912b
Cech, Thomas, 912b
Cell cycle, 862
Cell-mediated immunity, 89
Cells, 2, 114
Cell-to-cell channels, 406–407, 406f, 407f
Cellular immune response, 86
Cellular respiration
citric acid cycle in, 516–517, 517f
defined, 543
enzymes in, 144
in oxidative phosphorylation, 543–545
vs. photosynthesis, 587
regulation of, 573–579
Cellulose, 335–336, **336f**
Centrifugation

differential, 102, 102f
ultracentrifugation, 111
Cephalopods, 337
Ceramide
insulin resistance and, 743–744, 744f
as precursor, 820f
synthesis of, 819, 819f
Cerebroside, 357, **357**, 819, **820f**
CETCH cycle, 619–620
Cetuximab (Erbitux), 434, 434f, 996
cGMP, 980, **980f**
cGMP phosphodiesterase, 439, 439f
Chain, Ernest, 979
Chair form, 329–330, 329f
Changeux, Jean-Pierre, 78
Channelrhodopsin, 607, 607f
Channels, 382
Chaperones, 57
Charged tRNA, 921
Charpentier, Emmanuelle, 294b
Checkpoints, 862
Chemical modification reaction, 182
Chemical shifts, 133
Chemical space, 984
Chemiosmotic hypothesis, 562–563, 563f
Chemotroph, 447, 586
Cheng, Yung-Chi, 987
Cheng–Prusoff equation, 987
Chirality
of amino acids, 35, 769f, 770
establishment of, 767f
Chitin, 336–337, 337f
Chitosan, 337
Chlamydomonas, 911
Chloramphenicol, 942, 943t

Chlorobium thiosulfatophilum, 606
Chlorophyll *a*, 589–590, 602, 603f
absorbance spectrum, 590f
structure of, **589f**
Chlorophyll *b*, 602–603, **602**, 603f
Chlorophylls, 786
defined, 589
in photosynthesis, 589–593
light absorption by, 590, 590f
phytol, 589
structure of, 589
Chloroplasts
ATP synthase, 600–601
ATP synthesis in, 599–602
defined, 588
electron micrograph of, 588f
evolution of, 589
genome of, 589
in photosynthesis, 588–589, 588f
reaction center, 590–591, 591f
redox conditions, 601
structure of, 588, 588f
Cholecystokinin (CCK), 735, 735f, 735t
Cholera toxin, 344, 344f
Cholesterol
"bad," 832
carbon numbering, 834, 834f
defined, 355, 821
discovery of, 981
excess, effects of, 830, 830f
fatty acid chains and, 371–372, 372f
formation of, 825f
"good," 832
from lanosterol, **825f**

levels, clinical management of, 832–833
lipid rafts, 372–373, 372f
as membrane fluidity regulator, 371–372
in membrane lipid, 357–358, 821–823
as precursor, 833–841, 833f
as precursor for steroid hormones, 827, 834, 834f
as precursor for vitamin D, 839–840
structure of, 357–358, **357**
transport of, 827–829
Cholesterol homeostasis, 827
Cholesterol synthesis, 821–825, 822f
blocking of, 833, 981
condensation mechanism of, 823, 823f
defined, 822
isopentenyl pyrophosphate in, 822–823, 823f
liver in, 825, 828f
low-density (LDLs) in, 829–830
metabolism, 829–830
mevalonate in, 822, 822f, 823f, 827
as precursor for steroid hormones, 834, 834f
rate of, 825–827
regulation of, 825–833
site of, 827, 828f, 829
squalene in, 823, 824–825, 824f, 825f
stages of, 822–825
sterol regulatory element binding protein (SREBP) in, 825–827, 826f
Choline, 818
Chorismate in amino acid synthesis, 776–779, 777f
Chromatin, 961–967
defined, 893
in gene expression, 893, 961–967
higher-order, structure of, 958
histone tails and, 965–966, 965f
remodeling of, 961–967, 966f

structure of, **893f**
Chromatin-remodeling complexes, 966
Chromatography
affinity, 104–105, 104f, 110
gel-filtration, 103, 103f, 110
high-performance liquid (HPLC), 105, 105f
ion-exchange, 103–104, 104f
Chromogenic substrate, 182, 182f
Chromosomes
accessory, 272, 274
bacterial, 864, 864f
eukaryotic, 861, 861f, 863
in human genome, 283, 283f, 286f
yeast, 958
Chronic myelogenous leukemia (CML), 435, 435f
Chylomicron remnants, 828
Chylomicrons, 667–668, 668f, 828, 828t
Chymotrypsin
active site, 183f
catalysis kinetics, 182, 182f
catalytic mechanism, 181–182, 181f
catalytic triad in, 183–185
conformations of, 225, 225f
covalent catalysis in, 181, 181f, 183f
diisopropylphosphofluoridate (DIPF) and, 181–182, 182f
elastase and, 186, 186f
mammalian, 313
natural substrate for, 170, **170f**
oxyanion hole, 185, 185f
peptide hydrolysis by, 183, 184f
S_1 pockets of, 186f
serine residue, 181–182, 182f
specificity of, 181f
specificity pocket of, 185, 185f

structure of, 183–185, **313f**
substrate preferences of, 158–159, 158t
trypsin and, 186, 186f
Chymotrypsinogen
conformations of, 225, 225f
defined, 224
proteolytic activation of, 224f, 225–226
Ciproflaxin, 857, **857**
Circe effects, 159
Cirrhosis, 756
Cis configuration, peptide bonds, 44, 44f, 45f
Cis-acting elements, 896
Cisplatin, **871**
cis-Polyisoprene, **840f**
Citrate
in fatty acid metabolism, 690, 695f
in glyoxylate cycle, 537, 537f
isomerization of, 524–525, 525f
in isomerization reactions, 467
vs. phosphate, 459
phosphofructokinase inhibition by, 495
in polymerization, 695
synthesis of, 533
transport to cytoplasm, 533
Citrate synthase
in citric acid cycle, 522–523, 523f
conformational changes on binding, 523, 523f
defined, 523
mechanism of, 523–524, 524f
Citric acid cycle
acetyl CoA in, 502, 516, 518–520, 522–524, 524f, 535
aconitase in, 524–525, 525f
ADP in, 503
ATP in, 517, 526–531, 533, 534–535
biosynthetic roles of, 534–536, 534f

carbon oxidation in, 522–531
in cellular respiration, 516–517, 517f
citrate isomerization in, 524–525, 525f
citrate synthase in, 522–523, 523f
citryl CoA in, 522–524, 524f
components of, 530t
control sites of, 533, 533f
decarboxylation in, 518–519, 519f
defined, 516
entry to, 531–533
evolution of, 536
in exercise, 532
glycolysis and, 517–521, 518f
high-energy electron harvesting in, 516
illustrated, 529f
intermediates in, 534
isocitrate dehydrogenase in, 525, 533, 533f
isocitrate in, 524–525
α-ketoglutarate dehydrogenase complex in, 526, 533, 533f
α-ketoglutarate in, 525
ketone bodies in, 753–754, 754f
lipoamide in, 520–521, 522f
in mitochondria, 516, 516f
overview of, 459, 516–517, 517f
oxaloacetate in, 517, 522–523, 523f, 528–529, 534
oxidation by, 488
pathway integration, 535
pattern of, 517, 517f
phosphorylation in, 531–532, 532f
in photosynthesis. *See* dark reactions
pyruvate dehydrogenase complex in, 516, 517–521, 518f, 520f, 522f, 531–533, 531f, 532f
pyruvate dehydrogenase in, 531–533
pyruvate dehydrogenase phosphatase (PDP) in, 531

rate of the cycle, 533, 533f
reactions of, 528
regulation of, 531–532, 533, 533f
replenishment, 534–535
substrate channeling in, 530
succinate dehydrogenase in, 528–529
succinyl CoA in, 526–527, 527f
succinyl CoA synthetase in, 527
thiamine pyrophosphate (TPP) in, 518–519, 519f
Citrulline, 715–716, **715**
Citrullinemia, 727t
Citryl CoA (citryl coenzyme A), 522–524, 524f
Clamp loaders, 857–858, 859f
Clapham, David, 425b
Class I MHC proteins, 90, 90f
Classic galactosemia, 491
Clathrin, 375, 829
Clathrin-coated pit, 375
Cleavage
DNA. *See* DNA, cleavage of
protein, 121–123, 122f
Cleland, W. Wallace, 160
Clinical trials, 996–997, 997f
Cloned genes, 104–105
Clones, 113
Cloning
of cDNA, 394
expression, 279, 279f
plasmid vectors in, 274–275
in recombinant DNA technology, 277–278
Cloning vectors, 274
mutant λ phage as, 276, 276f
Clopidogrel (Plavix), 836, 836f
Closed promoter complex, 887, 887f

Clostridium perfringens, 488
Clotting. *See* Blood clotting
Clustered regularly interspaced palindromic repeats *See* CRISPRs
Coactivators, 965, 965f
Coat proteins (COPs), 942
Coated pits, 829
Cobalamin, 676–677, 676f, 677f, 678f. *See also* Vitamin B_{12}
Cobalt atom, 676–677
Cochlea, 440
Coding strand, 884
Codon-anticodon interactions, 921
Codons
    defined, 918
    maximizing number of, 921
    stop, 935–936, 935f
    in translation, 920–921, 921f
Coenzyme A, 462–463, **462f**, 486f
Coenzyme B_{12}, 676–677, **676f**, 677f, 678
Coenzyme Q, 528, 550, 551–552
Coenzyme Q_{10}, 840
Coenzymes
    defined, 144
    prosthetic groups, 144
    stoichiometric, 144
    types of, 144t
    vitamin, 463–464, 463t
Cofactors, 144
Cognate DNA, 194, 197–199, **198f**, 199f
Cohesive ends, DNA, 272–273, 273f
Coiled-coil proteins, 53, **53f**
Co-immunoprecipitation, 116, 117f
Colipase, 667
Collagen
    amino acid sequence of, 53–54, 54f

ascorbate and, 757
in cartilage, 340–341, 340f
defined, 53
structure of, **54f**
triple helix, 54
Color blindness, 442
Color vision, 440f
in animals, 442, 442f
cone receptors, 440
defective, 442
evolution of, 442, 442f
Combinatorial chemistry, 319, 982–983
Combinatorial control, 960
Committed step, 211, 494, 780, 780f
Common ancestor, 3, 3f, 25
Compactin, 981, **981**
Comparative genomics, 22–23, 22f
Compartmentalization, 468
Compartments, drug target, 990
Competitive inhibition. *See also* Enzyme inhibition
defined, 164–165
dissociation constant, 166–167
double-reciprocal plot, 156, 156f
kinetics of, 166–167, 167f
use of, 166
Complementarity-determining regions (CDRs), 86
Complementary DNA (cDNA)
cloning and sequencing of, 394
defined, 278
formation of, 278–279, 278f, 279f
screening of, 279, 279f
synthesis of, 289
Complementary sequences, 6, 6f
Complementary single-stranded ends, DNA, 272

Complex I, 549, 552, 553f, 559. *See also* NADH-Q oxidoreductase
Complex I mutations, 578
Complex II, 549, 553. *See also* Succinate-Q reductase
Complex III, 549, 554, 555f, 559. *See also* Q-cytochrome *c* oxidoreductase
Complex IV, 549, 556, 559. *See also* Cytochrome *c* oxidase
Complex V, 562
Concerted model
    allosteric enzymes, 215
    defined, 78, 215
    T and R states, 78f
    tetramers, 78–79
Condensing enzyme, 687
Cones, 438, 440, 442, 442f
Conformation selection, 151
Congenital disorders of glycosylation, 344–345
Congenital erythropoietic porphyria, 788
Congenital hemolytic anemia, 509
Congestive heart failure, 387
Conjugation in drug metabolism, 990–991, 991f
Connexin, 406
Connexons, 406
Consensus sequence, 220, 886
Conservative substitutions, 305, 307f, 308f
Conserved sequences, 886f
Constitutional isomers, 325, 326f
Controlled studies, 997
Controlled termination of replication, 267–268
Convergent evolution, 313, 313f
Cooperative binding
    concerted model, 78–79, 78f
    of oxygen, 76–77
    oxygen delivery and, 76–77, 77f
    sequential model, 78–79, 79f

Cooperative transition, 59
Copper ions in cytochrome c oxidase, 556
Coproporphyrin I, 788
Coproporphyrinogen III, 786, 787f
Core enzyme, 886
Corepressors, 955
Corey, Robert, 46
Cori, Carl, 509b, 661
Cori, Gerty, 509b, 661
Cori cycle, 509, 509f
Cori disease, 661t
Coronary artery disease, 830
Corrin ring, 676–677, 676f
Corticosteroids, 837, 837f
Corticosterone, **837f**
Cortisol, 222, 837, **837f**
Corynebacterium diptheriae, 943
Cotransporters, 390. *See also* Secondary transporters
Coulomb energy, 8
Coupled assays, 982, 982f
Coupling, 268
Covalent bonds
    in biological molecules, 7–8
    defined, 5
    multiple, 7–8
    as strongest bonds, 7–8
Covalent catalysis
    chymotrypsin as example, 181, 181f, 183f
    defined, 180
Covalent enzyme-bound intermediate, 481
Covalent modifications
    acetylation, 218, 219t
    common, 219t
    dephosphorylation, 218

in enzyme regulation, 218–223
irreversible, 218
phosphorylation, 219t
COVID-19, 26, 89, 437, 881. *See also* SARS-CoV-2
CpG island, 961
Crassulacean acid metabolism (CAM), 624, 624f
Creatine, **160**, **454**, **747**
Creatine kinase, 454
Creatine phosphate, 453–455, 454f, **454**, 747, 747t, **747**
Crick, Francis, 5, 6, 845
CRISPR-Cas system, 293, 294b, 294f, 868, 874
CRISPRs (clustered regularly interspaced palindromic repeats), 293, 294f
Cristae, 543, 565f
Critical Assessment of Structure Prediction (CASP), 61
Cro in genetic circuit formation, 957–958, 958f
Cross talk, 414
Cross-links, 43, 43f
Cross-peaks, 134
Crotonyl-CoA, **619**
Crown gall, 295
Cryo-crystallography, 938b
Cryo-electron microscopy (cryo-EM), 100, 135–136, 136f
Crystal violet dye, 373
CTP. *See* Cytidine triphosphate (CTP)
CTP-phosphocholine cytidylyltransferase (CCT), 818
C-type lectins, 347, 347f
Cumulative feedback inhibition, 781–782
Cumulative selection, 60
Cupriavidus necator, 606–607
Cushing syndrome, 222–223
Cushing's disease, 222–223
Cut and display, 89–90
Cyanide, 577, 577f

Cyanidiales, 317
Cyanobacteria, 589, 589f, 593
Cyanocobalamin, 676f, 677
Cyclins, 862–863
Cyclic AMP (cAMP)
activation of, 740
binding to regulatory subunit, 221
defined, 792
in eukaryotic cells, 221, 418
generation by adenylate cyclase, 418
in glycogen metabolism, 652–653, 657f
phosphorylation stimulation, 418
as second messenger, **413**, 424
in signal transduction, 412, 418–419
structure of, **221**
Cyclic electron flow, 592–593
Cyclic GMP (cGMP), **413**, 792
Cyclic nucleotides, 792
Cyclic photophosphorylation, 601, 601f
Cyclin-dependent protein kinases, 863
Cycloheximide, 943, 943t
Cyclooxygenase inhibitors, 366
Cyclooxygenases, 141
Cyclophosphamide, **871**, 991
Cys_2His_2 zinc-finger domains, 959
Cystathionase, 776
Cystathionine, 776
Cystathionine β-synthase, 776
Cysteine, **43f**, 719, 719f
in glycolysis, 483f
linked, 42
pyruvate formation from, 719f
structure of, **38f**, 39, **40t**, 41
synthesis of, 772, 776

Cysteine proteases, 188, 188f, **188f**
Cysteine thiyl radical, 803
Cystic fibrosis, 44, 341
Cystine, 43
Cytidine, 869f
Cytidine diphosphodiacylglycerol (CDP-diacylglycerol), **816**, 817, **817**
Cytidine monophosphate (CMP), 816, **817**
Cytidine triphosphate (CTP), 216f, 217f, 451
    ATCase inhibition by, 211, 211f, 807
    defined, 210, 211
    effect on ATCase kinetics, 216–217, 216f, 217f
    in pyrimidine synthesis, 796
    T state stabilization, 216, 216f, 217f
Cytidine triphosphate synthetase, 796
Cytochrome, in photosynthetic reaction center, 591f, 592–593, 593f
Cytochrome *b5*, 692–693, 693f
Cytochrome *bf* complex, 596, 596f, 605
Cytochrome *c*, in oxidative phosphorylation, 551, 551f
Cytochrome *c* oxidase, 549, 549f, 550t
    defined, 554
    electron flow in, 577
    heme, 557
    mechanism, 558, 558f
    peroxide bridge, 558, 558f
    proton transport by, 559, 559f
    in respiratory chain, 554–555, 556–559
    structure of, 557, 557f
    subunits, 556
Cytochrome P450, 865, 990, 990f
    defined, 835
    hydroxylation by, 834–836, 835f
    mechanism, 835
    protective function, 836, 836f
    research in, 836b

Cytochromes, 551
Cytoplasm, 502–503, 502f, 624, 641, 641f, 690, 690f
Cytoplasmic side, 544
Cytosine, **4**, **5**, **5f**, **783f**, 868–869
Cytoskeleton, 35, 206
Cytotoxic (killer) T cells, 86

D amino acids, 35, 35f
Dalgarno, Lynn, 930
Daltons, 43
Daly, Marie M., 357b
Dark reactions, 587
Darst, Seth, 881
Dawkins, Richard, 60
De novo pathways. *See also* Nucleotide synthesis
  defined, 792, 792f
  purine, 796f, 797, 797f, 798–799, 798f, 799t
  pyrimidine, 792, 792f, 796
Deamination
  agents, 865
  in amino acid degradation, 712
  example of, 865, 865f
  pyridoxal phosphate (PLP) in, 711
Death cap, 894f
Debranching enzyme, 646, 661
Decarboxylation
  in citric acid cycle, 518–519, 519f
  in gluconeogenesis, 502–503
  in pentose phosphate pathway, 624
  pyridoxal phosphate (PLP) in, 711
DeepMind, 61
Deficiency disorders, 63–64, 63f
Degrons, 704, 707
Dehydratases, 712
7-dehydrocholesterol (pro-vitamin D_3), 839–840, 839f

Deinococcus radiodurans, 864, 864f
Deleterious reactions, 480
Denaturation
of DNA, 17–18, 18f
of proteins, 56, 59, 59f, 162
Denisovans, 318, 319f
5′-deoxyadenosyl radical, 677, 677f

Deoxyguanylate, 801f
Deoxyhemoglobin
aβ dimers, 75
2,3-BPG binding to, 80f
carbon dioxide and, 82
defined, 78
quaternary structure of, **77f**, 78
structure of, 79f
Deoxymyoglobin, 73, **74f**
Deoxyribonuclease (DNase), 289
Deoxyribonucleic acid (DNA). *See* DNA
Deoxyribonucleoside 3′-phosphoramidites, 268, 268f, **269**

Deoxyribonucleoside triphosphate (dNTP), 847, 847f, 848, 848f
Deoxyribonucleotide synthesis
control of, 808–809
deoxyuridylate in, 804–805
dihydrofolate reductase in, 805
overview of, 801–802
ribonucleotide reductase in, 801–803, 802f, 804f, 808–809, 808f
thymidylate, 804–807, 805f, 806f
Deoxyribose, 4, 326f, 327
Deoxyribose phosphodiesterase, 867
Deoxyuridylate (dUMP), 804–805, 805f
Dephosphorylation, 218, 220, 221
Deprotonation
effect of buffer on, 193, 193f

water, kinetics of, 192f, 193
Designer genes, 281
Desmolase, 837
Desmopressin, 127f
Destroying angel, 894f
Development phase, of drug development, 978, 978f
α-dextrinase, 473
DHU loop, 919
Diabetes insipidus, 741
Diabetes mellitus
defined, 741
exercise and, 745
insulin in, 742–743
insulin resistance and, 741, 742–743, 743f
ketosis in, 682, 682f
monitoring of, 331
obesity and, 741–746
trans fats and, 679
type 1, 741, 746
type 2, 741, 743
Diabetic ketoacidosis, 682–683
Diabetic neuropathy (DN), 532–533
Diacylglycerol (DAG), 667f, 669, 743, 744f
in lipid synthesis, 815–816, 821
in signal transduction, 420–421, 420f
structure of, **413**
Diacylglycerol kinase, 815
Dialysis, 57
Dialysis in protein purification, 103, 103f
Diamond-Blackfan anemia, 938
Diastereoisomers, 325–326, 326f
Diazotrophic microorganisms, 764
Dicer, 972
Dictyostelium discoideum, 201, 201f

Dicyclohexylcarbodiimide (DCC), **128f**, 577
Diels-Alder reaction, 778
2,4-dienoyl CoA, 675, **675f**
Diet
    fatty acid metabolism and, 696
    ketogenic, 682
Differential centrifugation, 102, 102f
Diffusion
    facilitated, 382
    lateral, 369, 370, 370f
    lipid, 369
    membrane protein, 370
    simple, 382
    transverse, 370, 370f
Diffusion coefficient, 369, 370
Digestion
    of dietary proteins, 702, 702f
    enzymes in, 223, 224, 224f
    of lipids, 667–668, 667f
    proteolytic enzymes in, 223–228
Digestive enzymes, 63, 702
    chymotrypsinogen, 224–225, 224f
    synthesis of, 223
Digitalis, 387
Digitoxigenin, 387
Diglyceride acyltransferase, 816
Digoxin, 387, 387f
Dihedral angles, 45
Dihydrobiopterin, 723
Dihydrofolate reductase, 805
Dihydrolipoyl transacetylase, 518t, 520
Dihydropteridine reductase, 723
Dihydrotestosterone (DHT), 838
Dihydroxyacetone, 325, **325**, 326f
Dihydroxyacetone phosphate (DHAP), 332

in Calvin–Benson cycle, 616
in glycolysis, 466, 476f, 478, 479f, 489
in lipid synthesis, 815
structure of, **332**
Dihydroxyphenylalanine, **162**
Diisopropylphosphofluoridate (DIPF), 170, 170f, **170f**, 181–182, 182f
Dimerization arm, 431, 431f, 432f, 434
Dimethylallyl pyrophosphate, **823**
Dimethylbenzimidazole, 677
2,4-dinitrophenol (DNP), 577–578, **578**
2,4-dinitrophenylhydrazine, **727**
Dioxygenases, 724, 724f
Diphosphatidylglycerol, **356f**
Diphosphatidylglycerol (cardiolipin), 817, **817**
2,3-diphosphoglycerate (2,3-DPG). *See* 2,3-bisphosphoglycerate (2,3-BPG)
Diphthamide, 944, 944f
Diphtheria toxin, 943–944, 944f
Diplococcus pneumoniae, 280
Dipolar ions, 35
Dipoles, 9
Direct DNA repair, 867
Disaccharides
defined, 333
structure of, 333–334, 333f
types of, 333–334, 333f
Discovery phase, of drug development, 978, 978f
Diseases and disorders
albinism, 727t
alcaptonuria, 726
alcohol-related, 755–757, 757f
Alzheimer's disease, 62–63, 63f
amino acid sequences and, 44
amyotrophic lateral sclerosis (ALS), 271, 290

Anderson disease, 661t
anemia, 21, 83–84, 339
Angelman syndrome, 705
anthrax, 857
argininosuccinase deficiency, 717, 717f
arsenite poisoning, 535–536, 536f
atherosclerosis, 679, 827, 830–831, 832
autism, 705
B-cell leukemia, 898
beriberi, 535–536, 756
bronchitis, 341
Burkitt lymphoma, 898
cancer. *See* Cancer
carbamoyl phosphate synthetase deficiency, 717, 717f
carnitine deficiency, 672
cataracts, 491, 491f
cholera, 344, 344f
citrullinemia, 727t
congenital disorders of glycosylation, 344–345
congestive heart failure, 387
Cori disease, 661t
coronary artery disease, 830
Cushing syndrome, 222–223
cystic fibrosis, 44, 341
diabetes. *See* Diabetes mellitus
drug-resistant, 998–999
emphysema, 228
epigenetics and, 962
familial hypercholesterolemia, 830
galactosemia, 491
glucose 6-phosphate dehydrogenase deficiency, 634–636
glycogen-storage, 660–661, 661t, 749
gout, 810
Hartnup disease, 702

heart disease, 833, 981
hemolytic anemia, 634–635
Hers disease, 661t
HIV infection. *See* Human immunodeficiency virus (HIV) infection
homocystinuria, 727t
Huntington disease, 62, 703, 869
hyperammonemia, 717
hyperlysinemia, 727t
I-cell disease, 344–345
lactose intolerance, 492
Leber hereditary optic neuropathy (LHON), 578
Lesch-Nyhan syndrome, 810–811
long QT syndrome (LQTS), 404–405
Lynch syndrome, 870, 870t
maple syrup urine disease, 727
McArdle disease, 661, 661t, 749
mercury poisoning, 535–536
mitochondrial, 578–579
multidrug resistance in, 388–390
multiple myeloma, 113–114
mutations causing, 271–272
neurological, protein misfolding in, 62–63
ornithine transcarbamoylase deficiency, 717, 717f
osteoarthritis, 341
osteogenesis imperfecta, 54
Parkinson disease, 62, 703, 705, 817
phenylketonuria, 727–728
Pompe disease, 661, 661f, 661t
predisposition to, 23
protein aggregates in, 62–63
pyruvate carboxylase deficiency (PCD), 510–511
retinitis pigmentosa, 906
ricin poisoning, 944
rickets, 840

scurvy, 63, 756–757
severe combined immunodeficiency (SCID), 809–810
sickle-cell anemia, 21, 23, 44, 83, 83f
Tay-Sachs disease, 820–821
thalassemia, 906, 906f
triose phosphate isomerase deficiency (TPID), 509–510
tuberculosis, 538, 707
tyrosinemia, 727t
vitamin D deficiency, 464t, 840
von Gierke disease, 660–661, 661t
Wernicke-Korsakoff syndrome, 756
xeroderma pigmentosum, 870, 870t
Zellweger syndrome, 679
Dispensation sequence, 285
Displacement loop (D-loop), 873
Dissociation constant (K_d), 91–93, 92f, 95f, 157, 166–167, 986
Distal histidine, 74f, 79f, 82–83
Distant evolutionary relationships, 305–308
Distribution, drug, 989–990, 989f, 990f
Disulfide bonds
formation of, 43, 43f
reduction, 122–123, 123f
Dithiothreitol, 106
Diuron, **605**
Divergent evolution, 313
DNA
ancient, amplification and sequencing of, 318–319, 319f
bases in, 4, **4**, 11–12, 12f. *See also* Bases/base pairs
building blocks, 4–5
chemically synthesized linker, 274
coding strand of, 884
cognate, 194, 197–199, **198f**
cohesive ends, 272–273, 273f
complementary (cDNA), 278–279, 279f, 289, 394, 401

complementary single-stranded ends, 272
covalent structure, 4, 5f
damage to, 864–872, 864f
denaturation, 17–18, 18f
distortion of, 198, 199f
double helix of, 5, 6, 11–12, 17–18. *See also* Double helix
double-stranded, 282
electroporation and, 296, 296f
exchange between species, 317, 317f
fingerprint, 266
forensics and, 271, 271f
functions of, 2
heredity and, 6
ionic interactions, 11f
as linear polymer, 5f
linking number of, 852f, 853
methylation, 200
microinjection of, 288f, 289–290
promoter sites in, 882
proofreading of, 866–867, 866f
properties of, 4–6
proviral, 290
recombinant. *See* recombinant DNA technology
restriction fragment, 265–266
in storage of genetic information, 4, 6
structure of, 4–5, 6
sugars, 4
supercoiled, 851–857, 856f
synthesis of, 268–269, 268f
topoisomers of, 853, 853f
transferred (T-DNA), 296
unwinding of, 851–857, 882, 887, 887f, 888f
DNA, cleavage of, 272, 273f
by CRISPR-Cas system, 293, 294f

EcoRV endonuclease, 194
metal ion catalysis in, 196–197, 197f
restriction enzymes and, 194–200, 265–266
stereochemistry, 196, 196f
DNA fragments
covalent insertion of, 272
insertion and replication of, 274
insertional inactivation of, 274, 275f
joined by DNA ligases, 272
library of, 277–278, 277f
DNA gyrase, 857
DNA ligase, 867
defined, 849
DNA fragments joined by, 272
in DNA replication, 850, 862
in forming recombinant DNA molecules, 272–273
reaction, 849–850, 849f
DNA methylase, 200
DNA microarrays
defined, 288
gene-expression analysis with, 288–289, 288f, 289f
measuring gene expression using, 287f, 288
DNA photolyase, 867
DNA polymerase α, 862, 862t
DNA polymerase β, 862t
DNA polymerase δ, 862, 862t
DNA polymerase I, 846, **846f**, 859, 862t
DNA polymerase II, 862t
DNA polymerase III, 857–859, 857f, 858f, 862t
DNA polymerase switching, 862
DNA polymerases
common structural features, 846–847
defined, 846
DNA repair, 866–867

error-prone, 864–865
eukaryotic, 861–862, 862t
holoenzyme, 858, 859f, 860
mechanism, 846, 846f
metal ion catalysis in, 847, 847f
primer, 846, 848f
prokaryotic, 862t
proofreading activities, 866–867, 866f
specificity of, 847–848
structure of, 846–847, **846f**
template, 846
as template-directed enzymes, 846
types of, 862t
DNA probes
amino acid sequences in making, 124
defined, 266–267
generated from protein sequences, 277, 277f
as primer, 269
synthesis by automated solid-phase methods, 268–269
DNA recombination
in cell division, 874
defined, 872
functions of, 872–874
Holliday junctions in, 873–874, 873f
illustrated, 872, 872f
initiation of, 872–873, 873f
mechanism, 873, 873f
RecA in, 872–873
recombinases in, 873
strand invasion in, 872–873, 873f
synapse of, 874
DNA repair
base-excision, 867, 867f
direct, 867
double-strand, 868

in *E. coli*, 866–867, 867f
enzyme complexes in, 867f, 868
example of, 864, 864f
ligase in, 867
mismatch, 867, 867f
nonhomologous end joining (NHEJ) in, 868
nucleotide-excision, 868, 868f
overview of, 864, 864f, 866
proofreading in, 866–867, 866f
single-strand, 858–859
thymine in, 868–869
trinucleotide repeats and, 869, 869f
uracil DNA glycosylase in, 869
DNA replication, 6f, 846–851
ATP hydrolysis in, 850–851, 850f
cell cycle and, 861f, 862–863
clamp loaders in, 857–858, 859f
controlled termination of, 267–268, 267f
coordinated process in, 857–864
cross-linking in, 866, 866f
defective, in cancer, 869–871, 870t
DNA polymerase III in, 857–859, 859f
DNA polymerases in, 847, 860–861, 862t
in *E. coli*, 857, 860–861, 860f
errors in, 864–865
in eukaryotes, 861–862, 861f, 862f
in eukaryotic cell cycle, 862–863, 862t
helicases in, 850–851, 851f
lagging strand in, 849, 849f, 858–859, 858f
leading strand in, 849, 849f, 858–859, 858f
licensing factors in, 862
ligase in, 849–850, 849f, 862
minor-groove interactions in, 848, 848f
Okazaki fragments in, 849, 849f, 859

origin of, 860–861, 860f, 861f
origin of replication complexes (ORCs), 861–862, 861f
overview of, 846
polymerase switching in, 862
prepriming complex in, 860, 860f
primer in, 848, 848f
processivity in, 857–858
replication fork in, 849, 858, 858f, 859f
replicon, 861
RNA polymerases in, 848, 848f
shape complementarity in, 847–848, 848f
shape selectivity in, 848, 848f
sites of, 860–861
sliding DNA clamp in, 857–858, 857f
specificity of, 847–848
telomeres in, 863, 863f
template in, 846
termination of, 860, 861f
trombone model in, 859, 859f
tumor-suppressor genes in, 870
DNA sequencing, 123
amino acid sequences and, 123f
amplification by PCR, 269–270
ancient DNA, 318–319, 319f
by controlled termination of replication, 267–268, 267f
decreasing costs of, 22f
defined, 265
human migrations and, 23f
methods for, 21–22
next-generation (NGS), 284–286, 285f, 286f
pyrosequencing, 284
reversible terminator method, 285
semiconductor, 285, 286f
DNA vectors, 272, 274–276
DnaA, 860, 860f

DnaB, 858
DNA-binding domains, 960
DNA-binding proteins
basic-leucine zipper (bZip) in, 959, 959f
binding to regulatory sites in operons, 951–956
in eukaryotes, 958–960
helix-turn-helix motif in, 951, 951f
homeodomains in, 958, 958f
in prokaryotes, 950–956
symmetry matching in, 951
transcription inhibition by, 953
transcription simulation by, 955–956
zinc-finger domains in, 959, 959f
DNA-binding sites, 954f, 955, 961
DNA-encoded libraries, 984–985, 984f
Dolichol phosphate, **342**
Domains
acetyllysine-binding, 966, 966f
defined, 3
DNA-binding, 950–956, 958–960
homeodomains, 958, 958f
immunoglobulin, 86–87
nuclear-hormone receptor, 963–964, 964f
protein, 52, 52f
Doolittle, Russell, 318b
Dopamine, 785, 785f
Dopaquinone, **162**
Double helix, 5–6, 5f, 845
Acid–base reactions and, 17–18
base pairs, 11
destabilization, 17–18
as expression of rules of chemistry, 11–12
features of, 846
formation of, 6, 15–17, 15f
minor groove, 897

right-handed, 853
single-molecule methods of monitoring, 15–17, 15f, 16f
structure, 5, **5**
topoisomerases and, 853–854, 854f
in transcription, 897, 897f
unwinding of, 853–854
Double helix formation
from component strands, 5f, 6–7
entropy and, 14f
heat release in, 14–15
illustrated, 5f
principles of, 12
Double-blind studies, 997
Double-displacement reactions, 160–161
Double-reciprocal plot, 156, 156f, 167f
Double-stranded DNA, 282
Double-stranded RNA, 293, 294f
Doudna, Jennifer, 294b
Downstream core promoter element (DPE), 896
Doxycycline, 166
Drosophila melanogaster
bases and genes, 125
fluorescence micrograph of, 117f
in genetic studies, 866
genome of, 84, 283
Toll receptor in, 84
Drug candidates
absorption of, 988–989, 989f
ADME properties of, 988–989, 988f
administration routes for, 988–992
characteristics of, 986–995
distribution of, 989–990, 989f, 990f
effective concentrations of, 986–987, 987f
excretion of, 992
ligand binding in, 986, 986f

metabolism of, 990–991
oral bioavailability of, 988–989, 989f
potency of, 986–987
selectivity of, 986–987
side effects of, 987
therapeutic index of, 993
Drug development, 977–999
animal testing in, 993
clinical trials in, 996–997, 997f
combinatorial chemistry in, 982–983
criteria, 986–995
DNA-encoded libraries in, 984–985, 984f
high-throughput screening in, 981–982, 982f
lead molecules, 980–986, 982f, 984f, 985f, 994f
natural products in, 980–981
overview of, 978–980, 978f
phases of, 996–999
phenotypic screening approach, 985–986, 985f
screening libraries in, 982–983, 983f
serendipitous observations in, 979–980
split-pool synthesis in, 982–983, 983f, 984f
structure-based, 993–995, 994f
target-based screening approach, 985–986, 985f
Drug targets, 978–979, 978f
animal-model testing of, 993
compartments, 990
validation of, 978
Druggability, 978
Drugs
absorption of, 988–989, 989f
administration routes for, 988–992
delivery with liposomes, 361
discovery approaches, 978–986, 978f
distribution of, 989–990, 989f, 990f
excretion of, 992, 992f

half-life of, 992, 992f
metabolism of, 990–991, 991f
natural products in, 980–981
resistance to, 998–999
side effects of, 987
targets of, 978–979, 978f
therapeutic index of, 993
toxicity of, 992–993, 993f
Duodenum, 702
Dynamin, 375

E. coli. *See* *Escherichia coli (E. coli)*
E site, ribosomal, 929, 929f, 934
Ear, hair cells of, 440–441, 440f
EcoRV endonuclease
cleavage of DNA, 194, 196, 196f
magnesium ion-binding site in, 196–197, 197f
nonspecific and cognate DNA with, 199f
recognition site structure, 197f
twofold rotational symmetry, 197, 197f
Ectotherms, 162
Edman degradation, 120, 120f
Effective concentration, 986–987
EF-hand protein family, 423, 423f
EGF signaling, 431–433
Eicosanoids, 693–694, 693f, 694f
Elastase
blocking of, 228
catalytic triad in, 186, 187f
S_1 pockets of, 186f
Elasticity, 157
Electric dipoles, 9, 9f
Electrochemical potential, 383. *See also* Membrane potential
Electromagnetic radiation, and DNA damage, 866

Electron transfer
half-reactions in, 548
inhibitors, 577–578, 577f
in oxidative phosphorylation, 545–548, 561, 562f
in photosynthesis, 589–593
rate of, 561, 562f
uncoupling, 575–576
Electron-density maps, 131, 131f, 132f
Electron-proton transfer reactions, 553f
Electron-transferring flavoprotein (ETF), 672
Electron-transport chain, 517, 559, 559f
components of, 549f, 550t
defined, 543
in desaturation of fatty acids, 692–693, 693f
electron flow through, 543, 543f
FAD (flavin adenine dinucleotide) and, 517, 531
$FADH_2$ (flavin adenine dinucleotide reduced) and, 517, 531, 545, 553–554
inhibition of, 577
iron–sulfur clusters in, 551–552, 551f
NADH (nicotinamide adenine dinucleotide reduced) and, 517, 530, 545, 547, 548–549
oxidation by, 488
in oxidative phosphorylation, 543, 548–549, 569f
Electron-transport potential, 545
Electrophilic catalyst, 181
Electrophoresis
capillary, 268
gel, 105–107, 105f, 106f, 107f, 266–267, 266f, 363
SDS, 105f, 106–107
two-dimensional, 108–109, 108f, 109f
Electroporation, 296, 296f
Electrospray ionization (ESI), 118
Electrostatic repulsion, 453

Elion, Gertrude, 996b
Elongation factors
bacterial versus eukaryotic, 937
G (EF-G), 934, 934f
Ts (EF-Ts), 932
Tu (EF-Tu), 931–932, 931f
Elongation reactions, 692
Embden-Meyerhof-Parnas pathway, 473
Emphysema, 228
Enantiomers, 325, 326f
Endocytosis, 829
Endoplasmic reticulum (ER), 374, 374f
defined, 341
membrane, 692
protein glycosylation in, 341–342, 341f
protein synthesis in, 939–942
protein targeting from, 939–941
ribosome binding to, 939–942, 939f
rough, 939
smooth, 667, 668f, 939
stress in, 745
Endosomes, 376f
defined, 376, 829
LDL release in, 831, 831f
Endosymbiosis
mitochondria evolution from, 374
receptor-mediated, 375–376, 375f, 376f
Endosymbiotic event, 544–545
Endosymbiotic theory, 545
Endotherms, 162
Enediol intermediate in glycolysis, 479, 479f
Energy. *See also* Thermodynamics
activation, 148–149
binding, 151, 180

free. *See* Free energy
kinetic, 12
light, 606–607, 607f
potential, 12–13
status, 468
total, 12
Energy charge, 468f
defined, 468
in regulation, 575–576
Energy coupling agent, 481
Energy homeostasis. *See* Caloric homeostasis
Energy metabolism, 732–759
body weight regulation, 733–738
diabetes and obesity, 741–746
ethanol and, 755–759
exercise and, 746–752
fasted-fed cycle, 738–741
starvation, 752–754, 753t
Energy transfer
from accessory pigments to reaction centers, 603–604, 604f
resonance, 603–604, 603f, 604f
Enhancers
defined, 898, 962
experimental demonstration of, 963f
in gene expression, 962, 963f
probe for, 963f
in transcription, 898
Enol, 484
Enol intermediates, 524
Enol phosphate, 484
Enolase, 484
Enoyl CoA hydratase, 672–673
Enoyl reductase, 687
Ensemble studies, 163

Enterohepatic cycling, 992, 992f
Enteropeptidase, 226, 226f
Enterostatin, 735t
Enthalpy, 13
Entropy
    change during chemical reaction, 13
    double helix formation and, 14f
    overall, 14
    total, 13
Envelope form, 330, 330f
Enzymatic cascades, 228, 228f
Enzymatic velocity, 158
Enzyme inhibition
    affinity labels, 170, 170f
    competitive, 164–165, 167f
    by diisopropylphosphofluoridate (DIPF), 170, 170f
    illustrated, 170f
    irreversible, 164, 169–172
    mechanism-based (suicide), 171, 173f
    mixed noncompetitive, 166
    noncompetitive, 168
    pure noncompetitive, 166, 168f
    reversible, 164, 166–168, 166f, 167f
    by specific molecules, 164
    by transition-state analogs, 139f, 173f
    transition-state analogs in, 169
    type of, determining, 171b–172b
    uncompetitive, 166, 167f
Enzyme kinetics
    for allosteric enzyme, 161, 161f
    chymotrypsin, 182–183, 182f
    of competitive inhibitors, 166–167, 167f
    defined, 151
    in first-order reactions, 152
    Lineweaver-Burk plot, 156, 156f

maximal rate, 154–155, 156
Michaelis constant in, 154–157, 157t
Michaelis–Menten model for, 151–162, 167, 183
of noncompetitive inhibitors, 168, 168f
in pseudo-first-order reactions, 152
in second-order reactions, 152
sigmoidal, 212, 212f
specificity constant, 158–159
steady-state assumption and, 154–155
of uncompetitive inhibitors, 167–168, 167f, 168f
of water deprotonation, 192f, 193
Enzyme multiplicity, 781
Enzyme regulation, 210–232
by covalent modification, 218–223
of protein kinase A (PKA), 221–222, 222f
strategies, 210
Enzyme-linked immunosorbent assay (ELISA)
defined, 114
indirect, 115, 115f
sandwich, 115, 115f
Enzyme-pyridoxal phosphate complex (E-PLP), 710
Enzyme-pyridoxamine phosphate complex (E-PMP), 710
Enzymes, 34, 141–173
acceleration of reactions, 148–151
accessory enzyme systems, 692–694
activation energy and, 148, 148f, 149
active sites, 149, 150–151, 150f, 156
activity of, 101
allosteric, 161, 161f, 211. *See also* Allosteric enzymes
amount control, 210
amphitropic, 818
assay measurement of, 101
ATP hydrolysis and, 201
binding energy between substrate and, 151
branching, 655, 655f

catalytic activity, control of, 468
catalytic efficiency, 158–159, 158t
catalytic reaction, 149, 149f
in cellular respiration, 144
classes of, 143–144, 143t
cofactors for, 144, 144t
condensing, 687
debranching, 646, 661
defined, 142
digestive, 63, 223, 224–225, 224f, 702
energy-transducing, 14–15
ensemble studies, 163
free energy change, 145–147
Gibbs free energy and, 145–148
in gluconeogenesis, 535
of glycolysis, 474, 497
inhibition by molecules, 164–173
isozymes, 217–218, 218f
kinetic properties of, 151–162
kinetically perfect, 480
metabolism control of, 467
molecular dynamics, 165, 165f
multiple forms of, 210
overview of, 416
peptide-cleaving, 188–189
in photosynthesis, 144
as proteins, 142
proteolytic, 143, 210, 223–228
of purine nucleotide synthesis, 800
pyridoxal phosphate, 711–712, 712f
rate enhancement by, 142, 142t
reaction rate and, 148, 148f
regulatory, 821
restriction, 194–200, 265. *See also* Restriction enzymes (endonucleases)

reversible covalent modification, 210
from RNA, 912
single-molecule studies, 162–165, 163f, 164f
specificity, 142, 143f
spectroscopic characteristics of, 149
speed, 142
substituted intermediate, 161
substrate interaction, 150–151
temperature and, 161–162
ternary complex of, 159
transition state formation and, 148–151
turnover number of, 157, 157t
urea cycle, 716
Enzyme–substrate (ES) binding
in catalysis, 150–151
conformation selection, 151
induced-fit model of, 151, 151f
lock-and-key model of, 150–151, 151f
multiple weak attractions, 150
Enzyme–substrate (ES) complex, 168
defined, 149
diffusion-controlled encounter, 159
dissociation constant for, 157
evidence of existence, 149
fates, 153
formation in catalysis, 149, 149f
hydrogen bonds in, 150, 151f
reformed, 153
structure of, **150f**
Enzyme–substrate-inhibitor (ESI) complex, 167–168
Epidermal growth factor (EGF)
defined, 431
Ras activation and, 432, 432f
in signal transduction, 414f, 431–433
signaling pathway, 414f, 431–433, 432f, 433f

structure of, **430f**, 431
Epidermal growth factor receptor (EGFR)
defined, 432
dimerization of, 431f, 432
modulator structure of, 431f
overexpression of, 433
phosphorylation of carboxyl-terminal tail, 432
unactivated, structure of, 431f, 434
Epigenetics, 962
Epimers, 326f, 327
Epinephrine
defined, 414, 650
effects of, 221
in fatty acid metabolism, 695
in glycogen metabolism, 651–653, 651f, 656, 657f, 658, 658f
in signal transduction, 414–425, 414f, **414**, 416f, 419f
structure of, **650**
synthesis of, 783, 783f, 785f
Epitopes, 113
Equatorial bonds, 329–330, 329f
Equilibrium constant, 17
dissociation of water, 17
between enzyme-bound reactants and products, 204
metabolism and, 451
rate constants, 148
of reactions, 91–92, 146–147
standard free-energy change and, 147t
Equilibrium point, 148f
Equilibrium potential, 402, 402f, 403, 403b
Equilibrium reaction, 148
Erbitux, 996
Error-prone polymerases, 864–865
Erythromycin, 942–943, 943t
Erythropoietin (EPO), 339, 339f
Erythrose 4-phosphate, **627**, **628**

Escherichia coli (E. coli), 3
DNA polymerase I, 846, 846f
DNA recombination in, 872
DNA repair in, 866–867, 867f
DNA replication in, 857, 860–861, 860f
fatty acid synthesis in, 687
flagella movement of, 579–580
gene expression in, 950–956
genome of, 958
lac operon of, 953, 953f, 954f
membranes, 371
methionine repressor, 951, 951f
operons in, 955
primary RNA transcript, 898f
promoter sequences, 887f
pyruvate dehydrogenase complex in, 518t
RecA protein, 957
recombinant systems and, 112
restriction enzymes in, 194
ribonucleotide reductase of, 803
ribosomes in, 926
RNA polymerases in, 881, 881t, 882, 887f, 890
RNA sequence alignments, 314, 314f
sigma factors in, 890–892
translation in, 917
two-dimensional electrophoresis and, 108
Essential amino acids, 768f, 768t
defined, 702, 768
pathway steps, 768–769, 768f
table of, 702t
Estradiol
binding of, 70–71, 93–94, 93f
precursors, 838, 838f
receptors for, 71f

structure of, **70f**, **71**, **838f**, **963**
Estrogen response elements (EREs), 963–964
Estrogens
defined, 834
nuclear hormone receptors and, 963–964
pathways for formation of, 838f
receptors for, 70–72, 71f, 72f, 93–94, 93f, 95f
synthesis of, 837–838, 838f, **838f**
Estrone, 70, **70f**, 838, **838f**
Ethanol
cancer and, 758–759
fermentation of, 473f, 486–487
formation of, 486f
in glycolysis, 473
metabolism, 755–759
vitamin metabolism and, 756–757
Ethanolamine, 817–818, **818**
Eukarya, 3, 3f
Eukaryotes
ABC transporters in, 390
chromatin and, 893, 893f
chromosomes, 861, 861f, 863
defining characteristics, 3
DNA replication in, 861–862, 861f, 862f
DNA-binding proteins in, 958–960
fatty acid synthesis in, 687
gene expression in. *See* Gene expression (eukaryotes)
genomes of, 282–283
glycolysis in, 473, 476–477
membranes, 373–376
new genes, expression of, 289–290
nuclear envelope, 374, 374f
oxidative phosphorylation in, 543–544
photosynthesis in, 588–589, 593
primary transcripts in, 901f

promoters in, 895f
protein synthesis inhibition in, 943–944
ribosomes, 936–937
RNA polymerases in, 881, 881f, 894–895, 894t, 896f
RNA processing, 892–893, 908, 908f
transcription factors in, 896–898, 897f, 958–960
transcription in. *See* Transcription in eukaryotes
translation in, 892, 892f, 936–937, 937f
translation initiation in, 936–937, 937f
Eukaryotic cell cycle, 861f, 862–863
Eukaryotic genes
organization of, 958
quantitation and manipulation of, 287–296
Eukaryotic RNA polymerases, 881, **881f**
Eversion, 386
Evolution
of amino acid sequences, 44
of aminoacyl-tRNA synthetases, 926
ancient DNA amplification and sequencing in, 318–319, 319f
of blood types, 344
caloric homeostasis and, 734
of carbonic anhydrases, 193
of chloroplasts, 589
of citric acid cycle, 536
of color vision, 442, 442f
comparative genomics and, 25–27
convergent, 313, 313f
divergent, 313
of DNA-binding sites, 955
of drug resistance, 998–999
of globins, 316, 316f
of glycolysis, 511
of immune system, 84–86
in laboratory, 319, 320f
of metabolism, 468

molecular, 271, 318, 319–321
obesity and, 734
of proteasomes, 707, 707f
of sensory systems, 441–442, 441f
of vitamins, 464
Evolutionary relationships, 301, 302
distant, 305–308
three-dimensional structures and, 310–315
Evolutionary trees, 316–318, 316f
Excinuclease, 868
Excretion, drug, 992, 992f
Exemestane, 838, **839f**
Exercise
aerobic, 747
anaerobic, 747
ATP in, 454–455, 455f, 498–499, 747–749, 747t
caloric homeostasis and, 752b
citric acid cycle in, 532
creatine phosphate in, 747, 747t
diabetes and, 745
effects on muscle and whole-body metabolism, 750–751, 751t
energy metabolism and, 746–752
fatty acid metabolism in, 748, 750
fuel sources for, 746–750, 747t
gene expression in, 750, 751
glycolysis during, 499
long-distance running, fuel for, 748–749
middle-distance running, fuel for, 747–748
mitochondrial biogenesis and, 749–750, 750f
molecular adaptation to, 750–751, 750f
oxidative phosphorylation in, 747–749
oxygen concentration and, 77f
in proteins phosphorylation, 223
reactive oxygen species and, 561
running velocity, 748, 748f

sprinting, fuel for, 747
Exercise is Medicine initiative, 751
Exons, splicing, 901, 902f
Exonuclease, 846
Expression cloning, 279, 279f
Expression vectors, 275, 275f
Expressome, 935
Extracellular signal-regulated kinases (ERKs), 433
Extrinsic pathway, clotting, 228

2-^{18}F-2-D-deoxyglucose (FDG), 497, 498f

F_{ab} fragments, 87–88, 87f, 88f
Facilitated diffusion, 382
Facultative anaerobes, 488
FAD (flavin adenine dinucleotide)
as catalytic cofactor, 518
defined, 460
electron transfer potential of, 520
electron-transport chain and, 517, 531
structure of oxidized form, **461f**
structure of reactive components of, 461, **461f**
$FADH_2$ (flavin adenine dinucleotide reduced), 672–673
defined, 460
electron-transport chain and, 517, 531, 545, 553–554
structure of reactive components of, 461, **461f**
Familial hypercholesterolemia, 830–831, 832
Faraday constant, 383, 546
Farnesene, 841, 841t, **841**
Farnesyl pyrophosphate, 823, 824f, **824f**
Fast twitch muscle fibers, 487, 493
Fasted state, 739–740
Fasted-fed cycle, 738–741
defined, 738
postabsorptive state, 739–740

postprandial state, 739
refed state, 741
Fasting, 753
Fast-twitch muscle fibers, 649, 747
Fat
in adipose tissue, 748
body, energy storage in, 666
brown, 576
as fuel, 457f
neutral. *See* triacylglycerols
Fat cells, 666
Fatty acid chains
cholesterol and, 371–372, 372f
melting temperature, 371, 371t
packing of, 371, 371f, 372f
Fatty acid metabolism, 665–696
acetyl carnitine in, 671–672
acetyl CoA carboxylase in, 685, 694–696, 694f, 722
acetyl CoA in, 532, 670–671, 672–673, 690, 690f, 691
activation in, 670–671
acyl carrier protein (ACP) in, 685, 686f, 689, 689f
acyl CoA synthase in, 672
β-oxidation pathway in, 672f
chylomicrons in, 667–668, 668f
citrate in, 690, 695f
coenzyme B_{12} in, 676, 677f
degradation in, 667, 667f, 672f, 679f, 683–692
diet and, 696
enoyl CoA hydratase in, 672–673, 674f
epinephrine in, 695
in exercise, 748, 750
FADH2 in, 672–673
glucagon in, 695
hormones in, 693–694

inhibition of by NADH, 755
insulin in, 696
ketone bodies in, 679–683
lipases in, 668–669
lipid mobilization and transport in, 667–668, 668f
lipolysis in, 669, 670f
malonyl CoA in, 685, 695
methylmalonyl CoA in, 677–678, 678f
NADH in, 672–673
NADPH sources for, 691
overview of, 665
oxidation in, 669–670, 671–674, 673t, 678–679
palmitoyl CoA in, 674, 674f, 695
pancreatic lipases in, 667, 667f
pathway integration, 691, 691f
peroxisomes in, 678–679, 679f
phosphatidate and, 815–821, 815f
steps in, 667f
triacylglycerols in, 666–668, 669f
in tumor cells, 691–692
Fatty acid synthase
catalytic cycle of, 689, 689f
defined, 683, 685, 686
structure of, 688, 688f
Fatty acid synthesis
in animals, 687–689
in cytoplasm, 690, 690f
degradation versus, 684–685, 684f
by fatty acid synthase, 683–692
glucagon and, 740
malonyl CoA in, 685
maximal, 695
reactions in, 684–689, 686t, 687f
steps in, 667f, 686–687, 686t, 687f
Fatty acid thiokinase, 673t. *See also* Acyl CoA synthetase

Fatty acids
animals and, 683
β oxidation of, 753
chain length in, 354, 688
cholesterol and, 371–372, 372f
defined, 353
degree of unsaturation, 354, 371
derivatives, 665
desaturation of, 692–693, 693f
as fuel, 665, 668–674
generation by lipolysis, 670, 670f
in lipids, 353–354, 353f, 354t
in membrane lipids, 353–354, 353f, 354t
in muscle, 743–744, 748
naturally occurring, 354t
in obesity, 743–744, 744f
odd-chain, 675–676, 677f
pathological conditions by, 679
physiological roles of, 665
polyunsaturated, 674–675, 675f, 679, 693–694
saturated, 679
structures of, 353f, 354
unsaturated, 674–679, 674f, 675f, 692–694
Fatty liver, 755–756
Fatty-acid binding proteins (FABPs), 667
Fatty-acid transport proteins (FATPs), 667
Favism, 634
F_c fragment, 87f, 88
Feedback inhibition, 211, 468
in amino acid synthesis, 780–783, 780f
cumulative, 781–782
enzyme multiplicity and, 781
in nucleotide synthesis, 807–809
in purine synthesis control, 807–808, 808f

Feedforward activation, 494
Feedforward stimulation, 494
Fehling's solution, 331
FeMo cofactor, 765–766, 765f
Fermentation
of alcohol, 472, 486–487
as anaerobic process, 488
defined, 486
in glycolysis, 486–487
to lactic acid, 473, 487, 487f
starting and ending points, 488t
Ferredoxin, 597–598, 597f, 602, 765
Ferredoxin-$NADP^+$, 597f, 598
Ferredoxin-$NADP^+$ reductase, 598, 598f
Ferredoxin–thioredoxin reductase, 601
Ferritin, 48, 48f, 786, 970, **970f**
Ferrochelatase, 786
Fetal hemoglobin, 81, 81f
Fiber types, muscle, 649, 649t
Fibrils, 336
Fibrin, 229–230, 230f
Fibrin clots, 229–230, 230f
Fibrin monomer, 230
Fibrinogen
conversion by thrombin, 229–230
structure of, 229, **229f**
Fibrinopeptides, 230
Fibronectin, 370
Fibrous proteins, 53–54
Fidelis, Krzysztof, 61
50S subunit of ribosomes, 927, 927f, 929f, 931–932, 933, 935
Fight-or-flight response, 412, 414, 785
Filgrastim, 995
Fingerprint, DNA, 266

First Law of Thermodynamics, 12–13, 734
First-order reactions, 152
First-pass metabolism, 990
Fischer, Emil, 150, 993
5′ cap, 900–901, 902f

Five-carbon units, 840–841
Flagella
    bacterial, 579–580, 579f
    rotary movement of, 579–580
    structure of, 580, 580f
Flagellar motor
    components of, 580, 580f
    rotation of, 579–580
    schematic view of, 580f
    structure of, 580f
Flagellin, 579f
Flavin adenine dinucleotide (FAD), 867
Flavin mononucleotide (FMN), 461, 461f, 552, 552f, 891–892, 891f
Flavoproteins, 520, 553–554, 679, 679f
Fleming, Alexander, 979
FliG protein, 580
FliM protein, 580
FliN protein, 580
Flip-flop, 370, 370f
Flippases, 388
Florey, Howard, 979
Fluconazole, 990f
Fluid mosaic model, 370
Fluorescence microscopy, 117–118, 117f, 207, 207f
Fluorescence recovery after photobleaching (FRAP), 369, 370f
Fluorouracil, 806, 806f
Folding funnel, 60, 61f
Folic acid, 463t
Food production, 604

Foodstuffs, energy extraction from, 459, 459f
Formylglycinamidine ribonucleotide, 798
N-formylkynurenine, 724f, **724**
N-formylmethionine (fMet), 930–931
Formylmethionyl (fMet) peptide, **126**
Formylmethionyl-tRNA, 930, 930f
Formyltetrahydrofolate, 798, 798f, 799
43S preinitiation complex (PIC), 936
Fossil record, 316
Fourier transform, 131
Foxglove, 387, 387f
Fractional saturation, 73
Fragile X mental retardation protein (FMRP), 938
Framington Heart Study, 981
Franklin, Rosalind, 5, 129b
Frataxin, 552
Free energy
    ATP and, 449–456
    change during chemical reaction, 145–147, 455b–456b
    defined, 13
    Gibbs, 13, 145–148
    in membrane transport, 382–383, 382f
    negative, 14
    of oxidation of single-carbon compounds, 456, 457f
    in oxidation–reduction reactions, 546, 547–548
    of phosphorylated compounds, 454t
    of phosphorylation, 221
    standard change, 146–147
    standard free-energy change and, 147b
    thermodynamics of metabolism and, 449
Free radicals. *See* Reactive oxygen species (ROS)
Friedreich's ataxia, 552
Fructofuranose, 327–328, 328f
Fructokinase, 489–490

Fructopyranose, 328f, 329
Fructose, 325, 326f, 327
excessive consumption of, 489
in glycolysis, 489–490, 489f
metabolism, 489–490, 489f
ring structures, 327, 328f
Fructose 1,6-bisphosphate, 740, 740f
in gluconeogenesis, 500f, 503
in glycolysis, 466, 476f, 477, **477**
Fructose 1-phosphate in glycolysis, 489, 489f
Fructose 2,6-bisphosphate (F-2,6-BP), 740
activation of phosphofructokinase by, 495, 496f
in gluconeogenesis, 505f, 506–507, 506f, 507f, 508
in glycolysis, 495, 496f
regulation of phosphofructokinase by, 495, 495f
Fructose 6-phosphate, 619f, 740f
in Calvin–Benson cycle, 615, 615f, **616f**, 618, 619f
in gluconeogenesis, 500f, 503
in glycolysis, 477, **477**, 495
in pentose phosphate pathway, **627**, **628**
phosphorylation of, 477
Fructose bisphosphatase 2 (FBPase2), 506
Fucopyranose, **332f**
Fuel reserves in human body, 752, 752t
Fumarase, 528
Fumarate
in amino acid degradation, 718, 719f
in oxidation-reduction reactions, **465**
from phenylalanine, 724, 724f, **724**
in purine synthesis, 799
in urea cycle, 715, **716**
4-fumarylacetoacetate, 724, **724**
Functional groups, of proteins, 34
Fungi, polysaccharides of, 336–337, 337f

Funny current (I_f), 405
Furan, 327
Furanose, 327, 328, 328f, 329–330
Futile cycles, 508

G elongation factor (EF-G), 934, 934f
G proteins
  activation of, 415–418, 417f, 439f
  adenylate cyclase and, 423–424
  ATP synthase and, 569
  defined, 416
  in glycogen metabolism, 651–653
  heterotrimeric, 415–418, 417f
  resetting of, 419–420, 419f
  role in signaling pathways, 416
  seven-transmembrane-helix (7TM) receptor and, 424–425, 425f
  in signal transduction, 415–418, 417f
  small, 432
  subunits, 416, 417f, 424, 424f
Gain, 653
Galactitol, 491
Galactokinase, 490, 491
Galactolipids, 588
Galactose, 164f, 326f, 327
  defined, 490
  in glycolysis, 489f, 490–491
  missing transferase and, 491
  ring form, 329f
  structure of, **164**
Galactose 1-phosphate uridyl transferase, 491
Galactosemia, 491
β-galactosidase, 164, 165f, 274, 274f, 334, 951–952, 952f
β-galactosides, 954
Galacturonic acid, **336**

Galdieria sulphuraria, 317, 317f
Gamma helix, 46
Gamma phosphoryl group, 201–202
Gangliosides, 820f
    disorders of, 820–821
    structure of, 819f, **820**
    synthesis of, 819, 819f
Gap junctions, 406–407, 406f, 407f
Gas-phase ions, 118
Gastric H^+–K^+ ATPase, 384
Gastric inhibitory peptide, 735t
Gastrointestinal peptides, 735t
Gate opening, 706
Gatto, Gregory, 29
GC box, 896, 896f
GDP (guanosine diphosphate)
    in citric acid cycle, 526–527
    hydrolysis of, 451
    in olfaction, 436
    in signal transduction, 416, 432, 432f
    in translation, 932
    in vision, 439
Gel electrophoresis
    defined, 106
    isoelectric focusing and, 107–108, 108f
    polyacrylamide, 105f, 106–107, 106f
    protein separation by, 105–107, 105f, 106f, 107f
    restriction fragments separation by, 266–267
    SDS, 105f, 106–107
    SDS-PAGE, 106–107, 108
    two-dimensional electrophoresis and, 108–109, 108f, 109f
Gel-filtration chromatography, 103, 103f, 110
Gellert, Martin, 854
Gene disruption, 290–294, 292f, 294f

consequences of, 290–291, 291f
defined, 290
by homologous recombination, 290–291, 291f
Gene expression
analysis with microarrays, 288–289, 288f, 289f
bacterial, 935, 950–951
chromatin in, 893, 961–967
constitutive, 950
control of, 938, 949–972
epigenetics and, 962
exercise and, 750, 751
levels of, 287–289
methylation in, 961–962
nuclear hormone receptors in, 963–965
regulated, 950
regulatory circuits, 956–958
ribosomes and, 938
transcription factors in, 958–960
transcriptional, 935, 950
transcriptional, in eukaryotes, 967–972
transcriptional, in prokaryotes, 967–969
translational, 935, 970–971
Gene expression (eukaryotes), 958–960
activation domains in, 960
basic-leucine zipper (bZip) in, 959, 959f
chromatin remodeling in, 961–967
coactivators in, 965, 965f
combinatorial control in, 960
DNA methylation and, 961–962
DNA-binding structures in, 958–960
enhancers in, 962, 963f
homeodomain in, 958, 958f
hypomethylation in, 961
mediator in, 960, 960f
nuclear hormone receptors in, 963–965, 964f

overview of, 958
posttranscriptional, 970–971
at posttranscriptional level, 969
versus in prokaryotes, 958
regulation of, 958–960
transcription factors in, 958–960
zinc-finger domains in, 959, 959f
Gene expression (prokaryotes), 950–951
attenuation in, 967–969, 968f
catabolite activator protein (CAP) in, 955–956, 955f, 956f
catabolite repression in, 955
chromatin remodeling in, 966f
corepressors in, 955
DNA-binding proteins in, 950–951
DNA-binding sites in, 955, 955f, 956f
versus in eukaryotes, 958
helix-turn-helix motif, 951, 951f
lac operon in, 953, 953f
lac repressor in, 950, 953, 953f, 954f
λ repressor in, 957–958, 957f, 958f
ligand binding in, 954
operon model, 953
overview of, 949
posttranscriptional, 967–972
pur repressor in, 955, 955f
regulatory sites in, 950–951
RNA in, 880–881
symmetry matching in, 950–951
transcriptional, 950–951
"Gene guns," 296
Gene knockdown, 295
Gene knockout. *See* Gene disruption
Gene therapy, 296
Gene transfer, horizontal, 317–318, 317f

General acid–base catalysis, 180
General transcription factors, 898
Genes
cloned, 104–105
comparative analysis of, 286–287
designer, 281
horizontal transfer, 317–318, 317f
number of, in human genome, 283
protein-coding, 25
regulator, 952
reporter, 274
structural, 952
synthesis by automated solid-phase methods, 268–269
tumor suppressor, 870
Genetic code, aminoacyl-tRNA synthetases and, 921–926
Genetic recombination, 872. *See also* DNA recombination
Genetically modified organisms (GMOs), 296
Genomes
analysis of, 284–287
of *Arabidopsis thaliana*, 283
of *Caenorhabditis elegans*, 283
of chloroplasts, 589
comparative, 25–27, 286–287, 286f
complete, 282f
defined, 125
of *Drosophila melanogaster*, 84, 283
editing, 291–294, 292f
eukaryotic, 282–283
of *Haemophilus influenzae*, 282, 282f, 309
human, 283–284, 283f, 286–287, 286f
long interspersed elements, 284
of mice, 286f
of mitochondria, 544–545
next-generation sequencing, 284–286, 285f, 286f

noncoding DNA in, 284
number of genes in, 283
protein encoding, 25
proteome as functional representation, 125–126
of puffer fish, 286–287
of *Reclinomonas americana*, 545
of *Rickettsia prowazekii*, 545
of *Saccharomyces cerevisiae*, 283, 958
sequencing of, 21–22, 282–287
Genomic library, 277–278, 277f, 278f
Genomic variation, 22–24, 23f
Genomics
comparison, 22–23, 22f
revolution, 21–27
Gentamycin, 942
Geraniol, **436**
Geranyl pyrophosphate, 823, 823f
Geranyl transferase, 823
Ghrelin, 735t, 736
Gibbs, Josiah Willard, 13
Gibbs free energy, 13, 145–148
Gibbs free energy of activation, 148
Gigaseal, 393
Gilman, Alfred, 425b
Gla domain in prothrombin, 229, 229f
GlcNAcase, 339
Gleevec (imatinib mesylate), 435, 435f
Globin fold, 75
Globins. *See also* Hemoglobin; Myoglobin
defined, 303
evolution of, 316, 316f
sequence alignment in, 303–305
Globular proteins, 51–52
Glomeruli, 992

Glucagon
defined, 650
in essential enzyme regulation, 507–508, 507f
excess in type 1 diabetes, 746
in fatty acid metabolism, 695
in glycogen metabolism, 651–653, 656, 657f, 658, 658f
liver and, 739–740
in postabsorptive state, 739–740
secretion of, 735
Glucagon-like peptide 1 (GLP-1), 735, 735f, 735t
Glucocorticoids, 834
Glucogenic amino acids, 718, 719f
Glucokinase, 495–496, 739
Glucokinase regulatory protein (GKRP), 496
Gluconeogenesis, 499–504
acetoacetate in, 753–754
decarboxylation in, 502–503
defined, 473, 499
energy change and, 501
energy charge and, 505–506
evolution of, 511
fasting and, 753
fructose 1,6-bisphosphate in, 500f, 503
fructose 2,6-bisphosphate in, 505f, 506–507, 506f, 507f, 508
fructose 6-phosphate in, 500f, 503
glucagon and, 740
glucose 6-phosphate in, 500f, 503–504, 504f, 646, 648
glucose generation and, 503–504, 504f
glycolysis and, 499–501, 505–511, 505f
hormones in, 507–508
in liver, 499, 503, 506–508, 753
in muscle contraction, 508–509, 509f, 510f
overview of, 473–474, 499
oxaloacetate in, 499–503, 500f, 502f
pathway integration, 509, 510f

pathway of, 499, 500f
phosphoenolpyruvate (PEP) in, 500f
phosphorylation in, 502–503, 507
protein metabolism and, 725
pyruvate conversion in, 501–502, 502f
reactions of, 504t
reciprocal regulation in, 505–510, 505f
regulation of, 505–510, 505f, 740f, 746
stoichiometry of, 504
substrate cycles in, 508, 508f
urea cycle in, 716
Gluconeogenic pathway, 680
Glucophage, 745
Glucopryanose, 327–328, **327**
Glucose, 326f, 327
in brain, 740
as cellular fuel, 473
characteristics of, 473
complete oxidation of, 573–574, 574t
conversion into pyruvate, 485–486
as essential energy source, 325, 330
formation of, 473, 740
generation from glucose 6-phosphate, 503–504, 504f
generation of, 473–474
in glycogen, 335, 335f, 640, 641–642
homopolymers of, 335
levels of, 425f
in liver-glycogen metabolism, 659–660
metabolism, 447f, 473f
in postprandial period, 739
as reducing sugar, 330–331
in refed state, 741
ring form, 329f
storage forms of, 335, 335f
structure of, **2**, **327**

synthesis from noncarbohydrate precursors, 499–504
transporters, 474, 474t
Glucose 1-phosphate in glycogen metabolism, 642–643, **643**, 646
Glucose 6-phosphate dehydrogenase (G6PD), 626
deficiency, 635–636
in pentose phosphate pathway, 634–636
in reactive oxygen species protection, 634–636
Glucose 6-phosphate (G-6P), 332, **332**, 739, 740
galactose conversion into, 490–491
in gluconeogenesis, 500f, 503–504, 504f, 646, 648
in glycolysis, 476, **477**, 494, 495f
isomerization of, 477
in liver, 646–647, 661
metabolism of, 631–634, 641–642, 642f
in pentose phosphate pathway, 624, 631–634
transporter, 661
Glucose homeostasis
blood, 334
defined, 739
in diabetes, 741–746
starvation and, 752–754, 753t
Glucose transporters (GLUTs), 498, 498t, 742
Glucose-alanine cycle, 713, 713f
α-1,6-glucosidase, 661
α-1,6-glucosidase in glycogen metabolism, 645, 645f
Glutamate, **160**
chirality of, 767f
formation of, 708, 713, 720, 720f, 769–770
in nitrogen fixation, 766–767
oxidative deamination of, 708–709
structure of, 39, **39f**, **708**
synthesis of, 766–767, 771, 773f
Glutamate dehydrogenase, 708–709, 766–767
Glutamate synthase, 767
Glutamic acid, 39, **40t**

Glutamine, 766–767
carbon monoxide poisoning and, 83
in citric acid cycle, 535
degradation of, 720
in nitrogen transport, 713
in pyrimidine synthesis, 794, 794f
structure of, **38f**, 39
synthesis of, 766–767, 771
Glutamine phosphoribosyl amidotransferase, 797
Glutamine synthetase, 713, 767
in amino acid synthesis, 782–783, 782f
regulation of, 782–783, 782f
structure of, 782–783
Glutathione, 634
conjugation reaction, 991, **991f**
defined, 783–784
structure of, **784f**
Glutathione peroxidase, 635, 784, **784f**
Glutathione reductase, 635, 784
Glycan-binding proteins, 346
Glycated hemoglobin, 331
Glycation, 331
Glyceraldehyde, 325, **325**, 326f, 489
Glyceraldehyde 3-phosphate dehydrogenase (GAPDH), 480–481, 482f, **482f**, 483f, 622
Glyceraldehyde 3-phosphate (GAP), 332, **332**
in Calvin–Benson cycle, 615
catalytic mechanism of, 482
free-energy profiles for, 481, 481f
in fructose metabolism, 489
in glycolysis, 466, 476f, 478, 479f, 480–481, 480f, 481f
NADH generation, 487, 487f
oxidation of, 457–458, 482
in pentose phosphate pathway, 626, **627**, **628**
structure of, **457**

Glycerol
generation by lipolysis, 670, 670f
in gluconeogenesis, 499
in liver, 669–670
in phosphoglycerides, 356
release of, 740
structure of, **2**
Glycerol 3-phosphate, 739
in lipid synthesis, 815
reoxidation of, 571
Glycerol 3-phosphate shuttle, 570–571, 570f
Glycerol phosphate acyltransferase, 815
Glycine, 719, 719f
in Calvin–Benson cycle, 614f, 615
collagen chain and, 54, 54f
conversion into serine, 719, 719f
defined, 36
in liposomes, 360, 360f
porphyrins from, 786–787
pyruvate formation from, 719, 719f
structure of, **37f**
synthesis of, 772
Glycine cleavage enzyme, 774
Glycine synthase, 774
Glycine-glycine-glutamine (GGQ) sequence, 936
Glycobiology, 347b
Glycocholate, 667f, **833f**
Glycoforms, 338
Glycogen
branch point in, 335f
defined, 335, 640
glucose storage in, 335, 335f, 640, 641–642
in glycogen metabolism, 344–345, 651f, 652f
in liver, 641, 641f, 651, 740, 741
molecules, 640, 641f, 655f

in muscle, 641, 641f
phosphorolytic cleavage of, 643–645
remodeling, 645, 645f
storage efficiency, 656
storage sites of, 641, 641f
structure of, **336f**, **641f**, **643**
Glycogen lakes, 661f
Glycogen metabolism, 640–661
branching enzyme in, 655, 655f
cAMP in, 652–653, 657f
coordinate control of, 656, 657f
degradation of, 641–642
enzyme breakdown, 642–647
epinephrine in, 651–653, 651f, 656, 657f, 658, 658f
G proteins in, 651–653
glucagon in, 651–653, 656, 657f, 658, 658f
α-1,6-glucosidase in, 645f
glycogen in, 344–345, 651f, 652f
glycogen phosphorylase in, 642–643
glycogen synthase in, 654–655, 655f
glycogen synthase kinase (GSK) in, 655–656, 657f
glycogenin in, 654
hormones in, 651–653, 651f, 656–661, 657f
insulin in, 658–659, 659f
in liver, 646–647, 659–660, 659f, 660f
overview of, 640–642
pathway integration, 652f
phosphoglucomutase in, 646, 646f, 647f
phosphoglycerate mutase in, 646
phosphorolysis in, 642–645
phosphorylase in, 642–647, 645f, 659, 659f, 660f
protein kinase A (PKA) in, 651, 652f, 656, 657f, 658f
protein phosphatase 1 (PP1) in, 653, 656–658, 657f, 659
pyridoxal phosphate (PLP) in, 643–645, 644f
regulation of, 642, 656–661, 657f

regulatory cascade for, 651–653, 652f
7TM receptors in, 652, 652f
termination of, 653
transferase in, 645–646, 645f
UDP-glucose and, 654–655
Glycogen phosphorylase
a, 647–649, **647f**, 650, 650f
allosteric regulation of, 647–651, 648f
b, 647–649, **647f**, 650, 650f
carboxyl-terminal domain of, 643, 644f
defined, 642, 646
in glycogen metabolism, 642–647
glycogen-binding site of, 643–645, 644f
in liver, 647–649, 647f, 648f, 657f
in muscle, 648, 648f, 650f
regulation of, 647–651, 653
Glycogen synthase
α-1,6 linkages, 655, 655f
defined, 654
in glycogen synthesis, 655–656
isozymes of, 654–655
Glycogen synthase kinase (GSK), 742
defined, 655–656
in glycogen metabolism, 655–656, 657f
Glycogenin, 641, 654
Glycogen-storage diseases, 661f, 661t
Glycolate, 614f, 615
Glycolipids, 355, 357, 359
N-glycolylneuraminate, 819
Glycolysis, 447f
aerobic, 497–498, 531
aldehyde oxidation in, 480–481
anaerobic mode, 531, 747, 749
ATP formation in, 482–484

1,3-bisphosphoglycerate (1,3-BPG) in, 457–458, 480–481, 483–484
in cancer, 497–498
citric acid cycle and, 517–521, 518f
control of, 492–499
covalent enzyme-bound intermediate in, 481
defined, 473
dihydroxyacetone phosphate (DHAP) in, 466, 476f, 478, 479f, 489
as Embden-Meyerhof-Parnas pathway, 473
enediol intermediate in, 479, 479f
energy charge and, 505–506
as energy-conversion pathway, 474–492
enzymes of, 474, 497
in eukaryotic cells, 473, 476–477
evolution and, 511
fermentation in, 486–487
first stage of, 475f, 476f
fructose 1,6-bisphosphate in, 466, 476f, 477
fructose 1-phosphate in, 489, 489f
fructose 2,6-bisphosphate in, 495, 496f
fructose 6-phosphate in, 477, 495
fructose in, 489–490, 489f
galactose in, 489f, 490–491
gluconeogenesis and, 499–501, 505–511, 505f
glucose 6-phosphate (G-6P) in, 476, 477, 494, 495f
glucose transporters in, 498, 498t
glyceraldehyde 3-phosphate (GAP) in, 476f, 478, 479f, 480–481, 480f
hexokinase in, 476–477, 476f, 494, 495–496, 495f
historical perspective on, 473
isomerization of carbon sugars in, 477, 478
in liver, 494–497, 495f, 496f, 497f, 506–508
in muscle, 493–494, 495f
NAD^+ in, 482, 482f, 486–488, 487f

NADH in, 482, 486–487, 486f

overview of, 473f, 475f, 476f
pathway integration, 509, 510f
pentose phosphate pathway and, 624–628
phosphofructokinase (PFK) in, 493–495, 493f, 496f
3-phosphoglycerate in, 484–485
2-phosphoglycerate in, 484–485
3-phosphoglycerate in, 485–486
phosphoglycerate mutase in, 484
pyruvate in, 473, 473f, 476f, 485–486, 486f
pyruvate kinase in, 494, 495f, 496–497, 497f
reactions of, 485t
reciprocal regulation in, 505–511, 505f
regulation of, 740f, 746
second stage of, 475f, 480–481, 480f
stages of, 474–476, 475f, 480f
thioester intermediate in, 481, 481f, 482, 483f
triose phosphate isomerase (TPI) in, 478–480, 479f
Glycolytic intermediates, 633
Glycolytic pathway
glucokinase in, 495–496
hexokinase in, 495–496
phosphofructokinase (PFK) in, 493–495, 496f
pyruvate kinase in, 496–497, 497f
Glycopeptide transpeptidase, 173
Glycophorin, 348f, 369
Glycoproteins, 337–346
Glycosaminoglycans, 338, 339–340, 340f
Glycosidic bonds, 331–332, 332f, 336, 336f, 338
Glycosidic linkage, 331–332, 332f, 335f, 336f, 338f
O-glycosidic linkage, 332, 332f
N-glycosidic linkage, 332, 332f
Glycosylation, 331, 341–342
congenital disorders of, 344–345
errors in, 344–345

location of, 341f
in nutrient sensing, 339, 339f
Glycosyltransferases, 341–342, 343f
Glyoxylate, 537, 537f, 615
Glyoxylate cycle, 536–538, 537f
Glyoxysomes, 537
Glyphosate, 777
Glyset, 334
GMP (guanosine monophosphate)
in purine synthesis, 799–800, 799f
synthesis of, 807–808, 808f
GMP synthetase, 800
Golden rice, 296
Goldstein, Joseph, 830
Golgi complex, 341, 341f, 342f, 344, 942
Gout, 810
G-protein-coupled receptors (GPCRs), 418, 735–736
Gram, Hans Christian, 373
Gram negative bacteria, 373
Gram positive bacteria, 373
Gram staining technique, 373, 374f
Granulocyte colony-stimulating factor (G-CSF), 995
Granum, 588
Grb2, 432, 432f
Green fluorescent protein (GFP), 63, 64f, 117, 117f
Greider, Carol, 1, 27–28, 863
Group-specific reagents, 169–170, 170f
Group-transfer reactions, 465–466, 465t
GTP (guanosine triphosphate)
as energy source, 792
hydrolysis, 419–420
in olfaction, 436
in resetting G proteins, 419–420
in signal transduction, 416
in translation, 932

in vision, 439
GTPase-activating protein (GAP), 434
GTPases
defined, 433
Ras family of, 432
in signal transduction, 433
GTP-GDP cycle, 932, 932f
Guanidinium chloride, 59
Guanidinium group of arginine, 39, 39f
Guanine, **4**, **5**, **5f**, **18**
Guanine-nucleotide-exchange factor (GEF), 432
Guanosine triphosphate (GTP), 451
Guanylate, 800
Guide strand, 295
Guirard, Beverly, 770b
Gustation. *See* Taste
$G_{\beta\gamma}$ dimer, 424, 424f

H5N1 flu, 348
Haemophilus influenzae, 282, 282f, 309
Hair cells, 440–441, 440f, 441f
Hairpin turns. *See* Reverse turns
Half-life
of drugs, 992, 992f
of proteins, 703, 704, 705t
Half-reactions
defined, 546
in electron transport, 548
Halobacterium salinarum, 586, 586f
Hartnup disease, 702
Hatch-Slack pathway, 622
Haworth projections, 327–328
HCN channels, 405
HCN4 gene, 405–406, 405f

Hearing
hair cells in, 440–441, 440f, 441f
ion channels in, 440–441
signal transduction in, 440–441, 441f
Heart disease, 833, 981. *See also* Atherosclerosis
Heat
defined, 12
oxidative phosphorylation uncoupling in generation of, 575–576, 576f
release in double helix formation, 14–15
thermodynamics and, 12
Heat shock protein 70 (Hsp70), 310, **311f**
Heat-shock genes, 890–891
Heavy (H) chains
in antibody diversity, 89
defined, 86–87
in immunoglobulin classes, 87f
Heinz bodies, 635, 635f
Helicase DnaB, 860
Helicases
asymmetry, 851f
defined, 850
in DNA replication, 850–851
mechanism, 850, 850f, 851f
structure of, 850, **850f**
symmetry, 850, 850f
Helix-turn-helix motif, 52, 52f, 951, 951f
Heller, Jutta, 29
Hemagglutinin, 347–348, 348f
Heme, 69, **73f**
biosynthetic pathway, 786f
in cytochrome c oxidase, 557
degradation of, 788f
labeling of, 786, 786f
in oxygen-binding, 73–74

structural changes, 79–80
structure of, **557**, **589f**
synthesis of, 787f
Heme prosthetic group, 554–555
Hemiacetal intramolecular, **327**
Hemichannels, 406
Hemiketal intramolecular, 327, **327**
Hemoglobin, 21
alignment comparison, 305, 305f
alignment with gap insertion, 303, 304f
α chains, 75
$\alpha_2\beta_2$ tetramer of, 55, **55f**
αβ dimers, 75
amino acid sequences of, 303–305, 303f
β chains, 75, 82f, 83
Bohr effect, 81–83
2,3-BPG binding to, 81
comparative genomics and, 26, 26f
conformational changes in, 78, 78f
cooperative oxygen binding by, 76–77
cooperativity, 78–79
defined, 69, 303
fetal, 81, 81f
globin fold, 75
glucose and, 331
glutathione and, 635
glycated, 331
mutations and, 83–84
myoglobin comparison, 75
oxygen affinity of, 80–81, 80f, 81f, 82f
oxygen delivery by, 77f
oxygen transport by, 81
oxygen-binding, 73–74
oxygen-binding curve, 76, 76f, 77f

polypeptide chains, 75
purified, 80, 80f
quaternary structure of, 75–76, **76f**, 77–78, 77f
R state, 78, 78f
receptor-mediated endocytosis and, 375–376
sequence alignment of, 307f, 308f
sickle-cell, 83, 83f
space-filling model, 76f
subunits, 75–76, 76f
T state, 78, 78f, 82
tertiary structure of, 310–311, **310f**
Hemoglobin A (HbA), 75
Hemoglobin β-chain gene (HbB), 83
Hemoglobin S (HbS), 83–84, 84f
Hemolytic anemia, G6PD deficiency and, 634–635
Hemostasis, 228
Henderson–Hasselbalch equation, 19, 20b–21b
Heparin, 232
Hepatic steatosis, 743
Hepatocytes, 669
Heptad repeat, 53, **53f**
Heptoses, 325
HER2 receptor, 434, 434f
Herbicides, photosynthesis and, 605
Hereditary nonpolyposis colorectal cancer (HNPCC), 870
Herpes simplex infections, 797
Hers disease, 661t
Heterotrimeric G proteins, 415–418, 417f
Heterotrophs, 586
Heterotropic effects, 217
Hexokinase
defined, 476
in glycolysis, 476–477, 476f, 494, 495–496, 495f
inhibition of, 494
liver and glycolysis and, 495–496

metal ion requirement, 476
muscle and glycolysis and, 494
Hexose monophosphate pathway. *See* Pentose phosphate pathway
Hexose monophosphate pool, 615
Hexose phosphates, 615, 615f
Hexose sugars formation in Calvin–Benson cycle, 615–618, 616f
Hexoses, 325, 326f, 476, 616f
High-density lipoproteins (HDLs), 828t, 829
defined, 829
properties of, 832
protective effects and, 832
reverse cholesterol transport in, 832
High-performance liquid chromatography (HPLC), 105, 105f
High-throughput screening, 981–982, 982f
Hind, Geoffrey, 599b
Hines, Justin, 29
Hippocrates, 980
His 64 (distal histidine), **313f**
His tag, 105
Histamine, 783, **783f**
Histidine
degradation, 720, 720f
distal, 74, 79f, 82–83
ionization of, 39, 39f
proton shuttle, 193, 194f
proximal, 73, 79, 79f
residue, 183
structure of, **38f**, 39, 39f, **39f**, **40t**
Histidine operon, 969, 969f
Histone acetyltransferases (HATs), 965–966, **965f**
Histone code, 967
Histone deacetylases, 967
Histones
acetylation of, 965–966
amino-terminal tails of, 965–966

in gene regulation, 967t
homologous, 893
modifications, 967, 967t
modifications of, 967t
tails, 965–966, 965f
Hitchings, George, 996b
HIV. *See* Human immunodeficiency virus (HIV) infection
HMG-CoA reductase, 981
HMG-CoA reductase inhibitor, 981
Hodgkin, Alan, 392
Hodgkin, Dorothy, 677b
Hoffmann, Felix, 980
Holliday, Robin, 873
Holliday junctions, 873–874, 873f
Holoenzyme, 144, 886, 887f
Homeodomain, 958, 958f
Homeostasis, 467. *See also* Caloric homeostasis; Glucose homeostasis
Homo sapiens, 2f
Homocysteine
in activated methyl cycle, 774, 775f
in amino acid synthesis, 775
in cysteine synthesis, 776
levels, reducing, 776
structure of, 41
in vascular disease, 776
Homocystinuria, 727t
Homodimer, 55
Homogenate, 101–102
Homogenization in protein purification, 101–102
Homogentisate, 724, 726, **726**
Homogentisate oxidase, 724
Homologies
databases for, 308–309
defined, 302

detection of, 302–309
repeated motifs and, 311–312
sequence alignment in, 305, 305f, 311
shuffling in, 305, 305f
statistical analysis in, 305
substitution matrices in, 305–308
three-dimensional structures and, 311
Homologous recombination, 290–291, 291f
Homologous sequences, 308–309
Homologs, 302, 302f
Homology directed repair (HDR), 292, 292f
Homolytic cleavage reaction, 677, 677f
Homopolymers, 335
Homoserine, 41, **41f**
Homotropic effects, 215
Horizontal gene transfer, 317–318, 317f
Hormone receptors, 963–964, 964f
Hormone-receptor complex, 417
Hormones
in acetyl CoA carboxylase regulation, 694–696
androgens, 834, 837–838, 838f
antidiuretic, 126, 127f
eicosanoid, 693–694, 693f, 694f
in fatty acid metabolism, 693–694
in gluconeogenesis, 507–508
in glucose metabolism, 507
in glycogen metabolism, 651–653, 651f, 656–661, 657f
local, 694
metabolic functions of, 468
in signal transduction, 415–416
steroid, 827, 834–836, 834f
HT1171, **707**
Human genome, 283–284, 283f, 286–287, 286f
Human Genome Project, 22f
Human history, genome sequencing and, 22–23, 23f

Human immunodeficiency virus (HIV) infection
drug development effects, 994f
protease, 189, 189f
protease inhibitors, 189, 994, 994f, 998
zinc-finger domains and, 294
Human milk oligosaccharides, 335
Human papillomavirus (HPV), 705
Human ribonuclease, **302f**
Humoral immune response, 86
Huntington disease, 62, 703, 869
Huxley, Andrew, 392
Hybrid-biological-inorganic (HBI) system, 606–607
Hybridoma cells, 114, 114f
Hydrogen bonds, 9f
acceptors, 9, 18
in base pairs, 5
breaking with membranes, 367
covalent bonds, compared to, 9
donors, 9
in enzyme-substrate complex, 150, 150f, 151f
interaction, 9
as noncovalent bond, 5, 9, 9f, 10, 11
strength of, 9
water, 10, 11
Hydrogen ions
in acid–base reactions, 17
concentration in solutions, 17
oxygen release and, 81–82
Hydrogen-bond donors, 9
Hydrolases, 143t
Hydrolysis. *See also* ATP hydrolysis
GTP (guanosine triphosphate), 419–420
of lipids, 668–669
in metabolism, 451–452, 466
of peptide bonds, 180–181, 183, 184f

of phosphodiester bond, 194–195, 195f
Hydrolytic enzymes, 184f, 186–187, 186f
Hydrolytic reaction, 465t, 466
Hydronium ions, 17
Hydropathy index, 368
Hydropathy plots, 368, 368f
Hydrophilic amino acids, 38, 52
Hydrophilic moiety, 358, 359f
Hydrophobic amino acids, 51f, 52f
structures of, 37f
types of, 36–38
Hydrophobic effect, 10–11, 11f, 13, 38, 52
Hydrophobic interactions
defined, 11
as noncovalent bond, 9
Hydrophobic moiety, 358, 359f
3-hydroxy-3-methylglutaryl CoA, 722
3-hydroxy-3-methylglutaryl CoA reductase (HMG-CoA reductase), 822, 822f, 826, 827f, 833, 833f
3-hydroxyanthranilate, 724, **724**
D-3-Hydroxybutyrate, 753
3-hydroxykynurenine, 724f
Hydroxyl groups, 38–39, 63
Hydroxylation, 63
cytochrome P450 in, 835–836, 835f
steroid hormones, 834–836
P-hydroxymercuribenzoate, 212–213, 212f
P-hydroxyphenylpyruvate, 724, **724**, 778
P-hydroxyphenylpyruvate hydroxylase, 724
Hydroxyproline, 54, **63f**, 757, 757f
Hyperammonemia, 717
Hypercholesterolemia, 830–831. *See also* Familial hypercholesterolemia
Hyperglycemia, 533

Hyperlysinemia, 727t
Hyperpolarization-activated cyclic nucleotide-gated (HCN) channels, 405
Hyperpolarization-activated ion channels, 405–406, 405f
Hypersensitive sites, 961
Hypervariable loops, 86–88, 87f, 88f
Hypervariable regions, 86, 87f
Hypoglycemia, 510
Hypomethylation, 961
Hypoxanthine, 810, 865, 865f
Hypoxanthine-guanine phosphoribosyltransferase (HGPRT), 800, 810
Hypoxia
    defined, 498, 758
    tumor, 498, 499f
Hypoxia-inducible factor 1 (HIF-1), 498, 499, 499f, 751, 758
Ibuprofen, 166, 990, **990f**
Ice, 10, 10f
I-cell disease, 344–345
Identity, 303
IF2-GTP-initiator-tRNA complex, 931
Imatinib mesylate (Gleevec), 999
Imidazoles, 38f
Immune response, 86
Immune system
    adaptive, 86–88
    binding proteins and, 84–91
    evolution of, 84–86
    innate, 84–86
    MHC proteins in, 89–91
    overview of, 84
    T cells. *See* T cells, killer
    T-cell receptors. *See* T-cell receptors (TCRs)
Immunity, cell-mediated, 89
Immunoelectron microscopy, 118, 118f

Immunoglobulin A (IgA), 88, 88f
Immunoglobulin D (IgD), 88, 88f
Immunoglobulin domains, 86–87. *See also* Immunoglobulin fold
Immunoglobulin E (IgE), 88, 88f
Immunoglobulin fold, 86, **86f**
Immunoglobulin G (IgG)
    antigen binding of, 88
    cleavage of, 87, 87f
    defined, 86
    structure of, 86, **87f**
Immunoglobulin M (IgM), 88, 88f, 89
Immunoglobulins. *See also* Antibodies
    classes of, 88–89, 88f
    defined, 86
    heavy chains, 89
    light chains, 89
    myeloma and, 114
    sequences of, 86f
Immunologic techniques
    enzyme-linked immunosorbent assay (ELISA), 114–115, 115f
    fluorescence microscopy, 117–118, 117f
    hybridoma cells in, 114
    monoclonal antibodies in, 113–114, 113f, 114f
    polyclonal antibodies in, 113, 113f
    in protein studies, 112–118
    western blotting, 116, 116f, 265
Immunotoxins, 281
Indinavir (Crixivan), 189, 189f, 994–995
Indinavir complex, 189, 189f
Indirect ELISA, 115, 115f
Indole, 779
Indole groups, 37–38
Induced-fit model, 151, 151f, 180
Inducer, 954

Influenza virus, 347–348, 348f
Information science, 21
Ingram, Vernon, 83
Inhibition
competitive, 166–167, 167f
noncompetitive, 166, 168f
reversible, 166–168
uncompetitive, 167–168, 168f
Inhibition constant (K_i), 987, 987b–988b
Inhibitory concentration, 987
Inhibitory factor 1 (IF1), 575
Initiation factors, 931, 931f
Initiator element (Inr), 896
Initiator tRNA, 930
In-line displacement, 195
Innate immune system, 84–86
Inosinate, 799, 799f, 808
Inosine, 810, 921
Inositol, **817**
Inositol 1,4,5-trisphosphate (IP_3), **413**, 420–421, 420f
Insertional inactivation, 274, 275f
Insig, 826–827, 826f, 827f
Insulin, 735
adiponectin and, 737
amino acid sequence of, 43, 43f
binding of, 426–427, 427f, 430f
defined, 33, 425
in essential enzyme regulation, 507–508, 507f
in fatty acid metabolism, 696
formation of, 224
glucokinase and, 496
in glycogen metabolism, 658–659, 659f
levels of, 425f
MALDI-TOF mass spectrum of, 119f

pancreatic failure and, 744–745
in postprandial period, 739
recombinant human, 995
release of, 744, 745f
research in, 677b
secretion of, 735, 739
sensitivity to in athletes, 750
in signal transduction, 414f, 425–431, 742–743, 742f, 744f
Insulin receptor
activation of, 426–427, 427f
binding sites for, 742
defined, 426
structure of, 426, 427f
subunits, 426f, 427
Insulin resistance, 737
biochemical basis of, 742–743, 744f
ceramide and, 743–744, 744f
defined, 741
in muscle, 743–744
in pancreatic failure, 744–745, 745f
Insulin signaling, 425–431
illustrated, 427f
lipid kinase in, 428, 428f, 429f
pathway, 428, 430f
termination of, 430–431
Insulin-dependent diabetes. *See* Type 1 diabetes
Insulin-receptor kinase, 428–430, 429f
Insulin-receptor substrates (IRS), 428, 428f, 658, 742, 742f, 743
Insulin-signaling pathway, 742–743, 742f
Integral membrane proteins, 363, 363f, 364f
Intermediary metabolism. *See* Metabolism
Intermediate-density lipoproteins, 828, 828t
Intermembrane space (IM space), 543
Internal guide sequence (IGS), 910

Internal ribosome entry sites (IRES), 937
International Union of Biochemistry, 143
Intracellular pathogen, 89
Intramolecular hemiacetal, 327
Intramolecular hemiketal, 327
Intramolecular rearrangements, 677, 678
Intrinsic pathway, clotting, 228
Intrinsic termination signals, 888, 889f
Introns
    self-splicing, 909–910, 910f
    splicing, 901–902, 902f
Inverse PCR, 281, 281f
Invertase, 334
Inverted repeats, 197, 197f
Ion channels, 392–393
    acetylcholine receptor, 400–401, 401f, 402f
    action potentials and, 392, 392f, 402–404
    ball-and-chain model for inactivation, 399–400, 400f
    calcium, 396, 397, 397f
    cell-to-cell, 406–407, 406f, 407f
    defined, 392, 402
    disruption of, 404–405
    energetic basis of selectivity, 396, 397f
    equilibrium potential and, 402–404, 402f
    gap junction, 406–407, 406f, 407f
    in hearing, 440–441
    hyperpolarization-activated, 405–406, 405f
    inactivation of, 399–400, 400f
    ligand-gated, 400–401
    membrane permeability and, 399–400
    nerve impulses and, 392
    patch-clamp technique, 393, 393f, 394f
    potassium, 394–400, 395f, 396f, 397f, 398f, 399f, 405
    selectivity filter, 396, 397f
    sequence relations of, 394

shaker, 394
sodium, 392, 394, 396–397, 397f, 399–400, 404
structure of, 394f
in vision, 439, 439f, 440
voltage-gated, 398–399, 399f
Ion gradients, 458, 458f
Ion semiconductor sequencing, 285, 286f
Ion source, 118
Ion-exchange chromatography, 103–104, 104f
Ionic interactions, 8–9, 11f
IRE-binding protein (IRP), 970–971, 970f
Iron
metabolism of, 970–971
oxygen-binding and, 73–74, 79f
receptor-mediated endocytosis and, 375–376, 376f
structural transition in subunit, 79
Iron center of ribonucleotide reductase, 803, 804
Iron-response element (IRE), 970–971, 970f
Iron–sulfur clusters, 551–552, 551f
Iron–sulfur proteins, 525f
defined, 525, 551
in nitrogen fixation, 764–765, 765f
in oxidative phosphorylation, 552
structure of, **765f**
Irreversible inhibition. *See also* Enzyme inhibition
defined, 164
in mapping active site, 169–172
mechanism-based (suicide), 171, 173f
Islet-1 gene, 962
Isocitrate
in citric acid cycle, 525
in glyoxylate cycle, 537, 537f
in isomerization reactions, 467
Isocitrate dehydrogenase, in citric acid cycle, 525, 533, 533f
Isocitrate lyase, 537

Isoelectric focusing, 107–108, 108f
Isoelectric point, 107, 108f
Isoenzymes. *See* Isozymes
Isoform, 217
Isoleucine, 36, **37f**, 718
    degradation of, 722–723, 725b–726b
    in maple syrup urine disease, 727
    structure of, **37f**
Isomerases, 143t
Isomerization, 439–440, 439f
Isomerization reactions in metabolism, 465t, 467
Isomers
    constitutional, 325, 326f
    diastereoisomers, 325–326, 326f
    stereoisomers, 325, 326f
Isopentenyl pyrophosphate, 822–823, 822f, **823**
Isopeptide bonds, 703, 704f
Isoprene, **822**, 833–841
Isoprenoids, 840–841
Isopropylthiogalactoside (IPTG), 954, 954f
Isotope labeling studies, 530, 786, 786f, 822f
Isotrenes, 841f
Isovaleryl CoA, **722**
Isovaleryl CoA dehydrogenase, 722
Isozymes
    defined, 217
    distinguishing, 217–218
    of lactate dehydrogenase (LDH), 217, 218f
Itano, Harvey, 83

Jacob, François, 952
Jagendorf, André, 599, 599b
Jagendorf's demonstration, 599

K^+ ions. *See* Potassium ions

Kanamycin, 942
k_{cat} (rate constant), 157
k_{cat}/k_M (specificity constant), 158–159, 159f
K_d (rate constant) (dissociation constant), 157, 166
Kendrew, John, 51
Ketimine, **708**
α-ketoacids, 722–723, 769–770
β-ketoacyl synthase, 687
α-ketobutyrate, 721
Ketogenic amino acids, 718, 719f
Ketogenic diets, 682
Ketoglutarate, **160**
α-ketoglutarate, **160**
  in amino acid degradation, 718, 719, 719f, 720, 720f
  in amino acid synthesis, 766–767, 769
  in citric acid cycle, 525, **525**
  in double-displacement reactions, 160–161
  in glutamate synthesis, 766, 767
  in nitrogen fixation, 766
  oxidative decarboxylation of, 526
α-ketoglutarate dehydrogenase, 535
α-ketoglutarate dehydrogenase complex
  in citric acid cycle, 526, 533, 533f
  defined, 526
α-ketoisocaproate, 722
Ketone, **327**
Ketone bodies
  acetyl CoA formation from, 679–680
  brain and, 753–754
  in citric acid cycle, 753–754, 754f
  defined, 680
  in diabetes, 682, 682f

in fatty acid metabolism, 679–683
formation of, 680, 680f, 752–754
as fuel source, 679–683
high levels of, 682–683
in liver, 681, 681f, 753, 754f
starvation and, 752–754, 753f
as water soluble, 682
Ketoses
aldoses conversion to, 477, 615
defined, 325
Ketosis, 682, 682f
3-ketosphinganine, 819, **819**
β-ketothiolase, 673
K_i (inhibition constant), 987, 987b–988b
Kidney
drug excretion in, 992
gluconeogenesis in, 499
Killer T cells, 86
Kilocalories (kcal), 146
Kilodaltons (kDa), 43
Kilojoules (kJ), 146
Kinase fold, 222
Kinases, 476
Kinetic energy, 12
Kinetic perfection, 159
Kinetic proofreading, 924–925, 924f
Kinetics, 141
defined, 151
enzyme. *See* enzyme kinetics
as study of reaction rates, 152
of water deprotonation, 192f, 193
Klenow fragment, 846, 846f
Klug, Aaron, 893
K_M. *See* Michaelis constant

Knowledge-based methods, 61
Köhler, Georges, 113
Kornberg, Roger, 881
Krebs, Hans, 459, 528b
Krebs cycle. *See* Citric acid cycle
Kringle domain, 229
Kynurenine, 724f

L amino acids, 35, 35f, 43
Lac operon, 953, 953f, 954, 954f
Lac regulatory site, 950f
Lac repressor
    binding of, 953
    components of, 954
    defined, 950
    effects of IPTG on, 954f
    inhibition relief, 956
    structure of, 953, **953f**, 955
Lac repressor-DNA complex, 950–951, 950f
Lactase, 334, 474, 492
Lactate, **101**, **159**, 533
    in Cori cycle, 509, 509f
    formation from pyruvate, 487
    formation of, 486f, 487
    in gluconeogenesis, 499
    in glucose metabolism, 473f
    in glycolysis, 473
    in muscle contraction, 508–509, 509f
Lactate dehydrogenase (LDH), 217, 218f, 487f, 509
Lactic acid fermentation, 473, 487, 487f
Lactic acidosis, 510
Lactobacillus, 492f
Lactobacillus acidophilus, 488
Lactoferrin, 35f

β-lactoglobulin, 119f
Lactonases, 626
Lactose, 952f
    defined, 334
    in human milk, 335
    structure of, 333–334, **333f**
Lactose intolerance, 492
Lactose operon. See *Lac* operon; *Lac* repressor
Lactose permease, 390–392, 391f
LacZ gene, 274, 274f
Lagging strand
    defined, 849
    synthesis of, 849f, 858–859, 858f
    template, 859
λ phages
    alternative infection modes for, 275–276, 276f
    for DNA cloning, 272, 275–276
    mutant, as cloning vector, 276, 276f
λ repressor
    defined, 957
    in gene expression, 957–958
    in genetic circuit formation, 957f, 958, 958f
    structure of, **957f**
Lamprey, 316, 316f
Lanosterol, 824, **825f**, 827
Large subunit (50S) of ribosomes, 927, 927f, 929f, 931–932, 933, 935
Lateral diffusion, 369, 370, 370f
Lavoisier, Antoine, 764
Laws of thermodynamics, 12–14
Lead molecules, 980–986
    DNA-encoded libraries, 984–985, 984f
    high-throughput screening, 981–982, 982f
    from natural products, 980–981
    phenotypic screening, 985–986, 985f

screening libraries, 982–983, 983f
structure-based design, 993–995, 994f
target-based screening, 985–986, 985f
Lead optimization, 986
Leader peptide sequences, 969f
Leader sequences, 967–968, 969f
Leading strand
defined, 849
synthesis of, 849f, 858–859, 858f
Leaflets, 359
Leber hereditary optic neuropathy (LHON), 578
Lectins
as carbohydrate-binding proteins, 346–348
classes, 346–347
C-type, 347, 347f
defined, 346
in interactions between cells, 346
L-type, 347
Leghemoglobin
sequence alignment of, 307, 307f, 308f
tertiary structure of, 310, **310f**
Leptin
in caloric homeostasis, 736–737
defined, 736
effects in brain, 736, 736f
obesity and, 736–737, 736f
secretion of, 736
Leptin resistance, 737–738
Lerner, Michael, 903
Lesch–Nyhan syndrome, 810–811
Leucine, 36, 718
degradation of, 723
in maple syrup urine disease, 727
structure of, **37f**
Leucine-rich repeats (LRRs), 84, 85f

Leuconostoc citrovorum, 488
Leukemia, 497
Leukocyte antigen A2 (HLA-A2), 90
Leukotrienes, 693
Levinthal, Cyrus, 59
Levinthal's paradox, 59
Licensing factors, 862
Ligand binding
    concerted model, 78–79, 78f
    in drug development, 986, 986f
    sequential model, 78–79, 79f
    7TM receptor and, 415–418
Ligand-gated channels, 400–401
Ligands, 70f
    defined, 69, 191, 963, 986
    features of, 72f
    receptors and, 413, 964f
Ligases, 143t
Ligation reactions in metabolism, 465t, 467
Light
    absorption, 439–440, 589–590, 590f
    electromagnetic spectrum of, 438f
Light (L) chains, 87, 87f, 89
Light absorption, 439–440, 589–590, 590f
Light energy, 606–607, 607f
Light independent reactions, 587
Light reactions. *See also* Photosynthesis
    in Calvin–Benson cycle, 620, 620f
    defined, 587
    herbicides and, 605
    illustrated, 587f
    stoichiometry for, 602
Light-harvesting complexes, 604
Light-independent reactions. *See* Dark reactions

Limit dextrin, 473
Limonene, 840, **840f**
lin-4 gene, 971
Linear polymers, 5f, 41
Lineweaver–Burk plot, 156, 156f, 164, 164f, 167, 167f
α-1,6 linkages, 655, 655f
Linking number, 852f, 853
Linoleate, 675
Linoleoyl CoA, 675f
Lipases, 667, 667f
Lipid bilayers. *See also* Membrane lipids
    as cooperative structures, 360
    defined, 355, 359
    diagram, 359f
    formation of, 359–360
    as permeability barrier, 361–362, 361f
    self-assembly process, 359
    as self-sealing, 360
    stabilization of, 360
Lipid droplet, 666
Lipid metabolism
    diacylglycerol in, 821
    disruption of, 820–821
    liver in, 669
    phosphatidic acid phosphatase in, 821, 821f
Lipid phosphatases, 431
Lipid rafts, 372–373, 372f
Lipid vesicles, 360–361, 360f
Lipids
    defined, 353
    digestion of, 667–668, 667f
    energy storage in, 666–668
    fatty acids in, 353–354, 353f, 354t
    hydrolysis of, 668–669

membrane. *See* membrane lipids
metabolism of. *See* fatty acid metabolism
synthesis of, 815–816, 821
transport of, 667, 668f
Lipin 1, 821
Lipinski, Christopher A., 989
Lipinski's rules, 989, 989f
Lipmann, Fritz, 770b
Lipoamide in citric acid cycle, 520–521, 522f
Lipoic acid, 518, **518**
Lipolysis, 669–670, 670f
Lipophilic molecules, 382
Lipoprotein particles, 827–828
Lipoproteins
chylomicrons, 828, 828t
components of, 827
high-density (HDLs), 828t, 829, 832
intermediate-density (IDLs), 828, 828t
low-density (LDLs), 828, 828t, 829–832, 829f, 831f
metabolism, 829f
properties of, 828t
as transporters, 827–829
very-low-density (VLDLs), 828, 828f, 828t
Liposomes
defined, 360
formation of, 360–361, 360f
therapeutic applications of, 361
Lipoxygenase, 693, 693f
Liver
alcoholic injury of, 755–756
in amino acid degradation, 708–709, 712–713
in cholesterol synthesis, 825, 828f
cirrhosis of, 756
drug metabolism in, 990

ethanol metabolism in, 755–759
fatty, 755–756
glucagon and, 739–740
gluconeogenesis in, 499, 503, 506–508, 753
glucose 6-phosphate (G-6P) in, 646–647, 661
glucose and, 739
glucose levels and, 646–647
glucose sensor in, 659
glycerol in, 669–670
glycogen in, 641, 641f, 651, 740, 741
glycogen metabolism in, 646–647, 659–660, 659f, 660f
glycogen phosphorylase in, 647–649, 647f, 648f, 657f
glycolysis in, 494–497, 495f, 496f, 497f, 506–508
ketone bodies formed in, 680f
ketone bodies in, 681, 681f, 753, 754f
ketone body synthesis in, 753–754, 754f
in lipid metabolism, 669
peroxisomes in, 679f
in starvation, 753
transplant of, 832
in triacylglycerol synthesis, 816
Local hormones, 694
Lock-and-key model, 150–151, 151f
Long interspersed elements (LINES), 284
Long QT syndrome (LQTS), 404–405
Loops, 50, 50f
Lovastatin, 833, 833f, 981, **981**
Low-density lipoprotein receptor
absence of, 830–831
destruction of, 831
LDL release, 831, 831f
mutations in, 831
Low-density lipoproteins (LDLs), 828t, 829f
in cholesterol metabolism, 829–830, 829f
cycling of, 832

defined, 828
in familial hypercholesterolemia, 830–831
oxidized, 830
receptor-mediated endocytosis of, 829, 829f
schematic model of, 829f
L-type lectins, 347
Lupine leghemoglobin, 307–308
Lyases, 143t
Lycopenes, 841, 841f, **841f**
Lynch syndrome, 870, 870t
Lysine, 644f, 718
acetylated, **218**, 966
structure of, 39, 39f, **39f**, **40t**
synthesis of, 781
Lysogenic pathway, 275
Lysosomes
cholesterol synthesis and, 829
defined, 344–345
function of, 344–345, 345f
in I-cell disease, 344–345
with lipids, 820, 820f
in Pompe disease, 661f
Lysozyme, antibodies against, 87–88
Lytic pathway, 275

MacKinnon, Roderick, 395, 399
Macrophages, 830, 832
Macugen, 321
Magnesium ions
in ATP hydrolysis, 201–202
in Calvin–Benson cycle, 612–613, 613f, 621
in DNA cleavage, 194–196
RNA polymerases and, 882
Magnetic moment, 132
Main chains. *See* Backbones, in polypeptide chains

Major histocompatibility complex (MHC), 84
Major histocompatibility complex proteins, 89–91
anchor residues, 90
class I, 90, 90f
peptide presentation by, 89–91, 90f
structure of, 89–91
T-cell receptors and, 89–91, 91f
Malaria, 635–636
Malate, 537, 537f
in Calvin–Benson cycle, 622f, 623, 624
in citric acid cycle, 528
in gluconeogenesis, 502, 502f
in oxidation-reduction reactions, **465**
Malate dehydrogenase, 528, 691
Malate synthase, 537
Malate–aspartate shuttle, 571, 571f
Malathion, **182**
MALDI-TOF mass spectroscopy, 118–119, 119f, 345, 345f
4-maleylacetoacetate, **724**
Malic enzyme, 691
Malignant hyperthermia, 508
Malnutrition, 756
Malonyl ACP, 685, 686–687
Malonyl CoA, 685, 695
Malonyl transacylase, 686
Malonyl/acetyl transacylase (MAT), 688f, 689
Maltase, 334, 473
Maltase inhibitors, 334
Maltose, 333–334, **333f**
Mammalian fatty acid synthase, 688, **688f**, 689f
Mammalian liver homogenate, 871
Manganese, 595, 595f
Manganese center, 595, 595f
Mannose, 326f, 327
Mannose 6-phosphate, 345, 345f

Mannose 6-phosphate receptor, 346
Maple-syrup urine disease, 727
Margulis, Lynn, 545, 545b
Mass spectroscopy
    defined, 118
    MALDI-TOF, 118–119, 119f
    peptide sequencing by, 120–121, 121f
    in protein and peptide identification, 118–126
    proteomic analysis by, 125f, 126
    tandem, 121, 121f
Mass-to-charge ratio, 118
Mast cells, 232
Matrix, 118, 543
Matrix side, 544
Matrix-assisted laser desorption/ionization (MALDI), 118–119, 345
Maximal rate, 154–155, 156
McArdle disease, 661, 661t, 749
Mechanism-based (suicide) inhibition, 171
Mechanism-based toxicity, 992
Mediator, 960, 960f
Meiosis, 872
Melanin, 162, 783
Melanocyte-stimulating hormone (MSH), 736, 736f
Melanoma, 64f
Melatonin, 785, 785f
Melting temperature
    of fatty acid chains, 371, 371t
    of phospholipid membrane, 371, 371f
Membrane anchors, 367, 367f
Membrane channels
    ion, 382, 392–406
    membrane permeability to, 407–408, 408f
    water, 407–408, 408f
Membrane diffusion
    facilitated, 382

lateral, 369, 370, 370f
lipid, 369
protein, 370
Membrane lipids. *See also* Lipid bilayers
as amphipathic molecule, 358
archaeal, 358, 358f
carbohydrate moieties, 357
cholesterol, 357–358, 821–833
defined, 355
diffusion coefficient, 369
fatty acids in, 353–354, 353f, 354t
glycolipids, 357, 372
hydrophilicity of, 358, 359f
hydrophobicity of, 358, 359f, 360
lateral diffusion, 369, 370, 370f
metabolism, 821
movement in membranes, 370, 370f
permeability barrier, 361
phospholipids, 355–357
phospholipids, synthesis of, 815–821
rate of diffusion, 369
representations of, 359f
sphingolipids, synthesis of, 819, 819f
synthesis of, 814–841
triacylglycerols, synthesis of, 815–821
as two-dimensional solutions, 355
Membrane potential, 383
Membrane proteins. *See also specific proteins*
α helix of, 364, 364f, 365f, 367–369, 368f, 368t
ATP hydrolysis, 384–390
β strands of, 365f
carriers, 390
channels. *See* membrane channels
content variation, 362

defined, 355
diffusion, 370
function of, 362
gel patterns of, 363, 363f
hydropathy plots for, 368, 370f
hydrophobicity of, 367, 367f
integral, 363, 363f, 364f
membrane interaction, 363–367
peripheral, 363, 363f
pumps. *See* pumps
as two-dimensional solutions, 355
Membrane transport
ABC transporters in, 388–390, 388f, 389f
active, 382–383, 384
energetic cost of, 383b
free energy in, 382–383, 382f
passive, 382–383
potassium ion channels and, 397, 397f
primary active, 390
secondary active, 390
transporters. *See* transporters
Membranes, 352–376
archaeal, 358, 358f
as asymmetric, 355, 373, 373f
budding and fusion of, 375–376, 375f
common features of, 355
defined, 363
diffusion, 369–373
as electrically polarized, 355
endoplasmic reticulum (ER), 692
enzymatic activities, 373
fluidity of, 370–372
functions of, 352
ion gradients across, 458, 458f

lipid bilayer, 355, 359–362
mitochondria, 543–544
as noncovalent assemblies, 355
overview of, 363–364
permeability of, 360–361, 361f, 382
planar bilayer, 360, 361f
polarity scale for transmembrane helices, 368t
processes of, 362–369
protein interaction, 363–367
as sheetlike structures, 355
synthesis of, 373
Membrane-spanning α helices, 364, 364f, 365f, 368f, 369
Menten, Maud, 153, 154b
β-mercaptoethanol, 56–57, **56**, **56f**, 57f, 106
Mercury poisoning, 535–536
Merrifield, R. Bruce, 127
Metabolic pathways. *See also specific pathways*
amphibolic, 448
biosynthetic, 448
classes of, 448
defined, 448
degradative, 448
formation of, 449
illustrated, 447f
motifs, 460–468
regulation of, 448
thermodynamically favorable, 449
thermodynamically unfavorable, 449
Metabolic syndrome, 743, 743f
Metabolism, 446–468
activated carriers in, 460–463
AMPK in, 696
anabolic reactions in, 451–452
carbon bonds cleavage, 466

catabolic reactions in, 466
catalytic activity control and, 468
cholesterol synthesis, 829–830
common motifs in, 448, 460–468
defined, 447
drug, 990–991
enzyme control and, 467
evolution of, 468
first-pass, 990
free energy in, 449–450
fructose, 489–490, 489f
glucose, 447f
of glucose 6-phosphate, 631–634
group-transfer reactions in, 465–466
hormones and, 468
hydrolytic reactions in, 466
inborn error of, 509–511
integration of, 732–759
interconnected interactions in, 447–449, 447f
iron, 970–971
isomerization reactions in, 467
kinetic stability of, 462
ligation reactions in, 467
lipid, 821
lipoproteins, 828f
overview of, 447–448
oxidation-reduction reactions in, 465
of pyruvate, 486–488
regulation of, 467–468
substrate accessibility control and, 467–468
substrate cycles in, 508, 508f
thermodynamics of, 448–449
types of reactions in, 465t
Metabolites, 2, 672
Metabolomics, 447

Metal ion catalysis
in ATP hydrolysis, 201–202
in carbon dioxide hydrolysis, 191–192
defined, 180
in DNA cleavage, 196–197, 197f
Metal ions, 847, 847f, 882, 883f
Metalloproteases, 188f, 189
Metals, cofactor, 144t
Metformin, 745
Methionine
degradation, 721, 721f
from homocysteine, 774
metabolism, 721, 721f
oxidation of, 228, 228f
regeneration of, 775
structure of, 36, 37f, **37f**
synthesis of, 781
in translation, 929, 930, 930f
Methionine sulfoxide, 228, 228f
Methionine synthase, 775
Methotrexate, 806f, 807
Methylases, 200
Methylation
of adenine, 200, 200f
in amino acid synthesis, 774–775
DNA protection by, 199f, 200
in gene expression, 961–962
of phospholipids, 775
reaction, 676
3-methylbutane-1-thiol, **436**
2-methylbutyryl CoA, **725b**
Methylcobalamin, 676f, 775
β-methylcrotonyl CoA, 722
Methylglucopyranose, **332f**
β-methylglutaconyl CoA, 722

Methylglyoxal, 510, **510**
Methylmalonyl CoA, 677–678, 677f, 678f, **678f**
Metmyoglobin, 74
Mevalonate, 822, 822f, 823f, 827
Mice, genome of, 286f
Micelles, 359, 359f
Michaelis, Leonor, 153
Michaelis constant (K_M)
in Cheng–Prusoff equation, 987
defined, 154
determination of, 156
as enzyme characteristic, 156–157
physiological consequences of variations, 156
values of enzymes, 157t
Michaelis–Menten equation, 154–155, 155b, 161
Michaelis–Menten kinetics, 151–162, 153f, 167, 167f, 183, 212, 215, 215f
Microbiomes, 22f, 23–24, 24f, 682
MicroRNAs, 908, 909f, 971–972, 971f
Microsomal ethanol-oxidizing system (MEOS), 755
Miglitol, 334, **334**
Migrations, genome sequencing and, 23, 23f
Migratory birds, protein metabolism in, 725
Milstein, César, 113
Mineralocorticoids, 834
Minoxidil, 991
Mismatch DNA repair, 867, 867f
Mitchell, Peter, 562–563, 581, 599, 599b
Mitochondria
in apoptosis, 579
ATP synthase in, 564f, 570–571
brown fat, 576
in citric acid cycle, 516, 516f
electron entry via shuttles, 570–571

electron micrograph and diagram of, 544f
endosymbiotic origin of, 544–545
genome of, 544–545
matrix, 543
membrane, 543
membranes and, 374
oxidative phosphorylation in, 543–544, 562–564, 563f, 564f
properties of, 543–544
structure of, 543–544, 544f
transporters, 572–573, 572f, 573f
Mitochondrial ATP-ADP translocase, 572–573, 572f, 573f, 578
Mitochondrial ATPase, 562. *See also* ATP synthase
Mitochondrial biogenesis, 749–750, 750f
Mitochondrial diseases, 578–579
Mitochondrial mutants, 578
Mitochondrial outer membrane permeabilization (MOMP), 579
Mitochondrial porin, 544
Mitochondrial transporters
defined, 573f
illustrated, 573f
for metabolites, 572–573, 573f
structure of, 572, 572f
Mitosis, 862f
Mixed inhibition, 166. *See also* Enzyme inhibition
Mixed noncompetitive inhibition, 166
Mixed-function oxygenase, 723, 835
Mobile genetic elements, 284
Molecular clock hypothesis, 25–27, 26f, 316
Molecular evolution, 318, 319–321
Molecular imaging agents, 422
Molecular motors, flagella, 579–580
Molecular oxygen, toxic derivatives of, 560–561
Molecular recognition, 69, 71f
antibodies and, 88, 89

complementarity-determining regions and, 88
example of, 82
immune system and, 84
intracellular pathogens and, 91
utility of, 81
Molecules
amphipathic nature of, 359
homologous, 302
permeability of, 361, 361f
Moloney murine leukemia virus, 290
Monoacylglycerols, 667f, 668f
Monoclonal antibodies, 995–996, 995t
defined, 113
generation for proteins, 113–114
illustrated, 113f
preparation of, 114f
in signal transduction inhibition, 434, 434f
as therapeutic agents, 114
Monod, Jacques, 78, 952
Monomers, 5f
Monooxygenase, 723, 724f, 835
Monosaccharides. *See also* Carbohydrates
alcohols and, 331–332
aldoses, 325
amines and, 331–332
boat form of, 329–330, 329f
chair form of, 329–330, 329f
common, 326–327, 326f
defined, 325
diastereoisomers, 325–326, 326f
envelope form of, 330, 330f
glycosidic bonds, 331–332, 332f
isomers of, 325–326, 326f
ketoses, 325
linkage of, 333–337

modified, 331–332, 332f
nomenclature of, 325
reducing sugars, 330–331
ring forms of, 327–329, 327f, 329f
stereoisomers, 325, 326f
structure of, 325–327
Morphine, 989, **989f**
MotA–MotB pairs, 580, 580f
Motifs
defined, 52
helix-turn-helix, 52, 52f, 951, 951f
metabolism, 448
repeating, 124, 124f
Moult, John, 61
mRNA (messenger RNA)
cDNA prepared from, 278–279
5′ cap of, 900–901, 901f
FMN and, 891–892, 891f
poly(A) tail of, 900–901
precursors, 898–899, 903–906
RNA editing and, 908–909, 909f
structure of, 937, 937f
transcription and, 908, 908f
transferrin-receptor, 970–971, 970f
vaccines, 880–881
Mucins, 338, 341, 341f
Mucoprotein, 338
Mucus, 341
Muller, Hermann, 866
Mullis, Kary, 269
Multidrug resistance, 388–390
Multidrug resistance protein, 388
Multiple myeloma, 113–114
Multiple-drug resistance, 999

Multiple-substrate reactions
classes of, 159
defined, 159
double-displacement, 160–161
sequential, 159–160
Muscle
ATP in contraction, 493
biochemical adaptations to exercise, 750–751, 751t
excess fatty acids in, 743–744
fast twitch, 487, 493
fatty acids in, 743–744, 748
fiber types, 649, 649t
glycogen in, 641, 641f
glycogen phosphorylase in, 648, 648f, 650f
glycolysis in, 493–494, 495f
insulin resistance in, 743–744
PP1 regulation in, 657f, 658, 658f
signal transduction in, 742–743
Muscle contraction
alanine in, 509
ATP formation in, 747–749
fuel sources for, 746–750, 747t
gluconeogenesis in, 508–509, 509f, 510f
lactate in, 508–509, 509f
Muscle-relaxation pathway, 980, 980f
Mutagenesis
cassette, 281, 281f
by PCR, 281, 281f
site-directed, 187–188, 187f, 280, 280f
Mutagens, 865–866, 865f
Mutant λ phage, 276f
Mutarotation, 328
Mutase, 484
Mutations
defined, 25

deletion, 279, 281, 281f
disease-causing, functional effects of, 271–272
in genes encoding hemoglobin subunits, 83–84
hemoglobin and, 83–84
insertion, 279, 281
at level of function, 310
at level of sequence, 310
point, 280
in protein kinase A, 222–223
in recombinant DNA technology, 279–281
substitution, 279
MWC model, 78
myc gene, 898
Mycobacterium tuberculosis, 271, 538, 707
Myelin, 362, 362f
Myelin sheath, 352f
Myogenin, 291, 291f
Myoglobin, 69
alignment comparison, 305, 305f
alignment with gap insertion, 303, 304f
amino acid sequences of, 303–305, 303f
carbon monoxide and, 74–75, 75f
as compact molecule, 51, 51f
defined, 50–51, 69, 73, 303
distribution of amino acids in, 51f
oxygen and, 73–75
oxygen-binding curve, 73f, 76
receptor-mediated endocytosis and, 375–376
sequence alignment of, 307
structure of, 73, **73f**
tertiary structure of, 310, **310f**
three-dimensional structure of, **51f**
Myosin, 145
actin filaments and, 204–206, 205f, 206f

active sites, 204, 204f
altered conformation persistence, 203–207
ATP complex structure, 201, 201f
ATP hydrolysis and, 200–207
ATPase transition-state analog, 202, 202f
catalytic strategies of, 179, 200–207
conformational changes, 202f, 203, 203f
defined, 200
kinetic studies of, 201
as slow enzymes, 203
structure of, **201f**
two-headed structure, 206f
Myosin V, 205, 205f
Myosteatosis, 743
Myrcene, 840, **840f**

Na^+ ions. *See* Sodium ions

Na^+–K^+ ATPase, 384

Na^+–K^+ pumps, 384, 387, 387f

NAD^+ (nicotinamide adenine dinucleotide oxidized)

in glycolysis, 482, 482f, 486–488, 487f
light absorption and, 101
from metabolism of pyruvate, 486–488
reduction potential of, 547
regeneration of, 487, 487f, 488
structures of oxidized form of, 460–461, **460f**
synthesis of, 783, 783f
NADH (nicotinamide adenine dinucleotide reduced), 487f
in ATP generation, 461
electrons from, 570–571
electron-transport chain and, 517, 530, 545, 547, 548–549
ethanol metabolism in, 755
in fatty acid oxidation, 672–673

in glycolysis, 482, 486–487, 486f
light absorption, 101
in oxidative phosphorylation, 545, 547–548
pyruvate reduction by, 487
in respiratory chain, 552–553, 553f
structures of oxidized form of, 460
transport of, 570–571
NADH-cytochrome *b5* reductase, 692, 693f
NADH-Q oxidoreductase, 549, 549f, 550t, 552–553, 553f
$NADP^+$ (nicotinamide adenine dinucleotide phosphate), 626, 631
NADPH (nicotinamide adenine dinucleotide phosphate reduced), 835
in Calvin–Benson cycle, 610, 618, 622
dihydrofolate reductase and, 805
in fatty acid synthesis, 691
formation by photosystem I, 601
formation of, 624–630
in glucose 6-phosphate conversion, 624
oxidative generation of, 624
pathways requiring, 624t
in pentose phosphate pathway, 631–633
in reductive biosynthesis, 461
Nalidixic acid, 857, **857**
National Center for Biotechnology Information, 309
Native chemical ligation, 129, 129f
Native protein, 57
N-degron, 704
Neanderthals, 318, 319f
Neer, Eva, 425b
Negative nitrogen balance, 768
Negatively charged amino acids, 39–40, 39f
N-end rule, 704
Neomycin, 942
Neonatal Fc receptor (FcRn), 996
Nernst equation, 403

Nerve impulses, 392, 400
Neuraminidase, 348
Neuroglobin, 82–83
Neurological diseases. *See* Diseases and disorders
Neuron, myelination of, 362, 362f
Neuropeptide Y (NPY), 736, 736f
Neurotransmitter release, 375, 375f
Neurotransmitters, 400, 785
Neutral fat. *See* Triacylglycerols
Next-generation sequencing (NGS)
    defined, 284
    detection methods in, 284–286, 285f, 286f
    as highly parallel, 284
    ion semiconductor, 285, 286f
    pyrosequencing, 284
    reversible terminator method, 285
    RNA-seq, 289
NF-κB, 707
Niacin (vitamin B_3), 463t, 464f
Nicotinamide, 783, **783f**
Nitric oxide (NO)
    functions of, 784t
    synthesis of, 784–785, 784f
Nitrogen
    in amino acids, 764
    excess, disposal of, 713–718
    metabolism, 701, 716f, 783
    peripheral tissue transport of, 712–713
Nitrogen fixation
    in amino acid synthesis, 764–767, 764f
    ATP in, 765–769
    in bacteria, 764–767
    defined, 764
    FeMo cofactor in, 765, 765f

glutamate in, 766–767
glutamine in, 766–767
iron–sulfur proteins in, 765–766, 765f
P clusters in, 766
Nitrogenase, 764, 765–766, **765f**
Nitrogenase complex, 764–765
Nitrogenous bases. *See* Bases/base pairs
Nitrous acid, 865
N-linkage, 338, 338f, 341
N-linked oligosaccharides, 338, 338f, 345
Nonalcoholic fatty liver disease (NAFLD), 695
Noncompetitive inhibition. *See also* Enzyme inhibition
defined, 166
example of, 168
inhibitor binding, 168
kinetics of, 168, 168f
Nonconservative substitutions, 305, 307, 307f
Noncovalent bonds
in biological molecules, 7–11, 9f
hydrogen bonds, 5, 9, 9f, 10, 11
hydrophobic effect and, 10–11, 11f
types of, 8
van der Waals interactions, 9–10, 10f, 12
Nonessential amino acids, 768, 768f, 768t
Nonheme iron proteins, 525, 551–552
Non-homologous end joining (NHEJ), 292, 292f, 868
Nonphotochemical quenching (NPQ), 604
Nonpolar molecules, 11
Nonproteinogenic amino acids, 126
Nonshivering thermogenesis, 575, 577, 580–581
Norepinephrine, 785, 785f
Northern blotting, 267
Novobiocin, 857
Nuclear envelope, 374, 374f

Nuclear hormone receptors
defined, 963
domain structures, 964, 964f
in gene expression, 963–965
ligand-binding to, 963, 964f, 965f
Nuclear magnetic resonance (NMR) spectroscopy, 132–135, 132t
basis of, 133, 133f
chemical shifts, 133
defined, 132
NOESY and, 133–134, 134f, 135f
one-dimensional, 133, 133f
RNA structure, 320, 321f
signals, 133f
two-dimensional, 133–135
Nuclear membrane, gene expression and, 892
Nuclear Overhauser effect (NOE), 133–134
Nuclear Overhauser enhancement spectroscopy (NOESY), 134–135, 134f, 135f
Nuclear pores, 374
Nucleation-condensation model, 60, 60f
Nucleic acids, 265. *See also* DNA; RNA
Nucleophilic catalyst, 181
Nucleoside diphosphate kinase, 451, 796
Nucleoside diphosphokinase, 527
Nucleoside monophosphate, 451
Nucleoside monophosphate kinases, 451, 796
Nucleoside phosphorylases, 809
Nucleosides
defined, 792
nomenclature of, 792, 792t
Nucleosome, 893, **893f**
Nucleotidases, 809
Nucleotide synthesis, 791–812
de novo pathways in, 792, 798
deoxyribonucleotide, 801–807, 802f, 808–809, 808f

disorders of, 809–811
inosinate in, 808
overview of, 791–792
of purine, 783, 796–801, 797f, 807–808, 808f
of pyrimidine, 783, 792f, 793–797, 793f, 807
regulation of, 807–809
salvage pathways in, 792, 792f
substrate channeling in, 794
Nucleotide-excision repair, 868, 868f
Nucleotides
cyclic, 792
defined, 792
metabolism disruptions, 809–811
nomenclature of, 792, 792t
sequence of, 43
in signal transduction pathways, 792
NusA protein, 890

Obesity, 734
causes of, 734
diabetes and, 741–746
evolution and, 734
health consequences of, 734t
insulin in, 736
insulin resistance and, 743, 743f
leptin resistance in, 736f, 737–738
storage capacity of fat tissue, 743f
Obligate anaerobes, 488, 488t
Octadecanoic acid, 353
Odd-chain fatty acids, 675–676, 676f
Odorant receptors (ORs)
activation of, 436–437, 437f
evolution of, 441, 441f
in olfaction, 436–437
Off-diagonal peaks, 134

Off-target toxicity, 992
O-GlcNAc transferase, 339
Okazaki, Reiji, 849, 849b
Okazaki, Tsuneko, 849, 849b
Okazaki fragments, 849, 849f, 859
Oleate, 693
Olfaction. *See also* Sensory systems
    7TM receptors in, 436–437
    COVID-19 and, 437
    odorant receptors (ORs) in, 436–437, 437f, 441, 441f
    signal transduction in, 436–437, 436f, 437f
Olfactory neurons, 436
Oligomycin, 577
Oligopeptides. *See* Peptides
Oligosaccharide chain, 819
Oligosaccharides, 345f
    antigen structures, 343, 343f
    attached to erythropoietin, 339, 339f
    defined, 333
    enzymes responsible for assembly, 342–343
    human milk, 335
    mass spectroscopy and, 345, 345f
    N-linked, 338, 338f
    O-linked, 338, 338f
    sequencing of, 338, 339f
O-linkage, 338, 338f, 341
Omega (Ω) loop, 46
ω-carbon atom, 354
“On-bead” assays, 983f
Oncogenes, 433
One-dimensional NMR, 133, 133f
On-target toxicity, 992
Open promoter complex, 887, 887f
Open reading frames (ORFs), 309

Operator site, 952
Operon model, 952
Operons, 953f
in bacteria, 955
defined, 952
histidine, 969, 969f
lac, 953, 953f
structure of, 952, 953f
threonine, 969, 969f
trp, 968, 968f
Opsin, 438
Optogenetics, 607, 607f
Oral bioavailability, 988–989, 989f
Origin of replication complexes, 861–862
Origin of replication (oriC locus), 860, 861f
Ornithine, 715–716
Ornithine transcarbamoylase, 715, 717
Ornithine transcarbamoylase deficiency, 717f, 718–719
Orotate, 794–795
Orotate phosphoribosyltransferase, 795
Orotidylate, 795
Orotidylate decarboxylase, 795
Orthologs, 302, 302f
Orthophosphate, 453, **453f**, 482, 483f, 503, 642–643
Oseltamivir, 348
Osteoarthritis, 341
Osteogenesis imperfecta, 54
Overlap peptides, 122, 122f
Oxaloacetate, **160**
in amino acid degradation, 718, 719–720, 719f
in amino acid synthesis, 769
in Calvin–Benson cycle, 622, 622f
in citric acid cycle, 517, 522–523, 523f, 528–529, 534
conversion into phosphoenolpyruvate, 502–503

in fasting or diabetes, 680
formation of, 501–502
in gluconeogenesis, 499–503, 500f, 502f
in glyoxylate cycle, 537f
in ligation reactions, 467
in oxidation-reduction reactions, **465**
in starvation, 753–754
Oxidant, 546
Oxidation
activated carriers of electrons for, 460–461
of aldehydes, 480–481
carbon, 456–459
by citric acid cycle, 488
in drug metabolism, 990
by electron transport chain, 488
energy, 457–458
in fatty acid metabolism, 669–670, 671–674, 673t, 678–679
of fatty acids, 678–679
of glyceraldehyde 3-phosphate (GAP), 482
of membrane proteins, 674f
phase I transformations in, 990
pyruvate dehydrogenase complex and, 518–519
of succinate, 528–529
of unsaturated fatty acids, 674–675, 674f
Oxidation-reduction potential. *See* Reduction potential
Oxidation-reduction reactions
free-energy change in, 546, 547–548
in metabolism, 465, 465t
Oxidative phosphorylation, 542–581
ADP in, 572–573, 572f, 575f
ATP in, 573–574, 575f
ATP yield in, 573–574, 574t
ATP-ADP translocase in, 572–573, 572f, 573f, 578
cellular respiration in, 543–545
chemiosmotic hypothesis in, 562–563, 563f

defined, 458, 543
electron transfer in, 545–548, 561, 562f
electron-transport chain in, 543, 548–549, 569f
in eukaryotes, 543–544
in exercise, 747–749
inhibition of, 577–578
iron–sulfur clusters in, 551–552, 551f
in mitochondria, 543–544, 562–564, 563f, 564f
mitochondrial transporters in, 572–573, 572f
NADH in, 545, 547–548
overview of, 542, 543f
photosynthesis comparison, 600f
proton gradients in, 458, 458f, 543, 548–549, 562–569
proton-motive force in, 543, 562–563, 563f, 565–567, 565f
rate of, 574
reduction potential in, 545–548, 546f
respiratory chain in, 549–562
respiratory control in, 573–574, 575f
shuttles in, 570–573, 570f, 571f
transporters in, 570–573, 572f
uncoupling of, 575–576, 576f
Oxidized LDL (oxLDL), 830
Oxidized lipoamide, 520
Oxidizing agent, 546
Oxidoreductases, 143t
Oxidosqualene cyclase, 824
Oxoguanine-adenine base pair, 865, 865f
Oxyanion hole
of chymotrypsin, 185, 185f
defined, 185
of subtilisin, 186–187, 187f
Oxygen
affinity in red blood cells, 80–81, 80f, 81f, 82f
carbon monoxide and, 81, 82–83
concentration in tissues, 77, 77f

cooperative binding of, 76–77
cooperative release of, 76
hemoglobin quaternary structure and, 77–78, 77f
in hydroxylation function, 834–836
myoglobin and, 73–75
partial pressure, 76
pyruvate and, 486
reactive, 74
toxic derivatives of, 560–561
Oxygen affinity of hemoglobin, 80–81, 80f, 81f, 82f
Oxygen binding
cooperative, 76–77
by heme iron, 73–74
hemoglobin quaternary structure and, 75–76, 77f
iron and, 79f
pure hemoglobin, 80, 80f
sites, 73
Oxygenase reaction, 614–615, 614f
Oxygenases
in aromatic amino acid degradation, 723–724
mixed-function, 723
Oxygen-binding curve
defined, 73
fractional saturation, 73
for hemoglobin, 76, 76f, 77f
for myoglobin, 73f, 76
sigmoid, 76
T-to-R transition, 78, 78f, 80–81
Oxygenic photosynthesis, 586, 587f. *See also* Photosynthesis
Oxyhemoglobin, **77f**, 78, 79f
Oxymyoglobin, 73–74, **74f**

P clusters, 765f, 766
P site, ribosomal, 929, 929f, 931, 934, 935
p53, 705, 870

P450, 756
P680, 594, 595f
P700, 597–598, 597f
P960, 591, 592, 592f, 593f
Pacemakers, 405–406
Paclitaxel, 977
Paddles, 398–399
PALA, 213–214, **213f**, 214f, **214f**
Palindromes, 265
Palmitate, 673–674, 690
Palmitoleate, 674, 674f
Palmitoyl CoA, 674, 674f, 695
Pamaquine, 634
p-aminobenzoic acid (PABA), 166, **166**
Pancreas, β cells of, 735, 744
Pancreatic failure, 744–745
Pancreatic lipases, 667, 667f
Pancreatic trypsin inhibitor, 226–228, 227f
Pancreatic zymogens, 225f, 226, 226f
Pantothenic acid (vitamin B_5), 463t, 464f
Papain, 87, 143
Paracoccus denitrificans, 551
Paralogs, 302, 302f
Paraquat, 605
Park, James, 979
Parkinson disease, 62, 703, 705, 817
Partial pressure, oxygen, 76
Partition coefficient, 989
Passenger strand, 295
Passive membrane transport, 382–383
Pasteur, Louis, 472
Patch-clamp technique, 393, 393f, 394f
Pathogen-associated molecular patterns (PAMPs), 84–85, 85f
Pauling, Linus, 25, 46, 83, 169

PCSK9 (proprotein convertase subtilisin/kexin type), 832
Pectin, 296, 336
Pegfilgrastim, 995
Pegylation, 995
Penicillin, 979f
conformations of, 173, **173f**
mechanism of action, 172–173, 173f
reactive site of, 172–173, 172f
research in, 677b
structure of, **979**, **998**
Penicillium citrinum, 981
Penicilloyl-enzyme derivative, 173f
Pentose phosphate pathway
Calvin–Benson cycle and, 633–634
cell growth and, 633
decarboxylation in, 624
defined, 610, 624
erythrose 4-phosphate in, 627–628
fructose 6-phosphate in, 627, 628
glucose 6-phosphate dehydrogenase in, 634–636
glucose 6-phosphate in, 624, 631–634
glycolysis and, 624–628
illustrated, 625f
modes, 631–633, 632f
$NADP^+$ in, 631
NADPH in, 631–633
nonoxidative phase of, 624–630, 628t
overview of, 610
oxidative phase of, 624, 626f, 628t, 631
rate of, 631
reactions, 627–630, 629f, 630f
ribulose 5-phosphate in, 624, 626, 627, 631–633
sedoheptulose 7-phosphate in, 627
tissues with, 632t

transaldolase in, 626–628, 629–630, 630f
transketolase in, 626–628, 629f
Pentose shunt. *See* Pentose phosphate pathway
Pentoses, 325, 326–327, 326f
Peptide bonds
chemical nature of, 180
cis configuration, 44, 44f, 45f
cleavage of, 63–64, 185
defined, 41
formation in translation, 933–935, 934f
formation of, 42f
hydrolysis of, 180–181, 183, 184f
lengths, 44, 44f
as planar, 44, 44f
rigidity of, 46
rotation of, 45, 45f
stability of, 42
torsion angles, 45
trans configuration, 44–45, 44f, 45d
Peptide mass fingerprinting, 124, 125f
Peptide sequences, 59f
Peptide-ligation methods, 129
Peptides
mass spectroscopy for sequencing, 120–121, 121f
overlap, 122, 122f
presentation by MHC proteins, 89–91, 90f
sequencing of, 277
synthesis of, 126–129, 128f, 129f
Peptidoglycan, 173, 173f
Peptidyl transferase center, 932–933
Perilipin, 669
Peripheral membrane proteins, 363, 363f
Periplasm, 373
Periplasmic side, 591
Permeability

lipid bilayers, 360–361, 361f
membrane, 382, 406–407
of potassium ion channels, 396
Permeability coefficients, 361, 361f
Peroxide bridge in cytochrome *c* oxidase, 558, 558f
Peroxisome proliferator-activated receptor (PPARα), 756
Peroxisomes
in Calvin–Benson cycle, 615, 615f
defined, 615
electron micrograph of, 614f
in fatty acid oxidation, 678–679, 679f
Perutz, Max, 75
PEST sequences, 704
P-glycoprotein, 388
pH
buffers and, 19–20, 19f
carbon dioxide and, 82, 82f
defined, 17
effect on carbonic anhydrase activity, 190–191, 191f
effect on oxygen affinity of hemoglobin, 81f, 82f
ionization state as function of, 36f
Pharmacogenomics, 836
Pharmacology, 978. *See also* Drug development
Phase I transformations in oxidation, 990
Phase II transformations in conjugation, 990
Phenobarbital, 836
Phenotypic screening approach, 985–986, 985f
Phenyl isothiocyanate, 120
Phenylacetate, 717
Phenylacetyl CoA, 718
Phenylacetylglutamine, 718
Phenylalanine, 718
degradation of, 723–724, 724f, **724**, 768, 769
phenylketonuria and, 727–728

structure of, 37, 37f, **37f**, 38, **728**
synthesis of, 776–777, 778f
Phenylalanine hydroxylase, 724
Phenylalanine operon, 969f
Phenylketonuria, 727–728
Phenylpyruvate, **728**, 778
Phi (ϕ) angle, 45, 45f, 46f
Phosphatases
defined, 220, 503
in gluconeogenesis, 503
insulin signaling and, 430–431, 743
in phosphorylation, 219–220
PP2A, 220
Phosphate carrier, 572, 573, 573f
Phosphate esters, 458
Phosphates, 20, 458–459
Phosphatidate, 356
defined, 815
as intermediate, 815–821, 815f
structure of, **356f**, **816**
Phosphatidic acid phosphatase (PAP), 816, 821, 821f
Phosphatidylcholine, **356f**
Phosphatidylcholine, synthesis of, 818
Phosphatidylethanolamine, **356f**, 817–818, **818**
Phosphatidylethanolamine methyltransferase, 818
Phosphatidylinositol, **356f**, 816, **817**
Phosphatidylinositol 3,4,5-trisphosphate (PIP_3), 428, **428f**, 429f, 742, 742f
Phosphatidylinositol 4,5-bisphosphate (PIP_2)
in insulin signaling, 428, **428f**, 429f
in phosphoinositide cascade, 420, 420f
in signal transduction pathway, 742, 742f
synthesis of, 817
Phosphatidylinositol-dependent protein kinase (PDK), 742

Phosphatidylserine, **356f**, 818
Phosphite triester method, 268f, 269
Phosphocreatine, **160**
Phosphodiester bonds, 194–195, 195f, 882–884
Phosphoenolpyruvate (PEP)
formation of, 484, 501–503, 502f
in gluconeogenesis, 500f
in glycolysis, 466, 484–485
phosphoryl-transfer potential, 453–454, 454f, 484–485
Phosphoenolpyruvate carboxykinase (PEPCK), 502, 503
Phosphoenolpyruvate carboxylase, 623
Phosphofructokinase (PFK), 477, 740, 740f
activation of, 495
in liver, 494–495, 495f
in muscle, 493–494, 493f
regulation of, 494–495, 495f
Phosphofructokinase 2 (PFK2), 506–507, 507f
Phosphoglucomutase, 646, 646f, 647f
6-phosphogluconate dehydrogenase, 626
Phosphogluconate pathway. *See* Pentose phosphate pathway
6-phosphoglucono-δ-lactone, 626, 626f
Phosphoglucose isomerase, 477
2-phosphoglycerate, 466
3-phosphoglycerate
in Calvin–Benson cycle, 611–612, **611**, 612f, 613f, 615, 615f
in cysteine synthesis, 772
in glycine synthesis, 772
in glycolysis, 484–486
in oxygenase reaction, 614, 614f
in serine synthesis, 772
3-phosphoglycerate dehydrogenase, 780–781, **780f**, **781f**
2-phosphoglycerate in glycolysis, 482–484
Phosphoglycerate kinase, 482
Phosphoglycerate mutase, 484, 646

3-phosphoglyceric acid, **457**, **458**
Phosphoglycerides, 356, 356f, 359f
Phosphoglycolate, 614, 614f
Phosphoinositide 3-kinases (PI3Ks), 428, 742
Phosphoinositide cascade, 420–421, 420f, 421f, 653
Phosphoinositide-dependent kinase-1 (PDK1), 429–430, 430f
Phospholipase C, 420, 420f
Phospholipid synthesis
    from activated alcohol, 817–818
    activated intermediate, 816–817
    phosphatidate and, 815–821, 815f
    phosphatidylcholine, 818
    sources of intermediates in, 815–821
Phospholipids, 355–357
    alcohols and, 817–818
    base-exchange reactions in generation of, 818
    in bimolecular sheet formation, 359–362
    components of, 355f
    defined, 355
    flip-flop, 370, 370f
    lipid vesicles formed from, 360–361
    melting temperature, 371, 371f
    membrane, 355–357
    platform for, 356
    synthesis of, 815–821
Phosphopantetheine, 686f
Phosphopentose epimerase, 617, 617f
Phosphopentose isomerase, 309f, 617, 617f
Phosphoproteome, 223
Phosphoproteomics, 223
5-phosphoribosyl-1-pyrophosphate (PRPP)
    in purine synthesis, 797, 807–808
    in pyrimidine synthesis, 779, 795
Phosphoribulokinase, 622
Phosphorolysis in glycogen metabolism, 642–647

Phosphorothioates, 196, 196f
Phosphoryl group, 220
Phosphorylase. *See* Glycogen phosphorylase
Phosphorylase *a*, 647–649, **647f**, 650, 650f, 659, 660f, 739, 740
Phosphorylase *b*, 647–649, **647f**, 650, 650f
Phosphorylase kinase
    activation of, 650–651, 650f
    defined, 650
    subunits, 650, 650f
Phosphorylaspartate, **384**
Phosphorylation
    amplified effects of, 221
    ATP formation by, 601, 601f, 602
    cAMP stimulation of, 418
    of carboxyl-terminal domain (CTD), 897, 897f
    of carboxyl-terminal tail, 432
    in citric acid cycle, 531–532, 532f
    control of, 219–220
    in covalent modification, 218, 219t
    dephosphorylation and, 220
    EGF receptor, 432
    in enzyme regulation, 218, 219t
    free energy of, 221
    of fructose 6-phosphate, 477
    in gluconeogenesis, 502–503, 507
    in glycogen metabolism, 642–643
    in glycolysis, 476–477
    insulin binding in, 427, 428f
    in insulin signaling, 425–431
    in metabolism, 451, 458
    of nucleoside monophosphates, 451
    oxidative. *See* oxidative phosphorylation
    phosphoinositide-dependent kinase 1 (PDK1), 430f
    in phosphorylase activation, 650–651, 650f

in phosphorylase conversion, 650
of proteins, 223
in purine nucleotide synthesis, 797–799, 798f
of pyruvate dehydrogenase, 531–532, 532f
reactive intermediates, 333
of serine residue, 507
substrate-level, 482–483
sugars, 332–333
Phosphorylethanolamine, 818, **818**
Phosphoryl-transfer potential, 453–455, 454f, 457–458
Phosphoserine, **63f**
Phosphotriesters, 268f, 269
Photoinduced charge separation, 590, 590f, 592f
Photophosphorylation, cyclic, 601, 601f, 602
Photorespiration
in C_4 pathway, 622–623, 622f
in Calvin–Benson cycle, 614f, 615
Photosynthesis, 585–607
accessory pigments in, 602–605, 603f, 604f
artificial photosynthetic systems and, 606–607, 607f, 620, 620f
in autotrophs, 611
bacterial reaction center, 591f, 592–593, 592f, 593f
basic equation of, 586
biochemical principles of, 587
chlorophylls in, 589–593
in chloroplasts, 588–589, 588f
components of, location of, 605, 605f
in cyanobacteria, 593
cyclic photophosphorylation in, 601, 601f, 602
dark reactions, 587, 610
defined, 586
efficiency of, 604
electron transfer in, 589–593
energy conversion in, 586–588

enzymes in, 144
in eukaryotes, 588–589, 593
herbicide inhibition of, 605
in heterotrophs, 586
light absorption in, 590, 590f
light energy conversion in, 586–588
light reactions in, 587, 587f, 602, 605, 610
light-harvesting complexes in, 604, 604f
overview of, 586–588
oxidative phosphorylation comparison, 600f
photoinduced charge separation in, 590, 591f
photosystem I. *See* photosystem I
photosystem II. *See* photosystem II
in prokaryotes, 606t
proton-motive force in, 599
reaction centers in, 591f, 592–593, 593f, 596, 596f, 602–605, 604f
resonance energy transfer in, 603–604, 603f
vs. respiration, 587
in thylakoid membranes, 588–589
Z scheme of photosynthesis, 598, 599f
Photosynthetic systems, 606–607, 606t, 607f
Photosystem I. *See also* Photosynthesis
defined, 588, 594f
electron flow through, 601
ferredoxin generated by, 597–598, 597f
illustrated, 593f
inhibitors of, 605
link to photosystem II, 596, 596f
NADPH formation by, 601
reaction center, 597–598, 597f
structure of, 597–598, 597f
Z scheme of photosynthesis, 598, 599f
Photosystem II. *See also* Photosynthesis
defined, 588

electron flow through, 593–594, 595f
electron source, 593–594
illustrated, 593f
inhibitors of, 605
link to photosystem I, 596, 597f
location of, 596
photochemistry of, 594
proton release, 596f
reaction center, 594–596, 594f
structure of, 594f
Z scheme of photosynthesis, 598, 599f
Photosystems, 588
proton gradients in, 593–599
Phototroph, 447, 586
Phototrophic halobacteria, 585
Phototrophy
defined, 586
light energy conversion, 586–588
overview of, 586f
Photovoltaic cells, 606, 607f
Phytoene, 841, **841f**
Phytol, 589
Pichia pastoris, 112
Pickart, Cecile, 708b
Pig embryos, UCP-1 into, 577
Ping-pong reactions, 160–161
Pinnix, Chelsea, 29, 29f
pK_a values, 18, 40t
Placebo effect, 997
Planar bilayer membrane, 361, 361f
Plants
C_3, 623, 624f
C_4, 623, 624f
C_4 pathway and, 623

genetically engineered, 295–296, 295f
glyoxylate cycle in, 536–538, 537f
oxaloacetate synthesis, 683
photosynthesis in. *See* photosynthesis
polysaccharides of, 335–336
recombinant DNA technology in, 295–296, 295f
starch in, 618
sucrose synthesis in, 618, 619f
thylakoid membranes of, 605, 605f
Plaques in genomic library screening, 277, 278f
Plasma lipoproteins, 828t
Plasma-membrane proteins, 940, 940f
Plasmids
antibiotic resistance and, 998
defined, 272
engineered, 274
expression vectors, 275
genes, 274
microinjection of, 290, 290f, 291f
polylinker region, 274, 274f
Ti, 295–296, 295f
as vectors for DNA cloning, 274–275
Plastocyanin, 605
Plastoquinol, **594**, 596
Plastoquinone, 593–594, **594**, 595f, 596, 605
Pleckstrin homology domain, 428, 430
PLP-Schiff-base linkage, 643–644, 644f
Point mutation, 280
Poisoning
arsenite, 535–536, 536f
mercury, 535–536
ricin, 944
Polar amino acids, 38–39, 38f
Polar head group, 358
Polarity, 4

Poly(A) polymerase, 901, 901f
Poly(A) tail, 901
Poly(A) tail-binding protein I (PABPI), 937, 937f
Polyacrylamide gel electrophoresis (PAGE), 105f, 106–107, 106f
Polyacrylamide gels, 266
Polycistronic transcript, 953
Polyclonal antibodies, 113, 113f
Polycomb repressive complex-2 (PRC-2), 967
Polyenes, 841
Polygenic transcript, 953
Polylinker region, plasmid, 274, 274f
Polymerase chain reaction (PCR)
    cycle steps, 269–270, 269f, 270f
    defined, 265, 269
    DNA sequence amplification by, 269–270, 269f, 270f
    first cycle of, 269f
    as gene exploration tool, 265
    inverse, 281, 281f
    multiple cycles of, 270f
    mutagenesis by, 281, 281f
    quantitative (qPCR), 287, 287f
    uses of, 271
Polymerase switching, 862
Polymerases, processive, 857–858
Polymorphisms, 271
Polypeptide chains
    backbone, 42, 42f
    bond rotation in, 45, 45f
    cleavage of, 121, 122t
    components of, 42f
    cross-linked, 43, 43f
    directionality of, 42, 42f
    disulfide bonds of, 43, 43f
    flexibility of, 44–46
    formation of, 42

loops, 50, 50f
random-coil conformation, 56
residue, 42
reverse turns, 50, 50f
side chains, 42, 42f, 52
subunit structures, 55
Polypyrimidine tract, 902
Polysaccharides
defined, 335
of fungi and arthropods, 336–337, 337f
glycosidic bonds, 335f, 336f
glycosidic linkages, 336f
of plants, 335–336
Polysomes, 935, 935f
Polyunsaturated fatty acids, 674–675, 675f, 679, 693–694
Pompe disease, 661, 661f, 661t
Porin, 52f
amino acid distribution in, 52, 52f
amino acid sequence of, 364–365, 364f, 365f
defined, 364
hydropathy plot for, 369f, 370f
Porphobilinogen, 788
Porphobilinogen deaminase, 786
Porphyrias
disorders of, 788
synthesis of, 786–787
Positively charged amino acids, 39, 39f
Positron emission topography (PET) scanning, 63, 63f
Postabsorptive state, 739–740
Postmarketing surveillance, 997
Postprandial period, 735
Postprandial state, 739
Posttranscriptional gene expression
in eukaryotes, 970–971
in prokaryotes, 967–972

Posttranslational modifications, 63–64, 63f, 123
Potassium ion channels
as archetypical structure, 394–395
hERG, 405
inactivation of, 399–400, 400f
path through, 396f
permeability of, 400
purification of, 394
selectivity filter, 396, 396f, 397f
structure of, 394–397, 395f, 397f, 398
transport model, 397, 397f
voltage-gated, 398–399, 399f
Potassium ions
action potentials and, 393
dehydration of, 396, 397f
hydration of, 397f
Potential energy, 12–13
PP2A, 220
PPARα (peroxisome proliferator-activated receptor), 756
Precose, 334
Precursor ions, 120
Predisposition, 23
Pregnenolone, **837f**
androgen synthesis by, 837–838, 838f
corticosteroids from, 837, 837f
defined, 837
estrogen synthesis by, 837–838, 838f
progesterone from, 837, 837f
structure of, **837f**
synthesis of, 836–838
Pre-initiation complex (PIC), 897–898
Pre-mRNA processing, 900–901, 901f, 908, 908f
Pre-N-degrons, 704
Prephenate branch, 777–778
Prepriming complex, 860, 860f

Pre-rRNA, 900f
Primaquine, 634, 636
Primary active transport, 390
Primary antibody, 116
Primary messenger, 413
Primary protein structure, 34, 41–46
Primary transcripts, 901f
Primase, 848, 848f
Primers
annealing, 269
defined, 846
DNA probes as, 269
in DNA replication, 848, 848f
in polymerase chain reaction (PCR), 269–270, 269f
RNA, 859
Probes. *See* DNA probes
Procaspases, 224
Processivity
defined, 645, 857
in DNA replication, 857–858
Procollagen, 224
Prodrugs, 836
Product ions, 121
Proenzyme, 223
Progesterone, 834, 837, **837f**
Progestogen, 834
Programmed cell death. *See* Apoptosis
Progressive neuromuscular disorder, 509
Proinsulin, synthesis of, 224, 279, 279f, 744
Prokaryotes. *See also* Bacteria
ABC transporters in, 390
defined, 3
DNA-binding proteins in, 950–956
gene expression in. *See* Gene expression (prokaryotes)

glycolysis in, 473
photosynthetic, 606t
proteasomes, 707, 707f
RNA polymerases in, 881, 881f
transcription and translation in, 892f
transcription factors in, 958
Prokaryotic RNA polymerases, 881, **881f**
Proliferating cell nuclear antigen (PCNA), 862
Proline
degradation of, 720, 720f
structure of, 37, **37f**
synthesis of, 771
Prolyl hydroxylase, 758
Promoters
alternative sequences, 890–892, 890f
bacterial, 886–887, 886f, 887f
closed complex, 887, 887f
common elements, 895f
core, 886
defined, 882
open complex, 887, 887f
strong, 886
upstream of, 886
weak, 886
Pro-N-degrons, 704
Proofreading
in DNA repair, 866–867, 866f
kinetic, 924–925, 924f
in transcription, 885
in translation, 923–925, 924f, 970–971
Proopiomelanocortin (POMC), 736
Propionyl CoA, 675–676, 676f, 721, 722–723, **726b**
Prostacyclin, 693, 693f
Prostacyclin synthase, 693, 693f
Prostaglandin, 693, 693f

Prostaglandin H_2
defined, 365
formation of, 365, 366f
synthase-1, 365–366, 365f, 366f
Prostate-specific antigen (PSA), 186
Prosthetic groups, 144
Protease inhibitors, 189
α_1-antiproteinase, 227, 228f
drugs, 189, 189f
in HIV infection treatment, 189, 189f, 994, 994f, 998
initial design of, 994, 994f
pancreatic trypsin inhibitor, 226–228, 227f
serine, 228
Proteases, 346
active sites, 188f
applied to glycoproteins, 346
aspartyl, 188, **188f**
catalytic triad in, 186–187
cysteine, 188, **188f**
defined, 142, 181
metalloproteases, **188f**, 189
reaction facilitation, 180–189
serine, 179
Protease-substrate interactions, 185, 185f
Proteasomes. *See also* Amino acid degradation
19S regulatory unit, 705–706, 705f
20S, 705–706, 705f
26S, 705, 705f
in amino acid degradation, 705–707, 706f, 707f
defined, 705
evolution of, 707, 707f
free amino acid generation, 706f
prokaryotic, 707, 707f
Protein Data Bank (pdb), 136

Protein domains, 52, 52f
Protein folding, 25, 939
essence of, 60
funnel, 60, 61f
as highly cooperative process, 59
illustrated, 25f
Levinthal's paradox in, 59
misfolding and, 745
nucleation-condensation model, 60, 60f
pathway of chymotrypsin inhibitor, 60f
by progressive stabilization, 59–60
transition from folded to unfolded, 59f
typing-monkey analogy, 60, 60f
Protein identification
cleavage in, 121–123, 122f
co-immunoprecipitation in, 116, 117f
genomic and proteomic methods as complementary, 123
MALDI-TOF mass spectroscopy in, 118–119, 119f
mass spectroscopy in, 118–126, 119f, 121f, 125f
peptide mass fingerprinting, 124, 125f
in protein studies, 101
Protein kinase A (PKA)
cAMP activation of, 221–222, 222f
chains, 418
consensus sequence, 220
Cushing syndrome, 222–223
defined, 219
gene stimulation, 418
in glycogen metabolism, 651, 652f, 656, 657f, 658f
regulation of, 221–222, 222f
in signal transduction, 418–419, 424
Protein kinase B (PKB), 742, 742f
Protein kinase C (PKC), 421, 421f, 743
Protein kinase inhibitors, as anticancer drugs, 435
Protein kinases

defined, 219
in phosphorylation, 219–220, 220t
serine, 219–220, 220t
in signal transduction, 433
specificity, 220
threonine, 219–220, 220t
Protein phosphatase, 220
Protein phosphatase 1 (PP1)
functions of, 653, 656–658
in glycogen metabolism, 653, 656–658, 657f, 659
phosphorylase *a* and *b* and, 659–660, 660f
regulation in muscle, 657f, 658, 658f
regulation of glycogen synthesis by, 656–658, 657f
substrate for, 659
subunits, 658
Protein purification
affinity chromatography in, 104–105, 104f
assays in, 101
binding affinity and, 102–105
cell release and, 101–102
charge and, 102–105
dialysis in, 103, 103f
effectiveness, calculating, 110b–111b
electrophoretic analysis of, 109f
gel electrophoresis in, 105–107, 105f, 106f, 107f
gel-filtration chromatography in, 103, 103f
high-performance liquid chromatography (HPLC) in, 105, 105f
homogenization in, 101–102
ion-exchange chromatography in, 103–104, 104f
isoelectric focusing in, 107–108, 108f
in protein studies, 101
quantitative evaluation of, 109–111, 109t
recombinant DNA technology in, 112
salting out in, 102–103
SDS-PAGE in, 106–107, 107f, 108

sedimentation coefficient and, 111
sedimentation-equilibrium technique in, 111
separation of proteins in, 105–109
size and, 102–105
solubility and, 102–105
two-dimensional electrophoresis in, 108–109, 108f, 109f
ultracentrifugation and, 111
Protein sorting. *See also* Protein targeting
defined, 939
pathways, 941–942, 942f
Protein structures, 2–3
amino acid sequence as determinant, 55–64
amino acid sequences and, 39f, 42f
complex assembly, 34, 34f
determination by cryo-EM, 135–136, 136f
dictating function, 34f
elucidation of, 136
family of, 135, 135f
primary, 34, 41–46, 310–311
quaternary, 34, 55, 55f
secondary, 34, 46–50, 52, 58t
synthetic peptides and, 126
tertiary, 34, 50–54, 310–311, 310f
three-dimensional prediction from sequence, 61–62, 62f
Protein studies
enzyme-linked immunosorbent assay (ELISA) in, 114–115, 115f
fluorescence microscopy in, 117–118, 117f
immunology in, 112–118
mass spectroscopy in, 118–126, 119f, 121f, 125f
peptide synthesis, 126–129
purification methods for, 101–112
steps in, 100
western blotting in, 116, 116f
X-ray crystallography in, 129–132

Protein synthesis, 916–944. *See also* Translation
accuracy of, 917–918, 931
antibiotic inhibitors of, 942–944, 943f, 943t, 944f
endoplasmic reticulum (ER) in, 939–942
eukaryotic versus bacterial, 936–937
insulin and, 739
manipulation of, 938–939, 938f
peptide-ligation methods, 129
polypeptide-chain growth in, 917, 917f
ribosomes as site of, 917, 926–939
RNA in, 880
Protein targeting, 939–942
Protein turnover, regulation of, 703–707. *See also* Amino acid degradation
Protein wasting, 752–754, 754f
Proteinogenic amino acids, 126
Proteins, 33–64
acetylation of, 219–220
adaptor, 428
affinity tags and, 112, 170f
aggregated, in neurological diseases, 62–63, 63f
aggregation of, 703
allosteric, 210, 211–217
alpha helix of, 46–48, 47f
amino acids. *See* Amino acids
antibody generation to, 112–113
β pleated sheets of, 48–50, 49f, 50f
binding and, 70–72
binding partners of, 116
building blocks of, 2
cargo, 941–942
cellular, degradation of, 703
chaperone, 57
cleavage of, 121–123, 122f

coat proteins (COPs), 942
coiled-coil, 53, **53f**
covalent modification of, 218–223, 219t
crystallization of, 130
defined, 2, 43
degradation of, 754, 754f. *See also* Amino acid degradation
denatured, 56, 59, 59f, 162
dietary, digestion and absorption of, 702–703, 702f
disulfide bonds, 43
DNA-binding, 950–956
encoding, 25
enzymes as, 142
fibrous, 53–54
flexibility of, 35, 35f
folding of, 25, 25f
functional groups of, 34
functions of, 33–35
genetically engineered, 281
glycan-binding, 346
glycosylation of, 339
half-life of, 703, 704, 705t
interaction of, 34
internal repeats, 124, 124f
as linear polymers, 34, 41
loops, 50, 50f
membrane. *See* membrane proteins
misfolding of, 62–63
molecular weights of, 111t
native, 57
overview of, 100
phosphorylation of, 223
plasma-membrane, 940, 940f
posttranslational modifications, 63–64
properties of, 33–35

pure, 101
purification of, 101–112
refolding of, 57
regulatory, 954
repressor, 953
reverse turns, 50, 50f
ribosomal. *See* ribosomes
rigidity of, 35
S values of, 111t
secretory, 940, 940f
secretory pathway, 939
separation of, 100, 105–109
subunits of, 55
tagging for destruction, 703–705
translocation of, 940–941
unfolding of, 59, 59f
Proteoglycans
in cartilage, 340–341, 340f
defined, 338
properties of, 339–340
structural roles, 339–340
Proteolysis, 142, 753
Proteolytic activation, 223–228
apoptosis by, 224
of chymotrypsinogen, 224–225, 224f
zymogens, 225f, 226
Proteolytic enzymes
activation of, 223–228
in blood clotting, 228–229
chymotrypsinogen as, 224, 224f
in digestion, 224–225
function of, 143
inhibitors of, 226–228
Proteomes, 125–126
Proteomics, 125

Prothrombin, 228–229, 229f
Proton abstraction, 193
Proton dissociation, 18
Proton gradients
    across thylakoid membrane, 599–602
    in ATP synthesis, 562–569
    biochemical processes and, 579–581
    cytochrome *bf* contribution to, 596, 596f
    formation of, 548–549
    in oxidative phosphorylation, 458, 458f, 543, 548–549, 562–569
    in photosynthesis, 592
    photosystems and, 593–599
    power transmission by, 579–581, 581f
Proton shuttle, 193, 194f
Proton transport, 558–559, 559f
Proton-motive force
    ATP forms without, 565–566, 565f
    energy in, 599
    in oxidative phosphorylation, 543, 562–563, 563f, 565–567, 565f
    in photosynthesis, 599
Proto-oncogenes, 433
Protoplasts, 296
Protoporphyrin IX, 786, 787f
Protospacer-adjacent motif (PAM), 294
Proviral DNA, 290
Proximal histidine, 73, 79, 79f
Prusoff, William, 987
Pseudo-first-order reactions, 152
Pseudogenes, 283–284
Pseudosubstrate sequence, 222
Psi (ψ) angle, 45, 45f, 46f
Psoralens, 866, 866f
P-type ATPases
    defined, 384

as evolutionarily conserved, 387–388
roles of, 387–388
SERCA, 384–387
Puffer fish, genome of, 286–287
Pumps
ATP-driven, 384
calcium ion, 384–387, 385f
defined, 384
ion gradients, 382
MDR, 388
Na^+–K^+, 384, 387, 387f
purification of, 384
Pur repressor, 954f, 955
Pure noncompetitive inhibition, 166, 168f
Purine catabolism, 809f
Purine nucleotide synthesis, 783, 797–801
AMP in, 799–800, 799f
control of, 807–808, 808f
de novo pathway for, 796f, 797, 797f, 798–799, 798f, 799t
enzymes of, 800
GMP in, 799–800, 799f
5-phosphoribosyl-1-pyrophosphate (PRPP) in, 797, 807–808
phosphorylation in, 797–799, 798f
ribose phosphate in, 797
salvage pathway for, 797, 800
Purine nucleotides, 792, 797
Purine synthesis, 799–800, 799f
Purinosomes, 800, 800f
Puromycin, 943, 943t, **943f**
PurZ, 801, 801f
Pyran, 327
Pyranose, 327, 327f, 329–330
Pyridoxal phosphate enzymes
bond cleavage in, 712, 712f

reaction choice, 711–712, 711f, 712f
stereoelectronic effects, 712, 712f
Pyridoxal phosphate (PLP)
in amino acid degradation, 709–710, 711–712
in glycogen metabolism, 643–645, 644f
in Schiff-base intermediates formation, 709–710
in Schiff-base linkage, 769
structure of, **709**, **711f**
Pyridoxamine phosphate (PMP), 710, 710f, **710**, 769f, 770
Pyridoxine (vitamin B_6), 463t, 464f, 709–710, **709**
Pyrimidine nucleotide synthesis, 783, 793–797
carbamoyl phosphate in, 793f, 794
control of, 807
cytidine triphosphate (CTP) in, 796
de novo pathway for, 792, 792f, 796
glutamine in, 796
mono-, di-, and triphosphates in, 796
orotate in, 794–795
5-phosphoribosyl-1-pyrophosphate (PRPP) in, 779, 795
regulation of, 807
salvage pathway for, 796–797
substrate channeling in, 794
Pyrimidine nucleotides
defined, 792
recycling of, 796–797
Pyrimidines, 866, 866f
Pyrosequencing, 284, 285f
Pyrrolidine rings, 37, 54, 54f
Pyruvate
alcohols, formation from, 486–487
in amino acid degradation, 712–713, 718, 719, 719f
in amino acid synthesis, 769
in ATP formation, 484–485
carboxylation of, 501–502, 535

conversion into phosphoenolpyruvate, 484, 501–503, 502f
fates of, 486, 486f
formation of, 484–485, 719, 719f
glucose conversion into, 485–486
in glycolysis, 473, 473f, 476f, 485–486, 486f
in ligation reactions, 467
metabolism disruption, 535–536
oxaloacetate synthesis from, 467
reduction of, 487, 487f
structure of, **101**, **159**, **712**
Pyruvate carboxylase
in citric acid cycle, 534–535
in gluconeogenesis, 500f, 501–502, 501f, 502f
Pyruvate carboxylase deficiency (PCD), 510–511
Pyruvate decarboxylase, 486
Pyruvate dehydrogenase, 531–533, 532f, 535
diabetic neuropathy from inhibition of, 532–533
Pyruvate dehydrogenase complex, 515, 516
of *B. stearothermophilus*, 520f
carbon dioxide production, 518–521
in citric acid cycle, 516, 517–521, 518f, 520f, 522f, 531–533, 531f, 532f
components of, 518–521, 520f
of *E. coli*, 518t
mechanism, 518–520, 519f
reactions of, 520–521, 522f
regulation of, 531–532, 531f
response to energy change, 531, 532f
Pyruvate dehydrogenase, in citric acid cycle, 531–533
Pyruvate dehydrogenase phosphatase, 531
Pyruvate kinase
in glycolysis, 494, 495f, 496–497, 497f
liver and glycolysis and, 496–497, 496f
muscle and glycolysis and, 494

Pyruvate kinase isozyme (PKM), 633
Pyruvate kinase M, 498

Q cycle
    defined, 555
    in respiratory chain, 555–556, 555f
Q pool, 553
Q-cytochrome c oxidoreductase, 549, 549f, 550t
    defined, 554–555
    in respiratory chain, 554–555
    structure of, 554f, 555
Quantitative PCR (qPCR), 287, 287f
Quaternary protein structure, 34, 55, 55f
Quinones
    oxidative states of, 550–551, 550f
    in photosynthesis, 592, 592f
    ubiquitous, 561
Quinonoid intermediate, 710

R groups, 35, 37f. *See also* Amino acid side chains
R state of hemoglobin, 78, 78f, 79
Racemizations, 711
Raf, 432
Ramachandran, Gopalasamudram, 45
Ramachandran plot
    for angles of rotation, 46f
    β strands, 48f
    defined, 45–46
    for helices, 47, 47f
Random-coil conformation, 56
Ras
    activation of, 432, 432f
    affixation to cytoplasmic face, 218
    GTPase activity of, 432
    in protein kinase cascade initiation, 432–433

Ras genes, 271
Rate constants, 152
RBP4, 737
R-carvone, **436**
Reaction centers
accessory pigments and, 602–605, 603f, 604f
bacterial, 591f, 592–593, 592f, 593f
chloroplasts and, 590–591, 591f
cyclic electron flow in, 592–593
defined, 590
photosystem I, 597–598, 597f
photosystem II, 594–596, 594f
Reaction rates
defined, 152
enzymes and, 148, 148f
kinetics as study of, 152
rate constants, 152
Reactions
acid–base, 17–18
ATP hydrolysis, 204, 204f
bimolecular, 152
in Calvin–Benson cycle, 611–620, 617f
carbonic anhydrases and, 190–194
of citric acid cycle, 528
deleterious, 480
DNA ligase, 849–850, 849f
double-displacement, 160–161
elongation, 692
enzyme acceleration of, 148–151
equilibrium, 146–147
equilibrium constant of, 146
in fatty acid oxidation, 673t
in fatty acid synthesis, 684–689, 686t, 687f
first-order, 152

free-energy difference of, 145
of gluconeogenesis, 504t
group-transfer, 465–466
hydrolytic, 466
isomerization, 467
ligation, 467
multiple-substrate, 159–161
oxidation-reduction, 465
oxygenase, 614–615, 614f
pentose phosphate pathway, 627–630, 629f, 630f
pseudo-first-order, 152
reduction potentials of, 548
second-order, 152
sequential, 159–160
standard reduction potentials of, 547t
transaldolase, 629–630, 630f, 631f
transketolase, 627–628, 629f, 631f
velocity versus substrate concentration, 149, 149f
Reactive oxygen species (ROS)
accessory pigments and, 604
defined, 560
DNA damage and, 865
exercise and, 561
glucose 6-phosphate dehydrogenase in protection against, 634–635
pathological conditions that may entail injury, 560t
release prevention, 74
source of, 677
Reactive substrate analogs, 170, 170f
Real-time PCR, 287
RecA, 872–873, 957
Receptor tyrosine kinase, 426
Receptor-mediated endocytosis, 375–376, 375f, 376f, 829, 829f
Receptors, 413
Reclinomonas americana, 545

Recognition helix, 951
Recognition sequence, 194
Recognition sites (sequences)
in cognate and noncognate DNA, 197–199, 198f, 199f
defined, 194
distortion of, 198, 198f
EcoRV endonuclease, 197f, 198
structure of, 197, 197f
Recombinant DNA
formation of, 272–273
manipulation of, 272
Recombinant DNA technology
amino acid sequence information, 123
in biology, 272–281
blotting techniques in, 265, 266–267, 267f
cloning in, 277–278
cohesive-end method in, 272, 273f
complementary DNA (cDNA) in, 278–279, 278f, 279f
complete genome, 282–287, 282f
disease-causing mutations, functional effects of, 271–272
in disease-causing mutations identification, 271–272
DNA probes in, 266–267, 268–269
DNA sequencing in, 265, 267–268
DNA synthesis in, 268–269, 268f
electroporation in, 296, 296f
eukaryotic genes, 287–296
functional effects of disease-causing mutations and, 271–272
gel electrophoresis in, 266–267, 266f
gene disruption in, 290–294, 291f, 292f, 294f
gene expression analysis in, 287–289, 287f, 288f
gene insertion into eukaryotic cells, 289–290
gene therapy in, 296
genome comparison, 286–287, 286f
genome sequencing, 282–283
genomic libraries in, 277–278, 277f, 278f

human genome, 283–284, 283f
λ phage in, 275–276, 276f
mutation creation, 279–281
in mutation identification, 271–272
next-generation sequencing methods, 284–286, 285f, 286f
in plants, 295–296, 295f
plasmids in, 274–275
polymerase chain reaction (PCR) in, 265, 269–270, 269f, 270f
in protein purification, 112
restriction-enzyme analysis in, 265–266, 272–273
RNA interference in, 294–295, 295f
solid-phase approach in, 268–269, 268f
tools of, 265–272
transformed into animal cells, 289–290
transgenic animals in, 290, 291f
vectors in, 274–276
Recombinant human insulin, 995. *See also* Insulin
Recombinant proteins, 995, 995t
Recombinases, 873, 873f
Recombination, DNA. *See* DNA recombination
Recombination synapse, 874
Recovery, 369, 400
Red blood cells, 80–81, 80f, 81f, 82f
Red fluorescent protein (RFP), 64f
Redox balance, 486
Redox couples, 546
Redox potential. *See* Reduction potential
Reducing agent, 546
Reducing end, 333
Reducing sugars, 330–331
Reductant, 546
Reductase, 764, **765f**
5α-reductase, 838
Reductase mRNA in cholesterol regulation, 827

Reduction potential
measurement of, 546, 546f
of NAD^+, 547
in oxidative phosphorylation, 545–548, 546f
of reactions, 548
Refed state, 741
Refractory period, 404
Regulator genes, 952
Regulatory domains
in amino acid synthesis, 780–782, 781f
recurring, 781f
structures of, 780–781
Regulatory protein P_{II}, 782–783, 782f
Regulatory proteins, 954
Regulatory sites, 211
Release factors
bacterial, 937
ribosome (RRF), 935
translation termination by, 935–936, 935f
Relenza, 348
Renewable energy, 606–607, 607f
Repeating motifs, 124, 124f, 311–312, 312f
Replication factor C (RFC), 862
Replication fork, 859f. *See also* DNA replication
defined, 849
schematic view of, 858f
Replication protein A, 862
Replicon, 861
Reporter genes, 274
Repressors
corepressors, 955
lac, 953, 953f, 954f
λ, 957–958, 957f
protein, 952

pur, 955, 955f
Residue, 42, 53, 54
Resistin, 737
Resonance energy transfer, 603–604, 603f
Resonance structures
ATP (adenosine triphosphate), 453, 453f
defined, 8
depiction of, 8
of orthophosphate, 453f
Respirasome, 559, 559f
Respiration. *See* Cellular respiration
Respiratory chain
coenzyme Q in, 551–552
components of, 549f, 550t
cytochrome c oxidase in, 554–555, 556–559
defined, 543
electron transfer in, 561, 562f
NADH-Q oxidoreductase in, 552–553, 553f
in oxidative phosphorylation, 549–562
Q cycle in, 555–556, 555f
Q-cytochrome *c* oxidoreductase in, 554–555, 554f
succinate-Q reductase in, 553–554
Respiratory control, 573–574, 575f
Respiratory quotient (RQ), 748, 748f
Restriction endonucleases. *See* Restriction enzymes (endonucleases)
Restriction enzymes (endonucleases), 179
analysis, 265
catalytic strategies of, 179, 194–200
defined, 194, 265
in DNA cleavage, 194–200, 265–266
in *E. coli*, 194
in forming recombinant DNA molecules, 272–273
hydrolysis of phosphodiester bond, 194–195, 195f
inverted repeats, 197, 197f

recognition sites, 197, 197f, 198f
restriction-modification systems, 200
specificity, 197, 200, 266, 266f
type II, 194
Restriction fragments
separation by gel electrophoresis, 266–267, 266f
in Southern blotting, 266
Restriction-fragment-length polymorphisms (RFLPs), 271
Restriction-modification systems, 200
11-*cis*-retinal, 438–440, **438**, 439f
Retinitis pigmentosa, 906
Retinol (vitamin A), 464t, 756
Retrovir, 189
Retroviruses
in drug resistance evolution, 998
in gene introduction, 290
transduction of, 290
Reverse cholesterol transport, 832
Reverse transcriptase, 863
Reverse turns, 50, 57–59
Reversible covalent modification, 468, 782–783, 782f
Reversible inhibition, 164, 166–168, 166f, 167f. *See also* Enzyme inhibition
Reversible terminator method, 285
Revertants, 871
Rhinovirus, 55
Rhizobium bacteria, 764
Rho, 889–890, 889f, 890f
Rhodobacter capsulatus, 364
Rhodopseudomonas blastica, 364f, 365f
Rhodopseudomonas viridis, 590, 591f, 606
Rhodopsin, 370, 438–440, 439f
Rhodospirillum rubrum, 551
Riboflavin (vitamin B_2), 463t, 464f

Ribonuclease
amino acid sequences in, 56–57, 56f, 57f
denatured, 56
reduction and denaturation of, 56f
sequence comparison of, 302, **302f**
structure of, 56–57, 56f
Ribonuclease III (RNase III), 899
Ribonuclease P (RNase P), 899
Ribonucleic acid (RNA). *See* RNA
Ribonucleotide reductase
defined, 801
in deoxyribonucleotide synthesis, 801–803, 802f, 804f, 808–809, 808f
elements of, 802, 802f
mechanism, 803
regulation of, 808–809, 808f
stable radicals, 803–804, 804f
tyrosyl radicals, 802f, 803
Ribose, 326–327, 326f, 329f
Ribose phosphate, 797
Ribosomal initiator element (rInr), 895
Ribosome release factor (RRF), 936
Ribosomes
bacterial, 936–937
catalysis by proximity and orientation, 933
defined, 916, 921
endoplasmic reticulum bound, 939–942, 939f, 940f
eukaryotic, 936–937
gene expression and, 938
large subunit (50S) of, 927, 927f, 929f, 931–932, 933, 935
polysomal, 935, 935f
in protein synthesis, 916–917, 926–939
schematic representation, 930f
70S subunit of, 927, 927f, 929f, 931
sites of, 928–929, 929f

small subunit (30S) of, 927, 927f, 929f, 931
structure of, 927, 927f
subunits of, 927, 927f
in translation, 921, 926–939
tRNA-binding sites, 928–929, 929f
Riboswitches, 891, 891f
Ribozyme, 142, 909
Ribulose 1,5-bisphosphate, 611–612, **611**, 613f, 615–618, 617f
Ribulose 5-phosphate
in pentose phosphate pathway, 624, 626, **627**, 631–633
structure of, **626**
Ricin, 944
Ricinus communis, 944
Rickets, 840
Rickettsia prowazekii, 545
Rieske center, 555
Rifampicin, 538
Right operator, 957, 957f
RNA, 6. *See also* Transcription
ATP binding of, 320–321, 320f, 321f
compared to DNA, 85
double-stranded, 294–295, 295f
enzymes from, 912
guide strand, 295
messenger. *See* mRNA (messenger RNA)
micro, 908, 909f, 971–972, 971f
passenger strand, 295
primer, 859
ribosomal. *See* rRNA (ribosomal RNA)
roles of, 880–881
single guide (sgRNA), 293, 293f
small interference (siRNA), 295, 295f, 972
small nuclear (snRNA), 903–906
small regulatory, 908, 908f

splicing of, 902f, 903–906, 905f
structure of, 320, 321f
synthesis of, 882
transfer. *See* tRNA (transfer RNA)
RNA editing, 908–909, 909f
RNA interference (RNAi), 294–295, 295f, 971
RNA polymerase holoenzyme complex, 886, **887f**
RNA polymerase I, 894, 895f
promoter sequences, 895
in RNA synthesis, 894, 895, 895f
rRNA production, 899–900
RNA polymerase II, 894, 895f
promoter region, 896
promoter sequences, 895
in RNA synthesis, 894, 895f, 896
RNA polymerase III, 894, 895f, 897f, 899, 899f
promoter sequences, 895
tRNA (transfer RNA), 900
RNA polymerases, 896f
active site of, 882
backtracking and, 885, 885f
in bacteria, 886–887
catalytic action of, 881–890
defined, 881
in DNA replication, 848, 848f
DNA templates and, 882
in *E. coli*, 881, 881t, 882, 887f, 890
eukaryotic, 881, 881f, 894–895, 894t, 896f
eukaryotic promoter elements, 895–896, 896f
functions of, 881
metal ions and, 882, 883f
phosphodiester bonds, formation of, 882–884
prokaryotic, 881, 881f
promoter sites in, 886–887

in proofreading, 885
structure of, 881, **881f**
subunits of, 886
in transcription, 881–890
types of, 894–895, 894t
RNA processing
eukaryotic pre-rRNA, 899f, 900
of pre-mRNA, 899f, 900–901, 901f
in transcription of eukaryotes, 892–893, 908, 908f
tRNA, 898–899, 901f
RNA sequences, comparison of, 314, 314f, 315b, 316f
RNA splicing, 901–902, 902f. *See also* Splicing
RNA-DNA hybrid
backtracking, 885, 885f
during elongation, 888, 888f
lengths of, 885
separation, 885, 885f
translocation, 885, 885f
RNA-induced silencing complex (RISC), 295, 295f
RNA-seq, 289
Rodbell, Martin, 425b
Rods, 438, 438f
Rofecoxib (Vioxx), 997
Rotational catalysis in ATP synthase, 567, 567f
Rotenone, 577, 577f
rRNA (ribosomal RNA)
in base pairing, 927
folding of, 928
in structural scaffolding, 928
transcription of, 898–899, 899f, 900f
in translation, 927–928, 928f
Rubisco
in Calvin–Benson cycle, 611–615, 612f, 613f, 614f, 621
defined, 611
magnesium ion in, 612–613, 613f

oxygenase reaction, 613f, 614–615, 614f
structure of, 611–612, 612f

S_1 pockets, 185, 185f, 186
Saccharomyces cerevisiae, 283, 488, 881f, 958
Salicin, 980
Salicylic acid, 980, **980**
Salmonella test, 871–872, 871f
Salmonella typhimurium, 579–580, 579f
Salt fractionation, 110
Salting out, 102–103
Salvage pathways. *See also* Nucleotide synthesis
defined, 792, 792f
for IMP and GMP synthesis, 811
purine, 797, 800
pyrimidine, 796–797
Sample half-cell, 546
Sandwich ELISA, 115, 115f
Sanger, Frederick, 43, 267, 282
Sanger dideoxy method, 267, 267f
Sarcin-ricin loop (SRL), 931
Sarcoplasmic reticulum Ca^{2+} ATPase. *See* SERCA

Sarin, **182**
SARS-CoV-2, 89, 89f, 100, 880, 881. *See also* COVID-19
Saturated fatty acids, 679
S-carvone, **436**
Schiff bases
in amino acid degradation, 709–711, 711f
in amino acid synthesis, 766, 767f
in aminoacrylate, 779, **779**
linkage with PLP, 644f
in retinal, 438f
in transaldolase reaction, 629–630, 630f, 631f

Scissile bond, 185, 185f
Scoring system, 307, 307f
Screening libraries, 982–983, 983f
Screw sense, 47, 47f
scRNA-seq, 289
Scurvy, 63, 756–757
SDS (sodium dodecyl sulfate), 106
SDS–polyacrylamide gel electrophoresis (SDS-PAGE), 106–107, 107f, 109, 110, 363, 363f
Second Law of Thermodynamics, 13–15
Second messengers, 413–414, 413f, 421–422, 424–425
Secondary active transport, 390
Secondary antibody, 116
Secondary assays, 982
Secondary protein structure, 34, 46–50, 52, 58t
Secondary transporters, 390–392, 390f, 391f
Second-order reactions, 152
Secretory pathway, 939
Secretory proteins, 940, 940f
Sedimentation coefficients, 111
Sedimentation equilibrium, 111
Sedoheptulose 7-phosphate, **627**
Selectins, 347
Selectivity filter, 396, 397f
Self-splicing, 909–912
    defined, 909
    example of, 910, 910f
    intron structure, 910f
    mechanism, 910, 911f
Sense (+) strand, 884
Sensory systems
    evolution of, 441–442, 441f
    7TM receptor and, 436–437, 436f
    signal transduction and, 435–442, 436f
Sequence alignment

with conservative substitution, 307f
defined, 303
distant evolutionary relationships, 305–308
with gap insertion, 303, 304f
of hemoglobin, 307f, 308f
homologous sequences, 308–309
of identities only versus Blosum-62, 307f
of leghemoglobin, 307, 307f, 308f
of repeated motifs, 311–312, 312f
scoring system, 307f
shuffling and, 304f, 305, 305f
statistical analysis of, 302–305
statistical comparison of, 305, 305f
three-dimensional structures in evaluation of, 311
Sequence comparison methods, 302, 310
Sequence identities, 303
Sequence template, 311
Sequential model
allosteric enzymes, 215
of hemoglobin-oxygen binding, 78–79, 78f
Sequential reactions, 159–160
SERCA
defined, 384
P-type ATPase, 384–387
pumping by, 385–386, 385f
structure of, 385–386
Serine, **41f**, 719, 719f
in catalytic triads, 183–185, 183f
in chymotrypsin, 181–182, 182f
in cysteine synthesis, 772, 776
defined, 38
from glycine, 719, 719f
in glycine synthesis, 772
pyruvate formation from, 719, 719f
in sphingolipid synthesis, 819, 819f, **819**

sphingosine from, 783
structure of, **38f**, 41, 41f
synthesis of, 772, 776
Serine dehydratase, 712
Serine hydroxymethyltransferase, 772
Serine kinases, 219–220, 220t
Serine phosphatases, 431
Serine protease inhibitors, 226–227
Serine proteases
catalytic strategies of, 179, 183–185
convergent evolution and, 313, 313f
Serotonin, synthesis of, 783, **783f**, 785, 785f
Serpins, 226–227
Seven-transmembrane-helix (7TM) receptor
defined, 415
G proteins and, 424–425, 425f
in glycogen metabolism, 652, 652f
ligand binding to, 415–418
in olfaction, 436–437
phosphoinositide cascade activation, 420–421, 420f, 421f
sensory systems and, 436–437, 436f
in signal termination, 419f
in signal transduction, 415f, 419f, 420–421
70S initiation complex, 931, 931f
70S ribosomes, 927, 927f, 929f, 931
Severe Acute Respiratory Syndrome (SARS), 26
Severe combined immunodeficiency (SCID), 809–810
SgRNA (single guide RNA), 293, 293f
Shaker channel, 394, 399, 399f
Shaker gene, 394
Shape complementarity, 847–848, 847f
Shemin, David, 786
Shikimate in amino acid synthesis, 776–779
Shine, John, 930
Shine–Dalgarno sequences, 930

Short interspersed elements (SINES), 284
Shuffled sequences, 304f, 305, 305f
Sialic acids, **332f**, 819
Sick sinus syndrome, 405
Sickle-cell anemia, 21, 23, 44, 83, 83f
Sickled red blood cells, 83f
Side chains
    amino acid. *See* amino acid side chains
    hydrophilic, 52
    hydrophobic, 52
    polypeptide chains, 42, 42f, 52
Side effect, 987, 997
Sigma (σ) subunit, 886–887, 887f, 890–892
Sigmoid oxygen-binding curve, 76
Sigmoidal curve, 215, 215f
Sigmoidal kinetics, 212, 212f, 215
Signal peptidase, 940
Signal sequence, 940
Signal transduction, 412–442
    abnormalities in cancer, 433, 434, 434f, 435f
    adaptor proteins in, 428
    β-adrenergic receptor in, 415, 415f, 416f, 419f
    calcium ions in, 420–422, 422f
    calmodulin in, 420, 423, 423f
    cAMP in, 412, 418–419
    cross talk, 414
    defects, 433–435
    defined, 412
    EGF signaling, 431–433
    epidermal growth factor (EGF) in, 414f, 431–433, 432f, 433f
    epinephrine in, 414–425, 414f, 416f, 419f
    function of, 413, 414f
    G proteins in, 415–418, 417f
    in glycogen metabolism, 651–653

GTPases and, 433
in hearing, 440–441, 441f
insulin in, 414f, 425–431, 742–743, 742f, 744f
molecular circuits, 413–414
monoclonal antibodies as inhibitors, 434, 434f
nucleotides in, 792
in olfaction, 436–437, 436f, 437f
overview of, 413–414, 413f
primary messenger, 413
principles of, 413–414, 414f
protein kinase A in, 418–419, 424
protein kinases in, 433
Ras in, 432, 432f
second messengers, 413–414, 413f, 421–422, 424
sensory systems and, 435–442, 436f
7TM receptors, 415f, 419f, 420–421
in vision, 437–439, 439f
Signal-recognition-particle (SRP), 940, 940f
Sildenafil, 980, **980f**
Simple diffusion, 382
Single guide RNA (sgRNA), 293, 293f
Single-cell RNA-seq, 289
Single-molecule methods, 15–17, 16f
Single-molecule Michaelis–Menten equation, 164
Single-molecule studies, enzyme, 162–165, 163f
Single-particle analysis, 135
Single-stranded DNA, 266
Single-stranded-binding protein (SSB), 858, 858f
Sinoatrial (SA) node, 405
Site-directed mutagenesis, 187–188, 187f, 280, 280f
Sliding DNA clamp, 857, 857f
Slow-twitch muscle fibers, 649, 747
Small G proteins, 432
Small interference RNA (siRNA), 295, 295f, 972
Small nuclear ribonucleoprotein particles (snRNPs), 903–906, 903f

Small nuclear RNA (snRNA), 903–906
Small nucleolar ribonucleoprotein (snoRNPs), 899
Small subunit (30S) of ribosomes, 927, 927f, 929f, 931
Smell. *See* Olfaction
Smooth endoplasmic reticulum (SER), 667, 668f, 939
SNARE proteins, 376, 376f
Snell, Esmond, 770b
SOD1 gene, 272
Sodium dodecyl sulfate (SDS)
    in gel electrophoresis, 105f, 106–107
    PAGE, 106–107, 107f
Sodium ion channels, 396–397
    inactivation of, 399–400
    paddles, 404
    purification of, 394
    selectivity filter, 397f
Sodium ions, 393
Solid-phase DNA synthesis, 268–269, 268f
Solid-phase peptide synthesis, 127–129, 128f
Somatostatin, 735t
Sonicating, 360
Sos, 432, 432f
Southern, Edwin, 266
Southern blotting, 266, 267f, 290
Space-filling models, 76f
Special pair, 591, 592, 592f
Specific activity, 101
Specificity, dissociation constants and, 93–94
Specificity constant, 158–159
Sperm whale myoglobin, 73
Sphingolipids
    ceramide and, 819, 819f
    defined, 819
    diversity and, 821

gangliosides, 819
synthesis of, 819, 819f
Sphingomyelin, 359f
defined, 357, 819
structure of, **357f**, **820f**
Sphingosine, 356
defined, 357
structure of, **357f**, **819**
synthesis of, 783, **783f**
Spike protein, 89, 89f
Spliceosomes, 902
assembly and action, 903–906, 905f
catalytic center, 905, 905f
defined, 902
mRNA precursors and, 903–904
structure of, **904f**
Splicing
alternative, 906–907, 907f, 907t
branch points in, 902, 903f
catalytic center, 905, 905f
defined, 902
group I, 910, 911f
group II, 911, 911f, 912
mechanism, 902f, 905f
mRNA precursors, 903–906
mutations affecting, 906, 906f
pathways comparison, 911f
self-splicing and, 909–912, 910f, 911f
sites of, 902f, 903–906
snRNPs in, 903–906
spliceosomes in, 902–906, 905f
transesterification in, 902–903, 903f, 905f
Splicing factors, 903
Split-pool synthesis, 982–983, 983f, 984f
Squalene

cyclization of, 824–825, 825f
synthesis of, 823, 824–825, 824f, 825f
Squalene synthase, 823
SREBP (sterol regulatory element binding protein), 756, 825–827, 826f, 830
SREBP cleavage activating protein (SCAP), 826–827, 826f
SRP receptor, 940, 940f, 941f
Stable radicals, 803–804, 804f
Standard free-energy change, 146–147, 147b, 147t
Standard reference half-cell, 546
Staphylococcus aureus, 172–173, 173f, 979
Starch, 335, **336f**, 618
Starvation, metabolic adaptations in, 752–754, 753t
Statins, 166, 833
Stator, 566
Steady-state assumption
defined, 152–153
in enzyme kinetics, 152–153
Steady-state system, 152–153
Stearoyl CoA desaturase, 692, 693f
Steatorrhea, 667
Steitz, Joan, 903
Steitz, Tom, 846
Stereochemistry
of cleaved DNA, 196, 196f
observation of, 196
of proton addition, 769f, 770f
Stereocilia, 440–441, 440f, 441f
Stereoelectronic control, 712, 712f
Stereoisomers, carbohydrate, 325, 326f
Steric exclusion, 46
Steric repulsion, 44
Steroid hormones
binding and activation, 834
cholesterol as precursor, 827, 834, 834f

classes of, 834
defined, 834
hydroxylation of, 834–836
identification of, 834
synthesis of, 834–836, 834f
Sterol regulatory element binding protein (SREBP), 756, 825–827, 826f, 830
Sterol regulatory element (SRE), 825–826
Stewart, Sarah, 962b
Sticky ends, DNA, 272–273, 273f
Stochastic processes, 16
Stoichiometric coenzymes, 144
Stoichiometry
of gluconeogenesis, 504
for light reactions, 602
of palmitate synthesis, 690
Stoma, 623f, 624
Strand invasion, 872–873, 873f
Strand separation, 269, 269f
Streptococcus lactis, 488
Streptococcus pyogenes, 293, 294b
Streptococcus thermophilus, 488
Streptomyces achromogenes, 265
Streptomyces coelicolor, 891
Streptomyces lividans, 395
Streptomycin, 942, **942**, 943t
Stroma, 588, 594f, 596f
Stroma lamellae, 588
Strominger, Jack, 91, 979
Structural genes, 952
Structure-activity relationship (SAR), 994
Structure-based drug development, 993–995, 994f
Stryer, Lubert, 28
Stubbe, JoAnne, 804b

Substituted enzyme intermediates, 161
Substitution matrix, 305–308, 306f, 307f, 309f
Substitutions
in amino acid sequences, 305–308, 306f, 307f, 309f
conservative, 305, 307f, 308f
nonconservative, 305, 307f
Substrate binding
in catalysis, 151
conformation selection, 151
induced-fit model, 151, 151f, 180
lock-and-key model, 150–151, 151f
Substrate channeling
in amino acid synthesis, 779, 779f
defined, 497, 530
in pyrimidine synthesis, 794
Substrate cycles, 508, 508f
Substrate-induced cleft closing, 477
Substrate-level phosphorylation, 482–483
Substrates. *See also* Enzyme-substrate (ES) complex
accessibility of, controlling, 467–468
in biochemical reactions, 159–161
chromogenic, 182, 182f
concentration, 152f, 153–155, 153f, 156
defined, 142
enzyme interaction, 150–151
homotropic effect on allosteric enzymes, 215
multiple, in reactions, 159–161
reciprocal relation, 808
spectroscopic characteristics of, 149
Subtilisin
catalytic triad of, 186–187, 187f
oxyanion hole of, 186–187, 187f
site-directed mutagenesis of, 187, 187f
structure of, 313, **313f**
Subunit, polypeptide chain, 55

Succinate
in glyoxylate cycle, 537, 537f
oxidation of, 528–529
in oxidation-reduction reactions, **465**
Succinate dehydrogenase in citric acid cycle, 528–529
Succinate-Q reductase, 549, 549f, 550t, 553–554
Succinyl CoA
in amino acid degradation, 718, 719f, 721, 721f
in citric acid cycle, 526–527, 527f
formation of, 526, 677–678, 678f, **678f**
porphyrins from, 786–787
Succinyl CoA synthetase
in biochemical transformation, 527
reaction mechanism of, 527, 527f
Sucrase, 334, 474
Sucrose
defined, 334
structure of, 333–334, **333f**
synthesis of, 618, 619f
Sucrose 6-phosphate, 618, 619f
Sugars
in cyclic forms, 327–329
DNA, 4
five-carbon, 615–616, 616f, 624–630
monosaccharides. *See* Monosaccharides
N-linked, 341–342
nonoxidative interconversion of, 624
O-linked, 341–342
phosphorylation, 333
reducing, 330–331
Suicide inhibition, 171, 806, 806f, 810
Suicide inhibitors, 171
Sulfamethoxazole, 807
Sulfanilamide, 166, **166**

Sulfhydryl groups, 39
Sulfolipids, 588–589
Sulfolobus archaea, 2f
Sulfolobus shibatae, 855f
Summers, Michael, 28, 28f
Supercoiling
    ATP hydrolysis in, 855–857, 856f
    catalyzation of, 855
    defined, 851
    degree of, 851–853
    DNA, condenses, 853f
    linking number and, 852f, 853
    negative, 853f, 854, 855–857, 856f
    positive, 854
    relaxation of, 854–855, 854f
    right-handed, 852
    topoisomerases and, 854–857, 854f, 856f
    twist in, 852f, 853
    writhe in, 852f, 853
Superhelical cable, 54
Superoxide anion, 74
Superoxide dismutase, 560–561, 560f
Superoxide radicals, 560–561
Supersecondary structures, 52, 52f
Suppressors of cytokine signaling (SOCS), 737–738, 738f
Surface complementarity, 12
Surroundings, 12
Sutherland, Earl, 425b
Svedberg units, 111
Symmetry matching, 951
Symporters, 390, 390f
Synaptic cleft, 400, 400f
Synaptic vesicles, 375f
Synchrotron radiation, 130

Syngas, 692
Synthetic biology, 620, 620f
Synthetic oligonucleotides, 320–321
Synthetic peptides
    as antigens, 126
    construction of, 126–129, 128f
    as drugs, 126, 127f
    linking of, 129
    in receptor isolation, 126
    in three-dimensional structure of proteins, 126
Synthetic vaccines, 281
Systems, 12

T cells, killer, 86
T state of hemoglobin, 78, 78f, 82
Tamiflu, 348
Tamoxifen, **93**, 95f
Tandem mass spectroscopy, 121, 121f
Taq DNA polymerase, 270
Target, in drug development, 978
Target validation, in drug development, 978
Target-based screening approach, 985–986, 985f
Taste. *See* Sensory systems
TATA box, in transcription of eukaryotes, 896, 896f
TATA-box-binding protein associated factor (TAF), 966
TATA-box-binding protein (TBP), 312, 312f, 896–897, 897f, 966
Taurocholate, **833f**
Taxol, 977, **977**
Tay–Sachs disease, 820–821
T-cell receptors (TCRs)
    defined, 91
    MHC proteins and, 89–91
    structure of, **91f**
Telomerase, 863–864, 863f
Telomeres, 863, 863f

Temperature, 13, 161–162
Template, DNA
coding strands and, 884, 884f
defined, 846
DNA polymerases, 846
lagging strand, 859
in replication, 846
RNA polymerases and, 882
transcribed regions of, 888–889
transcription bubbles and, 888
Template strand, 884, 884f
Termination utilization substance (Tus), 860
Ternary complex, 159
Terpenes, 840, 840f
Tertiary protein structure, 34, 50–54, 310–311, 310f
Testosterone, 70–71, 71f, **71**, 834, 838, **838f**
Tetracycline, 943t
Tetrahydrobiopterin, 723
Tetrahydrofolate, 773f
in amino acid synthesis, 772–774, 773f
defined, 772
one-carbon groups carried by, 773f, 773t
Tetrahymena, 909, 910f, 911
Tetrapyrrole, 786
Tetraubiquitin chain, **704f**
Tetrodotoxin, **394**
Tetroses, 325
TFIID protein complex, 896–898, 897f
Thalassemia, 906, 906f
Therapeutic index, 993
Thermodynamics
of coupled reactions, 449, 451–452
laws of, 12–14, 734
of metabolism, 448–449
Thermogenin, 576

Thermus aquaticus, 270, 881f
Thiamine (vitamin B_1), 463t, 535, 756
Thiamine pyrophosphate (TPP), 615
in citric acid cycle, 518–519, 519f
deficiency, 535
defined, 535
structure of, **518**
in transketolase reaction, 629, 629f
Thioester intermediate, 481, 481f, 482, 483f
Thioesterase, 689
Thioesters, 462
Thioether groups, 36
Thiol groups, 39
Thioredoxin, 601
in Calvin–Benson cycle, 621–622, 621t, **621f**
enzyme activation by, 622f
enzymes regulated by, 621t
Thioredoxin reductase, 803
30S initiation complex, 931, 931f
3D genome, 863
Three-dimensional structure
conservation of, 310–311, 310f
convergent evolution, 313
repeated motifs, 312
RNA sequences, 314, 314f, 315b
in sequence alignment evaluation, 311
tertiary structure and, 310–311
in understanding evolutionary relationships, 308
Threonine
defined, 38
degradation of, 721–722
pyruvate and, 719
structure of, **38f**
synthesis of, 781

Threonine deaminase, 721–722, 780–781, 780f, **781f**
Threonine dehydratase, 712, 721
Threonine kinases, 219–220, 220t
Threonine operon, 969, 969f
Threonyl-tRNA synthetase, 922–923, **923f**
Threshold effects, 215f, 216
Thrombin, 143, **143f**
    antithrombin and, 232
    in blood clotting, 228–229, 231
    dual function of, 231
    inhibitors of, 232
Thromboxane synthase, 693
Thromboxanes, 693, 693f
Thunnus alalunga, 551
Thylakoid membranes, 594f
    defined, 588
    pH gradient across, 599
    photosynthesis in, 588–589
    photosystem II, 596f
    photosystem II and, 594
    proton gradient across, 599–602
    stacked, 605, 605f
    unstacked, 605, 605f
Thylakoid spaces, 588–589, 599
Thylakoids, 588
Thymidine, 796
Thymidine kinase, 796–797
Thymidine monophosphate (TMP), 804, 805f
Thymidine phosphorylase, 796
Thymidylate
    blocking synthesis of, 805–807, 806f
    defined, 804
    synthesis of, 804–805, 805f
Thymidylate synthase, 804, 805f
Thymine, 796

in DNA repair, 868–869
structure of, **4**, **5**, **5f**
synthesis of, 774
Thyroxine, **963**
Thyroxine, synthesis of, 783, **783f**
Time-of-flight (TOF) mass analyzer, 119, 119f
Tip links, 441, 441f
Tissue factor pathway inhibitor (TFPI), 232
Tissue factor (TF), 228
Titin, 43
Titration, 19
Toll-like receptors (TLRs)
defined, 84
extracellular domain of, 85
illustrated, 85f
PAMPs and, 85f
Topoisomerases
bacterial, 855–857
defined, 853–854
type I, 854–855, 854f
type II, 854, 855–857, **855f**, 856f
Topoisomers, 853, 853f
Torpedo marmorata, 401, 401f
Torsion angles, 45
Tosyl-l-phenylalanine chloromethyl ketone (TPCK), 170, **170**, **170f**, 171
Toxicity, drug, 992–993, 993f
Tractability, 978
Trans configuration, peptide bonds, 44–45, 45f
Trans fat, 679
Trans unsaturated fatty acids, 679
Transacetylase, 520–521, 521f
Transaldolase
in pentose phosphate pathway, 626–628, 629–630, 630f
reactions, 629–630, 630f, 631f
Transaminases

in amino acid degradation, 708–713
defined, 708
mechanism, 710, 710f
Transamination
in amino acid degradation, 709–711
amino acid synthesis by, 767, 769–770, 769f, 770f
Schiff-base intermediates in, 710
Transcription
ATP hydrolysis in, 905
in bacteria, 886, 935, 935f
chemistry of, 882
defined, 881
elongation, 882, 884, 884f, 888, 888f
in eukaryotes, 892–893, 892f
in gene expression, 935, 950
initiation of, 882
mRNA processing and, 908, 908f
nuclear hormone receptors in, 963–965
overview of, 881
in prokaryotes, 892f
promoters in, 882, 886, 886f
proofreading in, 885
regulation of, 890–898, 892f
repression of, 967
rho in, 889–890, 889f, 890f
riboswitches in, 891, 891f
RNA polymerases in, 881–890
of rRNA, 898–899, 899f, 900f
self-splicing in, 909–912, 910f, 911f
splicing in, 880, 902f, 903–906, 903f, 905f
stages of, 882
start site, 886
termination of, 882, 888–890, 889f, 890f
upstream promoter element (UPE) in, 886, 895

Transcription activator-like effector nucleases (TALENs), 292–293, 292f, 293f
Transcription bubbles
defined, 882
elongation at, 888, 888f
schematic representation, 888f
structure of, **883f**
Transcription factors
activation domain, 960
defined, 291, 896, 959
DNA-binding domains of, 958–960
ethanol metabolism and, 756
in eukaryotes, 896–898, 897f, 958–960
in gene expression, 958–960
nuclear hormone receptor, 963–964, 964f
in prokaryotes, 958
regulatory domains of, 960
Transcription in eukaryotes, 890–898
in bacteria versus, 892, 892f
CAAT box in, 896, 896f
carboxyl-terminal domain (CTD) in, 894
control of, 892–893
downstream core promoter element (DPE) in, 896
enhancers in, 898
eukaryotic promoter elements, 896f
GC box in, 896, 896f
initiation of, 892, 896–898, 897f
initiator element (Inr) in, 896
microRNAs in, 902f, 908
nuclear membrane in, 892
pre-mRNA processing and, 899–900, 901f, 908, 908f
products of, 898–909
RNA editing in, 908–909, 909f
RNA polymerases in, 896f
RNA processing and, 892–893, 908, 908f

splicing in, 905f
TATA box in, 896, 896f
transcription factors in, 896–898, 897f
translation and, 892, 892f
upstream promoter element (UPE) in, 895
Transcription initiation, 882
in bacteria, 886
de novo, 884–885
in eukaryotes, 892, 896–898, 897f
Transcription repressors, 960
Transcriptome, 288
Transducin, rhodopsin and, 439
Transduction, 290, 413
Transesterification reactions, 902–903
Transfection, 289
Transferases, 143t
Transferred DNA (T-DNA), 296
Transferrin, 376, 970
Transferrin receptor, 376, 376f, 970
Transferrin-receptor mRNA, 970–971, 970f
Transgenic mice, 290
Transglutaminase, 230
Transition state
ATP hydrolysis, 202–203
in catalysis, 149
collapse of, 151
defined, 148
formation facilitation of, 148–151
symbol, 148
Transition-state analogs, 169, 169f, 173f, 202, 202f
Transketolase, 535, 615
in Calvin–Benson cycle, 616, 616f, 618
in pentose phosphate pathway, 626–628, 629f
reaction, 628–629, 629f, 631f
Translation, 47, 917–921

accuracy of, 917–918, 917t
activation sites, 922–923, 923f
adenylation in, 921–922
aminoacyl-tRNA synthetase in, 921–926
anticodons in, 919–921, 921f
in bacteria, 930, 931f, 935, 935f, 936–937
base pairing in, 919–920, 927–928, 928f
codon-anticodon interactions in, 921
codons in, 920–921, 921f
defined, 917
direction of, 935
elongation factors in, 931–932, 931f, 937
in eukaryotes, 892, 892f, 936–937, 937f
eukaryotic initiation of, 936–937, 937f
formylmethionyl-tRNA in, 930, 930f
in gene expression, 935
initiation factors, 931, 931f
initiation of, 929–930, 930f, 931f, 936–937
initiation sites, 929–930, 930f
mRNA in, 937
organization in, 937
overview of, 916–917
peptide bond formation in, 932–933, 933f
proofreading in, 923–925, 924f, 970–971
reading frame, 931
release factors in, 935–936, 935f
ribosomes in, 921, 926–939
rRNA in, 927–928, 928f
Shine–Dalgarno sequences in, 930
signaling in, 940–941
termination of, 935–936, 935f, 937
translocation in, 933–935, 934f
tRNA in, 918–920, 929, 930f, 936–937
wobble hypothesis and, 920–921, 920t
Translesion polymerases, 864–865

Translocase, 934
Translocation
inhibition by antibiotics, 943–944, 944f
mechanism of action, 934
of proteins, 940–941
RNA-DNA hybrid, 885, 885f
signal sequences in, 940–941, 940f, 941f
in translation, 933–935, 934f
Translocon, 940–941
Transmembrane helices, 367–369
Transport vesicles, 941–942
Transporters
ABC, 388–390, 388f, 389f, 999
antiporters, 390, 390f
ATP-ADP, 572–573, 572f, 573f
dicarboxylate, 573, 573f
glucose, 390, 474, 474t, 498, 498t
glucose 6-phosphate, 661
mitochondrial, 572–573, 572f, 573f
in oxidative phosphorylation, 570–573
phosphate, 572, 573f
in photosynthesis, 589–593, 589f
secondary, 390–392
symporters, 390, 390f
tricarboxylate, 573, 573f
uniporters, 390, 390f
Transverse diffusion, 370, 370f
Trastuzumab (Herceptin), 114, 434
Tree of life, 3f
Triacylglycerol synthesis, 815–821
Triacylglycerol synthetase complex, 816
Triacylglycerols
in adipose tissue, 753
defined, 666–668
electron micrograph of, 666f

as energy source, 692
in fatty acid metabolism, 668–669, 669f
hydrolysis of, 499
pancreatic lipases and, 667f
structure of, **666**
synthesis of. *See* Triacylglycerol synthesis
transport of, 827–829
Tricarboxylic acid (TCA) cycle. *See* Citric acid cycle
Triglycerides. *See* Triacylglycerols
Trimethoprim, 807, **807**
Trinucleotide repeats, 869, 869f
Triose phosphate isomerase deficiency (TPID), 509–510
Triose phosphate isomerase (TPI)
catalytic mechanism of, 479f, 480
in glycolysis, 478–480, 479f
structure of, **479f**
Trioses, 325
Triple helix of collagen, 54f
tRNA (transfer RNA)
acceptor stem, 919
anticodons of, 918, 919–920
bases, 919–920
CCA terminal region of, 919, 919f
charged, 921
codons in, 920–921
common features of, 918–920
defined, 918
extra arm, 919
helix stacking in, 919, 919f
initiator, 936–937
inosine in, 921
molecule design, 918–920, 919f
precursors of, 900f, 919
recognition sites on, 925, 925f

RNA polymerase III and, 900
RNA processing, 898–899, 901f
structure of, **918f**, 919, 919f, **919f**
synthetase recognition of, 925, 925f
in translation, 918–920, 929, 930f, 936–937
translocation of, 933–935, 934f
wobble hypothesis and, 920–921, 920t
Trombone model, 859, 859f
Troponin complex, 419
Trp operon, 968, 968f
TRPV1, 136
Trypanosomes, 909
Trypsin, 143, **143f**
catalytic triad in, 186–187, 186f
chymotrypsin and, 186, 186f
defined, 226
generation of, 226
S_1 pockets, 186f
S_1 pockets of, 186f
structure of, 186f
Trypsin inhibitor, 226–228, 227f
Trypsinogen, 226
Tryptophan, 718, **724**
in alanine, 719
degradation of, 724, 724f
nicotinamide from, 783
as precursor for neurotransmitters, 785, 785f
serotonin from, 783
structure of, 37–38, 37f, **37f**
synthesis of, 778–779, 778f
Tryptophan synthase, 779, **779f**
Tryptophan synthetase, 794
Ts elongation factor (EF-Ts), 932
t-SNARE, 942

T-to-R equilibrium, 216–217, 216f, 217f
T-to-R state transition, ATCase, 214f, 215
T-to-R transition, 78f, 80–81
Tu elongation factor (EF-Tu), 931–932, 931f
Tuberculosis (TB), 538, 707
Tumor hypoxia, 498
Tumor-inducing (Ti) plasmids, 295–296, 295f
Tumor-suppressor genes, 433, 434, 870
Turnover number, 157, 157t
Twin studies, 23, 24t
Twist in supercoiling, 852f, 853
2′, 3′-dideoxy analog, 267, **267**
Two-dimensional electrophoresis, 108–109, 108f, 109f
Two-dimensional NMR, 133–135
Twofold rotational symmetry, 197, 197f
Type 1 diabetes
    defined, 741
    glucagon excess in, 746
    insulin insufficiency in, 746
    metabolic derangements in, 746
    treatment for, 746
Type 2 diabetes
    defined, 741
    exercise and, 746
    metabolic syndrome and, 743, 743f
    treatments for, 660, 745
Type I muscle fibers, 649
Type I topoisomerases, 854–855, 854f
Type II topoisomerases, 854, 855–857, **855f**, 856f
Type IIb muscle fibers, 649
Typing-monkey analogy, 60, 60f
Tyrosine phosphatases, 431
Tyrosine, 718
    defined, 38

degradation of, 723–724, 724f
from phenylalanine, 768, 769
phenylketonuria and, 728
as precursor for neurotransmitters, 785f
structure of, **38f**, **40t**, **162**, **724**
synthesis of, 776–777, 778f
thyroxine from, 783
Tyrosine kinases, 219–220, 426, 427f, 428f
Tyrosine phosphatase IB, 743
Tyrosinemia, 727t
Tyrosyl radical, 802f, 803, 804
Tyrosyl-tRNA synthetase, 924

Ubiquinol, 553–554, 672
Ubiquinone, 550, 672
Ubiquinone reductase, 672
Ubiquitin
conjugation, 703–704, 704f
defined, 703
pathway, 707
in protein tagging, 703–705
research in, 708b
structure of, **703f**
Ubiquitination, 704–705
Ubiquitin-conjugating enzyme (E2), 703, 704f
Ubiquitin-protein ligase (E3), 703–705, 704f
Ubiquitin-activating enzyme (E1), 703, 704f
UDP (uridine diphosphate), 656
UDP-galactose 4-epimerase, 491
UDP-glucose
defined, 490, 653, 792
in galactose conversion, 491
in glycogen synthesis, 654–655
synthesis of, 653–654
UDP-glucose pyrophosphorylase, 653

Ultracentrifugation, 111
Ultraviolet light, and DNA damage, 866, 866f
UMP kinase, 796
Uncompetitive inhibition, 166, 167f, 168f. *See also* Enzyme inhibition
Uncoupling proteins, 576, 576f
Unfolded protein response (UPR), 745
Unicellular red algae, 317, 317f
Uniporters, 390, 390f
Unnatural amino acids, 938–939, 938f
Unsaturated fatty acids, 674–679, 674f, 675f, 692–694
Upstream promoter element (UPE), 886, 895
Uracil DNA glycosylase, 869, 869f
Urate, 810
Urea, 56–57, **56**, 712
Urea cycle
    in amino acid degradation, 713–718
    carbamoyl phosphate in, 714–716
    disorders of, 717–718, 717f
    fumarate in, 715, **716**
    in gluconeogenesis, 716, 716f
    illustrated, 714f
Ureotelic, 718
Ureotelic organisms, 718
Uric acid, 718, **718**
Uridine diphosphate glucose (UDP-glucose), 653–654, **653**
Uridine monophosphate synthetase, 795
Uridine triphosphate (UTP), 211, 451, 653
Uridylate, 795
Uridylyl transferase (UT), 782f
Urine, disease diagnosis and, 726, 726f
Uroporphyrinogen III, 787f, 788

Vaccines
    adaptive immune system and, 89, 89f
    as biologics, 995t

mRNA (messenger RNA), 880–881
synthetic, 281
Vaccinia virus, 290
Valine
degradation of, 722–723
in maple syrup urine disease, 727
structure of, 36, **37f**, 38
van der Waals forces, 150
van der Waals interactions
contact distance, 10, 10f, 12
defined, 9
energy of, 10, 10f
hydrocarbon tails, 360
maximization of, 12
as noncovalent bond, 9–10, 10f, 12
protein stability and, 52
Variable number of tandem repeats (VNTR) region, 341, 341f
Vascular endothelial growth factor (VEGF), 321, 498
Vasopressin, 126, 127f
VDAC (voltage-dependent anion channel), 544
Vectors
cloning, 274, 275, 276f
defined, 272
expression, 275
plasmid, 274–275, 274f
viral, 290
Very-low-density lipoproteins (VLDLs), 828, 828f, 828t
Vibrio cholerae, 344
Vicine, 634, **635f**
Vioxx (rofecoxib), 997
Viral hepatitis, 711
Viral receptors, 348f
Viral vectors, 290
Virions, 275
Viruses

coats, 55, 55f
defined, 26
in gene introduction, 290
infectious mechanisms of, 347–348
influenza, 347–348, 348f
progeny, 275
retroviruses, 290, 998
RNA genomes in, 880
transduction of, 290
Visible light, 438f
Vision. *See also* Sensory systems
in animals, 442
color, 440, 440f, 442, 442f
color blindness and, 442
cones in, 440
evolution of, 442, 442f
ion channels in, 439, 439f, 440
light absorption in, 439–440
7TM receptors in, 437–439
signal transduction in, 437–439, 439f
Visual pigments, 438, 440, 440f
Vitamin A (retinol), 464t, 756
Vitamin B_1 (thiamine), 463t, 535, 756
Vitamin B_2 (riboflavin), 463t, 464f
Vitamin B_3 (niacin), 463t, 464f
Vitamin B_5 (pantothenic acid), 463t, 464f
Vitamin B_6 (pyridoxine), 463t, 464f, 709–710, **709**
Vitamin B_7 (biotin), 463t, 501, 501f
Vitamin B_9 (folic acid), 463t
Vitamin B_{12}, 463t, 677b
as coenzyme, 676–677, 676f, 678
corrin ring and cobalt atom, 676–677
in fatty acid metabolism, 676–677

Vitamin C (ascorbic acid)
deficiency, 464t
deficiency of, alcohol related, 756–757, 757f
forms of, 757, 757f
function of, 464t
Vitamin D (calcitriol)
biochemical role, 839, 840
cholesterol as precursor, 839–840
deficiency, 464t, 840
function of, 464t
synthesis of, 839–840, 839f
Vitamin E (α-tocopherol), 464t
Vitamin K
in blood clotting, 231, 231f, 464t
deficiency, 464t
structure of, **231f**
in γ-carboxyglutamate formation, 231, 231f
Vitamins
coenzyme, 463–464, 463t
defined, 463
evolution of, 464
metabolism of and ethanol, 756–757
noncoenzyme, 464t
in reducing homocysteine levels, 776
V_{max}, 156. *See also* Maximal rate
Voltage-gated ion channels, 398–399, 399f
von Gierke disease, 660–661, 661t
von Gierke, Edgar, 660
v-SNARE, 942
Wald, George, 439
Wang, James, 854
Warburg, Otto, 497
Warburg effect, 497, 575, 758
Warfarin, 231, **231f**

Water
attack, facilitating, 201–202, 202f
concentration of, 17
dissociation, equilibrium constant of, 17
as highly cohesive, 10
hydrogen bonds, 10, 11
as polar molecule, 10
properties of, 10
Water-oxidizing complex (WOC), 594f, 595, 595f, 596f
Watson, James, 5, 6, 845
Watson-Crick base pairs. *See* Bases/base pairs
Wernicke–Korsakoff syndrome, 756
Wernicke's encephalopathy, 535
Western blotting, 116, 116f, 265
Wet beriberi, 535
White adipose tissue (WAT), 575
Wiley, Don, 90, 91
Williams, Roger, 770b
Windows, 368
Withering, William, 387
Wobble hypothesis, 920–921, 920t
Woese, Carl, 3
Wood-Ljungdahl pathway, 692
Wool, 53
Wooly mammoth, 301f
Writhe in supercoiling, 852f, 853
Wyman, Jeffries, 78

Xanthine oxidase, 810
Xanthohumol, **578**
Xanthomas, 830
Xanthylate (XMP), 800
Xenobiotic compounds, 990–991, 990f
Xeroderma pigmentosum, 870, 870t
X-ray crystallography

defined, 129
diffraction patterns, 130–131, 130f
electron-density map, 131, 131f, 132f
experiment, 129–132, 130f
reflections, 130
resolution, 131, 132f
synchrotron radiation and, 130
X-rays, 866
Xylulose 5-phosphate, **627**, **628**

Yanofsky, Charles, 967
Yeast chromosomes, 958
Yonath, Ada, 938b

Z scheme of photosynthesis, 598, 599f
Zanamivir, 348
Zellweger syndrome, 679
Zinc
activation of water molecule, 191–192, 191f, 192f
in biological systems, 190
in carbonic anhydrase, 190–191, 191f
in translation, 923
Zinc-finger domains, 959, 959f
Zinc-finger nucleases (ZFNs), 292, 293f, 294
Zingiberene, **436**, 840, **840f**
Zwitterions, 35, 36f
Zymogens
cascade of activations, 228–229, 228f
conversion into proteases, 226
defined, 223
developmental process control by, 224
proteolytic activation, 226, 226f
secretion of, 224, 224f

Extended Descriptions

The cover page of the book titled “Biochemistry, Tenth edition” is shown
Logo of W. H. Freeman Macmillan learning
Structures of cell membrane and associated proteins
Reactions and its corresponding graph and related questions
Incomplete purification table along with the percent yield equation
New case study Mile High Stadium and Silent Killer: Hemoglobin Dysfunction
Logo of Macmillan learning
FIGURE 6.18 The active site of human carbonic anhydrase II includes a bound zinc ion
Photograph and a snippet of the accompanying text of a short profile of a scientist
FIGURE 12.38 Many cells take up molecules by receptor-mediated endocytosis
FIGURE 15.6 The sources of ATP change as exercise duration increases, even within the first few seconds
FIGURE 16.36 The Cori cycle allows the liver to better support other tissues, such as skeletal muscle
FIGURE 1.1 Despite tremendous biological diversity, there is remarkable similarity in the molecules that make up living organisms
Examples of metabolites
FIGURE 1.2 A possible timeline for biochemical evolution shows that life on Earth began approximately 3.5 billion years ago
FIGURE 1.3 The relationships of all modern organisms can be displayed on a tree of life with just three major branches
Structures of the four nitrogenous bases of D N A
FIGURE 1.4 The covalent structure of DNA is a linear polymer of monomeric units

FIGURE 1.5 The double helix has two antiparallel strands
FIGURE 1.6 The nitrogenous bases in DNA form specific Watson–Crick base pairs
FIGURE 1.7 Once separated, each strand of the DNA double helix can act as a template for the generation of its partner strand
FIGURE 1.8 When two DNA strands with complementary sequences are mixed, they spontaneously assemble to form a double helix
Resonance structures of adenine
FIGURE 1.9 Electric dipoles can form a variety of noncovalent interactions
FIGURE 1.10 Hydrogen bonds are weak noncovalent interactions between specific hydrogen atoms and lone pairs of electrons
An example of hydrogen bonding
FIGURE 1.11 The energy of a van der Waals interaction varies and is most favorable at the van der Waals contact distance
Electric dipole in a water molecule
FIGURE 1.12 The structure of ice involves extensive hydrogen bonding
FIGURE 1.13 The hydrophobic effect is due to the behavior of water molecules
FIGURE 1.14 Ionic interactions among phosphate groups oppose the formation of the DNA double helix
Example of a reversible reaction
FIGURE 1.15 Optimal base stacking allows many weak, but favorable, van der Waals contacts that drive double- helix formation
FIGURE 1.16 Double-helix formation entails a loss of entropy
FIGURE 1.17 DNA double-helix formation can be probed at the single-molecule level
A table corresponding to the experiments based on double helix formation
FIGURE 1.19 A plot of the running average of the number of experimental repetitions observing double-helix formation reveals eventual convergence on a stable value
Dissociation of water
FIGURE 1.20 DNA strands are separated by the addition of a base

Reversible reaction of guanine
FIGURE 1.21 Buffers resist changes in pH over a narrow pH range
FIGURE 1.22 Added hydrogen ions protonate buffer components rather than remaining free
Reversible deprotonation reaction of phosphoric acid
FIGURE 1.23 The cost to sequence a human genome has decreased dramatically over the past two decades
FIGURE 1.24 DNA sequences vary more within populations than they do between populations
FIGURE 1.25 Genomic information can confirm locations of ancestry
FIGURE 1.26 The human microbiome comprises many different bacterial and fungal species
FIGURE 1.27 Protein folding is primarily dictated by the specific sequence of amino acids
FIGURE 1.28 The similarities between hemoglobin sequences from different species provide evidence for a molecular clock
FIGURE 1.29 There are a variety of possible career paths for those involved in biochemical research
Fused structure of a benzene ring with a 5-membered heterocyclic ring
Types of insulin structure
FIGURE 2.1 The structure of a protein determines its function
FIGURE 2.2 Some proteins form complex assemblies
FIGURE 2.3 Conformational changes allow flexibility in protein function
FIGURE 2.4 The l and d isomers of amino acids are mirror images of each other
FIGURE 2.5 The ionization state of amino acids is altered by changes in pH
FIGURE 2.6 The hydrophobic amino acids have nonpolar R groups
FIGURE 2.7 The polar amino acids have polar but uncharged R groups at physiological pH
FIGURE 2.8 Histidine can bind or release protons near physiological pH

FIGURE 2.9 Two amino acids are positively charged at physiological pH. The guanidinium group in the arginine side chain is shown in red
FIGURE 2.10 Two amino acids are negatively charged at physiological pH
Ionization of an alpha-carboxyl group.
Ionization of an alpha-carboxyl group.
Ionization of a histidine amino acid
Reversible reaction of ammonia
Ionization of a mercapto group
Ionization of a hydroxyl group
Reversible reaction of ammonia
Ionization of an amine group
FIGURE 2.11 Some amino acids are not found in proteins because they are too reactive
FIGURE 2.12 The formation of the peptide bond linking two amino acids is accompanied by the loss of a molecule of water
FIGURE 2.13 Amino acid sequences have direction
FIGURE 2.14 A polypeptide chain consists of a constant backbone and variable side chains
FIGURE 2.15 The formation of a disulfide bond from two cysteine residues is an oxidation reaction
FIGURE 2.16 The primary structure of bovine insulin is its amino acid sequence
FIGURE 2.17 Peptide bonds are planar and have partial double-bond character
Peptide bond resonance structures
FIGURE 2.18 For most amino acids, the trans configuration of the peptide bond is strongly favored because of steric clashes that arise in the cis isomer.
FIGURE 2.19 For peptide bonds between proline and its preceding residue, cis bonds are as likely as trans bonds
FIGURE 2.20 The structure of each amino acid in a polypeptide adjusts by rotation about two single bonds
FIGURE 2.21 A Ramachandran plot shows that not all φ and ψ values are possible without collisions between atoms

FIGURE 2.22 Various depictions of an alpha helix reveal several of its key features
FIGURE 2.23 In an alpha helix, hydrogen bonds form between the CO group of residue I and the NH group of residue i + 4
FIGURE 2.24 Both right- and left-handed helices lie in regions of allowed conformations in the Ramachandran plot
FIGURE 2.25 There are two common ways to draw α helices. (A) A ribbon depiction. (B) A cylindrical (rod) depiction
FIGURE 2.27 β strands occupy an allowed region of the Ramachandran plot
FIGURE 2.28 The side chains of a beta strand project alternately above and below the plane of the strand
FIGURE 2.29 In an antiparallel beta sheet, adjacent beta strands run in opposite directions
FIGURE 2.30 In a parallel β sheet, adjacent β strands run in the same direction
FIGURE 2.31 In a mixed beta sheet, the beta strands have a combination of parallel and antiparallel pairings
FIGURE 2.32 The twisted shape of some beta sheets is more evident in a schematic depiction of strands
FIGURE 2.33 Fatty acid-binding protein is rich in beta sheets
FIGURE 2.34 In a reverse turn, the CO group of residue i of the polypeptide chain is hydrogen bonded to the NH group of residue i + 3
FIGURE 2.35 Loops are found on protein surfaces
FIGURE 2.36 Myoglobin folds into a compact structure
FIGURE 2.37 Hydrophobic amino acids are preferentially distributed in the interior of myoglobin.
FIGURE 2.38 Porin, found in the hydrophobic environment of the membrane, exhibits an “inside out” amino acid distribution
FIGURE 2.39 The helix-turn-helix motif is a supersecondary structural element found in many DNA-binding proteins
FIGURE 2.40 Domains are compact regions within proteins that are connected by flexible polypeptide segments

FIGURE 2.41 The alpha-helical coiled coil adopts an extended structure
FIGURE 2.42 Heptad repeats from each helix in a coiled-coil protein interact with one another
FIGURE 2.43 The amino acid sequence of a part of a collagen chain reveals that every third residue is a glycine.
FIGURE 2.44 A single strand of a collagen triple helix adopts an extended conformation
FIGURE 2.45 Glycine residues form the interior of the collagen triple helix
FIGURE 2.46 Quaternary structure refers to the arrangement of multiple polypeptide chains
FIGURE 2.47 Human hemoglobin is composed of an alpha 2 beta 2 tetramer
FIGURE 2.48 Viral coat proteins adopt complex quaternary structures with many copies of relatively few unique subunits
Urea and beta-mercaptoethanol
FIGURE 2.49 Bovine ribonuclease is a single polypeptide chain with four intramolecular disulfide bonds
FIGURE 2.50 Beta-Mercaptoethanol disrupts disulfide bonds
FIGURE 2.51 Ribonuclease is denatured with urea and β-mercaptoethanol
FIGURE 2.52 Native ribonuclease can be re-formed from scrambled ribonuclease in the presence of a trace of beta-mercaptoethanol
FIGURE 2.53 Many sequences can adopt alternative conformations in different proteins
FIGURE 2.54 The transition from folded to unfolded state is abrupt
FIGURE 2.55 At the denaturation midpoint, half the molecules are fully folded and half are fully unfolded
FIGURE 2.56 In the analogy of the typing monkey, the desired result is achieved more rapidly if individual correct keystrokes are retained
FIGURE 2.57 The proposed folding pathway of chymotrypsin inhibitor-2 demonstrates the nucleation-condensation model
FIGURE 2.58 The folding funnel depicts the thermodynamics of protein folding.

FIGURE 2.59 AlphaFold represents a significant step forward in protein folding prediction.
FIGURE 2.60 The structure of the Aβ amyloid fibril reveals its extensive β sheet network
FIGURE 2.61 The extent of amyloid fibril aggregation in the brain can predict the progression of Alzheimer disease
FIGURE 2.62 Posttranslational modifications to proteins include covalent attachments.
FIGURE 2.63 GFP is modified posttranslationally by the chemical rearrangement of three amino acids
Structure of 5-membered heterocyclic pentagonal ring
Structure of substituted benzene ring
Branched structure of substituted carboxylate ion
Branched structure of substituted carboxylate ion
Structure of a polypeptide
Structure of an amino acid
Structure of a substituted 5-membered heterocyclic pentagonal ring
Ball-and-stick model of an amino acid derivative
Ball-and-stick model of an amino acid derivative
Ball-and-stick model of an amino acid derivative
Ball-and-stick model of an amino acid derivative
Ball-and-stick model of an amino acid derivative
An image showing a large number of penguins
FIGURE 3.1 Comparing the percentage of receptor R bound to ligand L with the concentration of added L reveals how tightly R binds L
FIGURE 3.2 The binding of L to R can be characterized by L1/2
FIGURE 3.3 Estrogens are hormones that are bound by estrogen receptors
FIGURE 3.4 The steroid hormones β -estradiol and testosterone appear quite similar, yet receptors recognize the molecules as distinct
FIGURE 3.5 Proteins such as estrogen receptors include binding pockets that are complementary to the shapes of specific ligands
FIGURE 3.6 Even subtle features of ligands can be recognized

FIGURE 3.7 Dissociation and association are constantly occurring, even at equilibrium where the concentrations of all species are constant
FIGURE 3.8 Half saturation of human myoglobin occurs when the partial pressure of oxygen is 2 torr
FIGURE 3.9 The structure of myoglobin consists primarily of α helices surrounding a heme molecule
FIGURE 3.10 The structure of heme comprises four pyrrole rings that use their nitrogen atoms to bind to a central iron atom
FIGURE 3.11 Oxygen binding changes the position of the heme iron ion
FIGURE 3.12 The complex between iron and oxygen in myoglobin can be described by two resonance structures
FIGURE 3.13 Bound oxygen is stabilized through a hydrogen bond between the distal histidine and one of the oxygen atoms
FIGURE 3.14 Carbon monoxide can bind to the iron ion in myoglobin, blocking the oxygen-binding site
FIGURE 3.15 Hemoglobin is an assembly of four subunits, each of which is very similar to myoglobin
FIGURE 3.16 The oxygen-binding curve for hemoglobin, with its sigmoid (S-like) shape, is markedly different from that for myoglobin
FIGURE 3.17 Cooperativity enhances oxygen delivery by hemoglobin
FIGURE 3.18 Oxygen delivery by hemoglobin responds to exercise
FIGURE 3.19 Substantial quaternary structural changes occur in hemoglobin upon oxygen binding
FIGURE 3.20 A concerted model can explain cooperative oxygen binding by hemoglobin
FIGURE 3.21 The sigmoid oxygen-binding curve of hemoglobin can be seen as a combination of the T state binding curve and the R state binding curve
FIGURE 3.22 A sequential model can account for oxygen-binding cooperativity
FIGURE 3.23 Oxygen binding causes the iron to move into the porphyrin

FIGURE 3.24 The movement of the distal histidine and its associated α helix upon oxygen binding drives cooperativity
Structure of 2,3-Bisphosphoglycerate
FIGURE 3.25 The oxygen-binding curves for pure hemoglobin and hemoglobin in red blood are markedly different
FIGURE 3.26 2,3-Bisphosphoglycerate binds in the central cavity within deoxyhemoglobin
FIGURE 3.27 Fetal red blood cells obtain oxygen from maternal red blood cells by virtue of fetal hemoglobin's lower affinity for 2,3-BPG
FIGURE 3.28 Lowering the pH decreases the oxygen affinity of hemoglobin and facilitates the release of oxygen into metabolically active tissues
FIGURE 3.29 Ionic interactions involving the β chain C-terminal histidine are responsible for some of the pH sensitivity of hemoglobin oxygen affinity
FIGURE 3.30 The presence of carbon dioxide decreases the oxygen affinity of hemoglobin, even beyond the effect due to a decrease in pH
Formation of carbamate
FIGURE 3.31 Carbon monoxide is rapidly transferred from carboxyhemoglobin to N g b-H64Q
FIGURE 3.34 Two molecules of hemoglobin S interact through hydrophobic patches
FIGURE 3.35 The structure of the LRR domain from TLR3 reveals how many LRR units come together to form a structure with binding surfaces for potential partners
Thymine and uracil
FIGURE 3.36 The innate immunity component TLR3 recognizes its PAMP, a double stranded RNA
FIGURE 3.37 Immunoglobulin sequences include regions of extensive sequence variability
FIGURE 3.38 The immunoglobulin fold consists of a pair of β sheets linked by a disulfide bond

FIGURE 3.39 An IgG molecule has a Y-shaped structure comprising two identical arms with hypervariable regions at the end
FIGURE 3.40 Immunoglobulin G molecules can be cleaved into two F ab fragments and one F c fragment by treatment with papain
FIGURE 3.41 The structure of an F ab fragment reveals how the six hypervariable loops come together to form a binding surface
FIGURE 3.42 The structure of a complex between lysozyme and a specific F ab fragment reveals how the binding surface on the F ab interacts with the antigen
FIGURE 3.43 Five classes of immunoglobulin have the same light chain combined with a different heavy chain (γ, α, μ, δ, or ε)
FIGURE 3.44 Antibodies elicited against the spike protein of SARS-CoV-2 can bind to this protein and block the ability of the virus to infect cells
FIGURE 3.45 The structure of the extracellular domain of a class I MHC protein reveals a deep groove
FIGURE 3.46 In class I MHC proteins, peptides can bind in the groove
FIGURE 3.47 Each MHC class I protein presents peptides with some recurring features
FIGURE 3.48 The T-cell receptor recognizes specific class I MHC complexes, contacting both the MHC protein and the bound peptide
FIGURE 3.49 Binding can be monitored by measuring the fraction of receptors with ligand bound as a function of the amount of ligand added
FIGURE 3.50 At high enough concentrations, ligands with lower affinity for a receptor can compete for binding with high-affinity ligands
FIGURE 3.50 At high enough concentrations, ligands with lower affinity for a receptor can compete for binding with high-affinity ligands
Binding of a receptor to its ligand with the forward and reverse reaction rates
FIGURE 3.51 At equilibrium, the rates of the forward and reverse reactions are the same

FIGURE 3.52 A rate constant reflects the distribution of reaction times at the single molecule level
Binding of oxygen by hemoglobin
Two graphs for myoglobin and hemoglobin
Reversible reaction of oxygen binding in arthropods
Structure of choline
Structure of spermine
Structure of inositol Penta phosphate
Structure of indole
Ribbon diagram of SARS-CoV-2 spike protein bound to angiotensin-converting enzyme 2 and immunofluorescence photomicrographs of infected cells
Chemical equation for oxidation of lactate to pyruvate
FIGURE 4.1. Schematic illustration of differential centrifugation and photomicrographs of the pellets obtained at each step
FIGURE 4.2. Schematic illustration of dialysis to separate proteins from small molecules
FIGURE 4.3. Schematic illustration of gel-filtration chromatography to separate proteins on the basis of their size
FIGURE 4.4. Schematic illustration of ion-exchange chromatography to separate proteins based on their net charge
Chemical structure of ionized carboxymethyl group and protonated diethylaminoethyl group bound to cellulose or agarose bead
FIGURE 4.5. Schematic illustration of affinity chromatography to separate proteins based on their binding to a specific ligand
FIGURE 4.6. Graph showing H P L C mediated protein separation with high resolving power
FIGURE 4.7. Schematic illustration of polyacrylamide gel electrophoresis
FIGURE 4.8. Cross-linking reaction for polyacrylamide gel formation
Chemical structure of sodium dodecyl sulfate
FIGURE 4.9. Photograph of stained polyacrylamide gel showing protein bands
FIGURE 4.10. Electrophoresis graph for protein mass determination

FIGURE 4.11. Electrophoretic analysis for monitoring the progress of protein purification
FIGURE 4.12. Schematic illustration of isoelectric focusing mediated separation of proteins
FIGURE 4.13. Schematic illustration and actual image of two-dimensional gel electrophoresis for separation of complex protein mixtures
FIGURE 4.14. Photographic results of two dimensional gel electrophoresis showing alterations of protein level in normal and cancerous tissue
FIGURE 4.15. Schematic illustration of polyclonal and monoclonal antibodies with different number of epitopes
FIGURE 4.16. Schematic illustration of monoclonal antibody production
FIGURE 4.17. Schematic illustration of indirect and sandwich ELISA for antigen or antibody detection
FIGURE 4.18. Schematic illustration of western blotting to detect specific proteins
FIGURE 4.19. Schematic illustration of co-immunoprecipitation for the detection of protein binding partners
FIGURE 4.21. Fluorescence microscopy mediated detection of changes in protein localization inside a cell
FIGURE 4.23. Schematic illustration of MALDI-TOF mass spectrometer for measurement of ionized samples based on their mass-to-charge ratio
FIGURE 4.24. Mass spectrum obtained through MALDI-TOF mass spectrometry
FIGURE 4.25. Method of Edman degradation for peptide sequencing
FIGURE 4.26. Peptide sequencing with the help of tandem mass spectrometry
FIGURE 4.27. Use of overlapping peptides to establish the order of sequenced peptides
FIGURE 4.28. Use of reduction and alkylation reactions for the separation of disulfide-linked polypeptides before sequencing
FIGURE 4.29. Ribbon diagram and units of calmodulin protein

FIGURE 4.30. Mass spectrum showing peptide mass fingerprinting
Chemical structure of f Met peptide
FIGURE 4.31. Chemical structure of 8-arginine vasopressin and 1-Desamino-8-D-arginine vasopressin
FIGURE 4.32. Steps of solid-phase peptide synthesis involving repeated coupling and deprotection
Chemical structures of t-Butyloxycarbonyl amino acid and 9-Fluorenylmethyloxycarbonyl
Chemical structure of dicyclohexylcarbodiimide
FIGURE 4.33. Native chemical ligation reaction for linking two synthetic peptides
FIGURE 4.34. Schematic illustration of the fundamental steps of x-ray crystallography experiment
FIGURE 4.35. X-ray diffraction pattern of a protein crystal
FIGURE 4.36. Electron density map of a protein to determine position of atoms in the crystallized protein
FIGURE 4.37. Electron density map of a protein at different resolutions
FIGURE 4.38. Graph depicting different spin states of a nucleus in N M R spectroscopy
FIGURE 4.39. One-dimensional superscript 1 H NMR spectra shows chemical shift of protons in a sample
FIGURE 4.40. Identification of closely placed protons in a polypeptide due to nuclear overhauser effect
FIGURE 4.41. NOESY spectrum for a protein
FIGURE 4.42. Calculation of structures based on N M R constraints
FIGURE 4.43. Family of related structures produced by N M R spectroscopy
FIGURE 4.44. Projections of a protein complex captured through cryo-E M
Two-dimensional electrophoresis gel showing separation results
Chemical structure of phenylthiohydantoin derivative
Three different protein gels showing different banding patterns
Reaction showing cleavage of cystine by performic acid to produce two molecules of cysteic acid

Chemical equation showing the hydration of carbon dioxide
Chemical equation showing the hydrolysis of a peptide bond
Chemical equation showing the hydrolysis of ester bond
FIGURE 5.1. Chemical structures showing the high specificity of enzymes for their substrates and chemical reactions
Reaction catalyzed by nucleoside monophosphate kinase
Hypothetical chemical reaction
Chemical equation showing the conversion of dihydroxyacetone phosphate into glyceraldehyde-3-phosphate
FIGURE 5.2. Graphical representation of the unperturbed equilibrium point of a reaction in the presence and absence of an enzyme
Calculation of equilibrium constants for catalyzed and uncatalyzed reaction
FIGURE 5.3. Graphical representation of the enzyme-mediated acceleration of a reaction by lowering of the free energy of activation
FIGURE 5.4. Graphical representation of the maximal velocity attained by an enzyme-catalyzed reaction as the substrate concentration increases
FIGURE 5.5 Ribbon diagram and ball-and-stick model show a substrate surrounded by the active site residues of cytochrome P 450 enzyme
FIGURE 5.6. Ribbon diagram and schematic representation of the primary structure depict the coming together of distantly located amino acids in the active site of a folded protein
FIGURE 5.7. Hydrogen bonding between the side chains of active site residues and the substrate
FIGURE 5.8. Schematic illustration of the lock and key model and the induced-fit model
FIGURE 5.9. Graphical representation of the relation between initial velocity and substrate concentration
Model proposed by Michaelis and Menten for enzyme catalysis
Enzyme catalysis
FIGURE 5.10. Graphical representation of Michaelis-Menten kinetics
Reaction catalyzed by alcohol dehydrogenase
Reaction catalyzed by aldehyde dehydrogenase

FIGURE 5.11. The Lineweaver–Burk plot
Chemical structure of the side chain of valine
Chemical structure of the side chain of phenylalanine
Bisubstrate reaction
Chemical equation showing the oxidation of lactate to produce pyruvate
Cleland notation for the conversion of pyruvate into lactate
Chemical equation showing the conversion of creatine into phosphocreatine
Cleland notation for the conversion of creatine into phosphocreatine
Double displacement reaction between aspartate and alpha-ketoglutarate
Cleland notation for the conversion of aspartate into glutamate
FIGURE 5.12. Graphical representation of the allosteric enzyme activity
Graphical representation of the relation between enzyme activity and temperature
Chemical reaction showing the conversion of tyrosine into dopaquinone
FIGURE 5.13. Schematic illustration and graphical representation of molecular heterogeneity
FIGURE 5.14. Schematic illustration of the stochastic behavior of a single-enzyme molecule
Chemical equation showing the conversion of carbohydrate galactose to galactose
FIGURE 5.15. Chemical reaction showing the formation of a highly fluorescent product
FIGURE 5.16. Lineweaver-Burk plot comparing single-molecule kinetic studies and ensemble studies
FIGURE 5.17. Scatter plot indicating heterogeneity of beta-galactosidase at molecular level
FIGURE 5.18. Schematic illustration showing the binding of different types of reversible inhibitors to the enzyme
Chemical structure of sulfanilamide and P A B A

FIGURE 5.19. Michaelis–Menten plot showing the activity of a competitive inhibitor
FIGURE 5.20. Lineweaver–Burk plot depicts competitive inhibition
FIGURE 5.21.Michaelis–Menten plot showing the activity of an uncompetitive inhibitor
FIGURE 5.22. Lineweaver–Burk plot distinguishing uncompetitive inhibition
FIGURE 5.23. Michaelis–Menten plots show the activity of pure noncompetitive inhibitor
FIGURE 5.24. Lineweaver–Burk plot distinguishing a pure noncompetitive inhibition
FIGURE 5.25. The chemical structure of the transition state of a reaction and its analog
FIGURE 5.26. Schematic illustration of irreversible inhibition of an enzyme by D I P F, a group specific reagent
FIGURE 5.27. The chemical structure of the natural substrate of chymotrypsin and an affinity label that binds to chymotrypsin
Lineweaver–Burk plot shows enzyme activity at different concentrations of molecule X
FIGURE 5.28 Chemical structure and ball-and-stick model of penicillin and benzylpenicillin respectively
FIGURE 5.29. Schematic representation of a section of peptidoglycan in Staphylococcus aureus
FIGURE 5.30. Similar chemical structures of penicillin and transition state (R prime-D-Ala-D-Ala peptide) of the transpeptidase reaction
FIGURE 5.31. Schematic illustration showing the formation of penicilloyl-enzyme complex
Enzyme catalysis
Graphical representation of the reaction progress for two different reactions
Forward and reverse rate constants for the conversion of S into P
Protein binding to a small molecule and the formula for K subscript d
Michaelis–Menten plot
Double-reciprocal plots for three different enzyme concentrations
Michaelis–Menten curves for asparaginase from different sources

Sequential conversion of A to D
Photograph of a chess board and ball-and-stick model of an enzyme
Hydrolysis of a peptide
Chemical reaction
FIGURE 6.1. Chemical structure of a peptide with highlighted target amino acids and bonds cleaved by chymotrypsin
FIGURE 6.2. Schematic illustration of the irreversible inactivation of chymotrypsin by D I P F
Molecular structures of malathion and sarin
FIGURE 6.3. Chemical reaction for monitoring chymotrypsin action
FIGURE 6.4. Graphical representation of the two kinetic phases of chymotrypsin activity
FIGURE 6.5. Schematic illustration of hydrolysis by chymotrypsin
FIGURE 6.6. The ribbon diagram of chymotrypsin with active site serine residue
FIGURE 6.7. Schematic illustration of a catalytic triad in the active site of chymotrypsin and the polarization of hydroxyl group of serine residue
FIGURE 6.8. Schematic illustration of the mechanism of peptide hydrolysis
FIGURE 6.9. Schematic illustration of oxyanion hole-mediated stabilization of a tetrahedral intermediate formed during chymotrypsin catalysis
FIGURE 6.10. Space-filling model of the specificity pocket of chymotrypsin
FIGURE 6.11. Structure of a molecule
FIGURE 6.12. Similar structures of chymotrypsin and trypsin
FIGURE 6.13. Spacing filling models and schematic illustrations of the S 1 pockets of chymotrypsin, trypsin, and elastase
FIGURE 6.14. Ball-and-stick model of catalytic triad and oxyanion hole of subtilisin
FIGURE 6.15. Bar graph shows the activity of subtilisin enzyme for different mutations of the catalytic triad
FIGURE 6.16. Schematic illustration of the different catalytic strategies of (A) cysteine proteases, (B) aspartyl proteases, and (C)

metalloproteases
FIGURE 6.17. Ribbon diagram and ball-and-stick model of H I V protease with inhibitor indinavir
Reversible chemical reactions depicting the formation of carbonic acid
FIGURE 6.18. Ribbon diagram of carbonic anhydrase roman number 2 and the ball-and-stick model of its active site
FIGURE 6.19. Graphical representation of the dependence of carbonic anhydrase activity on p H
FIGURE 6.20. Reversible reaction consisting of one reactant and two products is shown
FIGURE 6.21.Electron density map of carbonic anhydrase active site and C O 2 binding site
FIGURE 6.22. Mechanism for the hydration of carbon dioxide by carbonic anhydrase
FIGURE 6.23. Chemical reaction shows the reversible deprotonation of water molecule bound to carbonic anhydrase active site and the ratio of rate constants for protonation and deprotonation
FIGURE 6.24. Reversible reaction shows the deprotonation of the zinc-bound water molecule in carbonic anhydrase aided by buffer
FIGURE 6.25. Graphical representation of the rate of carbon dioxide hydration by carbonic anhydrase as a function of buffer concentration
FIGURE 6.26. Schematic illustration of histidine 64 residue of carbonic anhydrase roman number 2 acting as a proton shuttle
FIGURE 6.27. Chemical reaction shows the restriction enzyme-mediated hydrolysis of phosphodiester bond
Two reversible reactions consisting of two reactants and two products are shown
Chemical reaction for the direct hydrolysis of D N A
Series of reversible reactions consisting of two reactants, two products, and an intermediate product are shown
FIGURE 6.28. Schematic representation of Eco R V cleavage site in a D N A sequences

FIGURE 6.29. Schematic illustration of the inversion of the stereochemical configuration of phosphorus atom after cleavage of D N A by Eco R V
FIGURE 6.30. Ball-and-stick model of the bridge formed by M g superscript 2 plus ion between the enzyme and substrate
FIGURE 6.31. Two fold rotational symmetry of recognition site for Eco R V
FIGURE 6.32. The ribbon diagram of Eco R V bound to a cognate D N A and the ball-and-stick model of C G and A T base pair
Ball-and-stick model of cognate D N A from Eco R V complex
FIGURE 6.34.Ribbon diagram illustrates the positions of the nonspecific and the cognate D N A within Eco R V
FIGURE 6.35. Energy level diagram showing D N A distortions due to an increase in binding energy
FIGURE 6.36. Schematic illustration of the methylation of the recognition sequence of Eco R V
FIGURE 6.37. Ball-and-stick model of asparagine 185 residue of Eco RV and methylated adenine hydrogen bonded to thymine
Reversible reaction consisting of two reactants and two products is shown
FIGURE 6.38. Schematic illustration of the structure of myosin
FIGURE 6.39. Schematic illustration of A T P bound to the myosin molecule
The structure of transition state of A T P
FIGURE 6.40. Ball-and-stick model of a transition-state analog of myosin
FIGURE 6.41. Chemical reaction shows the serine 236 mediated attack of water molecule on gamma-phosphoryl of A T P
FIGURE 6.42. Schematic illustration compares the overall structures of the myosin A T P ase domain with bound A T P and that with the transition-state analog A D P–vanadate
Chemical equation of A T P hydrolysis in the presence of with O superscript 18 labeled water
FIGURE 6.43. Schematic illustration of the reversible hydrolysis of A T P within the active site of myosin

FIGURE 6.44. Ribbon diagram and schematic illustration of actin filament
FIGURE 6.45. Graphical representation of the position of a single dimeric myosin roman number 5 molecule and a model of the movement of the dimeric molecule
FIGURE 6.46. Schematic illustration of the steps involved in the movement of myosin along an actin filament
FIGURE 6.47. Schematic illustration of the structure of myosin assembly in muscle
Chemical structure of the amide substrate of chymotrypsin
Molecular structure of the aldehyde derivative of the substrate of elastase
Chemical structure of a molecule A
Enzyme catalyzed reaction
A chemical reaction representing the committed step of pyrimidine synthesis
Graphical representation of the inhibition of A T C ase by C T P
Graph of the rate of formation of N-carbamoylaspartate as a function of aspartate concentration
Chemical reaction of p-Hydroxymercuribenzoate with a crucial cysteine residue of aspartate transcarbamoylase
Schematic illustration of the top and side views of the catalytic subunit trimer of A T C ase
Chemical equation for the formation of an intermediate compound in the A T C ase catalytic pathway and the structure of its analog P A L A
The ribbon structure of the catalytic trimer of A T C ase and the active site residues of one of the catalytic subunits bound to P A L A
Schematic illustration of the tense and relaxed states of A T C ase
Graphical representation of the change of state in a cooperative enzyme as a function of substrate concentration
Graphical representation of the velocity of reaction as a function of substrate concentration for allosteric and Michaelis-Menten enzymes
Schematic illustration of the stabilization of T state of A T C ase by C T P

A schematic illustration of the equilibrium between the R and T states of A T C ase
Graphical representation of the different effects of A T P and C T P on A T C ase kinetics
Schematic illustration of the timing of expression of isozymes of lactate dehydrogenase and their tissue specific concentrations respectively
Chemical structure of acetylated lysine
Chemical reaction of the phosphorylation of an amino acid residue catalyzed by a protein kinase enzyme is shown
Chemical reaction of dephosphorylation of a phosphorylated protein catalyzed by a protein phosphatase enzyme
Schematic illustration of the range of free energy between phosphorylated and dephosphorylated proteins
Chemical structure of cyclic adenosine monophosphate
A schematic illustration of the binding of c A M P to the regulatory subunits of P K A
Schematic illustration of the secretion of zymogens by acinar cells of the pancreas
Schematic illustration of the activation of chymotrypsinogen by proteolysis
Schematic illustration of the conversion of chymotrypsinogen into chymotrypsin
A flow chart of the cascade of activation of zymogens initiated by the activation of trypsin
The ribbon structures of free pancreatic trypsin inhibitor and the pancreatic trypsin inhibitor bound to trypsin
Chemical reaction of the oxidation of methionine to methionine sulphoxide
Schematic illustration of an enzymatic cascade leading to the clotting of blood
Schematic illustration of the protein domains of prothrombin
Schematic illustration of the binding of calcium ions to the g l a domain of prothrombin
Schematic illustration of the structure of fibrinogen

Schematic illustration of the cleavage of fibrinogen by thrombin to initiate fibrin clot formation
Cross-linking reaction between glutamine and lysine residue
Chemical structure of vitamin K and warfarin
Chemical reactions showing the synthesis of gamma-carboxyglutamate
Graph depicts the velocity curve of an allosteric enzyme and the effect of negative modifier
Graphical representation of the fraction of enzyme in the R state and the fraction of substrate-bound active sites as a function of substrate concentration.
Schematic illustration of a metabolic pathway
Three vertical bar graphs showing the results of control group (no inhibitor), P K A inhibitor, and P K G inhibitor
Graphical representation of the reaction rate as a function of the mole ratio of P A L A to A T C ase
Photograph of a family of dogs is accompanied by a ribbon diagram of a zinc finger protein bound to D N A
Schematic representation of central dogma
FIGURE 8.1. Schematic representation of the structure of nucleic acids
FIGURE 8.2. Chemical structures of ribose and deoxyribose found in R N A and D N A respectively
FIGURE 8.3. The chemical structure of D N A and R N A
FIGURE 8.4. Chemical structures of different purines are pyrimidines
FIGURE 8.5. Chemical structures of a nucleoside and a nucleotide
FIGURE 8.6. Photomicrograph compares the size of an E.coli cell to its coiled genome
FIGURE 8.7. Photomicrograph of the stained chromosomes of female Indian muntjac
FIGURE 8.8. Simplified schematic representation of a nucleic acid strand
FIGURE 8.10. The Watson–Crick model of double-helical D N A
FIGURE 8.11. Base-pairing of nucleotide bases

FIGURE 8.12. Schematic representation of the side view of D N A reveals the stacking of base pairs within the double helix
FIGURE 8.13. Schematic representation of the different structural forms of D N A
FIGURE 8.14. The structures of the sugars in the A and B forms of D N A
FIGURE 8.15. The major and minor grooves of a D N A double helix
FIGURE 8.16. Two photomicrographs show the relaxed and supercoiled forms of circular bacterial D N A
FIGURE 8.17. Stem-loop structures formed in single-stranded D N A and R N A molecules
FIGURE 8.18. Schematic representation of complex structure adopted by R N A molecule
FIGURE 8.19. Bands obtained by density-gradient centrifugation and corresponding graphs for N superscript 14 and N superscript 15 D N A
FIGURE 8.20. D N A banding pattern detected by density-gradient centrifugation across 4 generations
FIGURE 8.21. Schematic representation of the semi-conservative mode of D N A replication
FIGURE 8.22 Single-stranded DNA absorbs light more effectively than does double-helical DNA
Reaction catalyzed by D N A polymerase
FIGURE 8.23. Schematic illustration of D N A polymerization using the saw-tooth schematic
FIGURE 8.24 DNA polymerases catalyze the strand-elongation reaction in the 5'-to-3' direction
FIGURE 8.25. Schematic representation of D N A synthesis from R N A template in retroviruses
Reaction catalyzed by R N A polymerase
FIGURE 8.26. Ribbon structure of R N A polymerase
FIGURE 8.27. Schematic representation of the elongation of the R N A strand catalyzed by R N A polymerase using D N A as a template
FIGURE 8.28. Sequences of m R N A strand, template D N A strand, and coding D N A strand

FIGURE 8.29. Schematic representation of the prokaryotic and eukaryotic promoter sites
FIGURE 8.30. Stem-loop structure at the 3 prime end of an E.coli m R N A transcript
FIGURE 8.31. Schematic representation of mRNA in eukaryotes modified after transcription
FIGURE 8.32. Structure of a t R N A molecule
FIGURE 8.33. The structure of amino acyl-t R N A
FIGURE 8.34. Graphical representation of arginine codon usage preference in different species
FIGURE 8.35. Schematic representation of the prokaryotic and eukaryotic start signals for protein synthesis
FIGURE 8.36. Schematic illustration of structure of the beta-globin gene
FIGURE 8.37. Schematic representation of the splicing of a beta-globin m R N A
FIGURE 8.38. Schematic representation of the location of splice sites in an m R N A
FIGURE 8.39 The tissue plasminogen activator (TPA) gene was generated by exon shuffling
FIGURE 8.40. Schematic illustration of membrane-bound and soluble antibody molecules generated by alternative splicing
Chemical structure
Chemical structure
Chemical structure
Chemical structure
Chemical structure
Chemical structure
Three-dimensional structure of Cas 9 endonuclease
Cleavage site of a restriction enzyme
Cleavages sites for five different restriction endonucleases
Photograph of electrophoresis gel slab with stained D N A fragments
Schematic illustration of the steps of southern blotting
Schematic illustration of the steps of chain-terminating D N A sequencing method

Chemical Structure of 2 prime, 3 prime-dideoxy analog
Stepwise illustration of the Phosphite triester method of oligonucleotide synthesis
Structure of a deoxyribonucleoside 3 prime phosphoramidite with D M T and beta C E attached
Schematic illustration of the steps of the first cycle of Polymerase Chain Reaction
Schematic illustration of multiple cycles of Polymerase Chain Reaction
Photograph of gel electrophoresis slab of P C R in a forensic case
Schematic illustration of cohesive-end method of D N A ligation
Schematic illustration of addition of cohesive ends to a D N A fragment
Schematic illustration of unique restriction sites in a polylinker sequence of a plasmid
Schematic illustration of the steps of insertional inactivation of genes for identification of colonies
Structure of an expression vector
Schematic illustration of the lytic and lysogenic pathways of infection in lambda phage
Steps of development of mutant lambda phage to be used as cloning vector
Oligonucleotide probe designed from a target sequence
Schematic illustration of the creation of genomic library from a whole genome digest
Schematic illustration of the screening of a genomic library for a specific gene
Schematic illustration of double-stranded c D N A preparation from m R N A using reverse transcriptase
Schematic illustration of the screening of colonies in a c D N A library that express a protein of interest
Schematic illustration of designing a bacteria to express proinsulin by infection with proinsulin c D N A
Schematic illustration of site-directed mutagenesis in P C R
Schematic illustration of cassette mutagenesis

Schematic illustration of the application of P C R to generate mutations
Mapped genome of Haemophilus influenzae
The set of human chromosomes with the location of genes associated with important biochemical pathways marked
Schematic illustration of pyrosequencing
Light generation during the pyrosequencing process
Chemical reactions catalyzed by apyrase
Different approaches used in next-generation sequencing methods
Comparison of human and mouse genomes
Graphs depicting results of a quantitative P C R
Schematic illustration of the steps of D N A microarray analysis
Heat map of a microarray analysis of tumors
Micrograph of a cloned plasmid D N A being injected into a fertilized mouse egg
Schematic illustration of foreign D N A insertion by homologous recombination
Consequences of myogenin knockout in mice
Schematic illustration of non-homologous end joining and homology directed repair of D N A
Recognition of individual bases in D N A by TALE repeats
Schematic illustration of the introduction of double-stranded break into D N A by Z F N or TALEN
Structure of single guide R N A
Schematic illustration of D N A cleavage by CRISPR-Cas system
Mechanism of R N A interference
Schematic illustration of the steps of introduction of foreign D N A into plant cell by electroporation
Electrophoresis gel slab
Banding pattern in southern, northern, and western blots
Four chromatograms of the alpha chain variants of hemoglobin
Map of hypothetical p SAP plasmid
A time versus temperature plot
Cleavage sites in a D N A segment
Electrophoresis gel slab

Sequencing chromatogram
Cleavage sites of K p n roman number 1 and A c c 6 5 roman number 1.
Microarray data
FIGURE 10.1 Homologs can be divided into two classes
FIGURE 10.2 The amino acid sequences of human hemoglobin (chain) and human myoglobin will be used to demonstrate sequence alignments
FIGURE 10.3 Amino acid sequences are compared by sliding one sequence past the other, one amino acid at a time
FIGURE 10.4 Scoring method
FIGURE 10.6 Comparison of alignment scores reveals the statistical significance of an unshuffled alignment
FIGURE 10.7 The Blosum-62 substitution matrix enables scoring based on amino acid similarity
FIGURE 10.8 Conservative and nonconservative substitutions yield very different scores in the Blosum-62 matrix
FIGURE 10.9 Counting conservative substitutions reveals strong similarity between α-hemoglobin and myoglobin
FIGURE 10.10 Alignment using Blosum-62 can uncover more distant evolutionary relationships
FIGURE 10.11 Alignment of human myoglobin and lupine leghemoglobin reveals many conservative substitutions
FIGURE 10.12 Related protein sequences can be rapidly identified using online BLAST searches
FIGURE 10.13 Three-dimensional structure is more conserved than primary structure
FIGURE 10.14 The structures of actin and a large fragment of heat shock protein 70 (Hsp70) reveal an unexpected relationship
FIGURE 10.15 Internal repeats can be identified using a self-alignment
FIGURE 10.16 Mammalian chymotrypsin and bacterial subtilisin are examples of convergent evolution
FIGURE 10.17 RNA sequence alignments provide insights into structure based on conservation of base-pairing. (A) A comparison of

sequences in a part of ribosomal RNA taken from a variety of species
Sequences of R N A fragments
Sequences of R N A fragments
Sequences of R N A fragments
Stem loop structure of R N A
FIGURE 10.18 Sequence alignments enable the construction of an evolutionary tree
FIGURE 10.21 Proteins encoded within the G. sulphuraria genome with high homology to prokaryotic sequences are suggestive of horizontal gene transfer
FIGURE 10.22 DNA sequence comparisons enable the placement of Neanderthals and Denisovans on an evolutionary tree
FIGURE 10.23 Evolution can be studied in the laboratory setting
FIGURE 10.24 A conserved secondary structure is common to RNA molecules selected for ATP binding
FIGURE 10.25 Experimental molecular evolution yields an ATP-binding RNA molecule
Evolutionary tree of similar genes
Sequence of two proteins
Sequence alignments
An evolutionary tree
Structures of dihydroxyacetone, D-glyceraldehyde, and L-Glyceraldehyde
Classification of isomers
Molecular structures of common monosaccharides
Formation of hemiacetal from aldehyde and alcohol
Chemical structure of pyran
Formation of alpha-D-Glucopyranose and beta-D-Glucopyranose from D-Glucose
Formation of hemiketal from ketone and alcohol
Chemical structure of furan
Formation of alpha-D-Fructofuranose from D-Fructose
Four distinct ring structures adopted by D-fructose in solution
The ring structures of common monosaccharides
Structure of the chair and boat forms of beta-D-glucopyranose

Chair form of beta-D glucopyranose with steric hinderance
Structures of C-3 endo and C-2 endo forms of a puckered furanose ring
Oxidation of glucose
Chemical structures of alpha-D-Methylglucopyranose and adenosine monophosphate
Chemical structures of beta-L-Fucopyranose, beta-D-Acetylgalactosamine, beta-D-Acetylglucosamine, and sialic acid
Chemical structures of glucose 6-phosphate (G-6 P), dihydroxyacetone phosphate (D H A P), glyceraldehyde 3-phosphate (G A P)
Chemical structure of maltose
Chemical structures of sucrose, alpha-Lactose, and alpha-maltose
Chemical structures of acarbose (Precose) and miglitol (Glyset)
Chemical structure of glycogen
Straight chain of cellulose and bent structure of starch and glycogen
Chemical structure of galacturonic acid
Chemical structure of chitin repeating unit
Chemical structures of N-linked G l c N A c and O-linked G a l N A c
Schematic illustrations of N-linked oligosaccharides
Schematic illustration of erythropoietin with oligosaccharides linked to amino acid residues
Structure of beta-D-acetylglucosamine
Structures of chondroitin 6-sulfate, keratan sulfate, heparin, dermatan sulfate, and hyaluronate
An electron micrograph and schematic representation of proteoglycan
Schematic illustrations depict the mucoprotein and an oligosaccharide bound to the V N T R region of the protein
Structure of dolichol phosphate
Chemical structure of isoprene
Schematic illustration of protein sorting in the Golgi complex
Glycosyltransferase reaction
Schematic illustration of the structures of O antigen, A antigen, and B-antigen

Ribbon diagram of cholera toxin bound to O antigens depicted as ball-and-stick models
Stepwise formation of mannose 6-phosphate residue
Mass spectrums for the characterization of oligosaccharides
Ribbon diagram and ball and stick model depict the calcium ion mediated binding of C-type lectin to carbohydrates
Schematic illustrations depict the entry and exit of influenza virus from host cell
Chemical structures of beta L-Galactopyranose and beta L-Glucopyranose
Chemical structures of D-Erythrose, D-Ribose, D-Glyceraldehyde, Dihydroxyacetone, D-Erythrulose, D-Ribulose, and D-Fructose
Chemical structure of raffinose
Graphical representation of G A G concentration versus time in days
Space-filling model of sphingomyelin and scanning electron micrograph of the myelin sheath
Chemical structures of palmitate and oleate
Numbering of carbon atoms in a fatty acid chain
Structure of linolenate
Schematic representation of a phospholipid molecule
Chemical structure of phosphatidate
Chemical structures of common phosphoglycerides located in the membrane
Structures of serine, ethanolamine, choline, glycerol, and inositol
Structures of sphingosine and sphingomyelin
Chemical structure of cerebroside
Chemical structure of cholesterol
Structure of membrane lipid of the archaeon Methanococcus jannaschii
Space filling models of phosphoglyceride, sphingomyelin, and an archaeal lipid; and shorthand depiction of membrane lipid labeled (A) and (B) respectively
Schematic illustration of micelles
Schematic illustration of lipid bilayer
Schematic illustration of liposome

Production of liposomes containing glycine
Experimental study of the properties of planar bilayer membranes
The permeability coefficients (P) of ions and molecules in a lipid bilayer
Schematic illustration of the wrapping of Schwann cell membrane around an axon and an electron micrograph of myelin sheath around the axon
S D S gel patterns of membrane proteins from different cell types
Membrane proteins interact with lipid bilayers in different ways
Schematic illustration of the view of bacteriorhodopsin through the membrane and cytoplasmic side
Amino acid sequence of the membrane spanning helices of bacteriorhodopsin
Schematic illustration of the side view and periplasmic view of porin protein from Rhodopseudomonas blastica
Secondary structure of porin protein from Rhodopseudomonas blastica
Ribbon structure of prostaglandin H 2 synthase-1 attached to the membrane surface
Step-wise formation of prostaglandin H 2 from arachidonate
Ribbon structure of prostaglandin H 2 synthase-1 containing a hydrophobic channel
Acetyl group transfer to serine residue of prostaglandin H 2 synthase 1 by aspirin
Structures of S-Palmitoyl cysteine, C-terminal S-farnesyl cysteine methyl ester, and Glycosylphosphatidylinositol (G P I) anchor
Hydropathy plot for glycophorin A and the amino acid sequence and disposition of glycophorin A
Hydropathy plot for porin
Schematic representation of fluorescence bleaching and recovery and a graphical representation of fluorescence intensity versus time
Schematic illustration of lateral and transverse diffusion in lipid bilayer
Graph showing the melting temperature of a phospholipid membrane
Space-filling models labeled (A) and (B)

Schematic illustration of cholesterol inserted in lipid bilayer
Lipid raft and human monocytic cell stained with a fluorescent dye
Transport of ions by N a superscript plus-K superscript plus transport system in the lipid bilayer
Structure of the plasma membrane of gram positive and gram negative bacteria and their photomicrographs
Schematic illustration of nuclear and surrounding E R
Schematic representation and photomicrographs of the steps of receptor-mediated endocytosis
Fusion of vesicles to the plasma membrane to release neurotransmitter
Schematic illustration of receptor-mediated endocytosis of transferrin receptor and iron
Schematic illustration of the initiation of membrane fusion
Chemical structure of a fatty acid
Chemical structure of platelet-activating factor (P A F)
Different ways in which membrane proteins interact with lipid bilayers
Hydropathy plots of different proteins A, B, and C
Graphical representation of the fluidity of fatty acids in a phospholipid bilayer as a function of temperature
Bar graphs depict the effect of ibuprofen and indomethacin on prostaglandin H 2 synthesis
Two graphs depict the variation of free energy as a function of concentration ratio and membrane potential respectively
Chemical structure of phoshorylaspartate
Schematic representation of a conformational change of pump proteins during transport of a molecule
Schematic structure of S E R C A P-type A T P ase and the ball-and-stick model of amino acid residues in the transmembrane domain bound to calcium
Conformational change in the structure of S E R C A P-type A T P ase
Conformational change of S E R C A during a catalytic cycle
Chemical structure of digoxin and chemical reaction inhibited by cardiotonic steroids

Schematic structure of multidrug-resistance protein and bacterial lipid transport protein
Open and closed forms of bacterial lipid transporter M s b A
Mechanism of transport of molecules by A B C transporters
Schematic representation of antiporter, symporter, and uniporter
Side view and bottom view of E.coli lactose permease
Mechanism of transport of lactose by lactose permease
Graphical representation of action potential
Patch-clamp technique
Result of patch-clamp experiment
Sructure of Tetrodotoxin
Structural features of sodium and calcium channels, shaker potassium channel, and bacterial potassium channel
Different views of the bacterial potassium ion channel
Space-filling model of a potassium ion channel
Selectivity filter of potassium ion channel
Desolvation and resolvation energy of potassium and sodium ions
Calcium channel and sodium channel
Model of K superscript plus channel ion transport
View through the pore and side view of the voltage-gated potassium channel
Closed and open voltage-gated potassium channel
Graph of membrane current versus time after depolarization
Mechanism of channel inactivation
Structure of acetylcholine
Schematic representation of synapse
Model of acetylcholine receptor and a view of the receptor from outside the cell
Opening of the acetylcholine receptor due to ligand binding
Schematic representation of equilibrium potential
Graphs for membrane potential and current flow and schematic representation of the states of ion channels during an action potential
Graph depicts the percentage of activated H C N 4 channels as function of potential
Structure and orientation of connexon

Side and bottom view of aquaporin
Electrophysiological recordings of cells
Graphs depicting membrane potential in the presence or absence of a drug or compound
A graph and a photograph
Generalized signal-transduction pathway
Chemical structure of different secondary messengers
Physiological outcomes of different signal transduction pathways
Chemical structure of epinephrine
Schematic representation of 7 T M helix receptor
Schematic representation of the side view and top view of the beta-2 adrenergic receptor
Stabilization of the active conformation of beta-adrenergic receptor
Signaling pathway initiated by epinephrine
Ribbon diagram and schematic representation of the G protein subunits
Beta-2 A R bound to G protein and G D P and receptor bound forms of alpha subunit
Schematic representation of adenylate cyclase and ribbon diagram of adenylate cyclase bound to G subscript alpha S subunit
Flowchart shows events leading to cardiac muscle contraction
G protein resetting
Termination of beta-adrenergic receptor signaling
Cleavage of phosphatidylinositol 4,5-bisphosphate
Protein kinase C activation
Ball-and-stick model of calcium ion bound to oxygen atoms
Structure of Fura-2
Fluorescence spectra of Fura-2 and photographs of calcium ions spreading across an egg cell
E F hand motif
Conformational change in the apo form of calmodulin and its binding to protein kinase
Flow chart show events leading to smooth muscle contraction
Signal transduction by G protein beta gamma dimer

Generalized signaling pathway involving the three classes of G protein alpha subunits
Structure of adenosine
Chemical structure of caffeine
Graphical representation of glucose and insulin levels post meal
Insulin ribbon structure
Insulin receptor
Chemical reaction catalyzed by tyrosine kinase
Unactivated form of insulin receptor kinase
Conformational change in insulin receptor
Activation of insulin receptor
Schematic representation of the common amino acid sequence in I R S-1 and I R S-2
Formation of phosphatidyl 3,4,5-trisphosphate
Insulin signaling pathway
Ribbon diagram of the inactive conformation of P D K 1 and comparison of the activation loops of inactive and active forms
Insulin signaling pathway
Ribbon diagram of epidermal growth factor
Extracellular domain of the E G F receptor and its dimerization upon E G F binding
E G F receptor signaling
E G F signaling pathway
E G F receptor bound to cetuximab
Photomicrographs show the panel of breast cancer cells expressing normal and high levels of H E R 2
Formation of b c r- a b l gene
Ribbon structure of A b l kinase bound to imatinib
Structures of benzaldehyde, 3-methylbutane-1-thiol, geraniol, zingiberene, R-Carvone, and S-Carvone
Olfactory signal-transduction cascade
The structures of four sets of closely related compounds
Distinct patterns of olfactory-receptor activation
Electromagnetic spectrum

Structures of 11-cis-Retinal and 11-cis-Retinal connected to lysine through Schiff base
Scanning electron micrograph and schematic representation of retinal rod cells
Graphical representation of light absorption by rhodopsin
Isomerization of 11-cis-retinal in presence of light
Visual signal transduction
Absorption spectra of different light receptors from human cone cells
Scanning electron micrograph of stereocilia bundle on hair cells
Micrograph of tips of two stereocilia
Hair cell signal detection
Phylogenetic tree
Photograph shows several fruits and vegetables
Flow Chart for the cleavage of membrane lipid
Structure of A T P
Percentage of binding capacity of the receptor as a function of hormone concentration
Stimulation of adenylate cyclase as a percentage of maximum hormone concentration
Distinct patterns of olfactory-receptor activation
Flow chart depicting the transformation of glucose to pyruvate
Node diagram depicting metabolic pathways are interconnected series of enzyme-catalyzed reactions
Chemical reactions and their respective standard free energy changes
Structures of A T P, A D P, and A M P
A T P hydrolysis and standard free energy changes
Reversible reactions catalyzed by nucleoside monophosphate kinase and nucleoside diphosphate kinase
Reaction with its standard free energy change
Standard free energy changes of A T P and glycerol-3-phosphate hydrolysis
Structure of Glycerol 3-phosphate
Four resonance structures of orthophosphate separated by two-way arrows

Graphical representation of the compounds with high phosphoryl-transfer potential that can be used to make A T P from A D P
Structure of creatine phosphate
Structure of creatine
Graphical representation of the sources of A T P change as exercise duration increases
A T P and A D P cycle
Free energy of oxidation of single-carbon compounds increases with the degree of hydrogen saturation from most energy on the left to least energy on the right
Structures of glucose and saturated fatty acids
Reaction for oxidation of glyceraldehyde 3-phosphate to 3-Phosphoglyceric acid
Reaction for the formation of 1,3-Bisphosphoglycerate
Reaction for the formation of 3-phosphoglyceric acid
Proton gradients formed in the biological membrane using energy from either sunlight or chemical oxidation can power A T P synthesis
Three stages of extraction of energy from food to form A T P in aerobic organisms
Reaction for the formation of N A D H
Structure of oxidized forms of N A D superscript plus and N A D P superscript plus
Reaction for the formation of F A D H 2
Structure of flavin adenine dinucleotide
Reaction for the formation of reduced form (F A D H 2) from oxidized form (F A D)
Reaction for the biosynthesis of fatty acids
Structure of Acyl C o A and Acetyl C o A
Structure of coenzyme A
Reversible reaction depicts the formation of acetate from acetyl C o A and its standard free energy change
Structures of oxygen esters and thioesters
Structures of water-soluble B vitamins
Formation of Fumarate from Succinate
Formation of oxaloacetate from malate

Formation of glucose 6-phosphate and A D P
Hydrolytic reaction
Formation of Glyceraldehyde 3-phosphate from Fructose 1, 6-Bisphosphate
Formation of Phosphoenolpyruvate (P E P) from 2-Phosphoglycerate
Equilibrium reaction depicts the formation of isocitrate from citrate
Equilibrium reaction depicts the formation of oxaloacetate from pyruvate
Graphical representation of energy charge versus relative rate of A T P synthesis
Structure of Arginine phosphate
Reaction catalyzed by aldolase
Structures of Ethanol and Acetaldehyde
Structures of Lactate and Pyruvate
Structure of Succinate and Fumarate
Structure of Oxalosuccinate and Isocitrate
Structure of Malate and Oxaloacetate
Graphical representation of delta G for the hydrolysis of A T P varies as a function of the M g superscript 2 plus concentration
Schematic illustration of sources of A T P for muscle contraction
Schematic representation of glucose metabolism
Two stages of glycolytic pathway
Stage 1 of glycolytic pathway
Reversible conversion of glucose to glucose 6-phosphate
Conformational change in hexokinase upon glucose binding
Conversion of glucose 6-phosphate to fructose 6-phosphate
Reversible conversion of fructose 6-phosphate to fructose 1, 6-bisphosphate
Reversible conversion of fructose 1, 6-bisphosphate to dihydroxyacetone phosphate and glyceraldehyde 3-phosphate
Reversible conversion of dihydroxyacetone phosphate to glyceraldehyde 3-phosphate
Ribbon diagram of triose phosphate isomerase
Catalytic mechanism of triose phosphate isomerase
Conversion of enediol intermediate into methyl glyoxal

Stage 2 of glycolytic pathway
Reversible conversion of glyceraldehyde 3-phosphate to 1,3-bisphosphoglycerate
Chemical reactions depict the oxidation of an aldehyde and formation of acyl-phosphate production
Graphs depicting free energy profiles
Ribbon diagram of G A P D H
Catalytic mechanism of G A P D H
Chemical reaction shows the conversion of 1,3-bisphosphoglycerate to 3-phosphoglycerate
Conversion of 3-phosphoglycerate to pyruvate
Transfer of phosphoryl group from histidine residues of an enzyme to 3-phosphoglycerate
Removal of phosphoryl group from 2,3-bisphosphoglycerate
Conversion of phosphoenolpyruvate to pyruvate
Step 6 of glycolysis
Different fates of pyruvate molecule
Conversion of pyruvate to ethanol
Ball-and-stick model of zinc ion in the alcohol dehydrogenase active site and its binding partners
Reoxidation of N A D H
Chemical reaction shows the conversion of pyruvate to lactate
Regeneration of N A D superscript plus during lactic acid fermentation
Entry of additional sugars in the glycolytic pathway
Entry of fructose into the glycolytic pathway in the liver
Irreversible conversion of galactose to galactose 1-phosphate
Formation of U D P-glucose from galactose 1-phosphate and U D P-glucose
Chemical reaction shows the conversion of galactose to galactitol
Photographs comparing healthy eye and cataract affected eye
Breakdown of lactose into galactose and glucose
Ribbon diagram of E.coli phosphofructokinase
Graphical representation of the inhibition of phosphofructokinase activity

Flowcharts depict glycolysis regulation
Chemical structure of fructose 2, 6-bisphosphate and flow chart depicting allosteric activation of phosphofructokinase
Structure of fructose 2, 6-bisphosphate
Graphs depict fructose 1, 6-bisphosphate synthesis with respect to fructose 6-phosphate concentration
Regulation of pyruvate kinase activity
Pretherapy and post therapy PET scans
Hypoxia-induced gene expression alteration in tumors
Gluconeogenesis pathway
Formation of dihydroxyacetone phosphate from glycerol
Formation of oxaloacetate from pyruvate
Structures of biotin and carboxybiotin covalently bound to the epsilon-amino group of a lysine
First stage of pyruvate carboxylation
Final stage of pyruvate carboxylation
Ribbon diagrams of pyruvate carboxylase subunits
Formation of phosphoenolpyruvate from oxaloacetate
Transport of malate produced in the mitochondrial matrix to the cytoplasm and its conversion to oxaloacetate
Formation of free glucose in E R lumen
Step 6 of gluconeogenesis
Reciprocal regulation of glycolysis and gluconeogenesis
Schematic representation and ribbon diagram of the domains of P F K 2 slash F B P ase 2
Hormonal regulation of synthesis and degradation of fructose 2, 6-bisphosphate
Different rates of operation of a A T P-driven cycle
Cori cycle
Cooperation between glycolysis and gluconeogenesis during a sprint
Structure of methylglyoxal
Activity of P F K and F B P ase in different bumblebee species
Schematic representation of the citric acid cycle
Structure of acetyl coenzyme A or acetyl C o A
Electron micrograph and schematic illustration of a mitochondrion

Citric acid cycle
Citric acid cycle and oxidative phosphorylation in a mitochondrion
Connection between glycolysis and citric acid cycle
Structure of thiamine pyrophosphate (T P P) and lipoic acid
Stepwise conversion pyruvate to acetyl C o A
Formation of hydroxyethyl-T P P
Mechanism of E 1 decarboxylation reaction
Oxidation of hydroxyethyl-T P P
Formation of acetyl C o A
Regeneration of oxidized lipoamide
Structure of lipoamide
Photograph of bacterial pyruvate dehydrogenase complex
Ribbon diagram of a subunit of the transacetylase trimer
Activity of pyruvate dehydrogenase complex
Formation of citrate from oxaloacetate
Space filling model shows the binding of oxaloacetate to citrate synthesis
Citrate synthase mechanism
Conversion of citrate to isocitrate
Ribbon diagram of citrate synthase and ball-and-stick model of its iron-sulfur cluster connected to citrate and side chains of amino acids
Conversion of isocitrate to alpha-ketoglutarate
Oxidative decarboxylation of alpha-ketoglutarate
Conversion of succinyl C o A into succinate
Mechanism of action of succinyl C o A synthetase
Sequential reaction showing conversion of succinate to oxaloacetate
Conversion of fumarate into L-malate
Citric acid cycle
Conversion of glucose to C O 2 and fatty acids
Regulation of pyruvate dehydrogenase complex activity
Response of pyruvate dehydrogenase complex to changes in the energy of the cell
Regulation of citric acid cycle
Fates of the intermediates of citric acid cycle

Inhibition of pyruvate dehydrogenase by arsenite and its reversal by 2,3-dimercaptopropanol
Glyoxylate cycle
Structure of 2-vinyl-isocitrate
Structure of homopyruvoyl-modified isocitrate lyase
Structure of malonate
Structure of oxaloacetate
Colony-forming units in mice lungs in the weeks after an infection
Colony-forming units in mice lungs in the weeks after an infection
Schematic representation of proton flow across A T P synthase
Oxidative phosphorylation
FIGURE 18.2 Mitochondria (A) An electron micrograph and (B) a diagram
FIGURE 18.3 Redox potential can be precisely measured
FIGURE 18.4 Components of the electron-transport chain
FIGURE 18.5 Quinones can have three different oxidation states, two of which are stable
FIGURE 18.6. The three-dimensional structure of cytochrome c is remarkably conserved among distantly related species
FIGURE 18.7 Three different types of iron–sulfur clusters are commonly found in biological systems
FIGURE 18.8 Flavins have two oxidation states
FIGURE 18.9 Electron transfer through NADH-Q oxidoreductase is coupled to proton transfer reactions
Structure of reduced ubiquinone
FIGURE 18.10 Q-cytochrome c oxidoreductase is a homodimer, with each monomer consisting of 11 distinct polypeptide chains
FIGURE 18.11 The Q cycle allows the safe transfer of electrons from Q H 2 to cytochrome c
Chemical structure of copper ion bonded to histidine residue covalently linked to a tyrosine residue
FIGURE 18.12 The structure of bovine cytochrome c oxidase reveals 13 polypeptide chains and numerous electron carriers
Structure of heme A

FIGURE 18.13 The mechanism of cytochrome c oxidase prevents early oxygen release
FIGURE 18.14 Two metals form a peroxide bridge in cytochrome c oxidase
FIGURE 18.15 Proton transport by cytochrome c oxidase has two components
FIGURE 18.16 Electrons flow via two pathways through the electron-transport chain
FIGURE 18.17 Three complexes of the ETC associate to form the respirasome
Conversion of superoxide radical by enzyme superoxide dismutase
FIGURE 18.18 The superoxide dismutase mechanism has two phases
FIGURE 18.19 Proteins dramatically improve the rate of electron transfer
FIGURE 18.20 The chemiosmotic hypothesis states that electron-driven proton transport and ATP synthesis are coupled
FIGURE 18.21 The chemiosmotic hypothesis is supported by experiments using bacterial proton pumps
FIGURE 18.22 The structure of ATP synthase reveals a complex molecular rotational motor
FIGURE 18.23 Mitochondrial ATP synthase forms homodimers
FIGURE 18.24 ATP synthase assists in the formation of cristae
FIGURE 18.25 ATP-synthesis is catalyzed by ATP synthase
FIGURE 18.26 ATP forms without a proton-motive force but is not released
FIGURE 18.27 ATP synthase nucleotide-binding sites cycle through distinct conformational states
FIGURE 18.28 The binding-change mechanism involves the cycling of all three β subunits through three conformations
FIGURE 18.29 The ATP-driven rotation in ATP synthase has been directly observed
FIGURE 18.30 Components of the proton-conducting unit of ATP synthase include two half channels and a critical charged residue
FIGURE 18.31 Proton motion across the membrane drives rotation of the c ring

FIGURE 18.32 Protons must travel around the c ring to cross the membrane
FIGURE 18.33 An overview of oxidative phosphorylation shows the spatial relationship of the components
FIGURE 18.34 The glycerol 3-phosphate shuttle allows for rapid rates of oxidative phosphorylation at the cost of energetic efficiency
FIGURE 18.35 The malate–aspartate shuttle preserves all the chemical potential energy of cytoplasmically generated NADH
FIGURE 18.36 The ATP-ADP translocase catalyzes the exchange of entry of ADP and ATP
FIGURE 18.37 Structurally homologous mitochondrial transporters
FIGURE 18.38 ATP synthase depends upon the rest of the ATP synthesome, as well as the ETC and CAC
FIGURE 18.39 Mechanism of heat generation by U C P-1
FIGURE 18.40 P E T scan results of the uptake and distribution of F superscript 18-fluorodeoxyglucose in adipose tissue
FIGURE 18.41 Inhibitors of the electron transport chain
FIGURE 18.43 The flagellar motor is a complex structure containing as many as 40 distinct types of proteins
FIGURE 18.44 Rotation of the flagellum involves proton half-channels like ATP synthase
FIGURE 18.45 Proton gradient as an interconvertible form of free energy
Absorption spectra of the reduced and oxidized forms of cytochrome c
Results of an experiment using the X F technology
Phototrophic halobacteria are visible from the air in salt ponds near the San Francisco Bay and a schematic shows electron excitation and its transfer to acceptor
FIGURE 19.1 Phototrophy can be accomplished by the cooperation of just two proteins
FIGURE 19.2 The light reactions of oxygenic photosynthesis generate both A T P and reducing power
FIGURE 19.3 The anatomy of a chloroplast reveals complex membrane-enclosed structures

FIGURE 19.5: Structure of Chlorophyll alpha
FIGURE 19.6 Chlorophyll a has a distinct absorbance spectrum in the visible range
FIGURE 19.7 The absorption of light leads to the excitation of an electron from its ground state to a higher energy level
FIGURE 19.8 The key to photosynthesis is photoinduced charge separation
FIGURE 19.9 The photosynthetic reaction center in a nonsulfur purple bacterium is a large complex with many electron-carrying groups and one special pair
FIGURE 19.10 In the reaction center of nonsulfur purple bacteria, electrons flow from the special pair to a quinone
FIGURE 19.11 Cyclic electron flow in the bacterial reaction center allows the generation of A T P but not reducing power
FIGURE 19.12 In green plants, electrons can flow through two photosystems
Structures of Plastoquinone and Plastoquinol
FIGURE 19.13 Photosystem II is a large membrane protein complex with many chlorophyll molecules, one special pair, and the water-oxidizing complex
FIGURE 19.14 In photosystem II, electrons flow from manganese atoms to plastoquinone
FIGURE 19.15 The core of the water-oxidizing complex includes four manganese ions and one calcium ion
FIGURE 19.16 Four photons are required to generate one oxygen molecule after the first cycle
FIGURE 19.17 The model for the water-oxidizing complex explains the light-flash experiments
FIGURE 19.18 Photosystem II releases protons into the thylakoid lumen and takes them up from the stroma
FIGURE 19.19 Electron flow through cytochrome bf contributes to the proton gradient
FIGURE 19.20 Photosystem I is a protein complex with numerous chlorophyll molecules and one special pair.
FIGURE 19.21 In photosystem I, electrons flow to ferredoxin

FIGURE 19.22 Ferredoxin is an electron-carrying, iron-sulfur protein
FIGURE 19.23 Ferredoxin–N A D P + reductase transfers electrons from the protein ferredoxin to N A D P +
FIGURE 19.24 The “Z” scheme of photosynthesis is the linear path of electrons from H 2 O to N A D P +
FIGURE 19.25 Photosynthesis and oxidative phosphorylation have a similar layout but differ in a number of ways
Reversible reaction catalyzed by ferredoxin-thioredoxin reductase
FIGURE 19.26 Cyclic photophosphorylation allows A T P production without a need for an electron source
Structure of chlorophyll b
FIGURE 19.27 Chlorophylls a and b absorb light maximally at different wavelengths
Structure of Lycopene and beta carotene
FIGURE 19.28 Resonance energy transfer allows electrons to transfer energy over a distance
FIGURE 19.29 Energy is transferred from accessory pigments to reaction centers
FIGURE 19.30 Photosynthetic assemblies are differentially distributed in the stacked and unstacked regions of thylakoid membranes
FIGURE 19.31 Photovoltaic cells can drive artificial photosynthesis
FIGURE 19.32 Optogenetics allows neurons to be controlled using light
Graph depicts atmospheric C O 2 measured at Mauna Loa, Hawaii
FIGURE 20.1 The Calvin–Benson cycle consists of three stages
Sequential conversion of ribulose 1,5-bisphosphate to 3-phosphoglycerate
FIGURE 20.2 The enzyme ribulose 1,5-bisphosphate carboxylase slash oxygenase (Rubisco) comprises 16 subunits
Formation of carbamate from the lysine side chain and its binding to a magnesium ion
FIGURE 20.3 C O 2 fixation by magnesium-coordinated ribulose 1,5-bisphosphate
FIGURE 20.4 In stage 1 of the Calvin–Benson cycle, 3-phosphoglycerate is formed

FIGURE 20.5 The enediolate on Rubisco can react with oxygen in a wasteful side reaction
FIGURE 20.6 Photorespiration consumes O 2 and produces C O 2
FIGURE 20.8 In stage 2 of the Calvin–Benson cycle, hexose phosphate is formed
Aldose and ketose formation
Ketose formation
FIGURE 20.9 Five-carbon sugars are formed from six-carbon and three-carbon sugars
FIGURE 20.10 In stage 3 of the Calvin–Benson cycle, ribulose 1,5-bisphosphate is regenerated
FIGURE 20.11 The full Calvin–Benson cycle process for converting three molecules of C O 2 to dihydroxyacetone phosphate is complex
FIGURE 20.12 Carbohydrates are stored as sucrose
Conversion of crotonyl-C o A to ethylmalonyl-C o A and butyryl-C o A
FIGURE 20.13 Scientists have engineered artificial photosynthesis using alternative C O 2 fixation pathways
FIGURE 20.14 Light regulates the Calvin–Benson cycle
FIGURE 20.16 Thioredoxin can activate enzymes by reducing them
FIGURE 20.17 The C 4 pathway can concentrate C O 2
FIGURE 20.21 The pentose phosphate pathway consists of an oxidative and a nonoxidative phase
FIGURE 20.22 The oxidative phase of the pentose phosphate pathway yields two molecules of NADPH
Formation of ribose 5-phosphate
Reactions catalyzed by transketolase
Reaction catalyzed by transketolase
Formation of xylulose 5-phosphate
Reaction catalyzed by transaldolase
Reaction catalyzed by transketolase
FIGURE 20.23 The transketolase reaction takes place on thiamine pyrophosphate
FIGURE 20.24 The transaldolase reaction involves a Schiff base intermediate

FIGURE 20.25 For transketolase and transaldolase, a carbanion intermediate is stabilized by resonance
FIGURE 20.26 The pentose phosphate pathway can operate in four modes
Structure of reduced glutathione
Structure of pamaquine
Structure of primaquine
FIGURE 20.27 Fava beans produce a pyrimidine glycoside
Conversion of oxidized glutathione to reduced glutathione catalyzed by glutathione reductase
FIGURE 21.3 The fundamental structure of glycogen is a linear polymer with occasional branches
FIGURE 21.4 Glucose 6-phosphate can have many metabolic fates
Cleavage of glucose 1-phosphate residue from glycogen with n residues
FIGURE 21.5 Glycogen phosphorylase forms a homodimer with a pyridoxal phosphate (P L P) group in each active site
FIGURE 21.6 P L P forms a Schiff-base linkage with lysine
FIGURE 21.7 The mechanism of phosphorylase involves P L P and the formation of a carbocation
FIGURE 21.8 Glycogen remodeling requires three distinct catalytic activities
Action of alpha-1, 6-glucosidase
FIGURE 21.9 Phosphoglucomutase transfers a phosphoryl group to the substrate
FIGURE 21.10 Phosphorylase exists in two distinct quaternary states
FIGURE 21.11 Phosphorylase is regulated by phosphorylation
FIGURE 21.12 Liver phosphorylase is allosterically inhibited by glucose
FIGURE 21.13 Muscle phosphorylase is allosterically regulated by A T P, A M P, and glucose 6-phosphate
Amino acid sequence of glucagon
Structure of epinephrine
FIGURE 21.14 Phosphorylase kinase is activated by calcium ions and hormonally controlled phosphorylation

FIGURE 21.15 Glycogen breakdown is controlled by the combined effects of multiple hormones in a tissue specific manner
FIGURE 21.16 Glycogen degradation is stimulated by hormone binding to 7 T M receptors
Structure of uridine diphosphate glucose (U D P-glucose)
Formation of U D P-glucose from glucose 1-phosphate and U T P
Synthesis of U D P-glucose and the hydrolysis of pyrophosphate and the resulting reaction
Elongation of glycogen molecule by 1 glucose residue
FIGURE 21.17 Action of a branching enzyme
FIGURE 21.18 A cross section of a glycogen molecule reveals the basic branching structure
FIGURE 21.19 Glycogen metabolism is regulated in part by hormone-triggered cyclic A M P cascades
FIGURE 21.20 Glycogen synthesis is regulated by protein phosphatase 1 (P P 1)
FIGURE 21.21 P P 1 is regulated by hormonally controlled cascades
FIGURE 21.22 Insulin inactivates glycogen synthase kinase
FIGURE 21.23 Blood glucose regulates liver-glycogen metabolism
FIGURE 21.24 Glucose regulates liver-glycogen metabolism
FIGURE 21.25 An electron micrograph of a muscle cell from a patient with Pompe disease reveals enlarged lysosomes
Western blot photograph shows the separation of samples of glycogen
Western blot photograph shows the separation of samples of glycogen isolated from a cell line
Synthesis and degradation of fatty acids
Structure of triacylglycerol
FIGURE 22.2 Breakdown of triacylglycerol into monoacylglycerol and fatty acids by lipase
Structure of glycocholate
FIGURE 22.4 Fat absorption and transport is a complex process involving multiple proteins
Hydrolyzation of triacylglycerol to yield glycerol and isolated fatty acids

FIGURE 22.5 Triacylglycerols in adipose tissue are converted into free fatty acids in response to hormonal signals
FIGURE 22.6 Lipolysis generates fatty acids and glycerol
Stepwise conversion of glycerol to D-Glyceraldehyde 3-phosphate
Thioester linkage formation between fatty acid and coenzyme A
Structure of acyl adenylate
Conversion of fatty acid to acyl adenylate and acyl adenylate to acyl C o A
Formation of acyl carnitine from acyl C o A and carnitine
FIGURE 22.7 Acyl carnitine translocase mediates the entry of acyl carnitine into the mitochondrial matrix
FIGURE 22.8 The reaction sequence for the degradation of fatty acids has four sequential steps
Sequential transfer of electrons from substrate to ubiquinone
FIGURE 22.9 Each round of fatty acid degradation removes two carbons
FIGURE 22.10 The degradation of a monounsaturated fatty acid involves an additional enzymatic step
FIGURE 22.11 Multiple additional enzymes are necessary to oxidize polyunsaturated fatty acids
FIGURE 22.12 The final product of odd-numbered fatty acid degradation is converted into a C A C intermediate
FIGURE 22.13 Coenzyme B 12 (cobalamin) is a class of molecules with a complex structure
FIGURE 22.14 Cobalamin enzymes catalyze specific rearrangement reactions
FIGURE 22.15 Cobalamin enzymes accomplish homolytic bond cleavage to form a radical
FIGURE 22.16 Succinyl C o A is formed from methylmalonyl C o A by a rearrangement reaction
FIGURE 22.17 The active site of methylmalonyl C o A mutase reveals how radical formation is accomplished
FIGURE 22.18 Initiation of peroxisomal fatty acid degradation requires a flavoprotein

FIGURE 22.19 Ketone bodies are formed from acetyl C o A primarily in the liver
FIGURE 22.20 Pathway Integration: The liver supplies ketone bodies to the peripheral tissues
FIGURE 22.21 Acetoacetate can be used as a fuel to drive A T P formation
Formation of acetoacetate from D-3-hydroxybutyrate
FIGURE 22.22 Diabetic ketosis results when insulin signaling is impaired
FIGURE 22.23 The steps in fatty acid degradation and synthesis are chemically similar
FIGURE 22.24 Phosphopantetheine group in acyl carrier protein and coenzyme A
FIGURE 22.25 Like beta-oxidation, saturated fatty acid synthesis consists of four steps
FIGURE 22.26 Mammalian fatty acid synthase is a large, dimeric, multidomain protein complex
FIGURE 22.27 One catalytic cycle of mammalian fatty acid synthase consists of seven steps
FIGURE 22.28 Acetyl C o A can be transferred from the mitochondrial matrix to the cytoplasm
FIGURE 22.29 Pathway Integration: Fatty acid synthesis requires the cooperation of various pathways in different cellular compartments
FIGURE 22.30 Desaturation of fatty acids by an electron transport chain in the E R membrane
FIGURE 22.31 Several eicosanoid hormones are produced from arachidonate by distinct enzymatic pathways
FIGURE 22.32 Structures of different eicosanoids
FIGURE 22.33 Inhibition and activation of acetyl C o A carboxylase
FIGURE 22.35 The catalytic activity of acetyl C o A carboxylase depends upon the concentration of citrate
Acetyl C o A containing radioactive carbon and hydrogen atoms
Relationship between carnitine acyltransferase 1 activity and concentration of carnitine

Relationship between carnitine acyltransferase 1 activity and concentration of palmitoyl C o A
Relationship between carnitine acyltransferase 1 activity and concentration of malonyl C o A
Effect of various amounts of soraphen A on fatty acid synthesis
Effect of various amounts of soraphen A on fatty acid oxidation
Effect of various amounts of soraphen A on phospholipid synthesis
Effect of different concentrations of soraphen A on the viability of cancer cells
Schematic representation of the absorption of protein digestion products by a cell
FIGURE 23.1 The products of protein digestion are absorbed by the small intestine
FIGURE 23.2 Ubiquitin is a small, compact protein with seven lysines
Isopeptide bond between ubiquitin and the side chain of lysine residue of the target protein
FIGURE 23.3 Ubiquitin conjugation requires three enzymes
FIGURE 23.4 In a tetraubiquitin chain, four ubiquitin molecules are linked by isopeptide bonds
FIGURE 23.5 The 20 S proteasome is barrel-shaped and made up of 28 homologous subunits
FIGURE 23.6 The 26 S proteasome consists of one 20 S and two 19 S subunits
FIGURE 23.7 The proteasome and other proteases generate free amino acids
FIGURE 23.8 Proteasomes have become more complex in eukaryotes
Structure of bortezomib
Structure of H T 1171
Oxidative deamination in the liver
Transfer of the alpha-amino group from an alpha-amino acid to an alpha-ketoacid
Formation of alpha-ketoglutarate from glutamate
Conversion of an ammonium ion into urea in terrestrial vertebrates
Reversible conversion of P L P (phenol) to P L P (phenolate)
Formation of external aldimine from internal aldimine

FIGURE 23.9 Transaminations proceed through three steps to form P M P
Structure of pyridoxamine phosphate
FIGURE 23.10 The active site of aspartate aminotransferase reveals P L P bound to a lysine through a Schiff-base linkage
FIGURE 23.11 P L P enzymes labilize one of three bonds at the alpha-carbon atom of an amino acid substrate
FIGURE 23.12 Stereoelectronic effects determine specific bond cleavage
FIGURE 23.13 Bond orientation in the active site determines bond cleavage in different P L P enzymes
Deamination of serine
FIGURE 23.14 PATHWAY INTEGRATION: The glucose–alanine cycle allows muscle cells to use amino acids as fuel
FIGURE 23.15 The urea cycle eliminates both nitrogen and carbon waste products
Formation of carbamoyl phosphate from bicarbonate
Reaction catalyzed by N-acetylglutamate synthase
Reaction catalyzed by ornithine transcarbamoylase
Reaction catalyzed by argininosuccinate synthetase
Reaction catalyzed by argininosuccinase
Reaction catalyzed by arginase
FIGURE 23.16 Nitrogen metabolism is integrated with other pathways
FIGURE 23.17 Argininosuccinase deficiency can be managed by supplementing the diet with arginine
FIGURE 23.18 Both carbamoyl phosphate synthetase and ornithine transcarbamoylase deficiencies can be treated the same way
Structure of uric acid
FIGURE 23.19 The carbon skeletons of all 20 proteogenic amino acids enter central metabolism as just seven different molecules
FIGURE 23.20 Pyruvate is the metabolic entry point for the carbon skeletons from three-carbon amino acids
FIGURE 23.21 Four amino acids produce carbon skeletons that enter central metabolism as alpha-ketoglutarate
FIGURE 23.22 Stepwise conversion of histidine to glutamate

FIGURE 23.23 The degradation pathways for proline and arginine converge on a common intermediate
FIGURE 23.24 Succinyl C o A is formed from methionine, isoleucine, threonine, and valine
FIGURE 23.25 Methionine catabolism proceeds through the formation of S A M
Conversion of threonine to propionyl C o A
Conversion of leucine to isovaleryl C o A
Conversion of isovaleryl C o A to beta-methylglutaconyl C o A
Conversion of beta-methylglutaconyl C o A to acetyl C o A and acetoacetate
Reaction catalyzed by phenylalanine hydroxylase
Irreversible conversion of quinonoid dihydrobiopterin to tetrahydrobiopterin
FIGURE 23.26 Phenylalanine and tyrosine degradation produce both acetoacetate and fumarate
FIGURE 23.27 Tryptophan degradation requires multiple oxygenases and numerous steps
Structure of 2-methylbutyryl C o A
Structure of butyryl C o A
Beta-oxidation of 2-methylbutyryl C o A
Hydration and oxidation steps of beta-oxidation
Thiolysis of the product of the oxidation step of beta-oxidation
Conversion of homogentisate to a highly colored polymer
FIGURE 23.28 Urine has long been used to diagnose diseases due to the excretion of unusual biochemical products
Conversion of alpha-ketoacid to 2,4-dinitrophenylhydrazone derivative
Conversion of phenylalanine to phenylpyruvate
Chemical structure
Chemical structure
Chemical structure
Chemical structure
Variation of percentage of digestion of pentapeptide with minutes of incubation

Photograph of an event and schematic representation of integration of metabolic pathways for glucose homeostasis
Coordinated use of nutrient pools to maintain homeostasis
FIGURE 24.2 Signal molecules originating from the gut induce feelings of satiety in the brain
FIGURE 24.3 Leptin suppresses appetite by affecting the brain
FIGURE 24.4 Adipokines help to maintain systemic lipid and glucose homeostasis
FIGURE 24.5 Suppressors of cytokine signaling (S O C S) regulate insulin receptor function
FIGURE 24.6 Glycolysis and gluconeogenesis are reciprocally regulated
FIGURE 24.7 Insulin signaling activates A k t using the second messenger P I P 3
FIGURE 24.8 The storage capacity of fat tissue can be exceeded in obesity
FIGURE 24.9 Excess fat can disrupt signal-transduction pathways and lead to insulin insensitivity
FIGURE 24.10 Insulin release by the pancreas is regulated by blood-glucose concentration, using A T P as a second messenger
Irreversible reaction catalyzed by creatine kinase
FIGURE 24.11 Running velocity decreases dramatically as a function of the duration of the race
FIGURE 24.12 An idealized representation of fuel use and RQ illustrates major changes as a function of aerobic exercise intensity
FIGURE 24.13 Exercise results in mitochondrial biogenesis and enhanced fat metabolism
FIGURE 24.14 Biochemical adaptations to exercise vary over a range of time scales
FIGURE 24.15 The blood concentrations of ketone bodies glucose, and fatty acids during starvation
FIGURE 24.16 Fuel use during prolonged starvation changes after fat mass is depleted
FIGURE 24.17 Formation of 4-hydroxyproline requires ascorbate
Structure of ascorbic acid, ascorbate, and dehydroascorbic acid

Relation between blood-lactate levels, oxygen consumption, and heart rate during exercise of increasing intensity
Reaction sequence depicting the assimilation of N 2
FIGURE 25.1 The nitrogenase complex fixes nitrogen to ammonia
FIGURE 25.2 The F e protein, or reductase, transfers elections of high reducing power
FIGURE 25.3 The M o F e protein, or nitrogenase, catalyzes the reduction of N 2 to N H 3
Formation of glutamate
Formation of protonated Schiff base
Formation of glutamate from alpha-ketoglutarate
FIGURE 25.4 Glutamate chirality is established by hydride transfer to the Schiff base
Conversion of glutamate to glutamine
Irreversible reaction catalyzed by phenylalanine hydroxylase
FIGURE 25.6 Essential and nonessential amino acids can be distinguished by the required number of biosynthetic steps
FIGURE 25.7 Transamination is a critical step in the biosynthesis of most amino acids
FIGURE 25.8 Proton addition during transamination establishes amino acid stereochemistry
Conversion of aspartate to asparagine
Conversion of glutamate to glutamic gamma-semialdehyde
Formation of arginine and proline from glutamate
Formation of serine from 3-phosphoglycerate
Formation of glycine from serine
FIGURE 25.9 Tetrahydrofolate is an important carrier of activated one-carbon units
FIGURE 25.10 Interconversion of one carbon units attached to tetrahydrofolate
Formation of S-adenosylmethionine from methionine
Formation of homocysteine from S-adenosylmethionine
Reaction catalyzed by methionine synthase
FIGURE 25.11 The activated methyl cycle enables regeneration of methionine

Formation of alpha-ketobutyrate and cysteine
FIGURE 25.12 Chorismate is formed from phosphoenolpyruvate and erythrose 4-phosphate
Structure of glyphosate
FIGURE 25.13 Phenylalanine and tyrosine are formed in the prephenate branch
FIGURE 25.14 Tryptophan is formed in the anthranilate branch
Structure of 5-phosphoribosyl-1-pyrophosphate
FIGURE 25.15 Tryptophan synthase contains two remotely positioned catalytic domains
Reaction between Schiff base of aminoacrylate and indole
FIGURE 25.16 Tryptophan synthase uses substrate channeling to prevent loss of the indole intermediate
Inhibition of the first irreversible step of a biosynthetic pathway
FIGURE 25.17 3-Phosphoglycerate dehydrogenase is a homotetramer
FIGURE 25.18 Threonine deaminase is regulated by feedback inhibition and activation
FIGURE 25.19 The regulatory domains of 3-phosphoglycerate dehydrogenase and threonine deaminase are related structurally
Inhibition of enzymes by different products of a pathway
FIGURE 25.20 The three aspartokinases from E. coli have different regulatory domains
Structure of tyrosine residue modified by adenylylation
FIGURE 25.21 Glutamine synthetase is regulated by covalent modification
FIGURE 25.22 A diverse array of biomolecules are derived from amino acids
FIGURE 25.23 Glutathione structure
FIGURE 25.24 Ribbon diagram of glutathione peroxidase
FIGURE 25.25 Regeneration of selenolate active site after peroxide cleavage
FIGURE 25.26 Generation of nitric oxide from arginine
FIGURE 25.27 Tyrosine is a precursor for the catecholamines
FIGURE 25.28 The neurotransmitters serotonin and melatonin are synthesized from tryptophan

FIGURE 25.29 The origins of atoms in heme were revealed by isotope-labeling studies
Formation of delta-aminolevulinate
FIGURE 25.30 Heme is synthesized from eight molecules of delta-aminolevulinate
FIGURE 25.31 Heme is degraded into biliverdin and bilirubin
Structure of tryptophan
Formation of proline from ornithine
Schematic representation of a branched pathway
Ribbon diagram of A T P grasp domain
FIGURE 26.1 Nucleotides can be synthesized by de novo and salvage pathways
FIGURE 26.2 Pyrimidine nucleotides can be synthesized de novo
FIGURE 26.3 Carbamoyl phosphate synthetase 2 includes sites for three reactions
Formation of carbamic acid from bicarbonate
Formation of carbamoyl phosphate from carbamic acid
FIGURE 26.4 The three active sites of carbamoyl phosphate synthetase 2 are linked by a channel through which intermediates pass
Formation of orotate from carbamoyl phosphate
Reaction catalyzed by P R P P synthetase
Formation of orotidylate
Formation of uridylate from orotidylate
Formation of C T P from U T P
Structure of acyclovir
FIGURE 26.5 Purine nucleotides can be synthesized de novo
Formation of 5-phosphoribosyl-1-amine from P R P P
Activation of the carbonyl oxygen atom followed by the displacement of the phosphoryl group by a nucleophile
FIGURE 26.6 The de novo purine biosynthesis pathway involves nine steps
FIGURE 26.7 Inosinate can be converted to A M P and G M P
FIGURE 26.8 Hela cells in the presence and absence respectively of purine in the medium

Structure of inosinate
Structure of 2-aminoadenine
FIGURE 26.9 The nucleotide containing 2-aminoadenine is synthesized from deoxyguanylate
FIGURE 26.10 Ribonucleotide reductase uses a radical mechanism to produce deoxyribonucleotides
Oxidation of N A D P H coupled with the reduction of ribose substrate
FIGURE 26.11 The ribonucleotide reductase R 2 subunit contains a stable free radical on a tyrosine residue
FIGURE 26.12 Thymidylate synthase catalyzes the addition of a methyl group to d U M P to form T M P
Reduction of dihydrofolate to tetrahydrofolate
FIGURE 26.13 Enzymes crucial for nucleotide synthesis are anticancer drug targets
FIGURE 26.14 Fluoruracil acts by suicide inhibition
Generalized structure of aminopterin and methotrexate
Structure of trimethoprim
Regulation of aspartate transcarbamoylase
FIGURE 26.15 Purine biosynthesis is regulated at many steps
FIGURE 26.16 Ribonucleotide reductase is highly regulated to balance the pool of deoxyribonucleotides
FIGURE 26.17 Purines are catabolized for excretion
Structure of allopurinol
Structure of azaserine
Action of statins on cholesterol level and photograph of medicines targeting lipid biosynthesis
FIGURE 27.1 Phosphatidate is a key intermediate in lipid biosynthesis
A reaction depicting the conversion of glycerol 3-phosphate to phosphatidate
A reaction depicting the conversion of phosphatidate to triacylglycerol
Conversion of phosphatidate to C D P diacylglycerol
Conversion of C D P diacylglycerol to phosphatidylinositol and C M P
Structure of diphosphatidylglycerol (cardiolipin)
Conversion of ethanolamine to phosphatidylethanolamine

Formation of phosphatidylcholine
Structure of sphingosine
FIGURE 27.2 Biosynthesis of ceramide involves four steps
FIGURE 27.3 The ganglioside G subscript M 1 consists of five monosaccharides linked to ceramide
FIGURE 27.4 Ceramide can be converted into sphingomyelin, cerebroside, and gangliosides
Conversion of ganglioside G subscript M 2 to ganglioside G subscript M 3
FIGURE 27.6 Phosphatidic acid phosphatase is a key regulatory enzyme in lipid synthesis
FIGURE 27.7 Isotope-labeling experiments have revealed the source of carbon atoms in cholesterol synthesized from acetate
FIGURE 27.8 3-Hydroxy-3-methylglutaryl C o A has different fates
FIGURE 27.9 Mevalonate is converted into isopentenyl pyrophosphate
Structure of isoprene
Formation of dimethylallyl pyrophosphate from isopentenyl pyrophosphate
FIGURE 27.10 Condensation reactions build carbon–carbon bonds that eventually form the cholesterol skeleton
FIGURE 27.11 Two molecules of farnesyl pyrophosphate are linked to form squalene
FIGURE 27.12 Squalene cyclization leads to the steroid skeleton in the form of lanosterol
FIGURE 27.13 Cholesterol is formed from lanosterol
FIGURE 27.14 S R E B P regulates gene expression in response to cholesterol levels
FIGURE 27.15 Insig regulates S C A P-S R E B P movement
FIGURE 27.16 Insig facilitates the degradation of H M G-C o A reductase
FIGURE 27.18 L D L consists of a core of cholesterol esters surrounded by a single molecule of apolipoprotein B-100
FIGURE 27.19 L D L enters cells through receptor-mediated endocytosis

FIGURE 27.20 Arterial plaques are one of the effects of excess cholesterol
FIGURE 27.21 The L D L receptor releases L D L in the endosome
FIGURE 27.22 Structure of lovastatin
FIGURE 27.23 Bile salts are synthesized from cholesterol
FIGURE 27.24 Different classes of steroid hormones are derived from cholesterol
FIGURE 27.25 A common numbering system is used for cholesterol and other steroids
FIGURE 27.26 The reaction mechanism for cytochrome P 450 enzymes reveals how oxygen is inserted into R-H bonds
FIGURE 27.27 Cytochrome P 450 2 C 19 converts the prodrug clopidogrel to an active form
Conversion of cholesterol to pregnenolone
FIGURE 27.28 Pregnenolone is converted into progesterone, cortisol, and aldosterone
FIGURE 27.29 Progesterone is converted into testosterone and estradiol
Formation of 5 alpha-dihydrotestosterone
FIGURE 27.30 Structure of anastrozole and exemestane
FIGURE 27.31 Vitamin D is synthesized from 7-dehydrocholesterol in a process initiated by absorption of ultraviolet light
FIGURE 27.32 Some terpenes are familiar from everyday life
FIGURE 27.33 Two carotenoids responsible for the color of tomatoes and carrots are large isotrenes
Structure of farnesene
Formation of diacylglycerol from phosphatidate
Fused-ring core structure of a steroid
Structure of a compound
Structure of a compound
Structure of a compound
Structure of a compound
Structure of a compound
Ribbon diagram of D N A polymerase copying D N A

FIGURE 28.1 The structure of the E.coli D N A polymerase I Klenow fragment resembles a hand
FIGURE 28.2 Three metal ions (typically, M g superscript 2 plus) participate in the D N A polymerase reaction
FIGURE 28.3 Base analogs that have the same shape as normal bases can participate in D N A replication
FIGURE 28.4 Minor-groove interactions promote the specificity of D N A replication
FIGURE 28.5 Shape selectivity promotes the specificity of DNA replication
FIGURE 28.6 D N A polymerases require a primer
FIGURE 28.7 The lagging strand is made in short pieces called Okazaki fragments
FIGURE 28.8 D N A ligase catalyzes the joining of two D N A strands
FIGURE 28.9 Helicases are hexamers
Structure of A M P-P N P
FIGURE 28.10 Helicases have intrinsic asymmetry
FIGURE 28.11 Helicases unwind D N A
FIGURE 28.12 The linking number (L k), twist (T w), and writhe (W r) of circular DNA are related
FIGURE 28.14 Topoisomerase 1 binds to D N A
FIGURE 28.15 Topoisomerase 1 relaxes supercoiled D N A
Cleavage of phosphodiester bond by the tyrosine residue of topoisomerase
FIGURE 28.16 Topoisomerase 2 is a dimer
FIGURE 28.17 Topoisomerase 2 uses A T P hydrolysis to introduce negative supercoils into D N A
Structure of nalidixic acid and ciprofloxacin
FIGURE 28.18 The sliding clamp subunit of D N A polymerase 3 is a dimer
FIGURE 28.19 D N A synthesis at the replication fork is highly coordinated
FIGURE 28.20 The D N A polymerase holoenzyme consists of multiple subunits

FIGURE 28.21 The trombone model describes the coordination of D N A synthesis at the replication fork
FIGURE 28.22 The E. coli chromosome has a single origin of replication
FIGURE 28.23 The assembly of D n a A proteins initiates D N A replication
FIGURE 28.24 The prepriming complex prepares the template strands for D N A synthesis
FIGURE 28.25 Replication termination in E. coli occurs at T e r sites
FIGURE 28.26 Eukaryotic chromosomes have multiple origins of replication
FIGURE 28.27 Eukaryotic D N A replication and cell division are highly coordinated
FIGURE 28.28 Telomeres may form duplex loops
FIGURE 28.29 Telomerase uses its R N A template to synthesize the G-rich strand of telomeres
FIGURE 28.30 The bacterium Deinococcus radiodurans repairs DNA damage quickly
FIGURE 28.31 Damaged D N A bases can form base pairs
FIGURE 28.32 Adenine can be deaminated to form hypoxanthine
FIGURE 28.33 Aflatoxin can be activated into a mutagen
FIGURE 28.34 Chemical structure and ball-and-stick model of thymine dimer
FIGURE 28.35 Psoralen is a cross-linking agent
FIGURE 28.36 D N A polymerases have proofreading activities
FIGURE 28.37 D N A mismatch repair in E. coli involves multiple proteins
FIGURE 28.38 Base-excision repair enzymes remove damaged bases
FIGURE 28.39 Nucleotide-excision repair involves the removal of a section of damaged D N A
FIGURE 28.40 Excision and replacement of uridine bases in D N A by cytidine
FIGURE 28.41 Trinucleotide repeats can form structures that lead to their expansion during D N A replication
Structure of cyclophosphamide and cisplatin

FIGURE 28.42 The Ames test determines the mutagenicity of various compounds
FIGURE 28.43 D N A recombination
FIGURE 28.44 Strand invasion can initiate recombination
FIGURE 28.45 Holliday junctions are formed and resolved by recombinases
D N A banding pattern in lanes A, B, and C
Illustration of four agar plates used for Ames test
Electron micrograph and schematic representation of R N A synthesis and splicing respectively
FIGURE 29.1 R N A polymerase structures in prokaryotes and eukaryotes resemble each other
R N A synthesis using D N A as a template
FIGURE 29.2 The R N A polymerase active site contains metal ions
FIGURE 29.3 R N A polymerase separates a region of the double helix to form the transcription bubble
FIGURE 29.4 R N A transcript complementary to the template strand
Structure of a molecule
FIGURE 29.5 The elongation mechanism involves a series of steps
FIGURE 29.6 A structure within R N A polymerase forces the separation of the R N A–D N A hybrid
FIGURE 29.7 The R N A–D N A hybrid can occasionally backtrack within the R N A polymerase
Consensus sequence for the core promoter
FIGURE 29.8 Bacterial promoters contain conserved sequences
FIGURE 29.9 E. coli R N A polymerase holoenzyme complex binds to conserved promoter sequences
FIGURE 29.10 E. coli R N A polymerase binds to a promoter sequence
FIGURE 29.11 The transcription bubble moves with the R N A polymerase during elongation
FIGURE 29.12 Some genes contain intrinsic termination signals
FIGURE 29.13 Rho protein promotes the termination of transcription
FIGURE 29.14 Rho protein is an A T P-dependent helicase
FIGURE 29.15 Alternative promoters vary in their consensus sequences at conserved sites

FIGURE 29.16 Riboswitches use metabolite concentrations to regulate transcription
FIGURE 29.17 Transcription and translation are closely coupled in prokaryotes, whereas they are spatially and temporally separate in eukaryotes
FIGURE 29.19 The structure of the nucleosome consists of eight histone proteins surrounded by D N A
FIGURE 29.21 Eukaryotic promoters share common elements
FIGURE 29.22 The sequence of the T A T A box is highly conserved
FIGURE 29.23 The sequences of the C A A T box and G C box are also highly conserved
FIGURE 29.24 The T A T A-box-binding protein binds to D N A
FIGURE 29.25 General transcription factors are essential in initiating transcription by RNA polymerase 2
FIGURE 29.26 Cleavage of a primary R N A transcript in E. coli produces 5 S, 16 S, and 23 S r R N A molecules and a t R N A molecule
Modification of uridylate into ribothymidylate and pseudouridylate
FIGURE 29.27 The processing of eukaryotic pre-r R N A produces mature r R N As
FIGURE 29.28 Electron microscopy gives a window into r R N A transcription and processing in eukaryotes
FIGURE 29.29 Transfer R N A precursors are processed
FIGURE 29.30 The 5 prime ends of eukaryotic m R N As are capped
FIGURE 29.31 Primary transcripts in eukaryotes are polyadenylated
FIGURE 29.32 Splice sites are identified by conserved sequences
Reversible transesterification reaction
FIGURE 29.33 The splicing mechanism for m R N A precursors involves a lariat intermediate
FIGURE 29.34 The splicing branch point has a unique structure
FIGURE 29.35 The spliceosome consists of proteins and R N As
FIGURE 29.36 The spliceosome promotes the splicing of some genes
Base-pairing of the 5 prime splice site of the pre-m R N A with the conserved sequence of U 1 s n R N A
FIGURE 29.37 The spliceosome’s catalytic center includes two key magnesium ions

FIGURE 29.38 Mutations in splice sites can cause diseases such as thalassemia
FIGURE 29.39 Alternative splicing produces different m R N As
FIGURE 29.40 The C T D couples transcription to pre-m R N A processing
FIGURE 29.41 Small regulatory R N As are involved in gene regulation
FIGURE 29.42 R N A editing alters the coding sequence of m R N As
FIGURE 29.44 Self-splicing introns have a complex structure
FIGURE 29.45 The catalytic mechanism of the group 1 self-splicing intron includes a series of transesterification reactions
FIGURE 29.46 In self-splicing mechanisms, the catalytic site is formed by the intron itself
Three genes on a double-stranded D N A
Graphs for the liver, muscle, and brain indicating how much m R N A has attached to each D N A sequence
The ribosome, shown above, is a cellular machine that is not unlike a 3 D printer
FIGURE 30.1 Polypeptides are synthesized by the successive addition of amino acids to the carboxyl terminus
FIGURE 30.2 The secondary structure of all transfer R N A s resembles a cloverleaf
FIGURE 30.3 Transfer R N A s have an L-shaped tertiary structure
Structures of 5-methycytidine and dihydrouridine
FIGURE 30.4 The four double-stranded regions of a t R N A stack to form an L-shaped structure
FIGURE 30.5 Ester linkages couple amino acids to t R N A s
Anticodon and codon sequence
FIGURE 30.6 16 S r R N A monitors base-pairing between the codon and the anticodon
Structure of aminoacyl A M P
FIGURE 30.7 The amino acid-binding site of threonyl- t R N A synthetase contains a zinc ion
FIGURE 30.8 Threonyl- t R N A synthetase also contains an editing site
FIGURE 30.9 Amino acids move between the activation site and the editing site of an aminoacyl- t R N A synthetase

FIGURE 30.10 Kinetic proofreading can increase reaction specificity
FIGURE 30.11 Aminoacyl- t R N A synthetases bind to both the acceptor stem and the anticodon loop of a t R N A
FIGURE 30.12 t R N A s have multiple recognition sites for aminoacyl-t R N A synthetases
FIGURE 30.13 Class I and class II aminoacyl-t R N A synthetases recognize different faces of the t R N A molecule
FIGURE 30.14 The ribosome consists of a large subunit and a small subunit
FIGURE 30.15 Ribosomal R N A s form intramolecular base pairs
FIGURE 30.16 The ribosome has three binding sites for transfer R N A s
FIGURE 30.17 The key components of the translation machinery interact on an active ribosome
FIGURE 30.18 Initiator regions in m R N A determine where protein biosynthesis starts
FIGURE 30.19 Methionyl-t R N A is formylated to create a modified amino acid
FIGURE 30.20 Prokaryotic initiation factors aid the assembly of initiation complexes
FIGURE 30.21 The structure of elongation factor T u (E F-T u) and an aminoacyl-t R N A resembles those of other G proteins
FIGURE 30.22 The G T P ase E F T u binds aminoacyl t R N A only in its G T P form
FIGURE 30.23 Peptide-bond formation links amino acids
FIGURE 30.24 Protein biosynthesis is a cyclical process
FIGURE 30.25 Translocation repositions t R N A s and m R N A with respect to the ribosome
FIGURE 30.27 Release factors facilitate the termination of protein biosynthesis
Release of complete protein from t R N A
FIGURE 30.28 Translation initiation differs in eukaryotes as compared with prokaryotes
FIGURE 30.29 Protein interactions circularize eukaryotic m R N A

FIGURE 30.30 Unnatural amino acids can be incorporated into proteins
FIGURE 30.32 The signal sequences of eukaryotic secretory and plasma membrane proteins contain hydrophobic residues
FIGURE 30.33 The signal-recognition particle (S R P) consists of six proteins and one 300-nucleotide R N A
FIGURE 30.34 The S R P targeting cycle delivers nascent proteins containing a signal sequence to the E R
FIGURE 30.35 Protein-sorting pathways deliver proteins to their final destinations
Structure of streptomycin
FIGURE 30.36 The antibiotic puromycin resembles the aminoacyl terminus of an aminoacyl-t R N A
FIGURE 30.37 Diphtheria toxin inhibits protein biosynthesis in eukaryotes
The two basic mechanisms for the elongation of biomolecules are represented in the adjoining illustration
Graphical representation of optical density gradient for each fraction
Graphical representation of optical density gradient for each fraction
Graphical representation of optical density gradient for each fraction
Graphical representation of helices unwound versus time in minutes
Graphical representation of helicase activity
Graphical representation of effects of R N A R N A on helix stability
Structure of a t R N A
Structure of a t R N A
Complex biological processes often require coordinated control of the expression of many genes
FIGURE 31.1 The sequence of the lac regulatory site is a nearly perfect inverted repeat
FIGURE 31.2 The lac repressor binds to operator D N A
FIGURE 31.3 Sequence-specific D N A-binding proteins interact with D N A through a helix-turn-helix motif
FIGURE 31.4 Some D N A-binding proteins recognize specific D N A sequences through beta strands
Formation of galactose and glucose

FIGURE 31.5 The Beta-galactosidase reaction can be monitored using a colored indicator.
FIGURE 31.6 The production of β-galactosidase can be increased by the addition of lactose
FIGURE 31.7 Operons are clusters of genes under a common control
FIGURE 31.8 The lac repressor binds to D N A as a dimer
FIGURE 31.9 Binding of I P T G alters the lac repressor structure and affects its ability to bind D N A
FIGURE 31.10 The lac operon can be induced
FIGURE 31.11 Operator sites are not distributed evenly across the E. coli genome
FIGURE 31.12 The catabolite activator protein (CAP) binds to DNA as a dimer
The CAP dimer binds to D N A and to R N A polymerase
FIGURE 31.14 The lambda repressor binds to D N A as a dimer
FIGURE 31.15 The sequence of the lambda right operator is a binding target for regulatory proteins
FIGURE 31.16 The lambda repressor controls its own synthesis
FIGURE 31.17 The lambda repressor and Cro form a genetic circuit
FIGURE 31.18 Two different D N A-binding homeodomains can form a heterodimer
FIGURE 31.19 Two basic-leucine zipper proteins can form a heterodimer
FIGURE 31.20 Zinc-finger domains bind to D N A
FIGURE 31.21 The mediator complex binds to transcription factors and to R N A polymerase II
Structure of 5-methylcytosine
Structure of estradiol
Structure of all-trans-retinoic acid (a retinoid) and thyroxine (L-3,5,39,59-tetraiodothyronine) (a thyroid hormone)
FIGURE 31.24 Nuclear hormone receptors contain two important conserved domains
FIGURE 31.25 Nuclear hormone receptors interact with ligands
FIGURE 31.26 Nuclear hormone receptors recruit coactivators upon ligand binding

A chemical reaction
FIGURE 31.27 Histone acetyltransferase modifies histone tails
FIGURE 31.28 Bromodomains interact with acetyllysine
FIGURE 31.29 Gene regulation can involve chromatin remodeling
FIGURE 31.30 The leader region of t r p m R N A includes tryptophan codons
FIGURE 31.31 Attenuation regulates transcription
FIGURE 31.32 The leader sequences of several operons contain codons for the specific amino acid that they regulate
FIGURE 31.33 The structure of ferritin forms a sphere
FIGURE 31.34 Ferritin m R N A includes an iron-response element in its 5 prime untranslated region
FIGURE 31.35 Transferring receptor m R N A has a set of iron-response elements (I R E s) in its 3 prime untranslated region
FIGURE 31.36 The I R P is an aconitase
FIGURE 31.37 Micro R N A s bind to the Argonaute complex
FIGURE 31.38 Micro R N A–Argonaute complexes target specific m R N A molecules for cleavage
Structure of 5-azacytidine
Patterns of D N A fragments in Gel electrophoresis
Autoradiograph of lambda repressor concentration
Gel electrophoresis showing results of D N A from different organisms treated with H p a 2
Structure of Paclitaxel
FIGURE 32.1 The journey to an approved drug is divided into a discovery phase and a development phase
FIGURE 32.2 Drug targets span a variety of protein classes
Structure of Penicillin
FIGURE 32.3 Penicillin disrupts the biosynthesis of the bacterial cell wall
FIGURE 32.4 Structures of Sildenafil and c G M P
FIGURE 32.5 c G M P stimulates muscle relaxation
FIGURE 32.7 Coupled assays link the activity of an enzyme to the production of a fluorescent product

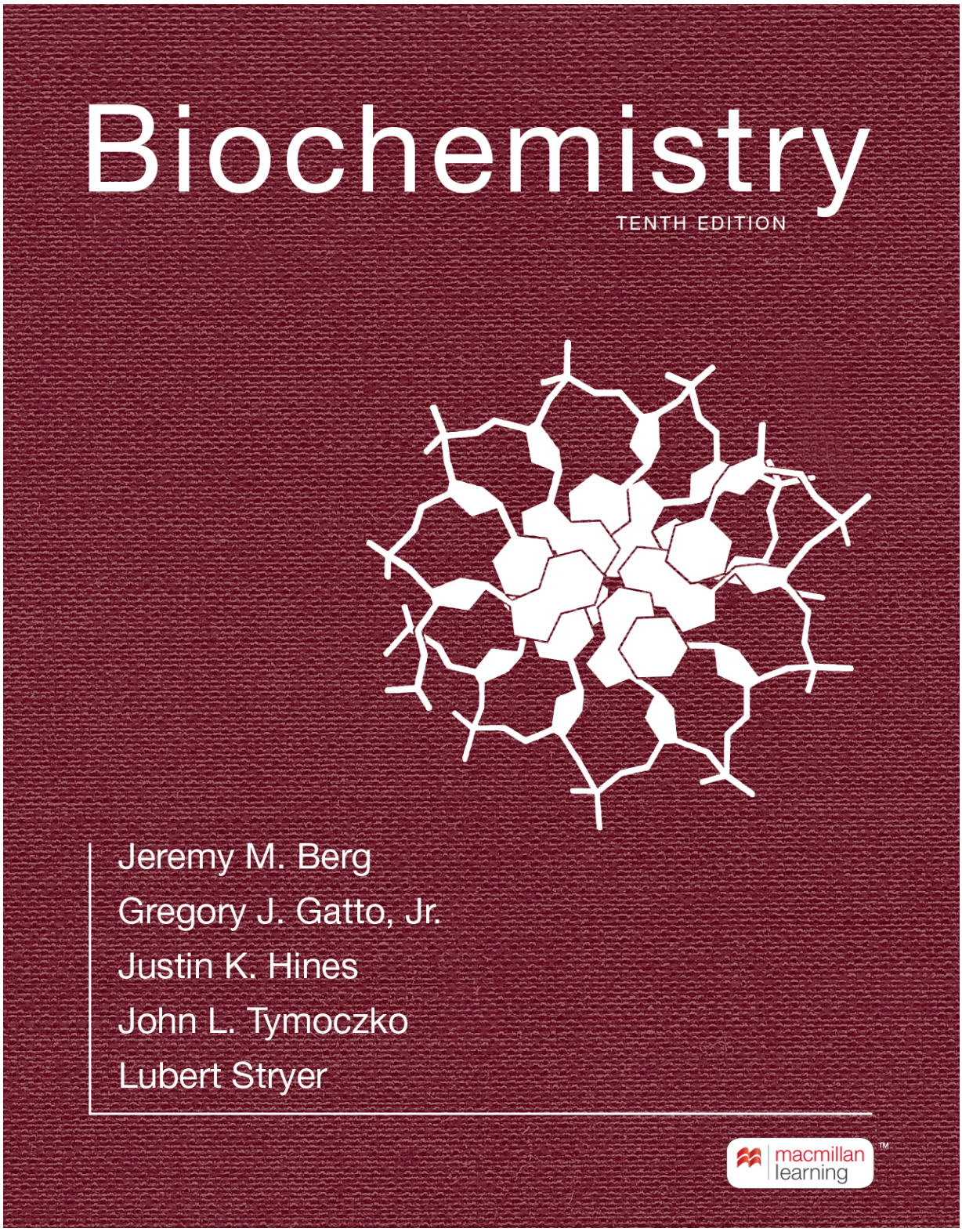
FIGURE 32.8 Compound libraries can be generated by split-pool synthesis
FIGURE 32.10 Diverse D N A-encoded libraries are generated by split pool synthesis
FIGURE 32.11 Target-based screening and phenotypic screening are two paths to early drug discovery
FIGURE 32.12 Simple ligand binding results in a hyperbolic curve
FIGURE 32.13 Effective concentration (E C) describes the amount of compound required to elicit a particular biological response
FIGURE 32.14 Inhibitors compete with substrates for enzyme active sites
FIGURE 32.15 The pharmacokinetics of a compound in a living organism is described by its absorption, distribution, metabolism, and excretion (A D M E) properties
FIGURE 32.16 Lipinski's rules serve as a guide to predict oral bioavailability
FIGURE 32.17 Albumin is abundant in the bloodstream and binds hydrophobic compounds
FIGURE 32.18 Once absorbed, compounds distribute to various organs within the body
FIGURE 32.19 Cytochrome P450 isozymes catalyze xenobiotic metabolic reactions such as hydroxylation
FIGURE 32.20 Compounds that have certain functional groups are often modified by conjugation reactions
Structures of Cyclophosphamide-glutathione conjugate, Morphine glucuronidate, and Minoxidil sulfate
FIGURE 32.21 Drugs can move between the intestine and the circulation via enterohepatic cycling
FIGURE 32.22 Drug excretion may be measured by its half-life
FIGURE 32.23 Acetaminophen metabolism results in its toxicity
FIGURE 32.24 Structural information led to the initial design of an H I V protease inhibitor
FIGURE 32.25. Optimizing lead molecules requires the balancing of multiple compound properties

FIGURE 32.26 Clinical trials proceed in phases examining safety and efficacy in increasingly large groups
Hydrolyzation of penicillin by Beta-Lactamase
Structure of Atenolol
Structure of Sildenafil
Structure of Indinavir
Structure of Compound A
Metabolism of Amphetamine
Structure of two fused rings
Variation of p H with the addition of O H superscript minus
Structure of a peptide
Structure of a peptide at p H 5.5
Structure of a peptide at p H 7.5
Chemical structure
Relationship between concentration and p H
Electrophoretic mobility of a protein with no disulfide bond or one disulfide bond
Reaction mechanism of aspartyl protease
Reaction mechanism of metalloprotease
Restriction map of a linear D N A
Formation of incompatible sticky ends
Three pairs of aligned protein sequences
Chemical structure
Flowchart depicts a signaling pathway
Citrate molecule undergoing a series of reactions
Illustration of an enzyme bound to a substrate
Two reactions and their overall summation
Reversible chemical reaction
Structure of alpha-ketoglutarate
Structure of pipecolate
Chemical structure of four fused rings
Formation of protosterol cation
Structure of labeled mevalonate and labeled isopentenyl pyrophosphate
Illustration of the replication fork

Oxidative deamination reaction
Chemical structure
Structure of methane and formaldehyde
Structure of a molecule with its Fischer projection and stereochemical rendering
FIGURE 1 Molecules are depicted in various ways
FIGURE 2 A space-filling model shows the atoms tightly packed
FIGURE 3 In a ball-and-stick model, bonds are represented by sticks
FIGURE 4 In a backbone model, only the backbone polypeptide chain is represented
FIGURE 5 In a simple ribbon diagram, the α helices are shown as coiled ribbons and a strands are depicted as arrows
FIGURE 6 An enhanced ribbon diagram may show functionally important areas using ball-and-stick
FIGURE 7 Structures of various functional groups
Reaction between ammonia, N H 3, and methyl iodide, H 3 C, single bond, I and its mechanism

Extended description for The cover page of the book

titled “Biochemistry, Tenth edition” is shown



An illustration of the chemical structure of the D N A double helix is depicted as observed when looked at from the terminus.

The names of the author are listed as follows:

Jeremy M. Berg
Gregory J. Gatto, Jr.
Justin L. Tymoczko
Lubert Stryer

The logo of Macmillan learning is in the lower right corner.

Return to The cover page of the book titled “Biochemistry, Tenth edition” is shown

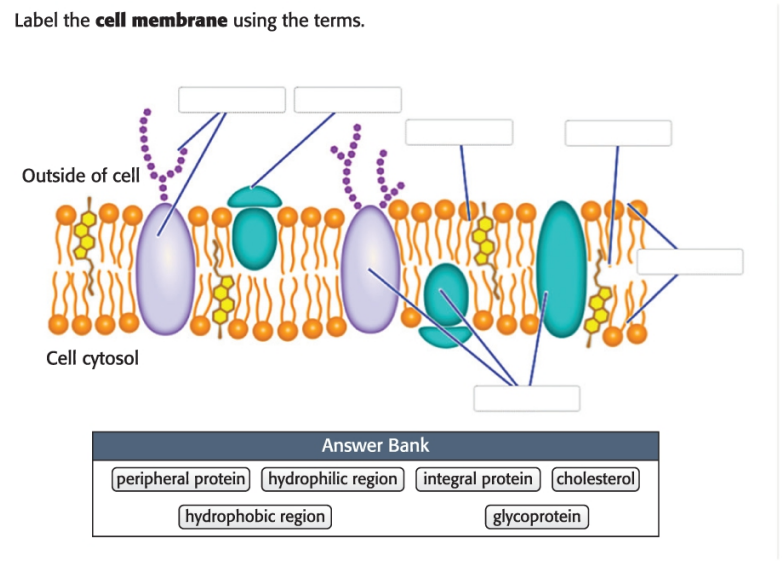
Extended description for Logo of W. H. Freeman Macmillan learning



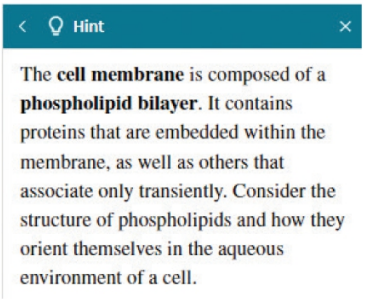
The logo includes two parts: the emblem and the wordmark. The emblem depicts a stylized open book and also resembling sea gulls or waves. Next to it, there is the phrase "w.h. freeman Macmillan learning". W.H. Freeman is in lowercase letters and is highlighted in black. Macmillan learning is below W.H. Freeman, in smaller font with letters M and L capitalized, highlighted in red.

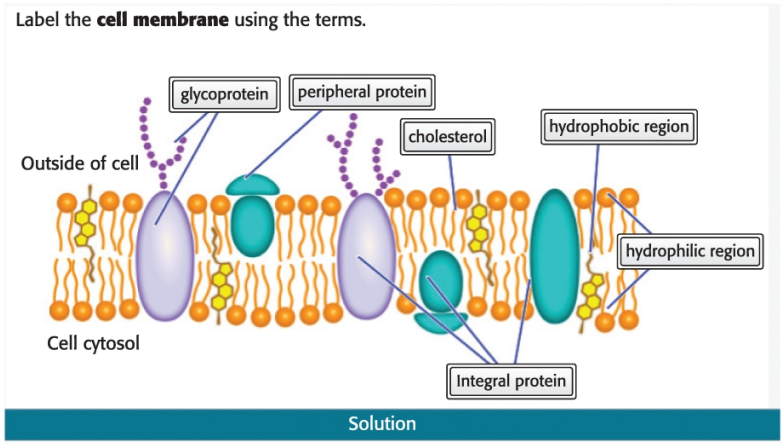
Return to Logo of W. H. Freeman Macmillan learning

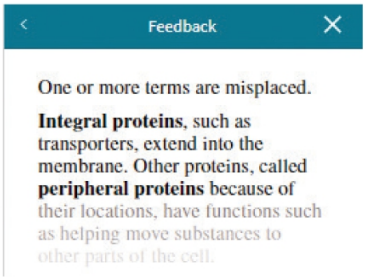
Extended description for Structures of cell membrane and associated proteins



© Macmillan Learning







First illustration: The schematic diagram shows the cell membrane composed of the phospholipid bilayer that separates the outside of the cell from the cell cytosol. The phospholipid bilayer is represented as small orange spherical structures arranged adjacent

to each other at intervals and bordering the layer above and below. The orange spherical structures are marked by a blank rectangular box. Each sphere is bound to a pair of stalks. The stalks of both spherical layers face each other toward the center and are marked by a blank rectangular box. Numerous proteins are shown embedded at an interval across the phospholipid bilayer of the cell membrane. The illustration shows an oval-shaped purple membrane-bound protein with a branched chain formed by a series of hexagonal molecules extending from the top of the protein toward the outside of the cell. The oval protein with a branched hexagon chain is marked by a blank rectangular box. Numerous fused yellow hexagonal structures with branches extending from them occurring at intervals are marked by a blank rectangular box and are shown spanning either the top half or bottom half of the phospholipid bilayer. The turquoise oval-shaped protein spanning the top half of the phospholipid bilayer is bound with a flat elliptical turquoise structure on the top toward the outside of the cell is marked by a blank rectangular box. The second oval-shaped purple membrane-bound protein with two branched chains formed by a series of hexagonal molecules extending from the top of the protein toward the outside of the cell. The second turquoise oval-shaped protein spanning the bottom half of the phospholipid bilayer is bound with a flat elliptical turquoise structure on the bottom toward the cell cytosol. An oblong oval turquoise protein spans the phospholipid bilayer of the membrane. The second purple oval protein, second turquoise protein, and oblong oval turquoise protein are collectively marked by a blank rectangular box.

The Answer bank terms provided inside the box are peripheral protein, hydrophilic region, integral protein, cholesterol, hydrophobic region, and glycoprotein. Label the cell membrane using the terms.

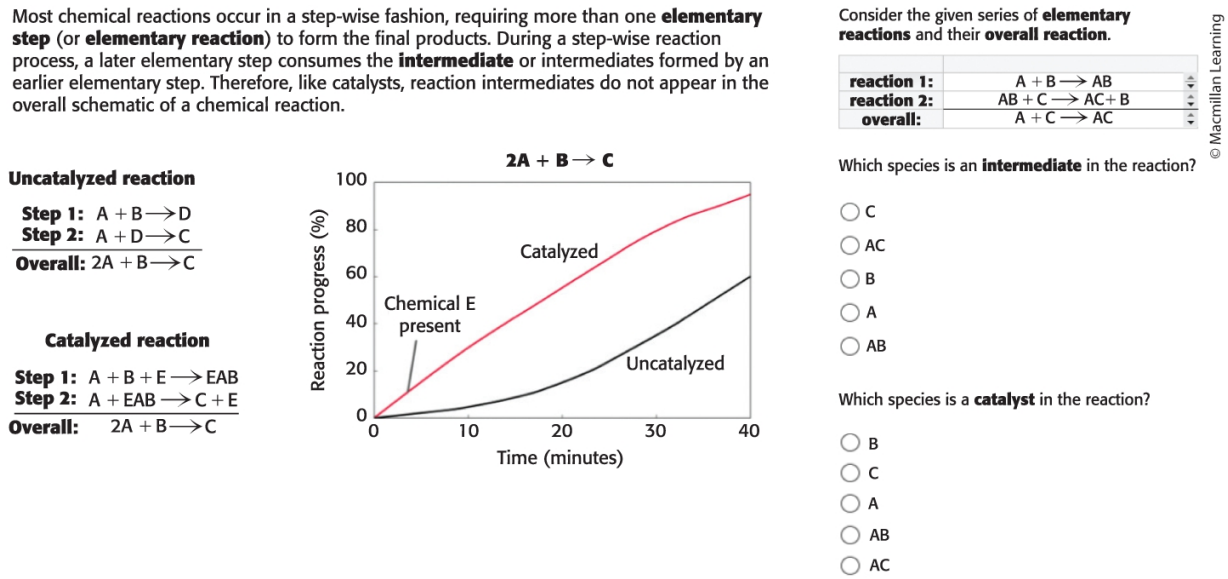
Second illustration: The schematic diagram shows the cell membrane composed of the phospholipid bilayer that separates the outside of the cell from the cell cytosol. The phospholipid bilayer is represented as small orange spherical structures arranged adjacent to each other at intervals and bordering the layer above and below. The orange spherical structures are marked by a rectangular box labeled “hydrophilic region.” Each sphere is bound to a pair of stalks. The stalks of both spherical layers face each other toward the center and are marked by a rectangular box labeled “hydrophobic region.” Numerous proteins are shown embedded at an interval across the phospholipid bilayer of the cell membrane. The illustration shows an oval-shaped purple membrane-bound protein with a branched chain formed by a series of hexagonal molecules extending from the top of the protein toward the outside of the cell. The oval protein with a branched hexagon chain is marked by a rectangular box labeled “glycoprotein.” Numerous fused yellow hexagonal structures with branches extending from them occurring at intervals are marked by a rectangular box labeled “cholesterol” and are shown spanning either the top half or bottom half of the phospholipid bilayer. The turquoise oval-shaped protein spanning the top half of the phospholipid bilayer is bound with a flat elliptical turquoise structure on the top toward the outside of the cell and is marked by a rectangular box labeled “peripheral protein.” The second oval-shaped purple membrane-bound protein with two branched chains formed by a series of hexagonal molecules extending from the top of the protein toward the outside of the cell. The second turquoise oval-shaped protein spanning the bottom half of the phospholipid bilayer is bound with a flat elliptical turquoise structure on the bottom toward the cell cytosol. An oblong oval turquoise protein spans the phospholipid bilayer of the membrane. The second purple oval protein, second turquoise protein, and oblong oval turquoise protein are collectively marked by a rectangular box labeled “Integral protein.”

A hint box is provided on the right that reads “The cell membrane is composed of a phospholipid bilayer. It contains proteins that are embedded within the membrane, as well as others that associate only transiently. Consider the structure of phospholipids and how they orient themselves in the aqueous environment of a cell.”

A feedback box on the bottom right reads “One or more terms are misplaced. Integral proteins, such as transporters, extend into the membrane. Other proteins, called peripheral proteins because of their locations, have functions such as helping move substances to other parts of the cell.”

Return to Structures of cell membrane and associated proteins

Extended description for Reactions and its corresponding graph and related questions



The paragraph text at the top of the left window reads,

Most chemical reactions occur in a step-wise fashion, requiring more than one elementary step (or elementary reaction) to form the final products. During a step-wise reaction process, a later elementary step consumes the intermediate or intermediates formed by an earlier elementary step. Therefore, like catalysts, reaction intermediates do not appear in the overall schematic of a chemical reaction.

Below the paragraph text, there are two steps uncatalyzed and catalyzed reactions along with a graph.

The uncatalyzed reaction reads,

Step-1: A plus B, right arrow, D

step-2: A plus D, right arrow, C

An underline below these steps gives the sum of step reactions which reads overall: 2 A plus B, right arrow, C.

The catalyzed reaction reads,

Step-1: A plus B plus E, right arrow, E A B

step-2: A plus E A B, right arrow, C plus E

An underline below these steps gives the sum of step reactions which reads overall: 2 A plus B, right arrow, C.

The graph is drawn for the overall reaction 2 A plus B, right arrow, C. The horizontal axis of the graph is labeled Time (in minutes). The vertical axis is labeled reaction progress (in percent). The horizontal axis ranges from 0 to 40 in increments of 10 units. The vertical axis ranges from 0 to 100 in increments of 20 units. The graph shows two curves. A red line curve for Catalyzed reaction starts from (0, 0) rises linearly till (33, 80), rises with a decreasing slope, and then terminates at (40, 95). A point on the curve at (3, 10) is labeled "Chemical E present". A black concave-up curve for uncatalyzed reaction starts from (0, 0), rises almost linearly till (13, 8), then curves up through (15, 11), (20, 18), and (25, 22). It then again rises linearly till (40, 56).Note: all numerical values in the graph are approximated.

The right-side window reads as follows:

Consider the given series of elementary reactions and their overall reaction.

Reaction-1: A plus B, right arrow, A B

Reaction-2: A B plus C, right arrow, A C plus B

overall: A plus C, right arrow, A C.

Below these reactions, there are two M C Q problems based on the reactions.

First problem:

Which species is an intermediate in the reaction?

1. C

2. A C

3. B

4. A

5. A B

Second problem:

Which species is a catalyst in the reaction?

1. B

2. C

3. A

4. A B

5. A C

Return to Reactions and its corresponding graph and related questions

Extended description for Incomplete purification table along with the percent yield equation

Complete the purification table: % yield

$$\% \text{ yield} = \frac{\text{total activity in step}}{\text{total activity step 1}} \times 100$$

step (procedure)	total protein (mg)	activity (units)	specific activity (units/mg)	% yield	purification factor
crude extract	20,000	4,000,000	200	100	
precipitation (salt)	5,000	3,000,000	600	75	
precipitation (pH)	4,000	1,000,000	250		
ion-exchange chromatography	200	800,000	4,000		
affinity chromatography	50	750,000	15,000		
size-exclusion chromatography	45	675,000	15,000		

The end user needs to fill the table using the percent yield equation. percent yield equals Start Fraction total activity inches step over total activity step 1 End Fraction multiplied by 100.

The table consists of 6 columns and 6 rows. The headings of the columns are as follows: step (procedure), total protein (milligrams), activity (units), specific activity (units per milligram), percent yield, and purification factor. The row entries are as follows.

Row 1: step (procedure): crude extract. total protein (milligrams): 20,000. activity (units): 4,000,000. specific activity (units per milligram): 200. percent yield: 100. Note: A human entry of 100 is shown here indicating that this value is calculated using the equation. purification factor: Blank.

Row 2: step (procedure): precipitation (salt). Note: A curved blue arrow points from Row 1 step (procedure) entry Crude extract to precipitation (salt). total protein (milligrams): 5,000. activity (units): 3,000,000. Note: This value is encircled in blue. specific activity (units per milligram): 600. percent yield: 75. Note: A human entry of 75 is shown here indicating that this value is calculated using the equation. purification factor: Blank.

Row 3: step (procedure): precipitation (pH). total protein (milligrams): 4,000. activity (units): 1,000,000. specific activity (units per milligram): 250. percent yield: Blank. purification factor: Blank.

Row 4: step (procedure): ion-exchange chromatography. total protein (milligrams): 200. activity (units): 800,000. specific activity (units per milligram): 4,000. percent yield: Blank. purification factor: Blank.

Row 5: step (procedure): affinity chromatography. total protein (milligrams): 50. activity (units): 750,000. specific activity (units per milligram): 15,000. percent yield: Blank. purification factor: Blank.

Row 6: step (procedure): size-exclusion chromatography. total protein (milligrams): 45. activity (units): 675,000. specific activity (units per milligram): 15,000. percent yield: Blank. purification factor: Blank. There are no entries under purification factor column.

Return to Incomplete purification table along with the percent yield equation

Extended description for New case study Mile High Stadium and Silent Killer: Hemoglobin Dysfunction

Mile High Stadium and the Silent Killer
Case Study on Hemoglobin Regulation and Dysfunction
By Justin Hines, Lafayette College



Photo Credit: Zoonar /A. Kravchenko /AGE Fotostock

Act 1 - Trouble at Mile High Stadium

Gino had hemoglobin on the mind. He had been embarrassed earlier when he failed to remember how pH was related to oxygen transport in the human body.

As an undergraduate in his junior year who hoped to go to medical school, Gino's day job shadowing emergency room physician Dr. Rose Smith was otherwise going well. But the routine patient visits were interrupted when he saw a large crowd gathered just outside in the hospital lobby. Most had flowers, but some, strangely, were carrying footballs and wearing jerseys.

"Dr. Smith, what's that all about?" Gino pointed to the noisy crowd.

"Oh that... yes, we have a patient up on three recovering from a sickle cell attack."

"But why so many people?" asked Gino. "And why do some have footballs? Is it a child or something?"

"No, actually he's an NFL star... plays defensive end. Most of those people are just fans. He played a game last night here in Denver at the new Mile High Stadium. The combination of vigorous exercise from sprinting all over a 100-yard field and the fact that the game was here in Denver triggered a sickle cell crisis. He'll probably never play in Denver again."

"He has sickle cell anemia and plays in the NFL??!"

"Actually, he has sickle cell *trait*, meaning he is heterozygous for the sickle cell allele, HbS. Some people with sickle cell trait can be top athletes. But, the right conditions can still bring about a crisis."

A photograph shows the Mile High Stadium. A text beside the photograph reads:

Mile High Stadium and the Silent Killer Case Study on Hemoglobin Regulation and Dysfunction By Justin Hines, Lafayette College

Act 1 - Trouble at Mile High Stadium

Gino had hemoglobin on the mind. He had been embarrassed

earlier when he failed to remember how pH was related to

oxygen transport in the human body.

As an undergraduate in his junior year who hoped to go to medical school, Gino's day job shadowing emergency room physician Dr. Rose Smith was otherwise going well. But the routine patient visits were interrupted when he saw a large crowd gathered just outside in the hospital lobby. Most had flowers, but some, strangely, were carrying footballs and wearing jerseys.

SPORTS

"Dr. Smith, what's that all about?" Gino pointed to the noisy crowd.

"Oh that. yes, we have a patient up on three recovering from a sickle cell attack."

"But why so many people?" asked Gino. "And why do some have footballs? Is it a child or something?"

"No, actually he's an N F L star. plays defensive end. Most of those people are just fans. He played a game last night here in Denver at the new Mile High Stadium. The combination of vigorous exercise from sprinting all over a 100-yard field and the fact that the game was here in Denver triggered a sickle cell crisis. He'll probably never play in Denver again."

"He has sickle cell anemia and plays in the N F L??!"

"Actually, he has sickle cell trait, meaning he is heterozygous for the sickle cell allele, H b S. Some people with sickle cell trait can be top athletes. But, the right conditions can still bring about a crisis."

"What does playing in Denver, Colorado have to do with sickle cell?"

"Oh Gino. you really need to go back and review your stuff on hemoglobin again. this is all straight out of undergraduate biochemistry !"

Return to New case study Mile High Stadium and Silent Killer: Hemoglobin Dysfunction

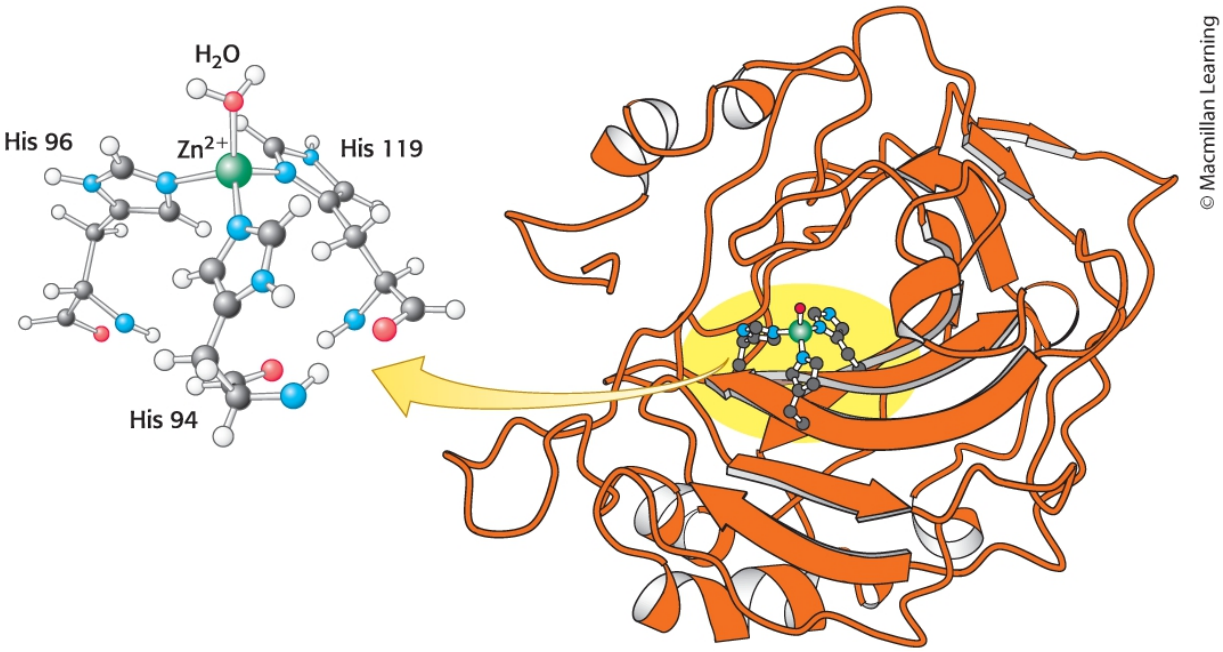
Extended description for Logo of Macmillan learning



The logo includes two parts: the emblem and the wordmark. The emblem depicts a stylized open book and also resembling sea gulls or waves. Next to it, there is the phrase "Macmillan learning" in lowercase letters. Macmillan is highlighted in red and learning is in black. Below it the different centers of macmillan are shown which are: Austin, Boston, New York, and Plymouth.

Return to Logo of Macmillan learning

Extended description for FIGURE 6.18 The active site of human carbonic anhydrase II includes a bound zinc ion



© Macmillan Learning

The three-dimensional ribbon diagram of human carbonic anhydrase 2 is composed of antiparallel beta-strands and a few coiled alpha-helices connected by thin thread-like loops. The core of the enzyme is composed of antiparallel beta-strands. The active site of the enzyme is present between the beta-strands and thread-like loops. It contains a zinc ion bound to the active site residues.

The ball-and-stick model shows a central Z n superscript 2 plus ion connected to the imidazole rings of three histidine residues. Z n superscript 2 plus ion is depicted as a green sphere and is connected above with an H 2 O molecule. The histidine residues are composed of black, blue, white, and red spheres. The model highlights the residues H i s 96, H i s 119, and H i s 94.

Return to FIGURE 6.18 The active site of human carbonic anhydrase II includes a bound zinc ion

Extended description for Photograph and a snippet of the accompanying text of a short profile of a scientist

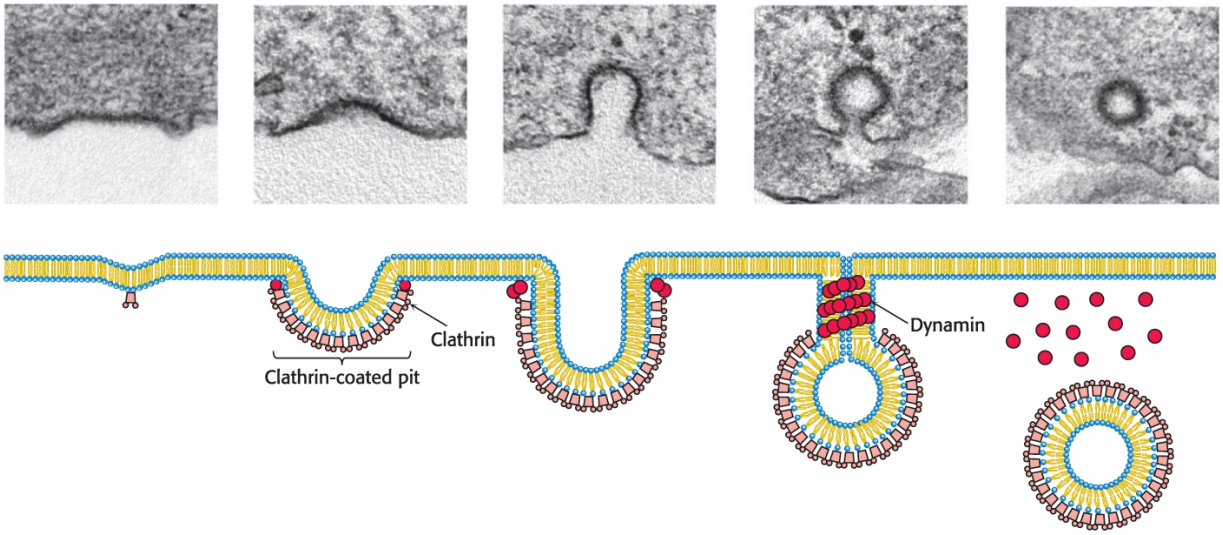


JAMES TENSUAN/The New York Times/Redux

A photograph of Carolyn Bertozzi. Snippet of accompanying text: Chemist Carolyn Bertozzi is a leader in developing the field of glycobiology and communicating its exciting possibilities. Initially planning to go to medical school, her interest in chemistry.

Return to Photograph and a snippet of the accompanying text of a short profile of a scientist

Extended description for FIGURE 12.38 Many cells take up molecules by receptor-mediated endocytosis



Credit: *Top*: Republished with permission of Company of Biologists, from Membrane remodeling in clathrin-mediated endocytosis. Volker Haucke, Michael M. Kozlov, J Cell Sci (2018) 131 (17): jcs216812. Figure 1. Permission conveyed through Copyright Clearance Center, Inc.; *Bottom*: Schmid SL. Reciprocal regulation of signaling and endocytosis: Implications for the evolving cancer cell. J Cell Biol. 2017 Sep 4;216(9):2623-2632. doi: 10.1083/jcb.201705017. Epub 2017 Jul 3. PMID: 28674108; PMCID: PMC5584184. Copyright © 2017 Schmid. Illustration by Marcel Mettlen. Used with permission.

The figure shows photomicrographs of receptor-mediated endocytosis on the top and corresponding steps of receptor-mediated endocytosis below.

The first micrograph shows the surface of the cell.

In the second micrograph, the surface begins to invaginate slightly.

In the third micrograph, the invagination becomes prominent.

In the fourth micrograph, the neck of the invagination starts to get closer.

In the fifth micrograph, the completely invaginated membrane appears as a sphere inside the cell.

The schematic illustration of the corresponding steps of receptor-mediated endocytosis is shown below the micrographs.

The lipid bilayer of the membrane consists of two parallel layers of lipids. Each lipid molecule has the yellow extensions aligned together and forms the core of the bilayer. The blue spheres are located away from each other.

Step 1: The plasma membrane forms a slight invagination. A clathrin molecule attaches to the inner surface of the invagination.

Step 2: The invagination becomes slightly deeper by concave folding, and the inner surface of the invagination is lined by a series of clathrin molecules. The invagination is labeled clathrin-coated pit. The clathrin molecule is depicted as a box-like structure fused to a sphere on the bottom left and bottom right.

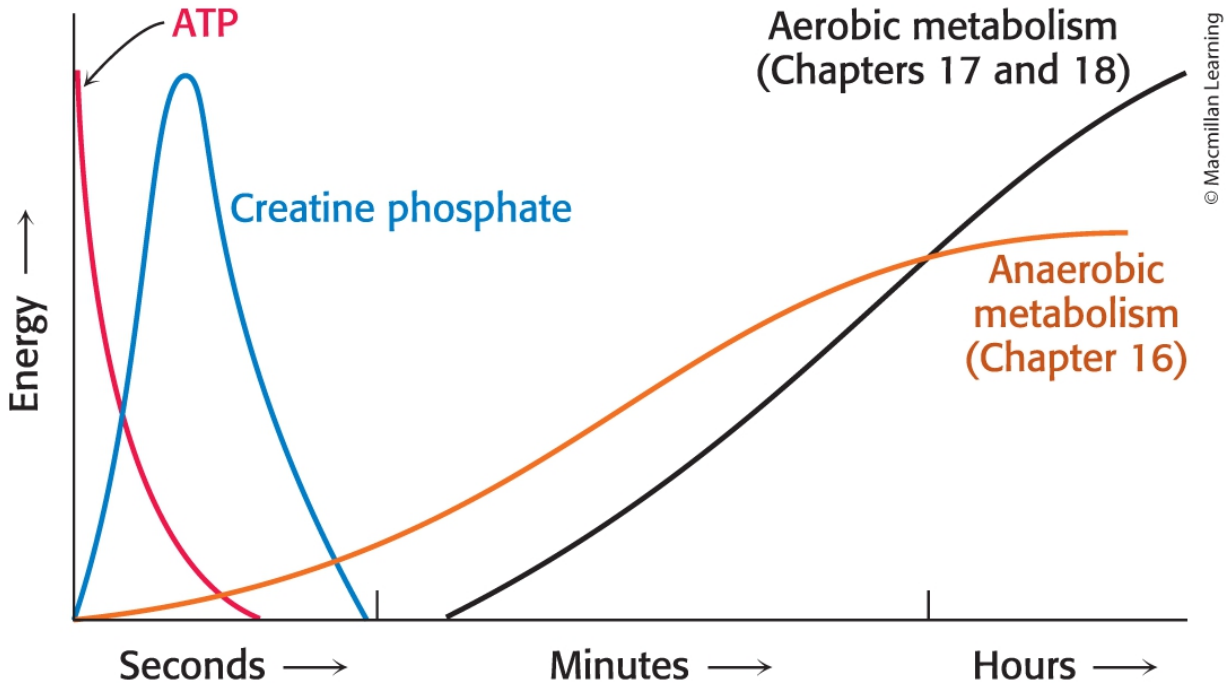
Step 3: The invagination becomes prominent as a U-shaped structure.

Step 4: The invagination becomes spherical and its neck is continuous with the membrane. Several spherical bead-like structures called dynamin zip the neck of the spherical invagination.

Step 5: The dynamin spheres are released and a spherical structure surrounded by a lipid bilayer and clathrin coating is released into the intracellular space.

Return to FIGURE 12.38 Many cells take up molecules by receptor-mediated endocytosis

Extended description for FIGURE 15.6 The sources of ATP change as exercise duration increases, even within the first few seconds

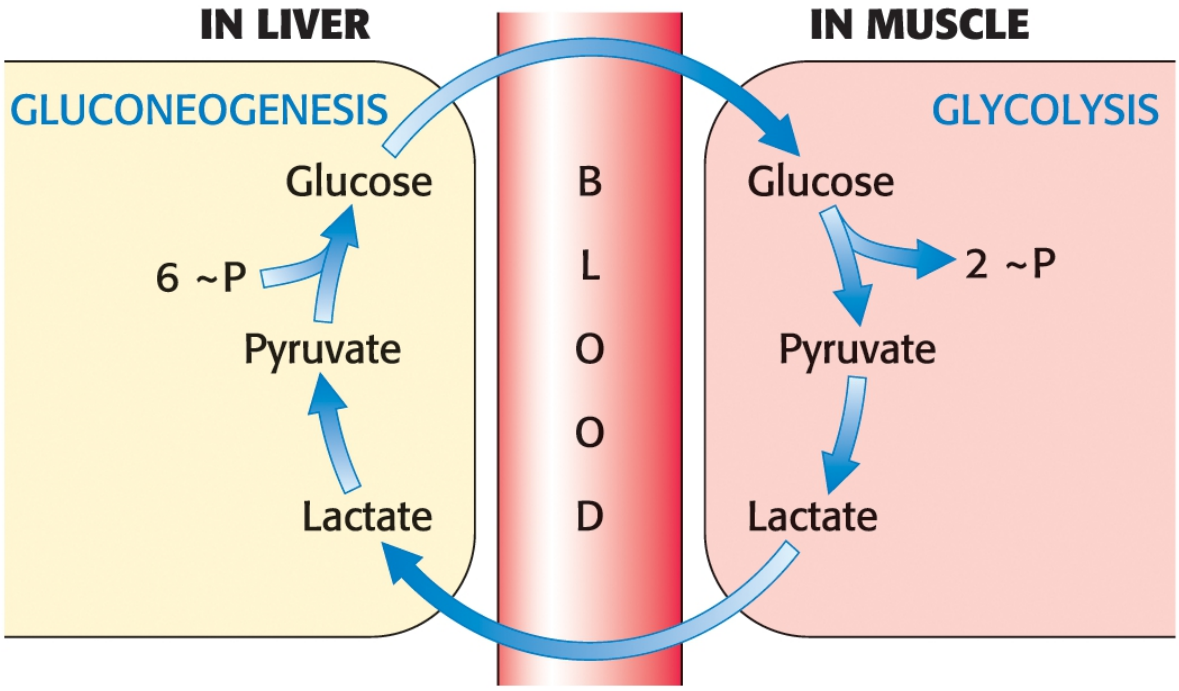


The vertical axis is labeled Energy indicated by an upward arrow. The horizontal and vertical axes intersect at the bottom left. The horizontal axis contains two markings from left to right. The first interval between the vertical axis and the first marking is labeled Seconds indicated by a rightward arrow. The second interval between the first and the second markings is labeled Minutes indicated by a rightward arrow. The third interval between the second and the third marking is labeled Hours indicated by a rightward arrow. A red curve representing A T P starts on high value of Energy on the vertical axis and falls concave upward to intersect the horizontal axis in the seconds interval. A blue curve representing Creatine phosphate starts at the intersection of the axes, rises almost linearly to a peak at high value of energy, and falls

concave upwards to intersect the horizontal axis at the first marking. An orange curve representing Anaerobic metabolism (Chapter 16) starts at the intersection of the axes, rises with an increasing slope till a low to mid value of energy, and rises further with a decreasing slope to mid value of energy in the hours interval. A black curve representing Aerobic metabolism (Chapters 17 and 18) starts on the horizontal axis to the right of the first marking, rises with an increasing slope till a low to mid value of energy, and rises further with a decreasing slope to mid value of energy in the hours interval.

Return to FIGURE 15.6 The sources of ATP change as exercise duration increases, even within the first few seconds

Extended description for FIGURE 16.36 The Cori cycle allows the liver to better support other tissues, such as skeletal muscle



© Macmillan Learning

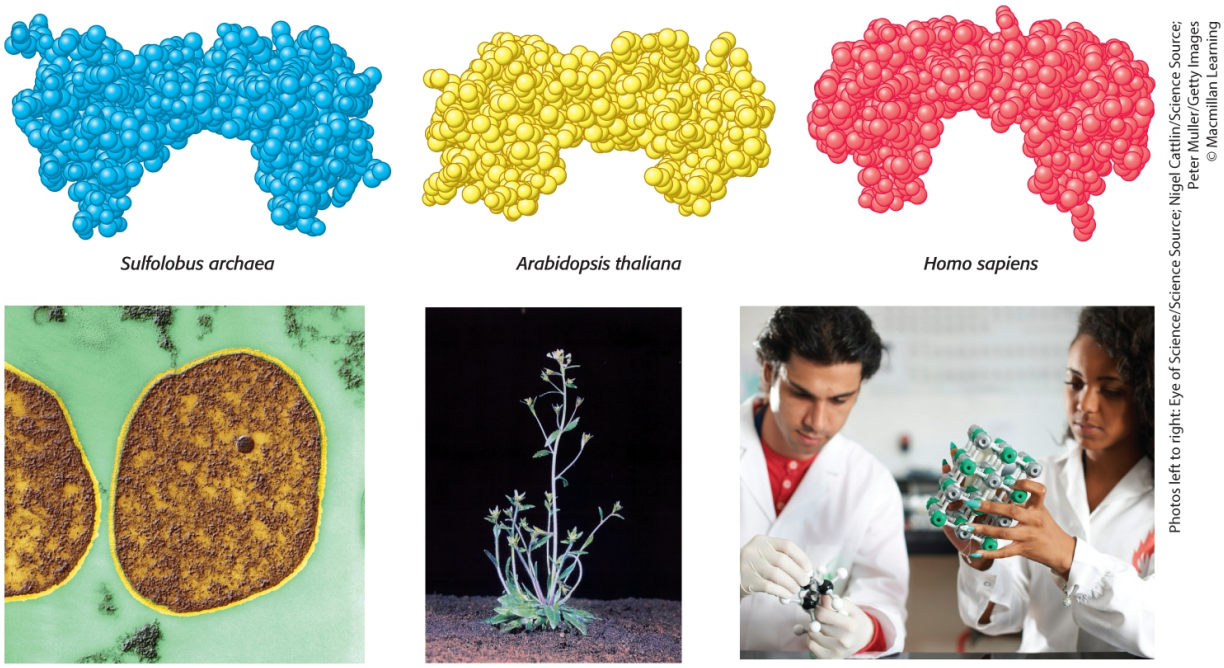
The illustration shows three different compartments. The central compartment is labeled blood and is long and cylindrical. The left compartment is a rounded half-rectangle labeled “IN LIVER.” The right compartment is also a rounded half-rectangle labeled “IN MUSCLE.” Each conversion is shown by sequential curved arrows.

In muscle, glycolysis is depicted as follows: Step 1: Glucose is converted into pyruvate coupled with the release of 2, wavy line, P represents 2 nucleoside triphosphates. Step 2: Pyruvate is further converted into lactate. Step 3: The lactate travels from the muscle compartment to the liver compartment through the blood compartment.

In the liver, gluconeogenesis is depicted as follows: Step 1: Lactate is converted into pyruvate. Step 2: Pyruvate is further converted into glucose with the coupled entry of 6, wavy line, P which represents 6 nucleoside triphosphates. Step 3: The glucose molecule travels back to the muscle compartment through the blood compartment.

Return to FIGURE 16.36 The Cori cycle allows the liver to better support other tissues, such as skeletal muscle

Extended description for FIGURE 1.1 Despite tremendous biological diversity, there is remarkable similarity in the molecules that make up living organisms



Photos left to right: Eye of Science/Science Source; Nigel Cattlin/Science Source; Peter Muller/Getty Images
© Macmillan Learning

The shape of the TATA-box binding protein in the three organisms has similar inverted horseshoe shapes.

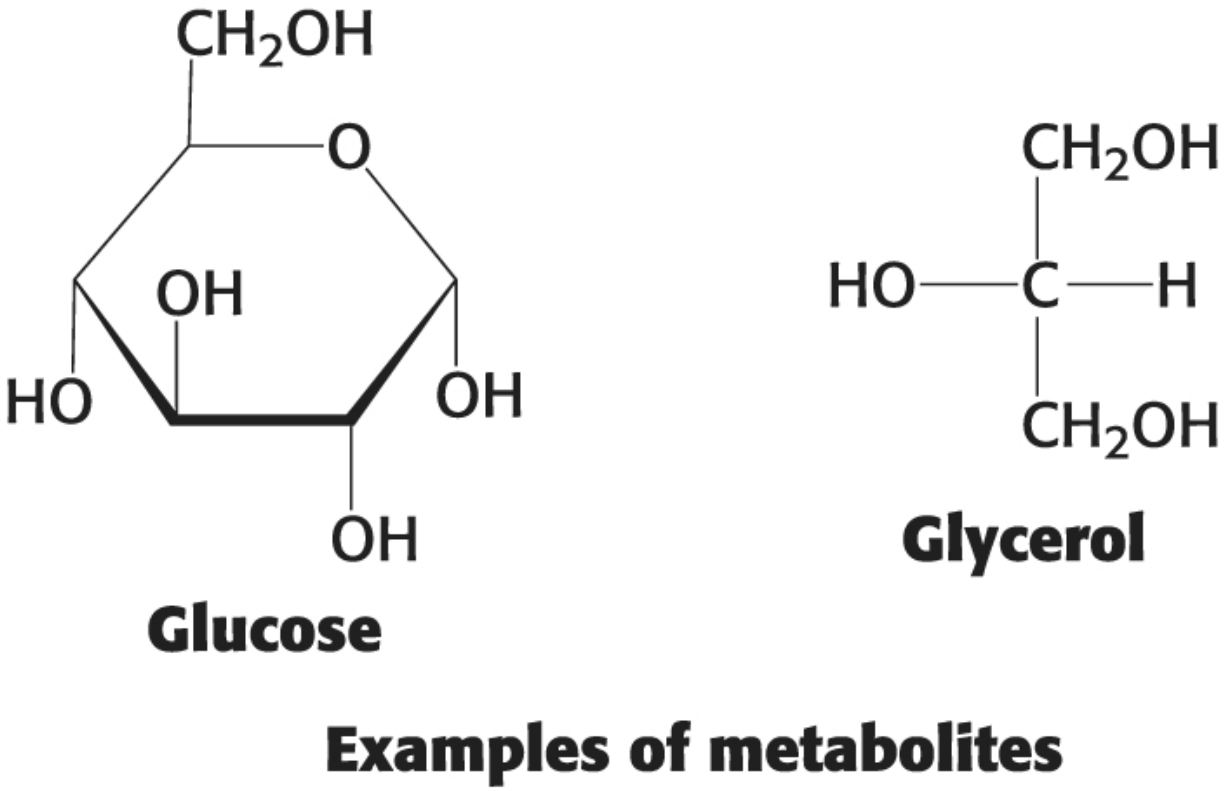
A micrograph of *Sulfolobus archaea* shows an oval-shaped cell with a small nucleus.

A photograph of *Arabidopsis thaliana* shows a plant with leaves around its base and small flowers blooming on long stalks growing from the base.

A photograph shows two people working on molecular models in a laboratory.

Return to FIGURE 1.1 Despite tremendous biological diversity, there is remarkable similarity in the molecules that make up living organisms

Extended description for Examples of metabolites

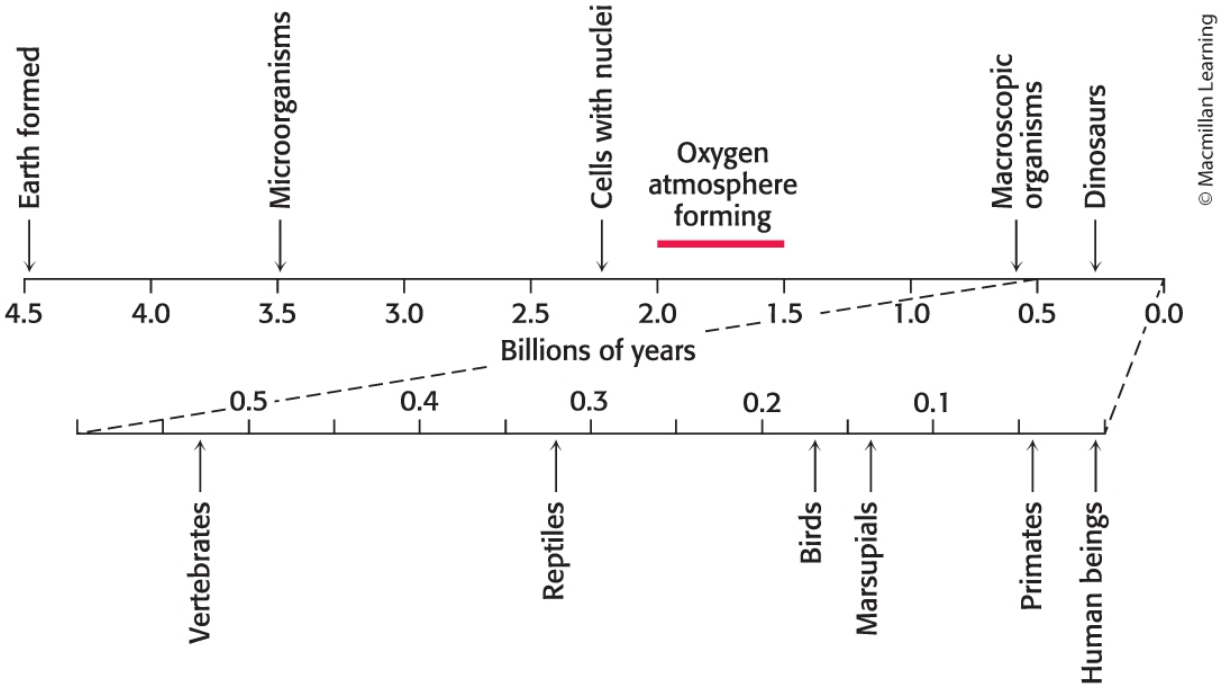


Glucose: A 6-membered heterocyclic hexagonal ring is in a horizontal orientation and consists of 1 O and 5 C atoms. The O atom occupies the first position, which is the top-right vertex. C 1, C 2, and C 4 are each single bonded to O H below. C 3 is single bonded to O H above. C 5 is single bonded to C H 2 O H above. C 2 and C 3 are toward the observer.

Glycerol: A central C atom is single bonded to C H 2 O H above and below, O H on the left, and H on the right.

Return to Examples of metabolites

Extended description for FIGURE 1.2 A possible timeline for biochemical evolution shows that life on Earth began approximately 3.5 billion years ago



The main timeline ranges from 4.5 to 0.0 billion years in decrements of 0.5 units. The following events are indicated on the timeline:

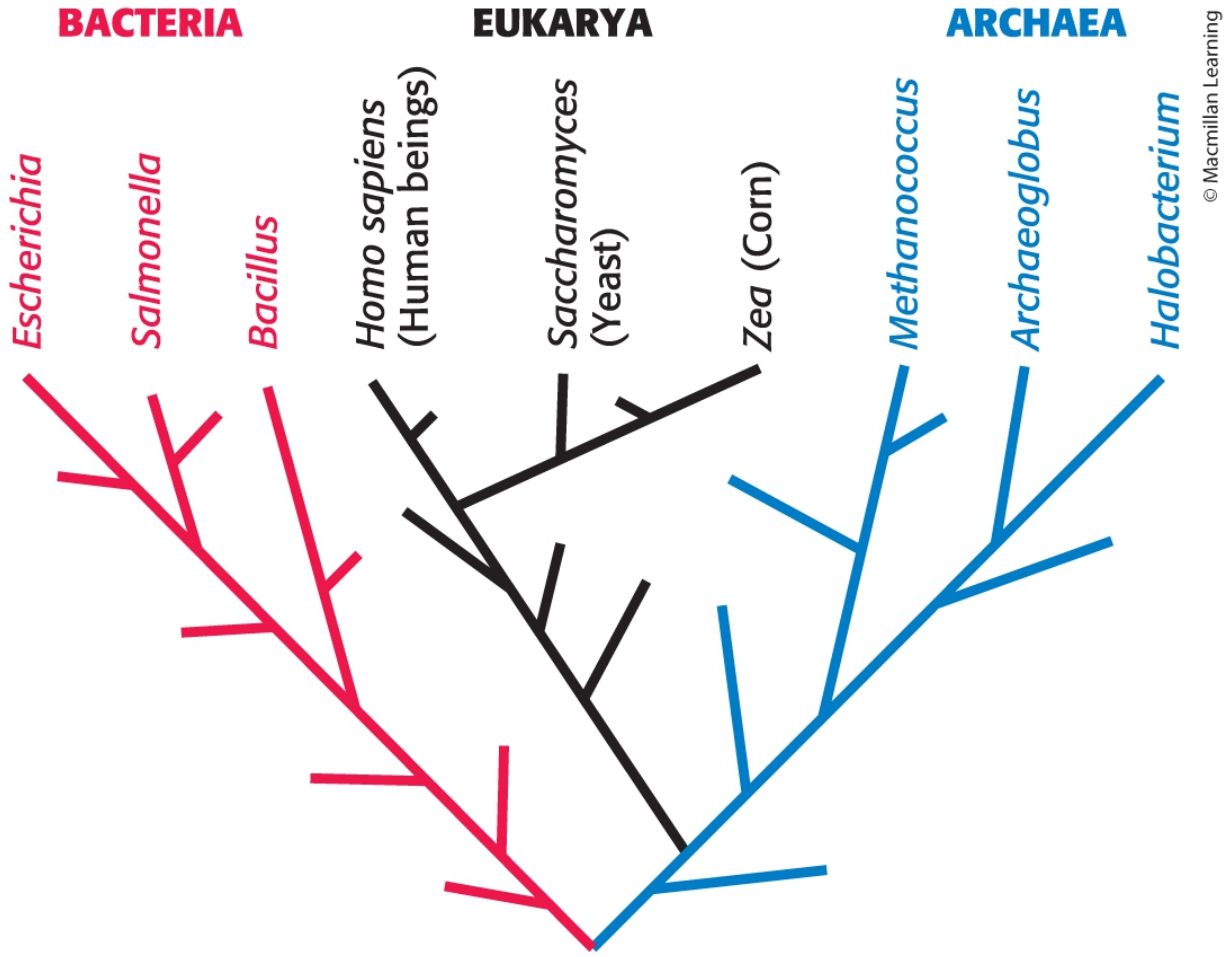
1. Earth formed: 4.5 billion years
2. Microorganisms: 3.5 billion years
3. Cells with nuclei: 2.2 billion years
4. Oxygen forming atmosphere: Between 2.0 and 1.5 billion years
5. Macroscopic organisms: 0.6 billion years
6. Dinosaurs: 0.3 billion years

A second timeline is shown below the main timeline, ranging from 0.6 to 0.0 billion years in decrements of 0.1 units. This timeline indicates the times of emergence of classes of animals as follows:

1. Vertebrates: 0.53 billion years
2. Reptiles: 0.32 billion years
3. Birds: 0.17 billion years
4. Marsupials: 0.14 billion years
5. Primates: 0.04 billion years
6. Human beings: 0.01 billion years

Return to FIGURE 1.2 A possible timeline for biochemical evolution shows that life on Earth began approximately 3.5 billion years ago

Extended description for FIGURE 1.3 The relationships of all modern organisms can be displayed on a tree of life with just three major branches



The tree begins at a point and has two main branches extending toward the upper left and upper right, respectively.

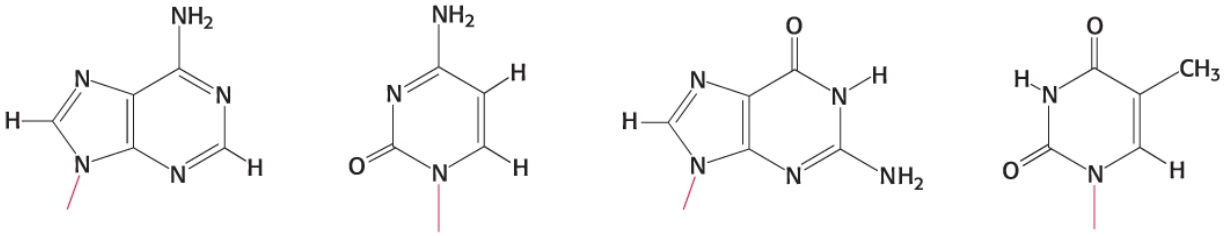
The branch toward the upper left pertains to Bacteria and ends at *Escherichia*. Two sub-branches extend from the main branch. One is closer to *Escherichia* and ends at *Salmonella* followed by the other that ends at *Bacillus*.

The branch toward the upper right pertains to Archaea and ends at *Halobacterium*. Two sub-branches extend from the main branch. One is closer to *Halobacterium* and ends at *Archaeoglobus* followed by the other that ends at *Methanococcus*.

The branch for Archaea contains a major sub-branch pertaining to Eukarya. The sub-branch extends from the base of the Archaea branch and extends toward the upper left to end at *Homo sapiens* (Human beings) such that it is close to *Bacillus*. A smaller sub-branch from the *Homo sapiens* sub-branch extends toward the upper right to end at *Zea* (Corn) such that it is close to *Methanococcus*. A small sub-branch on the *Zea* branch midway between *Homo sapiens* and *Zea* extends upward pertaining to *Saccharomyces* (yeast).

Return to FIGURE 1.3 The relationships of all modern organisms can be displayed on a tree of life with just three major branches

Extended description for Structures of the four nitrogenous bases of D N A



Adenine (A) has the following structure: A 5-membered heterocyclic pentagonal ring is in a horizontal orientation and consists of 2 N and 3 C atoms. The first N atom, highlighted, occupies the first position, which is the bottom-left vertex, and the second N atom occupies the third position, which is the top-left vertex. A double bond is present between C 1 and the second N atom and between C 2 and C 3. C 1 is single bonded to H. This ring is fused to a 6-membered heterocyclic hexagonal ring in a vertical orientation that consists of 2 N and 4 C atoms. The first N atom occupies the first position, which is the top-right vertex, and the second N atom occupies the third position, which is the bottommost vertex. A double bond is present between C 1 and the second N atom and between C 4 and the first N atom. C 1 is single bonded to H, and C 4 is single bonded to N H 2. The two rings are fused to each other such that C 2 and C 3 of the 5-membered ring are the C 3 and C 2 of the 6-membered ring, respectively.

Cytosine (C) has the following structure: A 6-membered heterocyclic hexagonal ring is in a vertical orientation and consists of 2 N and 4 C atoms. The first N atom, highlighted, occupies the first position, which is the bottommost vertex, and the second N atom occupies the third position, which is the top-left vertex. A double bond is

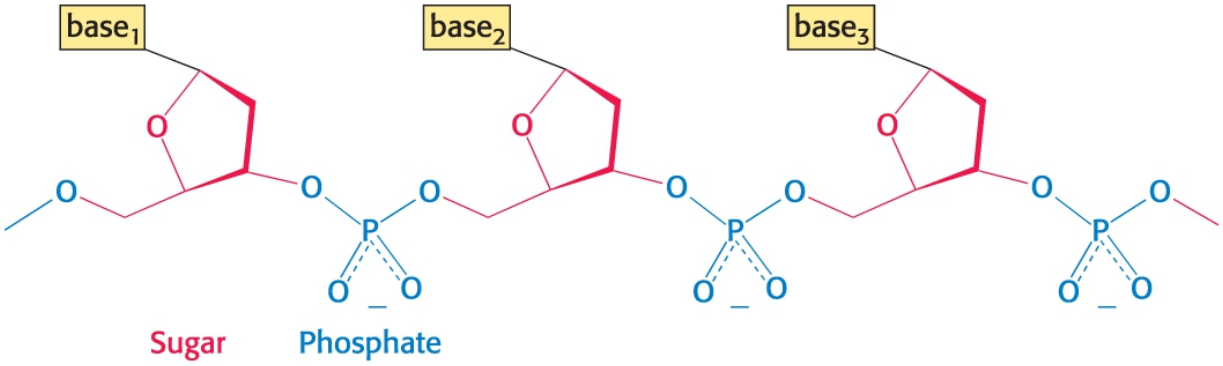
present between the second N atom and C 2 and between C 3 and C 4. C 1 is double bonded to O, C 2 is single bonded to N H 2, and C 3 and C 4 are each single bonded to H.

Guanine (G) has the following structure: A 5-membered heterocyclic pentagonal ring is in a horizontal orientation and consists of 2 N and 3 C atoms. The first N atom, highlighted, occupies the first position, which is the bottom-left vertex, and the second N atom occupies the third position, which is the top-left vertex. A double bond is present between C 1 and the second N atom and between C 2 and C 3. C 1 is single bonded to H. This ring is fused to a 6-membered heterocyclic hexagonal ring in a vertical orientation that consists of 2 N and 4 C atoms. The first N atom occupies the first position, which is the top-right vertex, and the second N atom occupies the third position, which is the bottommost vertex. A double bond is present between C 1 and the second N atom. The first N atom is single bonded to H, C 1 is single bonded to N H 2, and C 4 is double bonded to O. The two rings are fused to each other such that C 2 and C 3 of the 5-membered ring are the C 3 and C 2 of the 6-membered ring, respectively.

Thymine (T) has the following structure: A 6-membered heterocyclic hexagonal ring is in a vertical orientation and consists of 2 N and 4 C atoms. The first N atom, highlighted, occupies the first position, which is the bottommost vertex, and the second N atom occupies the third position, which is the top-left vertex. A double bond is present between C 3 and C 4. C 1 is double bonded to O, the second N atom is single bonded to H, C 2 is double bonded to O, C 3 is single bonded to C H 3, and C 4 is single bonded to H.

Return to Structures of the four nitrogenous bases of D N A

Extended description for FIGURE 1.4 The covalent structure of DNA is a linear polymer of monomeric units



Three sugar molecules are joined in a linear chain via phosphate groups.

The sugar has the following structure: A heterocyclic pentagonal ring is in a horizontal orientation and consists of 1 O and 5 C atoms. The O atom occupies the first position which is the leftmost vertex. C 1 of each sugar molecule is single bonded to a base. The first sugar molecule is bonded to base 1, the second sugar molecule is bonded to base 2, and the third sugar molecule is bonded to base 3.

The phosphate group has the following structure: A central P is single bonded to O on the upper left and O on the upper right. P is partially double bonded to O on the lower left and O on the lower right by means of a straight line and a dotted line. The phosphate group carries a negative charge. The single bonded to O on the upper left is single bonded to C 3 of a sugar molecule on the left. The single bonded to O on the upper right is single bonded to a C H 2 group on the lower right. The C H 2 group is single bonded to C 4 of the next sugar molecule on the upper right.

Return to FIGURE 1.4 The covalent structure of DNA is a linear polymer of monomeric units

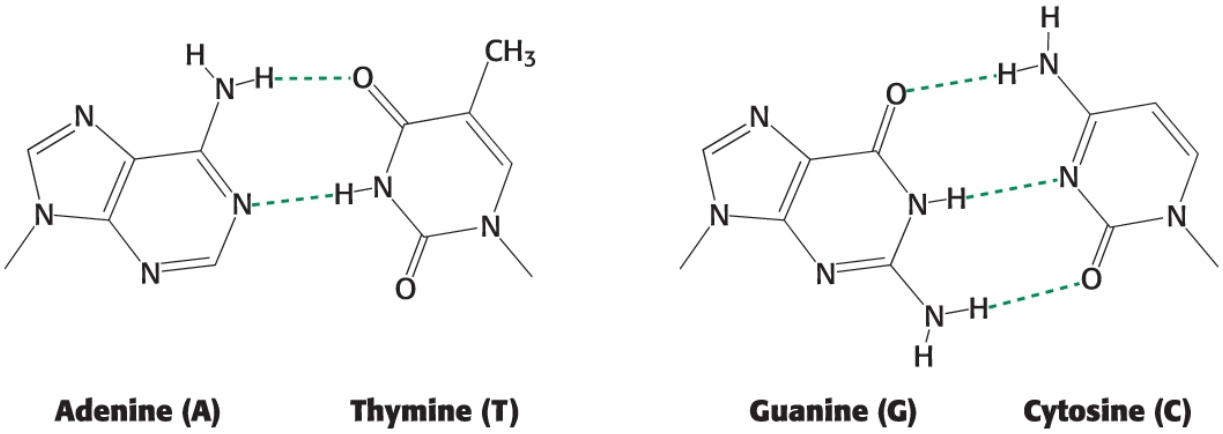
Extended description for FIGURE 1.5 The double helix has two antiparallel strands



Two ribbon-like strands of D N A are shown to be twisted to form a double-helix structure. A rightward arrow along one strand (red) and a leftward arrow along the other strand (blue) represent the antiparallel nature of the strands. Vertical lines, colored green, purple, orange, and yellow, between the two strands, show complementary bonding between the nitrogenous bases of the two strands.

Return to FIGURE 1.5 The double helix has two antiparallel strands

Extended description for FIGURE 1.6 The nitrogenous bases in DNA form specific Watson–Crick base pairs



Adenine (A) has the following structure: A 5-membered heterocyclic pentagonal ring is in a horizontal orientation and consists of 2 N and 3 C atoms. The first N atom occupies the first position, which is the bottom-left vertex, and the second N atom occupies the third position, which is the top-left vertex. A double bond is present between C 1 and the second N atom and between C 2 and C 3. The first N atom is single bonded to C H 3 in the form of a line. This ring is fused to a 6-membered heterocyclic hexagonal ring in a vertical orientation that consists of 2 N and 4 C atoms. The first N atom occupies the first position, which is the top-right vertex, and the second N atom occupies the third position, which is the bottommost vertex. A double bond is present between C 1 and the second N atom and between C 4 and the first N atom. C 4 is single bonded to N. This N atom is single bonded to H on the upper left and H on the upper right. The two rings are fused to each other such that C 2 and C 3 of the 5-membered ring are the C 3 and C 2 of the 6-membered ring, respectively.

Thymine (T) has the following structure: A 6-membered heterocyclic hexagonal ring is in a vertical orientation and consists of 2 N and 4 C atoms. The first N atom occupies the first position, which is the bottom-right vertex, and the second N atom occupies the third position, which is the bottom-left vertex. A double bond is present between C 3 and C 4. C 1 is double bonded to O, the second N atom is single bonded to H, C 2 is double bonded to O, C 3 is single bonded to C H 3, and the first N atom is single bonded to C H 3 in the form of a line.

A dashed green line is drawn between the first N atom of the 6-membered ring in adenine and the H single bonded to the second N atom in thymine. A second dashed green line is drawn between the H on the upper right in adenine and the O atom double bonded to C 2 in thymine.

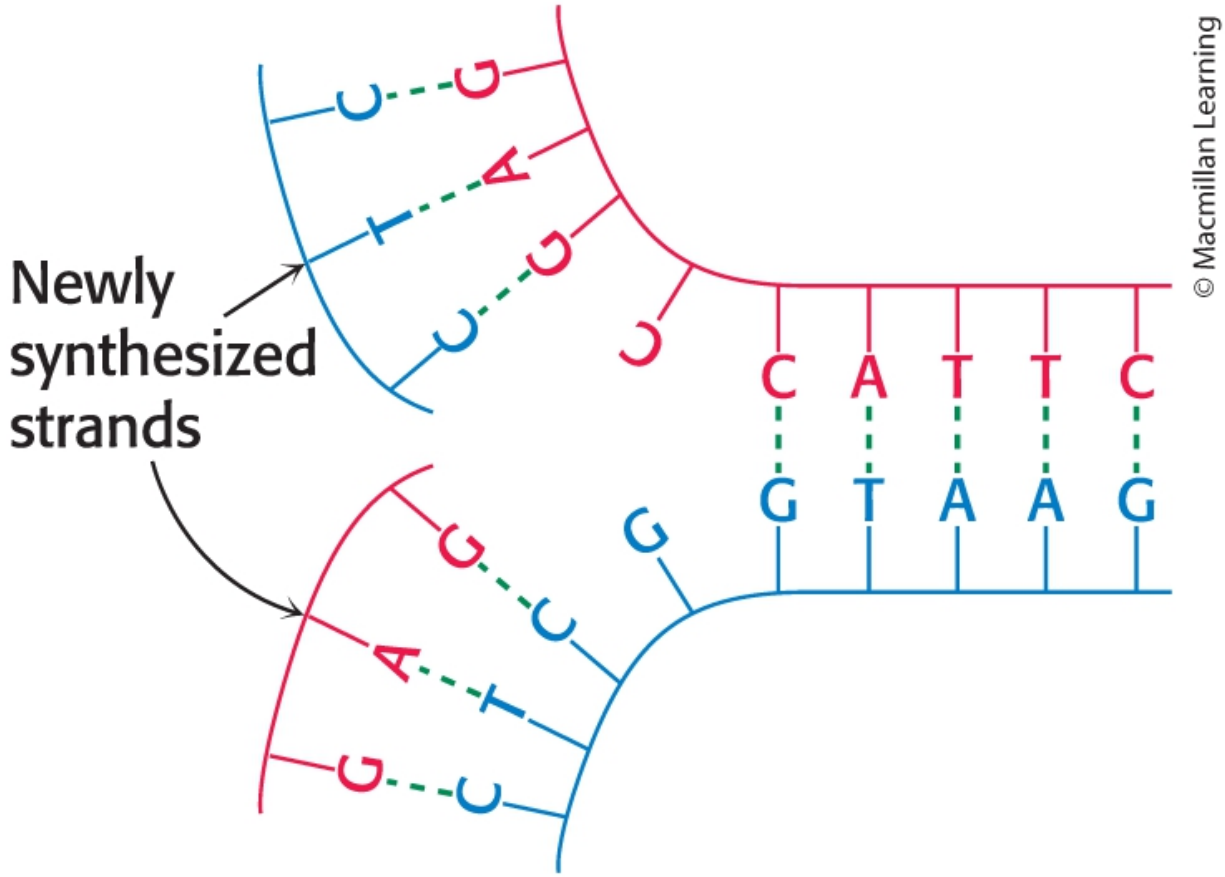
Guanine (G) has the following structure: A 5-membered heterocyclic pentagonal ring is in a horizontal orientation and consists of 2 N and 3 C atoms. The first N atom occupies the first position, which is the bottom-left vertex, and the second N atom occupies the third position, which is the top-left vertex. A double bond is present between C 1 and the second N atom and between C 2 and C 3. The first N atom is single bonded to C H 3 in the form of a line. This ring is fused to a 6-membered heterocyclic hexagonal ring in a vertical orientation that consists of 2 N and 4 C atoms. The first N atom occupies the first position, which is the top-right vertex, and the second N atom occupies the third position, which is the bottommost vertex. A double bond is present between C 1 and the second N atom. The first N atom is single bonded to H. C 1 is single bonded to N. This N atom is single bonded to H on the upper right and H on the lower left. C 4 is double bonded to O. The two rings are fused to each other such that C 2 and C 3 of the 5-membered ring are the C 3 and C 2 of the 6-membered ring, respectively.

Cytosine (C) has the following structure: A 6-membered heterocyclic hexagonal ring is in a vertical orientation and consists of 2 N and 4 C atoms. The first N atom, highlighted, occupies the first position, which is the bottom-right vertex, and the second N atom occupies the third position, which is the bottom-left vertex. A double bond is present between the second N atom and C 2 and between C 3 and C 4. The first N atom is single bonded to C H 3 in the form of a line. C 1 is double bonded to O. C 2 is single bonded to N. This N atom is single bonded to H above and H on the lower left.

A dashed green line is drawn between the O atom double bonded to C 4 of the 6-membered ring in guanine and the H atom on the lower left single bonded to N bound to C 2 in cytosine. A second dashed green line is drawn between the H atom single bonded to first N atom of the 6-membered ring in guanine and the second N atom in cytosine. A third dashed green line is drawn between the H on the upper right single bonded to N bound to C 1 in guanine and the O atom double bonded to C 1 in cytosine.

Return to FIGURE 1.6 The nitrogenous bases in DNA form specific Watson–Crick base pairs

Extended description for FIGURE 1.7 Once separated, each strand of the DNA double helix can act as a template for the generation of its partner strand

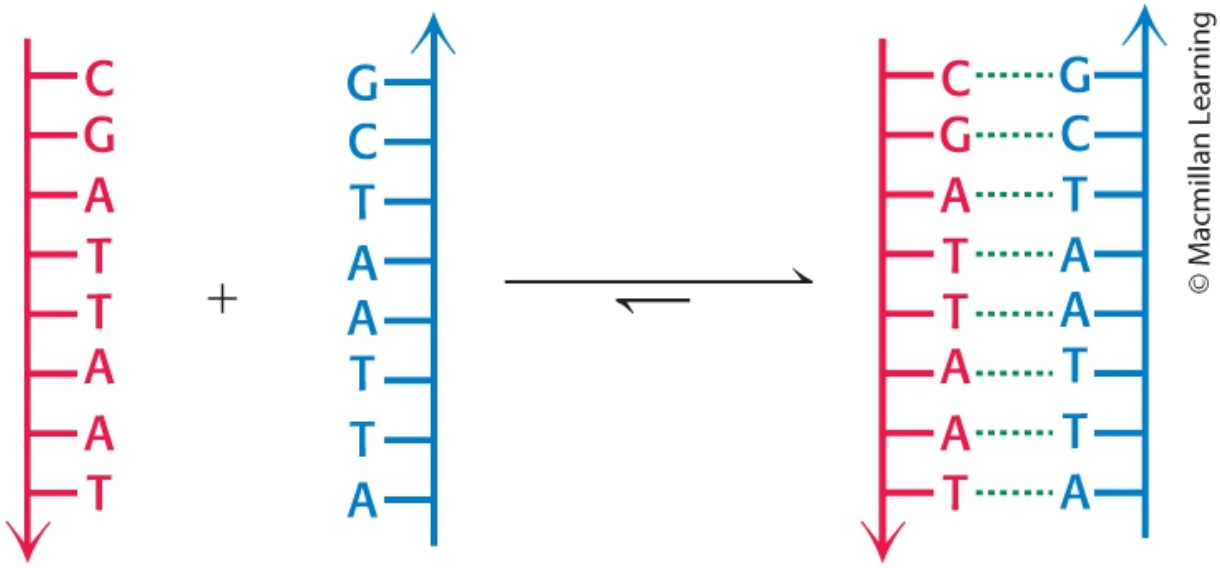


© Macmillan Learning

The parent D N A is illustrated to have two antiparallel strands of D N A held together by complementary base pairing between via hydrogen bonds represented by dashed green lines. The parent strands are shown to separate on the left end, forming a fork. The separated parent strands are each bonded to newly synthesized strands by complementary base pairing via hydrogen bonds represented by dashed green lines.

Return to FIGURE 1.7 Once separated, each strand of the DNA double helix can act as a template for the generation of its partner strand

Extended description for FIGURE 1.8 When two DNA strands with complementary sequences are mixed, they spontaneously assemble to form a double helix

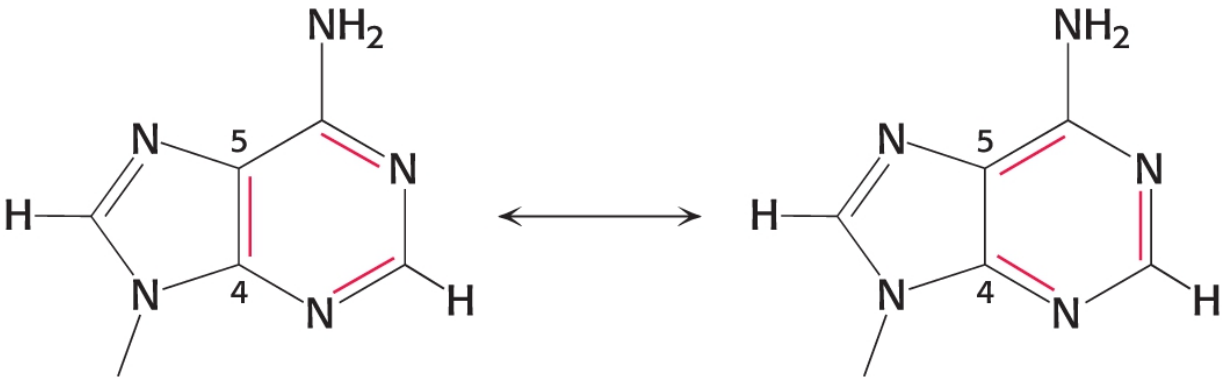


The reversible reaction consists of two reactants and one product. The product side is more preferred in the reaction.

The first reactant is a single stranded D N A (red) having a downward orientation. The second reactant is a single stranded D N A (blue) having an upward orientation. The corresponding nitrogenous bases of the two strands are complementary to each other. The product is a double stranded D N A formed by complementary base pairing of nitrogenous bases of the two reactant D N A strands. The two D N A strands are antiparallel to each other.

Return to FIGURE 1.8 When two DNA strands with complementary sequences are mixed, they spontaneously assemble to form a double helix

Extended description for Resonance structures of adenine

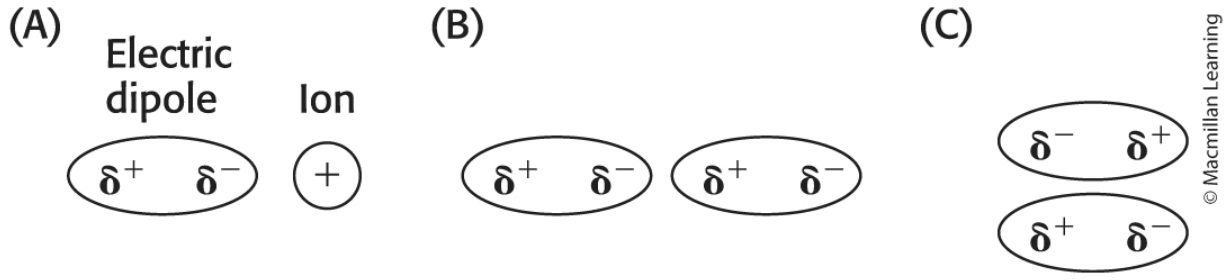


The first resonance structure is as follows: A 5-membered heterocyclic pentagonal ring is in a horizontal orientation and consists of 2 N and 3 C atoms. The first N atom occupies the first position, which is the bottom-left vertex, and the second N atom occupies the third position, which is the top-left vertex. C 2 and C 3 are numbered 5 and 4, respectively. A double bond is present between C 1 and the second N atom. The first N atom is single bonded to C H 3 in the form of a line. C 1 is single bonded to H. This ring is fused to a 6-membered heterocyclic hexagonal ring in a vertical orientation that consists of 2 N and 4 C atoms. The first N atom occupies the first position, which is the top-right vertex, and the second N atom occupies the third position, which is the bottommost vertex. A highlighted double bond is present between C 1 and the second N atom, C 2 and C 3, and C 4 and the first N atom. C 1 is single bonded to H, and C 4 is single bonded to N H 2. The two rings are fused to each other such that C 2 and C 3 of the 5-membered ring are the C 3 and C 2 of the 6-membered ring, respectively.

The second resonance structure is as follows: A 5-membered heterocyclic pentagonal ring is in a horizontal orientation and consists of 2 N and 3 C atoms. The first N atom occupies the first position, which is the bottom-left vertex, and the second N atom occupies the third position, which is the top-left vertex. C 2 and C 3 are numbered 5 and 4, respectively. A double bond is present between C 1 and the second N atom. The first N atom is single bonded to C H 3 in the form of a line. C 1 is single bonded to H. This ring is fused to a 6-membered heterocyclic hexagonal ring in a vertical orientation that consists of 2 N and 4 C atoms. The first N atom occupies the first position, which is the top-right vertex, and the second N atom occupies the third position, which is the bottommost vertex. A highlighted double bond is present between the first N atom and C 1, the second N atom and C 2, and C 3 and C 4. C 1 is single bonded to H, and C 4 is single bonded to N H 2. The two rings are fused to each other such that C 2 and C 3 of the 5-membered ring are the C 3 and C 2 of the 6-membered ring, respectively.

Return to Resonance structures of adenine

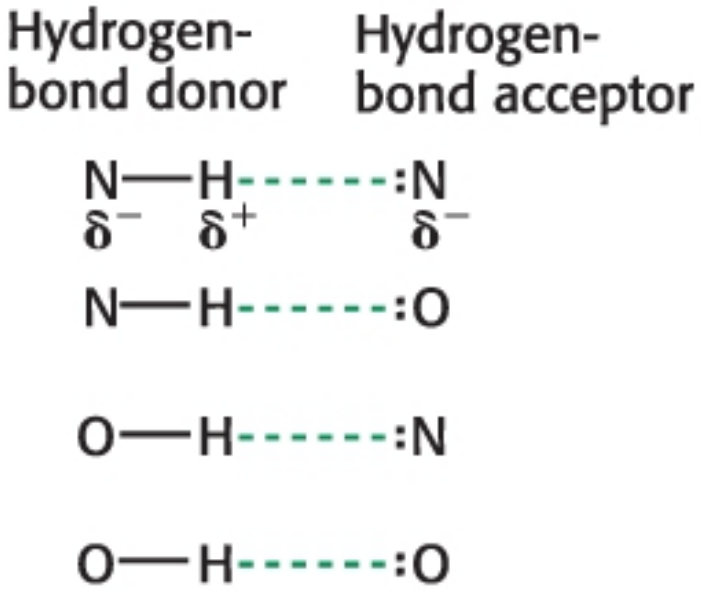
Extended description for FIGURE 1.9 Electric dipoles can form a variety of noncovalent interactions



Part (A): An oval capsule labeled electric dipole is illustrated with a delta plus charge at its left end and a delta minus charge at its right end. A circle labeled ion carrying a positive charge is illustrated to the right of the electric dipole.
Part (B): Two oval capsules representing electric dipoles are illustrated side-by-side. The first dipole carries a delta plus charge at its left end and a delta minus charge at its right end. The second dipole carries a delta plus charge at its left end and a delta minus charge at its right end.
Part (C): Two oval capsules representing electric dipoles are illustrated one below the other. The dipole at the top carries a delta minus charge at its left end and a delta plus charge at its right end. The dipole at the bottom carries a delta plus charge at its left end and delta minus charge at its right end.

Return to FIGURE 1.9 Electric dipoles can form a variety of noncovalent interactions

Extended description for FIGURE 1.10 Hydrogen bonds are weak noncovalent interactions between specific hydrogen atoms and lone pairs of electrons



Pair 1:

Hydrogen-bond donor: H, single bond, H. The first H carries a delta minus charge and the second H carries a delta plus charge.
Hydrogen-bond acceptor: N with a lone pair of electrons and a delta minus charge.
A dashed green line is drawn between the second H and the N with a lone pair of electrons.

Pair 2:

Hydrogen-bond donor: N, single bond, H.
Hydrogen-bond acceptor: O having a lone pair of electrons.
A dashed green line is drawn between H and O.

Pair 3:

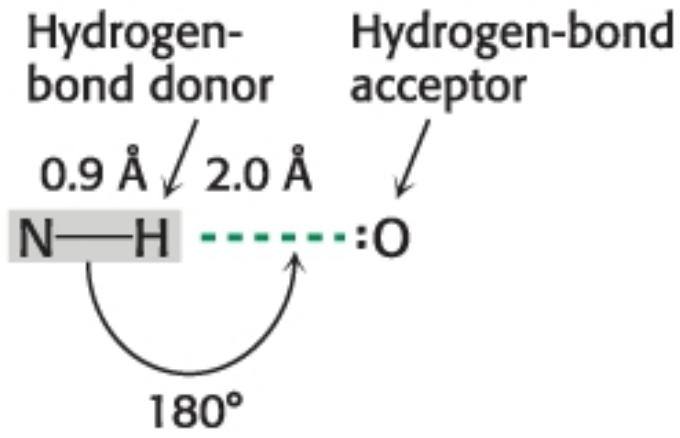
Hydrogen-bond donor: O, single bond, H.
Hydrogen-bond acceptor: N having a lone pair of electrons.
A dashed green line is drawn between H and N.

Pair 4:

Hydrogen-bond donor: O, single bond, H.
Hydrogen-bond acceptor: O having a lone pair of electrons.
A dashed green line is drawn between the O bonded to H and the O with a lone pair of electrons.

Return to FIGURE 1.10 Hydrogen bonds are weak noncovalent interactions between specific hydrogen atoms and lone pairs of electrons

Extended description for An example of hydrogen bonding



Hydrogen-bond donor: N, single bond, H. The bond length of the single bond is 0.9 Angstrom.

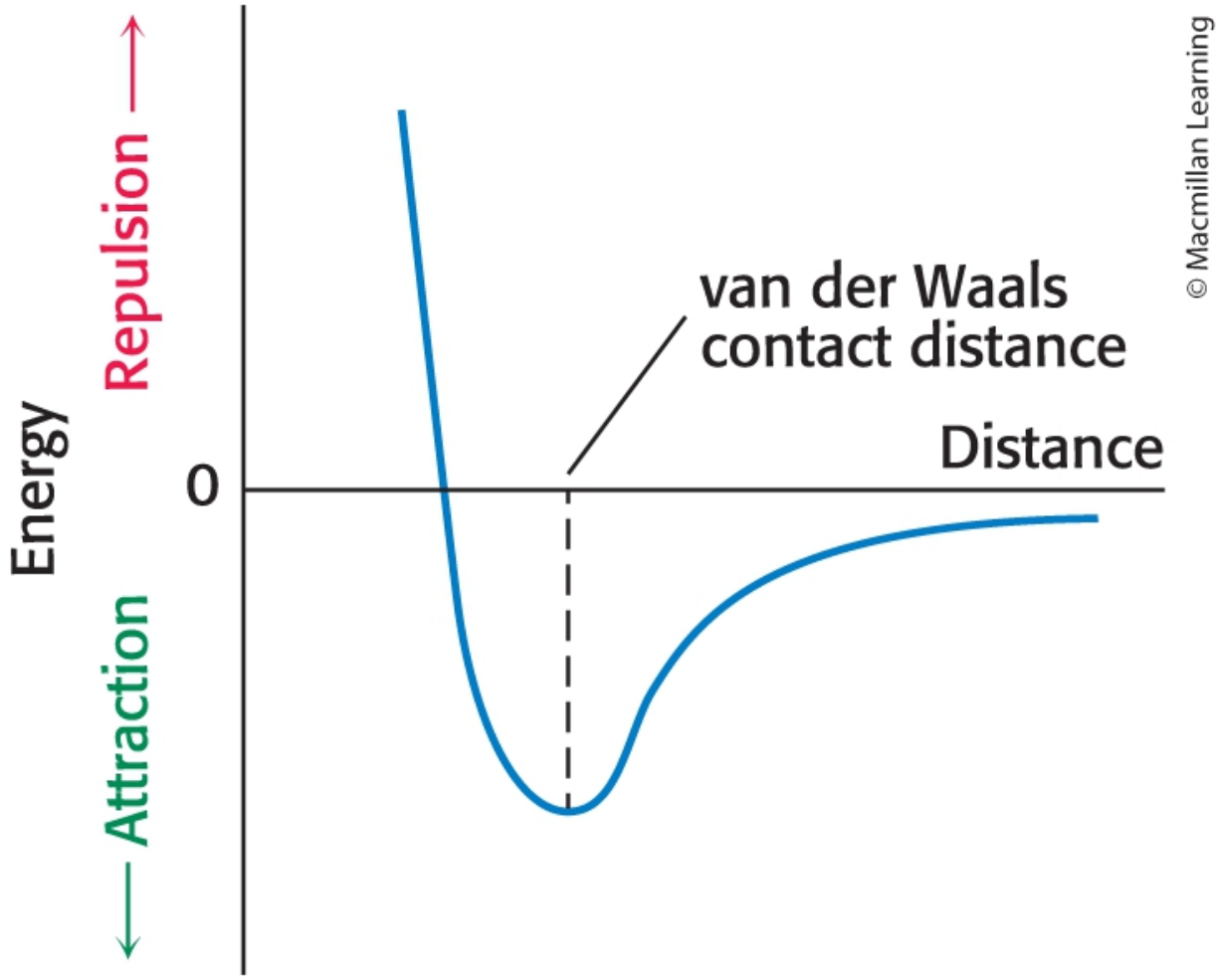
Hydrogen-bond acceptor: O with 2 lone pairs of electrons.

A dashed green line is drawn between H and O representing a hydrogen bond. The bond length of the hydrogen bond is 2.0 Angstrom.

The angle between the single bond between N and H and the hydrogen bond is 180 degrees.

Return to An example of hydrogen bonding

Extended description for FIGURE 1.11 The energy of a van der Waals interaction varies and is most favorable at the van der Waals contact distance

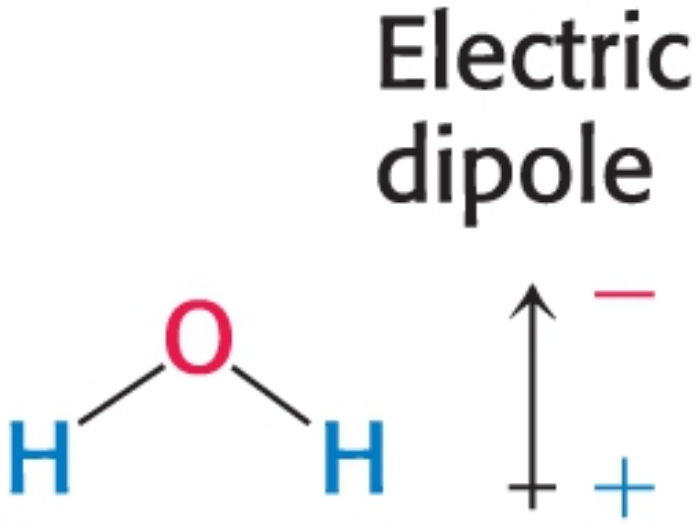


The horizontal axis is labeled Distance, and the vertical axis is labeled Energy with the positive vertical axis pertaining to Repulsion and the negative vertical axis pertaining to Attraction. The intersection of the axes is labeled 0. A curve starts at a point close to 0 distance and high on the repulsion axis and drops steeply to a point further on the distance axis and the midpoint of the attraction axis. The curve then rises gradually and becomes almost

parallel to the distance axis. The point on the distance axis that corresponds to the point of dip is labeled van der Waals contact distance.

Return to FIGURE 1.11 The energy of a van der Waals interaction varies and is most favorable at the van der Waals contact distance

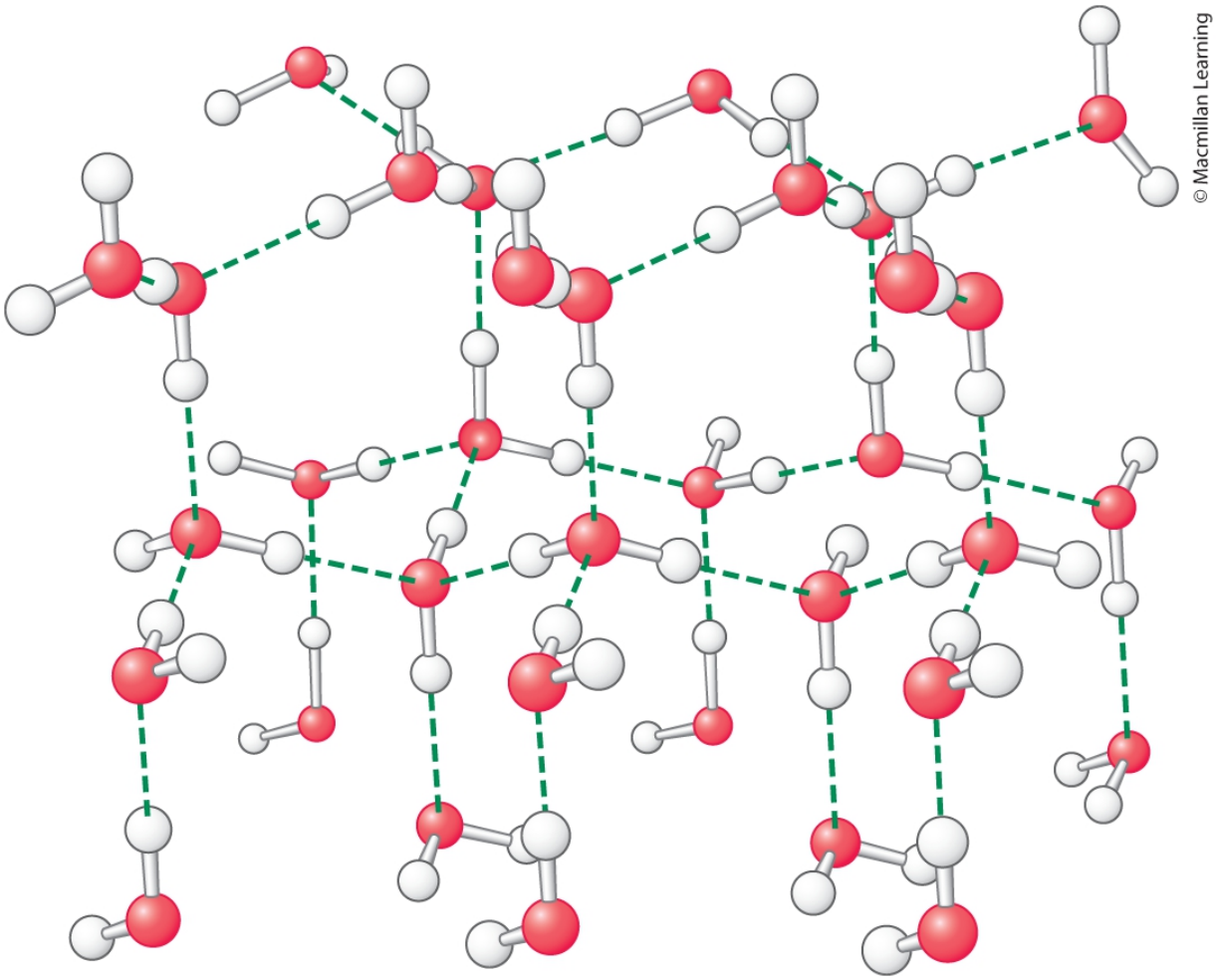
Extended description for Electric dipole in a water molecule



A central O atom is single bonded to H on the lower left and lower right. An upward arrow with a crossed tail is labeled electric dipole. The arrow tip is at O and carries a negative charge. The tail is at the H atoms and carries a positive charge.

Return to Electric dipole in a water molecule

Extended description for FIGURE 1.12 The structure of ice involves extensive hydrogen bonding

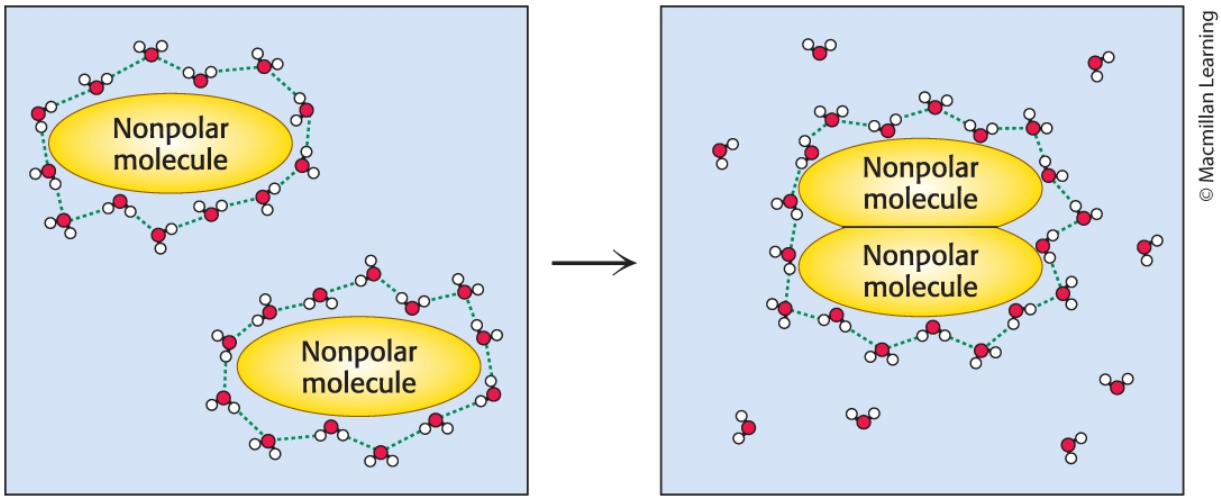


Ice is illustrated to be made up of water molecules. The ball-and-stick model of water molecules is as follows: A red sphere representing an O atom is bonded to a white sphere representing an H atom on the lower left and on the lower right. Dashed green lines are drawn between H and O atoms of adjacent water molecules, forming hexagonal shapes. Two parallel sheets of such fused hexagons are illustrated. Dashed green lines are drawn between H

and O atoms of adjacent water molecules of the top and the bottom sheet. The dashed green lines represent hydrogen bonds.

Return to FIGURE 1.12 The structure of ice involves extensive hydrogen bonding

Extended description for FIGURE 1.13 The hydrophobic effect is due to the behavior of water molecules



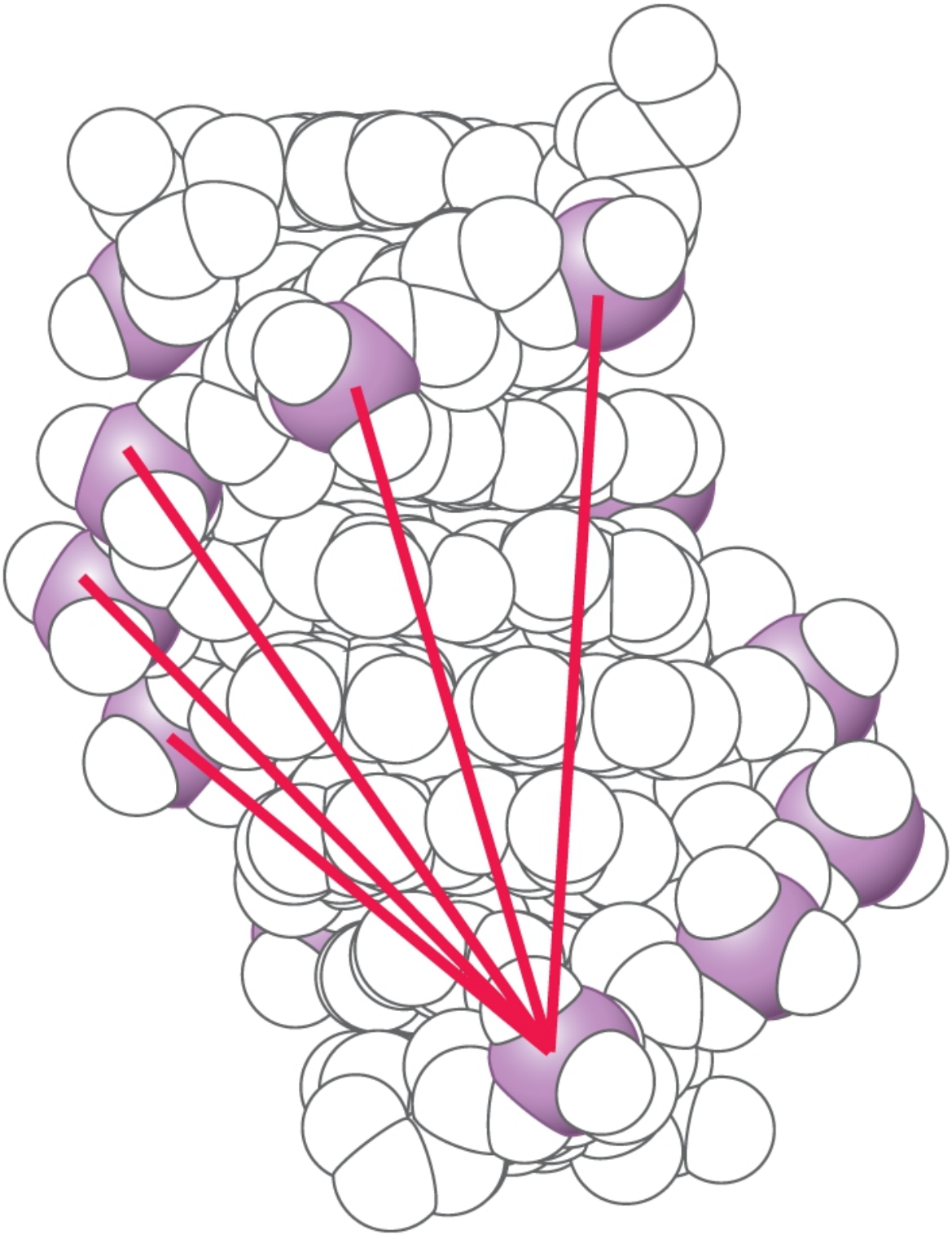
Two stages are shown as follows:

Stage 1: Two ovals labeled nonpolar molecules are shown far apart. Each nonpolar molecule is surrounded by ball-and-stick models of water molecules. Dashed green lines are drawn between the O atoms and H atoms of adjacent water molecules.
Stage 2: The nonpolar molecules are shown to aggregate together, one on top of the other. Ball-and-stick models of water molecules are shown to surround the aggregated nonpolar molecules. Dashed green lines are drawn between the O atoms and H atoms of adjacent water molecules. Some water molecules are shown to be suspended freely in the solution.

Return to FIGURE 1.13 The hydrophobic effect is due to the behavior of water molecules

Extended description for FIGURE 1.14 Ionic interactions among phosphate groups oppose the

formation of the DNA double helix

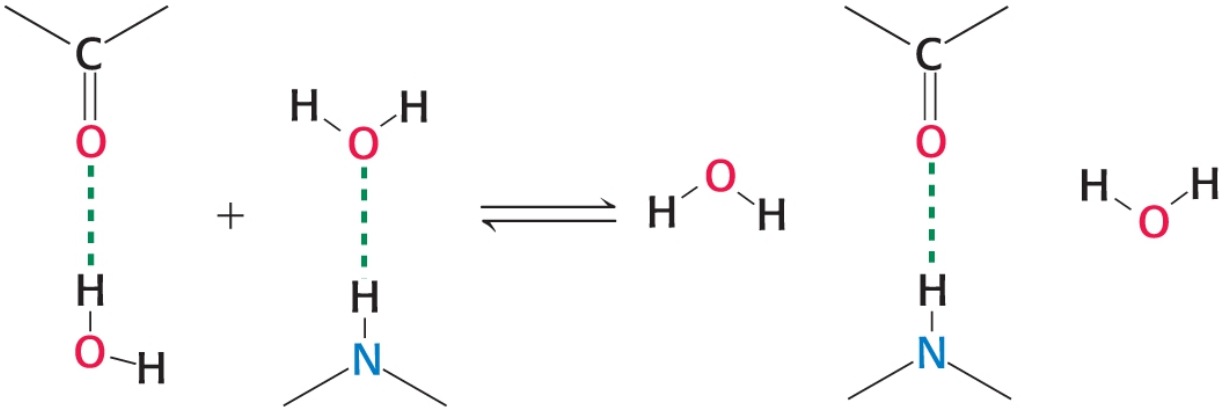


© Macmillan Learning

The space-filling model of a D N A double-helix structure is shown. The P atoms are represented by purple spheres and the other atoms are represented by white spheres. Red lines from one purple sphere are drawn to purple spheres of the groove above.

Return to FIGURE 1.14 Ionic interactions among phosphate groups oppose the formation of the DNA double helix

Extended description for Example of a reversible reaction



The reaction consists of three reactants and three products.

The first reactant has the following structure: A central C atom is single bonded to C H 3 on the upper left and C H 3 on the upper right each in the form of a line. The central C atom is double bonded to O, highlighted in red, below.

The second reactant has the following structure: A central O atom, highlighted in red, is single bonded to H above and H on the lower right. The second reactant is placed below the first reactant. A dashed green line is drawn between the O atom of the first reactant and the H above of the second reactant.

The third reactant has the following structure: A central N atom, highlighted in blue, is single bonded to C H 3 on the lower left and C H 3 on the lower right each in the form of a line. The central N atom is single bonded to H above.

Another molecule of the second reactant is placed above the third reactant. A dashed green line is drawn between the O atom of the second molecule and the H atom above of the third reactant.

The first product has the following structure: A central O atom, highlighted in red, is single bonded to H on the lower left and H on the lower right.

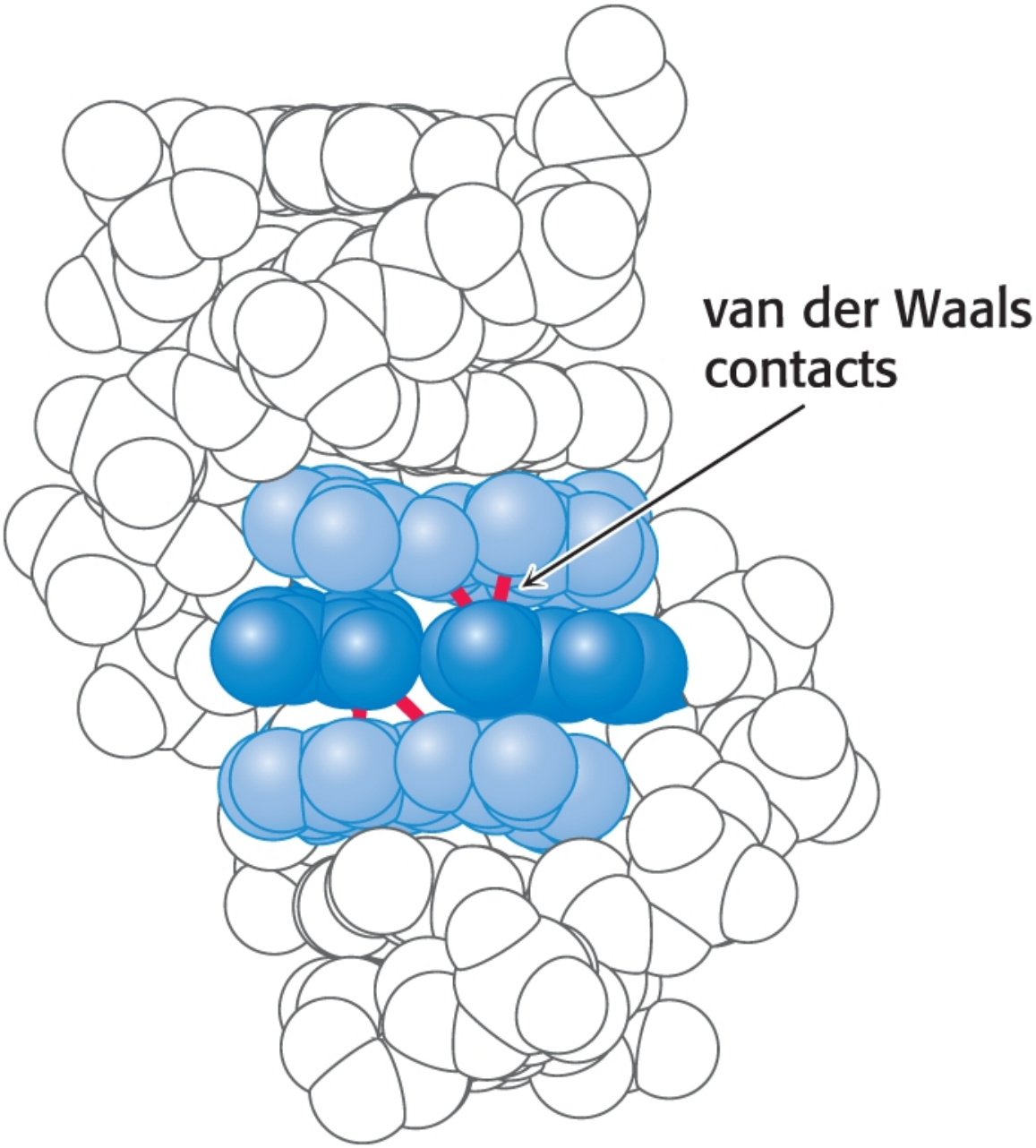
The second product is made of two molecules connected by a dashed green line. The first molecule has the following structure: A central C atom is single bonded to C H 3 on the upper left and C H 3 on the upper right each in the form of a line. The central C atom is double bonded to O, highlighted in red, below. The second molecule is placed below the first molecule and has the following structure: A central N atom, highlighted in blue, is single bonded to C H 3 on the lower left and C H 3 on the lower right each in the form of a line. The central N atom is single bonded to H above. The dashed green line is drawn between the O atom of the first molecule and the H atom above of the second molecule.

The third product has the following structure: A central O atom, highlighted in red, is single bonded to H on the upper left and H on the upper right.

The dashed green lines represent hydrogen bonds.

Return to Example of a reversible reaction

Extended description for FIGURE 1.15 Optimal base stacking allows many weak, but favorable, van der Waals contacts that drive double- helix formation



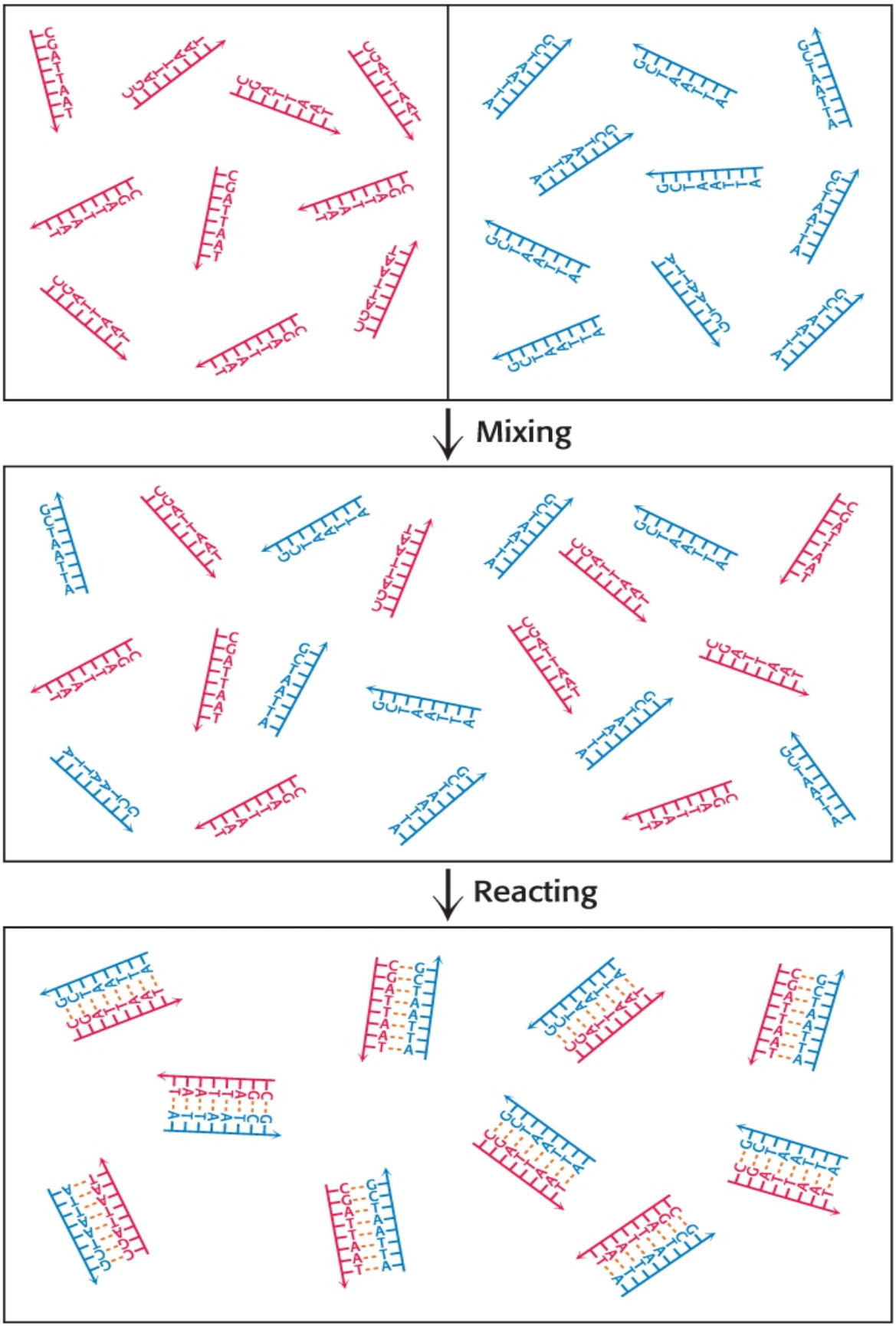
© Macmillan Learning

The space-filling model of a D N A double-helix structure is shown. In the middle portion, adjacent bases are shown to stack one on top of the other, forming three stacked layers. Atoms of the top and bottom layers are colored light blue and the atoms of the middle layer are colored dark blue. Short red lines labeled van der Waals contacts are drawn between spheres of two adjacent layers.

Return to FIGURE 1.15 Optimal base stacking allows many weak, but favorable, van der Waals contacts that drive double- helix formation

Extended description for FIGURE 1.16 Double-helix

formation entails a loss of entropy



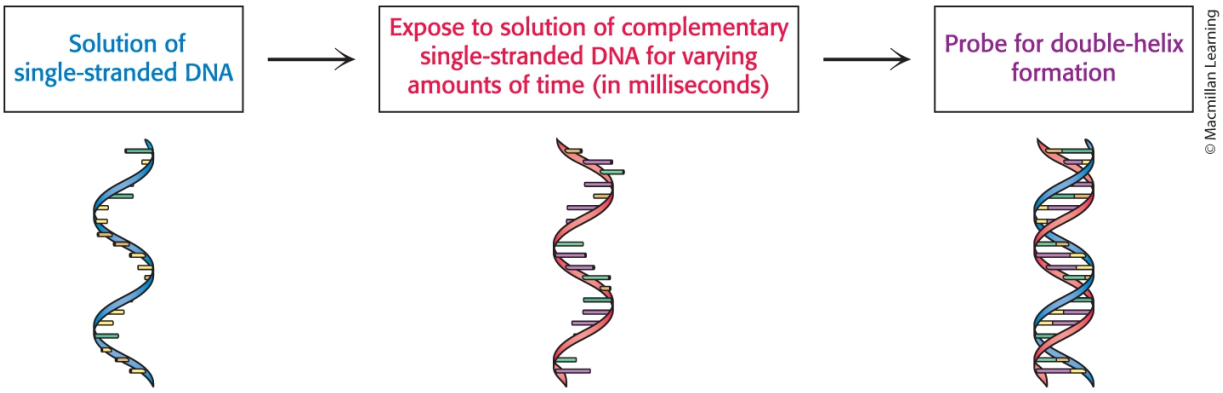
© Macmillan Learning

The process involves 2 steps as follows:

Step 1, mixing: Two solutions are shown. The first solution contains red single-stranded D N A molecules. The second solution contains blue single-stranded D N A molecules. The two solutions are shown to mix together.
Step 2, reacting: A complementary red and a blue strand of D N A are shown to come together to form a duplex.

Return to FIGURE 1.16 Double-helix formation entails a loss of entropy

Extended description for FIGURE 1.17 DNA double-helix formation can be probed at the single-molecule level

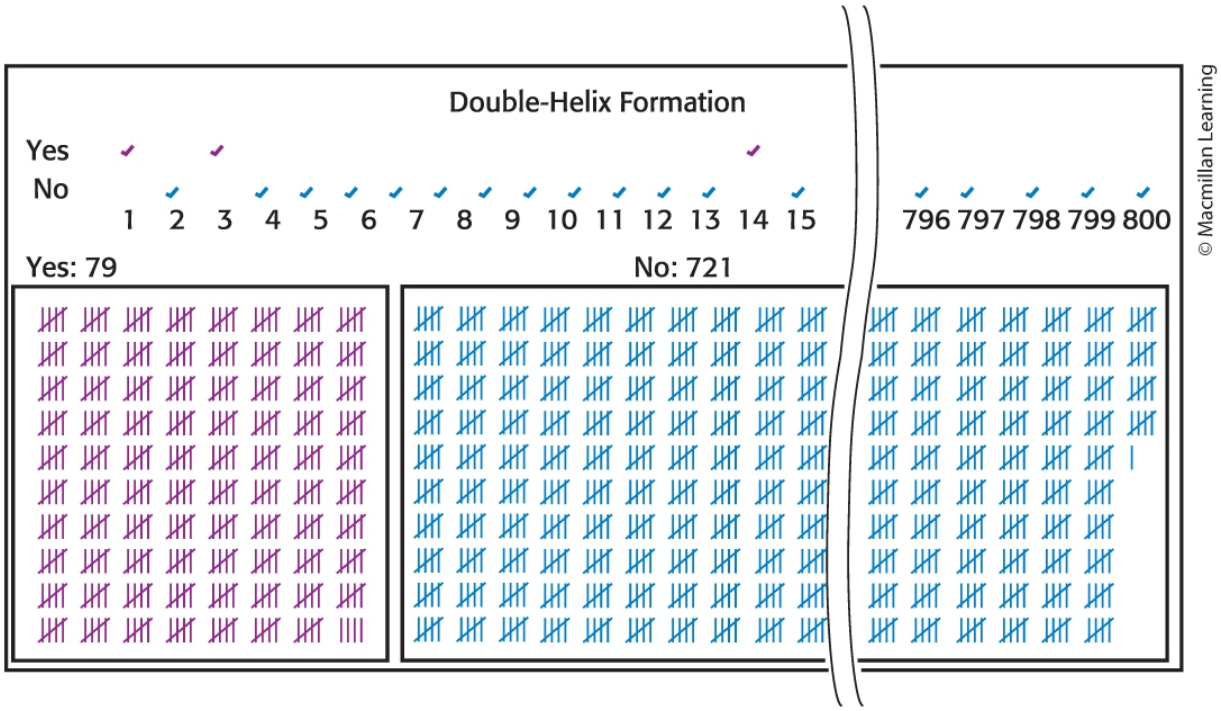


The process involves 3 steps as follows:

Step 1: Solution of single-stranded D N A. A blue helical single-stranded D N A is shown. The sugar-phosphate backbone is represented by a blue ribbon-like structure. The nitrogenous bases are represented by short blue lines, perpendicular to the backbone. Step 2: Expose to a solution of complementary single-stranded DNA for varying amounts of time (in milliseconds). A red helical single-stranded D N A molecule is shown. The sugar-phosphate backbone is represented by a red ribbon-like structure. The nitrogenous bases are represented by short red lines, perpendicular to the backbone. Step 3: Probe for double-helix formation. The red and blue helical single-stranded D N A molecules are shown to come together to form a D N A double helix by complementary base pairing. The red and the blue ribbon-like backbones of the single-stranded D N A molecules are shown to twist together to form a double helix. Adjacent complementary nitrogenous bases of the two strands are shown to join together, forming a ladder-like pattern.

Return to FIGURE 1.17 DNA double-helix formation can be probed at the single-molecule level

Extended description for A table corresponding to the experiments based on double helix formation



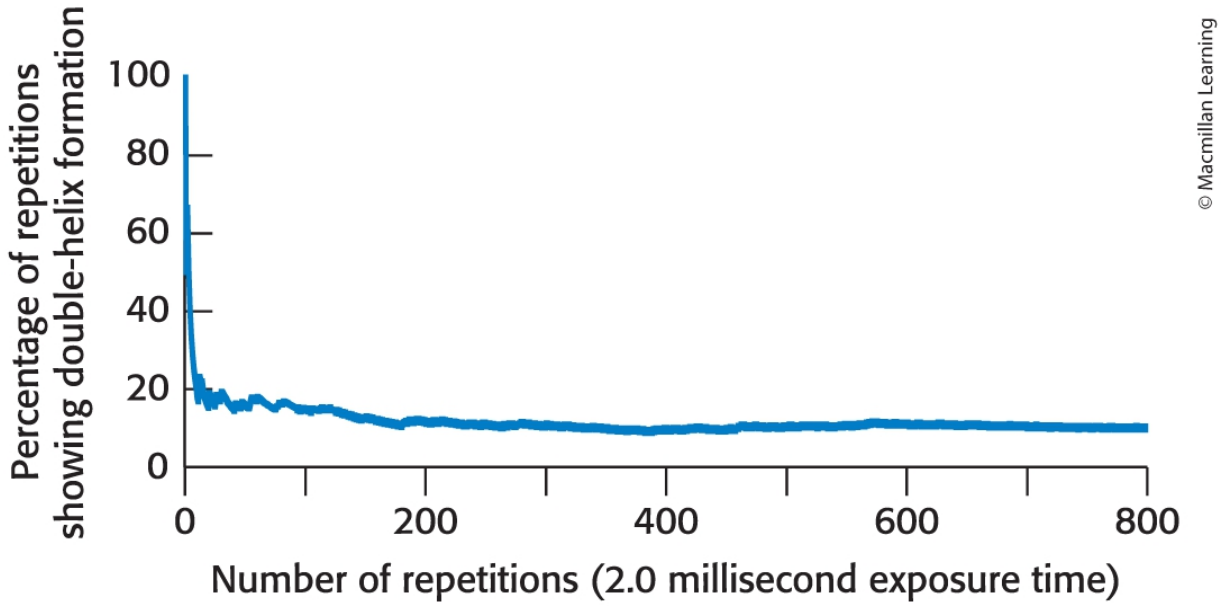
The table has a common heading titled Double-Helix Formation. A row labeled Yes followed by a row labeled No are shown for the individual trials ranging from 1 to 800.

A tally box for Yes ticked for trials 1, 3, and 14 is shown. The number of times the result was a Yes for the detection of a double helix is 79.

A tally box for No ticked for all trials except 1, 3, and 14 is shown. The number of times the result was a No for the detection of a double helix is 721.

[Return to A table corresponding to the experiments based on double helix formation]

Extended description for FIGURE 1.19 A plot of the running average of the number of experimental repetitions observing double-helix formation reveals eventual convergence on a stable value



© Macmillan Learning

The horizontal axis is labeled Number of repetitions (2.0 millisecond exposure time) and ranges from 0 to 800 in increments of 100 units. The vertical axis is labeled Percentage of repetitions showing the double-helix formation and ranges from 0 to 100 in increments of 20 units. A plotline starts at (0, 100) and sharply drops to (10, 20), followed by a gradual decline to nearly (800, 10).

Return to FIGURE 1.19 A plot of the running average of the number of experimental repetitions observing double-helix formation reveals eventual convergence on a stable value

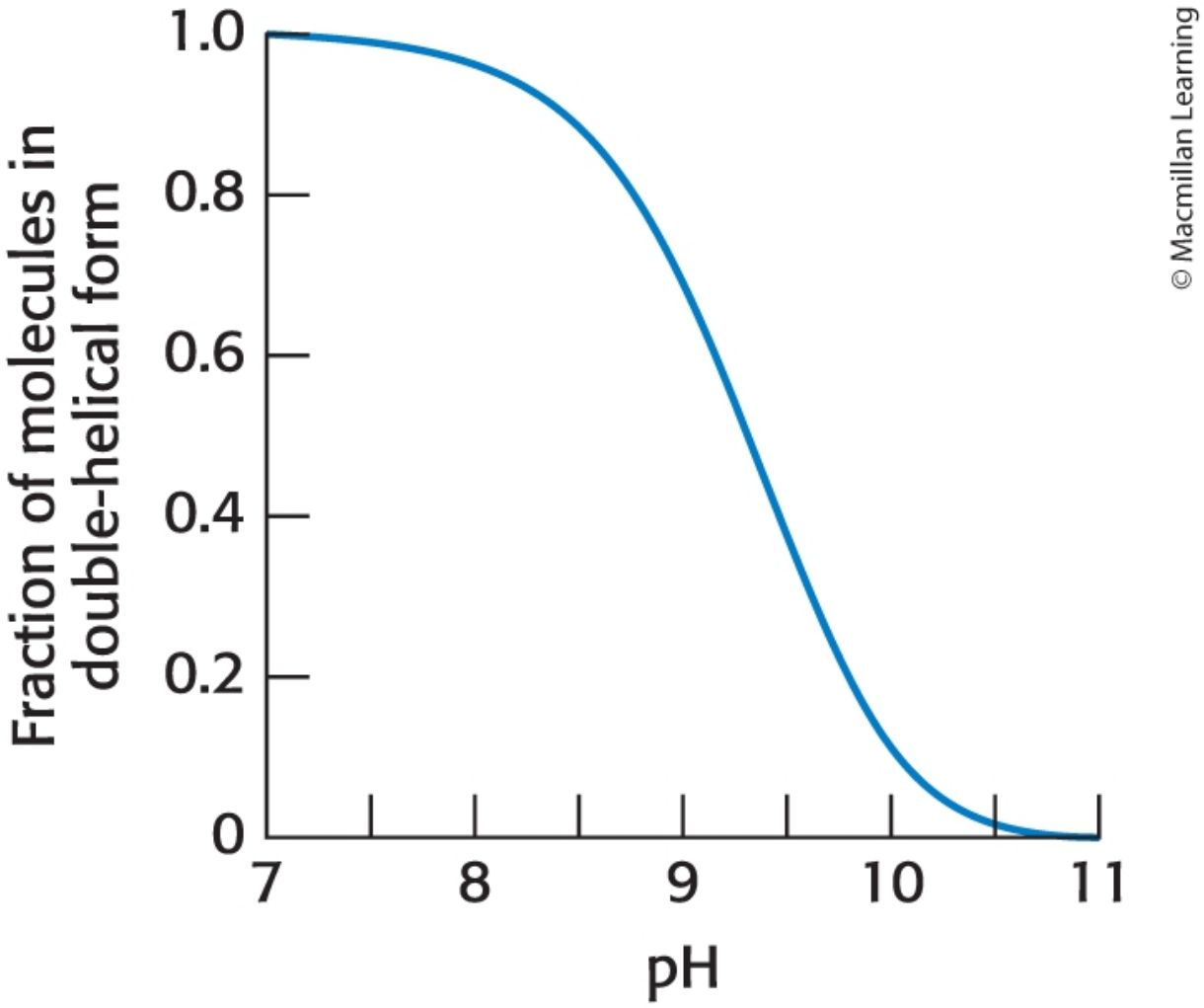
Extended description for Dissociation of water



The reaction consists of one reactant and two products. The reactant is H 2 O. A reversible reaction arrow leads to the products. The first product is H superscript plus. The second product is O H superscript minus.

Return to Dissociation of water

Extended description for FIGURE 1.20 DNA strands are separated by the addition of a base

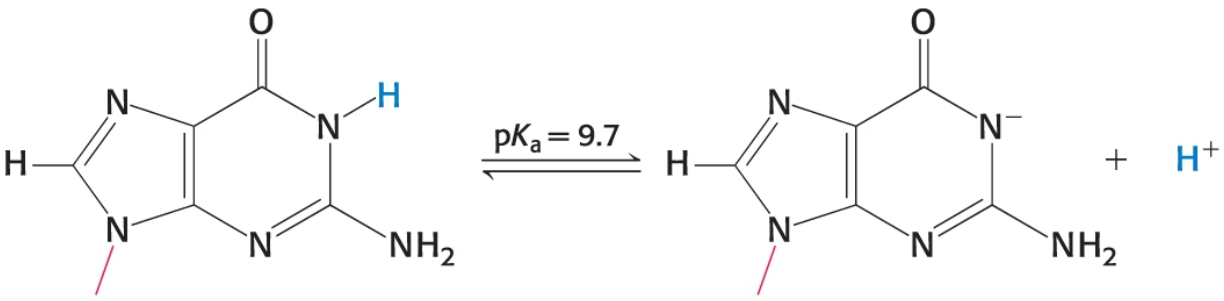


© Macmillan Learning

The horizontal axis is labeled p H and ranges from 7 to 11 in increments of 1 unit. The vertical axis is labeled Fraction of molecules in double-helical form and ranges from 0 to 1.0 in increments of 0.2 units. A curve starts at (7, 1.0), gradually drops to (9, 0.9), followed by a sharp decline to nearly (11, 0). The curve has an inverted S-shape.

Return to FIGURE 1.20 DNA strands are separated by the addition of a base

Extended description for Reversible reaction of guanine



Guanine (G)

The reaction consists of one reactant and two products.

The reactant labeled Guanine (G) has the following structure: A 5-membered heterocyclic pentagonal ring is in a horizontal orientation and consists of 2 N and 3 C atoms. The first N atom occupies the first position, which is the bottom-left vertex, and the second N atom occupies the third position, which is the top-left vertex. A double bond is present between C 1 and the second N atom and between C 2 and C 3. The first N atom is single bonded to C H 3 in the form of a red line. C 1 is single bonded to H. This ring is fused to a 6-membered heterocyclic hexagonal ring in a vertical orientation that consists of 2 N and 4 C atoms. The first N atom occupies the first position, which is the top-right vertex, and the second N atom occupies the third position, which is the bottommost vertex. A double bond is present between C 1 and the second N atom. The first N atom is single bonded to H (highlighted in blue), C 1 is single bonded to N H 2, and C 4 is double bonded to O. The two rings are fused to each other such that C 2 and C 3 of the 5-membered ring are the C 3 and C 2 of the 6-membered ring, respectively.

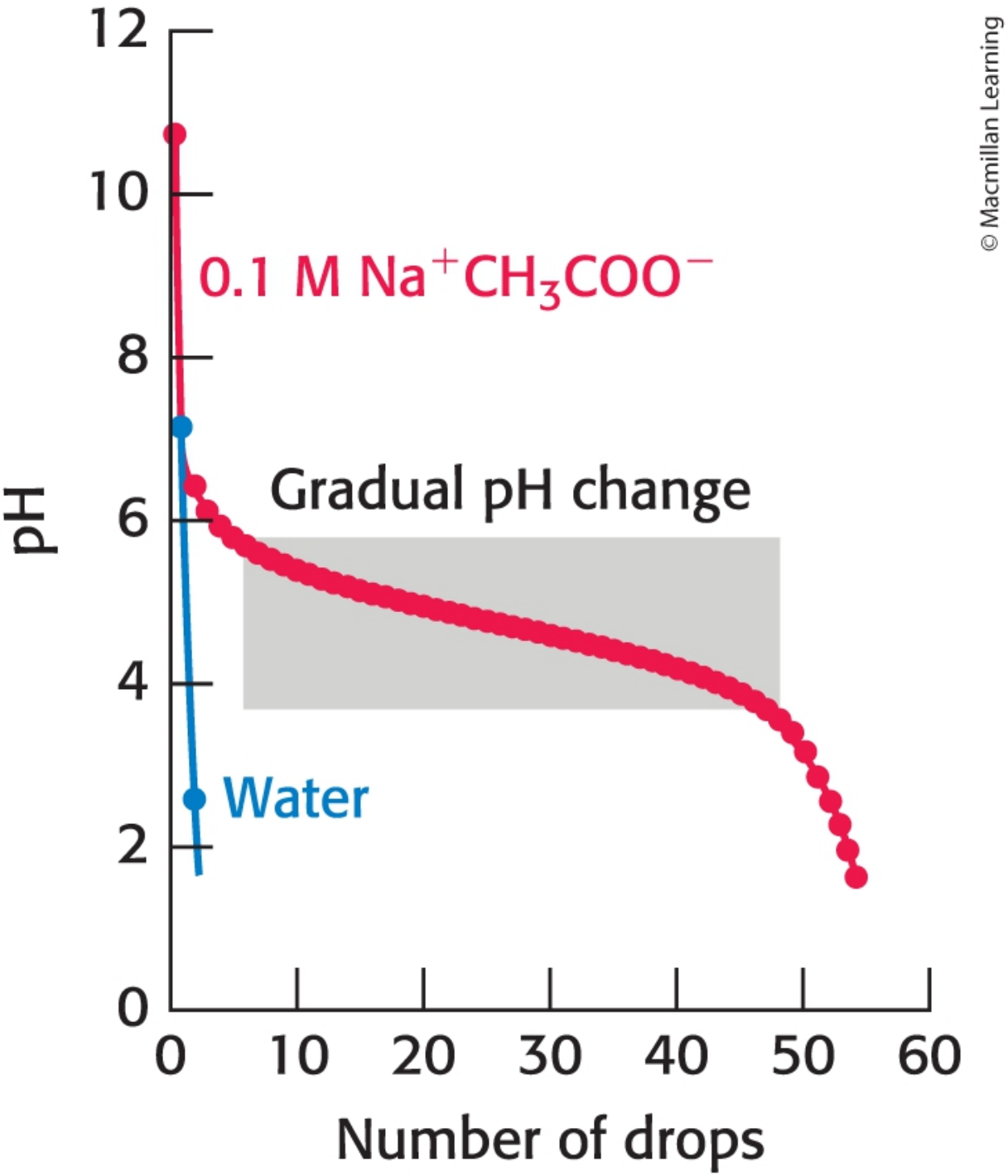
The reaction arrow is labeled p K subscript a equals 9.7.

The first product has the following structure: A 5-membered heterocyclic pentagonal ring is in a horizontal orientation and consists of 2 N and 3 C atoms. The first N atom occupies the first position, which is the bottom-left vertex, and the second N atom occupies the third position, which is the top-left vertex. A double bond is present between C 1 and the second N atom and between C 2 and C 3. The first N atom is single bonded to C H 3 in the form of a red line. C 1 is single bonded to H. This ring is fused to a 6-membered heterocyclic hexagonal ring in a vertical orientation that consists of 2 N and 4 C atoms. The first N atom occupies the first position, which is the top-right vertex, and the second N atom occupies the third position, which is the bottommost vertex. A double bond is present between C 1 and the second N atom. The first N atom carries a negative charge. C 1 is single bonded to N H 2, and C 4 is double bonded to O. The two rings are fused to each other such that C 2 and C 3 of the 5-membered ring are the C 3 and C 2 of the 6-membered ring, respectively.

The second product is H superscript plus, highlighted in blue.

Return to Reversible reaction of guanine

Extended description for FIGURE 1.21 Buffers resist changes in pH over a narrow pH range



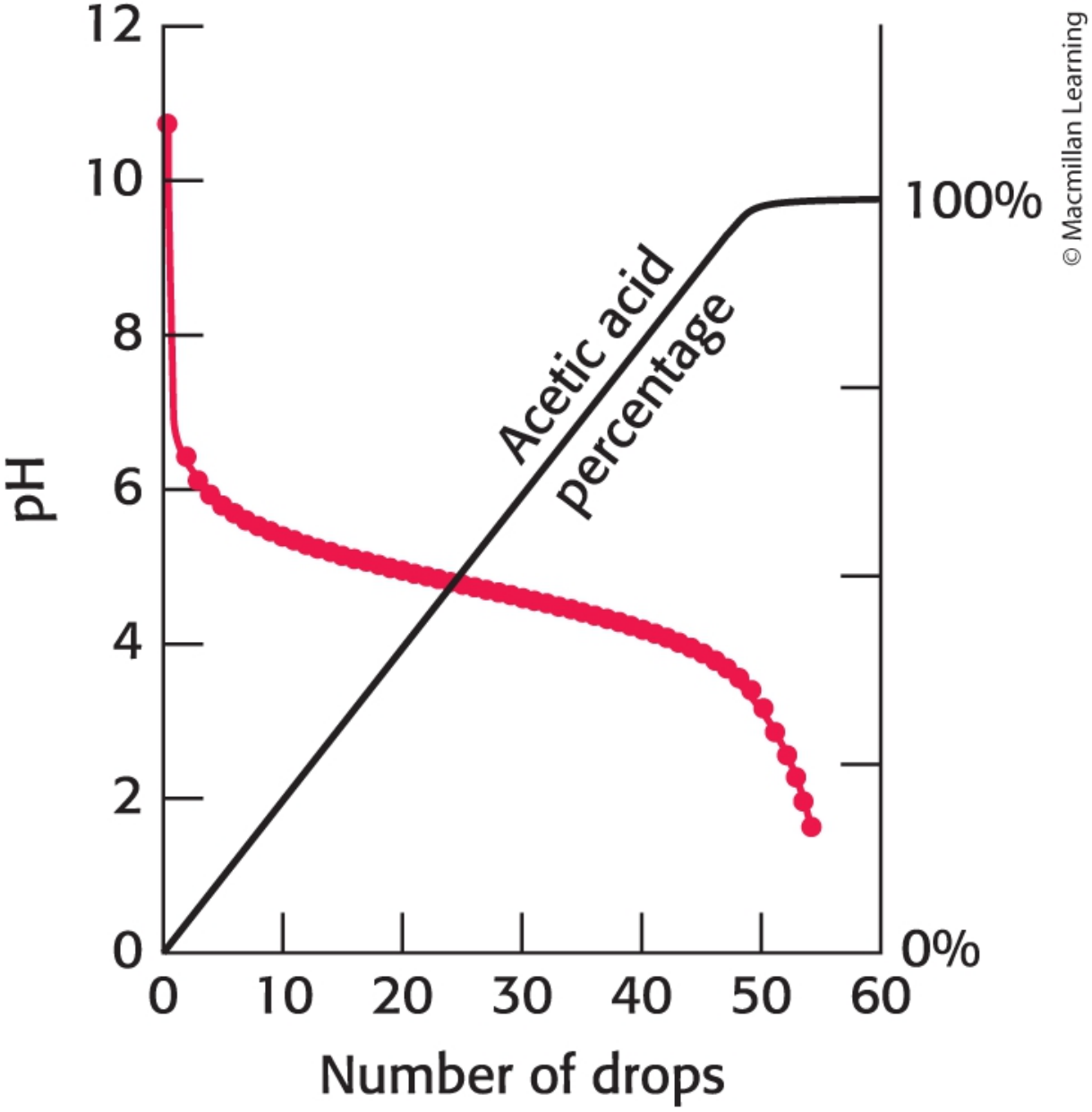
© Macmillan Learning

The horizontal axis is labeled Number of drops and ranges from 0 to 60 in increments of 10 units. The vertical axis is labeled p H and ranges from 0 to 12 in increments of 2 units.

Water: The trend line starts at (1, 7) and sharply drops to (2, 2.5).
0.1 M N a superscript plus C H 3 C O O superscript minus: The trendline starts at nearly (1, 11), sharply drops to (2, 6.5), gradually declines to nearly (50, 3.5), followed by a drop to nearly (55, 1.5).
A rectangle labeled Gradual p H change encloses the curve between 8 and 50 along the horizontal axis and between 5.5 and 6.5 along the vertical axis.

Return to FIGURE 1.21 Buffers resist changes in pH over a narrow pH range

Extended description for FIGURE 1.22 Added hydrogen ions protonate buffer components rather than remaining free



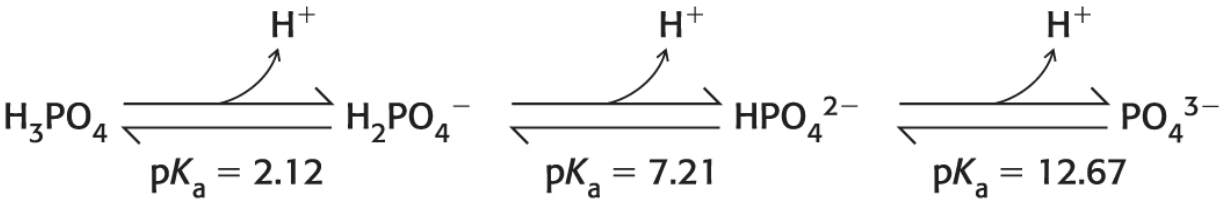
The horizontal axis is labeled Number of drops and ranges from 0 to 60 in increments of 10 units. The left vertical axis is labeled p H and

ranges from 0 to 12 in increments of 2 units. the right vertical axis represents acetic acid percentage and ranges from 0 percent to 100 percent.

Change in p H: The trendline starts at nearly (1, 11), sharply drops to (2, 6.5), gradually declines to nearly (50, 3.5), followed by a drop to nearly (55, 1.5).
Acetic acid percentage: The curve starts at (0, 0 percent), rises to nearly (50, 100 percent), and then runs parallel to the horizontal axis.

Return to FIGURE 1.22 Added hydrogen ions protonate buffer components rather than remaining free

Extended description for Reversible deprotonation reaction of phosphoric acid



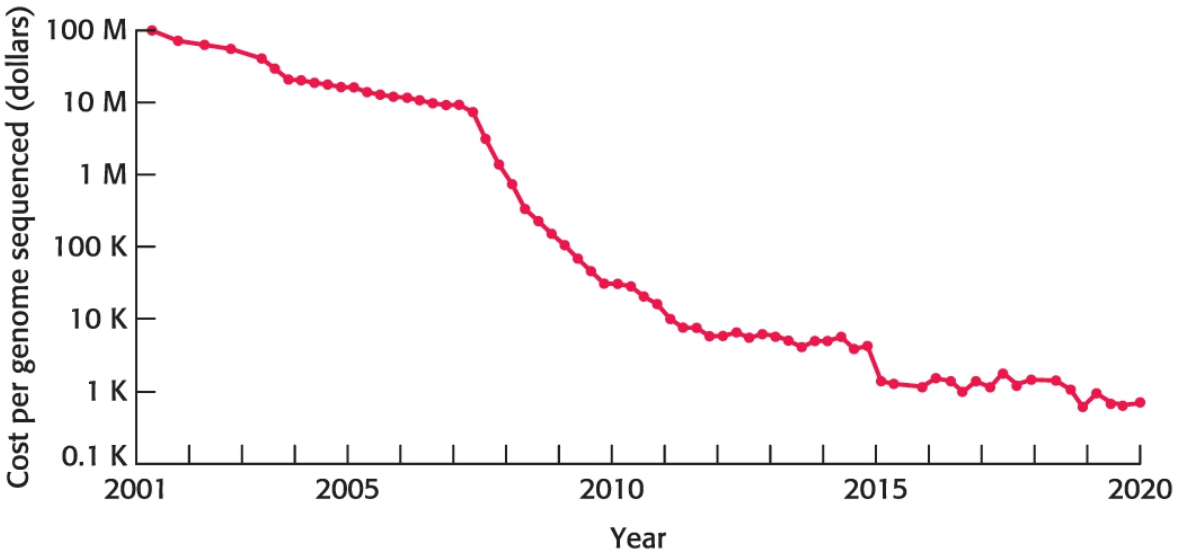
The first reactant is H 3 P O 4. One H superscript plus ion is lost to form the product, H 2 P O 4 superscript minus ion. The reaction arrow is labeled p K subscript a equals 2.12.

The product of the first reaction is the reactant of the second reaction. One H superscript plus ion is lost to form the product, H P O 4 superscript 2 minus ion. The reaction arrow is labeled p K subscript a equals 7.21.

The product of the second reaction is the reactant of the third reaction. One H superscript plus ion is lost to form the product, P O 4 superscript 3 minus ion. The reaction arrow is labeled p K subscript a equals 12.67.

Return to Reversible deprotonation reaction of phosphoric acid

Extended description for FIGURE 1.23 The cost to sequence a human genome has decreased dramatically over the past two decades

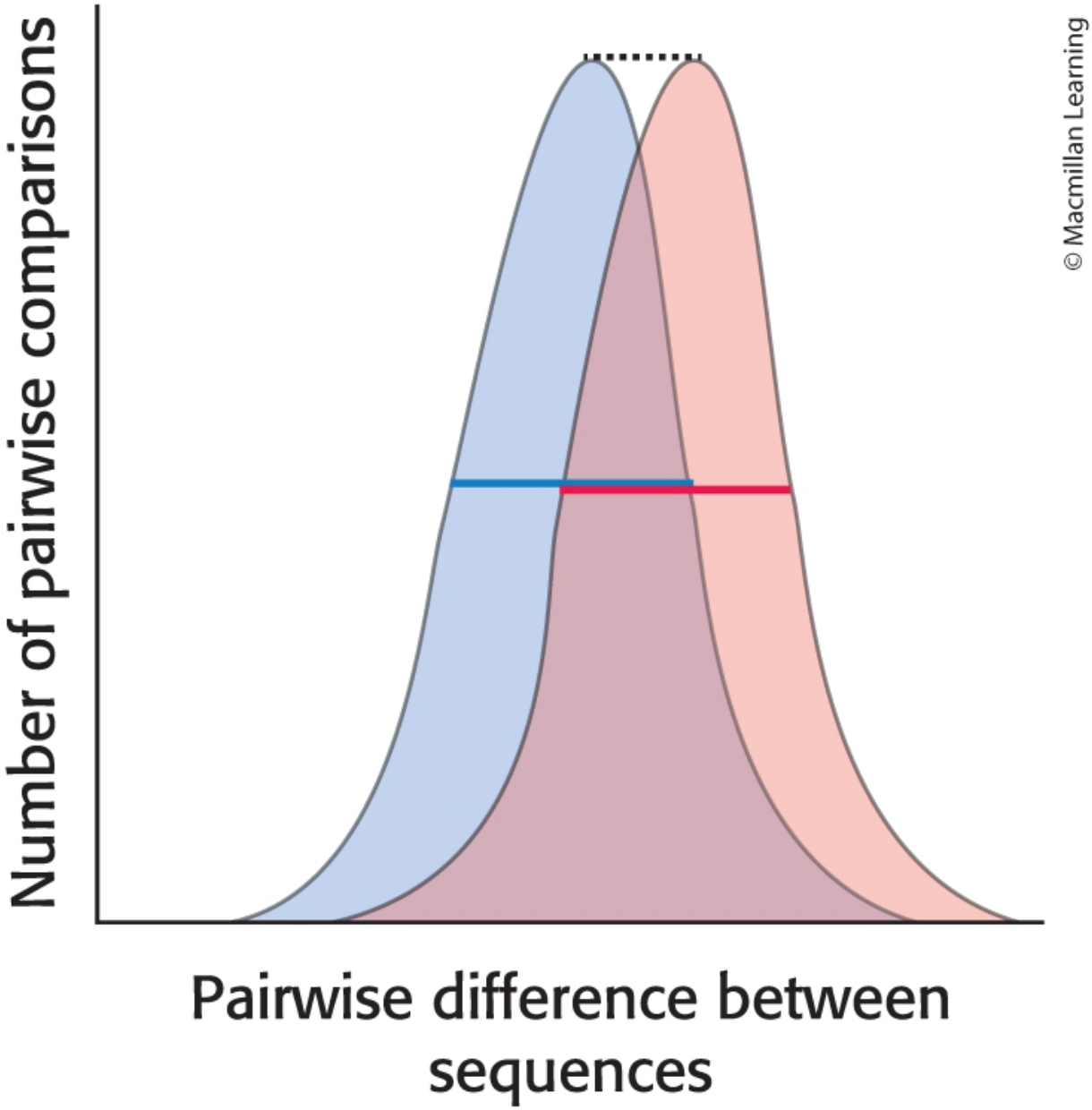


© Macmillan Learning

The horizontal axis is labeled Year and ranges from 2001 to 2020 in increments of 5 units. The vertical axis is labeled Cost per genome sequenced (dollars) and ranges from 0.1 K to 100 M in geometric increments of 10 units. A trendline starts at (2001, 100 M), gradually drops to nearly (2007, 10 M), followed by a decline to (2020, 0.1 K) with minor fluctuations.

Return to FIGURE 1.23 The cost to sequence a human genome has decreased dramatically over the past two decades

Extended description for FIGURE 1.24 DNA sequences vary more within populations than they do between populations

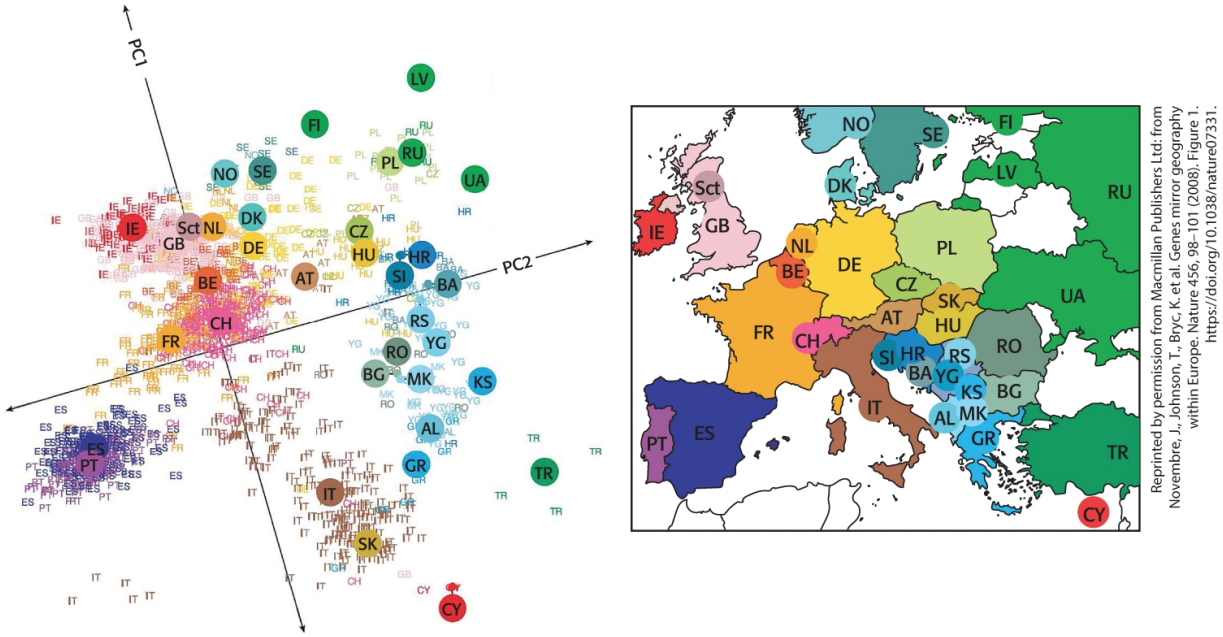


The horizontal axis is labeled Pairwise difference between sequences. The vertical axis is labeled Number of pairwise

comparisons. A blue bell-shaped curve has a peak corresponding to the upper end of the vertical axis. A red bell-shaped curve partially overlaps with the blue curve on the blue curve's left and has the same peak height. A black horizontal line is drawn between the peaks of the two curves. A blue horizontal line is drawn through the middle of the blue curve. A red horizontal is drawn through the middle of the blue curve. The red and the blue lines are longer than the black line.

Return to FIGURE 1.24 DNA sequences vary more within populations than they do between populations

Extended description for FIGURE 1.25 Genomic information can confirm locations of ancestry



A map of Europe is color-coded as follows:

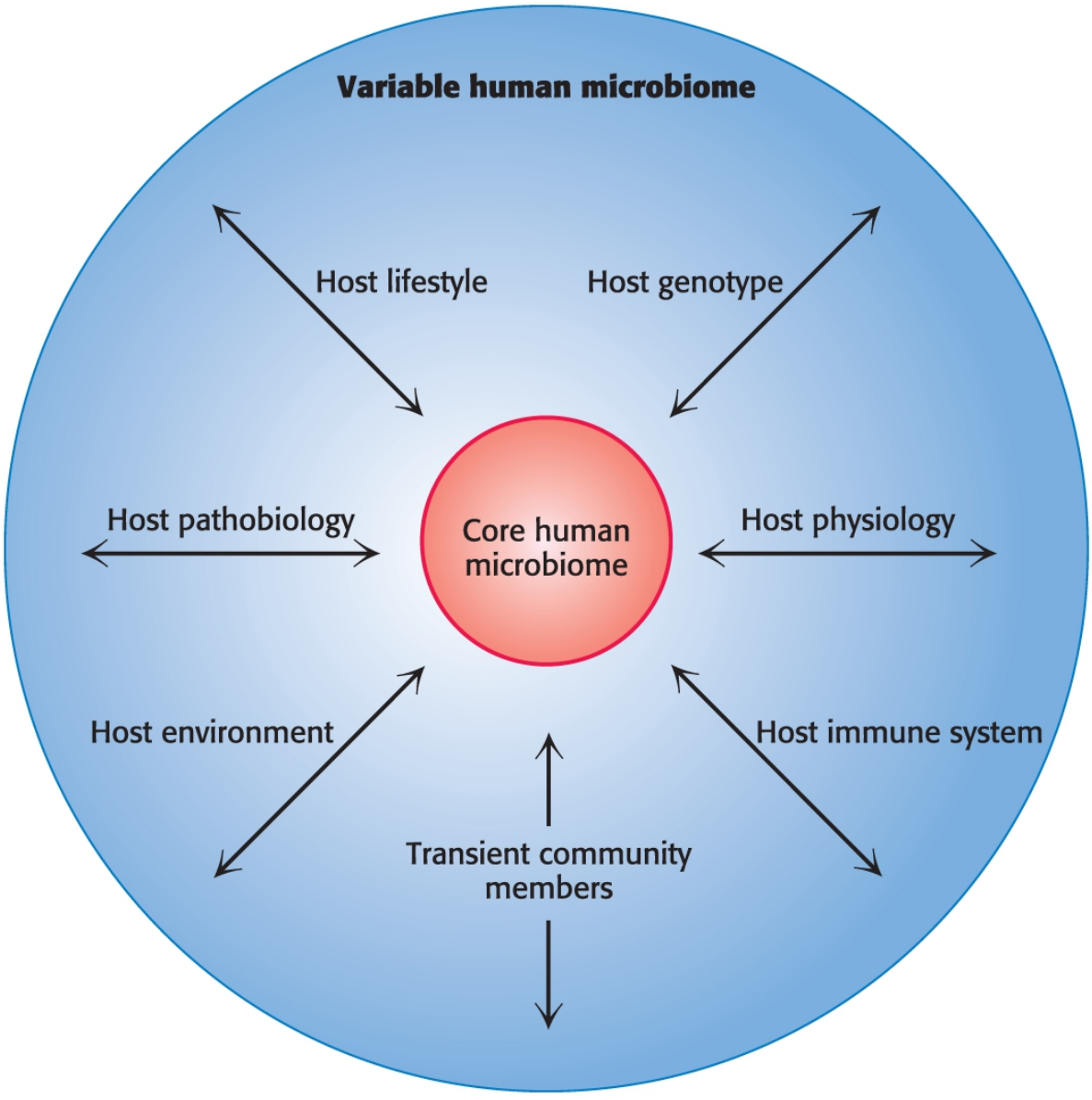
Poland, the Czech Republic, Ukraine, Turkey, Latvia, and Russia are colored in shades of green.
Romania, Bulgaria, Greece, Serbia, Hungary, etcetera are colored in shades of blue.
Italy is colored brown. France, Germany, Denmark, the Netherlands are colored in shades of yellow.
Portugal is colored purple.
Spain is colored indigo.
Ireland is colored red.
Scotland and Great Britain are colored in shades of pink.
Norway, Sweden, and Denmark are colored in shades of turquoise.

Statistical analysis shows a coordinate plane with mutually perpendicular axes. the vertical axis is labeled P C 1 and the

horizontal axis is labeled P C 2. The axes are slightly tilted to the left. Scatterplots on the plane roughly reproduce the map of Europe.

Return to FIGURE 1.25 Genomic information can confirm locations of ancestry

Extended description for FIGURE 1.26 The human microbiome comprises many different bacterial and fungal species



© Macmillan Learning

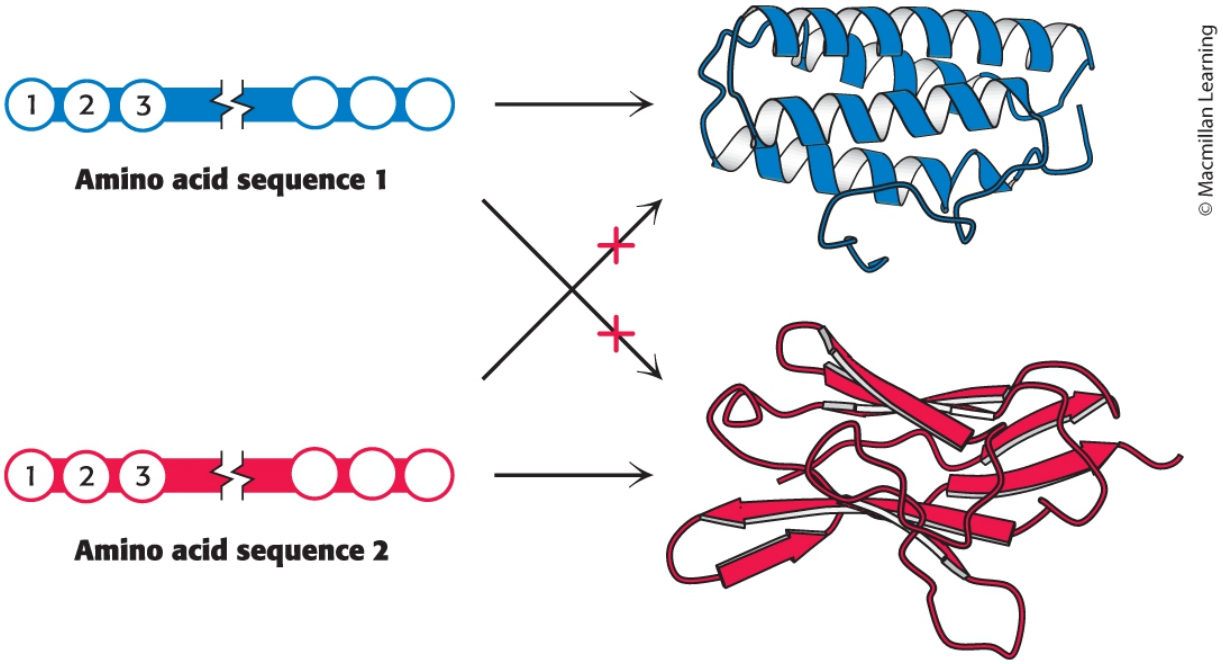
A large circle contains a smaller circle in its center. The smaller circle is labeled Core human microbiome. The periphery of the larger sphere is labeled Variable human microbiome. Double-

headed arrows between the central circle and the periphery of the large circle represent factors that influence the microbiome and are as follows:

Host lifestyle
Host genotype
Host physiology
Host immune system
Transient community members
Host environment
Host pathology

Return to FIGURE 1.26 The human microbiome comprises many different bacterial and fungal species

Extended description for FIGURE 1.27 Protein folding is primarily dictated by the specific sequence of amino acids



© Macmillan Learning

Two different amino acid sequences are shown. Amino acid sequence 1 is shown as a blue-colored linear chain of several amino acids. The three-dimensional structure of the protein with this amino acid sequence is shown as a few tightly coiled blue ribbons connected end-to-end by thread-like structures.

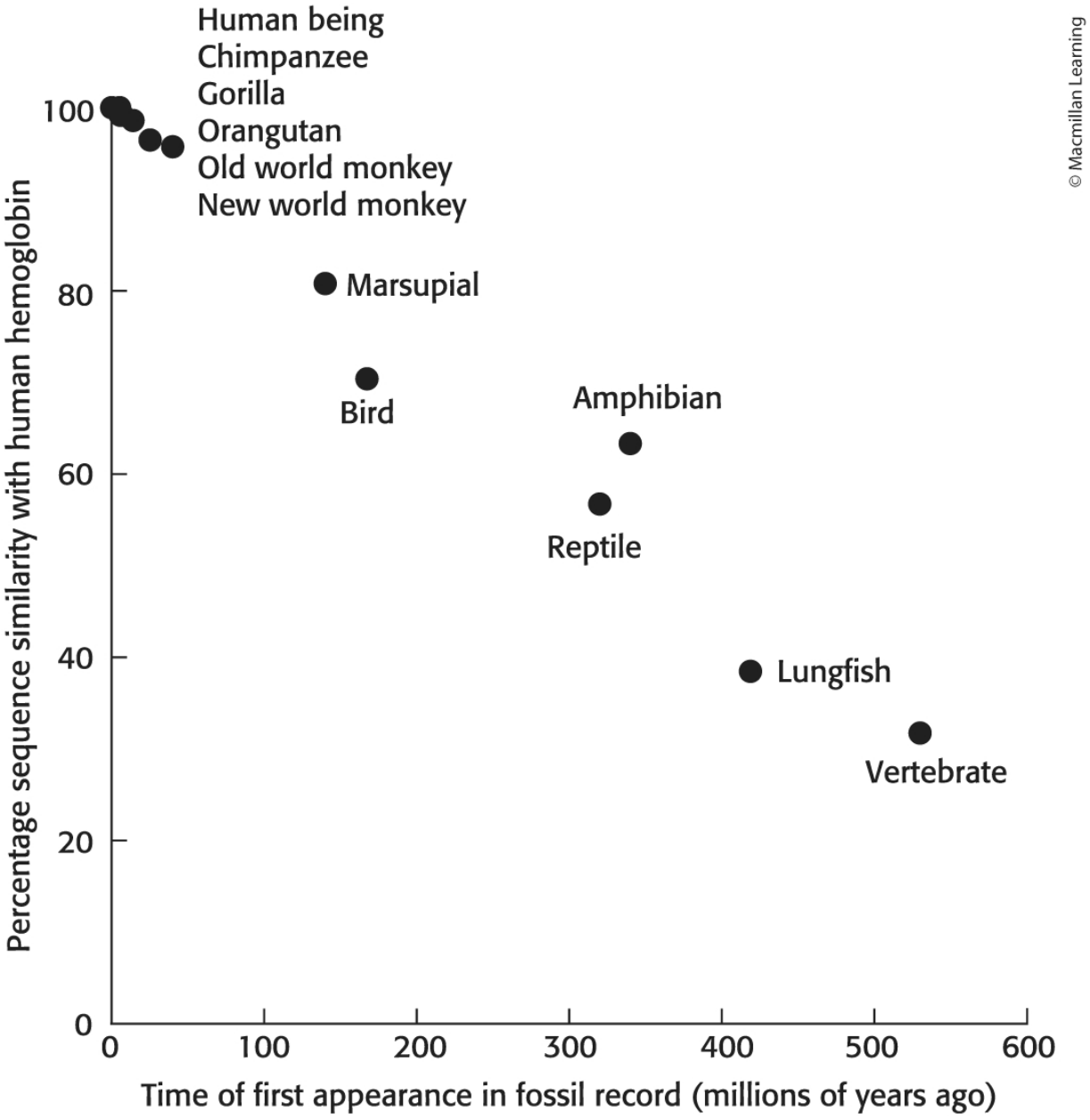
Amino acid sequence 2 is shown as a red-colored linear chain of several amino acids. The three-dimensional structure of the protein with this amino acid sequence is shown as a few thick red arrows connected end-to-end by thread-like structures.

Amino acid sequence 1 cannot give rise to the protein structure in red. Similarly, amino acid sequence 2 cannot give rise to the protein

structure in blue.

Return to FIGURE 1.27 Protein folding is primarily dictated by the specific sequence of amino acids

Extended description for FIGURE 1.28 The similarities between hemoglobin sequences from different species provide evidence for a molecular clock



© Macmillan Learning

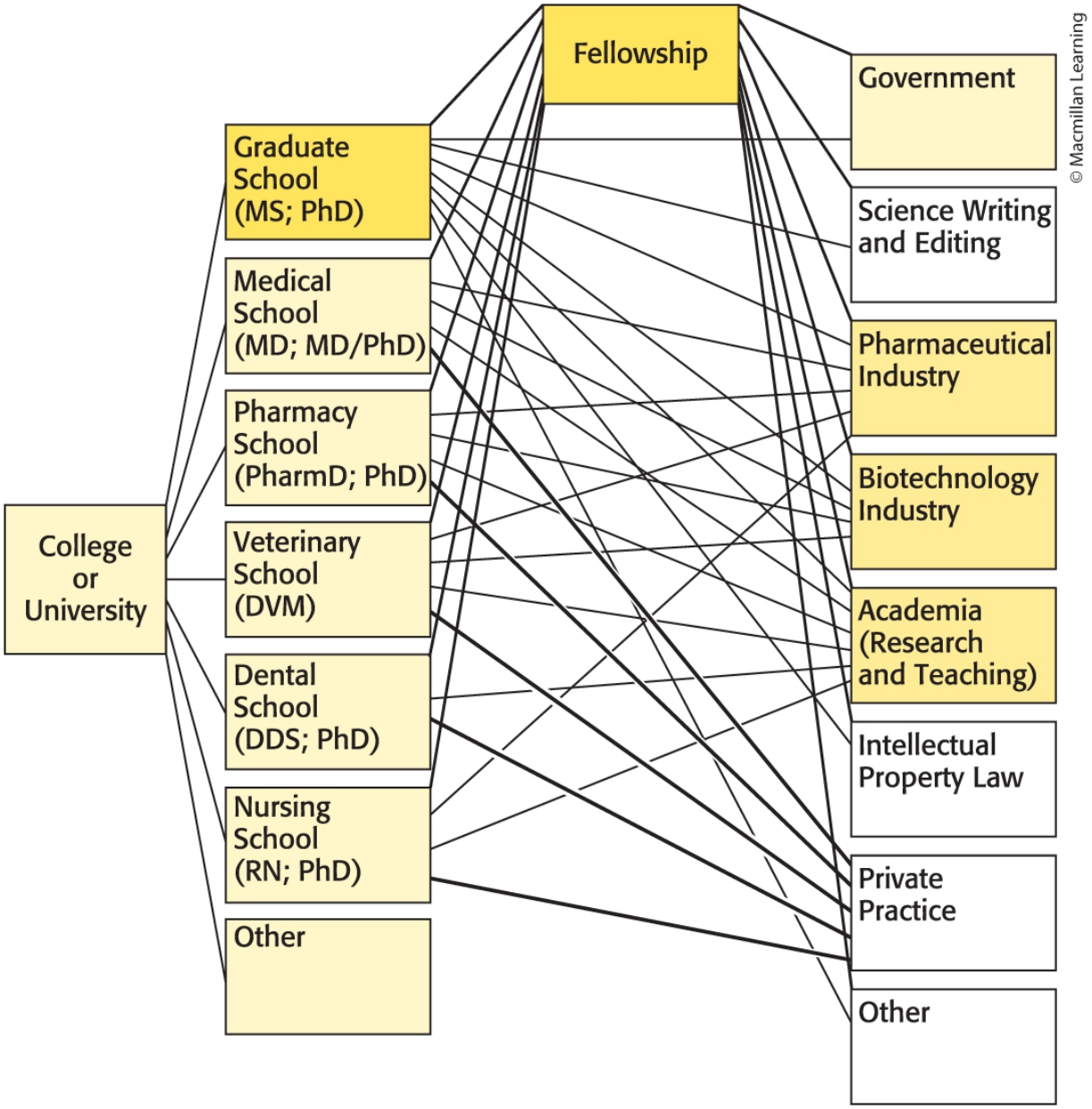
The horizontal axis is labeled Time of first appearance in fossil record (millions of years ago) and ranges from 0 to 600 in

increments of 100 units. The vertical axis is labeled Percentage sequence similarity with human hemoglobin and ranges from 0 to 100 in increments of 20 units. the plot points are as follows:

1. Human being, Chimpanzee, Gorilla, Orangutan, Old world monkey, and New world monkey: Ranging from (0, 100) to (60, 95)
2. Marsupial: (150, 80)
3. Bird: (170, 70)
4. Reptile: (320, 55)
5. Amphibian: (340, 63)
6. Lungfish: (410, 38)
7. Vertebrate: (520, 35)

Return to FIGURE 1.28 The similarities between hemoglobin sequences from different species provide evidence for a molecular clock

Extended description for FIGURE 1.29 There are a variety of possible career paths for those involved in biochemical research



A box labeled College or University (pale yellow) is connected to 7 boxes as follows:

Graduate School (M S; P h D) (dark yellow)
Medical School (M D; M D and P h D) (pale yellow)
Pharmacy School (Pharm D; P h D) (pale yellow)
Veterinary School (D M V) (pale yellow)
Dental school (D D S; P h D) (pale yellow)
Nursing School (R N; P h D) (pale yellow)
Other (pale yellow)

The first 6 of the 7 boxes above are connected to a box labeled Fellowship (dark yellow). Fellowship is connected to 8 boxes as follows:

Government (pale yellow)
Science Writing and Editing (white)
Pharmaceutical Industry (light yellow)
Biotechnology Industry (light yellow)
Academia (Research and Training) (light yellow)
Intellectual Property Law (white)
Private Practice (white)
Other (white)

Graduate School (M S; P h D) is connected to Government, Science Writing and Editing, Pharmaceutical Industry, Biotechnology Industry, Academia (Research and Training), Intellectual Property Law, and Other.

Medical School is connected to Pharmaceutical Industry, Biotechnology Industry, Academia (Research and Training), and Private Practice.

Pharmacy School is connected to Pharmaceutical Industry, Biotechnology Industry, Academia (Research and Training), and Private Practice.

Veterinary School is connected to Pharmaceutical Industry, Biotechnology Industry, Academia (Research and Training), and Private Practice.

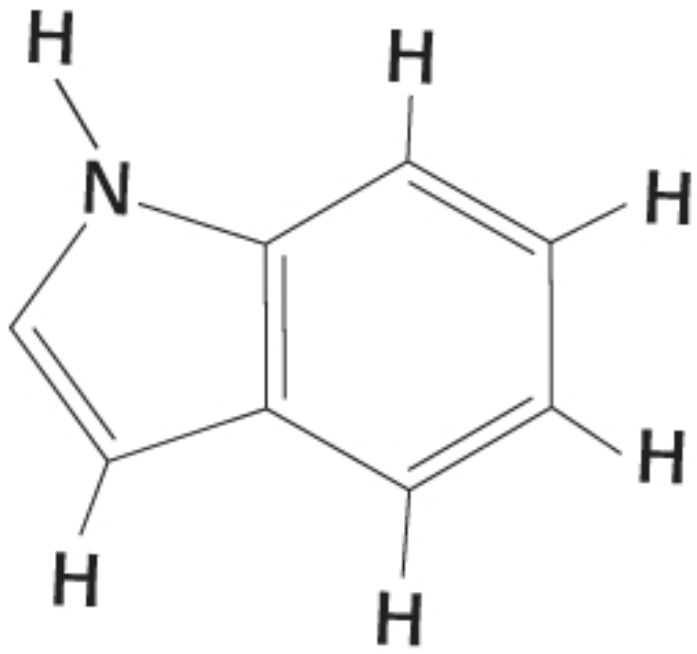
Dental School is connected to Academia (Research and Training) and Private Practice.

Nursing School is connected to Pharmaceutical Industry, Academia (Research and Training), and Private Practice.

The intensity of the yellow shading corresponds to the intensity of the biochemical research activity.

Return to FIGURE 1.29 There are a variety of possible career paths for those involved in biochemical research

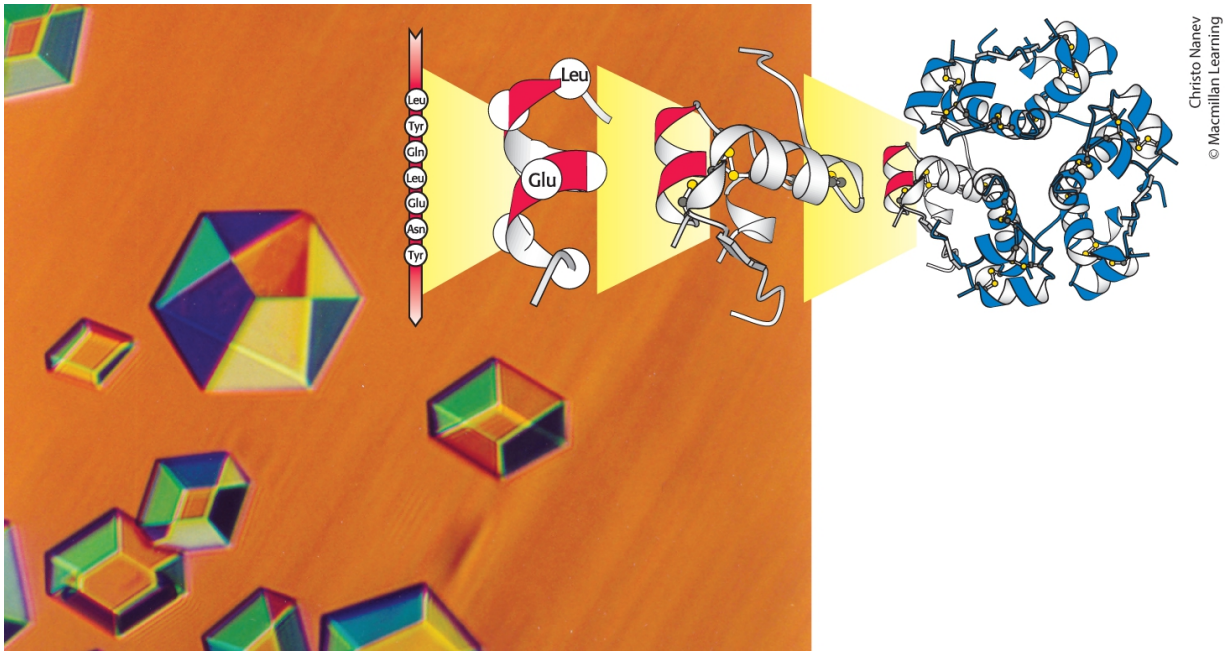
Extended description for Fused structure of a benzene ring with a 5-membered heterocyclic ring



A benzene ring is in a vertical orientation and consists of 3 alternating double bonds between C 1 and C 2, C 3 and C 4, and C 5 and C 6. C 1, C 2, C 3, and C 4 are each single bonded to H. The benzene ring is fused to a 5-membered heterocyclic ring in a horizontal orientation which consists of 1 N and 4 C atoms. The N atom occupies the first position, which is the top-right vertex. A double bond is present between C 1 and C 2 and C 3 and C 4. C 3 and N are each single bonded to H. The two rings are fused to each other such that C 1 and C 2 of the 5-membered ring are the C 6 and C 5 of the benzene ring, respectively.

Return to Fused structure of a benzene ring with a 5-membered heterocyclic ring

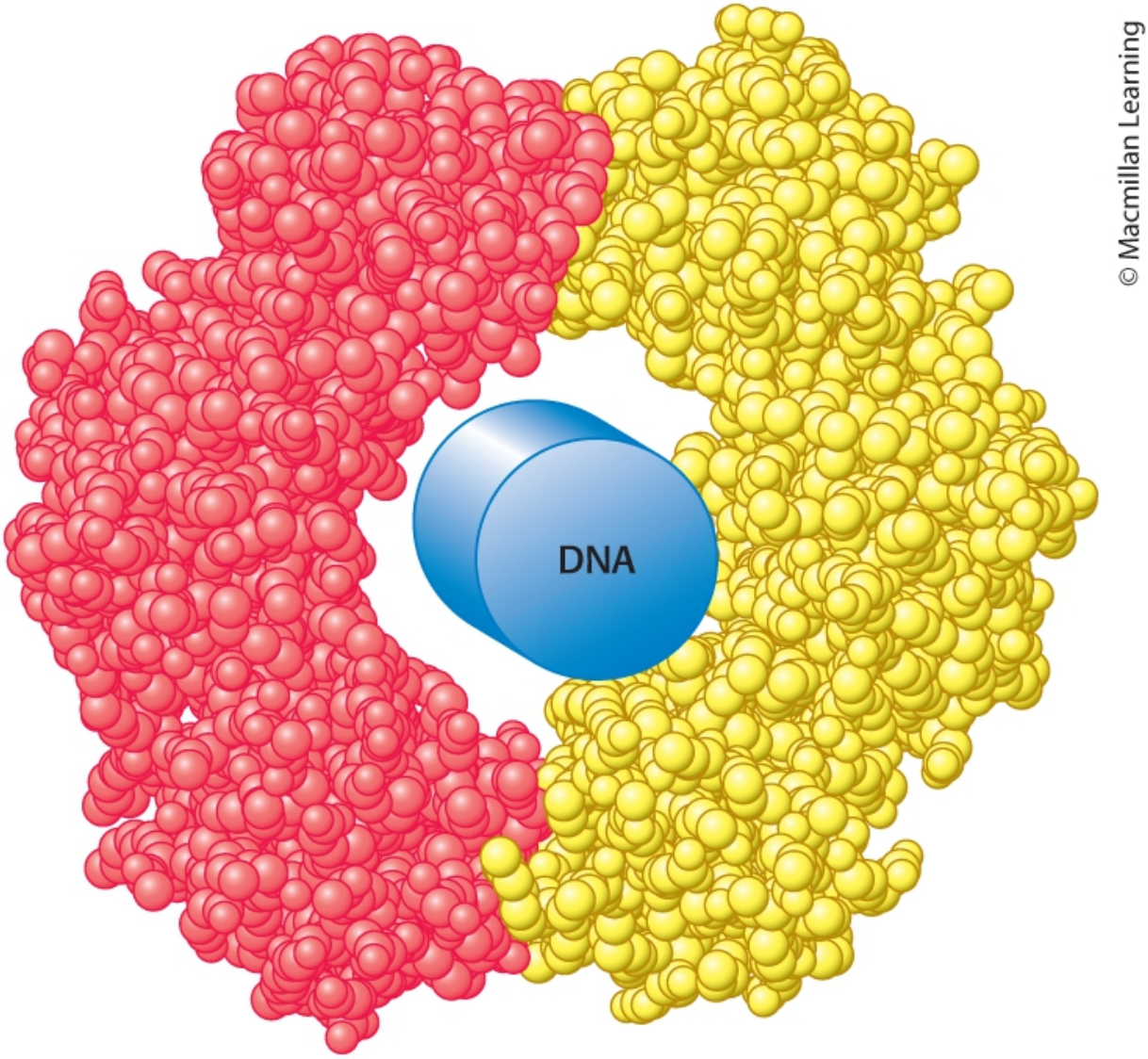
Extended description for Types of insulin structure



The primary structure illustrates the peptide sequence. The secondary structure illustrates the formation of alpha helices. The tertiary structure shows the alpha helices held together forming a three-dimensional unit. The quaternary structure shows three such units coming together.

Return to Types of insulin structure

Extended description for FIGURE 2.1 The structure of a protein determines its function

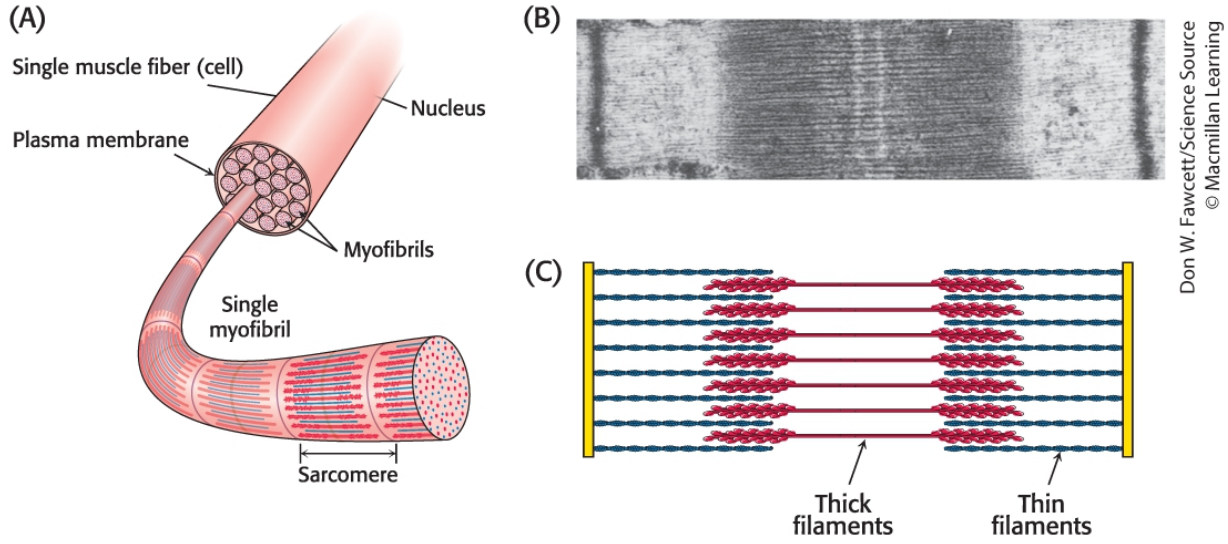


© Macmillan Learning

A rod-shaped structure labeled D N A is surrounded by a ring shaped-protein made up of multiple small spheres. Half of the ring on the left is colored red, and the other half on the right is colored yellow.

Return to FIGURE 2.1 The structure of a protein determines its function

Extended description for FIGURE 2.2 Some proteins form complex assemblies



Part (A): A single muscle fiber (cell) is magnified. It is a multinucleate cell surrounded by a cell membrane and contains numerous myofibrils. A magnified view of a myofibril shows it to be a highly ordered assemblage of thick myosin and thin actin filaments. One short unit of myofibril is labeled sarcomere. The cross-section of the myofibril near the middle of a sarcomere shows how actin and myosin filaments are organized in three dimensions. Each myofibril is formed by many such contracting sarcomere units.

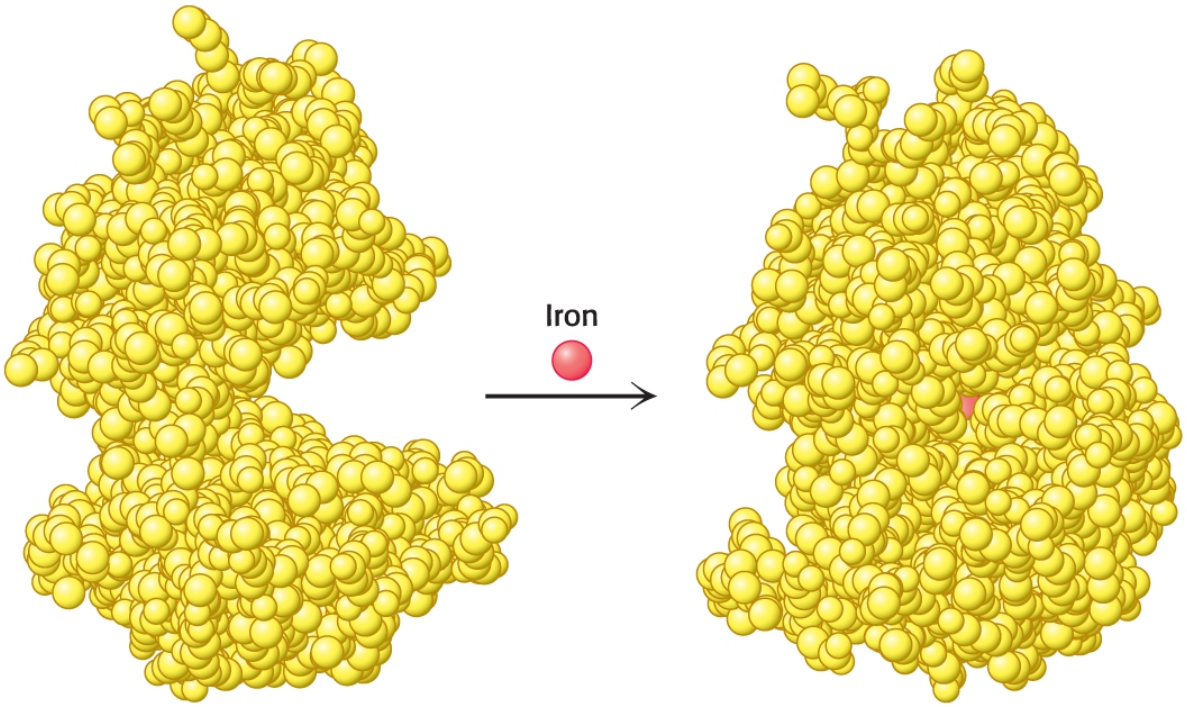
Part (B): The micrograph shows a thin light gray vertical strip in the middle flanked by two thick dark gray regions on both sides. The dark gray regions are followed by a thick light region which is followed by a thin dark gray line.

Part (C): The structure of a single sarcomere is represented as a two-dimensional line diagram. Two parallel vertical yellow bars are shown some distance apart. Blue parallel horizontal lines labeled

thin filaments extend from the yellow bars toward the middle. Parallel horizontal red lines labeled thick filaments are illustrated in the middle section. Small grape-like red structures emerge from the ends of the thick filaments and extend partially into the space between two adjacent thin filaments.

Return to FIGURE 2.2 Some proteins form complex assemblies

Extended description for FIGURE 2.3 Conformational changes allow flexibility in protein function

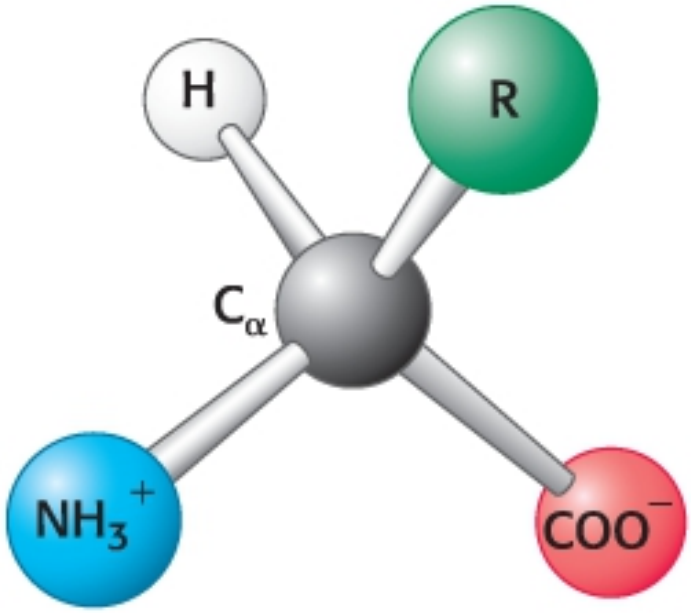


© Macmillan Learning

The starting 3-dimensional structure of the protein is illustrated to be roughly a C-shape. Upon binding of iron, represented by a red sphere, the protein undergoes a conformational change. The resultant 3-dimensional structure of the protein loses its C-shape with the iron atom at the center.

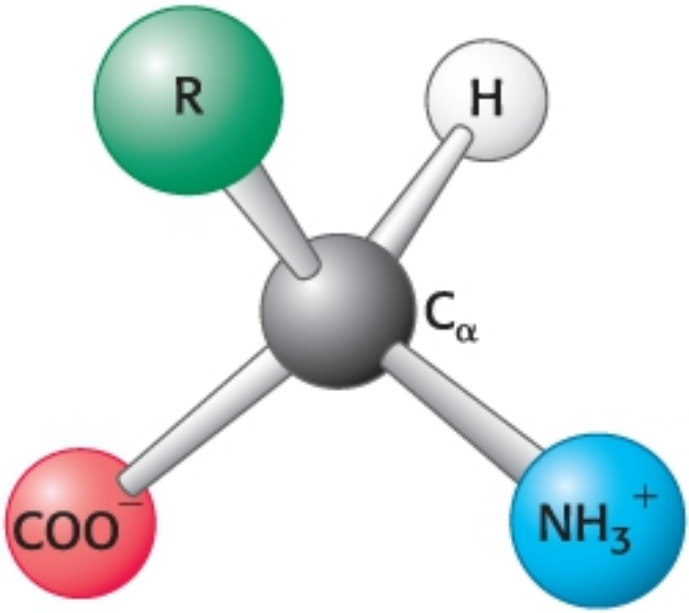
Return to FIGURE 2.3 Conformational changes allow flexibility in protein function

Extended description for FIGURE 2.4 The l and d isomers of amino acids are mirror images of each other



© Macmillan Learning

L isomer



D isomer

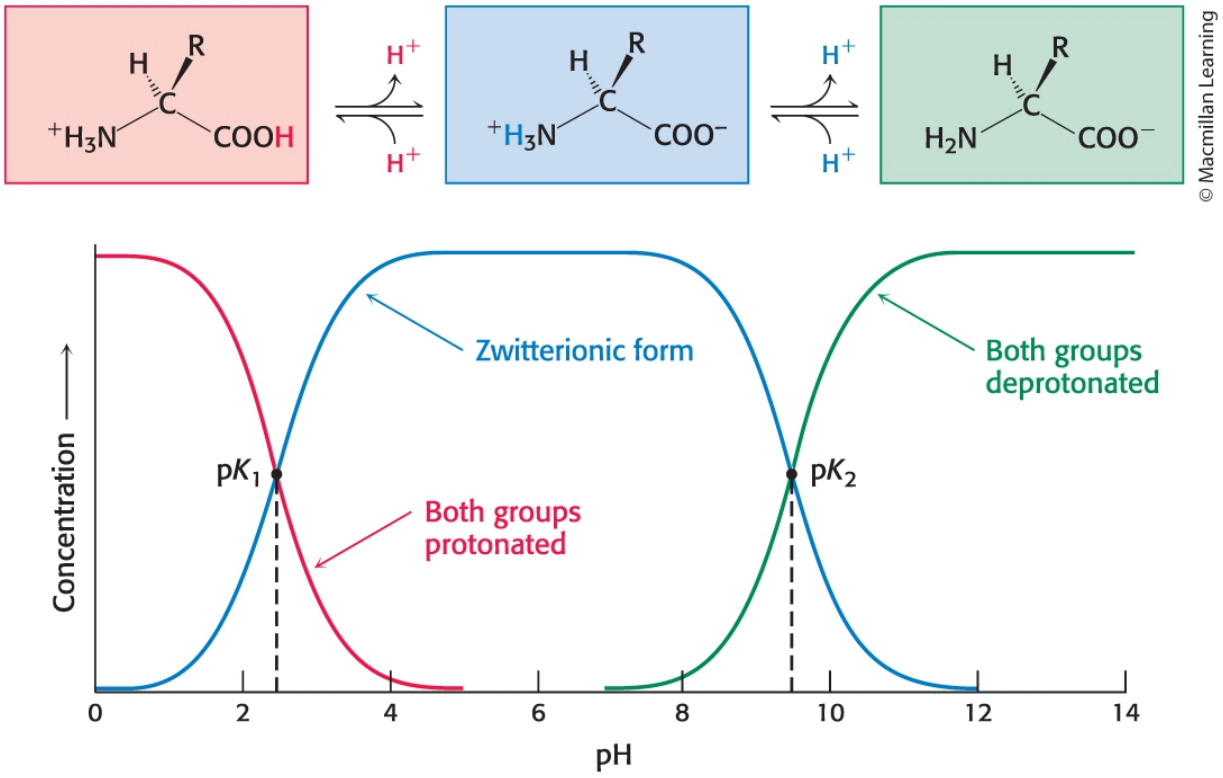
In the ball-and-stick model, the C alpha atom is depicted as a black sphere. N H 3 superscript plus ion is depicted as a blue sphere. R group is depicted as a green sphere. H atom is depicted as a small white sphere. C O O superscript minus ion is depicted as a red sphere.

The structure of the L isomer is as follows: A central C alpha atom is connected to an H atom on the upper left, R group on the upper right, N H 3 superscript plus on the lower left, and C O O superscript minus on the lower right. The R group and N H 3 superscript plus are toward the observer. The H atom is away from the observer.

The structure of the D isomer is as follows: A central C alpha atom is connected to the R group on the upper left, H atom on the upper right, C O O superscript minus on the lower left, and N H 3 superscript plus on the lower right. The R group and N H 3 superscript plus are toward the observer. The H atom is away from the observer.

Return to FIGURE 2.4 The l and d isomers of amino acids are mirror images of each other

Extended description for FIGURE 2.5 The ionization state of amino acids is altered by changes in pH



© Macmillan Learning

Within a red box, the following structure is illustrated: A central C atom is single bonded to C O O H on the lower right, N H 3 superscript plus on the lower left, dash bonded to H on the upper left, and wedge bonded to R on the upper right. H atom in C O O H is highlighted in red. A double-headed equilibrium arrow directs to a blue box from the red box. Loss of two H superscript plus ions takes place in the process.

Within the blue box, the following structure is illustrated: A central C atom is single bonded to C O O superscript minus on the lower right, N H 3 superscript plus on the lower left, dash bonded to H on the upper left, and wedge bonded to R on the upper right. H atom in

N H 3 is highlighted in blue. A double-headed equilibrium arrow directs to a green box from the blue box. Loss of two H superscript plus ions takes place in the process.

Within the green box, the following structure is illustrated: A central C atom is single bonded to C O O superscript minus on the lower right, N H 2 on the lower left, dash bonded to H on the upper left, and wedge bonded to R on the upper right.

The corresponding graph below plots the relative concentration of the three ionization states with changing p H. The horizontal axis is labeled p H and ranges from 0 to 14 in increments of 2 units. The vertical axis is labeled concentration and increases from bottom to top.

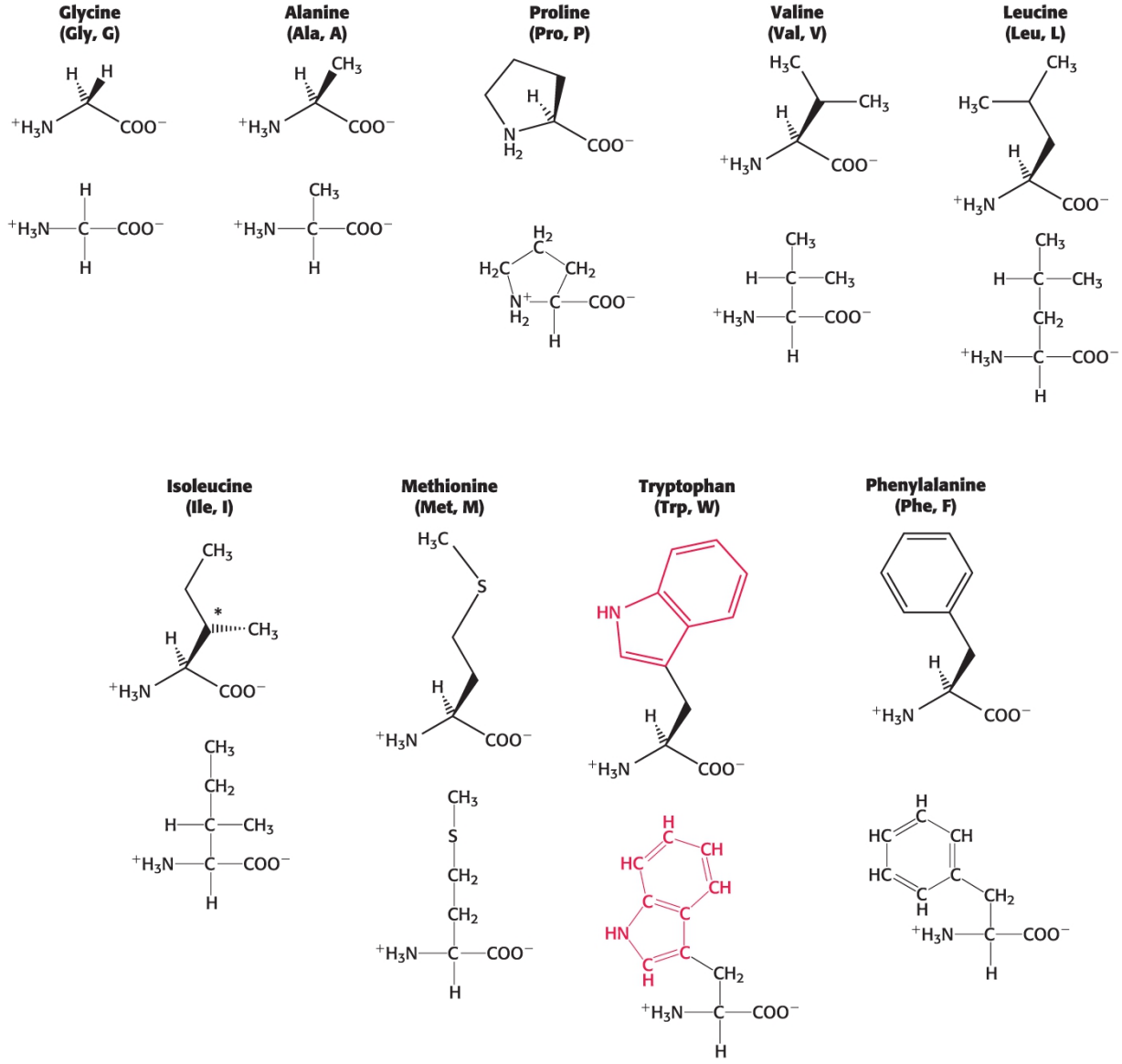
A red curve labeled both groups protonated starts from the top of the vertical axis at p H 0 and gradually moves down to 0 at p H 5. A blue curve labeled zwitterionic form starts from the origin, moves to the right, and rises to the top of the vertical axis at p H 4, stays constant till p H 8, and gradually drops to 0 at p H 12.

A green curve labeled both groups deprotonated starts from the horizontal axis at p H 5, moves to the right and gradually rises to the top of the vertical axis at p H 12, and remains constant till p H 14.

The point of the intersection of the red and the blue curves at the midpoint of the vertical axis at p H 2.5 is labeled p K subscript 1. The point of the intersection of the green and the blue curves at the midpoint of the vertical axis at p H 9.5 is labeled p K subscript 2.

Return to FIGURE 2.5 The ionization state of amino acids is altered by changes in pH

Extended description for FIGURE 2.6 The hydrophobic amino acids have nonpolar R groups



Glycine (G l y, G): Arrangement of bonds: A central C atom is wedge bonded to H on the upper right, dash bonded to H on the upper left, single bonded to N H 3 superscript plus on the lower left, and single bonded to C O O superscript minus on the lower right. Fischer projection: A central C atom is single bonded to H above and H

below, C O O superscript minus on the right, and N H 3 superscript plus on the left. Alanine (A l a, A): Arrangement of bonds: A central C atom is wedge bonded to C H 3 on the upper right, dash bonded to H on the upper left, single bonded to N H 3 superscript plus on the lower left, and single bonded to C O O superscript minus on the lower right. Fischer projection: A central C atom is single bonded to C H 3 above, H below, C O O superscript minus on the right, and N H 3 superscript plus on the left.

Proline (P r o, P): Arrangement of bonds: A 5-membered heterocyclic pentagonal ring is in a vertical orientation and consists of 1 N and 4 C atoms. The N atom bound to H 2 occupies the first position, which is the bottom left vertex. C 3 is wedge bonded to C 4. C 4 is dash bonded to H on the upper left and single bonded to C O O superscript minus on the lower right. Fischer projection: A 5-membered heterocyclic pentagonal ring is in a vertical orientation and consists of 1 N and 4 C atoms. The N atom bound to H 2 and carrying a positive charge occupies the first position, which is the bottom left vertex, and C atoms occupy the remaining positions. C 1, C 2, and C 3 are each bound to H 2. C 4 is single bonded to C O O superscript minus on the right and H below.

Valine (V a l, V): Arrangement of bonds: A central C atom is wedge bonded to C 2 of a 3-carbon alkane chain on the upper right, dash bonded to H on the upper left, single bonded to N H 3 superscript plus on the lower left, and single bonded to C O O superscript minus on the lower right. Fisher projection: A central C atom is single bonded to H below, C O O superscript minus on the right, N H 3 superscript plus on the left, and C above. The C above is single bonded to H on the left and C H 3 above and C H 3 on the right.

Leucine (L e u, L): Arrangement of bonds: A central C atom is wedge bonded to C 1 of a 3-carbon alkane chain on the upper right, dash bonded to H on the upper left, single bonded to N H 3 superscript

plus on the lower left, and single bonded to C O O superscript minus on the lower right. C 2 of the alkane chain in single bonded to C H 3 on the upper right. Fisher projection: A central C atom is single bonded to H below, C O O superscript minus on the right, N H 3 superscript plus on the left, and C H 2 above. C of the C H 2 above is single bonded to a central C atom above. The central C atom above is single bonded to H on the left, C H 3 above and C H 3 on the right.

Isoleucine (I l e, I): Arrangement of bonds: A central C atom is wedge bonded to C 1 of a 2-carbon alkane chain depicted as a line structure using 1 line on the upper right, dash bonded to H on the upper left, single bonded to N H 3 superscript plus on the lower left, and single bonded to C O O superscript minus on the lower right. C 1 of the alkane chain is marked with an asterisk and dash bonded to C H 3 on the right. C 2 of the alkane chain is single bonded to C H 3 on the upper right. Fisher projection: A central C atom is single bonded to H below, C O O superscript minus on the right, N H 3 superscript plus on the left, and a central C atom above. The central C atom above is single bonded to H on the left, C H 2 above, and C H 3 on the right. The C H 2 above is single bonded to C H 3 above.

Methionine (M e t, M): Arrangement of bonds: A central C atom is wedge bonded to C 1 of a 2-carbon alkane chain depicted as a line structure using 1 line on the upper right, dash bonded to H on the upper left, single bonded to N H 3 superscript plus on the lower left, and single bonded to C O O superscript minus on the lower right. C 2 of the alkane chain is single bonded to S on the upper right which is single bonded to C H 3 on the upper left. Fischer projection: C H 3, single bond, S, single bond, C H 2, single bond, C H 2, single bond, C, single bond, H in a vertical manner. C 4 is single bonded to N H 3 superscript plus on the left and C O O superscript minus on the right.

Tryptophane (T r p, W): Arrangement of bonds: A central C atom is wedge bonded to C H 2 on the upper right, dash bonded to H on the upper left, single bonded to N H 3 superscript plus on the lower left, and single bonded to C O O superscript minus on the lower right. C H 2 is single bonded to C 3 of 5-membered heterocyclic pentagonal ring in a vertical orientation on the upper left consisting of 1 N and 4 C atoms. The N atom bound to H occupies the first position, which is the top left vertex. A double bond is present between C 3 and C 4. The pentagonal ring is fused to a benzene ring in a horizontal orientation with C 1 occupying the rightmost vertex. The benzene ring contains alternating double bonds between C 1 and C 2, C 3 and C 4, and C 5 and C 6. The two rings are fused together such that C 1 and C 2 of the pentagonal ring are C 4 and C 3 of the benzene ring, respectively. The two rings are shown in red. Fisher projection: A central C atom is single bonded to H below, C O O superscript minus on the right, N H 3 superscript plus on the left, and C H 2 above. C in the C H 2 above is single bonded to C 3 of a 5-membered heterocyclic pentagonal ring in a vertical orientation on the upper left consisting of 1 N and 4 C atoms. The N atom bound to H occupies the first position, which is the top left vertex, and C atoms occupy the remaining positions. C 4 is bound to H and double bonded to C 3. The pentagonal ring is fused to a benzene ring in a horizontal orientation with a C atom occupying each vertex. C 1, C 4, C 5, and C 6 are each bound to H. The ring contains alternating double bonds between C 2 and C 3, C 4 and C 5, and C 6 and C 1. The two rings are fused together such that C 1 and C 2 of the pentagonal ring are C 4 and C 3 of the benzene ring, respectively. The two rings are shown in red.

Phenylalanine (P h 2, F): Arrangement of bonds: A central C atom is wedge bonded to C H 2 on the upper right, dash bonded to H on the upper left, single bonded to N H 3 superscript plus on the lower left, and single bonded to C O O superscript minus on the lower right. C H 2 is single bonded to C 2 of a benzene ring in a horizontal

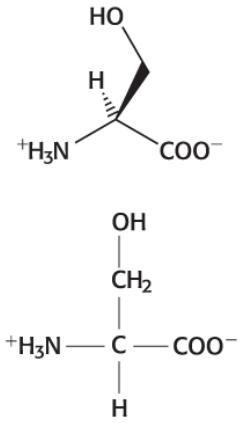
orientation with C 1 occupying the rightmost vertex. The ring contains alternating double bonds between C 1 and C 2, C 3 and C 4, and C 5 and C 6. Fischer projection: A central C atom is single bonded to H below, C O O superscript minus on the right, N H 3 superscript plus on the left, and a C H 2 above. The C H 2 above is single bonded to C 3 of a benzene ring in a vertical orientation with C 1 occupying the topmost vertex with a C atom occupying each vertex. C 1, C 2, C 4, C 5, and C 6 are each bound to H. The ring contains alternating double bonds between C 2 and C 3, C 4 and C 5, and C 6 and C 1.

Return to FIGURE 2.6 The hydrophobic amino acids have nonpolar R groups

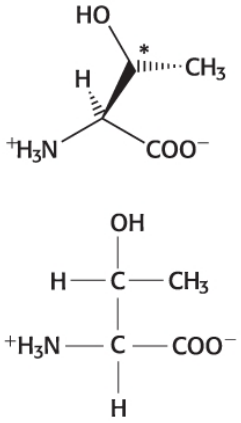
Extended description for FIGURE 2.7 The polar amino acids have polar but uncharged R groups at

physiological pH

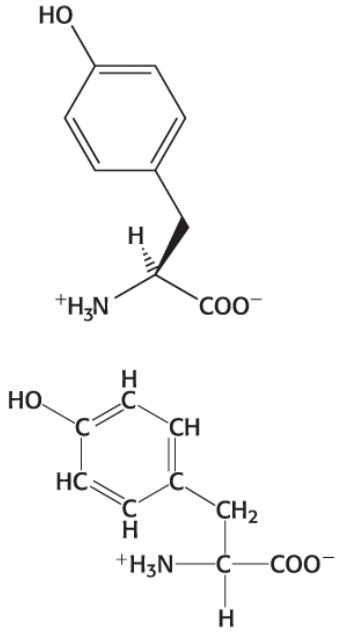
Serine (Ser, S)



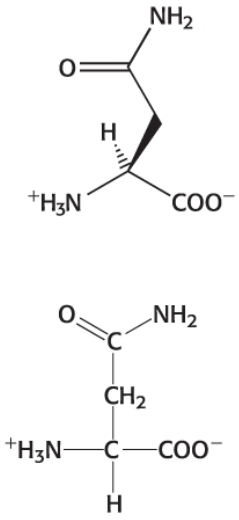
Threonine (Thr, T)



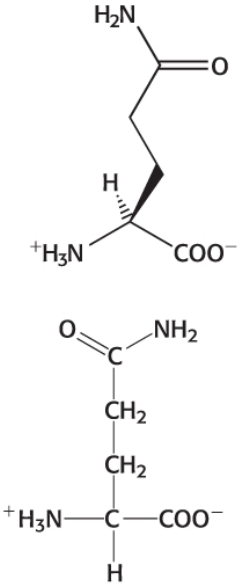
Tyrosine (Tyr, Y)



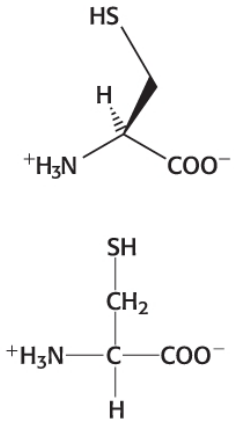
Asparagine (Asn, N)



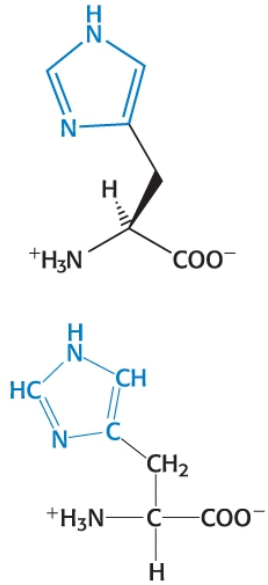
Glutamine (Gln, Q)



Cysteine (Cys, C)



Histidine (His, H)



Serine (S e r, S): Arrangement of bonds: A central C atom is wedge bonded to C H 2 on the upper right, dash bonded to H on the upper left, single bonded to N H 3 superscript plus on the lower left, and single bonded to C O O superscript minus on the lower right. C H 2 is single bonded to O H on the upper left. Fischer projection: A central C atom is single bonded to H below, single bonded to N H 3 superscript plus on the left, single bonded to C H 2 above, and single bonded to C O O superscript minus on the right. C H 2 is single bonded to O H above.

Threonine (T h r, T): Arrangement of bonds: A central C atom is wedge bonded to C H on the upper right marked with an asterisk, dash bonded to H on the upper left, single bonded to N H 3 superscript plus on the lower left, and single bonded to C O O superscript minus on the lower right. C H is single bonded to O H on the upper left and dash bonded to C H 3 on the right. Fischer projection: A central C atom is single bonded to H below, single bonded to N H 3 superscript plus on the left, single bonded to a central C atom above, and single bonded to C O O superscript minus on the right. The C atom above is single bonded to O H above, single bonded to H on the left, and single bonded to C H 3 on the right.

Tyrosine (T y r, Y): Arrangement of bonds: A central C atom is wedge bonded to C H 2 on the upper right, dash bonded to H on the upper left, single bonded to N H 3 superscript plus on the lower left, and single bonded to C O O superscript minus on the lower right. C H 2 is single bonded to C 2 of a benzene ring in a horizontal orientation with C 1 occupying the rightmost vertex. The ring contains alternating double bonds between C 1 and C 2, C 3 and C 4, and C 5 and C 6. C 5 is single bonded to O H. Fischer projection: A central C atom is single bonded to H below, single bonded to N H 3 superscript plus on the left, single bonded to a C H 2 above, and single bonded to C O O superscript minus on the right. The C H 2 above is single bonded to C 3 of a benzene ring in a vertical

orientation with C 1 occupying the topmost vertex and a C atom occupies each vertex. The ring contains alternating double bonds between C 2 and C 3, C 4 and C 5, and C 6 and C 1. C 1, C 2, C 4, C 5, and C 6 are each bound to H. C 5 is single bonded to O H.

Asparagine (A s n, N): Arrangement of bonds: A central C atom is wedge bonded to C 1 of 2-carbon alkane chain depicted as a line structure using one line on the upper right, dash bonded to H on the upper left, single bonded to N H 3 superscript plus on the lower left, and single bonded to C O O superscript minus on the lower right. C 2 of the alkane chain is double bonded to O on the left and single bonded to N H 2 on the upper right. Fisher projection: A central C atom is single bonded to H below, single bonded to N H 3 superscript plus on the left, single bonded to a C H 2 above, and single bonded to C O O superscript minus on the right. The C H 2 above is single bonded to a central C atom above. The central C atom above is double bonded to O on the upper left and single bonded to N H 2 on the upper right.

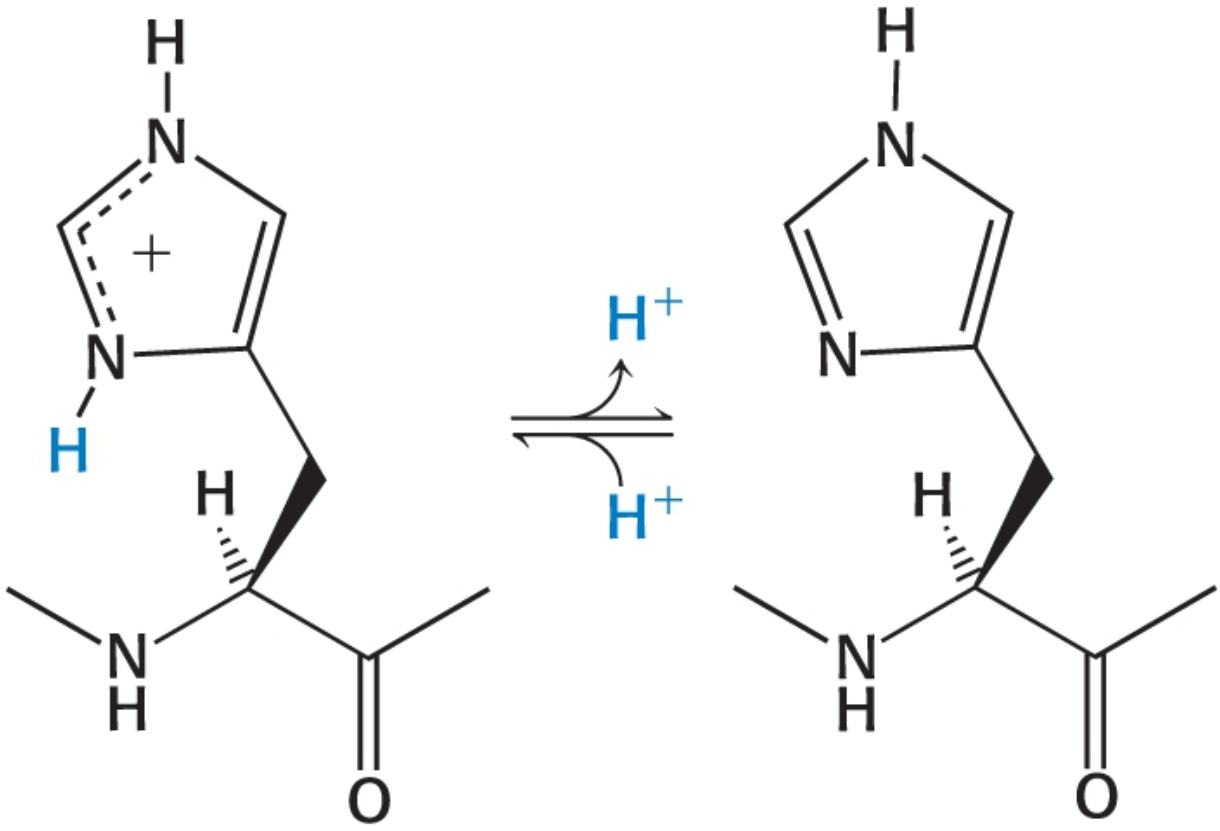
Glutamine (G l n, Q): Arrangement of bonds: A central C atom is wedge bonded to C 1 of 3-carbon alkane chain depicted as a line structure using 2 zigzag lines on the upper right, dash bonded to H on the upper left, single bonded to N H 3 superscript plus on the lower left, and single bonded to C O O superscript minus on the lower right. C 3 of the alkane chain is double bonded to O on the right and single bonded to N H 2 on the upper left. Fisher Projection: A central C atom is single bonded to H below, single bonded to N H 3 superscript plus on the left, single bonded to a C H 2 above, and single bonded to C O O superscript minus on the right. The C H 2 above is single bonded to C H 2 above which is single bonded to a central C atom above. The central C atom above is double bonded to O on the upper left and single bonded to N H 2 on the upper right.

Cysteine (C y s, C): Arrangement of bonds: A central C atom is wedge bonded to C H 2 on the upper right, dash bonded to H on the upper left, single bonded to N H 3 superscript plus on the lower left, and single bonded to C O O superscript minus on the lower right. C H 2 is single bonded to S H on the upper left. Fischer projection: A central C atom is single bonded to H below, single bonded to N H 3 superscript plus on the left, single bonded to a C H 2 above, and single bonded to C O O superscript minus on the right. The C H 2 above is single bonded to S H above.

Histidine (H I s, H): Arrangement of bonds: A central C atom is wedge bonded to C H 2 on the upper right, dash bonded to H on the upper left, single bonded to N H 3 superscript plus on the lower left, and single bonded to C O O superscript minus on the lower right. C H 2 is single bonded to C 3 of a 5-memebered heterocyclic pentagonal ring in a vertical orientation consisting of 2 N and 3 C atoms, on the upper left. The first N atom occupies the first position, which is the bottom left vertex. The second N bound to H occupies the third position, which is the topmost vertex. A double bond is present between the first N and C 1 and C 2 and C 3. Fischer projection: A central C atom is single bonded to H below, single bonded to N H 3 superscript plus on the left, single bonded to a C H 2 above, and single bonded to C O O superscript minus on the right. The C H 2 above is single bonded to C 3 of a 5-memebered heterocyclic pentagonal ring in a vertical orientation consisting of 2 N and 3 C atoms, on the upper left. The first N atom occupies the first position, which is the bottom left vertex. The second N bound to H occupies the third position, which is the topmost vertex, and the C atoms occupy the remaining positions. C 1 and C 2 are each bound to H. A double bond is present between the first N and C 1 and C 2 and C 3.

Return to FIGURE 2.7 The polar amino acids have polar but uncharged R groups at physiological pH

Extended description for FIGURE 2.8 Histidine can bind or release protons near physiological pH



The reaction consists of one reactant and one product. The reactant has the following structure: A 1 N and 4 C heteronuclear alkane chain is depicted as a line structure using 4 zigzag lines. The N atom bound to H occupies the second position. C 3 is double bonded to O below. C 2 is dash bonded to H on the upper left and wedge bonded to C H 2 on the upper right. C H 2 is single bonded to C 3 of a 5-memebered heterocyclic pentagonal ring in a vertical orientation on the upper left consisting of 2 N and 3 C atoms. The first N atom single bonded to H occupies the first position, which is the bottom left vertex. H atom is highlighted in blue. The second N atom single bonded to H occupies the third position, which is the topmost

vertex. A double bond is present between C 2 and C 3. A partial double bond is present across the first N atom, C 1, and the second N atom of the ring represented as a dotted line. A plus sign is shown across the dotted line.

An H superscript plus ion highlighted in blue is eliminated in the forward reaction.

The product has the following structure: A 1 N and 4 C heteronuclear alkane chain is depicted as a line structure using 4 zigzag lines. The N atom bound to H occupies the second position. C 3 is double bonded to O below. C 2 is dash bonded to H on the upper left and wedge bonded to C H 2 on the upper right. C H 2 is single bonded to C 3 of a 5-memebered heterocyclic pentagonal ring in a vertical orientation on the upper left consisting of 2 N and 3 C atoms. The first N atom occupies the first position, which is the bottom left vertex. The second N atom single bonded to H occupies the third position, which is the topmost vertex. A double bond is present between the first N atom and C 1 and C 2 and C 3.

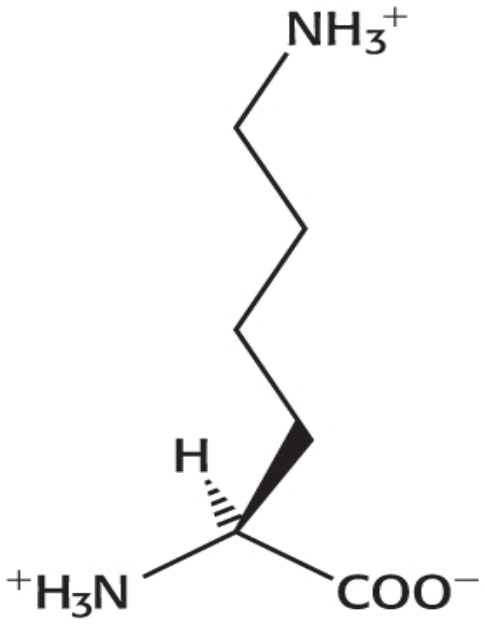
An H superscript plus ion highlighted in blue is added in the backward reaction.

Return to FIGURE 2.8 Histidine can bind or release protons near physiological pH

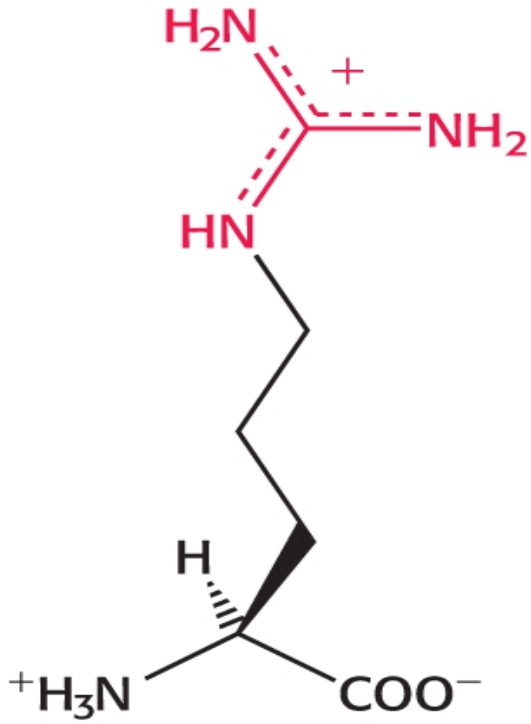
Extended description for FIGURE 2.9 Two amino acids are positively charged at physiological pH. The

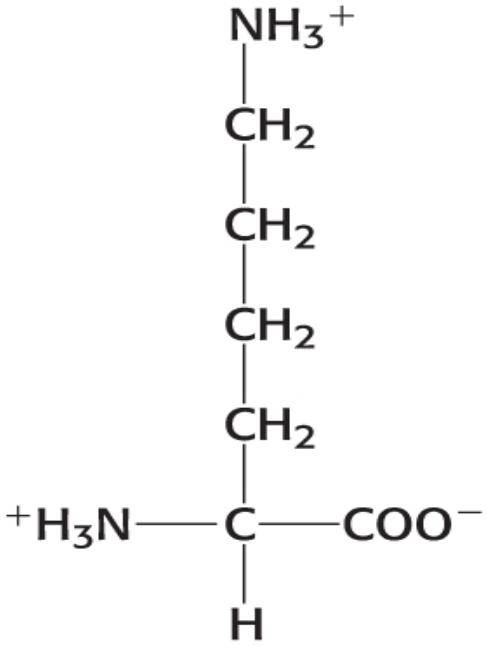
guanidinium group in the arginine side chain is shown in red

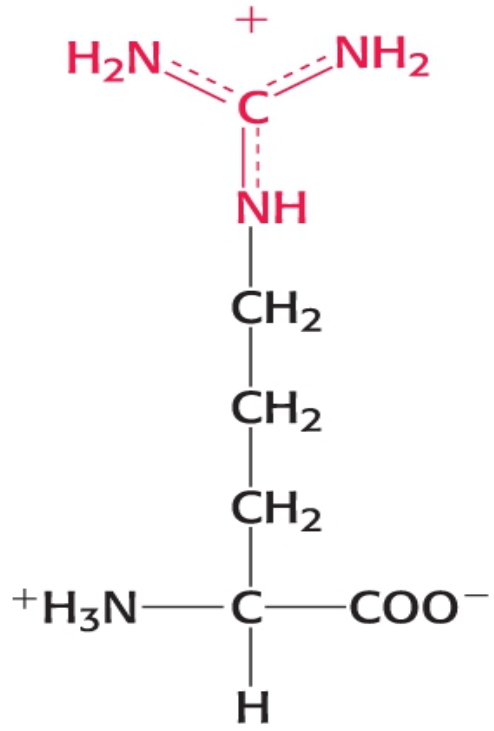
Lysine
(Lys, K)



Arginine
(Arg, R)







The first structure of lysine (L y s, K) is as follows: A 5-carbon alkane chain is depicted as a line structure in vertical orientation using 4 zigzag lines. C 1 is single bonded to N H 3 superscript plus on the upper right. C 4 is wedge bonded to C 5 on the lower left. C 5 is dash bonded to H on the upper left, single bonded to N H 3 superscript plus on the lower left, and single bonded to C O O superscript minus on the lower right.

The second structure of lysine is as follows: N H 3 superscript plus, single bond, C H 2, single bond, C H 2, single bond, C H 2, single bond, C H 2, single bond, C, single bond, H in a vertical orientation. C 5 is single bonded to N H 3 superscript plus on the left and C O O superscript minus on the right.

The first structure of arginine (A r g, R) is as follows: A 1 N and 5 C heteronuclear alkane is depicted as a line structure in vertical orientation using 5 zigzag lines. N occupies the second position and is bound to an H atom. C 1 is single bonded to N H 2 on the right and N H 2 on the upper left. A V-shaped dashed line goes from the N H 2 on the upper left to the N H 2 on the right. A plus sign is present at the center of the dashed line. A dashed line is present between C 1 and the N atom of the alkane chain. The N H 2 groups, dashed lines, plus sign, N H group of the alkane chain are highlighted in red. C 4 is wedge bonded to C 5 on the lower left. C 5 is dash bonded to H on the upper left, single bonded to N H 3 superscript plus on the lower left, and single bonded to C O O superscript minus on the lower right.

The second structure of arginine is as follows: C, single bond, N H, single bond, C H 2, single bond, C H 2, single bond, C H 2, single bond, C, single bond, H in a vertical orientation. C 1 is single bonded to N H 2 on the upper left and single bonded to N H 2 on the upper right. A V-shaped dashed line goes from the N H 2 on the upper left to the N H 2 on the upper right. A plus sign is present at

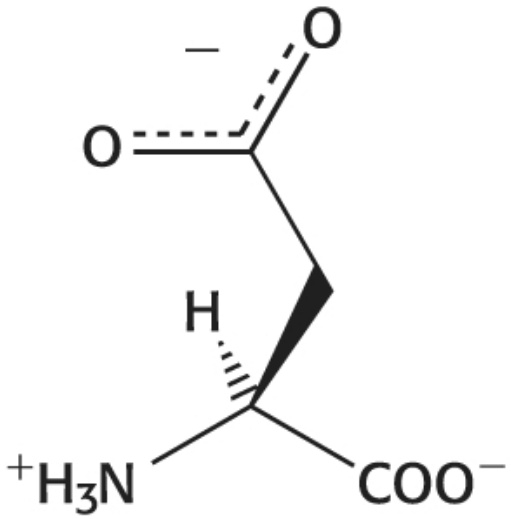
the center of the dashed line. A dashed line is present on the right of the single bond between C 1 and the first N atom of the alkane chain. The N H 2 groups, dashed lines, plus sign, N H group are highlighted in red. C 5 is single bonded to N H 3 superscript plus on the left and single bonded to C O O superscript minus on the right.

Return to FIGURE 2.9 Two amino acids are positively charged at physiological pH. The guanidinium group in the arginine side chain is shown in red

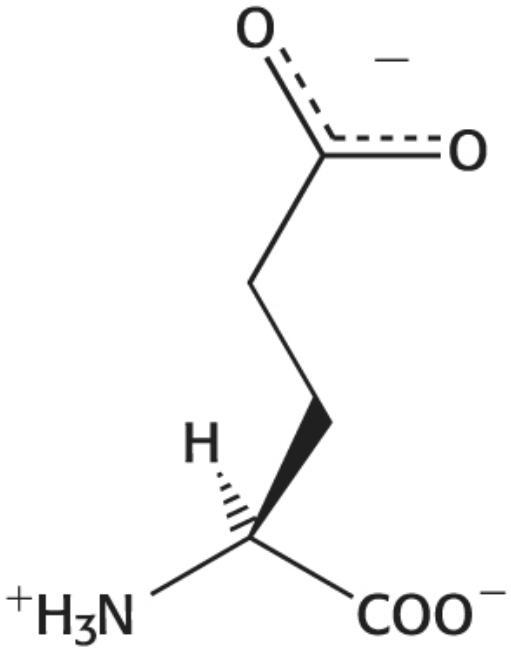
Extended description for FIGURE 2.10 Two amino acids

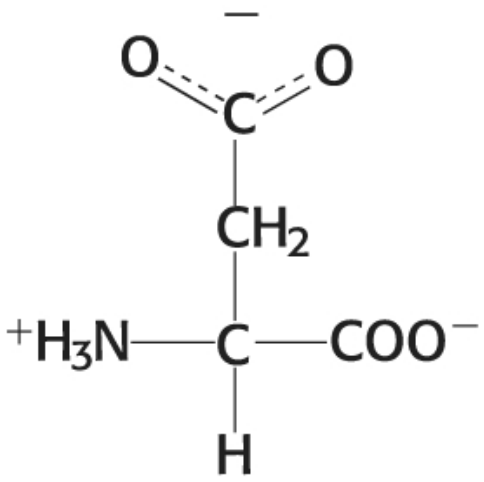
are negatively charged at physiological pH

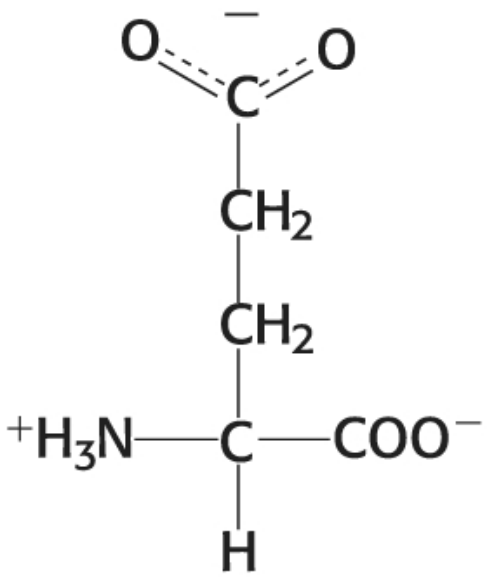
Aspartate (Asp, D)



Glutamate (Glu, E)







The first structure of aspartate (A s p, D) is as follows: A central C atom is single bonded to a C atom on the upper left and wedge bonded to a C atom on the lower left. C on the upper left is single bonded to an O atom on the upper right and O on the left. A V-shaped dashed line connects the two O atoms. A minus symbol is shown between the two O atoms. C on the lower left is dash bonded to H on the upper left, single bonded to N H 3 superscript plus on the lower left and C O O superscript minus on the lower right.

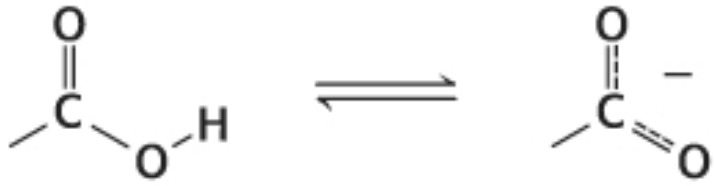
The second structure of aspartate is as follows: C, single bond, C H 2, single bond, C, single bond, H in a vertical orientation. C 1 is single bonded to an O atom on the upper left and upper right. A V-shaped dashed line connects the two O atoms. A minus symbol is shown between the two O atoms. C 3 is single bonded to N H 3 superscript plus on the left and C O O superscript minus on the right.

The first structure of glutamate (G l u, E) is as follows: A 3-carbon alkane chain is depicted as a line structure using 3 zigzag lines in a vertical orientation. C 1 is single bonded to an O atom on the upper left and upper right. A V-shaped dashed line connects the two O atoms. A minus symbol is shown between the two O atoms. C 3 is wedge bonded to a central C atom on lower left. This C atom is dash bonded to H on the upper left, single bonded to N H 3 superscript plus on the lower left and C O O superscript minus on the lower right.

The second structure of glutamate is as follows: C, single bond, C H 2, single bond, C H 2, single bond, C, single bond, H in a vertical orientation. C 1 is single bonded to an O atom on the upper left and upper right. A V-shaped dashed line connects the two O atoms. A minus symbol is shown between the two O atoms. C 4 is single bonded to N H 3 superscript plus on the left and C O O superscript minus on the right.

Return to FIGURE 2.10 Two amino acids are negatively charged at physiological pH

Extended description for Ionization of an alpha-carboxyl group.

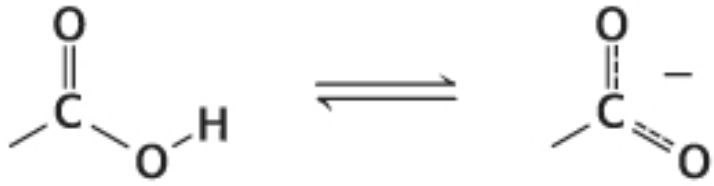


The reaction consists of one reactant and one product. The reactant has the following structure: A central C atom is single bonded to O on the lower right and double bonded to O above. The C atom has an open single bond on the lower left. The O atom on the lower right is single bonded to H on the upper right.

The product has the following structure: A central C atom is single bonded to O on the lower right and single bonded to O above. The C atom has an open single bond on the lower left. A dashed line is present between C and O on the lower right and C and O above. A minus sign is present adjacent to this dashed line.

Return to Ionization of an alpha-carboxyl group.

Extended description for Ionization of an alpha-carboxyl group.

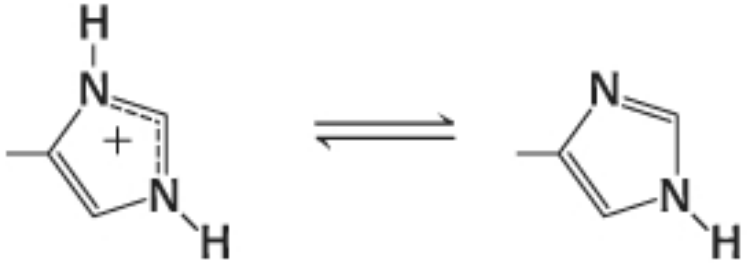


The reaction consists of one reactant and one product. The reactant has the following structure: A central C atom is single bonded to O on the lower right and double bonded to O above. The C atom has an open single bond on the lower left. The O atom on the lower right is single bonded to H on the upper right.

The product has the following structure: A central C atom is single bonded to O on the lower right and single bonded to O above. The C atom has an open single bond on the lower left. A dashed line is present between C and O on the lower right and C and O above. A minus sign is present adjacent to this dashed line.

Return to Ionization of an alpha-carboxyl group.

Extended description for Ionization of a histidine amino acid

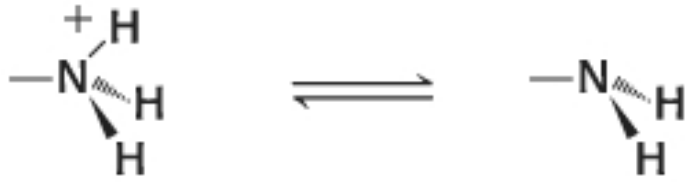


The reaction consists of one reactant and one product. The reactant has the following structure: A 5-membered heterocyclic pentagonal is in a vertical orientation and consists of 2 N and 3 C atoms. The first N atom is single bonded to H and occupies the first position, which is the topmost vertex. The second N atom is single bonded to H and occupies the third position, which is the bottom right vertex. C 2 is double bonded to C 3. A partial double bond is present across the first N, C 1, and the second N. C 3 has an open single bond on the left. A positive charge is shown inside the ring.

The product has the following structure: A 5-membered heterocyclic pentagonal is in a vertical orientation and consists of 2 N and 3 C atoms. The first N atom occupies the first position, which is the topmost vertex. The second N atom is single bonded to H and occupies the third position, which is the bottom right vertex. A double bond is present between the first N atom and C 1 and C 2 and C 3. C 3 has an open single bond on the left.

Return to Ionization of a histidine amino acid

Extended description for Reversible reaction of ammonia



The reaction consists of one reactant and one product. The reactant has the following structure: A central N superscript plus is wedge bonded to H on the lower right, dash bonded to H on the right, and single bonded to H on the upper right. It has an open single bond on the left. The product has the following structure: A central N atom is wedge bonded to H on the lower right, dash bonded to H on the right. It has an open single bond on the left.

Return to Reversible reaction of ammonia

Extended description for Ionization of a mercapto group



The reaction consists of one reactant and one product. The reactant has the following structure: S is single bonded to H on the upper right. S has an open single bond on the left. The product has the following structure: S superscript minus has an open single bond on the left.

Return to Ionization of a mercapto group

Extended description for Ionization of a hydroxyl group

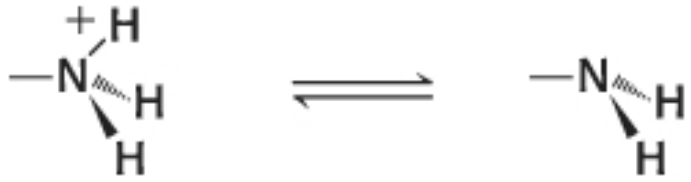


The reaction consists of one reactant and one product. The reactant has the following structure: A benzene ring is in a horizontal orientation with C 1 occupying the rightmost vertex. The ring contains alternating double bonds between C 1 and C 2, C 3 and C 4, and C 5 and C 6. C 1 is single bonded to O. This O atom is single bonded to H on the upper right. C 4 has an open single bond.

The product has the following structure: A benzene ring is in a horizontal orientation with C 1 occupying the rightmost vertex. The ring contains alternating double bonds between C 1 and C 2, C 3 and C 4, and C 5 and C 6. C 1 is single bonded to O superscript minus. C 4 has an open single bond.

Return to Ionization of a hydroxyl group

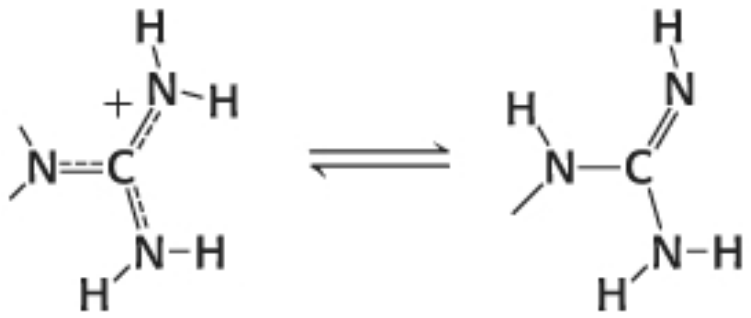
Extended description for Reversible reaction of ammonia



The reaction consists of one reactant and one product. The reactant has the following structure: A central N superscript plus is wedge bonded to H on the lower right, dash bonded to H on the right, and single bonded to H on the upper right. It has an open single bond on the left. The product has the following structure: A central N atom is wedge bonded to H on the lower right, dash bonded to H on the right. It has an open single bond on the left.

Return to Reversible reaction of ammonia

Extended description for Ionization of an amine group

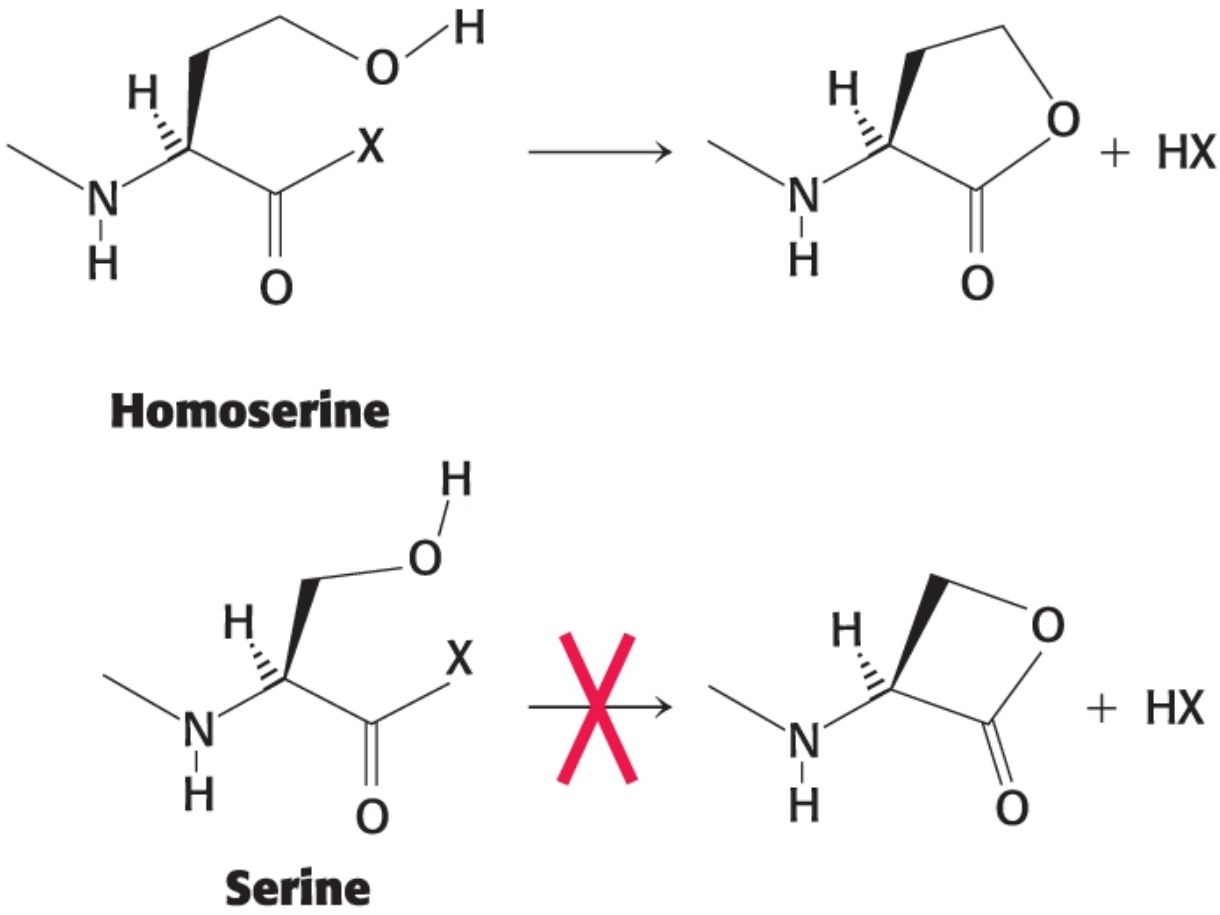


The reaction consists of one reactant and one product. The reactant has the following structure: A central C atom is single bonded to N on the left, single bonded to N on the upper right, and single bonded to N on the lower right. The N on the left has two open single bonds on the upper left and lower left. The N on the upper left is single bonded to H on the upper right and single bonded to H on the lower right. The N on the lower right is single bonded to H on the right and single bonded to H on the lower left. A partial double bond is present across the central C atom and each N atom, respectively. The central C atom carries a positive charge.

The product has the following structure: A central C atom is single bonded to N on the left, double bonded to N on the upper right, and single bonded to N on the lower right. The N on the left has an open single bond on the lower left and is single bonded to H on the upper left. The N on the upper right is single bonded to H above. The N on the lower right is single bonded to H on the right and single bonded to H on the lower left.

Return to Ionization of an amine group

Extended description for FIGURE 2.11 Some amino acids are not found in proteins because they are too reactive



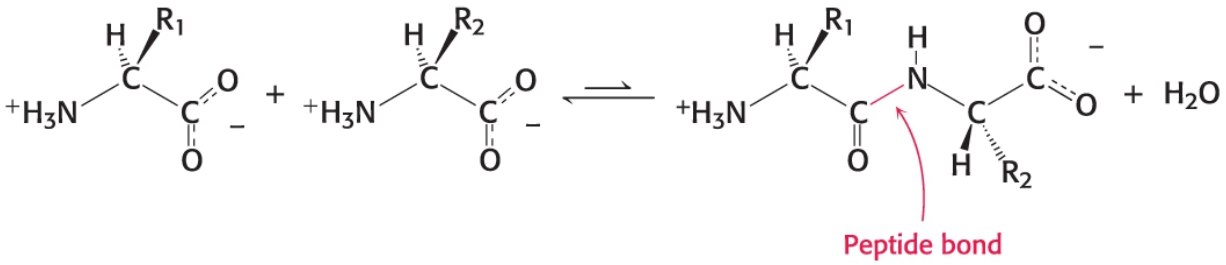
Cyclization of homoserine: The reaction consists of one reactant and two products. The reactant has the following structure: A 1 N and 3 C heteronuclear alkane chain is depicted as a line structure using 3 zigzag lines. N single bonded to H below occupies the second position. C 3 is double bonded to O below and single bonded to X on the upper right. C 2 is dash bonded to H on the upper left and wedge bonded to C 1 of a 2-carbon alkane chain depicted as a line structure using one line. C 2 of the second chain is single bonded to O on the

lower right which is single bonded to H on the upper right. The first product has the following structure: A 5-membered heterocyclic pentagonal ring is in a horizontal orientation and consists of 1 O and 4 C atoms. O occupies the first position, which is the rightmost vertex. C 1 is double bonded to O below. C 2 is wedge bonded to C 3. C 2 is dash bonded to H on the upper left and single bonded to N which is single bonded to H below and C H 3 on the upper left in the form of a line. The second product is H X.

Cyclization of serine: The reaction consists of one reactant and two products. The reactant has the following structure: A 1 N and 3 C heteronuclear alkane chain is depicted as a line structure using 3 zigzag lines. N single bonded to H below occupies the second position. C 3 is double bonded to O below and single bonded to X on the upper right. C 2 is dash bonded to H on the upper left and wedge bonded to C H 2 on the upper right. C H 2 is single bonded to O on the right which is single bonded to H on the upper right. The first product has the following structure: The first product has the following structure: A 4-membered heterocyclic ring is in a horizontal orientation and consists of 1 O and 3 C atoms. O occupies the first position, which is the rightmost vertex. C 1 is double bonded to O below. C 2 is wedge bonded to C 3. C 2 is dash bonded to H on the upper left and single bonded to N which is single bonded to H below and C H 3 on the upper left in the form of a line. The second product is as follows: H X. The reaction arrow is crossed out.

Return to FIGURE 2.11 Some amino acids are not found in proteins because they are too reactive

Extended description for FIGURE 2.12 The formation of the peptide bond linking two amino acids is accompanied by the loss of a molecule of water



The reaction consists of two reactants and two products. The first reactant has the following structure: A central C atom is single bonded to N H 3 superscript plus on the lower left, single bonded to C on the lower right, dash bonded to H on the upper left, and wedge bonded to R 1 on the upper right. The C on the lower right is single bonded to O on the upper right and single bonded to O below. A partial double bond is present between the C and O below and the C and O on the upper right. The C on the lower right carries a negative charge.

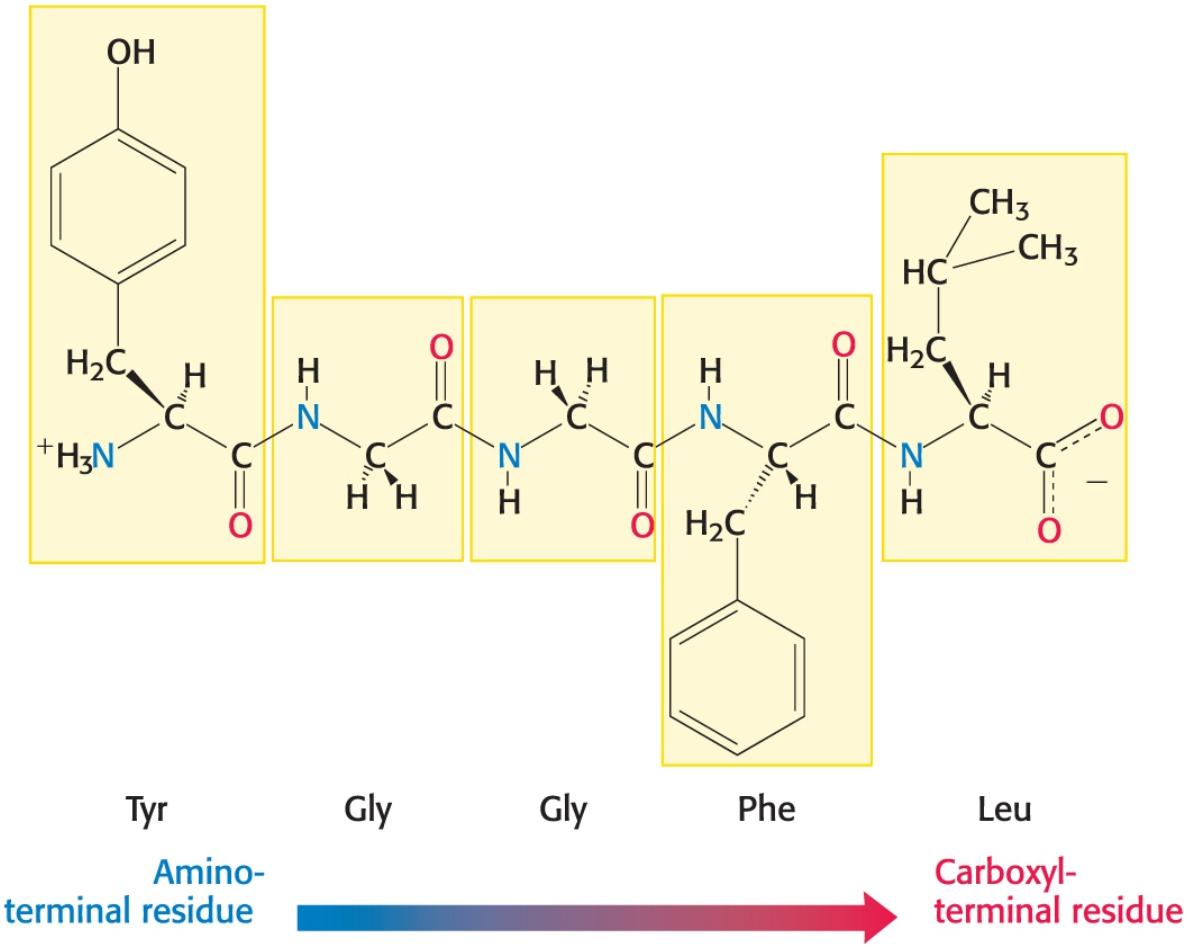
The second reactant has the following structure: A central C atom is single bonded to N H 3 superscript plus on the lower left, single bonded to C on the lower right, dash bonded to H on the upper left, and wedge bonded to R 2 on the upper right. The C on the lower right is single bonded to O on the upper right and single bonded to O below. A partial double bond is present between the C and O below and the C and O on the upper right. The C on the lower right carries a negative charge.

The backward reaction is more preferred than the forward reaction as indicated by the reversible reaction arrow.

The first product has the following structure: Superscript plus H 3 N, single bond, C, single bond, C, single bond, N, single bond, C, single bond, C, single bond, O. The chain is shown in a zigzag manner. The single bond between C 2 and N is highlighted in red and labeled peptide bond. C is dash bonded to H on the upper left and wedge bonded to R 1 on the upper right. C 2 is double bonded to O below. C 3 is wedge bonded to H on the lower left and dash bonded to R 2 on the lower right. C 4 is single bonded to O above and carries a negative charge. A partial double bond is present between C 4 and O above and the C 4 and O on the lower right. The second product is H 2 O.

Return to FIGURE 2.12 The formation of the peptide bond linking two amino acids is accompanied by the loss of a molecule of water

Extended description for FIGURE 2.13 Amino acid sequences have direction



© Macmillan Learning

The polypeptide chain has the following sequence: Tyrosine, Glycine, Glycine, Phenylalanine, and Leucine. The amino acids are linked by peptide bonds. The structure of tyrosine is as follows: A central C atom is single bonded to C on the lower right, single bonded to N H 3 superscript plus on the lower left, wedge bonded to C H 2 on the upper left, and dash bonded to H on the upper right. N is highlighted in blue. C of C H 2 is single bonded to C 4 of a benzene ring in a vertical orientation above, with C 1 occupying the topmost vertex. The ring contains alternating double bonds between C 1 and

C 2, C 3 and C 4, and C 5 and C 6. C 1 of the benzene ring is single bonded to O H. The C on the lower right is double bonded to O below and single bonded to N of the glycine residue. O is highlighted in red.

Glycine has the following structure: A central C atom is single bonded to N on the upper left, single bonded to C on the upper right, wedge bonded to H on the lower right, and dash bonded to H on the lower left. N is single bonded to H above and is highlighted in blue. The C on the upper right is double bonded to O above and single bonded to N of the second glycine residue. O above is highlighted in red.

The second glycine residue has the following structure: A central C atom is single bonded to N on the lower left, single bonded to C on the lower right, wedge bonded to H on the upper left, and dash bonded to H on the upper right. N is single bonded to H below and highlighted in blue. The C on the lower right is double bonded to O below and single bonded to N of the phenylalanine residue. O below is highlighted in red.

Phenylalanine has the following structure: A central C atom is single bonded to N on the upper left, single bonded to C on the upper right, wedge bonded to H on the lower right, and dash bonded to C H 2 on the lower left. N is highlighted in blue. C in C H 2 is single bonded to C 1 of a benzene ring in a vertical orientation below, with C 1 occupying the topmost vertex. The ring contains alternating double bonds between C 2 and C 3, C 4 and C 5, and C 6 and C 1. N is single bonded to H above. The C on the upper right is double bonded to O above and single bonded to N of the leucine residue. O above is highlighted in red.

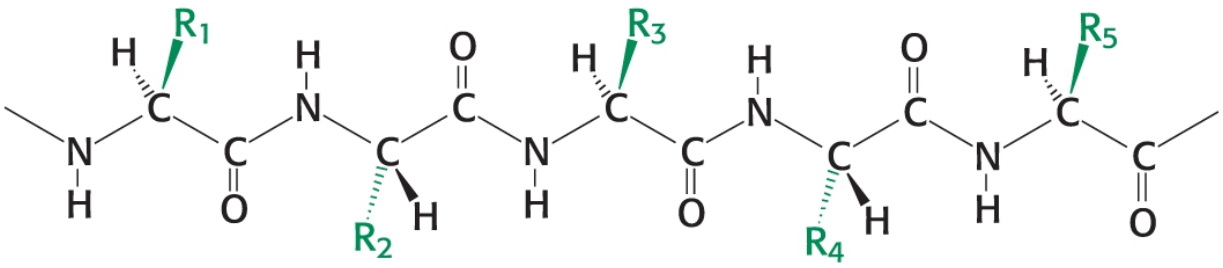
Leucine has the following structure: A central C atom is single bonded to C on the lower right, single bonded to N on the lower left,

wedge bonded to C H 2 on the upper left, and dash bonded to H on the upper right. C in C H 2 is single bonded to C H above. C in C H is single bonded to C H 3 on the right and single bonded to C H 3 on the upper right. N is single bonded to H below and is highlighted in blue. C on the lower right is single bonded to O on the upper right and single bonded to O below. A partial double bond is present across the O on the upper right, C, and the O below. The C atom carries a negative charge. Both O atoms are highlighted in red.

A right-pointing arrow from the tyrosine residue to the leucine residue has a color gradient from blue to red. The tail of the arrow at tyrosine is labeled amino-terminal residue. The arrowhead at the leucine residue is labeled carboxyl-terminal residue.

Return to FIGURE 2.13 Amino acid sequences have direction

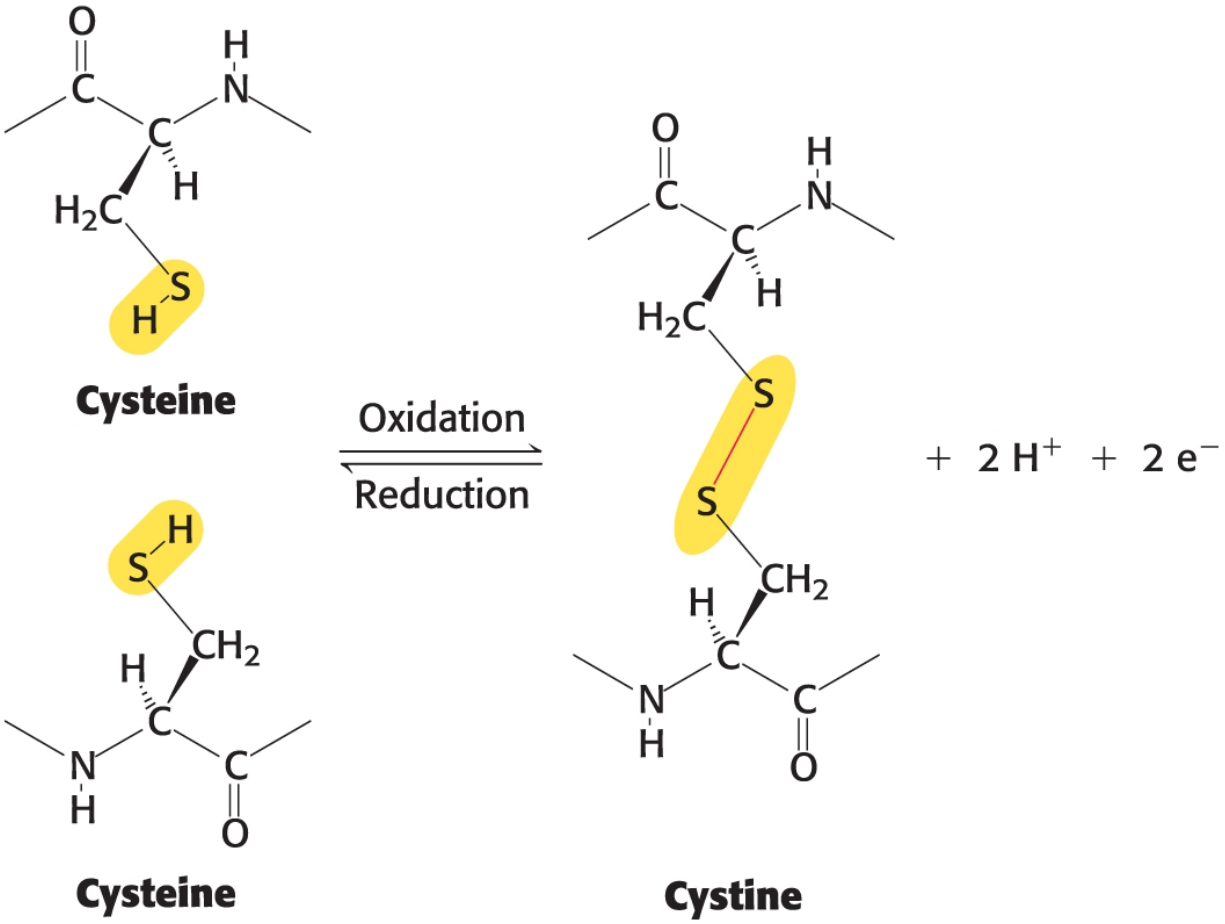
Extended description for FIGURE 2.14 A polypeptide chain consists of a constant backbone and variable side chains



The structure is as follows: open single bond, N, single bond, C, single bond, C, single bond, N, single bond, C, single bond, C, single bond, N, single bond, C, single bond, C, single bond, N, single bond, C, single bond, C, single bond, N, single bond, C, single bond, C, open single bond. The chain is shown in a zigzag manner. The first, third, and fifth N atoms are each single bonded to H below. The second and the fourth N atoms are each single bonded to H above. C 1, C 5, and C 9 are dash bonded to H on the upper left and wedge bonded to R 1, R 3, and R 5 on the upper right, respectively. C 3 and C 7 are wedge bonded to H on the lower right and dash bonded to R 2 and R 4 on the lower left, respectively. C 2, C 7, and C 10 are each double bonded to O below. C 4 and C 8 are each double bonded to O above. The R groups are highlighted in green.

Return to FIGURE 2.14 A polypeptide chain consists of a constant backbone and variable side chains

Extended description for FIGURE 2.15 The formation of a disulfide bond from two cysteine residues is an oxidation reaction



The reaction consists of one reactant and three products. The reactant is two molecules of cysteine amino acids. The structure of first cysteine amino acid is as follows: A 1 N and 2 C heteronuclear alkane chain is depicted as a line structure using 2 zigzag lines. N atom occupies the third position. N is single bonded to H above. N atom has an open single bond on the lower right. C 1 is double bonded to O above. C 1 has an open single bond on the lower left. C 2 is wedge bonded to C H 2 on the lower left and dash bonded to H

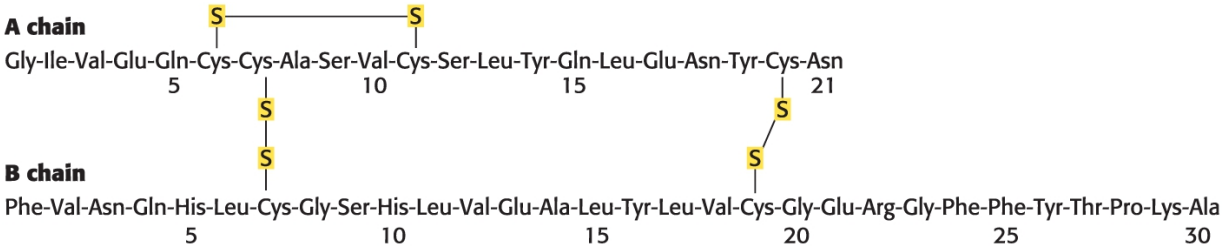
on the lower right. C H 2 on the lower left is single bonded to S on the lower right. S is single bonded to H on the lower left. S, single bond, H is highlighted in yellow. The structure of the second cysteine amino acid is as follows: A 1 N and 2 C heteronuclear alkane chain is depicted as a line structure using 2 zigzag lines. N atom occupies the first position. N is single bonded to H below. N atom has an open single bond on the upper left. C 1 is wedge bonded to C H 2 on the upper right and dash bonded to H on the upper left. C H 2 on the upper right is single bonded to S on the upper left. S is single bonded to H on the upper right. S, single bond, H is highlighted in yellow. C 2 is double bonded to O below. C 2 has an open single bond on the upper left.

The forward reaction arrow is labeled oxidation and the backward reaction arrow is labeled reduction.

The three products are one molecule of cystine, 2 H superscript plus ions, and 2 e superscript minus. The structure of cystine is as follows: A 1 N and 2 C heteronuclear alkane chain is depicted as a line structure using 2 zigzag lines. N atom occupies the third position. N is single bonded to H above. N atom has an open single bond on the lower right. C 1 is double bonded to O above. C 1 has an open single bond on the lower left. C 2 is wedge bonded to C H 2 on the lower left and dash bonded to H on the lower right. C H 2 on the lower left is single bonded to S on the lower right. S is single bonded to another S on the lower left. S, single bond, S is highlighted in yellow. The second S is single bonded to a C H 2 group on the lower right. This C H 2 is part of a second heteronuclear alkane chain. C H 2 is wedge bonded to C 1 of the second alkane chain. C 1 is wedge bonded to H on the upper left. The heteronuclear alkane chain consists of 1 N and 2 C atoms. N occupies the first position and is single bonded to H below. N has an open single bond on the upper left. C 2 is double bond to O below and has an open single bond on the upper right.

Return to FIGURE 2.15 The formation of a disulfide bond from two cysteine residues is an oxidation reaction

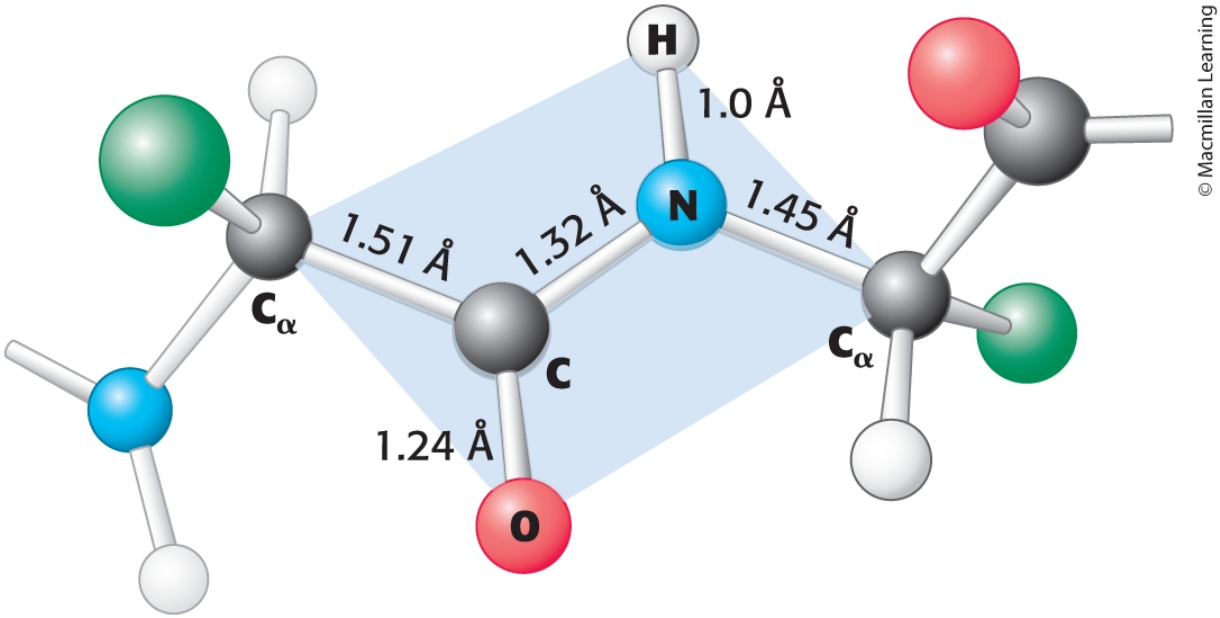
Extended description for FIGURE 2.16 The primary structure of bovine insulin is its amino acid sequence



Chain A is made up of 21 amino acids, and B chain is made up of 30 amino acids. Cysteine as the sixth and the eleventh position of chain A are each single bonded to S above. A single bond is present between the two S atoms above. Cysteine at the seventh position of chain A is single bonded to S below. This S is single bonded to S below, which is single bonded to cysteine at the seventh position of chain B below. Cysteine at the twentieth position of chain A is single bonded to S below. This S is single bonded to another S on the lower left, which is single bonded to cysteine at the nineteenth position of chain B below.

Return to FIGURE 2.16 The primary structure of bovine insulin is its amino acid sequence

Extended description for FIGURE 2.17 Peptide bonds are planar and have partial double-bond character



© Macmillan Learning

Two amino acids are linked together by a peptide bond shown on the same plane. The amino acids are represented using ball-and-stick models. In the ball-and-stick model, black spheres represent carbon atoms, blue spheres represent nitrogen atoms, white spheres represent hydrogen atoms, red spheres represent oxygen atoms, and green spheres represent side chains.

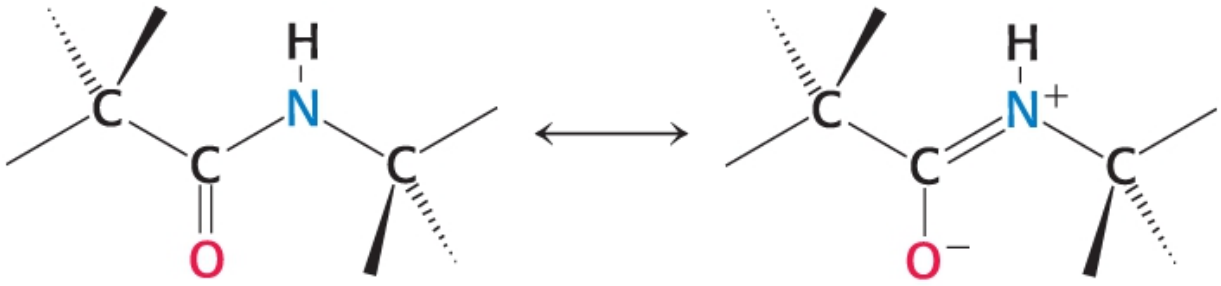
The first amino acid has the following structure: A central black sphere labeled C alpha is connected to a blue sphere on the lower left, another black sphere labeled C on the lower right, a large green sphere above and toward the observer, and a small white sphere above and away from the observer. The blue sphere is connected to a small white sphere below, and the black sphere on the lower right is connected to a red sphere labeled O below.

The second amino acid has the following structure: A central black sphere labeled C alpha is connected to a blue sphere on the upper left, another black sphere on the upper right, a large green sphere on the lower right and away from the observer, and a small white sphere below and toward from the observer. The blue sphere is connected to a small white sphere above labeled H and the black sphere labeled C in the previous amino acid. The black sphere on the upper right is connected to a red sphere labeled O toward the observer.

The bond length between C in the first amino acid and N in the second amino acid is 1.32 Angstrom. The bond length between C alpha and C in the first amino acid is 1.51 Angstrom. The bond length between C and O in the first amino acid is 1.24 Angstrom. The bond length between N and H in the second amino acid is 1.0 Angstrom. The bond length between N and C alpha in the second amino acid is 1.45 Angstrom.

Return to FIGURE 2.17 Peptide bonds are planar and have partial double-bond character

Extended description for Peptide bond resonance structures



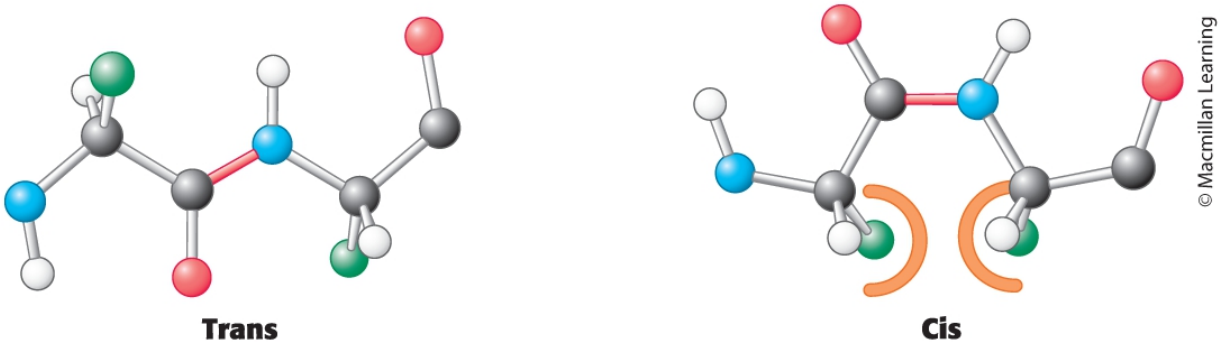
Peptide-bond resonance structures

The first resonance structure is as follows: Open single bond, C, single bond, C, single bond, N, single bond, C, open single bond. The chain is shown in a zigzag manner. N is single bonded to H above. N is highlighted in blue. C 1 has an open wedge bond on the upper right and an open dash bond on the upper left. C 2 is double bonded to O below. O is highlighted in red. C 3 has an open wedge bond on the lower left and an open dash bond on the lower right.

The second resonance structure is as follows: Open single bond, C, single bond, C, double bond, N superscript plus, single bond, C, open single bond. The chain is shown in a zigzag manner. N superscript plus is single bonded to H above. C 1 has a wedge bond on the upper right and a dash bond on the upper left. C 2 is single bonded to O superscript minus below which is highlighted in red. C 3 has a wedge bond on the lower left and a dash bond on the lower right.

Return to Peptide bond resonance structures

Extended description for FIGURE 2.18 For most amino acids, the trans configuration of the peptide bond is strongly favored because of steric clashes that arise in the cis isomer.



Trans: Two amino acids are linked together by a peptide bond highlighted in red. The amino acids are represented using ball-and-stick models. In the ball-and-stick model, black spheres represent carbon atoms, blue spheres represent nitrogen atoms, white spheres represent hydrogen atoms, red spheres represent oxygen atoms, and green spheres represent side chains.

In the first amino acid, a central black sphere is connected to another black sphere on the lower right, a blue sphere on the lower left, a green sphere above and toward the observer, and a white sphere above and away from the observer. The blue sphere is connected to a white sphere below. The black sphere on the lower right is connected to a red sphere below and connected to a blue sphere in the second amino acid on the upper right.

In the second amino acid, a central black sphere is connected to a blue sphere on the upper left, a black sphere on the upper right, a green sphere below and away from the observer, and a white sphere

below and toward the observer. The blue sphere is connected to a white sphere above. The black sphere on the upper right is connected to a red sphere above.

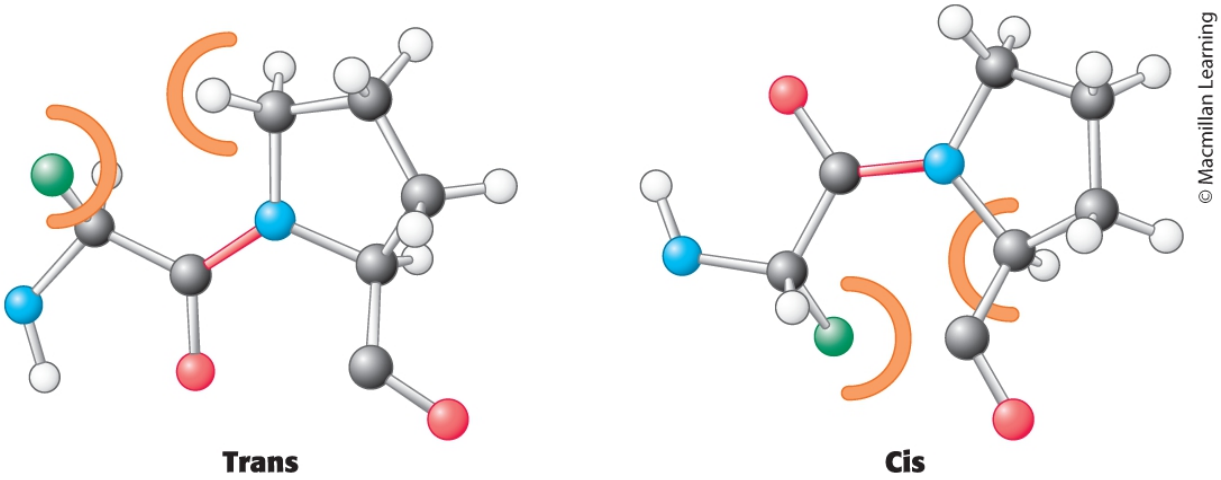
Cis: Two amino acids are linked together by a peptide bond highlighted in red. The amino acids are represented using ball-and-stick models. In the ball-and-stick model, black spheres represent carbon atoms, blue spheres represent nitrogen atoms, white spheres represent hydrogen atoms, red spheres represent oxygen atoms, and green spheres represent side chains.

In the first amino acid, a central black sphere is connected to a blue sphere on the left, a black sphere on the upper right, a green sphere on the lower right and away from the observer, and a white sphere below and toward the observer. The blue sphere is connected to a white sphere above. The black sphere on the upper right is connected to a red sphere on the upper left and connected to a blue sphere in the second amino acid on the upper right.

In the second amino acid, a central black sphere is connected to a blue sphere on the upper left, a black sphere on the upper right, a green sphere on the lower left and away from the observer, and a white sphere below and toward the observer. The blue sphere is connected to a white sphere on the upper right. The black sphere on the upper right is connected to a red sphere above. Orange semicircles are drawn around the side chains.

Return to FIGURE 2.18 For most amino acids, the trans configuration of the peptide bond is strongly favored because of steric clashes that arise in the cis isomer.

Extended description for FIGURE 2.19 For peptide bonds between proline and its preceding residue, cis bonds are as likely as trans bonds



Trans: Proline and the amino acid residue are linked together by a peptide bond highlighted in red. The amino acids are represented using ball-and-stick models. In the ball-and-stick model, black spheres represent carbon atoms, blue spheres represent nitrogen atoms, white spheres represent hydrogen atoms, red spheres represent oxygen atoms, and green spheres represent side chains.

In the first amino acid, a central black sphere is connected to another black sphere on the lower right, a blue sphere on the lower left, a green sphere on the upper left and toward the observer, and a white sphere above and away from the observer. The blue sphere is connected to a white sphere below. The black sphere on the lower right is connected to a red sphere below and connected to a blue sphere of a heterocyclic pentagonal ring on the upper right. The 5-membered heterocyclic pentagonal ring is in a vertical orientation and consists of 1 blue and 4 black spheres. The blue sphere occupies the first position, which is the bottom left vertex. Each black sphere

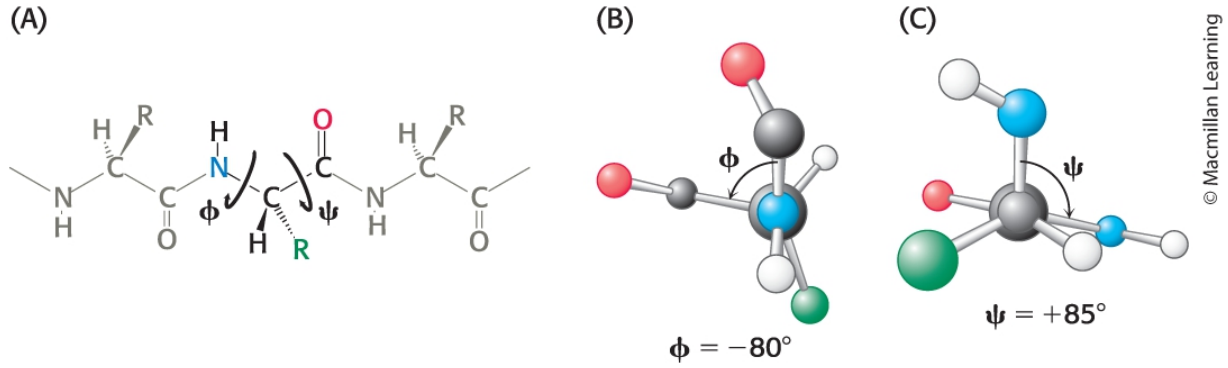
except for the one at the bottommost vertex is connected to two white spheres. The black sphere at the bottommost vertex is connected to a white sphere away from the observer and another black sphere below which is connected to a red sphere on the lower right. Orange semicircles are drawn around the green sphere of the first amino acid and the white spheres are connected to the black sphere at the top right vertex.

Cis: Proline and the amino acid residue are linked together by a peptide bond highlighted in red. The amino acids are represented using ball-and-stick models. In the ball-and-stick model, black spheres represent carbon atoms, blue spheres represent nitrogen atoms, white spheres represent hydrogen atoms, red spheres represent oxygen atoms, and green spheres represent side chains.

In the first amino acid, a central black sphere is connected via rods to a blue sphere on the left, a black sphere on the upper right, a green sphere on the lower right and away from the observer, and a white sphere below and toward the observer. The blue sphere is connected to a white sphere above. The black sphere on the upper right is connected to a red sphere on the upper left and connected to a blue sphere of a heterocyclic pentagonal ring on the right. The 5-membered heterocyclic pentagonal ring is in a horizontal orientation and consists of 1 blue and 4 black spheres. The blue sphere occupies the first position, which is the leftmost vertex. Each black sphere except for the one at the bottom left vertex is connected to two white spheres. The black sphere at the bottom left vertex is connected to a white sphere away from the observer and another black sphere on the lower left, which is connected to a red sphere on the lower right. Orange semicircles are drawn around the green sphere of the first amino acid and the white spheres are connected to the black sphere at the bottom left vertex.

Return to FIGURE 2.19 For peptide bonds between proline and its preceding residue, cis bonds are as likely as trans bonds

Extended description for FIGURE 2.20 The structure of each amino acid in a polypeptide adjusts by rotation about two single bonds



Part (A): Open single bond, N, single bond, C, single bond, C, single bond, N, single bond, C, single bond, C, single bond, N, single bond, C, single bond, C, open single bond. The first and the third N atoms are each single bonded to H below. The second N atom is single bonded to H above and is highlighted in blue. C 1 and C 5 are each dash bonded to H on the upper left and wedge bonded to R on the upper right. C 2 and C 6 are double bonded to O below. C 4 is double bonded to O above which is highlighted in red. C 3 is wedge bonded to H on the lower left and dash bonded to R on the lower right, which is highlighted in green. A rotating curved arrow around the single bond between C 3 and the second N is labeled phi. Another rotating curved arrow around the single bond between C 3 and C 4 is labeled psi.

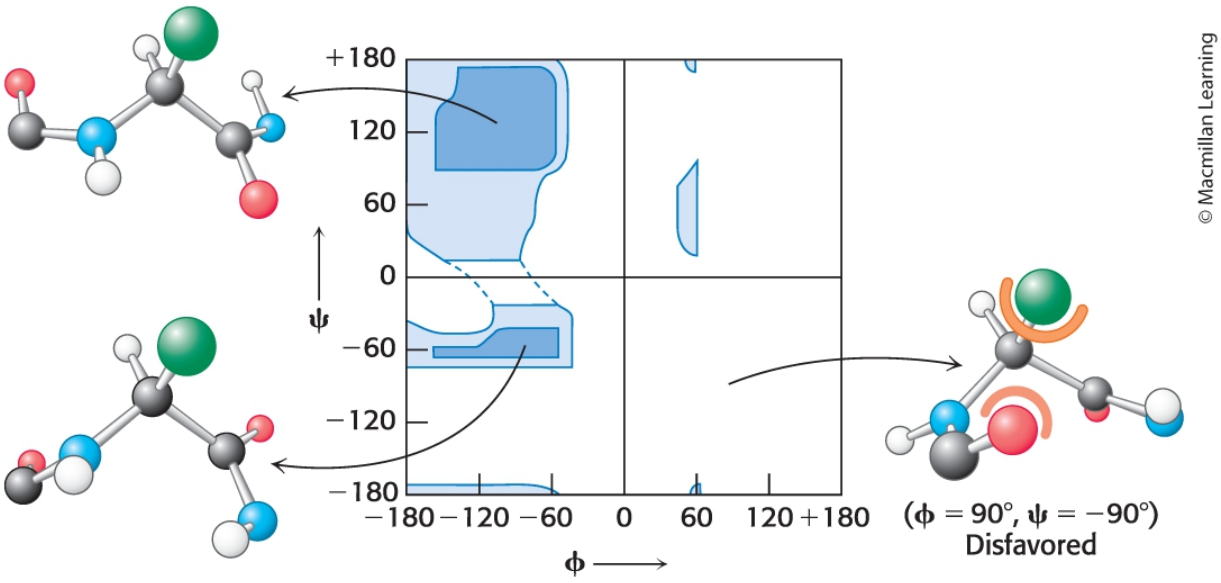
Part (B): A ball-and-stick model shows a central black sphere connected to a blue sphere in the front, a black sphere on the upper left, a small white sphere on the upper right away from the observer, and a green sphere on the lower right. The black sphere on the upper left is connected to a red sphere on the upper left. The blue

sphere is connected to a black sphere above and a small white sphere below. The black sphere above is connected to a red sphere above. The angle between the black sphere connected to the blue sphere and the black sphere connected to the central black sphere is labeled phi. Phi equals negative 80 degrees.

Part (C): A ball-and-stick model shows a central black sphere connected to a black sphere in the front, a red sphere on the left and away from the observer, and a blue sphere on the lower right. The blue sphere is connected to a small white sphere on the lower right. The black sphere in the front is connected to a blue sphere above, a small white sphere on the lower right, and a green sphere on the lower left and toward the observer. The blue sphere above is connected to a small white sphere on the upper left and toward the observer. The angle between the blue sphere above and the blue sphere on the lower right is labeled psi. Psi equals positive 85 degrees.

Return to FIGURE 2.20 The structure of each amino acid in a polypeptide adjusts by rotation about two single bonds

Extended description for FIGURE 2.21 A Ramachandran plot shows that not all φ and ψ values are possible without collisions between atoms



© Macmillan Learning

The Ramachandran plot consists of a horizontal axis and a vertical axis. The horizontal axis is labeled phi and has markings ranging from negative 180 to positive 180 in increments of 60 units. The vertical axis is labeled psi and has markings ranging from negative 180 to positive 180 in increments of 60 units.

The plot is divided into four quadrants with the help of a horizontal and a vertical line. The horizontal line begins from the marking 0 on the vertical axis. The vertical line begins from the marking 0 on the horizontal axis. The first quadrant is located at the top left. The second quadrant is located at the top right. The third quadrant is located at the bottom left. The fourth quadrant is located at the bottom right.

The first quadrant contains a light blue region that spans from a point just above 0 to positive 180 on the vertical axis and negative 180 to a point after negative 60 on the horizontal axis. The left side of the bottom portion of the light blue region narrows down from a point just below the positive 60 on the vertical axis. The right side of the bottom portion of the light blue region narrows down from a point between the positive 60 and positive 120 on the vertical axis. The bottom side of the light blue region spans from a point before negative 120 marking to a point before negative 60 on the horizontal axis. Within the top portion of the light blue region, a square-shaped dark blue region with an indentation on the top left is present. It spans from the midpoint of positive 120 and 60 to a point just below positive 180 on the vertical axis and a point before negative 120 to a point just after negative 60 on the horizontal axis.

An arrow from the dark blue region points toward a molecule depicted using a ball-and-stick model. The structure of the molecule is as follows: A black sphere is connected to another black sphere on the lower right, a blue sphere on the lower left, a green sphere on the upper right, and a white sphere on the upper left. The green sphere is toward the observer and the white sphere is away from the observer. The black sphere on the lower right is connected to a blue sphere on the right and a red sphere below. The red sphere is toward the observer. The blue sphere is away from the observer and is connected to a white sphere that is away from the observer. The blue sphere on the lower left is connected to a black sphere on the right and a white sphere in the center. The white sphere is toward the observer. The black sphere is connected to a red sphere above. The red sphere is away from the observer.

In the second quadrant, a tiny light blue region pointed downward is located on the top left at negative 180 above the positive 60 marking on the horizontal axis. An elongated light blue region is present on the bottom left. It has a pointed tip on the top. It spans from a point

just above 0 to a point below positive 120 on the vertical axis and two closely spaced points between 0 and 60 on the horizontal axis.

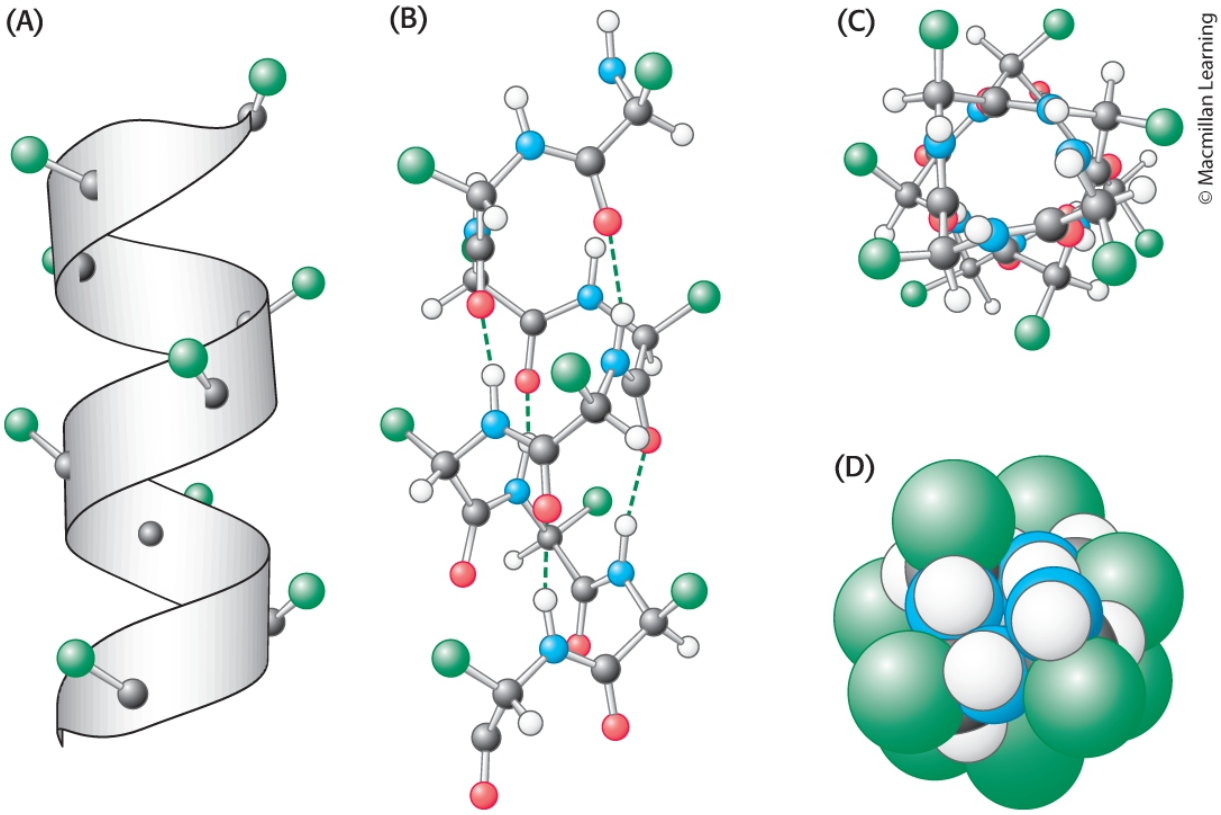
In the third quadrant, a narrow rectangular-shaped light blue region is present. This light blue region has a concave depression on the top left. It spans from a point just below negative 60 to a point below 0 on the vertical axis and negative 180 to a point just after negative 60 on the horizontal axis. The two pointed edges on the top right portion of the rectangular light blue region are connected to the corresponding two pointed edges on the bottom side of the light blue region in the first quadrant by two dashed lines. Within the light blue region, a smaller dark blue region is present. The dark blue region has a shape similar to the blue region. It spans from a point just below negative 60 to a point above negative 60 on the vertical axis and a point after negative 180 to a point just after negative 60 on the horizontal axis.

An arrow from the dark blue region points toward a molecule depicted using a ball-and-stick model. The structure of the molecule is as follows: A black sphere is connected to another black sphere on the lower right, a blue sphere on the lower left, a green sphere on the upper right, and a white sphere on the upper left. The green sphere is toward the observer. The white sphere is away from the observer. The black sphere on the lower right is connected to a blue sphere on the lower right and a red sphere on the upper right. The red sphere is away from the observer. The blue sphere is toward the observer and is connected to a white sphere on the lower left. The white sphere is toward the observer. The blue sphere on the lower left is connected to a white sphere toward the observer and a black sphere on the lower left. The black sphere on the lower left is connected to a red sphere behind. A narrow light blue region is located at the bottom left of the third quadrant. It spans from negative 180 to a point just above negative 180 on the vertical axis and negative 180 to negative 60 on the horizontal axis.

In the fourth quadrant, a tiny light blue pointed region is located at positive 60 on the horizontal axis. An arrow from the middle of the white region points toward a molecule depicted using a ball-and-stick model. The structure of the molecule is as follows: A black sphere is connected to a green sphere on the upper right, a white sphere on the upper left, a black sphere on the lower right, and a blue sphere on the lower left. The green sphere is toward the observer and is surrounded by a thick orange semi-circular line. The white sphere is away from the observer. The black sphere on the lower right is connected to a white sphere on the lower right, a blue sphere on the lower right and away from the observer, and a red sphere behind. The blue sphere on the lower left is connected to a white sphere on the left and a black sphere toward the observer. The black sphere is connected to a red sphere on the upper right. The red sphere is surrounded by a thick red semi-circular line. Note: phi is equal to 90 degrees, psi is equal to negative 90 degrees, disfavored.

Return to FIGURE 2.21 A Ramachandran plot shows that not all φ and ψ values are possible without collisions between atoms

Extended description for FIGURE 2.22 Various depictions of an alpha helix reveal several of its key features



Part (A): A ribbon-like structure forms a vertical helical structure. Green spheres connected to black spheres are attached to the helix at equal distances from top to bottom.

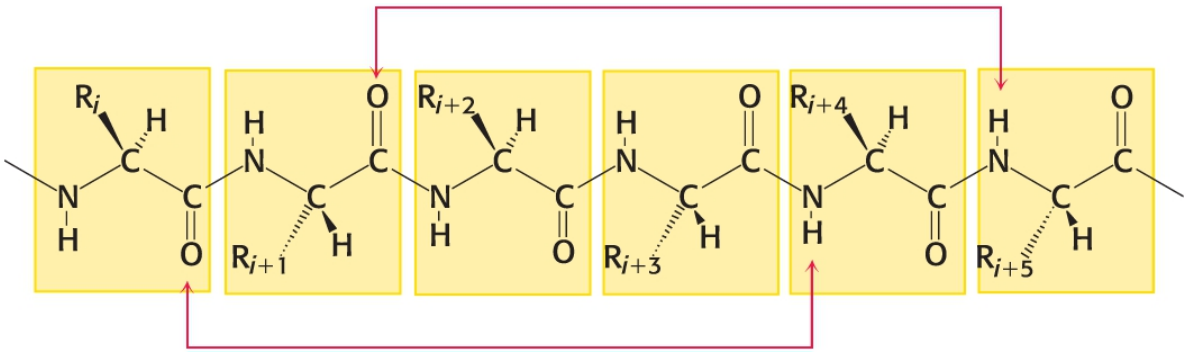
Part (B): A side-view of the ball-and-stick model of an alpha helix is illustrated. black spheres represent carbon atoms, blue spheres represent nitrogen atoms, white spheres represent hydrogen atoms, red spheres represent oxygen atoms, and green spheres represent side chains. Green dashed lines are drawn between the N H and C O groups of adjacent turns.

Part (C): An end-view of an alpha-helix shows a ring-like structure in which the side chains of the amino acids are oriented toward the periphery. Black spheres represent carbon atoms, blue spheres represent nitrogen atoms, white spheres represent hydrogen atoms, red spheres represent oxygen atoms, and green spheres represent side chains.

Part (D): An end-view of a space-filling model of an alpha-helix shows blue spheres fused to white spheres at the center and large green spheres at the periphery. Blue spheres represent nitrogen atoms, white spheres represent hydrogen atoms, and green spheres represent side chains.

Return to FIGURE 2.22 Various depictions of an alpha helix reveal several of its key features

Extended description for FIGURE 2.23 In an alpha helix, hydrogen bonds form between the CO group of residue I and the NH group of residue i + 4



Six amino acid residues are connected in a linear chain by peptide bonds. The basic structure of the peptide linkage between two amino acids is as follows: In the first amino acid, a central C atom is single bonded to C on the lower right, single bonded to N on the lower left, dash bonded to H on the upper right, and wedge bonded to R subscript i on the upper left. N is single bonded to H below and has an open single bond on the upper left. The C on the lower right is double bonded to O below and single bonded to N of the next amino acid.

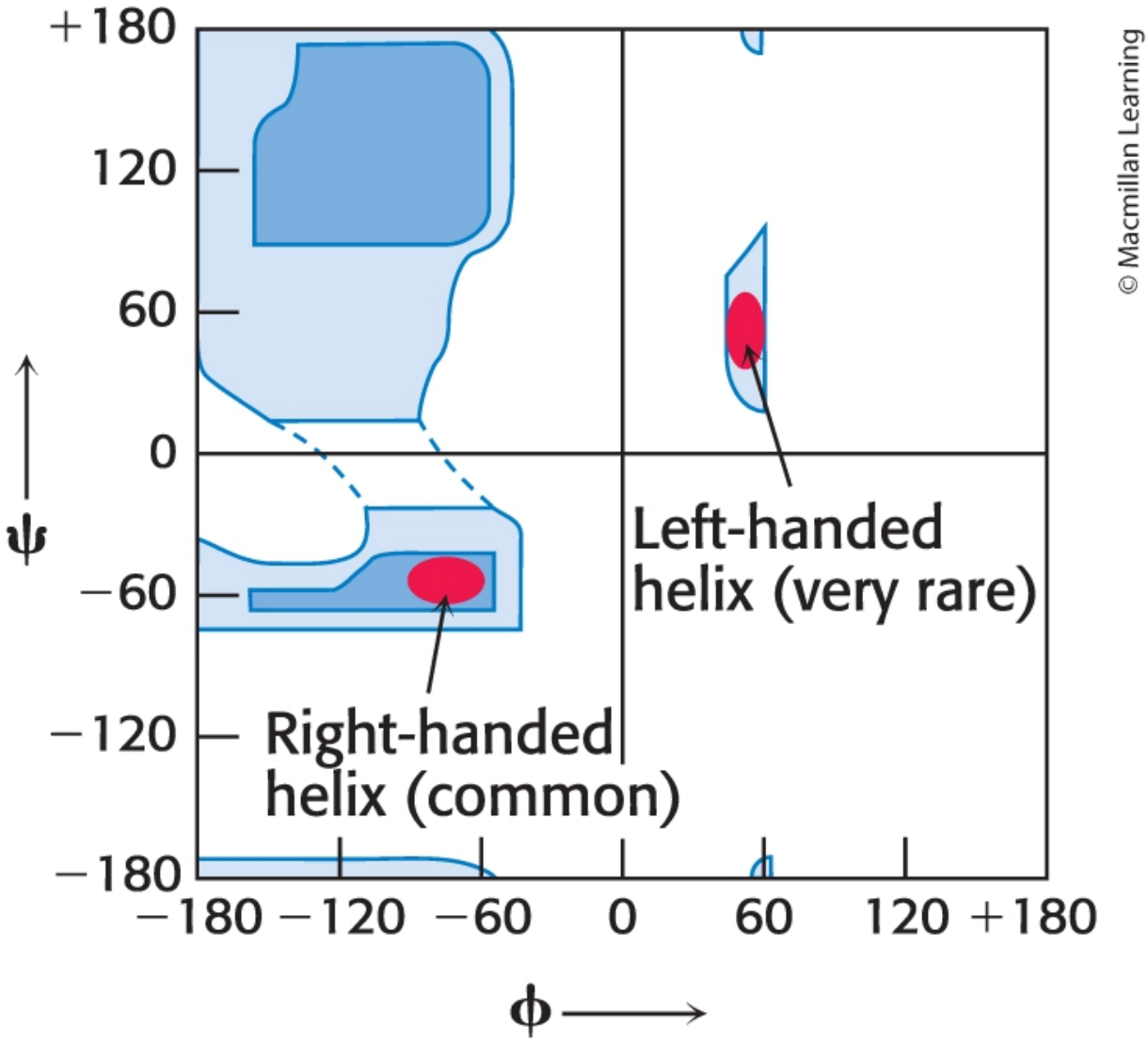
In the next amino acid, a central C atom is single bonded to C on the upper right, single bonded to N on the upper left, dash bonded to R subscript i plus 1 on the lower left, and wedge bonded to H on the lower right. N is single bonded to H above. C on the upper right is double bonded to O above and single bonded to N of the next amino acid.

Two such pairs of amino acids are linked in a series. The respective side chains of the next four amino acids are R subscript i plus 2, R

subscript i plus 3, R subscript i plus 4, and R subscript i plus 5. A double headed red arrow is shown between the O atom in the second amino acid and the H bonded to N above in the sixth amino acid. A double headed red arrow is shown between the O atom in the first amino acid and the H bonded to N below in the fifth amino acid.

Return to FIGURE 2.23 In an alpha helix, hydrogen bonds form between the CO group of residue I and the NH group of residue i + 4

Extended description for FIGURE 2.24 Both right- and left-handed helices lie in regions of allowed conformations in the Ramachandran plot



The Ramachandran plot consists of a horizontal axis and a vertical axis. The horizontal axis is labeled phi and has markings ranging from negative 180 to positive 180 in increments of 60 units. The

vertical axis is labeled psi and has markings ranging from negative 180 to positive 180 in increments of 60 units.

The plot is divided into four quadrants with the help of a horizontal and a vertical line. The horizontal line begins from the marking 0 on the vertical axis. The vertical line begins from the marking 0 on the horizontal axis. The first quadrant is located at the top left. The second quadrant is located at the top right. The third quadrant is located at the bottom left. The fourth quadrant is located at the bottom right.

The first quadrant contains a light blue region that spans from a point just above 0 to positive 180 on the vertical axis and negative 180 to a point after negative 60 on the horizontal axis. The left side of the bottom portion of the light blue region narrows down from a point just below the positive 60 on the vertical axis. The right side of the bottom portion of the light blue region narrows down from a point between the positive 60 and positive 120 on the vertical axis. The bottom side of the light blue region spans from a point before negative 120 marking to a point before negative 60 on the horizontal axis. Within the top portion of the light blue region, a square-shaped dark blue region with an indentation on the top left is present. It spans from the midpoint of positive 120 and 60 to a point just below positive 180 on the vertical axis and a point before negative 120 to a point just after negative 60 on the horizontal axis.

In the second quadrant, a tiny light blue region pointed downward is located at the top left at negative 180 above the positive 60 marking on the horizontal axis. An elongated light blue region is present at the bottom left. It has a pointy tip on the top. It spans from a point just above 0 to a point below positive 120 on the vertical axis and two closely spaced points between 0 and 60 on the horizontal axis. Within the elongated region, a red circular region labeled left-handed helix (very rare) is present. The red region fits inside the

elongated region. The red region spans from a point below positive 60 to a point just above positive 60 on the vertical axis.

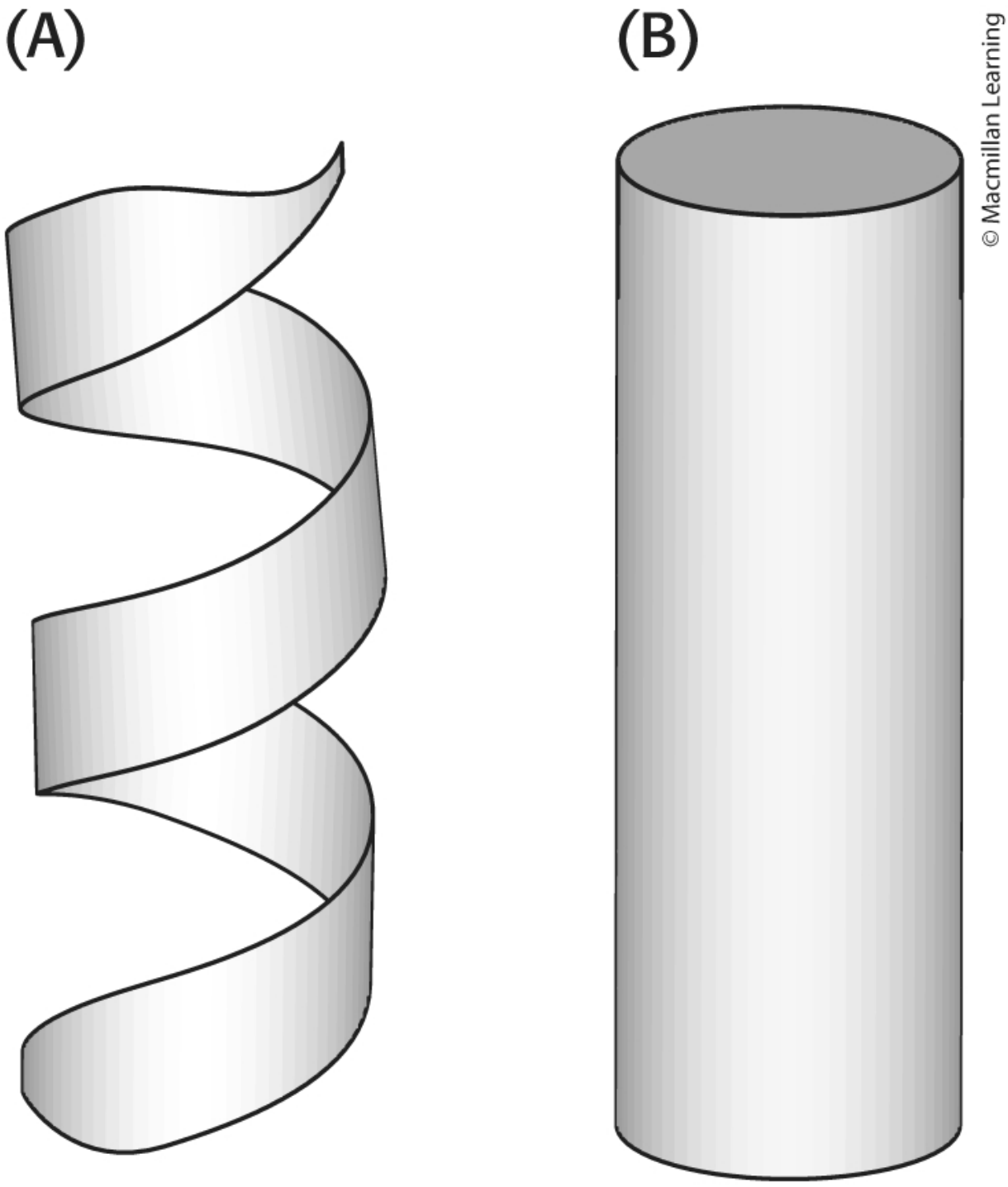
In the third quadrant, a narrow rectangular-shaped light blue region is present. This light blue region has a concave depression on the top left. It spans from a point just below negative 60 to a point below 0 on the vertical axis and negative 180 to a point just after negative 60 on the horizontal axis. The two pointed edges on the top right portion of the rectangular light blue region are connected to the corresponding two pointed edges on the bottom side of the light blue region in the first quadrant by two dashed lines. Within the light blue region, a smaller dark blue region is present. The dark blue region has a shape similar to the blue region. It spans from a point just below negative 60 to a point above negative 60 on the vertical axis and a point after negative 180 to a point just after negative 60 on the horizontal axis. Within the dark blue region, a red circular region labeled right-handed helix (common) is present on the right. The red region fits inside the dark blue region. It spans between a point before negative 60 to negative 60 on the horizontal axis. A narrow light blue region is located at the bottom left of the third quadrant. It spans from negative 180 to a point just above negative 180 on the vertical axis and negative 180 to negative 60 on the horizontal axis.

In the fourth quadrant, a tiny light blue pointed region is located at positive 60 on the horizontal axis.

Return to FIGURE 2.24 Both right- and left-handed helices lie in regions of allowed conformations in the Ramachandran plot

Extended description for FIGURE 2.25 There are two common ways to draw α helices. (A) A ribbon

depiction. (B) A cylindrical (rod) depiction

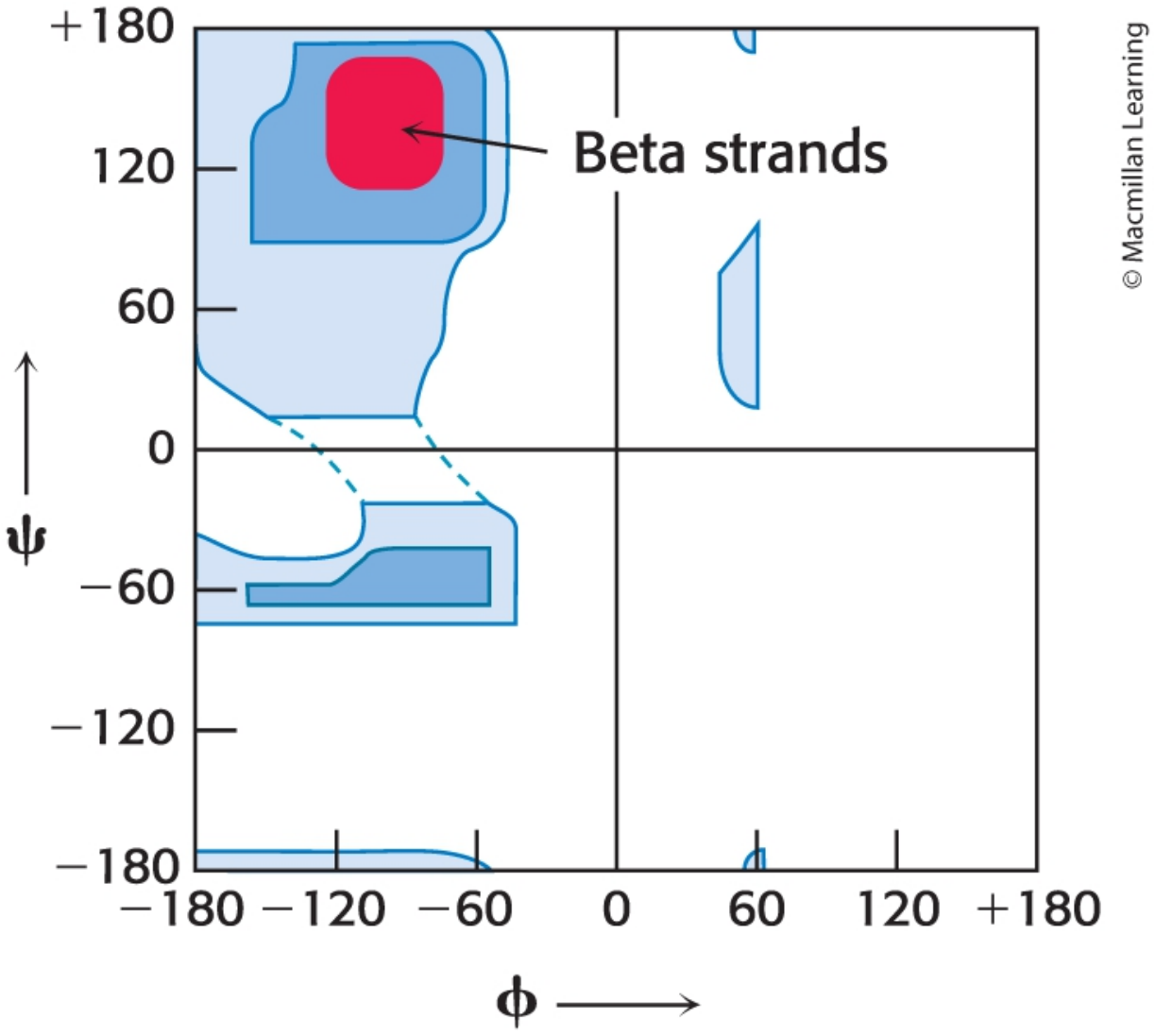


Part (A): The alpha helix is shown as a gray ribbon having 2.5 turns in a left handed manner.

Part (B): A gray solid cylinder is shown.

Return to FIGURE 2.25 There are two common ways to draw α helices. (A) A ribbon depiction. (B) A cylindrical (rod) depiction

Extended description for FIGURE 2.27 β strands occupy an allowed region of the Ramachandran plot



The Ramachandran plot consists of a horizontal axis and a vertical axis. The horizontal axis is labeled phi and has markings ranging from negative 180 to positive 180 in increments of 60 units. The vertical axis is labeled psi and has markings ranging from negative 180 to positive 180 in increments of 60 units.

The plot is divided into four quadrants with the help of a horizontal and a vertical line. The horizontal line begins from the marking 0 on the vertical axis. The vertical line begins from the marking 0 on the horizontal axis.

The first quadrant is located at the top left. The second quadrant is located at the top right. The third quadrant is located at the bottom left. The fourth quadrant is located at the bottom right. The first quadrant contains a light blue region that spans from a point just above 0 to positive 180 on the vertical axis and negative 180 to a point after negative 60 on the horizontal axis. The left side of the bottom portion of the light blue region narrows down from a point just below the positive 60 on the vertical axis. The right side of the bottom portion of the light blue region narrows down from a point between the positive 60 and positive 120 on the vertical axis. The bottom side of the light blue region spans from a point before negative 120 marking to a point before negative 60 on the horizontal axis. Within the top portion of the light blue region, a square-shaped dark blue region with an indentation on the top left is present. It spans from 90 to a point just below positive 180 on the vertical axis and negative 150 to a point just after negative 60 on the horizontal axis. Within the dark blue region, a small square-shaped red region labeled beta strands is present. The red region spans from a point below positive 180 to a point below positive 120 on the vertical axis and a point just before negative 120 to a point before negative 60 on the horizontal axis.

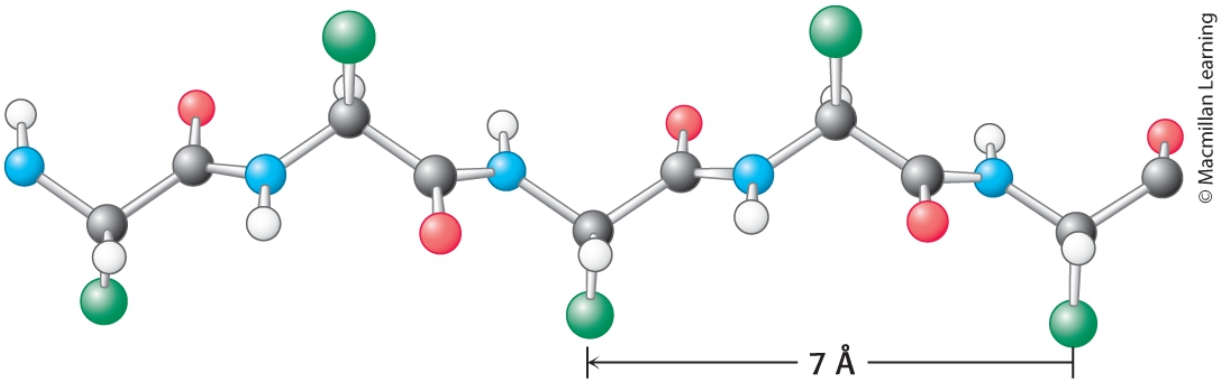
In the second quadrant, a tiny light blue region pointed downward is located on the top left at negative 180 above the positive 60 marking on the horizontal axis. An elongated light blue region is present on the bottom left. It has a pointy tip on the top. It spans from a point just above 0 to a point below positive 120 on the vertical axis and two closely spaced points between 0 and 60 on the horizontal axis.

In the third quadrant, a narrow rectangular-shaped light blue region is present. This light blue region has a concave depression on the top left. It spans from a point just below negative 60 to a point below 0 on the vertical axis and negative 180 to a point just after negative 60 on the horizontal axis. The two pointed edges on the top right portion of the rectangular light blue region are connected to the corresponding two pointed edges on the bottom side of the light blue region in the first quadrant by two dashed lines. Within the light blue region, a smaller dark blue region is present. The dark blue region has a shape similar to the light blue region. It spans from a point just below negative 60 to a point above negative 60 on the vertical axis and a point after negative 180 to a point just after negative 60 on the horizontal axis. A narrow light blue region is located at the bottom left of the third quadrant. It spans from negative 180 to a point just above negative 180 on the vertical axis and negative 180 to negative 60 on the horizontal axis.

In the fourth quadrant, a tiny light blue pointed region is located at positive 60 on the horizontal axis.

Return to FIGURE 2.27 β strands occupy an allowed region of the Ramachandran plot

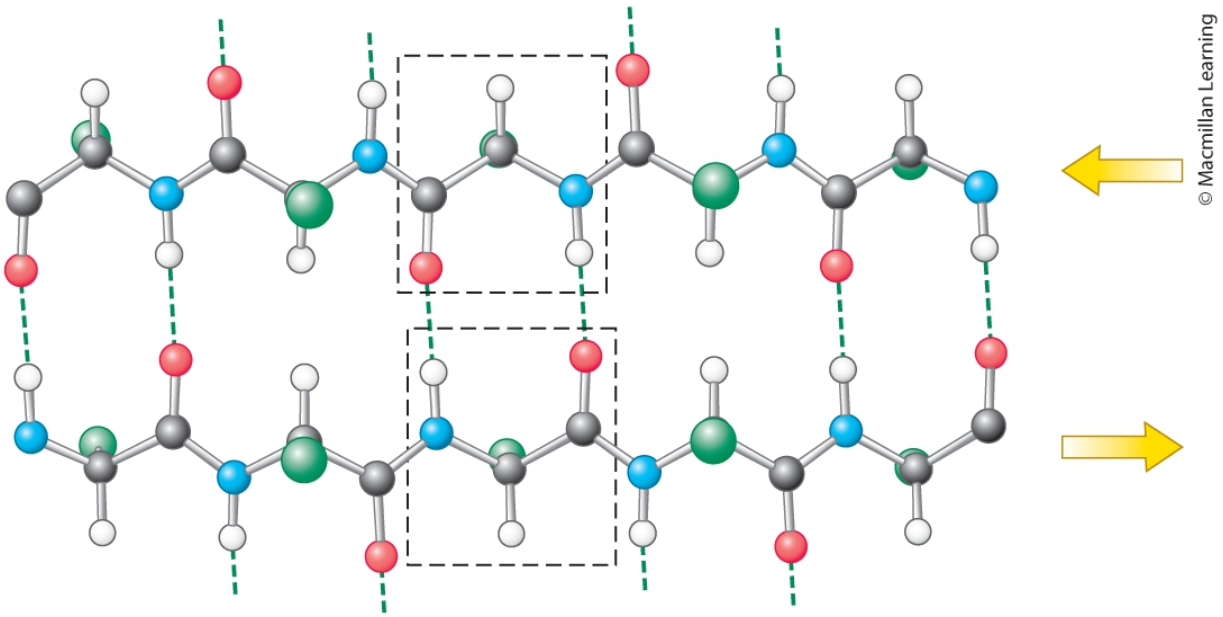
Extended description for FIGURE 2.28 The side chains of a beta strand project alternately above and below the plane of the strand



The ball-and-stick model is represented by a central black sphere connected to a blue sphere on the upper left and a black sphere on the upper right. The blue sphere is connected to a small white sphere. The second black sphere is connected to a red sphere. The central black sphere is connected to a small white sphere above and away from the observer and a large green sphere below. The second black sphere of one amino acid is connected to the blue sphere of the adjacent amino acid. Five such amino acids are linked such that the side chains of the adjacent amino acids are facing in vertically opposite directions. The distance between the side chains of two amino acids in alternate positions is 7 angstrom.

Return to FIGURE 2.28 The side chains of a beta strand project alternately above and below the plane of the strand

Extended description for FIGURE 2.29 In an antiparallel beta sheet, adjacent beta strands run in opposite directions



The structure of the ball-and-stick model is as follows: C atoms are depicted as black spheres, R groups are depicted as green spheres, H atoms are depicted as small white spheres, amino groups are depicted as small blue spheres, and carboxyl groups are depicted as small red spheres. The C and the N atoms form the zigzag-shaped backbone of the structure. Two peptide chains are shown above each other.

The first chain starts with a black sphere connected to another black sphere on the lower left, a blue sphere on the lower right, a white sphere above, and a green sphere behind. The blue sphere on the lower right is connected to a white sphere below and a black sphere on the upper right. The black sphere on the upper right is connected to a red sphere above and a black sphere on the lower right. The

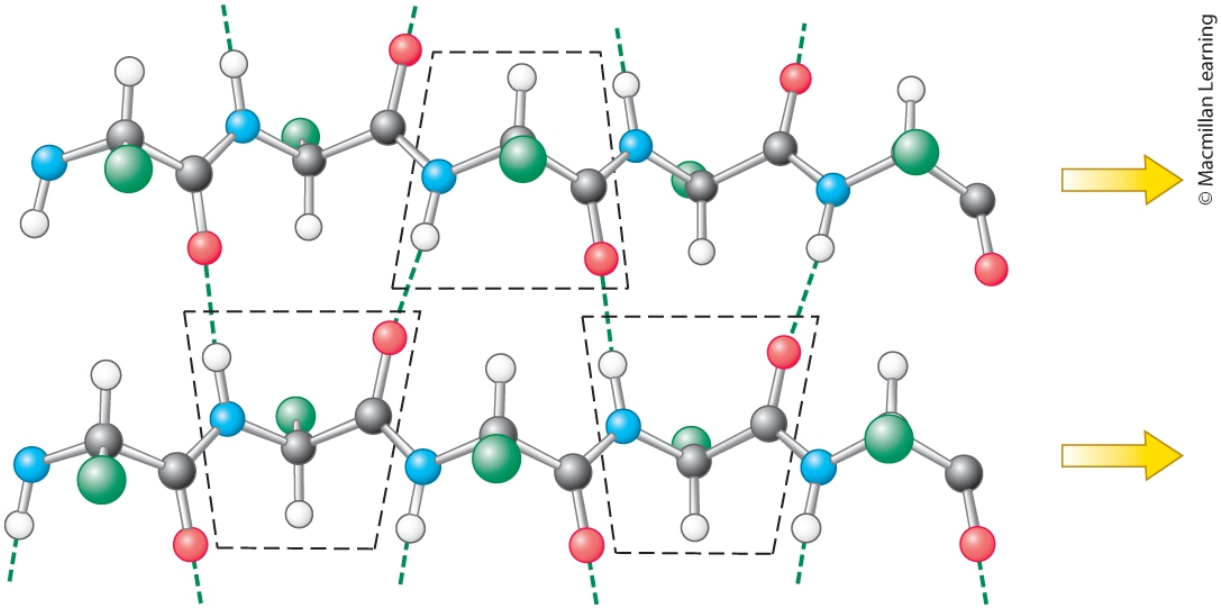
black sphere on the lower right is connected to a green sphere toward the observer, a white sphere below, and a blue sphere on the upper right.

These structures are present in an alternating manner in the first peptide. A rightward pointing arrow is present at the right of the first peptide chain. Vertical dashed lines arise upward from the first red sphere, second white sphere, second red sphere, and fourth white sphere. The second peptide chain starts with a black sphere connected to a blue sphere on the upper left, a black sphere on the upper right, a white sphere below, and a green sphere behind. The blue sphere on the upper left is connected to a white sphere above. The black sphere on the upper right is connected to a blue sphere on the lower right and a red sphere above. The blue sphere is connected to a black sphere on the upper right and a white sphere below. The black sphere on the upper right is connected to a black sphere on the lower right, a white sphere above, a green sphere toward the observer.

These structures are repeated alternately. A leftward pointing arrow is shown at the right of the second peptide chain. Vertical lines arise downward from the second white sphere, first red sphere, fourth white sphere, and second red sphere. Vertical dashed lines arising in the downward direction from the first red sphere, white sphere, second red sphere, third white sphere, third red sphere, and fifth white sphere located below the plane of the first peptide chain connect with the first white sphere, first red sphere, third white sphere, second red sphere, second red sphere, and third red sphere, respectively, located above the plane of the second peptide chain. The third molecule from the left is enclosed within dashed square boxes in both the chains.

Return to FIGURE 2.29 In an antiparallel beta sheet, adjacent beta strands run in opposite directions

Extended description for FIGURE 2.30 In a parallel β sheet, adjacent β strands run in the same direction



The structure of the ball-and-stick model is as follows: C atoms are depicted as black spheres, R groups are depicted as green spheres, H atoms are depicted as small white spheres, amino groups are depicted as small blue spheres, and carboxyl groups are depicted as small red spheres. The C and N atoms form the zigzag backbone of the structure. Two peptide chains are shown one above the other. Both the chains have the same structure.

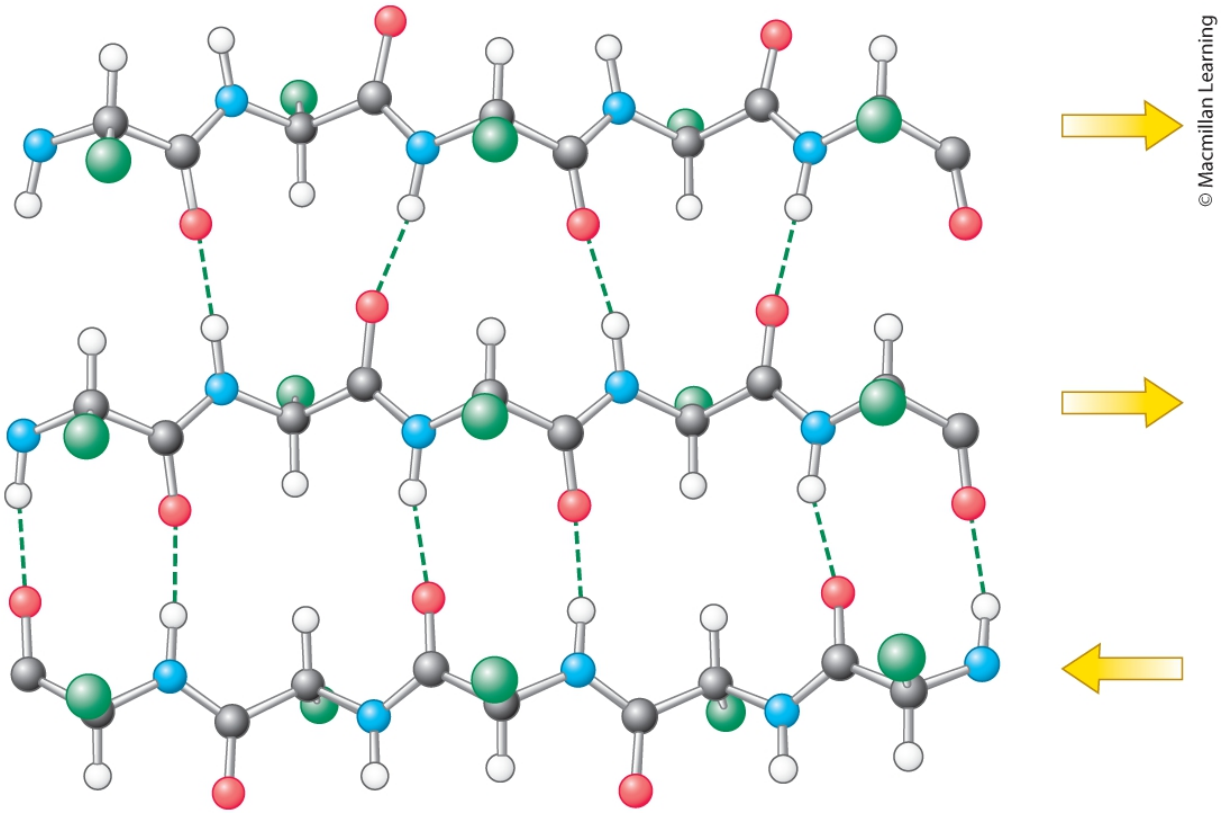
A black sphere is connected to another black sphere on the lower right, a blue sphere on the lower left, a white sphere above, and a green sphere toward the observer. The blue sphere on the lower left is connected to a white sphere below. The black sphere on the lower right is connected to a red sphere below and a blue sphere on the upper right. The blue sphere on the upper right is connected to a white sphere above and a black sphere on the lower right. The black

sphere is connected to a green sphere behind, a white sphere below, and a black sphere on the upper right.

These structures are present in an alternating manner in both the peptide chains. A right-pointing arrow is present at the right of both the peptides. Vertical dashed lines arise upward from the second white sphere above, the first red sphere, the fourth white sphere, and the second red sphere located above the plane of the first peptide. Vertical dashed lines arise downward from the first white sphere, first red sphere, third white sphere, second red sphere, fifth white sphere, and third red sphere located below the plane of the second peptide. Vertical dashed lines arising in the downward direction from the first red sphere, third white sphere, second red sphere, fifth white sphere, located below the plane of the first peptide connect with the second white sphere, first red sphere, fourth white sphere, second red sphere, and second red sphere, respectively, located above the plane of the second peptide chain. The third molecule from the left in the first peptide is enclosed within dashed boxes. The second and the fourth molecule from the left in the second peptide are enclosed within dashed boxes.

Return to FIGURE 2.30 In a parallel β sheet, adjacent β strands run in the same direction

Extended description for FIGURE 2.31 In a mixed beta sheet, the beta strands have a combination of parallel and antiparallel pairings



Three peptide chains are shown one below the other. The ball-and-stick model of an amino acid unit is as follows: Black spheres represent carbon atoms, blue spheres represent nitrogen atoms, white spheres represent hydrogen atoms, red spheres represent oxygen atoms, and green spheres represent side chains.

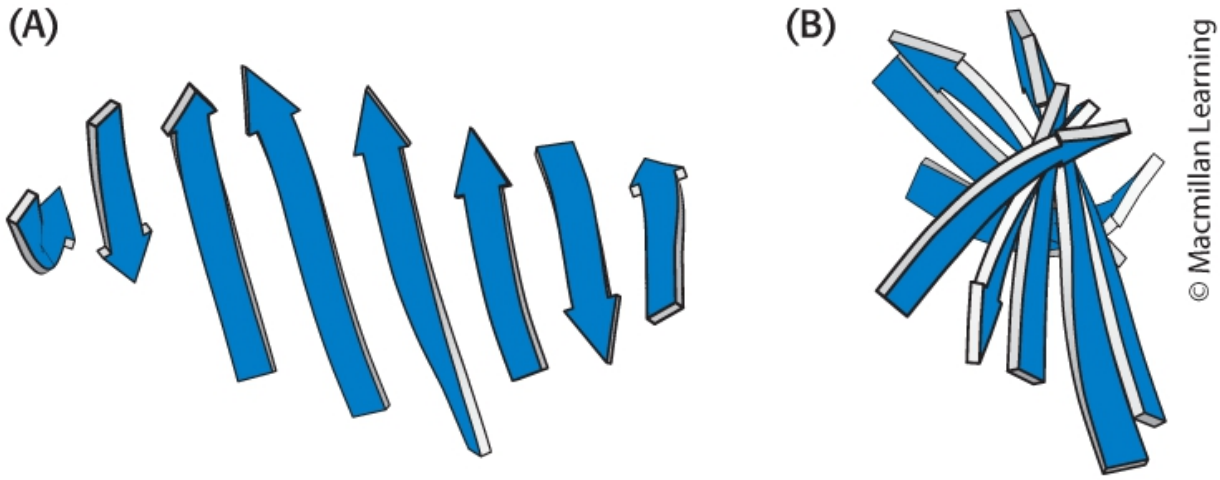
A black sphere is connected to another black sphere on the lower right, a blue sphere on the lower left, a white sphere above, and a green sphere toward the observer. The blue sphere on the lower left is connected to a white sphere below. The black sphere on the lower

right is connected to a red sphere below and a blue sphere on the upper right. The blue sphere on the upper right is connected to a white sphere above and a black sphere on the lower right. The black sphere is connected to a green sphere behind, a white sphere below, and a black sphere on the upper right.

The first and the second peptide chains are parallel to each other, and the third peptide chain is anti-parallel to the first two strands. Green dotted lines are drawn between a red and a white sphere of two peptide chains in close proximity. A right pointing arrow next to the first and the second chain indicates that the carboxy terminals of the peptide chains are oriented to the right. A left pointing arrow next to the third chain indicates that the carboxy terminal of the peptide chain is oriented to the left.

Return to FIGURE 2.31 In a mixed beta sheet, the beta strands have a combination of parallel and antiparallel pairings

Extended description for FIGURE 2.32 The twisted shape of some beta sheets is more evident in a schematic depiction of strands



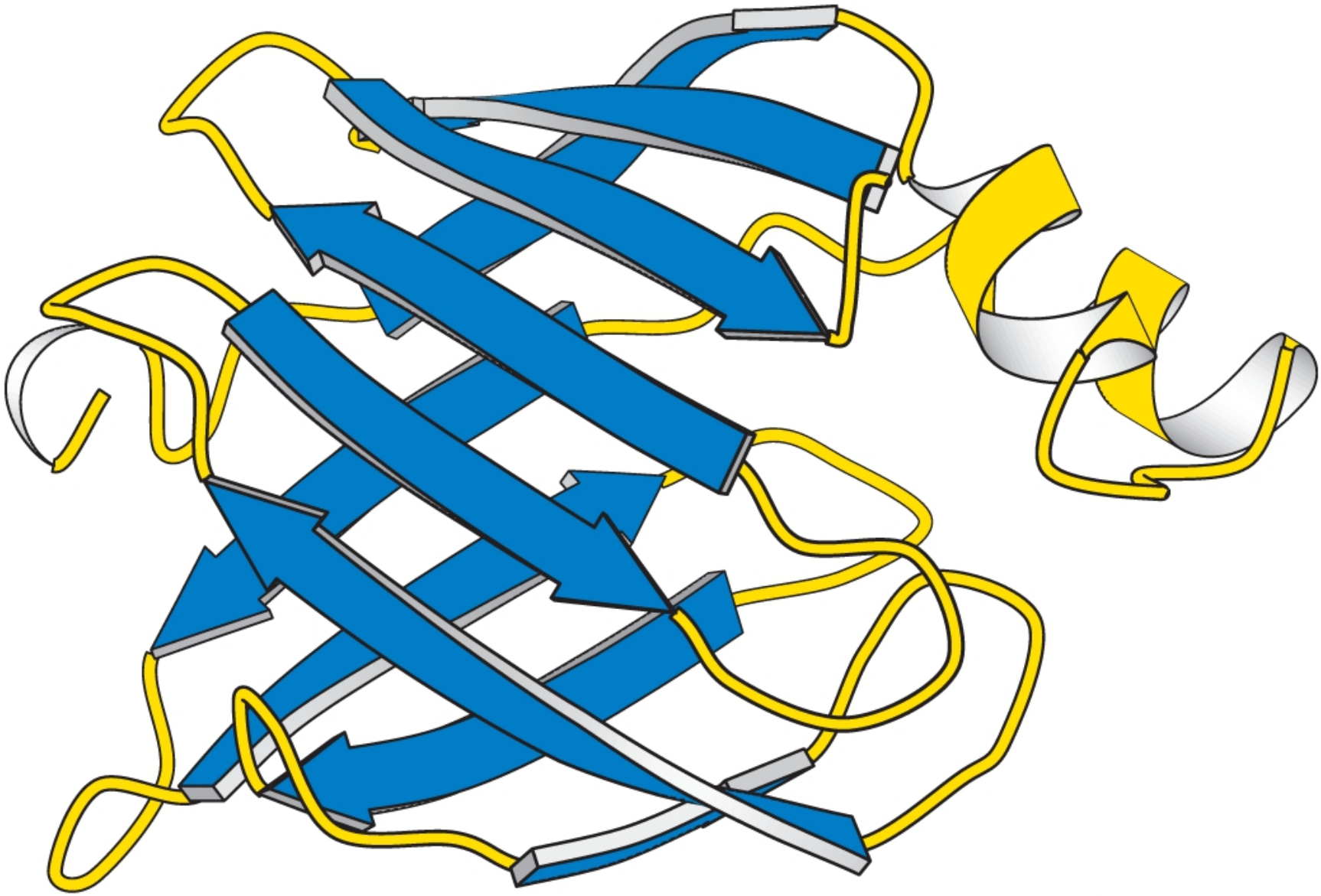
Part (A): Eight broad blue arrows are placed side by side. The first and the last arrows are twisted upward and are the shortest. The arrows look longer as they go from the ends to the middle. This diagram shows the twisted shape of beta sheets as seen from the front.

Part (B): Eight broad blue arrows are placed in a line from the front to back. The arrows gradually bend to the left from the right, from front to back. This diagram shows the twisted shape of beta sheets as seen from the side.

Return to FIGURE 2.32 The twisted shape of some beta sheets is more evident in a schematic depiction of strands

Extended description for FIGURE 2.33 Fatty acid-

binding protein is rich in beta sheets

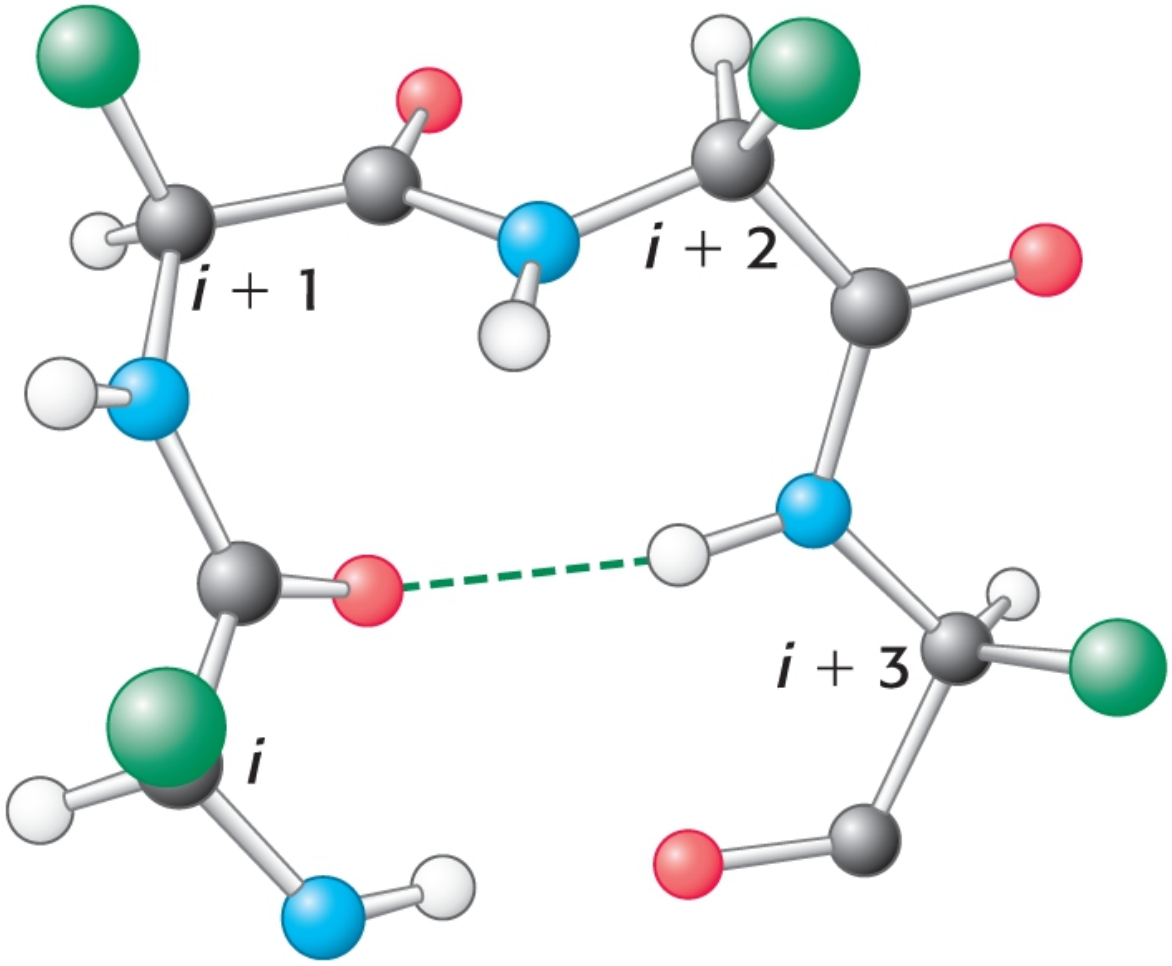


© Macmillan Learning

Broad blue arrows representing beta-sheets are arranged around an axis forming a barrel-like structure. The adjacent strands are oriented in opposite directions and connected by short tread-like loops. One of the arrows is connected to a yellow helix.

Return to FIGURE 2.33 Fatty acid-binding protein is rich in beta sheets

Extended description for FIGURE 2.34 In a reverse turn, the CO group of residue i of the polypeptide chain is hydrogen bonded to the NH group of residue i + 3



© Macmillan Learning

The ball-and-stick model of the residues in a reverse turn is shown. Each residue has the following structure: A central black sphere is connected to a black sphere on the lower right and a blue sphere on the lower left. The central black sphere is connected to a small white sphere away from the observer and a large green sphere above and toward the observer. The other black sphere is connected to a red sphere and the blue sphere is connected to a small white sphere.

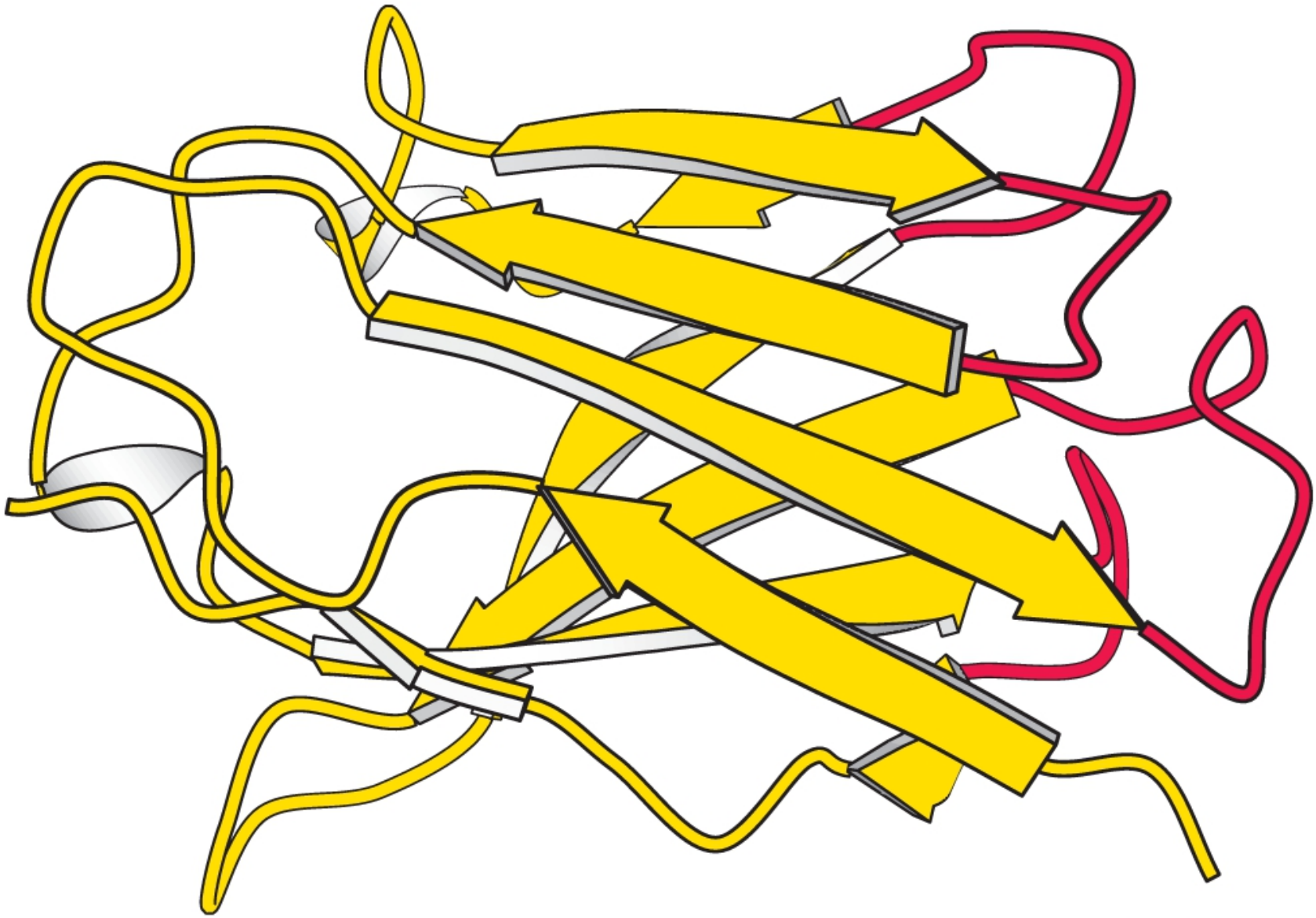
The second black sphere of one residue is connected to the blue sphere of the next residue.

Four such residues form an inverted U-shaped turn. The residues are labeled i, i plus 1, i plus 2, and i plus 3 in a clockwise direction, starting from the residue on the lower left. A dotted line is drawn between the red sphere of the first residue (i) and the small white sphere connected to the blue sphere of the fourth residue (i plus 3).

Return to FIGURE 2.34 In a reverse turn, the CO group of residue i of the polypeptide chain is hydrogen bonded to the NH group of residue i + 3

Extended description for FIGURE 2.35 Loops are found

on protein surfaces

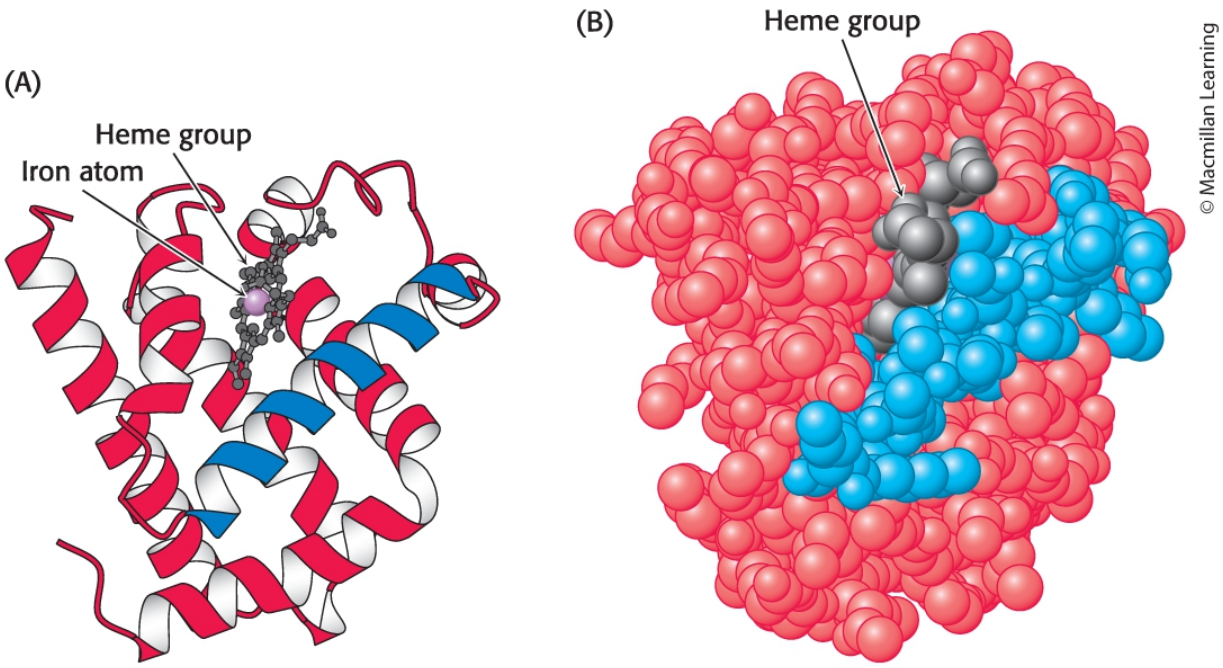


© Macmillan Learning

Antiparallel beta-sheets are shown at the center with the help of thick yellow arrows pointing in the upward and downward directions. The head and tail of the adjacent beta-strands at the bottom are connected by yellow thread-like structures forming curvy loops. The head and the tail of the adjacent beta-strands at the top are connected by red thread-like structures forming curvy loops.

Return to FIGURE 2.35 Loops are found on protein surfaces

Extended description for FIGURE 2.36 Myoglobin folds into a compact structure



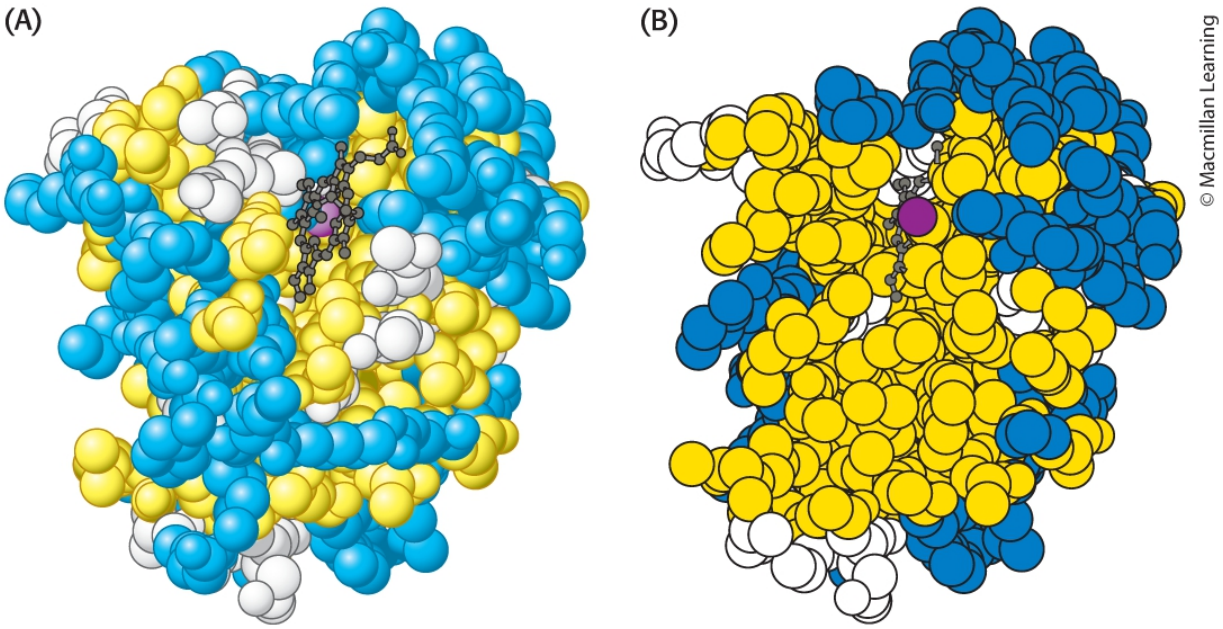
Part (A): The ribbon diagram of myoglobin is composed of six cylindrical spiral ribbons connected by thread-like loops. Four long red spiral ribbons are arranged vertically in a slanting orientation. They rest on the floor made up of one horizontal red spiral ribbon. A blue spiral ribbon crosses three vertical spiral ribbons diagonally. A molecule is present between the second and the third vertical spiral ribbon. It contains a central iron atom depicted as a light purple sphere. Several tiny black spheres cluster around the iron atom and are labeled heme group.

Part (B): The space-filling model of myoglobin is composed of red, black, and blue spheres. The red spheres form most of the myoglobin molecule. They form a broad and elongated structure. A thick cluster of blue spheres passes diagonally from the upper right

to the lower left of the myoglobin molecule. A small cluster of black spheres is present above the middle of the blue cluster and is labeled heme group.

Return to FIGURE 2.36 Myoglobin folds into a compact structure

Extended description for FIGURE 2.37 Hydrophobic amino acids are preferentially distributed in the interior of myoglobin.

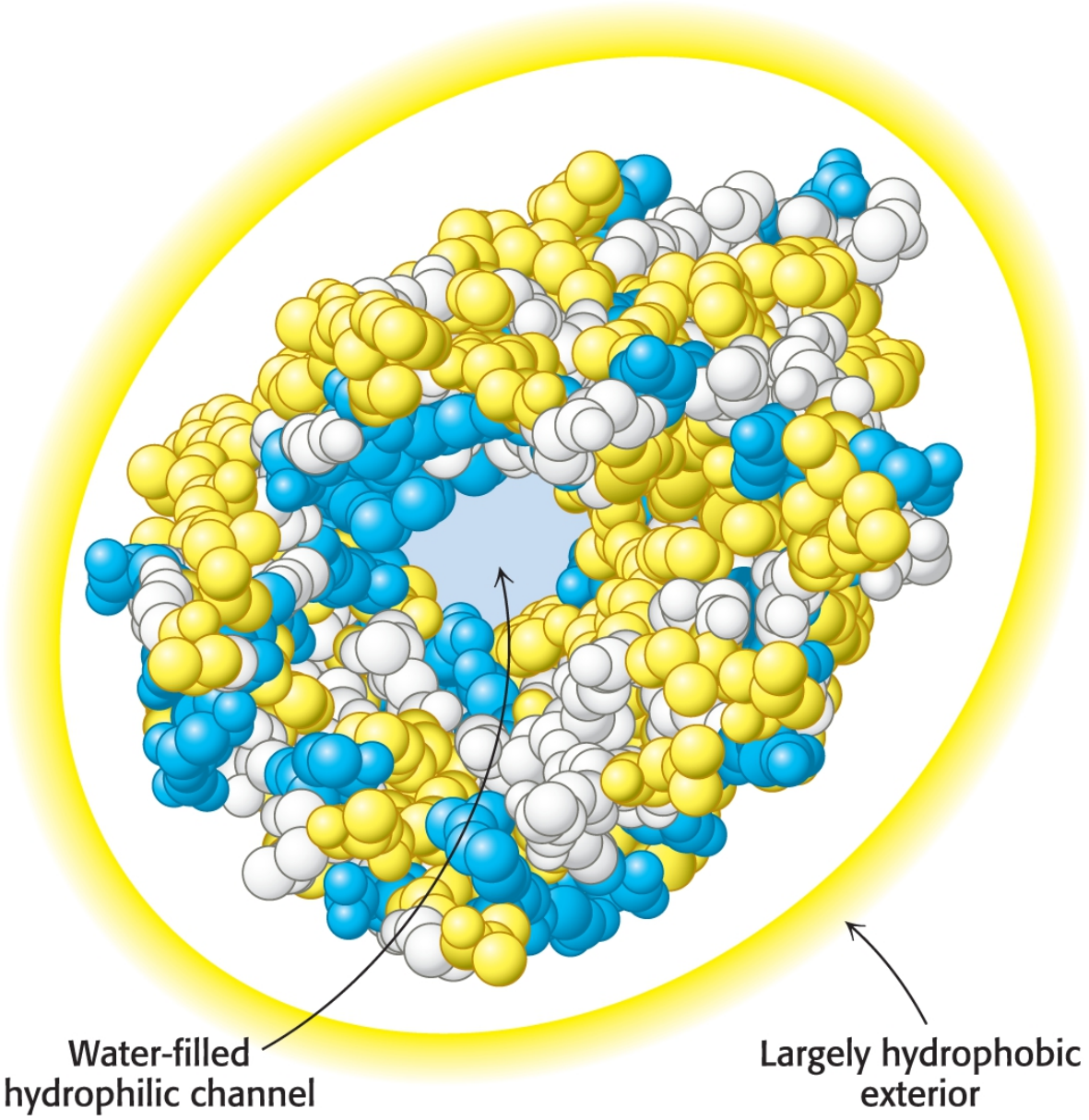


Part (A): The three-dimensional structure is roughly circular. The atoms are represented as spheres. The hydrophobic amino acids are shown in yellow, charged amino acids are shown in blue, and others are shown in white. The surface of the protein is covered with blue spheres interspaced with yellow and white spheres. A cluster of small black spheres at the center encloses a purple sphere.

Part (B): The cross-section of myoglobin shows a purple circle at the center. Most of the interior of the protein is filled with yellow circles.

Return to FIGURE 2.37 Hydrophobic amino acids are preferentially distributed in the interior of myoglobin.

Extended description for FIGURE 2.38 Porin, found in the hydrophobic environment of the membrane, exhibits an “inside out” amino acid distribution



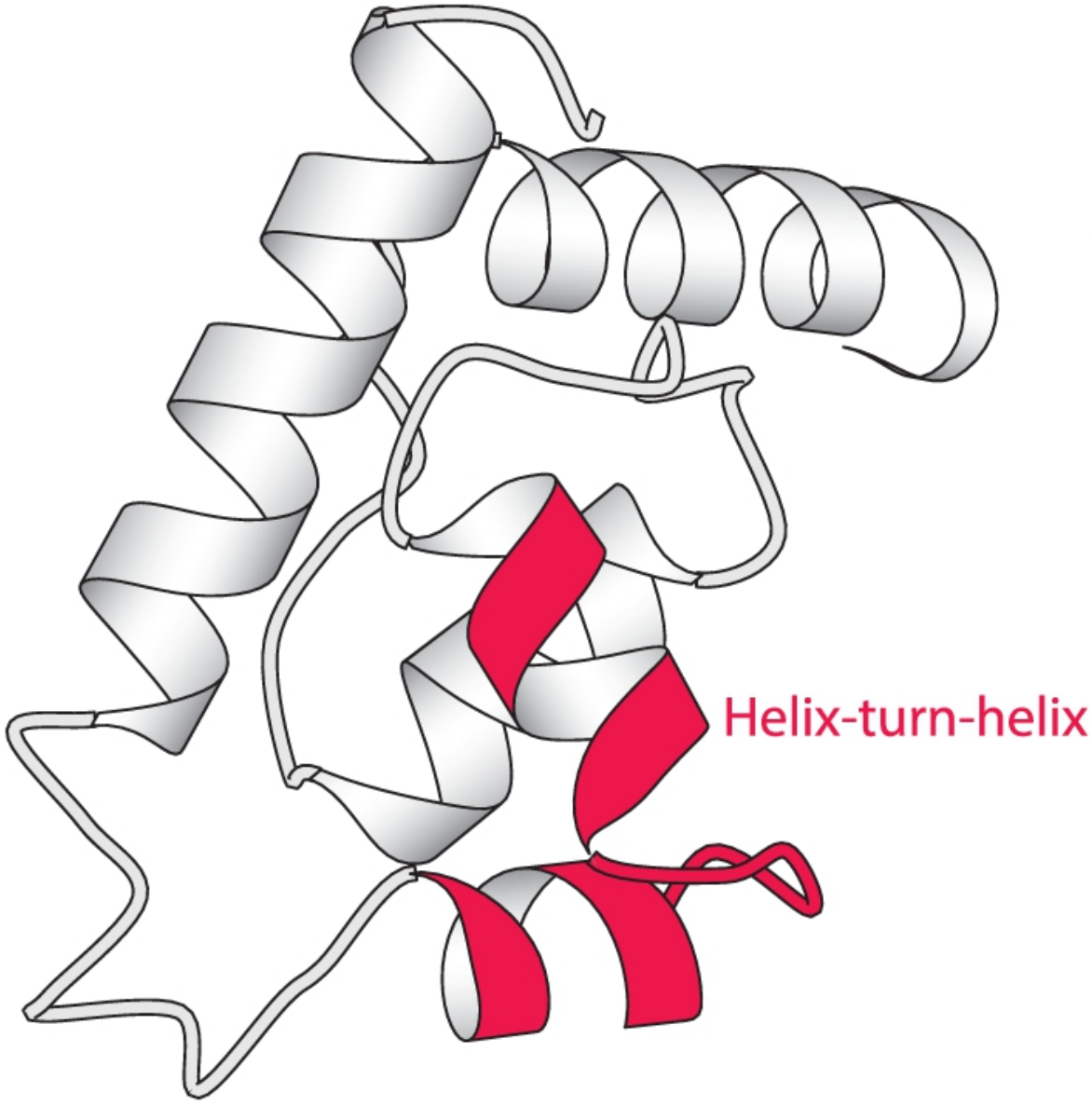
© Macmillan Learning

The structure is donut-shaped. The periphery of the structure is mostly made up of yellow spheres, which make up of hydrophobic

amino acids. The region around the central void is mostly made up of blue spheres which make up hydrophilic amino acids. The yellow and blue spheres are interspaced with white spheres. The void at the center is labeled water-filled hydrophilic channel. A circle around the protein is labeled largely hydrophobic exterior.

Return to FIGURE 2.38 Porin, found in the hydrophobic environment of the membrane, exhibits an “inside out” amino acid distribution

Extended description for FIGURE 2.39 The helix-turn-helix motif is a supersecondary structural element found in many DNA-binding proteins



© Macmillan Learning

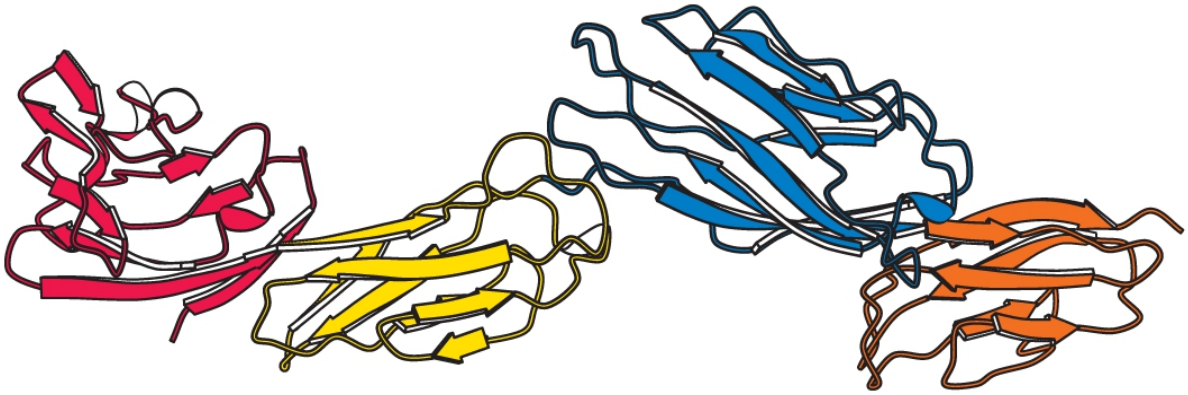
The diagram consists of 3 cylindrical white spiral ribbons. One ribbon is longer than the other two ribbons. One of the short ribbons is present horizontally on the top right of the long ribbon.

The second short ribbon is present vertically on the bottom right of the long ribbon. These ribbons are connected by thread-like loops.

A set of two short cylindrical red spiral ribbons are present in front of the short ribbon. These red spiral ribbons are arranged such that one red spiral ribbon forms a horizontal floor on which the second red spiral ribbon rests in a slanting orientation. These red spiral ribbons are connected by a red thread-like structure that forms a knotted loop. The short red spiral ribbons and the knotted loop are labeled helix-turn-helix.

Return to FIGURE 2.39 The helix-turn-helix motif is a supersecondary structural element found in many DNA-binding proteins

Extended description for FIGURE 2.40 Domains are compact regions within proteins that are connected by flexible polypeptide segments

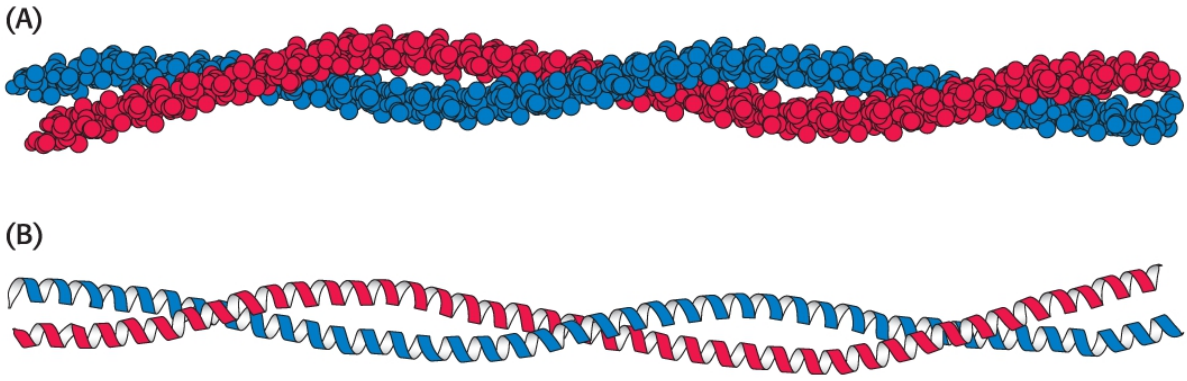


© Macmillan Learning

A set of 4 antiparallel beta-sheets are shown. The antiparallel beta-strands in each beta-sheet are shown as thick arrows pointing in opposite directions. The head and tail of the adjacent antiparallel beta-strands are connected by long, curved thread-like structures.

Return to FIGURE 2.40 Domains are compact regions within proteins that are connected by flexible polypeptide segments

Extended description for FIGURE 2.41 The alpha-helical coiled coil adopts an extended structure



© Macmillan Learning

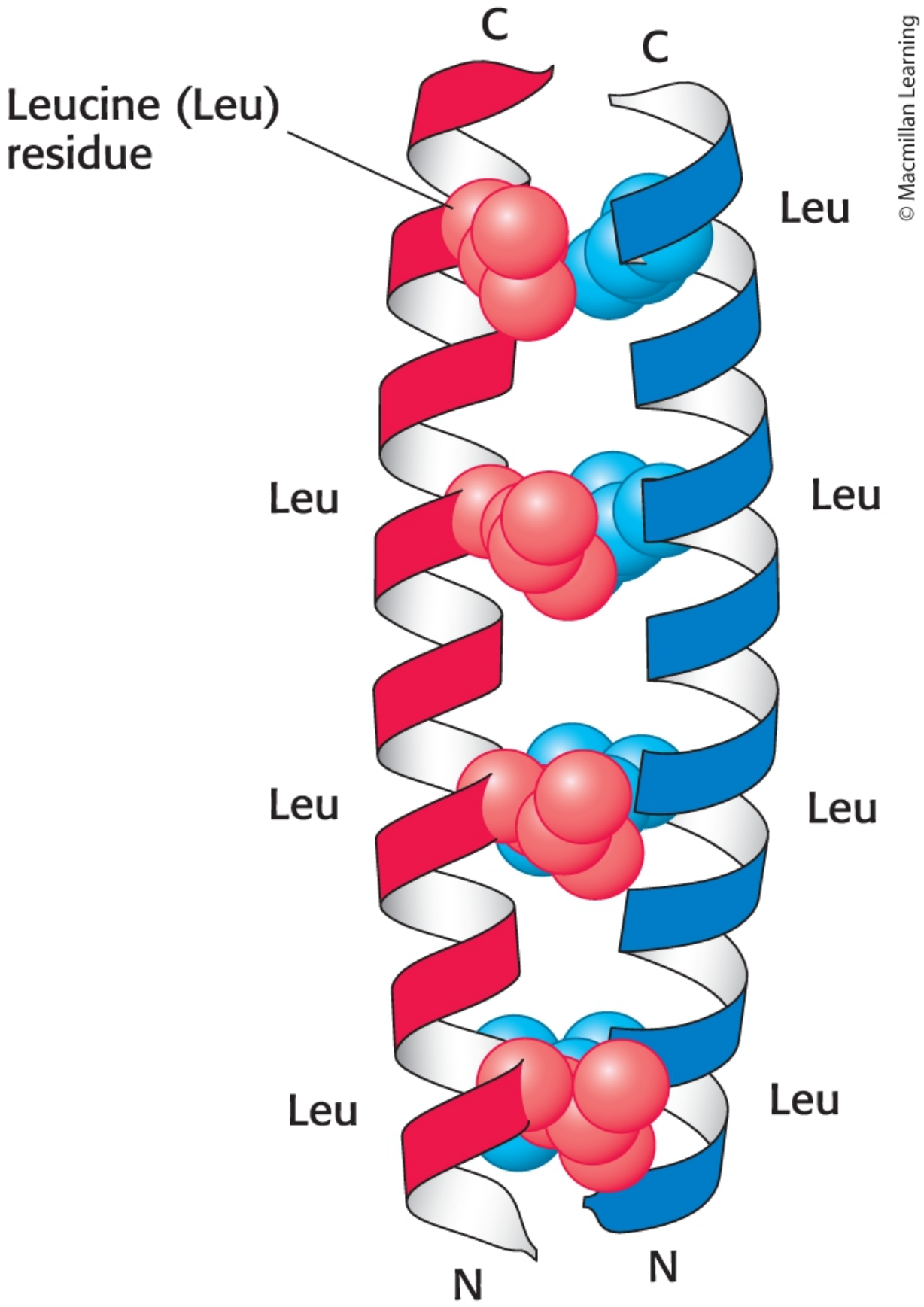
Part (A): Two alpha helices are made of red and blue spheres representing atoms, respectively. The two helices twist around each other to form a coiled structure.

Part (B): The two alpha helices are represented using two red and blue ribbons. The two ribbons twist around each other to form a coiled structure.

Return to FIGURE 2.41 The alpha-helical coiled coil adopts an extended structure

Extended description for FIGURE 2.42 Heptad repeats from each helix in a coiled-coil protein interact with

one another



© Macmillan Learning

Two protein helices are shown running parallel to each other. The left helix is red, and the right helix is blue. The helices have opposite turns, and the top terminals are labeled C, and the bottom terminals are labeled N. Four sets of four red spheres attached to the red helix interact with four sets of four blue spheres of the blue helix. Each set of spheres represents a leucine residue.

Return to FIGURE 2.42 Heptad repeats from each helix in a coiled-coil protein interact with one another

Extended description for FIGURE 2.43 The amino acid sequence of a part of a collagen chain reveals that every third residue is a glycine.

13
-Gly-Pro-Met-Gly-Pro-Ser-Gly-Pro-Arg-
22
-Gly-Leu-Hyp-Gly-Pro-Hyp-Gly-Ala-Hyp-
31
-Gly-Pro-Gln-Gly-Phe-Gln-Gly-Pro-Hyp-
40
-Gly-Glu-Hyp-Gly-Glu-Hyp-Gly-Ala-Ser-
49
-Gly-Pro-Met-Gly-Pro-Arg-Gly-Pro-Hyp-
58
-Gly-Pro-Hyp-Gly-Lys-Asn-Gly-Asp-Asp-

© Macmillan Learning

The first sequence starts from the thirteenth residue: Glycine, Proline, Methionine, Glycine, Proline, Serine, Glycine, Proline, Arginine

The second sequence starts from the twenty-second residue: Glycine, Leucine, Hydroxyproline, Glycine, Proline, Hydroxyproline, Glycine, Alanine, Hydroxyproline

The third sequence starts from the thirty-first residue: Glycine, Proline, Glutamine, Glycine, Phenylalanine, Glutamine, Glycine, Proline, Hydroxyproline

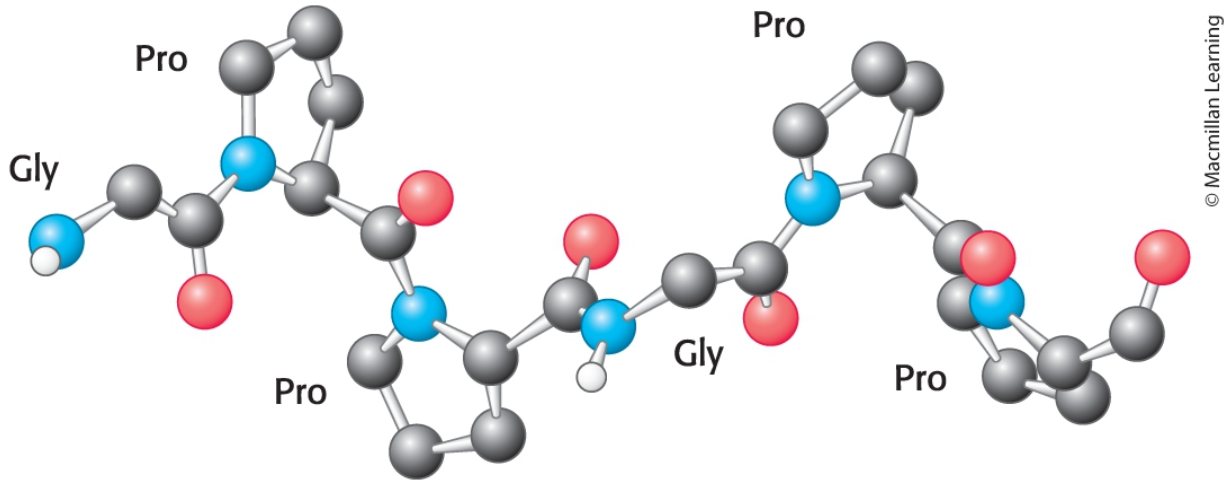
The fourth sequence starts from the fortieth residue: Glycine, Glutamine, Hydroxyproline, Glycine, Glutamine, Hydroxyproline, Glycine, Alanine, Serine

The fifth sequence starts from the forty-ninth residue: Glycine, Proline, Methionine, Glycine, Proline, Arginine, Glycine, Proline, Hydroxyproline

The sixth sequence starts from the fifty-eighth residue: Glycine, Proline, Hydroxyproline, Glycine, Lysine, Asparagine Glycine, Aspartic acid, Aspartic acid

Return to FIGURE 2.43 The amino acid sequence of a part of a collagen chain reveals that every third residue is a glycine.

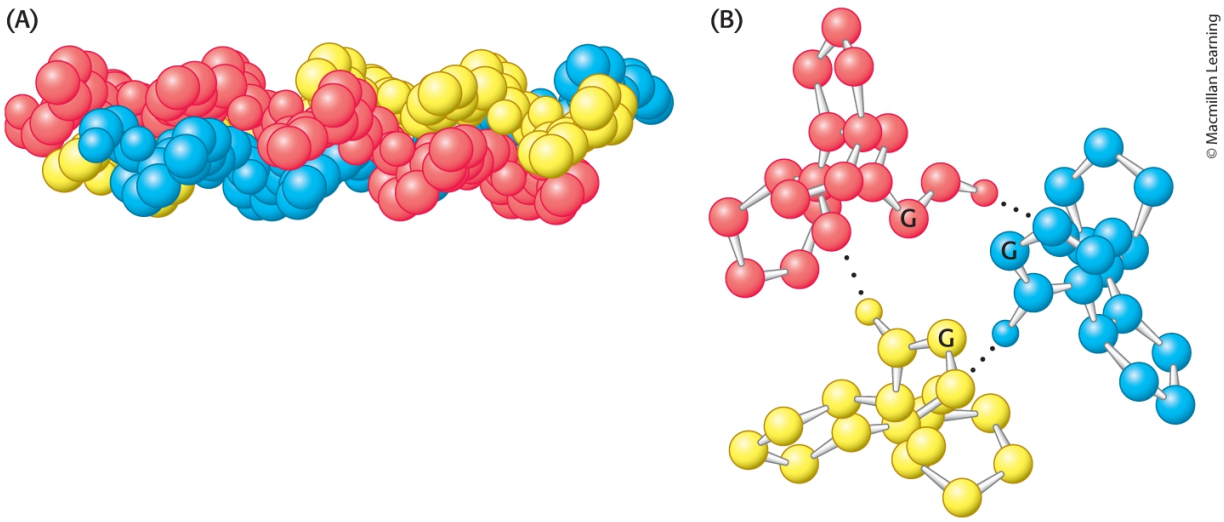
Extended description for FIGURE 2.44 A single strand of a collagen triple helix adopts an extended conformation



In the ball-and-stick model, the C atoms are represented as black spheres, oxygen atoms as red spheres, and nitrogen atoms as blue spheres. The sequence of the strand is as follows: Glycine, Proline, Proline, Glycine, Proline, Proline.

Return to FIGURE 2.44 A single strand of a collagen triple helix adopts an extended conformation

Extended description for FIGURE 2.45 Glycine residues form the interior of the collagen triple helix

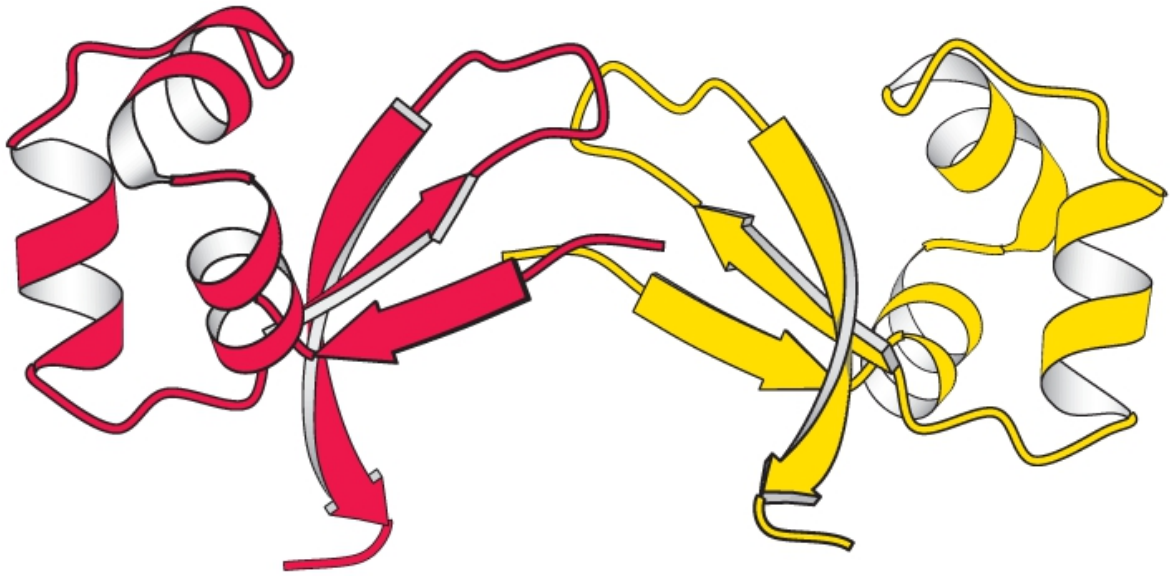


Part (A): Three chains of red, blue, and yellow spheres, respectively, are twisted forming a triple helical structure.

Part (B): A cross-section of a collagen triple-helix is shown. Glycine and pyroline residues of the red, blue, and yellow strands are shown arranged in a circle. Dotted lines representing hydrogen bonds are drawn between the adjacent stands. The alpha-C atoms of glycine residues of each strand are labeled and are oriented to the center of the triple-helix. The pyrrolidine rings of the proline residues are oriented toward the periphery.

Return to FIGURE 2.45 Glycine residues form the interior of the collagen triple helix

Extended description for FIGURE 2.46 Quaternary structure refers to the arrangement of multiple polypeptide chains



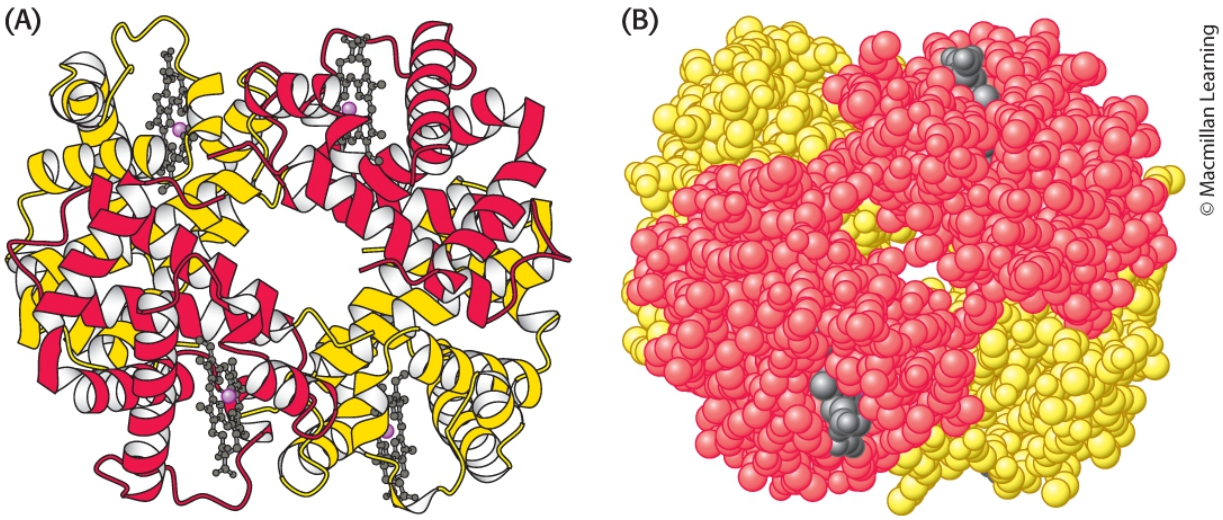
The homodimer consists of two identical structures facing each other. The first structure consists of two cylindrical spiral ribbons on the left. The cylindrical spiral ribbons are connected by narrow and wavy thread-like structures on the top. A thread from the left spiral connects it to the tail of a beta-sheet arrow on the right. The beta-sheet is composed of a pair of antiparallel beta-strands. The antiparallel beta-strands are depicted as thick arrows pointing in opposite directions.

The head and tail of the arrows are connected by a thread-like structure on the top. The downward-facing head of one arrow is attached to a free short thread-like structure. A thread from the right spiral connects to the head of a beta-strand arrow. The tail of the beta-strand arrow has a free short thread-like structure. The beat sheets of the first structure face the beat-sheets of the second

structure. The second structure is a mirror image of the first structure.

Return to FIGURE 2.46 Quaternary structure refers to the arrangement of multiple polypeptide chains

Extended description for FIGURE 2.47 Human hemoglobin is composed of an alpha 2 beta 2 tetramer

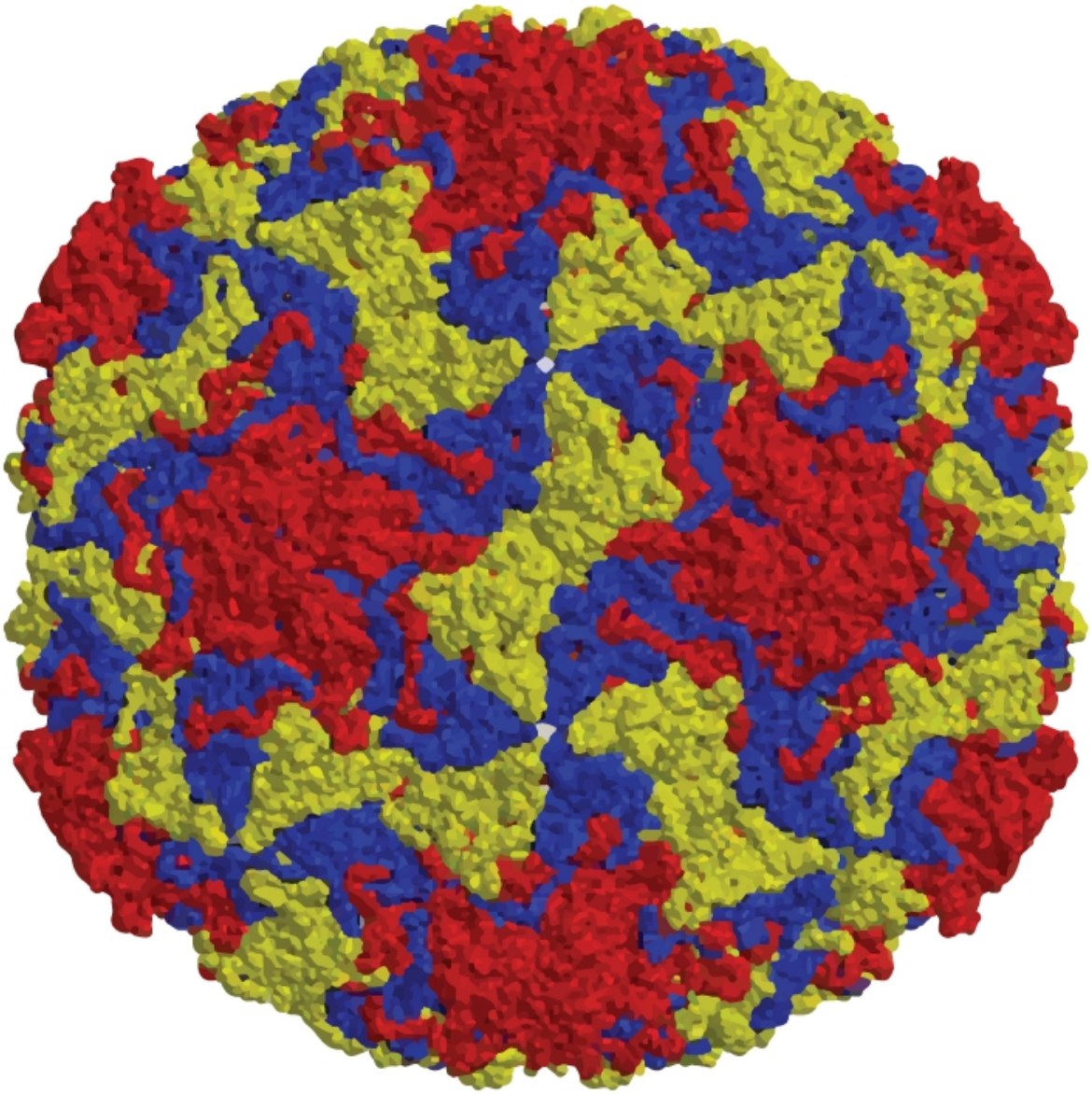


Part (A): Four similar units mainly composed of alpha helices are shown to aggregate together forming a donut shape. Out of the four units, two units are yellow and two units are red. A red unit is adjacent to a yellow unit. At the center of each unit is a heme group represented as a purple sphere enclosed in a cage of small black spheres.

Part (B): The space-filling model shows the same structure as described above. The units are made up of red and yellow spheres, respectively.

Return to FIGURE 2.47 Human hemoglobin is composed of an alpha 2 beta 2 tetramer

Extended description for FIGURE 2.48 Viral coat proteins adopt complex quaternary structures with many copies of relatively few unique subunits



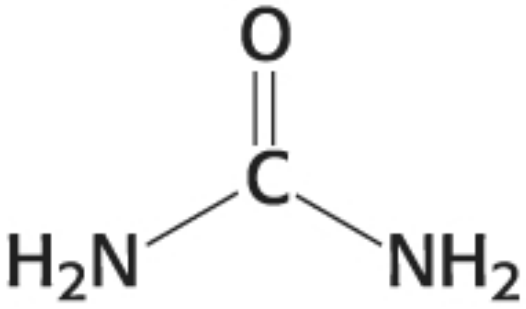
© Macmillan Learning

The quaternary structure has a hexagonal shape. The vertices of the hexagon are curved. Large blue star-shaped patches are present against a yellow background. The star-shaped patches have irregular

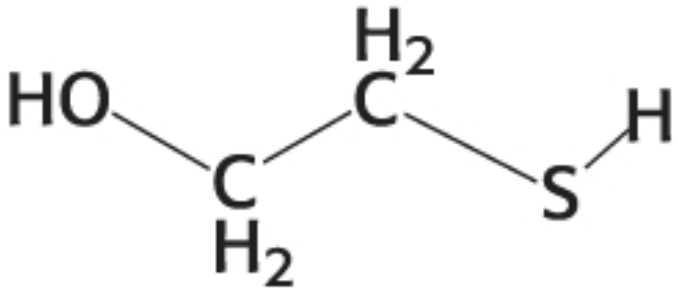
margins. Within the star-shaped patches, red patches are present at the center. All the patches have a rough bumpy texture.

Return to FIGURE 2.48 Viral coat proteins adopt complex quaternary structures with many copies of relatively few unique subunits

Extended description for Urea and beta-mercaptoethanol



Urea

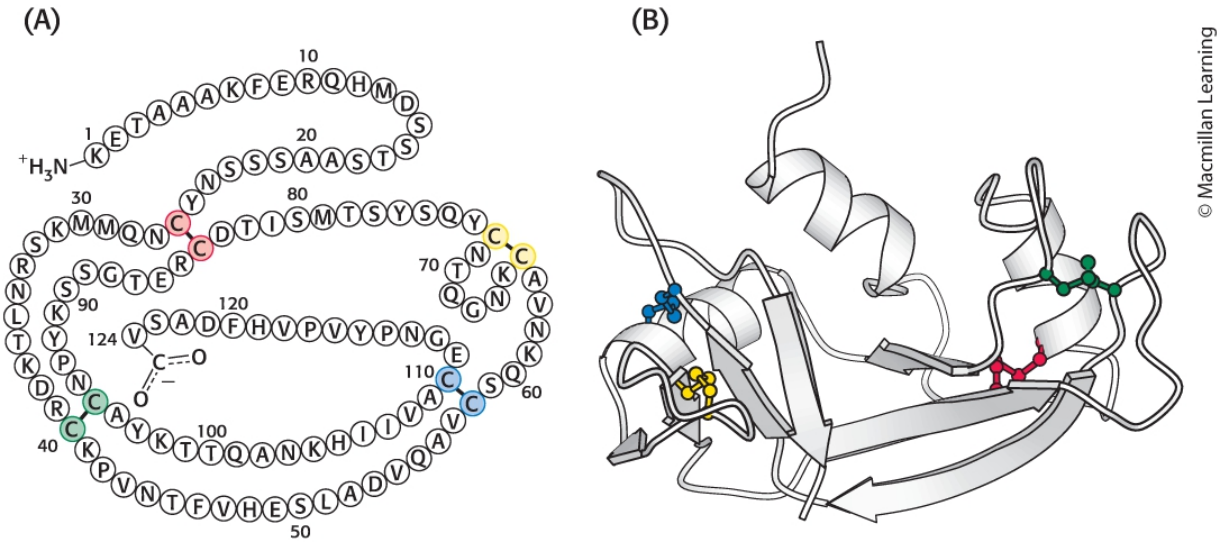


β-Mercaptoethanol

The structure of urea is as follows: A central C atom is single bonded to N H 2 on the lower left and N H 2 on the lower right, and double bonded to O above. The structure of beta-mercaptoethanol is as follows: O H, single bond, C, single bond, C, single bond, S, single bond, H in a zigzag manner. Both C atoms are bound by H 2.

Return to Urea and beta-mercaptoethanol

Extended description for FIGURE 2.49 Bovine ribonuclease is a single polypeptide chain with four intramolecular disulfide bonds

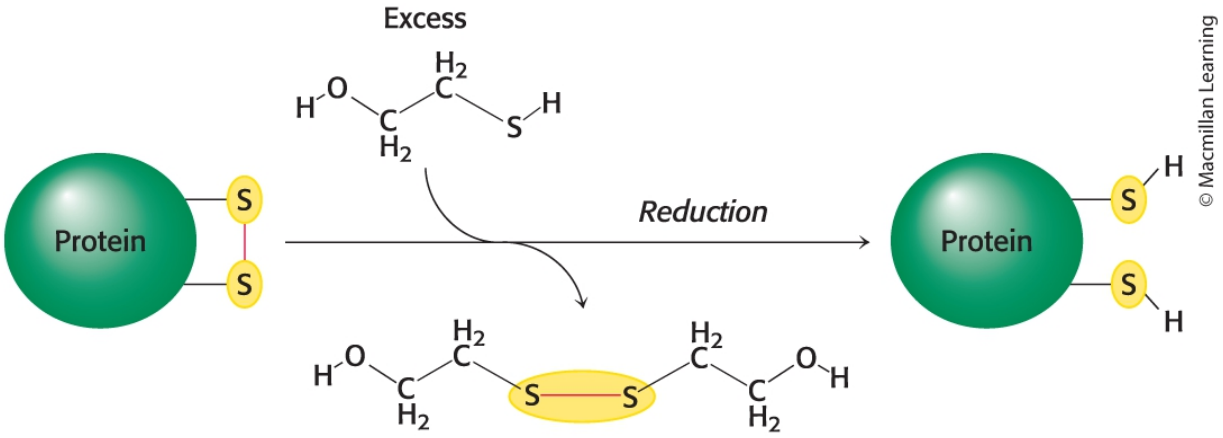


Part (A): The primary structure of bovine ribonuclease is illustrated as a string of circles representing amino acid residues folding into a roughly spiral shape. Some non-adjacent cysteine residues in the chain are linked to each other. Residue 26 is linked to residue 84, residue 40 is linked to residue 95, residue 110 is linked to residue 58, and residue 72 is linked to residue 65.

Part (B): The three-dimensional structure forms a roughly U-shape. It consists of some alpha-helices represented by helical ribbon-like structures and some beta sheets represented by broad arrows. These structures are connected by short thread-like loops. The linked cysteine residues are represented as clusters of red, yellow, green, and blue spheres.

Return to FIGURE 2.49 Bovine ribonuclease is a single polypeptide chain with four intramolecular disulfide bonds

Extended description for FIGURE 2.50 Beta-Mercaptoethanol disrupts disulfide bonds



The reaction consists of two reactants and two products. The first reactant has the following structure: A large green sphere labeled protein has two S atoms linked to it on its side. A red disulfide bond is present between the two S atoms. S atoms are highlighted in yellow. The second reactant is in excess and has the following structure: C H 2 is single bonded to C H 2 on the upper right. C 1 is single bonded to O on the upper left which is single bonded to H on the lower left. C 2 is single bonded to S on the lower right which is single bonded to H on the upper right.

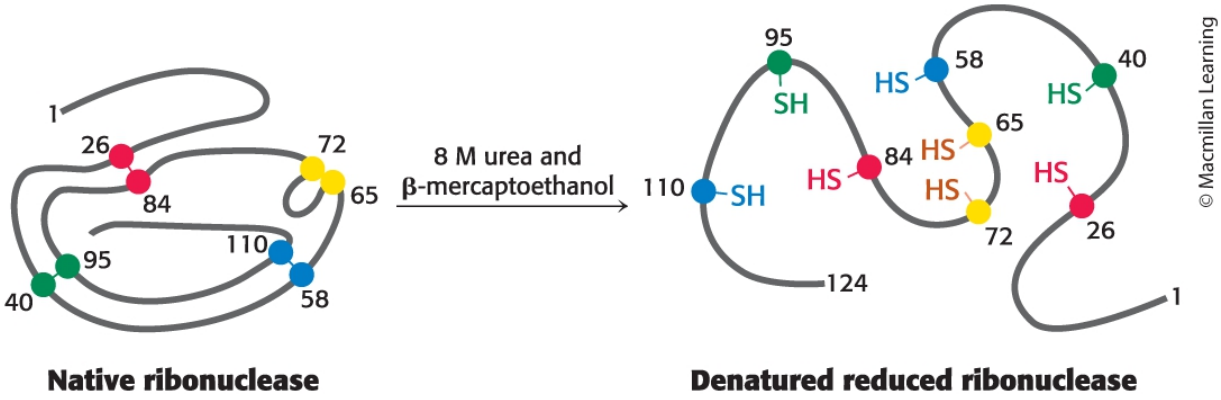
The reaction arrow is labeled reduction.

The first product has the following structure: A large green sphere labeled protein has two S atoms linked to it on its side. The S atoms are each single bonded to H atoms to the right, which are pointing away from each other. S atoms are highlighted in yellow. The second product has the following structure: Two molecules of the second reactant are placed side-by-side such that the respective S atoms are

facing each other. The S atoms are single bonded to each other highlighted in red and the bonding is shown within a yellow sphere.

Return to FIGURE 2.50 Beta-Mercaptoethanol disrupts disulfide bonds

Extended description for FIGURE 2.51 Ribonuclease is denatured with urea and β-mercaptoethanol



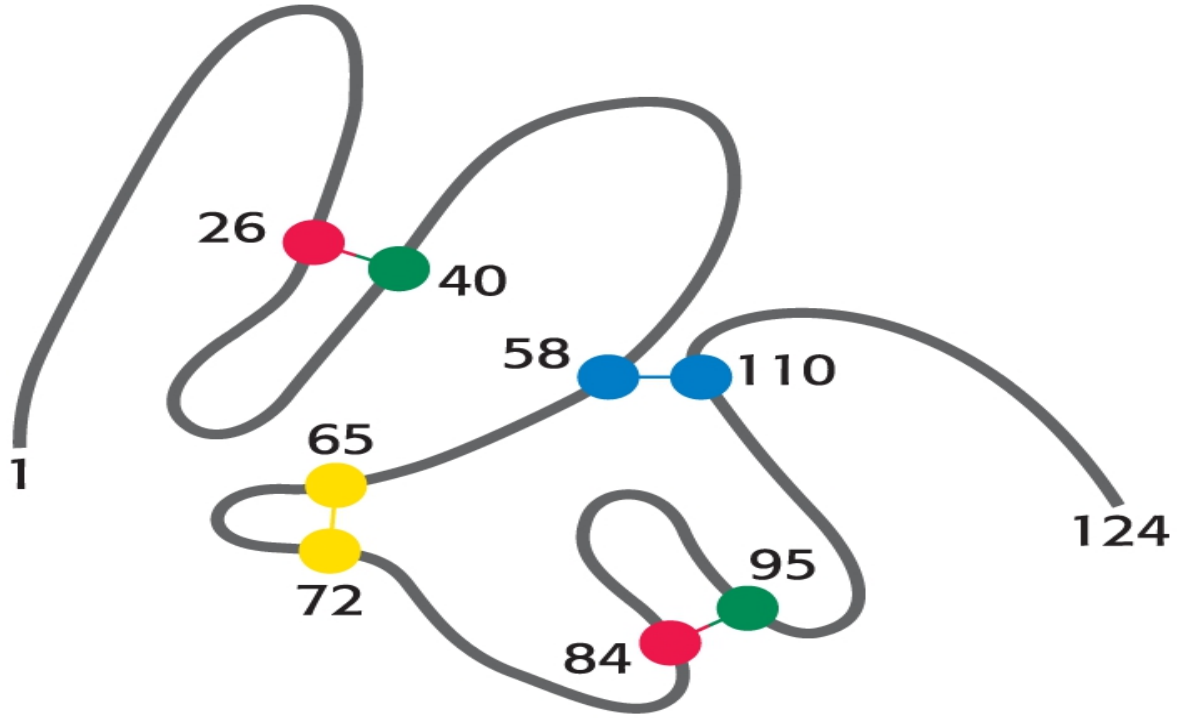
The reactant is native ribonuclease and is depicted as a curved gray line that folds inwards to form a loose coiled structure. The markings on the gray line from the extreme top end to the interior are as follows: 1, 26, 40, 58, 65, 72, 84, 95, and 110. The markings located adjacently are 26 and 84, 40 and 95, 65 and 72, and 58 and 110. The line makes an inward loop at the point of contact between the markings 65 and 72. The reaction arrow is labeled 8 M urea and beta-mercaptoethanol.

The product is denatured reduced ribonuclease and is depicted as a curved gray line that starts from the bottom left, forms two large loops, and ends at the bottom right. The markings on the gray line from the extreme right end to the extreme left end are 1, 26, 40, 58, 65, 72, 84, 95, 110, and 124. The markings 26, 40, 58, 65, 72, 84, 95, and 110 are each connected to an S H group.

Return to FIGURE 2.51 Ribonuclease is denatured with urea and β-mercaptoethanol

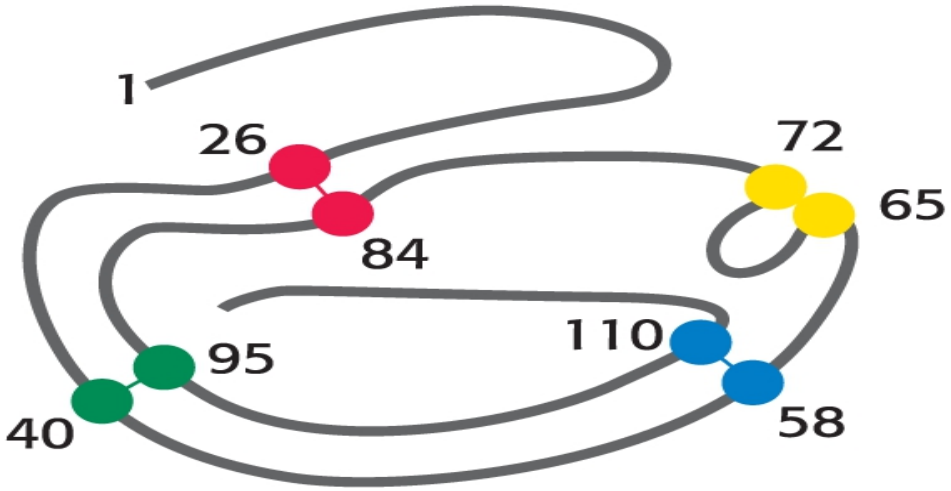
Extended description for FIGURE 2.52 Native ribonuclease can be re-formed from scrambled

ribonuclease in the presence of a trace of beta-mercaptoethanol



Scrambled ribonuclease

Trace of
β-mercaptoethanol



Native ribonuclease

© Macmillan Learning

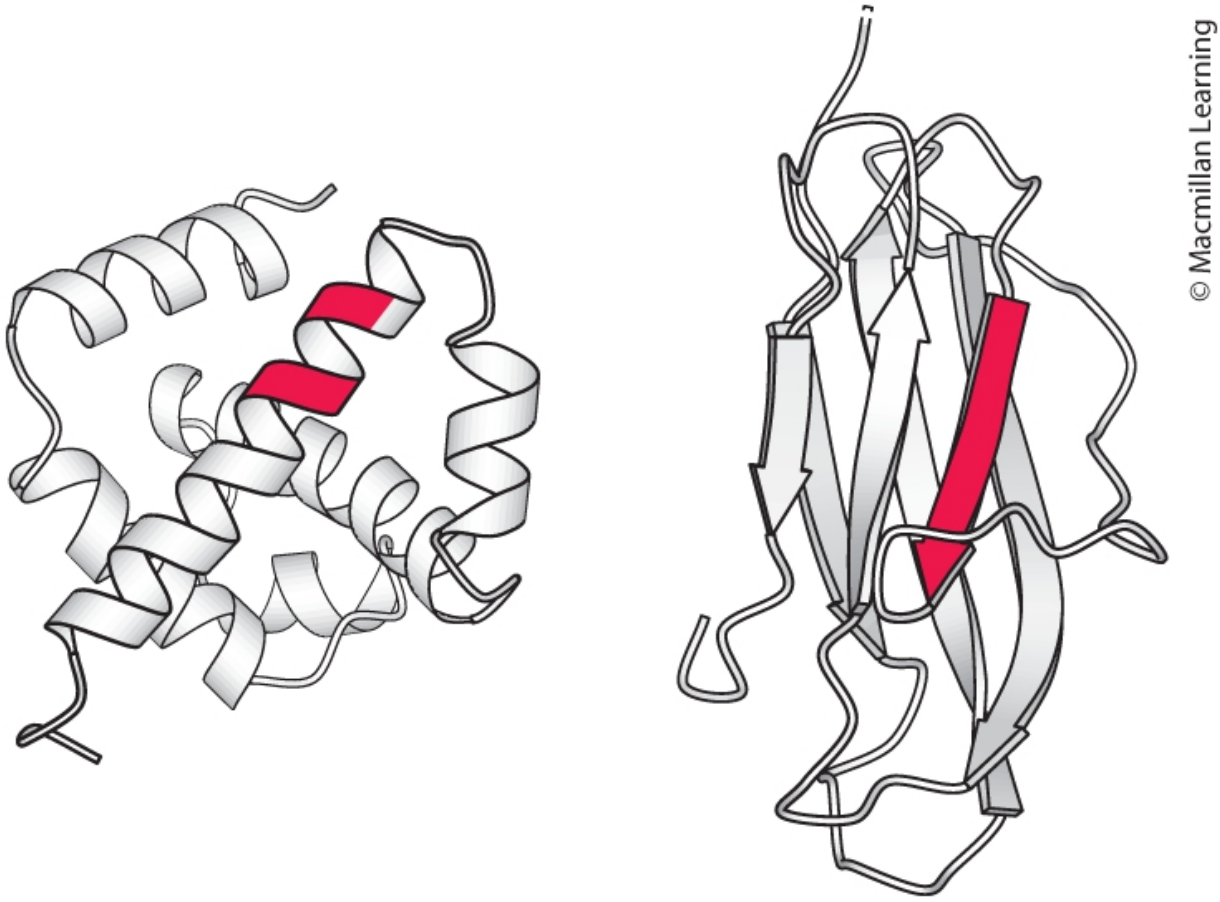
Scrambled ribonuclease is represented as a long string of amino acids. Residues 26 and 84 are highlighted in red. Residues 40 and 95 are highlighted in green. Residues 65 and 72 are highlighted in yellow. Residues 58 and 110 are highlighted in blue. Residue 26 is linked to residue 40. Residue 65 is linked to residue 72. Residue 58 is linked to residue 110. Residue 84 is linked to residue 95.

A downward arrow labeled trace of beta-mercaptoethanol points from scrambled ribonuclease to native ribonuclease.

In the native ribonuclease, residue 26 is linked to residue 84, residue 40 is linked to residue 95, residue 110 is linked to residue 58, and residue 72 is linked to residue 65. The amino acid string folds into a roughly spiral shape.

Return to FIGURE 2.52 Native ribonuclease can be re-formed from scrambled ribonuclease in the presence of a trace of beta-mercaptoethanol

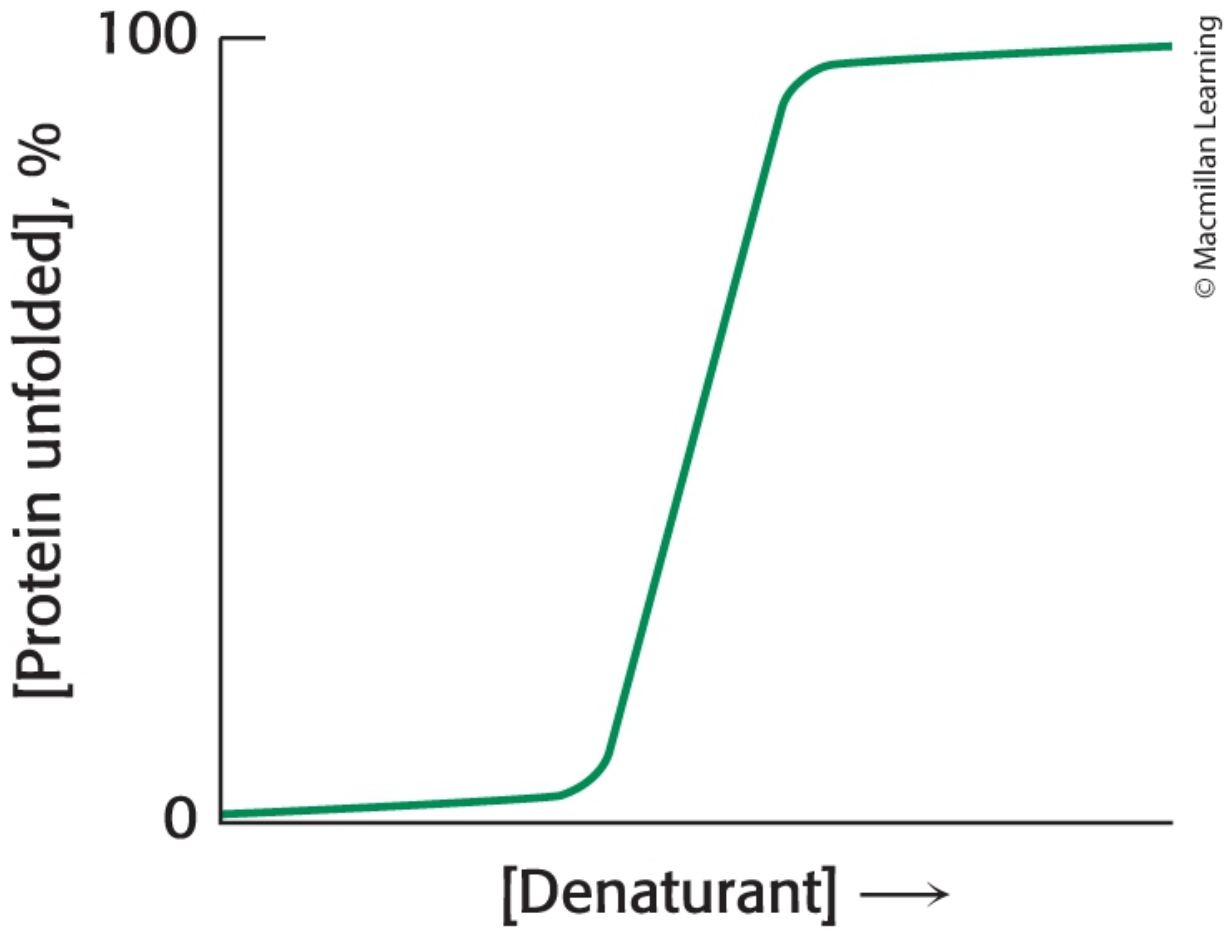
Extended description for FIGURE 2.53 Many sequences can adopt alternative conformations in different proteins



In the first protein, several alpha helices are connected by short thread-like loops. A short segment of one of the alpha helices is highlighted in red. In the second protein, several beta strands are connected by short thread-like loops. A short segment of one of the beta strands is highlighted in red. Both the red regions have the same amino acid sequences.

Return to FIGURE 2.53 Many sequences can adopt alternative conformations in different proteins

Extended description for FIGURE 2.54 The transition from folded to unfolded state is abrupt



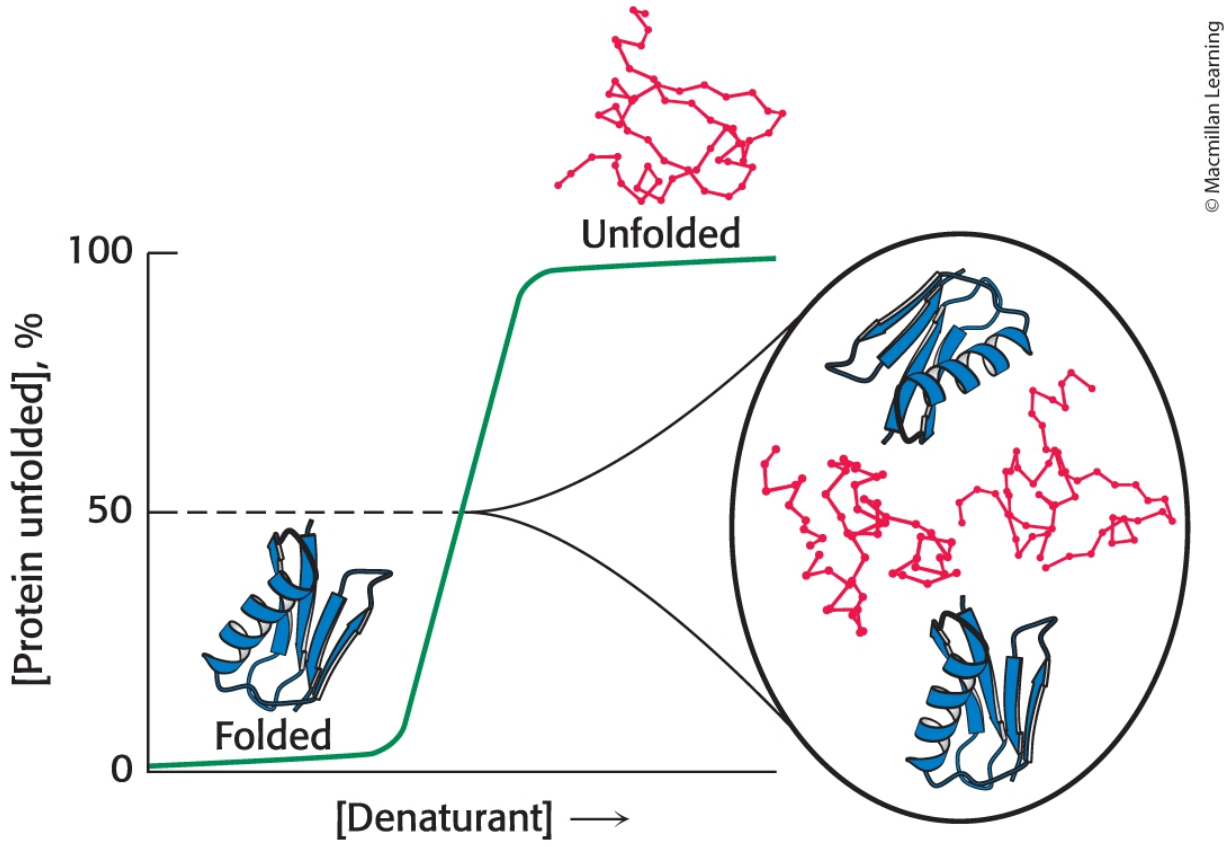
The horizontal axis is labeled concentration of denaturant and increases from left to right. The vertical axis is labeled concentration of protein unfolded, percentage and has two markings: 0 and 100. The marking 0 is located at the bottom and the marking 100 is located at the top of the vertical axis.

A curve begins at the 0 mark on the vertical axis and moves horizontally toward the right. It rises steeply toward the right at a point just before the mid point of the horizontal axis. The curve

continues rising until it reaches just below the 100 mark on the vertical axis. It then moves horizontally toward the right at a point after the mid point of the horizontal axis. The curve gradually reaches the 100 marking on the vertical axis.

Return to FIGURE 2.54 The transition from folded to unfolded state is abrupt

Extended description for FIGURE 2.55 At the denaturation midpoint, half the molecules are fully folded and half are fully unfolded



© Macmillan Learning

The horizontal axis is labeled concentration of denaturant and a rightward arrow indicates increasing concentration. The vertical axis is labeled concentration of protein unfolded, percentage and ranges from 0 to 100 in increments of 50 units. An S-shaped curve starts at the origin, gradually rises to nearly 5 percent, followed by a steep rise to nearly 100 percent, and then remains constant.

A diagrammatic representation of a folded protein with intact alpha helices and beta pleats is indicated near the lower arm of the curve. A diagrammatic representation of a completely unfolded protein is

represented as a folded string with no alpha helices or beta pleats indicated near the upper arm of the curve. A dotted line passing through the midpoint of the curve at 50 percent is drawn, and a corresponding diagram shows two folded proteins and two unfolded proteins.

Return to FIGURE 2.55 At the denaturation midpoint, half the molecules are fully folded and half are fully unfolded

Extended description for FIGURE 2.56 In the analogy of the typing monkey, the desired result is achieved more

rapidly if individual correct keystrokes are retained

```
 200 ?T(\G{+s x[A.N5~,#ATxSGpn`e□@
 400 oDr'Jh7s DFR:W41'u+^v6zpJseOi
 600 e2ih'8zs n527x8l8d_ih=H1dseb.
 800 S#dh>}/s ]tZqC%lP%DK<|!^aseZ.
1000 V0th>nLs ut/is]l_kwojjwMasef.
1200 juth+nvs it is[lukh?SCw=ase5.
1400 Iithdn4s it is0l/ks/IxwLase~.
1600 M?thinrs it is lXk?T"_woasel.
1800 MSthinWs it is lwkN7□Kw(asel.
2000 Mhthin`s it is likv,aww_asel.
2200 MMthinns it is lik+5avw1asel.
2400 MethinXs it is likydaqw)asel.
2600 Methin4s it is lik2daseasel.
2800 MethinHs it is like□aTweasel.
2883 Methinks it is like a weasel.
```

```
 200 )z~hg)W4{{cu!kO{d6jS!N1EyUx}p
 400 "W hi\kR.<&CfA%4-Y1G!iT$6({|6
 600 .L=hinkm4(uMGP^1AWoE6k1wW=yiS
 800  AthinkaPa_vYH liR\Hb,Uo4\-"(
1000 OFthinksP)@fZO li8v] /+Eln26B
1200 6ithinksMVt -V likm+gl#K~)BFk
1400 vxthinksaEt □w like.S1Geutks.
1600 :Othinks<it MC likesN2[eaVe4.
1800 uxthinksqit 0r likeQh)weaoeW.
2000 Y/thinks it id like7a1wea)e&.
2200 Methinks it iW like a[weaWel.
2400 Methinks it is like a:weasel.
2431 Methinks it is like a weasel.
```

© Macmillan Learning

In the first set of data, attempts 200 to 2883 are shown. The individual correct keystrokes in each attempt are retained in the next attempt. The correct line "Methinks it is a weasel" is obtained at attempt number 2883.

In the second set of data, attempts 200 to 2431 are shown. The individual correct keystrokes in each attempt are retained in the next attempt. The correct line "Methinks it is a weasel" is obtained at attempt number 2431.

Return to FIGURE 2.56 In the analogy of the typing monkey, the desired result is achieved more rapidly if individual correct keystrokes are retained

Extended description for FIGURE 2.57 The proposed folding pathway of chymotrypsin inhibitor-2 demonstrates the nucleation-condensation model

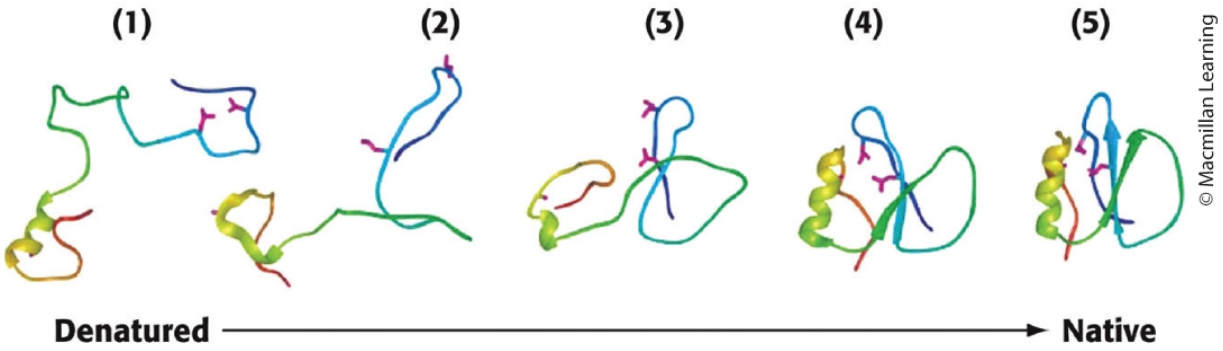


Diagram (1) consists of a cylindrical spiral ribbon. It is connected to a thread-like structure forming curved waves. This thread-like structure is present in a horizontal orientation. Two Y-shaped structures are present on the top right end of the thread-like structure. The spiral ribbon is connected to a smaller curved thread-like structure.

Diagram (2) shows a thread-like structure in a vertical orientation with a horizontal bottom. The cylindrical spiral ribbon is inverted such that it is connected to a smaller curved thread-like structure at the top.

Diagram (3) shows a thread-like structure in a more coiled form.

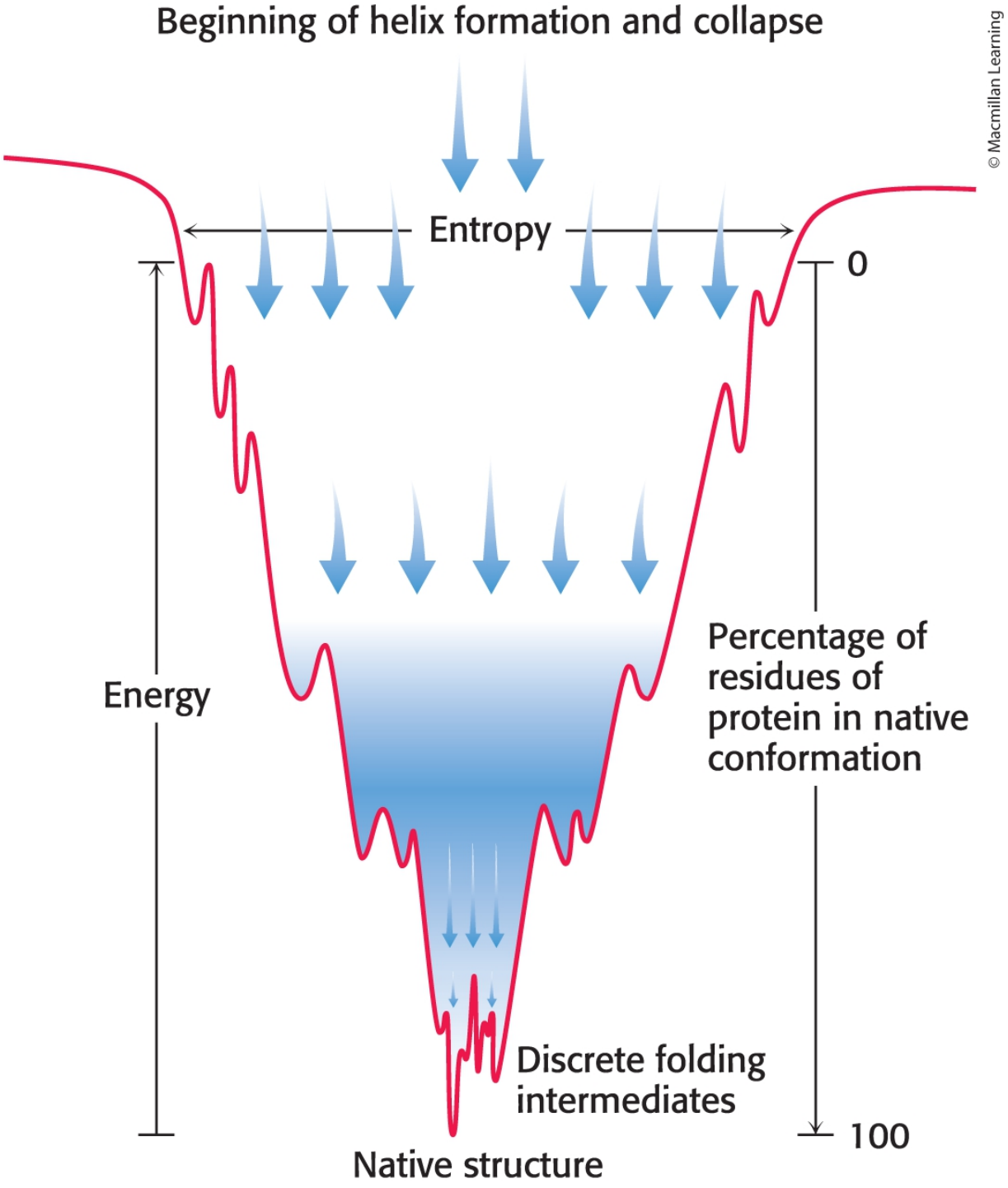
Diagram (4) shows the cylindrical ribbon having three turns. The thread-like structure is relatively more coiled.

Diagram (5) shows the spiral ribbon and the thread-like structure close together in a more compact form.

A rightward pointing arrow below spans from the diagram (1) to diagram (5). The head of the arrow is labeled native and the tail of the arrow is labeled denatured. The figure illustrates a ball-and-stick model of a parallel beta sheet.

Return to FIGURE 2.57 The proposed folding pathway of chymotrypsin inhibitor-2 demonstrates the nucleation-condensation model

Extended description for FIGURE 2.58 The folding funnel depicts the thermodynamics of protein folding.

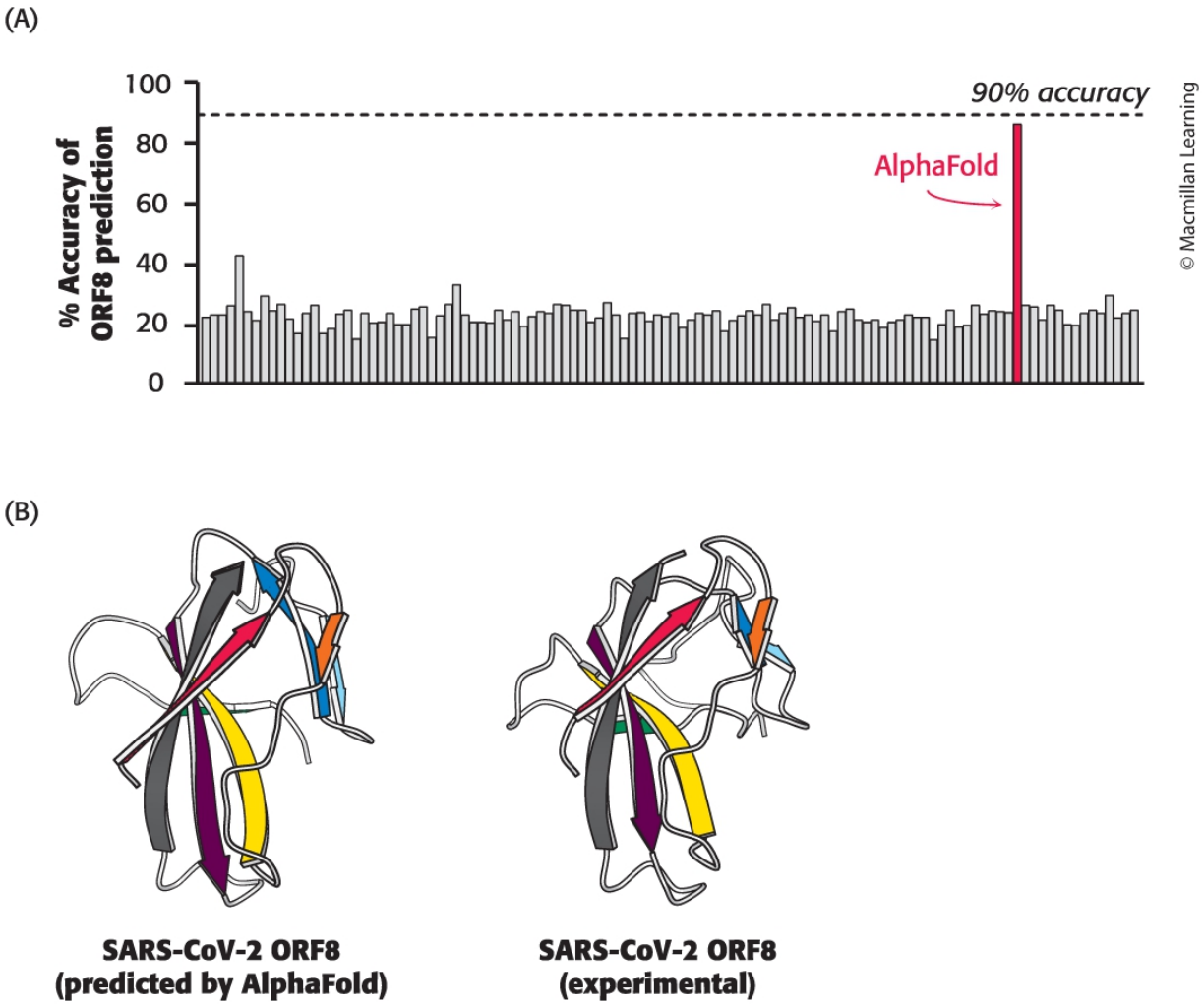


A funnel-shaped curve is illustrated with minor fluctuations and is labeled native structure. Two arrows pointing down are shown above the mouth of the funnel and are labeled the beginning of helix formation and collapse. A double-headed arrow spanning across the widest portion of the mouth of the funnel at the top is labeled entropy. Downward arrows are drawn from the mouth. The tip of the funnel is labeled discrete folding intermediates.

An upward arrow pointing from the tip of the funnel to the mouth of the funnel is labeled energy. A downward arrow pointing from the mouth of the funnel to the tip of the funnel at the bottom is labeled the percentage of residues of protein in native conformation and ranges from 0 to 100 from top to bottom. The mid-section of the funnel is colored blue which gradually gets lighter toward the tip. Downward arrows are indicted in this region pointing to the tip of the funnel.

Return to FIGURE 2.58 The folding funnel depicts the thermodynamics of protein folding.

Extended description for FIGURE 2.59 AlphaFold represents a significant step forward in protein folding prediction.

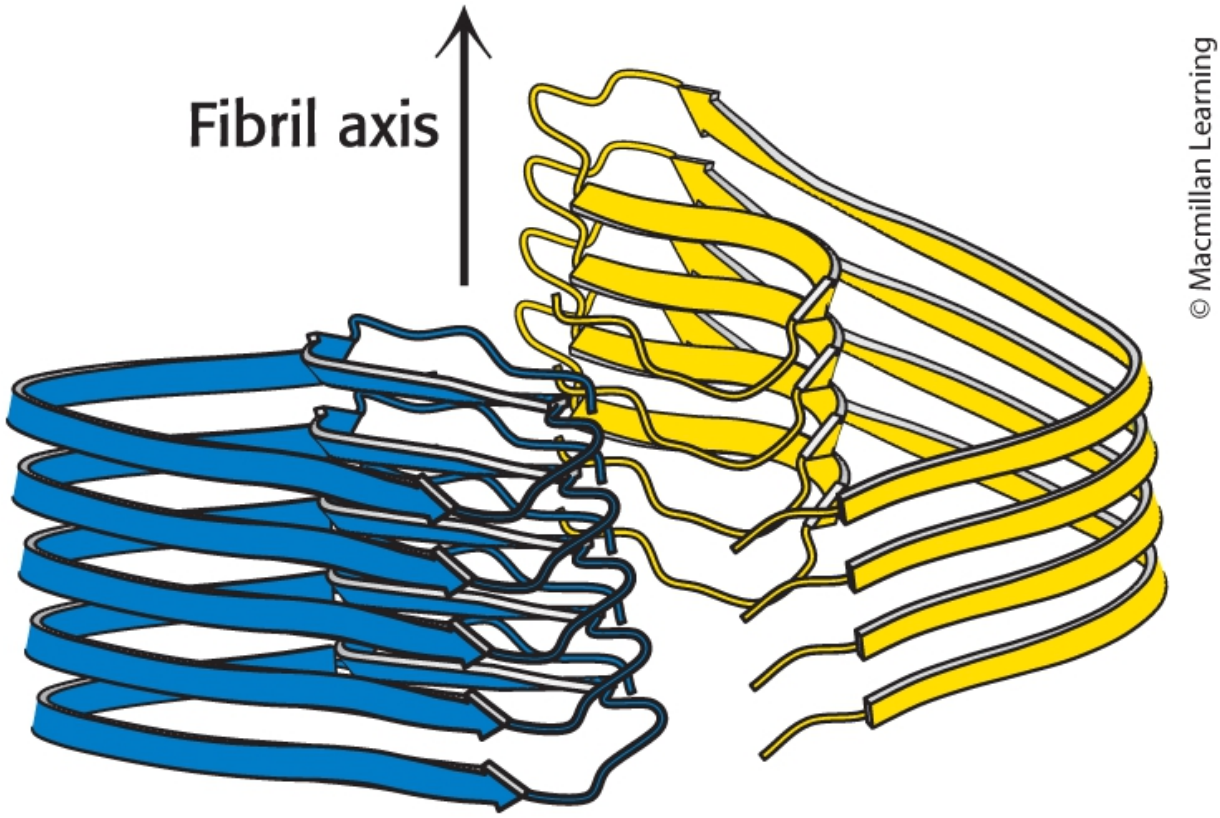


Part (A): The vertical axis is labeled percentage accuracy of O R F 8 prediction and ranges from 0 to 100 in increments of 20 units. Multiple data bars are shown along the horizontal axis and all lie below 45 percent. A red bar labeled alphaFold peaks at an accuracy of 90 percent.

Part (B): Two structures of the S A R S-Co V-2 O R F 8 are made up of beta sheets connected by short loops. The structure predicted by alphaFold is very similar to the experimentally determined structure.

Return to FIGURE 2.59 AlphaFold represents a significant step forward in protein folding prediction.

Extended description for FIGURE 2.60 The structure of the Aβ amyloid fibril reveals its extensive β sheet network



© Macmillan Learning

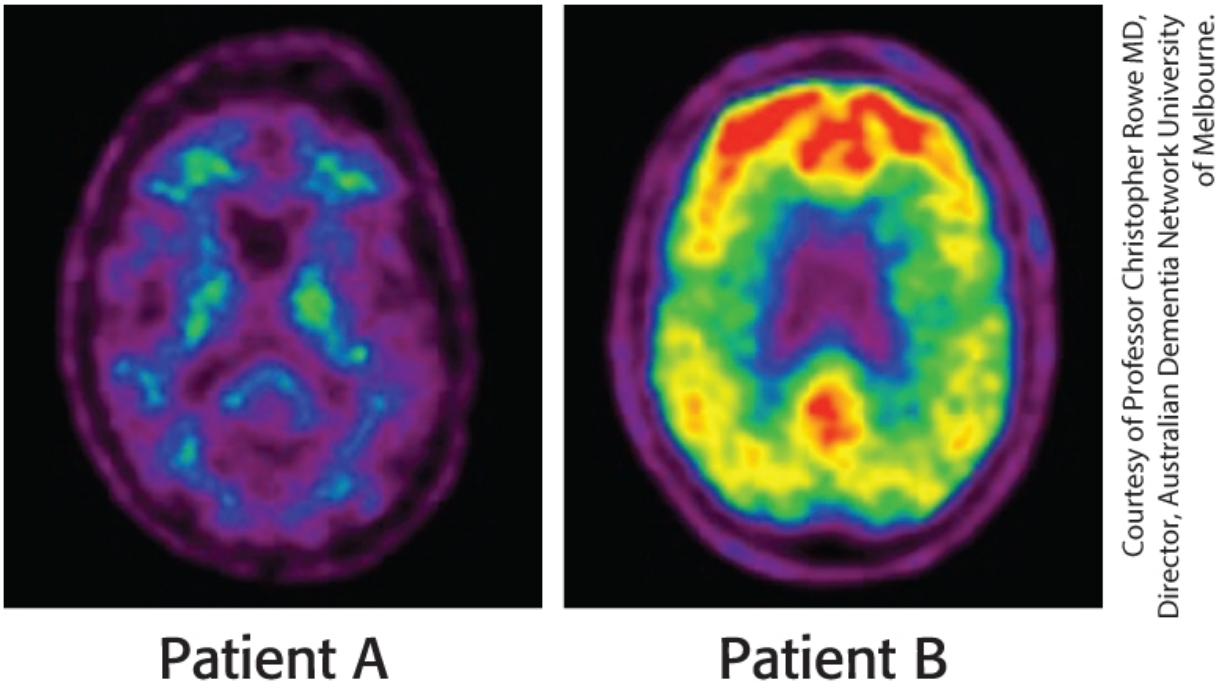
5 antiparallel beta sheets are shown on the left in blue. The peptides are depicted as thick arrows. The peptides are arranged one above the other and are curved at the center. The peptides on the outer side point toward the right. The peptides on the inner side point toward the back. The head of the outer peptides is connected to the corresponding tails of the inner peptides. Blue narrow thread-like structure connects the peptides.

4 antiparallel beta sheets are shown on the right in yellow. The peptides are arranged one above the other and are curved at the

center. The peptides on the outer side point toward the back. They are curved near the tail that faces the observer. The peptides on the inner side point toward the front. The head of the outer peptides is connected to the corresponding tails of the inner peptides. A yellow narrow thread-like structure connects the peptides. Short threads arise from the tails of the outer peptides. An upward arrow labeled fibril axis is present between the two sets of beta sheets.

Return to FIGURE 2.60 The structure of the Aβ amyloid fibril reveals its extensive β sheet network

Extended description for FIGURE 2.61 The extent of amyloid fibril aggregation in the brain can predict the progression of Alzheimer disease

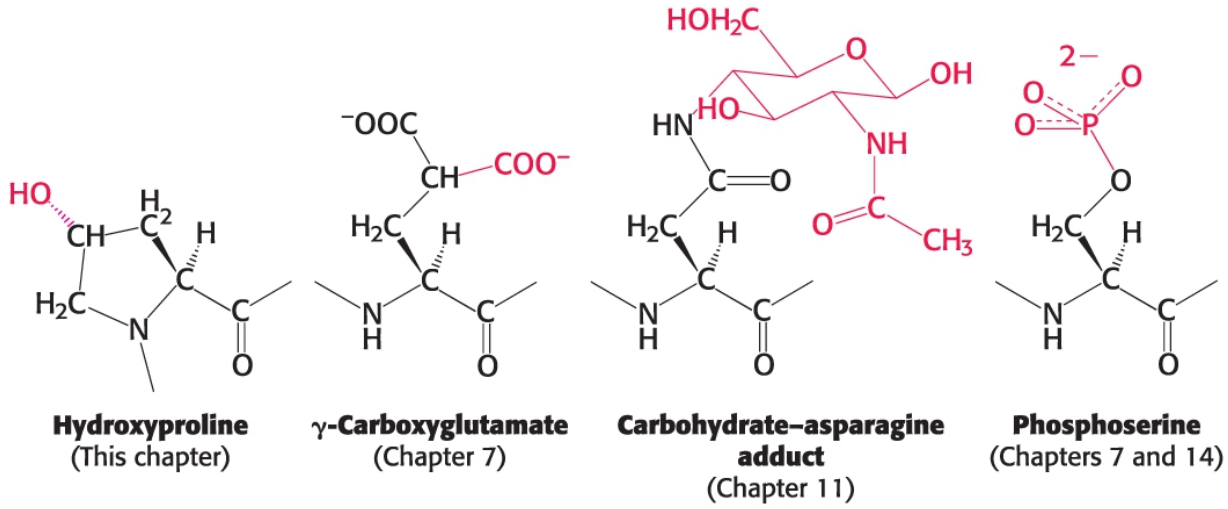


Patient A: Light green signal is detected in certain small regions in the brain indicating minimal accumulation of A beta fibrils.

Patient B: Green, yellow, and red signals are detected in major areas of the brain indicating a high accumulation of A beta fibrils.

Return to FIGURE 2.61 The extent of amyloid fibril aggregation in the brain can predict the progression of Alzheimer disease

Extended description for FIGURE 2.62 Posttranslational modifications to proteins include covalent attachments.



Hydroxyproline (This chapter): A 5-membered heterocyclic pentagonal ring is in a horizontal orientation and consists of 1 N and 4 C atoms. The N atom occupies the first position, which is the bottom right vertex and the C atoms occupy the remaining positions. N has an open single bond. C 1 and C 3 are each bound to H 2. C 2 is bound to H and dash bonded to O H highlighted in red. C 4 is dash bonded to H on the upper right and a central C atom on the lower right. The central C atom is double bonded to O below and has a single bond on the upper right.

Gamma-Carboxyglutamate (Chapter 7): A central C atom is single bonded to N H on the lower left, single bonded to C on the lower right, dash bonded to H on the upper right, and wedge bonded to C H 2 on the upper left. N in N H has an open single bond on the upper left. The C on the lower right is double bonded to O below and has an open single bond on the upper right. C H 2 is single bonded to C

H on the upper right. C H is single bonded to C O O superscript minus on the upper left. C H is single bonded to C O O superscript minus, highlighted in red, on the upper right.

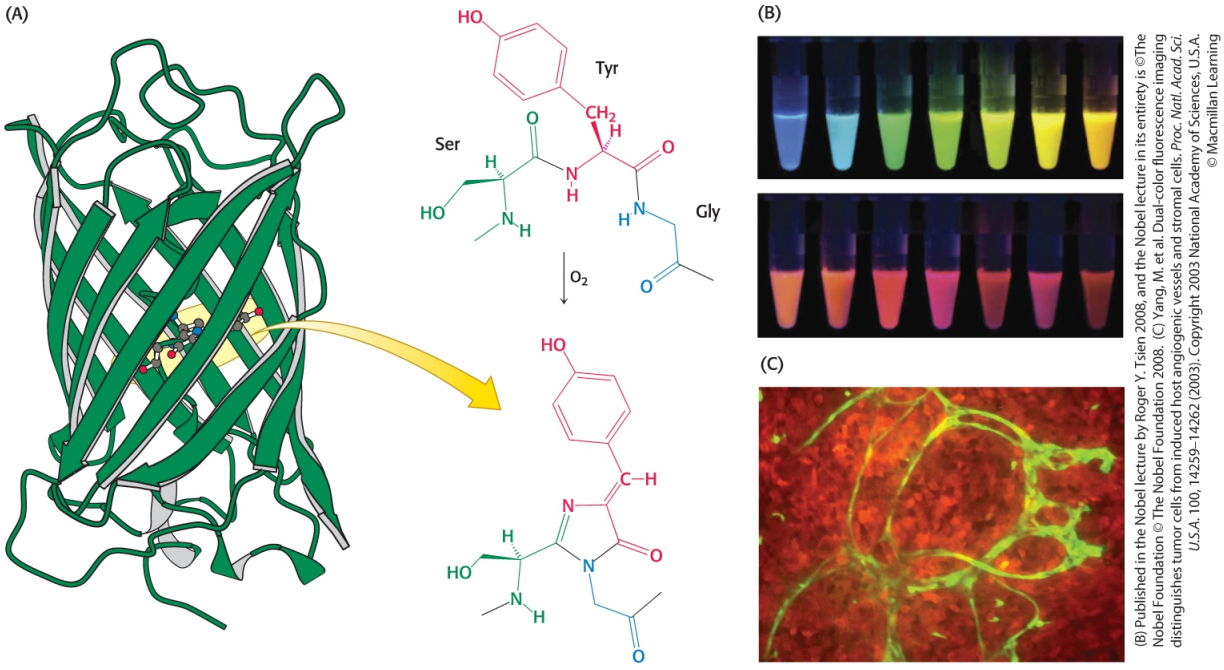
Carbohydrate-asparagine adduct (Chapter 11): A central C atom is single bonded to N H on the lower left, single bonded to C on the lower right, dash bonded to H on the upper right, and wedge bonded to C H 2 on the upper left. N in N H has an open single bond on the upper left. The C on the lower right is double bonded to O below and has an open single bond on the upper right. C H 2 is single bonded to C on the upper right which is double bonded to O on the right. C is single bonded to N H on the upper left which is single bonded to C 4 of a carbohydrate group, highlighted in red on the upper right. The carbohydrate group consists of a 5-membered heterocyclic ring in a chair conformation. The ring consists of 1 O and 5 C atoms. The O atom occupies the first position, which is the top right vertex. C atoms are numbered in a clockwise direction from O. C 2 and C 5 are close to each other. C 4 occupies the top left vertex. C 1 is single bonded to O H on the upper right. C 2 is single bonded to N H on the lower right. C 3 is single bonded to O H on the upper right. C 4 is single bonded to N H of asparagine on the lower left. C 5 is single bonded to C H 2 O H on the upper right. N H single bonded to C 2 is single bonded to a central C atom below. The central C atom is double bonded to O on the lower left and single bonded to C H 3 on the lower right.

Phosphoserine (Chapter 7 and 14): A central C atom is single bonded to N H on the lower left, single bonded to C on the lower right, dash bonded to H on the upper right, and wedge bonded to C H 2 on the upper left. N in N H has an open single bond on the upper left. The C on the lower right is double bonded to O below and has an open single bond on the upper right. C H 2 is single bonded to O on the upper right which is single bonded to P of a phosphate group carrying a negative 2 charge, highlighted in red, on the upper left.

The phosphate group consists of a central P atom with three resonating double bonds to O on the left, upper left, and upper right.

Return to FIGURE 2.62 Posttranslational modifications to proteins include covalent attachments.

Extended description for FIGURE 2.63 GFP is modified posttranslationally by the chemical rearrangement of three amino acids



Part (A): The G F P molecule is depicted using a ribbon diagram. It consists of a hollow cylindrical barrel-like structure formed by antiparallel beta-sheets. The beta-strands pass diagonally across the length of the barrel. The head and tail of the adjacent beta-strand are connected by curved thread-like structures. A cylindrical spiral ribbon is present below the barrel and is connected to it through a thread-like structure. A ball-and-stick model of a molecule is shown inside the barrel. The structure of the molecule is shown on the right. The molecule is produced by the oxidation of a tripeptide composed of serine, tyrosine, and glycine. The structure of the tripeptide is as follows: The serine molecule consists of a 3-carbon alkane chain depicted as a line structure using 2 zigzag lines. C 1 is single bonded to O H on the lower left. C 1 is wedge bonded to C 2. C

2 is dash bonded to H above and single bonded to N below. This N is single bonded to H on the lower right and C H 3 on the lower left in the form of a line. C 3 is double bonded to O above and single bonded to N on the lower right. This N is single bonded to H below and single bonded to the C atom of the tyrosine amino acid. The C atom is single bonded to H on the upper right and wedge bonded to C H 2 on the upper left. C H 2 is single bonded to the C 3 of a benzene ring in a vertical orientation. The benzene ring contains alternating double bonds between C 2 and C 3, C 4 and C 5, C 6 and C 1. C 6 of the benzene ring is single bonded to O H. The C atom of tyrosine is single bonded to C on the lower right. This C is double bonded to O on the upper right and single bonded to N atom of glycine. N is single bonded to H on the lower left and C on the lower right. The C atom is single bonded to C below. This C is double bonded to O on the lower left and single bonded to C H 3 on the lower right in the form of a line. A downward reaction arrow labeled O 2 is shown below the tripeptide.

The structure of the product is as follows: A central C atom is wedge bonded to C H 2 on the upper left that is single bonded to O H on the lower left. The central C atom is dash bonded to H above and single bonded to N below. This N is single bonded to H on the lower right and C H 3 on the lower left in the form of a line.

The central C atom is single bonded to C 1 of a 5-membered heterocyclic pentagonal ring in a horizontal orientation consisting of 2 N and 3 C atoms. The first N atom occupies the first position, which is the bottom left vertex. The second N atom occupies the second position, which is the top left vertex. A double bond is present between C 1 and the second N atom. C 3 is double bonded to O. The first N atom is single bonded to C 1 of a 3-carbon alkane chain depicted as a line structure using 2 zigzag lines. C 2 of the alkane chain is double bonded to O below. C 2 of the pentagonal ring is double bonded to C on the upper right. This C is single bonded to

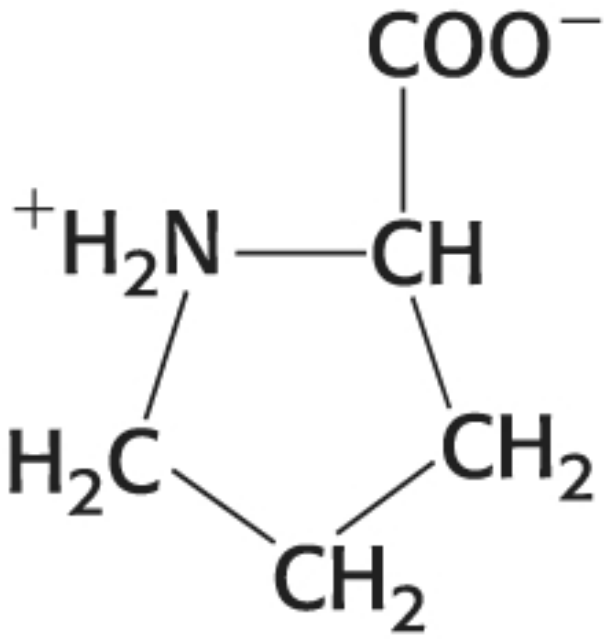
H on the right and C 2 of a benzene ring in a horizontal orientation on the upper left. The benzene ring contains alternating double bonds between C 1 and C 2, C 3 and C 4, C 5 and C 6. C 5 of the benzene ring is single bonded to O H.

Part (B): Two black rectangles are shown. In the first rectangle, seven Eppendorf are adjacently placed. Each Eppendorf is half-filled with a solution that displays fluorescence. From left to right, the first and the second Eppendorf's show light blue and dark blue fluorescence, respectively. The third and the fourth Eppendorf's display light green and yellowish-green fluorescence, respectively. The fifth, sixth, and seventh Eppendorf show yellowish green, dark yellow, and orangish-yellow fluorescence, respectively. In the second rectangle, seven Eppendorf are adjacently placed. Each Eppendorf is half-filled with a solution that displays fluorescence. From left to right, the first and the second Eppendorf show light orange and dark orange fluorescence, respectively. The third and the fourth Eppendorf display orangish pink and pink fluorescence, respectively. The fifth, sixth, and seventh Eppendorf show purplish orange, purplish pink, and reddish-orange fluorescence, respectively.

Part (C): A photomicrograph shows a background composed of tiny bright red cells. An irregular tubular network that forms a large circle in the center having branch-like extensions is present among these cells. This tubular network is bright green colored.

Return to FIGURE 2.63 GFP is modified posttranslationally by the chemical rearrangement of three amino acids

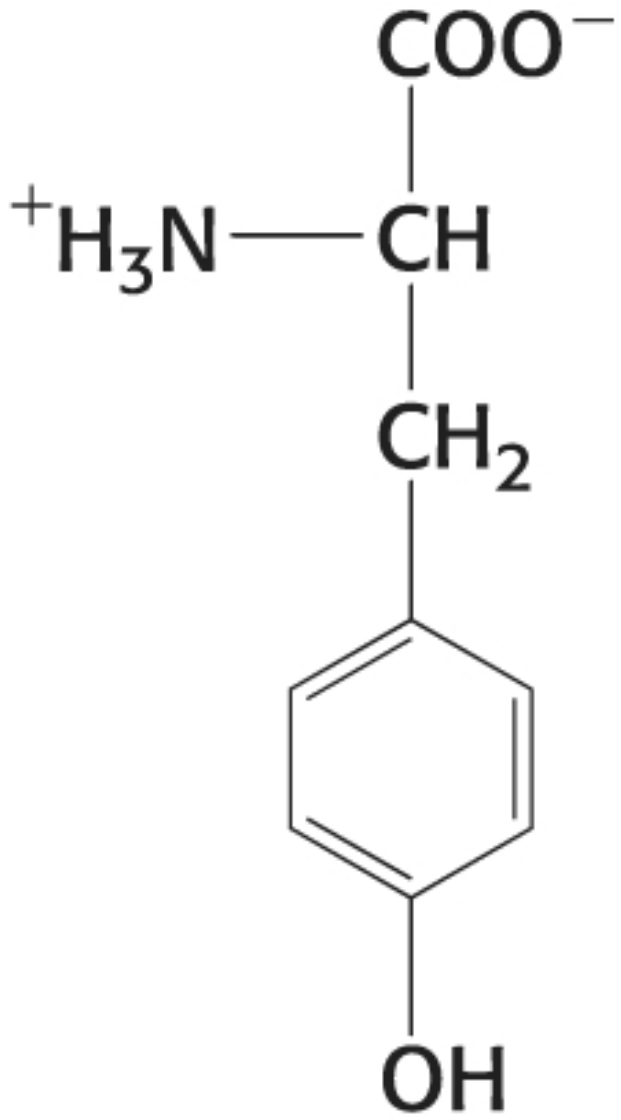
Extended description for Structure of 5-membered heterocyclic pentagonal ring



The structure is as follows: A 5-membered heterocyclic pentagonal ring is in vertical orientation and consists of 1 N and 4 C atoms. The N atom occupies the first position, which is the top left vertex and is bound to H 2 and carries a positive charge. C 1 is bound to H and single bonded to C O O superscript minus above. C 2, C 3, and C 4 are each bound to H 2.

Return to Structure of 5-membered heterocyclic pentagonal ring

Extended description for Structure of substituted benzene ring

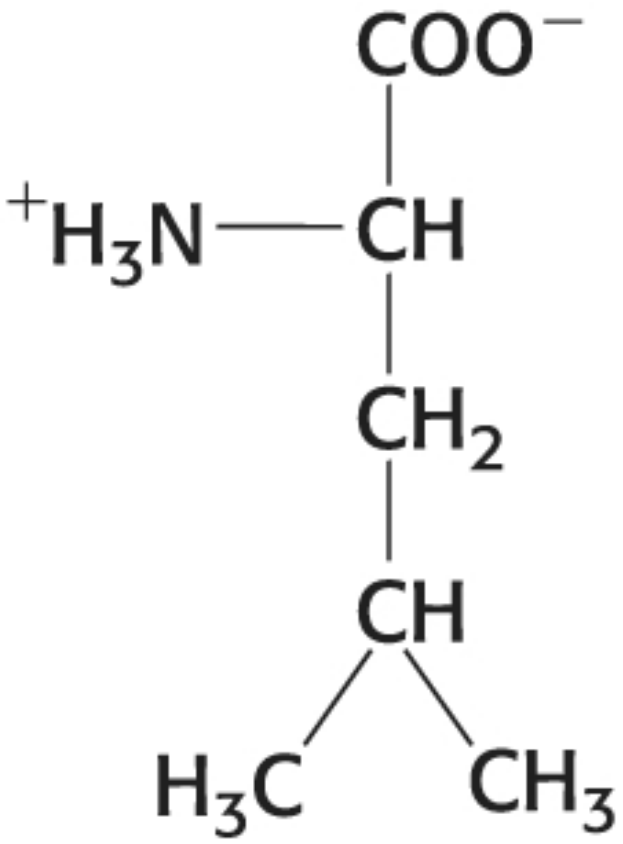


The molecule has the following structure: A benzene ring is in a vertical orientation with C 1 occupying the topmost vertex. The ring contains alternating double bonds between C 2 and C 3, C 4 and C 5, and C 6 and C 1. C 1 is single bonded to C H 2 single bond, C H, single bond, C O O superscript minus above. C 2 of this chain is

single bonded to N H 3 superscript plus on the left. C 4 is single bonded to O H.

Return to Structure of substituted benzene ring

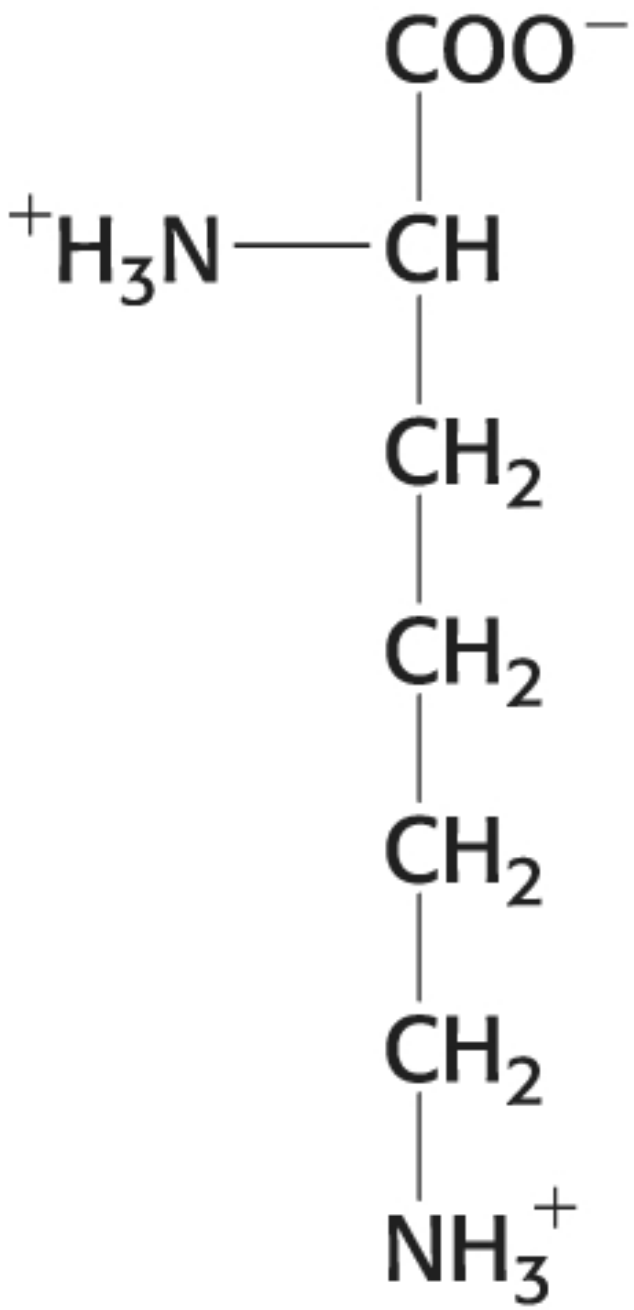
Extended description for Branched structure of substituted carboxylate ion



The structure of the molecule is as follows: C O O superscript minus, single bond, C H, singe bond, C H 2, single bond, C H in a vertical orientation. C 2 is single bonded to N H 3 superscript plus on the left. C 4 is single bonded to C H 3 on the lower left and C H 3 on the lower right.

Return to Branched structure of substituted carboxylate ion

Extended description for Branched structure of substituted carboxylate ion

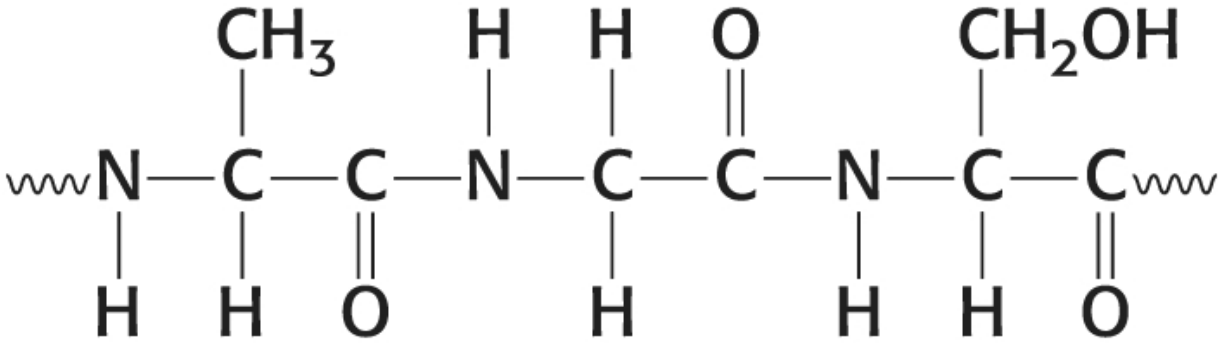


The molecule has the following structure: C O O superscript minus, single bond, C H, single bond, C H 2, single bond, C H 2, single

bond, C H 2, single bond, C H 2, single bond, N H 3 superscript plus. C in C H is single bonded to N H 3 superscript plus on the left.

Return to Branched structure of substituted carboxylate ion

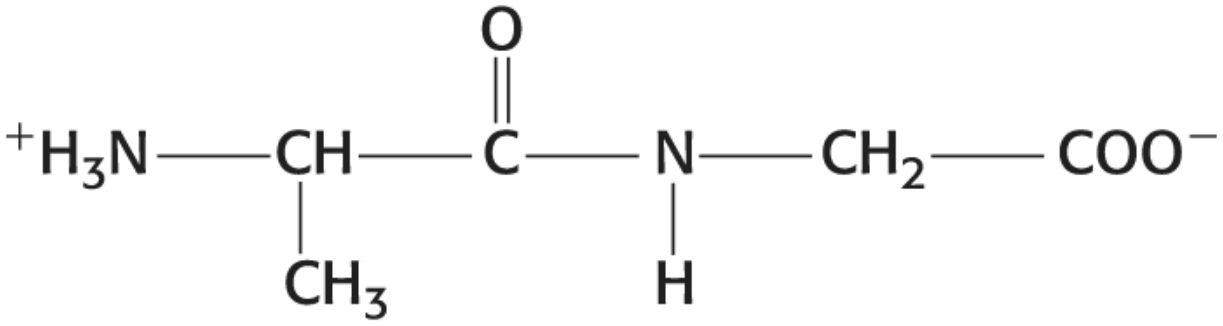
Extended description for Structure of a polypeptide



The structure is as follows: N, single bond, C, single bond, C, single bond, N, single bond, C, single bond C, single bond, N, single bond, C, single bond, C. The first N atom is single bonded to H below. C 1 is single bonded to C H 3 above and H below. C 2 is double bonded to O below. The second N atom is single bonded to H above. C 3 is single bonded to H above and below. C 4 is double bonded to O above. The first N atom is single bonded to H below. C 5 is single bonded to C H 2 O H above and H below. C 6 is double bonded to O below. The structure extends on both sides.

Return to Structure of a polypeptide

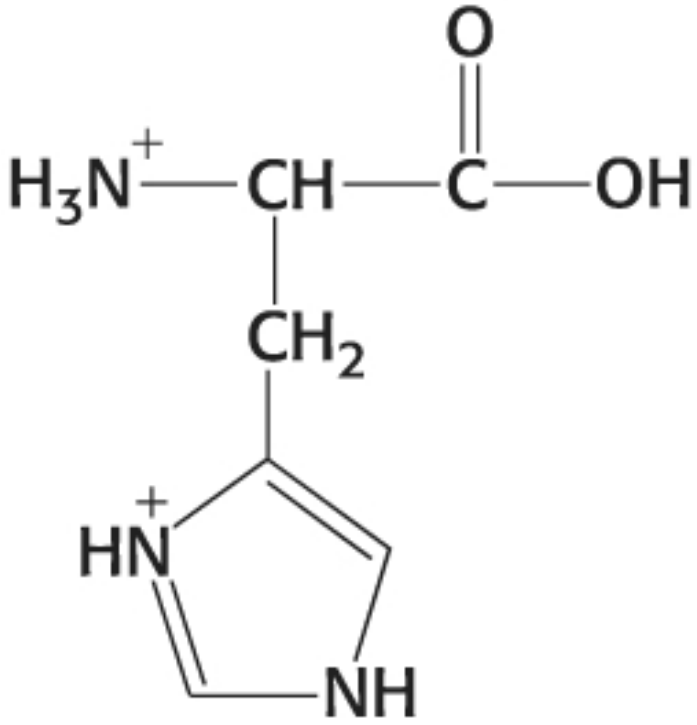
Extended description for Structure of an amino acid



The structure is as follows: N H 3 superscript plus, single bond, C H, single bond, C, single bond, C, single bond, N, single bond, C H 2, single bond, C O O superscript minus. C 1 is single bonded to C H 3 below. C 2 is double bonded to O above. The second N atom is single bonded to H below.

Return to Structure of an amino acid

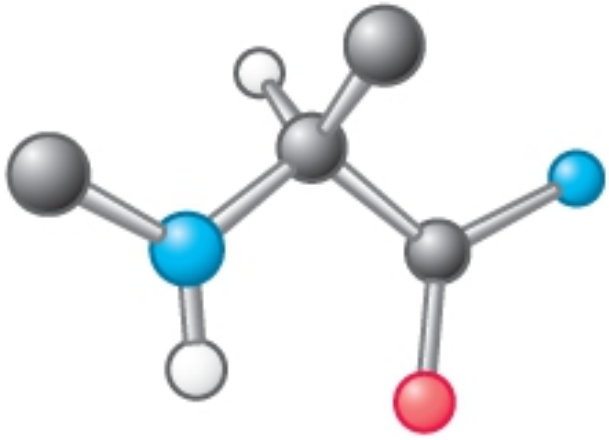
Extended description for Structure of a substituted 5-membered heterocyclic pentagonal ring



The structure is as follows: A 5-membered heterocyclic pentagonal ring is in a vertical orientation and consists of 2 N and 3 C atoms. The first N atom bound to H occupies the first position, which is the bottom right vertex. The second N bound to H and carrying a positive charge occupies the third position, which is the top left vertex. A double bond is present between C 1 and the second N and C 2 and C 3. C 2 is single bonded to C H 2 above which is single bonded to C H above. C in C H is single bonded to N H 3 superscript plus on the left and C on the right. This C is double bonded to O above and O H on the right.

Return to Structure of a substituted 5-membered heterocyclic pentagonal ring

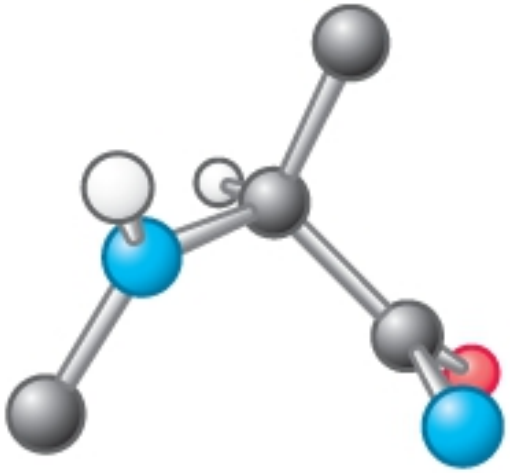
Extended description for Ball-and-stick model of an amino acid derivative



A central black sphere is connected to a blue sphere on the lower left, a black sphere on the lower right, a black sphere above and toward the observer, and a small white sphere above and away from the observer. The blue sphere is connected to a small white sphere below and a black sphere on the upper left. The black sphere on the lower right is connected to a red sphere below and a blue sphere on the upper right.

Return to Ball-and-stick model of an amino acid derivative

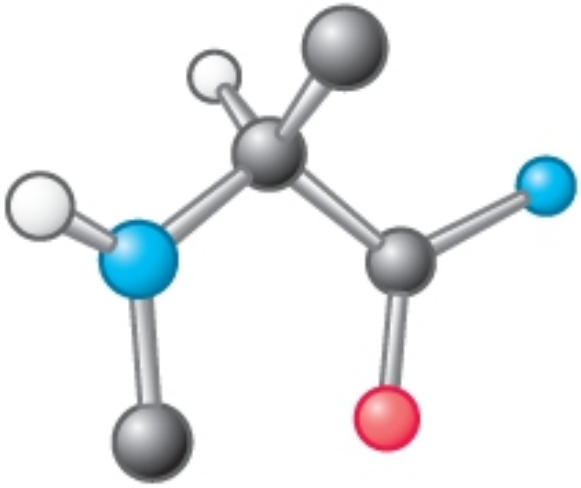
Extended description for Ball-and-stick model of an amino acid derivative



A central black sphere is connected to a black sphere on the upper right and toward the observer, a black sphere on the lower right, a blue sphere on the left toward the observer, and a small white sphere behind. The black sphere on the lower right is connected to a blue sphere on the lower right and toward the observer and a red sphere on the lower right and away from the observer. The blue sphere on the left is connected to a black sphere on the lower left and a white sphere above and toward the observer.

Return to Ball-and-stick model of an amino acid derivative

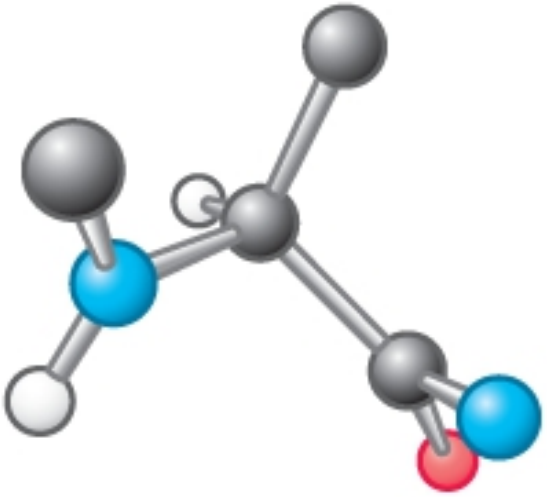
Extended description for Ball-and-stick model of an amino acid derivative



A central black sphere is connected to a blue sphere on the lower left, a black sphere on the lower right, a black sphere above and toward the observer, and a small white sphere above and away from the observer. The blue sphere is connected to a small white sphere on the lower left and away from the observer and a black sphere below. The black sphere on the lower right is connected to a red sphere below and a blue sphere on the upper right.

Return to Ball-and-stick model of an amino acid derivative

Extended description for Ball-and-stick model of an amino acid derivative

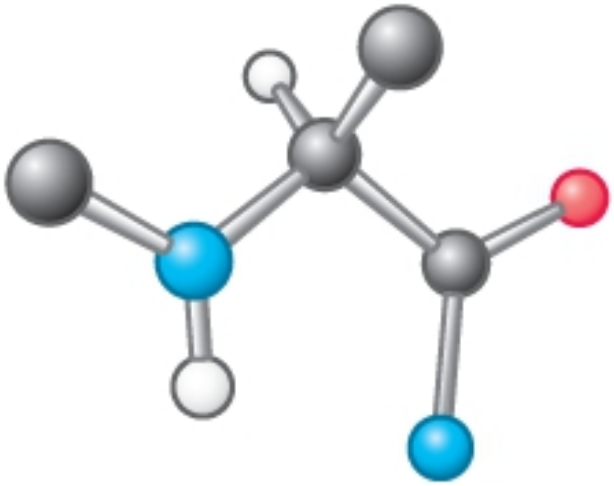


© Macmillan Learning

A central black sphere is connected to another black sphere on the upper right and toward the observer, a black sphere on the lower right, a blue sphere on the left toward the observer, and a small white sphere behind. The black sphere on the lower right is connected to a blue sphere on the lower right and toward the observer and a red sphere on the lower right and away from the observer. The blue sphere on the left is connected to a black sphere on the upper left and toward the observer and a white sphere on the lower left and away from the observer.

Return to Ball-and-stick model of an amino acid derivative

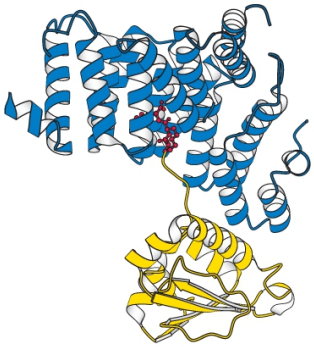
Extended description for Ball-and-stick model of an amino acid derivative



A central black sphere is connected to a blue sphere on the lower left, a black sphere on the lower right, a black sphere above and toward the observer, and a small white sphere above and away from the observer. The blue sphere is connected to a small white sphere below and a black sphere on the upper left and toward the observer. The black sphere on the lower right is connected to a red sphere on the upper right and away from the observer and a blue sphere below.

Return to Ball-and-stick model of an amino acid derivative

Extended description for An image showing a large number of penguins



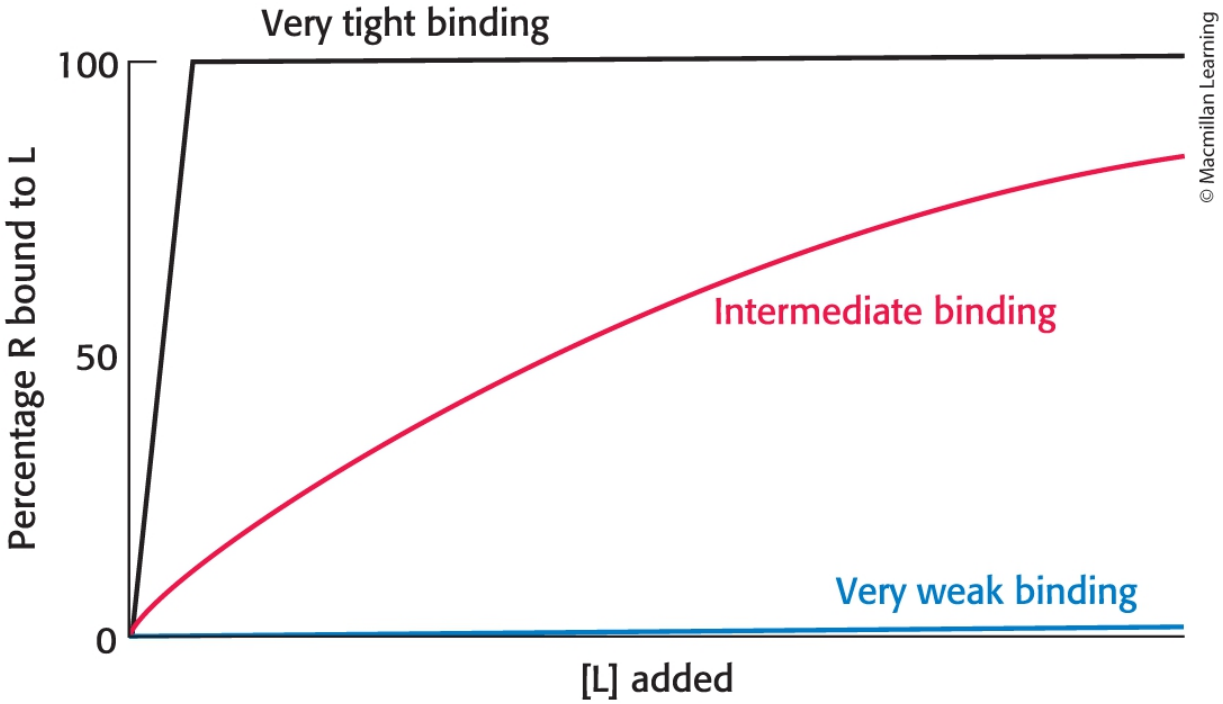


Stefan Christmann/naturepl.com
© Macmillan Learning

The receptor protein is shown in blue. It consists of several alpha-helices located adjacent to one another. They are connected by short thread-like loops. The target protein is shown in yellow, below the receptor protein. It consists of four alpha helices in a horizontal orientation above an anti-parallel beta-sheet. The beta-strands and alpha-helices are connected by short thread-like loops. A thread moves from the alpha-helix of the target protein into the center of the receptor protein. The terminal of this thread contains a short peptide depicted using a ball-and-stick model.

Return to An image showing a large number of penguins

Extended description for FIGURE 3.1 Comparing the percentage of receptor R bound to ligand L with the concentration of added L reveals how tightly R binds L



The horizontal axis is labeled concentration of L added. The vertical axis is labeled the percentage of R bound to L and ranges from 0 to 100 in increments of 50 units. R is receptor and L is ligand.

Three curves are shown on the graph. The first curve is labeled very tight binding. The curve begins at the origin and moves gradually to the upper right linearly until it reaches 100 on the vertical axis at very little concentration of ligand added. The curve then moves horizontally toward the right till the end of the horizontal axis.

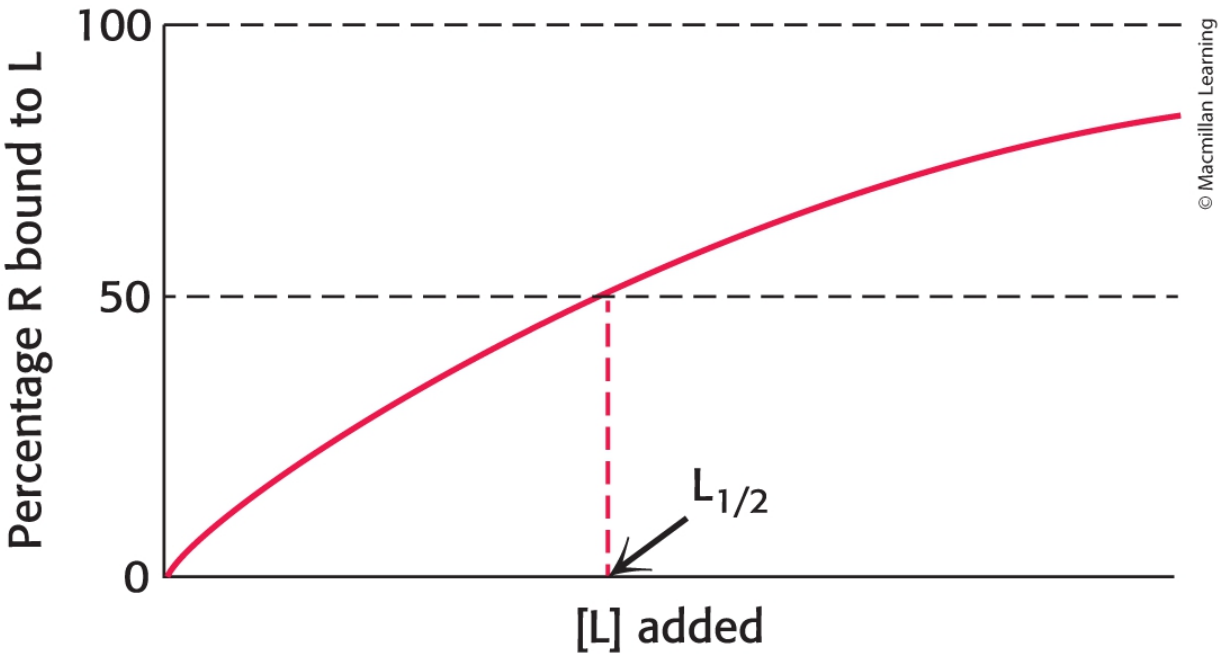
The second curve is labeled intermediate binding. The curve begins at the origin and moves gradually to the upper right until it reaches

approximately 80 percent on the vertical axis at the highest concentration of L added, and ends at the end of the horizontal axis.

The third curve is labeled very weak binding. The curve begins at the origin and overlaps with the horizontal axis along its way toward the right. The curve slightly rises above the horizontal axis near the end to reach approximately 1 percent on the vertical axis.

Return to FIGURE 3.1 Comparing the percentage of receptor R bound to ligand L with the concentration of added L reveals how tightly R binds L

Extended description for FIGURE 3.2 The binding of L to R can be characterized by L1/2

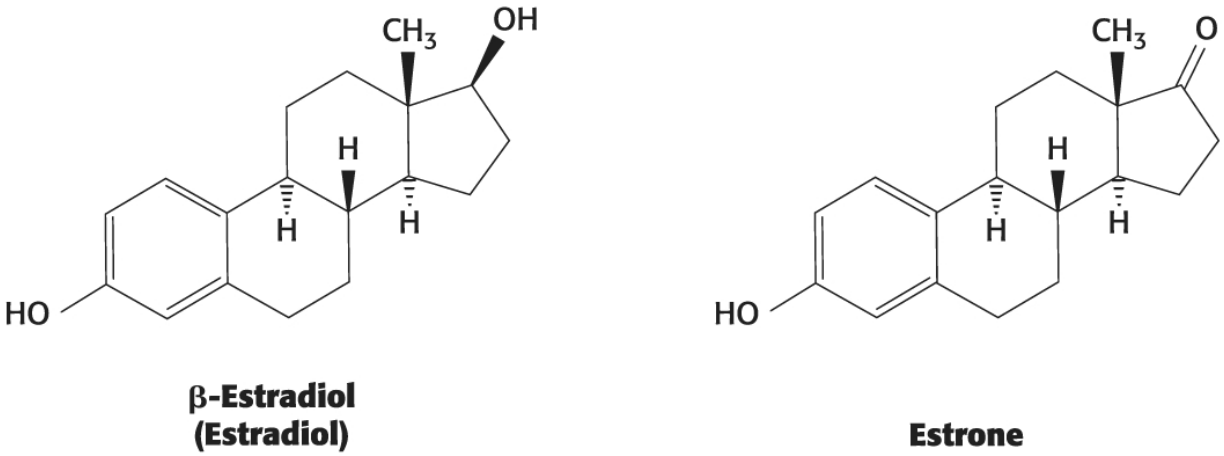


The horizontal axis is labeled concentration of L added. The vertical axis is labeled percentage R bound to L and ranges from 0 to 100 in increments of 50 units.

The curve begins at 0 and moves gradually upward to the right until it reaches approximately 80 percent on the vertical axis at the highest concentration of L added. A dotted horizontal line arises from the markings 50 and 100 on the vertical axis till the end of the horizontal axis. At the point of intersection between the horizontal line from the marking 50 and the curve, a red dotted vertical line extends till the horizontal axis. The point of contact of the red dotted line and the horizontal axis is labeled L superscript StartFraction 1 over 2 EndFraction.

Return to FIGURE 3.2 The binding of L to R can be characterized by L1/2

Extended description for FIGURE 3.3 Estrogens are hormones that are bound by estrogen receptors



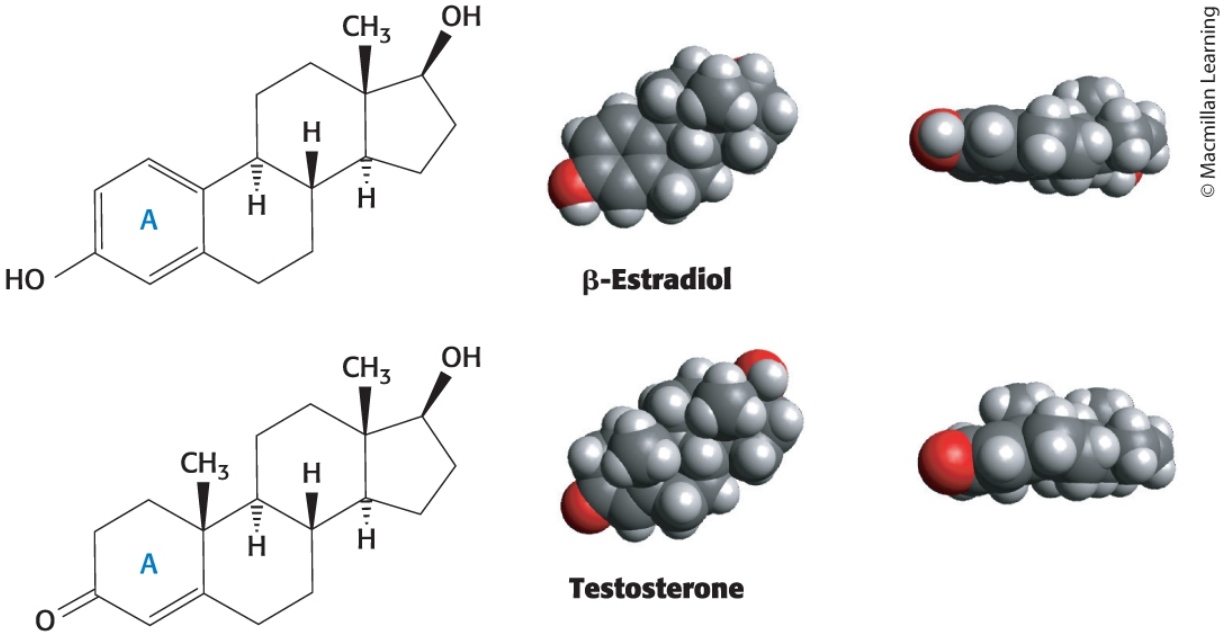
The structure of beta-estradiol or estradiol is as follows: A benzene ring, two hexagonal rings, and a pentagonal ring are fused together. The benzene ring is in a vertical orientation with C 1 occupying the topmost vertex. The ring contains alternating double bonds between C 1 and C 2, C 3 and C 4, and C 5 and C 6. C 5 is single bonded to O H on the lower left. The benzene ring is fused on the right to the first 6-carbon hexagonal ring in a vertical orientation with C 1 occupying the topmost vertex. The rings are fused together such that C 2 and C 3 of the benzene ring are C 6 and C 5 of the hexagonal ring, respectively. C 1 is dash bonded to H below. This hexagonal ring is fused to the second 6-carbon hexagonal ring in a vertical orientation with C 1 occupying the topmost vertex on the upper right. The rings are fused together such that C 1 and C 2 of the first ring are C 5 and C 4 of the second ring, respectively. C 2 is wedge bonded to C H 3 above. C 3 is dashed bonded to H below. C 4 is wedge bonded to H above. The second hexagonal ring is fused on the right to the 5-carbon pentagonal ring in a horizontal orientation with C 1 occupying the rightmost vertex. The two rings are fused together such that C 2 and C 3 of the second hexagonal ring are C 4 and C 3 of

the pentagonal ring, respectively. C 5 is wedge bonded to O H on the upper right.

The structure of estrone is as follows: A benzene ring, two hexagonal rings, and a pentagonal ring are fused together. The benzene ring is in a vertical orientation with C 1 occupying the topmost vertex. The ring contains alternating double bonds between C 1 and C 2, C 3 and C 4, and C 5 and C 6. C 5 is single bonded to O H on the lower left. The benzene ring is fused on the right to the first 6-carbon hexagonal ring in a vertical orientation with C 1 occupying the topmost vertex. The rings are fused together such that C 2 and C 3 of the benzene ring are C 6 and C 5 of the hexagonal ring, respectively. C 1 is dash bonded to H below. This hexagonal ring is fused to the second 6-carbon hexagonal ring in a vertical orientation with C 1 occupying the topmost vertex on the upper right. The rings are fused together such that C 1 and C 2 of the first ring are C 5 and C 4 of the second ring, respectively. C 2 is wedge bonded to C H 3 above. C 3 is dashed bonded to H below. C 4 is wedge bonded to H above. The second hexagonal ring is fused on the right to the 5-carbon pentagonal ring in a horizontal orientation with C 1 occupying the rightmost vertex. The two rings are fused together such that C 2 and C 3 of the second hexagonal ring are C 4 and C 3 of the pentagonal ring, respectively. C 5 is double bonded to O on the upper right.

Return to FIGURE 3.3 Estrogens are hormones that are bound by estrogen receptors

Extended description for FIGURE 3.4 The steroid hormones β -estradiol and testosterone appear quite similar, yet receptors recognize the molecules as distinct



The structure of beta-estradiol is as follows: A benzene ring, two hexagonal rings, and a pentagonal ring are fused together. The benzene ring is in a vertical orientation with C 1 occupying the topmost vertex. The ring contains alternating double bonds between C 1 and C 2, C 3 and C 4, and C 5 and C 6. The center of the ring is labeled A. C 5 is single bonded to O H on the lower left. The benzene ring is fused on the right to the first 6-carbon hexagonal ring in a vertical orientation with C 1 occupying the topmost vertex. The rings are fused together such that C 2 and C 3 of the benzene ring are C 6 and C 5 of the hexagonal ring, respectively. C 1 is dash bonded to H below. This hexagonal ring is fused to the second 6-carbon hexagonal ring in a vertical orientation with C 1 occupying the topmost vertex on the upper right. The rings are fused together

such that C 1 and C 2 of the first ring are C 5 and C 4 of the second ring, respectively. C 2 is wedge bonded to C H 3 above. C 3 is dashed bonded to H below. C 4 is wedge bonded to H above. The second hexagonal ring is fused on the right to the 5-carbon pentagonal ring in a horizontal orientation with C 1 occupying the rightmost vertex. The two rings are fused together such that C 2 and C 3 of the second hexagonal ring are C 4 and C 3 of the pentagonal ring, respectively. C 5 is wedge bonded to O H on the upper right.

The structure of testosterone is as follows: Three hexagonal rings and a pentagonal ring are fused together. A 6-carbon hexagonal ring is in a vertical orientation with C 1 occupying the topmost vertex. A double bond is present between C 3 and C 4. The center of the ring is labeled A. C 5 is double bonded to O on the lower left. C 2 is wedge bonded to C H 3 above. The first hexagonal ring is fused on the right to the second 6-carbon hexagonal ring in a vertical orientation with C 1 occupying the topmost vertex. The two rings are fused together such that C 2 and C 3 of the first ring are C 6 and C 5 of the second hexagonal ring, respectively. In the second hexagonal ring, C 1 is dash bonded to H below. The second hexagonal ring is fused on the upper right to the third 6-carbon hexagonal ring in a vertical orientation with C 1 occupying the topmost vertex. The two rings are fused together such that C 1 and C 2 of the second ring are C 5 and C 4 of the third ring, respectively. C 4 is wedge bonded to H above. The third hexagonal ring is fused to the 5-carbon pentagonal ring in a horizontal orientation with C 1 occupying the rightmost vertex. The two rings are fused together such that C 2 and C 3 of the third hexagonal ring are C 4 and C 3 of the pentagonal ring, respectively. C 3 is dash bonded to H below. C 4 is wedge bonded to C H 3 above. C 5 is wedge bonded to O H on the upper right.

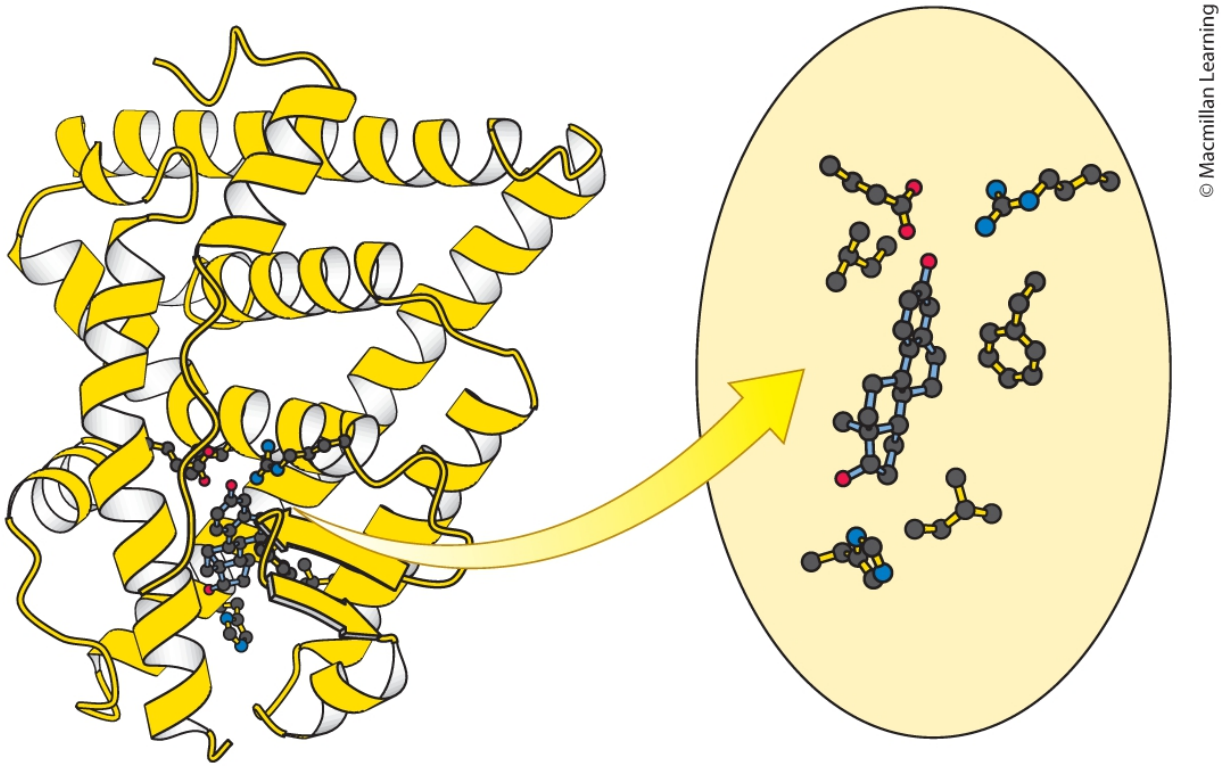
Two views of the space-filling model of both beta-estradiol and testosterone are shown. Beta-estradiol in the first view is depicted as a cluster of dark grey and light grey spheres. A red sphere is present

on the lower left. Beta-estradiol in the second view is depicted as a linear cluster of dark grey and light grey spheres. The red sphere is located on the left and away from the observer.

Testosterone in the first view is depicted as a cluster of dark and grey spheres. A red sphere is located on the upper right end and lower left end. The upper right red sphere is located away from the observer. Testosterone in the second view is depicted as a linear cluster of dark grey and light grey spheres. A red sphere is located on the left and toward the observer.

Return to FIGURE 3.4 The steroid hormones β -estradiol and testosterone appear quite similar, yet receptors recognize the molecules as distinct

Extended description for FIGURE 3.5 Proteins such as estrogen receptors include binding pockets that are complementary to the shapes of specific ligands



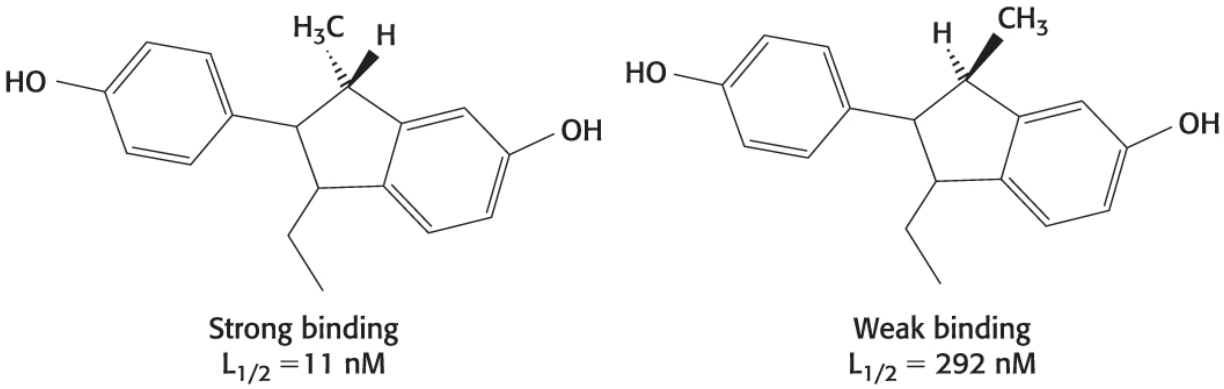
© Macmillan Learning

The estrogen receptor consists of 8 alpha helices and two beta-pleats in an antiparallel orientation. The alpha helices are connected by short thread-like loops. Two alpha helices are present in a horizontal orientation one above the other. The ends of the top alpha helix are connected to the alpha helix below. The left alpha helix moves toward the right to form a horizontal platform below the bottom horizontal alpha helix. The right alpha helix and a vertical alpha helix in front of the left alpha helix join near their end to create a pocket for an alpha helix on the ligand binding. The pocket is lined by amino acids depicted as ball-and-stick models. The ligand-

binding pocket of the receptor is enlarged that shows the estrogen at the center surrounded by side chains of amino acids.

Return to FIGURE 3.5 Proteins such as estrogen receptors include binding pockets that are complementary to the shapes of specific ligands

Extended description for FIGURE 3.6 Even subtle features of ligands can be recognized

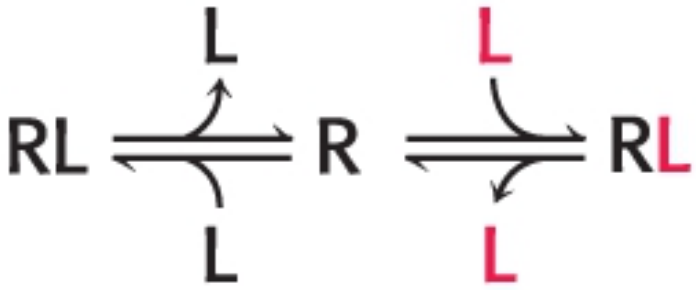


The structure of the first synthetic ligand is as follows: A benzene ring is in a horizontal orientation with C 1 occupying the rightmost vertex. The ring contains alternating double bonds between C 2 and C 3, C 4 and C 5, and C 6 and C 1. C 4 is single bonded to O H on the left. C 1 is single bonded to C 5 of a 5-carbon pentagonal ring in a vertical orientation, with C 1 occupying the topmost vertex. C 1 of the pentagonal ring is dash bonded to C H 3 on the upper left and wedge bonded to H on the upper right. C 4 is single bonded to C H 2 in the form of a line on the lower left. C of this C H 2 is single bonded to C H 3 in the form of a line on the lower right. The pentagonal ring is fused to a benzene ring on the right in a vertical orientation, with C 1 occupying the topmost vertex. The rings are fused together such that C 2 and C 3 of the pentagonal ring are C 6 and C 5 of the benzene ring, respectively. The ring contains alternating double bonds between C 2 and C 3, C 4 and C 5, and C 6 and C 1. C 2 is single bonded to O H on the upper right. Note: Strong binding, L subscript StartFraction 1 over 2 EndFraction equals 11 n M.

The structure of the second synthetic ligand is similar to the synthetic ligand on the left, except that the C 1 of the pentagonal ring is dash bonded to H on the upper left and wedge bonded to C H 3 on the upper right. Note: Weak binding, L subscript StartFraction 1 over 2 EndFraction equals 292 n M.

Return to FIGURE 3.6 Even subtle features of ligands can be recognized

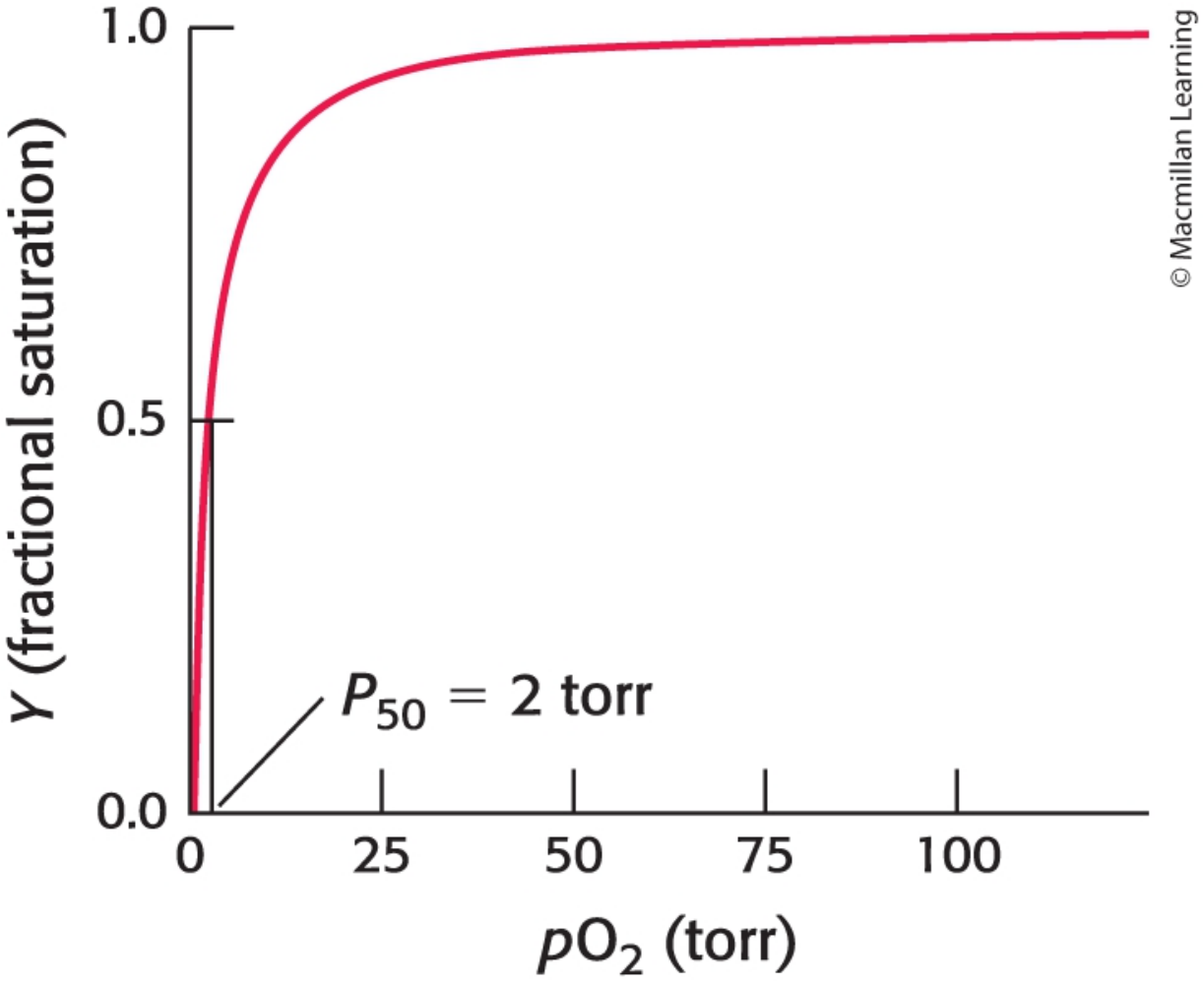
Extended description for FIGURE 3.7 Dissociation and association are constantly occurring, even at equilibrium where the concentrations of all species are constant



The receptor is depicted as R, the ligand is depicted as L, and the receptor-ligand complex is depicted as R L. The reversible reaction is a two-step reaction. The overall reaction shows reactant R L dissociates to produce R, which again gives R L. In the first step, L is eliminated in the forward reaction to give R and added in the backward reaction. In the second step, L is added in the forward reaction to give R L (L highlighted in red) and eliminated in the backward reaction to give R. L in the second step is highlighted in red.

Return to FIGURE 3.7 Dissociation and association are constantly occurring, even at equilibrium where the concentrations of all species are constant

Extended description for FIGURE 3.8 Half saturation of human myoglobin occurs when the partial pressure of oxygen is 2 torr



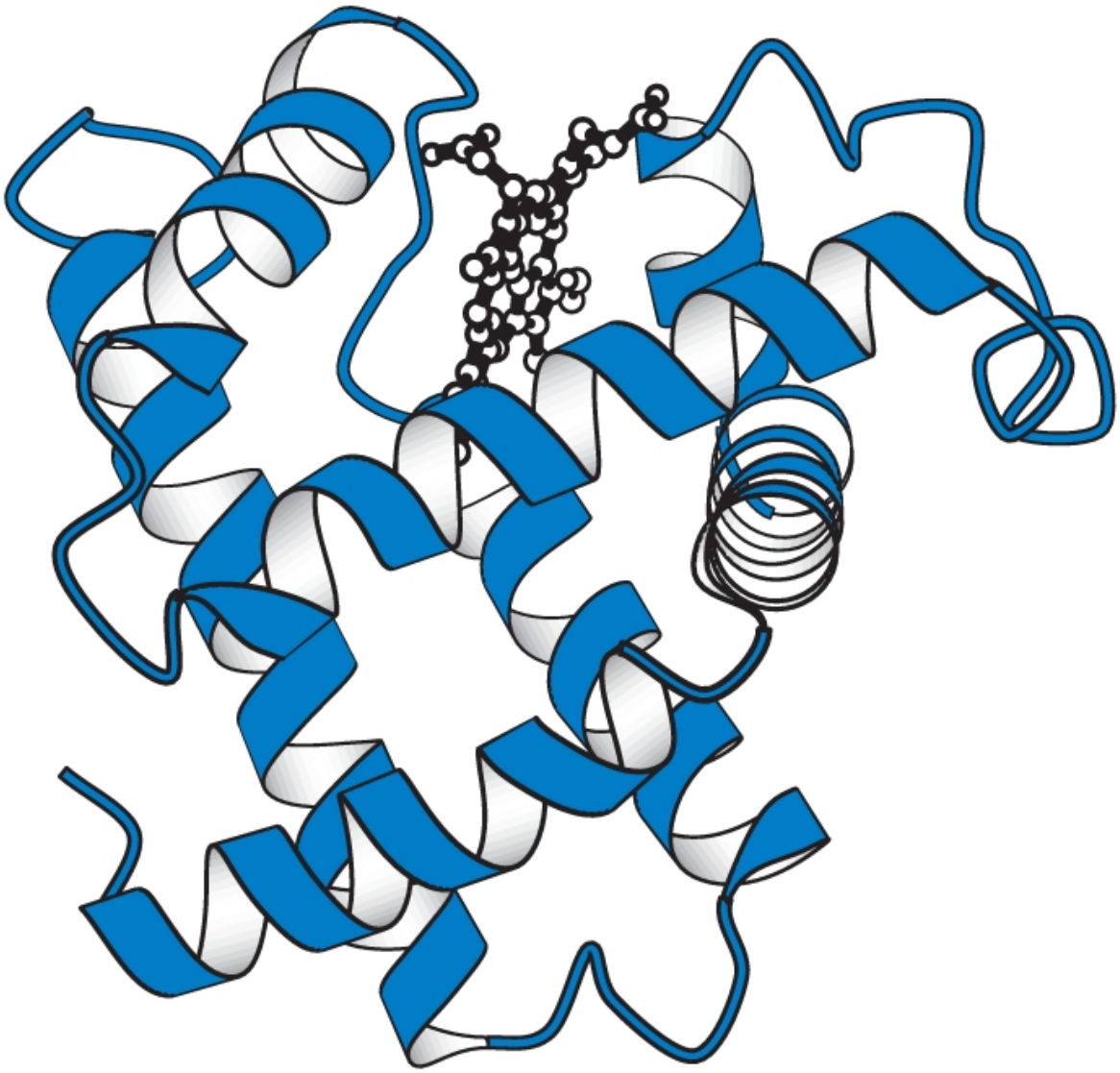
The horizontal axis is labeled p O subscript 2 (torr) and ranges from 0 to 100 in increments of 25 units. The vertical axis is labeled Y (fractional saturation) and ranges from 0.0 to 1.0 in increments of 0.5 units.

A curve shown on the graph has a hyperbolic shape. It begins at the origin and moves upward to point (2, 0.5). It then continues to the

upper right until it reaches approximately point (25, 0.9). The curve then moves horizontally toward the right till the end of the horizontal axis.

Return to FIGURE 3.8 Half saturation of human myoglobin occurs when the partial pressure of oxygen is 2 torr

Extended description for FIGURE 3.9 The structure of myoglobin consists primarily of α helices surrounding a heme molecule



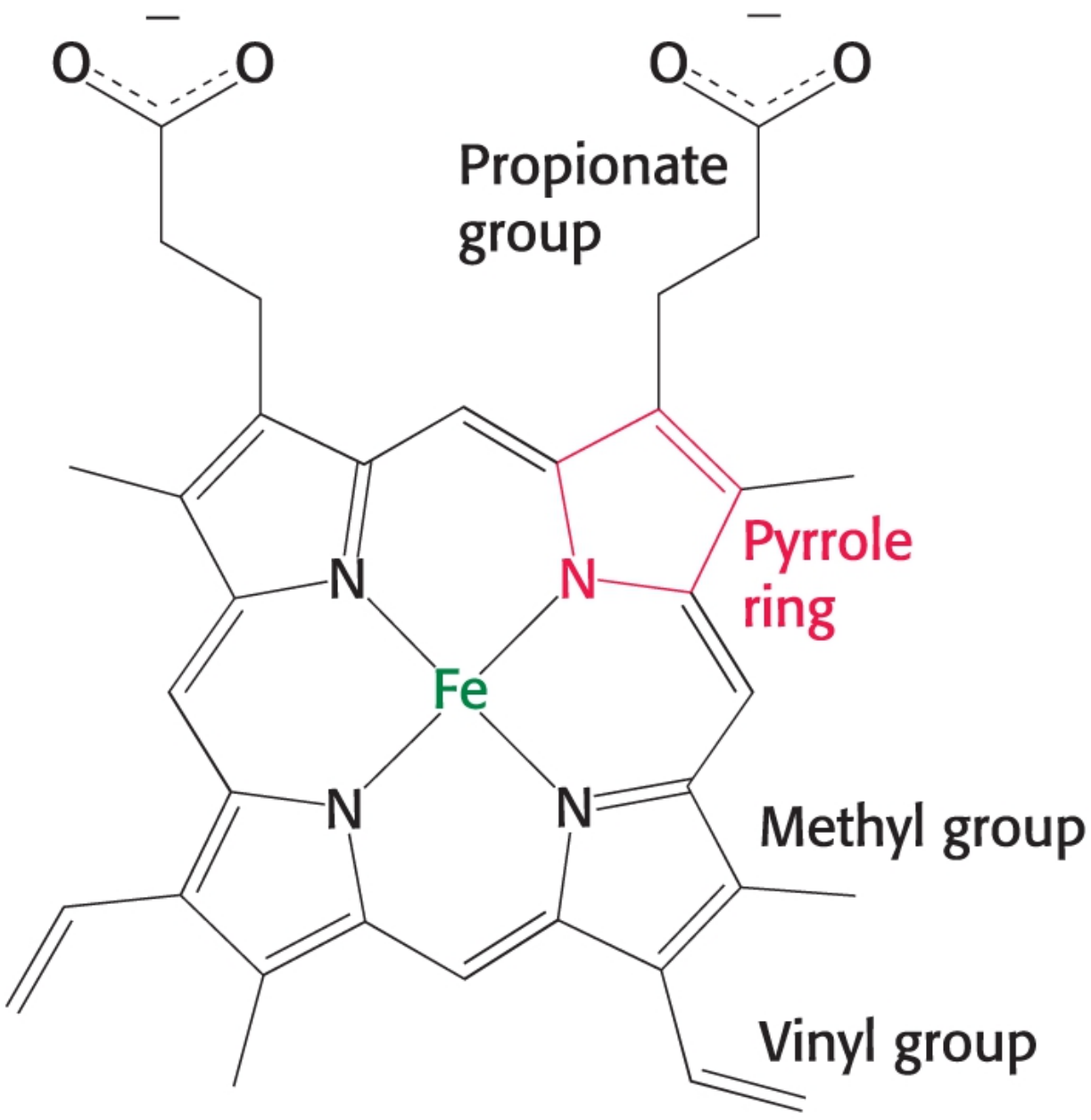
© Macmillan Learning

Myoglobin

The myoglobin protein is composed of 8 alpha-helices connected by short thread-like loops forming a compact globular structure. The heme molecule is depicted as a ball-and-stick model composed of white spheres. It is located inside a pocket having a long diagonal alpha-helix at the base and flanked by two short alpha-helices.

Return to FIGURE 3.9 The structure of myoglobin consists primarily of α helices surrounding a heme molecule

Extended description for FIGURE 3.10 The structure of heme comprises four pyrrole rings that use their nitrogen atoms to bind to a central iron atom

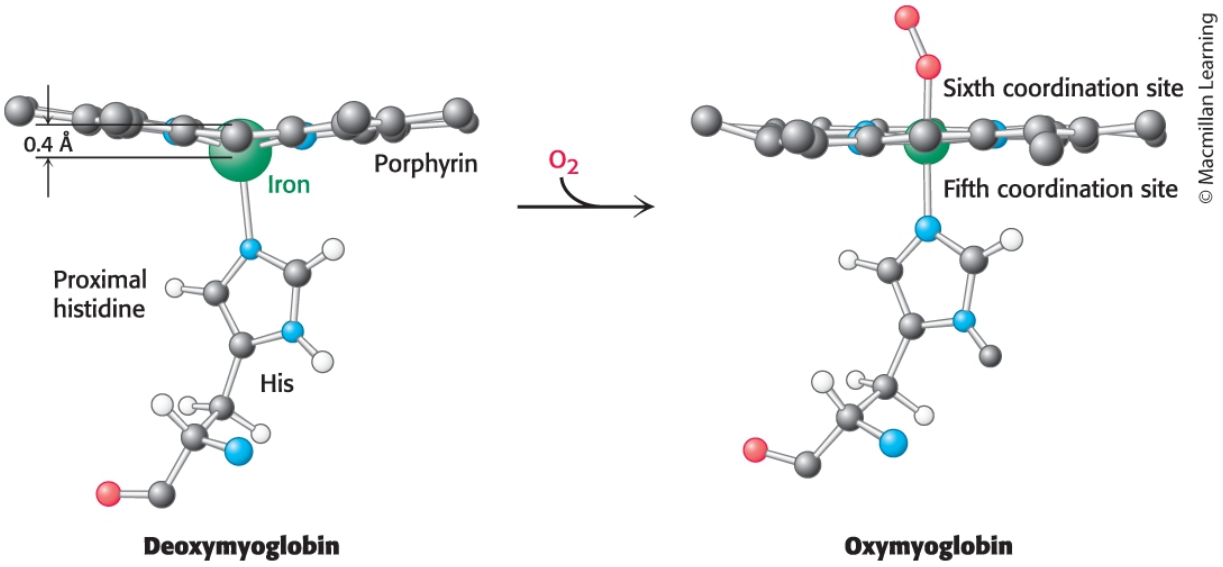


Heme (Fe-protoporphyrin IX)

Heme has the following structure: A central F e atom is single bonded to the N atom of a 5-membered heterocyclic ring on the upper right, lower right, lower left, and upper left, respectively. The 5-membered heterocyclic pentagonal ring consists of 1 N and 4 C atoms in different orientations. N occupies the first position, and N atoms of each ring face inward. The adjacent rings are connected to a common C H group in the middle. The ring is labeled pyrrole ring. In the ring on the lower right, C 2 is single bonded to a C H 3 in the form of a line, and C 3 is single bonded to a vinyl group. In the ring on the upper right, C 2 is single bonded to C 1 of a 3-carbon alkane chain depicted as a line structure using 2 zigzag lines. C 3 of this chain is partially double bonded to O on the upper right and upper left. A negative charge is present between the two O atoms. This group is labeled propionate group.

Return to FIGURE 3.10 The structure of heme comprises four pyrrole rings that use their nitrogen atoms to bind to a central iron atom

Extended description for FIGURE 3.11 Oxygen binding changes the position of the heme iron ion



In the ball stick model, carbon atoms are represented as black spheres, N atoms are represented as blue spheres, oxygen atoms are represented as red spheres, H atoms are represented as white spheres, and the iron atom is represented as a large green sphere.

The reaction consists of two reactants and one product. The first reactant is deoxymyoglobin. The ball-and-stick model shows the side view of the flat porphyrin ring. The black spheres connected to one another are visible to the observer. The ring contains a central green sphere slightly below the plane of the ring. The distance between the center of the green sphere and the plane of the ring is 0.4 Angstrom. The green sphere is connected to a blue sphere located at the topmost vertex of a heterocyclic pentagonal ring of histidine molecule. The black spheres are located at the top right vertex, bottom left vertex, and top left vertex of the ring. The second blue sphere is located at the bottom right vertex. The black sphere at the

top right vertex is connected to a white sphere. The black sphere at the top left vertex is connected to a white sphere. The blue sphere at the bottom right vertex is connected to a white sphere. The black sphere at the bottom left vertex is connected to another black sphere below. This black sphere is connected to a white sphere on the left and right. The black sphere below is connected to another black sphere located toward the observer. This black sphere is connected to a white sphere on the left and a blue sphere on the right. The black sphere located toward the observer is connected to another black sphere below which is connected to a red sphere on the left.

The second reactant is O 2 written over the reaction arrow.

The product is oxymyoglobin. The ball-and-stick model shows the side view of the flat porphyrin ring. The black spheres connected to one another are visible to the observer. The ring contains a central green sphere slightly in the plane of the ring. The green sphere is connected to a red sphere above the plane of the ring. This connection is labeled the sixth coordination site. This red sphere is connected to another red sphere on the upper left. This connection is labeled the fifth coordination site. The green sphere is connected below to a blue sphere located at the topmost vertex of a heterocyclic pentagonal ring of histidine molecule. The black spheres are located at the top right vertex, bottom left vertex, and top left vertex of the ring. The second blue sphere is located at the bottom right vertex. The black sphere at the top right vertex is connected to a white sphere. The black sphere at the top left vertex is connected to a white sphere. The blue sphere at the bottom right vertex is connected to a white sphere. The black sphere at the bottom left vertex is connected to another black sphere below. This black sphere is connected to a white sphere on the left and the right. The black sphere below is connected to another black sphere located toward the observer. This black sphere is connected to a white sphere on the left and a blue sphere on the right. The black

sphere located toward the observer is connected to another black sphere below which is connected to a red sphere on the left.

Return to FIGURE 3.11 Oxygen binding changes the position of the heme iron ion

Extended description for FIGURE 3.12 The complex between iron and oxygen in myoglobin can be described by two resonance structures

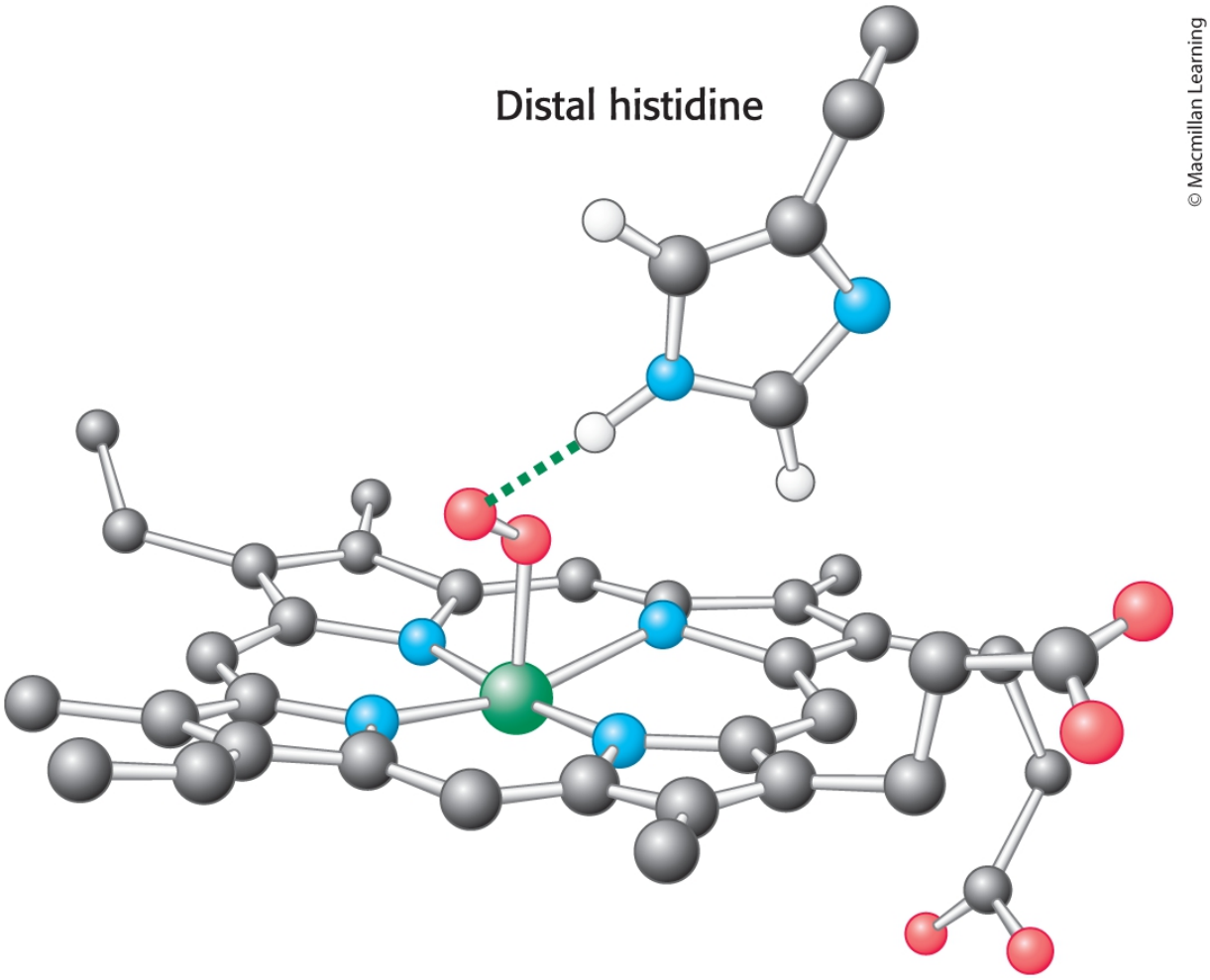


The first resonance structure is as follows: F e superscript 2 plus is single bonded to O above. O is double bonded to O on the upper right. The O atoms and the double bond are highlighted in red.

The second resonance structure is as follows: F e superscript 3 plus is single bonded to O above. O is partially double bonded to O superscript minus on the upper right. O atom, O superscript minus atom, and the partial double bond are highlighted in red and labeled superoxide ion.

Return to FIGURE 3.12 The complex between iron and oxygen in myoglobin can be described by two resonance structures

Extended description for FIGURE 3.13 Bound oxygen is stabilized through a hydrogen bond between the distal histidine and one of the oxygen atoms



© Macmillan Learning

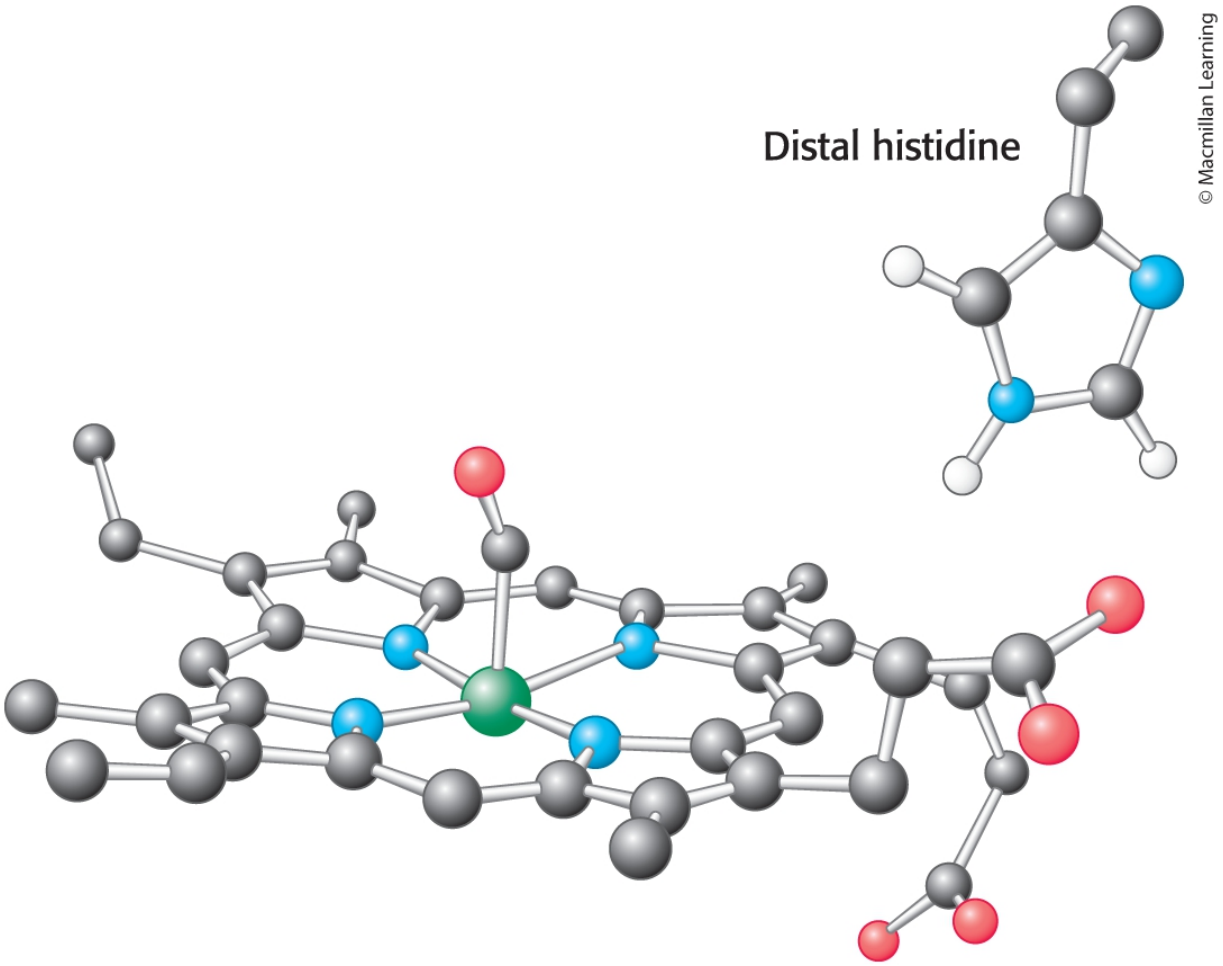
In the ball-and-stick model, carbon atoms are represented as black spheres, nitrogen atoms are represented as blue spheres, oxygen atoms are represented as red spheres, hydrogen atoms are depicted as white spheres, and the iron atom is depicted as a large green sphere.

The heme ring is flat and its top view is shown. A central green sphere is connected to a blue sphere on the upper left, lower left, upper right, and lower right. These blue spheres are a part of pyrrole rings located on the upper left, upper right, lower left, and lower right of the green sphere. The skeleton of the pyrrole ring is composed of 1 blue sphere and 4 black spheres. The side chain of the upper right and lower right rings contains a chain of 3 black spheres in which the terminal black sphere is connected to one red sphere on either side. The rings are connected through a black sphere. One black sphere on the upper left vertex of the upper left ring and the bottom left vertex of the lower left ring is connected to a chain of two black spheres. One black sphere at the topmost vertex of the upper left ring and the topmost vertex of the upper right ring is connected to a black sphere above. One black sphere at the top left vertex of the lower left ring and the bottommost vertex of the lower right ring is connected to a black sphere.

The central green sphere is connected to a red sphere above the plane of the ring. This red sphere is connected to another red sphere on the upper left. The red sphere on the upper left is connected to a white sphere on the upper right by a dotted lined. The white sphere is connected on the upper right to a blue sphere located on the bottom left vertex of a heterocyclic pentagonal ring of distal histidine consisting of 3 black spheres and two blue spheres. The black spheres are located at the topmost vertex, bottom right vertex, and top right vertex. The second blue sphere is located at the top right vertex. The black sphere at the lower right and upper left vertices are connected to a white sphere. The black sphere at the topmost vertex is connected to a chain of two black spheres above.

Return to FIGURE 3.13 Bound oxygen is stabilized through a hydrogen bond between the distal histidine and one of the oxygen atoms

Extended description for FIGURE 3.14 Carbon monoxide can bind to the iron ion in myoglobin, blocking the oxygen-binding site



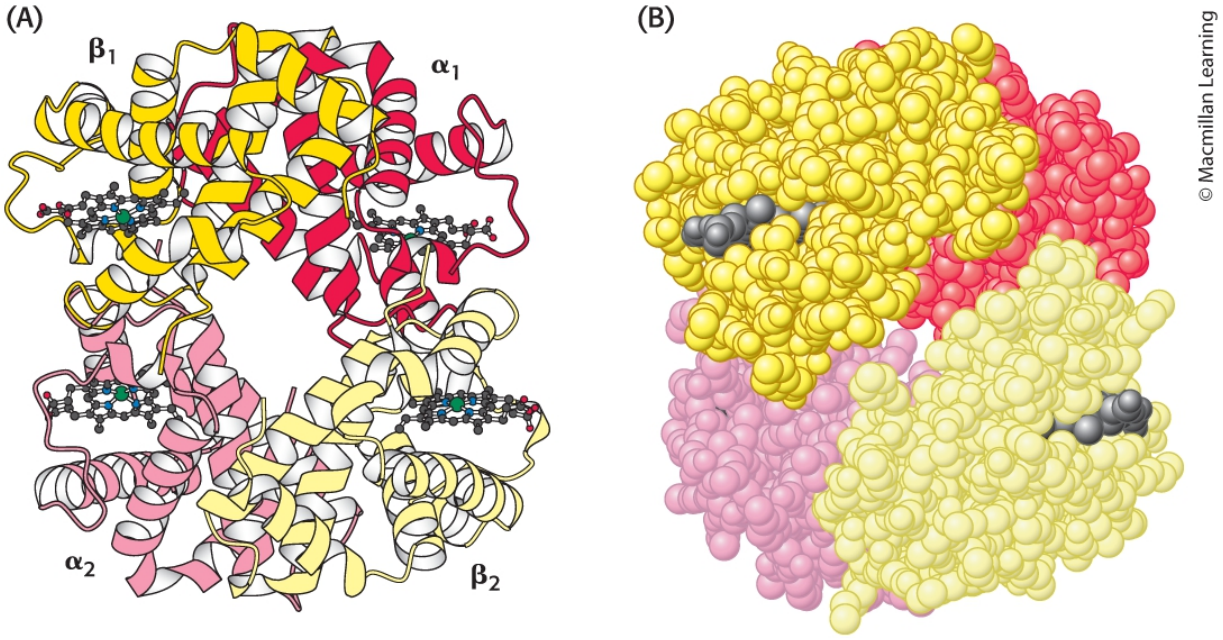
In the ball-and-stick model, carbon atoms are represented as black spheres, nitrogen atoms are represented as blue spheres, oxygen atoms are represented as red spheres, hydrogen atoms are represented as white spheres, and the iron atom is represented as a large green sphere.

The heme ring is flat and its top view is shown. A central green sphere is connected to a blue sphere on the upper left, lower left, upper right, and lower right. These blue spheres are part of pyrrole rings located on the upper left, upper right, lower left, and lower right of the green sphere. The skeleton of the pyrrole ring is composed of 1 blue sphere and 4 black spheres. The side chain of the upper right and lower right rings contain a chain of 3 black spheres in which the terminal black sphere is connected to one red sphere on either side. The rings are connected through a black sphere. One black sphere at the top left vertex of the upper left ring and the bottom left vertex of the lower left ring is connected to a chain of two black spheres. One black sphere at the topmost vertex the upper left ring, and the topmost vertex of the upper right is connected to a black sphere above. One black sphere at the top left vertex of the lower left ring and bottommost vertex of the lower right ring is connected to a black sphere.

The central green sphere is connected to a black sphere above the plane of the ring. This black sphere is connected to a red sphere on the upper left. The heterocyclic pentagonal ring in distal histidine is shown above the heme ring. It consists of 3 black spheres and 2 blue spheres. The black spheres are located at the topmost vertex, bottom right vertex, and top right vertex. The first and second blue spheres are located at the top right and bottom left vertex. The black spheres at the bottom right and top left vertices are connected to a white sphere. The blue sphere at the bottom left vertex is connected to a white sphere. The black sphere at the topmost vertex is connected to a chain of two black spheres above.

Return to FIGURE 3.14 Carbon monoxide can bind to the iron ion in myoglobin, blocking the oxygen-binding site

Extended description for FIGURE 3.15 Hemoglobin is an assembly of four subunits, each of which is very similar to myoglobin



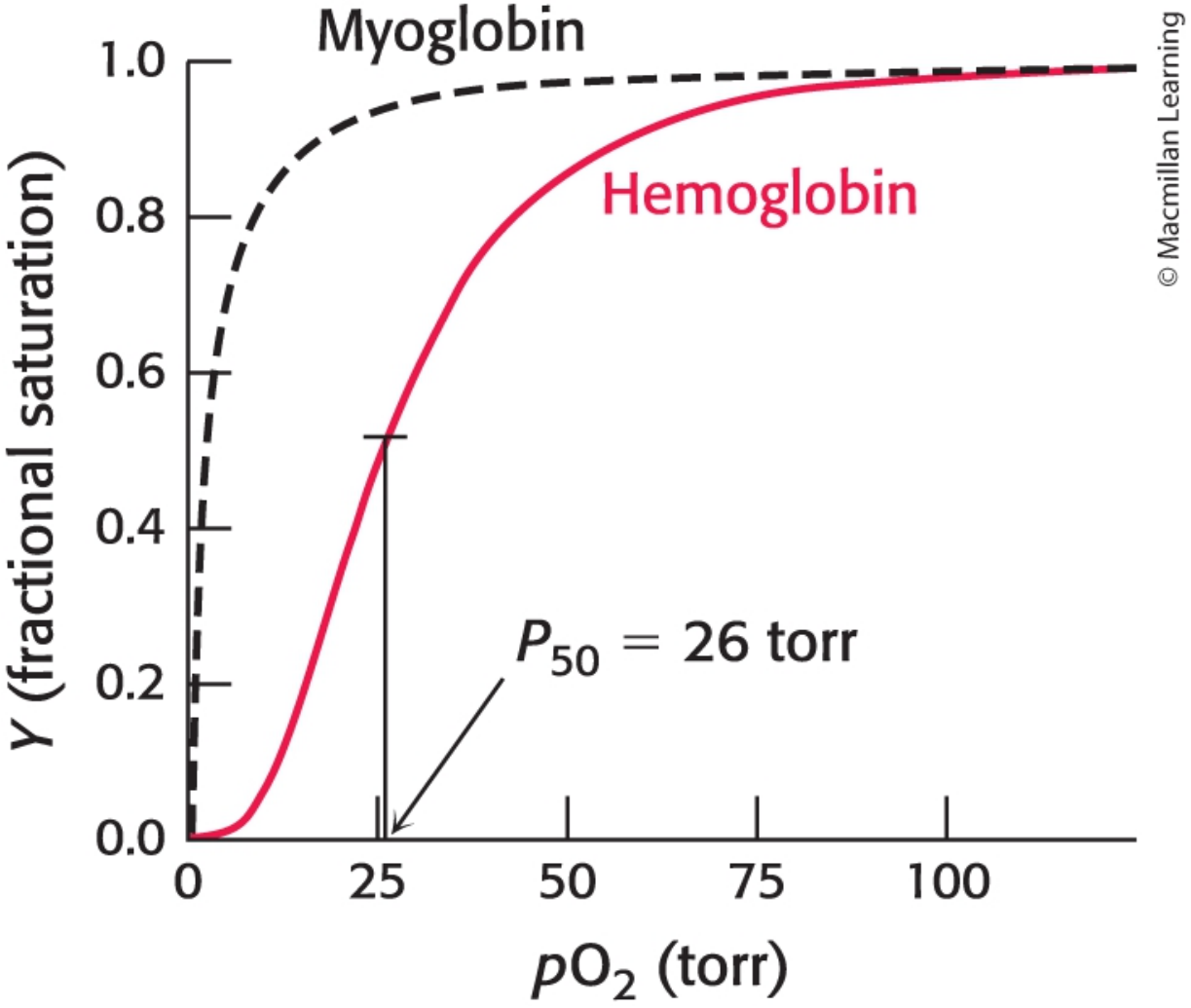
© Macmillan Learning

1. Part (A): Four units composed of alpha helices aggregate together form a donut shape with a hollow center. Out of the four units, the first unit on the upper left is dark yellow, the second unit on the upper right is red, the third unit on the lower right is light yellow, and the fourth unit on the lower left is pink. At the center of each unit is a heme group represented as a green sphere enclosed in a cage of small black spheres.
2. Part (B): The space-filling model shows a globular compact structure. It consists of four subunits that are dark yellow, red, light yellow, and pink. The dark yellow subunit located on the upper left has a cluster of dark yellow spheres. The red subunit on the upper right has a cluster of red spheres. The light yellow subunit on the lower right has a cluster of light yellow spheres. The pink subunit on the lower left has a cluster of pink spheres.

A small cluster of black spheres is embedded in the left and right ends of the dark yellow and light yellow subunits, respectively.

Return to FIGURE 3.15 Hemoglobin is an assembly of four subunits, each of which is very similar to myoglobin

Extended description for FIGURE 3.16 The oxygen-binding curve for hemoglobin, with its sigmoid (S-like) shape, is markedly different from that for myoglobin



The horizontal axis is labeled p O subscript 2 (torr) and ranges from 0 to 100 in increments of 25 units. The vertical axis is labeled Y (fractional saturation) and ranges from 0.0 to 1.0 in increments of 0.2 units.

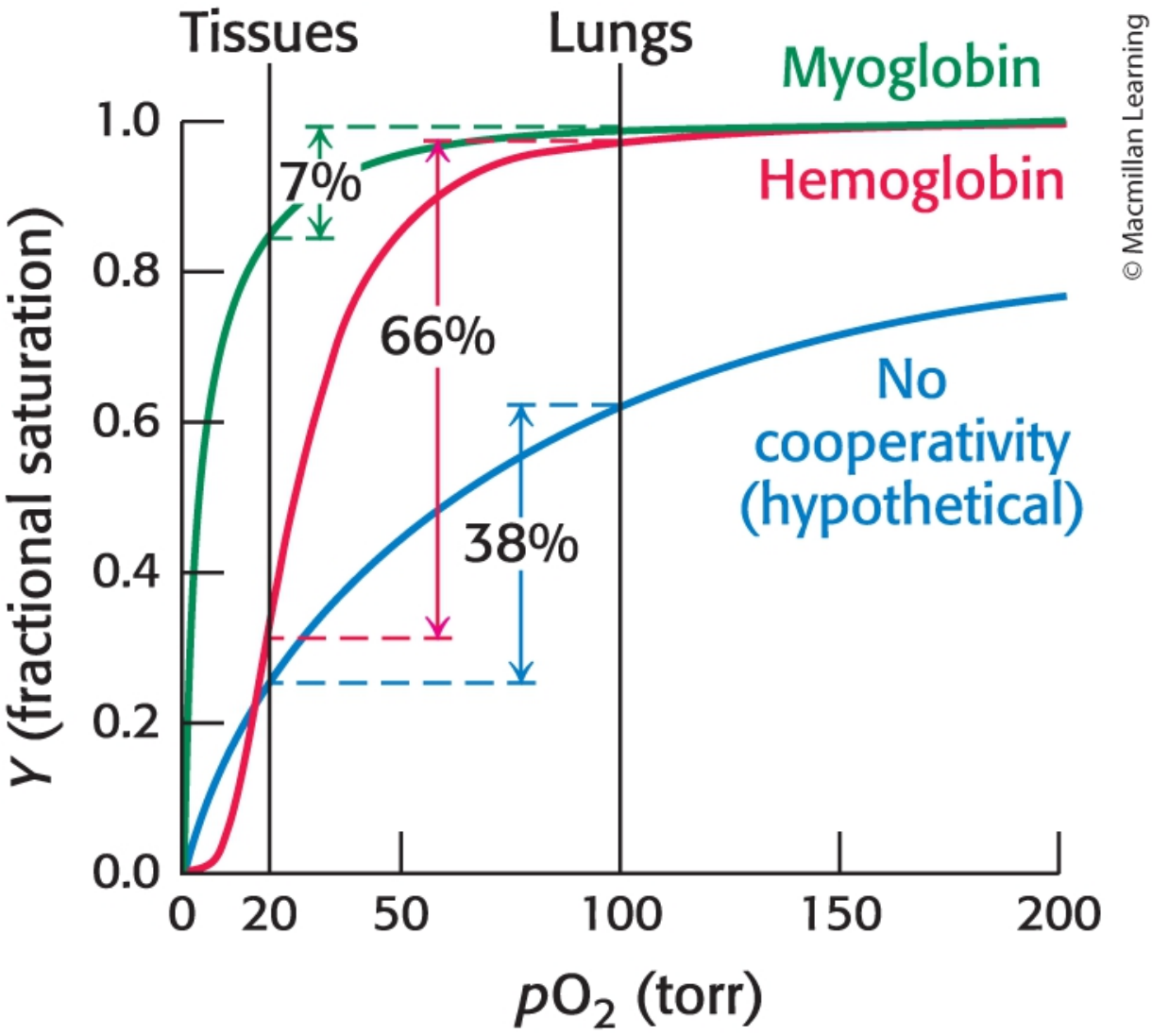
The oxygen binding curve for myoglobin has a hyperbolic shape. The curve begins at the origin and moves to the upper right until it reaches approximately point (25, 0.9). The curve then rises to 0.98 Y and moves horizontally to the right.

The oxygen binding curve for hemoglobin has a sigmoidal shape. It begins at the origin and moves horizontally to the right until approximately 2 torr. The curve then rises and moves toward the upper right until it reaches approximately point (75, 0.9). It then moves horizontally toward the right and merges with the myoglobin curve at approximately at 87.5 torr.

A vertical line begins at 26 torr and intersects with the hemoglobin curve. This line is labeled P subscript 50 is equal to 26 torr.

Return to FIGURE 3.16 The oxygen-binding curve for hemoglobin, with its sigmoid (S-like) shape, is markedly different from that for myoglobin

Extended description for FIGURE 3.17 Cooperativity enhances oxygen delivery by hemoglobin



The horizontal axis is labeled p O subscript 2 (torr) and ranges from 0 to 200 in increments of 50 units. The vertical axis is labeled Y (fractional saturation) and ranges from 0.0 to 1.0 in increments of 0.2 units. A vertical line begins at 20 torr on the horizontal axis and is labeled tissues. Another vertical line begins at 100 torr on the horizontal axis and is labeled lungs.

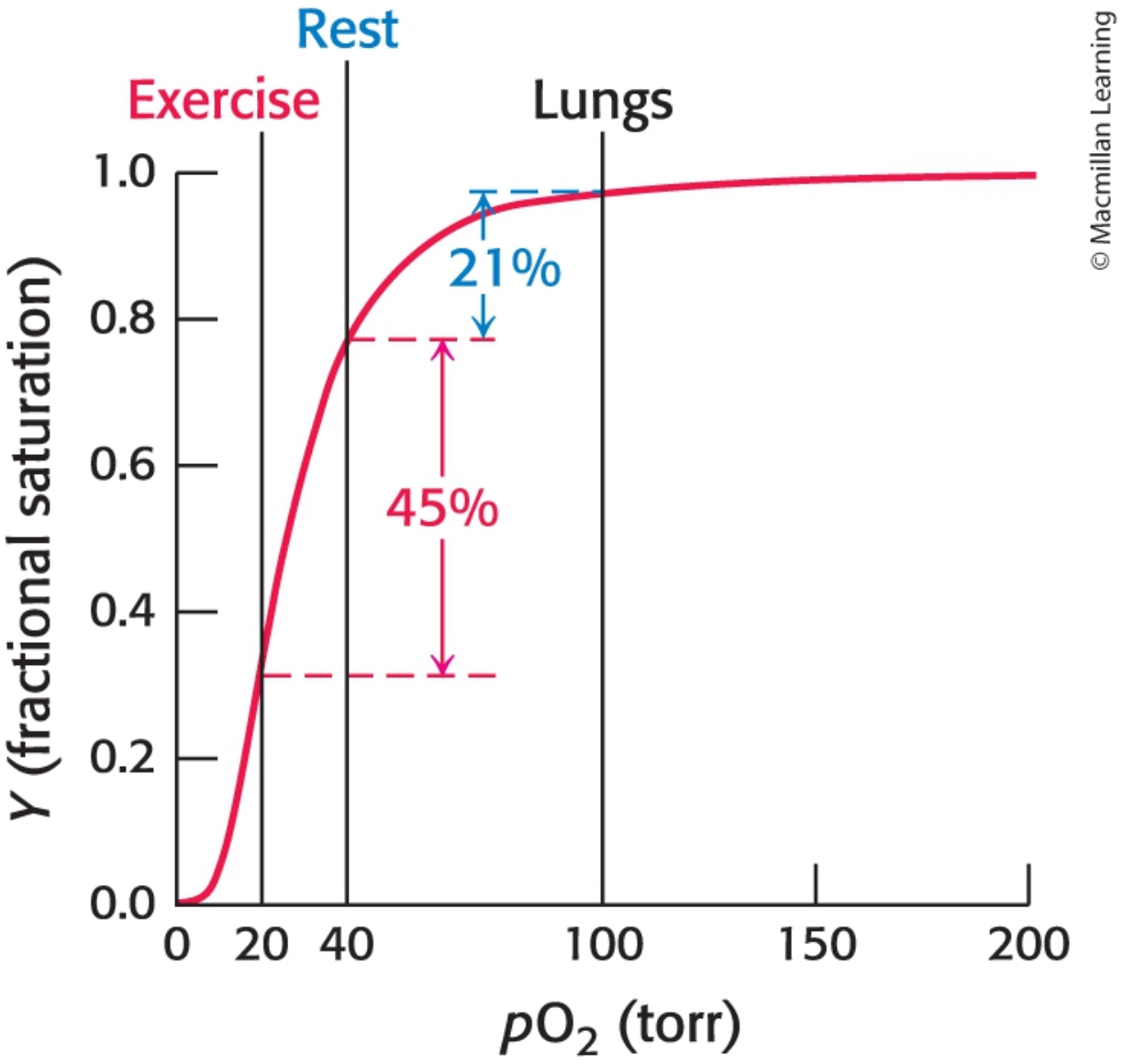
The oxygen binding curve for myoglobin has a hyperbolic shape. It begins at the origin and moves to the upper right until it reaches approximately point (25, 0.9). The curve then moves horizontally to the right. The region at which the curve makes a transition in the horizontal direction has a double-headed vertical arrow that spans from approximately markings 0.82 to 1.0 on the vertical axis. This arrow is labeled 7 percent.

The oxygen binding curve for hemoglobin has a sigmoidal shape. It begins at the origin and moves horizontally to the right until approximately 2 torr. The curve then rises and moves to the upper right until it reaches approximately point (75, 0.9). It then moves horizontally to the right and merges with the myoglobin curve at approximately at 110 torr. A double-headed vertical arrow spans from approximately markings 0.3 to 0.98 on the vertical axis at approximately 60 torr. This arrow is labeled 66 percent.

The oxygen binding curve for non-cooperative (hypothetical) protein begins at the origin. It rises upward in a curved manner and reaches approximately point (200, 0.78). A double-headed vertical arrow spans from approximately markings 0.25 to 0.6 on the vertical axis at approximately 75 torr. It is labeled 38 percent.

Return to FIGURE 3.17 Cooperativity enhances oxygen delivery by hemoglobin

Extended description for FIGURE 3.18 Oxygen delivery by hemoglobin responds to exercise



© Macmillan Learning

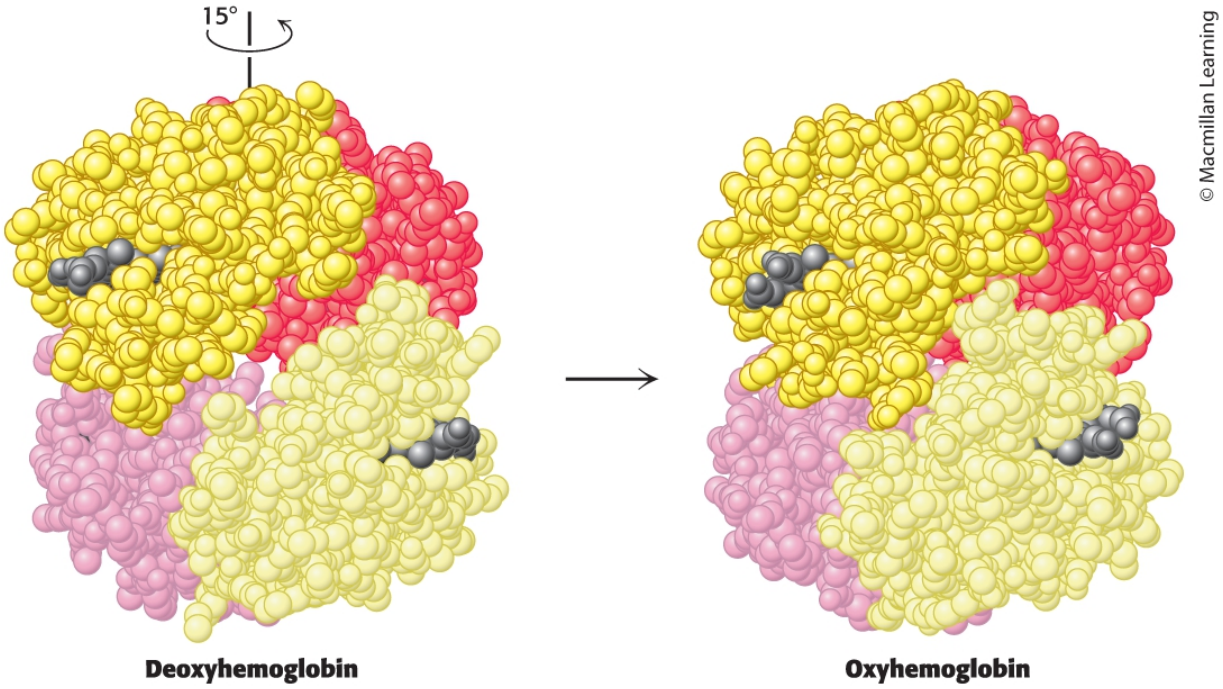
The horizontal axis is labeled p O subscript 2 (torr) and has markings 0, 20, 40, 100, 150, and 200. The vertical axis is labeled Y (fractional saturation) and ranges from 0.0 to 1.0 in increments of 0.2 units.

A vertical line begins at 20 torrs and is labeled exercise. A second vertical line begins at 40 torrs and is labeled rest. A third vertical line begins at 100 torrs and is labeled lungs.

The oxygen binding curve for hemoglobin has a sigmoidal shape and begins at the origin and moves horizontally to the right until approximately 2 torrs. The curve then rises, moves upward to the right until it reaches approximately point (75, 0.9), and then moves horizontally to the right. A double-headed vertical arrow spans from approximately 0.78 Y to 0.98 Y at approximately 70 torrs. This arrow is labeled 21 percent and is present in the region of the curve that shows the transition in the horizontal direction. A double-headed vertical arrow spans from approximately 0.3 Y to 0.78 Y at approximately 60 torrs. It is labeled 45 percent.

Return to FIGURE 3.18 Oxygen delivery by hemoglobin responds to exercise

Extended description for FIGURE 3.19 Substantial quaternary structural changes occur in hemoglobin upon oxygen binding



© Macmillan Learning

The space-filling model shows a globular compact structure of deoxyhemoglobin and oxyhemoglobin. Both structures consist of four subunits represented as dark yellow, red, light yellow, and pink. The dark yellow subunit located on the upper left is composed of a cluster of dark yellow spheres.

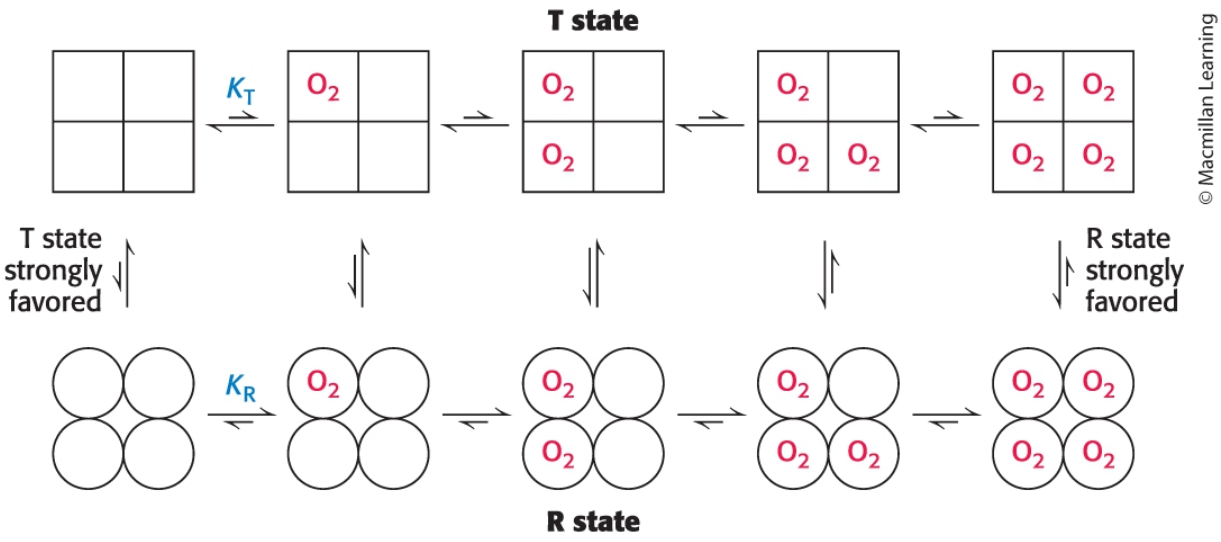
The red subunit on the upper right has a cluster of red spheres. The light yellow subunit on the lower right has a cluster of light yellow spheres. The pink subunit on the lower left has a cluster of pink spheres.

There is very little free space at the center of deoxyhemoglobin. A small cluster of black spheres is embedded in the left and right ends

of the dark yellow and light yellow subunits, respectively. A curved arrow in an anti-clockwise direction is shown above deoxyhemoglobin to depict a rotation of 15 degrees. In the oxyhemoglobin, there is no free space at the center. The upper left and upper right subunits in oxyhemoglobin are rotated 15 degrees with respect to the lower left and lower right subunits.

Return to FIGURE 3.19 Substantial quaternary structural changes occur in hemoglobin upon oxygen binding

Extended description for FIGURE 3.20 A concerted model can explain cooperative oxygen binding by hemoglobin



© Macmillan Learning

Five reversible T states are shown. Each T state is depicted as a square composed of two columns and two rows. Five reversible R states are shown below. Each R state is depicted as a cluster of four circles such that two circles are located side-by-side above and two circles below side-by-side touching each other. The T and R states are interconvertible.

The first T state is an empty square with two columns and two rows. A reversible reaction arrow is shown below and on its right. The right arrow is labeled K subscript T and shows the formation of the second T state. The arrow below is labeled T state strongly favored and shows the formation of the first R state.

The second T state is a square containing O 2 in the first row of the first column. The remaining rows and columns are empty. A reversible reaction arrow leads to the third T state.

The third T state is a square containing O 2 in the first and second row of the first column. The remaining rows and columns are empty. A reversible reaction arrow leads to the fourth T state.

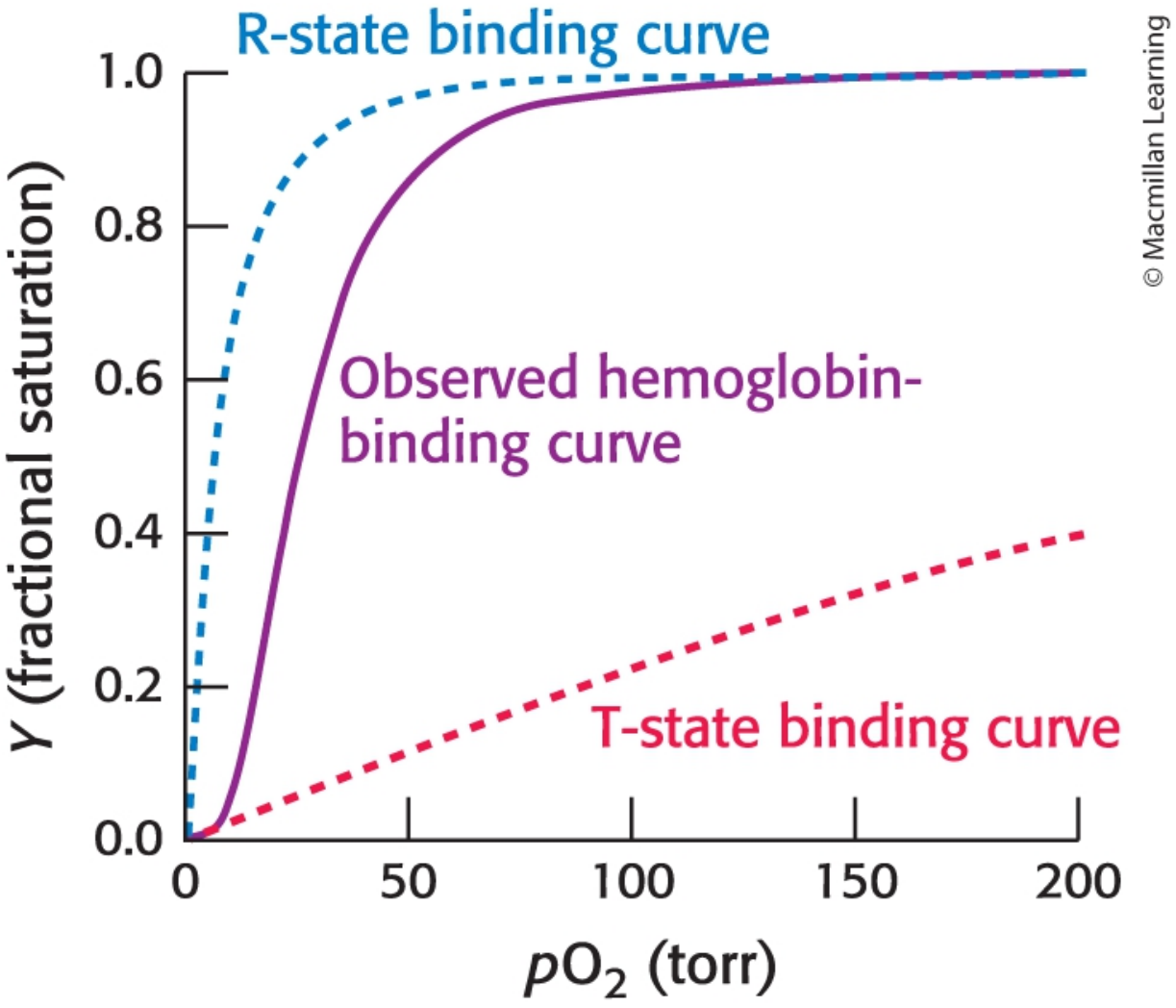
The fourth T state is a square containing O 2 in the first and second rows of the first column and the second row of the second column. A reversible reaction arrow leads to the fifth T state.

The fifth T state is a square containing O 2 in all the rows and columns. A reversible reaction arrow below is labeled R state strongly favored. It shows the formation of the fifth R state.

The first R state has all the circles empty. A reversible reaction arrow labeled K subscript R leads to the second R state. The second R state contains O 2 in the first circle of the top row. The remaining circles are empty. A reversible reaction arrow leads to the third R state. The third R state contains O 2 in the first circle of the top row and the first circle of the bottom row. The remaining circles are empty. A reversible reaction arrow leads to the fourth R state. The fourth R state contains O 2 in the first circle of the top row and both circles of the bottom row. The second circle of the top row is empty. A reversible reaction arrow leads to the fifth R state. The fifth R state contains O 2 in all the circles.

Return to FIGURE 3.20 A concerted model can explain cooperative oxygen binding by hemoglobin

Extended description for FIGURE 3.21 The sigmoid oxygen-binding curve of hemoglobin can be seen as a combination of the T state binding curve and the R state binding curve



The horizontal axis is labeled p O subscript 2 (torr) and ranges from 0 to 200 in increments of 50 units. The vertical axis is labeled Y (fractional saturation) and ranges from 0.0 to 1.0 in increments of 0.2 units.

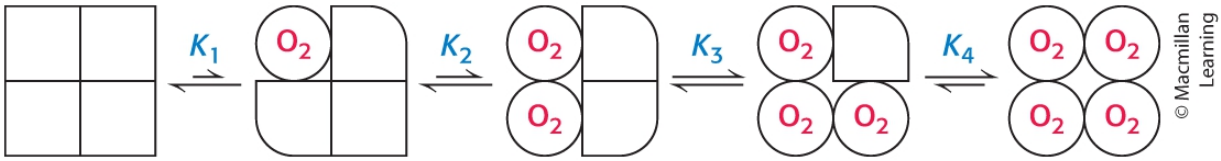
The R-state binding curve has a hyperbolic shape. The curve begins at the origin and moves to the upper right until it reaches approximately point (25, 0.9). The curve then reaches 0.98 Y and moves horizontally toward the right.

The observed hemoglobin oxygen binding curve has a sigmoidal shape. The curve begins at the origin and moves horizontally toward the right until approximately 2 torr. The curve then rises and moves toward the upper right until it reaches approximately point (60, 0.9). It then moves rises to 0.98 Y and moves horizontally toward the right to merge with the R-state binding curve at approximately 120 torr.

The T-state binding curve is a diagonal straight line that begins at the origin. It moves toward the upper right until it reaches the point (200, 0.38).

Return to FIGURE 3.21 The sigmoid oxygen-binding curve of hemoglobin can be seen as a combination of the T state binding curve and the R state binding curve

Extended description for FIGURE 3.22 A sequential model can account for oxygen-binding cooperativity



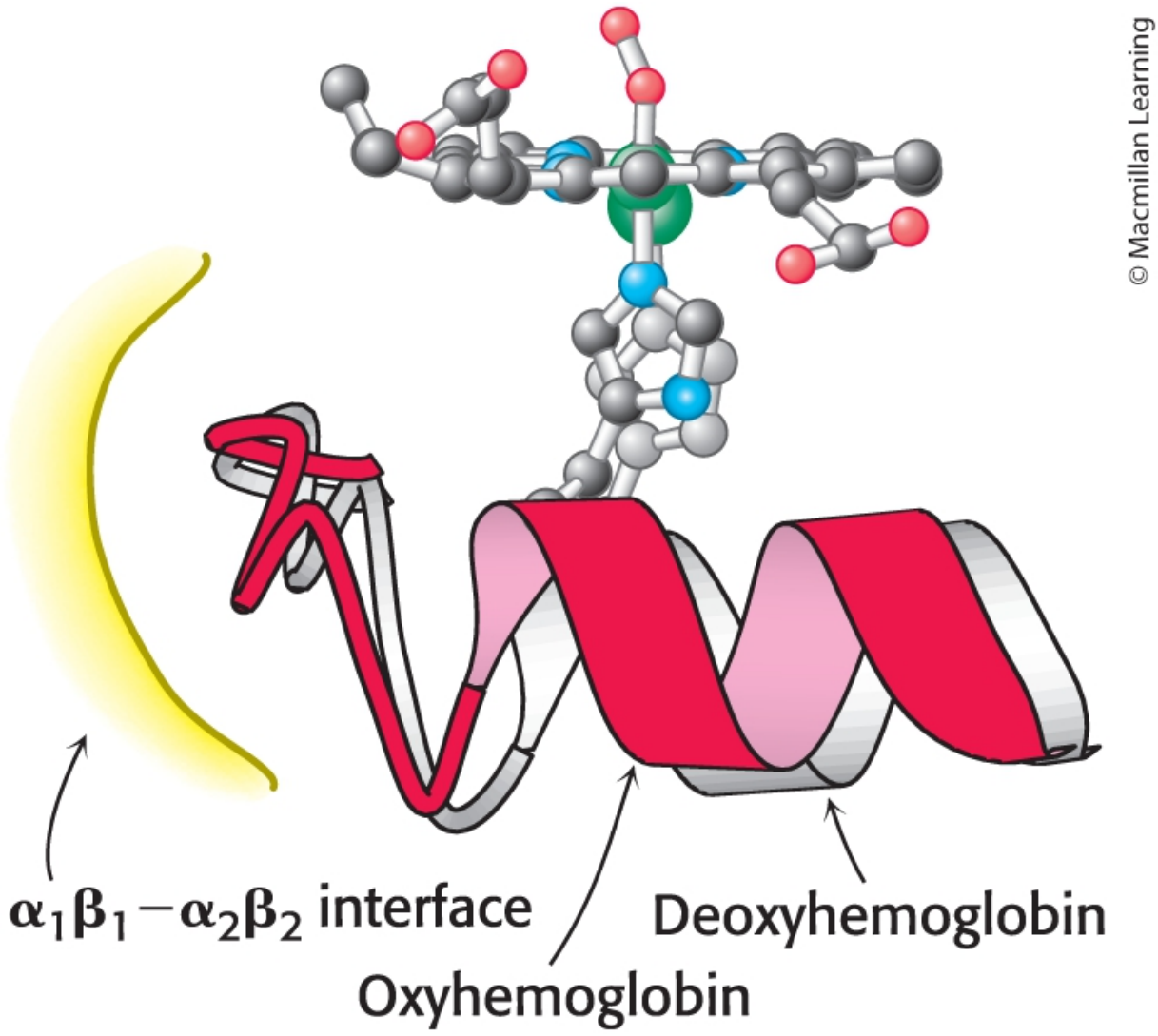
Five reversible states of hemoglobin are shown. The first state is depicted as an empty square composed of two rows and two columns. A reversible reaction arrow labeled K subscript 1 leads to the second hemoglobin state. The second hemoglobin state consists of a circle at the top left. The circle contains O 2. The top right and bottom left boxes of the square have a curved corner at the top right and bottom left, respectively. The bottom right box is square-shaped. A reversible reaction arrow labeled K subscript 2 leads to the third hemoglobin state.

The third hemoglobin state consists of a circle at the top left and bottom left. These circles contain O 2. The top right and bottom right boxes have a curved corner at the top right and bottom right, respectively. A reversible reaction arrow labeled K subscript 3 leads to the fourth hemoglobin state.

The fourth hemoglobin state consists of a circle at the top left, bottom left, and bottom right. These circles contain O 2. The top right box has a curved corner at the top right. A reversible reaction arrow labeled K subscript 4 leads to the fifth hemoglobin state. It consists of a circle at the top left, top right, bottom left, and bottom right. All the circles contain O 2.

Return to FIGURE 3.22 A sequential model can account for oxygen-binding cooperativity

Extended description for FIGURE 3.23 Oxygen binding causes the iron to move into the porphyrin



© Macmillan Learning

Deoxyhemoglobin is depicted as a grey horizontal helix, and oxyhemoglobin as a red horizontal helix. Grey and red thread like loops are shown at the left end of the deoxyhemoglobin and oxyhemoglobin helices, respectively. The deoxyhemoglobin molecule is shown behind the oxyhemoglobin molecule.

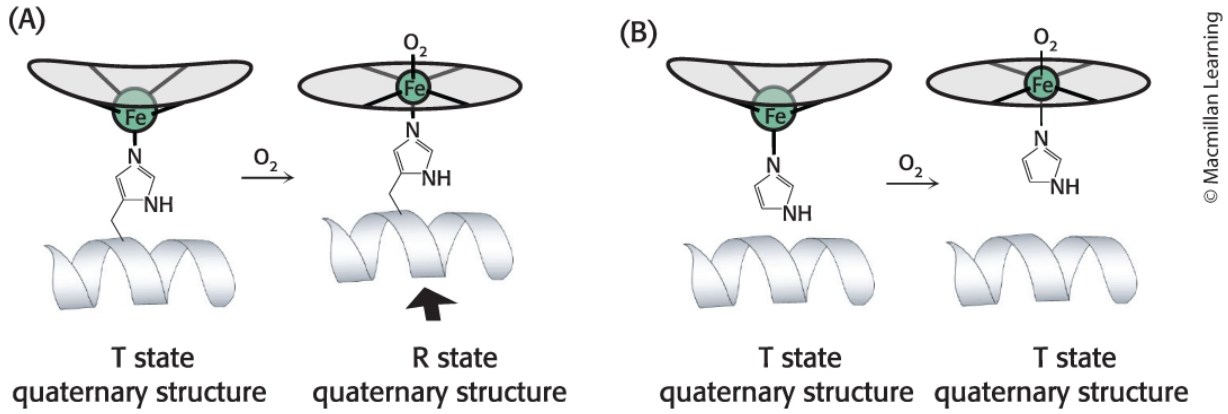
A ball-and-stick model of the proximal histidine and heme rings is shown on the top of both the molecules. The proximal histidine above the deoxyhemoglobin molecule is composed of a ring of 5 grey spheres. The bottom left grey sphere is connected to the deoxyhemoglobin helix below. The proximal histidine above the oxyhemoglobin molecule is composed of a ring of 3 black and 2 blue spheres. The black sphere on the bottom left is connected to a black sphere on the lower left. The topmost blue sphere of the proximal histidine of oxyhemoglobin is connected to a central green sphere of the heme ring.

This green sphere is located in the plane of the heme ring and connected to a red sphere above. The red sphere above is connected to another red sphere on the upper left. The topmost grey sphere of the proximal histidine of deoxyhemoglobin is connected to the central green sphere of the heme ring. This green sphere is located slightly below the plane of the heme ring. The proximal histidine of deoxyhemoglobin is located below the proximal histidine of oxyhemoglobin. The heme ring is depicted as a flat cage-like structure composed of a skeleton of black spheres.

A brown curved line is shown on the left of the oxyghemoglobin and deoxyhemoglobin molecule. The left region of the line is highlighted in yellow and labeled alpha 1 beta 1- alpha 2 beta 2 interface.

Return to FIGURE 3.23 Oxygen binding causes the iron to move into the porphyrin

Extended description for FIGURE 3.24 The movement of the distal histidine and its associated α helix upon oxygen binding drives cooperativity



© Macmillan Learning

1. Part (A): T state quaternary structure: A downward curved bean-shaped structure contains a green sphere at the center labeled F e. The green sphere is located below the plane of the bean-shaped structure. The green sphere is single bonded to N below a 5-membered heterocyclic pentagonal ring in a horizontal orientation and consists of 2 N and 3 C atoms. The first N atom occupies the first position, which is the topmost vertex. The second N atom occupies the third position, which is the bottom right vertex and is bound to H. A double bond is present between the first N atom and C 1 and C 2 and C 3. C 2 is single bonded to C H 2 below in the form of a line. The C atom of this C H 2 is single bonded to an alpha-helix in a horizontal orientation. A rightward pointing arrow is labeled O 2.

   R state quaternary structure: An oval-shaped structure contains a green sphere at the center labeled F e. The green sphere is located in the plane of the oval. It is single bonded to O 2 above. The green sphere is single bonded to N below a 5-membered heterocyclic pentagonal ring in a horizontal orientation and

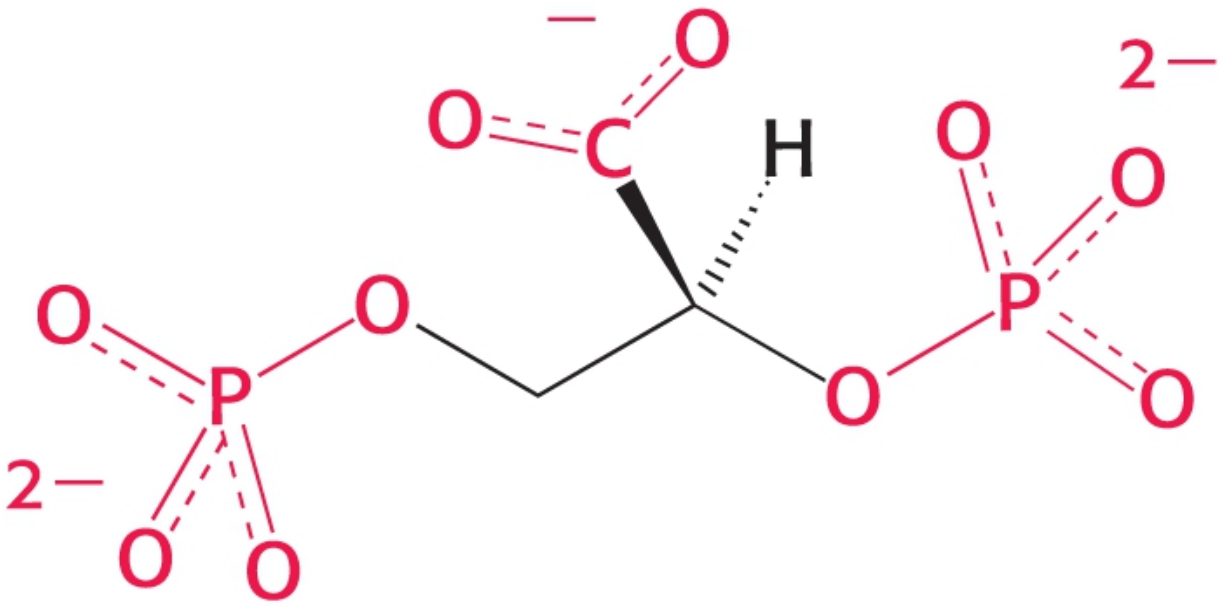
consists of 2 N and 3 C atoms. The first N atom occupies the first position, which is the topmost vertex. The second N atom occupies the third position, which is the bottom right vertex and is bound to H. A double bond is present between the first N atom and C 1 and C 2 and C 3. C 2 is single bonded to C H 2 below in the form of a line. The C atom of this C H 2 is single bonded to an alpha-helix in a horizontal orientation. A thick arrow points toward the alpha helix.

2. Part (B): T state quaternary structure: A downward curved bean-shaped structure contains a green sphere at the center labeled F e. The green sphere is located below the plane of the bean-shaped structure. The green sphere is single bonded to N below a 5-membered heterocyclic pentagonal ring in a horizontal orientation and consists of 2 N and 3 C atoms. The first N atom occupies the first position, which is the topmost vertex. The second N atom occupies the third position, which is the bottom right vertex and is bound to H. A double bond is present between the first N atom and C 1 and C 2 and C 3. This ring is present above an alpha-helix in a horizontal orientation. A rightward pointing arrow is labeled O 2.

   T state quaternary structure: An oval-shaped structure contains a green sphere at the center labeled F e. The green sphere is located in the plane of the oval. It is single bonded to O 2 above. The green sphere is single bonded to N below a 5-membered heterocyclic pentagonal ring in a horizontal orientation and consists of 2 N and 3 C atoms. The first N atom occupies the first position, which is the topmost vertex. The second N atom occupies the third position, which is the bottom right vertex and is bound to H. A double bond is present between the first N atom and C 1 and C 2 and C 3. The ring is located above an alpha helix in horizontal orientation.

Return to FIGURE 3.24 The movement of the distal histidine and its associated α helix upon oxygen binding drives cooperativity

Extended description for Structure of 2,3-Bisphosphoglycerate



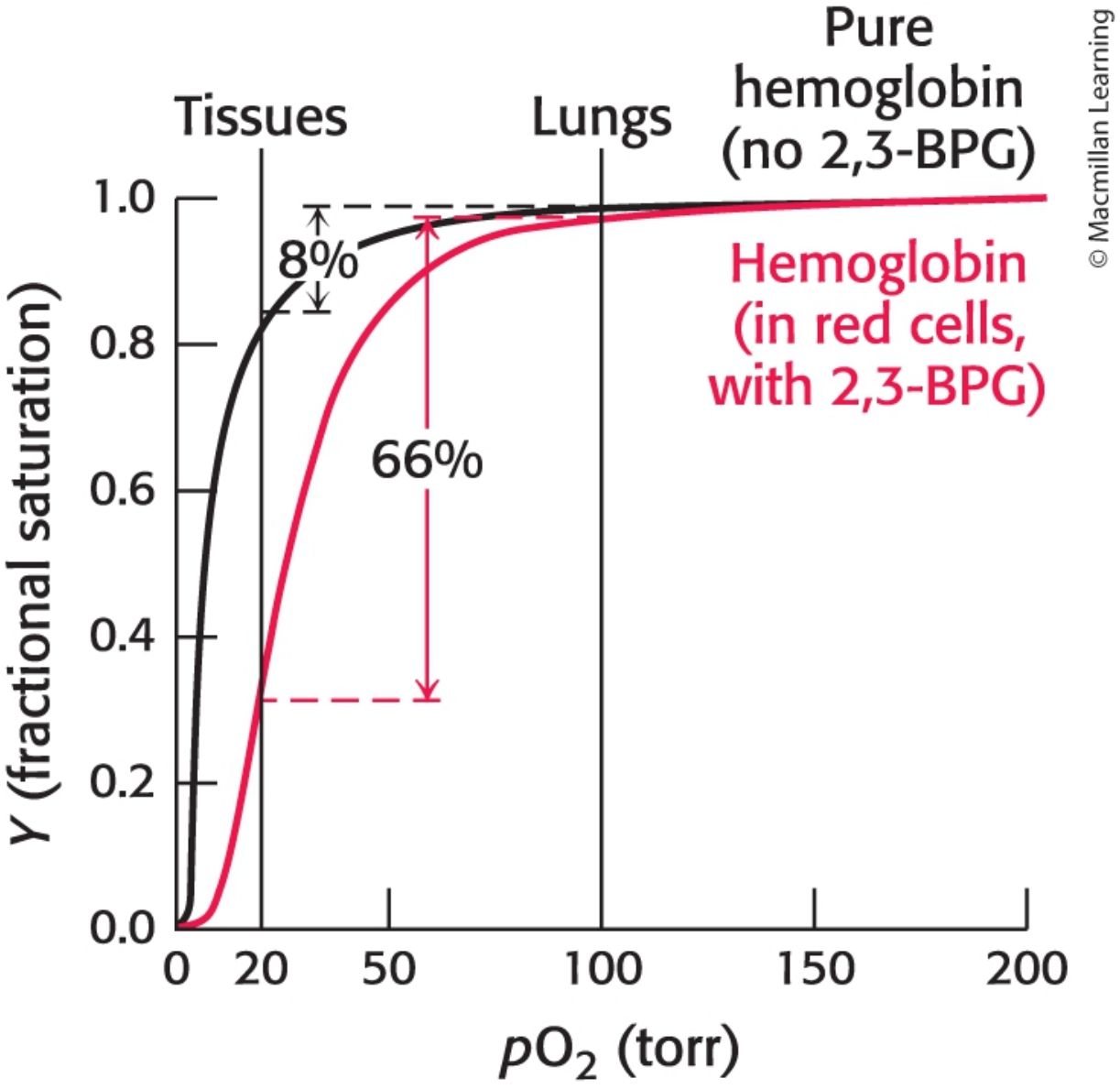
2,3-Bisphosphoglycerate (2,3-BPG)

2,3-Bisphosphoglycerate (2,3-B P G) has the following structure: A 2 O and 2 C heteronuclear alkane chain is depicted as a line structure using 3 zigzag lines. The first O atom occupies the first position and the second O atom occupies the fourth position. The first O atom is single bonded to P on the lower left. P is partially double bonded to O on the upper left, O on the lower left, and O on the lower right. A charge of negative 2 is present between the oxygen atoms on the upper left and lower left. C 2 is wedged bonded C on the upper left and dash bonded to H on the upper right. This C atom is partially double bonded to O on the upper left and O on the upper right. A negative charge is present between the two O atoms. The second O

atom is single bonded to P on the upper right. P is partially double bonded to O on the upper left, O on the upper right, and O on the lower right. A charge negative 2 is present on the top of the oxygen atom at the upper right. Except for the alkane chain and the H atom on C 2 are highlighted in red.

Return to Structure of 2,3-Bisphosphoglycerate

Extended description for FIGURE 3.25 The oxygen-binding curves for pure hemoglobin and hemoglobin in red blood are markedly different



The horizontal axis is labeled p O subscript 2 (torr) and has markings 0, 20, 50, 100, 150, and 200. The vertical axis is labeled Y

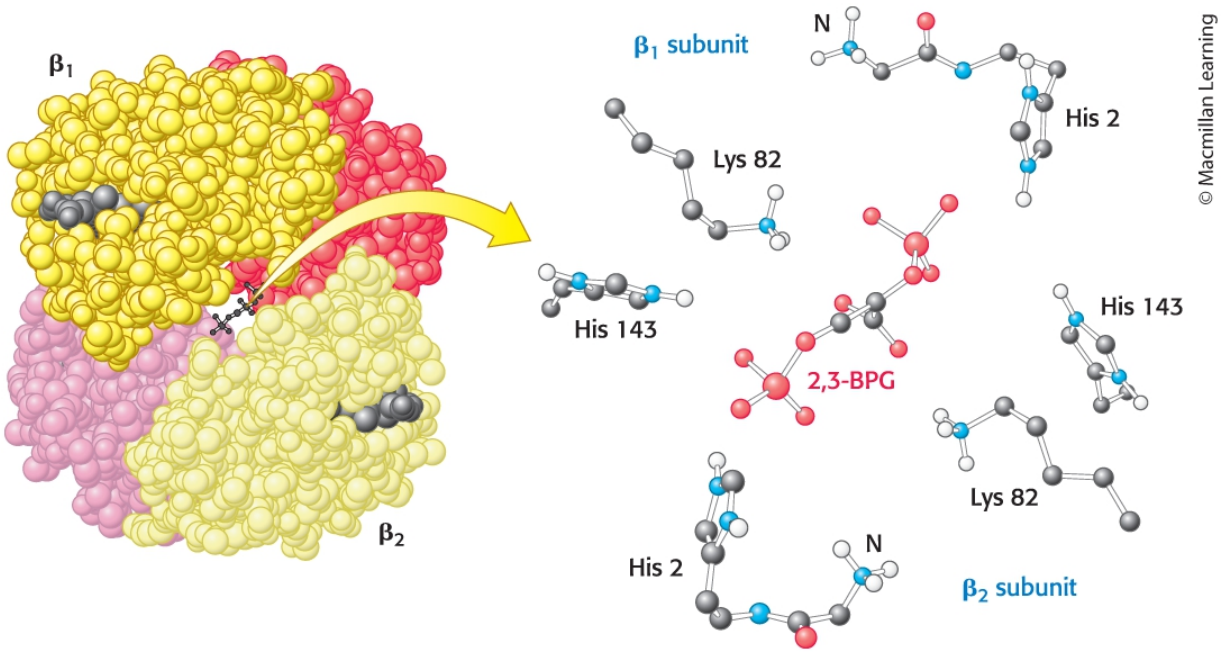
(fractional saturation) and ranges from 0.0 to 1.0 in increments of 0.2 units.

A vertical line begins at 20 torr and is labeled tissues. Another vertical line begins at 100 torr and is labeled lungs. The oxygen binding curve for pure hemoglobin (no 2, 3-B P G) has a hyperbolic shape. It begins at the origin and moves upward to the right until it reaches approximately point (35, 0.9). The curve then moves horizontally to the right. The region at which the curve makes a transition in the horizontal direction has a double-headed vertical arrow that spans from approximately 0.82 Y to 1.0 Y. This arrow is labeled 8 percent on the right of the vertical line labeled tissues.

The oxygen binding curve for hemoglobin (in red cells, with 2, 3- B P G) has a sigmoidal shape. It begins at the origin and moves horizontally to the right until approximately 2 torr. The curve then rises and moves upward to the right until it reaches approximately point (70, 0.9). It then moves horizontally to the right and merges with the pure hemoglobin curve at approximately at 110 torr. A double-headed vertical arrow spans from approximately 0.3 Y to 0.98 Y on the pure hemoglobin curve at approximately 60 torr. This arrow is labeled 66 percent.

Return to FIGURE 3.25 The oxygen-binding curves for pure hemoglobin and hemoglobin in red blood are markedly different

Extended description for FIGURE 3.26 2,3-Bisphosphoglycerate binds in the central cavity within deoxyhemoglobin

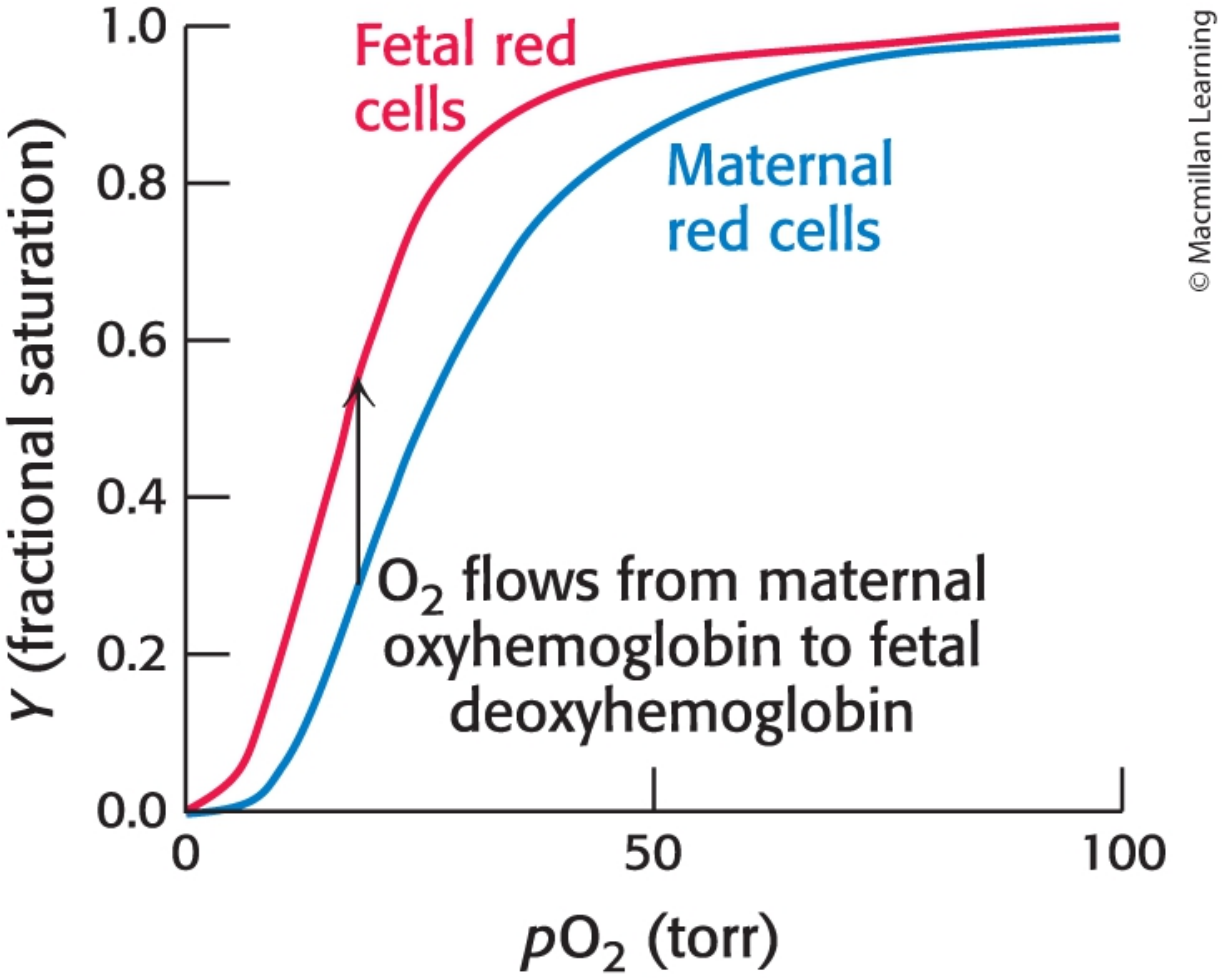


The space-filling model shows a globular compact structure of deoxyhemoglobin. It consists of four subunits that are dark yellow, red, light yellow, and pink in color. The dark yellow subunit located at the upper left is labeled beta 1, and is composed of a cluster of the dark yellow sphere. The red subunit located at the upper right is composed of a cluster of red spheres. The light yellow subunit located at the lower right is labeled beta 2 and is composed of a cluster of light yellow spheres. The pink subunit located at the lower left is composed of a cluster of pink spheres. A small cluster of black spheres is embedded in the left and the right end of the dark yellow and the light yellow subunits, respectively. There is a free space at the center of the deoxyhemoglobin molecule.

This space is the central cavity and is enlarged on the right. The enlarged figure shows a ball-and-stick model of 2, 3- B P G composed of red and black spheres in a diagonal orientation at the center. It is surrounded by the amino acid residues histidine 2, histidine 143, lysine 82, histidine 2, histidine 143, and lysine 82 from the bottom left to the bottom right. Histidine 2, histidine 143, and lysine 82 at the bottom left, left, and top left is part of the beta 1 subunit. The remaining histidine 2, histidine 143, and lysine 82 are part of the beta 2 subunit.

Return to FIGURE 3.26 2,3-Bisphosphoglycerate binds in the central cavity within deoxyhemoglobin

Extended description for FIGURE 3.27 Fetal red blood cells obtain oxygen from maternal red blood cells by virtue of fetal hemoglobin's lower affinity for 2,3-BPG



© Macmillan Learning

The horizontal axis is labeled p O subscript 2 (torr) and ranges from 0 to 100 in increments of 50 units. The vertical axis is labeled Y (fractional saturation) and ranges from 0.0 to 1.0 in increments of 0.2 units.

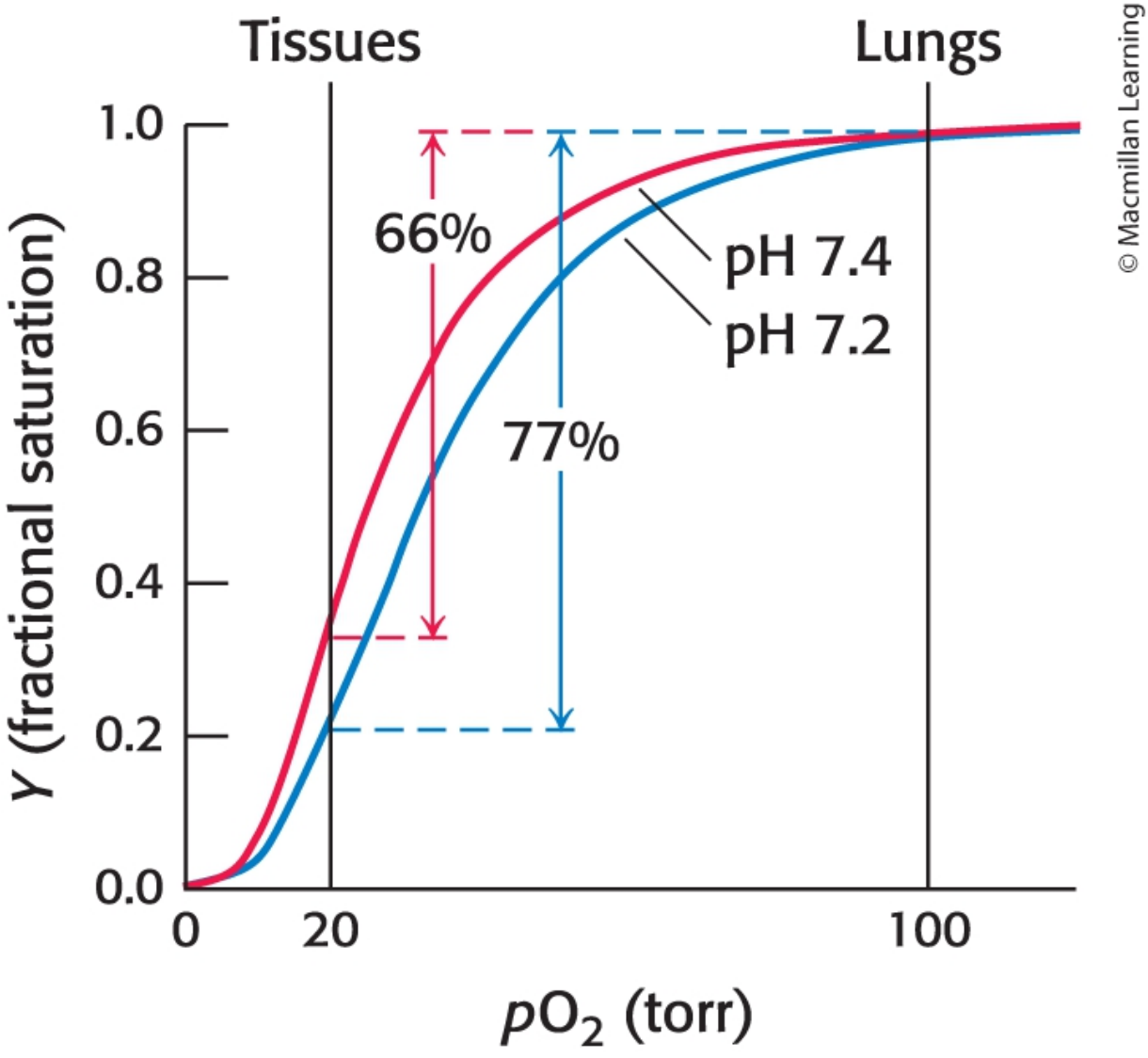
Two curves labeled fetal red cells, and maternal red cells are shown. The fetal red cell curve begins at the origin and moves upward to the

right to reach approximately point (4, 0.05). It moves steeply upward till approximately point (40, 0.98). The curve then moves horizontally to the right. A point on this curve approximately at point (20, 0.52) is labeled O 2 flows from maternal oxyhemoglobin to fetal deoxyhemoglobin.

The maternal red cells curve begins at the origin and moves horizontally to the right until approximately 6 torr. The curve then rises and moves upward on the right of the fetal red cells curve until it reaches approximately point (75, 0.98). It then moves horizontally to the right below the fetal red cells curve.

Return to FIGURE 3.27 Fetal red blood cells obtain oxygen from maternal red blood cells by virtue of fetal hemoglobin's lower affinity for 2,3-BPG

Extended description for FIGURE 3.28 Lowering the pH decreases the oxygen affinity of hemoglobin and facilitates the release of oxygen into metabolically active tissues



The horizontal axis is labeled p O subscript 2 (torr) and has markings 0, 20, and 100. Markings 20 and 100 are at a greater distance than markings 0 and 20. The vertical axis is labeled Y

(fractional saturation) and ranges from 0.0 to 1.0 in increments of 0.2 units.

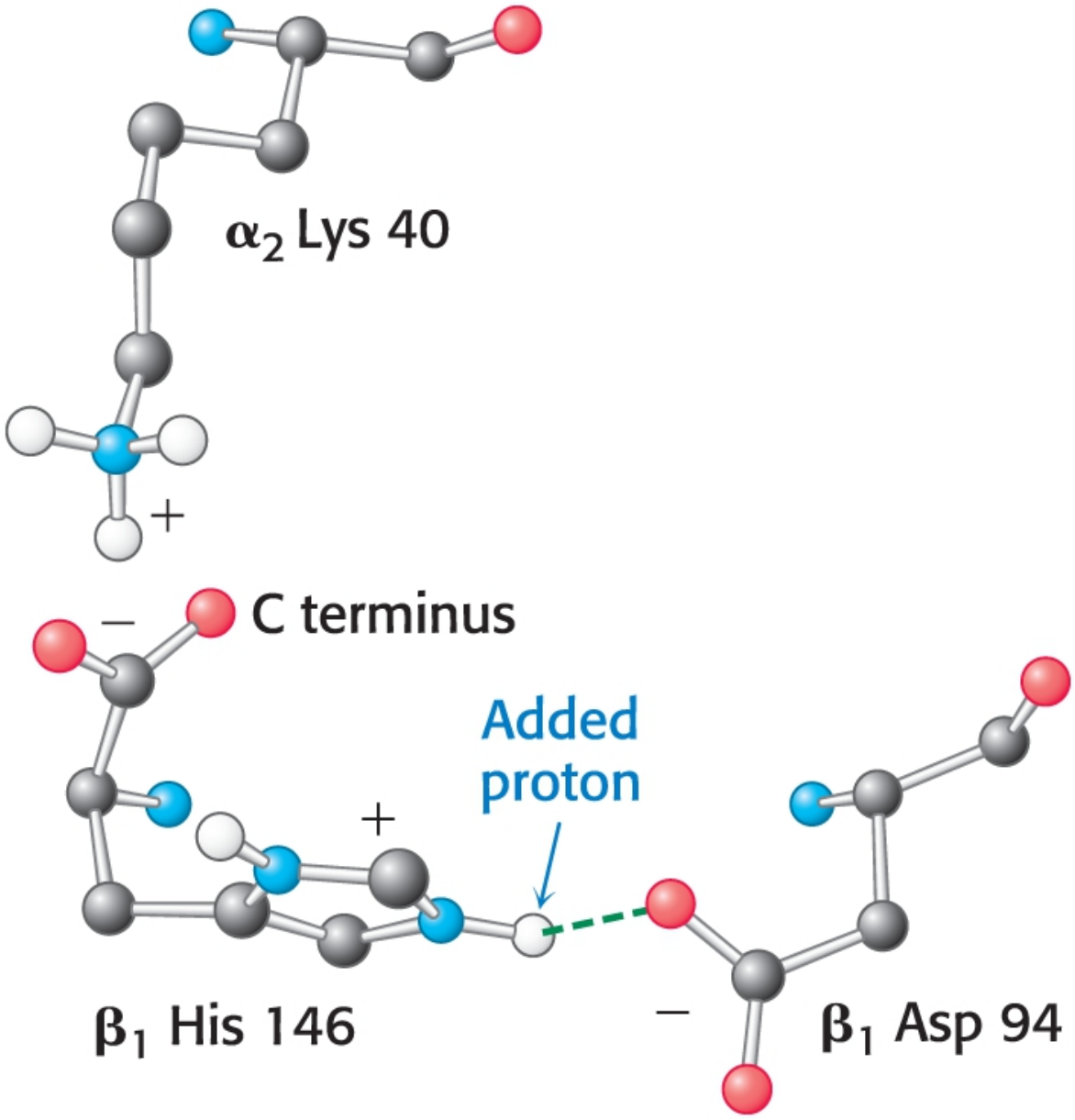
A vertical line begins at 20 torr and is labeled tissues. Another vertical line begins at 100 torr and is labeled lungs. The oxygen binding curve for hemoglobin at p H 7.4 has a sigmoidal shape. It begins at the origin and moves upward to the right until it reaches approximately point (70, 0.98). The curve then rises to 1.0 Y and moves horizontally toward the right.

The oxygen binding curve for hemoglobin at p H 7.2 has a sigmoidal shape. This curve is located toward the right of the oxygen binding curve for hemoglobin at p H 7.4. It begins at the origin, merges with the first curve, and moves almost horizontally toward the right until approximately 8 torr. The curve then rises and moves upward to the right until it reaches approximately point (70, 0.9). It then moves horizontally toward the right and merges with the first curve at approximately at 90 torr.

A double-headed vertical arrow spans from approximately 0.3 Y to 1.0 Y at approximately 35 torr. This arrow is labeled 66 percent. Another double-headed vertical arrow spans from approximately 0.2 Y to 1.0 Y at approximately 50 torr. This arrow is labeled 77 percent.

Return to FIGURE 3.28 Lowering the pH decreases the oxygen affinity of hemoglobin and facilitates the release of oxygen into metabolically active tissues

Extended description for FIGURE 3.29 Ionic interactions involving the β chain C-terminal histidine are responsible for some of the pH sensitivity of hemoglobin oxygen affinity



© Macmillan Learning

In the ball-and-stick model, C atoms are represented as black spheres, N atoms are represented as blue spheres, O atoms are represented as red spheres, and H atoms are represented as white spheres.

The C-terminal of the beta 1 chain consisting of aspartic acid 94 and histidine 146 is shown. Aspartic acid 94 consists of a chain of 4 black spheres connected in a zigzag manner. The first black sphere from the left is connected to a red sphere on the upper left and lower left. A negative charge is present between the two red spheres. The third black sphere is connected to a blue sphere on the left. The fourth black sphere is connected to a red sphere on the upper right. The red sphere on the upper left is connected through a dashed line to a white sphere labeled added proton on the left. The white sphere is connected to a blue sphere located at the leftmost vertex of a flat heterocyclic pentagonal ring consisting of 2 blue and 3 black spheres. The second blue sphere is located at the top left vertex and connected to a white sphere. The remaining positions are occupied by black spheres. A positive charge is present above the black sphere on the top right vertex of the ring.

The black sphere on the bottom left vertex is connected to another black sphere on the left. This black sphere is connected to a vertical chain of two black spheres. The bottom black sphere of this chain is connected to a blue sphere on the right. The top black sphere of this chain is connected to a red sphere on the upper left and upper right. This region is labeled C terminus. A negative charge is present between the two red spheres. The lysine 40 side chain of the alpha 2 chain is shown above the C terminus of the beta 1 chain.

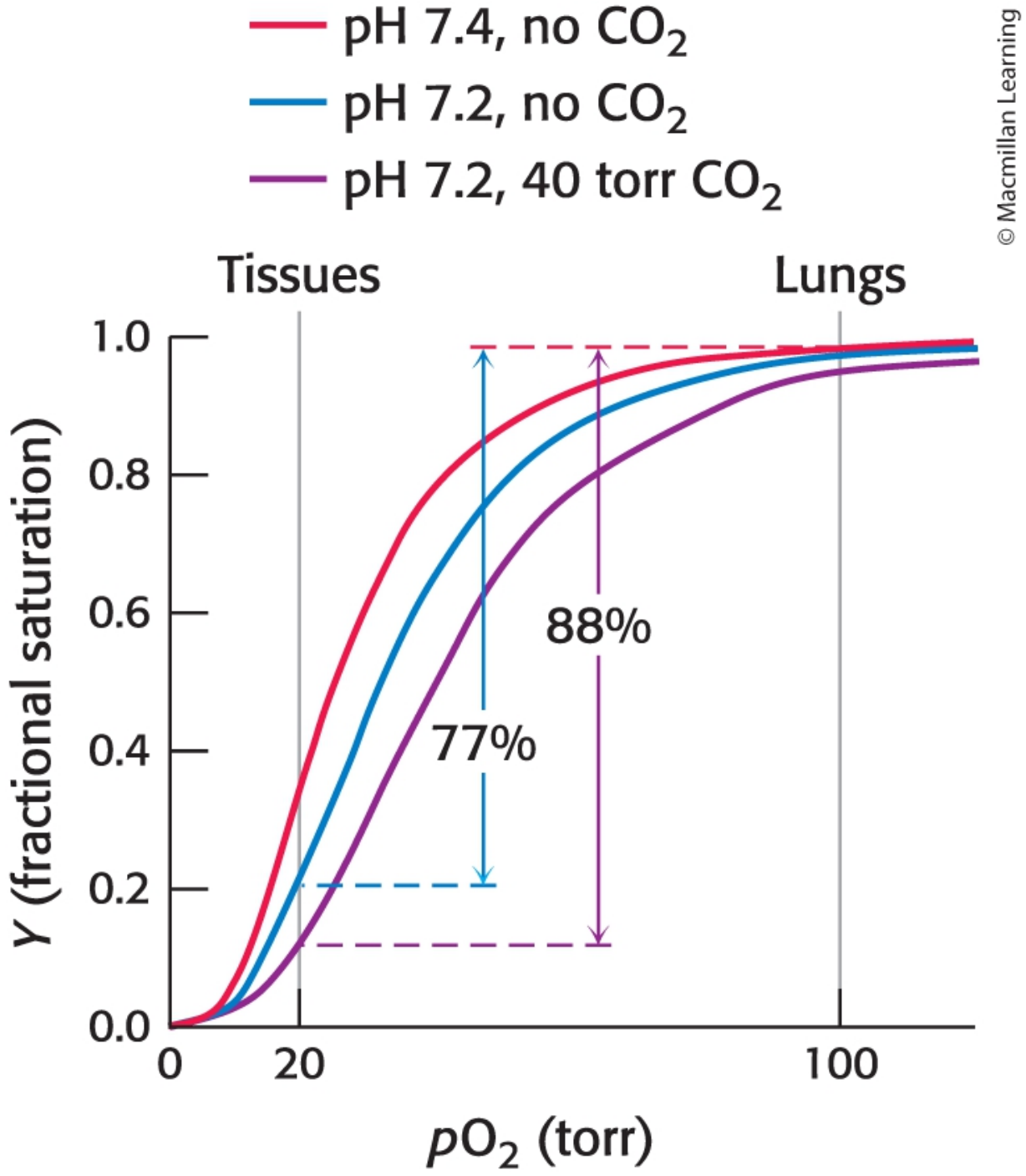
The structure of this side chain is as follows: A central blue sphere is connected to a white sphere on the left, below, and right. A positive charge is present between the white spheres on the right and bottom. The blue sphere is connected above to a chain of 3 black

spheres in a vertical orientation. The topmost black sphere of the chain is connected to a zigzag chain of 3 black spheres on the right. The rightmost black sphere of the chain is connected to a red sphere on the right. The second black sphere of the chain is connected to a blue sphere on the left.

Return to FIGURE 3.29 Ionic interactions involving the β chain C-terminal histidine are responsible for some of the pH sensitivity of hemoglobin oxygen affinity

Extended description for FIGURE 3.30 The presence of carbon dioxide decreases the oxygen affinity of

hemoglobin, even beyond the effect due to a decrease in pH



The horizontal axis is labeled p O subscript 2 (torr) and has markings 0, 20, and 100. The vertical axis is labeled Y (fractional saturation) and ranges from 0.0 to 1.0 in increments of 0.2 units.

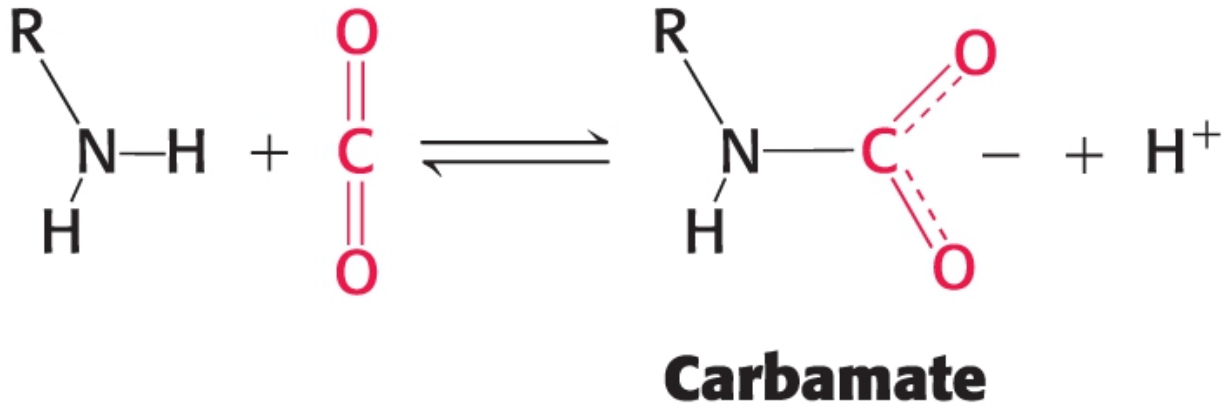
A vertical line begins at 20 torrs and is labeled tissues. Another vertical line begins at 100 torrs and is labeled lungs. The oxygen binding curve for hemoglobin at p H 7.4 and no C O 2 is depicted using a red line. The oxygen binding curve for hemoglobin at p H 7.2 and no C O 2 is depicted using a blue line. The oxygen binding curve for hemoglobin at p H 7.2 and 40 torr C O 2 is depicted using a purple line. All the curves have a sigmoidal shape.

The red curve begins at the origin and moves horizontally to the right until 8 torrs. It then moves upward to the right until it reaches approximately point (70, 0.98). The curve then rises to 1.0 Y and moves horizontally to the right. The blue curve begins at the origin, merges with the red curve, and moves almost horizontally to the right until approximately 10 torrs. The curve then rises and moves upward to the right until it reaches approximately point (70, 0.9). It then moves horizontally to the right and merges with the red curve approximately at 90 torrs. The purple begins at the origin merges with the red and blue curves and moves almost horizontally to the right until approximately 12 torrs. The curve then rises and moves upward to the right until it reaches approximately point (90, 0.9). It then moves horizontally to the right below the blue curve.

A double-headed vertical arrow spans from approximately 0.2 Y to 1.0 Y at approximately 65 torrs. This arrow is labeled 77 percent. Another double-headed vertical arrow spans from approximately 0.1 Y to 1.0 Y at approximately 60 torrs. This arrow is labeled 88 percent.

Return to FIGURE 3.30 The presence of carbon dioxide decreases the oxygen affinity of hemoglobin, even beyond the effect due to a decrease in pH

Extended description for Formation of carbamate

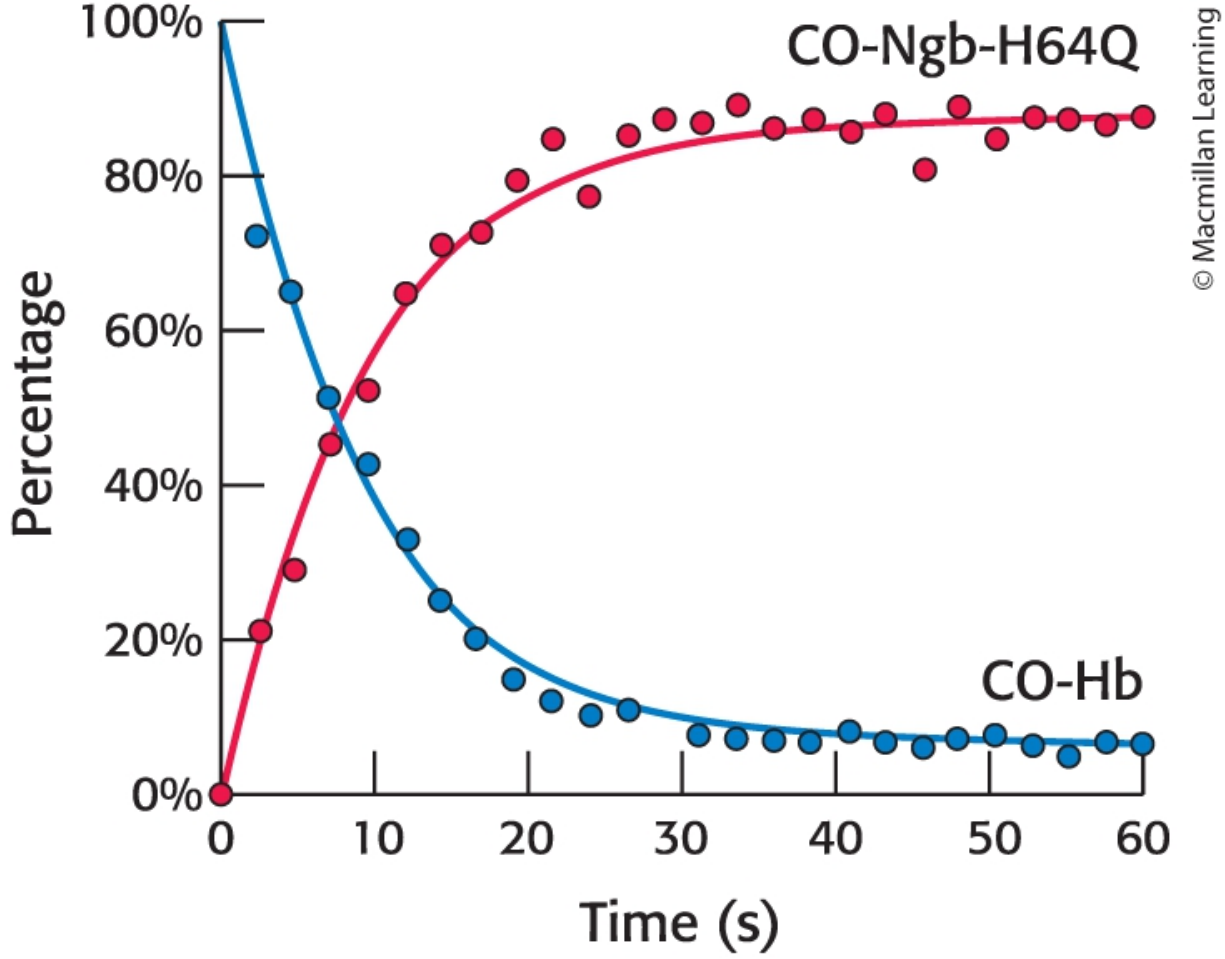


The reversible reaction consists of two reactants and two products. The first reactant has the following structure: N, single bond, H. N is single bonded to R on the upper left and single bonded to H on the lower left. The second reactant has the following structure: O, double bond, C, double bond, O in a vertical orientation. The second reactant is highlighted in red.

The first product labeled carbamate has the following structure: N, single bond, C. N is single bonded to R on the upper left and single bonded to H on the lower left. C is partially double bonded to O on the upper right and lower right. A minus sign is present between the two O atoms. The C atom and the two O atoms are highlighted in red. The second product is H superscript plus.

Return to Formation of carbamate

Extended description for FIGURE 3.31 Carbon monoxide is rapidly transferred from carboxyhemoglobin to N g b-H64Q



The horizontal axis is labeled time (s) and ranges from 0 to 60 in increments of 10 units. The vertical axis is labeled percentage and ranges from 0 to 100 in increments of 20 units.

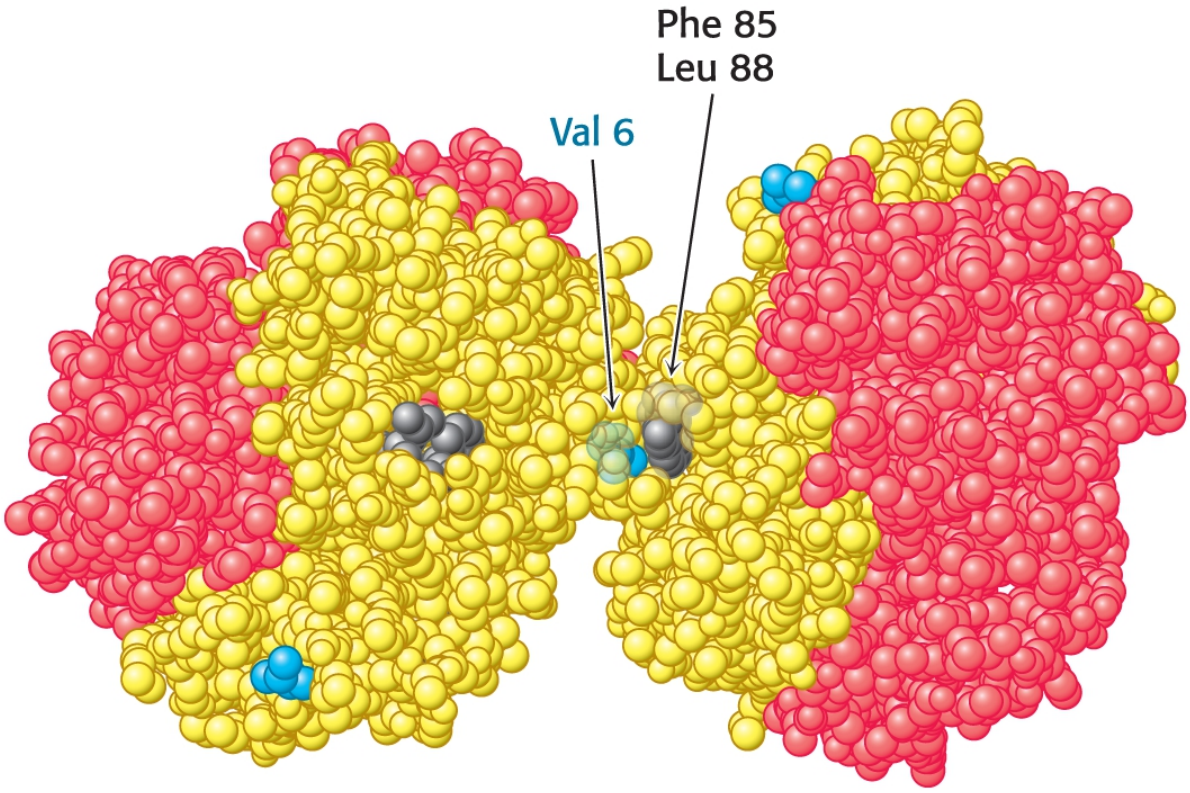
Two curves are shown on the graph. The first curve is labeled C O - H b. It begins at 100 percent on the vertical axis and moves downward toward the lower right until it reaches approximately

point (40, 10). It forms a curved slope between 10 to 30 seconds. At 10 seconds, the percentage is approximately 30. At 20 seconds, the percentage is approximately 18. At 30 seconds, the percentage is approximately 11 percent. After 40 seconds, the curve moves horizontally toward the right and ends at the end of the horizontal axis. Several points are marked on and around the curve.

The second curve is labeled C O - N g b - H 6 4 Q. It begins at the origin and moves to the upper right until it reaches approximately point (30, 82). It forms a curved slope between approximately 12 seconds and 30 seconds. At 10 seconds, the percentage is approximately 58. At 20 seconds, the percentage is approximately 79. At 30 seconds, the percentage is 81. Several points are marked on and around the curve.

Return to FIGURE 3.31 Carbon monoxide is rapidly transferred from carboxyhemoglobin to N g b-H64Q

Extended description for FIGURE 3.34 Two molecules of hemoglobin S interact through hydrophobic patches



© Macmillan Learning

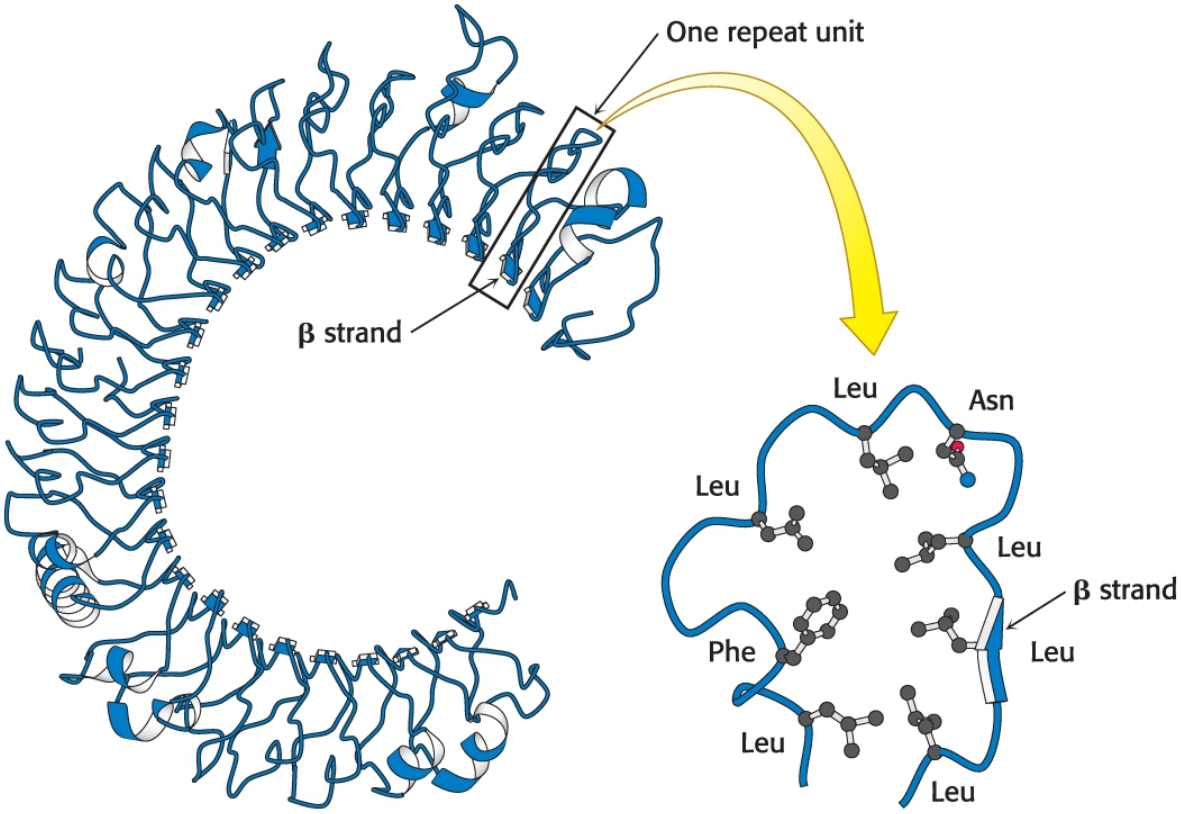
The space-filling model shows a globular compact structure of two hemoglobin S molecules side-by-side. Both structures consists of two subunits that are dark yellow and red. A small cluster of four blue spheres is located at the bottom of the dark yellow subunit of the left hemoglobin S molecule. A small cluster of three blue spheres is located at the top of the dark yellow subunit of the right hemoglobin S molecule.

A small cluster of black sphere is located at the center of the dark yellow subunit of left hemoglobin S molecule. The dark yellow subunits of the two hemoglobin S molecules face each other and are attached at the center. Valine 6, phenylalanine 85, and leucine 88 are

located at the point of attachment of the two subunits. Valine is depicted as a small cluster of light blue transparent spheres. Phenylalanine and leucine are depicted as small clusters of transparent gray spheres.

Return to FIGURE 3.34 Two molecules of hemoglobin S interact through hydrophobic patches

Extended description for FIGURE 3.35 The structure of the LRR domain from TLR3 reveals how many LRR units come together to form a structure with binding surfaces for potential partners



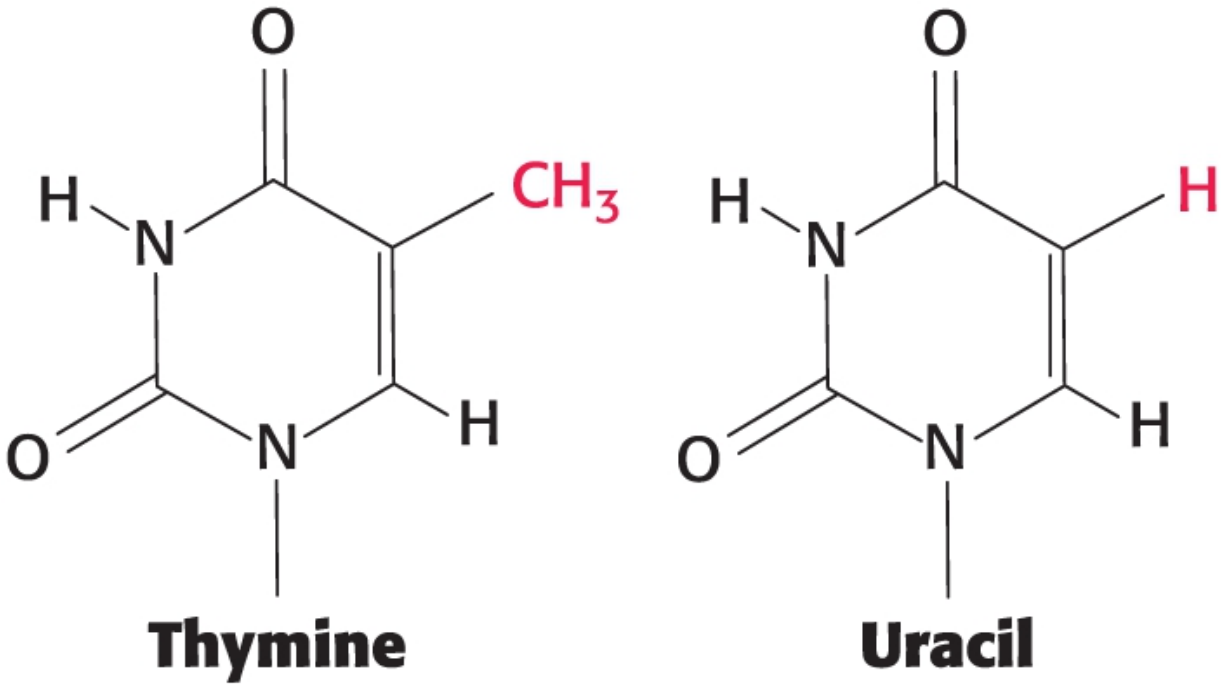
© Macmillan Learning

The L R R domain is depicted as a large C-shaped structure composed of several L R R repeats. Each L R R unit is composed of a beta-strand at the base connected to a circular loop-like structure above. The structure of the L R R unit is enlarged to show a circular loop with an open bottom. A beta-strand in an upward orientation is at the bottom right of the loop. From the bottom left to the bottom right, the order of amino acids is leucine, phenylalanine, leucine, leucine, asparagine, leucine, leucine, and leucine. The beta-strand is below the leucine residue. The beta-strand also contains a leucine

residue. A leucine residue is at the bottom right end of the loop below the beta-strand. The side chains of the amino acid residues face the hollow interior of the loop. They are depicted as a ball-and-stick model.

Return to FIGURE 3.35 The structure of the LRR domain from TLR3 reveals how many LRR units come together to form a structure with binding surfaces for potential partners

Extended description for Thymine and uracil



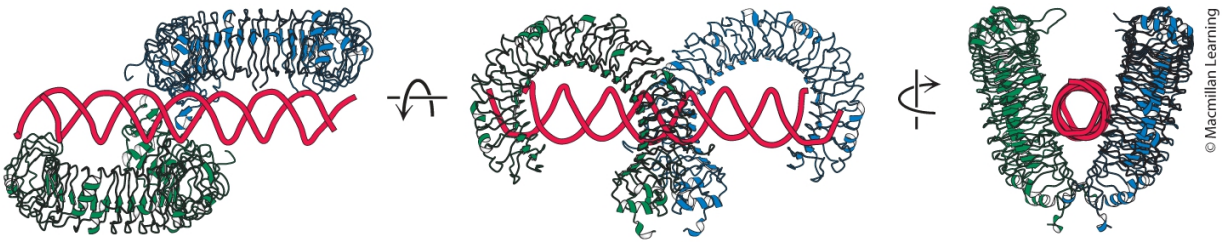
The structure of thymine is as follows: A 6-membered heterocyclic hexagonal ring is in a vertical orientation and consists of 2 N and 4 C atoms. The first N atom occupies the first position, which is the bottommost vertex. The second N atom occupies the third position, which is the top left vertex. The first N atom has an open single bond below. The second N atom is single bonded to H on the upper left. A double bond is present between C 3 and C 4. C 1 is double bonded to O on the lower left. C 2 is double bonded to O above. C 3 is single bonded to C H 3 on the upper right which is highlighted in red. C 4 is single bonded to H on the lower right.

The structure of uracil is as follows: A 6-membered heterocyclic hexagonal ring is in a vertical orientation and consists of 2 N and 4 C atoms. The first N atom occupies the first position, which is the bottommost vertex. The second N atom occupies the third position,

which is the top left vertex. The first N atom has an open single bond below. The second N 2atom is single bonded to H on the upper left. A double bond is present between C 3 and C 4. C 1 is double bonded to O on the lower left. C 2 is double bonded to O above. C 3 is single bonded to H on the upper right which is highlighted in red. C 4 is single bonded to H on the lower right.

Return to Thymine and uracil

Extended description for FIGURE 3.36 The innate immunity component TLR3 recognizes its PAMP, a double stranded RNA



First view: The side view of a double-stranded R N A in horizontal orientation is shown. It is sandwiched between two extracellular domains of T L R 3 protein in a horizontal orientation. The blue domain is on the upper right of the R N A molecule. The green domain is on the lower left of the R N A molecule. The domains are composed of beta-sheets and alpha helices. Long thread-like loops connect these secondary structures. The bottom left portion of the beta-sheet of the top blue domain moves into the center of the helix. The top right portion of the beta-sheet of the bottom green domain moves into the center of the helix.

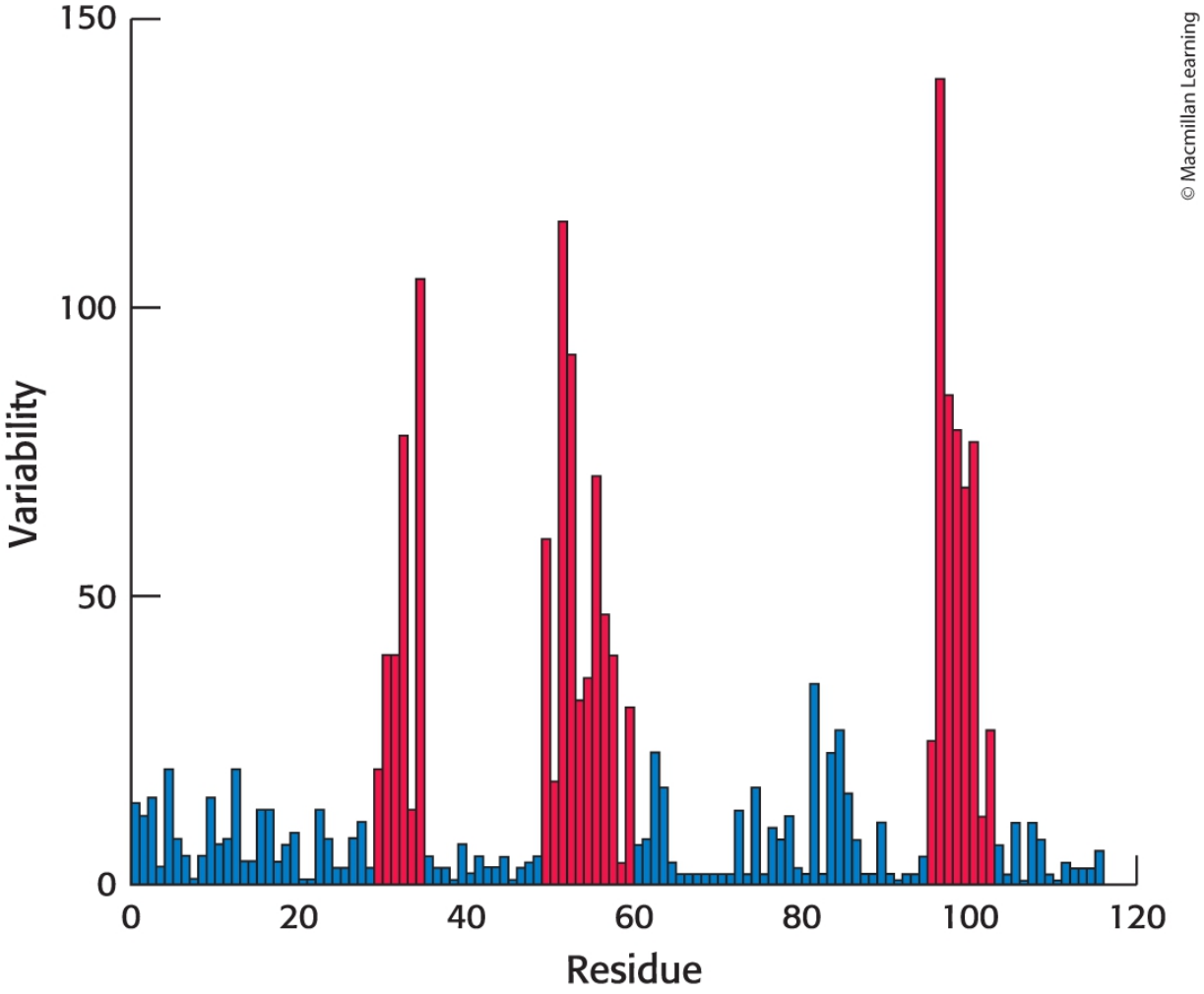
Second view: The first view rotates 180 degrees in an anti-clockwise direction across the horizontal plane to form the second view. It consists of a double-stranded R N A in a horizontal orientation. The green and blue domains form an arch-shaped structure on the upper left and upper right of the R N A helix such that the left portion of the green domain and the right portion of the blue domain merge at the center of the R N A helix. They continue downward and diverge below the R N A helix.

Third view: The second view rotates 180 degrees in a clockwise direction across a vertical plane to form the third view. The top view

of the R N A helix is shown in the center such that it consists of a coiled circular structure. It is flanked by the green domain on the left and the blue domain on the right each in a vertical orientation. The domains are slightly slanted such that they touch at their lower terminals below the R N A helix.

Return to FIGURE 3.36 The innate immunity component TLR3 recognizes its PAMP, a double stranded RNA

Extended description for FIGURE 3.37 Immunoglobulin sequences include regions of extensive sequence variability



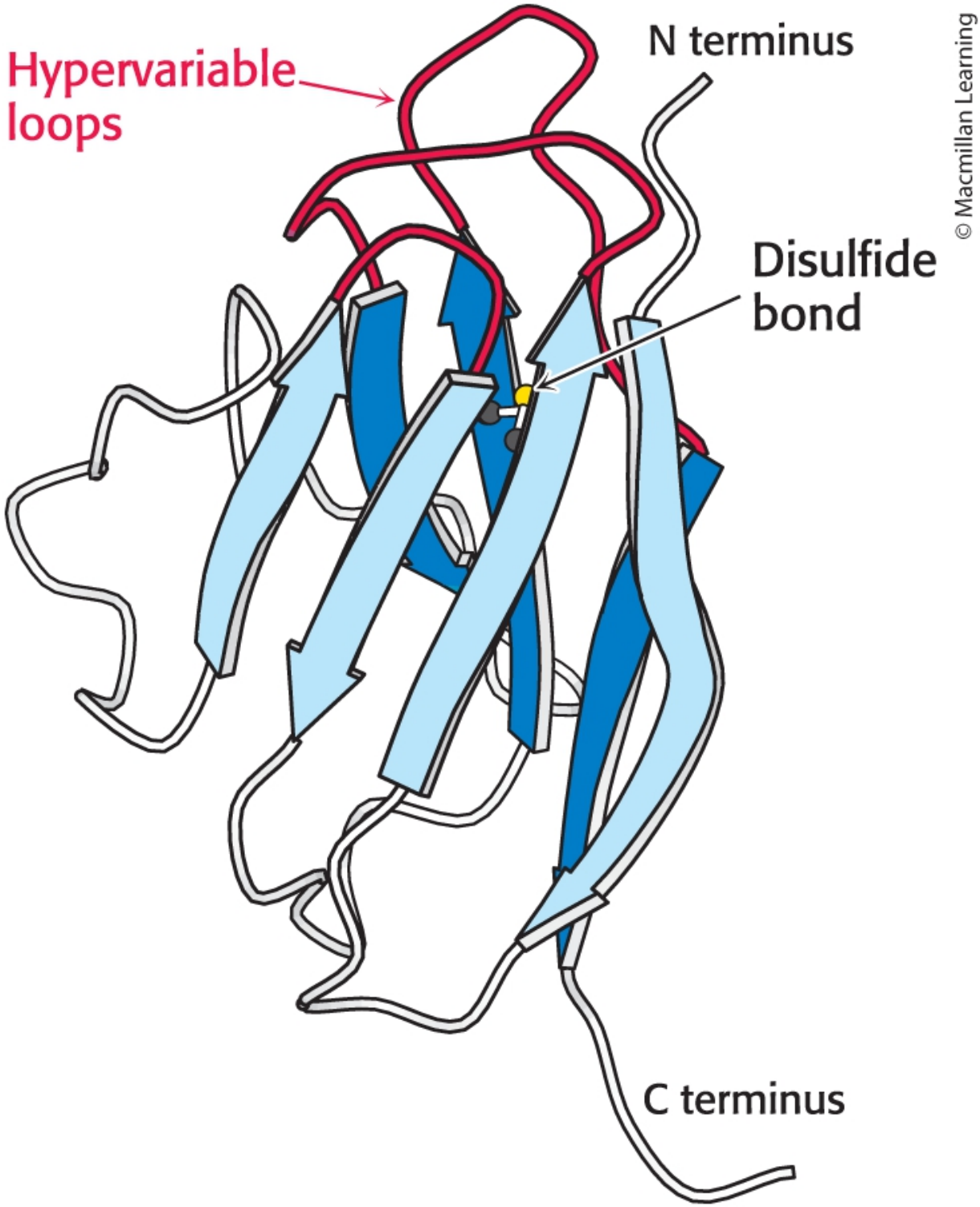
The horizontal axis is labeled residue and ranges from 0 to 120 in increments of 20 units. The vertical axis is labeled variability and ranges from 0 to 150 in increments of 50 units. Several blue and red bars are shown on the graph. The red bars are clustered between 30 to 35 residues, 50 to 60 residues, and 95 to 102 residues. All the blue bars and several red bars show variability much less than 50. The

red bar show variability greater than 50 at the residue 33, 50, 53, 56, 97, 98, 99, and 100 and greater than 100 at residue 35, 52, and 96.

Return to FIGURE 3.37 Immunoglobulin sequences include regions of extensive sequence variability

Extended description for FIGURE 3.38 The immunoglobulin fold consists of a pair of β sheets

linked by a disulfide bond

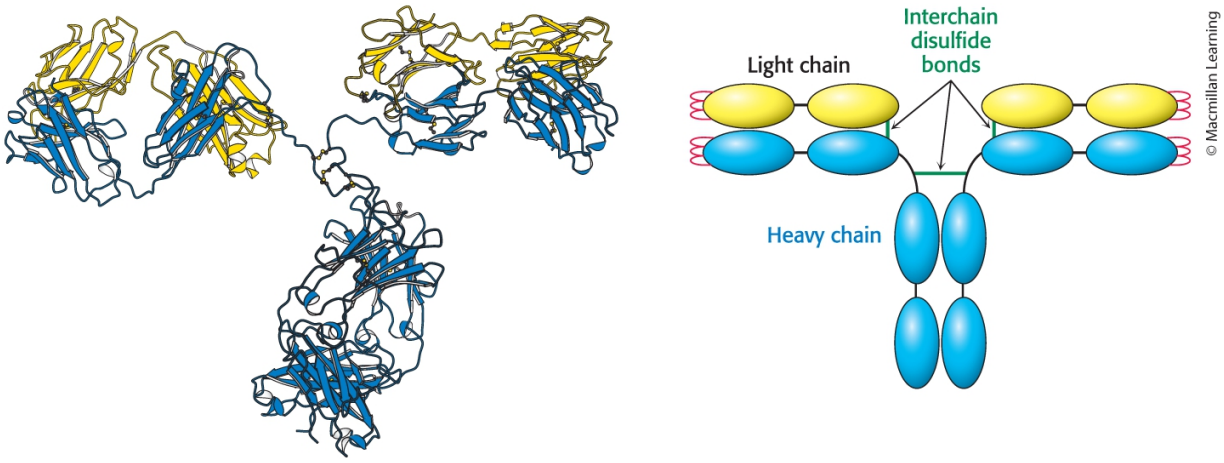


The immunoglobulin fold consists of a pair of an anti-parallel beta-sheet containing 7 beta-strands. The vertical beta-strands are alternately oriented in the upward and the downward directions. They are depicted as thick light blue and dark blue arrows. Short thread-like loops connect the beta-strands. The red loops at the top are labeled hypervariable loops. White loops are located at the bottom. A white short thread at the top of a beta-strand oriented downward is labeled N terminus. A white short thread at the bottom of another beta-strand oriented downward is labeled C terminus.

A ball-and-stick model labeled disulfide bond is shown above the immunoglobulin fold. It consists of a small yellow sphere above connected to a black sphere on either side.

Return to FIGURE 3.38 The immunoglobulin fold consists of a pair of β sheets linked by a disulfide bond

Extended description for FIGURE 3.39 An IgG molecule has a Y-shaped structure comprising two identical arms with hypervariable regions at the end



The immunoglobulin G molecule is depicted as a T-shaped structure. The vertical part of the molecule labeled heavy chain is composed of two layers located side-by-side, and each layer is composed of two blue ovals in a vertical orientation. The left and right arms of the molecule labeled light chain consists of a layer of two yellow ovals located above the layer of two blue ovals, each in a horizontal orientation. There is a space between the two arms. The ovals are connected with lines.

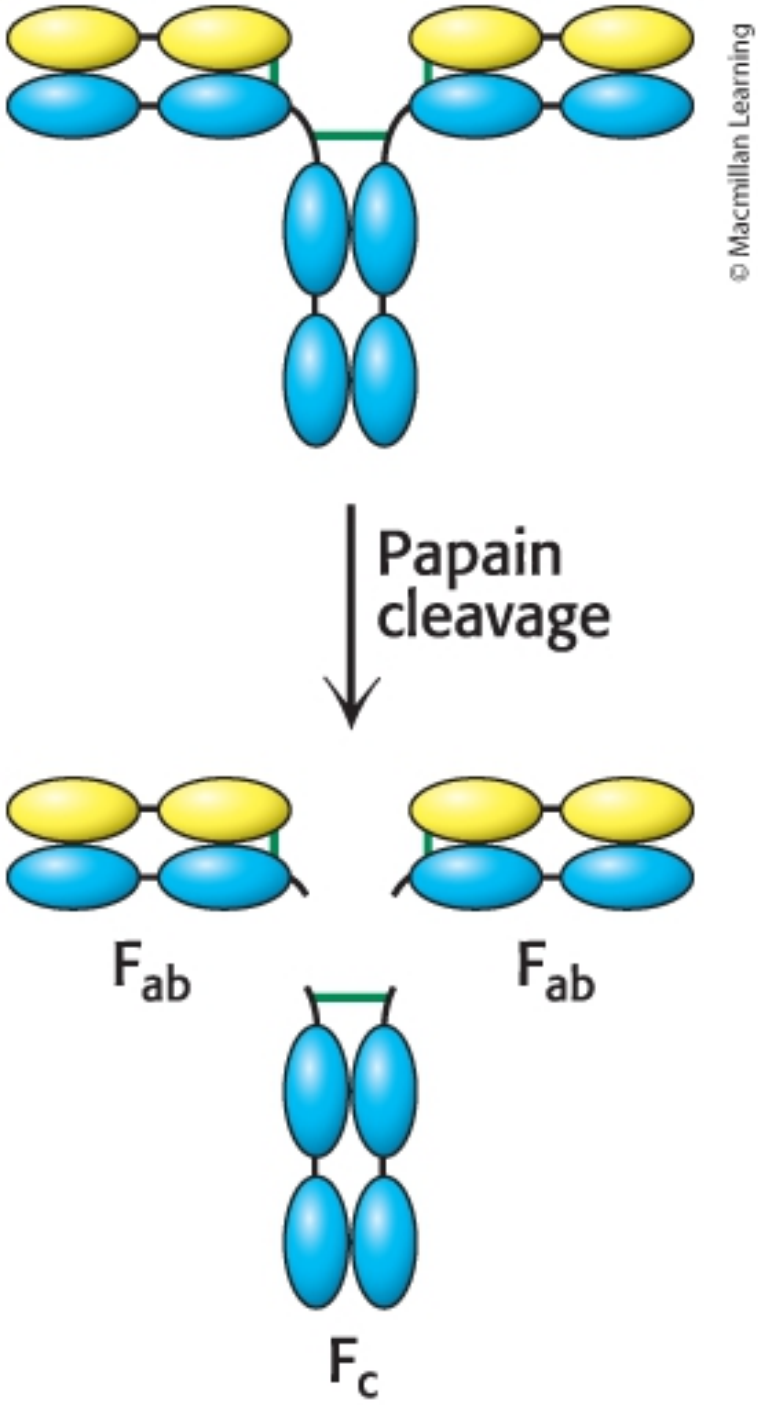
A vertical line connects the left yellow oval of the top layer to the left blue oval of the bottom layer of the left arm and the left yellow oval of the top layer with the left blue oval of the bottom layer of the right arm. A horizontal line connects the two layers of the vertical chain. These lines are labeled interchain disulfide bonds.

The ribbon diagram of the I g G molecule is depicted as a Y-shaped structure. The two arms of the Y-shaped structure are composed of 2

pairs of beta-sheets connected by thread-like loops. Each pair consists of a yellow beta-sheet located above a blue beta-sheet. The thread-like structure from both the pairs connects below to a pair of a blue beta-sheet. The pair consists of a blue beta-sheet located above another blue beta-sheet. These beta sheets are connected by thread-like loops.

Return to FIGURE 3.39 An IgG molecule has a Y-shaped structure comprising two identical arms with hypervariable regions at the end

Extended description for FIGURE 3.40 Immunoglobulin G molecules can be cleaved into two F ab fragments and one F c fragment by treatment with papain



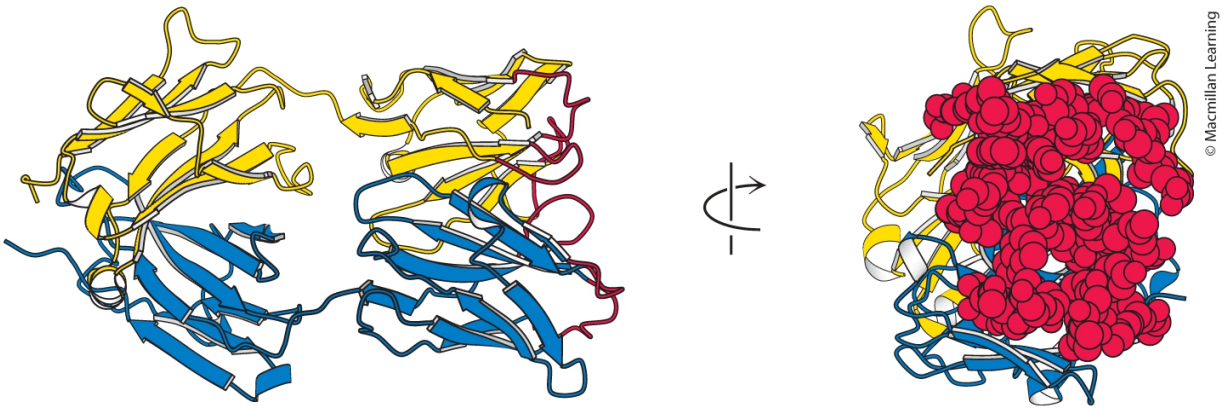
© Macmillan Learning

The immunoglobulin G molecule is depicted as T-shaped structure. The vertical part of the molecule is composed of two layers located side-by-side, and each layer is composed of two blue ovals in a vertical orientation. The left and right arms of the molecule consists of a layer of two yellow ovals located above the layer of two blue ovals, each in a horizontal orientation. There is an empty space between the two arms.

The ovals are connected with lines. The products of papain cleavage are two F subscript ab fragments and one F subscript c fragment. The F subscript ab fragment consists of a layer of two yellow ovals located above the layer of two blue ovals, each in a horizontal orientation. The F subscript c fragment consists of two layers located side-by-side, and each layer is composed of two blue ovals in a vertical orientation.

Return to FIGURE 3.40 Immunoglobulin G molecules can be cleaved into two F ab fragments and one F c fragment by treatment with papain

Extended description for FIGURE 3.41 The structure of an F ab fragment reveals how the six hypervariable loops come together to form a binding surface

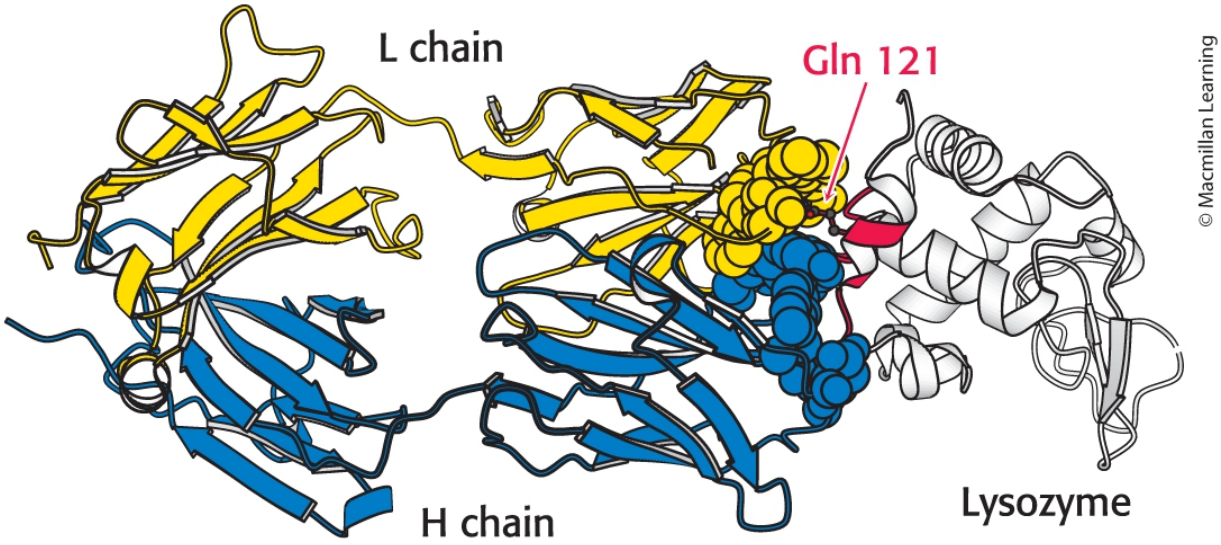


Side view: Two pairs of beta-sheets are connected by thread-like loops. Each pair consists of a yellow anti-parallel beta-sheet above a blue anti-parallel beta-sheet. Thread-like structures from both the pairs connect them. The red loop-like structures are present on the right of the right pair of beta-sheet.

End view: The side view is rotated 180 degrees across the vertical plane to form the end view. It consists of a pair of anti-parallel beta-sheets. Their surface is covered with clumped red spheres.

Return to FIGURE 3.41 The structure of an F ab fragment reveals how the six hypervariable loops come together to form a binding surface

Extended description for FIGURE 3.42 The structure of a complex between lysozyme and a specific F ab fragment reveals how the binding surface on the F ab interacts with the antigen



© Macmillan Learning

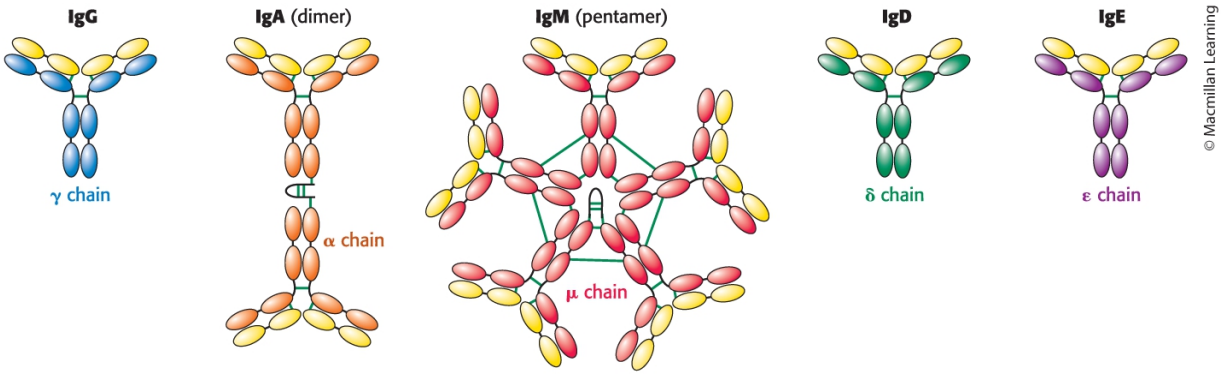
Two pairs of beta-sheets are connected by thread-like loops. Each pair consists of a yellow anti-parallel beta-sheet above a blue anti-parallel beta-sheet. Thread-like structures from both the pairs connect them. The top yellow beta sheets are labeled L chain. The bottom blue beta sheets are labeled H chain. A loop on the right of the yellow beta-sheet of the right pair contains a cluster of yellow spheres. One yellow sphere is labeled glutamine 121.

A loop on the right of the blue beta-sheet of the right pair contains a cluster of blue spheres. The lysozyme molecule consists of 5 alpha-helices, of which 2 are large and 3 small. These helices are connected to an anti-parallel beta-sheet composed of two beta-strands through long thread-like loops. One large and two small

alpha-helices of lysozyme interact with the cluster of yellow and blue spheres.

Return to FIGURE 3.42 The structure of a complex between lysozyme and a specific F ab fragment reveals how the binding surface on the F ab interacts with the antigen

Extended description for FIGURE 3.43 Five classes of immunoglobulin have the same light chain combined with a different heavy chain (γ,α, μ, δ, or ε)



The immunoglobulins are depicted as T-shaped structures.

I g G: The vertical region of the molecule labeled gamma chain is composed of two layers one above the other. Each layer is composed of two blue ovals in a vertical orientation. The left and right arms of the molecule are composed of a layer of two yellow ovals in a horizontal orientation located above a layer of two blue ovals in a horizontal orientation. The ovals are connected by vertical and horizontal lines.

I g A (dimer): The vertical region of the molecule labeled alpha chain is composed of two layers one above the other. Each layer is composed of two orange ovals in a vertical orientation. The left and right arms of the molecule are composed of a layer of two yellow ovals in a horizontal orientation located above a layer of two orange ovals in a horizontal orientation. The ovals are connected by lines. Vertical and horizontal lines connect the ovals. This entire structure constitutes an I g A monomer. It is connected below to another I g A monomer in an inverted orientation through a U-shaped pin-like

structure in a horizontal orientation. Two vertical lines are present inside the U-shaped structure.

I g M (pentamer): The vertical region of the molecule labeled mu chain is composed of two layers one above the other. Each layer is composed of two pink ovals in a vertical orientation. The left and right arms of the molecule are composed of a layer of two yellow ovals in a horizontal orientation located above a layer of two pink ovals in a horizontal orientation. The ovals are connected by lines. Vertical and horizontal lines connect the ovals. This entire structure constitutes an I g M monomer. The vertical regions of five different I g M monomers are organized such that they occupy the vertices of a pentagon. The bottom layer of the vertical region of the I g M monomer on the bottom left and bottom right vertices are connected through an inverted U-shaped pin-like structure. Two horizontal lines are present inside the U-shaped structure.

I g D: The vertical region of the molecule labeled delta chain is composed of two layers one above the other. Each layer is composed of two green ovals in a vertical orientation. The left and right arms of the molecule are composed of a layer of two yellow ovals in a horizontal orientation located above a layer of two green ovals in a horizontal orientation. The ovals are connected by lines. Vertical and horizontal lines connect the ovals.

I g E: The vertical region of the molecule labeled epsilon chain is composed of two layers one above the other. Each layer is composed of two purple ovals in a vertical orientation. The left and right arms of the molecule are composed of a layer of two yellow ovals in a horizontal orientation located above a layer of two purple ovals in a horizontal orientation. The ovals are connected by lines. Vertical and horizontal lines connect the ovals.

Return to FIGURE 3.43 Five classes of immunoglobulin have the same light chain combined with a different heavy chain (γ,α, μ, δ, or ε)

Extended description for FIGURE 3.44 Antibodies elicited against the spike protein of SARS-CoV-2 can

bind to this protein and block the ability of the virus to infect cells

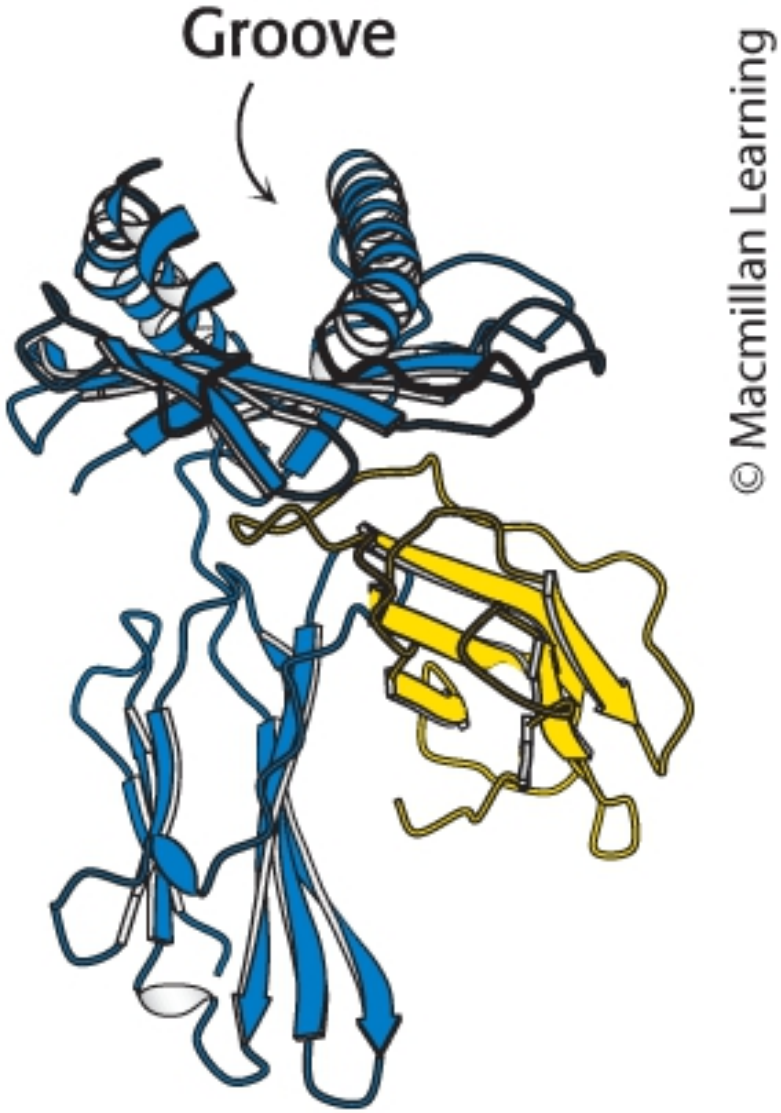


© Macmillan Learning

The trimeric spike protein consists of several vertically orientated alpha-helices that form its core. Some helices are at the bottom surface. Anti-parallel beta-sheets are at the top surface, top left surface, left surface, top right surface, right surface, and at the bottom. The beta-sheets at the top surface, top right surface, and right surface form a concave depression. Thread-like loops from the surface of the top right beta-sheet touch the beta-strands of the blue beta-sheet of the left pair of the F subscript a b fragment.

Return to FIGURE 3.44 Antibodies elicited against the spike protein of SARS-CoV-2 can bind to this protein and block the ability of the virus to infect cells

Extended description for FIGURE 3.45 The structure of the extracellular domain of a class I MHC protein reveals a deep groove

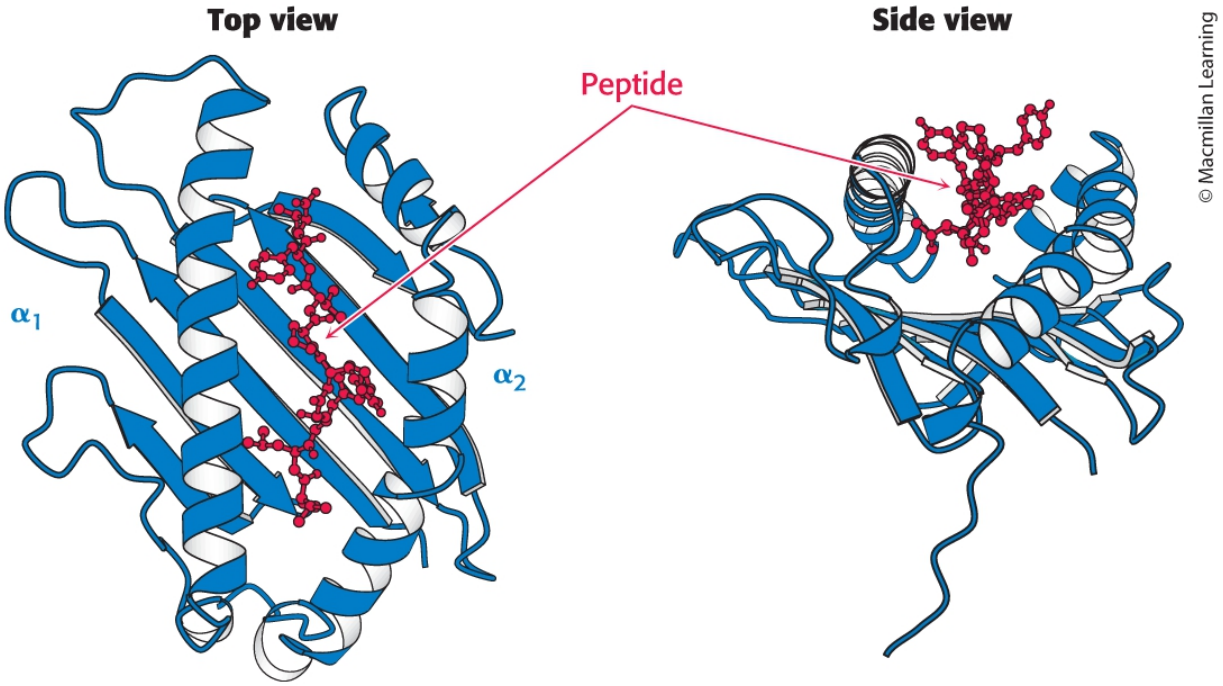


The extracellular domain is composed of two distinct polypeptides shown in yellow and blue. The blue polypeptides consist of two adjacent anti-parallel beta-sheets containing beta-strands in a vertical orientation. These are connected at the top to a flat anti-

parallel beta-sheet in a horizontal orientation. Two alpha-helices on the left and an alpha helix on the right, flank a deep groove at the top center of the horizontal beta-sheet. The beta sheets are interconnected by short thread-like loops. The yellow polypeptide is located on the right of the junction between the top horizontal and the bottom vertical beta-sheets of the blue polypeptide. It is composed of an anti-parallel beta-sheet in a horizontal orientation. Short-thread-like loops connected the individual beta-strands.

Return to FIGURE 3.45 The structure of the extracellular domain of a class I MHC protein reveals a deep groove

Extended description for FIGURE 3.46 In class I MHC proteins, peptides can bind in the groove

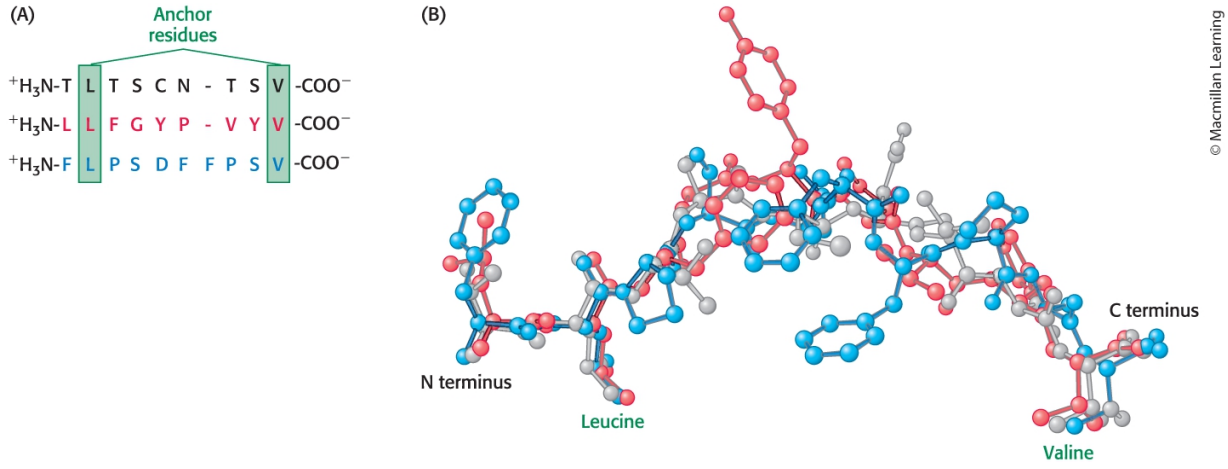


Top view: Two alpha-helices flank an anti-parallel beta-sheet in a diagonal orientation. The left alpha-helix labeled alpha 1 is longer than the right alpha-helix. The right alpha-helix labeled alpha 2 is smaller and is connected on the top to a shorter helix. The beta-strands of the beta-sheet are connected by long thread-like loops. A peptide in a vertical orientation is between the alpha helices in front of the beta-sheet.

Side view: A flat beta-sheet is shown. Two alpha helices are shown on its top such that they create a central groove. Peptide is shown inside the groove created the alpha-helices.

Return to FIGURE 3.46 In class I MHC proteins, peptides can bind in the groove

Extended description for FIGURE 3.47 Each MHC class I protein presents peptides with some recurring features



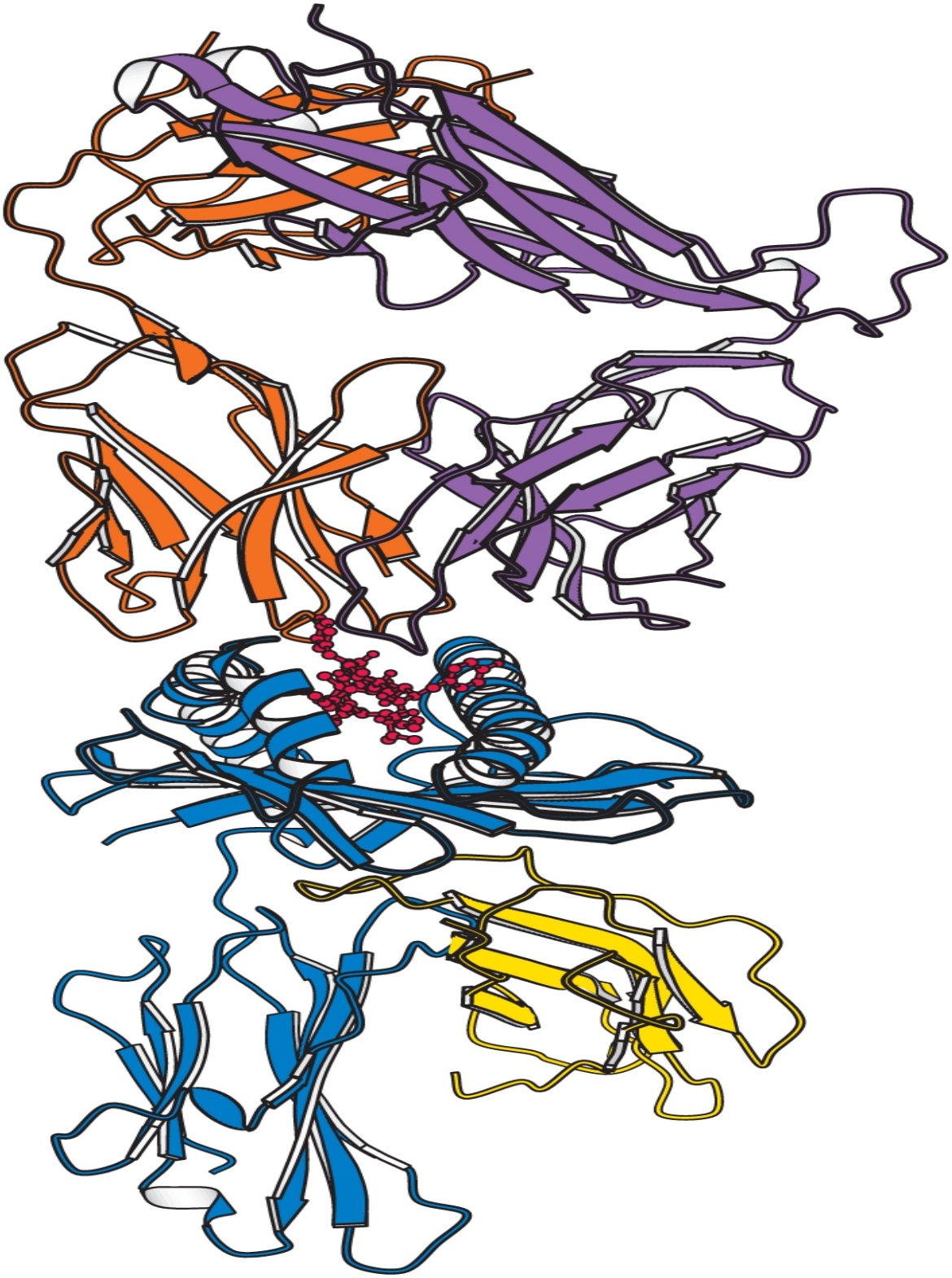
1. Part (A): The sequence of the first peptide is as follows: Superscript plus H 3 N, single bond, T, L T, S, C, N, dash, T, S, V, single bond, C O O superscript minus. The sequence of the second peptide is as follows: Superscript plus H 3 N, single bond, L, L, F, G, Y, P, dash, V, Y, V, single bond, C O O superscript minus. The sequence of the third peptide is as follows: Superscript plus H 3 N, single bond, F, L, P, S, D, F, F, P, S, V, single bond, C O O superscript minus. From the left, the second and tenth residue of each peptide are highlighted in green and labeled anchor residues.
2. Part (B): Three overlapping ball-and-stick models of the three peptides are shown. It shows that the N-terminus, C-terminus, and the side chains of leucine and valine residues are at the same position. The remaining structure is different due to the presence of different side chains of different amino acid residues at the corresponding positions of the peptides.

Return to FIGURE 3.47 Each MHC class I protein presents peptides with some recurring features

Extended description for FIGURE 3.48 The T-cell receptor recognizes specific class I MHC complexes,

contacting both the MHC protein and the bound peptide

T-cell receptor



MHC class I

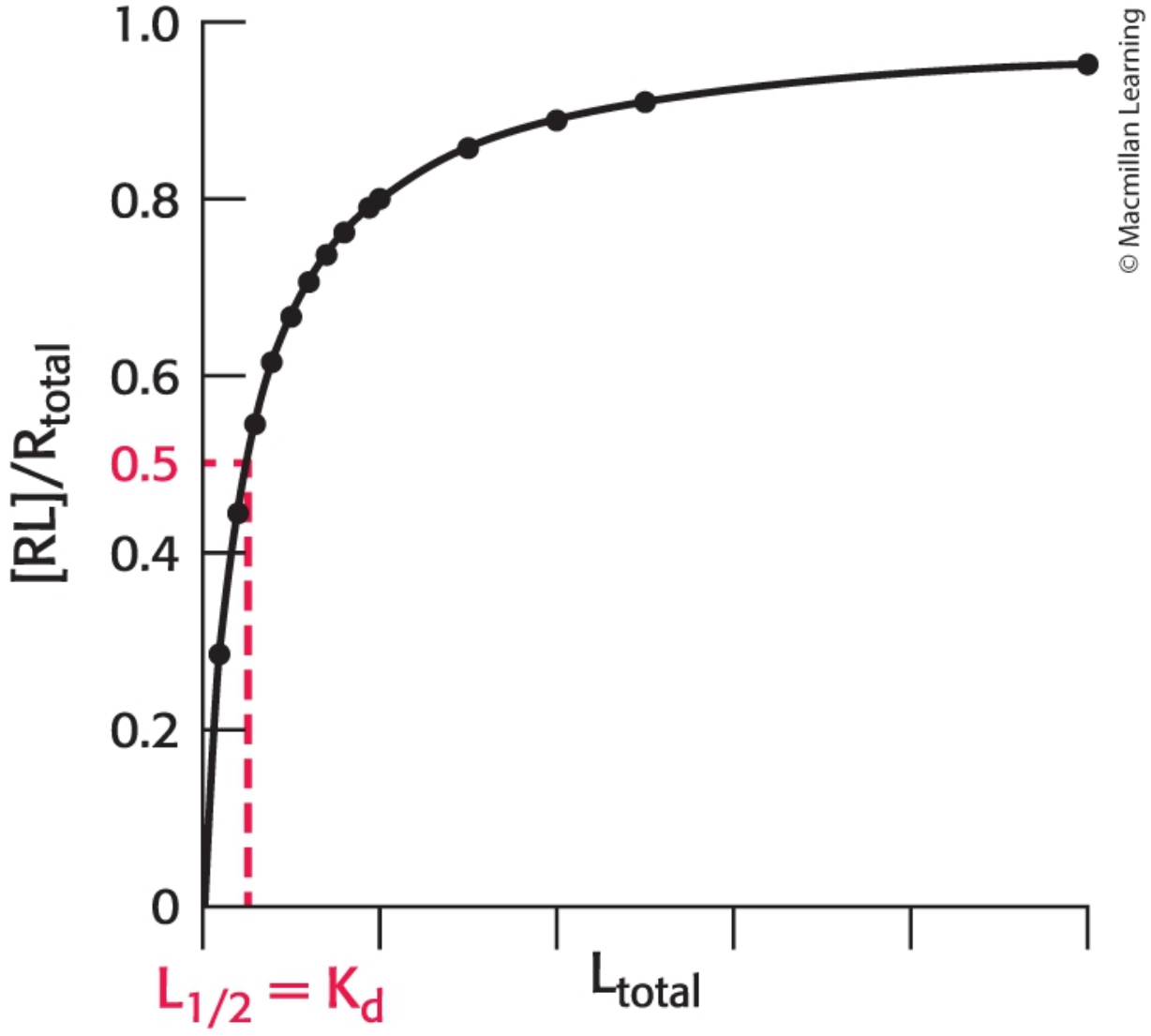
© Macmillan Learning

The M H C class 1 complex is composed of two distinct polypeptides shown in yellow and blue. The blue polypeptides consist of two adjacent anti-parallel beta-sheets containing beta-strands in a vertical orientation. These are connected at the top to a flat anti-parallel beta-sheet in a horizontal orientation. Two alpha helices on the left and an alpha helix on the right flank a deep groove at the top center of the horizontal beta-sheet. The beta sheets are interconnected by short thread-like loops.

The yellow polypeptide is on the right of the junction between the top horizontal and bottom vertical beta-sheets of the blue polypeptide. It is composed of an anti-parallel beta-sheet in a horizontal orientation. Short thread-like loops connect the individual beta-strands. The T-cell receptor is above the M H C class 1 complex. It consists of two pairs of beta-sheets one above the other. In each pair, an orange anti-parallel beta-sheet on the left is associated with a purple anti-parallel beta-sheet on the right. Short thread-like loops connect the beta-strands of the beta-sheets.

Return to FIGURE 3.48 The T-cell receptor recognizes specific class I MHC complexes, contacting both the MHC protein and the bound peptide

Extended description for FIGURE 3.49 Binding can be monitored by measuring the fraction of receptors with ligand bound as a function of the amount of ligand added



The horizontal axis is labeled L subscript total and has 5 unlabeled equidistant markings. The vertical axis is labeled StartFraction

concentration of R L over R subscript total EndFraction and ranges from 0 to 1.0 in increments of 0.2 units.

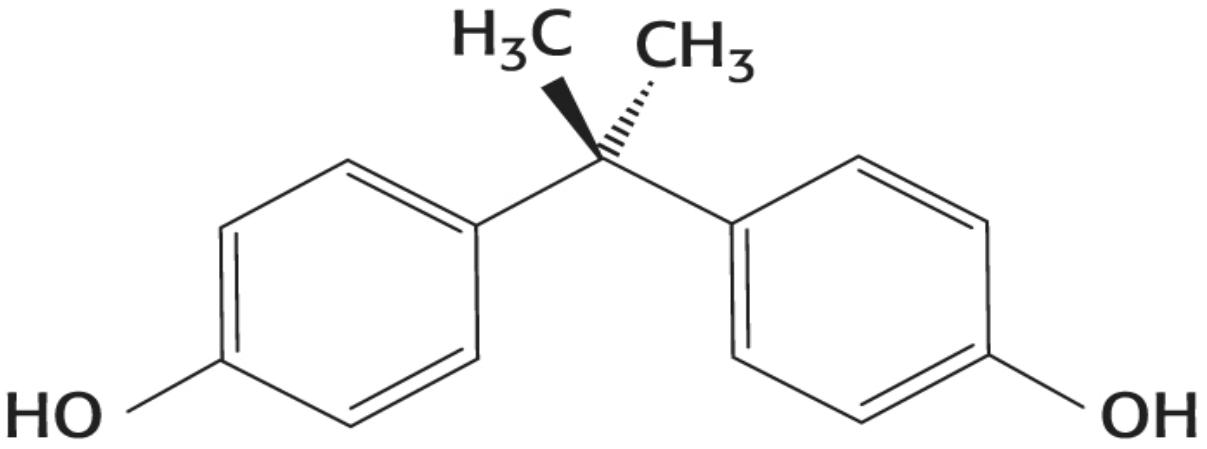
A hyperbolic curve begins at the origin and moves gradually to the upper right. It forms a curve between the markings 0.7 and 0.9 on the vertical axis. The curve then moves almost horizontally after the second marking on the horizontal axis till the end of the horizontal axis. Several points are marked on the curve represented as thick black dots.

A red dotted line starts from the 0.5 marking on the vertical axis and intersects the curve. At the point of intersection, a red dotted vertical line moves toward the horizontal axis. The point of intersection of the vertical line with the horizontal axis is labeled L subscript StartFraction 1 over 2 EndFraction equals K subscript d.

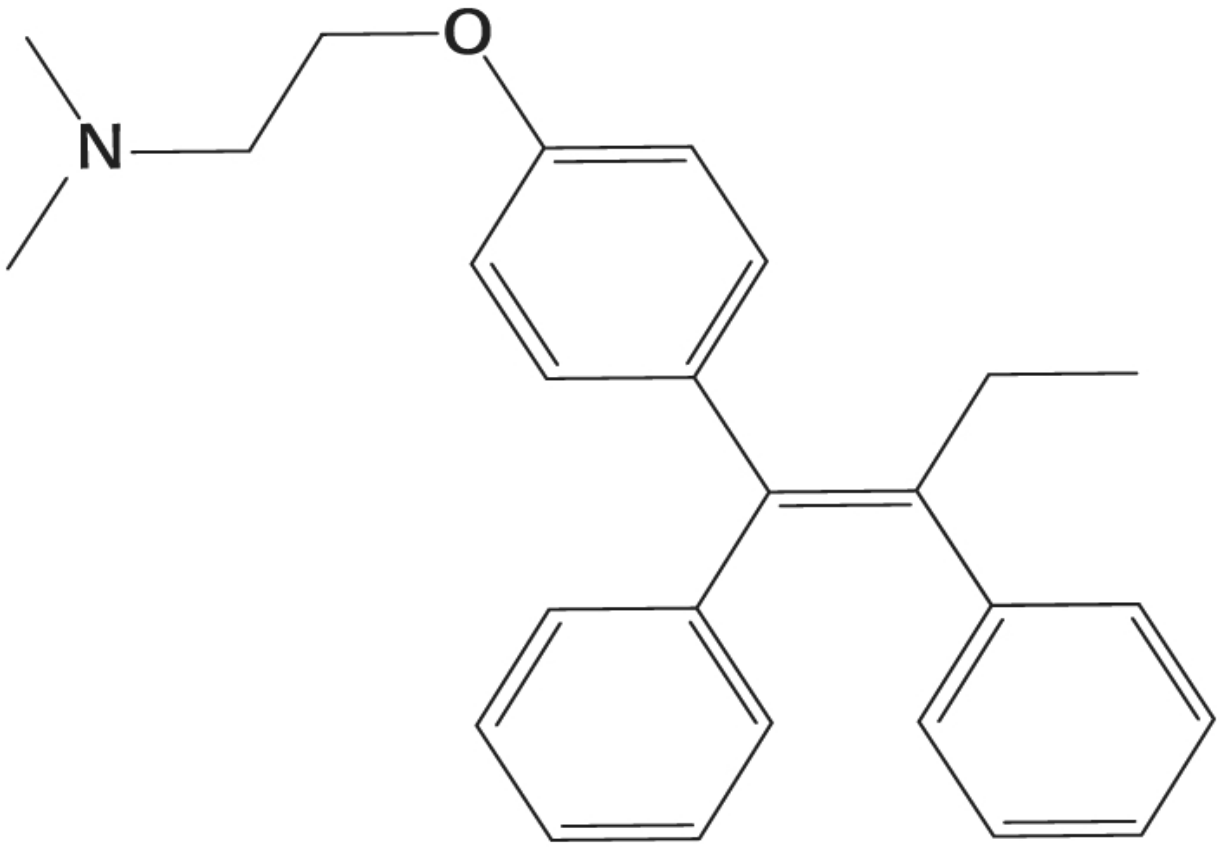
Return to FIGURE 3.49 Binding can be monitored by measuring the fraction of receptors with ligand bound as a function of the amount of ligand added

Extended description for FIGURE 3.50 At high enough concentrations, ligands with lower affinity for a

receptor can compete for binding with high-affinity ligands



Bisphenol A (BPA)



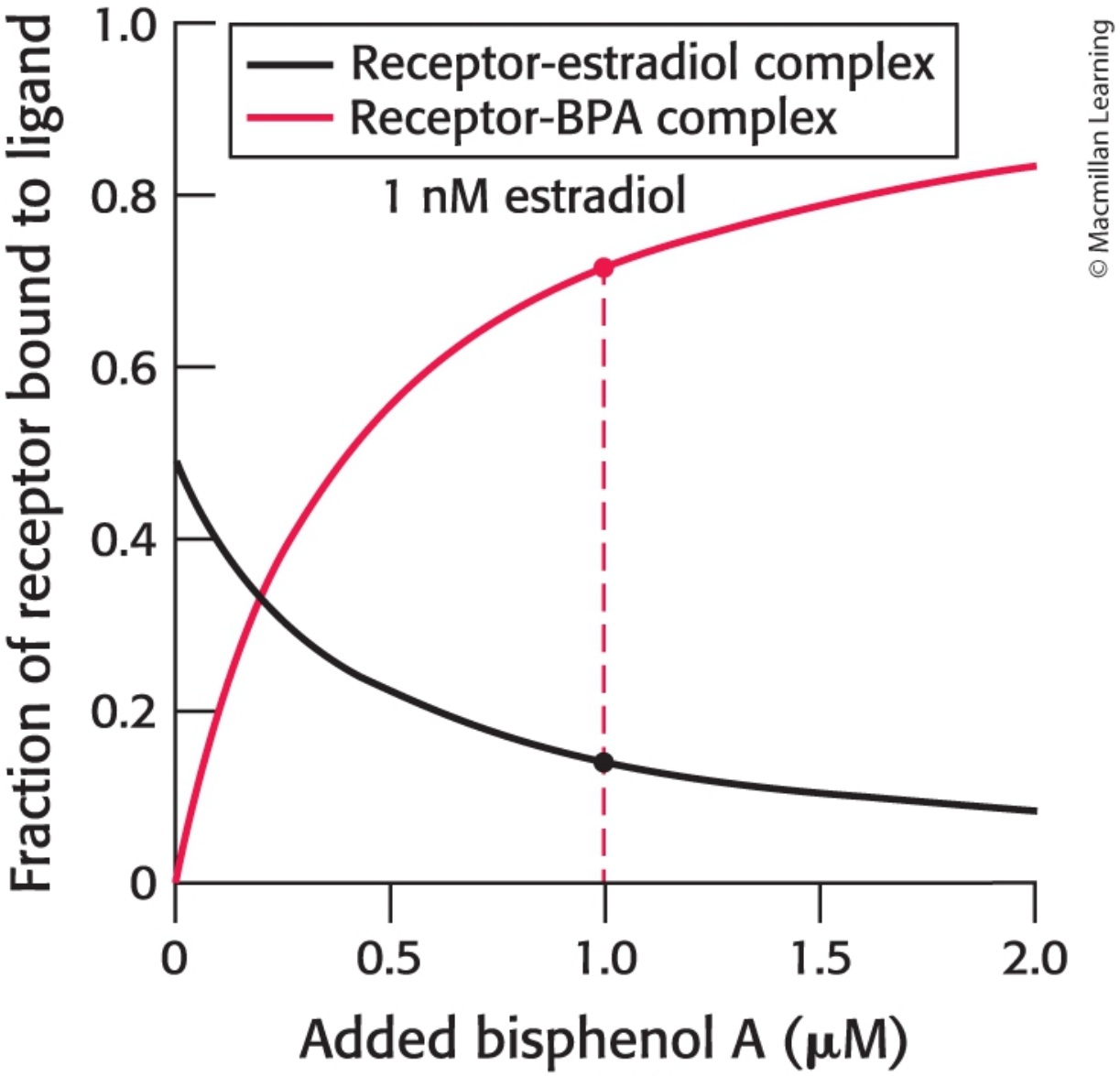
Tamoxifen

Bisphenol A (B P A) has the following structure: A benzene ring is in a vertical orientation, with C 1 occupying the topmost vertex. The ring contains alternating double bonds between C 1 and C 2, C 3 and C 4, and C 5 and C 6. C 5 is single bonded to O H on the lower left. C 2 is single bonded to a central C atom on the upper right. This C is single bonded on the lower right to C 5 of a second benzene ring in a vertical orientation, with C 1 occupying the topmost vertex. The ring contains alternating double bonds between C 1 and C 2, C 3 and C 4, and C 5 and C 6. The central C atom is wedge bonded to C H 3 on the upper left and dash bonded to C H 3 on the upper right. C 3 of the second benzene ring is single bonded to O H on the lower right.

Tamoxifen has the following structure: A benzene ring is in a horizontal orientation, with C 1 occupying the rightmost vertex. The ring contains alternating double bonds between C 1 and C 2, C 3 and C 4, and C 5 and C 6. C 5 is single bonded to O on the upper left. This O is single bonded on the left to C 1 of a 2-carbon alkane chain depicted as a line structure using 1 line. C 2 of the chain is single bonded to a central N atom on the left. This N atom is single bonded to C H 3 on the upper left and C H 3 on the lower left, each in the form of a line. C 2 of this ring is single bonded on the lower right to C 1 of a 2-carbon alkene chain depicted as two parallel lines. C 2 of this chain is single bonded to C 1 of a second 2-carbon alkane chain depicted as a line structure using 1 line. C 1 and C 2 of the alkene chain are each single bonded to a benzene ring on the lower left and the lower right, respectively. The benzene ring is in a horizontal orientation, with C 1 occupying the rightmost vertex. The ring contains alternating double bonds between C 2 and C 3, C 4 and C 5, and C 6 and C 1.

Return to FIGURE 3.50 At high enough concentrations, ligands with lower affinity for a receptor can compete for binding with high-affinity ligands

Extended description for FIGURE 3.50 At high enough concentrations, ligands with lower affinity for a receptor can compete for binding with high-affinity ligands



The horizontal axis is labeled added bisphenol A (micro molar) and ranges from 0 to 2.0 in increments of 0.5 units. The vertical axis is

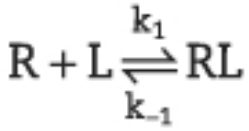
labeled fraction of receptor bound to ligand and ranges from 0 to 1.0 in increments of 0.2 units.

A curve for receptor-estradiol complex begins approximately at point (0, 0.48) and then moves down to the lower right until it reaches point (1.0, 0.14). It then gradually moves down to the right until it reaches point (2.0, 1.0).

The curve for receptor-B P A complex begins at the origin. The curve moves upward to the right till point (1.0, 0.7). The curve moves gradually upward to the right until it reaches point (2.0, 0.84). A dotted vertical line begins from 1.0 on the horizontal axis, intersects the two curves, and is labeled 1 nanomolar estradiol.

Return to FIGURE 3.50 At high enough concentrations, ligands with lower affinity for a receptor can compete for binding with high-affinity ligands

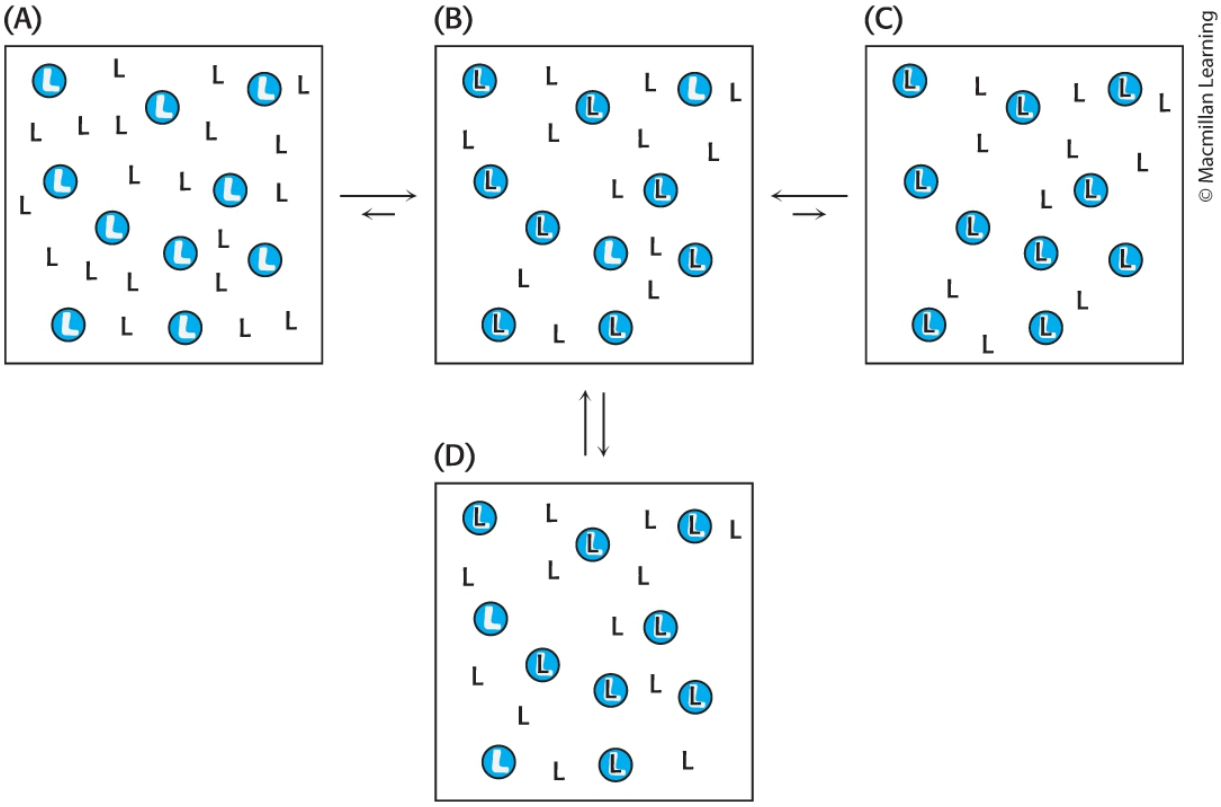
Extended description for Binding of a receptor to its ligand with the forward and reverse reaction rates



The reaction has two reactants and one product. The reactants are R and L. The product is R L. The forward reaction rate shown above the top forward arrow is lowercase K subscript 1. The reverse reaction rate shown below the bottom backward arrow is lowercase k subscript minus 1.

Return to Binding of a receptor to its ligand with the forward and reverse reaction rates

Extended description for FIGURE 3.51 At equilibrium, the rates of the forward and reverse reactions are the same



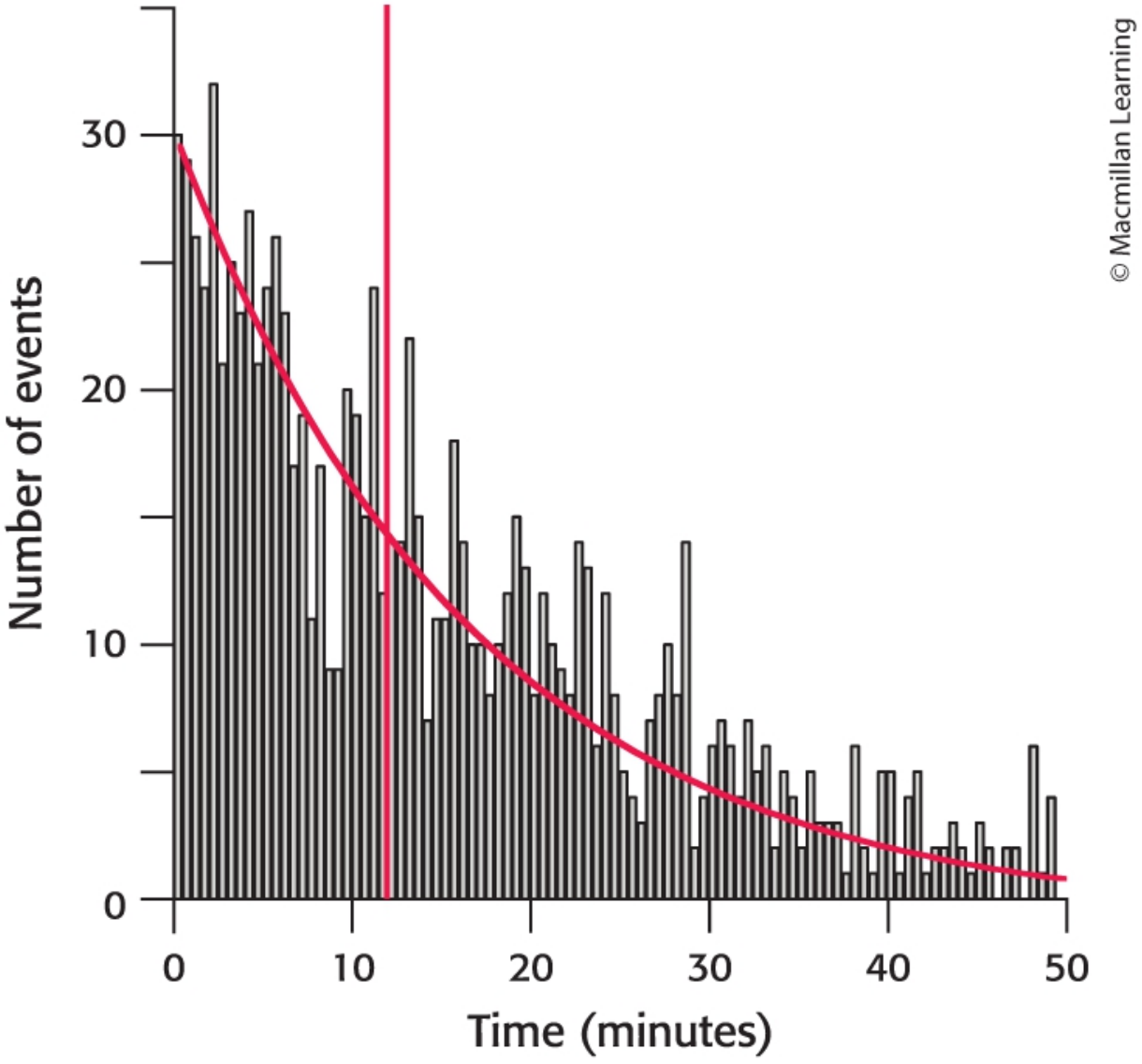
Each part consists of a square containing blue circles and several L letters. Parts (A) and (B), (B) and (C), and (B) and (D) are interconvertible shown by reversible reaction arrows.

1. Part (A): 10 blue circles labeled L are present randomly inside the square. These L labeling are shown in white. The L letters depicted in black exceed the number of blue circles, and present randomly around the circles.
2. Part (B): 8 black L letters occupies the L labeling inside 8 blue circles. The L labeling of two blue circles are empty.

3. Part (C): 10 black L letters occupies the black L labeling in all the circles.
4. Part (D): 8 black L letters occupies the L labeling inside 8 blue circles. The L labeling of two blue circles are empty.

Return to FIGURE 3.51 At equilibrium, the rates of the forward and reverse reactions are the same

Extended description for FIGURE 3.52 A rate constant reflects the distribution of reaction times at the single molecule level



© Macmillan Learning

The horizontal axis is labeled time (minutes) and ranges from 0 to 50 in increments of 10 units. The vertical axis is labeled number of events and ranges from 0 to 30 in increments of 10 units.

Several bars are shown at different times. The number of events decreases as time increases. A red curve begins from 30 events and gradually moves toward the lower right to read approximately 2 events at 50 minutes. A red vertical line originates from the base of the bar located at 12 minutes and goes beyond 30 events.

Return to FIGURE 3.52 A rate constant reflects the distribution of reaction times at the single molecule level

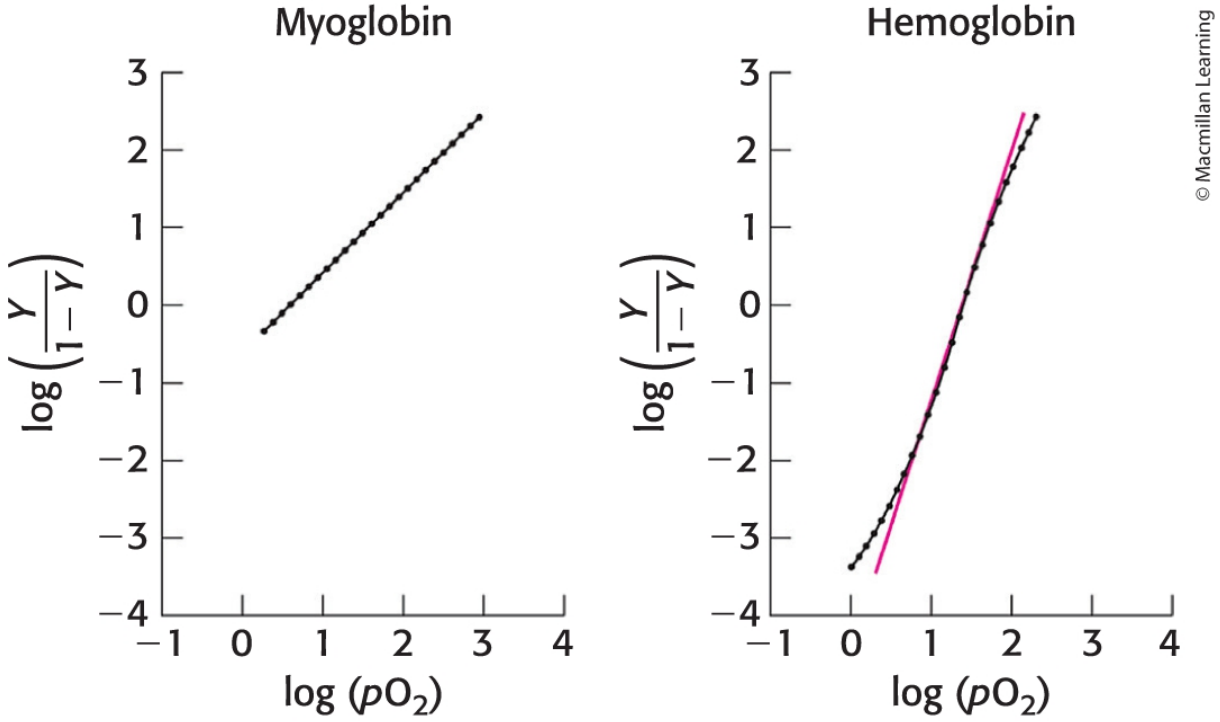
Extended description for Binding of oxygen by hemoglobin



The reaction consists of two reactants and one product. The first reactant is H b. The second reactant is n O 2. A reversible reaction arrow leads to the product. The product is H b open parenthesis O 2 close parenthesis with subscript n.

Return to Binding of oxygen by hemoglobin

Extended description for Two graphs for myoglobin and hemoglobin



© Macmillan Learning

Myoglobin Hill plot: The horizontal axis is labeled log p O subscript 2 and ranges from negative 1 to 4 in increments of 1 unit. The vertical axis is labeled log StartFraction y over 1 minus y EndFraction and ranges from negative 4 to 3 in increments of 1 unit.

A straight line begins at approximately negative 0.5 on the vertical axis at log p O subscript 2 of approximately 0.25 and moves upward to the right until it reaches approximately point (3, 2.5). The straight line has several data points.

Hemoglobin Hill plot: The horizontal axis is labeled log p O subscript 2 and ranges from negative 1 to 4 in increments of 1 unit.

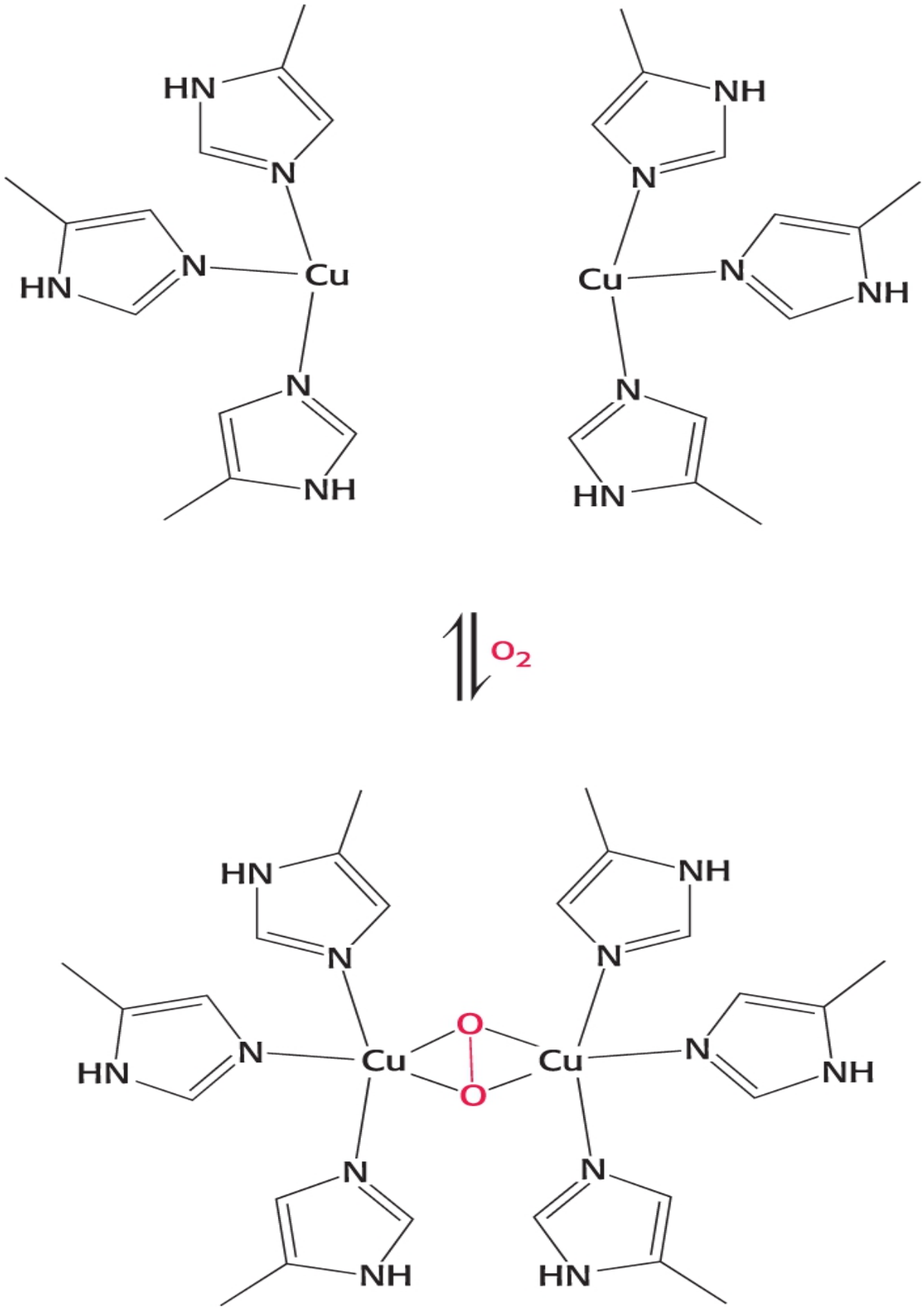
The vertical axis is labeled log StartFraction y over 1 minus y EndFraction and ranges from negative 4 to 3 in increments of 1 unit.

A diagonal curve is shown. A red diagonal passes through the curve such that it overlaps with the curve. The curve begins at approximately negative 3.5 on the vertical axis at log p O subscript 2 of 0 and moves upward to the right until it reaches approximately point (2.2, 2.5). The straight line has several data points.

Return to Two graphs for myoglobin and hemoglobin

Extended description for Reversible reaction of oxygen

binding in arthropods


HN
N
HN
N
Cu
N
NH
NH
N
Cu
N
NH
N
HN
O2
HN
N
HN
N
Cu
O
O
Cu
N
NH
N
NH
N
HN

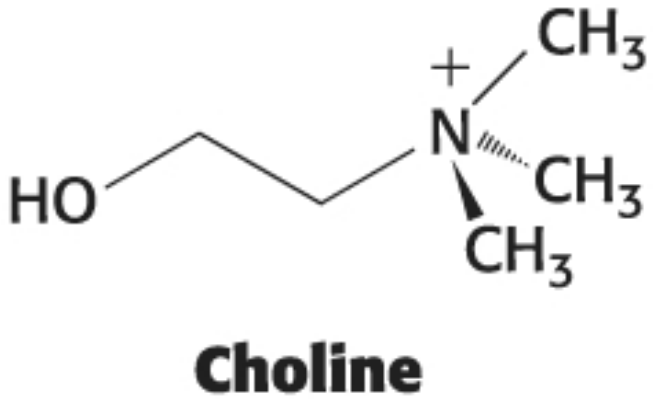
The reversible reaction consists of two reactants and one product. The first reactant has the following structure: A central C u atom is single bonded to the N atoms of three heterocyclic pentagonal rings above, below, and on the left. The structure of the pentagonal ring is as follows: A 5-membered heterocyclic pentagonal ring consists of 2 N and 3 C atoms. Three such rings are oriented in different directions. The first N atom occupies the first position and the second N atom occupies the third position. A double bond is present between the first N atom and C 1 and C 2 and C 3. C 2 has an open single bond.

Two molecules of the first reactant are used. The second molecule is the mirror image of the first molecule. The second reactant is O 2.

The product has the following structure: O, single bond, O is arranged in a vertical orientation. Each O atom is single bonded to a common C u atom on either side. The two molecules of the reactant are connected through an O 2 molecule.

Return to Reversible reaction of oxygen binding in arthropods

Extended description for Structure of choline

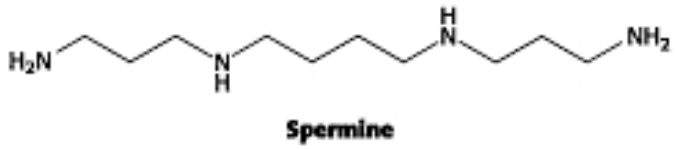


Choline

The structure of choline is as follows: A 2-carbon alkane chain is depicted as a line structure using 1 line. C 1 is single bonded to O H on the lower left. C 2 is single bonded to N superscript plus on the upper right. The N atom is single bonded to C H 3 on the upper right, dash bonded to C H 3 on the lower right, and wedge bonded to C H 3 below.

Return to Structure of choline

Extended description for Structure of spermine

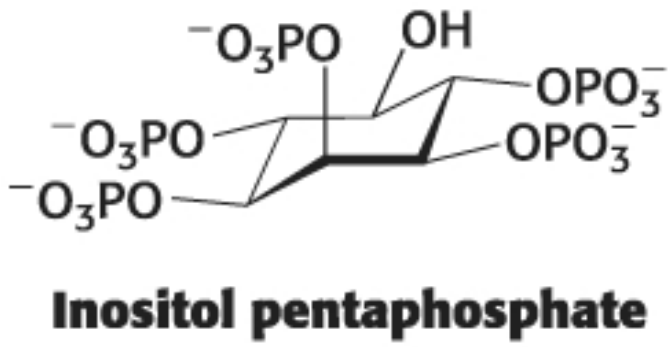


Spermine

The structure of spermine is as follows: A 2 N and 10 C heteronuclear alkane chain is depicted as a line structure using 11 zigzag lines. The first N atom occupies the fourth position and the second N atom occupies the ninth position. C 1 is single bonded to N H 2 on the lower left. Each N atom is bound to H. C 10 is single bonded to N H 2 on the upper right.

Return to Structure of spermine

Extended description for Structure of inositol Penta phosphate

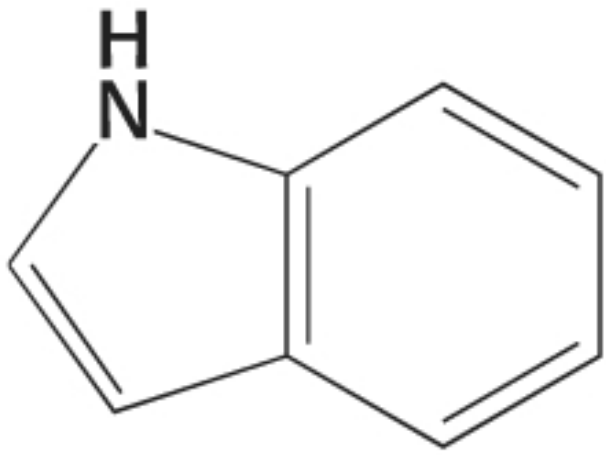


Inositol pentaphosphate

Inositol Penta phosphate has the following structure: A 6-carbon ring in horizontal orientation is shown as a boat conformation. C 1 occupies the top right vertex. C 3 and C 6 are close to each other. C 4 occupies the bottom left vertex. C 1, C 2, C 3, C 4, and C 5 are each single bonded to O P O 3 superscript minus. C 6 is single bonded to O H. The ring is in a plane perpendicular to the plane of the paper such that C 2 and C 3 are toward the observer.

Return to Structure of inositol Penta phosphate

Extended description for Structure of indole

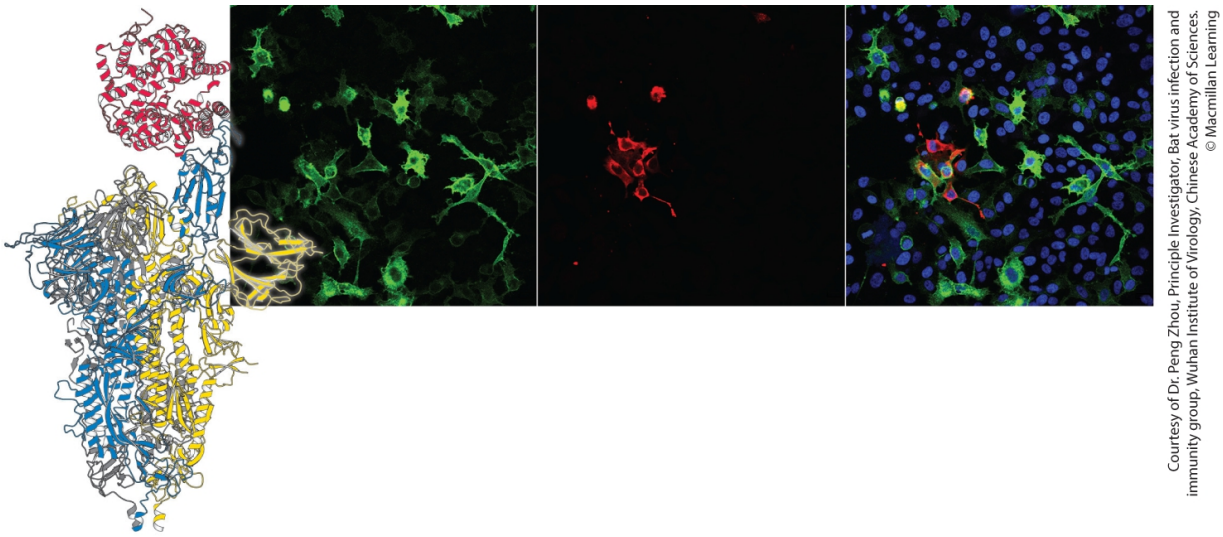


Indole

Indole has the following structure: A 5-membered pentagonal ring and a benzene ring are fused together side-by-side. The 5-membered heterocyclic pentagonal ring is in a horizontal orientation and consists of 1 N and 4 C atoms. N occupies the first position, which is the top left vertex and is bound to H. A double bond is present between C 3 and C 4. The pentagonal ring is fused to the benzene ring in a vertical orientation, with C 1 occupying the topmost vertex. The ring contains alternating double bonds between C 1 and C 2, C 3 and C 4, and C 5 and C 6. The two rings are fused together such that C 2 and C 3 are C 6 and C 5 of the benzene ring, respectively.

Return to Structure of indole

Extended description for Ribbon diagram of SARS-CoV-2 spike protein bound to angiotensin-converting enzyme 2 and immunofluorescence photomicrographs of infected cells



Courtesy of Dr. Peng Zhou, Principle Investigator, Bat virus infection and immunity group, Wuhan Institute of Virology, Chinese Academy of Sciences.
© Macmillan Learning

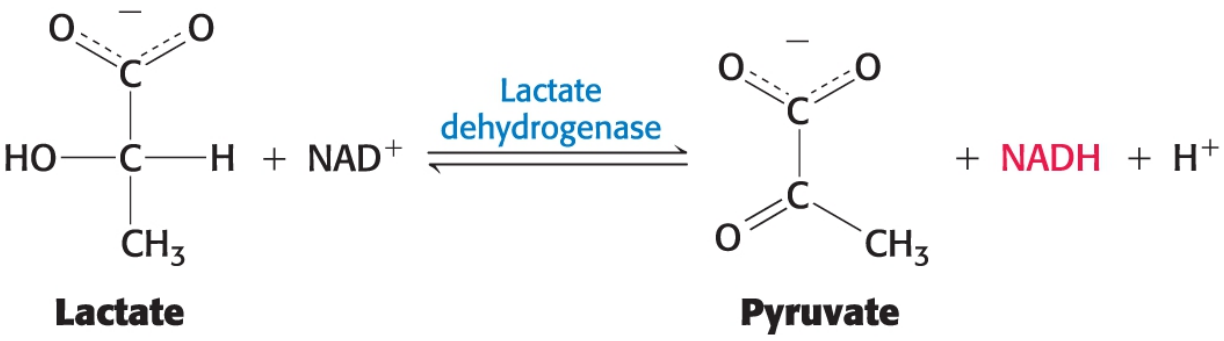
The spike protein is shown to be composed of beta strands connected by short loops. It has an elongated structure.

The three immunofluorescence micrographs are as follows:

The first micrograph shows cells expressing the angiotensin-converting enzyme 2 labeled in green.
The second micrograph shows virus particles labeled in red and concentrated toward the left.
The third micrograph is a combined image of the first two. Nuclei of the cells are visible and are labeled in blue.

Return to Ribbon diagram of SARS-CoV-2 spike protein bound to angiotensin-converting enzyme 2 and immunofluorescence photomicrographs of infected cells

Extended description for Chemical equation for oxidation of lactate to pyruvate



The reversible reaction consists of two reactants and three products.

The first reactant is lactate and has the following structure: H O, single bond, C, single bond, H. C is single bonded to C H 3 below and single bonded to C above which is partially double bonded to O on the upper left and partially double bonded to O on the upper right. The C O O group above carries a negative charge.

The second reactant is N A D superscript plus.

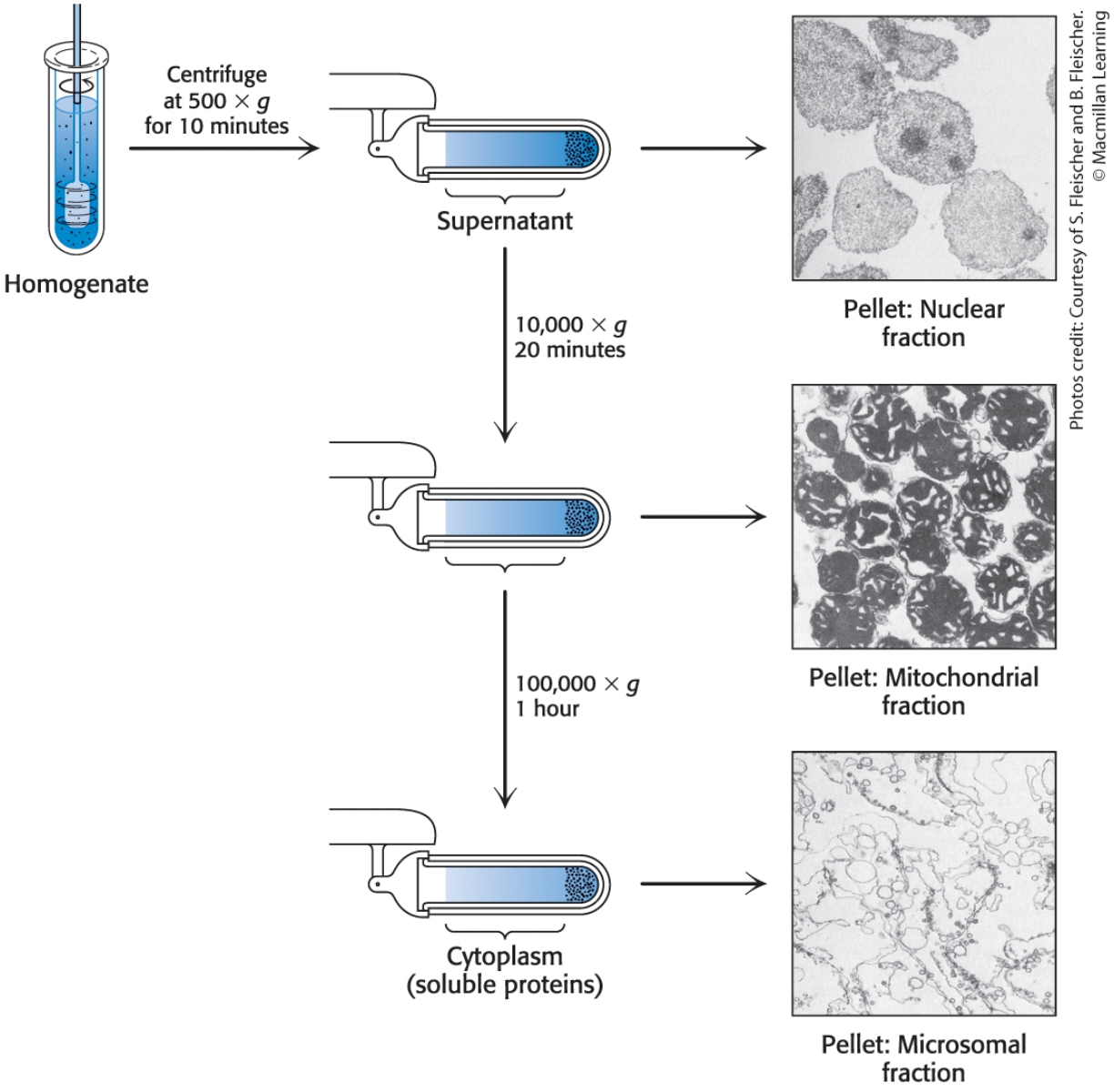
The first product has the following structure: A C atom is single bonded to C above. C 1 is single bonded to C H 3 on the lower right and double bonded to O on the lower left. C 2 is partially double bonded to O on the upper left and partially double bonded to O on the upper right. The C O O group above carries a negative charge.

The second product is N A D H.

The third product is H superscript plus ion.

Return to Chemical equation for oxidation of lactate to pyruvate

Extended description for FIGURE 4.1. Schematic illustration of differential centrifugation and photomicrographs of the pellets obtained at each step

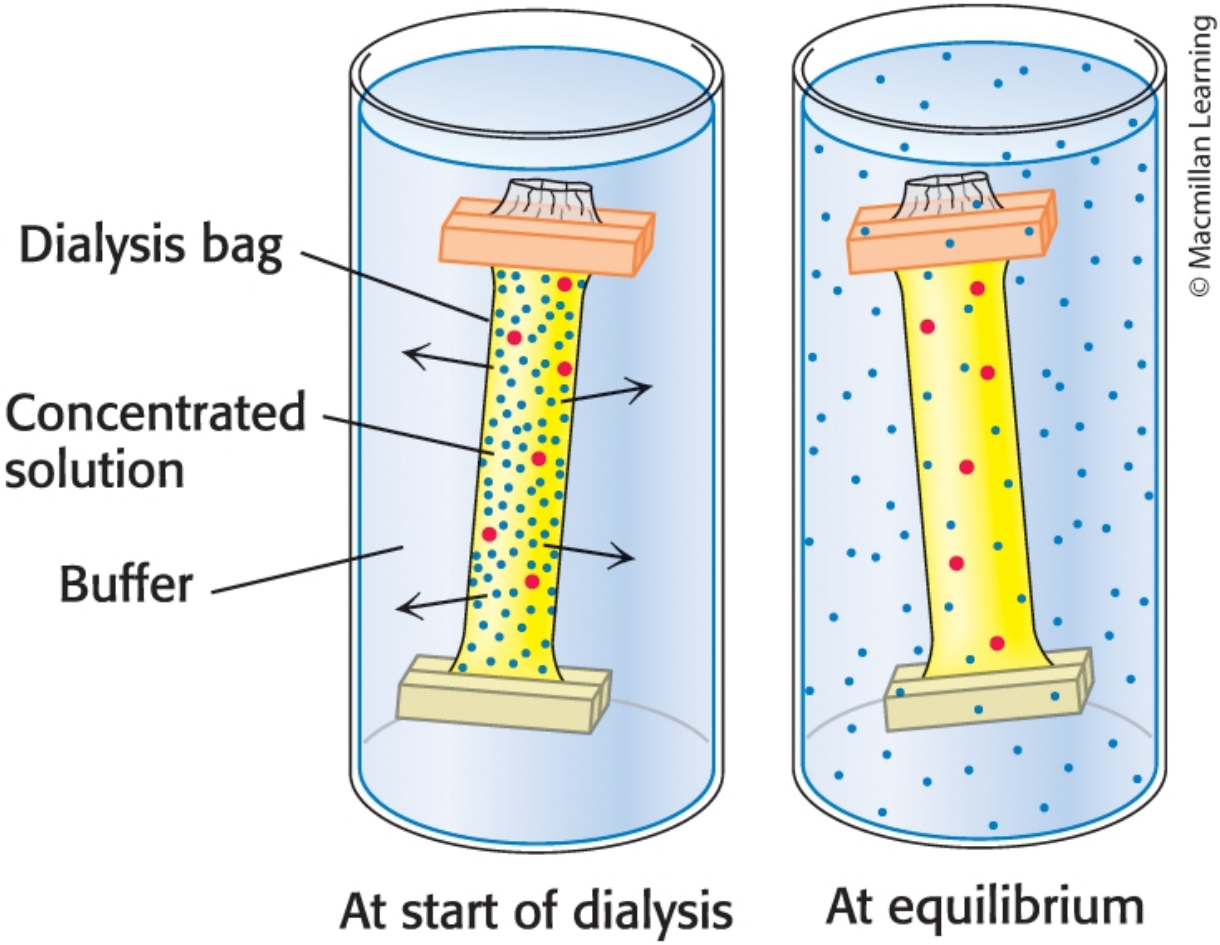


1. A test tube homogenizer containing a cell homogenate is shown. The homogenate is then centrifuged at 500 g for 10 minutes.

2. A centrifuge tube is shown in a horizontal orientation. It has a pellet at the base and the fluid supernatant fills the rest of the tube. A corresponding micrograph is labeled "Pellet: Nuclear fraction." It shows conglomerates comprising chromatin and other nuclear material.
3. The supernatant is then again centrifuged at 10,000 g for 20 minutes.
4. The centrifuge tube is shown in a horizontal orientation which contains supernatant and a pellet. A corresponding micrograph is labeled "Pellet: Mitochondrial fraction." It shows conglomerates comprising several mitochondria.
5. The supernatant is then again centrifuged at 10,000 g for 20 minutes.
6. The supernatant is then again centrifuged at 100,000 g for 1 hour.
7. The centrifuge tube is shown in a horizontal orientation which contains supernatant and a pellet. The supernatant is labeled "Cytoplasm (soluble proteins)." A corresponding micrograph is labeled "Pellet: Microsomal fraction." It shows small bead-like particles.

Return to FIGURE 4.1. Schematic illustration of differential centrifugation and photomicrographs of the pellets obtained at each step

Extended description for FIGURE 4.2. Schematic illustration of dialysis to separate proteins from small molecules

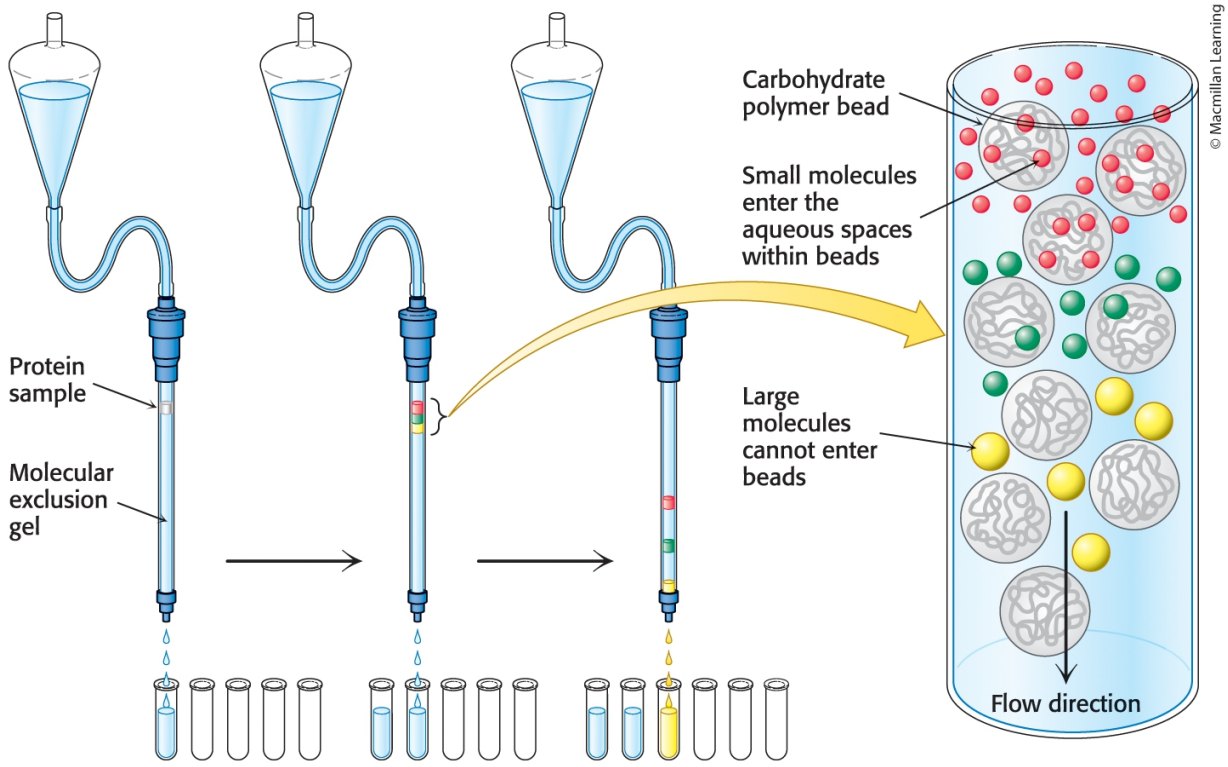


At the start of dialysis: A container filled with a buffer is shown. A column labeled "Dialysis bag" is shown suspended in the buffer and clipped on both ends. Several small blue dots interspaced with moderately sized green dots and larger red dots are shown inside the dialysis bag and is labeled "Concentrated solution." Outward arrows are directed from the concentrated solution in the dialysis bag toward the buffer outside.

At equilibrium: The blue dots earlier inside the dialysis bag are now shown to be in the buffer. On the green and red dots are shown to remain in the dialysis bag.

Return to FIGURE 4.2. Schematic illustration of dialysis to separate proteins from small molecules

Extended description for FIGURE 4.3. Schematic illustration of gel-filtration chromatography to separate proteins on the basis of their size



Three stages of the chromatographic separation technique is shown.

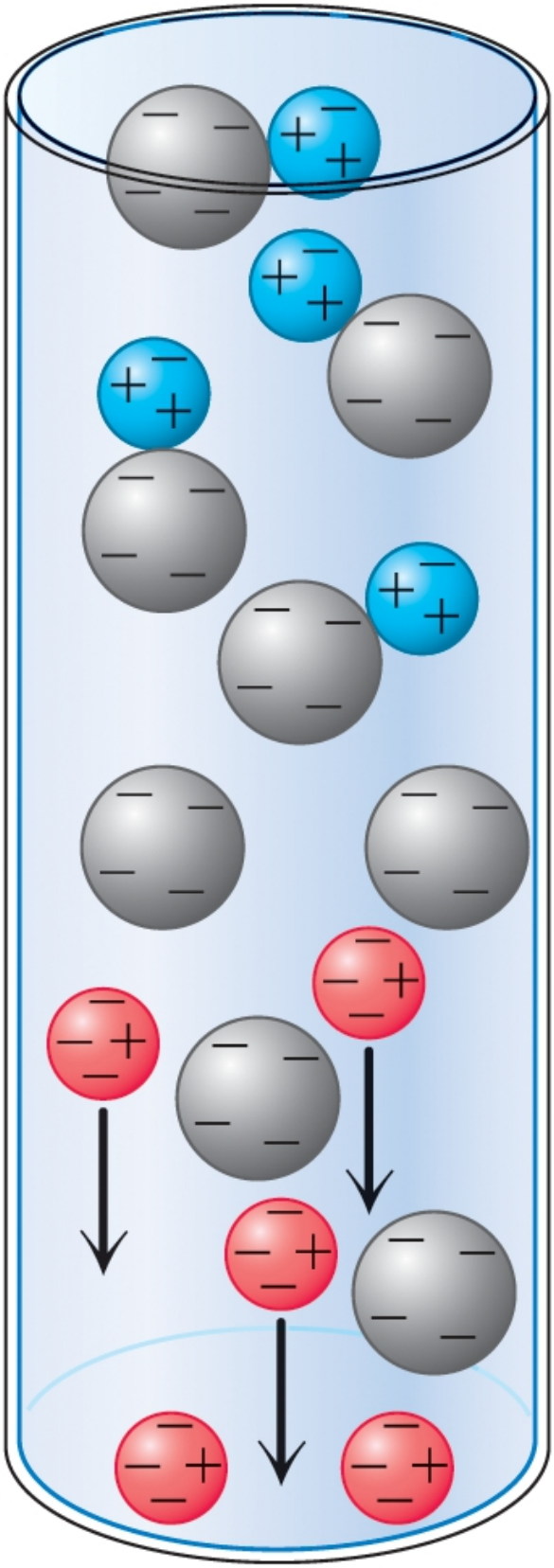
The first stage shows a funnel drip. A swan-neck tube from the funnel drip is connected to a vertical column. The apparatus is filled with molecular exclusion gel. A small white section is seen in the column and is labeled "Protein sample." The contents passing through the column is collected in a test-tube below.
The second stage shows the column having three consecutive sections colored red, green, and yellow. The contents passing through the column is collected in a test-tube below. A magnified view of these sections is shown. It shows the column filled with spherical beads labeled "Carbohydrate polymer beads." The flow

direction is indicated from the top to bottom. Small red spheres are shown at the top of the column and a callout reads, "Small molecules enter the aqueous spaces within beads." Moderate sized green beads are shown in the middle portion of the column. Larger yellow spherical beads are shown is the bottom portion of the column and a callout reads, "Large molecules cannot enter beads." The third stage shown the three colored segments separate along the length of the column. The yellow molecules are shown to be collected in a test-tube below.

Return to FIGURE 4.3. Schematic illustration of gel-filtration chromatography to separate proteins on the basis of their size

Extended description for FIGURE 4.4. Schematic illustration of ion-exchange chromatography to

separate proteins based on their net charge



Positively charged protein binds to negatively charged bead

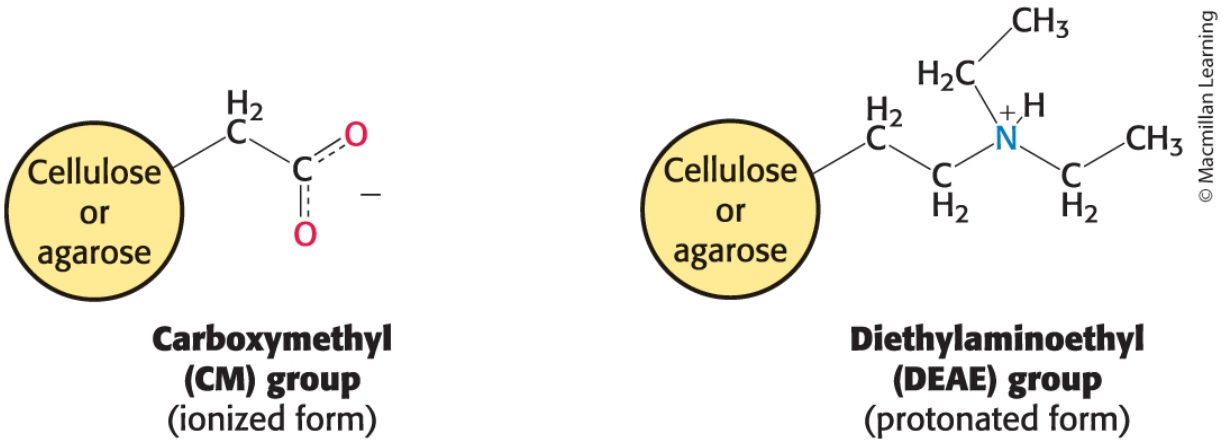
Negatively charged protein flows through

© Macmillan Learning

A column is shown to contain negatively charged beads. Blue spheres carrying a net positive charge are shown to adhere to the beads. A callout reads, "Positively charged protein binds to negatively charged bead." Red spheres carrying a net negative charge are shown to elute out of the column. A callout reads, "Negatively charged protein flows through."

Return to FIGURE 4.4. Schematic illustration of ion-exchange chromatography to separate proteins based on their net charge

Extended description for Chemical structure of ionized carboxymethyl group and protonated diethylaminoethyl group bound to cellulose or agarose bead



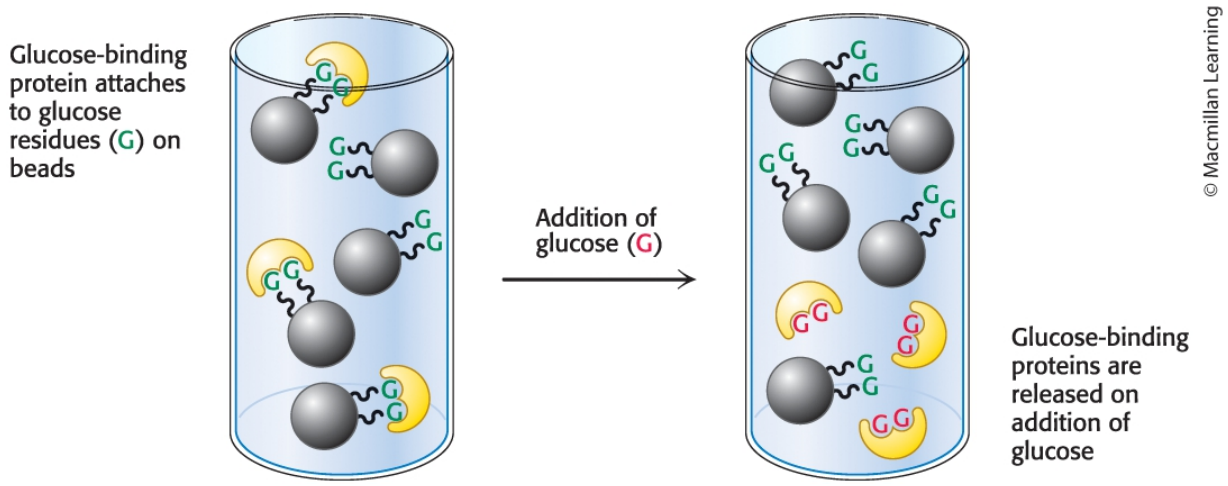
Carboxymethyl (C M) group (ionized form): C, single bond, C. C 1 is bound to H 2 and single bonded to a large bead labeled "Cellulose or agarose" on the lower left. C 2 is partially double bonded to O on the upper right and partially double bonded to O below. The terminal C O O group carries a negative charge.

Diethylaminoethyl (DEAE) group (protonated form): C, single bond, C, single bond, N, single bond, C, single bond, C H 3. C 1, C 2, and C 3 are each bound to H 2. C 1 is single bonded to a large bead labeled "Cellulose or agarose" on the lower left. N carries a positive charge and is single bonded to h on the upper right and single bonded to C H 2 on the upper left which is further single bonded to C H 3 on the upper right.

Return to Chemical structure of ionized carboxymethyl group and protonated diethylaminoethyl group bound to cellulose or agarose

bead

Extended description for FIGURE 4.5. Schematic illustration of affinity chromatography to separate proteins based on their binding to a specific ligand



A column is shown to contain spherical beads with glucose residues (shown in green) covalently attached to their surface. Crescent-shaped proteins, concanavalin A, are shown to attach to these glucose residues on the beads. A callout reads, "Glucose-binding protein attaches to glucose residues on beads."

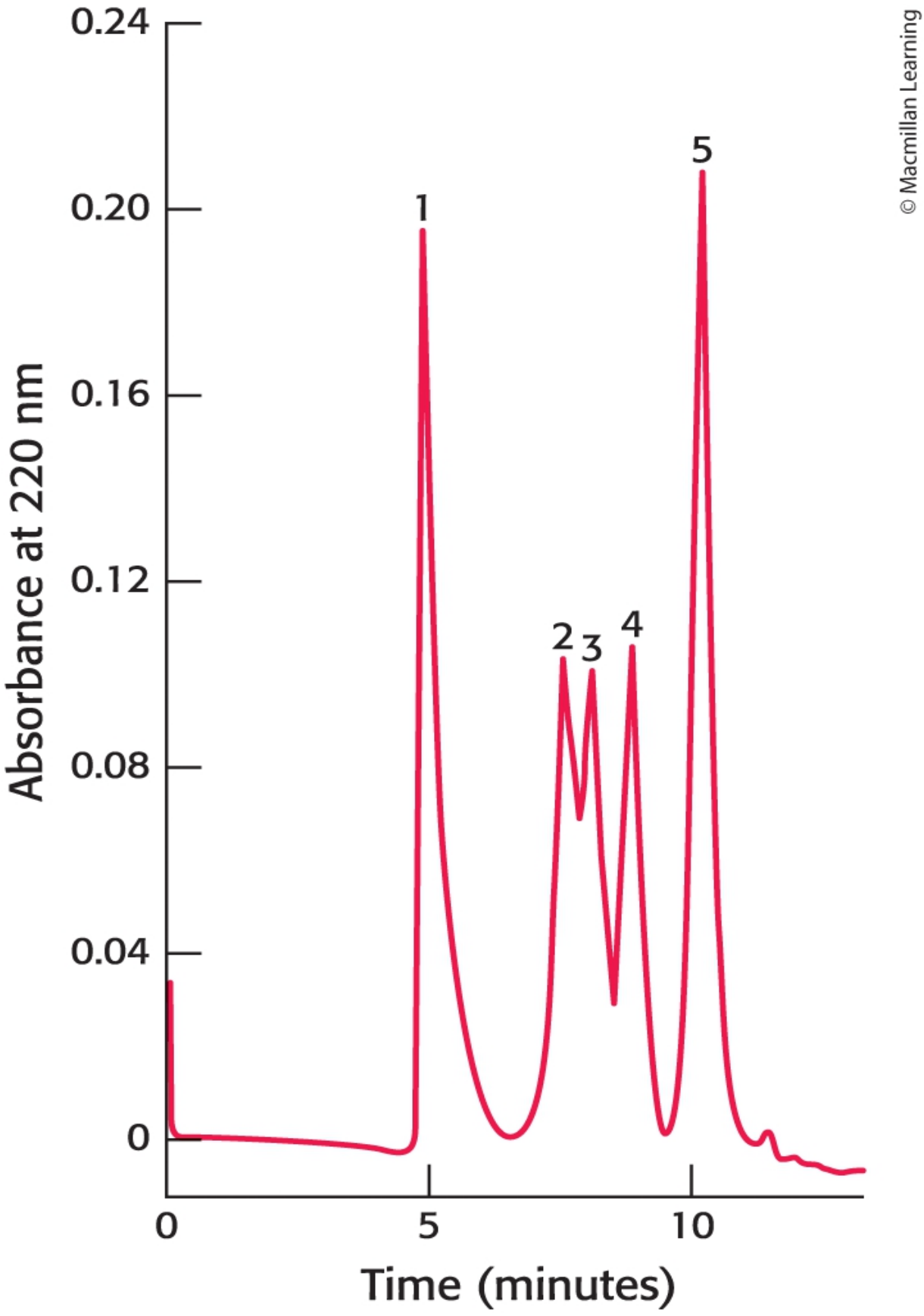
Glucose (shown in red) is shown to be added to the column.

After addition of glucose, the proteins are shown to detach from the beads and bind to the added glucose. A callout reads, "Glucose-binding proteins are released on addition of glucose."

Return to FIGURE 4.5. Schematic illustration of affinity chromatography to separate proteins based on their binding to a specific ligand

Extended description for FIGURE 4.6. Graph showing H P L C mediated protein separation with high resolving

power



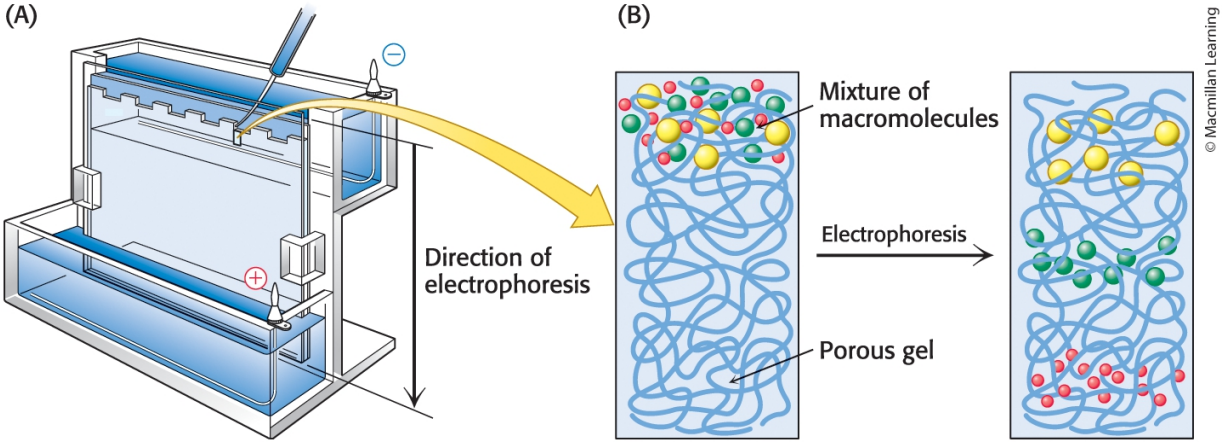
© Macmillan Learning

The horizontal axis is labeled Time (minutes) and ranges from 0 to 10 in increments of 5 units. The vertical axis is labeled Absorbance at 220 n m and ranges from 0 to 0.24 in increments of 0.04 units. Five peaks are labeled on the graph from 1 through 5 as follows:

Peak 1 at (5, 0.20)
Peak 2 at (7.5, 0.10)
Peak 3 at (8, 0.95)
Peak 4 at (9, 0.10)
Peak 5 at (10, 0.21)

Return to FIGURE 4.6. Graph showing H P L C mediated protein separation with high resolving power

Extended description for FIGURE 4.7. Schematic illustration of polyacrylamide gel electrophoresis

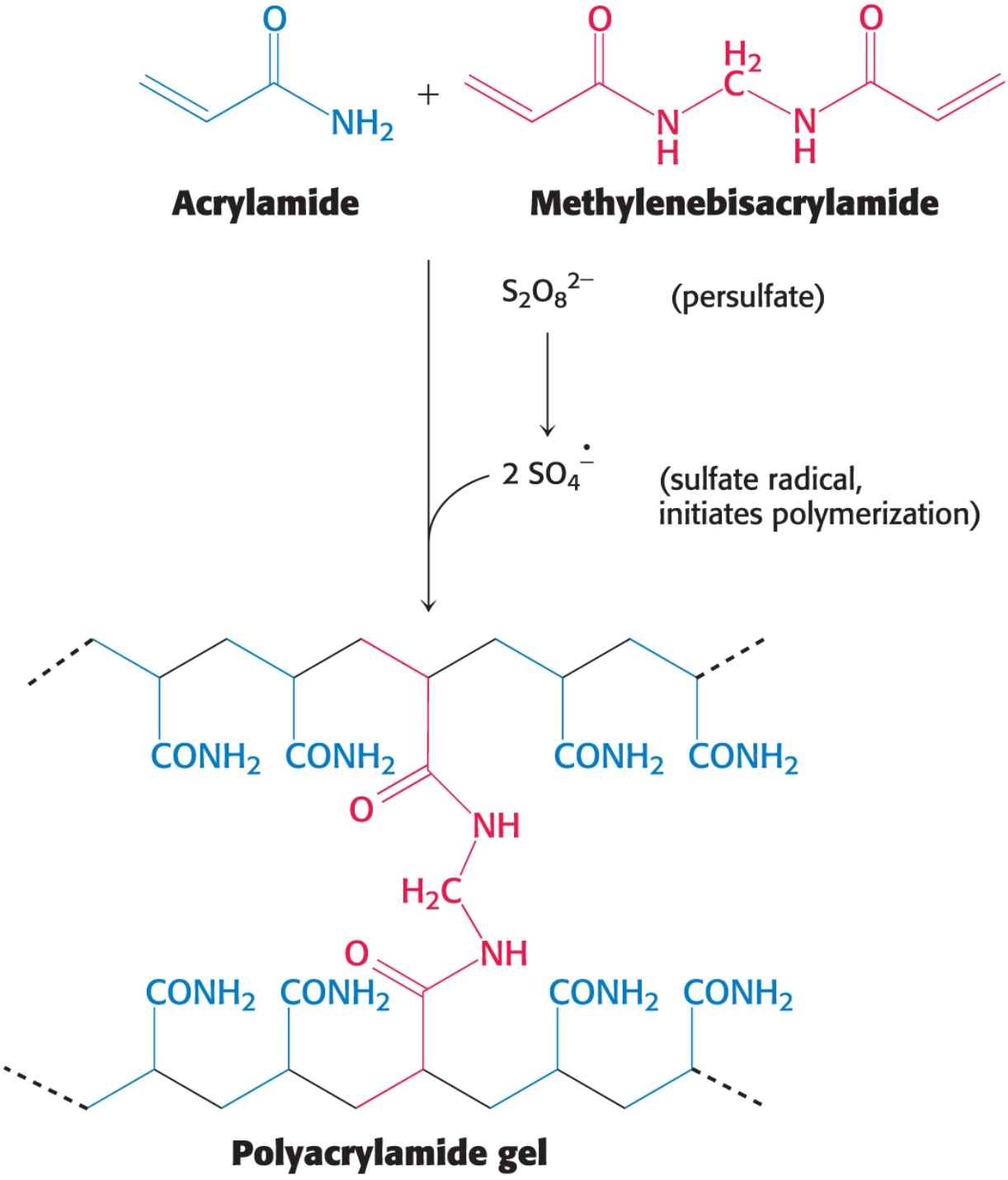


Part (A): A polyacrylamide gel electrophoresis set-up is shown. The gel is mounted vertically. It has several small wells at the top into which the sample is shown to be loaded by a pipette. The direction of electrophoresis is shown to be from the top to bottom. A tank with a buffer is present at the top, behind the gel. This has a negative electrode. Another tank with a buffer is present at the bottom, in front of the gel. This has a positive electrode.

Part (B): A magnified view of the well loaded with the sample is shown. It shows a mesh-like matrix made up of intertwined rope-like structures. Pockets in the matrix is labeled "Porous gel". A mixture of macromolecules are shown at the top portion of the gel and consists of large yellow spheres, moderate-sized green spheres, and small red spheres. A rightward arrows from this is labeled "Electrophoresis" which points at the separated macromolecules. The large yellow spheres are shown to be trapped toward the top of the gel. The intermediate-sized green spheres are trapped in the middle. The small red spheres are trapped at the bottom of the gel.

Return to FIGURE 4.7. Schematic illustration of polyacrylamide gel electrophoresis

Extended description for FIGURE 4.8. Cross-linking reaction for polyacrylamide gel formation



The first reactant is Acrylamide and has the following structure: A 3-carbon alkene chain is depicted as a line structure using 2 zigzag lines. C 1 is double bonded to C 2. C 3 is double bonded to O above and single bonded to N H 2 on the lower right.

The second reactant is Methylenebisacrylamide and has the following structure: A 3-carbon alkene chain is depicted as a line structure using 2 zigzag lines. C 1 is double bonded to C 2. C 3 is double bonded to O above and single bonded to N bound to H on the lower right. N is single bonded to C bound to H 2 on the upper right. C is single bonded to N bound to H on the lower right. N is single bonded to C 1 of a 3-carbon alkene chain depicted using 2 zigzag lines on the upper right. C 1 is double bonded to O above. C 2 is double bonded to C 3.

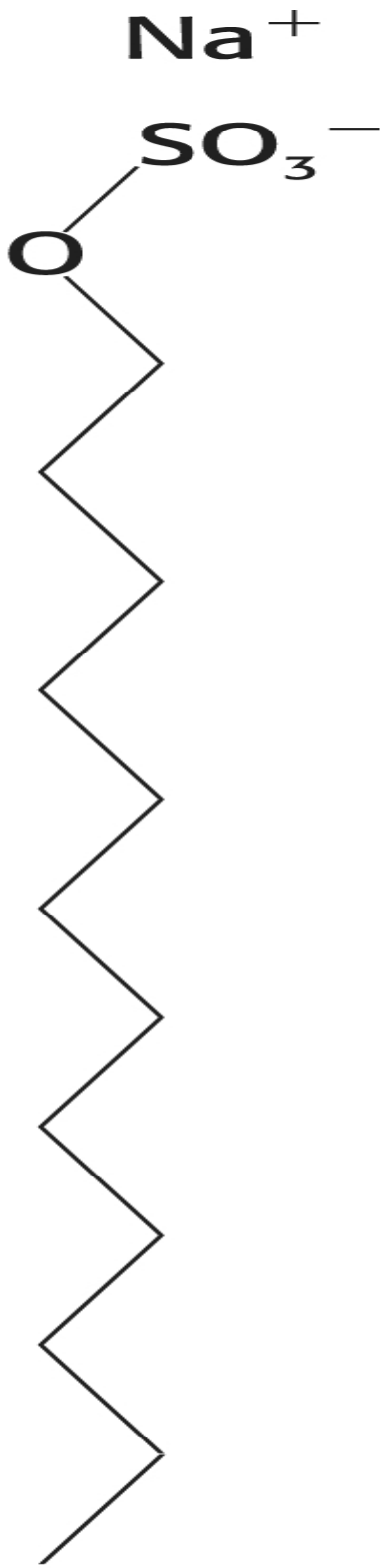
S 2 O 8 superscript 2 minus (persulfate) is shown to form 2 S O 4 superscript minus with a lone electron (sulfate radical). The sulfate radical is indicated to initiate polymerization.

The product is Polyacrylamide gel which has the following structure: A polymeric units is shown to consist of a 10-carbon alkane chain depicted as a line structure using 9 zigzag lines. C 2, C 4, C 8, and C 10 are each single bonded to C O N H 2 below. C 6 is single bonded to a C atom below. The C atom is double bonded to O on the lower left and single bonded to N H on the lower right. N H is single bonded to C H 2 on the lower left which is single bonded to N H on the lower right. N H is single bonded to a central C atom on the lower left which is double bonded to O on the upper left and single bonded to C 6 of another 10-carbon alkane chain below. The alkane chain is depicted as a line structure using 9 zigzag lines. C 2, C 4, C 8, and C 10 are each single bonded to C O N H 2 above. The group linking the two alkane chains is highlighted in red.

Return to FIGURE 4.8. Cross-linking reaction for polyacrylamide gel formation

Extended description for Chemical structure of sodium

dodecyl sulfate

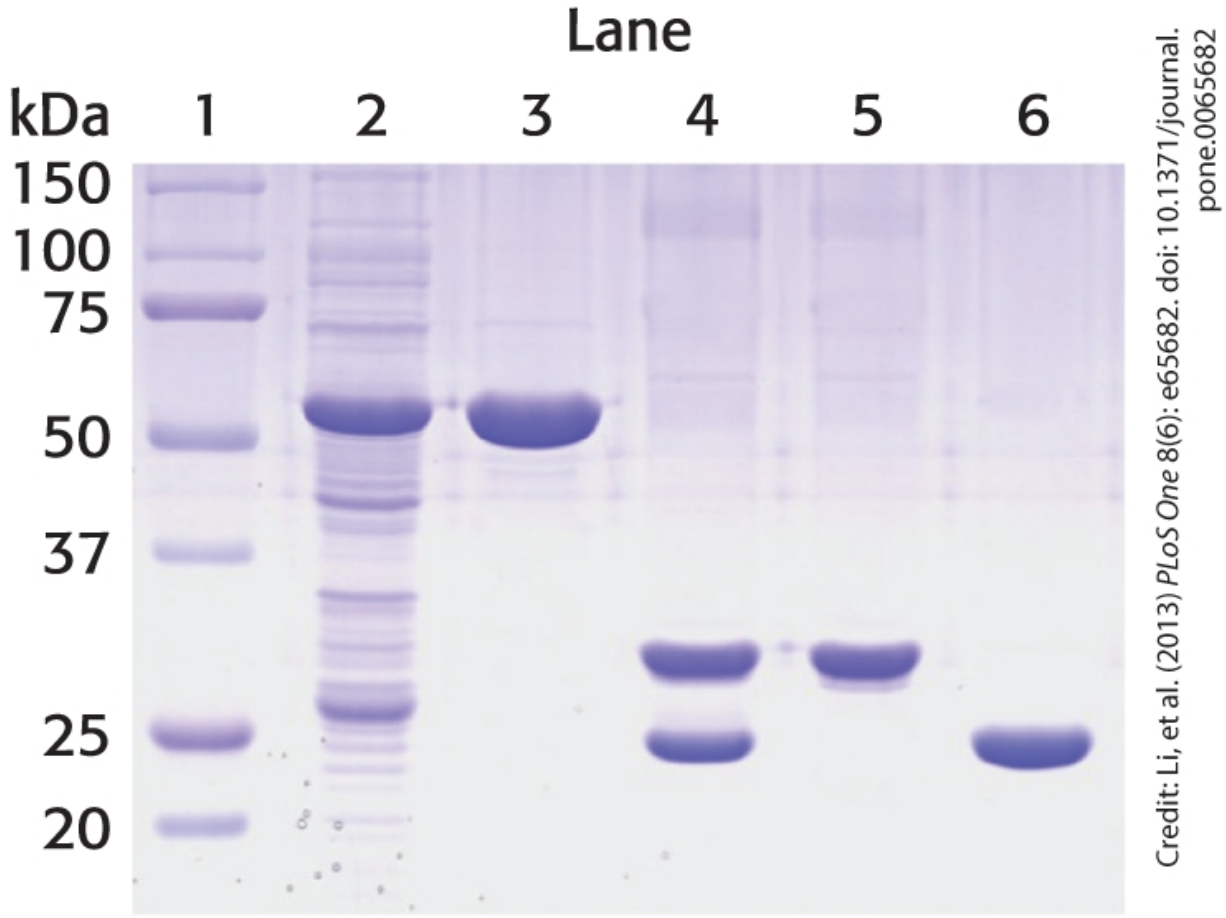


Sodium dodecyl sulfate (SDS)

The structure of sodium dodecyl sulfate (S D S) is as follows: S O 3 superscript minus is single bonded to O on the lower left. O is single bonded to C 1 of a 12-carbon alkane chain depicted as a line structure using 11 zigzag lines. N a superscript plus is present above S O 3 superscript minus as a counter-ion.

Return to Chemical structure of sodium dodecyl sulfate

Extended description for FIGURE 4.9. Photograph of stained polyacrylamide gel showing protein bands



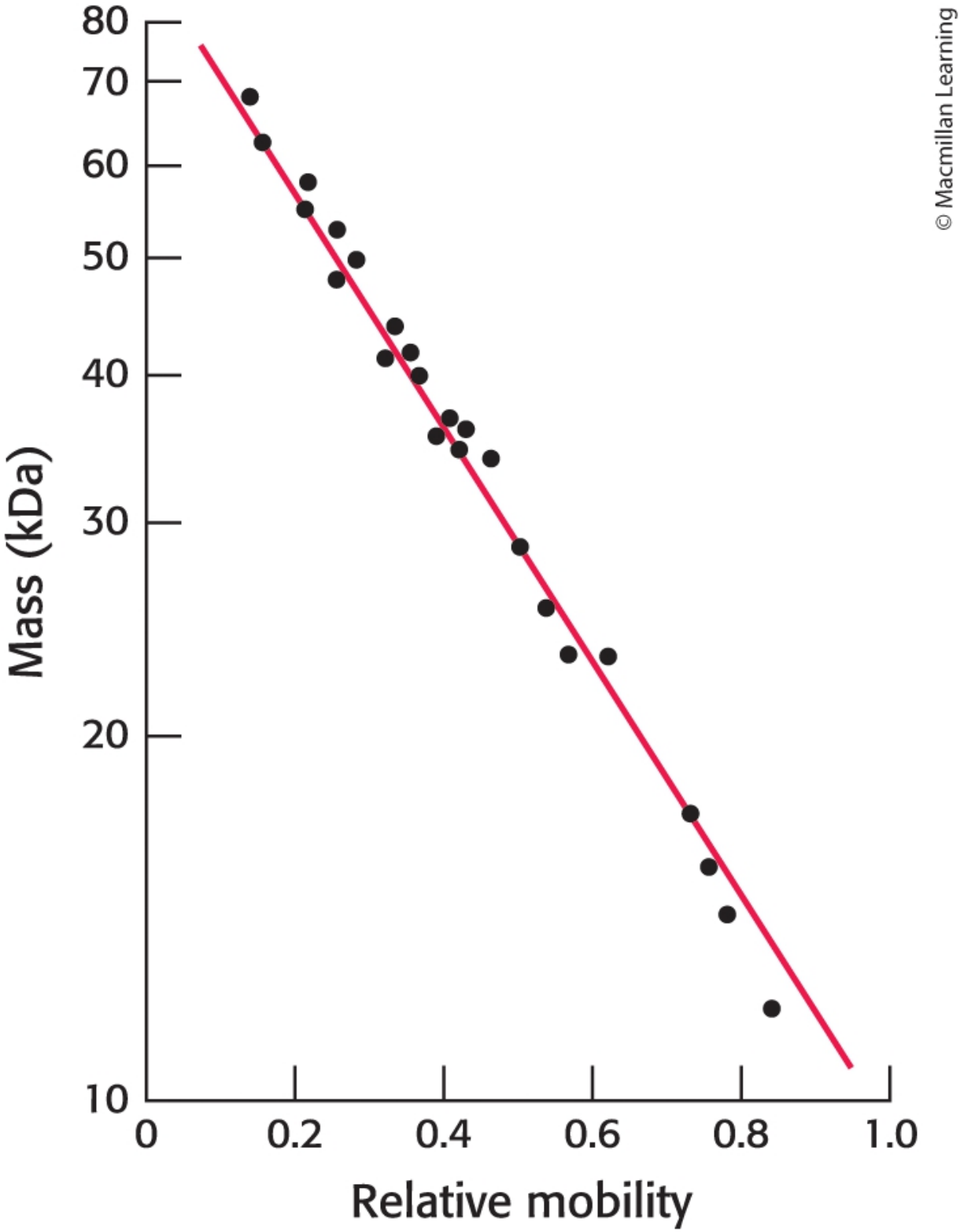
Credit: Li, et al. (2013) *PLoS One* 8(6): e65682. doi: 10.1371/journal.pone.0065682

The photograph shows six vertical lanes that are labeled 1 through 6. Lane 1 is shown to represent a protein ladder which functions as a reference. It contains proteins of various sizes ranging from 20 to 150 kilo Dalton, from bottom to top. The rest of the lanes show the separate proteins in the samples. Some of the bands appear significantly darker than the rest.

Return to FIGURE 4.9. Photograph of stained polyacrylamide gel showing protein bands

Extended description for FIGURE 4.10. Electrophoresis

graph for protein mass determination

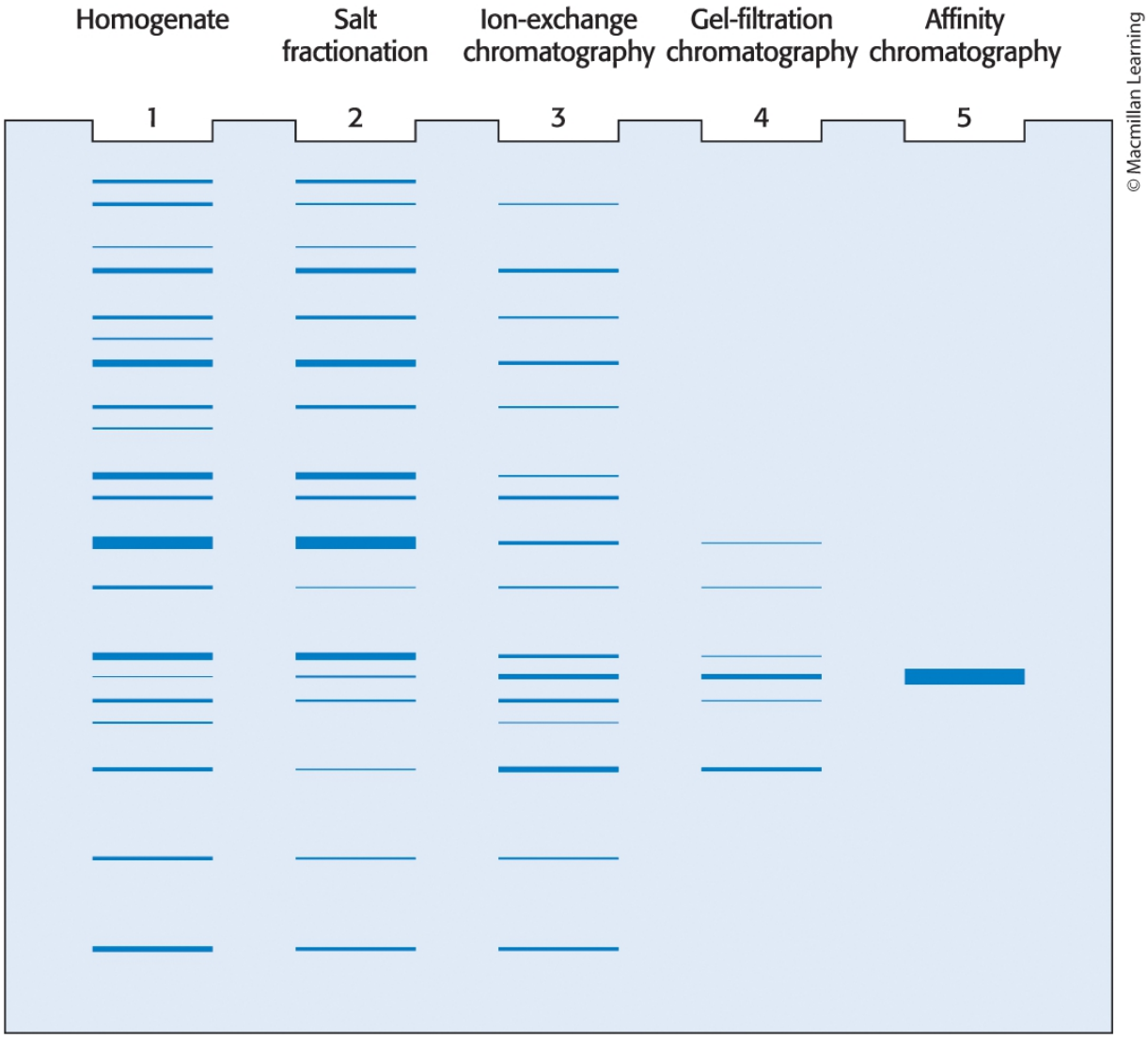


© Macmillan Learning

The horizontal axis is labeled Relative mobility and ranges from 0 to 1.0 in increments of 0.2 units. The vertical axis is labeled Mass (kilo Dalton) and ranges from 10 to 80 in unequal increments. The trendline has a negative slope which starts at (0.1, 75) and ends at (0.95, 11). Plot points are shown to lie near the trendline.

Return to FIGURE 4.10. Electrophoresis graph for protein mass determination

Extended description for FIGURE 4.11. Electrophoretic analysis for monitoring the progress of protein purification

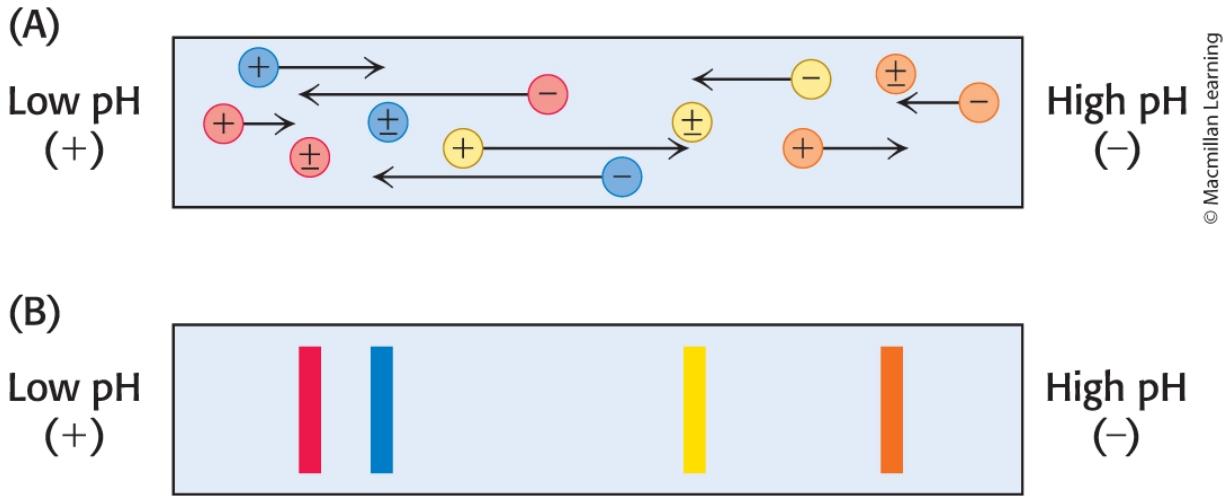


The gel is shown to have 5 lanes, from left to right, labeled Homogenate, Salt fractionation, Ion-exchange chromatography, Gel-filtration chromatography, and Affinity chromatography.

The band corresponding to the protein of interest is shown be present approximately in the middle. The number of bands obtained at each subsequent step is shown to decrease. The band corresponding to protein of interest is shown to get thicker along the purification process. In the final lane, only the band corresponding to the protein of interest is visible.

Return to FIGURE 4.11. Electrophoretic analysis for monitoring the progress of protein purification

Extended description for FIGURE 4.12. Schematic illustration of isoelectric focusing mediated separation of proteins



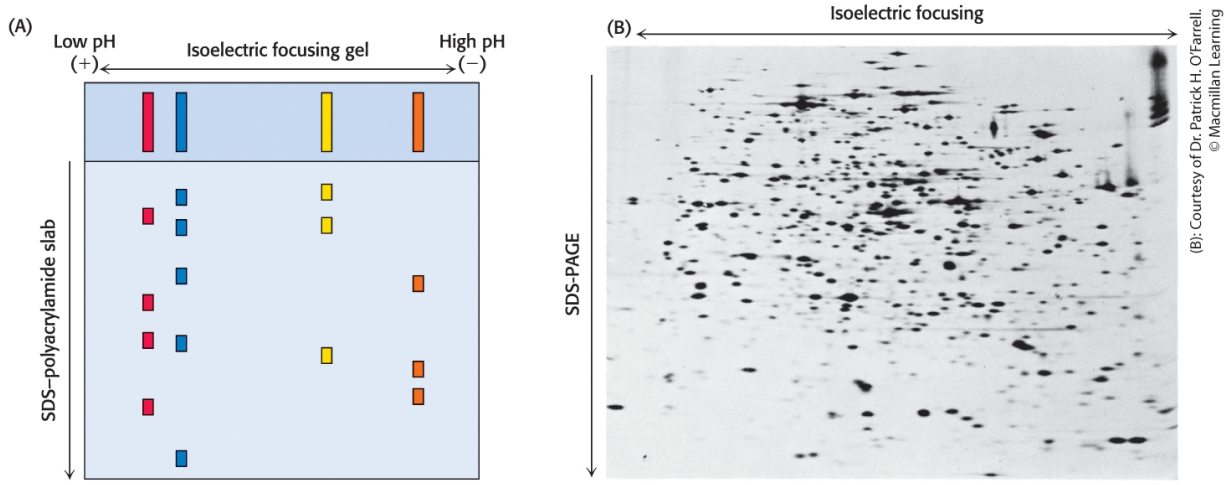
© Macmillan Learning

Part (A): A p H gradient is shown across the gel. The left end is labeled low p H (plus) and the right end is labeled high p H (minus). Several red, blue, yellow, and orange spheres are shown carrying the following charges: positive, negative, and both positive and negative. The spheres carrying a positive charge are shown to migrate toward the right terminal. The spheres carrying a negative charge are shown to migrate toward the left terminal. Spheres carrying both positive and negative charges are shown to remain stagnant.

Part (B): Several vertical protein bands are shown along the gel. Red and blue bands are present closer to the positive left terminal. An orange band is present closer to the negative right terminal. A yellow band is present almost in the middle but slightly closer to the right terminal.

Return to FIGURE 4.12. Schematic illustration of isoelectric focusing mediated separation of proteins

Extended description for FIGURE 4.13. Schematic illustration and actual image of two-dimensional gel electrophoresis for separation of complex protein mixtures



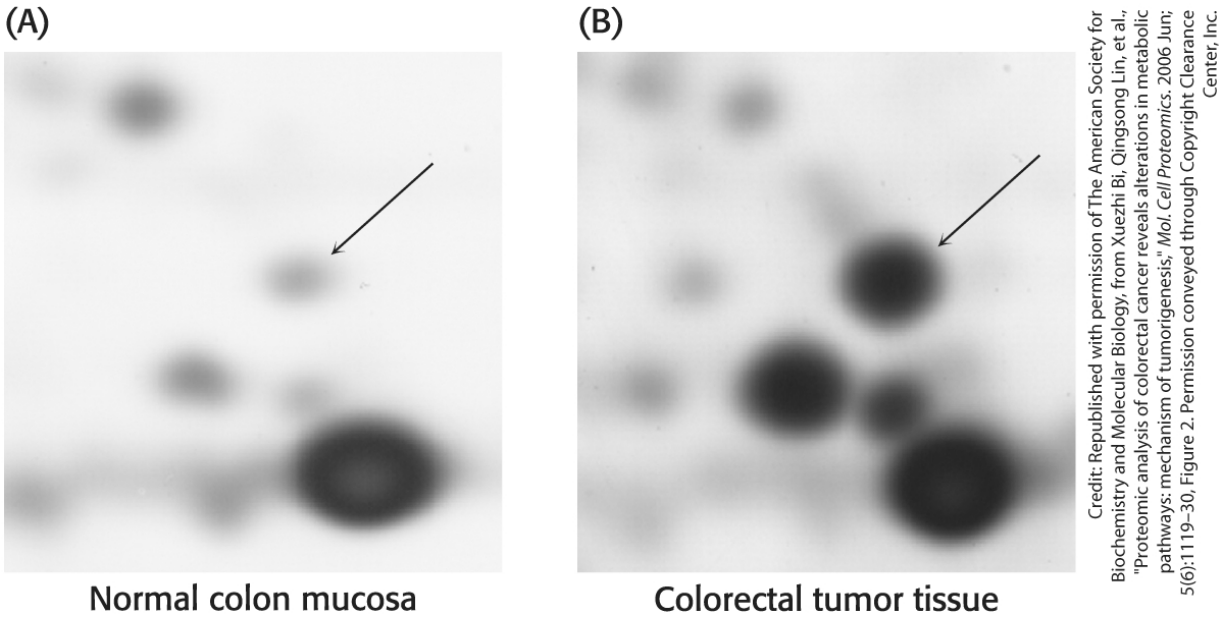
Part (A): The figure illustrates an isoelectric focusing gel slab at the top joined to a larger S D S-polyacrylamide gel slab at the bottom. A double-headed arrow is shown above the isoelectric focusing gel, indicating that the separation is horizontal. A downward arrow is shown along the S D S-polyacrylamide gel, indicating that the separation is vertical. A p H gradient is shown across the gel. The left end is labeled low p H (plus) and the right end is labeled high p H (minus). Several vertical protein bands are shown along the gel. Red and blue bands are present closer to the positive left terminal. An orange band is present closer to the negative right terminal. A yellow band is present almost in the middle but slightly closer to the right terminal. Below each band, corresponding small separated segments are shown in the S D S-polyacrylamide gel.

Part (B): A photograph of two-dimensional gel electrophoresis shows several dark spots corresponding to respective proteins. The

spots are mostly present in the middle portion and toward the top half of the gel.

Return to FIGURE 4.13. Schematic illustration and actual image of two-dimensional gel electrophoresis for separation of complex protein mixtures

Extended description for FIGURE 4.14. Photographic results of two dimensional gel electrophoresis showing alterations of protein level in normal and cancerous tissue



Photograph (A) shows proteins isolated from normal colon mucosa. A faint black spot is indicated in the gel among several spots of varying intensities.

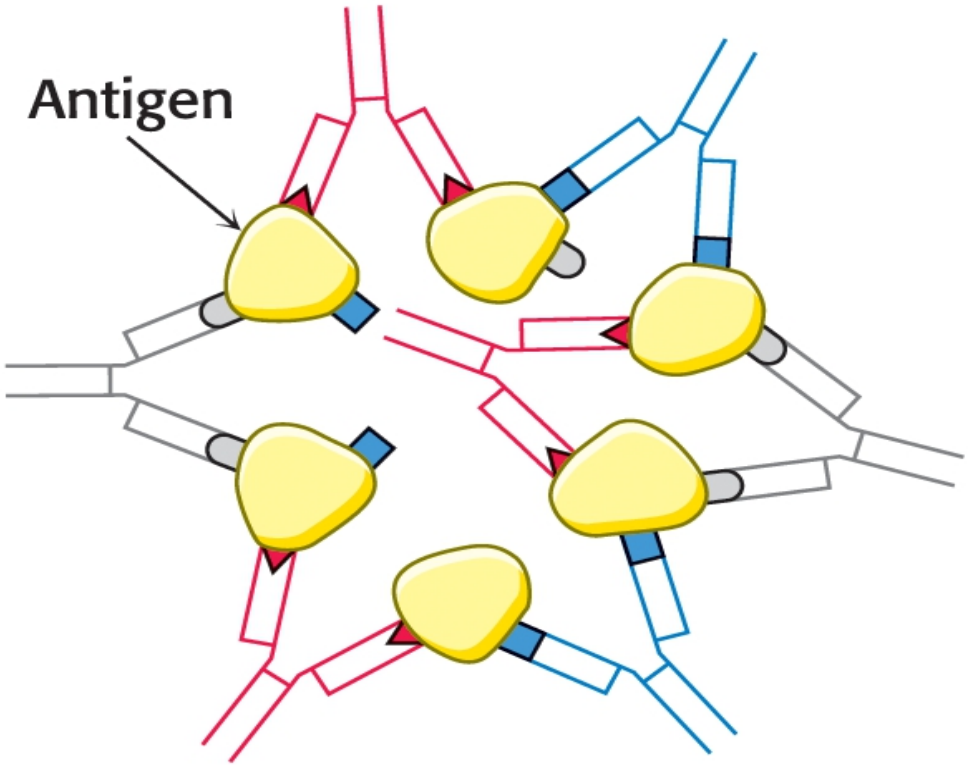
Photograph (B) shows proteins isolated from colorectal tumor tissue. The faint spot in the previous photograph is shown to be darker and larger in this sample.

Return to FIGURE 4.14. Photographic results of two dimensional gel electrophoresis showing alterations of protein level in normal and cancerous tissue

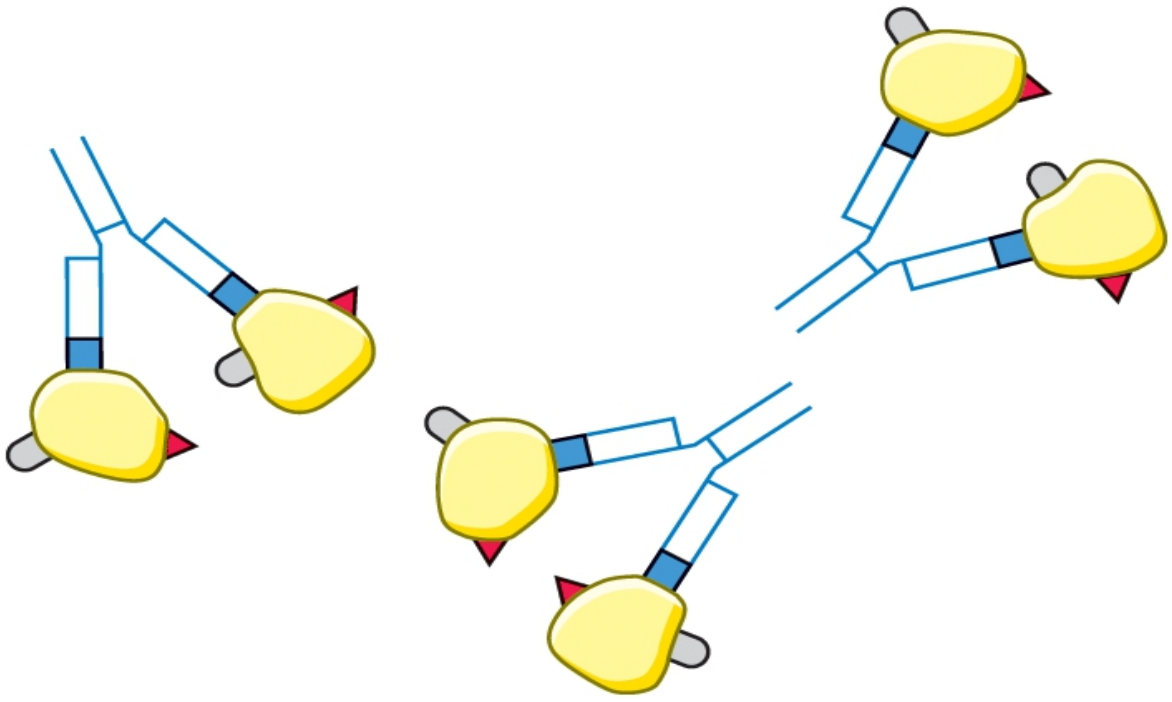
Extended description for FIGURE 4.15. Schematic illustration of polyclonal and monoclonal antibodies

with different number of epitopes

Polyclonal antibodies



Monoclonal antibodies



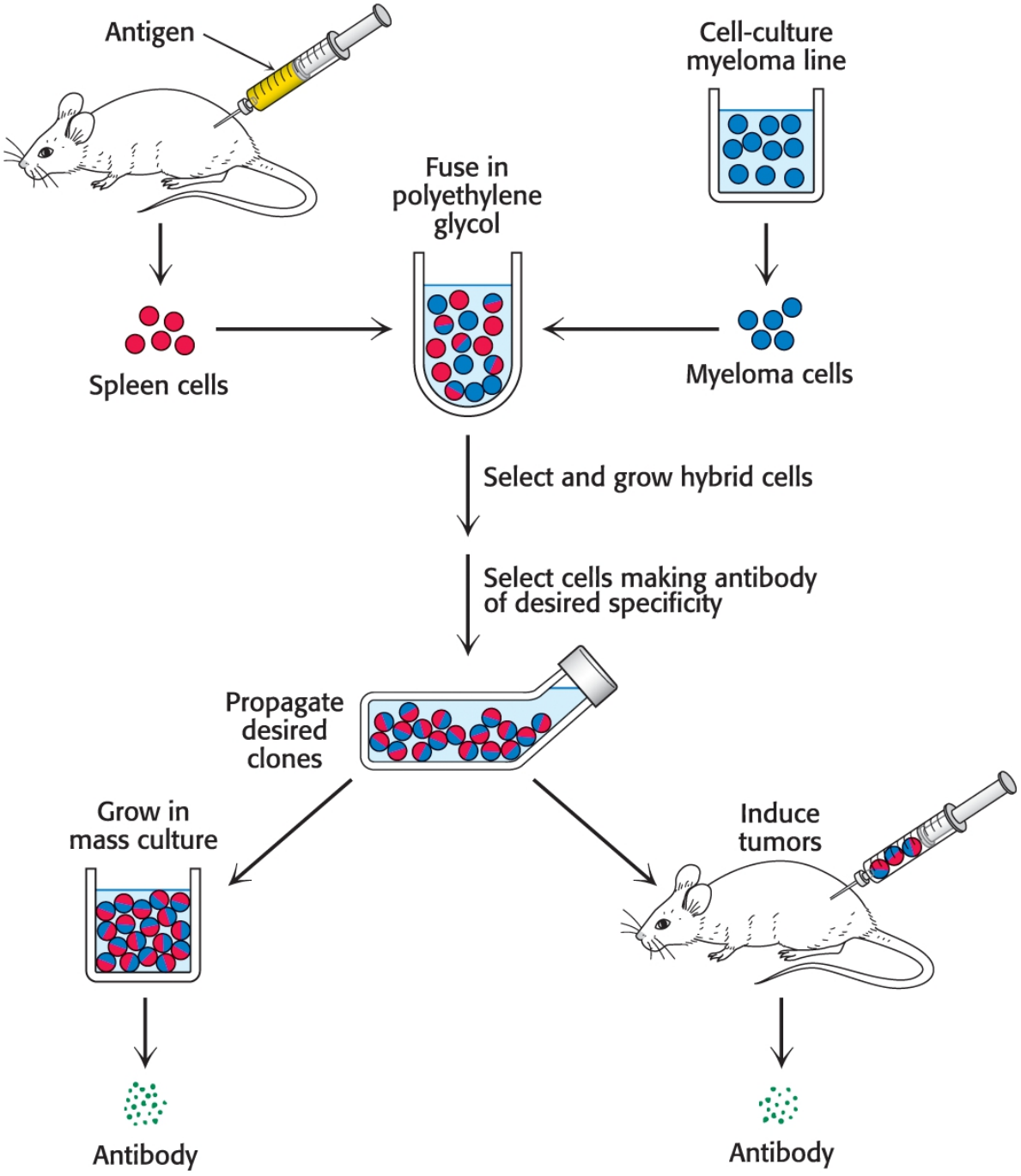
© Macmillan Learning

Polyclonal antibodies: The antibodies are represented by Y-shaped structures colored red, blue, and gray. Cells are shown to express the following epitopes on their surface: red triangles, blue squares, and gray circles. Each antibody is shown to bind to an antigen of the corresponding color. The two arms of each antibody bind to corresponding epitopes on two cells.

Monoclonal antibodies: The antibodies are represented by Y-shaped structures colored blue. Cells are shown to express the following epitopes on their surface: red triangles, blue squares, and gray circles. The two arms of each antibody bind to corresponding blue epitopes on two cells.

Return to FIGURE 4.15. Schematic illustration of polyclonal and monoclonal antibodies with different number of epitopes

Extended description for FIGURE 4.16. Schematic illustration of monoclonal antibody production



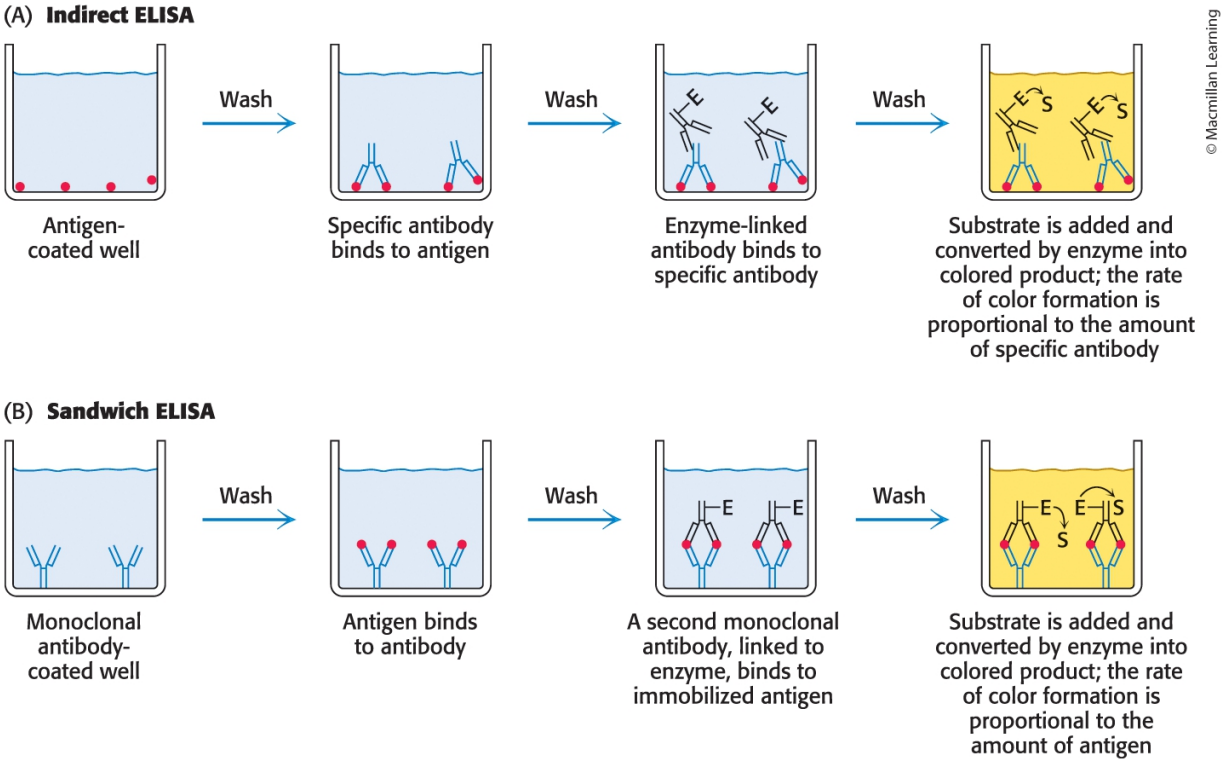
© Macmillan Learning

1. A mouse is shown to be injected with antigen.

2. Spherical red spleen cells are shown to be harvested from the mouse.
3. Myeloma cell line is shown to be expanded by cell culture.
4. Spherical blue myeloma cells are shown to be obtained from the cell culture.
5. A tube filled with polyethylene glycol is shown. The tube is shown to contain the spleen and myeloma cells which fuse to produce hybrid cells. The hybrid cells are shown to be half blue and half red.
6. The hybrid cells are selected and grown.
7. The cells making antibody of desired specificity and selected.
8. A cell culture flask is shown to be used to propagate desired clones.
9. The clones are shown to be grown in mass culture of injected into mouse to induce tumors. Antibodies are obtained from both the mass culture and the tumor induced mouse.

Return to FIGURE 4.16. Schematic illustration of monoclonal antibody production

Extended description for FIGURE 4.17. Schematic illustration of indirect and sandwich ELISA for antigen or antibody detection



Part (A): Indirect ELISA.

1. Antigen-coated well: A well containing a buffer is shown. The floor of the well is shown to be coated with red spherical antigens. The well is then washed.
2. Specific antibody binds to antigen: Arms of the Y-shaped antibodies are shown to bind to antigens in the well. The well is then washed.
3. Enzyme-linked antibody binds to specific antibody: An arm of Y-shaped secondary antibody is shown to bind to the stem of the primary antibody bound to antigens. The stem of the

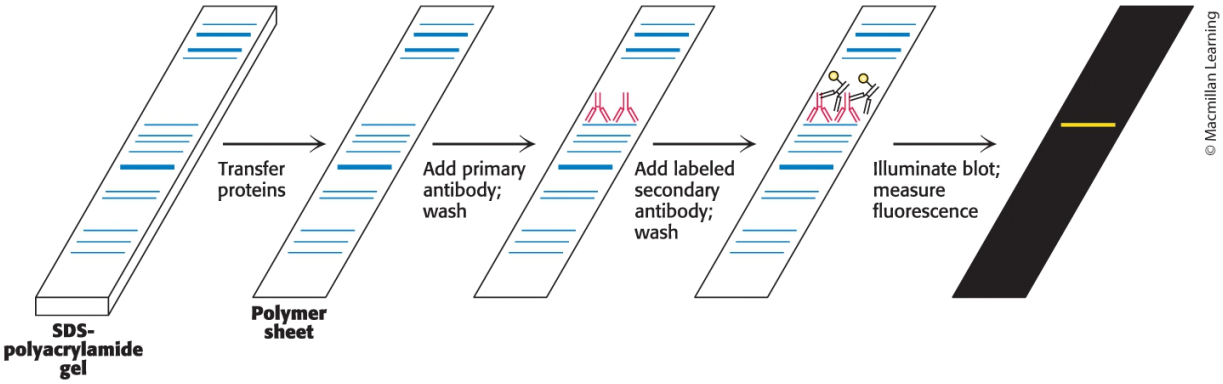
secondary antibody is linked to an enzyme. The well is then washed.
4. Substrate is added and converted by enzyme into colored product; the rate of color formation is proportional to the amount of specific antibody: The enzyme linked to the antibody-antigen complex is shown to convert the substrate to a yellow colored product.

Part (B): Sandwich ELISA.

1. Monoclonal antibody-coated well: well containing a buffer is shown. The floor of the well is shown to be coated with Y-shaped antibodies. The well is then washed.
2. Antigen binds to antibody: Red spherical antigens are shown to bind to the arms of the antibodies. The well is then washed.
3. A second monoclonal antibody, linked to enzyme, binds to immobilized antigen: The arms of the Y-shaped secondary antibody are shown to bind to the antigens bound to the primary antibody. The stem of the secondary antibody is linked to an enzyme. The well is then washed.
4. Substrate is added and converted by enzyme into colored product; the rate of color formation is proportional to the amount of specific antibody: The enzyme linked to the antibody-antigen complex is shown to convert the substrate to a yellow colored product.

Return to FIGURE 4.17. Schematic illustration of indirect and sandwich ELISA for antigen or antibody detection

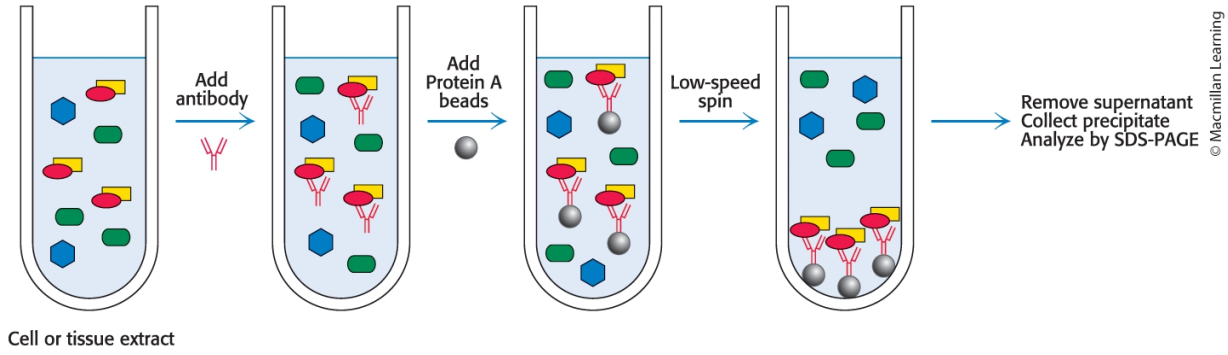
Extended description for FIGURE 4.18. Schematic illustration of western blotting to detect specific proteins



1. A long slab of S D S-polyacrylamide gel I shown. Several horizontal bands of proteins are shown on the gel. The bands are of varying thickness.
2. The proteins are shown to transferred to a polymer sheet. The bands on the polymer sheet have the exact same arrangement and thickness as those on the gel.
3. Y-shaped primary antibodies are added to the sheet. The antibodies are shown to bind specifically to only one band on the sheet. The sheet is then washed.
4. Labeled Y-shaped secondary antibodies are shown to be added to the sheet. These secondary antibodies are show to bind to the primary antibodies. The sheet is then washed.
5. The immunoblot is illuminated. Only the antibody-bound protein band is visible as a bright yellow band against a dark background. The fluorescence is measured.

Return to FIGURE 4.18. Schematic illustration of western blotting to detect specific proteins

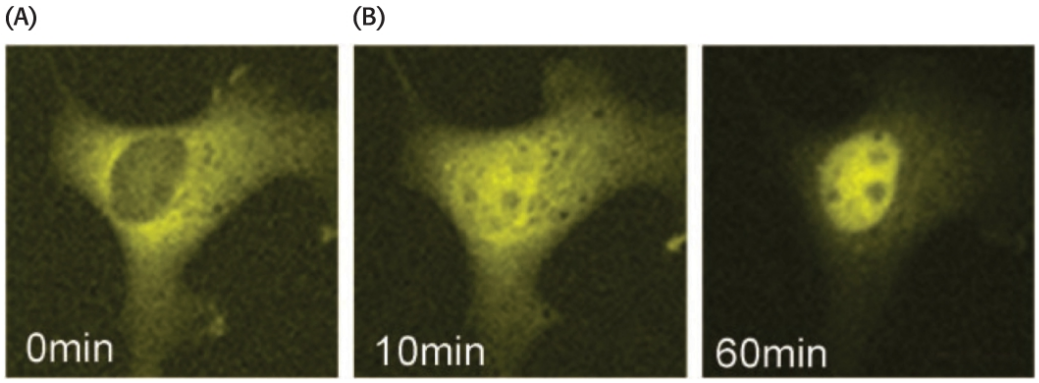
Extended description for FIGURE 4.19. Schematic illustration of co-immunoprecipitation for the detection of protein binding partners



A test tube is shown to contain a cell or tissue extract. Several particles are seen as follows: a blue hexagon, a green oval, a red oval fused to a yellow rectangle. Y-shaped antibody are shown to be added to the tube. The antibodies are shown to bind to the ovals fused to the rectangles. Spherical Protein A beads are shown to bind to the stem of the antibodies. The antibodies bound to the beads and the protein of interest are shown to precipitate at the bottom of the tube upon low-speed spin. The supernatant is removed and the precipitate is analyzed by SDS-PAGE.

Return to FIGURE 4.19. Schematic illustration of co-immunoprecipitation for the detection of protein binding partners

Extended description for FIGURE 4.21. Fluorescence microscopy mediated detection of changes in protein localization inside a cell



Credit: Republished with permission of Society for Neuroscience, from Nishi, M. et al., "Visualization of Glucocorticoid Receptor and Mineralocorticoid Receptor Interactions in Living Cells with GFP-Based Fluorescence Resonance Energy Transfer," *The Journal of Neuroscience*, 24, 21, 2004, 4918-27, Figure 7. Permission conveyed through Copyright Clearance Center, Inc.

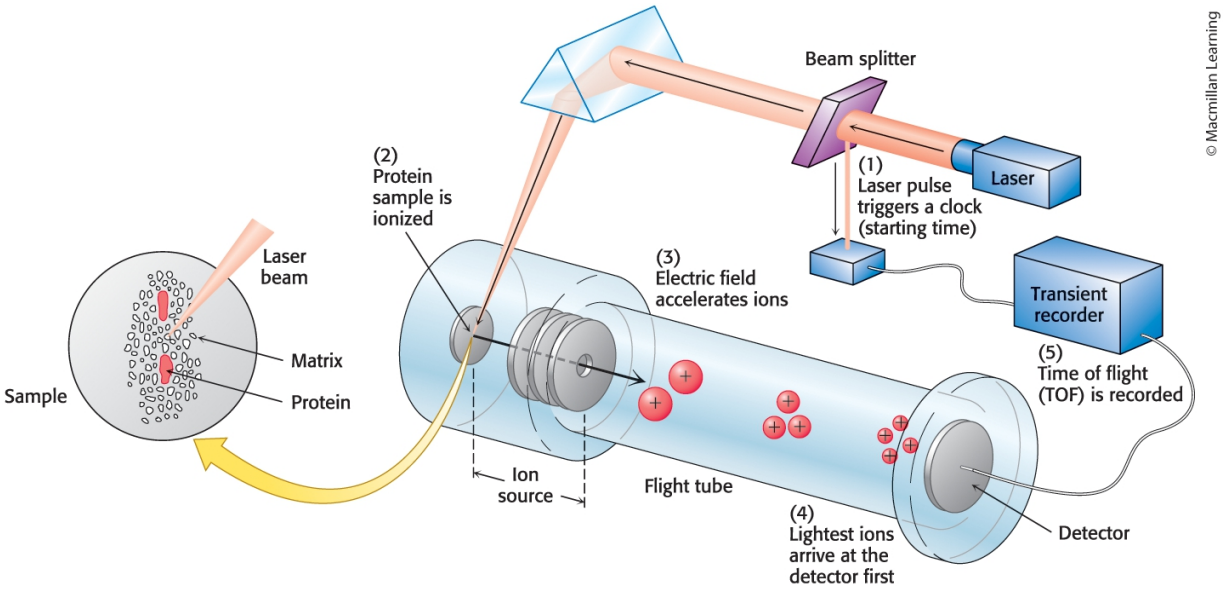
Part (A): At 0 minutes. Yellow fluorescence is shown to be predominantly detected in the cytoplasm while the nucleus appears as a dark circle at the center.

Part (B): At 10 minutes, the intensity of the yellow fluorescence is shown to decrease in the cytoplasm and increase in the nucleus.

Part (C): At 60 minutes, yellow fluorescence is observed only in the nucleus.

Return to FIGURE 4.21. Fluorescence microscopy mediated detection of changes in protein localization inside a cell

Extended description for FIGURE 4.23. Schematic illustration of MALDI-TOF mass spectrometer for measurement of ionized samples based on their mass-to-charge ratio



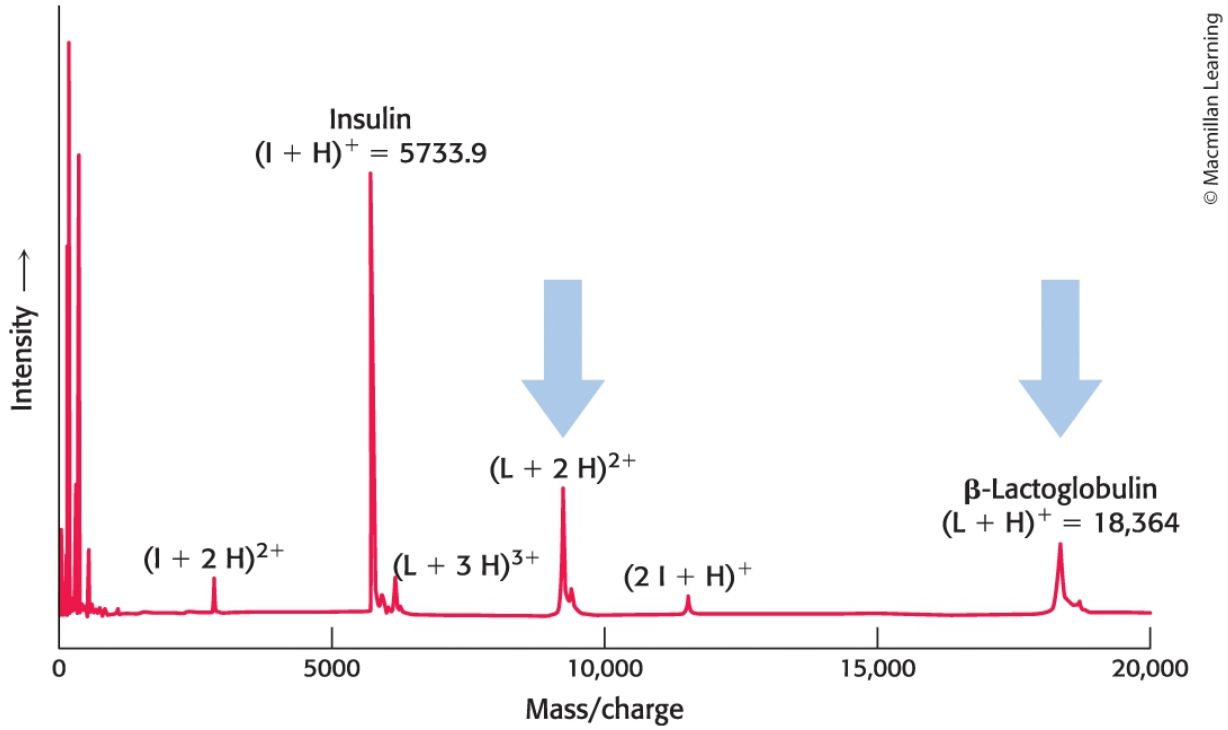
A laser is projected as a rectangular slab labeled "Beam splitter." A laser beam passes through the beam splitter to enter a glass prism in front of the beam splitter. A fraction of the laser pulse is directed down from the beam splitter to a clock that starts time. The laser beam is refracted inside the prism and then it hits a plate in the ionizer where the protein sample is ionized. This ionizing setup consists of a small plate inside a cylindrical enclosure. The ionized sample from this small plate then passes through central apertures of a series of larger discs. This setup of the discs inside the enclosure is labeled "Ion source." The enclosure is connected to a long tube with a smaller diameter labeled "Flight tube." Ions are shown to pass through this tube. Lighter ions pass ahead of the heavier ions to reach the detector at the other end of the flight tube. The detector is connected to a transient recorder which records the

time of flight of the ions (T O F). The recorder is connected to the clock.

A magnified view of the plate where the sample is ionized is shown. The sample is shown to be present on a matrix and the laser beam is shown to hit the sample.

Return to FIGURE 4.23. Schematic illustration of MALDI-TOF mass spectrometer for measurement of ionized samples based on their mass-to-charge ratio

Extended description for FIGURE 4.24. Mass spectrum obtained through MALDI-TOF mass spectrometry



© Macmillan Learning

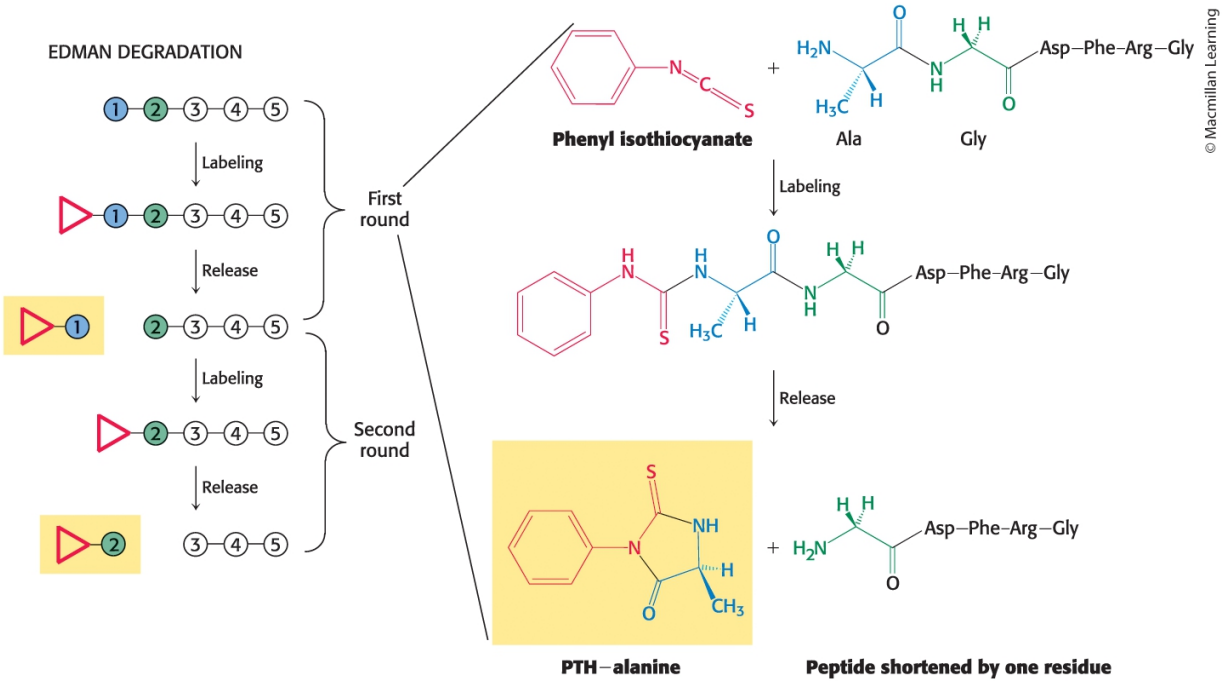
The horizontal axis is labeled Mass over charge and ranges from 0 to 20,000 in increments of 5000 units. The vertical axis is labeled intensity. The following peaks are observed:

1. open parenthesis I plus 2 H close parenthesis superscript 2 plus at 2700 has a short peak
2. open parenthesis I plus 2 H close parenthesis superscript plus equals 5733.9 at 5500 has a very tall peak and is labeled insulin
3. open parenthesis L plus 3 H close parenthesis superscript 3 plus at 6000 has a short peak
4. open parenthesis L plus 2 H close parenthesis superscript 2 plus at 9000 has a relative taller peak and has a bold arrow pointing at it

5. open parenthesis 2 I plus H close parenthesis superscript plus at 12000 has a short peak
6. open parenthesis L plus H close parenthesis superscript plus at 18,500 has a relatively taller peak and is labeled beta-lactoglobulin. It has a bold arrow pointing at it.

Return to FIGURE 4.24. Mass spectrum obtained through MALDI-TOF mass spectrometry

Extended description for FIGURE 4.25. Method of Edman degradation for peptide sequencing



1. Stage 1: A peptide chain is shown to consist of 5 amino acid residues. The first two are labeled in blue and green respectively. An arrow points down to the next stage and is labeled “Labeling.”
2. Stage 2: A red triangle is shown to be connected to the first residue. An arrow points down to the next stage and is labeled “Release.”
3. Stage 3: The red triangle connected to the first amino acid residue is shown to separate from the peptide. An arrow points down to the next stage and is labeled “Labeling.”
4. Stage 4: A red triangle is shown to be connected to the second residue of the shortened peptide. An arrow points down to the next stage and is labeled “Labeling.”
5. Stage 5: The red triangle connected to the second amino acid residue is shown to separate from the peptide.

The steps until stage 3 are labeled “First round” and the steps preceding these are labeled “Second round.”

The steps involved in the first round are shown as two reactions:

The first reactant is Phenyl isothiocyanate which has the following structure: A benzene ring in a horizontal orientation consists of three alternating double bonds between C 1 and C 2, C 3 and C 4, and C 5 and C 6. C 2 is single bonded to N on the right which is double bonded it C on the lower right. C is double bonded to S on the lower right.

The second reactant is the peptide chain with the first two residues being alanine and glycine followed by aspartic acid, phenylalanine, arginine, and glycine. Alanine has the following structure: A central C atom is single bonded to N H 2 on the upper left, single bonded to C H 3 on the lower left, wedge bonded to H on the lower right, and single bonded to a central C atom on the upper right. The central C atom on the upper right is double bonded to O above and single bonded to N on the glycine residue. Glycine has the following structure: A central C atom is single bonded to N H on the lower left, wedge bonded to H on the upper left, dash bonded to h on the upper right, and single bonded to a central C atom on the lower right. The central C atom is double bonded to O below and single bonded to the aspartic acid residue. The reaction arrow is labeled “Labeling.”

The product has the following structure: A benzene ring in a vertical orientation consists of 3 alternating double bonds between C 1 and C 2, C 3 and C 4, and C 5 and C 6. C 2 is single bonded to N H on the upper right which is single bonded to a central C atom below. The central C atom is double bonded to S below and single bonded to N of the alanine residue of the peptide.

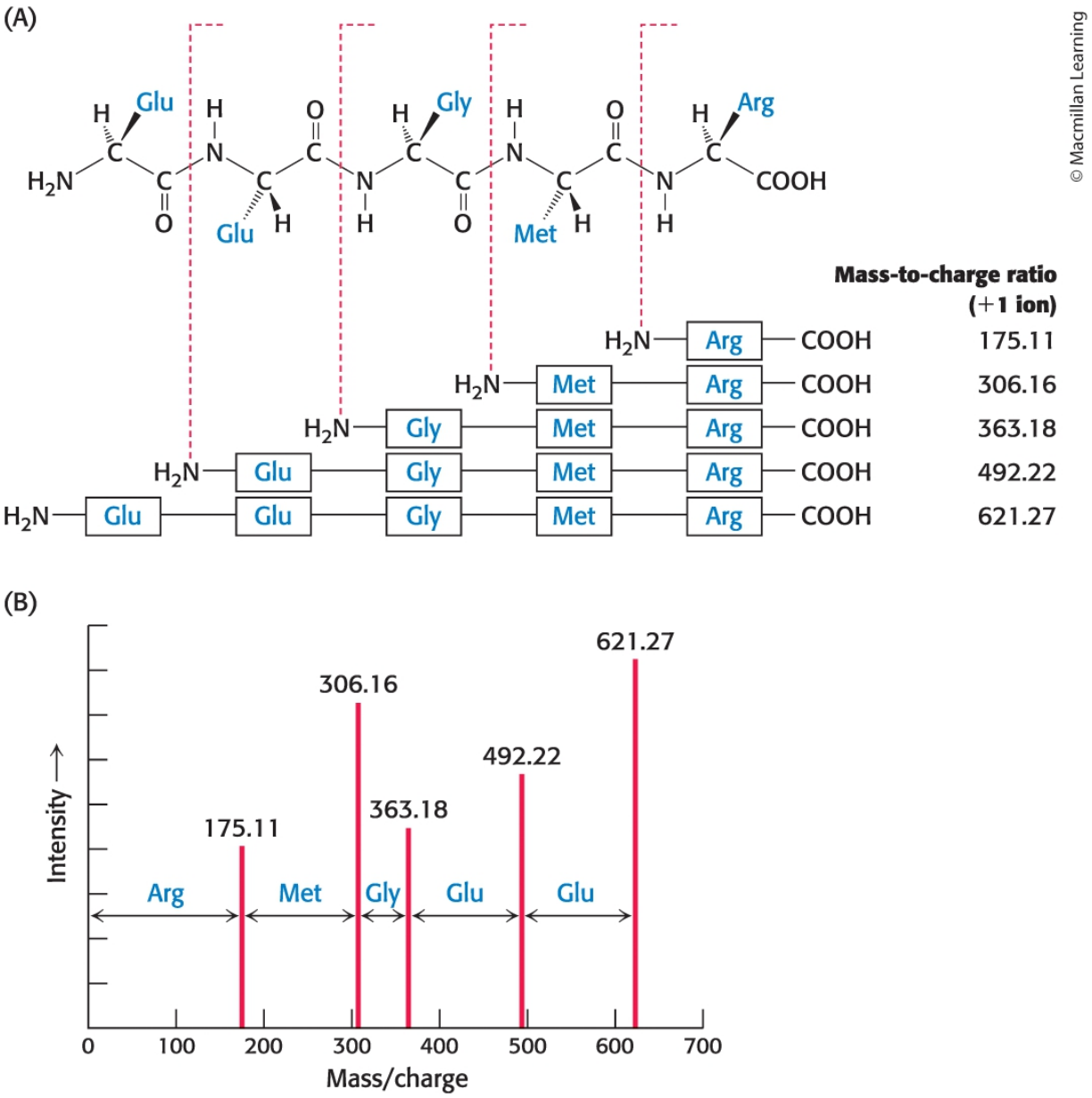
The reaction arrow from this product is labeled “release.”

The first product has the following structure: A benzene ring in a horizontal orientation consists of three alternating double bonds between C 1 and C 2, C 3 and C 4, and C 5 and C 6. C 2 is single bonded to the first N of a 5-membered pentagonal ring in a vertical orientation. The pentagonal ring consists of 2 N and 3 C atoms. the first N atom occupies the first position which is the rightmost vertex. The second N bound to H occupies the third position which is the leftmost vertex. C 1 occupies the topmost vertex and is double bonded to S. C 2 is dash bonded to H on the right and wedge bonded to C H 3 on the lower right. C 3 is double bonded to O on the lower left. This product is labeled P T H alanine.

The second product is the shortened peptide consisting of glycine, aspartic acid, phenylalanine, arginine, and glycine.

Return to FIGURE 4.25. Method of Edman degradation for peptide sequencing

Extended description for FIGURE 4.26. Peptide sequencing with the help of tandem mass spectrometry



© Macmillan Learning

Part (A): A peptide is shown to have the following sequence from the amino to the carboxy terminal: Glutamic acid, Glutamic acid,

Glycine, Methionine, Arginine.

The mass to charge ratio (plus 1 ion) for the fragmented peptide is as follows:

Arginine: 175.11
Methionine, Arginine: 306.16
Glycine, Methionine, Arginine: 363.18
Glutamic acid, Glycine, Methionine, Arginine: 492.22
Glutamic acid, Glutamic acid, Glycine, Methionine, Arginine: 621.27

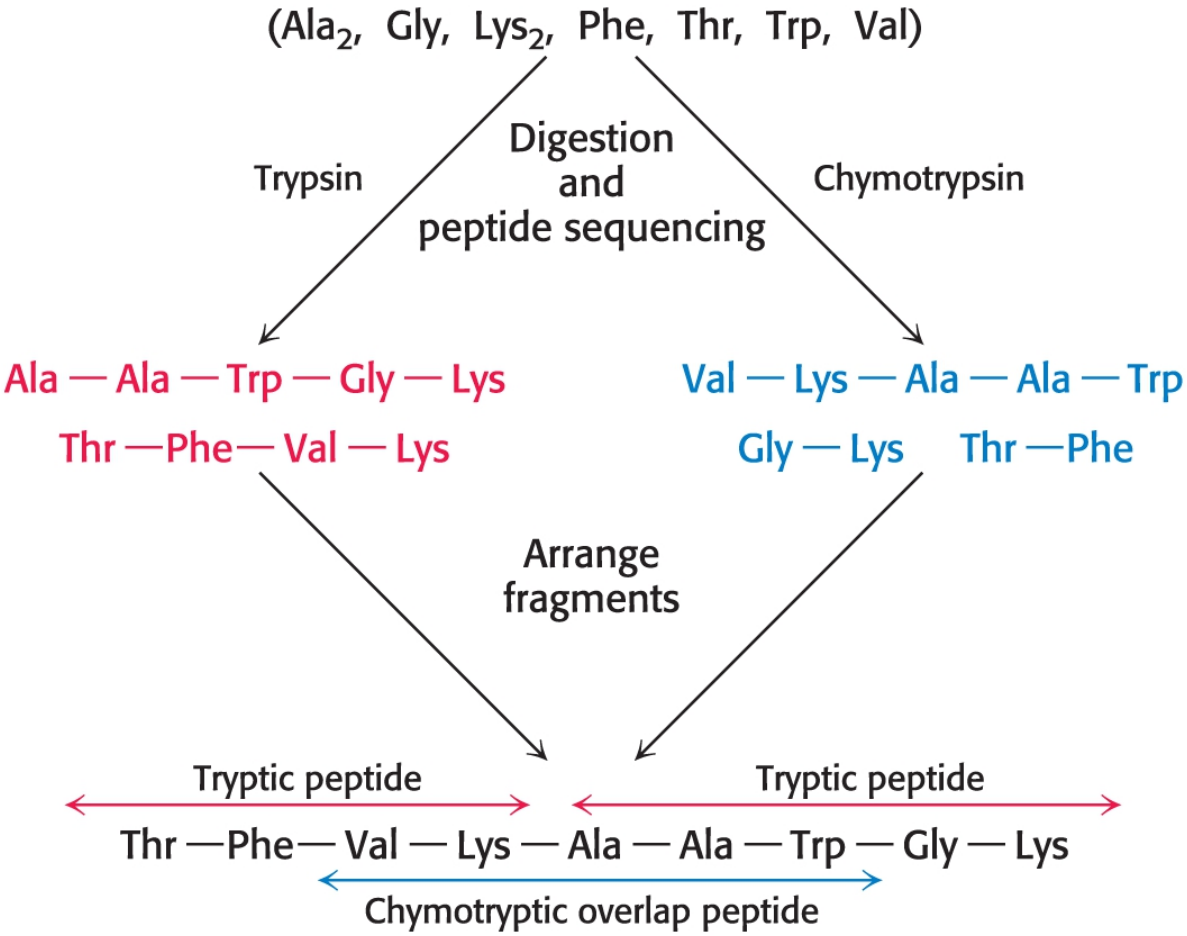
Part (B): A mass spectrum is shown. The horizontal axis is labeled mass over charge and ranges from 0 to 700 in increments of 100 units. The vertical axis is labeled intensity. The peaks are observed as follows:

The first peak (175.11) is at 185. The horizontal distance between the vertical axis is this peak is labeled Arginine.
The second peak (306.16) is at 305. The horizontal distance between the first peak is this peak is labeled Methionine.
The third peak (363.18) is at 370. The horizontal distance between the second peak is this peak is labeled Glycine.
The fourth peak (492.22) is at nearly 500. The horizontal distance between the third peak is this peak is labeled Glutamic acid.
The fifth peak (621.27) is at 615. The horizontal distance between the first peak is this peak is labeled Glutamic acid.

The peaks are of varying heights.

Return to FIGURE 4.26. Peptide sequencing with the help of tandem mass spectrometry

Extended description for FIGURE 4.27. Use of overlapping peptides to establish the order of sequenced peptides



© Macmillan Learning

A peptide sequence is as follows: Alanine subscript 2, Glycine, Lysine subscript 2, Phenylalanine, Threonine, Tryptophan, Valine

The peptide is digested and sequenced.

Trypsin digestion yields the following two sets of peptides:

Alanine, Alanine, Tryptophan, Glycine, Lysine

Threonine, Phenylalanine, Valine, Lysine

Chymotrypsin digestion yields the following three sets of peptides:

Valine, Lysine, Alanine, Alanine, Tryptophan
Glycine, Lysine
Threonine, Phenylalanine

After arranging the fragments obtained by both the digestions, the following sequence is obtained:

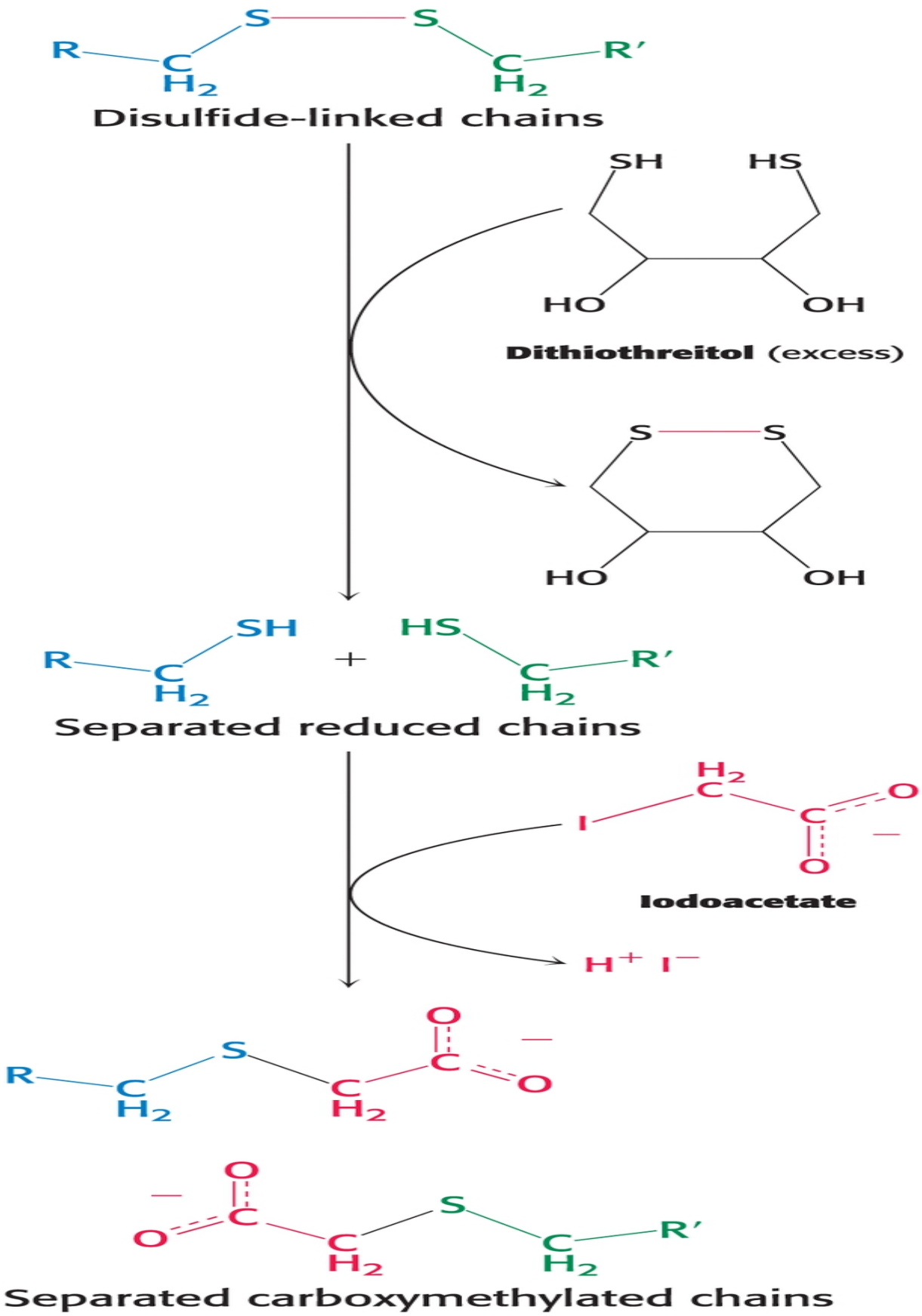
Threonine, Phenylalanine, Valine, Lysine, Alanine, Alanine, Tryptophan, Glycine, Lysine

Residue 1 to 4 and 5 to 9 are labeled tryptic peptide. Residue 3 to 7 are labeled chymotryptic overlap peptide.

Return to FIGURE 4.27. Use of overlapping peptides to establish the order of sequenced peptides

Extended description for FIGURE 4.28. Use of reduction and alkylation reactions for the separation of disulfide-

linked polypeptides before sequencing


Disulfide-linked chains
Dithiothreitol (excess)
Separated reduced chains
Iodoacetate
Separated carboxymethylated chains

The first reactant is disulphide-linked chains which has the following structure: A central C atom bound to H 2 is single bonded to R on the left and single bonded to s on the upper right. S is single bonded to S on the right. The second S is single bonded to a C bound to H 2 on the lower right which is single bonded to R dash on the right. The disulphide bond is highlighted in red. The group to the left of the disulphide link is shown in blue and the group to the right is shown in green.

The formation of disulphide link in dithiothreitol (excess) is shown next to the reaction arrow. The structure of dithiothreitol is as follows: A 4-carbon alkane chain is depicted as a line structure using 3 zigzag lines such that it forms an U-shape. C 1 and C 4 are each single bonded to S H above. C 2 is single bonded to O H on the lower left. C 3 is single bonded to O H on the lower right. The product shows a single bond representing the disulphide linkage between the two S atoms.

The reaction leads to the formation of separated reduced chains.

The first product has the following structure: A central C atom bound to H 2 is single bonded to R on the upper left and S H on the upper right. This is shown in blue.

The second product has the following structure: A central C atom bound to H 2 is single bonded to S H on the upper left and single bonded to R dash on the upper right. This is shown in green.

A reaction arrow from these products leads to the separated carboxymethylated chains. The conversion of iodoacetate to H I is shown next to the reaction arrow. The structure of iodoacetate is as follows: I is single bonded to C bound to H 2 on the upper right which is single bonded to C on the lower right. C is partially double

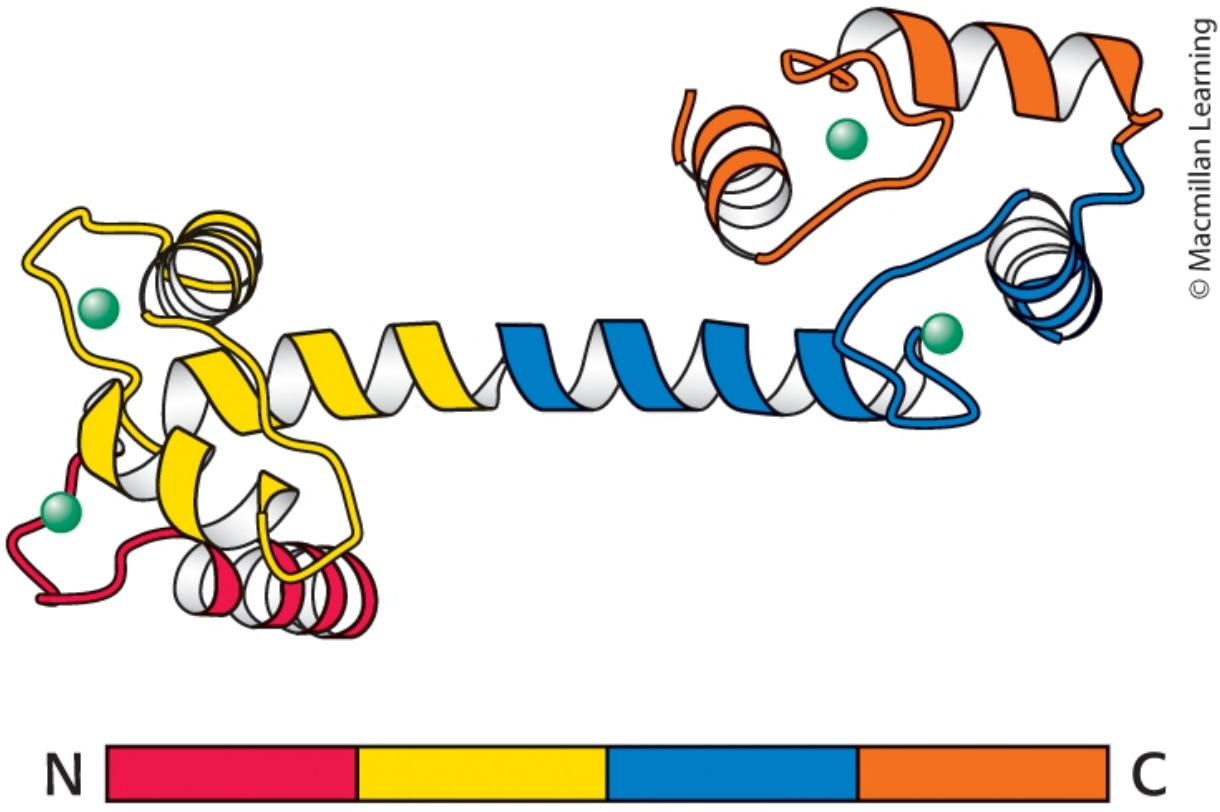
bonded to O below and partially double bonded to O on the upper right. The C O O group carries a negative charge. The converted product is H superscript plus I superscript minus. The components of this conversion are shown in red.

The first product of the alkylation reaction has the following structure: A central C atom bound to H 2 is single bonded to R on the upper left and S on the upper right. This is shown in blue. S is single bonded to C bound to H 2 on the lower right which is single bonded to C on the upper right. C is partially double bonded to O above and partially double bonded to O on the lower right. The C O O group carries a negative charge. This is shown in red.

The second product of the alkylation reaction has the following structure: A central C atom bound to H 2 is single bonded to S on the upper left and single bonded to R dash on the upper right. This is shown in green. S is single bonded to C bound to H 2 on the lower left which is single bonded to c on the upper left. C is partially double bonded to O above and partially double bonded to O on the lower left. The C O O group carries a negative charge. This is shown in green.

Return to FIGURE 4.28. Use of reduction and alkylation reactions for the separation of disulfide-linked polypeptides before sequencing

Extended description for FIGURE 4.29. Ribbon diagram and units of calmodulin protein

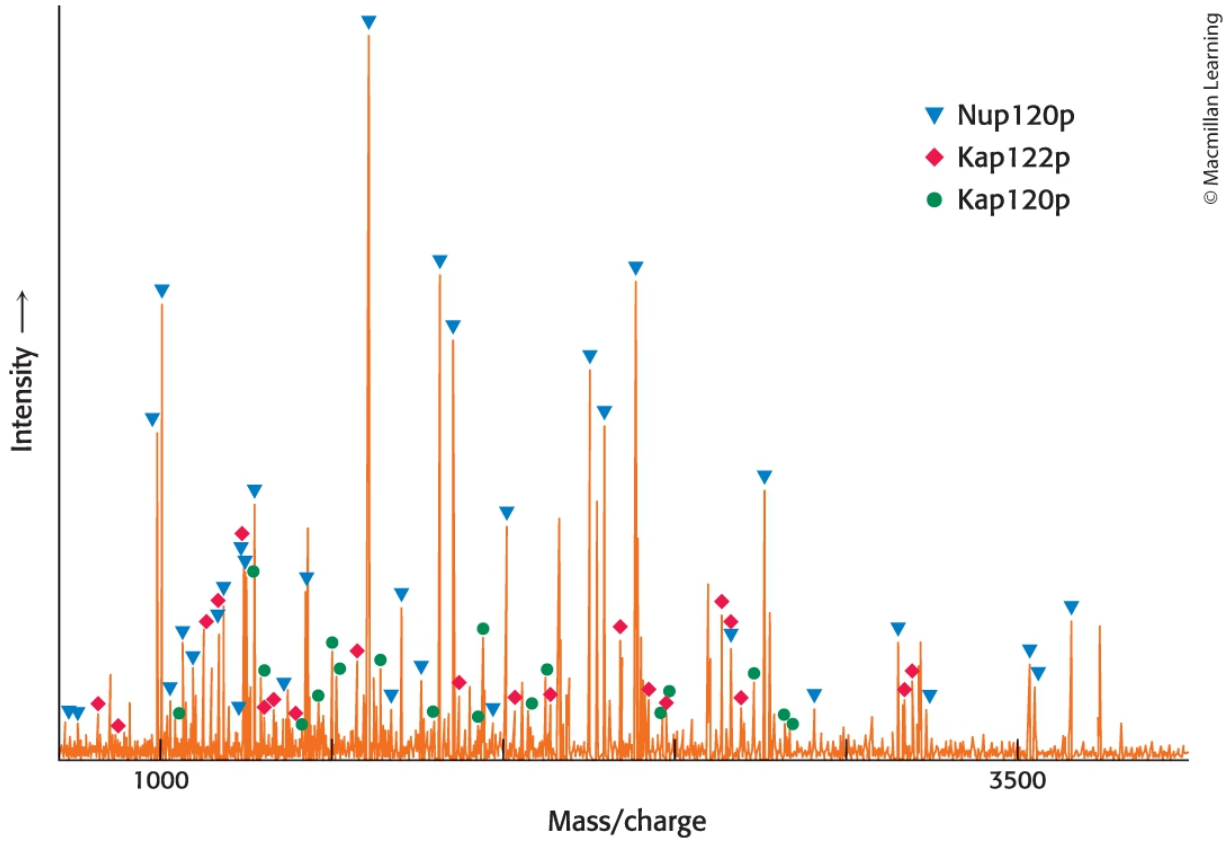


© Macmillan Learning

Starting from the N to C terminal, the units are colored red, yellow, blue, and orange. Each unit consists of a alpha helix connected to next unit by short loops. Small green spheres bound to each unit represent calcium ions.

Return to FIGURE 4.29. Ribbon diagram and units of calmodulin protein

Extended description for FIGURE 4.30. Mass spectrum showing peptide mass fingerprinting



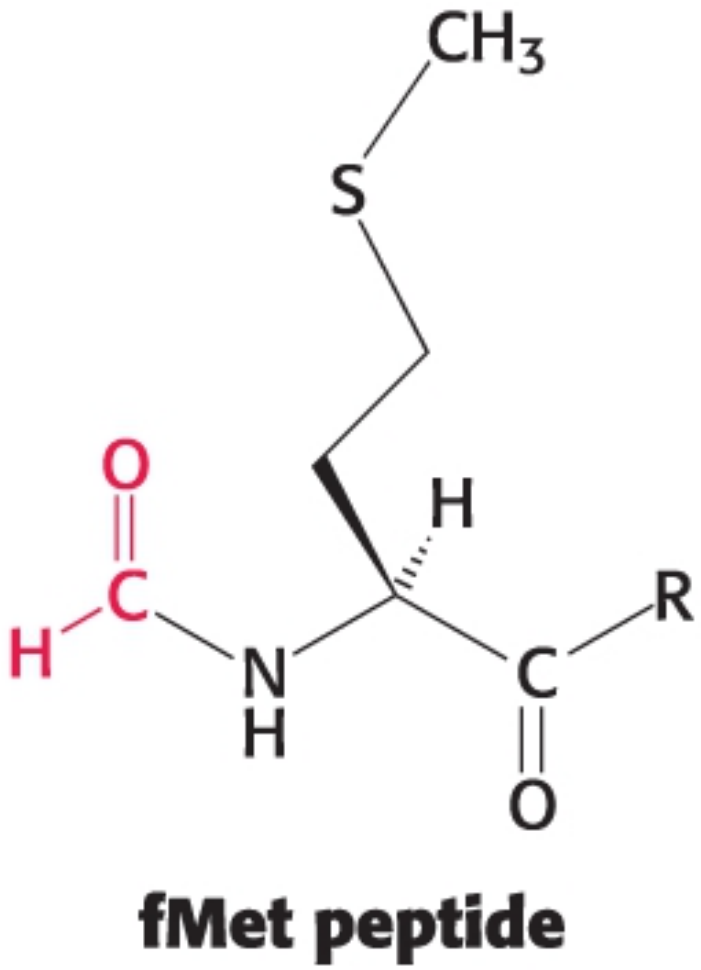
The horizontal axis is labeled mass over charge. The vertical axis is labeled Intensity. Several peaks of varying heights are seen in the spectrum. The following are indicated:

Blue triangle: Nup 120 p
Red diamond: Kap 122 p
Green circle: Kap 120 p

The peaks with the blue triangles are significantly taller than the rest. The peaks for the other two proteins are low lying.

Return to FIGURE 4.30. Mass spectrum showing peptide mass fingerprinting

Extended description for Chemical structure of f Met peptide



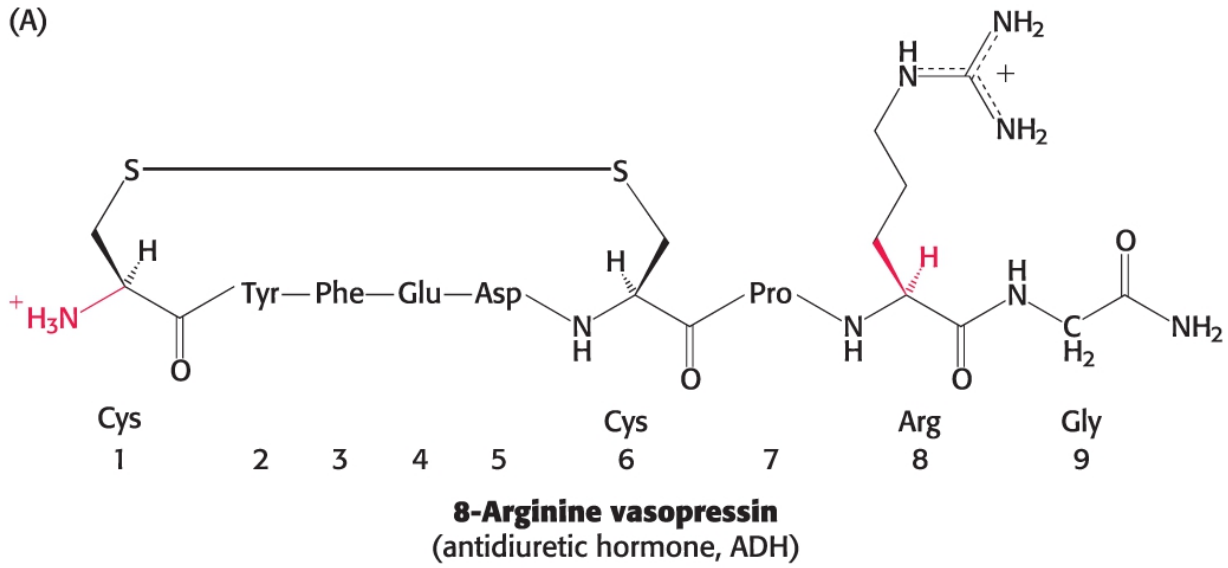
fMet peptide

The structure is as follows: A C atom is dash bonded to H on the upper right, single bonded to C on the lower right, single bonded to N H on the lower left, and wedge bonded to C 1 of a 3-membered heteronuclear alkane chain above. The alkane chain consists of 2 C and 1 S atoms and is depicted by a line structure using 2 zigzag lines. The S atom occupies the third position and is single bonded to C H 3 on the upper right. The C on the lower right is single bonded to R on the upper right and double bonded to O below. The N on the lower

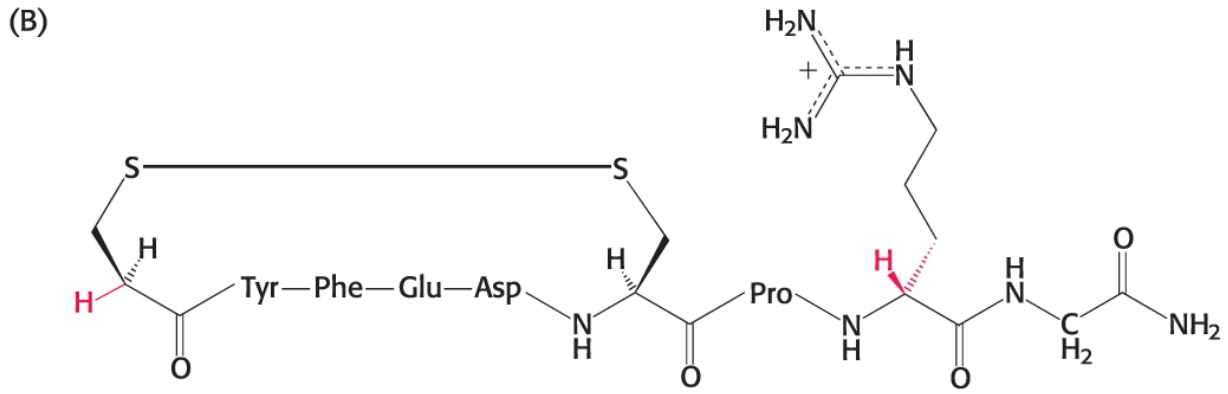
left is single bonded to a C atom on the upper left which is single bonded to H on the lower left and double bonded to O above. The C O H group is highlighted in red.

Return to Chemical structure of f Met peptide

Extended description for FIGURE 4.31. Chemical structure of 8-arginine vasopressin and 1-Desamino-8-D-arginine vasopressin



8-Arginine vasopressin
(antidiuretic hormone, ADH)



1-Desamino-8-D-arginine vasopressin
(Desmopressin)

The structure of antidiuretic hormone (A D H), 8-Arginine vasopressin is as follows: It consists of 9 amino acid residues- Cysteine, Tyrosine, Phenylalanine, Glutamic acid, Aspartic acid, Cysteine, Proline, Arginine, Glycine. The structure of cysteine is as follows: a central C atom is single bonded to C on the lower right,

single bonded to N H 3 superscript plus on the lower left, wedge bonded to C H 2 on the upper left, and dash bonded to H on the upper right. The C atom on the lower right is double bonded to O below and single bonded to Tyrosine at the second position. C H 2 is single bonded to S on the upper right. This S atom is single bonded to S of the cysteine residue at the sixth position. Cysteine has the following structure: a central C atom is single bonded to C on the lower right, single bonded to N H on the lower left, wedge bonded to C H 2 on the upper right, and dash bonded to H on the upper left. C on the lower right is double bonded to O below and single bonded to proline at the seventh position. C H 2 is single bonded to S on the upper left which is bonded to S of cysteine at the first position. Arginine at the eighth position has the following structure: A central C atom is single bonded to C on the lower right, single bonded to N H on the lower left, wedge bonded to C H 2 on the upper left, and dash bonded to H on the upper right. C on the lower right is double bonded to O below and single bonded to N H of glycine at the ninth position. C H 2 on the upper left is single bonded to C 1 of 3-carbon alkane chain depicted as a line structure using two zigzag lines. C 3 of the alkane chain is single bonded to N bound to H on the upper right. N is partially double bonded to C on the right which is partially double bonded to N H 2 on the upper right and partially double bonded to N H 2 on the lower right. This group carries a positive charge. Glycine at the ninth position has the following structure: A central C H 2 group is single bonded to N H on the upper left and single bonded to C on the upper right. C on the upper right is single bonded to N H 2 on the lower right and double bonded to O above.

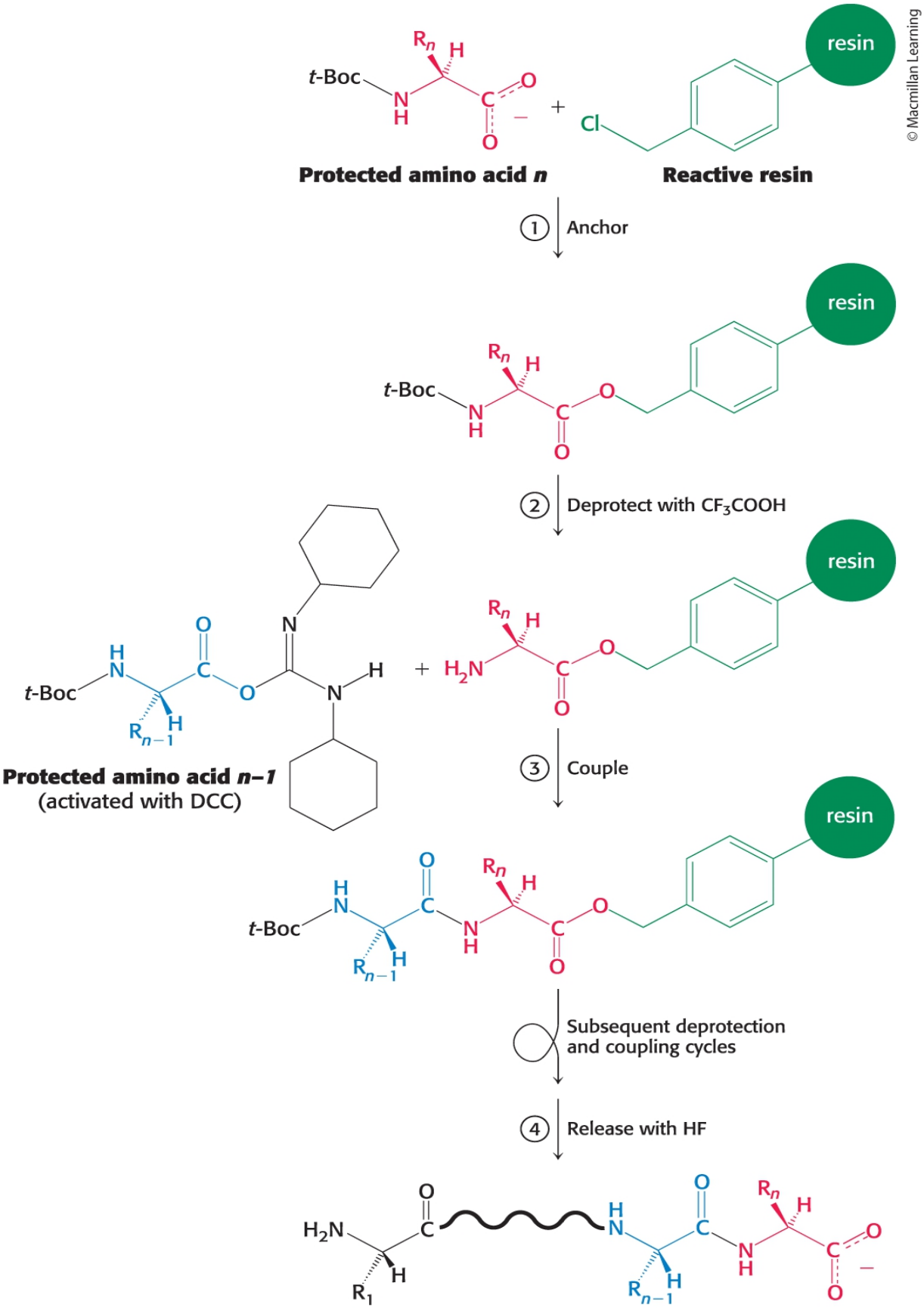
The structure of 1-Desamino-8-D-Arginine vasopressin, Desmopressin, is as follows: It has the same structure at A D H except for the position of the side chain of arginine at the eight position. The central C atom of arginine is wedge bonded to H on the upper left and dash bonded to C 1 of 3-carbon alkane chain

depicted as a line structure using two zigzag lines. C 3 of the alkane chain is single bonded to N bound to H on the upper left. N is partially double bonded to C on the left which is partially double bonded to N H 2 on the upper left and partially double bonded to N H 2 on the lower left. This group carries a positive charge.

Return to FIGURE 4.31. Chemical structure of 8-arginine vasopressin and 1-Desamino-8-D-arginine vasopressin

Extended description for FIGURE 4.32. Steps of solid-phase peptide synthesis involving repeated coupling

and deprotection



© Macmillan Learning

Step 1: Anchor. The first reactant is Protected amino acid n, which has the following structure: A central C atom is single bonded to N H on the lower left, single bonded to C on the lower right, dash bonded to H on the upper right, and wedge bonded to R n on the upper left. N H is single bonded to t-B o c on the upper left. The C on the lower right is partially double bonded to O on the upper right and partially double bonded to O below. The C O O group carries a negative charge. The second reactant is Reactive resin, which has the following structure: A benzene ring in a vertical orientation consists of 3 alternating double bonds between C 1 and C 2, C 3 and C 4, and C 5 and C 6. C 2 is single bonded to a resin. C 5 is single bonded to C H 2 which is single bonded to C l on the upper left. The product has the following structure: A central C atom is single bonded to N H on the lower left, single bonded to C on the lower right, dash bonded to H on the upper right, and wedge bonded to R n on the upper left. N H is single bonded to t-B o c on the upper left. The C on the lower right is single bonded to O on the upper right and double bonded to O below. The O on the upper right is single bonded to C H 2 on the lower right. C H 2 is single bonded to C 5 of a benzene ring in a vertical orientation. It consists of 3 alternating double bonds between C 1 and C 2, C 3 and C 4, and C 5 and C 6. C 2 is single bonded to a resin.

Step 2: Deprotect with C F 3 C O O H. The product of step 1 is the reactant here. The first product is Protected amino acid m minus 1 (activated with D C C), which has the following structure: A central C atom is single bonded to N H on the upper left, single bonded to C on the upper right, wedge bonded to H on the lower right, and dash bonded to R n minus 1 on the lower left. N H is single bonded to t-B o c on the lower left. C on the upper right is double bonded to O above and single bonded to O on the lower right. The O on the lower right is single bonded to C on the upper right which is double bonded to N above and single bonded to N on the lower right. The N above is single bonded to C 3 of a 6-carbon hexagonal ring in a

horizontal orientation. The N on the lower right is single bonded to H on the upper right and single bonded to C 1 of a 6-Carbon hexagonal ring below. The second product has the following structure: A central C atom is single bonded to N H 2 on the lower left, single bonded to C on the lower right, dash bonded to H on the upper right, and wedge bonded to R n on the upper left. The C on the lower right is single bonded to O on the upper right and double bonded to O below. The O on the upper right is single bonded to C H 2 on the lower right. C H 2 is single bonded to C 5 of a benzene ring in a vertical orientation. It consists of 3 alternating double bonds between C 1 and C 2, C 3 and C 4, and C 5 and C 6. C 2 is single bonded to a resin.

Step 3: Couple. The products of step 2 are the reactants of step 3. The product has the following structure: A central C atom is single bonded to N H on the upper left, single bonded to C on the upper right, wedge bonded to H on the lower right, and dash bonded to R n minus 1 on the lower left. N H is single bonded to t-B o c on the lower left. C on the upper right is double bonded to O above and single bonded to N H on the lower right. N H is single bonded to a central C atom on the upper right. This C atom is wedge bonded to R n on the upper left, dash bonded to H on the upper right, and single bonded to C on the lower right. The C on the lower right is single bonded to O on the upper right and double bonded to O below. The O on the upper right is single bonded to C H 2 on the lower right. C H 2 is single bonded to C 5 of a benzene ring in a vertical orientation. It consists of 3 alternating double bonds between C 1 and C 2, C 3 and C 4, and C 5 and C 6. C 2 is single bonded to a resin.

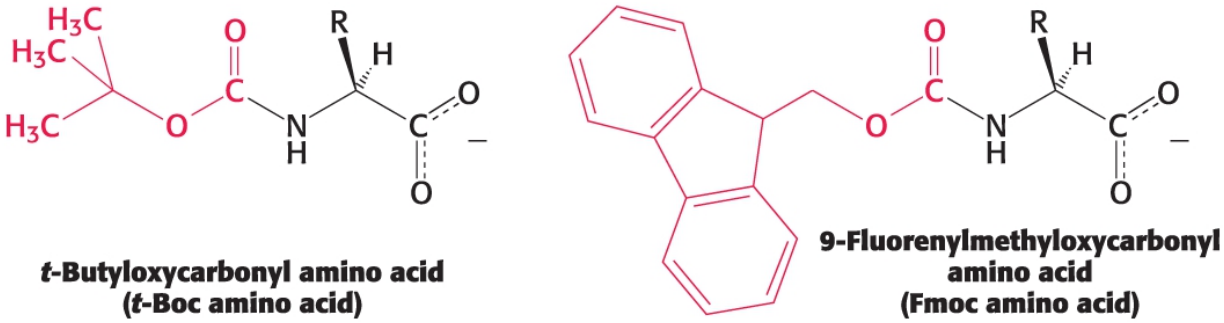
This product undergoes subsequent deprotection and coupling cycles.

Step 4: Release with H F. The product has the following structure: A central C atom is single bonded to N H 2 on the upper left, dash

bonded to R 1 on the lower left, wedge bonded to H on the lower right, and single bonded to C on the upper right. The C on the upper right is double bonded to O above and linked to N H of a peptide by a wavy bond. The second last amino acid has a central C atom single bonded to N H on the upper left, dash bonded to R n minus 1 on the lower left, wedge bonded to H on the lower right, and single bonded to C on the upper right. The C on the upper right is double bonded to O above and single bonded to N H of the last amino acid. The last amino acid has a central C atom single bonded to N H on the lower left, wedge bonded to R n on the upper left, dash bonded to H on the upper right, and single bonded to C on the lower right. The C on the lower right is partially double bonded to O on the upper right and partially double bonded to O below. This C O O group carries a negative charge.

Return to FIGURE 4.32. Steps of solid-phase peptide synthesis involving repeated coupling and deprotection

Extended description for Chemical structures of t-Butyloxycarbonyl amino acid and 9-Fluorenylmethyloxycarbonyl



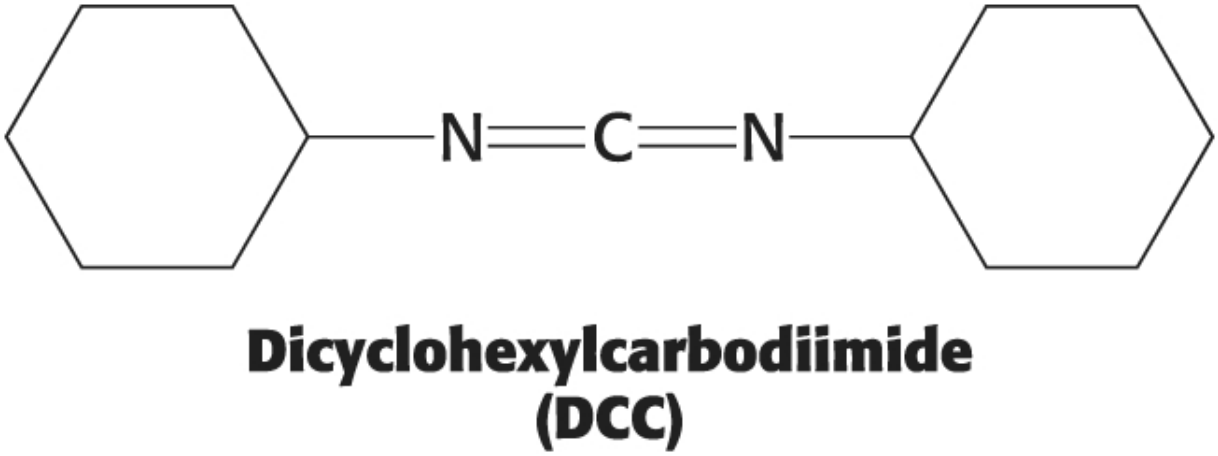
t-Butyloxycarbonyl amino acid has the following structure: A central C atom is single bonded to N bound to H on the lower left, single bonded to C on the lower right, dash bonded to H on the upper right, dash bonded to R on the upper left. The C on the lower right is partially double bonded to O on the upper right and partially double bonded to O below. The C O O group carries a negative charge. N is single bonded to C on the upper left which is double bonded to O above and single bonded to O on the lower left. The O on the lower left is single bonded to a central c atom on the upper left. The central C atom is single bonded to C H 3 on the lower left, single bonded to C H 3 on the upper left, and single bonded to C H 3 above. This entire group bonded to The amino acid is shown in red.

9-Fluorenylmethyloxycarbonyl has the following structure: A central C atom is single bonded to N bound to H on the lower left, single bonded to C on the lower right, dash bonded to H on the upper right, dash bonded to R on the upper left. The C on the lower right is partially double bonded to O on the upper right and partially double bonded to O below. The C O O group carries a negative charge. N is single bonded to C on the upper left which is double bonded to O

above and single bonded to O on the lower left. The O on the lower left is single bonded to a C H 2 group on the upper left. C H 2 is single bonded to C 2 of a 5-membered pentagonal ring in a vertical orientation. The ring consists of 5-C atoms. The pentagonal ring is fused to a benzene ring in a vertical orientation such that C 1 and C 5 of the pentagonal ring are C 3 and C 4 of the benzene ring, respectively. The benzene ring consists of 3 alternating double bonded between C 1 and C 2, C 3 and C 4, and C 5 and C 6. The pentagonal ring is fused to a second benzene ring in a horizontal orientation such that C 3 and C 4 of the pentagonal ring are C 6 and C 5 of the benzene ring, respectively. The benzene ring consists of 3 alternating double bonded between C 1 and C 2, C 3 and C 4, and C 5 and C 6. The entire group bonded to the amino acid is shown in red.

Return to Chemical structures of t-Butyloxycarbonyl amino acid and 9-Fluorenylmethyloxycarbonyl

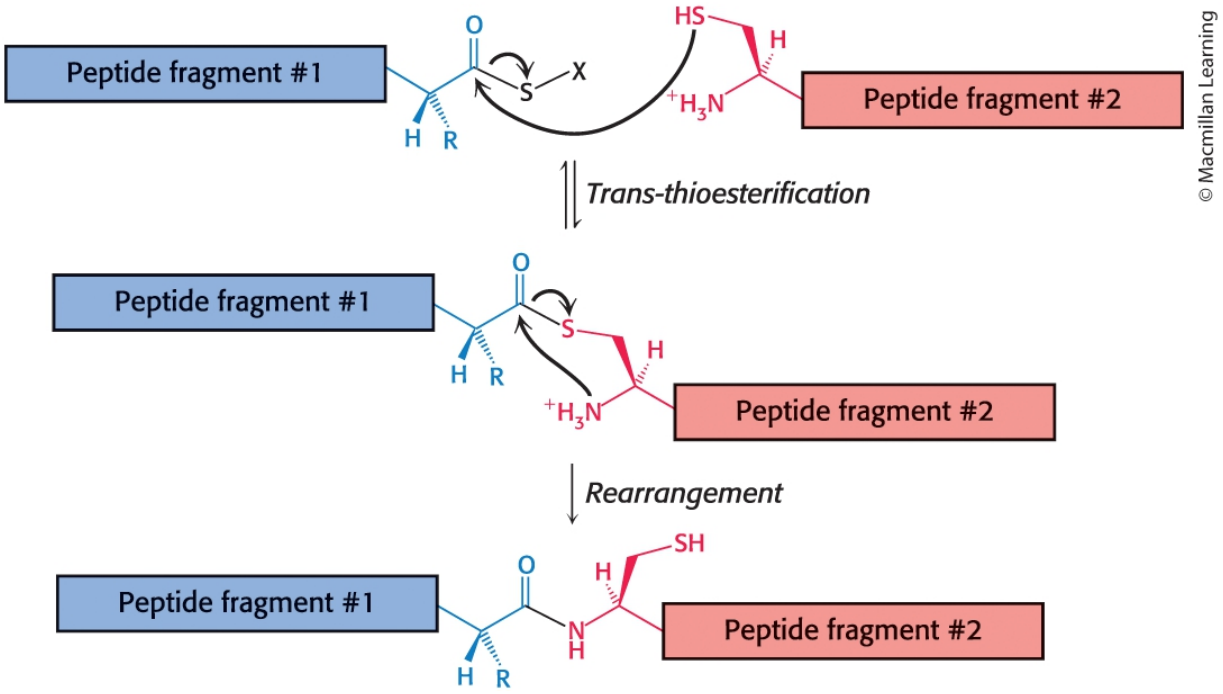
Extended description for Chemical structure of dicyclohexylcarbodiimide



Dicyclohexylcarbodiimide, D C C, has the following structure: C 1 of a 6-carbon hexagonal ring in a horizontal orientation is single bonded to N. N is double bonded to C on the right which is double bonded to N on the right. The second N is single bonded to C 4 of a 6-Carbon hexagonal ring in a horizontal orientation.

Return to Chemical structure of dicyclohexylcarbodiimide

Extended description for FIGURE 4.33. Native chemical ligation reaction for linking two synthetic peptides



© Macmillan Learning

The first reactant is Peptide fragment number 1 which has the following structure: A central C atom is single bonded to C on the upper right, dash bonded to R on the lower right, wedge bonded to H on the lower left, and has a single bond on the upper left. The C on the upper right is double bonded to O above and single bonded to S on the lower right which is single bonded to X on the upper right. The second reactant is Peptide fragment number 2 which has the following structure: A central C atom is single bonded to N H 3 superscript plus on the lower left, wedge bonded to C H 2 on the upper left, dash bonded to H on the upper right, and has a single bon on the lower right. The C H 2 on the upper right is single bonded to S H on the left.

An arrow points from S H of peptide fragment number 2 to the C double bonded to O on peptide fragment number 1. Another arrow points from the C double bonded to O on peptide fragment number 1 to S of the same fragment.

A reversible reaction arrow from these reactants is labeled Trans-thioesterification.

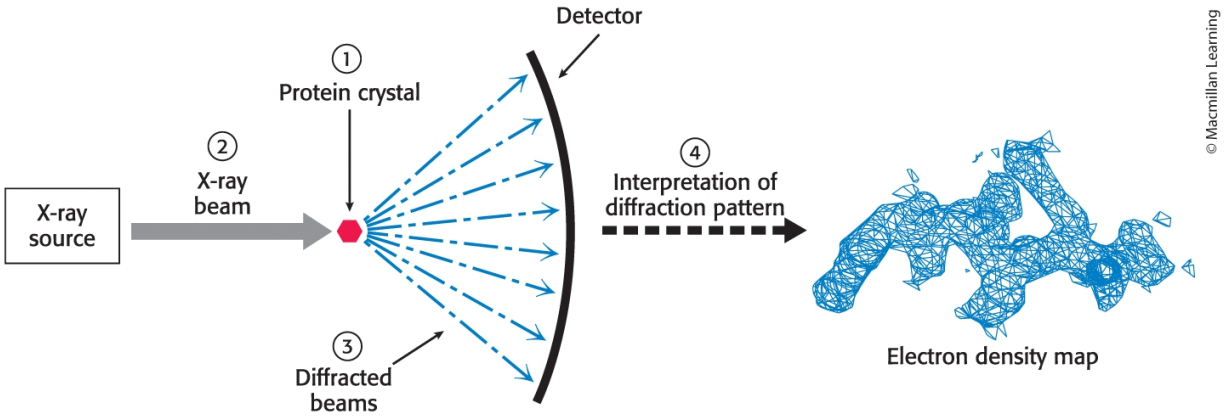
In the product, S of the first fragment is single bonded to C H 2 of the second fragment.

A reaction arrow from this product is labeled Rearrangement.

In the product of rearrangement, the C double bonded to O of the first fragments is single bonded to N H of the second fragment. In the second fragment, the central C atom is dash bonded to H on the upper left and wedge bonded to C H 2 on the upper right which is single bonded to S H on the right.

Return to FIGURE 4.33. Native chemical ligation reaction for linking two synthetic peptides

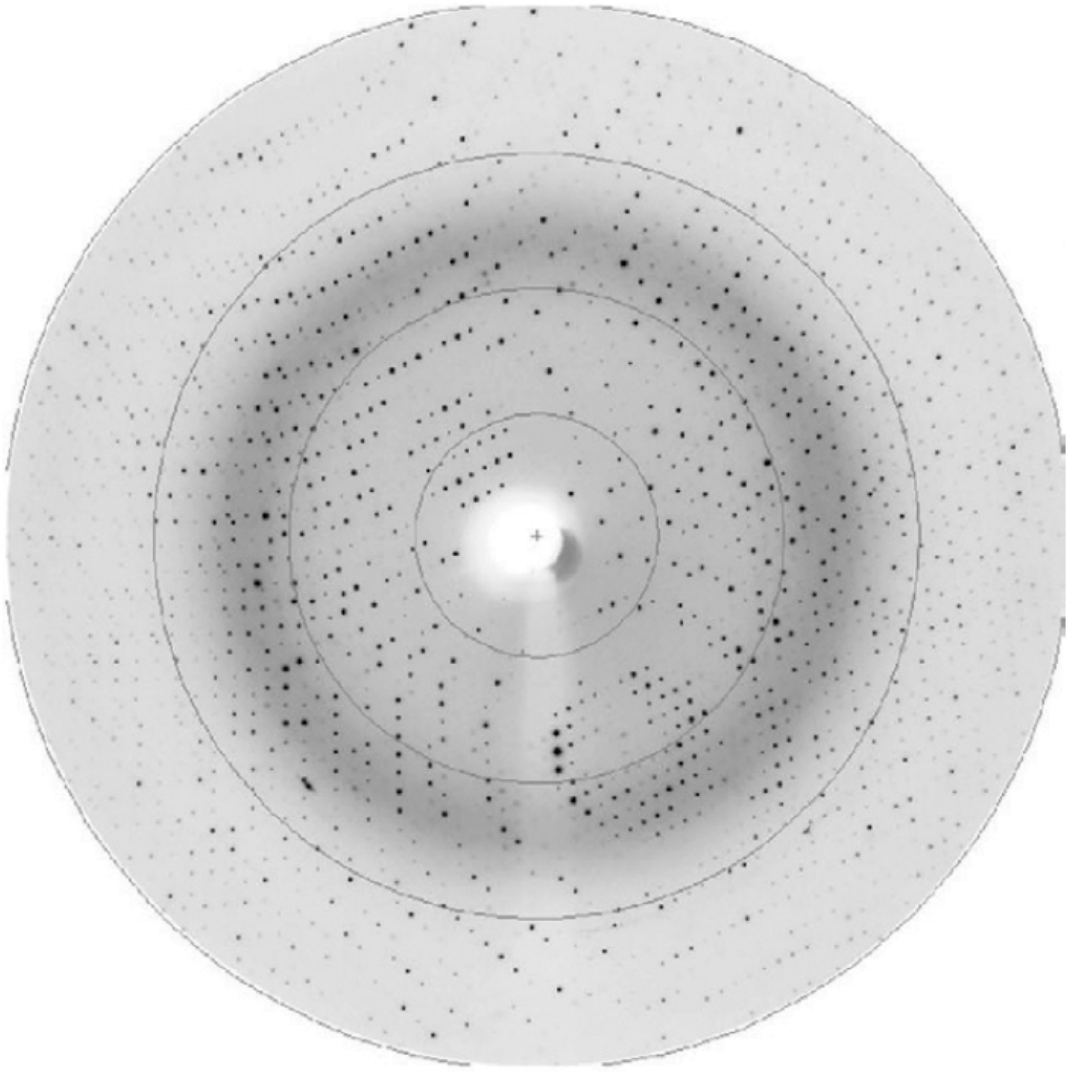
Extended description for FIGURE 4.34. Schematic illustration of the fundamental steps of x-ray crystallography experiment



An X-ray beam from an X-ray source is shown to hit a protein crystal represented by a red hexagon. Diffracted beam from the protein crystal are shown to hit an inverted C-shaped (concave) detector. A dashed arrow from the detector is labeled interpretation of diffraction pattern. The arrow points at the electron density map of the protein. It is a three-dimensional image which is represented by a mesh-like cage, which mimics the structure of the protein.

Return to FIGURE 4.34. Schematic illustration of the fundamental steps of x-ray crystallography experiment

Extended description for FIGURE 4.35. X-ray diffraction pattern of a protein crystal

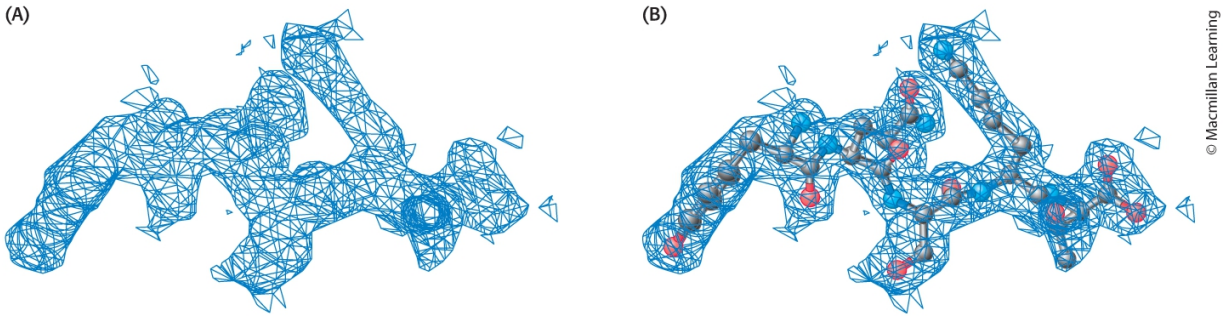


Credit: Reproduced with permission of the International Union of Crystallography, from Ellis et al., Resolution improvement from `in situ annealing' of copper nitrite reductase crystals, *Acta Cryst.* D58: 456–8, 2002, Fig.1B. © 2002 IUCr (https://journals.iucr.org/). https://doi.org/10.1107/S0907444902000136

It shows concentric rings of varying darkness. A dark gray ring is present in the middle. Several spots are seen on this surface and are more concentrated near the dark gray circle.

Return to FIGURE 4.35. X-ray diffraction pattern of a protein crystal

Extended description for FIGURE 4.36. Electron density map of a protein to determine position of atoms in the crystallized protein

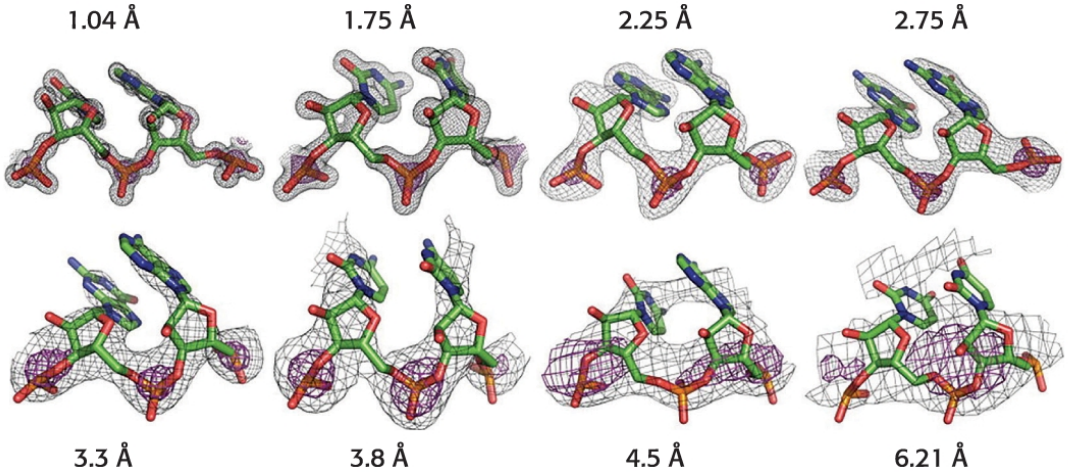


Part (A): It is a three-dimensional image which is represented by a mesh-like cage, which mimics the structure of the protein.

Part (B): The atoms of the protein are placed within the cage.

Return to FIGURE 4.36. Electron density map of a protein to determine position of atoms in the crystallized protein

Extended description for FIGURE 4.37. Electron density map of a protein at different resolutions



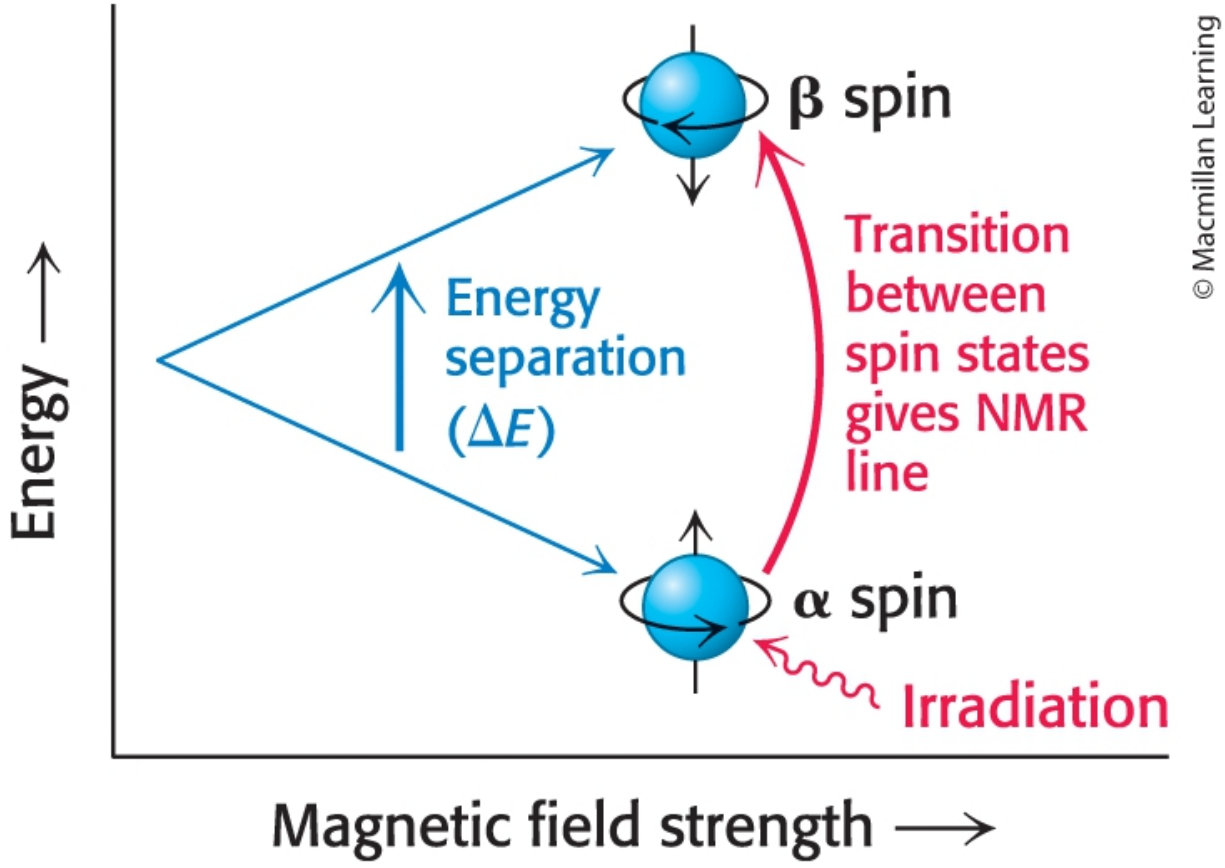
Credit: Kevin S Keating, Anna Marie Pyle, "Semiautomated model building for RNA crystallography using a directed rotameric approach," Figures 1B–1I from https://www.pnas.org/content/107/18/8177 *Proc. Natl. Acad. Sci. U.S.A.* 2010 May 4; 107(18): 8177–8182. doi: 10.1073/pnas.0911888107.

The electron density maps are shown for the following resolutions: 1.04 Angstrom, 1.75 Angstrom, 2.25 Angstrom, 2.75 Angstrom, 3.3 Angstrom, 3.8 Angstrom, 4.5 Angstrom, and 6.21 Angstrom.

The protein is roughly M-shaped. The electron-density map is shown to be more diffused at lower resolutions. The electron-density maps are more defined at higher resolutions.

Return to FIGURE 4.37. Electron density map of a protein at different resolutions

Extended description for FIGURE 4.38. Graph depicting different spin states of a nucleus in N M R spectroscopy



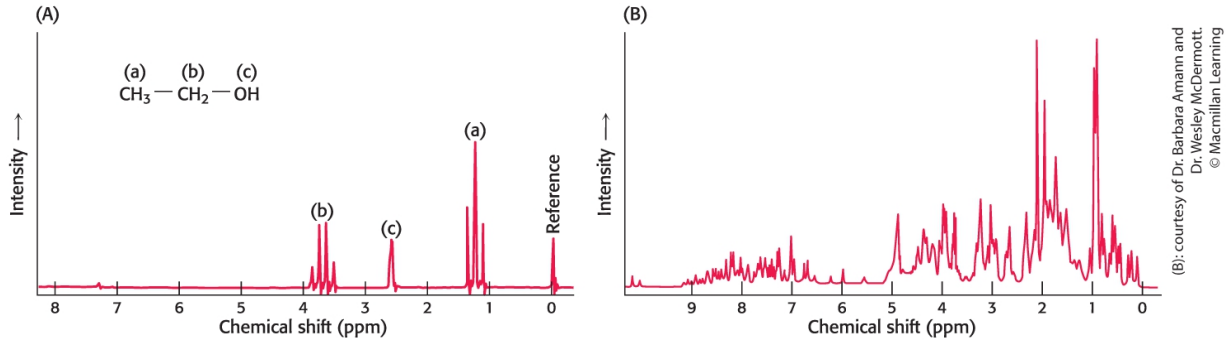
© Macmillan Learning

The horizontal axis is labeled Magnetic field strength. The vertical axis is labeled Energy. A sphere representing a magnetic nucleus is shown at low energy and high magnetic field strength. An upward arrow passes through the sphere and a counter-clockwise arrow is shown around the sphere. This sphere is labeled alpha spin. A wavy arrow representing irradiation is pointed at the sphere. Another sphere exactly above the first sphere is shown. The second sphere is shown at high energy and high magnetic field. A downward arrow passes through the sphere and a clockwise arrow is shown around the sphere. This sphere is labeled beta spin. An arrow from the alpha to beta spin magnetic nucleus is labeled transition between

spin state gives N M R line. Two divergent arrows from a point near the midpoint of the vertical axis points at the alpha and beta spin magnetic nucleus, respectively. The vertical distance between the two divergent arrows is labeled Energy separation, delta E.

Return to FIGURE 4.38. Graph depicting different spin states of a nucleus in N M R spectroscopy

Extended description for FIGURE 4.39. One-dimensional superscript 1 H NMR spectra shows chemical shift of protons in a sample



Part (A): The horizontal axis is labeled Chemical shift (p p m) and ranges from 8 to 0 in decrements of 1 unit. The vertical axis is labeled Intensity. A molecule is shown on the spectra: C H 3, single bond, C H 2, single bond, O H. C H 3 is labeled (a), C H 2 is labeled (b), and O H is labeled (c).

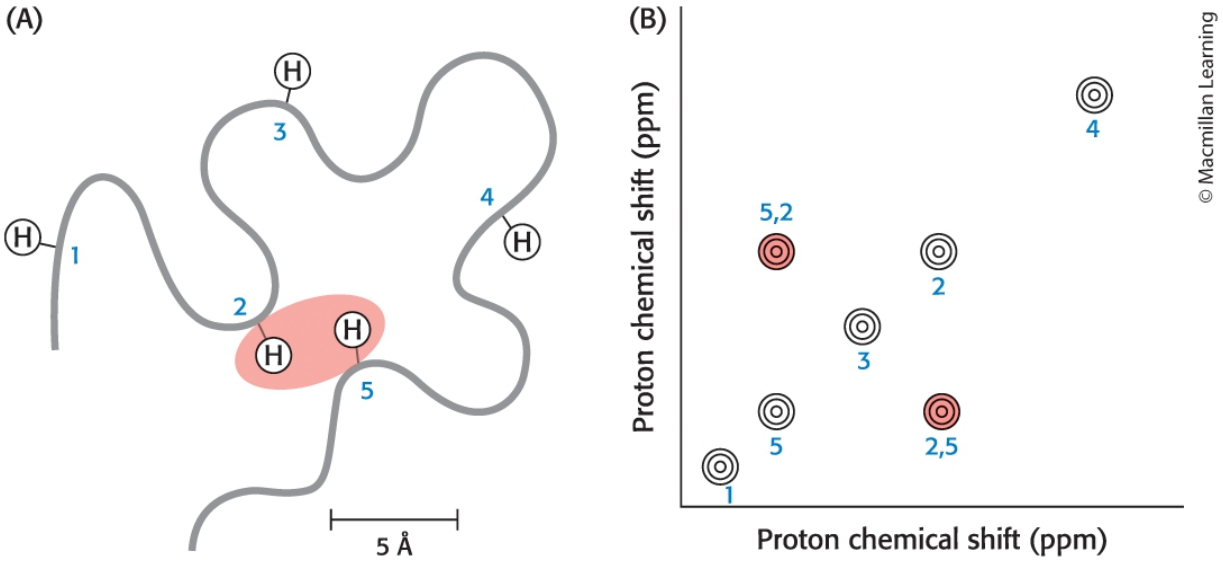
Reference: A medium peak is observed at 0.

1. For (a): A group of three high peaks, with the middle one being the tallest, is observed between 1.5 and 1.
2. For (b): A group of four moderate peaks, with the middle two being the tallest, is observed between 4 and 3.5.
3. For (c): A single moderate peak with a slightly broader base is observed near 2.5.

Part (B): The horizontal axis is labeled Chemical shift (p p m) and ranges from 9 to 0 in decrements of 1 unit. The vertical axis is labeled Intensity. Several peaks are shown to gradually increase in height from 9 to 2. Two very high peaks are observed at 2 and 1.

Return to FIGURE 4.39. One-dimensional superscript 1 H NMR spectra shows chemical shift of protons in a sample

Extended description for FIGURE 4.40. Identification of closely placed protons in a polypeptide due to nuclear overhauser effect

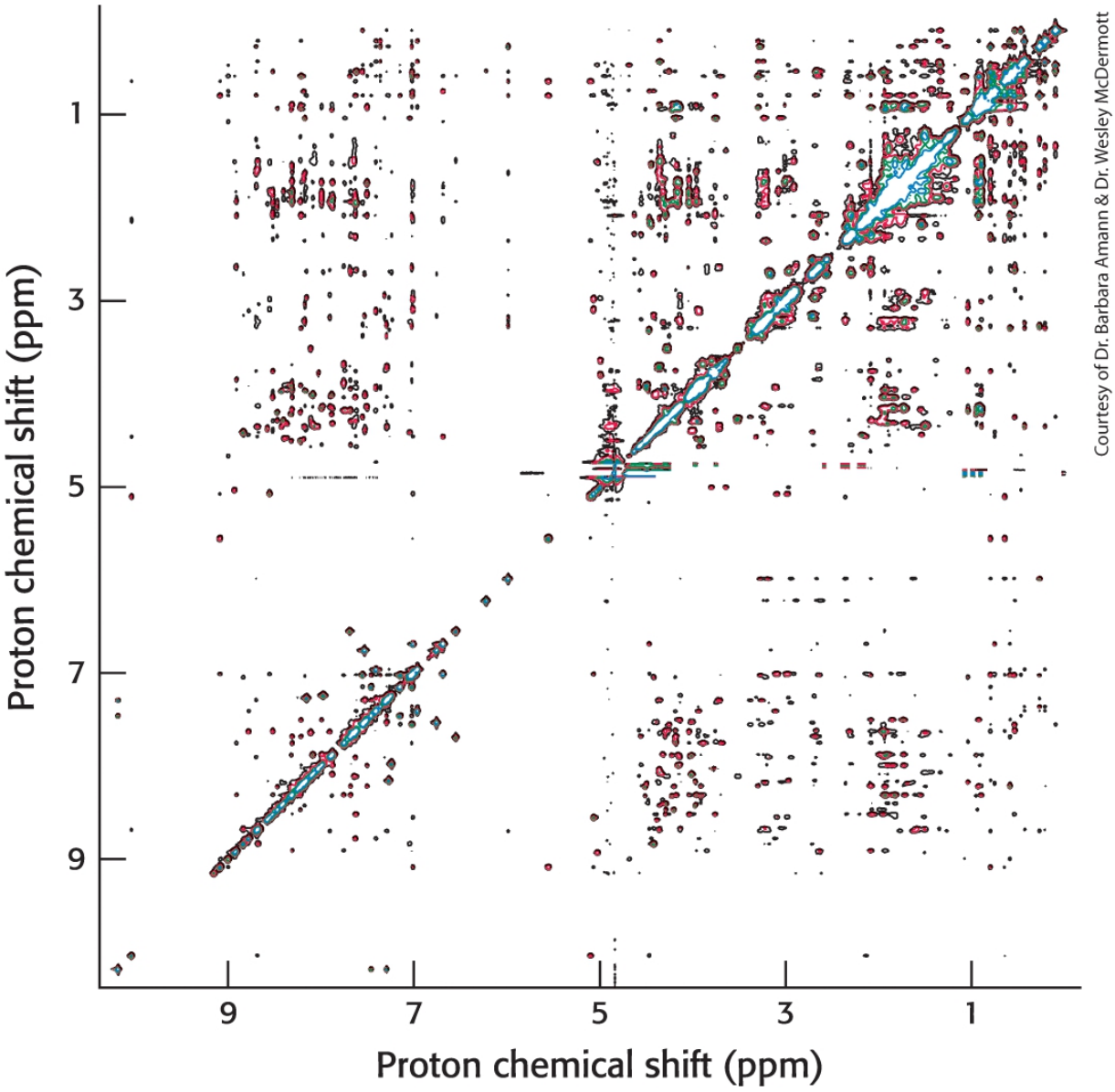


Part (A): A polypeptide is represented by a folded rope-like structure. Protons (H) are shown at position 1 through 5. The protons at positions 2 and 5 are shown to be in close proximity and are enclosed within an oval.

Part (B): A N O E S Y spectrum is shown. The horizontal axis is labeled Proton chemical shift (p p m). The vertical axis is labeled Proton chemical shift (p p m). Data points for the five protons align along a diagonal at nearly 45 degrees. A point above the diagonal is labeled 5, 2. Another point below the diagonal is labeled 2, 5.

Return to FIGURE 4.40. Identification of closely placed protons in a polypeptide due to nuclear overhauser effect

Extended description for FIGURE 4.41. NOESY spectrum for a protein

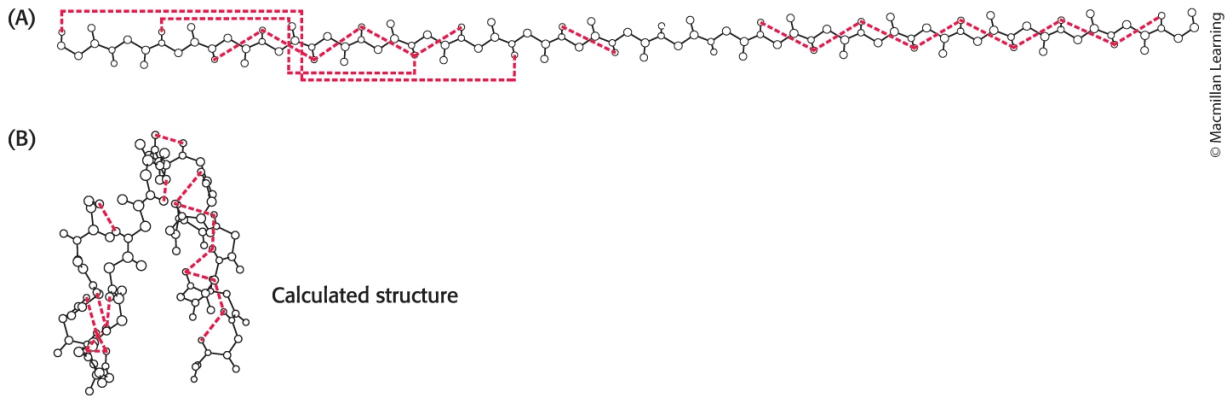


The horizontal axis is labeled Proton chemical shift (p p m) and ranges from 9 to 1 in decrements of 2 units. The vertical axis is labeled Proton chemical shift (p p m) and ranges from 9 to 1 in decrements of 2 units. If the area of the spectrum is divided in four

quadrants, most of the dots are scattered in the top right quadrant. Some of the points align along a diagonal at nearly 45 degrees where the intensity of the points is high.

Return to FIGURE 4.41. NOESY spectrum for a protein

Extended description for FIGURE 4.42. Calculation of structures based on N M R constraints

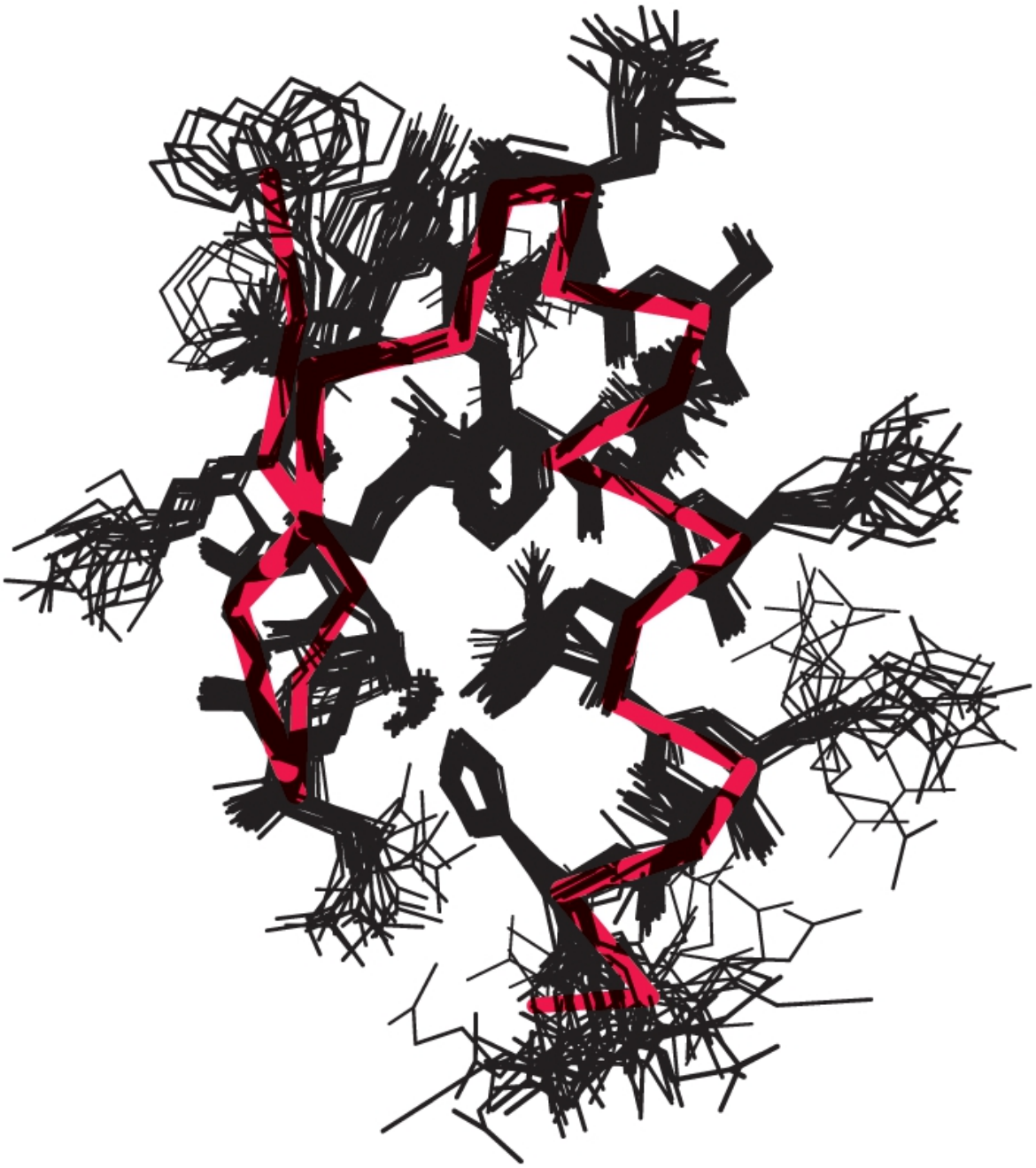


Part (A): A long linear polypeptide chain is shown. Dotted red lines drawn along the length of the peptide and between two distant amino acids show protons that are in close proximity in space.

Part (B): The calculated structure is shown to have an inverted C-shape. Red dotted lines between protons show their proximity in space.

Return to FIGURE 4.42. Calculation of structures based on N M R constraints

Extended description for FIGURE 4.43. Family of related structures produced by N M R spectroscopy

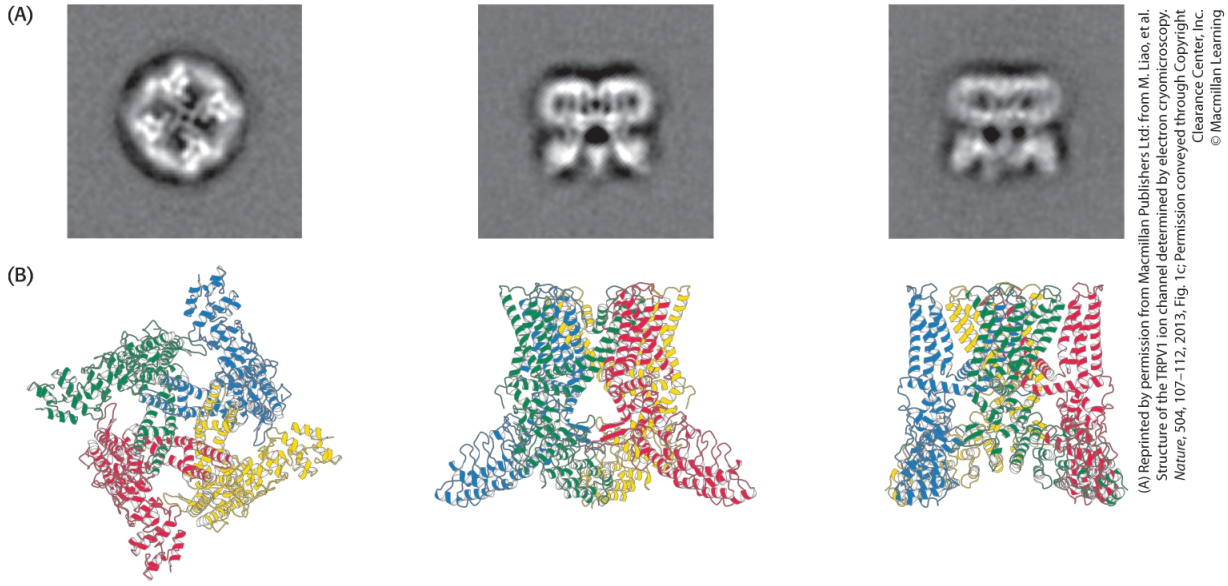


Courtesy of Dr. Barbara Amann

The structure of the protein domain is generated using data from N M R spectroscopy. The domain is inverted U-shaped as traced by a red line.

Return to FIGURE 4.43. Family of related structures produced by N M R spectroscopy

Extended description for FIGURE 4.44. Projections of a protein complex captured through cryo-E M



(A) Reprinted by permission from Macmillan Publishers Ltd: from M. Liao, et al. Structure of the TRPV1 ion channel determined by electron cryomicroscopy. *Nature*, 504, 107–112, 2013, Fig. 1c; Permission conveyed through Copyright Clearance Center, Inc. © Macmillan Learning

Part (A):

The first photograph shows the protein to have a swastika shaped structure.
The second photograph shows the protein to have a structure resembling two crescent shapes joined back to back. The shaped are again connected by a domain at the bottom leaving at hole at the center.
The third photograph shows the protein to have a rectangular structure with an inverted U-shaped groove at the bottom and two holes to the upper left and upper right of the groove.

Part (B): Three-dimensional ribbon diagrams corresponding to each photograph of part (A) are shown.

Return to FIGURE 4.44. Projections of a protein complex captured through cryo-E M

Extended description for Two-dimensional

electrophoresis gel showing separation results

© Macmillan Learning

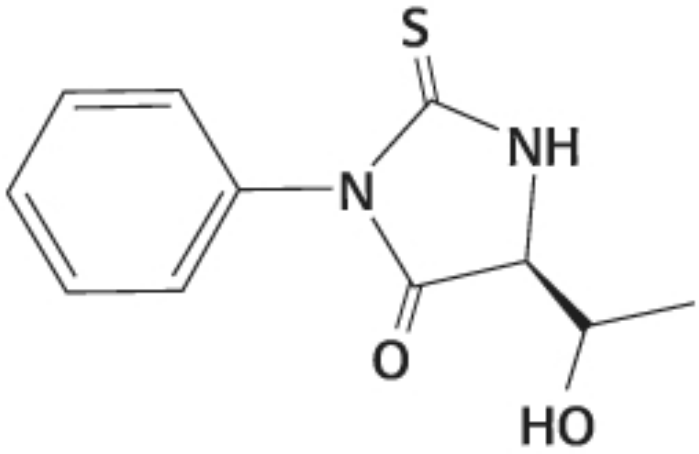
The figure illustrates an isoelectric focusing gel slab at the top joined to a larger S D S-polyacrylamide gel slab at the bottom. A double-headed arrow is shown above the isoelectric focusing gel. The left end is labeled p H 5 and the right end is labeled p H 9. A downward arrow is shown along the S D S-polyacrylamide gel.

Five ovals in vertical orientation are shown along the length of the isoelectric focusing gel slab with equal spacing between adjacent ovals.

Five ovals in horizontal orientation are shown scattered across the S D S-polyacrylamide gel slab. Oval (a) is toward the extreme right and lies almost in the middle. Oval (b) is to the right and higher up than (a). Oval (c) is exactly below (b) but lower down than (a). Oval (d) is to the extreme right and lies at a level between (a) and (b). Oval (e) is exactly below (d) and higher up than (c) but lower down than (a).

Return to Two-dimensional electrophoresis gel showing separation results

Extended description for Chemical structure of phenylthiohydantoin derivative



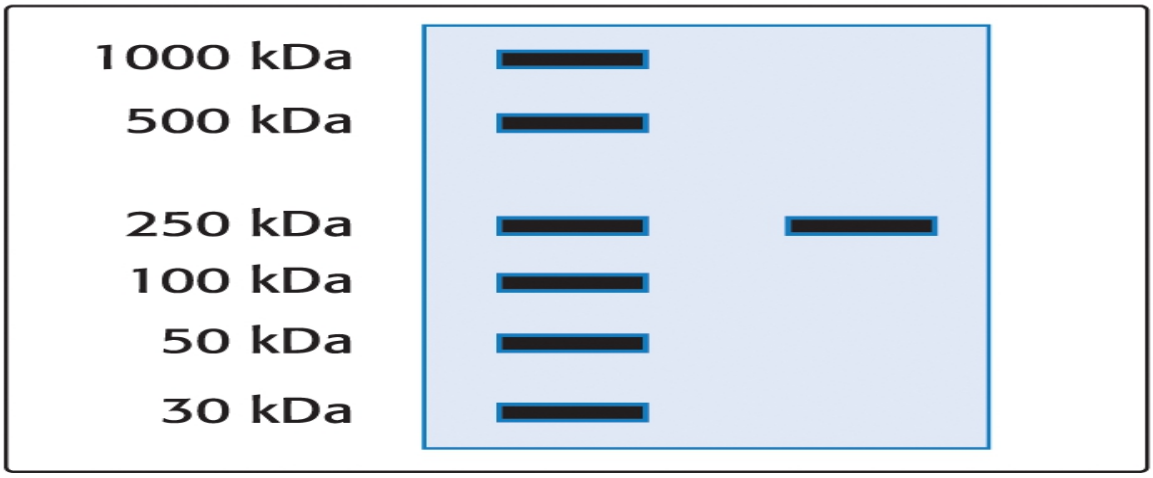
A benzene ring in a horizontal orientation consists of 3 alternating double bonds between C 1 and C 2, C 3 and C 4, and C 5 and C 6. C 1 is single bonded to the first N of a 5-membered heterocyclic pentagonal ring in a vertical orientation. The pentagonal ring consists of 2 N and 3 C atoms. The first N atom occupies the first position which is the top left vertex. The second N is bound to H and occupies the third position which is the top right vertex. C 1 at the topmost vertex is double bonded to S. C 2 is wedge bonded to a C H group which is single bonded to O H n the lower left and single bonded to C H 3 on the upper right depicted by a line. C 3 is double bonded to O.

Return to Chemical structure of phenylthiohydantoin derivative

Extended description for Three different protein gels

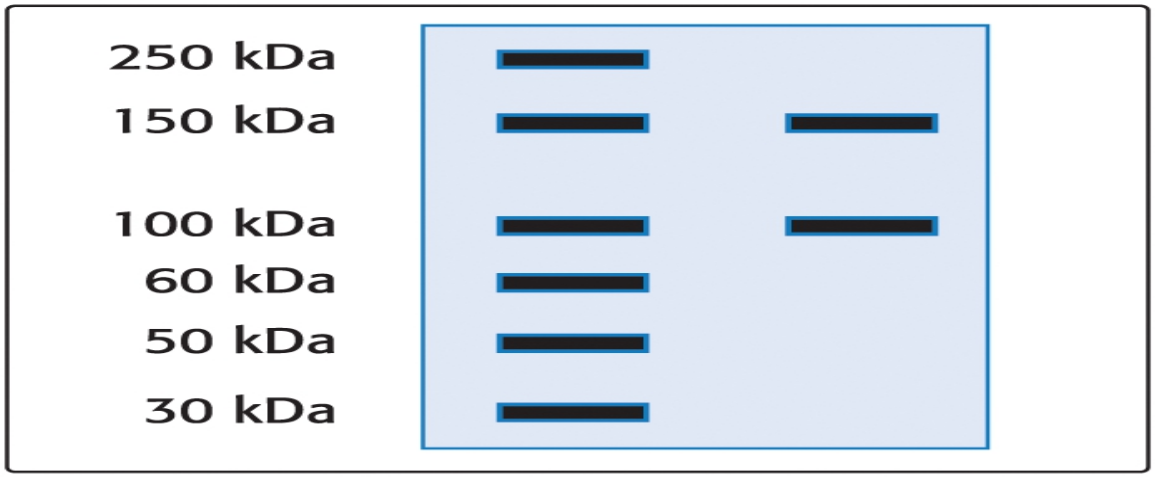
showing different banding patterns

(A)

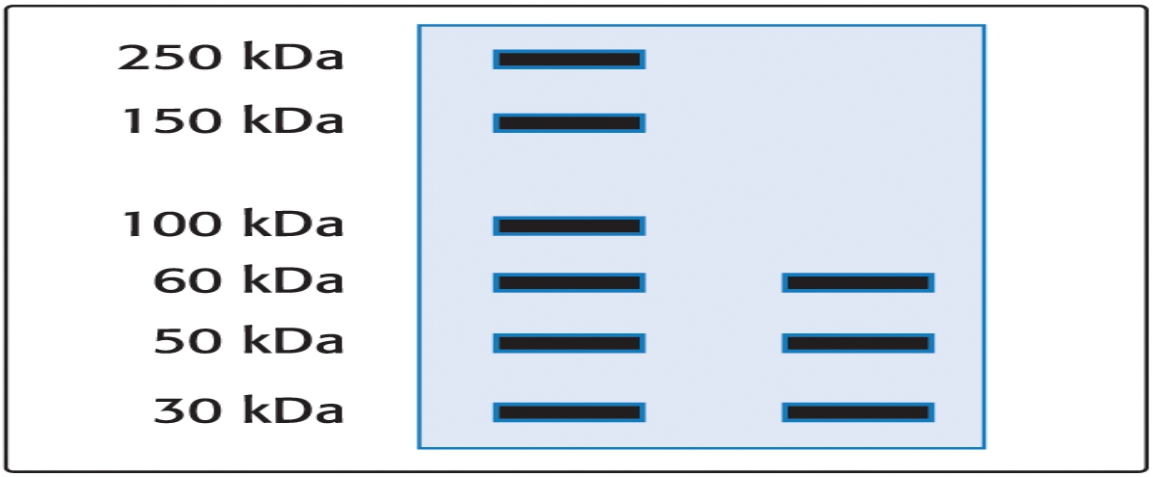


© Macmillan Learning

(B)



(C)



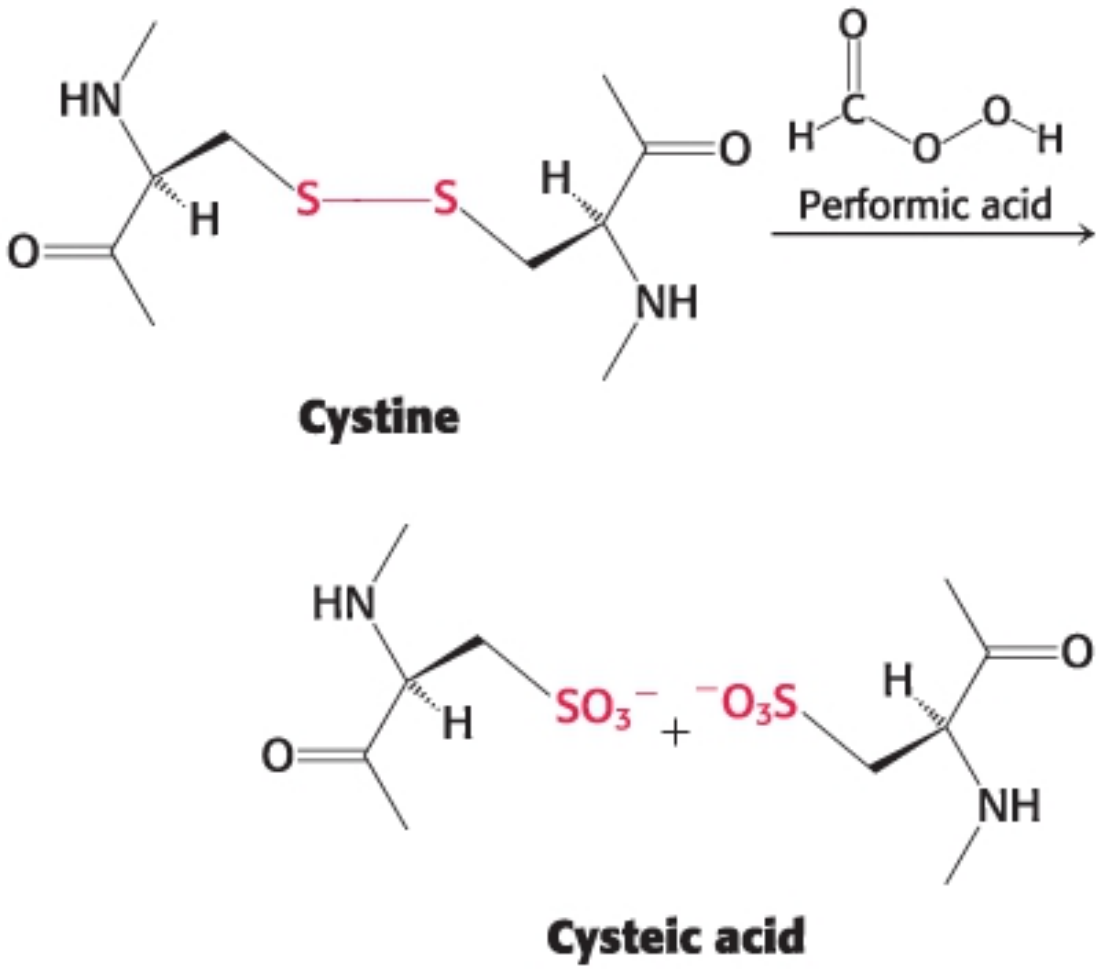
Option (A): An electrophoresis gel is shown. In the first lane, a protein ladder is shown which includes bands corresponding to the following sizes, in kilo Daltons, from top to bottom: 1000, 500, 250, 100, 50, and 30. In the second lane, a single band is present which corresponds to 250 kilo Daltons.

Option (B): An electrophoresis gel is shown. In the first lane, a protein ladder is shown which includes bands corresponding to the following sizes, in kilo Daltons, from top to bottom: 250, 150, 100, 60, 50, and 30. In the second lane, two bands are present which correspond to 150 and 100 kilo Daltons, respectively.

Option (C): An electrophoresis gel is shown. In the first lane, a protein ladder is shown which includes bands corresponding to the following sizes, in kilo Daltons, from top to bottom: 250, 150, 100, 60, 50, and 30. In the second lane, three bands are present which correspond to 60, 50, and 30 kilo Daltons, respectively.

Return to Three different protein gels showing different banding patterns

Extended description for Reaction showing cleavage of cystine by performic acid to produce two molecules of cysteic acid



The reactant has the following structure: A central C atom is single bonded to N H on the upper left, wedge bonded to C H 2 on the upper right, dash bonded to H on the lower right, and single bonded to C on the lower left. The N H on the upper right has a single bond on the upper right. The C on the lower left is double bonded to O on the left and has a single bond on the lower right. C H 2 on the upper right is single bonded to S on the lower right. S is single bonded to

another S on the right. The second S is single bonded to C H 2 on the lower right. C H 2 is single bonded to a central C atom on the upper right. The central C atom is dash bonded to H on the upper left, single bonded to C on the upper right, and single bonded to N H on the lower right. The C on the upper right is double bonded to O on the right and has a single bonded on the upper left. The N H on the lower right has a single bond on the lower left.

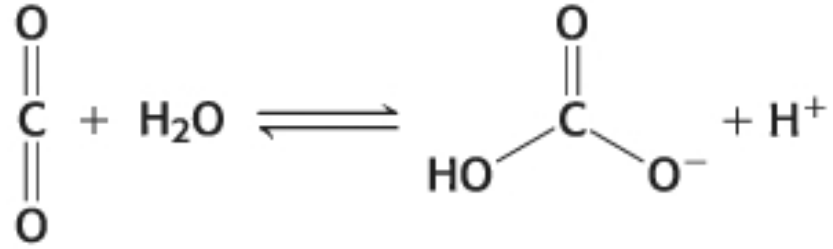
The reaction arrow is labeled Performic acid, which has the following structure: H, single bond, C, single bond, O, single bond, O, single bond, H. C is double bonded to O above.

The products are labeled Cysteic acid. The first product has the following structure: A central C atom is single bonded to N H on the upper left, wedge bonded to C H 2 on the upper right, dash bonded to H on the lower right, and single bonded to C on the lower left. The N H on the upper right has a single bond on the upper right. The C on the lower left is double bonded to O on the left and has a single bond on the lower right. C H 2 on the upper right is single bonded to S O 3 superscript minus on the lower right.

The second product has the same structure as the first product but is flipped along its axis.

Return to Reaction showing cleavage of cystine by performic acid to produce two molecules of cysteic acid

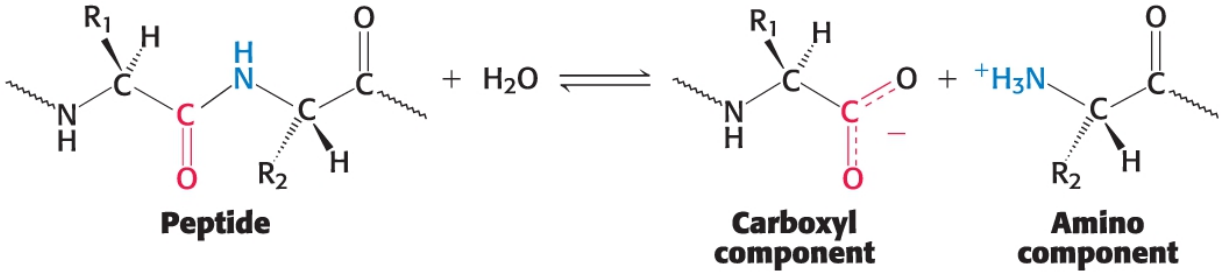
Extended description for Chemical equation showing the hydration of carbon dioxide



The reaction is reversible and consists of two reactants and two products. The first reactant has the following structure: A central C atom is double bonded to O above and below. The second reactant is H 2 O. The first product has the following structure: A central C atom is single bonded to O superscript minus on the lower right, single bonded to O H on the lower left, and double bonded to O above. The second product is H superscript plus ion.

Return to Chemical equation showing the hydration of carbon dioxide

Extended description for Chemical equation showing the hydrolysis of a peptide bond



The reaction is reversible and consists of two reactants and two products.

The first reactant is a peptide which has the following structure: A 2 N and 4 C heteronuclear alkane chain is depicted as a line structure using 5 zigzag lines. The N atoms occupy the first and fourth position. The first N atom is single bonded to H below. It has a zigzag line on the upper left. C 1 is wedge bonded to R subscript 1 on the upper left and dash bonded to H on the upper right. C 2 is double bonded to O below and is highlighted in red. The second N atom is bound to H above and highlighted in blue. C 3 is dash bonded to R subscript 2 on the lower left and wedge bonded to H on the lower right. C 4 is double bonded to O above. It has an open single bond on the lower right.

The second reactant is H 2 O.

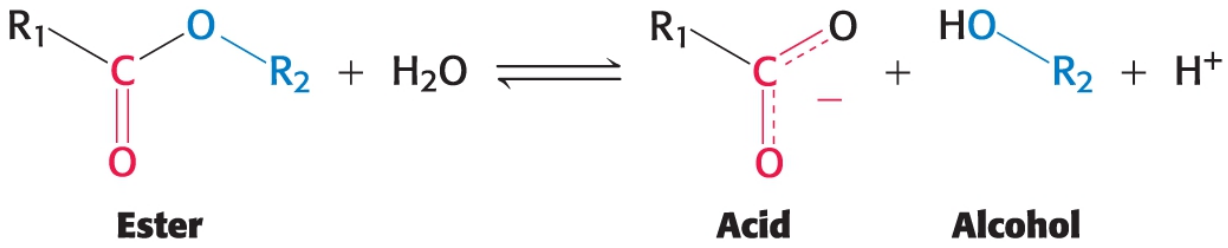
The first product is the carboxyl component which has the following structure: A 1 N and 2 C heteronuclear alkane chain is depicted as a line structure using 2 zigzag lines. The N atom occupies the first position and is single bonded to H below. It has an open single bond on the upper left. C 1 is wedge bonded to R subscript 1 on the upper

left and dash bonded to H on the upper right. C 2 is single bonded to O below and on the upper right with a resonance bond shared between C and the O atoms. C 2 and its associated bonds are highlighted in red.

The second product is the amino component which has the following structure: A 1 N and 2 C heteronuclear alkane chain is depicted as a line structure using 2 zigzag lines. The N atom occupies the first position. It is bound to H 3 superscript plus. This N H 3 superscript plus group is highlighted in blue. C 1 is dash bonded to R subscript 2 on the lower left and wedge bonded to H on the lower right. C 2 is double bonded to O above. It has zigzag line on the lower right.

Return to Chemical equation showing the hydrolysis of a peptide bond

Extended description for Chemical equation showing the hydrolysis of ester bond

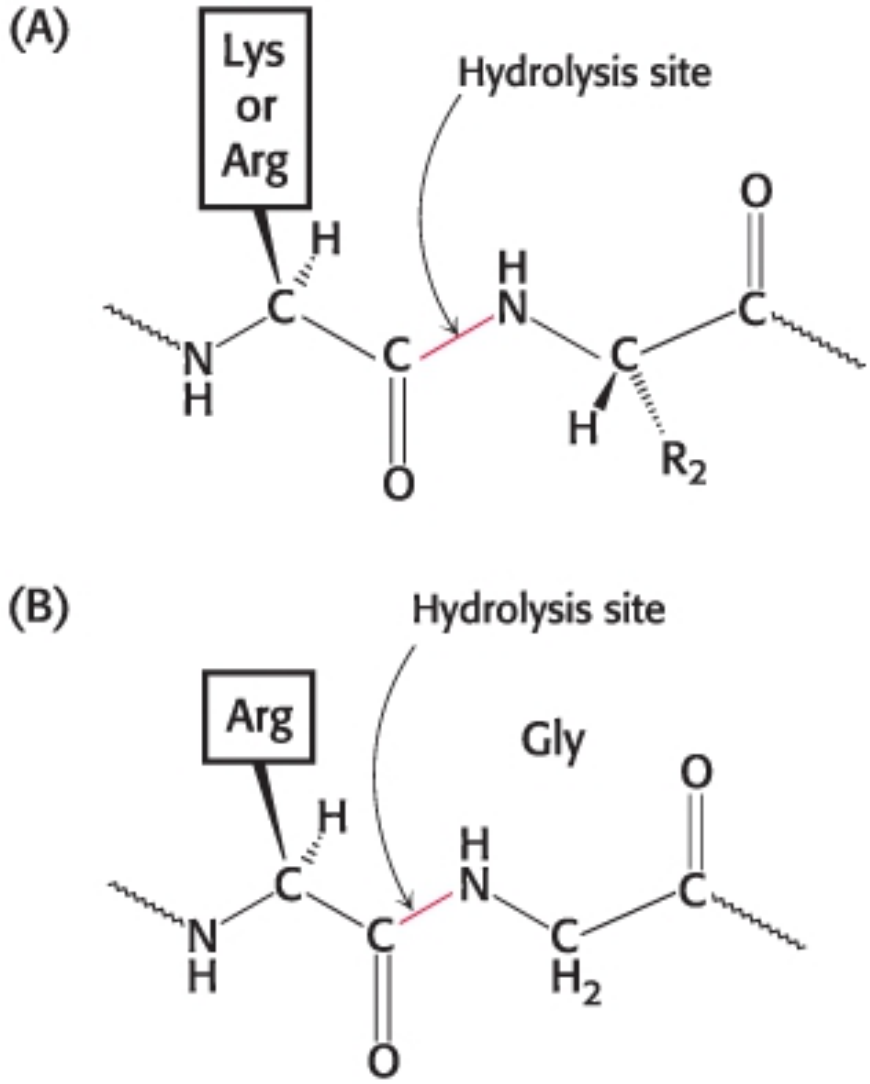


The reaction is reversible and consists of two reactants and three products. The first reactant is an ester and has the following structure: A central C atom is single bonded to R subscript 1 on the upper left, single bonded to O on the upper right, and double bonded to O below. The O atom on the upper right is single bonded to R subscript 2 on the lower right. C, double bond, O is highlighted in red while O, single bond, R subscript 2 is highlighted in blue. The second reactant is H 2 O.

The first product is an acid that has the following structure: A central C atom is single bonded to R subscript 1 on the upper left and single bonded to O below and on the upper right with a resonance bond shared between C and the two O atoms. The C and O atom below and their associated bonds are highlighted in red. The second product is an alcohol which has the following structure: O H, single bond, R subscript 2. The O atom of the O H group, single bond, and R subscript 2 are highlighted in blue. The third product is H superscript plus ion.

Return to Chemical equation showing the hydrolysis of ester bond

Extended description for FIGURE 5.1. Chemical structures showing the high specificity of enzymes for their substrates and chemical reactions



Part (A): It shows the structure of a peptide and hydrolysis site cleaved by trypsin.

The structure of the peptide is as follows: A 2 N and 4 C heteronuclear alkane chain is depicted as a line structure using 5

zigzag lines. The N atoms occupy the first and fourth positions. The first N atom is bound to H below. It has a zigzag line on the upper left. C 1 is wedge bonded to either lysine or arginine on the upper left and dash bonded to H on the upper right. C 2 is double bonded to O below. The second N atom is single bonded to H above. C 3 is dash bonded to R subscript 2 on the lower right and wedge bonded to H on the lower left. C 4 is double bonded to O above. It has a zigzag line on the lower right. The single bond between C 2 and the second N atom is labeled hydrolysis site and is highlighted in red.

Part (B): It shows the structure of a peptide and hydrolysis site cleaved by thrombin.

The structure of the peptide is as follows: A 2 N and 4 C heteronuclear alkane chain is depicted as a line structure using 5 zigzag lines. The N atoms occupy the first and fourth positions. The first N atom is single bonded to H below. It has a zigzag line on the upper left. C 1 is wedge bonded to arginine on the upper left and dash bonded to H on the upper right. C 2 is double bonded to O below. The second N atom is bound to H above. C 3 is single bonded to H 2 below. C 4 is double bonded to O above. It has a zigzag line on the lower right. The single bond between C 2 and the second N atom is labeled hydrolysis site and is highlighted in red. There is a glycine residue above C 3.

Return to FIGURE 5.1. Chemical structures showing the high specificity of enzymes for their substrates and chemical reactions

Extended description for Reaction catalyzed by nucleoside monophosphate kinase



The reaction consists of two reactants and two products. The first reactant is A T P. The second reactant is N M P. A reversible reaction arrow leads to the products. The first product is A D P. The second product is N D P.

Return to Reaction catalyzed by nucleoside monophosphate kinase

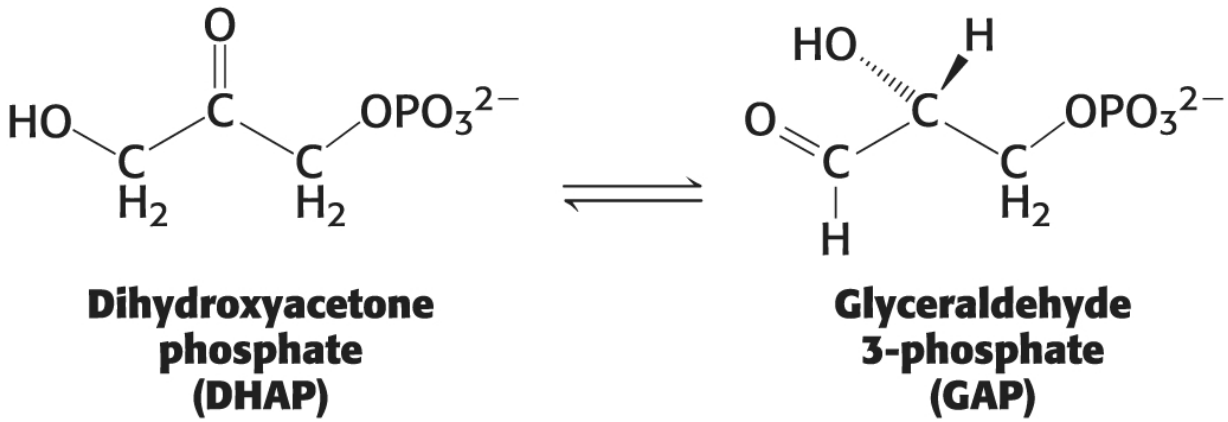
Extended description for Hypothetical chemical reaction



The reaction consists of two reactants and two products. The first reactant is A. The second reactant is B. A reversible reaction arrow leads to the products. The first product is C. The second product is D.

Return to Hypothetical chemical reaction

Extended description for Chemical equation showing the conversion of dihydroxyacetone phosphate into glyceraldehyde-3-phosphate



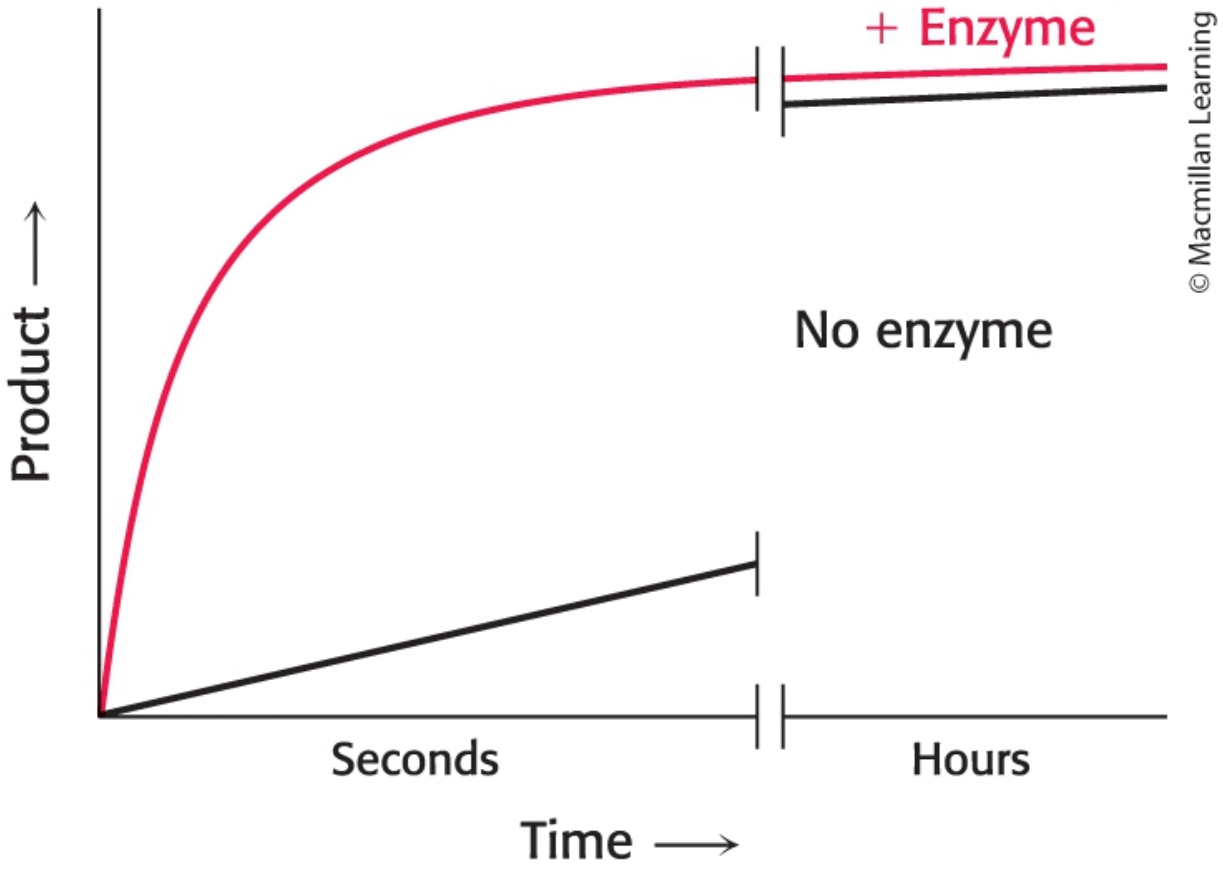
The reaction is reversible and consists of one reactant and one product.

The reactant is dihydroxyacetone phosphate (D H A P) and has the following structure: A three-carbon alkane chain is depicted as a line structure using two zigzag lines. C 1 is single bonded to O H on the upper left and bound to H 2 below. C 2 is double bonded to O above. C 3 is single bonded to O P O 3 superscript 2 minus on the upper right and bound to H 2 below.

The product is glyceraldehyde 3-phosphate (G A P) and has the following structure: A three-carbon alkane chain is depicted as a line structure using two zigzag lines. C 1 is double bonded to O on the upper left and single bonded to H below. C 2 is dash bonded to O H on the upper left and wedge bonded to H on the upper right. C 3 is single bonded to O P O 3 superscript 2 minus on the upper right and bound to H 2 below.

Return to Chemical equation showing the conversion of dihydroxyacetone phosphate into glyceraldehyde-3-phosphate

Extended description for FIGURE 5.2. Graphical representation of the unperturbed equilibrium point of a reaction in the presence and absence of an enzyme



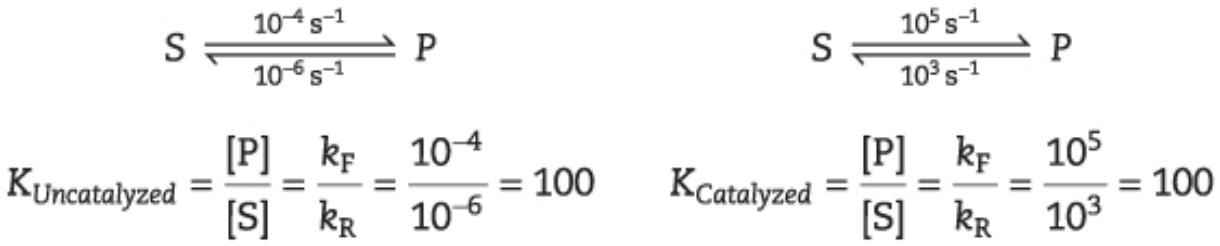
The horizontal axis is labeled time. The first half of this axis is labeled seconds and the second half is labeled hours. The two halves are separated by an axis break. The vertical axis is labeled product.

In the presence of an enzyme, the product formation curve rises rapidly (up to roughly 95 percent) in the seconds phase and then plateaus in the hours phase. In the absence of an enzyme, the product formation curve rises linearly up to less than the half of the product concentration at the end of the seconds phase. A break is

shown as short vertical line at the tip of the straight line. The remaining product is formed in the hours phase. It is depicted as a straight horizontal line, just below the plateau of the first curve in the hours phase. Both curves still terminate at the same point.

Return to FIGURE 5.2. Graphical representation of the unperturbed equilibrium point of a reaction in the presence and absence of an enzyme

Extended description for Calculation of equilibrium constants for catalyzed and uncatalyzed reaction



The first reaction shows the reversible conversion of S to P. The top forward arrow is labeled 10 superscript minus 4 baseline s superscript minus 1. The bottom backward arrow is labeled 10 superscript minus 6 baseline s superscript minus 1.

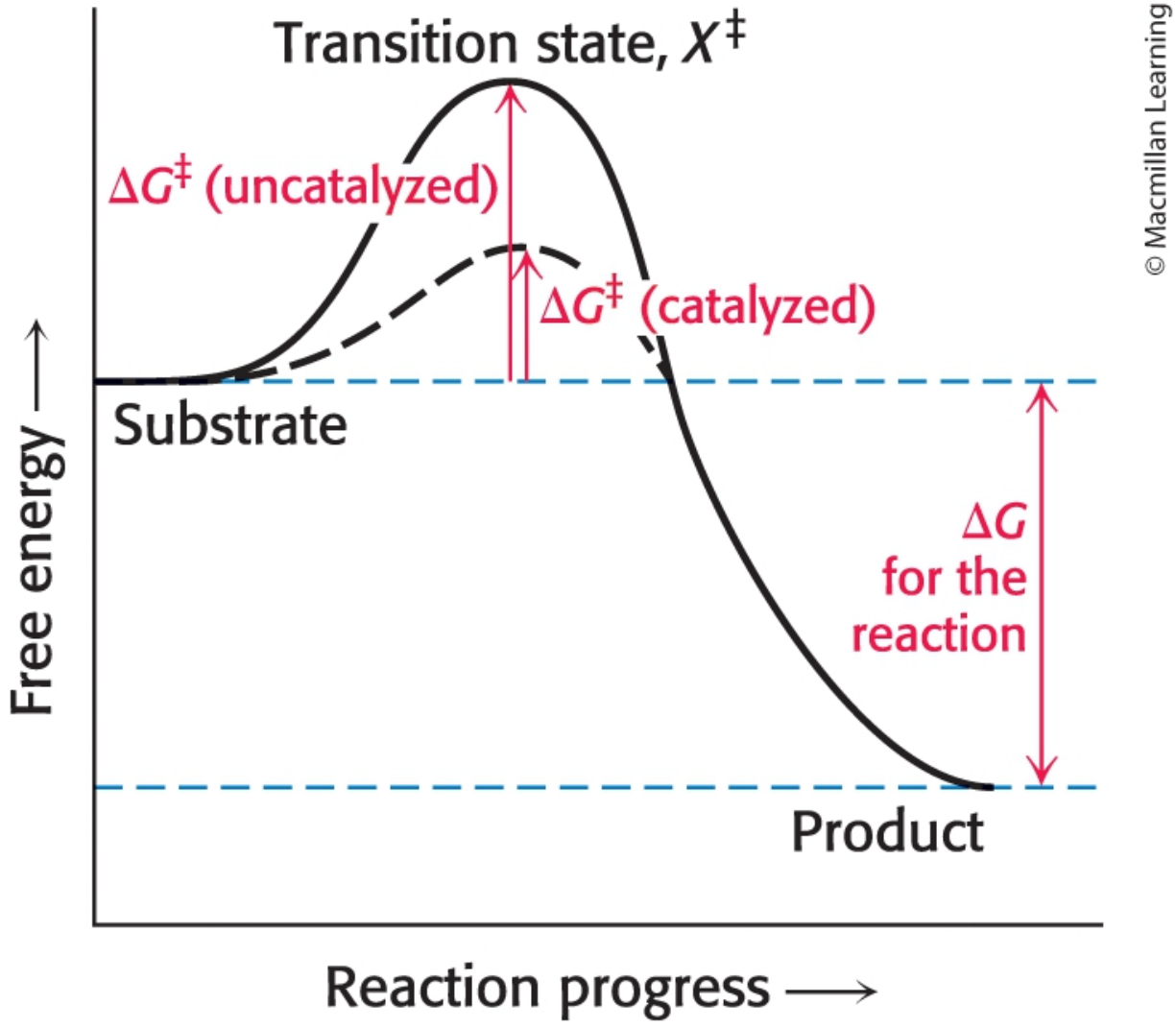
The calculation of K subscript uncatalyzed is depicted as follows: K subscript uncatalyzed baseline equals the concentration of P over concentration of S equals StartFraction lowercase k subscript F over lowercase k subscript R EndFraction equals 10 superscript minus 4 over 10 superscript minus 6 equals 100.

The second reaction shows the reversible conversion of S to P. The top forward arrow is labeled 10 superscript 5 baseline s superscript minus 1. The bottom backward arrow is labeled 10 superscript 3 baseline s superscript minus 1.

The calculation of K subscript catalyzed is depicted as follows: K subscript catalyzed baseline equals the concentration of P over concentration of S equals StartFraction lowercase k subscript F over lowercase k subscript R EndFraction equals 10 superscript 5 over 10 superscript 3 equals 100.

Return to Calculation of equilibrium constants for catalyzed and uncatalyzed reaction

Extended description for FIGURE 5.3. Graphical representation of the enzyme-mediated acceleration of a reaction by lowering of the free energy of activation



The horizontal axis is labeled reaction progress. The vertical axis is labeled free energy. Two dashed lines run parallel to the horizontal axis. The first line is extremely close to the horizontal axis and is labeled product on the extreme right. The second line is located just

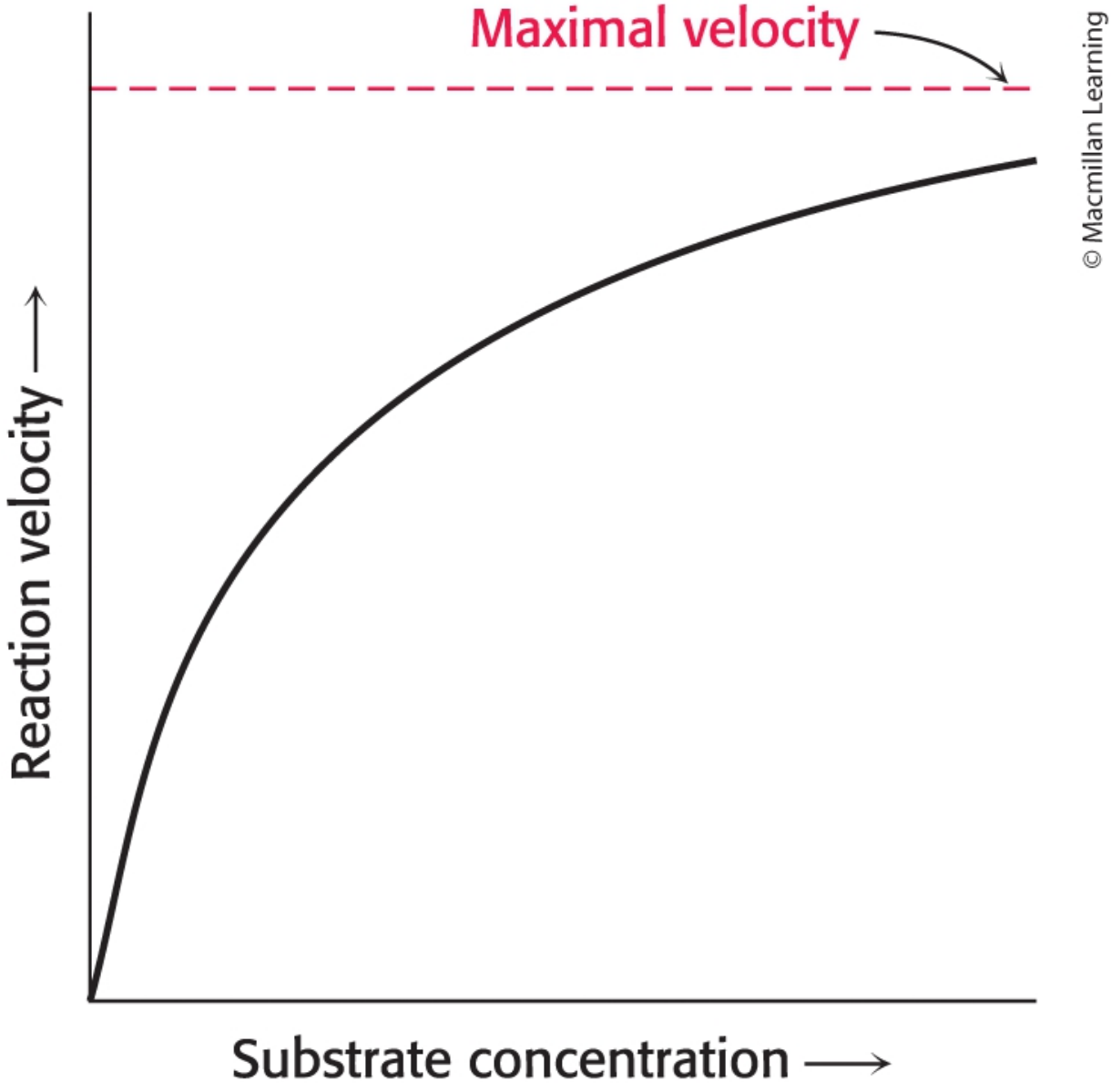
above the mid point of the vertical axis and is labeled substrate on the extreme left. The distance between two lines is labeled delta G for the reaction.

A solid curve labeled delta G superscript double dagger (uncatalyzed) is present. It rises steadily from the substrate line at the start of the reaction to a highest free energy labeled transition state, X superscript double dagger. This state is achieved in the middle of the reaction. The curve then falls to the product line by the end of the reaction.

A dashed curve labeled delta G superscript double dagger (catalyzed) is also present. It follows the same path as the solid curve, but only attains half the height of the peak of the solid curve.

Return to FIGURE 5.3. Graphical representation of the enzyme-mediated acceleration of a reaction by lowering of the free energy of activation

Extended description for FIGURE 5.4. Graphical representation of the maximal velocity attained by an enzyme-catalyzed reaction as the substrate concentration increases



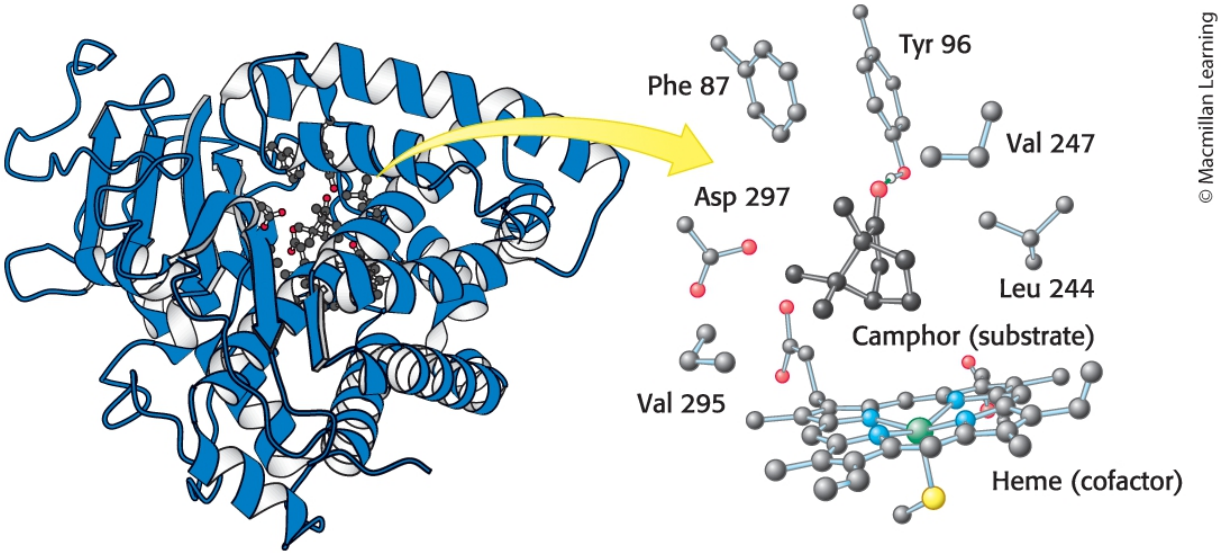
The horizontal axis is labeled substrate concentration. The vertical axis is labeled reaction Velocity. A dashed line parallel to the

horizontal axis is labeled maximal velocity. It is located at the highest reaction velocity.

An upward convex curve rises rapidly from the origin and plateaus just below the maximal Velocity line.

Return to FIGURE 5.4. Graphical representation of the maximal velocity attained by an enzyme-catalyzed reaction as the substrate concentration increases

Extended description for FIGURE 5.5 Ribbon diagram and ball-and-stick model show a substrate surrounded by the active site residues of cytochrome P 450 enzyme



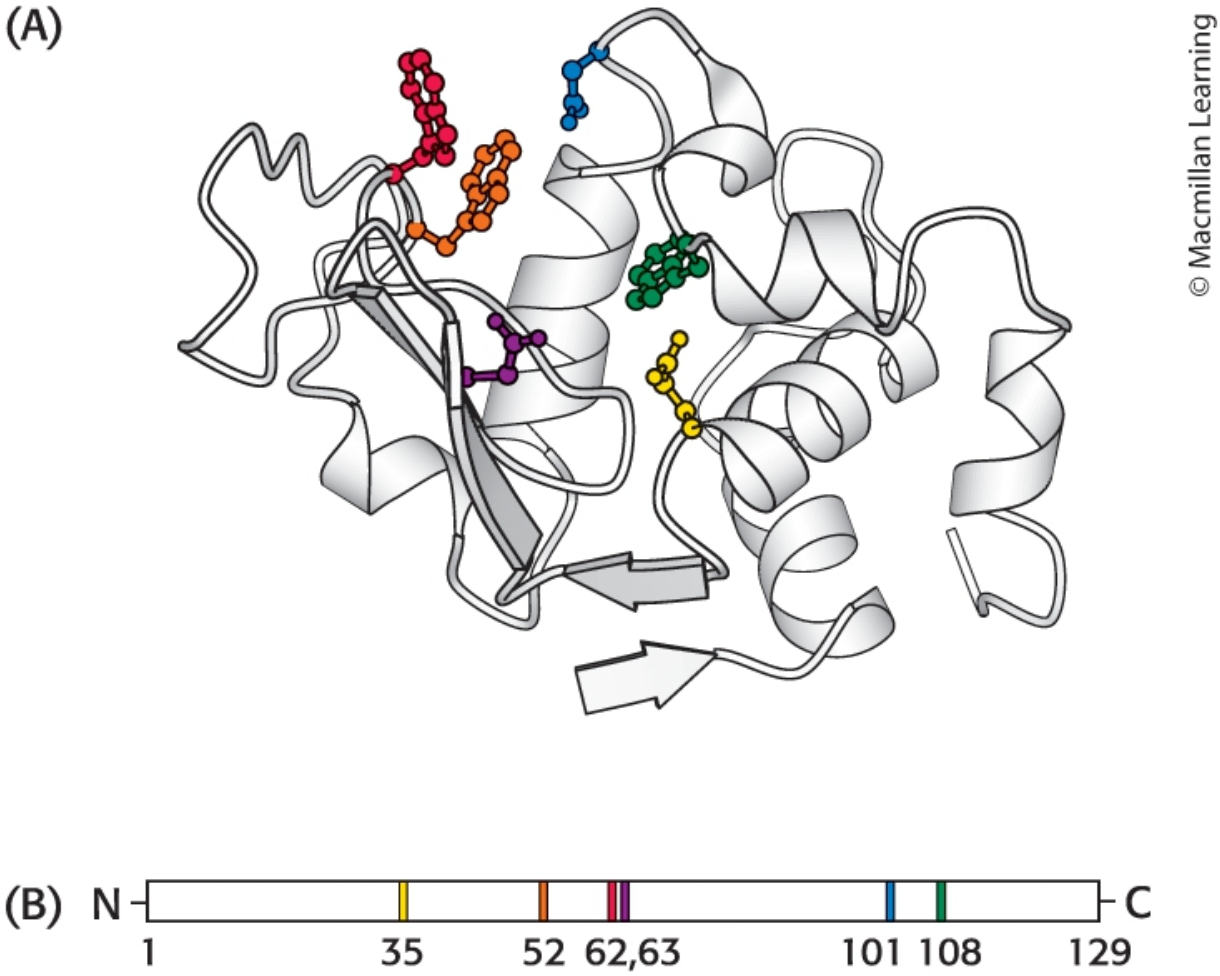
© Macmillan Learning

Ribbon diagram: The protein structure consists of interconnected motifs such as ribbon-shaped alpha helices and arrow-shaped beta sheets. The ball-and-stick model of camphor, the substrate, is shown as several interconnected black spheres. It is located inside a cavity located between the alpha helices and beta-sheets.

Ball and stick model: One black sphere of camphor is connected to a chain of a red, white, and red sphere, which is then connected at the top to a residue labeled T y r 96. A planar arrangement of interconnected black, spheres labeled Heme (cofactor) is present below the substrate. Heme contains four blue spheres inside the interconnected network of black spheres. The blue spheres are connected to a single green sphere at the center. Various residues labeled V a l 295, A s p 297, P h e 87, V a l 247, and Le u 244 are present around the substrate from bottom left to bottom right.

Return to FIGURE 5.5 Ribbon diagram and ball-and-stick model show a substrate surrounded by the active site residues of cytochrome P 450 enzyme

Extended description for FIGURE 5.6. Ribbon diagram and schematic representation of the primary structure depict the coming together of distantly located amino acids in the active site of a folded protein



© Macmillan Learning

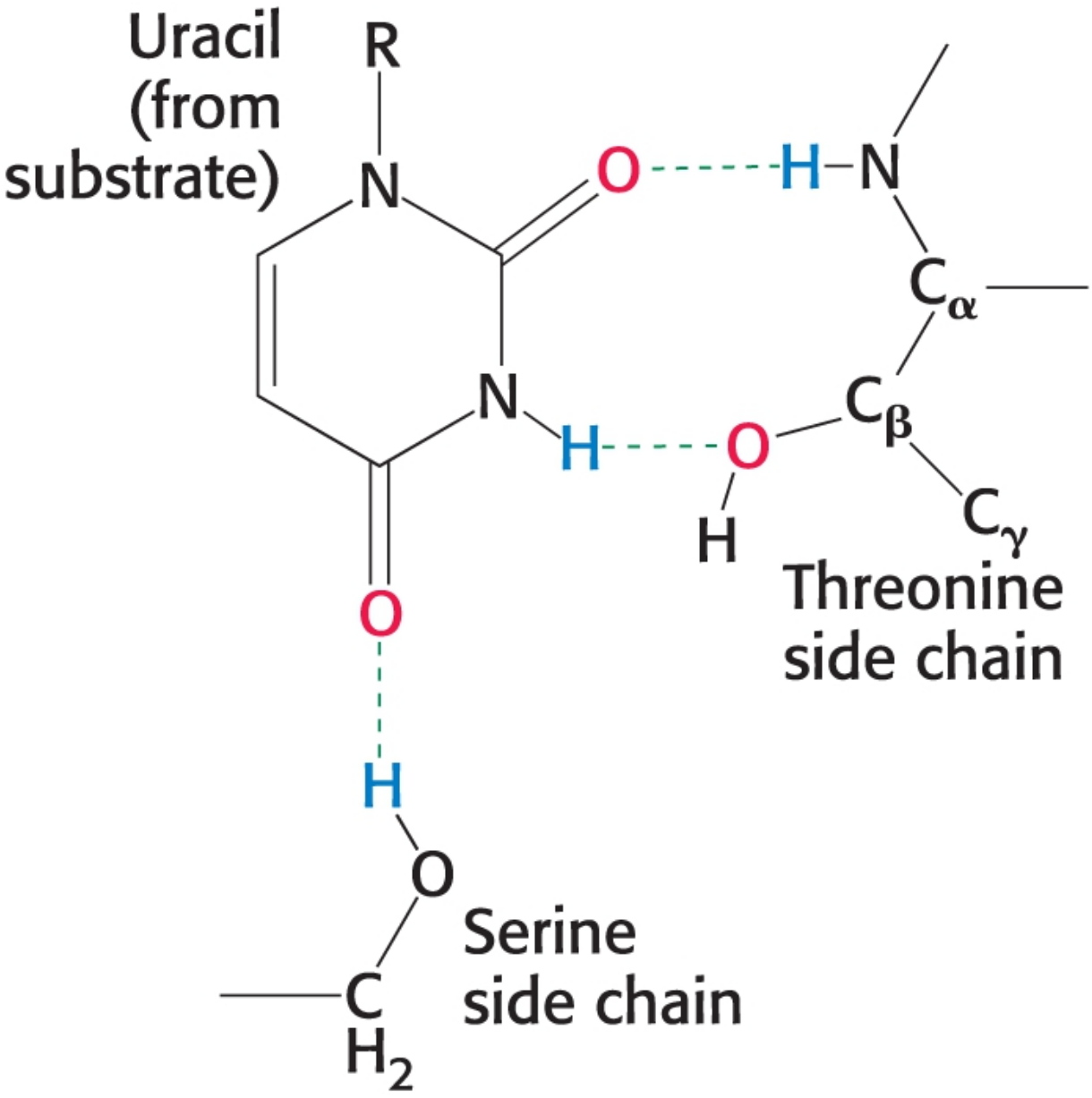
(A): The ribbon diagram of lysozyme consists of interconnected motifs such as ribbon-shaped alpha helices and arrow-shaped beta-sheets. The alpha helices and the beta-strands are connected by thread-like loops. The active site residues are shown as different clusters composed of interconnected colored spheres. Each cluster has a different color like red, orange, blue, purple, green, and

yellow. They are located on different alpha-helices, thread-like loops, and beta-strand. They are brought together by the folding of the protein.

(B): The primary structure of lysozyme is depicted as a horizontal narrow rectangular structure. It is made up of 129 and its left and right end are labeled N and C respectively. It has the markings 1, 35, 52, 62, 63, 101, 108, and 129 to show the location of different amino acid residues. The residues 35, 52, 62, 63, 101, and 108 are shown as tiny vertical bars having yellow, orange, red, purple, blue, and green colors respectively.

Return to FIGURE 5.6. Ribbon diagram and schematic representation of the primary structure depict the coming together of distantly located amino acids in the active site of a folded protein

Extended description for FIGURE 5.7. Hydrogen bonding between the side chains of active site residues and the substrate



Three interacting compounds are shown:

1. Uracil (from substrate): A heterocyclic hexagonal ring composed of 2 N and 4 C is present in a vertical orientation. The first N atom occupies the first position, which is the topmost vertex. The second N atom occupies the third position, which is the bottom right vertex. A double bond is present between C 3 and C 4. The first N atom is single bonded to R above. C 1 is double bonded to O on the upper right. The second N atom is single bonded to H on the lower right. C 2 is double bonded to O below.

2. Threonine side chain: A 1 N and 3 C heteronuclear alkane chain is depicted as a line structure using 3 zigzag lines. It is present in a vertical orientation. The N atom occupies the first position, C 1 is represented as C subscript alpha, C 2 is represented as C subscript beta, and C 3 is represented as C subscript gamma. The N atom is single bonded to H on the left. It has an open single bond on the upper right. C subscript alpha has an open single bond on the right. C subscript beta is single bonded to O on the lower left. This O is single bonded to H on the lower left.

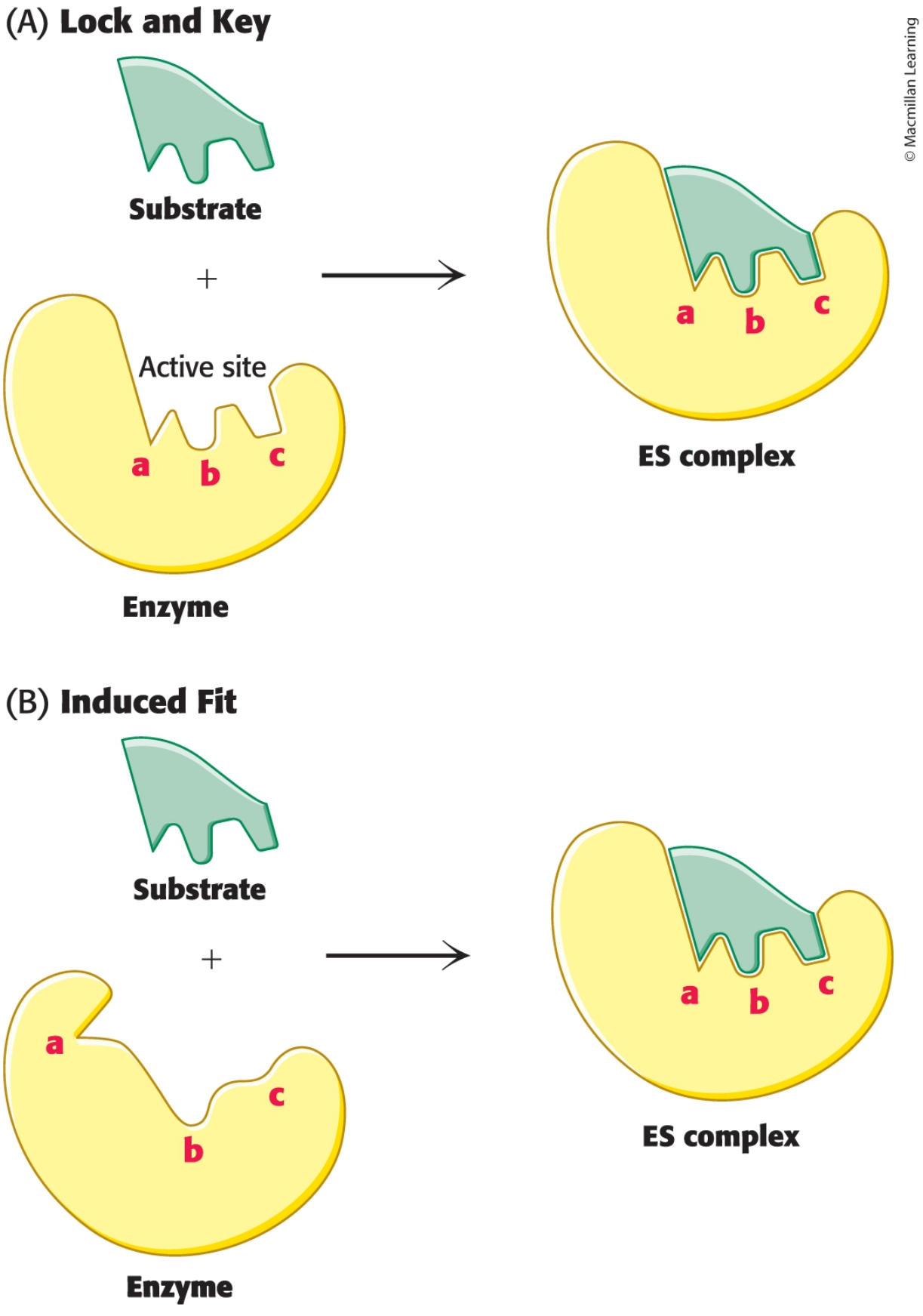
3. Serine side chain: H, single bond, O, single bond, C H 2 is present in a vertical orientation. C has an open single bond on the left.

A dashed line connects the O atom double-bonded to C 2 of the uracil component with the first H atom of the serine side chain. A second dashed line connects the O atom double-bonded to C 1 of the uracil component with the H atom single bonded to the first N atom of the threonine side chain. A third dashed line connects the H atom single bonded to the second N atom of the uracil component with the O atom single bonded to the C subscript beta of the threonine side chain.

Return to FIGURE 5.7. Hydrogen bonding between the side chains of active site residues and the substrate

Extended description for FIGURE 5.8. Schematic illustration of the lock and key model and the induced-

fit model



© Macmillan Learning

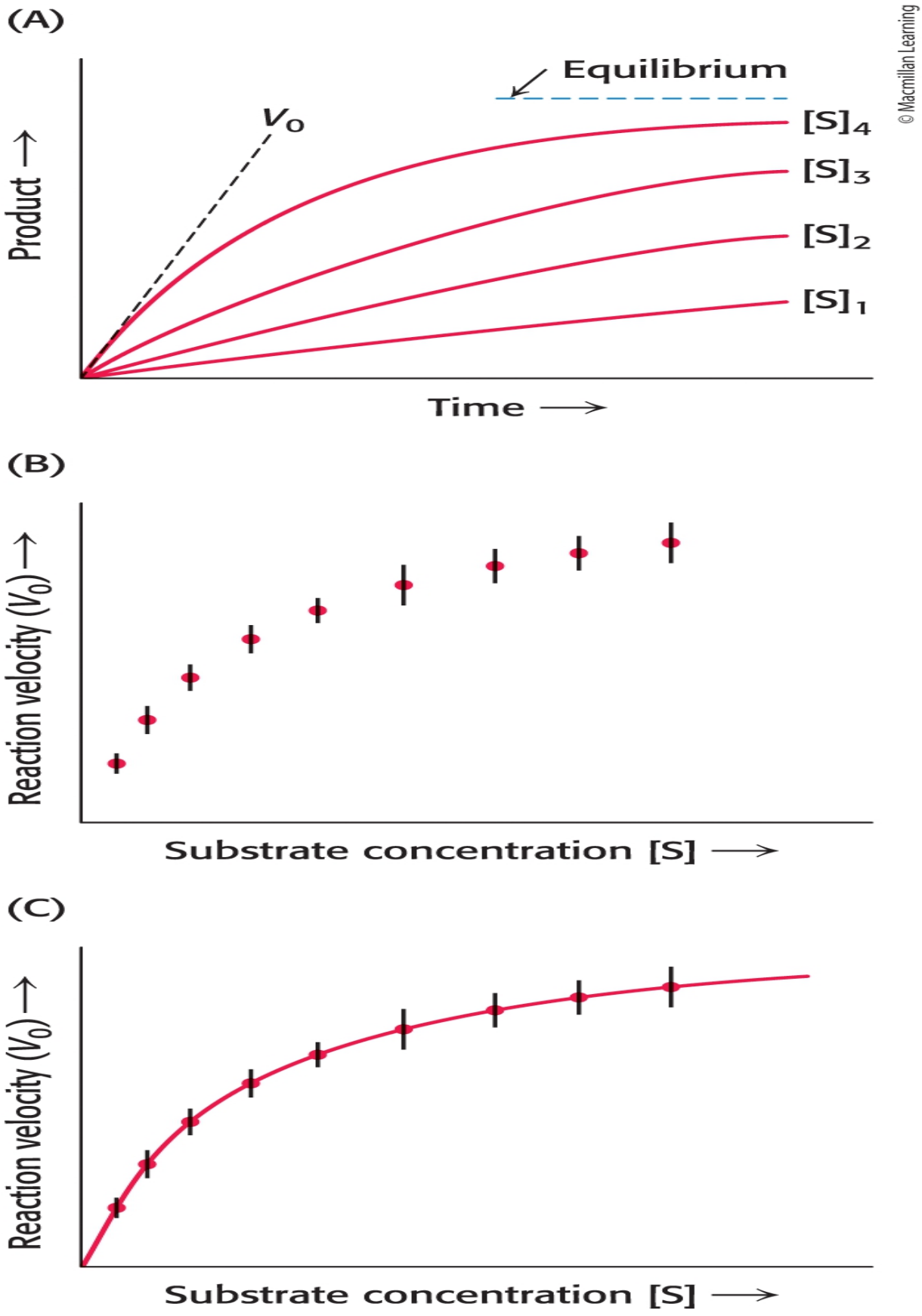
(A) Lock and Key Model: The substrate and the active site of the enzyme are perfectly complementary to each other such that the three projections of the substrate fit perfectly in the three grooves of the enzyme active site labeled a, b, and c. The enzyme and substrate combine to form an E S (enzyme-substrate) complex.

(B) Induced Fit Model: The substrate and the active site of the enzyme are originally not perfectly complementary to each other. The enzyme later modifies shape of its active site such that the three projections of the substrate fit perfectly in the three grooves of the active site. The enzyme and substrate combine to form an E S complex.

Return to FIGURE 5.8. Schematic illustration of the lock and key model and the induced-fit model

Extended description for FIGURE 5.9. Graphical representation of the relation between initial velocity

and substrate concentration



© Macmillan Learning

Graph (A): The horizontal axis is labeled time. The vertical axis is labeled product. A dashed line labeled equilibrium runs parallel to the horizontal axis at the highest concentration of product on the vertical axis. A dashed straight line labeled V naught rises steeply from the origin at an angle of roughly 60 degrees. The graph consists of four curves:

1. substrate concentration subscript 1: The curve is a straight line that rises gradually from the origin at an angle of roughly 15 degrees. It stops at a product concentration much less than half of the maximum product concentration given in the vertical axis.

2. substrate concentration subscript 2: The curve is a straight line that rises gradually from the origin at an angle of roughly 20 degrees. It then plateaus slightly in the end. It stops at a product concentration just below half of the maximum product concentration given in the vertical axis.

3. substrate concentration subscript 3: The curve is a straight line that rises gradually from the origin at an angle of roughly 45 degrees. It then plateaus slightly in the end. It stops at a product concentration just above half of the maximum product concentration given in the vertical axis.

4. substrate concentration subscript 4: The curve is slightly hyperbolic. It rises gradually from the origin at an angle of roughly 60 degrees. It then plateaus slightly in the second half of the graph just below the equilibrium point.

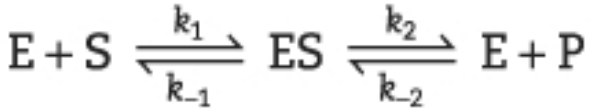
(B) The graph is a scatterplot. The horizontal axis is labeled substrate concentration substrate concentration. The vertical axis is labeled Reaction velocity (V naught). The data points are presented such that they form an upward convex curve that starts from the

origin and plateaus at the highest reaction velocity, in the upper right corner of the graph.

(C) The graph is a scatterplot. The horizontal axis is labeled Substrate concentration substrate concentration. The vertical axis is labeled Reaction velocity (V naught). The data points are presented such that they form an upward convex curve similar to graph (B). They start from the origin and plateau at the highest reaction velocity, in the upper right corner of the graph. A line connects the data points.

Return to FIGURE 5.9. Graphical representation of the relation between initial velocity and substrate concentration

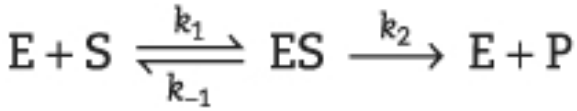
Extended description for Model proposed by Michaelis and Menten for enzyme catalysis



The chemical equation is depicted as follows: E plus S is reversibly converted into E S. The top forward arrow is labeled lowercase k subscript 1. The bottom backward arrow is labeled lowercase k subscript minus 1. E S is further reversibly converted into E plus P. The top forward arrow is labeled lowercase k subscript 2. The bottom backward arrow is labeled lowercase k subscript minus 2.

Return to Model proposed by Michaelis and Menten for enzyme catalysis

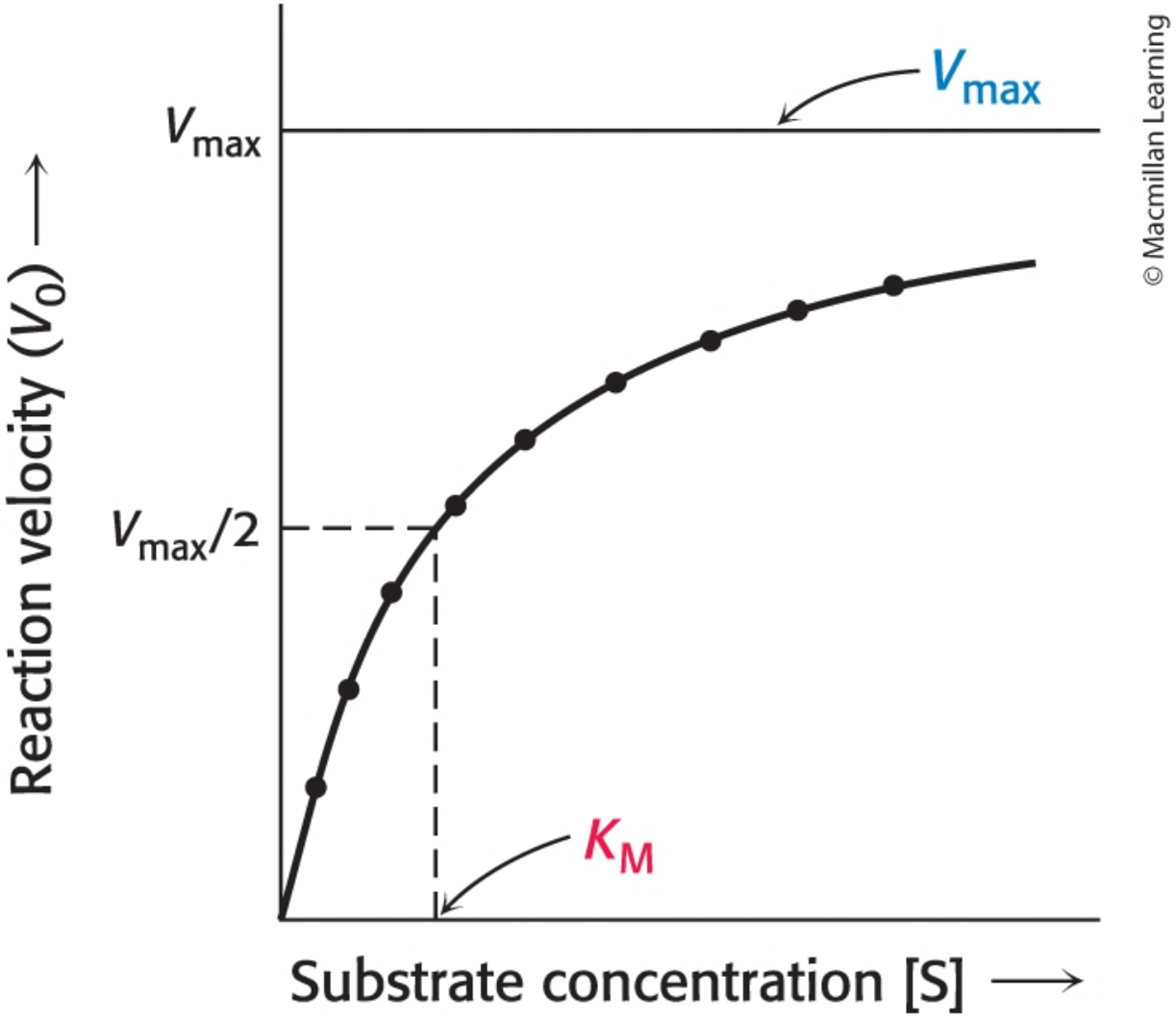
Extended description for Enzyme catalysis



The chemical equation is depicted as follows: E plus S is reversibly converted into E S. The top forward arrow is labeled lowercase k subscript 1. The bottom backward arrow is labeled lowercase k subscript minus 1. E S is further irreversibly converted into E plus P. The forward arrow is labeled lowercase k subscript 2.

Return to Enzyme catalysis

Extended description for FIGURE 5.10. Graphical representation of Michaelis-Menten kinetics

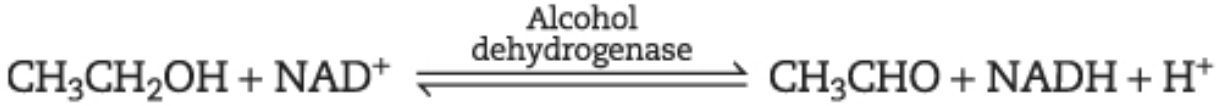


The graph contains a hyperbolic curve. The horizontal axis is labeled substrate concentration. The vertical axis is labeled reaction velocity (V naught). A solid line labeled V subscript max runs parallel to the horizontal axis at the highest reaction velocity on the vertical axis. A dashed line labeled StartFraction V subscript max over 2 EndFraction runs parallel to the horizontal axis at half the height of the V subscript max line. Another dashed line labeled K

subscript M runs parallel to the vertical axis at a very low substrate concentration. It originates at a point from the curve where the StartFraction V subscript max over 2 EndFraction line touches the curve. The several data points represented as thick dots are shown in the hyperbolic curve.

Return to FIGURE 5.10. Graphical representation of Michaelis-Menten kinetics

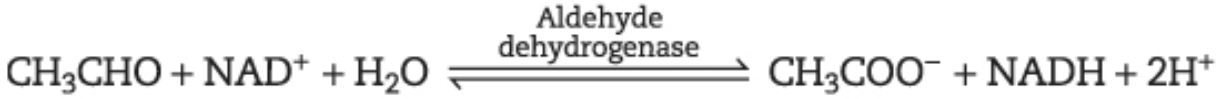
Extended description for Reaction catalyzed by alcohol dehydrogenase



The reaction consists of two reactants and three products. The first reactant is C H 3 C H 2 O H. The second reactant is N A D superscript plus. A reversible reaction arrow labeled "Alcohol dehydrogenase" leads to the products. The first product is C H 3 C H O. The second product is N A D H. The third product is H superscript plus.

Return to Reaction catalyzed by alcohol dehydrogenase

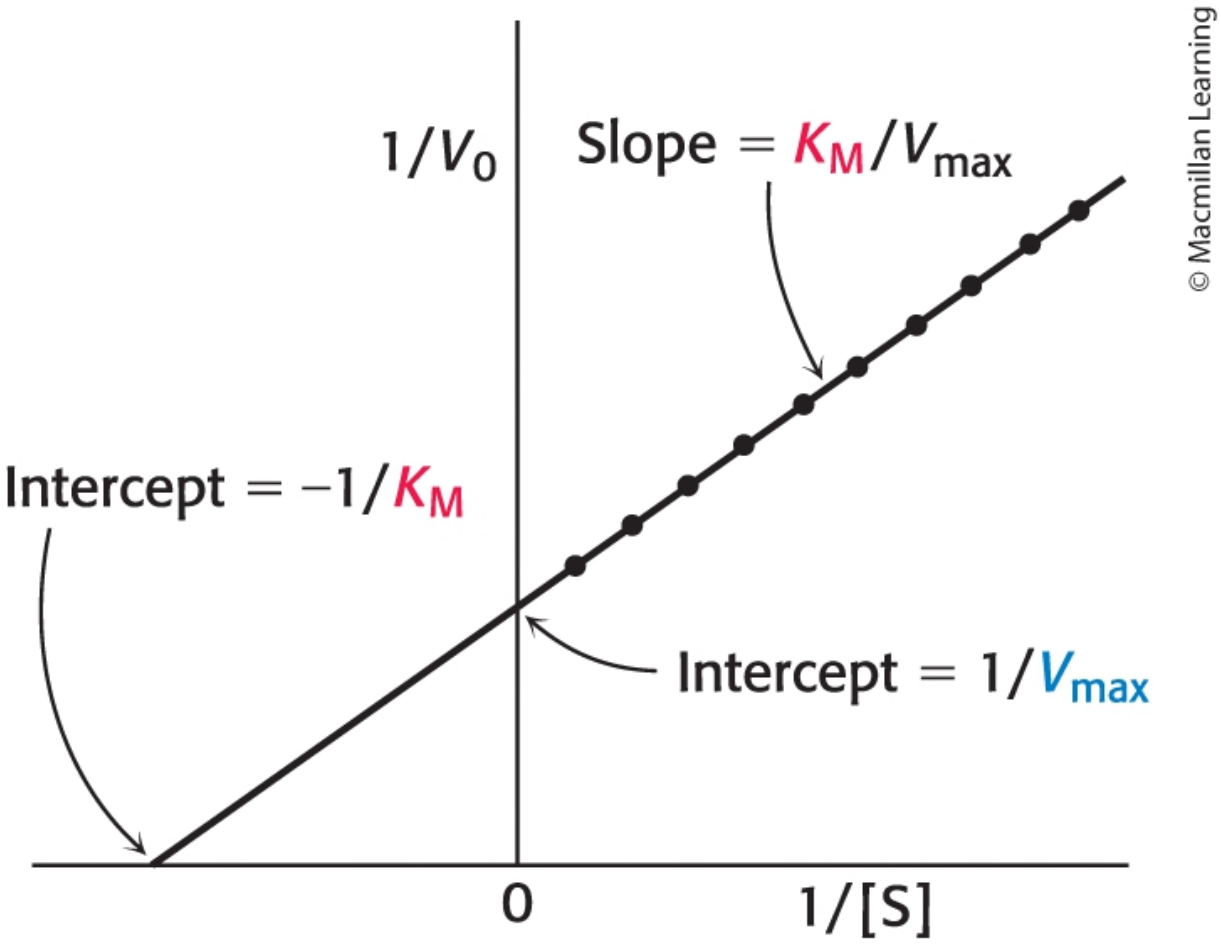
Extended description for Reaction catalyzed by aldehyde dehydrogenase



The reaction consists of three reactants and three products. The first reactant is C H 3 C H O. The second reactant is N A D superscript plus. The third reactant is H 2 O. A reversible reaction arrow labeled "Aldehyde dehydrogenase" leads to the products. The first product is C H 3 C O O superscript minus. The second product is N A D H. The third product is 2 H superscript plus.

Return to Reaction catalyzed by aldehyde dehydrogenase

Extended description for FIGURE 5.11. The Lineweaver–Burk plot

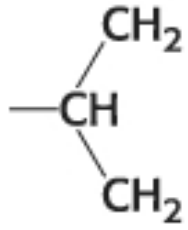


© Macmillan Learning

The horizontal axis is labeled StartFraction 1 over substrate concentration EndFraction. The vertical axis is labeled StartFraction 1 over V naught EndFraction. A linear slope runs from a point on the negative side of the horizontal axis with an intercept value of StartFraction negative 1 over K subscript M EndFraction. It crosses the vertical axis with an intercept value of StartFraction 1 over V subscript max EndFraction. The slope in the positive quadrant has a value of StartFraction K subscript M over V subscript max EndFraction.

Return to FIGURE 5.11. The Lineweaver–Burk plot

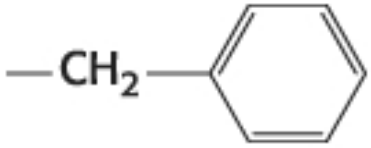
Extended description for Chemical structure of the side chain of valine



The structure of the side chain is as follows: A central C atom is single bonded to C H 2 on the upper right and C H 2 on the lower right. The central C atom is bound to H and has an open single bond on the left.

Return to Chemical structure of the side chain of valine

Extended description for Chemical structure of the side chain of phenylalanine



The structure of the side chain is as follows: A benzene ring is in a horizontal orientation with C 1 occupying the rightmost vertex. It consists of alternating with double bonds between C 2 and C 3, C 4 and C 5, and C 6 and C 1. C 4 is single bond to C H 2 on the left. C H 2 has an open single bond on the left.

Return to Chemical structure of the side chain of phenylalanine

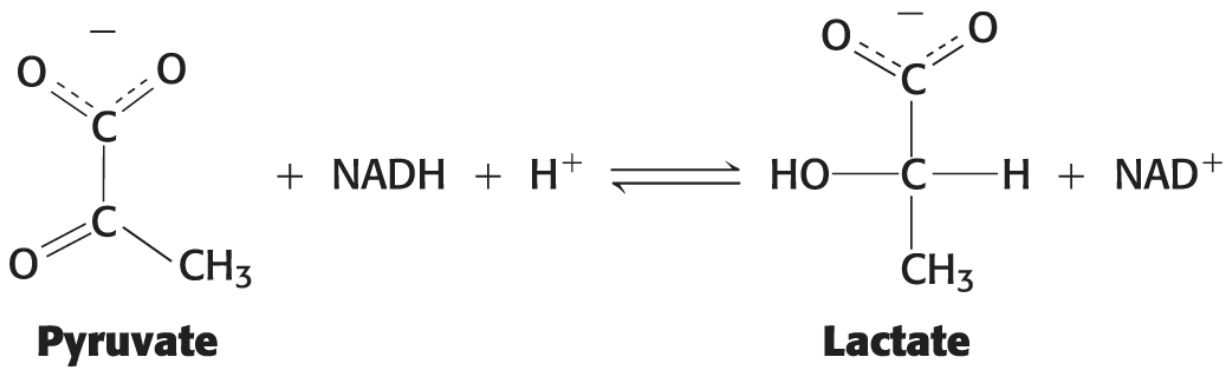
Extended description for Bisubstrate reaction



The reaction consists of two reactants and two products. The reactants are A and B. A reversible reaction arrow leads to the products. The products are P and Q.

Return to Bisubstrate reaction

Extended description for Chemical equation showing the oxidation of lactate to produce pyruvate



The reaction is reversible and consists of three reactants and two products.

The first reactant is pyruvate and has the following structure: A central C atom is double bonded to O on the lower left, single bonded to C H 3 on the lower right, and single bonded to C above. The C atom above is single bonded to an O atom on the upper right and the upper left with a resonance bond shared between them.

The second reactant is N A D H.

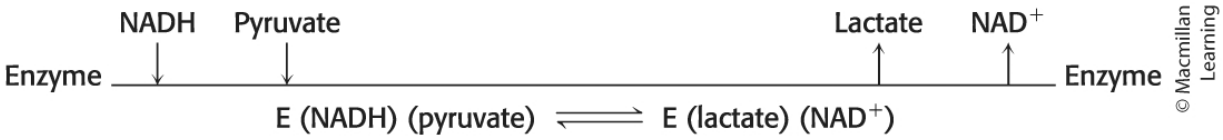
The third reactant is H superscript plus ion.

The first product is lactate and has the following structure: A central C atom is single bonded to O H on the left, H on the right, C H 3 below, and C above. The C atom above is single bonded to an O atom on the upper right and upper left with a resonance bond shared between them.

The second product is N A D superscript plus.

Return to Chemical equation showing the oxidation of lactate to produce pyruvate

Extended description for Cleland notation for the conversion of pyruvate into lactate



The mechanism observes the following sequence:

1. Enzyme

2. Addition of N A D H

3. Addition of Pyruvate

4. The reversible conversion of E (enzyme), N A D H, and pyruvate into E, lactate, and N A D superscript plus.

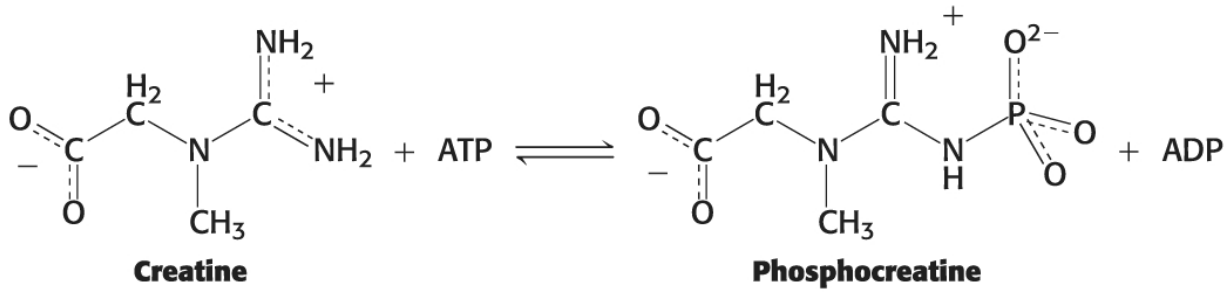
5. Removal of lactate.

6. Removal of N A D superscript plus.

7. Enzyme

Return to Cleland notation for the conversion of pyruvate into lactate

Extended description for Chemical equation showing the conversion of creatine into phosphocreatine



The reaction is reversible and consists of two reactants and two products.

The first reactant is creatine and has the following structure: A 1 N and 3 C heteronuclear alkane chain is depicted as a line structure using 4 zigzag lines. The N atom occupies the third position. The C atoms occupy the remaining positions. C 1 is single bonded to an O atom below and on the upper left with a resonance bond shared between them. This end of the molecule carries an overall negative charge. C 2 is bound to H 2. The first N atom is single bonded to C H 3 below. C 3 is single bonded to an N H 2 group above and on the lower right with a resonance bond shared between them. This end of the molecule carries an overall positive charge.

The second reactant is an A T P molecule.

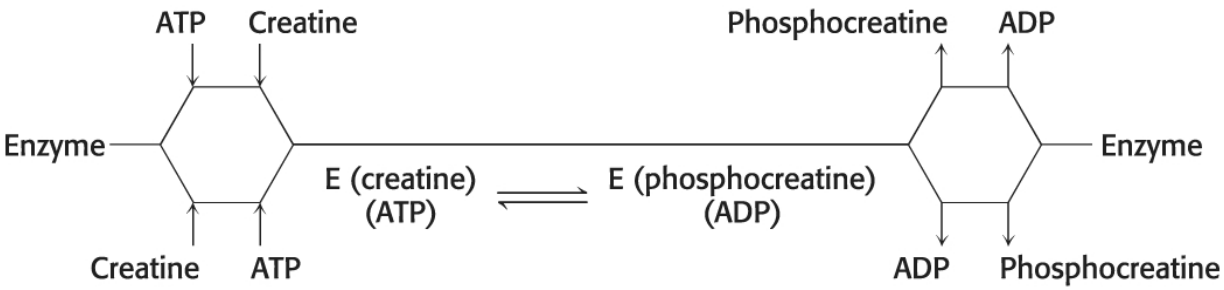
The first product is phosphocreatine and has the following structure: A 2 N and 3 C heteronuclear alkane chain is depicted as a line structure using 4 zigzag lines. The first N atom occupies the third position and the second N atom occupies the fifth position. The C atoms occupy the remaining positions. C 1 is single bonded to an O atom below and on the upper left with a resonance bond

shared between them. This end of the molecule carries an overall negative charge. C 2 is bound to H 2. The first N atom is single bonded to C H 3 below. C 3 is single bonded to an N H 2 group above. The second N atom is bound to H and single bonded to a central P atom on the upper right. P atom is single bonded to an O superscript 2 minus ion above, and an O atom on the right and the lower right. Resonance bonds are shared between central P atom and O atoms.

The second product is an A D P.

Return to Chemical equation showing the conversion of creatine into phosphocreatine

Extended description for Cleland notation for the conversion of creatine into phosphocreatine



The mechanism observes the following sequence:

1. Enzyme

2. Addition of either A T P or Creatine

3. Addition of either Creatine or A T P.

4. The reversible conversion of the E (enzyme), creatine, and A T P into E, phosphocreatine, and A D P.

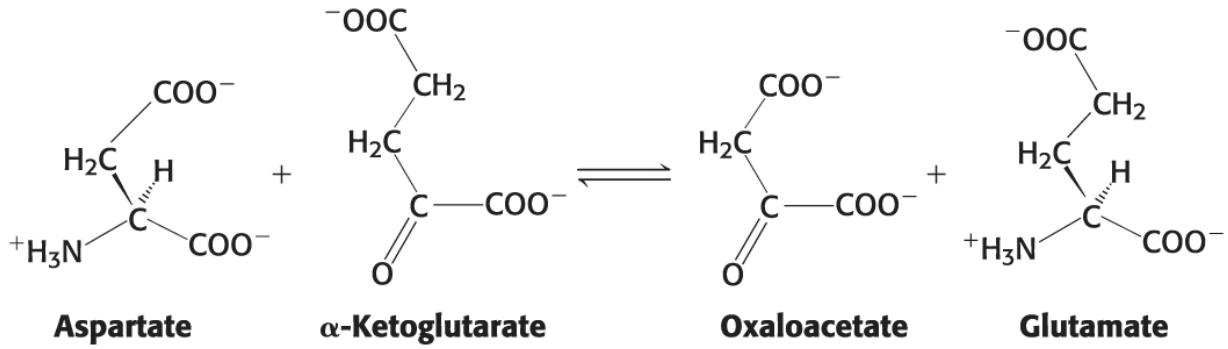
5. Removal of either A D P or phosphocreatine.

6. Removal of either phosphocreatine or A D P.

7. Release of enzyme.

[Return to Cleland notation for the conversion of creatine into phosphocreatine]

Extended description for Double displacement reaction between aspartate and alpha-ketoglutarate



The reaction is reversible and consists of two reactants and two products.

The first reactant is aspartate and has the following structure: A central C atom is single bonded to C O O superscript minus group on the lower right, single bonded to N H 3 superscript plus on the lower left, dash bonded to H on the upper right, and wedge bonded to C H 2 on the upper left. The C H 2 group is further single bonded to another C O O superscript minus group on the upper right.

The second reactant is alpha-ketoglutarate and has the following structure: A three carbon alkane chain is depicted as a line structure using two zigzag lines in a vertical orientation. C 1 is single bonded to a C O O superscript minus group on the right and double bonded to an O atom on the lower left. C 2 is bound to H 2. C 3 is bound to H 2 and single bonded to another C O O superscript minus group on the upper left.

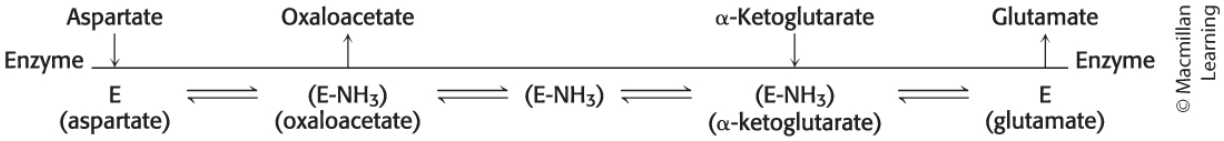
The first product is oxaloacetate and has the following structure: A central C atom is single bonded to a C O O superscript minus group on the right and double bonded to an O atom on the lower left. C 2 is

bound to H 2 and single bonded to another C O O superscript minus group on the upper right.

The second product is glutamate and has the following structure: A central C atom is single bonded to C O O superscript minus group on the lower right, single bonded to N H 3 superscript plus on the lower left, dash bonded to H on the upper right, and wedge bonded to C H 2 on the upper left. The C H 2 group on the upper left is single bonded to another C H 2 group on the upper right which is further single bonded to another C O O superscript minus group on the upper left.

Return to Double displacement reaction between aspartate and alpha-ketoglutarate

Extended description for Cleland notation for the conversion of aspartate into glutamate



The mechanism observes the following sequence:

1. Enzyme

2. Addition of aspartate

3. Formation of an enzyme-aspartate complex.

4. The reversible conversion of the enzyme-aspartate complex into an enzyme-N H 3-oxaloacetate complex or enzyme-N H 3 complex.

5. Removal of oxaloacetate.

6. Addition of alpha-ketoglutarate.

7. The reversible conversion of the enzyme-N H 3 complex into an enzyme-N H 3-alpha-ketoglutarate complex.

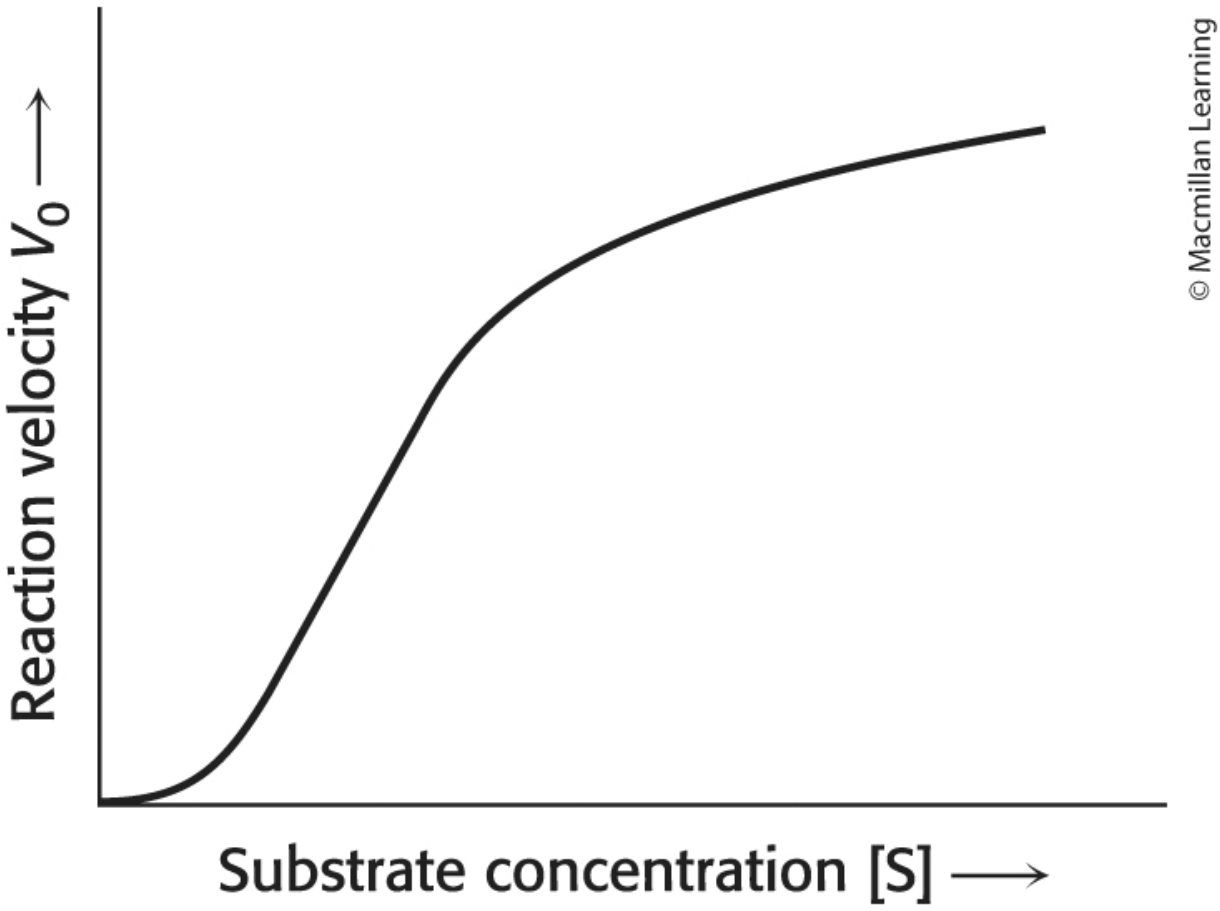
8. The reversible conversion of the enzyme-N H 3-alpha-ketoglutarate complex into an enzyme-glutamate complex.

9. Removal of glutamate.

10. Enzyme

Return to Cleland notation for the conversion of aspartate into glutamate

Extended description for FIGURE 5.12. Graphical representation of the allosteric enzyme activity

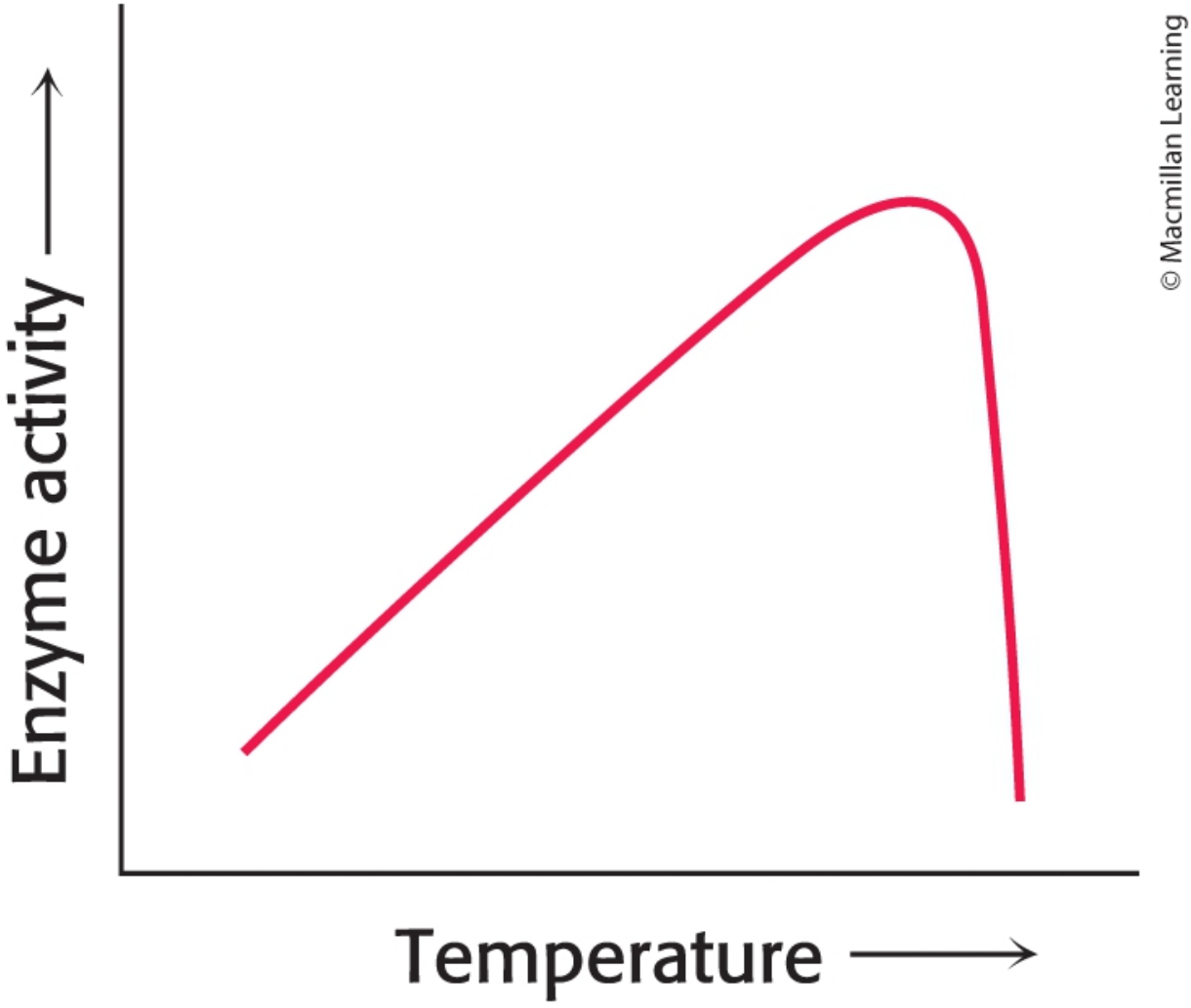


© Macmillan Learning

The horizontal axis is labeled substrate concentration substrate concentration. The vertical axis is labeled reaction velocity V naught. A sigmoidal curve rises rapidly from the origin, plateaus slightly, and then rises gradually toward the upper right corner.

Return to FIGURE 5.12. Graphical representation of the allosteric enzyme activity

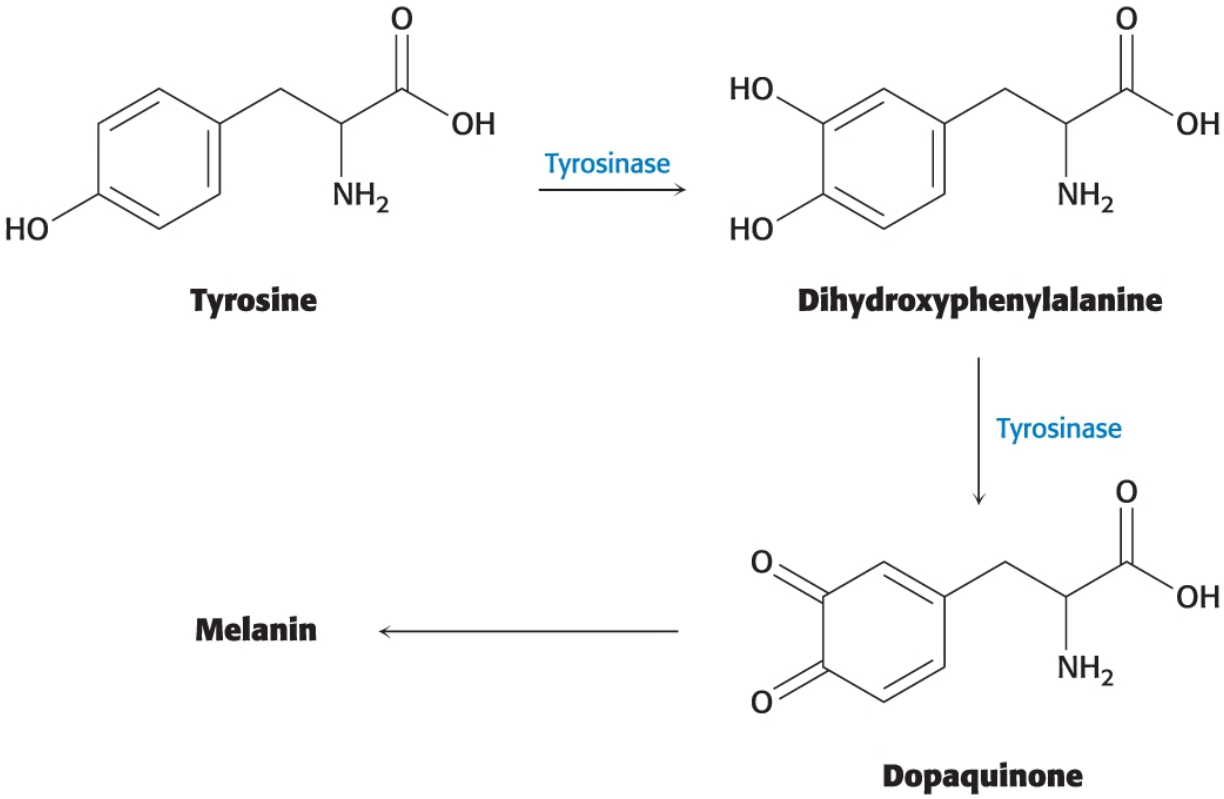
Extended description for Graphical representation of the relation between enzyme activity and temperature



The horizontal axis is labeled temperature. The vertical axis is labeled enzyme activity. A curve rises linearly, peaks in the upper right corner of the graph at the highest enzyme activity, and then drops sharply in a nearly vertical fashion.

Return to Graphical representation of the relation between enzyme activity and temperature

Extended description for Chemical reaction showing the conversion of tyrosine into dopaquinone



The reaction consists of three steps, each with one reactant and one product. The initial two steps are catalyzed by tyrosinase.

Step 1: The reactant is tyrosine and has the following structure: A benzene ring is present in a vertical orientation with C 1 occupying the topmost vertex. Alternating double bonds are present between C 2 and C 3, C 4 and C 5, and C 6 and C 1. C 5 atom of the benzene ring is single bonded to O H. C 2 atom of the ring is single bonded to C 1 atom of a 3 carbon alkane chain depicted as a line structure using 2 zigzag lines. C 2 atom of the chain is single bonded to N H 2 below. C 3 atom of the chain is double bonded to O above and single bonded

to O H on the lower right. The reaction is catalyzed by the enzyme tyrosinase.

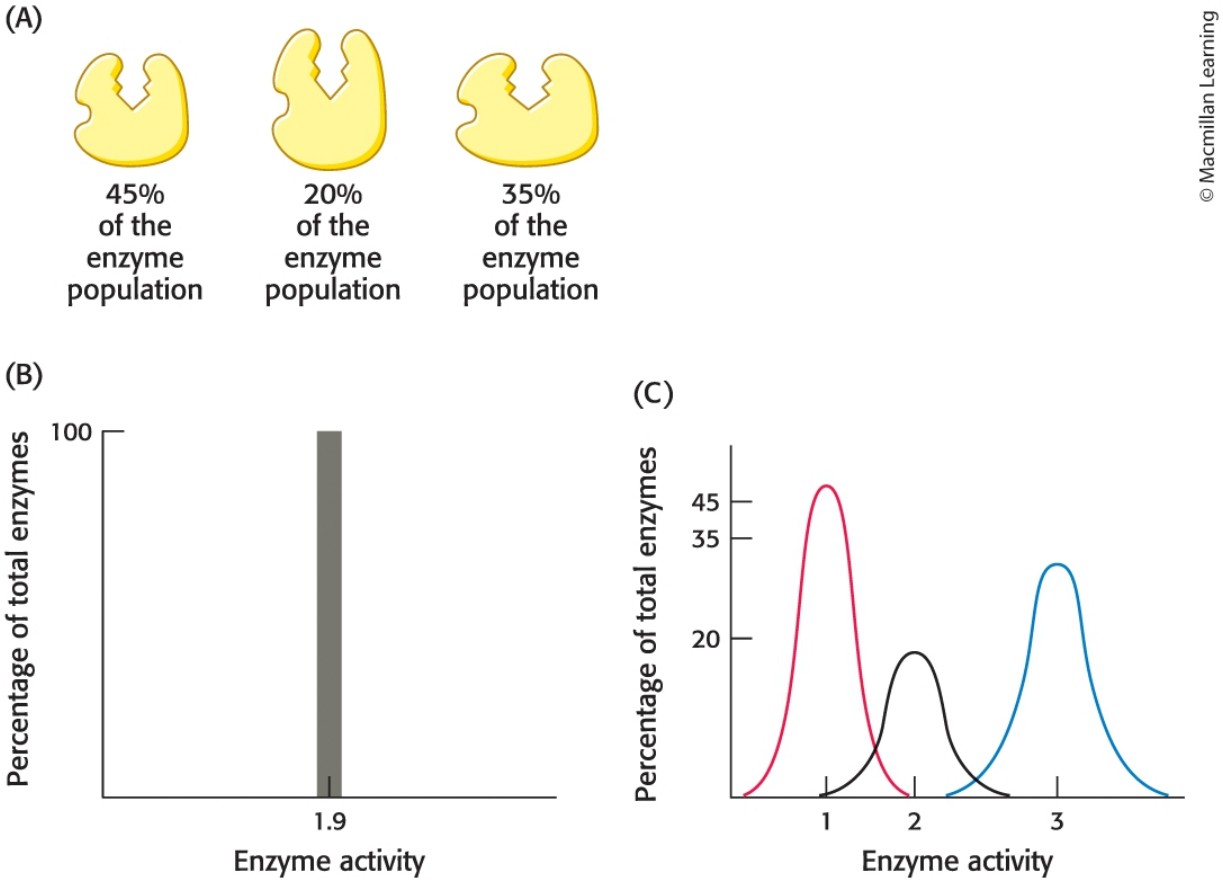
The product is dihydroxyphenylalanine and has the following structure: A benzene ring is present in a vertical orientation with C 1 occupying the topmost vertex. Alternating double bonds are present between C 2 and C 3, C 4 and C 5, and C 6 and C 1. C 5 is single bonded to O H on the lower left. C 6 is single bonded to O H on the upper left. C 2 atom of the ring is single bonded to C 1 atom of a 3 carbon alkane chain depicted as a line structure using 2 zigzag lines. C 2 atom of the chain is single bonded to N H 2 below. C 3 atom of the chain is double bonded to O above and single bonded to O H on the lower right.

Step 2: The reactant is Dihydroxyphenylalanine. The reaction occurs in catalyzed by tyrosinase. The product is dopaquinone and has the following structure: A 6 C hexagonal ring is present in a vertical orientation with C 1 occupying the topmost vertex. Double bonds are present between C 1 and C 2 and C 3 and C 4. C 5 is double bonded to O on the lower left. C 6 is double bonded to O on the upper left. C 2 atom of the ring is single bonded to C 1 atom of a 3 carbon alkane chain depicted as a line structure using 2 zigzag lines. C 2 atom of the chain is single bonded to N H 2 below. C 3 atom of the chain is double bonded to O above and single bonded to O H on the lower right

Step 3: The reactant is dopaquinone. The product is melanin.

Return to Chemical reaction showing the conversion of tyrosine into dopaquinone

Extended description for FIGURE 5.13. Schematic illustration and graphical representation of molecular heterogeneity



© Macmillan Learning

Part (A): Three of the major shapes used by enzymes are shown:

1. Roughly square-shaped: 45 percent of the enzyme population.

2. Elongated in height: 20 percent of the enzyme population.

3. Elongated in width: 35 percent of the enzyme population.

Part (B): A bar graph is shown. The horizontal axis is labeled enzyme activity and is marked 1.9 at the midpoint. The vertical axis is labeled percentage of total enzymes. It has the marking 100 at the top. At the 1.9 unit mark, a vertical bar having a height of 100 units is shown.

Part (C): A graph containing three curves is shown. The horizontal axis is labeled enzyme activity. It has marking ranging from 0 to 3 in increments of 1 unit. The vertical axis is labeled percentage of total enzymes. It has markings 20, 35, and 45. The graph consists of three bell-shaped curves:

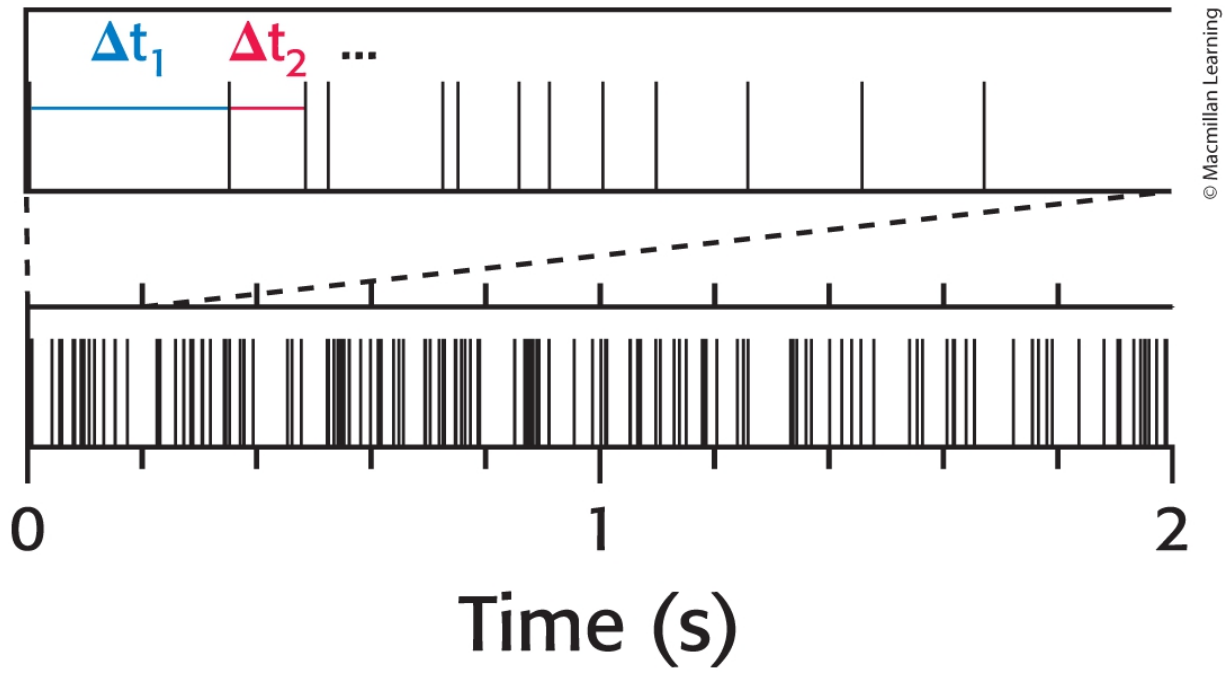
1. The first curve rises rapidly from the origin, peaks at (1, 45), and falls to (2, 0).

2. The second rises rapidly from (1,0), peaks at (2, 19), and falls to (2.5, 0).

3. The third curve rises rapidly from (2.3, 0), peaks at (3, 33), and falls to (3.5, 0).

Return to FIGURE 5.13. Schematic illustration and graphical representation of molecular heterogeneity

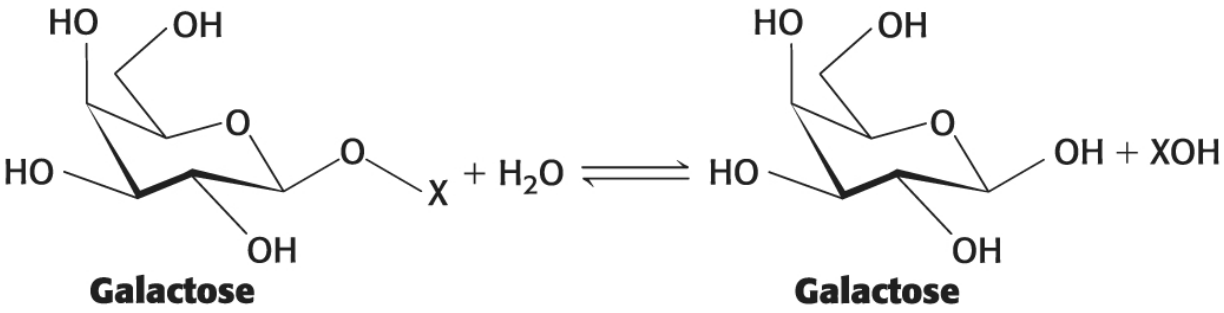
Extended description for FIGURE 5.14. Schematic illustration of the stochastic behavior of a single-enzyme molecule



A horizontal barcode like image is shown. It consists of several short thick and thin vertical lines. The barcode is divided into 10 sections. The horizontal axis is labeled time (s) that ranges from 0 to 2 in increments of 1 unit. The initial section of the barcode is enlarged on the top. It consists of vertical lines separated by irregular gaps. Variable time increments labeled delta t subscript 1, delta t subscript 2 are shown in the enlarged view. The gap between the distantly placed first and second vertical line is labeled delta t subscript 1. The gap between the closely spaced second and third line is labeled delta t subscript 2.

Return to FIGURE 5.14. Schematic illustration of the stochastic behavior of a single-enzyme molecule

Extended description for Chemical equation showing the conversion of carbohydrate galactose to galactose



The reaction is reversible and consists of two reactants and two products.

The first reactant is labeled galactose and has the following structure: A six-membered heterocyclic ring consisting of 1 O and 5 C atoms is in a chair conformation. O atom occupies the top-right vertex. C 1 is single bonded to O on the upper right. This O atom is single bonded to X on the lower right. C 2 is single bonded to O H on the lower right. C 3 is single bonded to O H on the upper left. C 4 is single bonded to O H above. C 5 is single bonded to C H 2 on the upper left in the form of a line. This C H 2 is single bonded to O H on the upper right.

The second reactant is H 2 O.

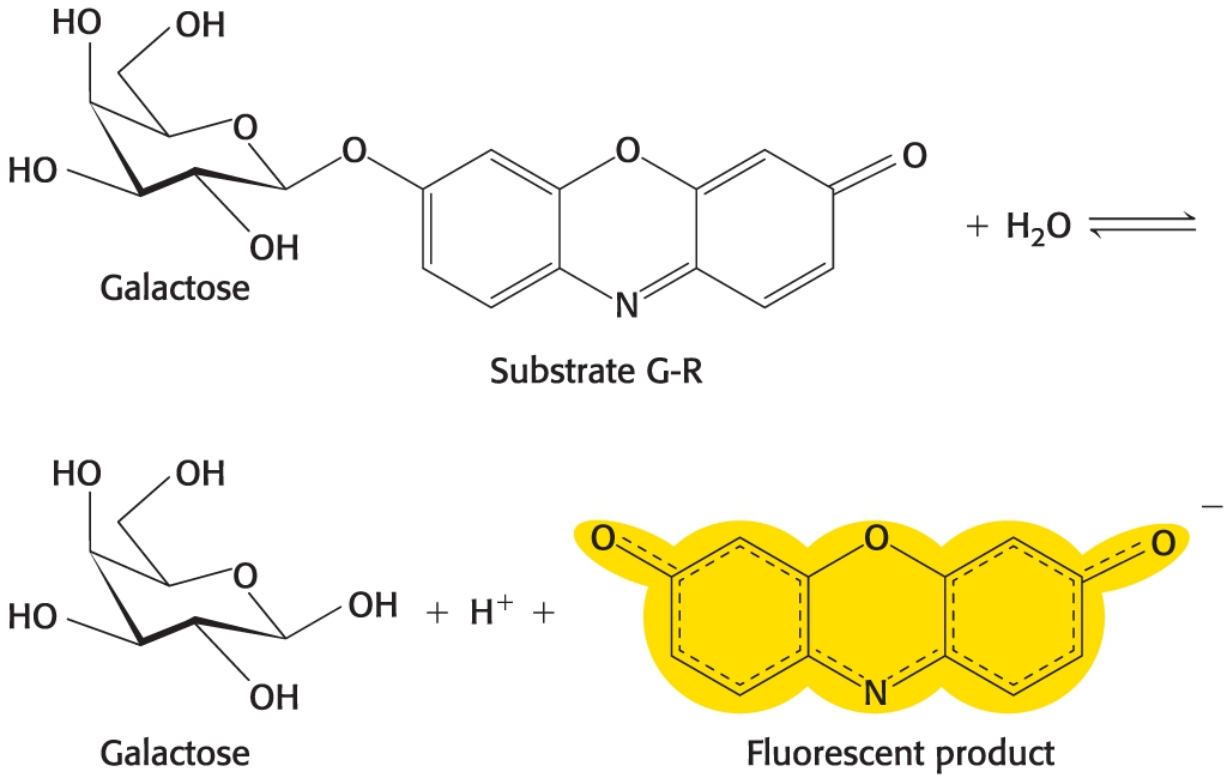
The first product is also labeled galactose and has the following structure: A six-membered heterocyclic ring consisting of 1 O and 5 C atoms is in a chair conformation. O atom occupies the top-right vertex. C 1 is single bonded to O H on the upper right. C 2 is single bonded to O H on the lower right. C 3 is single bonded to O H on the upper left. C 4 is single bonded to O H above. C 5 is single bonded to

C H 2 on the upper left in the form of a line. This C H 2 is single bonded to O H on the upper right.

The second product is X O H.

Return to Chemical equation showing the conversion of carbohydrate galactose to galactose

Extended description for FIGURE 5.15. Chemical reaction showing the formation of a highly fluorescent product



The reaction is reversible and has two reactants and three products.

The first reactant is the substrate G-R molecule. It is composed of three fused rings connected to a galactose molecule.

The galactose molecule has the following structure: A six-membered heterocyclic ring consisting of 1 O and 5 C atoms is in a chair conformation. O atom occupies the top-right vertex. C 2 is single bonded to O H on the lower right. C 3 is single bonded to O H on the upper left. C 4 is single bonded to O H above. C 5 is single bonded to

C H 2 on the upper left in the form of a line. This C H 2 is single bonded to O H on the upper right.

The fused rings have the following structure: A 6 C hexagonal ring is in a vertical orientation with C 1 occupying the topmost vertex. A double bond is present between C 1 and C 2 and C 3 and C 4. C 1 is single bonded to O on the upper left. This O atom is single bonded to the C 1 atom of the galactose molecule. This hexagonal ring is fused on the right to a 6-membered heterocyclic hexagonal ring such that C 2 and C 3 of the first ring are C 4 and C 3 of the second ring respectively. The second ring consists of 1 O, 1 N, and 4 C atoms. O occupies the first position, which is the topmost vertex. N occupies the second position, which is the bottom-most vertex. A double bond is present between C 2 and N atoms. The second hexagonal ring is fused on the right to a third 6 C hexagonal ring such that C 1 and C 2 of the second ring are C 6 and C 5 respectively of the third ring. C 1 occupies the topmost vertex of the third ring. A double bond is present between C 3 and C 4, and C 6 and C 1. C 2 is double bonded to O on the upper right.

The second reactant is H 2 O.

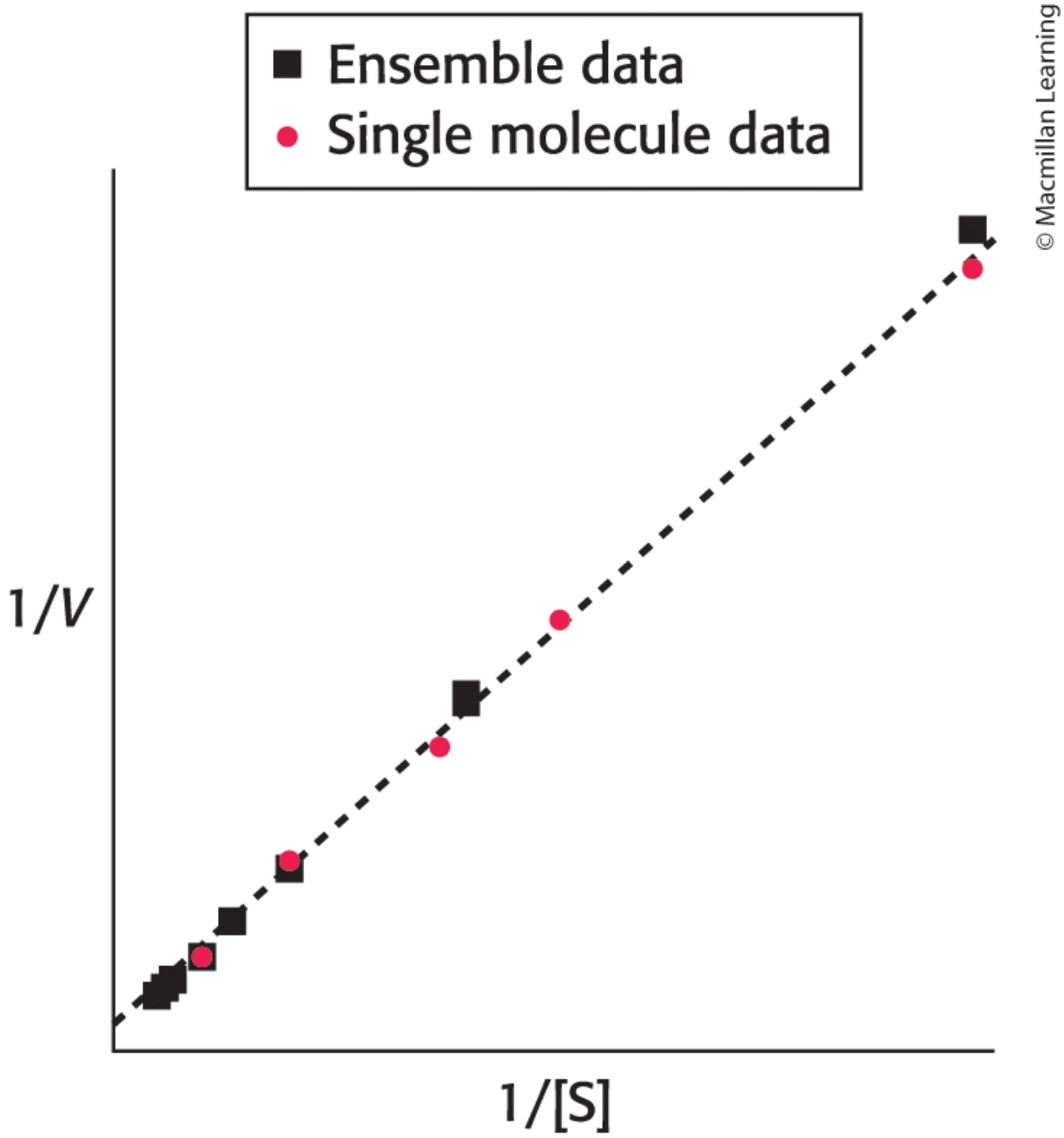
The first product is galactose which has the following structure: A six-membered heterocyclic ring consisting of 1 O and 5 C atoms is in a chair conformation. O atom occupies the top-right vertex. C 2 is single bonded to O H on the lower right. C 3 is single bonded to O H on the upper left. C 4 is single bonded to O H above. C 5 is single bonded to C H 2 on the upper left in the form of a line. This C H 2 is single bonded to O H on the upper right.

The second product is H superscript plus ion.

The third product is labeled fluorescent product and has the following structure: A 6 C hexagonal ring is in a vertical orientation with C 1 occupying the topmost vertex. The resonating bonds in the ring are depicted as a dashed hexagon inside the ring. C 6 is bonded to the O atom on the upper left through a resonance bond. This hexagonal ring is fused on the right to a 6-membered heterocyclic hexagonal ring such that C 2 and C 3 of the first ring are C 4 and C 3 of the second ring respectively. The second ring consists of 1 O, 1 N, and 4 C atoms. O occupies the first position, which is the topmost vertex. N occupies the second position, which is the bottom-most vertex. A resonance bond is present between C 2 and N, and N and C 3. The second hexagonal ring is fused on the right to a third 6 C hexagonal ring such that C 1 and C 2 of the second ring are C 6 and C 5 respectively of the third ring. C 1 occupies the topmost vertex of the third ring. The resonating bonds in the ring are depicted as a dashed hexagon inside the ring. C 2 is bonded to O on the upper right through a resonance bond.

Return to FIGURE 5.15. Chemical reaction showing the formation of a highly fluorescent product

Extended description for FIGURE 5.16. Lineweaver-Burk plot comparing single-molecule kinetic studies and ensemble studies



© Macmillan Learning

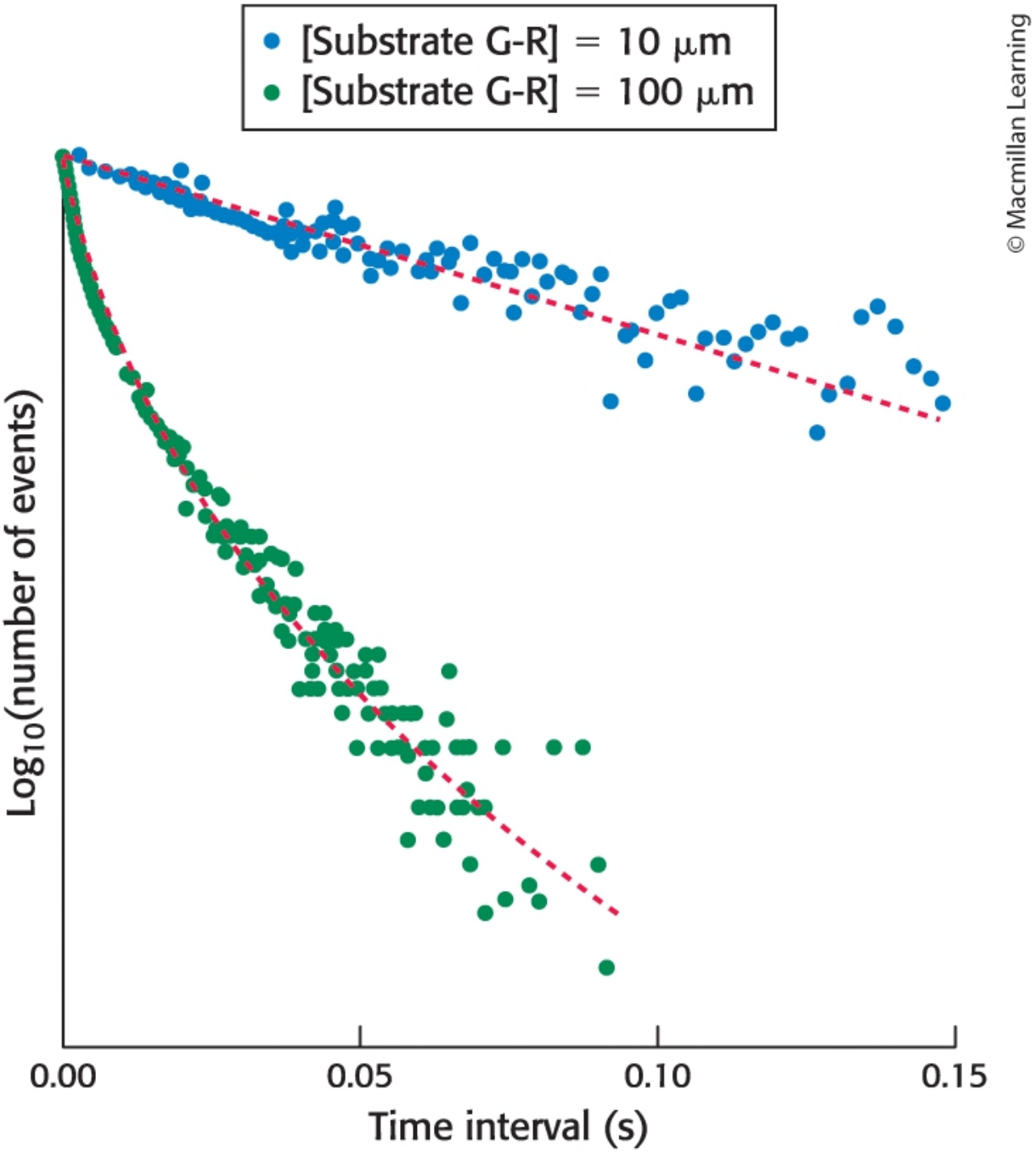
The horizontal axis is labeled StartFraction 1 over substrate concentration EndFraction. The vertical axis is labeled StartFraction 1 over V EndFraction. Two scatter plots are shown:

1. Ensemble data: The data points are represented as small black squares. All the data points fall on a dashed straight line that rises uniformly from the origin toward the upper right corner of the graph.

2. Single-molecule data: The data points are represented as small red dots. All the data points fall on a dashed straight line that rises uniformly from the origin toward the upper right corner of the graph.

Return to FIGURE 5.16. Lineweaver-Burk plot comparing single-molecule kinetic studies and ensemble studies

Extended description for FIGURE 5.17. Scatter plot indicating heterogeneity of beta-galactosidase at molecular level



© Macmillan Learning

The horizontal axis is labeled time interval (s) that ranges from 0.00 to 0.15 in increments of 0.05 units. The vertical axis is labeled log subscript 10 (number of events). Two scatter plots are shown:

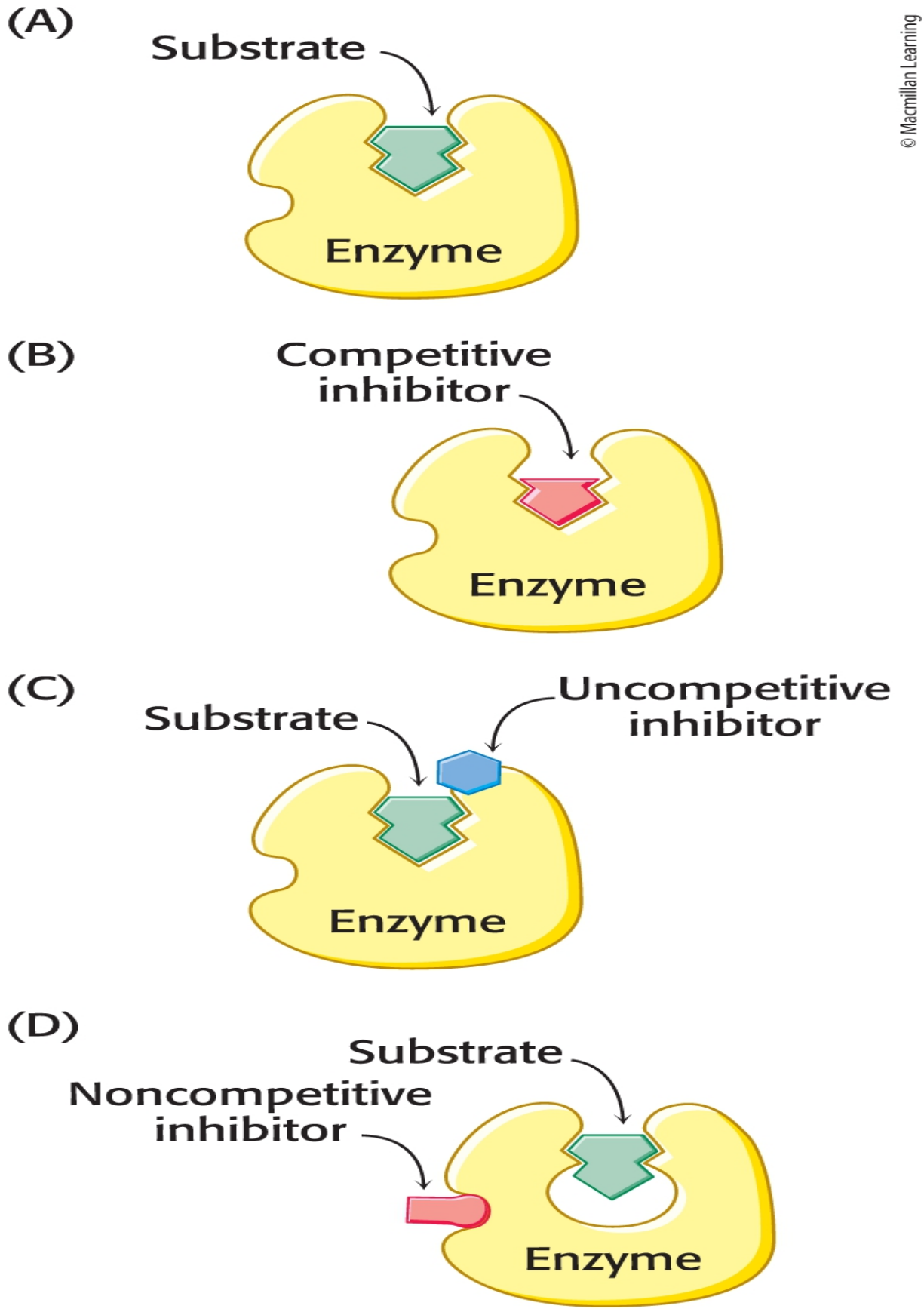
1. Substrate G-R equals 10 micromolar: The data points are depicted as blue dots clustered around a trendline. The trendline decreases gradually from the highest log number of events to more than half of the highest log number of events at 0.15 seconds.

2. Substrate G-R equals 100 micrometers: The data points are depicted as green dots clustered around trendline. The trendline rapidly moves downward from the highest log number of events to reach the lowest log number of events at around 0.09 seconds.

Return to FIGURE 5.17. Scatter plot indicating heterogeneity of beta-galactosidase at molecular level

Extended description for FIGURE 5.18. Schematic illustration showing the binding of different types of

reversible inhibitors to the enzyme



© Macmillan Learning

Part (A) The substrate fits perfectly inside the groove of the enzyme molecule.

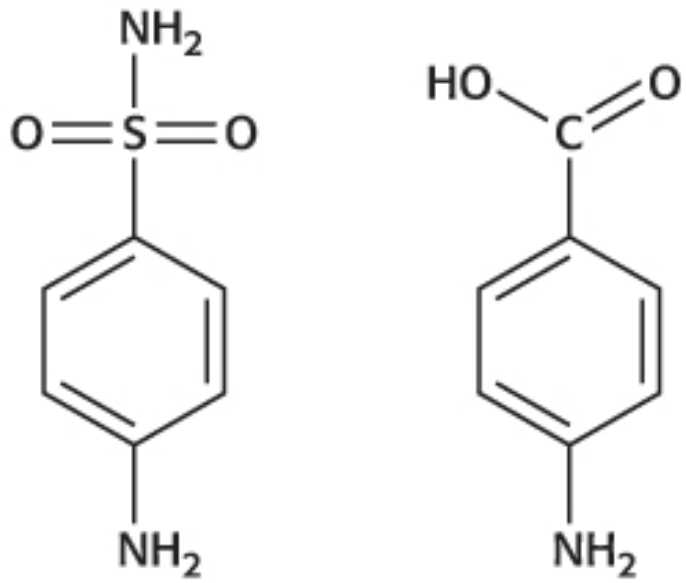
(B) The competitive inhibitor is not the perfect fit for the enzyme groove but fits well enough to block the substrate.

(C) The uncompetitive inhibitor fits perfectly on a different groove of the enzyme. This groove is located above the main groove bound by the substrate.

(D) The noncompetitive inhibitor fits perfectly on a different groove located on the side of the enzyme. This changes the shape of the main groove designated for the substrates. The substrate binds to the main groove but does not fit perfectly into it.

Return to FIGURE 5.18. Schematic illustration showing the binding of different types of reversible inhibitors to the enzyme

Extended description for Chemical structure of sulfanilamide and P A B A



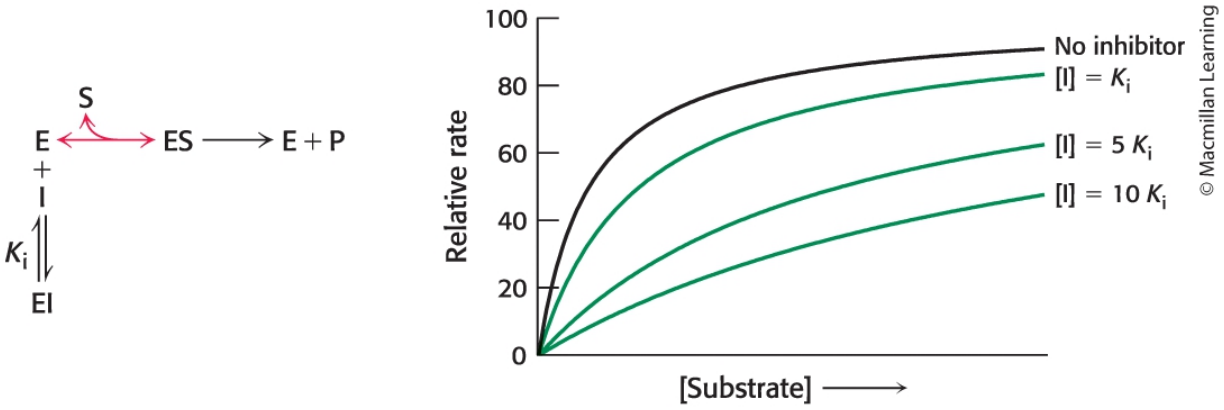
Sulfanilamide **PABA**

Sulfanilamide: A benzene ring is in a vertical orientation with C 1 occupying the topmost vertex. Alternating double bonds are present between C 2 and C 3, C 4 and C 5, and C 6 and C 1. C 1 is single bonded to a central S atom above. This S atom is single bonded to N H 2 above and double bonded to O on the left and right. C 4 is single bonded to N H 2 below.

P A B A: A benzene ring is in a vertical orientation with C 1 occupying the topmost vertex. Alternating double bonds are present between C 2 and C 3, C 4 and C 5, and C 6 and C 1. C 1 is single bonded to a central C atom above. This C atom is single bonded to O H on the upper left and double bonded to O on the upper right. C 4 is single bonded to N H 2 below.

Return to Chemical structure of sulfanilamide and P A B A

Extended description for FIGURE 5.19. Michaelis–Menten plot showing the activity of a competitive inhibitor



The horizontal axis is labeled concentration of substrate. The vertical axis is labeled relative rate. It has markings ranges from 0 to 100 in increments of 20 units. Four curves are shown:

1. No inhibitor: The curve rises rapidly to 75 units on the vertical axis then plateaus at around 85 units.

2. Concentration of I equals K subscript i: The curve rises rapidly to 60 units and then plateaus around 80 units.

3. Concentration of I equals 5 K subscript i: The curve rises almost linearly to 60 units.

4. Concentration of I equals 10 K subscript i: The curve rises almost linearly to approximately units.

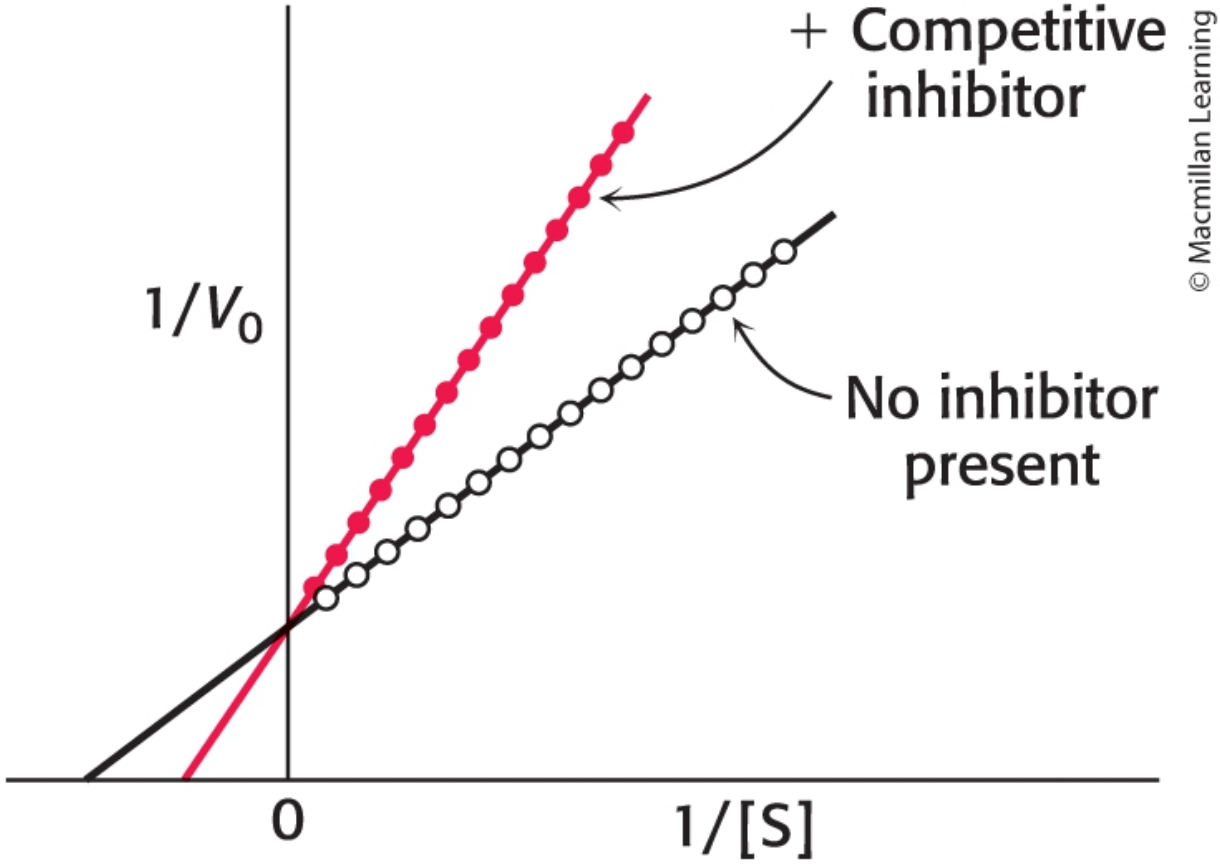
Two equations are shown that depict the two reactions that an enzyme may undergo:

1. E, double-headed arrow and removal of S, E S, forward reaction arrow, E plus P.

2. E plus I, reversible reaction arrow in the presence of K subscript i, E I.

Return to FIGURE 5.19. Michaelis–Menten plot showing the activity of a competitive inhibitor

Extended description for FIGURE 5.20. Lineweaver–Burk plot depicts competitive inhibition



The horizontal axis is labeled StartFraction 1 over substrate concentration EndFraction. The vertical axis is labeled 1 over V naught. Two straight line plots are shown:

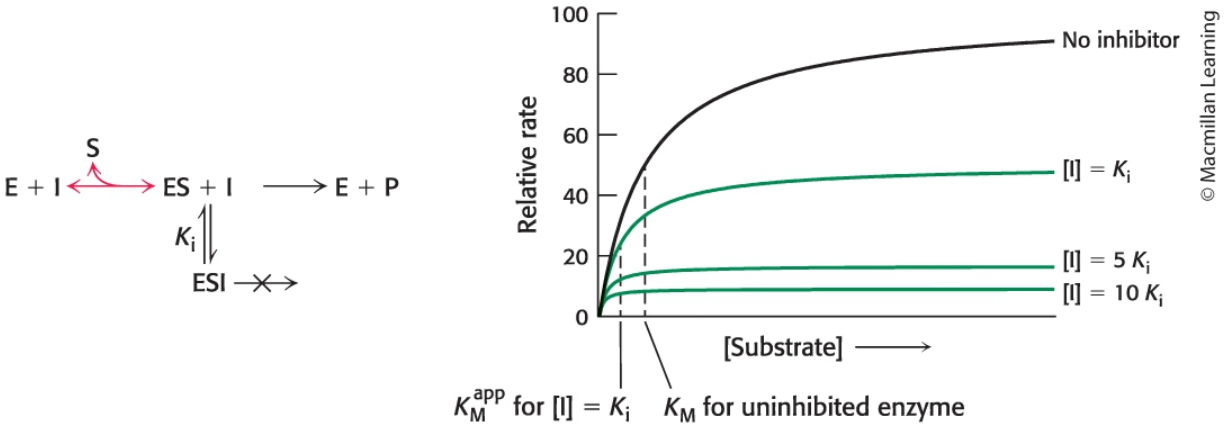
No inhibitor present: A straight line with a linear slope runs from a point on the negative side of the horizontal axis. It crosses the vertical axis into the positive quadrant.

Competitive inhibitor: A straight line with a steeper slope runs from a point slightly closer to the origin, on the negative side of the

horizontal axis. It crosses the vertical axis into the positive quadrant.

Return to FIGURE 5.20. Lineweaver–Burk plot depicts competitive inhibition

Extended description for FIGURE 5.21.Michaelis–Menten plot showing the activity of an uncompetitive inhibitor



The horizontal axis is labeled substrate concentration. The vertical axis is labeled relative rate. It has markings ranging from 0 to 100 in increments of 20 units. Four hyperbolic curves are shown:

1. No inhibitor: The hyperbolic curve rises rapidly to 75 units on the vertical axis and then plateaus around 85 units on the vertical axis.

2. Concentration of I equals K subscript i: The hyperbolic curve rises rapidly to 40 units on the vertical axis and then plateaus at the same value.

3. Concentration of I equals 5 K subscript i: The hyperbolic curve rises to 10 units on the vertical axis and then plateaus at the same value.

4. Concentration of I equals 10 K subscript i: The hyperbolic curve rises to around 7 units on the vertical axis and then plateaus at the same value.

A dashed vertical line rises from the horizontal axis, near the origin, and intersects with curve 2 at approximately 25 units. This line is labeled K superscript app subscript M for concentration of I equals K subscript i.

Another dashed vertical line rises from the horizontal axis, on the right of the first dashed line, and intersects with the first curve at approximately 50 units. This line is labeled K subscript M for uninhibited enzyme.

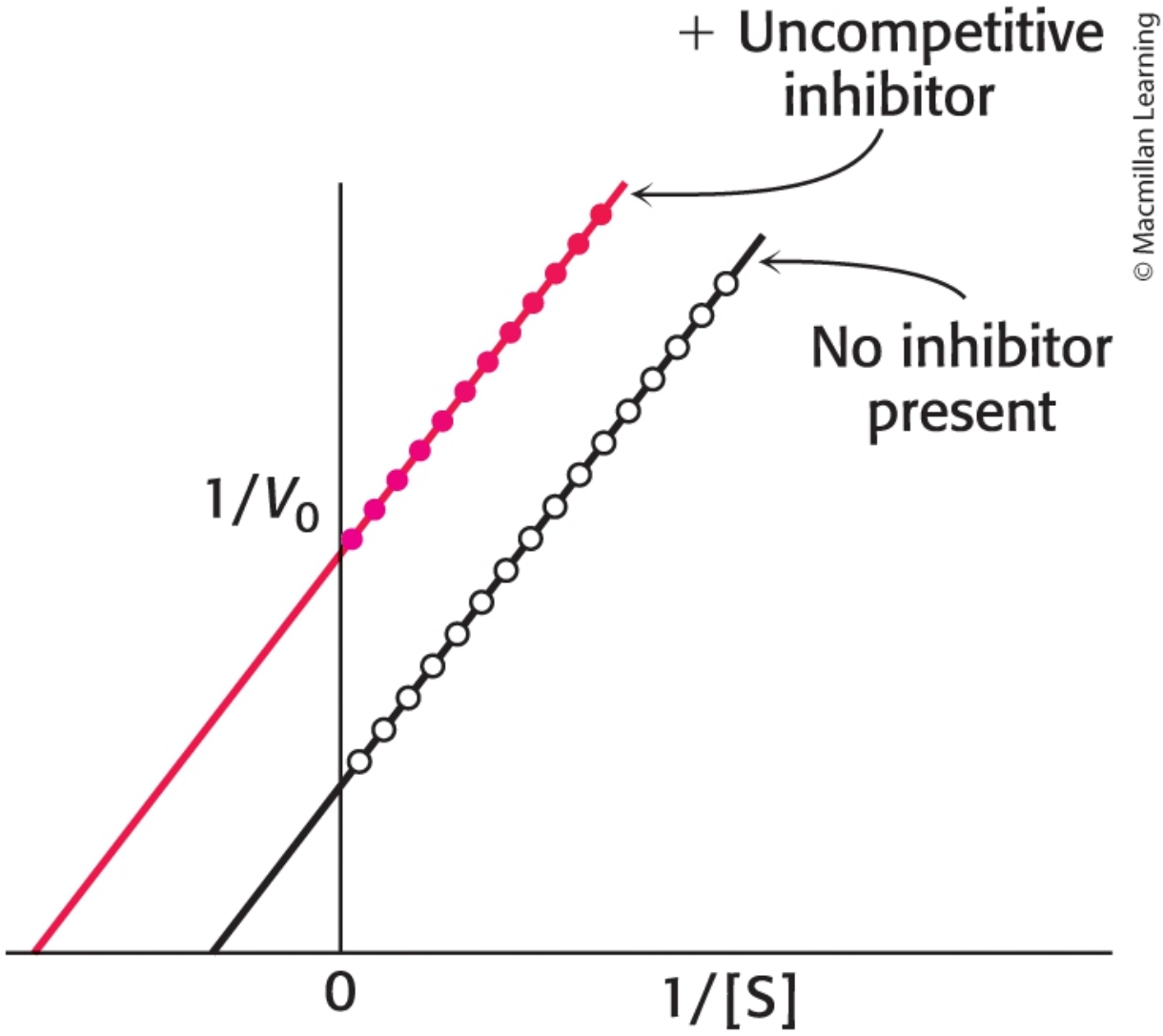
Two equations are shown that depict the two reactions that an enzyme may undergo:

1. E plus I, double-headed arrow and removal of S, E S plus I, forward arrow, E plus P.

2. E S plus I, reversible reaction arrow in the presence of K subscript i, E S I, forward reaction arrow crossed out.

Return to FIGURE 5.21.Michaelis–Menten plot showing the activity of an uncompetitive inhibitor

Extended description for FIGURE 5.22. Lineweaver–Burk plot distinguishing uncompetitive inhibition



© Macmillan Learning

The horizontal axis is labeled StartFraction 1 over substrate concentration EndFraction. The vertical axis is labeled 1 over V naught. Two straight line plots are shown:

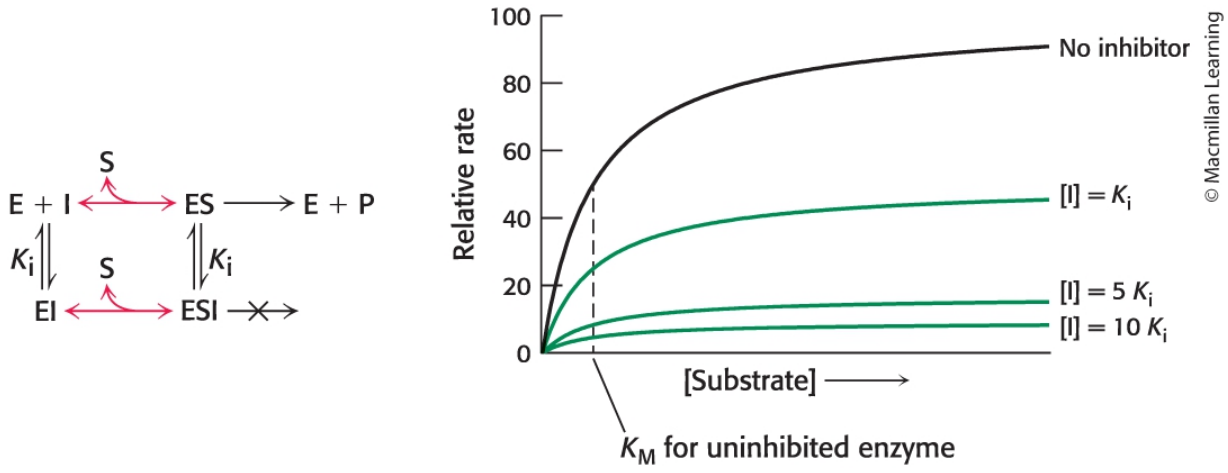
No inhibitor present: A straight line runs from a point on the negative side of the horizontal axis. It crosses the vertical axis into

the positive quadrant.

Uncompetitive inhibitor: A straight line runs from a point further away from the origin, on the negative side of the horizontal axis. It crosses the vertical axis into the positive quadrant. Two straight lines are perfectly parallel.

Return to FIGURE 5.22. Lineweaver–Burk plot distinguishing uncompetitive inhibition

Extended description for FIGURE 5.23. Michaelis–Menten plots show the activity of pure noncompetitive inhibitor



The horizontal axis is labeled concentration of substrate. The vertical axis is labeled relative rate. It has markings ranging from 0 to 100 in increments of 20 units. Four hyperbolic curves are shown:

1. No inhibitor: The hyperbolic curve rises rapidly to 75 units on the vertical axis and then plateaus around 85 units.

2. Concentration of I equals K subscript i: The hyperbolic curve rises to 40 units and then plateaus at the same value.

3. Concentration of I equals 5 K subscript i: The hyperbolic curve rises to a height of 10 units and then plateaus at the same value.

4. Concentration of I equals 10 K subscript i: The hyperbolic curve rises to 5 units and then plateaus at the same value.

A dashed vertical line rises from the horizontal axis, near the origin, and intersects with curve 1 at approximately 50 units. This line is labeled K subscript M for uninhibited enzyme.

Three equations are shown, depicting the three reactions that an enzyme may undergo:

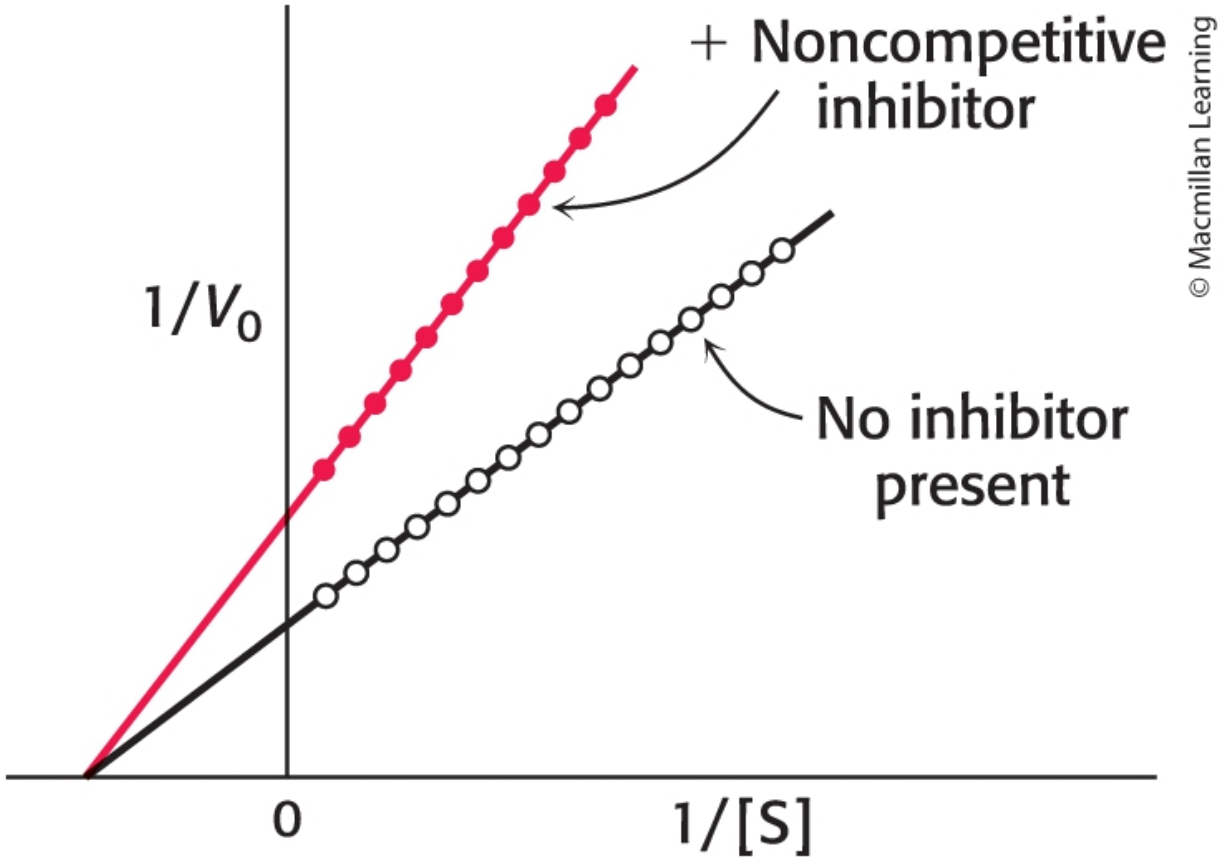
1. E plus I, double-headed arrow and removal of S, E S, forward reaction arrow, E plus P.

2. E plus I, reversible reaction arrow in the presence of K subscript i, E I, double-headed arrow and removal of S, E S I, forward reaction arrow crossed out.

3. E S, reversible reaction arrow in the presence of K subscript i, E S I, forward reaction arrow crossed out.

Return to FIGURE 5.23. Michaelis–Menten plots show the activity of pure noncompetitive inhibitor

Extended description for FIGURE 5.24. Lineweaver–Burk plot distinguishing a pure noncompetitive inhibition



© Macmillan Learning

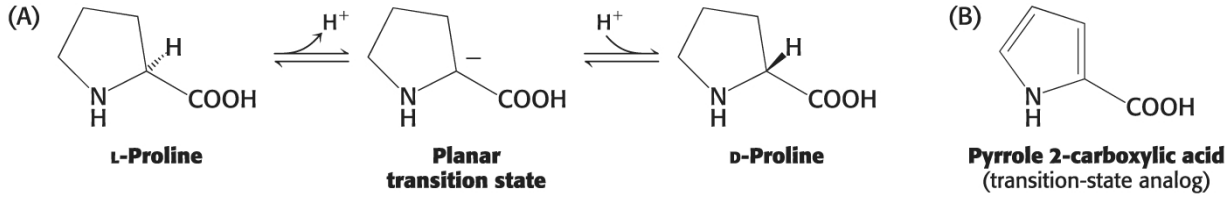
The horizontal axis is labeled StartFraction 1 over substrate concentration EndFraction. The vertical axis is labeled 1 over V naught. Two straight line plots are shown:

No inhibitor present: A straight line with a linear slope runs from a point on the negative side of the horizontal axis. It crosses the vertical axis into the positive quadrant.

Noncompetitive inhibitor: A straight line with steeper slope runs from the same point on the negative side of the horizontal axis. It crosses the vertical axis into the positive quadrant.

Return to FIGURE 5.24. Lineweaver–Burk plot distinguishing a pure noncompetitive inhibition

Extended description for FIGURE 5.25. The chemical structure of the transition state of a reaction and its analog



Part (A) The reaction consists of two steps:

Step 1: This reaction is reversible and consists of one reactant and one product. The reactant is L-Proline and has the following structure: A five-membered heterocyclic pentagonal ring consisting of 1 N and 4 C atoms is in a vertical orientation. N atom occupies the first position, which is the bottom-most vertex. The N atom is bound to H. C 4 is single bonded to C O O H on the lower right and dash bonded to H on the upper right. The product is labeled planar transition state and has the following structure: A five-membered heterocyclic pentagonal ring consisting of 1 N and 4 C atoms is in a vertical orientation. N atom occupies the bottom-most vertex. The N atom is bound to H. C 4 is single bonded to C O O H on the lower right and carries a negative charge. H superscript plus ion is released as a byproduct in this reaction.

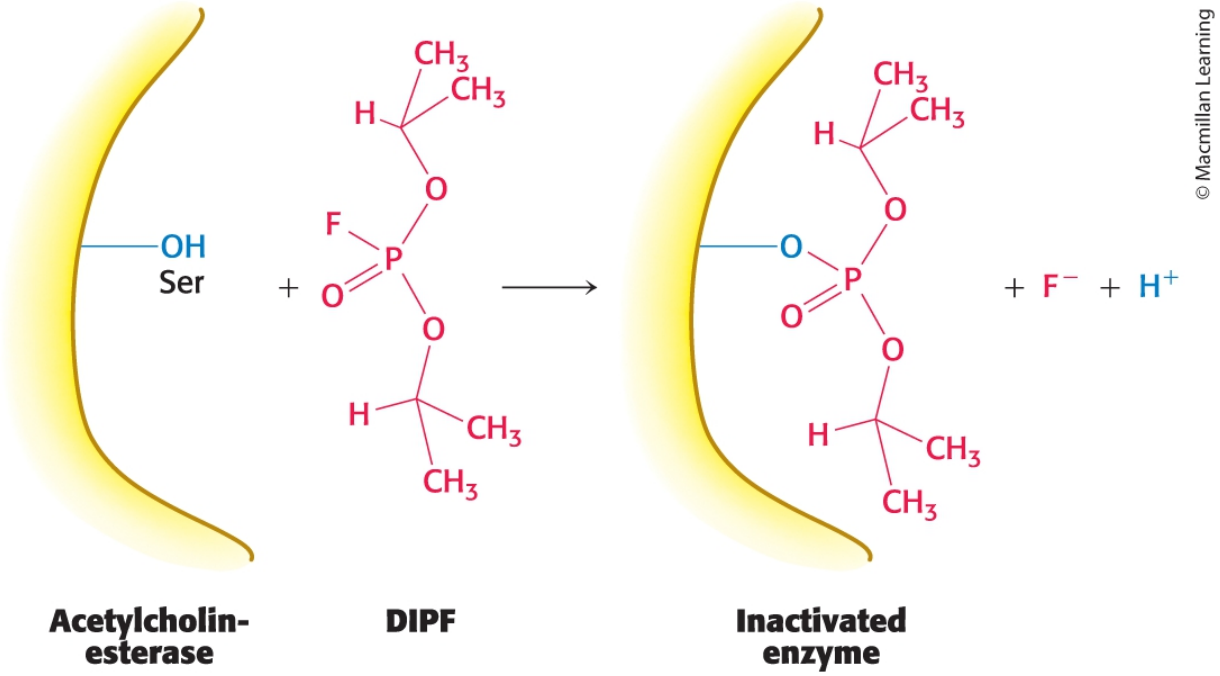
Step 2: This reaction is reversible and consists of one reactant and one product. The reactant is labeled planar transition state. The product is D-Proline and has the following structure: A five-membered heterocyclic pentagonal ring consisting of 1 N and 4 C atoms is in a vertical orientation. N atom occupies the bottommost vertex and is bound to H. C 4 is single bonded to C O O H on the

lower right and wedge bonded to H on the upper right. H superscript plus ion is consumed in this reaction.

Part (B) Pyrrole 2-carboxylic acid (transition-state analog): A five-membered heterocyclic pentagonal ring consisting of 1 N and 4 C atoms is in a vertical orientation. N atom occupies the bottom-most vertex and is bound to H. A double bond is present between C 1 and C 2, and C 3 and C 4. C 4 is single bonded to C O O H on the lower right.

Return to FIGURE 5.25. The chemical structure of the transition state of a reaction and its analog

Extended description for FIGURE 5.26. Schematic illustration of irreversible inhibition of an enzyme by D I P F, a group specific reagent



© Macmillan Learning

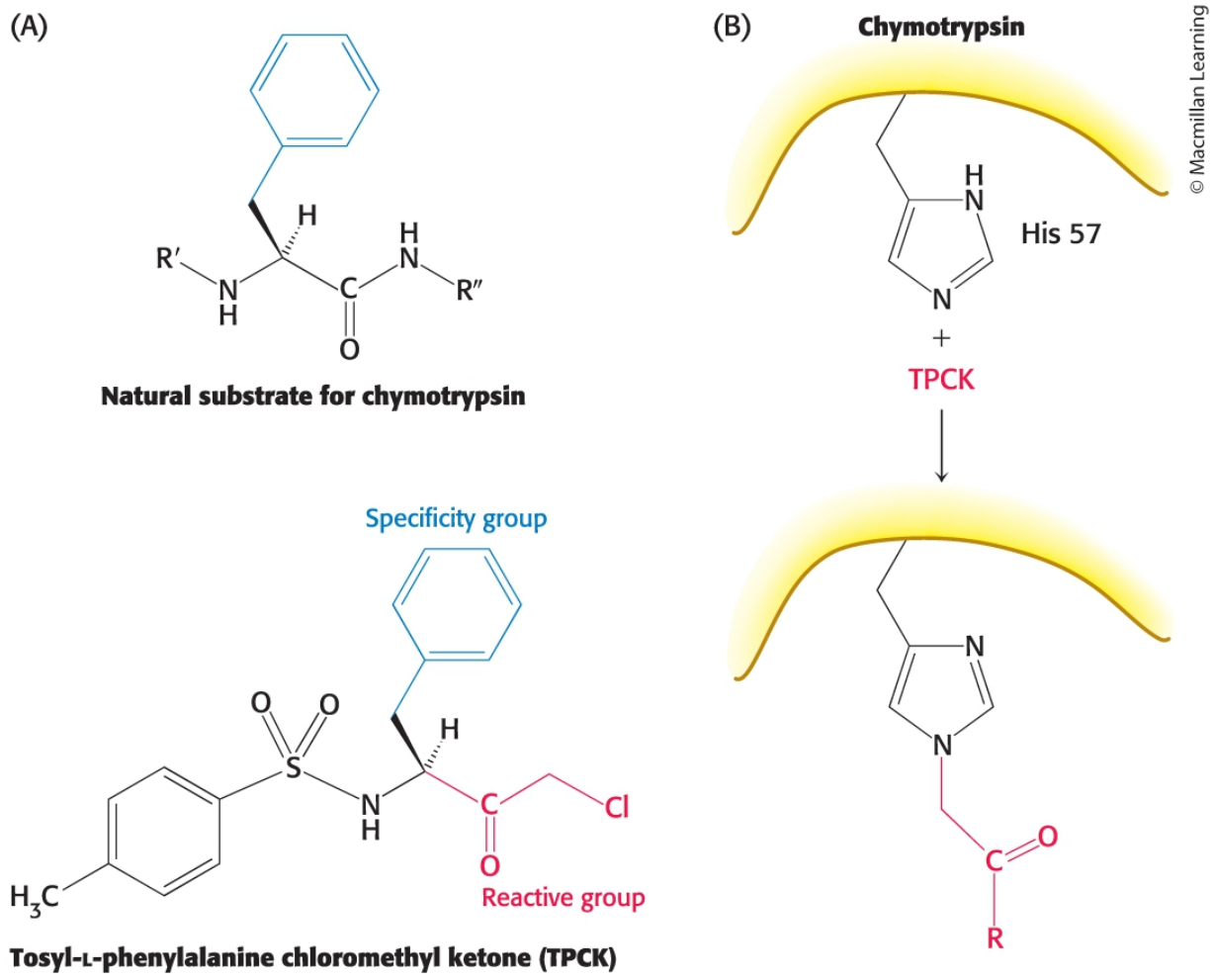
The acetylcholinesterase enzyme is depicted as a vertical curved line with a yellow highlight. It is connected to O H of a serine residue at the center. O H group is highlighted in blue.

Diisopropylphosphofluoridate (D I P F) has the following structure: A 2 O, 1 P, and 2 C heteronuclear alkane chain is depicted as a line structure using 4 zigzag lines in a vertical orientation. The O atoms occupy the second and fourth positions. P atom occupies the third position. C 1 is single bonded to C H 3 above, on the upper right and H on the upper left. The P atom is single bonded to F on the upper left and double bonded to O on the lower left. C 2 is single bonded to C H 3 below, on the lower right, and H on the lower left. The entire molecule is highlighted in red.

The product is labeled Inactivated enzyme and has the following structure: The O atom (blue) of the O H group of the serine residue loses its H atom and forms a single bond with the P atom of D I P F (red) which has lost its F atom. The second product is F superscript minus which is highlighted in red. The third product is H superscript plus which is highlighted in blue.

Return to FIGURE 5.26. Schematic illustration of irreversible inhibition of an enzyme by D I P F, a group specific reagent

Extended description for FIGURE 5.27. The chemical structure of the natural substrate of chymotrypsin and an affinity label that binds to chymotrypsin



Part(A) Chemical structures:

1. The natural substrate for chymotrypsin: A 2 N and 2 C heteronuclear alkane chain is depicted as a line structure using 3 zigzag lines. The N atoms occupy the first and fourth positions while the C atoms occupy the remaining positions. The first N atom is bound to H below and single bonded to R prime on the upper left. C

1 is dash bonded to H on the upper right and wedge bonded to a C atom on the upper left. The wedge bonded C atom is single bonded to C 4 of a benzene ring in a vertical orientation. It contains alternating double bonds between C 1 and C 2, C 3 and C 4, and C 5 and C 6. C 2 of the heteronuclear chain is double bonded to O below. The second N atom is bound to H above and single bonded to R double prime on the lower right. The benzene ring and the single bond at C 4 are highlighted in blue.

2. Tosyl-L-phenylalanine chloromethyl ketone (T P C K): A 1 S, 1 N and 3 C heteronuclear alkane chain is depicted as a line structure using 4 zigzag lines. The S atom occupies the first position and is double bonded to O on the upper right and the upper left. It is single bonded to C 2 of a benzene ring in a vertical orientation with C 1 occupying the topmost vertex. The ring contains alternating double bonds between C 1 and C 2, C 3 and C 4, and C 5 and C 6. C 5 of this ring is single bonded to C H 3 on the lower left. The N atom occupies the second position in the alkane chain and is bound to H. C 1 is dash bonded to H on the upper right and wedge bonded to a C atom on the upper left. This C atom is single bonded to C 4 of a benzene ring in a vertical orientation with C 1 occupying the topmost vertex. The ring contains alternating double bonds between C 1 and C 2, C 3 and C 4, and C 5 and C6. C 2 of the heteronuclear chain is double bonded to O below. C 3 is single bonded to C l on the lower right. The benzene ring and the single bond at C 4 are highlighted in blue and collectively labeled specificity group. C 2 and C 3 of the chain, along with their associated bonds, are highlighted in red and labeled reactive group.

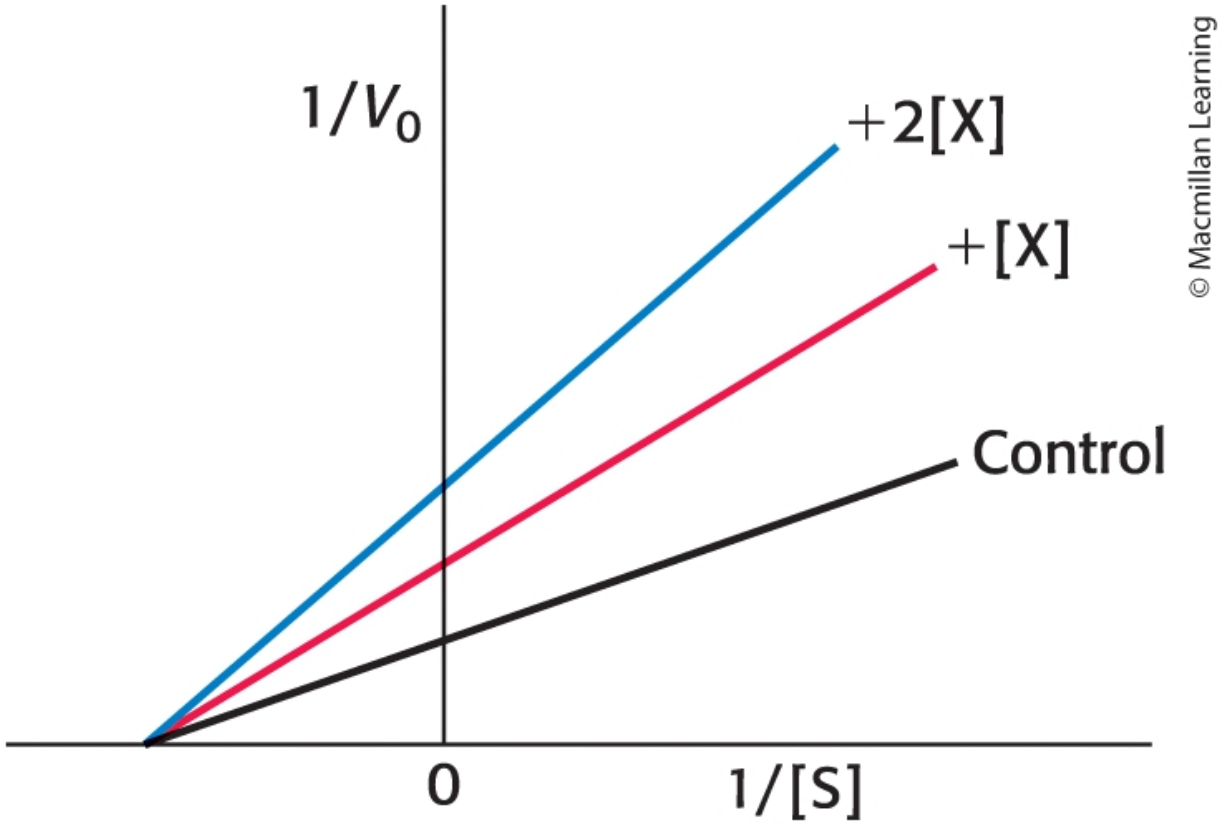
(B) The histidine residue of the chymotrypsin molecule is labeled His 57 and has the following structure: A five membered heterocyclic pentagonal ring consisting of 2 N and 3 C atoms is in a horizontal orientation. The first N atom occupies the first position, which is top left vertex. The second N atom occupies the third

position, which is the bottom-most vertex. C 1 occupies the bottom right vertex. A double bond is present between C 1 and the second N atom and C 2 and C 3. The second N atom is bound to H. C 3 is single bonded to C H 2 in the form of a line which in turn is connected to chymotrypsin. The chymotrypsin molecule is depicted as an upward curved line with a yellow highlight.

The His 57 residue reacts with T P C K and undergoes the following modification. The modified product consists of a five-membered heterocyclic pentagonal ring composed of 2 N and 3 C atoms is in a horizontal orientation. The first N atom occupies the first position, which is the top right vertex. The second N atom occupies the third position, which is the bottom-most vertex. A double bonds are present between the first N atom and C 1, and C 1 and C 3. The second N atom is single bonded to C H 2 below in the form of a line which is further single bonded to a C atom below. This C atom is double bonded to O on the upper right and single bonded to R below. The modified portion is also highlighted in red.

Return to FIGURE 5.27. The chemical structure of the natural substrate of chymotrypsin and an affinity label that binds to chymotrypsin

Extended description for Lineweaver–Burk plot shows enzyme activity at different concentrations of molecule X



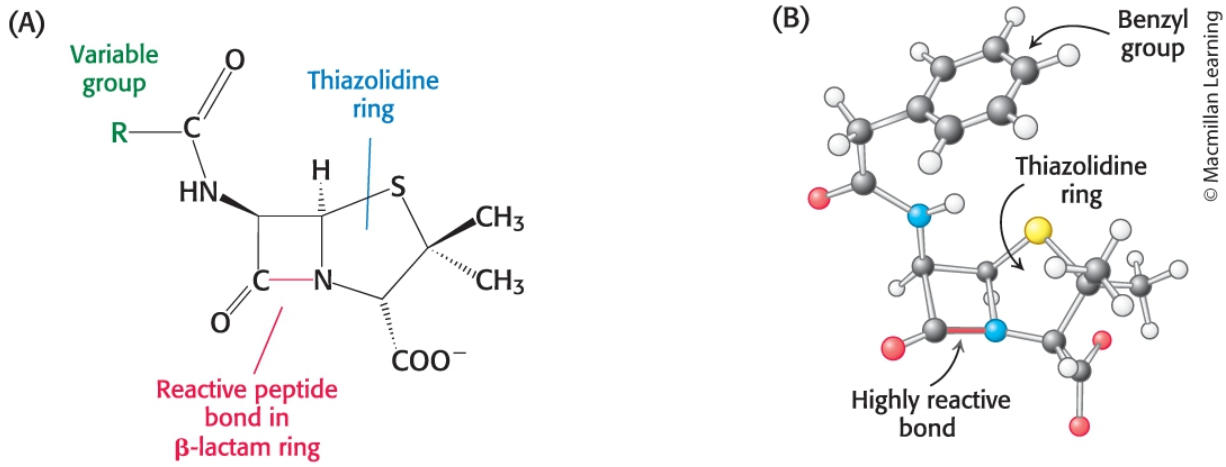
The horizontal axis is labeled StartFraction 1 over substrate concentration EndFraction. The vertical axis is labeled 1 over V naught. Three straight-line plots are shown:

Control: A straight line with a linear slope runs from a point on the negative side of the horizontal axis. It crosses the vertical axis into the positive quadrant. Plus concentration of X: A straight line with a steeper slope runs from the same point on the negative side of the horizontal axis. It crosses the vertical axis into the positive quadrant.

Plus 2 concentration of X: A straight line with an even steeper slope runs from the same point on the negative side of the horizontal axis. It crosses the vertical axis into the positive quadrant.

Return to Lineweaver–Burk plot shows enzyme activity at different concentrations of molecule X

Extended description for FIGURE 5.28 Chemical structure and ball-and-stick model of penicillin and benzylpenicillin respectively



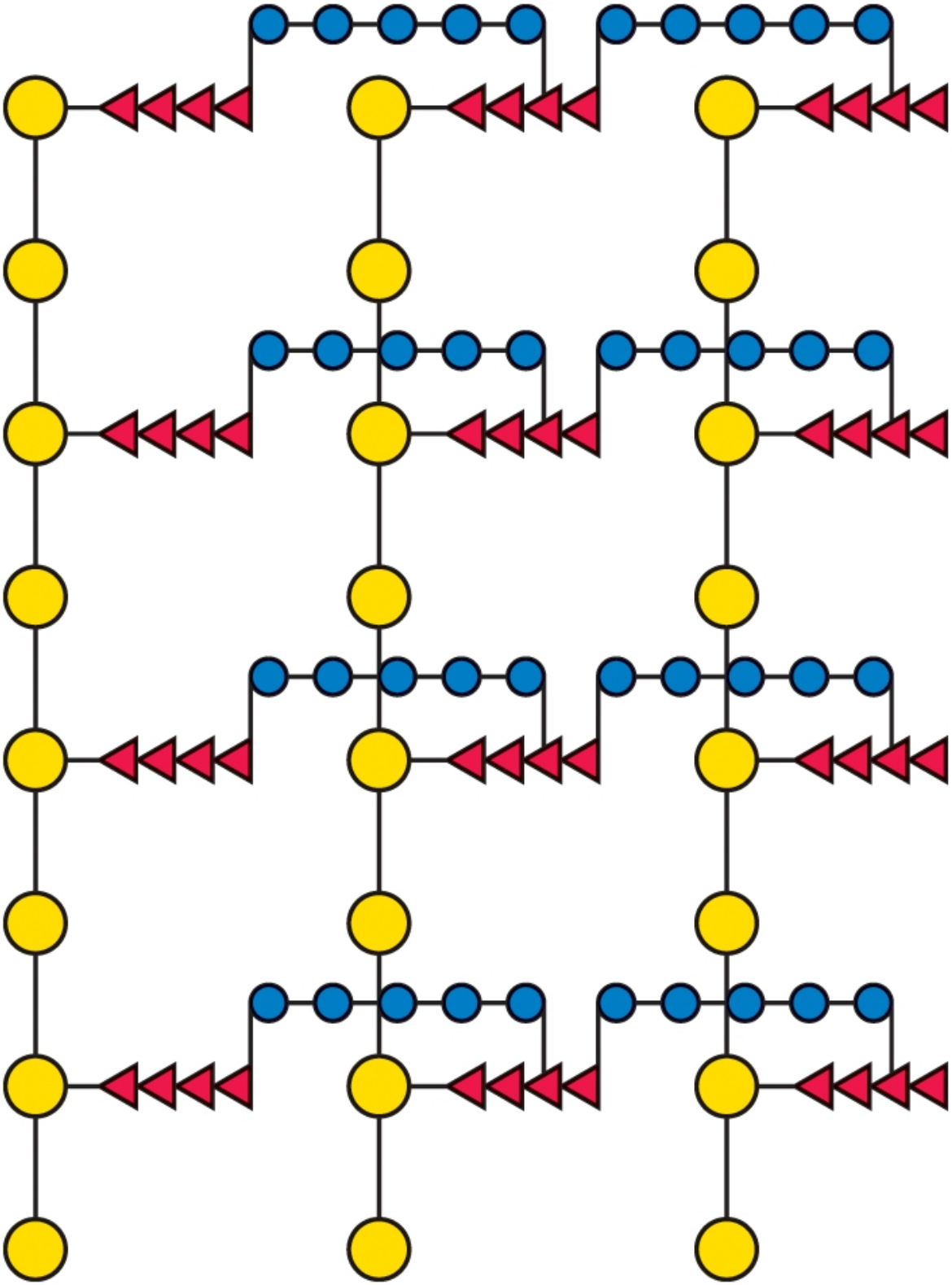
Part (A): A central C atom is single bonded to R (variable group) on the left, double-bonded to O on the upper right, and single bonded to N H on the lower right. N is wedge bonded to C 2 of a 1 N and 3 C heterocyclic quadrilateral ring. N occupies the first position, which is the bottom right vertex. C 1 occupies the bottom left vertex and is double bonded to O on the lower left. The bond between C and N is labeled reactive peptide bond in the beta-lactam ring. The quadrilateral ring is fused to a 1 S, 1 N, and 3 C containing heterocyclic pentagonal ring labeled thiazolidine ring such that C 3 and N of the quadrilateral ring are C 1 and N respectively of the pentagonal ring. The pentagonal ring is in a horizontal orientation. N occupies the first position, which is the bottom right vertex. S occupies the topmost vertex. C 1 is dash bonded to H above. C 2 is wedge bonded and dash bonded to a C H 3 group on the upper right and lower right, respectively. C 3 is dash bonded to C O O superscript minus on the lower right.

(B) In the ball-and-stick model, C atoms are depicted as black spheres, N atoms are depicted as blue spheres, O atoms are depicted as red spheres, H atoms are depicted as small white spheres, and S atom is depicted as a yellow sphere. A benzyl group composed of a ring of 6 black spheres is present in the position of the variable group R. All black spheres except one are connected to a white sphere. The remaining structure of the molecule is similar to (A) except atoms are replaced by spheres. The highly reactive bond is highlighted in red and the thiazolidine ring is shown with an arrow.

Return to FIGURE 5.28 Chemical structure and ball-and-stick model of penicillin and benzylpenicillin respectively

Extended description for FIGURE 5.29. Schematic representation of a section of peptidoglycan in

Staphylococcus aureus



© Macmillan Learning

Three types of fibers are shown:

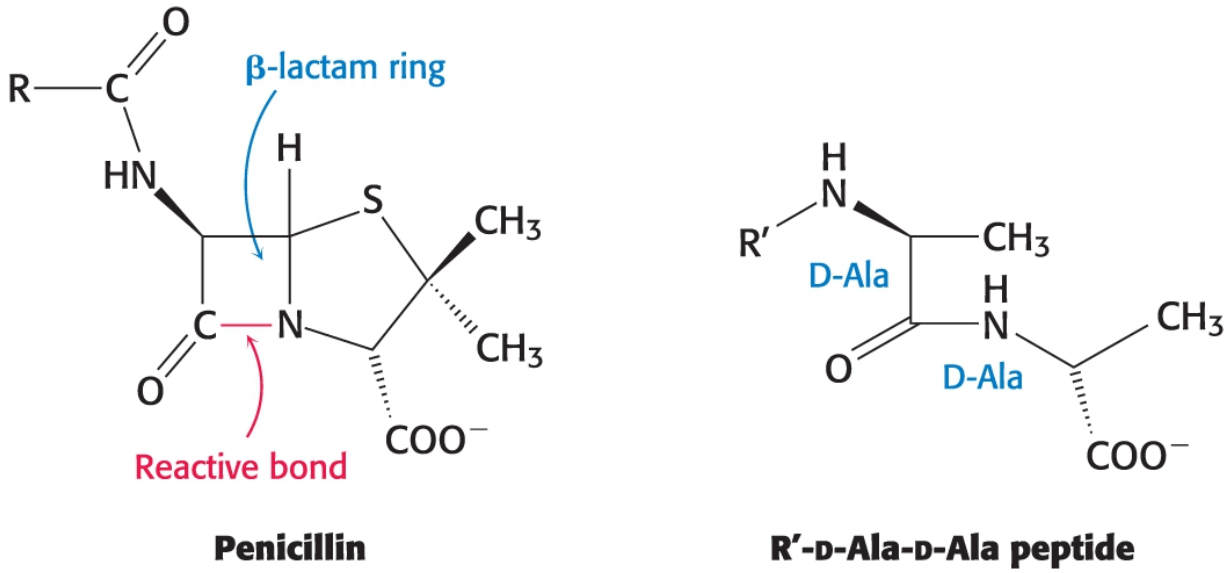
1. Sugars (yellow): They form three equidistant vertical lines in the diagram. Each line is composed of 8 yellow circles separated by equal-sized gaps.

2. Tetrapeptides (red): Short horizontal chains composed of 4 small triangles are connected to every alternate unit of each sugar (yellow) fiber.

3. Pentaglycine bridges (blue): Short horizontal chains composed of five blue circles interconnect individual rows of tetrapeptides (red).

Return to FIGURE 5.29. Schematic representation of a section of peptidoglycan in *Staphylococcus aureus*

Extended description for FIGURE 5.30. Similar chemical structures of penicillin and transition state (R prime-D-Ala-D-Ala peptide) of the transpeptidase reaction



Penicillin **R′-D-Ala-D-Ala peptide**

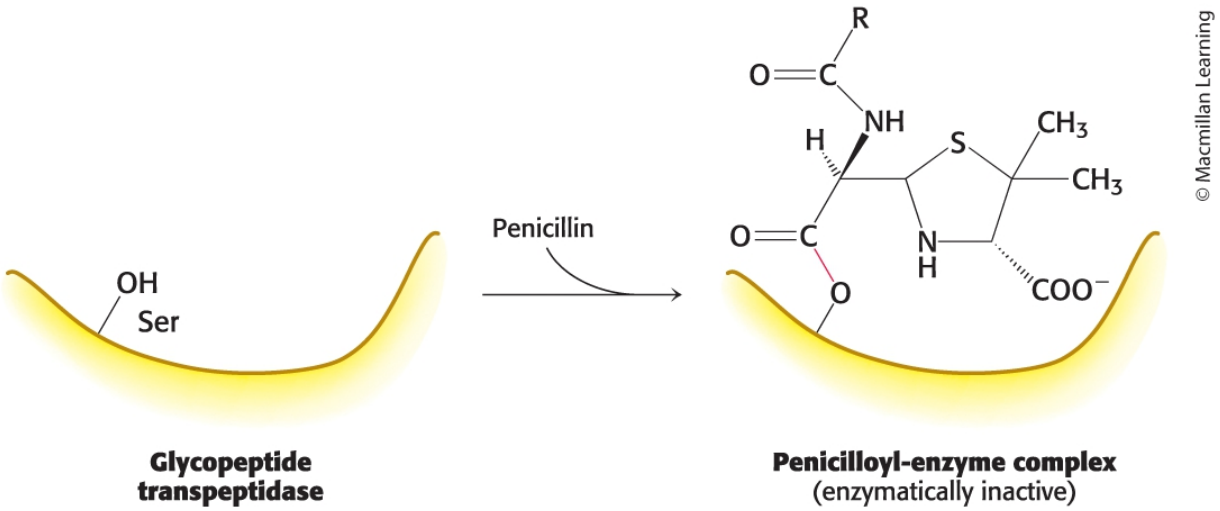
Penicillin: A central C atom is single bonded to R on the left, double-bonded to O on the upper right, and single bonded to N H on the lower right. N is wedge bonded to C 2 of a 1 N and 3 C heterocyclic quadrilateral ring. N occupies the first position, which is the bottom right vertex. C 1 occupies the bottom left vertex and is double bonded to O on the lower left. The bond between C and N is labeled reactive bond. The quadrilateral ring labeled beta-lactam ring is fused to a 1 S, 1 N, and 3 C containing heterocyclic pentagonal ring such that C 3 and N of the quadrilateral ring are C 1 and N respectively of the pentagonal ring. The pentagonal ring is in a horizontal orientation. N occupies the first position, which is the bottom right vertex. S occupies the topmost vertex. C 1 is single bonded to H above. C 2 is wedge bonded and dash bonded to a C H 3

group on the upper right and lower right, respectively. C 3 is dash bonded to C O O superscript minus on the lower right.

R prime-D-Ala-D-Ala peptide: R prime, single bond, N, wedge bond, C is present in a zigzag manner. N is bound to H. C is single bonded to C H 3 on the right and single bonded to C below in the form of a vertical line. The C atom below is double bonded to O on the lower left, and single bonded to N on the right. This part of the molecule is labeled D-Ala. The N atom is bound to H and is single bonded to C on the lower right in the form of a line. The C atom is single bonded to C H 3 on the upper right and dash bonded to C O O superscript minus below. This part of the molecule is also labeled D-Ala.

Return to FIGURE 5.30. Similar chemical structures of penicillin and transition state (R prime-D-Ala-D-Ala peptide) of the transpeptidase reaction

Extended description for FIGURE 5.31. Schematic illustration showing the formation of penicilloyl-enzyme complex



The reaction consists of one reactant and one product.

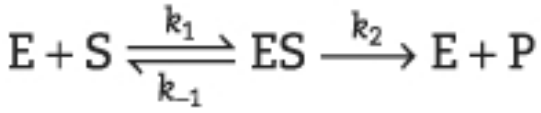
The reactant is an enzyme labeled glycopeptide transpeptidase. It is depicted as a downward curved horizontal line with a yellow highlight. A serine residue with an available O H group is connected to the enzyme. The reaction occurs in the presence of penicillin.

The product is labeled penicilloyl-enzyme complex (enzymatically inactive) and has the following structure: A 1 N and 3 C heteronuclear alkane chain is depicted as a line structure using 3 zigzag lines. It is present in a vertical orientation. The N atom occupies the second position. C 1 is double bonded to O on the left and single bonded to R on the upper right. The N atom is bound to H and wedge bonded to C 2. C 2 is dash bonded to H on the upper left, and single bonded to C 1 of a five-membered heterocyclic pentagonal ring in a horizontal orientation. The ring consists of 1 S,

1 N, and 3 C atoms. N atom occupies the first position, which is the bottom left vertex. It is bound to H. S atom occupies the first position, which is the topmost vertex. C 2 of this ring is single bonded to C H 3 on the upper right and on the right. C 3 is dash bonded to C O O superscript minus on the lower right. C 3 of the heteronuclear alkane chain is double bonded to O on the left. The O atom of the serine residue of glycopeptide transpeptidase loses its H bond and forms a single bond with the C 3 atom of the heteronuclear alkane chain.

Return to FIGURE 5.31. Schematic illustration showing the formation of penicilloyl-enzyme complex

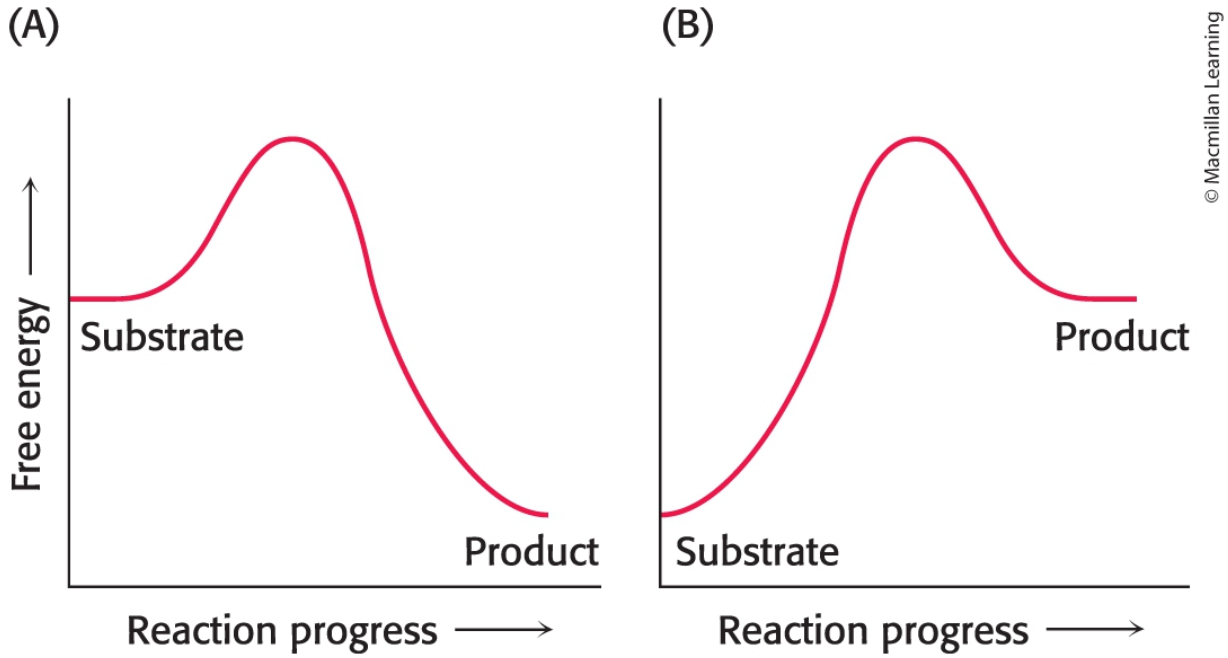
Extended description for Enzyme catalysis



The chemical equation is depicted as follows: E plus S is reversibly converted into E S. The top forward arrow is labeled lowercase k subscript 1. The bottom backward arrow is labeled lowercase k subscript minus 1. E S is further irreversibly converted into E plus P. The forward arrow is labeled lowercase k subscript 2.

Return to Enzyme catalysis

Extended description for Graphical representation of the reaction progress for two different reactions



© Macmillan Learning

The horizontal axis is labeled reaction progress. The vertical axis is labeled free energy. Two energy levels are shown in each case.

(A): The first level is extremely close to the right end of the horizontal axis and is labeled Product. The second level is at four times the height of the product level and is located above the left end of the horizontal axis. It is labeled substrate.

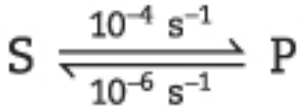
A solid curve rises steadily from the substrate level at the start of the reaction to a higher level in the middle of the reaction and forms a peak. The curve then falls to the product level by the end of the reaction.

(B): The first level is extremely close to the left end of horizontal axis and is labeled Substrate. The second level is at four times the height of the substrate level, above the right end of the horizontal axis, and is labeled product.

A solid curve rises rapidly from the substrate level at the start of the reaction to a higher level in the middle of the reaction and forms a peak. The curve then falls slightly to the product level by the end of the reaction.

Return to Graphical representation of the reaction progress for two different reactions

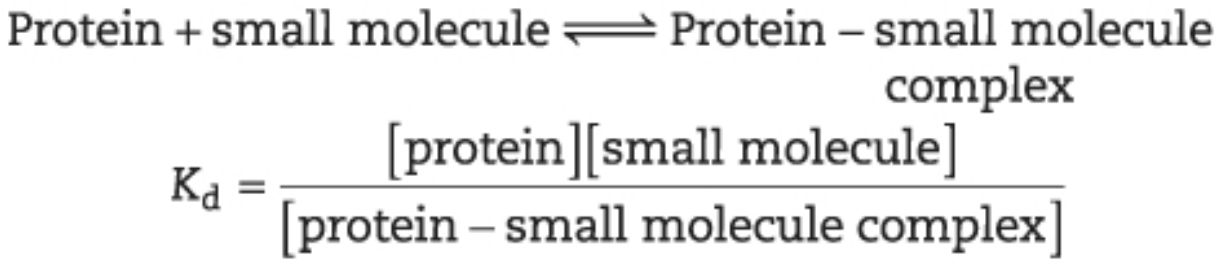
Extended description for Forward and reverse rate constants for the conversion of S into P



The reaction shows the reversible conversion of S to P. The forward rate constant shown above the forward arrow is 10 superscript minus 4 baseline s superscript minus 1. The reverse rate constant shown below the backward arrow is 10 superscript minus 6 baseline s superscript minus 1.

Return to Forward and reverse rate constants for the conversion of S into P

Extended description for Protein binding to a small molecule and the formula for K subscript d



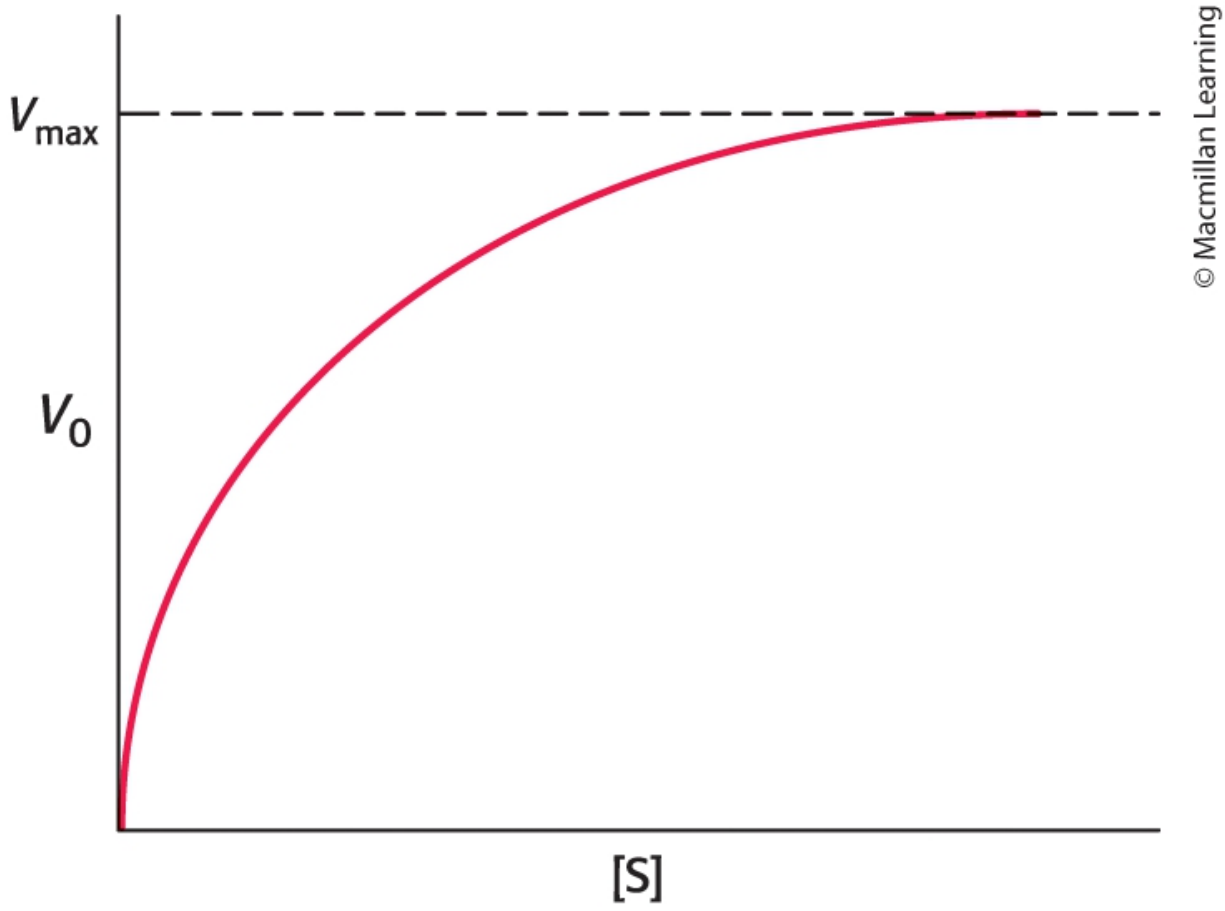
The chemical reaction consists of two reactants and one product. The first reactant is protein. The second reactant is small molecule. A reversible reaction arrow leads to the product. The product is the protein-small molecule complex.

The formula for K subscript d is as follows:

K subscript d equals StartFraction concentration of protein into concentration of small molecule over concentration of protein-small molecule complex EndFraction.

Return to Protein binding to a small molecule and the formula for K subscript d

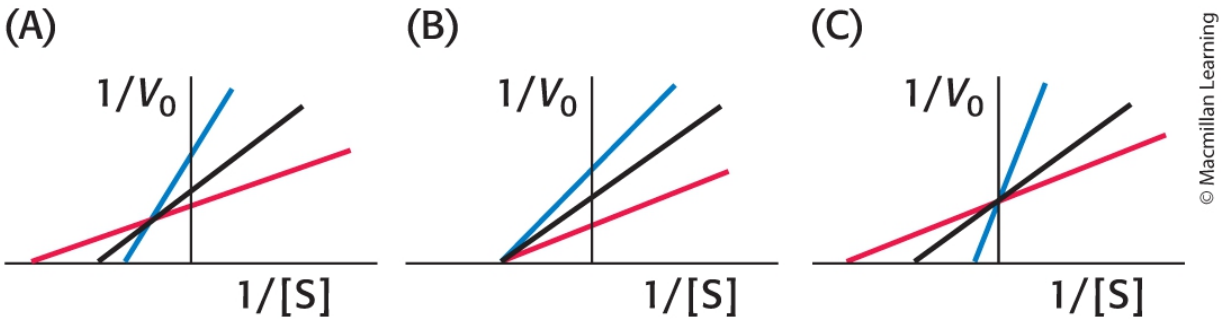
Extended description for Michaelis–Menten plot



The graph shows an upward convex curve. The horizontal axis is labeled substrate concentration. The vertical axis is labeled V naught. A dashed line labeled V subscript max runs parallel to the horizontal axis at the highest point of the vertical axis. An upward convex curve starts from the origin and plateaus near the dashed-line at a high substrate concentration.

Return to Michaelis–Menten plot

Extended description for Double-reciprocal plots for three different enzyme concentrations



© Macmillan Learning

The horizontal axis is labeled StartFraction 1 over substrate concentration EndFraction. The vertical axis is labeled StartFraction 1 over V naught EndFraction. Three straight line plots are shown in each graph:

(A) All the straight lines intercept each other at a point to the left of the vertical axis, just above the origin.

Red: A straight line runs from a point on the negative side of the horizontal axis. It crosses the vertical axis into the positive quadrant.

Black: A steeper straight line from a point slightly closer to the origin, on the negative side of the horizontal axis. It crosses the vertical axis into the positive quadrant.

Blue: An even steeper straight line runs from a point even closer to the origin, on the negative side of the horizontal axis. It crosses the vertical axis into the positive quadrant.

(B) Red: A straight line runs from a point on the negative side of the horizontal axis. It crosses the vertical axis into the positive quadrant.

Black: A steeper straight line runs from the same point on the negative side of the horizontal axis. It crosses the vertical axis into the positive quadrant.

Blue: An even steeper straight line runs from the same point on the negative side of the horizontal axis. It crosses the vertical axis into the positive quadrant.

(C) All the straight lines cross the vertical axis at the same point.

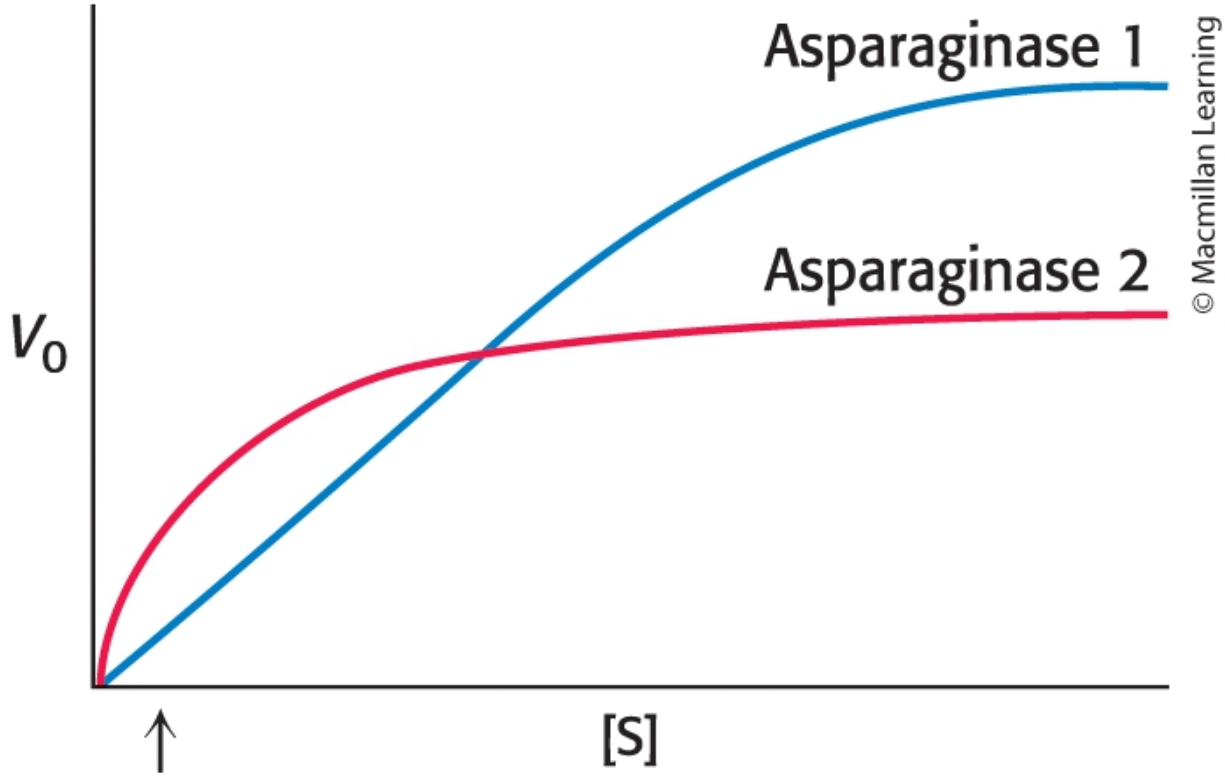
Red: A straight line runs from a point on the negative side of the horizontal axis. It crosses the vertical axis into the positive quadrant.

Black: A steeper straight runs from a point slightly closer to the origin, on the negative side of the horizontal axis. It crosses the vertical axis into the positive quadrant.

Blue: An even steeper straight line runs from a point slightly even closer to the origin, on the negative side of the horizontal axis. It crosses the vertical axis into the positive quadrant.

Return to Double-reciprocal plots for three different enzyme concentrations

Extended description for Michaelis–Menten curves for asparaginase from different sources



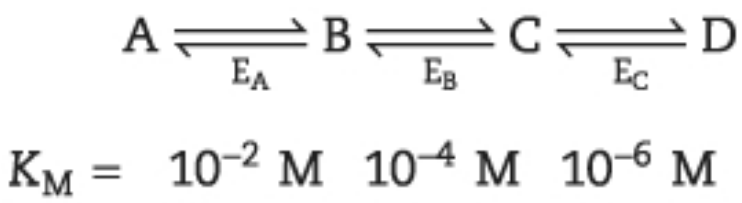
The horizontal axis is labeled substrate concentration. The vertical axis is labeled V naught. A hyperbolic curve and a line curve are shown:

1. Asparaginase 1: The line curve rises linearly until three-fourth of the maximum value of V naught on the vertical axis, and then plateaus at the highest concentration of substrate.

2. Asparaginase 2: The hyperbolic curve rises rapidly until one-half of the value of V naught on the vertical axis, and then plateaus at a substrate concentration less than half of the maximum value.

Return to Michaelis–Menten curves for asparaginase from different sources

Extended description for Sequential conversion of A to D



The pathway is depicted as follows: A is reversibly converted into B. The bottom backward arrow is labeled E subscript A. B is then reversibly converted into C. The bottom backward arrow is labeled E subscript B. C is further reversibly converted into D. The bottom backward arrow is labeled E subscript C.

The value of K subscript M for the different enzymes is as follows:

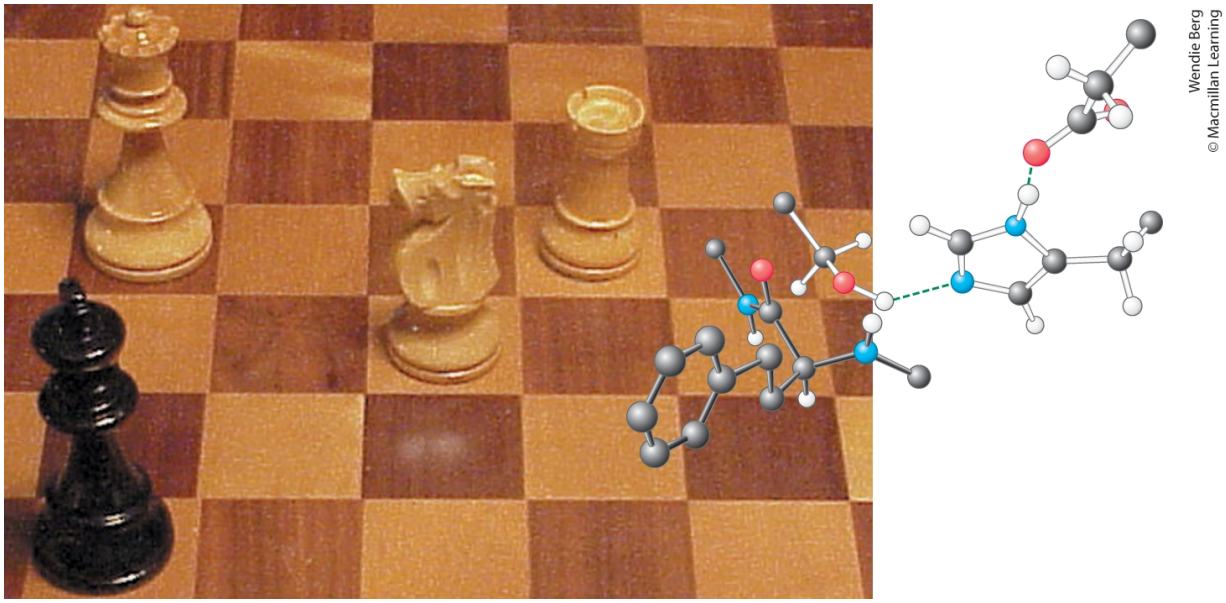
E subscript A: 10 superscript minus 2 molar.

E subscript B: 10 superscript minus 4 molar.

E subscript C: 10 superscript minus 6 molar.

Return to Sequential conversion of A to D

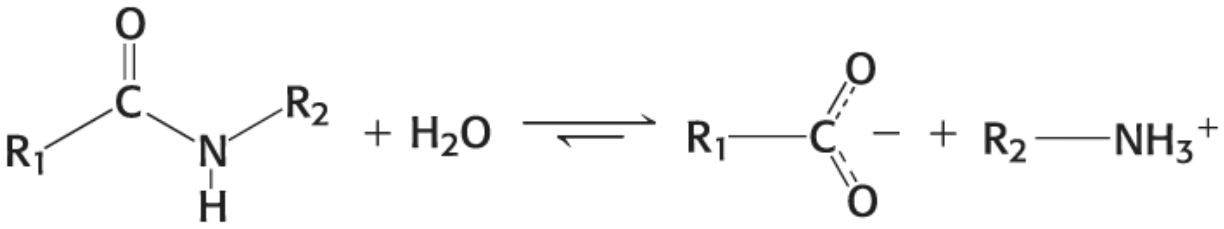
Extended description for Photograph of a chess board and ball-and-stick model of an enzyme



The chess board contains three white-colored chess pieces and one black color chess piece. The ball-and-stick model of the enzyme consists of several interconnected red, blue, white, and black spheres.

Return to Photograph of a chess board and ball-and-stick model of an enzyme

Extended description for Hydrolysis of a peptide



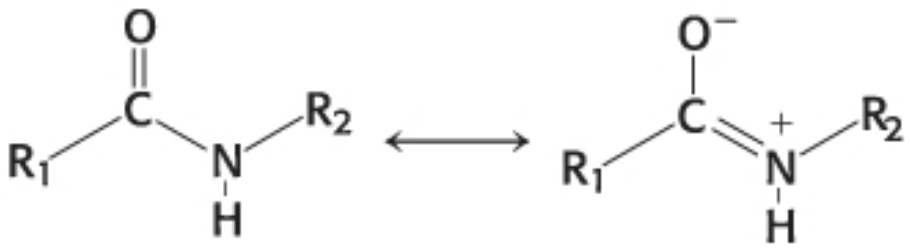
The hydrolysis reversible reaction consists of two reactants and two products.

The first reactant has the following structure: A central C atom is double bonded to O above, single bonded to R subscript 1 on the lower left, and N on the lower right. N is single bonded to R subscript 2 on the upper right and H below. The second reactant is H 2 O.

The first product has the following structure: A central C atom is single bonded to R subscript 1 on the left. The central C atom is single bonded to O on the upper right and shares a resonance bond with O. The central C atom is single bonded to a second O atom on the lower right and shares a resonance bond with the second O atom. The second product has the following structure: R subscript 2, single bond, N H 3 superscript plus.

Return to Hydrolysis of a peptide

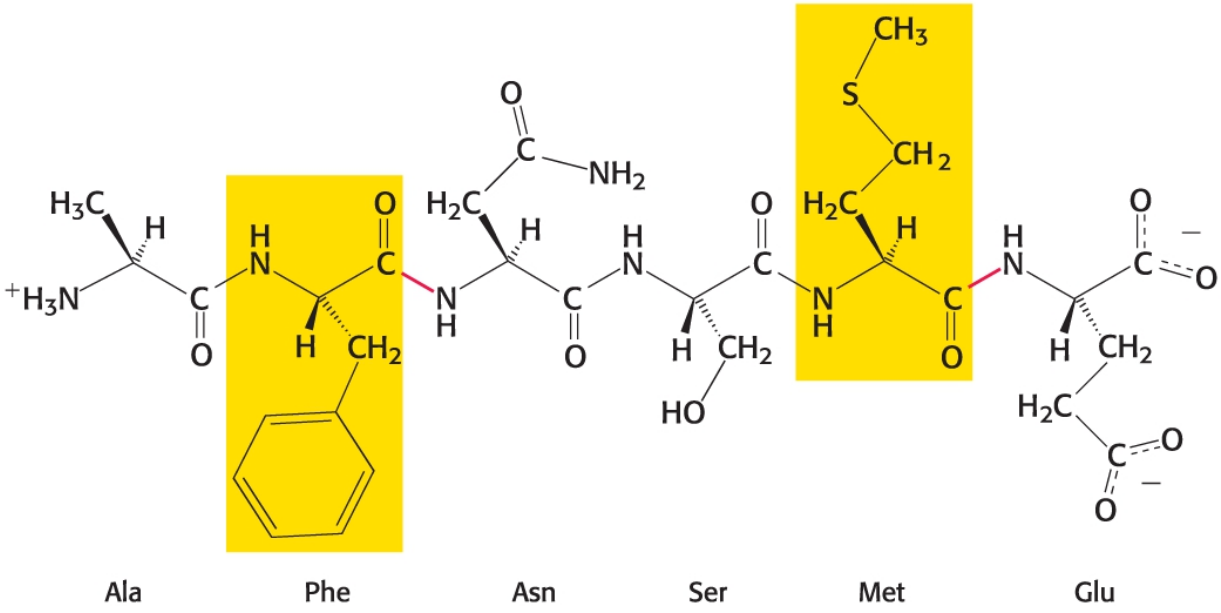
Extended description for Chemical reaction



The reaction consists of one reactant and one product. The first reactant has the following structure: A central C atom is double bonded to O above, single bonded to N on the lower right, and single bonded to R subscript 1 on the lower left. The N atom on the lower right is single bonded to R subscript 2 on the upper right and H below. The product has the following structure: A central C atom is single bonded to O superscript script minus above, double-bonded to N superscript plus on the lower right, and single bonded to R subscript 1 on the lower left. The N atom on the lower right is single bonded to R subscript 2 on the upper right and H below.

Return to Chemical reaction

Extended description for FIGURE 6.1. Chemical structure of a peptide with highlighted target amino acids and bonds cleaved by chymotrypsin



The peptide is composed of amino acids A l a, P h e, A s n, S e r, M e t, and G l u.

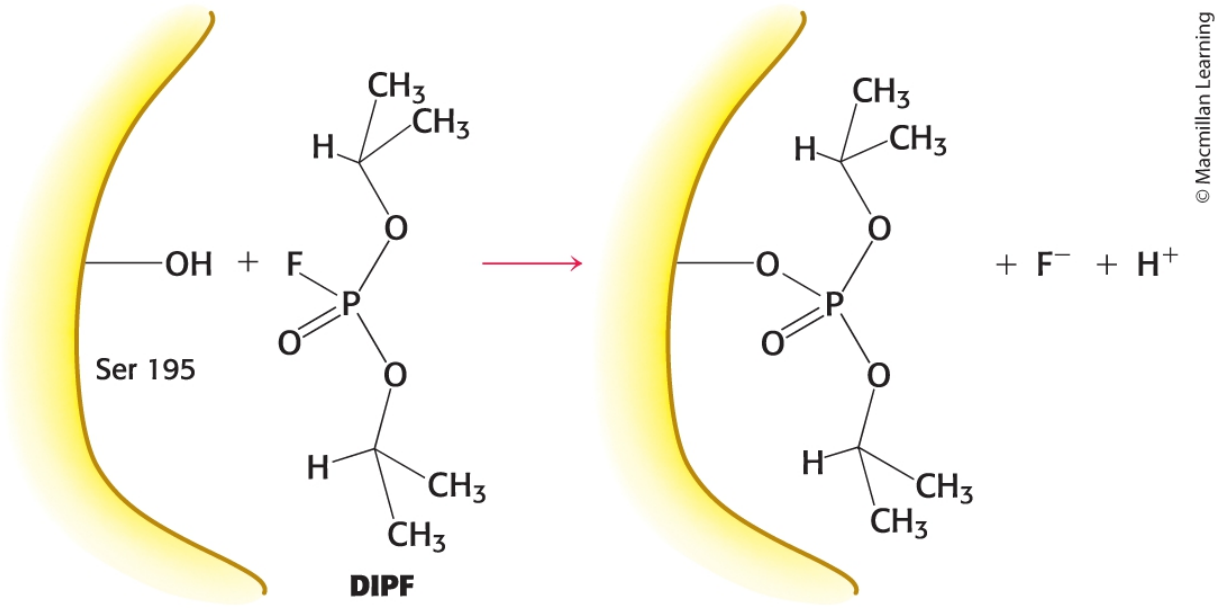
The structure of the peptide is as follows: A 5 N and 1 2 C heteronuclear alkane chain is depicted as a line structure using 16 zigzag lines. The first N bound to H occupies the third position. The second N bound to the H atom occupies the sixth position. The third N bound to H occupies the ninth position. The fourth N bound to H occupies the twelfth position. The fifth N bound to H occupies the fifteenth position. C 1 is wedge bonded to C H 3 on the upper left, dash bonded to H on the upper right, and single bonded to N H 3 superscript plus on the lower left. C 2 is double bonded to O below. C 3 is wedge bonded to H on the lower left and dash bonded to C H 2 on the lower right. C H 2 is single bonded to C 6 of a benzene ring in

a horizontal orientation with C 1 occupying the rightmost vertex. The ring contains alternating double bonds between C 1 and C 2, C 3 and C 4, and C 5 and C 6. C 4 of the alkane chain is double bonded to O above. C 5 of the alkane chain is dash bonded to H on the upper right and wedge bonded to C H 2 on the upper left. C H 2 is single bonded to a central C atom on the upper right. The central C atom is double bonded to O on the upper left and single bonded N H 2 on the lower right. C 6 is double bonded to O below. C 7 is wedge bonded to H on the lower left and dash bonded to C H 2 on the lower right. C H 2 single bonded to O H on the lower left. C 8 is double bonded to O above. C 9 is dash bonded to H on the upper right and wedge bonded to C H 2 on the upper left. C H 2 is single bonded to C H 2 on the upper right, which is again single bonded to S on the upper left. S is single bonded to C H 3 on the upper right. C 10 is double bonded to O below. C 11 is dash bonded to C H 2 on the lower left and wedge bonded to H on the lower right. C H 2 is single bonded to C H 2 on the lower left, which is again single bonded to C on the lower right. This C atom is partially double bonded to O on the upper right and O lower left. C 12 is partially double bonded to O above and O on the lower right. This C O O group has a net negative charge.

P h e amino acid highlighted in yellow includes the first N atom, C 3, and its associated benzene ring. M e t amino acid highlighted in yellow includes the fourth N atom, C 9 and its associated chain, and C 10. The single bond between C 4 and second N atom and C 10 and fifth N atom is highlighted in red.

Return to FIGURE 6.1. Chemical structure of a peptide with highlighted target amino acids and bonds cleaved by chymotrypsin

Extended description for FIGURE 6.2. Schematic illustration of the irreversible inactivation of chymotrypsin by D I P F



The irreversible inactivation of chymotrypsin by D I P F is shown as a chemical reaction consisting of two reactants and three products.

The first reactant is S e r 195 bound to the enzyme. The enzyme is depicted as a vertical concave surface with a yellow highlight. The O H group of S e r 195 is single-bonded to the enzyme. The second reactant is D I P F which has the following structure: A 1 P, 2 O, and 2 C heteronuclear alkane chain is depicted as a line structure using 4 zigzag lines. The first O atom occupies the second position and the second O atom occupies the fourth position. The P atom occupies the third position. C 1 is single bonded to C H 3 on the lower right, and below, and single bonded to H on the lower left. The P atom is single-bonded to F on the upper left and double-bonded to O on the

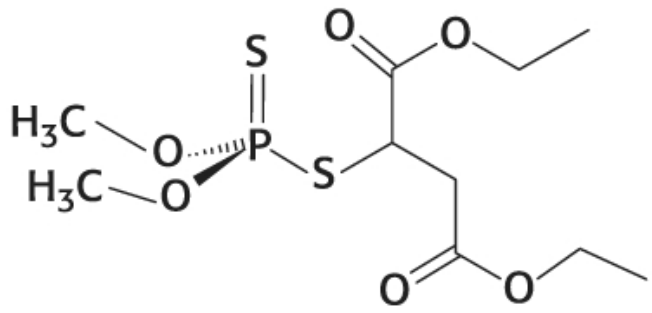
lower left. C 2 is single bonded to C H above, upper right, and single bonded to H on the left.

A forward reaction arrow is shown.

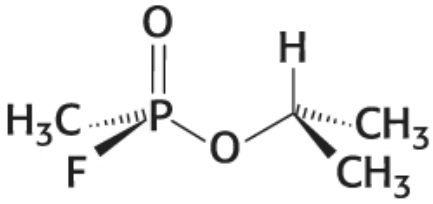
The first product consists of D I P F bound to the enzyme. It has the following structure: The O atom of the S e r 195 residue loses its H atom and forms a single bond with the P atom of D I P F which has lost its F atom. The second product is F superscript minus ion. The third product is H superscript plus ion.

Return to FIGURE 6.2. Schematic illustration of the irreversible inactivation of chymotrypsin by D I P F

Extended description for Molecular structures of malathion and sarin



Malathion



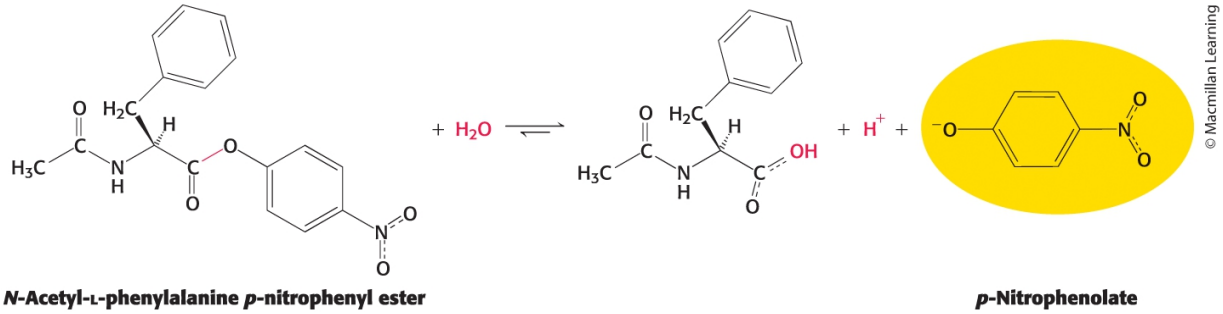
Sarin

The structure of malathion is as follows: A 1 P, 1 S, and 2 C heteronuclear alkane chain is depicted as a line structure using 3 zigzag lines. P atom occupies the first position. S atom occupies the second position. P is double bonded to S above, dash bonded O, single bond, C H 3 on the left, and wedge bonded to O, single bond, C H 3 on the lower left. C 1 is single bonded above to C 1 of another 1 O and 3 C heteronuclear alkane chain depicted as a line structure using 3 zigzag lines. O atom occupies the second position. C 1 is double bonded to O on the upper left. C 2 of the main chain is single bonded below to C 1 a 1 O and 3 C heteronuclear alkane chain depicted as a line structure using 3 zigzag lines. O occupies the second position. C 1 is double bonded to O on the lower left.

The structure of sarin is as follows: A 1 P, 1 O, and 1 C heteronuclear alkane chain is depicted as a line structure using 2 zigzag lines. P occupies the first position. O occupies the second position. P is double bonded to O above, dash bonded to C H 3 on the left, and wedge bonded to F on the lower left. C 1 is single bonded to H above, dash bonded to C H 3 on the lower right, and wedge bonded to C H 3 below.

Return to Molecular structures of malathion and sarin

Extended description for FIGURE 6.3. Chemical reaction for monitoring chymotrypsin action



The reaction consists of two reactants and three products.

The first reactant is N-Acetyl-L-phenylalanine p-nitrophenyl ester has the following structure: A 1 N and 4 C heteronuclear alkane chain is depicted as a line structure using 4 zigzag lines. N occupies the third position and is bound to H. C 1 is bound to H 3. C 2 is double bonded to O above. C 3 is dash bonded to H on the upper right and wedge bonded to C H 2 on the upper left. C H 2 is single bonded to C 3 of a benzene ring in a horizontal orientation with C 1 occupying the right most vertex. The ring contains alternating double bonds between C 2 and C 3, C 4 and C 5, and C 6 and C 1. C 4 of the heteronuclear chain is single bonded to O on the upper right and double bonded to O below. The O atom on the upper right is single bonded to C 6 of a benzene in a vertical orientation with C 1 occupying the topmost vertex. Alternating double bonds are present between C 1 and C2, C 3 and C 4, and C 5 and C 6. C 3 of the benzene ring is single bonded to N on the lower right. The N atom is single bonded to O on the upper right and O below with a resonance bond shared between them.

The second reactant is a H 2 O.

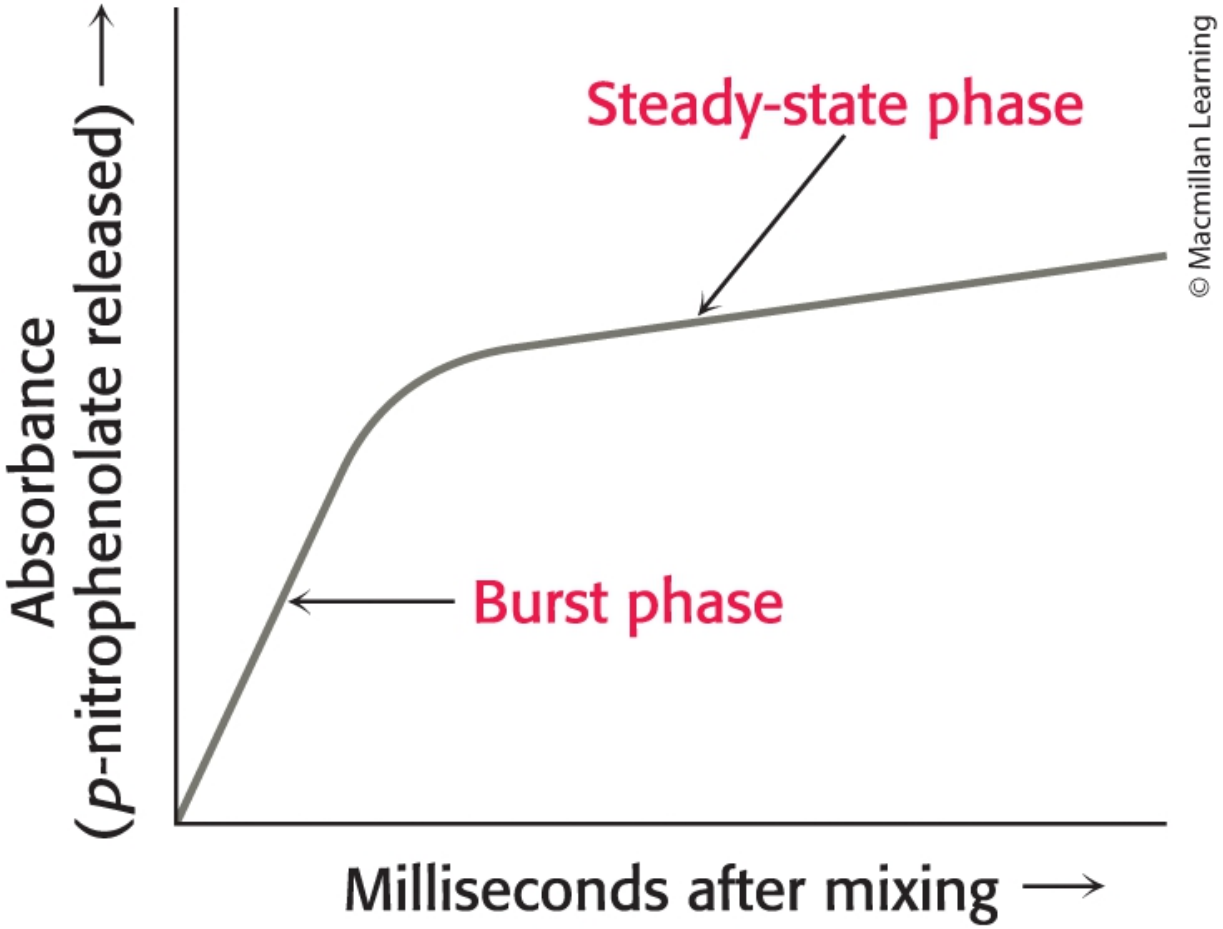
The structure of the first product is as follows: A 1 N and 4 C heteronuclear alkane chain is depicted as a line structure using 4 zigzag lines. N occupies the third position and is bound to H. C 1 is bound to H 3. C 2 is double bonded to O above. C 3 is dash bonded to H on the upper right and wedge bonded to C H 2 on the upper left. C H 2 is single bonded to C 3 of a benzene ring in a horizontal orientation with C 1 occupying the right most vertex. The ring contains alternating double bonds between C 2 and C 3, C 4 and C 5, and C 6 and C 1. C 4 of the heteronuclear alkane chain is single bonded to O H on the upper right and O on the lower left with a resonance bond shared between them.

The second product is H superscript plus ion.

The third product is p-Nitrophenolate whose structure is as follows: A benzene ring is in a horizontal orientation with C 1 occupying the rightmost vertex. The ring contains alternating double bonds between C 1 and C 2, C 3 and C 4, and C 5 and C 6. C 1 is single bonded to N on the right. The N atom is single bonded to O on the upper right and O on the lower right with a resonance bond shared between them. C 4 is single bonded to O superscript minus on the left. The entire molecule is enclosed in a yellow circle.

Return to FIGURE 6.3. Chemical reaction for monitoring chymotrypsin action

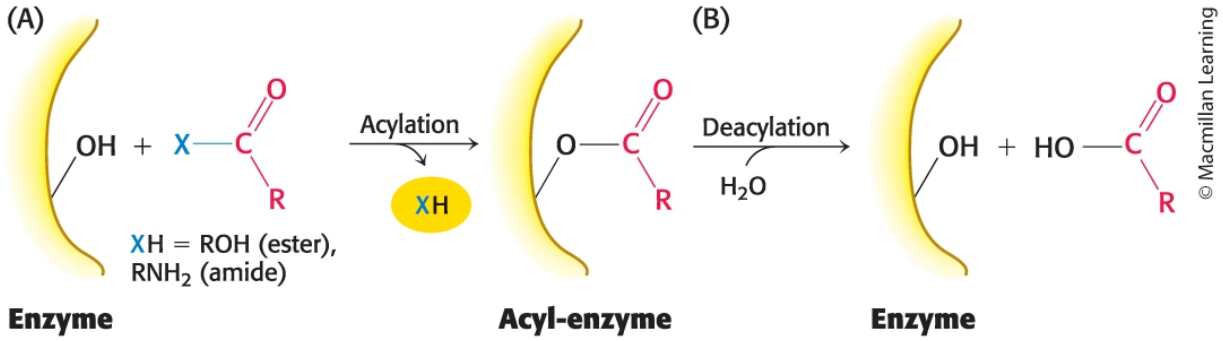
Extended description for FIGURE 6.4. Graphical representation of the two kinetic phases of chymotrypsin activity



The horizontal axis is labeled milliseconds after mixing. The vertical axis is labeled absorbance (p-nitrophenolate released). A black curve begins at origin moves gradually toward the upper right in a straight line and is labeled burst phase. The curve then moves almost horizontally and very slowly reaches the upper right and is labeled steady-state phase.

Return to FIGURE 6.4. Graphical representation of the two kinetic phases of chymotrypsin activity

Extended description for FIGURE 6.5. Schematic illustration of hydrolysis by chymotrypsin



The chymotrypsin enzyme is depicted as a vertical concave surface with a yellow highlight.

Part (A): It shows the formation of an acyl-enzyme intermediate in an acylation reaction.

The structure of the first reactant is as follows: The chymotrypsin enzyme single bonded to an O H group in the concave depression is shown. The structure of the second reactant is as follows: A central C atom is single double bonded to O on the upper right, single bonded to R on the lower right, and X on the left. X is highlighted in blue color.

Note: X H equals R O H (ester) and R N H 2 (amide).

A forward reaction arrow is labeled acylation and X H leaves the reaction.

The structure of acyl-enzyme is as follows: A central C atom is double bonded to O on the upper right, single bonded to R on the

lower right, and single bonded to O on the left. The O atom on the left is single bonded to the enzyme.

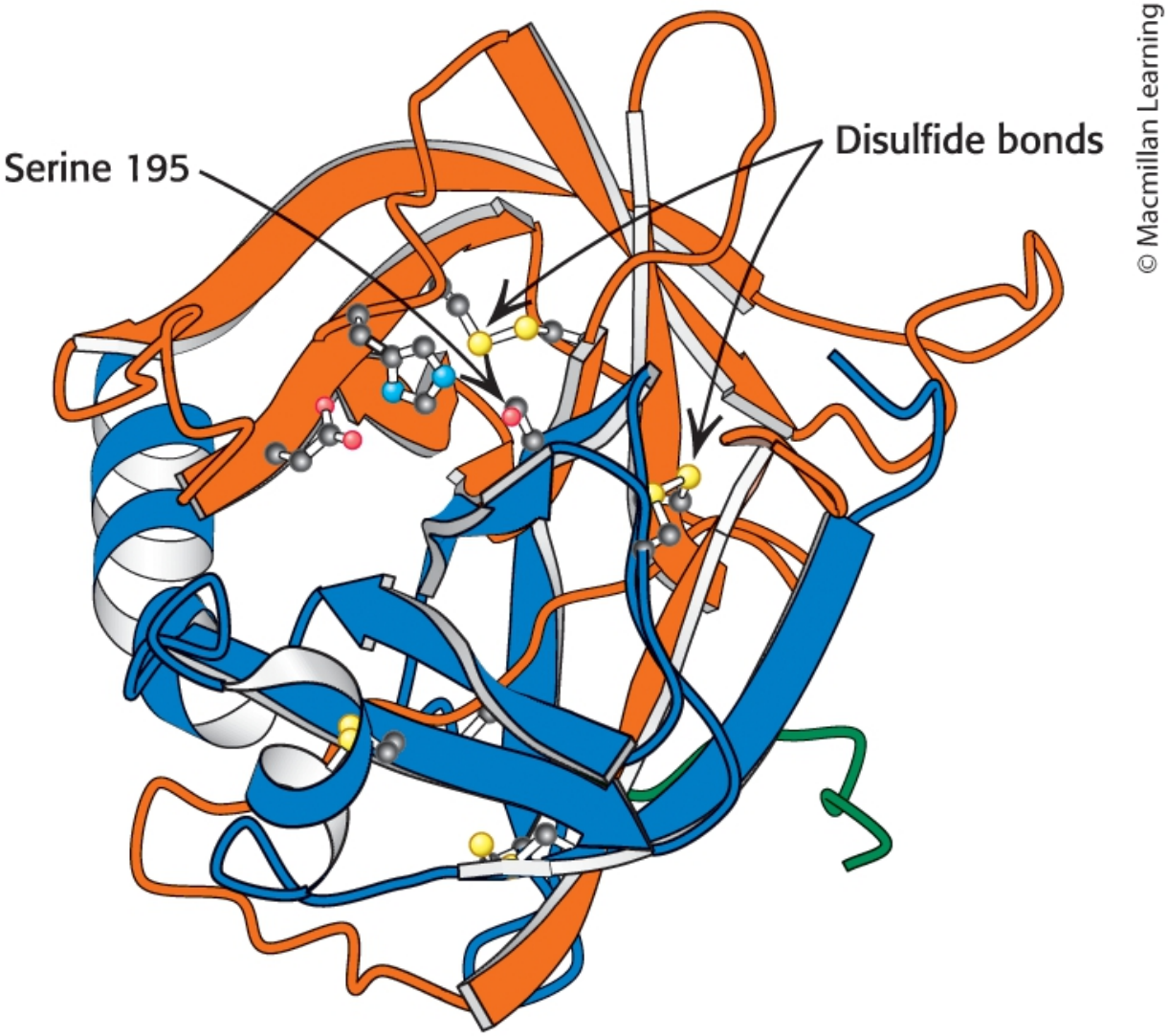
Part (B): The acyl-enzyme is converted into a free enzyme by deacylation reaction.

A forward reaction arrow is labeled deacylation. H 2 O enters the reaction.

The structure of the first product is as follows: The enzyme molecule single bonded to an O H group is shown. The structure of the second product is as follows: A central C atom is double bonded to O on the upper right, single bonded to R on the lower right, and single bonded to O H on the left.

Return to FIGURE 6.5. Schematic illustration of hydrolysis by chymotrypsin

Extended description for FIGURE 6.6. The ribbon diagram of chymotrypsin with active site serine residue

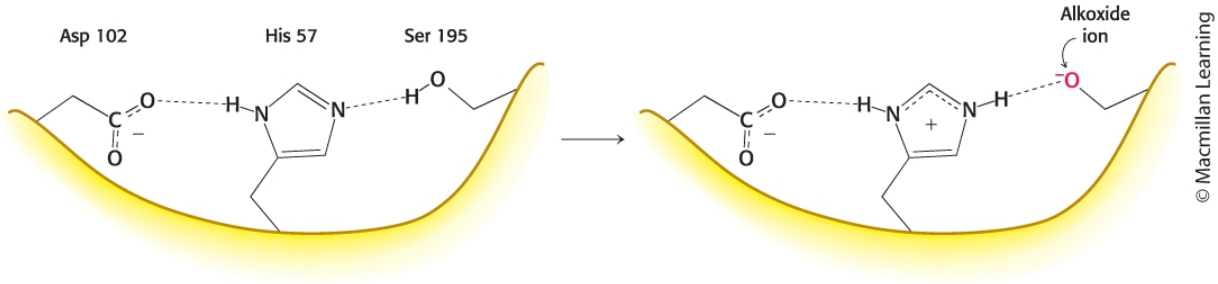


The chymotrypsin consists of three chains. The three chains of chymotrypsin are represented in orange, blue, and green colors. The orange and blue chains consist of beta-strands and alpha-helix connected by a thread-like loop. Serine 195 is located in a cleft on

the surface of chymotrypsin. The ball-and-stick models of disulfide bonds are shown at the top and rightmost region of chymotrypsin.

Return to FIGURE 6.6. The ribbon diagram of chymotrypsin with active site serine residue

Extended description for FIGURE 6.7. Schematic illustration of a catalytic triad in the active site of chymotrypsin and the polarization of hydroxyl group of serine residue

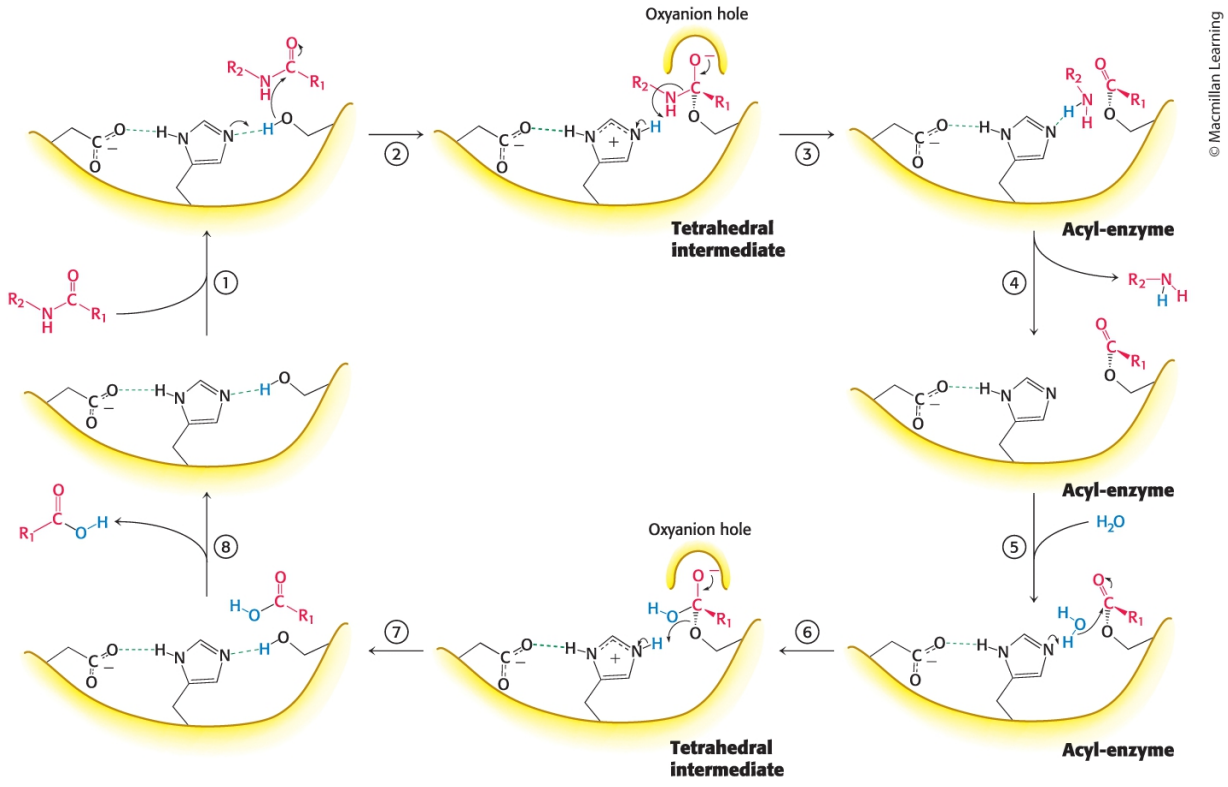


The enzyme is depicted as a concave surface with a yellow highlight. The catalytic triad consists of A s p 102, H i s 57, and S e r 195 residues. The A s p 102 residue consists of a central C atom partially bonded to O on the upper right and O below. The C O O group has a net negative charge. C is single bonded to C H 2 on the upper left in the form of a line. C H 2 is single-bonded to the enzyme. The O atom on the upper right is hydrogen-bonded to an H atom. The H atom is single bonded to the first N atom of H i s 57 residues. The H i s 57 residue consists of a 5-membered heterocyclic pentagonal ring in a vertical orientation consisting of 2 N and 3 C atoms. The first N atom occupies the first position, which is the top-left vertex. The second N atom occupies the third position, which is the top-right vertex. C 1 occupies the topmost vertex. A double is present between C 1 and second N and C 2 and C 3. C 3 is single bonded to C H 2 on the lower left in the form of a line. C H 2 is single-bonded to the enzyme. The second N is hydrogen-bonded to an H atom on the upper right. The H atom is again single bonded to O of S e r 195 residue on the upper right. The O atom is single-bonded to C H 2 on the lower right in the form of a line. C H 2 is single-bonded to the enzyme.

A forward reaction arrow shows the polarization of the O H group of S e r 195 residue. The second N atom of H is 57 residue is single-bonded to H on the upper right. This H atom is hydrogen-bonded to O superscript minus ion of S e r 195 side chain. O superscript minus ion is labeled alkoxide ion.

Return to FIGURE 6.7. Schematic illustration of a catalytic triad in the active site of chymotrypsin and the polarization of hydroxyl group of serine residue

Extended description for FIGURE 6.8. Schematic illustration of the mechanism of peptide hydrolysis



The mechanism is shown in a series of 8 irreversible steps. The enzyme active site is depicted as a concave surface with a yellow highlight. The active site of the enzyme contains a catalytic triad composed of aspartate, histidine, and serine interconnected by hydrogen bonds.

Step 1:

A peptide with the following structure enters the active site: A central C atom is double bonded to O above, single bonded to R 1 on the lower right, and single bonded to N on the lower left. N is bound to H below and single bonded to R 2 on the upper left.

The second N atom of the heterocyclic pentagonal ring of histidine donates electrons toward the hydrogen-bonded H atom. An arrow from the single bond between the H and O atom of serine residue points toward the central C atom of the peptide. An arrow from the C atom points toward the double-bonded O atom.

Step 2:

A Tetrahedral intermediate is formed.

The pentagonal ring of histidine acquires a net positive charge. The second N of the ring becomes single bonded to H. An arrow from the H atom points toward the N atom. The central C atom is single bonded to O superscript minus above. O superscript minus is located inside an oxyanion hole. An arrow from the O superscript minus atom points toward the C atom. A counter-clockwise arrow points from the single bond between N and C of the peptide toward the H atom bound to N.

Step 3:

An acyl-enzyme complex is formed.

The second N atom of the pentagonal ring of histidine becomes hydrogen-bonded to H. This H atom is single-bonded to N of the peptide. N is single bonded to R 2 above and H below. The bond between N and C of the peptide is broken. C atom becomes dashed bonded to O atom of a serine residue. C is double bonded to O above and wedge bonded to R 1 on the lower right.

Step 4:

A molecule having the following structure leaves the active site: R 2, single bond, N. N is single bonded to H below and H on the lower right. The second N of the pentagonal ring of the histidine residue is not bonded to any atom.

Step 5:

H 2 O molecule enters the active site. The second N of the pentagonal ring of histidine transfers electrons toward the H atom of a H 2 O molecule. An arrow from the single bond between this H and O atom points toward a C atom dash bonded to the O atom of a serine residue. An arrow points from this C atom to double-bonded O above.

Step 6:

A tetrahedral intermediate is formed.

C atom is a single bonded O superscript minus which is located inside an oxyanion hole. An arrow from O superscript minus points toward the C atom. An arrow from the dash bond between the C atom and O atom of serine residue points toward the H atom single bonded to the second N of histidine pentagonal ring. The pentagonal ring of histidine has a net positive charge.

Step 7:

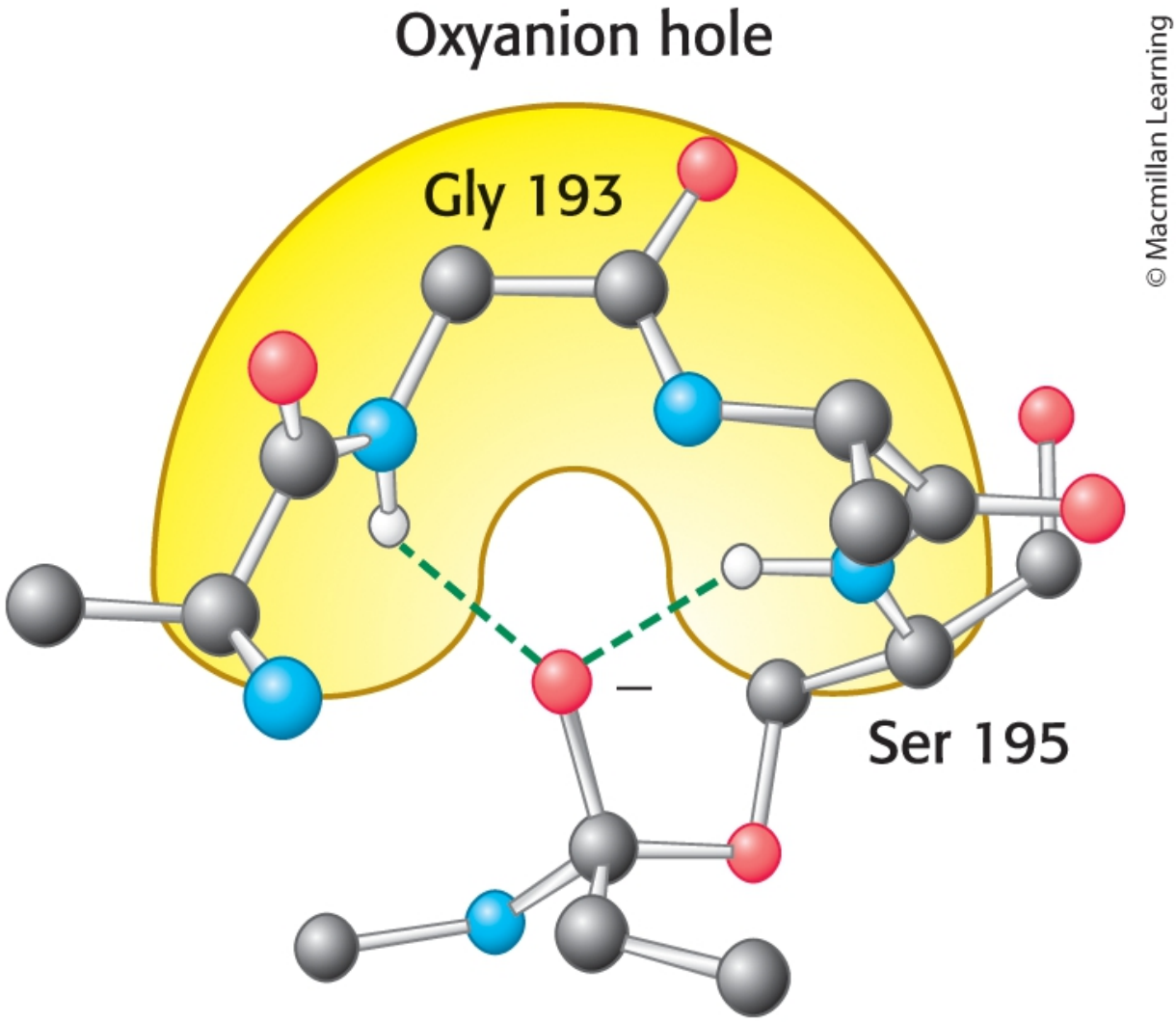
The catalytic triad re-attains its original bonding pattern. A molecule having the following structure is located above the active site: A central C atom is double bonded to O above, single bonded to O on the lower left, and single bonded to R 1 on the lower right. O atom is single bonded to H on the upper left.

Step 8:

The molecule in step 7 leaves the active site.

Return to FIGURE 6.8. Schematic illustration of the mechanism of peptide hydrolysis

Extended description for FIGURE 6.9. Schematic illustration of oxyanion hole-mediated stabilization of a tetrahedral intermediate formed during chymotrypsin catalysis

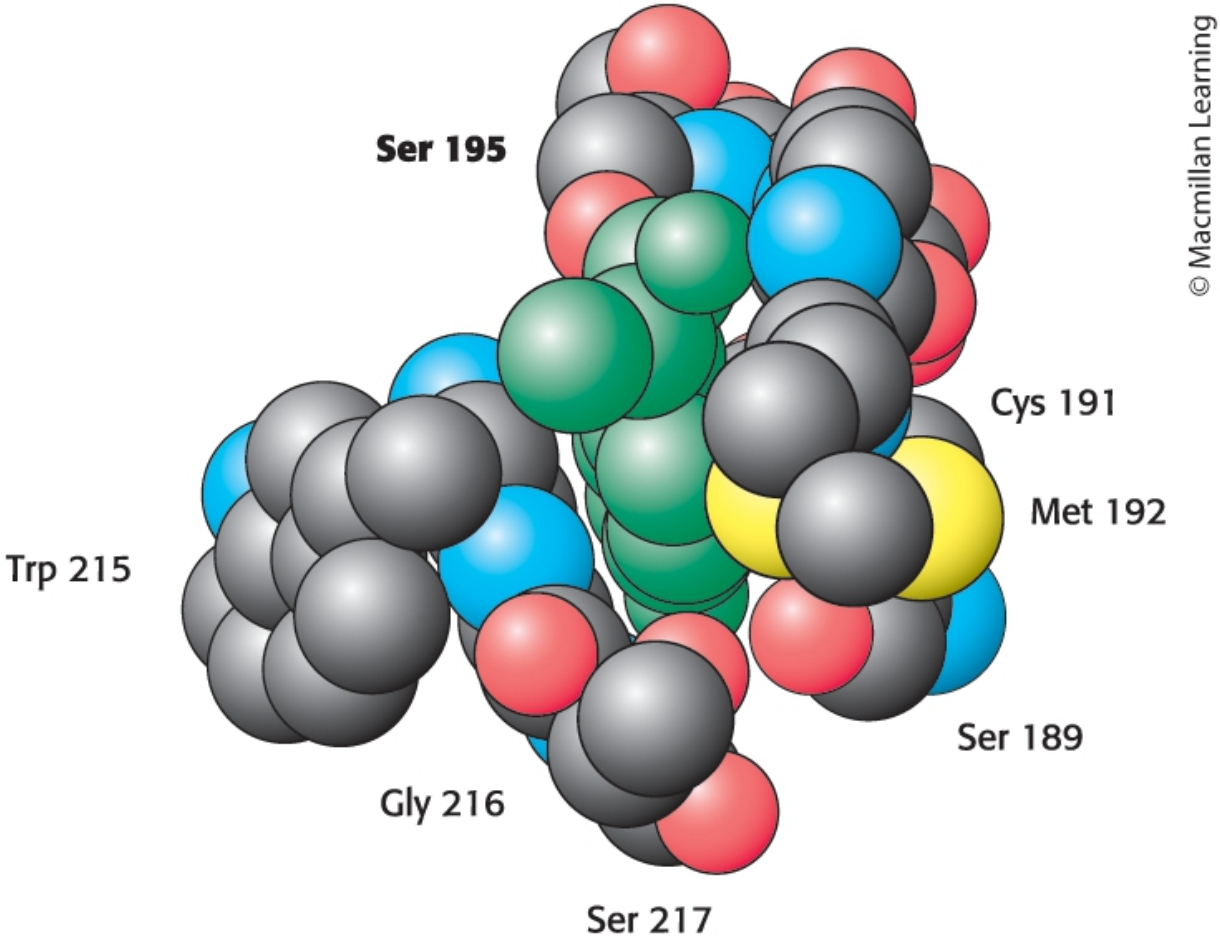


The oxyanion hole is depicted as a large bean-shaped structure with a cleft at the bottom center. The ball-and-stick model of the amino acid residues and the substrate are shown. They are composed of blue, black, red, and white spheres. G l y 193 is located at the center

of the hole. S e r 195 is located at the bottom right end of the hole. A white sphere connected to the S e r 195 residue depicting the oxygen atom is hydrogen-bonded to the red sphere of the tetrahedral intermediate located below the hole. This red sphere has a negative charge and is hydrogen-bonded on the upper left to a white sphere connected to an amino acid residue at the bottom left end of the hole.

Return to FIGURE 6.9. Schematic illustration of oxyanion hole-mediated stabilization of a tetrahedral intermediate formed during chymotrypsin catalysis

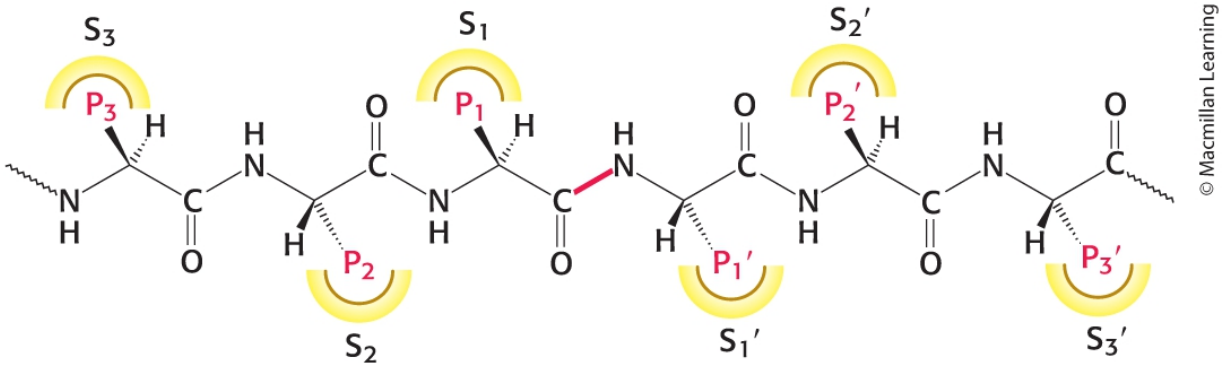
Extended description for FIGURE 6.10. Space-filling model of the specificity pocket of chymotrypsin



The space-filling model is composed of several interconnected red, blue, yellow, green, and black spheres. All the spheres are placed close to each other to form a compact structure. The model highlights T r p 215, G l y 216, S e r 217 from left to bottom, and S e r 189, M e t 192, C y s 191, and S e r 195 from bottom right to top.

Return to FIGURE 6.10. Space-filling model of the specificity pocket of chymotrypsin

Extended description for FIGURE 6.11. Structure of a molecule

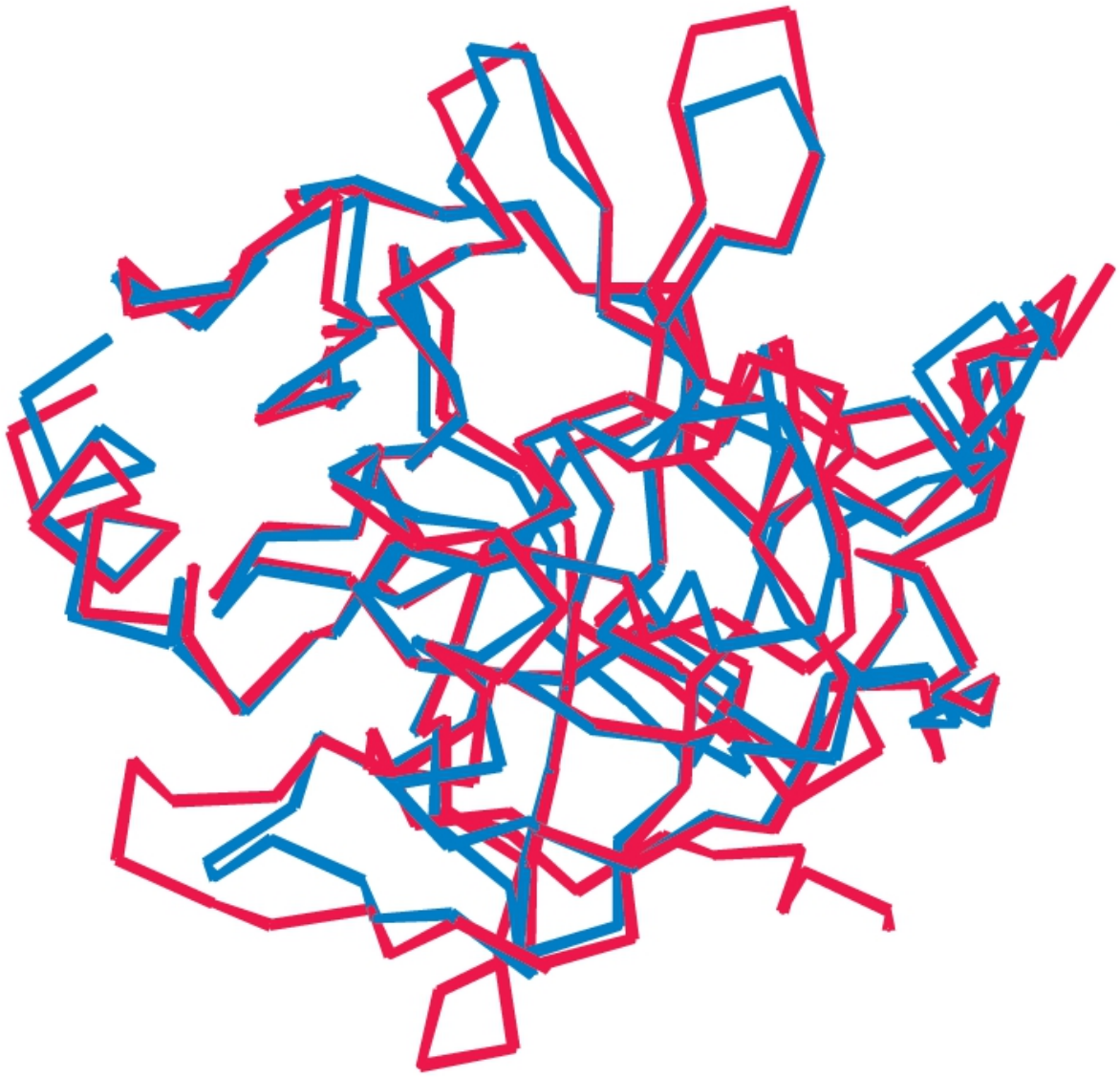


The structure of the molecule is as follows: A 6 N and 1 2 C heteronuclear alkane is depicted as a line structure using 17 zigzag lines. The first N bound to H occupies the first position. It has an open single bond on the upper left. The second N atom bound to H occupies the fourth position. The third N atom bound to H occupies the seventh position. The fourth N bound to H occupies the tenth position. The fifth N bound to H occupies the thirteenth position. The sixth N bound to H occupies the sixteenth position. C 1 is wedge bonded to P subscript 3 on the upper left and dash bonded to H on the upper right. P subscript 3 is located inside an inverted U-shaped pocket labeled S subscript 3. C 2 is double bonded to O below. C 3 is wedge bonded to H on the lower left and dash bonded to P subscript 2 on the lower right highlighted in red color. P subscript 2 is located inside a U-shaped pocket labeled S subscript 2. C 4 is double bonded to O above. C 5 is wedge bonded to P subscript 1 on the upper left and dash bonded to H on the upper right. P subscript 1 is located inside an inverted U-shaped pocket labeled S subscript 1. C 6 is double bonded to O below. C 7 is wedge bonded to H on the lower left and dash bonded to P prime subscript 1 on the lower right. P prime subscript 1 is located inside a U-shaped pocket labeled S subscript 1. C 8 is double bonded to O above. C 9 is wedge bonded to

P prime subscript 2 on the upper left and dash bonded to H on the upper right. P prime subscript 2 is located inside an inverted U-shaped pocket labeled S prime subscript 2. C 1 0 is double bonded to O below. C 11 is wedge bonded to H on the lower left and dash bonded to P prime subscript 3 on the lower right. P prime subscript 3 is located in a U-shaped pocket labeled S prime subscript 3. C 12 is double bonded to O above and has an open single-bonded on the lower right.

Return to FIGURE 6.11. Structure of a molecule

Extended description for FIGURE 6.12. Similar structures of chymotrypsin and trypsin

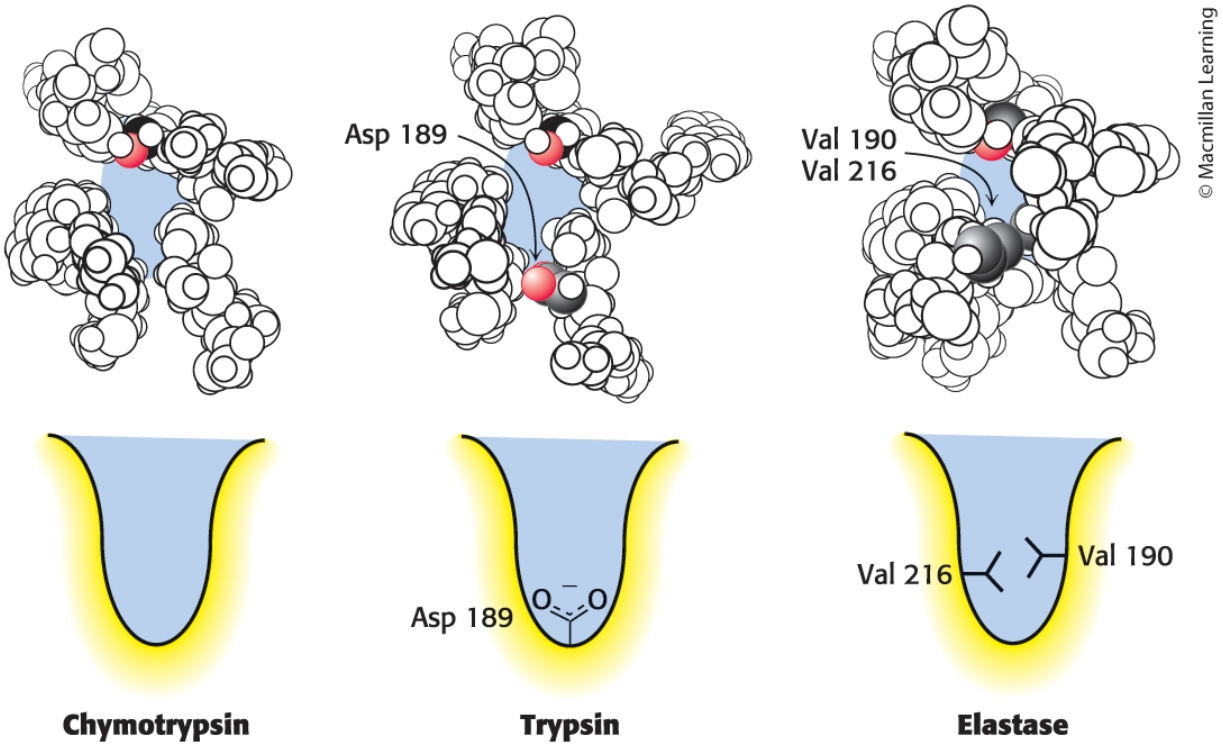


© Macmillan Learning

A red zigzag line represents structure of chymotrypsin and a blue zigzag line represents the structure of trypsin. The blue and red zigzag lines overlap each other and form a compact structure.

Return to FIGURE 6.12. Similar structures of chymotrypsin and trypsin

Extended description for FIGURE 6.13. Spacing filling models and schematic illustrations of the S 1 pockets of chymotrypsin, trypsin, and elastase



© Macmillan Learning

Space-filling model of chymotrypsin: Two clusters composed of white spheres are separated by a small gap. A black and red sphere is located on the top of the right cluster.

Schematic illustration of chymotrypsin: The pocket is depicted as a deep U-shaped pit-like structure. It has a yellow highlighted outline. The pit is empty.

Space-filling model of trypsin: Two clusters composed of white spheres are separated by a small gap. A black and red sphere is located on the top of the right cluster. Another black and a red

sphere is located at the bottom of the right cluster and is labeled A s p 189.

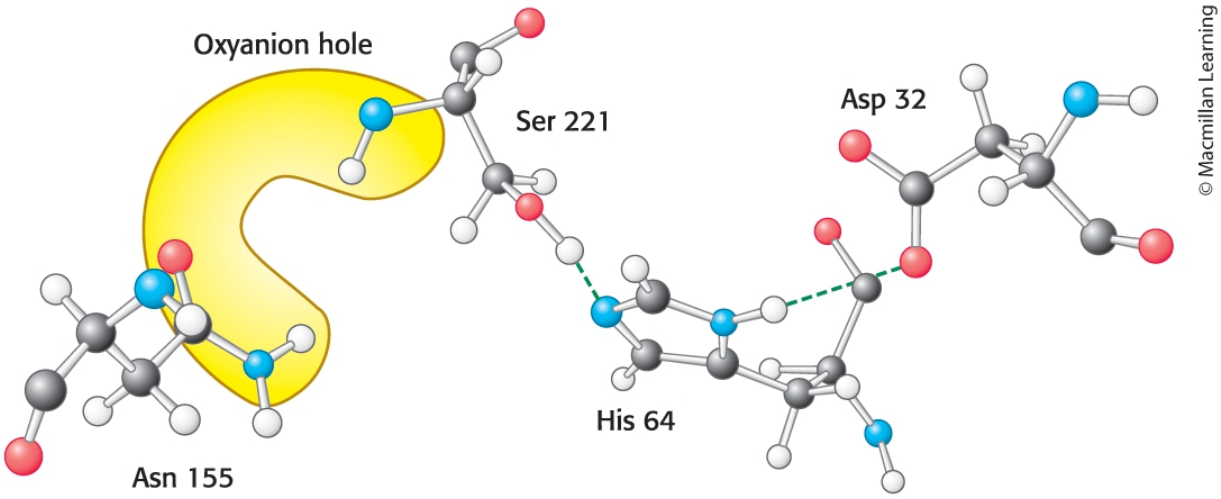
Schematic illustration of trypsin: The pocket is depicted as a deep U-shaped pit-like structure. It has a yellow highlighted outline. The side chain of A s p 189 residue is shown at the base of the pit. It consists of a central C atom partially double bonded O on the upper left and upper right. C is single bonded to the base of the pit. The C O O group has an overall negative charge.

Space-filling model of elastase: Two clusters composed of white spheres are separated by a small gap. A black and red sphere is located on the top of the right cluster. Two black spheres located at the bottom of the left cluster are labeled V a l 190 and V a l 216.

Schematic illustration of elastase: The pocket is depicted as a deep U-shaped pit-like structure. It has a yellow highlighted outline. The side chains of V al 216 and V a l 190 residues are shown at the left and right sidewalls of the pit respectively. The side of V a l 216 residue consists of a central C atom single bonded to C H 3 on the upper right and lower right in the form of a line. The side chain of V a l 190 residue consists of a central C atom single bonded to C H 3 on the upper left and C H 3 on the lower left in the form of a line.

Return to FIGURE 6.13. Spacing filling models and schematic illustrations of the S 1 pockets of chymotrypsin, trypsin, and elastase

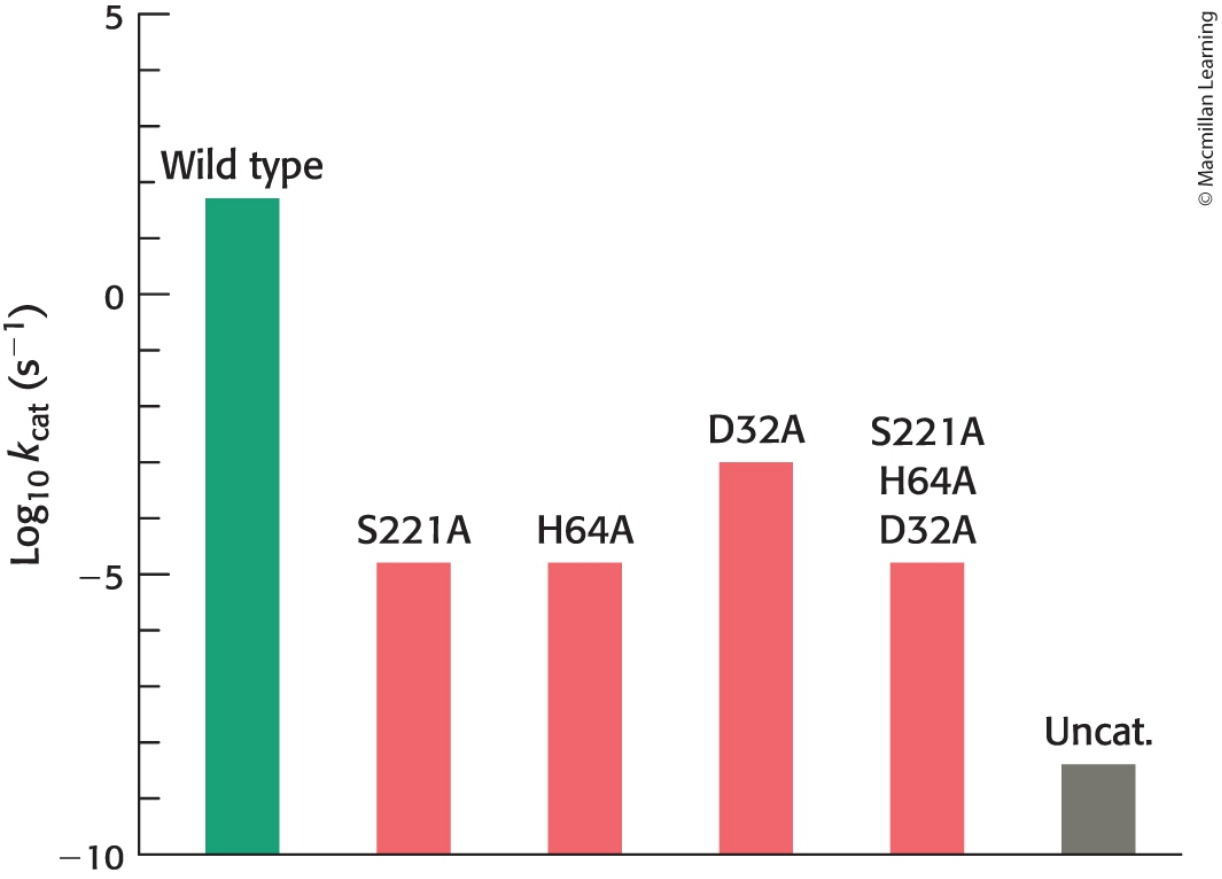
Extended description for FIGURE 6.14. Ball-and-stick model of catalytic triad and oxyanion hole of subtilisin



The ball-and-stick model consists of several interconnected red, blue, white and black spheres. The model highlights A s n 155, S e r 221, H is 64, and A s p 32 residues. The oxyanion hole is depicted as a thick yellow inverted U-shaped structure. The side chain of A s n 155 is located at the bottom end of the oxyanion hole The side chain of S e r 221 is located at the top end of the hole.

Return to FIGURE 6.14. Ball-and-stick model of catalytic triad and oxyanion hole of subtilisin

Extended description for FIGURE 6.15. Bar graph shows the activity of subtilisin enzyme for different mutations of the catalytic triad



© Macmillan Learning

The vertical axis is labeled log base 10 k subscript cat (s superscript minus 1). It has markings ranging from negative 10 to 5 in increments of 5 units. Several vertical bars of varying height are shown in the graph.

First green color bar: Wild type, 2 s superscript minus 1.

Second red bar: S 221 A, negative 5 s superscript minus 1.

Third red bar: H 64 A, negative 5 s superscript minus 1.

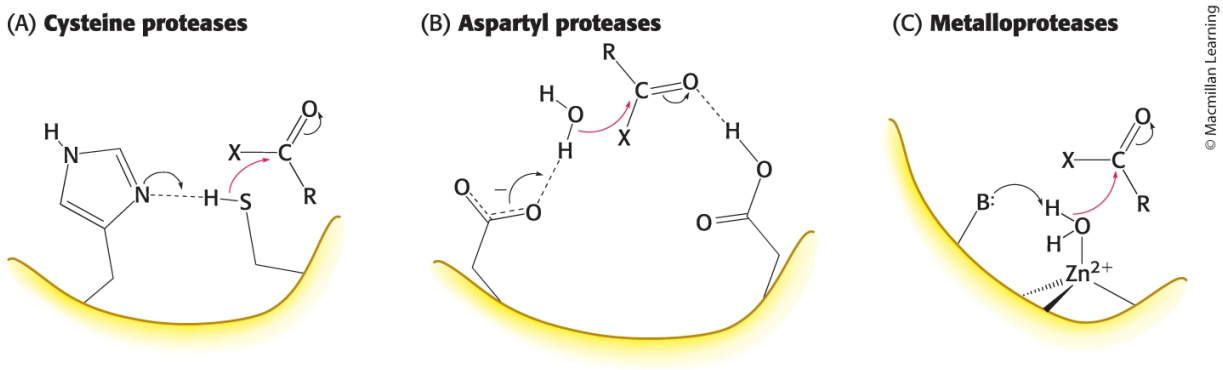
Fourth red bar: D 32 A, negative 3 s superscript minus 1.

Fifth red bar: S 221 A, H 64 A, D 32 A, negative 5 s superscript minus 1.

Sixth grey bar: Uncatalyzed, negative 8.5 s superscript minus 1.

Return to FIGURE 6.15. Bar graph shows the activity of subtilisin enzyme for different mutations of the catalytic triad

Extended description for FIGURE 6.16. Schematic illustration of the different catalytic strategies of (A) cysteine proteases, (B) aspartyl proteases, and (C) metalloproteases



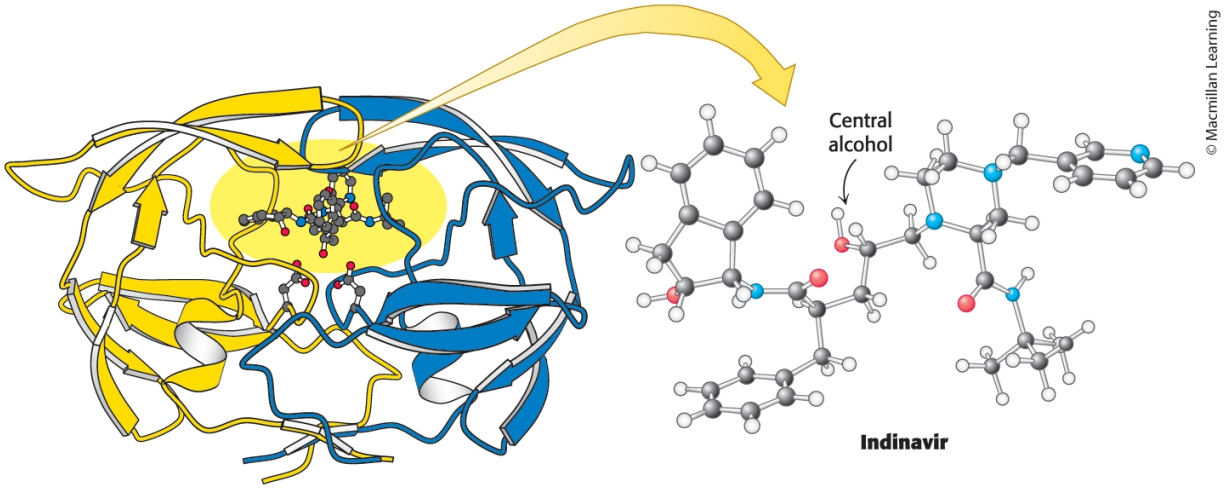
(A) Cysteine proteases: The enzyme is depicted as a horizontal concave surface with a yellow highlight. A five-membered heterocyclic pentagonal ring consisting of 2 N and 3 C atoms is in a vertical orientation with C 1 occupying the topmost vertex. The first N atom occupies the first position, which is the top-left vertex. The second N atom occupies the third position, which is the top-right vertex. A double bond is present between C 1 and second N, and C 2 and C 3. The first N is single bonded to H on the upper left. C 3 is single bonded to C H 2 on the lower left in the form of a line. C H 2 is single bonded to the enzyme. The second N is connected to a dashed line to an H atom. A black arrow moves from the second N to H. This H atom is single bonded to S. This S is single bonded to C H 2 on the lower right in the form of a line. C H 2 is single bonded to the enzyme. A red arrow from H, single bond, S points toward a central C atom. The C atom is double bonded to O on the upper right, single bonded to R on the lower right, and single bonded to X on the lower left. A black arrow moves from the central C atom to O.

(B) Aspartyl proteases: The enzyme is depicted as a horizontal concave surface with a yellow highlight. A central C atom is partially double bonded to O on the upper left and upper right. The C O O group has a net negative charge. The central C atom is single bonded to C H 2 on the lower left in the form of a line. C H 2 is single bonded to the enzyme. The O atom on the upper right is hydrogen-bonded to a water molecule. The structure of the water molecule is as follows: O is single bonded to H on the upper left and H on the lower left. A red arrow from O, single bond, H points toward a central C atom of another molecule. The central C atom is double bonded to O on the upper right, single bonded to X on the lower left, and single bonded to R on the upper left. O is hydrogen-bonded to H on the lower right. H is single bonded to O on the lower right. O is single bonded to a central C atom. C is double bonded to O on the lower left and single bonded to C H 2 on the lower right in the form of a line. C H 2 is single bonded to the enzyme.

(C) Metalloproteases: The enzyme is depicted as a horizontal concave surface with a yellow highlight. A central Z n superscript 2 ion is associated with the enzyme through a single bond, wedge, bond, and dash bond. The Z n ion is single bonded to O above. This O atom is single bonded to H on the upper left and lower left. A red arrow from O, single bond, H points toward a central C atom of another molecule. The central C atom is double bonded to O on the upper right, single bonded to R on the lower right, and single bonded to X on the right. An atom B is single bonded to the enzyme. B has a single lone pair of electrons. A black arrow moves from B to H atom on the upper left.

Return to FIGURE 6.16. Schematic illustration of the different catalytic strategies of (A) cysteine proteases, (B) aspartyl proteases, and (C) metalloproteases

Extended description for FIGURE 6.17. Ribbon diagram and ball-and-stick model of H I V protease with inhibitor indinavir

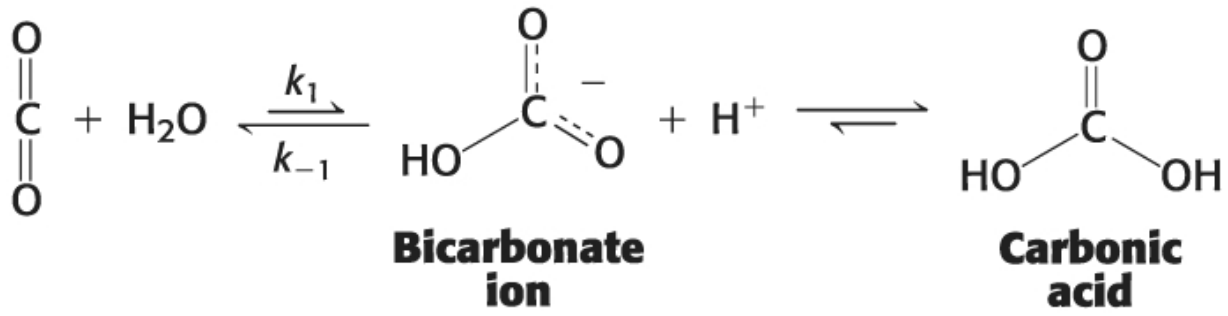


The ribbon diagram of H I V protease consists of yellow and blue colored beta-strands connected by thread-like loops. The protease shows two-fold symmetry. The inhibitor indinavir is bound to the active site.

The ball-and-stick model of indinavir consists of several interconnected red, blue, white, and black spheres. The model highlights the central alcohol molecule.

Return to FIGURE 6.17. Ribbon diagram and ball-and-stick model of H I V protease with inhibitor indinavir

Extended description for Reversible chemical reactions depicting the formation of carbonic acid



The first reversible reaction consists of two reactants and one product. The structure of the first reactant is as follows: A central C atom is double bonded to O above and O below. The second reactant is a H 2 O molecule. A reversible reaction arrow is labeled k subscript 1 above and k subscript minus 1 below.

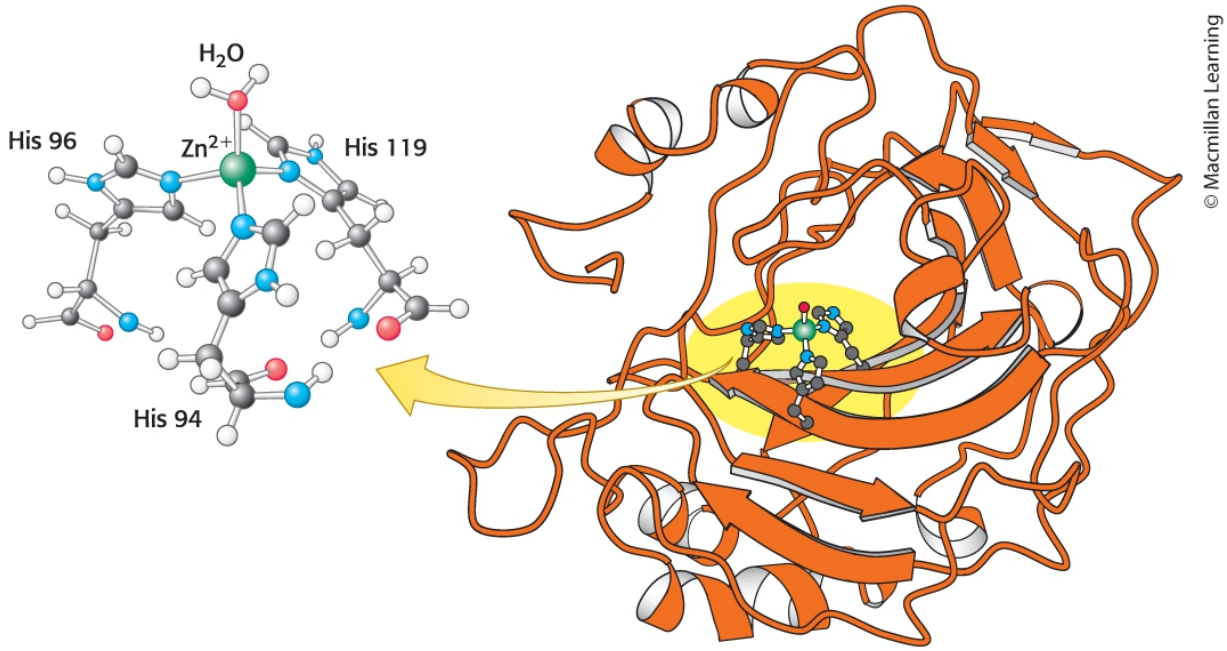
The first product is a bicarbonate ion whose structure is as follows: A central C atom is partially double bonded to O above, partially double bonded to O on the lower right, and single bonded to O H on the lower left. The second product is H superscript plus ion. A reversible reaction arrow is shown.

The forward reaction arrow is longer than the backward reaction arrow. The products of the first reversible reaction are the reactants of the second reversible reaction.

The product is carbonic acid whose structure is as follows: A central C atom is double bonded to O above, single bonded to O H on the lower right, and O H on the lower left.

Return to Reversible chemical reactions depicting the formation of carbonic acid

Extended description for FIGURE 6.18. Ribbon diagram of carbonic anhydrase roman number 2 and the ball-and-stick model of its active site

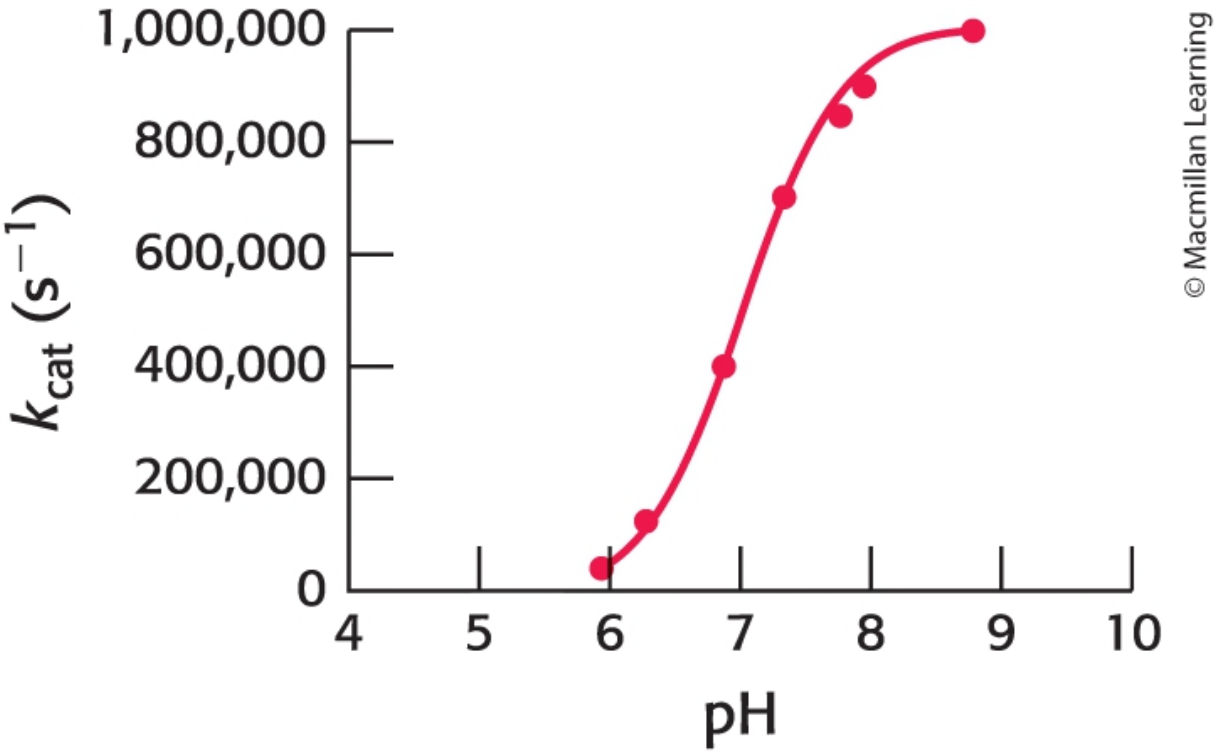


The ribbon diagram of human carbonic anhydrase roman number 2 is composed of anti-parallel beta-strands and a few alpha-helices connected by thread-like loops. The core of the enzyme is composed of beta-strands. The active site of the enzyme is present between the beta-strands and thread-like loops. It contains a zinc ion bound to the active site residues.

The ball-and-stick model shows a central Z n superscript ion connected to the imidazole rings of three histidine residues. Z n ion is depicted as a green sphere and is connected above to a H 2 O molecule. The histidine residues are composed of black, blue, white, and red spheres. The model highlights the residues H i s 96, H i s 119, and H i s 94.

Return to FIGURE 6.18. Ribbon diagram of carbonic anhydrase roman number 2 and the ball-and-stick model of its active site

Extended description for FIGURE 6.19. Graphical representation of the dependence of carbonic anhydrase activity on p H

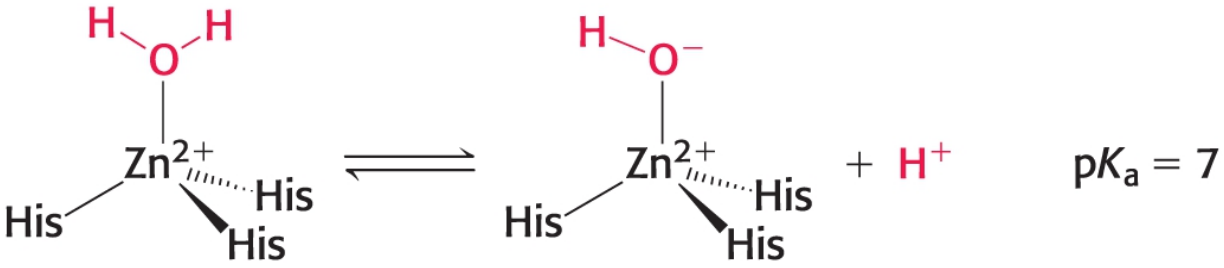


The horizontal axis is labeled p H. It has markings ranging from 4 to 10 in increments of 1 unit. The vertical axis is labeled k subscript cat in s superscript minus 1. It has markings ranging from 200,000 to 1,000,000 in increments of 200,000 units. A red curve rises from (6, 0) and moves steeply toward upper right to reach (9, 1,000,000). The data points marked on the curve are: (6, 0), (6.2,100,000), (7, 400,000), (7.2,700,000), (8, 900,000), (8, 950,000), and (9, 1,000,000).

All numerical values are estimated.

Return to FIGURE 6.19. Graphical representation of the dependence of carbonic anhydrase activity on p H

Extended description for FIGURE 6.20. Reversible reaction consisting of one reactant and two products is shown

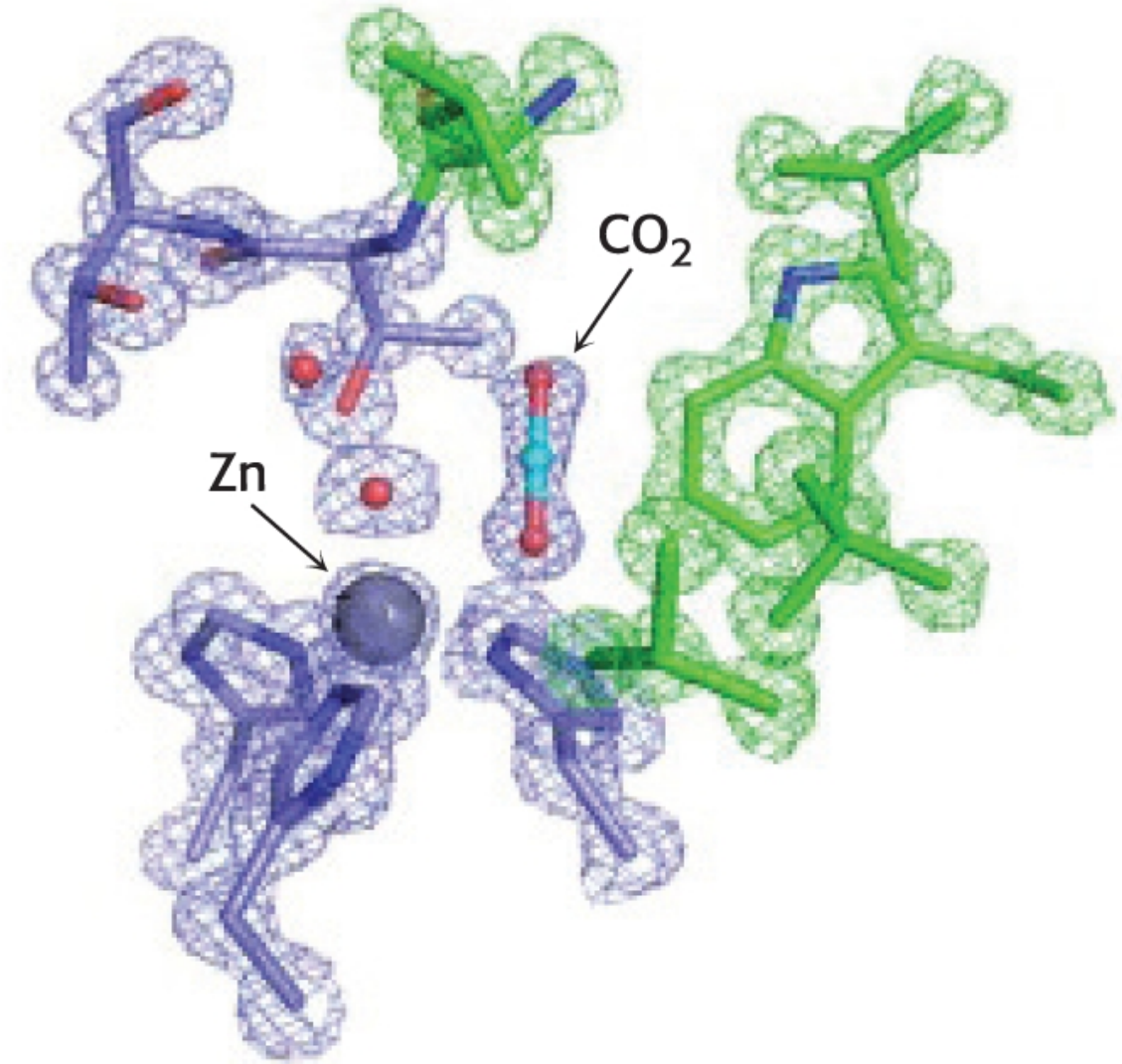


The reversible reaction consists of one reactant and two products.

The structure of the first reactant is as follows: A central Z n superscript 2 plus ion is single bonded to O above, which is again single bonded to H on the upper left and H on the upper right. The central Z n superscript 2 plus ion is dash bonded to His on the right, wedge bonded to His on the lower right, and single bonded to His on the lower left. The structure of the first product is as follows: The central Z n superscript 2 plus ion is single bonded to O superscript minus above, which is again single bonded to H on the upper left. The central Z n superscript 2 plus ion is dash bonded to His on the right, wedge bonded to His on the lower right, and single bonded to His on the lower left. The second product is H superscript plus ion. Note: p K subscript a is equal to 7.

Return to FIGURE 6.20. Reversible reaction consisting of one reactant and two products is shown

Extended description for FIGURE 6.21.Electron density map of carbonic anhydrase active site and C O 2 binding site



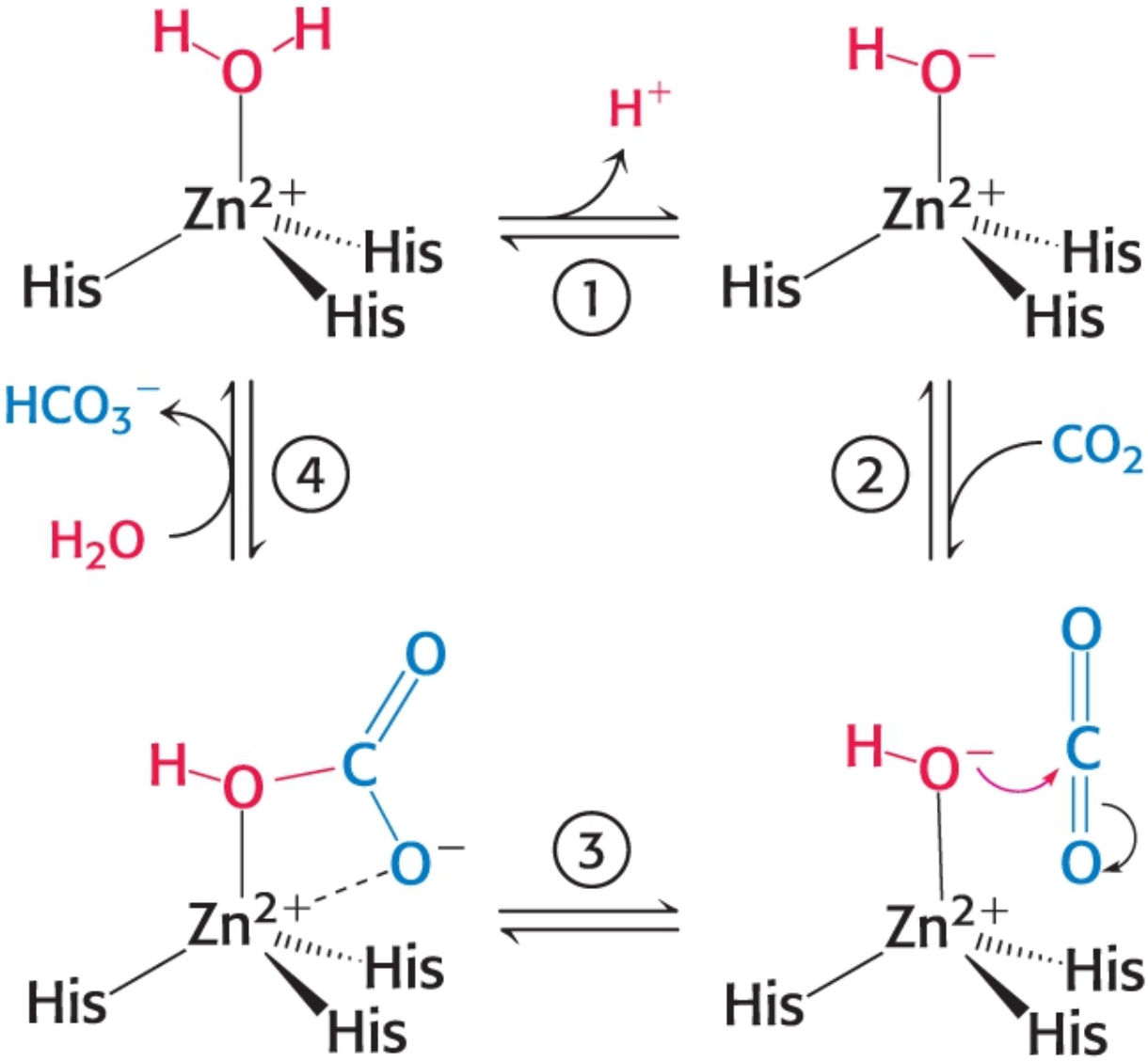
© Macmillan Learning

The electron density map is depicted as a cage-like structure outlining the shapes of the residues and molecules in the active site and C O 2 binding site. The hydrophobic amino acids are shown in green and hydrophilic amino acids are shown in purple. A vertically

oriented straight C O 2 molecule is located above the purple and green residues. Z n atom is depicted as a medium-sized sphere bound to cyclic rings shown in purple. Z n is located on the lower left of the C O 2 molecule.

Return to FIGURE 6.21.Electron density map of carbonic anhydrase active site and C O 2 binding site

Extended description for FIGURE 6.22. Mechanism for the hydration of carbon dioxide by carbonic anhydrase



The hydration of carbon dioxide takes place in four steps.

Step 1: The reversible reaction consists of one reactant and one product.

The structure of the reactant is as follows: A central Z n superscript 2 plus ion is single bonded to O above. This O atom is single bonded to H on the upper left and H on the upper right. The O and H atoms are highlighted in red. The Z n ion is dash bonded to His on the right, wedge bonded to His on the lower right, and single bonded to His on the lower left.

A reversible reaction arrow is shown. H superscript plus ion leaves the reaction.

The structure of the product is as follows: A central Z n superscript 2 plus ion is single bonded to O superscript minus above, which is single bonded to H on the upper left. The O and H atoms are highlighted in red. The Z n ion is dash bonded to His on the right, wedge bonded to His on the lower right, and single bonded to His on the lower left.

A reversible reaction arrow is shown. C O 2 enters the reaction.

Step 2: The reversible reaction consists of one reactant and one product.

The reactant of step 2 is the product of step 1.

The structure of the product is as follows: A central Z n superscript 2 plus ion is single bonded to O superscript minus above, which is single bonded to H on the upper left. The O and H atoms are highlighted in red. The Z n ion is dash bonded to His on the right, wedge bonded to His on the lower right, and single bonded to His on the lower left. A red arrow from O superscript minus atom points toward the central C atom of a C O 2 molecule. C is double bonded to O above and O below. The C O 2 molecule is highlighted in blue.

A reversible reaction arrow is shown.

Step 3: The reversible reaction consists of one reactant and one product.

The reactant of step 3 is the product of step 2.

The structure of the product is as follows: A central Z n superscript 2 plus ion is single bonded to O above, which is single bonded to H on the upper left. The O and H atoms are highlighted in red. The O atom is single bonded to C on the upper right. C is double bonded to O on the upper right and single bonded to O superscript minus on the lower right. A dashed blue line connects O superscript minus to the Z n ion. The Z n ion is dash bonded to His on the right, wedge bonded to His on the lower right, and single bonded to His on the lower left.

A reversible reaction arrow is shown. H 2 O enters and H C O 3 superscript minus leaves the reaction.

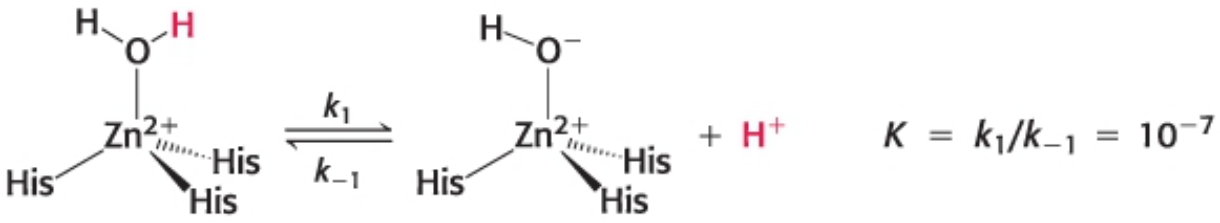
Step 4: The reversible reaction consists of one reactant and one product.

The reactant of step 4 is the product of step 3.

The structure of the product is as follows: A central Z n superscript 2 plus ion is single bonded to O above. The O atom is single bonded to H on the upper left and H on the upper right. The O and H atoms is highlighted in red. The Z n ion is dash bonded to His on the right, wedge bonded to His on the lower right, and single bonded to His on the lower left.

Return to FIGURE 6.22. Mechanism for the hydration of carbon dioxide by carbonic anhydrase

Extended description for FIGURE 6.23. Chemical reaction shows the reversible deprotonation of water molecule bound to carbonic anhydrase active site and the ratio of rate constants for protonation and deprotonation



The reversible reaction consists of one reactant and two products. The structure of the first reactant is as follows: A central Z n superscript 2 plus ion is single bonded to O above. O is single bonded to H on the upper left and H on the upper right. The H atom on the upper right is highlighted in red. The central Z n superscript 2 plus ion is dash bonded to H i s on the lower right, wedge bonded to H i s on the lower right, and single bonded to H i s on the lower left.

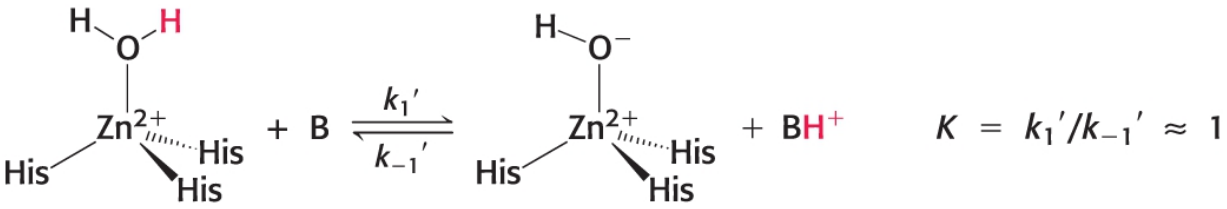
The forward reaction arrow is labeled k subscript 1. The reverse reaction arrow is labeled k subscript negative 1.

The structure of the first product is as follows: A central Z n superscript 2 plus ion is single bonded to O superscript minus above, which is single bonded to H on the upper left. The Z n superscript 2 plus ion is dash bonded to H i s on the lower right, wedge bonded to H i s on the lower right, and single bonded to H i s on the lower left. The second product is the H superscript plus ion which is highlighted in red.

Note: K equals StartFraction k subscript 1 over k subscript negative 1 EndFraction equals 10 raised to the negative 7th power.

Return to FIGURE 6.23. Chemical reaction shows the reversible deprotonation of water molecule bound to carbonic anhydrase active site and the ratio of rate constants for protonation and deprotonation

Extended description for FIGURE 6.24. Reversible reaction shows the deprotonation of the zinc-bound water molecule in carbonic anhydrase aided by buffer



The reversible reaction contains two reactants and two products.

The structure of first reactant is as follows: A central Z n superscript 2 plus ion is single bonded to O above. This O atom is single bonded to H on the upper left and H on the upper right. The H atom on the upper right is highlighted in red. The central Z n ion is dash bonded to His on the right, wedge bonded to His on the lower right, and single bonded to His on the lower left.

The second reactant is B.

A reversible reaction arrow is shown. The top forward reaction arrow is labeled k prime subscript 1. The bottom backward reaction arrow is labeled k prime subscript minus 1.

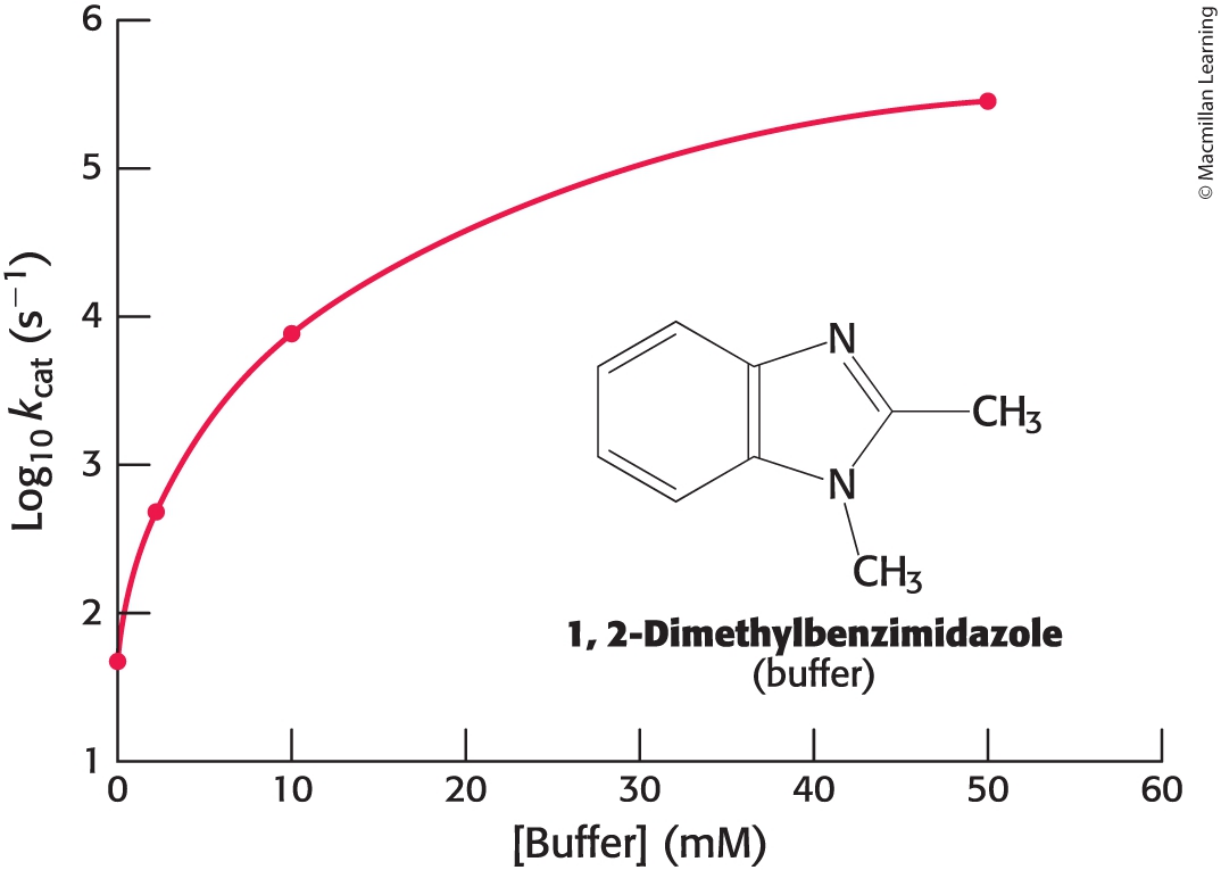
The structure of first product is as follows: A central Z n superscript 2 plus ion is single bonded to O superscript minus above. This O superscript minus atom is single bonded to H on the upper left. The central Z n ion is dash bonded to His on the right, wedge bonded to His on the lower right, and single bonded to His on the lower left.

The second product is B H superscript plus molecule. H superscript plus is highlighted in red.

Note: K equals StartFraction k prime subscript 1 over k prime subscript minus 1 EndFraction which is approximately equal to 1.

Return to FIGURE 6.24. Reversible reaction shows the deprotonation of the zinc-bound water molecule in carbonic anhydrase aided by buffer

Extended description for FIGURE 6.25. Graphical representation of the rate of carbon dioxide hydration by carbonic anhydrase as a function of buffer concentration



© Macmillan Learning

The horizontal axis is labeled the concentration of buffer in millimolar. It has markings ranging from 1 to 6 in increments of 1 unit. The vertical axis is labeled log base 10 k subscript cat close (s superscript minus 1).

A red concave down curve starts from (0, 1.8) and ends at (50, 5.4).

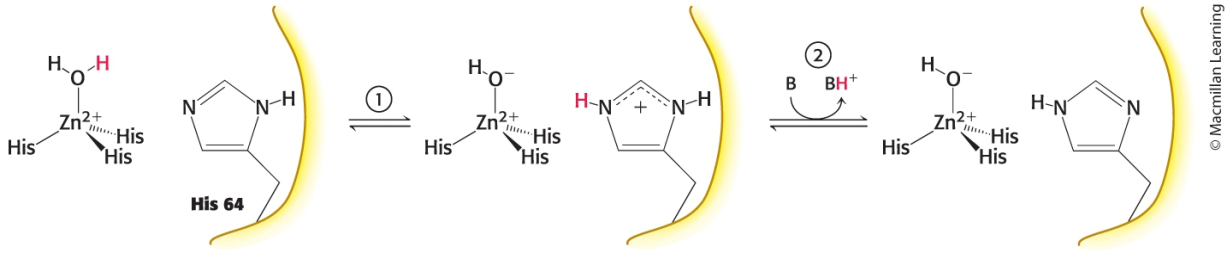
The data points on the curve are (0, 1.8), (2, 2.8), (10, 3.9), and (50, 5.4).

All numerical values are estimated.

The structure of 1, 2-Dimethylbenzimidazole (buffer) is as follows: A benzene ring is in a vertical orientation with C 1 occupying the topmost vertex. It contains alternating double bonds between C 2 and C 3, C 4 and C 5, and C 6 and C 1. The benzene ring is fused to a 5-membered heterocyclic pentagonal ring in a horizontal orientation consisting of 2 N and 3 C atoms such that C 2 and C 3 of the benzene ring are C 3 and C 2 respectively of the pentagonal ring. In the pentagonal ring, the first N atom occupies the first position, which is the topmost vertex. The second N atom occupies the third position, which is the bottom right vertex. A double bond is present between the first N and C 1. C 1 is single bonded to C H 3 on the right. The second N atom is single bonded to C H 3 on the lower right.

Return to FIGURE 6.25. Graphical representation of the rate of carbon dioxide hydration by carbonic anhydrase as a function of buffer concentration

Extended description for FIGURE 6.26. Schematic illustration of histidine 64 residue of carbonic anhydrase roman number 2 acting as a proton shuttle



The carbonic anhydrase roman number 2 enzyme is depicted as a vertical concave surface with a yellow highlight.

The structure of the first reactant is as follows: A central Z n superscript 2 plus ion is single bonded to O above. The O atom is single bonded to H on the upper left and H on the upper right. The H atom on the upper right is highlighted in red. The Z n ion is dash bonded to His on the right, wedge bonded to His on the lower right and single bonded to His on the lower left.

The structure of the second reactant is as follows: A five membered heterocyclic pentagonal ring consisting of 2 N and 3 C atoms is in a vertical orientation with C 1 occupying the topmost vertex. The first N atom occupies the first position, which is the top left vertex. The second N atom occupies the third position, which is the top right vertex. A double bond is present between C 2 and C 3, and the first N atom and C 1. The second N atom is single bonded to H on the upper right. C 2 of the pentagonal ring is single bonded to C H 2 on the lower right in the form of a line. C H 2 is single bonded to the enzyme. The pentagonal ring single bonded to the enzyme is labeled His 64.

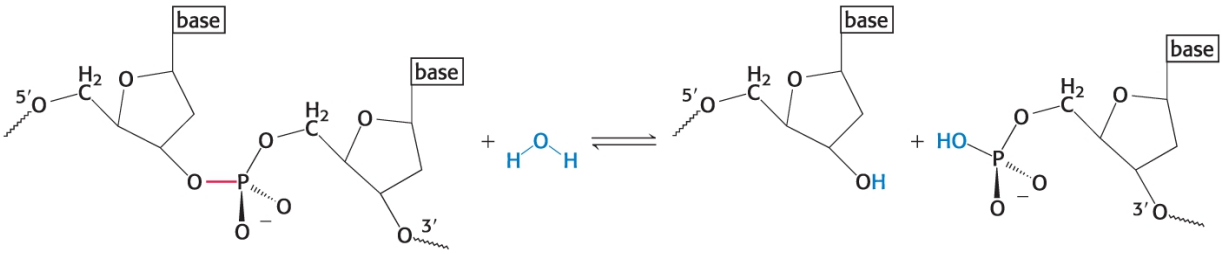
Step 1: After the removal of a proton from the zinc-bound water molecule a new structure formed is as follows: A central Z n superscript 2 plus ion is single bonded to O superscript minus above. The O atom is single bonded to H on the upper left. The Z n ion is dash bonded to His on the right, wedge bonded to His on the lower right, and single bonded to His on the lower left. A five membered heterocyclic pentagonal ring consisting of 2 N and 3 C atoms is in a vertical orientation with C 1 occupying the topmost vertex. The first N atom occupies the first position, which is the top left vertex. The second N atom occupies the third position, which is the top right vertex. A double bond is present between C 2 and C 3. A resonance bond is shared between the first N, C 1, and the second N. A net positive charge is present in the ring. The first N atom is single bonded to H on the upper left. This H atom is highlighted in red. The second N atom is single bonded to H on the upper right. C 2 of the pentagonal ring is single bonded to C H 2 on the lower right in the form of a line. C H 2 is single bonded to the enzyme. The pentagonal ring single bonded to the enzyme is labeled His 64.

Step 2: The proton single bonded to the first N is transferred to the buffer molecules in the solution. A reversible reaction arrow is shown. B enters the reaction and leaves as B H superscript plus. H superscript plus is highlighted in red. The structure of the first products is as follows: A central Z n superscript 2 plus ion is single bonded to O superscript minus above. This O superscript minus atom is single bonded to H on the upper left. The Z n ion is dash bonded to His on the right, wedge bonded to His on the lower right, and single bonded to His on the lower left. The structure of the second product is as follows: A five membered heterocyclic pentagonal ring consisting of 2 N and 3 C atoms is in a vertical orientation with C 1 occupying the topmost vertex. The first N atom occupies the first position, which is the top left vertex. The second N occupies the third position, which is the top right vertex. A double bond is present between C 2 and C 3, and C 1 and second N atom. C 2

of the pentagonal ring is single bonded to C H 2 on the lower right in the form of line. C H 2 is single bonded to the enzyme.

Return to FIGURE 6.26. Schematic illustration of histidine 64 residue of carbonic anhydrase roman number 2 acting as a proton shuttle

Extended description for FIGURE 6.27. Chemical reaction shows the restriction enzyme-mediated hydrolysis of phosphodiester bond



The reversible reaction consists of two reactants and two products.

The structure of the first reactant is as follows: A five-membered heterocyclic pentagonal ring consisting of 1 O and 4 C atoms is in a vertical orientation. O occupies the first position, which is the top-left vertex. C 1 occupies the topmost vertex and is single bonded to the base enclosed in a box above. C 4 is single bonded to C bound to H 2 on the upper left. C H 2 is single bonded to O on the lower left. The O atom has an open single bond and is labeled 5 prime. C 3 is single bonded to O on the lower right. This O is single-bonded to a central P atom through a red line. The P atom is wedge bonded to O superscript minus below, dash bonded to O on the lower right, and single bonded to O on the upper right. The O atom on the upper right is single bonded to C H 2 above. C H 2 is single bonded to C 4 of another heterocyclic pentagonal ring in a vertical orientation. The ring consists of 1 O and 4 C atoms. O occupies the top-left vertex. C 1 of the pentagonal ring is single bonded to the base enclosed in a box above. C 3 of the pentagonal ring is single bonded to O on the lower right. This O atom has an open single bond and is labeled 3 prime.

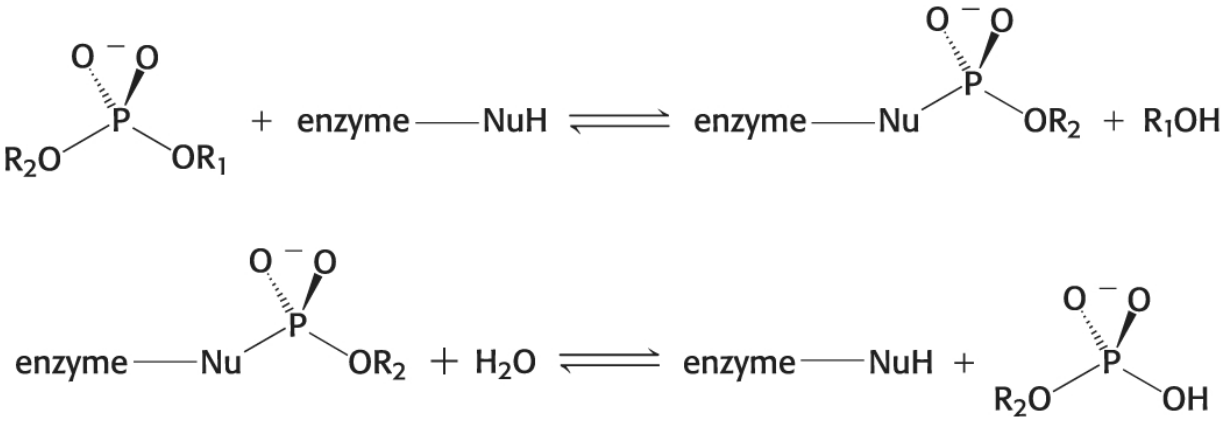
The structure of the second reactant is as follows: A central O atom is single-bonded to H on the lower left and H on the lower right. The entire molecule is highlighted in blue.

The structure of the first product is as follows: A five-membered heterocyclic pentagonal ring consisting of 1 O and 4 C atoms is in a vertical orientation. O occupies the first position, which is the top-left vertex. C 1 is single bonded to the base enclosed in a box above. C 3 is single bonded to O H on the lower right. H atom is highlighted in blue. C 4 is single bonded to C H 2 on the upper left. C H 2 is single bonded to O on the lower left. The O atom has an open single bond on the lower left and is labeled 5 prime.

The structure of the second reactant is as follows: A five-membered heterocyclic pentagonal ring is in a vertical orientation and consists of 1 O and 4 C atoms. O occupies the first position, which is the top-left vertex. C 1 is single bonded to the base enclosed in a box above. C 3 is single bonded to O on the lower right. This O atom has an open single bond and is labeled 3 prime. C 4 is single bonded to C H 2 on the upper left. C H 2 is single bonded to O on the lower left. O is single bonded to a central P atom below. P is single bonded to O H on the upper left, dash bonded to O on the lower right, and wedge bonded to O superscript minus below. The O H group is highlighted in blue.

Return to FIGURE 6.27. Chemical reaction shows the restriction enzyme-mediated hydrolysis of phosphodiester bond

Extended description for Two reversible reactions consisting of two reactants and two products are shown



The first reversible reaction consists of two reactants and two products.

The structure of the first reactant is as follows: A central P atom is dash bonded to O superscript minus on the upper left, wedge bonded to O on the upper right, single bonded to R subscript 2 O on the lower left, and O R subscript 1 on the lower right. The structure of the second reactant is as follows: Enzyme, single bond, N u H.

The first product has the following structure: The central P atom is dash bonded to O superscript minus on the upper left, wedge bonded to O on the upper right, single bonded to O R subscript 2 on the lower right, and N u on the lower left, which is again single bonded to the enzyme on the left. The second product is R subscript 1 O H.

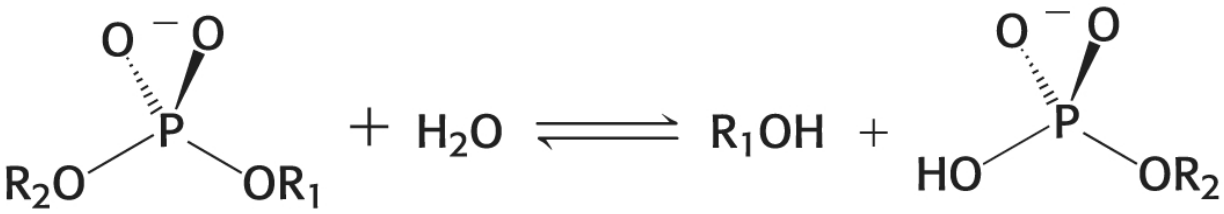
The second reversible reaction consists of two reactants and two products.

The structure of the first reactant is as follows: A central P atom is dash bonded to O superscript minus on the upper left, wedge bonded to O on the upper right, single bonded to O R subscript 2 on the lower right, and single bonded to N u on the lower left, which is again single bonded to the enzyme on the left. The second reactant is H 2 O molecule.

The first product is enzyme, single bond, N u H. The second product has the following structure: The central P atom is dash bonded to O superscript minus on the upper left, wedge bonded to O on the upper right, single bonded to R subscript 2 O on the lower left, and single O H on the lower right.

Return to Two reversible reactions consisting of two reactants and two products are shown

Extended description for Chemical reaction for the direct hydrolysis of D N A

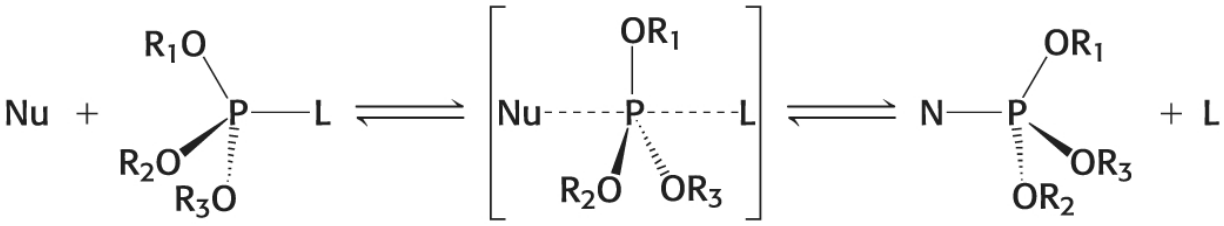


The reversible chemical reaction consists of two reactants and two products. The first reactant has the following structure: A central P atom is dash bonded to O superscript minus on the upper left, wedge bonded to O on the upper right, single bonded to R subscript 2 O on the lower left, and single bonded to O R subscript 1 on the lower right. The second reactant is H 2 O.

The first product has the following structure: R subscript 1 O H. The second product has the following structure: A central P atom is dash bonded to O superscript minus on the upper left, wedge bonded to O on the upper right, single bonded to O H on the lower left, and single bonded to O R subscript 2 on the lower right.

Return to Chemical reaction for the direct hydrolysis of D N A

Extended description for Series of reversible reactions consisting of two reactants, two products, and an intermediate product are shown



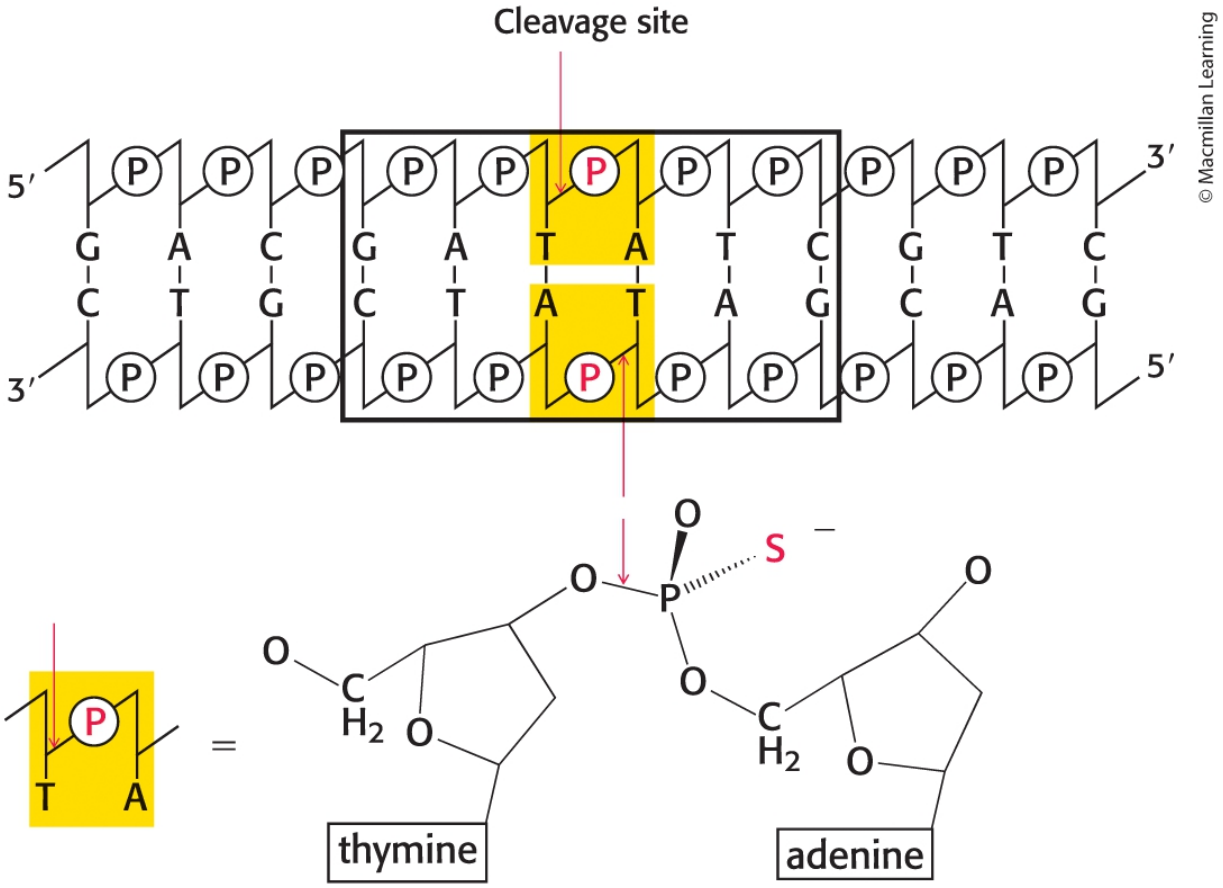
The first reactant is N u. The structure of the second reactant is as follows: P is single bonded to R subscript 1 O on the upper left, single bonded to L on the right, dash bonded to R subscript 3 O below, and wedge bonded to R subscript 2 O on the lower left.

The structure of the intermediate is as follows: A central P atom is single bonded to O R subscript 1 above, L on the right, and N u on the left. P is dash bonded to O R subscript 3 on the lower right and wedge bonded to R subscript 2 O on the lower left.

The structure of the first product is as follows: A central P atom is single bonded to O R subscript 1 on the upper right, wedge bonded to O R subscript 3 on the lower right, dash bonded to O R subscript 2 below, and single bonded to N on the left. The second product is L.

Return to Series of reversible reactions consisting of two reactants, two products, and an intermediate product are shown

Extended description for FIGURE 6.28. Schematic representation of Eco R V cleavage site in a D N A sequences



© Macmillan Learning

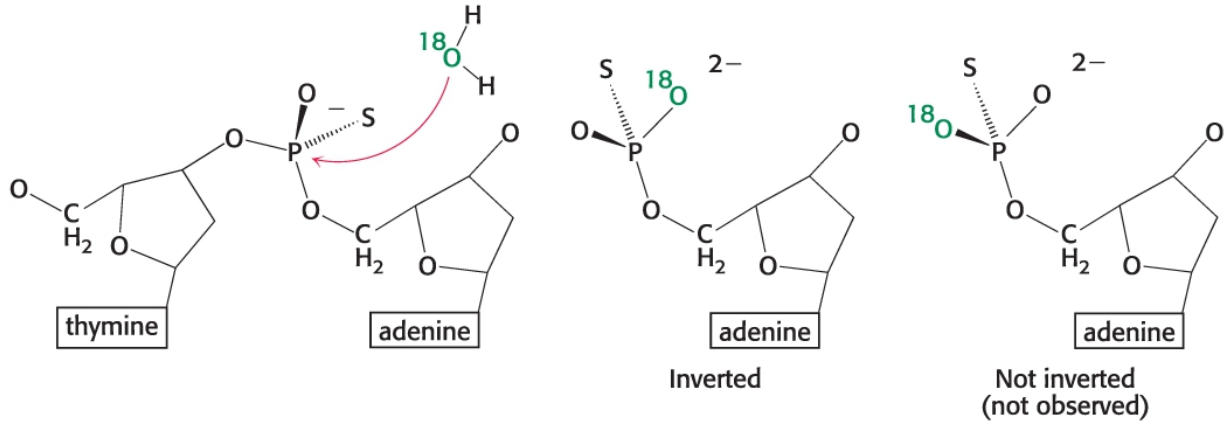
The two DNA strands are present in 5 prime to 3 prime and 3 prime to 5 prime orientation. The first sequence is G A C G A T A T C G T C. The second sequence is C T G C T A T A G C A G. The cleavage site is enclosed in a rectangular box. The sequence enclosed in the box is G A T A T C and C T A T A G. The sequences T A and A T are enclosed in yellow color.

The T A sequence is enlarged to show the structure of thymine connected to adenine through a phosphodiester bond. C 2 of the

pentagonal ring of thymine residue is single bonded to O. This O is single bonded to a central P atom. An arrow points toward this single bond. P is wedge bonded to O above and dash bonded to S superscript minus on the upper right. P is single bonded to O below. This O is single bonded to adenine residue.

Return to FIGURE 6.28. Schematic representation of Eco R V cleavage site in a D N A sequences

Extended description for FIGURE 6.29. Schematic illustration of the inversion of the stereochemical configuration of phosphorus atom after cleavage of D N A by Eco R V



A chemical structure of a dinucleotide composed of thymine and adenine is shown.

The structure of the dinucleotide is as follows: A 5-membered heterocyclic pentagonal ring is in a vertical orientation with C 1 occupying the top left vertex. It consists of 1 O and 4 C atoms. O occupies the first position, which is the bottom left vertex. C 1 is single bonded to C H 2. C H 2 is single bonded to O on the upper left. C 4 is single bonded to thymine on the lower left. C 2 is single bonded to O on the upper right. This O is single bonded to a central P atom. This P is wedge bonded to O superscript minus above, dash bonded to S on the upper right, and single bonded to O below. This O atom is single bonded to C H 2 on the lower right. C H 2 is single bonded to C 1 of a 5-membered heterocyclic pentagonal ring in a vertical orientation. It consists of 1 O and 4 C atoms. O occupies the first position which is the bottom left vertex. C 2 is single bonded to

O on the upper right. C 4 is single bonded to adenine on the lower left.

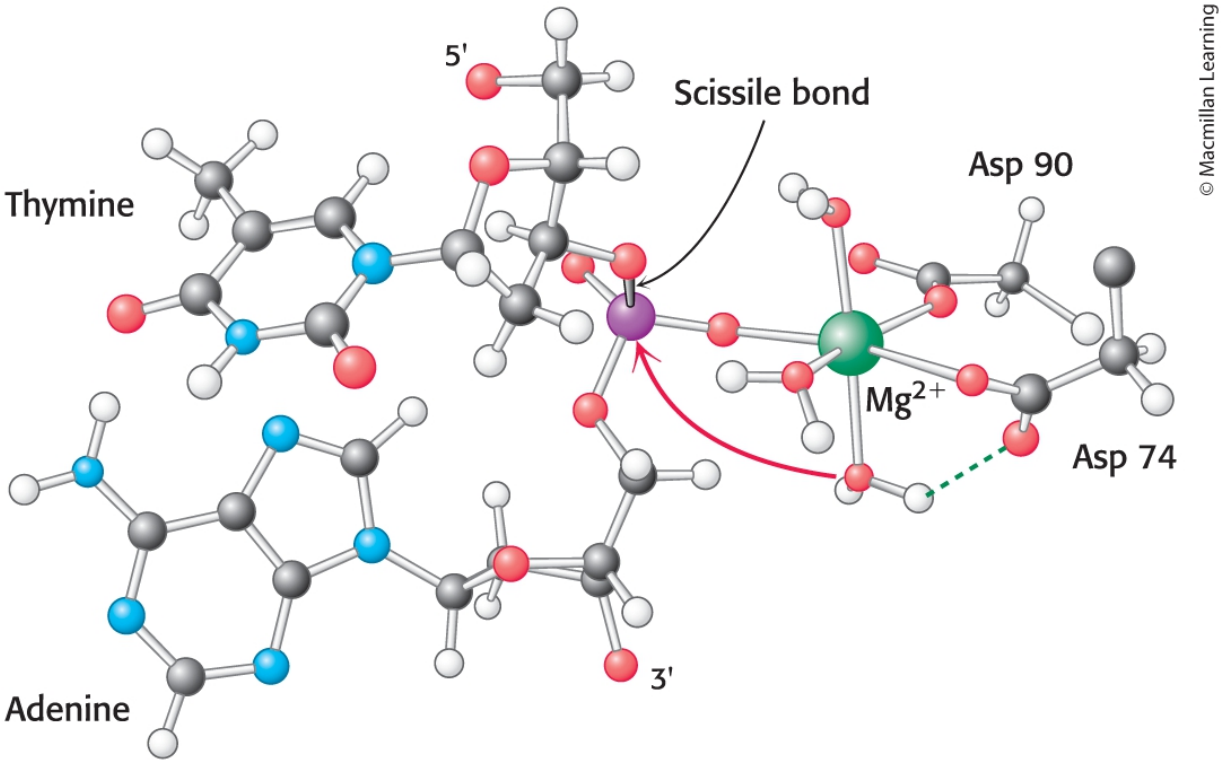
H 2 O molecule has the following structure: A central O superscript 18 atoms highlighted in green is single bonded to H on the upper right and lower right. A red arrow moves from the O superscript 18 atom toward the central P atom. This attack of water on the P atom leads to the formation of two products.

The first product is inverted and has the following structure: A 5-membered heterocyclic pentagonal ring is in a vertical orientation with C 1 occupying the top left vertex. It consists of 1 O and 4 C atoms. O occupies the first position, which is the bottom left vertex. C 1 is single bonded to C H 2 on the left. C H 2 is single bonded to O on the upper left. This O atom is single bonded to a central P atom above. This P is wedge bonded to O on the upper left, dash bonded to S above, and single bonded to O superscript 18 with a negative charge of 2 minus on the upper right. C 2 is single bonded to O on the upper right. C 4 is single bonded to adenine on the lower left.

The second product is not inverted (not observed) and has the following structure: A 5-membered heterocyclic pentagonal ring in a vertical orientation. It consists of 1 O and 4 C atoms. O occupies the first position which is the bottom left vertex. C 1 is single bonded to C H 2 on the left. C H 2 is single bonded to O on the upper left. This O atom is single bonded to a central P atom above. This P is wedge bonded to O superscript 18 on the upper left, dash bonded to S above, and single bonded to O superscript 2 minus on the upper right. C 2 is single bonded to O on the upper right. C 4 is single bonded to adenine on the lower left.

Return to FIGURE 6.29. Schematic illustration of the inversion of the stereochemical configuration of phosphorus atom after cleavage of D N A by Eco R V

Extended description for FIGURE 6.30. Ball-and-stick model of the bridge formed by M g superscript 2 plus ion between the enzyme and substrate



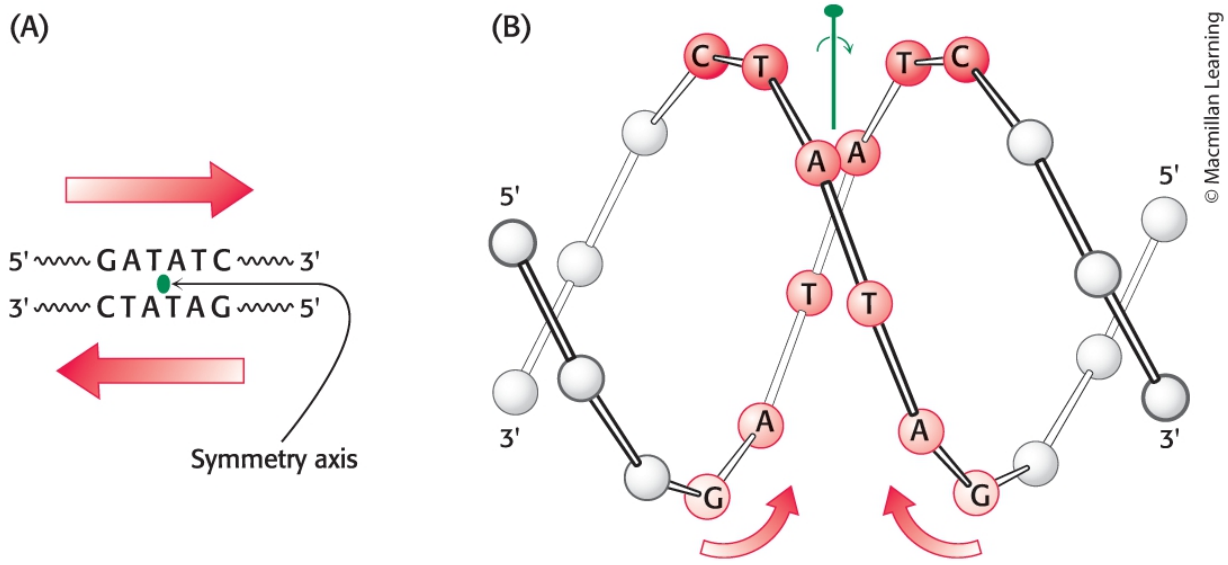
© Macmillan Learning

The ball-and-stick model consists of several interconnected red, blue, white and black spheres. The model highlights thymine residue, adenine residue, 5 prime end, and 3 prime end in the substrate. A scissile bond is shown between a purple sphere and red sphere in the substrate molecule. The purple sphere is connected to thymine and adenine residue through a red sphere. A s p 90, A s p 74, and M g superscript 2 plus ion are highlighted in the enzyme. M g superscript 2 plus ion is depicted as green sphere connected to a water molecule above, below and on the front. It is connected to a red sphere on the left, right, and back. The left red sphere is connected to the purple sphere. The water molecule consists of a

central red sphere connected to two white spheres. The white sphere of the water molecule present below is connected to the red sphere of A s p 74 residue through a dashed-line. The red sphere of this water molecule attacks the purple sphere as depicted by a red arrow.

Return to FIGURE 6.30. Ball-and-stick model of the bridge formed by M g superscript 2 plus ion between the enzyme and substrate

Extended description for FIGURE 6.31. Two fold rotational symmetry of recognition site for Eco R V



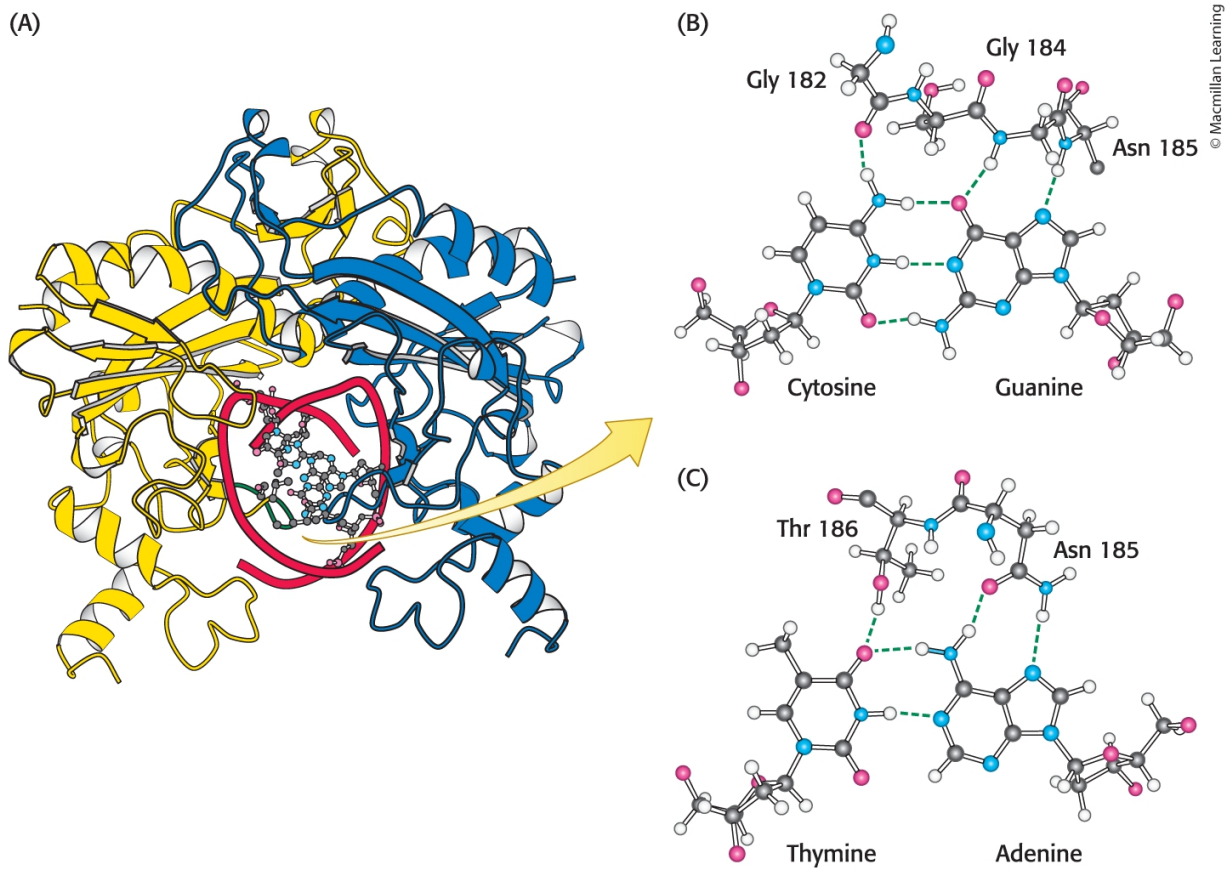
Part (A): The double stranded D N A sequence is 5 prime, zigzag line, G A T A T C, zigzag line, 3 prime. 3 prime, zigzag line, C T A T A G, zigzag line, 5 prime. A rightward arrow is given on the top and a leftward arrow is given on the bottom. The axis of rotation labeled symmetry axis is located between T A in the top sequence and A T in the bottom sequence.

Part (B): A section of a D N A double helix in a horizontal orientation composed of one complete turn is shown. The two D N A strands run in opposite directions that is 5 prime to 3 prime and 3 prime to 5 prime. The red and white spheres indicate different bases in the sequence. The sequences G A T A T C and C T A T A G are depicted as red spheres. The top strand in 3 prime to 5 prime orientation contains the sequence C T A in one half of the turn and T A G in the remaining half of the turn. The bottom strand in 5 prime to 3 prime orientation contains the sequence G A T in one half of the turn and

A T C n the remaining half of the turn. The two-fold symmetry is depicted as a vertical line with a clockwise arrow above the two halves of the D N A molecule. Two curved arrows at the bottom of the two halves of the D N A molecule point upward.

Return to FIGURE 6.31. Two fold rotational symmetry of recognition site for Eco R V

Extended description for FIGURE 6.32. The ribbon diagram of Eco R V bound to a cognate D N A and the ball-and-stick model of C G and A T base pair



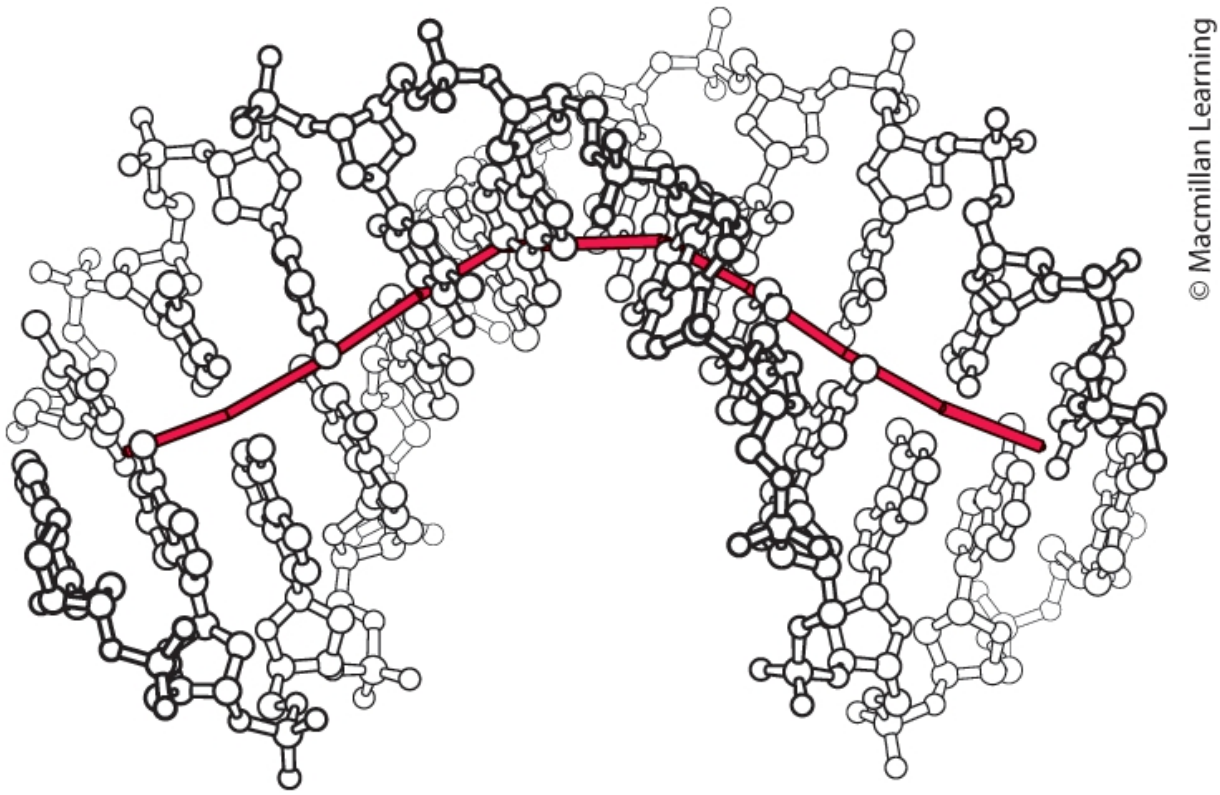
Part (A): The two ribbon-shaped protein subunits are represented in yellow and blue colors. They consist of beta-strands and alpha-helices connected by thread-like loops. The D N A backbone is represented as the red hollow circular structure at the center of the protein subunits.

Part (B): The ball-and-stick model highlights G l y 182, G l y 184, and A s n 185 residues. These residues are hydrogen-bonded to the C G base pair.

Part (C): The ball-and-stick model highlights T h r 186 and A s n 185 residues. These residues are hydrogen-bonded to T A base pair.

Return to FIGURE 6.32. The ribbon diagram of Eco R V bound to a cognate D N A and the ball-and-stick model of C G and A T base pair

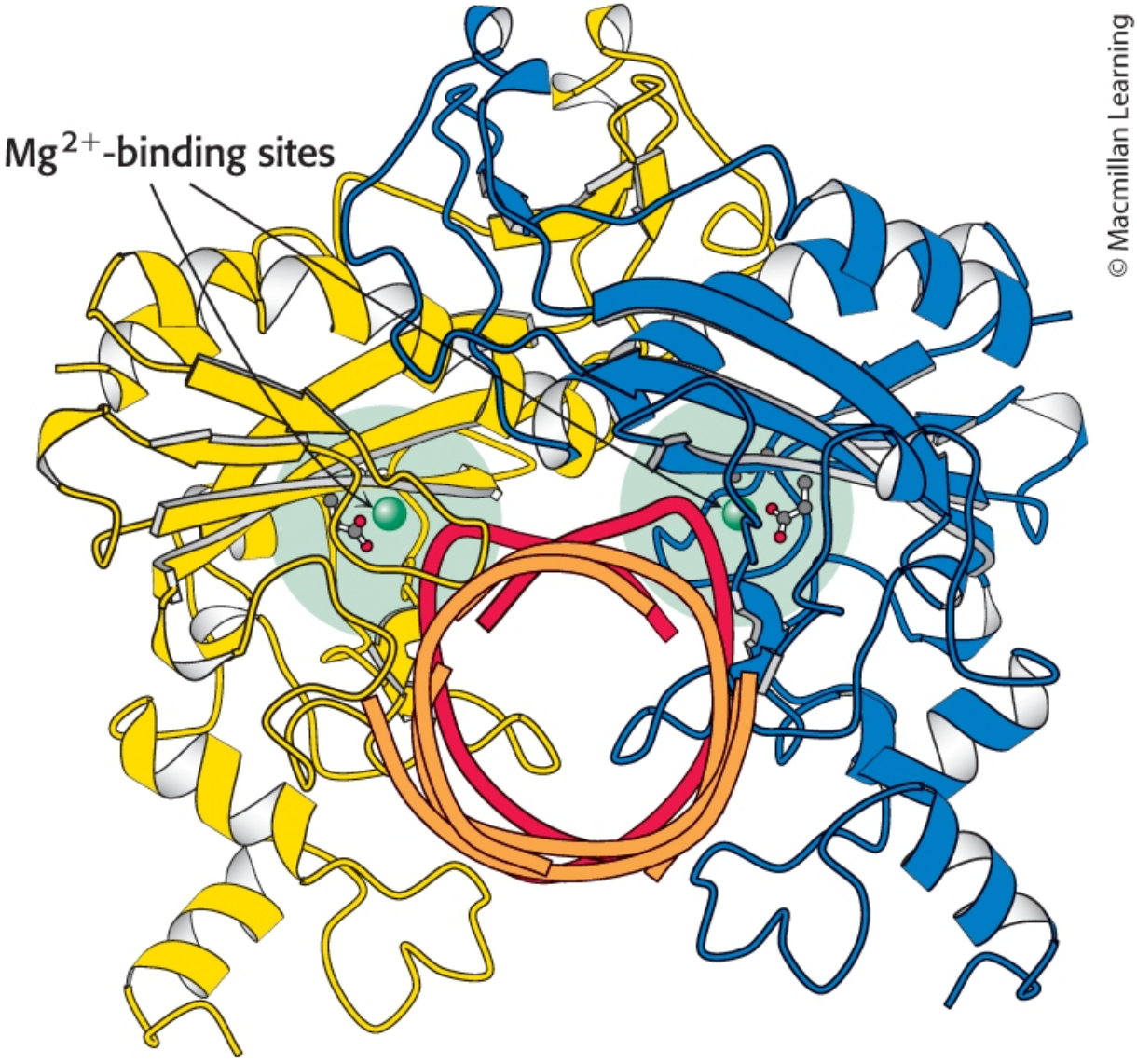
Extended description for Ball-and-stick model of cognate D N A from Eco R V complex



The D N A molecule is represented as a ball-and-stick model. The structure of D N A is distorted and bent downward at either end. A red downward curved line represents the path of the D N A helical axis.

Return to Ball-and-stick model of cognate D N A from Eco R V complex

Extended description for FIGURE 6.34.Ribbon diagram illustrates the positions of the nonspecific and the cognate D N A within Eco R V

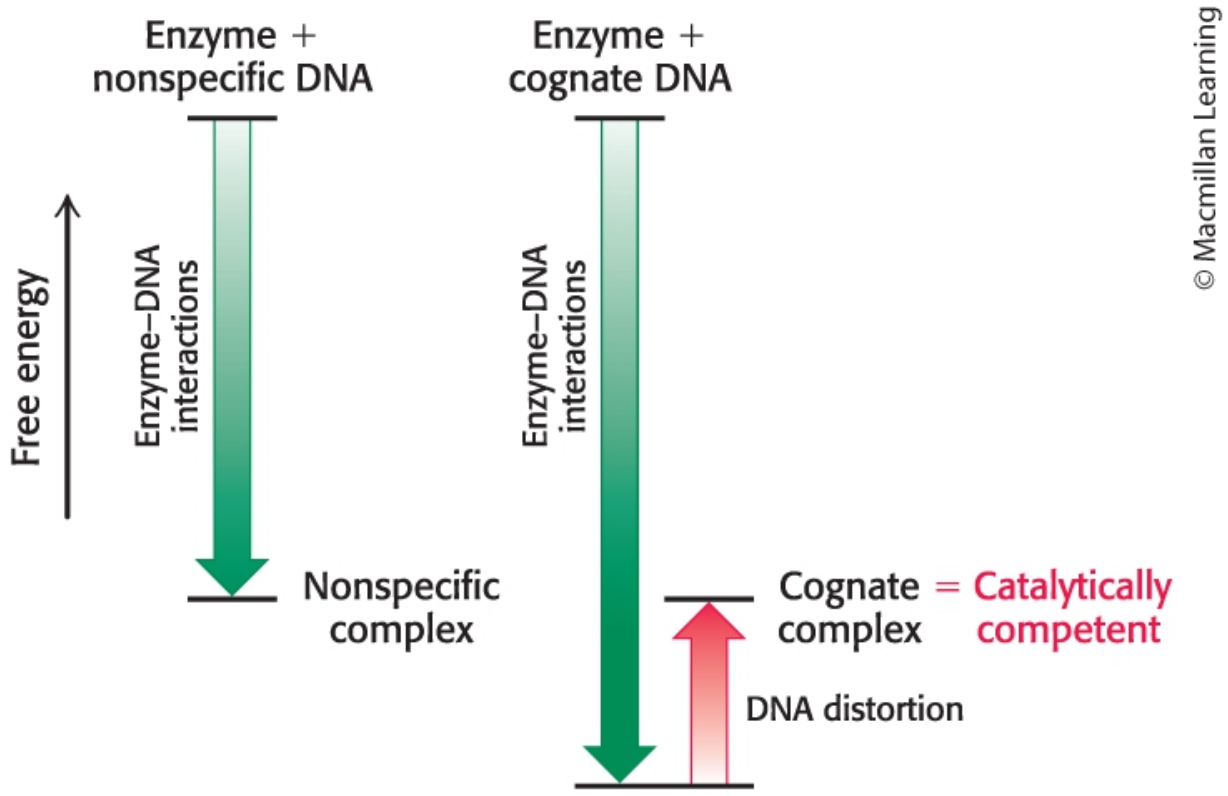


The nonspecific and specific complexes are shown as overlapping structures. The D N A backbone in the nonspecific complex is depicted as a circular coiled orange-colored structure. The D N A backbone in the specific complex is depicted as a circular coiled red-

colored structure. These D N A backbones are surrounded by the Eco R V protein. Eco R V is composed of two monomers flanking the D N A backbones. Each monomer is composed of alpha-helices and beta-strands connected by short loops. An M g superscript 2 plus binding site is present in each monomer. The D N A backbone in the nonspecific complex is far away from these sites. The D N A backbone in the specific complex has distortions at the top left and top right that allows it to reach the M g binding sites.

Return to FIGURE 6.34.Ribbon diagram illustrates the positions of the nonspecific and the cognate D N A within Eco R V

Extended description for FIGURE 6.35. Energy level diagram showing D N A distortions due to an increase in binding energy



An upward-pointing arrow is labeled free energy which increases from the bottom to the top. A thick green downward pointing arrow is shown adjacent to the free energy arrow. The tail of the green arrow labeled enzyme plus nonspecific D N A extends much above the head of the free energy arrow. The head of the green arrow labeled nonspecific complex extends much below the tail of the free energy arrow. The middle of the green arrow is labeled enzyme-D N A interactions.

A second green downward pointing arrow, much longer than the first green arrow, is shown on its right. The tail of the second arrow

is labeled enzyme plus cognate D N A. Its middle portion is labeled enzyme-D N A interactions. The head of the second green arrow extends much below the head of the first green arrow. A short red upward-pointing arrow is present between the heads of the two green arrows. It is labeled D N A distortion. The head of the red arrow is labeled cognate complex equals catalytically competent.

Return to FIGURE 6.35. Energy level diagram showing D N A distortions due to an increase in binding energy

Extended description for FIGURE 6.36. Schematic illustration of the methylation of the recognition sequence of Eco R V



The structure of cleaved D N A is as follows: 5 prime, zigzag line, G A T A T C, zigzag line, 3 prime. A red vertical line is present between first A and first T. 3 prime, a zigzag line, C T A T A G, a zigzag line, 5 prime. A red vertical line is present between second T and second A.

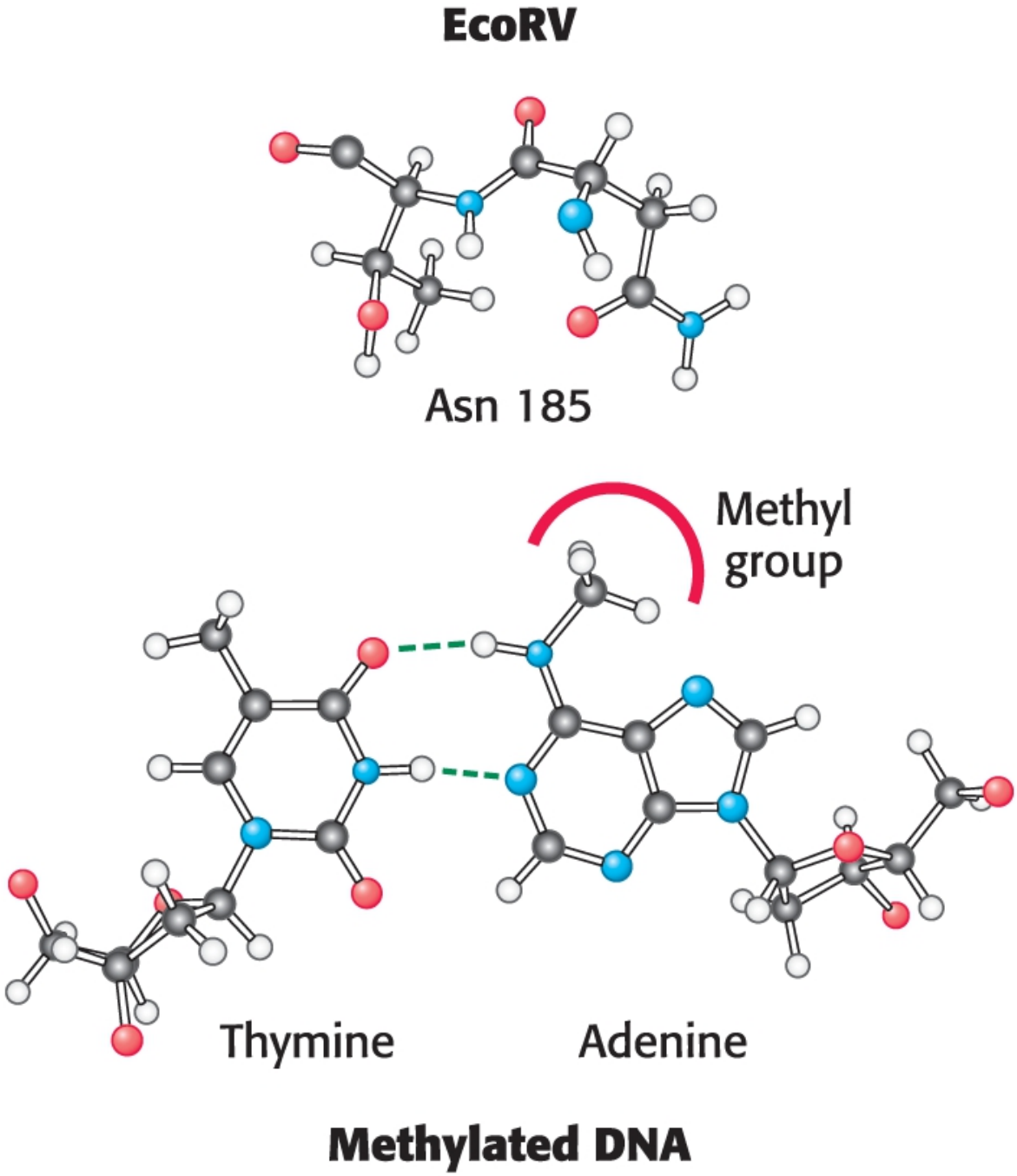
The structure of not cleaved D N A is as follows: 5 prime, zigzag line, G A T A T C, zigzag line, 3 prime. The first A is marked with an asterisk. 3 prime, zigzag line, C T A T A G, zigzag line, 5 prime. The second A is marked with an asterisk.

A residue marked with an asterisk is methylated adenosine whose structure is as follows: A 6-membered heterocyclic hexagonal ring is in a vertical orientation and consists of 2 N and 4 C atoms. The first N occupies the first position, which is the bottom-most vertex. The second N occupies the third position, which is the top-left vertex. A double bond is present between C 3 and C 4, first N and C 1, and second N and C 2. C 1 is single bonded to H on the lower left. C 2 is single bonded to N above. This N atom is single bonded to C H 3 on

the upper right and H on the upper left. C H 3 is labeled added methyl group. The hexagonal ring is fused to a 5-membered heterocyclic pentagonal ring in a horizontal orientation such that C 3 and C 4 of the hexagonal ring are C 3 and C 2 respectively of the pentagonal ring. The pentagonal ring consists of 2 N and 3 C atoms. The first N occupies the first position, which is the topmost vertex. The second N occupies the third position, which is the bottom-most vertex. C 1 is single bonded to H on the right. A double bond is present between the first N and C 1. The second N atom is single bonded to deoxyribose.

Return to FIGURE 6.36. Schematic illustration of the methylation of the recognition sequence of Eco R V

Extended description for FIGURE 6.37. Ball-and-stick model of asparagine 185 residue of Eco RV and methylated adenine hydrogen bonded to thymine



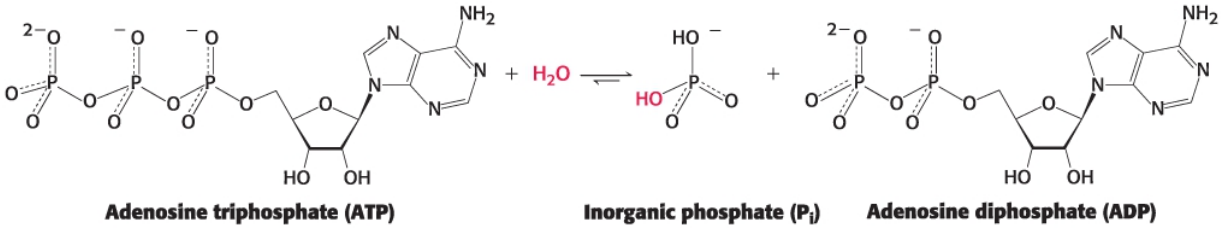
© Macmillan Learning

A s n 185: The ball-and-stick model of A s n 185 consists of several interconnected red, blue, white, and black spheres.

Methylated adenine hydrogen-bonded to thymine: The ball-and-stick model consists of several interconnected white, red, blue, and black spheres. The model highlights thymine hydrogen-bonded to adenine. A methyl group is connected to the adenine residue.

Return to FIGURE 6.37. Ball-and-stick model of asparagine 185 residue of Eco RV and methylated adenine hydrogen bonded to thymine

Extended description for Reversible reaction consisting of two reactants and two products is shown



The structure of the first reactant adenosine triphosphate (A T P) is as follows: A 5-membered heterocyclic pentagonal ring is in a vertical orientation and consists of 1 O and 4 C atoms. The O atom occupies the first position, which is the top vertex. C 1 is single bonded to the first N of a second 5-membered heterocyclic pentagonal ring. The pentagonal ring is in a horizontal orientation and contains 2 N and 3 C atoms with C 1 occupying the top left vertex. The first N atom occupies the topmost vertex. The second N atom occupies the bottom left vertex. A double bond is present between C 1 and second N and C 2 and C 3. The second pentagonal ring is fused to a 6-membered heterocyclic hexagonal ring such that C 2 and C 3 of the pentagonal ring are C 3 and C 2 respectively of the hexagonal ring. The 6-membered heterocyclic hexagonal ring is in a vertical orientation and consists of 2 N and 4 C atoms. The first N atom occupies the top-right vertex. The second N atom occupies the bottom-most vertex. A double bond is present between C 1 and second N and C 4 and first N. C 1 of the hexagonal ring is single bonded to N H 2 above. C 4 of the first pentagonal ring is single bonded to C H 2 on the upper left, which is again single bonded to O on the lower left. O is single bonded to P on the upper left. P is partially double bonded to O superscript minus above, O on the lower left, and single bonded to O on the lower left. This O atom is again single bonded to P on the upper left. P is partially double

bonded to O superscript minus above and O on the lower left. P is single bonded to O on the lower left, which is again single bonded to P on the upper left. P is partially bonded to O superscript 2 minus above, O on the lower left and O on the lower right. The second reactant is H 2 O highlighted in red.

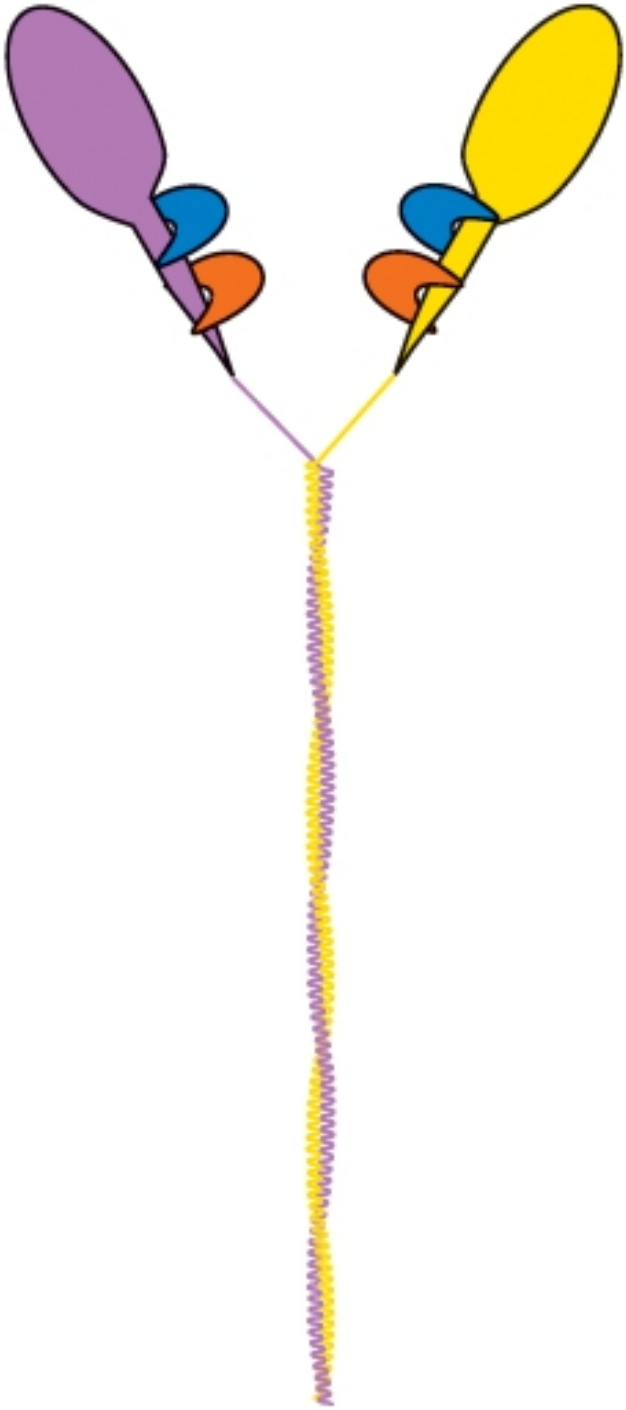
The first product is inorganic phosphate (P subscript i) whose structure is as follows: A central P atom is single bonded to O H superscript minus above and O H on the lower-left highlighted in red color. The P atom is partially double bonded to O on the lower left and lower right.

The second product is adenosine diphosphate (A D P) whose structure is as follows: A 5-membered heterocyclic pentagonal ring is in a horizontal orientation and consists of 1 O and 4 C atoms. The O atom occupies the first position, which is the top vertex. C 1 is wedge bonded to the first N of a second 5-membered heterocyclic pentagonal ring. The pentagonal ring is in a horizontal orientation and contains 2 N and 3 C atoms with C 1 occupying the left-most vertex. The first N atom occupies the bottom left vertex. The second N atom occupies the topmost vertex. A double bond is present between C 1 and second N and C 2 and C 3. The second pentagonal ring is fused to a 6-membered heterocyclic hexagonal ring such that C 2 and C 3 of the pentagonal ring are C 3 and C 2 respectively of the hexagonal ring. The 6-membered heterocyclic hexagonal ring is in a vertical orientation and consists of 2 N and 4 C atoms. The first N atom occupies the top-right vertex. The second N atom occupies the bottom-most vertex. A double bond is present between C 1 and second N and C 4 and first N. C 4 of the hexagonal ring is single bonded to N H 2 above. C 4 of the first pentagonal ring is single bonded to C H 2 on the upper left, which is again single bonded to O on the lower left. O is single bonded to P on the upper left. P is partially double bonded to O superscript minus above and O on the lower left. P is single bonded to O on the lower left, which is again

single bonded to P on the upper left. P is partially double bonded to O superscript 2 minus above, O on the lower left, and O below.

Return to Reversible reaction consisting of two reactants and two products is shown

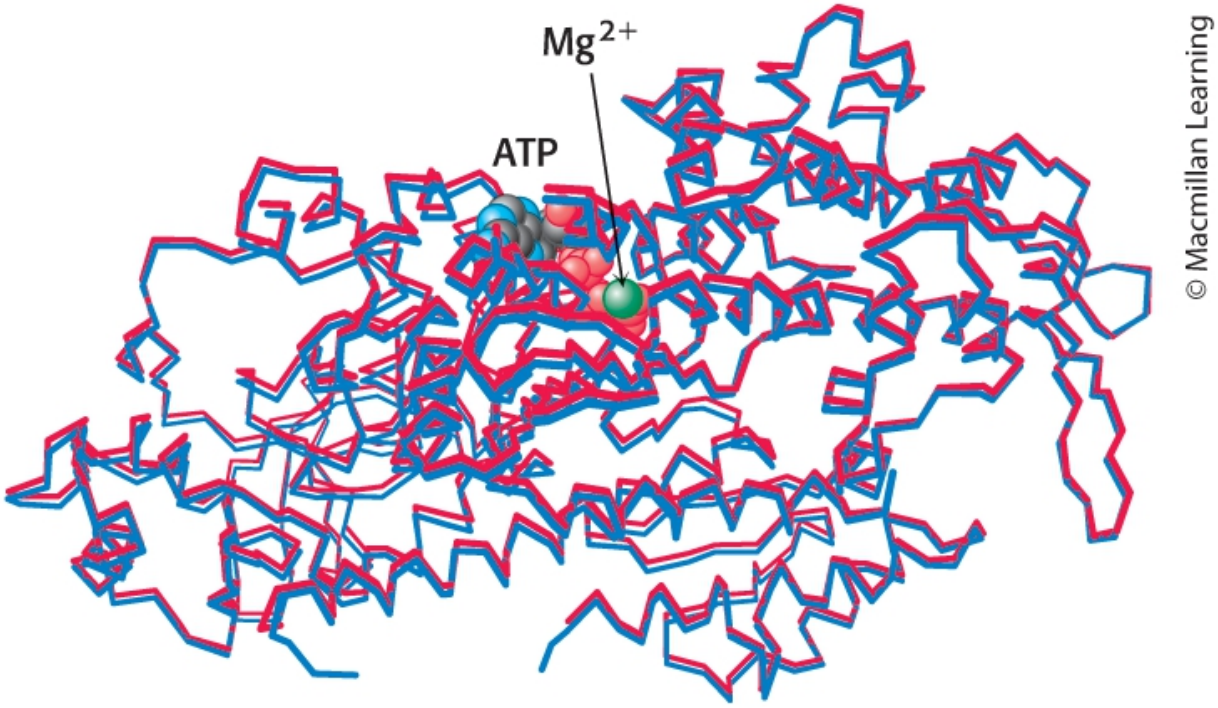
Extended description for FIGURE 6.38. Schematic illustration of the structure of myosin



Two heavy chains and two light chains are present. The two heavy chains are represented in purple and yellow colors. The two light chains are represented in blue and orange colors.

Return to FIGURE 6.38. Schematic illustration of the structure of myosin

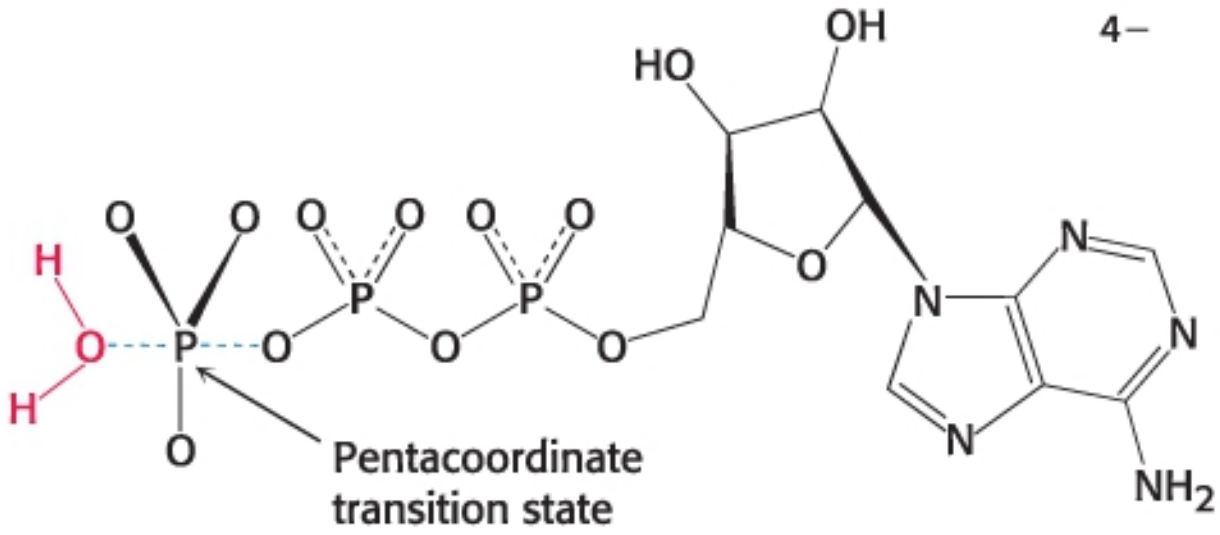
Extended description for FIGURE 6.39. Schematic illustration of A T P bound to the myosin molecule



Myosin is depicted as a compact structure composed of overlapping blue and red zigzag lines. The M g superscript 2 plus ion represented as a green sphere is located at the center. The A T P molecule is depicted as a cluster of a differently colored spheres located adjacent to the M g ion.

Return to FIGURE 6.39. Schematic illustration of A T P bound to the myosin molecule

Extended description for The structure of transition state of A T P



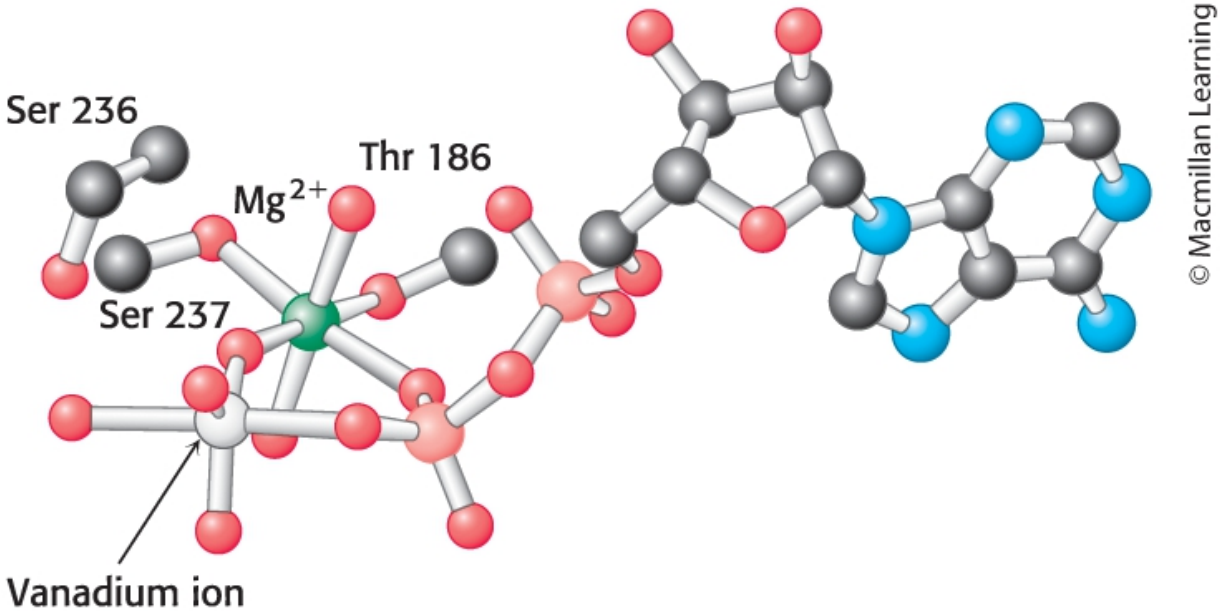
The structure of the molecule is as follows:

A 5-membered heterocyclic pentagonal ring is in a horizontal orientation and consists of 1 O and 4 C atoms. The O atom occupies the first position, which is the bottom-most vertex. C 1 is single bonded to C H 2 on the lower left in the form of a line. C H 2 is again single bonded to O on the lower left. O is single bonded to P on the upper left. P is partially double bonded to O on the upper left and upper right. P is single bonded to O on the lower left, which is again single bonded to P on the upper left. P is partially double bonded to O on the upper left and upper right. P is single bonded to O on the lower left, which is again single bonded to P on left. This P is wedge bonded to O on the upper left and upper right. P is single bonded to O on the left and below. The O atom on the left is single-bonded to H on the upper left and lower left. The terminal P atom is labeled pentacoordinate transition state.

C 2 of the pentagonal ring is single bonded to O H on the upper left. C 3 is single bonded to O H on the upper right. C 4 is wedge bonded to the second N of a 5-membered heterocyclic pentagonal ring. The 5-membered pentagonal ring is in a horizontal orientation and consists of 2 N and 3 C atoms. C 1 occupies the left-most vertex. The first N atom occupies the bottom left vertex. The second N atom occupies the top vertex. A double bond is present between C 1 and first N and C 2 and C 3. The second pentagonal ring is fused to a 6-membered heterocyclic hexagonal ring such that C 2 and C 3 of the pentagonal ring are C 4 and C 3 of the hexagonal ring respectively. The 6-membered heterocyclic hexagonal ring is in a vertical orientation and consists of 2 N and 4 C atoms. The first N atom occupies the top vertex. The second N atom occupies the bottom right vertex. A double bond is present between the first N and C 1, and the second N and C 2. C 2 of the hexagonal ring is single bonded to N H 2 below.

Return to The structure of transition state of A T P

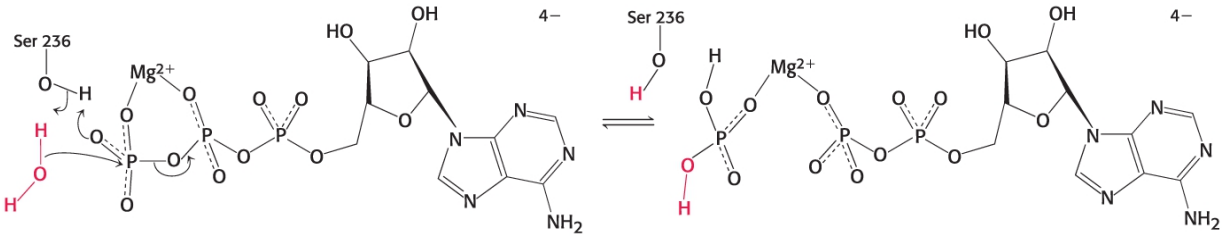
Extended description for FIGURE 6.40. Ball-and-stick model of a transition-state analog of myosin



The ball-and-stick model of a molecule is composed of several interconnected red, blue, black, white, and green spheres. Three rings are located at the extreme right end of the molecule. A white sphere represents the vanadium ion. The model highlights S e r 236, S e r 237, M g superscript 2 plus ion, and T h r 186. These residues are located at the extreme left of the molecule.

Return to FIGURE 6.40. Ball-and-stick model of a transition-state analog of myosin

Extended description for FIGURE 6.41. Chemical reaction shows the serine 236 mediated attack of water molecule on gamma-phosphoryl of A T P



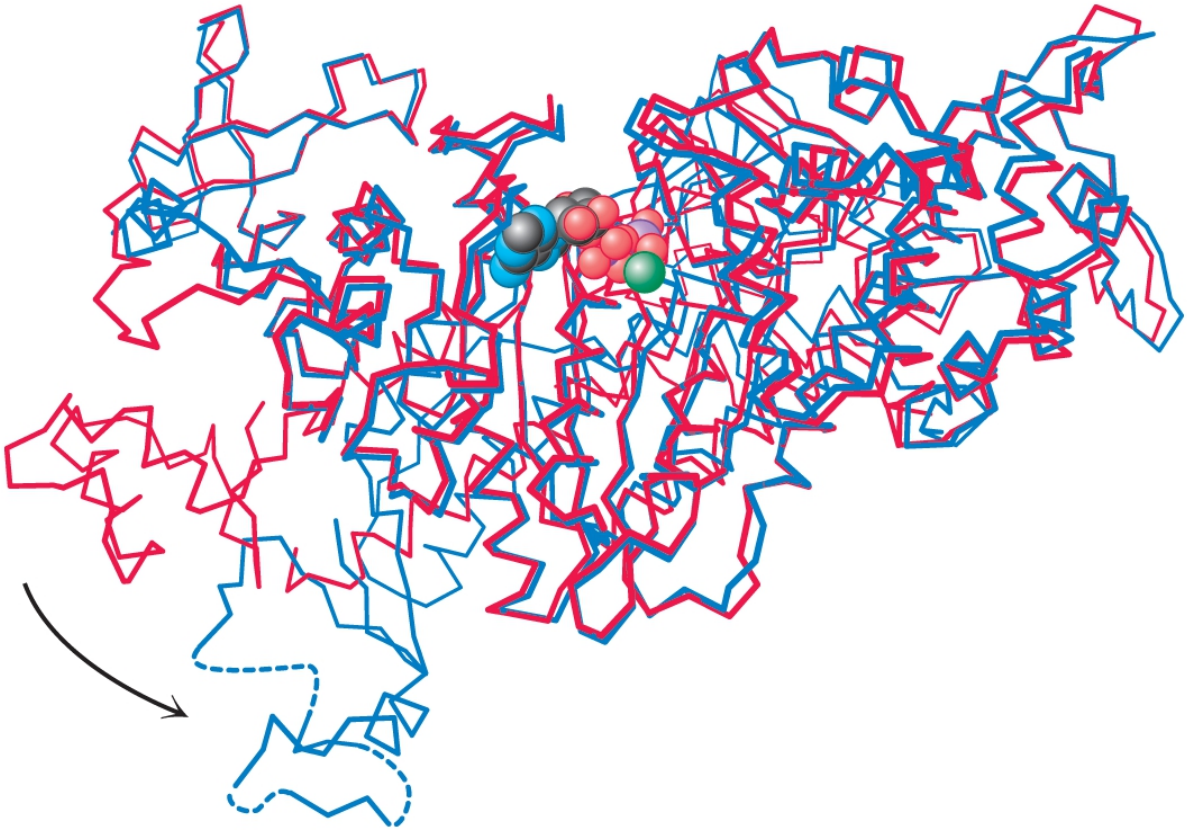
The side chain of serine 236 consists of a single bond, O, single bond, H. The O atom of the beta and gamma-phosphoryl group of A T P is single bonded to M g superscript 2 plus ion. An arrow from the single bond between the O and H atom of the serine side chain moves toward the H atom of the H 2 O molecule. The H 2 O molecule is highlighted in red. An arrow from the single bond between the H and O atom of the H 2 O molecule points toward the P atom of the gamma-phosphoryl group. An arrow from O partially double bonded to the P atom on the left moves toward the H atom of the serine side chain. An arrow points from the single bond between P and O (right) of the gamma-phosphoryl group toward the O, single bond, P atom of the beta-phosphoryl group.

A reversible reaction arrow is shown.

Serine 236 is single bonded to O, single bond, H. H is highlighted in red. The central P atom of the gamma-phosphoryl group is single-bonded to O on the left. O is single bonded to H on the lower left. The O and H atoms are highlighted in red.

Return to FIGURE 6.41. Chemical reaction shows the serine 236 mediated attack of water molecule on gamma-phosphoryl of A T P

Extended description for FIGURE 6.42. Schematic illustration compares the overall structures of the myosin A T P ase domain with bound A T P and that with the transition-state analog A D P–vanadate


© Macmillan Learning

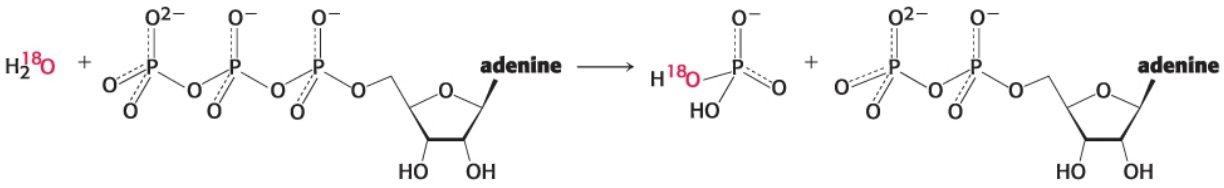
Myosin A T P ase domain with bound A T P is depicted as a compact structure composed of overlapping blue and red zigzag lines. A T P is shown as a cluster of tiny red spheres.

Myosin A T P ase domain with the transition-state analog ADP–vanadate is depicted as a structure composed of overlapping blue and red zigzag lines. A dramatic conformational change of a region at the carboxyl-terminus of the domain is shown. This region is

loosely coiled and shifted away from the main body of the myosin A T P ase domain.

Return to FIGURE 6.42. Schematic illustration compares the overall structures of the myosin A T P ase domain with bound A T P and that with the transition-state analog A D P–vanadate

Extended description for Chemical equation of A T P hydrolysis in the presence of with O superscript 18 labeled water



The irreversible reaction consists of two reactants and two products.

The first reactant is H 2 O superscript 18 highlighted in red.

The second reactant is A T P whose structure is as follows: A 5-membered heterocyclic pentagonal ring is in a vertical orientation and consists of 1 O and 4 C atoms. The O atom occupies the first position, which is the topmost vertex. C 1 is single bonded to adenine on the upper right. C 2 and C 3 are single bonded to O H below. C 4 is single bonded to C H 2 on the upper left in the form of a line. C H 2 is single bonded to O on the lower left. O is single bonded to P on the upper left. P is partially double bonded to O superscript minus above, partially double bonded to O on the lower left, and single bonded to O on the lower left. This O atom is single bonded to another P on the upper left. This P is partially double bonded to O superscript minus above, partially double bonded to O on the lower left, and single bonded to O on the lower left. This O atom is single bonded to another P on the upper left. This P is partially double bonded to O superscript 2 minus above, partially double bonded to O on the lower left, and partially double bonded to O below.

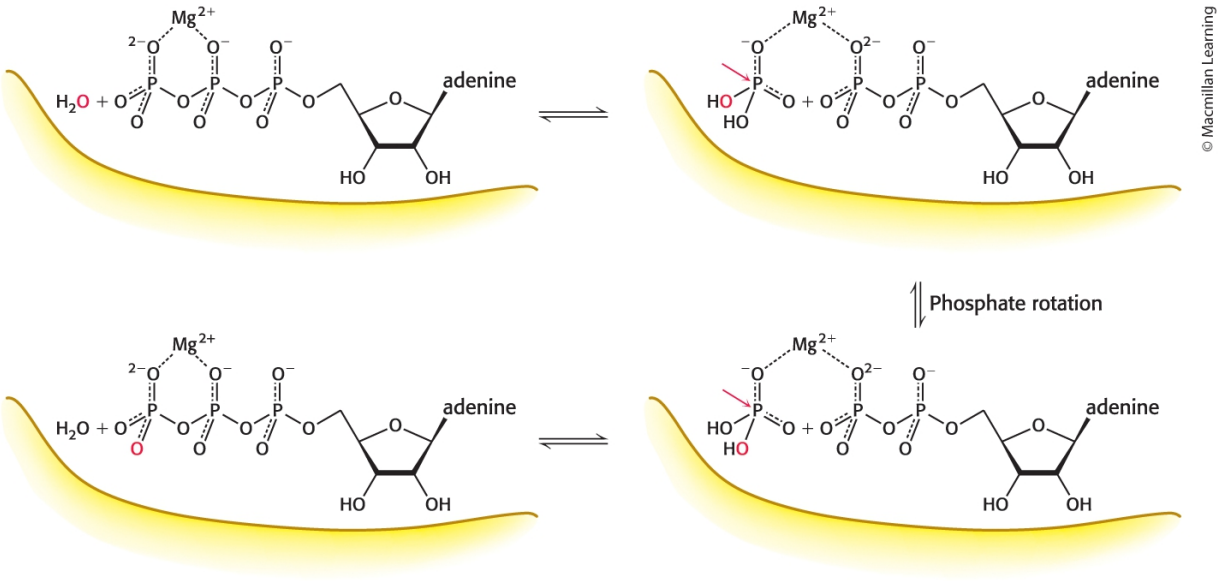
The structure of the first product is as follows: A central P atom is partially double bonded to O superscript minus above, partially

double bonded to O on the lower right P is single bonded to O H on the lower left, and H O superscript 18 on the lower left.

The structure of the second product is as follows: A 5-membered heterocyclic pentagonal ring is in a vertical orientation and consists of 1 O and 4 C atoms. The O atom occupies the first position, which is the topmost vertex. C 1 is single bonded to adenine on the upper right. C 2 and C 3 are single bonded to O H below. C 4 is single bonded to C H 2 on the upper left in the form of a line. C H 2 is single bonded to O on the lower left. O is single bonded to P on the upper left. P is partially double bonded to O superscript minus above, partially double bonded to O on the lower left, and single bonded to O on the lower left. This O atom is single bonded to another P on the upper left. This P is partially double bonded to O superscript 2 minus above, partially double bonded to O below, and partially double bonded to O on the lower left.

Return to Chemical equation of A T P hydrolysis in the presence of with O superscript 18 labeled water

Extended description for FIGURE 6.43. Schematic illustration of the reversible hydrolysis of A T P within the active site of myosin



© Macmillan Learning

The hydrolysis of A T P is shown in 3 reversible steps. The A T P molecule is shown inside the active site of the myosin depicted as a concave surface with a yellow highlight.

First reversible step:

The structure of the reactant is as follows: A 5-membered heterocyclic pentagonal ring is in a vertical orientation and consists of 1 O and 4 C atoms. The O atom occupies the first position, which is the topmost vertex. C 1 is wedge bonded to adenine on the upper right. C 2 and C 3 are single bonded to O H below. C 4 is single bonded to C H 2 on the upper left in the form of a line. C H 2 is single bonded to O on the lower left. O is single bonded to P on the upper left. P is partially double bonded to O superscript minus above, partially double bonded to O on the lower left, and single

bonded to O on the lower left. This O atom is single-bonded to another P on the upper left. This P is partially double bonded to O superscript minus above, partially double bonded to O on the lower left, and single bonded to O on the lower left. This O atom is single-bonded to another P on the upper left. This P is partially double bonded to O superscript 2 minus above, partially double bonded to O on the lower left, and partially double bonded to O below. M g superscript 2 plus ion is connected to two O above through a dashed line. A water molecule having the formula H 2 O is present inside the active site. O atom is highlighted in red.

The structure of the first product is as follows: A 5-membered heterocyclic pentagonal ring is in a vertical orientation and consists of 1 O and 4 C atoms. The O atom occupies the first position, which is the topmost vertex. C 1 is wedge bonded to adenine on the upper right. C 2 and C 3 are single bonded to O H below. C 4 is single bonded to C H 2 on the upper left in the form of a line. C H 2 is single bonded to O on the lower left. O is single bonded to P on the upper left. P is partially double bonded to O superscript minus above, partially double bonded to O on the lower left, and single bonded to O on the lower left. This O atom is single-bonded to another P on the upper left. This P is partially double bonded to O superscript 2 minus above, partially double bonded to O on the lower left, and partially bonded to O on the lower left.

The second product is the phosphate group whose structure is as follows: A central P atom is partially double bonded to O superscript minus above, partially double bonded to O on the lower right, single bonded to O H on the lower left and left. The O atom of the O H group on the left is highlighted in red. P has an open single bond on the upper left. M g superscript 2 plus ion is connected to O atom double-bonded to the free phosphate group and terminal P atom through a dashed line.

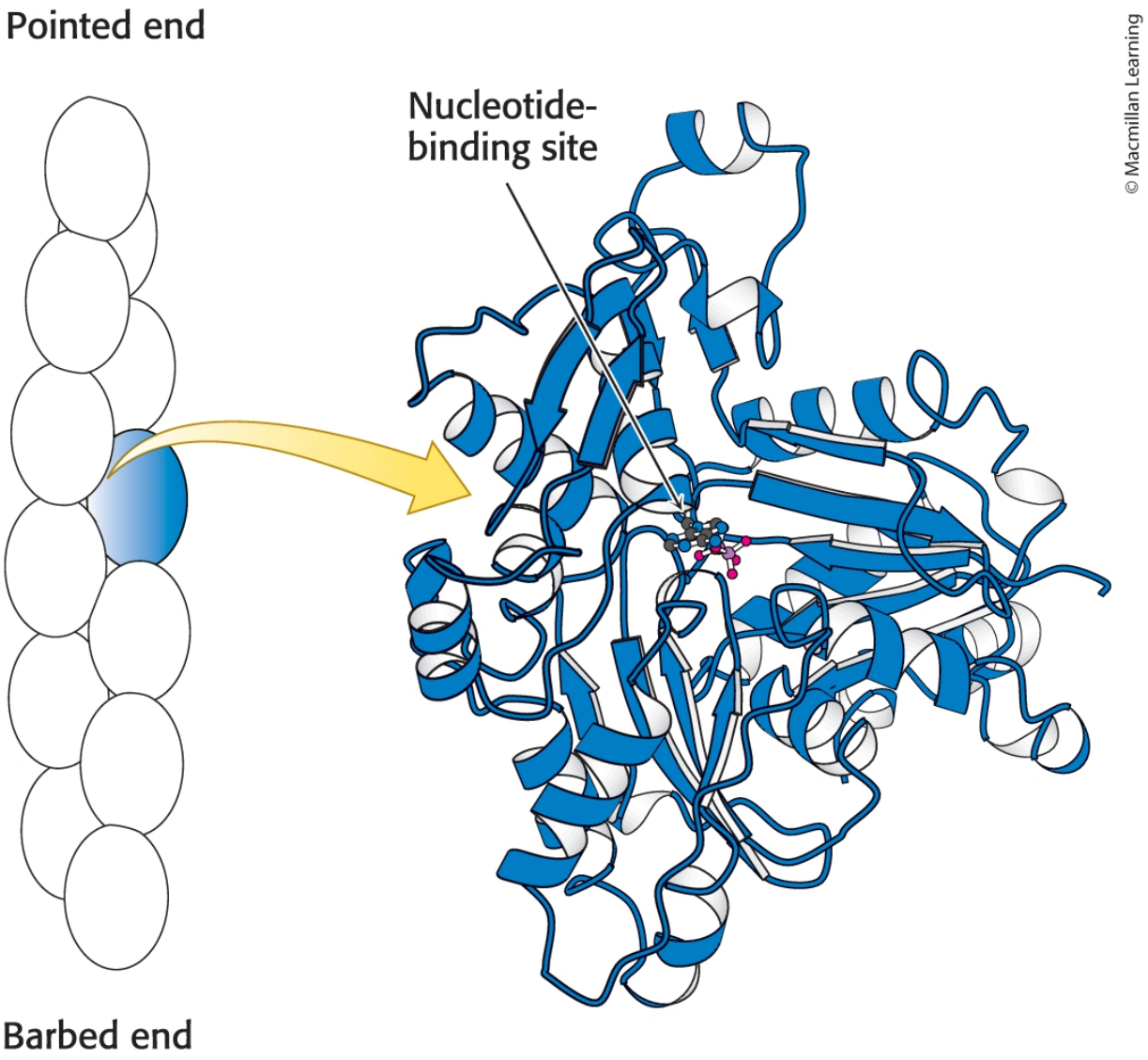
The second reversible step is labeled phosphate rotation. The structure of the product is the same as the product of the first step except that the O atom of the O H group on the lower left is highlighted in red. An arrow points toward the P atom.

Third reversible step:

The structure of the product is as follows: A 5-membered heterocyclic pentagonal ring is in a vertical orientation and consists of 1 O and 4 C atoms. The O atom occupies the first position, which is the topmost vertex. C 1 is wedge bonded to adenine on the upper right. C 2 and C 3 are single bonded to O H below. C 4 is single bonded to C H 2 on the upper left in the form of a line. C H 2 is single bonded to O on the lower left. O is single bonded to P on the upper left. P is partially double bonded to O superscript minus above, partially double bonded to O on the lower left, and single bonded to O on the lower left. This O atom is single-bonded to another P on the upper left. This P is partially double bonded to O superscript minus above, partially double bonded to O on the lower left, and single bonded to O on the lower left. This O atom is single-bonded to another P on the upper left. This P is partially double bonded to O superscript 2 minus above, partially double bonded to O on the lower left, and partially double bonded to O below. The O atom below is highlighted in red. M g superscript 2 plus ion is connected to two O above through a dashed line. A water molecule having the formula H 2 O is present.

Return to FIGURE 6.43. Schematic illustration of the reversible hydrolysis of A T P within the active site of myosin

Extended description for FIGURE 6.44. Ribbon diagram and schematic illustration of actin filament



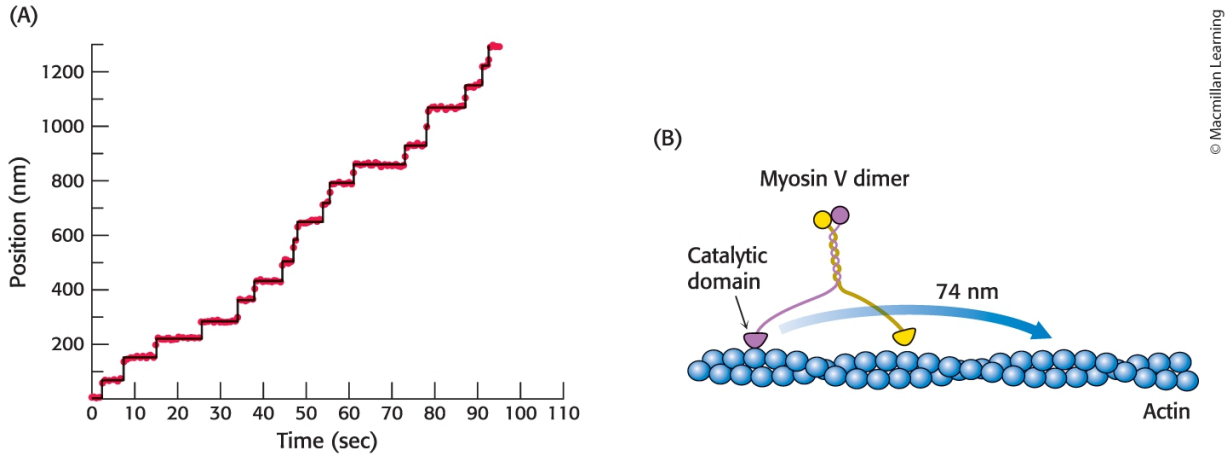
© Macmillan Learning

The schematic illustration of actin is composed of a vertical linear array of monomers. The monomers are depicted as oval-shaped structures. The top and bottom ends of the actin molecule are labeled pointed and barbed ends respectively. The ribbon diagram of an actin monomer is represented in blue color. It is composed of

beta-strands and alpha-helices connected by short thread-like loops. The nucleotide-binding site is located at the center.

Return to FIGURE 6.44. Ribbon diagram and schematic illustration of actin filament

Extended description for FIGURE 6.45. Graphical representation of the position of a single dimeric myosin roman number 5 molecule and a model of the movement of the dimeric molecule

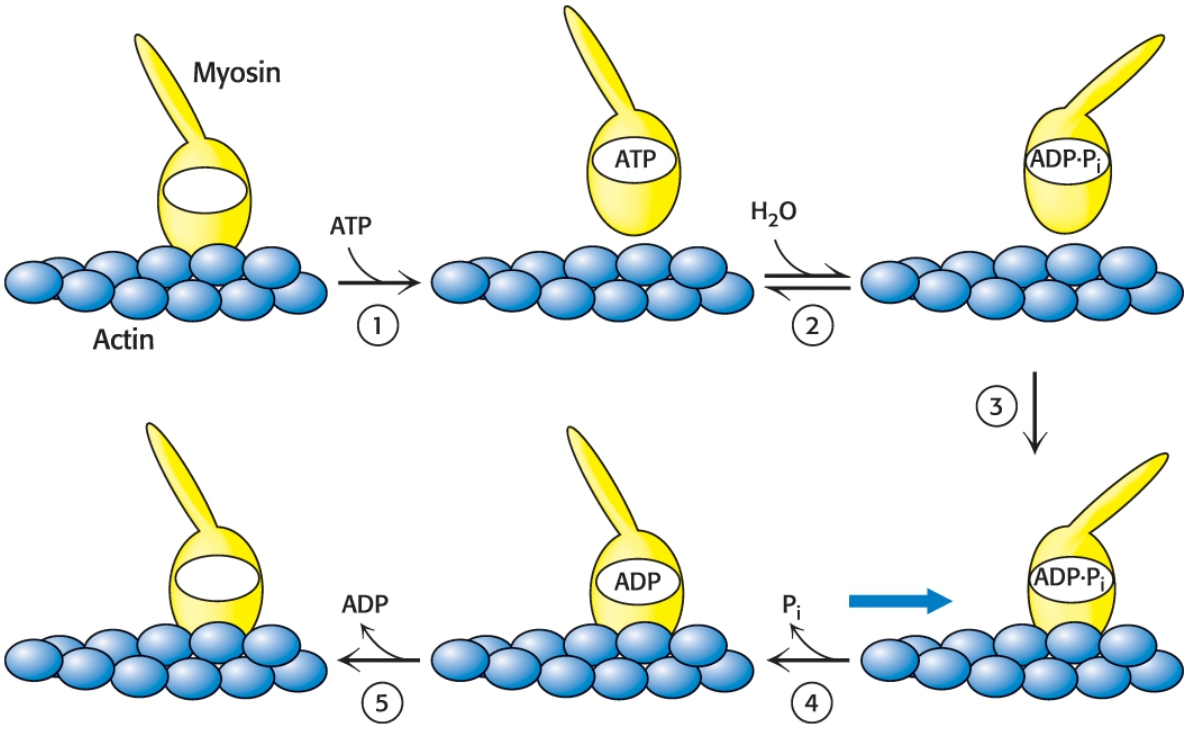


Part (A): The horizontal axis is labeled time in seconds. It has markings ranging from 0 to 110 in increments of 10 units. The vertical axis is labeled position nanometers. It has markings ranging from 200 to 1200 in increments of 200 units. A red-black plot rises from the origin (0,0) and moves toward the upper right in a zigzag ladder-like pattern.

Part (B): The actin filament is represented as a pair of horizontal structure twisted around each other. Each structure is composed of a linear array of tiny blue spheres. Myosin V dimer is represented as a coiled structure having two spheres (yellow and purple) at the top and two cone-shaped structures (yellow and purple) at the bottom. The purple cone-shaped structure is attached to the actin molecule and is labeled catalytic domain. An arrow from the catalytic domain moves toward the right end of actin and is labeled 74 nanometers.

Return to FIGURE 6.45. Graphical representation of the position of a single dimeric myosin roman number 5 molecule and a model of the movement of the dimeric molecule

Extended description for FIGURE 6.46. Schematic illustration of the steps involved in the movement of myosin along an actin filament



Myosin is represented as a yellow sphere with a horizontal oval-shaped groove at the center and a short tubular projection at the top. The actin filament is represented as a horizontal linear structure composed of an array of blue spheres. Myosin is attached to the surface of the actin filament. The groove is empty and the tubular projection is oriented toward the upper left.

Step 1: ATP enters and binds to the groove of myosin protein. The myosin protein is detached from the actin surface. This step is irreversible.

Step 2: H 2 O molecule enters. An A D P-P subscript i complex is formed in the groove. The tubular projection is oriented toward the upper right. The myosin protein remains detached from the actin surface. This step is reversible.

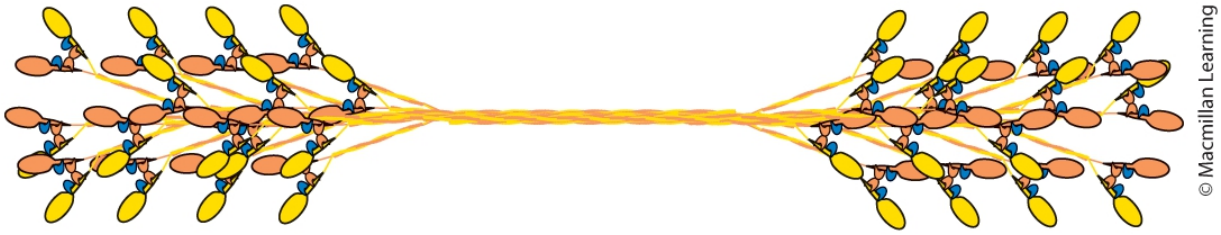
Step 3: The myosin protein with A D P-P subscript i complex in the groove attaches to the actin surface. The tubular projection is oriented toward the upper right. A rightward pointing blue arrow is shown adjacent to the myosin protein. This step is irreversible.

Step 4: P subscript i atom leaves the groove. The myosin protein with A D P in the groove is attached to the actin surface. The tubular projection is oriented toward the upper left. This step is irreversible.

Step 5: A D P is released from the groove. The myosin protein with an empty groove is attached to the actin surface. This step is irreversible.

Return to FIGURE 6.46. Schematic illustration of the steps involved in the movement of myosin along an actin filament

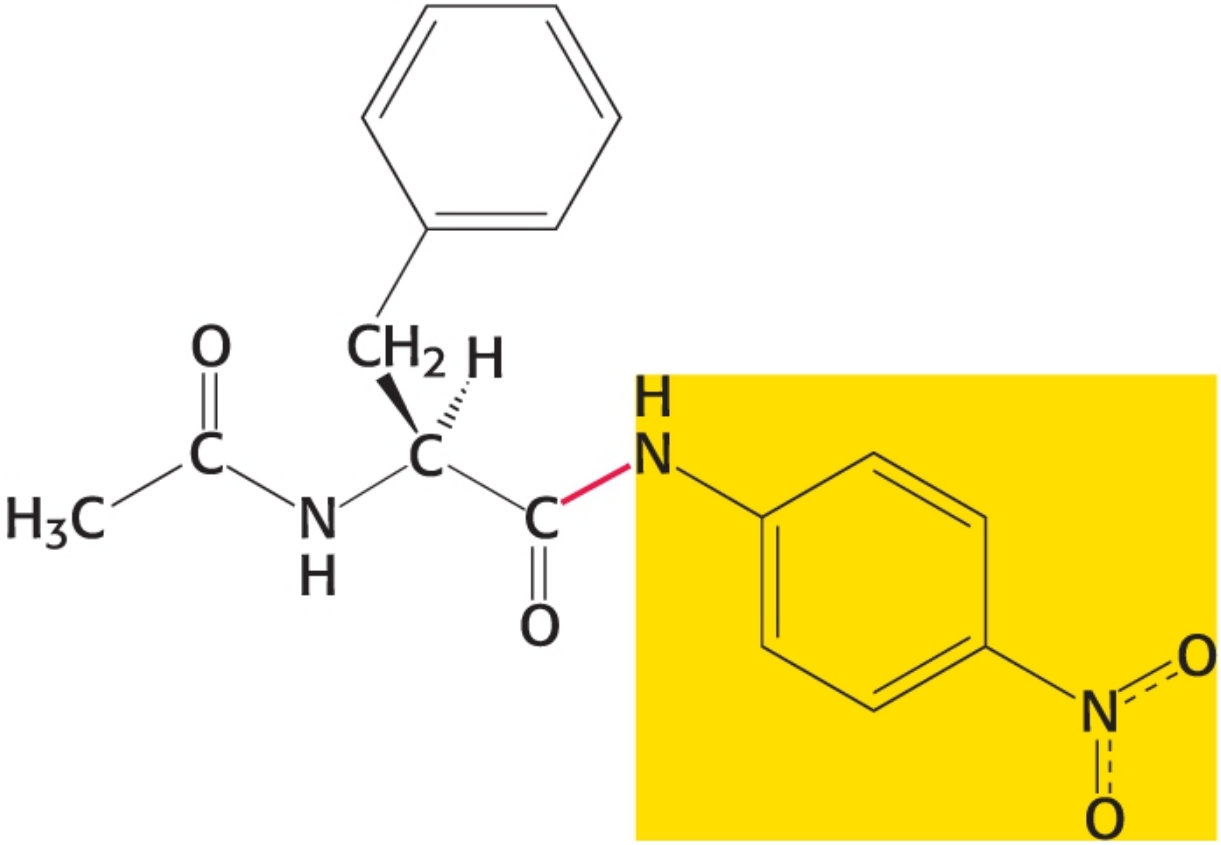
Extended description for FIGURE 6.47. Schematic illustration of the structure of myosin assembly in muscle



The dimeric myosin filaments are represented in yellow and orange colors. Multiple myosin dimers join together to form a thick filament. The globular heads protrude above and below from the left and right ends of a central thick filament.

Return to FIGURE 6.47. Schematic illustration of the structure of myosin assembly in muscle

Extended description for Chemical structure of the amide substrate of chymotrypsin

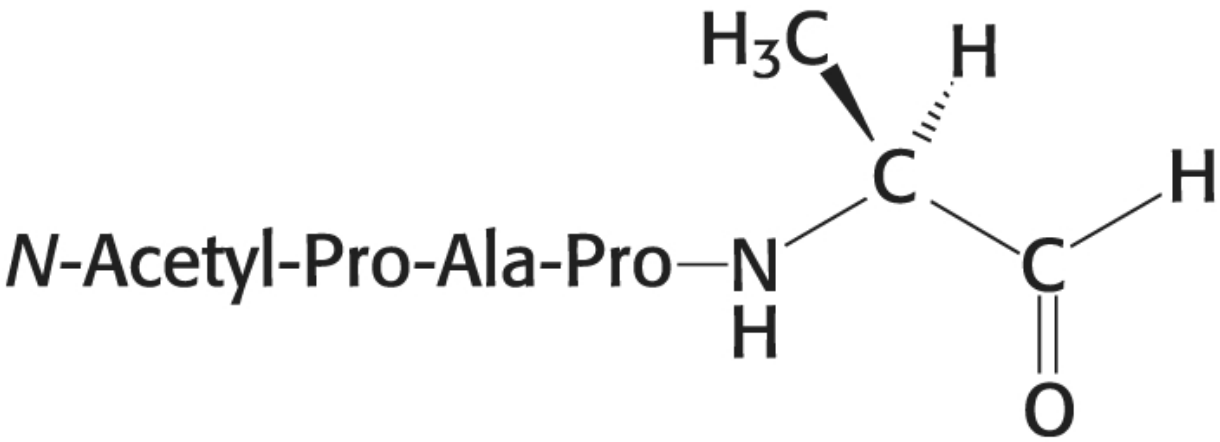


The substrate has the following structure: A 1 N and 4 C heteronuclear alkane chain is depicted as a line structure using 4 zigzag lines. N occupies the third position and is bound to H. C 1 is bound to H 3. C 2 is double bonded to O above. C 3 is dash bonded to H on the upper right and wedge bonded to C H 2 on the upper left. C H 2 is single bonded to C 3 of a benzene ring in a horizontal orientation with C 1 occupying the right most vertex. The ring contains alternating double bonds between C 2 and C 3, C 4 and C 5, and C 6 and C 1. C 4 of the heteronuclear chain is single bonded to N on the upper right and double bonded to O below. The single bond between C 4 and N is highlighted in red. The N atom is bound to H

and single bonded to C 6 of a benzene in a vertical orientation with C 1 occupying the topmost vertex. Alternating double bonds are present between C 1 and C2, C 3 and C 4, and C 5 and C 6. C 3 of the benzene ring is single bonded to N on the lower right. The N atom is single bonded to O on the upper right and O below with a resonance bond shared between them. The N atom on the upper right and benzene ring with its associated N O 2 group is highlighted in yellow.

Return to Chemical structure of the amide substrate of chymotrypsin

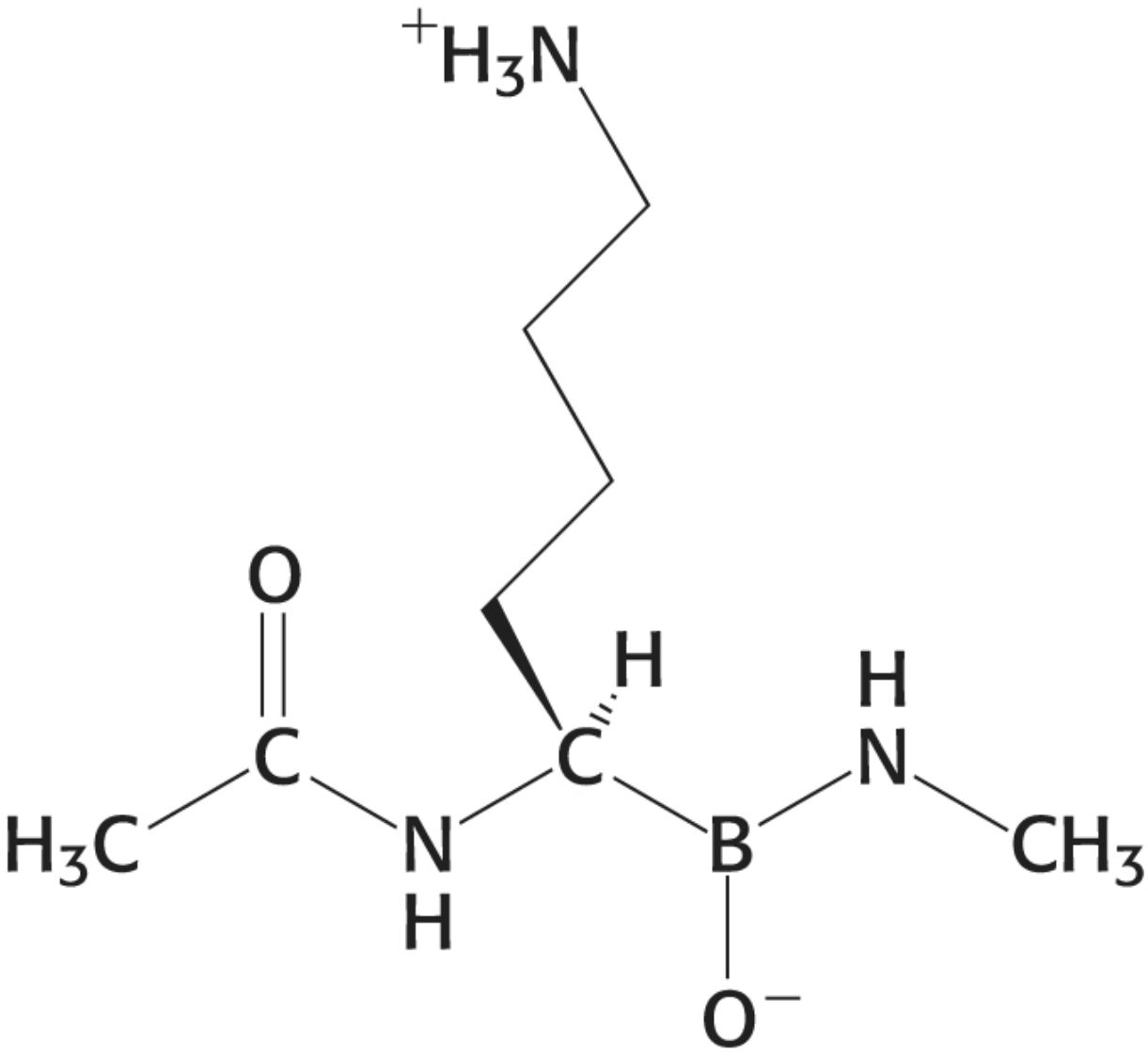
Extended description for Molecular structure of the aldehyde derivative of the substrate of elastase



The aldehyde derivative has the following structure: A central C atom is wedge bonded to C H 3 on the upper left, dash bonded to H on the upper right, single bonded to N on the lower left, and single bonded to C on the lower right. N is bound to H atom. C atom on the lower right is single bonded to H on the upper right and double bonded to O below. N is single bonded on the left to P r o, single bond, A l a, single bond, P r o, single bond, N-acetyl.

Return to Molecular structure of the aldehyde derivative of the substrate of elastase

Extended description for Chemical structure of a molecule A



Molecule A

The structure of molecule A is as follows: A 1 B, 2 N, and 2 C heteronuclear alkane chain is depicted as a line structure using 4 zigzag lines. The first and second N atoms occupy the second and

fifth positions respectively. B atom occupies the fourth position. C 1 is double bonded to O above and single bonded to C H 3 on the lower left. The first N atom is bound to H below. C 2 is dash bonded to H on the upper right and wedge bonded to C 1 of a 4 C alkane chain depicted as a line structure using 3 zigzag lines. C 4 of this chain is single bonded to N H 3 superscript plus on the upper left. B is single bonded to O superscript minus below. The second N is bound to H above and is single bonded to C H 3 on the lower right.

Return to Chemical structure of a molecule A

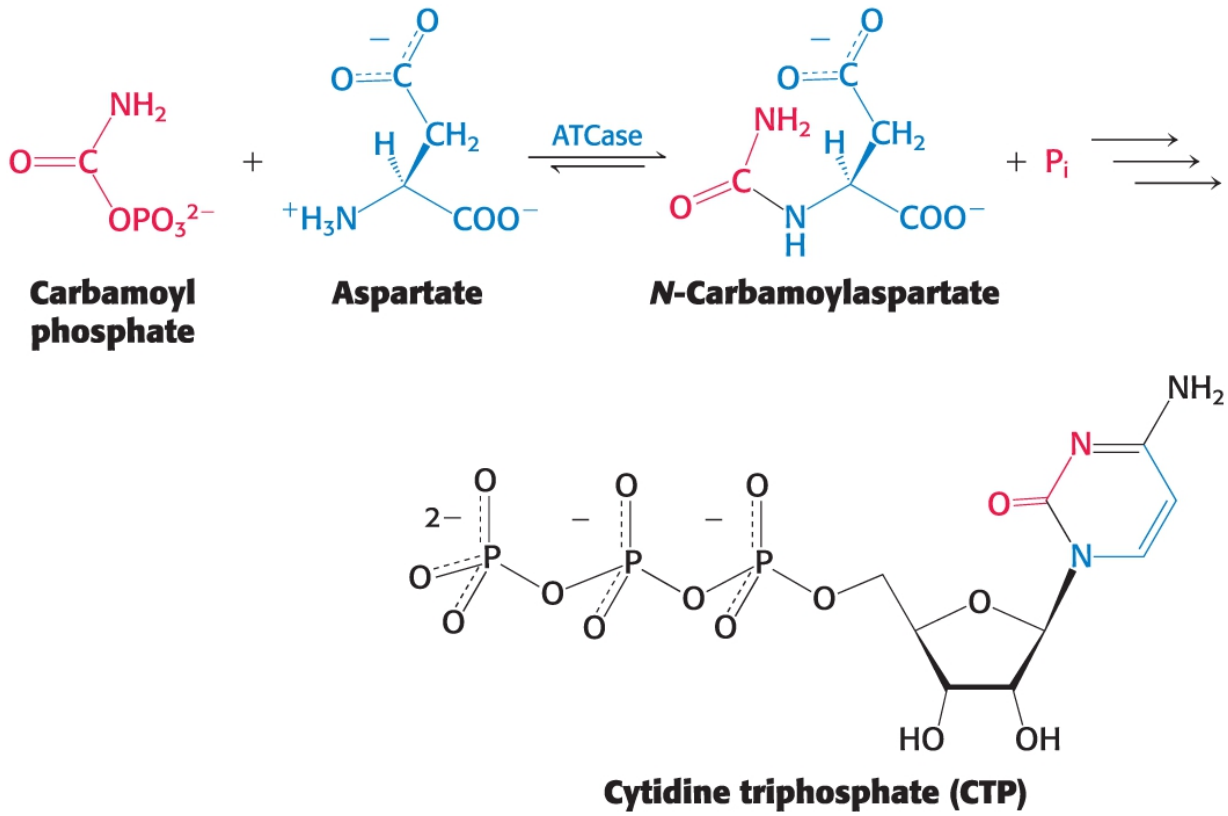
Extended description for Enzyme catalyzed reaction



The chemical reaction consists of two reactants and two products. The ball-and-stick model for each is shown. The enzyme is catalyzed by A T C ase. The first product is shown to produce C T P through a multistep pathway. C T P is shown to inhibit A T C ase in turn.

[Return to Enzyme catalyzed reaction]

Extended description for A chemical reaction representing the committed step of pyrimidine synthesis



A reversible reaction consists of two reactants and two products.

The first reactant is carbamoyl phosphate, which has the following structure: A central C atom is double bonded to O on the left, single bonded to N H 2 on the upper right, and single bonded to O P O 3 superscript 2 minus on the lower right.

The second reactant is aspartate, which has the following structure: A central C atom is single bonded to C O O superscript minus on the lower right, single bonded to N H 3 superscript plus on the lower

left, dash bonded to H on the upper left, and wedge bonded to C H 2 on the upper right. C H 2 is single bonded to C on the upper left. This C is partially double bonded to O on the left and partially double bonded to O on the upper right. This C O O group carries a negative charge.

A reversible reaction arrow is labeled A T C ase. The forward reaction arrow is longer than the backward reaction arrow.

The first product is N-carbamoylaspartate, which has the following structure: A central C atom is single bonded to C O O superscript minus on the lower right, single bonded to N H on the lower left, dash bonded to H on the upper left, and wedge bonded to C H 2 on the upper right. N H is single bonded to C on the upper left which is single bonded to N H 2 on the upper right and double bonded to O on the lower left. The C atom of C H 2, wedge bonded to the central C atom, is partially double bonded to O on the left and partially double bonded to O on the upper right. This C O O group carries a negative charge.

The second product is P subscript i.

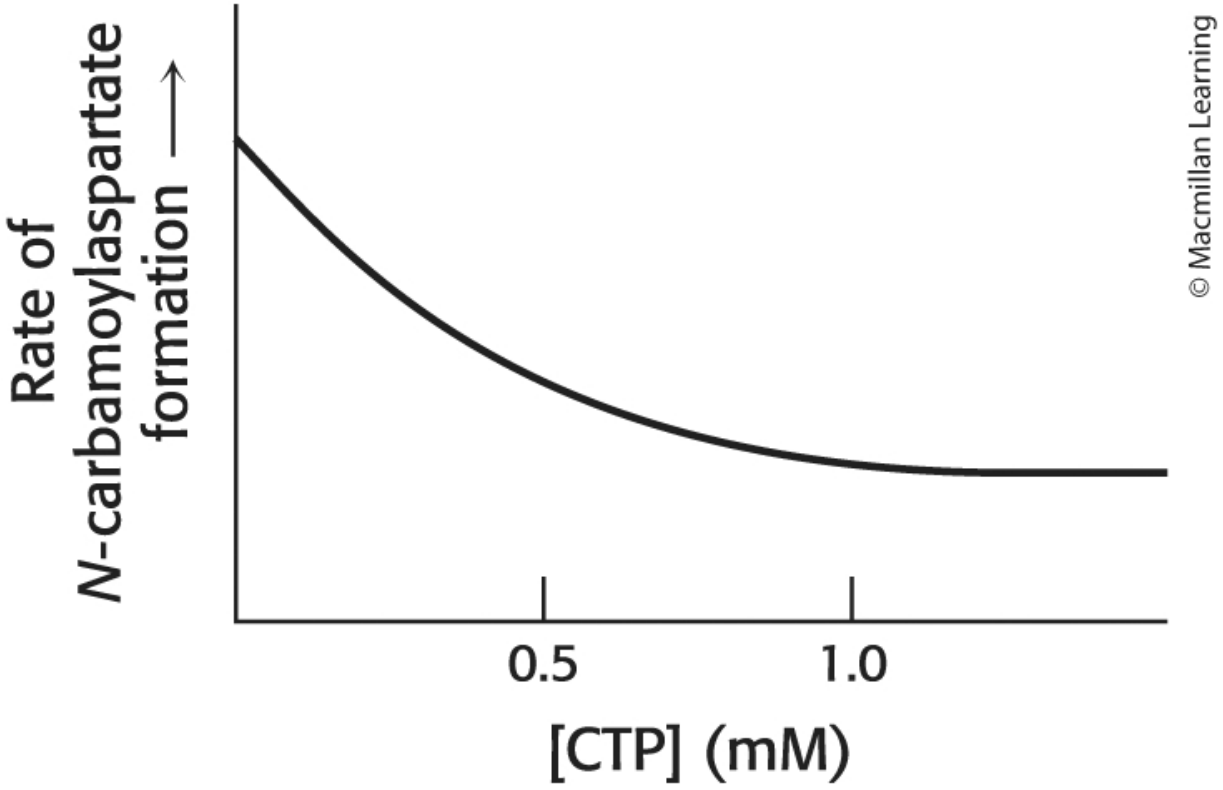
Three parallel arrows from the products indicate subsequent steps.

The final product is cytidine triphosphate (C T P), which has the following structure: A 5-membered heterocyclic pentagonal ring in a vertical orientation consists of 1 O and 4 C atoms. O occupies the first position, which is the topmost vertex. C 2 and C 3 are each single bonded to O H below. C 1 is wedge bonded to the first N of a 6-membered heterocyclic hexagonal ring in a horizontal orientation consisting of 2 N and 4 C atoms. The first N atom occupies the first position which is the bottom left vertex and the second N atom occupies the third position which is the top-left vertex. C 1 occupies

the leftmost vertex and is double bonded to O on the left. A double bond is present between the second N and C 2, and C 3 and C 4. C 2 is single bonded to N H 2 on the upper right. C 4 of the pentagonal ring is single bonded to C H 2 in the form of a line. C H 2 is single bonded to O of a triphosphate group on the left. Each phosphate group has a central P atom single bonded to O on the lower right, single bonded to O on the lower left, partially double bonded to O above, and partially double bonded to O below. The single bond to O atoms is shared between two adjacent phosphate groups. The terminal phosphate group is partially double bonded to O on the lower left and carries a negative charge of 2 minus. The other two phosphate groups each carry a negative charge.

Return to A chemical reaction representing the committed step of pyrimidine synthesis

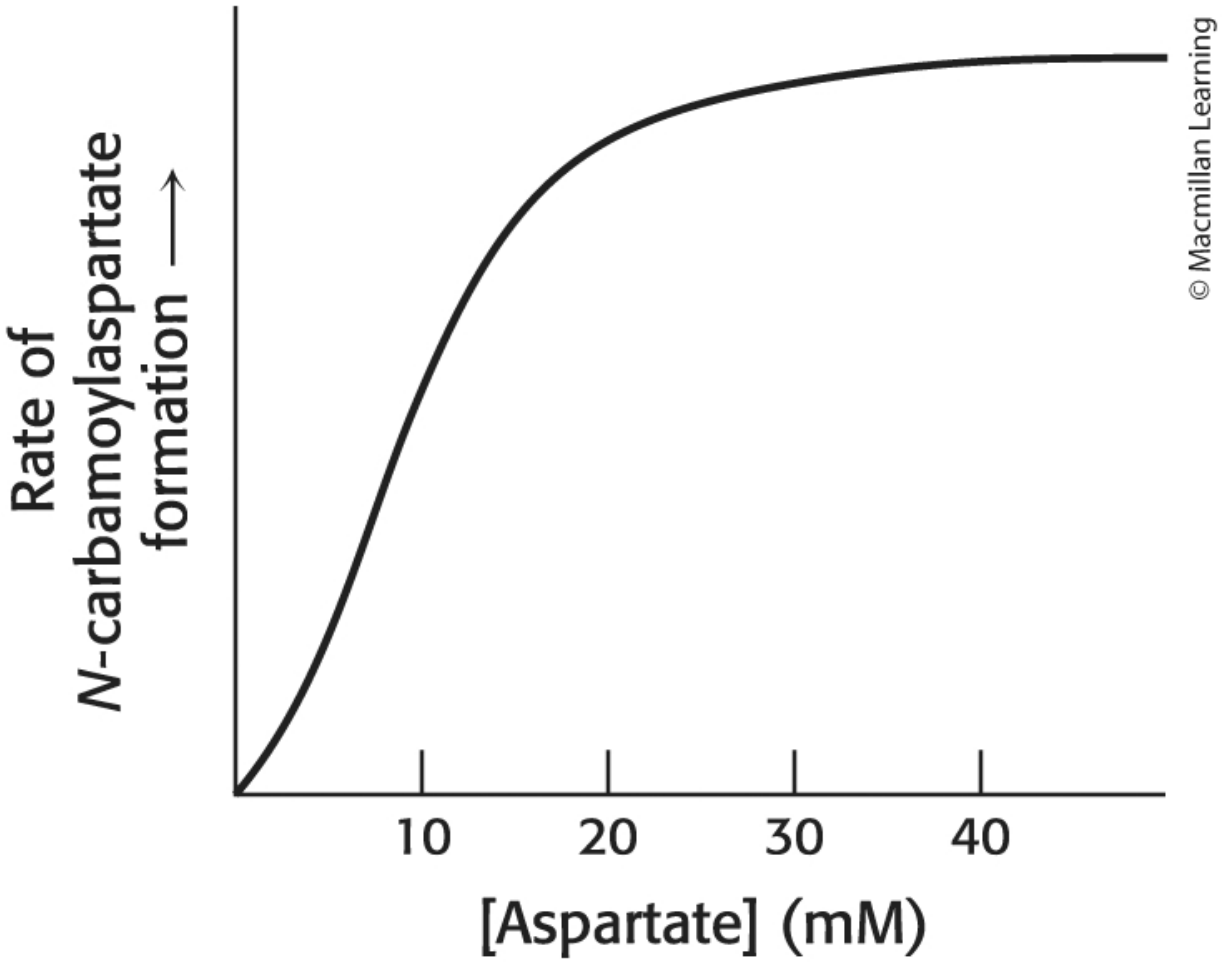
Extended description for Graphical representation of the inhibition of A T C ase by C T P



The horizontal axis is labeled C T P concentration in millimolar and ranges from 0.5 to 1.0 in increments of 0.5 units. The vertical axis is labeled the rate of N-carbamoylaspartate formation. The curve starts near the upper end of the vertical axis and then gradually falls below the midpoint of the vertical axis at a C T P concentration of 1 and then it remains constant beyond this point.

Return to Graphical representation of the inhibition of A T C ase by C T P

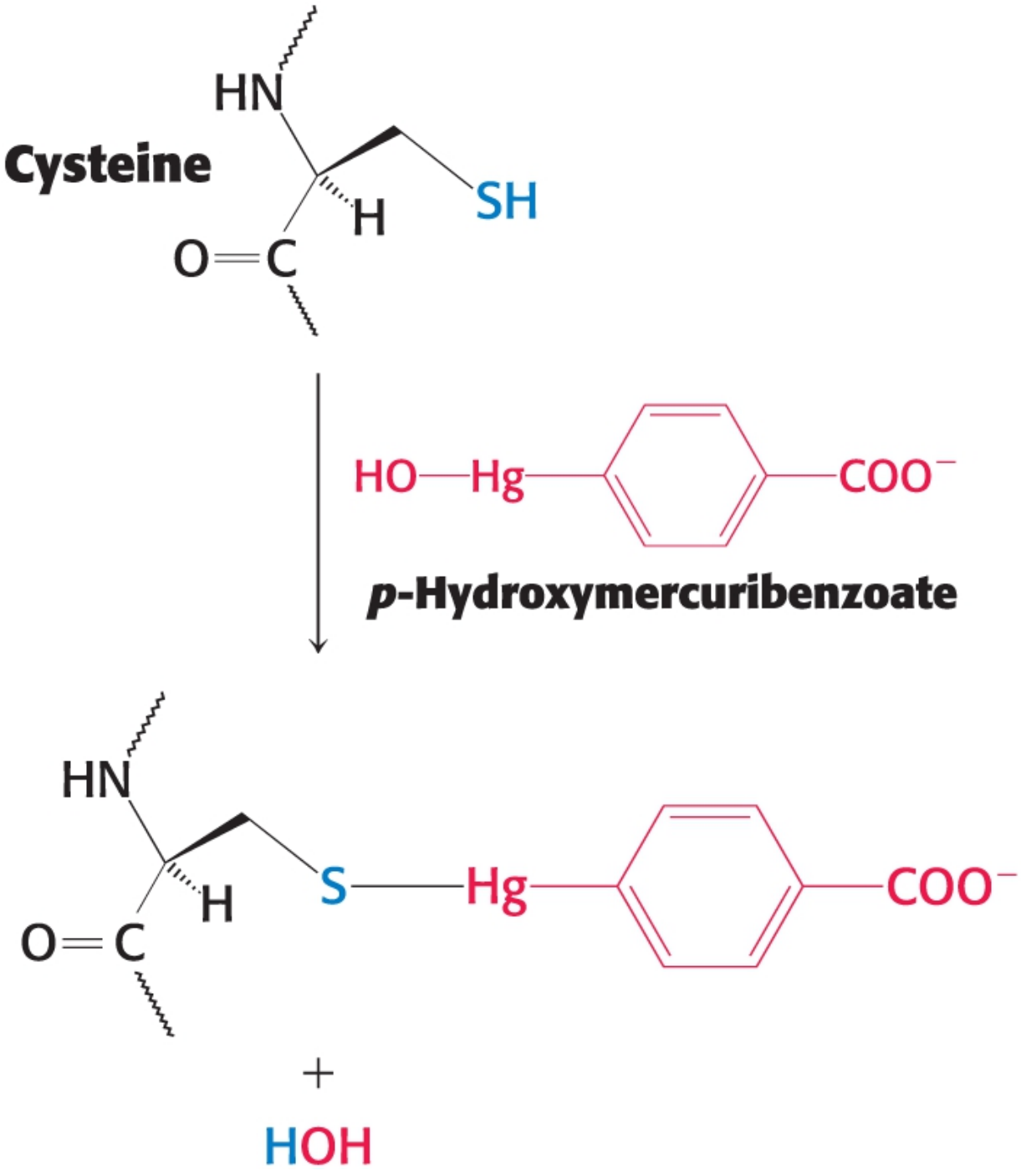
Extended description for Graph of the rate of formation of N-carbamoylaspartate as a function of aspartate concentration



The horizontal axis is labeled aspartate concentration in millimolar. It has markings ranging from 0 to 40 in increments of 10 units. The vertical axis is labeled the rate of formation of N-carbamoylaspartate formation. The curve starts at the origin and steeply rises to a point corresponding to 20 milli moles aspartate at the top of the vertical axis. This is followed by a gradual plateau formation. The curve has a sigmoidal shape.

Return to Graph of the rate of formation of N-carbamoylaspartate as a function of aspartate concentration

Extended description for Chemical reaction of p-Hydroxymercuribenzoate with a crucial cysteine residue of aspartate transcarbamoylase



The reaction consists of two reactants and two products.

The first reactant is the cysteine residue of aspartate transcarbamoylase, which has the following structure: A central C atom is single bonded to C on the lower left, single bonded to N H on the upper left, wedge bonded to C H 2 on the upper right, and dash bonded to H on the lower right. N H has an open single bond on the upper right. C on the lower left is double bonded to O on the left and has an open single bond on the lower right. C H 2 on the upper right is single bonded to S H on the lower right. S H is highlighted in blue.

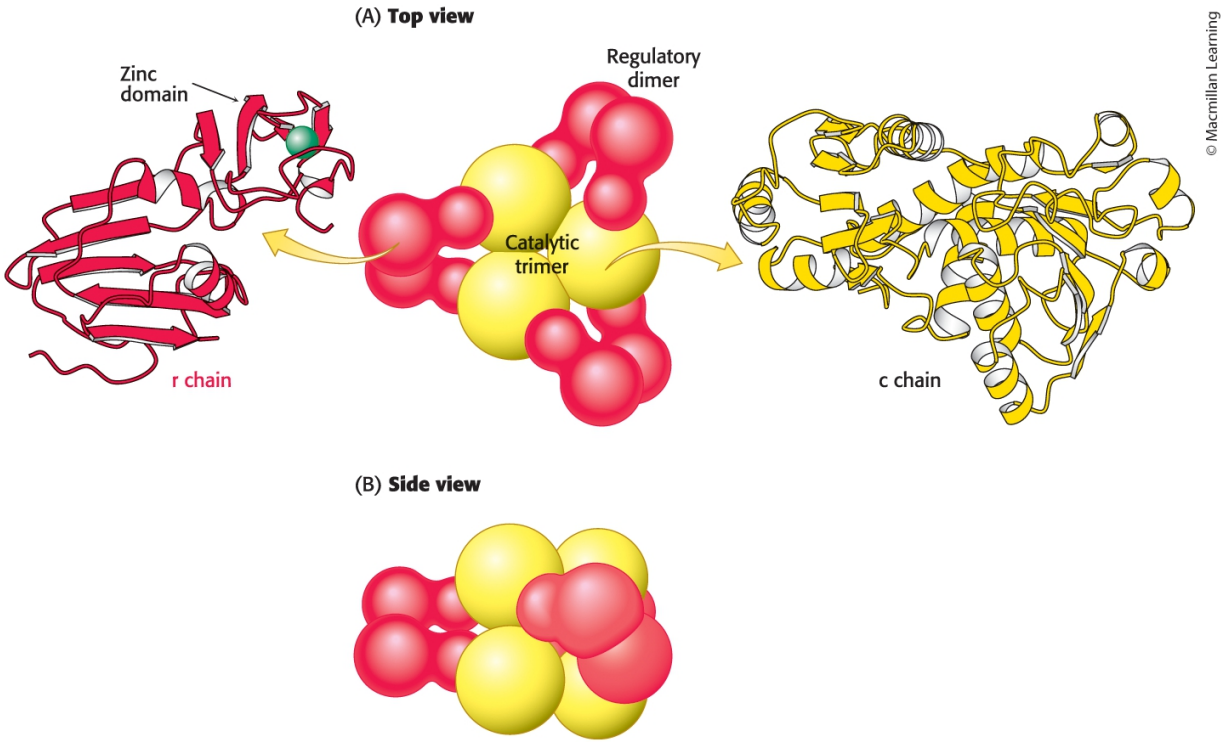
The reaction arrow is labeled p-Hydroxymercuribenzoate, which is the second reactant having the following structure: A benzene ring is in a horizontal orientation. It contains alternating double bonds between C 1 and C 2, C 3 and C 4, and C 5 and C 6. C 1 is single bonded to C O O superscript minus on the right. C 4 is single bonded to H g, single bond, O H on the left.

The first product has the following structure: A central C atom is single bonded to C on the lower left, single bonded to N H on the upper left, wedge bonded to C H 2 on the upper right, and dash bonded to H on the lower right. N H has an open single bond on the upper right. C on the lower left is double bonded to O on the left and has an open single bond on the lower right. C H 2 on the upper right is single bonded to S on the lower right, which is highlighted in blue. S is single bonded to H g on the right. H g is single bonded to C 4 of a benzene ring in a horizontal orientation. The benzene ring consists of alternating double bonds between C 1 and C 2, C 3 and C 4, and C 5 and C 6. C 1 is single bonded to C O O superscript minus.

The second product is H O H. The left H atom is highlighted in blue.

Return to Chemical reaction of p-Hydroxymercuribenzoate with a crucial cysteine residue of aspartate transcarbamoylase

Extended description for Schematic illustration of the top and side views of the catalytic subunit trimer of A T C ase

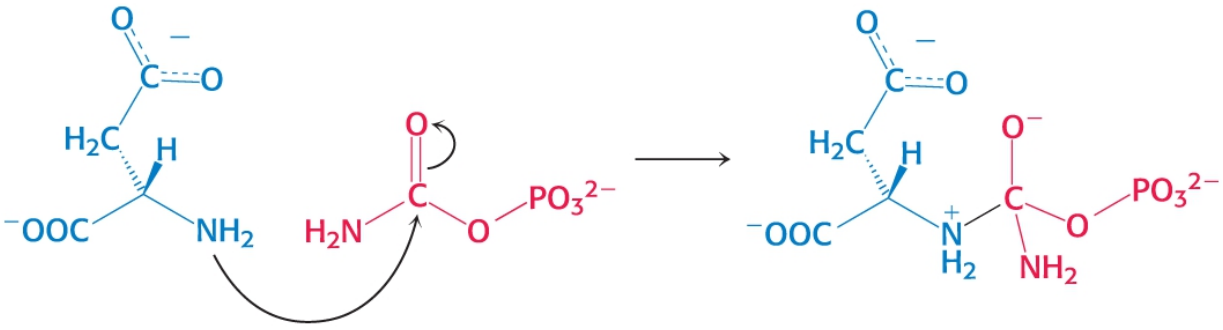


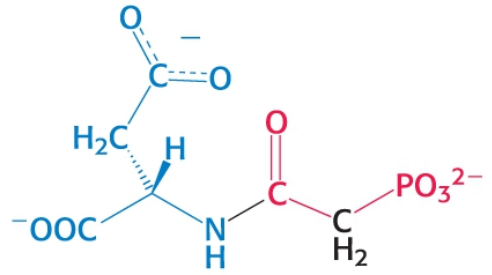
Part (A): Top view. One catalytic subunit is shown to have a central yellow spherical structure with two arms at upward inclined angles. Each arm is made up of a pair of fused red spheres. The yellow structure is labeled c chain and the ribbon diagram shows it to comprise alpha helices and some beta strands connected by short loops. The red arms are labeled r chain and are shown to primarily consist of antiparallel beta-strands and an alpha helix joined by short loops. One small green sphere is associated with the top part of the r chain and is labeled zinc domain. The three subunits are arranged around a central axis with the yellow spheres at the center and the red arms toward the periphery. Adjacent arms are accommodated by positioning one above the other.

Part (B): Side view. A catalytic trimer is shown above another similar trimer. Two yellow spheres of each trimer are visible to the observer.

Return to Schematic illustration of the top and side views of the catalytic subunit trimer of A T C ase

Extended description for Chemical equation for the formation of an intermediate compound in the A T C ase catalytic pathway and the structure of its analog P A L A





The reaction consists of two reactants and one product.

The first reactant has the following structure: A central C atom is single bonded to C O O superscript minus on the lower right, single bonded to N H 2 on the lower left, wedge bonded to H on the upper right, and dash bonded to C H 2 on the upper left. C H 2 is single bonded to C on the upper right. This C is partially double bonded to O on the right and partially double bonded to O on the upper left. This C O O group carries a negative charge.

The second reactant has the following structure: A central C atom is double bonded to O above, single bonded to N H 2 on the lower left, and single bonded to O on the lower right. O atom on the lower right is single bonded to P O 3 superscript 2 minus on the upper right.

A curved arrow is pointed from the N H 2 group of the first reactant to the central C atom of the second reactant. Another curved arrow is pointed from the central C atom of the second reactant to the double-bonded O above.

The reactants are labeled bound substrates.

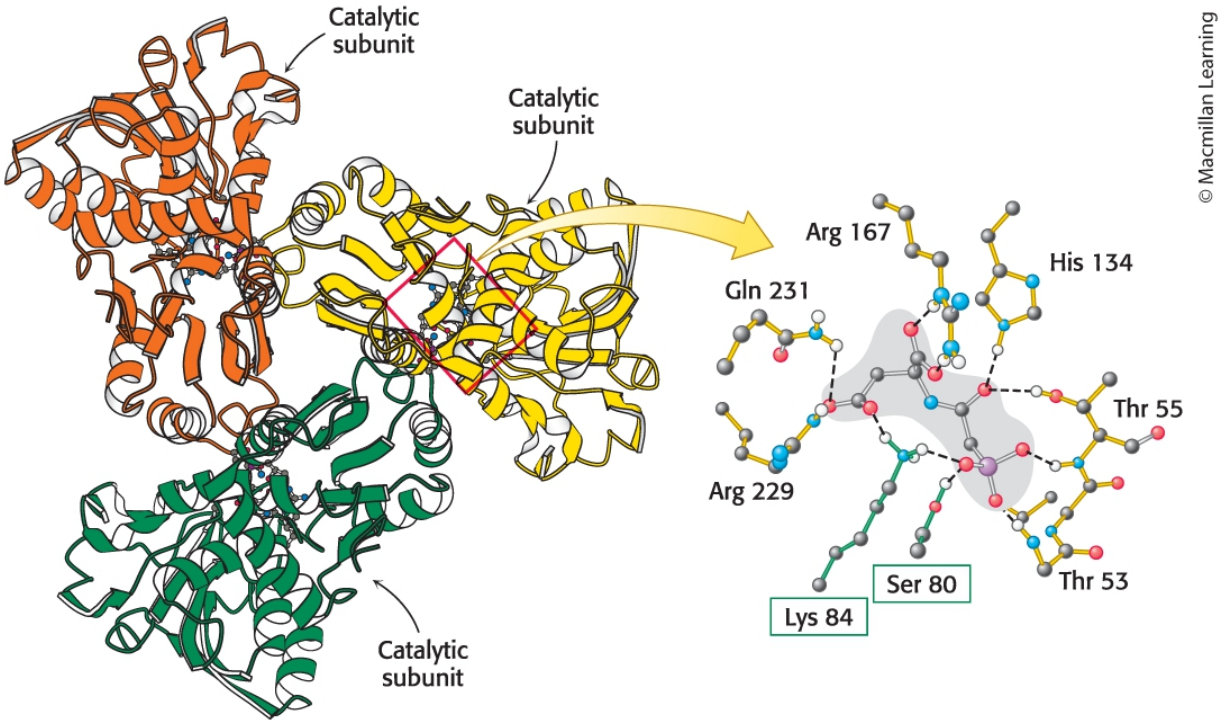
The product is labeled reaction intermediate, which has the following structure: A central C atom is single bonded to C O O superscript minus on the lower right, single bonded to N H 2 superscript plus on the lower left, wedge bonded to H on the upper right and dash bonded to C H 2 on the upper left. C H 2 is single bonded to C on the upper right. This C is partially double bonded to O on the right and partially double bonded to O on the upper left. This C O O group carries a negative charge. N H 2 superscript plus is single bonded to a C atom on the upper right. This C atom is single bonded to O superscript minus above, single bonded to N H 2 below, and single bonded to O on the lower right. The O atom on the lower right is single bonded to P O 3 superscript 2 minus on the upper right.

The structure of N-(Phosphonacetyl)-L-aspartate (P A L A) is as follows: A central C atom is single bonded to C O O superscript minus on the lower right, single bonded to N H on the lower left, wedge bonded to H on the upper right and dash bonded to C H 2 on the upper left. C H 2 is single bonded to C on the upper right. This C is partially double bonded to O on the right and partially double bonded to O on the upper left. This C O O group carries a negative charge. N H is single bonded to a C atom on the upper right. This C

atom is double bonded to O above, single bonded to C H 2 on the lower right which is single bonded to P O 3 superscript 2 minus on the upper right.

Return to Chemical equation for the formation of an intermediate compound in the A T C ase catalytic pathway and the structure of its analog P A L A

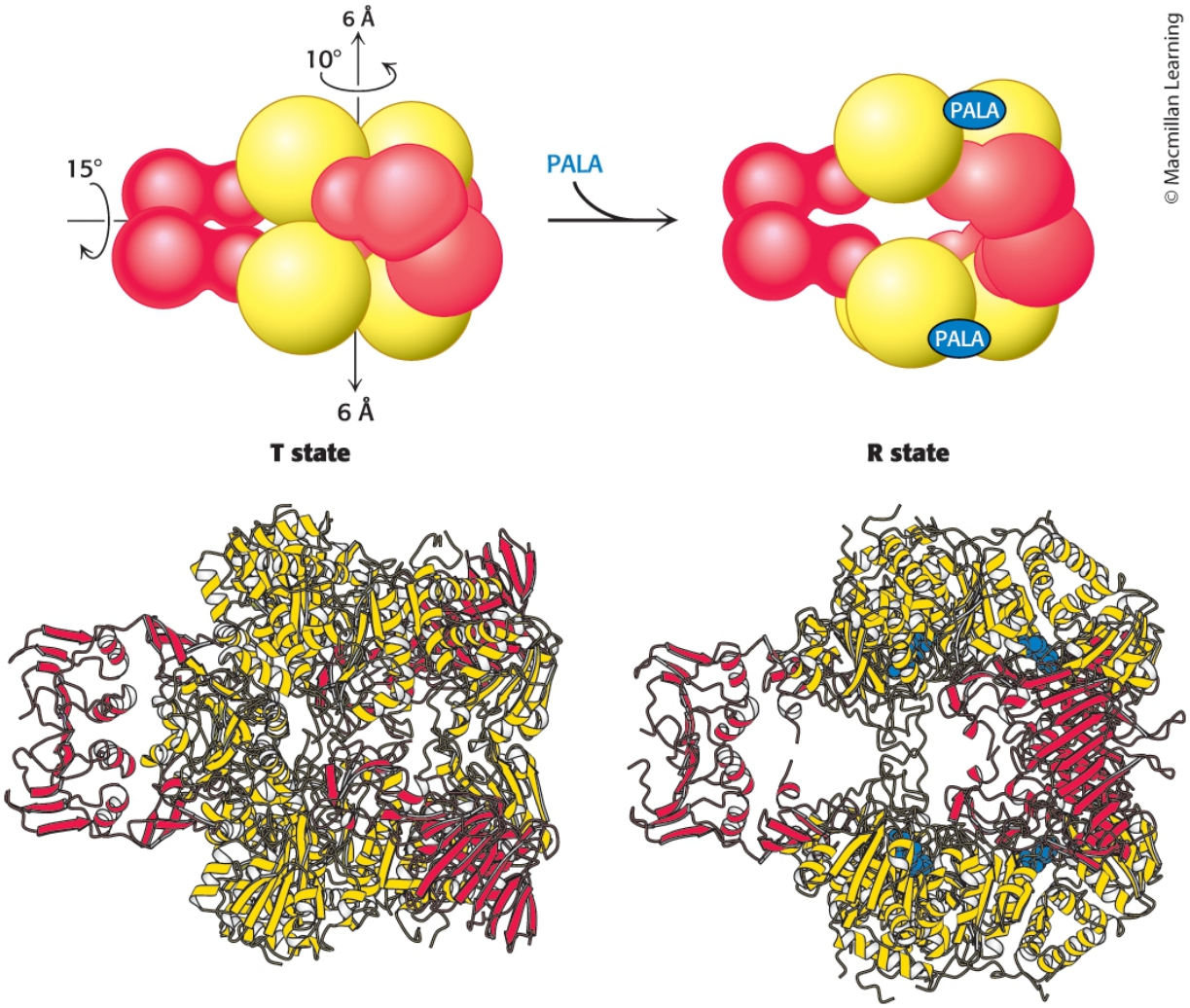
Extended description for The ribbon structure of the catalytic trimer of A T C ase and the active site residues of one of the catalytic subunits bound to P A L A



The catalytic trimer is shown to consist of three catalytic subunits colored orange, yellow, and green, respectively. Each subunit consists of alpha helices and beta strands joined by short loops. The catalytic subunits are connected around a central axis. The active site residues of the yellow subunit are shown in magnification. A central elongated gray shaded region highlights the ball-and-stick model of P A L A. It is surrounded by the following residues of the yellow subunit at the top: A r g 229, G l n 231, A r g 167, H i s 134, T h r 55, and T h r 53. The following residues of the green subunits are present at the bottom of P A L A: L y s 84 and S e r 80.

Return to The ribbon structure of the catalytic trimer of A T C ase and the active site residues of one of the catalytic subunits bound to P A L A

Extended description for Schematic illustration of the tense and relaxed states of A T C ase



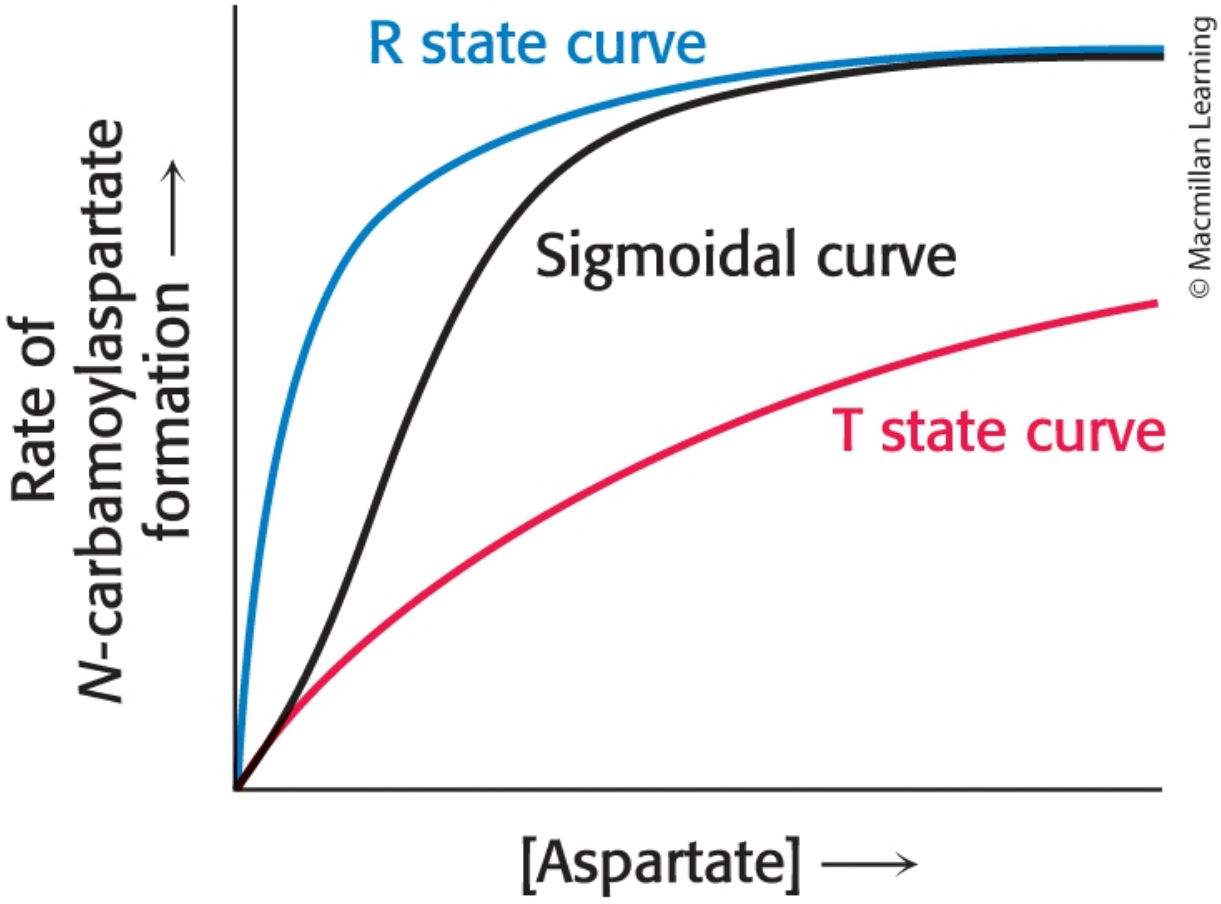
Tense state (T). One catalytic subunit is shown to have a central yellow spherical structure with two arms at upward inclined angles. Each arm is made up of a pair of fused red spheres. The side view of the trimer shows the three subunits arranged around a central vertical axis with the yellow spheres at the center and the red arms to the periphery. Adjacent arms are accommodated by positioning one above the other. One trimer is positioned above the other and

there is no gap in between. An upward arrow along the vertical axis is labeled 6 Angstrom and a counter-clockwise arrow around the axis is labeled 10 degrees. A downward arrow along the vertical axis is labeled 6 Angstrom. A clockwise arrow around the horizontal axis is labeled 15 degrees. The ribbon structure shows the two catalytic trimers forming a vase-shaped structure tilted 90 degrees to the left. There is a minimal gap in between.

Relaxed state: Binding of P A L A to the catalytic trimer produces a relaxed state. The arrangement is almost identical to the tense state but there is more gap between the top and bottom trimers. The ribbon structure shows the two catalytic trimers forming a vase-shaped structure tilted 90 degrees to the left. There are enlarged gaps near the neck.

Return to Schematic illustration of the tense and relaxed states of A T C ase

Extended description for Graphical representation of the change of state in a cooperative enzyme as a function of substrate concentration



The horizontal axis is labeled aspartate concentration. The vertical axis is labeled the rate of N-carbamoylaspartate formation. The following three curves are shown:

T state curve (shown in red): It starts at the origin and rises almost linearly to a point corresponding to the midpoint of the vertical axis. It has a slight downward curve.

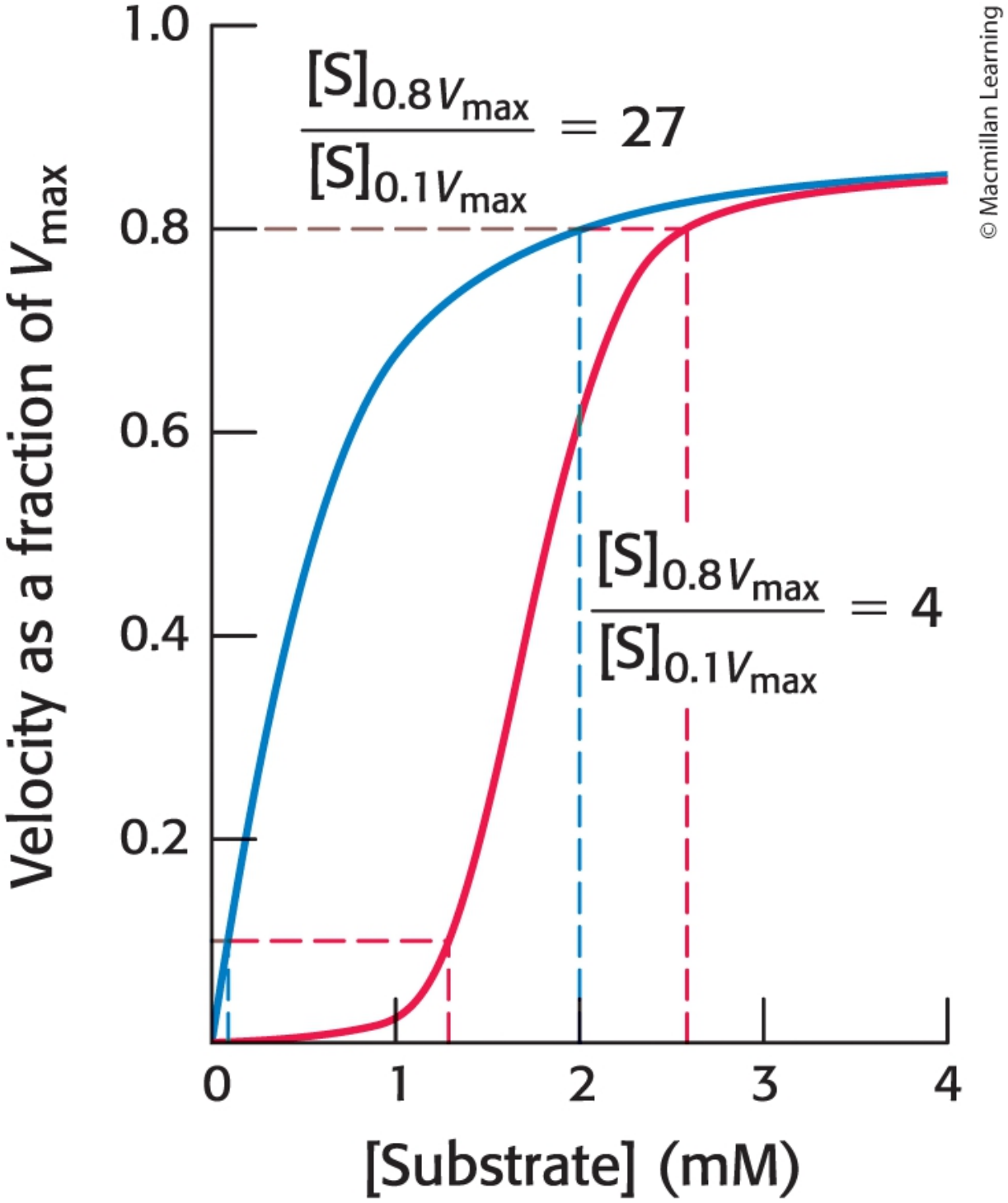
Sigmoidal curve (shown in black): It starts from the origin and rises steeply toward the top of the vertical axis and then plateaus. It has a slight S-shape.

R state curve (shown in blue): It starts from the origin and rises parallel to the sigmoidal curve but has a steeper slope. It then plateaus to meet the sigmoidal curve. It is a hyperbolic curve.

Return to Graphical representation of the change of state in a cooperative enzyme as a function of substrate concentration

Extended description for Graphical representation of the velocity of reaction as a function of substrate

concentration for allosteric and Michaelis-Menten enzymes



The horizontal axis is labeled substrate concentration in millimolar. It has markings ranging from 0 to 4 in increments of 1 unit. The vertical axis is labeled velocity as a fraction of V max. It has markings ranging from 0 to 1.0 in increments of 0.2 units.

Two curves are shown as follows:

Red curve: It is a sigmoidal curve that starts at the origin, slowly rises to (1, 0.05), followed by a steep rise to nearly (2.6, 0.8) and it gradually plateaus. An equation next to the curve reads that the ratio of substrate concentration subscript 0.8 V max to substrate concentration subscript 0.1 V max equals 4.

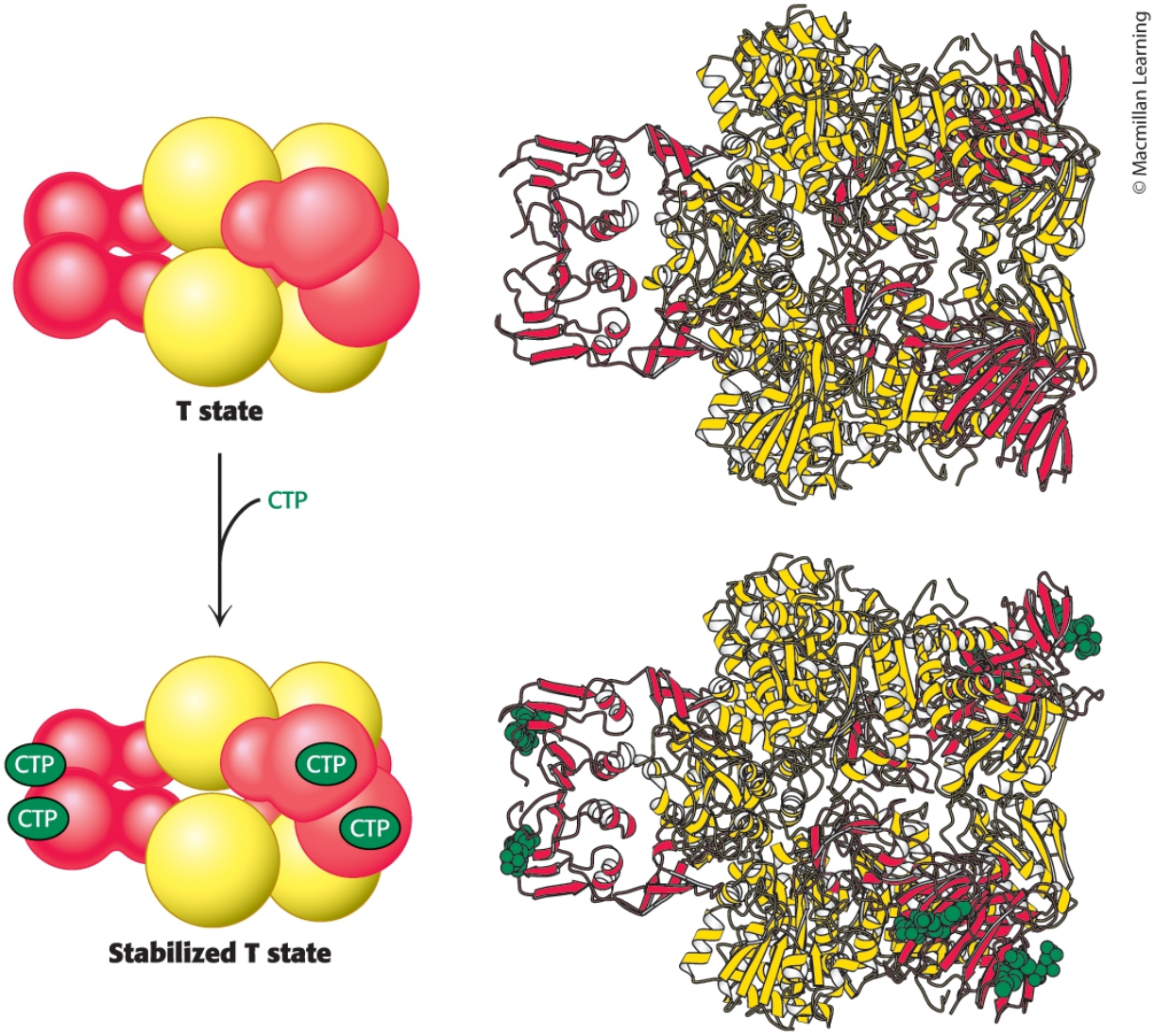
Blue curve: It starts at the origin, steeply rises to (2, 0.8), and then gradually plateaus to meet the red curve. An equation next to the curve reads that the ratio of substrate concentration subscript 0.8 V max to substrate concentration subscript 0.1 V max equals 27.

A vertical red dotted line is drawn up from 1.3 on the horizontal axis to meet the red curve at a point. A horizontal red dotted line is drawn from this point to the vertical axis at 0.1. Another vertical red line is drawn from 2.6 on the horizontal axis to meet the red curve at a point. A horizontal red dotted line is drawn from this point to the vertical axis at 0.8. A vertical blue line is drawn from 2 on the horizontal axis to meet the blue curve at a point. A horizontal blue dotted line is drawn from this point to the vertical axis at 0.8, which is overlapping the horizontal red dotted line.

All the numerical values are estimated.

Return to Graphical representation of the velocity of reaction as a function of substrate concentration for allosteric and Michaelis-Menten enzymes

Extended description for Schematic illustration of the stabilization of T state of A T C ase by C T P



© Macmillan Learning

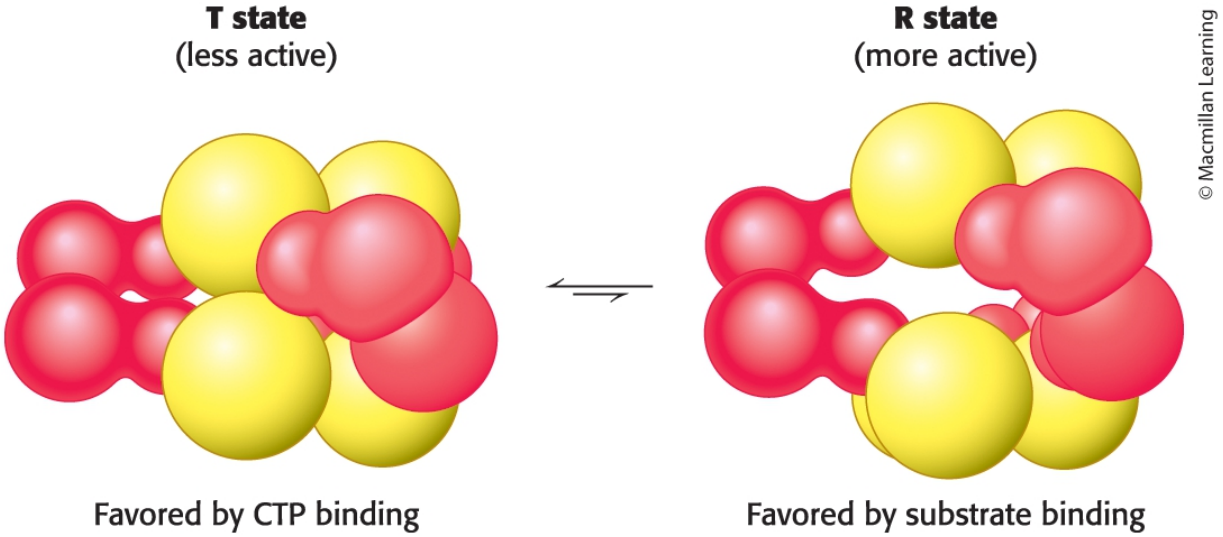
Tense state (T). One catalytic subunit is shown to have a central yellow spherical structure with two arms at upward inclined angles. Each arm is made up of a pair of fused red spheres. The side view of the trimer shows the three subunits arranged around a central vertical axis with the yellow spheres at the center and the red arms toward the periphery. Adjacent arms are accommodated by

positioning one above the other. One trimer is positioned above the other and there is no gap in between. The ribbon structure shows the two catalytic trimers forming a vase-shaped structure tilted 90 degrees to the left. There is a minimal gap in between.

Stabilized T state: C T P binds to the r chains of the catalytic trimers thereby stabilizing the T state. The arrangement is almost identical to the tense state. The ribbon structure shows the two catalytic trimers forming a vase-shaped structure tilted 90 degrees to the left. The structure is more compact.

Return to Schematic illustration of the stabilization of T state of A T C ase by C T P

Extended description for A schematic illustration of the equilibrium between the R and T states of A T C ase

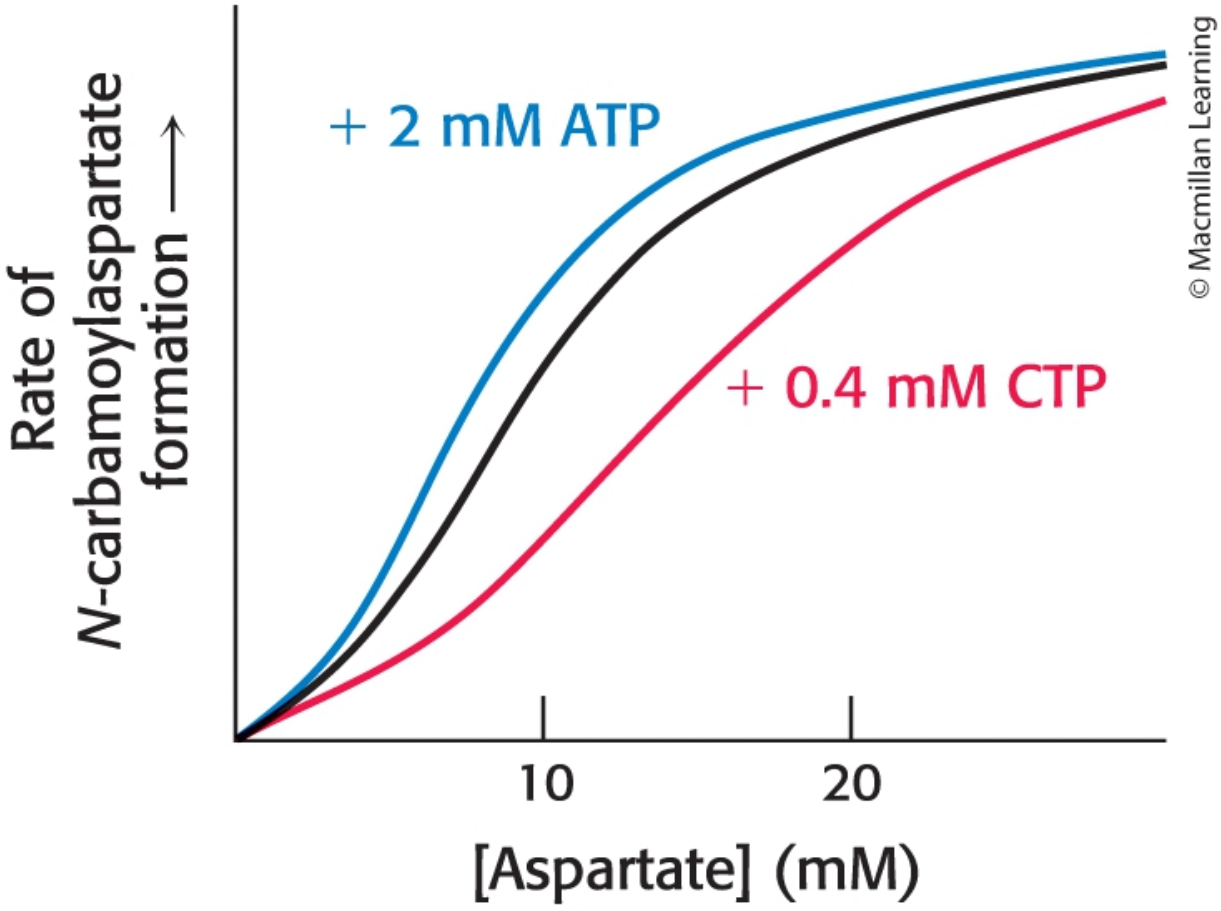


T state (less active): It is favored by C T P binding. One catalytic subunit is shown to have a central yellow spherical structure with two arms at upward inclined angles. Each arm is made up of a pair of fused red spheres. The side view of the trimer shows the three subunits arranged around a central vertical axis with the yellow spheres at the center and the red arms to the periphery. Adjacent arms are accommodated by positioning one above the other. One trimer is positioned above the other and there is no gap in between.

R state (more active): It is favored by substrate binding. The arrangement is almost identical to the tense state but there is more gap between the top and bottom trimers.

Return to A schematic illustration of the equilibrium between the R and T states of A T C ase

Extended description for Graphical representation of the different effects of A T P and C T P on A T C ase kinetics



The horizontal axis is labeled aspartate concentration in millimolar. It has markings ranging from 0 to 20 in increments of 10 units. The vertical axis is labeled the rate of N-carbamoylaspartate formation. The following three curves are shown:

Red curve: It starts at the origin and rises almost linearly to a point corresponding to the midpoint of the vertical axis. It has a slight S-shape. It is labeled plus 0.4 millimolar C T P.

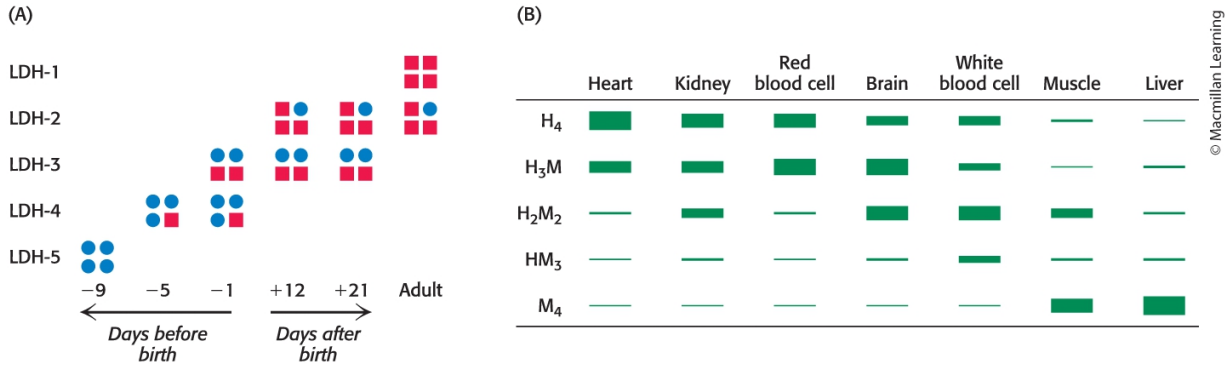
Black curve: It starts from the origin and rises steeply toward the top of the vertical axis and then plateaus. It is located on the left of the red curve and has a slight S-shape.

Blue curve: It starts from the origin and rises parallel to the left of the black curve but has a steeper slope. It then plateaus to meet the black curve. It is labeled plus 2 millimolar A T P.

The black curve is closer to the blue curve.

Return to Graphical representation of the different effects of A T P and C T P on A T C ase kinetics

Extended description for Schematic illustration of the timing of expression of isozymes of lactate dehydrogenase and their tissue specific concentrations respectively



Part (A): Along the vertical axis, the following are marked from left to right: negative 9, negative 5, negative 1, positive 12, positive 21, Adult. A leftward arrow from negative 1 to negative 9 is labeled days before birth. A rightward arrow from positive 12 to positive 21 is labeled days after birth. The L D H profile is represented to consist of four quadrants. The H isozyme is represented by squares and the M isozyme by circles. The profiles for the following five isozymes are shown:

L D H 1: All the four quadrants are red squares. Expressed in Adults.

L D H 2: The top right quadrant is a blue circle and the other three quadrants are red squares. They are expressed at positive 12 and positive 21 days, and in adults.

L D H 3: The top left and top right quadrants are blue circles and the rest two quadrants are red squares. They are expressed at positive 12, positive 21, and negative 1 days.

L D H 4: The top left, top right, and bottom left quadrants are blue circles and the last quadrant is a red square. They are expressed at negative 1 and negative 5 days.

L D H 5: All the four quadrants are blue circles. They are expressed at negative 9 day.

Part (B): Green bars represent the concentration of L D H isozymes in the following tissues:

Heart: Thickest bar for H subscript 4, thinner bar for H subscript 3 M, and thin lines for H subscript 2 M subscript 2, H M subscript 3, and M subscript 4.

Kidney: Thickest bar for H subscript 4, slightly thinner bar for H subscript 3 M subscript, relatively more thinner bar for H subscript 2 M 2, and thin lines for H M subscript 3 and M subscript 4.

Red blood cell: Thickest bar for H subscript 3 M, slightly thinner bar for H subscript 4, and thin lines for H subscript 2 M subscript 2, H M subscript 3, and M subscript 4.

Brain: Thickest bar for H subscript 3 M, slightly thinner bar for H subscript 2 M subscript 2, thinner bar for H subscript 4, and thin lines for H M subscript 3 and M subscript 4.

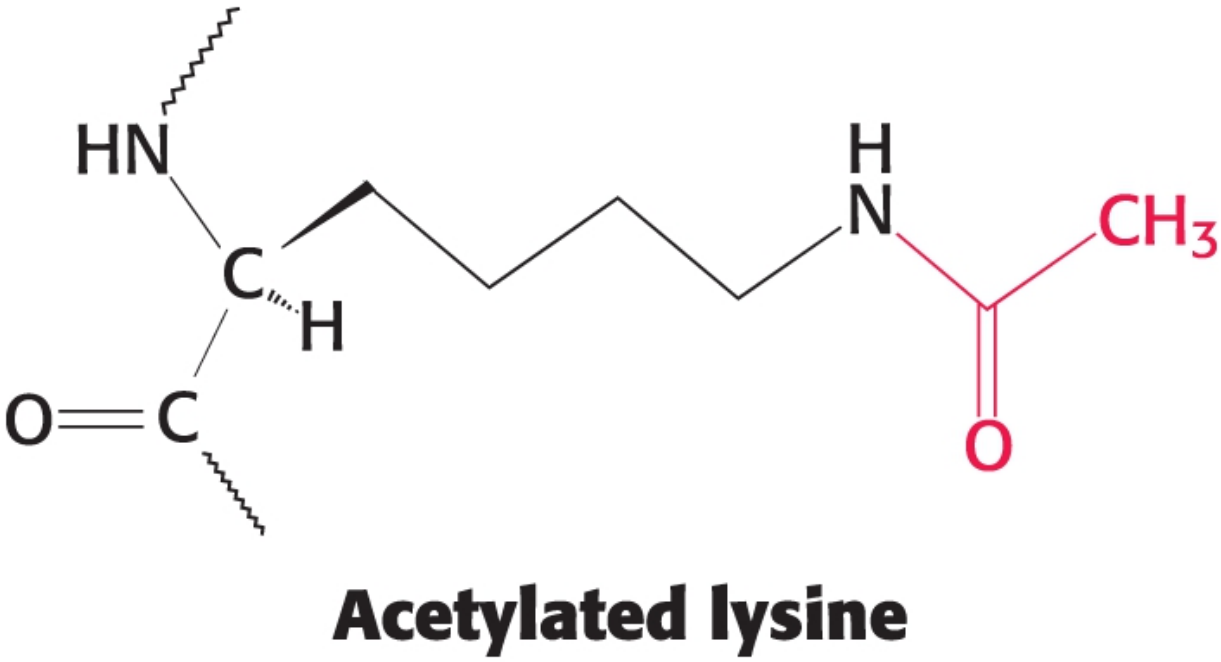
White blood cell: Thickest bar for H subscript 2 M subscript 2, thinner bar for H subscript 4, slightly thinner bars for H subscript 3 and H M subscript 3, and a thin line for M subscript 4.

Muscle: Thickest bar for M subscript 4, thinner bar for H subscript 2 M subscript 2, and thin lines for H subscript 4, H subscript 3 M, and H M subscript 3.

Liver: Thickest bar for M subscript 4 and thin lines for H subscript 4, H subscript 3 M, H subscript 2 M subscript 2, and H M subscript 3.

Return to Schematic illustration of the timing of expression of isozymes of lactate dehydrogenase and their tissue specific concentrations respectively

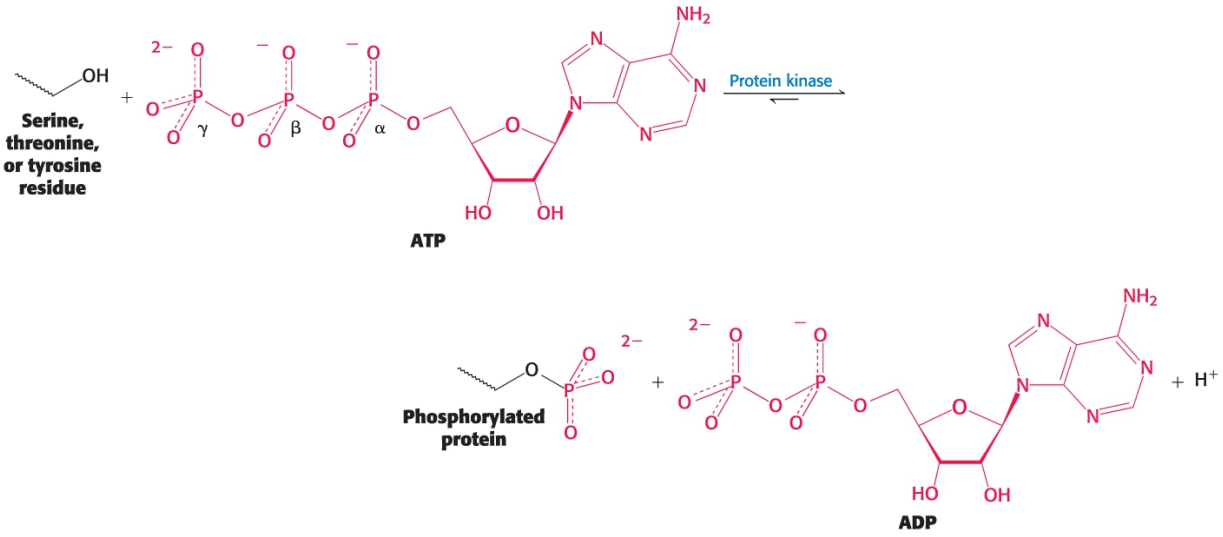
Extended description for Chemical structure of acetylated lysine



A central C atom is single bonded to N H on the upper left, single bonded to C on the lower left, dash bonded to H on the lower right, and wedge bonded to C 1 of a 4-carbon alkane chain on the upper right. N H has an open bond on the upper right. C on the lower left is double bonded to O on the left and has an open bond on the lower right. The 4 carbon alkane chain is depicted as a line structure using 3 zigzag lines. C 4 of the alkane chain is single bonded to N H on the upper right. N H is single bonded to C on the lower right which is double bonded to O below and single bonded to C H 3 on the upper right.

Return to Chemical structure of acetylated lysine

Extended description for Chemical reaction of the phosphorylation of an amino acid residue catalyzed by a protein kinase enzyme is shown



The reversible reaction consists of two reactants and three products.

The first reactant is serine, threonine, or tyrosine residue, which has the following structure: A central C H 2 group is single bonded to O H on the upper right and has an open bond on the upper left.

The second reactant is A T P, which has the following structure: A 5-membered heterocyclic pentagonal ring in a vertical orientation consists of 1 O and 4 C atoms. The O atom occupies the first position which is the topmost vertex. C 2 and C 3 are each single bonded to O H. C 1 is wedge bonded to the first N of a 5-membered heterocyclic pentagonal ring in a vertical orientation consisting of 2 N and 3 C atoms. The first N atom occupies the first position which is the bottom left vertex and the second N atom occupies the third position which is the topmost vertex. A double bond is present between the second N and C 1, and C 2 and C 3. This ring is fused to a

heterocyclic hexagonal ring is a vertical orientation consisting of 2 N and 4 C atoms. The first N occupies the first position which is the top-right vertex and the second N occupies the third position which is the bottom-most vertex. A double bond is present between C 4 and the first N and C 1 and the second N. C 4 is single bonded to N H 2 above. The rings are fused such that C 2 and C 3 of the pentagonal ring are C 3 and C 2 of the hexagonal ring, respectively. C 4 of the heterocyclic pentagonal ring, composed of 1 O and 4 C atoms, is single bonded to C H 2 in the form of a line. C H 2 is single bonded to O of a triphosphate group. Each phosphate group has a central P atom single bonded to O on the lower right, single bonded to O on the lower left, partially double bonded to O above, and partially double bonded to O below. The single bond to O atoms is shared between two adjacent phosphate groups. The terminal phosphate group is partially double bonded to O on the lower left and carries a negative charge of 2 minus. The other two phosphate groups each carry a negative charge. Starting from the terminal phosphate group, the phosphate groups are labeled gamma, beta, and alpha.

The reversible reaction arrow is labeled protein kinase. The forward reaction arrow is longer than the backward reaction arrow.

The first product is phosphorylated protein, which has the following structure: A central C H 2 group is single bonded to O on the upper right and has an open single bond on the upper left. O is single bonded to P on the lower right. P is partially double bonded to O on the upper right, partially double bonded to O on the right, and partially double bonded to O below. The P O 3 group carries a negative charge of 2 minus.

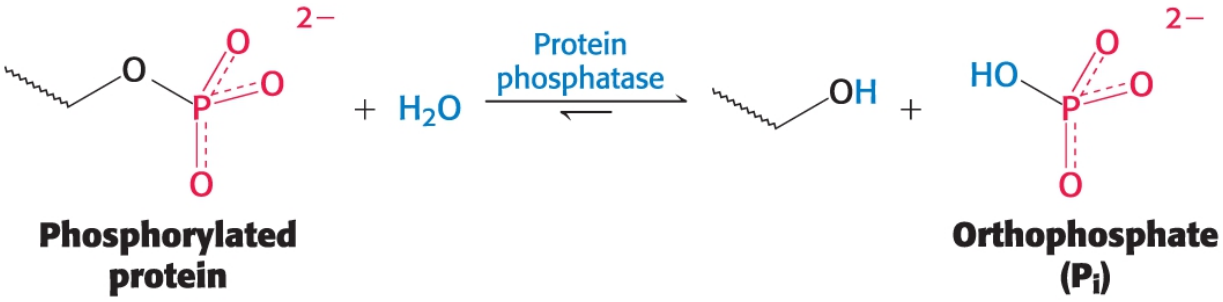
The second product is A D P, which has the following structure: A 5-membered heterocyclic pentagonal ring in a vertical orientation consists of 1 O and 4 C atoms. The O atom occupies the first position which is the topmost vertex. C 2 and C 3 are each single bonded to O

H below. C 1 is wedge bonded to the first N of a 5-membered heterocyclic pentagonal ring in a vertical orientation consisting of 2 N and 3 C atoms. The first N atom occupies the first position which is the bottom left vertex and the second N atom occupies the third position which is the topmost vertex. A double bond is present between the second N and C 1 and C 2 and C 3. This ring is fused to a heterocyclic hexagonal is a vertical orientation consisting of 2 N and 4 C atoms. The first N occupies the first position which is the top-right vertex and the second N occupies the third position which is the bottom-most vertex. A double bond is present between C 4 and the first N and C 1 and the second N. C 4 is single bonded to N H 2 above. The rings are fused such that C 2 and C 3 of the pentagonal ring are C 3 and C 2 of the hexagonal ring, respectively. C 4 of the heterocyclic pentagonal ring, composed of 1 O and 4 C atoms, is single bonded to C H 2 which is single bonded to O of a diphosphate group. Each phosphate group has a central P atom single bonded to O on the lower right, single bonded to O on the lower left, partially double bonded to O above, and partially double bonded to O below. The single bond to O atoms is shared between two adjacent phosphate groups. The terminal phosphate group carries a negative charge of 2 minus and the other phosphate group carries a negative charge.

The third product is H superscript plus ion.

Return to Chemical reaction of the phosphorylation of an amino acid residue catalyzed by a protein kinase enzyme is shown

Extended description for Chemical reaction of dephosphorylation of a phosphorylated protein catalyzed by a protein phosphatase enzyme



The reversible reaction consists of two reactants and two products.

The first reactant is phosphorylated protein, which has the following structure: A central C H 2 group is single bonded to O on the upper right and has an open single bond on the upper left. O is single bonded to P on the lower right. P is partially double bonded to O on the upper right, partially double bonded to O on the right, and partially double bonded to O below. The P O 3 group carries a negative charge of 2 minus.

The second reactant is H 2 O.

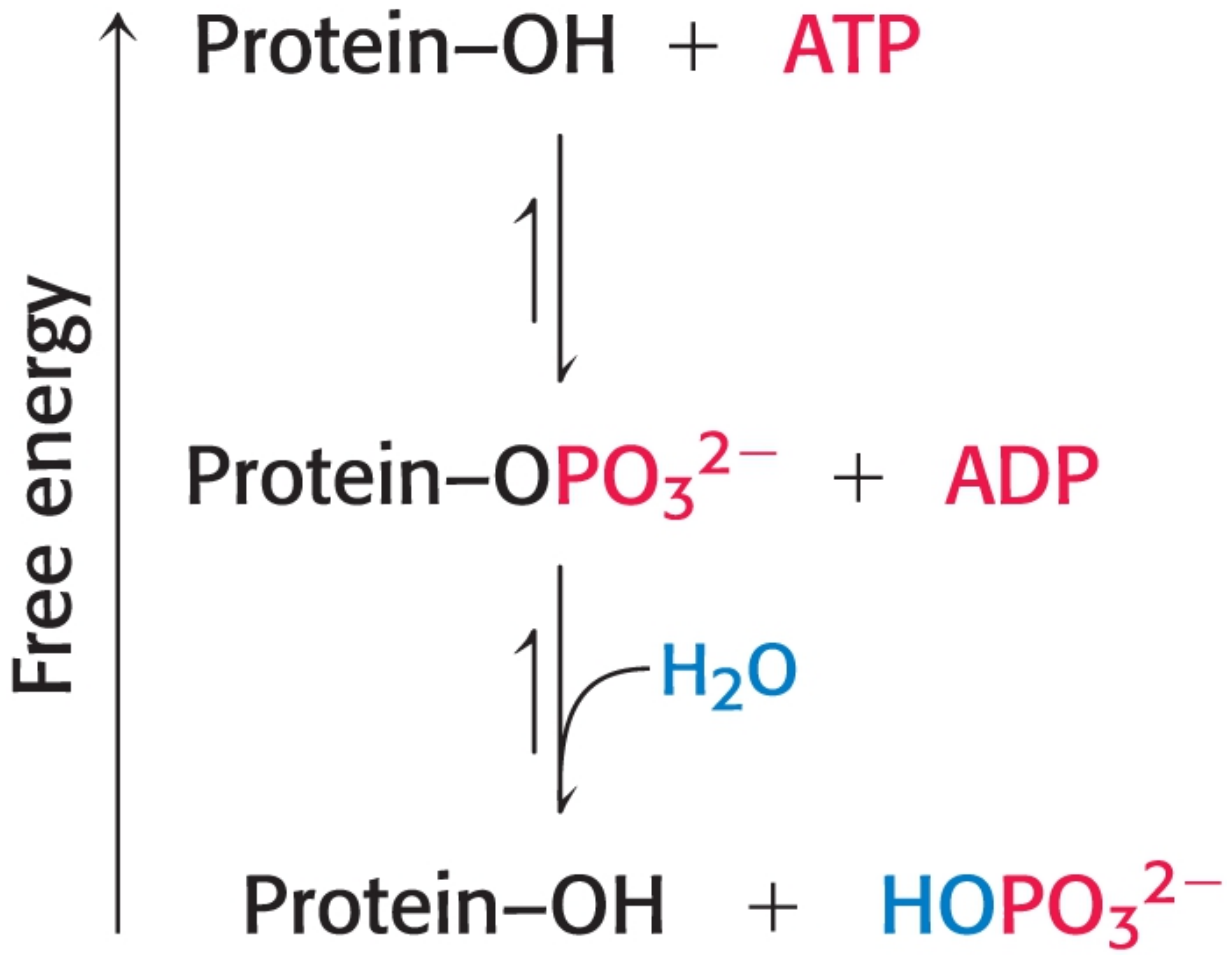
The reversible reaction arrow is labeled protein phosphatase. The forward reaction arrow is longer than the backward reaction arrow.

The first product has the following structure: A central C H 2 group is single bonded to O H on the upper right and has an open bond on the upper left.

The second product is orthophosphate (P subscript i), which has the following structure: A central P atom is single bonded to O H on the upper left, partially double bonded to O on the upper right, partially double bonded to O on the right, and partially double bonded to O below. The P O 3 group carries a negative charge of 2 minus.

Return to Chemical reaction of dephosphorylation of a phosphorylated protein catalyzed by a protein phosphatase enzyme

Extended description for Schematic illustration of the range of free energy between phosphorylated and dephosphorylated proteins



Two reversible reactions are shown. The first reaction shows the dephosphorylation of a protein. The products of this reaction are the reactants of the next dephosphorylation reaction.

The first reactant has the following structure: Protein, single bond, O H. The second reactant is A T P.

The forward reaction arrow is longer than the backward reaction arrow.

The first product has the following structure: Protein, single bond, O P O 3 superscript 2 minus. The second product is A D P. These products are the reactants of the next reaction.

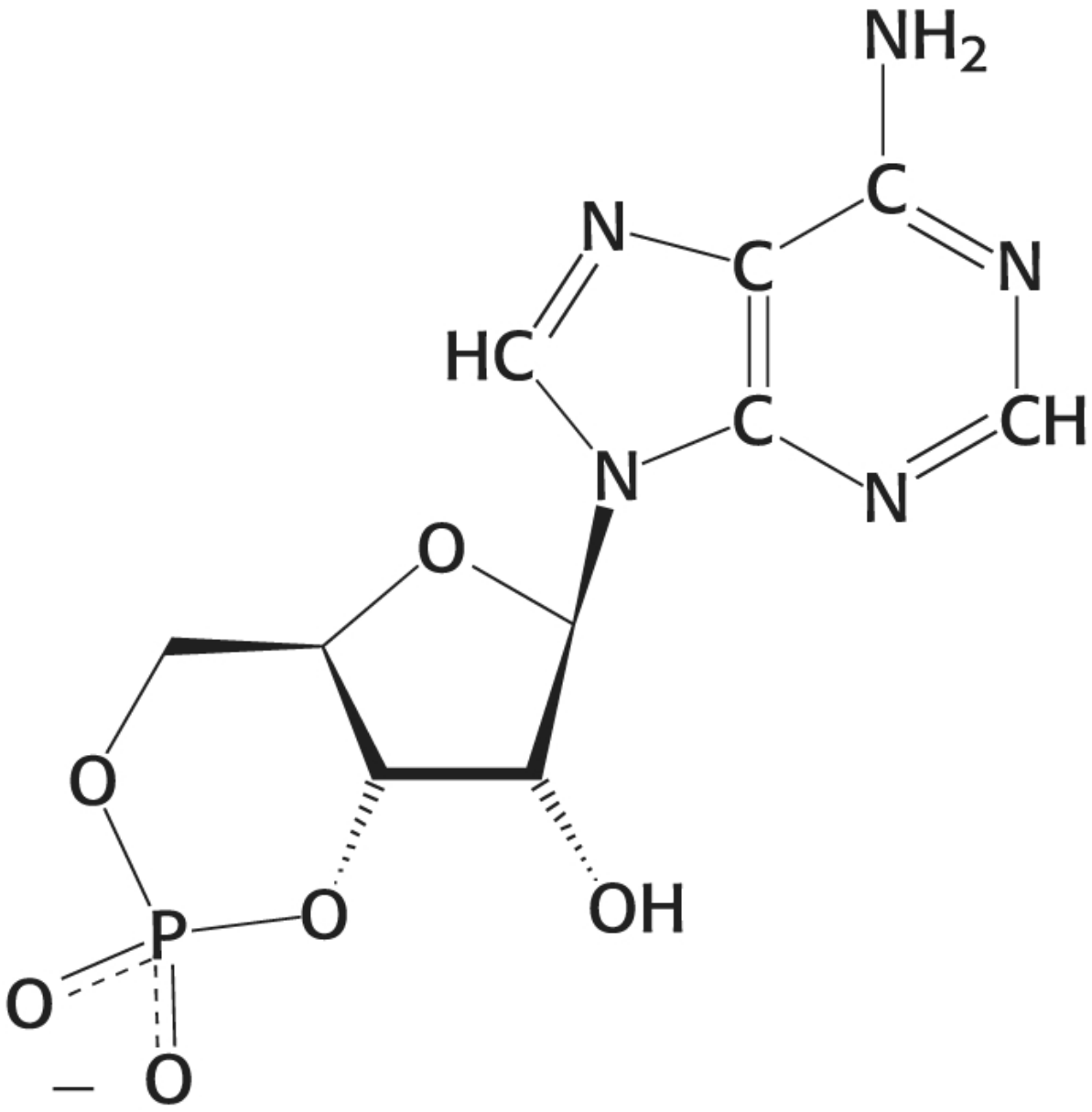
The forward reaction arrow is longer than the backward reaction arrow. H 2 O reacts with the phosphorylated protein.

The first product has the following structure: Protein, single bond, O H. The second product is H O P O 3 superscript 2 minus.

The free energy is shown to increase from the dephosphorylated protein at the bottom to the original protein at the top. The phosphorylated protein lies in the middle.

Return to Schematic illustration of the range of free energy between phosphorylated and dephosphorylated proteins

Extended description for Chemical structure of cyclic adenosine monophosphate

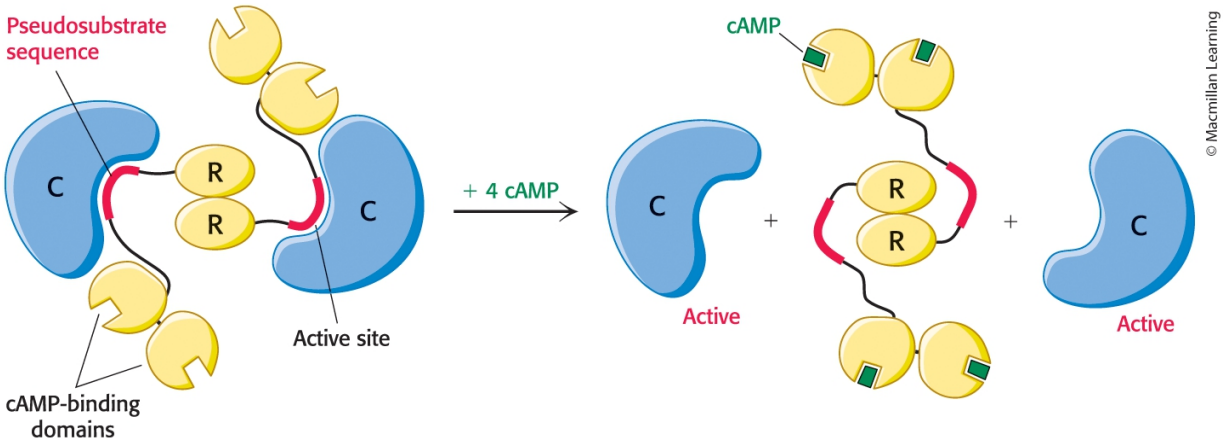


Cyclic adenosine monophosphate (cAMP)

A heterocyclic pentagonal ring in a vertical orientation consists of 1 O and 4 C atoms. The O atom occupies the first position which is the topmost vertex. C 2 is dash bonded to O H. C 3 is dash bonded to O and C 4 is wedge bonded to C H 2 which is single bonded to O on the lower left. These two O atoms are single bonded to a central P atom on the lower left. This P atom is partially double bonded to O on the lower left and partially double bonded to O below. The P O 2 group carries a negative charge. C 1 of the pentagonal ring is wedge bonded to the first N of a heterocyclic pentagonal ring in a horizontal orientation consisting of 2 N and 3 C atoms. The first N occupies the first position which is the bottom left vertex, the second N occupies the third position which is the top-left vertex, and C atoms occupy the remaining positions. C 1 is bound to H and is double bonded to the second N. This pentagonal ring is fused to a 6-membered heterocyclic ring in a vertical orientation which consists of 2 N and 4 C atoms. The first N atom occupies the first position which is the top-right vertex, the second N atom occupies the third position which is the bottom-most vertex, and C atoms occupy the remaining positions. C 1 is bound to H and C 4 is single bonded to N H 2. Alternating double bonds are present between C 1 and the second N, C 2 and C 3, and C 4 and the first N. The ring are fused such that C 2 and C 3 of the pentagonal ring are C 3 and C 2 of the hexagonal ring, respectively.

Return to Chemical structure of cyclic adenosine monophosphate

Extended description for A schematic illustration of the binding of c A M P to the regulatory subunits of P K A



The holoenzyme is shown to have the following structure: Two kidney-shaped catalytic subunits labeled C are shown to face each other. Two ovoid regulatory subunits, labeled R, are placed one on top of the other and are present in the space between the two catalytic subunits. The top regulatory unit is connected by a chain to a pair of spherical structures with clefts. These clefts are labeled c A M P binding domains. A short region in the chain near the groove of the catalytic subunit is shown in red and labeled pseudosubstrate sequence. Another such chain is bound to the bottom regulatory subunit with the c A M P binding domains facing down.

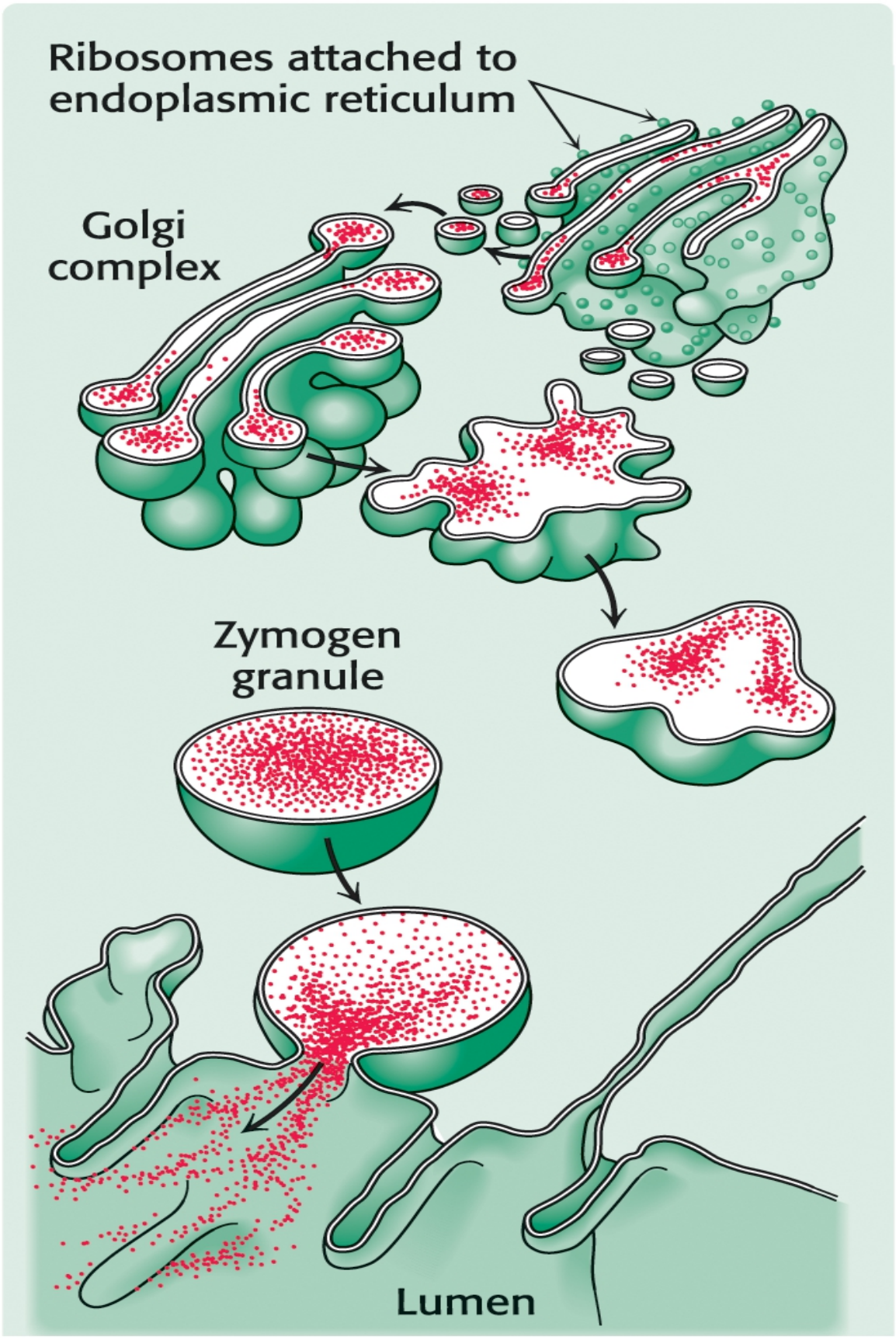
An arrow labeled plus 4 c A M P points from the holoenzyme to the activated enzyme.

In the activated enzyme, the c A M P molecules are shown to bind to the c A M P binding domains of the regulatory subunits. The kidney-shaped catalytic subunits are shown to separate from the regulatory subunits and become activated.

Return to A schematic illustration of the binding of c A M P to the regulatory subunits of P K A

Extended description for Schematic illustration of the

secretion of zymogens by acinar cells of the pancreas

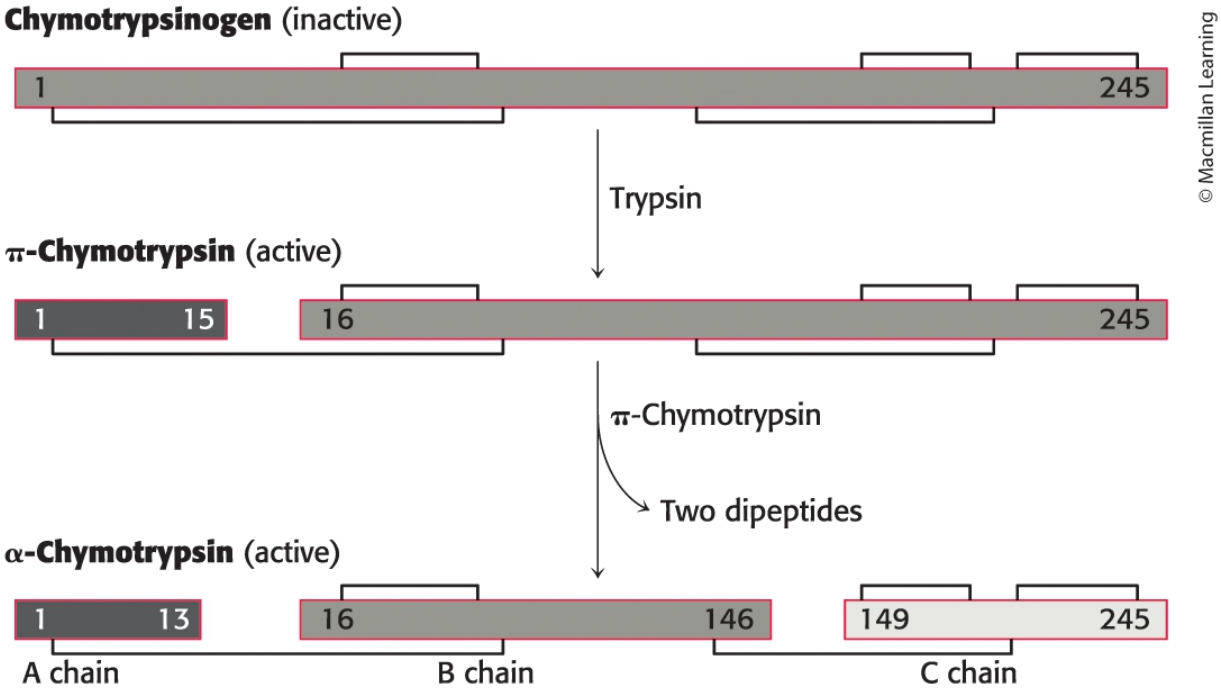


© Macmillan Learning

The following steps are shown to take place in the cytoplasm of the acinar cells: The endoplasmic reticulum is shown as folded membranous structures with granules on their surface which are ribosomes. Cup-shaped vesicles filled with zymogen are shown to bud from the endoplasmic reticulum and fuse with the stacked flattened pouch-shaped Golgi complex. Irregular-shaped structures packed with zymogen are shown to exit the Golgi apparatus and gradually become large cup-shaped zymogen granules. These zymogen granules are shown to fuse with the folded plasma membrane of the cell and secrete their contents into the lumen outside the cell.

Return to Schematic illustration of the secretion of zymogens by acinar cells of the pancreas

Extended description for Schematic illustration of the activation of chymotrypsinogen by proteolysis



© Macmillan Learning

Chymotrypsinogen (inactive): It is shown as a long ribbon made up of 245 amino acids. Five intrachain disulfide bonds are shown, two in the left half and three in the right half.

Trypsin cleaves the chymotrypsinogen to give pi-Chymotrypsin.

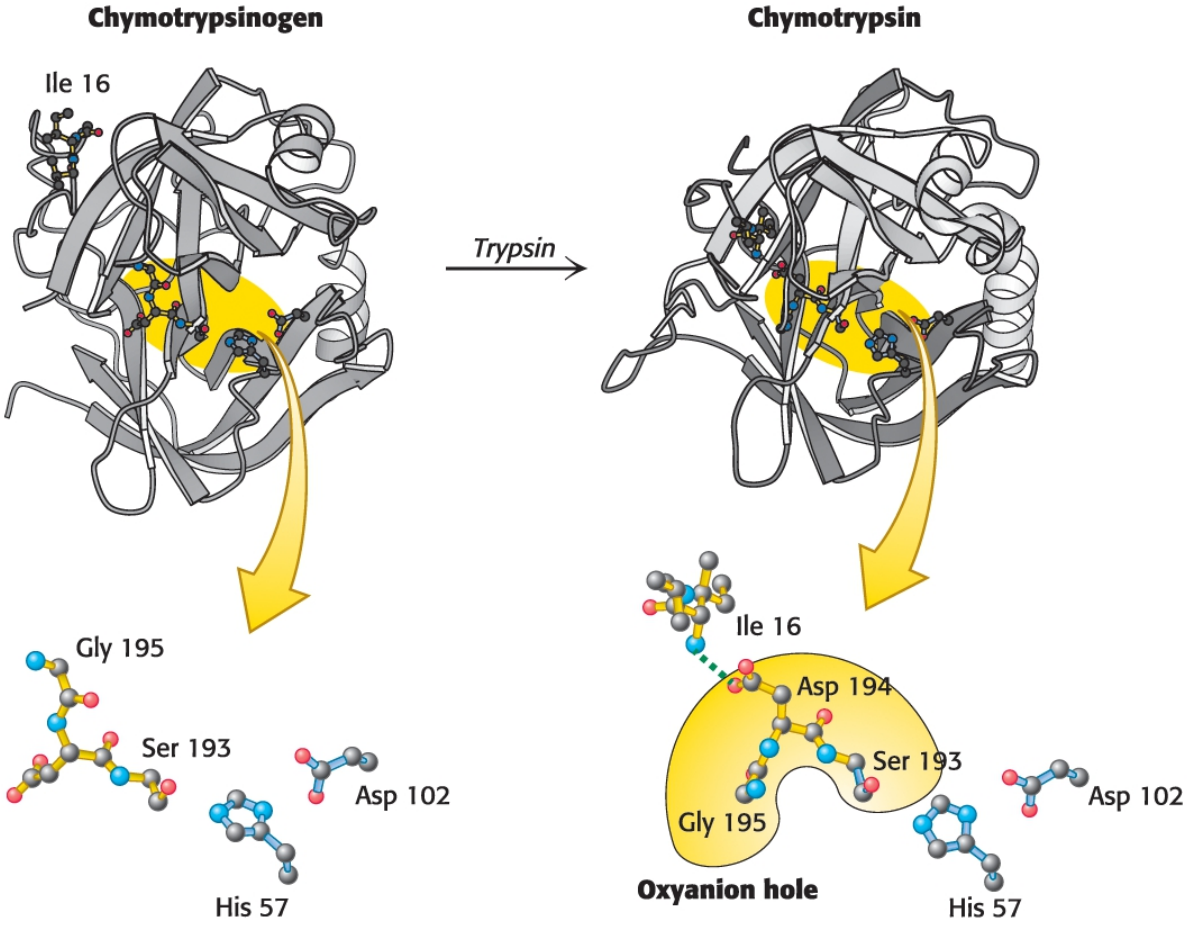
pi-Chymotrypsin (active): This is created by cleavage of the peptide bond joining the amino acids at positions 15 and 16. An interchain disulfide bond is shown to link the two peptide chains. Four intrachain disulfide bonds are shown in the longer peptide chain.

pi-Chymotrypsin cleaves another pi-Chymotrypsin to give an alpha-Chymotrypsin and two dipeptides are released in the process.

Alpha-Chymotrypsin (active): This is created by cleavage of the peptide bonds in bond the short and long peptide chains of pi-Chymotrypsin. The following three chains are formed: A chain consisting of amino acids 1 to 13, B chain consisting of amino acids 16 to 146, and C chain consisting of amino acids 149 to 245. An interchain disulfide bond is present between chain A and chain B, and chain B and chain C, respectively. One intrachain disulfide bond is present in chain B and two intrachain disulfide bonds are present in chain C.

Return to Schematic illustration of the activation of chymotrypsinogen by proteolysis

Extended description for Schematic illustration of the conversion of chymotrypsinogen into chymotrypsin



© Macmillan Learning

The ribbon structures of the enzymes are shown.

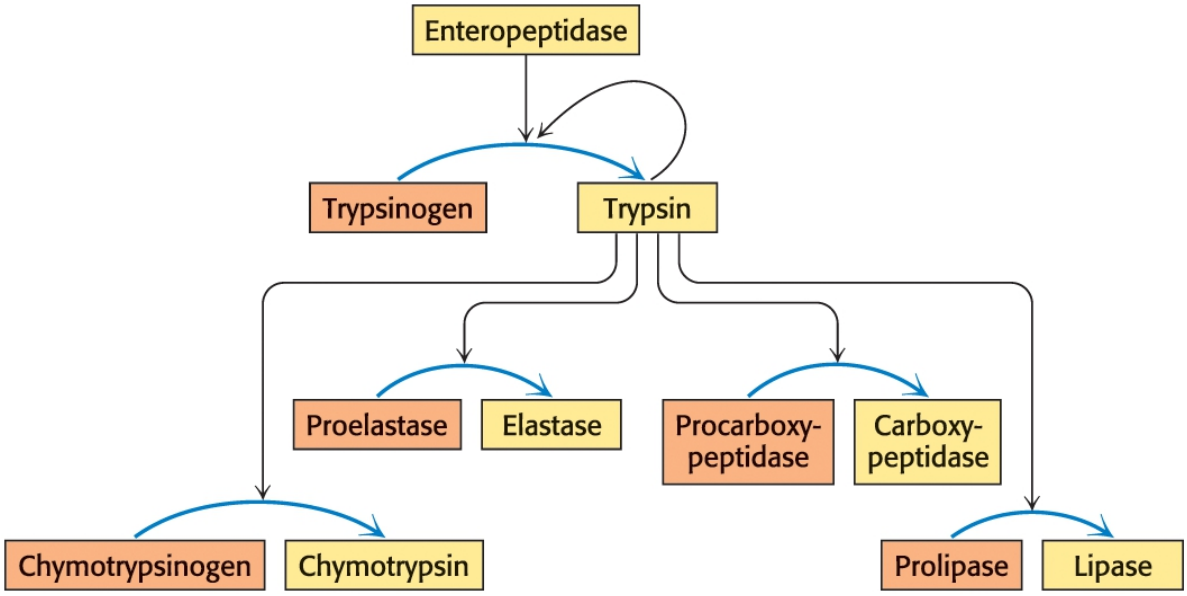
Chymotrypsinogen is shown to have a globular structure made up of several beta-strands and a few alpha helices connected by short loops. Isoleucine 16 residue is shown to be positioned away from the central active site. A magnified view of the amino acid residues at the catalytic site shows Glycine 195 and Serine 193 residues together at the top left, Histidine 57 below, and Aspartate 102 on the right.

Trypsin is shown to act on chymotrypsinogen to produce chymotrypsin.

Chymotrypsin is shown to have a more compact globular structure compared to chymotrypsinogen. A magnified view of the catalytic site shows the inverted U-shaped oxyanion hole comprising Glycine 195, Aspartate 194, and Serine 193 residues. The Isoleucine 16 residue is present on the top left of the oxyanion hole. Histidine 57 is present to the lower right and Aspartate 102 is present to the right of the oxyanion hole.

Return to Schematic illustration of the conversion of chymotrypsinogen into chymotrypsin

Extended description for A flow chart of the cascade of activation of zymogens initiated by the activation of trypsin



© Macmillan Learning

Enteropeptidase (yellow) is shown to aid the conversion of trypsinogen (orange) to trypsin (yellow).

Trypsin is shown to aid in the following conversions:

Trypsinogen to trypsin

Chymotrypsinogen (orange) to chymotrypsin (yellow)

Proelastase (orange) to elastase (yellow)

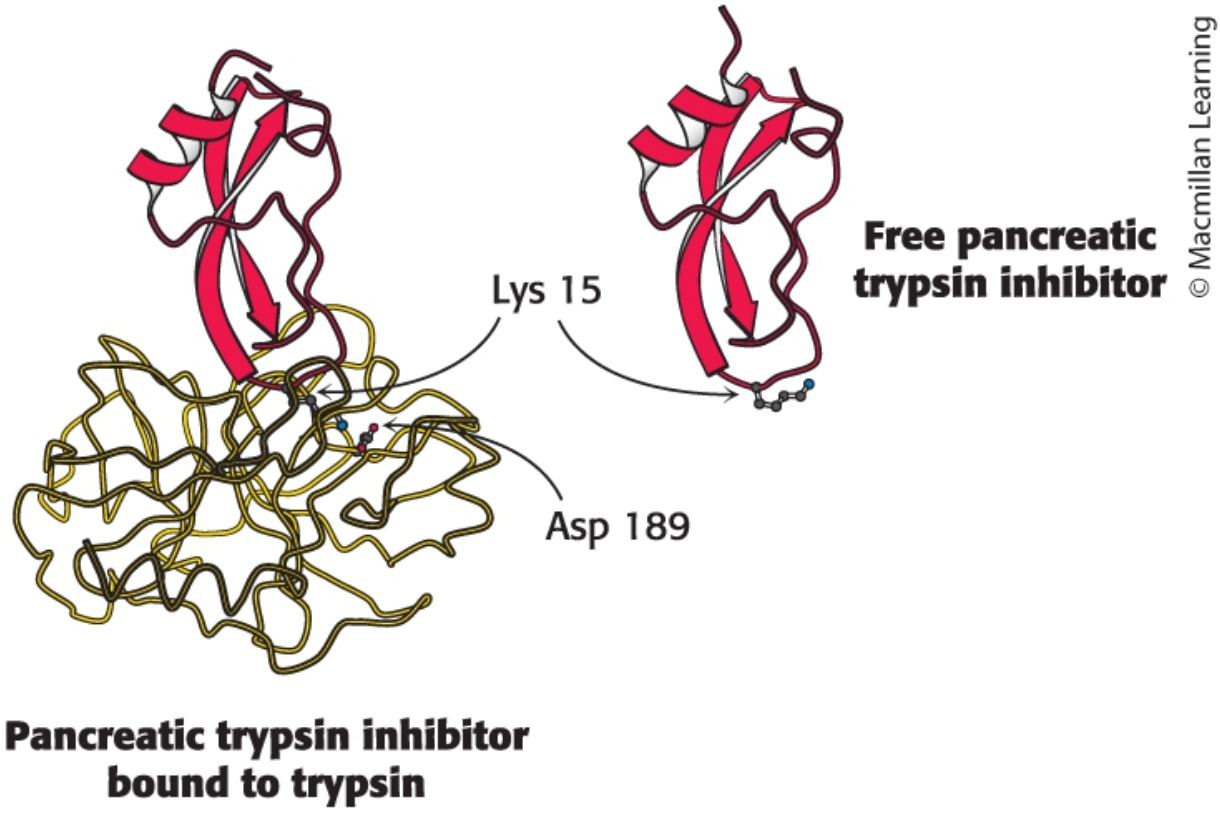
Procarboxypeptidase (orange) to carboxypeptidase (yellow)

Prolipase (orange) to lipase (yellow)

Active enzymes are shown in yellow and zymogens are shown in orange.

Return to A flow chart of the cascade of activation of zymogens initiated by the activation of trypsin

Extended description for The ribbon structures of free pancreatic trypsin inhibitor and the pancreatic trypsin inhibitor bound to trypsin

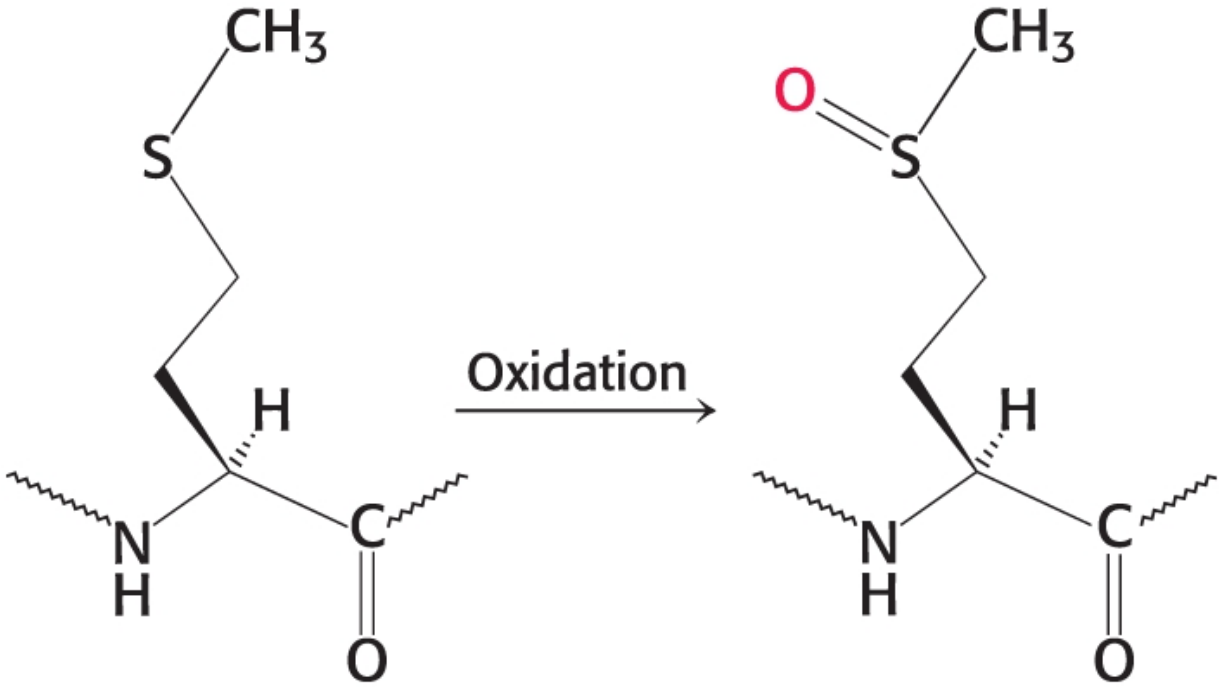


Free pancreatic trypsin inhibitor: It is shown to consist of two antiparallel beta strands and an alpha helix connected by short loops. A lysine 15 residue is present at the bottom.

Pancreatic trypsin inhibitor bound to trypsin: The pancreatic trypsin inhibitor is connected to trypsin below which is shown to be a globular structure made up of intertwined peptide chains. The lysine 15 residue of the pancreatic trypsin inhibitor is shown to protrude into the catalytic site of trypsin. Lysine 15 forms an ionic bond with aspartate 189 of trypsin.

Return to The ribbon structures of free pancreatic trypsin inhibitor and the pancreatic trypsin inhibitor bound to trypsin

Extended description for Chemical reaction of the oxidation of methionine to methionine sulphoxide



The reaction consists of one reactant and one product.

The reactant has the following structure: A central C atom is dash bonded to H on the upper right, single bonded to C on the lower right, single bonded to N H on the lower left, and wedge bonded to C 1 of a heteronuclear alkane chain on the upper left. The C on the lower right is double bonded to O below and has an open single bond on the upper right. The N H on the lower left has an open single bond on the upper left. The heteronuclear alkane chain is depicted as a line structure using two zigzag lines and consists of 1 S and 2 C atoms. The S atom occupies the third position and is single bonded to C H 3 on the upper right.

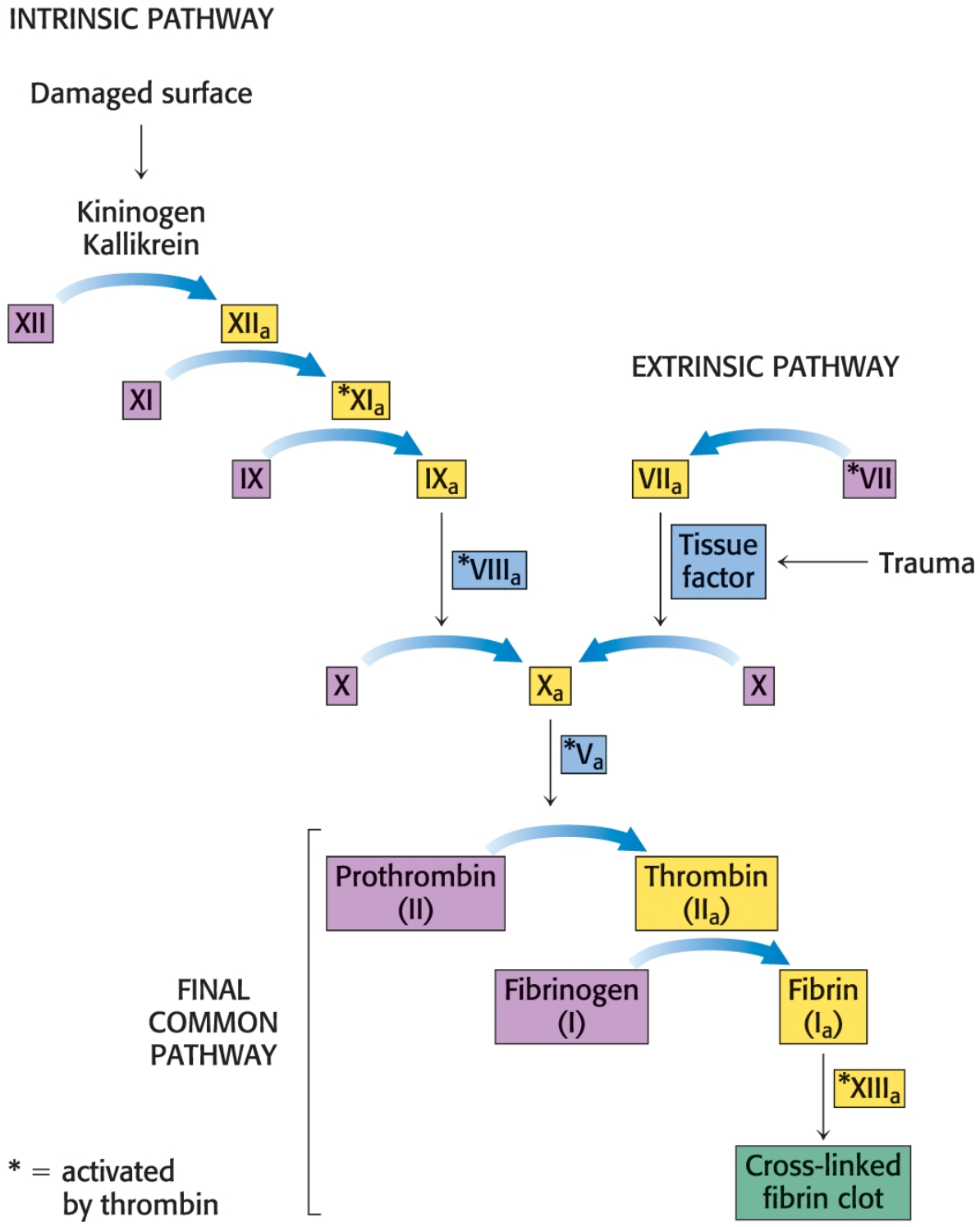
The forward reaction arrow is labeled oxidation.

The product has the following structure: A central C atom is dash bonded to H on the upper right, single bonded to C on the lower right, single bonded to N H on the lower left, and wedge bonded to C 1 of a heteronuclear alkane chain on the upper left. The C on the lower right is double bonded to O below and has an open single bond on the upper right. The N H on the lower left has an open single bond on the upper left. The heteronuclear alkane chain is depicted as a line structure using two zigzag lines and consists of 1 S and 2 C atoms. The S atom occupies the third position and is double bonded to O on the upper left and single bonded to C H 3 on the upper right.

Return to Chemical reaction of the oxidation of methionine to methionine sulphoxide

Extended description for Schematic illustration of an

enzymatic cascade leading to the clotting of blood



Two pathways are shown as follows:

Intrinsic pathway:

Damaged surface leads to Kininogen Kallikrein catalyzing the conversion of Factor 12 (purple) to Factor 12 subscript a (yellow).

Factor 12 subscript a catalyzes the conversion of Factor 11 (purple) to asterisk Factor 11 subscript a (yellow).

Asterisk factor 11 subscript a catalyzes the conversion of Factor 9 (purple) to Factor 9 subscript a (yellow).

Factor 9 subscript a forms a complex with asterisk Factor 8 subscript a (blue). This complex catalyzes the conversion of Factor 10 (purple) to factor 10 subscript a.

Extrinsic pathway:

Asterisk Factor 7 (purple) is converted to Factor 7 subscript a (yellow).

Trauma leads to the release of tissue factor (blue) which forms a complex with Factor 7 subscript a. This complex catalyzes the conversion of Factor 10 (purple) to factor 10 subscript a (yellow).

Factor 10 subscript a forms a complex with asterisk Factor 5 subscript a (blue). This complex catalyzes the conversion of Prothrombin 2 (purple) to Thrombin roman number 2 subscript a (yellow) and initiates the final common pathway.

Thrombin 2 subscript a catalyzes the conversion of Fibrinogen 1 (purple) to Fibrin 1 subscript a (yellow). Fibrin 1 subscript a forms a complex with asterisk Factor 13 subscript a (yellow). This complex leads to the formation of the cross-linked fibrin clot.

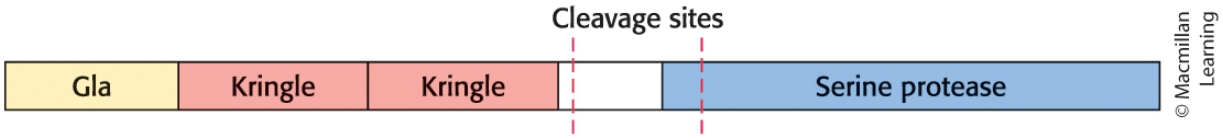
Inactive forms of clotting factors are shown in purple and their activated counterparts are shown in yellow.

Stimulatory proteins that are not themselves enzymes are shown in blue. All the numbers are given as roman numbers.

Note: Asterisk denotes activated by thrombin.

Return to Schematic illustration of an enzymatic cascade leading to the clotting of blood

Extended description for Schematic illustration of the protein domains of prothrombin

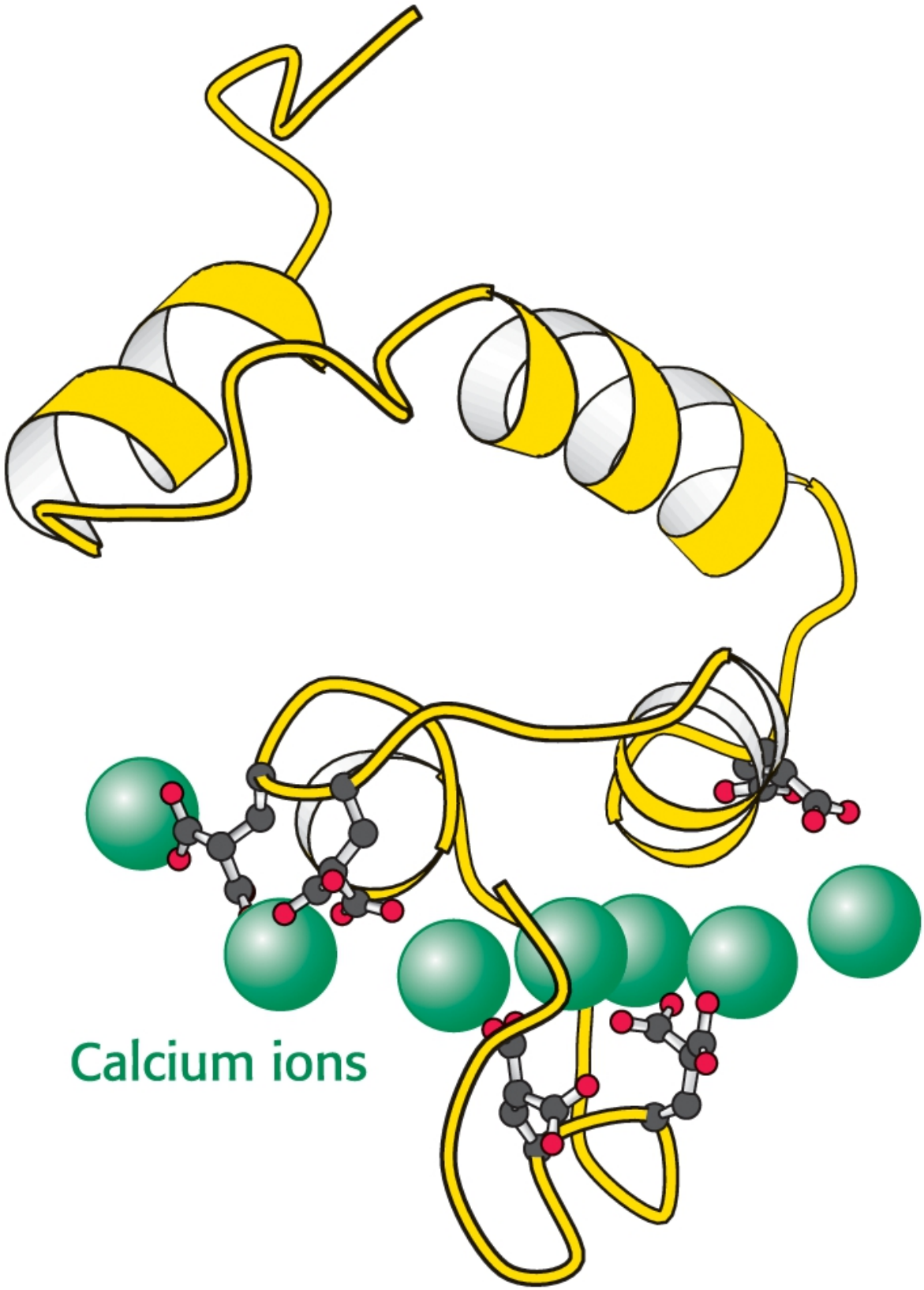


The following protein domains are shown from left to right: G l a, Kringle, Kringle, Serine protease. An unlabeled domain is present between second Kringle and serine protease. Cleavage sites are indicated toward the left end of the unlabeled domain and the left end of the serine protease domain. The serine protease domain is the longest domain.

Return to Schematic illustration of the protein domains of prothrombin

Extended description for Schematic illustration of the binding of calcium ions to the g l a domain of

prothrombin

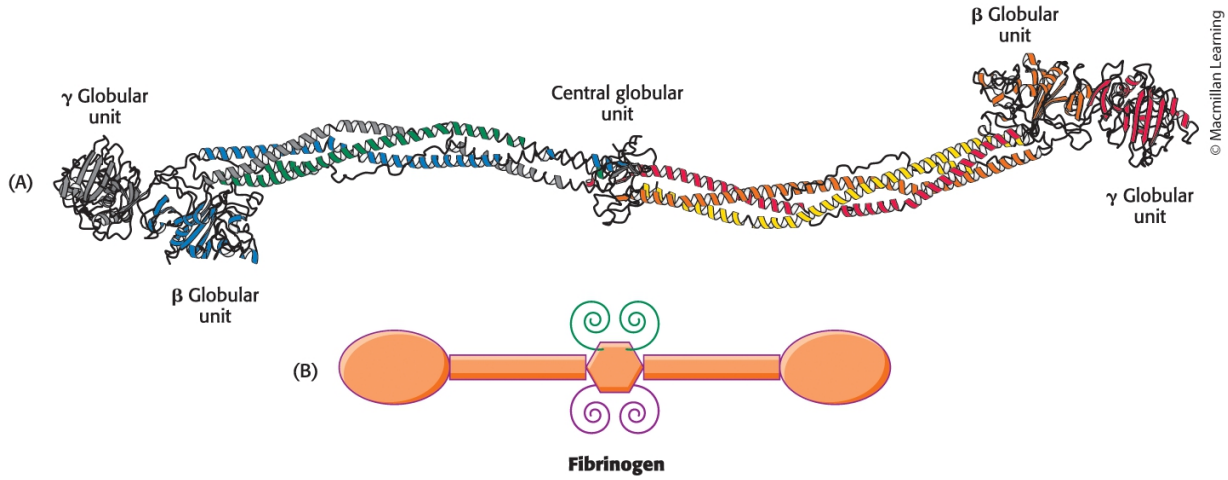


© Macmillan Learning

The ribbon structure of the protein is shown to have three alpha helices connected by short loops. The bottom terminus has a long peptide chain consisting of gamma-carboxyglutamate residues, shown in red. Several spherical calcium ions are shown to bind to these gamma-carboxyglutamate residues.

Return to Schematic illustration of the binding of calcium ions to the g l a domain of prothrombin

Extended description for Schematic illustration of the structure of fibrinogen

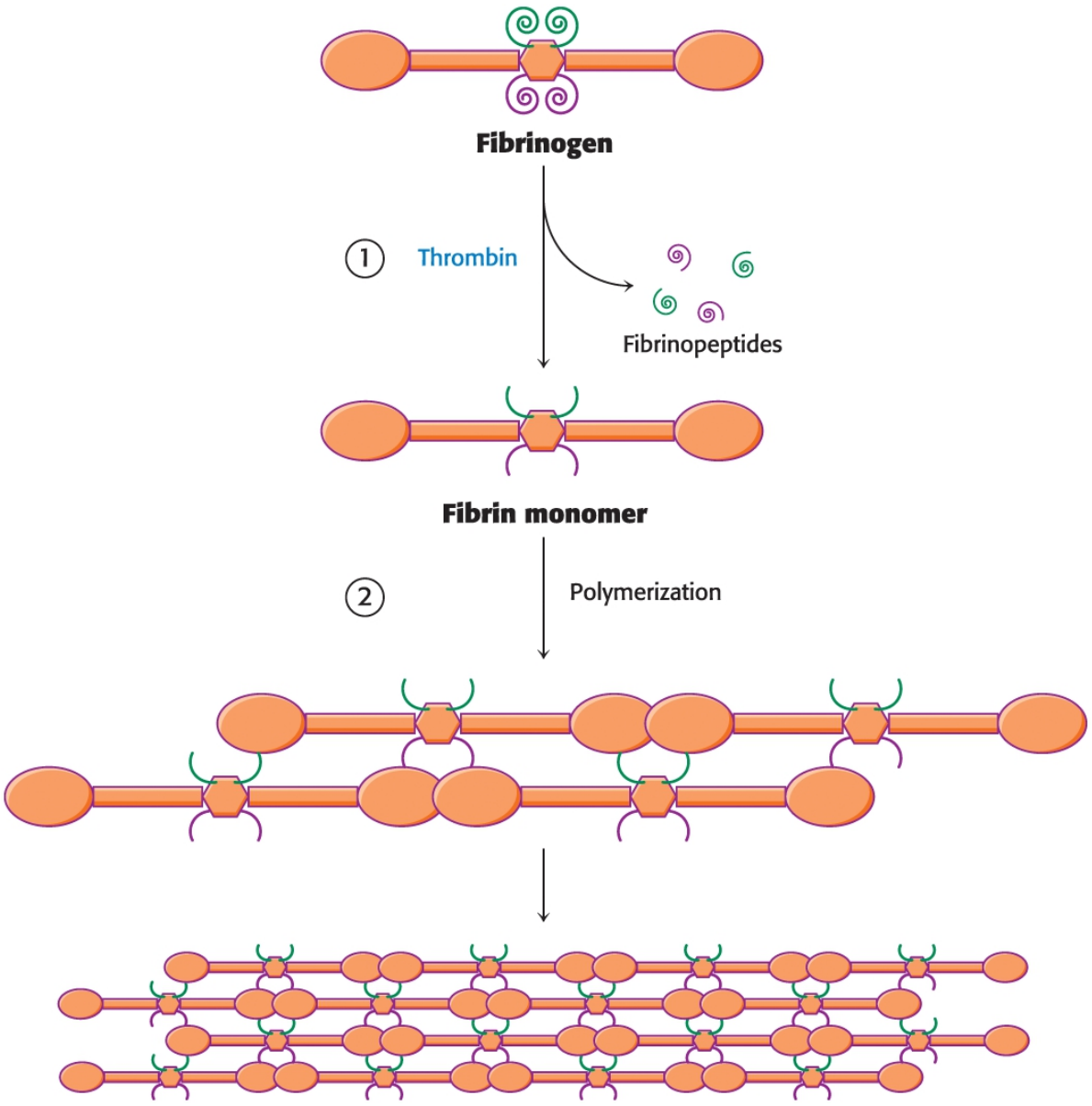


Part (A): The ribbon structure of fibrinogen consists of two long rod-shaped regions made up of alpha-helical coiled-coil structures. The two rods are connected in the middle by central globular units. The terminals of each rod consist of two globular units labeled gamma and beta globular units. The relative position of the identical terminal globular units is trans.

Part (B): A central hexagon is connected to two oval structures on the left and right by long rods, respectively. A pair of green comma-shaped fibrinopeptides facing each other are present at the top of the hexagonal unit. Similarly, a pair of red fibrinopeptides are present at the bottom of the hexagonal unit.

Return to Schematic illustration of the structure of fibrinogen

Extended description for Schematic illustration of the cleavage of fibrinogen by thrombin to initiate fibrin clot formation



© Macmillan Learning

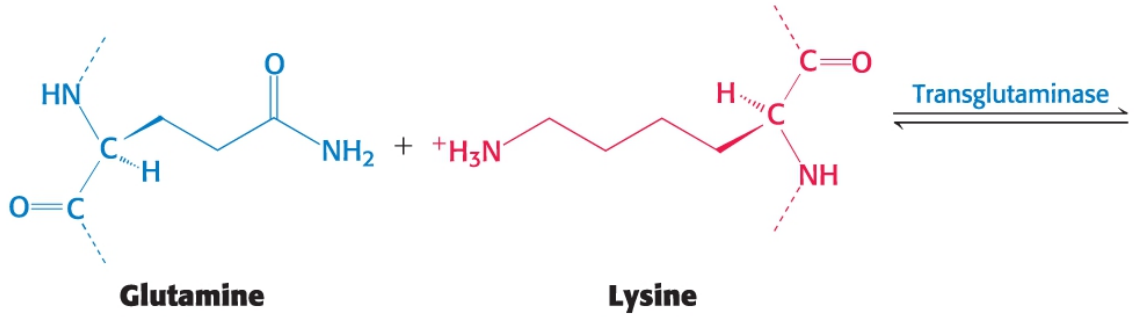
Step 1: A fibrinogen unit is shown. A central hexagon is connected to two oval structures on the left and right by long rods, respectively. A pair of green comma-shaped fibrinopeptides facing each other are

present at the top of the hexagonal unit. Similarly, a pair of red fibrinopeptides are present at the bottom of the hexagonal unit. Thrombin is shown to remove the comma-shaped heads of the fibrinopeptides leaving behind short bent arms. This unit is labeled fibrin monomer.

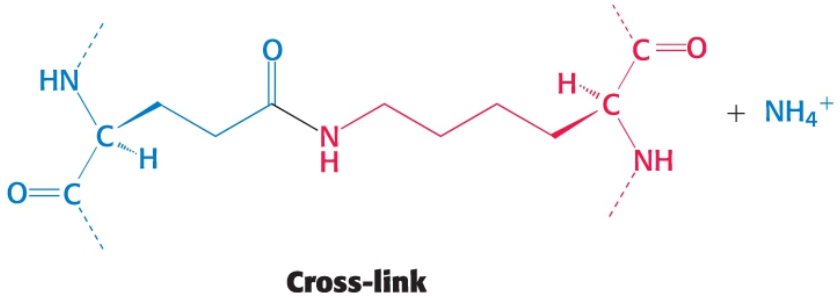
Step 2: Several fibrin monomers are shown to polymerize. The adjacent oval structures of two monomers are shown to overlap. The short bent arms of one monomer are shown to attach to the overlapping oval structures of fibrin chains below. This is shown to grow in size to form an extended mesh.

Return to Schematic illustration of the cleavage of fibrinogen by thrombin to initiate fibrin clot formation

Extended description for Cross-linking reaction between glutamine and lysine residue



Glutamine **Lysine**



Cross-link

The reaction consists of two reactants and two products.

The first reactant is glutamine, which has the following structure: A central C atom is single bonded to N H on the upper left, single bonded to C on the lower left, dash bonded to H on the lower right, and wedge bonded to C 1 of a 3-carbon alkane chain on the upper right. N H has an open single bond on the upper right. C on the lower left is double bonded to O on the left and has an open single bond on the lower right. The alkane chain is depicted as a line structure using 2 zigzag lines. C 3 of the alkane chain is double bonded to O above and single bonded to N H 2 on the lower right.

The second reactant is lysine, which has the following structure: A central C atom is single bonded to N H on the lower right, single

bonded to C on the upper right, dash bonded to H on the upper left, and wedge bonded to C 1 of a 4-carbon alkane chain on the lower left. N H has an open single bond on the lower left. C on the upper right is double bonded to O on the right and has an open single bond on the upper left. The alkane chain is depicted as a line structure using 3 zigzag lines. C 4 of the alkane chain is single bonded to N H 3 superscript plus on the lower left.

The reversible reaction arrow is labeled transglutaminase.

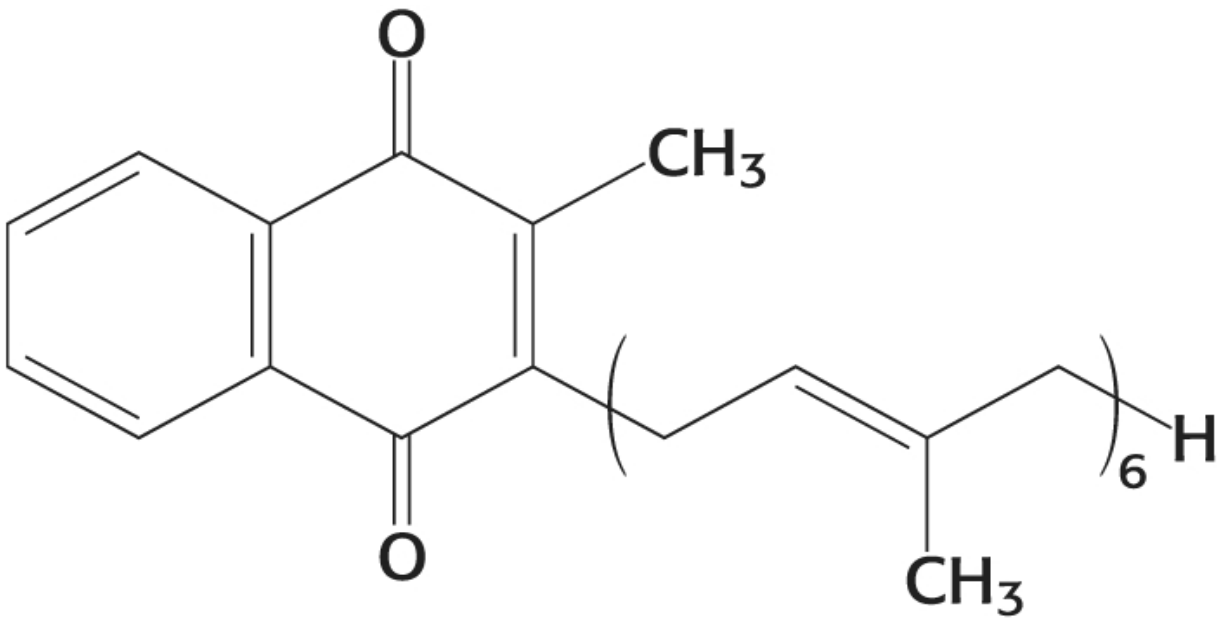
The first product is labeled cross-link and has the following structure: A central C atom is single bonded to N H on the upper left, single bonded to C on the lower left, dash bonded to H on the lower right, and wedge bonded to C 1 of an 8-membered heteronuclear alkane chain on the upper right. N H has an open single bond on the upper right. C on the lower left is double bonded to O on the left and has an open single bond on the lower right. The heteronuclear alkane chain is depicted as a line structure using 7 zigzag lines and consists of 1 N and 7 C atoms. The N atom occupies the fourth position and is bound to H. C 3 of the alkane chain is double bonded to O above. C 7 is wedge bonded to a central C atom on the upper right. The central C atom is single bonded to N H on the lower right, single bonded to C on the upper right, and dash bonded to H on the upper left. N H has an open single bond on the lower left. C on the upper right is double bonded to O on the right and has an open single bond on the upper left.

The second product is N H 4 superscript plus.

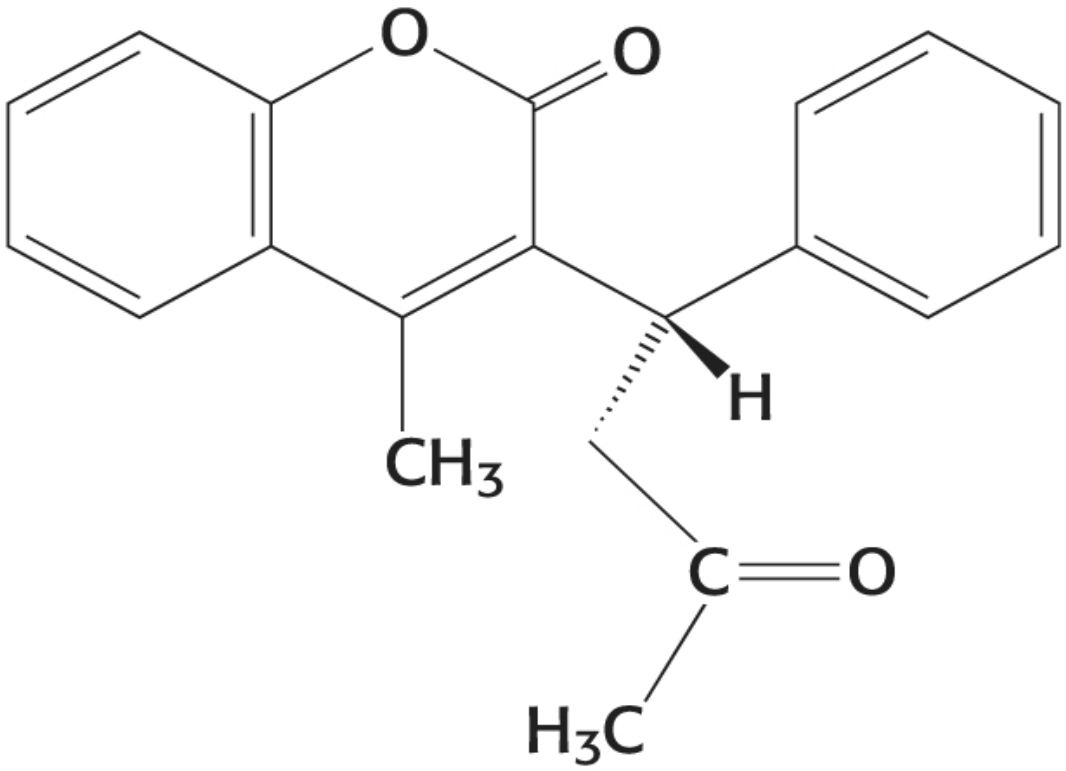
Return to Cross-linking reaction between glutamine and lysine residue

Extended description for Chemical structure of vitamin

K and warfarin



Vitamin K



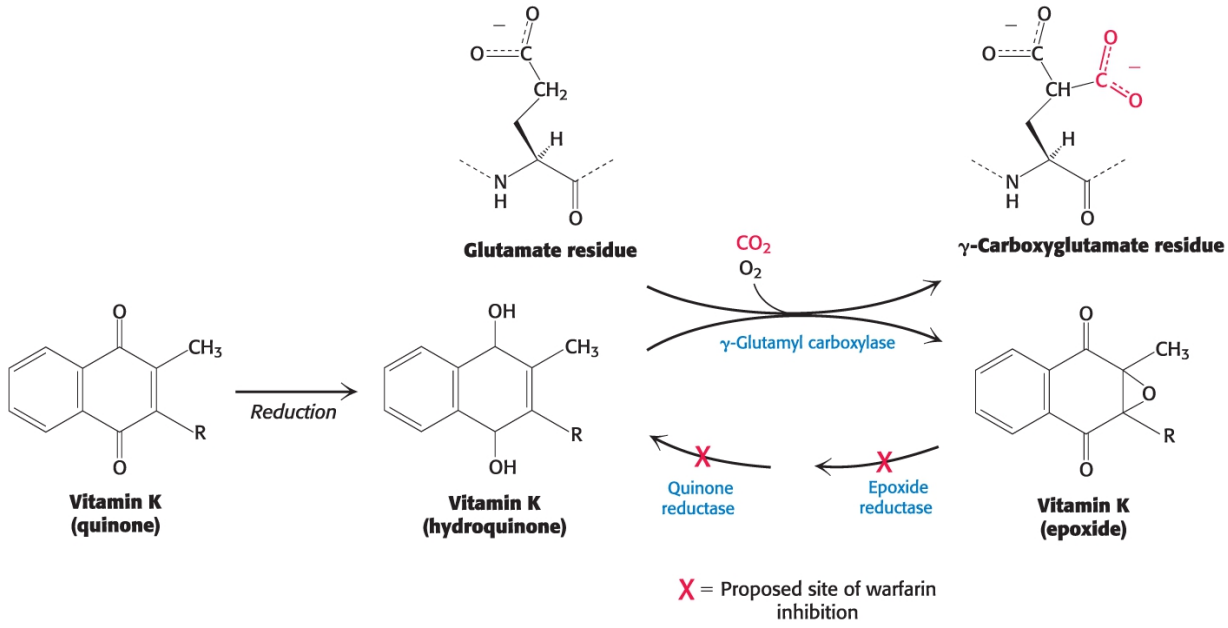
Warfarin

Vitamin K has the following structure: A benzene ring in a vertical orientation consists of alternating double bonds between C 2 and C 3, C 4 and C 5, and C 6 and C 1. The benzene ring is fused to a 6-carbon hexagonal ring in a vertical orientation. C 2 is double bonded to C 3. C 1 is double bonded to O above. C 2 is single bonded to C H 3 on the upper right. C 3 is single bonded to C 1 of a polymeric chain consisting of 6 monomeric units. C 4 is double bonded to O below. The two rings are fused such that C 2 and C 3 of the benzene ring are C 6 and C 5 of the hexagonal ring, respectively. The monomeric unit is a 4-carbon alkene chain depicted as a line structure using 3 zigzag lines. A double bond is present between C 2 and C 3. C 3 is single bonded to C H 3 below. C 4 of the terminal monomer is single bonded to H on the lower right.

Warfarin has the following structure: A benzene ring in a vertical orientation consists of alternating double bonds between C 2 and C 3, C 4 and C 5, and C 6 and C 1. The benzene ring is fused to a 6-membered heterocyclic hexagonal ring in a vertical orientation. The ring consists of 1 O and 5 C atoms. The O atom occupies the first position, which is the topmost vertex. C 2 is double bonded to C 3. C 1 is double bonded to O on the upper right. C 2 is single bonded to a central C atom. C 3 is single bonded to C H 3 below. The two rings are fused such that C 2 and C 3 of the benzene ring are C 5 and C 4 of the hexagonal ring, respectively. The central C atom is single bonded to C 5 a benzene ring in a vertical orientation on the upper right. The ring consists of alternating double bonds between C 2 and C 3, C 4 and C 5, and C 6 and C 1. The central C atom is wedge bonded to H on the lower right and dash bonded to C H 2 on the lower left. C H 2 is single bonded to C on the lower right. This C atom is double bonded to O on the right and single bonded to C H 3 on the lower left.

Return to Chemical structure of vitamin K and warfarin

Extended description for Chemical reactions showing the synthesis of gamma-carboxyglutamate



Reduction of vitamin K (quinone) to vitamin K (hydroquinone):

The reactant vitamin K (quinone) has the following structure: A benzene ring in a vertical orientation consists of three alternating double bonds between C 2 and C 3, C 4 and C 5, and C 6 and C 1. The benzene ring is fused to a 6-carbon hexagonal ring in a vertical orientation. C 2 is double bonded to C 3. C 1 is double bonded to O. C 2 is single bonded to C H 3. C 3 is single bonded to R. C 4 is double bonded to O. The two rings are fused such that C 2 and C 3 of the benzene ring are C 6 and C 5 of the hexagonal ring, respectively.

The product is vitamin K (hydroquinone), which has the following structure: A benzene ring in a vertical orientation consists of three alternating double bonds between C 2 and C 3, C 4 and C 5, and C 6 and C 1. The benzene ring is fused to a 6-carbon hexagonal ring in a

vertical orientation. C 2 is double bonded to C 3. C 1 is single bonded to O H. C 2 is single bonded to C H 3. C 3 is single bonded to R. C 4 is single bonded to O H. The two rings are fused such that C 2 and C 3 of the benzene ring are C 6 and C 5 of the hexagonal ring, respectively.

Conversion of vitamin K (hydroquinone) to vitamin K (epoxide):

The reaction arrow is labeled gamma-glutamyl carboxylase.

Vitamin K (epoxide) has the following structure: A benzene ring in a vertical orientation consists of three alternating double bonds between C 2 and C 3, C 4 and C 5, and C 6 and C 1. The benzene ring is fused to a 6-carbon hexagonal ring in a vertical orientation. C 1 is double bonded to O. C 2 is single bonded to C H 3 on the upper right and single bonded to O on the lower right. C 3 is single bonded to R on the lower right and single bonded on the upper right to the same O atom which is single bonded to C 2. C 4 is double bonded to O below. The two rings are fused such that C 2 and C 3 of the benzene ring are C 6 and C 5 of the hexagonal ring, respectively.

The conversion of glutamate residue to gamma-carboxyglutamate residue takes place simultaneously and C O 2 and O 2 are consumed.

The structure of glutamate residue is as follows: A central C atom is dash bonded to H on the upper right, single bonded to C on the lower right, single bonded to N H on the lower left, and wedge bonded to C H 2 on the upper left. The C on the lower right is double bonded to O below and has an open bond on the upper right. The N H group on the lower left has an open bond on the upper left. C H 2 on the upper left is single bonded to C H 2 on the upper right which is single bonded to C on the upper left. This C is partially double

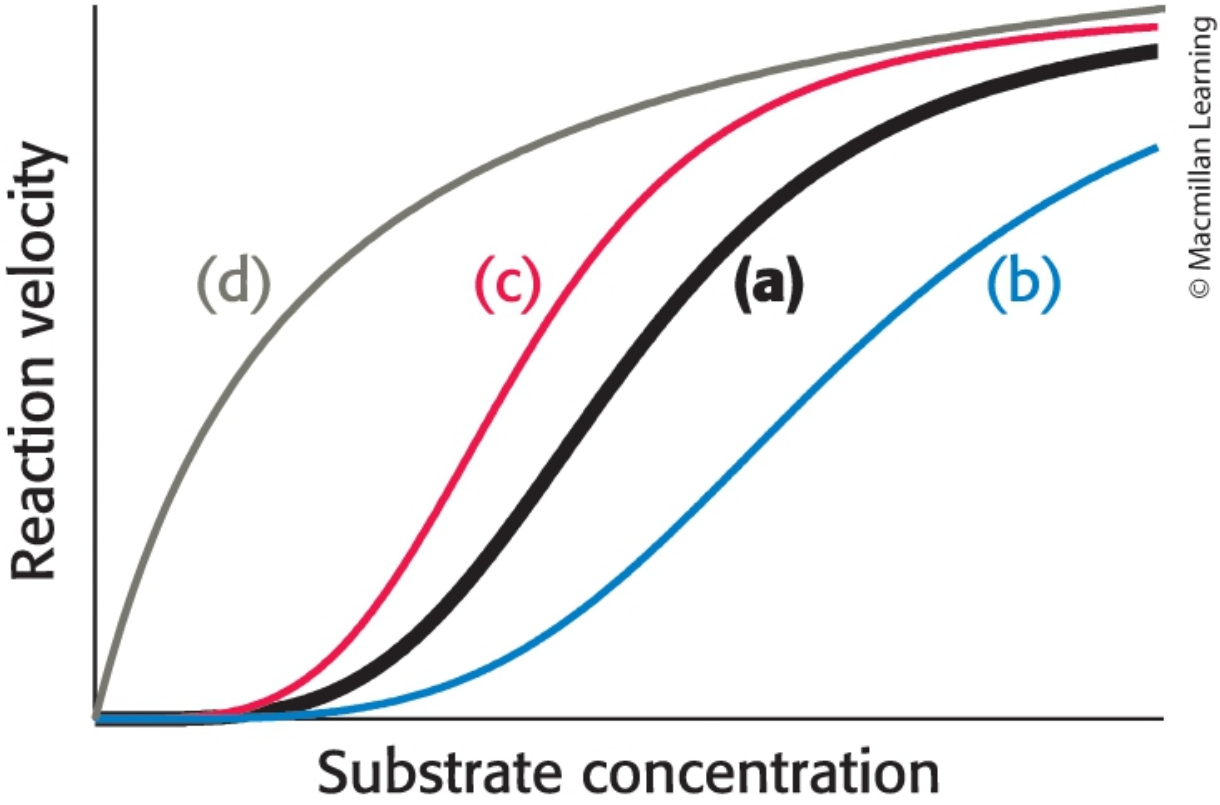
bonded to O above and partially double bonded to O on the left, and this C O O group carries a negative charge.

The structure of gamma-Carboxyglutamate residue is as follows: A central C atom is dash bonded to H on the upper right, single bonded to C on the lower right, single bonded to N H on the lower left, and wedge bonded to C H 2 on the upper left. The C on the lower right is double bonded to O below and has an open bond on the upper right. The N H on the lower left has an open single bond on the upper left. C H 2 on the upper left is single bonded to C H on the upper right which is single bonded to C on the upper left and single bonded to C on the upper right. The C on the upper left is partially double bonded to O above and partially double bonded to O on the left, and this C O O group carries a negative charge. The C on the upper right is partially double bonded to O above and partially double bonded to O on the lower right, and this C O O group carries a negative charge.

Two reaction arrows from vitamin K (epoxide) to vitamin K (hydroquinone) are crossed out indicating the proposed site of warfarin inhibition. The first reaction arrow is labeled epoxide reductase. The second reaction arrow is labeled quinone reductase.

Return to Chemical reactions showing the synthesis of gamma-carboxyglutamate

Extended description for Graph depicts the velocity curve of an allosteric enzyme and the effect of negative modifier



The horizontal axis is labeled substrate concentration. The vertical axis is labeled reaction velocity. The following four curves are shown:

Curve (a), solid black: It starts from the origin and runs along the horizontal axis before rising steeply to a point near the top end of the vertical axis, followed by a short plateau. It has a sigmoidal shape.

Curve (b), blue: It starts from the origin and runs along the horizontal axis before rising linearly to a point near the top end of the vertical axis. The slope of this curve is less steep than the curve (a). This curve is located toward the right of the curve (a).

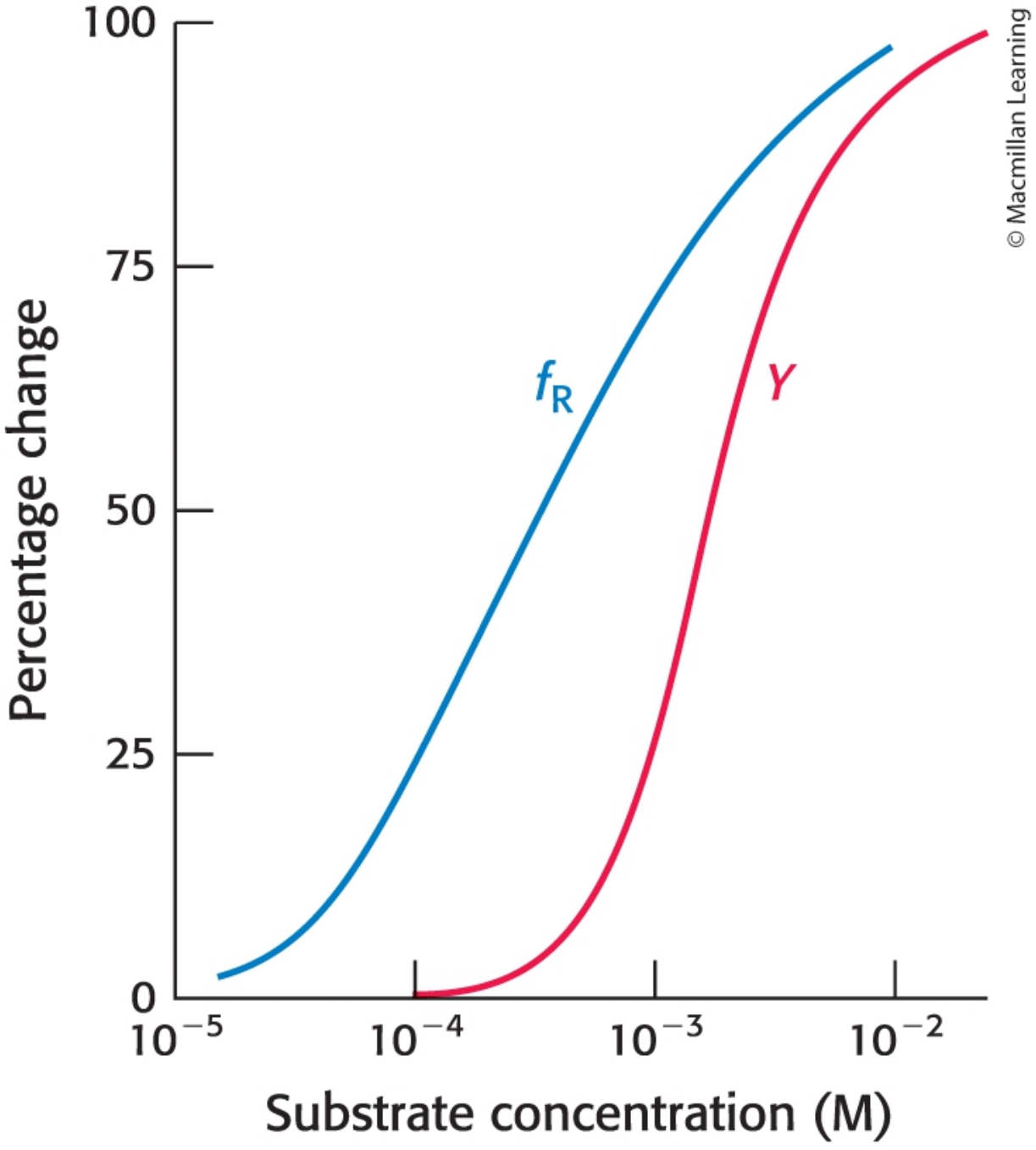
Curve (c), red: It starts from the origin and runs along the horizontal axis, and rises steeply before curve (a) to reach a point near the top end of the vertical axis, followed by a plateau. It has a sigmoidal shape and its slope is steeper than curve (a).

Curve (d), gray: It starts from the origin and rises steeply to a point near the top end of the vertical axis and then gradually plateaus. It is a hyperbolic curve.

Return to Graph depicts the velocity curve of an allosteric enzyme and the effect of negative modifier

Extended description for Graphical representation of the fraction of enzyme in the R state and the fraction of

substrate-bound active sites as a function of substrate concentration.



The horizontal axis is labeled substrate concentration in molar. It has markings ranging from 10 raised to the power negative 5 to 10

raised to the power negative 2 in geometric increments of 10 units. The vertical axis is labeled percentage change. It has markings ranging from 0 to 100 in increments of 25 units.

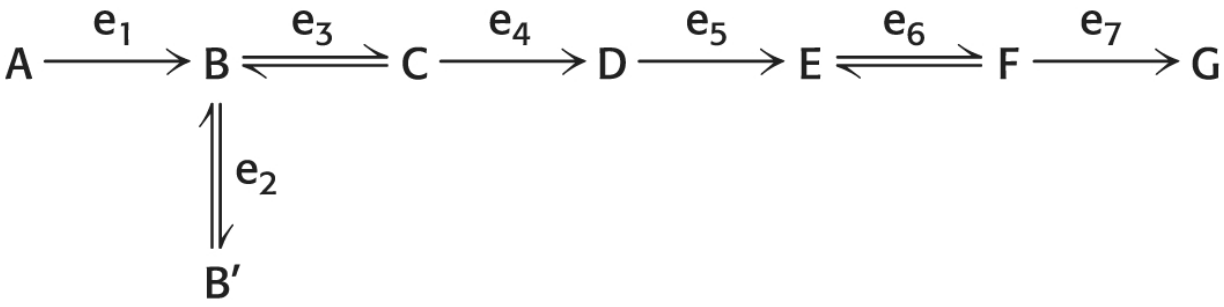
Curve Y (red): It starts from (10 raised to the power negative 4, 0) and moves slightly horizontally toward the right. It then rises steeply to nearly (10 raised to the power negative 2, 95). It has a sigmoidal shape.

Curve f subscript R (blue): It starts near the origin and linearly rises to nearly (10 raised to the power negative 2, 100). It has a slightly sigmoidal shape but the slope is less steep than the red curve.

All the numerical values are estimated.

Return to Graphical representation of the fraction of enzyme in the R state and the fraction of substrate-bound active sites as a function of substrate concentration

Extended description for Schematic illustration of a metabolic pathway



Reactant A forms product B. The forward reaction arrow is labeled e subscript 1.

B forms product B dash. The reversible reaction arrow is labeled e subscript 2.

B forms product C. The reversible reaction arrow is labeled e subscript 3.

C forms product D. The forward reaction arrow is labeled e subscript 4.

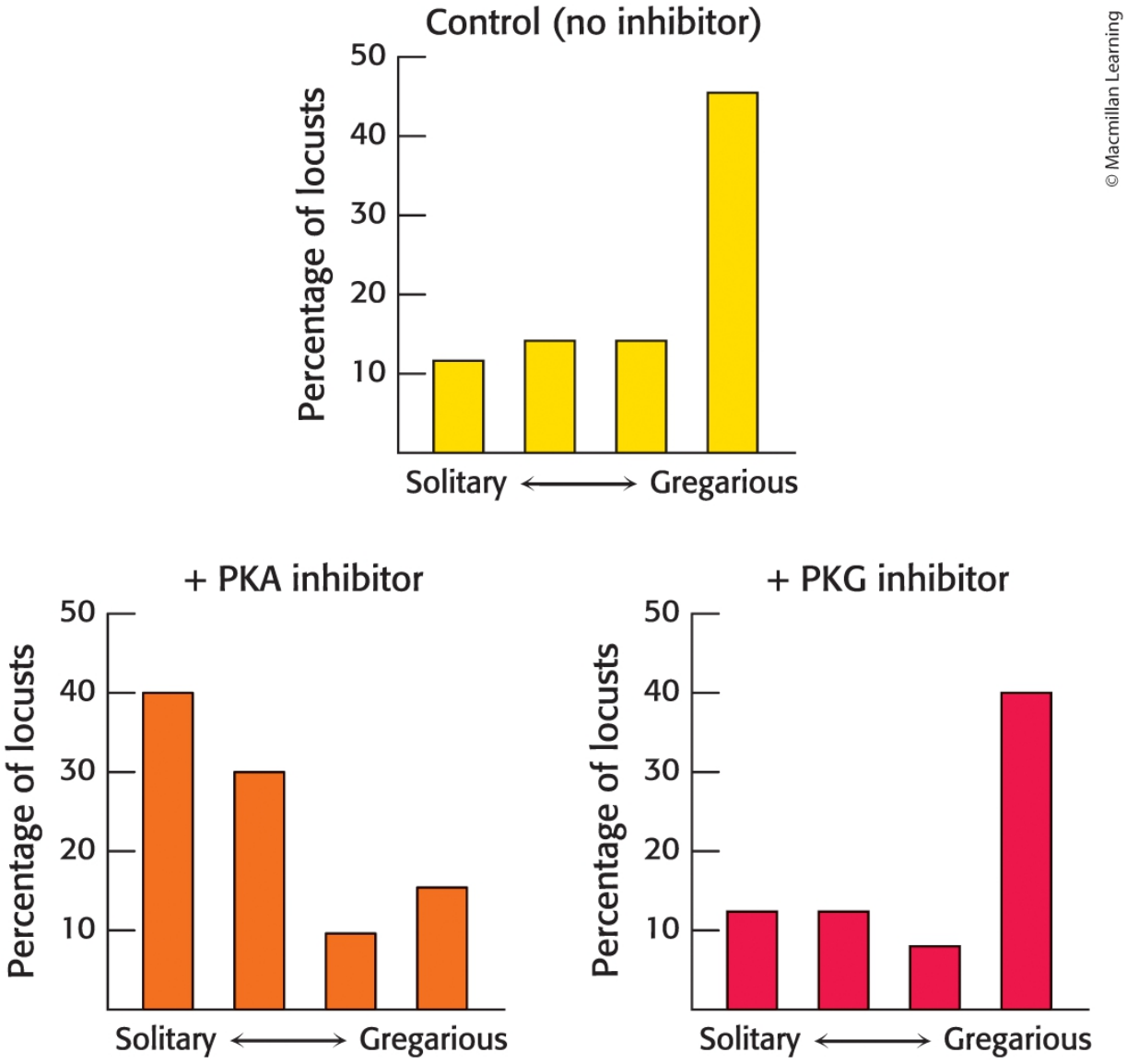
D forms product E. The forward reaction arrow is labeled e subscript 5.

E forms products F. The reversible reaction arrow is labeled e subscript 6.

F forms product G. The forward reaction arrow is labeled e subscript 7.

Return to Schematic illustration of a metabolic pathway

Extended description for Three vertical bar graphs showing the results of control group (no inhibitor), P K A inhibitor, and P K G inhibitor



© Macmillan Learning

The vertical axes represent a range from solitary to gregarious, from the left to right. The vertical axes are labeled the percentage of locusts. It has markings ranging from 0 to 50 in increments of 10 units.

Control (no inhibitor): Four vertical bars are shown to have the following height, from left to right: 11, 15, 15, and 45.

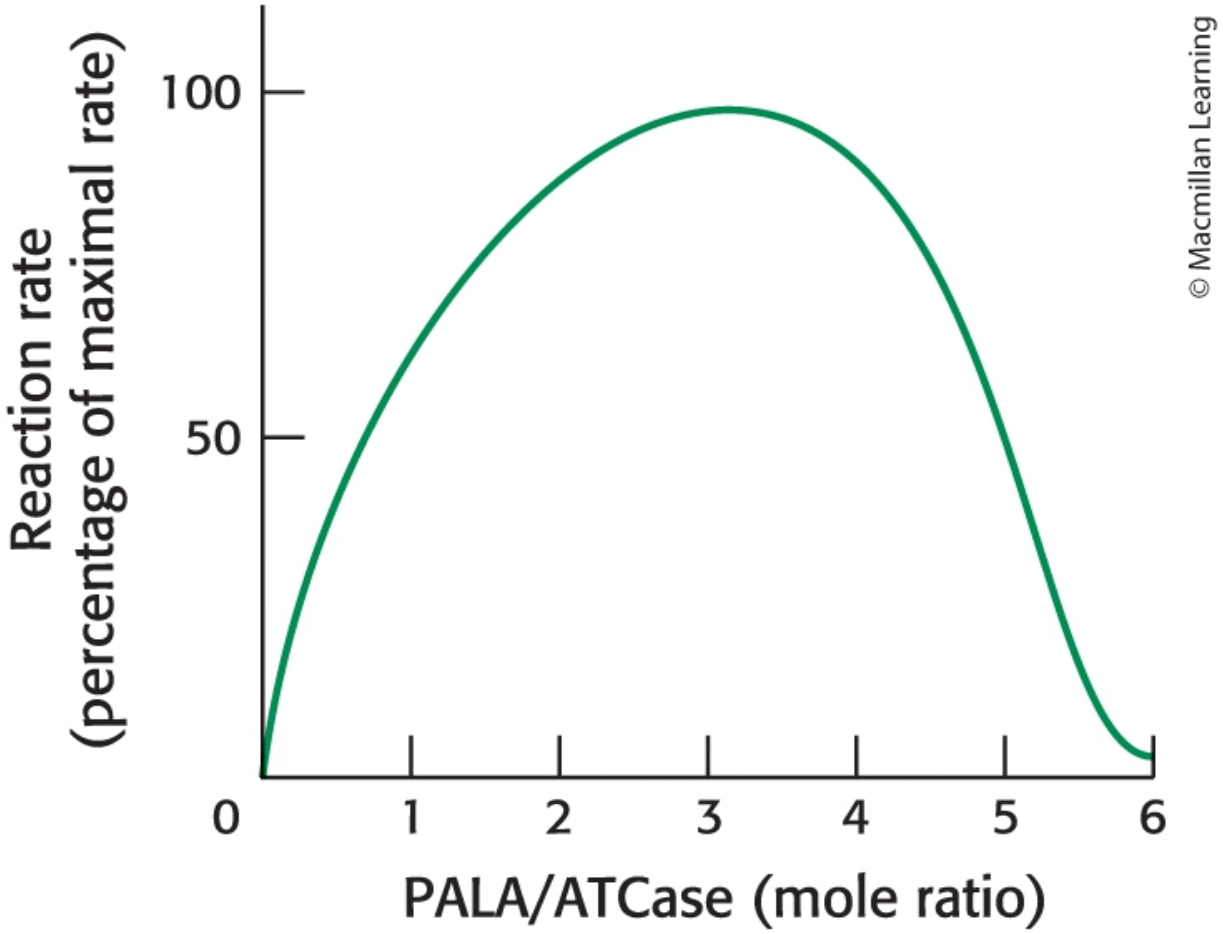
P K A inhibitor: Four vertical bars are shown to have the following height, from left to right: 40, 30, 10, and 15.

P K G inhibitor: Four vertical bars are shown to have the following height, from left to right: 12, 12, 8, and 40.

All numerical values are estimated.

Return to Three vertical bar graphs showing the results of control group (no inhibitor), P K A inhibitor, and P K G inhibitor

Extended description for Graphical representation of the reaction rate as a function of the mole ratio of P A L A to A T C ase



The horizontal axis is labeled P A L A over A T C ase (mole ratio). It has markings ranging from 0 to 6 in increments of 1 unit. The vertical axis is labeled reaction rate (percentage of maximal rate). It has markings ranging from 0 to 100 in increments of 50 units. A broad bell-shaped curve starts from the origin, peaks at nearly (3, 100), and ends at (6, 0).

All numerical values are estimated.

Return to Graphical representation of the reaction rate as a function of the mole ratio of P A L A to A T C ase

Extended description for Photograph of a family of dogs is accompanied by a ribbon diagram of a zinc finger protein bound to D N A

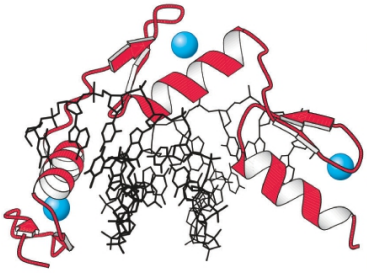




Photo: Lelusy/Shutterstock
© Macmillan Learning

In the photograph, one parent has a complete black fur coat and the other parent has a white fur coat with black patches. The puppy is shown to have a head with black fur and the body is white with black patches.

The zinc finger protein is shown to comprise alpha helices and beta strands connected by short loops. Three blue spheres linked to the protein represent zinc ions. A control region of D N A is shown in black. The zinc-finger protein is shown to sit at the top of the D N A.

Return to Photograph of a family of dogs is accompanied by a ribbon diagram of a zinc finger protein bound to D N A

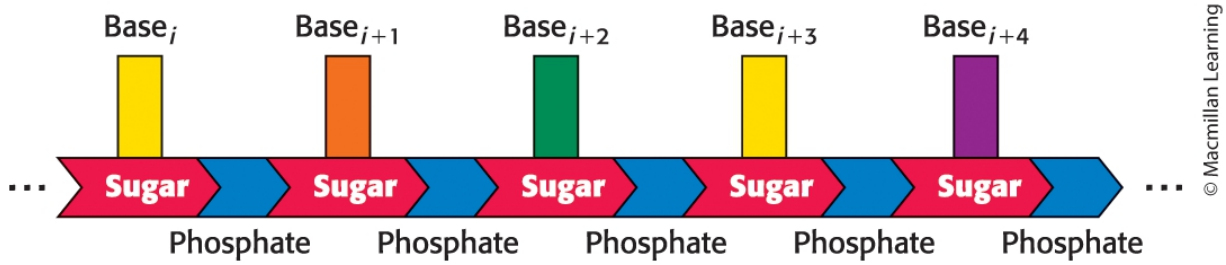
Extended description for Schematic representation of central dogma



An arrow from D N A to R N A is labeled transcription. An arrow from R N A to protein is labeled translation. A curved arrow starting from and ending at D N A is labeled replication.

Return to Schematic representation of central dogma

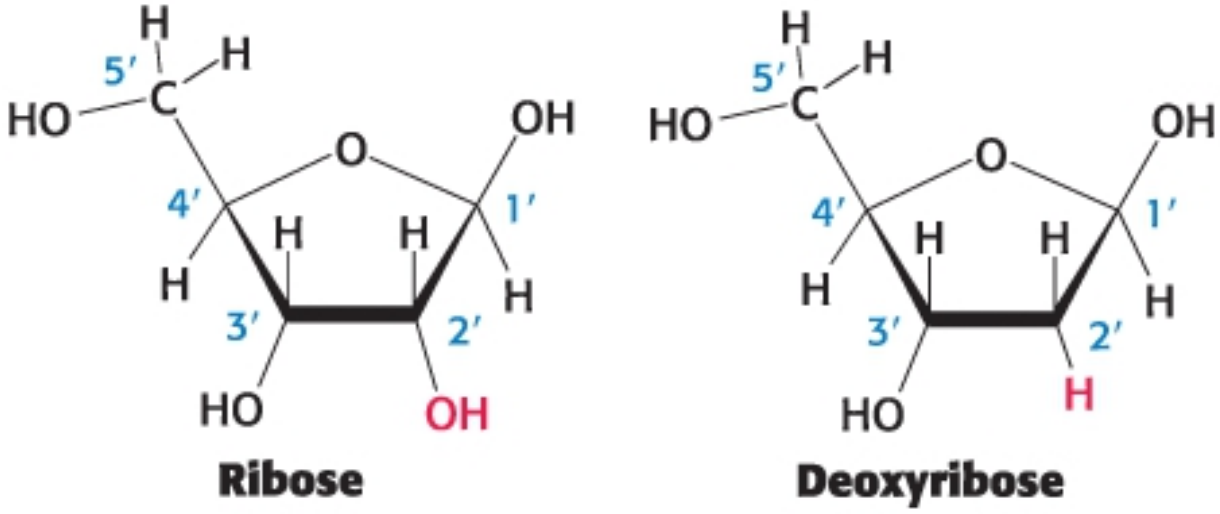
Extended description for FIGURE 8.1. Schematic representation of the structure of nucleic acids



A nucleic acid chain is shown to have a linear backbone linked to bases. The backbone is made up of sugars interspersed by phosphates. Vertical bars on top of each sugar are labeled Base. There are four such units shown labeled Base subscript i through Base subscript i plus 4.

Return to FIGURE 8.1. Schematic representation of the structure of nucleic acids

Extended description for FIGURE 8.2. Chemical structures of ribose and deoxyribose found in R N A and D N A respectively



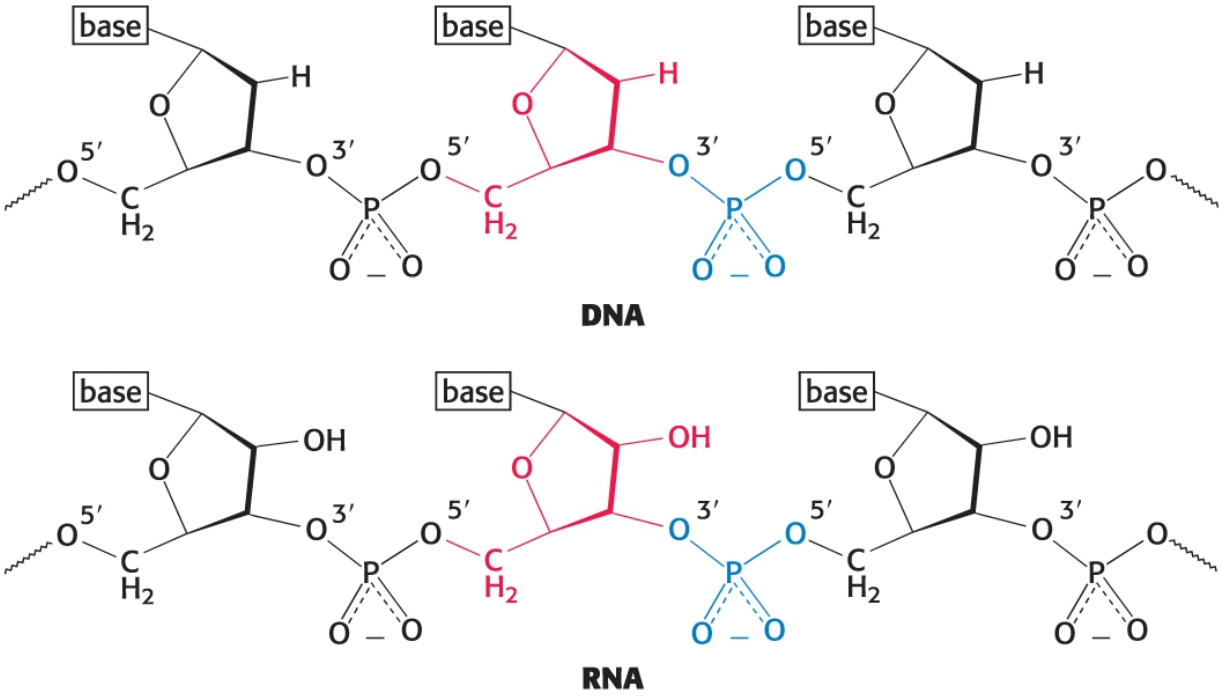
Ribose: A 5-membered heterocyclic pentagonal ring in a vertical orientation consists of 1 O and 4 C atoms. The O atom occupies the first position which is the topmost vertex. C 1, labeled 1 prime, is single bonded to an O H on the upper right and single bonded to H on the lower right. C 2, labeled 2 prime, is single bonded to H above and single bonded to O H on the lower right, which is highlighted in red. C 3, labeled 3 prime, is single bonded to O H on the lower left and single bonded to H above. C 4, labeled 4 prime, is single bonded to H on the lower left and single bonded to C on the upper left which is labeled 5 prime. This 5 prime C is single bonded to H on the upper right, single bonded to H above, and single bonded to O H on the lower left.

Deoxyribose: A 5-membered heterocyclic pentagonal ring in a vertical orientation consists of 1 O and 4 C atoms. The O atom occupies the first position which is the topmost vertex. C 1, labeled 1

prime, is single bonded to an O H on the upper right and single bonded to H on the lower right. C 2, labeled 2 prime, is single bonded to H above and single bonded to H on the lower right, which is highlighted in red. C 3, labeled 3 prime, is single bonded to O H on the lower left and single bonded to H above. C 4, labeled 4 prime, is single bonded to H on the lower left and single bonded to C on the upper left which is labeled 5 prime. This 5 prime C is single bonded to H on the upper right, single bonded to H above, and single bonded to O H on the lower left.

Return to FIGURE 8.2. Chemical structures of ribose and deoxyribose found in R N A and D N A respectively

Extended description for FIGURE 8.3. The chemical structure of D N A and R N A



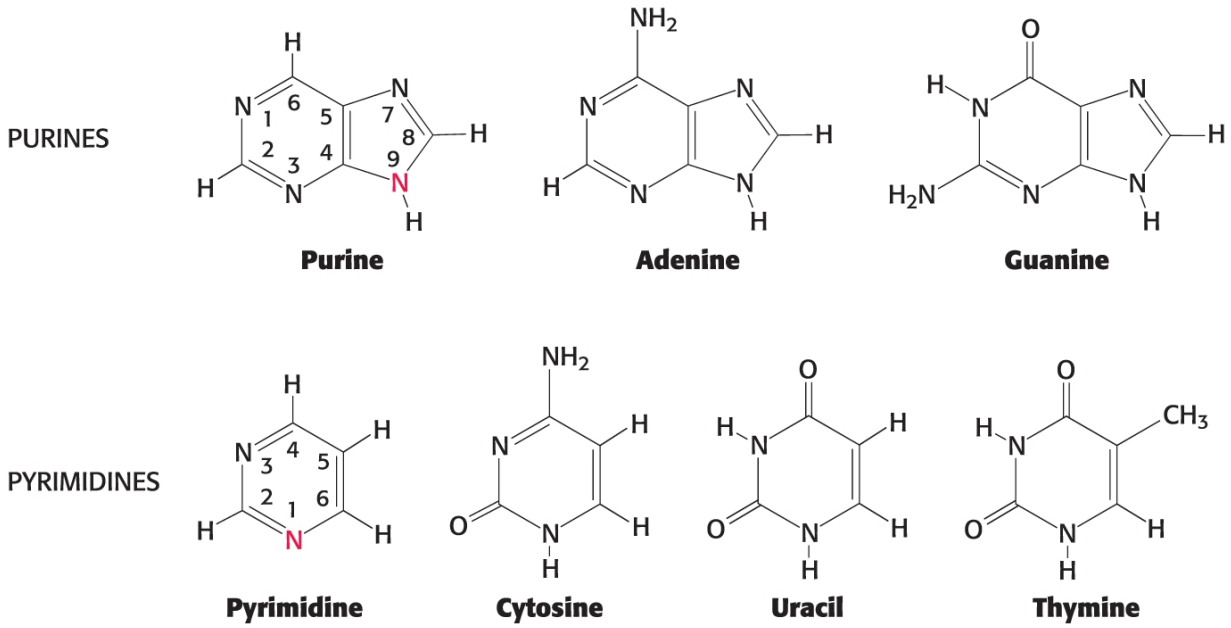
D N A: Three nucleotide units are joined in a linear horizontal fashion. Each nucleotide unit has the following structure: A 5-membered heterocyclic pentagonal ring in a horizontal orientation consists of 1 O and 4 C atoms. The O atom occupies the first position which is the leftmost vertex. C 1 is single bonded to a base. C 2 is single bonded to H. C 3 is single bonded to O which is labeled 3 prime. This O atom is single-bonded to P on the lower right. P is single bonded to O on the upper right which is labeled 5 prime, partially double bonded to O on the lower right, and partially double bonded to O on the lower left. These partially double-bonded O atoms carry a negative charge. C 4 is single bonded to C H 2 which is single bonded to O on the upper left which is labeled 5 prime. Two adjacent nucleotides are linked by a phosphodiester bond formed between the 3 prime end of the left nucleotide and the 5 prime end

of the right nucleotide. The pentagonal ring of the second nucleotide is highlighted in red and the P O 4 group carrying a negative charge is highlighted in blue.

R N A: Three ribonucleotide units are joined in a linear horizontal fashion. Each ribonucleotide unit has the following structure: A 5-membered heterocyclic pentagonal ring in a horizontal orientation consists of 1 O and 4 C atoms. The O atom occupies the first position which is the leftmost vertex. C 1 is single bonded to a base. C 2 is single bonded to O H. C 3 is single bonded to O which is labeled 3 prime. O is single bonded to P on the lower right. P is single bonded to O on the upper right which is labeled 5 prime, partially double bonded to O on the lower right, and partially double bonded to O on the lower left. These partially double-bonded O atoms carry a negative charge. C 4 is single bonded to C H 2 which is single bonded to O on the upper left which is labeled 5 prime. Two adjacent ribonucleotides are linked by a phosphodiester bond formed between the 3 prime end of the left nucleotide and the 5 prime end of the right nucleotide. The pentagonal ring of the second ribonucleotide is highlighted in red and the P O 4 group carrying a negative charge is highlighted in blue.

Return to FIGURE 8.3. The chemical structure of D N A and R N A

Extended description for FIGURE 8.4. Chemical structures of different purines are pyrimidines



Purines:

The general structure of purine: A 6-membered heterocyclic hexagonal ring in a vertical orientation consists of 2 N and 4 C atoms. The first N atom occupies the first position, which is the bottom-most vertex. The second N atom occupies the third position, which is the top-left vertex. C 1 and C 2 are each single bonded to H. Double bonds are present between the first N and C 1 and the second N and C 2. This ring is fused to a 5-membered heterocyclic pentagonal ring in a horizontal orientation. The pentagonal ring consists of 2 N and 3 C atoms. The first N atom occupies the first position which is the top-right vertex and the second N atom occupies the third position which is the bottom-right vertex which is highlighted in red. C 1 and the second N atom are each single bonded to H. Double bonds are present between the first N and C 1

and C 2 and C 3. The rings are fused such that C 3 and C 4 of the hexagonal ring are C 3 and C 2 of the pentagonal ring, respectively. The atoms of the hexagonal ring are numbered 1 to 6 in an anticlockwise direction starting from the top-left vertex. In the pentagonal ring, the first N atom is labeled 7, C 1 is labeled 8, and the second N atom is labeled 9.

Adenine: A 6-membered heterocyclic hexagonal ring in a vertical orientation consists of 2 N and 4 C atoms. The first N atom occupies the first position, which is the bottom-most vertex. The second N atom occupies the third position, which is the top-left vertex. C 1 is single bonded to H and C 2 is single bonded to N H 2 above. Double bonds are present between the first N and C 1 and the second N and C 2. This ring is fused to a 5-membered heterocyclic pentagonal ring in a horizontal orientation. The pentagonal ring consists of 2 N and 3 C atoms. The first N atom occupies the first position which is the top-right vertex and the second N atom occupies the third position which is the bottom-right vertex. C 1 and the second N atom are each single bonded to H. Double bonds are present between the first N and C 1 and C 2 and C 3. The rings are fused such that C 3 and C 4 of the hexagonal ring are C 3 and C 2 of the pentagonal ring, respectively.

Guanine: A 6-membered heterocyclic hexagonal ring in a vertical orientation consists of 2 N and 4 C atoms. The first N atom occupies the first position, which is the bottom-most vertex. The second N atom occupies the third position, which is the top-left vertex. The second N atom is single bonded to H. C 1 is single bonded to N H 2 on the lower left. C 2 is single bonded to O above. A double bond is present between the first N and C 1. This ring is fused to a 5-membered heterocyclic pentagonal ring in a horizontal orientation. The pentagonal ring consists of 2 N and 3 C atoms. The first N atom occupies the first position which is the top right vertex and the second N atom occupies the third position which is the bottom right

vertex. C 1 and the second N atom are each single bonded to H. Double bonds are present between the first N and C 1 and C 2 and C 3. The rings are fused such that C 3 and C 4 of the hexagonal ring are C 3 and C 2 of the pentagonal ring, respectively.

Pyrimidines:

The general structure of pyrimidine is as follows: A 6-membered heterocyclic hexagonal ring in a vertical orientation consists of 2 N and 4 C atoms. The first N atom occupies the first position which is the bottom-most vertex and the second N atom occupies the third position which is the top-left vertex. Three alternating double bonds are present between the first N and C 1, the second N and C 2, and C 3 and C 4. C 1, C 2, C 3, and C 4 are each single bonded to H. The atoms of the hexagonal ring are numbered 1 to 6 in a clockwise direction starting from the bottom-most vertex.

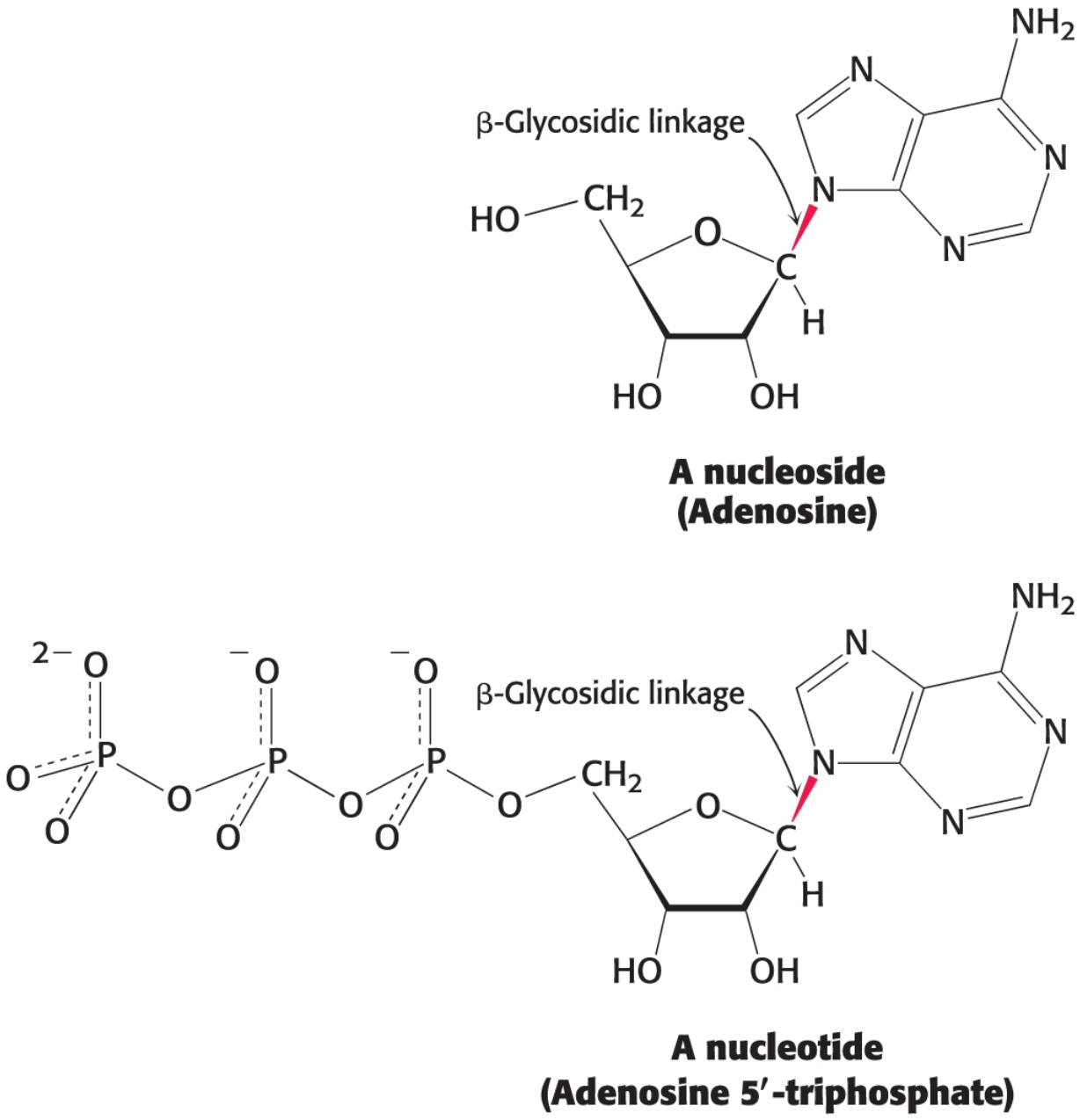
Cytosine: A 6-membered heterocyclic hexagonal ring in a vertical orientation consists of 2 N and 4 C atoms. The first N atom occupies the first position which is the bottom-most vertex and the second N atom occupies the third position which is the top-left vertex. Double bonds are present between the second N and C 2 and C 3 and C 4. C 1 is double bonded to O on the lower left. The first N atom is single-bonded to H below. C 2 is single bonded to N H 2 above. C 3 and C 4 are each single bonded to H.

Uracil: A 6-membered heterocyclic hexagonal ring in a vertical orientation consists of 2 N and 4 C atoms. The first N atom occupies the first position which is the bottom-most vertex and the second N atom occupies the third position which is the top-left vertex. A double bond is present between C 3 and C 4. C 1 is double bonded to O on the lower left. The first N atom is single-bonded to H below. The second N atom is single-bonded to H on the upper left. C 2 is double bonded to O above. C 3 and C 4 are each single bonded to H.

Thymine: A 6-membered heterocyclic hexagonal ring in a vertical orientation consists of 2 N and 4 C atoms. The first N atom occupies the first position which is the bottom-most vertex and the second N atom occupies the third position which is the top-left vertex. A double bond is present between C 3 and C 4. C 1 is double bonded to O on the lower left. The first N atom is single-bonded to H below. The second N atom is single-bonded to H on the upper left. C 2 is double bonded to O above. C 3 is single bonded to C H 3 on the upper right. C 4 is single bonded to H on the lower right.

Return to FIGURE 8.4. Chemical structures of different purines are pyrimidines

Extended description for FIGURE 8.5. Chemical structures of a nucleoside and a nucleotide



A nucleoside (Adenosine): A 5-membered heterocyclic pentagonal ring in a vertical orientation consists of 1 O and 4 C atoms. The O atom occupies the first position, which is the topmost vertex. C 2

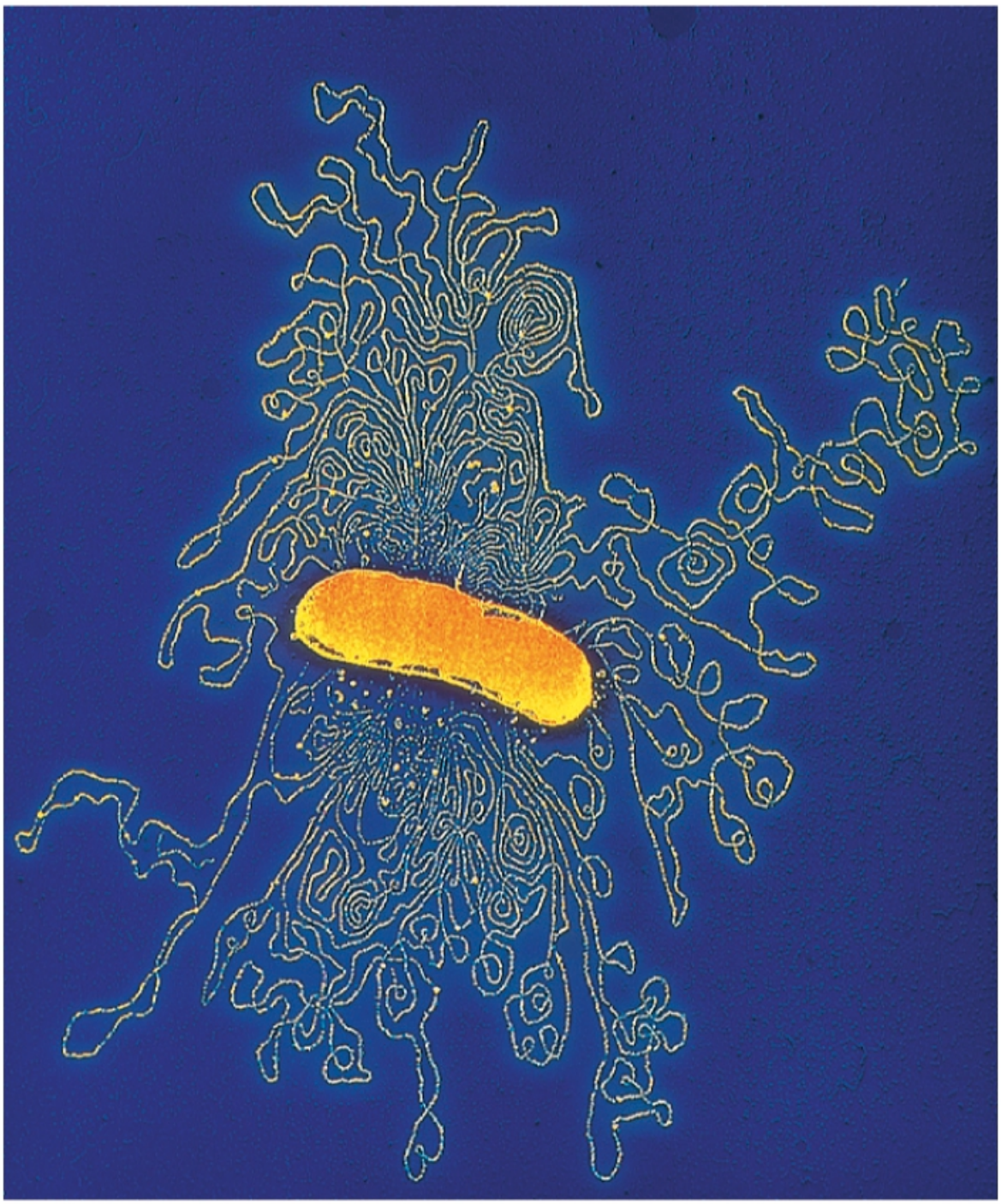
and C 3 are each single bonded to O H. C 1 is single bonded to H on the lower right and wedge bonded to the first N of a 5-membered heterocyclic pentagonal ring in a horizontal orientation on the upper right. The wedge bond is highlighted in red and labeled beta-Glycosidic linkage. The pentagonal ring consists of 2 N and 3 C atoms. The first N atom occupies the first position which is the bottom left vertex and the second N atom occupies the third position which is the topmost vertex. A double bond is present between the second N and C 1 and C 2 and C 3. This ring is fused to a heterocyclic hexagonal in a vertical orientation consisting of 2 N and 4 C atoms. The first N atom occupies the first position which is the top right vertex and the second N atom occupies the third position which is the bottom-most vertex. A double bond is present between C 4 and the first N and C 1 and the second N. C 4 is single bonded to N H 2 above. The rings are fused such that C 2 and C 3 of the pentagonal ring are C 3 and C 2 of the hexagonal ring, respectively. C 4 of the pentagonal ring consisting of 1 O and 4 C atoms is single bonded to C H 2 which is single bonded to O H on the lower left.

A nucleotide (Adenosine 5 prime-triphosphate): A 5-membered heterocyclic pentagonal ring in a vertical orientation consists of 1 O and 4 C atoms. The O atom occupies the first position, which is the topmost vertex. C 2 and C 3 are each single bonded to O H. C 1 is single bonded to H on the lower right and wedge bonded to the first N of a 5-membered heterocyclic pentagonal ring in a horizontal orientation on the upper right. The wedge bond is highlighted in red and labeled beta-Glycosidic linkage. The pentagonal ring consists of 2 N and 3 C atoms. The first N atom occupies the first position which is the bottom left vertex and the second N atom occupies the third position which is the topmost vertex. A double bond is present between the second N and C 1 and C 2 and C 3. This ring is fused to a heterocyclic hexagonal in a vertical orientation consisting of 2 N and 4 C atoms. The first N atom occupies the first position which is the top right vertex and the second N atom occupies the third position

which is the bottom-most vertex. A double bond is present between C 4 and the first N and C 1 and the second N. C 4 is single bonded to N H 2 above. The rings are fused such that C 2 and C 3 of the pentagonal ring are C 3 and C 2 of the hexagonal ring, respectively. C 4 of the pentagonal ring consisting of 1 O and 4 C atoms is single bonded to C H 2 which is single bonded to O atom of a triphosphate group. Each phosphate group has a central P atom single bonded to O on the lower right, single bonded to O on the lower left, partially double bonded to O above, and partially double bonded to O below. The single bonded O atoms are shared between two adjacent phosphate groups. The terminal phosphate group carries a negative charge of 2 minus as it is partially double bonded to O above, left, and on the lower left. The other two phosphate groups each carry a negative charge.

Return to FIGURE 8.5. Chemical structures of a nucleoside and a nucleotide

Extended description for FIGURE 8.6. Photomicrograph compares the size of an *E.coli* cell to its coiled genome



Dr. Gopal Murti/Science Source

The extensively coiled and intertwined D N A of E.coli is shown to fill most of the space in the photomicrograph. A rod-shaped E.coli cell is shown in the center and occupies a much lesser area. The cell is surrounded by the D N A network.

Return to FIGURE 8.6. Photomicrograph compares the size of an *E.coli* cell to its coiled genome

Extended description for FIGURE 8.7. Photomicrograph of the stained chromosomes of female Indian muntjac

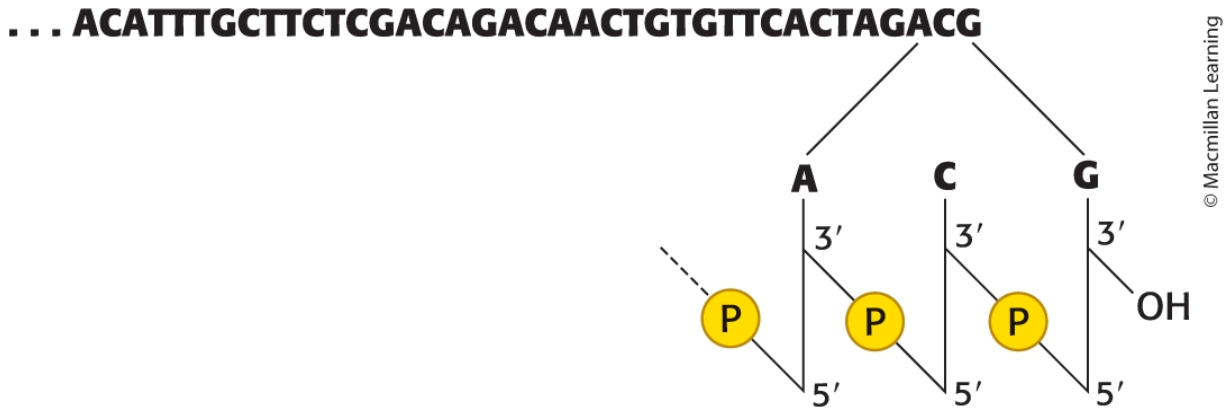


Credits: (Left) Super Prin/Shutterstock; (Right) Reprinted by permission from Macmillan Publishers Ltd: *Nature Genetics*, J-Y Lee, M. Koi, E.J. Stanbridge, M. Oshimura, A.T. Kumamoto, & A.P. Feinberg, Simple purification of human chromosomes to homogeneity using muntjac hybrid cells, vol. 7, pp. 29–33, ©1994, Figure 2b. Permission conveyed through Copyright Clearance Center, Inc.

The photomicrograph shows three pairs of long X-shaped chromosomes stained orange. Two pairs of human chromosomes are also seen in green which are much smaller and appears like large blots.

[Return to FIGURE 8.7. Photomicrograph of the stained chromosomes of female Indian muntjac]

Extended description for FIGURE 8.8. Simplified schematic representation of a nucleic acid strand

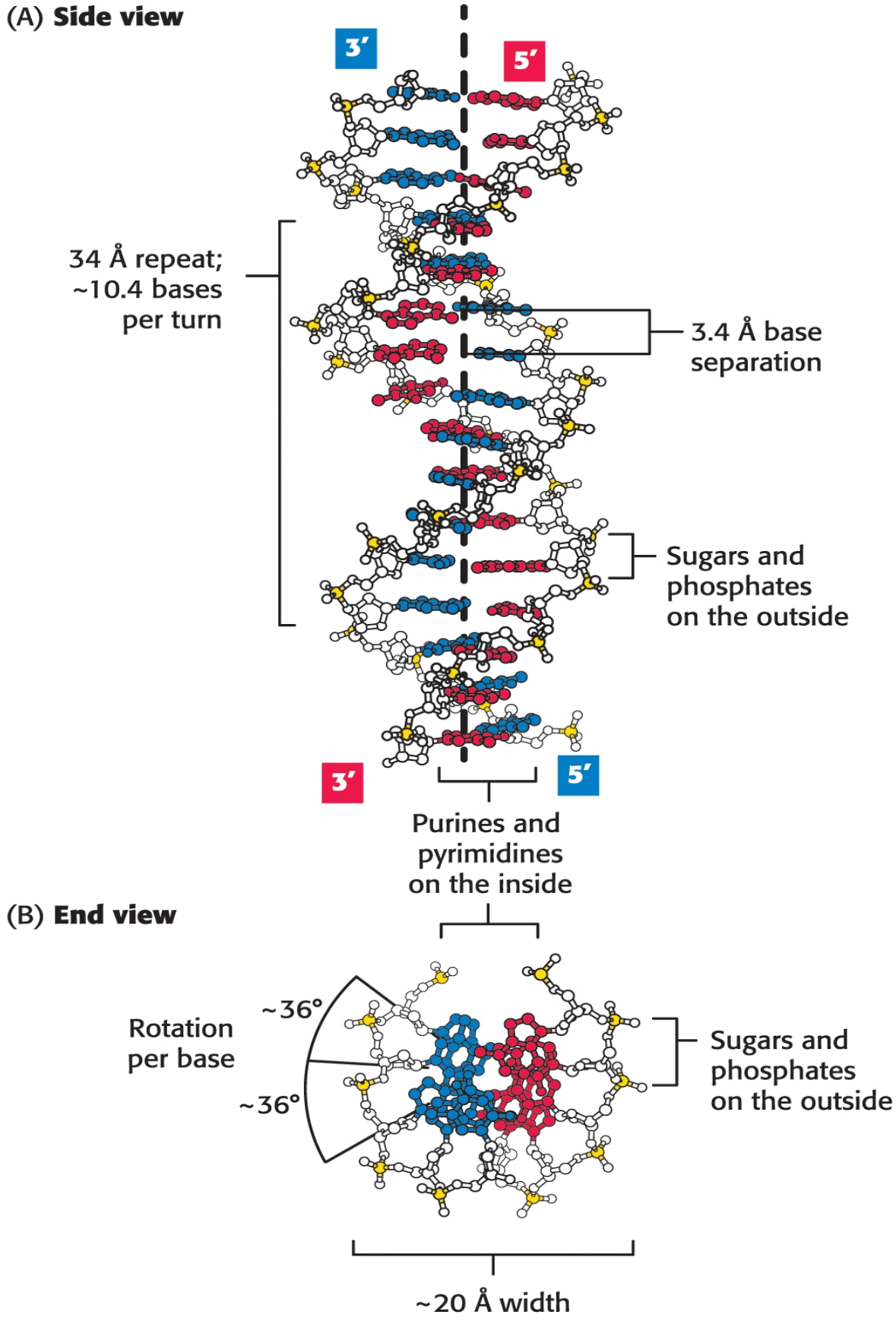


A nucleic acid sequence is shown: A C A T T T G C T T C T C G A C A G A C A A C T G T G T T C A C T A G A C G. The last three bases are A C G, which are shown in magnification. The magnified portion shows three equally spaced vertical lines. The top of lines are labeled A, C, and G, from the left to right. The top end of each vertical line is labeled 3 prime and the bottom end is labeled 5 prime. A phosphoryl group represented by P in a yellow circle is bonded to 3 prime of the left vertical line and 5 prime of the right vertical line. The 3 prime end of the terminal G base is single bonded to O H. This entire arrangement of the strand resembles a saw tooth structure.

Return to FIGURE 8.8. Simplified schematic representation of a nucleic acid strand

Extended description for FIGURE 8.10. The Watson–

Crick model of double-helical D N A



© Macmillan Learning

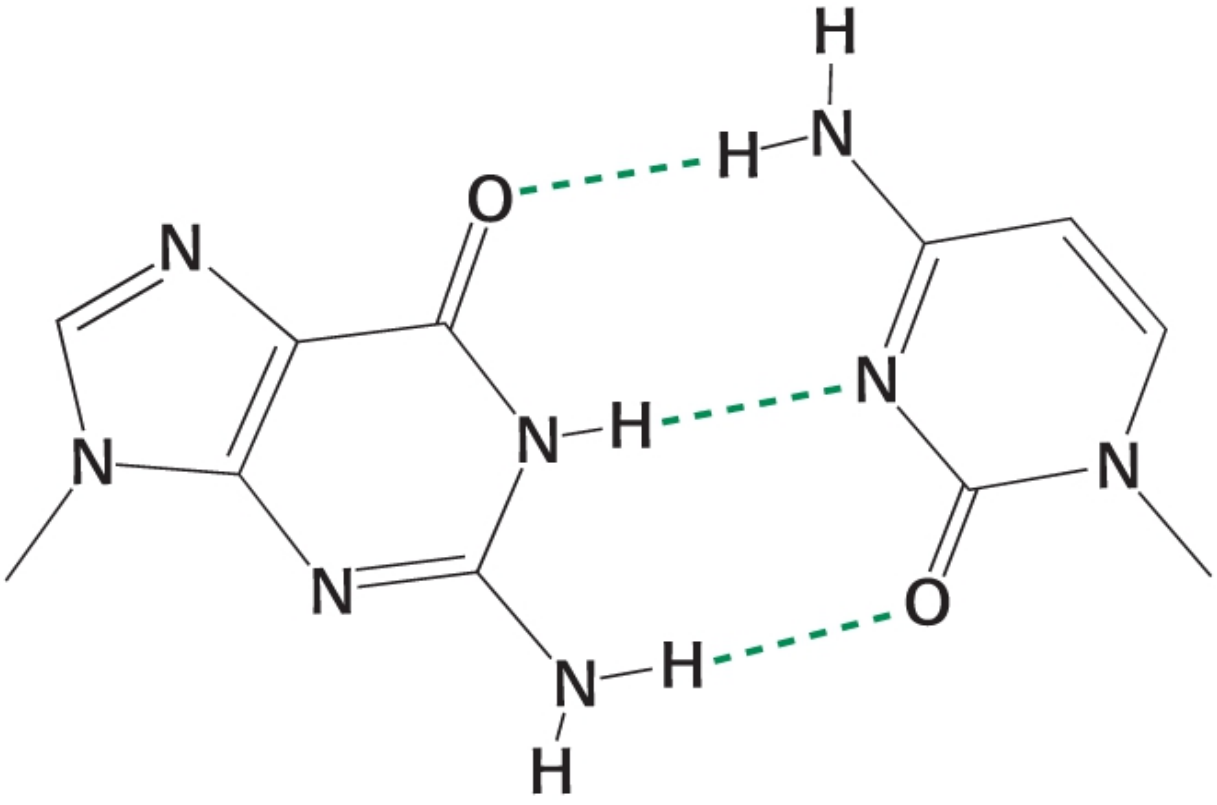
Part (A): Side view. The double helix is left-handed. The purine and pyrimidine bases are inside and pointed toward the central vertical axis of the double helix, and the sugar-phosphate backbone is located outside toward the periphery. The bases of one strand are shown in red and the bases of the other strand are shown in blue. The orientation of the red strand is 3 prime to 5 prime from the bottom to top. The orientation of the blue strand is 5 prime to 3 prime from the bottom to top. One turn is labeled 34 Angstrom repeat; approximately 10.4 bases per turn. Base separation is 3.4 Angstrom.

Part (B): End view. The purine and pyrimidine bases are buried inside the helix. The blue bases are shown on the left and the red bases is shown on the right. The two bases resemble C-shapes facing each other. The sugar-phosphate backbone forms an incomplete circle around the bases. Rotation per base is approximately 36 degrees. The width of the helix is approximately 20 Angstrom.

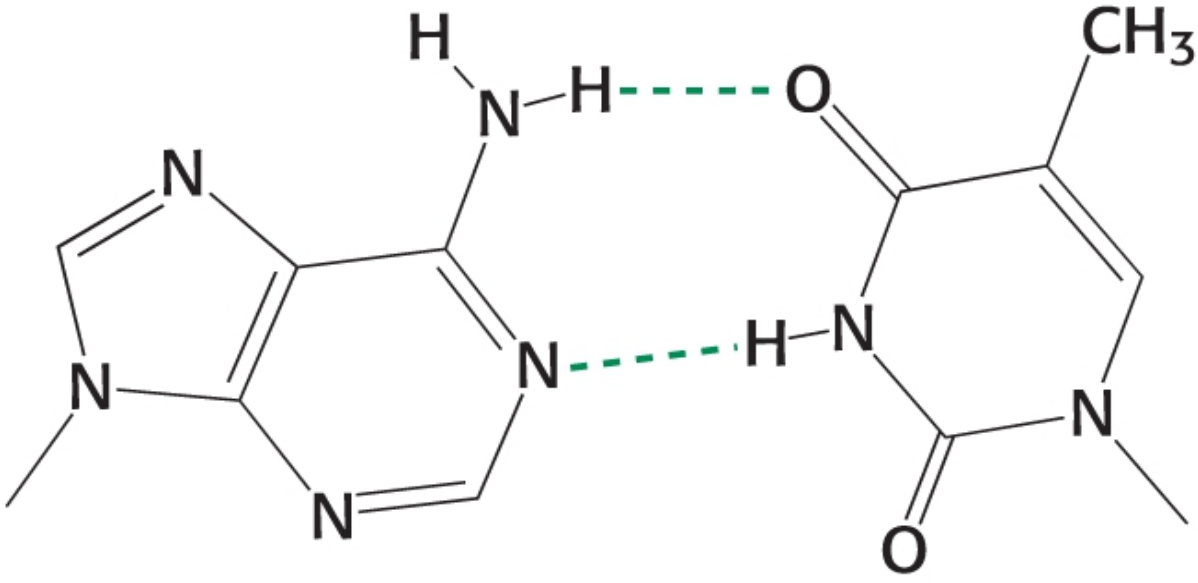
Return to FIGURE 8.10. The Watson–Crick model of double-helical D N A

Extended description for FIGURE 8.11. Base-pairing of

nucleotide bases



Guanine **Cytosine**



Adenine **Thymine**

Guanine and Cytosine: Three hydrogen bonds are formed between these two bases.

Cytosine has the following structure: A 6-membered heterocyclic hexagonal ring is in a horizontal orientation and consists of 2 N and 4 C atoms. The first N atom occupies the first position, which is the bottom right vertex, and the second N atom occupies the third position, which is the leftmost vertex. Double bonds are present between the second N and C 2 and C 3 and C 4. C 1 is double bonded to O on the lower left. C 2 is single bonded to N on the upper left which is single bonded to H above and single bonded to H on the left. The second N has an open single bond on the lower right.

Guanine has the following structure: A 6-membered heterocyclic hexagonal ring and a 5-membered pentagonal ring are fused. The six-membered heterocyclic hexagonal ring is in a vertical orientation and consists of 2 N and 4 C atoms. The first N atom occupies the first position, which is the top-left vertex and the second N atom single bonded to H occupies the third position, which is the bottom-most vertex. A double bond is present between the second N and C 1. C 1 is single bonded to N on the lower right which is single bonded to H below and single bonded to H on the right. C 4 is double bonded to O above. The 6-membered hexagonal ring is fused to a 5-membered heterocyclic ring in a vertical orientation which consists of 2 N and 3 C atoms. The first N atom occupies the first position, which is the bottom left vertex and the second N atom occupies the third position, which is the topmost vertex. A double bond is present between the second N and C 1 and C 2 and C 3. The first N has an open single bond on the lower left. The rings are fused such that C 2 and C 3 of the hexagonal ring are the C 3 and C 2 of the pentagonal ring, respectively.

The first hydrogen bond is present between N H single bonded to C 2 of cytosine and O double bonded to C 4 of the hexagonal ring of

guanine. The second hydrogen bond is present between the second N of cytosine and the first N bound to H of the hexagonal ring of guanine. The third hydrogen bond is present between the O atom double-bonded to C 1 of cytosine and N H single-bonded to C 1 of the hexagonal ring of guanine.

Adenine and Thymine: Two hydrogen bonds are formed between these two bases.

Thymine has the following structure: A 6-membered heterocyclic hexagonal ring in a horizontal orientation consists of 2 N and 4 C atoms. The first N atom occupies the first position, which is the bottom right vertex. The second N atom bound to H occupies the third position, which is the leftmost vertex. A double bond is present between C 3 and C 4. C 3 is single bonded to C H 3 on the upper right. C 1 is double bonded to O on the lower left. C 2 is double bonded to O on the upper left. The first N atom has an open single bond on the lower right.

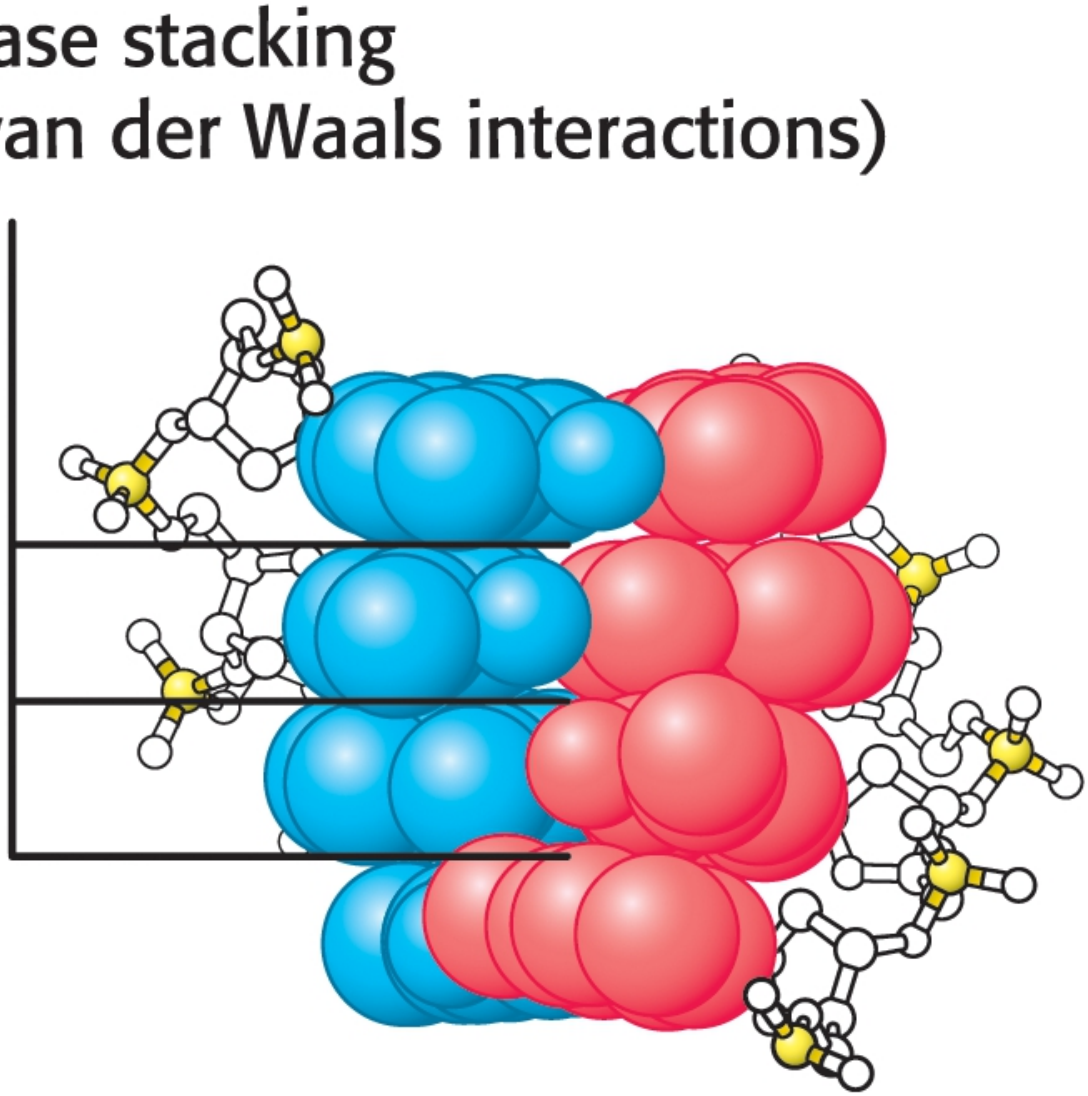
Adenine has the following structure: A 6-membered heterocyclic hexagonal ring and a 5-membered pentagonal ring are fused. The six-membered heterocyclic hexagonal ring is in a vertical orientation and consists of 2 N and 4 C atoms. The first N atom occupies the first position, which is the top-right vertex, and the second N atom occupies the third position, which is the bottom-most vertex. Double bonds are present between the first N and C 4 and the second N and C 1. C 4 is single bonded to N which is single bonded to H on the upper left and single bonded to H on the upper right. The 6-membered ring is fused to a 5-membered heterocyclic pentagonal ring in a horizontal orientation which consists of 2 N and 3 C atoms. The first N atom occupies the first position, which is the bottom left vertex, and the second N atom occupies the third position, which is the topmost vertex. A double bond is present between the second N and C 1 and C 2 and C 3. The first N has an

open single bond on the lower left. The rings are fused such that C 2 and C 3 of the hexagonal ring are the C 3 and C 2 of the pentagonal ring, respectively.

The first hydrogen bond is present between the H bound to the second N of thymine and the first N atom of the hexagonal ring of adenine. The second hydrogen bond is present between the O atom double-bonded to C 2 of thymine and N H single bonded to C 4 of the hexagonal ring of adenine.

Return to FIGURE 8.11. Base-pairing of nucleotide bases

Extended description for FIGURE 8.12. Schematic representation of the side view of D N A reveals the stacking of base pairs within the double helix



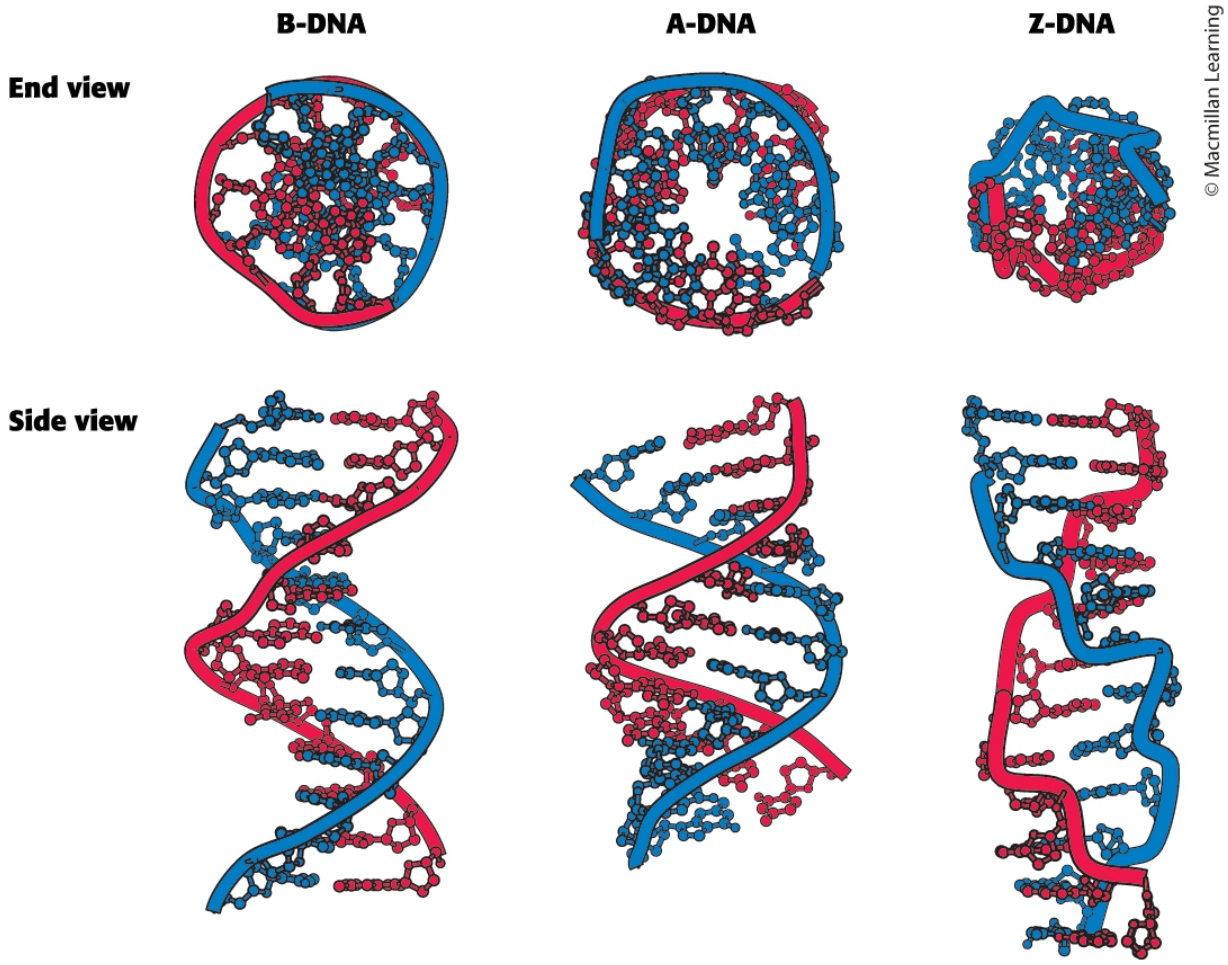
© Macmillan Learning

A D N A double helix is diagrammatically represented. The space-filling model of the bases is shown. The bases of the left strand are shown as blue spheres and those of the right strand are shown as red spheres. They coil around each other along the vertical axis. The bases of each strand are stacked almost perfectly one above the

other. The ball-and-stick model of the sugar-phosphate backbone is shown on the outside. Base stacking is shown to be via van der Waals interactions.

Return to FIGURE 8.12. Schematic representation of the side view of D N A reveals the stacking of base pairs within the double helix

Extended description for FIGURE 8.13. Schematic representation of the different structural forms of D N A



B-D N A:

End view: It resembles a wheel. Half of the circumference is red and the other half is blue, and this represents the sugar-phosphate backbone. The bases are arranged such that they resemble the spokes of the wheel and form a central donut shape around the central axis.

Side view: The double helix is left-handed. The purine and pyrimidine bases are inside and point toward the central vertical axis of the double helix, and the sugar-phosphate backbone is outside toward the periphery. The bases and the backbone of one strand are shown in red and the bases and the backbone of the other strand are shown in blue.

A-D N A:

End view: It is shaped like a large donut. Half of the circumference is red and the other half is blue, and this represents the sugar-phosphate backbone. The bases are oriented toward the central axis. The central hole is much larger compared to that of B-D N A.

Side view: The width of the double helix is greater than that of B-D N A.

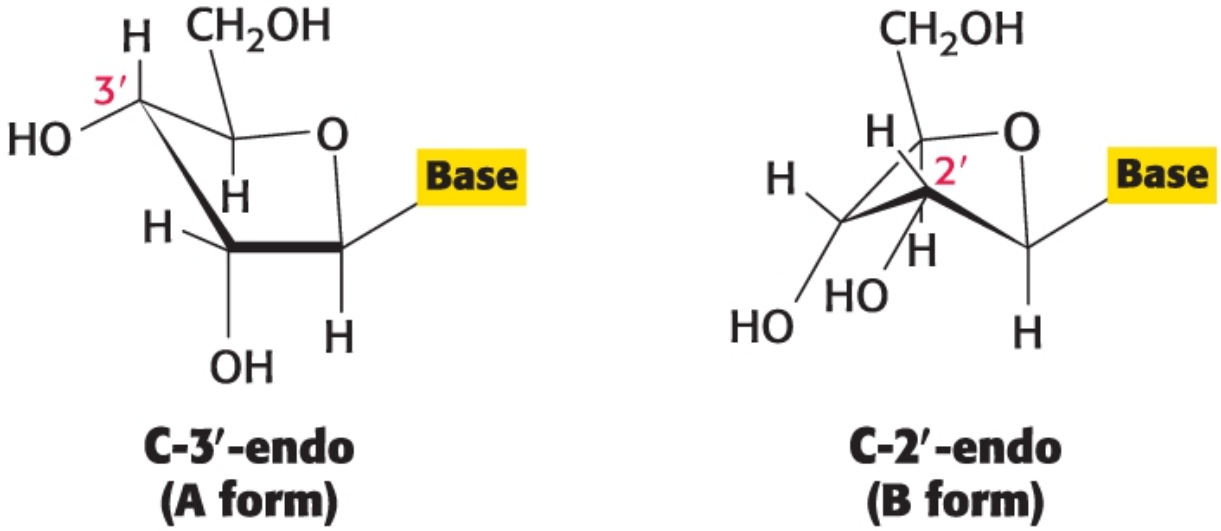
Z-D N A:

End view: It is shaped like a small donut. Half of the circumference is red and the other half is blue, and this represents the sugar-phosphate backbone. The backbone is wrinkled. The bases are oriented toward the central axis and are much more staggered compared to the other two forms.

Side view: The width of the double helix is smaller than that of B-D N A. The sugar-phosphate backbone is zigzag along the vertical axis.

Return to FIGURE 8.13. Schematic representation of the different structural forms of D N A

Extended description for FIGURE 8.14. The structures of the sugars in the A and B forms of D N A



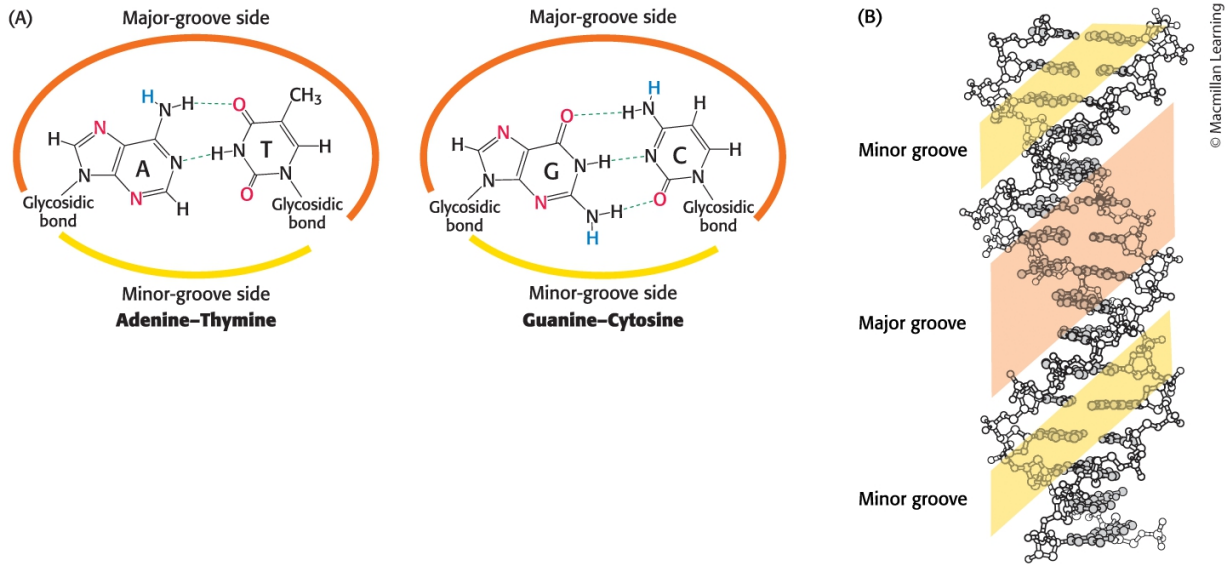
C-3 prime-endo (A form): The puckered sugar is a 5-membered ring consisting of 1 O and 4 C atoms. The O atom occupies the first position which is the top right vertex. O is single bonded to C 1 below. C 1 is single bonded to Base on the upper right, single bonded to H below, and single bonded to C 2 on the left. C 1 and C 2 are toward the observer. C 2 is single bonded to O H below, single bonded to H on the upper left, and wedge bonded to C 3 on the upper left. C 3 is labeled 3 prime and is single bonded to H above, single bonded to O H on the lower left, and single bonded to C 4 on the lower right. C 4 is single bonded to H below, single bonded to C H 2 O H on the upper left, and single bonded to O at the first position on the right.

C-2 prime-endo (B form): The puckered sugar is a 5-membered ring consisting of 1 O and 4 C atoms. The O atom occupies the first position which is the top right vertex. O is single bonded to C 1 below. C 1 is single bonded to Base on the upper right, single bonded

to H below, and wedge bonded to C 2 on the upper left. C 2 is labeled 2 prime and is single bonded to O H on the lower left, single bonded to H on the upper left, and wedge bonded to C 3 on the lower left. C 3 is single bonded to O H on the lower left, single bonded to H on the upper left, and single bonded to C 4 on the upper right. C 4 is single bonded to C H 2 O H on the upper left, single bonded to H below, and single bonded to O at the first position on the right.

Return to FIGURE 8.14. The structures of the sugars in the A and B forms of D N A

Extended description for FIGURE 8.15. The major and minor grooves of a D N A double helix



Part (A): The major and minor grooves in an adenine-thymine and guanine-cytosine base pair are shown.

Adenine-thymine base pair:

Thymine has the following structure: A 6-membered heterocyclic hexagonal ring in a horizontal orientation consists of 2 N and 4 C atoms. The first N atom occupies the first position, which is the bottom right vertex. The second N atom bound to H occupies the third position, which is the left-most vertex. A double bond is present between C 3 and C 4. C 3 is single bonded to C H 3. C 1 is double bonded to O (red) on the lower left. C 2 is double bonded to O (red) on the upper left. The first N has a glycosidic bond on the lower right. C 4 is single bonded to H.

Adenine has the following structure: A 6-membered heterocyclic hexagonal ring and a 5-membered pentagonal ring are fused. The six-membered heterocyclic hexagonal ring is in a vertical orientation and consists of 2 N and 4 C atoms. The first N atom occupies the first position, which is the top-right vertex. The second N atom (red) occupies the third position, which is the bottom-most vertex. Double bonds are present between the first N and C 4 and the second N and C 1. C 4 is single bonded to N which is single bonded to H (blue) on the upper left and single bonded to H on the upper right. C 1 is single bonded to H. The 6-membered ring is fused to a 5-membered heterocyclic pentagonal ring in a horizontal orientation which consists of 2 N and 3 C atoms. The first N atom occupies the first position, which is the bottom left vertex. The second N atom (red) occupies the third position, which is the topmost vertex. A double bond is present between the second N and C 1 and C 2 and C 3. The first N has a glycosidic bond on the lower left. The rings are fused such that C 2 and C 3 of the hexagonal ring are the C 3 and C 2 of the pentagonal ring, respectively.

The first hydrogen bond is present between the H bound to the second N of thymine and the first N of the hexagonal ring of adenine. The second hydrogen bond is present between the O atom double-bonded to C 2 of thymine and N H single bonded to C 4 of the hexagonal ring of adenine. A large arc joining the glycosidic bond of adenine and thymine, over the base pair, is labeled the major-groove side. A smaller arc joining the glycosidic bond of adenine and thymine, below the base pair, is labeled minor-groove side.

Guanine-Cytosine base pairing:

Cytosine has the following structure: A 6-membered heterocyclic hexagonal ring is in a horizontal orientation and consists of 2 N and 4 C atoms. The first N atom occupies the first position, which is the bottom right vertex. The second N atom occupies the third position,

which is the left-most vertex. Double bonds are present between C 3 and C 4 and the second N and C 2. C 1 is double bonded to O (red) on the lower left. C 2 is single bonded to N on the upper left which is single bonded to H (blue) above and single bonded to H on the left. The first N has a glycosidic bond on the lower right. 3 and C 4 are each single bonded to H.

Guanine has the following structure: A 6-membered heterocyclic hexagonal ring and a 5-membered pentagonal ring are fused. The six-membered heterocyclic hexagonal ring is in a vertical orientation and consists of 2 N and 4 C atoms. The first N atom single bonded to H occupies the first position, which is the top vertex. The second N atom (red) occupies the third position, which is the bottom-most vertex. A double bond is present between the second N and C 1. C 1 is single bonded to N on the lower right which is single bonded to H (blue) below and single bonded to H on the upper right. C 4 is double bonded to O (red) above. The 6-membered hexagonal ring is fused to a 5-membered heterocyclic ring in a horizontal orientation which consists of 2 N and 3 C atoms. The first N atom occupies the first position, which is the bottom left vertex. The second N atom (red) occupies the third position, which is the topmost vertex. A double bond is present between the second N and C 1 and C 2 and C 3. C 1 is single bonded to H. The first N has a glycosidic bond on the lower left. The rings are fused such that C 2 and C 3 of the hexagonal ring are the C 3 and C 2 of the pentagonal ring, respectively.

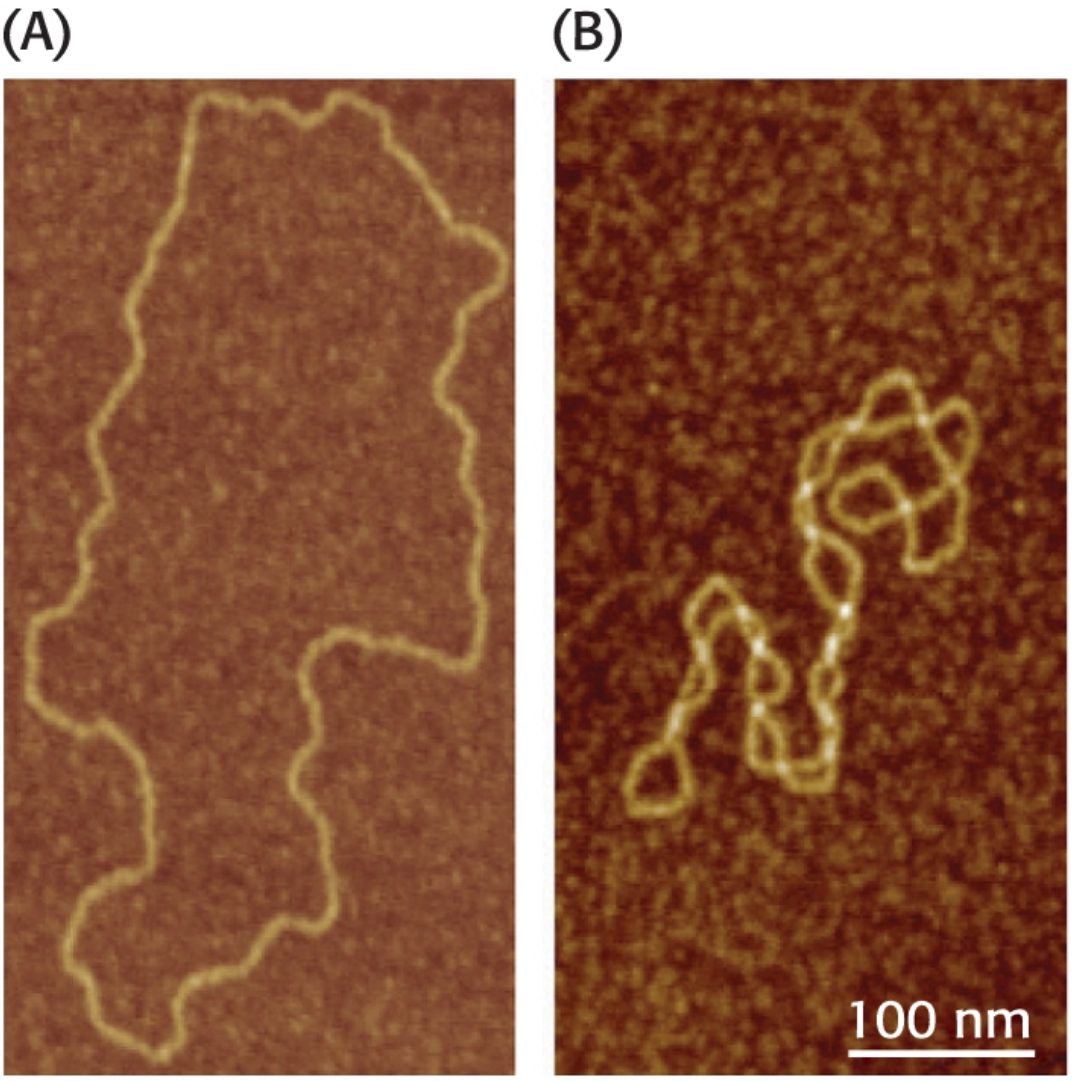
The first hydrogen bond is present between N H single bonded to C 2 of cytosine and O double bonded to C 4 of the hexagonal ring of guanine. The second hydrogen bond is present between the second N of cytosine and H single bonded to the first N of the hexagonal ring of guanine. The third hydrogen bond is present between the O atom double-bonded to C 1 of cytosine and N H single-bonded C 1 of the hexagonal ring of guanine. A large arc joining the glycosidic

bond of guanine and cytosine, over the base pair, is labeled the major-groove side. A smaller arc joining the glycosidic bond of guanine and cytosine, below the base pair, is labeled minor-groove side.

Part (B): A side view of the D N A double helix is illustrated. A thick wedge across the middle turn (turning toward the top left) is labeled major groove. A thinner wedge is shown across the regions (turning toward the top right) above and below the thick wedge, respectively. The thinner wedges are labeled minor groove.

Return to FIGURE 8.15. The major and minor grooves of a D N A double helix

Extended description for FIGURE 8.16. Two photomicrographs show the relaxed and supercoiled forms of circular bacterial D N A



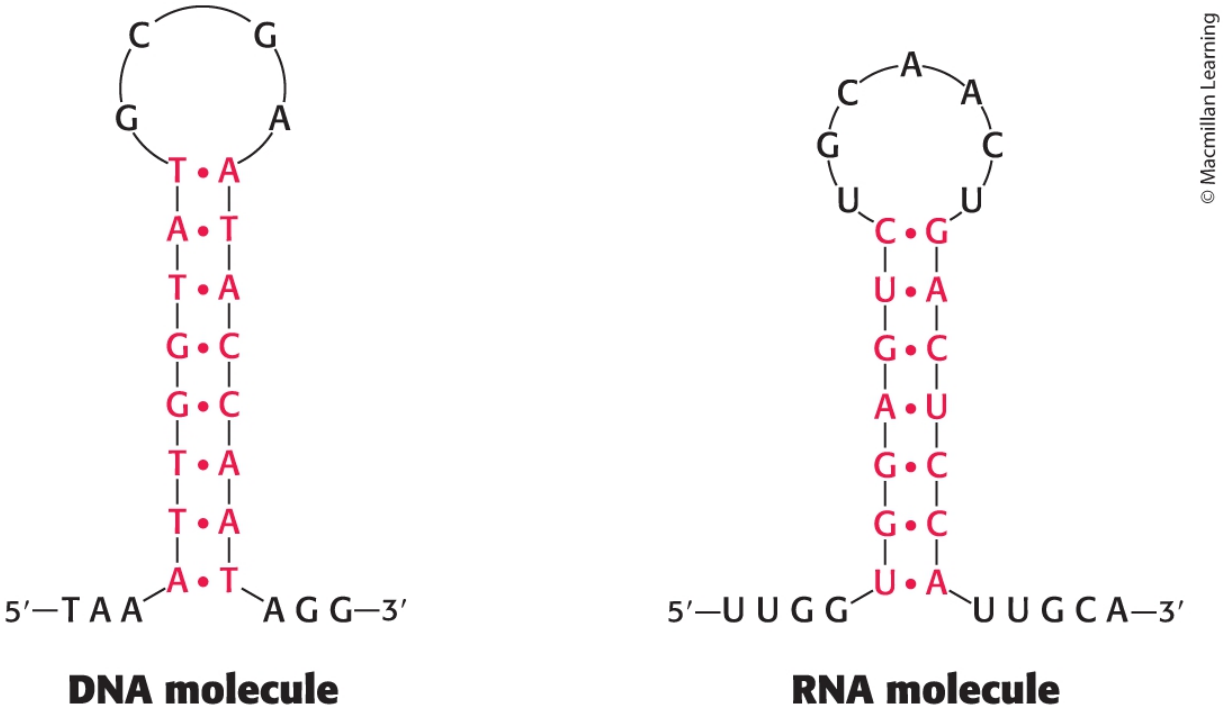
Credit: Republished with permission of Oxford University Press, from Witz, Guillaume; Stasiak, Andrzej, "DNA supercoiling and its role in DNA decatenation and unknotting," (2010) *Nuc. Acids Res.* 38(7) 2119-2133, Figure 1. Permission conveyed through Copyright Clearance Center, Inc.

Part (A): Relaxed form: The circular D N A is a single thread-like structure that forms an irregular closed loop.

Part (B): The circular D N A is a single thread-like structure that forms a tightly coiled shape. The scale is 100 nanometers.

Return to FIGURE 8.16. Two photomicrographs show the relaxed and supercoiled forms of circular bacterial D N A

Extended description for FIGURE 8.17. Stem-loop structures formed in single-stranded D N A and R N A molecules



© Macmillan Learning

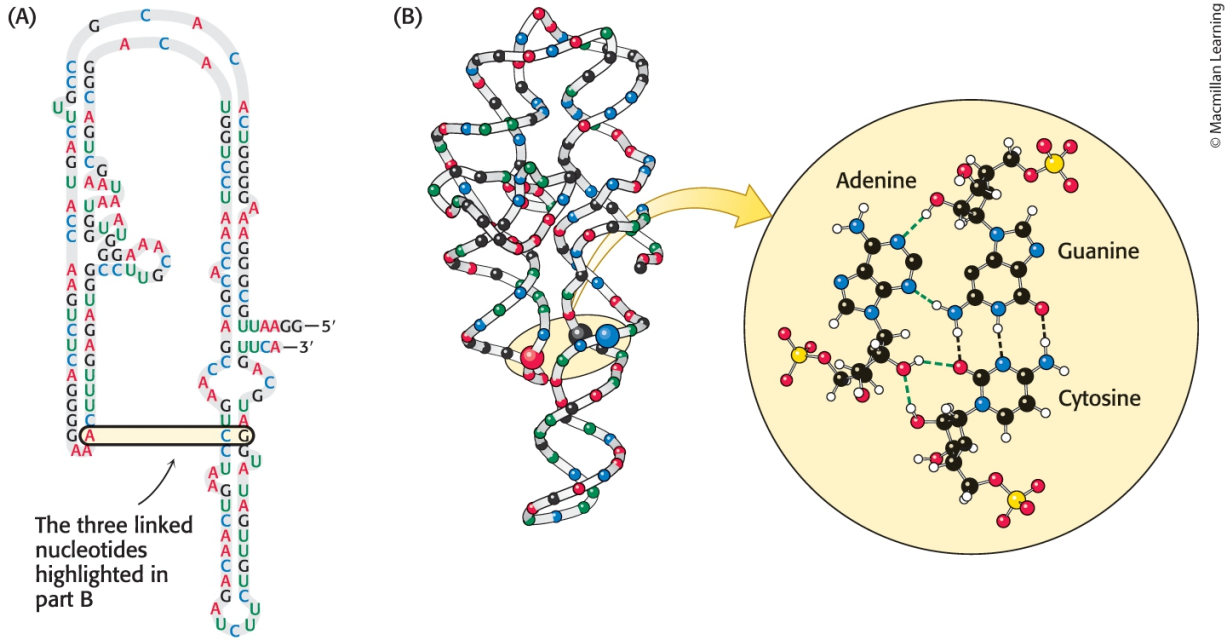
Single-stranded D N A: The stem-loop structure has a 5 prime trail end to the left and a 3 prime trail end to the right. The nucleotides of the stem are shown in red. Base pairing between A and T and G and C are shown by red dots. The loop has 4 nucleotides G, C, G, and A in a clockwise direction starting from the bottom left. They are shown in black.

Single-stranded R N A: The stem-loop structure has a 5 prime trail end to the left and a 3 prime trail end to the right. The nucleotides of the stem are shown in red. Base pairing between A and U and G and C are shown by red dots. The loop has 7 nucleotides U, G, C, A, A, C,

and U in a clockwise direction starting from the bottom left. They are shown in black.

Return to FIGURE 8.17. Stem-loop structures formed in single-stranded D N A and R N A molecules

Extended description for FIGURE 8.18. Schematic representation of complex structure adopted by R N A molecule



Part (A): Stem-loop structure. A single-stranded R N A molecule is shown to fold back on itself to form a structure resembling a double-stranded structure. This further is shown to fold to form an inverted U-shape, with the left arm longer than the right arm. A nucleotide (A) of the left arm is linked horizontally to two adjacent nucleotides (C and G) on the inner and outer region of the right arm.

Part (B): Three-dimensional stem-loop structure. The stem-loop structure is represented as a twisted rope made up of a series of colored spheres. The linkage of the nucleotides in the two arms is also highlighted. A magnified view of this linkage is shown. The ball-and-stick models of the nucleotides are shown. Guanine at the top is shown to be linked to cytosine at the bottom by three hydrogen bonds shown as black dashed lines. Cytosine is linked to adenine on

the top left by two hydrogen bonds shown as green dashed lines. Adenine is also linked to guanine on the right by two hydrogen bonds shown as green dashed lines.

Return to FIGURE 8.18. Schematic representation of complex structure adopted by R N A molecule

Extended description for FIGURE 8.19. Bands obtained by density-gradient centrifugation and corresponding graphs for N superscript 14 and N superscript 15 D N A

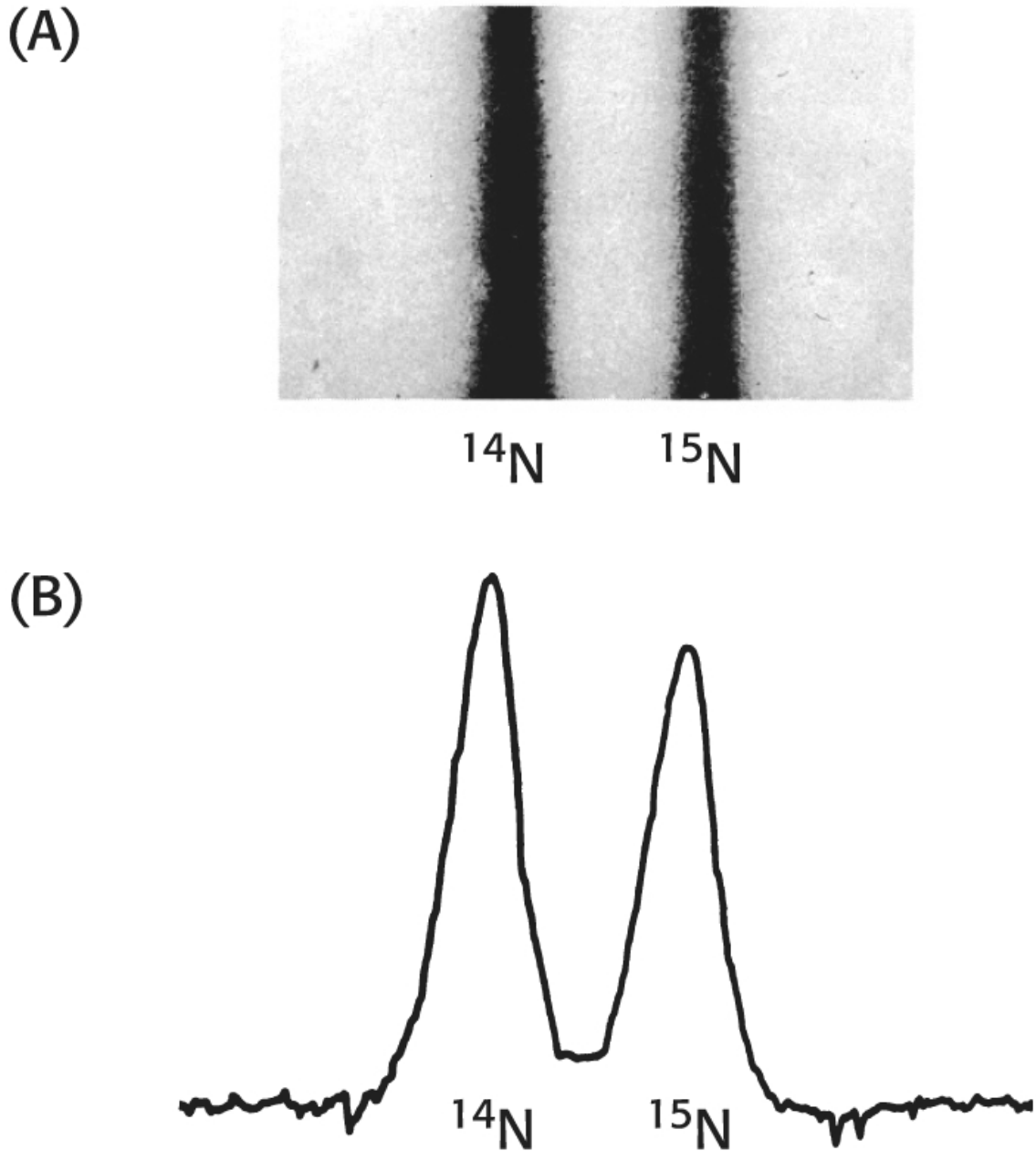


Photo credit: M. Meselson and F.W. Stahl. *Proc. Nat. Acad. Sci.* 44(1958):671.
© Macmillan Learning

Part (A): Two dark bands are seen for N superscript 14 and N superscript 15. The band for N superscript 14 is slightly thicker.

Part (B): The absorption plot shows two peaks at N superscript 14 and N superscript 15. The peak at N superscript 14 is slightly taller.

Return to FIGURE 8.19. Bands obtained by density-gradient centrifugation and corresponding graphs for N superscript 14 and N superscript 15 D N A

Extended description for FIGURE 8.20. D N A banding pattern detected by density-gradient centrifugation across 4 generations

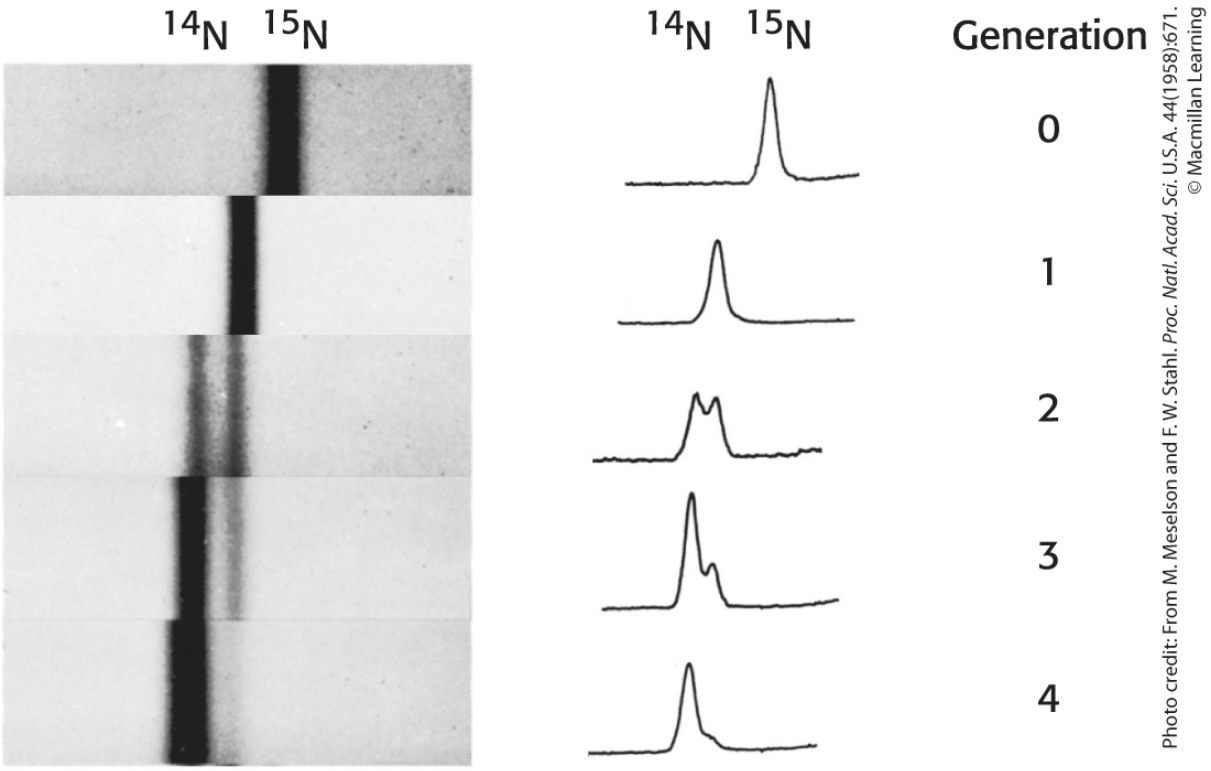


Photo credit: From M. Meselson and F. W. Stahl. *Proc. Natl. Acad. Sci.* U.S.A. 44(1958):671.
© Macmillan Learning

Band patterns are shown for N superscript 14 and N superscript 15 isotopes. Graphs with corresponding peaks are also shown.

Generation 0: A thick, dark band is seen for N superscript 15. A corresponding peak is seen in the graph at N superscript 15.

Generation 1: A thinner, dark band is seen between N superscript 14 and N superscript 15. A corresponding shorter peak is seen in the graph between N superscript 14 and N superscript 15.

Generation 2: Two faint, thin bands are seen for N superscript 14 and between N superscript 14 and N superscript 15. Two corresponding short peaks are seen in the graph at N superscript 14 and between N superscript 14 and N superscript 15.

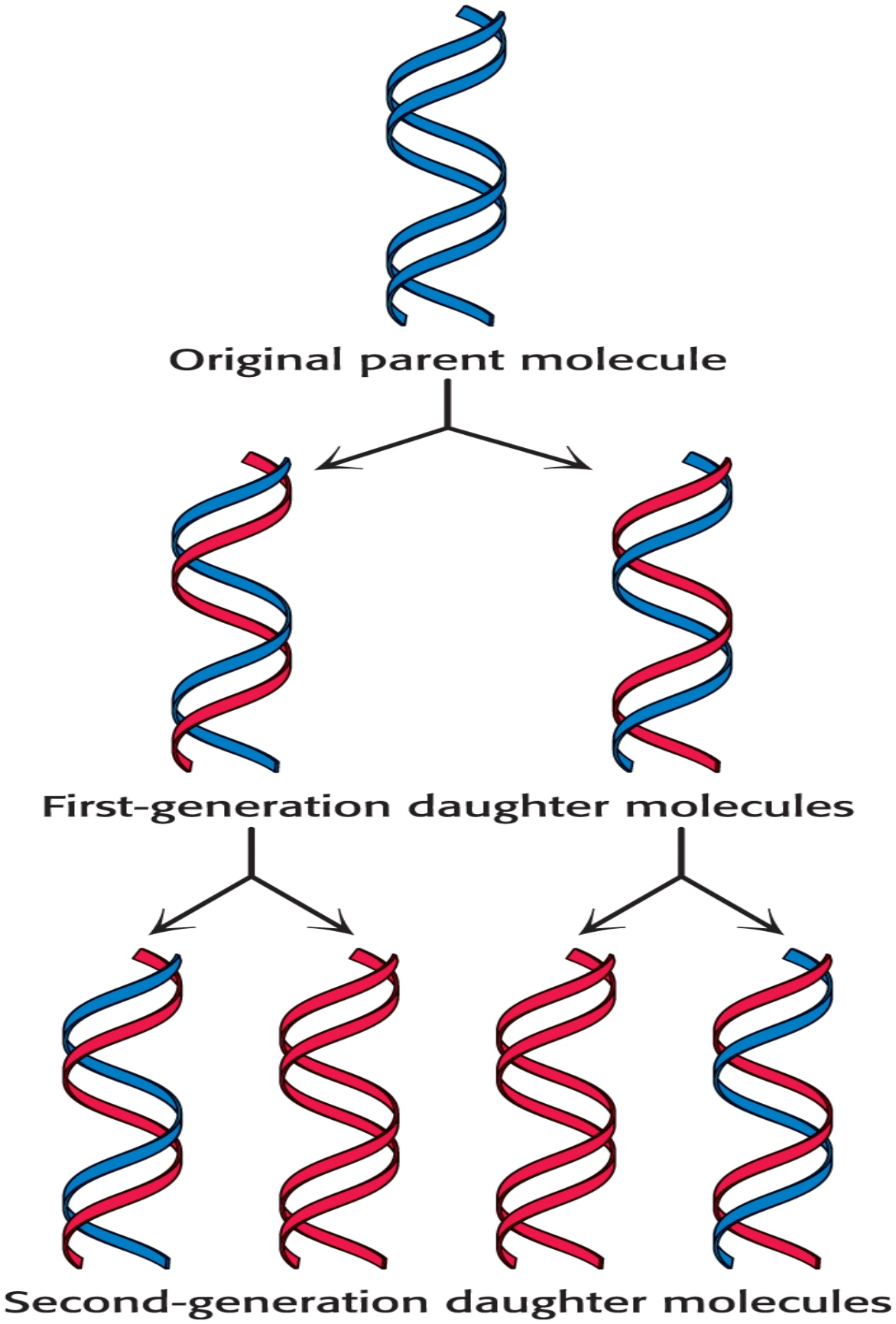
Generation 3: A thick, dark band is seen for N superscript 14 and a thin faint band is seen between N superscript 14 and N superscript 15. A corresponding tall peak at N superscript 14 and a short peak between N superscript 14 and N superscript 15 are seen on the graph.

Generation 4: A thicker, dark band is seen for N superscript 14 and an extremely faint band is seen between N superscript 14 and N superscript 15. A corresponding peak is seen in the graph at N superscript 14.

Return to FIGURE 8.20. D N A banding pattern detected by density-gradient centrifugation across 4 generations

Extended description for FIGURE 8.21. Schematic representation of the semi-conservative mode of D N A

replication

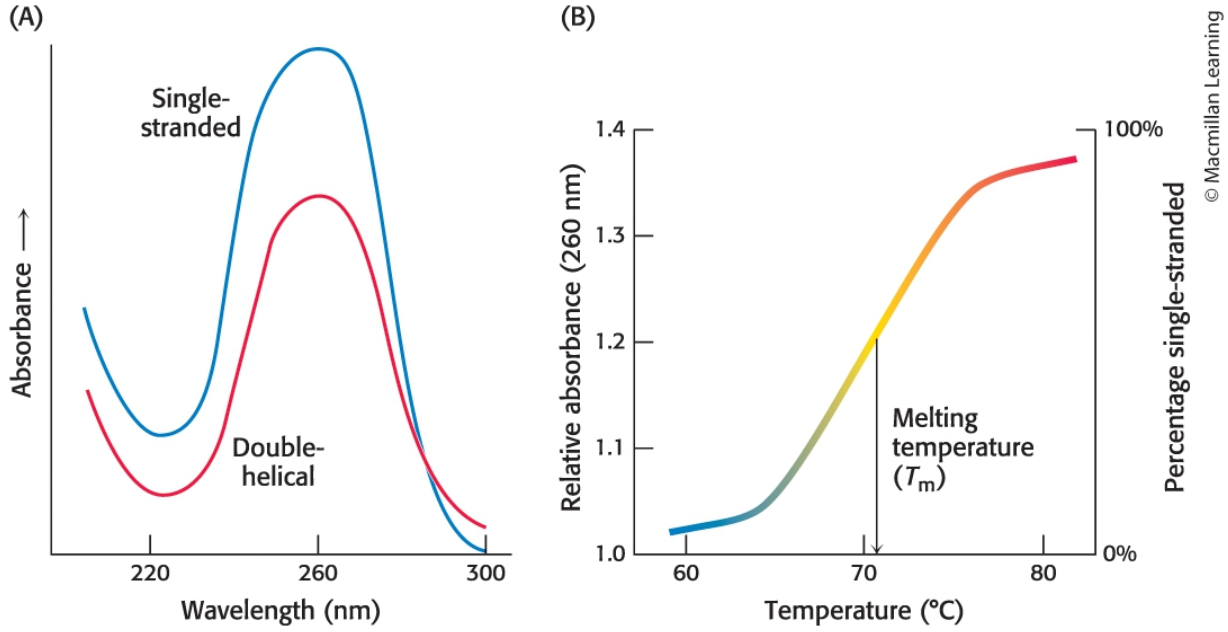


© Macmillan Learning

The original parent molecule is represented by a double helix with both strands colored blue. The original parent gives rise to two first generation daughter molecules. Each daughter molecule is represented by a double helix having one blue colored strand and the other red colored strand. Each first generation daughter molecule gives rise to two second generation daughter molecules. The second generation daughter molecules are each represented by a double helix. Half of the second generation daughter molecules have one blue and one red strand. The remaining daughter molecules have two red strands.

Return to FIGURE 8.21. Schematic representation of the semi-conservative mode of D N A replication

Extended description for FIGURE 8.22 Single-stranded DNA absorbs light more effectively than does double-helical DNA



Part (A): The horizontal axis is labeled Wavelength (n m) and ranges from 220 to 300 in increments of 40 units. The vertical axis is labeled Absorbance. The following two curves are shown:

Single-stranded (blue): It starts near the mid-point of the vertical axis and drops slightly at 220 n m, and rises to a high peak at 260 n m before dropping to a minimum at 300 n m.

Double-helical (red): It starts slightly below the blue curve and follows nearly the same trajectory as that of the blue curve but lies below it. The curve intersects the blue curve near the end before terminating at a point slightly higher than that of the blue curve at 300 n m.

Part (B): The horizontal axis is labeled temperature in degrees Celsius and ranges from 60 to 80 in increments of 10 units. The left vertical axis is labeled Relative absorbance (260 n m) and ranges from 1 to 1.4 in increments of 0.1 units. The right vertical axis is labeled Percentage single-stranded and ranges from 0 to 100 percent. The curve has a rainbow color gradient starting as blue and ending as red. The curve has a sigmoid shape. It starts just above (60, 1), rises slightly followed by a steep rise to (77, 1.35), then it gradually plateaus. The curve rises from 0 percent to 100 percent along the right vertical axis. A vertical arrow is drawn from the mid-point of the slope of the curve to the horizontal axis at nearly 71 degrees Celsius and is labeled Melting temperature (T subscript m).

All numerical values are estimated.

Return to FIGURE 8.22 Single-stranded DNA absorbs light more effectively than does double-helical DNA

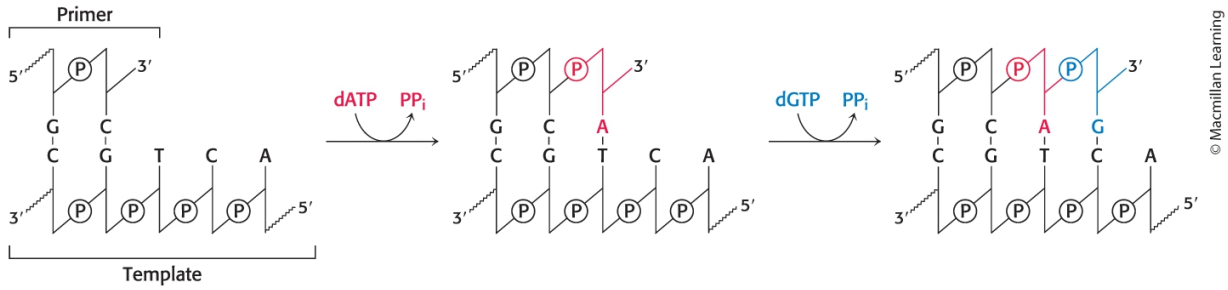
Extended description for Reaction catalyzed by D N A polymerase



The reaction consists of two reactants and two products. The first reactant is open parenthesis D N A close parenthesis with subscript n. The second reactant is d N T P. A reversible reaction arrow leads to the products. The first product is open parenthesis D N A close parenthesis with subscript n plus 1. The second product is P P subscript i.

Return to Reaction catalyzed by D N A polymerase

Extended description for FIGURE 8.23. Schematic illustration of D N A polymerization using the saw-tooth schematic



The template is shown to have the following sequence: 3 prime, C, G, T, C, A, 5 prime. The primer is bound to the template at the top near the 3 prime end and has the following sequence: 5 prime, G, C, 3 prime.

The reaction arrow shows the consumption of d A T P (red) and release of P P subscript i.

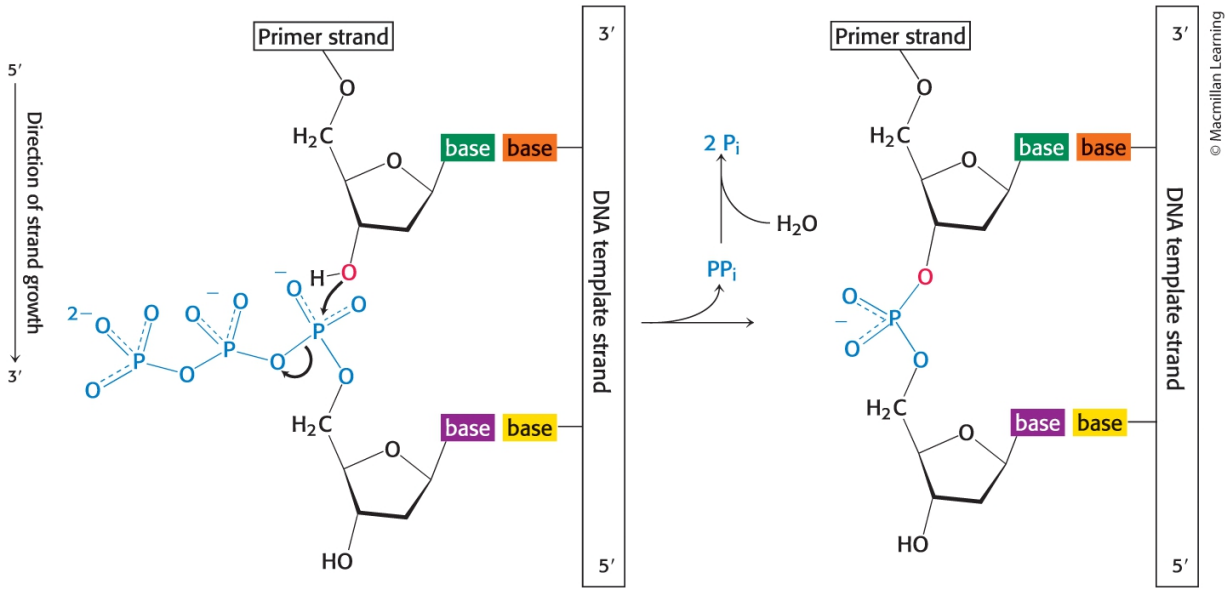
The product shows the growing primer with the following sequence: 5 prime, G, C, A (red), 3 prime.

The reaction arrow shows the consumption of d G T P (blue) and release of P P subscript i.

The product shows the growing primer with the following sequence: 5 prime, G, C, A (red), G (blue) 3 prime.

Return to FIGURE 8.23. Schematic illustration of D N A polymerization using the saw-tooth schematic

Extended description for FIGURE 8.24 DNA polymerases catalyze the strand-elongation reaction in the 5'-to-3' direction



The direction of polymerization is from the 5 prime to the 3 prime end. A vertical strip represents the D N A template strand with the top end labeled 3 prime and the bottom end labeled 5 prime. Two bases are highlighted in orange and yellow along the length of the template strand, from top to bottom. The primer strand is shown to the left of the template strand and is anti-parallel to the template strand. The 3 prime terminal nucleotide of the primer strand is base-paired with the orange base of the template strand.

The terminal primer nucleotide has the following structure: A 5-membered heterocyclic pentagonal ring in a vertical orientation consists of 1 O and 4 C atoms. The O atom occupies the first position which is the topmost vertex. C 1 is single bonded to the base (green). C 3 is single bonded to O (red) which is single bonded to H on the lower left. C 4 is single bonded to C H 2 which is single bonded to O

on the upper right which is single bonded to the primer strand on the upper left.

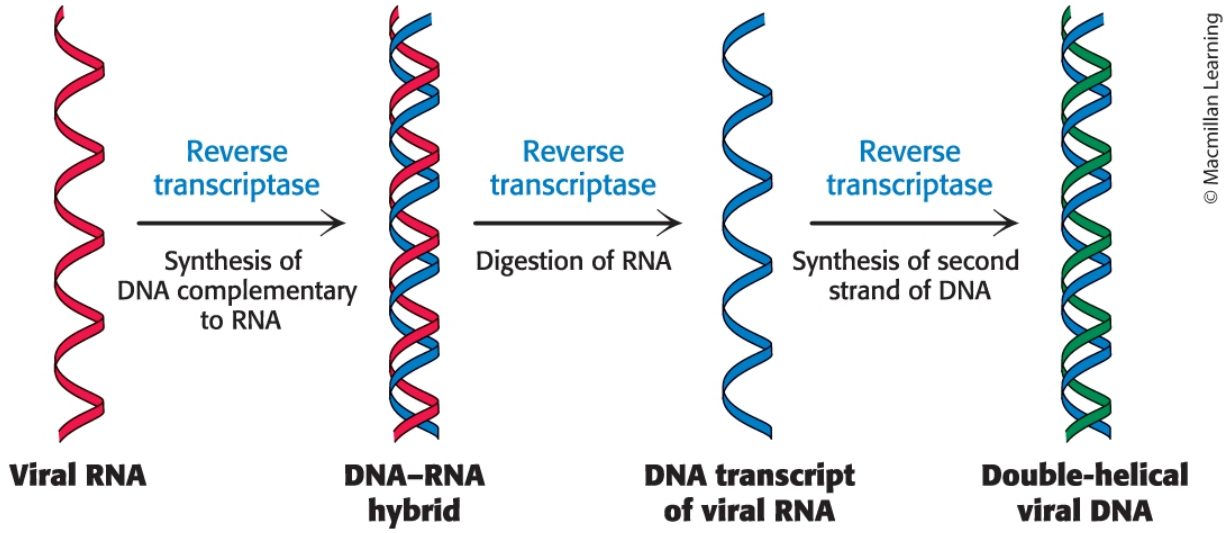
A nucleotide triphosphate is shown to react with the terminal primer nucleotide. The nucleotide triphosphate has the following structure: A 5-membered heterocyclic pentagonal ring in a vertical orientation consists of 1 O and 4 C atoms. The O atom occupies the first position, which is the topmost vertex. C 1 is single bonded to the base (purple). The base is aligned with the bottom base of the template strand. C 3 is single bonded to O H on the lower left. C 4 is single bonded to C H 2 which is single bonded to O of a triphosphate group on the upper right. Each phosphate group has a central P atom single bonded to O on the lower right, single bonded to O on the lower left, partially double bonded to O on the upper left, and partially double bonded to O on the upper right. The single bonded O atoms are shared between two adjacent phosphate groups. The terminal phosphate group carries a negative charge of 2 minus and the other two phosphate groups each carries a negative charge. An arrow points from the O of the O H group of the terminal primer nucleotide to the alpha P of the triphosphate. Another arrow points from this P to the single-bonded O on the lower left.

The reaction arrow shows the release of P P subscript i. P P subscript i reacts with H 2 O to give 2 P subscript i.

The product shows the formation of a 3 prime to 5 prime phosphodiester bond between the two nucleotides in the growing primer strand. The purple base of the primer strand is paired with the yellow base of the template strand.

Return to FIGURE 8.24 DNA polymerases catalyze the strand-elongation reaction in the 5'-to-3' direction

Extended description for FIGURE 8.25. Schematic representation of D N A synthesis from R N A template in retroviruses



Synthesis of D N A complementary to R N A. The viral R N A is represented by a red single helix. An arrow from the viral R N A to the D N A-R N A hybrid is labeled Reverse transcriptase. The D N A-R N A hybrid is represented by a double helix with one red and one blue strand.

Digestion of R N A: An arrow from the D N A-R N A hybrid to the D N A transcript of viral R N A is labeled Reverse transcriptase. The D N A transcript of viral R N A is represented by a blue single helix.

Synthesis of second strand of D N A: An arrow from the D N A transcript of viral R N A to double-helical viral D N A is labeled Reverse transcriptase. The double-helical viral D N A is represented by a double helix with one blue and one green strand.

Return to FIGURE 8.25. Schematic representation of D N A synthesis from R N A template in retroviruses

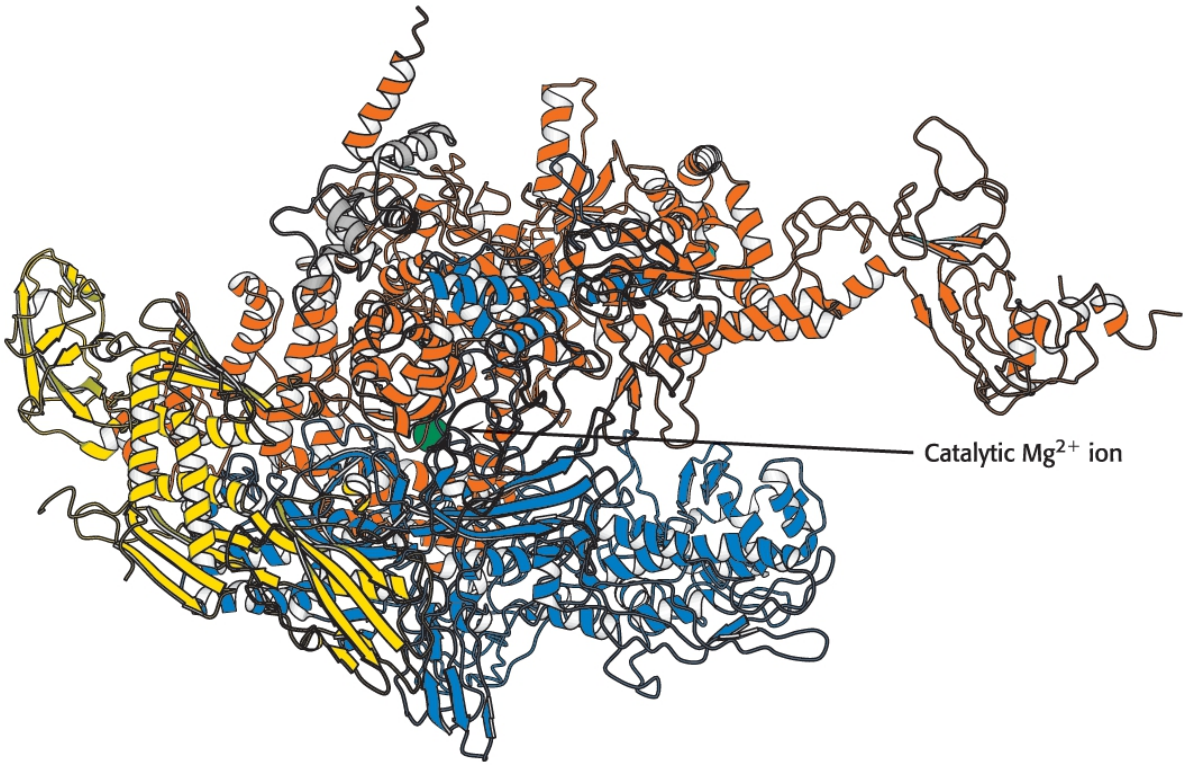
Extended description for Reaction catalyzed by R N A polymerase

$$(\mathrm{RNA})_{n\ \mathrm{residues}} + \mathrm{ribonucleoside\ triphosphate} \rightleftharpoons (\mathrm{RNA})_{n+1\ \mathrm{residues}} + \mathrm{PP_i}$$

The reaction consists of two reactants and two products. The first reactant is open parenthesis R N A close parenthesis with subscript n residues. The second reactant is ribonucleoside triphosphate. A reversible reaction arrow leads to the products. The first product is open parenthesis R N A close parenthesis with subscript n plus 1 residues. The second product is P P subscript i.

Return to Reaction catalyzed by R N A polymerase

Extended description for FIGURE 8.26. Ribbon structure of R N A polymerase

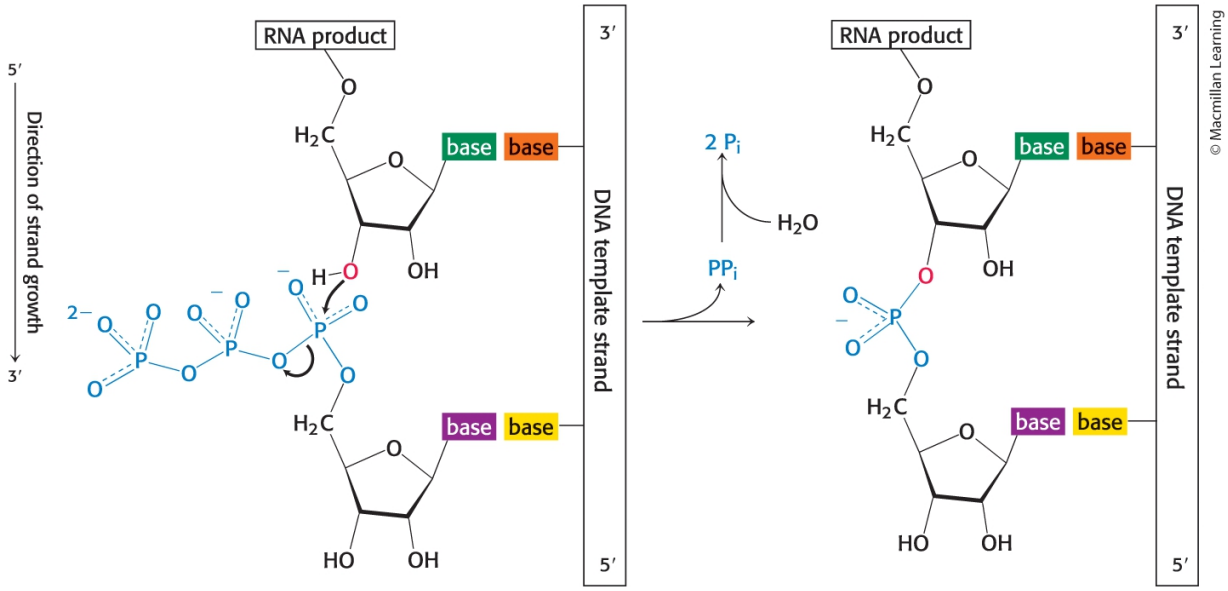


© Macmillan Learning

The multisubunit R N A polymerase enzyme consists of yellow, orange, and blue subunits. The overall shape of the enzyme resembles a crab claw. A green sphere embedded in the center of the enzyme is labeled catalytic M g superscript 2 plus ion.

Return to FIGURE 8.26. Ribbon structure of R N A polymerase

Extended description for FIGURE 8.27. Schematic representation of the elongation of the R N A strand catalyzed by R N A polymerase using D N A as a template



The direction of R N A strand growth is from the 5 prime to the 3 prime end. A vertical strip represents the D N A template strand with the top end labeled 3 prime and the bottom end labeled 5 prime. Two bases are highlighted in orange and yellow along the length of the template strand, from top to bottom. The R N A product strand is shown to the left of the template strand and is anti-parallel to the template strand. The 3 prime terminal nucleotide of the R N A product strand is base-paired with the orange base of the template strand.

The terminal primer nucleotide has the following structure: A 5-membered heterocyclic pentagonal ring in a vertical orientation consists of 1 O and 4 C atoms. The O atom occupies the first

position, which is the topmost vertex. C 1 is single bonded to the base (green). C 2 is single bonded to O H. C 3 is single bonded to O (red) which is single bonded to H on the lower left. C 4 is single bonded to C H 2 which is single bonded to O on the upper right which is single bonded to the R N A product strand on the upper left. A nucleotide triphosphate is shown to react with the terminal R N A product nucleotide.

The nucleotide triphosphate has the following structure: A 5-membered heterocyclic pentagonal ring in a vertical orientation consists of 1 O and 4 C atoms. The O atom occupies the first position, which is the topmost vertex. C 1 is single bonded to the base (purple). C 2 and C 3 are each single bonded to O H. C 4 is single bonded to C H 2 which is single bonded to O of a triphosphate group on the upper right. Each phosphate group has a central P atom single bonded to O on the lower right, single bonded to O on the lower left, partially double bonded to O on the upper left, and partially double bonded to O on the upper right. The single bonded O atoms are shared between two adjacent phosphate groups. The terminal phosphate group carries a negative charge of 2 minus and the other two phosphate groups each carry a negative charge.

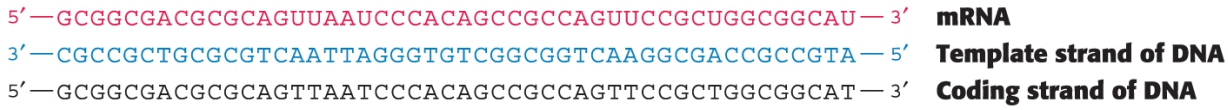
An arrow points from the O atom of the O H group bound to C 3 of the R N A product nucleotide to the alpha P of the triphosphate. Another arrow points from this P to the single-bonded O on the lower left.

The reaction arrow shows the release of P P subscript i. P P subscript i reacts with H 2 O to give 2 P subscript i.

The product shows the formation of a 3 prime to 5 prime phosphodiester bond between the two nucleotides in the growing R N A product strand. The purple base of the R N A product strand is paired with the yellow base of the D N A template strand.

Return to FIGURE 8.27. Schematic representation of the elongation of the R N A strand catalyzed by R N A polymerase using D N A as a template

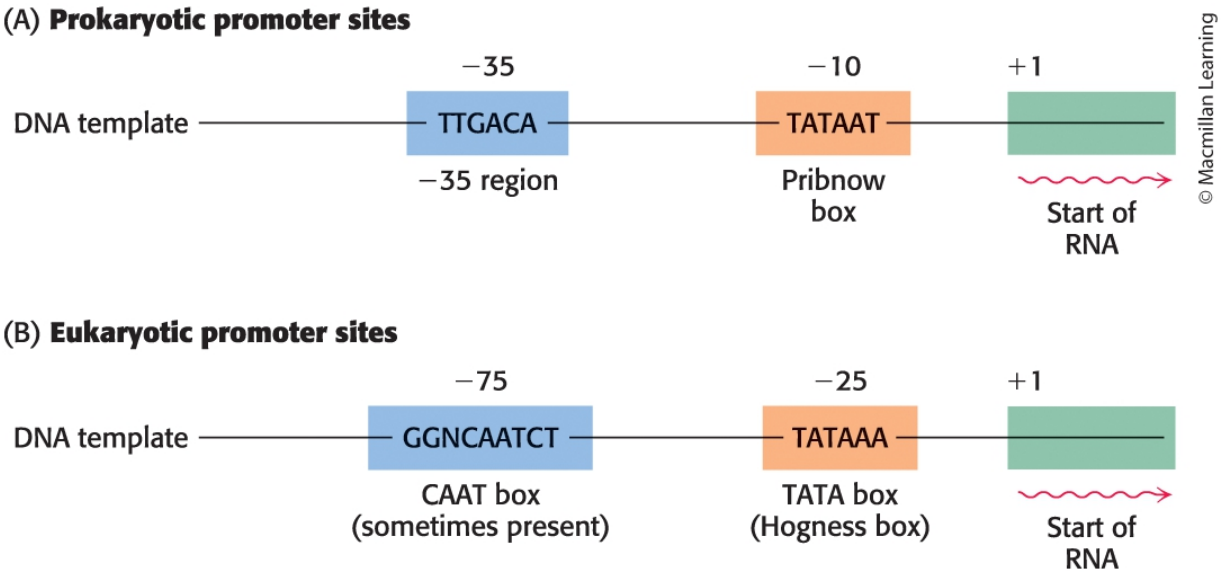
Extended description for FIGURE 8.28. Sequences of m R N A strand, template D N A strand, and coding D N A strand



The orientation of the m R N A strand is 5 prime to 3 prime, from the left to right. It is composed of G, C, A, and U bases. The orientation of the template D N A strand is 3 prime to 5 prime, from the left to right. It is composed of G, C, A, and T bases. The orientation of the coding D N A strand is 5 prime to 3 prime, from the left to right. It is composed of G, C, A, and T bases. The m R N A strand is complementary to the template strand. In the m R N A strand, G is present opposite to C in the template D N A strand, U is present opposite to A in the template D N A strand, and T is present opposite to A in the template D N A strand. The m R N A is identical to the coding D N A strand except for the U replaced with T in the D N A strand. The template strand is complementary to the coding strand.

Return to FIGURE 8.28. Sequences of m R N A strand, template D N A strand, and coding D N A strand

Extended description for FIGURE 8.29. Schematic representation of the prokaryotic and eukaryotic promoter sites

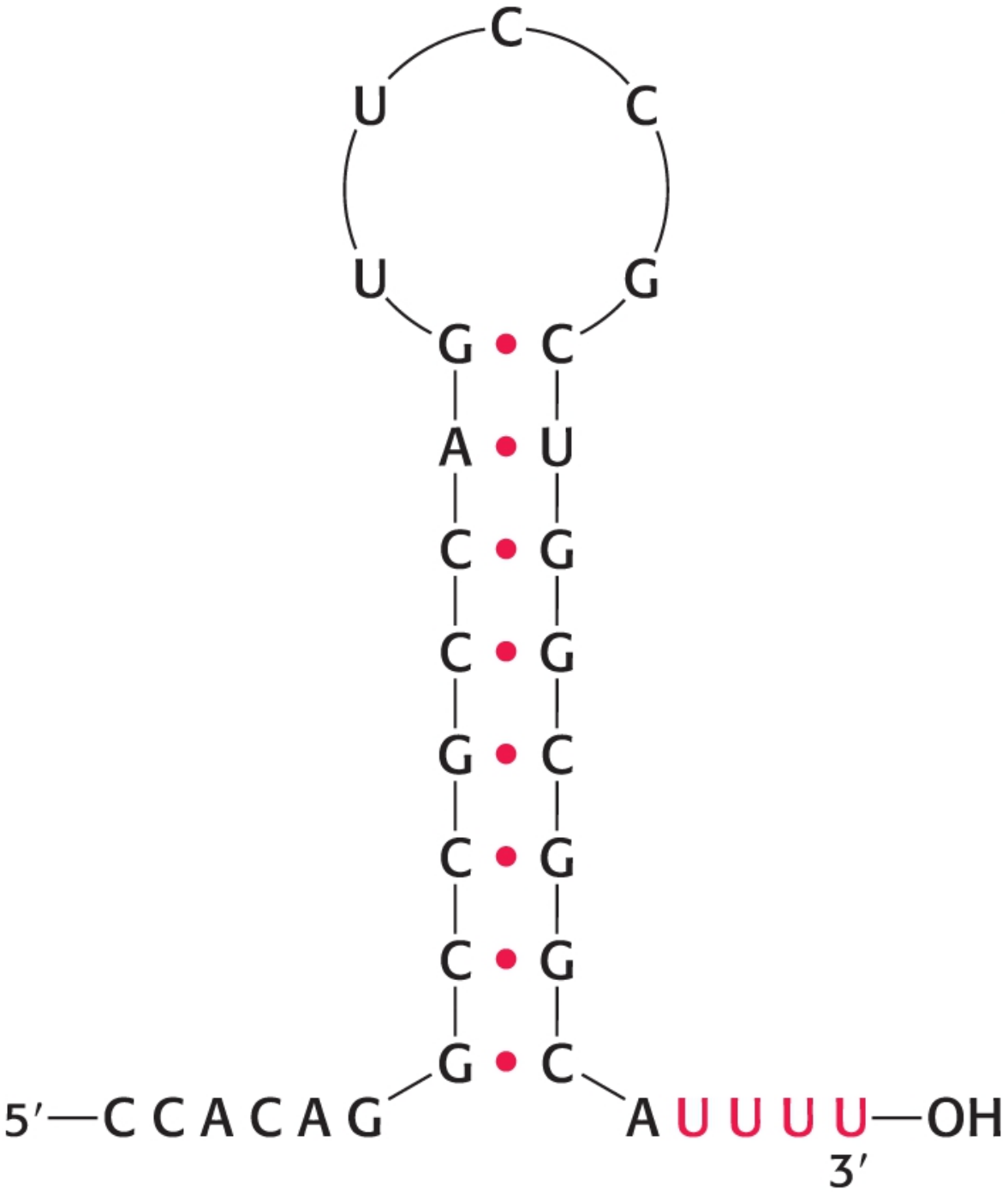


Part (A): Prokaryotic promoter sites. The D N A template is shown to extend to a minus 35 region (blue) with the sequence T T G A C A. This is followed by the Pribnow box (orange) at minus 10 with the sequence T A T A A T. This is followed by a green box labeled plus 1 at the start. The plus 1 mark denotes the start of R N A synthesis.

Part (B): Eukaryotic promoter sites. The D N A template is shown to extend to the C A A T box region (blue) which is sometimes present at minus 75 and has the sequence G G N C A A T C T. This is followed by the TATA box (orange) at minus 25 with the sequence T A T A A A. This is followed by a green box labeled plus 1 at the start. The plus 1 mark denotes the start of R N A synthesis.

Return to FIGURE 8.29. Schematic representation of the prokaryotic and eukaryotic promoter sites

Extended description for FIGURE 8.30. Stem-loop structure at the 3 prime end of an *E.coli* m R N A transcript

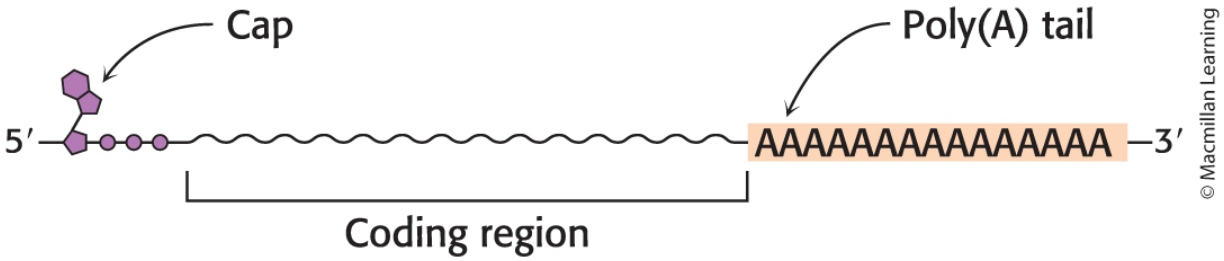


© Macmillan Learning

The stem-loop structure has a 5 prime trail end to the left and a 3 prime trail end to the right. Base pairing between A and U and G and C are shown by red dots along the stem. The loop has 5 nucleotides, U, U, C, C, and G in a clockwise direction starting from the bottom left. The 3 prime end of the stem-loop has a repeating U sequence with an O H terminal. The sequence at the 5 prime end is C C A C A G.

Return to FIGURE 8.30. Stem-loop structure at the 3 prime end of an *E.coli* m R N A transcript

Extended description for FIGURE 8.31. Schematic representation of mRNA in eukaryotes modified after transcription

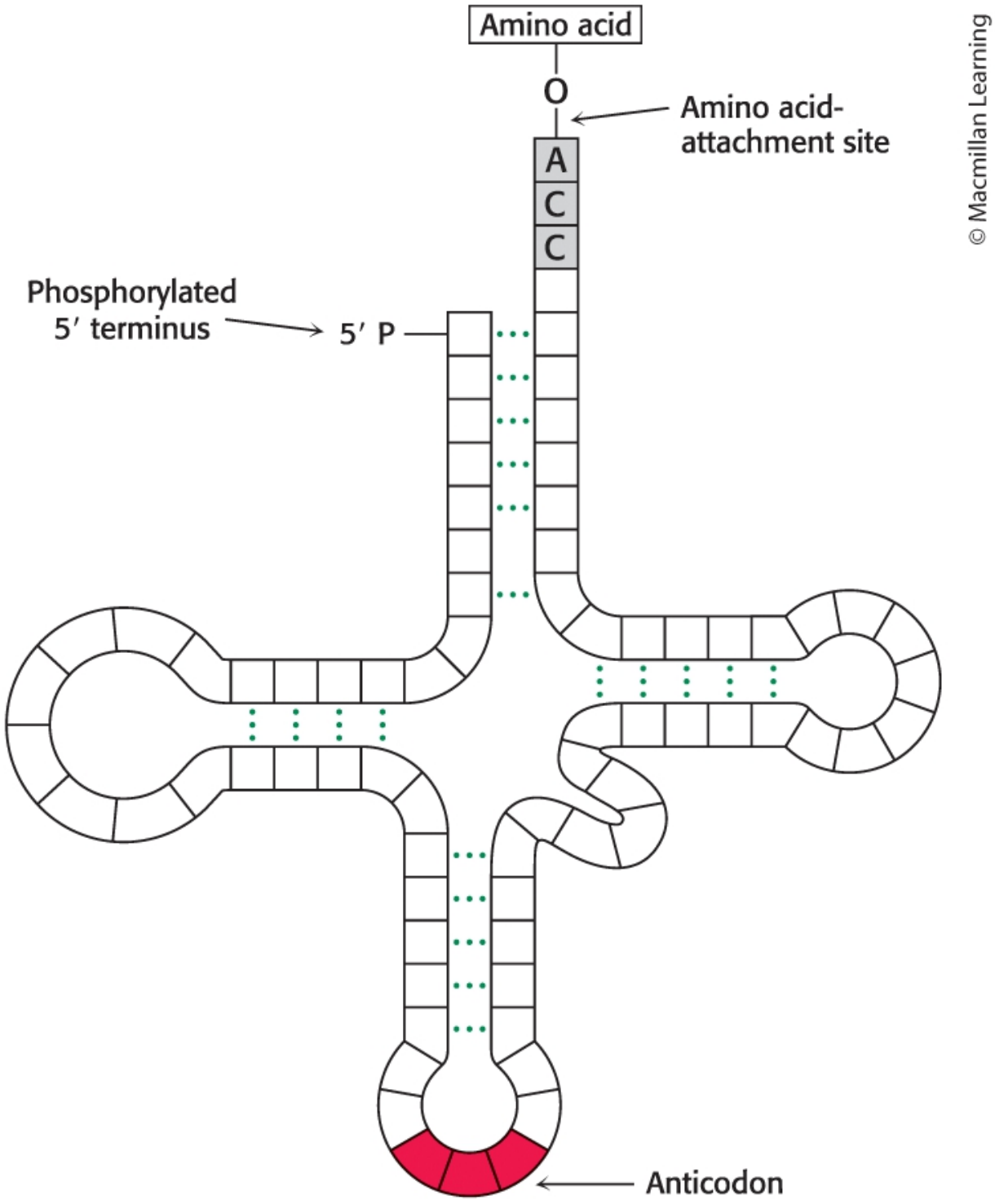


The coding region in the middle is flanked by a cap at the 5 prime end (left) and a Poly (A) tail at the 3 prime end (right). The cap is shown as a purine nucleotide. The poly (A) tail is shown as a repeating A sequence.

Return to FIGURE 8.31. Schematic representation of mRNA in eukaryotes modified after transcription

Extended description for FIGURE 8.32. Structure of a t

R N A molecule



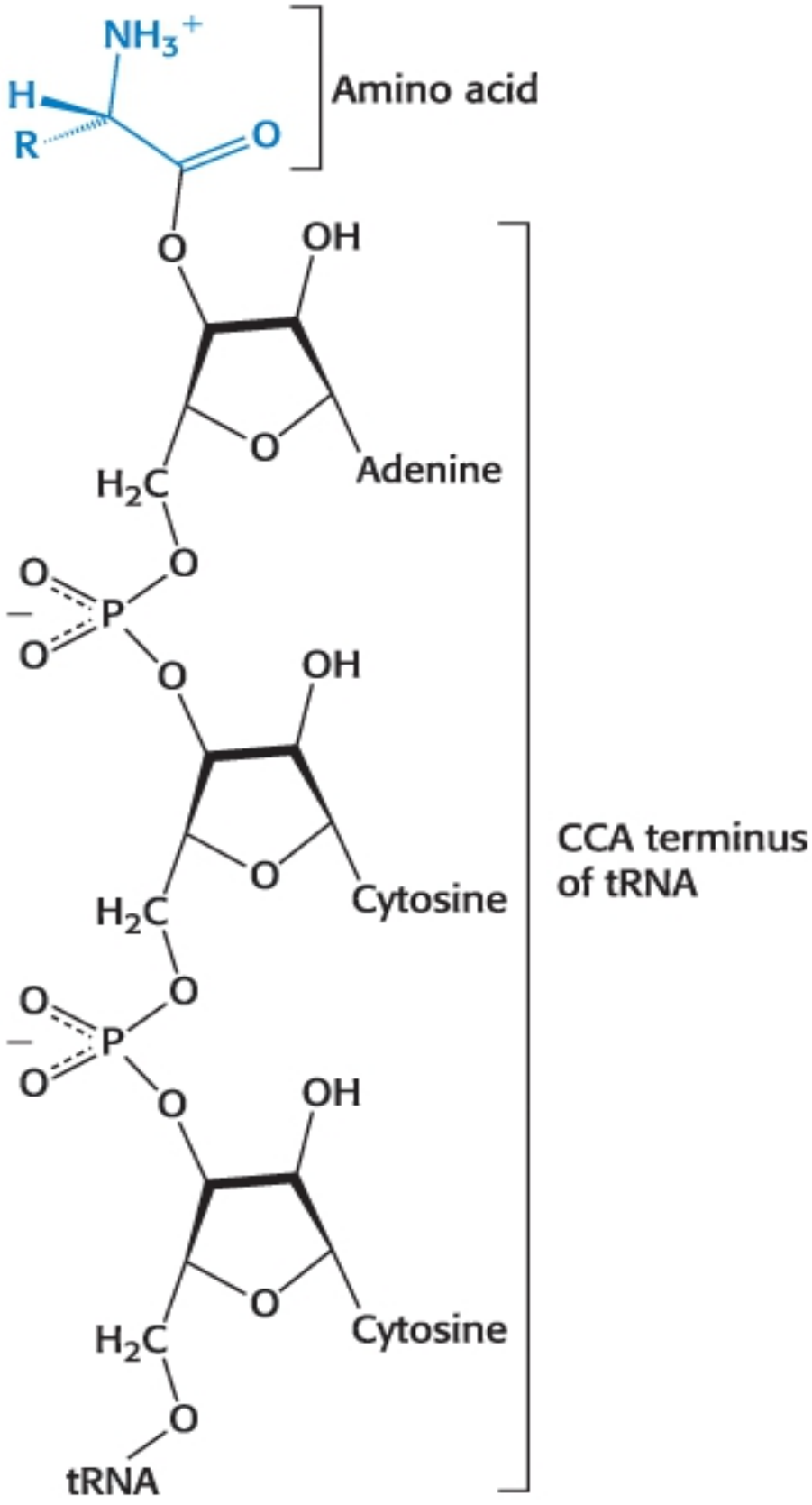
The t R N A molecule is shown to comprise several stem-loop structures formed by a single-strand of R N A via intramolecular hydrogen bonding. The three-dimensional structure resembles a clover leaf structure with 4 arms- 3 long and 1 short arm. The terminal of the left segments of the extended top portion is labeled phosphorylated 5 prime terminus. The left segment has a terminal C C A sequence. An amino acid is single bonded to O which is single bonded to the terminal base A. This site is labeled amino-acid attachment site. The three bases at the bottom loop are highlighted in red and labeled anticodon. A short loop is present between the right and bottom loops.

Return to FIGURE 8.32. Structure of a t R N A molecule

Extended description for FIGURE 8.33. The structure of

amino acyl-t R N A

Aminoacyl-tRNA



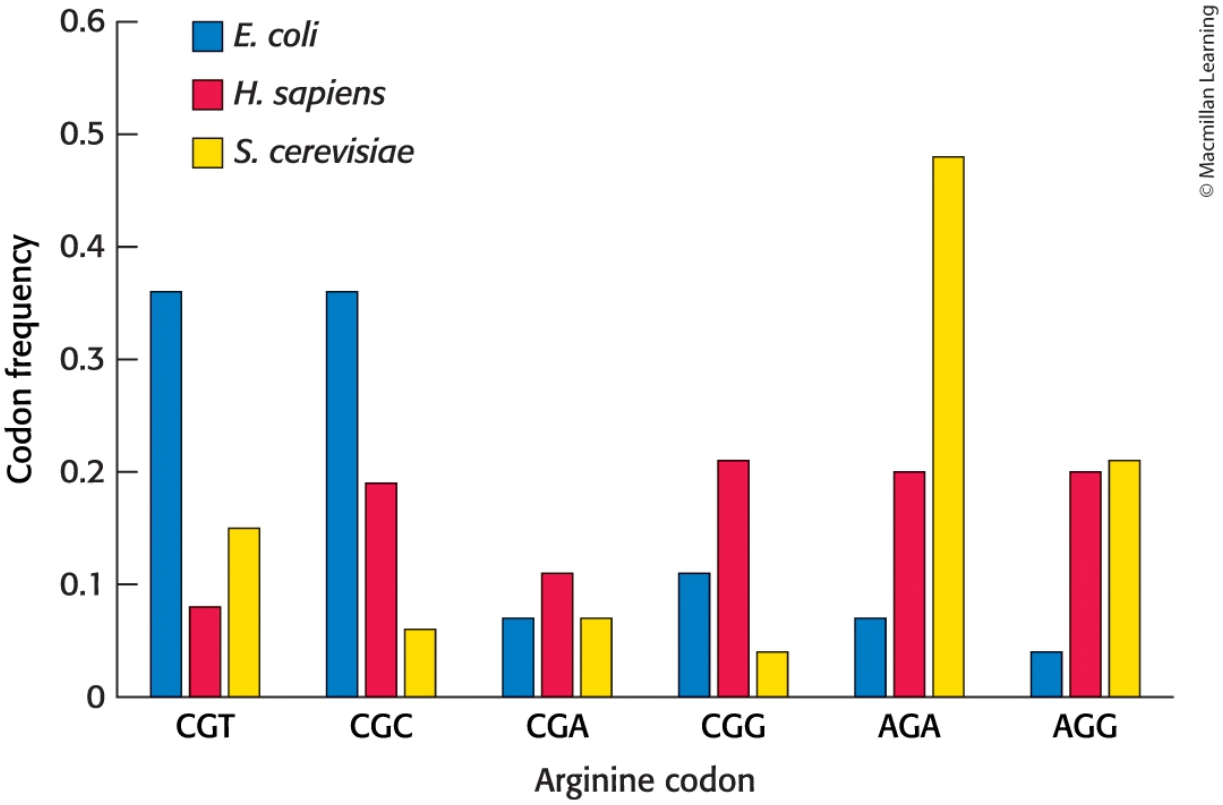
Amino acyl-t R N A:

The amino acid (blue) has the following structure: A central C atom is single bonded to N H 3 superscript plus above, wedge bonded to H on the left, dash bonded to R on the lower left, and single bonded to a central C atom on the lower right. This C atom is double bonded to O on the upper right and single bonded to O of a nucleotide of the C C A terminus of t R N A below.

The nucleotide has the following structure: A 5-membered heterocyclic pentagonal ring in a vertical orientation consists of 1 O and 4 C atoms. The O atom occupies the first position which is the bottom-most vertex. C 1 is single bonded to C H 2. C 2 is single bonded to O which is single bonded to the amino acid. C 3 is single bonded to O H. C 4 is single bonded to Adenine on the lower right. C H 2 bonded to C 1 is single bonded to O on the lower right which is single bonded to P on the lower left. P is partially double bonded to O on the upper left, partially double bonded to O on the lower left, and single bonded to O on the lower right. The partially double-bonded O atoms carry a negative charge. The O on the lower right is single bonded to C 2 of the pentagonal ring of the next nucleotide, cytosine. This is further linked to another cytosine below.

Return to FIGURE 8.33. The structure of amino acyl-t R N A

Extended description for FIGURE 8.34. Graphical representation of arginine codon usage preference in different species



© Macmillan Learning

The horizontal axis is labeled arginine codon. The vertical axis is labeled codon frequency and ranges from 0 to 0.6 in increments of 0.1 units. *E. coli* is shown in blue, *H. sapiens* in red, and *S. cerevisiae* in yellow. The following 6 markings are indicated along the horizontal axis:

C G T: *E. coli,* 0.36. *H. sapiens,* 0.08. *S. cerevisiae,* 0.15

C G C: *E. coli,* 0.36. *H. sapiens,* 0.2. *S. cerevisiae,* 0.05

C G A: *E. coli,* 0.07. *H. sapiens,* 0.12. *S. cerevisiae,* 0.07

C G G: *E. coli,* 0.12. *H. sapiens,* 0.22. *S. cerevisiae,* 0.03

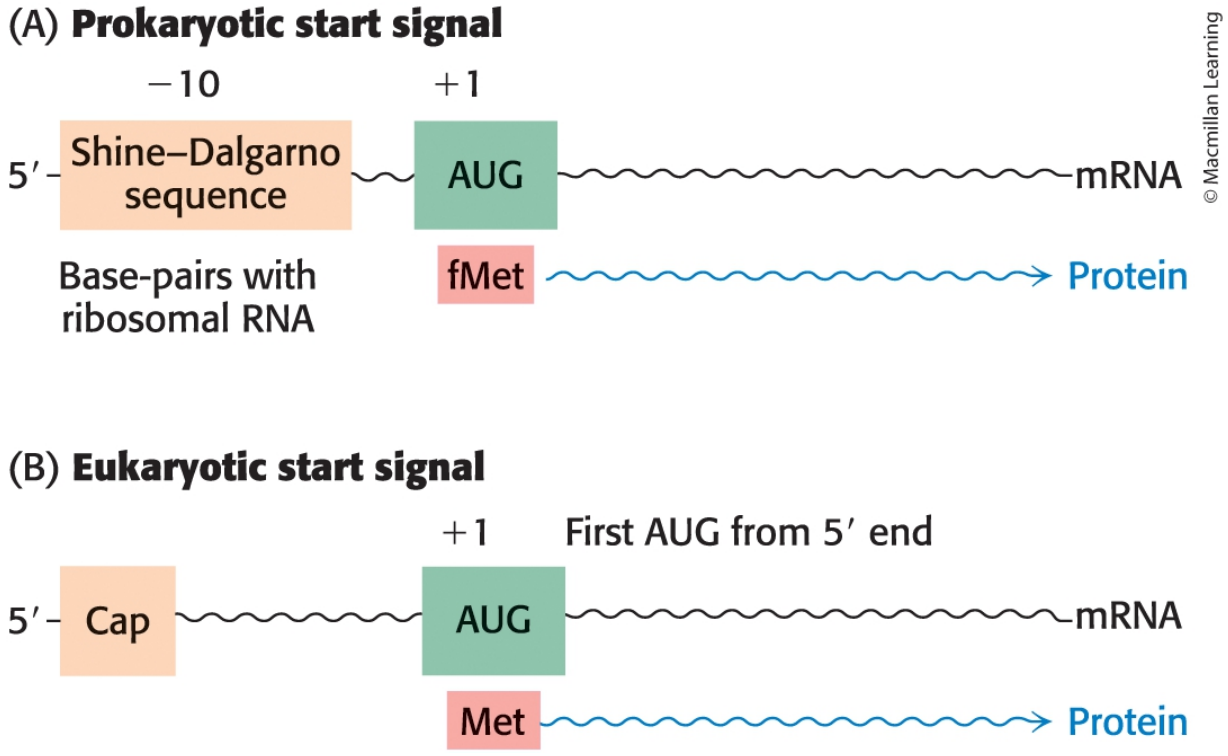
A G A: *E. coli,* 0.06. *H. sapiens,* 0.2. *S. cerevisiae,* 0.5

A G G: *E. coli,* 0.03. *H. sapiens,* 0.2. *S. cerevisiae,* 0.22

All numerical values are estimated.

Return to FIGURE 8.34. Graphical representation of arginine codon usage preference in different species

Extended description for FIGURE 8.35. Schematic representation of the prokaryotic and eukaryotic start signals for protein synthesis



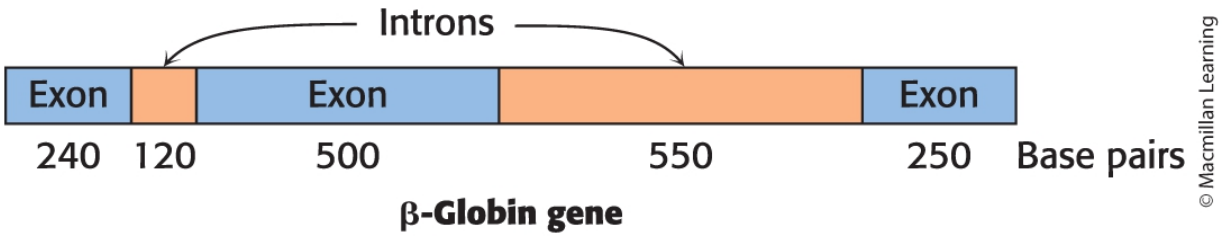
Part (A): Prokaryotic start signal. The 5 prime terminal is at the left followed by the Shine-Dalgarno sequence at minus 10. The next is A U G starting at plus 1 which extends into the m R N A sequence. The Shine-Dalgarno sequence base-pairs with ribosomal R N A. A U G codes for f Methionine and extends into the protein coded by the m R N A sequence.

Part (B): Eukaryotic start signal. The 5 prime terminal is at the left followed by a Cap. The Cap is followed by an m R N A sequence till A U G starting at plus 1. This extends into the rest of the m R N A

sequence. The first A U G from 5 prime end codes for methionine and extends into the protein coded by the m R N A sequence.

Return to FIGURE 8.35. Schematic representation of the prokaryotic and eukaryotic start signals for protein synthesis

Extended description for FIGURE 8.36. Schematic illustration of structure of the beta-globin gene

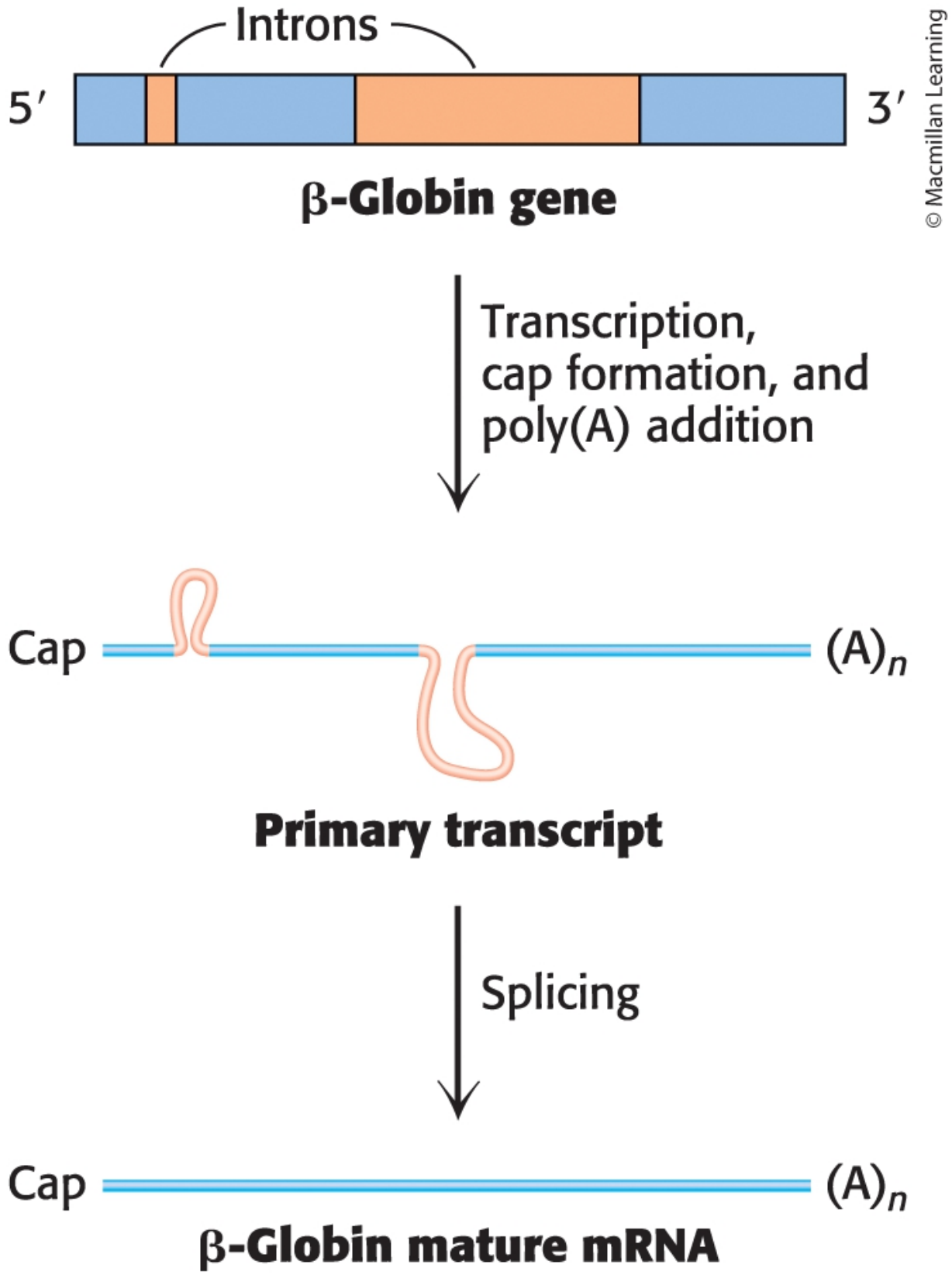


The gene is discontinuous with exons (blue) interspersed with introns (orange). The segments, from left to right are as follows: Exon (240 base pairs), Intron (120 base pairs), Exon (500 base pairs), Intron (550 base pairs), and Exon (250 base pairs).

Return to FIGURE 8.36. Schematic illustration of structure of the beta-globin gene

Extended description for FIGURE 8.37. Schematic

representation of the splicing of a beta-globin m R N A



© Macmillan Learning

Beta-globin gene: The 5 prime terminal is on the left and the 3 prime terminal is on the right. Two orange segments labeled introns are shown in between blue m R N A segments. The introns are of varying sizes.

An arrow from the beta-globin gene is pointed at the primary transcript. The arrow is labeled transcription, cap formation, and poly-A addition.

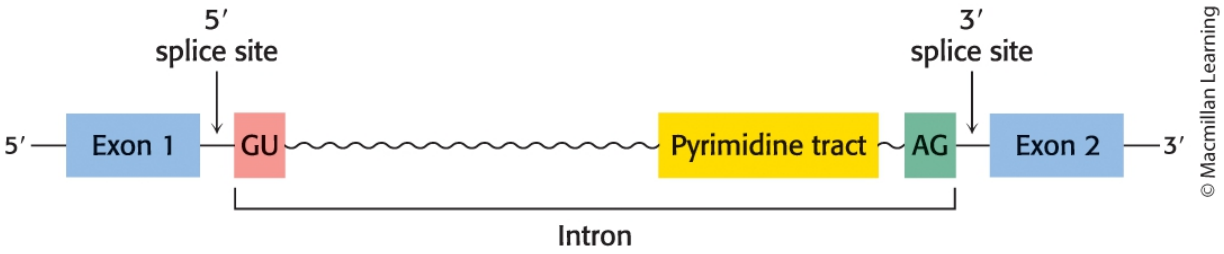
Primary transcript: The m R N A is shown as a solid blue line with a cap at the left terminal and (A) subscript n at the right terminal. Two pink loops are seen at the position of the introns in the beta-globin gene.

An arrow from the primary transcript is pointed at the beta-globin mature m R N A. The arrow is labeled splicing.

Beta-globin mature m R N A: A continuous long stretch of blue mature m R N A is shown with the cap at the left terminal and (A) subscript n at the right terminal.

Return to FIGURE 8.37. Schematic representation of the splicing of a beta-globin m R N A

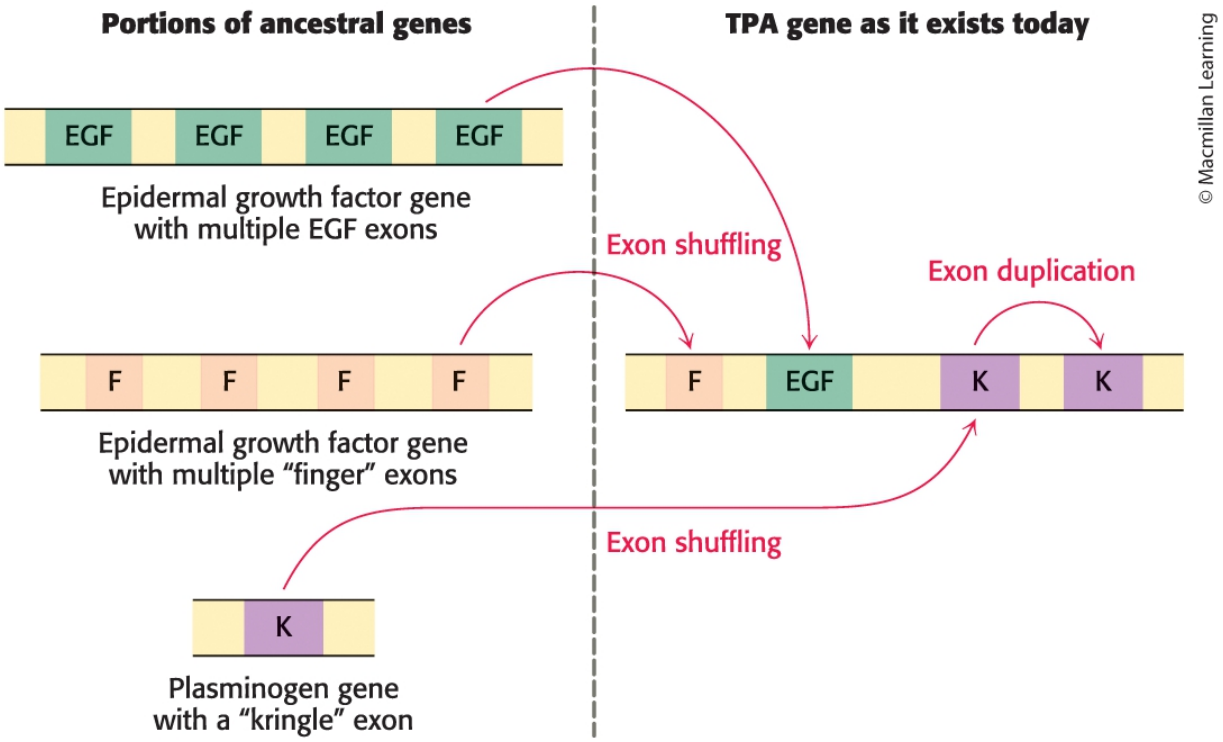
Extended description for FIGURE 8.38. Schematic representation of the location of splice sites in an m R N A



The order of sequences from the 5 prime to the 3 prime end in the left to right direction are as follows: Exon 1 (blue), 5 prime splice site, G U (red), m R N A stretch, pyrimidine tract (yellow), A G (green), 3 prime splice site, exon 2 (blue). The region of m R N A between the 5 prime and the 3 prime splice site is labeled intron.

Return to FIGURE 8.38. Schematic representation of the location of splice sites in an m R N A

Extended description for FIGURE 8.39 The tissue plasminogen activator (TPA) gene was generated by exon shuffling



Portions of ancestral genes:

Epidermal growth factor gene with multiple E G F exons: A stretch of a gene is shown with E G F exons (green) interspersed with short introns.

Epidermal growth factor gene with multiple "finger" exons: A stretch of a gene is shown with short F exons (pink) interspersed with introns.

Plasminogen gene with a "kringle" exon: A gene is shown with one K exon (purple) flanked by two introns on either side.

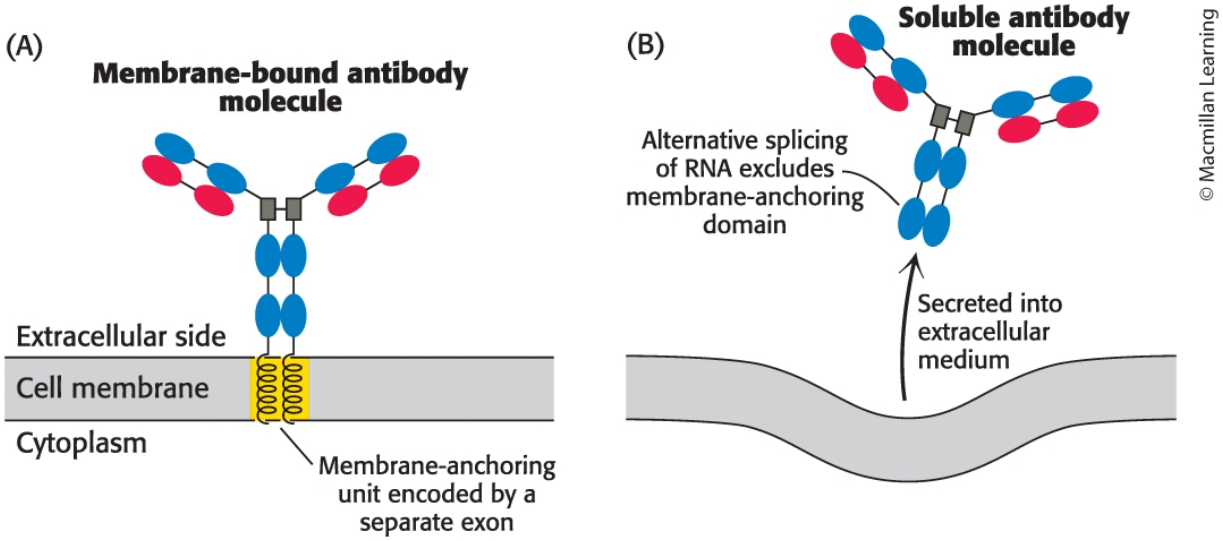
T P A gene as it exists today:

An arrow each from the E G F exon, F exon, and K exon to the T P A gene is labeled Exon shuffling.

The sequence of the T P A gene is as follows: Intron, F exon, intron, E G F exon, intron, K exon, intron, K exon, intron. An arrow from the first K exon to the next K exon in the T P A gene is labeled Exon duplication.

Return to FIGURE 8.39 The tissue plasminogen activator (TPA) gene was generated by exon shuffling

Extended description for FIGURE 8.40. Schematic illustration of membrane-bound and soluble antibody molecules generated by alternative splicing

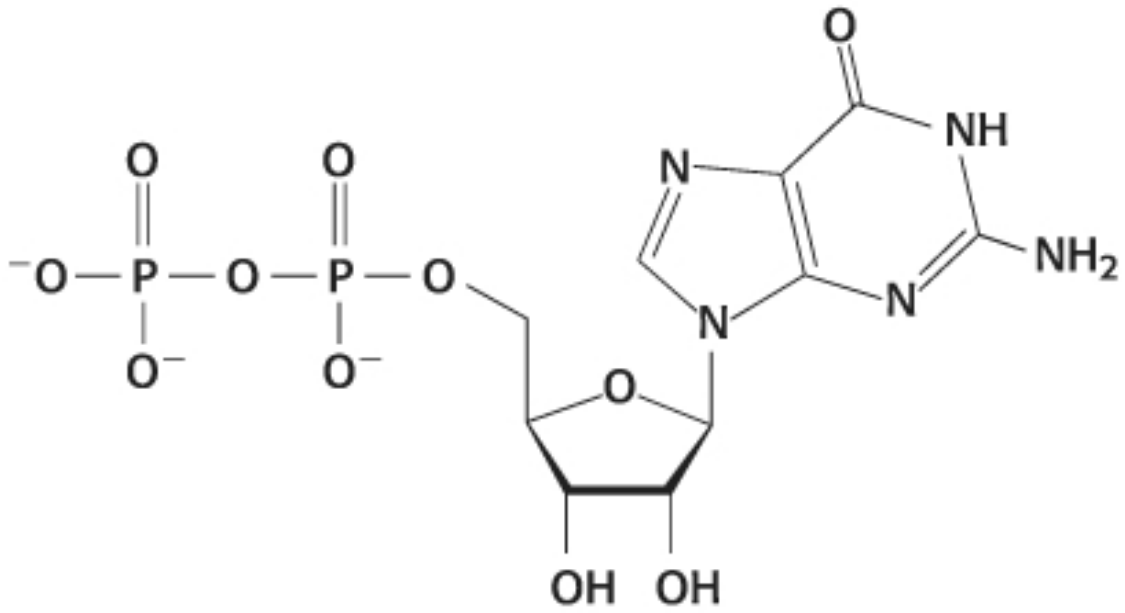


Part (A): Membrane-bound antibody molecule. A horizontal strip is labeled Cell membrane which separates the extracellular side above from the Cytoplasm below. A pair of vertical yellow coils are shown embedded in the cell membrane and labeled Membrane-anchoring unit encoded by a separate exon. A Y-shaped antibody molecule is shown adhered to the membrane-anchoring units. The antibody has two blue heavy chains forming the Y-shape. A short red light chain is linked in parallel to each top arm of the heavy chain.

Part (B): Soluble antibody molecule. The cell membrane is shown to curve slightly inward forming a bowl shape. The Y-shaped antibody molecule is shown to be secreted into the extracellular medium. An arrow directed to the bottom of the antibody is labeled Alternative splicing of R N A excludes membrane-anchoring domain.

Return to FIGURE 8.40. Schematic illustration of membrane-bound and soluble antibody molecules generated by alternative splicing

Extended description for Chemical structure

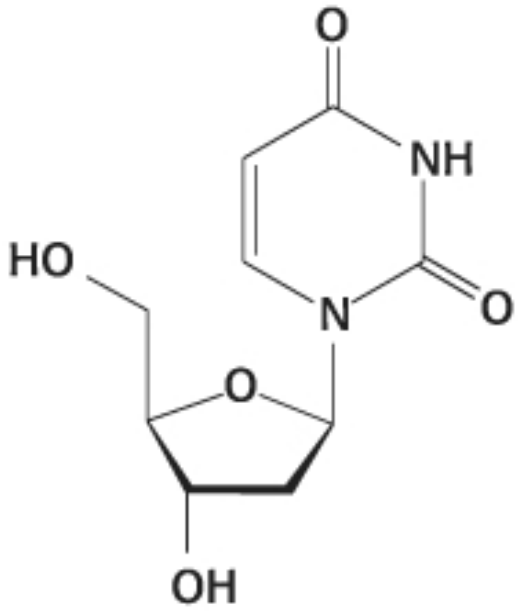


The structure is as follows: A 5-membered heterocyclic pentagonal ring in a vertical orientation consists of 1 O and 4 C atoms. The O atom occupies the first position, which is the topmost vertex. C 2 and C 3 are single bonded to O H below. C 4 is single bonded to C H 2 above in the form of a line that is further single bonded to O on the upper left. O is single bonded to P, single bond, O, single bond, P, single bond, O superscript minus. Each P is double bonded to O above and single bonded to O superscript minus below. C 1 is single bonded to the first N of a 5-membered heterocyclic pentagonal ring in a horizontal orientation. The ring consists of 2 N and 3 C atoms. The first N occupies the first position which is the bottom left vertex and the second N occupies the third position which is the top left vertex. C 1 occupies the leftmost vertex. A double bond is present between C 1 and the second N. The pentagonal ring is fused to a 6-membered heterocyclic hexagonal ring in a vertical orientation such that C 2 and C 3 of the pentagonal ring are C 3 and C 2 of the hexagonal ring respectively. The hexagonal ring consists of 2 N and 4

C atoms. The first N atom bound to H occupies the first position, which is the top right vertex and the second N atom occupies the third position, which is the bottom-most vertex. C 1 occupies the bottom right vertex. A double bond is present between C 1 and the second N and C 2 and C 3. C 1 is single bonded to N H 2 on the lower right. C 4 is double bonded to O above.

Return to Chemical structure

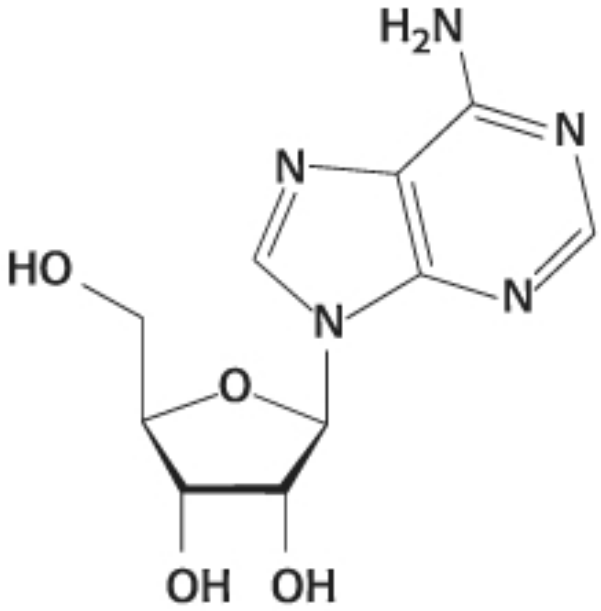
Extended description for Chemical structure



The structure is as follows: A 5-membered heterocyclic pentagonal ring in a vertical orientation consists of 1 O and 4 C atoms. The O atom occupies the first position, which is the topmost vertex. C 3 is single bonded to O H below. C 4 is single bonded to C H 2 above in the form of a line that is further single bonded to O H on the upper left. C 1 is single bonded to the second N of a 6-membered heterocyclic hexagonal ring in a vertical orientation. The hexagonal ring consists of 2 N and 4 C atoms. The first N atom bound to H occupies the first position, which is the top right vertex and the second N atom occupies the third position, which is the bottom-most vertex. C 1 and C 4 are each double bonded to O. A double bond is present between C 2 and C 3.

Return to Chemical structure

Extended description for Chemical structure

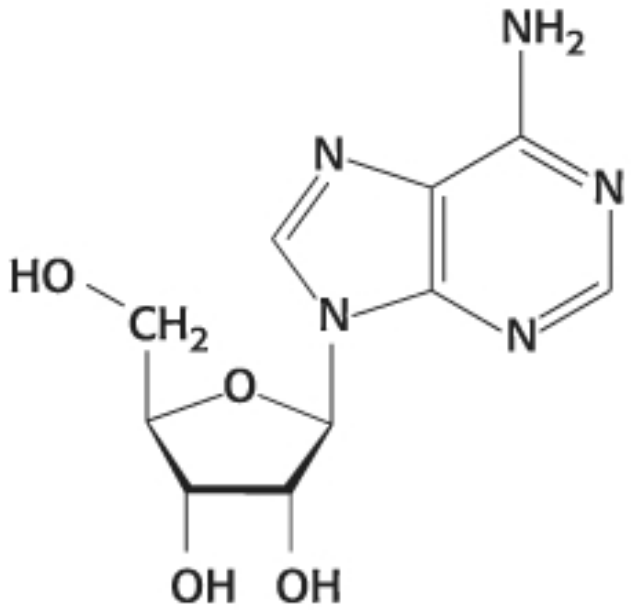


The structure is as follows: A 5-membered heterocyclic pentagonal ring in a vertical orientation consists of 1 O and 4 C atoms. The O atom occupies the first position, which is the topmost vertex. C 2 and C 3 are each single bonded to O H below. C 4 is single bonded to C H 2 above in the form of a line that is further single bonded to O H on the upper left. C 1 is single bonded to the first N of a 5-membered heterocyclic pentagonal ring in a horizontal orientation. The ring consists of 2 N and 3 C atoms. The first N occupies the first position, which is the bottom left vertex and the second N occupies the third position, which is the topmost vertex. A double bond is present between C 1 and the second N. The pentagonal ring is fused to a 6-membered heterocyclic hexagonal ring in a vertical orientation such that C 2 and C 3 of the pentagonal ring are C 3 and C 2 of the hexagonal ring respectively. The hexagonal ring consists of 2 N and 4 C atoms. The first N atom occupies the first position, which is the top right vertex and the second N atom occupies the third position, which is the bottom-most vertex. C 1 occupies the bottom right

vertex. Alternating double bonds are present between C 1 and the second N, C 2 and C 3, and C 4 and the first N. C 4 is single bonded to N H 2 above.

Return to Chemical structure

Extended description for Chemical structure

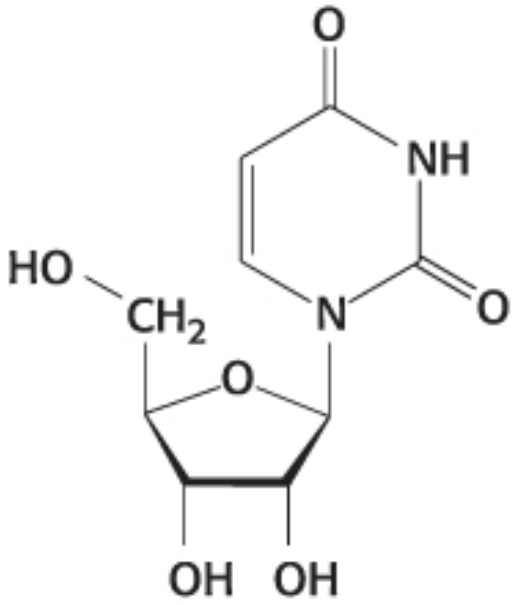


The structure is as follows: A 5-membered pentagonal ring in a vertical orientation consists of 1 O and 4 C atoms. The O atom occupies the first position, which is the topmost vertex. C 2 and C 3 are each single bonded to O H below. C 4 is single bonded to C H 2 which is single bonded to O H on the upper left. C 1 is single bonded to the first N of a 5-membered heterocyclic pentagonal ring in a horizontal orientation. The ring consists of 2 N and 3 C atoms. The first N occupies the first position which is the bottom left vertex and the second N occupies the third position which is the top left vertex. A double bond is present between C 1 and the second N. The pentagonal ring is fused to a 6-membered heterocyclic hexagonal ring in a vertical orientation. The ring consists of 2 N and 4 C atoms. The first N atom occupies the first position which is the top right vertex and the second N atom occupies the third position which is the bottom-most vertex. Three alternating double bonds are present between C 1 and second N, C 2 and C 3, and C 4 and the first N. C 4 is single bonded to N H 2 above. The rings are fused such that C 2 and

C 3 of the pentagonal ring are C 3 and C 2 of the hexagonal ring respectively.

Return to Chemical structure

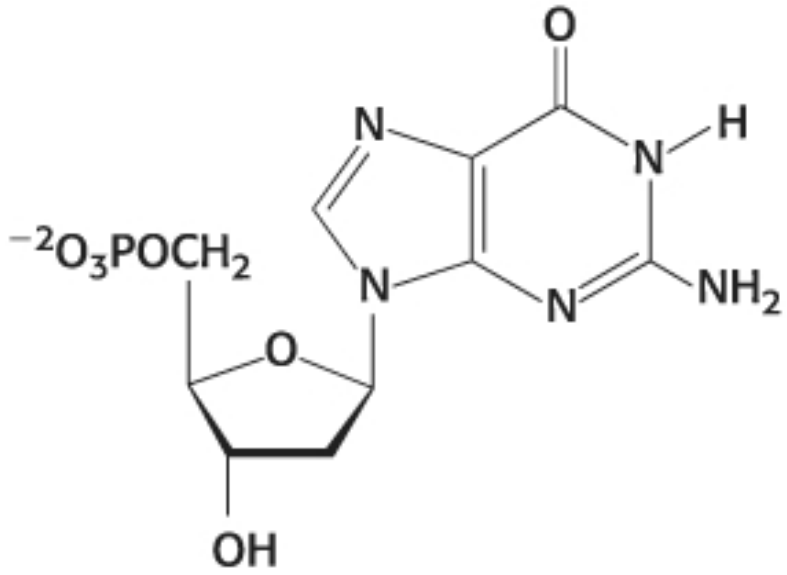
Extended description for Chemical structure



The structure is as follows: A 5-membered pentagonal ring in a vertical orientation consists of 1 O and 4 C atoms. The O atom occupies the first position, which is the topmost vertex. C 2 and C 3 are each single bonded to O H below. C 4 is single bonded to C H 2 which is single bonded to O H on the upper left. C 1 is single bonded to the second N of a 6-membered heterocyclic hexagonal ring in a vertical orientation. The hexagonal ring consists of 2 N and 4 C atoms. The first N bound to H occupies the first position which is the top right vertex and the second N occupies the third position which is the bottom-most vertex. C 1 and C 4 are each double bonded to O. A double bond is present between C 2 and C 3.

Return to Chemical structure

Extended description for Chemical structure



The structure is as follows: A 5-membered pentagonal ring in a vertical orientation consists of 1 O and 4 C atoms. The O atom occupies the first position, which is the topmost vertex. C 3 is single bonded to O H below. C 4 is single bonded to C H 2 O P O 3 superscript 2 minus. C 1 is single bonded to the first N of a 5-membered heterocyclic pentagonal ring in a horizontal orientation. The ring consists of 2 N and 3 C atoms. The first N occupies the first position which is the bottom left vertex and the second N occupies the third position which is the top left vertex. A double bond is present between C 1 and the second N. The pentagonal ring is fused to a 6-membered heterocyclic hexagonal ring in a vertical orientation. The ring consists of 2 N and 4 C atoms. The first N atom occupies the first position which is the top right vertex and the second N atom occupies the third position which is the bottom-most vertex. Two double bonds are present between C 1 and the second N and C 2 and C 3. C 1 is single bonded to N H 2 on the lower right. The first N is single bonded to H. C 4 is double bonded to O above. The

rings are fused such that C 2 and C 3 of the pentagonal ring are C 3 and C 2 of the hexagonal ring respectively.

Return to Chemical structure

Extended description for Three-dimensional structure of Cas 9 endonuclease

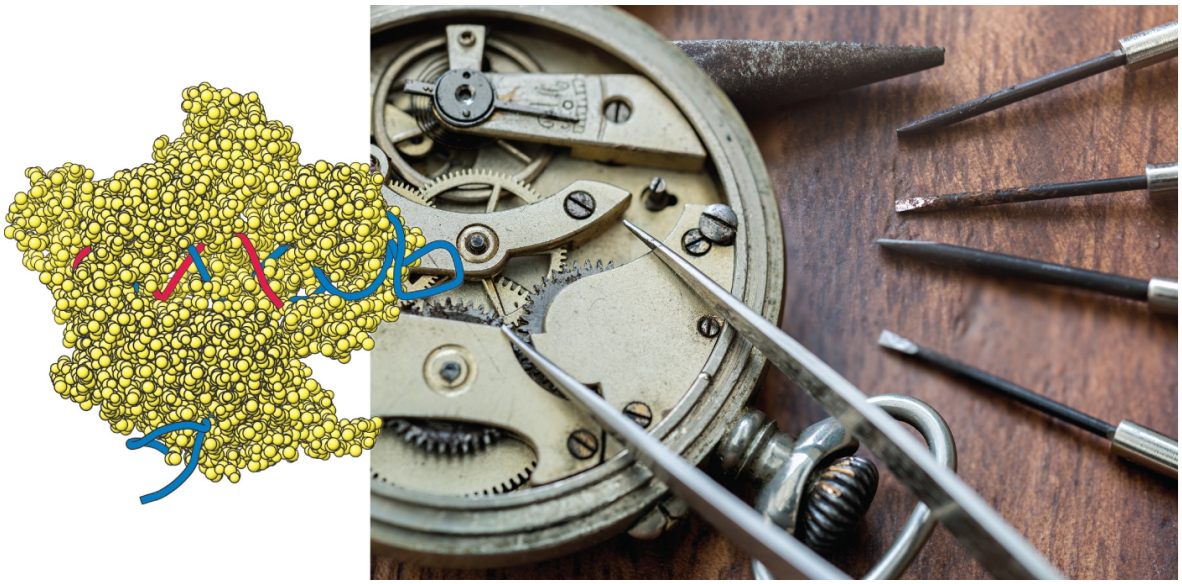
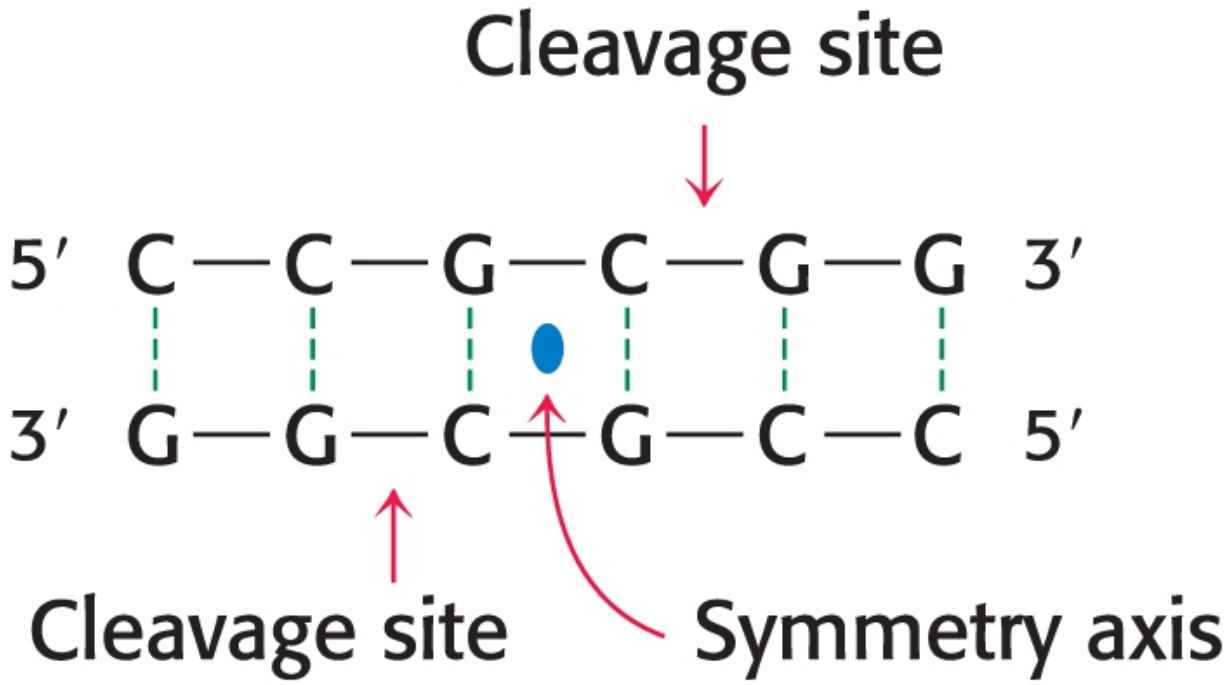


Photo: Gitanna/Shutterstock
© Macmillan Learning

The Cas 9 endonuclease is shown to bind to a genomic D N A sequence shown as red and blue strands.

Return to Three-dimensional structure of Cas 9 endonuclease

Extended description for Cleavage site of a restriction enzyme

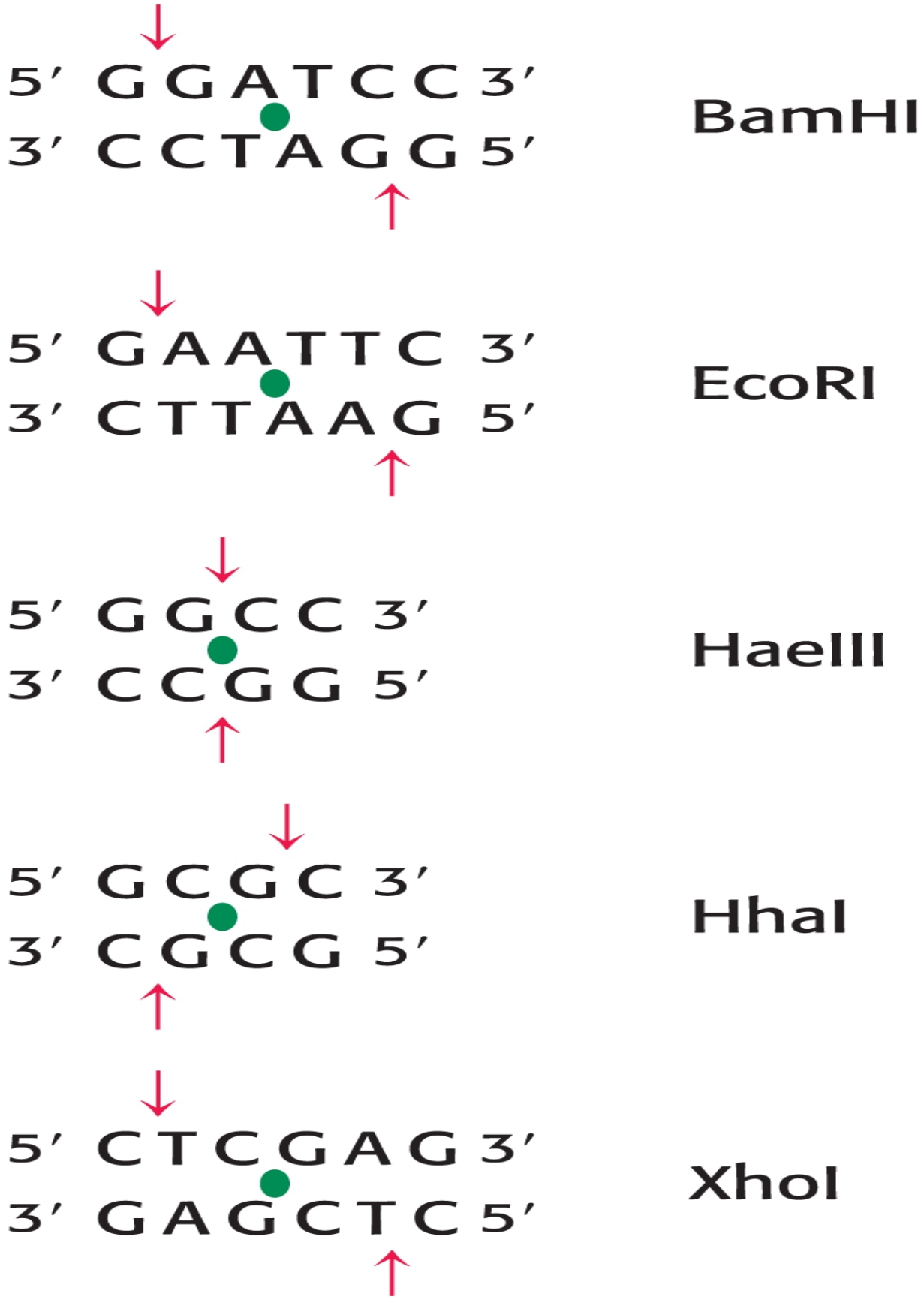


A segment of a double stranded D N A strand. The orientation of the top strand is 5 prime to 3 prime, from left to right, and has the following sequence: C, C, G, C, G, G. The orientation of the bottom strand is anti-parallel to the top strand and has the complementary sequence. Dotted green lines between G and C bases of the two strands represent intramolecular hydrogen bonding. A blue dot in the middle of the sequence between the third and the fourth base is labeled symmetry axis. The phosphodiester linkage between C and G at the second and third positions from the 3 prime end, respectively, in the top strand is labeled cleavage site. Similarly, the linkage between G and C at the second and third positions from the 3 prime end, respectively, in the bottom strand is labeled cleavage site.

Return to Cleavage site of a restriction enzyme

Extended description for Cleavages sites for five

different restriction endonucleases


5′ G G A T C C 3′
3′ C C T A G G 5′
BamHI
5′ G A A T T C 3′
3′ C T T A A G 5′
EcoRI
5′ G G C C 3′
3′ C C G G 5′
HaeIII
5′ G C G C 3′
3′ C G C G 5′
HhaI
5′ C T C G A G 3′
3′ G A G C T C 5′
XhoI

Double stranded palindromic D N A sequences are shown along with the corresponding cleavage sites of the following enzymes:

Bam H roman number 1: The D N A sequence in the 3 prime to 5 prime direction is C, C, T, A, G, G. The symmetry axis is indicated to be between T and A at the third and fourth positions, respectively, from the 3 prime end. The cleavage site on each strand is between G and G at the first and second positions, respectively, from the 5 prime end.

Eco R roman number 1: The D N A sequence in the 3 prime to 5 prime direction is C, T, T, A, A, G. The symmetry axis is indicated to be between T and A at the third and fourth positions, respectively, from the 3 prime end. The cleavage site on each strand is between G and A at the first and second positions, respectively, from the 5 prime end.

H a e roman number 3: The D N A sequence in the 3 prime 5 prime direction is C, C, G, G. The symmetry axis is indicated to be between C and G at the second and third positions, respectively, from the 3 prime end. The cleavage site on each strand is between C and G at the second and third positions, respectively, from the 3 prime end.

H h a roman 1: The D N A sequence in the 3 prime to 5 prime direction is C, G, C, G. The symmetry axis is indicated to be between G and C at the second and third positions, respectively, from the 3 prime end. The cleavage site on each strand is between C and G at the first and second positions, respectively, from the 3 prime end.

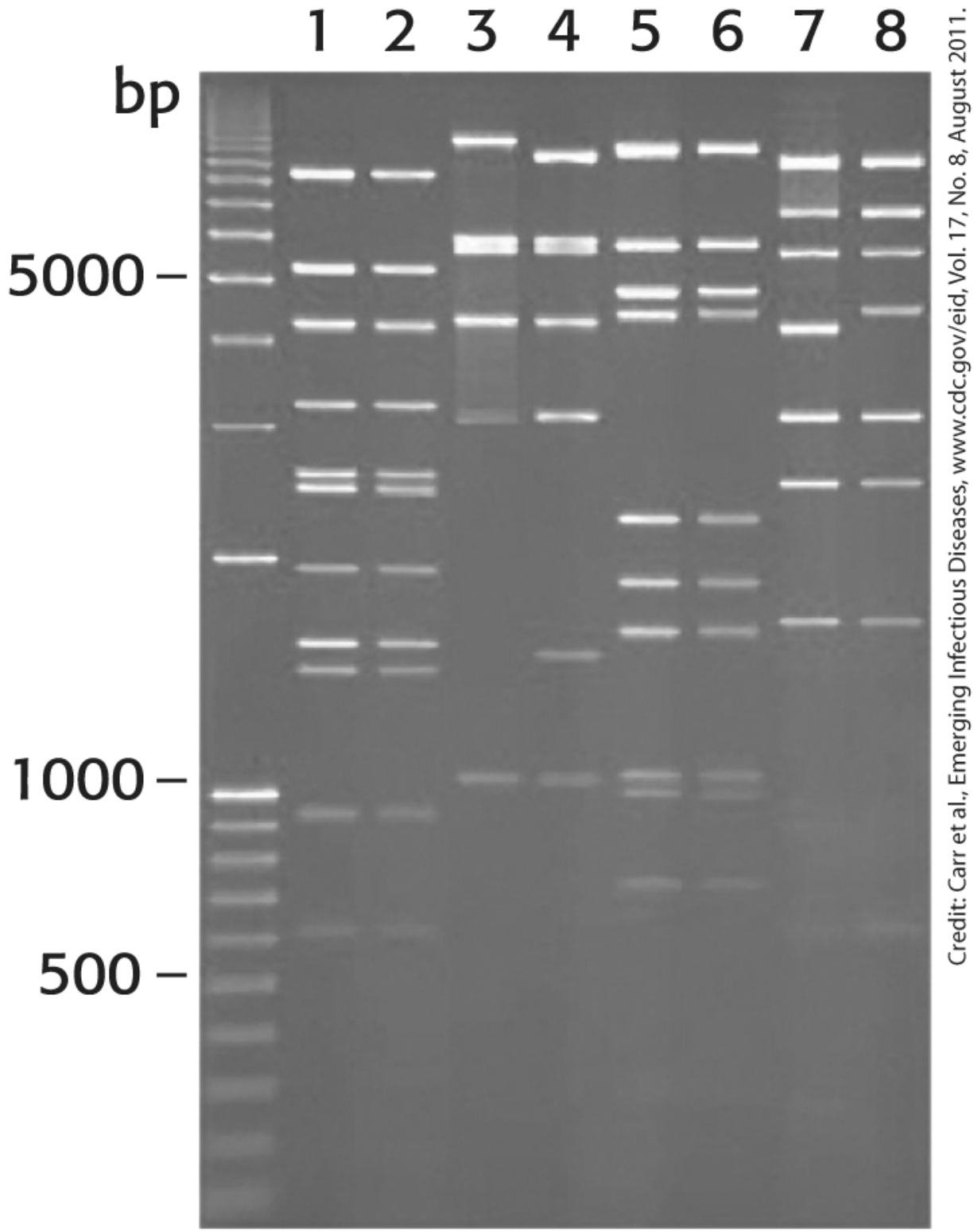
X h o 1: The D N A sequence in the 3 prime to 5 prime direction is G, A, G, C, T, C. The symmetry axis is indicated to be between G and C at the third and fourth positions, respectively, from the 3 prime end.

The cleavage site on each strand is between T and C at the fifth and sixth positions, respectively, from the 3 prime end.

Return to Cleavages sites for five different restriction endonucleases

Extended description for Photograph of

electrophoresis gel slab with stained D N A fragments

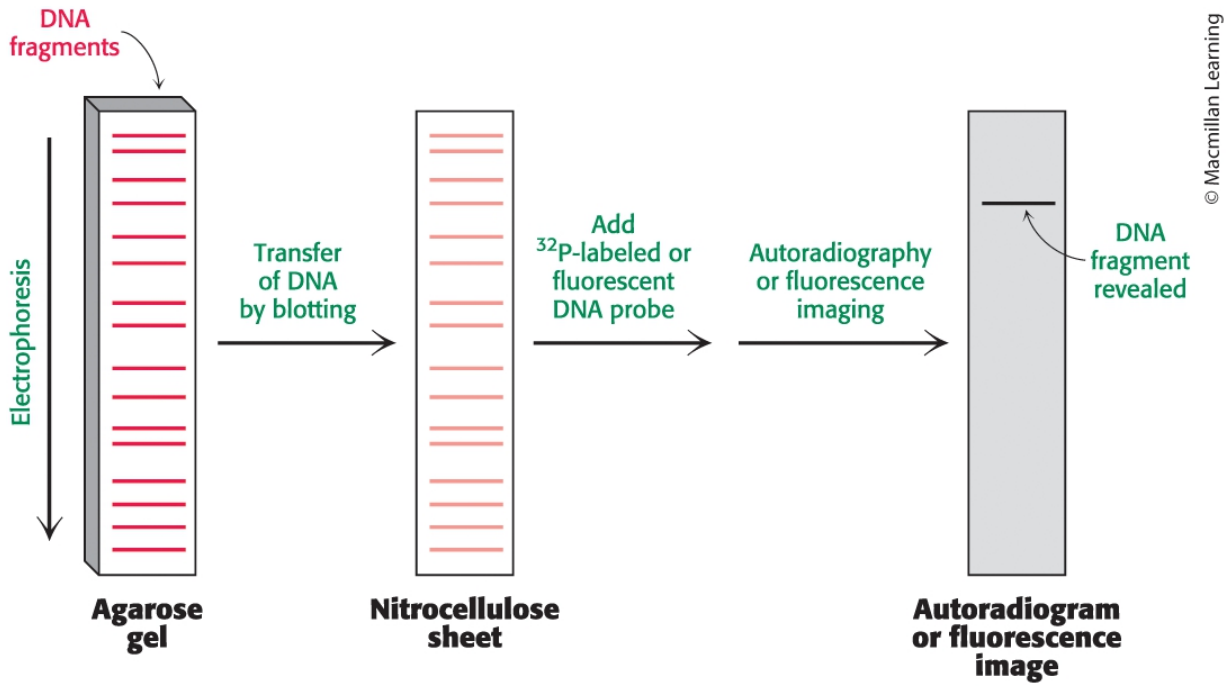


Credit: Carr et al., Emerging Infectious Diseases, www.cdc.gov/eid, Vol. 17, No. 8, August 2011.

The gel is shown to have eight vertical lanes numbered 1 through 8, from left to right. A D N A ladder is seen to the left of the first lane. Bands corresponding to 5000, 1000, and 500 base pairs are indicated on the D N A ladder, from top to bottom. Each lane has several bands of varying intensities. The banding pattern is almost identical with minor variations for each adjacent pair of lanes, from left to right.

Return to Photograph of electrophoresis gel slab with stained D N A fragments

Extended description for Schematic illustration of the steps of southern blotting



Step 1: Electrophoresis. A vertical agarose electrophoresis gel slab is illustrated. The direction of electrophoresis is from top to bottom. Several red horizontal bands are seen along the length of the gel slab.

Step 2: Transfer of D N A by blotting. A vertical strip of nitrocellulose sheet is illustrated. The transferred D N A from the agarose gel forms an identical banding pattern on the sheet.

Step 3: Add P superscript 32 labeled or fluorescent D N A probe.

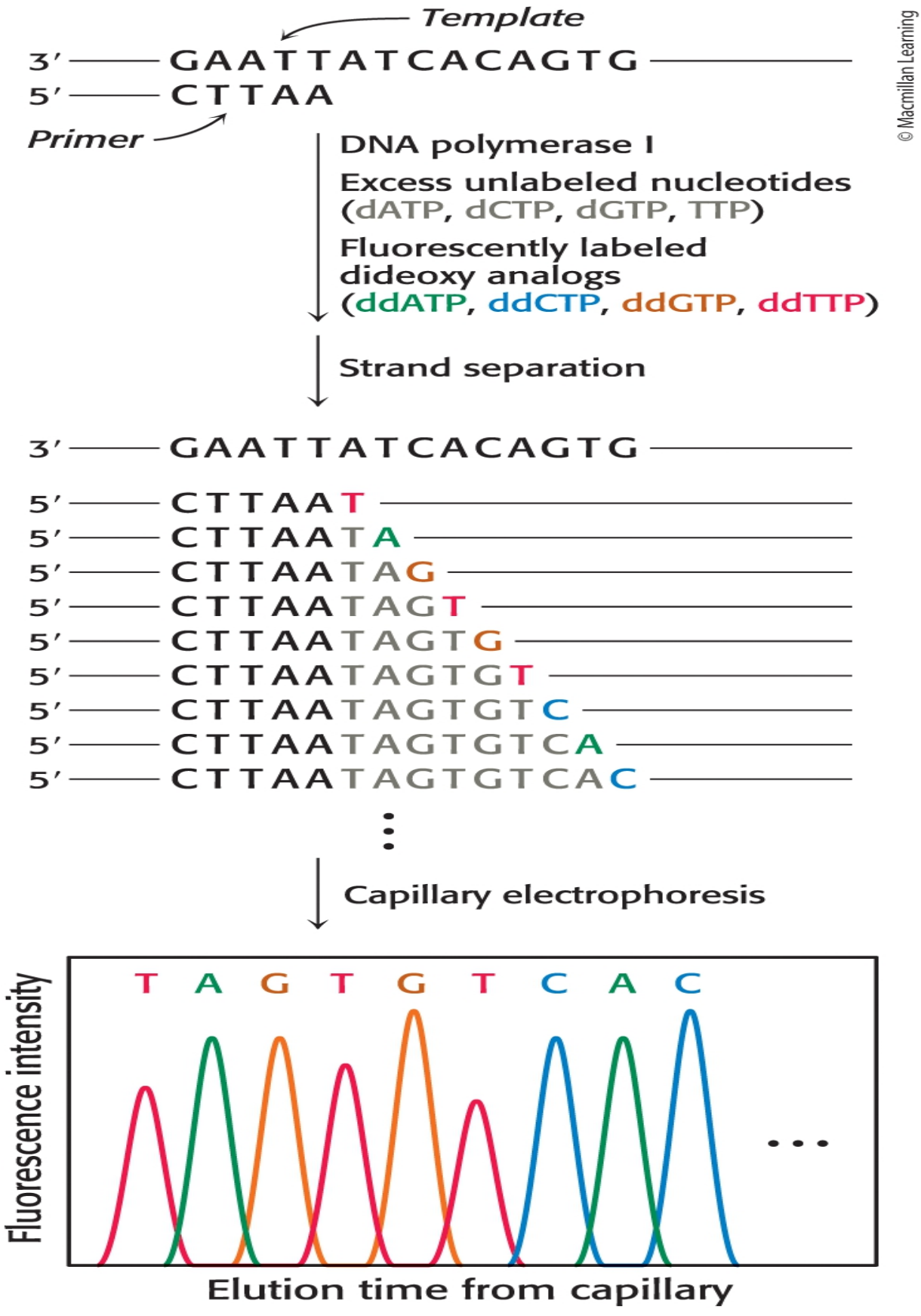
Step 4: Autoradiography or fluorescence imaging. A vertical autoradiogram or fluorescence image of the sheet is illustrated. Only

one horizontal black band is seen in the image at the top and is labeled D N A fragment revealed.

Return to Schematic illustration of the steps of southern blotting

Extended description for Schematic illustration of the

steps of chain-terminating D N A sequencing method


Template
3′ GAATTATCACAGTG
5′ CTTAA
Primer
DNA polymerase I
Excess unlabeled nucleotides
(dATP, dCTP, dGTP, TTP)
Fluorescently labeled
dideoxy analogs
(ddATP, ddCTP, ddGTP, ddTTP)
Strand separation
3′ GAATTATCACAGTG
5′ CTTAAT
5′ CTTAATA
5′ CTTAATAG
5′ CTTAATAGT
5′ CTTAATAGTG
5′ CTTAATAGTGT
5′ CTTAATAGTGTC
5′ CTTAATAGTGTCA
5′ CTTAATAGTGTCAC
Capillary electrophoresis
T A G T G T C A C
Fluorescence intensity
Elution time from capillary
© Macmillan Learning

Step 1: The template strand has the following sequence in the 3 prime to 5 prime direction, from left to right: G, A, A, T, T, A, T, C, A, C, A, G, T, G. The complementary primer has the following sequence in the 5 prime to 3 prime direction, from left to right: C, T, T, A, A. D N A Polymerase roman number 1 is added along with excess unlabeled nucleotides (d A T P, d C T P. d G T P, T T P). Fluorescently labeled dideoxy analogs are also added and color coded as follows: d d A T P (green), d d C T P (blue), d d G T P(orange), and d d T T P (red).

Step 2: Strand separation.

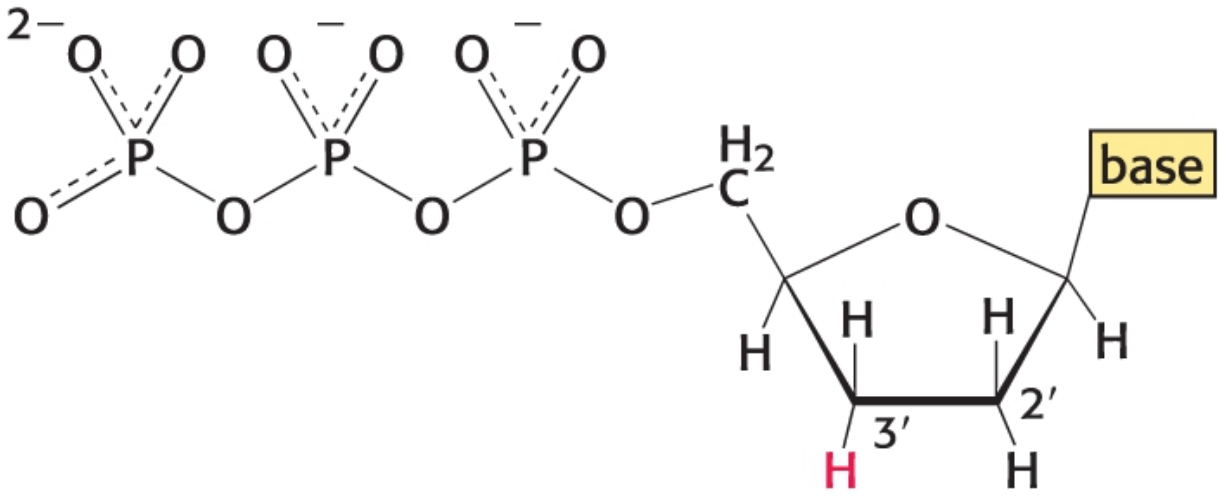
Step 3: The template strand is illustrated at the top. This is followed by the newly synthesized strands in increasing order of length, from top to bottom, such that the successive strands terminate at a base one position further down the preceding strand along the 5 prime to 3 prime direction. For each new strand, the terminal nucleotide is labeled with a dideoxy analog.

Step 4: Capillary electrophoresis.

Step 5: A graph depicts the sequence of the newly synthesized strand as the primer is extended. The horizontal axis is labeled elution time from capillary. The vertical axis is labeled fluorescence intensity. Peaks of varying height are observed whose colors correspond to the respective terminating dideoxy analog. The order of the peaks represents the sequence of the complement, which is as follows: T, A, G, T, G, T, C, A, C.

Return to Schematic illustration of the steps of chain-terminating D N A sequencing method

Extended description for Chemical Structure of 2 prime, 3 prime-dideoxy analog



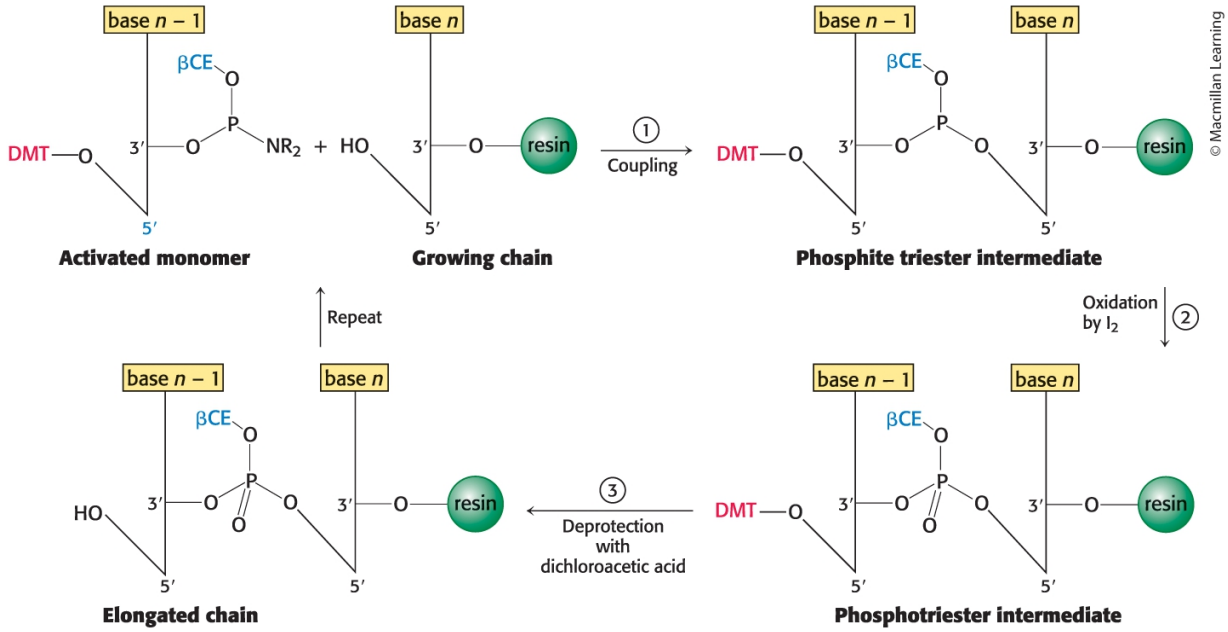
2′, 3′-Dideoxy analog

The structure is as follows: A 5-membered heterocyclic pentagonal ring in a vertical orientation consists of 1 and 4 C atoms. The O atom occupies the first position which is the topmost vertex. C 1 is single bonded to a base at the top right and single bonded to H on the bottom right. C 2 is labeled 2 prime and is single bonded to H above and single bonded to H on the lower right. C 3 is labeled 3 prime and is single bonded to H above and single bonded to H on the lower left which is colored red. C 4 is single bonded to H on the lower left and single bonded to C H 2 on the upper left. C H 2 is single bonded to O of a triphosphate group. The terminal phosphate group carries 2 minus charge and has a central P atom that is partially double bonded to O on the upper left, partially double bonded to O on the upper right, partially double bonded to O on the lower left, and single bonded to O on the lower right. Each of the other two phosphate groups has a central P atom single bonded to O on the lower right, single bonded to O on the lower left, partially double

bonded to O on the upper left, and partially double bonded to O on the upper right. The single bonded O atoms are shared between two adjacent phosphate groups. These two phosphate groups each carry a negative charge.

Return to Chemical Structure of 2 prime, 3 prime-dideoxy analog

Extended description for Stepwise illustration of the Phosphite triester method of oligonucleotide synthesis



Step 1: Coupling. The reaction consists of two reactants and one product. The first reactant is labeled Activated monomer and has the following structure: The sugar is represented by a vertical line with the top labeled 3 prime and the bottom labeled 5 prime. The 3 prime carbon is single bonded to base n minus 1 above and single bonded to O on the right. O is single bonded to P on the upper right. P is single bonded to N R 2 on the lower right and single bonded to O above which is single bonded to beta C E (blue) on the upper left. The 5 prime carbon is single bonded to O on the upper left which is single bonded to D M T (red) on the left. The second reactant is labeled growing chain and has the following structure: The sugar is represented by a vertical line with the top labeled 3 prime and the bottom labeled 5 prime. The 3 prime carbon is single bonded to base n above and single bonded to O on the right. O is single bonded to resin represented by a green circle on the right. The 5 prime carbon

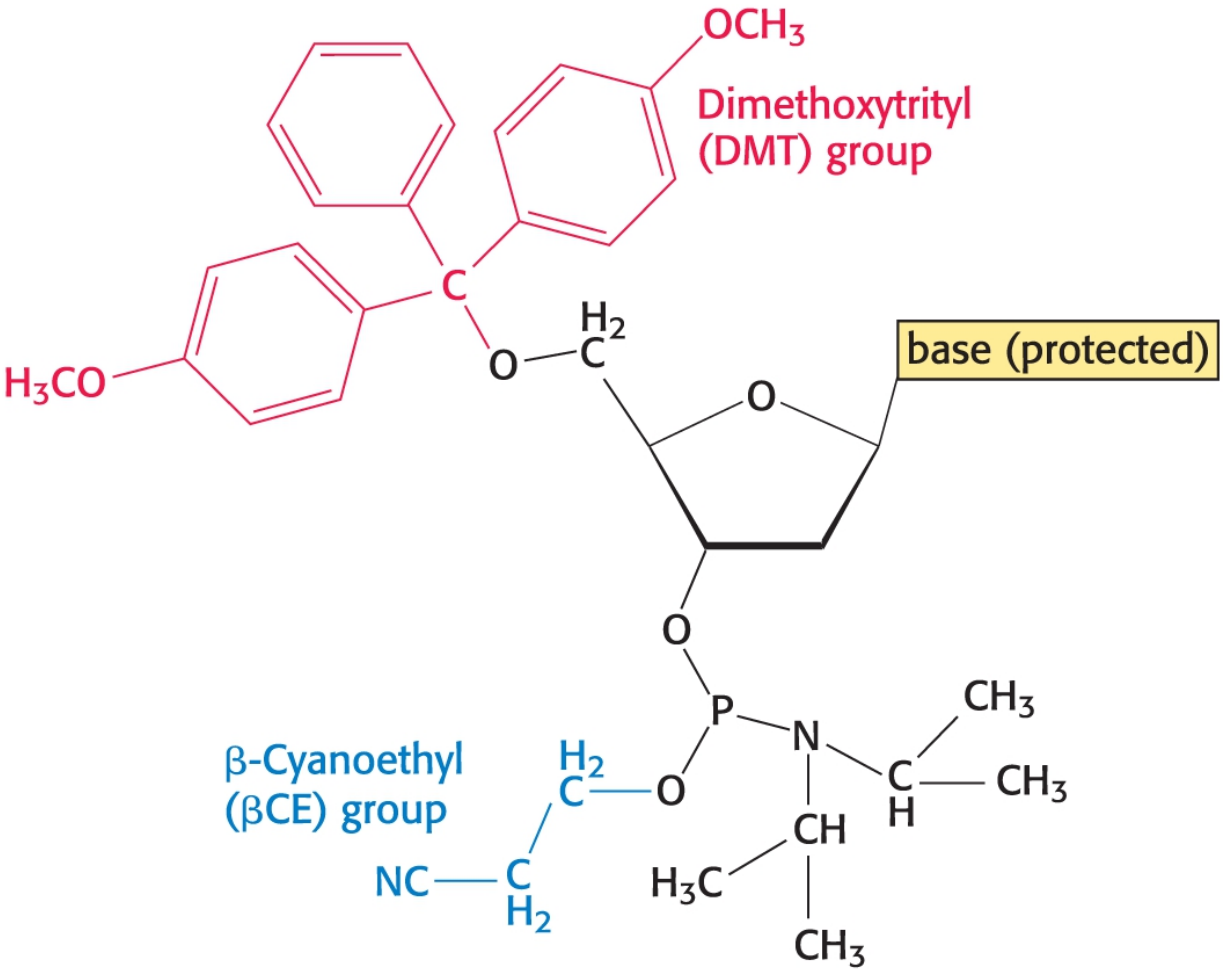
is single bonded to O H on the upper left. The product is labeled phosphite triester intermediate and has the following structure: It is represented by the formation of a link between the two reactants. The P of the activated monomer is single bonded to O on the lower right which is single bonded to the 5 prime carbon of the growing chain.

Step 2: Oxidation by I 2. Phosphite triester intermediate is converted into phosphotriester intermediate, which has a similar structure to the former except that P is also double bonded to O on the lower left.

Step 3: Deprotection with dichloroacetic acid. Phosphotriester intermediate forms the product, elongated chain, which has a similar structure to the former except the O atom single bonded to the 5 prime carbon of the n minus 1 nucleotide is bound to H instead of D M T. An arrow from this product points at the reactants of step 1 and is labeled Repeat.

Return to Stepwise illustration of the Phosphite triester method of oligonucleotide synthesis

Extended description for Structure of a deoxyribonucleoside 3 prime phosphoramidite with D M T and beta C E attached



A deoxyribonucleoside 3′-phosphoramidite with DMT and βCE attached

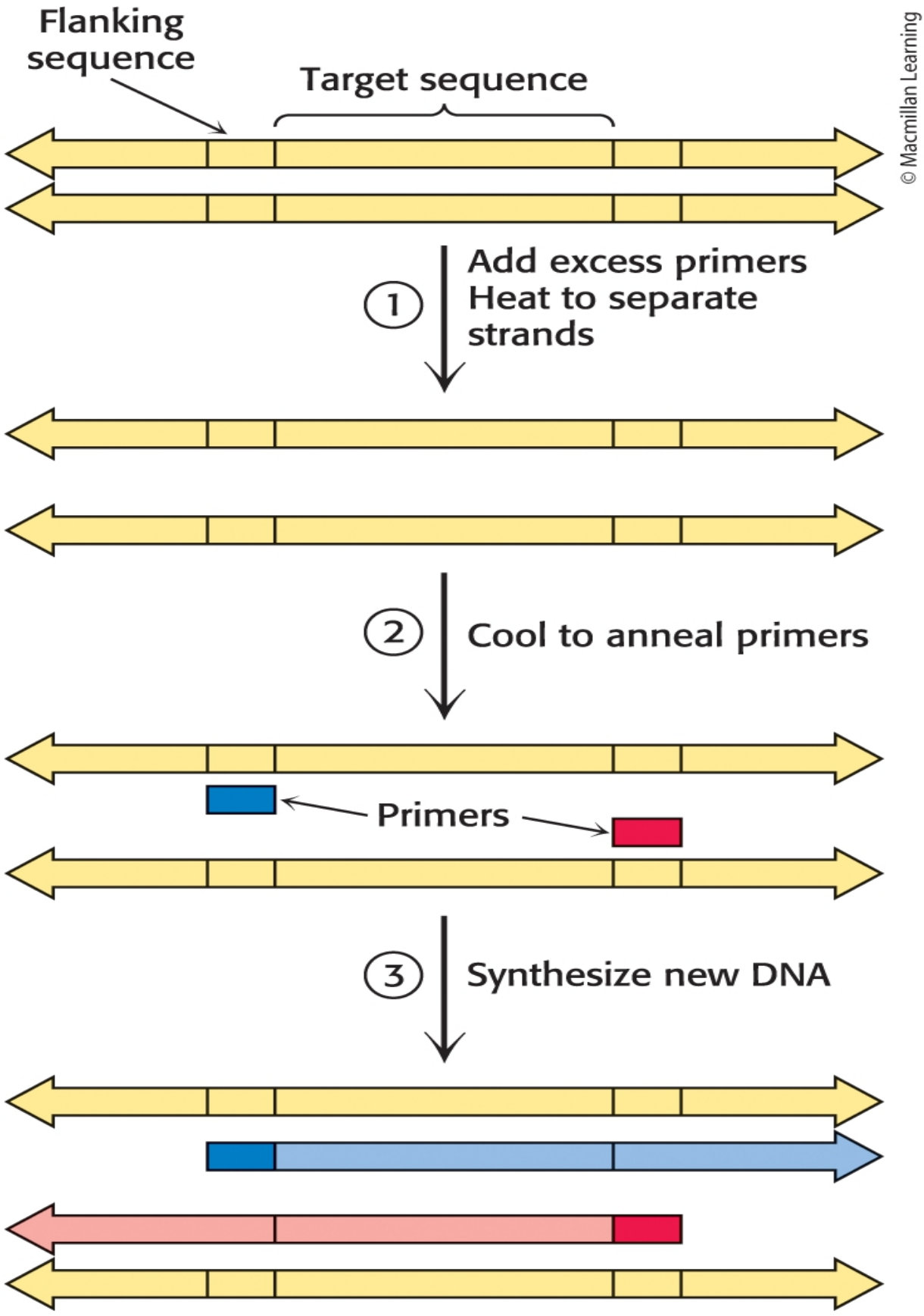
A 5 carbon heterocyclic pentagonal ring in a vertical orientation consists of 1 O and 4 C atoms. The O atom occupies the first position, which is the topmost vertex. C 1 is single bonded to a protected base on the upper right. C 3 is single bonded to O which is single bonded to P on the lower right. P is single bonded to O on the

lower left and single bonded to N on the lower right. The O on the lower left is single bonded to C H 2 on the left which is single bonded to C H 2 on the lower left which again is single bonded to C N on the left. The C H 2, single bond, C H 2, single bond, C N group is highlighted in blue and labeled beta-Cyanoethyl group or beta C E group. The N atom single bonded to P is single bonded to C H on the lower right and single bonded to C H below. The C H on the lower right is single bonded to C H 3 on the upper right and single bonded to C H 3 on the right. The C H below is single bonded to C H 3 below and single bonded to C H 3 on the lower left. C 4 of the pentagonal ring is single bonded to C H 2 which is single bonded to O on the lower left. O is bonded to a dimethoxytrityl group or D M T group highlighted in red. O is single bonded to a central C atom. C is single bonded to C 4 of a benzene ring in a horizontal orientation on the upper right. The benzene ring has three alternating double bonds between C 1 and C 2, C 3 and C 4, and C 5 and C 6. C 1 of the benzene ring is single bonded to O C H 3. The central C atom is single bonded to C 4 of another benzene ring in a horizontal orientation on the left. This benzene ring has three alternating double bonds between C 1 and C 2, C 3 and C 4, and C 5 and C 6. C 1 is single bonded to O C H 3 on the left. The central C atom is single bonded to C 4 of another benzene ring in a vertical orientation. This benzene ring has three alternating double bonds between C 1 and C 2, C 3 and C 4, and C 5 and C 6.

Return to Structure of a deoxyribonucleoside 3 prime phosphoramidite with D M T and beta C E attached

Extended description for Schematic illustration of the

steps of the first cycle of Polymerase Chain Reaction



© Macmillan Learning

Step 1: Add excess primers. Heat to separate strands. Two parallel double headed arrows represent a double-stranded D N A molecule. A region in the middle of both the strands is labeled Target sequence. Each target sequence is flanked on both sides by short sequences labeled Flanking sequence. The strands are shown to separate upon heating.

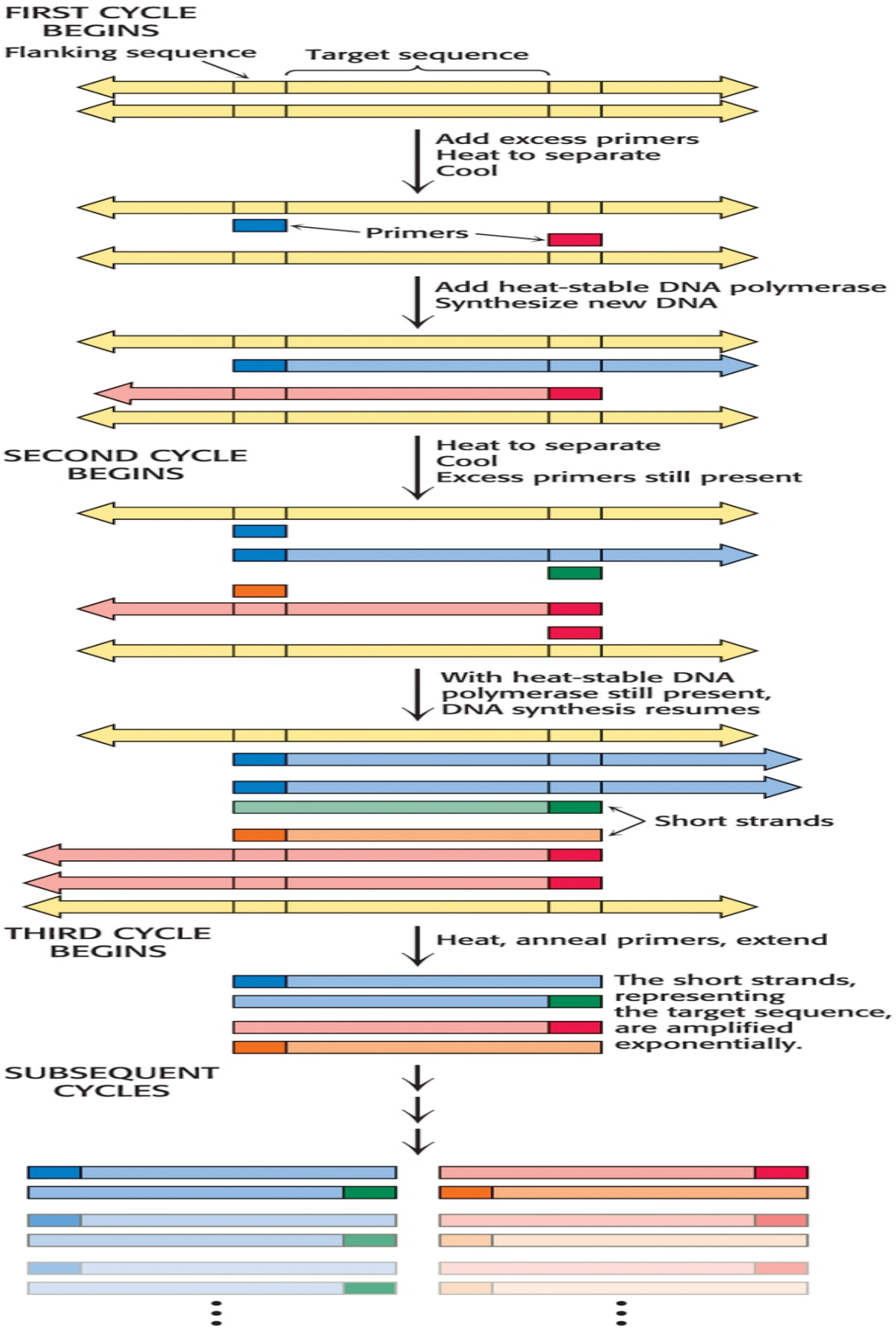
Step 2: Cool to anneal primers. A short primer colored blue is shown to anneal to the left flanking sequence of the top strand. A short primer colored red is shown to anneal to the right flanking sequence of the bottom strand.

Step 3: Synthesize new D N A. The blue primer annealed to the top strand is shown to extend in the rightward direction. The red primer annealed to the bottom strand is shown to extend in the leftward direction. This gives two D N A molecules.

Return to Schematic illustration of the steps of the first cycle of Polymerase Chain Reaction

Extended description for Schematic illustration of

multiple cycles of Polymerase Chain Reaction


FIRST CYCLE BEGINS
Flanking sequence
Target sequence
Add excess primers
Heat to separate
Cool
Primers
Add heat-stable DNA polymerase
Synthesize new DNA
SECOND CYCLE BEGINS
Heat to separate
Cool
Excess primers still present
With heat-stable DNA polymerase still present, DNA synthesis resumes
Short strands
THIRD CYCLE BEGINS
Heat, anneal primers, extend
The short strands, representing the target sequence, are amplified exponentially.
SUBSEQUENT CYCLES
© Macmillan Learning

First cycle begins:

Step 1: Add excess primers. Heat to separate strands. Cool. Two parallel double headed arrows represent a double-stranded D N A molecule. A region in the middle of both the strands is labeled Target sequence. Each target sequence is flanked on both sides by short sequences labeled Flanking sequence. The strands are shown to separate upon heating. A short primer colored blue is shown to anneal to the left flanking sequence of the top strand. A short primer colored red is shown to anneal to the right flanking sequence of the bottom strand.

Step 2: Add heat-stable D N A polymerase. Synthesize new D NA. The blue primer annealed to the top strand is shown to extend in the rightward direction. The red primer annealed to the bottom strand is shown to extend in the leftward direction. This gives two D N A molecules.

Second cycle begins:

Step 3: Heat to separate. Cool. Excess primers are still present. The newly synthesized strands are shown to separate. A blue primer is shown to anneal to the left flanking sequence of the top strand. A green primer is shown to anneal to the right flanking sequence of the newly synthesized blue strand. An orange primer is shown to anneal to the left flanking sequence of the newly synthesized red strand. A red primer is shown to anneal to the right flanking sequence of the bottom strand. With heat-stable D N A polymerase still present, D N A synthesis resumes. The blue primer is shown to extend in the rightward direction and the red primer is shown to extend in the leftward direction. The green primer extends leftward until the left flanking sequence and the orange primer extends rightward until the right flanking sequence. The green and orange

strands are labeled short strands which include the target sequence and the flanking sequences.

Third cycle begins:

Step 4: Heat, anneal primers, extend. The short strands representing the target sequence are shown to be amplified exponentially. Two short double stranded D N A molecules are shown.

Subsequent cycles:

Several short double stranded D N A molecules representing the target and flanking sequence are shown.

Return to Schematic illustration of multiple cycles of Polymerase Chain Reaction

Extended description for Photograph of gel

electrophoresis slab of P C R in a forensic case



Martin Shields/Science Source

Seven vertical lanes of D N A are indicated, from the left to right as follows:

Sizing Marker: It is a D N A ladder with 12 D N A bands of different sizes.

Victim: A single dark band is seen between the fifth and sixth bands of the sizing marker from the top.

Suspect 1: Two faint bands are seen between the second and third bands and the eighth and ninth bands of the sizing marker, respectively.

Suspect 2: Two very faint bands are seen corresponding to the fourth and eighth bands of the sizing marker, respectively.

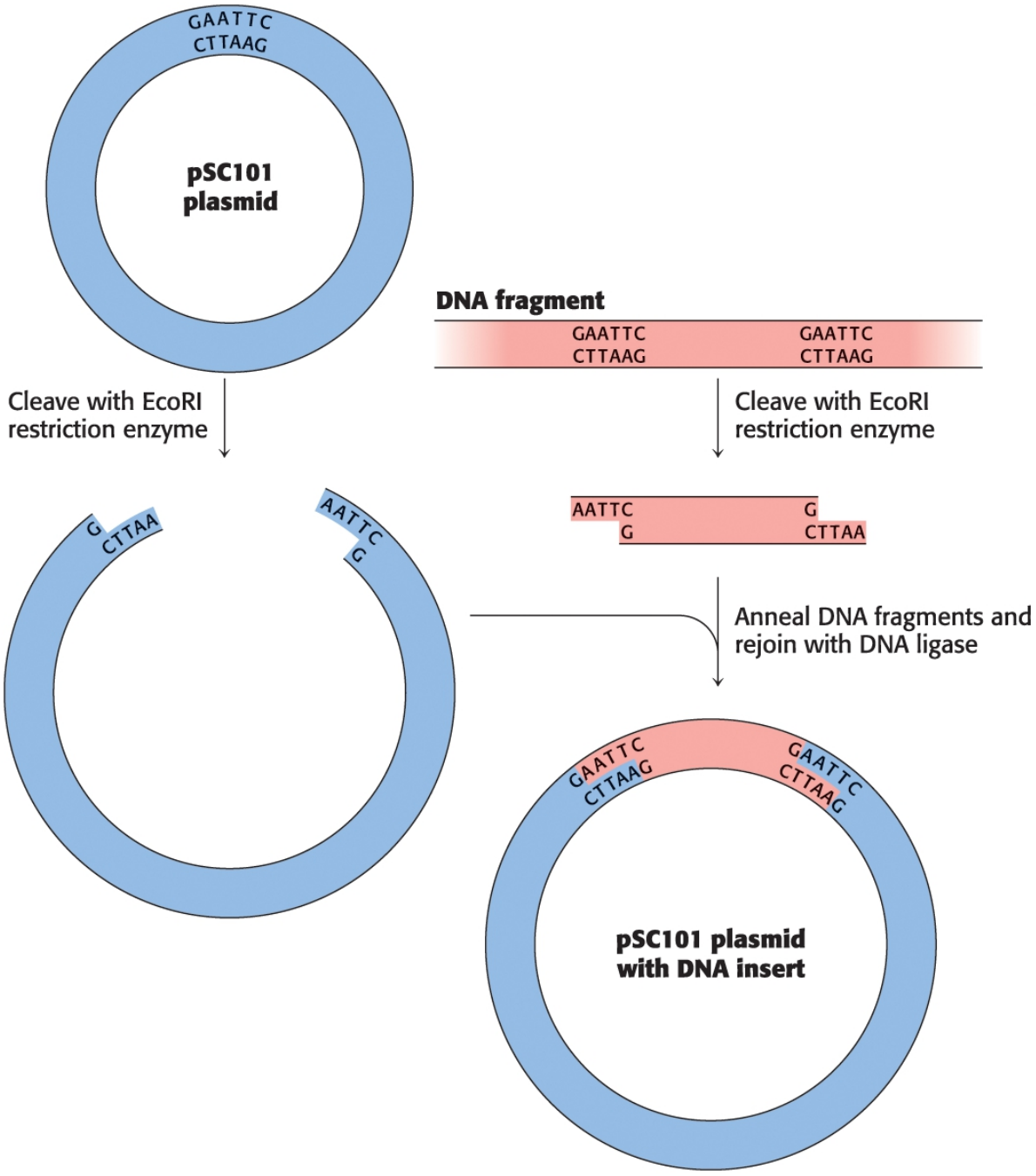
Female cells: A band is seen between the fifth and sixth bands of the sizing marker.

Sperm D N A: Two faint bands are seen between the second and third bands and the eighth and ninth bands of the sizing marker, respectively.

Sizing marker: It is a D N A ladder with 12 D N A bands of different sizes. It is identical to the first sizing marker.

Return to Photograph of gel electrophoresis slab of P C R in a forensic case

Extended description for Schematic illustration of cohesive-end method of D N A ligation



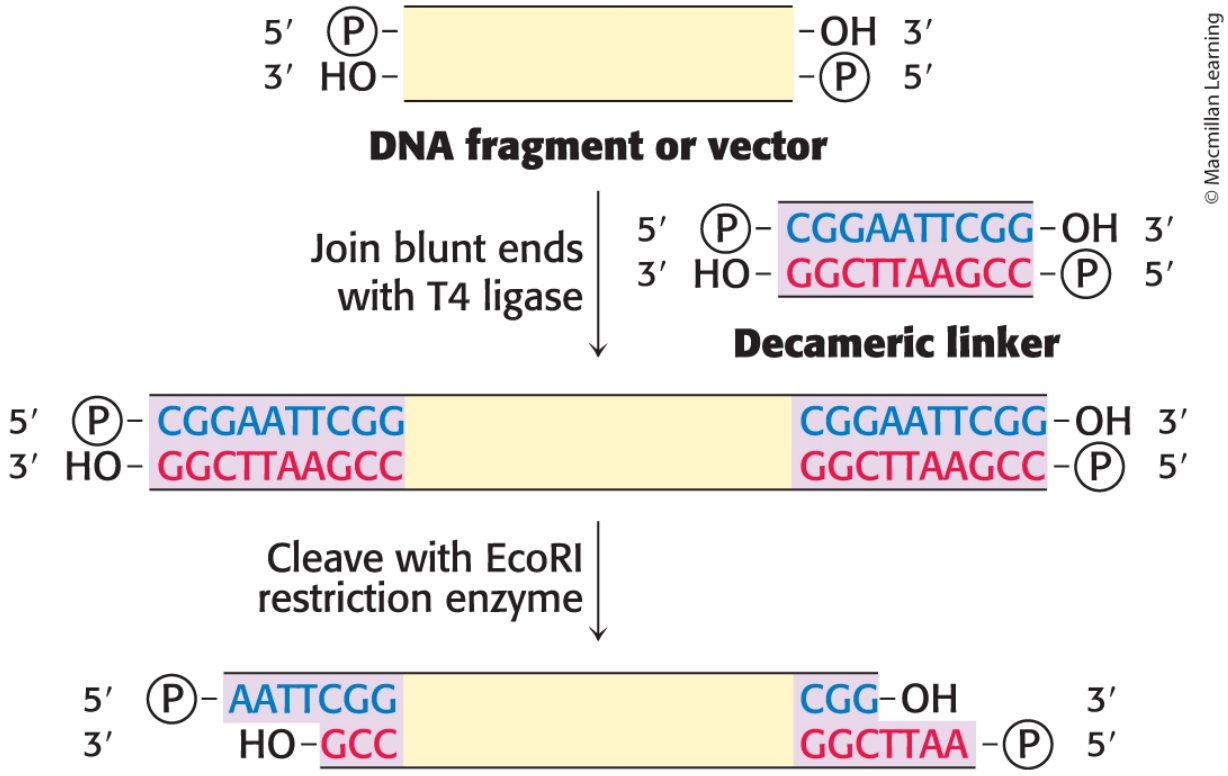
© Macmillan Learning

Step 1: Cleave with Eco R roman number 1 restriction enzyme. A circular plasmid labeled p S C 1 0 1 is shown in blue. The palindromic recognition sequence, in the clockwise direction, in the outer strand is G A A T T C. The cleavage is shown to take place between G and A leaving complementary cohesive ends on both the inner and outer strands. A straight D N A fragment is shown in red. It has the same recognition sequence as that of the plasmid. The D N A fragment has two of the recognition sequence spaced by a short D N A segment. It is cleaved with Eco R roman number 1. The cleavage is shown to take place between G and A leaving complementary cohesive ends on both the upper and lower strands.

Step 2: Anneal D N A fragment and rejoin with D N A ligase. The cleaved D N A fragment has cohesive ends that are complementary to those of the cleaved plasmid. The D N A fragment is shown to ligate with the plasmid at the restriction site. The ligated plasmid is labeled p S C 1 0 1 plasmid with D N A insert.

Return to Schematic illustration of cohesive-end method of D N A ligation

Extended description for Schematic illustration of addition of cohesive ends to a D N A fragment



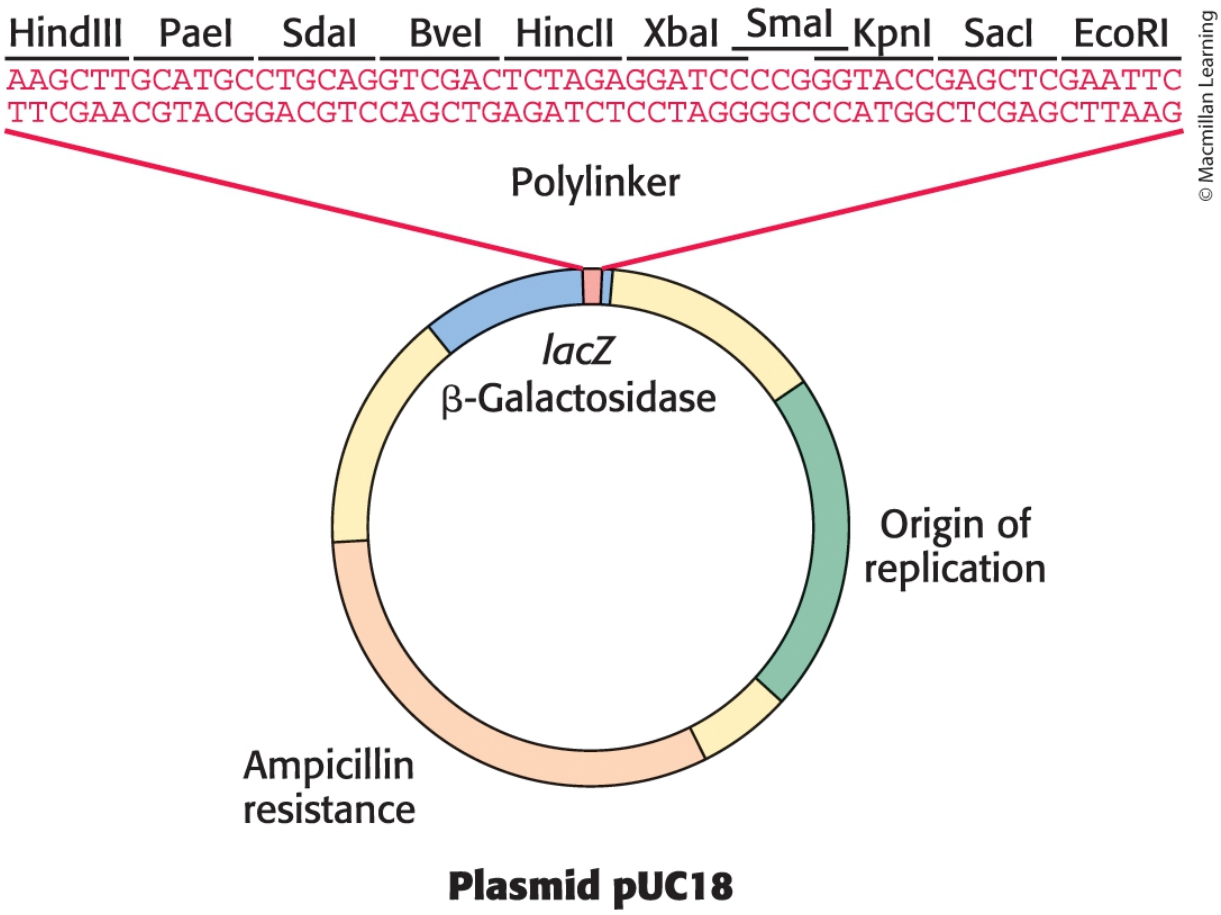
© Macmillan Learning

Step 1: Join blunt ends with T 4 ligase. A D N A fragment or vector is shown as a double stranded molecule with blunt ends. In both strands, the 5 prime terminal has a phosphate group and the 3 prime terminal has an O H group. A decameric linker is shown as another short D N A fragment having a palindromic sequence. The sequence, in the 5 prime to 3 prime direction, is as follows: C G G A A T T C G G. In both strands, the 5 prime terminal has a phosphate group and the 3 prime terminal has an O H group. The top strand is shown in blue and the bottom strand is shown in red. Two decameric linkers are shown to ligate to the D N A fragment in such a way that they flank the fragment.

Step 2: Cleave with Eco R 1 restriction enzyme. Eco R 1 is shown to cleave between G and A in both the flanking linker sequences thereby leaving cohesive ends. The sequence at the 5 prime terminal is phosphate group, single bond, A A T T C G G. The sequence at the 3 prime terminal O H, single bond, G C C.

Return to Schematic illustration of addition of cohesive ends to a D N A fragment

Extended description for Schematic illustration of unique restriction sites in a polylinker sequence of a plasmid



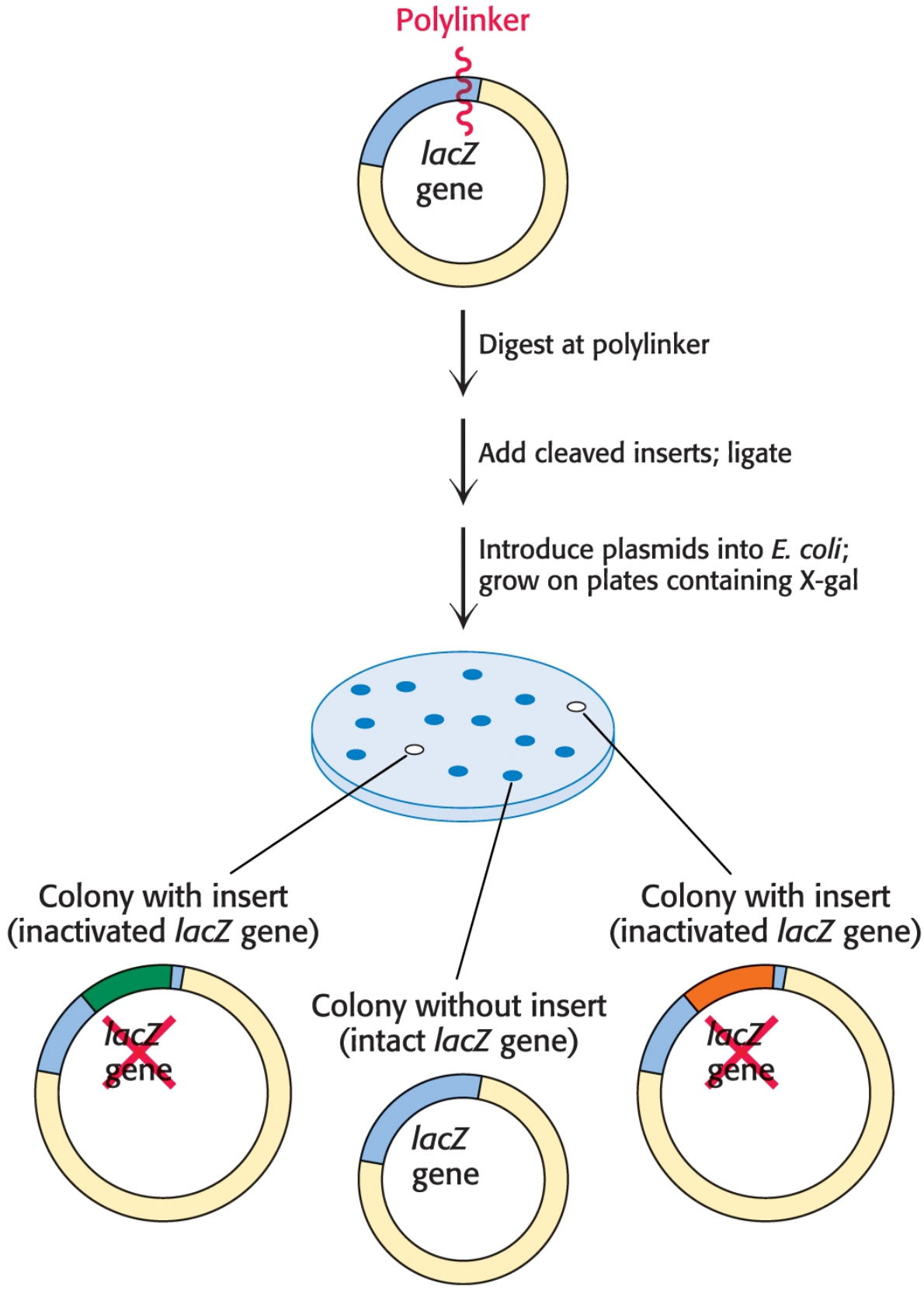
The plasmid labeled p U C 18 is shown to have the following highlighted sequences: Origin of replication, lac Z beta galactosidase, and ampicillin resistance. A short sequence within the lac Z gene is labeled polylinker. The polylinker sequence is magnified to indicate the following unique restriction sites: Hind roman number 3, P a e Roman number 1, S d a Roman number 1, B v e Roman number 1, H i n c Roman number 2, X b a Roman

number 1, S m a Roman number 1, K p n roman number 1, S a c Roman number 1, and Eco R Roman number 1.

Return to Schematic illustration of unique restriction sites in a polylinker sequence of a plasmid

Extended description for Schematic illustration of the steps of insertional inactivation of genes for

identification of colonies



© Macmillan Learning

A plasmid is shown with the lac Z gene highlighted. Cleavage at the polylinker site within the lac Z gene is highlighted in red.

Digest at polylinker.

Add cleaved inserts; ligate.

Introduce plasmids into E. coli; grow on plates containing X-gal.

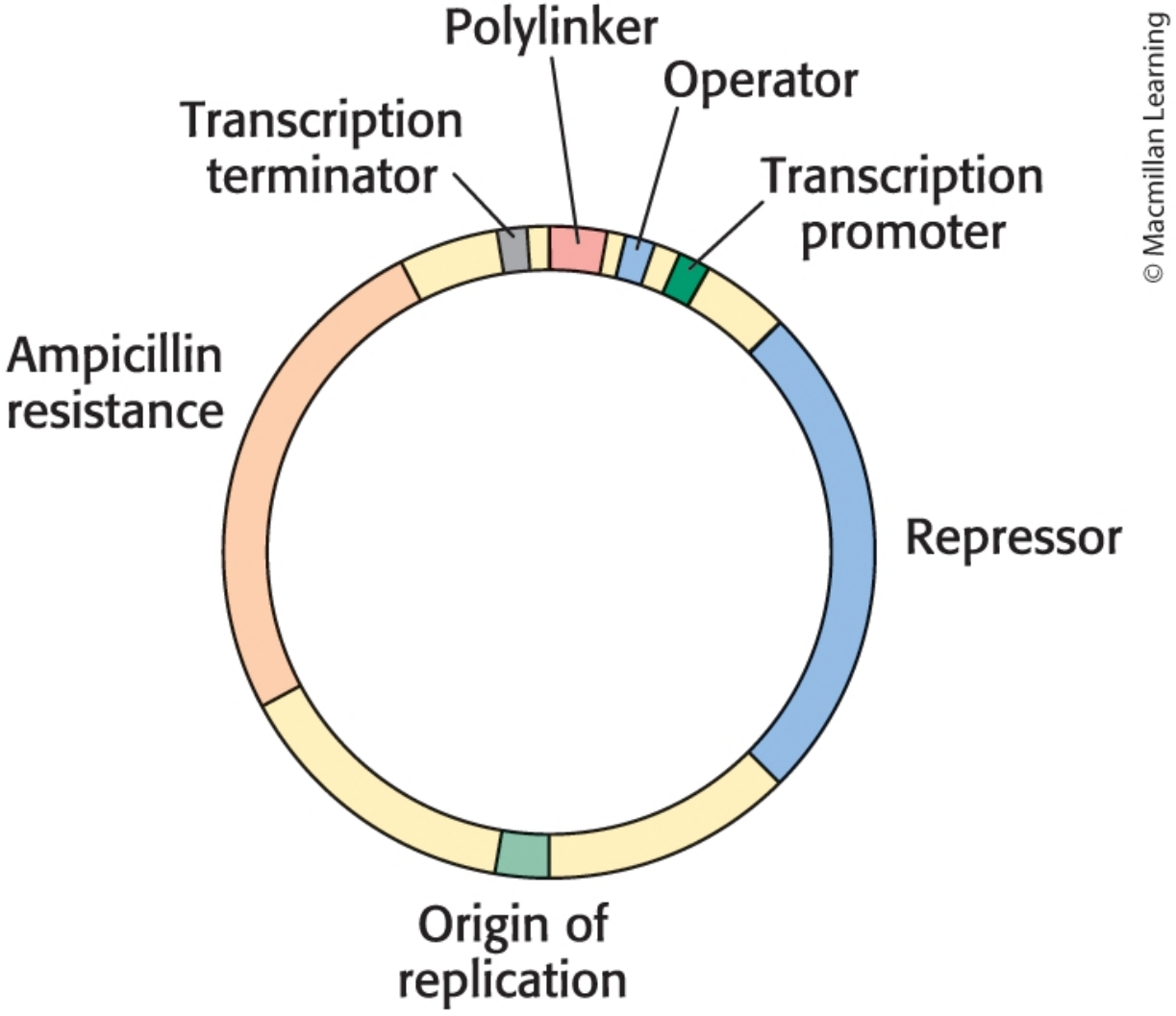
A culture plate is shown with several colonies. Two colonies are shown in white and the rest are shown in blue.

The plasmid of one of the white colonies is shown to have a short green D N A insert within the lac Z gene thereby inactivating the gene. The plasmid of the other white colony is shown to have an orange insert within the lac Z gene thereby inactivating the gene.

The plasmid of the blue colonies is shown to have an intact lac Z gene with no D N A inserts.

Return to Schematic illustration of the steps of insertional inactivation of genes for identification of colonies

Extended description for Structure of an expression vector



The following sequences of varying sizes are highlighted in the expression vector in a clockwise direction starting from the bottom:

Origin of replication

Ampicillin resistance

Transcription terminator

Polylinker

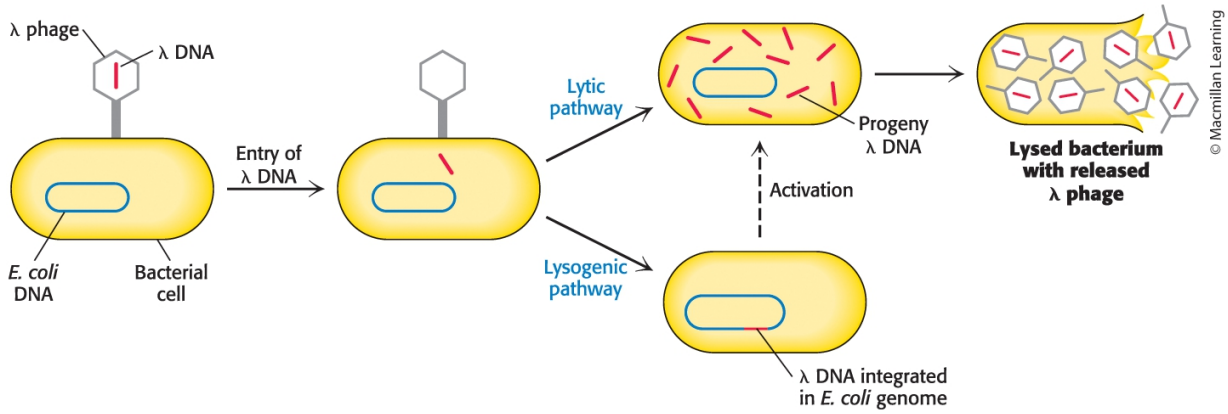
Operator

Transcription promoter

Repressor

Return to Structure of an expression vector

Extended description for Schematic illustration of the lytic and lysogenic pathways of infection in lambda phage



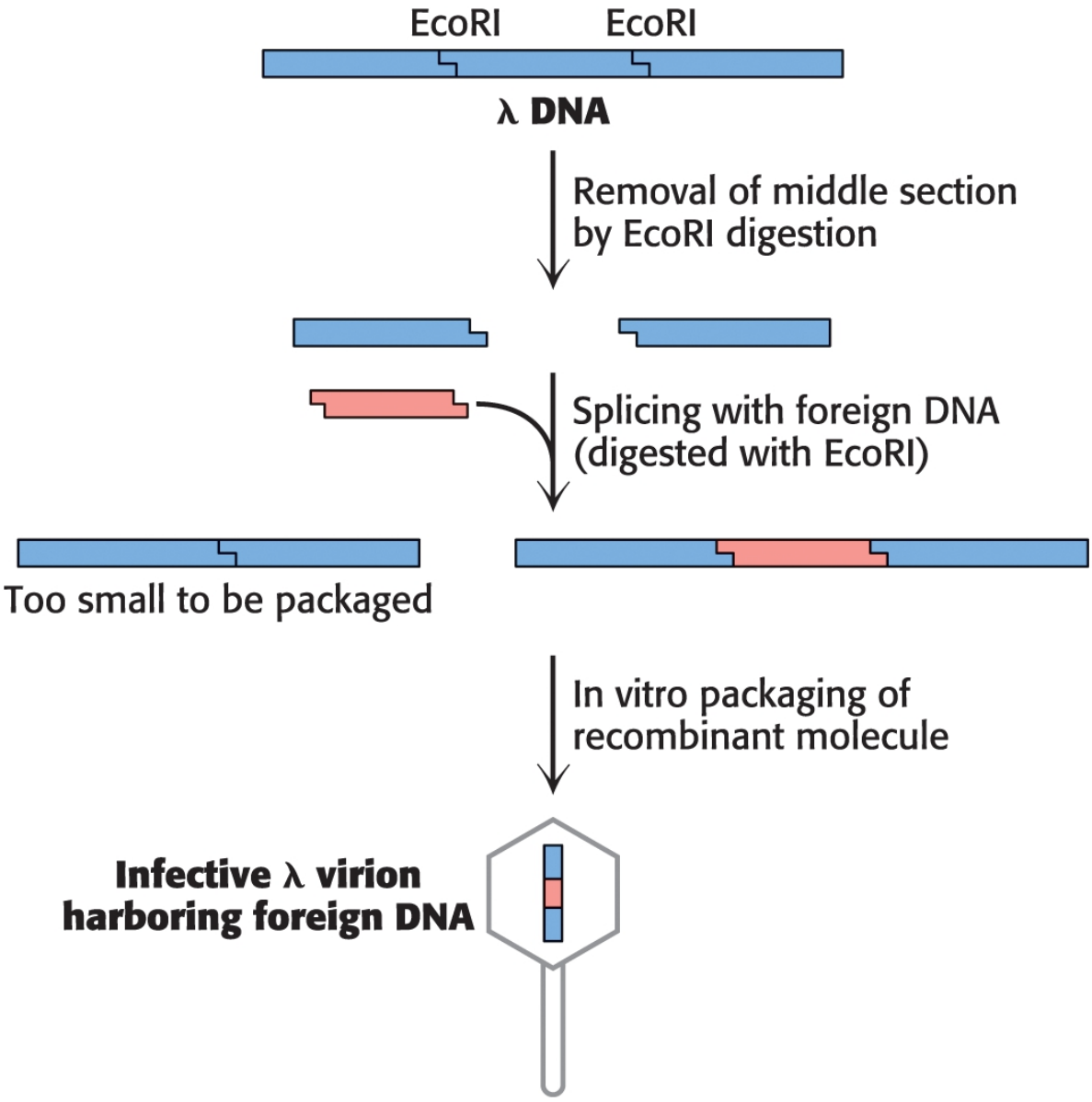
A rod-shaped bacterial cell (E. coli) is shown. The E. coli D N A is depicted as a small blue oval ring. A lambda phage is shown to adhere to the bacterial cell. The phage has a hexagonal head on top of a cylindrical tail which attaches to the bacterial cell. The phage head is shown to contain a short red D N A labeled lambda D N A. The lambda D N A is shown to be injected into bacterial cell by the phage.

Lytic pathway: The injected lambda D N A is shown to amplify within the bacterial cell. The new lambda D N A molecules are labeled progeny lambda D N A. New phage particles are shown to assemble within the bacterial cell which are eventually released from the lysed bacterium.

Lysogenic pathway: The lambda D N A is shown to be integrated into the E. coli D N A.

Return to Schematic illustration of the lytic and lysogenic pathways of infection in lambda phage

Extended description for Steps of development of mutant lambda phage to be used as cloning vector



© Macmillan Learning

Step 1: Removal of the middle section by Eco R 1 digestion. A lambda D N A is shown to have three sections interspaced by two Eco R 1 restriction sites. After Eco R 1 digestion, the left and right segments are shown to have cohesive ends. The right end is cohesive

for the left segment and the left end is cohesive for the right segment.

Step 2: Splicing with foreign D N A (digested with Eco R 1). A foreign D N A segment is shown with cohesive ends on both terminals. The following two modified lambda D N A are shown:

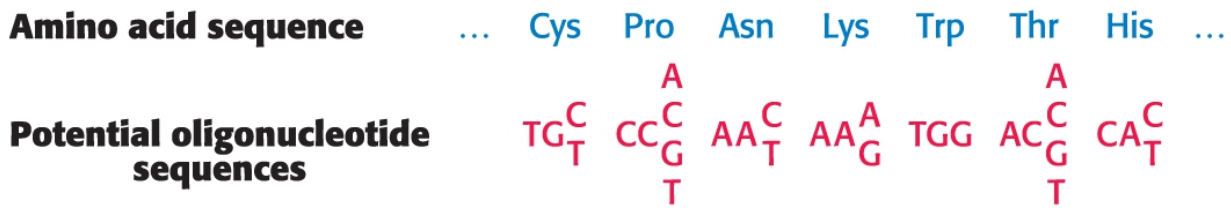
The two sections of lambda D N A after Eco R 1 digestion are shown to be ligated. This ligated D N A is too small to be packaged into a virion.

The foreign D N A is inserted in between the two sections of Eco R 1 digested lambda D N A. This gives a recombinant D N A of favorable size.

Step 3: In vitro packaging of the recombinant molecule. The lambda D N A with the foreign insert is shown to be packed into the head of an infective lambda virion.

Return to Steps of development of mutant lambda phage to be used as cloning vector

Extended description for Oligonucleotide probe designed from a target sequence



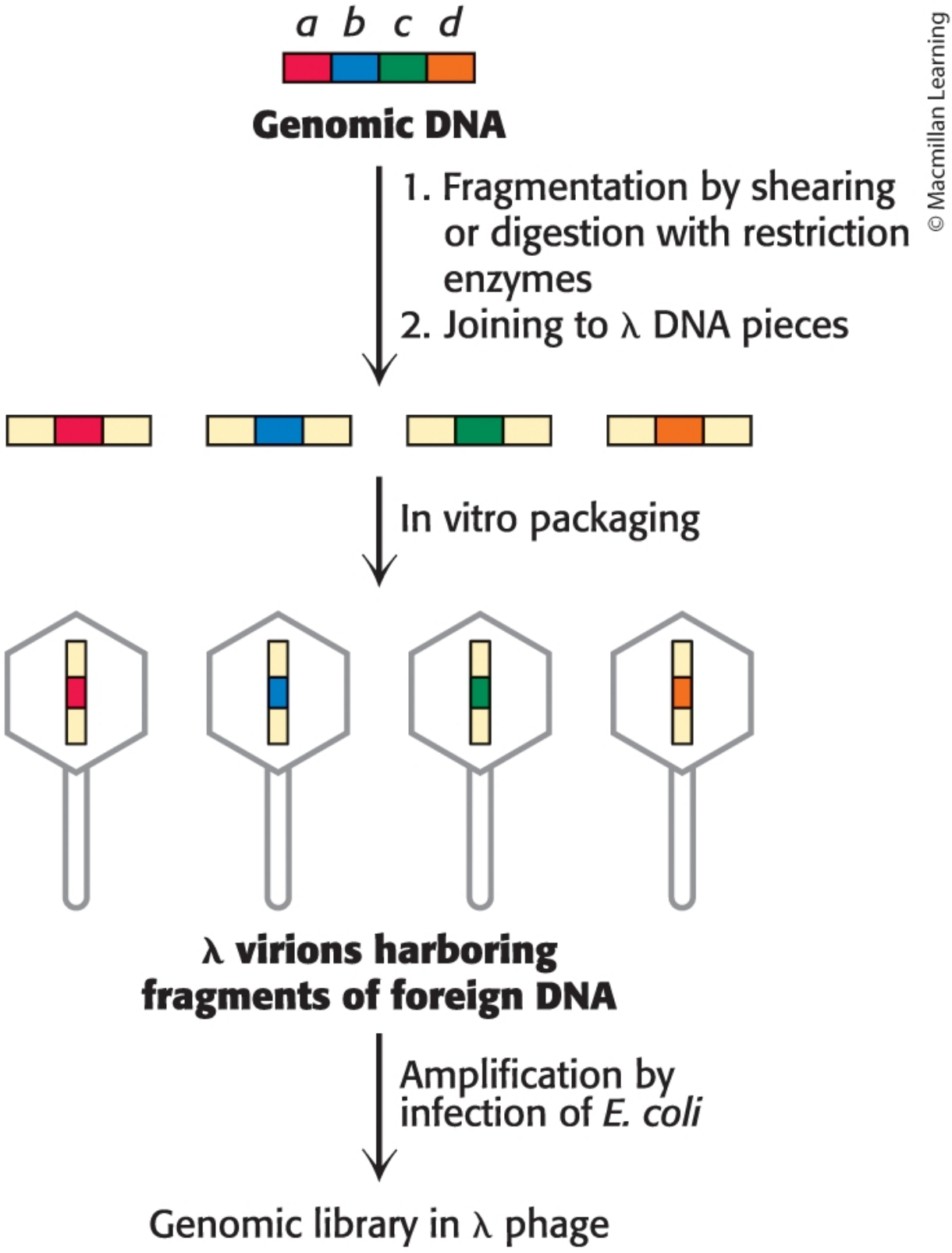
The amino acid sequence is as follows: Cysteine, Praline, Asparagine, Lysine, Tryptophan, Threonine, and Histidine.

The potential oligonucleotide sequences are as follows: T G, C or T, C C, A or C or G or T, A A, C or T, A A, A or G, T G G A C, A or C or G or T, C A, C or T.

Return to Oligonucleotide probe designed from a target sequence

Extended description for Schematic illustration of the creation of genomic library from a whole genome

digest



© Macmillan Learning

A genomic D N A is shown to have the following overlapping sequences: a (red), b (blue), c (green), and d (orange).

Step 1: Fragmentation by shearing or digestion with restriction enzymes.

Step 2: Joining lambda D N A pieces.

Four recombinant lambda D N A are shown with inserts corresponding to a, b, c, and d segments of the genomic D N A, respectively.

Step 3: In vitro packaging.

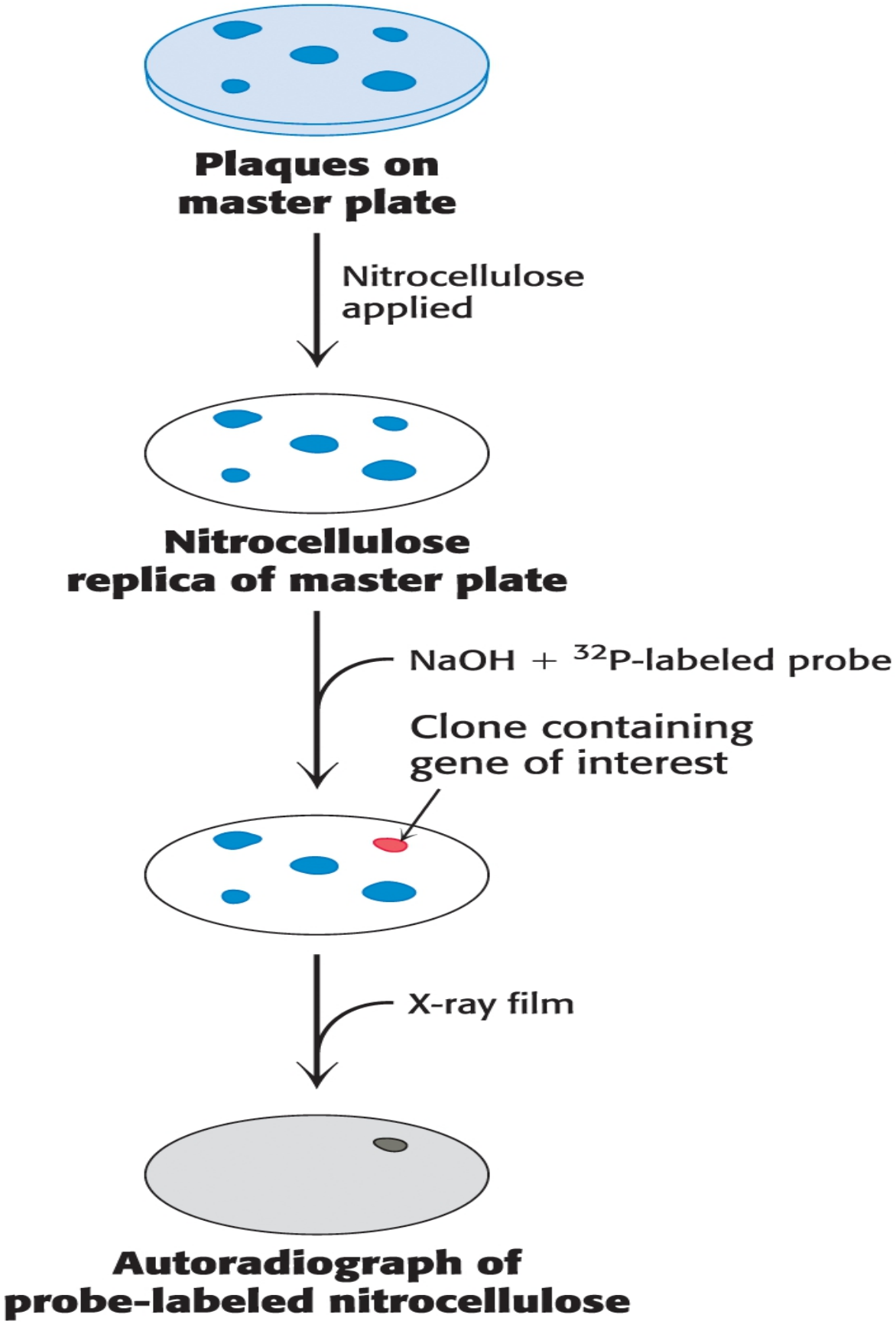
The recombinant lambda D N A is shown to be packed into the hexagonal heads of lambda virions, respectively.

Step 4: Amplification by infection of E. coli. This gives a genomic library in lambda phage.

Return to Schematic illustration of the creation of genomic library from a whole genome digest

Extended description for Schematic illustration of the

screening of a genomic library for a specific gene



© Macmillan Learning

A master culture plate is shown with five blue plaques of varying sizes.

Step 1: Nitrocellulose applied.

The nitrocellulose replica of the master plate is shown to have the same pattern of plaques as the master plate.

Step 2: Treatment with N a O H and P superscript 32 labeled probe.

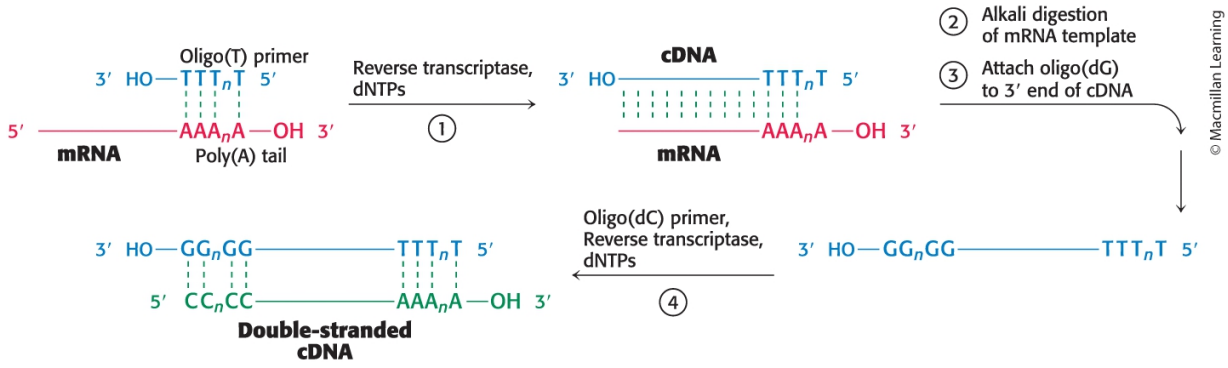
A plaque in the nitrocellulose replica is shown in red. This plaque is labeled clone containing gene of interest.

Step 3: Development of X-ray film.

The autoradiograph of the probe-labeled nitrocellulose shows only one spot at a position corresponding to the red labeled plaque.

Return to Schematic illustration of the screening of a genomic library for a specific gene

Extended description for Schematic illustration of double-stranded c D N A preparation from m R N A using reverse transcriptase



A single stranded red m R N A is shown. The 3 prime end of the m R N A has a poly A tail (repeating sequence of adenine) terminating in an O H group. An oligo T primer is shown to bind to the poly A tail of the m R N A. The primer has a repeating sequence of thymine terminating in an O H group at the 3 prime end. Hydrogen bonding between T and A is shown by dotted green lines.

Step 1: Addition of reverse transcriptase and d N T Ps.

The oligo T primer is shown to be extended in the 5 prime to 3 prime direction giving c D N A which is hydrogen bonded to the m R N A.

Step 2: Alkali digestion of m R N A template.

Step 3: Attach oligo d G to 3 prime end of c D N A.

The c D N A is shown to have a repeating sequence of guanine residues terminating in O H at the 3 prime end and a repeating sequence of thymine residues at the 5 prime end.

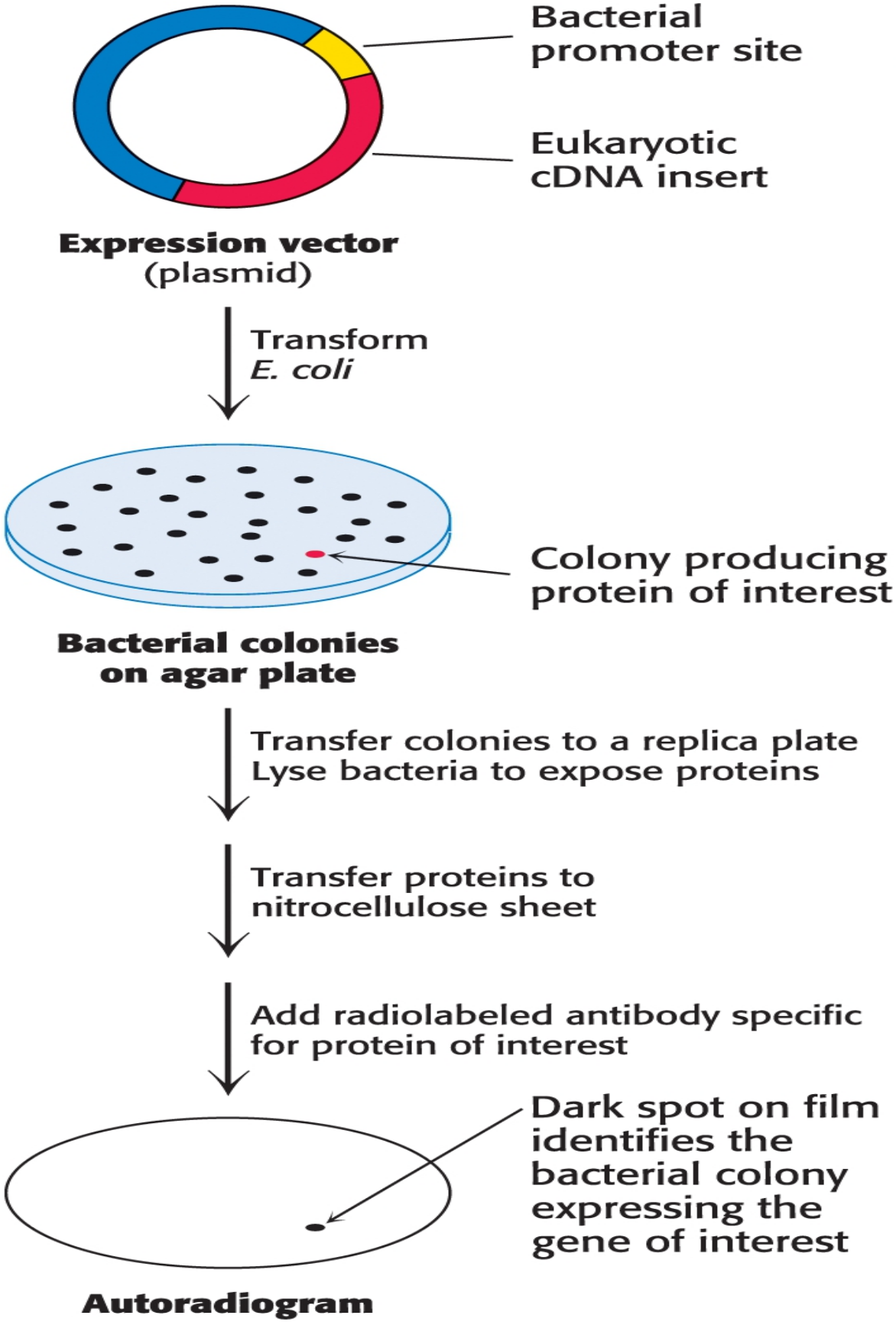
Step 4: Addition of Oligo d C primer, reverse transcriptase, and d N T Ps.

A double-stranded c D N A is shown. The c D N A strand from the previous step is hydrogen bonded to a new strand below. The new strand has a repeating sequence of adenine residues terminating in O H at the 3 prime end and a repeating sequence of cytosine residues at the 5 prime end.

Return to Schematic illustration of double-stranded c D N A preparation from m R N A using reverse transcriptase

Extended description for Schematic illustration of the screening of colonies in a c D N A library that express a

protein of interest



© Macmillan Learning

An expression vector (plasmid) is shown to have a circular D N A with a short sequence labeled bacterial promoter site followed by another longer sequence labeled eukaryotic c D N A insert.

Step 1: Transform E. coli.

An agar culture plate is shown with several bacterial colonies. One of the colonies is shown in red and labeled colony producing protein of interest.

Step 2: Transfer colonies to a replica plate. Lyse bacteria to expose proteins.

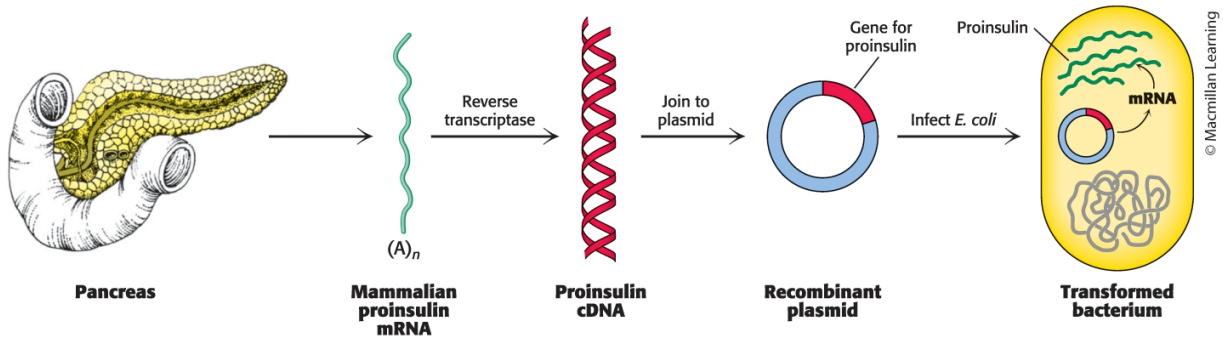
Step 3: Transfer proteins to nitrocellulose sheet.

Step 4: Add radiolabeled antibody specific to the protein of interest.

An autoradiogram is shown with a single spot corresponding to the labeled red colony in the agar plate. This dark spot on the film identifies the bacterial colony expressing the gene of interest.

Return to Schematic illustration of the screening of colonies in a c D N A library that express a protein of interest

Extended description for Schematic illustration of designing a bacteria to express proinsulin by infection with proinsulin c D N A



A human pancreas is illustrated.

A single-stranded mammalian proinsulin m R N A with a poly A tail is illustrated.

It is treated with reverse transcriptase.

A double-stranded helical proinsulin c D N A is produced by reverse transcriptase activity.

It is joined to a plasmid.

A circular recombinant plasmid with the inserted gene for proinsulin is illustrated.

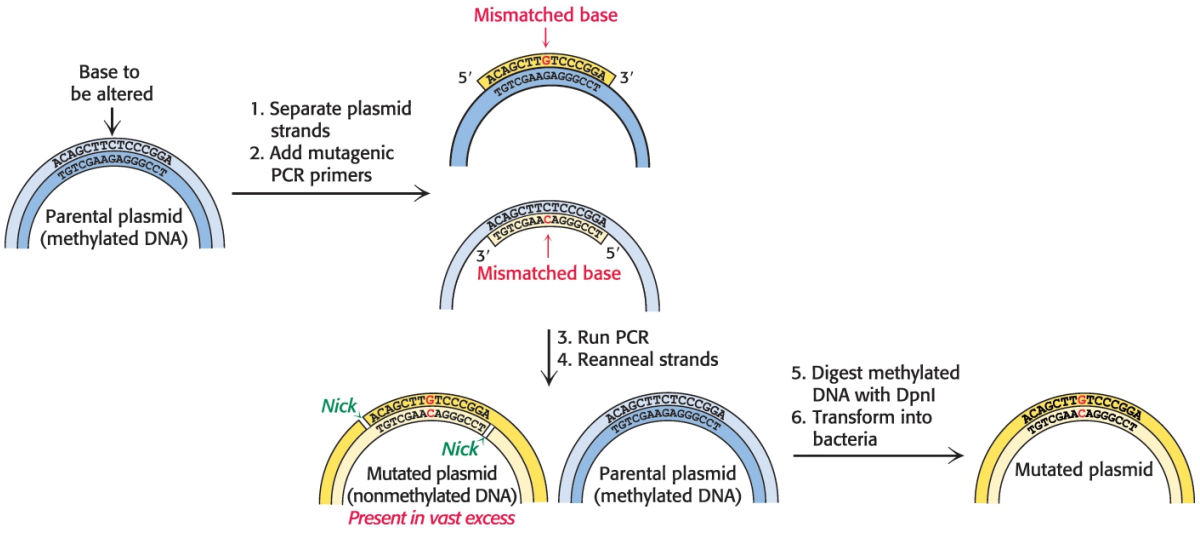
E. coli is infected with this recombinant plasmid.

Arod-shaped transformed bacterium with the recombinant plasmid is illustrated. Proinsulin m R N A is shown to be synthesized within

the cytoplasm of the bacterium.

Return to Schematic illustration of designing a bacteria to express proinsulin by infection with proinsulin c D N A

Extended description for Schematic illustration of site-directed mutagenesis in P C R



A parental plasmid (methylated D N A) is shown. The eighth base in the highlighted 15 bases long D N A segment is to be altered which is C in the outer strand and G in the inner strand.

Step 1: Separate plasmid strands.

Step 2: Add mutagenic P C R primers.

A complementary primer sequence with G (mismatched base) at the eighth position is shown to anneal to the inner strand.

A complementary primer sequence with C (mismatched base) at the eighth position is shown to anneal to the outer strand.

Step 3: Run P C R.

Step 4: Reanneal strands.

Mutated plasmid (nonmethylated D N A) is present in vast excess in the P C R product. The plasmid has G in the outer strand and C in the inner strand at the eighth position. A nick is present in both strands where the 5 prime end of the primer was present.

Parental plasmid (methylated D N A) has the original sequence.

Step 5: Digest methylated D N A with D p n roman number 1.

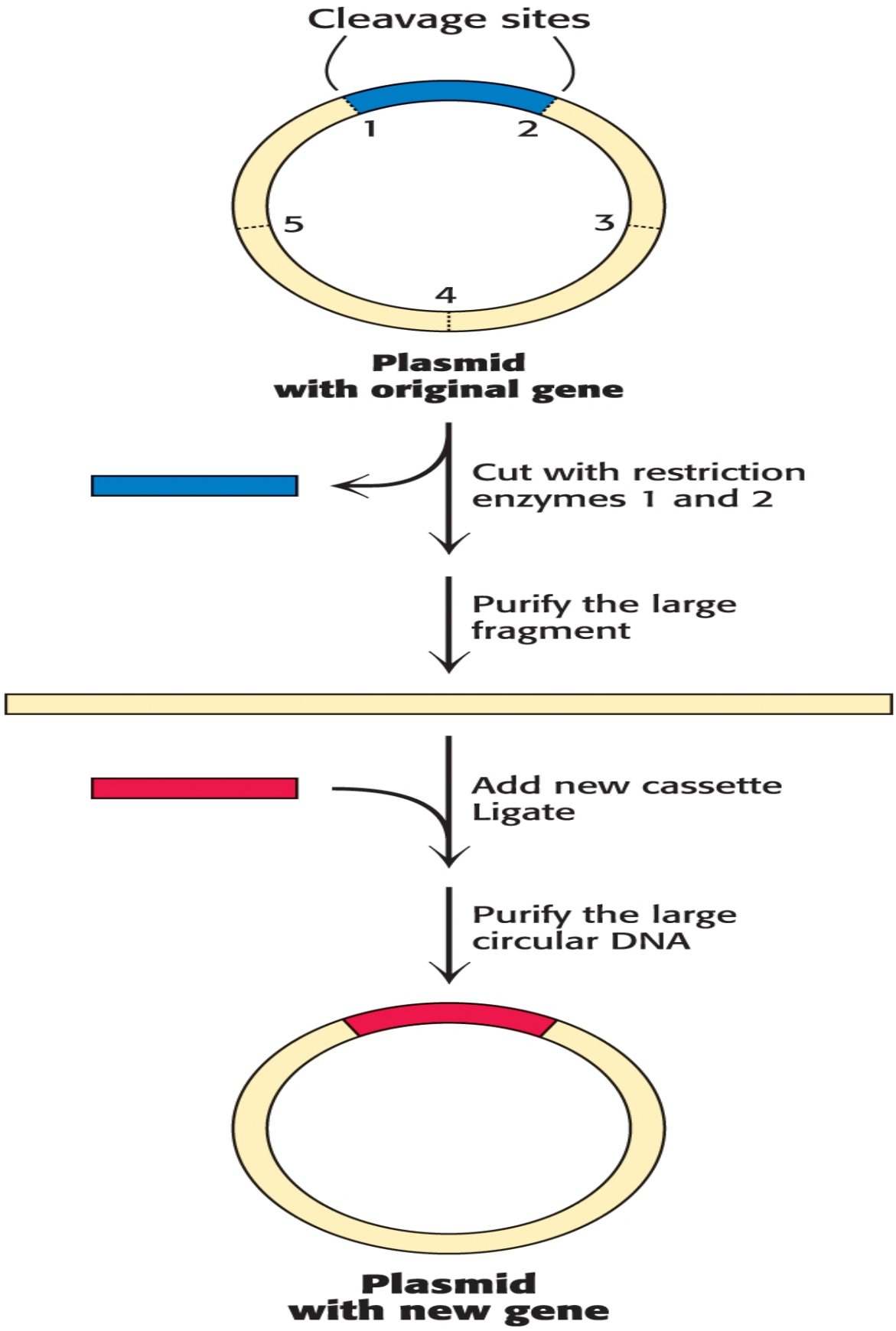
Step 6: Transform bacteria.

The final result is shown to be the mutated plasmid.

Return to Schematic illustration of site-directed mutagenesis in P C R

Extended description for Schematic illustration of

cassette mutagenesis



© Macmillan Learning

A plasmid with the original gene is shown. Five unique restriction sites numbered 1 to 5 are indicated in the plasmid. The segment between sites 1 and 2 is highlighted in blue to indicate the gene to be replaced.

Step 1: Cut with restriction enzymes 1 and 2.

Step 2: Purify large fragment.

The blue gene is shown to be removed. The remaining plasmid is shown as a linear D N A molecule.

Step 3: Add new cassette ligate.

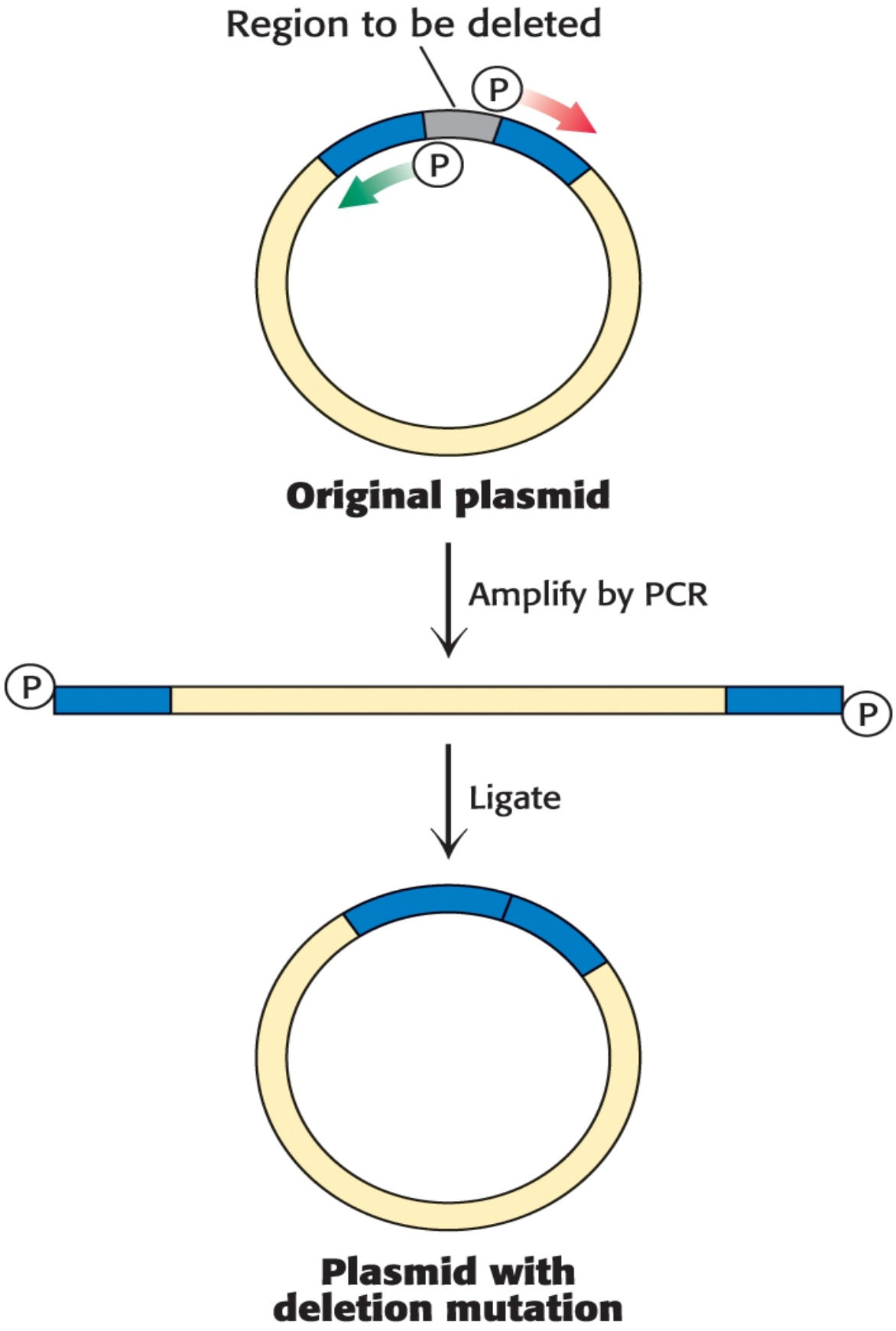
Step 4: Purify the large circular D N A.

The circular plasmid with the new gene is shown with a red D N A cassette inserted in the place of the original blue gene.

Return to Schematic illustration of cassette mutagenesis

Extended description for Schematic illustration of the

application of P C R to generate mutations



© Macmillan Learning

An original circular plasmid is shown. The region in the plasmid to be deleted is shown in grey. This region is flanked by two blue segments on both sides. Primers containing a phosphate group are shown to anneal to the flanking segments.

Step 1: Amplify by P C R.

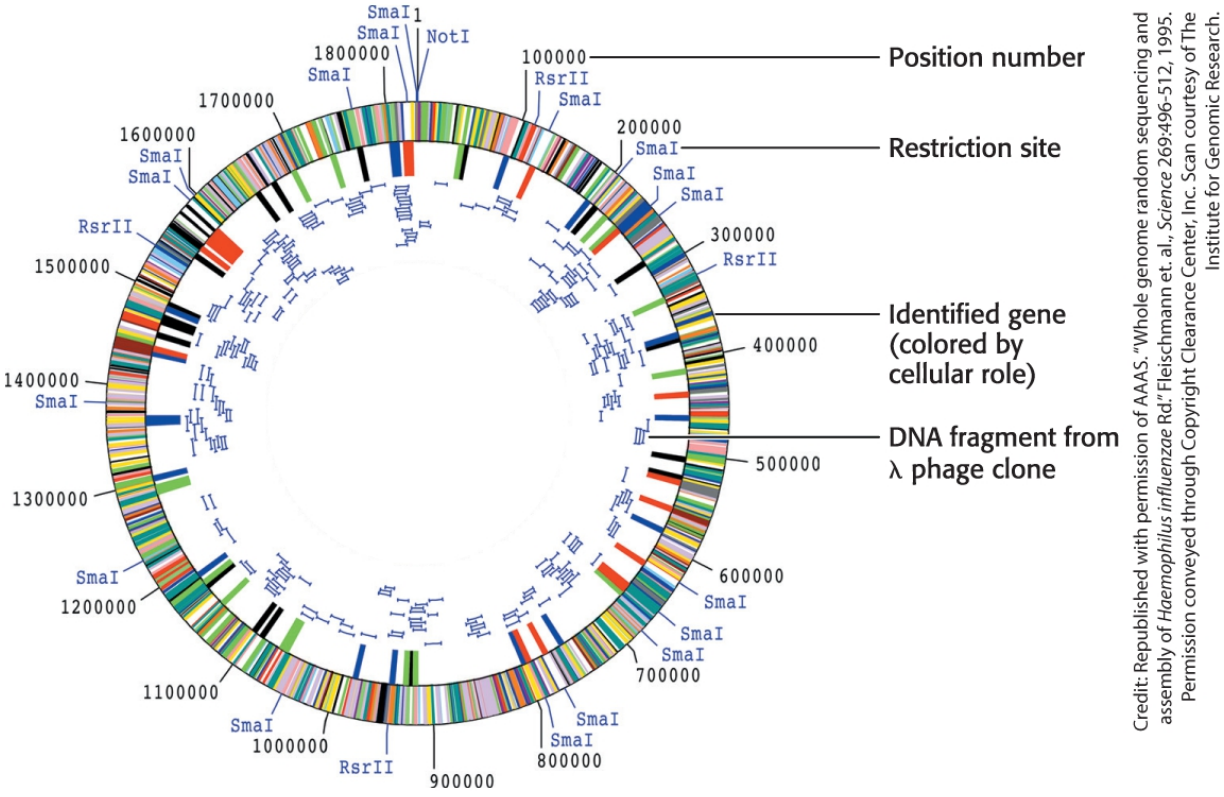
A linear D N A is shown with the blue flanking segments. Both the segments have a phosphate group at the free end.

Step 2: Ligate.

The product is a circular plasmid with deletion mutation. The ends of the blue flanking segments are ligated and grey region is removed.

Return to Schematic illustration of the application of P C R to generate mutations

Extended description for Mapped genome of *Haemophilus influenzae*

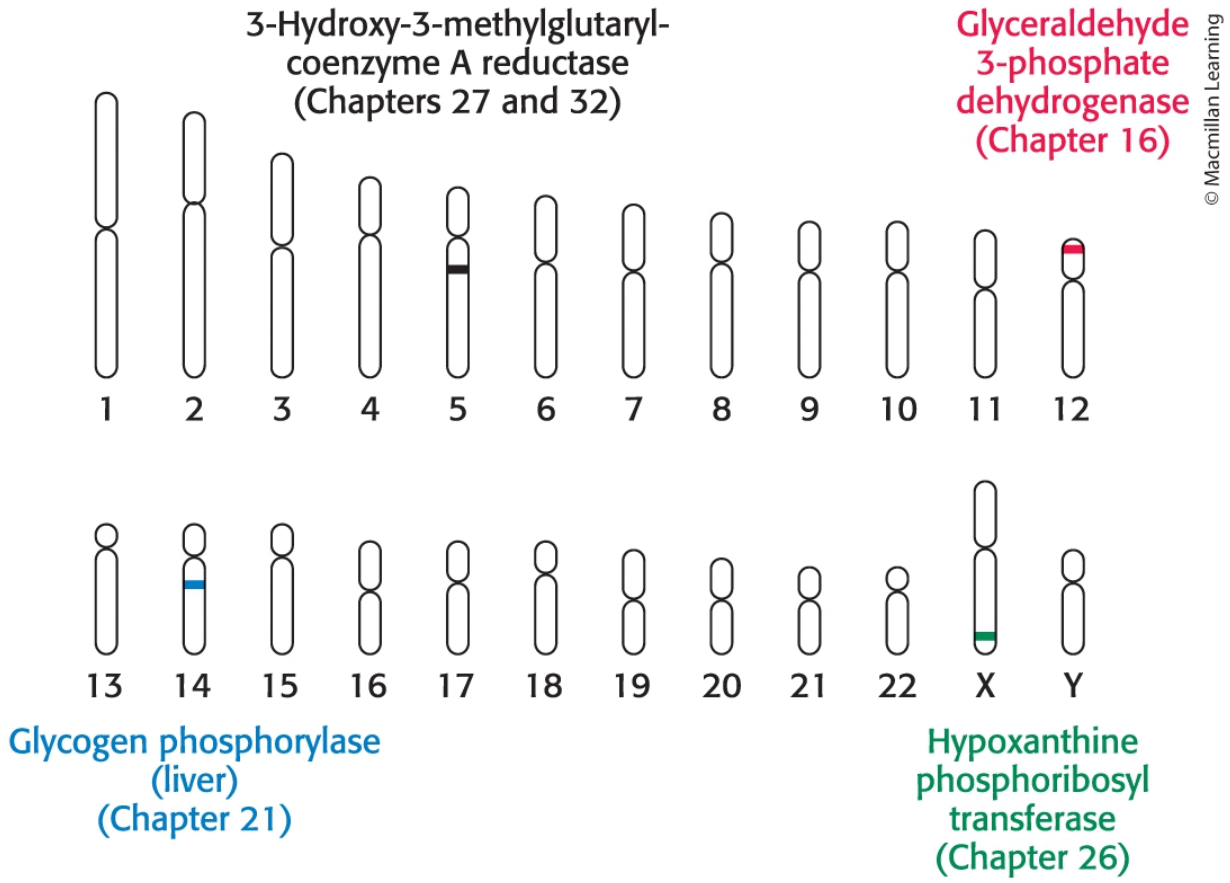


Credit: Republished with permission of AAAS. "Whole genome random sequencing and assembly of *Haemophilus influenzae* Rd." Fleischmann et. al., *Science* 269:496-512, 1995. Permission conveyed through Copyright Clearance Center, Inc. Scan courtesy of The Institute for Genomic Research.

The genome is shown to be circular. The identified genes are shown as color coded segments on the outer circle. They are colored according to their cellular role. Bars corresponding to D N A fragment from the lambda phage clone are shown along the inner circle. The position number and restriction sites with the genome are also indicated.

Return to Mapped genome of *Haemophilus influenzae*

Extended description for The set of human chromosomes with the location of genes associated with important biochemical pathways marked



Each chromosome is shown to have a long and a short arm joined at the centromere. The chromosomes vary in size. The following genes are highlighted:

3-Hydroxy-3-methylglutaryl-coenzyme A reductase (Chapters 27 and 32): On the long arm near the centromere of Chromosome 5.

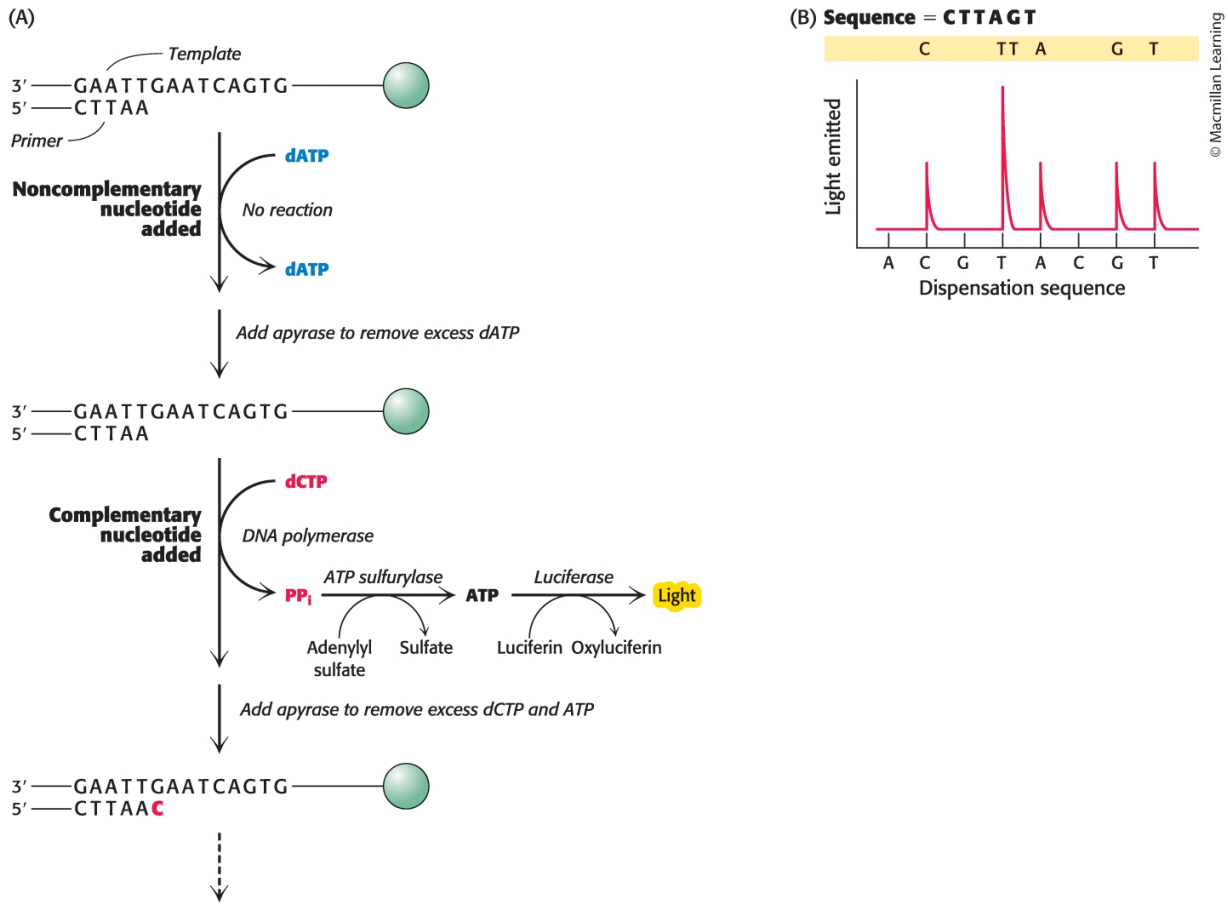
Glyceraldehyde-3-phosphate dehydrogenase (Chapter 16): On the tip of the short arm of Chromosome 12.

Glycogen phosphate (liver) (Chapter 21): On the long arm near the centromere of Chromosome 14.

Hypoxanthine phosphoribosyl transferase (Chapter 26): On the tip of the long arm of the X Chromosome.

Return to The set of human chromosomes with the location of genes associated with important biochemical pathways marked

Extended description for Schematic illustration of pyrosequencing



Part (A): Steps of pyrosequencing.

The template D N A sequence in the 3 prime to 5 prime direction is as follows: G A A T T G A A T C A G T G. The D N A template is tethered to a solid spherical support at the 5 prime end. The primer sequence annealed to the template is as follows: 5 prime C T T A A.

Noncomplementary nucleotide added: d A T P is added but no reaction takes place and d A T P leaves. Apyrase is added to remove excess d A T P. The primer is not extended in this case.

Complementary nucleotide added: d C T P is added in the presence of D N A polymerase. C is added to the primer. P P subscript i is released which is converted to A T P by A T P sulfurylase and in the process adenyl sulfate is converted to sulfate. A T P is then converted into light by luciferase and in the process luciferin is converted into oxyluciferin.

Apyrase is again added to remove excess d C T P and A T P.

The primer extends by the addition of a complementary C nucleotide base.

Part (B): A graph shows the determination of the sequence by pyrosequencing. The vertical axis is labeled Light emitted. The horizontal axis is labeled Dispensation sequence and has the following markings:

A: No peak

C: Short peak

G: No peak

T: A tall peak

A: Short peak

C: No peak

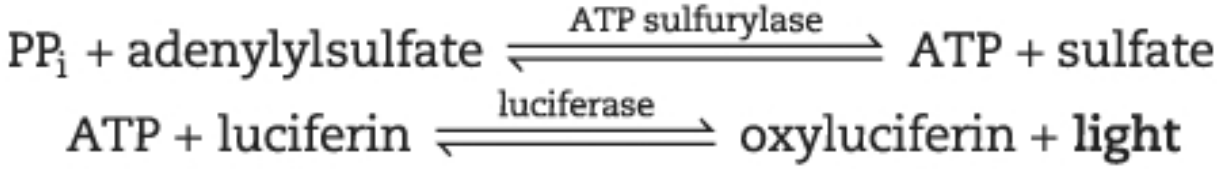
G: Short peak

T: Short peak

Sequence equals C T T A G T.

Return to Schematic illustration of pyrosequencing

Extended description for Light generation during the pyrosequencing process

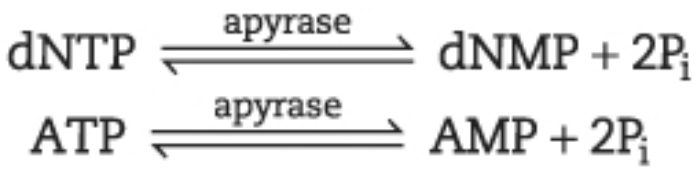


The first chemical reaction consists of two reactants and two products. The first reactant is P P subscript i. The second reactant is adenylylsulfate. A reversible reaction arrow labeled "A T P sulfurylase" leads to the products. The first product is A T P. The second product is sulfate.

The second chemical reaction consists of two reactants and two products. The first reactant is A T P. The second reactant is luciferin. A reversible reaction arrow labeled "luciferase" leads to the products. The first product is oxyluciferin. The second product is light.

Return to Light generation during the pyrosequencing process

Extended description for Chemical reactions catalyzed by apyrase



Reaction 1: The reversible reaction consists of 1 reactant and 2 products.

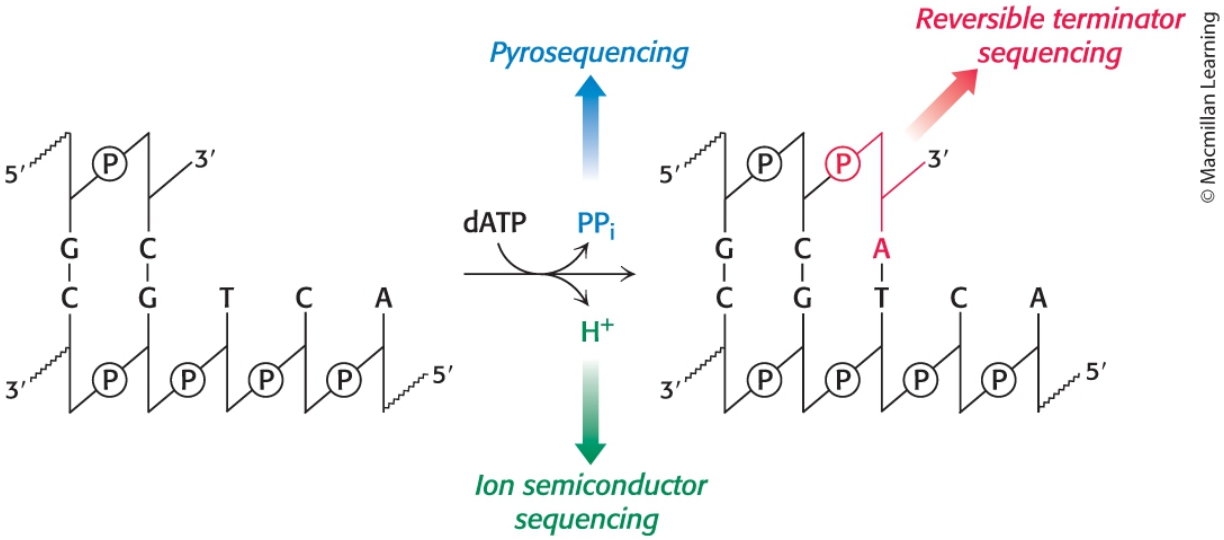
The reactant is d N T P. The first product is d N M P. The second product is 2 P subscript i. The reversible reaction arrow is labeled apyrase.

Reaction 2: The reversible reaction consists of 1 reactant and 2 products.

The first reactant is A T P. The first product is A M P. The second product is 2 P subscript i. The reversible reaction arrow is labeled apyrase.

Return to Chemical reactions catalyzed by apyrase

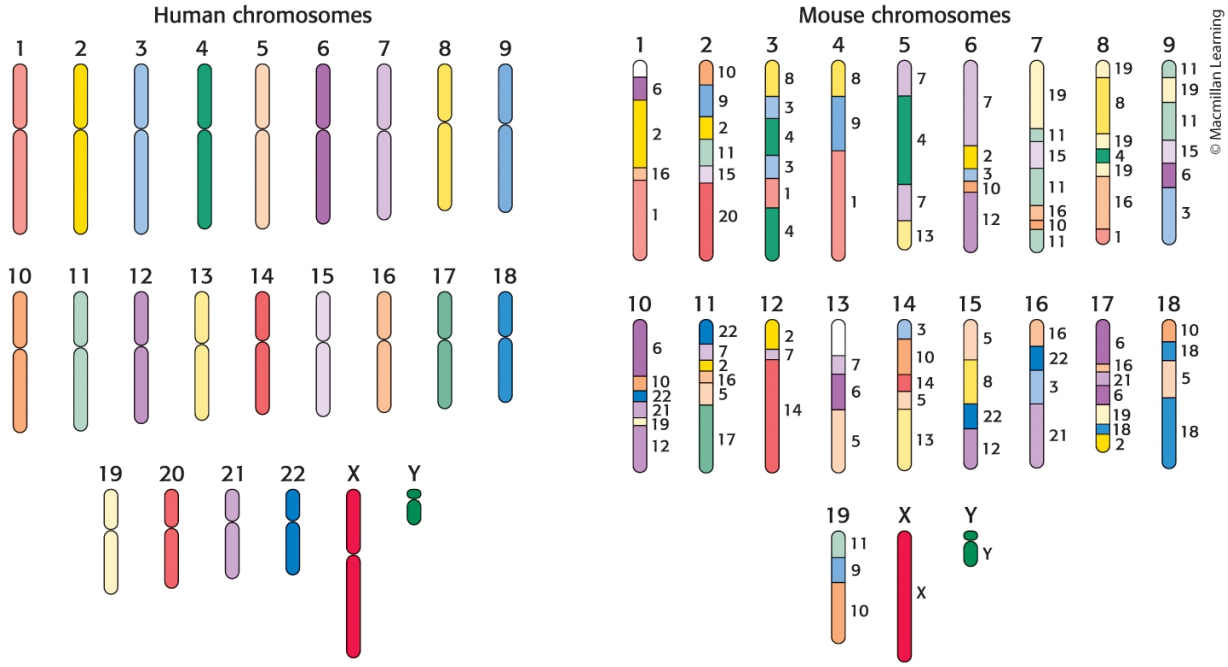
Extended description for Different approaches used in next-generation sequencing methods



The template D N A has the following sequence in the 3 prime to 5 prime direction: C G T C A. The primer has the following sequence in the 5 prime to 3 prime direction: G C. d A T P is added to extend the primer by adding A to the 3 prime end. This approach is used in reversible terminator sequencing. During this addition, P P subscript i and H superscript ions are released. P P subscript i is utilized in pyrosequencing. H superscript plus is utilized in ion semiconductor sequencing.

Return to Different approaches used in next-generation sequencing methods

Extended description for Comparison of human and mouse genomes



The human autosomes and the X and Y chromosomes are shown.

The mouse chromosomes are shown to indicate each region closely related to that of humans, from top to bottom, as follows:

Chromosome 1: Human chromosomes 6, 2, 16, and 1.

Chromosome 2: Human chromosomes 10, 9, 2, 11, 15, and 20.

Chromosome 3: Human chromosomes 8, 3, 4, 3, 1, and 4.

Chromosome 4: Human chromosomes 8, 9, and 1.

Chromosome 5: Human chromosomes 7, 4, 7, and 13.

Chromosome 6: Human chromosomes 7, 2, 3, 10, and 12.

Chromosome 7: Human chromosomes 19, 11, 15, 11, 16, 10, and 11.

Chromosome 8: Human chromosomes 19, 8, 19, 4, 19, 16, and 1.

Chromosome 9: Human chromosomes 11, 19, 11, 15, 6, and 3.

Chromosome 10: Human chromosomes 6, 10, 22, 21, 19, and 12.

Chromosome 11: Human chromosomes 22, 7, 2, 16, 5, and 17.

Chromosome 12: Human chromosomes 2, 7, and 14.

Chromosome 13: Human chromosomes 7, 6, and 5.

Chromosome 14: Human chromosomes 3, 10, 14, 5, and 13.

Chromosome 15: Human chromosomes 5, 8, 22, and 12.

Chromosome 16: Human chromosomes 16, 22, 3, and 21.

Chromosome 17: Human chromosomes 6, 16, 21, 6, 19, 18, and 2.

Chromosome 18: Human chromosomes 10, 18, 5, and 18.

Chromosome 19: Human chromosomes 11, 9, and 10.

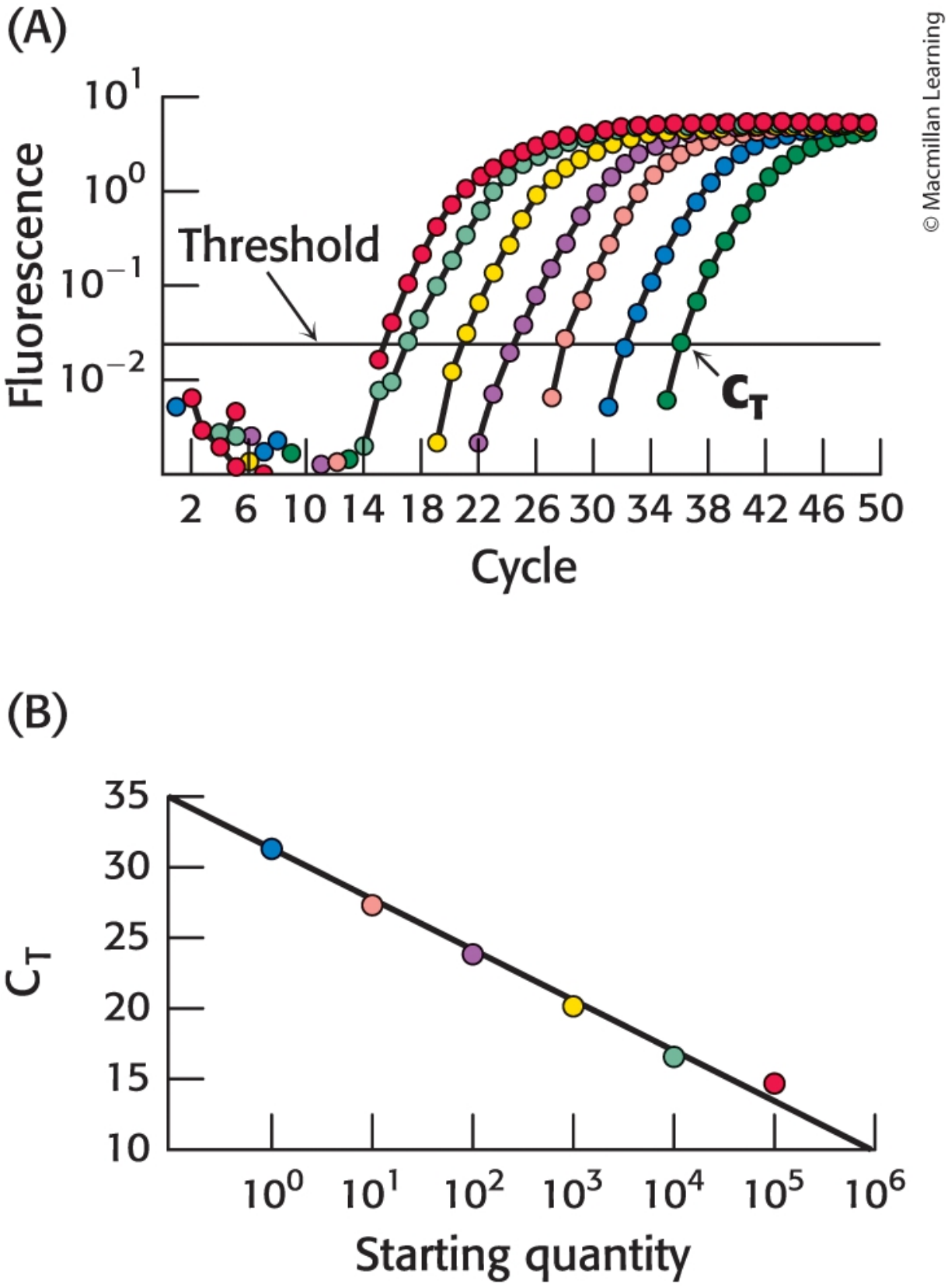
Chromosome X: Human chromosome X.

Chromosome Y: Human chromosome Y.

Return to Comparison of human and mouse genomes

Extended description for Graphs depicting results of a

quantitative P C R



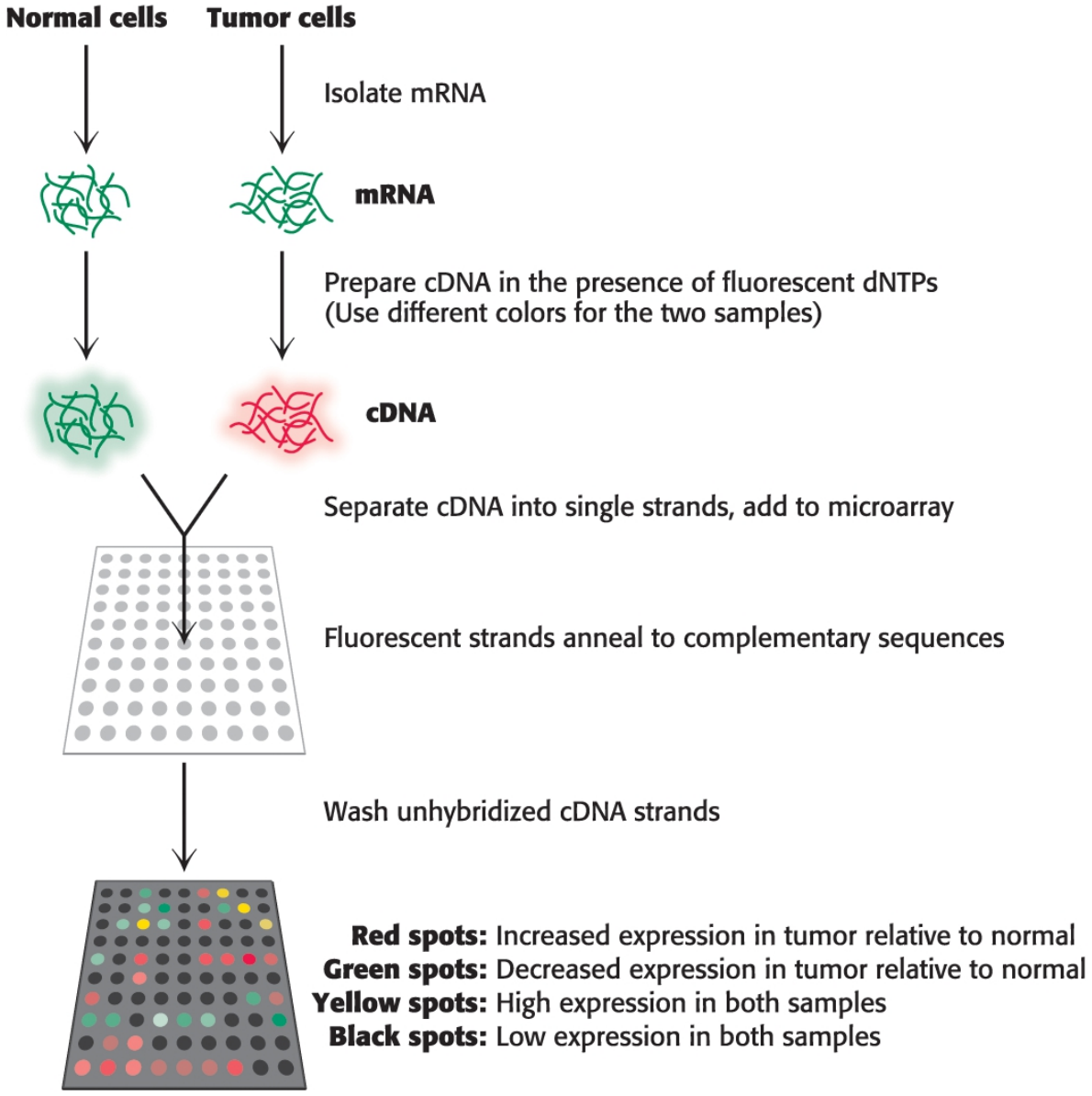
© Macmillan Learning

Graph (A): The horizontal axis is labeled cycle and ranges from 2 to 50 in increments of 4 units. The vertical axis is labeled fluorescence and ranges from 10 raised to the power minus 2 to 10 raised to the power in geometric increments of 10 units. A horizontal line labeled threshold passes through a point just above 10 raised to the power minus 2. Seven color coded curves corresponding to different samples are shown to have an S-shape and plateau to the same point. The points at which the curves cross the threshold is labeled C subscript T value. The arrangement of curves in the increasing order of C subscript T values is as follows: Red, turquoise, yellow, purple, pink, blue, and green.

Part (B): The horizontal axis is labeled Starting quantity and ranges from 10 raised to the power 0 to 10 raised to the power 6 in geometric increments of 10 units. The vertical axis is labeled C subscript T and ranges from 10 to 35 in increments of 5 units. A straight trendline starts at (0, 35) and ends at (10 raised to the power 6, 0). The color coded points lie on the trendline corresponding to their C subscript T values as mentioned above.

Return to Graphs depicting results of a quantitative P C R

Extended description for Schematic illustration of the steps of D N A microarray analysis



© Macmillan Learning

Step 1: Isolate m R N A from normal and tumor cells.

Step 2: Prepare c D N A in the presence of fluorescent d N TPs (use different colors for two samples). Normal cell c D N A is shown in

green. Tumor cell c D N A is shown in red.

Step 4: Separate c D N A into single strands and add to microarray. Fluorescent strands anneal to complementary sequences.

The microarray plate is shown to have several wells arranged in a row-wise pattern.

Step 5: Wash unhybridized c D N A strands.

The resultant microarray plate is shown to show the following spots:

Red spots: Increased expression in tumor relative to normal.

Green spots: Decreased expression in tumor relative to normal.

Yellow spots: High expression in both samples.

Black spots: Low expression in both samples.

Return to Schematic illustration of the steps of D N A microarray analysis

Extended description for Heat map of a microarray

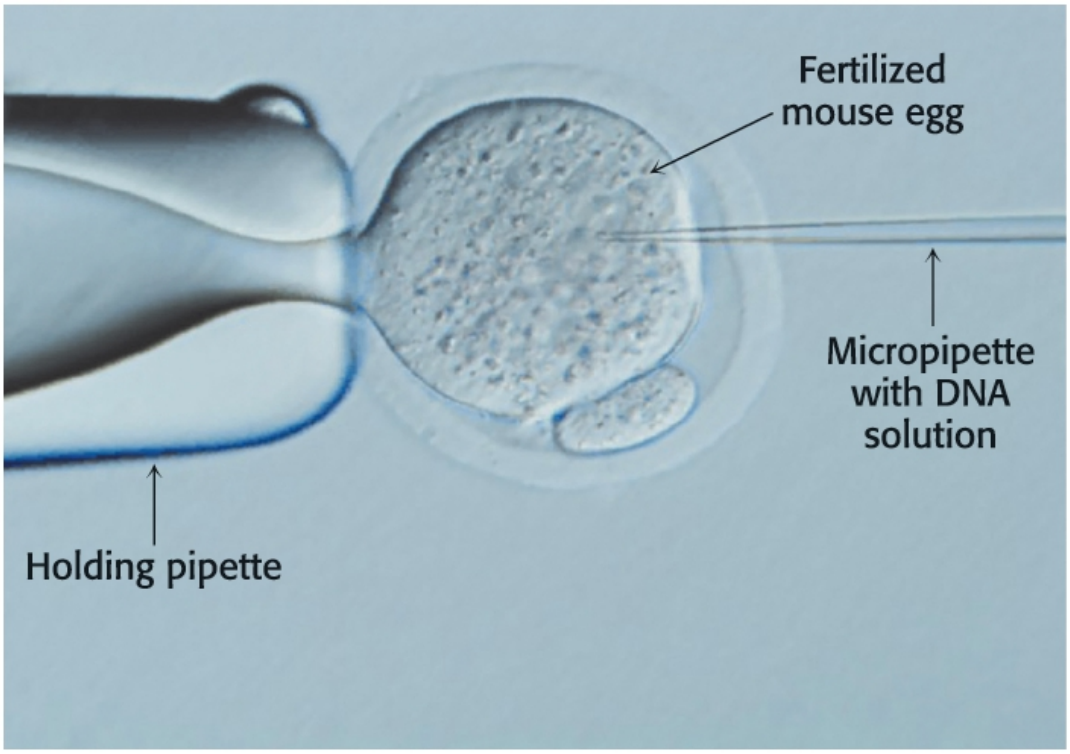
analysis of tumors

Credit: Kao J, Salari K, Bocanegra M, Choi YL, Girard L, Gandhi J, Kwei KA, Hernandez-Boussard T, Wang P, Gazdar AF, Minna JD, Pollack JR. Molecular profiling of breast cancer cell lines defines relevant tumor models and provides a resource for cancer gene discovery. February 2009. *PLoS One* 4(7):e6146, Figure 1B. DOI:10.1371/journal.pone.0006146.

The horizontal axis is labeled different tumors. The vertical axis is labeled different genes. Seven horizontal rectangles of varying thickness are shown one below the other. Each rectangle contains a cluster of red and green spots in a random arrangement. The red spots are clustered toward the left in the first, second, and third rectangles from the top. From the fourth to seventh rectangles, the cluster of red spots moves from the middle region toward the right. The green spots are clustered toward the right in the first, second, and third rectangles. From the fourth to seventh rectangles, the cluster of green spots moves from the right end toward the left.

Return to Heat map of a microarray analysis of tumors

Extended description for Micrograph of a cloned plasmid D N A being injected into a fertilized mouse egg

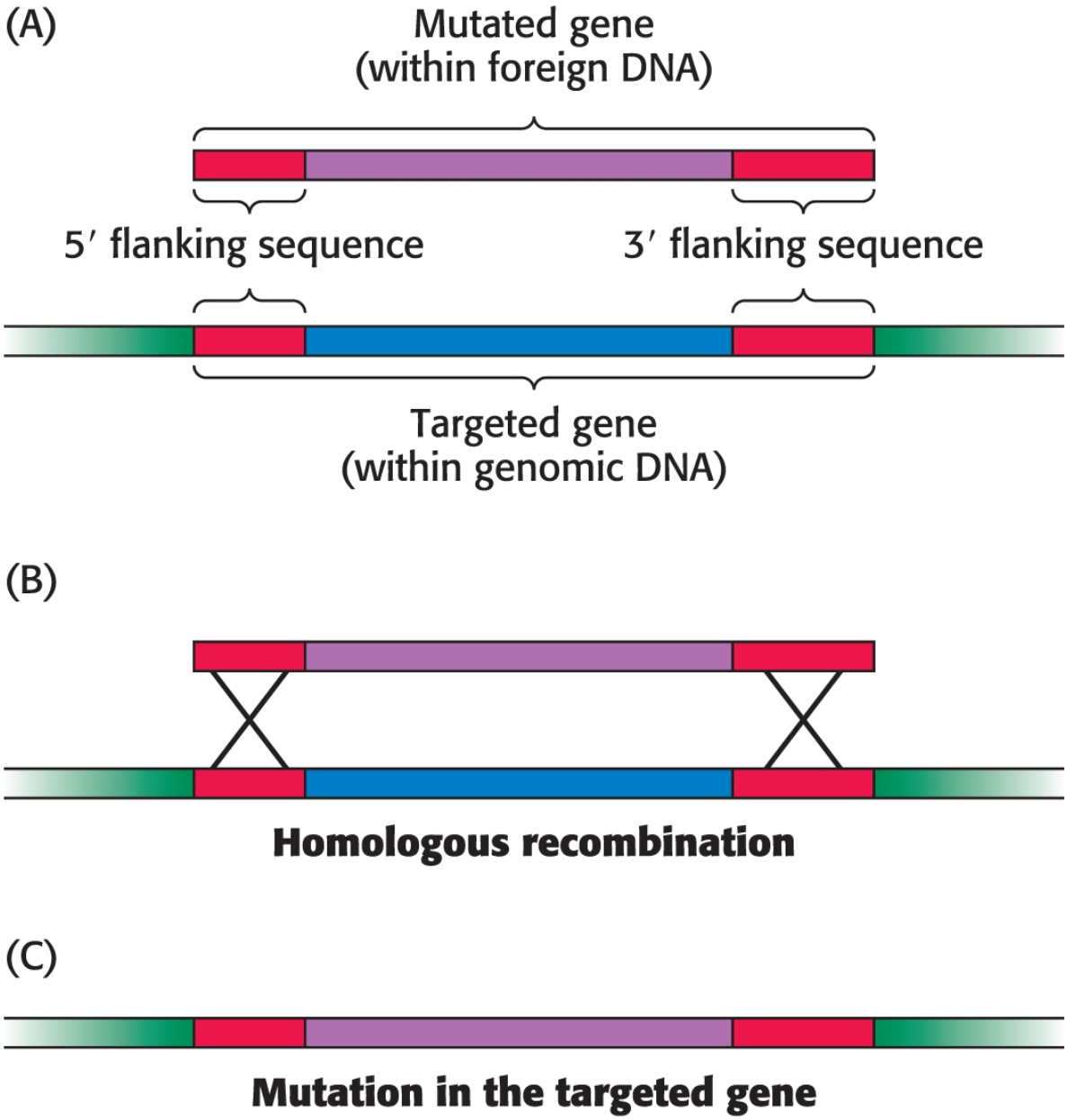


Credit: Marh et al, Hyperactive self-inactivating piggyBac for transposase-enhanced pronuclear microinjection transgenesis, PNAS, Vol 109, no. 47, pp. 19184–19189. Copyright 2012 National Academy of Sciences.

The fertilized mouse egg is shown to be held in place by a holding pipette. A thin micropipette is shown to inject the D N A solution into the egg.

Return to Micrograph of a cloned plasmid D N A being injected into a fertilized mouse egg

Extended description for Schematic illustration of foreign D N A insertion by homologous recombination



© Macmillan Learning

Part (A): A mutated gene within foreign D N A is shown in purple and is flanked by a 5 prime and 3 prime flanking sequence on either ends. The targeted gene within genomic D N A is shown in blue. The

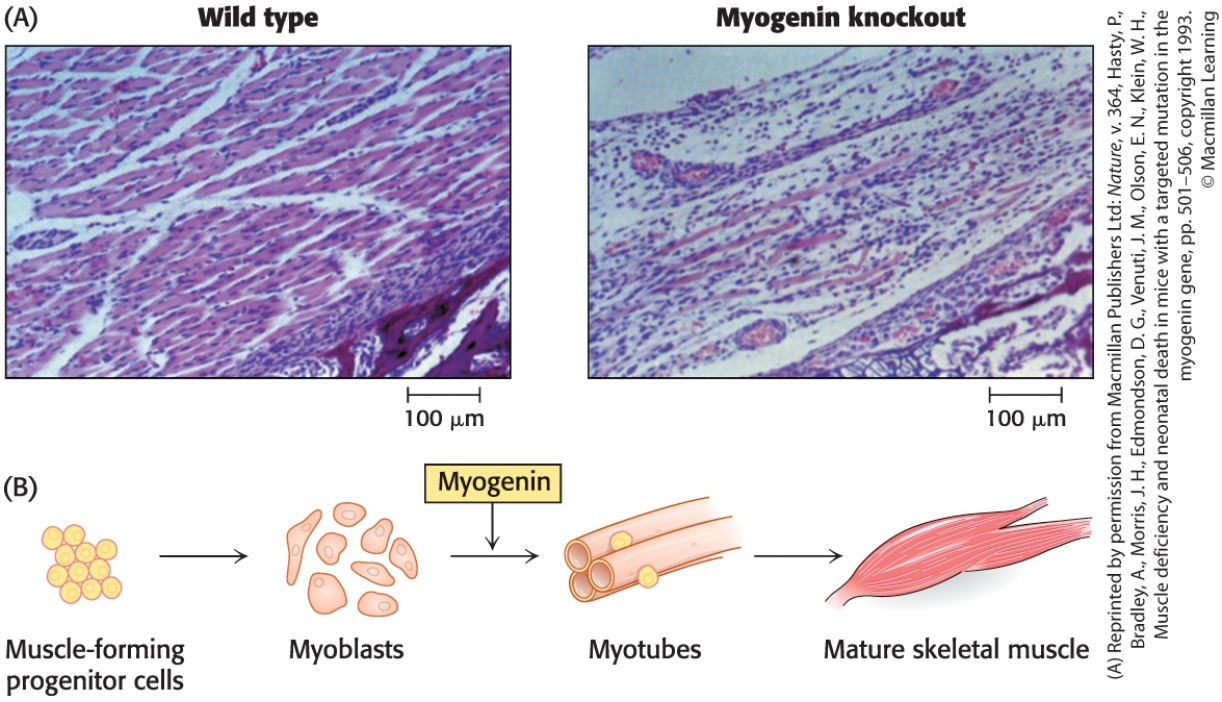
target sequence is also flanked by a 5 prime and 3 prime flanking sequence on either ends. The flanking sequences are shown in red. The genomic D N A is shown in green.

Part (B): A cross-joining of the corresponding flanking sequences of the mutated gene and the target gene shows homologous recombination.

Part (C): The purple mutated gene is shown to replace the target gene within the genomic D N A and is flanked by the 5 prime and 3 prime flanking sequences on either ends.

Return to Schematic illustration of foreign D N A insertion by homologous recombination

Extended description for Consequences of myogenin knockout in mice

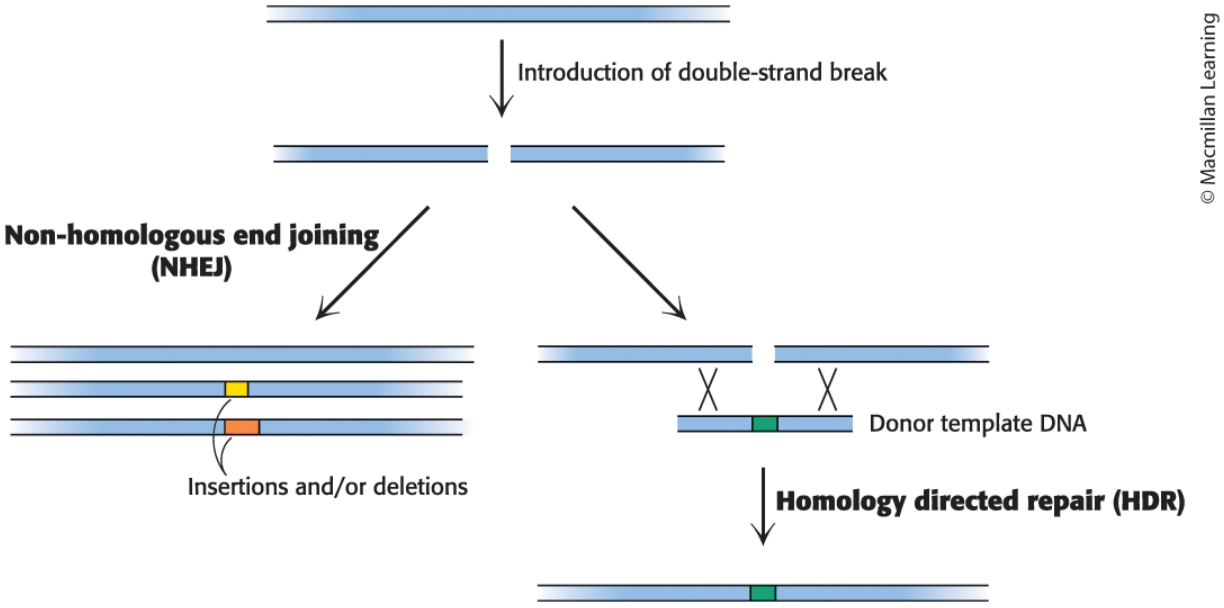


Part (A): A micrograph of muscle in wild type mice shows properly formed muscle tissue. A micrograph of muscle in myogenin knockout mice shows underdeveloped muscle tissue. The scale bar is 100 micrometers.

Part (B): A cluster of yellow spherical cells are labeled muscle-forming progenitor cells. These give rise to irregularly shaped myoblasts. Myogenin stimulates myoblasts to form tubular-shaped myotubules. These aggregate to form mature skeletal muscle.

Return to Consequences of myogenin knockout in mice

Extended description for Schematic illustration of non-homologous end joining and homology directed repair of D N A



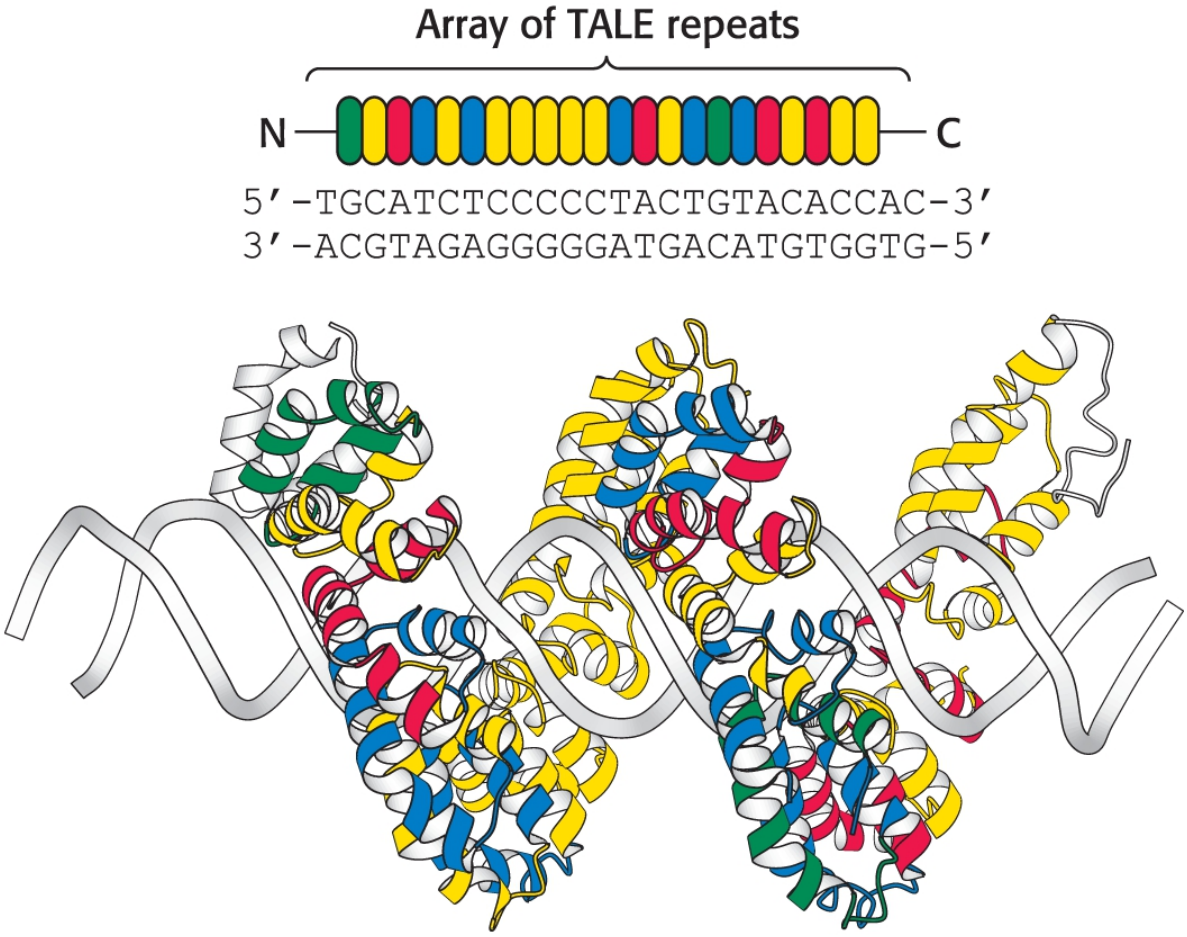
A linear double-stranded D N A is shown. A double-stranded break is introduced into the linear D N A.

Non-homologous end joining (N H E J): The repaired D N A can be of three types: identical to the original strand, joined with insertions, and slash or deletions in the strand.

Homology directed repair (H D R): A donor template D N A with a short green sequence in middle is shown to undergo homologous recombination with the original strand having a break. The resultant strand is shown to have the short green sequence incorporated into the repaired strand.

Return to Schematic illustration of non-homologous end joining and homology directed repair of D N A

Extended description for Recognition of individual bases in D N A by TALE repeats



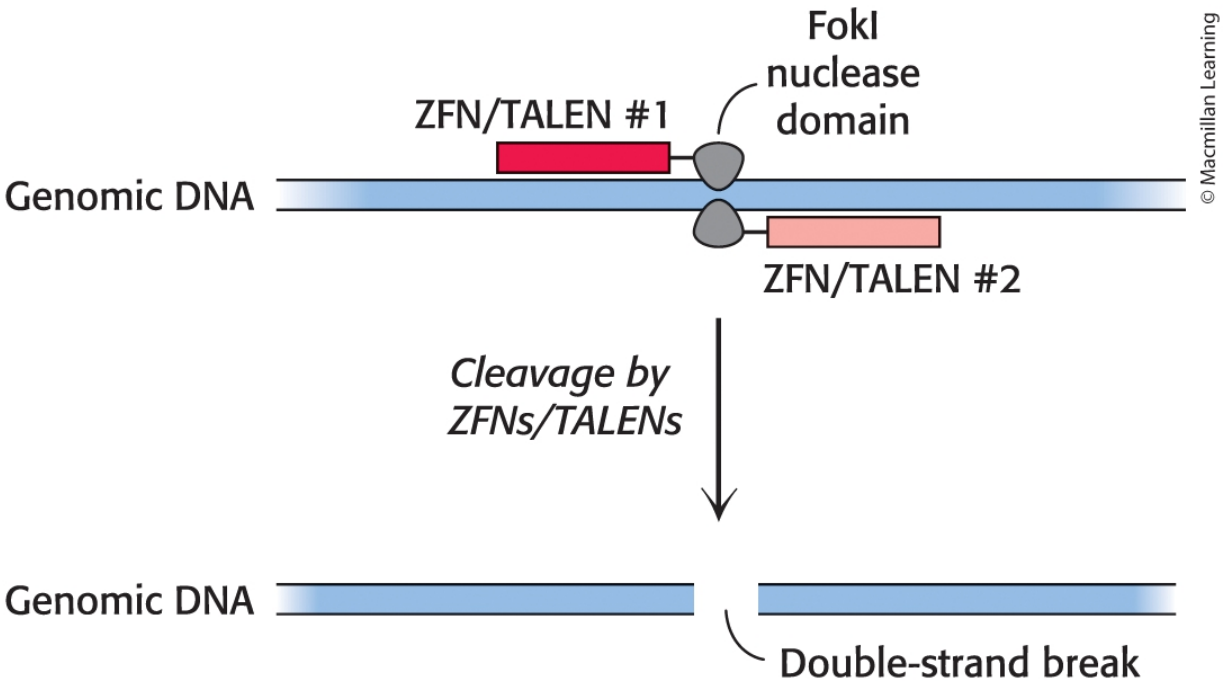
© Macmillan Learning

The D N A sequence in the 3 prime to 5 prime direction is T G C A T C T C C C C C T A C T G T A C A C C A C. The array of TALE repeats is a protein sequence aligned to the D N A sequence. The amino acid residues are color coded for each base as follows: G is green, C is yellow, A is red, and T is blue.

A double stranded D N A is shown to be bound by a TALE protein consisting of alpha helices connected by short loops.

Return to Recognition of individual bases in D N A by TALE repeats

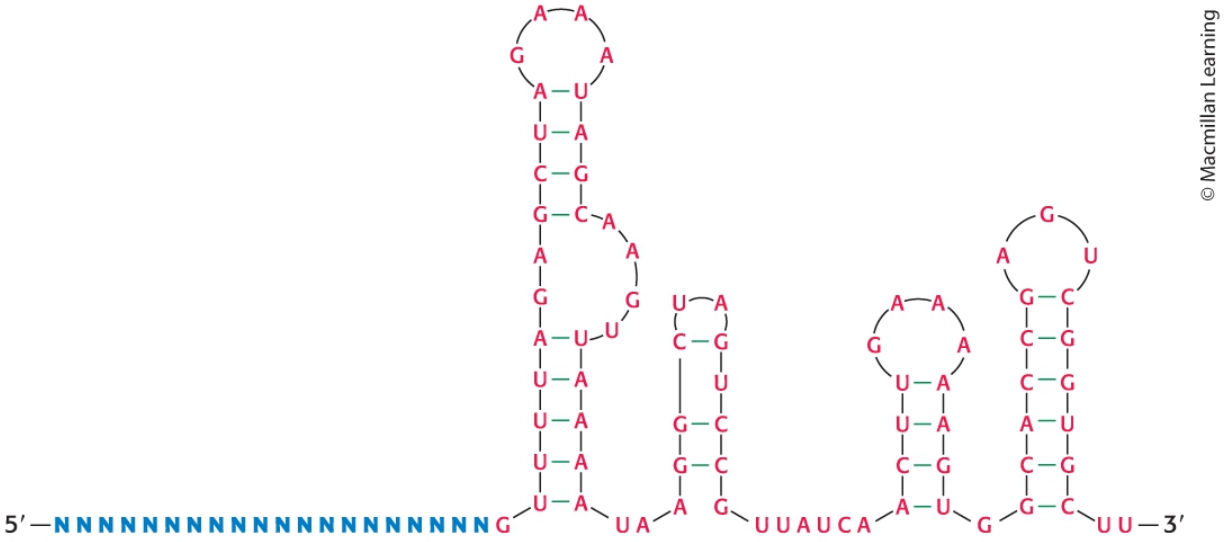
Extended description for Schematic illustration of the introduction of double-stranded break into D N A by Z F N or TALEN



A linear double-stranded genomic D N A is shown. Two triangular F o k roman number 1 nuclease domains are shown attached to the top and bottom strand on the D N A, respectively. A red bar labeled Z F N slash TALEN number 1 is linked to the left of the F o k 1 nuclease domain attached to the top strand. Similarly, a pink bar labeled Z F N slash TALEN number 2 is linked to the right of the F o k roman number 1 nuclease domain attached to the bottom strand. This introduces a double-stranded break at the D N A site.

Return to Schematic illustration of the introduction of double-stranded break into D N A by Z F N or TALEN

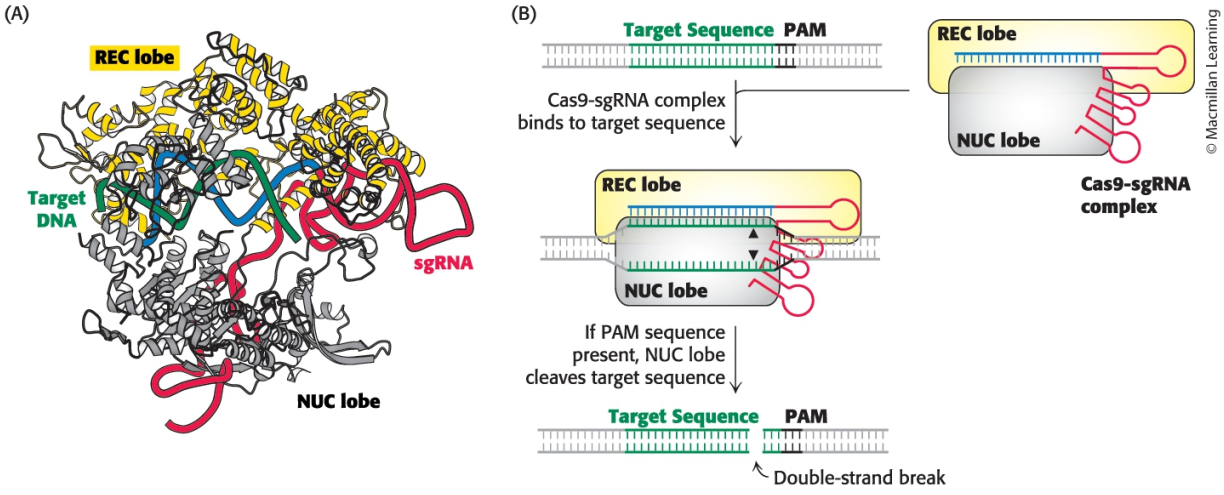
Extended description for Structure of single guide R N A



Twenty nucleotide residues (N) are present at the 5 prime end of the R N A. This is followed by four loops-stem structures toward the 3 prime end.

[Return to Structure of single guide R N A]

Extended description for Schematic illustration of D N A cleavage by CRISPR-Cas system



Part (A): Cas 9- s g R N A complex: The target D N A is shown as a green and blue double helix. The s g R N A shown in red is bound to one end of the target D N A. Some of the loops of the s g R N A are bound to the N U C lobe below. The N U C lobe shown in grey encircles the D N A. The R E C lobe shown in yellow covers the D N A from the top.

Part (B): D N A cleavage by CRISPR-Cas system:

The target sequence in a D N A segment in highlighted in green. A short PAM sequence to the right of the target sequence is highlighted in black.

The Cas 9- s g R N A complex is shown to have a rectangular R E C lobe. A short rectangular N U C lobe overlaps the R E C lobe above. The 20 nucleotide sequence (blue) of the s g R N A is shown linearly above the N U C lobe and within the R E C lobe. The first loop

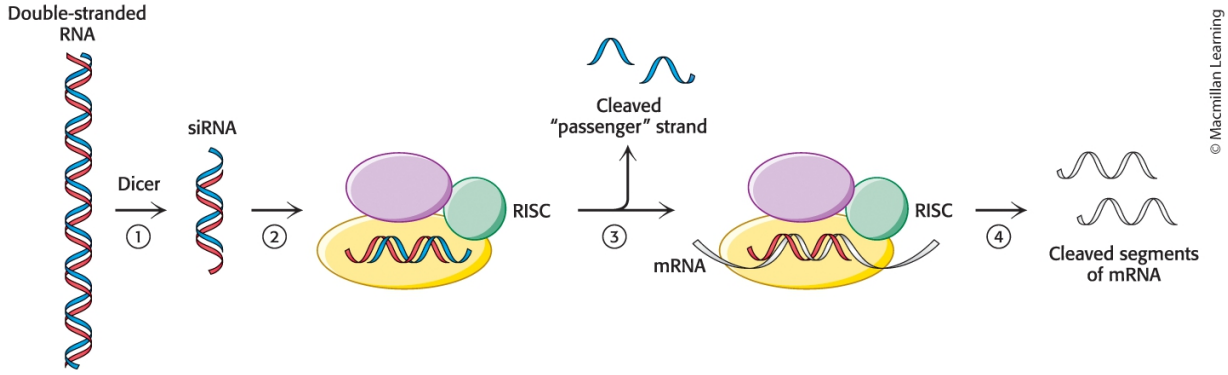
connected to the 20 nucleotides is shown to be horizontal and the other three loops bend into the N U C lobe.

The Cas 9- s g R N A complex binds to the target sequence. The strands at the target sequence and PAM are shown to separate. The blue 20 nucleotide sequence of the Cas 9- s g R N A complex is shown to bind to the top strand.

If PAM sequence is present, N U C lobe cleaves the target sequence. Two black triangles indicate the cleavage site in both strands. A double-stranded break in the target sequence is shown at a few bases upstream of the PAM sequence.

Return to Schematic illustration of D N A cleavage by CRISPR-Cas system

Extended description for Mechanism of R N A interference



Step 1: It is catalyzed by dicer. A long double-stranded R N A is shown to consist of a red and a blue strand. This long stretch on R N A is shown to be diced into a much smaller section labeled s i R N A.

Step 2: The fragmented s i R N A is shown to be incorporated into the R I S C. R I S C consists of three globular subunits and the s i R N A.

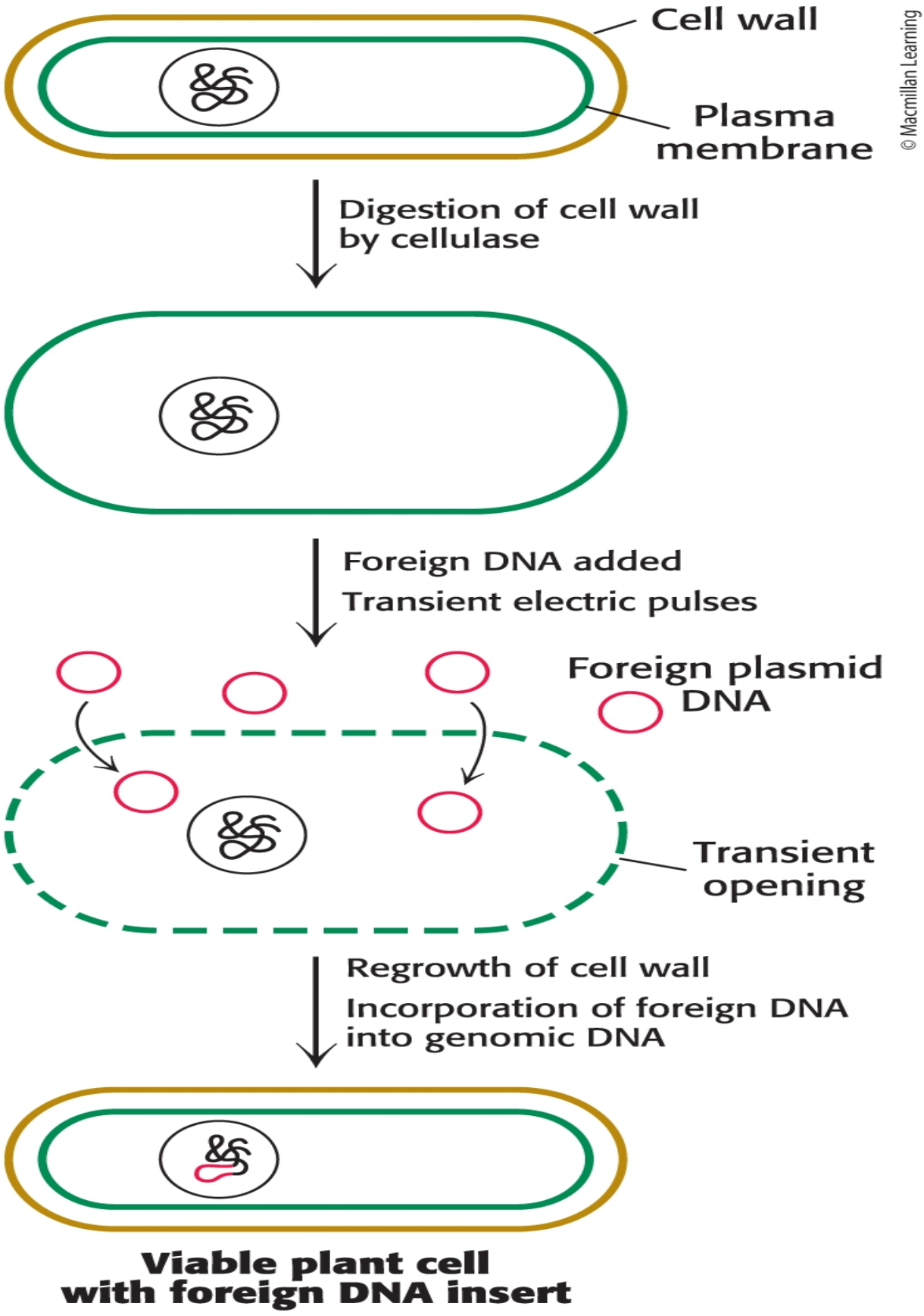
Step 3: The passenger strand (blue) of the s i R N A is cleaved and the red strand binds to an m R N A molecule.

Step 4: The m R N A molecule is cleaved by the R I S C into short segments.

[Return to Mechanism of R N A interference]

Extended description for Schematic illustration of the steps of introduction of foreign D N A into plant cell by

electroporation



© Macmillan Learning

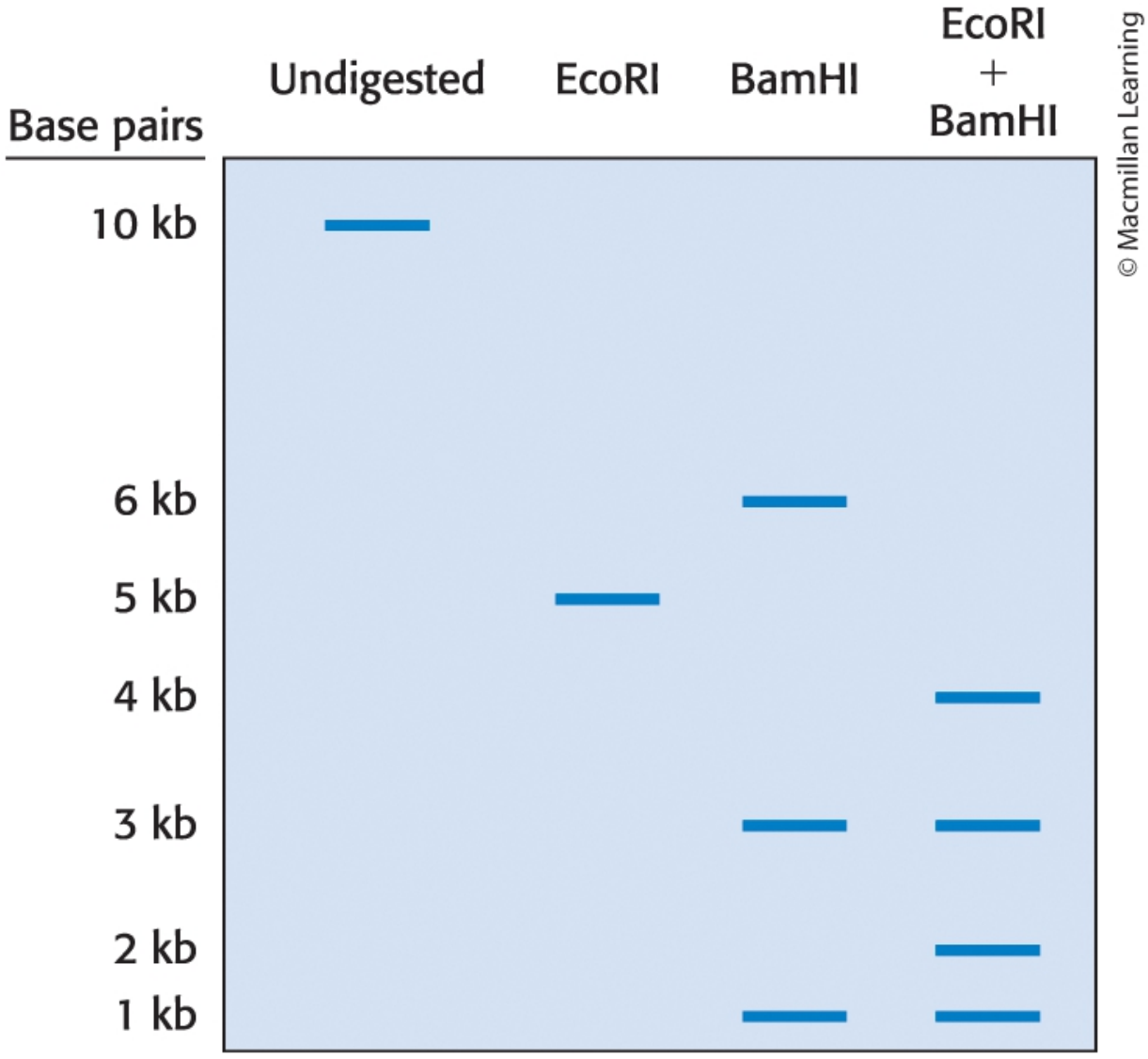
Step 1: Digestion of cell wall by cellulase. A plant cell is illustrated to have a plasma membrane enveloped by a cell wall. The nucleus containing the genome is present within the cell. The cell wall is shown to be digested leaving the plasma membrane exposed.

Step 2: Foreign D N A added and transient electric pulses are given to the plant cell. Foreign plasmid D N A molecules are shown as red rings. Electric pulses are shown to create transient openings in the cell membrane allowing the plasmids to enter the cell.

Step 3: Regrowth of cell wall. Incorporation of foreign D N A into genomic D N A. A viable plant cell with an intact cell wall and plasma membrane is shown to have the foreign D N A incorporated into its genomic D N A in the nucleus.

Return to Schematic illustration of the steps of introduction of foreign D N A into plant cell by electroporation

Extended description for Electrophoresis gel slab



The gel slab has four lanes with bands of varying sizes as follows:

Undigested: One band at 10 k b.

Eco R Roman number 1: One band at 5 k b.

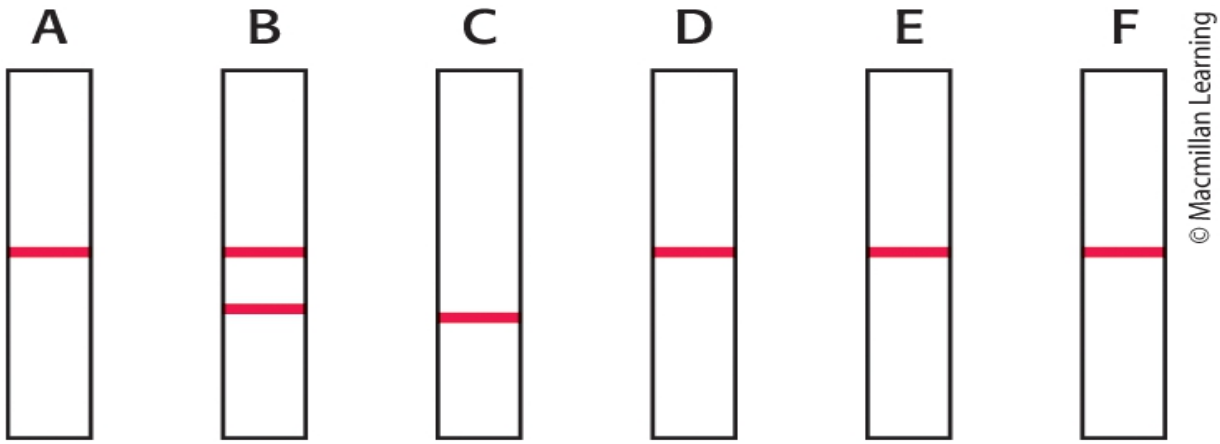
Bam H Roman number 1: Three bands at 6 k b, 3 k b, and 1 k b respectively.

Eco R Roman number 1 plus Bam H Roman number 1: Four bands at 4 k b, 3 k b, 2 k b, and 1 k b.

Return to Electrophoresis gel slab

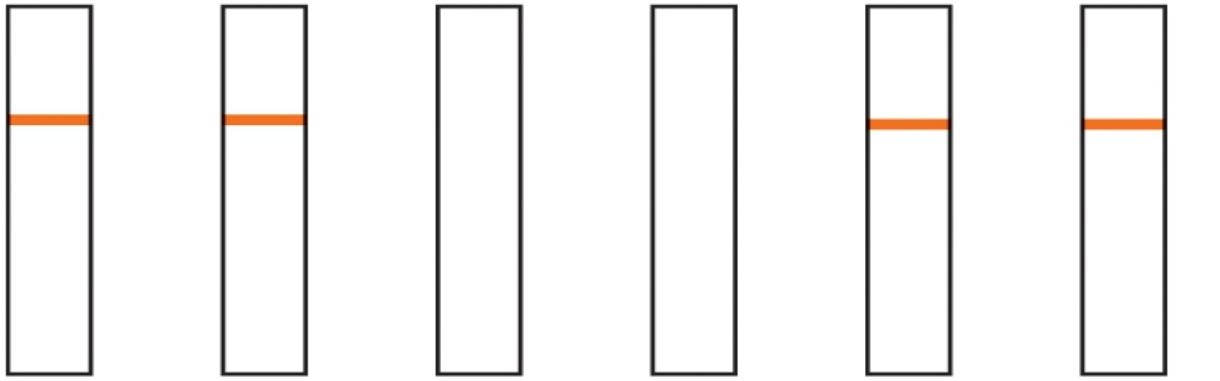
Extended description for Banding pattern in southern,

northern, and western blots

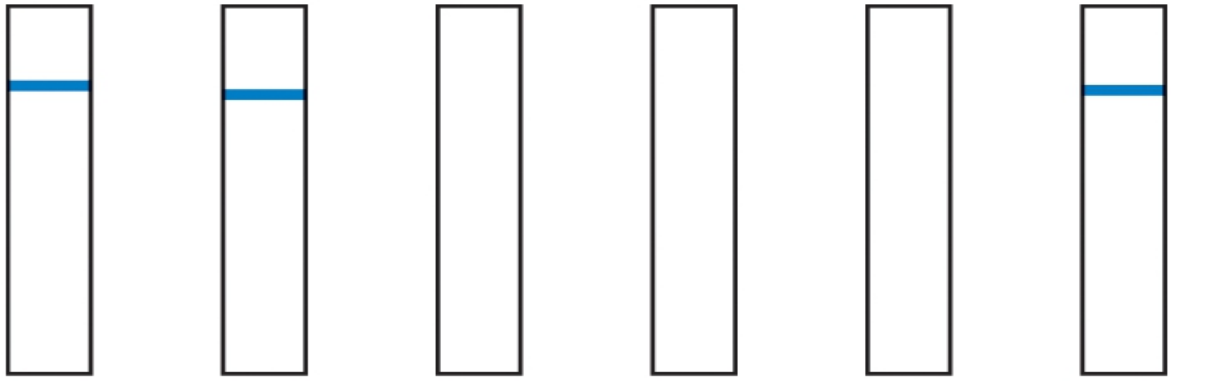


© Macmillan Learning

Southern blots



Northern blots



Western blots

The blot patterns for six individuals labeled A through F are given as follows:

Southern blot:

A: One red band in the middle.

B: One red band at the same level as A and one below.

C: One red band at the same level as the lower band of B.

D: One red band at the same level as A

E: One red band at the same level as A

F: One red band at the same level as A

Northern blot:

A: One orange band slightly above the midpoint.

B: One orange band at the same level as A.

C: No band.

D: No band.

E: One orange band at the same level as A.

F: One orange band at the same level as A.

Western blot:

A: One blue band below the top end.

B: One blue band at the same level as A.

C: No band.

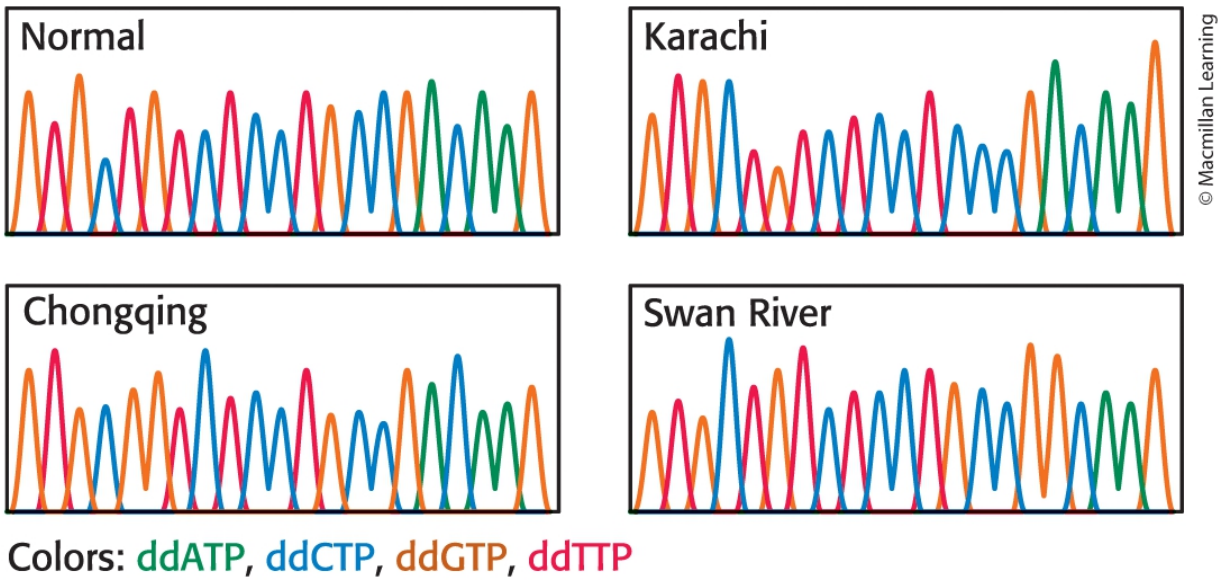
D: No band.

E: No band.

F: One blue band at the same level as A.

Return to Banding pattern in southern, northern, and western blots

Extended description for Four chromatograms of the alpha chain variants of hemoglobin



© Macmillan Learning

The d d N T P are color coded as follows:

d d A T P: green

d d C T P: blue

d d G T P: orange

d d T T P: red

The chromatograms are labeled Normal, Karachi, Chongqing, and Swan River.

The peaks observed from left to right are as follows:

Normal: Orange, red, orange, blue, red, orange, red, blue, red, blue, blue, red, orange, blue, blue, orange, green, blue, green, green, orange.

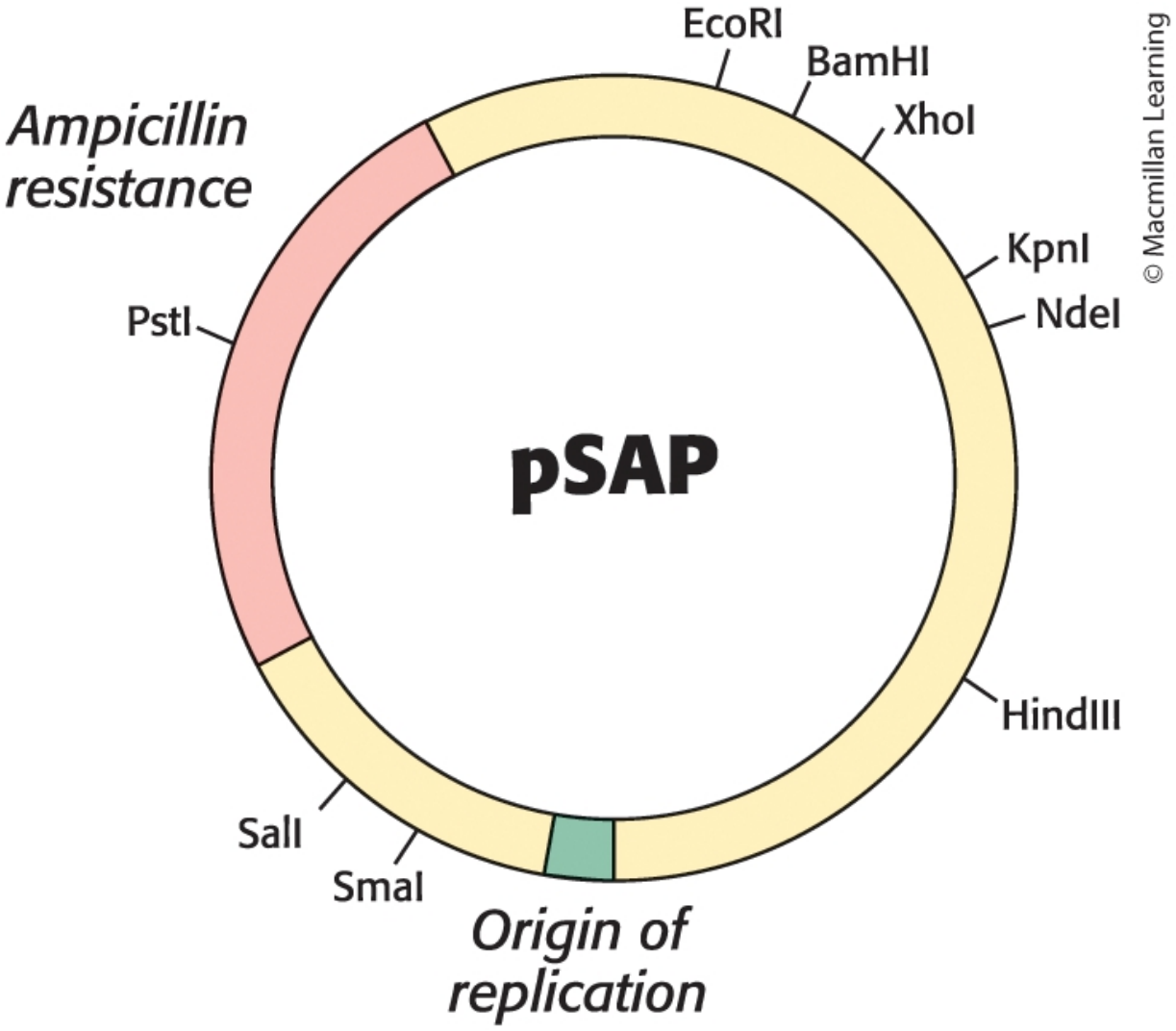
Karachi: Orange, red, orange, blue, red, orange, red, blue, red, blue, blue, red, blue, blue, blue, orange, green, blue, green, green, orange.

Chongqing: Orange, red, orange, blue, orange, orange, red, blue, red, blue, blue, red, orange, blue, blue, orange, green, blue, green, green, orange.

Swan River: Orange, red, orange, blue, red, orange, red, blue, red, blue, blue, red, orange, blue, blue, orange, orange, blue, green, green, orange.

Return to Four chromatograms of the alpha chain variants of hemoglobin

Extended description for Map of hypothetical p SAP plasmid



The circular plasmid has four segments of varying sizes and three of them have restriction sites. The restriction sites, in the clockwise direction, are as follows:

Segment 1 (yellow): Eco R roman number 1, Bam H roman number 1, X h o roman number 1, K p n roman number 1, N d e roman

number 1, Hind roman number 3.

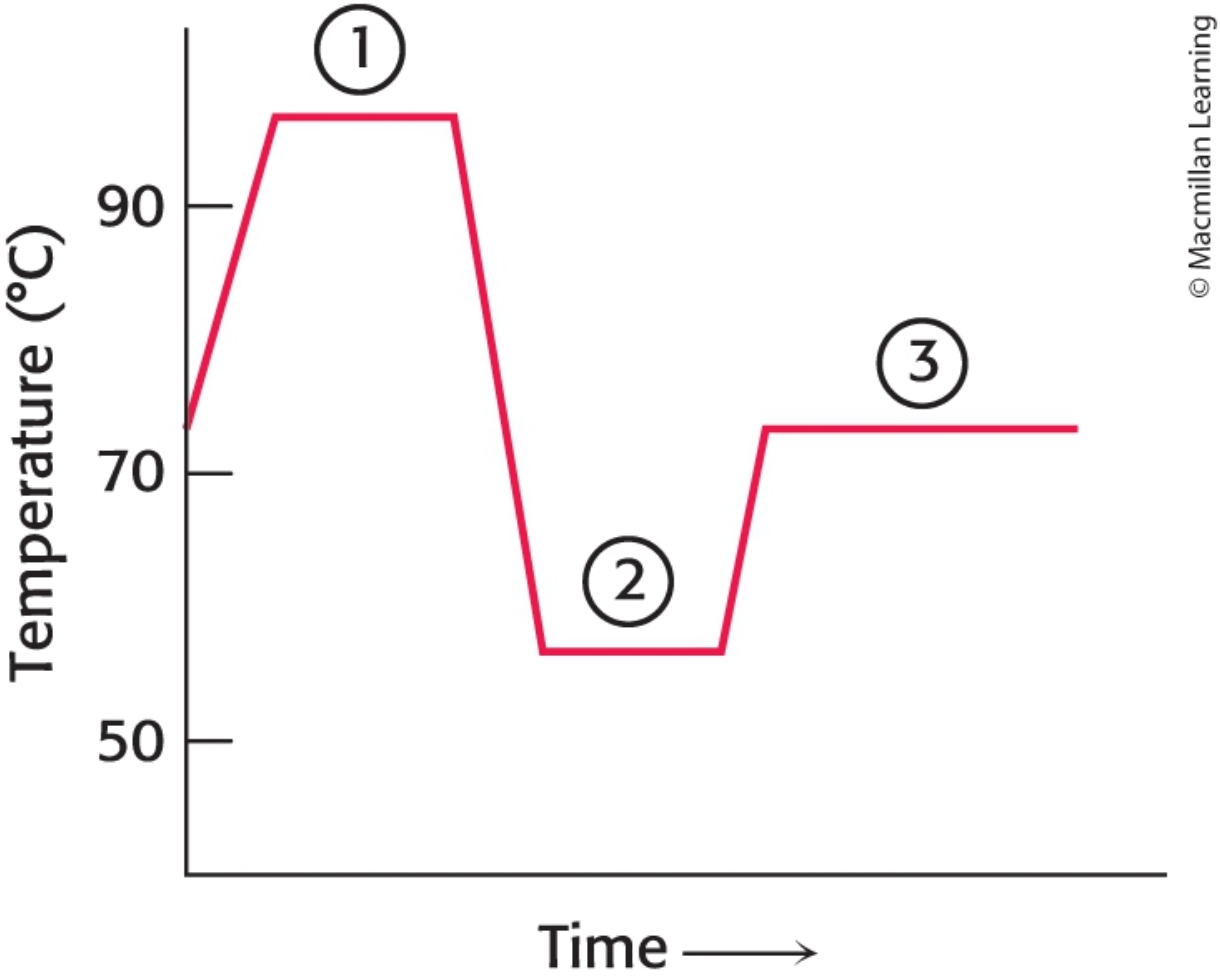
Segment 2 (green) is the origin of replication and has no restriction site.

Segment 3 (yellow): S m a roman number 1 and Sa l roman number 1.

Segment 4 (red): It is an ampicillin resistance gene that contains a P s t roman number 1 restriction site.

Return to Map of hypothetical p SAP plasmid

Extended description for A time versus temperature plot



© Macmillan Learning

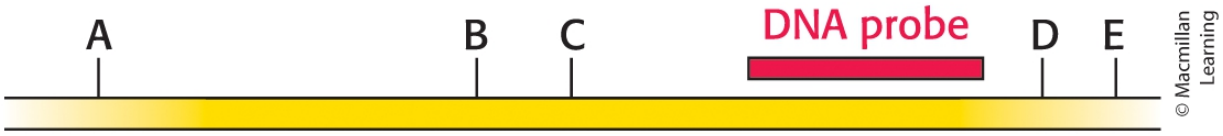
The horizontal axis is labeled time. The vertical axis is labeled temperature (degree Celsius) and ranges from 50 to 90 in increments of 20 units.

A red plot line starts from nearly 75 on the vertical axis and rises steeply to a plateau above 90. The plateau is labeled 1. The plot then falls sharply to another plateau below 60. The plateau is labeled 2.

The plot then rises sharply to another plateau just above 70. The plateau is labeled 3.

Return to A time versus temperature plot

Extended description for Cleavage sites in a D N A segment

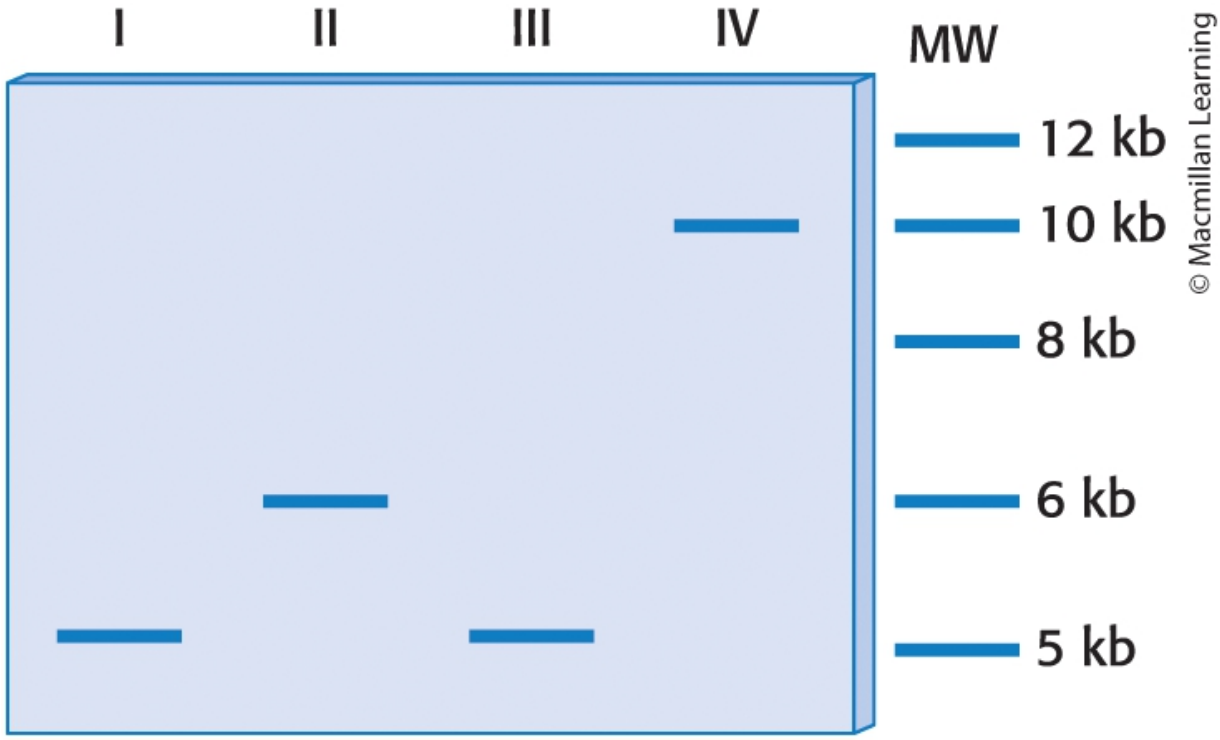


The D N A segment from the left to right is labeled Athrough E. The distance between A and B is large. The distance between B and C is one-fourth of that between A and B. The distance between C and D is greater than that between A and B. The distance between D and E is slightly less than that between B and C.

A D N A probe is complementary to a region between C and D and is closer to D.

Return to Cleavage sites in a D N A segment

Extended description for Electrophoresis gel slab



The gel slab has four lanes with bands of varying sizes as follows:

Lane 1: One band at 5 k b.

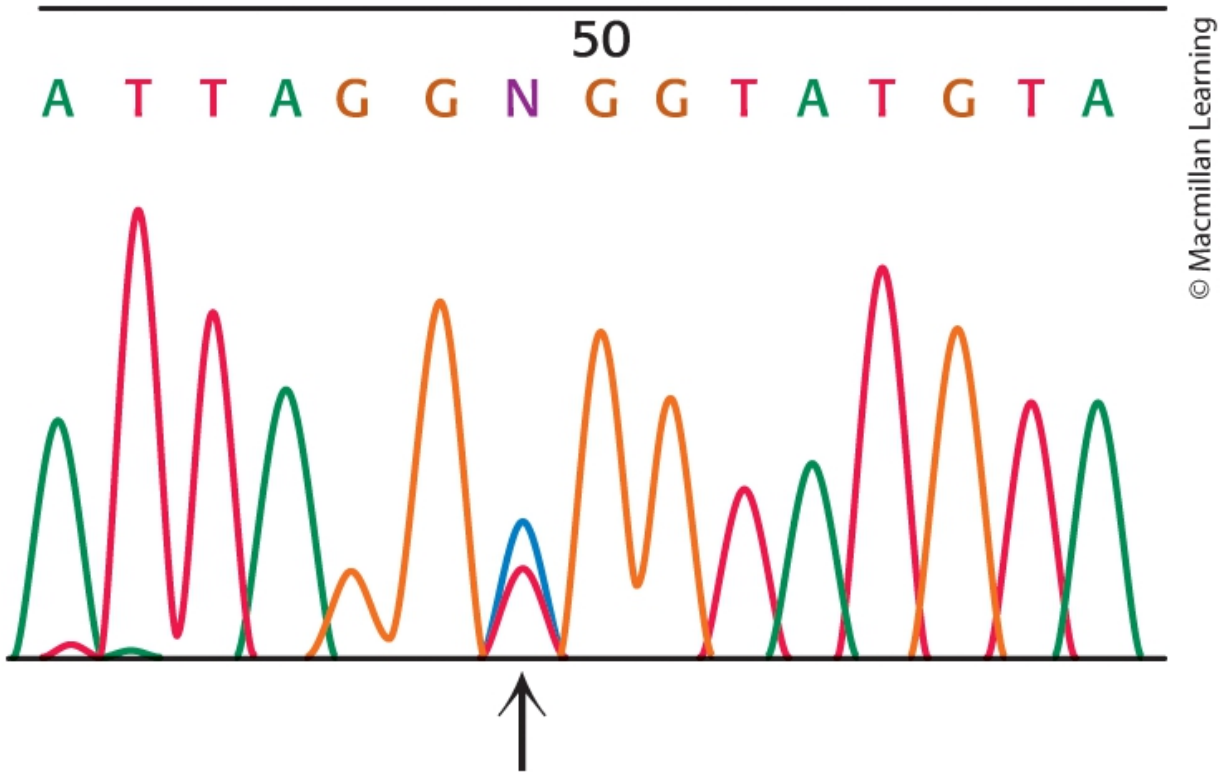
Lane 2: One band at 6 k b.

Lane 3: One band at 5 k b.

Lane 4: One band at 10 k b.

Return to Electrophoresis gel slab

Extended description for Sequencing chromatogram



The nucleotides are color coded as follows:

A: green

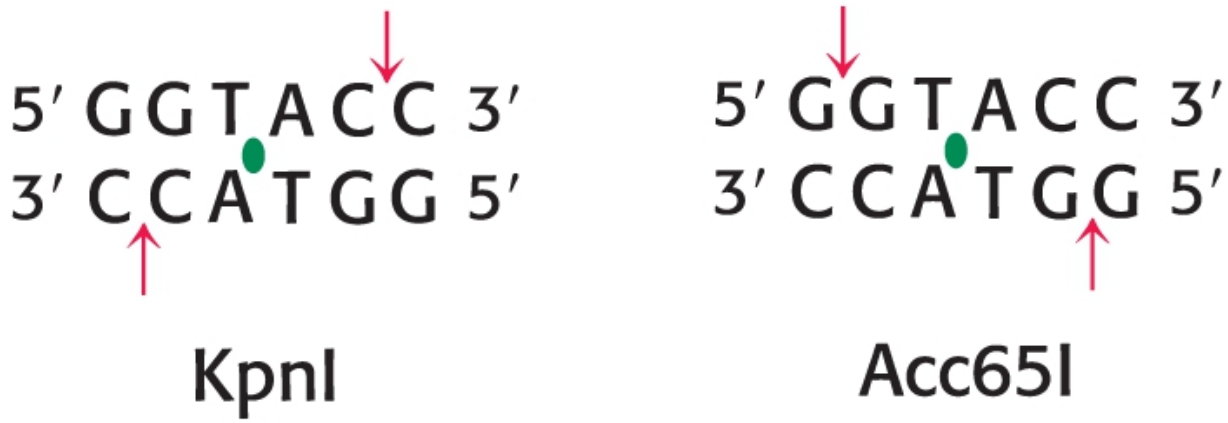
T: red

G: orange

At position 49 two overlapping peaks are observed. A short red peak and a slightly higher blue peak. The corresponding nucleotide is labeled N in purple.

Return to Sequencing chromatogram

Extended description for Cleavage sites of K p n roman number 1 and A c c 6 5 roman number 1.



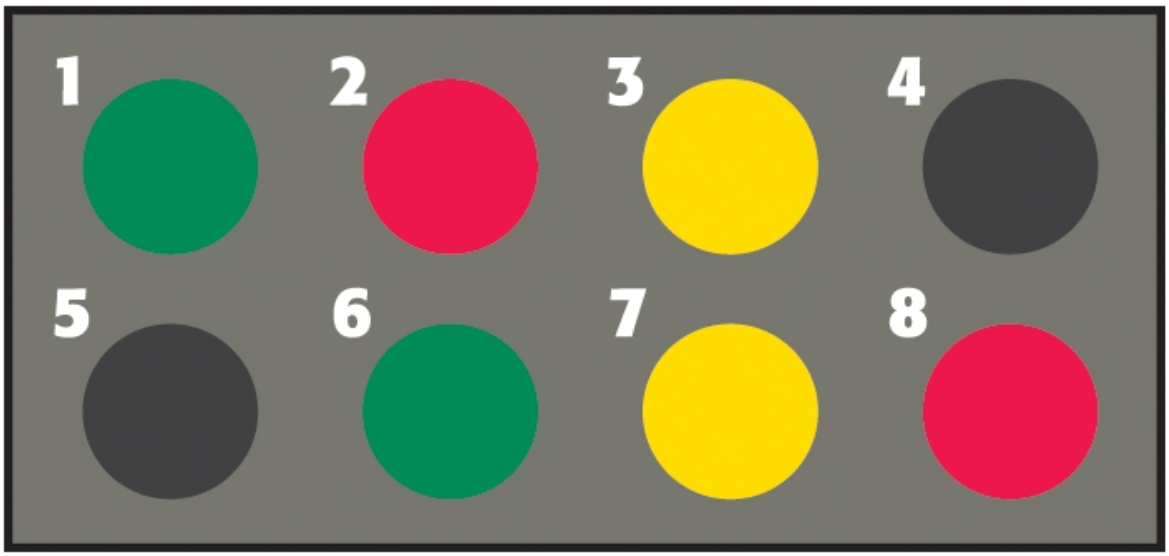
Two double-stranded palindromic D N A sequences are shown along with the corresponding cleavage sites of the following enzymes:

K p n Roman number 1: The D N A sequence in the 5 prime to 3 prime direction is G G T A C C. The symmetry axis is indicated to be between T and A at the third and fourth positions, respectively, from the 5 prime end. The cleavage site on each strand is between C and C at the first and second positions, respectively, from the 3 prime end.

A c c 6 5 Roman number 1: The D N A sequence in the 5 prime to 3 prime direction is G G T A C C. The symmetry axis is indicated to be between T and A at the third and fourth positions, respectively, from the 5 prime end. The cleavage site on each strand is between G and G at the first and second positions, respectively, from the 5 prime end.

Return to Cleavage sites of K p n roman number 1 and A c c 6 5 roman number 1.

Extended description for Microarray data



© Macmillan Learning

The microarray has two rows:

Top row:

Spot 1: Green

Spot 2: Red

Spot 3: Yellow

Spot 4: Black

Bottom row:

Spot 5: Black

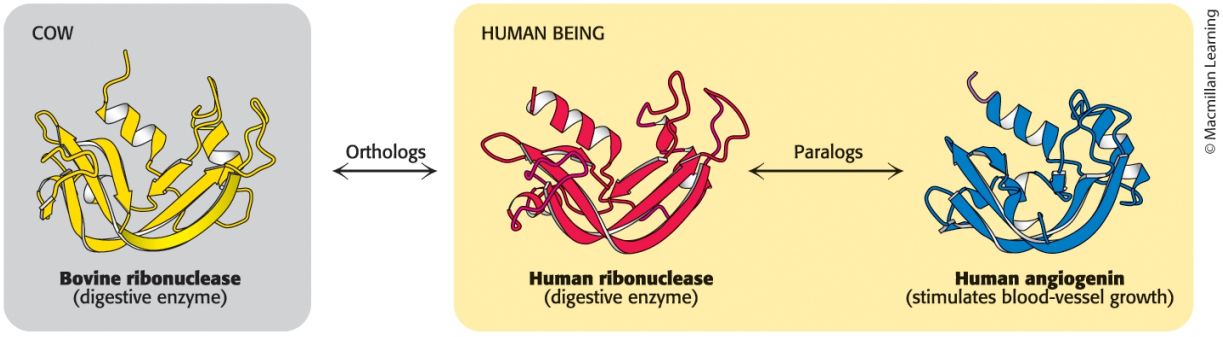
Spot 6: Green

Spot 7: Yellow

Spot 8: Red

Return to Microarray data

Extended description for FIGURE 10.1 Homologs can be divided into two classes



Bovine ribonuclease (digestive enzyme) has a cup shaped structure and consists of both beta sheets and alpha helices connected by short loops. It is followed by a double headed arrow labeled orthologs that points toward human ribonuclease (digestive enzyme). Human ribonuclease has a very similar structure to that of bovine ribonuclease but is slightly more compact. It is again followed by a double headed arrow labeled paralogs that points toward human angiogenin (stimulates blood-vessel growth). It has a similar structure to that of human ribonuclease.

Return to FIGURE 10.1 Homologs can be divided into two classes

Extended description for FIGURE 10.2 The amino acid sequences of human hemoglobin (chain) and human myoglobin will be used to demonstrate sequence alignments

Human hemoglobin (α chain)

VLSPADKTNVKAAWGKVGAHAGEYGAEALERMFLSFPTTKTYFPHFDLSHG
SAQVKGHGKKVADALTNAVAHVDDMPNALSALSDLHAHKLRVDPVNFKLLS
HCLLVTLAAHLPAEFTPAVHASLDKFLASVSTVLTSKYR

Human myoglobin

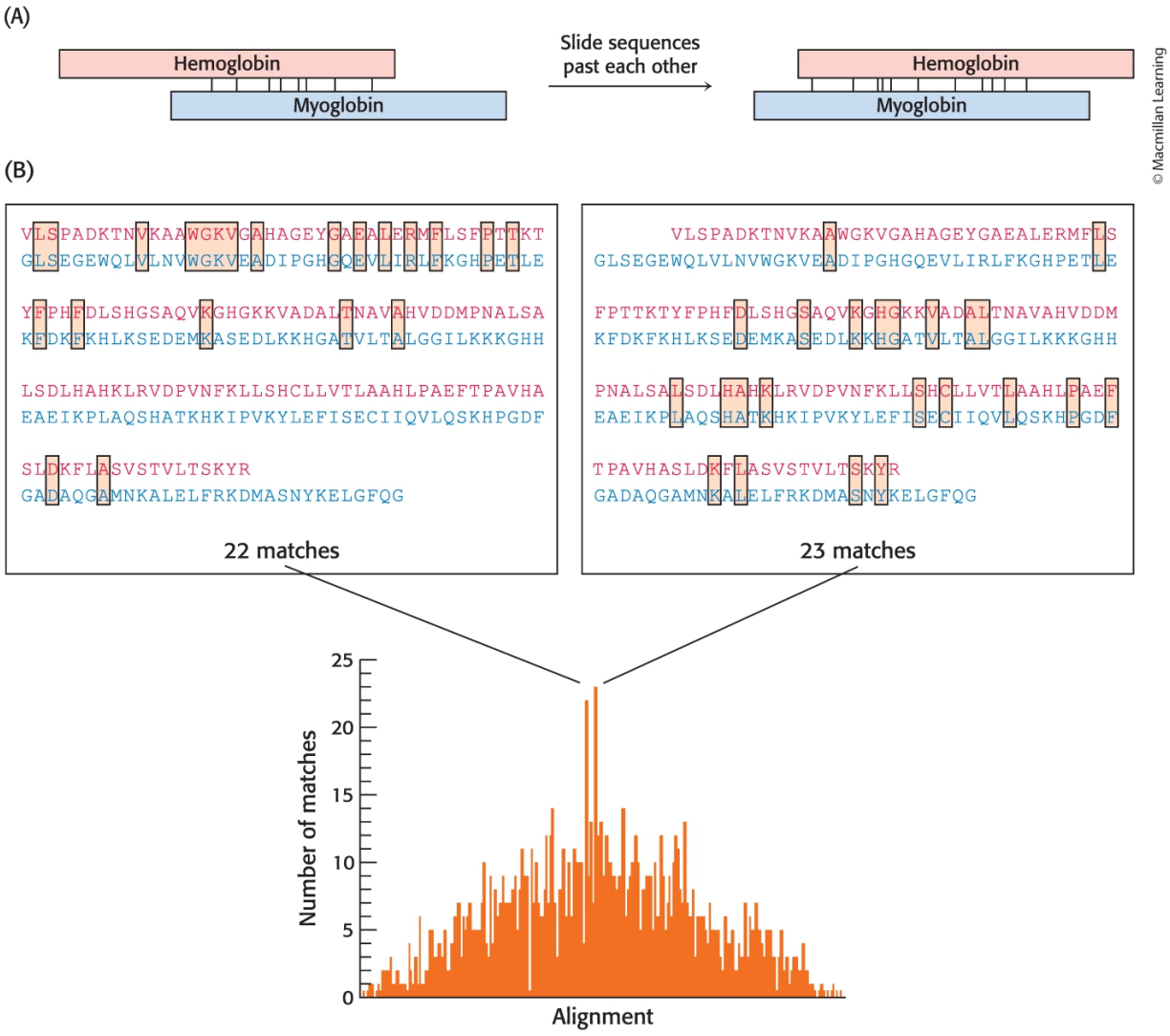
GLSDGEWQLVLNVWGKVEADIPGHGQEVLIRLFKGHPETLEKFDKFKHLKS
EDEMKASEDLKKHGATVLTALGGILKKKGHHEAEIKPLAQSHATKHKIPVK
YLEFISECIIQVLQSKHPGDFGADAQGAMNKALELFRKDMASNYKELGFQG

Human hemoglobin (alpha chain) has the following sequence: V L S P A D K T N V K A A W G K V G A H A G E Y G A E A L E R M F L S F P T T K T Y F P H F D L S H G S A Q V K G H G K K V A D A L T N A VA H V D D M P N A L S A L S D L H A H K L R V D P V N F K L L S H C L L V T L A A H L P A E F T P A V H A S L D K F L A S V S T V L T S K Y R.

Human myoglobin has the following structure: G L S D G E W Q L V L N V W G K V E A D I P G H G Q E V L I R L F K G H P E T L E K F D K F K H L K S E D E M K A S E D L K K H G A T V L T A L G G I L K K K G H H E A E I K P L A Q S H A T K H K I P V K Y L E F I S E C I I Q V L Q S K H P G D F G A D A Q G A M N K A L E L F R K D M A S N Y K E L G F Q G.

Return to FIGURE 10.2 The amino acid sequences of human hemoglobin (chain) and human myoglobin will be used to demonstrate sequence alignments

Extended description for FIGURE 10.3 Amino acid sequences are compared by sliding one sequence past the other, one amino acid at a time



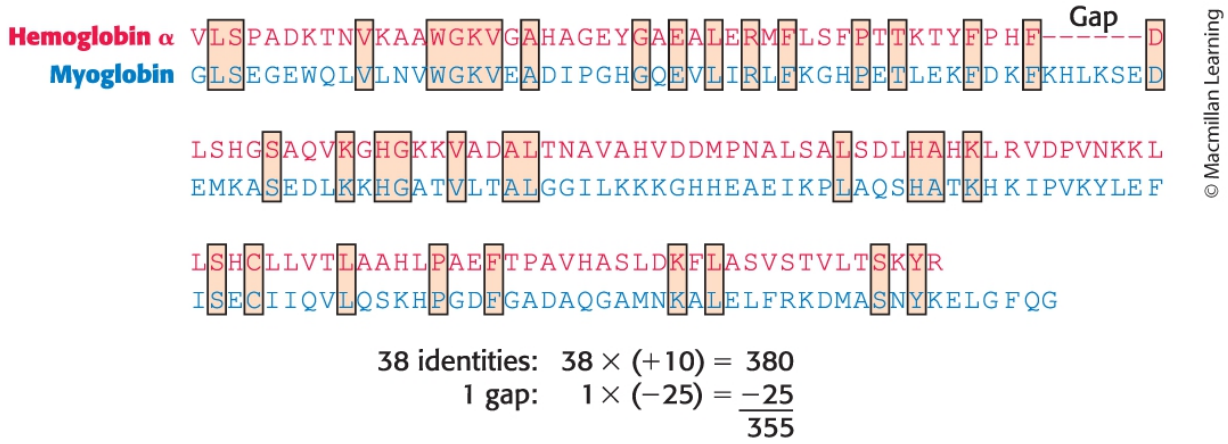
Part (A): The hemoglobin sequence is aligned above the myoglobin sequence. The hemoglobin sequence is placed slightly to the left and is only partially overlapped with the myoglobin sequence. After sliding sequences past each other, the hemoglobin sequence is

placed slightly to the right and is only partially overlapped with the myoglobin sequence.

Part (B): A histogram is shown. The horizontal axis is labeled Alignment. The vertical axis is labeled Number of matches and ranges from 0 to 25 in increments of 5 units. The histogram has a mountain shape with two tall peaks in the center. The first peak corresponds to 22 matches when hemoglobin is to the left of myoglobin. The second peak corresponds to 23 matches when hemoglobin is to the right of myoglobin after sliding. The matching amino acid residues are shown within boxes in both alignments. There is a short gap in the hemoglobin sequence when aligned with myoglobin.

Return to FIGURE 10.3 Amino acid sequences are compared by sliding one sequence past the other, one amino acid at a time

Extended description for FIGURE 10.4 Scoring method



The amino acid sequences of hemoglobin alpha and myoglobin are aligned. Several identical amino acids are identified across the aligned sequences and enclosed in rectangular boxes. The identical amino acids either occur singly or in a cluster of 2 to 3. A gap is shown in the hemoglobin alpha sequence. It is flanked by F and D amino acids and occurs between amino acid positions 47 and 52 in the myoglobin sequence. A calculation is shown as follows:

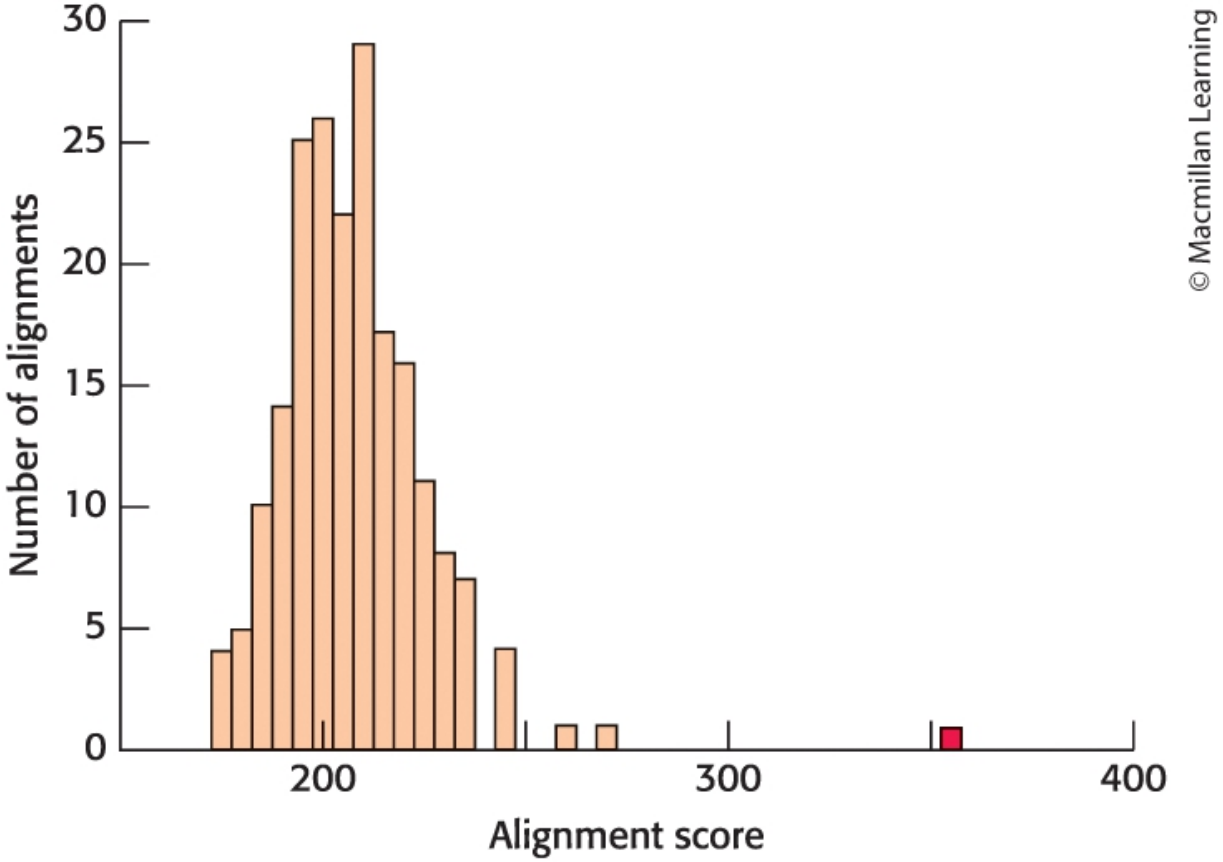
Line 1: 38 identities: 38 times positive 10 equals 380

Line 2: 1 gap: 1 times negative 25 equals negative 25

The sum of 380 and negative 25 is 355.

Return to FIGURE 10.4 Scoring method

Extended description for FIGURE 10.6 Comparison of alignment scores reveals the statistical significance of an unshuffled alignment



© Macmillan Learning

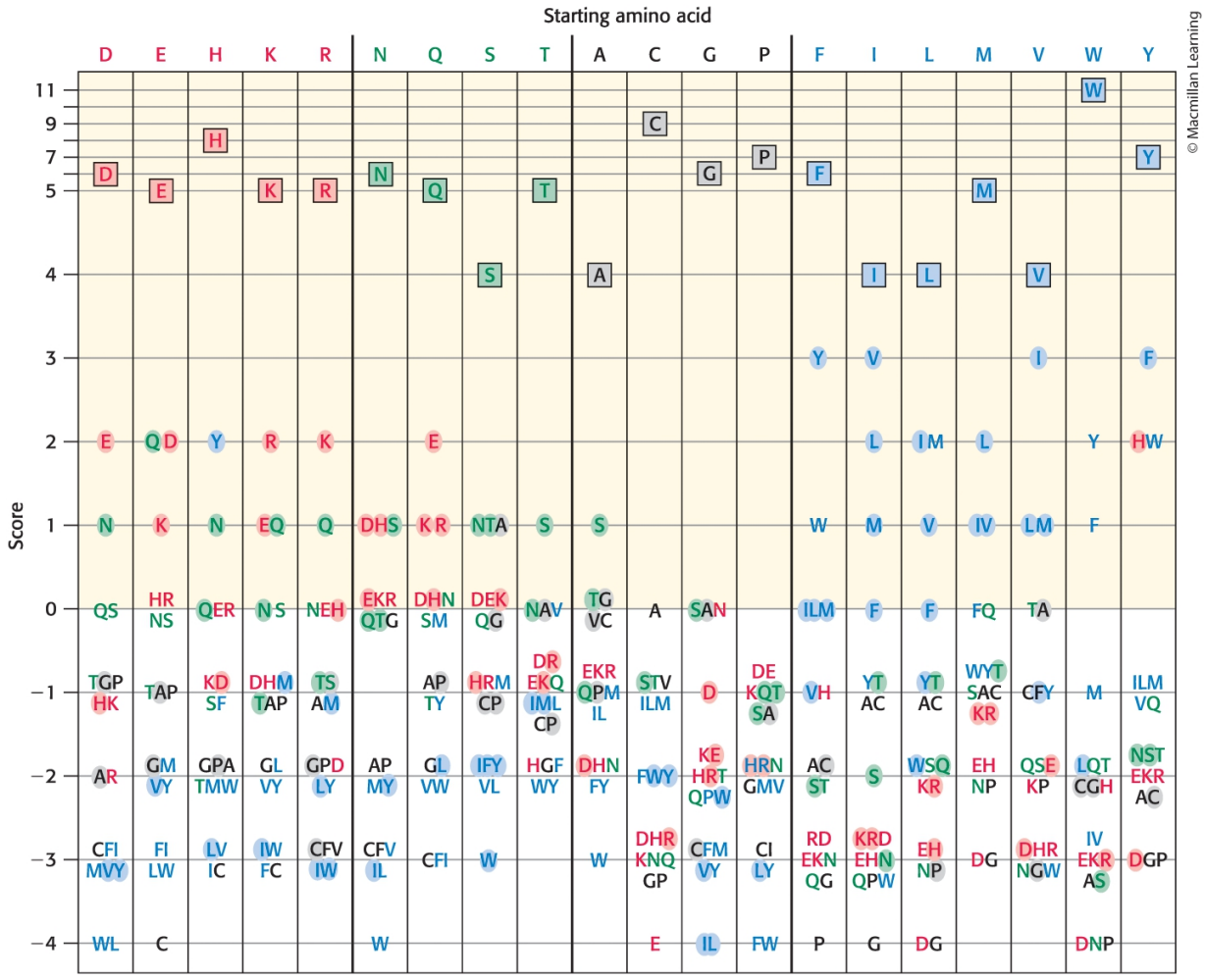
The horizontal axis is labeled Alignment score and ranges from 0 to 400 in increments of 100 units. The vertical axis is labeled Number of alignments and ranges from 0 to 30 in increments of 5 units.

Shuffled sequence: The histogram starts at nearly (100, 4), peaks at nearly (215, 29), and falls to (270, 2).

Unshuffled sequence: A single bar at almost (355, 2). All values are estimated.

Return to FIGURE 10.6 Comparison of alignment scores reveals the statistical significance of an unshuffled alignment

Extended description for FIGURE 10.7 The Blosum-62 substitution matrix enables scoring based on amino acid similarity



The columns are labeled Starting amino acid. There are 20 columns, from left to right as follows: D, E, H, K, R, N, Q, S, T, A, C, G, P, F, I, L, M, V, W, and Y. D, E, H, K, and R are labeled in red. N, Q, S, and T are labeled in green. A, C, G, and P are labeled in black. F, I, L, M, V, W, and Y are labeled in blue.

The rows are labeled Score and range from 11, 9, 7 5,4, 3, 2, 1, 0,-1, -2, -3 and -4, from top to bottom.

Substitutions scores are as follows:

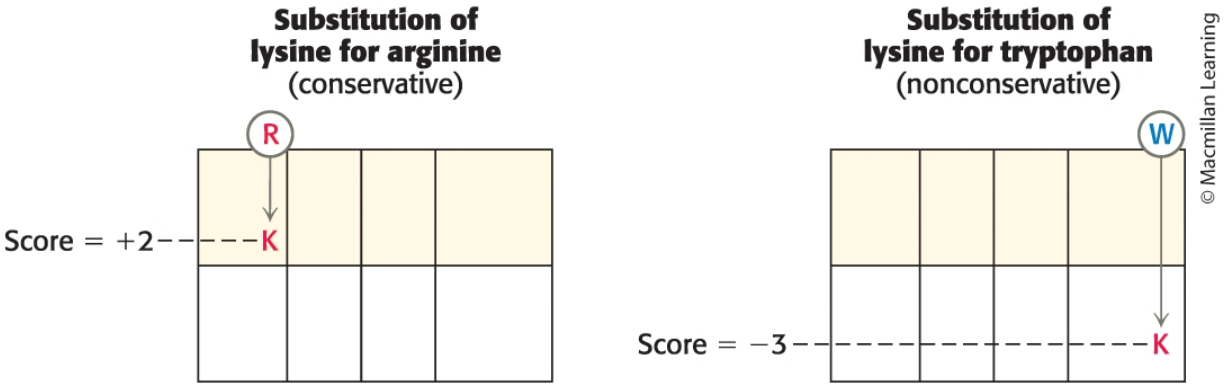
The rows entries for column D are as follows:

D shaded within a box is 6, E shaded is 2, N shaded is 1, Q S is 0, T G (shaded) P H (shaded) K is negative 1, A (shaded) R is negative 2, C F I M V (shaded) Y (shaded) is negative 3, W L is negative 4.

Similarly, the scores are given for the rest of the 19 amino acids.

Return to FIGURE 10.7 The Blosum-62 substitution matrix enables scoring based on amino acid similarity

Extended description for FIGURE 10.8 Conservative and nonconservative substitutions yield very different scores in the Blosum-62 matrix



Substitution of lysine for arginine (conservative): A matrix of 2 rows and 4 columns is shown. R (red) is substituted by K (red) in row 1 and column 1. The score is positive 2.

Substitution of lysine for tryptophan (nonconservative): A matrix of 4 rows and 2 columns is shown. W (blue) is substituted by K (red) in row 1 column 4. The score is negative 3.

Return to FIGURE 10.8 Conservative and nonconservative substitutions yield very different scores in the Blosum-62 matrix

Extended description for FIGURE 10.9 Counting conservative substitutions reveals strong similarity between α-hemoglobin and myoglobin

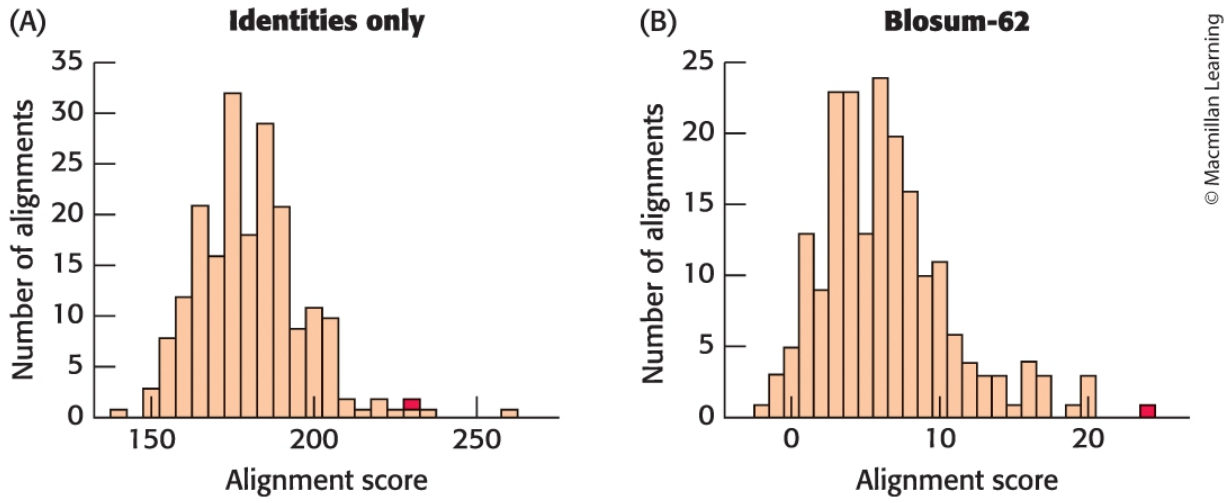


Conservative substitutions are indicated by yellow shading. The count of conservative substitutions is 19, which are as follows: D E, Y H, M L, V L, V L, L I, S A, R A, V I, K E, L I, L I, L I, A S, S A, L M, D N, L M, and R K.

Identities are indicated by orange boxes. The count of identities is 38, which are as follows: L L, S S, V V, W W, G G, K K, V V, A A, G G, E E, L L, R R, F F, P P, T T, F F, F F, D D, S S, K K, H H, G G, V V, A A, L L, L L, H H, A A, K K, S S, C C, L L, P P, F F, K K, L L, S S, and Y Y.

Return to FIGURE 10.9 Counting conservative substitutions reveals strong similarity between α-hemoglobin and myoglobin

Extended description for FIGURE 10.10 Alignment using Blosum-62 can uncover more distant evolutionary relationships



Part (A) is labeled Identities only. The horizontal axis is labeled Alignment score and ranges from 150 to 250 in increments of 50 units. The vertical axis is labeled Number of alignments and ranges from 0 to 35 in increments of 5 units.

Shuffled sequence: The histogram starts at (130, 1), peaks at (100, 32), and then falls to (270, 1).

Unshuffled sequence: A single bar at (225, 2).

Part (B) is labeled Biosum-62. The horizontal axis is labeled Alignment score and ranges from 0 to 20 increments of 10 units. The vertical axis is labeled Number of alignments and ranges from 0 to 25 in increments of 5 units.

Shuffled sequence: The histogram starts at (negative 2, 1), peaks at (6, 24), and then falls to (20, 4).

Unshuffled sequence: A single bar at (23, 2).

Return to FIGURE 10.10 Alignment using Blosum-62 can uncover more distant evolutionary relationships

Extended description for FIGURE 10.11 Alignment of human myoglobin and lupine leghemoglobin reveals many conservative substitutions

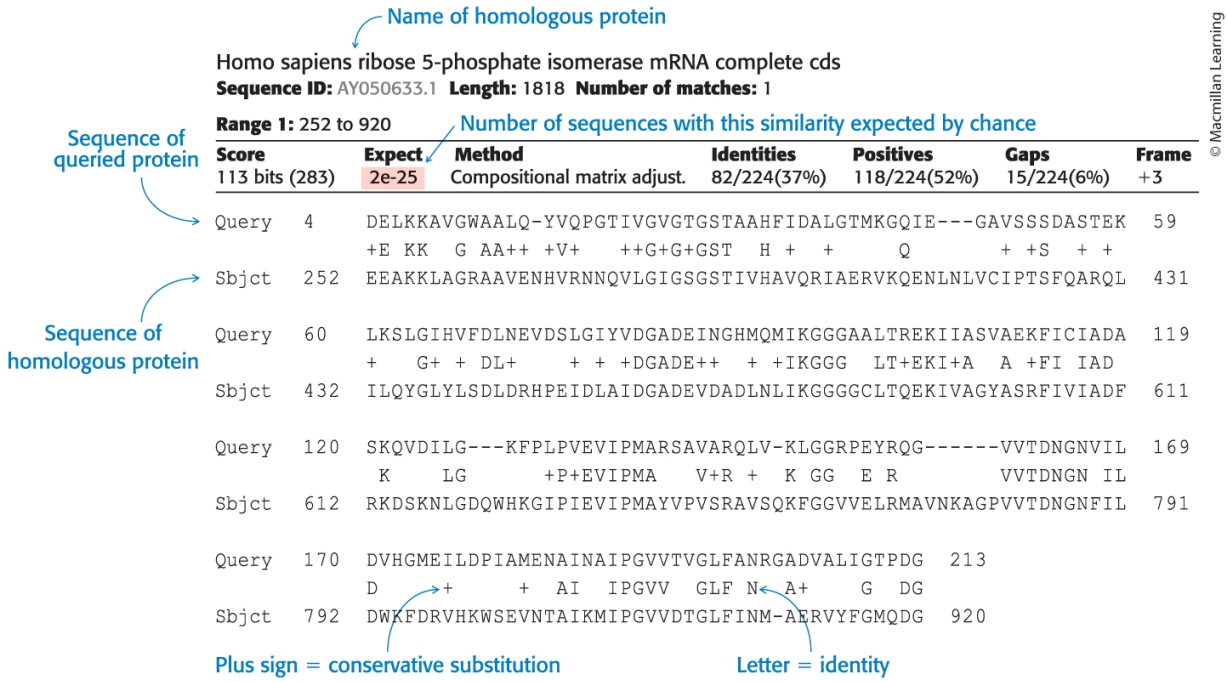


Conservative substitutions are indicated by yellow shading. The count of conservative substitutions is 29, which are as follows: S T, D E, E Q, N S, K W, D N, L V, K E, M V, S N, D E, K Q, L V, K E, E D, I L, T S, I V, Y H, I V, I L, Q K, L I, Q K, M L, L I, D E, M L, and L M.

Identities are indicated by orange boxes. The count of identities is 34, which are as follows: L L, L L, V V, W W, A A, I I, P P, H H, I I, P P, D D, F F, L L, K K, E E, L L, H H, V V, L L, G G, A A, K K, L L, H H, K K, E E, I I, G G, A A, N N, A A, A A, K K, and E E.

Return to FIGURE 10.11 Alignment of human myoglobin and lupine leghemoglobin reveals many conservative substitutions

Extended description for FIGURE 10.12 Related protein sequences can be rapidly identified using online BLAST searches



© Macmillan Learning

The table consists of 7 columns and 8 rows. The headings of the columns are as follows: Score 1 13 bits open parenthesis 283 close parenthesis, Expect 2 e hyphen 25, Method: compositional matrix adjust. Identities: 82 by 224 open parenthesis 37 percent close parenthesis, Plus: 118 by 224 open parenthesis 52 percent close parenthesis, Gaps: 25 by 224 open parenthesis 6 percent close parenthesis and Frame plus 3.

The row entries are as follows.

Row 1: Query 4: D E L K K A V G W A A L Q hyphen Y V Q P G T I V G V G T G S T A A H F I D A L G T M K G Q I E hyphen G A V S S S D A S

T E K plus E K K G A A plus plus plus V plus plus plus G plus G plus G S T H plus plus Q plus plus S plus plus, 59.

Row 2: S b j c t. 252: E E A K K L A G R A A V E N H V R N N Q V L G I G S G S T I V H A V Q R I A E R V K Q E N L N L V C I P T S F Q A R Q L, 431.

Row 3: Query 60: L K S L G I H V F D L N E V D S L G I Y V D G A D E I N G H M O M I K G G G A A L T R E K I I A S V A E K F I C I A D A plus G plus plus D L plus plus plus plus D G A D E plus plus plus plus I K G G G L T plus E K I plus A A + F I I A D, 119.

Row 4: S b j c t. 432: I L Q Y G L Y L S D L D R H P E I D L A I D G A D E V D A D L N L I K G G G G C L T Q E K I V A G Y A S R F I V I A D F, 611.

Row 5: Query 120: S K Q V D I L G hyphen K F P L P V E V I P M A R S A V A R Q L V hyphen K L G G R P E Y R Q G hyphen V V T D N G N V I L K L G plus P plus E V I P M A V plus R plus K G G E R V V T D N G N I L, 169.

Row 6: S b j c t. 612: R K D S K N L G D O W H K G I P I E V I P M A Y V P V S R A V S Q K F G G V V E L R M A V N K A G P V V T D N G N F I L, 791.

Row 7: Query 170: D V H G M E I L D P I A M E N A I N A I P G V V T V G L F A N R G A D V A L I G T P D G, 213.

Row 8: S b j c t. 792: D W K F D R V H K W S E V N T A I K M I P G V V D T G L F I N M hyphen A E R V Y F G M Q D G, 920.

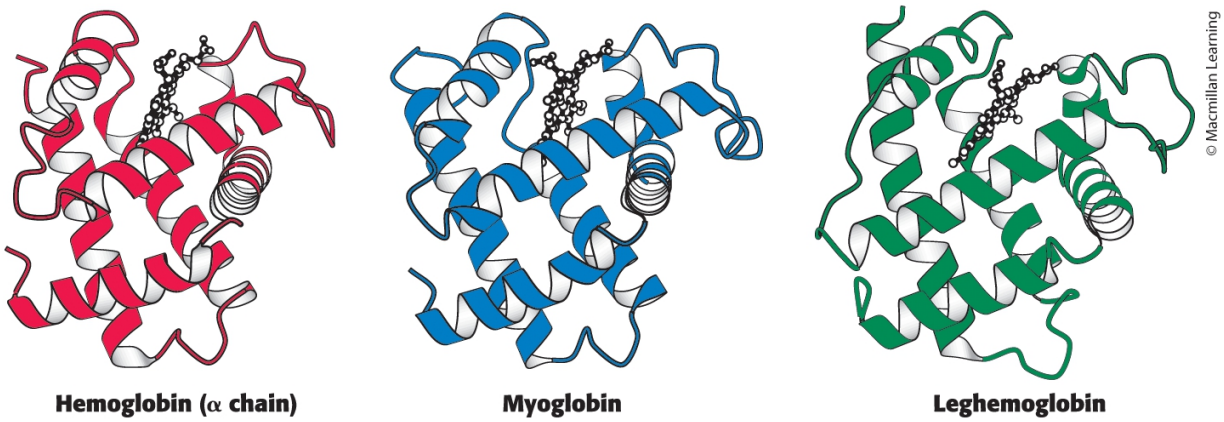
At the top of the table a note labeled “Name of homologous protein” reads: Homo sapiens ribose 5-phosphate isomerase mRNA complete

c d s, Sequence ID: A Y 0 5 0 6 3 3.1, Length: 1818, Number of matches: 1.

All the queries are labeled “Sequence of queried protein.” All the s b j c t are labeled “Sequence of homologous protein.” All the plus signs are equal to conservative substitution. All the letters are equal to the identity.

Return to FIGURE 10.12 Related protein sequences can be rapidly identified using online BLAST searches

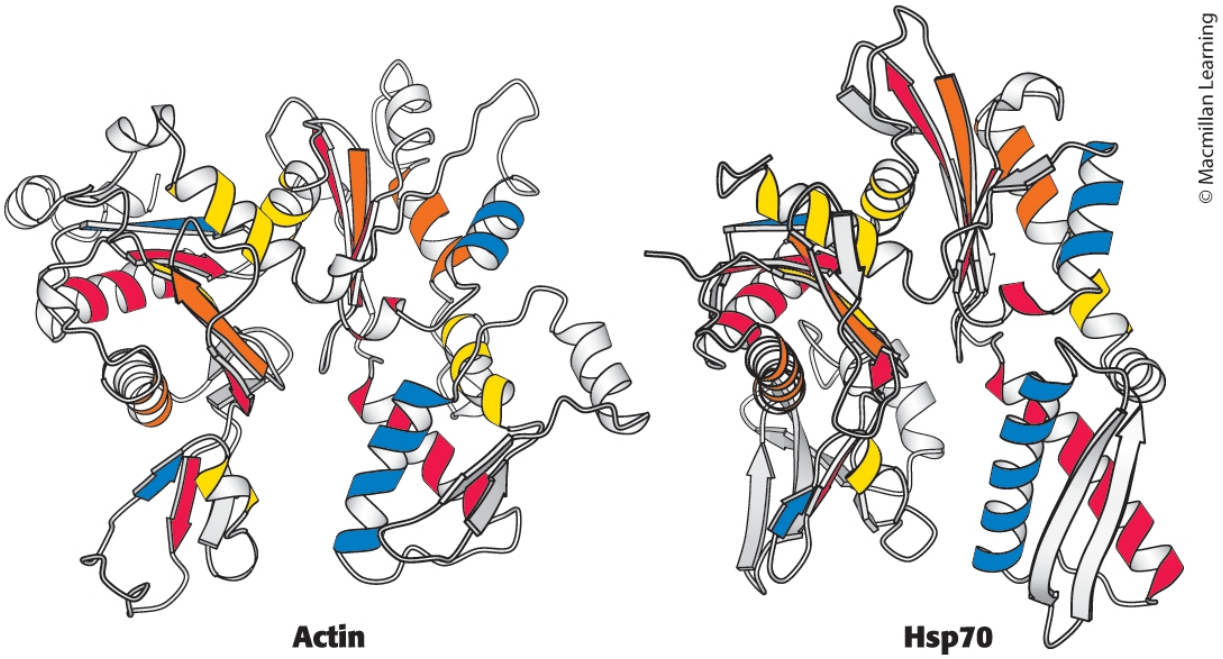
Extended description for FIGURE 10.13 Three-dimensional structure is more conserved than primary structure



The three-dimensional ribbon structures of the three proteins are very similar. They consist of alpha helices connected by short loops. The ribbon structure of hemoglobin is shaded in red. The ribbon structure of myoglobin is shaded in blue. The ribbon structure of leghemoglobin is shaded in green.

Return to FIGURE 10.13 Three-dimensional structure is more conserved than primary structure

Extended description for FIGURE 10.14 The structures of actin and a large fragment of heat shock protein 70 (Hsp70) reveal an unexpected relationship

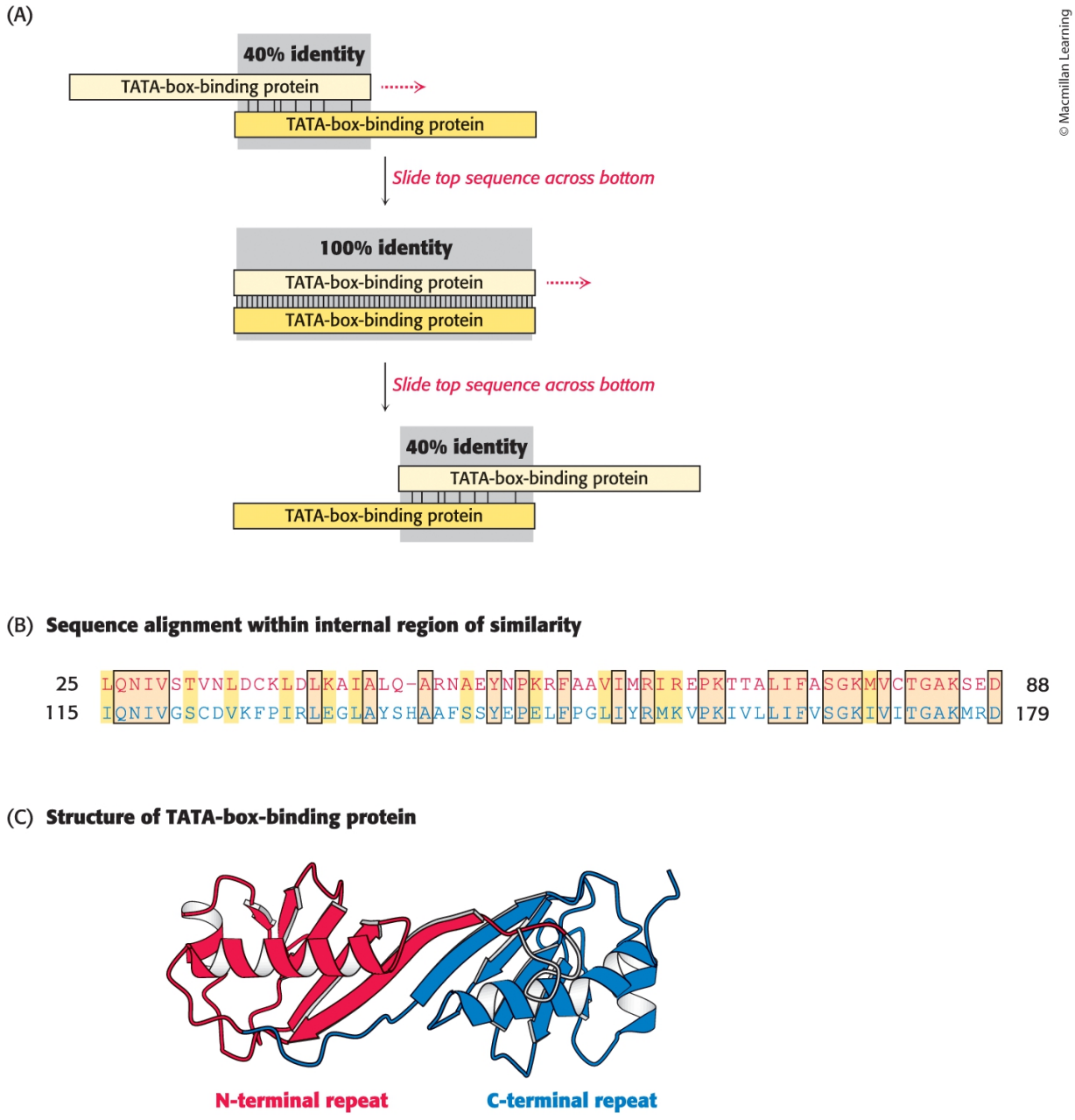


© Macmillan Learning

Both are three-dimensional structures that form an inverted U-shape. They consist of alpha helices and beta sheets connected by short loops. H s p 70 has a narrower groove as compared to actin.

Return to FIGURE 10.14 The structures of actin and a large fragment of heat shock protein 70 (Hsp70) reveal an unexpected relationship

Extended description for FIGURE 10.15 Internal repeats can be identified using a self-alignment



Part (A): The sequence of TATA-box-binding protein is sliding over the same sequence. When the top sequence is shifted to the left and

partially overlaps the sequence below, there is 40 percent identity. When the top sequence completely overlaps the bottom sequence, 100 percent identity is observed. When the top sequence is positioned to the right and partially overlaps the sequence below, 40 percent identity is observed.

Part (B): Sequence alignment within the internal region of similarity

Amino acid residues 25 to 88 (red) are placed above residues 115 to 179 (blue).

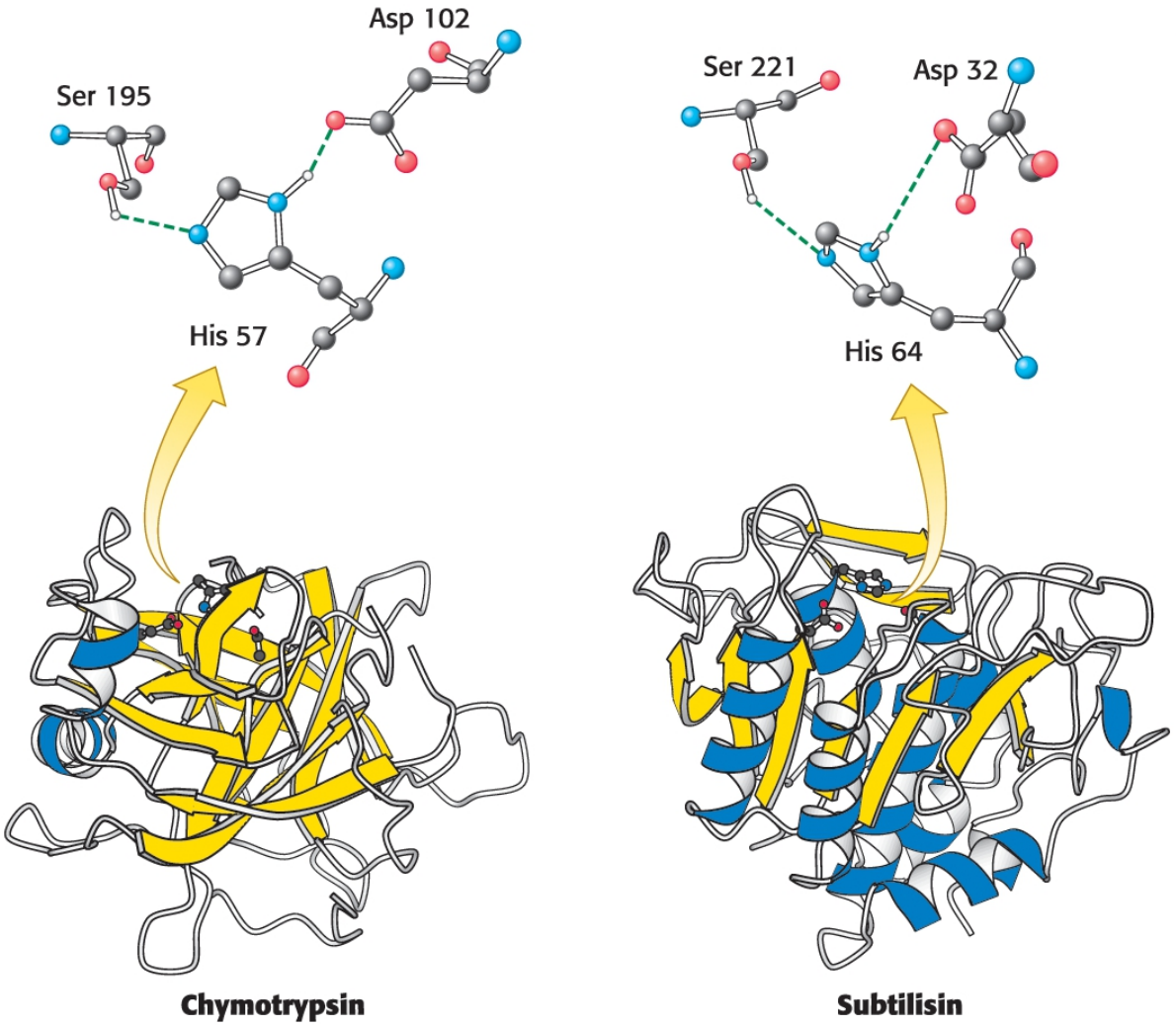
Conservative substitutions are indicated by yellow shading. The count is 12, which are as follows: L I, T S, L V, L I, K E, I L, A S, K E, V L, I M, R K, and M I.

Identities are indicated by orange boxes. The count is 26. They are as follows: Q Q, N N, I I, V V, L L, A A, A A, Y Y, P P, F F, I I, R R, P P, K K, L L, I I, F F, S S, G G, K K, V V, T T, G G, A A, K K, and D D.

Part (C): Structure of TATA-box-binding protein. The N-terminal repeat is shown, which has a similar three-dimensional ribbon structure as the C-terminal repeat. Each terminal consists of alpha helices and beta sheets connected by short loops.

Return to FIGURE 10.15 Internal repeats can be identified using a self-alignment

Extended description for FIGURE 10.16 Mammalian chymotrypsin and bacterial subtilisin are examples of convergent evolution



© Macmillan Learning

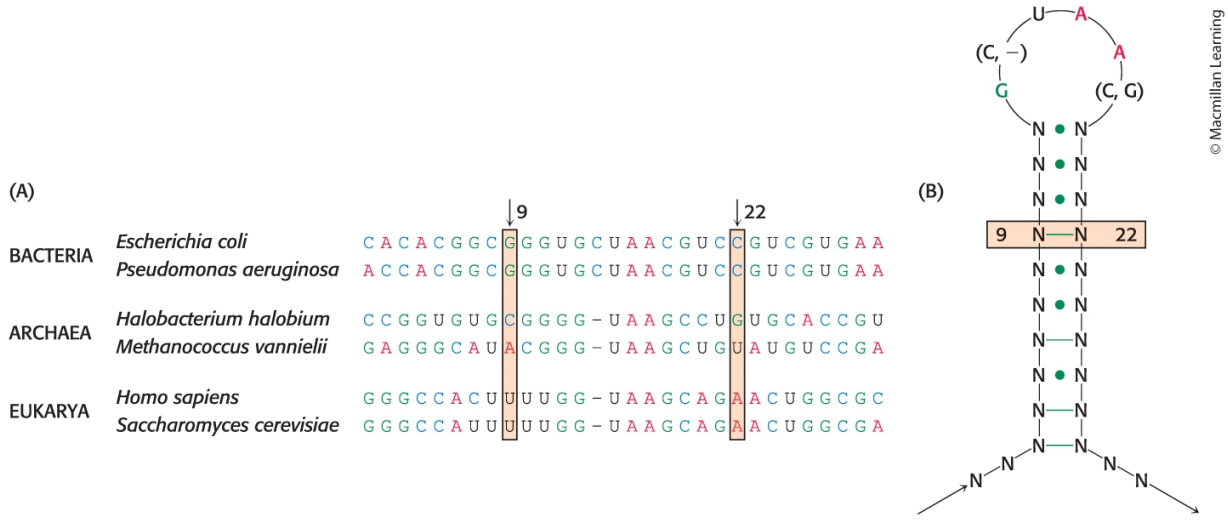
Both chymotrypsin and subtilisin have globular structures.

Chymotrypsin: The catalytic residues are Serine 195, Aspartate 102, and Histidine 57. Histidine below is hydrogen bonded to Serine on the upper left and Aspartate on the upper right.

Subtilisin: The catalytic residues are Serine 221, Aspartate 32, and Histidine 64. Histidine below is hydrogen bonded to Serine on the upper left and Aspartate on the upper right.

Return to FIGURE 10.16 Mammalian chymotrypsin and bacterial subtilisin are examples of convergent evolution

Extended description for FIGURE 10.17 RNA sequence alignments provide insights into structure based on conservation of base-pairing. (A) A comparison of sequences in a part of ribosomal RNA taken from a variety of species



Part (A):

Bacteria: Eschericia coli and Pseudomonas aeruginosa.

Archaea: Halobacterium halobium and Methanococcus vannielii.

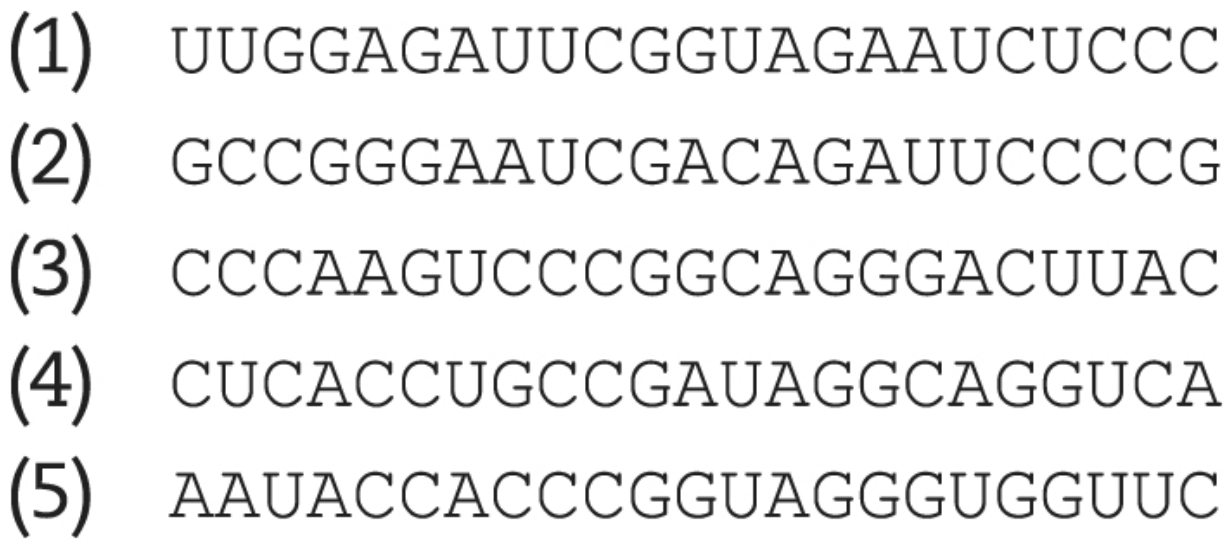
Eukarya: Homo sapiens and Saccharomyces cerevisiae.

The nucleotides at the ninth and twenty-second positions in all the organisms are identities that are indicated by orange boxes. The identities at the ninth position are: G G, C A, and U U. The identities at the twenty-second are: C C, G U, and A A.

Part (B): The secondary structure is a stem-loop structure. The Watson-Crick base pairing between the bases at the ninth and the twenty-second positions is shown to be conserved.

Return to FIGURE 10.17 RNA sequence alignments provide insights into structure based on conservation of base-pairing. (A) A comparison of sequences in a part of ribosomal RNA taken from a variety of species

Extended description for Sequences of R N A fragments



The five sequences are as follows:

Part 1: U U G G A G A U U C G G U A G A A U C U C C C

Part 2: G C C G G G A A U C G A C A G A U U C C C C G

Part 3: C C C A A G U C C C G G C A G G G A C U U A C

Part 4: C U C A C C U G C C G A U A G G C A G G U C A

Part 5: A A U A C C A C C C G G U A G G G U G G U U C

Return to Sequences of R N A fragments

Extended description for Sequences of R N A fragments



The five sequences are as follows:

Part 1: U U G G A G A U U C (red) G G U A G (blue) A A U C U C C C

Part 2: G C C G G G A A U C (red) G A C A G (blue) A U U C C C C G

Part 3: C C C A A G U C C C (red) G G C A G (blue) G G A C U U A C

Part 4: C U C A C C U G C C (red) G A U A G (blue) G C A G G U C A

Part 5: A A U A C C A C C C (red) G G U A G (blue) G G U G G U U C

Return to Sequences of R N A fragments

Extended description for Sequences of R N A fragments



The five sequences are as follows:

Part 1: U U G G A G A U U (red) C G G U A G A (blue) A U C U C C C

Part 2: G C C G G G A A U (red) C G A C A G A (blue) U U C C C C G

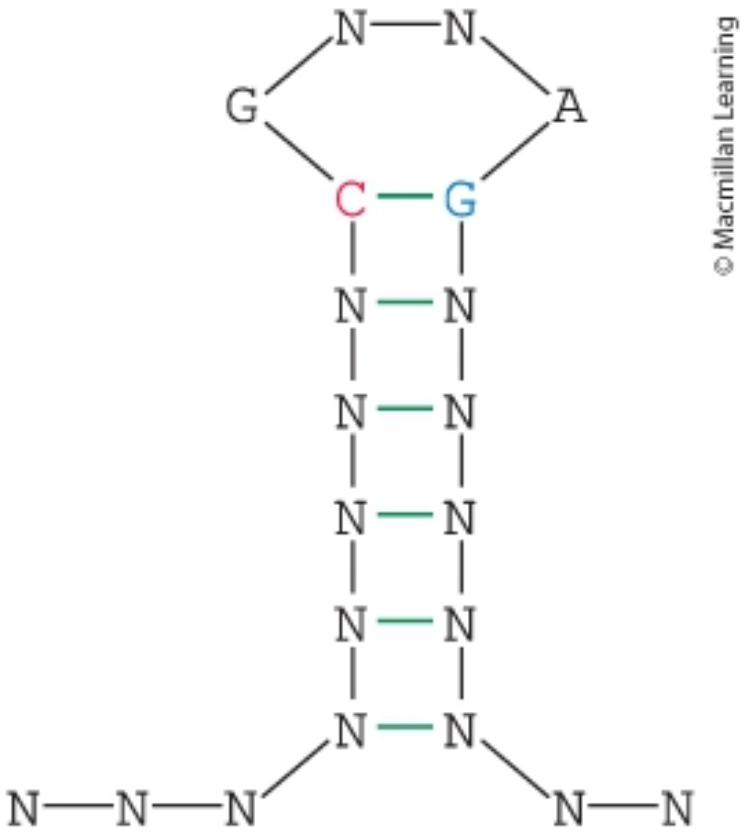
Part 3: C C C A A G U C C C (red) G G C A G G (blue) G A C U U A C

Part 4: C U C A C C U G C C (red) G A U A G G (blue) C A G G U C A

Part 5: A A U A C C A C C C (red) C G G U A G G (blue) G U G G U U C

Return to Sequences of R N A fragments

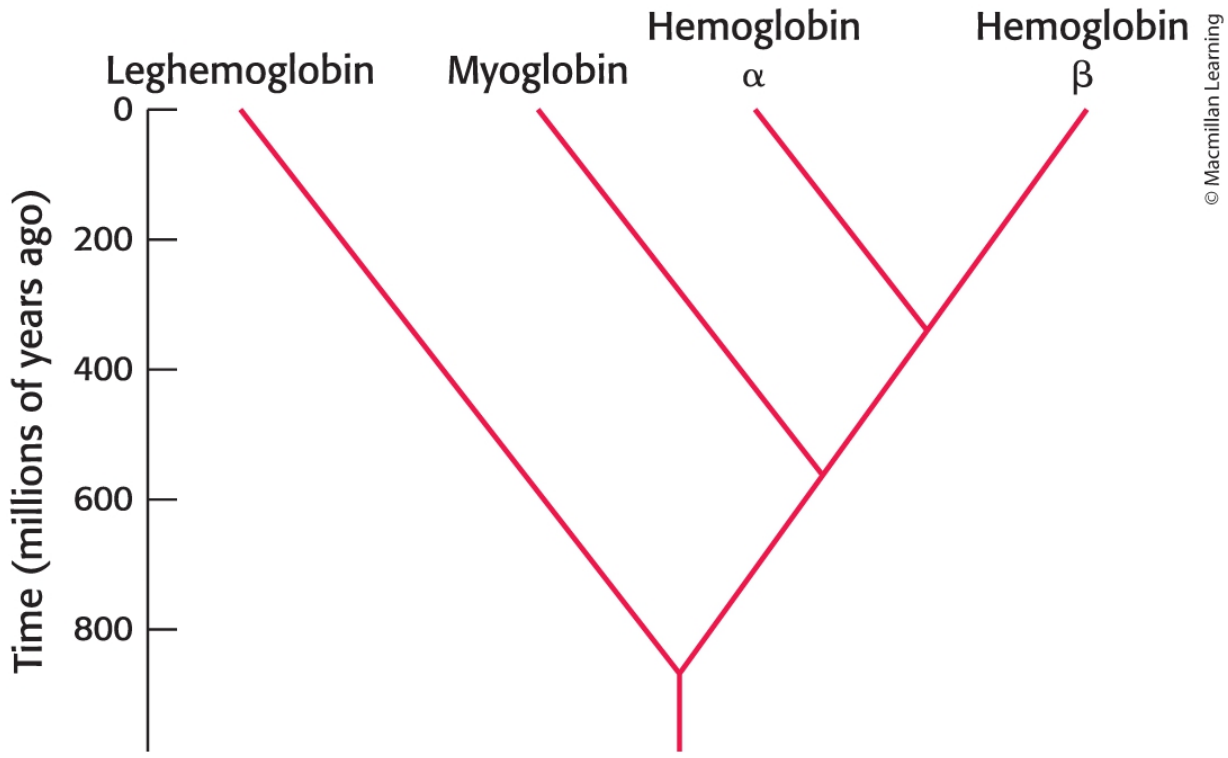
Extended description for Stem loop structure of R N A



A stem-loop structure is shown. It contains a trail of N residues at the left and right ends. The stem is composed of a pair of 5 N residues and a G C pair hydrogen bonded to each other from bottom to top. The loop part contains the residues G, N, N, and A arranged in a clockwise direction from bottom left to bottom right.

Return to Stem loop structure of R N A

Extended description for FIGURE 10.18 Sequence alignments enable the construction of an evolutionary tree



The vertical evolutionary tree is shown next to a vertical axis labeled Time (millions of years ago) and ranges from 800 to 0 in decrements of 200 units.

The root of the evolutionary tree is at 900 and it splits into two level-1 branches just before 800.

The first level-1 branch terminates in Leghemoglobin at 0.

The second level-1 branch splits into two level-2 branches just after 600.

The first level-2 branch terminates in myoglobin at 0.

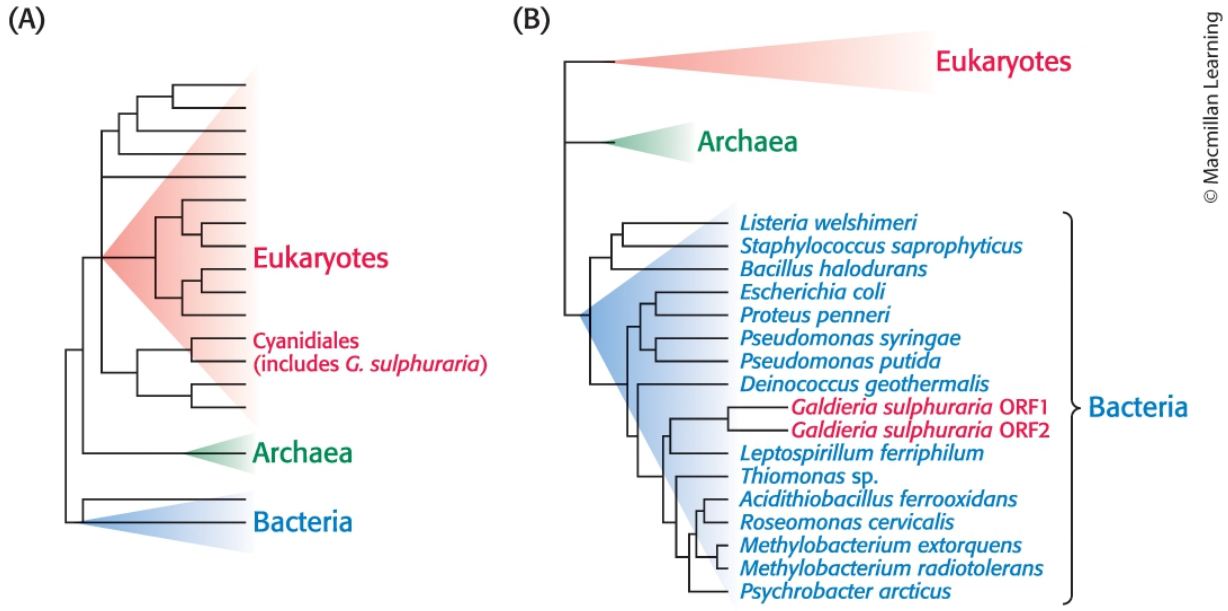
The second level-2 branch splits into two level-3 branches just after 400.

The first level-3 branch terminates in hemoglobin alpha at 0.

The second level-3 branch terminates in hemoglobin beta at 0.

Return to FIGURE 10.18 Sequence alignments enable the construction of an evolutionary tree

Extended description for FIGURE 10.21 Proteins encoded within the G. sulphuraria genome with high homology to prokaryotic sequences are suggestive of horizontal gene transfer



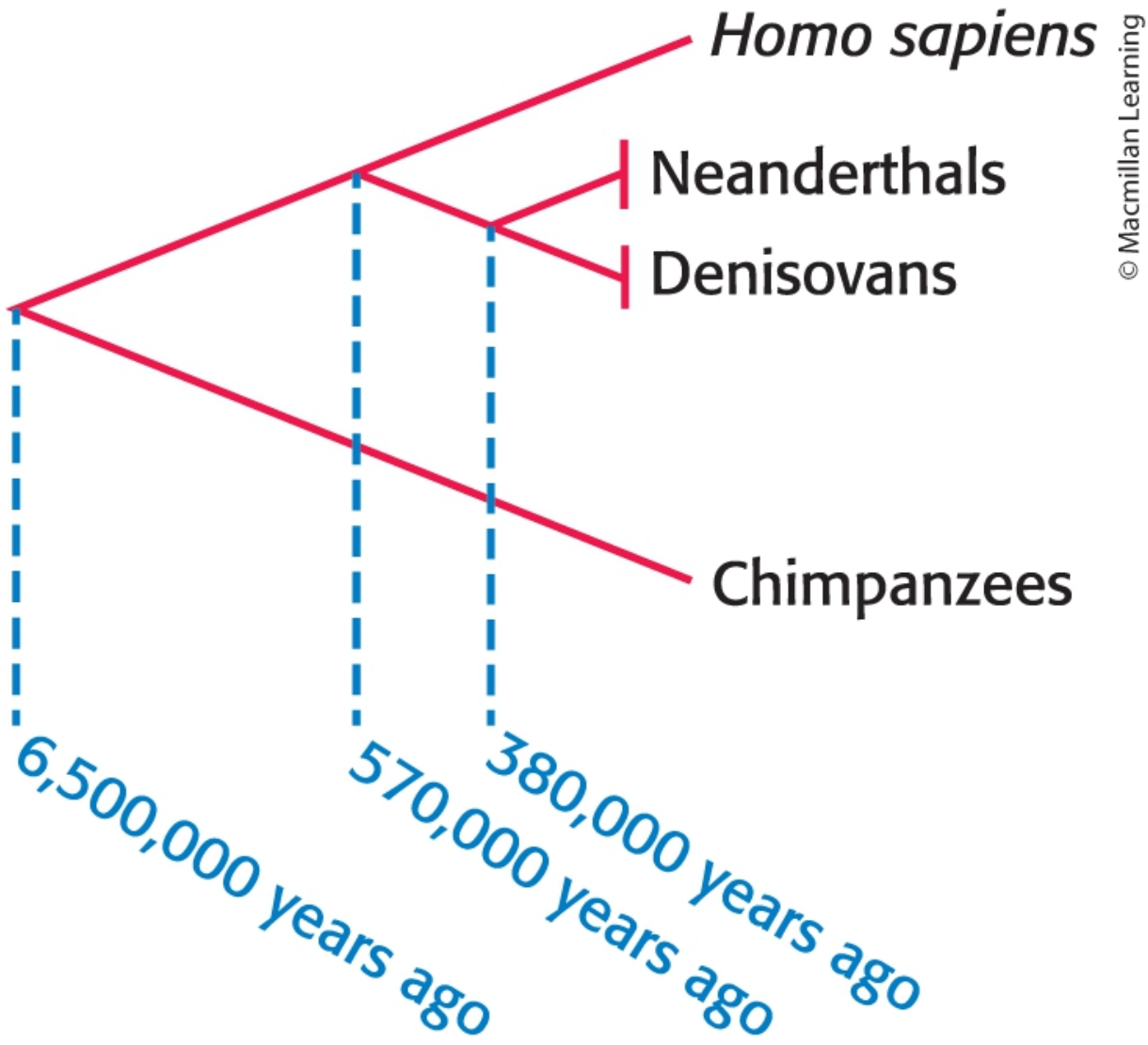
Part (A): A common ancestor gives rise to two level-1 branches. From bottom to top, the first level-1 branch splits into two level-2 branches that represent bacteria. The second level-1 branch splits into two level-2 branches. The first level-2 branch represents Archaea. The second level-2 branch splits into three level-3 branches. The first and second level-3 branches subsequently split into multiple branches that represent eukaryotes. The third level-3 branch subsequently splits into multiple branches that represent Cyanidiales (includes G. suphuraria).

Part (B): There are three level-1 branches. From top to bottom, the first level-1 branch represents eukaryotes. The second level-1 branch represents Archaea. The third level-3 branch subsequently splits

into multiple branches that represent bacteria named: *Listeria welshimeri, Staphylococcus saprophyticus, Bacillus halodurans, Escherichia coli, Proteus penneri, Pseudomonas syringae, Pseudomonas putida, Deinococcus geothermalis, Leptospirillum ferriphilum, Thiomonas sp., Acidithiobacillus ferrooxidans, Roseomonas cervicalis, Methylobacterium extorquens, Methylobacterium radiotolerans, Psychrobacter arcticus*. Two terminal branches in between represent *Galdieria sulphuraria* O R F 1 and *Galdieria sulphuraria* O R F 2.

Return to FIGURE 10.21 Proteins encoded within the G. sulphuraria genome with high homology to prokaryotic sequences are suggestive of horizontal gene transfer

Extended description for FIGURE 10.22 DNA sequence comparisons enable the placement of Neanderthals and Denisovans on an evolutionary tree

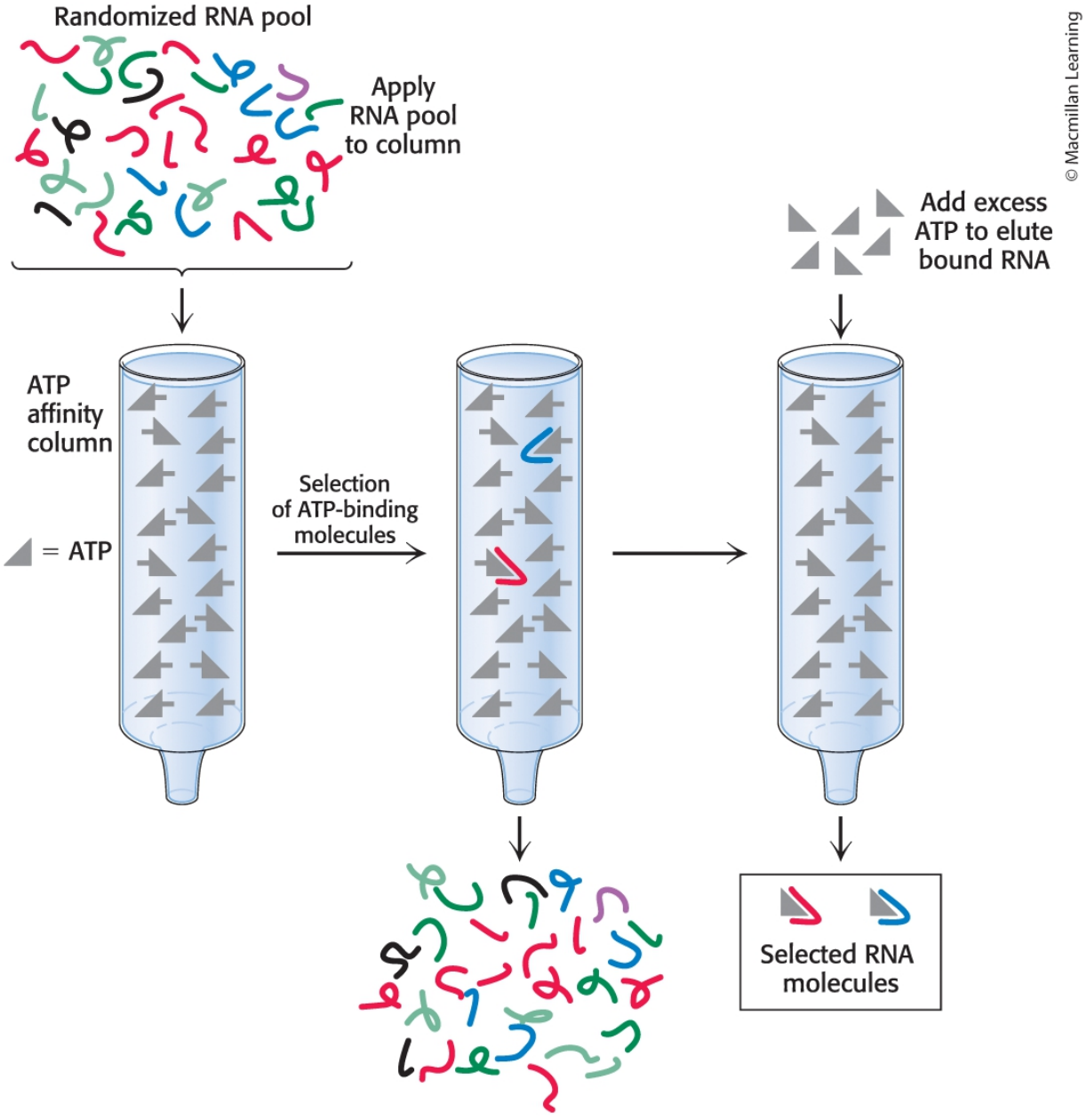


The common ancestor existed 6,500,000 years ago. This splits into two level-1 branches. The first level-1 branch is Chimpanzees. The second level-1 branch split into two level-2 branches 570,000 years ago. The first level-2 branch is Homo sapiens. The second level-2 branch split into two level-3 branches 380,000 years ago. The first

level-3 branch is the Neanderthals. The second level-3 branch is Denisovans.

Return to FIGURE 10.22 DNA sequence comparisons enable the placement of Neanderthals and Denisovans on an evolutionary tree

Extended description for FIGURE 10.23 Evolution can be studied in the laboratory setting



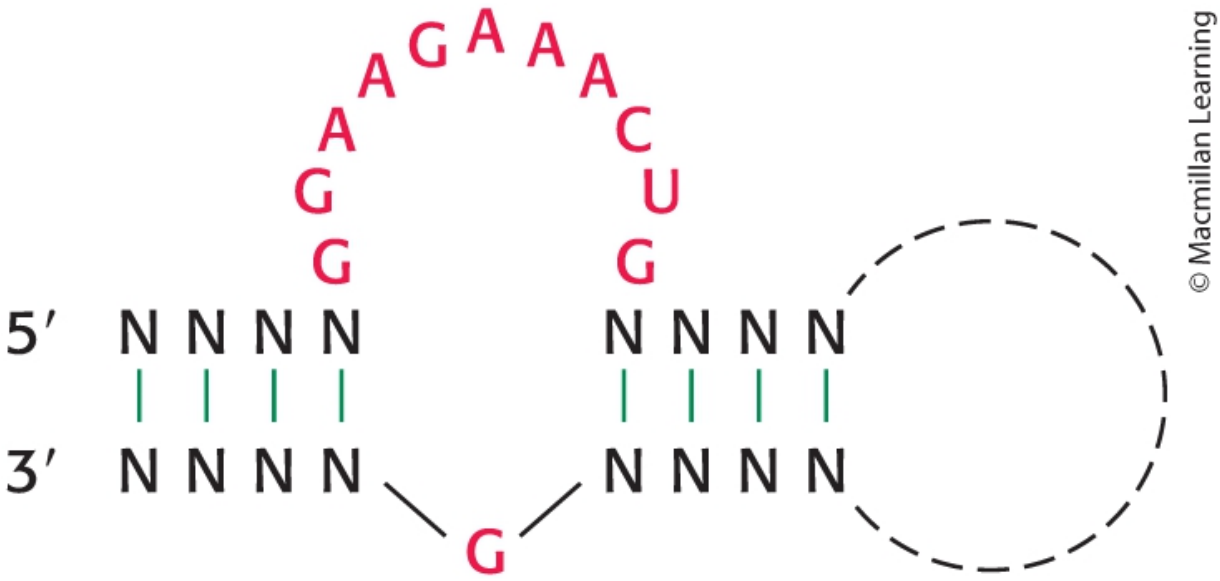
A randomized R N A pool with several R N A molecules is shown. A vertical column labeled A T P affinity column is shown. The column is layered with A T P molecules. The R N A pool is applied to the A T

P affinity column. The selection of A T P binding molecules is done by selecting the R N A molecules that bind to the A T P in the column. The unbound R N A molecules are released from the column.

Excess A T P is added to the column to elute out the selected R N A molecules.

Return to FIGURE 10.23 Evolution can be studied in the laboratory setting

Extended description for FIGURE 10.24 A conserved secondary structure is common to RNA molecules selected for ATP binding



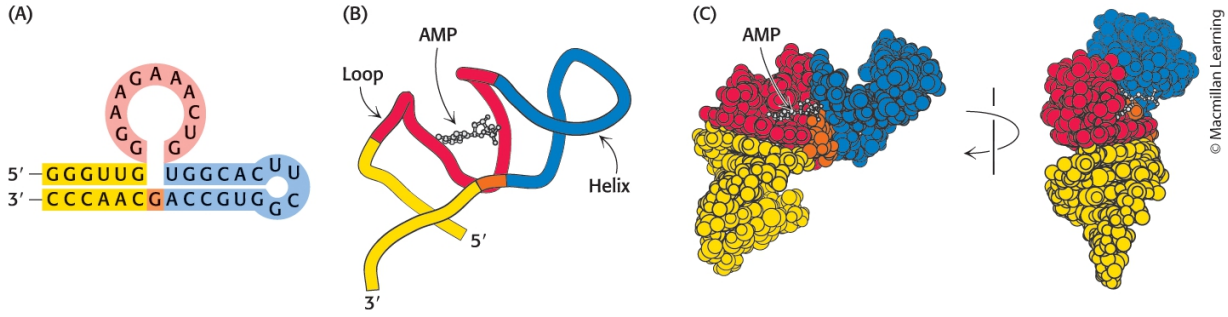
© Macmillan Learning

The sequence from the 3 prime end to loop is as follows: N N N N G G A A G A A A C U G N N N N loop.

The bases that are not conserved following the loop are paired with the top stem and have the following structure: N N N N G N N N N. The conserved bases are base paired.

Return to FIGURE 10.24 A conserved secondary structure is common to RNA molecules selected for ATP binding

Extended description for FIGURE 10.25 Experimental molecular evolution yields an ATP-binding RNA molecule



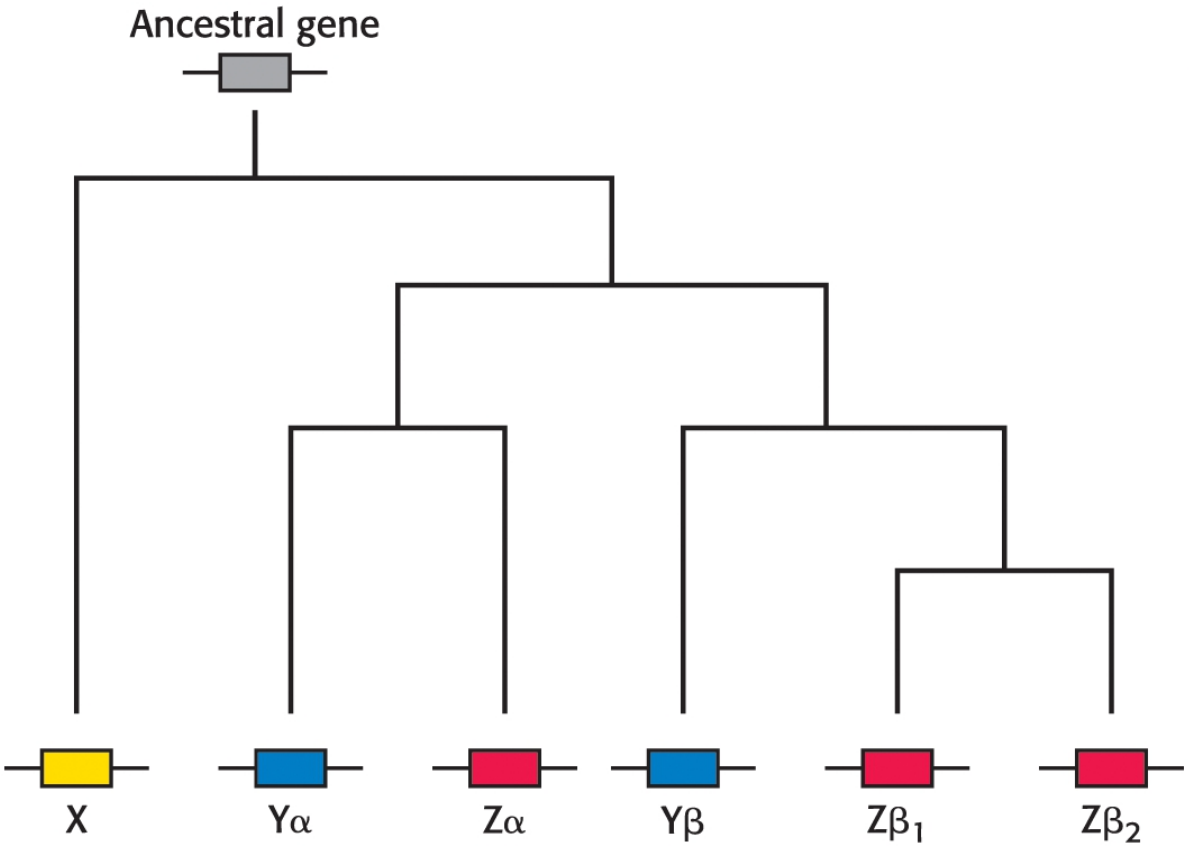
Part (A): The primary structure shows a horizontal stem loop structure. The left end of the stem is colored yellow containing the sequences C C C A A C at the 3 prime end and G G G U U G at the 5 prime end. The terminal loop at the right end is colored blue and contains the sequence U G G C A C U U C G G U G C C A G. A central loop of the upper strand is colored red and contains the sequence G G A A G A A A C U G.

Part (B): The N M R-structure reveals the blue region to be a helix. An A M P molecule is shown to be wedged within the red loop.

Part (C): The three-dimensional space-filling model shows a tightly bound helical structure with the distinct A M P binding region.

Return to FIGURE 10.25 Experimental molecular evolution yields an ATP-binding RNA molecule

Extended description for Evolutionary tree of similar genes



© Macmillan Learning

The ancestral gene is shown in gray, and it splits into two level-1 branches.

The first level-1 branch represents gene X shown in yellow.

The second level-1 branch splits into two level-2 branches.

The first level-2 branch splits into two level-3 branches.

The first level-3 branch represents gene Y alpha, shown in blue.

The second level-3 branch represents gene Z alpha, shown in red.

The second level-2 branch splits into two level-3 branches.

The first level-3 branch represents gene Y beta, shown in blue.

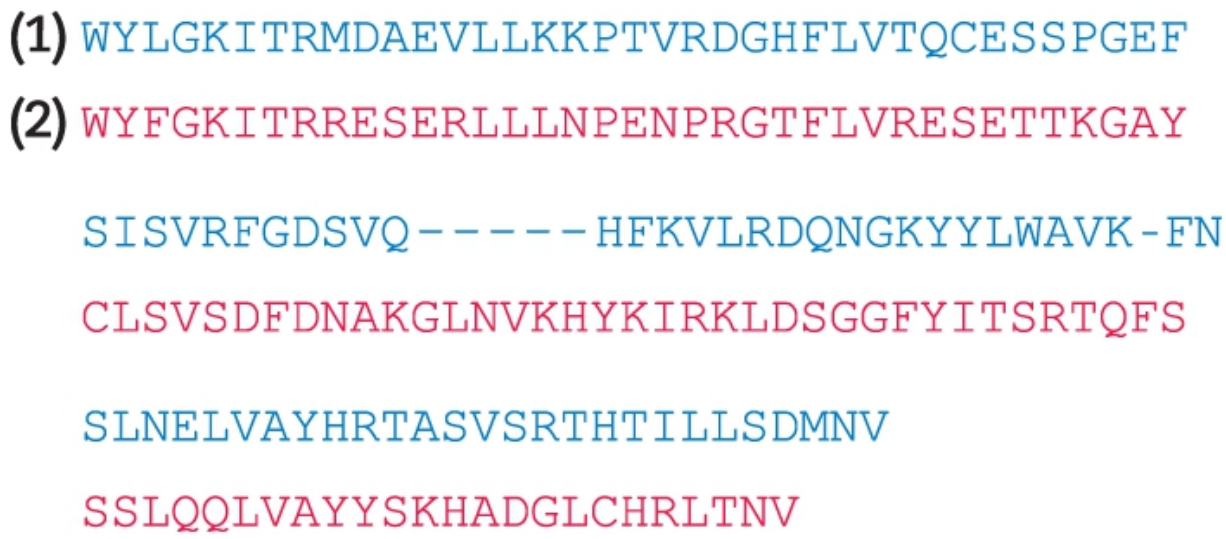
The second level-3 branch splits into two level-4 branches.

The first level-4 branch represents gene Z beta 1, shown in red.

The second level-4 branch represents gene Z beta 2, shown in red.

Return to Evolutionary tree of similar genes

Extended description for Sequence of two proteins



Protein 1: Segment shown in blue with a sequence: W Y L G K I T R M D A E V L L K K P T V R D G H F L V T Q C E S S P G E F

Protein 2: Segment shown in red with a sequence: W Y F G K I T R R E S E R L L L N P E N P R G T F L V R E S E T T K G A Y

Segment shown in blue: S I S V R F G D S V Q gap H F K V L R D Q N G K Y Y L W A V K gap F N

Segment shown in red: C L S V S D F D N A K G L N V K H Y K I R K L D S G G F Y I T S R T Q F S

Segment shown in blue: S L N E L V A Y H R T A S V S R T H T I L L S D M N V

Segment shown in red: S S L Q Q L V A Y Y S K H A D G L C H R L T N V

Return to Sequence of two proteins

Extended description for Sequence alignments



Alignment 1:

The sequence in blue: A hyphen S N L F D I R L I G

The sequence in red: G S N D F Y E V K I M D

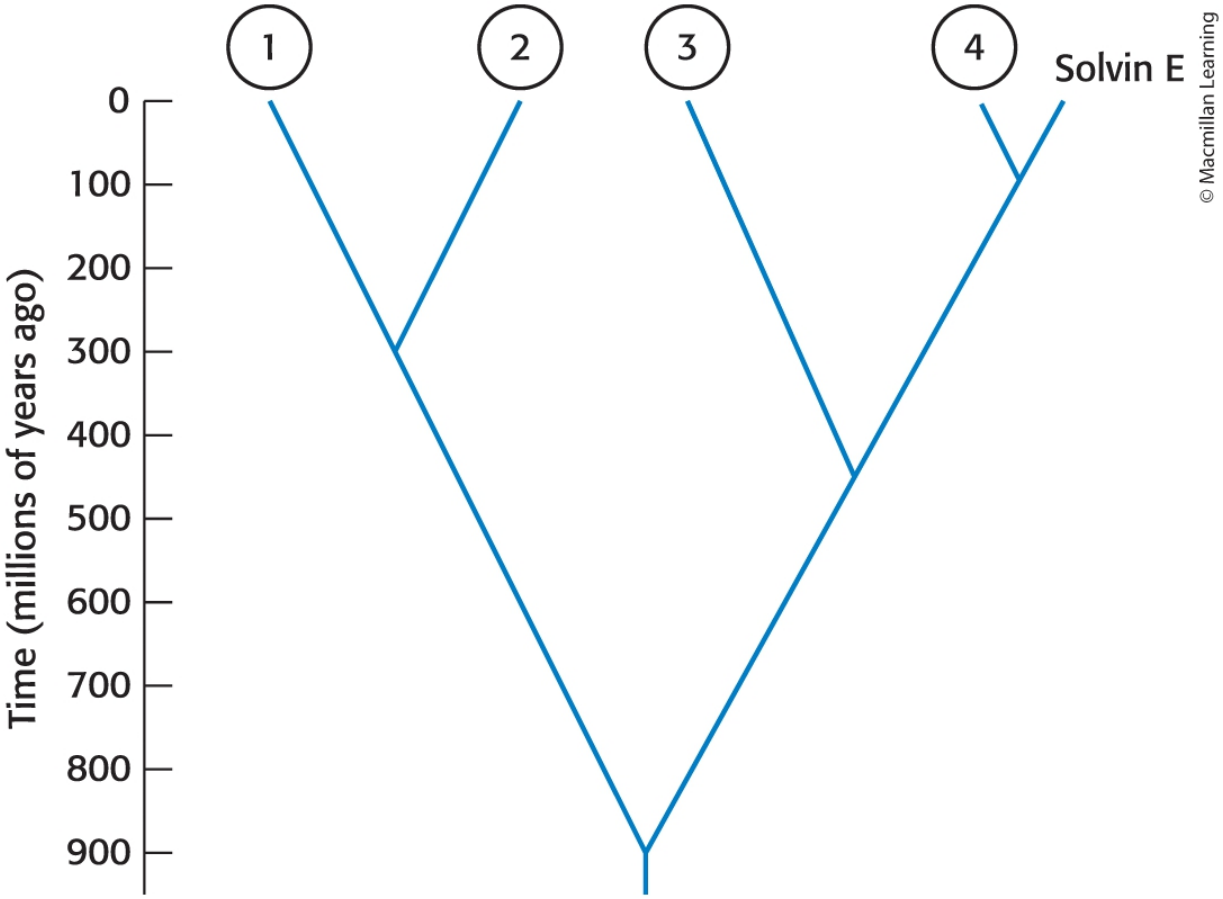
Alignment 2:

The sequence in blue: A S N L F D I R L I hyphen G

The sequence in red: G S N D F Y E V K I M D

Return to Sequence alignments

Extended description for An evolutionary tree

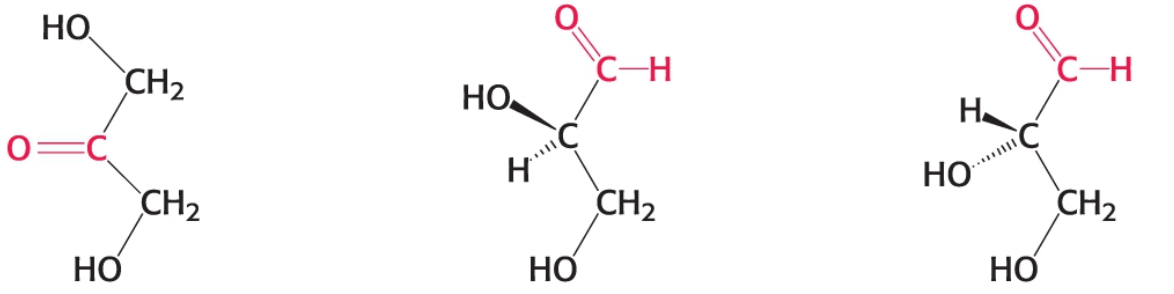


The vertical axis labeled Time (millions of years ago) is shown alongside the evolutionary tree and ranges from 900 to 0 in decrements of 100 units.

The root of the tree lies at 900 and splits into two level-1 branches. The first level-1 branch splits into two level-2 branches at 300. The first level-2 branch is labeled 1. The second level-2 branch is labeled 2. The second level-1 branch splits into two level-2 branches just after 550. The first level-2 branch is labeled 3. The second level-2 branch splits into two level-3 branches at 100. The first level-3 branch is labeled 4. The second level-3 branch represents Solvin E.

Return to An evolutionary tree

Extended description for Structures of dihydroxyacetone, D-glyceraldehyde, and L-Glyceraldehyde



Dihydroxyacetone
(a ketose)

D-Glyceraldehyde
(an aldose)

L-Glyceraldehyde
(an aldose)

The structure of dihydroxyacetone (a ketose) is as follows: A 3-carbon alkane chain is depicted as a vertical line structure using 2 zigzag lines. C 1 and C 3 are bound to H 2. C 1 is single bonded to O H on the upper left. C 2 is double bonded to O on the left. C 2 and O are highlighted in red. C 3 is single bonded to O H on the lower left.

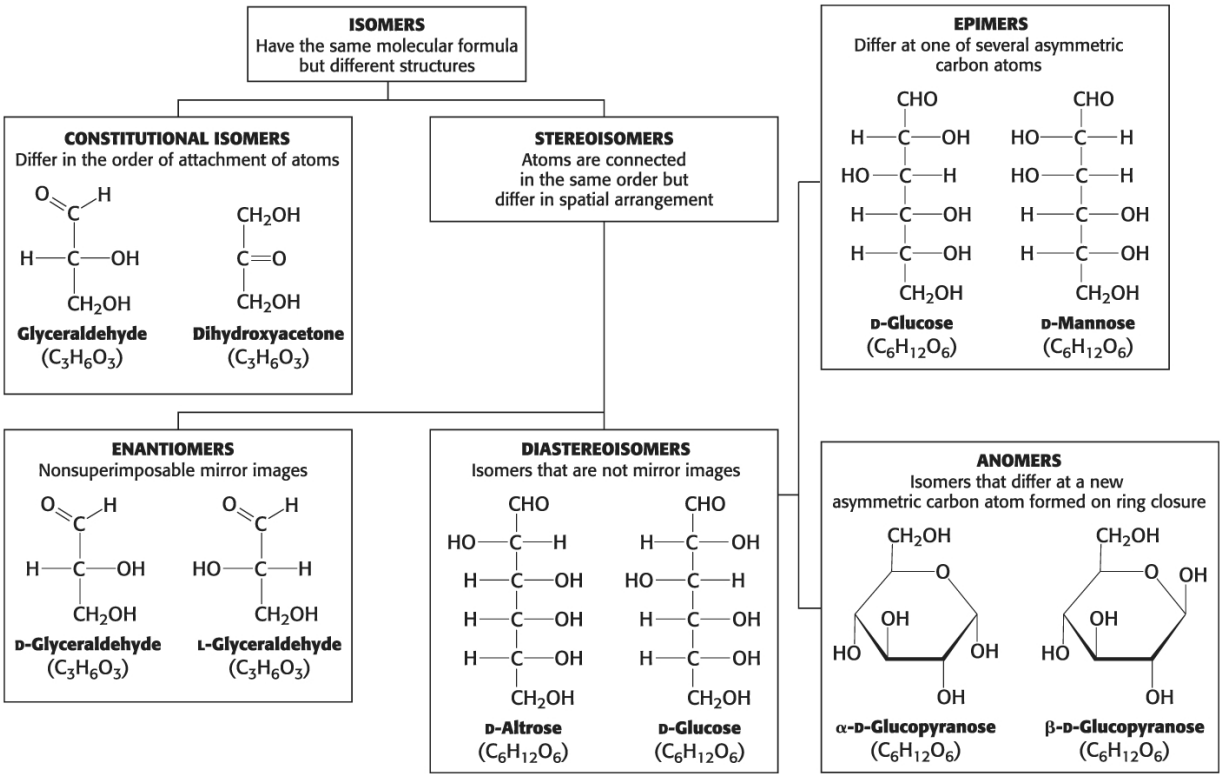
The structure of D-Glyceraldehyde (an aldose) is as follows: A 3-carbon alkane chain is depicted as a vertical line structure using 2 zigzag lines. C 3 is bound to H 2. C 1 is single bonded to H on the right and double bonded to O on the upper left. C 1 and the bonded H and O atoms are highlighted in red. C 2 is wedge bonded to H on the upper left and dash bonded to H on the lower left. C 3 is single bonded to O H on the lower left.

The structure of L-Glyceraldehyde (an aldose) is as follows: A 3-carbon alkane chain is depicted as a vertical line structure using 2 zigzag lines. C 3 is bound to H 2. C 1 is single bonded to H on the right and double bonded to O on the upper left. C 1 and the bonded

H and O atoms are highlighted in red. C 2 is wedge bonded to H on the upper left and dash bonded to O H on the lower left. C 3 is single bonded to O H on the lower left.

Return to Structures of dihydroxyacetone, D-glyceraldehyde, and L-Glyceraldehyde

Extended description for Classification of isomers



A flowchart starts with isomers that have the same molecular formula but different structures. These isomers are constitutional isomers that differ in the order of attachment of atoms and stereoisomers in which atoms are connected in the same order but differ in spatial arrangement. Constitutional isomers have two structures labeled glyceraldehyde (C 3 H 6 O 3) and dihydroxyacetone (C 3 H 6 O 3). The structure of glyceraldehyde is as follows: A central C atom is single bonded to H on the left, O H on the right, C H 2 O H below, and C above. The C atom above is double bonded to O on the upper left and single bonded to H on the upper right. The structure of dihydroxyacetone is as follows: A central C atom is single bonded to C H 2 O H above, C H 2 O H below, and double bonded to O on the right.

Stereoisomers are divided into enantiomers which are non-superimposable mirror images and diastereoisomers are isomers that are not mirror images. Enantiomers have two structures labeled D-Glyceraldehyde (C 3 H 6 O 3) and L-glyceraldehyde (C 3 H 6 O 3). The structure of D-Glyceraldehyde is as follows: A central C atom is single bonded to H on the left, O H on the right, C H 2 O H below, and C above. The C atom above is double bonded to O on the upper left and single bonded to H on the upper right. The structure of L-Glyceraldehyde is as follows: A central C atom is single bonded to O H on the left, H on the right, C H 2 O H below, and C above. The C atom above is double bonded to O on the upper left and single bonded to H on the upper right.

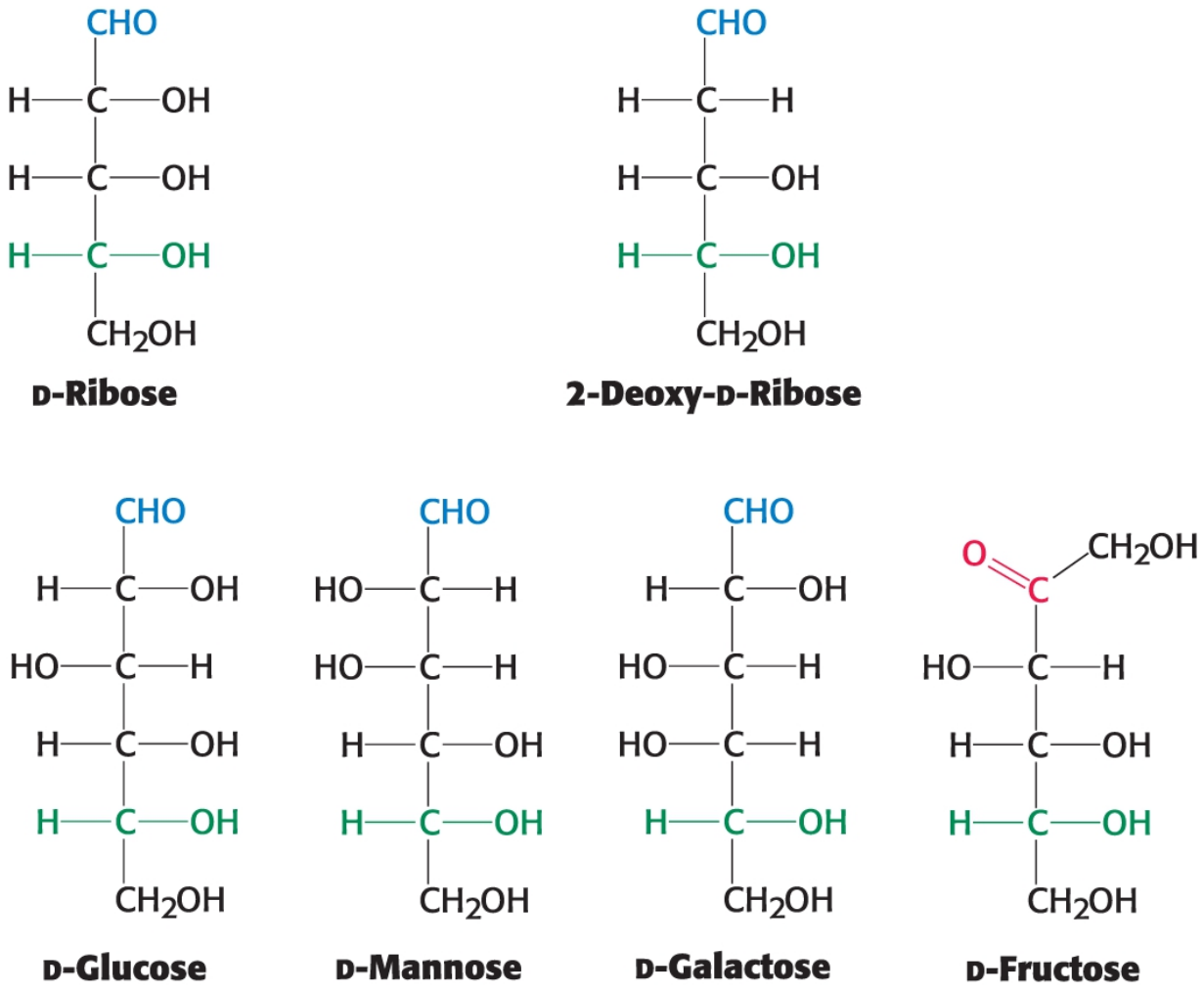
Diastereoisomers have two structures labeled D-Altrose (C 6 H 12 O 6) and D-Glucose (C 6 H 12 O 6). The structure of D-Altrose is as follows: The Fischer projection consists of a vertical line with C H O above and C H 2 O H below. The projection contains four C atoms placed one below the other on the vertical line. The C atoms are numbered from top to bottom. C 2 is single bonded to O H on the left and H on the right. C 3, C 4, and C 5 are each single bonded H on the left and O H on the right. The structure of D-Glucose is as follows: The Fischer projection consists of a vertical line with C H O above and C H 2 O H below. The projection contains four C atoms placed one below the other on the vertical line. The C atoms are numbered from top to bottom. C 2, C 4, and C 5 are each single bonded to H on the left and O H on the right. C 3 is single bonded to O H on the left and H on the right.

Diastereoisomers are classified into epimers that differ at one of several asymmetric carbon atoms and anomers are isomers that differ at a new asymmetric carbon atom formed on ring closure. Epimers have two structures labeled D-Glucose (C 6 H 12 O 6) and D-Mannose (C 6 H 12 O 6). The structure of D-Glucose is as follows: The Fischer projection consists of a vertical line with C H O above and C

H 2 O H below. The projection contains four C atoms placed one below the other on the vertical line. The C atoms are numbered from top to bottom. C 2, C 4, and C 5 are each single bonded to H on the left and O H on the right. C 3 is single bonded to O H on the left and H on the right. The structure of D-Mannose is as follows: The Fischer projection consists of a vertical line with C H O above and C H 2 O H below. The projection contains four C atoms placed one below the other on the vertical chain. The C atoms are numbered from top to bottom. C 2 and C 3 are each single bonded to O H on the left and H on the right. C 4 and C 5 are each single bonded to H on the left and O H on the right. Anomers have two structures labeled alpha-D-Glucopyranose (C 6 H 12 O 6) and beta-D-Glucopyranose (C 6 H 12 O 6). The structure of alpha-D-Glucopyranose is as follows: A 6-membered heterocyclic hexagonal ring is in a horizontal orientation and consists of 1 O and 5 C atoms. The O atom occupies the first position, which is the top right vertex. C 1, C 2, and C 4 are each single bonded to O H below. C 3 is single bonded to O H above. C 5 is single bonded to C H 2 O H above. The structure of beta-D-Glucopyranose is as follows: A 6-membered heterocyclic hexagonal ring is in a horizontal orientation and consists of 1 O and 5 C atoms. The O atom occupies the first position, which is the top right vertex. C 1 and C 3 are each single bonded to O H above. C 2 and C 4 are each single bonded to O H below. C 5 is single bonded to C H 2 O H above.

Return to Classification of isomers

Extended description for Molecular structures of common monosaccharides



The structure of D-Ribose is as follows: The Fischer projection consists of a vertical line with C H O above and C H 2 O H below. The projection contains three C atoms placed one below the other on the vertical line. The C atoms are numbered from top to bottom. C 2, C 3, and C 4 are each single bonded to H on the left and O H on the right. C H O is highlighted in blue. C 4 and the H atom and O H group bonded to it are highlighted in green.

The structure of 2-Deoxy-D-Ribose is as follows: The Fischer projection consists of a vertical line with C H O above and C H 2 O H below. The projection contains three C atoms placed one below the other on the vertical line. The C atoms are numbered from top to bottom. C 2 is single bonded to H on the left and H on the right. C 3 and C 4 are each single bonded to H on the left and O H on the right. C H O is highlighted in blue. C 4 and the H atom and O H group bonded to it are highlighted in green.

The structure of D-Glucose is as follows: The Fischer projection consists of a vertical line with C H O above and C H 2 O H below. The projection contains four C atoms placed one below the other on the vertical line. The C atoms are numbered from top to bottom. C 2, C 4, and C 5 are single bonded to H on the left and O H on the right. C 3 is single bonded to O H on the left and H on the right. C H O is highlighted in blue. C 5 and the H atom and O H group bonded to it are highlighted in green.

The structure of D-Mannose is as follows: The Fischer projection consists of a vertical line with C H O above and C H 2 O H below. The projection contains four C atoms placed one below the other on the vertical line. The C atoms are numbered from top to bottom. C 2 and C 3 are single bonded to O H on the left and H on the right. C 4 and C 5 are each single bonded to H on the left and O H on the right. C H O is highlighted in blue. C 5 and the H atom and O H group bonded to it are highlighted in green.

The structure of D-Galactose is as follows: The Fischer projection consists of a vertical line with C H O above and C H 2 O H below. The projection contains four C atoms placed one below the other on the vertical line. The C atoms are numbered from top to bottom. C 2 and C 5 are single bonded to H on the left and O H on the right. C 3 and C 4 are each single bonded to O H on the left and H on the right. C H O

is highlighted in blue. C 5 and the H atom and O H group bonded to it are highlighted in green.

The structure of D-Fructose is as follows: The Fischer projection consists of a vertical line with C above and C H 2 O H below. The projection contains three C atoms placed one below the other on the vertical line. The C atoms are numbered from top to bottom. C 1 is double bonded to O on the upper left and single bonded to C H 2 O H on the upper right. C 2 is single bonded to O H on the left and H on the right. C 3 and C 4 are each single bonded to H on the left and O H on the right. C 1 double bonded to O is highlighted in red. C 4 and the H atom and O H group bonded to it are highlighted in green.

Return to Molecular structures of common monosaccharides

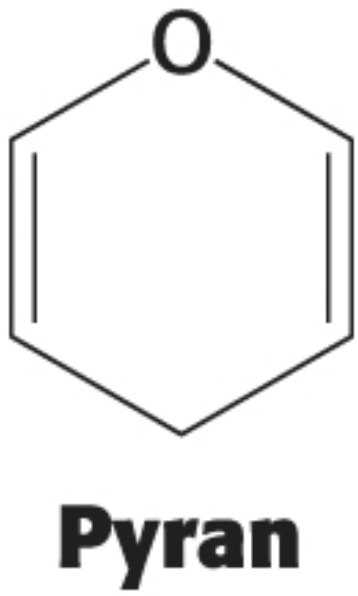
Extended description for Formation of hemiacetal from aldehyde and alcohol



The reaction consists of two reactants and one product. The first reactant is aldehyde whose structure is as follows: A central C atom is single bonded to R on the lower left, H on the lower right, and double bonded to O above. The second reactant is alcohol whose formula is H O R dash highlighted in red. The product is hemiacetal whose structure is as follows: A central C atom is single bonded to O H on the upper left, O R dash on the upper right, R on the lower left, and H on the lower right. The H atom of the O H group is highlighted in red. The O R dash group is highlighted in red.

Return to Formation of hemiacetal from aldehyde and alcohol

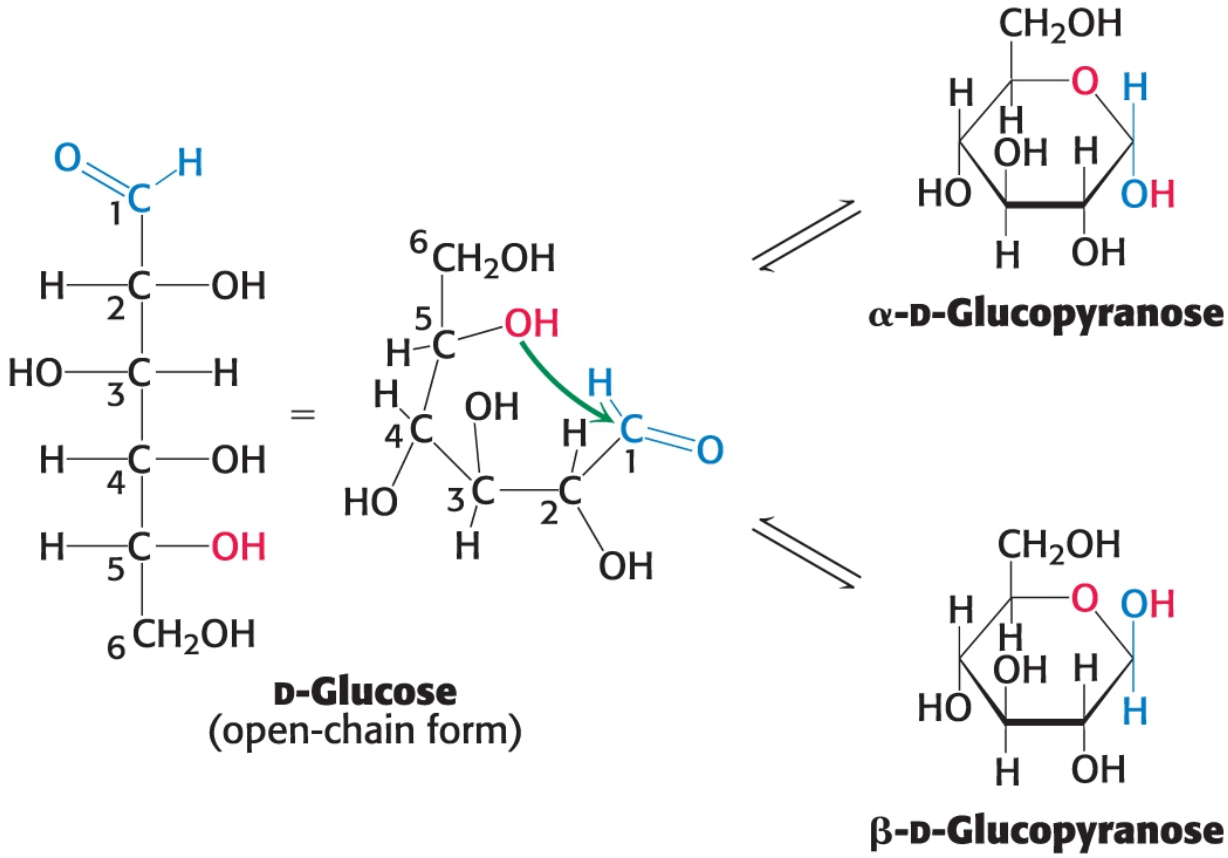
Extended description for Chemical structure of pyran



The structure is as follows: A 6-membered heterocyclic hexagonal ring labeled pyran is in a vertical orientation and consists of 1 O and 5 C atoms. O occupies the first position, which is the topmost vertex. A double bond is present between C 1 and C 2, and, C 4 and C 5.

Return to Chemical structure of pyran

Extended description for Formation of alpha-D-Glucopyranose and beta-D-Glucopyranose from D-Glucose



The structure of the open-chain form of D-Glucose is as follows: The Fischer projection consists of a vertical line with C above and C H 2 O H below. The projection contains four C atoms placed one below the other on the vertical line. The C atoms are numbered from top to bottom. C 1 is double bonded to O on the upper left and single bonded to H on the upper right. C 2, C 4, and C 5 are single bonded to H on the left and O H on the right. C 3 is single bonded to O H on the left and H on the right. C 1 and its bonded O and H atoms are highlighted in blue. The O H group bonded to C 5 is highlighted in red.

An equal symbol on the right of D-glucose shows the formation of a ring-like structure as follows: C 1 to C 5 atoms of the open-chain form fold to produce an open ring-like structure. C 1 to C 5 atoms are located in a clockwise direction starting from the right. The red highlighted O H group bonded to C 5 attacks C 1. C 6 is located above the open ring-like structure.

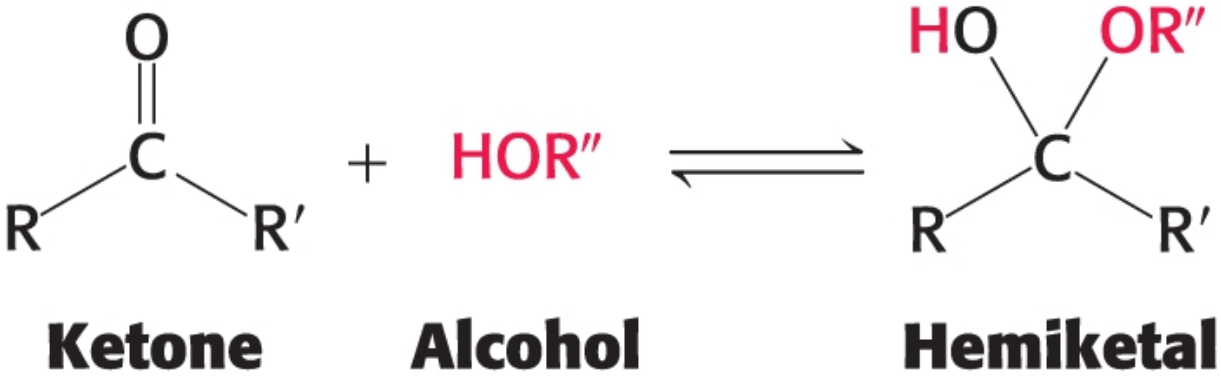
Two reversible reaction arrows show the formation of alpha-D-Glucopyranose and beta-D-glucopyranose.

The structure of alpha-D-Glucopyranose is as follows: A 6-membered heterocyclic hexagonal ring is in a horizontal orientation and consists of 1 O and 5 C atoms. The O atom occupies the first position, which is the top right vertex. It is highlighted in red. C 1, C 2, C 4 are each single bonded to H above and O H below. C 3 is single bonded to O H above and H below. C 5 is single bonded to C H 2 O H above and H below. The H atom above and O atom of O H group bonded to C 1 are highlighted in blue. The H atom of O H group is highlighted in red.

The structure of beta-D-glucopyranose is as follows: A 6-membered heterocyclic hexagonal ring is in a horizontal orientation and consists of 1 O and 5 C atoms. The O atom occupies the first position, which is the top right vertex. It is highlighted in red. C 1 and C 3 are each single bonded to O H above and H below. C 2 and C 4 are each single bonded to H above and O H below. C 5 is single bonded to C H 2 O H above and H below. The H atom below and the O atom of O H group bonded to C 1 are highlighted in blue. The H atom of the O H group is highlighted in red.

Return to Formation of alpha-D-Glucopyranose and beta-D-Glucopyranose from D-Glucose

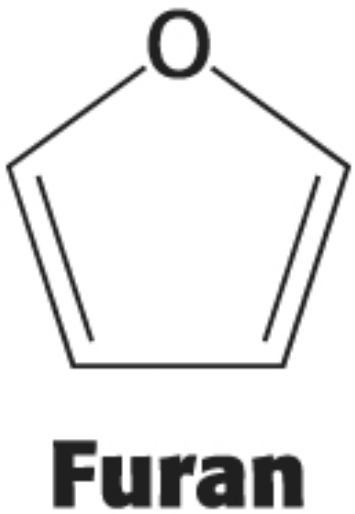
Extended description for Formation of hemiketal from ketone and alcohol



The chemical reaction consists of two reactants and one product. The first reactant is ketone whose structure is as follows: A central C atom is single bonded to R on the lower left, R dash on the lower right, and double bonded to O above. The second reactant is alcohol whose formula is H O R double dash highlighted in red. The product is hemiketal whose structure is as follows: A central C atom is single bonded to O H on the upper left, O R double dash on the upper right, R on the lower left, and R dash on the lower right. The H atom of the O H group is highlighted in red. The O R double dash group is highlighted in red.

Return to Formation of hemiketal from ketone and alcohol

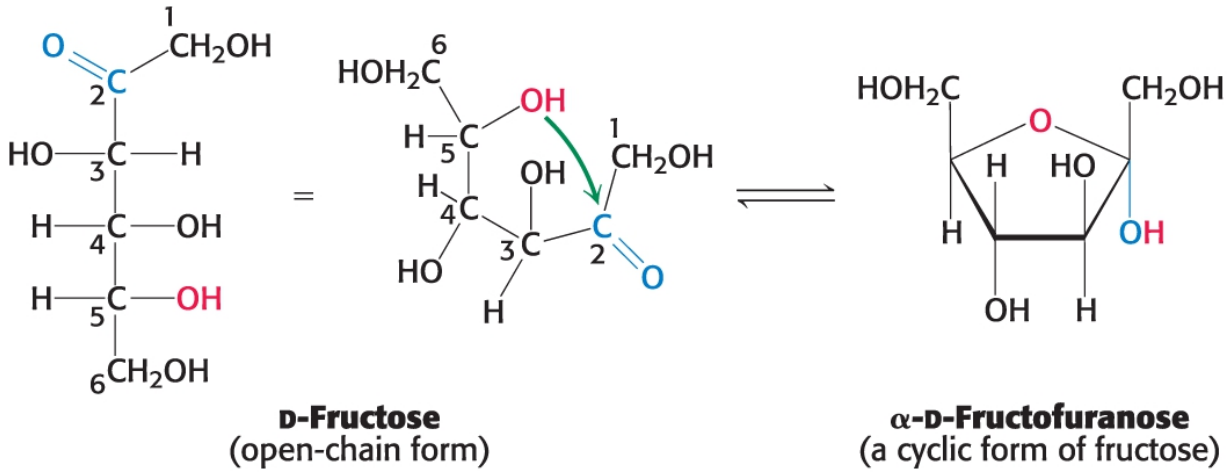
Extended description for Chemical structure of furan



The structure is as follows: A 5-membered heterocyclic pentagonal ring labeled furan is in a vertical orientation and consists of 1 O and 4 C atoms. O occupies the first position, which is the topmost vertex. A double bond is present between C 1 and C 2, and, C 3 and C 4.

Return to Chemical structure of furan

Extended description for Formation of alpha-D-Fructofuranose from D-Fructose



The structure of open-chain form of D-Fructose is as follows: The Fischer projection consists of a vertical line with C above and C H 2 O H below. The projection contains four C atoms placed one below the other on the vertical line. The C atoms are numbered from 2 to 6 from the top to bottom. C 2 is double bonded to O on the upper left and single bonded to C H 2 O H on the upper right. The C atom of C H 2 O H group is numbered 1. C 3 is single bonded to O H on the left and H on the right. C 4 and C 5 are each single bonded to H on the left and O H on the right. The O H group bonded to C 5 is highlighted in red.

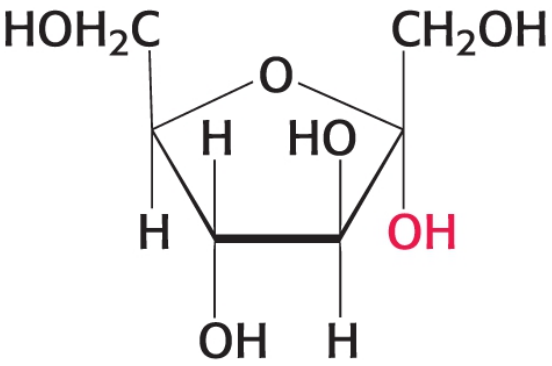
An equal symbol on the right of D-fructose shows the formation of a ring-like structure as follows: C 2 to C 5 atoms of the open-chain form fold to produce an open pentagonal ring-like structure. C 2 to C 5 atoms are located in a clockwise direction starting from the bottom right. The red highlighted O H group bonded to C 5 attacks C 2. C 6 is located above the open ring-like structure. C 1 is located above C 2, outside the ring-like structure.

A reversible reaction arrow is shown.

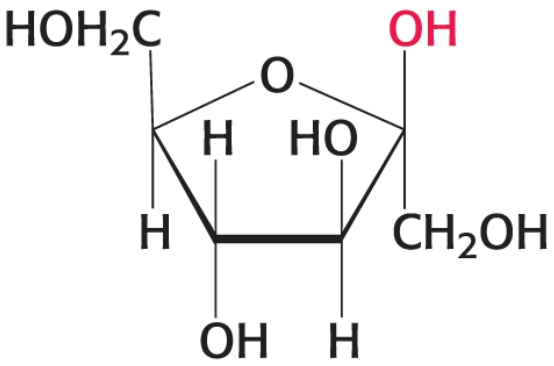
The structure of alpha D-Fructofuranose (a cyclic form of fructose) is as follows: A 5-membered heterocyclic pentagonal ring is in a vertical orientation and consists of 1 O and 4 C atoms. C 1 occupies the top right vertex. The O atom highlighted in red occupies the first position, which is the topmost vertex. C 1 is single bonded to C H 2 O H above and O H below. The O and H atoms of O H group are highlighted in blue and red respectively. C 2 is single bonded to O H above and H below. C 3 is single bonded to H above and O H below. C 4 is single bonded to C H 2 O H above and H below.

Return to Formation of alpha-D-Fructofuranose from D-Fructose

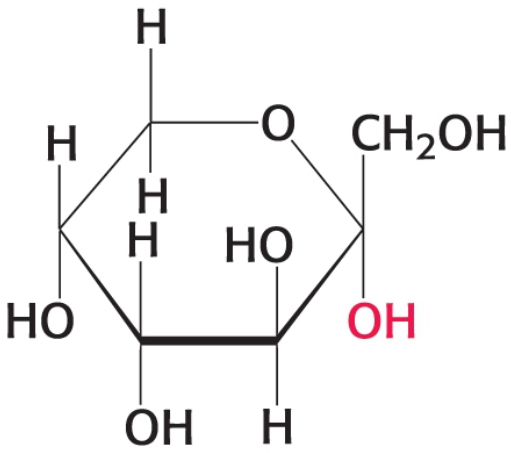
Extended description for Four distinct ring structures adopted by D-fructose in solution



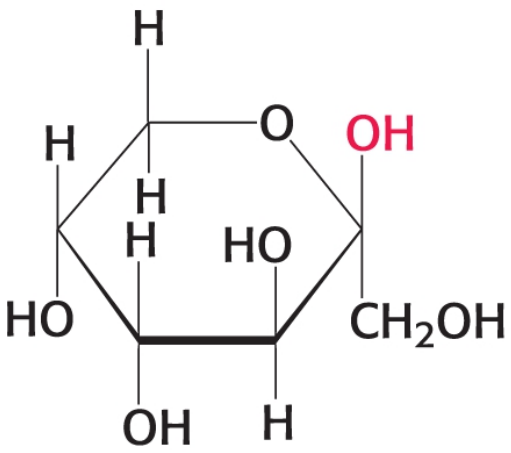
α-D-Fructofuranose



β-D-Fructofuranose



α-D-Fructopyranose



β-D-Fructopyranose

The four ring structures are alpha-D-Fructofuranose, beta-D-Fructofuranose, alpha-D-Fructopyranose, beta-D-Fructopyranose.

The structure of alpha-D-Fructofuranose is as follows: A 5-membered heterocyclic pentagonal ring is in a vertical orientation and consists of 1 O and 4 C atoms. The O atom occupies the first

position, which is the topmost vertex. C 1 is single bonded to C H 2 O H above and O H below. C 2 is single bonded to O H above and H below. C 3 is single bonded to H above and O H below. C 4 is single bonded to C H 2 O H above and H below.

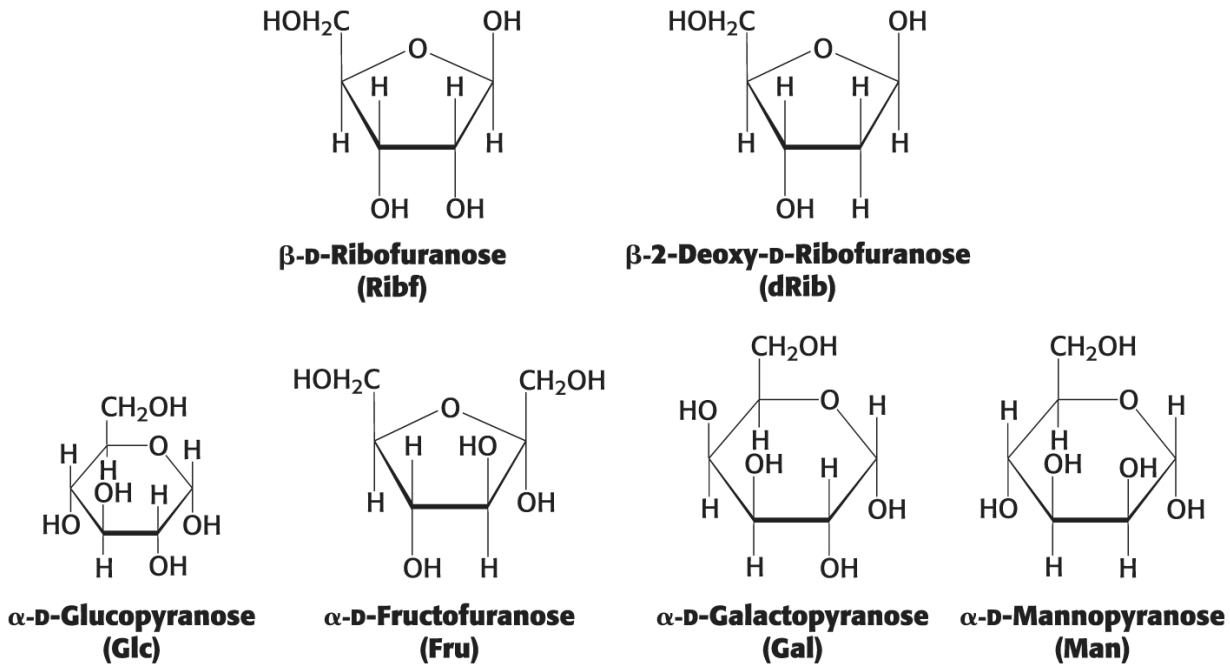
The structure of beta-D-Fructofuranose is as follows: A 5-membered heterocyclic pentagonal ring is in a vertical orientation and consists of 1 O and 4 C atoms. The O atom occupies the first position, which is the topmost vertex. C 1 is single bonded to O H above and C H 2 O H below. O H is highlighted in red. C 2 is single bonded to O H above and H below. C 3 is single bonded to H above and O H below. C 4 is single bonded to C H 2 O H above and H below.

The structure of alpha-D-Fructopyranose is as follows: A 6-membered heterocyclic hexagonal ring is in a horizontal orientation and consists of 1 O and 5 C atoms. The O atom occupies the first position, which is the top right vertex. C 1 is single bonded to C H 2 O H above and O H below. O H is highlighted in red. C 2 is single bonded to O H above and H below. C 3 and C 4 are each single bonded to H above and O H below. C 5 is single bonded to H above and H below.

The structure of beta-D-Fructopyranose is as follows: A 6-membered heterocyclic hexagonal ring is in a horizontal orientation and consists of 1 O and 5 C atoms. The O atom occupies the first position, which is the top right vertex. C 1 is single bonded to O H above and C H 2 O H below. O H is highlighted in red. C 2 is single bonded to O H above and H below. C 3 and C 4 are each single bonded to H above and O H below. C 5 is single bonded to H above and H below.

Return to Four distinct ring structures adopted by D-fructose in solution

Extended description for The ring structures of common monosaccharides



The structure of beta-D-Ribofuranose (R i b f) is as follows: A 5-membered heterocyclic pentagonal ring is in a vertical orientation and consists of 1 O and 4 C atoms. The O atom occupies the first position, which is the topmost vertex. C 1 is single bonded to O H above and H below. C 2 and C 3 are each single bonded to H above and O H below. C 4 is single bonded to C H 2 O H above and H below.

The structure of beta-2-Deoxy-D-Ribofuranose (d R i b) is as follows: A 5-membered heterocyclic pentagonal ring is in a vertical orientation and consists of 1 O and 4 C atoms. The O atom occupies the first position, which is the topmost vertex. C 1 is single bonded to O H above and H below. C 2 is single bonded to H above and H below. C 3 is single bonded to H above and O H below. C 4 is single bonded to C H 2 O H above and H below.

The structure of alpha-D-Glucopyranose (G l c) is as follows: A 6-membered heterocyclic hexagonal ring is in a horizontal orientation and consists of 1 O and 5 C atoms. The O atom occupies the first position, which is the top right vertex. C 1, C 2, and C 4 are each single bonded to H above and O H below. C 3 is single bonded to O H above and H below. C 5 is single bonded to C H 2 O H above and H below.

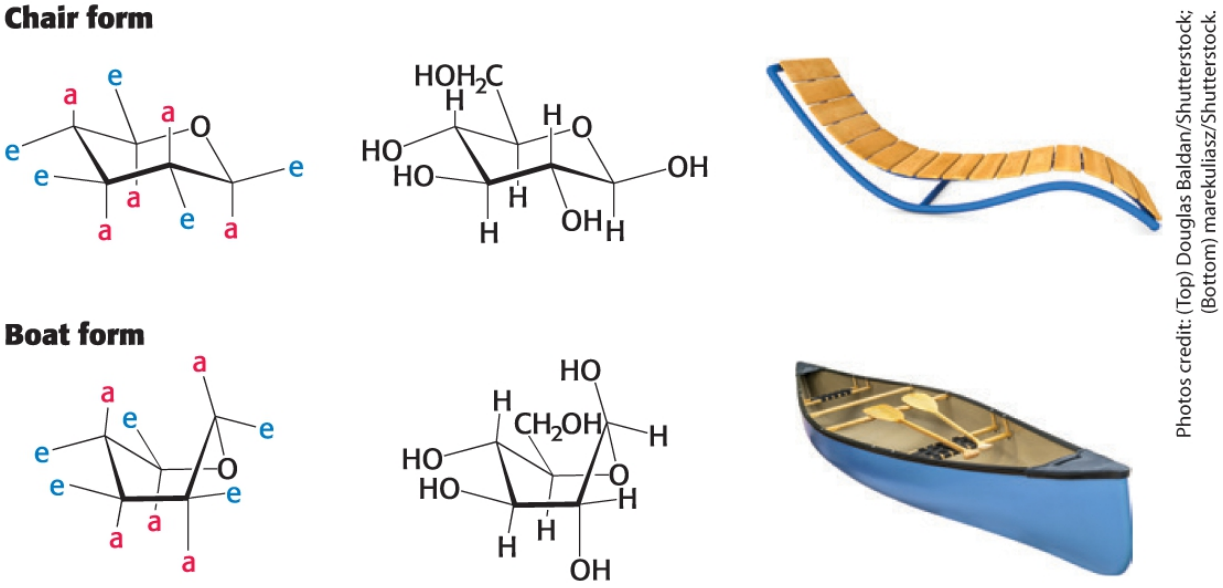
The structure of alpha-D-Fructofuranose (F r u) is as follows: A 5-membered heterocyclic pentagonal ring is in a vertical orientation and consists of 1 O and 4 C atoms. The O atom occupies the first position, which is the topmost vertex. C 1 is single bonded to C H 2 O H above and H below. C 2 is single bonded to O H above and H below. C 3 is single bonded to H above and O H below. C 4 is single bonded to C H 2 O H above and H below.

The structure of alpha-D-Galactopyranose (G a l) is as follows: A 6-membered heterocyclic hexagonal ring is in a horizontal orientation and consists of 1 O and 5 C atoms. The O atom occupies the first position, which is the top right vertex. C 1 and C 2 are each single bonded to H above and O H below. C 3 are C 4 are each single bonded to O H above and H below. C 5 is single bonded to C H 2 O H above and H below.

The structure of alpha-D-Mannopyranose (M a n) is as follows: A 6-membered heterocyclic hexagonal ring is in a horizontal orientation and consists of 1 O and 5 C atoms. The O atom occupies the first position, which is the top right vertex. C 1 and C 4 are each single bonded to H above and O H below. C 2 are C 3 are each single bonded to O H above and H below. C 5 is single bonded to C H 2 O H above and H below.

Return to The ring structures of common monosaccharides

Extended description for Structure of the chair and boat forms of beta-D-glucopyranose



Photos credit: (Top) Douglas Baldan/Shutterstock; (Bottom) marekuliasz/Shutterstock.

The chair form of beta-D-glucopyranose:

The structure of the first ring is as follows: A 6-membered heterocyclic ring is in a chair conformation and consists of 1 O and 5 C atoms. The O atom occupies the first position, which is the top right vertex. C 2 and C 5 are close to each other. C 4 occupies the top left vertex. C 1 is single bonded to e on the upper right and a below. C 2 is single bonded to a above and e on the lower right. C 3 is single bonded to e on the left and a below. C 4 is single bonded to e on the lower left and a above. C 5 is single bonded to e on the upper left and a below. a is highlighted in red and e is highlighted in blue.

The structure of the second ring is as follows: A 6-membered heterocyclic ring is in a chair conformation and consists of 1 O and 5 C atoms. The O atom occupies the first position, which is the top right vertex. C 2 and C 5 are close to each other. C 4 occupies the top

left vertex. C 1 is single bonded to O H on the upper right and H below. C 2 is single bonded to H above and O H on the lower right. C 3 is single bonded to O H on the left and H below. C 4 is single bonded to O H on the lower left and H above. C 5 is single bonded to C H 2 O H on the upper left and H below.

A photograph of a pool lounge chair is shown alongside the rings.

The boat form of beta-D-glucopyranose:

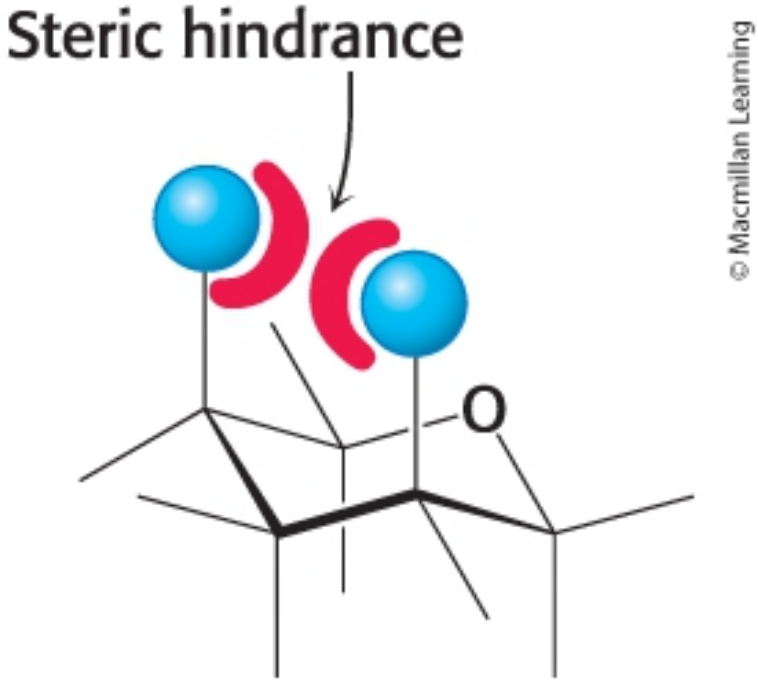
The structure of the first ring is as follows: A 6-membered heterocyclic hexagonal ring is in a boat conformation and consists of 1 O and 5 C atoms. The O atom occupies the first position, which is the top right vertex. C 2 and C 3 are close to each other. O and C 5 are located in the same plane. C 1, C 2, C 3, and C 4 are located in the same plane above the plane of O and C 5. C 1 is single bonded to e on the right and a above. C 2 is single bonded to a below and e on the right. C 3 is single bonded to a below and e on the upper left. C 4 is single bonded to a above and e on the right. C 5 is single bonded to e on the upper left and a below.

The structure of the second ring is as follows: A 6-membered heterocyclic hexagonal ring is in a boat conformation and consists of 1 O and 5 C atoms. The O atom occupies the first position, which is the top right vertex. C 2 and C 3 are close to each other. O and C 5 are located in the same plane. C 1, C 2, C 3, and C 4 are located in the same plane above the plane of O and C 5. C 1 is single bonded to O H above and H on the lower right. C 2 is single bonded to H on the right and O H below. C 3 is single bonded to O H on the upper left and H below. C 4 is single bonded to O H on the left and H above. C 5 is single bonded to C H 2 O H above and H on the lower right.

A photograph of a boat is shown alongside the rings.

Return to Structure of the chair and boat forms of beta-D-glucopyranose

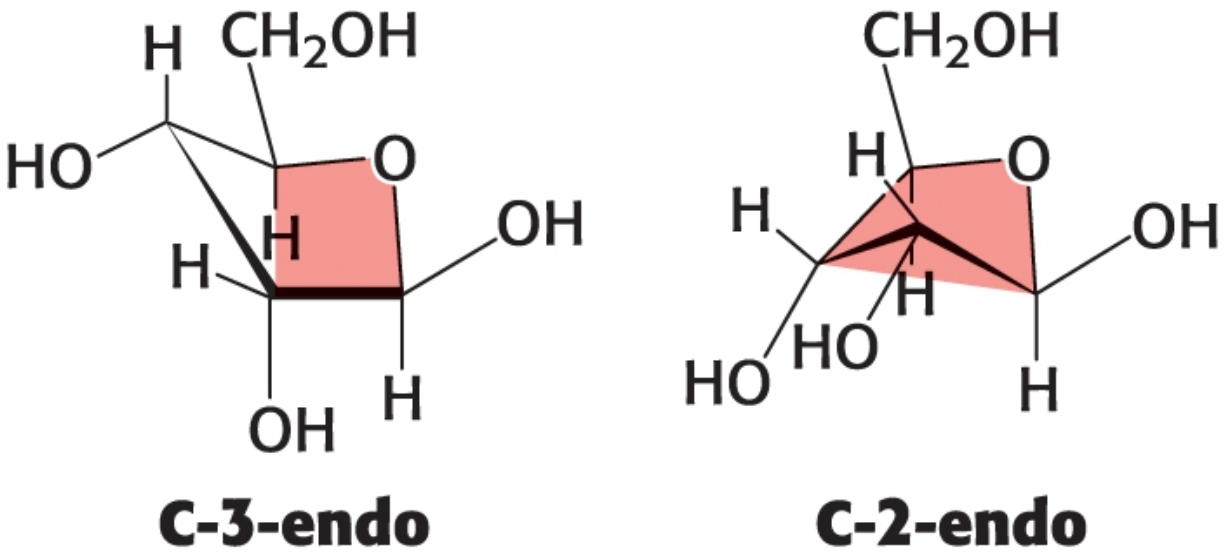
Extended description for Chair form of beta-D glucopyranose with steric hinderance



The structure of the chain form of beta-D glucopyranose is as follows: A 6-membered heterocyclic hexagonal ring is in a horizontal orientation with C 1 occupying the bottom right vertex. It consists of 1 O and 5 C atoms. O occupies the top right vertex. C 1 has an open single bond on the right and below. C 2 is single bonded to a blue sphere above and has an open single bond below. C 3 has an open single bond on the left and below. C 4 is single bonded to a blue sphere above and has an open single bond on the lower left. C 5 has an open single bond above and below. The blue spheres are located above the plane of the ring. A curved bean-shaped structure covers the sides of the blue spheres facing each other. A small gap is present between these curved structures and is labeled steric hindrance.

Return to Chair form of beta-D glucopyranose with steric hinderance

Extended description for Structures of C-3 endo and C-2 endo forms of a puckered furanose ring



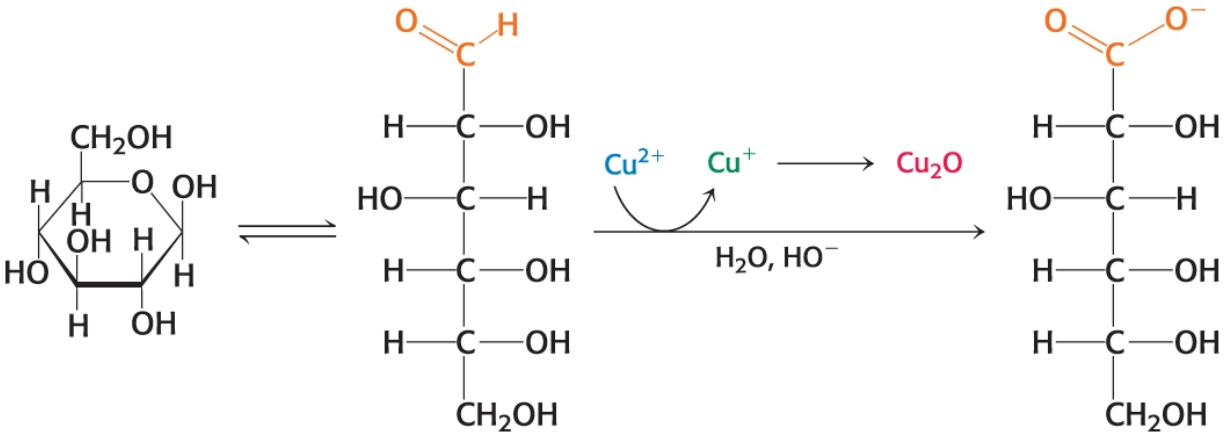
C-3 endo: The ring consists of 1 O and 4 C atoms. O is single bonded to C 1 below. C 1 is single bonded to C 2 on the left. C 2 is wedge bonded to C 3 on the upper left. C 3 is single bonded to C 4 on the lower right. C 4 is single bonded to O on the right. O, C 1, C 2, and C 4 are located in the same plane. C 3 is located above the plane. C 1 is single bonded to O H on the upper right and H below. C 2 is single bonded to H on the upper left and O H below. C 3 is single bonded to H above and O H on the lower left. C 4 is single bonded to C H 2 O H above and H below.

C-2 endo: The ring consists of 1 O and 4 C atoms. O is single bonded to C 1 below. C 1 is wedge bonded to C 2 on the upper left. C 2 is wedge bonded to C 3 on the lower left. C 3 is single bonded to C 4 on the upper right. C 4 is single bonded to O on the right. O, C 1, C 3, and C 4 are located in the same plane. C 2 is located above the plane of the ring. C 1 is single bonded to O H on the upper right and H below. C 2 is single bonded to H on the upper left and O H on the

lower left. C 3 is single bonded to H on the upper left and O H on the lower left. C 4 is single bonded to C H 2 O H above and H below.

Return to Structures of C-3 endo and C-2 endo forms of a puckered furanose ring

Extended description for Oxidation of glucose



The ring form of glucose is reversibly converted into open-chain form. The structure of the ring form of glucose is as follows: A 6-membered heterocyclic hexagonal ring is in a horizontal orientation and consists of 1 O and 5 C atoms. The O atom occupies the first position, which is the top right vertex. C 1 and C 3 are each single bonded to O H above and H below. C 2 and C 4 are each single bonded to H above and O H below. C 5 is single bonded to C H 2 O H above and H below.

The structure of the open-chain form is as follows: The Fischer projection consists of a vertical line with C above and C H 2 O H below. The projection contains four C atoms placed one below the other on the vertical line. The C atoms are numbered from top to bottom. C 1 is double bonded to O on the upper left and single bonded to H on the upper right. C 2, C 4, and C 5 are each single bonded to H on the left and O H on the right. C 3 is single bonded to O H on the left and H on the right.

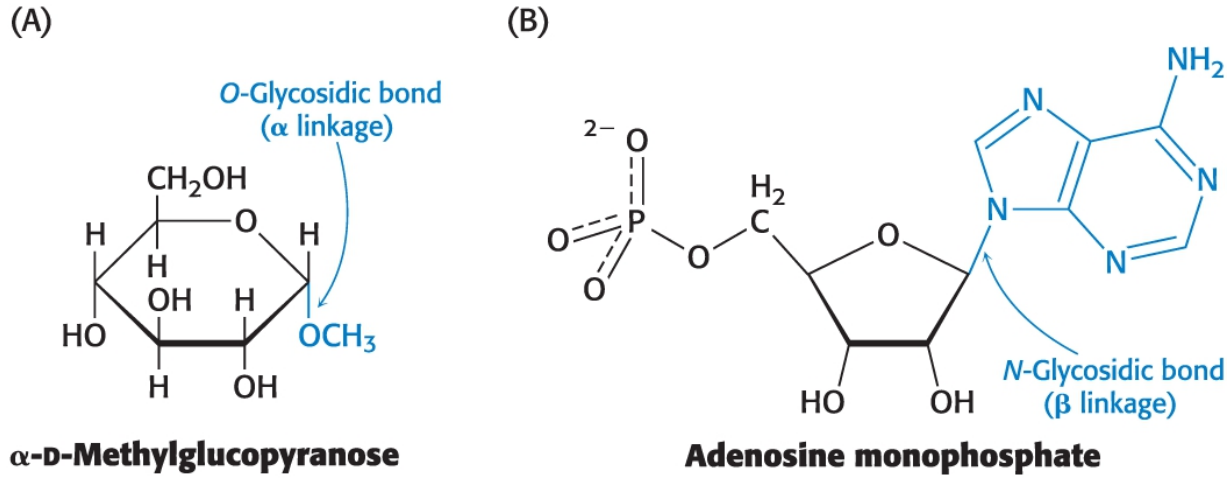
A forward reaction arrow is labeled H 2 O, H O superscript minus below. C u superscript 2 plus ion highlighted in blue enters the

reaction and C u superscript plus highlighted in green leaves the reaction. C u superscript plus is later converted into C u 2 O.

The structure of the oxidized product is as follows: The Fischer projection consists of a vertical line with C above and C H 2 O H below. The projection contains four C atoms placed one below the other on the vertical line. The C atoms are numbered from top to bottom. C 1 is double bonded to O on the upper left and single bonded to O superscript minus on the upper right. C 2, C 4, and C 5 are each single bonded to H on the left and O H on the right. C 3 is single bonded to O H on the left and H on the right.

Return to Oxidation of glucose

Extended description for Chemical structures of alpha-D-Methylglucopyranose and adenosine monophosphate



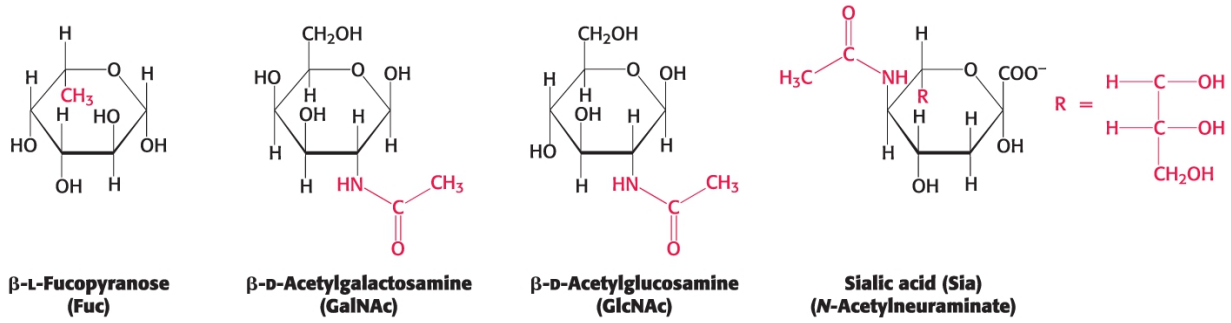
(A) The structure of alpha-D-Methylglucopyranose is as follows: A 6-membered heterocyclic hexagonal ring is in a horizontal orientation and consists of 1 O and 5 C atoms. The O atom occupies the first position, which is the top right vertex. C 1 is single bonded to H above and O C H 3 below. The single bond between C 1 and O C H 3 is labeled O-Glycosidic bond (alpha linkage). C 2 and C 4 are each single bonded to H above and O H below. C 3 is single bonded to O H above and H below. C 5 is single bonded to C H 2 O H above and H below.

(B) The structure of adenosine monophosphate is as follows: A 5-membered heterocyclic pentagonal ring is in a vertical orientation and consists of 1 O and 4 C atoms. The O atom occupies the first position, which is the topmost vertex. C 1 is single bonded to N 1 of a 5-membered pentagonal ring in a horizontal orientation on the top right. The single bond between C 1 and N 1 is labeled the N-glycosidic bond (beta linkage). C 2 and C 3 are single bonded to O H

below. C 4 is single bonded to C H 2, single bond, O, single bond, P on the top left. The P atom is partially double bonded to O above, O on the left, and O on the lower left. The 5-membered pentagonal ring on the top right has two N atoms. First N occupies the first position, which is the bottom left vertex. Second N occupies the third position, which is the topmost vertex. A double bond is present between C 1 and N 2 and C 2 and C 3. This ring is fused to a 6-membered heterocyclic hexagonal ring in a vertical orientation such that C 2 and C 3 of the pentagonal ring are C 3 and C 2 respectively of the hexagonal ring. The hexagonal ring consists of 2 N and 4 C atoms. C 1 occupies the bottom right vertex. First N occupies the top right vertex. Second N occupies the bottom-most vertex. C 4 is single bonded to N H 2 above. A double bond is present between C 1 and N 2 and C 4 and N 1.

Return to Chemical structures of alpha-D-Methylglucopyranose and adenosine monophosphate

Extended description for Chemical structures of beta-L-Fucopyranose, beta-D-Acetylgalactosamine, beta-D-Acetylglucosamine, and sialic acid



The structure of beta-L-Fucopyranose (F u c) is as follows: A 6-membered heterocyclic hexagonal ring is in a horizontal orientation and consists of 1 O and 5 C atoms. The O atom occupies the first position, which is the top right vertex. C 1, C 3, and C 4 are each single bonded to H above and O H below. C 2 is single bonded to O H above and H below. C 5 is single bonded to H above and C H 3 below.

The structure of beta-D-Acetylgalactosamine (G a l N A c) is as follows: A 6-membered heterocyclic hexagonal ring is in a horizontal orientation and consists of 1 O and 5 C atoms. The O atom occupies the first position, which is the top right vertex. C 1, C 3, and C 4 are each single bonded to O H above and H below. C 2 is single bonded to H above and N H below. C 5 is single bonded to C H 2 O H above and H below. The N H bonded to C 2 is single bonded to C on the lower right. This C is single bonded to C H 3 on the upper right and double bonded to O below.

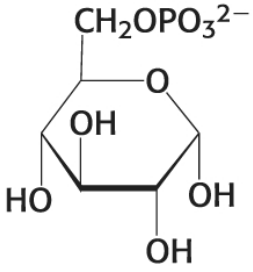
The structure of beta-D-Acetylglycosamine (G l c N A c) is as follows: A 6-membered heterocyclic hexagonal ring is in a horizontal orientation and consists of 1 O and 5 C atoms. The O atom occupies

the first position, which is the top right vertex. C 1 and C 3 are each single bonded to O H above and H below. C 2 is single bonded to H above and N H below. C 4 is single bonded to H above and O H below. C 5 is single bonded to C H 2 O H above and H below. The N H group bonded to C 2 is single bonded to C on the lower right. This C is single bonded to C H 3 on the upper right and double bonded to O below.

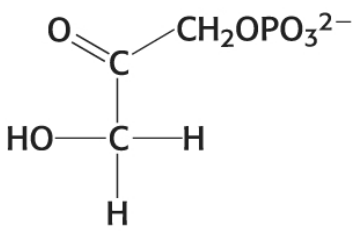
The structure of sialic acid (S i a) (N-Acetylneuraminate) is as follows: A 6-membered heterocyclic hexagonal ring is in a horizontal orientation and consists of 1 O and 5 C atoms. The O atom occupies the first position, which is the top right vertex. C 1 is single bonded to C O O minus above and O H below. C 2 is single bonded to H above and H below. C 3 is single bonded to H above and O H below. C 4 is single bonded to N H above and H below. C 5 is single bonded to H above and R below. N H bonded to C 4 is single bonded to C on the top left. This C is single bonded to C H 3 on the bottom left and double bonded to O above. On the right, the structure of R is depicted. The structure of R is as follows: C, single bond, C, single bond, C H 2 O H. C 1 and C 2 are single bonded to H on the left and O H right.

Return to Chemical structures of beta-L-Fucopyranose, beta-D-Acetylgalactosamine, beta-D-Acetylglucosamine, and sialic acid

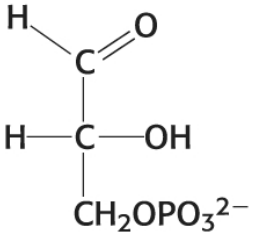
Extended description for Chemical structures of glucose 6-phosphate (G-6 P), dihydroxyacetone phosphate (D H A P), glyceraldehyde 3-phosphate (G A P)



Glucose 6-phosphate (G-6P)



Dihydroxyacetone phosphate (DHAP)



Glyceraldehyde 3-phosphate (GAP)

The structure of glucose 6-phosphate is as follows: A 6-membered heterocyclic hexagonal ring is in a horizontal orientation and consists of 1 O and 5 C atoms. The O atom occupies the first position, which is the top right vertex. C 1, C 2, and C 4 are each single bonded to O H below. C 3 is single bonded to O H above. C 5 is single bonded to C H 2 O P O 3 superscript 2 minus above.

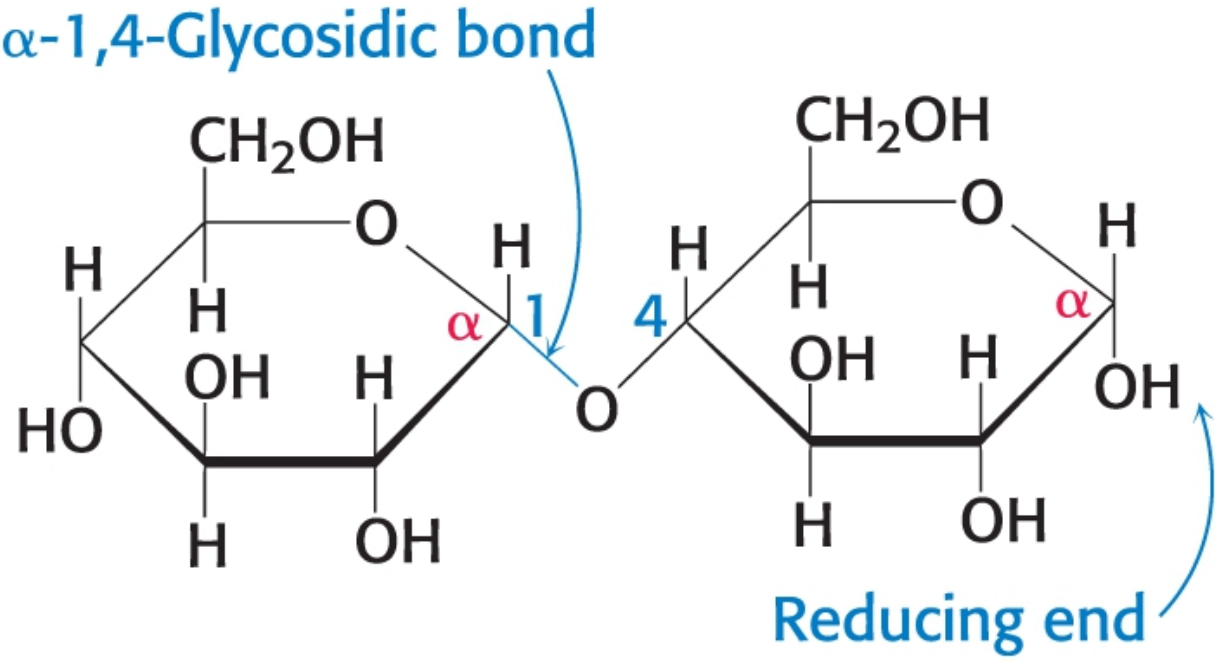
The structure of dihydroxyacetone phosphate is as follows: A central carbon atom is single-bonded to O H on the left, H on the right, H below, and C above. The C atom above is double bonded to O on the upper left and single bonded to C H 2 O P O 3 superscript 2 minus on the upper right.

The structure of glyceraldehyde 3-phosphate is as follows: A central carbon atom is single bonded to C H 2 O P O 3 superscript 2 minus below, O H on the right, H on the left, and C above. The C atom

above is double bonded to O on the upper right and single bonded to H on the upper left.

Return to Chemical structures of glucose 6-phosphate (G-6 P), dihydroxyacetone phosphate (D H A P), glyceraldehyde 3-phosphate (G A P)

Extended description for Chemical structure of maltose



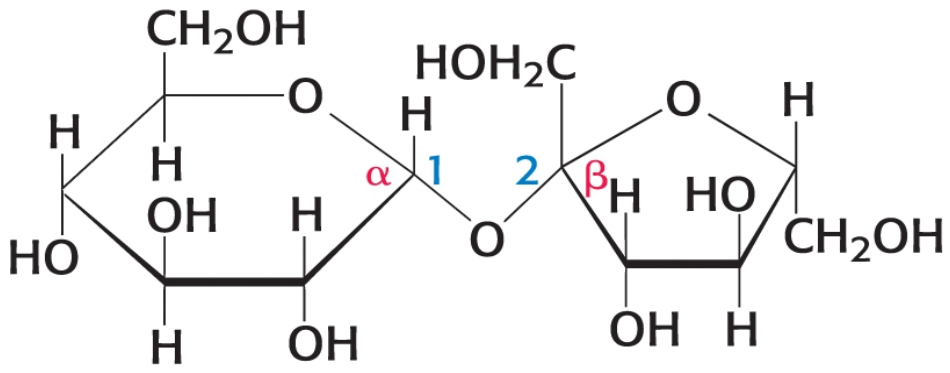
The structure of maltose is as follows: A 6-membered heterocyclic hexagonal ring is in a horizontal orientation and consists of 1 O and 5 C atoms. The O atom occupies the first position, which is the top right vertex. C 1 is single bonded to H above. C 2 and C 4 are each single bonded to H above. C 3 is single bonded to O H above and H below. C 5 is single bonded to C H 2 O H above and H below. C 1 labeled alpha is single bonded to O below and the bond is labeled alpha 1, 4-Glycosidic bond. O is single bonded to C 4 of a 6-membered heterocyclic ring in a horizontal orientation consisting of 1 O and 5 C atoms. The O atom occupies the first position, which is the top right vertex. C 1 and C 2 are each single bonded to H above and O H below. C 1 is labeled alpha. C 3 is single bonded to O H above and H below. C 4 is single bonded to H above. C 5 is single bonded to C H 2 O H above and H below. C 1 end of this ring is

labeled reducing end. The single bond between C 1 and O is labeled 1. The single bond between C 4 and O is labeled 4.

Return to Chemical structure of maltose

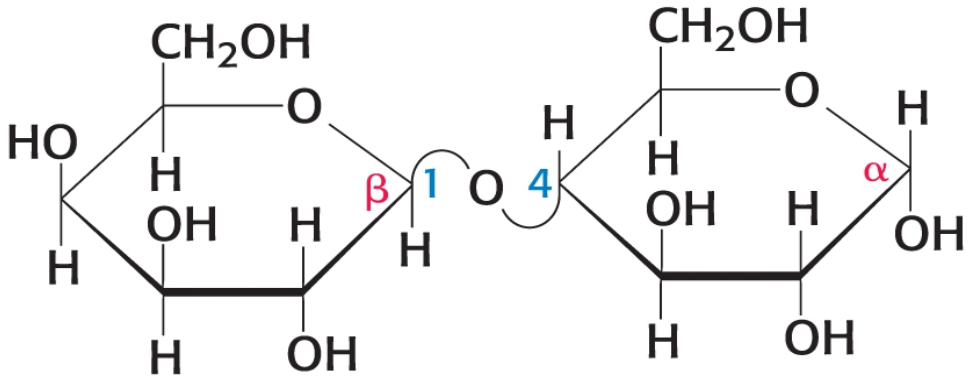
Extended description for Chemical structures of

sucrose, alpha-Lactose, and alpha-maltose



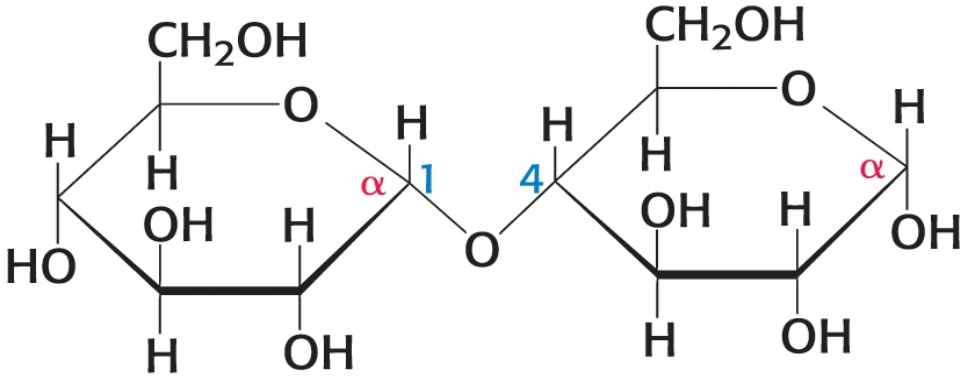
Sucrose

(α-D-Glucopyranosyl-(1→2)-β-D-Fructofuranose)



α-Lactose

(β-D-Galactopyranosyl-(1→4)-α-D-Glucopyranose)



α-Maltose

(α-D-Glucopyranosyl-(1→4)-α-D-Glucopyranose)

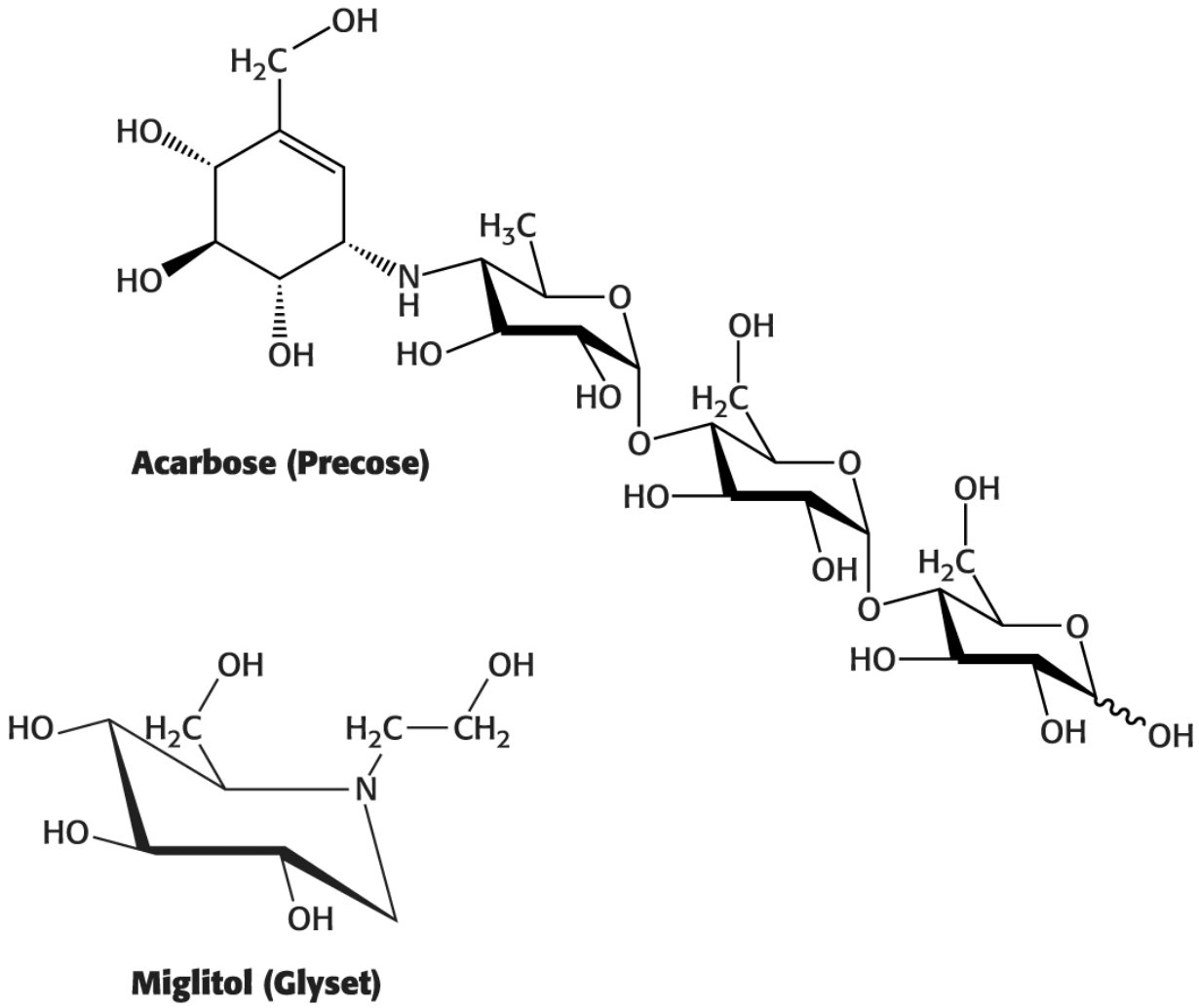
The structure of sucrose (alpha-D-Glucopyranosyl-(1 to 2)-beta-D-Fructofuranose) is as follows: A 6-membered heterocyclic hexagonal ring is in a horizontal orientation and consists of 1 O and 5 C atoms. The O atom occupies the first position, which is the top right vertex. C 1 is single bonded to H above and labeled alpha. C 2 and C 4 are each single bonded to H above and O H below. C 3 is single bonded to O H above and H below. C 5 is single bonded to C H 2 O H above and H below. C 1 is single bonded to O on the lower right. This O is single bonded to C 4 of a 5-membered heterocyclic pentagonal ring in a vertical orientation consisting of 1 O and 4 C atoms. The O atom occupies the first position, which is the topmost vertex. C 1 is single bonded to H above and C H 2 O H below. C 2 is single bonded to O H above and H below. C 3 is single bonded to H above and O H below. C 4 is single bonded to C H 2 O H above and labeled beta. The single bond between C 1 and O is labeled 1. The single bond between C 4 and O is labeled 2.

The structure of alpha-Lactose (beta-D-Galactopyranosyl-(1 to 4)-alpha-Glucopyranose is as follows: A 6-membered heterocyclic hexagonal ring is in a horizontal orientation and consists of 1 O and 5 C atoms. The O atom occupies the first position, which is the top right vertex. C 1 is single bonded to H below and labeled beta. C 2 is single bonded to H above and O H below. C 3 and C 4 are each single bonded to O H above and H below. C 5 is single bonded to C H 2 O H above and H below. C 1 is single bonded to O on the right. This O is single bonded to C 4 of a 6-membered heterocyclic hexagonal ring in a horizontal orientation consisting of 1 O and 5 C atoms. The O atom occupies the first position, which is the top right vertex. C 1 and C 2 are each single bonded to H above and O H below. C 1 is labeled alpha. C 3 is single bonded to O H above and H below. C 5 is single bonded to C H 2 O H above and H below. C 4 is single bonded to H above. The single bond between C 1 and O is labeled 1. The single bond between C 4 and O is labeled 4.

The structure of alpha-Maltose (D-Glucopyranosyl-(1 to 4)-alpha-D-Glucopyranose is as follows: A 6-membered heterocyclic hexagonal ring is in a horizontal orientation and consists of 1 O and 5 C atoms. The O atom occupies the first position, which is the top right vertex. C 1 labeled alpha is single bonded to H above. C 2 and C 4 are each single bonded to H above and O H below. C 3 is single bonded to O H above and H below. C 5 is single bonded to C H 2 O H above and H below. C 1 is single bonded to O below. This O is single bonded to C 4 of a 6-membered heterocyclic ring in a horizontal orientation consisting of 1 O and 5 C atoms. The O atom occupies the first position, which is the top right vertex. C 1 and C 2 are each single bonded to H above and O H below. C 1 is labeled alpha. C 3 is single bonded to O H above and H below. C 4 is single bonded to H above. C 5 is single bonded to C H 2 O H above and H below. The single bond between C 1 and O is labeled 1. The single bond between C 4 and O is labeled 4.

Return to Chemical structures of sucrose, alpha-Lactose, and alpha-maltose

Extended description for Chemical structures of acarbose (Precose) and miglitol (Glyset)



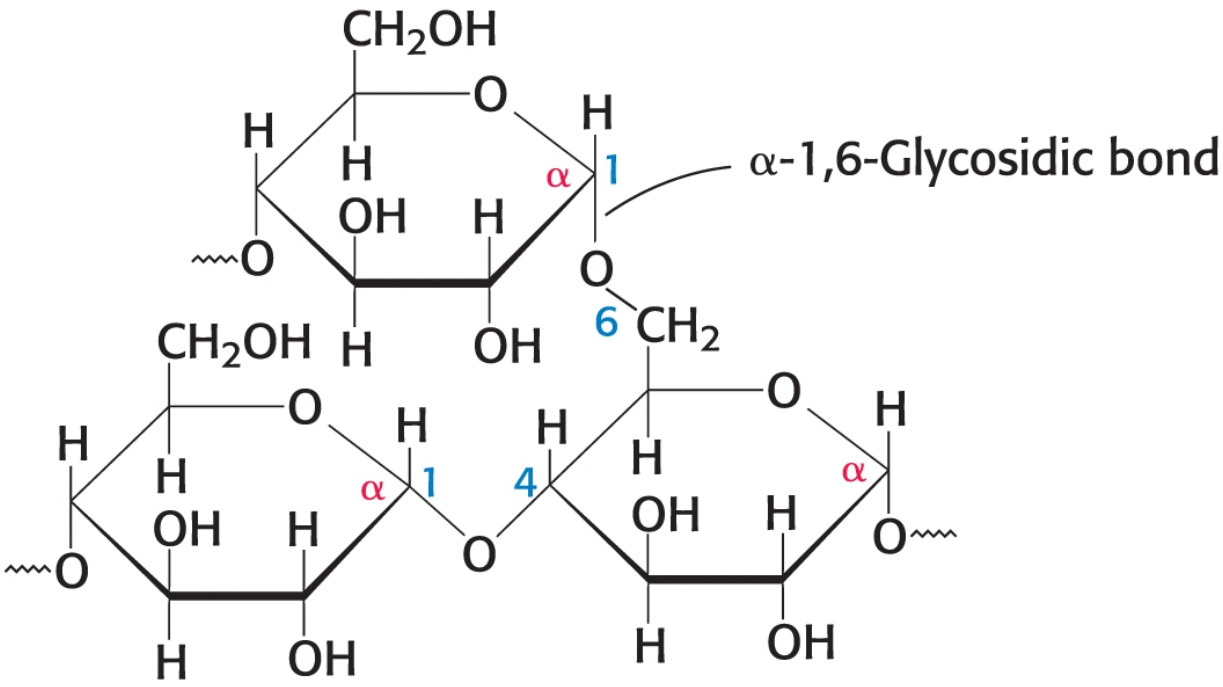
The structure acarbose (Precose) is as follows: A 6-carbon homocyclic ring in a vertical orientation has C 1 on the topmost vertex. A double bond is present between C 1 and C 2. C 1 is single bonded to C H 2 above and this C H 2 is single bonded to O H on the upper right. C 4 and C 6 are each dash bonded to O H. C 5 is wedge bonded to O H on the lower left. C 3 is dash bonded to N H on the bottom right. This N H is single bonded to C 4 of the first 6-

membered heterocyclic ring in a chair conformation that consists of 1 O and 5 C atoms. The O atom occupies the first position, which is the top right vertex. C 1 occupies the bottom right vertex. C 2 and C 5 are close to each other. C 4 occupies the top left vertex. C 1 is single bonded to O below. C 2 is single bonded to O H on the lower right. C 3 is single bonded to O H on the lower left. C 5 is single bonded to C H 3 on the upper left. The O atom bonded to C 1 is single bonded to the C 4 atom of a second 6-membered heterocyclic ring in a chair conformation that consists of 1 O and 5 C atoms. The O atom occupies the first position, which is the top right vertex. C 1 occupies the bottom-right vertex. C 2 and C 5 are close to each other. C 4 occupies the top left vertex. C 1 is single bonded to O below. C 2 is single bonded to O H on the lower right. C 3 is single bonded to O H on the left. C 5 is single bonded to C H 2 above and this C H 2 is single bonded to O H above. The O atom bonded to C 1 is single bonded to C 4 of a third 6-membered heterocyclic ring in a chair conformation that consists of 1 O and 5 C atoms. The O atom occupies the first position, which is the top right vertex. C 2 and C 5 are close to each other. C 4 occupies the top left vertex. C 1 is single bonded to O H on the lower right. C 2 is single bonded to O H on the lower right. C 3 is single bonded to O H on the left. C 5 is single bonded to C H 2 above and this C H 2 is single bonded to O H above.

The structure miglitol (Glyset) is as follows: A 6-membered heterocyclic hexagonal ring is in a chair conformation and consists of 1 N and 5 C atoms. The N atom occupies the first position, which is the top right vertex. C 1 occupies the bottom right vertex. N is single bonded to C H 2 on the upper right. This C H 2 is single bonded to another C H 2 on the right. This C H 2 is single bonded to O H on the upper right. C 2 and C 5 are close to each other. C 4 occupies the top left vertex. C 2 is single bonded to O H below. C 3 and C 4 are single bonded to O H on the left. C 5 is single bonded to C H 2 above and this C H 2 is single bonded to O H on the upper right.

Return to Chemical structures of acarbose (Precose) and miglitol (Glyset)

Extended description for Chemical structure of glycogen



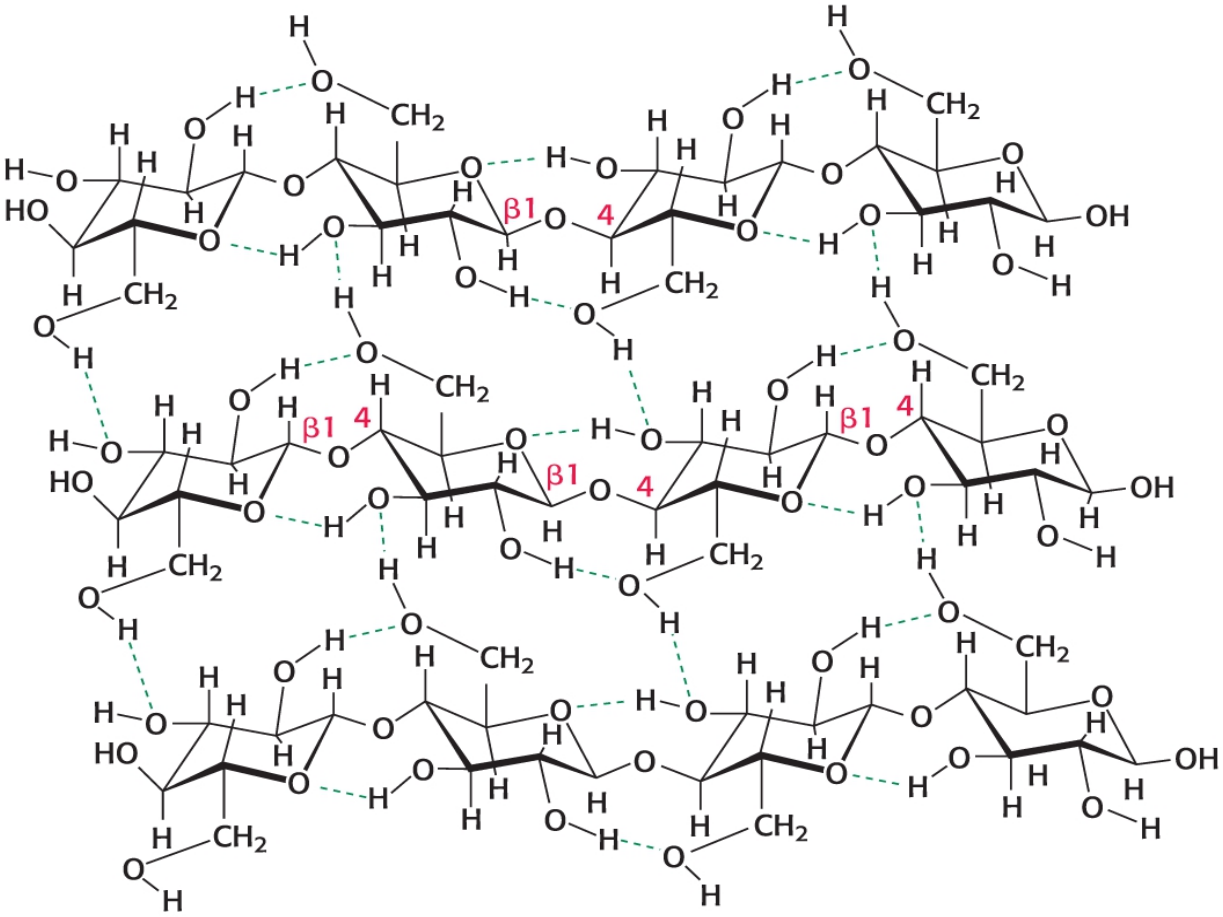
The structure of glycogen is as follows: A 6-membered heterocyclic hexagonal ring is in a horizontal orientation and consists of 1 O and 5 C atoms. The O atom occupies the first position, which is the top right vertex. C 1 is single bonded to H above. C 2 is single bonded to H above and O H below. C 3 is single bonded to O H above and H below. C 4 is single bonded to H above and O below. This O has an open single bond on the left. C 5 is single bonded to C H 2 O H above and H below. C 1 is single bonded to O below. This O is single bonded to C 4 of a 6-membered heterocyclic hexagonal ring in a horizontal orientation consisting of 1 O and 5 C atoms. The O atom occupies the first position, which is the top right vertex. C 1 is single bonded to H above and O below. This O has an open single bond on the right. C 2 is single bonded to H above and O H below. C 3 is single bonded to O H above and H. C 4 is single bonded to H above.

C 5 is single bonded to C H 2 above and H below. C H 2 is single bonded to O on the upper left. This O is single bonded to C 1 of another 6-membered heterocyclic hexagonal ring in a horizontal orientation consisting of 1 O and 5 C atoms. The single bond between O and C 1 is labeled alpha 1, 6-Glycosidic bond. The O atom occupies the first position which is the top right vertex. C 1 is single bonded to H above. C 2 is single bonded to H above and O H below. C 3 is single bonded to O H above and H below. C 4 is single bonded to H above and O below. This O has an open single bond on the left. C 5 is single bonded to C H 2 O H above and H below.

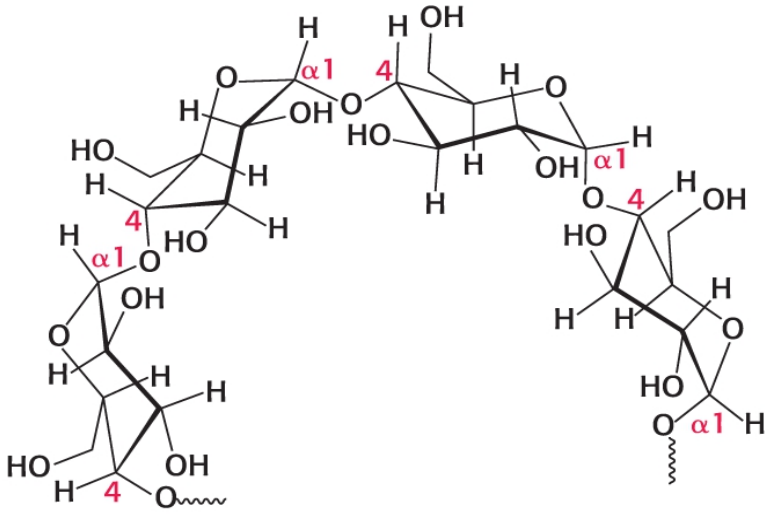
Return to Chemical structure of glycogen

Extended description for Straight chain of cellulose

and bent structure of starch and glycogen



Cellulose
(β-1,4 linkages)



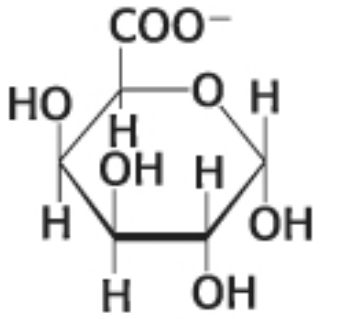
Starch and glycogen
(α-1,4 linkages)

Cellulose (beta-1, 4 linkages): Three straight chains of glucose molecules in a chair conformation connected by beta 1 to 4 glycosidic bonds are shown. The O atom of glucose residues in each chain alternatively occupies the bottom right and top right vertices. In the beta 1 to 4 glycosidic bond, C 1 and C 4 of adjacent glucose residues are single-bonded to a common O atom. The O atom is located above the plane of C 1 and C 4 atoms. Hydrogen bonds are present between O and H atoms of adjacent glucose residues within the same chain and between the adjacent chains. They are depicted as dashed lines.

Starch and glycogen (alpha-1, 4 linkages): A downward curved chain composed of glucose molecules in a chair conformation is shown. The O atom of each glucose residue occupies the top right vertex. The adjacent glucose residues are connected by alpha-1, 4 glycosidic bonds. In this bond, C 1 and C 4 of adjacent glucose residues are single-bonded to a common O atom. The O atom is located below the plane of C 1 and C 4 atoms.

Return to Straight chain of cellulose and bent structure of starch and glycogen

Extended description for Chemical structure of galacturonic acid

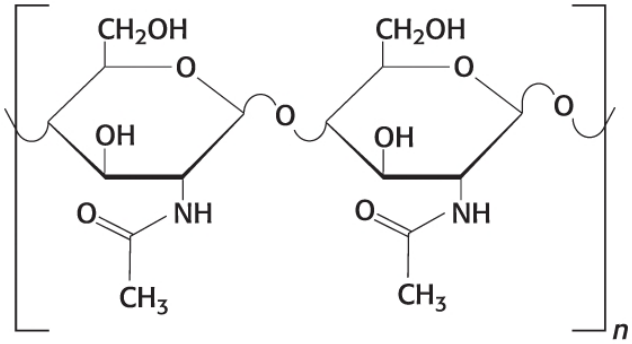


Galacturonic acid

The structure is as follows: A 6-membered heterocyclic hexagonal ring is in a horizontal orientation and consists of 1 O and 5 C atoms. The O atom occupies the first position, which is the top right vertex. The ring is in a plane perpendicular to the plane of the paper such that C 5 and O are away from the observer and C 2 and C 3 are toward the observer. C 1 and C 2 are each single bonded to H above and O H below. C 3 and C 4 are each single bonded to O H above and H below. C 5 is single bonded to C O O superscript minus above and H below.

Return to Chemical structure of galacturonic acid

Extended description for Chemical structure of chitin repeating unit





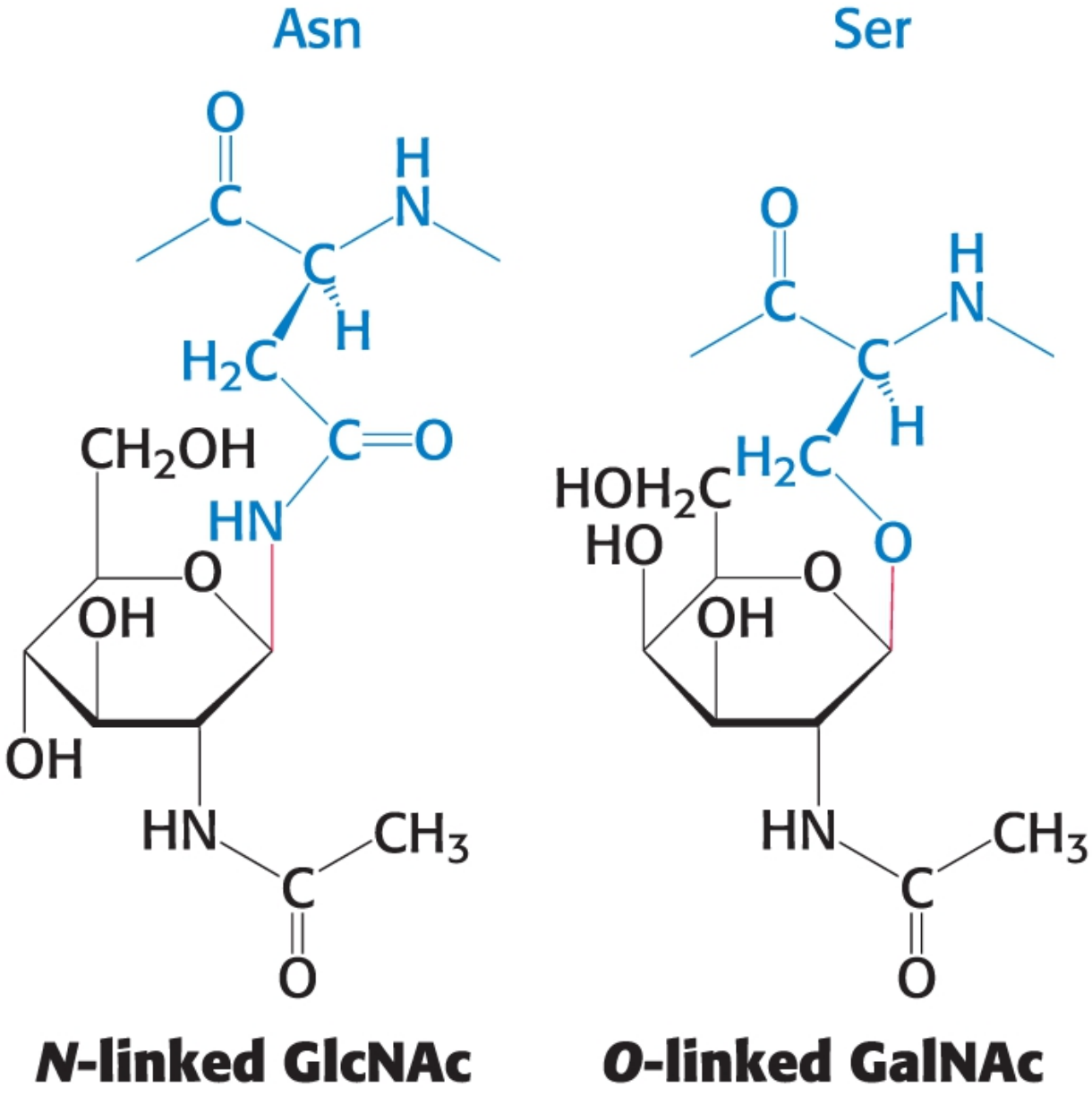
Charles Curtis/Shutterstock

The structure of the repeating unit is as follows: A 6-membered heterocyclic hexagonal ring is in a horizontal orientation and consists of 1 O and 5 C atoms. The O atom occupies the first position, which is the top right vertex. C 2 is single bonded to N H below. This N H is single bonded to C on the lower left. This C is double bonded to O on the upper left and single bonded to C H 3 below. C 3 is single bonded to O H above. C 5 is single bonded to C H 2 O H above. C 4 has an open single bond on the left. C 1 is single bonded to O on the right which is further single bonded to C 4 of a 6-membered heterocyclic hexagonal ring in a horizontal orientation consisting of 1 O and 5 C atoms. The O atom occupies the first position, which is the topmost vertex. C 1 is single bonded to O on the right. This O has an open single bond on the right. C 2 is single bonded to N H below. This N H is single bonded to C on the lower left. This C is double bonded to O on the upper left and single bonded to C H 3 below. C 3 is single bonded to O H above. C 5 is

single bonded to C H 2 O H above. The repeating unit is enclosed within brackets with subscript n.

Return to Chemical structure of chitin repeating unit

Extended description for Chemical structures of N-linked G l c N A c and O-linked G a l N A c



The structure of N-linked G l c N A c is as follows: A 6-membered heterocyclic hexagonal ring is in a horizontal orientation and consists of 1 O and 5 C atoms. The O atom occupies the first position, which is the top right vertex. C 1 is single bonded to N H on

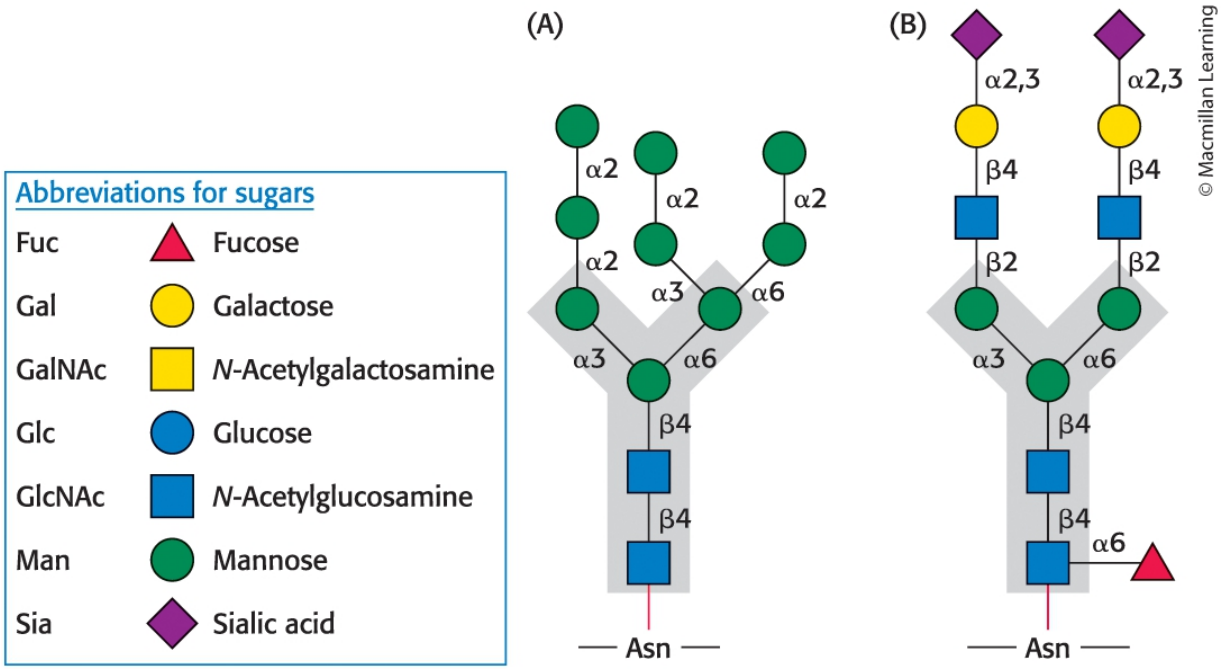
the top. C 2 is single bonded to N H below. C 3 is single bonded to O H above. C 4 is single bonded to O H below. C 5 is single bonded to C H 2 O H above. N H bonded to C 1 is further single bonded to C on the upper right. This C is double bonded to O on the right and single bonded to C H 2 on the upper left. C H 2 is wedge bonded to C on the upper right. This C is dash bonded to H on the lower right, single bonded to N H on the upper right, and single bonded to C on the upper left. This C is double bonded to O on the top and has an open single bond on the lower left. N H has an open single bond on the lower right. This group connected to C 1 of the ring through N H is labeled A s n.

N H bonded to C 2 is further single bonded to C on the lower right. This C is single bonded to C H 3 on the upper right and double bonded to O below.

The structure of O-linked G a l N A c is as follows: A 6-membered heterocyclic hexagonal ring is in a horizontal orientation and consists of 1 O and 5 C atoms. The O atom occupies the first position, which is the top right vertex. C 1 is single bonded to O on the top. C 2 is single bonded to N H below. C 3 and C 4 are each single bonded to O H above. C 5 is single bonded to C H 2 O H above. O bonded to C 1 is further single bonded to C H 2 on the upper left. This C H 2 is wedge bonded to C on the upper right. This C atom is single bonded to N H on the upper right, single bonded to C on the upper left, and dash bonded to H on the lower right. The C atom on the upper left is double bonded to O on the top and has an open single bond on the lower left. N H has an open single bond on the lower right. This group connected to C 1 of the ring through O is labeled S e r. The N H group bonded to C 2 is further single bonded to C on the lower right. This C is single bonded to C H 3 on the upper right and double bonded to O below.

Return to Chemical structures of N-linked G l c N A c and O-linked G a l N A c

Extended description for Schematic illustrations of N-linked oligosaccharides



(A) The structure of the first N-linked oligosaccharide from bottom to top is as follows: A s n, single bond, blue square, single bond labeled beta 4, blue square, single bond labeled beta 4, green circle. A s n has an open single bond on the left and right. The green circle is single bonded to a green circle on the upper left and upper right. The single bond on the upper left and upper right are labeled alpha 3 and alpha 6 respectively. The green circle on the upper left is single bonded to a green circle above. The single bond is labeled alpha. The green circle above is further single bonded to a green circle. The single bond is labeled alpha 2.

The green circle on the upper right is single bonded to a green circle on the upper left and upper right. The single bond on the upper left and upper right are labeled alpha 3 and alpha 6 respectively. Each of

the green circles is single bonded to a green circle above. The single bond is labeled alpha 2.

A grey-colored Y-shape covers the blue squares and the three green circles from bottom to top.

(b) The structure of the second N-linked oligosaccharide from bottom to top is as follows: A s n, single bond, blue square, single bond labeled beta 4, blue square, single bond labeled beta 4, green circle. A s n has an open single bond on the left and right. The first blue square is single bonded to a red triangle on the right. The single bond is labeled alpha 6. The green circle is single bonded to a green circle on the upper left and upper right. The single bond on the upper left and upper right are labeled alpha 3 and alpha 6 respectively. Each of these green circles is single bonded above to blue square, single bond, yellow circle, single bond, purple rhombus. The single bond between the green circle and blue square is labeled beta 2. The single bond between blue square and yellow circle is labeled beta 4. The single bond between the yellow circle and purple rhombus is labeled alpha 2, 3.

A grey-colored Y-shape covers the blue squares and the three green circles from bottom to top.

The chart for abbreviations for sugars on the left is as follows:

F u c - Red triangle - Fucose

G a l - Yellow circle - Galactose

G a l N A c - Yellow square - N-Acetylgalactosamine

G l c - Blue circle - Glucose

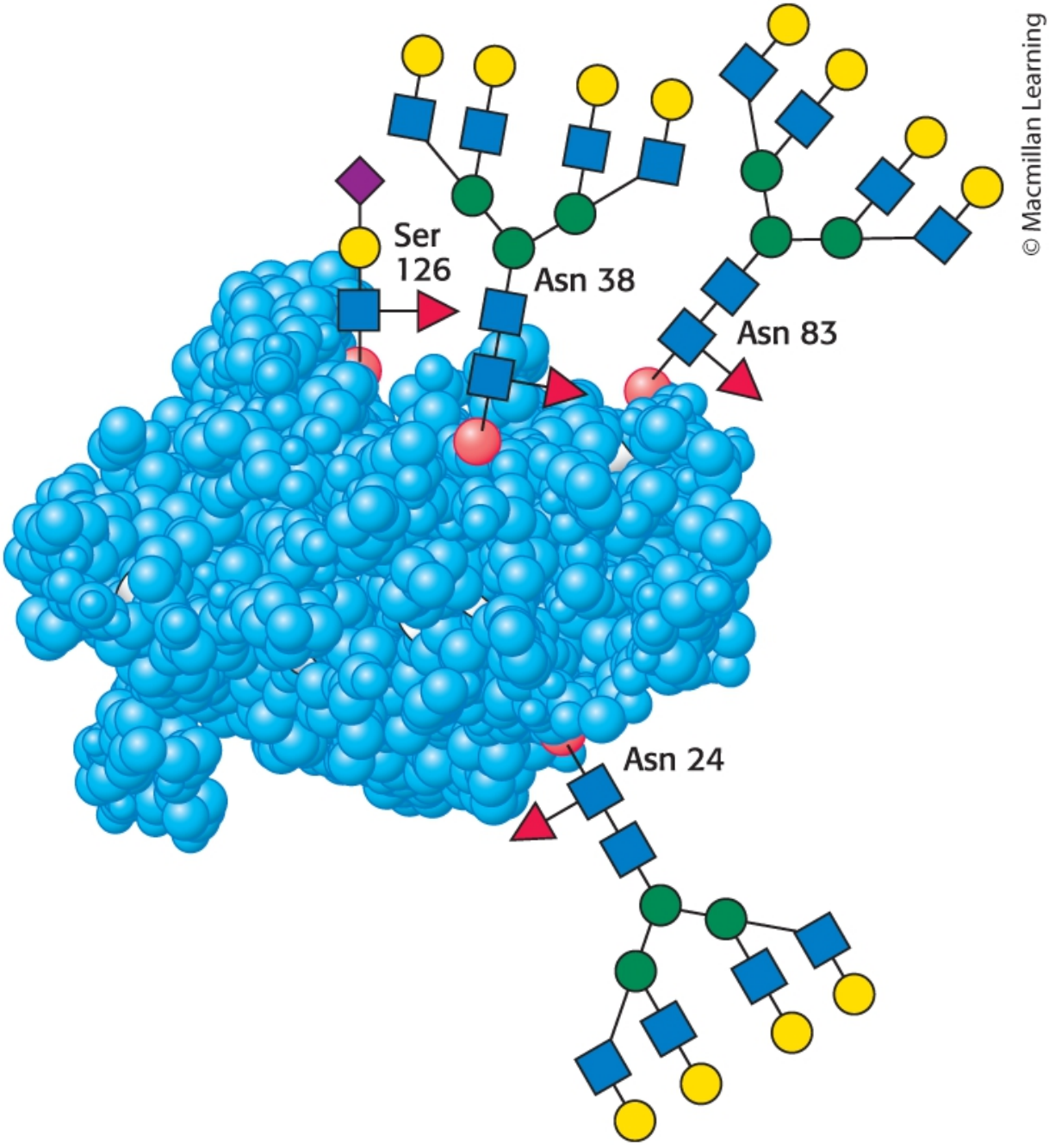
G l c N A c - Blue square - N-Acetylglucosamine

M a n - Green circle - Mannose

S i a - Purple rhombus - Sialic acid.

Return to Schematic illustrations of N-linked oligosaccharides

Extended description for Schematic illustration of erythropoietin with oligosaccharides linked to amino acid residues



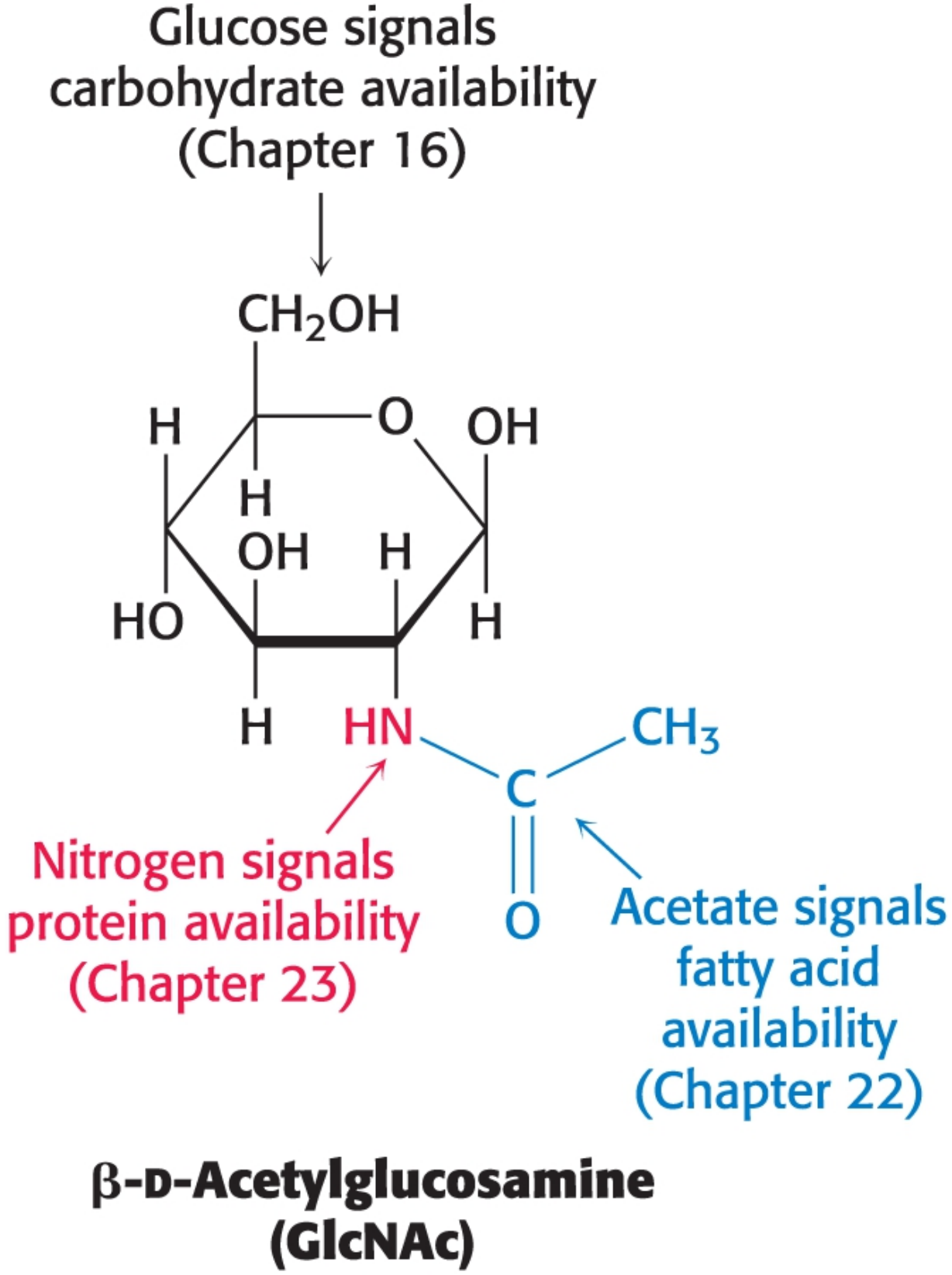
Erythropoietin is depicted as a compact cluster of blue spheres. Each of the amino acid residues; S e r 126, A s n 38, A s n 83, and A s n 24; is depicted as red sphere at the surface of erythropoietin. S e r 126, A s n 38, and A s n 83 are located at the top surface. A s n 24 is located at the bottom surface. Each of these amino acid residues are bound to oligosaccharides. The structure of oligosaccharide bound to S e r 126 is as follows: Red sphere, single bond, blue square, single bond, yellow circle, single bond, purple rhombus. The blue square is single bonded to a red triangle on the right.

The structure of oligosaccharide bound to A s n 38, A s n 83, and A s n 24 is as follows: Red sphere, single bond, blue square, single bond, blue square, single bond, green circle. The first blue square is single bonded to a red triangle. The green circle is single bonded to two green circles. Each green circle is single bonded to two blue squares. Each blue square is single bonded to a yellow circle.

Return to Schematic illustration of erythropoietin with oligosaccharides linked to amino acid residues

Extended description for Structure of beta-D-

acetylglucosamine

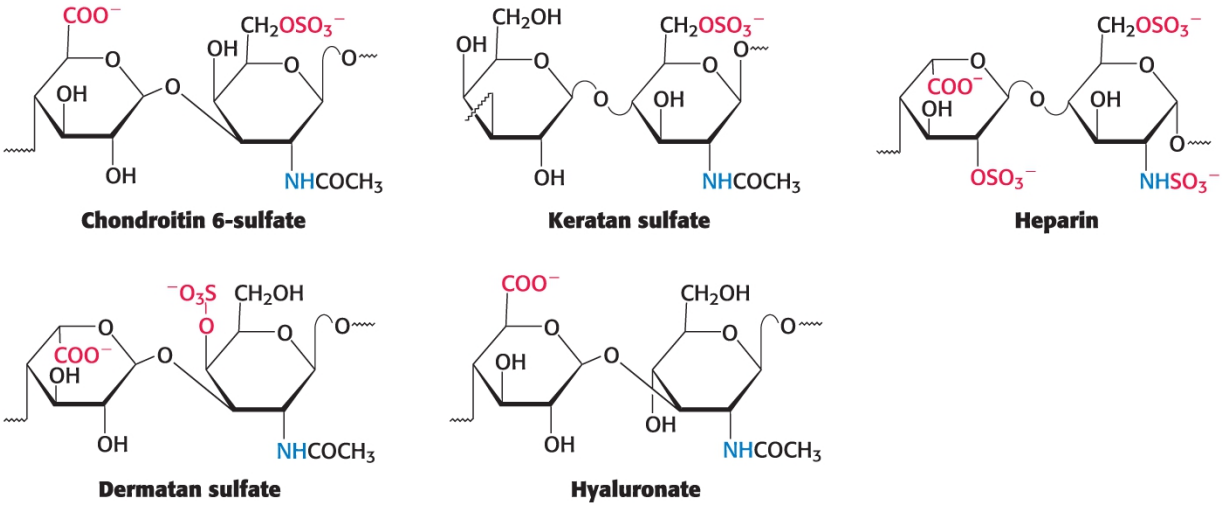


β-D-Acetylglucosamine (GlcNAc)

The structure of beta-D-acetylglucosamine (G l c N A c) is as follows: A 6-membered heterocyclic hexagonal ring is in a horizontal orientation and consists of 1 O and 5 C atoms. The O atom occupies the first position, which is the top right vertex. C 1 and C 3 are each single bonded to O H above and H below. C 2 is single bonded to H above and N H below. N H is highlighted in red. C 4 is single bonded to H above and O H below. C 5 is single bonded to C H 2 O H above and H below. The ring is labeled "glucose signals carbohydrate availability (Chapter 16)". N H bonded to C 2 is further single bonded to C on the lower right and is labeled "nitrogen signals protein availability (chapter 23)". The C atom on the lower right is single bonded to C H 3 on the upper right and double bonded to O below. The C atom, O atom, C H 3 group, and their associated bonds are highlighted in blue. They are labeled "acetate signals fatty acid availability (Chapter 22)".

Return to Structure of beta-D-acetylglucosamine

Extended description for Structures of chondroitin 6-sulfate, keratan sulfate, heparin, dermatan sulfate, and hyaluronate



The structure of chondroitin 6-sulfate is as follows: A 6-membered heterocyclic hexagonal ring is in a horizontal orientation and consists of 1 O and 5 C atoms. The O atom occupies the first position, which is the top right vertex. C 2 is single bonded to O H below. C 3 is single bonded to O H above. C 5 is single bonded to C O O superscript minus above. C 4 has an open single bond below. C 1 is single bonded to O on the upper right. This O is single bonded to C 3 of a 6-membered heterocyclic hexagonal ring in a horizontal orientation consisting of 1 O and 5 C atoms. The O atom occupies the first position, which is the top right vertex. C 1 is single bonded to O above. O has an open single bond on the right. C 2 is single bonded to N H C O C H 3 below. C 4 is single bonded to O H above. C 5 is single bonded to C H 2 O S O 3 superscript minus above. C O O superscript minus and O S O 3 superscript minus are highlighted in red. N H group of N H C O C H 3 is highlighted in blue.

The structure of keratan sulfate is as follows: A 6-membered heterocyclic hexagonal ring is in a horizontal orientation and consists of 1 O and 5 C atoms. The O atom occupies the first position, which is the top right vertex. C 2 is single bonded to O H below. C 3 is single bonded to C H 2 above in the form of a line. This C H 2 group has an open single bond on the lower left. C 4 is single bonded to O H above. C 5 is single bonded to C H 2 O H above. C 1 is single bonded to O on the right. This O is single bonded to C 4 of a 6-membered heterocyclic hexagonal ring in a horizontal orientation consisting of 1 O and 5 C atoms. The O atom occupies the first position, which is the top right vertex. C 1 is single bonded to O above. O has an open single bond on the right. C 2 is single bonded to N H C O C H 3 below. C 3 is single bonded to O H above. C 5 is single bonded to C H 2 O S O 3 superscript minus above. O S O 3 superscript minus is highlighted in red. N H group of N H C OC H 3 is highlighted in blue.

The structure of heparin is as follows: A 6-membered heterocyclic hexagonal ring is in a horizontal orientation and consists of 1 O and 5 C atoms. The O atom occupies the first position, which is the top right vertex. C 2 is single bonded to O S O 3 superscript minus below. C 3 is single bonded to O H above. C 4 is single bonded to C H 2 below in the form of a line. This C H 2 has an open single bond on the left. C 5 is single bonded to C O O superscript minus below. C 1 is single bonded to O on the upper right. This O is single bonded to C 4 of a 6-membered heterocyclic hexagonal ring in a horizontal orientation consisting of 1 O and 5 C atoms. The O atom occupies the first position, which is the top right vertex. C 1 is single bonded to O below. O has an open single bond on the right. C 2 is single bonded to N H S O 3 superscript minus below. C 3 is single bonded to O H above. C 5 is single bonded to C H 2 O S O 3 superscript minus above. C O O superscript minus, O S O 3 superscript minus and S O 3 superscript minus are highlighted in red. N H group of N H S O 3 superscript minus is highlighted in blue.

The structure of dermatan sulfate is as follows: A 6-membered heterocyclic hexagonal ring is in a horizontal orientation and consists of 1 O and 5 C atoms. The O atom occupies the first position, which is the top right vertex. C 2 is single bonded to O H below. C 3 is single bonded to O H above. C 4 is single bonded to C H 2 below in the form of a line. This C H 2 group has an open single bond on the left. C 5 is single bonded to C O O superscript minus below. C 1 is single bonded to O on the upper right. This O is single bonded to C 3 of a 6-membered heterocyclic hexagonal ring in a horizontal orientation consisting of 1 O and 5 C atoms. The O atom occupies the first position, which is the top right vertex. C 1 is single bonded to O above. O has an open single bond on the right. C 2 is single bonded to N H C O C H 3 below. C 4 is single bonded to O above. This O is single bonded to S O 3 superscript minus above. C 5 is single bonded to C H 2 O H above. C O O superscript minus and O, single bond, S O 3 superscript minus are highlighted in red. N H group of N H C OC H 3 is highlighted in blue.

The structure of hyaluronate is as follows: A 6-membered heterocyclic hexagonal ring is in a horizontal orientation and consists of 1 O and 5 C atoms. The O atom occupies the first position, which is the top right vertex. C 2 is single bonded to O H below. C 3 is single bonded to O H above. C 4 is single bonded to C H 2 below. This C H 2 has an open single bond on the right. C 5 is single bonded to C O O superscript minus below. C 1 is single bonded to O on the upper right. This O is single bonded to C 3 of a 6-membered heterocyclic hexagonal ring in a horizontal orientation consisting of 1 O and 5 C atoms. The O atom occupies the first position, which is the top right vertex. C 1 is single bonded to O above. O has an open single bond on the right. C 2 is single bonded to N H C O C H 3 below. C 4 is single bonded to O H below. C 5 is single bonded to C H 2 O H above. C O O superscript minus is highlighted in red. N H group of N H C OC H 3 is highlighted in blue.

Return to Structures of chondroitin 6-sulfate, keratan sulfate, heparin, dermatan sulfate, and hyaluronate

Extended description for An electron micrograph and schematic representation of proteoglycan

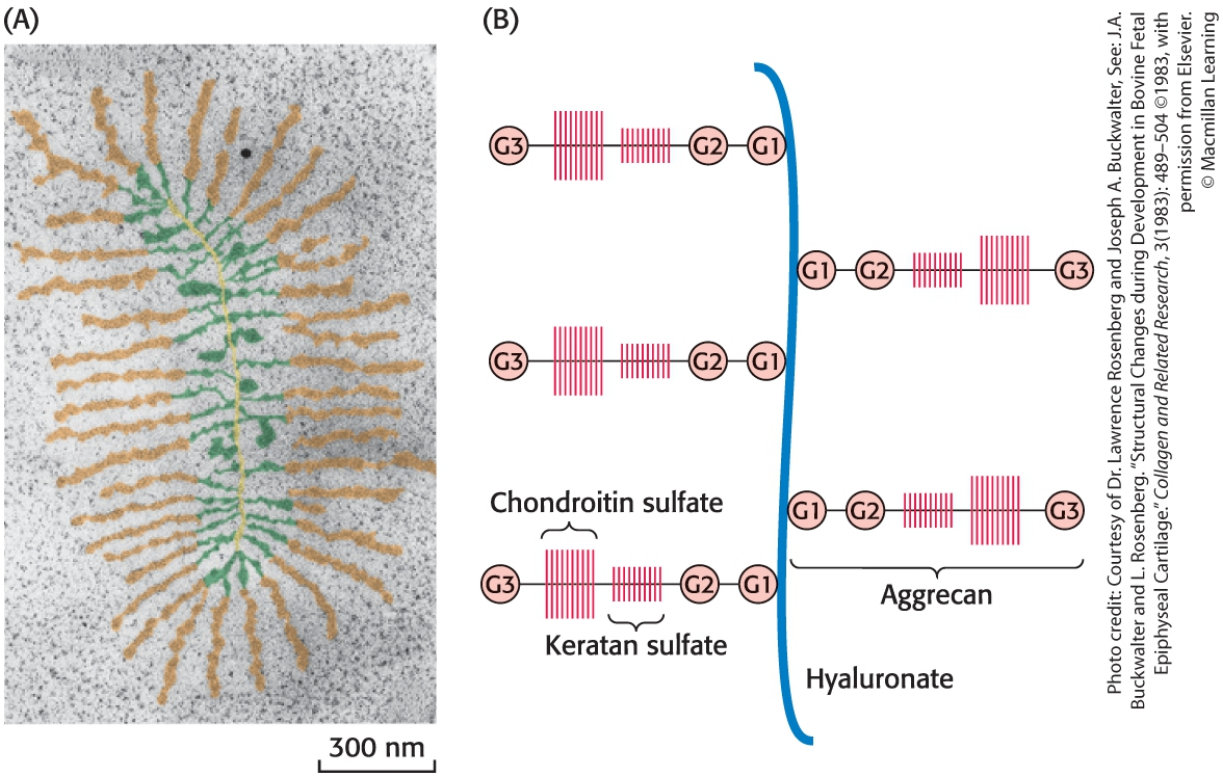
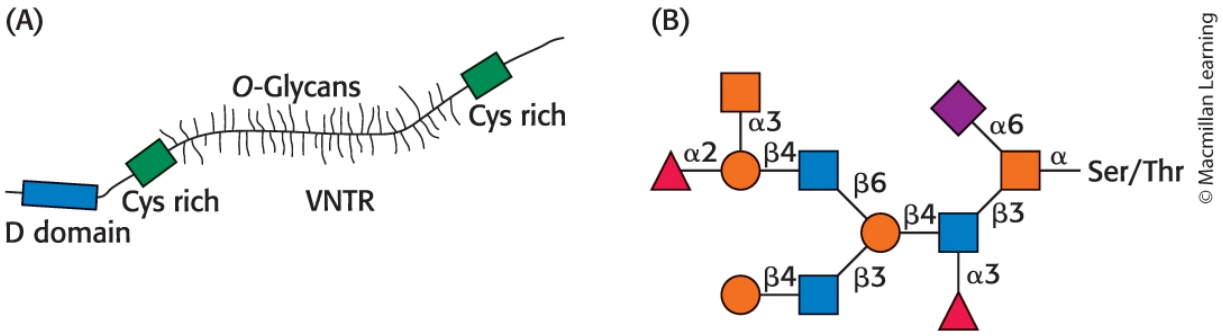


Photo credit: Courtesy of Dr. Lawrence Rosenberg and Joseph A. Buckwalter, See: J.A. Buckwalter and L. Rosenberg. "Structural Changes during Development in Bovine Fetal Epiphyseal Cartilage." *Collagen and Related Research*, 3(1983): 489–504 ©1983, with permission from Elsevier.
© Macmillan Learning

(A) A series of medium-sized extensions emerge from a central yellow line. These extensions are colored green near their origin from the yellow line. The remaining portion of the extensions is colored orange. (B) A central solid blue line is labeled hyaluronate. The extensions labeled aggrecan originate alternatively from the left and right of the blue line along its entire length. The aggrecan consists of two evenly spaced pink circles labeled G 1 and G 2 near its origin from the blue line and a pink circle labeled G 3 at the free end. G 1 is attached to the origin. A set of short vertical and parallel lines and long vertical and parallel lines are located between G 2 and G 3. There is a small gap between the set of long and short lines.

Return to An electron micrograph and schematic representation of proteoglycan

Extended description for Schematic illustrations depict the mucoprotein and an oligosaccharide bound to the V N T R region of the protein



(A) The protein is depicted as a wavy line. From left to right, the components of the protein are as follows:

A blue rectangle at the left end of the line is labeled D domain.

A green rectangle on the right of the blue rectangle is labeled C y s rich.

Another green rectangle labeled C y s rich is located toward the right end of the line.

A series of short irregular lines protrude above and below the wavy line between the two green rectangles. This region is labeled O-glycans.

(B) An orange square is single bonded to serine slash threonine on right. The single bond is labeled alpha. It is single-bonded to a purple square on the upper left. The single bond is labeled alpha 6.

It is single-bonded to a blue square on the lower left. The single bond is labeled beta 3.

The blue square is single bonded to a red triangle below. The single bond is labeled alpha 3. It is single bonded to an orange circle on the left. The single bond is labeled beta 4.

The orange circle is single bonded to a blue square on the upper left. The single bond is labeled beta 6. It is single-bonded to another blue square on the lower left. The single bond is labeled beta 3.

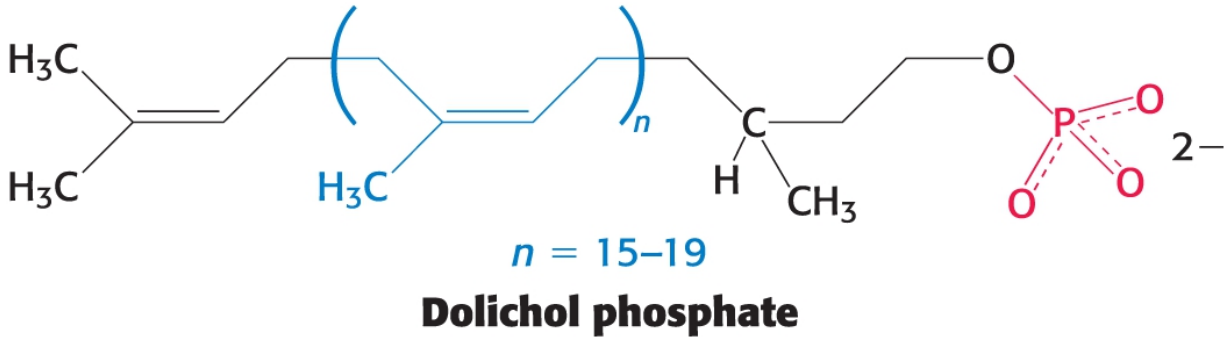
The blue square on the lower left is further single bonded to an orange circle on the left. The single bond is labeled beta 4.

The blue square on the upper left is single bonded to an orange circle. The single bond is labeled beta 4.

The orange circle is further single bonded to an orange square above. The single bond is labeled alpha 3. It is single bonded to a red triangle on the left. The single bond is labeled alpha 2.

Return to Schematic illustrations depict the mucoprotein and an oligosaccharide bound to the V N T R region of the protein

Extended description for Structure of dolichol phosphate



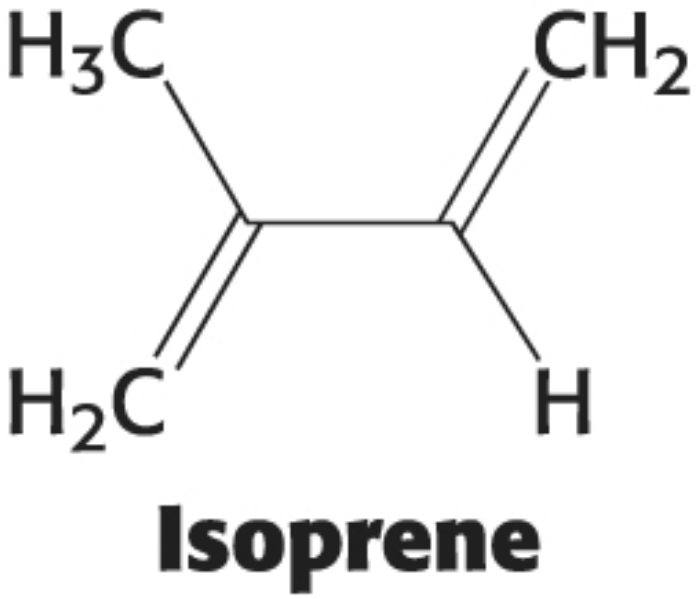
n = 15–19

Dolichol phosphate

The structure of dolichol phosphate is as follows: An 11-carbon alkene chain is depicted as a line structure using 10 zigzag lines. The alkene chain contains double bonds between C 1 and C 2 and C 5 and C 6. C 1 is single bonded to C H 3 on the upper left and C H 3 on the lower left. C 5 is single bonded to C H 3 on the lower left. C 4 to C 7 is enclosed in parentheses with subscript n. C 9 is single bonded to H on the lower left and C H 3 on the lower right. C 11 is single bonded to O on the right. O is single bonded to P on the lower right. P is partially double-bonded to O on the upper right, lower right, and lower left. This group has an overall negative charge of 2 minus.

Return to Structure of dolichol phosphate

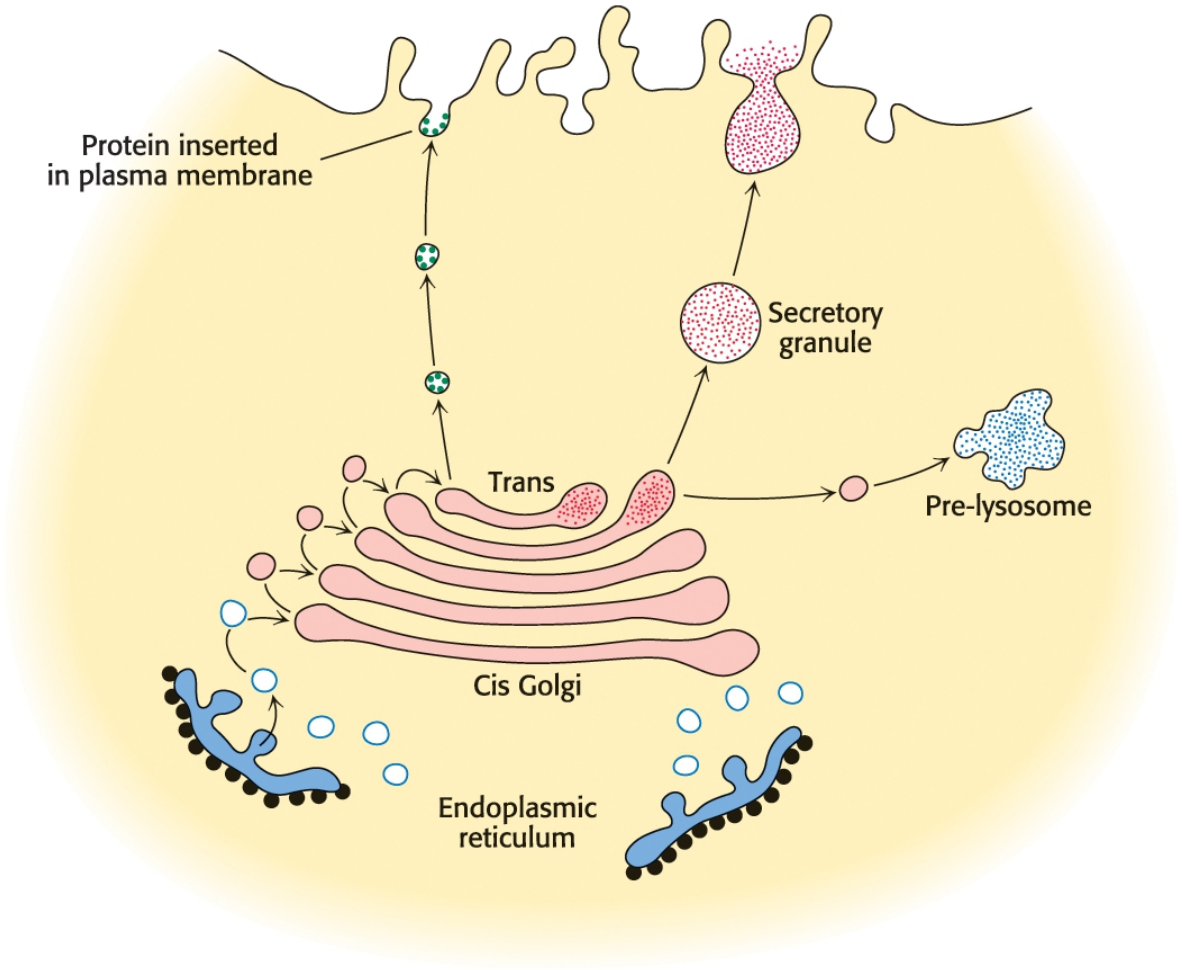
Extended description for Chemical structure of isoprene



The structure of isoprene is as follows: C, single bond, C. C 1 is single bonded to C H 3 on the upper left and double bonded to C H 2 on the lower left. C 2 is double bonded to C H 2 on the upper right and single bonded to H on the lower right.

Return to Chemical structure of isoprene

Extended description for Schematic illustration of protein sorting in the Golgi complex



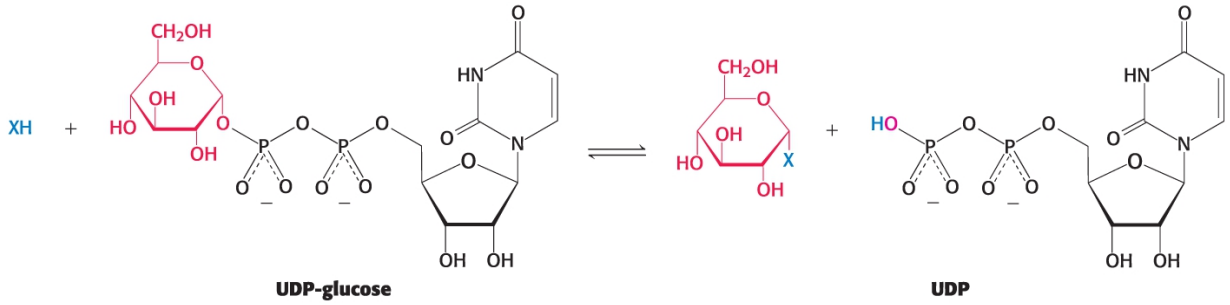
© Macmillan Learning

The endoplasmic reticulum is depicted as a tubular flat structure lined by thick black dots on the bottom surface. Round vesicles protrude from the top surface of endoplasmic reticulum and move toward the Cis Golgi compartment. The Golgi complex consists of 5 flat tubular sacs located one above the other. The size of these sacs decreases from bottom to top. The topmost face of the Golgi complex is labeled trans. Tiny vesicles emerge from each sac of Golgi complex and move to the next sac located above. The interior

of a vesicle emerging from the trans face of Golgi is lined with green dots that represent proteins. This vesicle fuses with the surface of the cell leading to the insertion of the protein (green dots) in plasma membrane. A tiny vesicle emerging from the second sac of the trans face moves toward a pre-lysosome. Another large vesicle emerging from this sac is labeled secretory granule. It is filled with tiny red colored granules. It fuses with the cell surface to release the granules into the exterior.

Return to Schematic illustration of protein sorting in the Golgi complex

Extended description for Glycosyltransferase reaction



The reaction consists of two reactants and two products. The first reactant is X H. The second reactant is U D P glucose whose structure is as follows: A 6-membered heterocyclic hexagonal ring is in a horizontal orientation and consists of 1 O and 5 C atoms. The O atom occupies the first position, which is the top right vertex. C 1 is single bonded to O below. C 2 and C 4 are each single bonded to O H below. C 3 is single bonded O H above. C 5 is single bonded to C H 2 O H above. The O bonded to C 1 is further single bonded to P, single bond, O, single bond, P, single bond, O, single bond, C H 2 in the form of a line. P 1 and P 2 are each partially double bonded to O on the lower left and lower right. The O atoms bonded to P have an overall negative charge. C H 2 is single bonded to C 4 of a 5-membered pentagonal ring in a vertical orientation. The heterocyclic pentagonal ring has 1 O and 5 C atoms with O occupying the topmost vertex. C 2 and C 3 are each single bonded to O H below. C 1 is single bonded to N 1 of a 6 membered heterocyclic hexagonal ring in a vertical orientation. It consists of 2 N and 4 C atoms. C 1 occupies the bottom left vertex and is double bonded to O on the lower left. First N occupies the first position, which is the bottom-most vertex. Second N bound to H occupies the second position, which is the top left vertex. C 2 is double bonded to O above. A double bond is present between C 3 and C 4.

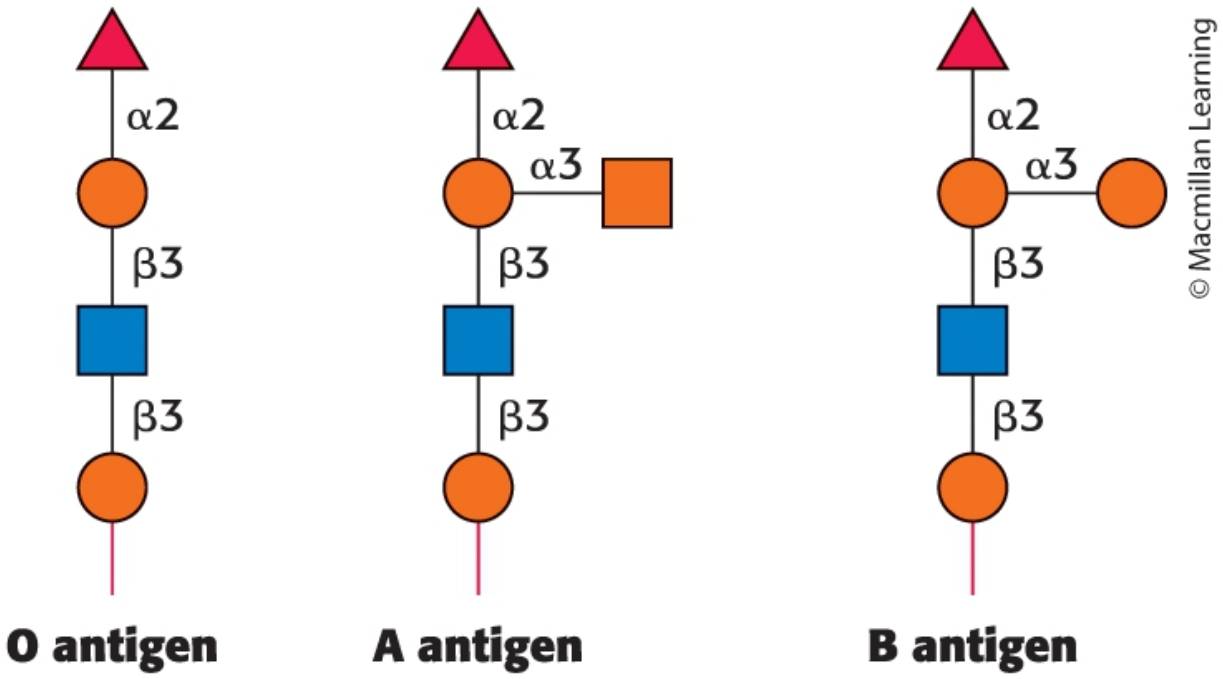
A reversible reaction arrow is shown.

The structure of the first product is as follows: A 6-membered heterocyclic hexagonal ring is in a horizontal orientation and consists of 1 O and 5 C atoms. The O atom occupies the first position, which is the top right vertex. C 1 is single bonded to X below. C 2 and C 4 are each single bonded to O H below. C 3 is single bonded to O H above. C 5 is single bonded to C H 2 O H above.

The second product is U D P whose structure is as follows: A 5-membered heterocyclic pentagonal ring in vertical orientation has 1 O and 4 C atoms with C 1 occupying the top right vertex. O occupies the topmost vertex. C 2 and C 3 are each single bonded to O H below. C 4 is single bonded to C H 2 above in the form of a line. C H 2 is single bonded to O, single bond, P, single bond, O, single bond, P, single bond, O H. P 1 and P 2 are each partially double bonded to O on the lower left and lower right. C 1 is single bonded to N 1 of a 6 membered heterocyclic hexagonal ring in a vertical orientation. It consists of 2 N and 4 C atoms. C 1 occupies the bottom left vertex and is double bonded to O on the lower left. First N occupies the first position, which is the bottom-most vertex. Second N bound to H occupies the second position, which is the top left vertex. C 2 is double bonded to O above. A double bond is present between C 3 and C 4.

Return to Glycosyltransferase reaction

Extended description for Schematic illustration of the structures of O antigen, A antigen, and B-antigen



The structure of O antigen is as follows: A red triangle is single bonded below to an orange circle by alpha 2. The orange circle is single bonded to below blue square by beta 3. The blue square is single bonded to orange circle by beta 3.

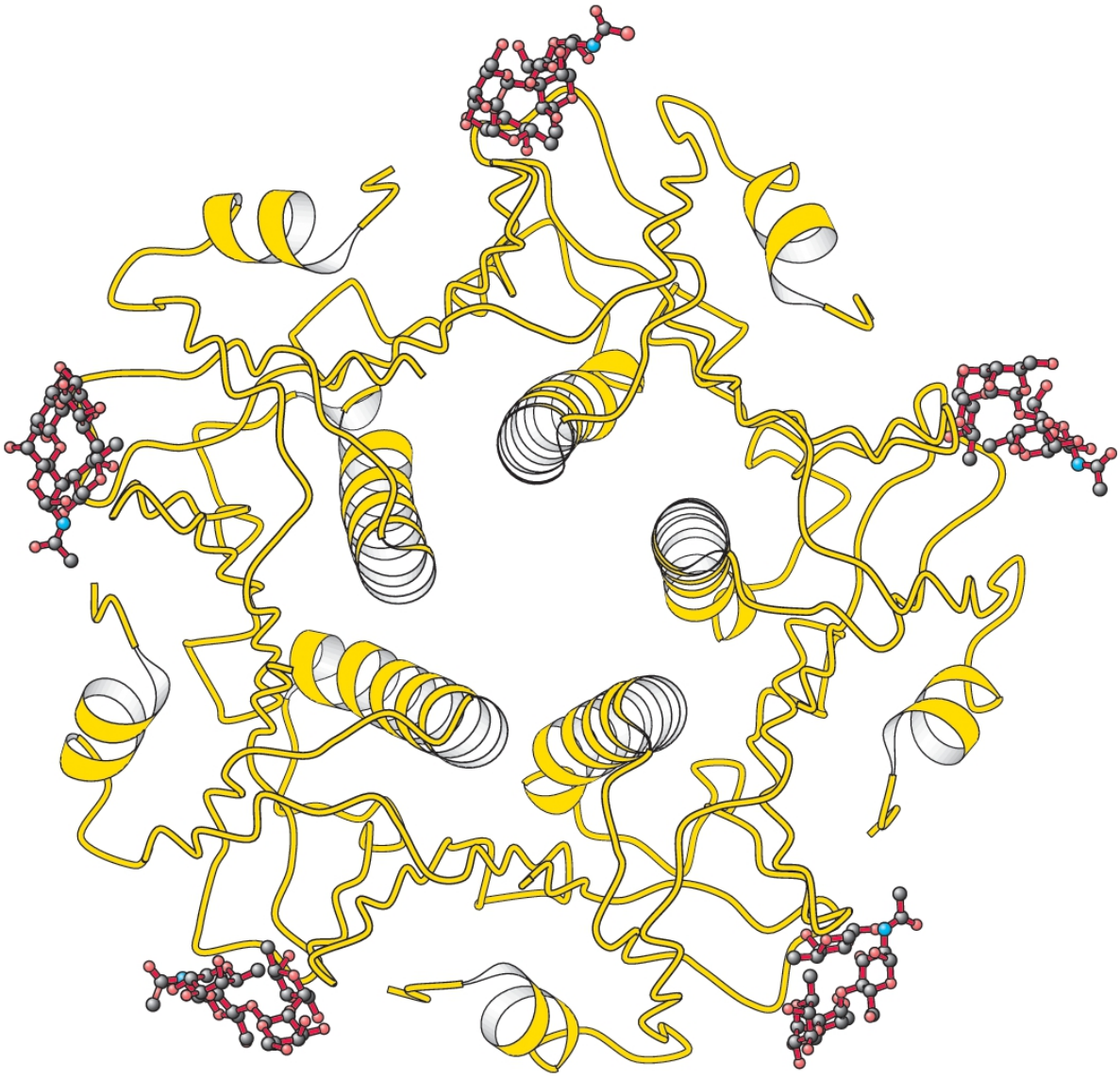
The structure of A antigen is as follows: A red triangle is single bonded below to an orange circle by alpha 2. The orange circle is single bonded below to blue square by beta 3. The blue square is single bonded below to an orange circle by beta 3. The first orange circle is single bonded to an orange square on the right by alpha 3.

The structure of B antigen is as follows: A red triangle is single bonded below to an orange circle by alpha 2. The orange circle is single bonded below to a blue square by beta 3. The blue square is

single bonded below to an orange circle by beta 3. The first orange circle is single bonded to an orange circle by alpha 3.

Return to Schematic illustration of the structures of O antigen, A antigen, and B-antigen

Extended description for Ribbon diagram of cholera toxin bound to O antigens depicted as ball-and-stick models



© Macmillan Learning

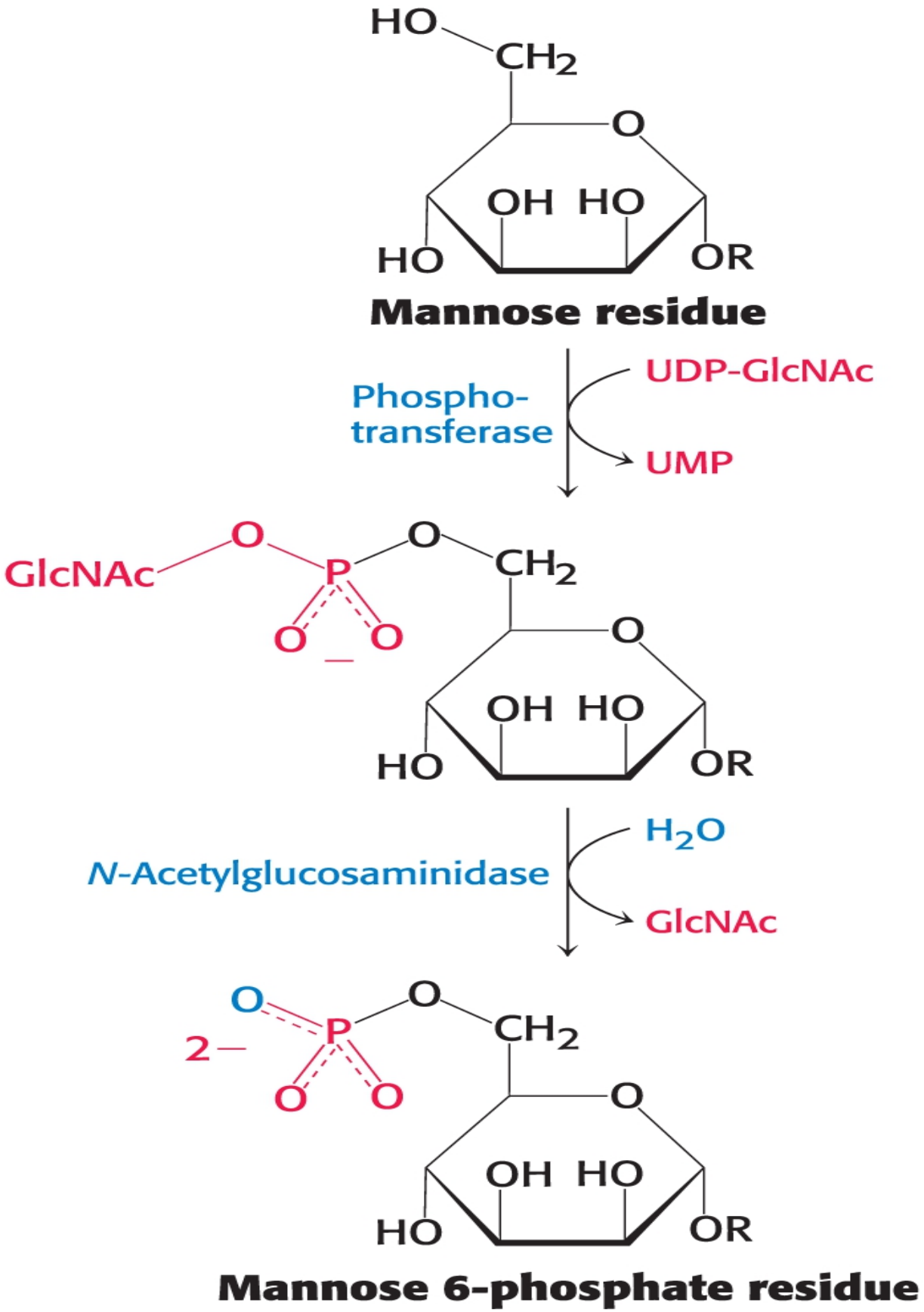
The ribbon diagram consists of an alpha-helix at the top, top left, top right, bottom left, and bottom right. A central hollow space is present between these helices. These alpha-helices are interconnected by long thread-like loops. These loops form a

pentagonal shape around the alpha-helices. The loop on each side is connected to a short alpha-helix. A ball and stick model of O antigen is attached to each of the vertices of the pentagonal shape formed by the loops.

Return to Ribbon diagram of cholera toxin bound to O antigens depicted as ball-and-stick models

Extended description for Stepwise formation of

mannose 6-phosphate residue


HO
CH2
O
OH HO
HO
OR
Mannose residue
Phospho-
transferase
UDP-GlcNAc
UMP
GlcNAc
O
P
O
O
O
CH2
O
OH HO
HO
OR
N-Acetylglucosaminidase
H2O
GlcNAc
2 —
O
P
O
O
O
CH2
O
OH HO
HO
OR
Mannose 6-phosphate residue

Step 1: It is catalyzed by phosphotransferase. The reactant is mannose residue whose structure is as follows: A 6-membered heterocyclic hexagonal ring is in a horizontal orientation and consists of 1 O and 5 C atoms. The O atom occupies the first position, which is the top right vertex. C 1 is single bonded to O R below. C 2 and C 3 are each single bonded to O H above. C 4 is single bonded to O H below. C 5 is single bonded to C H 2, single bond, O H above.

A forward reaction arrow shows the conversion of U D P-G l c N A c to U M P and the product.

The structure of the product is as follows: A 6-membered heterocyclic hexagonal ring is in a horizontal orientation and consists of 1 O and 5 C atoms. The O atom occupies the first position, which is the top right vertex. C 1 is single bonded to O R below. C 2 and C 3 are each single bonded to O H above. C 4 is single bonded to O H below. C 5 is single bonded to C H 2 above. This C H 2 is single bonded on the upper left to O, single bond, P, single bond, O, single bond, G l c N A c. The P atom is partially double bonded to O on the lower left and lower right. The O atom have an overall negative charge.

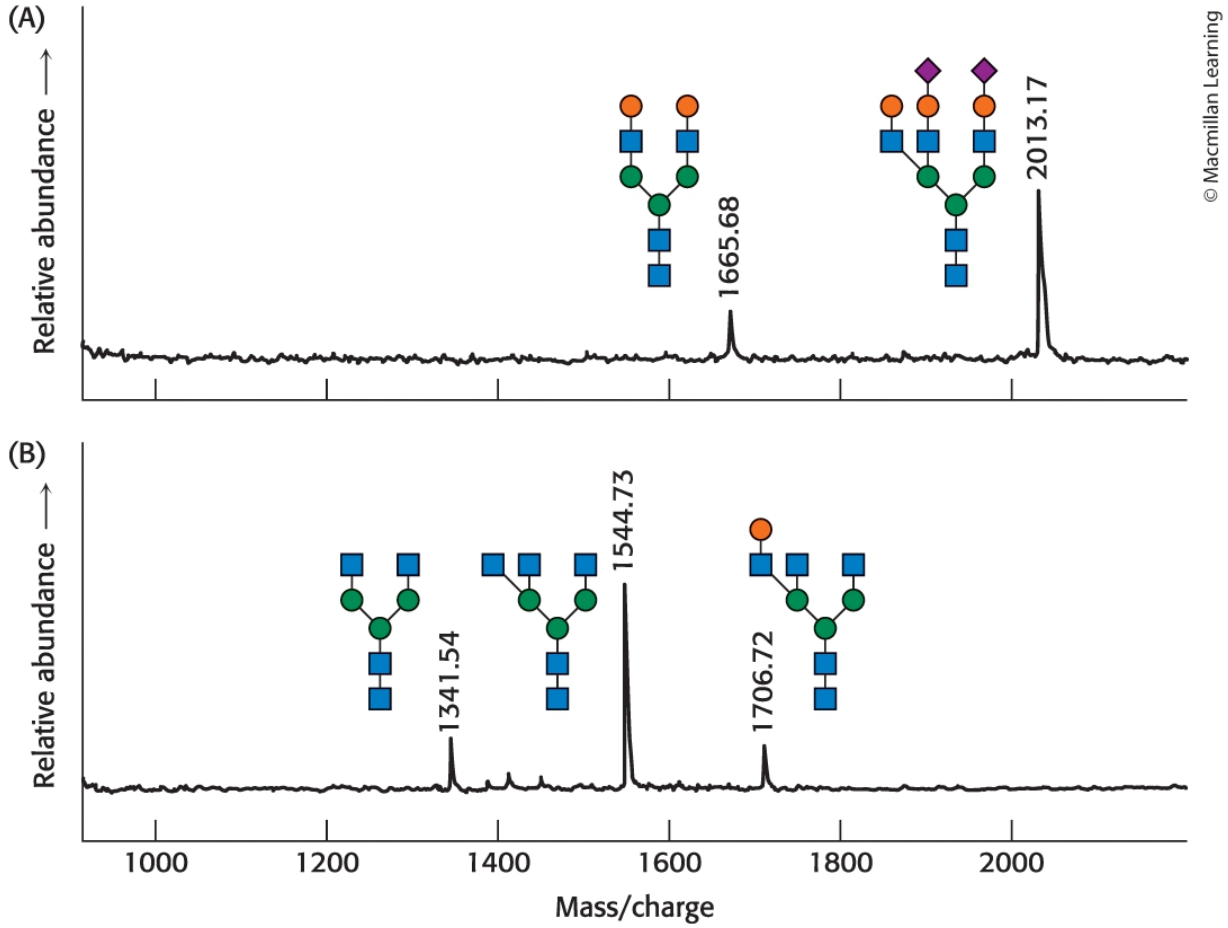
Step 2: The product formed in step 1 is converted into mannose 6-phosphate residue. It is catalyzed by N-acetylglucosaminidase. A forward reaction arrow is shown below the first product. It shows the entry of H 2 O and exit of G l c N A c.

The structure of mannose 6-phosphate residue is as follows: A 6-membered heterocyclic hexagonal ring is in a horizontal orientation and consists of 1 O and 5 C atoms. The O atom occupies the first position, which is the upper right vertex. C 1 is single bonded to O R below. C 2 and C 3 are each single bonded to O H above. C 4 is single bonded to O H below. C 5 is single bonded to C H 2 above. This C H 2

is single bonded on the upper left to O, single bond, P, partial double bond, O. The P atom is partially double bonded to O on the lower left and lower right. This group has an overall negative charge of 2 minus.

Return to Stepwise formation of mannose 6-phosphate residue

Extended description for Mass spectrums for the characterization of oligosaccharides



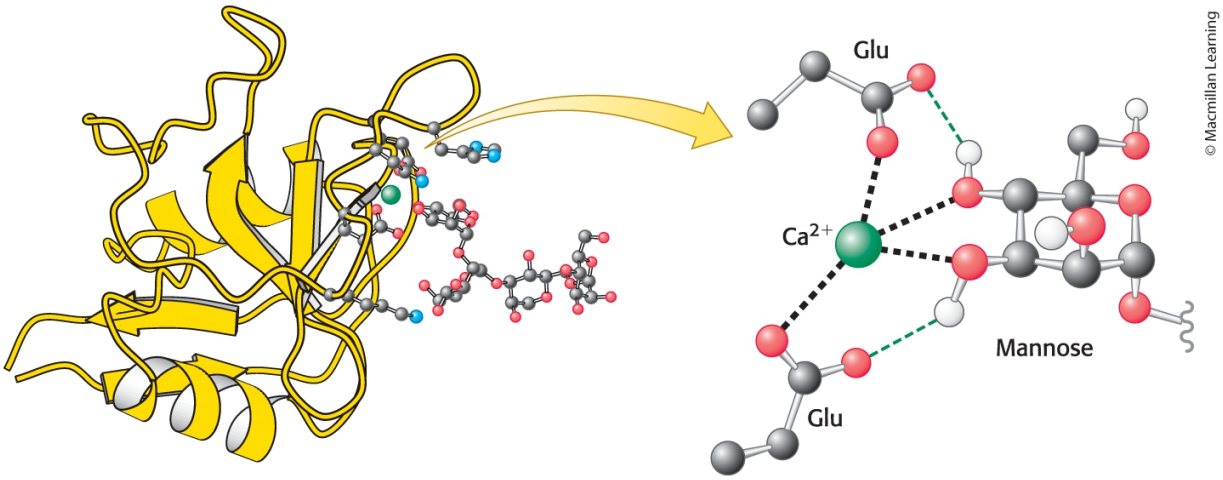
(A) The vertical axis is labeled relative abundance which increases from the bottom to the top. The horizontal axis has a series of evenly spaced markings. A line starts from the lowest relative abundance and moves horizontally toward the right. A tiny peak labeled 1665.68 is formed between the fourth and fifth marking on the horizontal axis. An oligosaccharide composed of four blue squares, three green circles, and two orange circles is shown along this peak. A relatively longer peak labeled 2013.17 is formed after the sixth marking on the horizontal axis. An oligosaccharide composed of five blue squares,

three green circles, three orange circles, and two purple rhombi is shown along the peak.

(B) The vertical axis is labeled relative abundance which increases from the bottom to the top. The horizontal axis is labeled mass over charge. It has markings ranging from 1000 to 2000 in increments of 200 units. A line starts from the lowest relative abundance and moves horizontally toward the right. A first tiny peak labeled 1341.54 is formed between 1200 and 1400 on the horizontal axis. An oligosaccharide composed of four blue squares and three green circles is shown along this peak. A relatively longer peak labeled 1544.73 is formed between 1400 and 1600 on the horizontal axis. An oligosaccharide composed of five blue squares and three green circles is shown along the peak. A third tiny peak slightly smaller than the first tiny peak is formed between 1600 and 1800. It is labeled 1706.72. An oligosaccharide composed of five blue squares, three green circles, and one orange circle is shown along the peak.

Return to Mass spectrums for the characterization of oligosaccharides

Extended description for Ribbon diagram and ball and stick model depict the calcium ion mediated binding of C-type lectin to carbohydrates



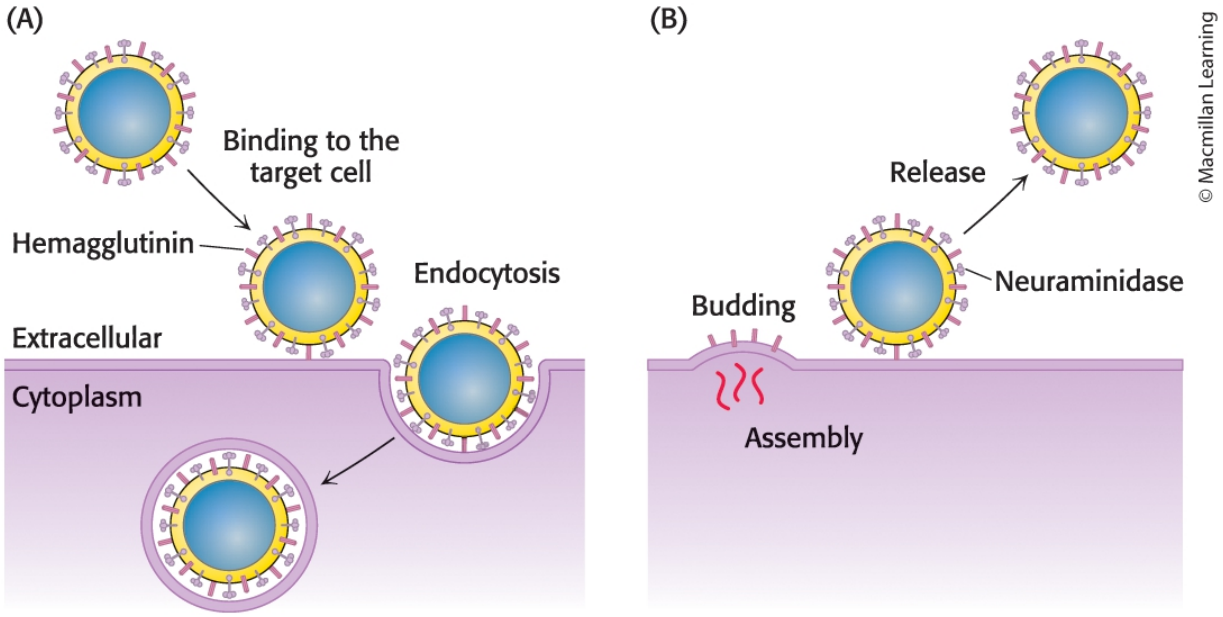
The ribbon diagram of C-type lectin consists of several beta-strands at the top and an alpha-helix at the bottom. These secondary structures are interconnected by long thread-like loops. A cluster of long thread-like loops at the right is connected to the ball-and-stick models of amino acid side chains, carbohydrates, and a green sphere.

These ball and stick models are enlarged on the right. A central green sphere is labeled C a superscript 2 plus. The side chains of G l u are shown above and below the green sphere. They are composed of 3 black and two red spheres. A red sphere of each side chain above and below is connected to the central grey sphere through a dashed line. A ball and stick model of mannose is shown on the right of the central green sphere. It is composed of a ring of one red and 5 black spheres. The black spheres of the ring are connected to black spheres or red spheres. The top left and bottom left black spheres of the ring are each connected to a red sphere on the left.

Each of these red spheres is connected to the central green sphere through a dashed line. A white sphere connected to each of these red spheres is further connected to the corresponding red sphere of G l u side chain above and below respectively through a dashed line.

Return to Ribbon diagram and ball and stick model depict the calcium ion mediated binding of C-type lectin to carbohydrates

Extended description for Schematic illustrations depict the entry and exit of influenza virus from host cell



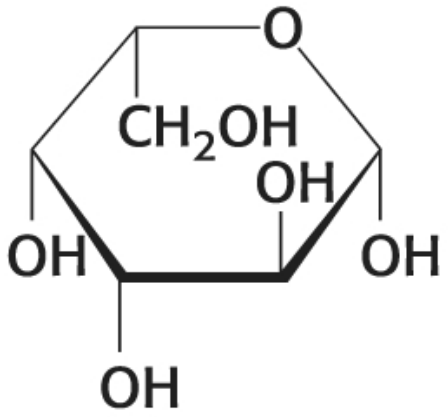
(a) The virus particle is depicted as a blue circle with a thick yellow border. It is located in the extracellular space. A series of surface proteins protrude from the yellow border, above the surface of the virus particle. The virus particle binds to the surface of the target cell through a surface protein labeled hemagglutinin. A semicircular invagination is formed on the surface of the target cell. The virus particle then fits inside this invagination. This process is labeled endocytosis. The virus particle enters inside the cytoplasm and is enclosed inside a circular portion of the target cell membrane.

(b) A slightly raised surface is shown on the target cell membrane. A series of viral surface proteins protrude outside from this raised surface. Three short irregular lines are located below this surface. The red lines depict the process of assembly. The raised surface

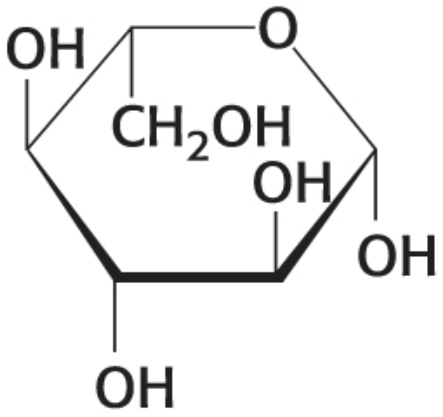
depicts the process of budding. A mature virus particle produced by budding is shown attached to the target cell membrane through hemagglutinin. The action of neuraminidase, a second set of viral surface proteins, causes the release of the virus.

Return to Schematic illustrations depict the entry and exit of influenza virus from host cell

Extended description for Chemical structures of beta L-Galactopyranose and beta L-Glucopyranose



β–L–Galactopyranose



β–L–Glucopyranose

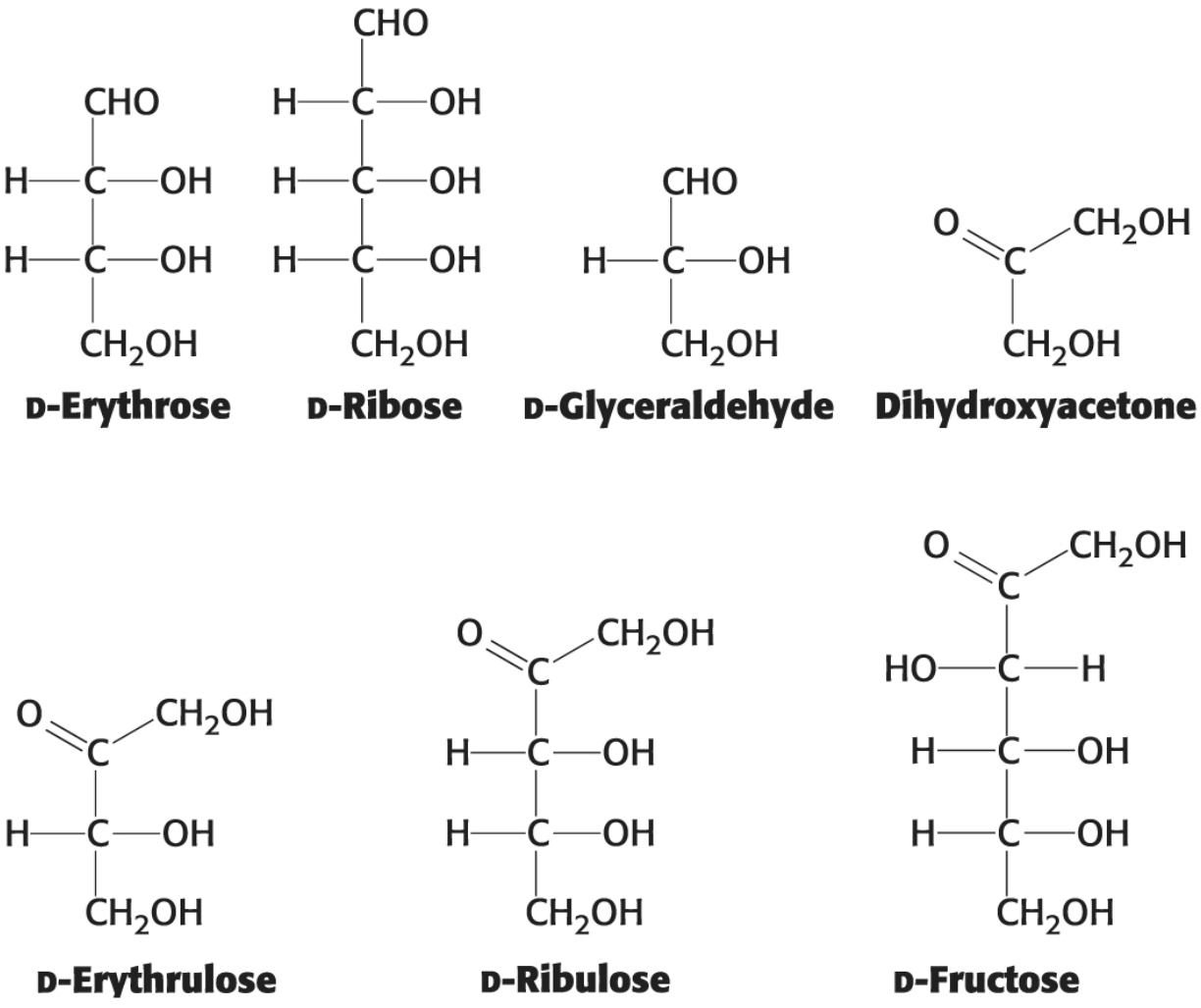
The structure of beta L-Galactopyranose is as follows: A 6-membered heterocyclic hexagonal ring is in a horizontal orientation and consists of 1 O and 5 C atoms. C 1 occupies the rightmost vertex. The O atom occupies the first position, which is the top right vertex. The ring is in a plane perpendicular to the plane of the paper such that C 5 and O are away from the observer and C 2 and C 3 are toward the observer. C 1, C 3, and C 4 are each single bonded to O H below. C 2 is single bonded to O H above. C 5 is single bonded to C H 2 O H below.

The structure of beta L-Glucopyranose is as follows: A 6-membered heterocyclic hexagonal ring is in a horizontal orientation and consists of 1 O and 5 C atoms. C 1 occupies the rightmost vertex. The O atom occupies the first position, which is the top right vertex. The ring is in a plane perpendicular to the plane of the paper such that C 5 and O are away from the observer and C 2 and C 3 are toward the observer. C 1 and C 3 are each single bonded to O H below. C 2 and C

4 are each single bonded to O H above. C 5 is single bonded to C H 2 O H below.

Return to Chemical structures of beta L-Galactopyranose and beta L-Glucopyranose

Extended description for Chemical structures of D-Erythrose, D-Ribose, D-Glyceraldehyde, Dihydroxyacetone, D-Erythrulose, D-Ribulose, and D-Fructose



The structure of D-Erythrose is as follows: The Fischer projection consists of a vertical line with C H O above and C H 2 O H below. The projection contains two C atoms placed one below the other on the vertical line. The C atoms are numbered from top to bottom. C 2 and C 3 each are single bonded to O H on the right and H on the left.

The structure of D-Ribose is as follows: The Fischer projection consists of a vertical line with C H O above and C H 2 O H below. The projection contains three C atoms placed one below the other on the vertical line. The C atoms are numbered from top to bottom. C 2, C 3, and C 4 each are single bonded to H on the left and O H on the right.

The structure of D-Glyceraldehyde is as follows: The Fischer projection consists of a vertical line with C H O above and C H 2 O H below. The projection contains a C atom at the center of the vertical line. The C atom is single-bonded to H on the left and O H on the right.

The structure of Dihydroxyacetone is as follows: A central carbon atom is double bonded to O on the upper left, single bonded to C H 2 O H on the upper right, and single bonded to C H 2 O H below.

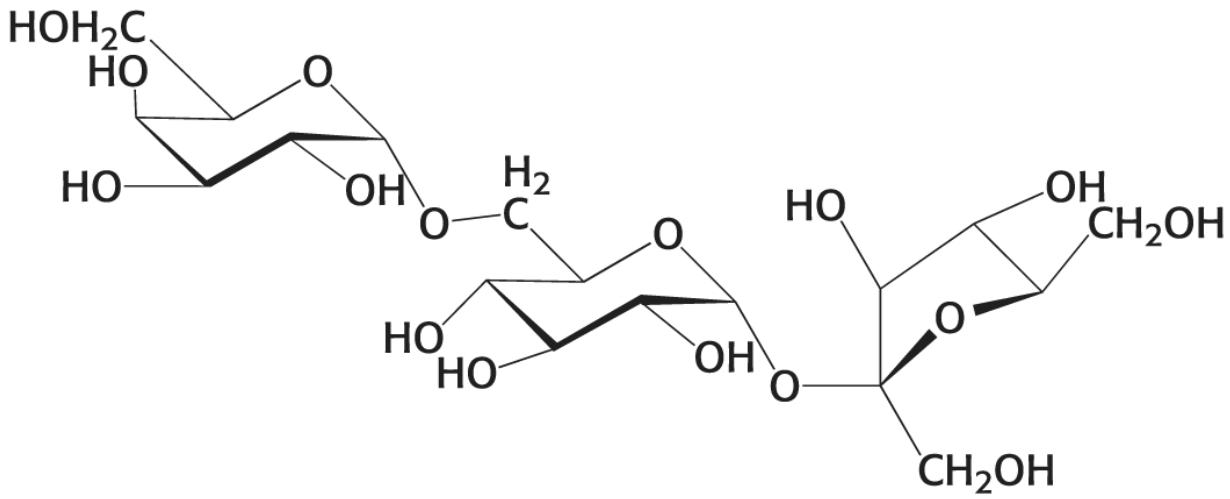
The structure of D-Erythrulose is as follows: The Fischer projection consists of a vertical chain with C above and C H 2 O H below. The projection contains a C at the center of the vertical line. C 1 is double bonded to O on the upper left and single bonded to C H 2 O H on the upper right. C 2 is single bonded to H on the left and O H on the right.

The structure of D-Ribulose is as follows: The Fischer projection consists of a vertical chain with C above and C H 2 O H below. The projection contains two C atoms placed one below the other on the vertical chain. The C atoms are numbered from top to bottom. C 1 is double bonded to O on the upper left and single bonded to C H 2 O H on the upper right. C 2 and C 3 are each single bonded to H on the left and O H on the right.

The structure of D-Fructose is as follows: The Fischer projection consists of a vertical chain with C above and C H 2 O H below. The projection contains three C atoms placed one below the other on the vertical chain. The C atoms are numbered from top to bottom. C 1 is double bonded to O on the upper left and single bonded to C H 2 O H on the upper right. C 2 is single bonded to O H on the left and H on the right. C 3 and C 4 are each single bonded to H on the left and O H on the right.

Return to Chemical structures of D-Erythrose, D-Ribose, D-Glyceraldehyde, Dihydroxyacetone, D-Erythrulose, D-Ribulose, and D-Fructose

Extended description for Chemical structure of raffinose



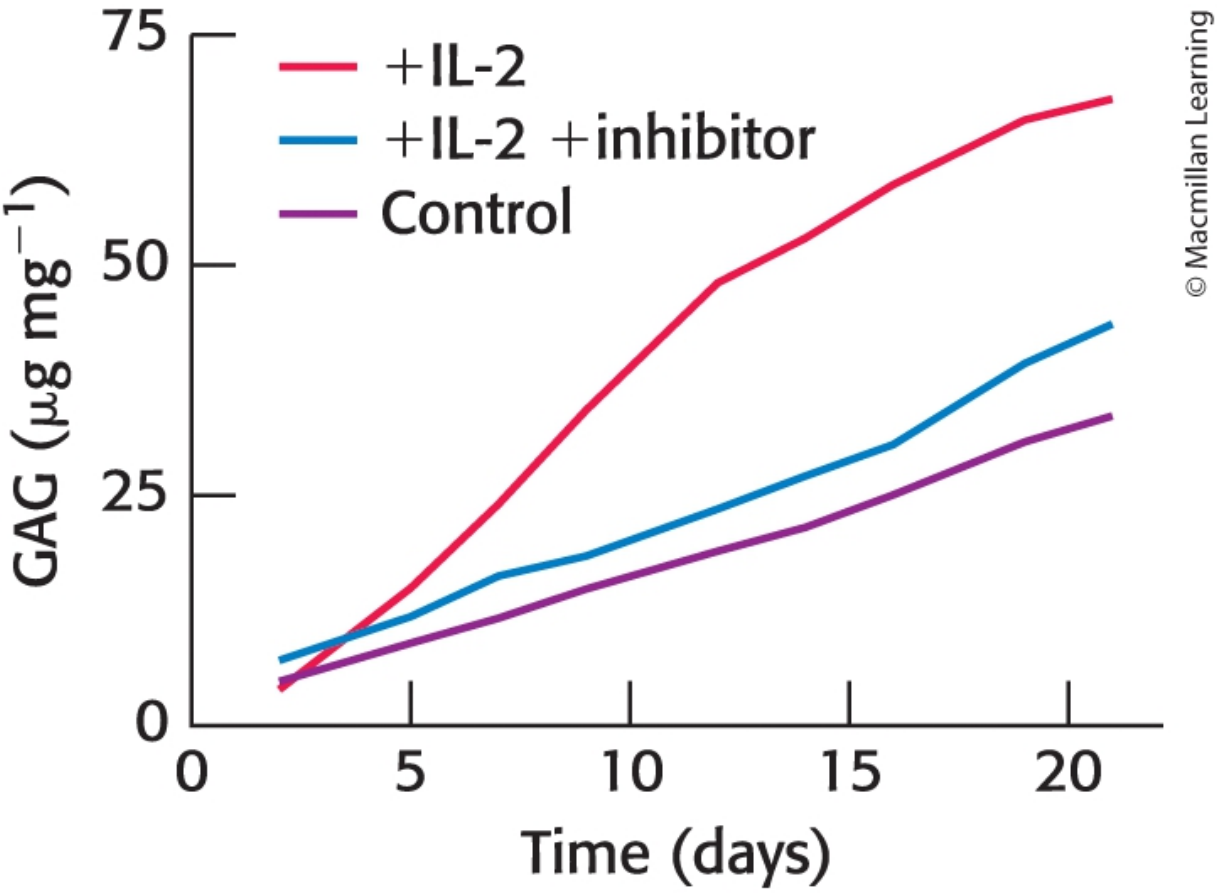
Raffinose

The structure of raffinose is as follows: A 6-membered heterocyclic hexagonal ring is in a chair conformation and consists of 1 O and 5 C atoms. The O atom occupies the first position, which is the top right vertex. C 2 and C 5 are close to each other. C 4 occupies the top left vertex. C 1 is single bonded to O, single bond, C H 2 on the lower right. C 2 is single bonded to O H on the lower right. C 3 is single bonded to O H on the left. C 4 is single bonded to O H above. C 5 is single bonded to C H 2 O H on the upper left. The C H 2 group bonded to C 1 through O is single bonded to C 5 of another 6-membered heterocyclic hexagonal ring in a chair conformation that consists of 1 O and 5 C atoms. The O atom occupies the first position, which is the top right vertex. C 2 and C 5 are close to each other. C 4 occupies the top left vertex. C 1 is single bonded to O on the lower right. C 2 is single bonded to O H on the lower right. C 3 is single bonded to O H on the left. C 4 is single bonded to O H on the lower left. The O atom bonded to C 1 is single bonded to C 1 of a 5-membered heterocyclic pentagonal ring that consists of 1 O and 4 C

atoms. C 1 occupies the bottom left vertex. O occupies the bottom-most vertex. C 1 and C 4 are wedge bonded to O atom. C 2 is single bonded to O H above. C 3 is single bonded to O H on the right. C 4 is single bonded to C H 2 O H on the upper right.

Return to Chemical structure of raffinose

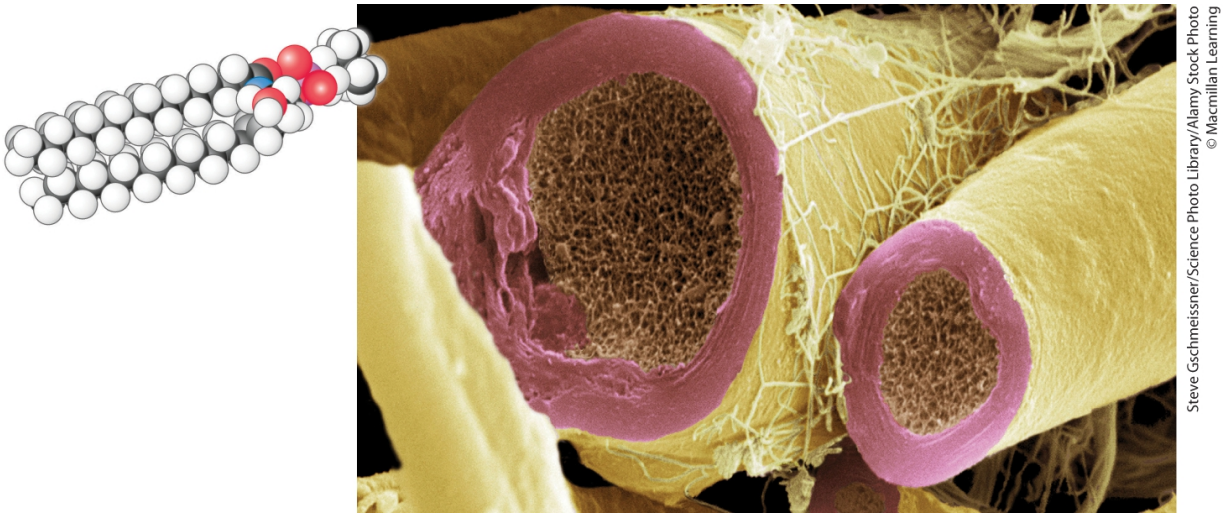
Extended description for Graphical representation of G A G concentration versus time in days



The horizontal axis is labeled time in days. It has markings ranging from 0 to 20 in increments of 5 units. The vertical axis is labeled G A G microgram m g superscript minus 1. It has markings ranging from 0 to 75 in increments of 25 units. The graph shows three increasing lines for plus I L 2, plus I L 2 plus inhibitor, and control. The line for plus I L 2 starts from (2.5, 5) and terminates at (20, 70). The line for plus I L 2 plus inhibitor starts from (2.5, 6) and terminates at (20, 35). The line for control starts from (2.5, 5) and terminates at (20, 30). All values are approximated.

Return to Graphical representation of G A G concentration versus time in days

Extended description for Space-filling model of sphingomyelin and scanning electron micrograph of the myelin sheath

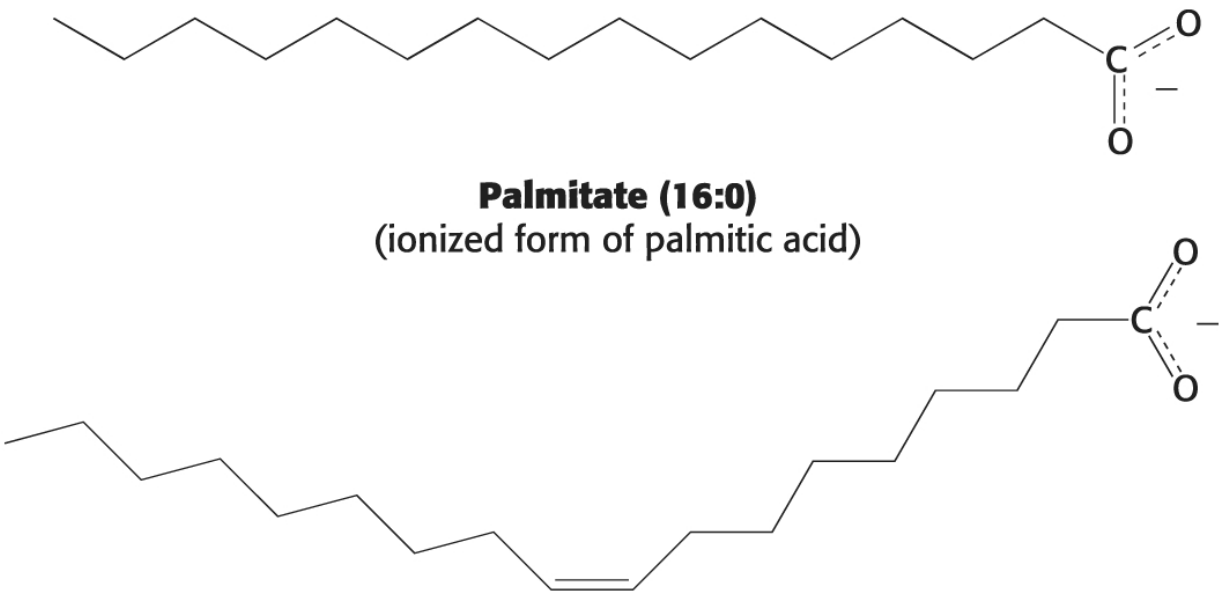


The space-filling model consists of two chains of black spheres fused side by side. Each black sphere is fused with three small white spheres. The white spheres cover the entire surface. The chains continue into a cluster composed of red spheres, a blue sphere, and a purple sphere. This cluster of red spheres is fused to a small cluster of black spheres on the right which is further fused to white spheres. The white spheres cover the entire surface of this cluster.

In the scanning electron micrograph, the cross-section of the myelin sheath is depicted as a cylindrical structure with a thick pink layer and a sponge-like interior.

Return to Space-filling model of sphingomyelin and scanning electron micrograph of the myelin sheath

Extended description for Chemical structures of palmitate and oleate

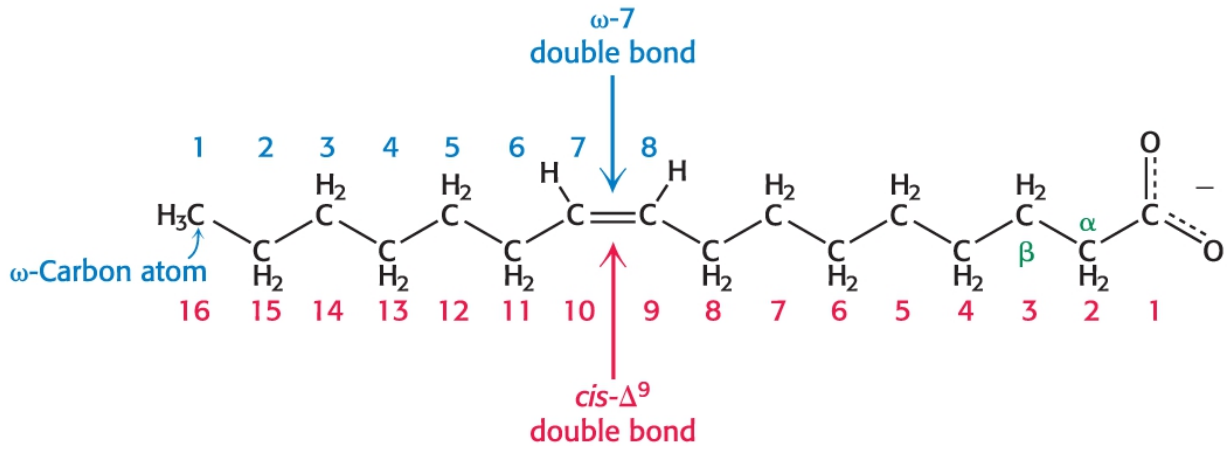


Palmitate is ionized form of palmitic acid. Its structure is as follows: A 16-carbon alkane chain is depicted as a line structure using 15 zigzag lines. C 16 is partially double bonded to O below and O on the upper right. The O atoms have an overall negative charge.

Oleate is the ionized form of oleic acid. Its structure is as follows: An 18-carbon alkene chain is depicted as a line structure using 17 zigzag lines. A double bond is present between C 9 and C 10. C 18 is partially double bonded to O on the upper right and lower right. The O atoms have an overall negative charge.

Return to Chemical structures of palmitate and oleate

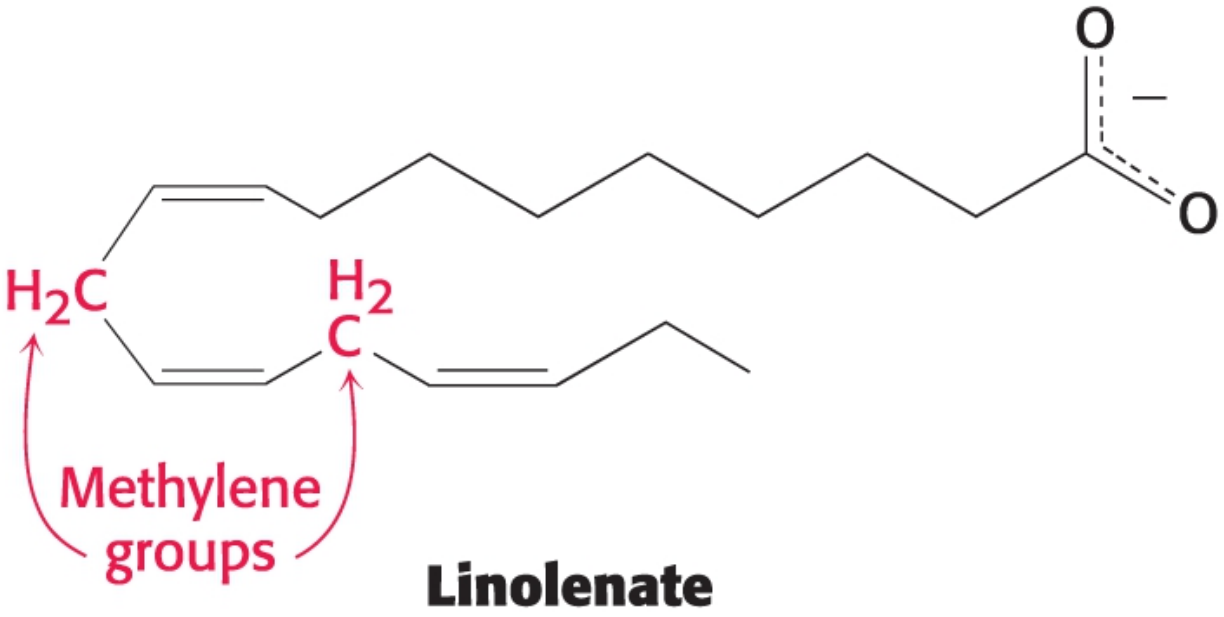
Extended description for Numbering of carbon atoms in a fatty acid chain



A 16 C alkene chain is depicted as a line structure using 15 zigzag lines. A double bond is present between C 7 and C 8. C 2, C 3, C 4, C 5, C 6, C 9, C 10, C 11, C 12, C 13, C 14 and C 15 are bound to H 2. C 1 is bound to H 3. C 7 and C 8 are each single bonded to H on the upper left and upper right respectively. C 16 is partially double bonded to O above and O on the lower right. The C O O group has an overall negative charge. C 1 is labeled omega-carbon atom. The double bond between C 7 and C 8 is labeled "omega-7 double bond". C 16 to C 1 are numbered 1 to 16 from right to left. These numbers are highlighted in red. C 2 and C 3 in this order are labeled alpha are labeled alpha and beta respectively. The double bond between C 9 and C 10 in this order is labeled "cis-delta superscript 9 double bond"

Return to Numbering of carbon atoms in a fatty acid chain

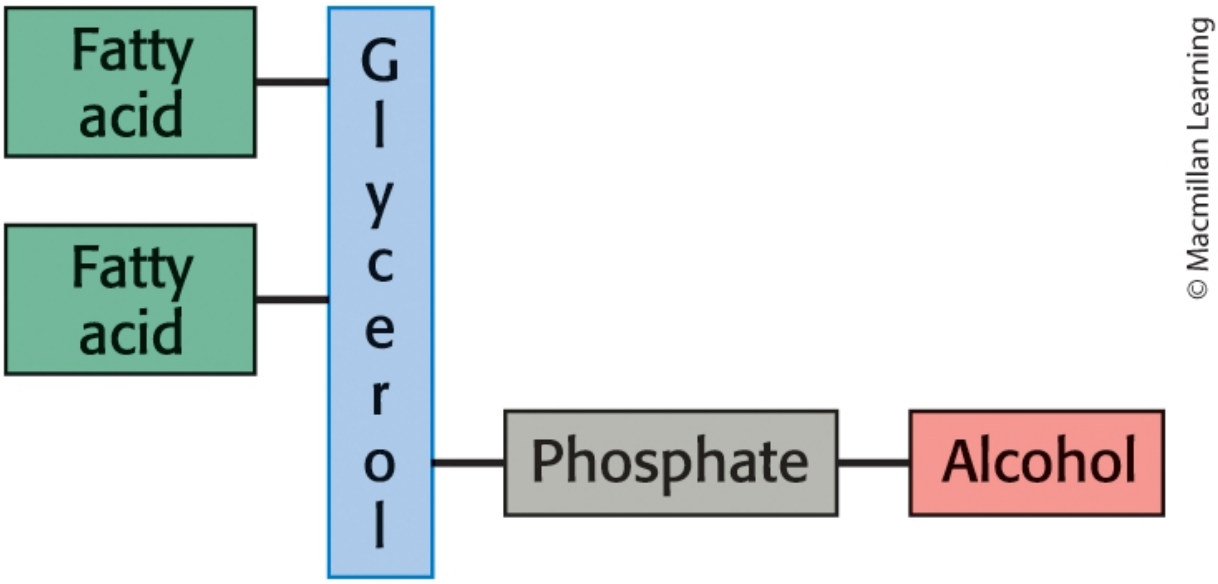
Extended description for Structure of linolenate



The structure of linolenate is as follows: An 18 C homonuclear alkene chain is depicted as a line structure using 17 zigzag lines. C 11 and C 14 are bound to H 2 and labeled methylene groups. A double bond is present between C 9 and C 10, C 12 and C 13, and C 15 and C 16. C 1 is partially double bonded to O above and O on the lower right. This C O O group has an overall negative charge. The chain folds at C 11.

Return to Structure of linolenate

Extended description for Schematic representation of a phospholipid molecule

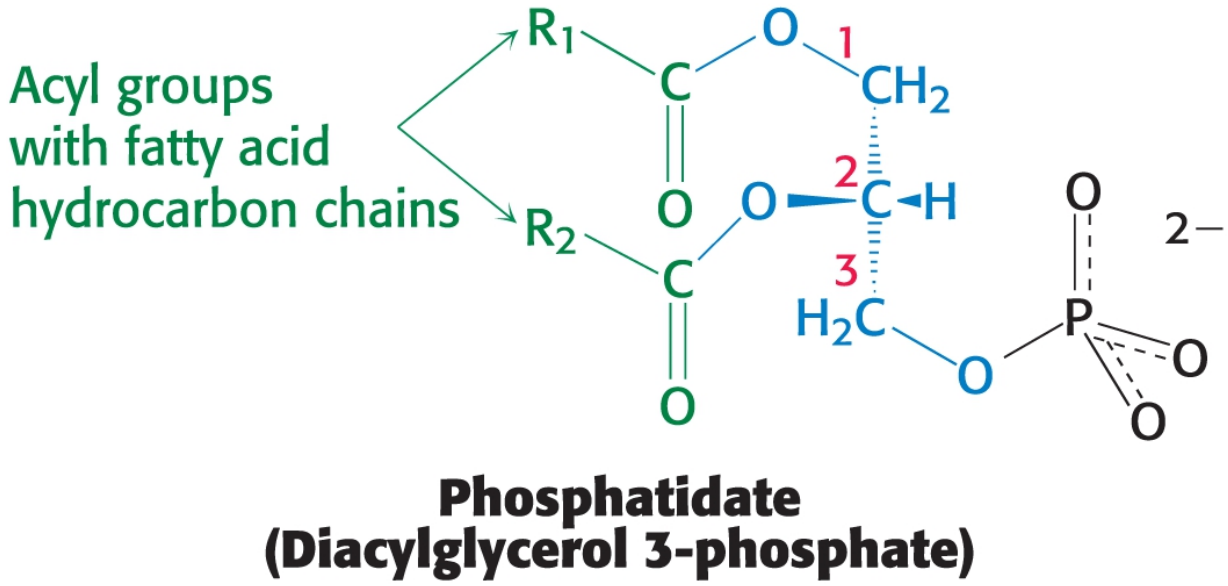


© Macmillan Learning

The glycerol molecule is depicted as a blue vertical bar. It is connected to a green square labeled fatty acid on the top left and middle left. It is connected to a grey rectangle labeled phosphate on the bottom right. The grey rectangle is further connected to a red rectangle on the right labeled alcohol.

Return to Schematic representation of a phospholipid molecule

Extended description for Chemical structure of phosphatidate



Phosphatidate
(Diacylglycerol 3-phosphate)

Phosphatidate is also called diacylglycerol 3-phosphate. Its structure is as follows: A central C atom is dash bonded to C H 2 above and C H 2 below. These C atoms are numbered 1 to 3 from top to bottom with the central C atom labeled 2. C 1 is single bonded to O on the upper left. This O atom is single bonded to C on the lower left. The C atom is double bonded to O below and single bonded to R 1 on the upper left.

C 2 is wedge bonded to H on the right and wedge bonded to O on the left. The O atom is single bonded to C on the lower left. This C atom is double bonded to O below and single bonded to R 2 on the upper left.

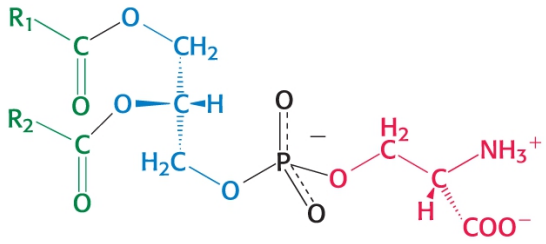
R 1 and R 2 are labeled “acyl groups with fatty acid hydrocarbon chains ”.

C 3 is single bonded to O on the lower right. This O atom is single bonded to P on the upper right. The P atom is partially double bonded to O above, O on the right, and O on the lower right. The P O 3 group has an overall negative charge of 2 minus.

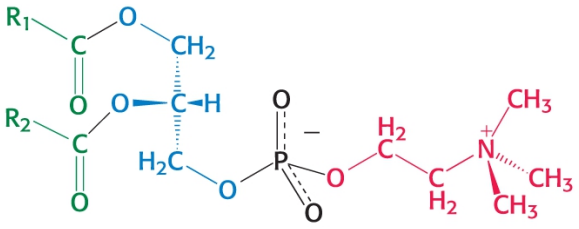
C 1 to C 3 and the O atoms bonded to them are highlighted in blue. The C O groups bonded to R 1 and these O atoms are highlighted in green. The P O 3 group is highlighted in black.

Return to Chemical structure of phosphatidate

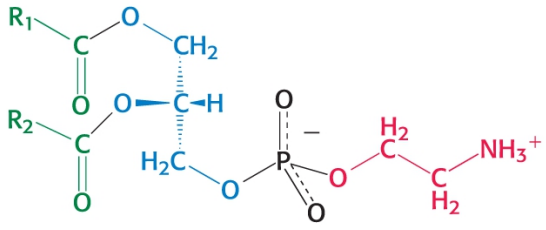
Extended description for Chemical structures of common phosphoglycerides located in the membrane



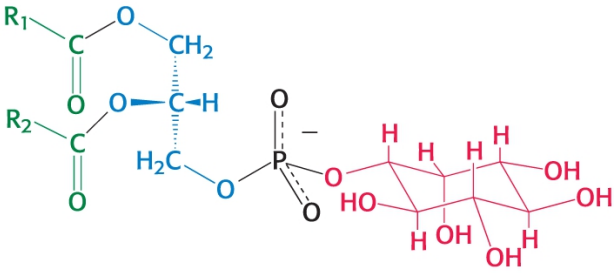
Phosphatidylserine



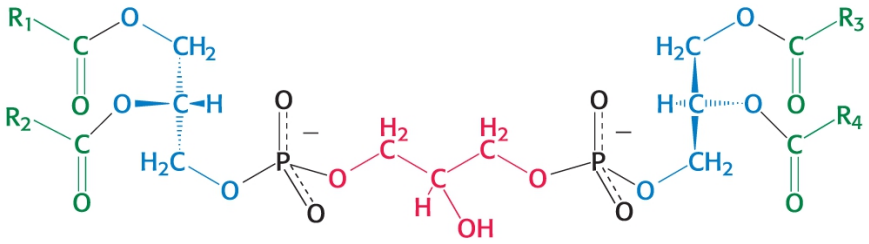
Phosphatidylcholine



Phosphatidylethanolamine



Phosphatidylinositol



Diphosphatidylglycerol (cardiolipin)

The common phosphoglycerides in the membrane are phosphatidylserine, phosphatidylcholine, phosphatidylethanolamine, phosphatidylinositol, and diphosphatidylglycerol (cardiolipin).

The structure of phosphatidylserine is as follows: A central C atom is dash bonded to C H 2 above, dash bonded to C H 2 below, wedge bonded to O on the left, and wedge bonded to H on the right. This O

atom is single bonded to C on the lower left. The C atom is double bonded to O below and single bonded to R 2 on the upper left.

The C H 2 group above is single bonded to O on the upper left. The O atom is single bonded to C on the lower left. This C atom is double bonded to O below and single bonded to R 1 on the upper left.

C H 2 group below is single bonded to O on the lower right. This O atom is single bonded to P on the upper right. The P atom is partially double bonded to O above, partially double bonded to O on the lower right, and single bonded to O on the right. The partially double bonded O atoms have an overall negative charge. The O atom on the right is single bonded to a 2-carbon alkane chain depicted as C H 2, single bond, C. C 2 of this chain is single bonded to N H 3 superscript plus on the upper right, dash bonded to C O O superscript minus on the lower right, and wedge bonded to H below.

The structure of phosphatidylcholine is as follows: A central C atom is dash bonded to C H 2 above, dash bonded to C H 2 below, wedge bonded to O on the left, and wedge bonded to H on the right. This O atom is single bonded to C on the lower left. The C atom is double bonded to O below and single bonded to R 2 on the upper left.

The C H 2 group above is single bonded to O on the upper left. The O atom is single bonded to C on the lower left. This C atom is double bonded to O below and single bonded to R 1 on the upper left.

C H 2 group below is single bonded to O on the lower right. This O atom is single bonded to P on the upper right. The P atom is partially double bonded to O above, partially double bonded to O on the lower right, and single bonded to O on the right. The partially double bonded O atoms have an overall negative charge. The O atom on the right is single bonded to a 2-carbon alkane chain depicted as

C H 2, single bond, C H 2. C 2 of this chain is single bonded to N superscript plus on the upper right. The N superscript plus atom is single bonded to C H 3 on the upper right, dash bonded to C H 3 on the lower right, and wedge bonded to C H 3 below.

The structure of phosphatidylethanolamine is as follows: A central C atom is dash bonded to C H 2 above, dash bonded to C H 2 below, wedge bonded to O on the left, and wedge bonded to H on the right. This O atom is single bonded to C on the lower left. The C atom is double bonded to O below and single bonded to R 2 on the upper left.

The C H 2 group above is single bonded to O on the upper left. The O atom is single bonded to C on the lower left. This C atom is double bonded to O below and single bonded to R 1 on the upper left.

C H 2 group below is single bonded to O on the lower right. This O atom is single bonded to P on the upper right. The P atom is partially double bonded to O above, partially double bonded to O on the lower right, and single bonded to O on the right. The partially double bonded O atoms have an overall negative charge. The O atom on the right is single bonded to a 2-carbon alkane chain depicted as C H 2, single bond, C H 2. C 2 of this chain is single bonded to N H 3 superscript plus on the upper right.

The structure of phosphatidylinositol is as follows: A central C atom is dash bonded to C H 2 above, dash bonded to C H 2 below, wedge bonded to O on the left, and wedge bonded to H on the right. This O atom is single bonded to C on the lower left. The C atom is double bonded to O below and single bonded to R 2 on the upper left.

The C H 2 group above is single bonded to O on the upper left. The O atom is single bonded to C on the lower left. This C atom is double

bonded to O below and single bonded to R 1 on the upper left.

C H 2 group below is single bonded to O on the lower right. This O atom is single bonded to P on the upper right. The P atom is partially double bonded to O above, partially double bonded to O on the lower right, and single bonded to O on the right. The partially double bonded O atoms have an overall negative charge. The O atom on the right is single bonded to C 5 of a 6-carbon homocyclic hexagonal ring in a chair conformation. In the ring, C 3 and C 6 are located closer. C 1 occupies the top right vertex. C 1 is single bonded to H above and O H on the right. C 2 is single bonded to O H on the right and H below. C 3 is single bonded to H above and O H on the lower right. C 4 is single bonded to O H on the left and H below. C 5 is single bonded to H above. C 6 is single bonded to H on the upper left and O H below.

The structure of diphosphatidylglycerol (cardiolipin) is as follows: A central C atom is dash bonded to C H 2 above, dash bonded to C H 2 below, wedge bonded to O on the left, and wedge bonded to H on the right. This O atom is single bonded to C on the lower left. The C atom is double bonded to O below and single bonded to R 2 on the upper left.

The C H 2 group above is single bonded to O on the upper left. The O atom is single bonded to C on the lower left. This C atom is double bonded to O below and single bonded to R 1 on the upper left.

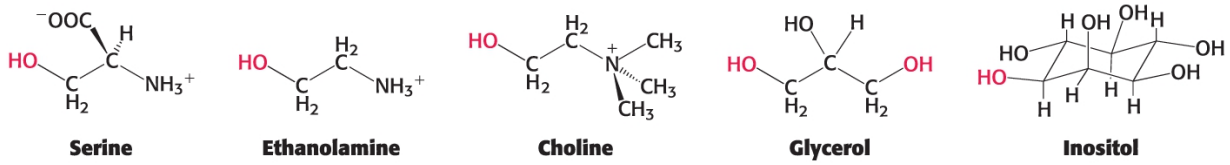
C H 2 group below is single bonded to O on the lower right. This O atom is single bonded to P on the upper right. The P atom is partially double bonded to O above, partially double bonded to O on the lower right, and single bonded to O on the right. The partially double bonded O atoms have an overall negative charge. The O atom on the right is single bonded to a 3-carbon alkane chain depicted as C H 2, single bond, C, single bond, C H 2. C 2 of this chain is single

bonded to H on the lower left and O H on the lower right. C 3 is single bonded to O on the lower right. This O atom is single bonded to P on the upper right. The P atom is partially double bonded to O above, partially double bonded to O below, and single bonded to O on the lower right. The O atom on the lower right is single bonded to C H 2 on the upper right.

C H 2 is wedge bonded above to C, wedge bond, C H 2. C 1 of this chain is dash bonded to H on the right and dash bonded to O on the right. The O atom is single bonded to C on the lower right. This C atom is double bonded to O below and single bonded to R 4 on the upper right. C 2 of the chain is single bonded to O on the upper right. The O atom is further single bonded to C on the lower right. The C atom is double bonded to O below and single bonded to R 3 on the upper right.

Return to Chemical structures of common phosphoglycerides located in the membrane

Extended description for Structures of serine, ethanolamine, choline, glycerol, and inositol



The structure of serine is as follows: A central C atom is wedge bonded to C O O superscript minus on the upper left, dash bonded to H on the upper right, single bonded to N H 3 superscript plus on the lower right, and single bonded to C H 2 on the lower left. The C H 2 group is single bonded to O H on the upper left.

The structure of ethanolamine is as follows: A central C atom bound to H 2 is single bonded to N H 3 superscript plus on the lower right and single bonded to C H 2 on the lower left. The C H 2 group is single bonded to O H on the upper left.

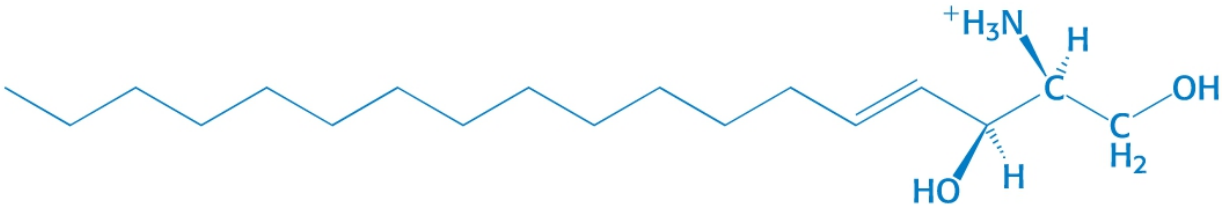
The structure of choline is as follows: A central C atom bound to H 2 is single bonded to N superscript plus on the lower right and single bonded to C H 2 on the lower left. The C H 2 group is single bonded to O H on the upper left. The N superscript plus atom is single bonded to C H 3 on the upper right, dash bonded to C H 3 on the lower right, and wedge bonded to C H 3 below.

The structure of glycerol is as follows: A 3-carbon alkane chain is depicted as a line structure using 2 zigzag lines. C 1 and C 3 are each bound to H 2. C 1 is single bonded to O H on the upper left. C 2 is single bonded to O H on the upper left and single bonded to H on the upper right. C 3 is single bonded to O H on the upper right.

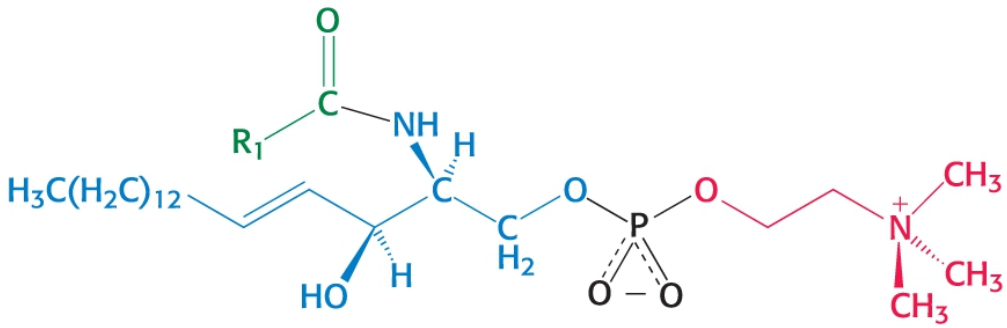
The structure of inositol is as follows: A 6-carbon homocyclic hexagonal ring is in a chair conformation. C 3 and C 6 are located close to each other. C 2, C 3, and C 4 are located toward the observer. C 1, C 5, and C 6 are located away from the observer. C 1 is single bonded to H above and O H on the lower right. C 2 is single bonded to O H on the upper right and H below. C 3 is single bonded to O H above and H below. C 4 is single bonded to O H on the upper left and H below. C 5 is single bonded to H above and O H on the lower right. C 6 is single bonded to O H on the upper right and H below.

Return to Structures of serine, ethanolamine, choline, glycerol, and inositol

Extended description for Structures of sphingosine and sphingomyelin



Sphingosine



Sphingomyelin

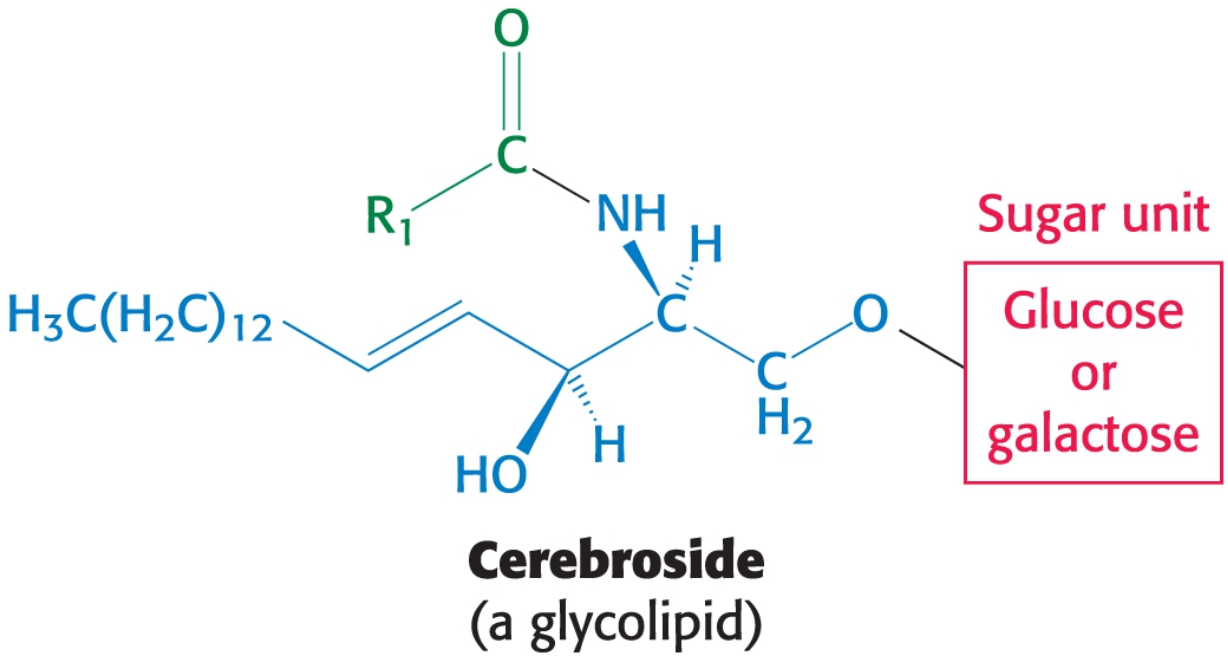
Sphingosine: A 17 Carbon homonuclear alkene chain is depicted as a line structure using 16 zigzag lines. A double bond is present between C 14 and C 15. C 16 is wedge bonded to O H on the lower left and dash bonded to H on the lower right. C 17 is wedge bonded to N H 3 superscript plus on the upper left and dash bonded to H on the upper right. C 17 is also single bonded to C H 2 on the lower right. C H 2 is single bonded to O H on the upper right.

Sphingomyelin: A 1 N, 1 P, 2 O, and 7 C heteronuclear alkene chain is depicted as a line structure using 10 zigzag lines. A double bond is present between C 1 and C 2. C 1 is single bonded to open bracket C H 2 close bracket with subscript 12 C H 3 on the upper left. The O atoms occupy the sixth and eighth positions. P occupies the seventh position. The N atom has an overall positive charge and occupies the

eleventh position. It is single bonded to C H 3 on the upper right, dash bonded to C H 3 on the lower right, and wedge bonded to C H 3 below. C 3 is wedge bonded to O H on the lower left and dash bonded to H on the lower right. C 4 is dash bonded to H on the upper right and wedge bonded to N H on the upper left. N H is single bonded to a central C atom that is double bonded to O above and single bonded to R 1 on the lower left. P is partially double bonded to O on the lower left and O on the lower right. The P O O group has an overall negative charge.

Return to Structures of sphingosine and sphingomyelin

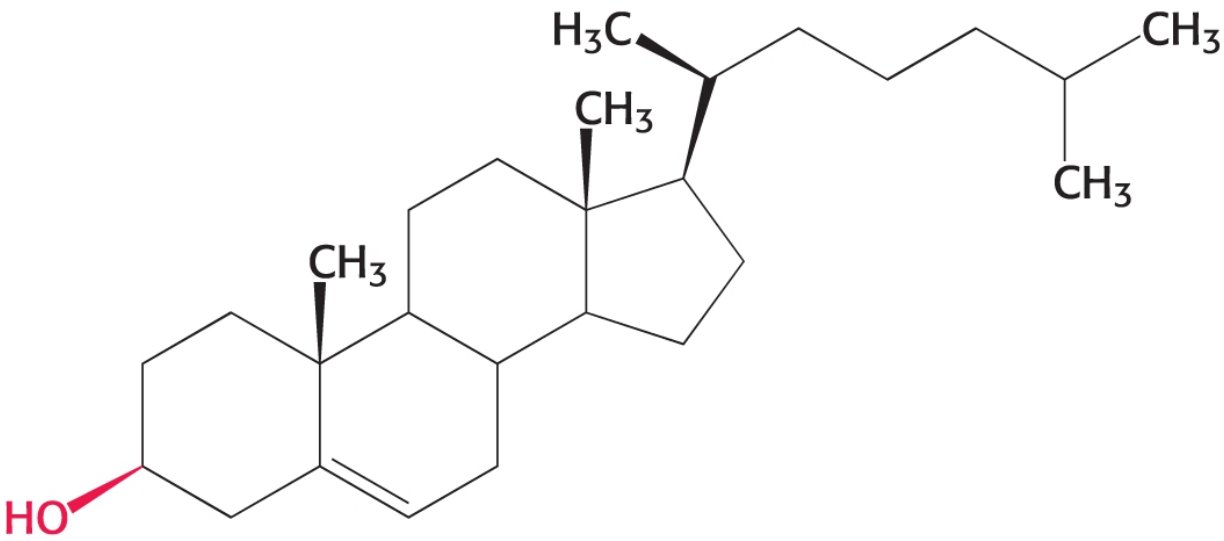
Extended description for Chemical structure of cerebroside



The structure of cerebroside is as follows: A 1 O and 5 C heteronuclear alkene chain is depicted as a line structure using 5 zigzag lines. O occupies the sixth position. A double bond is present between C 1 and C 2. C 1 is single bonded to open bracket C H 2 close bracket with subscript 12 C H 3 on the upper right. C 3 is wedge bonded to O H on the lower left and dash bonded to H on the lower right. C 4 is wedge bonded to N H on the upper left and dash bonded to H on the upper right. C 5 is bound to H 2. O is single bonded to a glucose or galactose molecule on the lower right. The glucose or galactose molecule is labeled sugar unit. The N H group on the upper left is single bonded to C on the upper left. This C atom is double bonded to O above and single bonded to R 1 on the lower right.

Return to Chemical structure of cerebroside

Extended description for Chemical structure of cholesterol



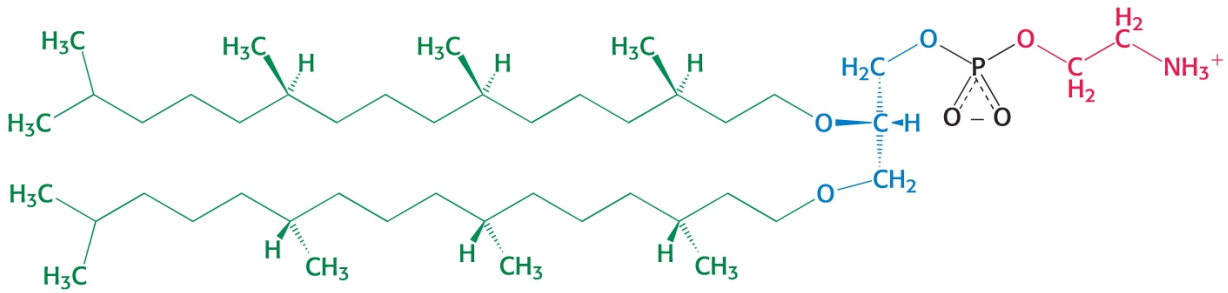
Cholesterol

The structure of cholesterol is as follows: A 6-carbon homocyclic hexagonal ring is in a vertical orientation with C 1 occupying the topmost vertex. C 5 is wedge bonded to O H on the lower left. O H and its wedge bond are highlighted in red. It is fused to a second 6-carbon homocyclic hexagonal ring in a vertical orientation such that C 2 and C 3 of the first ring are C 6 and C 5 respectively of the second ring. In the second ring, C 6 is wedge bonded to C H 3 above. A double bond is present between C 4 and C 5. The second ring is fused to a third 6-carbon homocyclic hexagonal ring in a vertical orientation such that C 1 and C 2 of the second ring are C 5 and C 4 respectively of the third ring. The third ring is fused to a 5-carbon homocyclic pentagonal ring in a horizontal orientation such that C 2 and C 3 of the third ring are C 4 and C 3 respectively of the pentagonal ring. C 4 is wedge bonded to C H 3 above. C 5 is wedge bonded to C 1 of a 5 carbon alkane chain depicted as a line structure

using 4 zigzag lines. C 1 is wedge bonded to C H 3 on the upper left. C 5 is single bonded to C H 3 on the upper right and C H 3 below.

Return to Chemical structure of cholesterol

Extended description for Structure of membrane lipid of the archaeon *Methanococcus jannaschii*



Membrane lipid from the archaeon *Methanococcus jannaschii*

The structure of the membrane lipid is as follows: A vertical chain consists of C H 2, dash bond, C, dash bond, C H 2. C 1 of this chain is single bonded to O 1 of a 1 P, 2 O, and 2 C alkane chain depicted as a line structure using 4 zigzag lines. The first O occupies the first position. The second O occupies the third position. P occupies the second position. C 4 and C 5 are each bound to H 2. P is partially double bonded to O on the lower right and lower left. The P O O group has an overall negative charge. C 5 is single bonded to N H 3 superscript plus on the lower right.

C 2 of the vertical chain is wedge bonded to H on the right and wedge bonded to O on the left. The O atom is single bonded to C 16 of a 16 carbon alkane chain depicted as a line structure using 15 zigzag lines. C 1 is single bonded to C H 3 on the lower left and C H 3 above. C 5, C 9, and C 13 are each wedge bonded to C H 3 on the upper left and dash bonded to H on the upper right.

C 3 of the vertical chain is single bonded to O of an 1 O and 15 C alkane chain depicted as a line structure using 15 zigzag lines. C 1 is single bonded to C H 3 on the upper left and C H 3 below. C 5, C 9, C

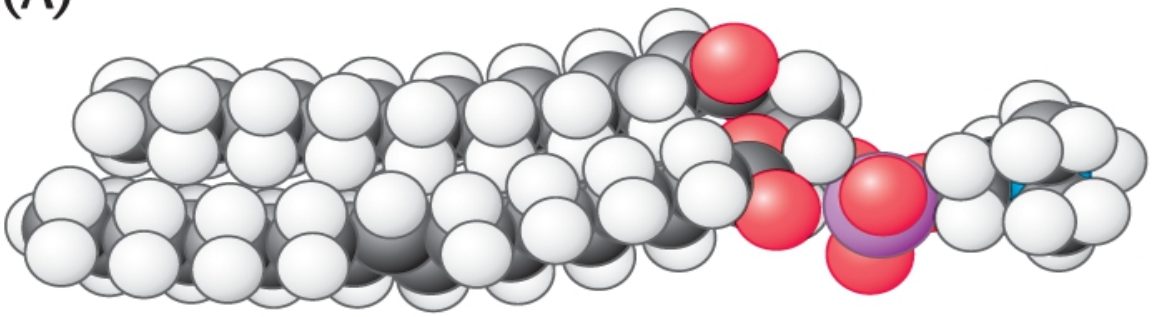
13 are each wedge bonded to H on the lower left and dash bonded to C H 3 on the lower right.

Return to Structure of membrane lipid of the archaeon *Methanococcus jannaschii*

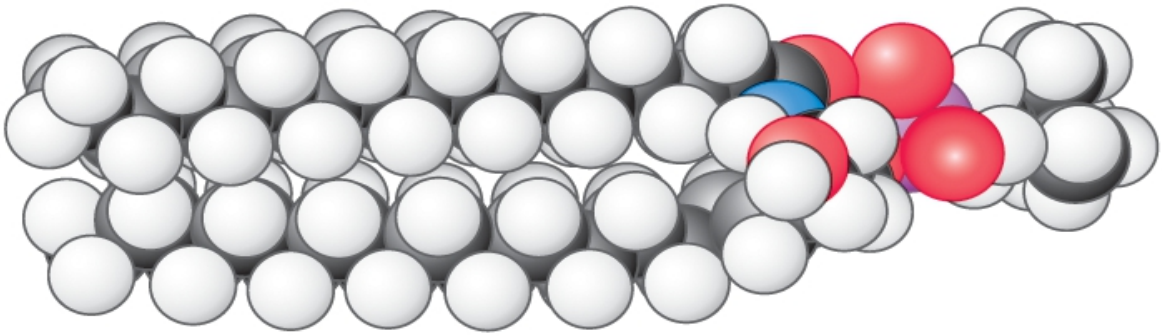
Extended description for Space filling models of phosphoglyceride, sphingomyelin, and an archaeal

lipid; and shorthand depiction of membrane lipid labeled (A) and (B) respectively

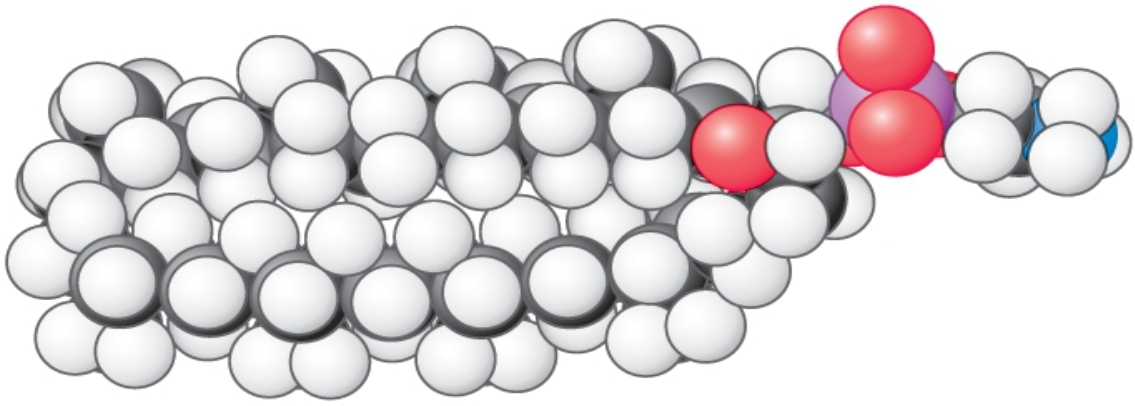
(A)



Phosphoglyceride

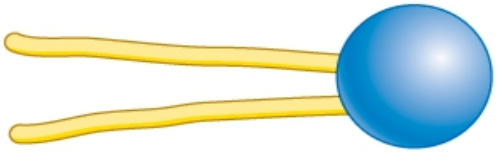


Sphingomyelin



Archaeal lipid

(B)



© Macmillan Learning

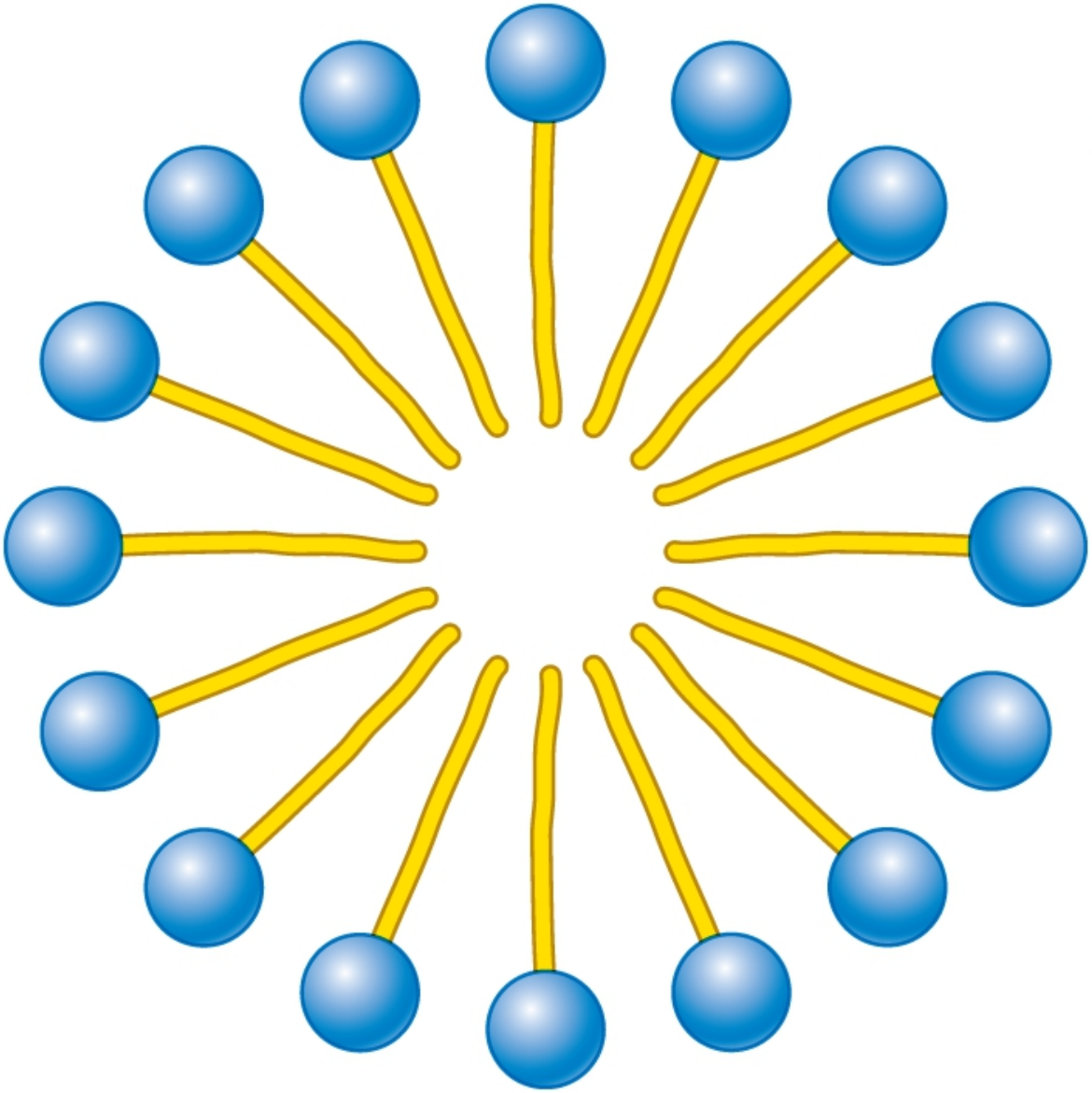
Part (A): The space-filling model consists of two chains of black spheres fused side by side. Each black sphere is fused with three small white spheres. The white spheres cover the entire surface. These chains of black spheres in phosphoglyceride are fused to a cluster of red spheres with a purple sphere in the center. This cluster of red spheres is fused to a small cluster of black spheres which are further fused to white spheres. The white spheres cover the entire surface of the cluster. In sphingomyelin, the chains continue into a cluster composed of red spheres, a blue sphere, and a purple sphere. This cluster of red spheres is fused to a small cluster of black spheres which is further fused to white spheres. The white spheres cover the entire surface of the cluster.

In archaeal lipid, the chains of black sphere continue into a cluster of four red spheres containing a purple sphere in the center. This cluster of red spheres is fused to a small cluster of black spheres which are further fused to white spheres. The white spheres cover the entire surface of the cluster.

Part (B): A blue sphere is connected to two horizontal and anti-parallel yellow extensions.

Return to Space filling models of phosphoglyceride, sphingomyelin, and an archaeal lipid; and shorthand depiction of membrane lipid labeled (A) and (B) respectively

Extended description for Schematic illustration of micelles



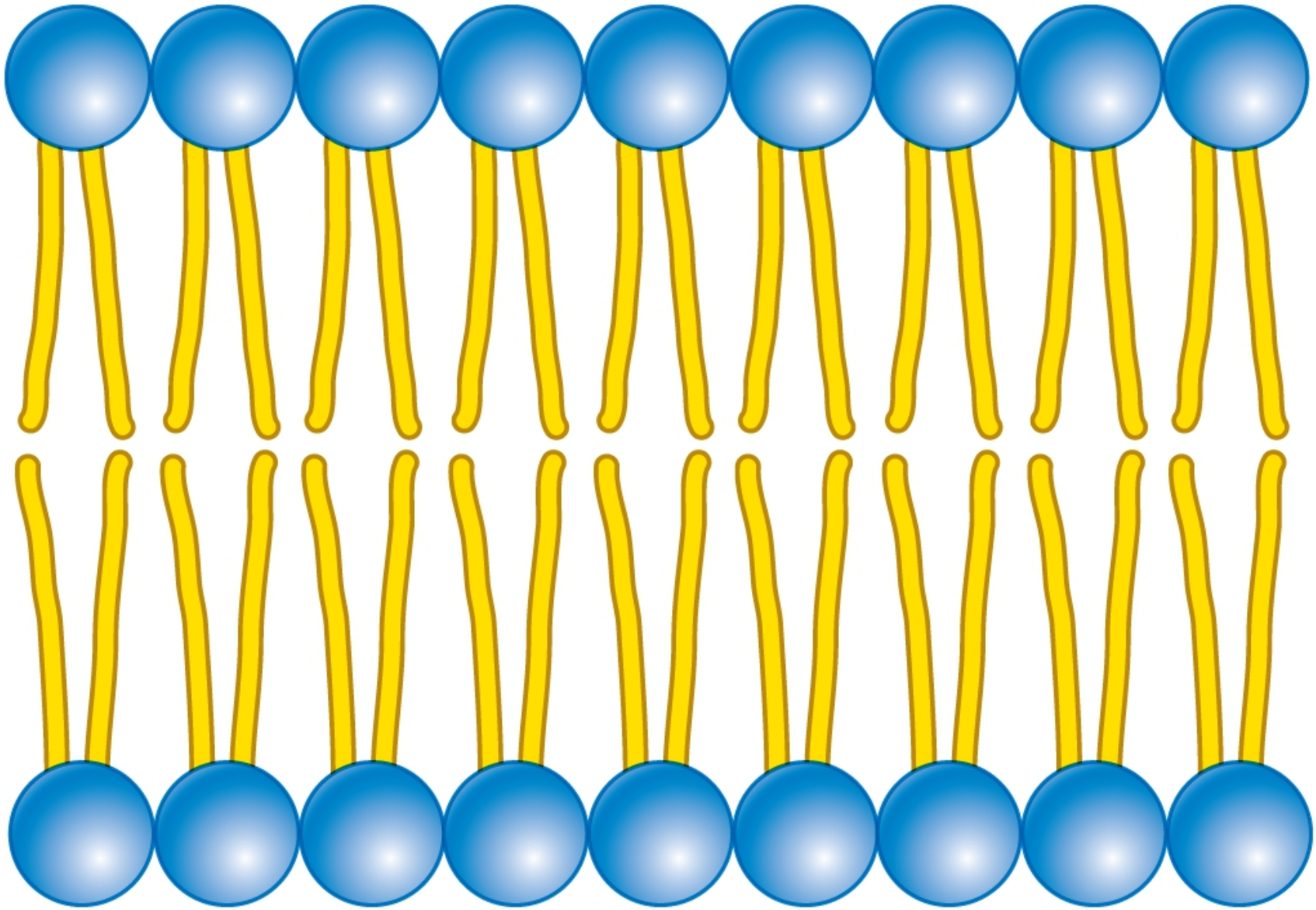
The micelle is depicted as a circular structure composed of 16 ionized fatty acids with single tails. Each ionized fatty acids with single tail is depicted as a blue sphere connected to a long and narrow yellow extension. They are radially arranged such that blue

spheres form the border of the circular structure and yellow extensions form the core.

Return to Schematic illustration of micelles

Extended description for Schematic illustration of lipid

bilayer

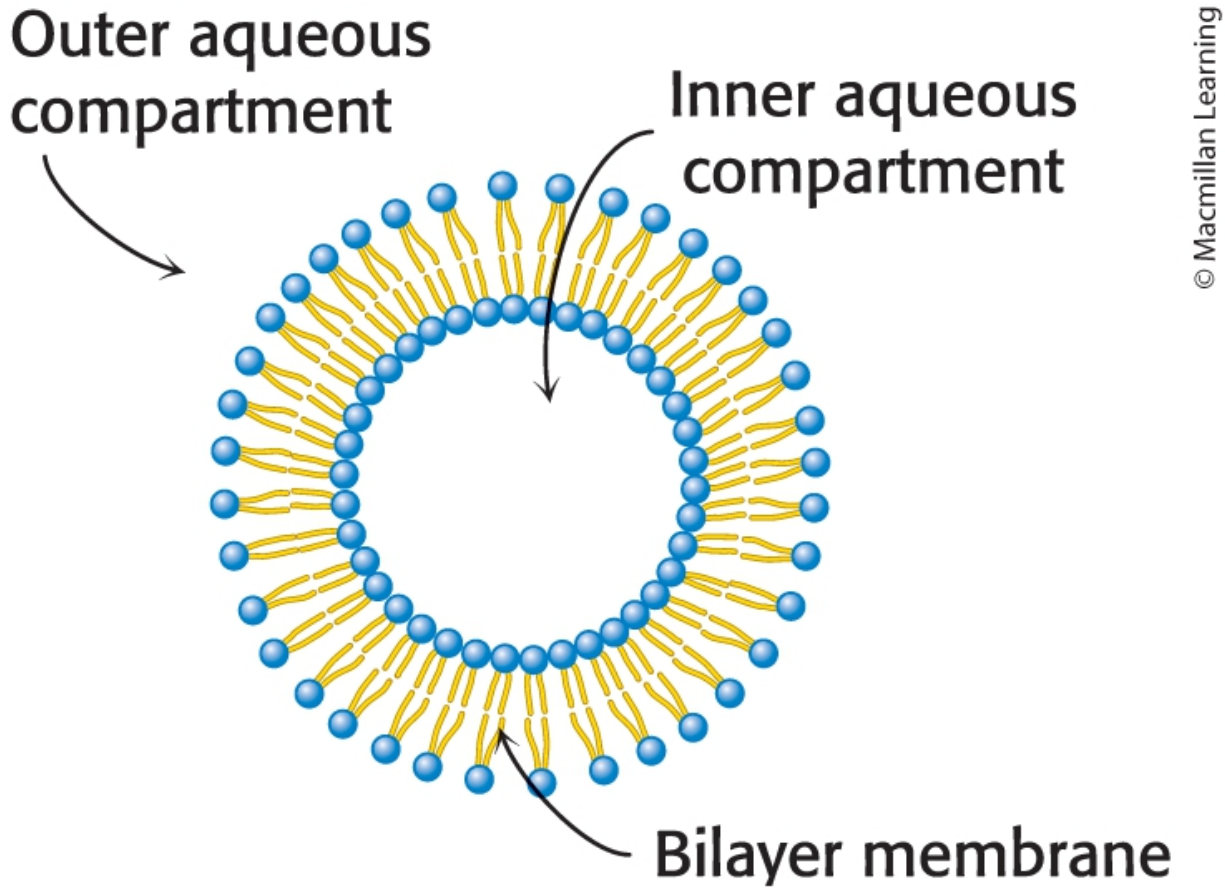


© Macmillan Learning

The lipid bilayer consists of two parallel layers of lipids. Each layer consists of 9 lipid molecules vertically stacked together. The lipid molecules are shown in a shorthand depiction. The yellow extensions of the shorthand depiction from the two layers are aligned together and form the core of the bilayer. The blue spheres of the two layers are located away from each other such that they form the left and right borders of the bilayer.

Return to Schematic illustration of lipid bilayer

Extended description for Schematic illustration of liposome

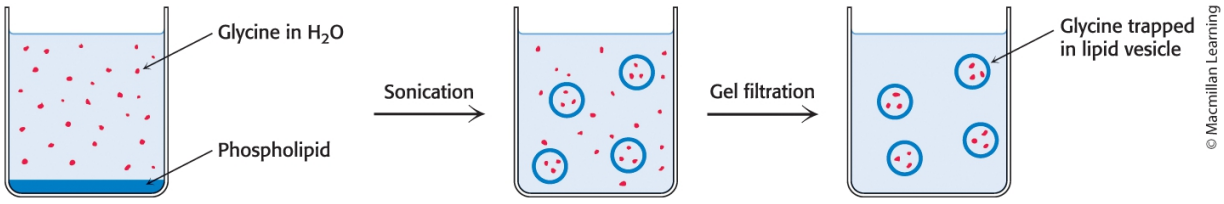


© Macmillan Learning

The liposome is depicted as a circular structure having a lipid bilayer outline and an empty core. The empty core is labeled the inner aqueous compartment. The lipid bilayer is labeled as a bilayer membrane. The space outside the bilayer is labeled the outer aqueous compartment. The blue spheres of the bilayer line the inner and outer surface of the liposome.

Return to Schematic illustration of liposome

Extended description for Production of liposomes containing glycine



A square-shaped vessel is shown to contain water and a layer of phospholipid settled at the bottom. Glycine molecules are suspended in water and are depicted as tiny red particles. Phospholipid is depicted as a thick blue layer.

The procedure is divided into two steps:

Step 1: Sonication.

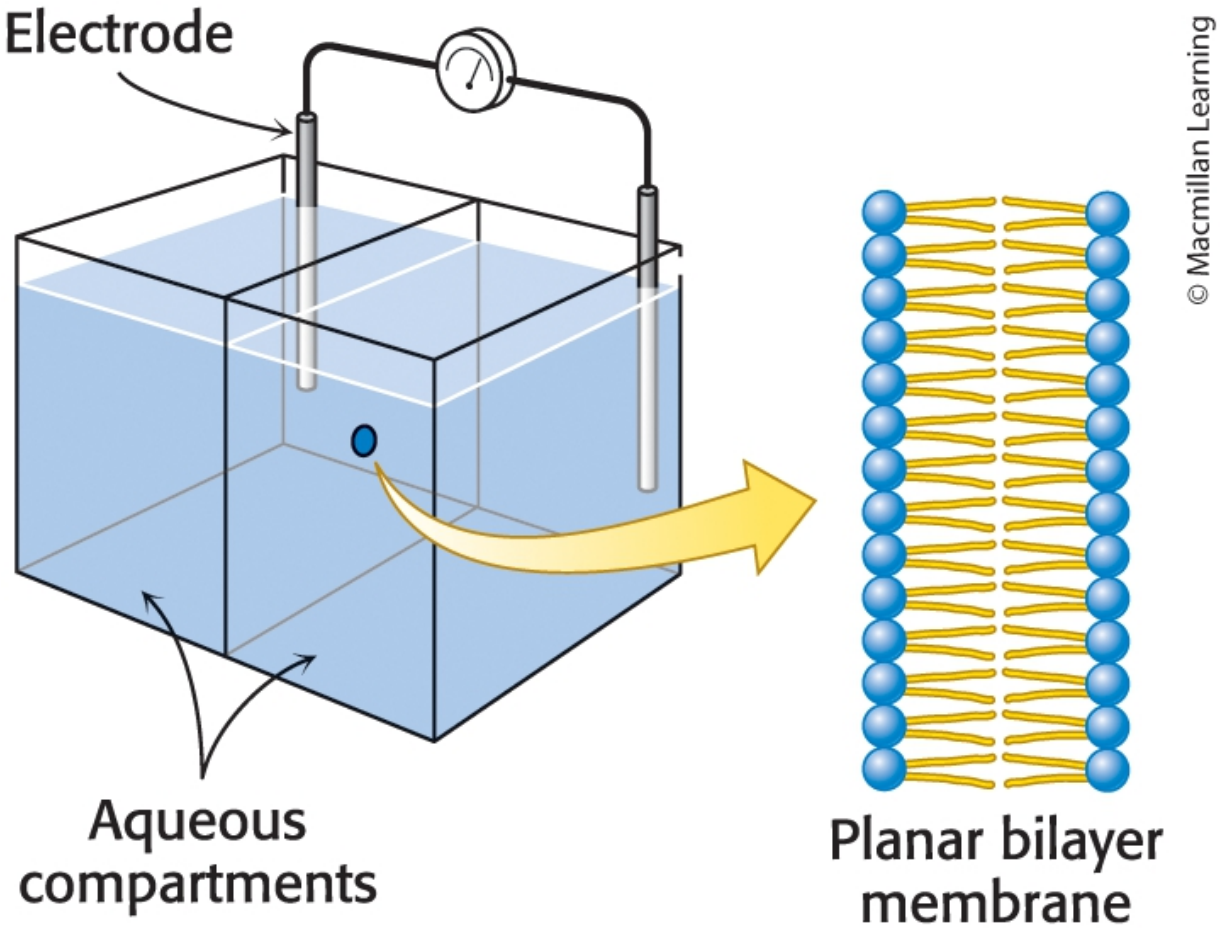
The vessel contains 4 circles with a thick blue border. Each of these circles contain three tiny red particles. Some red particles are suspended in the water outside.

Step 2: Gel filtration

The water in the vessel becomes clear and devoid of any red particles. The glycine trapped in lipid vesicles depicted as circles with thick blue border is highlighted by an arrow.

Return to Production of liposomes containing glycine

Extended description for Experimental study of the properties of planar bilayer membranes

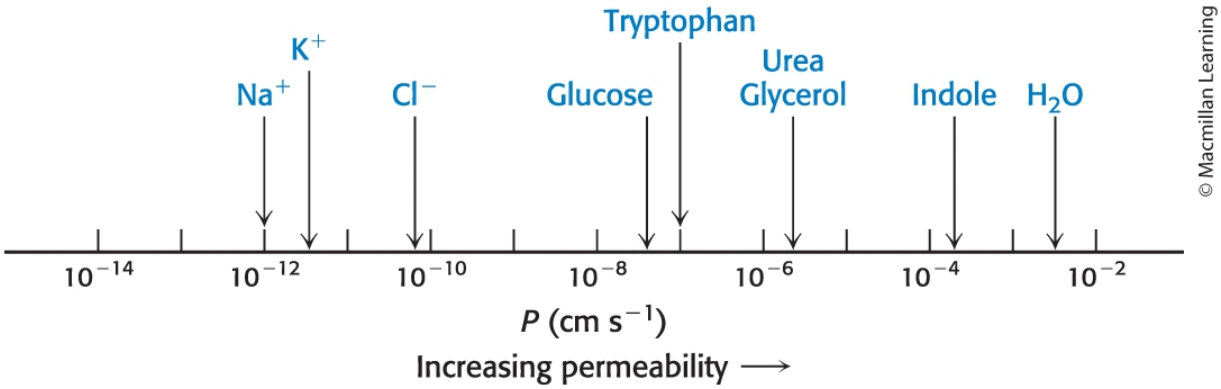


The figure has two parts. The first part shows an experimental setup consisting of a large tank. The tank is separated into two compartments with the help of a septum. Both the compartments are filled equally with water and are labeled aqueous compartments. An electrode is dipped inside each compartment. The electrodes are connected to each other through a meter. The center of the septum contains a tiny blue circle representing the hole. An arrow from hole points toward a planar bilayer membrane. The planar bilayer membrane consists of two vertically parallel layers of lipids. Each

layer consists of 14 lipid molecules stacked together. Each lipid molecule is shown in a shorthand depiction. The yellow extensions of the shorthand depiction are aligned together and form the core of the bilayer. The blue spheres are located away from each other.

Return to Experimental study of the properties of planar bilayer membranes

Extended description for The permeability coefficients (P) of ions and molecules in a lipid bilayer



© Macmillan Learning

The figure shows a horizontal scale labeled “permeability (centimeter second superscript negative 1)”. It increases from left to right. The scale has markings ranging from 10 superscript negative 14 to 10 superscript negative 2 in multiples of 10 superscript 2. The permeability of different ions and molecules is represented with the help of downward arrows on this scale. The permeability of different ions and molecules are as follows:

N a superscript plus: 10 superscript negative 12.

K superscript plus: 5 times 10 superscript negative 12.

C l superscript minus: 9 times 10 superscript negative 11.

Glucose: 6 times 10 superscript negative 8.

Tryptophan: 10 superscript negative 7.

Urea Glycerol: 3 times 10 superscript negative 6.

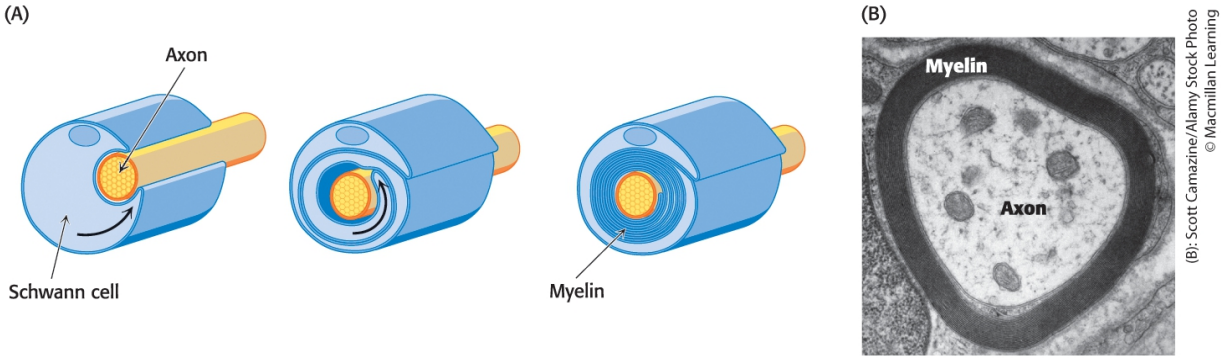
Indole: 3 times 10 superscript negative 4.

H 2 O: 5 times 10 superscript negative 3.

All values are approximated.

Return to The permeability coefficients (P) of ions and molecules in a lipid bilayer

Extended description for Schematic illustration of the wrapping of Schwann cell membrane around an axon and an electron micrograph of myelin sheath around the axon



Part (A): It shows the wrapping of Schwann cell membrane around an axon in three steps.

Step 1: A cross-section of tubular axon is wrapped by a thick Schwann cell half-way through. A curved upward arrow shows the direction of wrapping of the Schwann cell membrane.

Step 2: The tubular axon is surrounded by 2 layers of the cell membrane as the wrapping continues in the inward direction.

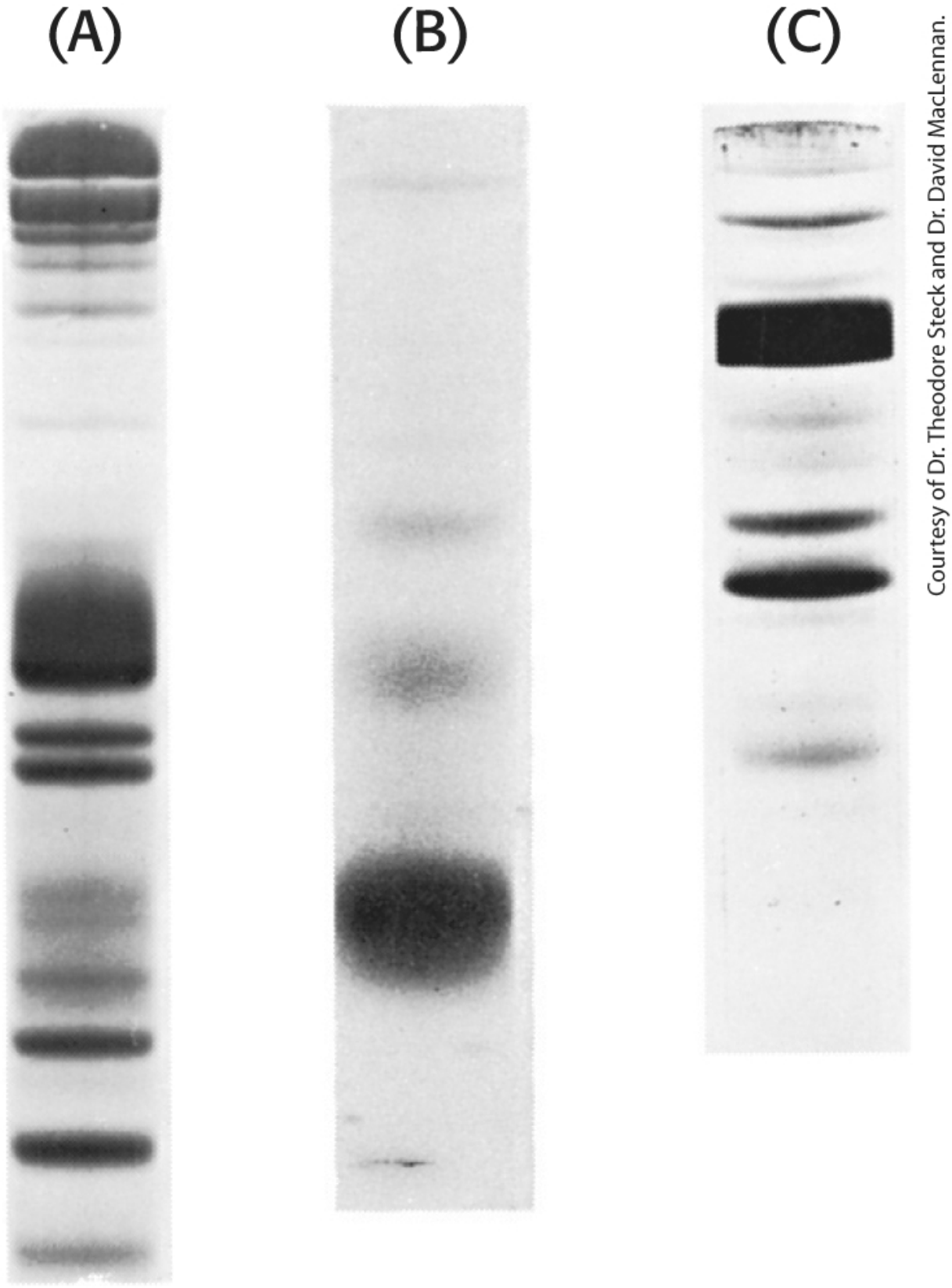
Step 3: The axon cross-section is surrounded by multiple layers of Schwann cell membrane. This thick layer of membrane is labeled myelin.

Part (B): A cross-section of axon is surrounded by a thick and dark layer of myelin.

Return to Schematic illustration of the wrapping of Schwann cell membrane around an axon and an electron micrograph of myelin sheath around the axon

Extended description for S D S gel patterns of

membrane proteins from different cell types



Courtesy of Dr. Theodore Steck and Dr. David MacLennan.

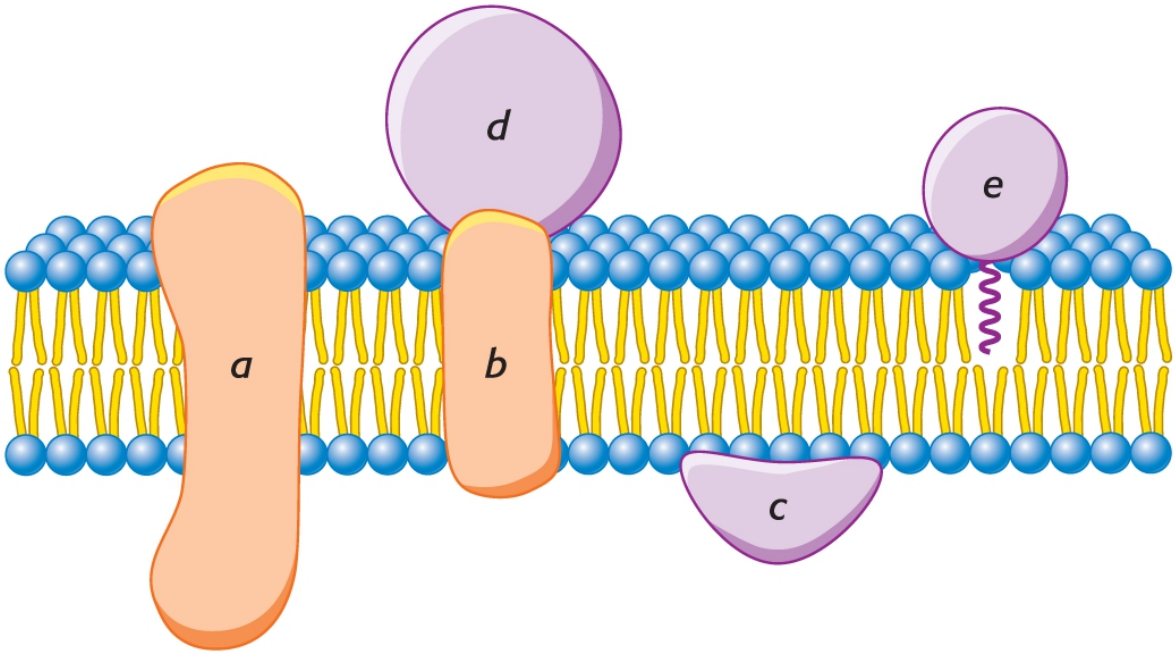
(A): The S D S gel pattern consists of a series of dark and light bands having narrow to medium thickness.

(B): The S D S gel pattern consists of a thick dark band near the bottom and two faint bands above it.

(C): The S D S gel pattern consists of a thick dark and rectangular band near the top. Two dark bands of medium thickness are seen below it. Two narrow and faint bands are seen above it. A narrow faint band is located below the medium thickness bands.

Return to S D S gel patterns of membrane proteins from different cell types

Extended description for Membrane proteins interact with lipid bilayers in different ways



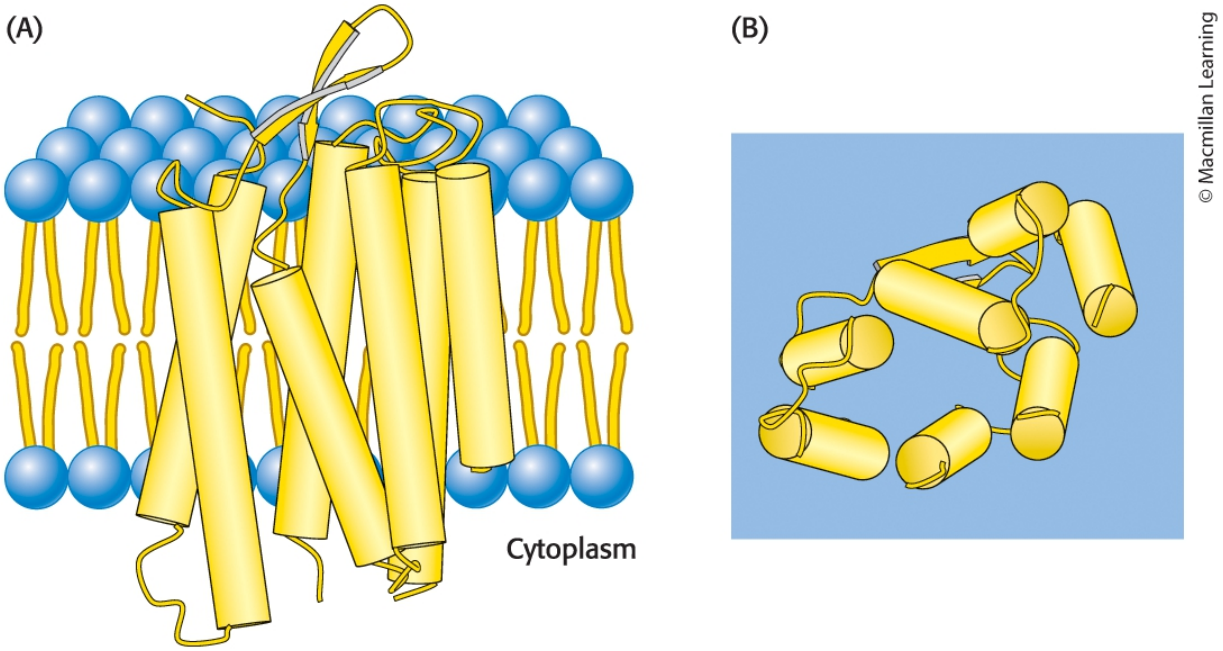
© Macmillan Learning

The lipid bilayer consists of two horizontally parallel layers of lipids. The upper layer consists of three rows of lipid molecules packed together compactly. Each lipid molecule is shown in a shorthand depiction. The yellow extensions of the shorthand depiction are aligned together and form the core of the bilayer. The blue spheres are located away from each other. The lipid bilayer shows five membrane proteins. The first membrane protein labeled "a" resembles a sausage. It traverses the lipid bilayer and extends above and below the bilayer. The second protein labeled "b" also resembles a sausage. Its size is relatively short than "a" and it also traverses the bilayer but does not extend above and below the bilayer. The third protein labeled "c" resembles an inverted triangle. This protein is attached to the lower surface of the lipid bilayer. The fourth oval-shaped protein labeled "d" is attached to the blue spheres of the outer leaflet of the lipid bilayer and protein b. The fifth oval-shaped

protein labeled "e" is attached to the top surface of the lipid bilayer through a zigzag anchor that penetrates the core of the bilayer halfway through.

Return to Membrane proteins interact with lipid bilayers in different ways

Extended description for Schematic illustration of the view of bacteriorhodopsin through the membrane and cytoplasmic side



Part (A): The membrane is depicted as a lipid bilayer. It is composed of shorthand depictions of lipids. The bacteriorhodopsin is composed of seven vertical cylindrical structures and a pair of anti-parallel beta-strands interconnected by thread-like loops. The cylindrical structures pass vertically through the membrane and the beta-strands project into the external space above the membrane surface.

Part (B): The bacteriorhodopsin is composed of a cluster of 5 short cylindrical structures interconnected to each other and the remaining two cylinders and a pair of beta-strands through thread-like loops. The 5 cylinders form a circular shape with a hollow space in the center.

Return to Schematic illustration of the view of bacteriorhodopsin through the membrane and cytoplasmic side

Extended description for Amino acid sequence of the membrane spanning helices of bacteriorhodopsin



The amino acid sequence is as follows:

First line: A Q I T G R P E W I W L A L G T A L M G L G T L Y F L V K G M G V S D P D A K K F Y A I T T L V P A. The sequences R P E W I W L A L G T A L M G L G T L Y F L V K and D P D A K K F Y A I T T L V P A are highlighted. In the first sequence R, E, and K are highlighted in red. In the second sequence, 2 D and 2 K are highlighted in red.

Second line: I A F T M Y L S M L L G Y G L T M V P F G G E Q N P I Y W A R Y A D W L F T T P L L L L D L A L L V. The sequences I A F T M Y L S M L and W A R Y A D W L F T T P L L L L D L A L are highlighted. An E residue between the two sequences is highlighted in red. In the second sequence, R and 2 D are highlighted in red.

Third line: D A D Q G T I L A L V G A D G I M I G T G L V G A L T K V Y S Y R F V W W A I S T A A M L Y I L Y V. The sequences D Q G T I L A L V G A, G I M I G T G L V G A L and Y S Y R F V W W A I S T A A M L Y I L Y V are highlighted. The first, second, and third D are highlighted in red. K residue between the two sequences is highlighted in red. An R residue in the second sequence is highlighted in red.

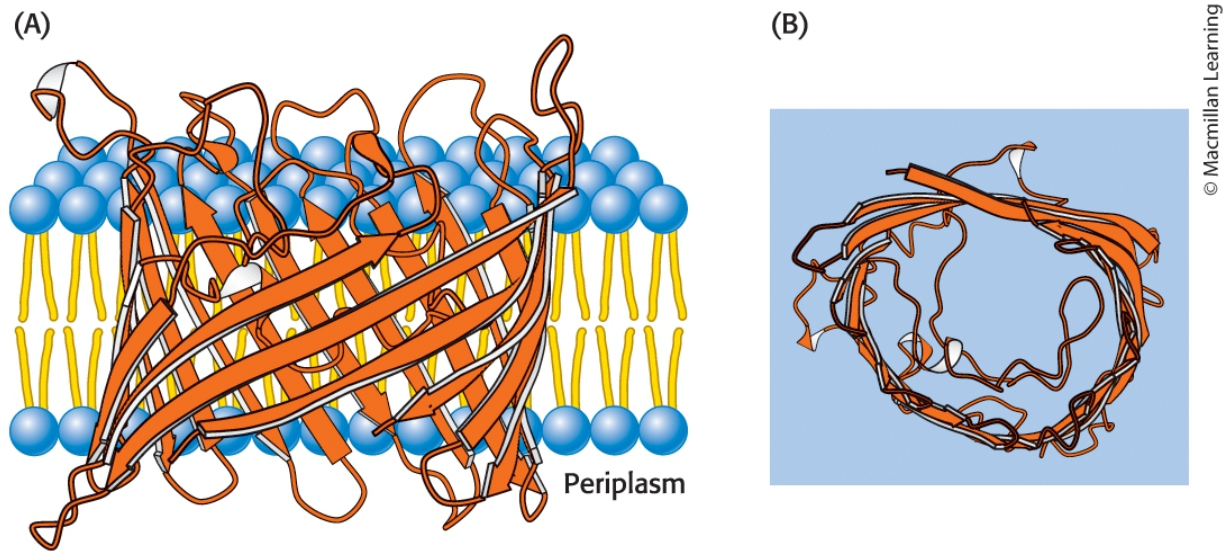
Fourth line: L F F G F T S K A E S M R P E V A S T F K V L R N V T V V L W S A Y V V V W L I G S E G A G I V P L. The sequence A S T F K V L

R N V T V V L W S A Y V V V W L I is highlighted. All the K, E, and R residues are highlighted in red. The last L is highlighted in yellow.

Fifth line: N I E T L L F M V L D V S A K V G F G L I L L R S R A I F G E A E A P E P S A D G A A A T S. The sequence N I E T L L F M V L D V S A K V G F G L I L L R is highlighted. All the E, D, K, R, and P residues are highlighted in red.

Return to Amino acid sequence of the membrane spanning helices of bacteriorhodopsin

Extended description for Schematic illustration of the side view and periplasmic view of porin protein from *Rhodopseudomonas blastica*

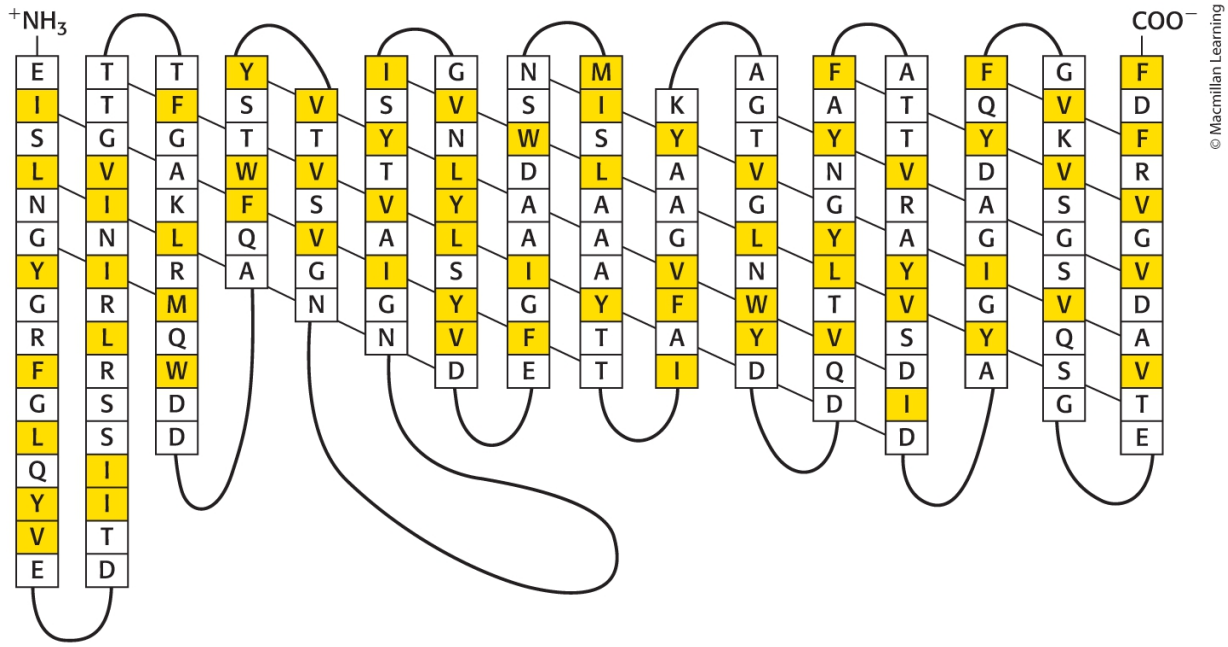


Part (A): The membrane is depicted as a lipid bilayer. It is composed of shorthand depictions of lipids. The porin protein has a barrel-shaped structure that is open at the top and bottom. It is composed of diagonally orientated anti-parallel beta strands interconnected by thread-like loops. The loops extend above and below the external and periplasmic surface respectively.

Part (B): The porin protein is depicted as a circular structure with a border composed of beta-strands. Some thread-like loops extend into the hollow interior of the protein.

Return to Schematic illustration of the side view and periplasmic view of porin protein from *Rhodopseudomonas blastica*

Extended description for Secondary structure of porin protein from *Rhodopseudomonas blastica*



The secondary structure of porin contains 16 vertical chains arranged side by side. Each of these chains has a different sequence. Their sequence from top to bottom is as follows:

Sequence 1: E I S L N G Y G R F G L Q Y V E.

Sequence 2: T T G V I N I R L R S S I I T D.

Sequence 3: T F G A K L R M Q W D D.

Sequence 4: Y S T W F Q A.

Sequence 5: V T V S V G N.

Sequence 6: I S Y T V A I G N.

Sequence 7: G V N L Y L S Y V D.

Sequence 8: N S W D A A I G F E.

Sequence 9: M I S L A A A Y T T.

Sequence 10: K Y A A G V F A I.

Sequence 11: A G T V G L N W Y D.

Sequence 12: F A Y N G Y L T V Q D.

Sequence 13: A T T V R A Y V S D I D.

Sequence 14: F Q Y D A G I G Y A.

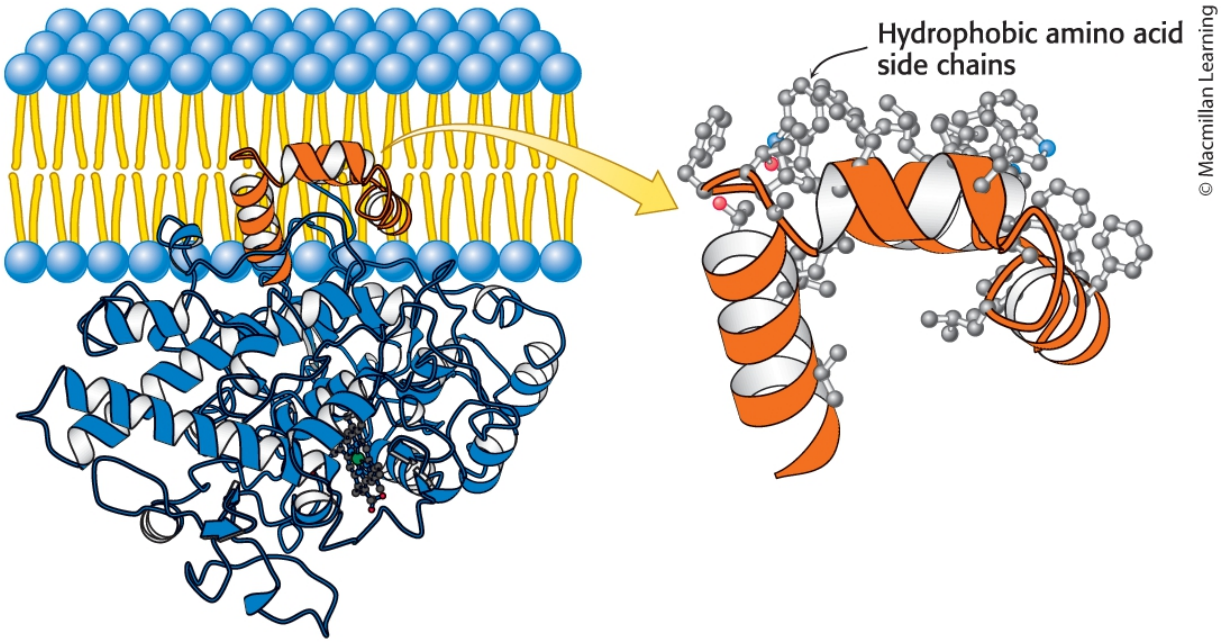
Sequence 15: G V K V S G S V Q S G.

Sequence 16: F D F R V G V D A V T E.

The first E residue of sequence 1 is single bonded to N H 3 superscript plus and the first F residue of sequence 16 is single bonded to C O O superscript minus. The wavy lines connect the adjacent chains from top and bottom in an alternating manner. Diagonal lines are drawn across the chains indicating hydrogen bonding. The hydrophobic residues F I L M V W and Y are highlighted in yellow.

Return to Secondary structure of porin protein from *Rhodopseudomonas blastica*

Extended description for Ribbon structure of prostaglandin H 2 synthase-1 attached to the membrane surface

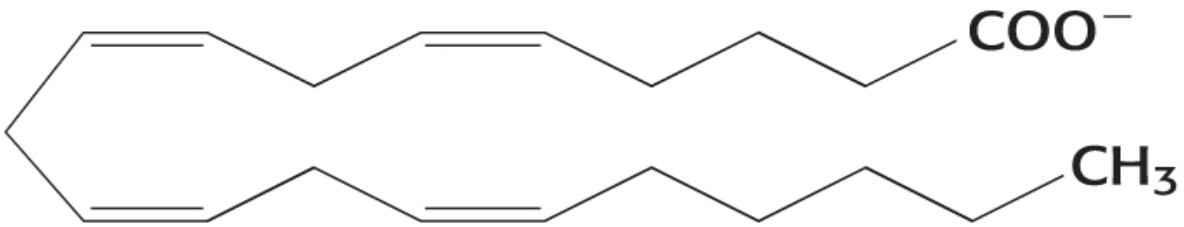


The membrane is depicted as a lipid bilayer. It is composed of shorthand depictions of lipids. The prostaglandin H 2 synthase-1 is composed of several alpha helices and a few beta-strands interconnected by thread-like loops. It is connected to the membrane through three alpha-helices at the top shown in orange. These alpha-helices are integrated into the yellow extensions of the lipid molecules. An arrow shows the enlarged view of the three orange alpha-helices interacting with ball-and-stick models of hydrophobic amino acid side chains. The ball-and-stick models are composed of grey spheres.

Return to Ribbon structure of prostaglandin H 2 synthase-1 attached to the membrane surface

Extended description for Step-wise formation of

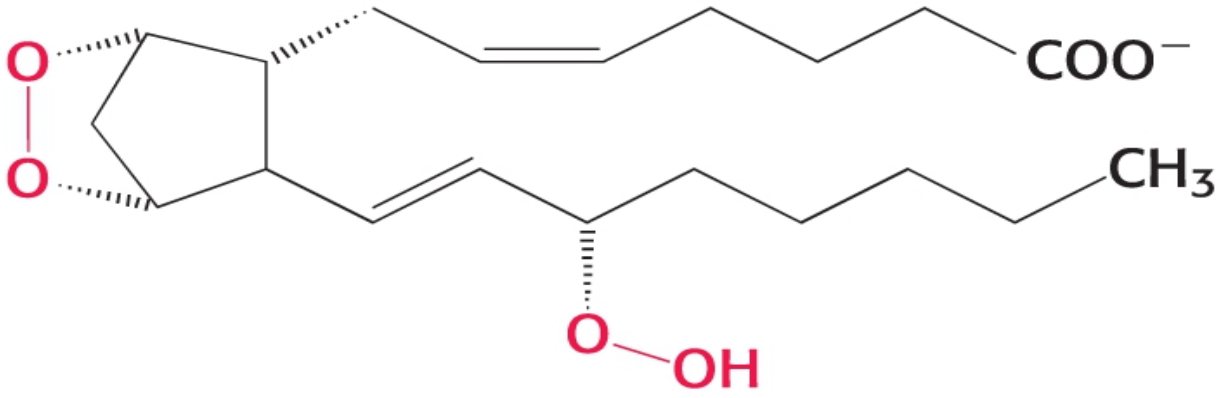
prostaglandin H 2 from arachidonate



Arachidonate

Cyclooxygenase

2 O_2

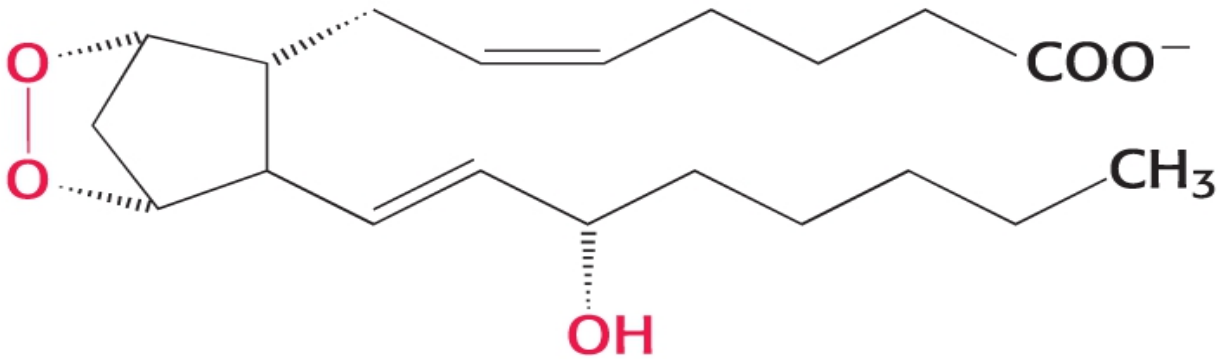


Prostaglandin G_2

Peroxidase

2 H^+ + 2 e^-

H_2O



Prostaglandin H_2

The conversion of arachidonate to prostaglandin H 2 occurs in two steps.

First step: The conversion of arachidonate to prostaglandin G 2 is catalyzed by cyclooxygenase and involves the addition of 2 O 2.

The structure of arachidonate is as follows: An 18-carbon alkene chain is depicted as a line structure using 17 zigzag lines. A double bond is present between C 4 and C 5, C 7 and C 8, C 10 and C 11, and C 13 and C 14. C 1 is single bonded to C O O superscript minus on the upper right. C 18 is single bonded to C H 3 on the upper right. The alkene chain is folded at C 9.

The structure of prostaglandin G 2 is as follows: A 5 carbon homocyclic pentagonal ring is in a horizontal orientation with C 1 occupying the leftmost vertex. C 2 is dash bonded to O on the lower left. C 5 is dash bonded to O on the upper left. The O's are single bonded to each other. C 3 is dash bonded to C 6 of a 6 carbon alkene chain depicted as a line structure using 5 zigzag lines. A double bond is present between C 4 and C 5. C 1 is single bonded to C O O superscript minus on the lower right. C 4 of the pentagonal ring is single bonded to C 7 of a 7 carbon alkene chain depicted as a line structure using 6 zigzag lines. A double bond is present between C 6 and C 7. C 5 is dash bonded to O below. This O is single bonded to O H on the lower right. C 1 is single bonded to C H 3 on the upper right.

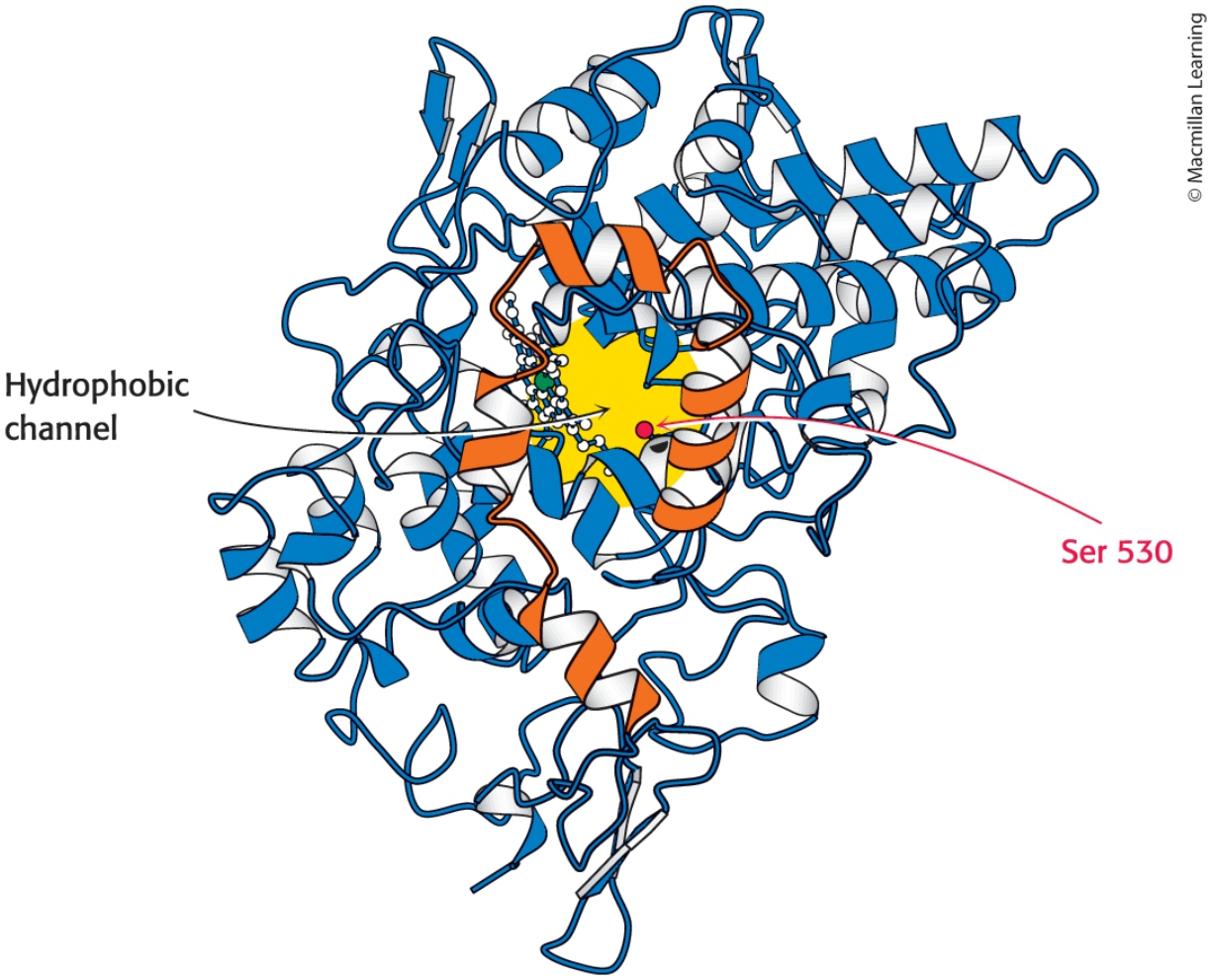
Second step: The conversion of prostaglandin G 2 to prostaglandin H 2 is catalyzed by peroxidase. It also involves the formation of H 2 O from 2 H superscript plus and 2 electrons.

The structure of prostaglandin H 2 is as follows: A 5 carbon homocyclic pentagonal ring is in a horizontal orientation with C 1

occupying the leftmost vertex. C 2 is dash bonded to O on the lower left. C 5 is dash bonded to O on the upper left. The O's are single bonded to each other. C 3 is dash bonded to C 6 of a 6 carbon alkene chain depicted as a line structure using 5 zigzag lines. A double bond is present between C 4 and C 5. C 1 is single bonded to C O O superscript minus on the lower right. C 4 of the pentagonal ring is single bonded to C 7 of a 7 carbon alkene chain depicted as a line structure using 6 zigzag lines. A double bond is present between C 6 and C 7. C 5 is dash bonded to O H below. C 1 is single bonded to C H 3 on the upper right.

Return to Step-wise formation of prostaglandin H 2 from arachidonate

Extended description for Ribbon structure of prostaglandin H 2 synthase-1 containing a hydrophobic channel



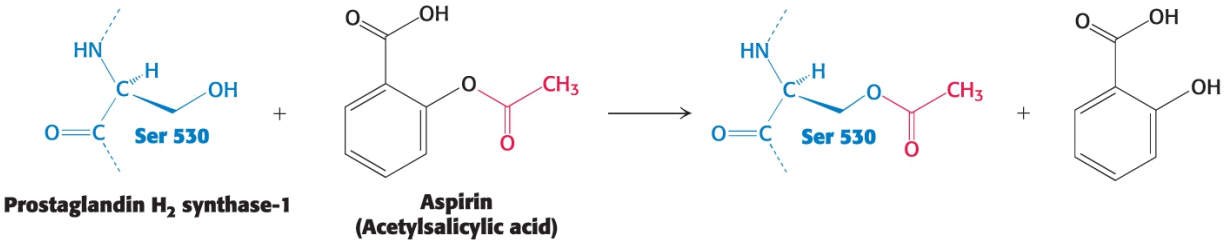
© Macmillan Learning

The ribbon structure shows the membrane-facing side of prostaglandin H 2 synthase-1. It is composed of several alpha-helices and a few beta-strands interconnected by thread-like loops. A central hollow space lined by the helices is highlighted in yellow and labeled hydrophobic channel. A set of three orange alpha-helices are located around the hydrophobic channel. A serine 530 residue attached to one of the alpha-helix around the channel is

depicted as a tiny red circle. A ball-and-stick model consisting of a green sphere and a several white spheres is connected to a few alpha-helices around the channel.

Return to Ribbon structure of prostaglandin H 2 synthase-1 containing a hydrophobic channel

Extended description for Acetyl group transfer to serine residue of prostaglandin H 2 synthase 1 by aspirin



The reaction consists of two reactants and two products. The first reactant is prostaglandin H 2 synthase-1 and its structure is as follows: A central carbon atom is single bonded to N H on the upper left. N H has an open single bond on the top right. The central C atom is dash bonded to H on the upper right, wedge bonded to C H 2 on the lower right, and single bonded to C on the lower left. The C atom on the lower left is double bonded to O on the left and has an open single bond on the lower right. C H 2 group is single bonded to O H on the upper right. The entire structure is labeled S e r 530.

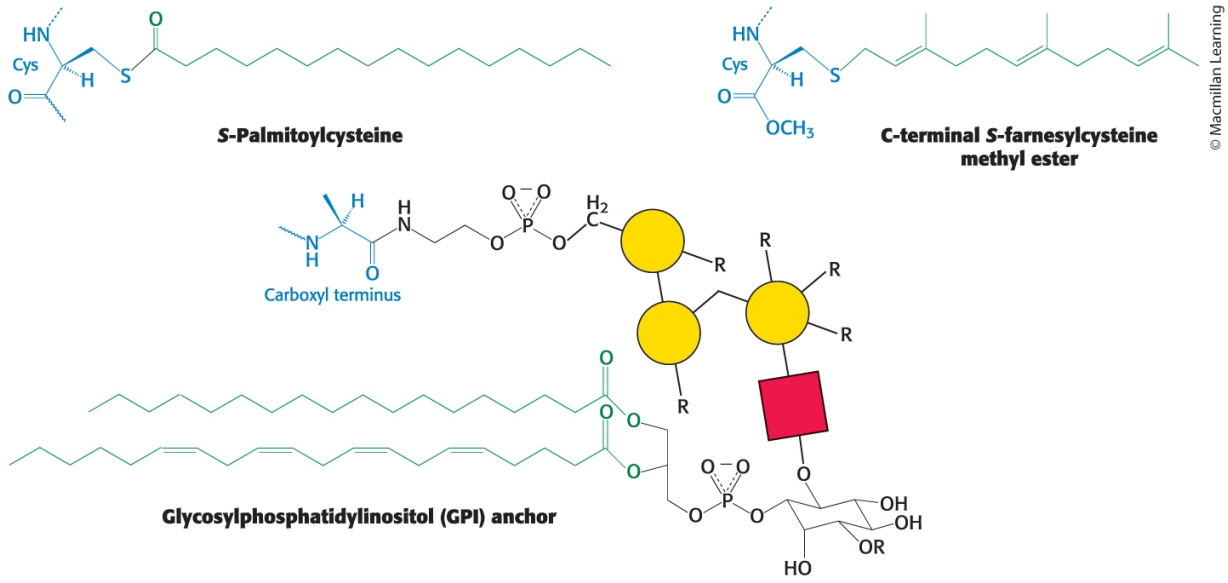
The second reactant is aspirin and its structure is as follows: A benzene ring is in a vertical orientation with C 1 occupying the topmost vertex. A double bond is present between C 2 and C 3, C 4 and C 5, and C 6 and C 1. C 1 is single bonded to a central C atom above in the form of a line. The central C atom is double bonded to O on the upper left and single bonded to OH on the upper right. C 2 is single bonded to O atom of an 1 O and 1 C heteronuclear alkane chain depicted as a line structure using 1 line. O occupies the first position. C atom of this alkane chain is double bonded to O below and single bonded to C H 3 on the upper right. The C O C H 3 group is highlighted in red.

The structure of the first product is as follows: A central carbon atom is single bonded to N H on the upper left. N H has an open single bond on the top right. The central C atom is dash bonded to H on the upper right, wedge bonded to C H 2 on the lower right, and single bonded to C on the lower left. The C atom on the lower left is double bonded to O on the left and has an open single bond on the lower right. C H 2 group is single bonded to the O atom of a 1 O and 1 C heteronuclear alkane chain depicted as a line structure using 1 line. O occupies the first position. C 1 of this alkane chain is double bonded to O below and single bonded to C H 3 on the upper right. The C O C H 3 group is highlighted in red.

The structure of the second product is as follows: A benzene ring is in a vertical orientation with C 1 occupying the topmost vertex. Alternating double bonds are present between C 2 and C 3, C 4 and C 5, and C 6 and C 1. C 1 is single bonded to a central C atom above in the form of a line. The central C atom is double bonded to O on the upper left and single bonded to O H on the upper right. C 2 is single bonded to O H on the upper right.

Return to Acetyl group transfer to serine residue of prostaglandin H 2 synthase 1 by aspirin

Extended description for Structures of S-Palmitoyl cysteine, C-terminal S-farnesyl cysteine methyl ester, and Glycosylphosphatidylinositol (G P I) anchor



The structure of S- Palmitoyl cysteine is as follows: A 16-carbon alkane chain is depicted as a line structure using 15 zigzag lines. C 1 is single bonded to S on the lower left and double bonded to O above. S is single bonded to C on the upper left. This C atom is wedge bonded on the lower left to a central C atom of cysteine residue. The central C atom is dash bonded to H on the lower left, single bonded to N H on the upper left, and single bonded to another C atom on the lower left in the form of a line. N H has an open single bond on the top right. The C atom on the lower left is double bonded to O on the left and single bonded to C H 3 on the lower right in the form of a line.

The structure of C-terminal S-farnesyl cysteine methyl ester is as follows: A 13-carbon alkene chain is depicted as a line structure using 12 zigzag lines. A double bond is present between C 2 and C 3,

C 6 and C 7, C 10 and C 11. C 1 is single bonded to S on the lower left. C 3, C 7 and C 11 are each single bonded to C H 3 above in the form of a line. S is single bonded C on the upper left. This C is wedge bonded to a central C atom of cysteine residue on the lower left. The central C is dash bonded to H on the lower left, single bonded to N H on the upper left, and single bonded to another C atom on the lower left in the form of a line. N H has an open single bond on the top right. The C atom on the lower left is double bonded to O on the left and single bonded to O C H 3 on the lower right.

The structure of glycosylphosphatidylinositol (G P I) anchor is as follows: A 1 P, 2 O, 2 N, and 5 C alkane chain depicted as a line structure using 9 zigzag lines. O atoms occupy the seventh and ninth positions. P occupies the eighth position. N occupies the first and fourth positions and are bound to H atoms. N 1 has an open single bond on the upper left. P is partially double bonded to O on the upper left and O on the upper right. The P O O group has an overall negative charge. C 2 is dash bonded to H on the upper right and wedge bonded to C H 3 on the upper left in the form of a line. C 3 is double bonded to O below. C 10 is bound to H 2 and is single bonded to a yellow circle on the right.

This yellow circle is single bonded to another yellow circle below. Both the yellow circles are single bonded to R. The yellow circle below is single bonded to C H 2 on the upper right in the form of a line. This C H 2 group is single bonded to a third yellow circle on the lower right. The third yellow circle is single bonded to R above, R on the upper right, and R on the lower right. It is single bonded to a red square below.

The red square is single bonded to O below. This O atom is single bonded to C 6 of a 6-carbon homocyclic ring in a chair conformation. In this ring, C 3 and C 6 are located closer. C 1 and C 2 are each single bonded to O H on the right. C 3 is single bonded to O

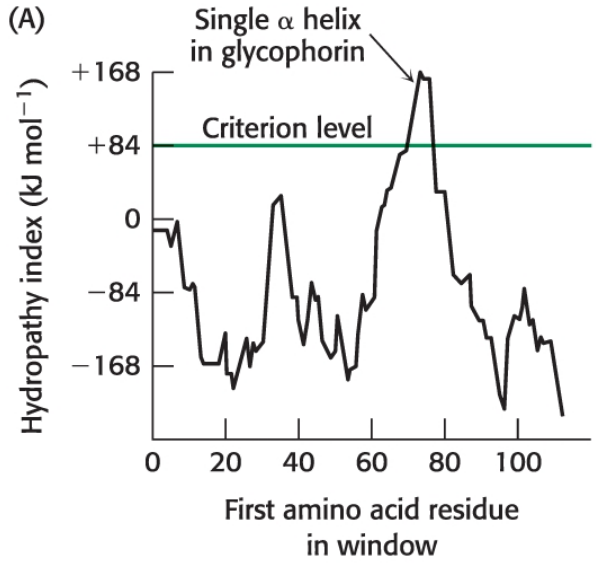
R on the lower right. C 4 is single bonded to O H below. C 5 is single bonded to O on the lower left. This O atom is single bonded to a P atom on the upper left. This P atom is partially double bonded to O on the upper left and O on the upper right The P O O group has an overall negative charge. The P atom is single bonded to O on the lower left. This O atom is single bonded to C 3 of a 3-carbon vertical chain.

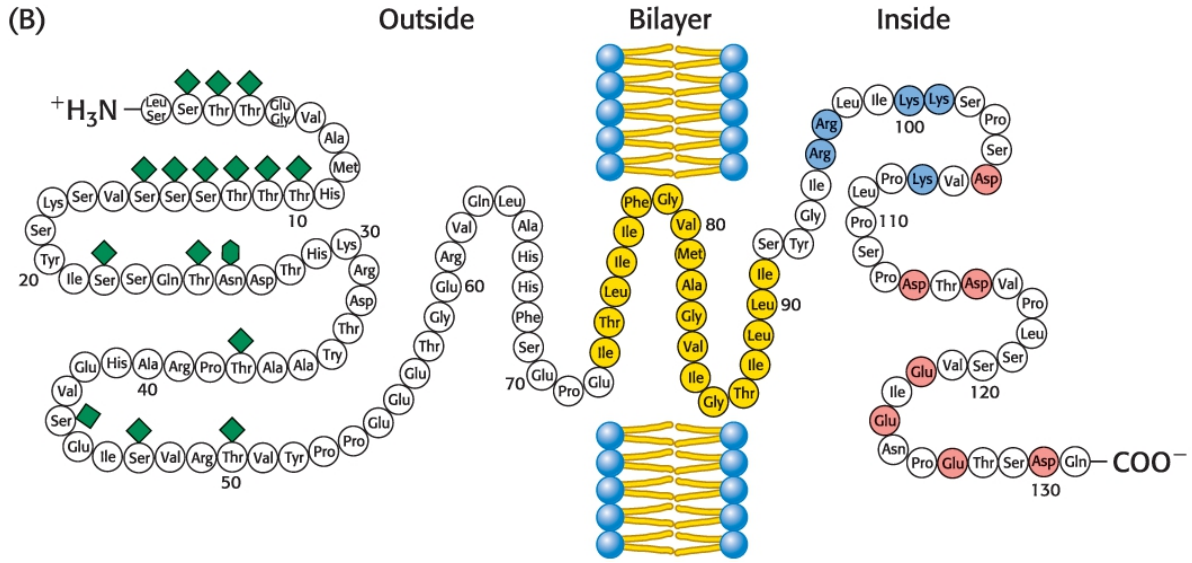
C 2 of the vertical chain is single bonded to O atom of a 1 O and 20 C heteronuclear alkene chain depicted as a line structure using 20 zigzag lines. A double bond is present between C 6 and C 7, C 9 and C 10, C 12 and C 13, C 15 and C 16. O occupies the twenty-first position. C 20 is double bonded to O above.

C 1 of the vertical chain is single bonded to O atom of an 1 O and 18 C heteronuclear alkane chain depicted as a line structure using 18 zigzag lines. C 1 8 is double bonded to O above.

Return to Structures of S-Palmitoyl cysteine, C-terminal S-farnesyl cysteine methyl ester, and Glycosylphosphatidylinositol (G P I) anchor

Extended description for Hydropathy plot for glycophorin A and the amino acid sequence and disposition of glycophorin A





© Macmillan Learning

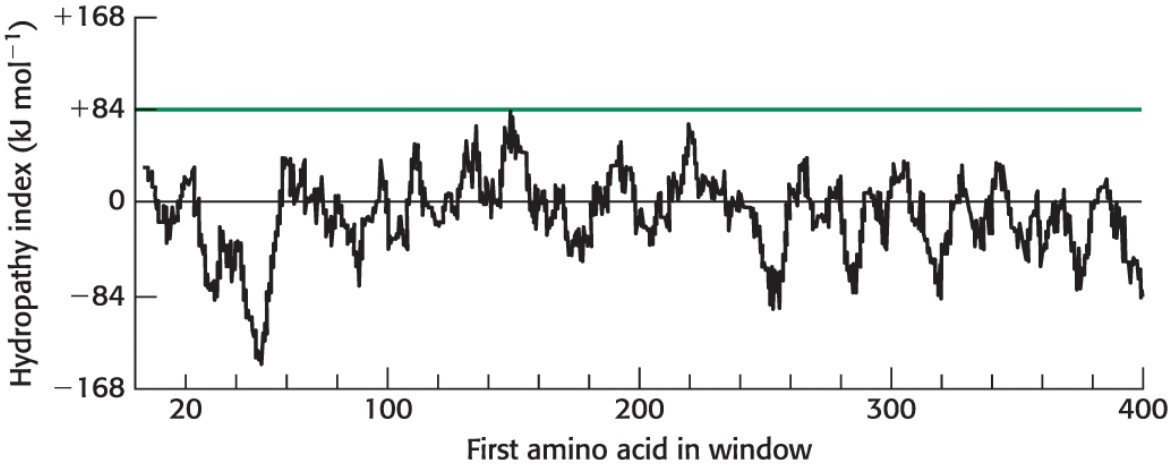
Part (A): The horizontal axis is labeled “First amino acid residue in window”. It has markings ranging from 0 to 100 in increments of 20 units. The vertical axis is labeled hydropathy index (k J mole

superscript minus 1). It has markings ranging from negative 168 to plus 168 in increments of 84 units. A green horizontal line parallel to the horizontal axis is drawn from the marking plus 84 on the vertical axis. A line curve starts from (0, negative 10) on the vertical axis and moves horizontally toward the right till (5, negative 10). It then forms a series of short and long peaks. The longest peak is seen at (80, plus 150) and is labeled single alpha helix in glycophorin.

Part (B): The amino acid sequence of glycophorin is divided into three regions: outside, bilayer, and inside. The outside region is composed of the first 73 amino acid residues from the N H 3 superscript plus terminal. It contains amino acids like leucine, serine, threonine, glutamic acid, glycine, valine, alanine, methionine, histidine, lysine, isoleucine, tyrosine, glutamine, asparagine, arginine, proline, and phenylalanine. Serine 2, threonine 3, threonine 4, threonine 10 to 12, serine 13 to 15, serine 22, threonine 25, threonine 37, serine 44, serine 47, and threonine 50 residues are labeled with a small green rhombus. The asparagine 26 residue is labeled with a small green hexagon. The amino acid residues from 74 to 91 pass through the lipid bilayer. It includes isoleucine, threonine, leucine, glycine, valine, methionine, and alanine. The inside region includes the C O O superscript minus terminal consisting of the amino acid residues from 92 to 131. These residues are serine, tyrosine, glycine, isoleucine, arginine, leucine, proline, aspartic acid, valine, lysine, threonine, glutamic acid, asparagine, and glutamine. Two arginine and three lysine residues are highlighted in blue. Four aspartic acid and three glutamic acid residues are highlighted in red.

Return to Hydropathy plot for glycophorin A and the amino acid sequence and disposition of glycophorin A

Extended description for Hydropathy plot for porin

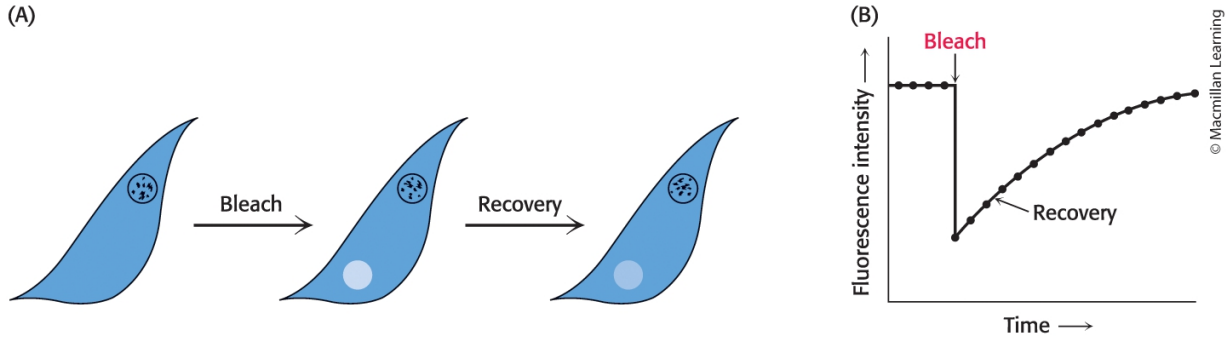


© Macmillan Learning

The horizontal axis is labeled first amino acid in window. It has markings 20, 100, 200, 300, and 400. The vertical axis is labeled hydropathy index in K J per mol. It has markings ranging from negative 168 to positive 168 in increments of 84 units. The graph shows two horizontal lines parallel to the horizontal axis starting from 0 and positive 84 on the vertical axis. The graph shows a line forming series of peaks and depressions without any strong peaks. It starts from (0, 40) shows a gradual downward fall to reach (50, negative 158) and raises upward to (60, 42). It then moves toward the right and forms several peaks and depressions. Several sharp falls are seen at (260, negative 90), (290, negative 84), (320, negative 84), (380, negative 70). The line terminates at (400, negative 80). All values are approximated.

Return to Hydropathy plot for porin

Extended description for Schematic representation of fluorescence bleaching and recovery and a graphical representation of fluorescence intensity versus time

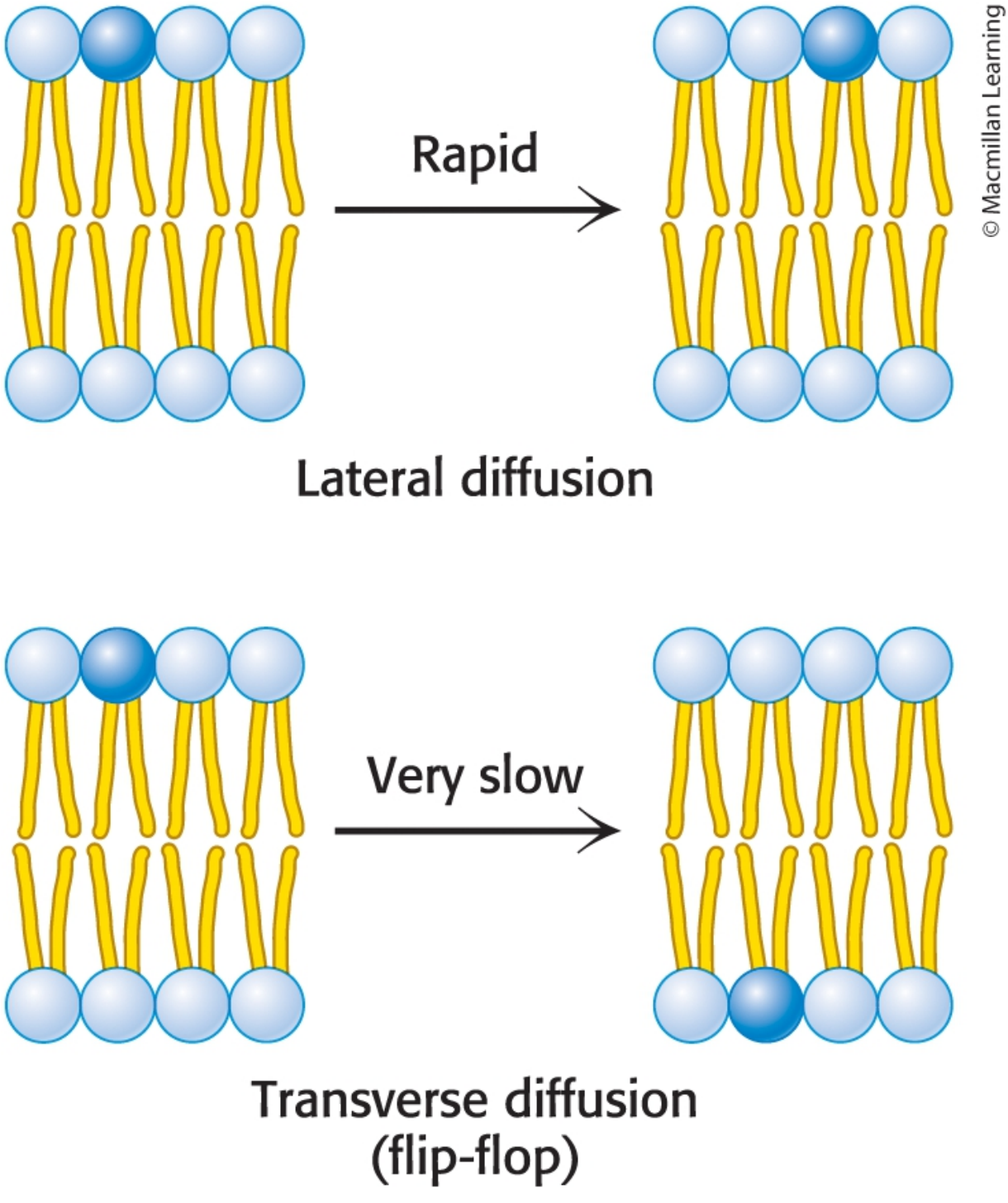


Part (A): It shows a spindle-shaped cell. The cell has a small circular structure containing a cluster of black dots in it. The cell undergoes bleaching leading to the formation of a circular white patch on the cell. The cell undergoes recovery and the bleached part starts to disappear slowly.

Part (B): The horizontal axis is labeled time and the vertical axis is labeled fluorescence intensity. The graph shows a line that starts from a point well above the middle of the vertical axis. It moves horizontally toward the right and is labeled bleach. The line then moves vertically downward up to a point much below the middle of the vertical axis. It again rises upward in a concave down fashion and this curve is labeled recovery.

Return to Schematic representation of fluorescence bleaching and recovery and a graphical representation of fluorescence intensity versus time

Extended description for Schematic illustration of lateral and transverse diffusion in lipid bilayer



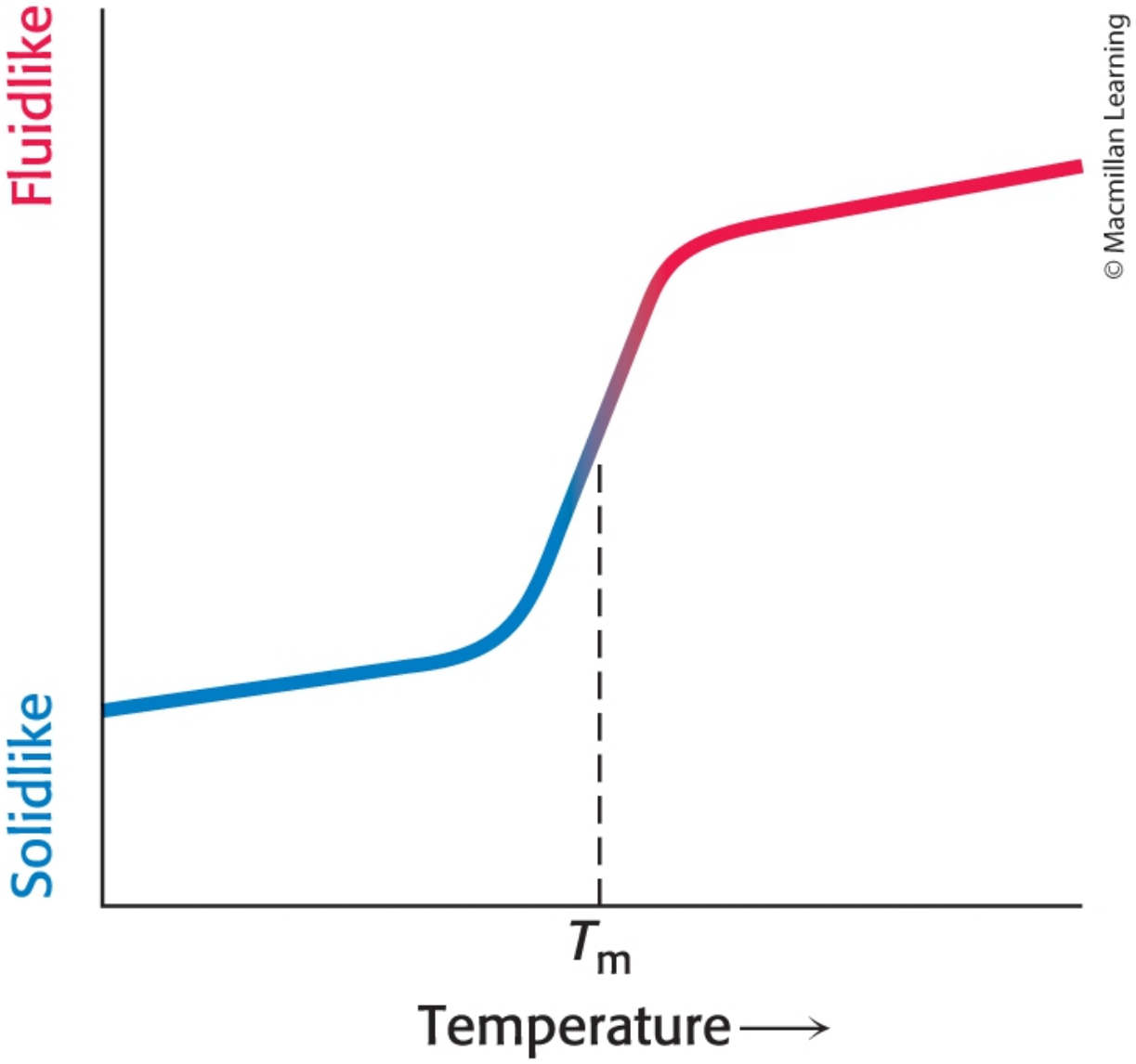
The lipid bilayer before diffusion consists of two layers of lipid molecules shown in shorthand depiction. Each layer consists of 4 lipid molecules. The spherical groups of all lipid molecules are light blue except for one lipid located at the second position of the top layer. The spherical group of this lipid is dark blue colored.

Lateral diffusion: It occurs very rapidly. The position of the lipid molecule having blue spherical group changes from second to third in the top layer.

Transverse diffusion (flip-flop): It occurs very slowly, The position of the lipid molecule having blue spherical group changes from second in the top layer to second in the bottom layer.

Return to Schematic illustration of lateral and transverse diffusion in lipid bilayer

Extended description for Graph showing the melting temperature of a phospholipid membrane

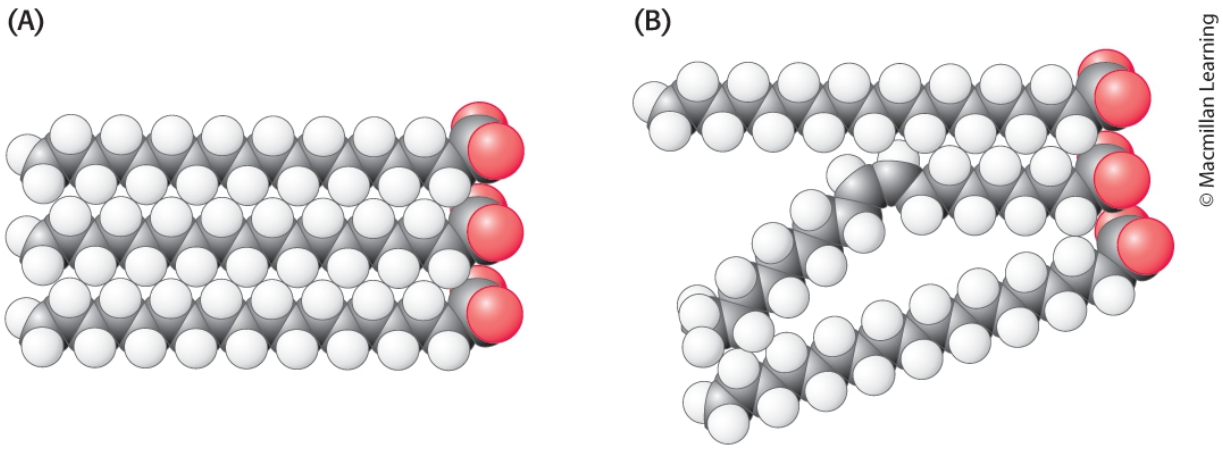


The horizontal axis is labeled temperature. The vertical axis is labeled solidlike at the bottom and fluidlike at the top. The sigmoidal curve starts from solidlike region and moves toward the right and suddenly rises upward near the mid point of the horizontal axis. It then terminates on the right near the fluidlike region. The midpoint

along the upward transition of the curve has a dashed vertical line touching the mid point of the horizontal axis and is labeled T subscript m.

Return to Graph showing the melting temperature of a phospholipid membrane

Extended description for Space-filling models labeled (A) and (B)



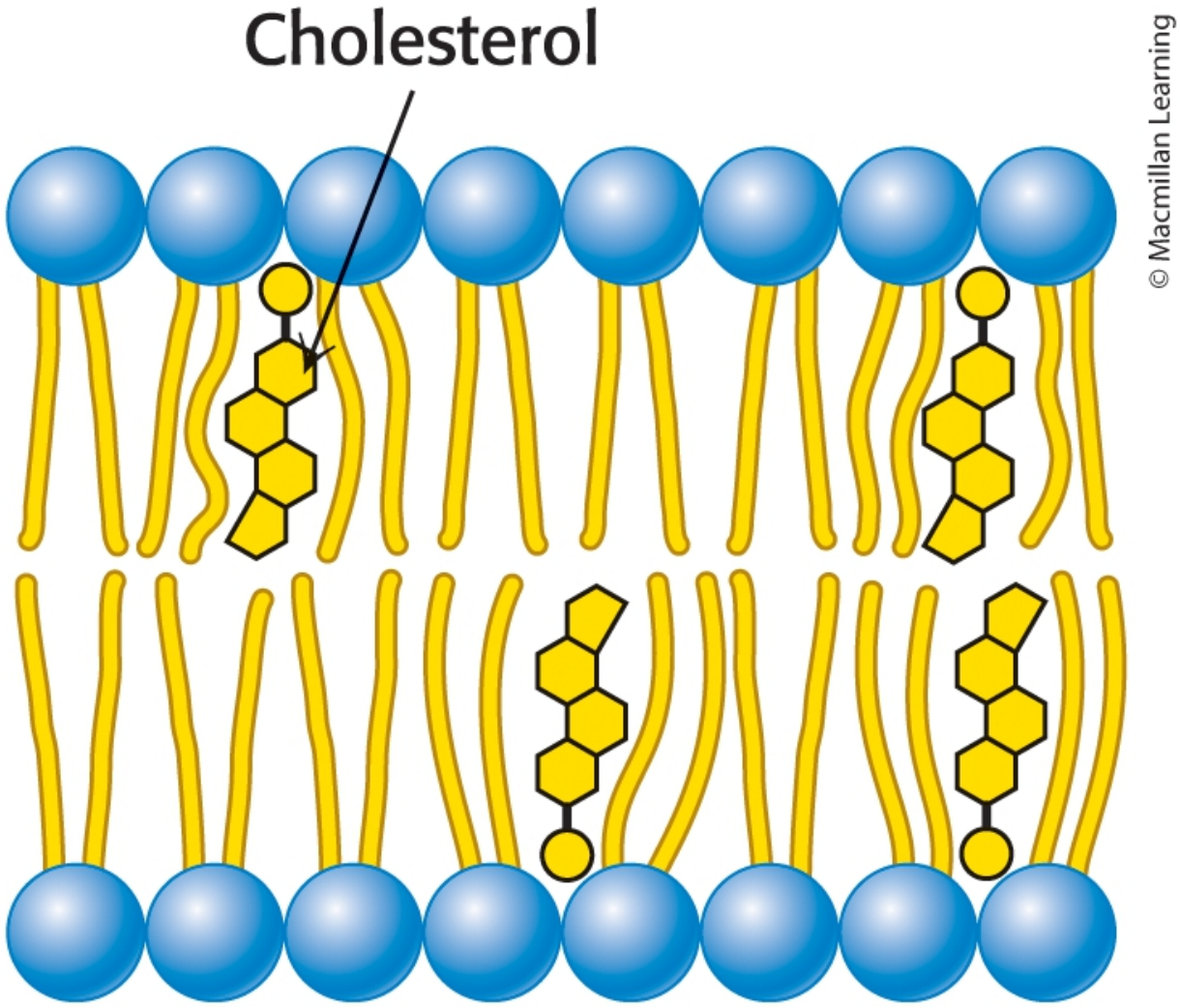
Space-filling model (A): It shows three horizontally oriented models stacked one above the other. Each model is composed of a linear chain of 18 fused black spheres. The second to seventeenth black spheres are fused to a white sphere, all located toward the observer. These white spheres are oriented upward or downward in an alternating manner. The first black sphere is fused with two white spheres. One white sphere is located away from the observer and another one is located toward the observer. The eighteenth black sphere is fused with two red spheres. One red sphere is located toward the observer and another one is located away from the observer.

Space filling model (B): It shows three models. The topmost model is in a horizontal orientation. The middle model has a kink at the tenth black sphere. The bottom-most model has a diagonal orientation. The eighteenth black spheres of all the three models are stacked one above the other. Each model is composed of a chain of 18 fused black spheres. The second to seventeenth black spheres are fused to a white sphere, all located toward the observer. These white spheres

are oriented upward or downward in an alternating manner. The first black sphere is fused with two white spheres. The eighteenth black sphere is fused with two red spheres. One red sphere is located toward the observer and another one is located away from the observer.

Return to Space-filling models labeled (A) and (B)

Extended description for Schematic illustration of cholesterol inserted in lipid bilayer



A lipid bilayer composed of lipid molecules in a shorthand depiction is shown. The cholesterol molecules are inserted between the yellow extensions of adjacent lipid molecules. A cholesterol molecule is depicted as a yellow circle connected to three fused hexagons. The insertion of a cholesterol molecule introduces a kink in the yellow extensions.

Return to Schematic illustration of cholesterol inserted in lipid bilayer

Extended description for Lipid raft and human monocytic cell stained with a fluorescent dye

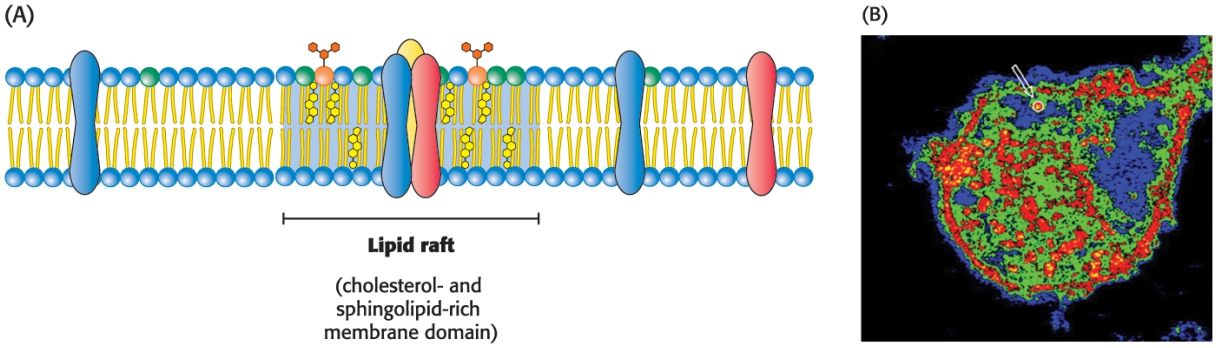


Photo credit: Katharina Gaus, Enrico Gratton, Eleanor P. W. Kable, et al., "Visualizing lipid structure and raft domains in living cells with two-photon microscopy." PNAS December 23, 2003 100 (26) 15554–15559; https://doi.org/10.1073/pnas.2534386100, Figure 1B. Copyright (2003) National Academy of Sciences, U.S.A.
© Macmillan Learning

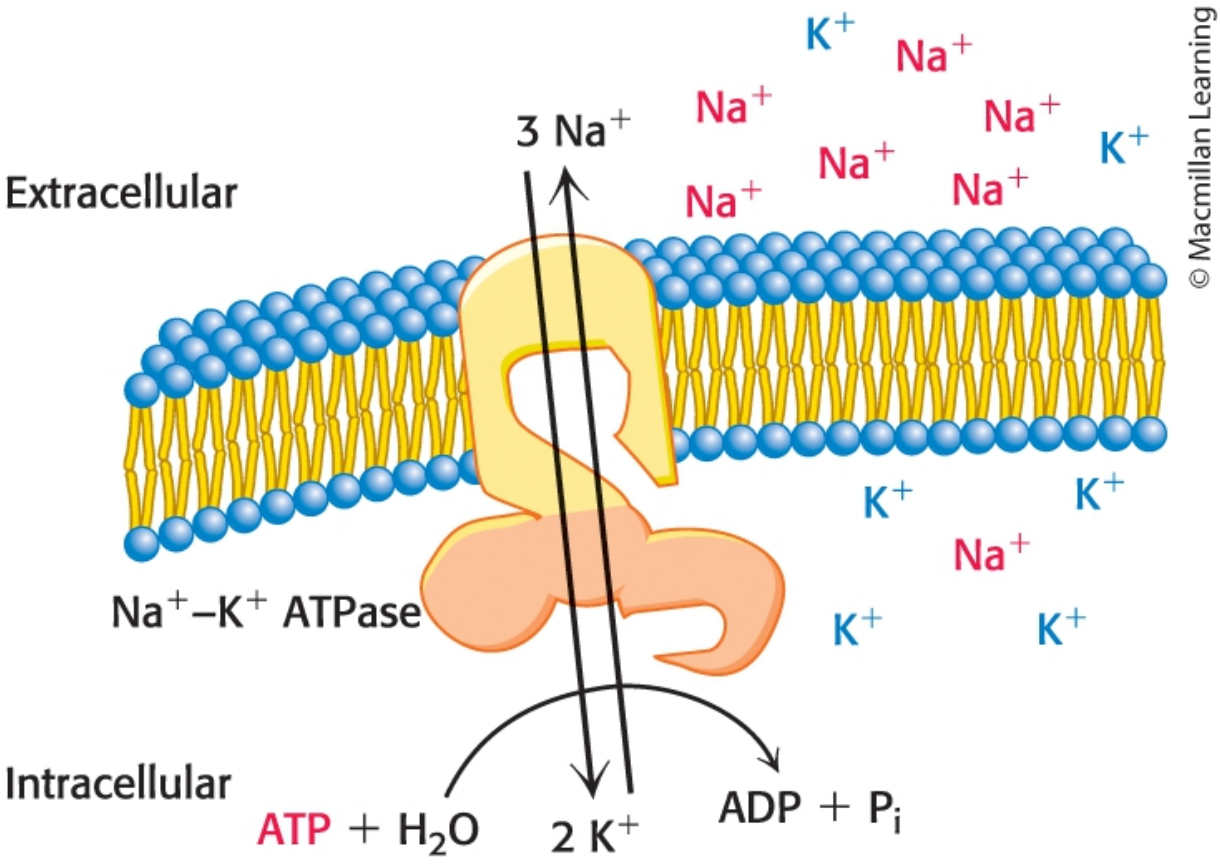
Part (A): It shows a lipid bilayer consisting of two horizontally parallel layers of lipids arranged compactly. Each lipid molecule is shown in a shorthand depiction. The yellow extensions of the shorthand depiction are aligned together and form the core of the bilayer. The spherical groups are blue, green, and orange colored. The lipid raft is a cholesterol-sphingolipid rich membrane domain. The orange and green spherical groups are concentrated in the outer leaflet of the lipid bilayer in the lipid raft. Cholesterol molecules depicted as fused hexagons are inserted between the yellow extensions of the lipid bilayer in the raft. The orange spherical groups are connected to a cluster of three orange hexagons. The bilayer also consists of 3 blue and 2 red dumble-shaped membrane proteins that traverse the bilayer. The lipid raft contains a cluster of yellow, blue, and red dumble-shaped membrane proteins.

Part (b): It shows a micrograph of circular human monocytic cell stained with fluorescent dye that is sensitive to the level of disorder. The cell shows small irregular-shaped red patches across a green

background. It shows a blue outline and a few large and small irregular-shaped blue patches. Some of the red patches contain a tiny yellow spot at center. An arrow points at a red patch surrounded by a medium-sized blue patch. The red patch contains a tiny yellow spot.

Return to Lipid raft and human monocytic cell stained with a fluorescent dye

Extended description for Transport of ions by N a superscript plus-K superscript plus transport system in the lipid bilayer



The lipid bilayer consists of two horizontally parallel layers of lipids. The outer leaflet consists of three rows of lipid molecules packed together compactly. Each lipid molecule is shown in a shorthand depiction. The yellow extensions of the shorthand depiction are aligned together and form the core of the bilayer. The blue spheres are located away from each other. The lipid bilayer consists of a transport system that extends from the extracellular region above the bilayer to the intracellular region below the bilayer. This transport system is labeled N a superscript plus-K superscript plus A

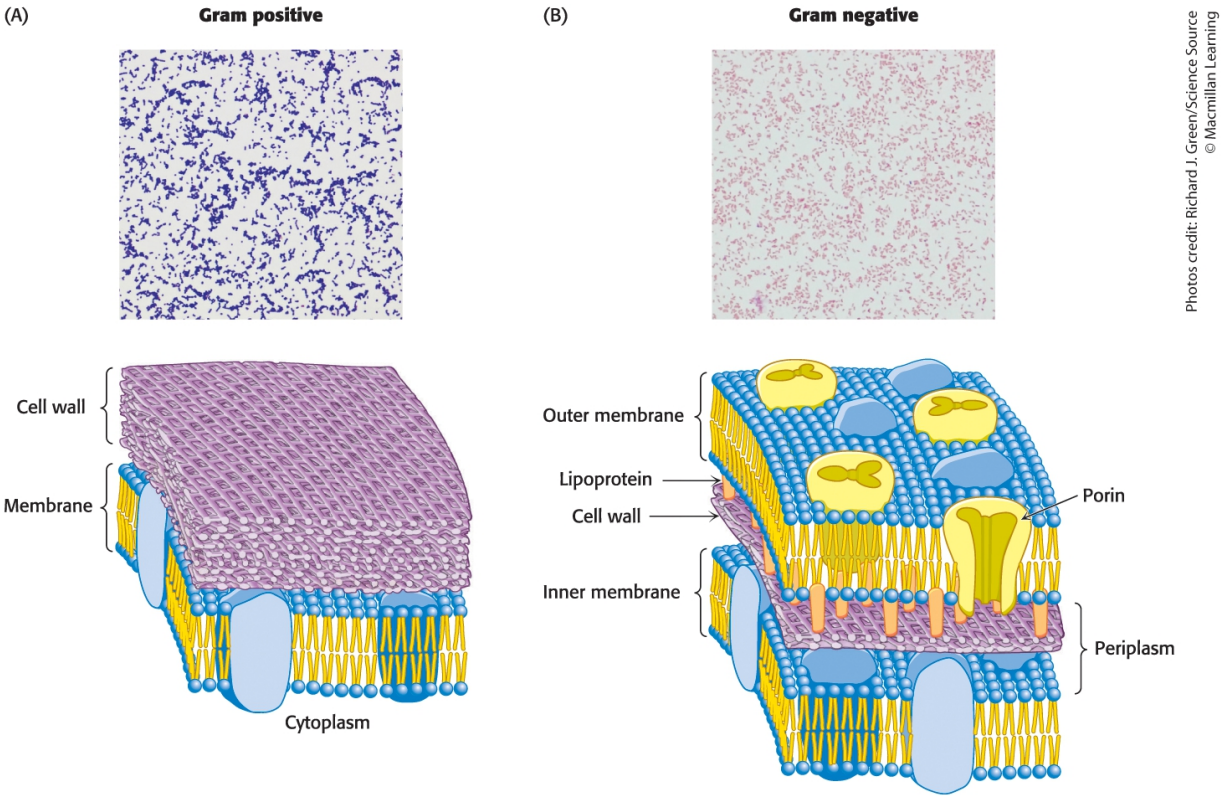
T P ase. The number of N a superscript plus ions in the extracellular region is much higher than the intracellular region. The number of K superscript plus ions in the intracellular region is much higher than the extracellular region.

A downward arrow across the A T P ase shows the movement of 2 K superscript plus ions into the intracellular region. An upward arrow across the A T P ase shows the movement of 3 N a superscript plus ions into the extracellular region.

The intracellular space below the A T P ase shows the conversion of A T P and H 2 O to A D P and P subscript i as the transport of ions occurs.

Return to Transport of ions by N a superscript plus-K superscript plus transport system in the lipid bilayer

Extended description for Structure of the plasma membrane of gram positive and gram negative bacteria and their photomicrographs

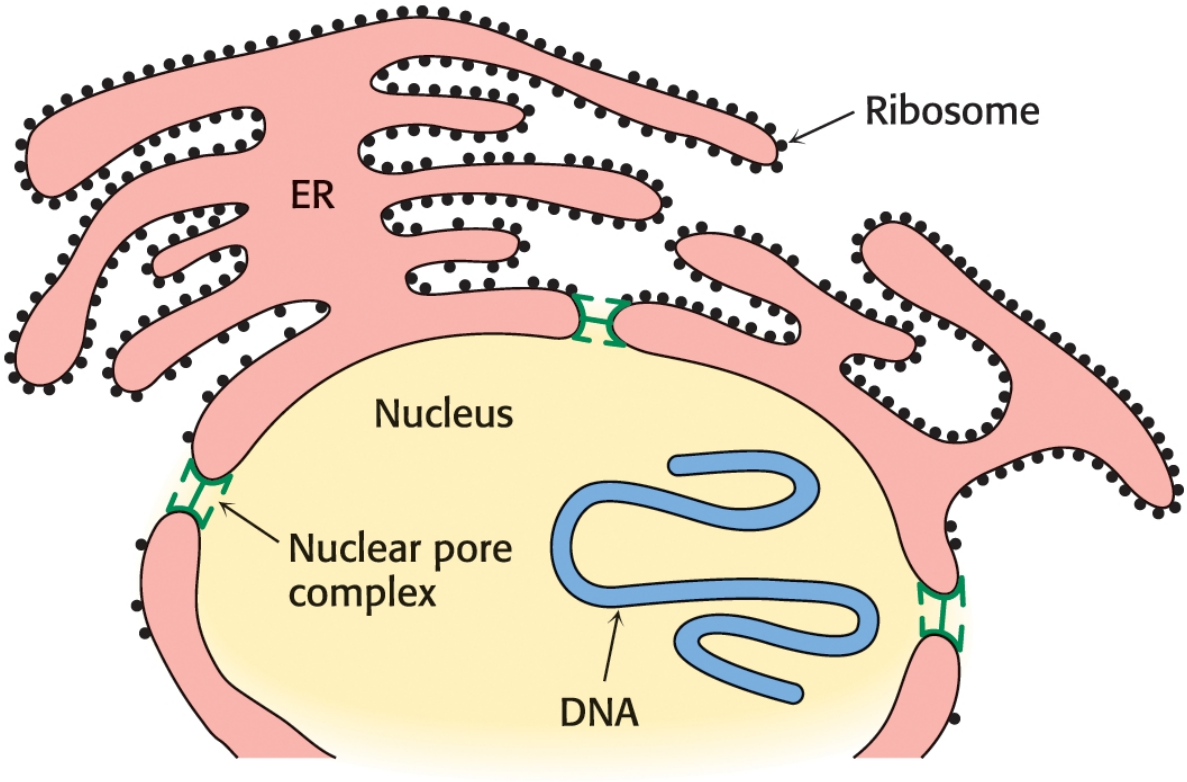


Part (A): It shows a photomicrograph of purple-stained gram-positive bacteria. The 3-D structure of the plasma membrane of the gram-positive bacteria is shown below the photomicrograph. The plasma membrane consists of two parallel layers of lipids. Both the layers consist of several rows of lipid molecules packed together compactly. Each lipid molecule is shown in a shorthand depiction. The yellow extensions of the shorthand depiction are aligned together and form the core of the bilayer. The blue spheres are located away from each other. The bilayer consists of two membrane proteins. A thick mesh-like purple-colored cell wall is present above the bilayer.

Part (B): It shows a photomicrograph of pink-stained gram-negative bacteria. The 3-D structure of the plasma membrane of the gram-negative bacteria is shown below the photomicrograph. These bacteria have two separate lipid bilayers. Each lipid bilayer consists of several rows of lipid molecules packed together compactly. Each lipid molecule is shown in a shorthand depiction. The yellow extensions of the shorthand depiction are aligned together and form the core of the bilayer. The blue spheres are located away from each other. The upper bilayer is labeled outer membrane and the bilayer at the bottom is labeled inner membrane. A thin mesh-like cell wall is present between the outer and inner membrane. Several short tube-like structures connecting the outer and inner membrane are labeled lipoproteins. The space between the two membranes is labeled periplasm. The outer membrane consists of channel-like structures labeled porin.

Return to Structure of the plasma membrane of gram positive and gram negative bacteria and their photomicrographs

Extended description for Schematic illustration of nuclear and surrounding E R

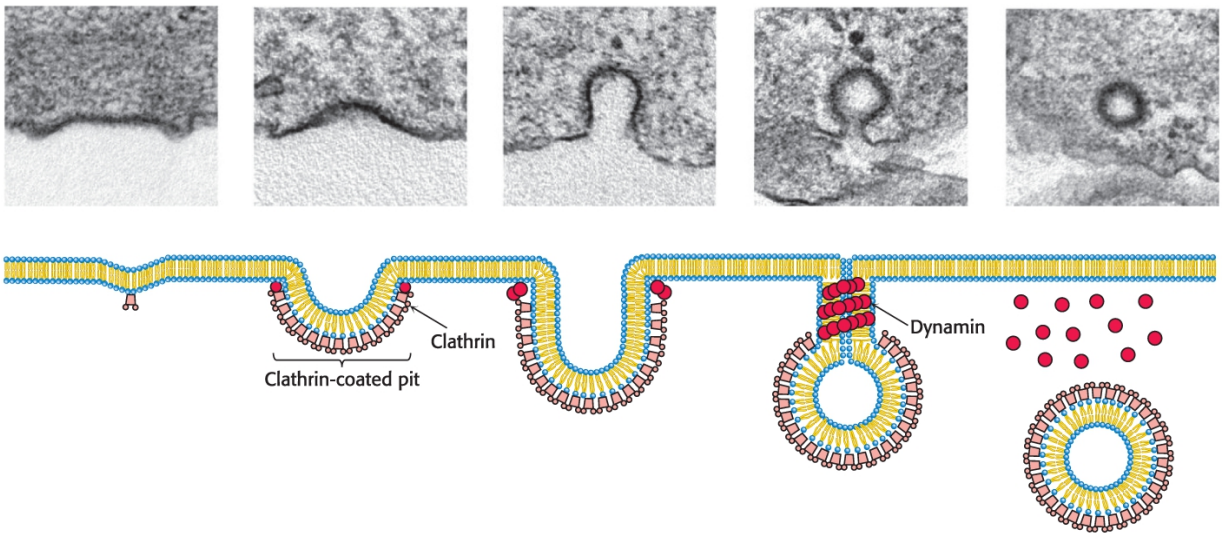


© Macmillan Learning

The nucleus is a circular structure containing a D N A molecule. The D N A molecule is depicted as a zigzag blue strand. The nucleus is surrounded by a double membrane nuclear envelope having a narrow lumen between them. A nuclear pore complex depicted as a narrow channel is present in the double membrane. At these complexes, the outer and inner membrane of the envelope becomes continuous. The outer membrane of the nuclear envelope continues into a network of membranes in the cytoplasm labeled E R. The surface of E R is lined by tiny black dots labeled ribosomes. The E R encloses a lumen that is continuous with the lumen of nuclear envelope.

Return to Schematic illustration of nuclear and surrounding E R

Extended description for Schematic representation and photomicrographs of the steps of receptor-mediated endocytosis



Credit: *Top*: Republished with permission of Company of Biologists, from Membrane remodeling in clathrin-mediated endocytosis. Volker Haucke, Michael M. Kozlov, J Cell Sci (2018) 131 (17): jcs216812. Figure 1. Permission conveyed through Copyright Clearance Center, Inc.; *Bottom*: Schmid SL. Reciprocal regulation of signaling and endocytosis: Implications for the evolving cancer cell. J Cell Biol. 2017 Sep 4;216(9):2623-2632. doi: 10.1083/jcb.201705017. Epub 2017 Jul 3. PMID: 28674108; PMCID: PMC5584184. Copyright © 2017 Schmid. Illustration by Marcel Mettlen. Used with permission.

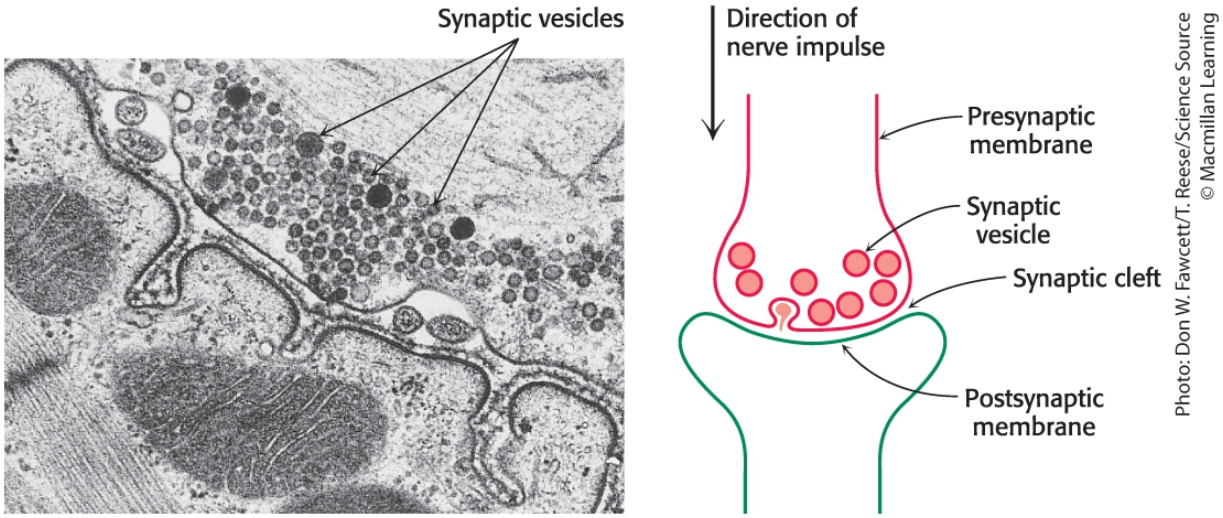
The figure shows photomicrographs of endocytosis on the top and corresponding steps of endocytosis below. The first photomicrograph shows the surface of the cell. In the second photomicrograph, the surface begins to invaginate slightly. In the third photomicrograph, the invagination becomes prominent. In the fourth photomicrograph, the neck of the invagination starts to get closer. In the fifth photomicrograph, the completely invaginated membrane appears as a sphere inside the cell.

The schematic illustration of the corresponding steps of endocytosis is shown below the photomicrographs. The lipid bilayer of the membrane consists of two parallel layers of lipids. Each lipid molecule is shown in a shorthand depiction. The yellow extensions of the shorthand depiction are aligned together and form the core of

the bilayer. The blue spheres are located away from each other. In the first step, the plasma membrane forms a slight invagination. A clathrin molecule attaches to the inner surface of the invagination. In the second step, the invagination becomes slightly deeper and the inner surface of the invagination is lined by a series of clathrin molecules. This invagination is labeled clathrin-coated pit. The clathrin molecule is depicted as a box-like structure fused to a sphere on the bottom left and bottom right. In the third step, the invagination becomes prominent. In the fourth step, the invagination becomes spherical and its neck is continuous with the membrane. Several spherical bead-like structures called dynamin zip the neck of the spherical invagination. In the fifth step, the dynamin spheres are released and a spherical structure surrounded by a lipid bilayer is released into the intracellular space.

Return to Schematic representation and photomicrographs of the steps of receptor-mediated endocytosis

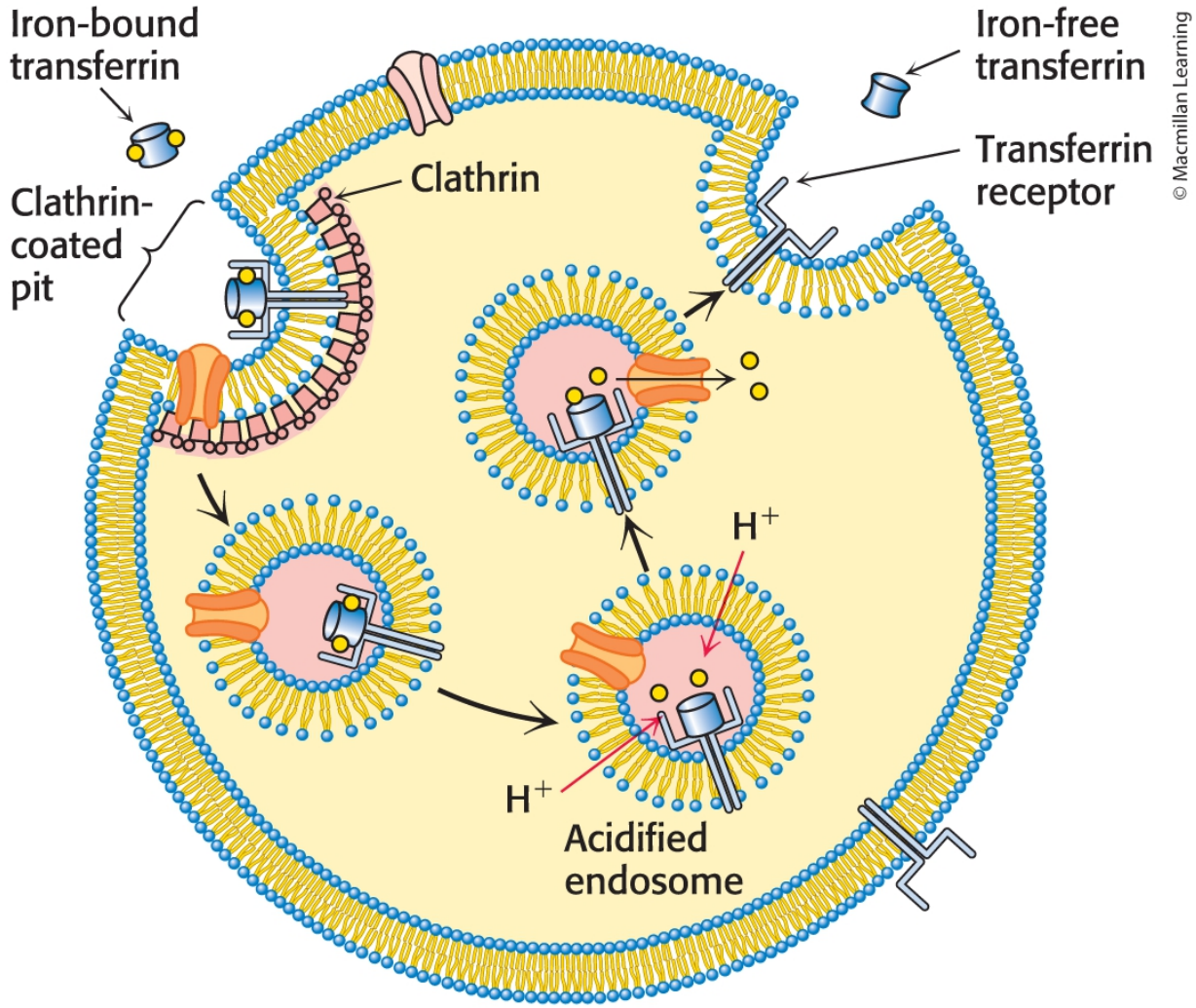
Extended description for Fusion of vesicles to the plasma membrane to release neurotransmitter



The figure has two parts. The first part shows the photomicrograph of two closely apposed cell membranes. Several spherical structures labeled synaptic vesicles are located close to the top membrane. The second part shows an elongated structure with a broad top having an inwardly curved surface. Its outline is labeled postsynaptic membrane. A bulb-like structure with an outline labeled presynaptic membrane sits in the depression of the postsynaptic membrane. The space between the presynaptic and postsynaptic membrane is labeled synaptic cleft. A downward arrow above the presynaptic membrane depicts the direction of nerve impulse. The presynaptic membrane contains several spheres labeled synaptic vesicles. A small invagination is present on the presynaptic membrane opposite the postsynaptic membrane to show the release of neurotransmitters into the synaptic cleft.

[Return to Fusion of vesicles to the plasma membrane to release neurotransmitter]

Extended description for Schematic illustration of receptor-mediated endocytosis of transferrin receptor and iron



A large circular cell surrounded by a lipid bilayer is shown. The bilayer contains a transferrin receptor and a protein channel. A clathrin-coated pit is created on the top left of the cell. In this pit, the lipid bilayer invaginates and the inner surface of the invagination is lined by a series of identical molecules. The protein channel is inserted into a portion of the invaginated bilayer. A short

cylindrical structure bound to a yellow sphere on either side is labeled “iron-bound transferrin”. The yellow spheres depict iron atoms. The iron-bound transferrin associated with the transferrin receptor in the clathrin-coated pit.

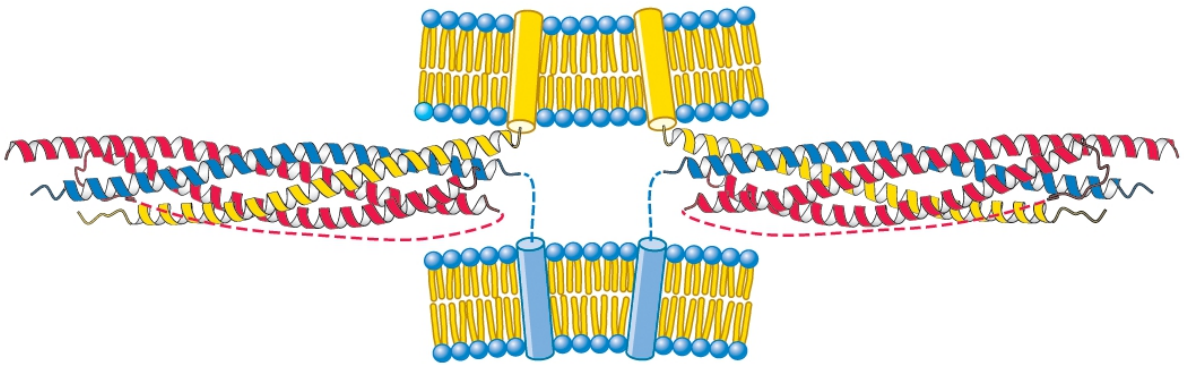
The pit forms a lipid vesicle having the protein channel and iron-bound transferrin associated with the transferrin receptor.

The lipid vesicle matures into an acidified endosome containing H superscript plus ions. This leads to the dissociation of yellow spheres from the transferrin protein.

The dissociated yellow spheres move into the cytoplasm through the protein channel in the endosomal membrane. The endosome then fuses with the lipid bilayer leading to the release of iron-free transferrin into the exterior and insertion of the transferrin receptor in the lipid bilayer.

Return to Schematic illustration of receptor-mediated endocytosis of transferrin receptor and iron

Extended description for Schematic illustration of the initiation of membrane fusion

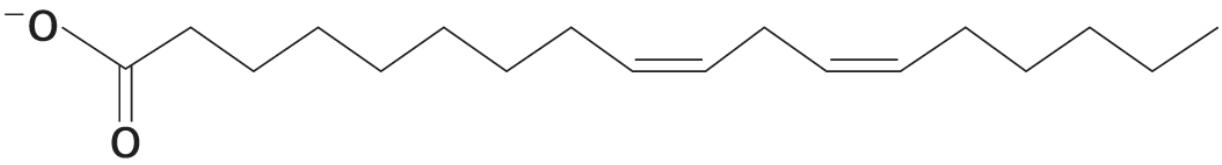


© Macmillan Learning

Two sections of lipid bilayers are shown one above the other. They are separated by a gap. Two yellow vertical cylindrical structures separated by a small space are inserted in the top bilayer. The bottom surface of each of these cylindrical structures are connected to a long yellow alpha-helix. Two blue vertical cylindrical structures separated by a small space are inserted in the bottom bilayer. The top surface of each of these cylindrical structures are connected to a long blue alpha-helix. The blue cylinders in the bottom bilayer are aligned with the yellow cylinders in the top bilayer. The blue and yellow helices form two tight bundles with two red alpha-helices.

Return to Schematic illustration of the initiation of membrane fusion

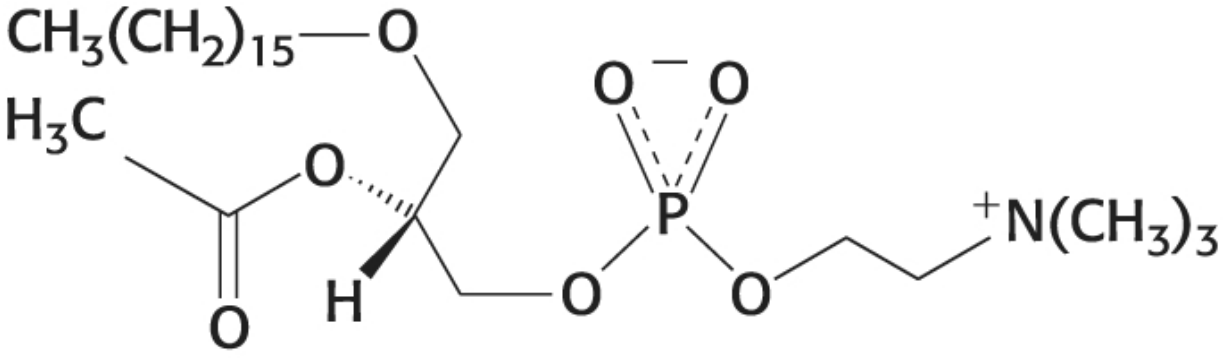
Extended description for Chemical structure of a fatty acid



The structure of the fatty acid is as follows: A 18-carbon alkene chain is depicted as a line structure using 17 zigzag lines. A double bond is present between C 9 and C 10, C 12 and C 13. C 1 is single bonded to O superscript minus on the upper left and double bonded to O below.

Return to Chemical structure of a fatty acid

Extended description for Chemical structure of platelet-activating factor (P A F)



Platelet-activating factor (PAF)

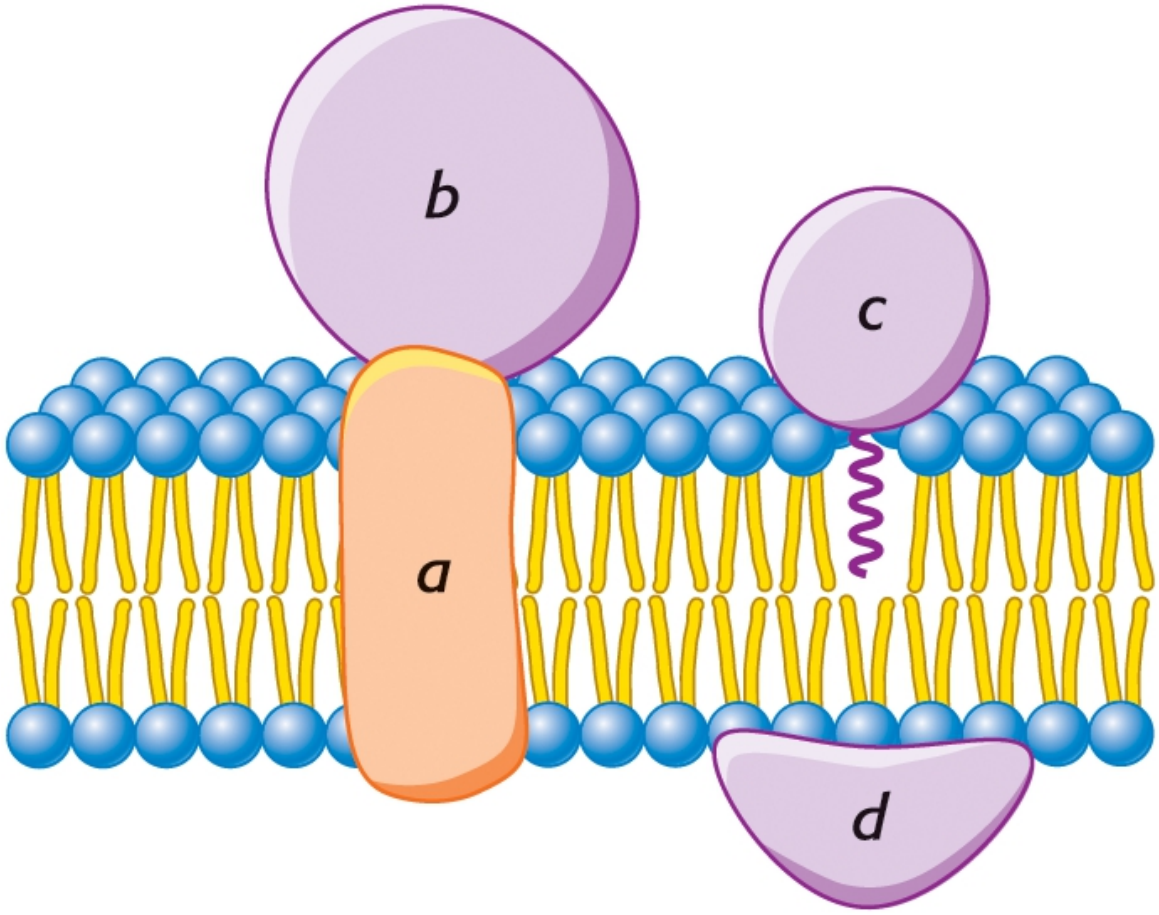
The structure of the platelet-activating factor is as follows: A central P atom is partially double bonded to O on the upper left, partially double bonded to O on the upper right, single bonded to O on the lower left, and single bonded to O on the lower right. Both the partially double-bonded O atoms have an overall negative charge. The O atom on the lower left is single-bonded to C H 2 in the form of a line on the left. This C H 2 is single bonded to C on the upper left. This C atom is wedge bonded to H on the lower left, dash bonded to O on the upper left, and single bonded to C H 2 above in the form of a line. The C H 2 group is single-bonded to O on the upper left. This O atom is single bonded to open bracket C H 2 close bracket with subscript 15 C H 3 on the left. The dash bonded O atom is single bonded to C on the lower left. This C atom is single bonded to C H 3 on the upper left and double bonded to O below.

The O atom on the lower that is right single bonded to P is further single bonded to a 2 carbon alkane chain depicted as a line structure

using a line. C 2 of this chain is single bonded to N superscript plus open bracket C H 3 close bracket with subscript 3 on the upper right.

Return to Chemical structure of platelet-activating factor (P A F)

Extended description for Different ways in which membrane proteins interact with lipid bilayers



© Macmillan Learning

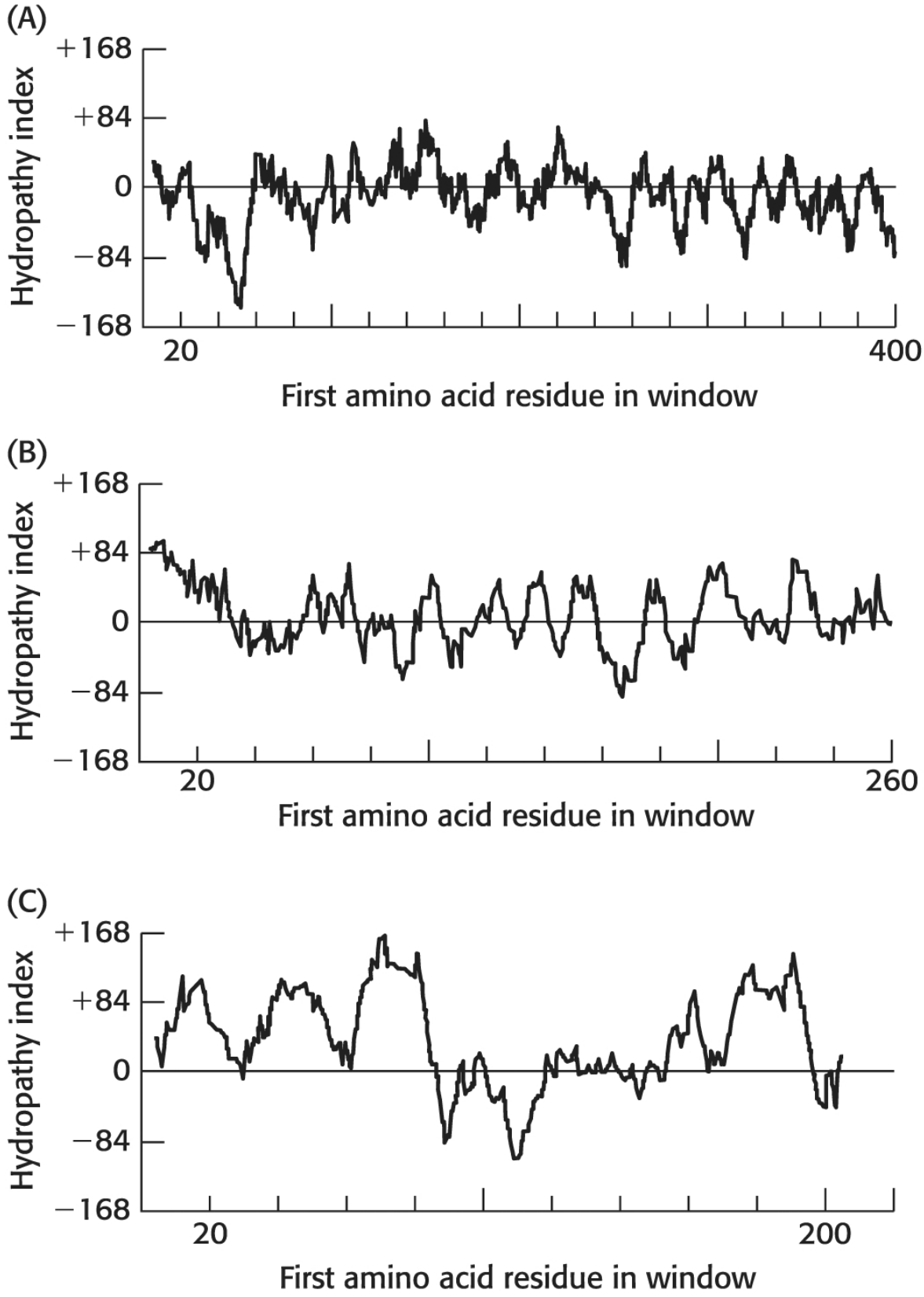
The lipid bilayer consists of two horizontally parallel layers of lipids. The upper layer consists of three rows of lipid molecules packed together compactly. Each lipid molecule is shown in a shorthand depiction. The yellow extensions of the shorthand depiction are aligned together and form the core of the bilayer. The blue spheres are located away from each other. The lipid bilayer shows four membrane proteins. The first membrane protein labeled "a" resembles a sausage and traverses the bilayer but does not extend above and below the bilayer. The second spherical protein labeled

"b" is attached to the blue spheres of the outer leaflet of the lipid bilayer and protein a. The third protein labeled "c" s attached to the top surface of the lipid bilayer through a zigzag anchor that penetrates the core of the bilayer halfway through. The fourth protein labeled "d" has an inverted triangular shape. It is attached to the lower surface of the lipid bilayer.

Return to Different ways in which membrane proteins interact with lipid bilayers

Extended description for Hydropathy plots of different

proteins A, B, and C



© Macmillan Learning

Hydropathy plot for protein A: The horizontal axis is labeled first amino acid in window. It has markings 20 and 400. 20 is on the extreme left and 400 is on the extreme right. The vertical axis is labeled hydropathy index. It has markings ranging from negative 168 to positive 168 in increments of 84 units. The graph shows a horizontal line parallel to the horizontal axis starting from 0 on the vertical axis. The graph shows a line forming series of peaks and depressions without any strong peaks. It starts at (0, 40) and shows a gradual downward fall to reach (50, negative 158) and again rises upward to (60, 20). It then moves toward the right and forms several peaks and depressions. Several sharp falls are seen at (260, negative 90), (290, negative 84), (320, negative 84), (380, negative 70). The line terminates at (400, minus 80). All values are approximated.

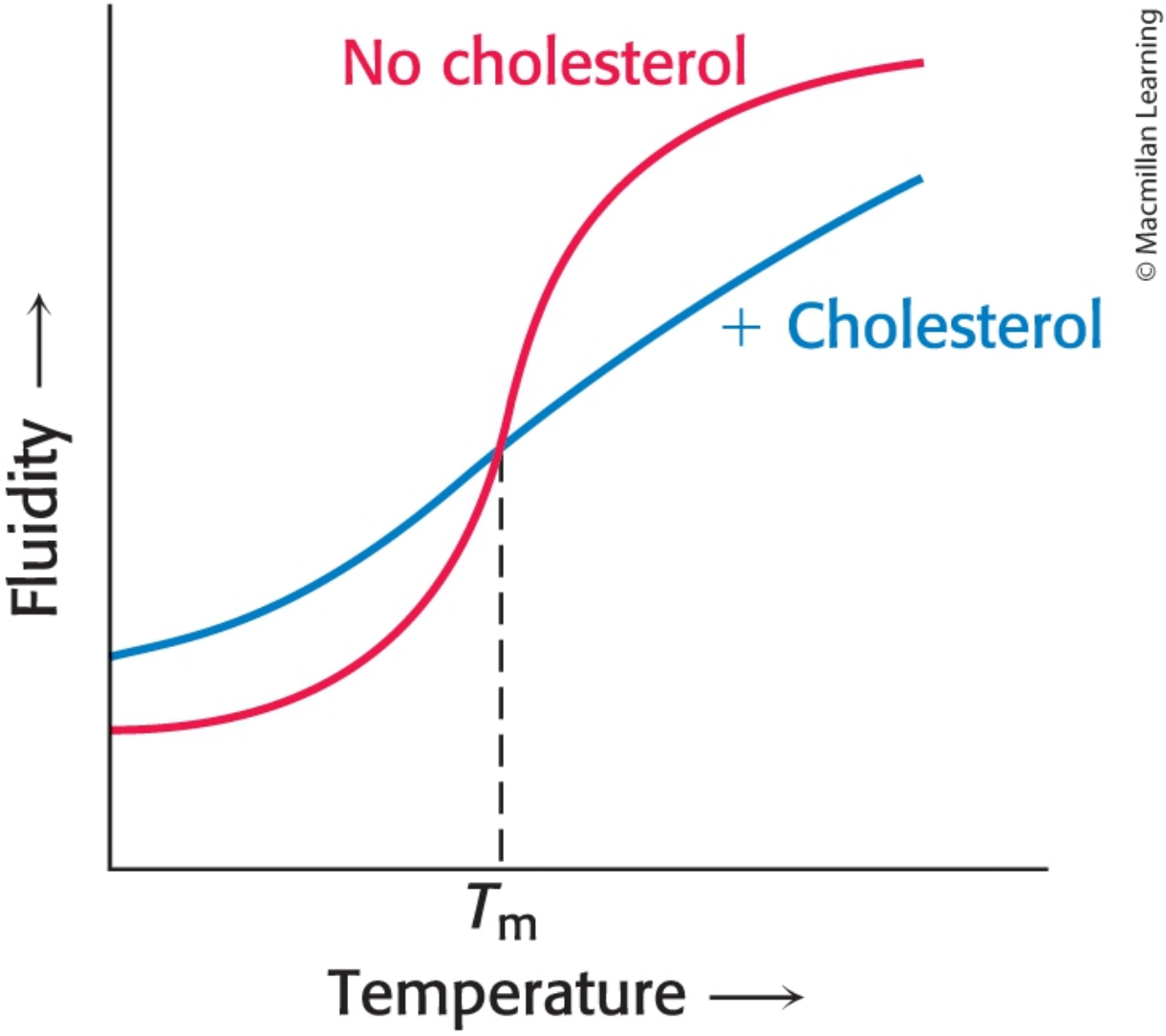
Hydropathy plot for protein B: The horizontal axis is labeled first amino acid in window. It has markings 20 and 400. 20 is on the extreme left and 260 is on the extreme right. The vertical axis is labeled hydropathy index. It has markings ranging from negative 168 to positive 168 in increments of 84 units. The graph shows a horizontal line parallel to the horizontal axis starting from 0 on the vertical axis. The graph shows a line forming series of peaks and depressions without any strong peaks. It starts from (0, 84) shows a gradual downward fall to reach (40, negative 40). It again rises upward to (75, 70) and then moves toward the right. It forms several peaks and depressions and terminates at (260, 0). All values are approximated.

Hydropathy plot for protein C: The horizontal axis is labeled first amino acid in window. It has markings 20 and 200. 20 is on the extreme left and 200 is on the extreme right. The vertical axis is labeled hydropathy index. It has markings ranging from negative 168 to positive 168 in increments of 84 units. The graph shows a horizontal line parallel to the horizontal axis starting from 0 on the vertical axis. The graph shows a line forming series of peaks and

depressions without any strong peaks. It starts from (10, 0) and shows an upward rise to (20, positive 90). It again falls downward to (30, 0). It then moves toward the right and forms several peaks and depressions. Sharp falls are seen at (90, negative 84), (110, negative 84), and terminates at (200, minus 0). All values are approximated.

Return to Hydropathy plots of different proteins A, B, and C

Extended description for Graphical representation of the fluidity of fatty acids in a phospholipid bilayer as a function of temperature



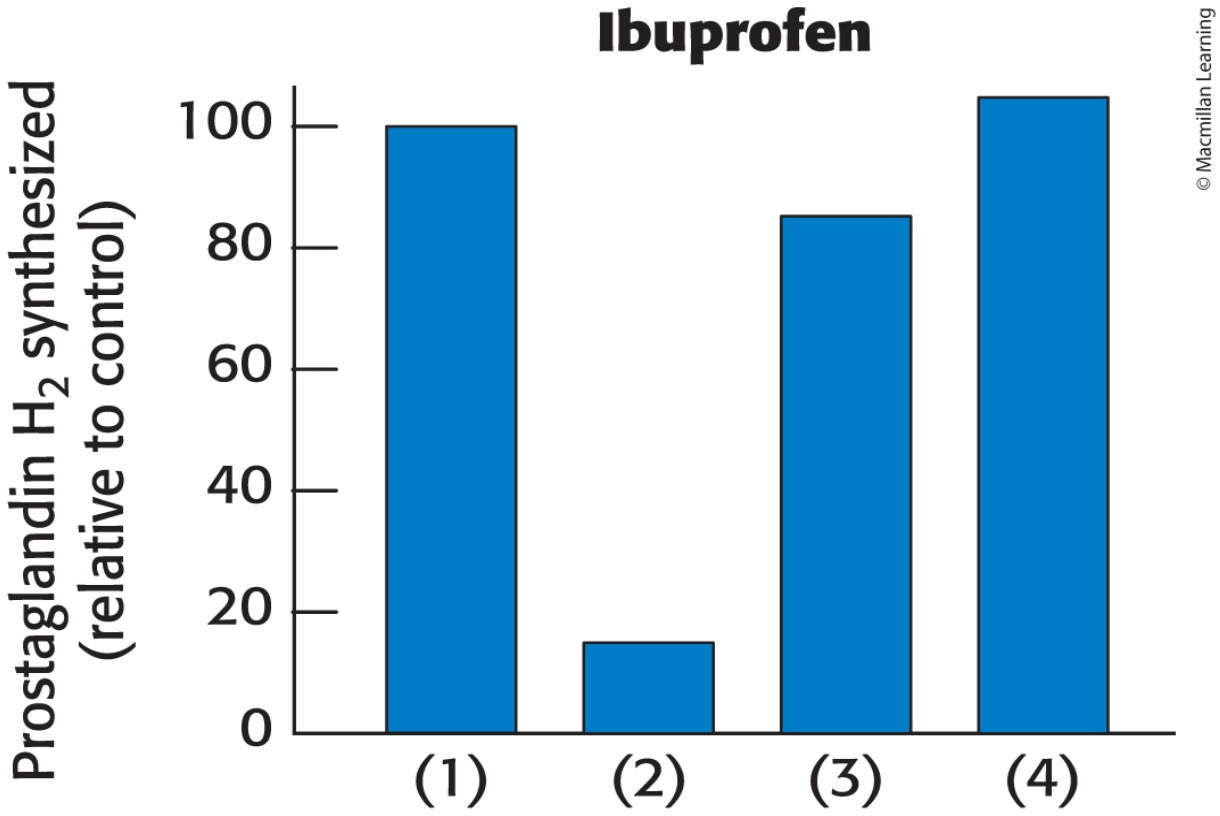
The horizontal axis is labeled temperature which increases from left to right. The vertical axis is labeled fluidity which increases from bottom to top. An increasing blue line curve labeled plus cholesterol starts at a fluidity value below the mid point of the vertical axis. It gradually moves toward the upper right. A red S-shaped curve is

labeled no cholesterol. It start below the blue line and terminates above the blue line at the highest fluidity. A vertical dashed line is drawn from the point of intersection of the blue line curve and the red curve to the mid point of the vertical axis. This dashed line is labeled T subscript m.

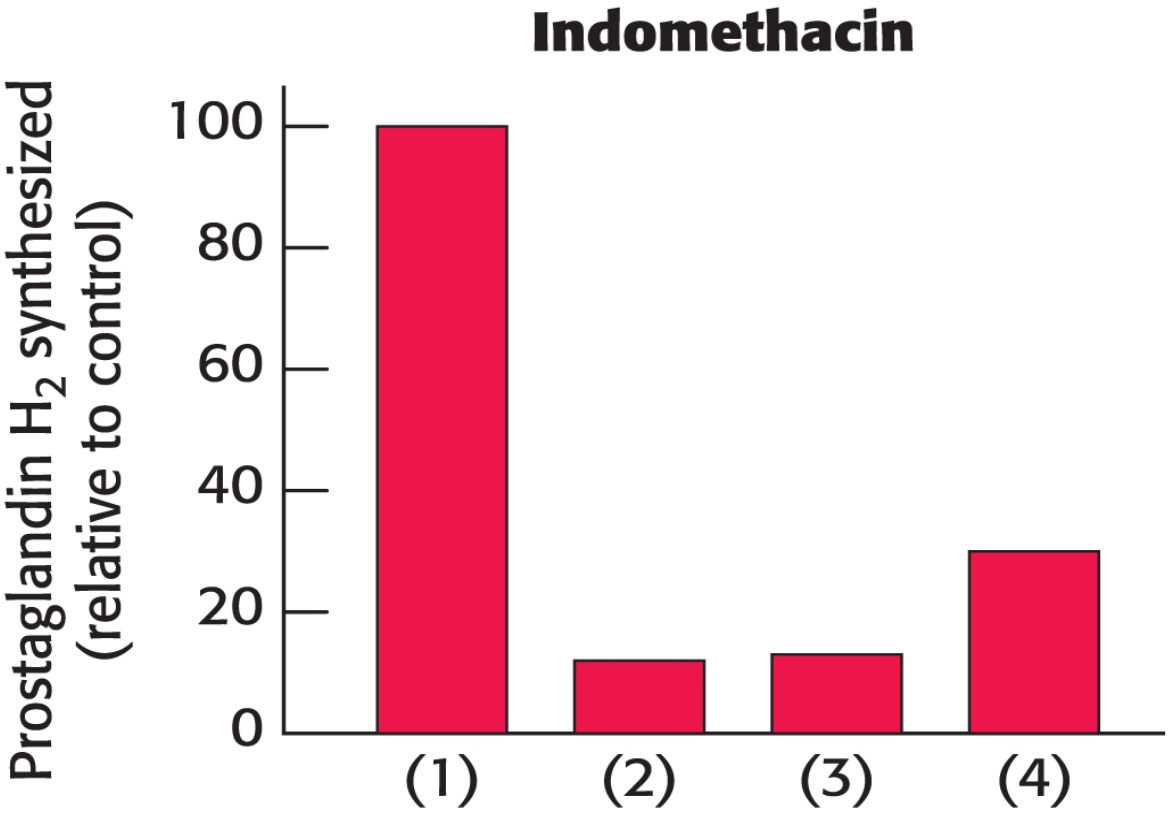
Return to Graphical representation of the fluidity of fatty acids in a phospholipid bilayer as a function of temperature

Extended description for Bar graphs depict the effect of ibuprofen and indomethacin on prostaglandin H 2

synthesis



© Macmillan Learning



The first bar graph is labeled as Ibuprofen. The horizontal axis has the markings (1), (2), (3), and (4). The vertical axis is labeled prostaglandin H 2 synthesized (relative to control). It has markings ranging from 0 to 100 in increments of 20 units. Four vertical bars are shown at (1),(2), (3), and (4). The coordinates of the vertical bars are as follows:

First bar: (1), 100; Second bar: (2), 18; Third bar: (3), 82; Fourth bar: (4), 120.

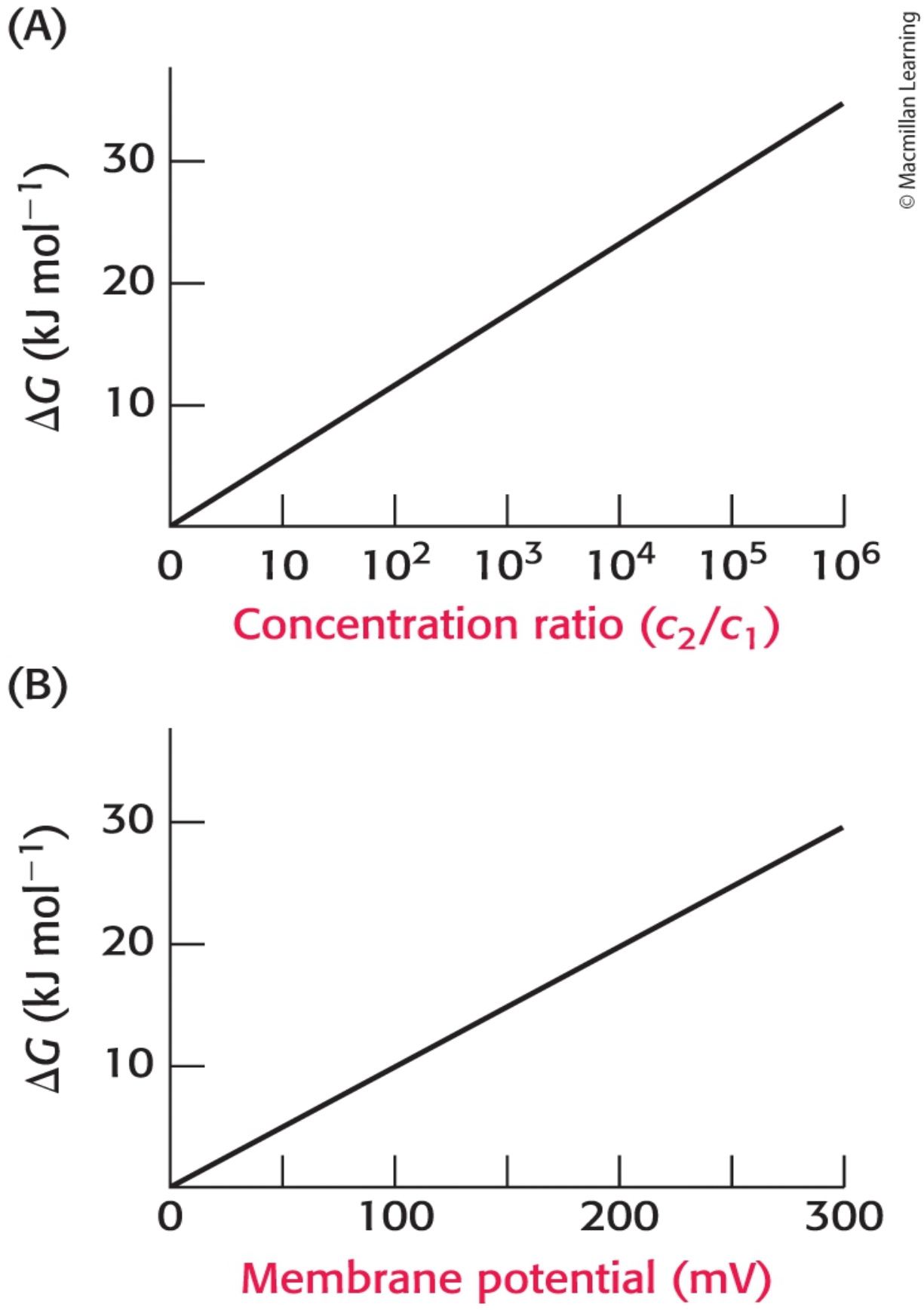
The second bar graph is labeled as Indomethacin. The horizontal axis has the markings (1), (2), (3), and (4). The vertical axis is labeled prostaglandin H 2 synthesized (relative to control). It has markings ranging from 0 to 100 in increments of 20 units. Four vertical bars are shown at (1), (2), (3), and (4). The coordinates of the vertical bars are as follows:

First bar: (1), 100; Second bar: (2), 10; Third bar: (3), 12; Fourth bar: (4), 30.

Return to Bar graphs depict the effect of ibuprofen and indomethacin on prostaglandin H 2 synthesis

Extended description for Two graphs depict the variation of free energy as a function of concentration

ratio and membrane potential respectively



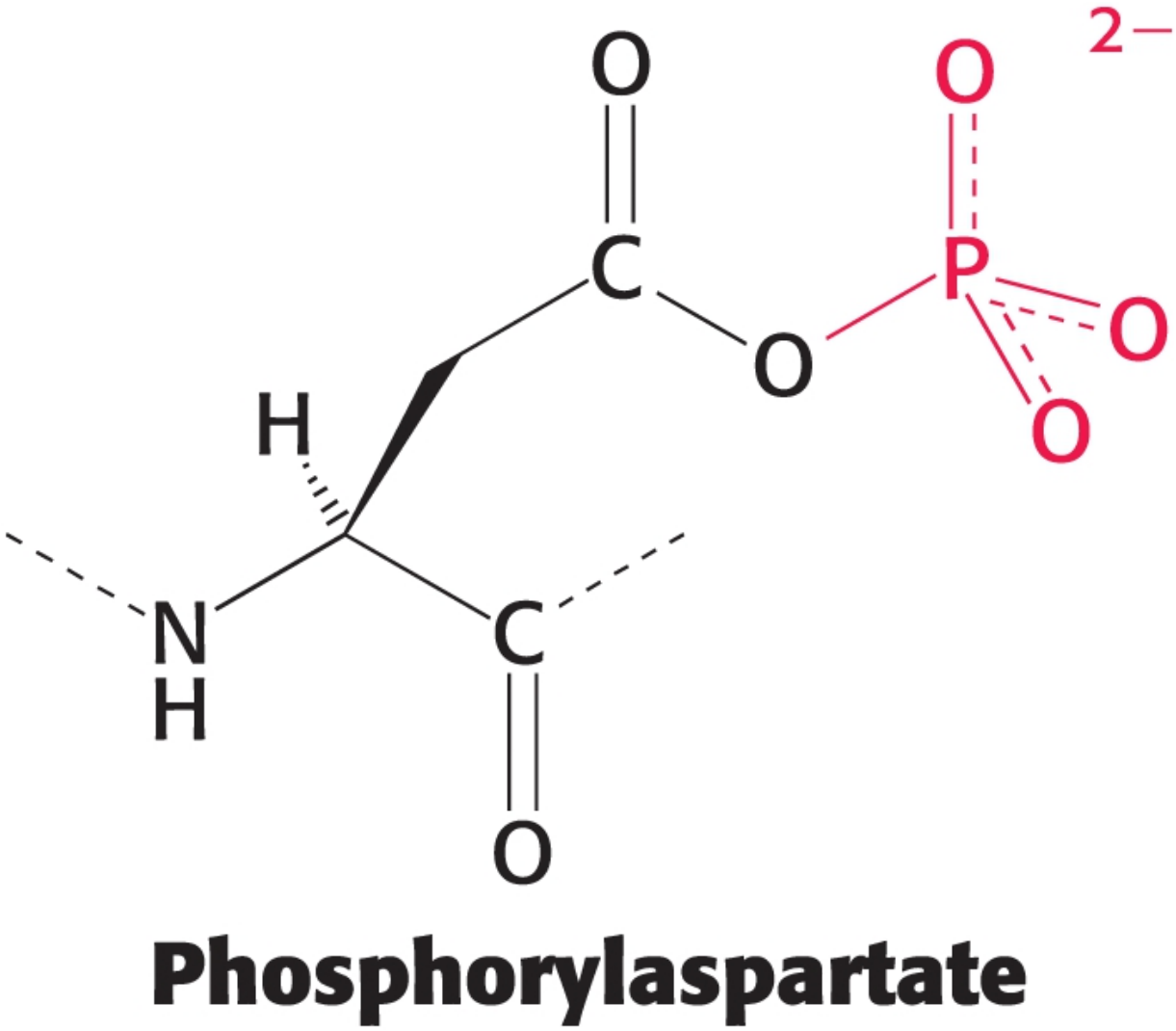
© Macmillan Learning

Graph (A): The horizontal axis is labeled concentration ratio (C 2 over C 1). It has markings ranging from 0 to 10 superscript 6 in multiples of 10 units. The vertical axis is labeled delta G (k J per mole). It has markings ranging from 10 to 30 in increments of 10 units. An increasing straight line starts from (0, 0) and ends (10 superscript 6, 40).

Graph (B): The horizontal axis is labeled membrane potential (m V). It has markings ranging from 0 to 300 in increments of 100 units. The vertical axis is labeled delta G (k J per mole). It has markings ranging from 10 to 30 in increments of 10 units. An increasing straight line starts from (0, 0) and ends at (300, 30).

Return to Two graphs depict the variation of free energy as a function of concentration ratio and membrane potential respectively

Extended description for Chemical structure of phoshorylaspartate

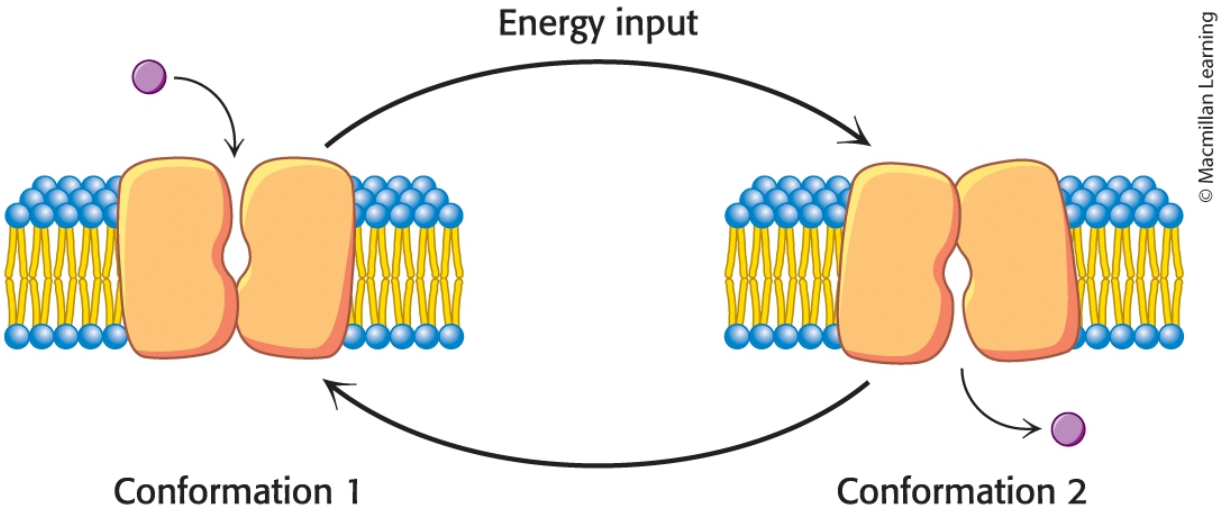


The structure of phosphorylaspartate is as follows: A 1 O, 1 C, and 1 P heteronuclear alkane chain is depicted as a line structure using 2 zigzag lines. O occupies the second position. P occupies the third position. C 1 is double bonded to O above. P is partially double bonded to O above, O on the lower right, and O below. The P O O group carries an overall negative charge of 2 minus. C 1 is single

bonded to C H 2 on the lower left. The C H 2 group is wedge bonded to a central C atom. This C atom is dash bonded to H on the upper left, single bonded to N H on the lower left, and single bonded to C on the lower right. This C atom is double bonded to O below and has an open single bond on the upper right. The N atom also has an open single bond on the upper left.

Return to Chemical structure of phoshorylaspartate

Extended description for Schematic representation of a conformational change of pump proteins during transport of a molecule



Conformation 1: A pair of integral membrane proteins are shown to span across a lipid bilayer. A groove is located at the center of the proteins that can accommodate a tiny circular molecule. A narrow channel is created between the top portion of the proteins to allow the entry of the molecule into the groove. The bottom portions of the proteins are attached tightly together.

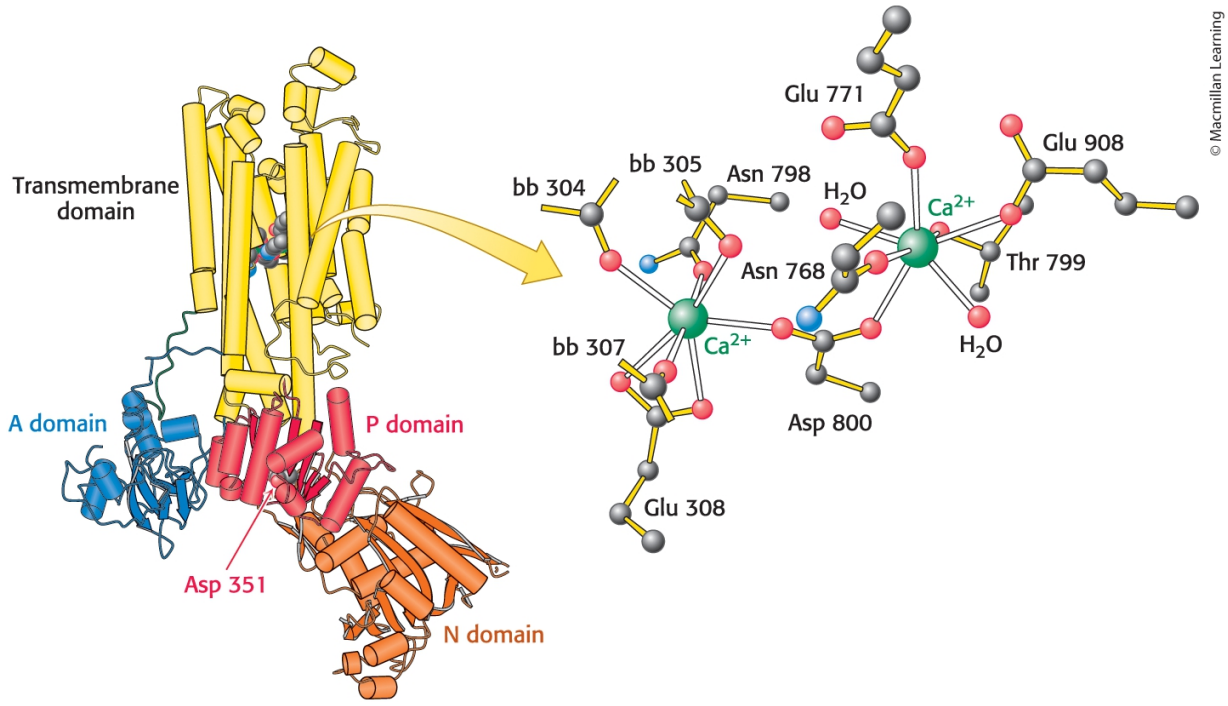
An energy input causes a conformational change to conformation 2

Conformation 2: The molecule is released into another side of the lipid bilayer. The top portion of the proteins is attached tightly together. A narrow channel is created between the bottom portion of the proteins to allow the release of the molecule from the groove.

The proteins again under a conformational change to conformation 1.

Return to Schematic representation of a conformational change of pump proteins during transport of a molecule

Extended description for Schematic structure of S E R C A P-type A T P ase and the ball-and-stick model of amino acid residues in the transmembrane domain bound to calcium



The S E R C A P-type A T P ase is composed of 4 domains from top to bottom. These domains are the transmembrane domain, A domain, P domain, and N domain. A and P domains are located in the middle. The transmembrane domain consists of long and short cylindrical structures interconnected by thread-like loops. A cluster of spheres is shown in the center of the transmembrane domain. The A domain consists of short cylindrical structures and beta-strands interconnected by thread-like loops. The P domain consists of medium to short cylindrical structures and beta-strands interconnected by thread-like loops. A cluster of spheres located in the center of the P domain is labeled A s p 531. The N domain has

long, medium, and short cylindrical structures and a few beta-strands interconnected by thread-like loops. It is oriented toward the bottom right.

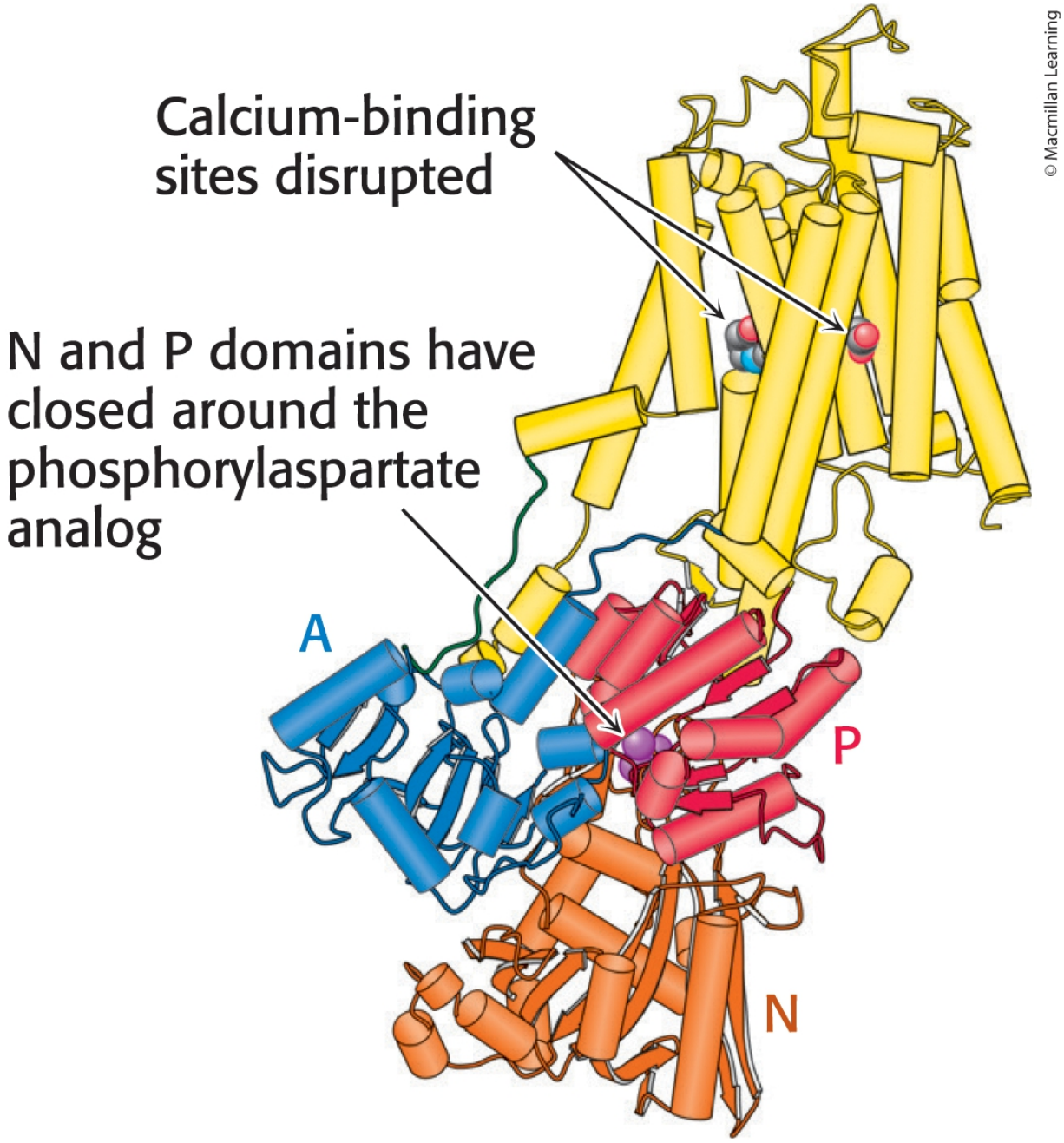
An arrow from the cluster of spheres in the center of the transmembrane points toward a ball-and-stick model. The model shows two C a superscript 2 plus ions connected to H 2 O, side chains of amino acid residues, and backbone carbonyl groups written as b b.

The first C a superscript 2 plus ion depicted as a green sphere is connected to a red sphere of G l u 771, G l u 908, T h r 799, H 2 O, A s p 800, A s n 768, and H 2 O in a clockwise direction starting from the top.

The second C a superscript 2 plus ion depicted as a green sphere is connected to a red sphere of A s n 798, a red sphere of b b 305, a red sphere of A s p 800, two red spheres of G l u 308, a red sphere of b b 307, and a red sphere of b b 304 in a clockwise direction starting from the top. A s n 798 and bb 305 are both oriented toward the upper right. G l u 308 and b b 307 are both oriented toward the lower left.

Return to Schematic structure of S E R C A P-type A T P ase and the ball-and-stick model of amino acid residues in the transmembrane domain bound to calcium

Extended description for Conformational change in the structure of S E R C A P-type A T P ase

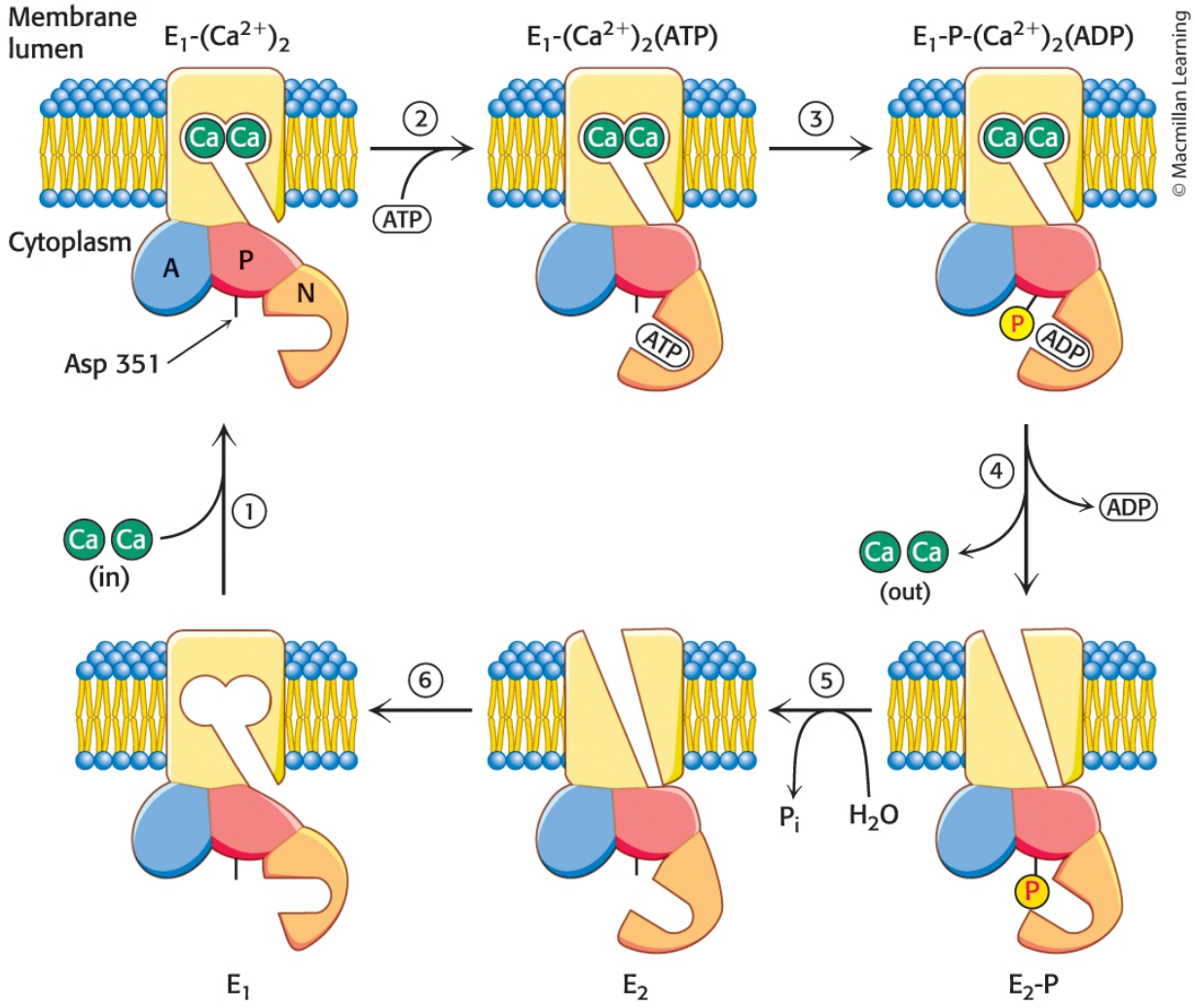


The structure of the A T P ase is altered such that the calcium-binding sites in the transmembrane domain are disrupted. The

orientation of cylindrical structures in the transmembrane domain is altered. Two clusters of spheres are shown in the center of the domain. The clusters are separated by two diagonally oriented long cylinders. The A and P domains have become closer and surround a phosphorylaspartate analog in the center of P domain. The orientation of N domain is shifted toward the bottom from bottom right.

Return to Conformational change in the structure of S E R C A P-type A T P ase

Extended description for Conformational change of S E R C A during a catalytic cycle



S E R C A is inserted into a membrane through a square-shaped domain having a pair of circular grooves in the center and a narrow channel connected to it. The circular groove allows C a ion binding and the channel opens into the cytoplasm. The square-shaped domain is fused below to the A and P domains located in the cytoplasm. The A and P domains are fused sideways. The P domain

is fused to the N domain. The N domain has a wide groove to allow the binding of A T P.

The catalytic cycle is divided into 6 steps.

Step 1:

E 1-open parenthesis C a superscript 2 plus close parenthesis with subscript 2: Two C a ions enter and bind to the circular grooves in the transmembrane domain of S E R C A. The A s p 351 residue of the P domain is depicted as a short thick line.

Step 2:

E 1-open parenthesis C a superscript 2 plus close parenthesis with subscript 2 A T P: The circular grooves in the transmembrane domain of S E R C A are bound to two C a ions. The wide groove in the N domain is bound to an A T P molecule. This causes a conformational change in the N domain and shifts the side bound to A T P toward the A s p 351 residue.

Step 3:

E 1-P-open parenthesis C a superscript 2 plus close parenthesis with subscript 2 A D P: The circular grooves in the transmembrane domain of S E R C A are bound to two C a ions. The wide groove in the N domain is bound to an A D Pmolecule. The A s p 351 residue of the P domain is phosphorylated.

Step 4:

E 2-P: The circular grooves of the transmembrane domain disappear as the two Ca ions are released. A diagonal channel is created in this

domain. The groove of the N domain also becomes empty as the A D P molecule is released. The N domain becomes attached to the phosphorylated A s p 351 residue.

Step 5:

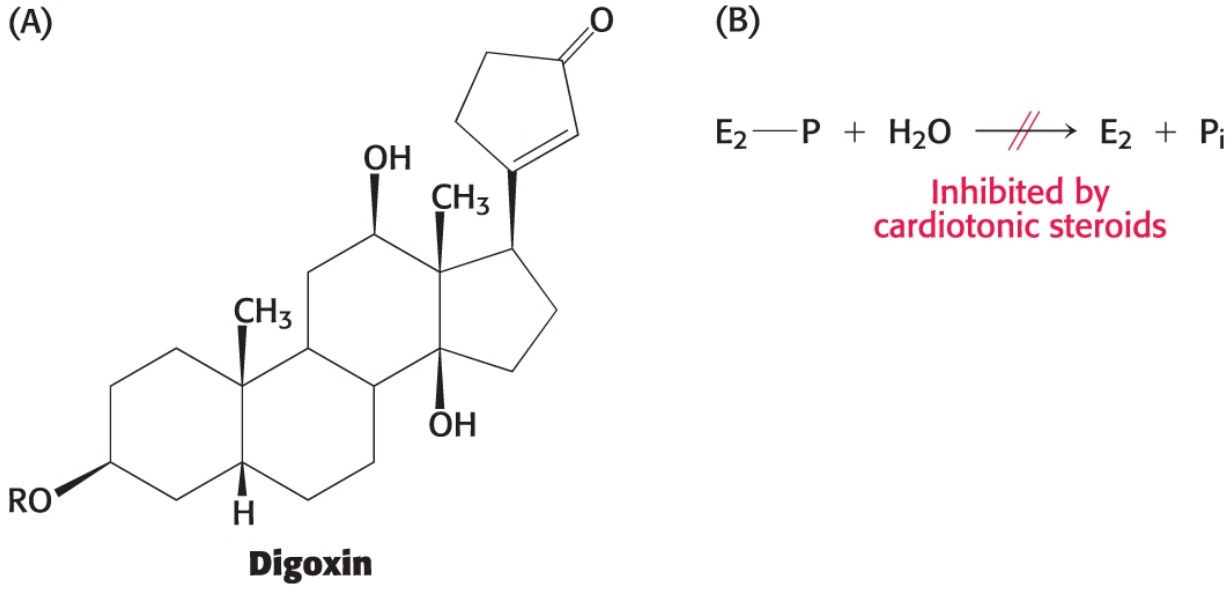
E 2: H 2 O enters and P subscript i is released. The A s p 351 residue is dephosphorylated.

Step 6:

E 1: The pair of circular grooves connected to a narrow channel is created again in the transmembrane domain. The N domain shifts away from the P domain.

Return to Conformational change of S E R C A during a catalytic cycle

Extended description for Chemical structure of digoxin and chemical reaction inhibited by cardiotonic steroids



Part (A):

The structure of digoxin is as follows: A 6-carbon homocyclic hexagonal ring is in a vertical orientation with C 1 occupying the topmost vertex. C 5 is wedge bonded to O R on the lower left. It is fused to a second 6-carbon homocyclic hexagonal ring in a vertical orientation such that C 2 and C 3 of the first ring are C 6 and C 5 respectively of the second ring. In the second ring, C 5 is wedge bonded to H below and C 6 is wedge bonded to C H 3 above. The second ring is fused to a third 6-carbon homocyclic hexagonal ring in a vertical orientation such that C 1 and C 2 of the second ring are C 5 and C 4 respectively of the third ring. In the third ring, C 1 is wedge bonded to O H above. The third ring is fused to a 5-carbon homocyclic pentagonal ring in a horizontal orientation such that C 2 and C 3 of the third ring are C 4 and C 3 respectively of the pentagonal ring. C 3 is wedge bonded to O H below and C 4 is wedge

bonded to C H 3 above. C 5 is wedge bonded to C 3 of a 5-carbon homocyclic pentagonal ring in a vertical orientation. In the pentagonal ring, C 1 is double bonded to O on the upper right. A double bond is present between C 2 and C 3.

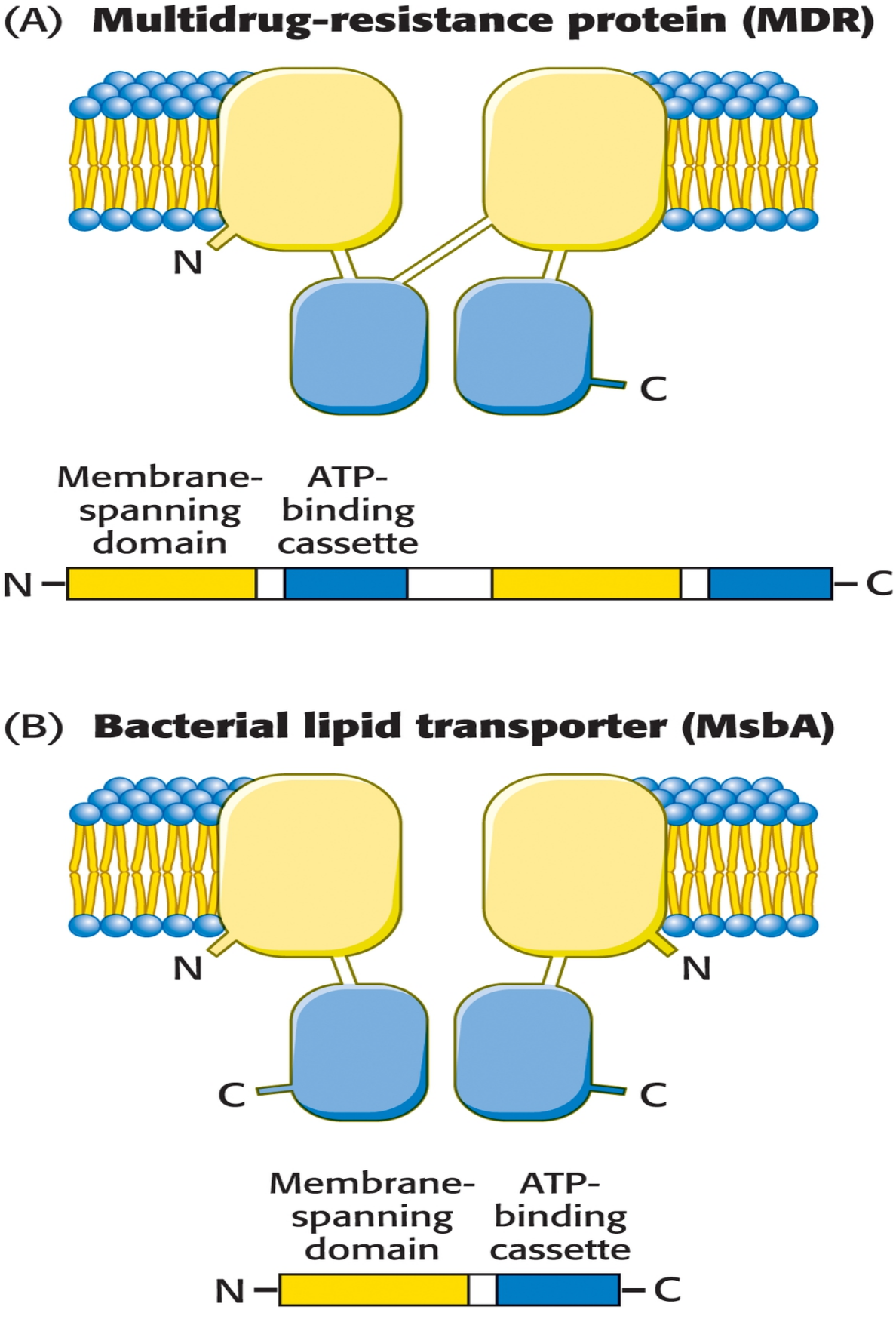
Part (B): The chemical reaction consists of two reactants and two products. The first reactant is E 2, single bond, P. The second reactant is H 2 O. A forward reaction arrow has two short and parallel red lines drawn across it. The red lines are labeled “Inhibited by cardiotonic steroids”. The first product is E 2. The second product is P subscript i.

Return to Chemical structure of digoxin and chemical reaction inhibited by cardiotonic steroids

Extended description for Schematic structure of multidrug-resistance protein and bacterial lipid

transport protein

© Macmillan Learning



Part (A): Multidrug-resistance protein (M D R). M D R consists of two large square-shaped transmembrane domains. A tiny extension on the bottom left of the left transmembrane domain is labeled N. An extension from the bottom right of the left transmembrane domain and the bottom left of the right transmembrane domain are connected to a small blue square-shaped domain in the cytoplasm. An extension at the bottom of the right transmembrane domain connects it to another small blue square-shaped domain in the cytoplasm. This square-shaped domain has an extension on the bottom right labeled C.

A long and narrow horizontal rectangular structure is shown. Its left end is labeled N and the right end is labeled C. From N to C, the domains are colored as follows: yellow, white, blue, white, yellow, white, and blue. The yellow domains are longer than the blue domains. The white domains are the shortest. The yellow domain is labeled the membrane-spanning domain. The blue domain is labeled A T P-binding cassette.

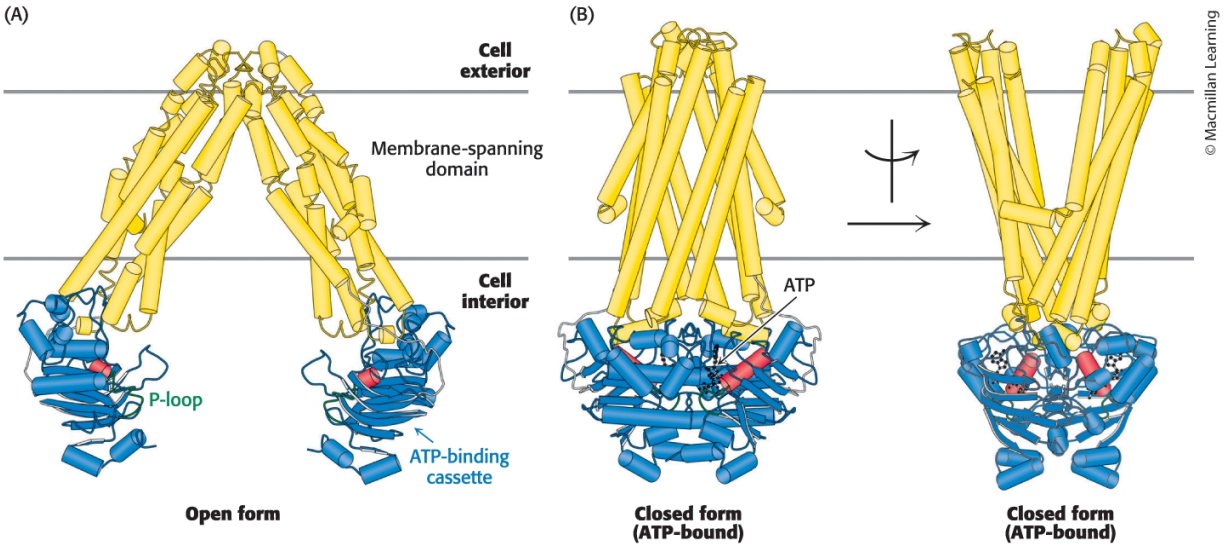
Part (B): Bacterial lipid transporter (M s b A). M s b A consists of two large square-shaped transmembrane domains. A tiny extension on the bottom left of the left transmembrane domain is labeled N. An extension from the bottom right of the left transmembrane domain is connected to a small blue square-shaped domain in the cytoplasm. An extension at the bottom of the right transmembrane domain connects it to another small blue square-shaped domain in the cytoplasm. Both of these small square-shaped domains have an extension at the bottom labeled C.

A long and narrow horizontal rectangular structure is shown. The left end is labeled N and the right end is labeled C. From N to C, the domains are colored as follows: Yellow, white, and blue.

The yellow domain is longer than the blue domain. The white domain is the shortest. The yellow domain is labeled the membrane-spanning domain. The blue domain is labeled A T P-binding cassette.

Return to Schematic structure of multidrug-resistance protein and bacterial lipid transport protein

Extended description for Open and closed forms of bacterial lipid transporter M s b A



Part (A) open form: Two horizontal lines separated by a large gap are shown. The region above the top line is labeled cell exterior. The region below the bottom line is labeled cell interior. An inverted V-shaped structure composed of short, medium, and long cylindrical structures pass the two horizontal lines. It extends into the cell exterior and interior. The region of this structure enclosed between the two lines is labeled membrane-spanning domain. In the cell interior, the extensions of the inverted structure are each bound to a small cluster of short and medium cylindrical structures and beta-strands interconnected by thread-like loops. A small loop from the left cluster is labeled P-loop. An arrow points toward an A T P-binding cassette in the right cluster.

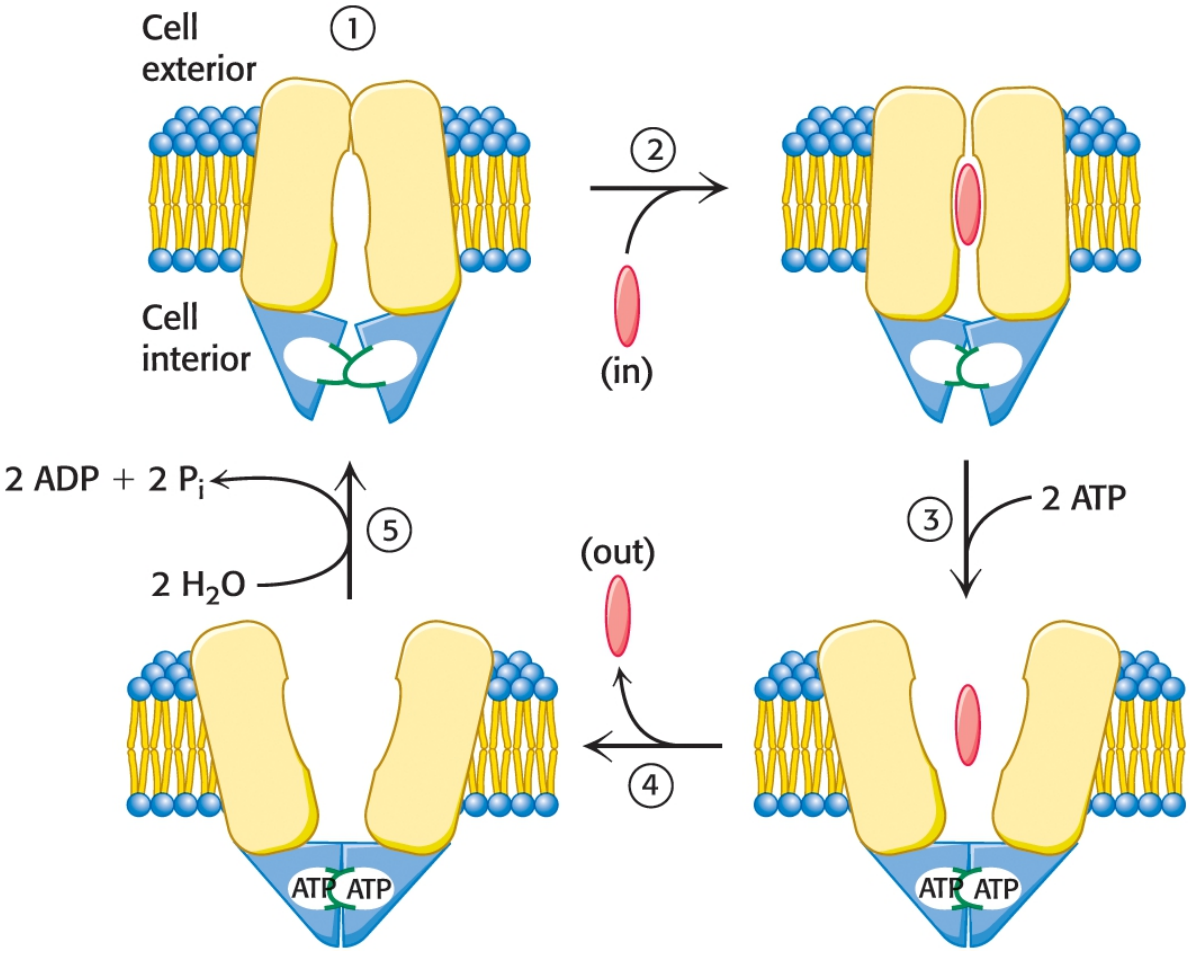
Part (B): It shows two views of the closed-form of M s b A protein bound to A T P. In the first view, a cluster of diagonally orientated long and a few short cylindrical structures pass through the two horizontal lines. They extend in the cell exterior and interior. The

extension into the cell interior is bound to a large cluster of short and medium cylindrical structures and beta-strands interconnected by thread-like loops. An A T P molecule is bound to the center of this cluster.

The first view is rotated by 90 degrees to get the second view. In the second view, an erect V-shaped structure composed of long cylindrical structures passes the two horizontal lines. It extends into the cell exterior and interior. The extension into the cell interior is bound to a large cluster of short and medium cylindrical structures and beta-strands interconnected by thread-like loops.

Return to Open and closed forms of bacterial lipid transporter M s b A

Extended description for Mechanism of transport of molecules by A B C transporters



© Macmillan Learning

The mechanism is divided into five steps as follows:

Step 1: A pair of large transmembrane domains are open toward the cell interior and closed toward the cell exterior. Each of the transmembrane domains is attached to a cytoplasmic domain having a wide empty groove. The grooves of the two cytoplasmic domains face each other.

Step 2: An oval-shaped molecule binds to a central groove formed between the transmembrane domains. This causes a conformational change as the transmembrane domains become closed at their intracellular region. The cytoplasmic domains also come closer.

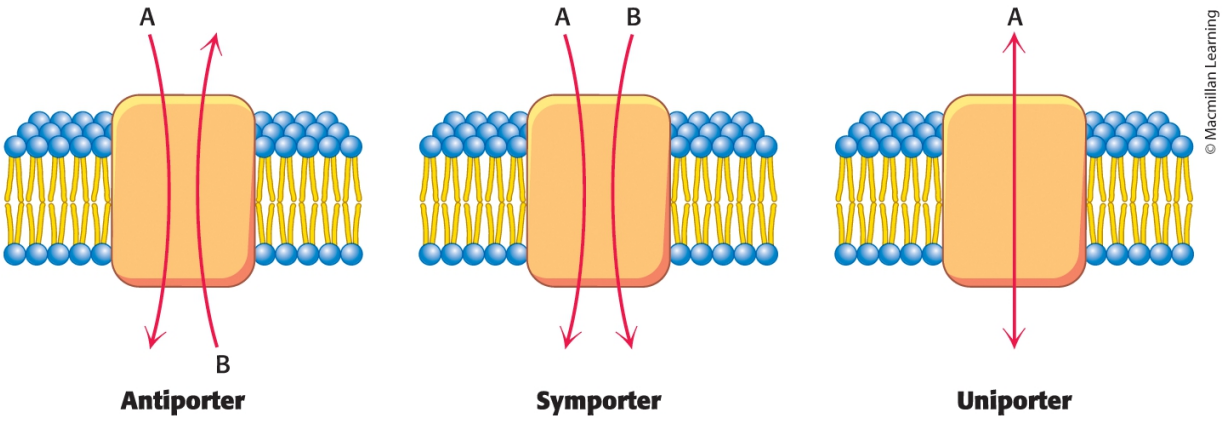
Step 3: 2 A T P molecules enter and bind to the grooves of the cytoplasmic domains. This causes a conformational change in the structure of the transmembrane domain such that it opens toward the cell exterior.

Step 4: The oval-shaped molecule is released from the central groove of the transmembrane domain. The A T P molecules are still bound to the groove of the cytoplasmic domains.

Step 5: 2 H 2 O molecules enter and 2 A D P plus 2 P subscript i are released.

Return to Mechanism of transport of molecules by A B C transporters

Extended description for Schematic representation of antiporter, symporter, and uniporter



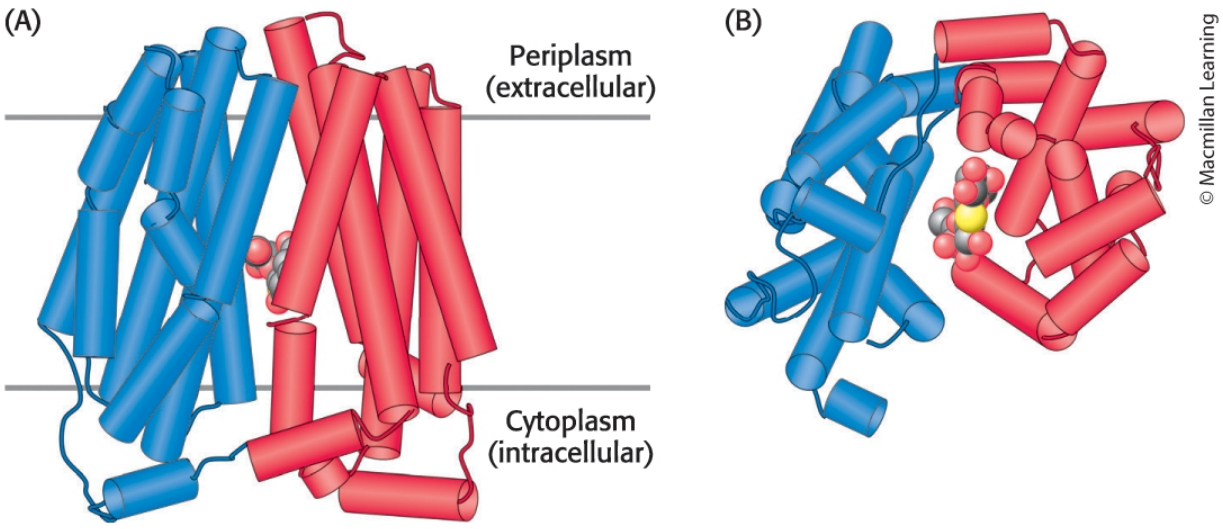
Antiporter: A large rectangular transmembrane protein is shown. It passes through a lipid bilayer. A downward arrow across the protein shows the inward movement of “A”. An upward arrow across the protein shows the outward movement of “B”.

Symporter: A large rectangular transmembrane protein is shown. It passes through a lipid bilayer. Two downward arrows across the protein show the inward movement of “A” and “B”.

Uniporter: A large rectangular transmembrane protein is shown. It passes through a lipid bilayer. A double-headed vertical arrow passing across the protein shows the inward and outward movement of A.

Return to Schematic representation of antiporter, symporter, and uniporter

Extended description for Side view and bottom view of *E.coli* lactose permease

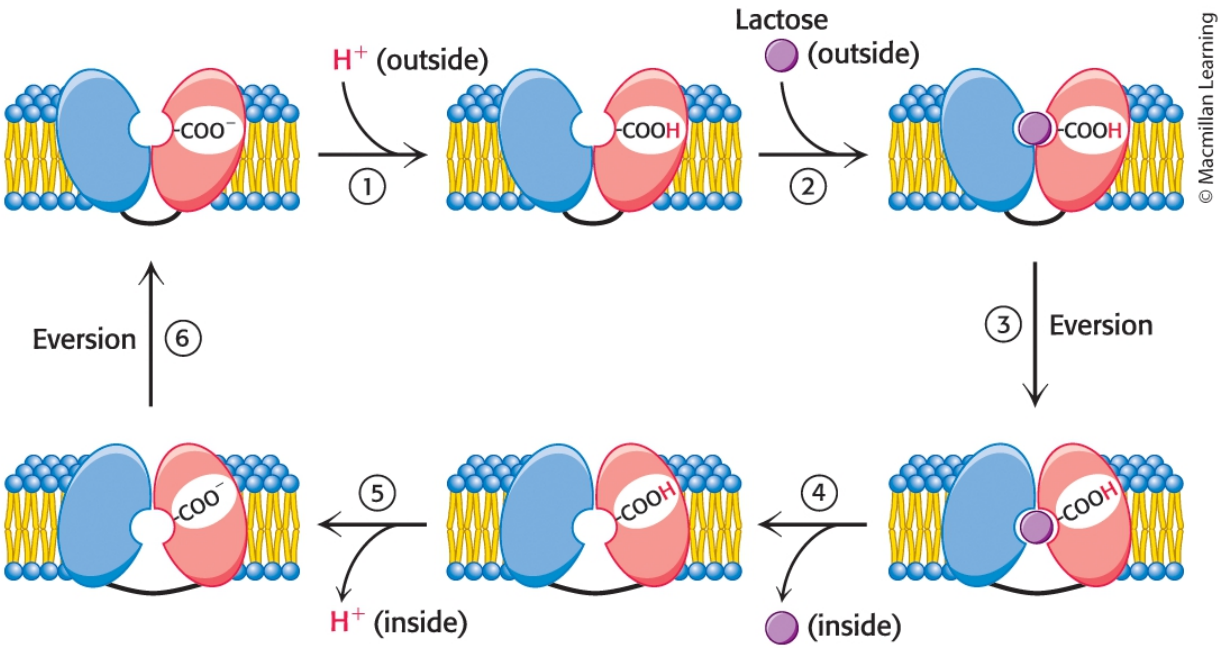


Part (A): Two horizontal lines separated by a large gap are shown. The region above the top line is labeled periplasm (extracellular). The region below the bottom line is labeled cytoplasm (intracellular). The lactose permease consists of a cluster of medium and long cylindrical structures passing through the gap between the two lines. They extend into the periplasm and cytoplasm. The cylindrical structures are connected by thread-like loops and a few medium cylindrical structures are located in the cytoplasm. The left half of the permease is colored blue and the right half is colored red.

Part (B): The bottom view shows a cluster of blue short and long cylindrical structures on the left and a cluster of red short and long cylindrical structures on the right. They surround a cluster of yellow, black, red, and grey spheres in the center.

Return to Side view and bottom view of *E.coli* lactose permease

Extended description for Mechanism of transport of lactose by lactose permease



The mechanism is divided into six steps as follows:

Step 1: A pair of oval-shaped transmembrane proteins are embedded in a lipid bilayer. A central groove located between the two proteins forms a circular shape. The groove of the right transmembrane protein is single bonded to C O O superscript minus inside the protein. The paired transmembrane proteins form an open face at the external surface. An H superscript plus ion enters and binds to C O O superscript minus to form a C O O H group.

Step 2: A purple circle labeled lactose binds to the circular central groove.

Step 3: This step is labeled eversion. It shows a conformational change in the transmembrane proteins as they form an open face at

the cytoplasmic surface.

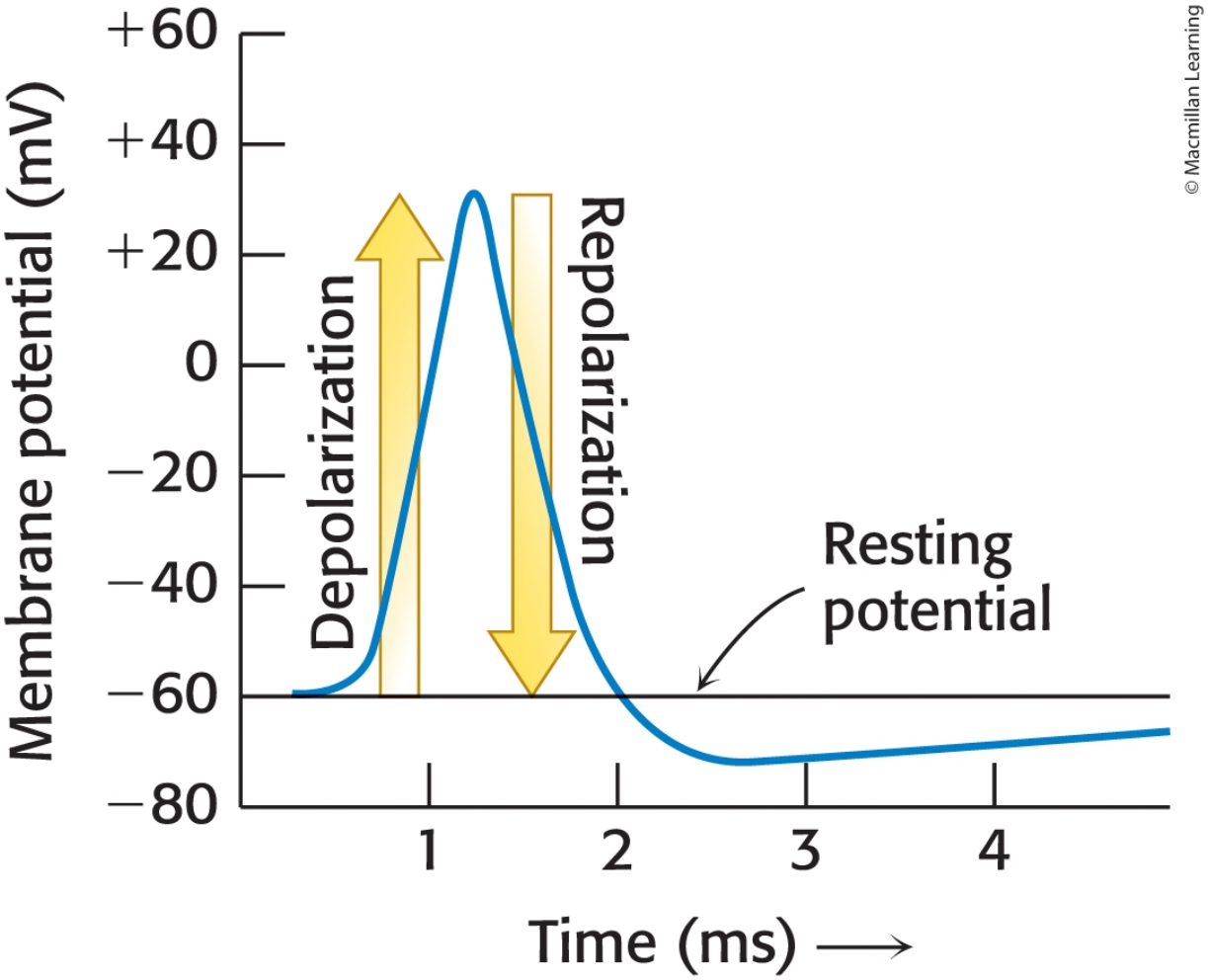
Step 4: The lactose molecule leaves the circular groove and moves inside.

Step 5: The H superscript plus ion leaves and a carboxylate group C O O superscript minus is formed again.

Step 6: This step is labeled eversion. It shows a conformational change in the transmembrane proteins as they form an open face at the external surface.

Return to Mechanism of transport of lactose by lactose permease

Extended description for Graphical representation of action potential



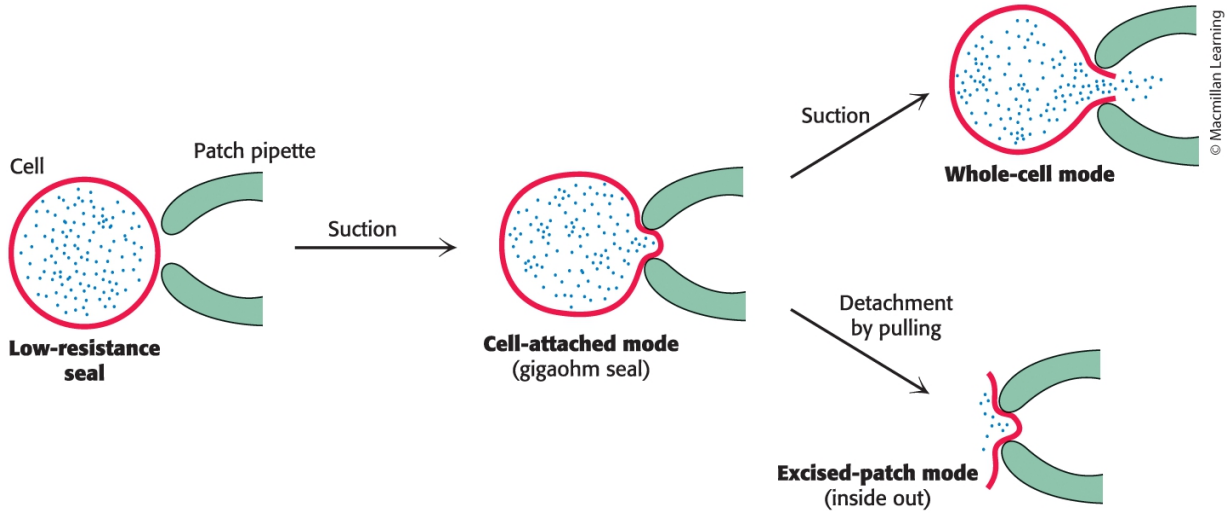
© Macmillan Learning

The horizontal axis is labeled time in milliseconds. It has markings ranging from 1 to 4 in increments of 1 unit. The vertical axis is labeled membrane potential in m V. It has markings ranging from negative 80 to positive 60 in increments of 20 units. A horizontal line parallel to the horizontal axis starts from negative 60 on the vertical axis. This line is labeled resting potential. A line curve starts at (0.4, negative 60) and shows upward movement to reach (1.3, positive 35). It then falls steeply to reach (2.5, negative 70) and continues moving

almost horizontally toward the right. An upward arrow labeled depolarization is shown along the upward slope of the curve. A downward arrow labeled repolarization is shown along the downward slope of the curve.

Return to Graphical representation of action potential

Extended description for Patch-clamp technique



A circular cell with a red outline contains tiny scattered dots. The red outline depicts the membrane. A patch pipette is located close to the red outline of the cell to form a low-resistance seal.

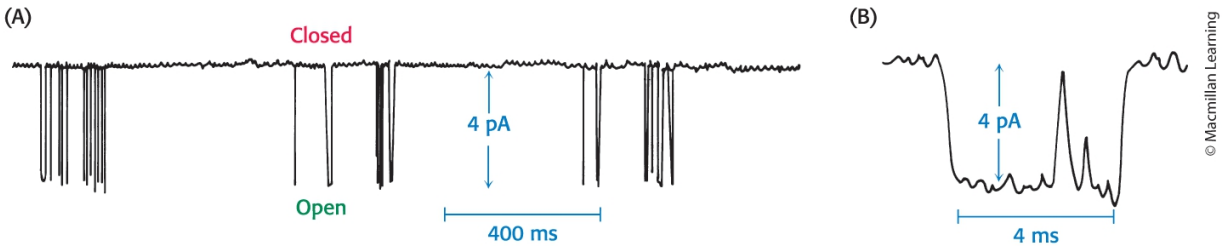
The pipette sucks a small portion of the cell in a cell-attached mode configuration. This produces a gigaohm seal.

The further suction of the cell portion causes it to burst open and release blue dots into the pipette. This configuration is the whole-cell mode.

However, pipette pulling leads to the detachment of a small section of the cell membrane and its cytoplasmic content. This configuration is an excised-patch mode (inside out).

[Return to Patch-clamp technique]

Extended description for Result of patch-clamp experiment

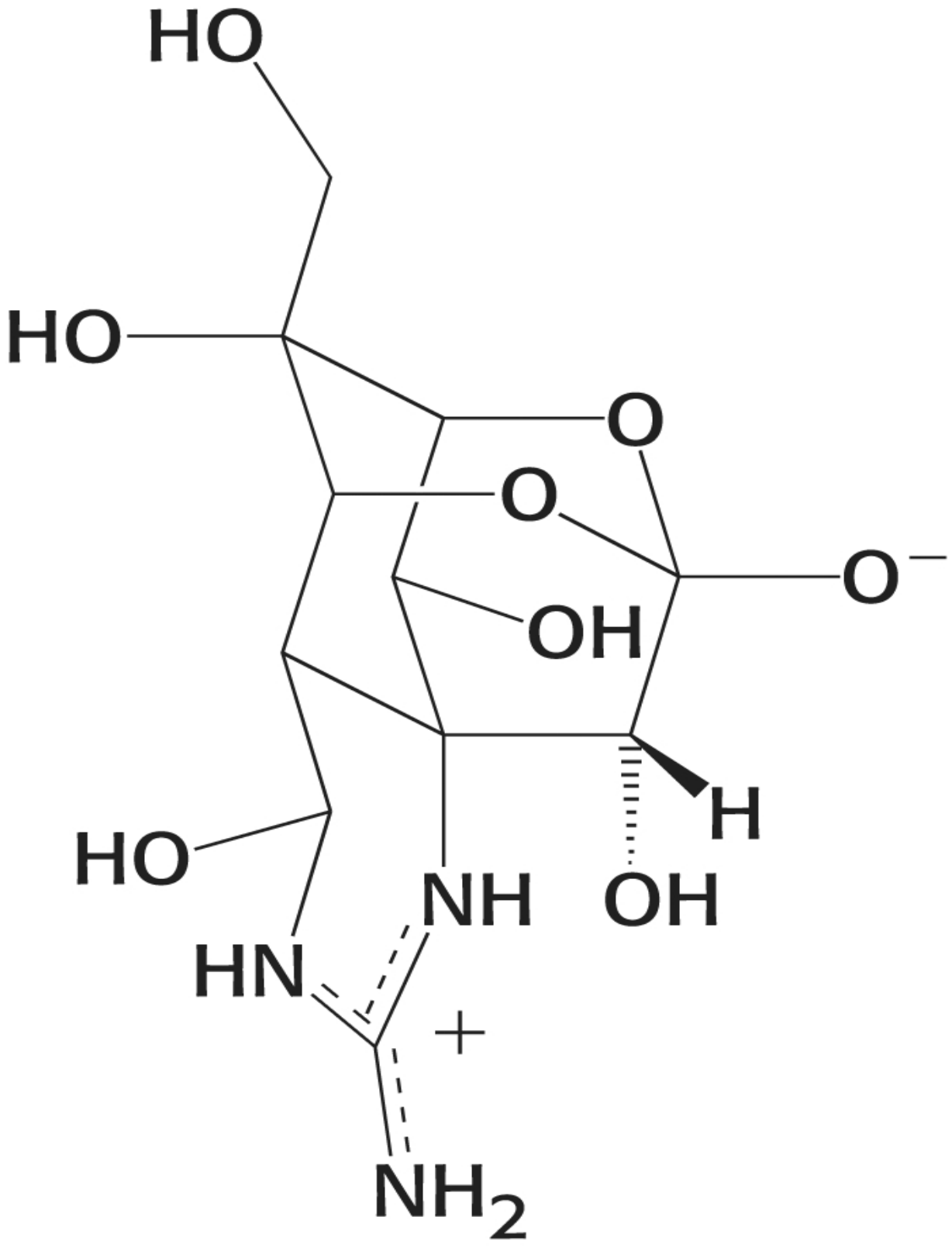


(A) A graph from patch-clamp experiment shows downward spikes with few gaps in between. The downward spikes indicate transitions between closed and open states of single ion channels. The length of a spike depicts 4 picoamperes and the time length between two spikes is 400 milliseconds.

(B) A zoomed-in view of one of the spikes is shown. It shows a series of small peaks and a single long peak. The time length from left to right for these peaks is 4 milliseconds.

Return to Result of patch-clamp experiment

Extended description for Sructure of Tetrodotoxin

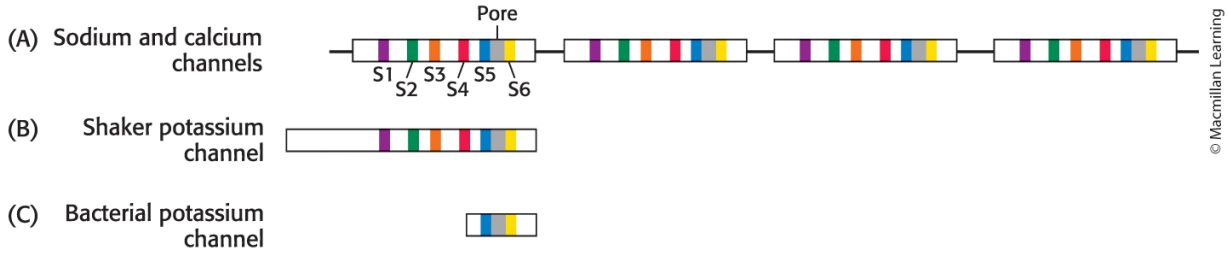


Tetrodotoxin

A 5-carbon vertical alkane chain is depicted as a line structure using 4 zigzag lines. C 1 is single bonded to O H on the upper left. C 2 is single bonded to O H on the left. C 5 is single bonded to O H on the lower left and N H on the lower left. C 2 is single bonded on the lower right to C 5 of a 6-membered heterocyclic hexagonal ring in a horizontal orientation consisting of 1 O and 5 C atoms. In the ring, O occupies the first position, which is the top right vertex. C 3 of the alkane chain is single bonded to O on the right. O is single bonded on the lower right to C 1 of the ring. C 4 of the alkane chain is single bonded on the lower right to C 3 of the ring. C 1 of the ring is single bonded to O superscript minus on the right. C 2 of the ring is wedge bonded to H on the lower right and dash bonded to O H below. C 4 of the ring is single bonded to O H on the lower right. C 3 of the ring is single bonded to a second N H group below. The first and the second N H groups are each partially double bonded to a common central C H group, on the lower right, and on the lower left, respectively, each in the form of a line. A positive charge is indicated near the second N H group. The central C H group is partially double bonded to N H 2 on the lower right.

Return to Sructure of Tetrodotoxin

Extended description for Structural features of sodium and calcium channels, shaker potassium channel, and bacterial potassium channel



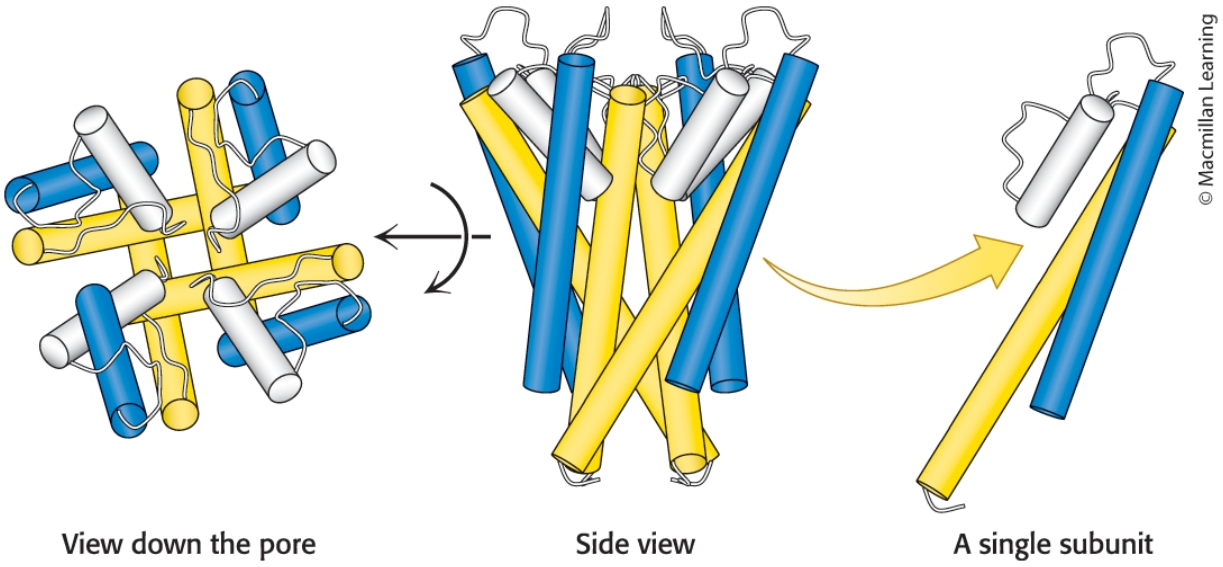
(A) The structure of sodium and calcium channels is as follows: The channel shows four interconnected horizontal bars. Each bar has a series of colored bands. From left to right the colors are violet, green, orange, red, blue, grey, and yellow. The bands with colors blue, grey, and yellow do not have spacing between them. The other bands are separated by spaces. The bands are labeled S 1, S 2, S 3, S 4, S 5, pore, and S 6 from left to right.

(B) The structure of the shaker potassium channel is as follows: The channel shows a horizontal bar. The bar has a series of colored bands. From left to right the colors are violet, green, orange, red, blue, grey, and yellow. The bands with colors blue, grey, and yellow do not have spacing between them. The other bands are separated by gaps.

(C) The structure of the bacterial potassium channel is as follows: The channel shows a horizontal bar. The bar has a series of colored bands. From left to right the colors are blue, grey, and yellow. These bands are not separated by a gap.

Return to Structural features of sodium and calcium channels, shaker potassium channel, and bacterial potassium channel

Extended description for Different views of the bacterial potassium ion channel



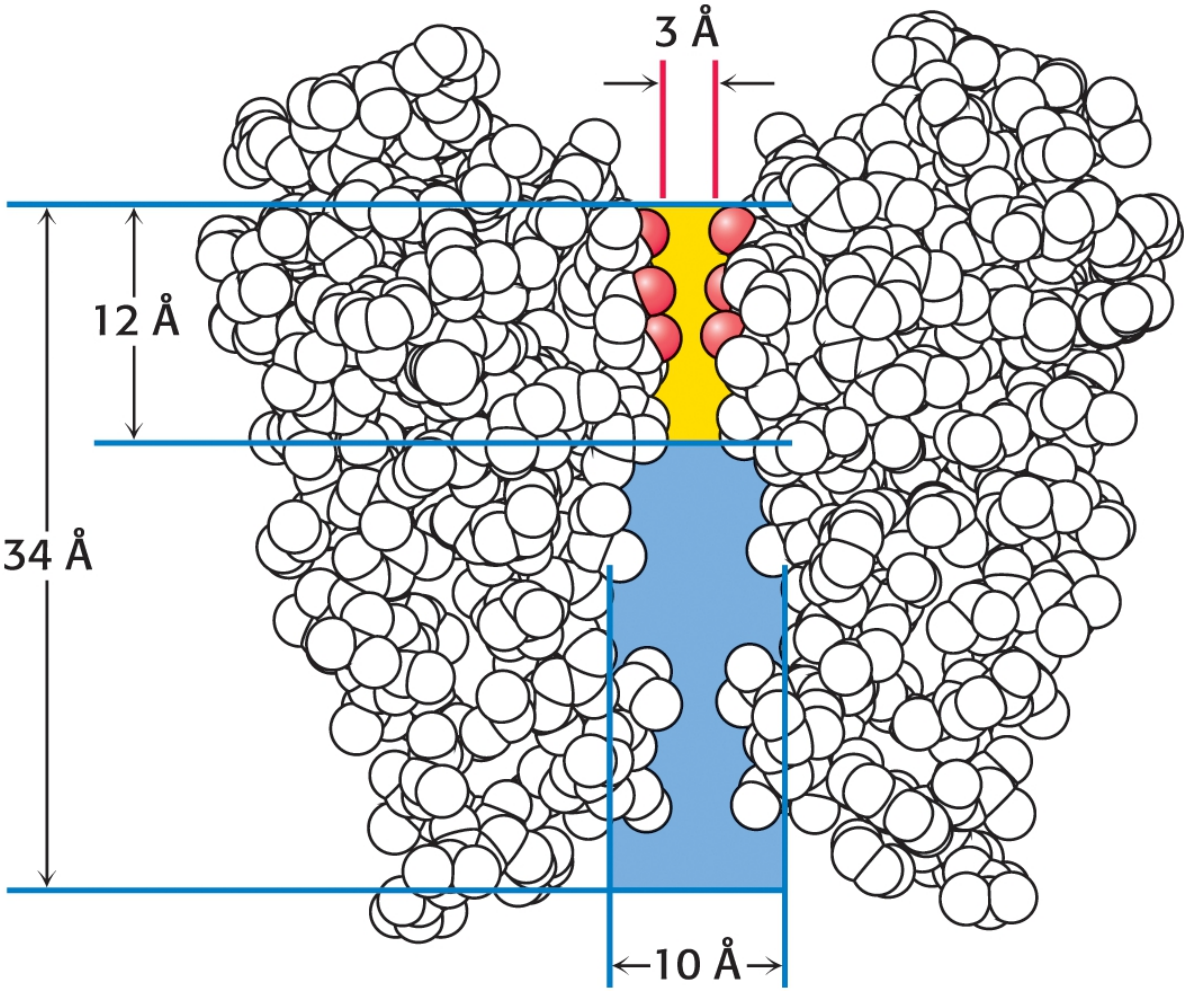
The structure of view down the pore is as follows: It shows four identical subunits. Each subunit consists of white, blue, and yellow elongated cylinders attached by threads. The four subunits are arranged such that they form a square with a pore in the center. The rotation of this view gives the side view.

The structure of the side view is as follows: It shows four identical subunits. Each subunit consists of white, blue, and yellow elongated cylinders attached by threads. The four subunits are arranged vertically.

The structure of a single subunit is as follows: It shows a single subunit with white, blue, and yellow elongated cylinders attached by threads.

Return to Different views of the bacterial potassium ion channel

Extended description for Space-filling model of a potassium ion channel



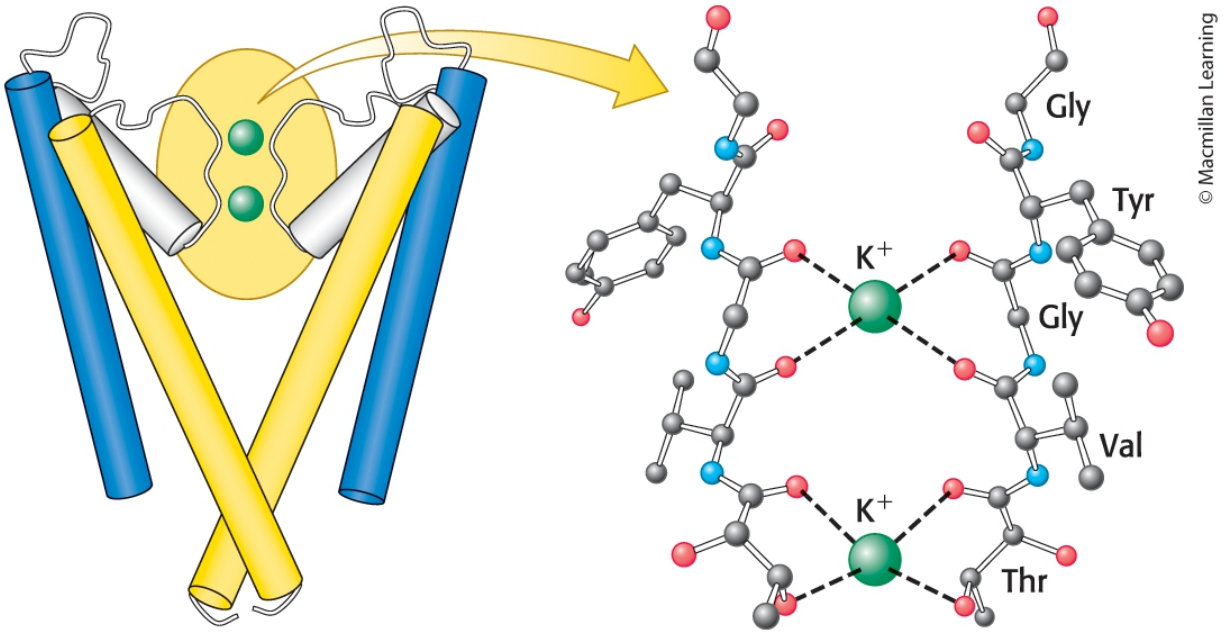
© Macmillan Learning

The figure shows two clusters of white spheres that are vertically separated by a gap. These clusters represent the potassium channel. The inner surface of the upper region of the clusters is separated by a gap of 3 angstroms. This gap is depicted by a yellow background and is lined by red spheres. The inner surface of the lower region of the clusters is separated by a 10-angstrom gap depicted by a blue background. The vertical length of the 3-angstrom gap is 12

angstrom. The vertical length of the entire gap from top to bottom is 34 angstrom.

Return to Space-filling model of a potassium ion channel

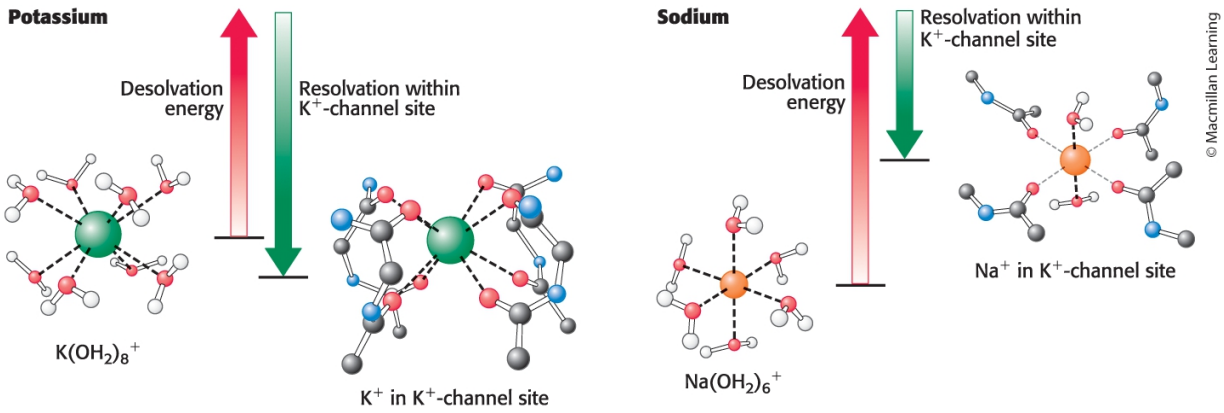
Extended description for Selectivity filter of potassium ion channel



The figure has two parts. The first part shows two identical subunits. Each subunit consists of white, blue, and yellow elongated cylinders attached by thread-like loops. The subunits form a V-shaped structure. The pore on the upper surface of the subunit is depicted as an oval with two green spheres. An arrow from this part point toward the next part on the right. In the second part, a ball and stick model of amino acid residues connected to two K superscript plus ions is shown. The first K superscript plus ion depicted as a green sphere is connected to a red sphere of different amino acid residues like tyrosine and glycine on either side. Tyrosine is connected to glycine above and glycine below. This glycine is connected to valine. Valine is further connected to threonine below. The second K superscript ion is connected to the red spheres of valine and threonine on either side. The amino acids are symmetrical and are attached in the same manner on the other side.

Return to Selectivity filter of potassium ion channel

Extended description for Desolvation and resolvation energy of potassium and sodium ions



The figure shows four structures.

The ball and stick model for K (O H 2) subscript 8 superscript plus is as follows: A central green sphere depicting potassium ion is connected to 8 red spheres. The 8 spheres represent the oxygen atoms of water molecules. Each red sphere is connected to two white spheres that represent hydrogen atoms oriented away from the green sphere.

The ball and stick model for K superscript plus ion in K superscript plus ion channel site is as follows: A central green K sphere is connected to 8 red spheres. The 8 red spheres are part of the side chains of amino acid residues oriented away from the central green sphere.

A red arrow from the right side of the K (O H 2) subscript 8 superscript plus points upward and is labeled desolvation energy. A downward green arrow beside the red arrow extends slightly below

the tail of the red arrow and is labeled resolvation within K superscript plus ion channel site.

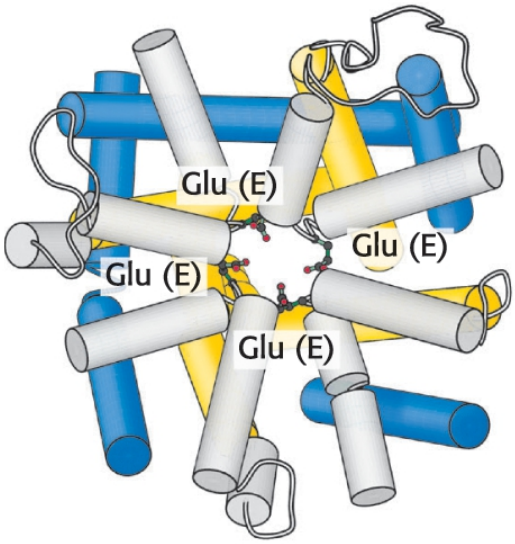
The ball and stick model for N a (O H 2) subscript 6 superscript plus is as follows: A central orange sphere depicting sodium ion is connected to 6 red spheres. The red spheres depict O atoms of water molecules. Each red sphere is connected to two white spheres that represent hydrogen atoms oriented away from the sodium ion.

The ball and stick model for N a superscript plus ion in K superscript plus ion channel site is as follows: A central orange sphere is connected to 6 red spheres. The red spheres above and below depict the O atom of water molecules and are further connected to 2 white spheres representing H atoms. The red spheres on the top left, top right, bottom left, and bottom right are part of the side chains of amino acid resides.

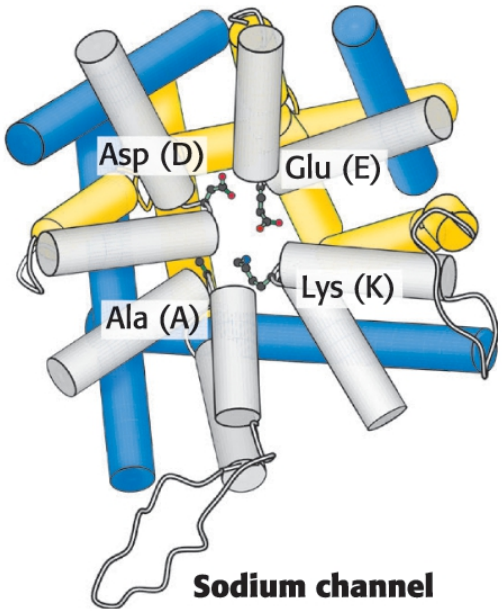
A red upward arrow from the right side of N a (O H 2) subscript 6 superscript plus is labeled desolvation energy. A downward green arrow beside the red arrow stops halfway near the middle of the first red arrow. The green arrow is labeled resolvation within K superscript plus ion channel site.

Return to Desolvation and resolvation energy of potassium and sodium ions

Extended description for Calcium channel and sodium channel



Calcium channel



Sodium channel

© Macmillan Learning

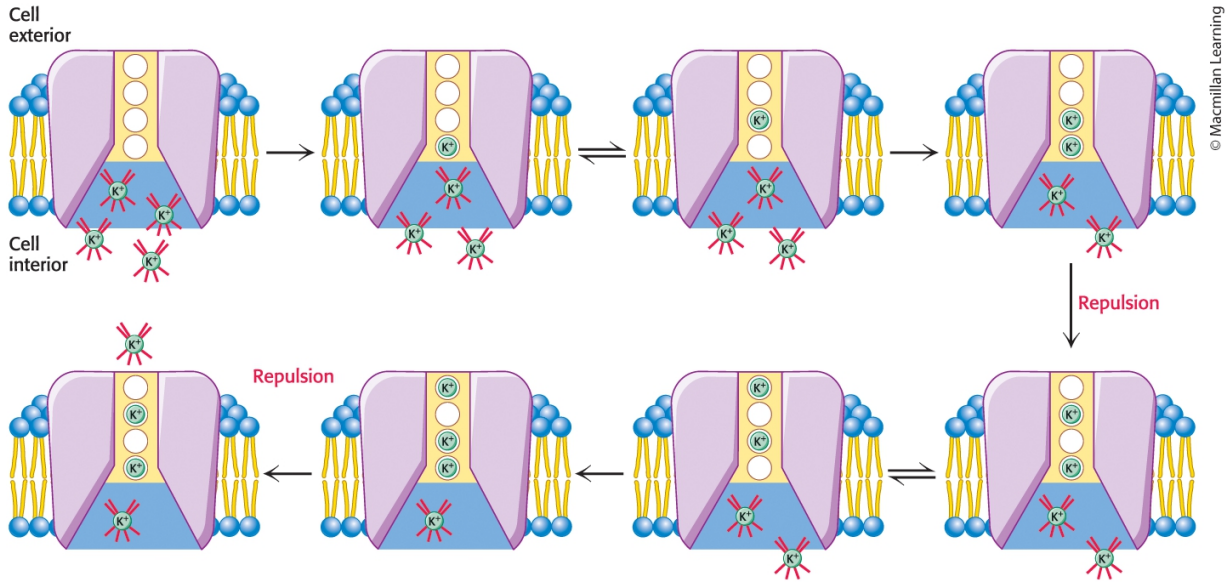
The structure of the calcium channel is as follows: The channel consists of 8 radially oriented white cylindrical structures surrounding a central pore. A similar orientation of yellow cylindrical structures is shown behind it, away from the observer. A few blue cylindrical structures are shown behind the yellow structures. These cylindrical structures are interconnected by thread-like loops. Four glutamate (E) residues line the central pore of the calcium channel.

The structure of the sodium channel is as follows: The channel consists of 8 radially oriented white cylindrical structures surrounding a central pore. A similar orientation of yellow cylindrical structures is shown behind it, away from the observer. A few blue cylindrical structures are shown behind the yellow structures. These cylindrical structures are interconnected by

thread-like loops. Aspartic acid (D), glutamic acid (E), alanine (A), and lysine (K) residues line the central pore of the sodium channel.

Return to Calcium channel and sodium channel

Extended description for Model of K superscript plus channel ion transport



The mechanism occurs in eight steps. In the first step, an inverted Y-shaped membrane channel is embedded in a lipid bilayer. The upper portion is labeled cell exterior and the inner portion is labeled cell interior. The interior of the cell contains four K superscript plus ions bound by water molecules depicted as red sticks. A forward arrow from this step points toward the second step.

In the second step, one of the K superscript plus ions enters the channel. Once it enters the channel, the water molecules are lost. A reversible reaction arrow points to the third step.

In the third step, the K superscript plus ion moves through the ion channel. Aforward arrow points toward the fourth step.

In the fourth step, two K superscript plus ions are depicted inside the ion channel. The K superscript plus ions lose their bound water molecules. An arrow from the fourth step points toward the fifth step and is labeled repulsion.

In the fifth step, the two K superscript plus ions in the channel repel one another and are present away from each other. A reversible reaction arrow points to the sixth step.

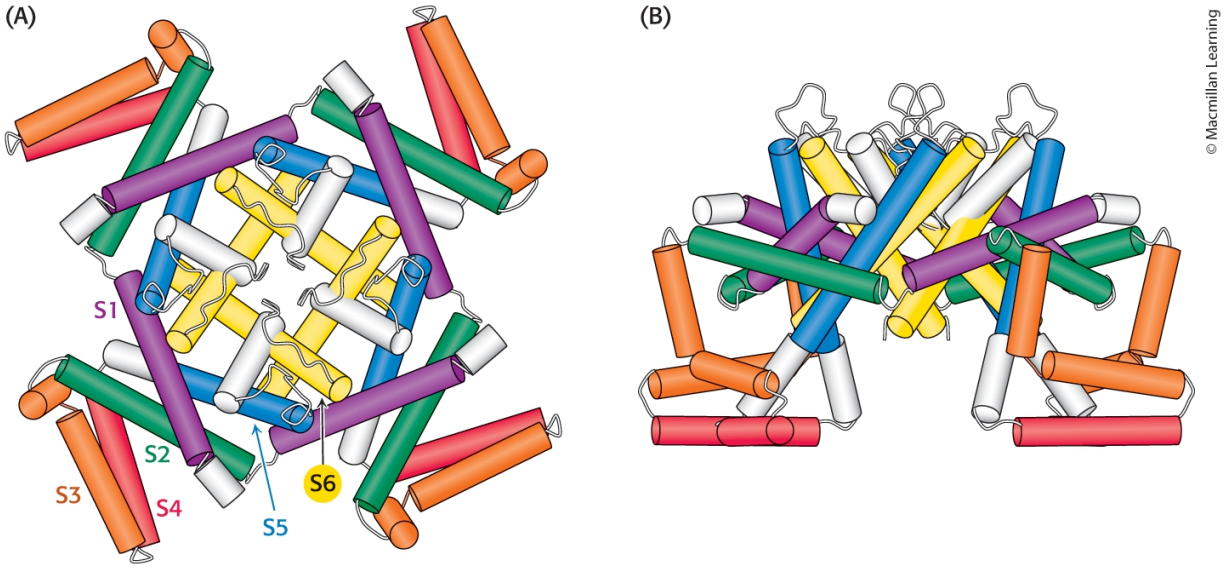
In the sixth step, out of the two K superscript plus ions in the channel one ion reaches the upper portion of the channel. An arrow from the sixth step points toward the seventh step.

In the seventh step, 3 K superscript plus ions without water molecules are seen inside the ion channel. An arrow from the seventh step points toward the eighth step.

In the eighth step, one of the K superscript plus ion bound to water molecules depicted as red sticks is seen in the cell exterior. 2 K plus ions without water molecules are seen inside the channel, and 1 K superscript plus ion bound to water molecules is seen in the cell interior.

Return to Model of K superscript plus channel ion transport

Extended description for View through the pore and side view of the voltage-gated potassium channel

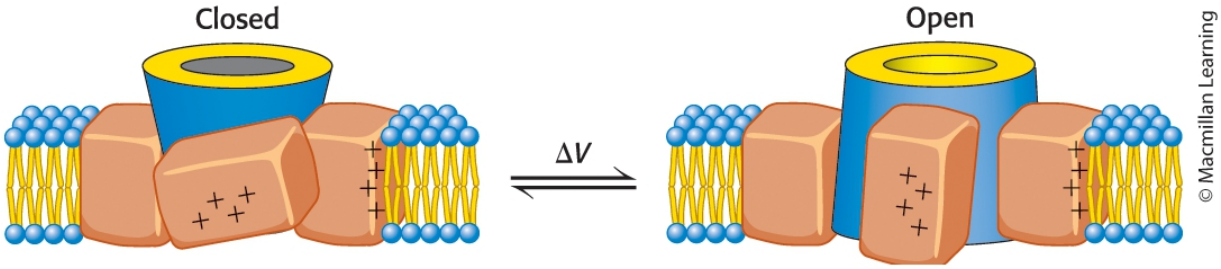


Part (A): The view looking down through the pore of the voltage-gated potassium channel is as follows: The channel consists of 6 identical subunits of S 1, S 2, S 3, S 4, S 5, and S 6 depicted as cylindrical structures. S 1 is purple, S 2 is green, S 3 is orange, S 4 is pink, S 5 is blue, and S 6 is yellow. Each subunit is arranged in such a way that a central square-shaped pore is formed. The subunits are attached by thread-like loops.

Part (B): The side view of the voltage-gated potassium channel is as follows: The channel consists of 6 identical subunits of S 1, S 2, S 3, S 4, S 5, and S 6 depicted as cylindrical structures. S 1 is purple, S 2 is green, S 3 is orange, S 4 is pink, S 5 is blue, and S 6 is yellow. The subunits form an arch-like structure.

Return to View through the pore and side view of the voltage-gated potassium channel

Extended description for Closed and open voltage-gated potassium channel

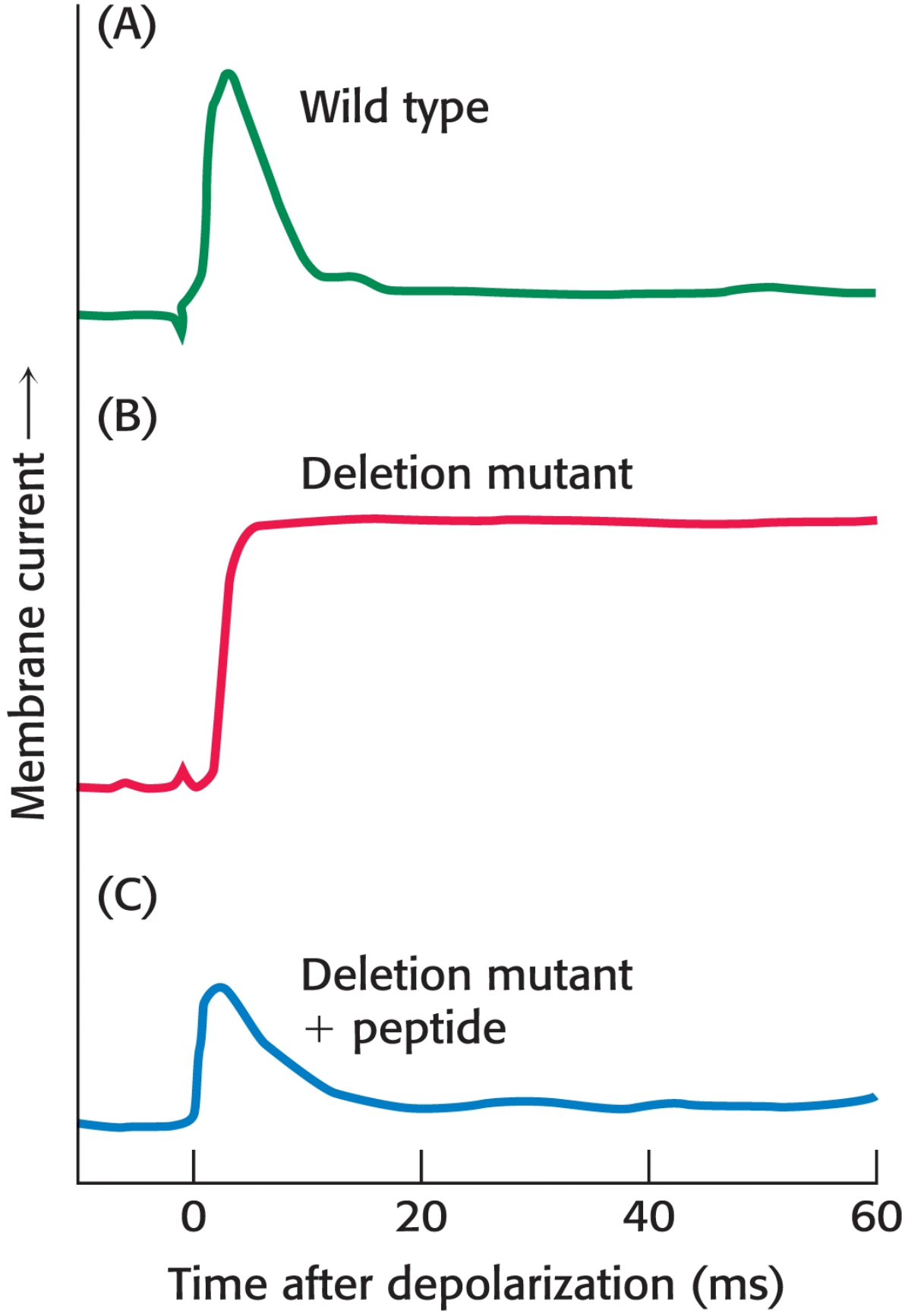


The structure of the closed voltage-gated potassium channel is as follows: The closed voltage-gated channel consists of a closed cylindrical channel that is surrounded by three rectangular block-like voltage sensing paddles with a positive charge. The voltage sensing paddles are embedded in a lipid bilayer. The structure of the open voltage-gated potassium channel is as follows: The open voltage-gated channel consists of an open cylindrical channel that is surrounded by vertical block-like voltage sensing paddles with a positive charge. The voltage sensing paddles are embedded in a lipid bilayer. The closed and open forms are separated by a reversible reaction arrow labeled delta V.

Return to Closed and open voltage-gated potassium channel

Extended description for Graph of membrane current

versus time after depolarization



© Macmillan Learning

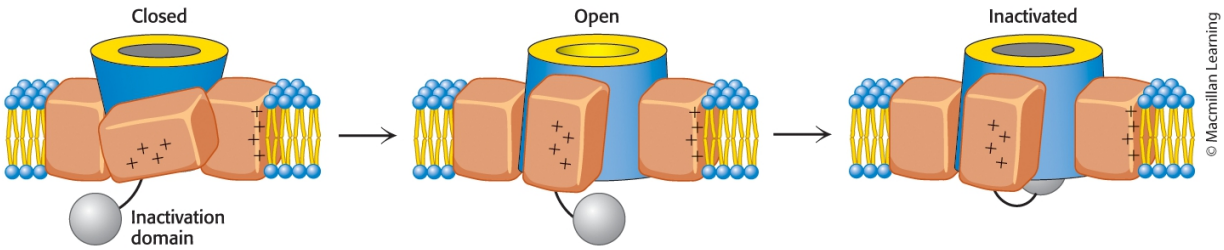
The horizontal axis is labeled time after depolarization in milliseconds. It has markings ranging from 0 to 60 in increments of 20 units. The vertical axis is labeled membrane current which increases from bottom to top. Three line curves labeled (A), (B), and (C) are shown in green, red, and blue colors. The green curve located at the top is labeled wild type. The red curve located in the middle is labeled deletion mutant. The blue curve located at the bottom is labeled deletion mutation plus peptide. The green curve starts at a membrane current above the midpoint of the vertical axis and moves almost horizontally till 0 milliseconds. It shows a slight dip before 0 milliseconds and then rises vertically upward to peak at the highest membrane current. It falls to a value of membrane current slightly above the initial value at 16 milliseconds. The line then moves horizontally toward the right.

The red curve starts at a value of membrane current just below the midpoint of the vertical axis and moves horizontally toward the right till 0 milliseconds. It shows a very tiny peak before 0 milliseconds and then rises vertically upward to a membrane current value above the midpoint of the vertical axis. The curve then continues moving horizontally toward the right.

The blue curve starts at the lowest membrane current and moves horizontally toward the right till 0 milliseconds. It then rises vertically upward to a point much below the midpoint of the vertical axis at 0 milliseconds. It then falls gradually downward to reach a membrane current value slightly higher than the initial value at 17 milliseconds. The line then moves horizontally toward the right.

Return to Graph of membrane current versus time after depolarization

Extended description for Mechanism of channel inactivation



The ball-and-chain model shows a channel in closed, open, and inactivated forms.

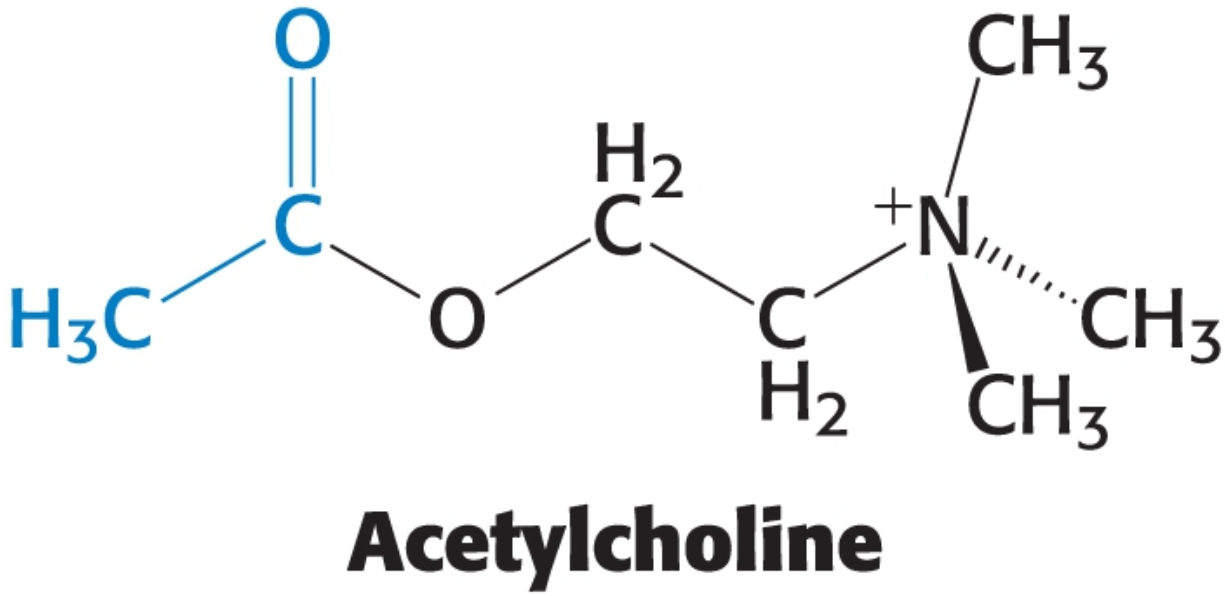
Closed form: The channel is embedded in a membrane with the broad side facing upward. It is surrounded by three rectangular blocks. Two vertical rectangular blocks are attached to the sides of the channel. The third rectangular block is located in front of the channel in a diagonal orientation. It is connected to a flexible chain which is further attached to a grey sphere labeled “inactivation domain”. The sphere is located away from the channel. The front and right rectangular blocks are positively charged.

Open form: The broad side of the channel faces downward. The orientation of the front rectangular block becomes vertical. The grey sphere is located toward the channel.

Inactivated: The grey sphere moves into the pore of the channel thereby blocking it.

Return to Mechanism of channel inactivation

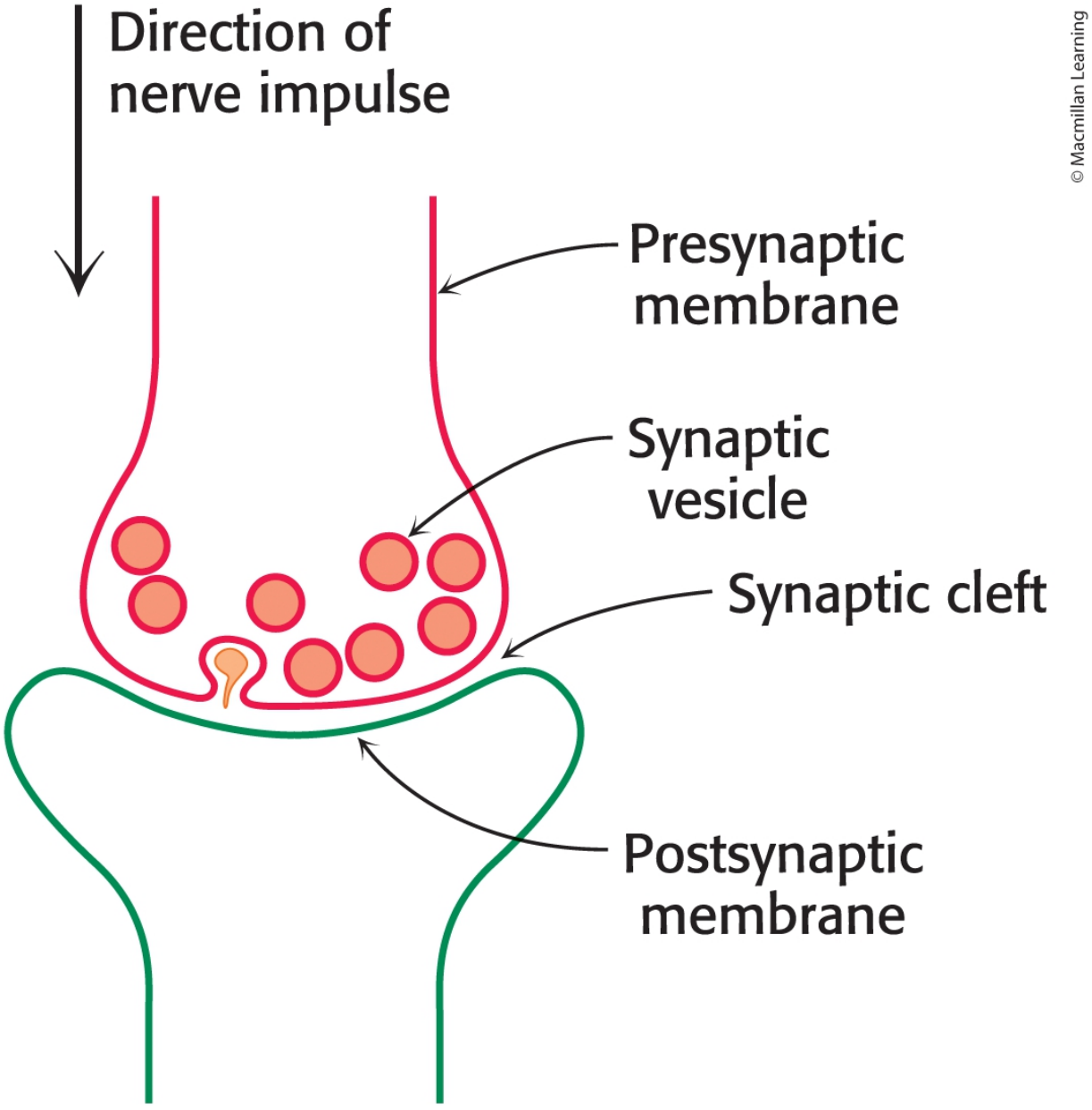
Extended description for Structure of acetylcholine



The structure of acetylcholine is as follows: A 1 O, 1 N, and 3 C heteronuclear alkane chain is depicted as a line structure using 4 zigzag lines. O occupies the second position. N occupies the fifth position and has an overall positive charge. C 1 is double bonded to O above and single bonded to C H 3 on the lower left. C 3 and C 4 are each bound to H 2. N is single bonded to C H 3 on the upper right, dash bonded to C H 3 on the lower right, and wedge bonded to C H 3 below.

Return to Structure of acetylcholine

Extended description for Schematic representation of synapse



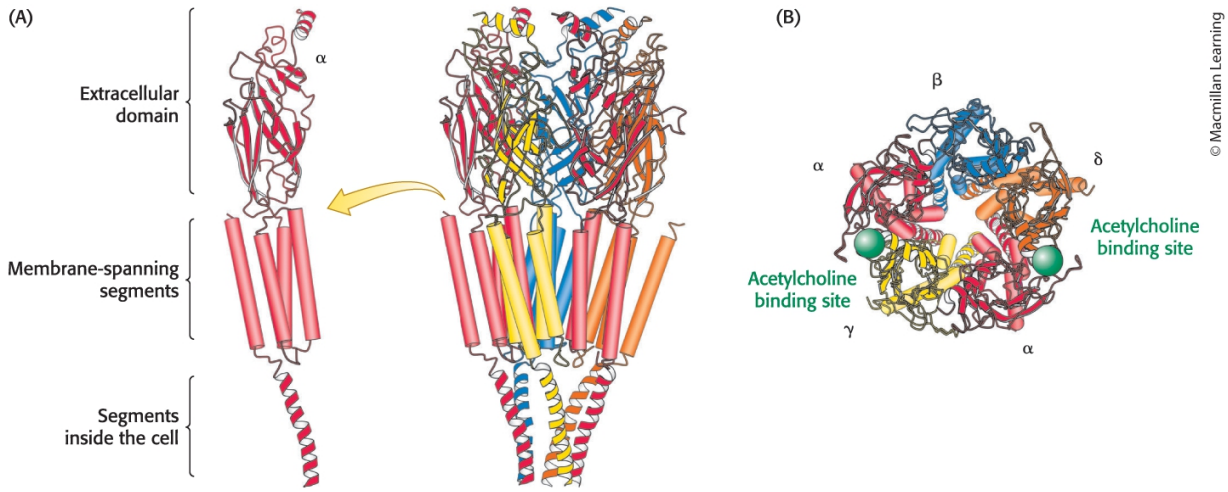
© Macmillan Learning

An elongated structure with a broad top having an inwardly curved surface is shown. Its outline is labeled postsynaptic membrane. A bulb-like structure with an outline labeled presynaptic membrane

sits in the depression of the postsynaptic membrane. The space between the presynaptic and postsynaptic membrane is labeled synaptic cleft. A downward arrow above the presynaptic membrane depicts the direction of nerve impulse. The presynaptic membrane encloses several spheres labeled synaptic vesicles. A small invagination is present on the presynaptic membrane opposite the postsynaptic membrane to show the release of neurotransmitters into the synaptic cleft.

Return to Schematic representation of synapse

Extended description for Model of acetylcholine receptor and a view of the receptor from outside the cell

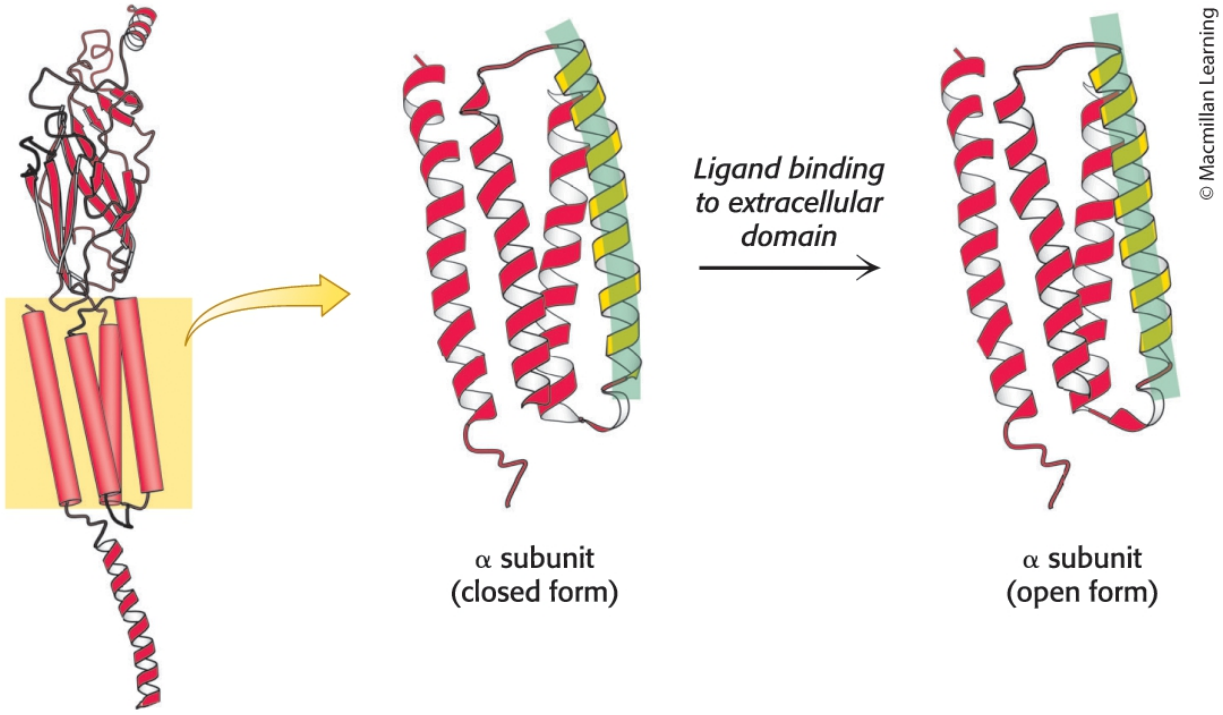


Part (A): The acetylcholine receptor consists of three parts from top to bottom: extracellular domain, membrane-spanning segments, and segments inside the cell. The extracellular domain consists of several beta-strands and a few alpha-helices. The membrane-spanning segments are depicted as vertically oriented long cylindrical structures shown in red, yellow, orange, and blue colors. These cylindrical structures are interconnected by short thread-like loops. Some of them are connected below to a few vertically oriented alpha-helices that are 5 in total. An arrow from the model of acetylcholine receptor points toward the model of its alpha subunit. In the alpha subunit, the extracellular domain consists of several beta-strands and one alpha-helix at the top interconnected by thread-like loops. The membrane-spanning segment consists of four long vertical cylindrical structures. One such structure is connected below to a vertical alpha helix.

Part (B): It shows two alpha, one beta, one gamma, and one delta subunit arranged in a circular cluster with a hollow core. The alpha subunit occupies the top left and bottom right region. The delta and gamma subunits occupy the top right and bottom left regions respectively. The beta subunit occupies the topmost region. A green sphere labeled “acetylcholine binding site” is bound to the gamma subunit and the alpha subunit at the bottom right. Each of the subunits consists of a few beta-strands and alpha-helices and randomly oriented cylindrical structures.

Return to Model of acetylcholine receptor and a view of the receptor from outside the cell

Extended description for Opening of the acetylcholine receptor due to ligand binding

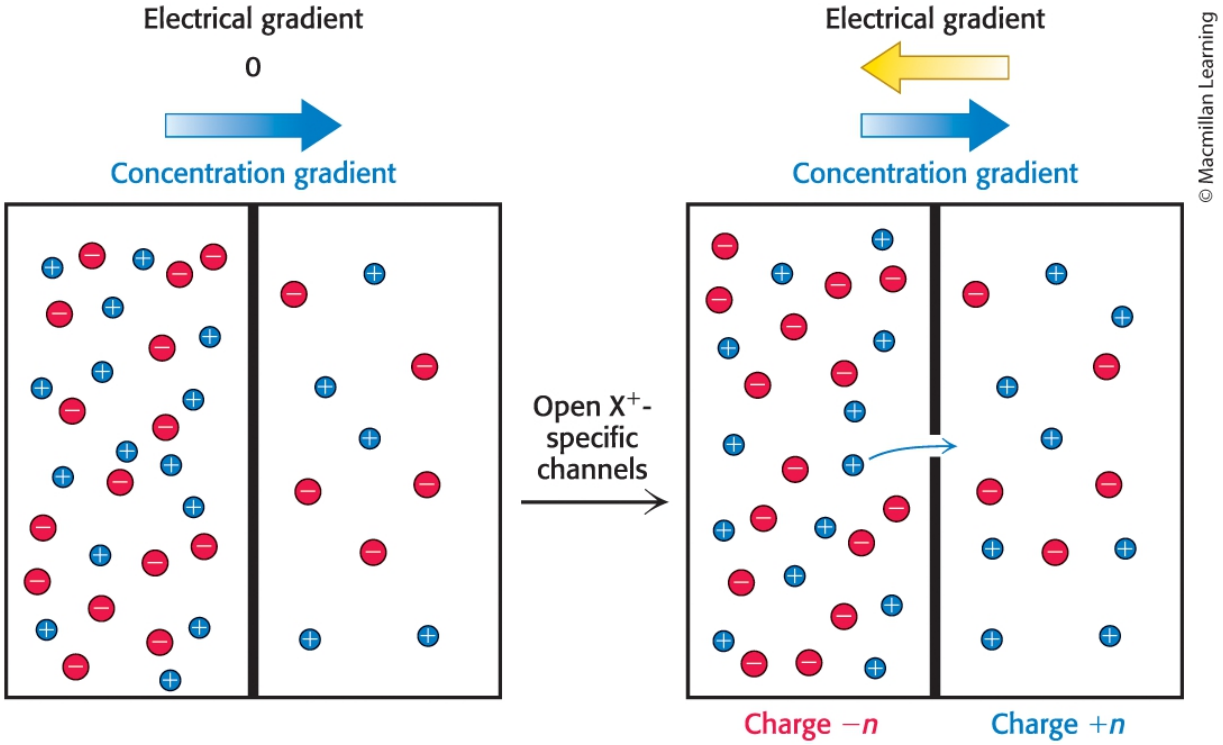


The alpha-subunit of the acetylcholine receptor is shown. An arrow from the alpha-subunit shows the enlarged view of the alpha subunit in close form. The close form consists of four vertical orientated long alpha-helices interconnected by short thread-like loops. The rightmost alpha-helix is shown in green. A vertical light green bar across this helix shows that the helix is slightly curved.

A forward arrow labeled "ligand binding to extracellular domain leads to the open form of alpha-subunit. In the open form, a vertical light green bar across the rightmost helix shows that the helix has straightened.

Return to Opening of the acetylcholine receptor due to ligand binding

Extended description for Schematic representation of equilibrium potential



© Macmillan Learning

A square box is separated into two compartments. The left compartment contains several red and blue circles. The red circles are negatively charged. The blue circles are positively charged. The size of the blue circles is smaller than the red circles. The right compartment contains five red and five blue randomly scattered circles. An arrow at the top of the square box is labeled concentration gradient. It moves from the left compartment toward the right compartment. The electrical gradient is zero at this point.

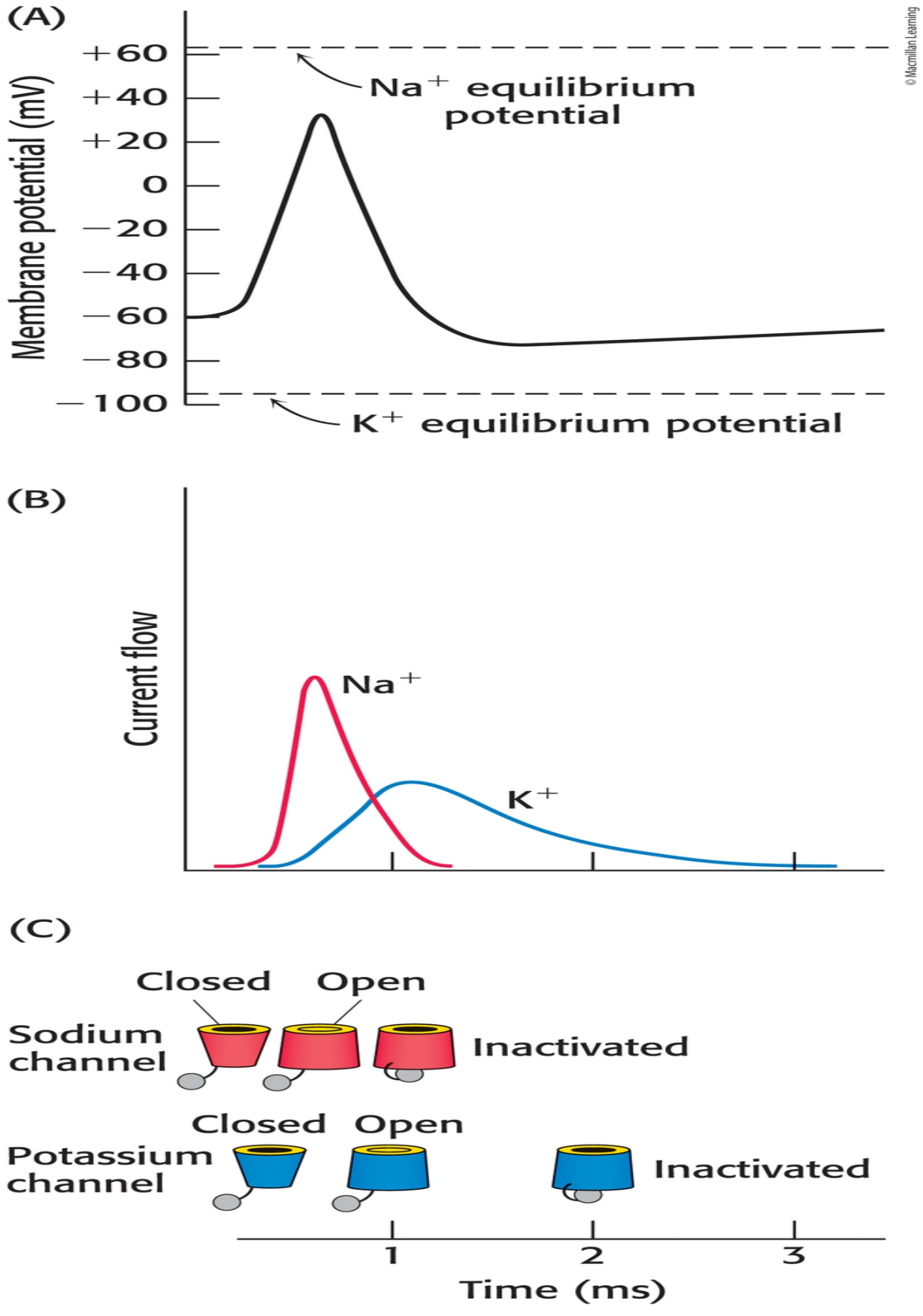
An arrow labeled “open X superscript plus specific channels” leads to another compartmentalized square box.

A narrow slit is shown in the center of the septum that separates the two compartments. The left compartment is labeled charge negative n. The right compartment is labeled charge positive n. An arrow from the left compartment moves toward the right compartment through the slit. An arrow at the top of the square is labeled concentration gradient. It moves from the left compartment toward the right compartment. Another arrow above it is labeled electrical gradient. This arrow moves from the right compartment toward the left compartment.

Return to Schematic representation of equilibrium potential

Extended description for Graphs for membrane potential and current flow and schematic

representation of the states of ion channels during an action potential



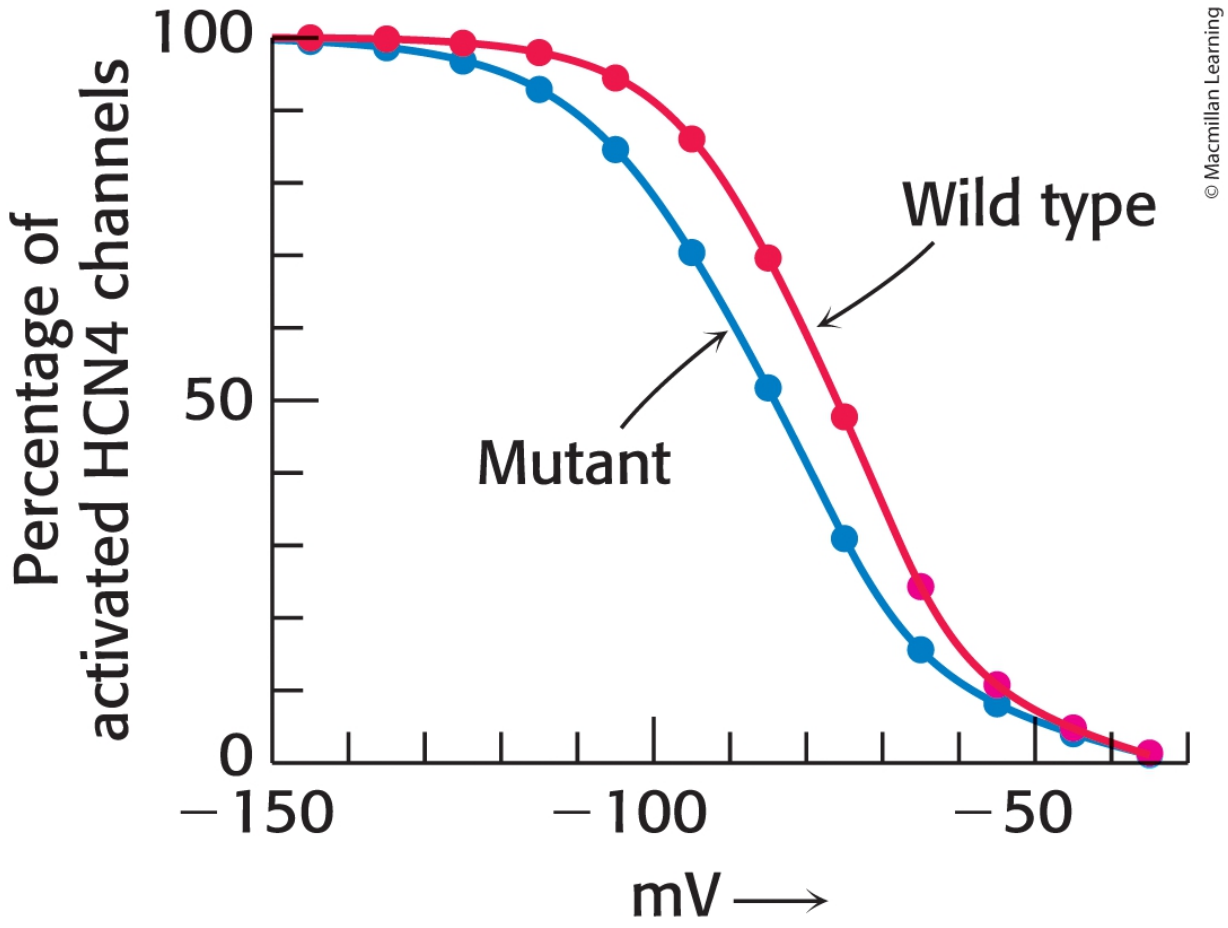
© Macmillan Learning

Graph (A): The vertical axis is labeled membrane potential (m V). It has markings ranging from negative 100 to positive 60 in increments of 20 units. A dashed horizontal line originates from approximately positive 62 m V on the vertical axis. This line is labeled N a superscript plus equilibrium potential. A dashed horizontal line originates from approximately negative 96 on the vertical axis. This line is labeled K superscript plus equilibrium potential. A line curve starts at negative 60 on the vertical axis. It moves horizontally for a short while and then moves gradually upward to peak at approximately 37 m V. It then falls gradually downward to reach approximately negative 70 m V and later moves almost horizontally toward the right. Graph (B): The vertical axis is labeled current flow. The horizontal axis has three equally spaced markings. The graph shows two lines curves in red and blue color. The red line curve starts near (0, 0) and moves horizontally for a short while. It shows steep upward movement to form a peak at a point above the midpoint of the vertical axis. It then falls vertically downward to reach a point on the right of the first marking on the horizontal axis. The blue line curve starts just toward the right of the red curve. It gradually moves upward to peak around the first marking on the horizontal axis at a point on the vertical axis much below its midpoint. The curve then moves gradually down to reach the lowest current flow at the third marking on the horizontal axis. Part (C): The sodium and potassium channels are depicted as rubber stopper-like structures shown in red and blue respectively. A scale for the time in milliseconds is shown. It has markings ranging from 1 to 3 in increments of 1 unit. The sodium channels in three orientations are shown from 0 to 1.2 milliseconds. A closed sodium channel is shown at 0 milliseconds with the broad side facing upward. A grey sphere is connected to the bottom of the channel through a curved line. An open sodium channel is shown at 0.5 milliseconds. It is relatively wider than the closed channel. An inactivated sodium channel is shown at 1.2 milliseconds. The grey sphere is attached to the bottom surface of the channel. The potassium channels in three

orientations are shown from 0 to 2 milliseconds. A closed potassium channel is shown at 0 milliseconds with the broad side facing upward. A grey sphere is connected to the bottom of the channel through a curved line. An open potassium channel is shown at 1 millisecond. It is relatively wider than the closed channel. An inactivated potassium channel is shown at 2 milliseconds. The grey sphere is attached to the bottom surface of the channel.

Return to Graphs for membrane potential and current flow and schematic representation of the states of ion channels during an action potential

Extended description for Graph depicts the percentage of activated H C N 4 channels as function of potential

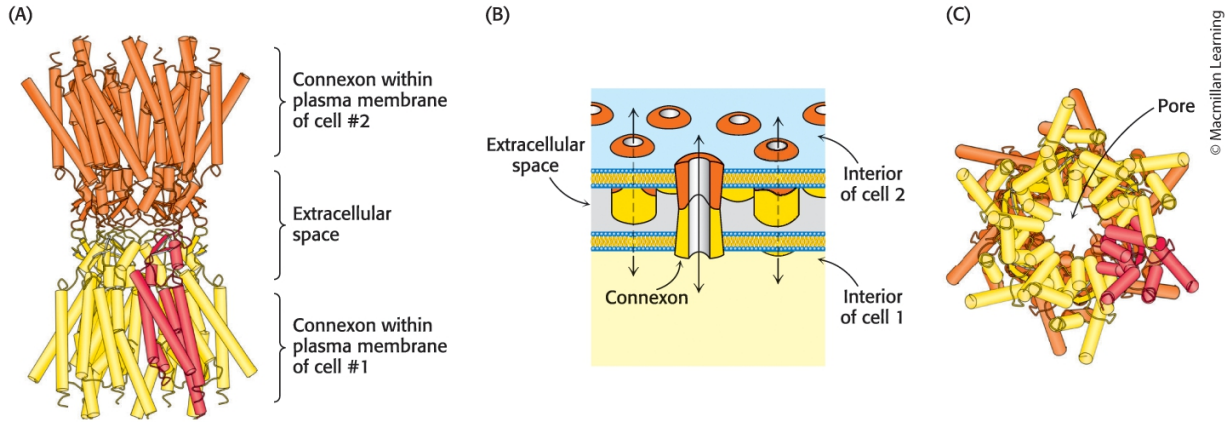


The horizontal axis labeled “m V” has markings ranging from negative 150 to negative 50 in increments of 50 units. The vertical axis labeled “percentage of activated H C N 4 channels” has markings ranging from 0 to 100 in increments of 50 units. The graph shows two decreasing curves. The blue curve is labeled mutant and the red curve is labeled wild type. The mutant curve starts from (negative 150, 100) moves toward the right to (negative 110, 100), and slopes downward passing through coordinates (negative 95, 70), (negative 75, 30), and terminates at (negative 40, 0). The wild-type curve starts from (negative 150, 100) moves toward the right to

(negative 120, 95), and slopes downward passing through coordinates (negative 90, 70), (negative 75, 30), and terminates at (negative 40, 0). All values are approximated.

Return to Graph depicts the percentage of activated H C N 4 channels as function of potential

Extended description for Structure and orientation of connexon



Part (A): The connexon is divided into three parts from top to bottom as follows: connexon within plasma membrane of cell number 2, extracellular space, and connexon within plasma membrane of cell number 1. The top and bottom parts consist of a cluster of vertically oriented long cylindrical structures connected by short thread-like loops. The middle part that resides in the extracellular space consists of a cluster of short cylindrical structures at the top and bottom connected by short thread-like loops located in the center.

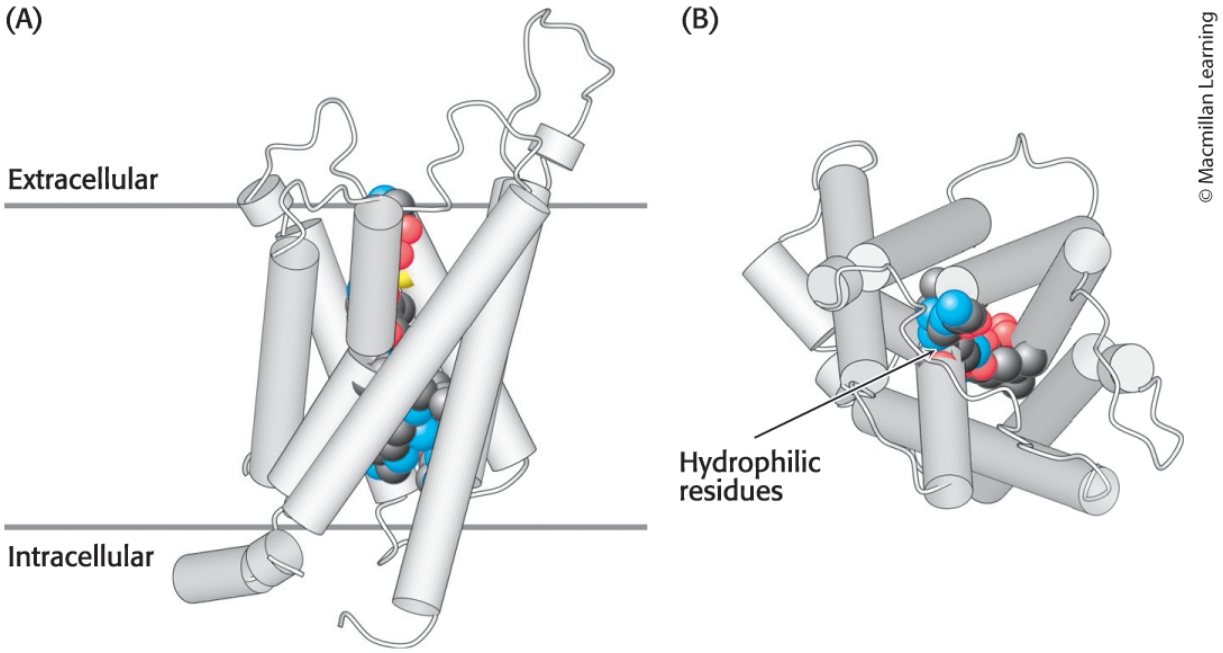
Part (B): Several connexons are depicted as long and hollow cylindrical structures spanning from one membrane to another membrane. The middle portion of the connexons is located in the extracellular space between the two membranes. The top surface of the upper membrane is labeled interior of cell 2. The bottom surface of the lower membrane is labeled interior of cell 1.

Part (C): It shows the bottom view of a connexon. The connexon is depicted as a star-shaped structure outlined by a cluster of short

cylindrical structures. A central pore is located in the connexon.

Return to Structure and orientation of connexon

Extended description for Side and bottom view of aquaporin

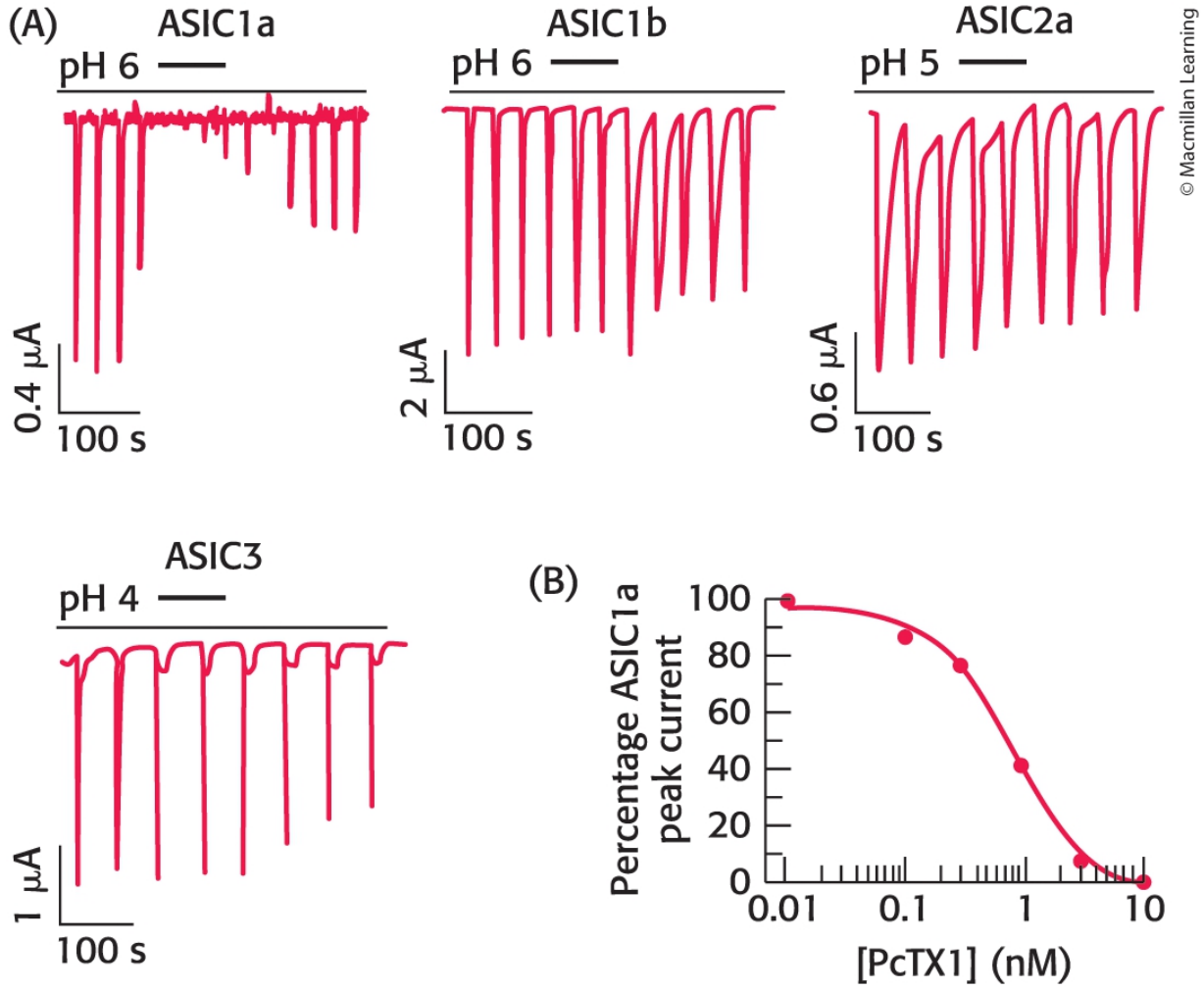


Part (A): The aquaporin consists of a few short, medium, and long cylindrical structures in a diagonal orientation interconnected by thread-like loops. Most of the portion of aquaporin is embedded within the plasma membrane depicted as two horizontal grey lines separated by a gap. The thread-like loops and a few short cylindrical structures extend into the extracellular region above. The bottom portion of aquaporin extends into the intracellular region below. The transmembrane portion of aquaporin contains a cluster of black, blue, red, and yellow spheres.

Part (B): It shows the top view of aquaporin. The top view consists of several cylindrical structures interconnected by thread-like loops. A cluster of black, blue, and red spheres is shown in the center of the aquaporin. The cluster is labeled hydrophilic residues.

Return to Side and bottom view of aquaporin

Extended description for Electrophysiological recordings of cells



Part (A):

First electrophysiological recording: It is labeled A S I C 1 a, p H 6. A series of downward spikes are shown on the left and right. The middle region does not contain any downward spike. The size of the spike on the extreme right is much smaller than the extreme left spikes. The length of time for 4 spikes is 100 seconds and the current is 0.4 microamperes.

Second electrophysiological recording:

It is labeled A S I C 1 b, p H 6. A series of downward spikes are shown from left to right. They have almost equal lengths. The length of time for 3 spikes is 100 seconds and the current is 2 microamperes.

Third electrophysiological recording:

It is labeled A S I C 2 a, p H 5. A series of downward spikes are shown from left to right. Their length decreases from left to right. The length of time for 2 spikes is 100 seconds and the current is 0.6 microamperes.

Fourth electrophysiological recording:

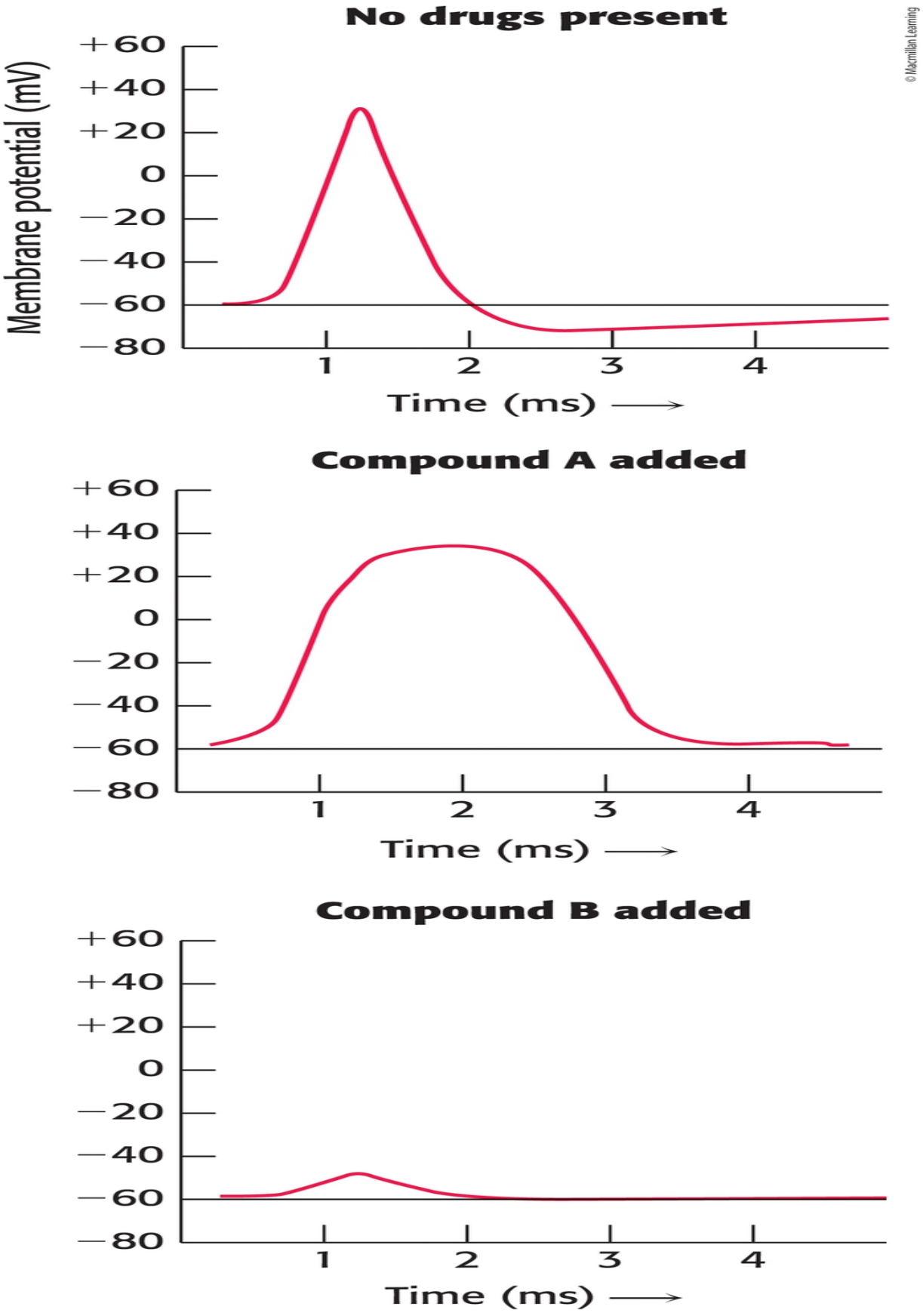
It is labeled A S I C 3, p H 4. A series of widely spaced downward spikes are shown from left to right. Their length decreases from left to right. The length of time for 2 spikes is 100 seconds and the current is 1 microampere.

Part (B): A graph is shown. The horizontal axis is labeled concentration of P c T X 1 in nanomolar. It has the markings 0.01, 0.1, 1, and 10. The vertical axis is labeled percentage A S I C 1 a peak current. It has markings ranging from 0 to 100 in increments of 10 units. A decreasing line curve begins at (0.01, 100) and moves almost horizontally till (0.1, 90). It then falls gradually downward through the points (0.3, 80), (0.9, 40), and (3, 10). It ultimately terminates at (10, 0). All values are estimated.

Return to Electrophysiological recordings of cells

Extended description for Graphs depicting membrane potential in the presence or absence of a drug or

compound



© Macmillan Learning

Graph 1: It is labeled “No drugs present”. The horizontal axis is labeled time in milliseconds. It has markings ranging from 1 to 4 in increments of 1 unit. The vertical axis is labeled membrane potential (m V). It has markings ranging from negative 80 to positive 60 in increments of 20 units. A horizontal line starts from negative 60 on the vertical axis. A line curve starts at (0.4, negative 60) and shows upward movement to reach (1.3, positive 35). It then falls steeply to reach (2.5, negative 70) and continues moving almost horizontally toward the right.

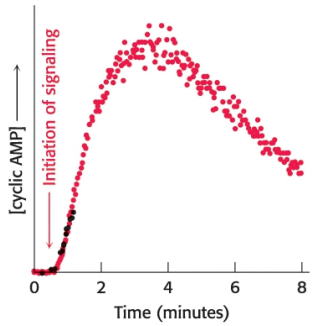
Graph 2: It is labeled “Compound A added”. It has markings ranging from 1 to 4 in increments of 1 unit. The vertical axis is labeled membrane potential (m V). It has markings ranging from negative 80 to positive 60 in increments of 20 units. A horizontal line starts from negative 60 on the vertical axis. A line curve starts at (0.2, negative 60) and rises upward to form a broad peak at positive 35 m V from 1.5 to 2.2 milliseconds. The curve then falls to reach (3.8, negative 61) and continues moving horizontally toward the right.

Graph 3: It is labeled “Compound B added”. It has markings ranging from 1 to 4 in increments of 1 unit. The vertical axis is labeled membrane potential (m V). It has markings ranging from negative 80 to positive 60 in increments of 20 units. A horizontal line starts from negative 60 on the vertical axis. A line curve starts at (0.2, negative 60) and moves horizontally toward the right for a while. It then gradually rises upward to peak at (1.2, negative 52) and then moves gradually downward to (2, negative 60). The curve then continues moving horizontally toward the right along the horizontal line.

All values are estimated.

Return to Graphs depicting membrane potential in the presence or absence of a drug or compound

Extended description for A graph and a photograph



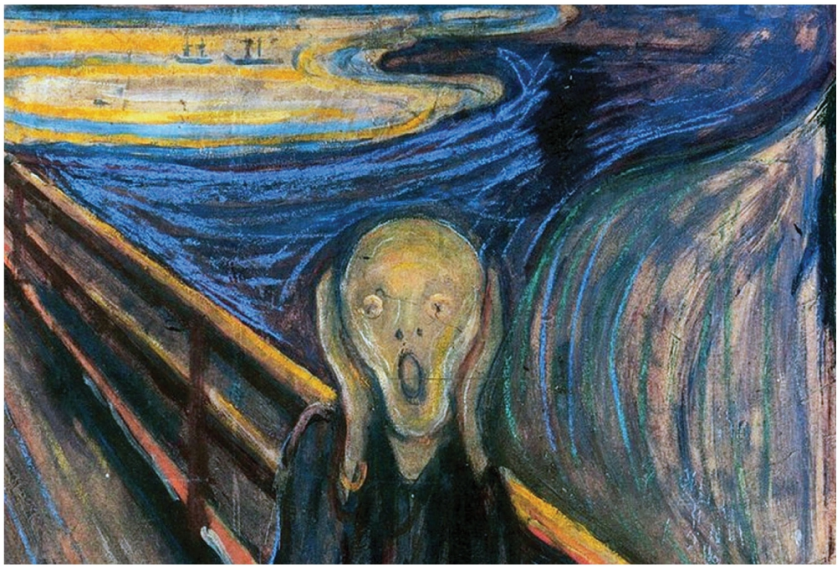
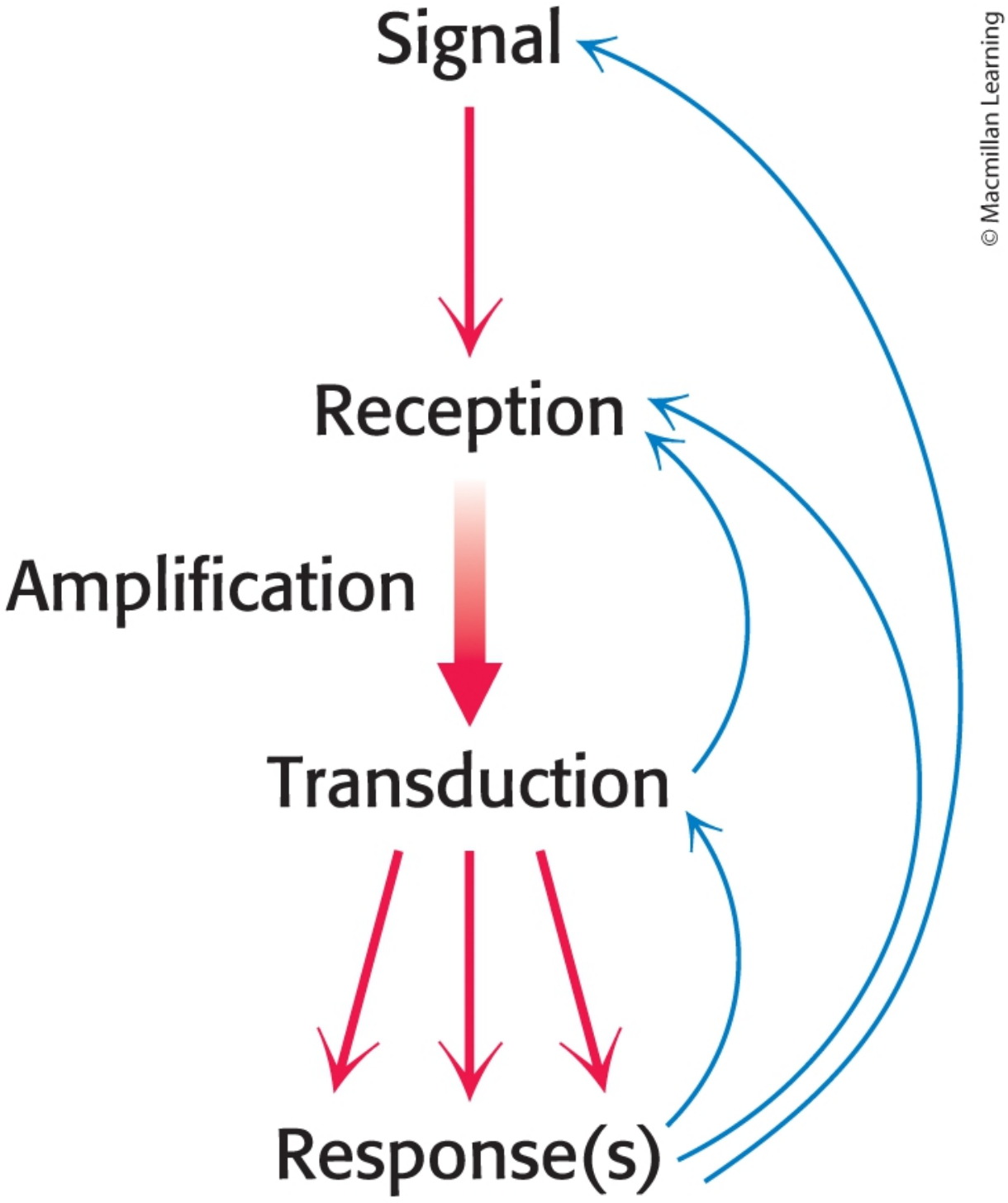


Photo12/Universal Images Group/Getty Images
© Macmillan Learning

The figure has two parts. The first part is a graph illustrating time in minutes on the horizontal axis. It has markings ranging from 0 to 8 in increments of 2 units. The vertical axis shows the concentration of cyclic A M P enclosed which increases from bottom to top. The data points depicted as red dots form a red curve. The curve starts at 0 on the horizontal axis and moves horizontally toward the right till it reaches 1 on the horizontal axis. The curve then rises steeply till it reaches a maximum point at 4 on the horizontal axis and then it starts decreasing gradually till at a point of 8 on the horizontal axis and the middle of the vertical axis. The curve is bell-shaped and the starting horizontal portion of the curve is marked with an arrow and labeled "Initiation of signaling." The second part shows an artistic painting.

Return to A graph and a photograph

Extended description for Generalized signal-transduction pathway

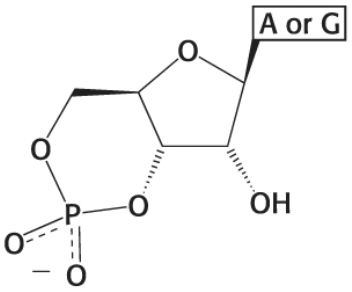


© Macmillan Learning

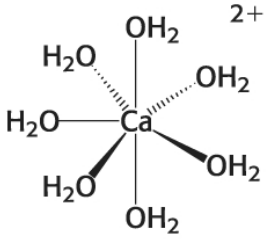
The flow chart is depicted as follows: signal, downward arrow, reception, downward arrow labeled amplification, transduction, three downward arrows, response open parenthesis S close parenthesis.

Return to Generalized signal-transduction pathway

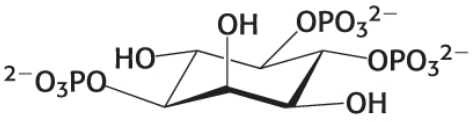
Extended description for Chemical structure of different secondary messengers



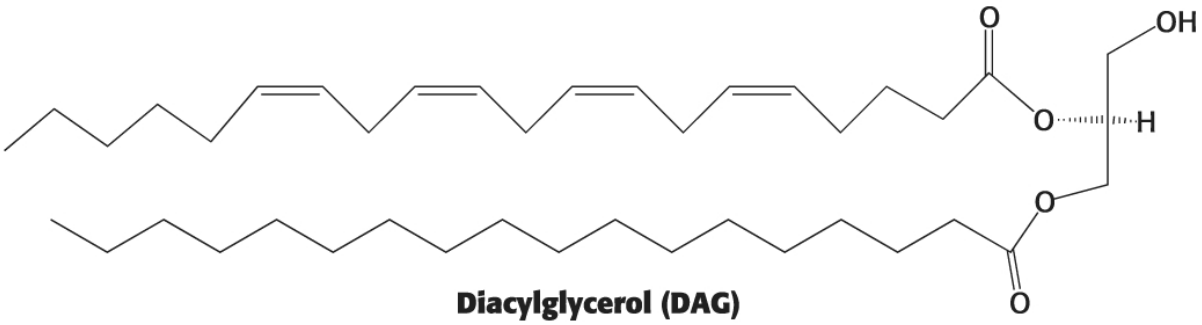
cAMP, cGMP



Calcium ion



Inositol 1,4,5-trisphosphate (IP_3)



Diacylglycerol (DAG)

The structure of c A M P or c G M P is as follows: A 5-membered heterocyclic pentagonal ring is in a vertical orientation and consists of 1 O and 4 C atoms. O occupies the topmost vertex. C 1 occupies the top right vertex and is wedge bonded to A or G on the upper right. C 2 is dash bonded to O H on the lower right. C 3 is dash bonded to O on the lower left. C 4 is wedge bonded to C H 2 on the left. This C H 2 is single bonded to O on the lower left. The O atoms of the C 3 and C H 2 group are single-bonded to a common P atom. This P atom is partially double bonded to O on the lower left and below. The P O O group has an overall negative charge.

The structure of calcium ion bound to water is as follows: A central C a atom is single bonded to O H 2 above, O H 2 below, H 2 O on the left, dash bonded to O H 2 on the upper right, dash bonded to H 2 O

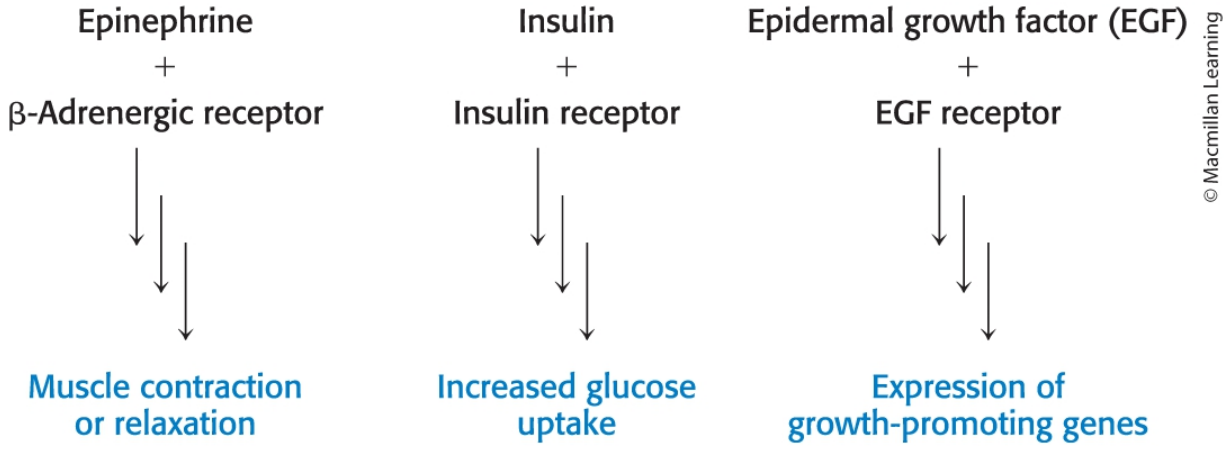
on the upper left, wedge bonded to O H 2 on the lower right, and wedge bonded to H 2 O on the lower right. This structure has an overall positive charge of 2 plus.

The structure of inositol 1,4,5-triphosphate (I P 3) is as follows: A 6-membered homocyclic hexagonal ring is in a chair conformation. The ring is in a plane perpendicular to the plane of paper such that C 2 and C 4 are located toward the observer and C 1 and C 5 are located away from the observer. C 3 and C 6 are located close to each other. C 1 is single bonded to O P O 3 superscript 2 minus. C 2 is single bonded to O H on the right. C 3 is single bonded to O H above. C 4 is single bonded to O P O 3 superscript 2 minus on the upper left. C 5 is single bonded to O H on the left. C 6 is single bonded to O P O 3 superscript 2 minus on the upper right.

The structure of diacylglycerol (D A G) is as follows: A vertical chain consists of three C atoms. C 1 is single bonded to O H on the upper right. C 2 is dash bonded to O on the left and H on the right. C 3 is single bonded to O on the lower left. The O atom bonded to C 2 is single bonded to a 20 carbon alkene chain depicted as a line structure using 19 zigzag lines. In this alkane chain, C 1 atom closer to the O atom is double bonded to O above. A double bond is present between C 5 and C 6, C 8 and C 9, C 11 and C 12, C 14 and C 15. The O atom bonded to C 3 of the vertical chain is single bonded to an 18-carbon alkane chain depicted as a line structure using 17 zigzag lines. C 1 closer to the O atom is double bonded to O below.

Return to Chemical structure of different secondary messengers

Extended description for Physiological outcomes of different signal transduction pathways



© Macmillan Learning

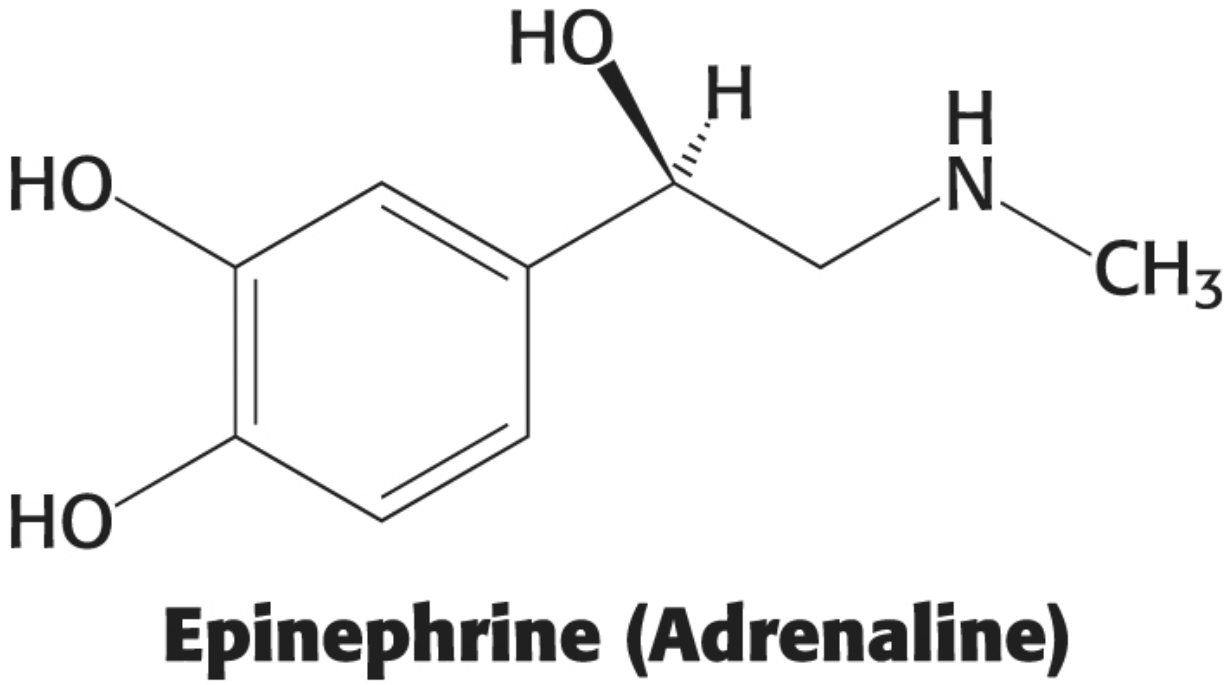
First pathway: Epinephrine plus beta-adrenergic receptor, three downward arrows, muscle contraction or relaxation.

Second pathway: Insulin plus insulin receptor, three downward arrows, increased glucose uptake.

Third pathway: Epidermal growth factor (E G F) plus E G F receptor, three downward arrows, expression of growth-promoting genes.

Return to Physiological outcomes of different signal transduction pathways

Extended description for Chemical structure of epinephrine

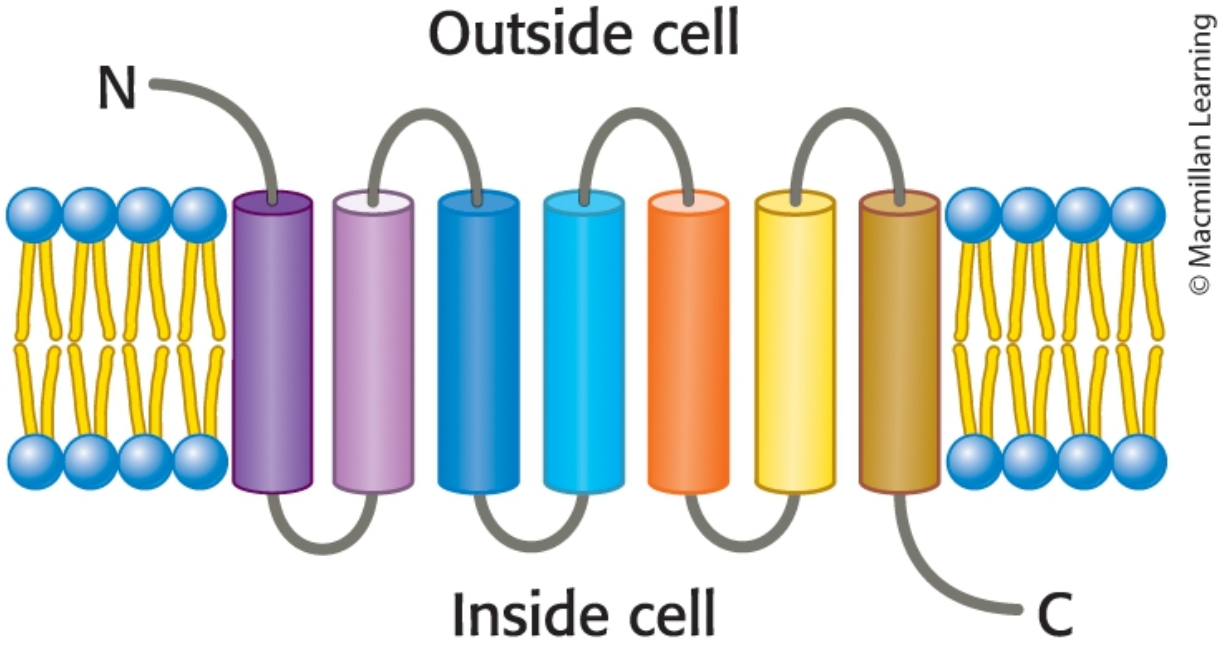


The structure of epinephrine or adrenaline is as follows: A benzene ring is in a vertical orientation with C 1 occupying the topmost vertex. It contains alternating double bonds between C 1 and C 2, C 3 and C 4, and C 5 and C 6. C 2 is single bonded to C 1 of a 1 N and 2 C heteronuclear alkane chain depicted as a line structure using 2 zigzag lines. N bound to H occupies the third position. C 1 is wedge bonded to O H on the upper left and dash bonded to H on the upper right. N is single bonded to C H 3 on the lower right.

C 5 of the benzene ring is single bonded to O H on the lower left. C 6 is single bonded to O H on the upper left.

Return to Chemical structure of epinephrine

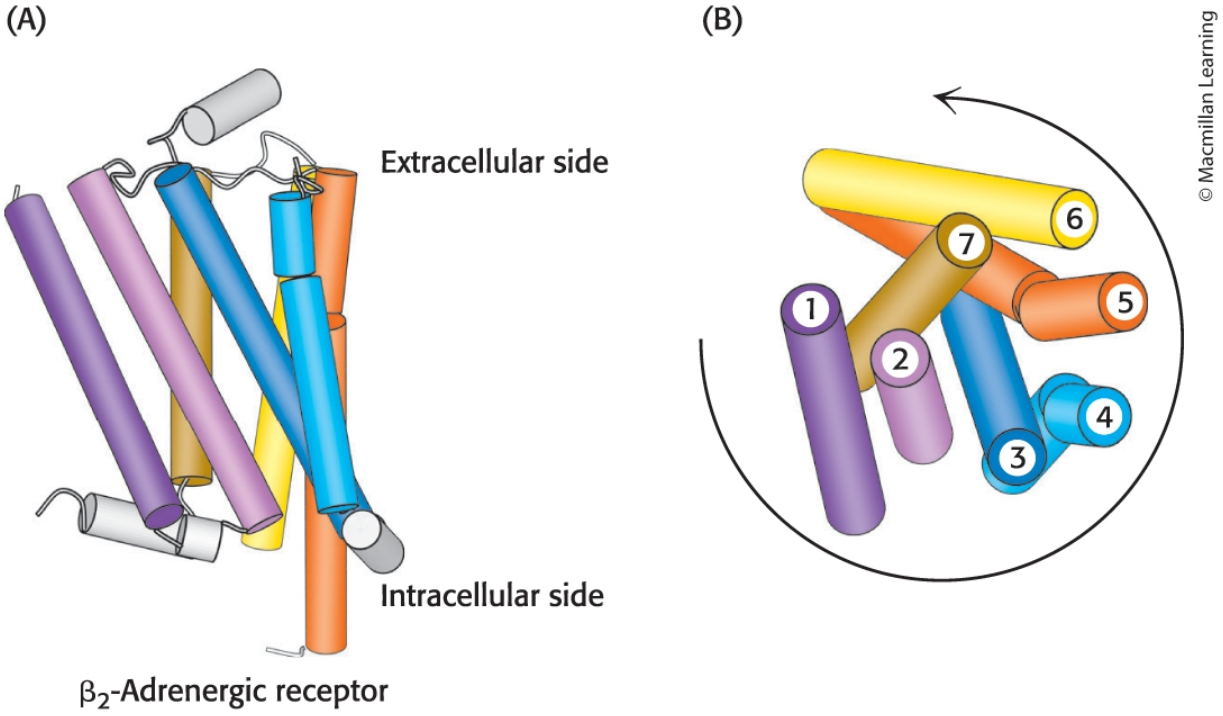
Extended description for Schematic representation of 7 T M helix receptor



The 7 T M helix receptor consists of 7 vertically oriented cylindrical structures that span through a lipid bilayer. The cylindrical structures are placed adjacent to each other in a tandem arrangement. The leftmost cylindrical structure has a short thread-like extension at the top labeled "N" which is located outside the cell. The rightmost cylindrical structure has a short thread-like extension at the bottom labeled "C" which is located inside the cell. The adjacent cylindrical structures are connected by curved thread-like loops at the bottom or top in an alternating manner.

Return to Schematic representation of 7 T M helix receptor

Extended description for Schematic representation of the side view and top view of the beta-2 adrenergic receptor

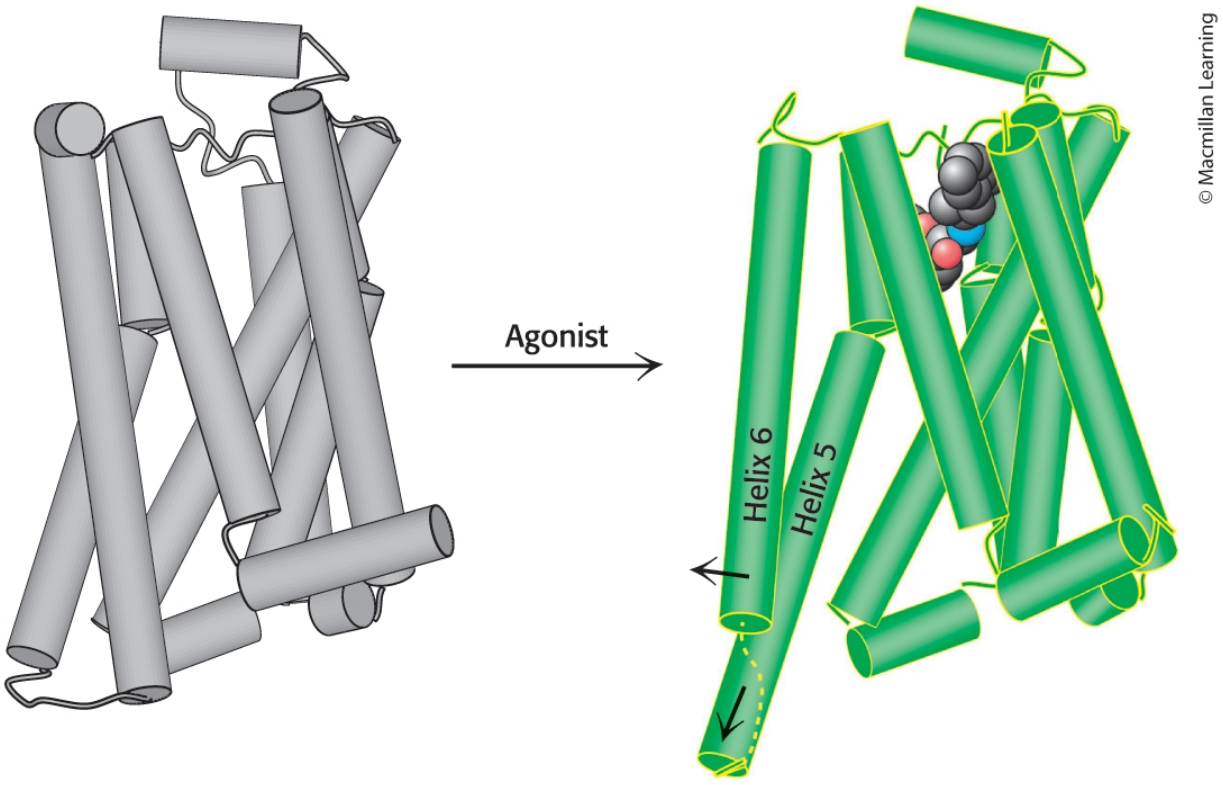


Part (A): The side view of the beta 2-adrenergic receptor shows a cluster of slightly diagonally oriented or vertically oriented long cylindrical structures. Their top is labeled extracellular side and the bottom is labeled intracellular side. They are interconnected by short thread-like loops. An irregular thread at the top of this cluster is connected to a short cylindrical structure at the extracellular side. A few short cylindrical structures are located on the intracellular side.

Part (B): The top view shows a cluster of randomly oriented seven long or short cylindrical structures labeled 1 to 7. These structures are arranged in an anticlockwise direction starting from the left.

Return to Schematic representation of the side view and top view of the beta-2 adrenergic receptor

Extended description for Stabilization of the active conformation of beta-adrenergic receptor



© Macmillan Learning

The beta 2-adrenergic receptor consists of a cluster of slightly diagonally oriented or vertically oriented long cylindrical structures. They are interconnected by short thread-like loops. An irregular thread at the top of this cluster is connected to a short cylindrical structure. A few short cylindrical structures are located at bottom of the receptor.

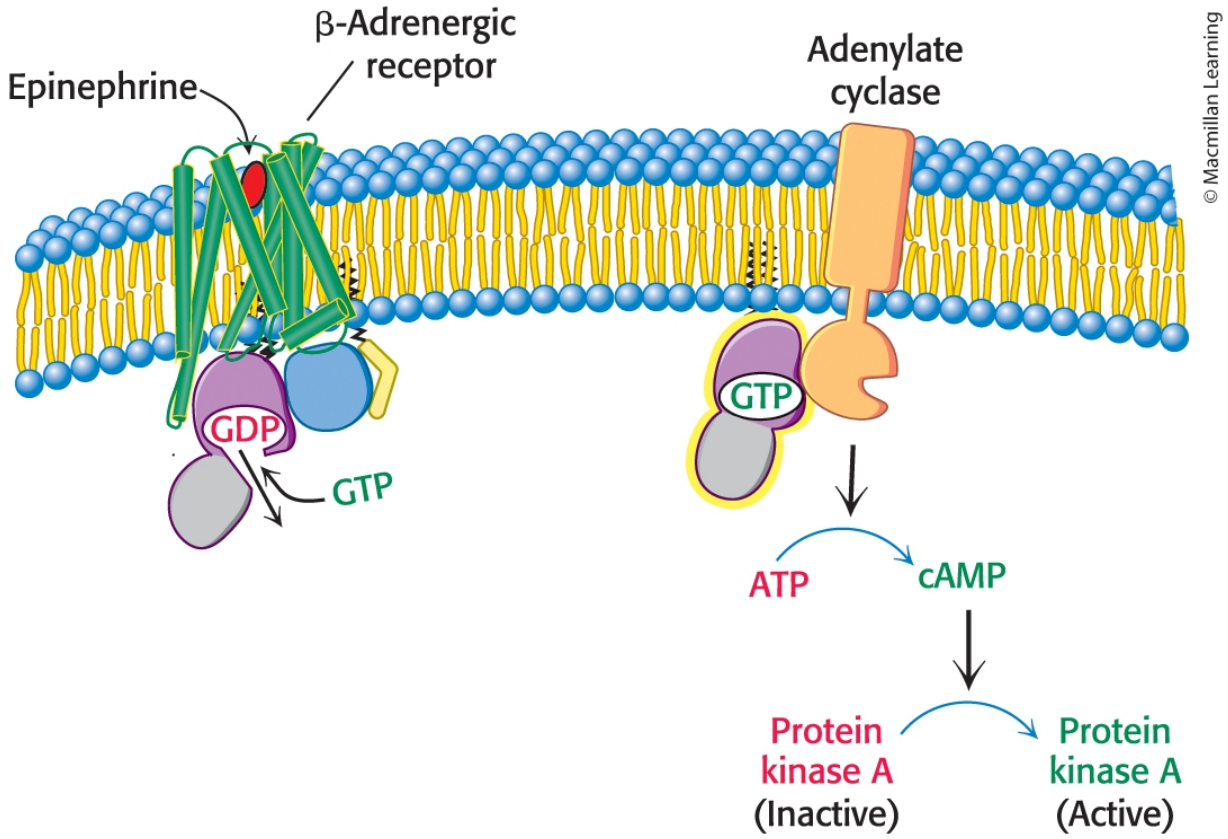
A forward arrow labeled agonist leads to the stabilized activated form of the receptor.

The orientation of some cylindrical structures on the left has altered as they are separated by a gap. A space-filling model composed of

black, red, and blue spheres is bound to the top groove of the receptor. The leftmost cylindrical structure is labeled helix 6 and its adjacent cylindrical structure is labeled helix 5. A leftward arrow is shown at the bottom of helix 6. A downward arrow is shown at the bottom of helix 5. These arrows depict the movement of helix 6 away from the receptor and the downward extension of helix 5 into the cell.

Return to Stabilization of the active conformation of beta-adrenergic receptor

Extended description for Signaling pathway initiated by epinephrine



A section of a horizontally oriented lipid bilayer is shown. The beta-adrenergic receptor is embedded in the lipid bilayer. It is composed of long and a few short cylindrical structures interconnected by thread-like loops. Epinephrine depicted as a red oval-shaped structure is bound to the top groove of the receptor. The cytoplasmic side of the receptor is bound to a trimeric structure. This structure is composed of a blue rounded-square-shaped structure associated with a purple round structure having a wide groove at the bottom labeled G D P. The purple round structure is further connected to a round and relatively smaller grey structure. The grey structure is located at the lower left of the purple structure such that a small

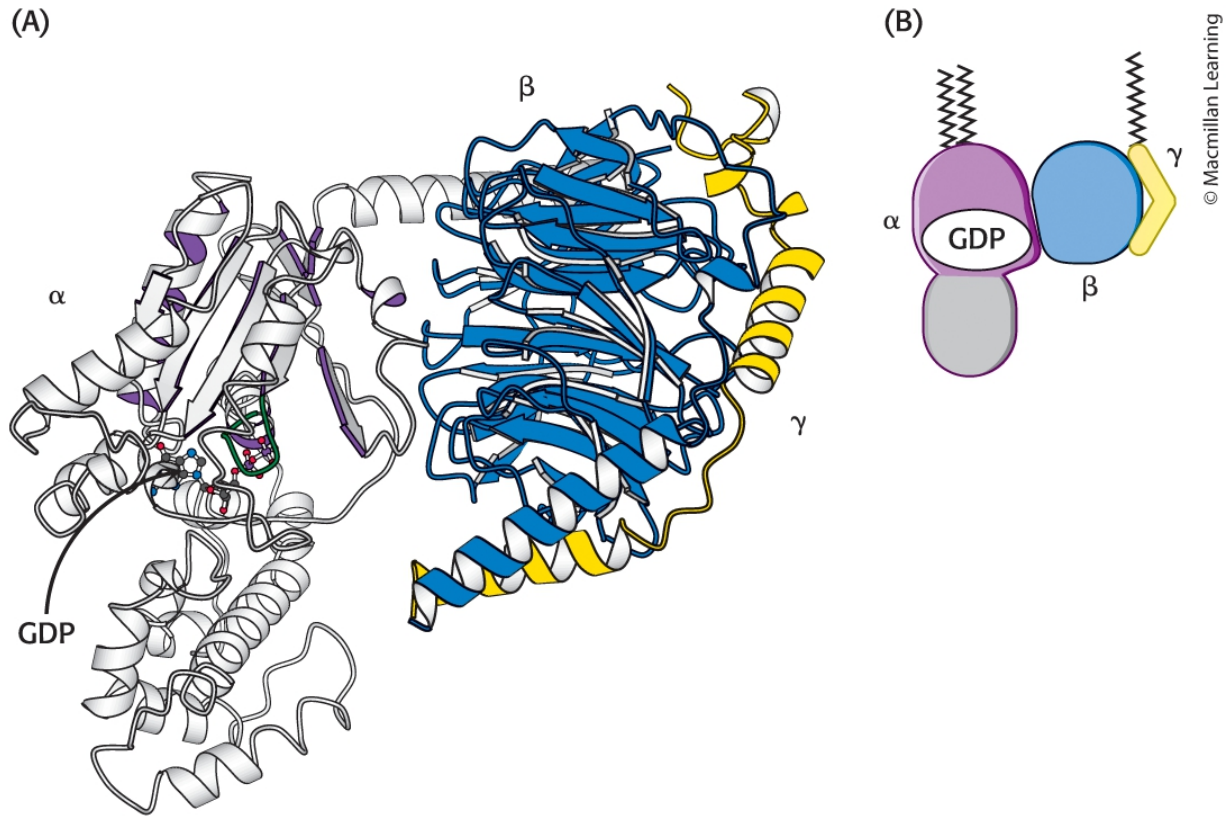
passage is created for the exit of G D P and entry of G T P into the groove of the purple structure. The blue rounded square is associated with a short yellow kinked structure that is attached to the inner leaflet of the bilayer through a zigzag line embedded in the bilayer. Likewise, the purple structure is attached to the inner leaflet of the bilayer through a zigzag line embedded within the bilayer.

On the right side, adenylate cyclase is shown embedded in the same bilayer. It is composed of a rectangular membrane-spanning region and a cytoplasmic round region having a tiny groove. The complex of purple and grey structure is bound to the cytoplasmic round region of adenylate cyclase. The purple structure is bound to G T P and its groove is closed by the grey sphere located below it.

A downward arrow below the cytoplasmic region of adenylate cyclase shows the conversion of A T P to c A M P. c A M P further helps in the conversion of inactive protein kinase A to active protein kinase A.

Return to Signaling pathway initiated by epinephrine

Extended description for Ribbon diagram and schematic representation of the G protein subunits



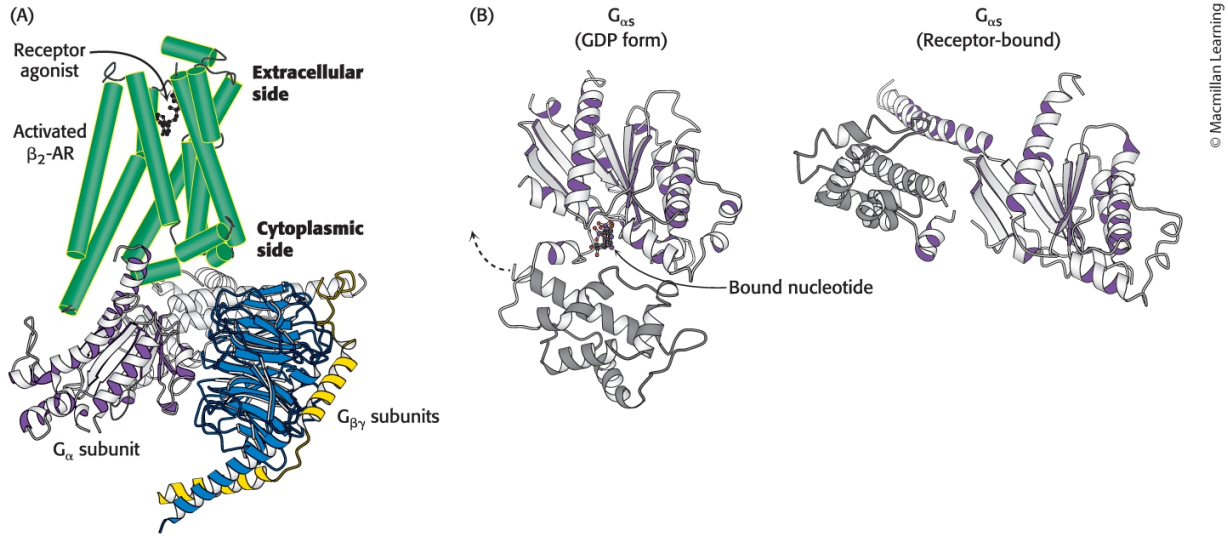
Part (A): The G protein is composed of alpha, beta, and gamma subunits. The beta and gamma subunits are closely associated to form a dimer. The beta subunit is composed of several horizontal beta-strands stacked together and a long alpha helix at the bottom. The gamma subunit consists of three alpha-helices out of which two are long and are associated with the bottom and right periphery of the beta subunit. The alpha subunit is located at a certain gap from the beta-gamma dimer. The beta-subunit of the dimer faces the alpha subunit. The alpha subunit is composed of several alpha-helices and few-beta strands. The beta-strands form the core of the top portion of the alpha subunit. The ball-and-stick model of G D P

is bound to a groove in the top region of the alpha subunit. An alpha-helix from the top region extends horizontally into the beta-subunit.

Part (B): The G protein is composed of a blue rounded-square-shaped structure labeled beta associated with a complex of purple round and grey round structures on the left labeled alpha and a yellow structure on the right labeled gamma. The purple structure has a wide groove at the bottom labeled G D P. The purple round structure is further connected to a round and relatively smaller grey structure below such that its groove is closed. The blue rounded square is associated with a short yellow kinked structure having a vertical zigzag line at the top. The purple structure of the alpha subunit has two vertical zigzag lines at the top.

Return to Ribbon diagram and schematic representation of the G protein subunits

Extended description for Beta-2 A R bound to G protein and G D P and receptor bound forms of alpha subunit



Part (A): A receptor agonist is bound to the top groove of the activated beta-2 A R. The top and bottom of the receptor are labeled extracellular side and cytoplasmic side respectively. The cytoplasmic side is associated with the ribbon diagram of G protein. The G protein is composed of G subscript alpha subunit and G subscript beta gamma subunits. The alpha-helices of the G subscript alpha subunit directly interact with the cytoplasmic side of activated beta-2 A R. The G subscript beta gamma subunits are associated with the G subscript alpha subunit.

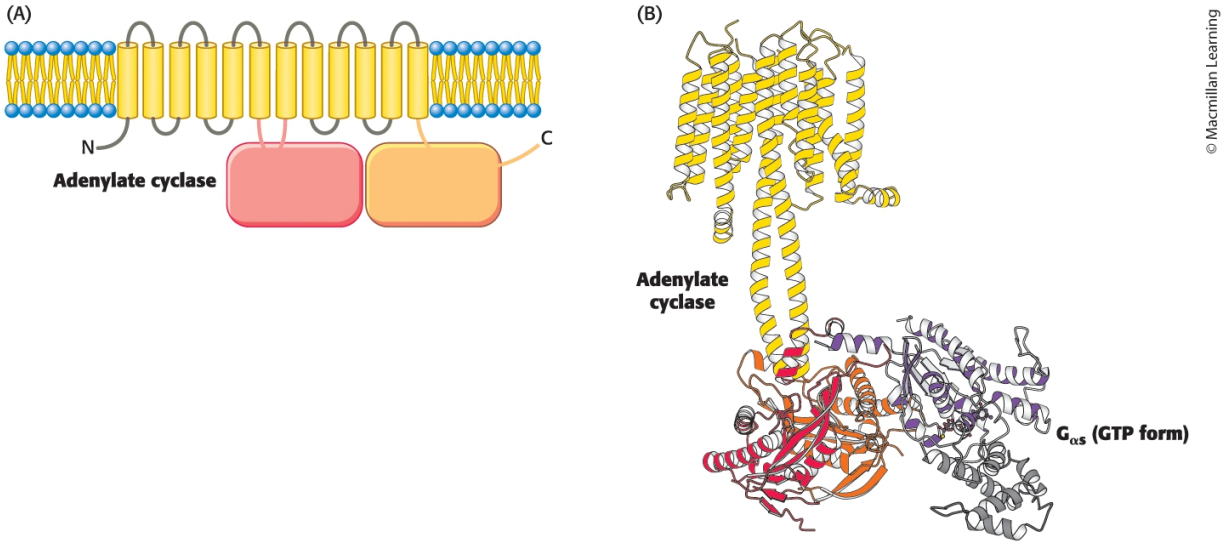
Part (B): The G alpha S (G D P form) is composed of top and bottom portions. The top portion contains three crisscrossing beta-strands circularly surrounded by alpha-helices. The secondary structures are interconnected by thread-like loops. The bottom portion is composed of a few loosely arranged alpha-helices interconnected by long threads. The ball-and-stick model of nucleotide is bound to alpha-helices at the bottom side of the top portion. An upward

curved dashed arrow is shown above a diagonally oriented central alpha-helix of the bottom portion.

The G subscript alpha S (receptor-bound) subunit shows that the bottom portion of the G D P form has moved to the left side of the top portion. This exposes the bottom side of the top portion.

Return to Beta-2 A R bound to G protein and G D P and receptor bound forms of alpha subunit

Extended description for Schematic representation of adenylate cyclase and ribbon diagram of adenylate cyclase bound to G subscript alpha S subunit



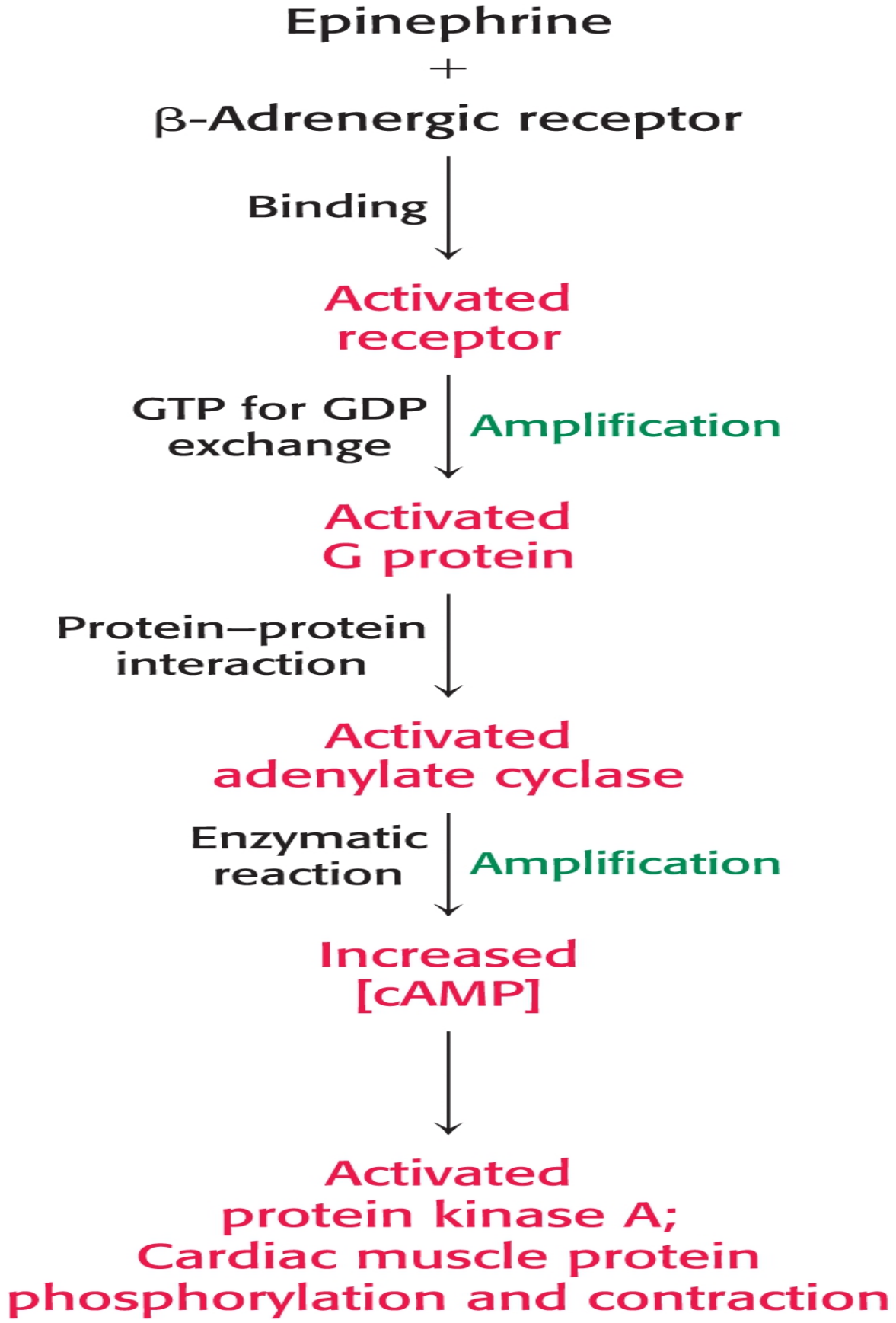
Part (A): A section of a horizontal lipid bilayer is shown. The adenylate cyclase protein consists of 12 vertically oriented cylindrical structures that span through the lipid bilayer. The cylindrical structures are placed adjacent to each other in a tandem arrangement. The leftmost cylindrical structure has a short thread-like extension in the cytoplasm labeled “N.” The rightmost cylindrical structure has a short thread-like extension in the cytoplasm labeled “C.” The adjacent cylindrical structures are connected by curved thread-like loops at the top or bottom in an alternating manner. The third bottom loop connecting the sixth and seventh structure is associated with a red rounded rectangle and the extension “C” is associated with an orange rounded rectangle. The red and orange rectangles are located side by side in the cytoplasm, below the lipid bilayer.

Part (B): The adenylate cyclase protein is depicted as a cluster of vertically oriented yellow alpha-helices. Two long yellow alpha-helices at the center of the cluster extend below into a small cluster composed of several alpha-helices and beta-strands shown in red or orange color. The ribbon diagram of G subscript alpha S (G T P form) is bound to the orange alpha-helices of the cluster. An alpha-helix at the top of the G subscript alpha S subunit is attached to the long yellow vertical alpha-helix extending below.

Return to Schematic representation of adenylate cyclase and ribbon diagram of adenylate cyclase bound to G subscript alpha S subunit

Extended description for Flowchart shows events

leading to cardiac muscle contraction

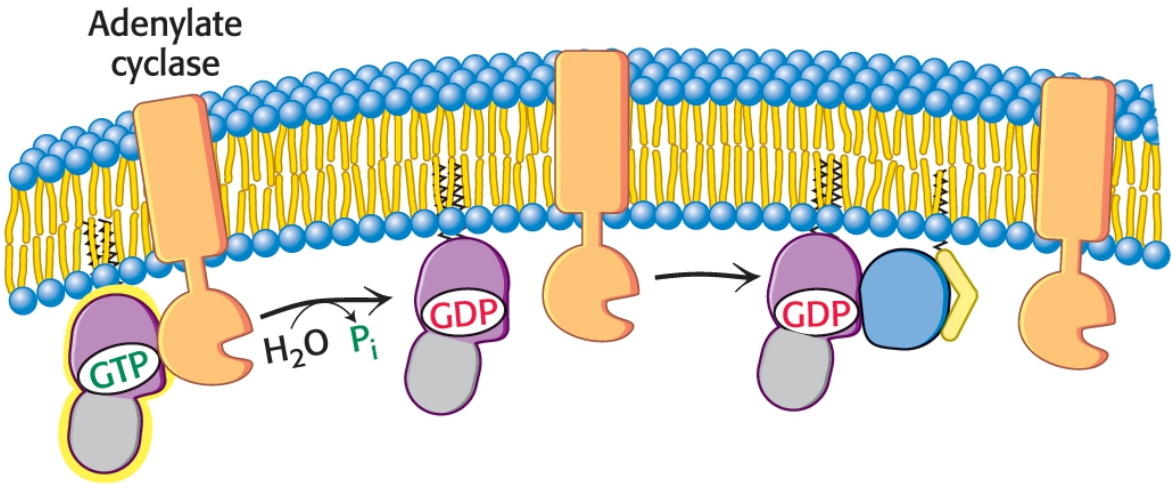


© Macmillan Learning

The flowchart is depicted as follows: Epinephrine plus beta-adrenergic receptor, downward arrow labeled “binding,” activated receptor, downward arrow labeled “amplification” and “G T P for G D P exchange,” activated G protein, downward arrow labeled “protein-protein interaction,” activated adenylate cyclase, downward arrow labeled “amplification” and “enzymatic reaction,” increased concentration of c A M P, downward arrow, activated protein kinase; cardiac muscle protein phosphorylation and contraction.

Return to Flowchart shows events leading to cardiac muscle contraction

Extended description for G protein resetting



© Macmillan Learning

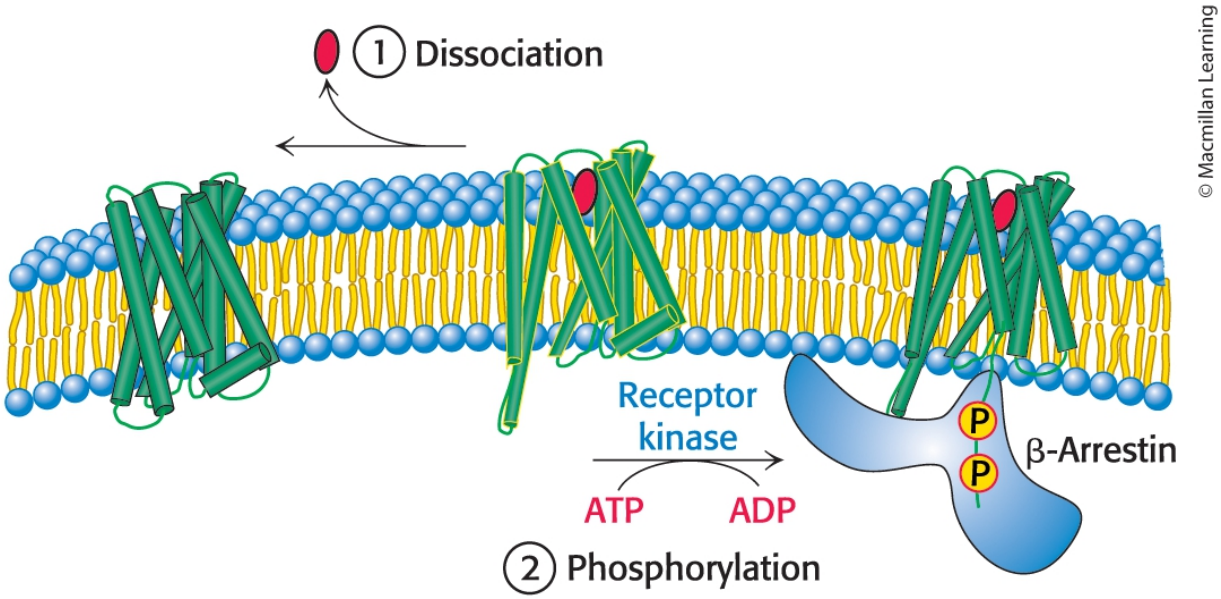
A section of a lipid bilayer is shown. The adenylate cyclase protein is shown embedded in the same bilayer. It is composed of a rectangular membrane-spanning region and a cytoplasmic round region having a tiny groove. A complex of purple and grey round structures is bound to the cytoplasmic round region of adenylate cyclase. The purple structure directly interacts with the cytoplasmic region of adenylate cyclase. The purple structure has a groove bound to G T P. This groove is closed by the grey sphere located below. Two zigzag lines at the top of the purple structure are embedded in the lipid bilayer.

A forward arrow leads to the purple structure bound to G D P and a grey structure below. It also shows the entry of H 2 O and exit of P subscript i. The complex of purple structure bound to G D P and a grey structure below is detached from the cytoplasmic region of adenylate cyclase. It is still attached to the inner leaflet of the lipid bilayer through two zigzag lines at the top.

A forward arrow leads to the trimeric G protein complex composed of G D P bound purple structure and its associated grey structure bound to a blue oval structure on the right. The blue structure is bound to a short yellow kinked structure on the right. The yellow structure is attached to the inner leaflet of the lipid bilayer through a zigzag line at the top embedded in the bilayer. The unbounded adenylate cyclase is shown embedded in the lipid bilayer on the right of the trimeric complex.

Return to G protein resetting

Extended description for Termination of beta-adrenergic receptor signaling



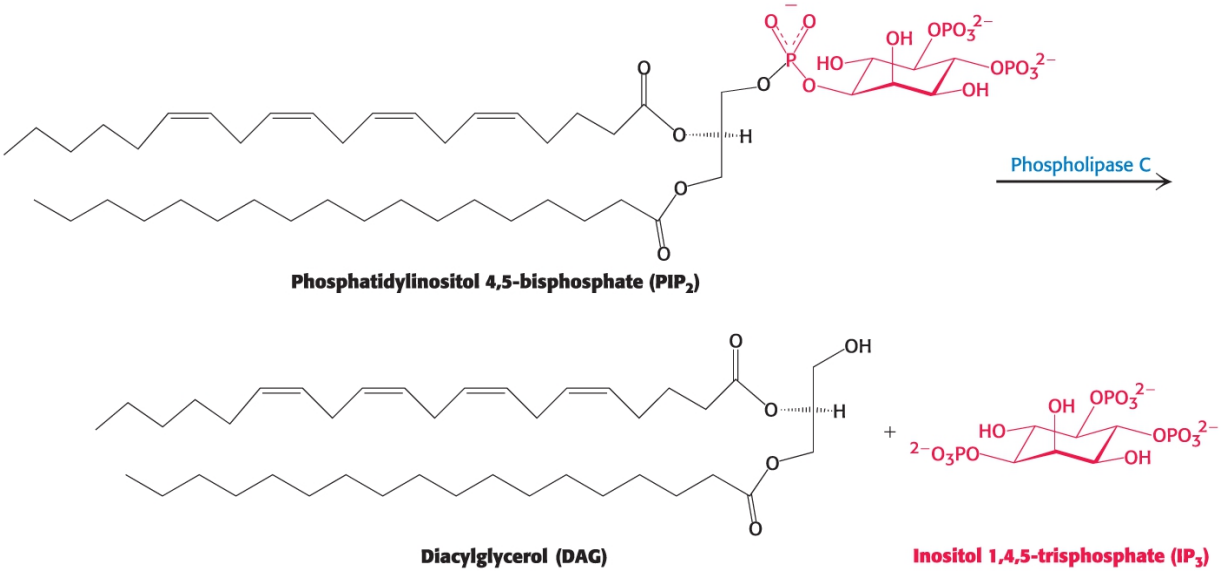
© Macmillan Learning

A section of a lipid bilayer is shown. The beta-adrenergic receptor is shown embedded in the center of the lipid bilayer. Its top groove is bound to a red tiny oval-shaped structure. A leftward arrow shows (1) dissociation of the red oval-shaped structure from the receptor to show an unbound receptor on the left.

A rightward arrow below the centrally located receptor shows (2) phosphorylation catalyzed by receptor kinase. During phosphorylation, A T P is converted into A D P. This arrow leads to the receptor bound to beta-arrestin at the cytoplasmic side. The beta-arrestin molecule contains two P atoms.

Return to Termination of beta-adrenergic receptor signaling

Extended description for Cleavage of phosphatidylinositol 4,5-bisphosphate



The chemical reaction consists of one reactant and two products. The reactant phosphatidylinositol 4,5-bisphosphate (P I P 2) has the following structure: A vertical chain consists of 3 C atoms. C 1 is single bonded to O on the right. This O atom is single-bonded to P on the upper right. P is further single bonded to O on the lower right and partially double bonded to O on the upper left and upper right. The partially double-bonded O atoms have an overall negative charge. The O atom on the lower right is single bonded to C 4 of a 6-membered homocyclic hexagonal ring in a chair conformation. The ring is in a plane perpendicular to the plane of paper such that C 1 and C 5 are located away from the observer and C 2 and C 4 are located toward the observer. C 3 and C 6 are located close to each other. C 1 is single bonded to O P O 3 superscript 2 minus on the lower right. C 2 is single bonded to O H on the upper right. C 3 is single bonded to O H above. C 5 is single bonded to O H on the lower

left. C 6 is single bonded to O P O 3 superscript 2 minus on the upper right.

C 2 of the vertical chain is dash bonded to H on the right and dash bonded to O on the left. This O atom is single bonded to C 1 of a 20-carbon alkene chain depicted as a line structure using 19 zigzag lines. C 1 of the chain is double bonded to O above. A double bond is present between C 5 and C 6, C 8 and C 9, C 11 and C 12, and C 14 and C 15.

C 3 of the vertical chain is single bonded to O on the lower left. This O is single bonded to C 1 of an 18-carbon alkane chain depicted as a line structure using 17 zigzag lines. C 1 of the chain is double bonded to O below.

A forward arrow labeled phospholipase C shows the products.

The first product is diacylglycerol (D A G) whose structure is as follows: A vertical chain consists of 3 C atoms. C 1 is single bonded to O H on the upper right. C 2 of the vertical chain is dash bonded to H on the right and dash bonded to O on the left. This O atom is single bonded to C 1 of a 20-carbon alkene chain depicted as a line structure using 19 zigzag lines. C 1 of the chain is double bonded to O above. A double bond is present between C 5 and C 6, C 8 and C 9, C 11 and C 12, and C 14 and C 15.

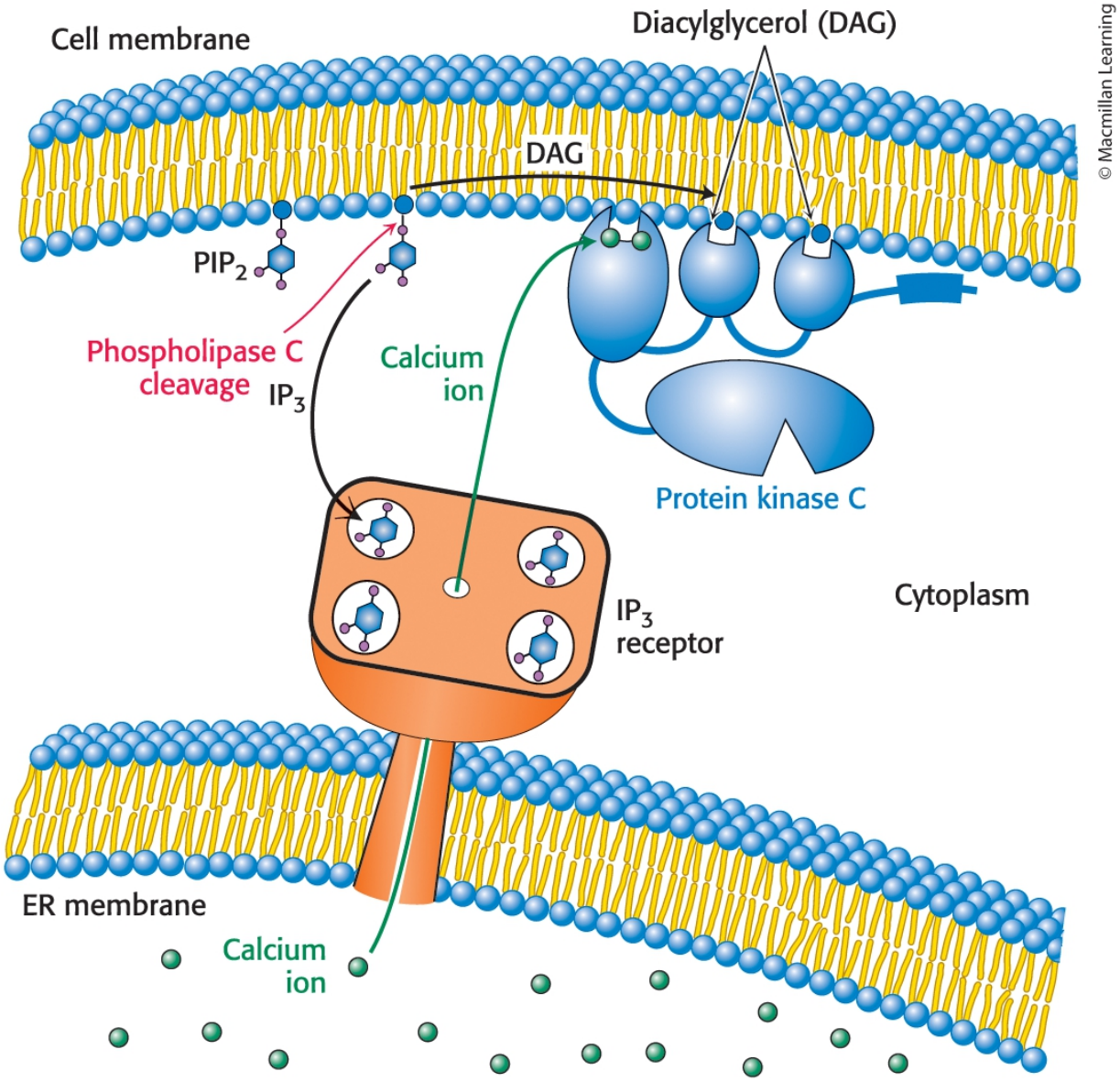
C 3 of the vertical chain is single bonded to O on the lower left. This O is single bonded to C 1 of an 18-carbon alkane chain depicted as a line structure using 17 zigzag lines. C 1 of the chain is double bonded to O below.

The second product is inositol 1,4,5-triphosphate (I P 3) whose structure is as follows: A 6-membered homocyclic hexagonal ring in

a chair conformation. The ring is in a plane perpendicular to the plane of paper such that C 1 and C 5 are located away from the observer and C 2 and C 4 are located toward the observer. C 3 and C 6 are located close to each other. C 1 is single bonded to O P O 3 superscript 2 minus on the lower right. C 2 is single bonded to O H on the upper right. C 3 is single bonded to O H above. C 4 is single bonded to O P O 3 superscript 2 minus on the upper left. C 5 is single bonded to O H on the lower left. C 6 is single bonded to O P O 3 superscript 2 minus on the upper right.

Return to Cleavage of phosphatidylinositol 4,5-bisphosphate

Extended description for Protein kinase C activation



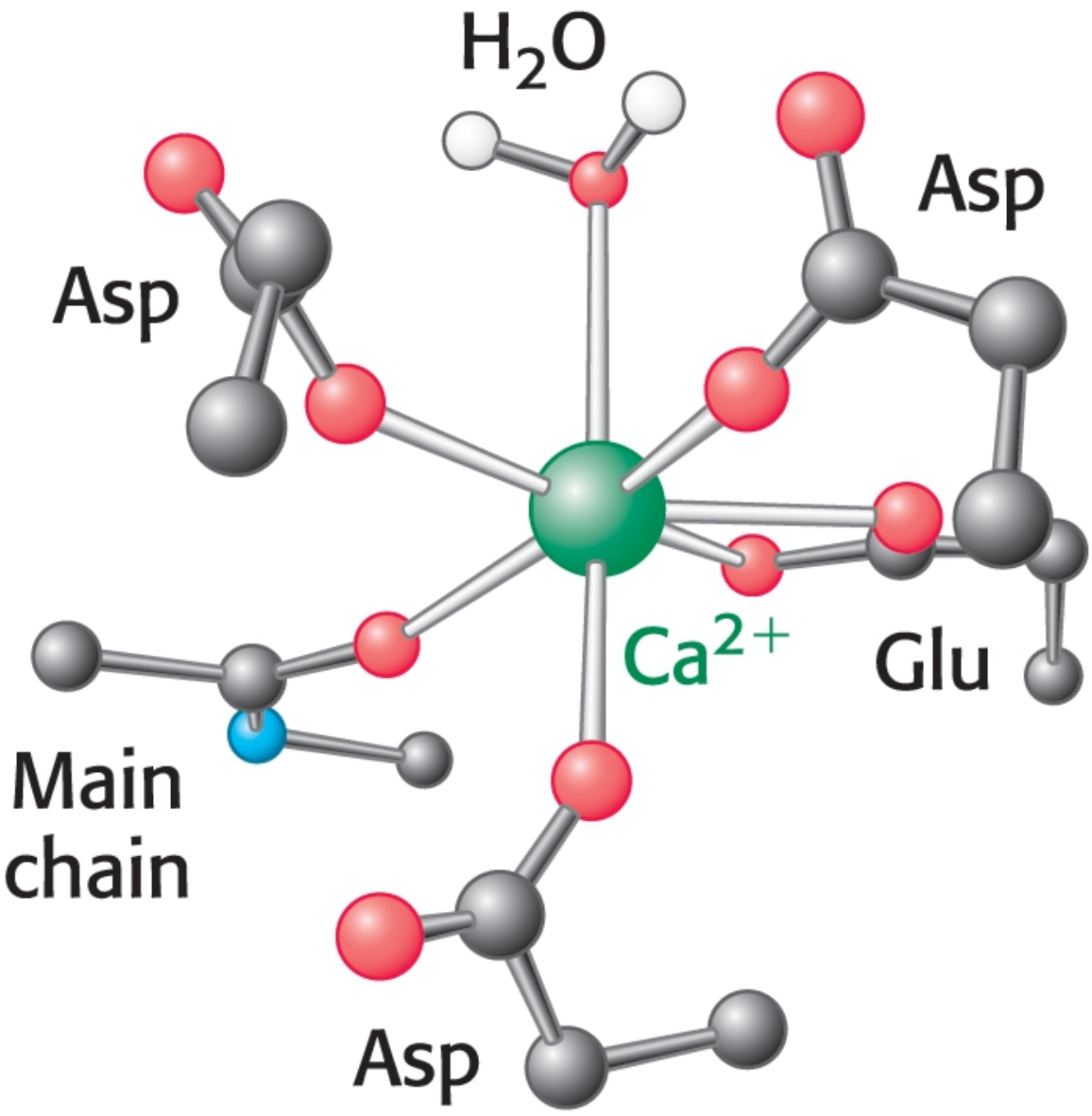
Two lipid bilayers separated by a large gap labeled cytoplasm are shown. The top bilayer is labeled cell membrane. The bottom bilayer is labeled E R membrane. P I P 2 in the inner leaflet of the cell membrane is cleaved into D A G and I P 3 by phospholipase C. P I P 2 is represented as a hexagon with its bottom-most vertex,

bottom left vertex, and topmost vertex connected to a tiny circle. The top tiny circle is connected to a circle in the inner leaflet. In P I P 2, phospholipase C breaks the linkage between the topmost tiny circle and the circle located in the inner leaflet.

I P 3 is depicted as a hexagon with its bottom-most vertex, bottom-left vertex, and topmost vertex connected to a tiny circle. It binds to four circular grooves of the I P 3 receptor embedded in the E R membrane. Several tiny green spheres depicting calcium ions are scattered below the E R membrane. One calcium ion passes through the transmembrane domain of the I P 3 receptor and enters the cytoplasm. The protein kinase is composed of four domains each containing a single groove connected by threads. A thread extending from the last domain of protein kinase C has a tiny rectangular domain. The three domains are attached to the inner leaflet of the cell membrane and the fourth domain is located in the cytoplasm. The shapes of the three domains are oval and round. Two calcium ions bind to the groove of the oval domain of protein kinase C attached to the inner leaflet. The grooves of the remaining two round domains bind to diacylglycerol.

Return to Protein kinase C activation

Extended description for Ball-and-stick model of calcium ion bound to oxygen atoms



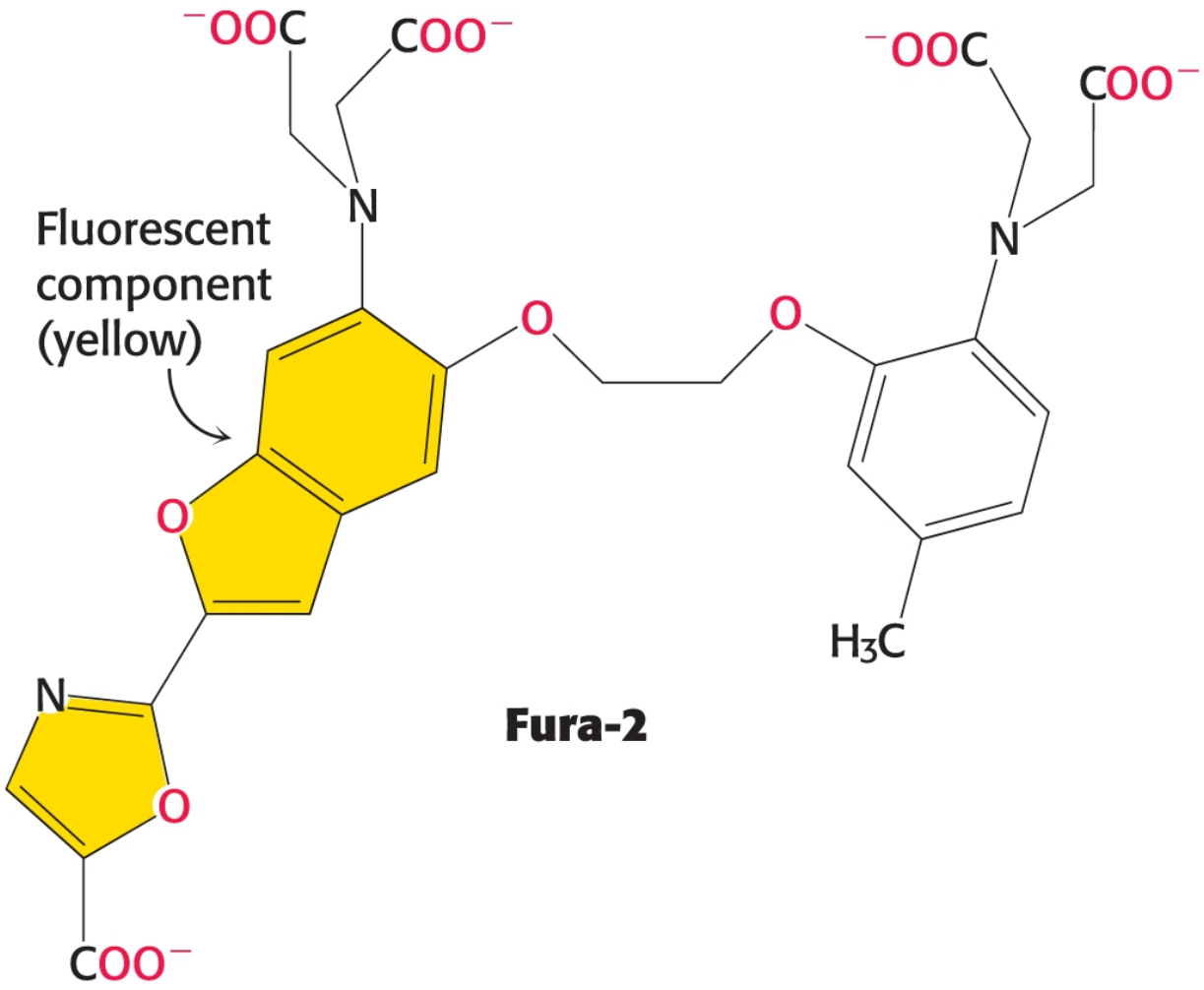
© Macmillan Learning

A central green sphere representing C a superscript 2 plus ion is connected to a red sphere above, on the upper right, right, lower right, below, on the lower left, and upper left. The red spheres represent O atoms. The red sphere above is connected to a white

sphere on the upper left and upper right that are part of H 2 O. The red spheres on the upper right and lower right are connected to a chain of dark grey spheres which are part of aspartic acid and glutamic acid residues respectively. The red sphere below is connected to a dark grey sphere on the lower left which is further connected to a red sphere on the left and a dark grey sphere on the lower right. The dark grey sphere on the lower right is further connected to another dark grey sphere on the right. These dark grey and red spheres located below are part of the aspartic acid residue. The red sphere on the lower right is connected to a chain of dark grey spheres. The first dark grey sphere is connected to a chain of blue and dark grey spheres below that are part of the main chain. The red sphere on the upper left is connected to a cluster of three dark grey spheres and one red sphere that is part of the aspartic acid residue.

Return to Ball-and-stick model of calcium ion bound to oxygen atoms

Extended description for Structure of Fura-2



Fura-2

The structure of Fura-2 is as follows: A 5-membered heterocyclic pentagonal ring shown in yellow is in a vertical orientation and consists of 1 N, 1 O, and 3 C atoms. C 1 occupies the top right vertex. N occupies the topmost vertex. O occupies the bottom right vertex. A double bond is present between N and C 1, and C 2 and C 3. C 2 is single bonded to C O O superscript minus below. C 1 is single bonded to C 4 of another 5-membered heterocyclic pentagonal ring in a vertical orientation consisting of 1 O and 4 C atoms. O occupies the top left vertex. A double bond is present between C 3 and C 4.

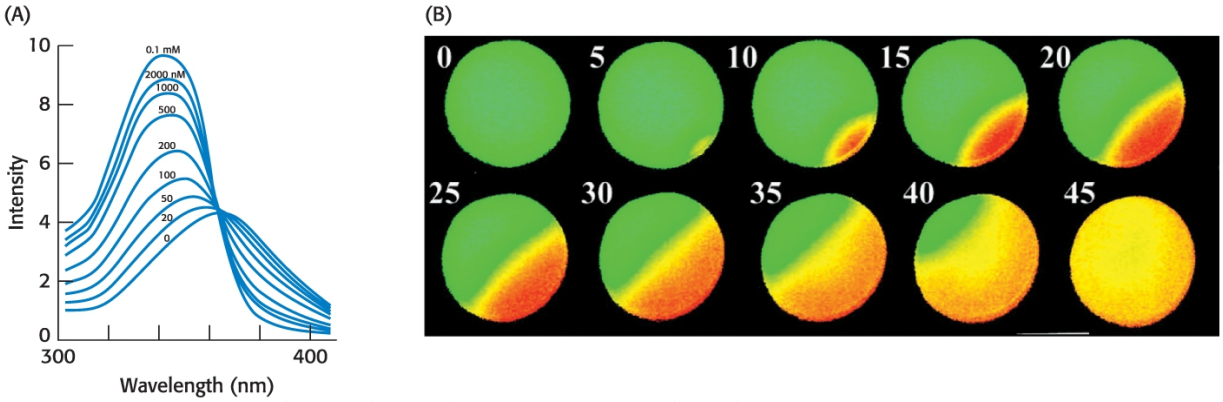
This pentagonal ring is fused to a benzene ring in a vertical orientation such that C 1 and C 2 of the pentagonal ring are C 5 and C 4, respectively, of the benzene ring. The benzene ring contains alternating double bonds between C 2 and C 3, C 4 and C 5, and C 6 and C 1.

C 1 is single bonded to N above. N is further single bonded to two different C H 2 groups on the upper left in the form of a line. Each C H 2 group is single bonded to C O O superscript minus above. The fused pentagonal ring and benzene ring are shown in yellow and labeled “Fluorescent component (yellow).”

C 2 of the benzene ring is single bonded to O 1 of a 2 O and 2 C heteronuclear alkane chain depicted as a line structure using 3 lines. O 2 occupies the fourth position of the alkane chain and is single bonded to C 6 of another benzene ring on the right. This benzene ring is in a vertical orientation and contains alternating double bonds between C 1 and C 2, C 3 and C 4, and C 5 and C 6. C 1 is single bonded to N above. N is further single bonded to C H 2 above and C H 2 on the upper right in the form of a line. Each C H 2 group is single bonded to C O O superscript minus above. C 4 is single bonded to C H 3 below.

Return to Structure of Fura-2

Extended description for Fluorescence spectra of Fura-2 and photographs of calcium ions spreading across an egg cell



(B) Credit: Republished with permission of Company of Biologists, from Exploring the mechanism of action of the sperm-triggered calcium-wave pacemaker in ascidian zygotes, Carroll, M. et al., December 15, 2003, *J Cell Sci* 116: 4997–5004; permission conveyed through Copyright Clearance Center, Inc. Courtesy Alex McDougall.
© Macmillan Learning

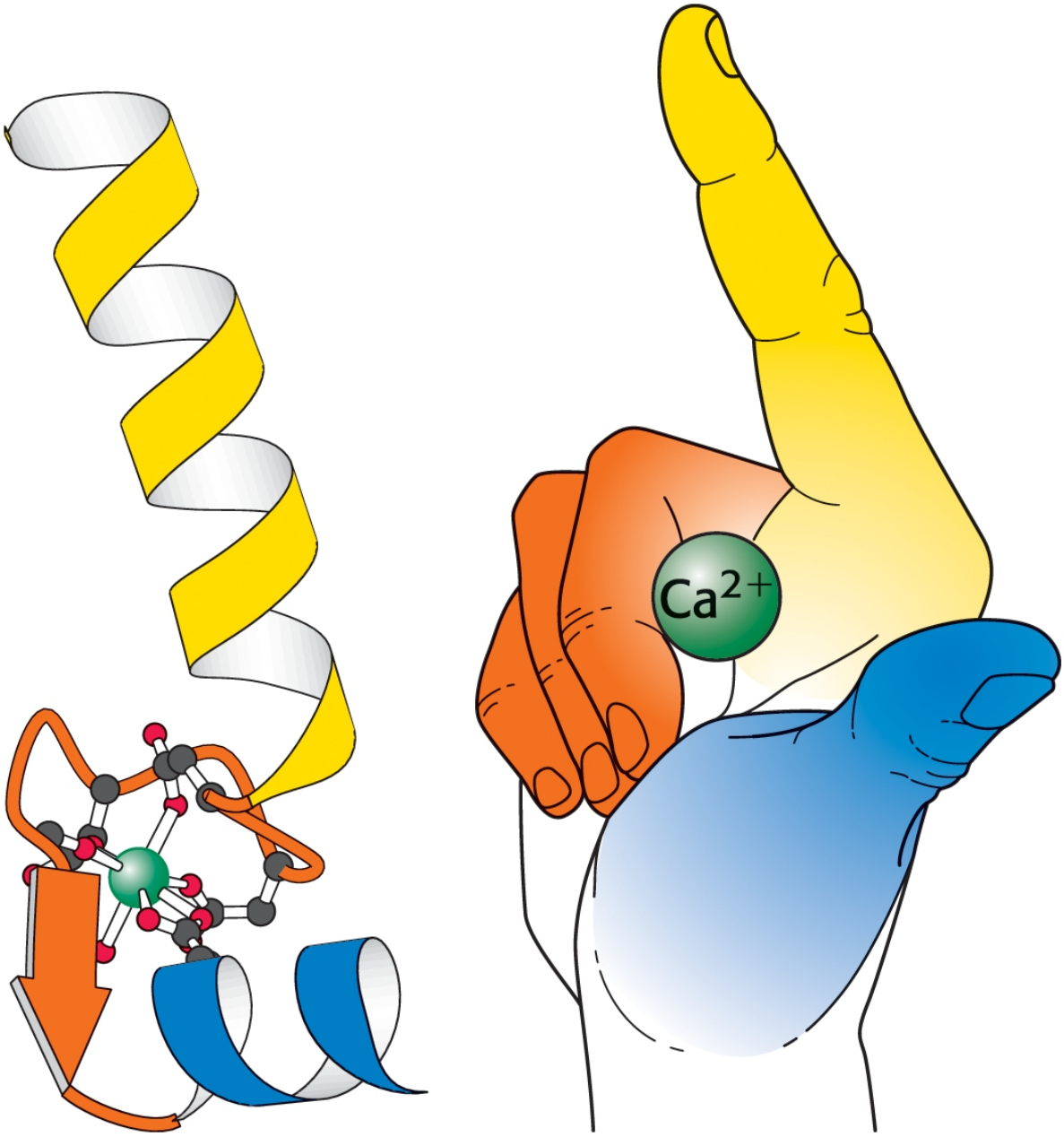
Part (A): It shows a graph with different curves. The horizontal axis is labeled wavelength in nanometers. It has markings ranging from 300 to 400 in increments of 100 units. The vertical axis is labeled intensity. It has markings ranging from 0 to 10 in increments of 2 units. The graph shows a series of bell-shaped curves arranged in ascending order of peak size from the bottom to the top. The topmost curve has a peak size of 10 at 350 nanometers. From bottom to top, the curves shift gradually shift toward the left. The bottommost curve has a peak size of 4.2 at 370 nanometers. From bottom to top, the curves are labeled 0, 20, 50, 100, 200, 500, 1000, 2000 nanomolar, and 0.1 millimolar.

Part (B): It shows 10 circular views of C a superscript 2 plus ion spreading across an egg cell at 0, 5, 10, 15, 20, 25, 30, 35, 40, and 45 seconds. At 0 seconds, the entire view is green-colored. At 5 seconds, a tiny yellow-orange patch is seen at the bottom right. From 10 to 40 seconds, the yellow-orange patch becomes

progressively larger and ultimately covers the entire view at 45 seconds.

Return to Fluorescence spectra of Fura-2 and photographs of calcium ions spreading across an egg cell

Extended description for E F hand motif



© Macmillan Learning

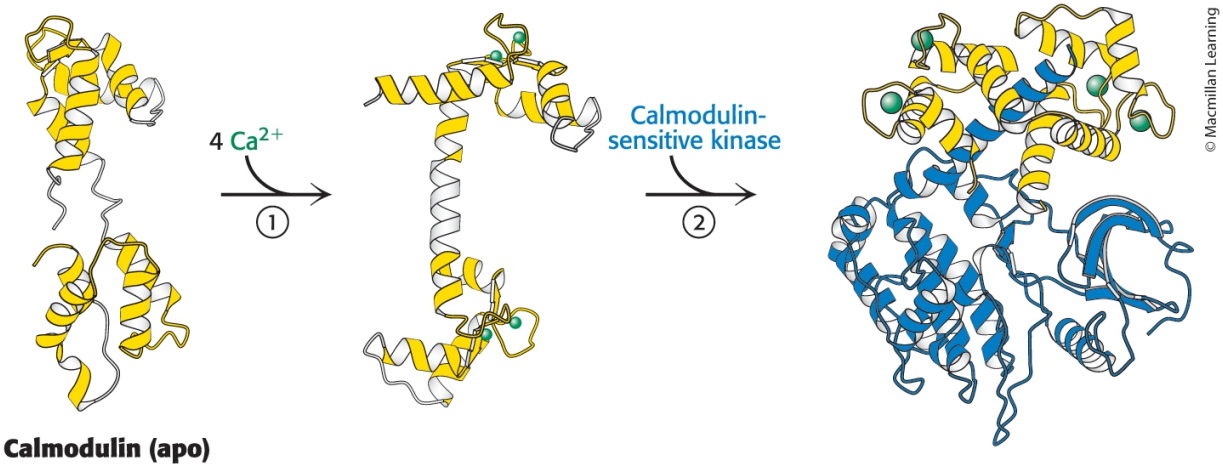
A long yellow alpha-helix is shown in diagonal orientation with its top tilted toward the top left. It is connected to a long orange loop. The loop is connected to an orange beta-strand represented as a downward arrow. The arrowhead is connected to a short orange

thread further connected to a short and horizontally oriented blue alpha-helix on the right.

A diagram of the right hand is shown on the right. The index finger is shown in yellow color and points toward the top right. The remaining fingers shown in orange are curled around a green sphere labeled C a superscript 2 plus in the palm. The thumb, shown in blue color, points toward the right.

Return to E F hand motif

Extended description for Conformational change in the apo form of calmodulin and its binding to protein kinase



The apo form of calmodulin consists of 4 alpha-helices and a beta-strand at the top connected through a long thread to a cluster of four loosely arranged alpha-helices at the bottom.

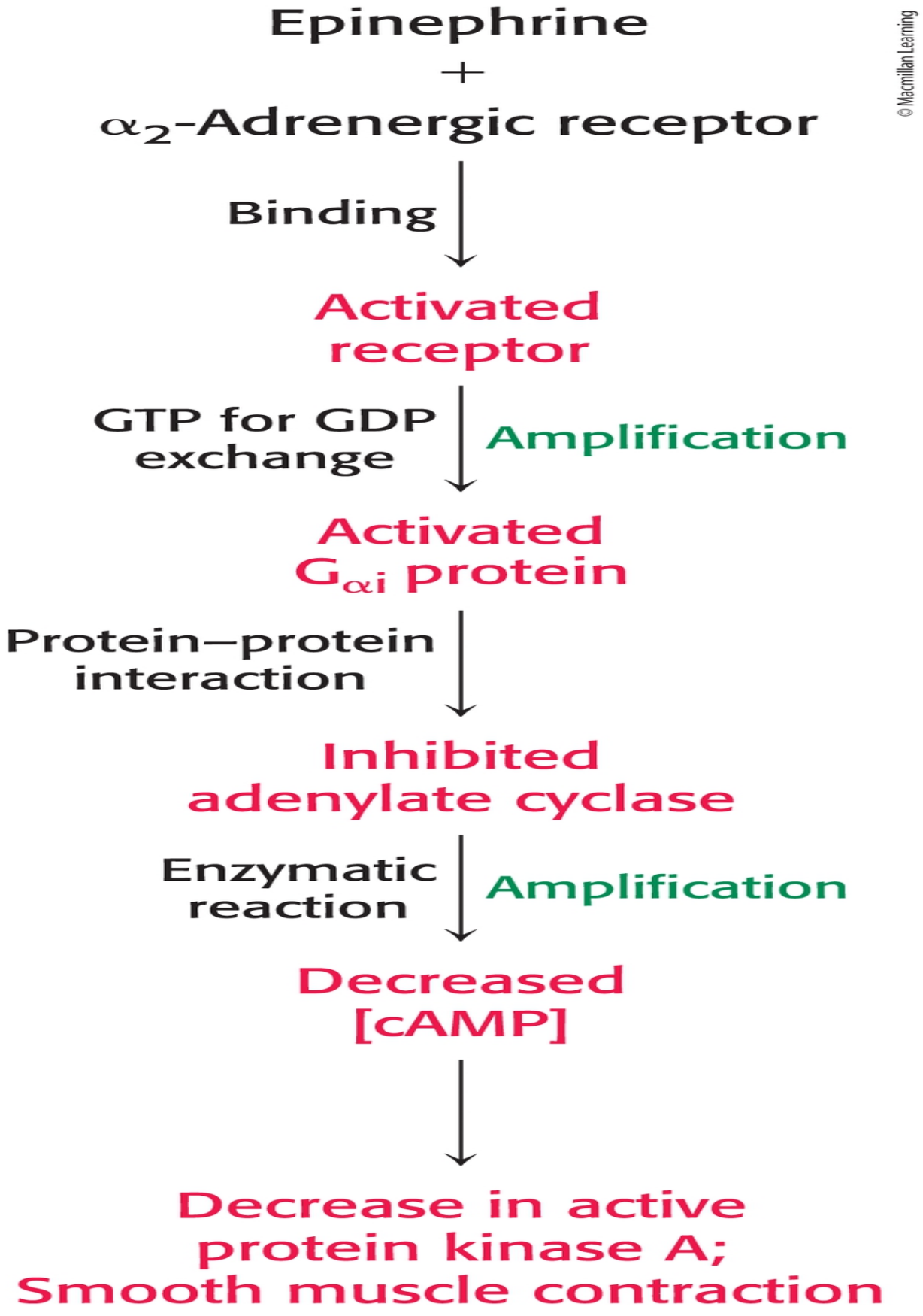
A forward arrow labeled 1 shows the entry of 4 C a superscript 2 plus ions. The C a superscript 2 plus ions are depicted as tiny green spheres. Two green spheres bind to the top portion and the remaining two bind to the bottom portion. A long vertical alpha helix connects the top and bottom portions.

A forward arrow labeled 2 shows the entry of calmodulin-sensitive kinase. The protein kinase is composed of several alpha-helices and a few beta-strands on the right. The calcium-bound calmodulin is clamped around an alpha-helix at the top surface of the protein kinase.

Return to Conformational change in the apo form of calmodulin and its binding to protein kinase

Extended description for Flow chart show events

leading to smooth muscle contraction

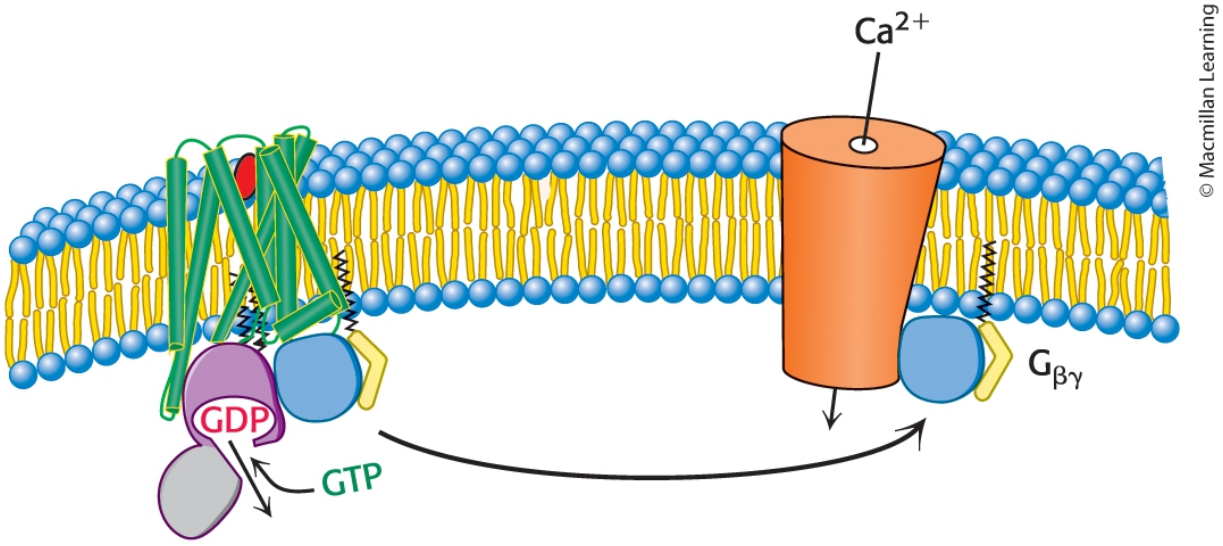


© Macmillan Learning

The flowchart is depicted as follows: Epinephrine plus alpha 2-adrenergic receptor, downward arrow labeled “binding,” activated receptor, downward arrow labeled “amplification” and “G T P for G D P exchange,” activated G subscript alpha i protein, downward arrow labeled “protein-protein interaction,” inhibited adenylate cyclase, downward arrow labeled “amplification” and “enzymatic reaction,” decreased concentration of c A M P, downward arrow, decrease in active protein kinase A; smooth muscle contraction.

Return to Flow chart show events leading to smooth muscle contraction

Extended description for Signal transduction by G protein beta gamma dimer

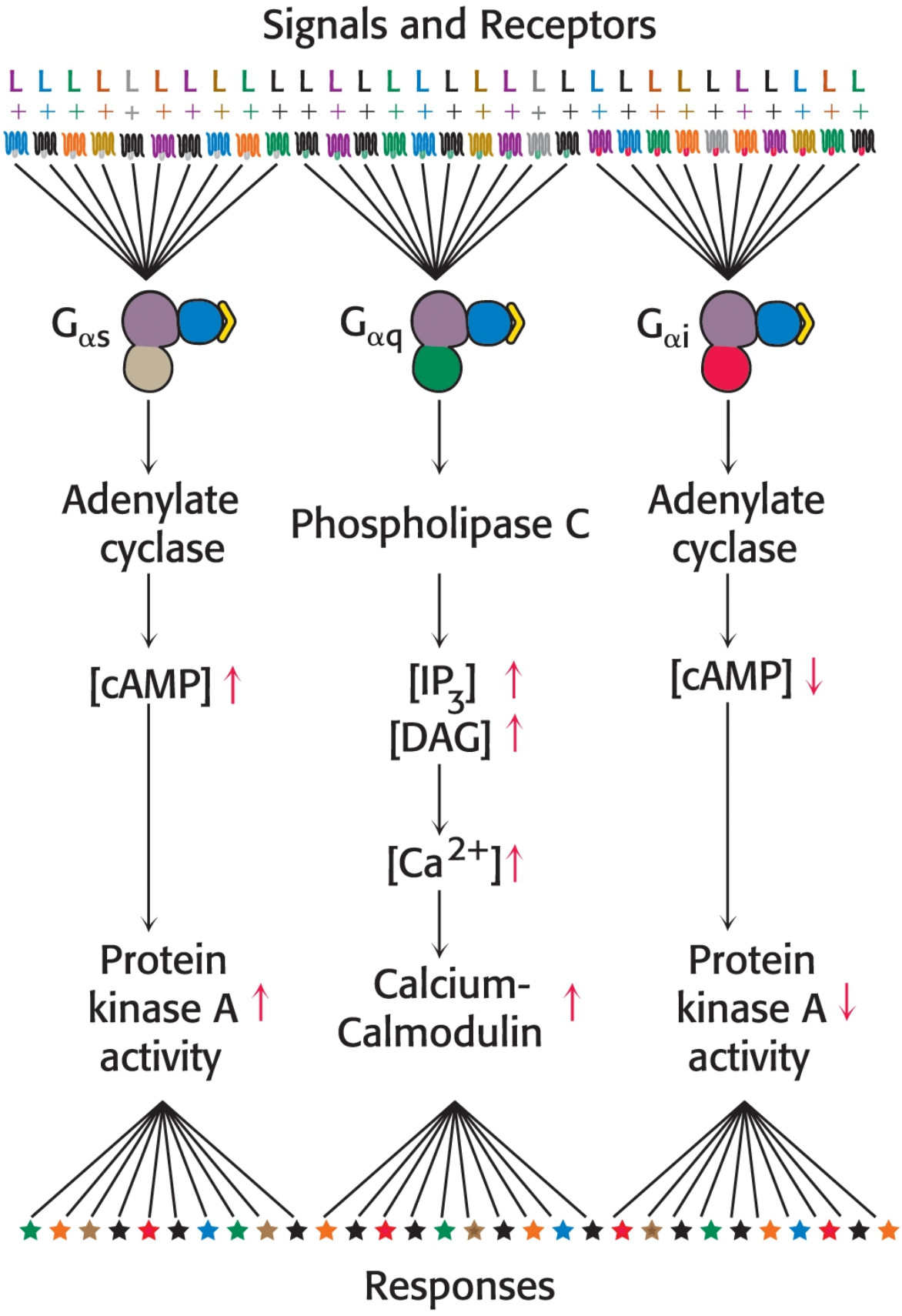


A horizontal section of a lipid bilayer is shown. The beta-adrenergic receptor bound to a red oval-shaped structure at the top is shown embedded in the bilayer. The cytoplasmic side of the receptor is bound to the trimeric G protein. The grey structure associated with the purple round structure is displaced toward the lower left to allow the exit of G D P and entry of G T P into the groove of the purple round structure. An arrow shows the G subscript beta gamma subunit associated with the cytoplasmic region of a cork-shaped structure embedded on the right of the same bilayer. G subscript beta gamma subunit consists of a blue rounded square and a short yellow kinked structure having a zigzag line at the top embedded in the lipid bilayer. The blue structure is directly associated with the cork-shaped structure. A downward arrow across the central channel of the cork-shaped structure shows the inward movement of C a superscript 2 plus.

Return to Signal transduction by G protein beta gamma dimer

Extended description for Generalized signaling pathway involving the three classes of G protein alpha

subunits



© Macmillan Learning

Three classes of the G protein alpha subunits are G subscript alpha S, G subscript alpha q, and G subscript alpha i. Ten different “7 T M” receptors bound to a ligand L are shown above each type of subunit to show signals and receptors. The 7 T M receptor is depicted as a tiny structure with zigzag turns. Lines from each of the receptor-ligand complex converge together and point below to a particular type of G protein alpha subunit.

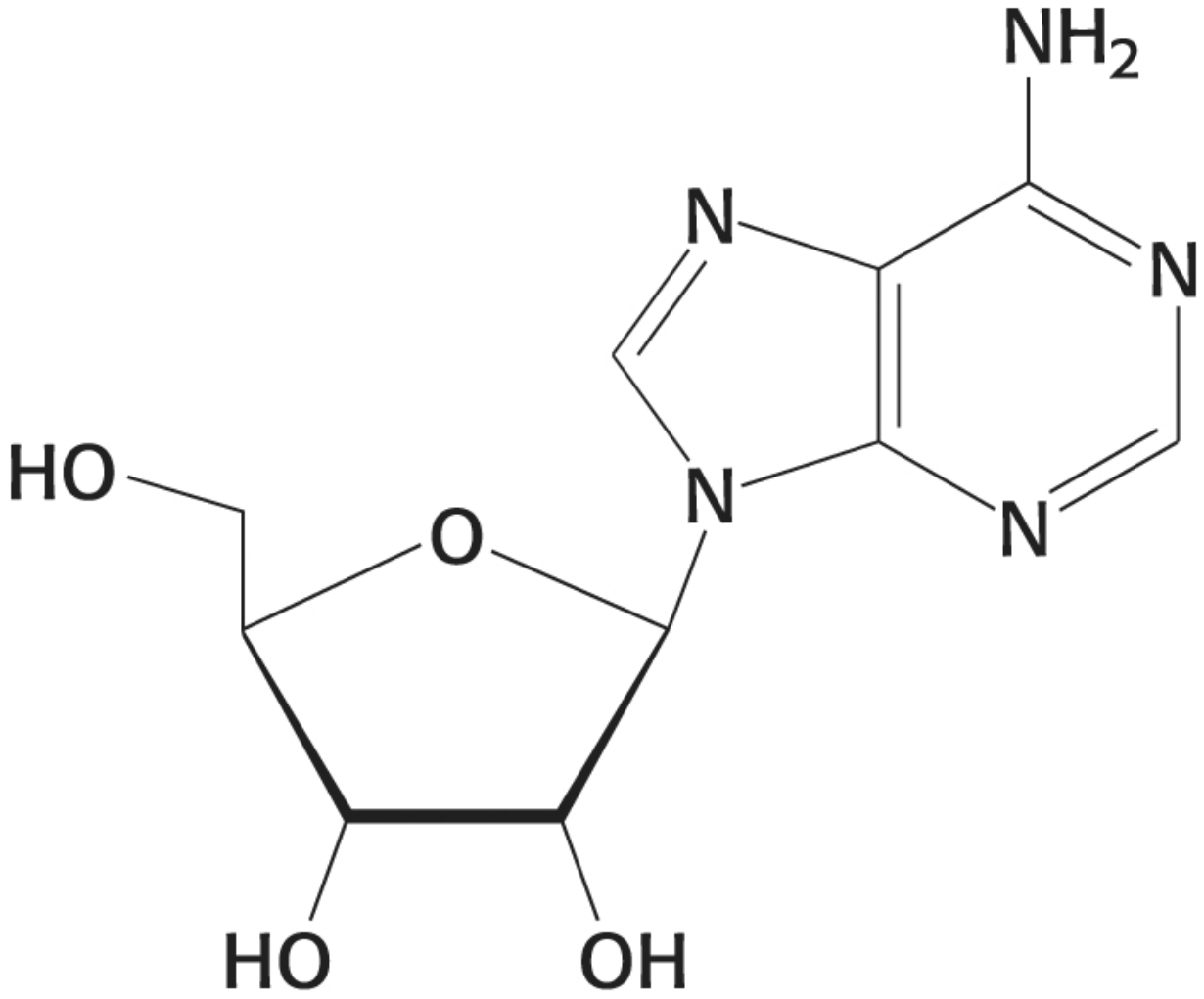
The signaling pathway initiated by the G subscript alpha S subunit is as follows: adenylate cyclase, concentration of c A M P increases, downward arrow, protein kinase A activity increases, 10 downward lines each pointing toward a differently colored star symbol to show the different responses.

The signaling pathway initiated by the G subscript alpha q subunit is as follows: Phospholipase C, downward arrow, concentration of I P 3 and D A G increases, downward arrow, concentration of C a superscript 2 plus ion increases, downward arrow, calcium-calmodulin increases, 10 downward lines each pointing toward a differently colored star symbol to show the different responses.

The signaling pathway initiated by the G subscript alpha i subunit is as follows: Adenylate cyclase, downward arrow, concentration of c A M P increases, downward arrow, protein kinase A activity decreases, 10 downward lines each pointing toward a differently colored star symbol to show the different responses.

Return to Generalized signaling pathway involving the three classes of G protein alpha subunits

Extended description for Structure of adenosine



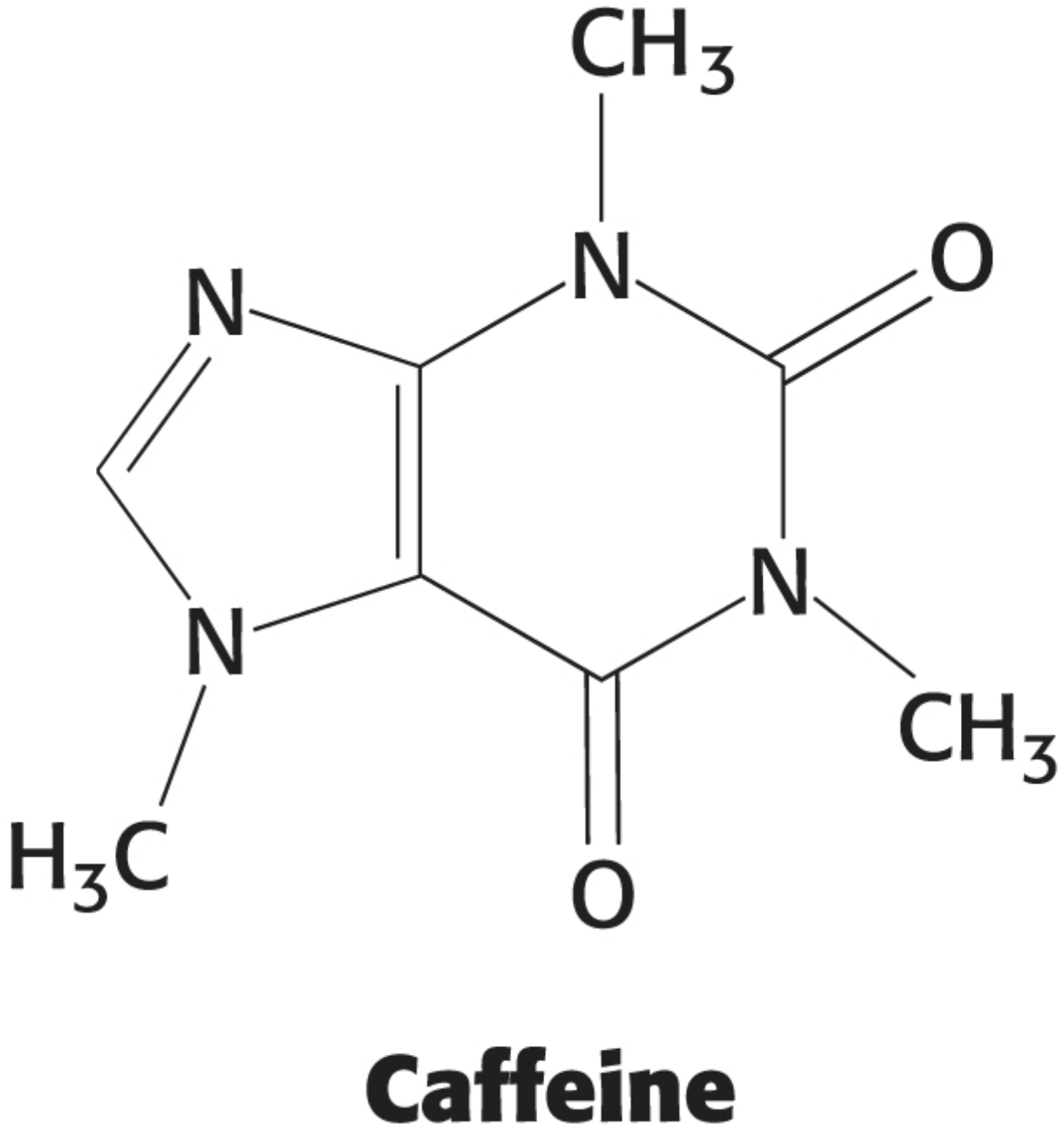
Adenosine

The structure of adenosine is as follows: A 5-membered heterocyclic pentagonal is in a vertical orientation and consists of 1 O and 4 C atoms. O occupies the topmost vertex. C 1 is single bonded to N 1 of a 5-membered heterocyclic pentagonal ring in a horizontal orientation consisting of 2 N and 3 C atoms. The first N atom occupies the first position, which is the bottom left vertex. The second N atom occupies the third position, which is the top left

vertex. C 1 occupies the rightmost vertex. A double bond is present between C 1 and N 2. This pentagonal ring is fused to a 6-membered heterocyclic hexagonal such that C 2 and C 3 of the pentagonal are C 3 and C 2 respectively of the hexagonal ring. The first N occupies the first position, which is the top right vertex. The second N occupies the third position, which is the bottom-most vertex. A double bond is present between C 1 and N 2, C 2 and C 3, C 4 and N 1. C 4 is single bonded to N H 2 above. C 2 and C 3 of the first pentagonal ring are each single bonded to O H below. C 4 is single bonded to C H 2 above in the form of a line. C H 2 is further single bonded to O H on the upper left.

Return to Structure of adenosine

Extended description for Chemical structure of caffeine

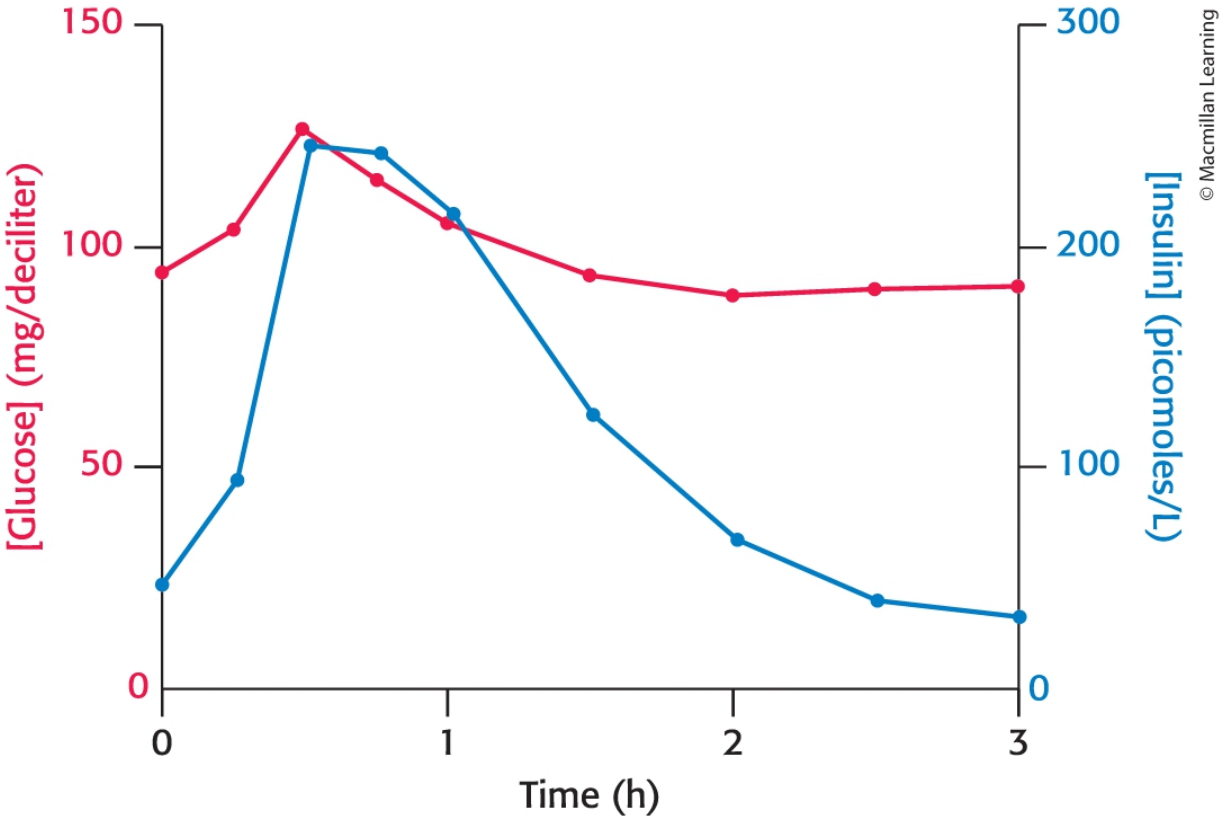


The structure of caffeine is as follows: A 5-membered heterocyclic pentagonal ring is in a horizontal orientation with C 1 occupying the

rightmost vertex. It consists of 2 N and 3 C atoms. First N occupies the first position, which is the bottom left vertex. Second N occupies the third position, which is the top left vertex. N 1 is single bonded to C H 3 on the lower left. A double bond is present between C 1 and N 2, and C 2 and C 3. It is fused to a 6-membered heterocyclic hexagonal ring such that C 2 and C 3 of the pentagonal ring are C 4 and C 3 of the hexagonal ring respectively. In the hexagonal ring, first N occupies the first position, which is the topmost vertex. Second N occupies the third position, which is the bottom right vertex. N 2 is single bonded to C H 3 on the lower right. N 1 is single bonded to C H 3 above. C 1 is double bonded to O on the upper right. C 2 is double bonded to O below.

Return to Chemical structure of caffeine

Extended description for Graphical representation of glucose and insulin levels post meal

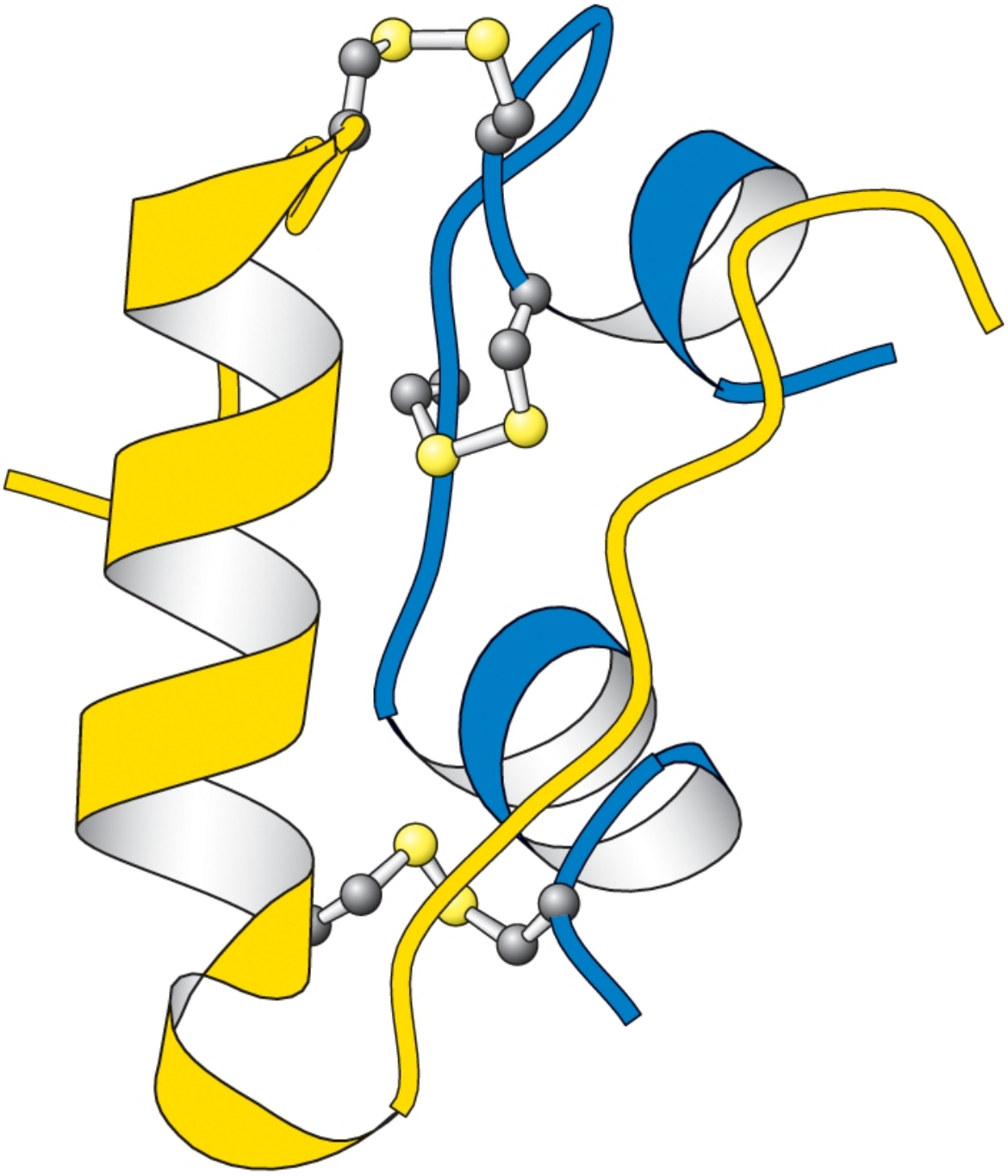


The horizontal axis is labeled time in hours. It has markings ranging from 0 to 3 in increments of 1 unit. The left vertical axis is labeled concentration of glucose in milligram per deciliter. It has markings ranging from 0 to 150 in increments of 50 units. The right vertical axis is labeled concentration of insulin in picomoles per liter. It has markings ranging from 0 to 300 in increments of 100 units. The graph contains two curves shown in blue and red. The red curve represents glucose concentration and has the following data points: (0, 95), (0.3, 105), (0.5, 130), (0.8, 115), (1, 106),(1.5, 95), (2, 92), (2.5, 90), and (3, 91).

The blue curve represents insulin concentration and has the following data points: (0, 50), (0.3, 100), (0.52, 250), (0.8, 248), (1, 220), (1.5, 120), (2, 80), (2.5, 45), and (3, 40).

Return to Graphical representation of glucose and insulin levels post meal

Extended description for Insulin ribbon structure



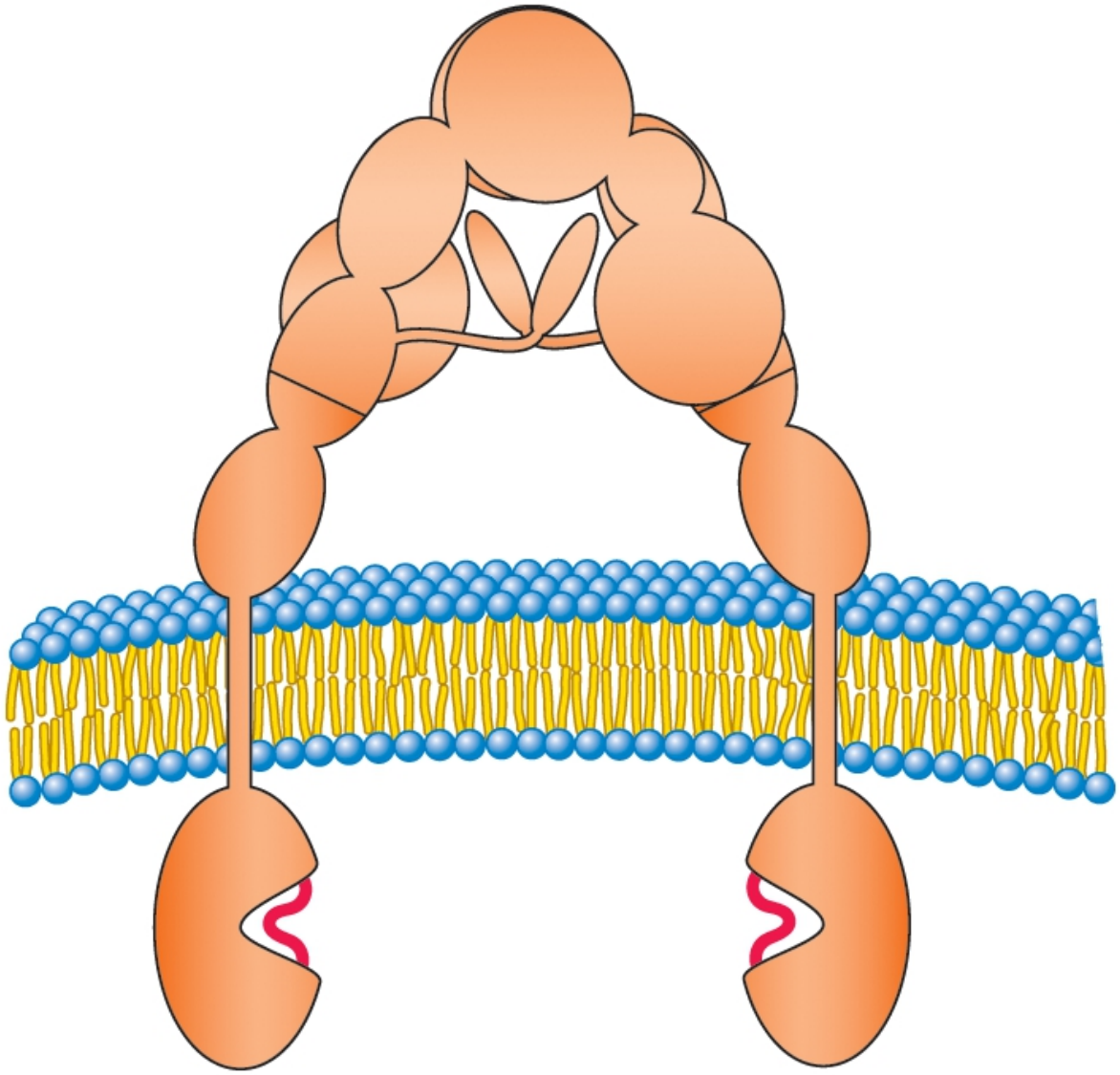
© Macmillan Learning

A vertical yellow alpha-helix is shown on the left. Long threads originate from the top and bottom portions of the alpha-helix. Two

short blue alpha-helices interconnected by a long blue thread are shown on the right. The long yellow thread of the left helix extends toward the upper right. Two ball-and-stick models connect the top portion of the yellow alpha-helix with the blue thread and bottom portion of the yellow alpha-helix with the second short blue alpha-helix. A third ball-and-stick model connects the different sections of the blue thread. The ball-and-stick model is composed of a chain of two black spheres connected to a yellow sphere. The yellow sphere is connected to another yellow sphere which is further connected to a chain of two black spheres.

Return to Insulin ribbon structure

Extended description for Insulin receptor



© Macmillan Learning

A section of a horizontal lipid bilayer is shown. The insulin receptor consists of two subunits each consisting of two different chains shown in dark orange and light orange colors. The dark orange chain consists of an oval-shaped domain located above the bilayer, a thin tubular domain spanning the bilayer, and a large oval-shaped

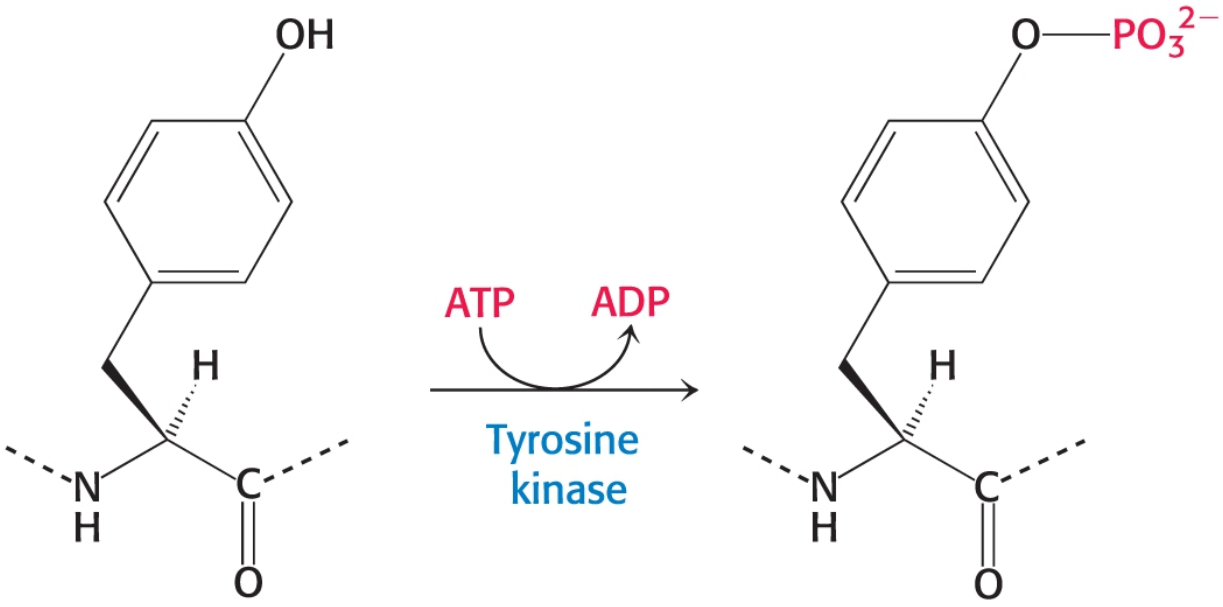
domain below the bilayer. The oval-shaped domain above the bilayer is connected to a half oval domain above. The large oval-shaped domain has a triangular groove. A wavy red line within the groove connects the ends of the groove.

The light orange chain consists of four globular domains and a half-globular domain at the bottom that is connected to the half oval domain of the dark orange chain located above the bilayer.

The light orange chains of the two subunits fold over one another to form an arch-shaped structure. A short extension having a leaf-shaped structure at the end originates from the half globular domain of each of the light orange chain. These leaf-shaped structures cross each other just below the arch formed by light orange chains.

Return to Insulin receptor

Extended description for Chemical reaction catalyzed by tyrosine kinase



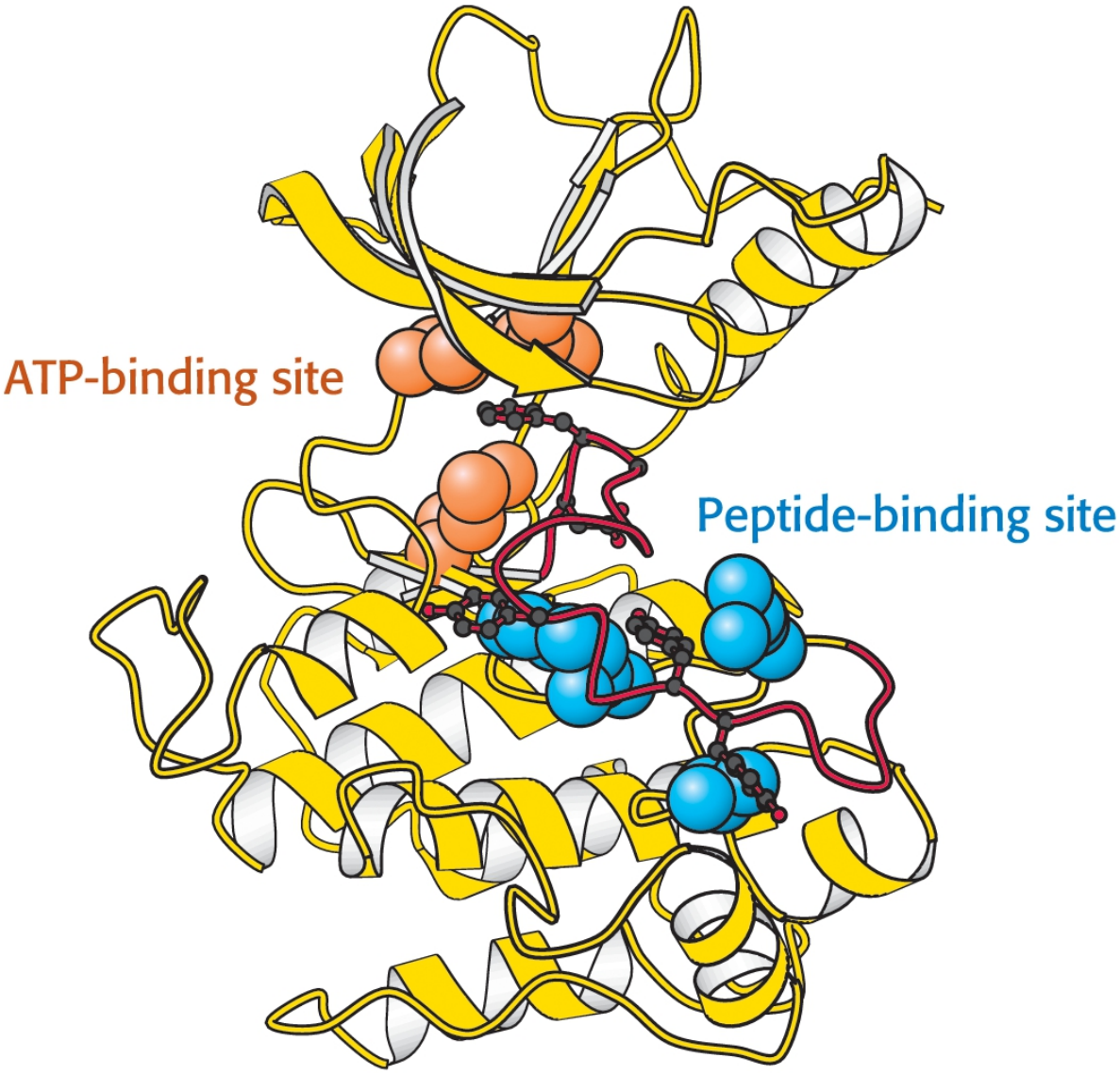
The chemical reaction consists of one reactant and one product. The reactant has the following structure: A benzene ring is in a horizontal orientation with C 1 occupying the rightmost vertex. It contains alternating double bonds between C 2 and C 3, C 4 and C 5, and C 6 and C 1. C 6 is single bonded to O H on the upper right. C 3 is single bonded to C H 2 in the form of a line on the lower left. This C H 2 is wedge bonded to C 1 of a 1 N and 2 C heteronuclear alkane chain depicted as a line structure using 2 zigzag lines. In the alkane chain, N bound to H occupies the first position and has a dashed line on the upper left. C 1 is dash bonded to H on the upper right. C 2 is double bonded to O below and has a dashed line on the upper right.

A forward arrow labeled tyrosine kinase shows the product. A curved arrow above the forward arrow shows the simultaneous conversion of A T P into A D P.

The structure of the product is as follows: A benzene ring is in a horizontal orientation with C 1 occupying the rightmost vertex. It contains alternating double bonds between C 2 and C 3, C 4 and C 5, and C 6 and C 1. C 6 is single bonded to O, single bond, P O 3 superscript 2 minus on the upper right. C 3 is single bonded to C H 2 in the form of a line on the lower left. This C H 2 is wedge bonded to C 1 of a 1 N and 2 C heteronuclear alkane chain depicted as a line structure using 2 zigzag lines. In the alkane chain, N bound to H occupies the first position and has a dashed line on the upper left. C 1 is dash bonded to H on the upper right. C 2 is double bonded to O below and has a dashed line on the upper right.

Return to Chemical reaction catalyzed by tyrosine kinase

Extended description for Unactivated form of insulin receptor kinase



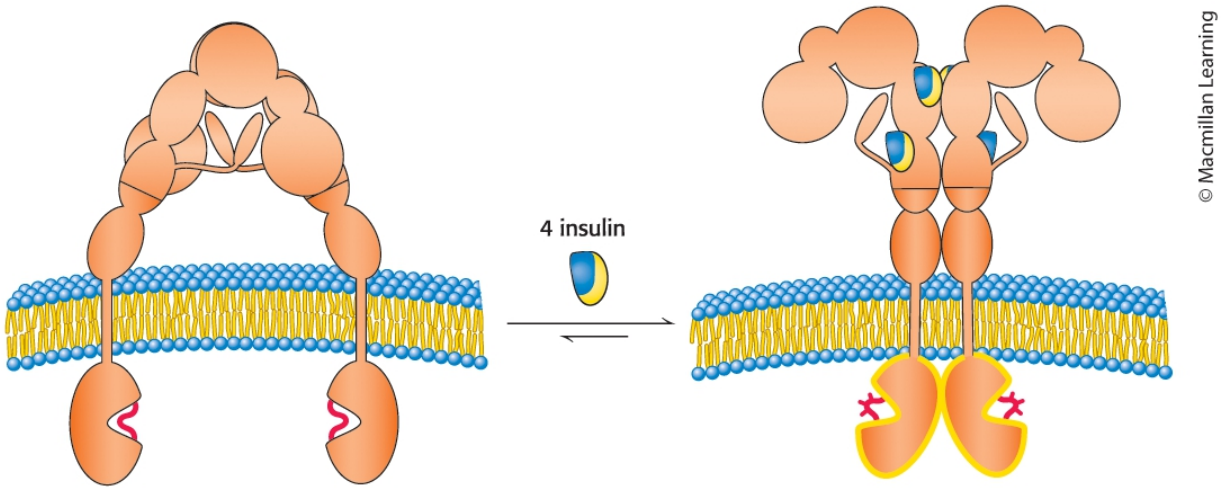
© Macmillan Learning

The unactivated insulin receptor kinase consists of several alpha-helices in the bottom portion and a few beta-strands and an alpha helix in the top portion. Several threads are located between the top and bottom portions. A cluster of orange spheres is located inside the beta-strands of the top portion and the top surface of the bottom

portion. These orange spheres depict residues from the A T P-binding site. Three clusters of blue spheres are shown around the top right of the bottom portion of the kinase. These blue spheres represent the peptide binding site. A long and wavy loop highlighted in red spans from the bottom portion to the junction between the top and bottom portion. The red loop passes across the blue and orange clusters and contains 5 ball-and-stick models of amino acid side chains.

Return to Unactivated form of insulin receptor kinase

Extended description for Conformational change in insulin receptor



© Macmillan Learning

A section of a horizontal lipid bilayer is shown. The insulin receptor consists of two subunits each consisting of two different chains shown in dark orange and light orange colors. The dark orange chain consists of an oval-shaped domain located above the bilayer, a thin tubular domain spanning the bilayer, and a large oval-shaped domain below the bilayer. The oval-shaped domain above the bilayer is connected to a half oval domain above. The large oval-shaped domain has a triangular groove. A wavy red line within the groove connects the ends of the groove.

The light orange chain consists of four globular domains and a half-globular domain at the bottom that is connected to the half oval domain of the dark orange chain located above the bilayer.

The light orange chains of the two subunits fold over one another to form an arch-shaped structure. The dark orange chains of the two subunits are located at a gap. A short extension having a leaf-shaped structure at the end originates from the half globular domain of

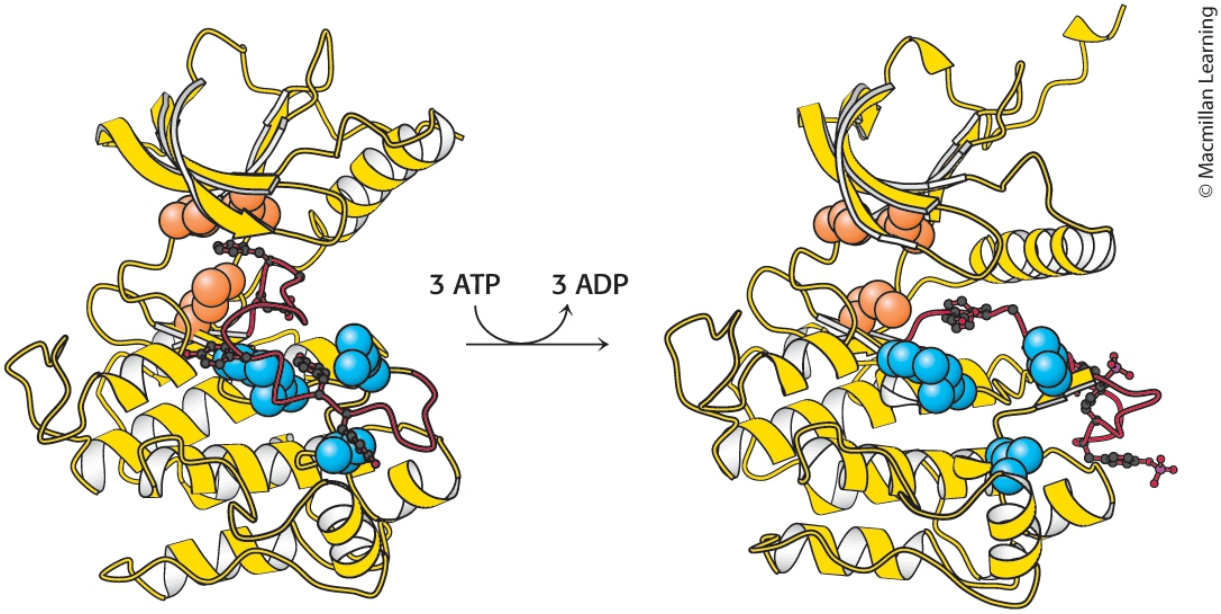
each of the light orange chains. These leaf-shaped structures cross each other just below the arch formed by light orange chains.

A reversible arrow labeled 4 insulin is shown and it leads to an altered conformation of the insulin receptor.

The insulin molecule is bound to the globular domains of the light orange chain located closer to the dark orange chain. The dark orange chains have come close together. The grooves of the large oval-shaped domains of the dark orange chain face away from each other and these domains contact each other. Before insulin binding, the grooves were facing each other and these domains were located at a large gap. Except for the three terminal globular domains of the light orange chain, the remaining domains, and the dark orange chain are located close together. The terminal globular domains of the left subunit hang toward the lower left and that of the right subunit hang toward the lower right.

Return to Conformational change in insulin receptor

Extended description for Activation of insulin receptor



© Macmillan Learning

The unactivated insulin receptor kinase consists of several alpha-helices in the bottom portion and a few beta-strands and an alpha helix in the top portion. Several threads are located between the

top and bottom portions. A cluster of orange spheres is located inside the beta-strands of the top portion and the top surface of the bottom portion. These orange spheres depict residues from the A T P-binding site. Three clusters of blue spheres are shown around the top right of the bottom portion of the kinase. These blue spheres represent the peptide binding site. A long and wavy loop highlighted in red spans from the bottom portion to the junction between the top and bottom portion. The red loop passes across the blue and orange clusters and contains 5 ball-and-stick models of amino acid side chains.

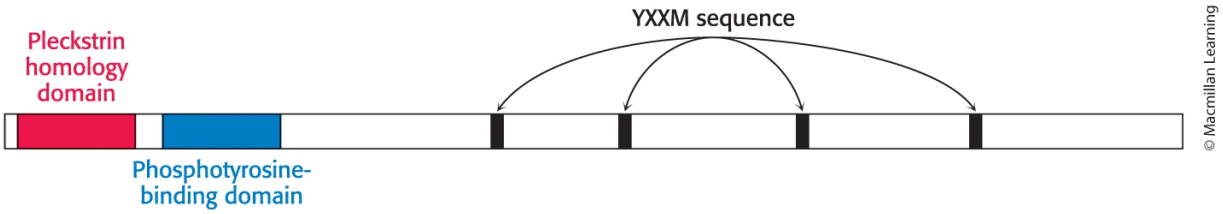
A forward arrow leads to the activated insulin receptor kinase. A curved arrow above the forward arrow shows the simultaneous

conversion of 3 A T P to 3 A D P.

In the activated protein kinase, the orientation of an alpha-helix in the top portion is changed from diagonal to horizontal. The conformation of the red loop is changed as it is displaced slightly away from the bottom portion.

Return to Activation of insulin receptor

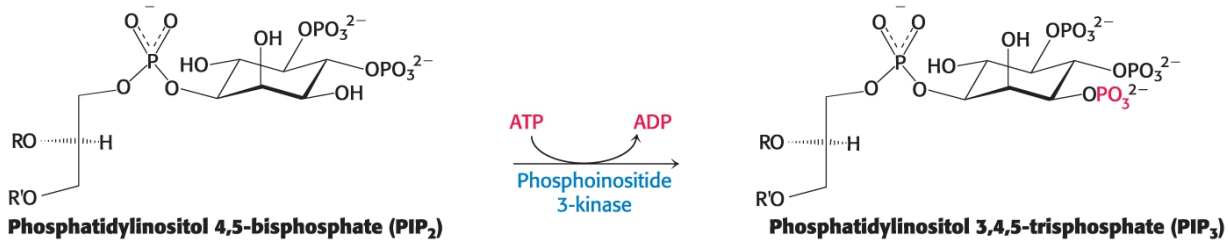
Extended description for Schematic representation of the common amino acid sequence in I R S-1 and I R S-2



A long and narrow rectangle is shown. The pleckstrin homology domain is shown in red color near the left end. The phosphotyrosine binding domain is shown in blue color adjacent to the pleckstrin homology domain. Four black stripes separated by some gap are shown toward the right of the phosphotyrosine binding domain. These stripes are labeled Y X X M sequence.

Return to Schematic representation of the common amino acid sequence in I R S-1 and I R S-2

Extended description for Formation of phosphatidyl 3,4,5-trisphosphate



The chemical reaction consists of one reactant and one product.

The reactant is phosphatidylinositol 4, 5-bisphosphate (P I P 2) whose structure is as follows: A vertical chain consists of 3 C atoms. C 1 is single bonded to O on the right. This O atom is single-bonded to P on the upper right. P is further single bonded to O on the lower right and partially double bonded to O on the upper left and upper right. The partially double-bonded O atoms have an overall negative charge. The O atom on the lower right is single bonded to C 4 of a 6-membered homocyclic hexagonal ring in a chair conformation. The ring is in a plane perpendicular to the plane of paper such that C 1 and C 5 are located away from the observer and C 2 and C 4 are located toward the observer. C 3 and C 6 are located close to each other. C 1 is single bonded to O P O 3 superscript 2 minus on the lower right. C 2 is single bonded to O H on the upper right. C 3 is single bonded to O H above. C 5 is single bonded to O H on the lower left. C 6 is single bonded to O P O 3 superscript 2 minus on the upper right.

C 2 of the vertical chain is dash bonded to O R on the left and H on the right. C 3 of the vertical chain is single bonded to O R prime on the lower left.

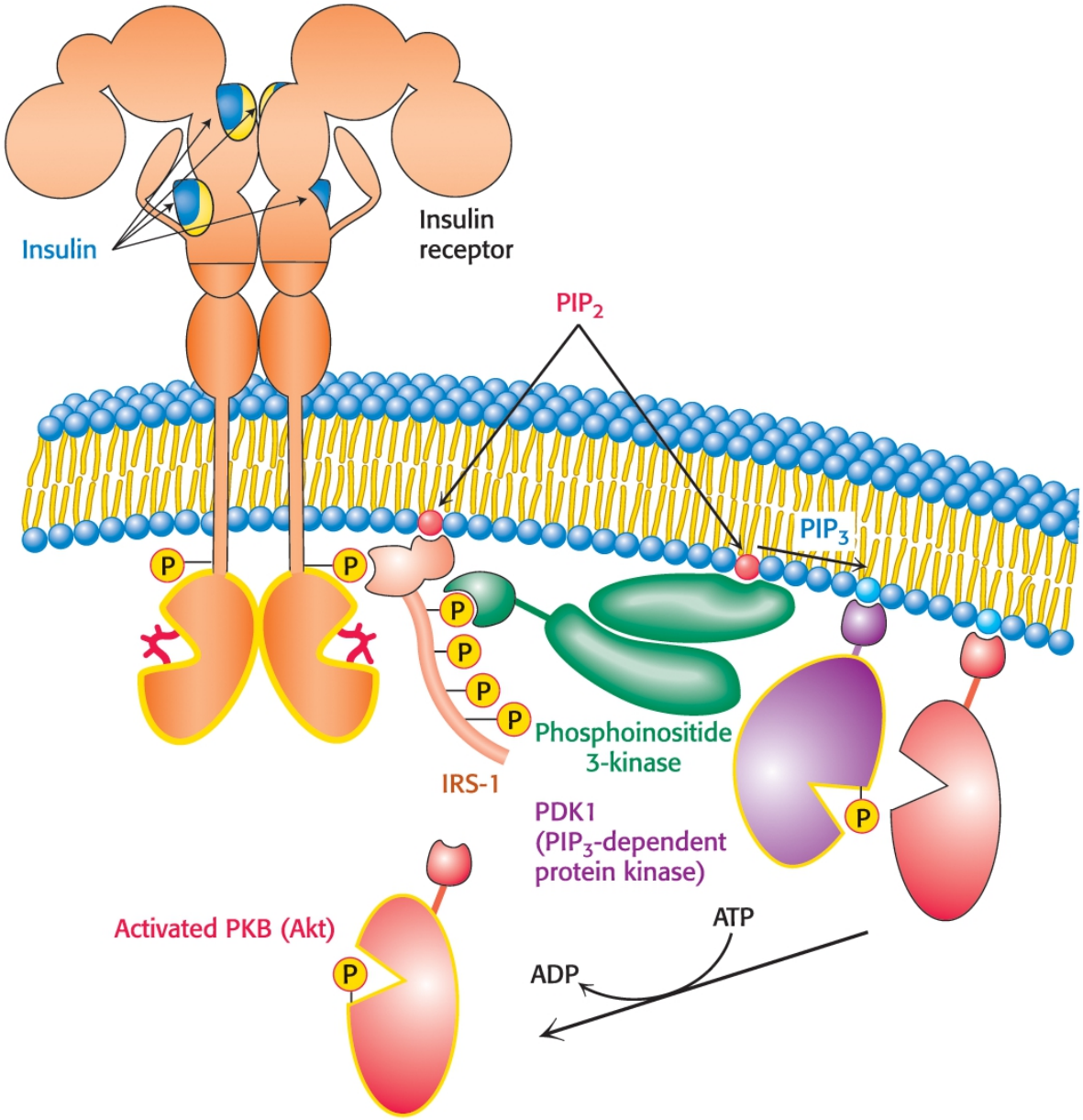
A forward arrow labeled phosphoinositide 3-kinase shows the product. A curved arrow above the forward arrow shows the simultaneous conversion of A T P to A D P.

The product is phosphatidylinositol 3,4,5-triphosphate (P I P 3) whose structure is as follows: A vertical chain consists of 3 C atoms. C 1 is single bonded to O on the right. This O atom is single-bonded to P on the upper right. P is further single bonded to O on the lower right and partially double bonded to O on the upper left and upper right. The partially double-bonded O atoms have an overall negative charge. The O atom on the lower right is single bonded to C 4 of a 6-membered homocyclic hexagonal ring in a chair conformation. The ring is in a plane perpendicular to the plane of paper such that C 1 and C 5 are located away from the observer and C 2 and C 4 are located toward the observer. C 3 and C 6 are located close to each other. C 1 is single bonded to O P O 3 superscript 2 minus on the lower right. C 2 is single bonded to O P O 3 superscript 2 minus on the upper right. C 3 is single bonded to O H above. C 5 is single bonded to O H on the lower left. C 6 is single bonded to O P O 3 superscript 2 minus on the upper right.

C 2 of the vertical chain is dash bonded to O R on the left and H on the right. C 3 of the vertical chain is single bonded to O R prime on the lower left.

Return to Formation of phosphatidyl 3,4,5-trisphosphate

Extended description for Insulin signaling pathway



© Macmillan Learning

An activated insulin receptor bound to 3 insulin molecules is shown spanning through a lipid bilayer. The cytoplasmic portion of the thin transmembrane domain of the dark orange chain is single-bonded to the P atom, just above the large oval-shaped domains in the cytoplasm.

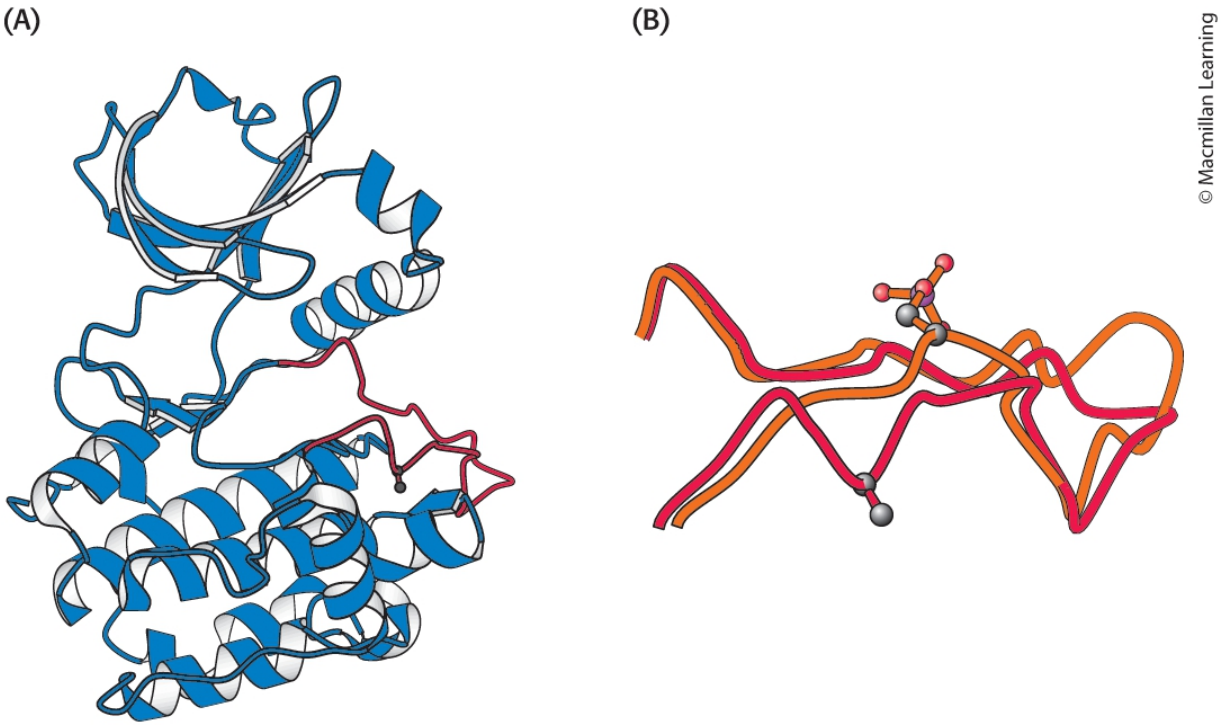
A small irregular-shaped protein with a long tail single bonded to 4 different P atoms is labeled I R S-1. It is shown in close proximity to the cytoplasmic region of the activated insulin receptor. The P atom single bonded to one of the dark orange chains fits inside the groove of I R S -1. Another groove on the top of I R S-1 surrounds a red sphere, labeled P I P 2, in the inner leaflet of the bilayer.

The phosphoinositide 3-kinase consists of a dimer. One subunit of this dimer has a globular domain with a groove surrounding the topmost P atom single bonded to the tail of I R S-1, and a long elongated domain connected to the globular domain by a thin thread. Another subunit is elongated and located above the first subunit. It has a tiny groove that surrounded P I P 2 in the inner leaflet of the bilayer.

P I P 2 is converted into P I P 3 depicted as a light blue sphere in the inner leaflet. A tiny globular domain of P D K 1 (P I P 3-dependent protein kinase) is bound to P I P 3. This domain is connected to a large oval-shaped domain of P D K 1. A triangular groove in P D K 1 is single-bonded to the P atom. An inactivated P K B (A k t) is located in close proximity to P D K 1. A tiny globular domain of P K B is bound to P I P 3 and its large oval-shaped domain has an empty triangular groove facing P D K 1. An arrow from inactivated P K B points toward activated P K B (A k t). A curved arrow above this arrow shows the simultaneous conversion of A T P to A D P. The triangular groove of the activated P K B is single bonded to P and detaches from P I P 3 in the inner leaflet.

Return to Insulin signaling pathway

Extended description for Ribbon diagram of the inactive conformation of P D K 1 and comparison of the activation loops of inactive and active forms



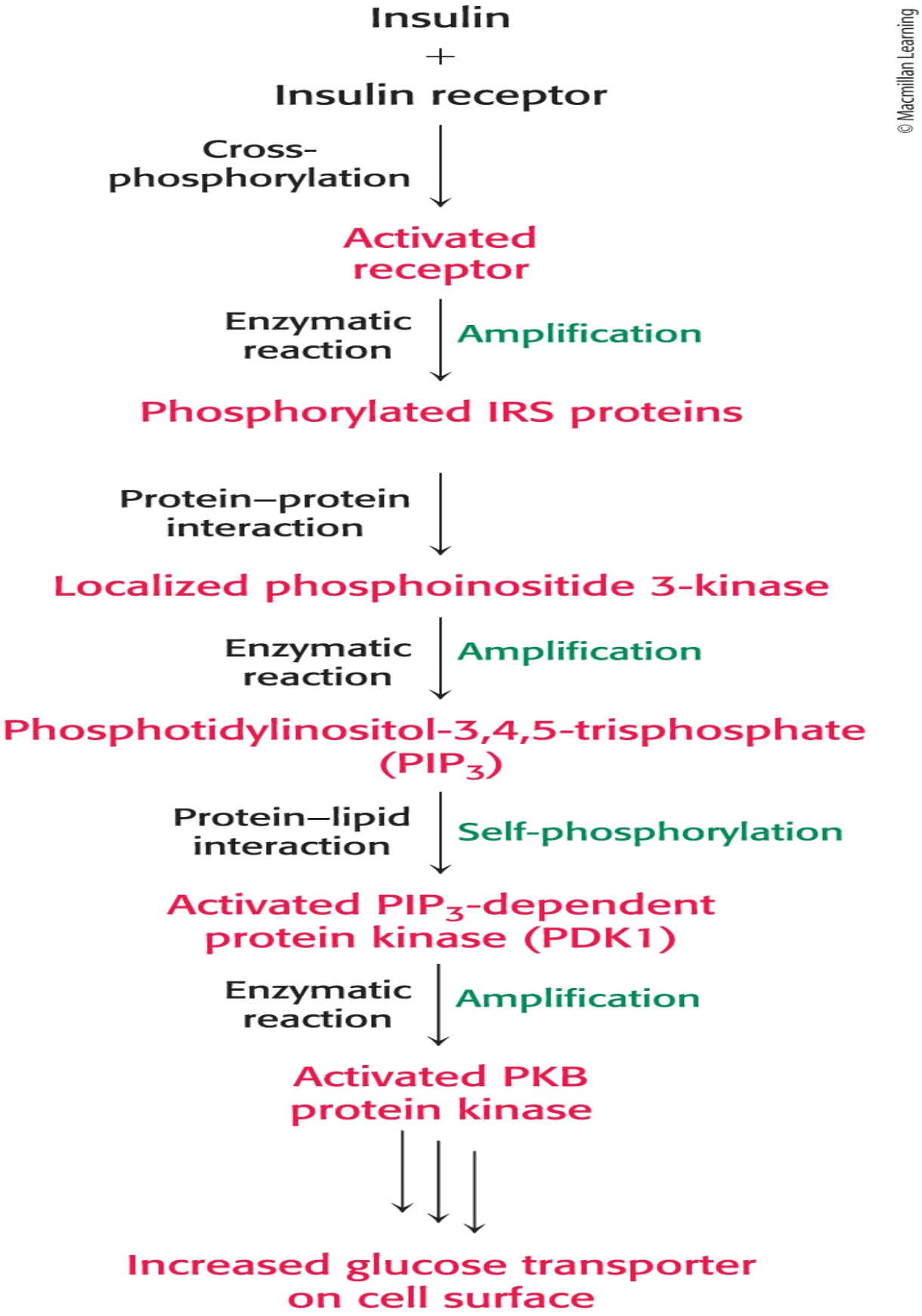
Part (A): The ribbon diagram of P D K 1 consists of top and bottom portions. The top portion consists of a few beta strands forming a concave groove and free short alpha-helices. The bottom portion consists of several alpha-helices and a few beta strands. The top and bottom portions are interconnected by long threads. A wavy red highlighted folded loop is shown near the top portion. It is located toward the top right of the bottom portion.

Part (B): Two superimposed activation loops of the active and inactive forms of P D K 1 are shown. The activation loop of the inactive form is shown in red and that of the active form is shown in orange. The right ends of the loops are entangled together. The

orange loop shows a small upward raised region near the middle of the bottom arm. The red loop shows a downward depression having a triangular shape in the bottom arm, toward the left of the raised region.

Return to Ribbon diagram of the inactive conformation of P D K 1 and comparison of the activation loops of inactive and active forms

Extended description for Insulin signaling pathway

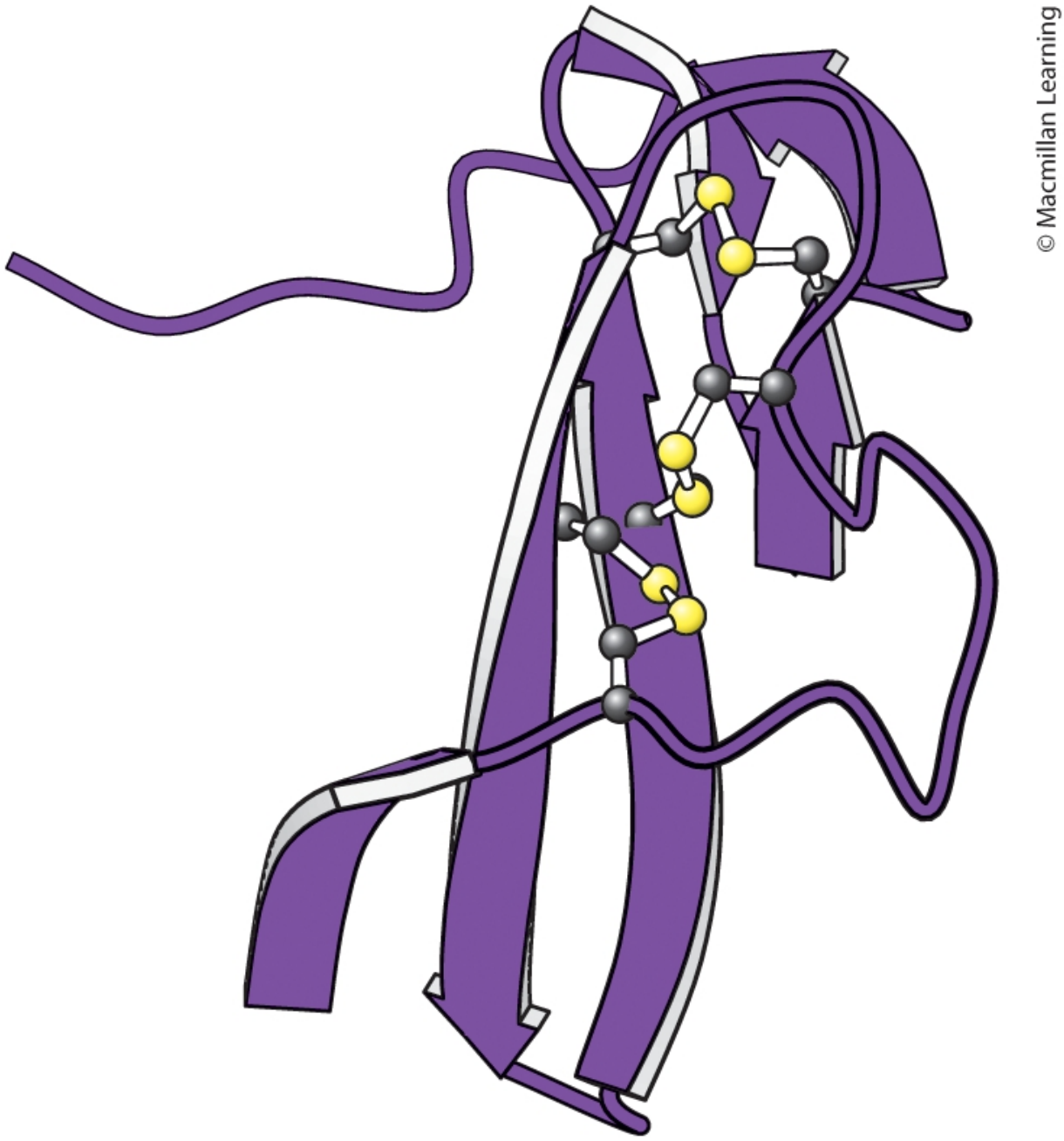


© Macmillan Learning

The flowchart is depicted as follows: Insulin plus insulin receptor, downward arrow labeled “cross-phosphorylation,” activated receptor, downward arrow labeled “amplification” and “enzymatic reaction,” phosphorylated I R S proteins, downward arrow labeled “protein-protein interaction,” localized phosphoinositide 3-kinase, downward arrow labeled “amplification” and “enzymatic reaction,” phosphatidylinositol-3,4,5-trisphosphate (P I P 3), downward arrow labeled “self-phosphorylation” and “protein-lipid interaction,” activated P I P 3-dependent protein kinase (P D K 1), downward arrow labeled “amplification” and “enzymatic reaction,” activated P K B protein kinase, three downward arrows, increased glucose transporter on cell surface.

Return to Insulin signaling pathway

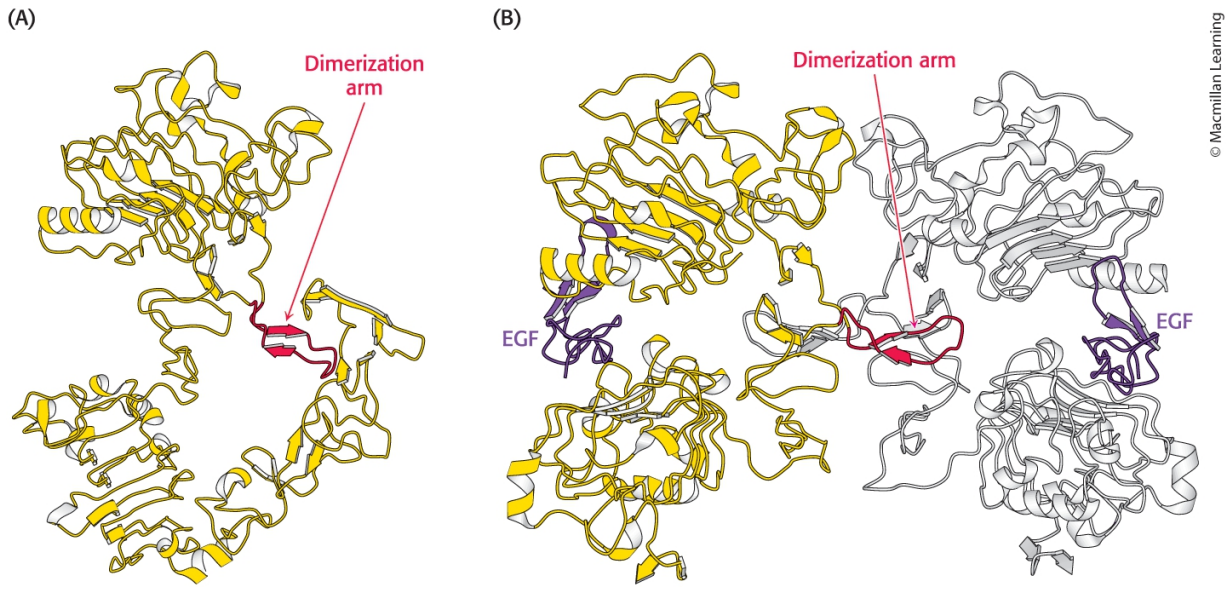
Extended description for Ribbon diagram of epidermal growth factor



The ribbon diagram consists of a few long and short beta-strands interconnected by long thread-like loops. Two long antiparallel beta strands are shown in the center. A short upward pointing beta-strand is located on the lower left of the central strands. A cluster of three short beta-strands is located at the top right of the central strands. The three disulfide bonds are depicted through three ball-and-stick models composed of a chain of two black spheres connected to a yellow sphere. The yellow sphere is connected to another yellow sphere which is further connected to a chain of two black spheres.

Return to Ribbon diagram of epidermal growth factor

Extended description for Extracellular domain of the E G F receptor and its dimerization upon E G F binding

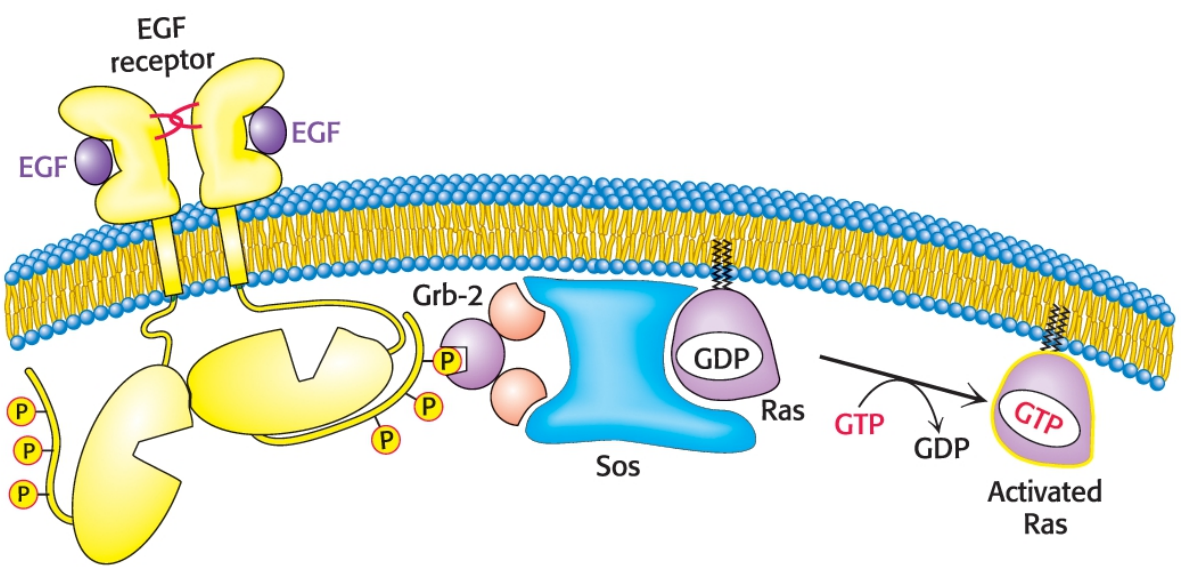


Part (A): The ribbon diagram of the extracellular domain consists of a top portion and a bottom portion. The top portion contains beta-strands and a few alpha-helices interconnected by long thread-like loops. The bottom portion has a roughly circular shape with a large hollow gap in the center. It is lined by several beta-strands and a few alpha-helices interconnected by long threads. A dimerization arm composed of two short antiparallel beta-strands is located inside the top opening of the bottom portion.

Part (B): Two extracellular domains have dimerized. The dimerization arm has extended outward into the center of the junction between the extracellular domains. An E G F molecule is bound to the outer periphery of the junction between the top and bottom portions of each domain. The E G F molecule consists of two antiparallel beta-strands surrounded by long thread-like loops.

Return to Extracellular domain of the E G F receptor and its dimerization upon E G F binding

Extended description for E G F receptor signaling



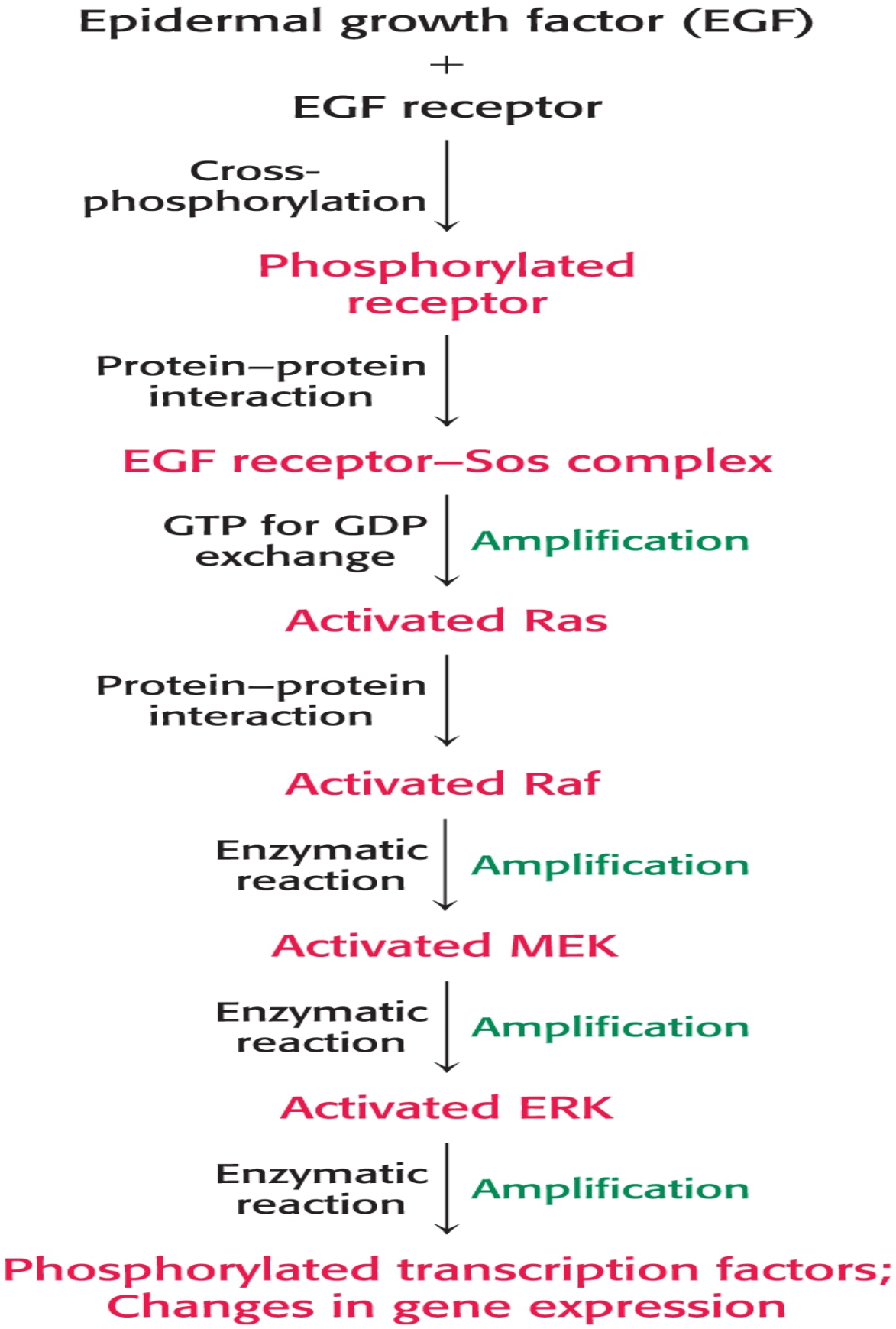
© Macmillan Learning

A horizontal section of a lipid bilayer is shown. An E G F receptor dimer is shown as a transmembrane protein. Each subunit of the dimer consists of an extracellular domain located above the bilayer and bound to a purple oval structure labeled E G F. The extracellular domains are linked by red curved lines. It is followed by a thin transmembrane domain connected below to a long thread which is further connected to a large oval-shaped domain located below the bilayer. Each domain has a wide groove and a tail single bonded to three P atoms.

One of the P atoms bonded to the tail is bound to the groove of a subunit of the trimeric G r b-2 protein. The remaining two subunits of G r b-2 have a groove that is bound to S o s. A large groove on the right side of S o s protein accommodates Ras protein bound to G D P and attached to the inner leaflet of the bilayer through two zigzag lines at the top. A forward arrow shows an activated Ras bound to G T P as G T P enters and G D P leaves.

Return to E G F receptor signaling

Extended description for E G F signaling pathway



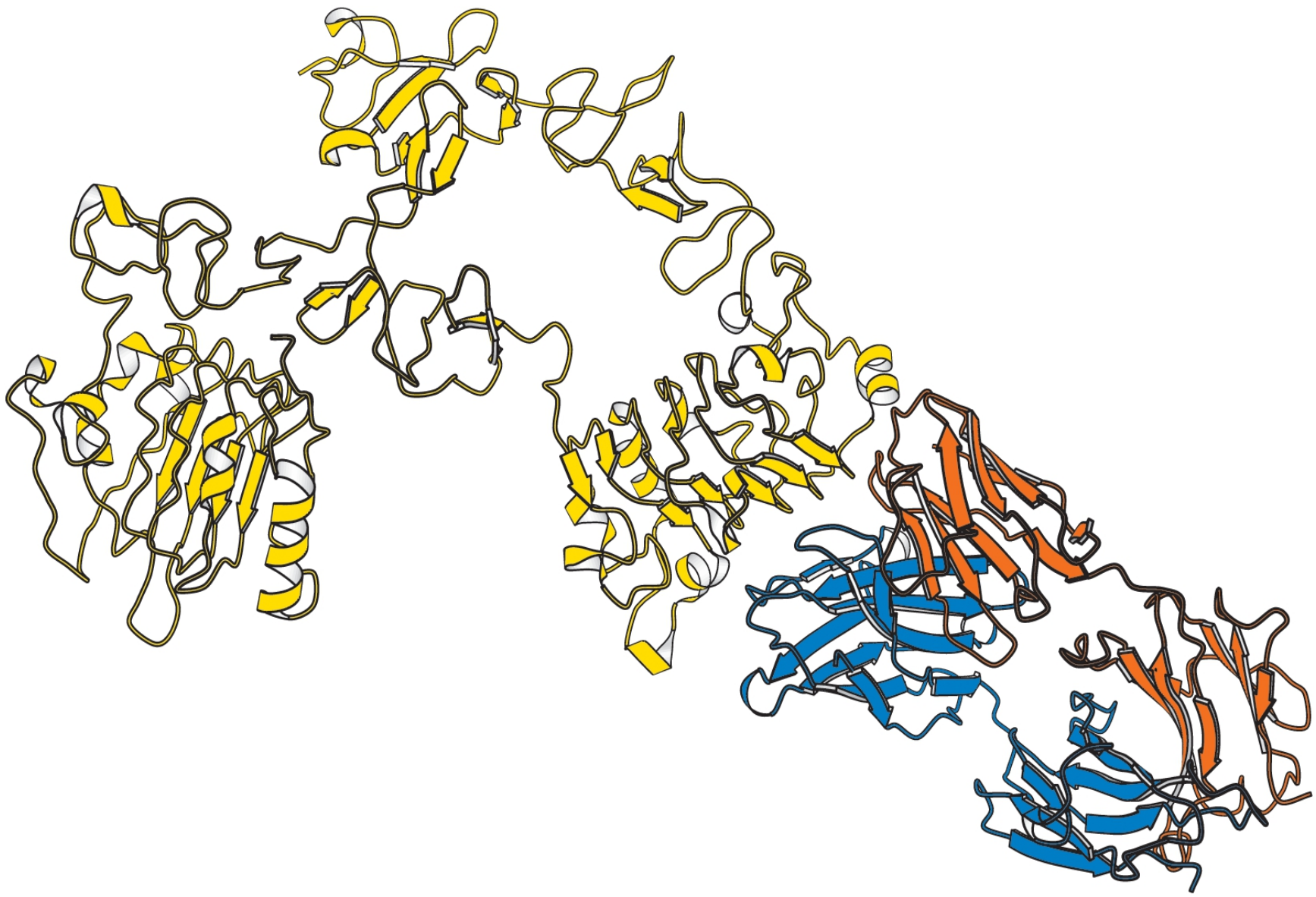
© Macmillan Learning

The flow chart is depicted as follows: Epidermal growth factor (E G F) plus E G F receptor, downward arrow labeled “cross-phosphorylation,” phosphorylated receptor, downward arrow labeled “protein-protein interaction,” E G F receptor-S o s complex, downward arrow labeled “amplification” and “G T P for G D P exchange,” activated Ras, downward arrow labeled “protein-protein interaction,” activated Raf, downward arrow labeled “amplification” and “enzymatic reaction,” activated M E K, downward arrow labeled “amplification” and “enzymatic reaction,” activated E R K, downward arrow labeled “amplification” and “enzymatic reaction,” phosphorylated transcription factors; changes in gene expression.

Return to E G F signaling pathway

Extended description for E G F receptor bound to

cetuximab

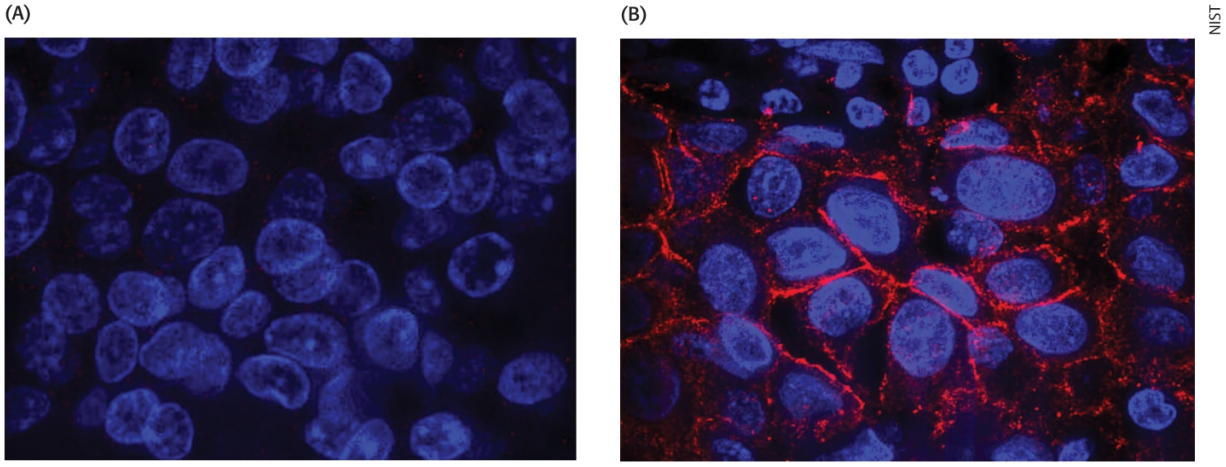


© Macmillan Learning

The ribbon diagram of the E G F receptor consists of a top portion and a bottom portion. The top portion contains several beta-strands and the bottom portion contains several beta-strands and a few helices. They are connected by long thread-like loops. The top and bottom portions are widely spaced. Long ribbons interconnecting these portions have a few beta-strands in the middle. Cetuximab is a paired cluster in which each cluster is composed of several randomly oriented beta-strands. There is a small gap between the clusters and one cluster of the pair interacts with the top portion of the E G F receptor.

Return to E G F receptor bound to cetuximab

Extended description for Photomicrographs show the panel of breast cancer cells expressing normal and high levels of H E R 2

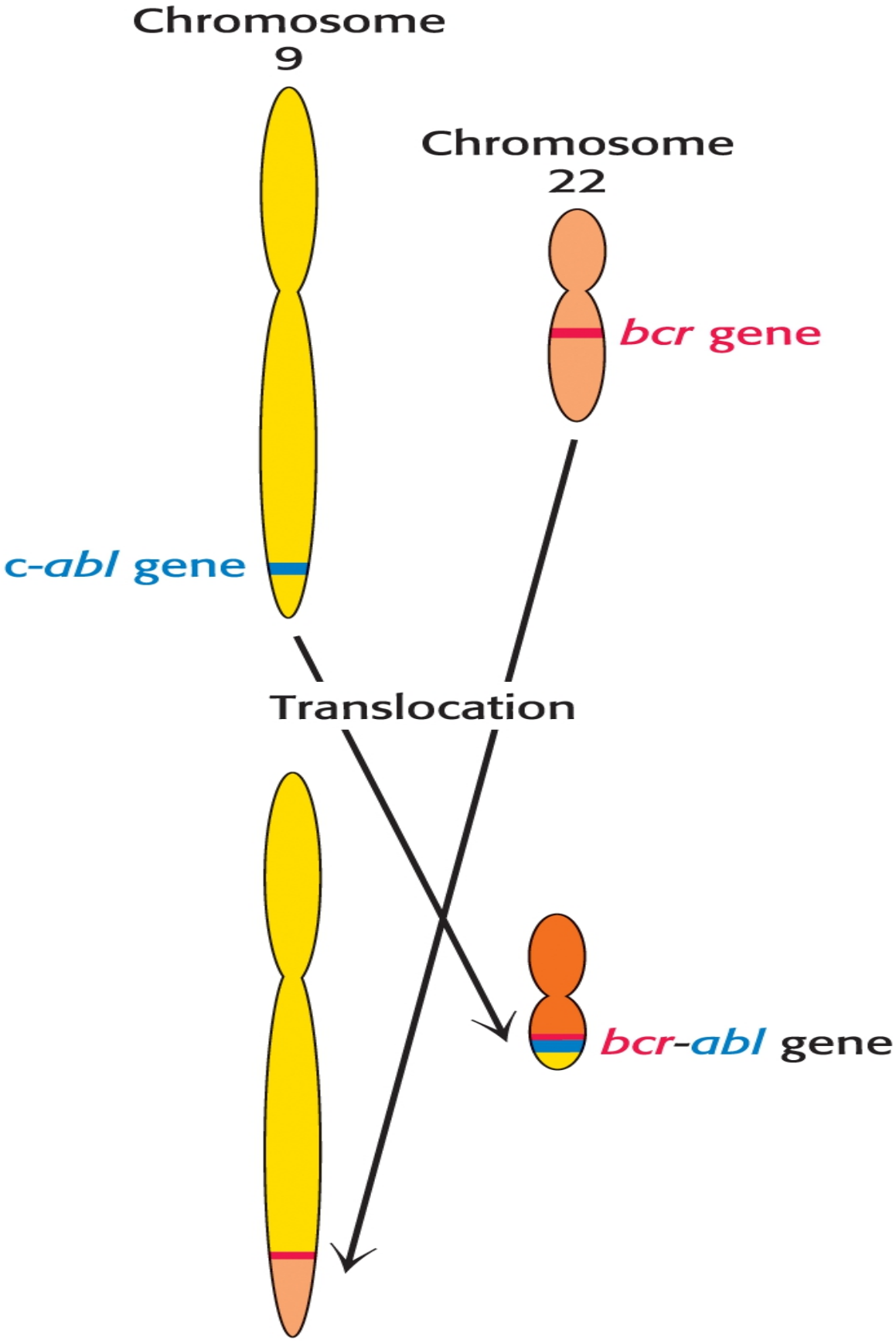


Photomicrograph (A): It shows several blue oval-shaped structures against a dark background.

Photomicrograph (B): It shows several blue oval-shaped structures surrounded by thin and granular red outlines against a dark background.

Return to Photomicrographs show the panel of breast cancer cells expressing normal and high levels of H E R 2

Extended description for Formation of b c r- a b l gene



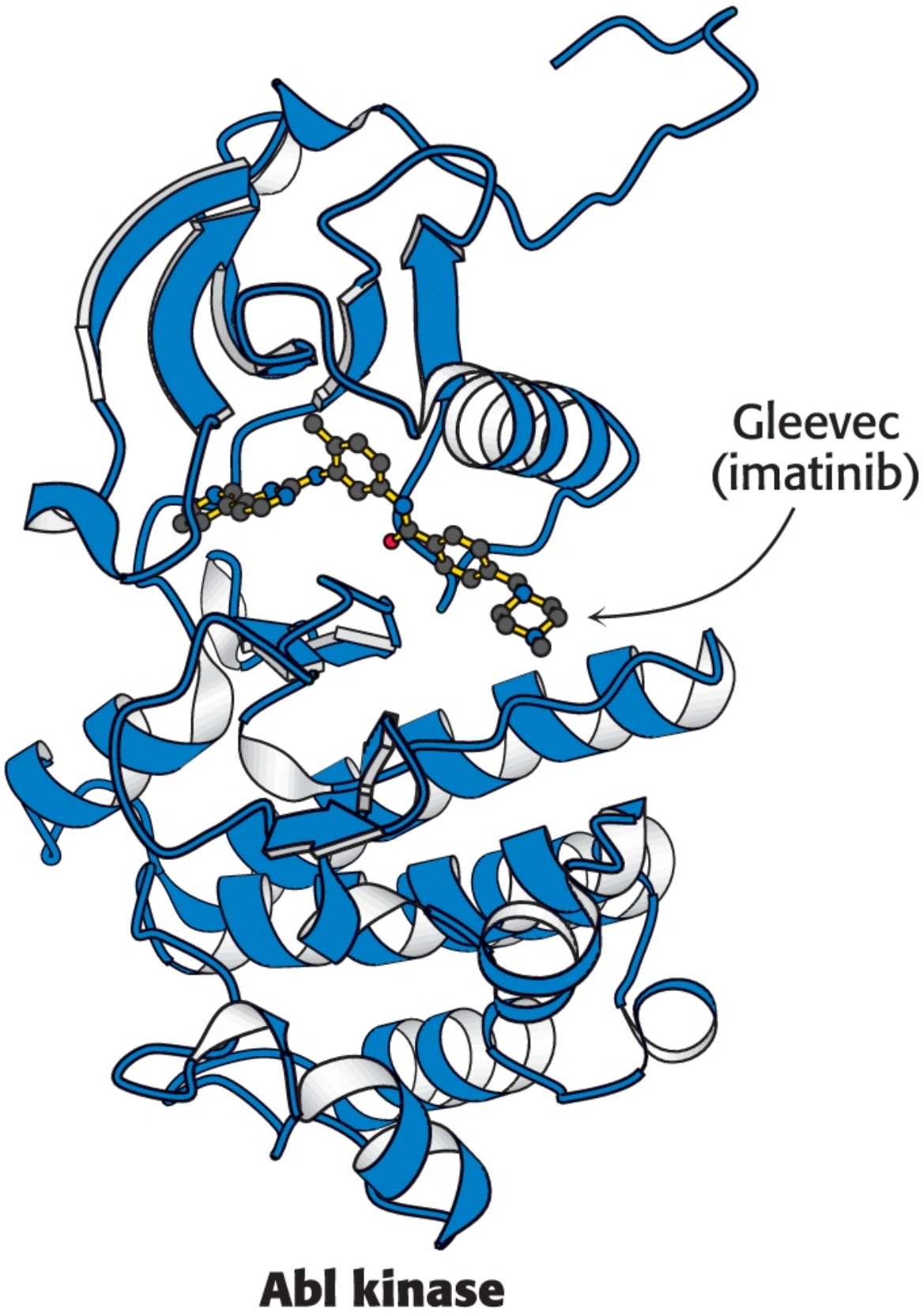
© Macmillan Learning

The long chromosome 9 contains the c-a b l gene in the long arm. The short chromosome 22 contains the b c r gene in the long arm. An arrow shows the movement of the bottom portion of the long arm of chromosome 22 containing the b c r gene toward the long arm of chromosome 22. This produces chromosome 9 having a long arm containing the bottom portion of chromosome 22 and b c r gene. Another arrow shows the movement of the bottom portion of the long arm of chromosome 9 containing the c-a b l gene toward the long arm of chromosome 22. This produces chromosome 22 having a long arm containing the bottom portion of chromosome 9 and the fused b c r-a b l gene.

Return to Formation of b c r- a b l gene

Extended description for Ribbon structure of A b l

kinase bound to imatinib



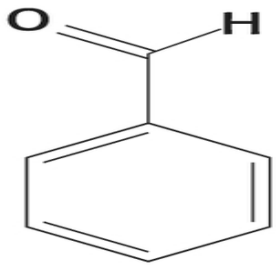
© Macmillan Learning

The ribbon structure of A b I kinase is composed of several alpha-helices at the bottom and beta-strands at the top interconnected through thin blue-colored threads. Small blue-colored spheres arranged in a hexagonal ring shape along with the long substituent chain are present in the groove between the top and bottom portions. They occupy the groove and block the A T P binding sites. The chain occupying the open groove is marked with an arrow and labeled Gleevac (imatinib).

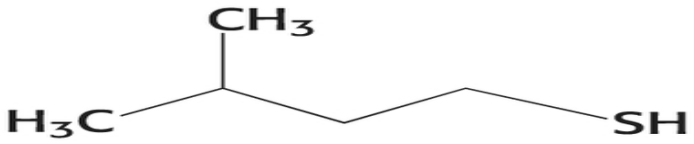
Return to Ribbon structure of A b l kinase bound to imatinib

Extended description for Structures of benzaldehyde, 3-methylbutane-1-thiol, geraniol, zingiberene, R-

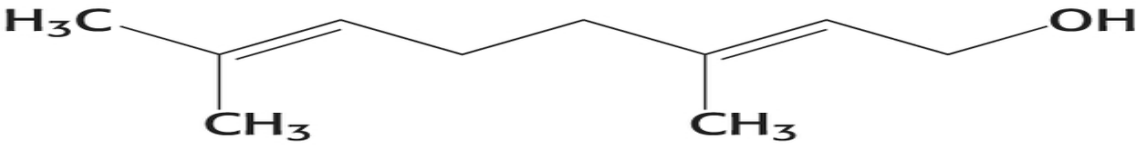
Carvone, and S-Carvone



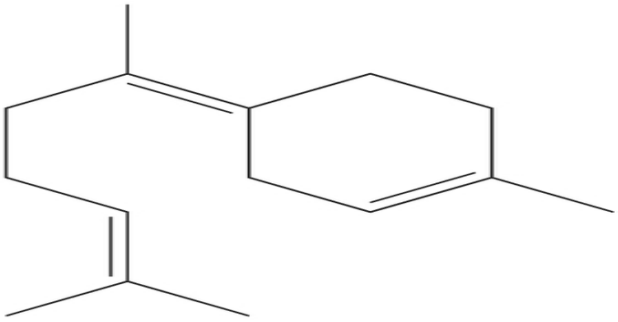
Benzaldehyde
(Almond)



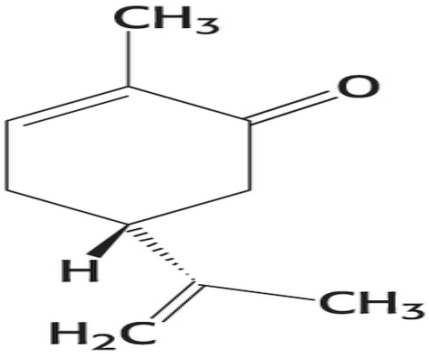
3-Methylbutane-1-thiol
(Skunk)



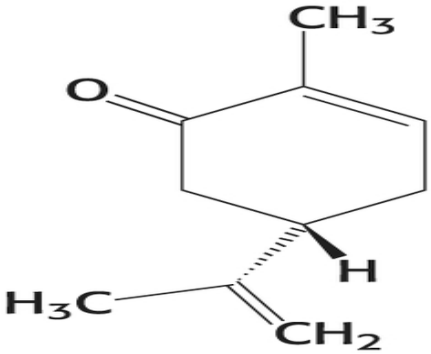
Geraniol
(Rose)



Zingiberene
(Ginger)



***R*-Carvone**
(Spearmint)



***S*-Carvone**
(Caraway)

The structure of benzaldehyde (Almond) is as follows: A benzene ring is in a vertical orientation with C 1 occupying the topmost vertex. Alternating double bonds are present between C 2 and C 3, C 4 and C 5, and C 6 and C 1. C 1 is single bonded to a central C atom above in the form of a line. The central C atom is double bonded to O on the upper left and single bonded to H on the upper right.

The structure of 3-Methylbutane-1-thiol (Skunk) is as follows: A 3-carbon alkane chain is depicted as a line structure using 2 zigzag lines. C 1 is single bonded to C H 3 above and C H 3 on the lower left. C 3 is single bonded to S H on the lower right.

The structure geraniol (Rose) is as follows: A 7-carbon alkene chain is depicted as a line structure using 6 zigzag lines. A double bond is present between C 1 and C 2 and C 5 and C 6. C 1 and C 5 are each single bonded to C H 3 below. C 1 is single bonded to H 3 C on the upper left. C 7 is single bonded to O H on the upper right.

The structure of zingiberene (Ginger) is as follows: A 6-carbon homocyclic hexagonal ring is in a vertical orientation with C 1 occupying the topmost vertex. A double bond is present between C 3 and C 4. C 3 is single bonded to C H 3 on the lower right in the form of a line. C 6 is double bonded to C 1 of a 4-carbon alkane side chain depicted as a line structure using 3 lines that resemble the left half of a vertical hexagon. C 1 of the side chain is single bonded to C H 3 above in the form of a line. C 4 is double bonded to C 2 of a second 3-carbon alkane side chain below, depicted as a line structure using 2 zigzag lines.

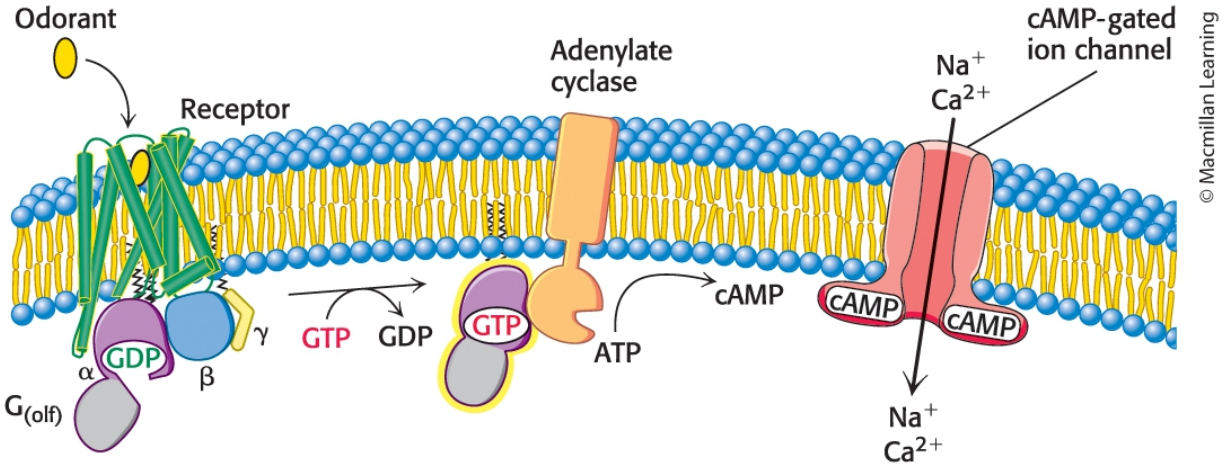
The structure of R-Carvone (spearmint) is as follows: A 6-carbon homocyclic hexagonal ring is in a vertical orientation with C 1 occupying the topmost vertex. A double bond is present between C 6 and C 1. C 1 is single bonded to C H 3 above. C 2 is double bonded to O on the upper right. C 4 is wedge bonded to H on the lower left and

dash bonded to a C atom in the form of a line on the lower right. The C atom is double bonded to C H 2 on the lower left and single bonded to C H 3 on the lower right.

The structure of S-Carvone (Caraway) is as follows: A 6-carbon hexagonal ring is in a vertical orientation with C 1 occupying the topmost vertex. A double bond is present between C 1 and C 2. C 1 is single bonded to C H 3 above. C 6 is double bonded to O on the upper left. C 4 is wedge bonded to H on the lower right and dash bonded to a C atom in the form of a line on the lower left. The C atom is double bonded to C H 2 on the lower right and single bonded to C H 3 on the lower left.

Return to Structures of benzaldehyde, 3-methylbutane-1-thiol, geraniol, zingiberene, R-Carvone, and S-Carvone

Extended description for Olfactory signal-transduction cascade

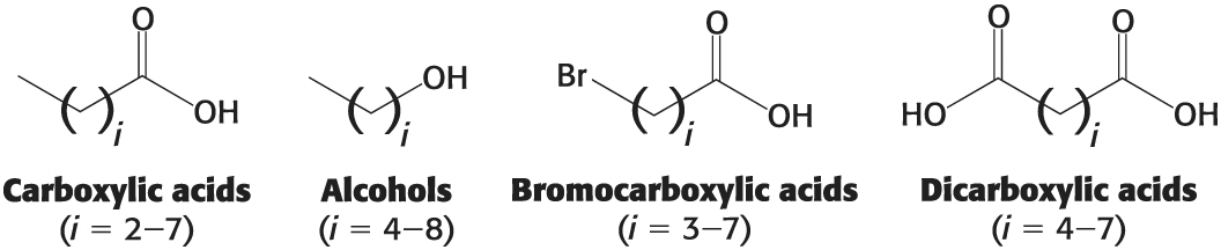


A section of a lipid bilayer is shown. The receptor bound to a yellow oval-shaped odorant at the top is shown embedded in the bilayer. The cytoplasmic side of the receptor is bound to the trimeric G subscript o l f protein composed of alpha, beta, and gamma subunits. In the alpha subunit, the grey structure associated with the purple round structure is displaced toward the lower left to allow the exit of G D P and entry of G T P into the groove of the purple round structure. The adenylate cyclase protein is shown embedded in the same bilayer. It is composed of a rectangular membrane-spanning region and a cytoplasmic round region having a tiny groove. The alpha subunit bound to G T P is associated with the cytoplasmic round region of adenylate cyclase. The purple structure directly interacts with the cytoplasmic region of adenylate cyclase. The purple structure has a groove bound to G T P. This groove is closed by the grey sphere located below. A curved arrow across the groove of adenylate cyclase shows the conversion of A T P to c A M P. Two zigzag lines at the top of the purple structure is embedded in the lipid bilayer. c A M P - gated ion channel is embedded in the lipid bilayer. It has a long transmembrane channel and two rectangular

grooves on the cytoplasmic side. Both grooves are bound to c A M P. A long downward vertical arrow passes through the transmembrane channel to show the inward movement of N a superscript plus and C a superscript 2 plus ions.

Return to Olfactory signal-transduction cascade

Extended description for The structures of four sets of closely related compounds



Carboxylic acids (i = 2–7)

Alcohols (i = 4–8)

Bromocarboxylic acids (i = 3–7)

Dicarboxylic acids (i = 4–7)

Carboxylic acids (i equals 2 to 7): A 3-carbon alkane chain is depicted as a line structure using 2 zigzag lines. C 3 is double bonded to O above and single bonded to O H on the lower right. C 2 is enclosed in brackets with subscript i.

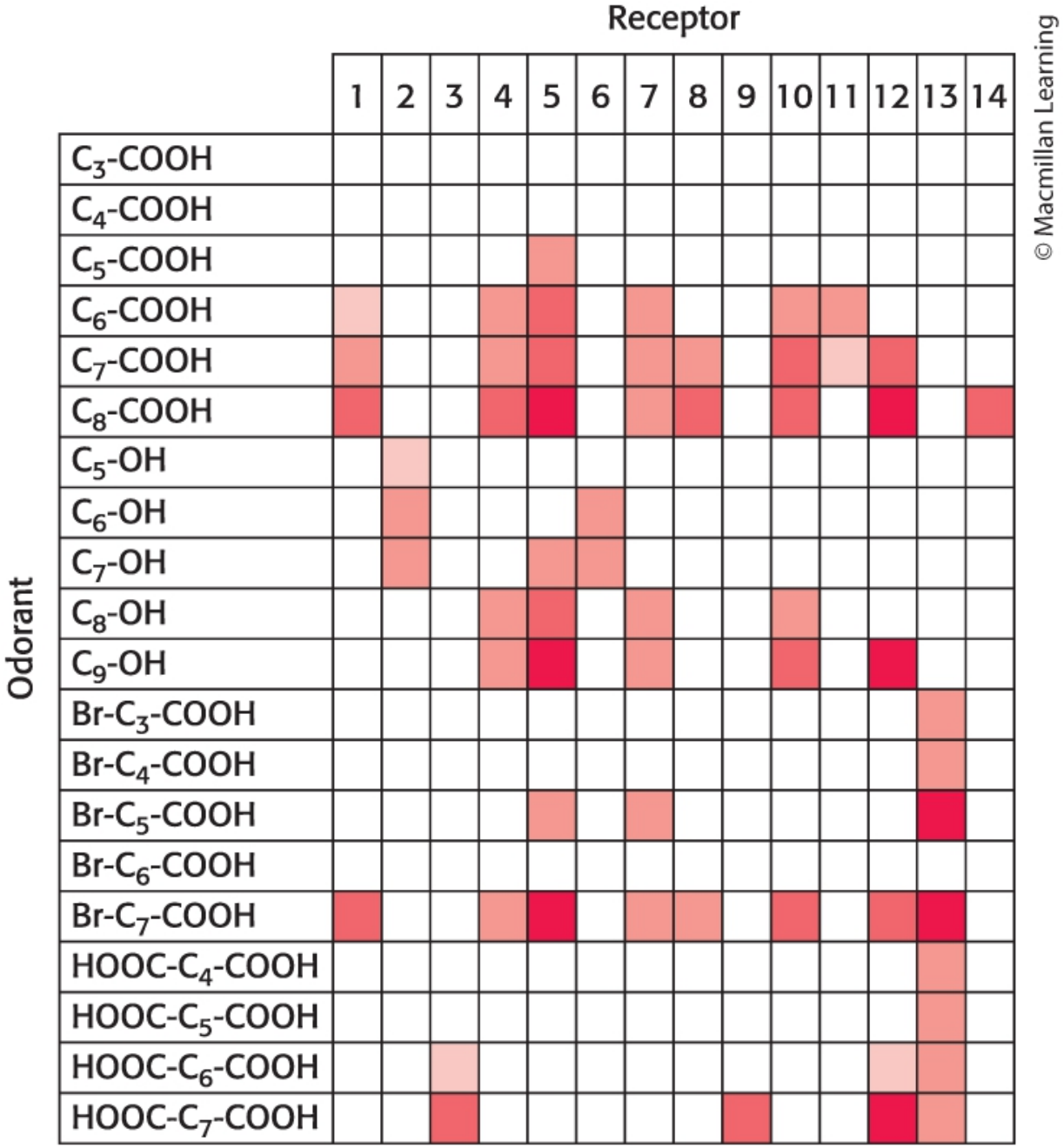
Alcohols (i equals 4 to 8): A 2-carbon alkane chain is depicted as a line structure using 1 line. C 2 is enclosed in brackets with subscript i and single bonded to O H on the upper right.

Bromocarboxylic acids (i equals 3 to 7): A 2-carbon alkane chain is depicted as a line structure using 1 line. C 1 is enclosed in brackets with subscript i and single bonded to B r on the upper left. C 2 is double bonded to O above and single bonded to O H on the lower right.

Dicarboxylic acids (i equals 4 to 7): A 3-carbon alkane chain is depicted as a line structure using 2 zigzag lines. C 1 and C 3 are each double bonded to O above. C 2 is enclosed in brackets with subscript i. C 1 is single bonded to O H on the lower left and C 3 is single bonded to O H on the lower right.

Return to The structures of four sets of closely related compounds

Extended description for Distinct patterns of olfactory-receptor activation



© Macmillan Learning

The table consists of 14 columns and 20 rows. The columns represent receptors and the rows represent odorants. The column headings are as follows: First column: 1, Second column: 2, Third column: 3, Fourth column: 4, Fifth column: 5, Sixth column: 6, Seventh column: 7, Eighth column: 8, Ninth column: 9, Tenth column: 10, Eleventh column: 14, Twelfth column: 12, Thirteenth column: 13, and Fourteenth column: 14

The row entries are as follows:

Row 1: C 3, single bond, C O O H; 1: blank; 2: blank; 3: blank; 4: blank; 5: blank; 6: blank; 7: blank; 8: blank; 9: blank; 10: blank; 11: blank; 12: blank; 13: blank; 14: blank.

Row 2: C 4, single bond, C O O H; 1: blank; 2: blank; 3: blank; 4: blank; 5: blank; 6: blank; 7: blank; 8: blank; 9: blank; 10: blank; 11: blank; 12: blank; 13: blank; 14: blank.

Row 3: C 5, single bond, C O O H; 1: blank; 2: blank; 3: blank; 4: blank; 5: light red; 6: blank; 7: blank; 8: blank; 9: blank; 10: blank; 11: blank; 12: blank; 13: blank; 14: blank.

Row 4: C 6, single bond, C O O H; 1: very light red; 2: blank; 3: blank; 4: light red; 5: medium red; 6: blank; 7: blank; 8: blank; 9: blank; 10: blank; 11: blank; 12: blank; 13: blank; 14: blank.

Row 5: C 7, single bond, C O O H; 1: light red; 2: blank; 3: blank; 4: light red; 5: medium red; 6: blank; 7: light red; 8: light red; 9: blank; 10: medium red; 11: very light red; 12: medium red; 13: blank; 14: blank.

Row 6: C 8, single bond, C O O H; 1: medium red; 2: blank; 3: blank; 4: medium red; 5: dark red; 6: blank; 7: light red; 8: medium red; 9:

blank; 10: medium red; 11: blank; 12: dark red; 13: blank; 14: medium red.

Row 7: C 5, single bond, O H; 1: blank; 2: very light red; 3: blank; 4: blank; 5: blank; 6: blank; 7: blank; 8: blank; 9: blank; 10: blank; 11: blank; 12: blank; 13: blank; 14: blank.

Row 8: C 6, single bond, O H; 1: blank; 2: light red; 3: blank; 4: blank; 5: blank; 6: light red; 7: blank; 8: blank; 9: blank; 10: blank; 11: blank; 12: blank; 13: blank; 14: blank.

Row 9: C 7, single bond, O H; 1: blank; 2: light red; 3: blank; 4: blank; 5: light red; 6: light red; 7: blank; 8: blank; 9: blank; 10: blank; 11: blank; 12: blank; 13: blank; 14: blank.

Row 10: C 8, single bond, O H; 1: blank; 2: blank; 3: blank; 4: light red; 5: medium red; 6: blank; 7: light red; 8: blank; 9: blank; 10: light red; 11: blank; 12: blank; 13: blank; 14: blank.

Row 11: C 9, single bond, O H; 1: blank; 2: blank; 3: blank; 4: light red; 5: dark red; 6: blank; 7: light red; 8: blank; 9: blank; 10: medium red; 11: blank; 12: dark red; 13: blank; 14: blank.

Row 12: B r, single bond, C 3, single bond, C O O H; 1: blank; 2: blank; 3: blank; 4: blank; 5: blank; 6: blank; 7: blank; 8: blank; 9: blank; 10: blank; 11: blank; 12: blank; 13: light red; 14: blank.

Row 13: B r, single bond, C 4, single bond, C O O H; 1: blank; 2: blank; 3: blank; 4: blank; 5: blank; 6: blank; 7: blank; 8: blank; 9: blank; 10: blank; 11: blank; 12: blank; 13: light red; 14: blank.

Row 14: B r, single bond, C 5, single bond, C O O H; 1: blank; 2: blank; 3: blank; 4: blank; 5: light red; 6: blank; 7: light red; 8: blank;

9: blank; 10: blank; 11: blank; 12: blank; 13: dark red; 14: blank.

Row 15: B r, single bond, C 6, single bond, C O O H; 1: blank; 2: blank; 3: blank; 4: blank; 5: blank; 6: blank; 7: blank; 8: blank; 9: blank; 10: blank; 11: blank; 12: blank; 13: blank; 14: blank.

Row 16: B r, single bond, C 7, single bond, C O O H; 1: medium red; 2: blank; 3: blank; 4: light red; 5: dark red; 6: blank; 7: light red; 8: light red; 9: blank; 10: medium red; 11: blank; 12: medium red; 13: dark red; 14: blank.

Row 17: H O O C, single bond, C 4, single bond, C O O H; 1: blank; 2: blank; 3: blank; 4: blank; 5: blank; 6: blank; 7: blank; 8: blank; 9: blank; 10: blank; 11: blank; 12: blank; 13: light red; 14: blank.

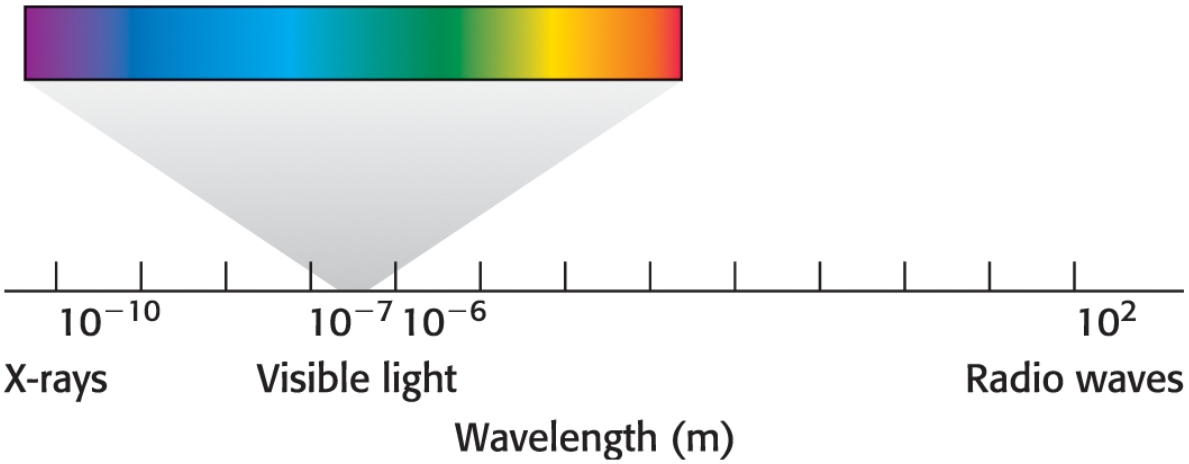
Row 18: H O O C, single bond, C 5, single bond, C O O H; 1: blank; 2: blank; 3: blank; 4: blank; 5: blank; 6: blank; 7: blank; 8: blank; 9: blank; 10: blank; 11: blank; 12: blank; 13: light red; 14: blank.

Row 19: H O O C, single bond, C 6, single bond, C O O H; 1: blank; 2: blank; 3: very light red; 4: blank; 5: blank; 6: blank; 7: blank; 8: blank; 9: blank; 10: blank; 11: blank; 12: very light red; 13: light red; 14: blank.

Row 20: H O O C, single bond, C 7, single bond, C O O H; 1: blank; 2: blank; 3: medium red; 4: blank; 5: blank; 6: blank; 7: blank; 8: blank; 9: medium red; 10: blank; 11: blank; 12: dark red; 13: light red; 14: blank.

Return to Distinct patterns of olfactory-receptor activation

Extended description for Electromagnetic spectrum

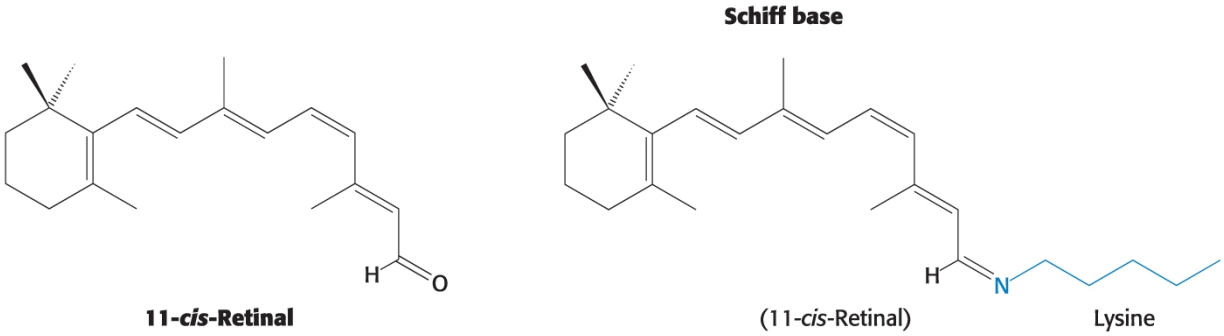


© Macmillan Learning

A horizontal line is labeled wavelength in meters and has 13 short vertical markings. The first marking from the left is labeled 10 superscript negative 10. The fourth, fifth, and thirteenth markings are labeled 10 superscript negative 7, 10 superscript negative 6, and 10 superscript 2 respectively. The left end of the line is labeled X-rays. The right end of the line is labeled radiowaves. The markings 10 superscript negative 7 and 10 superscript negative 6 are labeled visible light. The region between the fourth and fifth marking is enlarged to show a horizontal bar having colors violet, indigo, blue, green, yellow, orange, and red from left to right.

Return to Electromagnetic spectrum

Extended description for Structures of 11-cis-Retinal and 11-cis-Retinal connected to lysine through Schiff base



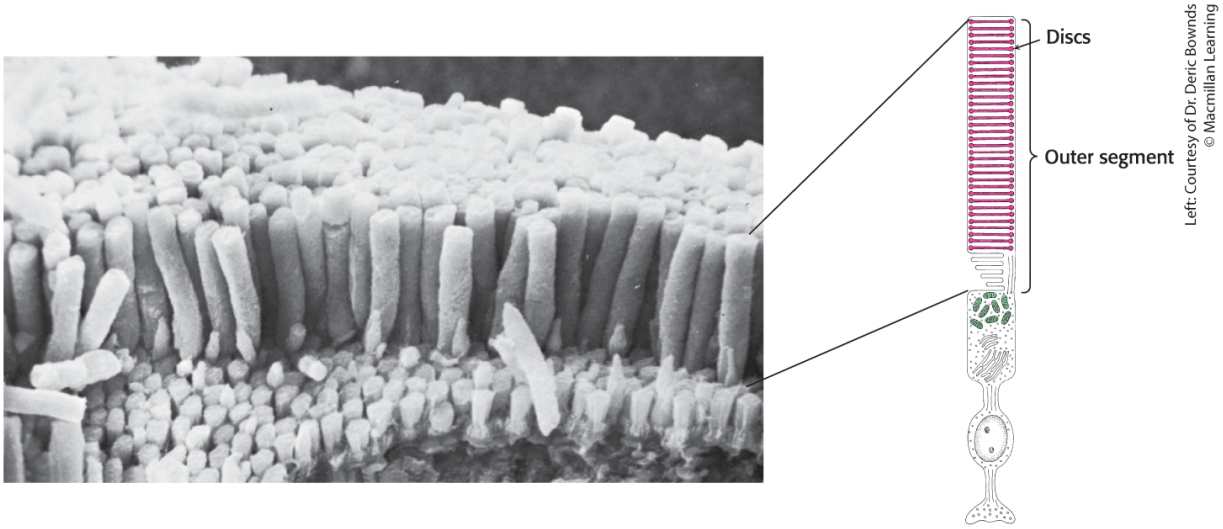
The structure of 11-cis-Retinal is as follows: A 6-carbon homocyclic hexagonal ring is in a vertical orientation with C 1 occupying the topmost vertex. A double bond is present between C 2 and C 3. C 1 is wedge bonded to C H 3 on the upper left in the form of a wedged line and dash bonded to C H 3 on the upper right in the form of a dashed line. C 3 is single bonded to C H 3 on the lower right in the form of a line. C 2 is single bonded to a 6-carbon alkene side chain depicted as a line structure using 5 zigzag lines. A double bond is present between C 1 and C 2, C 3 and C 4, and C 5 and C 6. C 3 of an alkene chain is single bonded to C H 3 above in the form of a line. C 6 of the alkene side chain is single bonded to C 2 of a second 3-carbon alkene side chain below. The second 3-carbon alkene side chain is depicted as a line structure using 2 zigzag lines. A double bond is present between C 2 and C 3. C 3 of the second alkene side chain is single bonded C below. This C atom located below is single-bonded to H on the lower left and double-bonded to O on the lower right.

The structure of 11-cis-Retinal connected to lysine through Schiff base is as follows: A 6-carbon homocyclic hexagonal ring is in a vertical orientation with C 1 occupying the topmost vertex. A double

bond is present between C 2 and C 3. C 1 is wedge bonded to C H 3 on the upper left in the form of a wedged line and dash bonded to C H 3 on the upper right in the form of a dashed line. C 3 is single bonded to C H 3 on the lower right in the form of a line. C 2 is single bonded to a 6-carbon alkene chain depicted as a line structure using 5 zigzag lines. A double bond is present between C 1 and C 2, C 3 and C 4, and C 5 and C 6. C 3 of an alkene chain is single bonded to C H 3 above in the form of a line. C 6 of the alkene side chain is single bonded to C 2 of the second 3-carbon alkene side chain below. The second 3-carbon alkene side chain is depicted as a line structure using 2 zigzag lines. A double bond is present between C 2 and C 3. C 3 of the second alkene side chain is single bonded to C below. This C atom located below is further single bonded to H on the lower left and double bonded to N on the lower right. N is single bonded to C 1 of a third 5-carbon alkane side chain depicted as a line structure using 4 zigzag lines. The third alkane side chain along with N is colored blue and labeled Lysine.

Return to Structures of 11-cis-Retinal and 11-cis-Retinal connected to lysine through Schiff base

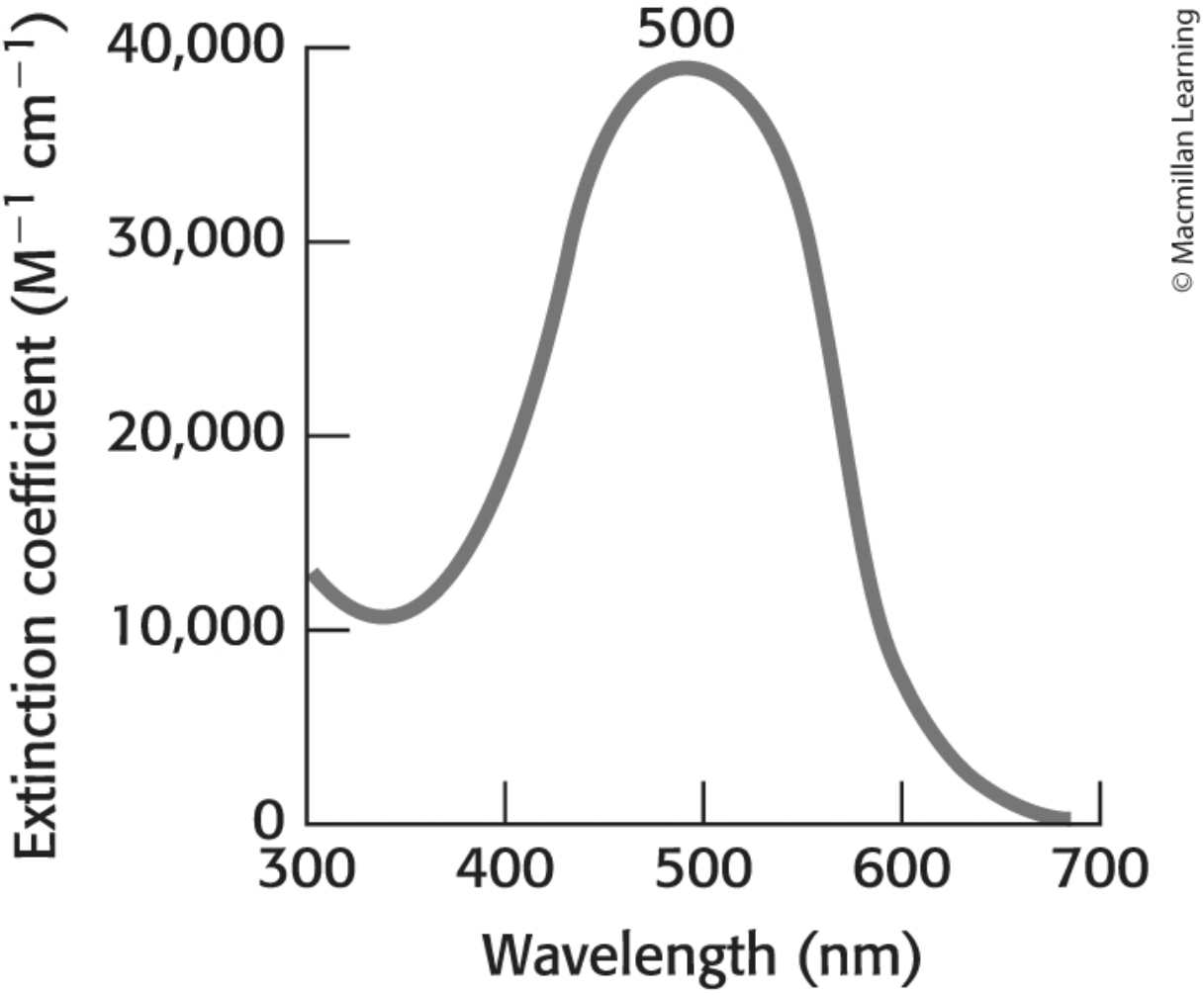
Extended description for Scanning electron micrograph and schematic representation of retinal rod cells



The scanning electron micrograph of retinol rod cells depicts white-long slender tubes densely arranged next to each other. The micrograph also shows some of the broken tubes of very small lengths. A schematic representation of the retinal rod cell shows a slender and elongated structure composed of a stack of several discs at the top. These discs are pink colored and labeled outer segment. The bottom part of the rod cell has a short cylinder filled with capsules and tube-like structures. The cylinder then has a white circular shape below it with a white colored circle enclosing two small black colored balls. The bottom cylindrical shape is filled with small black colored dots. An extension below the cylindrical shape has a broad base.

Return to Scanning electron micrograph and schematic representation of retinal rod cells

Extended description for Graphical representation of light absorption by rhodopsin

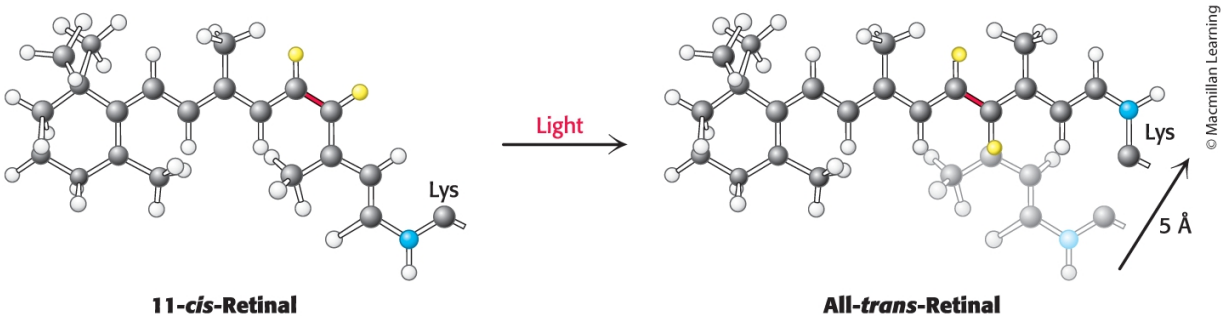


© Macmillan Learning

The horizontal axis is labeled wavelength in nanometers. It has markings ranging from 300 to 700 in increments of 100 units. The vertical axis is labeled extinction coefficient in molar inverse centimeter inverse. It has markings ranging from 0 to 40,000 in increments of 10,000 units. A bell-shaped structure is shown in the graph. It starts at (300, 12,000), moves to (340, 10,000), and then rises vertically upward to peak at (500, 40,000). It then falls vertically downward to reach (680, 0). All the values are estimated.

Return to Graphical representation of light absorption by rhodopsin

Extended description for Isomerization of 11-cis-retinal in presence of light



The reaction contains one reactant and one product. The reactant labeled 11-cis-retinal has the following structure: In the ball and stick model the C atoms are depicted as large black spheres and H atoms are depicted as small grey spheres. Six black spheres are connected in the form of a hexagonal ring in a vertical orientation with the first black sphere occupying the topmost position. The black sphere at the bottom right vertex is connected to another black sphere on the lower right. This black sphere is connected to two white spheres on the upper right, one away and one toward the observer, and a white sphere below. The black sphere at the bottom-most vertex is connected to a white sphere below and a second white sphere on the lower left and away from the observer. The black sphere at the bottom right is connected to the white sphere on the lower left and connected to the second white sphere above. The black sphere at the top left vertex is connected to the white sphere on the upper left and connected to the white sphere on the lower right and away from the observer. The black sphere at the topmost vertex is connected to the first black sphere on the upper left and toward the observer and connected to the second black sphere on the upper right and away from the observer. The first black sphere is connected to a white sphere on the upper left and connected to a white sphere on the upper right. The second black sphere is

connected to three white spheres on the upper left, upper right, and lower right. The black sphere at the top right vertex is connected to the first black sphere of a chain composed of 6 black spheres arranged in a zigzag manner. The first black sphere of the side chain is connected to a white sphere above. The second black sphere is connected to a white sphere below. The third black sphere is connected to another black sphere above which is further connected to three white spheres. The fourth black sphere is connected to a white sphere below. The fifth black sphere is single-bonded to a small yellow sphere above. The sixth black sphere is connected to a small yellow sphere on the upper right and connected to another black sphere below. The bond between the fifth and sixth black sphere is shown in red. The black sphere located below is connected to two black spheres on the lower left and lower right. The lower right black sphere is connected to a black sphere below. The black sphere below is connected to the white sphere on the lower left and connected to the blue sphere on the lower right. The blue-colored small sphere is connected to the black sphere on the upper right and a white sphere below. The black sphere on the upper right is labeled L y s.

A forward arrow labeled light leads to the product.

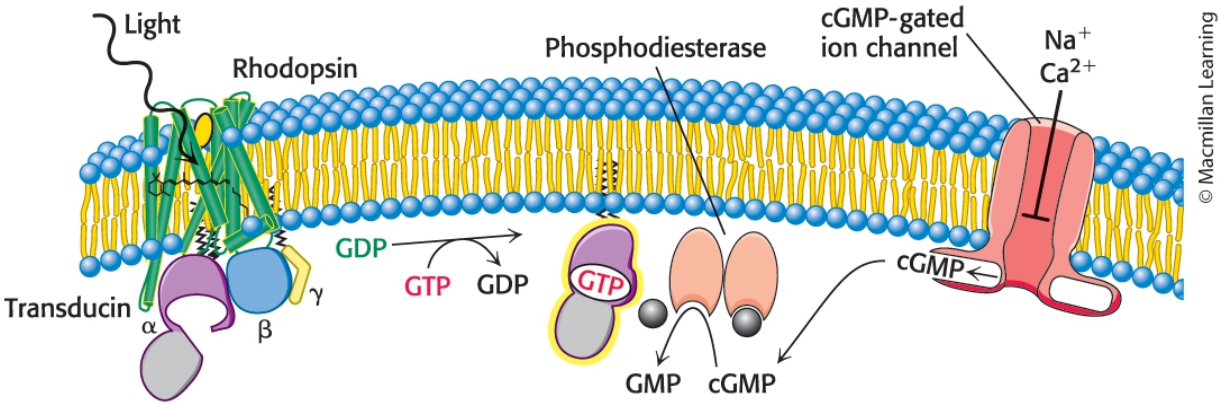
The product labeled All-trans-Retinal has the following structure: In the ball and stick model the C atoms are depicted as large black spheres and H atoms are depicted as small grey spheres. Six black spheres are connected in the form of a hexagonal ring in a vertical orientation with the first black sphere occupying the topmost position. The bottom right black sphere is connected to another black sphere on the lower right. This black sphere is connected to two white spheres on the upper right, one located away and another located toward the observer, and a white sphere below. The bottom-most black sphere is connected to a white sphere below and a second white sphere on the lower left and away from the observer.

The bottom left black sphere is connected to the white sphere on the lower left and connected to the second white sphere above. The top left is connected to the white sphere on the upper left and connected to the white sphere on the lower right and away from the observer. The topmost black sphere is connected to the first black sphere on the upper left and toward the observer and connected to the second black sphere on the upper right and away from the observer. The first black sphere is connected to three white spheres. The second black sphere is connected to three white spheres. The top right black sphere is connected to the first black sphere of a chain composed of 9 black spheres arranged in a zigzag manner. The first black sphere of the side chain is connected to a white sphere above. The second black sphere is connected to a white sphere below. The third black sphere is connected to another black sphere above which is further connected to three white spheres. The fourth black sphere is connected to a white sphere below. The fifth black sphere is single-bonded to a small yellow sphere above. The sixth black sphere is connected to a small yellow sphere below. The seventh black sphere is connected to a black sphere above. The black sphere above is connected to three white spheres. The eighth black sphere is connected to the white sphere below. The ninth black sphere is connected to a white sphere above and connected to a small blue sphere on the lower right. The blue sphere is connected to a white sphere on the upper right and connected to another black sphere below.

The rotation of Lys is marked with an arrow labeled 5 angstroms.

Return to Isomerization of 11-cis-retinal in presence of light

Extended description for Visual signal transduction



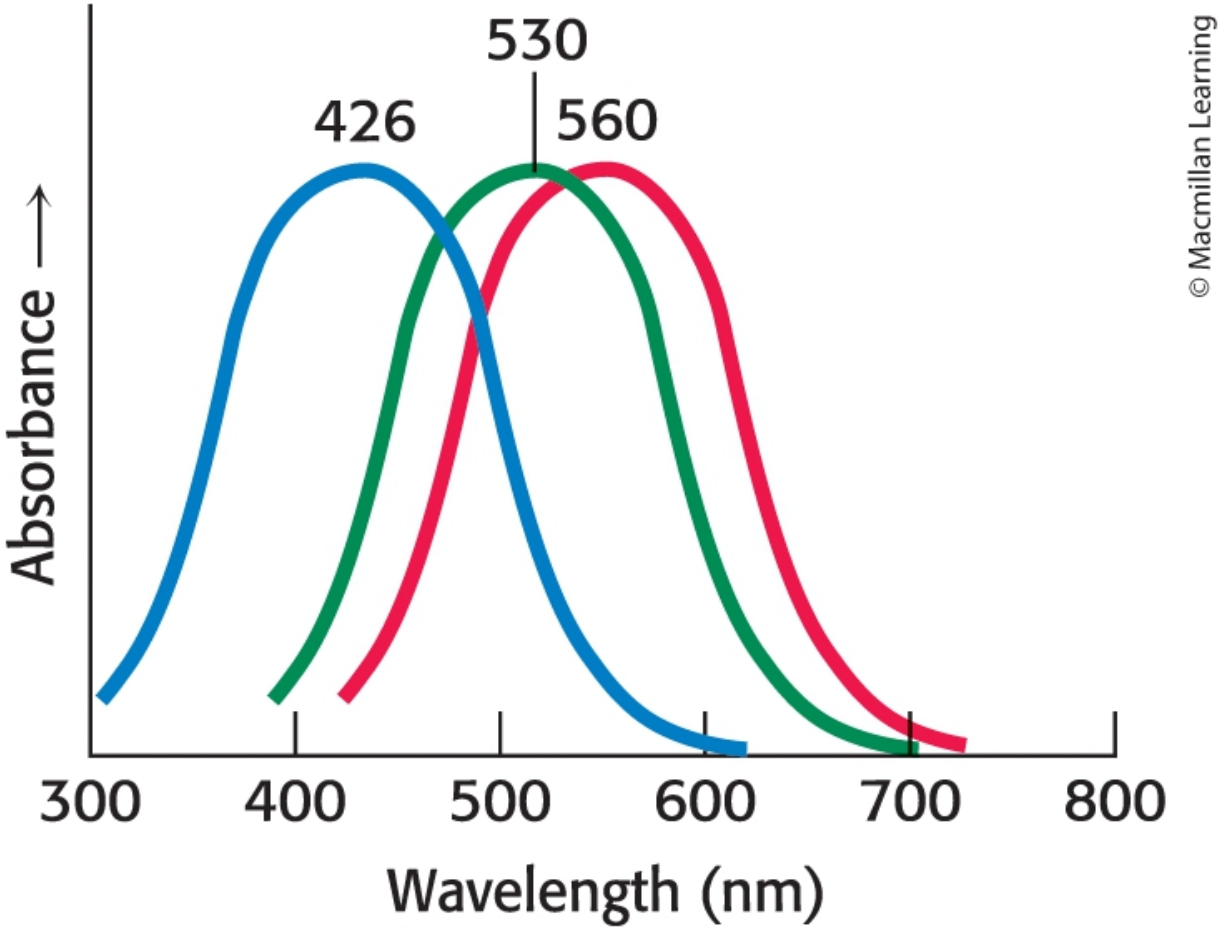
A section of a lipid bilayer is shown. Rhodopsin bound to a yellow oval-shaped structure at the top is shown embedded in the bilayer. The cytoplasmic side of the rhodopsin is bound to the trimeric G protein composed of alpha, beta, and gamma subunits. A wavy line labeled light strikes rhodopsin. In the alpha subunit, the grey structure associated with the purple round structure is displaced toward the lower left to allow the exit of G D P and entry of G T P into the groove of the purple round structure. Two zigzag lines at the top of the purple structure are embedded in the lipid bilayer.

c A M P - gated ion channel is embedded in same the lipid bilayer, toward the right. It has a long transmembrane channel and two rectangular grooves on the cytoplasmic side. A long vertical line with a minus symbol is shown inside the channel to depict the blockage of the entry of N a superscript plus and C a superscript 2 plus ions into the cell. The right groove of the channel is empty and the left groove contains c G M P. An arrow shows the displacement of this c G M P. The c G M P molecule moves toward the empty groove of phosphodiesterase.

The independent alpha subunit of G protein bound to G T P is shown attached to the inner leaflet through two zigzag lines at the top of the purple structure. A pair of oval-shaped structures labeled phosphodiesterase having a circular groove at the bottom surface are associated with the alpha subunit. The groove of the right oval is bound to a black sphere. The black sphere is displaced from the groove of the right oval structure. An arrow shows the conversion of c G M P, displaced from the left groove of c G M P-gated ion channel, to G M P in this groove.

Return to Visual signal transduction

Extended description for Absorption spectra of different light receptors from human cone cells



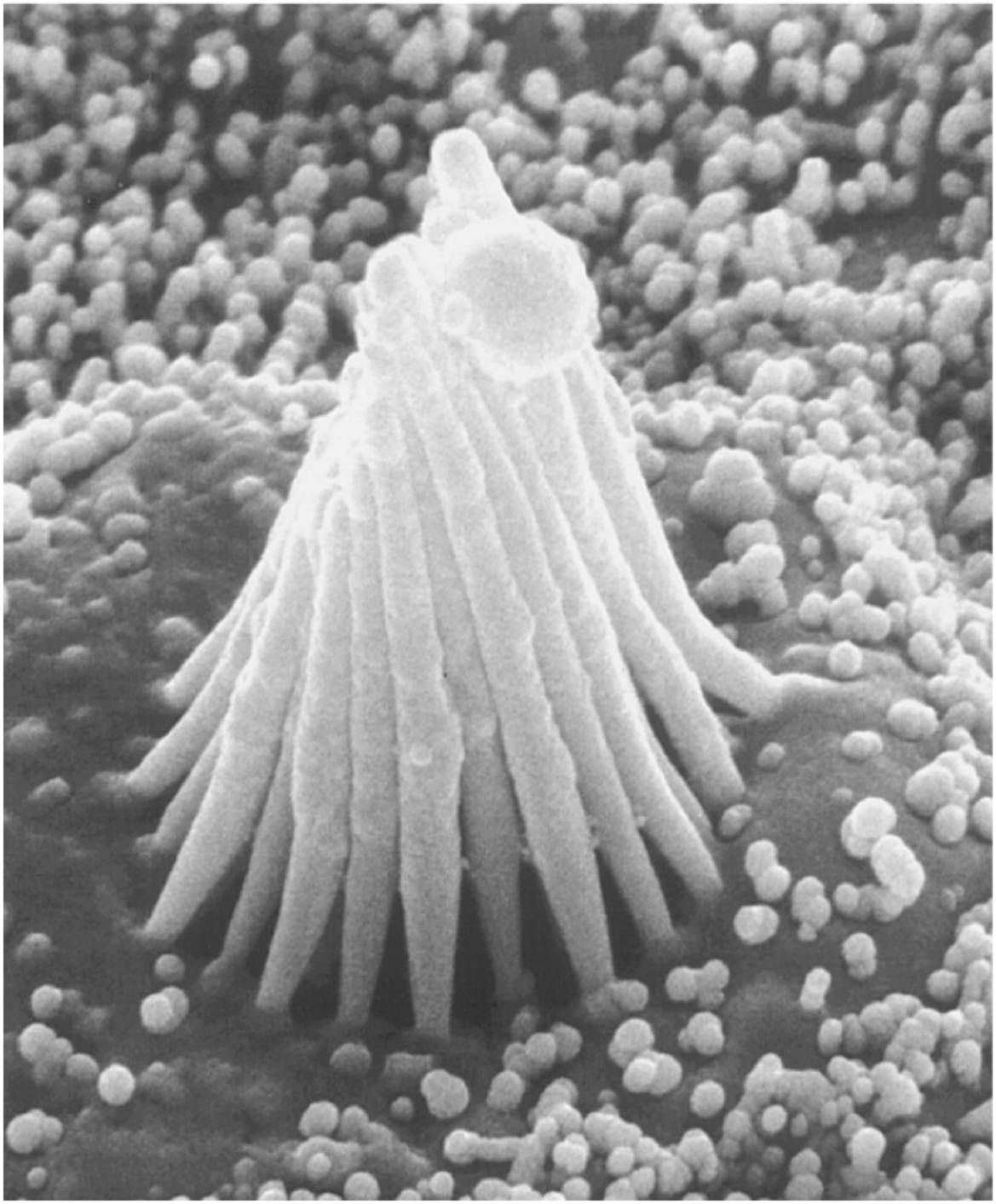
© Macmillan Learning

The horizontal axis is labeled wavelength in nanometers. It has markings ranging from 300 to 800 in increments of 100 units. The vertical axis is labeled absorbance. It increases from the bottom to the top. The graph contains three bell-shaped curves shown in blue, green, and red colors. The blue curve starts near the origin, forms a peak at 426 nanometers, and then falls vertically downward to reach the lowest absorbance at 610 nanometers. The green curve starts just above the lowest absorbance at 390 nanometers, forms a peak at 530 nanometers, and then falls vertically downward to reach the

lowest absorbance at 700 nanometers. The red curve starts just above the lowest absorbance at 410 nanometers, forms a peak at 560 nanometers, and then falls vertically downward to reach the lowest absorbance at 710 nanometers.

Return to Absorption spectra of different light receptors from human cone cells

Extended description for Scanning electron micrograph of stereocilia bundle on hair cells



Courtesy of R. Jacobs and A.J. Hudspeth

The scanning electron micrograph depicts stereocilia as a bundle of white-colored tubes in vertical orientation arranged around each other to form a conical shape. The base of the conical shape is located inside a depression on the surface. The conical arrangement has a large white-colored sphere on the top. Small white-colored spherical balls are scattered on the surface.

Return to Scanning electron micrograph of stereocilia bundle on hair cells

Extended description for Micrograph of tips of two stereocilia

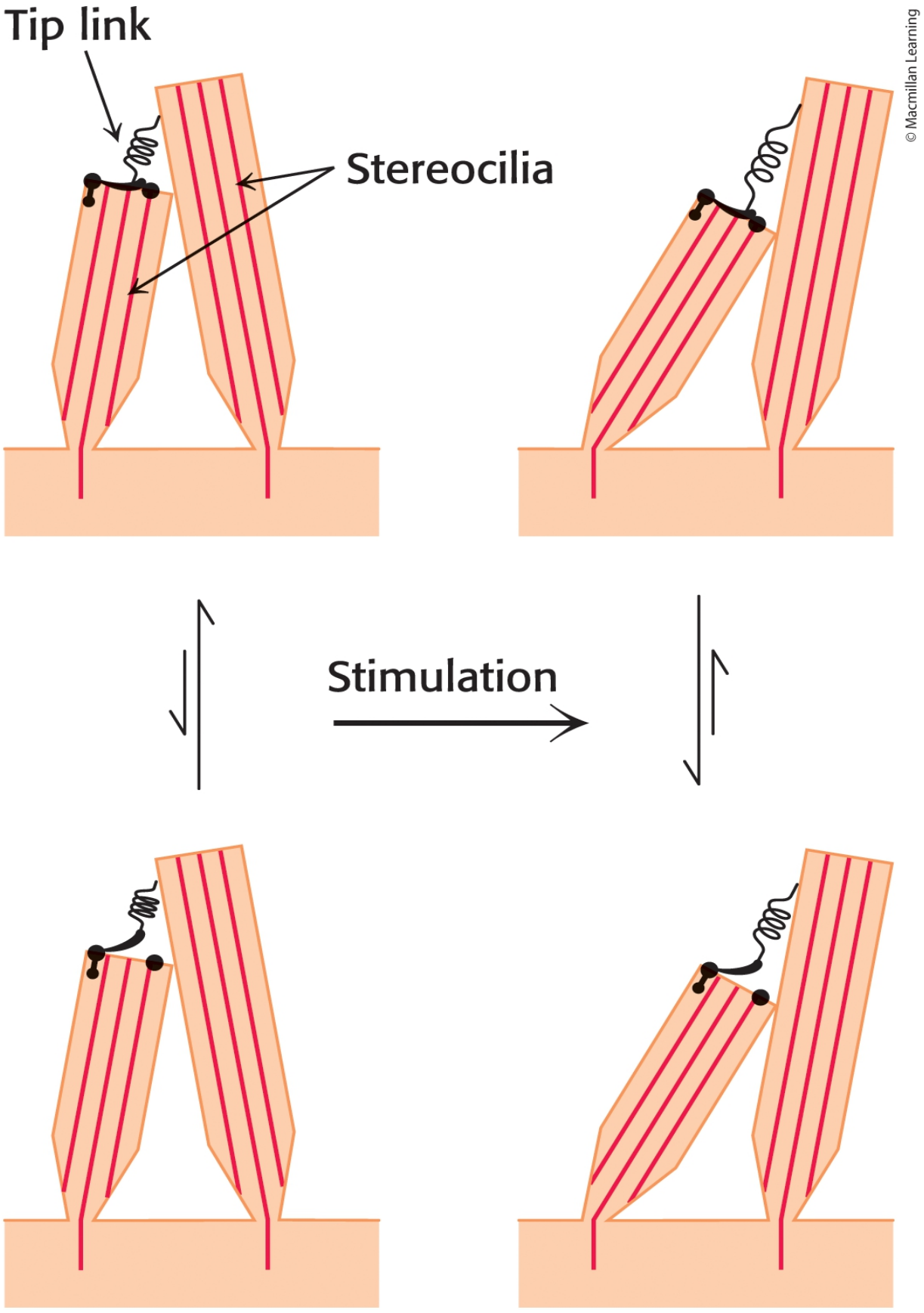


Courtesy of R. Jacobs and A.J. Hudspeth

The scanning electron micrograph shows the tips of two stereocilia. Stereocilia are depicted as grey-colored tubes. The tip of one tube is linked to another tube through a very thin thread. The thread is marked with an arrow.

Return to Micrograph of tips of two stereocilia

Extended description for Hair cell signal detection

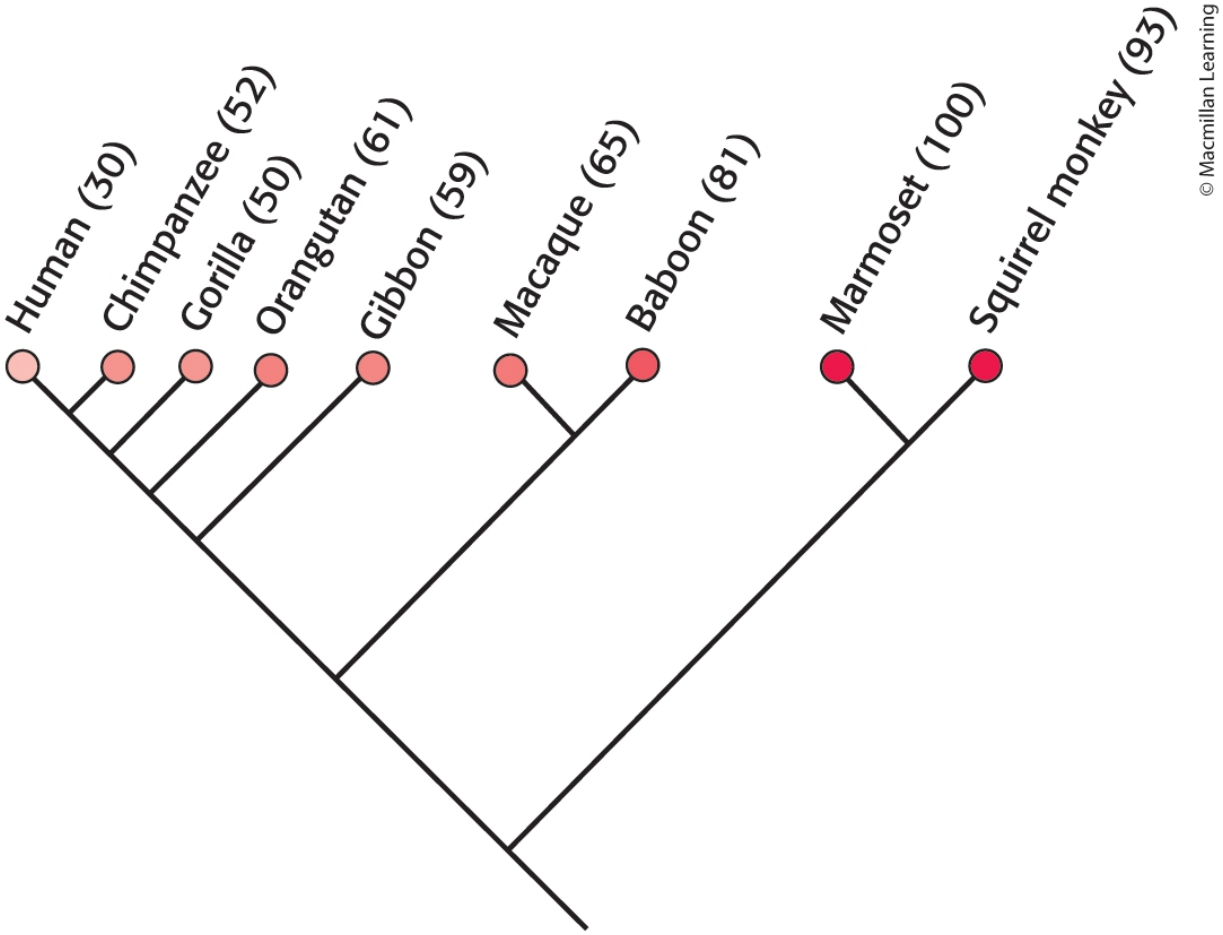


© Macmillan Learning

The stereocilia are depicted as two pencil-shaped structures with their tips embedded in the surface. One of the stereocilia is taller than the other. Their tips are linked through a spring-like structure. The spring-like structure is connected to an ion channel at the tip of the shorter stereocilia. In the first arrangement on the top left, the two stereocilia are inclined toward each other in the middle and the spring is in a compressed form and the gates of the ion channel are closed. In the second arrangement on the bottom left, the short stereocilia are inclined toward the right and the tall stereocilia are inclined toward the left such that the compressed spring pulls open the ion channel. In the third arrangement on the top right, the tall stereocilia are inclined toward the left and the smaller stereocilia are inclined toward the tall stereocilia. The spring connecting them is stretched and the ion channel is closed. In the fourth arrangement on the bottom right, both the stereocilia are inclined toward the right but the inclination of the smaller stereocilia is more than the inclination of the taller stereocilia, and the spring is stretched to open the ion channel. The first and second arrangements and the third and fourth arrangements are interconvertible as depicted by reversible reaction arrows. A forward arrow from the left reversible arrow to the right reversible arrow is labeled stimulation.

Return to Hair cell signal detection

Extended description for Phylogenetic tree



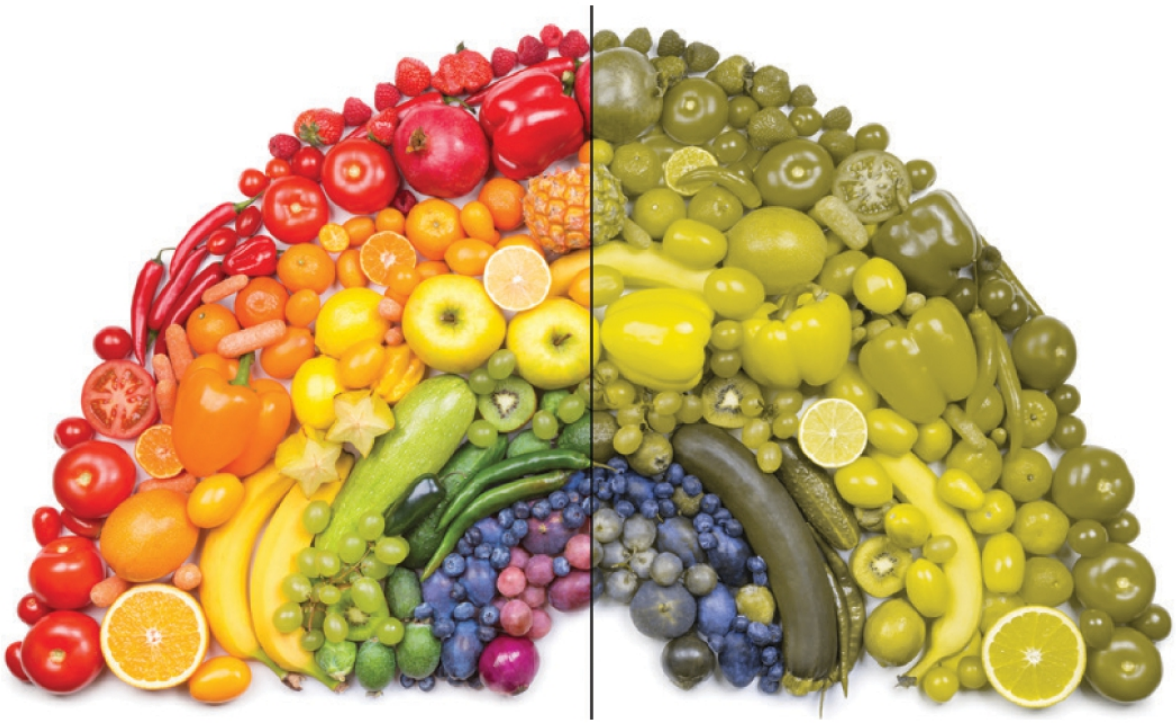
© Macmillan Learning

The root of the phylogenetic tree splits into two level 1 branch. The first level 1 branch splits into two level 2 branches. The first level 2 branch is marmoset open parenthesis 100 close parenthesis. The second level 2 branch is squirrel monkey open parenthesis 93 close parenthesis. The second level 1 branch splits into two level 2 branches. The first level 2 branch further splits into two level 3 branches. The first level 3 branch is macaque open parenthesis 65 close parenthesis. The second level 3 branch is baboon open parenthesis 81 close parenthesis.

The second level 2 branch further splits into two level 3 branches. The first level 3 branch is gibbon open parenthesis 59 close parenthesis. The second level 3 branch further splits into two level 4 branches. The first level 4 branch is the orangutan open parenthesis 61 close parenthesis. The second level 4 branch further splits into two level 5 branches. The first level 5 branch is gorilla open parenthesis 50 close parenthesis. The second level 5 branch further splits into two level 6 branches. The first level 6 branch is chimpanzee open parenthesis 52 close parenthesis. The second level 6 branch is human open parenthesis 30 close parenthesis.

Return to Phylogenetic tree

Extended description for Photograph shows several fruits and vegetables

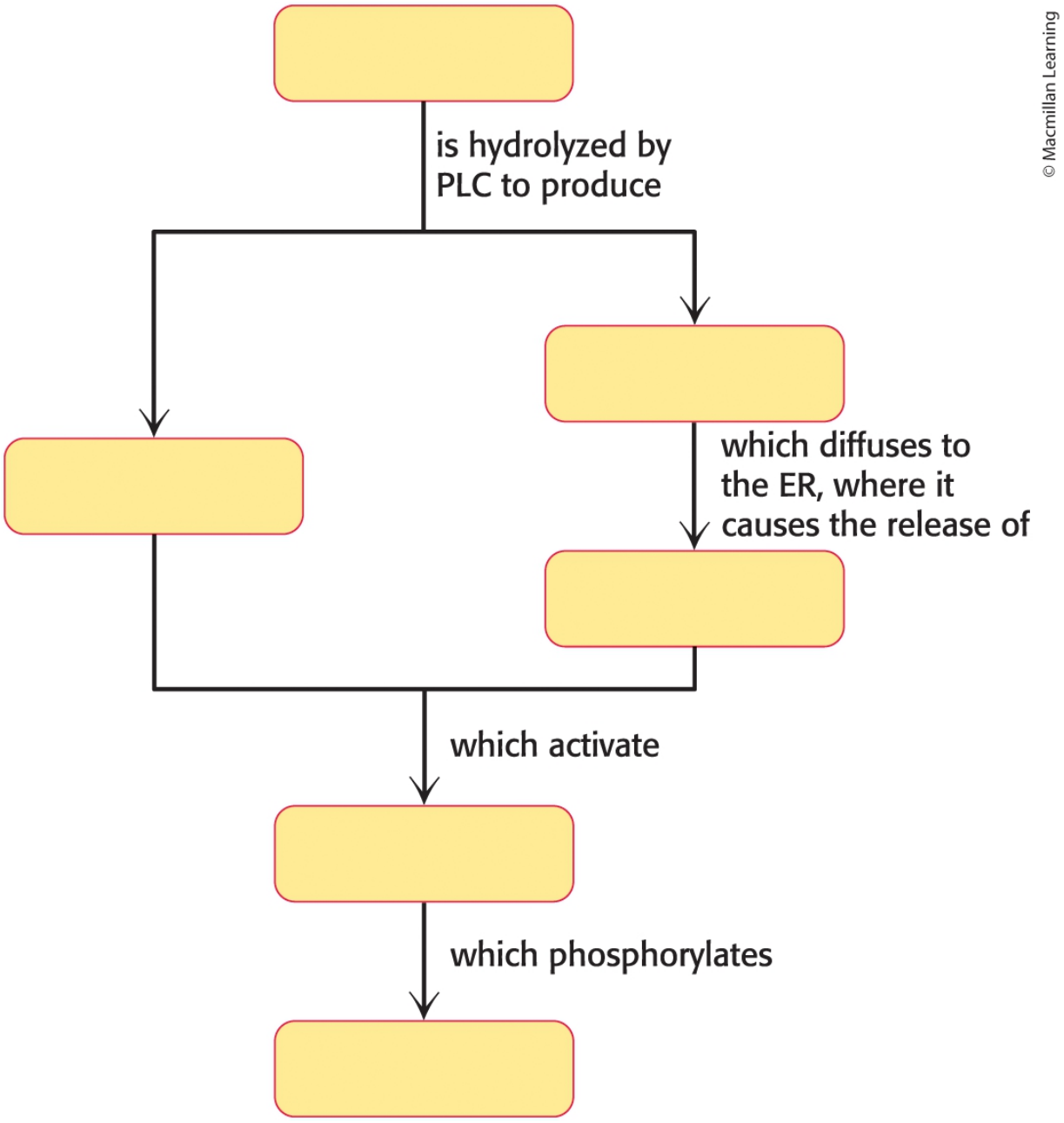


Viktar Malyshchyts/Shutterstock

A vertical line divides the arrangement of the fruits and vegetables into two equal left and right sections. The left section shows red tomatoes, red chilis, red bell peppers, orange bell peppers, orange carrots, orange pineapple, orange lime, yellow banana and other yellow fruits, green kiwi, green grapes, green cucumbers, green zucchini, green chilis, blueberries, red grapes, black grapes, and red plum among others. The right section shows all fruits and vegetables in shades of green, pale green, and yellow color. Some dark-colored fruits like blueberries are also shown.

Return to Photograph shows several fruits and vegetables

Extended description for Flow Chart for the cleavage of membrane lipid



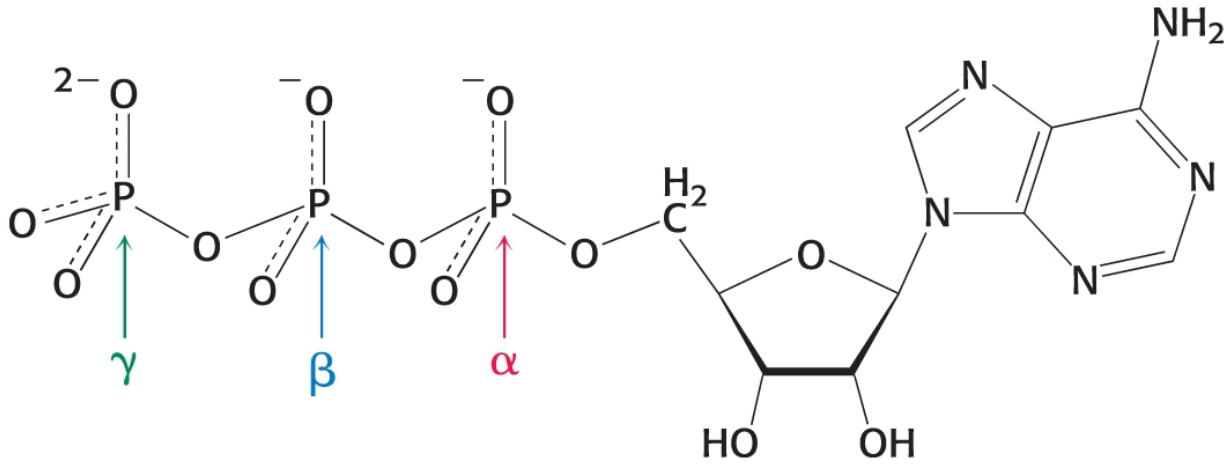
© Macmillan Learning

The flow chart has a yellow-colored rectangular box on the top middle with a vertical line below divided into two downward-facing

arrows with the first arrow on the left and the second arrow on the right. The vertical line is labeled “is hydrolyzed by P L C to produce,” on the right. The left arrow and right arrow each have an empty yellow-colored rectangular box below. The empty yellow-colored rectangular box on the right has a downward-facing arrow labeled “which diffuses to the E R, where it causes the release of.” The arrow leads to a second yellow-colored rectangular box on the right. The vertical lines from both the left and right rectangle meet together in the middle and merge with a downward-facing arrow leading to a second yellow-colored rectangular box in the middle. The downward-facing arrow is labeled “which activates.” A downward-facing arrow from the second yellow-colored rectangular box points to a third yellow-colored rectangular box in the middle. The downward facing arrow between the second and third boxes is labeled “which phosphorylates.”

Return to Flow Chart for the cleavage of membrane lipid

Extended description for Structure of A T P



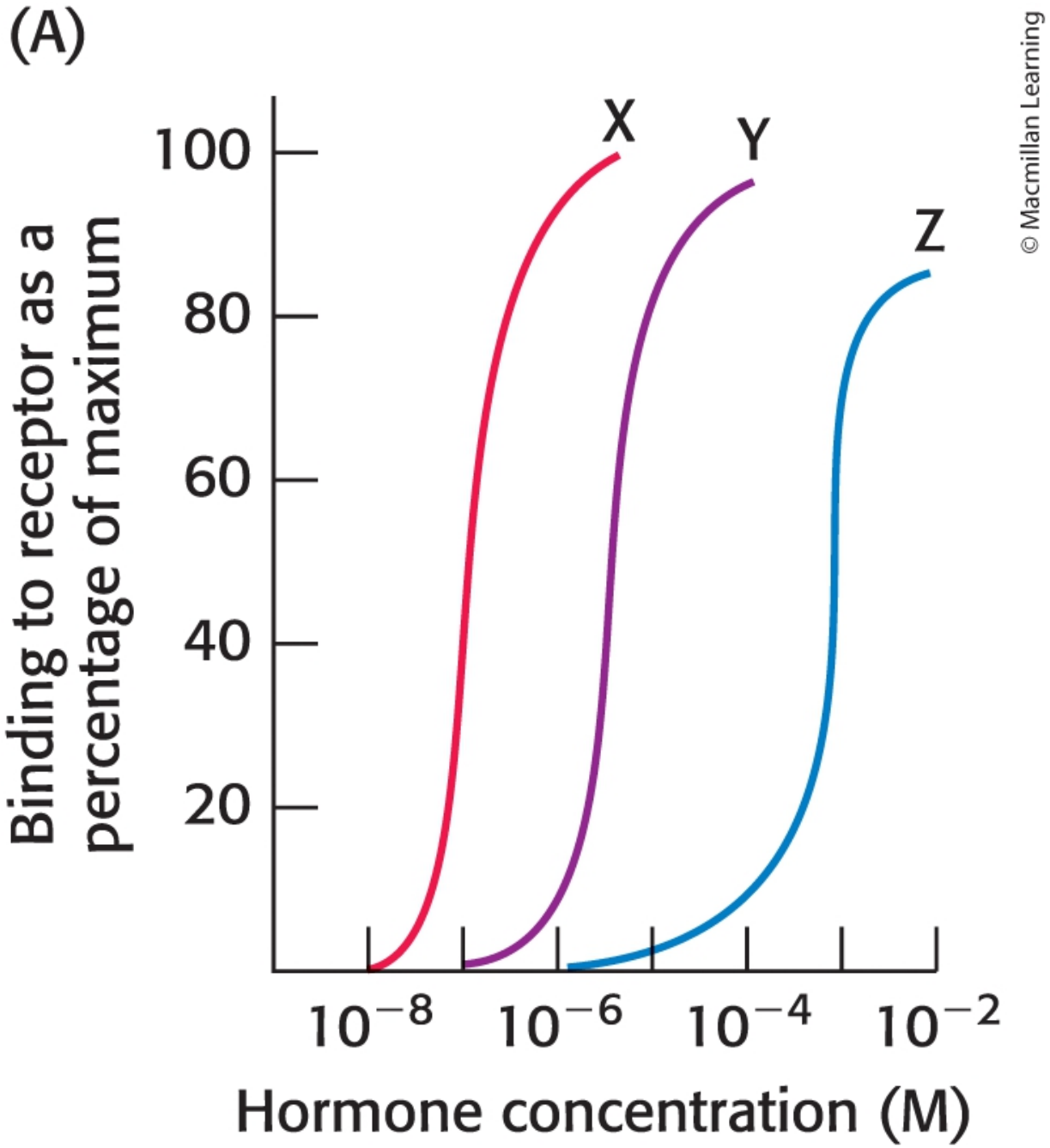
The structure of A T P is as follows: A 5-membered heterocyclic pentagonal ring is in a vertical orientation and consists of 1 Oand 4 C atoms. O occupies the first position, which is the topmost vertex. The ring is in a plane perpendicular to the plane of the paper such that C 2 and C 3 are toward the observer and O is away from the observer. C 1 is single bonded to above the first N atom of a second 5-membered heterocyclic pentagonal ring in a horizontal orientation consisting of 2 N and 3 C atoms. In the second pentagonal ring, the first N atom occupies the first position, which is the bottom left vertex, and the second N atom occupies the third position, which is the top left vertex. A double bond is present between C 1 and the second N atom and C 2 and C 3. The second pentagonal ring is fused to a 6-membered heterocyclic hexagonal ring in a vertical orientation consisting of 2 N and 4 C atoms. In the hexagonal ring, the first N atom occupies the first position, which is the top right vertex, and the second N atom occupies the third position, which is the bottommost vertex. The two rings are fused to each other such that C 2 and C 3 of the second pentagonal ring are the C 3 and C 2 of the hexagonal ring, respectively. In the hexagonal ring, a double bond is present between C 1 and the second N atom,

C 2 and C 3, and C 4 and first N. In the hexagonal ring, C 4 is single bonded to N H 2 above.

C 3 and C 4 of the first pentagonal ring are each single bonded to O H below. C 4 of the first pentagonal ring is single bonded to C H 2 above. C H 2 is single bonded to the first O atom of the following zigzag chain: O, single bond, P, single bond, O, single bond, P, single bond, O, single bond, P, partial double bond, O. P 1 and P 2 are each partially double bonded to O superscript minus above and partially double bonded to O on the lower left. P 3 is partially double bonded to O superscript minus above and partially double bonded to O on the lower left. The first P atom is labeled alpha, the second P atom is labeled beta and the third P atom is labeled gamma.

Return to Structure of A T P

Extended description for Percentage of binding capacity of the receptor as a function of hormone concentration

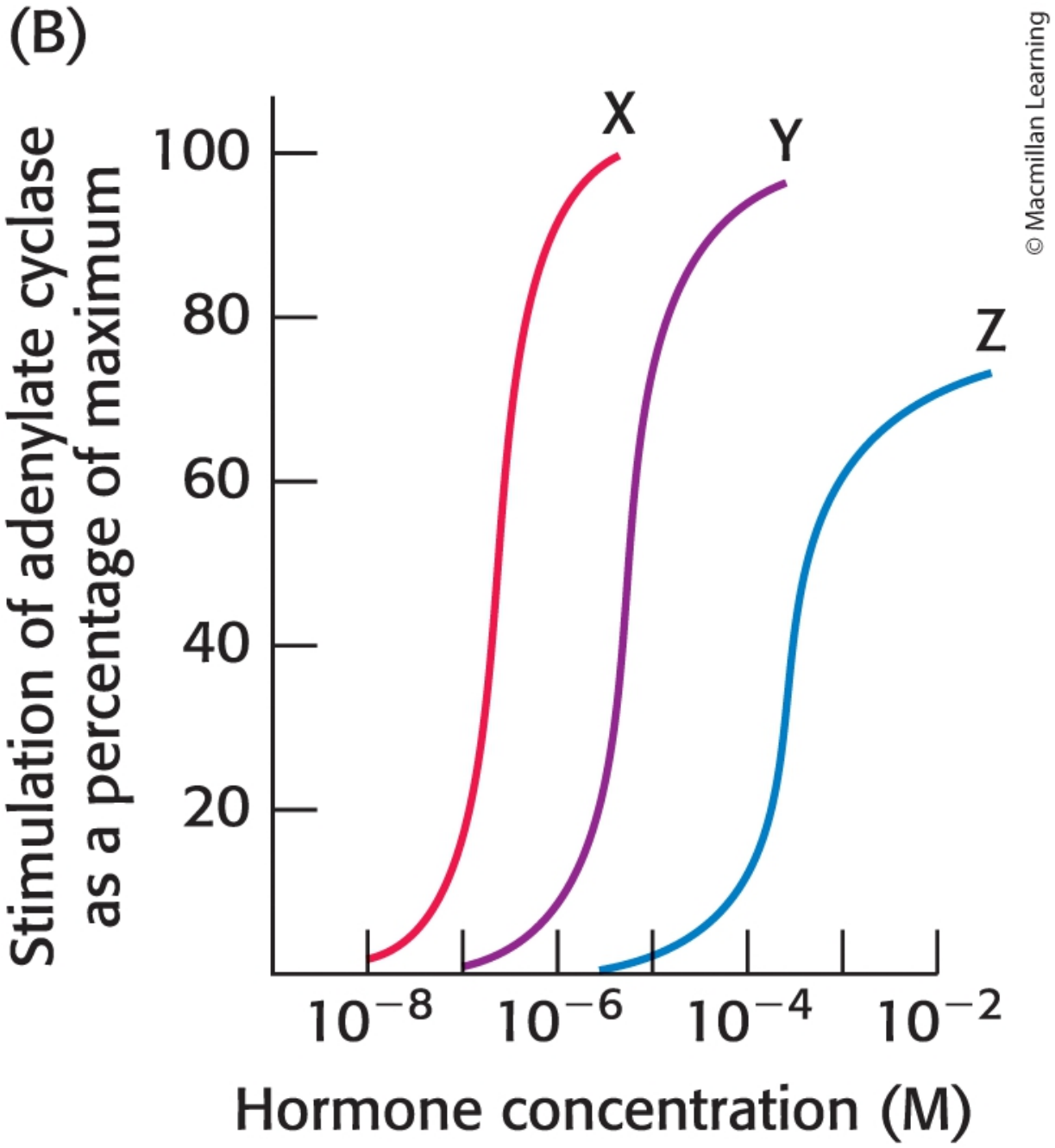


© Macmillan Learning

The horizontal axis represents the hormone concentration in molar. It has markings ranging from 10 raised to the power negative 8 to 10 raised to the power negative 2 in multiples of 10 raised to the power 2 units. The vertical axis represents the binding to receptor as a percentage of maximum. It has markings ranging from 20 to 100 in increments of 20 units. A red curve starts at 10 raised to the power negative 8 on the horizontal axis and rises steeply till it reaches a maximum point of 100 on the vertical axis at 10 raised to the power negative 6. The red curve is labeled X. A purple curve starts at 10 raised to the power negative 7 on the horizontal axis and rises gradually till it reaches 10 raised to the power of negative 6 on the horizontal axis. It then rises steeply till it reaches a maximum point of 100 on the vertical axis at 10 raised to the power negative 4. The purple curve is labeled Y. A blue curve starts at 10 raised to the power negative 6 on the horizontal axis and rises gradually till it reaches 10 raised to the power negative 3 on the horizontal axis. It then rises steeply till it reaches a maximum point of 80 on the vertical axis at 10 raised to the power negative 2. The blue curve is labeled Z.

Return to Percentage of binding capacity of the receptor as a function of hormone concentration

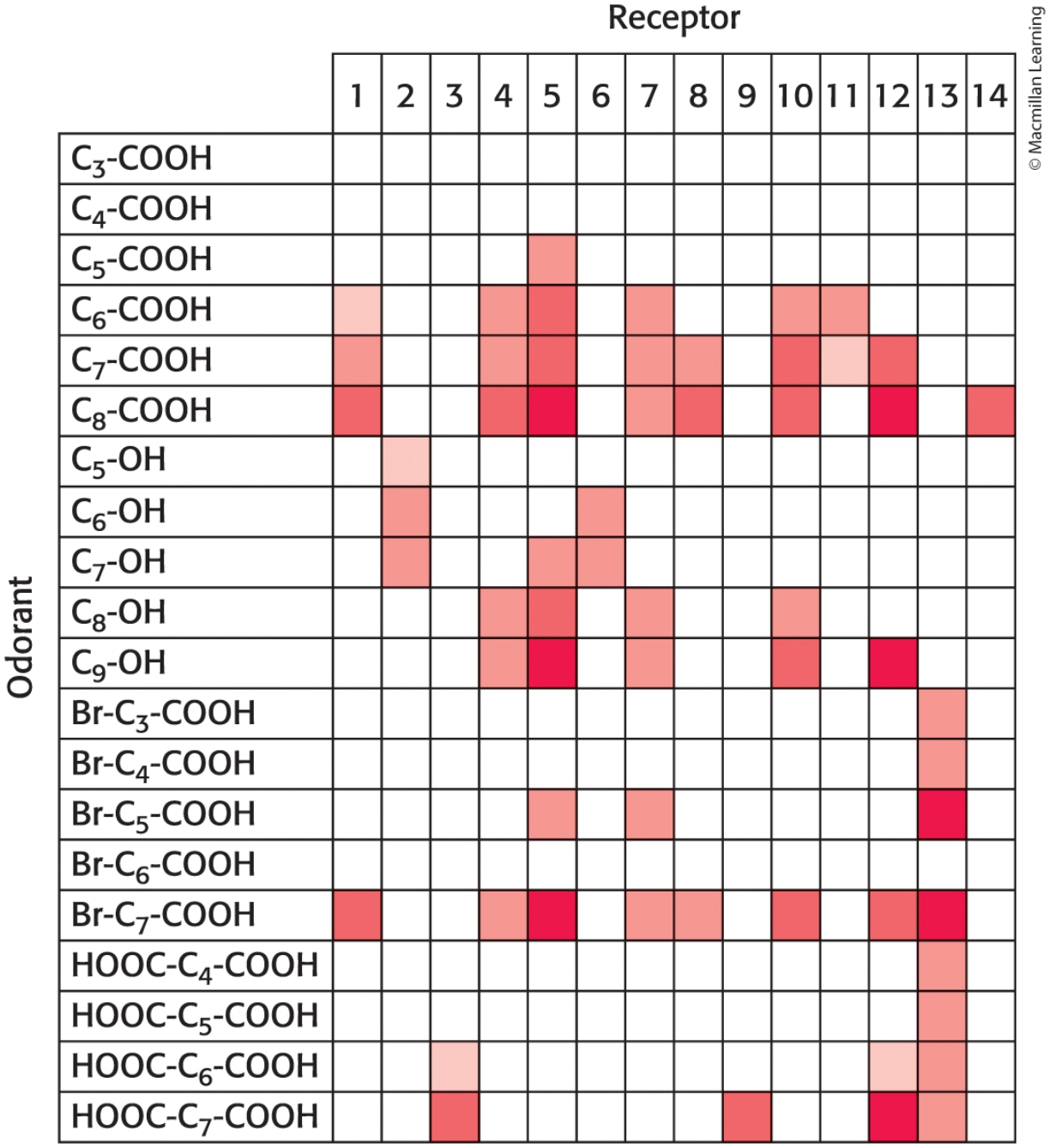
Extended description for Stimulation of adenylate cyclase as a percentage of maximum hormone concentration



The horizontal axis represents the hormone concentration in molar. It has markings ranging from 10 raised to the power negative 8 to 10 raised to the power negative 2 in multiples of 10 raised to the power 2 units. The vertical axis represents the stimulation of adenylate cyclase as a percentage of maximum. It has markings ranging from 20 to 100 in increments of 20 units. A red curve starts at 10 raised to the power negative 8 on the horizontal axis and rises gradually till it reaches point 10 raised to the power negative 7 on the horizontal axis. It then rises steeply till it reaches a maximum point of 100 on the vertical axis at 10 raised to the power negative 6. The red curve is labeled X. A purple curve starts at 10 raised to the power negative 7 on the horizontal axis and rises gradually till it reaches 10 raised to the power negative 6.5 on the horizontal axis. It then rises steeply till it reaches a maximum point of 100 on the vertical axis at 10 raised to the power negative 4. The purple curve is labeled Y. A blue curve starts at 10 raised to the power negative 6.5 on the horizontal axis and rises gradually till it reaches 10 raised to the power negative 4 on the horizontal axis. It then rises steeply to reach a maximum point of 70 on the vertical axis at 10 raised to the power negative 2. The blue curve is labeled X.

Return to Stimulation of adenylate cyclase as a percentage of maximum hormone concentration

Extended description for Distinct patterns of olfactory-receptor activation



© Macmillan Learning

The table consists of 14 columns and 20 rows. The columns represent receptors and the rows represent odorants. The column headings are as follows: First column: 1, Second column: 2, Third column: 3, Fourth column: 4, Fifth column: 5, Sixth column: 6, Seventh column: 7, Eighth column: 8, Ninth column: 9, Tenth column: 10, Eleventh column: 14, Twelfth column: 12, Thirteenth column: 13, and Fourteenth column: 14

The row entries are as follows:

Row 1: C 3, single bond, C O O H; 1: blank; 2: blank; 3: blank; 4: blank; 5: blank; 6: blank; 7: blank; 8: blank; 9: blank; 10: blank; 11: blank; 12: blank; 13: blank; 14: blank.

Row 2: C 4, single bond, C O O H; 1: blank; 2: blank; 3: blank; 4: blank; 5: blank; 6: blank; 7: blank; 8: blank; 9: blank; 10: blank; 11: blank; 12: blank; 13: blank; 14: blank.

Row 3: C 5, single bond, C O O H; 1: blank; 2: blank; 3: blank; 4: blank; 5: light red; 6: blank; 7: blank; 8: blank; 9: blank; 10: blank; 11: blank; 12: blank; 13: blank; 14: blank.

Row 4: C 6, single bond, C O O H; 1: very light red; 2: blank; 3: blank; 4: light red; 5: medium red; 6: blank; 7: blank; 8: blank; 9: blank; 10: blank; 11: blank; 12: blank; 13: blank; 14: blank.

Row 5: C 7, single bond, C O O H; 1: light red; 2: blank; 3: blank; 4: light red; 5: medium red; 6: blank; 7: light red; 8: light red; 9: blank; 10: medium red; 11: very light red; 12: medium red; 13: blank; 14: blank.

Row 6: C 8, single bond, C O O H; 1: medium red; 2: blank; 3: blank; 4: medium red; 5: dark red; 6: blank; 7: light red; 8: medium red; 9:

blank; 10: medium red; 11: blank; 12: dark red; 13: blank; 14: medium red.

Row 7: C 5, single bond, O H; 1: blank; 2: very light red; 3: blank; 4: blank; 5: blank; 6: blank; 7: blank; 8: blank; 9: blank; 10: blank; 11: blank; 12: blank; 13: blank; 14: blank.

Row 8: C 6, single bond, O H; 1: blank; 2: light red; 3: blank; 4: blank; 5: blank; 6: light red; 7: blank; 8: blank; 9: blank; 10: blank; 11: blank; 12: blank; 13: blank; 14: blank.

Row 9: C 7, single bond, O H; 1: blank; 2: light red; 3: blank; 4: blank; 5: light red; 6: light red; 7: blank; 8: blank; 9: blank; 10: blank; 11: blank; 12: blank; 13: blank; 14: blank.

Row 10: C 8, single bond, O H; 1: blank; 2: blank; 3: blank; 4: light red; 5: medium red; 6: blank; 7: light red; 8: blank; 9: blank; 10: light red; 11: blank; 12: blank; 13: blank; 14: blank.

Row 11: C 9, single bond, O H; 1: blank; 2: blank; 3: blank; 4: light red; 5: dark red; 6: blank; 7: light red; 8: blank; 9: blank; 10: medium red; 11: blank; 12: dark red; 13: blank; 14: blank.

Row 12: B r, single bond, C 3, single bond, C O O H; 1: blank; 2: blank; 3: blank; 4: blank; 5: blank; 6: blank; 7: blank; 8: blank; 9: blank; 10: blank; 11: blank; 12: blank; 13: light red; 14: blank.

Row 13: B r, single bond, C 4, single bond, C O O H; 1: blank; 2: blank; 3: blank; 4: blank; 5: blank; 6: blank; 7: blank; 8: blank; 9: blank; 10: blank; 11: blank; 12: blank; 13: light red; 14: blank.

Row 14: B r, single bond, C 5, single bond, C O O H; 1: blank; 2: blank; 3: blank; 4: blank; 5: light red; 6: blank; 7: light red; 8: blank;

9: blank; 10: blank; 11: blank; 12: blank; 13: dark red; 14: blank.

Row 15: B r, single bond, C 6, single bond, C O O H; 1: blank; 2: blank; 3: blank; 4: blank; 5: blank; 6: blank; 7: blank; 8: blank; 9: blank; 10: blank; 11: blank; 12: blank; 13: blank; 14: blank.

Row 16: B r, single bond, C 7, single bond, C O O H; 1: medium red; 2: blank; 3: blank; 4: light red; 5: dark red; 6: blank; 7: light red; 8: light red; 9: blank; 10: medium red; 11: blank; 12: medium red; 13: dark red; 14: blank.

Row 17: H O O C, single bond, C 4, single bond, C O O H; 1: blank; 2: blank; 3: blank; 4: blank; 5: blank; 6: blank; 7: blank; 8: blank; 9: blank; 10: blank; 11: blank; 12: blank; 13: light red; 14: blank.

Row 18: H O O C, single bond, C 5, single bond, C O O H; 1: blank; 2: blank; 3: blank; 4: blank; 5: blank; 6: blank; 7: blank; 8: blank; 9: blank; 10: blank; 11: blank; 12: blank; 13: light red; 14: blank.

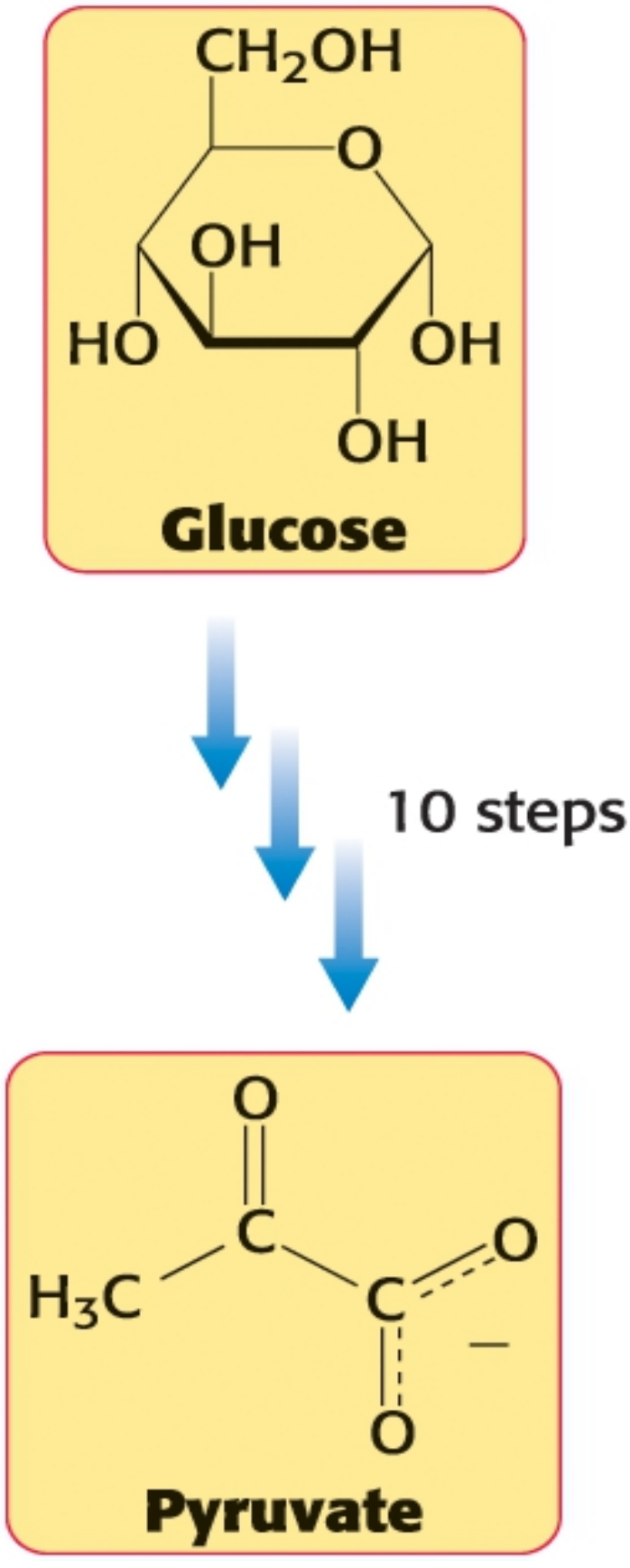
Row 19: H O O C, single bond, C 6, single bond, C O O H; 1: blank; 2: blank; 3: very light red; 4: blank; 5: blank; 6: blank; 7: blank; 8: blank; 9: blank; 10: blank; 11: blank; 12: very light red; 13: light red; 14: blank.

Row 20: H O O C, single bond, C 7, single bond, C O O H; 1: blank; 2: blank; 3: medium red; 4: blank; 5: blank; 6: blank; 7: blank; 8: blank; 9: medium red; 10: blank; 11: blank; 12: dark red; 13: light red; 14: blank.

Return to Distinct patterns of olfactory-receptor activation

Extended description for Flow chart depicting the

transformation of glucose to pyruvate



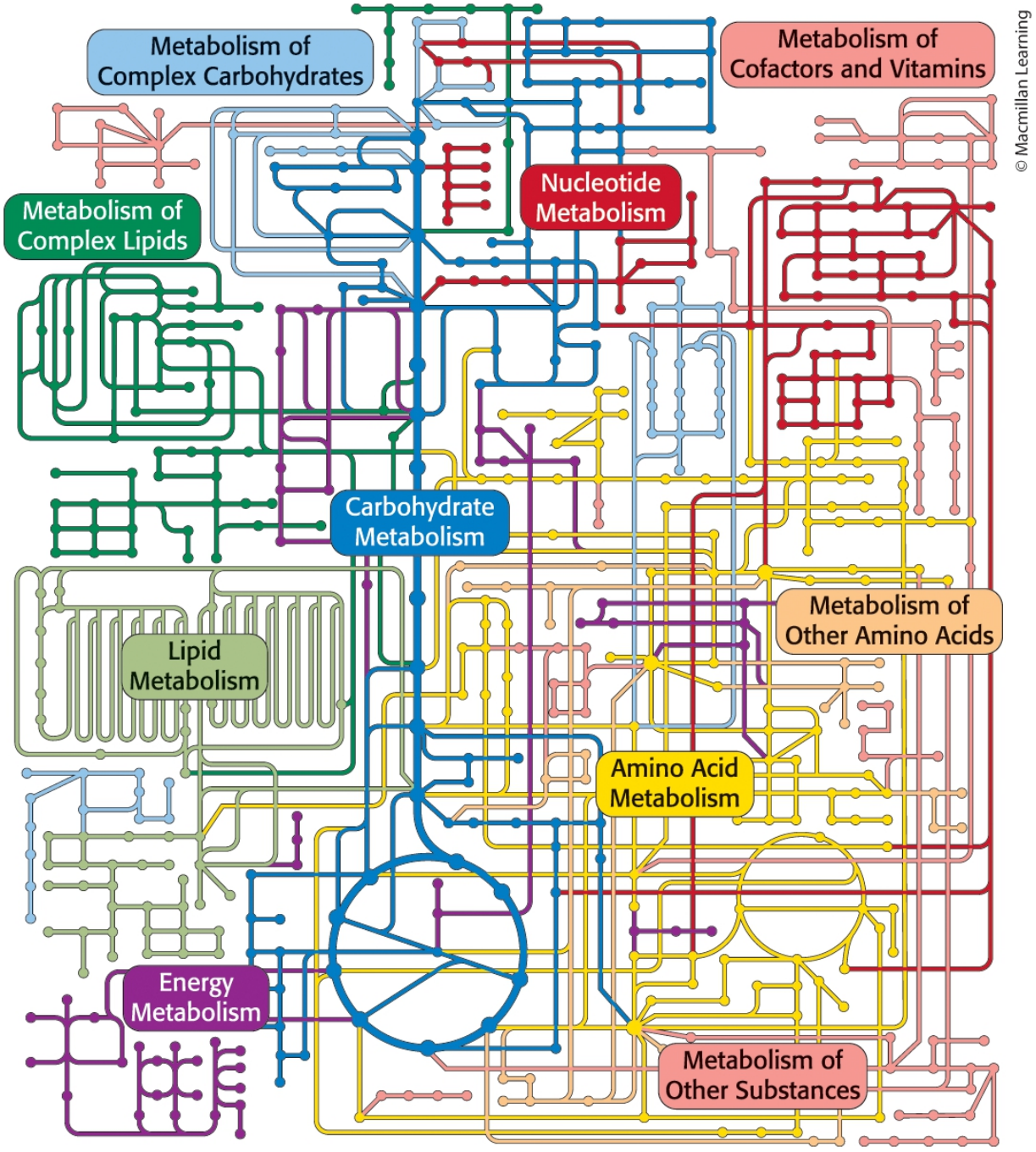
© Macmillan Learning

The flow chart has two steps. Glucose undergoes transformation to form pyruvate. Three step-like downward arrows labeled “10 steps” from glucose point to pyruvate. The structure of glucose is as follows: A 6-membered heterocyclic hexagonal ring is in a horizontal orientation and consists of 1 O and 5 C atoms. The O atom occupies the first position, which is the top right vertex. C 1, C 2, and C 4 are each single bonded to O H below. C 3 is single bonded to O H above. C 5 is single bonded to C H 2 O H above.

The structure of pyruvate is as follows: A 2-carbon alkane chain is depicted as a line structure using one line. C 1 is single bonded to C H 3 on the lower left and double bonded to O above. C 2 is partially double bonded to O on the upper right and partially double bonded to O below and has a negative sign as a counter sign.

Return to Flow chart depicting the transformation of glucose to pyruvate

Extended description for Node diagram depicting metabolic pathways are interconnected series of enzyme-catalyzed reactions



The names of different metabolic pathways at different locations are shown including the metabolism of complex carbohydrates, metabolism of cofactors and vitamins, metabolism of complex lipids, nucleotide metabolism, carbohydrate metabolism, lipid metabolism, metabolism of other amino acids, amino acid metabolism, energy metabolism, and metabolism of other substances. All these metabolic pathways are interconnected by different colored nodes and lines. Each node in the diagram represents a specific metabolite, whereas lines connecting nodes represent enzyme-catalyzed reactions.

Return to Node diagram depicting metabolic pathways are interconnected series of enzyme-catalyzed reactions

Extended description for Chemical reactions and their respective standard free energy changes

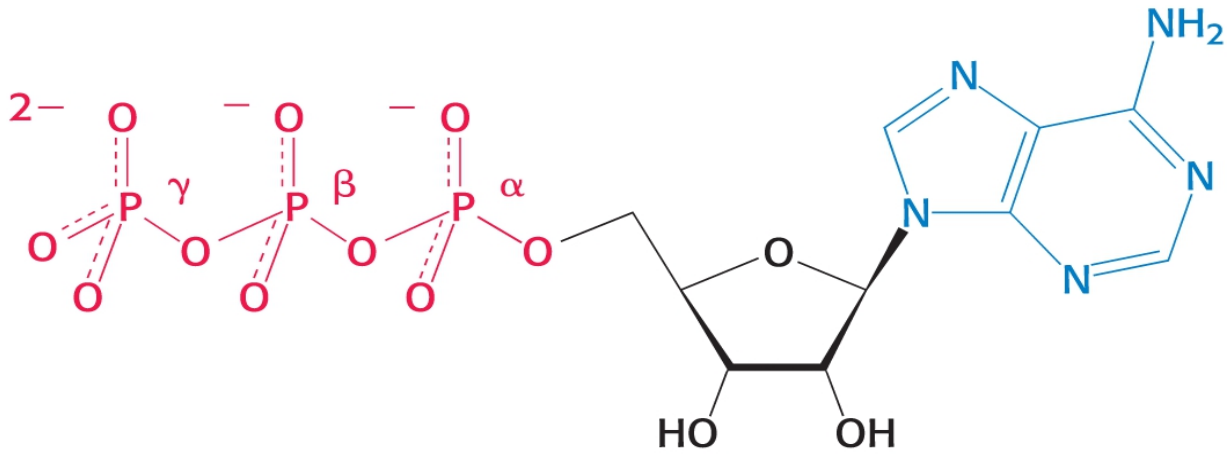
$A \rightleftharpoons B + C$	$\Delta G^{\circ\prime} = +21\ kJ\ mol^{-1}\ (+5\ kcal\ mol^{-1})$
$B \rightleftharpoons D$	$\Delta G^{\circ\prime} = -34\ kJ\ mol^{-1}\ (-8\ kcal\ mol^{-1})$
$A \rightleftharpoons C + D$	$\Delta G^{\circ\prime} = -13\ kJ\ mol^{-1}\ (-3\ kcal\ mol^{-1})$

The first reaction consists of one reactant and two products. The reactant is A. A reversible reaction arrow leads to products B and C. The value of delta G nought prime is positive 21 kilojoules per mole or positive 5 kilocalories per mole. The second reaction consists of one reactant and one product. The reactant is B. A reversible reaction arrow leads to product D. The value of delta G nought prime is negative 34 kilojoules per mole or negative 8 kilocalories per mole. The summation reaction consists of one reactant and two products. The reactant is A. A reversible reaction arrow leads to the products C and D. The value of delta G nought prime is 13 kilojoules per mole or negative 3 kilocalories per mole.

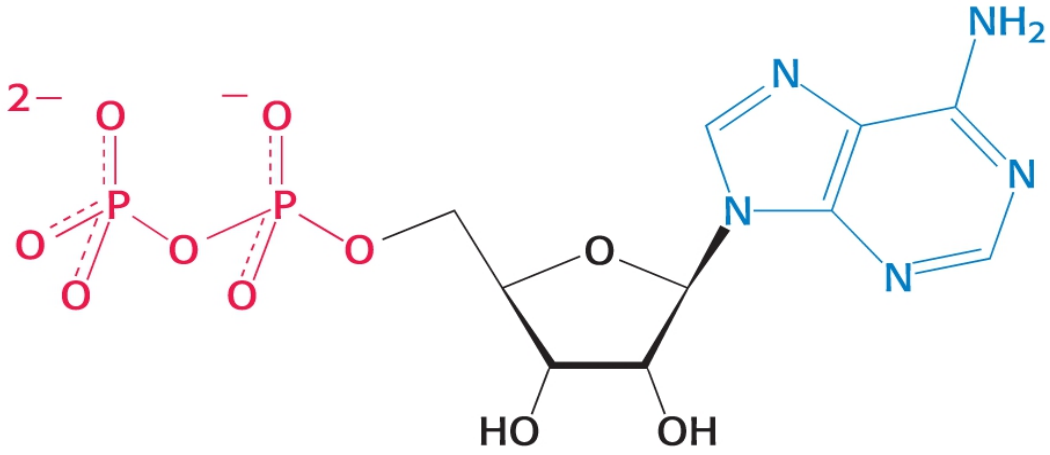
Return to Chemical reactions and their respective standard free energy changes

Extended description for Structures of A T P, A D P, and

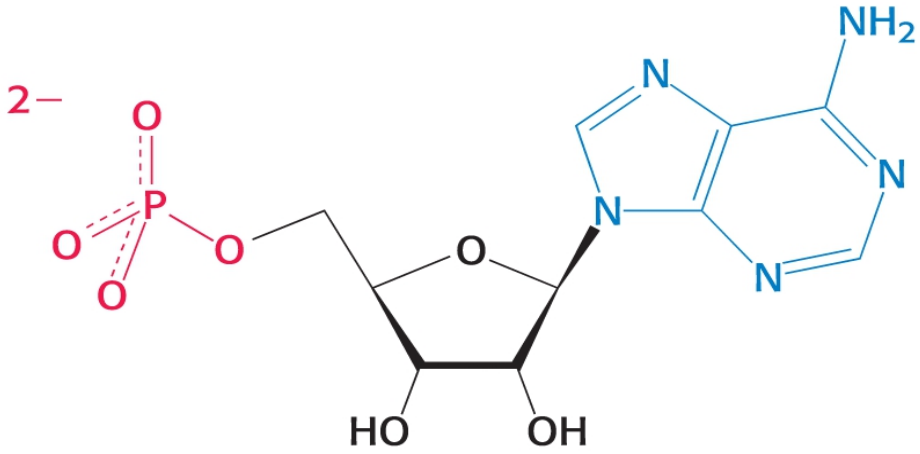
AMP



Adenosine triphosphate (ATP)



Adenosine diphosphate (ADP)



Adenosine monophosphate (AMP)

Adenosine triphosphate (A T P) has the following structure: A 5-membered heterocyclic pentagonal ring is in a vertical orientation and consists of 1 O and 4 C atoms. The O atom occupies the first position, which is the topmost vertex. The ring is in a plane perpendicular to the plane of the paper such that C 2 and C 3 are toward the observer and O is away from the observer. C 2 is single bonded to O H on the lower right. C 3 is single bonded to O H on the lower left. C 1 is single bonded to the first N atom of a second 5-membered heterocyclic pentagonal ring in a vertical orientation and consisting of 2 N and 3 C atoms. In the second 5-membered ring, the first N atom occupies the first position which is the bottom left vertex and the second N atom occupies the third position which is the topmost vertex. In the second 5-membered ring, a double bond is present between C 1 and the second N atom and C 2 and C 3. The second pentagonal ring is fused to a 6-membered heterocyclic hexagonal ring in a horizontal orientation consisting of 2 N and 4 C atoms. In the 6-membered ring, the first N atom occupies the first position which is the rightmost vertex and the second N atom occupies the third position which is the bottom left vertex. The two rings are fused to each other such that C 2 and C 3 of the second pentagonal ring are the C 3 and C 2 of the hexagonal ring, respectively. In the hexagonal ring, a double bond is present between C 1 and the second N atom and C 4 and the first N atom. C 4 of the hexagonal ring is single bonded to N H 2. C 4 of the first pentagonal ring is single bonded to C H 2 on the upper left in the form of a line, which is again single bonded on the lower left to the fourth O atom of the following zigzag horizontal chain: O, partial double bond, P, single bond, O, single bond, P, single bond, O, single bond, P, single bond, O. In the zigzag horizontal chain, the first P atom is partially double bonded to O superscript 2 minus above and an O atom on the lower left. In the zigzag horizontal chain, the second and third P atoms are each partially double bonded to O superscript minus above and an O atom on the lower left. The zigzag

horizontal chain is highlighted in pink and the second pentagonal ring and hexagonal ring are highlighted in blue.

Adenosine diphosphate (A D P) has the following structure: A 5-membered heterocyclic pentagonal ring is in a vertical orientation and consists of 1 O and 4 C atoms. The O atom occupies the first position, which is the topmost vertex. The ring is in a plane perpendicular to the plane of the paper such that C 2 and C 3 are toward the observer and O is away from the observer. C 2 is single bonded to O H on the lower right. C 3 is single bonded to O H on the lower left. C 1 is single bonded to the first N atom of a second 5-membered heterocyclic pentagonal ring in a vertical orientation and consisting of 2 N and 3 C atoms. In the second 5-membered ring, the first N atom occupies the first position which is the bottom left vertex and the second N atom occupies the third position which is the topmost vertex. In the second 5-membered ring, a double bond is present between C 1 and the second N atom and C 2 and C 3. The second pentagonal ring is fused to a 6-membered heterocyclic hexagonal ring in a horizontal orientation consisting of 2 N and 4 C atoms. In the 6-membered ring, the first N atom occupies the first position which is the rightmost vertex and the second N atom occupies the third position which is the bottom left vertex. The two rings are fused to each other such that C 2 and C 3 of the second pentagonal ring are the C 3 and C 2 of the hexagonal ring, respectively. In the hexagonal ring, a double bond is present between C 1 and the second N atom and C 4 and the first N atom. C 4 of the hexagonal ring is single bonded to N H 2. C 4 of the first pentagonal ring is single bonded to C H 2 on the upper left in the form of a line, which is again single bonded on the lower left to the third O atom of the following zigzag horizontal chain: O, partial double bond, P, single bond, O, single bond, P, single bond, O. In the zigzag horizontal chain, the first P atom is partially double bonded to O superscript 2 minus above and an O atom on the lower left. In the zigzag horizontal chain, the second P atom is partially double

bonded to O superscript minus above and an O atom on the lower left. The zigzag horizontal chain is highlighted in pink and the second pentagonal ring and hexagonal ring are highlighted in blue.

Adenosine monophosphate (A T P) has the following structure: A 5-membered heterocyclic pentagonal ring is in a vertical orientation and consists of 1 O and 4 C atoms. The O atom occupies the first position, which is the topmost vertex. The ring is in a plane perpendicular to the plane of the paper such that C 2 and C 3 are toward the observer and O is away from the observer. C 2 is single bonded to O H on the lower right. C 3 is single bonded to O H on the lower left. C 1 is single bonded to the first N atom of a second 5-membered heterocyclic pentagonal ring in a vertical orientation and consisting of 2 N and 3 C atoms. In the second 5-membered ring, the first N atom occupies the first position which is the bottom left vertex and the second N atom occupies the third position which is the topmost vertex. In the second 5-membered ring, a double bond is present between C 1 and the second N atom and C 2 and C 3. The second pentagonal ring is fused to a 6-membered heterocyclic hexagonal ring in a horizontal orientation consisting of 2 N and 4 C atoms. In the 6-membered ring, the first N atom occupies the first position which is the rightmost vertex and the second N atom occupies the third position which is the bottom left vertex. The two rings are fused to each other such that C 2 and C 3 of the second pentagonal ring are the C 3 and C 2 of the hexagonal ring, respectively. In the hexagonal ring, a double bond is present between C 1 and the second N atom and C 4 and the first N atom. C 4 of the hexagonal ring is single bonded to N H 2. C 4 of the first pentagonal ring is single bonded to C H 2 on the upper left in the form of a line, which is again single bonded on the lower left to the second O atom of the following zigzag horizontal chain: O, partial double bond, P, single bond, O. In the zigzag horizontal chain, P is partially double bonded to O superscript 2 minus above and an O atom on the lower left. The zigzag horizontal chain is highlighted in

pink and the second pentagonal ring and hexagonal ring are highlighted in blue.

Return to Structures of A T P, A D P, and A M P

Extended description for A T P hydrolysis and standard free energy changes

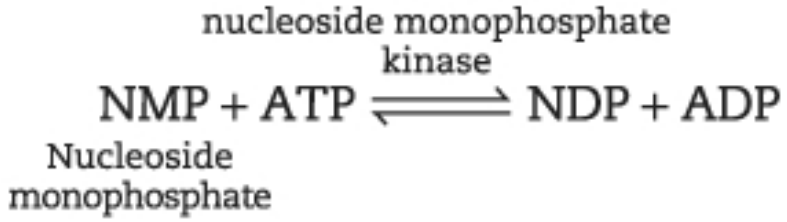
$$ATP + H_2O \rightleftharpoons ADP + P_i$$
$$\Delta G^{\circ\prime} = -30.5 \text{ kJ mol}^{-1} (-7.3 \text{ kcal mol}^{-1})$$

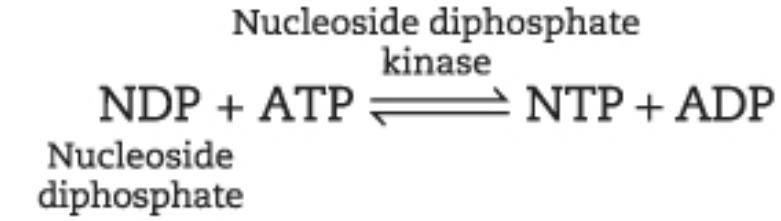
$$ATP + H_2O \rightleftharpoons AMP + PP_i$$
$$\Delta G^{\circ\prime} = -45.6 \text{ kJ mol}^{-1} (-10.9 \text{ kcal mol}^{-1})$$

The first reversible reaction consists of two reactants and two products. The reactants are A T P and H 2 O. The products are A D P and P subscript i. The value of delta G nought prime is negative 30.5 kilojoules per mole or negative 7.3 kilocalories per mole. The second reversible reaction consists of two reactants and two products. The reactants are A T P and H 2 O. The products are A M P and P P subscript i. The value of delta G nought prime is negative 45.6 kilojoules per mole or negative 10.9 kilocalories per mole.

Return to A T P hydrolysis and standard free energy changes

Extended description for Reversible reactions catalyzed by nucleoside monophosphate kinase and nucleoside diphosphate kinase





The reaction catalyzed by nucleoside monophosphate kinase consists of two reactants and two products. The reactants are N M P (nucleoside monophosphate) and A T P. The products are N D P and A D P. The reaction catalyzed by nucleoside diphosphate kinase consists of two reactants and two products. The reactants are N D P (nucleoside diphosphate) and A T P. The products are N T P and A D P.

Return to Reversible reactions catalyzed by nucleoside monophosphate kinase and nucleoside diphosphate kinase

Extended description for Reaction with its standard free energy change

$$A + ATP + H_2O \rightleftharpoons B + ADP + P_i$$

$$\Delta G^{\circ\prime} = -13.8 \text{ kJ mol}^{-1} (-3.3 \text{ kcal mol}^{-1})$$

The reaction consists of three reactants and three products. The reactants are A, A T P, and H 2 O. The products are B, A D P, and P subscript i. The value of delta G nought prime is negative 13.8 kilojoules per mole or negative 3.3 kilocalories per mole.

Return to Reaction with its standard free energy change

Extended description for Standard free energy changes of A T P and glycerol-3-phosphate hydrolysis

$$ATP + H_2O \rightleftharpoons ADP + P_i$$
$$\Delta G^{\circ\prime} = -30.5 \text{ kJ mol}^{-1} (-7.3 \text{ kcal mol}^{-1})$$

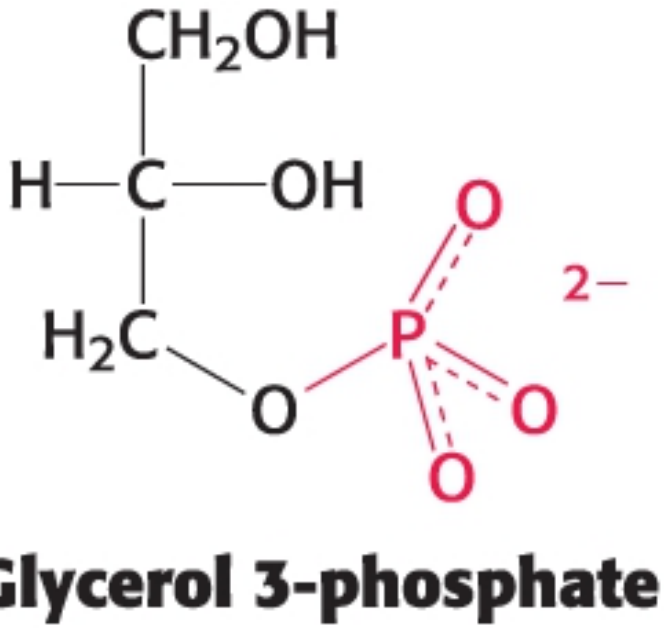
$$\text{Glycerol 3-phosphate} + H_2O \rightleftharpoons \text{glycerol} + P_i$$
$$\Delta G^{\circ\prime} = -9.2 \text{ kJ mol}^{-1} (-2.2 \text{ kcal mol}^{-1})$$

A T P hydrolysis reaction consists of two reactants and two products. The reactants are A T P and H 2 O. The products are A D P and P subscript i. The value of delta G nought prime is negative 30.5 kilojoules per mole or negative 7.3 kilocalories per mole.

Glycerol 3-phosphate reaction consists of two reactants and two products. The reactants are glycerol-3-phosphate and H 2 O. The products are glycerol and P subscript i. The value of delta G nought prime is negative 9.2 kilojoules per mole or negative 2.2 kilocalories per mole.

Return to Standard free energy changes of A T P and glycerol-3-phosphate hydrolysis

Extended description for Structure of Glycerol 3-phosphate

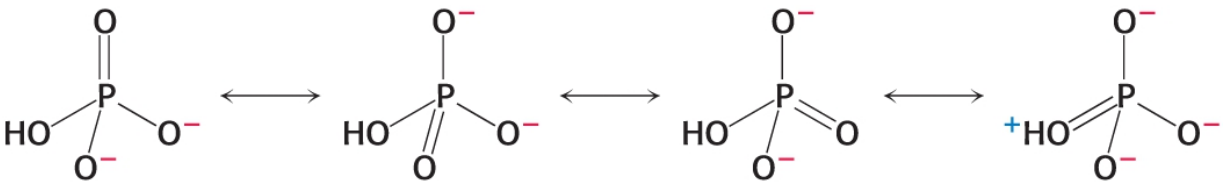


Glycerol 3-phosphate

The structure of glycerol 3-phosphate is as follows: A central C atom is single bonded to C H 2 O H above, H on the left, O H on the right, and C H 2 below. C H 2 is further single bonded to O on the lower right. This O is single bonded to P on the upper right. This P is partially double bonded to O on the upper right, O on the right, and O on the lower right. It has a counter 2 superscript minus on the right. The P atom and 3 O atoms are highlighted in red.

Return to Structure of Glycerol 3-phosphate

Extended description for Four resonance structures of orthophosphate separated by two-way arrows



The structure of the first resonance orthophosphate is as follows: A central P atom is double bonded to O above, single bonded to O H on the lower left, O superscript minus below, and O superscript minus on the lower right.

The structure of the second resonance orthophosphate is as follows: A central P atom is single bonded to O superscript minus above, single bonded to O H on the lower left, double bonded to O below, and single bonded to O superscript minus on the lower right.

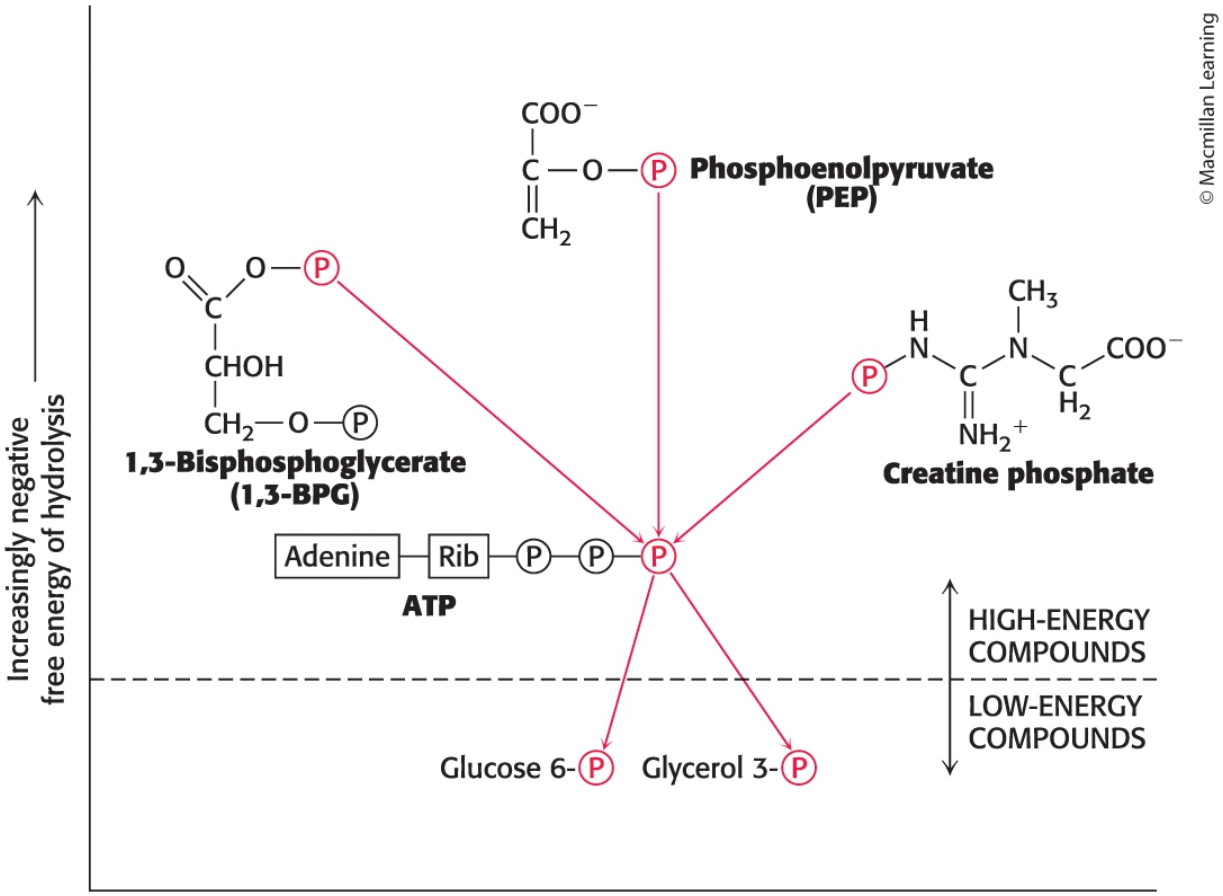
The structure of the third resonance orthophosphate is as follows: A central P atom is single bonded to O superscript minus above, single bonded to O H on the lower left, single bonded to O superscript minus below, and double bonded to O on the lower right.

The structure of the fourth resonance orthophosphate is as follows: A central P atom is single bonded to O superscript minus above, double bonded to O H superscript plus on the lower left, single bonded to O superscript minus below, and single bonded to O superscript minus on the lower right. Minus is highlighted in red and plus is highlighted in blue.

Three double headed arrows are placed between these four structures.

Return to Four resonance structures of orthophosphate separated by two-way arrows

Extended description for Graphical representation of the compounds with high phosphoryl-transfer potential that can be used to make A T P from A D P

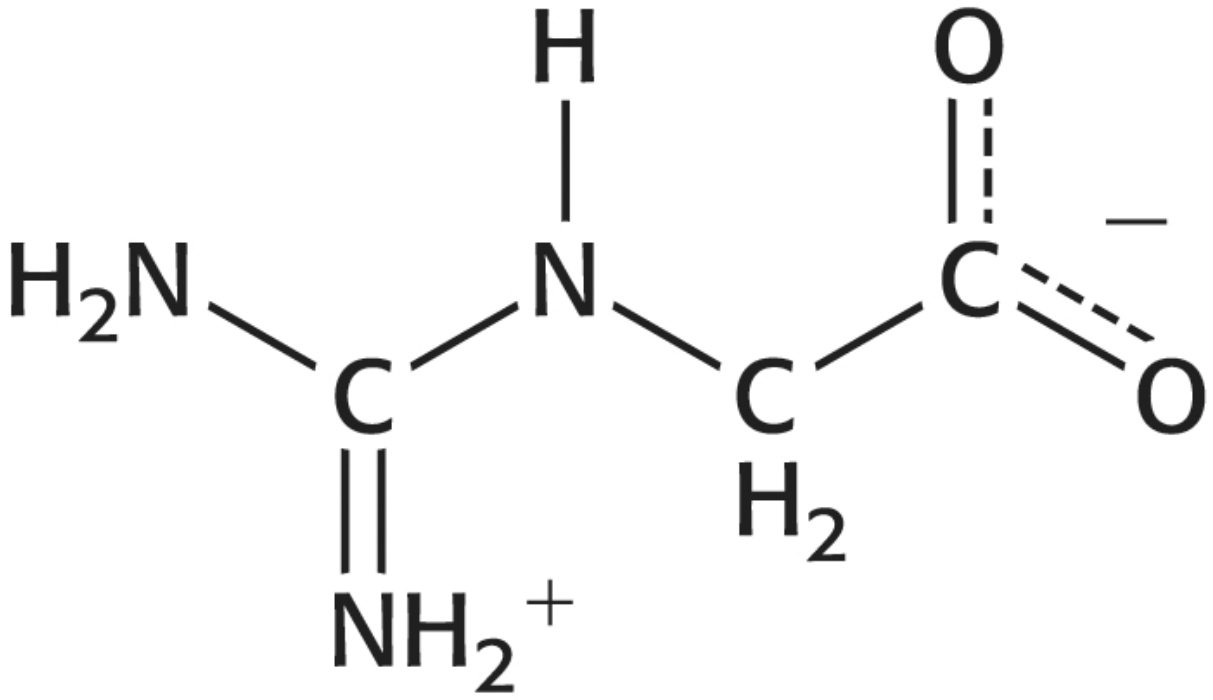


The vertical axis of the graph is labeled increasingly negative free energy of hydrolysis. The graph shows a horizontal dotted line well above the origin. A double-headed vertical arrow across the dotted line reads low-energy compounds below and high-energy compounds above. A compound above the dotted line labeled A T P has the following structure: adenine, single bond, R i b, single bond P, single bond, P, single bond, P. The compound 1, 3-Bisphosphoglycerate (1,3-B P G) above A T P has the following structure: A vertical chain is illustrated by C, single bond, C H O H,

single bond, C H 2. C 1 is double bonded to O on the upper left and single bonded to a second O atom on the upper right. The second O atom is single bonded to P on the right. C 3 is single bonded to a third O atom on the right which is single bonded to a second P atom on the right. The compound creatine phosphate on the right side of 1,3-Bisphosphoglycerate (1,3- B P G) has the following structure: A zigzag horizontal chain is illustrated by P, single bond, N H, single bond, C, single bond, N, single bond, C H 2, single bond, C O O superscript minus. C1 is double bonded to N H 2 below. The second N atom is single bonded to C H 3 above. The structure between 1,3-B P G, and creatine phosphate is labeled Phosphoenolpyruvate (P E P) and has the following structure: A vertical chain is illustrated by C O O superscript minus, single bond, C, double bond, C H 2. C 2 is single bonded to O on the right which is single bonded to P on the right. Two structures below the dotted lines read glucose 6, single bond, P and Glycerol 3, single bond, P. Arrows each from the first P atom of 1,3 B P G, and the P atoms from P E P, and creatinine phosphate point to the third P atom in A T P. Arrows each from the third P atom of A T P point to the P atoms of glucose 6, single bond, P and Glycerol 3, single bond, P. All the 6 P atoms that are connected by arrows are circled and highlighted in red.

Return to Graphical representation of the compounds with high phosphoryl-transfer potential that can be used to make A T P from A D P

Extended description for Structure of creatine phosphate

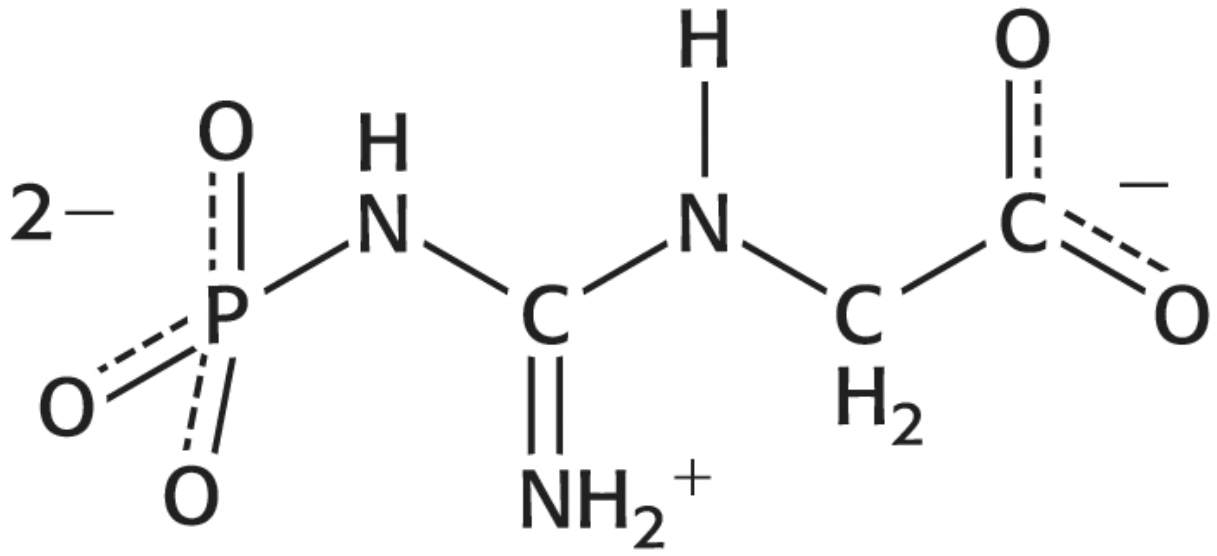


Creatine

The structure of creatine phosphate is as follows: A 1 N and 3 C heteronuclear alkane chain is depicted as a line structure using 3 zigzag lines. N occupies the second position. C 1 is single bonded to N H 2 on the top left and double bonded to N H 2 superscript plus below. N is single bonded to H above. C 2 is bound to H 2. C 3 is partially double bonded to O above and O on the lower right and has a counter negative sign.

Return to Structure of creatine phosphate

Extended description for Structure of creatine

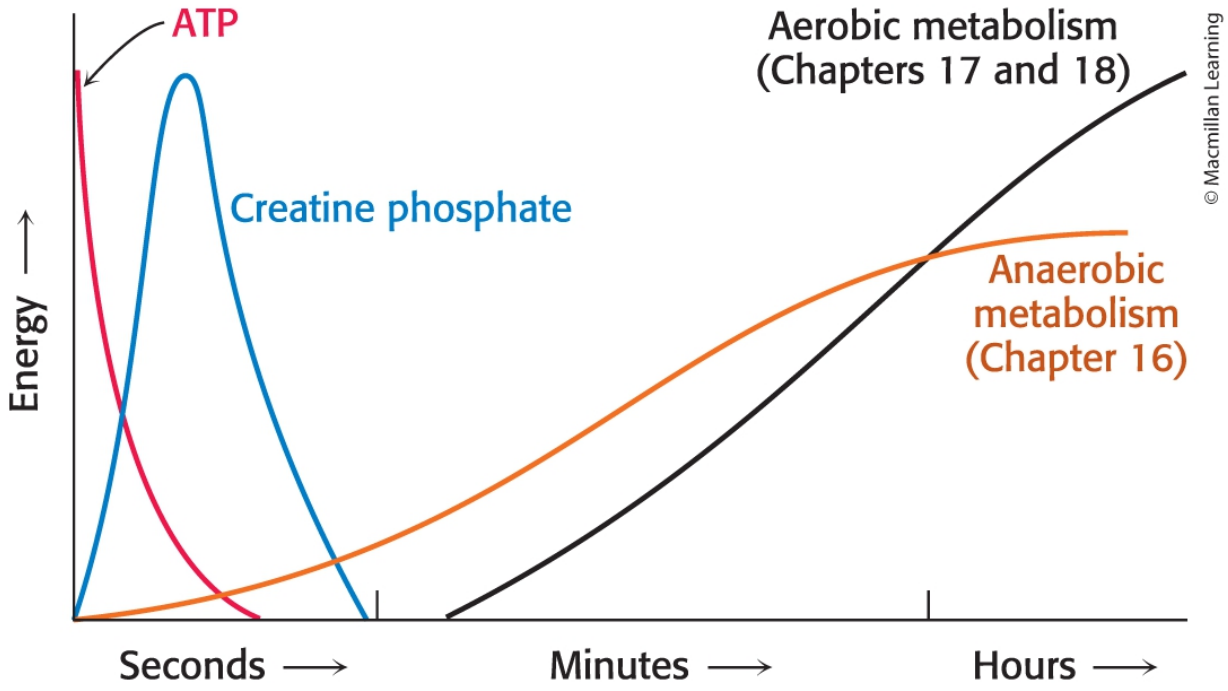


Creatine phosphate

The structure of creatine is as follows: A 2 N and 3 C heteronuclear alkane chain is depicted as a line structure using 4 zigzag lines. N 1 occupies the first position and N 2 occupies the third position. N 1 is bound to H above. N 1 is single bonded to P on the lower left. This P is partially double bonded to O above, O on the lower left, and O below and has a counter 2 minus sign. C 1 is double bonded to N H 2 superscript plus below. N 2 is single bonded to H above. C 2 is bound to H 2 below. C 3 is partially double bonded to O above and O on the lower right and has a counter negative sign.

Return to Structure of creatine

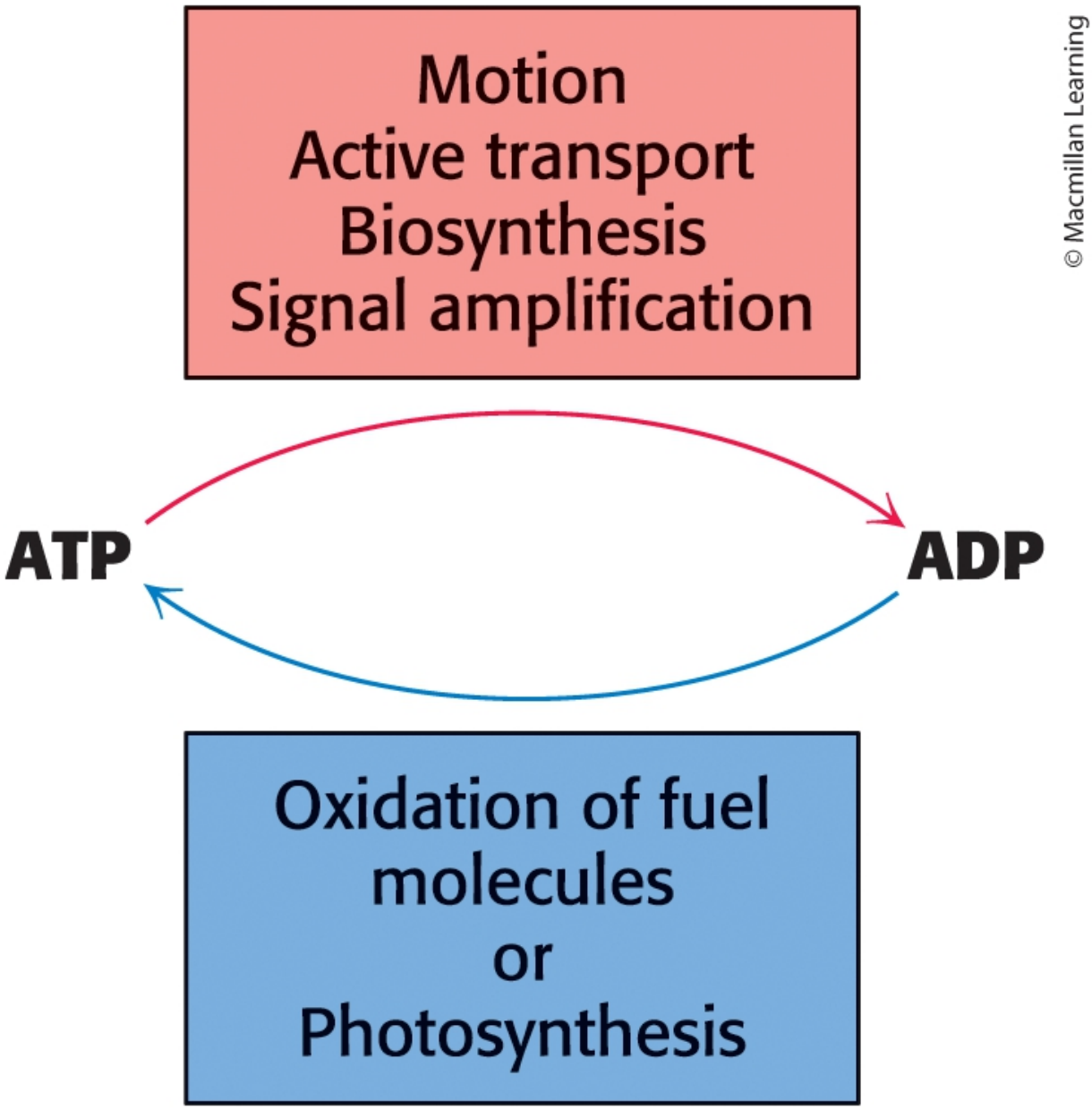
Extended description for Graphical representation of the sources of A T P change as exercise duration increases



The horizontal axis has markings from left to right labeled second, minutes, and hours. The vertical axis is labeled energy. The graph shows four curves. The first curve is an S-shaped orange curve labeled anaerobic metabolism (Chapter 16) that starts from the origin and ends at hours and mid energy. The second curve is an S-shaped black curve labeled aerobic metabolism (chapters 17 and 18) that starts between seconds and minutes on the horizontal axis and moves toward the upper right at hours and high energy. The third curve is blue and labeled creatinine phosphate. The curve starts from origin, rises to a peak at seconds on the horizontal axis, and falls steeply between seconds and minutes on the horizontal axis. The fourth pink curve starts at high energy on the vertical axis and exponentially decreases to seconds on the horizontal axis.

Return to Graphical representation of the sources of A T P change as exercise duration increases

Extended description for A T P and A D P cycle



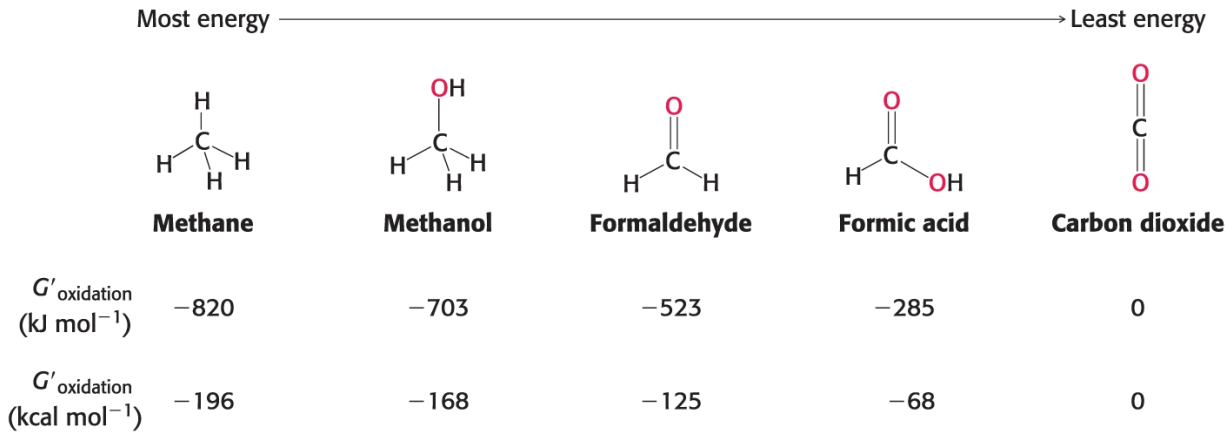
© Macmillan Learning

The figure reads A T P on the left and A D P on the right. A red curvy arrow from A T P points to A D P. A blue curvy arrow from A D P points to A T P. The text placed in a box above the red arrow reads: “Motion active transport biosynthesis signal amplification.” The text

placed in a box below the blue arrow reads: “Oxidation of fuel molecules or photosynthesis.”

Return to A T P and A D P cycle

Extended description for Free energy of oxidation of single-carbon compounds increases with the degree of hydrogen saturation from most energy on the left to least energy on the right



The compounds from left to right include methane, methanol, formaldehyde, formic acid, and carbon dioxide.

The structure of methane is as follows: A central C atom is single bonded to H above, H on the lower left, H below, and H on the lower right.

The structure of methanol is as follows: A central C atom is single bonded to O H above, H on the lower left, H below, and H on the lower right. The O atom from O H is highlighted in red.

The structure of formaldehyde is as follows: A central C atom is double bonded to O above, single bonded to H on the lower left, and single bonded to H on the lower right. O atom above is highlighted in red.

The structure of formic acid is as follows: A central C atom is double bonded to O above, single bonded to H on the lower left, and single bonded to O H on the lower right. The O atom above and O from O H on the lower right are highlighted in red.

The structure of carbon dioxide is as follows: A central C atom is double bonded to O above and double bonded to O below. Both the O atoms are highlighted in red.

The G dash oxidation in K J mol superscript minus 1 for methane is negative 820 and G dash oxidation in k c a l mol superscript minus 1 for methane is negative 196.

The G dash oxidation in K J mol superscript minus 1 for methanol is negative 703 and G dash oxidation in k c a l mol superscript minus 1 for methanol is negative 168.

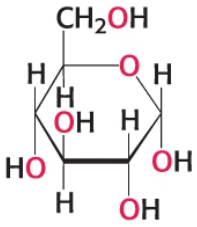
The G dash oxidation in K J mol superscript minus 1 for formaldehyde is negative 523 and G dash oxidation in k c a l mol superscript minus 1 for formaldehyde is negative 125.

The G dash oxidation in K J mol superscript minus 1 for formic acid is negative 285 and G dash oxidation in k c a l mol superscript minus 1 for formic acid is negative 68.

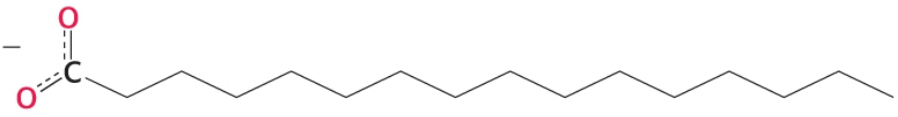
The G dash oxidation in K J mol superscript minus 1 for carbon dioxide is 0 and G dash oxidation in k c a l mol superscript minus 1 for carbon dioxide is 0.

Return to Free energy of oxidation of single-carbon compounds increases with the degree of hydrogen saturation from most energy on the left to least energy on the right

Extended description for Structures of glucose and saturated fatty acids



Glucose



Saturated fatty acid

The structure of glucose is as follows: A 6-membered heterocyclic hexagonal ring is in a horizontal orientation and consists of 1 O and 5 C atoms. The O atom occupies the first position, which is the top right vertex. C 1, C 2, and C 4 are each single bonded to H above and O H below. C 3 is single bonded to O H above and H below. C 5 is single bonded to C H 2 O H above and H below. All the O atoms in the heterocyclic ring are highlighted in red.

The structure of saturated fatty acid is as follows: A 16-carbon alkane chain is depicted as a line structure using 15 zigzag lines. C 1 is partially double bonded to the O atom above and partially double bonded to another O atom on the lower left. O atoms are highlighted in red.

Return to Structures of glucose and saturated fatty acids

Extended description for Reaction for oxidation of glyceraldehyde 3-phosphate to 3-Phosphoglyceric acid



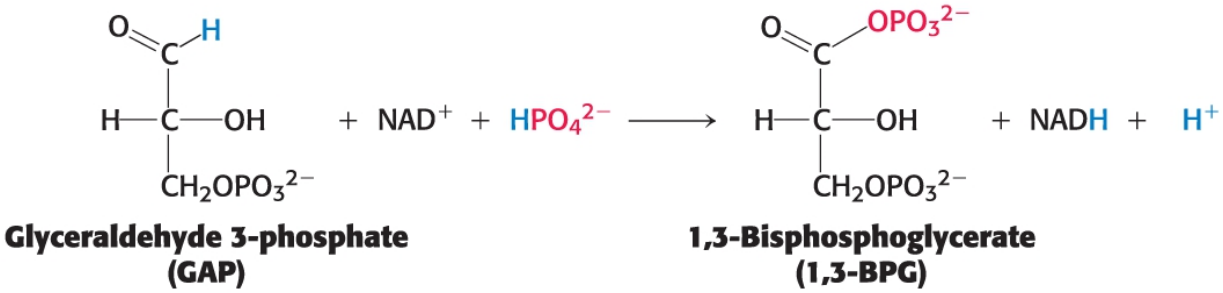
Glyceraldehyde 3-phosphate **3-Phosphoglyceric acid**

The structure of Glyceraldehyde 3-phosphate is as follows: The Fischer projection consists of a vertical chain with C above and C H 2 O P O 3 superscript 2 minus below. The projection contains a C atom at the center of the vertical line. The C atoms are numbered from top to bottom. C 1 is highlighted in red. C 1 is double bonded to O on the upper left and single bonded to H on the upper right. C 2 is single bonded to H on the left and O H on the right.

The structure of 3-Phosphoglyceric acid is as follows: The Fischer projection consists of a vertical chain with C above and C H 2 O P O 3 superscript 2 minus below. The projection contains a C atom at the center of the vertical line. The C atoms are numbered from top to bottom. C 1 is highlighted in red. C 1 is double bonded to O on the upper left and single bonded to H on the upper right. C 2 is single bonded to H on the left and O H on the right.

Return to Reaction for oxidation of glyceraldehyde 3-phosphate to 3-Phosphoglyceric acid

Extended description for Reaction for the formation of 1,3-Bisphosphoglycerate



Glyceraldehyde 3-phosphate reacts with N A D superscript plus and H P O 4 superscript 2 minus to give rise to 1,3-Bisphosphoglycerate plus N A D H plus H superscript plus.

The structure of glyceraldehyde 3-phosphate (G A P) is as follows: The Fischer projection consists of a vertical chain with C above and C H 2 O P O 3 superscript 2 minus below. The projection contains a C atom at the center of the vertical line. The C atoms are numbered from top to bottom. C 1 is double bonded to O on the upper left and single bonded to H on the upper right. The H on the upper right is highlighted in blue. C 2 is single bonded to H on the left and O H on the right.

In the third reactant H P O 4 superscript 2 minus, H is highlighted in blue and P O 4 superscript 2 minus is highlighted in red.

The structure of 1,3-Bisphosphoglycerate (1,3-B P G) is as follows: The Fischer projection consists of a vertical chain with C above and C H 2 O P O 3 superscript 2 minus below. The projection contains a C atom at the center of the vertical line. The C atoms are numbered from top to bottom. C 1 is double bonded to O on the upper left. C 1 is single bonded to O P O 3 superscript 2 minus on the upper right

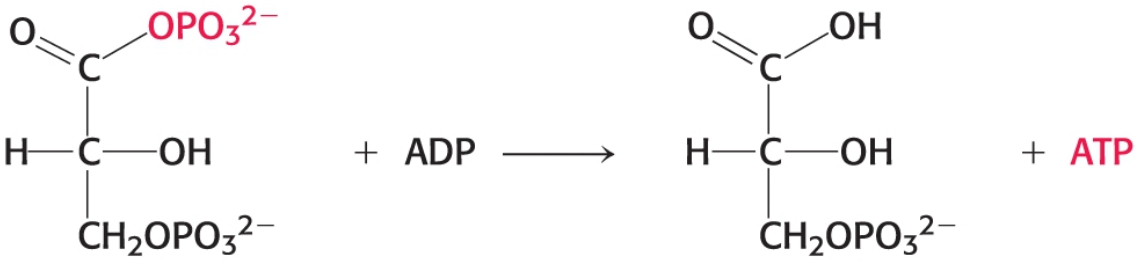
and highlighted in red. C 2 is single bonded to H on the left and O H on the right.

In the second product N A D H, H is highlighted in blue.

In the third product H superscript plus is highlighted in blue.

Return to Reaction for the formation of 1,3-Bisphosphoglycerate

Extended description for Reaction for the formation of 3-phosphoglyceric acid



1,3-Bisphosphoglycerate **3-Phosphoglyceric acid**

1,3-Bisphosphoglycerate reacts with A D P to form 3-phosphoglyceric acid and A T P.

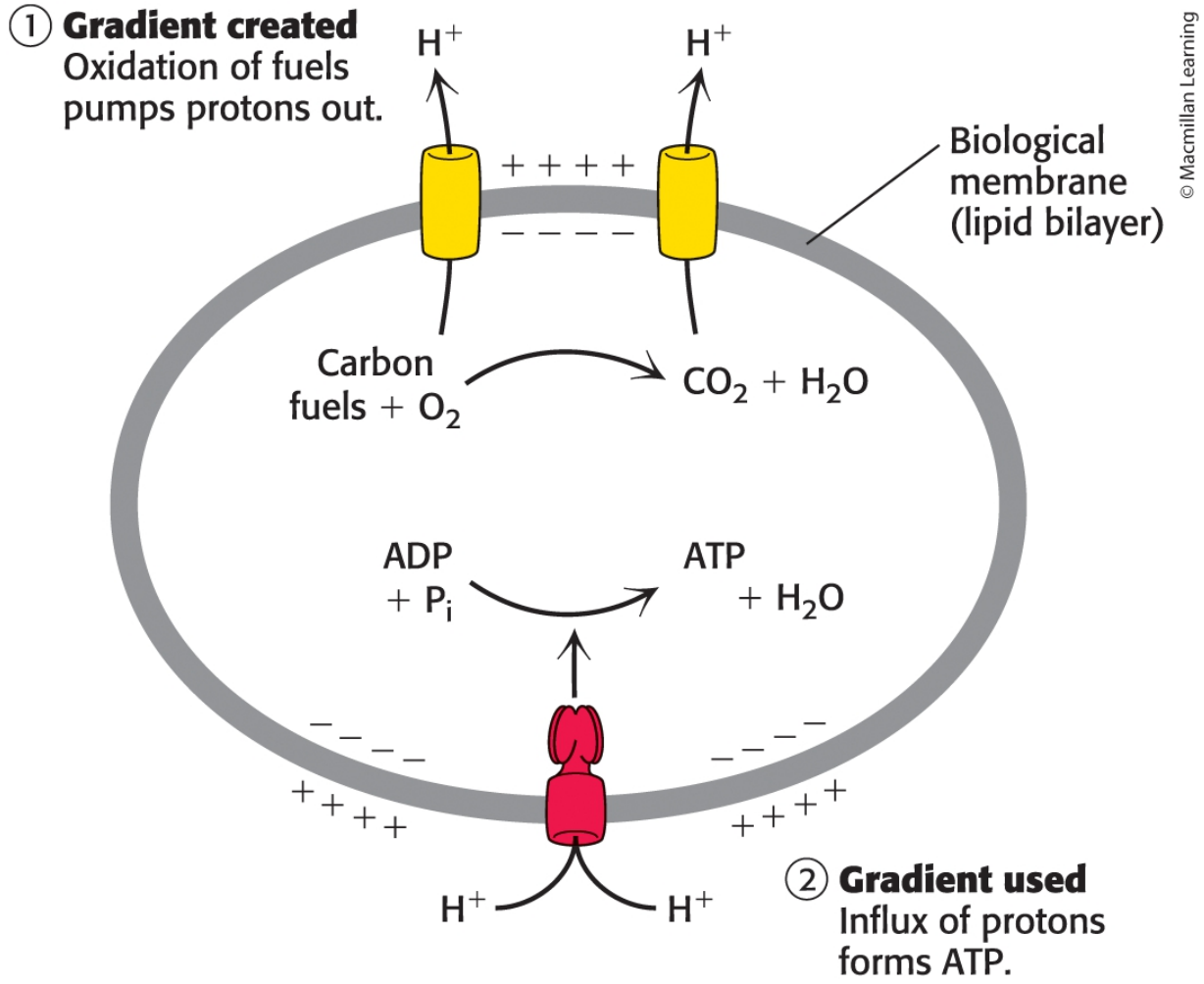
The structure of 1,3-Bisphosphoglycerate is as follows: The Fischer projection consists of a vertical chain with C above and C H 2 O P O 3 superscript 2 minus below. The projection contains a C atom at the center of the vertical line. The C atoms are numbered from top to bottom. C 1 is double bonded to O on the upper left. C 1 is single bonded to O P O 3 superscript 2 minus on the upper right and highlighted in red. C 2 is single bonded to H on the left and O H on the right.

The structure of 3-Phosphoglyceric acid is as follows: The Fischer projection consists of a vertical chain with C above and C H 2 O P O 3 superscript 2 minus below. The projection contains a C atom at the center of the vertical line. The C atoms are numbered from top to bottom. C 1 is double bonded to O on the upper left and O H on the upper right. C 2 is single bonded to H on the left and O H on the right.

The second product A T P is highlighted in red.

Return to Reaction for the formation of 3-phosphoglyceric acid

Extended description for Proton gradients formed in the biological membrane using energy from either sunlight or chemical oxidation can power A T P synthesis

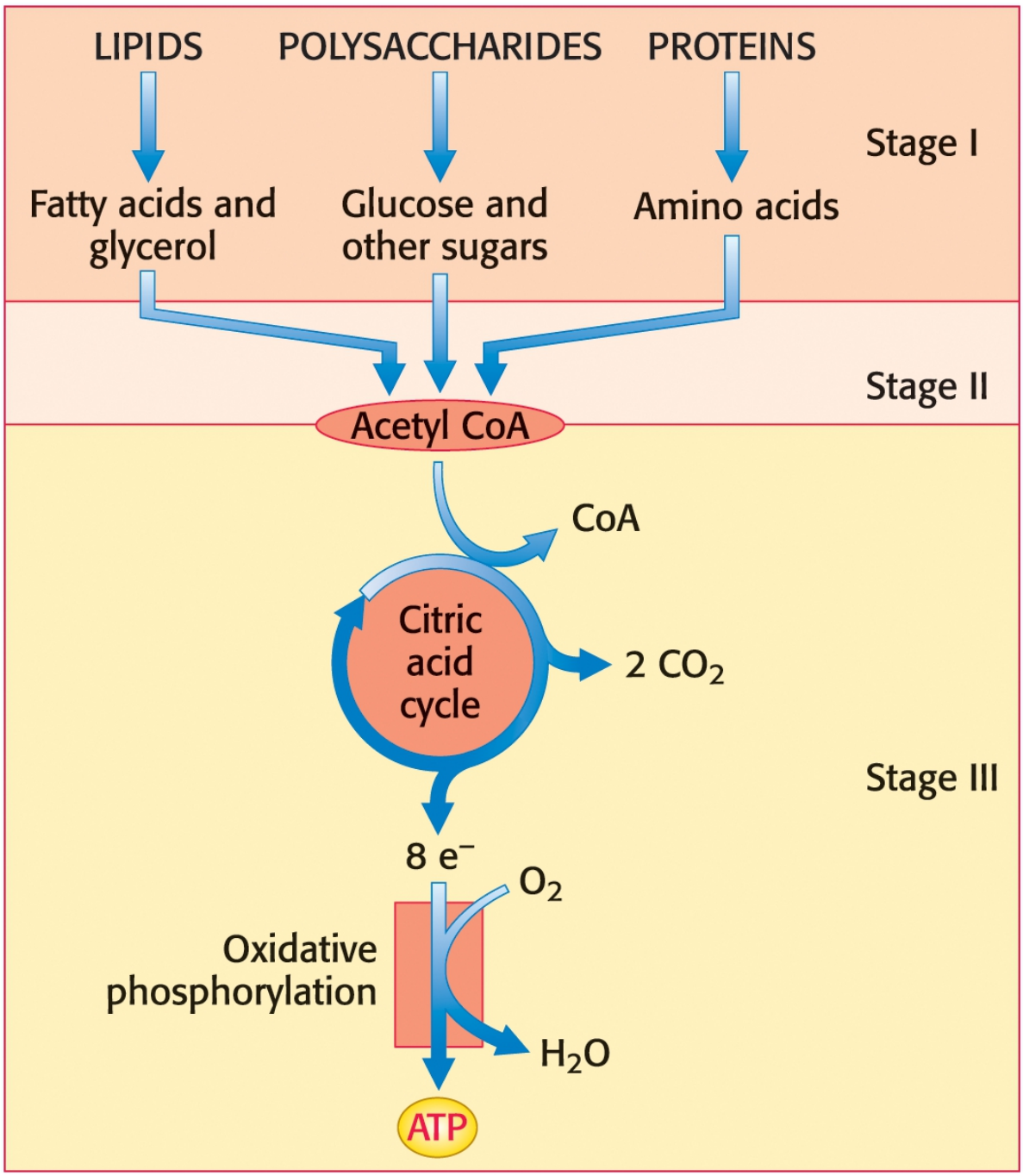


The figure shows a thick oval structure labeled biological membrane (lipid bilayer). The upper portion of the oval has two yellow cylindrical structures that depict proton pumps. The lower portion has a red cylindrical structure that depicts A T P synthesizing enzyme complex. Arrows from two yellow cylinders emerge outside.

The head of the arrow reads H superscript plus. The upper outer surface of the oval has four positive charges aligned in a row and the inner surface of the oval has four negative charges aligned in a row. An equation inside the oval close to the yellow cylinders reads Carbon fuels plus O 2 gives C O 2 plus H 2 O. Two H superscript plus ions from the lower region of the biological membrane enter the membrane through the red cylinder and point to an equation inside the oval that reads A D P plus P i gives A T P plus H 2 O. A text on the top left reads gradient created oxidation of fuels pumps protons out. A text on the bottom right reads gradient used influx of protons forms A T P.

Return to Proton gradients formed in the biological membrane using energy from either sunlight or chemical oxidation can power A T P synthesis

Extended description for Three stages of extraction of energy from food to form A T P in aerobic organisms

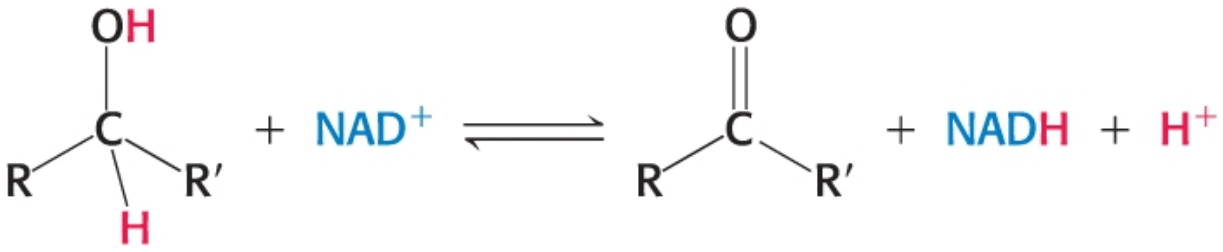


© Macmillan Learning

The flow chart starts with stage 1. In stage 1, lipids are hydrolyzed to fatty acids and glycerol, polysaccharides are hydrolyzed to glucose and other sugars, and proteins are hydrolyzed to amino acids. These products are converted to Acetyl C o A in stage 2. The acetyl C o A then enters the citric acid cycle in stage 3 where C o A, 2 C O 2, and 8 electrons are liberated. The 8 electrons undergo oxidative phosphorylation to produce A T P by converting O 2 to H 2 O.

Return to Three stages of extraction of energy from food to form A T P in aerobic organisms

Extended description for Reaction for the formation of N A D H



The two reactants combine by equilibrium reaction to form three products.

The structure of the first reactant is as follows: A central C atom is single bonded to O H above, R on the lower left, H below, and R dash on the lower right. H from O H above and H below are highlighted in red.

The second reactant N A D superscript plus is highlighted in blue.

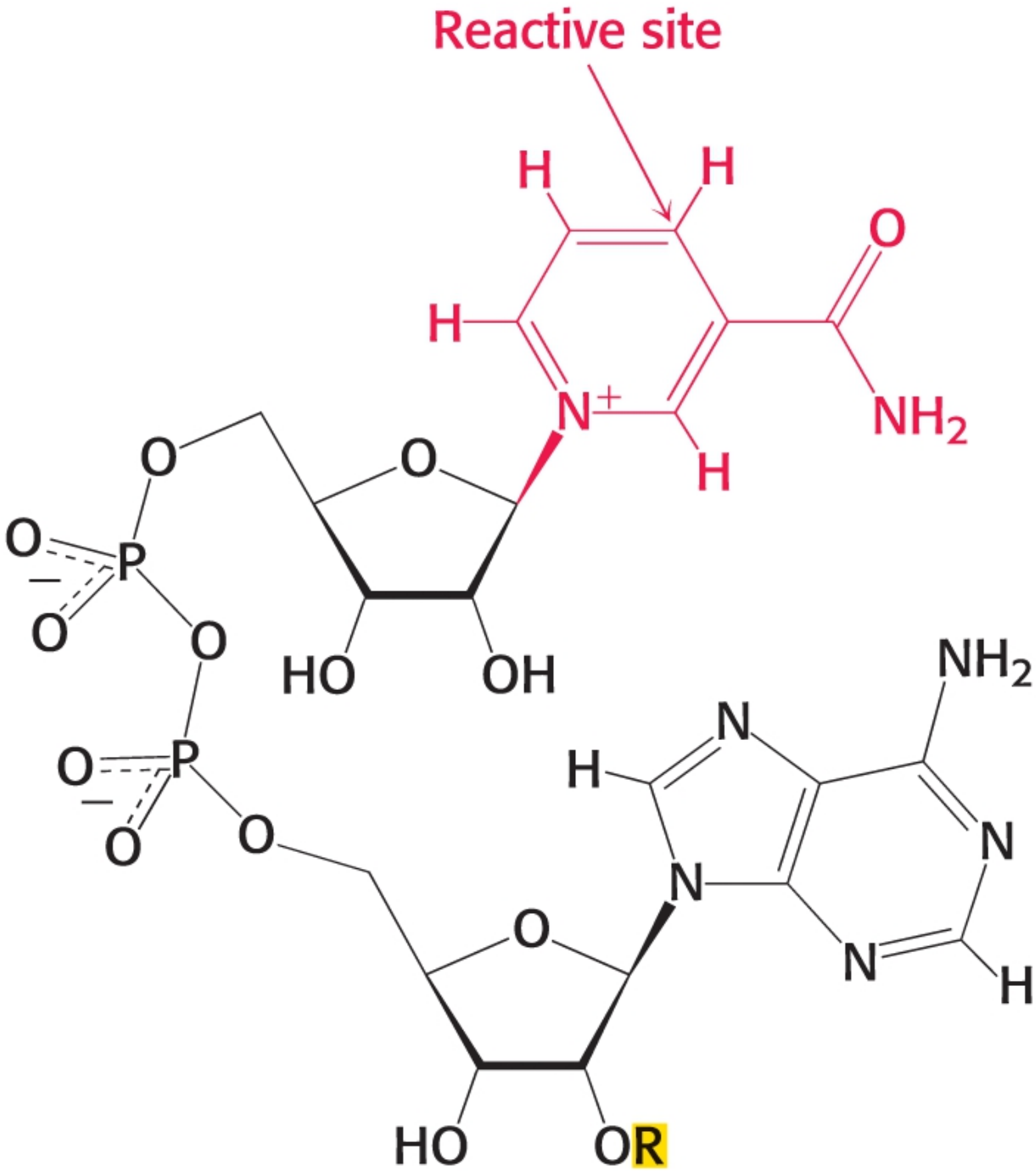
The structure of the first product is as follows: A central C atom is double bonded to O above, single bonded to R on the lower left, and R dash on the lower right.

In the second product, N A D H, N A D is highlighted in blue and H is highlighted in red.

The third product H superscript plus is highlighted in red.

Return to Reaction for the formation of N A D H

Extended description for Structure of oxidized forms of N A D superscript plus and N A D P superscript plus

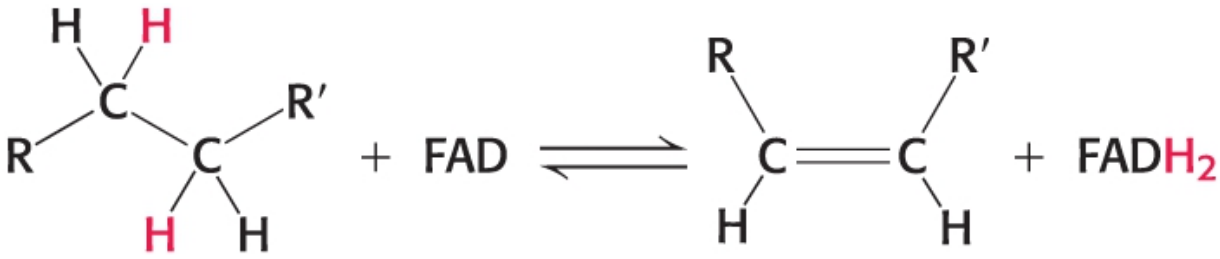


A 6-membered heterocyclic hexagonal ring is in a horizontal orientation and consists of 1 N and 5 C atoms with N superscript plus occupying the first position which is the bottom left vertex. Double bonds are present between N superscript plus and C 1, C 2 and C 3, and C 4 and C 5 atoms. C 1, C 2, C 3, and C 5 are each single bonded to H. C 3 is labeled reactive site. C 4 is single bonded to C on the right in the form of a line. This C is double bonded to O on the top right and single bonded to N H 2 on the bottom right. The 6-membered ring is highlighted in red. N superscript plus is wedge bonded to C 1 of a 5-membered heterocyclic pentagonal ring in a vertical orientation consisting of 1 O and 4 C atoms. O occupies the first position, which is the topmost vertex. The 5-membered ring is in a plane perpendicular to the plane of the paper such that C 2 and C 3 are toward the observer and O is away from the observer. C 2 and C 3 are single bonded to O H. C 4 is single bonded to C H 2 on the top left in the form of a line. This C H 2 is single bonded to O on the bottom left. The O atom is single bonded to P on the lower left. P atom is partially double bonded to O superscript minus on the upper left and O on the lower left. P is also single bonded to O in the lower right. This O is single bonded to P below. This P atom is partially double bonded to O on the left and O superscript minus on the bottom left. P is also single bonded to O on the lower right. This O is single bonded to C H 2 in the form of a line which in turn is single bonded to C 4 of a second 5-membered heterocyclic pentagonal ring in a vertical orientation consisting of 1 O and 4 C atoms. O occupies the first position, which is the topmost vertex. The 5-membered ring is in a plane perpendicular to the plane of the paper such that C 2 and C 3 are toward the observer and O is away from the observer. C 2 is single bonded to O R and C 3 is single bonded to O H. C 1 is wedge bonded to the first N atom of a third 5-membered heterocyclic pentagonal ring in a vertical orientation consisting of 2 N and 3 C atoms. The first N atom occupies the first position which is the bottom left vertex and the second N atom occupies the third position which is the topmost vertex. Double bonds are present between C 1

and the second N atom, and C 2 and C 3. C 1 is single bonded to H. The 5-membered ring is fused to a second 6-membered heterocyclic hexagonal ring in a vertical orientation consisting of 2 N and 4 C atoms. The first N atom occupies the first position which is the top right vertex and the second N atom occupies the third position which is the bottommost vertex. Double bonds are present between C 1 and the second N atom and C 4 and the first N atom. C 1 is single bonded to H and C 4 is single bonded to N H 2. The two rings are fused such that C 1 and C 2 of the third 5-membered ring are C 3 and C 2 of the second 6-membered ring, respectively.

Return to Structure of oxidized forms of N A D superscript plus and N A D P superscript plus

Extended description for Reaction for the formation of F A D H 2



The two reactants combine by equilibrium reaction to form two products.

The structure of the first product is as follows: A 2-carbon alkane chain is depicted as a line structure using one line. C 1 is single bonded to R on the lower left, H on the upper left, and H on the upper right. H on the upper right is highlighted in red. C 2 is single bonded to R dash on the upper right, H on the lower right, and H on the lower left. H on the lower left is highlighted in red.

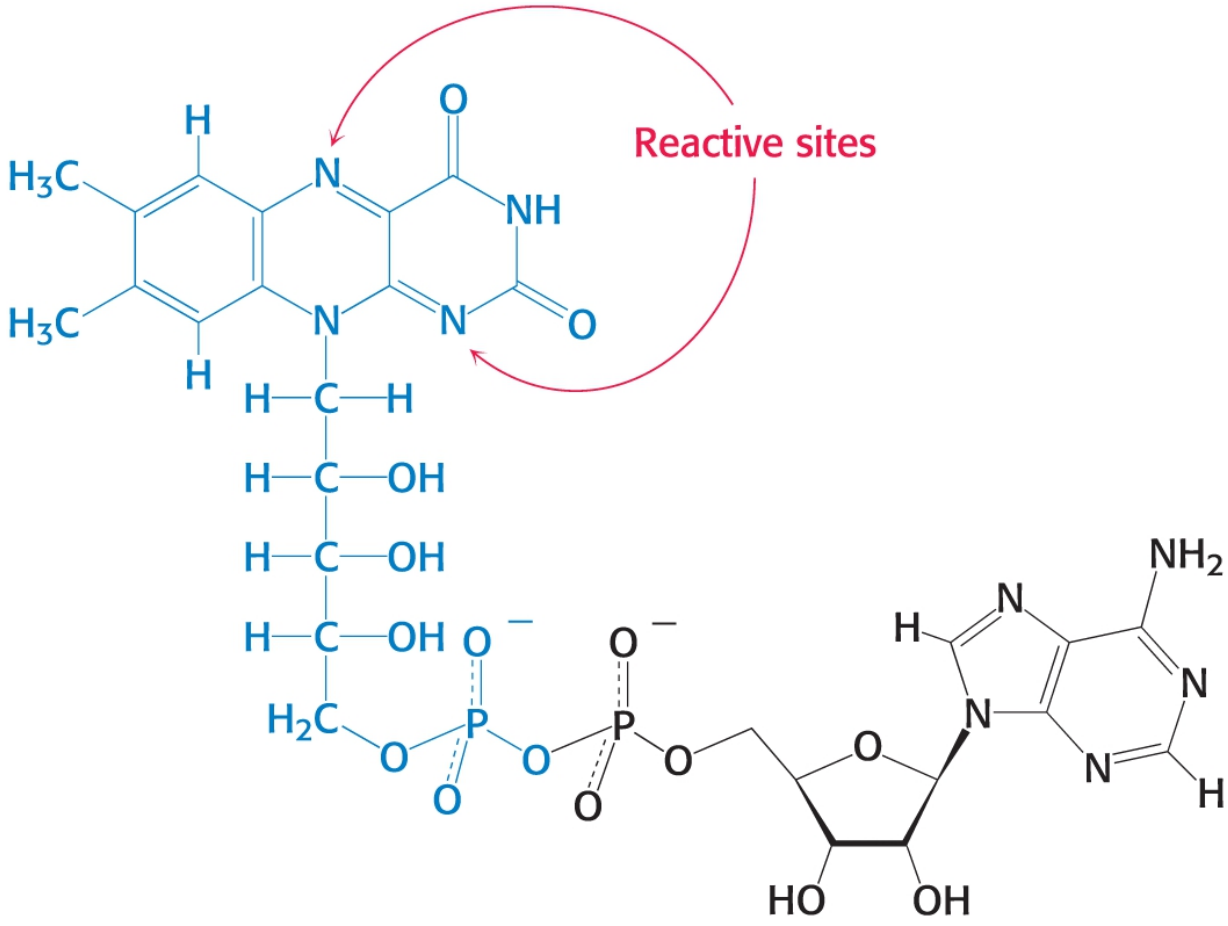
The second reactant is F A D.

The structure of the first product is as follows: C, double bond, C. C 1 is single bonded to R on the upper left and H on the lower left. C 2 is single bonded to R dash on the upper right and H on the lower right.

In the second product F A D H 2, H 2 is highlighted in red.

Return to Reaction for the formation of F A D H 2

Extended description for Structure of flavin adenine dinucleotide



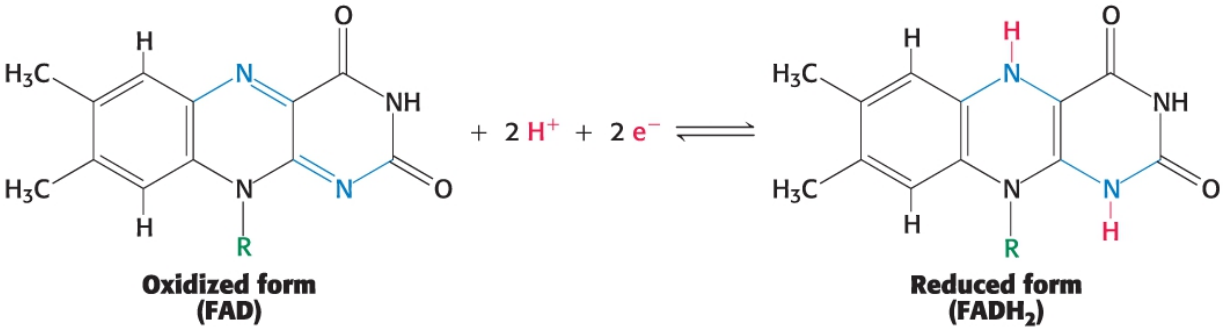
A benzene ring in a vertical orientation with C 1 occupying the topmost vertex is fused to a 6-membered heterocyclic hexagonal ring in a vertical orientation consisting of 2 N and 4 C atoms. The first N atom occupies the first position, which is the topmost vertex and the second N atom occupies the fourth position which is the bottommost vertex. The two rings are fused to each other such that C 2 and C 3 of the benzene ring are the C 4 and C 3 of the 6-membered ring, respectively. The benzene ring contains alternating double bonds between C 2 and C 3, C 4 and C 5, and C 6 and C 1. C 1

and C 4 are each single bonded to H. C 5 and C 6 are each single bonded to C H 3. In the 6-membered ring, a double bond is present between the first N atom and C 1. The heterocyclic hexagonal ring is fused to a second 6-membered heterocyclic hexagonal ring in a vertical orientation consisting of 2 N and 4 C atoms. The first N atom bound to H occupies the first position which is the top right vertex. The second N atom occupies the third position which is the bottommost vertex. The two rings are fused to each other such that C 1 and C 2 of the first heterocyclic ring are C 3 and C 2 of the second heterocyclic ring, respectively. A double bond is present between the second N atom and C 2. C 1 and C 4 are each double bonded to O. The first N atom of the first heterocyclic ring and the second N atom of the second heterocyclic ring are labeled reactive sites. The second N atom of the first heterocyclic ring is single bonded below to C 1 of a vertical chain consisting of 5 C atoms placed vertically. C 1 is single bonded to H on the left and H on the right. C 2, C 3, and C 4 are each single bonded to H on the left and O H on the right. C 5 bound to H 2 is single bonded to O on the lower right. O is single bonded to a P atom on the upper right. The P atom is partially double bonded to O superscript minus above and O on the lower left. P is also single bonded to O on the lower right. The structures until this point are highlighted in blue. The structures beyond this are highlighted in black. The O atom is single bonded to P on the upper right. The P atom is partially double bonded to O superscript minus above and O on the lower left. P is also single bonded to O on the lower right. The O atom is single bonded to C H 2 on the upper right in the form of a line. This C H 2 is single bonded to C 4 of a 5-membered pentagonal ring in a vertical orientation with O occupying the topmost vertex. The pentagonal ring is in a plane perpendicular to the plane of the paper such that C 2 and C 3 are toward the observer and O is away from the observer. C 2 and C 3 are each single bonded to O H. C 1 is wedge bonded to N of a second 5-membered pentagonal heterocyclic ring in a vertical orientation consisting of 2 N and 3 C atoms such that the first N atom occupies the first position which is

the bottom left vertex and the second N atom occupies the third position which is the topmost vertex. C 1 is single bonded to H. Double bonds are present between C 1 and the second N atom, and C 2 and C 3. This 5-membered ring is fused to a third 6-membered heterocyclic hexagonal ring consisting of 2 N and 4 C atoms. The first N atom occupies the first position which is the top right vertex. The second N atom occupies the third position which is the bottommost vertex. A double bond is present between C 4 and the first N atom and C 1 and the second N atom. C 1 is single bonded to H. C 4 is single bonded to N H 2. The two rings are fused to each other such that C 2 and C 3 of the second pentagonal ring are C 3 and C 2 of the third 6-membered heterocyclic ring.

Return to Structure of flavin adenine dinucleotide

Extended description for Reaction for the formation of reduced form (F A D H 2) from oxidized form (F A D)



The reaction shows that oxidized form (F A D) reacts with 2 H superscript plus and 2 electrons to produce the reduced form (F A D H 2).

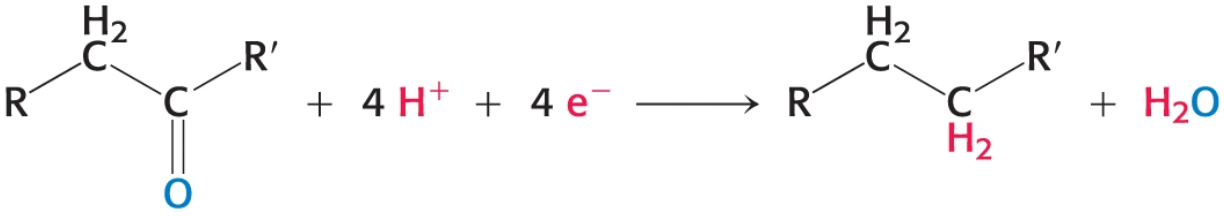
The structure of oxidized form (F A D) is as follows: A benzene ring in a vertical orientation with C 1 occupying the topmost vertex is fused to a 6-membered heterocyclic hexagonal ring in a vertical orientation consisting of 2 N and 4 C atoms. The first N atom occupies the first position, which is the topmost vertex and the second N atom occupies the fourth position which is the bottommost vertex. The second N atom is single bonded to R. The first N atom, C 1, and C 4 are highlighted in blue. The two rings are fused to each other such that C 2 and C 3 of the benzene ring are the C 4 and C 3 of the 6-membered ring, respectively. The benzene ring contains alternating double bonds between C 2 and C 3, C 4 and C 5, and C 6 and C 1. C 1 and C 4 are each single bonded to H. C 5 and C 6 are each single bonded to C H 3. In the 6-membered ring, a double bond is present between the first N atom and C 1. The heterocyclic hexagonal ring is fused to a second 6-membered heterocyclic hexagonal ring in a vertical orientation consisting of 2 N and 4 C atoms. The first N atom bound to H occupies the first position which

is the top right vertex. The second N atom occupies the third position which is the bottommost vertex. The two rings are fused to each other such that C 1 and C 2 of the first heterocyclic ring are C 3 and C 2 of the second heterocyclic ring. C 1, the second N atom, and C 2 are highlighted in blue. A double bond is present between the second N atom and C 2. C 1 and C 4 are each double bonded to O.

The structure of reduced form (F A D H 2) is as follows: A benzene ring in a vertical orientation with C 1 occupying the topmost vertex is fused to a 6-membered heterocyclic hexagonal ring in a vertical orientation consisting of 2 N and 4 C atoms. The first N atom occupies the first position, which is the topmost vertex and the second N atom occupies the fourth position which is the bottommost vertex. The first N atom is single bonded to H highlighted in red. The second N atom is single bonded to R. The first N atom and C 4 are highlighted in blue. The two rings are fused to each other such that C 2 and C 3 of the benzene ring are the C 4 and C 3 of the 6-membered ring, respectively. The benzene ring contains alternating double bonds between C 2 and C 3, C 4 and C 5, and C 6 and C 1. C 1 and C 4 are each single bonded to H. C 5 and C 6 are each single bonded to C H 3. The heterocyclic hexagonal ring is fused to a second 6-membered heterocyclic hexagonal ring in a vertical orientation consisting of 2 N and 4 C atoms. The first N atom bound to H occupies the first position which is the top right vertex. The second N atom occupies the third position which is the bottommost vertex. The two rings are fused to each other such that C 1 and C 2 of the first heterocyclic ring are C 3 and C 2 of the second heterocyclic ring. C 1, the second N atom, and C 2 are highlighted in blue. C 1 and C 4 are each double bonded to O. The second N atom is single bonded to H highlighted in red.

Return to Reaction for the formation of reduced form (F A D H 2) from oxidized form (F A D)

Extended description for Reaction for the biosynthesis of fatty acids



The three reactants combine to form two products.

The structure of the first product is as follows: A 2-carbon alkane chain is depicted as a line structure using one line. C 1 bound to H 2 is single bonded to R on the lower left. C 2 is single bonded to R dash on the upper right and double bonded to O below. O is highlighted in blue.

The second reactant is 4 H superscript plus. H superscript plus is highlighted in red.

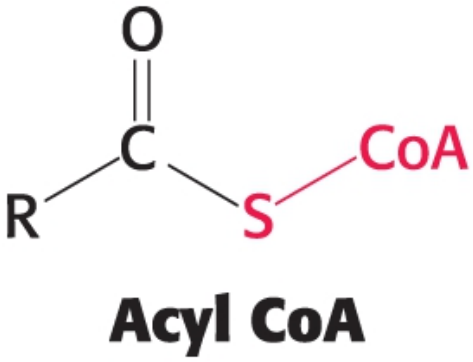
The third reactant 4 e superscript minus. e superscript minus is highlighted in red.

The structure of the first product is as follows: A 2-carbon alkane chain is depicted as a line structure using one line. C 1 bound to H 2 is single bonded to R on the lower left. C 2 bound to H 2 is single bonded to R dash on the upper right. H 2 bound to C 2 is highlighted in red.

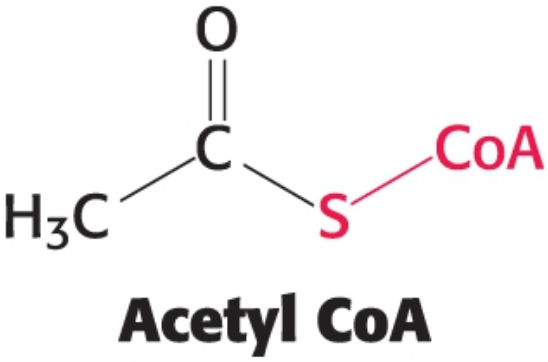
In the second product H 2 O, H 2 is highlighted in red and O is highlighted in blue.

Return to Reaction for the biosynthesis of fatty acids

Extended description for Structure of Acyl C o A and Acetyl C o A



Acyl CoA



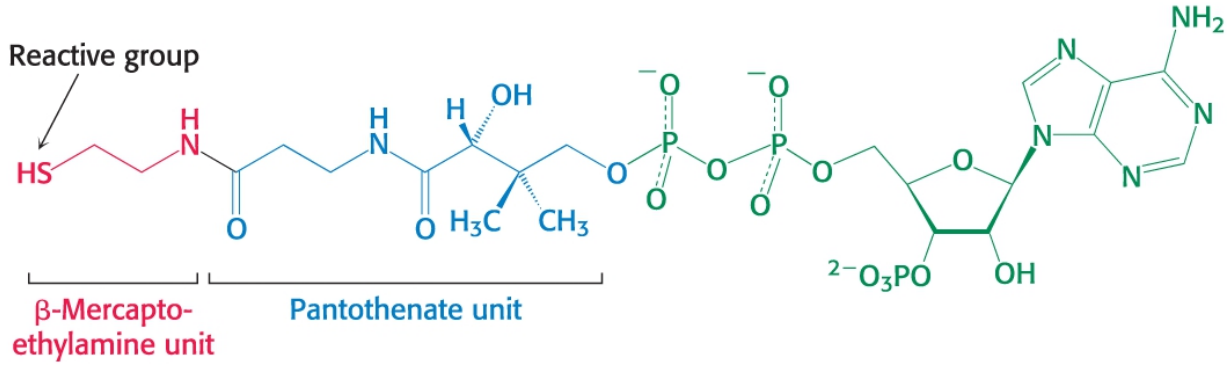
Acetyl CoA

The structure of Acyl C o A is as follows: A central C atom is double bonded to O above. C is single bonded to R on the lower left and S on the lower right. S is further single bonded to C o A on the upper right. S and C o A are highlighted in red.

The structure of Acetyl C o A is as follows: A central C atom is double bonded to O above. C is single bonded to C H 3 on the lower left and S on the lower right. S is further single bonded to C o A on the upper right. S and C o A are highlighted in red.

Return to Structure of Acyl C o A and Acetyl C o A

Extended description for Structure of coenzyme A



A 2-carbon alkane chain is depicted as a line structure using one line. C 1 is single bonded to S H on the lower left and C 2 is single bonded to N H 2 on the upper right. This is labeled beta-mercaptoethylamine unit and highlighted in red. S H is labeled reactive group. N H is single bonded to a 1 N and 7 C alkane chain depicted as a line structure using 7 zigzag lines. N occupies the fourth position and is bound to N H. C 1 and C 4 are each double bonded to O below. C 5 is wedge bonded to H on the upper left and dash bonded to O H on the upper right. C 6 is wedge bonded to C H 3 on the lower left and dash bonded to C H 3 on the lower right. C 7 is single bonded to O on the lower right. This structure is labeled panthothenate unit and is highlighted in blue. The O atom is single bonded to P on the upper right, single bond, O, single bond, P, single bond O in the form of a zigzag line. P 1 and P 2 are each partially double bonded to O superscript minus above and O on the lower left. The second O atom in the zigzag line is single bonded to C. This C atom is single bonded to C 4 of a 5-membered heterocyclic pentagonal ring in vertical orientation consisting of 1 O and 4 C atoms with O occupying the topmost vertex. C 2 is single bonded to O H and C 3 is single bonded to O 3 superscript 2 minus P O. C 1 is wedge bonded to N 2 of a 5-membered heterocyclic pentagonal ring consisting of 2 N and 3 C atoms. N 1 occupies the first position which

is the topmost vertex and N 2 occupies the fourth position which is the bottom left vertex. Double bonds are present between C 1 and C 2, and C 3 and N 1. The 5-membered ring is fused with a 6-membered heterocyclic hexagonal ring in a vertical orientation such that it contains 2 N and 4 C atoms. N 1 occupies the first position which is the top right vertex and N 2 occupies the third position which is the bottommost vertex. Double bonds are present between C 1 and N 2 and C 4 and N 1. C 1 is single bonded to N H 2. The two rings are fused such that C 1 and C 2 of the 5-membered ring are C 3 and C 2 of the 6-membered ring respectively. The structure beyond panthothenate is highlighted in green.

Return to Structure of coenzyme A

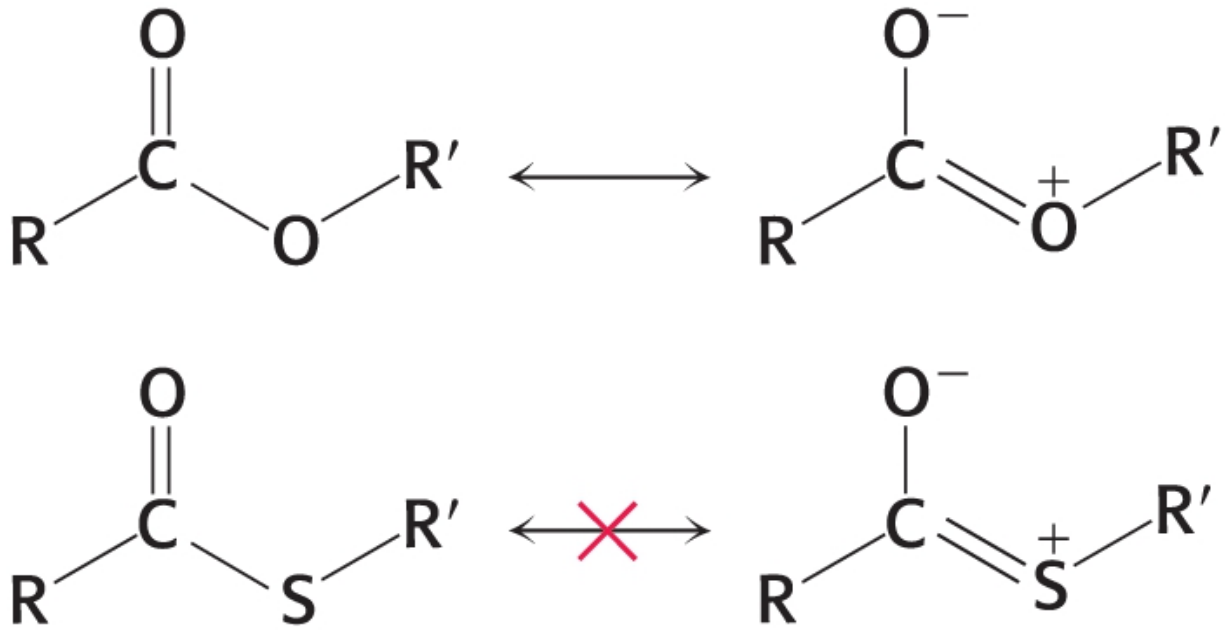
Extended description for Reversible reaction depicts the formation of acetate from acetyl C o A and its standard free energy change

$$\text{Acetyl CoA} + H_2O \rightleftharpoons \text{acetate} + \text{CoA} + H^+$$
$$\Delta G^{\circ\prime} = -31.4 \text{ kJ mol}^{-1} \ (-7.5 \text{ kcal mol}^{-1})$$

The reaction consists of two reactants and three products. The reactants are acetyl C o A and H 2 O. The products are acetate, C o A, and H superscript plus. The value of delta G nought prime is negative 31.4 kilojoules per mole or negative 7.5 kilocalories per mole.

Return to Reversible reaction depicts the formation of acetate from acetyl C o A and its standard free energy change

Extended description for Structures of oxygen esters and thioesters



Oxygen esters are stabilized by resonance structures not available to thioesters.

On the top, the figure shows two resonance structures of oxygen esters that are separated by double headed arrows.

The structure of the first oxygen ester on the left is as follows: A central C atom is double bonded to O above, single bonded to R on the lower left and single bonded to O on the lower right. This O is single bonded to R dash on the upper right.

The structure of the second oxygen ester on the left is as follows: A central C atom is single bonded to O superscript minus above, single

bonded to R on the lower left, and double bonded to O superscript plus on the lower right. This O superscript plus is single bonded to R dash on the upper right.

At the bottom, the figure shows two resonance structures of thioesters that are separated by double headed arrows and a cross is placed above this arrow.

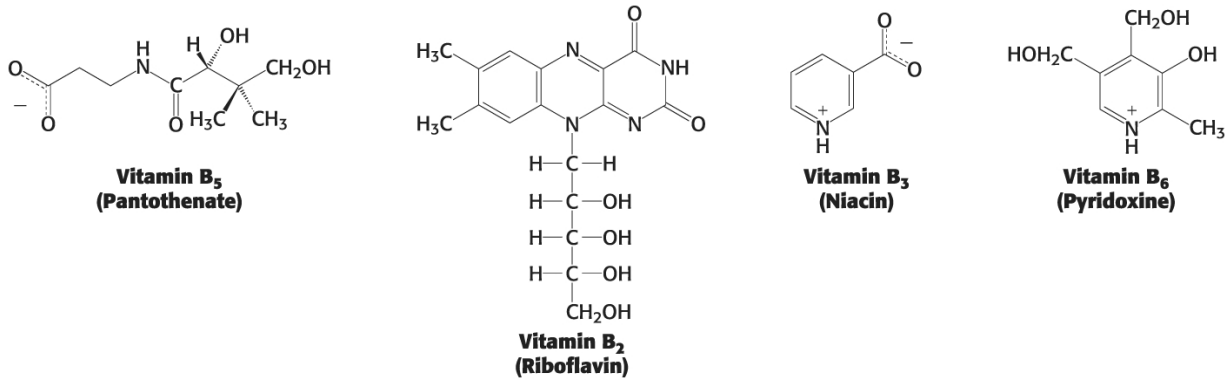
The structure of the first thioester on the left is as follows: A central C atom is double bonded to O above, single bonded to R on the lower left, and single bonded to S on the lower right. This S is single bonded to R dash on the upper right.

The structure of the second thioester on the left is as follows: A central C atom is single bonded to O superscript minus above, single bonded to R on the lower left and double bonded to S superscript plus on the lower right. This S superscript plus is single bonded to R dash on the upper right.

A text below reads: “Oxygen esters are stabilized by resonance structures not available to thioesters.”

Return to Structures of oxygen esters and thioesters

Extended description for Structures of water-soluble B vitamins



The structure of Vitamin B 5 (Panthotenate) is as follows: A 1 N and 6 C heteronuclear alkane chain is depicted as a line structure using 7 zigzag lines. N occupies the fourth position and is bound to H. C 1 is partially double bonded to O on the upper right and partially double bonded to O superscript minus below. C 4 is double bonded to O below. C 5 is wedge bonded to H on the upper left and dash bonded to O H on the upper right. C 6 is wedge bonded to C H 3 on the lower left and dash bonded to C H 3 on the lower right. C 6 is also single bonded to C H 2 O H on the upper right.

The structure of Vitamin B 2 (Riboflavin) is as follows: A benzene ring in a vertical orientation with C 1 occupying the topmost vertex is fused to another 6-membered heterocyclic hexagonal ring in vertical orientation consisting of 2 N and 4 C atoms. N 1 occupies the first position, which is the topmost vertex and N 2 occupies the fourth position which is the bottommost vertex. The two rings are fused to each other such that C 2 and C 3 of the benzene ring are the C 4 and C 3 of the 6-membered ring, respectively. The benzene ring contains alternating double bonds between C 2 and C 3, C 4 and C 5, and C 6 and C 1. C 5 and C 6 are each single bonded to C H 3. In the

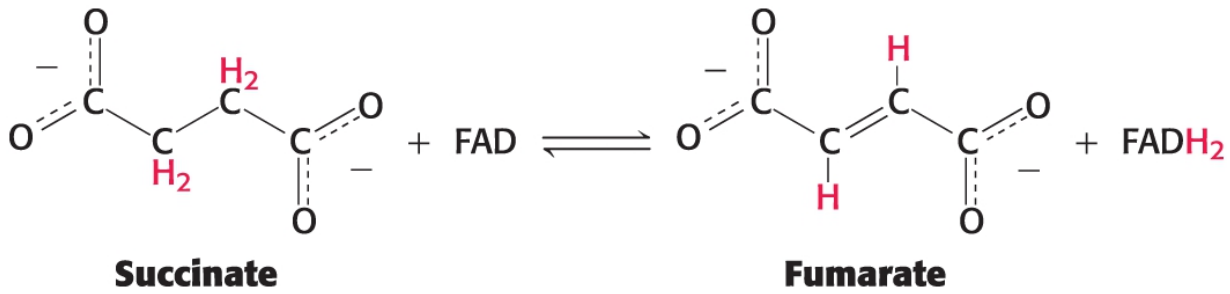
6-membered ring, a double bond is present between N 1 and C 1. The heterocyclic hexagonal ring is fused to another hexagonal ring in vertical orientation consisting of 2 N and 4 C atoms. The two rings are fused to each other such that C 1 and C 2 of the first heterocyclic ring are C 3 and C 2 of the second heterocyclic ring. N 1 bound to H occupies the first position which is the top right vertex. N 2 occupies the third position which is the bottommost vertex. A double bond is present between N 2 and C 2. C 1 and C 4 are each double bonded to O. N 2 of the first heterocyclic ring is attached to a Fischer projection consisting of a vertical line with 4 C atoms placed vertically with C H 2 O H at the bottom. The C atoms are numbered from top to bottom. C 1 is single bonded to H on the left and H on the right. C 2, C 3, and C 4 are each single bonded to H on the left and O H on the right.

The structure of Vitamin B 3 (Niacin) is as follows: A 6-membered hexagonal heterocyclic ring is in a vertical orientation consisting of 1 N and 5 C atoms with N H superscript plus occupying the first position which is the bottommost vertex. Double bonds are present between N H superscript plus and C 1, C 2 and C 3, and C 4 and C 5. C 4 is single bonded to a central C atom on the top right. The central C atom is partially double bonded to O above and O on the lower right and has a counter negative sign.

The structure of Vitamin B 6 (Pyridoxine) is as follows: A 6-membered hexagonal heterocyclic ring is in a vertical orientation consisting of 1 N and 5 C atoms. N atom bound to H superscript plus occupies the first position which is the bottommost vertex. Double bonds are present between N H superscript plus and C 1, C 2 and C 3, and C 4 and C 5. C 2 and C 3 are each single bonded to C H 2 O H. C 4 is single bonded to O H on the top right. C 5 is single bonded to C H 3 on the bottom right.

Return to Structures of water-soluble B vitamins

Extended description for Formation of Fumarate from Succinate



Succinate reacts with F A D through equilibrium reaction to produce Fumarate and F A D H 2.

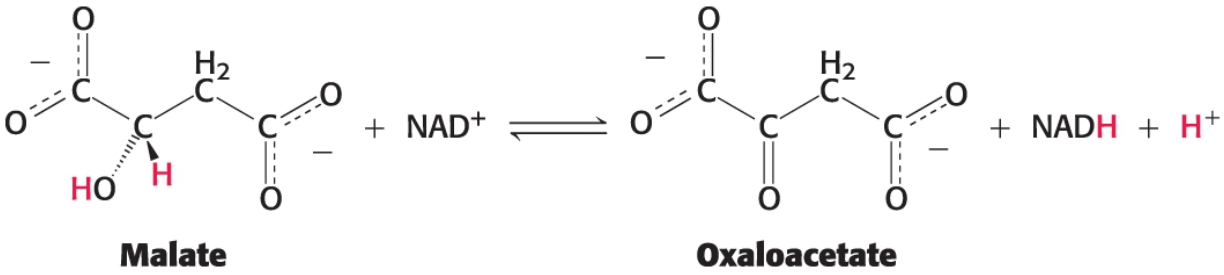
The structure of Succinate is as follows: A 4-carbon alkane chain is depicted as a line structure using 3 zigzag lines. C 1 is partially double bonded to O above and O on the lower left and has a counter negative sign. C 2 and C 3 are each bound to H 2 and these H 2 are highlighted in red. C 4 is partially double bonded to O on the upper right and O below and has a counter negative sign.

The structure of Fumarate is as follows: A 4-carbon alkene chain is depicted as a line structure using 3 zigzag lines. A double bond is present between C 2 and C 3. C 1 is partially double bonded to O above and O on the lower left and has a counter negative sign. C 2 is single bonded to H below and highlighted in red. C 3 is single bonded to H above and highlighted in red. C 4 is partially double bonded to O on the upper right and O below and has a counter negative sign.

In the product F A D H 2, H 2 is highlighted in red.

Return to Formation of Fumarate from Succinate

Extended description for Formation of oxaloacetate from malate



Malate reacts with N A D superscript plus through equilibrium reaction to produce oxaloacetate, N A D H and H superscript plus.

The structure of Malate is as follows: A 4-carbon alkane chain is depicted as a line structure using 3 zigzag lines. C 1 is partially double bonded to O above and O on the lower left and has a counter negative sign. C 2 is dash bonded to O H on the lower left and wedge bonded to H on the lower right. The H from O H on the lower left and H on the lower right are highlighted in red. C 3 is bound to H 2. C 4 is partially double bonded to O on the upper right and O below and has a counter negative sign.

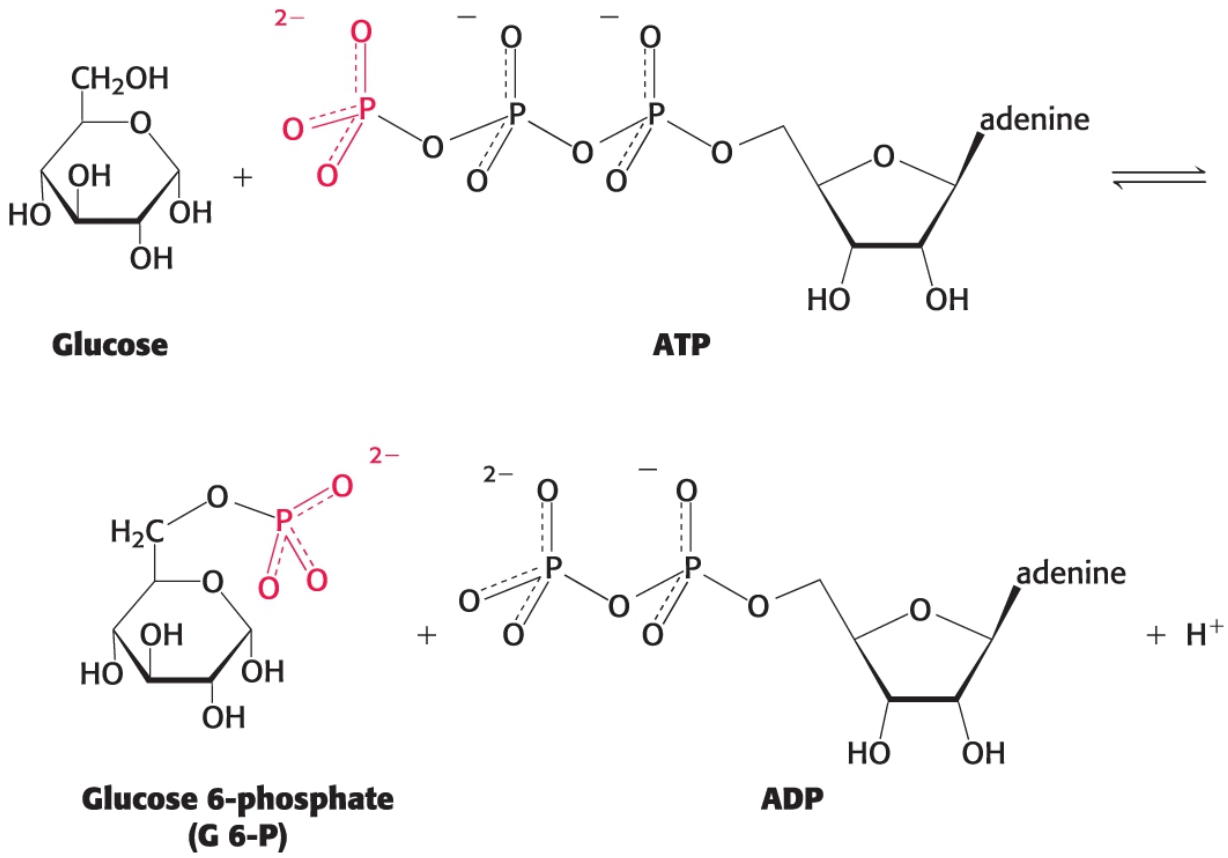
The structure of Oxaloacetate is as follows: A 4-carbon alkane chain is depicted as a line structure using 3 zigzag lines. C 1 is partially double bonded to O above and O on the lower left and has a counter negative sign. C 2 is double bonded to O below. C 3 is bound to H 2. C 4 is partially double bonded to O on the upper right and O below and has a counter negative sign.

In the second product N A D H, H is highlighted in red.

The third product H superscript plus is highlighted in red.

Return to Formation of oxaloacetate from malate

Extended description for Formation of glucose 6-phosphate and A D P



The reaction between glucose and A T P leads to the formation of glucose 6-phosphate, ADP, and hydrogen ion.

The reversible reaction consists of two reactants and three products.

The first reactant is glucose whose structure is as follows: A 6-membered heterocyclic hexagonal ring is in a horizontal orientation and consists of 1 O and 5 C atoms. The O atom occupies the first position, which is the top right vertex. C 1, C 2, and C 4 are each single bonded to O H below. C 3 is single bonded to O H above. C 5 is single bonded to C H 2 O H above.

The second reactant is A T P whose structure is as follows: A 5-membered heterocyclic pentagonal ring is in a vertical orientation and consists of 1 O and 4 C atoms. The O atom occupies the first position, which is the topmost vertex. C 1 is single bonded to adenine on the upper right. C 2 and C 3 are single bonded to O H below. C 4 is single bonded to C H 2 on the upper left in the form of a line. C H 2 is single bonded to O on the lower left. O is single bonded to P on the upper left. P is partially double bonded to O superscript minus above, partially double bonded to O on the lower left, and single bonded to O on the lower left. This O atom is single bonded to another P on the upper left. This P is partially double bonded to O superscript minus above, partially double bonded to O on the lower left, and single bonded to O on the lower left. This O atom is single bonded to another P on the upper left. This P is partially double bonded to O superscript 2 minus above, partially double bonded to O on the lower left, and partially double bonded to O below.

The first product is glucose 6-phosphate. The structure of glucose 6-phosphate is as follows: A 6-membered heterocyclic hexagonal ring is in a horizontal orientation and consists of 1 O and 5 C atoms. The O atom occupies the first position, which is the top right vertex. C 1, C 2, and C 4 are each single bonded to O H below. C 3 is single bonded to O H above. C 5 is single bonded to C H 2 above. The C atom of C H 2 is further single bonded to O atom on the upper right. The O atom is further single bonded to P atom on the lower right. This P is partially double bonded to O superscript 2 minus on the upper right, partially double bonded to O below, and partially double bonded to O on the lower right.

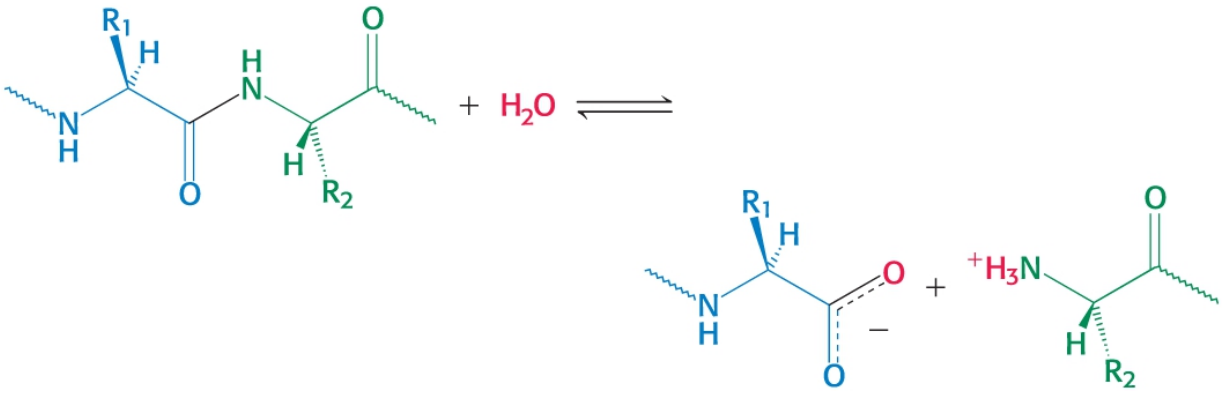
The structure of the second product, that is A D P is as follows: A 5-membered heterocyclic pentagonal ring is in a vertical orientation and consists of 1 O and 4 C atoms. The O atom occupies the first position, which is the topmost vertex. C 1 is single bonded to adenine on the upper right. C 2 and C 3 are single bonded to O H

below. C 4 is single bonded to C H 2 on the upper left in the form of a line. C H 2 is single bonded to O on the lower left. O is single bonded to P on the upper left. P is partially double bonded to O superscript minus above, partially double bonded to O on the lower left, and single bonded to O on the lower left. This O atom is single bonded to another P on the upper left. This P is partially double bonded to O superscript 2 minus above, partially double bonded to O below, and partially double bonded to O on the lower left.

The third product is H superscript positive ion.

Return to Formation of glucose 6-phosphate and A D P

Extended description for Hydrolytic reaction



The two reactants combine by equilibrium reaction to form two products.

The structure of the first reactant is as follows: A 2 N and 4 C heteronuclear alkane chain is depicted as a line structure using 5 zigzag lines. N 1 occupies the first position and N 2 occupies the fourth position. N 1 and N 2 are each bound to H. N 1 has an open wavy bond. C 1 is wedge bonded to R 1 on the upper left and dash bonded to H on the upper right. C 2 is double bonded to O below. The structures upto this point are highlighted in blue. C 3 is wedge bonded to H on the lower left and dash bonded to R 2 on the lower right. C 4 is double bonded to O above and has an open wavy bond on the right. The structures from N 2 are highlighted in green.

The second reactant H 2 O is highlighted in red.

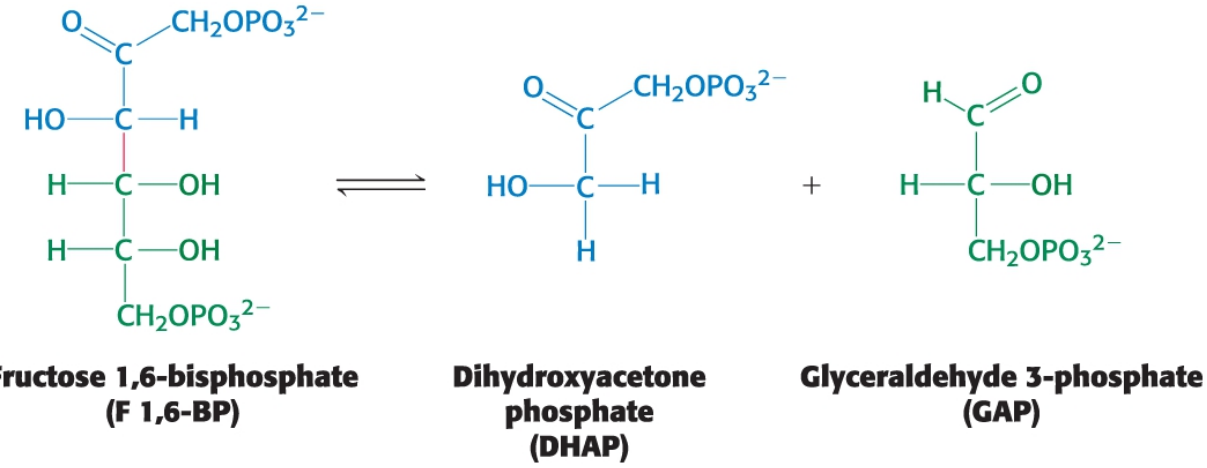
The structure of the first product is as follows: A 1 N and 2 C heteronuclear alkane chain is depicted as a line structure using 2 zigzag lines. N bound to H occupies the first position. C 1 is wedge bonded to R 1 on the upper left and dash bonded to H on the upper right. C 2 is partially double bonded to O on the upper right and O

below and has a counter negative sign. N has an open wavy bond on the left. The O atom single bonded to C 2 on the top right is highlighted in red and the rest of the structure is highlighted in blue.

The structure of the second product is as follows: A 1 N and 2 C heteronuclear alkane chain is depicted as a line structure using 2 zigzag lines. N bound to H 3 superscript plus occupies the first position. H 3 superscript plus is highlighted in red. C 1 is wedge bonded to H on the lower left and dash bonded to R 2 on the lower right. C 2 is double bonded to O above and has an open wavy bond on the left. The entire structure is highlighted in green.

Return to Hydrolytic reaction

Extended description for Formation of Glyceraldehyde 3-phosphate from Fructose 1, 6-Bisphosphate



The reaction reads fructose 1, 6-bisphosphate (F 1, 6-B P) equilibrium reaction arrow dihydroxyacetone phosphate (D H A P) and Glyceraldehyde 3-phosphate (G A P).

The structure of Fructose 1, 6-bisphosphate (F 1, 6-B P) is as follows: The Fischer projection consists of a vertical chain with C above and C H 2 O P O 3 superscript 2 minus below. The projection contains four C atoms placed one below the other on the vertical chain. The C atoms are numbered from top to bottom. C 1 is double bonded to O on the upper left and single bonded to C H 2 O P O 3 superscript 2 minus on the upper right. C 2 is single bonded to O H on the left and H on the right. C 3 and C 4 are each single bonded to H on the left and O H on the right. C 1 and C 2 are highlighted in blue and structures below this are highlighted in green. The vertical line between C 2 and C 3 is highlighted in red.

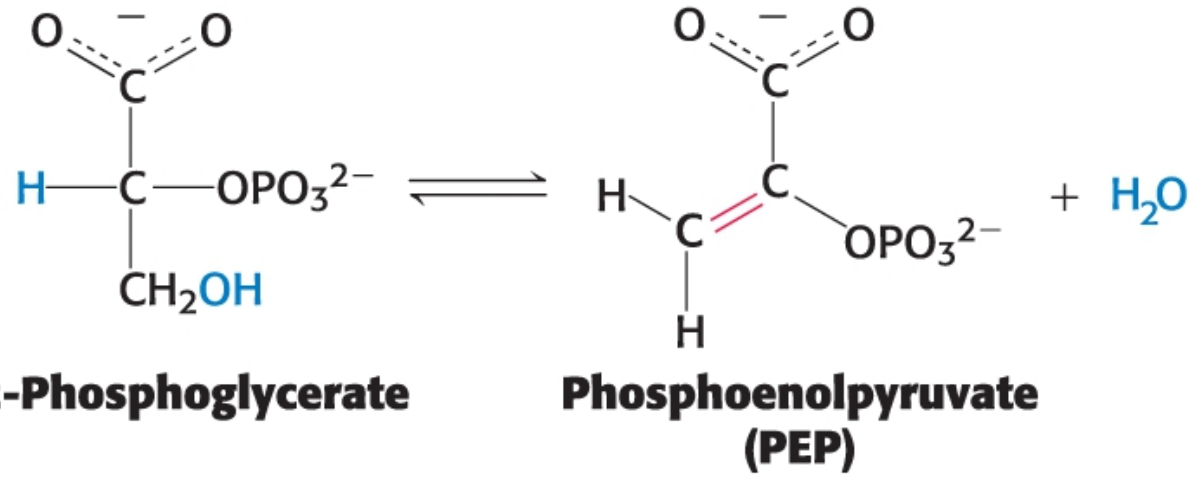
The structure of Dihydroxyacetone phosphate (D H A P) is as follows: The Fischer projection consists of a vertical chain with C

above and H below. The projection contains 1 C atom at the center. C 1 is double bonded to O on the left and single bonded to C H 2 O P O 3 superscript 2 minus on the right. C 2 is single bonded to O H on the left and H on the right. The entire structure is highlighted in blue.

The structure of Glyceraldehyde 3-phosphate (G A P) is as follows: The Fischer projection consists of a vertical chain with C above and C H 2 O P 3 superscript 2 minus below. The projection contains 1 C atom at the center. C 1 is single bonded to H on the left and double bonded to O on the right. C 2 is single bonded to H on the left and O H on the right. The entire structure is highlighted in green.

Return to Formation of Glyceraldehyde 3-phosphate from Fructose 1, 6-Bisphosphate

Extended description for Formation of Phosphoenolpyruvate (P E P) from 2-Phosphoglycerate



The reaction reads 2-Phosphoglycerate equilibrium arrow phosphoenolpyruvate (P E P) plus H 2 O.

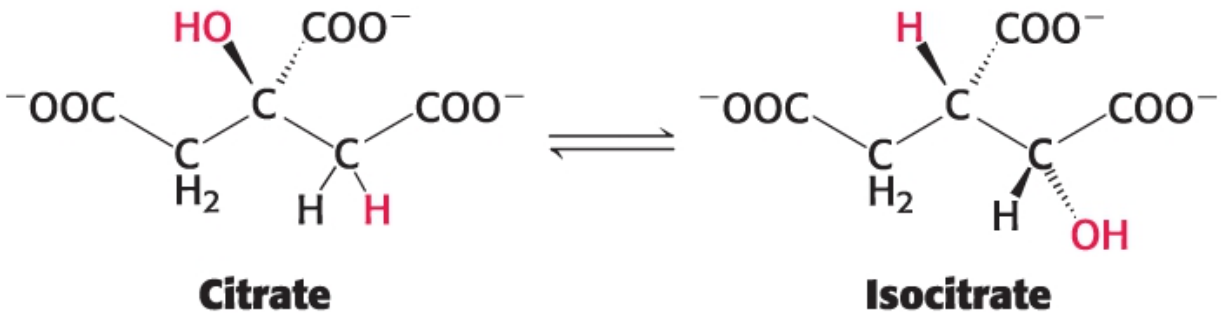
The structure of 2-Phosphoglycerate is as follows: The Fischer projection consists of a vertical chain with C above and C H 2 O H below. The projection contains 1 C atom at the center. C 1 is partially double bonded to O on the upper left and O on the upper right and has a counter negative sign. C 2 is single bonded to H on the left and O P O 3 superscript 2 minus on the right. H on the left side of C 1 and O H from C H 2 O H below are highlighted in blue.

The structure of phosphoenolpyruvate (P E P) is as follows: The Fischer projection consists of a vertical chain with C above and C below. C 1 is partially double bonded to O on the upper left and O on the upper right and has a counter negative sign. C 2 is single bonded to O P 3 superscript 2 minus on the lower right and double bonded to C on the lower left. The C atom is single bonded to H on the upper left and H below. The double bond is highlighted in red.

The second product H 2 O is highlighted in blue.

Return to Formation of Phosphoenolpyruvate (P E P) from 2-Phosphoglycerate

Extended description for Equilibrium reaction depicts the formation of isocitrate from citrate

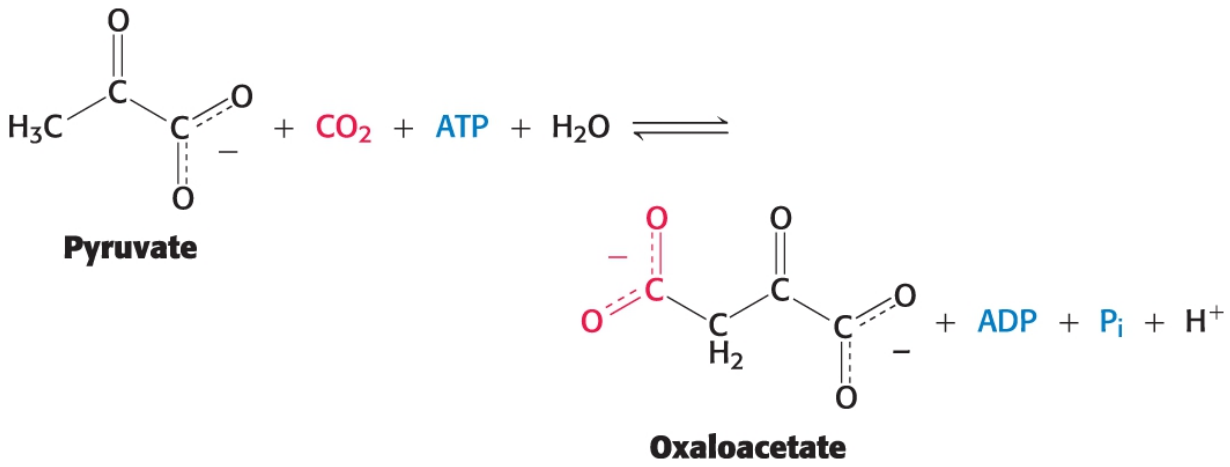


The structure of citrate is as follows: A 3-carbon alkane chain is depicted as a line structure using 2 zigzag lines. C 1 bound to H 2 is single bonded to C O O superscript minus on the upper left. C 2 is wedge bonded to O H on the upper left and dash bonded to C O O superscript minus on the upper right. O H on the upper left is highlighted in red. C 3 is single bonded to C O O superscript minus on the upper right, H on the lower left, and H on the lower right. H on the lower right is highlighted in red.

The structure of isocitrate is as follows: A 3-carbon alkane chain is depicted as a line structure using 2 zigzag lines. C 1 bound to H 2 is single bonded to C O O superscript minus on the upper left. C 2 is wedge bonded to H on the upper left and dash bonded to C O O superscript minus on the upper right. H on the upper left is highlighted in red. C 3 is single bonded to C O O superscript minus on the upper right. C 3 is wedge bonded to H on the lower left, and dash bonded to O H on the lower right. O H on the lower right is highlighted in red.

Return to Equilibrium reaction depicts the formation of isocitrate from citrate

Extended description for Equilibrium reaction depicts the formation of oxaloacetate from pyruvate



The reaction reads pyruvate plus C O 2 plus A T P plus H 2 O equilibrium reaction arrow oxaloacetate plus A D P plus P i plus H superscript plus.

The structure of Pyruvate is as follows: A 3-carbon alkane chain is depicted as a line structure using 2 zigzag lines. C 1 is bound to H 3. C 2 is double bonded to O above. C 3 is partially double bonded to O on the upper right and O below and has a counter negative sign.

The second reactant C O 2 is highlighted in red.

The third reactant A T P is highlighted in blue.

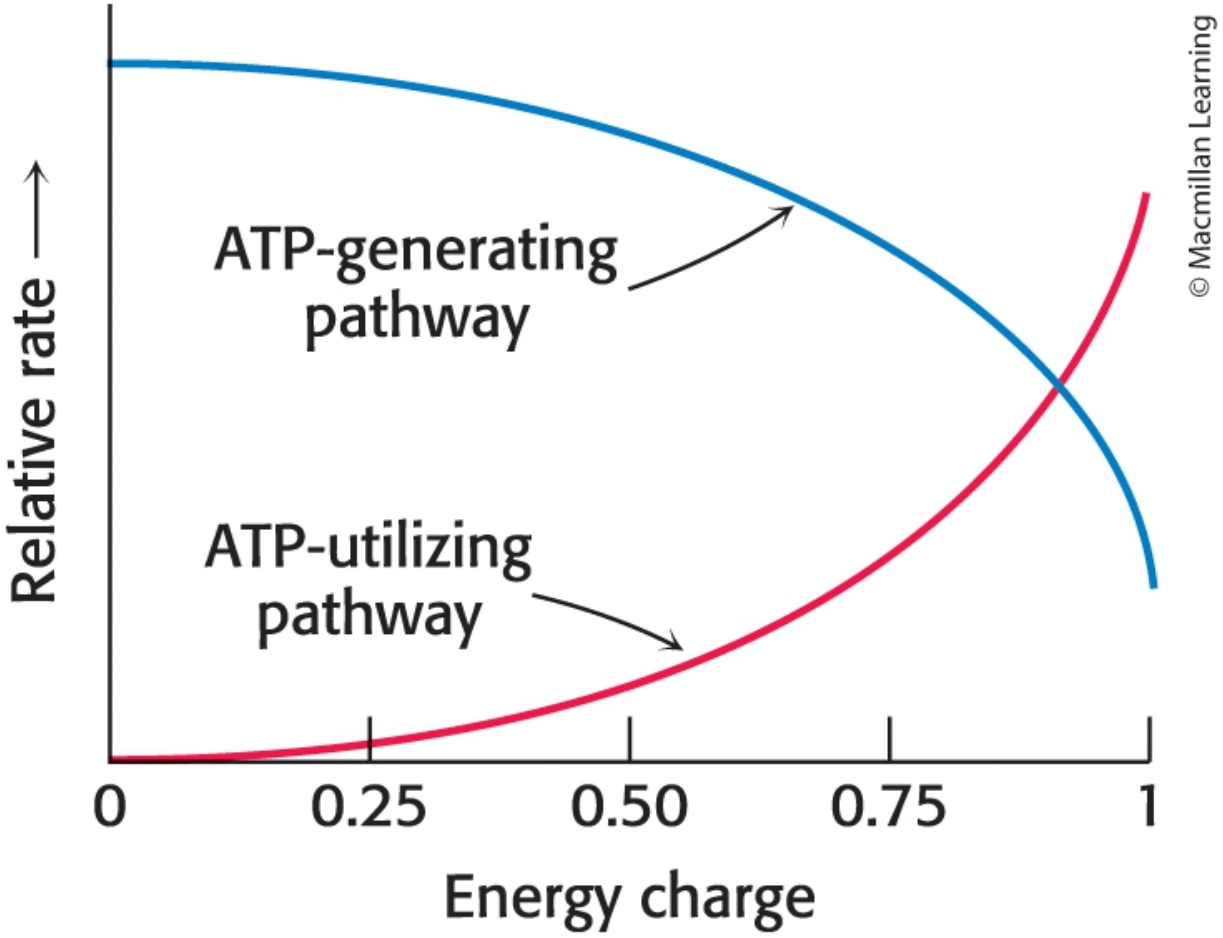
The structure of Oxaloacetate is as follows: A 4-carbon alkane chain is depicted as a line structure using 3 zigzag lines. C 1 is partially double bonded to O above and O on the lower left and has a counter negative sign. C 2 is bound to H 2. C 3 is double bonded to O above. C 4 is partially double bonded to O on the upper right and O below and

has a counter negative sign. C 1 and the O atoms attached to it are highlighted in red.

The second and third products A D P and P i are highlighted in blue.

Return to Equilibrium reaction depicts the formation of oxaloacetate from pyruvate

Extended description for Graphical representation of energy charge versus relative rate of A T P synthesis

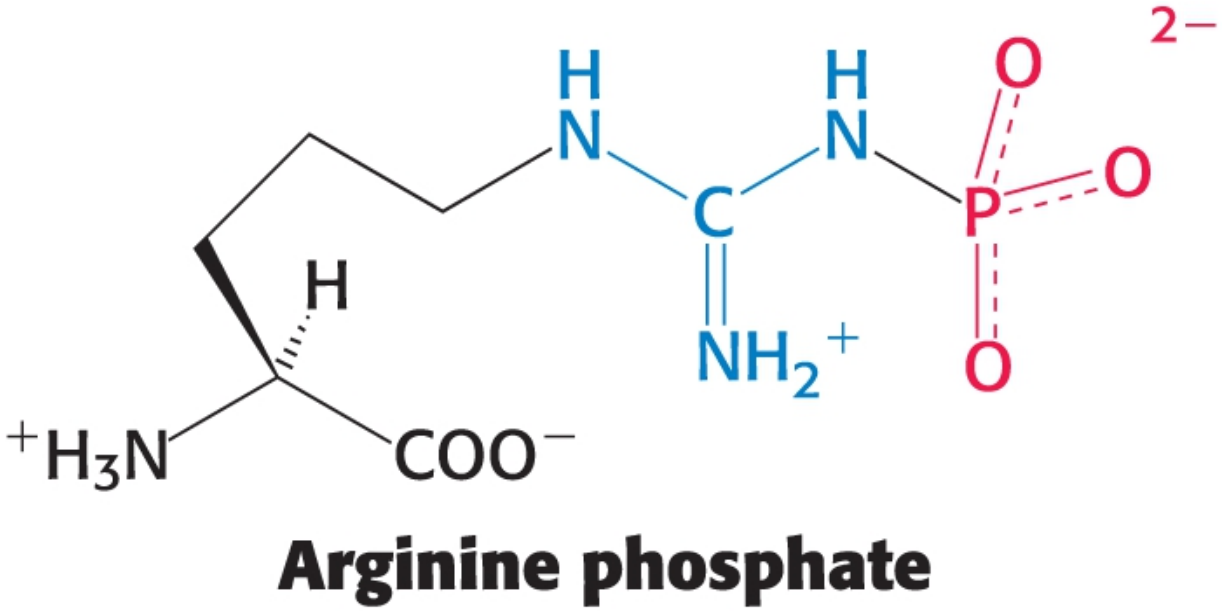


The horizontal axis of the graph labeled "energy charge" has markings ranging from 0 to 1 in increments of 0.25. The vertical axis is labeled "relative rate." The graph shows an increasing curve labeled A T P utilizing pathway that starts from the origin, takes a curve between 0.50 and 0.75 on the horizontal axis, and terminates well above the middle of the graph at marking 1 on the horizontal axis. The graph shows a decreasing curve labeled A T P generating pathway that starts well above the middle of the graph, slopes down

between 0.50 and 0.75, intersects with the first curve, and terminates well above the horizontal axis at marking 1.

Return to Graphical representation of energy charge versus relative rate of A T P synthesis

Extended description for Structure of Arginine phosphate

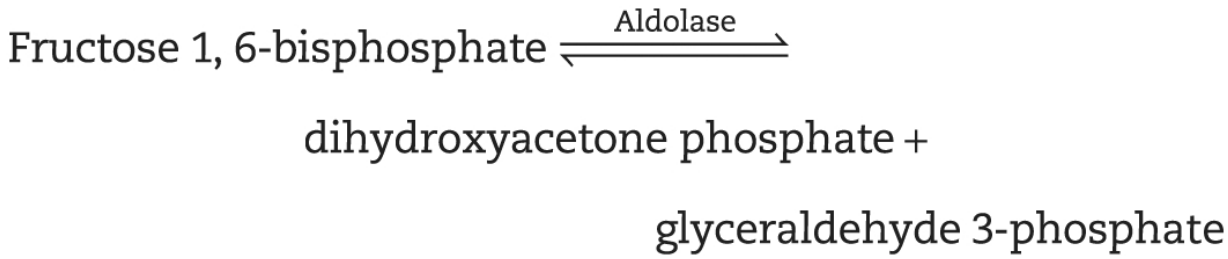


Arginine phosphate

The structure of Arginine phosphate is as follows: A 2 N and 4 C heteronuclear alkane chain is depicted as a line structure using 5 zigzag lines. N 1 occupies the fourth position and N 2 occupies the sixth position. N 1 and N 2 are each bound to H above. C 1 is wedge bonded on the lower right to a central C atom in the form of a line. The central C atom is dash bonded to H on the upper right, single bonded to N H 3 superscript plus on the lower left and C O O superscript minus on the lower right. C 4 is double bonded to N H 2 superscript plus below. N 2 is single bonded to P on the lower right. This P is partially double bonded to O above, O below, and O on the upper right and has a counter 2 negative sign. The structures from N 1 to N 2 are highlighted in blue. P and O atoms attached to it are highlighted in red.

Return to Structure of Arginine phosphate

Extended description for Reaction catalyzed by aldolase



The reaction consists of one reactant and two products. The reactant is fructose-1, 6-bisphosphate. The products are dihydroxyacetone phosphate and glyceraldehyde 3-phosphate.

Return to Reaction catalyzed by aldolase

Extended description for Structures of Ethanol and Acetaldehyde

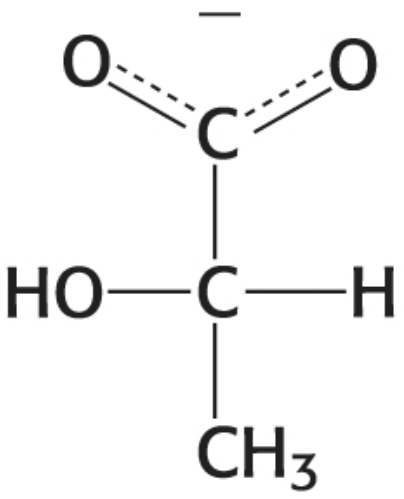


On the left, the structure of Ethanol is as follows: A central C atom is single bonded to O H on the upper right, H on the upper left, H on the lower left, and C H 3 below.

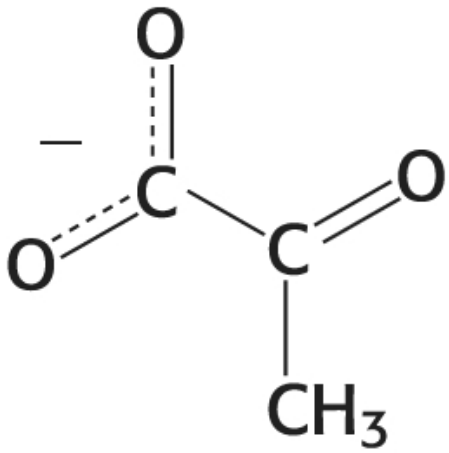
On the left, the structure of Acetaldehyde is as follows: A central C atom is single bonded to H on the upper left, double bonded to O on the upper right, and single bonded to C H 3 below.

Return to Structures of Ethanol and Acetaldehyde

Extended description for Structures of Lactate and Pyruvate



Lactate



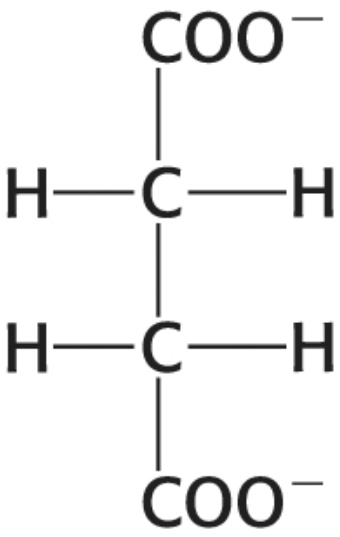
Pyruvate

The structure of Lactate is as follows: The Fischer projection of Lactate consists of a vertical chain with C above and C H 3 below. The projection contains 1 C atom at the center. C 1 is partially double bonded to O on the upper left and O on the upper right and has a counter negative sign. C 2 is single bonded to O H on the left and H on the right.

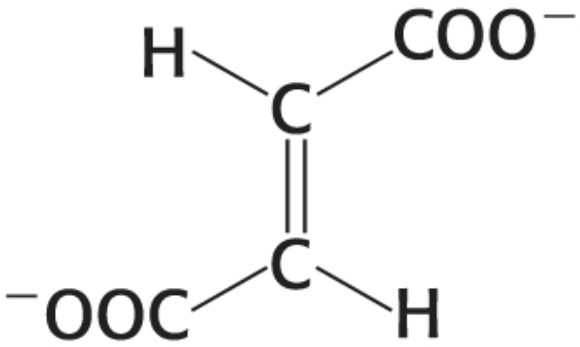
The structure of Pyruvate is as follows: A 2-carbon alkane chain is depicted as a line structure using a line. C 1 is partially double bonded to O above and O on the lower left and has a counter negative sign. C 2 is single bonded to C H 3 below and double bonded to O on the upper right.

Return to Structures of Lactate and Pyruvate

Extended description for Structure of Succinate and Fumarate



Succinate



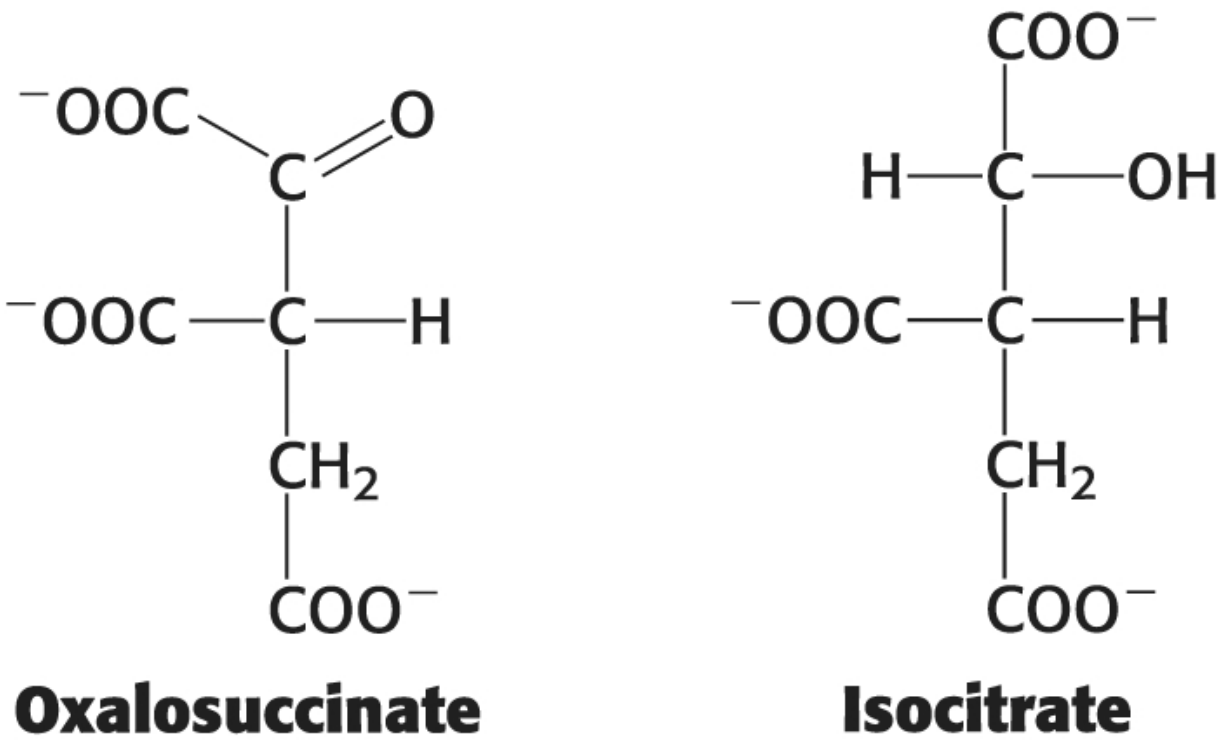
Fumarate

The structure of Succinate is as follows: The Fischer projection of Succinate consists of a vertical chain with C O O superscript minus above and C O O superscript minus below. The projection contains two C atoms placed one below the other on the vertical chain. The C atoms are numbered from top to bottom. C 1 and C 2 are each single bonded to H on the left and right.

The structure of Fumarate is as follows: Two C atoms are vertically double bonded. The C atoms are numbered from top to bottom. C 1 is single bonded to H on the upper left and C O O superscript minus on the upper right. C 2 is single bonded to C O O superscript minus on the lower left and H on the lower right.

Return to Structure of Succinate and Fumarate

Extended description for Structure of Oxalosuccinate and Isocitrate



Oxalosuccinate **Isocitrate**

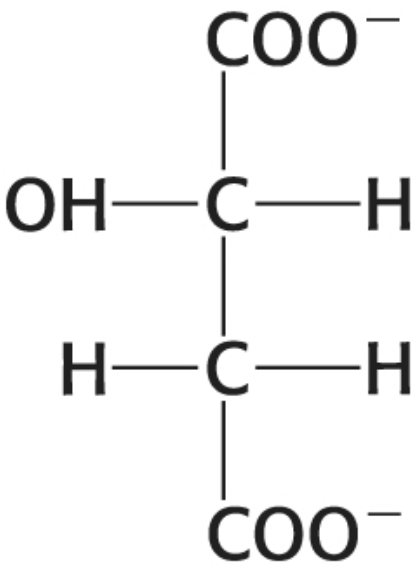
The structure of Oxalosuccinate is as follows: The Fischer projection of Oxalosuccinate consists of a vertical chain with C above and C O O superscript minus below. The projection contains two C atoms placed one below the other on the vertical chain. The C atoms are numbered from top to bottom. C 1 is single bonded to C O O superscript minus on the upper left and double bonded to O on the upper right. C 2 is single bonded to C O O superscript minus on the left and H on the right. C 3 is bound to H 2.

The structure of Isocitrate is as follows: The Fischer projection of Isocitrate consists of a vertical chain with C O O superscript minus above and C O O superscript minus below. The projection contains three C atoms placed one below the other on the vertical chain. The

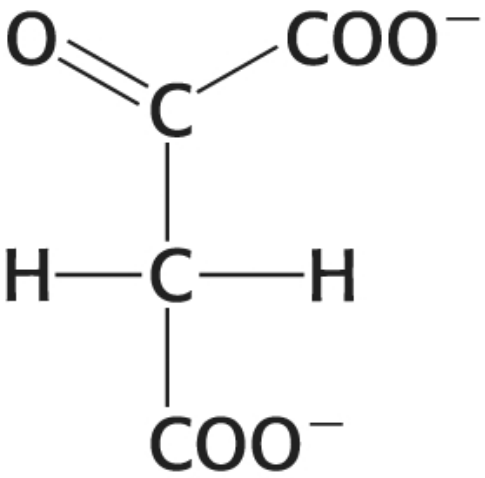
C atoms are numbered from top to bottom. C 1 is single bonded to H on the left and O H on the right. C 2 is single bonded to C O O superscript minus on the left and H on the right. C 3 is bound to H 2.

Return to Structure of Oxalosuccinate and Isocitrate

Extended description for Structure of Malate and Oxaloacetate



Malate



Oxaloacetate

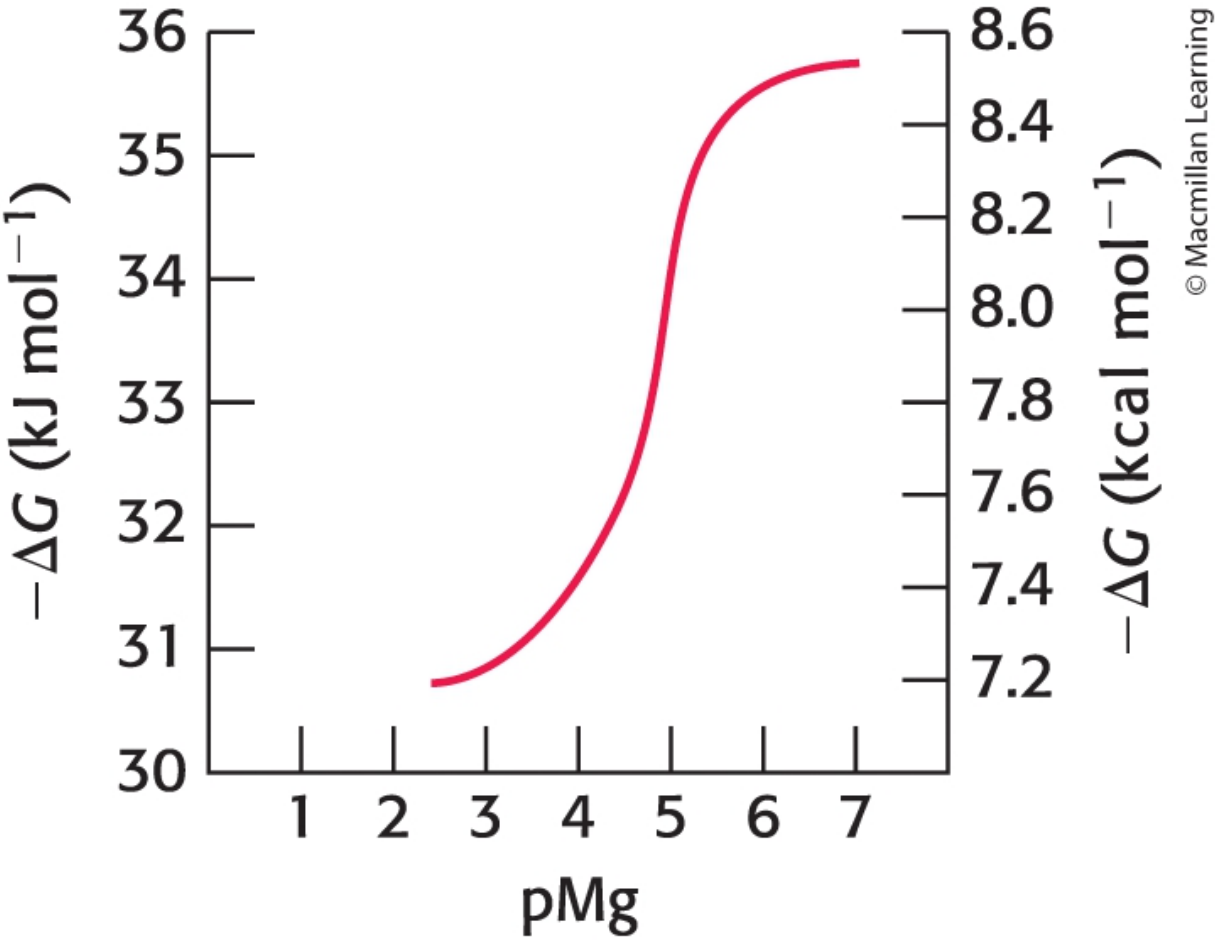
The structure of Malate is as follows: The Fischer projection of Malate consists of a vertical chain with C O O superscript minus above and C O O superscript minus below. The projection contains two C atoms placed one below the other on the vertical chain. The C atoms are numbered from top to bottom. C 1 is single bonded to O H on the left and H on the right. C 2 is single bonded to H on the left and H on the right.

The structure of Oxaloacetate is as follows: The Fischer projection of Oxaloacetate consists of a vertical chain with C above and C O O superscript minus below. The projection contains a C atom at the center. The C atoms are numbered from top to bottom. C 1 is double bonded to O on the upper left and single bonded to C O O

superscript minus on the upper right. C 2 is single bonded to H on the left and H on the right.

Return to Structure of Malate and Oxaloacetate

Extended description for Graphical representation of delta G for the hydrolysis of A T P varies as a function of the M g superscript 2 plus concentration



The horizontal axis of the graph labeled “p M g” has markings ranging from 1 to 7 in increments of 1 unit. The vertical axis on the left labeled “negative delta G in Kilojoule per mol” has markings ranging from 30 to 36 in increments of 1 unit. The vertical axis on the right labeled “negative delta G in Kilocalorie per mol” has markings ranging from 7.2 to 8.6 in increments of 0.2 units. The graph shows an S-shaped curve that starts roughly between 2 and 3 on the horizontal axis and between 30 and 31 on the left vertical

axis. The graph rises upwards and shows a curve at 5 on the horizontal axis and 33 on the left vertical axis. The graph terminates at 7 on the horizontal axis and at 36 on the left vertical axis. All values are approximated.

Return to Graphical representation of delta G for the hydrolysis of A T P varies as a function of the M g superscript 2 plus concentration

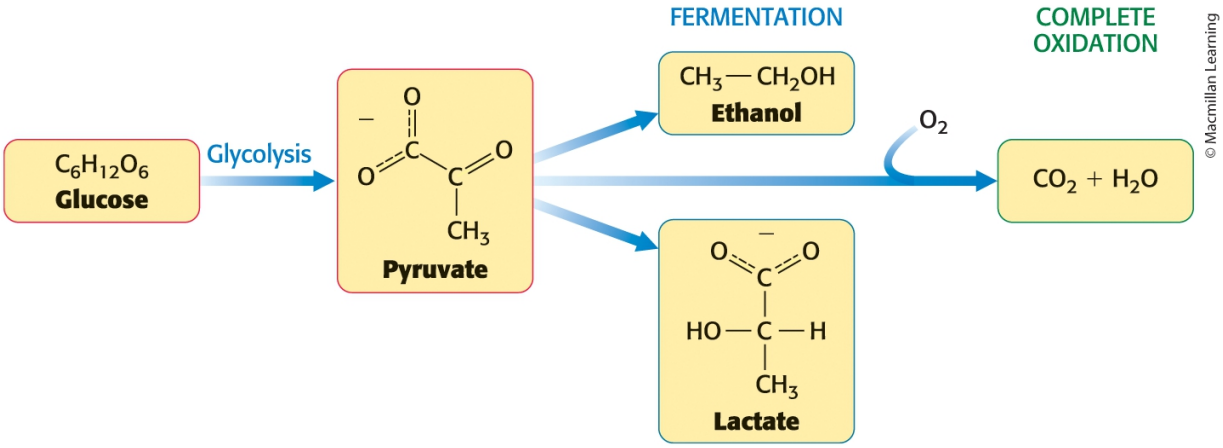
Extended description for Schematic illustration of sources of A T P for muscle contraction



In the schematic illustration, glucose is converted into pyruvate via glycolysis in the cytoplasm. The A T P generated during glycolysis moves toward the muscle fiber. The muscle fiber consists of a series of thick horizontal lines in the middle interdigitated with thin horizontal and parallel lines on either side. There are two fates of pyruvate that is A and B. In fate A, pyruvate is converted into lactate in the cytoplasm. In fate B, pyruvate moves inside the mitochondrion and is converted into C O 2 plus H 2 O and A T P. This A T P moves from the mitochondrion toward the muscle fiber.

Return to Schematic illustration of sources of A T P for muscle contraction

Extended description for Schematic representation of glucose metabolism



Glucose C 6 H 12 O 6 is converted into pyruvate via glycolysis. The structure of pyruvate is as follows: A central C atom is double bonded to O on the upper right, single bonded to C H 3 below, and single bonded to C on the upper left. This C atom is partially double bonded to O above and O on the lower left. This C O O group has an overall negative charge.

Pyruvate has three fates as follows:

It can be converted into ethanol via fermentation. The structure of ethanol is C H 3, single bond, C H 2 O H.

It can be converted into C O 2 plus H 2 O via complete oxidation in presence of O 2.

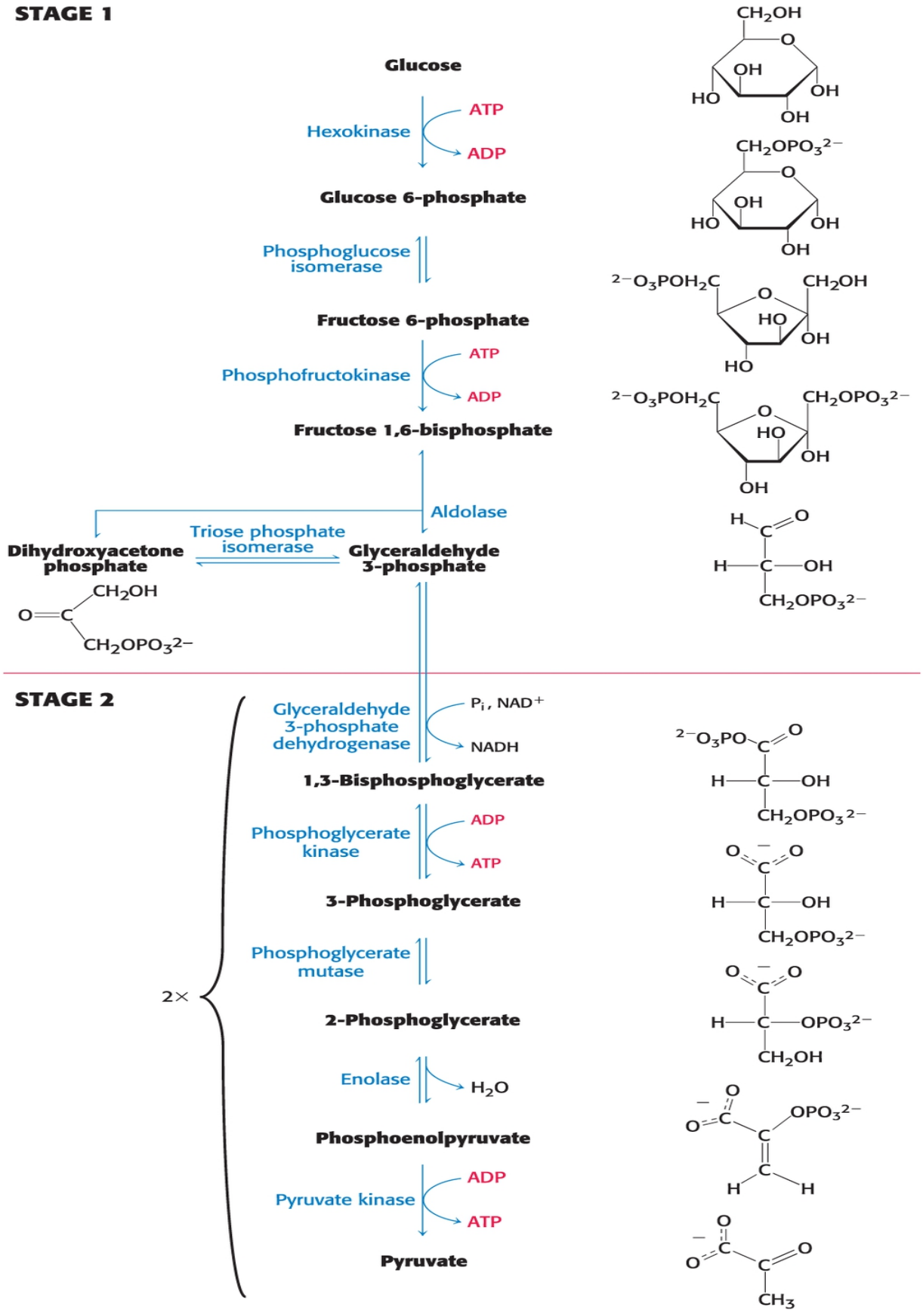
It can be converted into lactate. The structure of lactate is as follows: C, single bond, C, single bond, C H 3. C 1 is partially double bonded to O on the upper left and O on the upper right. This C O O group has

an overall negative charge. C 2 is single bonded to O H on the left and H on the right.

Return to Schematic representation of glucose metabolism

Extended description for Two stages of glycolytic

pathway


STAGE 1
Glucose
Hexokinase
ATP
ADP
Glucose 6-phosphate
Phosphoglucose isomerase
Fructose 6-phosphate
Phosphofructokinase
ATP
ADP
Fructose 1,6-bisphosphate
Aldolase
Triose phosphate isomerase
Dihydroxyacetone phosphate
Glyceraldehyde 3-phosphate
STAGE 2
2×
Glyceraldehyde 3-phosphate dehydrogenase
Pi, NAD+
NADH
1,3-Bisphosphoglycerate
Phosphoglycerate kinase
ADP
ATP
3-Phosphoglycerate
Phosphoglycerate mutase
2-Phosphoglycerate
Enolase
H2O
Phosphoenolpyruvate
Pyruvate kinase
ADP
ATP
Pyruvate

The glycolytic pathway is divided into stage 1 and stage 2.

Stage 1 is depicted as follows:

Glucose is irreversibly converted into glucose 6-phosphate by hexokinase. This conversion requires the breakdown of A T P to A D P.

The structure of glucose is as follows: A 6-membered heterocyclic hexagonal ring is in a horizontal orientation and consists of 1 O and 5 C atoms. O occupies the top right vertex. C 1 occupies the rightmost vertex and is single bonded to O H below. C 2 is single bonded to O H below. C 3 is single bonded to O H above. C 4 is single bonded to O H below. C 5 is single bonded to C H 2 O H above.

The structure of glucose 6-phosphate is as follows: A 6-membered heterocyclic hexagonal ring is in a horizontal orientation and consists of 1 O and 5 C atoms. O occupies the top right vertex. C 1 occupies the rightmost vertex and is single bonded to O H below. C 2 is single bonded to O H below. C 3 is single bonded to O H above. C 4 is single bonded to O H below. C 5 is single bonded to C H 2 O P O 3 superscript 2 minus above.

Glucose 6-phosphate is reversibly converted into fructose 6-phosphate by phosphoglucose isomerase.

The structure of fructose 6-phosphate is as follows: A 5-membered heterocyclic pentagonal ring is in a vertical orientation and consists of 1 O and 4 C atoms. O occupies the topmost vertex. C 1 occupies the rightmost vertex and is single bonded to C H 2 O H above and O H below. C 2 is single bonded to O H above. C 3 is single bonded to O H below. C 4 is single bonded to C H 2 O P O 3 superscript 2 minus above.

Fructose 6-phosphate is irreversibly converted into fructose 1, 6-bisphosphate by phosphofructokinase. This conversion requires the breakdown of A T P to A D P.

The structure of fructose 1, 6-bisphosphate is as follows: A 5-membered heterocyclic pentagonal ring is in a vertical orientation and consists of 1 O and 4 C atoms. O occupies the topmost vertex. C 1 occupies the rightmost vertex and is single bonded to C H 2 O P O 3 superscript 2 minus above and O H below. C 2 is single bonded to O H above. C 3 is single bonded to O H below. C 4 is single bonded to C H 2 O P O 3 superscript 2 minus above.

Fructose 1, 6-bisphosphate is irreversibly converted into glyceraldehyde 3-phosphate or dihydroxyacetone phosphate by aldolase.

The structure of glyceraldehyde 3-phosphate is as follows: C, single bond, C, single bond, C H 2 O P O 3 superscript 2 minus. C 1 is single bonded to H on the upper left and double bonded to O on the upper right. C 2 is single bonded to H on the left and O H on the right.

The structure of dihydroxyacetone phosphate is as follows: A central C atom is single bonded to C H 2 O H on the upper right, double bonded to O on the left, and single bonded to C H 2 O P O 3 superscript 2 minus on the lower right.

Glyceraldehyde 3-phosphate is reversibly converted into dihydroxyacetone phosphate by triose phosphate isomerase.

Stage 2 is depicted as follows:

Glyceraldehyde 3-phosphate is reversibly converted into 1,3-bisphosphoglycerate by glyceraldehyde 3-phosphate dehydrogenase.

This conversion requires the reduction of N A D superscript plus to N A D H and entry of P subscript i.

The structure of 1,3-bisphosphoglycerate is as follows: C, single bond, C, single bond, C H 2 O P O 3 superscript 2 minus. C 1 is single bonded to O P O 3 superscript 2 minus on the upper left and double bonded to O on the upper right. C 2 is single bonded to H on the left and O H on the right.

1,3-bisphosphoglycerate is reversibly converted into 3-phosphoglycerate by phosphoglycerate kinase. This conversion involves the formation of A T P from A D P.

The structure of 3-phosphoglycerate is as follows: C, single bond, C, single bond, C H 2 O P O 3 superscript 2 minus. C 1 is partially double bonded to O on the upper left and O on the upper right. This C O O group has an overall negative charge. C 2 is single bonded to H on the left and O H on the right.

3-phosphoglycerate is reversibly converted into 2-phosphoglycerate by phosphoglycerate mutase.

The structure of 2-phosphoglycerate is as follows: C, single bond, C, single bond, C H 2 O H. C 1 is partially double bonded to O on the upper left and O on the upper right. This C O O group has an overall negative charge. C 2 is single bonded to H on the left and O P O 3 superscript 2 minus on the right.

2-phosphoglycerate is reversibly converted into phosphoenolpyruvate by enolase. An H 2 O molecule is released during this conversion.

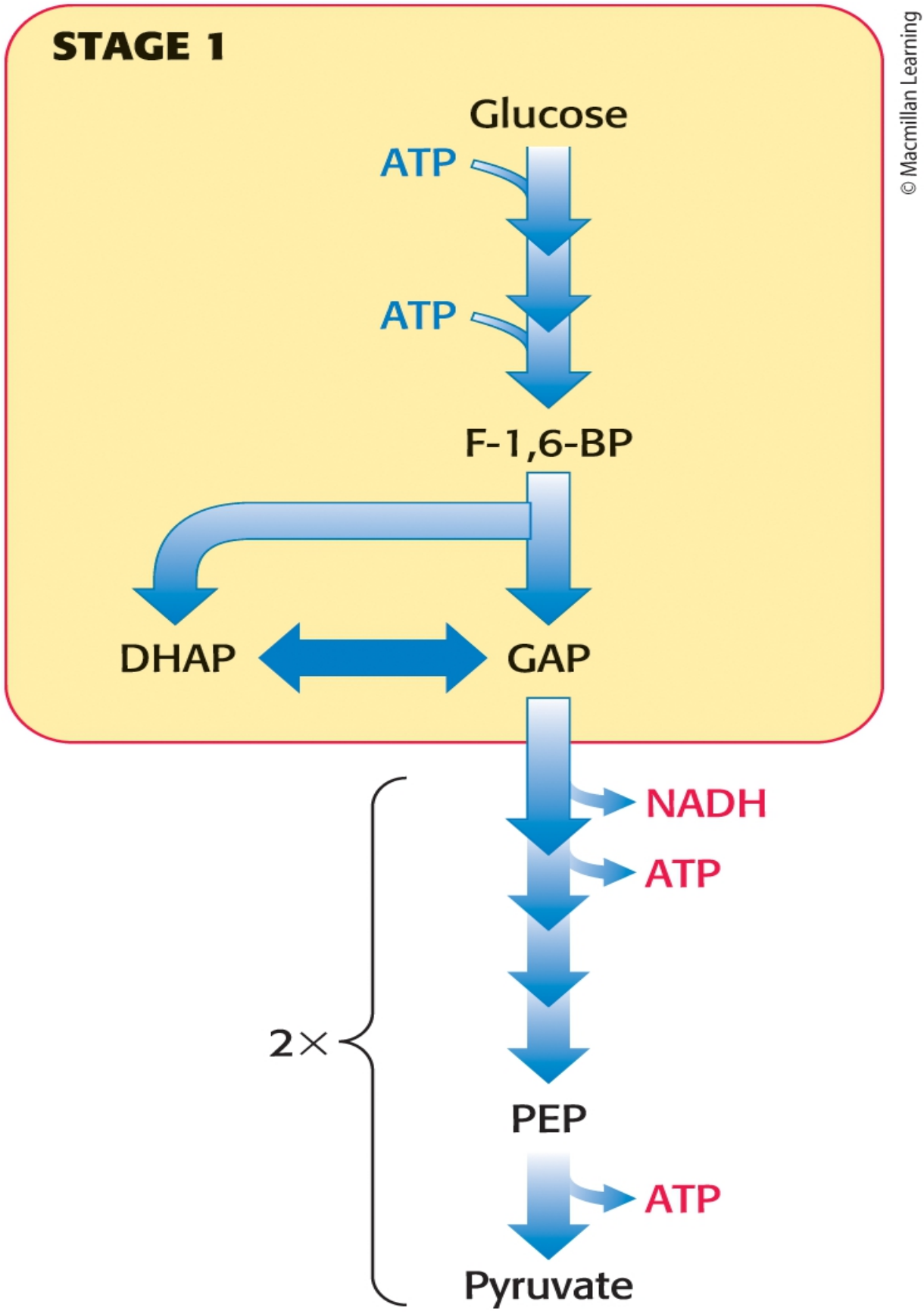
The structure of phosphoenolpyruvate is as follows: A central C atom is double bonded to C below, single bonded to O P O 3 superscript 2 minus on the upper right, and single bonded to C on the upper left. The C atom below is single-bonded to H on the lower left and H on the lower right. The C atom on the upper left is partially double bonded to O above and O on the lower left. This C O O group has an overall negative charge.

Phosphoenolpyruvate is irreversibly converted into pyruvate by pyruvate kinase. A D P is converted into A T P simultaneously.

The structure of pyruvate is as follows: A central C atom is double bonded to O on the upper right, single bonded to C H 3 below, and single bonded to C on the upper left. This C atom is partially double bonded to O above and O on the lower left. This C O O group has an overall negative charge.

Return to Two stages of glycolytic pathway

Extended description for Stage 1 of glycolytic pathway



© Macmillan Learning

The flowchart is depicted as follows:

Glucose, three downward arrows, F-1, 6-B P. The first and third downward arrows show the entry of A T P.

F-1, 6-B P, one downward arrow and one curved leftward arrow.

The downward arrow leads to G A P. The curved leftward arrow leads to D H A P. A double-headed arrow is shown between G A P and D H A P.

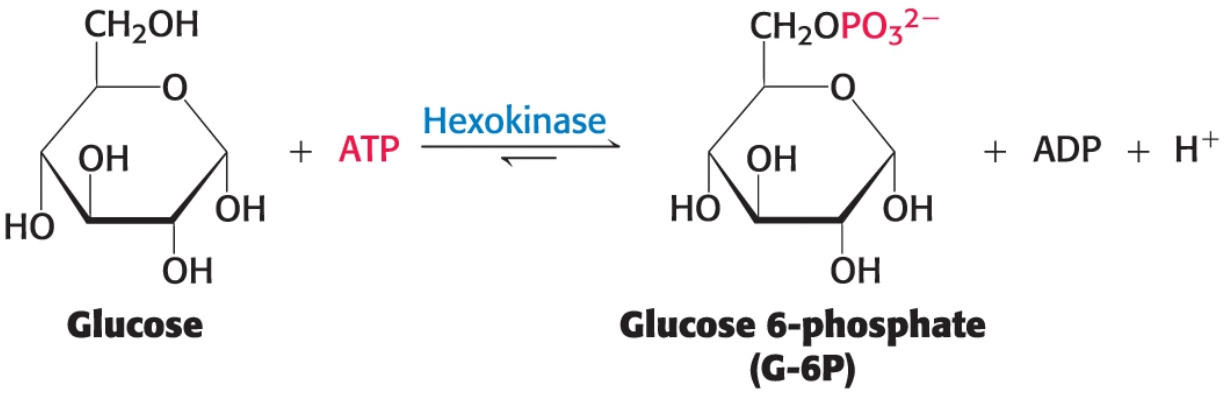
G A P, four downward arrows, P E P. The first and second downward arrow show the release of N A D H and A T P respectively.

P E P, one downward arrow, pyruvate. The downward arrow shows the release of A T P. The steps from the first downward arrow below G A P to the final pyruvate molecule are enclosed by left curly bracket labeled 2 times.

Note: The steps involving the conversion of glucose to D H A P and G A P are enclosed in a yellow rectangle labeled stage 1.

Return to Stage 1 of glycolytic pathway

Extended description for Reversible conversion of glucose to glucose 6-phosphate



The chemical reaction consists of two reactants and three products. The first reactant is glucose whose structure is as follows: A 6-membered heterocyclic hexagonal ring is in a horizontal orientation and consists of 1 O and 5 C atoms. O occupies the top right vertex. The ring is in a plane perpendicular to the plane of paper such that O and C 5 are located away from the observer and C 2 and C 3 are located toward the observer. C 1, C 2, and C 4 are each single bonded to O H below. C 3 is single bonded to O H above. C 5 is single bonded to C H 2 O H. The second reactant is A T P.

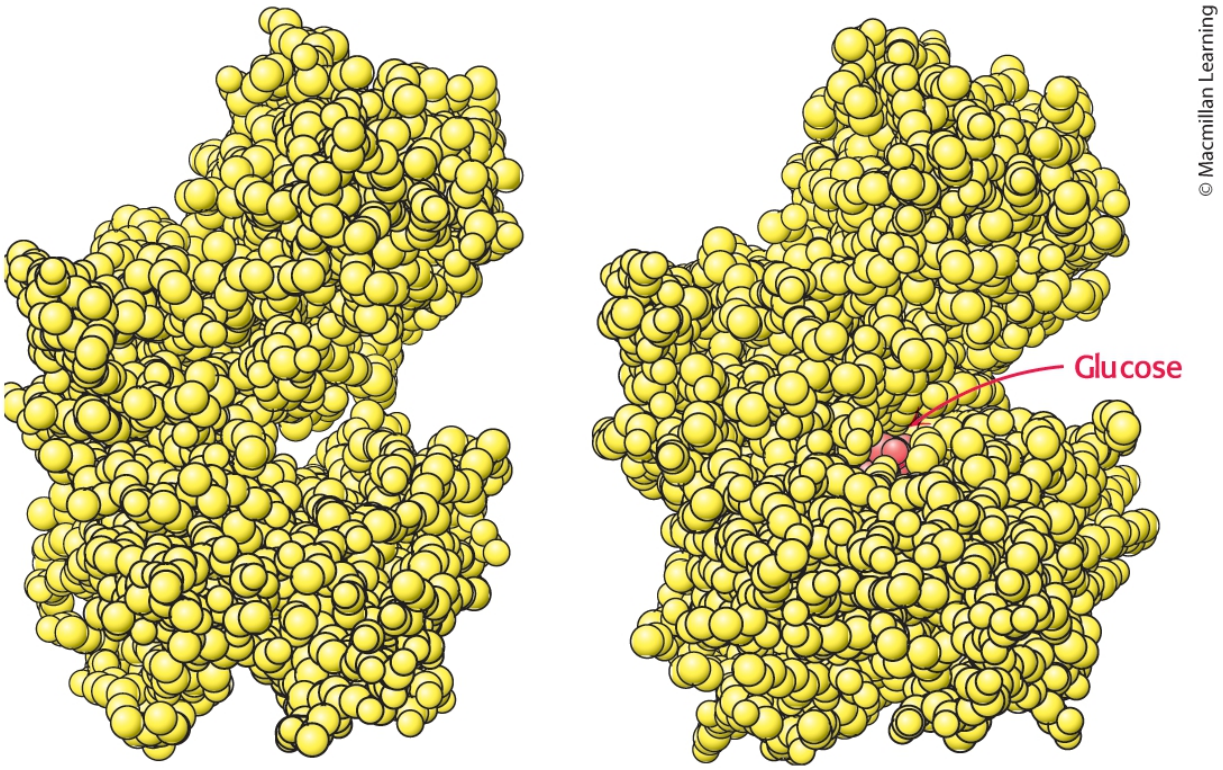
A reversible reaction arrow labeled hexokinase leads to the products.

The first product is glucose 6-phosphate (G-6 P) whose structure is as follows: A 6-membered heterocyclic hexagonal ring is in a horizontal orientation and consists of 1 O and 5 C atoms. O occupies the top right vertex. The ring is in a plane perpendicular to the plane of paper such that O and C 5 are located away from the observer and C 2 and C 3 are located toward the observer. C 1, C 2, and C 4 are each single bonded to O H below. C 3 is single bonded to O H above.

C 5 is single bonded to C H 2 O P O 3 superscript 2 minus above. The second product is A D P. The third product is H superscript plus.

Return to Reversible conversion of glucose to glucose 6-phosphate

Extended description for Conformational change in hexokinase upon glucose binding

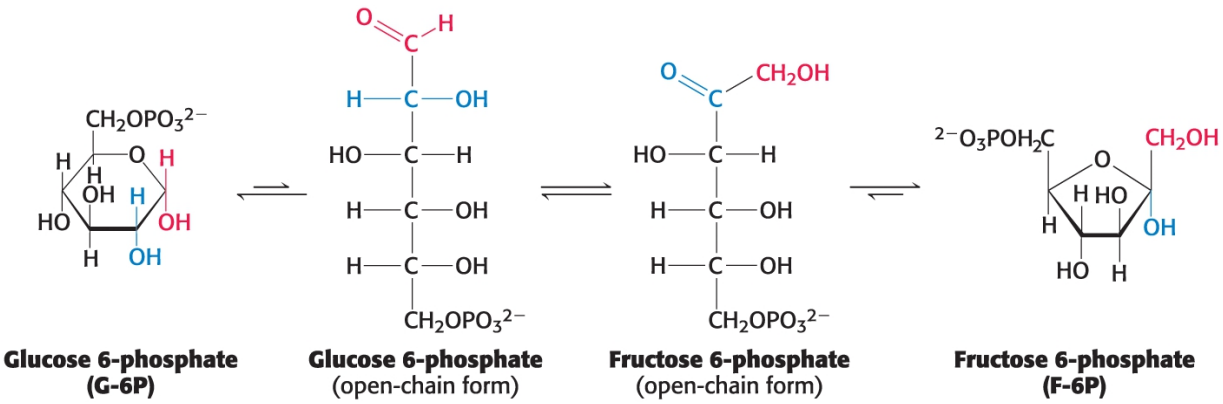


© Macmillan Learning

The hexokinase enzyme is depicted as a space-filling model composed of a large cluster of yellow spheres. The free hexokinase has two lobes with a tiny groove in the center. The groove is later occupied by a glucose molecule depicted as a cluster of red spheres. In the glucose-bound hexokinase, the two lobes are located close together.

Return to Conformational change in hexokinase upon glucose binding

Extended description for Conversion of glucose 6-phosphate to fructose 6-phosphate



The conversion of glucose 6-phosphate to fructose 6-phosphate takes place in 3 reversible steps.

The first step involves the reversible conversion of the cyclic form of glucose 6-phosphate (G-6 P) to its open-chain form.

The structure of the cyclic form of glucose 6-phosphate is as follows: A 6-membered heterocyclic hexagonal ring is in a horizontal orientation and consists of 1 O and 5 C atoms. O occupies the top right vertex. The ring is in a plane perpendicular to the plane of paper such that O and C 5 are located away from the observer and C 2 and C 3 are located toward the observer. C 1, C 2, and C 4 are each single bonded to H above and O H below. The H atom and O H group bonded to C 1 are highlighted in red. The H atom and O H group bonded to C 2 are highlighted in blue. C 3 is single bonded to O H above and H below. C 5 is single bonded to C H 2 O P O 3 superscript 2 minus above and H below.

The structure of glucose 6-phosphate (open-chain form) is as follows: C, single bond, C, single bond, C, single bond, C, single

bond, C, single bond, C H 2 O P O 3 superscript 2 minus. C 1 highlighted in red is double bonded to O on the upper left and single bonded to H on the upper right, both highlighted in red. C 2 highlighted in blue is single bonded to H on the left and O H on the right, both highlighted in blue. C 3 is single bonded to O H on the left and H on the right. C 4 and C 5 are each single bonded to H on the left and O H on the right.

In the second step, the open-chain form of glucose 6-phosphate is reversibly converted into the open-chain form of fructose 6-phosphate.

The structure of fructose 6-phosphate (open-chain form) is as follows: C, single bond, C, single bond, C, single bond, C, single bond, C H 2 O P O 3 superscript 2 minus. C 1 highlighted in blue is double bonded to O on the upper left and C H 2 O H on the upper right. The O atom is highlighted in blue and the C H 2 O H group is highlighted in red. C 2 is single bonded to O H on the left and H on the right. C 3 and C 4 are each single bonded to H on the left and O H on the right.

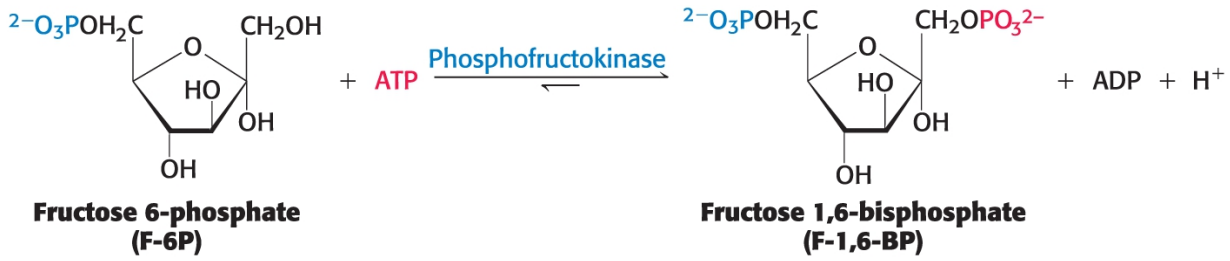
In the third step, the open-chain form of fructose 6-phosphate is reversibly converted into the cyclic form of fructose 6-phosphate (F-6 P).

The structure of the cyclic form of fructose 6-phosphate (F-6 P) is as follows: A 5-membered heterocyclic pentagonal ring is in a vertical orientation and consists of 1 O and 4 C atoms. The ring is in a plane perpendicular to the plane of the paper such that O is located away from the observer and C 2 and C 3 are located toward the observer. C 1 is single bonded to C H 2 O H above and O H below. C H 2 O H is highlighted in red. O H is highlighted in blue. C 2 is single bonded to O H above and H below. C 3 is single bonded to H above and O H

below. C 4 is single bonded to C H 2 O P O 3 superscript 2 minus above and H below.

Return to Conversion of glucose 6-phosphate to fructose 6-phosphate

Extended description for Reversible conversion of fructose 6-phosphate to fructose 1, 6-bisphosphate



Fructose 6-phosphate (F-6P)

Fructose 1,6-bisphosphate (F-1,6-BP)

The chemical reaction consists of two reactants and three products. The first reactant is fructose 6-phosphate (F-6 P) whose structure is as follows: A 5-membered heterocyclic pentagonal ring is in a vertical orientation and consists of 1 O and 4 C atoms. The ring is in a plane perpendicular to the plane of the paper such that O is located away from the observer and C 2 and C 3 are located toward the observer. C 1 is single bonded to C H 2 O H above and O H below. C 2 is single bonded to O H above. C 3 is single bonded to O H below. C 4 is single bonded to C H 2 O P O 3 superscript 2 minus above. P O 3 superscript 2 minus group is highlighted in blue.

The second reactant is A T P highlighted in red.

A reversible reaction arrow labeled phosphofructokinase shows the products.

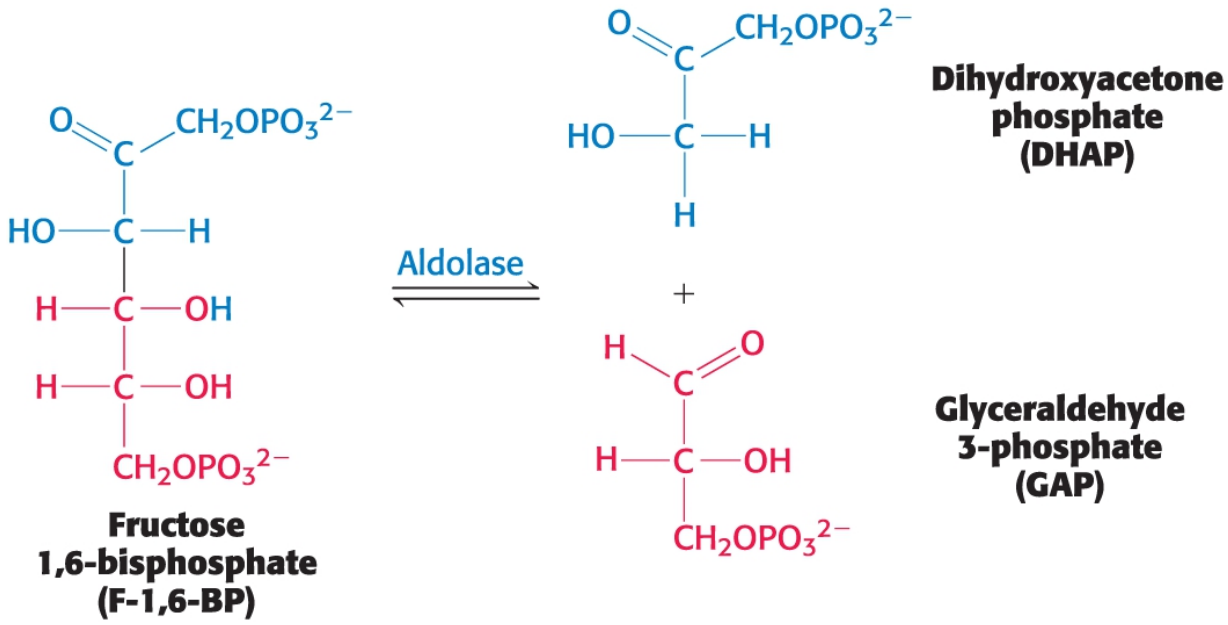
The first product is fructose 1, 6-bisphosphate (F-1, 6-B P) whose structure is as follows: A 5-membered heterocyclic pentagonal ring is in a vertical orientation and consists of 1 O and 4 C atoms. The ring is in a plane perpendicular to the plane of the paper such that O is located away from the observer and C 2 and C 3 are located toward the observer. C 1 is single bonded to C H 2 O P O 3 superscript 2

minus above and O H below. The P O 3 superscript 2 minus is highlighted in red. C 2 is single bonded to O H above. C 3 is single bonded to O H below. C 4 is single bonded to C H 2 O P O 3 superscript 2 minus above. P O 3 superscript 2 minus group is highlighted in blue.

The second product is A D P. The third reactant is H superscript plus.

Return to Reversible conversion of fructose 6-phosphate to fructose 1, 6-bisphosphate

Extended description for Reversible conversion of fructose 1, 6-bisphosphate to dihydroxyacetone phosphate and glyceraldehyde 3-phosphate



The structure of fructose 1, 6-bisphosphate (F-1,6 B P) is as follows: C, single bond, C, single bond, C, single bond, C, single bond, C H 2 O P O 3 superscript 2 minus. C 1 highlighted in blue is double bonded to O on the upper left and single bonded to C H 2 O P O 3 superscript 2 minus on the upper right, both highlighted in blue. C 2 highlighted in blue is single bonded to O H on the left and H on the right, both highlighted in blue. C 3 highlighted in red is single bonded to H on the left and O H on the right. The H atom is highlighted in red. The O atom of the O H group is highlighted in red and the H atom is highlighted in blue. C 4 highlighted in red is single bonded to H on the left and O H on the right, both highlighted in red. C H 2 O P O 3 superscript 2 minus group is also highlighted in red.

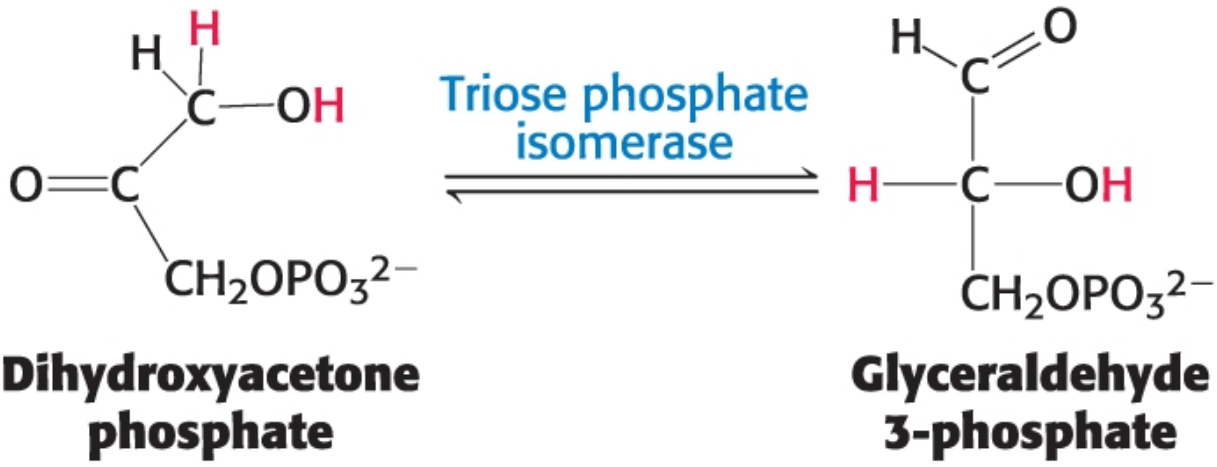
A reversible reaction arrow labeled aldolase leads to dihydroxyacetone phosphate and glyceraldehyde 3-phosphate.

The structure of dihydroxyacetone phosphate (D H A P) is as follows: C, single bond, C, single bond, H. C 1 is double bonded to O on the upper left and single bonded to C H 2 O P O 3 superscript 2 minus on the upper right. C 2 is single bonded to O H on the left and H on the right. The entire molecule is highlighted in blue.

The structure of glyceraldehyde 3-phosphate is as follows: C, single bond, C, single bond, C H 2 O P O 3 superscript 2 minus. C 1 is single bonded to H on the upper left and double bonded to O on the upper right. C 2 is single bonded to H on the left and O H on the right. The entire molecule is highlighted in red.

Return to Reversible conversion of fructose 1, 6-bisphosphate to dihydroxyacetone phosphate and glyceraldehyde 3-phosphate

Extended description for Reversible conversion of dihydroxyacetone phosphate to glyceraldehyde 3-phosphate



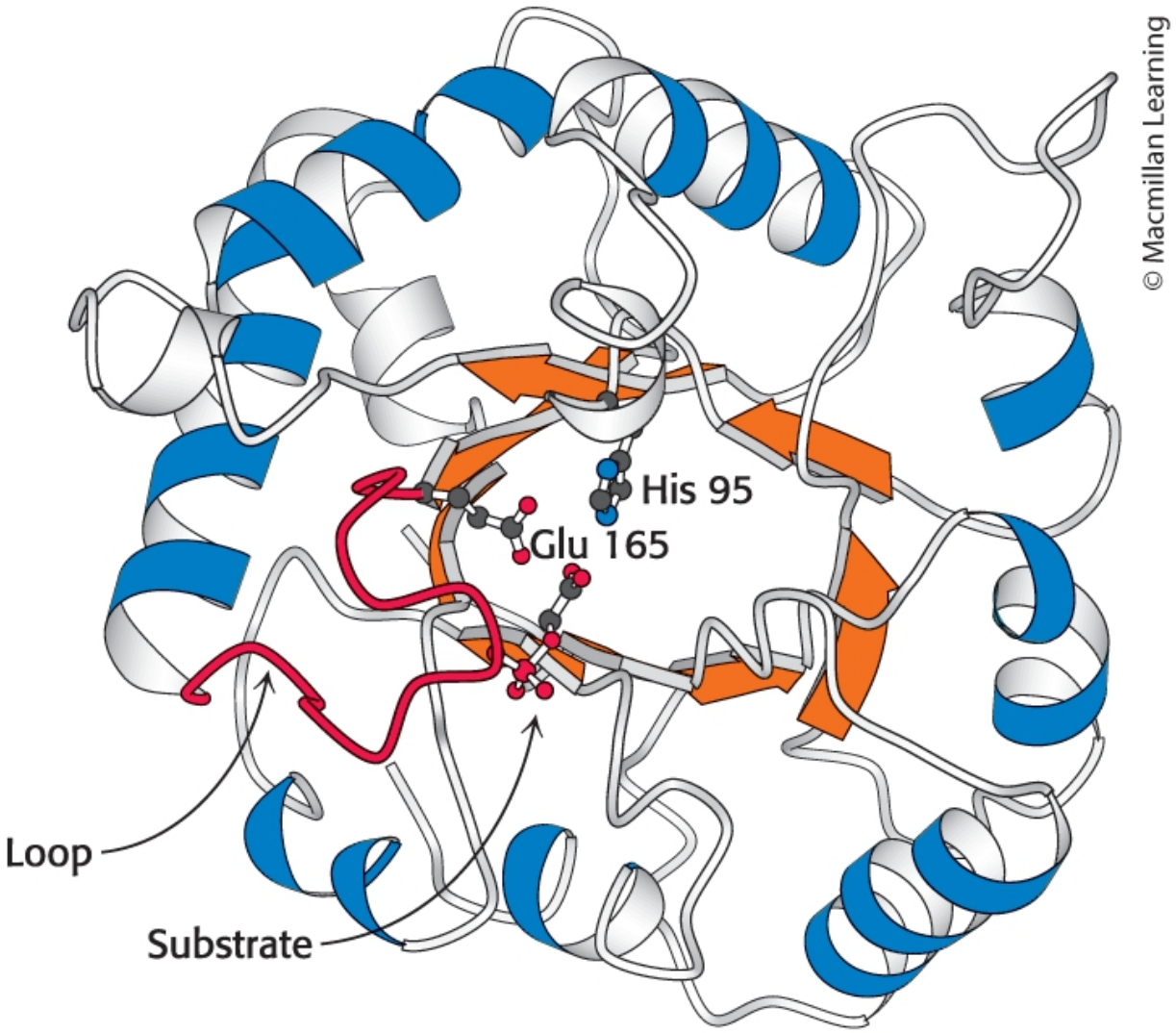
The structure of dihydroxyacetone phosphate is as follows: A central C atom is single bonded to C on the upper right, double bonded to O on the left, and single bonded to C H 2 O P O 3 superscript 2 minus on the lower right. The C atom on the upper right is single bonded to H on the upper left, single bonded to H above highlighted in red, and single bonded to O H on the right. The H atom of the O H group is highlighted in red.

A reversible reaction arrow labeled triose phosphate isomerase leads to glyceraldehyde 3-phosphate.

The structure of glyceraldehyde 3-phosphate is as follows: C, single bond, C, single bond, C H 2 O P O 3 superscript 2 minus. C 1 is single bonded to H on the upper left and double bonded to O on the upper right. C 2 is single bonded to H on the left highlighted in red and single bonded to O H on the right. The H atom of the O H group is highlighted in red.

Return to Reversible conversion of dihydroxyacetone phosphate to glyceraldehyde 3-phosphate

Extended description for Ribbon diagram of triose phosphate isomerase

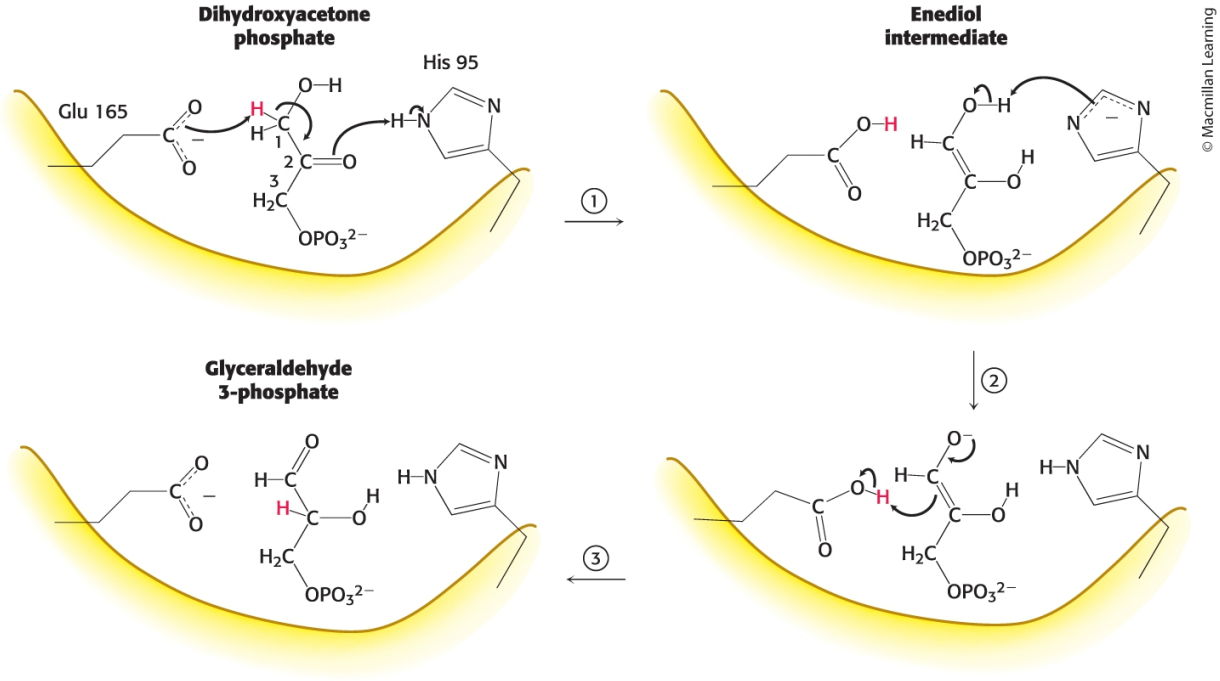


The ribbon diagram consists of a central core of 8 parallel beta-strands arranged in a circular fashion. These beta-strands are surrounded by a similar circular arrangement of eight alpha-helices. They are interconnected by long thread-like loops that extend into the space between the beta-strands and alpha-helices. The ball-and-stick model of H i s 95 and G l u 165 are located inside the hollow

center enclosed by the beta-strands. A wavy red loop connected to G l u 95 moves toward the lower left.

Return to Ribbon diagram of triose phosphate isomerase

Extended description for Catalytic mechanism of triose phosphate isomerase



The enzyme active site is depicted as a concave depression outlined by an orange line with a yellow highlight. The active site contains the side chains of G l u 165 on the upper left and H i s 95 on the upper right. The side chain of G l u 165 is as follows: A 2-carbon alkane chain is depicted as a line structure using 1 line. C 2 is single bonded to C which is further partially double bonded to O on the upper right and lower right. This C O O group has an overall negative charge. The side chain of H i s 95 is as follows: A 5-membered heterocyclic pentagonal ring is in a vertical orientation and consists of 2 N and 3 C atoms. First N occupies the top left vertex. Second N occupies the top right vertex. N 1 is single bonded to H on the left. A double bond is present between C 1 and N 2, and C 2 and C 3.

A dihydroxyacetone phosphate molecule is shown between G l u 165 and H i s 95 side chain. The structure of dihydroxyacetone phosphate is as follows: C, single bond, C, single bond, C H 2, single bond, O P O 3 superscript 2 minus. C 1 is single bonded to O, single bond, H on the upper right, H on the upper left, and H on the lower right. C 2 is double bonded to O on the right.

A black curved arrow moves from the C atom of the C O O group of G l u 165 toward the upper left H atom bonded to C 1 of dihydroxyacetone phosphate. Another black downward curved arrow moves the single bond between C 1 and the upper left H atom of dihydroxyacetone phosphate toward the single bond between C 1 and C 2. Another black arrow moves from the double bond between C 2 and O of the dihydroxyacetone phosphate molecule toward the H atom bonded to N 1 of H i s 95 side chain.

A forward arrow labeled 1 shows the enediol intermediate inside the active site of the enzyme.

The side chain of G l u 165 is as follows: A 2-carbon alkane chain is depicted as a line structure using 1 line. C 2 is single bonded to C which is further single bonded to O, single bond, H on the upper right, and double bonded to O lower right. The side chain of H i s 95 is as follows: A 5-membered heterocyclic pentagonal ring is in a vertical orientation and consists of 2 N and 3 C atoms. First N occupies the top left vertex. Second N occupies the top right vertex. A double bond is present between C 2 and C 3. A partial double bond is present between C 1 and N 1 and C 1 and N 1 thereby imparting a negative charge.

The structure of the intermediate is as follows: C, double bond, C, single bond, C H 2, single bond, O P O 3 superscript 2 minus. C 1 is single bonded to H on the left and single bonded to O, single bond,

H on the upper right. C 2 is single bonded to O, single bond, H on the right.

A black arrow moves from the partial double bond between C 1 and N 1 of H i s 95 toward the H atom of the O H group bonded to C 1 of the intermediate. Another arrow moves from the single bond between the O and H atom of the O H group toward the O atom.

A forward arrow labeled 2 shows the next intermediate inside the active site.

The side chain of G l u 165 is as follows: A 2-carbon alkane chain is depicted as a line structure using 1 line. C 2 is single bonded to C which is further single bonded to O, single bond, H on the upper right, and double bonded to O below. The side chain of H i s 95 is as follows: A 5-membered heterocyclic pentagonal ring is in a vertical orientation and consists of 2 N and 3 C atoms. First N occupies the top left vertex. Second N occupies the top right vertex. N 1 is single bonded to H. A double bond is present between C 1 and N 2, and C 2 and C 3.

The structure of the intermediate is as follows: C, double bond, C, single bond, C H 2, single bond, O P O 3 superscript 2 minus. C 1 is single bonded to H on the left and single bonded to O superscript minus on the upper right. C 2 is single bonded to O, single bond, H on the right.

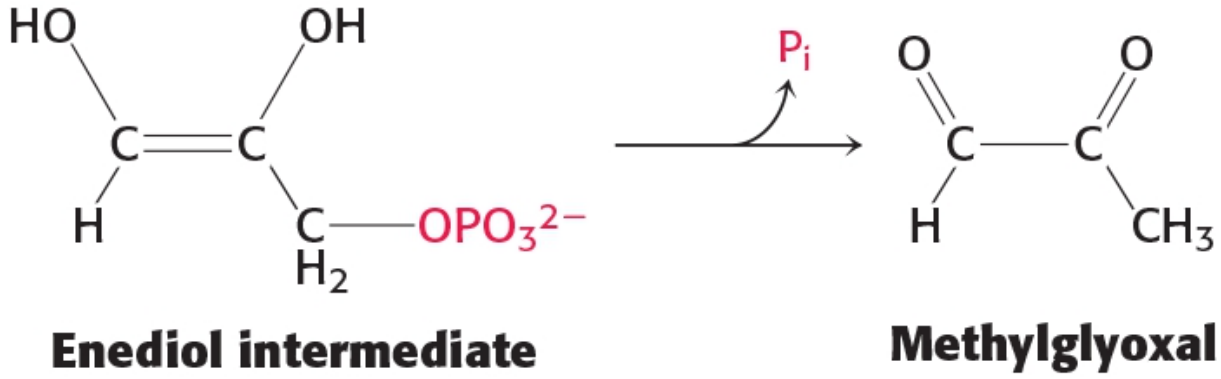
A curved arrow moves from O superscript minus toward its single bond with C 1 of the intermediate. Another arrow moves from the double bond between C 1 and C 2 moves toward the H atom of the O H group of G l u 165. Another arrow moves from the single bond between the O and H atom of the O H group toward the O atom.

A forward arrow labeled 3 shows the product glyceraldehyde 3-phosphate between the side chains of G l u 165 and H i s 95.

The structure of the product is as follows: C, single bond, C, single bond, C H 2, single bond, O P O 3 superscript 2 minus. C 1 is double bonded to O on the upper right and single bonded to H on the left. C 2 is single bonded to O, single bond, H on the right and H on the upper left.

Return to Catalytic mechanism of triose phosphate isomerase

Extended description for Conversion of enediol intermediate into methylglyoxal



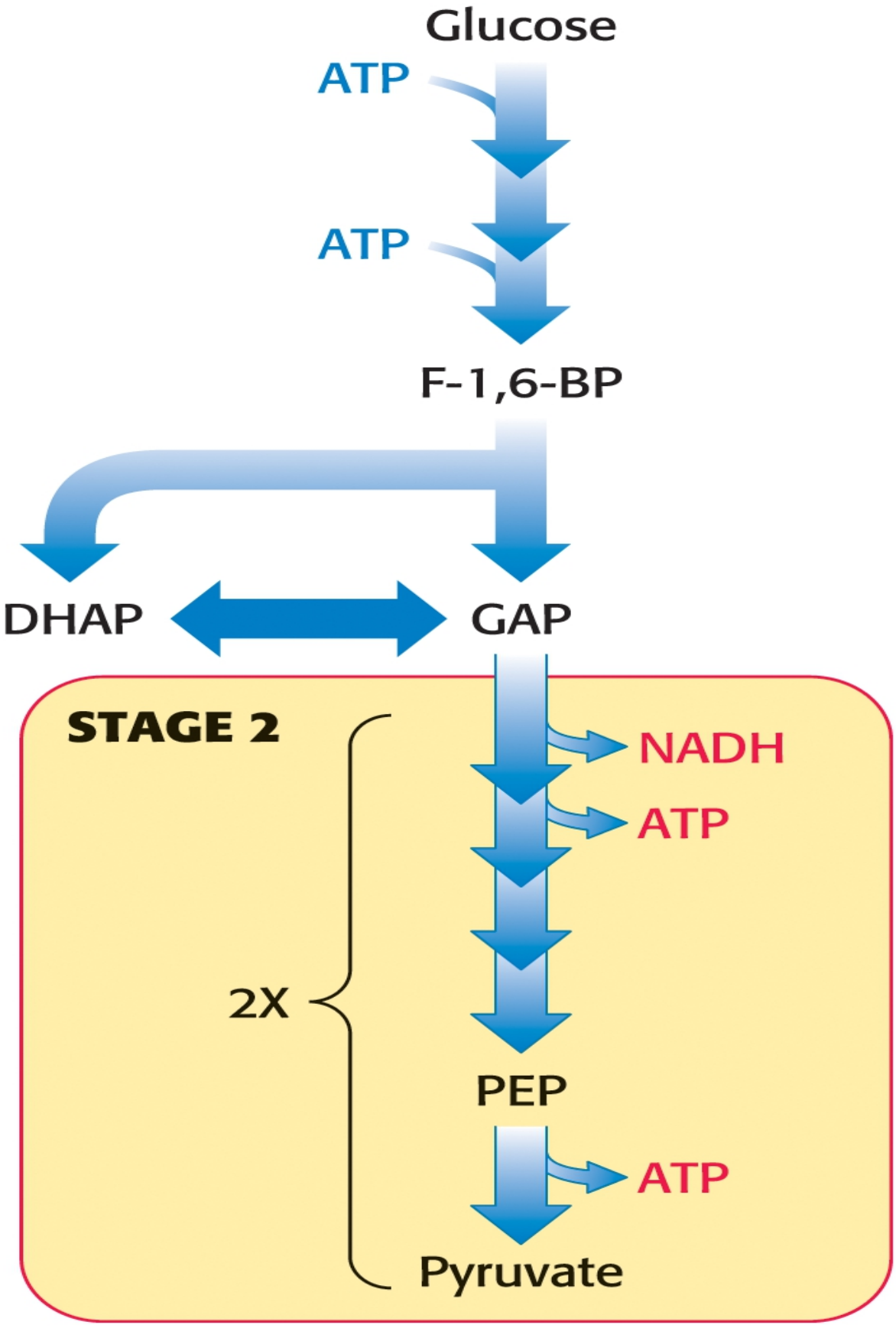
The chemical reaction consists of one reactant and one product. The reactant is enediol intermediate whose structure is as follows: C, double bond, C. C 1 is single bonded to O H on the upper left and H on the lower right. C 2 is single bonded to O H on the upper right and C H 2, single bond, O P O 3 superscript 2 minus on the lower right.

A forward reaction arrow leads to the product and shows the simultaneous release of P subscript i.

The product is methylglyoxal whose structure is as follows: C, single bond, C. C 1 is double bonded to O on the upper left and single bonded to H on the lower left. C 2 is double bonded to O on the upper right and single bonded to C H 3 on the lower right.

Return to Conversion of enediol intermediate into methylglyoxal

Extended description for Stage 2 of glycolytic pathway



© Macmillan Learning

The flowchart is depicted as follows:

Glucose, three downward arrows, F-1, 6-B P. The first and third downward arrows show the entry of A T P.

F-1, 6-B P, one downward arrow and one curved leftward arrow.

The downward arrow leads to G A P. The curved leftward arrow leads to D H A P. A double-headed arrow is shown between G A P and D H A P.

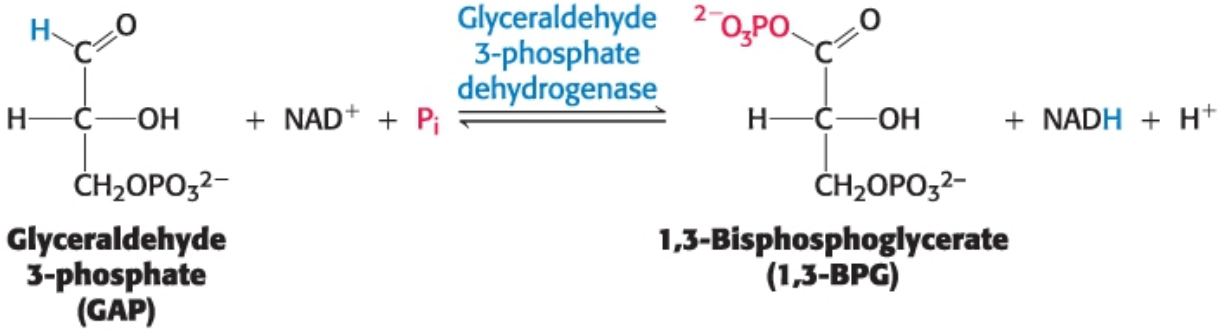
G A P, four downward arrows, P E P. The first and second downward arrow show the release of N A D H and A T P respectively.

P E P, one downward arrow, pyruvate. The downward arrow shows the release of A T P. The steps from the first downward arrow below G A P to the final pyruvate molecule are enclosed by left curly bracket labeled 2 times.

Note: The steps involving the conversion of G A P to pyruvate are enclosed in a yellow rectangle labeled stage 2.

Return to Stage 2 of glycolytic pathway

Extended description for Reversible conversion of glyceraldehyde 3-phosphate to 1,3-bisphosphoglycerate



The chemical reaction consists of three reactants and three products. The first reactant is glyceraldehyde 3-phosphate (G A P) whose structure is as follows: C, single bond, C, single bond, C H 2 O P O 3 superscript 2 minus. C 1 is single bonded to H on the upper left highlighted in blue and double bonded to O on the upper right. C 2 is single bonded to H on the left and O H on the right.

The second reactant is N A D superscript plus. The third reactant is P subscript i.

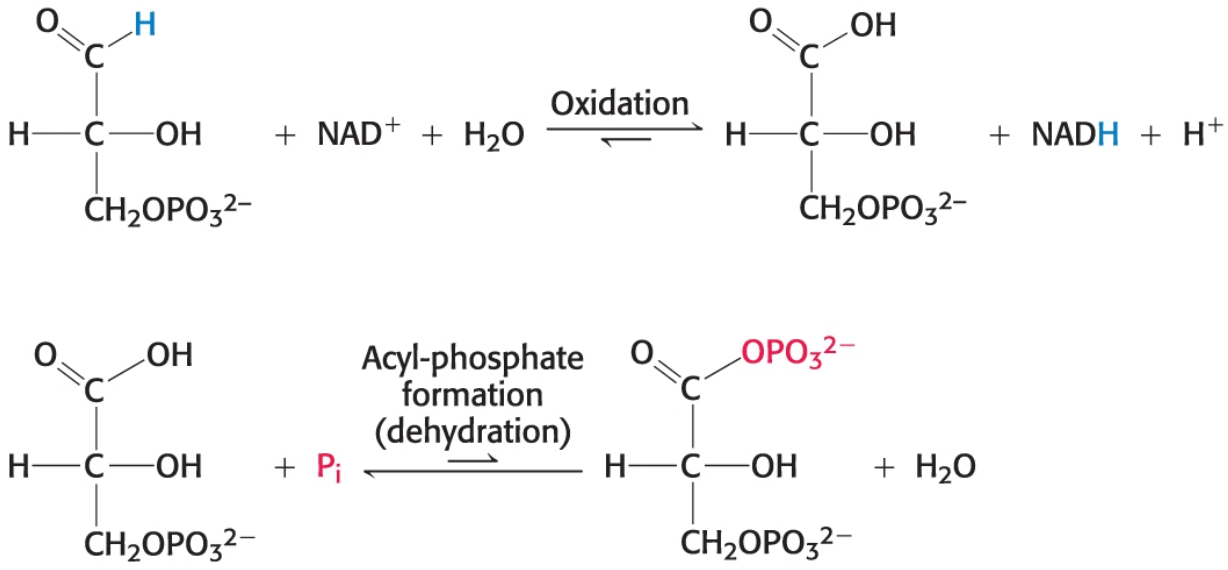
A reversible reaction arrow labeled glyceraldehyde 3-phosphate dehydrogenase leads to the products.

The first product is 1,3-bisphosphoglycerate (1,3-B P G) whose structure is as follows: C, single bond, C, single bond, C H 2 O P O 3 superscript 2 minus. C 1 is single bonded to O P O 3 superscript 2 minus on the upper left highlighted in red and double bonded to O on the upper right. C 2 is single bonded to H on the left and O H on the right.

The second product is N A D H with H highlighted in blue. The third product is H superscript plus.

Return to Reversible conversion of glyceraldehyde 3-phosphate to 1,3-bisphosphoglycerate

Extended description for Chemical reactions depict the oxidation of an aldehyde and formation of acyl-phosphate production



The first chemical reaction consists of three reactants and three products. The structure of the first reactant is as follows: C, single bond, C, single bond, C H 2 O P O 3 superscript 2 minus. C 1 is double bonded to O on the upper left and single bonded to H on the upper right highlighted in blue. C 2 is single bonded to H on the left and O H on the right.

The second reactant is N A D superscript plus. The third reactant is H 2 O.

A reversible reaction arrow labeled oxidation leads to the products.

The structure of the first product is as follows: C, single bond, C, single bond, C H 2 O P O 3 superscript 2 minus. C 1 is double bonded

to O on the upper left and single bonded to O H on the upper right. C 2 is single bonded to H on the left and O H on the right.

The second product is N A D H with H highlighted in blue. The third product is H superscript plus.

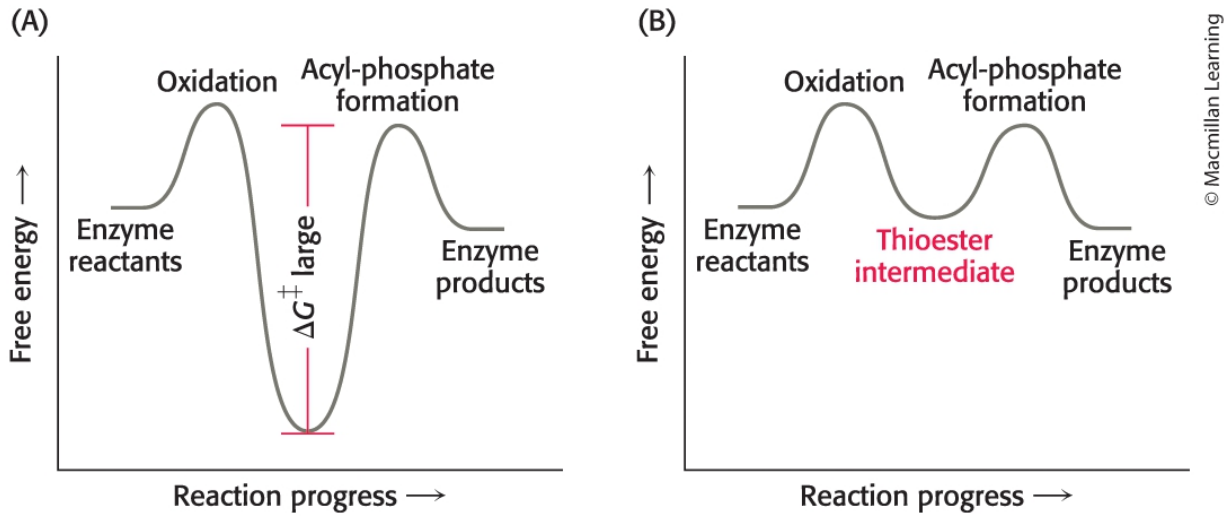
The second chemical reaction consists of two reactants and two products. The structure of the first reactant is as follows: C, single bond, C, single bond, C H 2 O P O 3 superscript 2 minus. C 1 is double bonded to O on the upper left and single bonded to O H on the upper right. C 2 is single bonded to H on the left and O H on the right. The second reactant is P subscript i highlighted in red.

A reversible reaction arrow labeled acyl-phosphate formation (dehydration) leads to the products.

The structure of the first product is as follows: C, single bond, C, single bond, C H 2 O P O 3 superscript 2 minus. C 1 is double bonded to O on the upper left and single bonded to O P O 3 superscript 2 minus on the upper right highlighted in red. C 2 is single bonded to H on the left and O H on the right. The second product is H 2 O.

Return to Chemical reactions depict the oxidation of an aldehyde and formation of acyl-phosphate production

Extended description for Graphs depicting free energy profiles



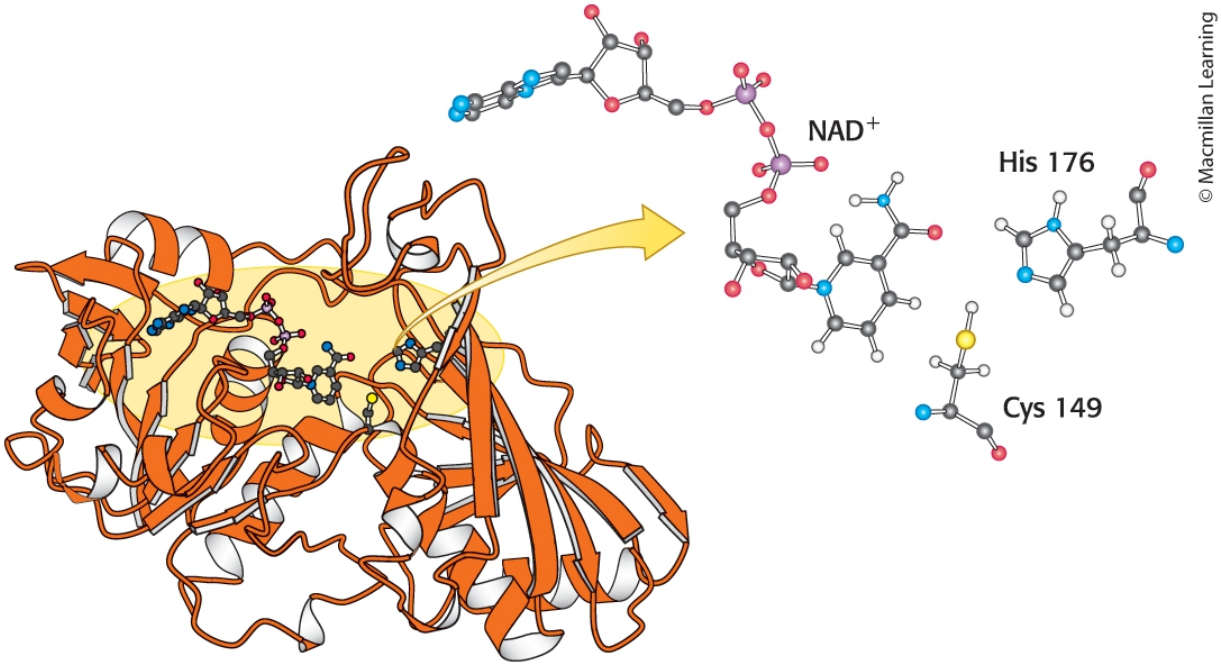
Graph (A): The horizontal axis is labeled reaction progress. The vertical axis is labeled free energy which increases from the bottom to the top. The curve begins at a point above the midpoint of the vertical axis and then moves horizontally for a short duration. This section of the curve is labeled “enzyme reactants.” It then rises steeply to form the first peak labeled “oxidation” at the highest free energy and then falls steeply to form a depression at the lowest free energy in the middle of the horizontal axis. It again rises vertically upward to form a second peak labeled “acyl-phosphate formation” just below the first peak. It then falls down to reach the same level as enzyme reactants and starts moving horizontally toward the right. This horizontal section is labeled “enzyme products.” The vertical length of the depression in the curve is labeled delta G superscript plus plus large.

Graph (B): The horizontal axis is labeled reaction progress. The vertical axis is labeled free energy which increases from the bottom

to the top. The curve begins at a point above the midpoint of the vertical axis and then moves horizontally for a short duration. This section of the curve is labeled “enzyme reactants.” It then rises steeply to form the first peak labeled “oxidation” at the highest free energy and then falls steeply to form a depression labeled “thioester intermediate” at the same free energy as the enzyme reactants, in the middle of the horizontal axis. It again rises vertically upward to form a second peak labeled “acyl-phosphate formation” just below the first peak. It then falls down to reach the same level as enzyme reactants and starts moving horizontally toward the right. This horizontal section is labeled “enzyme products.”

Return to Graphs depicting free energy profiles

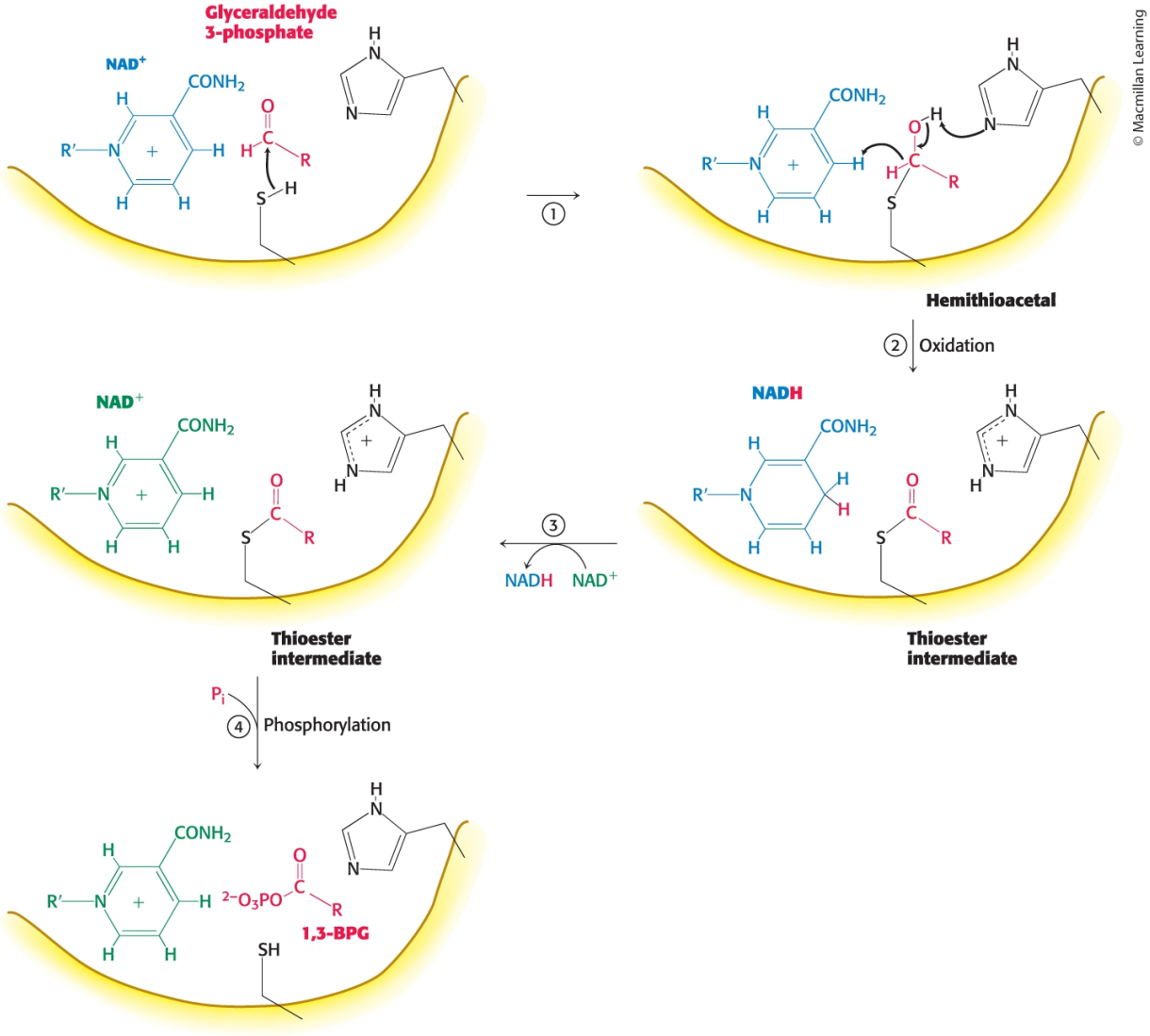
Extended description for Ribbon diagram of G A P D H



The ribbon diagram consists of several beta-strands and alpha-helices interconnected by thread-like loops. A groove is located at the top of the diagram. A loose cluster of long and curved threads like loops are located at the top of the groove. A few ball-and-stick models are located inside the groove. An arrow shows the magnified view of the ball-and-stick models of H i s 176, C y s 149, and N A D superscript plus located in the groove. N A D superscript plus is located on the left and H i s 176 and C y s 149 are located on the right and lower right respectively.

Return to Ribbon diagram of G A P D H

Extended description for Catalytic mechanism of G A P D H



The enzyme active site is depicted as a concave depression outlined by an orange line with a yellow highlight. The active site has side chains of two unlabeled amino acids located at the bottom and top right.

The side chain of the first amino acid residue is as follows: C H 2, single bond, S, single bond, H.

The side chain of the second amino acid residue is as follows: C H 2 is single bonded to C 2 of a 5-membered heterocyclic pentagonal ring in a horizontal orientation. First N occupies the bottom left vertex. The second N bound to H occupies the topmost vertex. C 1 occupies the leftmost vertex. A double bond is present between N 1 and C 1, and C 2 and C 3.

The active site is bound to N A D superscript plus and glyceraldehyde 3-phosphate. For simplification, only the aldehyde group of glyceraldehyde 3-phosphate is shown. The structure of the aldehyde group is as follows: A central C atom is double bonded to O above, single bonded to H on the lower left, and single bonded to R on the lower right.

The structure of N A D superscript plus is as follows: A 6-membered heterocyclic hexagonal ring is in a horizontal orientation and consists of 1 N and 5 C atoms. N occupies the leftmost vertex and is single bonded to R prime on the left. A double bond is present between N 1 and C 1, C 2 and C 3, C 4 and C 5. C 1, C 3, C 4, and C 5 are each single bonded to H. C 2 is single bonded to C O N H 2. A plus symbol is shown at the center of the ring.

An arrow from the single bond between S and H atoms of one of the amino acid residues points toward the central C atom of the aldehyde group.

A forward reaction arrow labeled 1 shows the formation of hemithioacetal.

The S atom of the amino acid residue becomes single-bonded to the central C atom of the aldehyde group. This C atom is single bonded to O, single bond, H above, and single bonded to H on the lower left and R on the lower right.

A curved arrow points from N 1 atom of the pentagonal ring of an amino acid residue toward the H atom of the O H group of the aldehyde group. Another arrow points from the single bond between the O and H atoms of this group toward the single bond between the O and C atoms.

Another arrow points from the central C atom toward the H atom bonded to C 3 of N A D superscript plus.

A forward arrow labeled 2 and oxidation shows the thioester intermediate.

N A D superscript plus bound to the active site is converted into N A D H. C 3 of N A D H is single bonded to two different H atoms.

The thioester intermediate consists of an S atom of one of the amino acid residues single bonded to C on the upper right. This C atom is double bonded to O above and single bonded to R on the lower right.

The pentagonal ring of the second amino acid residue attains a positive charge. C 1 is partially double bonded to N 1 and N 2. Both N 1 and N 2 are single-bonded to the H atom.

A forward arrow labeled 3 shows the thioester intermediate bound to the active site. N A D superscript plus molecule enters and N A D H is released.

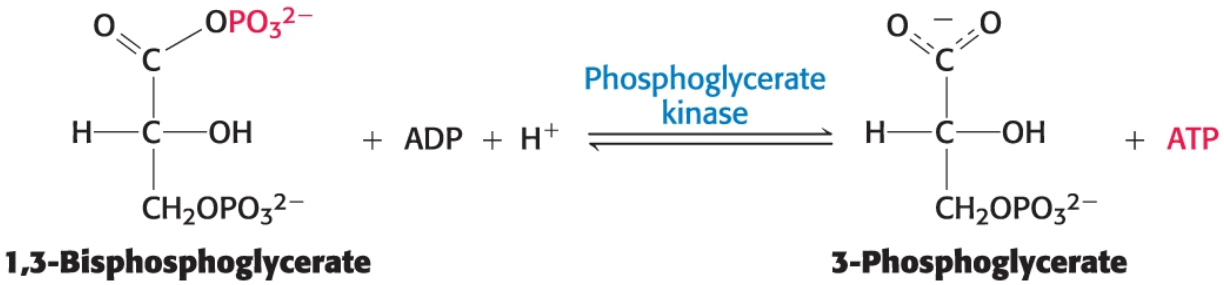
A forward arrow labeled 4 and phosphorylation shows the formation of 1,3-B P G. It also involves the entry of P subscript i.

The structure of 1, 3-B P G is depicted as follows: A central C atom is double bonded to O above, single bonded to O P O 3 superscript 2 minus on the lower left, and single bonded to R on the lower right.

The S atom of one of the amino acid residues is bound to H. The pentagonal ring of the second amino acid residue becomes neutral.

Return to Catalytic mechanism of G A P D H

Extended description for Chemical reaction shows the conversion of 1,3-bisphosphoglycerate to 3-phosphoglycerate



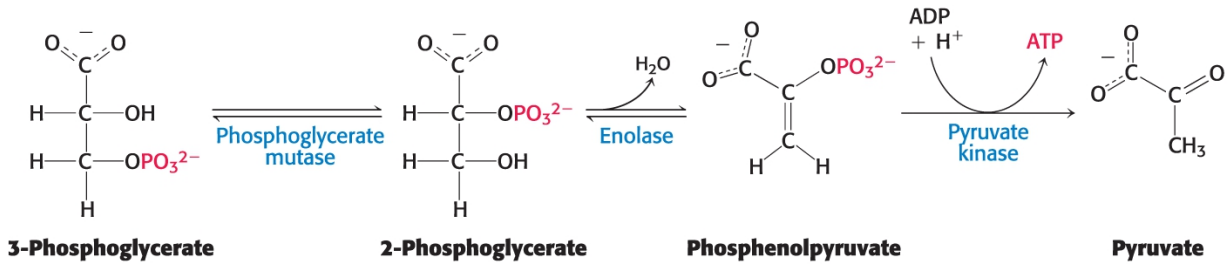
The chemical reaction consists of three reactants and two products. The first reactant is 1,3-bisphosphoglycerate whose structure is as follows: C, single bond, C, single bond, C H 2 O P O 3 superscript 2 minus. C 1 is double bonded to O on the upper left and single bonded to O P O 3 superscript 2 minus on the upper right. C 2 is single bonded to H on the left and O H on the right. The second reactant is A D P. The third reactant is H superscript plus.

A reversible reaction arrow labeled phosphoglycerate kinase leads to the products.

The first product is 3-phosphoglycerate whose structure is as follows: C, single bond, C, single bond, C H 2 O P O 3 superscript 2 minus. C 1 is partially double bonded to O on the upper left and O on the upper right. This C O O group has an overall negative charge. C 2 is single bonded to H on the left and O H on the right. The second product is A T P.

Return to Chemical reaction shows the conversion of 1,3-bisphosphoglycerate to 3-phosphoglycerate

Extended description for Conversion of 3-phosphoglycerate to pyruvate



The conversion of 3-phosphoglycerate to pyruvate takes place in three steps.

The first step involves the reversible conversion of 3-phosphoglycerate to 2-phosphoglycerate.

The structure of 3-phosphoglycerate is as follows: C, single bond, C, single bond, C, single bond, H. C 1 is partially double bonded to O on the upper left and O on the upper right. This C O O group has an overall negative charge. C 2 is single bonded to H on the left and O H on the right. C 3 is single bonded to H on the left and O P O 3 superscript 2 minus on the right. The P O 3 superscript 2 minus group is highlighted in red.

A reversible reaction arrow labeled phosphoglycerate mutase leads to the product 2-phosphoglycerate.

The structure of 2-phosphoglycerate is as follows: C, single bond, C, single bond, C, single bond, H. C 1 is partially double bonded to O on the upper left and O on the upper right. This C O O group has an overall negative charge. C 2 is single bonded to H on the left and O P O 3 superscript 2 minus on the right. The P O 3 superscript 2 minus

group is highlighted in red. C 3 is single bonded to H on the left and O H on the right.

The second step involves the reversible conversion of 2-phosphoglycerate to phosphoenolpyruvate.

A reversible reaction arrow labeled enolase leads to phosphoenolpyruvate from 2-phosphoglycerate. A curved upward pointing arrow above it shows the release of H 2 O.

The structure of phosphoenolpyruvate is as follows: A central C atom is double bonded to C below, single bonded to O P O 3 superscript 2 minus on the upper right, and single bonded to C on the upper left. The P O 3 superscript 2 minus group is highlighted in red. The C atom below is single-bonded to H on the lower left and H on the lower right. The C atom on the upper left is partially double bonded to O above and O on the lower left. This C O O group has an overall negative charge.

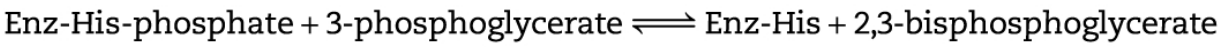
The third step involves the irreversible conversion of phosphoenolpyruvate to pyruvate.

A forward reaction arrow labeled pyruvate leads to pyruvate from phosphoenolpyruvate. A curved arrow above it shows the simultaneous conversion of A D P plus H superscript plus to A T P highlighted in red.

The structure of pyruvate is as follows: A central C atom is double bonded to O on the upper right, single bonded to C H 3 below, and single bonded to C on the upper left. This C atom is partially double bonded to O above and O on the lower left. This C O O group has an overall negative charge.

Return to Conversion of 3-phosphoglycerate to pyruvate

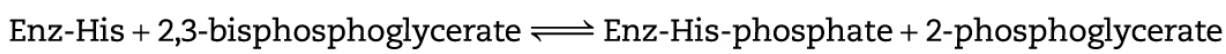
Extended description for Transfer of phosphoryl group from histidine residues of an enzyme to 3-phosphoglycerate



The reaction consists of two reactants and two products. The reactants are enzyme, single bond, histidine, single bond, phosphate, and 3-phosphoglycerate. The products are enzyme, single bond, histidine, and 2,3-bisphosphoglycerate.

Return to Transfer of phosphoryl group from histidine residues of an enzyme to 3-phosphoglycerate

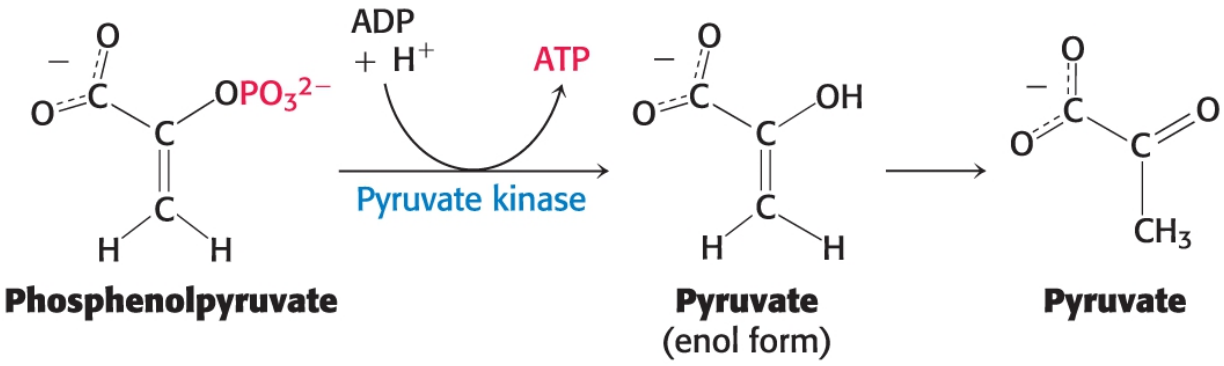
Extended description for Removal of phosphoryl group from 2,3-bisphosphoglycerate



The reaction consists of two reactants and two products. The reactants are enzyme, single bond, histidine, and 2,3-bisphosphoglycerate. The products are enzyme, single bond, histidine, single bond, phosphate, and 2-phosphoglycerate.

Return to Removal of phosphoryl group from 2,3-bisphosphoglycerate

Extended description for Conversion of phosphoenolpyruvate to pyruvate



The conversion of phosphoenolpyruvate to pyruvate takes place in three irreversible steps.

The first step involves the conversion of phosphoenolpyruvate to pyruvate (enol form).

The structure of phosphoenolpyruvate is as follows: A central C atom is double bonded to C below, single bonded to O P O 3 superscript 2 minus on the upper right, and single bonded to C on the upper left. The P O 3 superscript 2 minus group is highlighted in red. The C atom below is single-bonded to H on the lower left and H on the lower right. The C atom on the upper left is partially double bonded to O above and O on the lower left. This C O O group has an overall negative charge.

A forward reaction arrow labeled pyruvate kinase leads to pyruvate. A curved arrow above it shows the simultaneous conversion of A D P plus H superscript plus to A T P highlighted in red.

The structure of pyruvate (enol form) is as follows: A central C atom is double bonded to C below, single bonded to O H on the upper right, and single bonded to C on the upper left. The C atom below is single-bonded to H on the lower left and H on the lower right. The C atom on the upper left is partially double bonded to O above and O on the lower left. This C O O group has an overall negative charge.

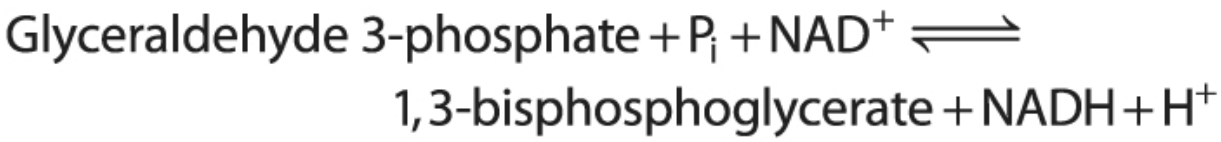
The second step involves the conversion of the enol form of pyruvate to pyruvate.

A forward reaction arrow leads to pyruvate from the enol form of pyruvate.

The structure of pyruvate is as follows: A central C atom is double bonded to O on the upper right, single bonded to C H 3 below, and single bonded to C on the upper left. This C atom is partially double bonded to O above and O on the lower left. This C O O group has an overall negative charge.

Return to Conversion of phosphoenolpyruvate to pyruvate

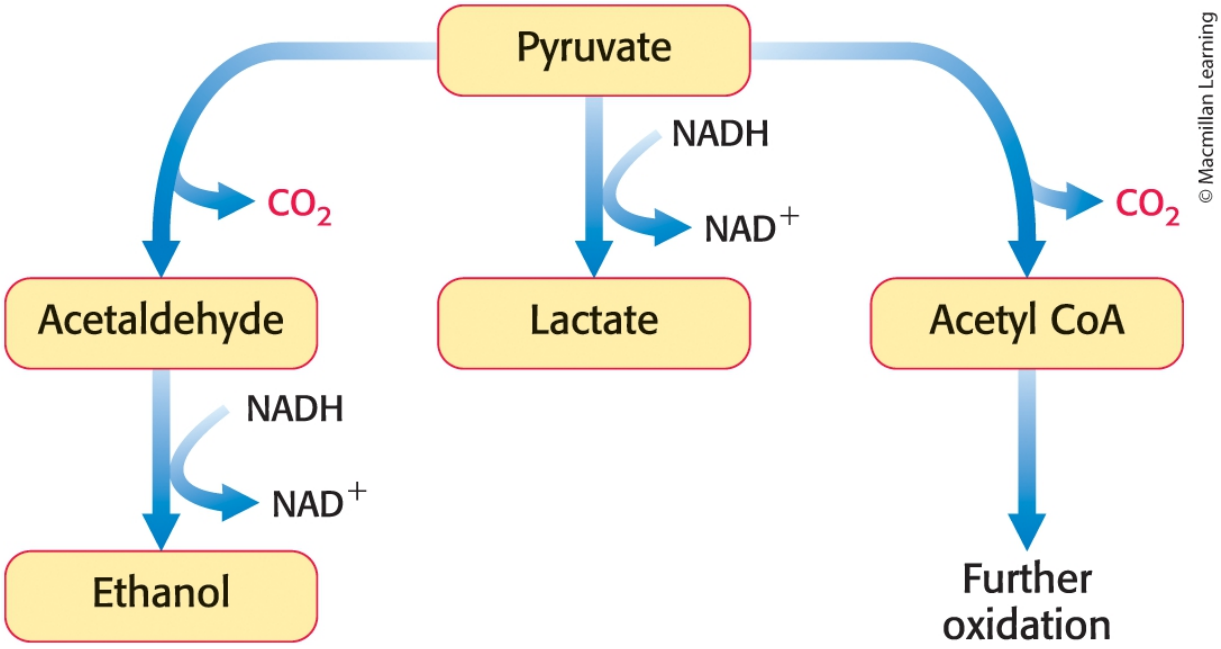
Extended description for Step 6 of glycolysis



The reaction consists of 3 reactants and 3 products. The reactants are glyceraldehyde 3-phosphate, P subscript i, and N A D superscript plus. The products are 1,3-bisphosphoglycerate, N A D H, and H superscript plus.

Return to Step 6 of glycolysis

Extended description for Different fates of pyruvate molecule



The flowchart is depicted as follows:

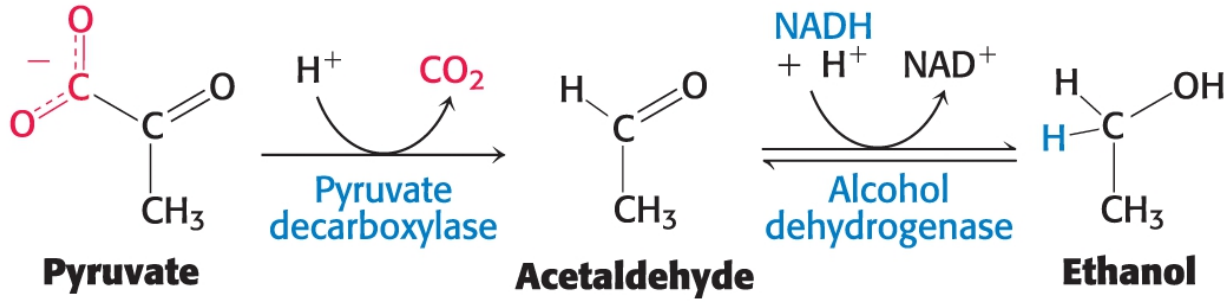
Pyruvate is shown at the top center. A leftward curved below pyruvate leads to acetaldehyde and shows the release of C O 2. A rightward curved arrow below pyruvate leads to acetyl-C o A and shows the release of C O 2. A downward arrow below pyruvate leads to lactate and shows the oxidation of N A D H to N A D superscript plus.

A downward arrow below acetaldehyde leads to ethanol. It also shows the oxidation of N A D H to N A D superscript plus.

A downward arrow below acetyl C o A leads to further oxidation.

Return to Different fates of pyruvate molecule

Extended description for Conversion of pyruvate to ethanol



In the first chemical reaction, pyruvate is converted into acetaldehyde. The structure of pyruvate is as follows: A central C atom is double bonded to O on the upper right, single bonded to C H 3 below, and single bonded to C on the upper left. This C atom is partially double bonded to O above and O on the lower left. This C O O group has an overall negative charge.

A forward reaction arrow labeled pyruvate decarboxylase leads to acetaldehyde. A curved arrow above it shows the simultaneous entry of H superscript plus and exit of C O 2.

The structure of acetaldehyde is as follows: A central C atom is single bonded to H on the upper left, double bonded to O on the upper right, and single bonded to C H 3 below.

In the second chemical reaction, acetaldehyde is further converted into ethanol.

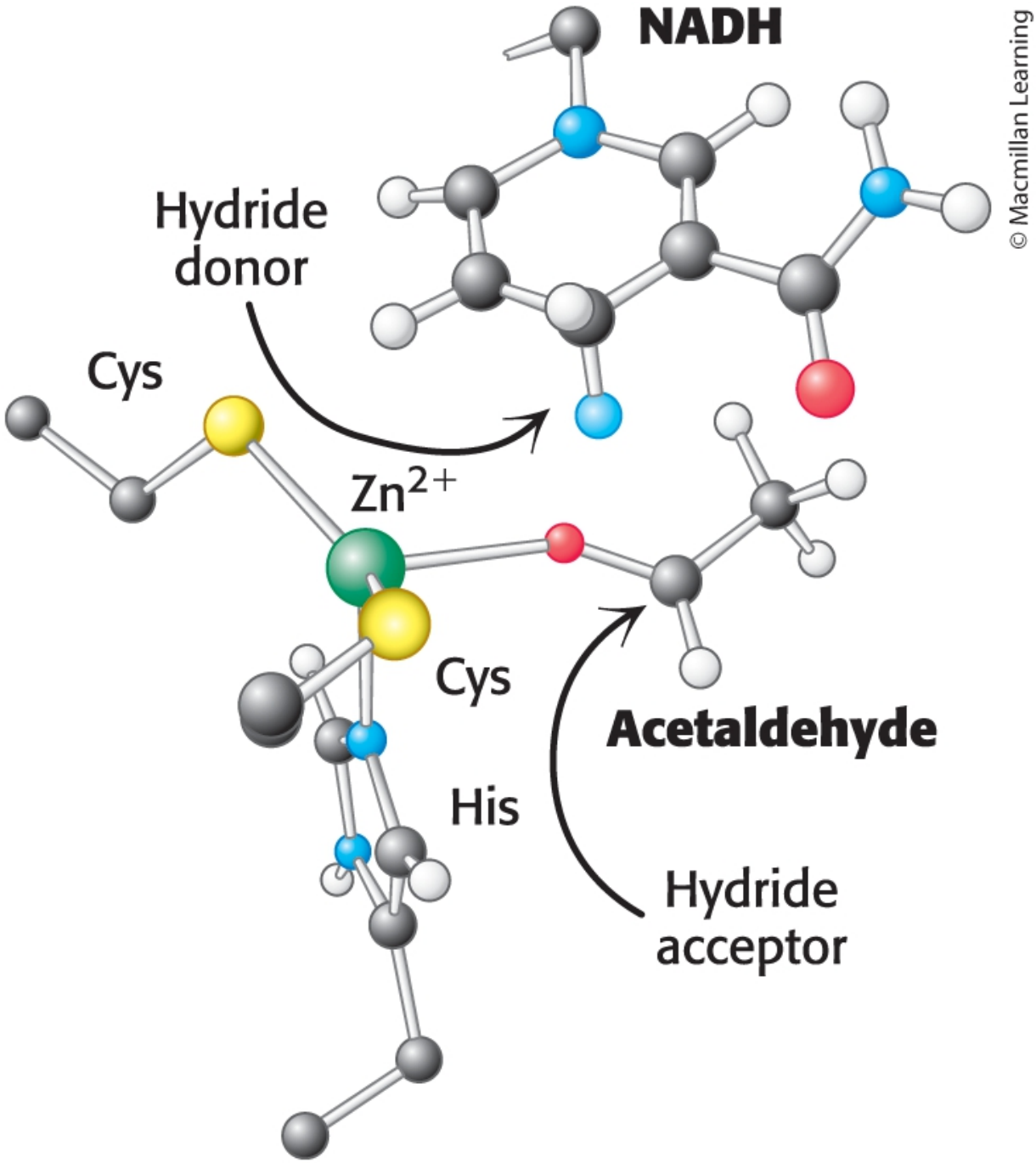
A reversible reaction arrow labeled alcohol dehydrogenase leads to ethanol from acetaldehyde. A curved arrow above it shows the

simultaneous oxidation of N A D H plus H superscript plus to N A D superscript plus.

The structure of ethanol is as follows: A central C atom is single bonded to H highlighted in blue on the left, single bonded to H on the upper left, single bonded to O H on the upper right, and single bonded to C H 3 below.

Return to Conversion of pyruvate to ethanol

Extended description for Ball-and-stick model of zinc ion in the alcohol dehydrogenase active site and its binding partners

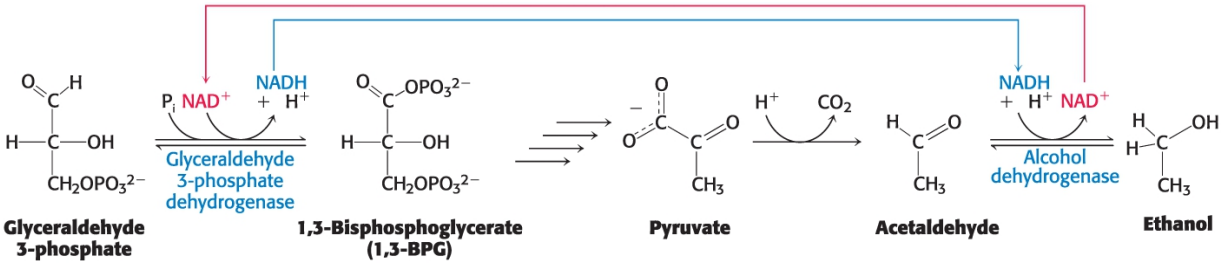


The Z n superscript 2 plus ion is depicted as a green sphere. It is connected to a yellow sphere of a cysteine residue located on the upper left and in the front, toward the observer. The yellow sphere of each cysteine residue is further connected to a chain of two black spheres. The Z n superscript 2 plus ion is connected to the blue sphere of the pentagonal ring of a histidine residue below. The ring consists of 2 blue and 3 black spheres. The bottom-most black sphere is connected to a chain of two black spheres below. The remaining spheres are connected to a white sphere. The Z n superscript 2 plus ion is also connected to a small red sphere of an acetaldehyde molecule labeled hydride acceptor. The red sphere is further connected to a chain of two black spheres. The first black sphere is connected to a white sphere below. The second black sphere is connected to three white spheres.

N A D H molecule labeled hydride donor is located above the acetaldehyde molecule. The ball-and-stick model of N A D H consists of a hexagonal ring composed of 1 blue and 5 black spheres. The blue sphere occupies the topmost vertex and is connected to a black sphere above. The bottom-most black sphere is connected to a blue sphere below. The top right and top left black spheres are connected to a white sphere. The bottom left black sphere is connected to a white sphere on the left and lower right. The bottom right black sphere is connected to a chain composed of a black sphere and a blue sphere. The black sphere of this chain is connected to a red sphere below. The blue sphere is connected to a white sphere above and a white sphere on the lower right.

Return to Ball-and-stick model of zinc ion in the alcohol dehydrogenase active site and its binding partners

Extended description for Reoxidation of N A D H



The figure shows a series of reactions. The first reaction consists of one reactant and one product. The reactant is glyceraldehyde 3-phosphate whose structure is as follows: C, single bond, C, single bond, C H 2 O P O 3 superscript 2 minus. C 1 is double bonded to O on the upper right and single bonded to H on the upper left. C 2 is single bonded to H on the left and O H on the right.

A reversible reaction arrow labeled glyceraldehyde 3-phosphate dehydrogenase leads to the product 1,3-bisphosphoglycerate (1,3-B P G). It shows the entry of P subscript i and a curved arrow above it shows the simultaneous reduction of N A D superscript plus to N A D H plus H superscript plus.

The structure of the product 1,3-bisphosphoglycerate (1,3-B P G) is as follows: C, single bond, C, single bond, C H 2 O P O 3 superscript 2 minus. C 1 is double bonded to O on the upper right and single bonded to O P O 3 superscript 2 minus on the upper right. C 2 is single bonded to H on the left and O H on the right.

Four parallel forward arrows are shown next to the product.

The second reaction consists of one reactant and one product. The reactant is pyruvate whose structure is as follows: A central C atom

is double bonded to O on the upper right, single bonded to C H 3 below, and single bonded to C on the upper left. This C atom is partially double bonded to O above and O on the lower left. This C O O group has an overall negative charge.

A forward reaction arrow leads to the product acetaldehyde. A curved arrow above it shows the simultaneous entry of H superscript plus and exit of C O 2.

The structure of the product acetaldehyde is as follows: A central C atom is single bonded to H on the upper left, double bonded to O on the upper right, and single bonded to C H 3 below.

The third reaction consists of one reactant and one product. The reactant is acetaldehyde. A reversible arrow labeled alcohol dehydrogenase leads to the product ethanol. A curved arrow above it shows the simultaneous reoxidation of N A D H plus H superscript plus to N A D superscript plus.

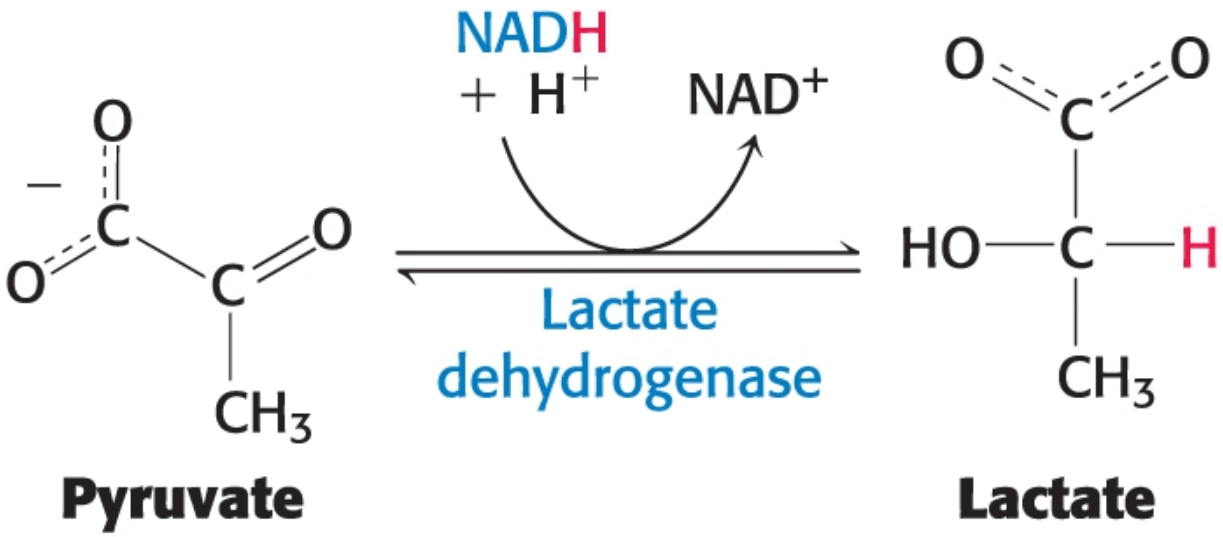
The structure of the product ethanol is as follows: A central C atom is single bonded to H on the lower left, H on the upper left, O H on the upper right, and C H 3 below.

An arrow moves from N A D H plus H superscript plus in the first reaction toward N A D H plus H superscript plus in the third reaction.

Another arrow moves from N A D superscript plus in the third reaction toward N A D superscript plus in the first reaction.

Return to Reoxidation of N A D H

Extended description for Chemical reaction shows the conversion of pyruvate to lactate



The chemical reaction consists of one reactant and one product. The reactant is pyruvate whose structure is as follows: A central C atom is double bonded to O on the upper right, single bonded to C H 3 below, and single bonded to C on the upper left. This C atom is partially double bonded to O above and O on the lower left. This C O O group has an overall negative charge.

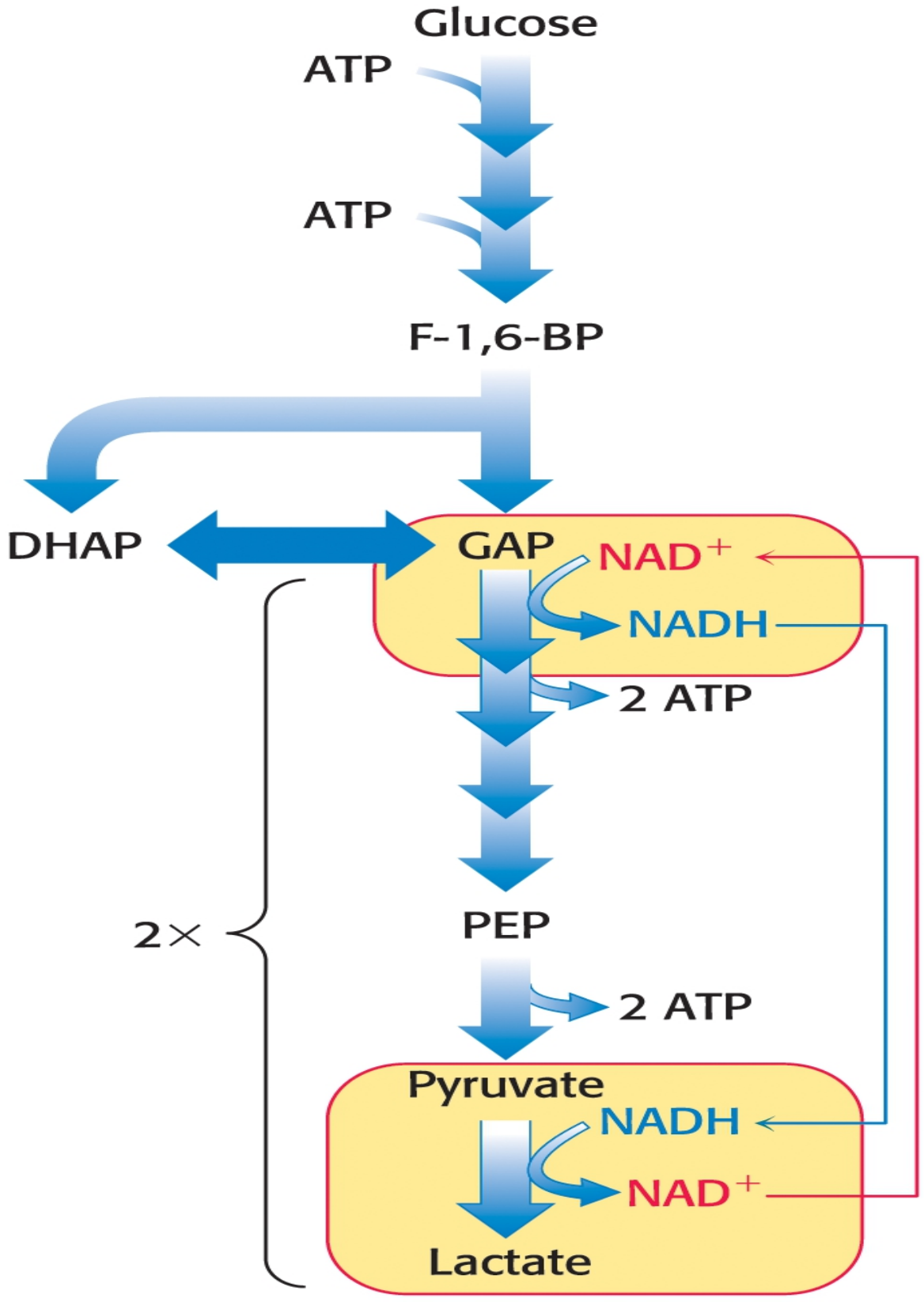
A reversible reaction arrow labeled lactate dehydrogenase leads to the product. A curved arrow above it shows the simultaneous oxidation of N A D H plus H superscript plus to N A D superscript plus. The H atom of N A D H is highlighted in red.

The product is lactate whose structure is as follows: C, single bond, C, single bond, C H 3. C 1 is partially double bonded to O on the upper left and O on the upper right. C 2 is single bonded to O H on the left and single bonded to H on the right highlighted in red.

Return to Chemical reaction shows the conversion of pyruvate to lactate

Extended description for Regeneration of N A D

superscript plus during lactic acid fermentation



© Macmillan Learning

Regeneration of NAD^+

The flowchart is depicted as follows:

Glucose, three downward arrows, F-1, 6-B P. The first and third downward arrows show the entry of A T P.

F-1, 6-B P, one downward arrow and one curved leftward arrow.

The downward arrow leads to G A P. The curved leftward arrow leads to D H A P. A double-headed arrow is shown between G A P and D H A P.

G A P, four downward arrows, P E P. The first downward arrow shows the reduction of N A D superscript plus to N A D H. It is enclosed along with G A P in a yellow rectangle. The second downward arrow shows the release of 2 A T P.

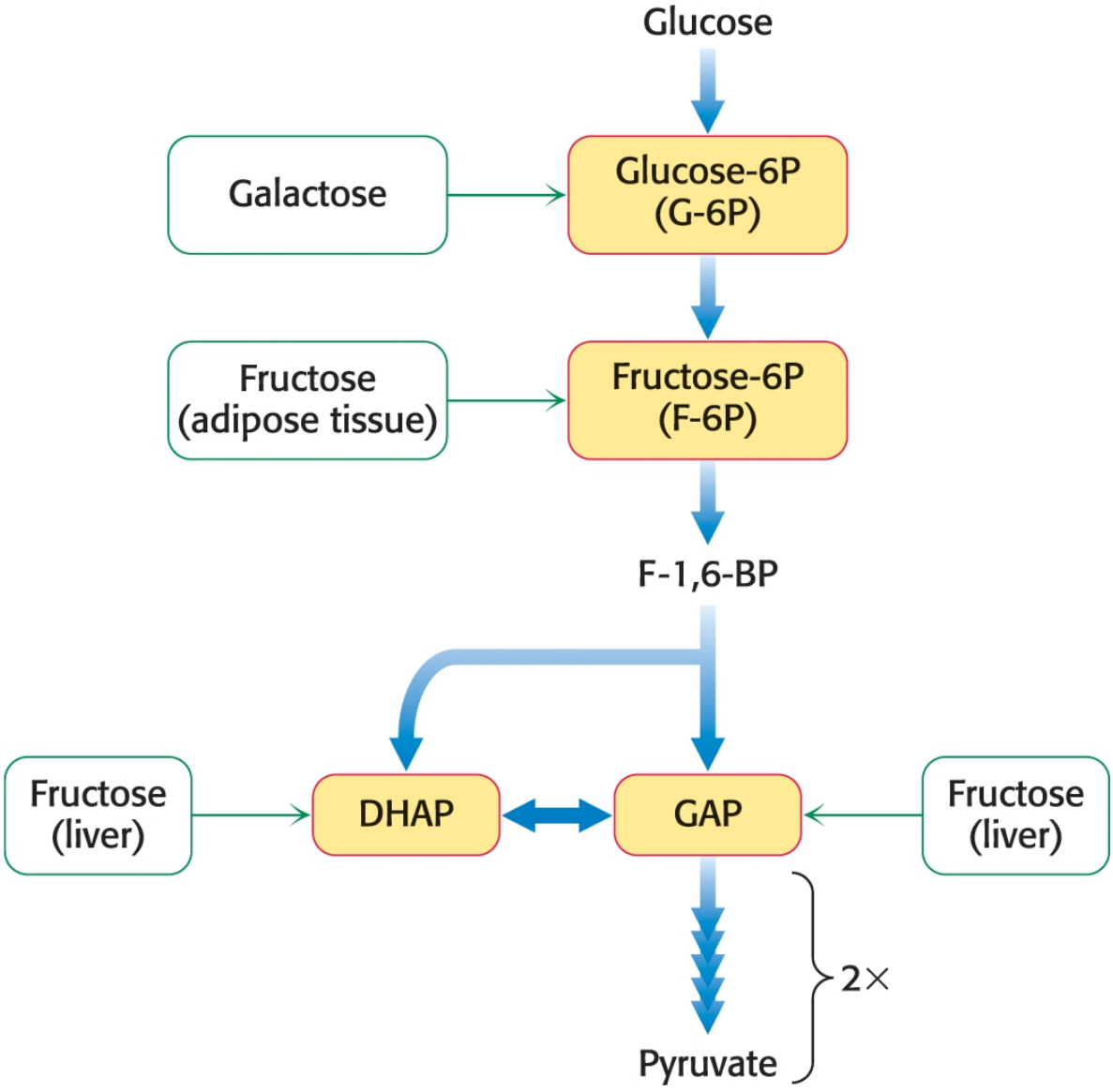
P E P, one downward arrow, pyruvate. The downward arrow shows the release of 2 A T P.

Pyruvate, one downward arrow, lactate. The downward arrow shows the reoxidation of N A D H to N A D superscript plus. These are enclosed in a yellow rectangle labeled regeneration of N A D superscript plus.

The steps from the first downward arrow below G A P to the lactate molecule are enclosed by a left curly bracket labeled 2 times.

Return to Regeneration of N A D superscript plus during lactic acid fermentation

Extended description for Entry of additional sugars in the glycolytic pathway



© Macmillan Learning

The flowchart is depicted as follows:

Glucose, downward arrow, yellow rectangle labeled glucose-6 P (G- 6 P), downward arrow, yellow rectangle labeled fructose-6 P (F-6 P),

downward arrow, F-1, 6-B P, one downward arrow, and one leftward curved arrow.

The leftward curved arrow leads to a yellow rectangle labeled D H A P.

The downward arrow leads to a yellow rectangle labeled G A P.

A double-headed arrow is located between D H A P and G A P.

G A P, a downward arrow with 5 arrowheads, pyruvate. The downward arrow with 5 arrowheads and pyruvate is enclosed in a right curly bracket labeled 2 times.

An arrow from a rectangle labeled galactose points toward the yellow rectangle labeled glucose-6 P (G- 6 P).

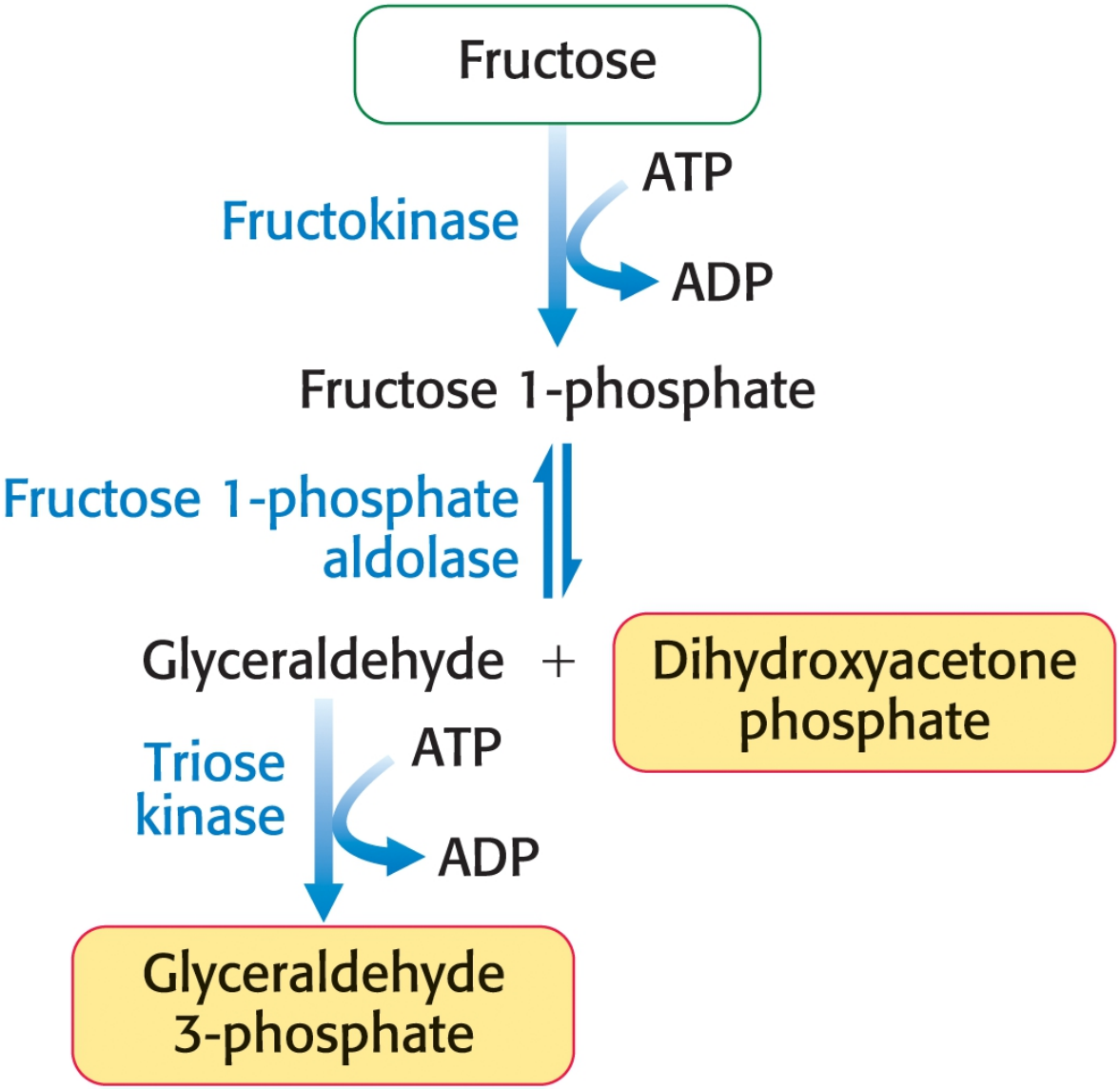
An arrow from a rectangle labeled fructose (adipose tissue) points toward the yellow rectangle labeled fructose-6 P (F-6 P).

An arrow from a rectangle labeled fructose (liver) points toward the yellow rectangle labeled D H A P.

An arrow from a rectangle labeled fructose (liver) points toward the yellow rectangle labeled G A P.

Return to Entry of additional sugars in the glycolytic pathway

Extended description for Entry of fructose into the glycolytic pathway in the liver



© Macmillan Learning

The flowchart is depicted as follows:

Fructose, a downward arrow labeled fructokinase, fructose 1-phosphate, reversible reaction arrow labeled fructose 1-phosphate aldolase, glyceraldehyde plus yellow rectangle labeled

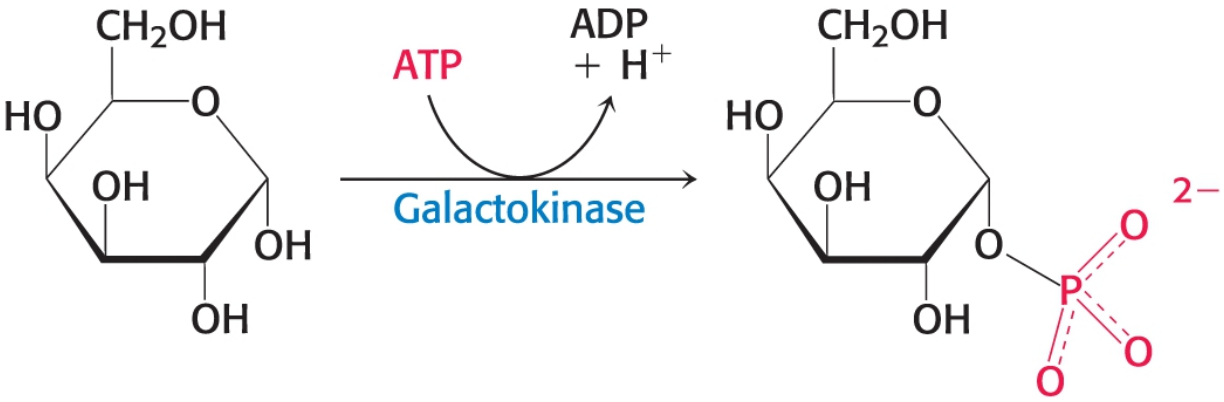
dihydroxyacetone phosphate, downward arrow below glyceraldehyde labeled triose kinase, yellow rectangle labeled glyceraldehyde 3-phosphate.

The downward arrow labeled fructokinase shows the simultaneous breakdown of A T P to A D P.

The downward arrow labeled triose kinase shows the simultaneous breakdown of A T P to A D P.

Return to Entry of fructose into the glycolytic pathway in the liver

Extended description for Irreversible conversion of galactose to galactose 1-phosphate



Galactose **Galactose 1-phosphate**

The structure of galactose is as follows: A 6-membered heterocyclic hexagonal ring is in a horizontal orientation and consists of 1 O and 5 C atoms. O occupies the top right vertex. The ring is in a plane perpendicular to the plane of the paper such that O and C 5 are located away from the observer and C 2 and C 3 are located toward the observer. C 1 and C 2 are each single bonded to O H below. C 3 and C 4 are each single bonded to O H above. C 5 is single bonded to C H 2 O H above.

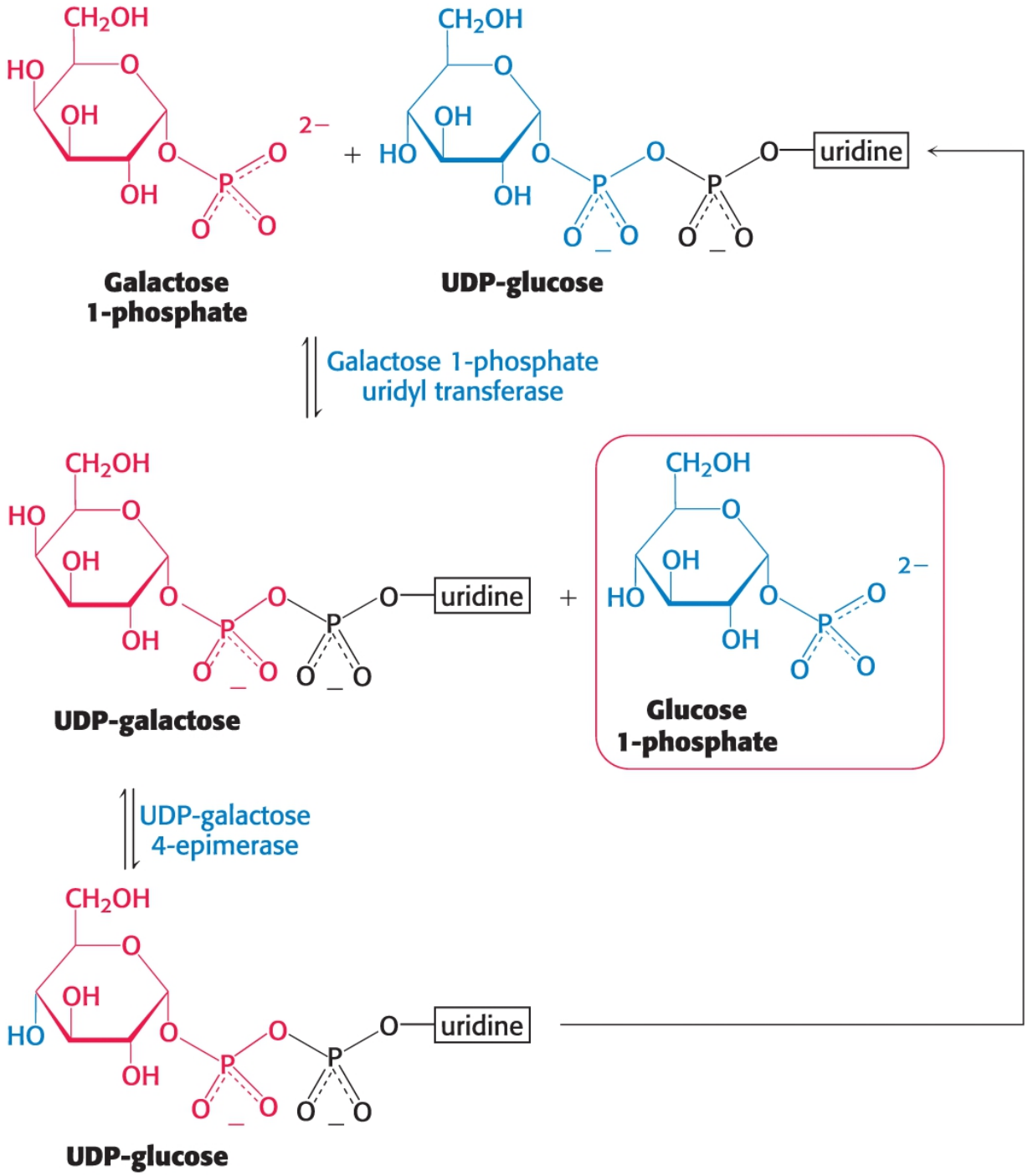
A forward reaction arrow labeled galactokinase leads to galactose 1-phosphate. A curved arrow above it shows the simultaneous breakdown of A T P highlighted in red to A D P plus H superscript plus.

The structure of galactose 1-phosphate is as follows: A 6-membered heterocyclic hexagonal ring is in a horizontal orientation and consists of 1 O and 5 C atoms. O occupies the top right vertex. The ring is in a plane perpendicular to the plane of the paper such that O

and C 5 are located away from the observer and C 2 and C 3 are located toward the observer. C 1 is single bonded to O below. This O is single-bonded to a central P atom highlighted in red. The P atom is partially double bonded to O on the upper right, O on the lower right, and O on the lower left. The O atoms have an overall negative charge of 2 minus. C 2 is single bonded to O H below. C 3 and C 4 are each single bonded to O H above. C 5 is single bonded to C H 2 O H above.

Return to Irreversible conversion of galactose to galactose 1-phosphate

Extended description for Formation of U D P-glucose from galactose 1-phosphate and U D P-glucose



The formation of U D P-glucose takes place in two steps. The first step involves the formation of U D P-galactose and glucose 1-phosphate from galactose 1-phosphate and U D P-glucose.

The structure of galactose 1-phosphate is as follows: A 6-membered heterocyclic hexagonal ring is in a horizontal orientation and consists of 1 O and 5 C atoms. O occupies the top right vertex. The ring is in a plane perpendicular to the plane of the paper such that O and C 5 are located away from the observer and C 2 and C 3 are located toward the observer. C 1 is single bonded to O below. This O is single-bonded to a central P atom. The P atom is partially double bonded to O on the upper right, O on the lower right, and O on the lower left. The O atoms have an overall negative charge of 2 minus. C 2 is single bonded to O H below. C 3 and C 4 are each single bonded to O H above. C 5 is single bonded to C H 2 O H above.

The structure of U D P-glucose is as follows: A 6-membered heterocyclic hexagonal ring is in a horizontal orientation and consists of 1 O and 5 C atoms. O occupies the top right vertex. The ring is in a plane perpendicular to the plane of the paper such that O and C 5 are located away from the observer and C 2 and C 3 are located toward the observer. C 1 is single bonded to O below. This O is single-bonded to a zigzag chain composed of P, single bond, O, single bond, P, single bond, O, single bond, uridine. Each P atom is partially double bonded to O on the lower left and lower left. These O atoms have an overall negative charge. C 2 and C 4 are each single bonded to O H below. C 3 is single bonded to O H above. C 5 is single bonded to C H 2 O H above.

A reversible reaction arrow labeled galactose 1-phosphate uridyl transferase leads to U D P-galactose and glucose 1-phosphate.

The structure of U D P-galactose is as follows: A 6-membered heterocyclic hexagonal ring is in a horizontal orientation and

consists of 1 O and 5 C atoms. O occupies the top right vertex. The ring is in a plane perpendicular to the plane of the paper such that O and C 5 are located away from the observer and C 2 and C 3 are located toward the observer. C 1 is single bonded to O below. This O is single-bonded to a zigzag chain composed of P, single bond, O, single bond, P, single bond, O, single bond, uridine. Each P atom is partially double bonded to O on the lower left and lower left. These O atoms have an overall negative charge. C 2 is single bonded to O H below. C 3 and C 4 are single bonded to O H above. C 5 is single bonded to C H 2 O H above.

The structure of glucose 1-phosphate is as follows: A 6-membered heterocyclic hexagonal ring is in a horizontal orientation and consists of 1 O and 5 C atoms. O occupies the top right vertex. The ring is in a plane perpendicular to the plane of the paper such that O and C 5 are located away from the observer and C 2 and C 3 are located toward the observer. C 1 is single bonded to O below. This O is single-bonded to a central P atom. The P atom is partially double bonded to O on the upper right, O on the lower right, and O on the lower left. The O atoms have an overall negative charge of 2 minus. C 2 and C 4 are each single bonded to O H below. C 3 is single bonded to O H above. C 5 is single bonded to C H 2 O H above.

The second step involves the formation of U D P-glucose from U D P-galactose and glucose 1-phosphate.

A reversible reaction arrow below U D P-galactose and glucose 1-phosphate lead to U D P-glucose. The arrow is labeled U D P-galactose 4-epimerase.

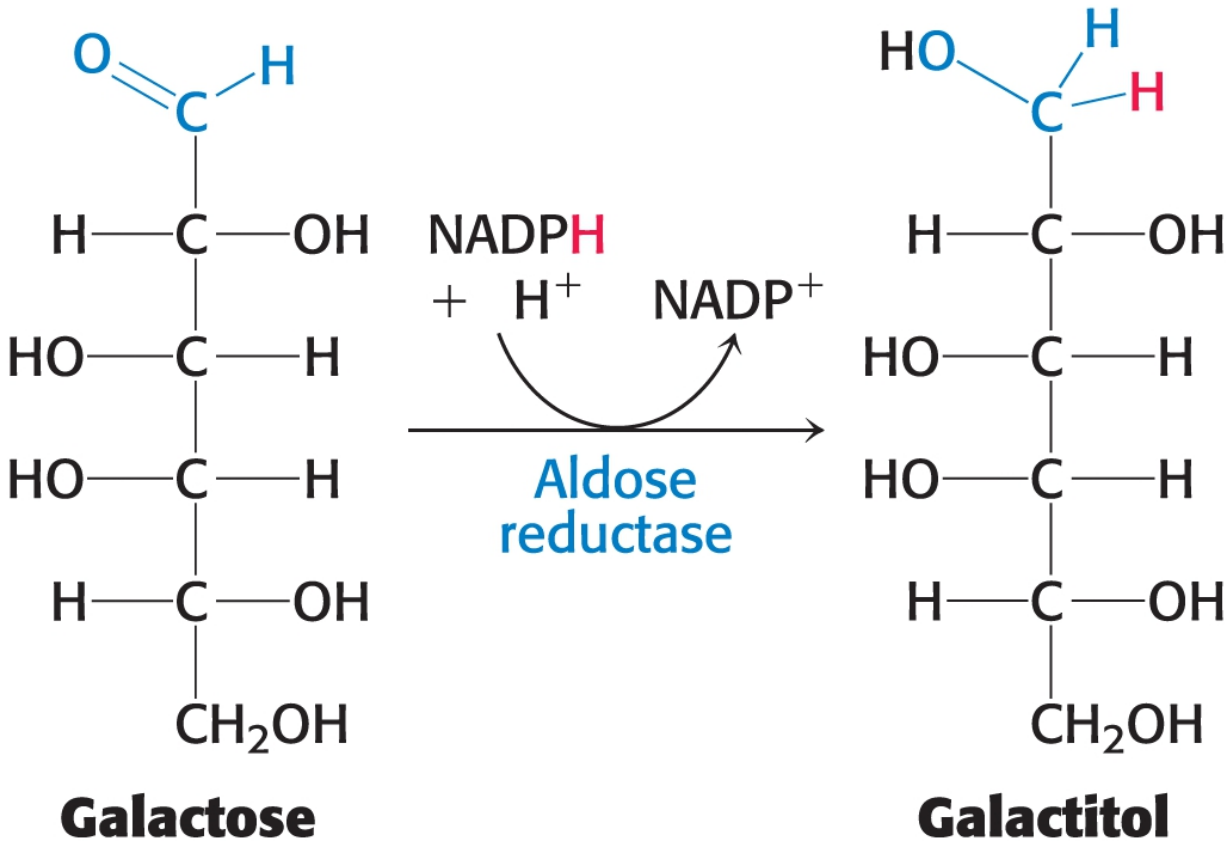
The structure of U D P-glucose is as follows: A 6-membered heterocyclic hexagonal ring is in a horizontal orientation and consists of 1 O and 5 C atoms. O occupies the top right vertex. The ring is in a plane perpendicular to the plane of the paper such that O

and C 5 are located away from the observer and C 2 and C 3 are located toward the observer. C 1 is single bonded to O below. This O is single-bonded to a zigzag chain composed of P, single bond, O, single bond, P, single bond, O, single bond, uridine. Each P atom is partially double bonded to O on the lower left and lower left. These O atoms have an overall negative charge. C 2 and C 4 are each single bonded to O H below. C 3 is single bonded to O H above. C 5 is single bonded to C H 2 O H above.

An arrow from U D P-glucose points toward galactose 1-phosphate and U D P-glucose at the top.

Return to Formation of U D P-glucose from galactose 1-phosphate and U D P-glucose

Extended description for Chemical reaction shows the conversion of galactose to galactitol



The chemical reaction consists of one reactant and one product. The reactant is galactose whose structure is as follows: C, single bond, C, single bond, C, single bond, C, single bond, C, single bond, C H 2 O H. C 1 is double bond to O on the upper left and single bonded to H on the upper right. C 1, O, and H are highlighted in blue.

A forward reaction arrow labeled aldose reductase leads to the product. A curved arrow above it shows the simultaneous oxidation of N A D P H plus H superscript plus to N A D P superscript plus. The H atom of N A D P H is highlighted in red.

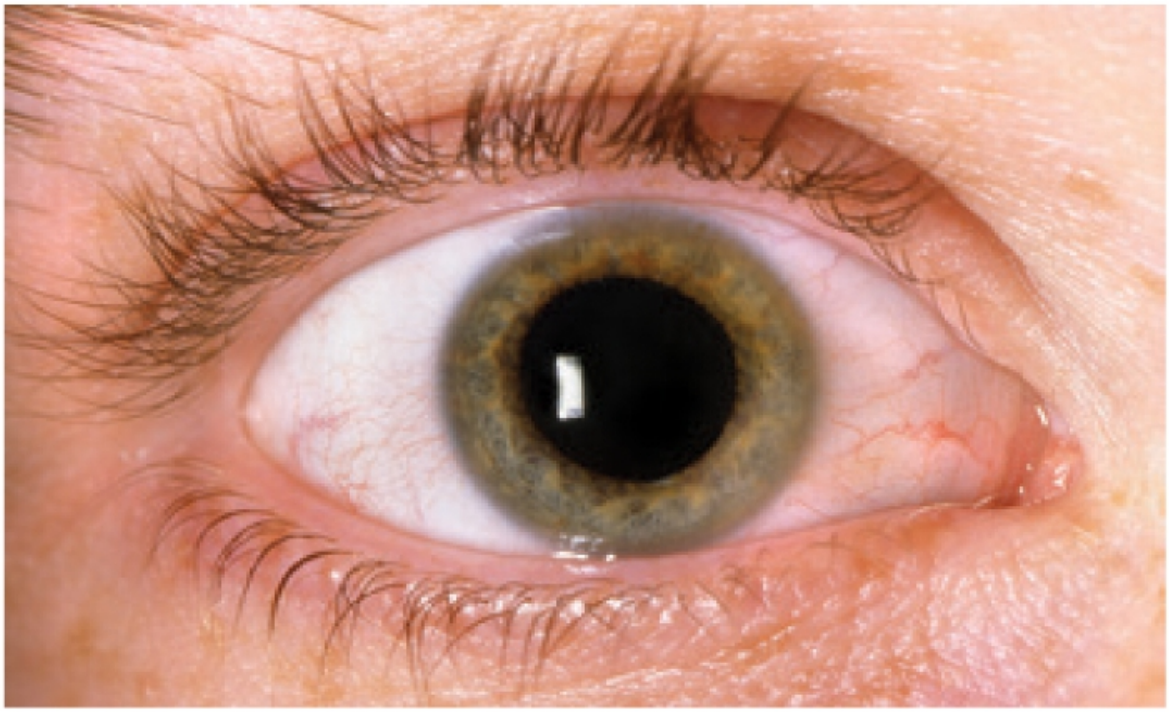
The product is galactitol whose structure is as follows: C, single bond, C, single bond, C, single bond, C, single bond, C, single bond, C H 2 O H. C 1 is single bonded to O H on the upper left, H on the upper right, and H on the right. The H atom on right is highlighted in red. C 1, H on the upper right, and the O atom of the O H group is highlighted in blue.

Return to Chemical reaction shows the conversion of galactose to galactitol

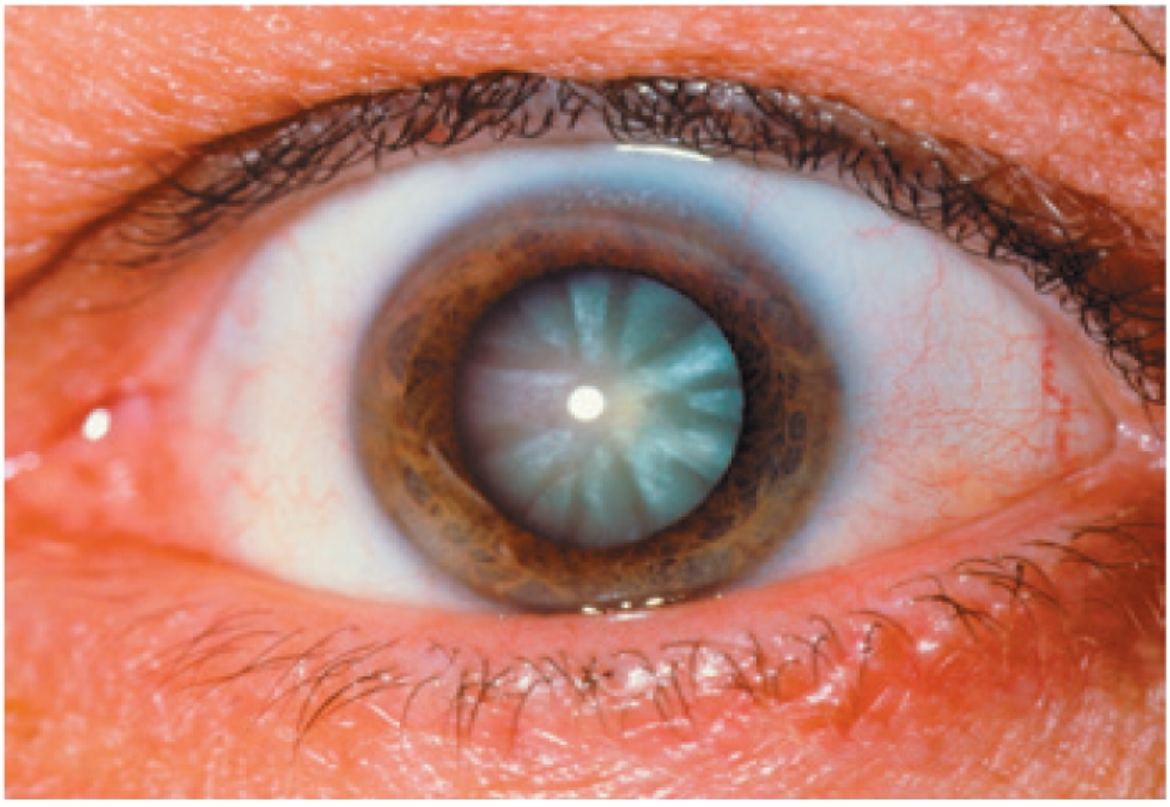
Extended description for Photographs comparing

healthy eye and cataract affected eye

(A)



(B)



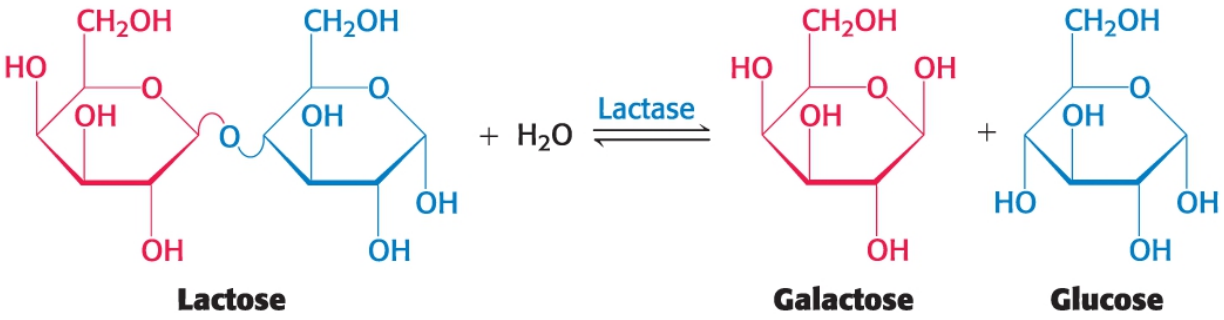
A: Tim Mainiero/Shutterstock; B: SPL/Science Source

Photograph (A): The eye has a black-colored circular pupil surrounded by a grey-colored iris.

Photograph (B): The eye has a cloudy appearing circular pupil with radial blue markings. It is surrounded by a brown-colored iris.

Return to Photographs comparing healthy eye and cataract affected eye

Extended description for Breakdown of lactose into galactose and glucose



The chemical reaction consists of two reactants and two products. The first reactant is lactose whose structure is as follows: A 6-membered heterocyclic hexagonal ring is in a horizontal orientation and consists of 1 O and 5 C atoms. O occupies the top right vertex. C 1 occupies the rightmost vertex. C 2 is single bonded to O H below. C 3 and C 4 are each single bonded to O H above. C 5 is single bonded to C H 2 O H above. C 1 is single bonded to O through a curved line. This O is further single bonded to C 4 of another 6-membered heterocyclic hexagonal ring in a horizontal orientation. This ring consists of 1 O and 5 C atoms. O occupies the top right vertex. C 1 and C 2 are each single bonded to O H below. C 3 is single bonded to O H above. C 5 is single bonded to C H 2 O H above.

The second reactant is H 2 O.

A reversible reaction arrow labeled lactase leads to the products.

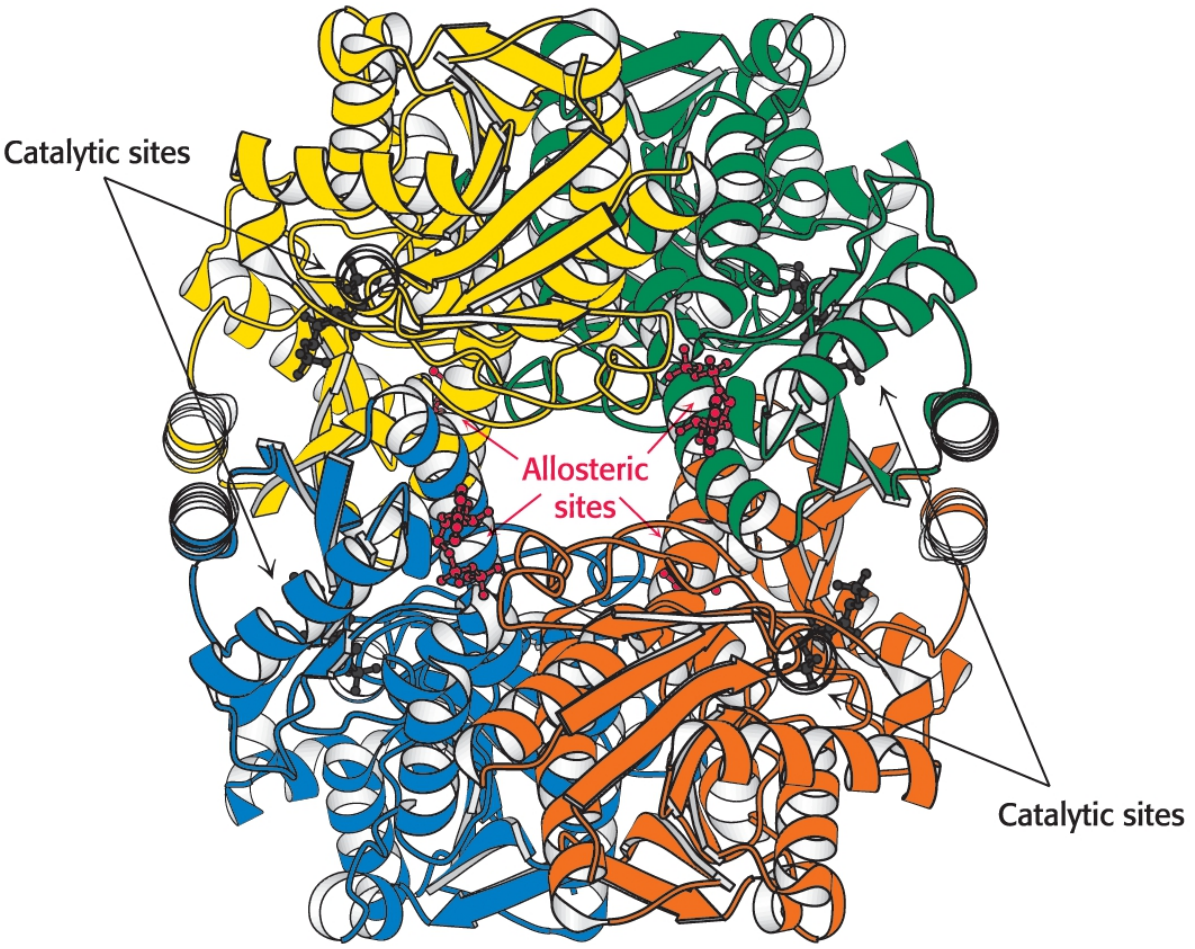
The first product is galactose whose structure is as follows: A 6-membered heterocyclic hexagonal ring is in a horizontal orientation and consists of 1 O and 5 C atoms. O occupies the top right vertex. C 1 occupies the rightmost vertex and is single bonded to O H above. C

2 is single bonded to O H below. C 3 and C 4 are each single bonded to O H above. C 5 is single bonded to C H 2 O H above.

The second product is glucose whose structure is as follows: A 6-membered heterocyclic hexagonal ring is in a horizontal orientation and consists of 1 O and 5 C atoms. O occupies the top right vertex. C 1 and C 2 are each single bonded to O H below. C 3 is single bonded to O H above. C 4 is single bonded to O H below. C 5 is single bonded to C H 2 O H above.

Return to Breakdown of lactose into galactose and glucose

Extended description for Ribbon diagram of *E.coli* phosphofructokinase



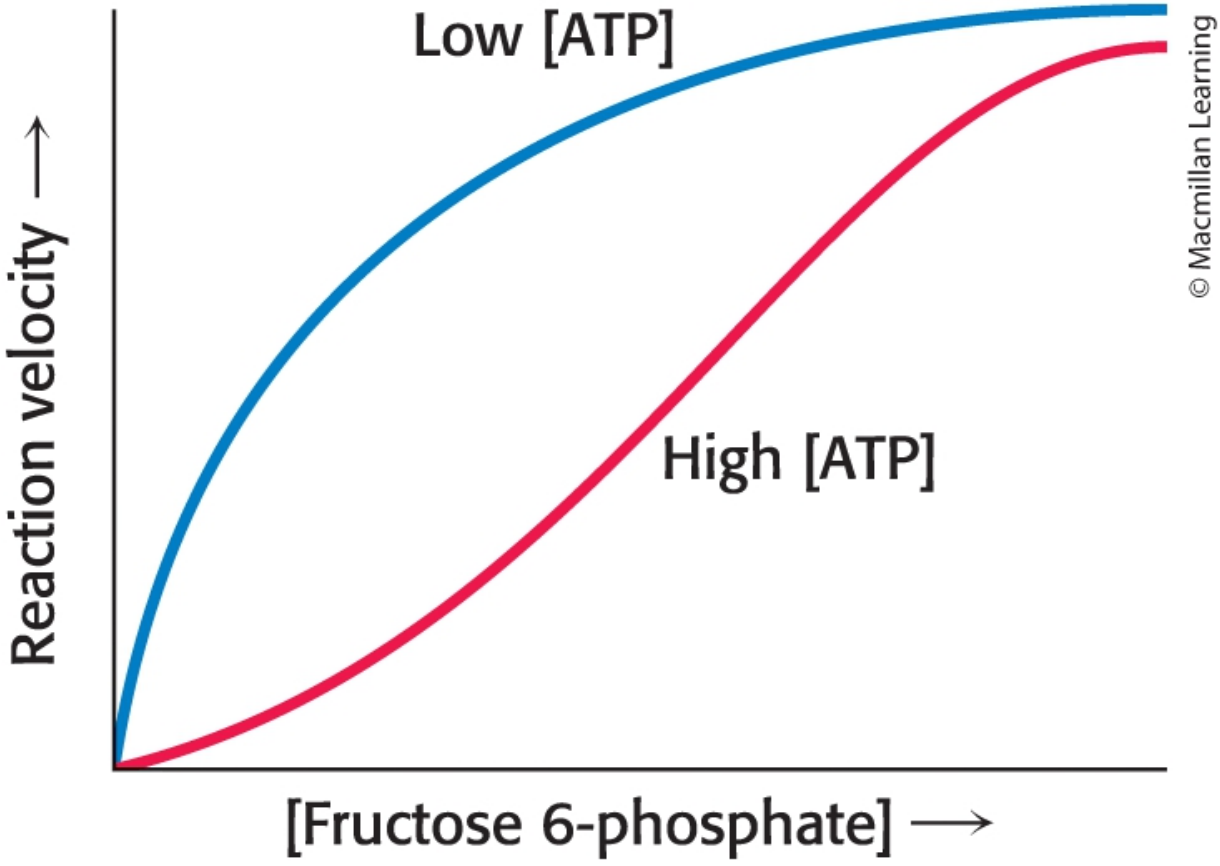
© Macmillan Learning

The ribbon diagram has a circular shape with a hollow core. It consists of four identical subunits shown in yellow, green, orange, and blue color. Each subunit is composed of alpha-helices and beta-strands. Each subunit has a tiny groove labeled catalytic site. A thread from the top left and bottom left subunit move toward each other and independently undergo coiling on the left periphery of the enzyme. Similarly, a thread from the top right and bottom right subunit moves toward each other and independently undergoes

coiling on the right periphery of the enzyme. An allosteric site is present in each subunit toward the hollow core.

Return to Ribbon diagram of *E.coli* phosphofructokinase

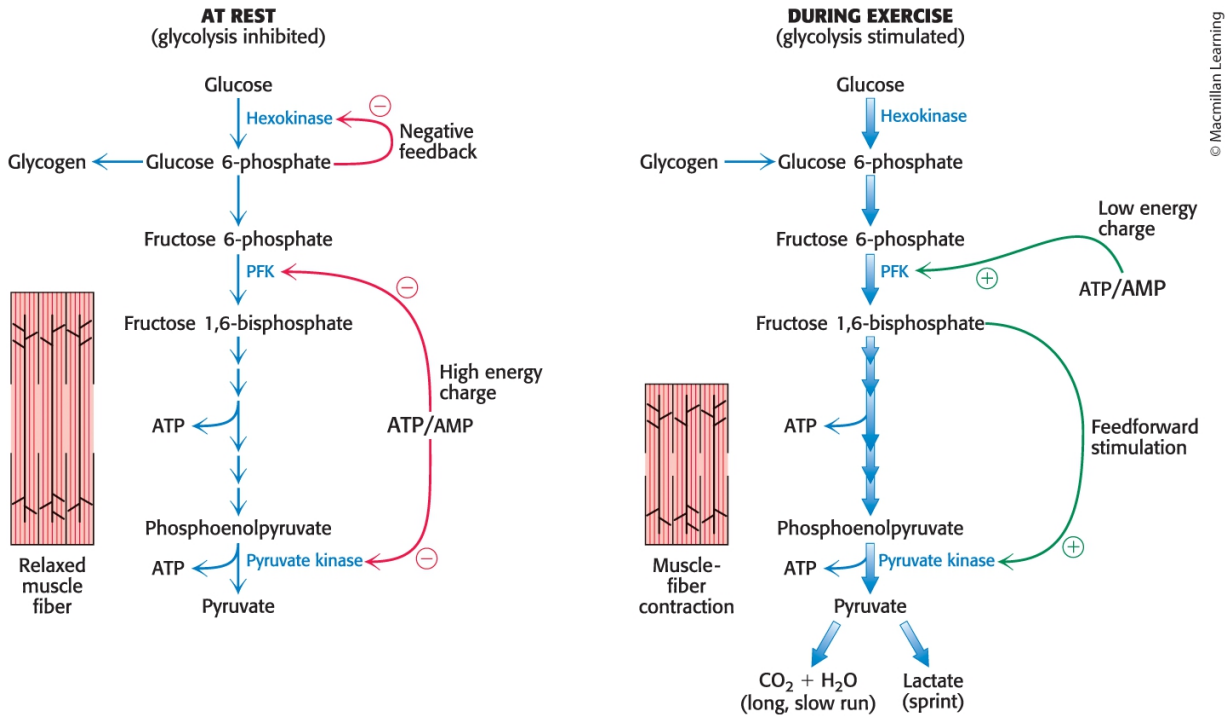
Extended description for Graphical representation of the inhibition of phosphofructokinase activity



The horizontal axis is labeled concentration of fructose 6-phosphate which increases from left to right. The vertical axis is labeled reaction velocity which increases from the bottom to the top. The graph shows two curves. The blue curve labeled “low A T P concentration” starts from the origin and moves gradually toward the upper right in a concave-down manner. It then forms a plateau at the highest reaction velocity. The red curve labeled “high A T P concentration” starts at the origin and moves almost linearly toward the upper right. It then forms a small plateau at the highest reaction velocity, near the extreme right end of the horizontal axis.

Return to Graphical representation of the inhibition of phosphofructokinase activity

Extended description for Flowcharts depict glycolysis regulation



The first flowchart is labeled “At rest (glycolysis inhibited)” and is depicted as follows.

Glucose, downward arrow labeled hexokinase, glucose 6-phosphate, downward arrow, fructose 6-phosphate, downward arrow labeled P F K, fructose 1, 6-bisphosphate, five downward arrows, phosphoenolpyruvate, downward arrow labeled pyruvate kinase, pyruvate.

A leftward arrow from glucose 6-phosphate leads to glycogen. The third downward arrow between fructose 1, 6-bisphosphate and phosphoenolpyruvate shows the release of A T P.

The downward arrow labeled pyruvate kinase shows the release of A T P.

A curved red arrow with a minus symbol is labeled “negative feedback” and it points from glucose 6-phosphate to hexokinase.

A double-headed red arrow with a minus symbol is labeled “A T P over A M P high energy charge” and it points toward P F K and pyruvate kinase.

A schematic illustration of the relaxed muscle fiber is shown alongside the flow chart. It shows elongated muscle fibers.

The second flowchart is labeled “During exercise (glycolysis stimulated)” and is depicted as follows:

Glucose, downward arrow labeled hexokinase, glucose 6-phosphate, downward arrow, fructose 6-phosphate, downward arrow labeled P F K, fructose 1, 6-bisphosphate, five downward arrows, phosphoenolpyruvate, downward arrow labeled pyruvate kinase, pyruvate, two downward arrows. The lower left downward arrow leads to C O 2 plus H 2 O (long, slow run). The lower right downward arrow leads to lactate (sprint).

A rightward arrow from glycogen leads to glucose 6-phosphate. The third downward arrow between fructose 1, 6-bisphosphate and phosphoenolpyruvate shows the release of A T P.

The downward arrow labeled pyruvate kinase shows the release of A T P.

A green arrow with a minus symbol is labeled “A T P over A M P low energy charge” and it points toward P F K.

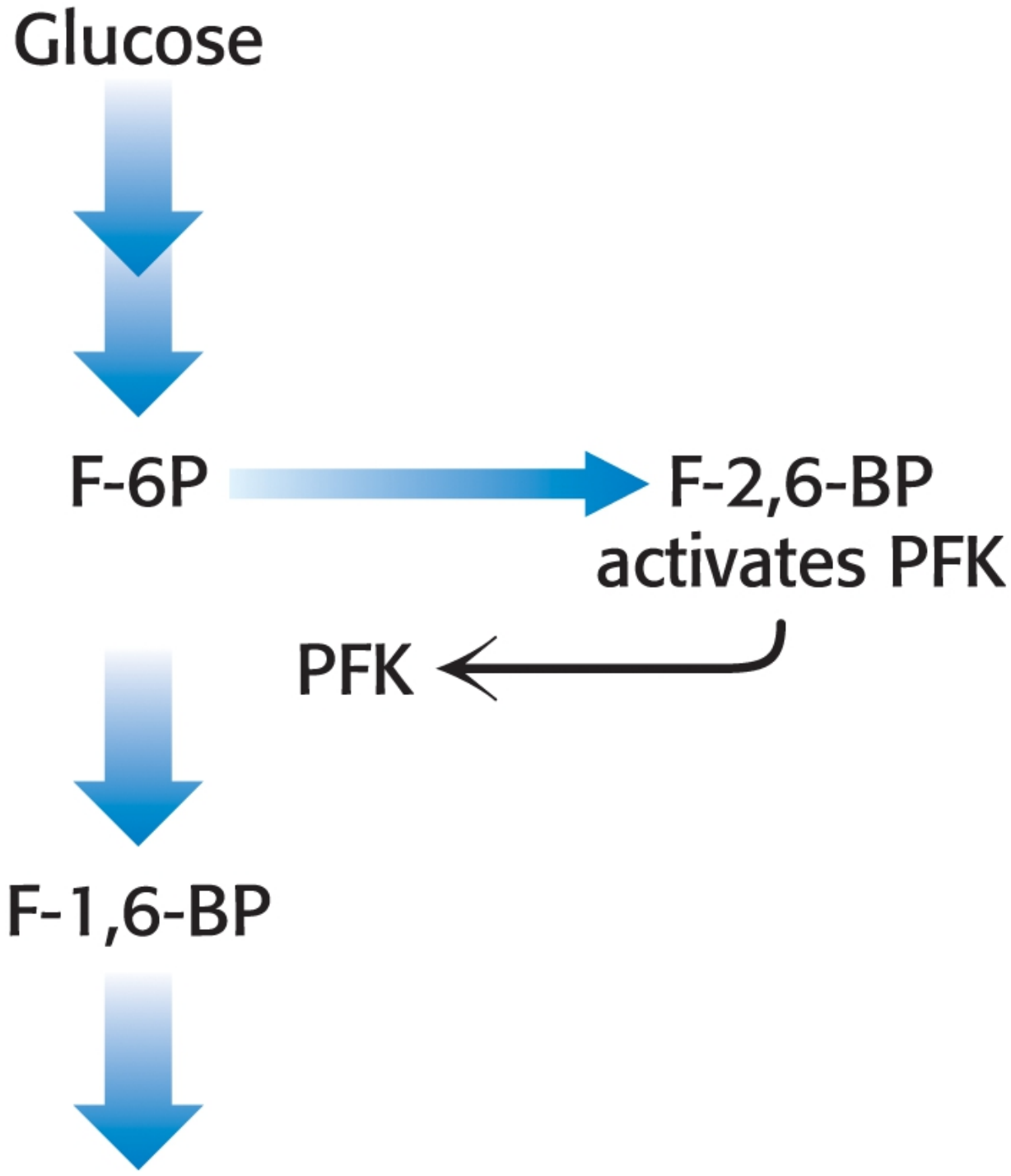
A curved green arrow with a plus symbol is labeled “feedforward stimulation” and it points from fructose 1, 6-bisphosphate toward pyruvate kinase.

A schematic illustration of the muscle-fiber contraction is shown alongside the flow chart. It shows shortened muscle fibers.

Return to Flowcharts depict glycolysis regulation

Extended description for Chemical structure of fructose 2, 6-bisphosphate and flow chart depicting

allosteric activation of phosphofructokinase



The structure of fructose 2, 6-bisphosphate (F-2, 6-B P) is as follows: A 5membered heterocyclic pentagonal ring is in a vertical

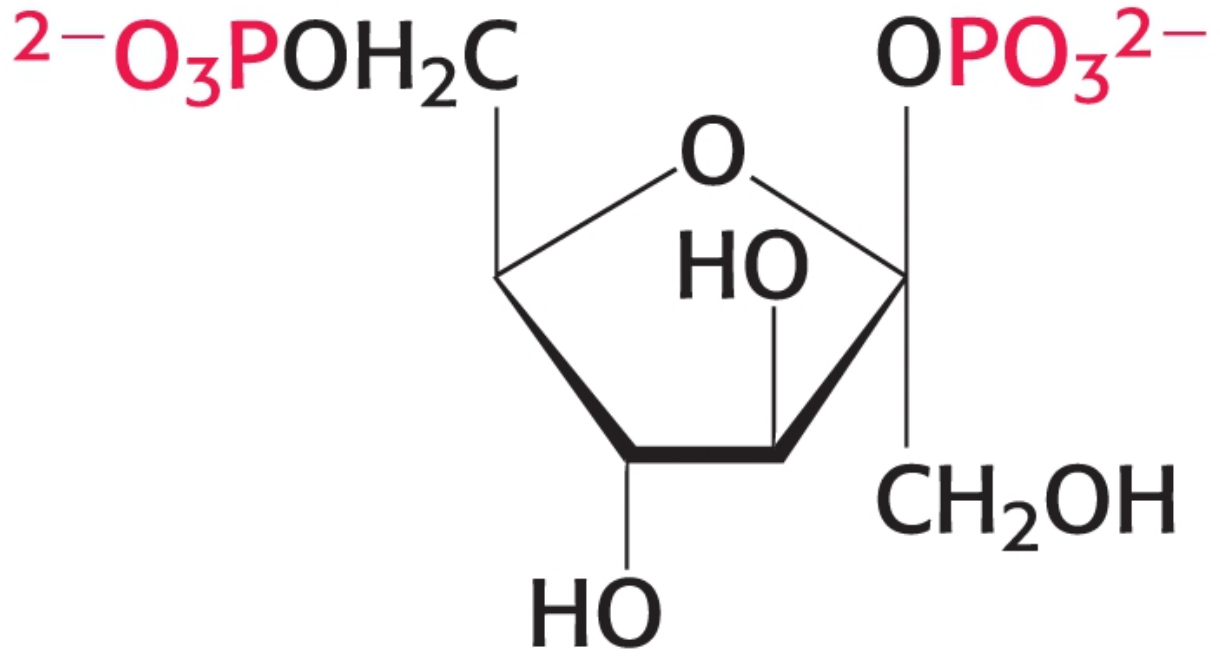
orientation and consists of 1 O and 4 C atoms. O occupies the topmost vertex. C 1 is single bonded to O P O 3 superscript 2 minus above and single bonded to C H 2 O H below. C 2 is single bonded to O H above. C 3 is single bonded to O H below. C 4 is single bonded to C H 2 O P O 3 superscript 2 minus above.

The flow chart is depicted as follows:

Glucose, two downward arrows, F-6 P, downward arrow, F-1, 6-B P, downward arrow. A rightward arrow from F-6 P leads to F-2, 6-B P activates P F K. A curved black arrow from F-2, 6-B P activates P F K leads to P F K.

Return to Chemical structure of fructose 2, 6-bisphosphate and flow chart depicting allosteric activation of phosphofructokinase

Extended description for Structure of fructose 2, 6-bisphosphate

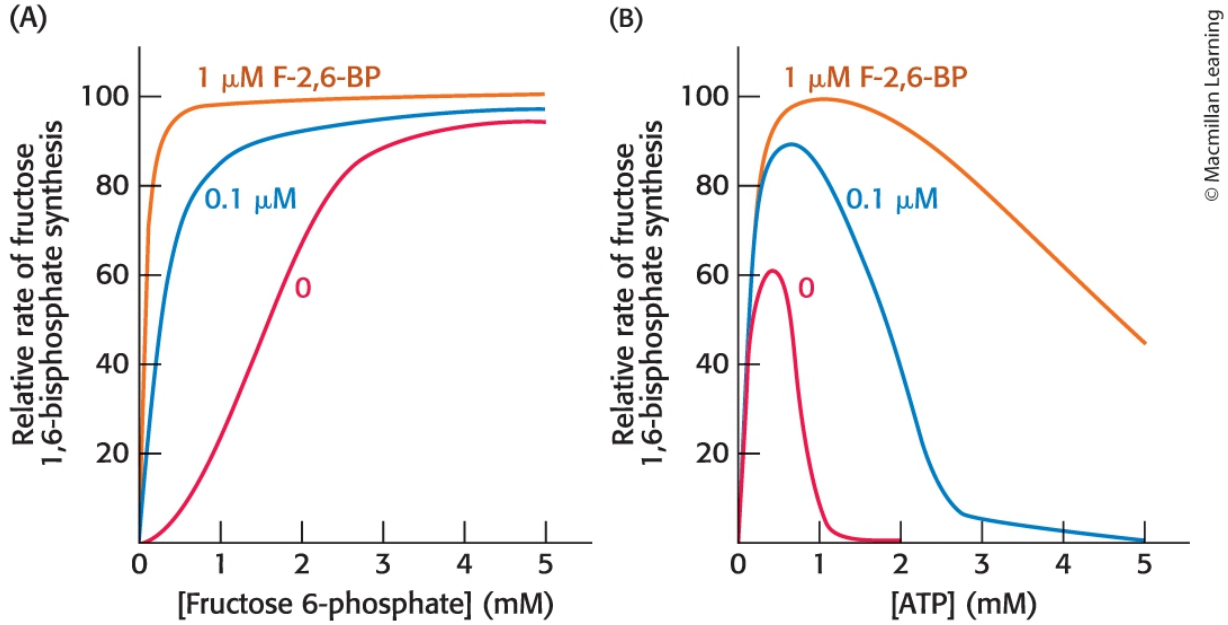


Fructose 2,6-bisphosphate (F-2,6-BP)

The structure is as follows: A 5-membered heterocyclic pentagonal ring is in a vertical orientation. It consists of 1 O and 4 C atoms. The ring is perpendicular to the plane of paper such that O is located away from the observer and C 2 and C 3 are located toward the observer. O occupies the topmost vertex. C 1 is single bonded to O P O 3 superscript 2 minus above and C H 2 O H below. C 2 is single bonded to O H above. C 3 is single bonded to O H below. C 4 is single bonded to C H 2 O P O 3 superscript 2 minus.

Return to Structure of fructose 2, 6-bisphosphate

Extended description for Graphs depict fructose 1, 6-bisphosphate synthesis with respect to fructose 6-phosphate concentration

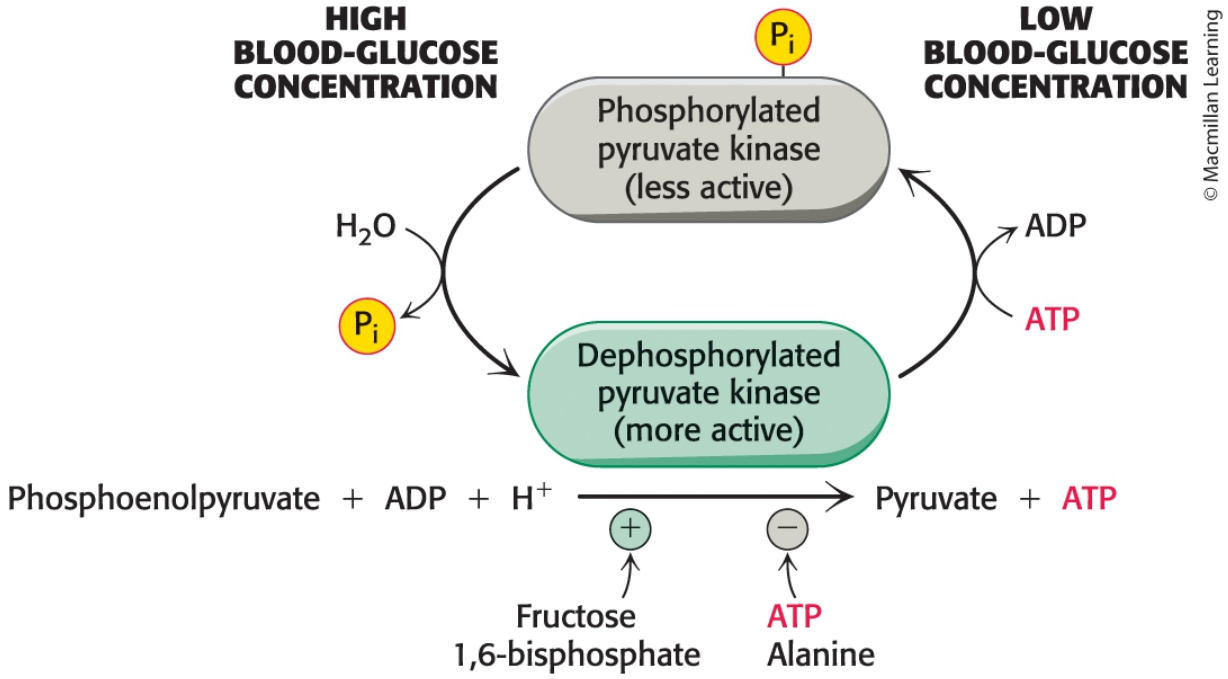


Part (A): The horizontal axis is labeled concentration of fructose 6-phosphate in millimolar. It has markings ranging from 0 to 5 in increments of 1 unit. The vertical axis is labeled the relative rate of fructose 1, 6-bisphosphate synthesis. It has markings ranging from 0 to 100 in increments of 20 units. The graph contains three curves shown in orange, blue, and red colors. The orange curve is labeled 1 micromolar F-2, 6-B P. It starts from the origin, rises steeply to reach the point (0.5, 99), and then starts moving horizontally toward the right. The blue curve is labeled 0.1 micromolar. It starts from the origin, rises steeply to reach the point (1, 90), and then moves gradually to reach (2, 95). The curve then starts moving horizontally toward the right. The red curve is labeled 0. It also begins from the origin, rises linearly toward the upper right to reach (3, 93), and then starts moving horizontally toward the right.

Part (B): The horizontal axis is labeled concentration of A T P in millimolar. It has markings ranging from 0 to 5 in increments of 1 unit. The vertical axis is labeled relative rate of fructose 1, 6-bisphosphate synthesis. It has markings ranging from 0 to 100 in increments of 20 units. The graph contains three curves shown in orange, blue, and red colors. The orange curve is labeled 1 micromolar F-2, 6-B P. It starts at the origin, moves vertically upward, forms a peak at (1.5, 100), and then starts declining toward the lower right to terminate at (5, 45). The blue curve is labeled 0.1 micromolar. It begins at the origin, moves vertically upward, forms a peak at (1, 88), and then starts declining toward the lower right to reach (2.8, 8). It then gradually declines to reach (5, 0). The red curve is labeled 0. It starts from the origin, moves vertically upward, forms a peak at (0.5, 60), and then starts declining toward the lower right to reach (1.4, 0). It then moves horizontally toward the right to reach (2, 0). All values are estimated.

Return to Graphs depict fructose 1, 6-bisphosphate synthesis with respect to fructose 6-phosphate concentration

Extended description for Regulation of pyruvate kinase activity

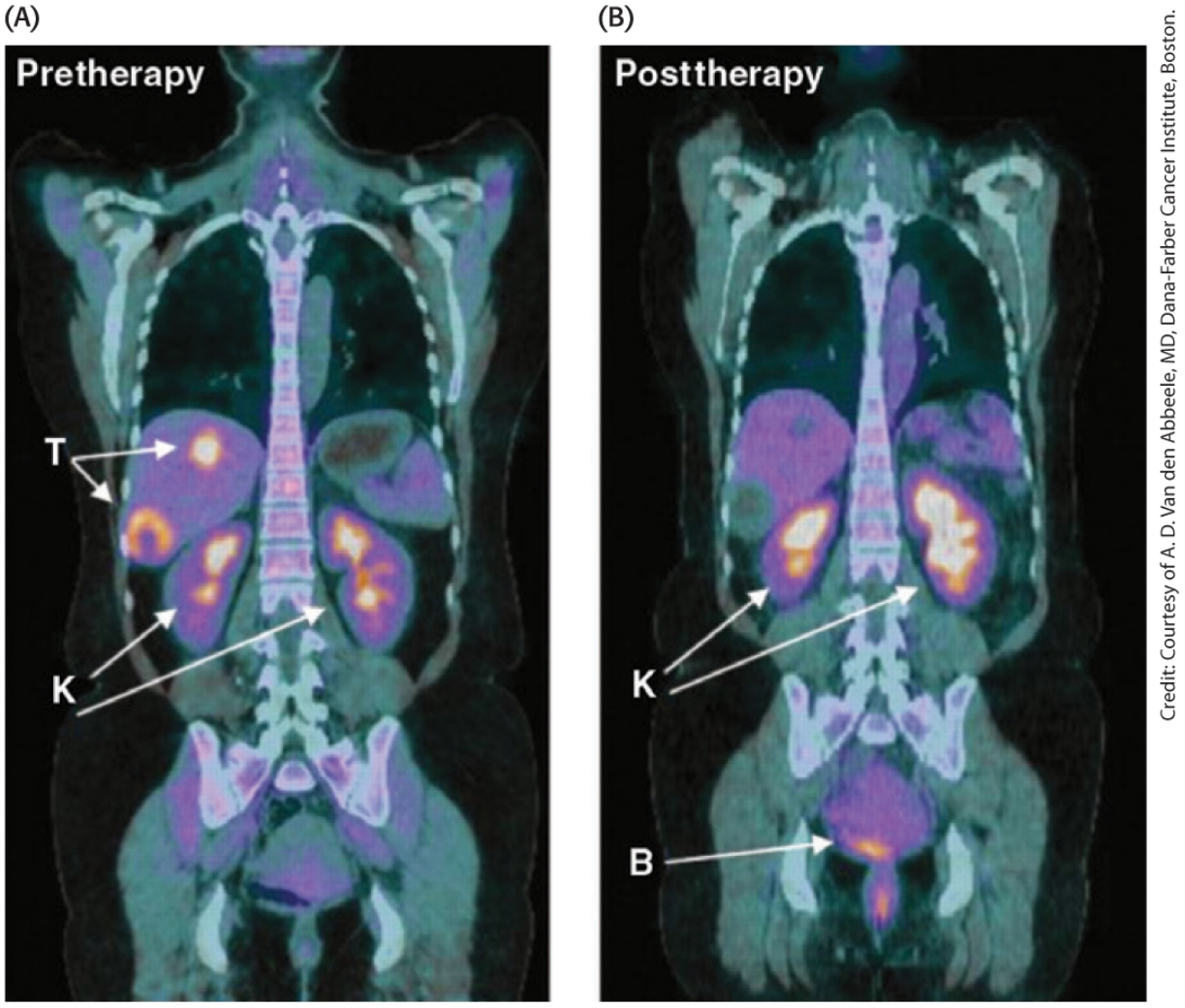


A grey rounded rectangle is labeled “phosphorylated pyruvate kinase (less active)” and it is single bonded to P subscript i above. A green rounded rectangle labeled “dephosphorylated pyruvate kinase (more active)” is located below it. The region toward the top left of the grey rectangle shows “high blood-glucose concentration”. The region toward the top right of the grey rectangle shows “Low blood-glucose concentration”. A curved downward arrow on the left moves from the grey rectangle to the green rectangle. Another curved arrow adjacent to it shows the simultaneous entry of H 2 O and the release of P subscript i. A curved upward arrow on the right moves from a green rectangle to a grey rectangle. Another curved arrow adjacent to it shows the conversion of A T P to A D P.

A reaction is shown below. It consists of 3 reactants and 2 products. The first reactant is phosphoenolpyruvate. The second reactant is A D P. The third reactant is H superscript plus. A forward arrow leads to the products. It has a plus and minus symbol. An arrow labeled “fructose 1, 6-bisphosphate” points toward the plus symbol. An arrow labeled “A T P alanine” points toward the minus symbol. The products are pyruvate and A T P.

Return to Regulation of pyruvate kinase activity

Extended description for Pretherapy and post therapy PET scans



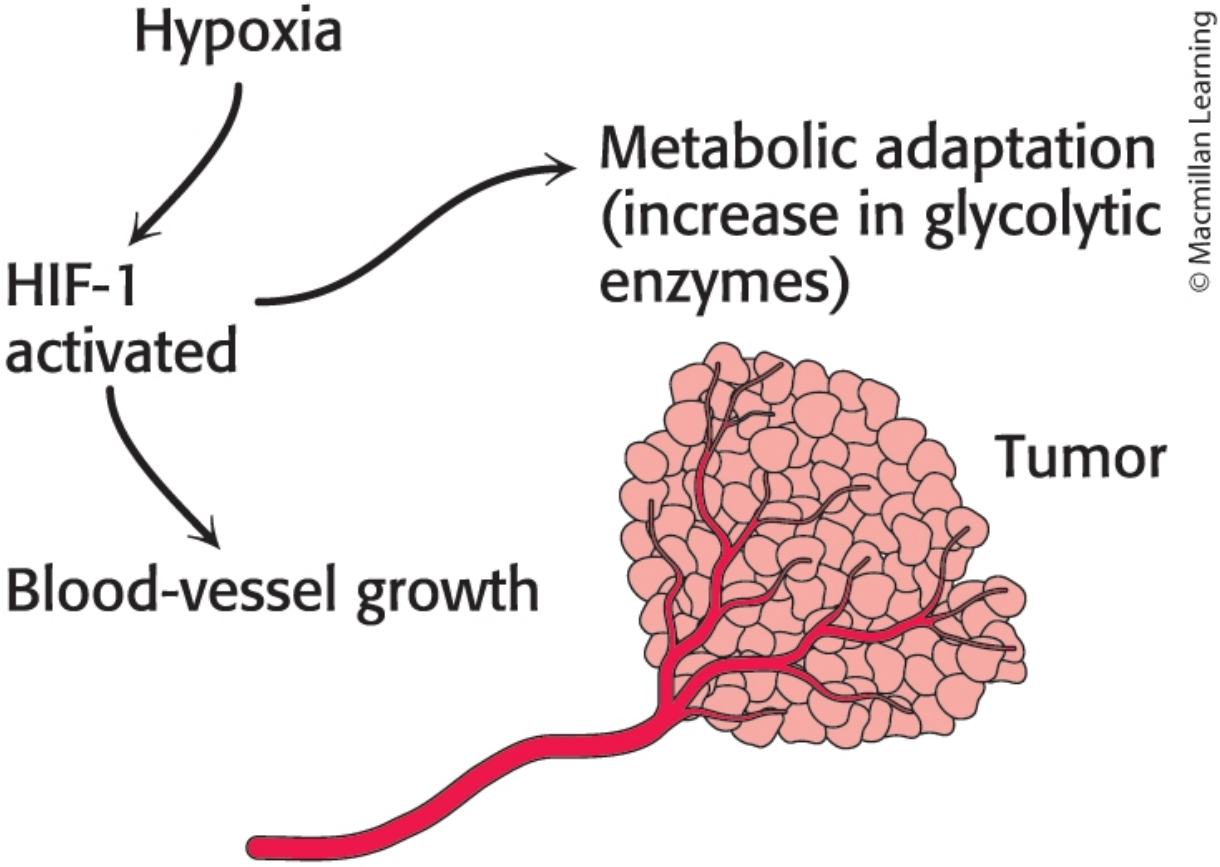
Credit: Courtesy of A. D. Van den Abbeele, MD, Dana-Farber Cancer Institute, Boston.

The scans show the posterior view of the thorax, abdomen, and pelvic region. In the pretherapy scan, two arrows labeled K point toward the kidneys. Two arrows labeled T point toward two bright yellow spots with an orange border in a large balloon-shaped structure located above the left kidney. The kidney also contains these bright yellow spots. In the post-therapy scan, two arrows labeled K point toward the kidney. An arrow labeled B points toward

the urinary bladder. Both the kidney and the bladder contain bright yellow spots with an orange border. The balloon-shaped structure above the left kidney does not contain any yellow spots.

Return to Pretherapy and post therapy PET scans

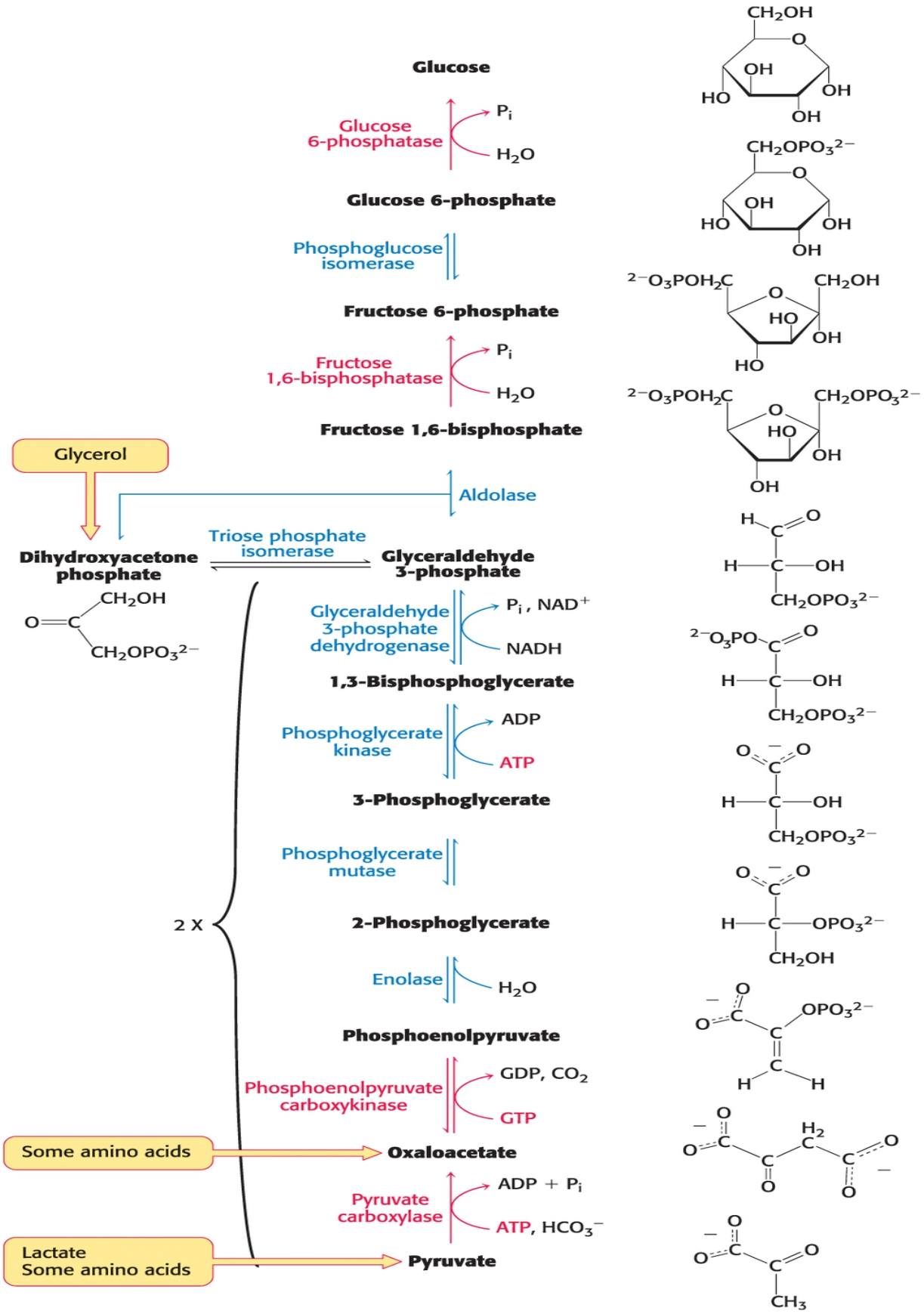
Extended description for Hypoxia-induced gene expression alteration in tumors



An arrow from hypoxia leads to H I F-1 activated. Two arrows from H I F-1 activated lead to "blood-vessel growth" and "metabolic adaptation (increase in glycolytic enzymes)." A schematic illustration shows a tumor containing a branched network of tiny blood vessels. These blood vessels branch off from a single large blood vessel located outside the tumor. The tumor is depicted as a large cluster of tiny irregular-shaped structures.

Return to Hypoxia-induced gene expression alteration in tumors

Extended description for Gluconeogenesis pathway


Glucose
Glucose 6-phosphatase
Pi
H2O
Glucose 6-phosphate
Phosphoglucose isomerase
Fructose 6-phosphate
Fructose 1,6-bisphosphatase
Pi
H2O
Fructose 1,6-bisphosphate
Glycerol
Aldolase
Dihydroxyacetone phosphate
Triose phosphate isomerase
Glyceraldehyde 3-phosphate
Glyceraldehyde 3-phosphate dehydrogenase
Pi, NAD+
NADH
1,3-Bisphosphoglycerate
Phosphoglycerate kinase
ADP
ATP
3-Phosphoglycerate
Phosphoglycerate mutase
2-Phosphoglycerate
2 X
Enolase
H2O
Phosphoenolpyruvate
Phosphoenolpyruvate carboxykinase
GDP, CO2
GTP
Some amino acids
Oxaloacetate
Pyruvate carboxylase
ADP + Pi
ATP, HCO3−
Lactate
Some amino acids
Pyruvate

The pathway is depicted as follows from the bottom to the top:

Pyruvate is irreversibly converted into oxaloacetate by pyruvate carboxylase. This conversion requires the entry of A T P, H C O 3 superscript, and release of A D P plus P subscript i.

An arrow from a yellow rectangle labeled “lactate some amino acids” points toward pyruvate. An arrow from a yellow rectangle labeled “some amino acids” points toward oxaloacetate.

The structure of pyruvate is as follows: A central C atom is double bonded to O on the upper right, single bonded to C H 3 below, and single bonded to C on the upper left. This C atom is partially double bonded to O above and O on the lower left. This C O O group has an overall negative charge.

The structure of oxaloacetate is as follows: A 4-carbon alkane chain is depicted as a line structure using 3 zigzag lines. C 3 is bound to H 2. C 1 is partially double bonded to O above and O on the lower right. This C O O group has an overall negative charge. C 2 is double bonded to O below. C 4 is partially double bonded to O on the upper right and O below. This C O O group has an overall negative charge.

Oxaloacetate is reversibly converted into phosphoenolpyruvate by phosphoenolpyruvate carboxykinase. This conversion requires the breakdown of GT P to G D P and the release of C O 2.

The structure of phosphoenolpyruvate is as follows: A central C atom is double bonded to C below, single bonded to O P O 3 superscript 2 minus on the upper right, and single bonded to C on the upper left. The C atom below is single-bonded to H on the lower left and H on the lower right. The C atom on the upper left is

partially double bonded to O above and O on the lower left. This C O O group has an overall negative charge.

Phosphoenolpyruvate is reversibly converted into 2-phosphoglycerate by enolase. This conversion requires the entry of H 2 O.

The structure of 2-phosphoglycerate is as follows: C, single bond, C, single bond, C H 2 O H. C 1 is partially double bonded to O on the upper left and O on the upper right. This C O O group has an overall negative charge. C 2 is single bonded to H on the left and O P O 3 superscript 2 minus on the right.

2-phosphoglycerate is reversibly converted into 3-phosphoglycerate by phosphoglycerate mutase.

The structure of 3-phosphoglycerate is as follows: C, single bond, C, single bond, C H 2 O P O 3 superscript 2 minus. C 1 is partially double bonded to O on the upper left and O on the upper right. This C O O group has an overall negative charge. C 2 is single bonded to H on the left and O H on the right.

3-phosphoglycerate is reversibly converted into 1,3-bisphosphoglycerate by phosphoglycerate kinase. This conversion requires the breakdown of A T P to A D P.

The structure of 1,3-bisphosphoglycerate is as follows: C, single bond, C, single bond, C H 2 O P O 3 superscript 2 minus. C 1 is single bonded to O P O 3 superscript 2 minus on the upper left and double bonded to O on the upper right. C 2 is single bonded to H on the left and O H on the right.

1,3-bisphosphoglycerate is reversibly converted into glyceraldehyde 3-phosphate by glyceraldehyde 3-phosphate dehydrogenase. This conversion requires the oxidation of N A D H to N A D superscript plus and release of P subscript i.

The structure of glyceraldehyde 3-phosphate is as follows: C, single bond, C, single bond, C H 2 O P O 3 superscript 2 minus. C 1 is single bonded to H on the upper left and double bonded to O on the upper right. C 2 is single bonded to H on the left and O H on the right.

Glyceraldehyde 3-phosphate is reversibly converted into dihydroxyacetone phosphate by triose phosphate isomerase. A yellow rectangle labeled glycerol points toward dihydroxyacetone phosphate.

The structure of dihydroxyacetone phosphate is as follows: A central C atom is single bonded to C H 2 O H on the upper right, double bonded to O on the left, and single bonded to C H 2 O P O 3 superscript 2 minus on the lower right.

Glyceraldehyde 3-phosphate and dihydroxyacetone phosphate are reversibly converted into fructose 1, 6-bisphosphate.

The structure of fructose 1, 6-bisphosphate is as follows: A 5-membered heterocyclic pentagonal ring is in a vertical orientation and consists of 1 O and 4 C atoms. O occupies the topmost vertex. C 1 occupies the rightmost vertex and is single bonded to C H 2 O P O 3 superscript 2 minus above and O H below. C 2 is single bonded to O H above. C 3 is single bonded to O H below. C 4 is single bonded to C H 2 O P O 3 superscript 2 minus above.

Fructose 1, 6-bisphosphate is irreversibly converted into fructose 6-phosphate by fructose 1, 6-bisphosphatase. This conversion requires

the entry of H 2 O and exit of P subscript i.

The structure of fructose 6-phosphate is as follows: A 5-membered heterocyclic pentagonal ring is in a vertical orientation and consists of 1 O and 4 C atoms. O occupies the topmost vertex. C 1 occupies the rightmost vertex and is single bonded to C H 2 O H above and O H below. C 2 is single bonded to O H above. C 3 is single bonded to O H below. C 4 is single bonded to C H 2 O P O 3 superscript 2 minus above.

Fructose 6-phosphate is reversibly converted into glucose 6-phosphate by phosphoglucose isomerase.

The structure of glucose 6-phosphate is as follows: A 6-membered heterocyclic hexagonal ring is in a horizontal orientation and consists of 1 O and 5 C atoms. O occupies the top right vertex. C 1 occupies the rightmost vertex and is single bonded to O H below. C 2 is single bonded to O H below. C 3 is single bonded to O H above. C 4 is single bonded to O H below. C 5 is single bonded to C H 2 O P O 3 superscript 2 minus above.

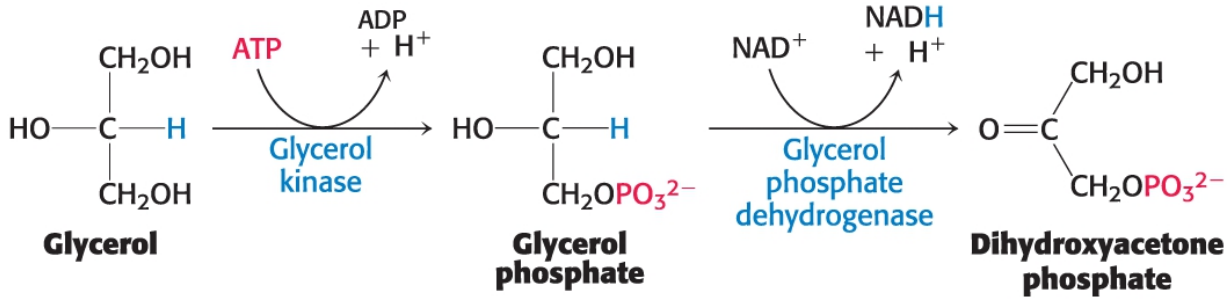
Glucose 6-phosphate is irreversibly converted into glucose by glucose 6-phosphatase. This conversion requires the entry of H 2 O and the release of P subscript i.

The structure of glucose is as follows: A 6-membered heterocyclic hexagonal ring is in a horizontal orientation and consists of 1 O and 5 C atoms. O occupies the top right vertex. C 1 occupies the rightmost vertex and is single bonded to O H below. C 2 is single bonded to O H below. C 3 is single bonded to O H above. C 4 is single bonded to O H below. C 5 is single bonded to C H 2 O H above.

The steps from pyruvate to glyceraldehyde 3-phosphate are enclosed by a left curly bracket labeled 2 times.

Return to Gluconeogenesis pathway

Extended description for Formation of dihydroxyacetone phosphate from glycerol



The formation of dihydroxyacetone phosphate from glycerol takes place in two irreversible steps.

In the first step, glycerol is converted into glycerol phosphate. The structure of glycerol is as follows: C H 2 O H, single bond, C, single bond, C H 2 O H. C 2 is single bonded to O H on the left and H on the right.

A forward reaction arrow labeled glycerol kinase leads to glycerol phosphate. A curved arrow above it shows the simultaneous breakdown of A T P into A D P plus H superscript plus.

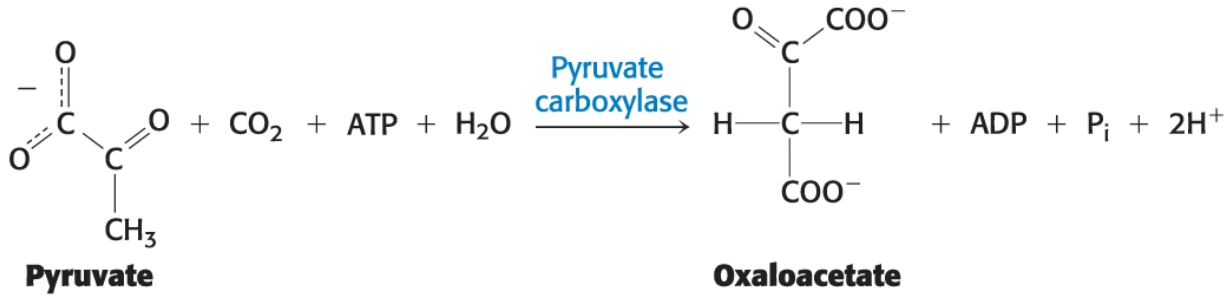
The structure of glycerol phosphate is as follows: C H 2 O H, single bond, C, single bond, C H 2 O P O 3 superscript 2 minus. C 2 is single bonded to O H on the left and H on the right. In the second step, glycerol phosphate is converted into dihydroxyacetone phosphate.

A forward reaction arrow labeled glycerol phosphate dehydrogenase leads to dihydroxyacetone phosphate from glycerol phosphate. A curved arrow above it shows the simultaneous reduction of N A D superscript plus to N A D H plus H superscript plus.

The structure of dihydroxyacetone phosphate is as follows: A central C atom is single bonded to C H 2 O H on the upper right, double bonded to O on the left, and single bonded to C H 2 O P O 3 superscript 2 minus on the lower right.

Return to Formation of dihydroxyacetone phosphate from glycerol

Extended description for Formation of oxaloacetate from pyruvate



The chemical reaction consists of four reactants and four products. The first reactant is pyruvate whose structure is as follows: A central C atom is double bonded to O on the upper right, single bonded to C H 3 below, and single bonded to C on the upper left. This C atom is partially double bonded to O above and O on the lower left. This C O O group has an overall negative charge. The second reactant is C O 2. The third reactant is A T P. The fourth reactant is H 2 O.

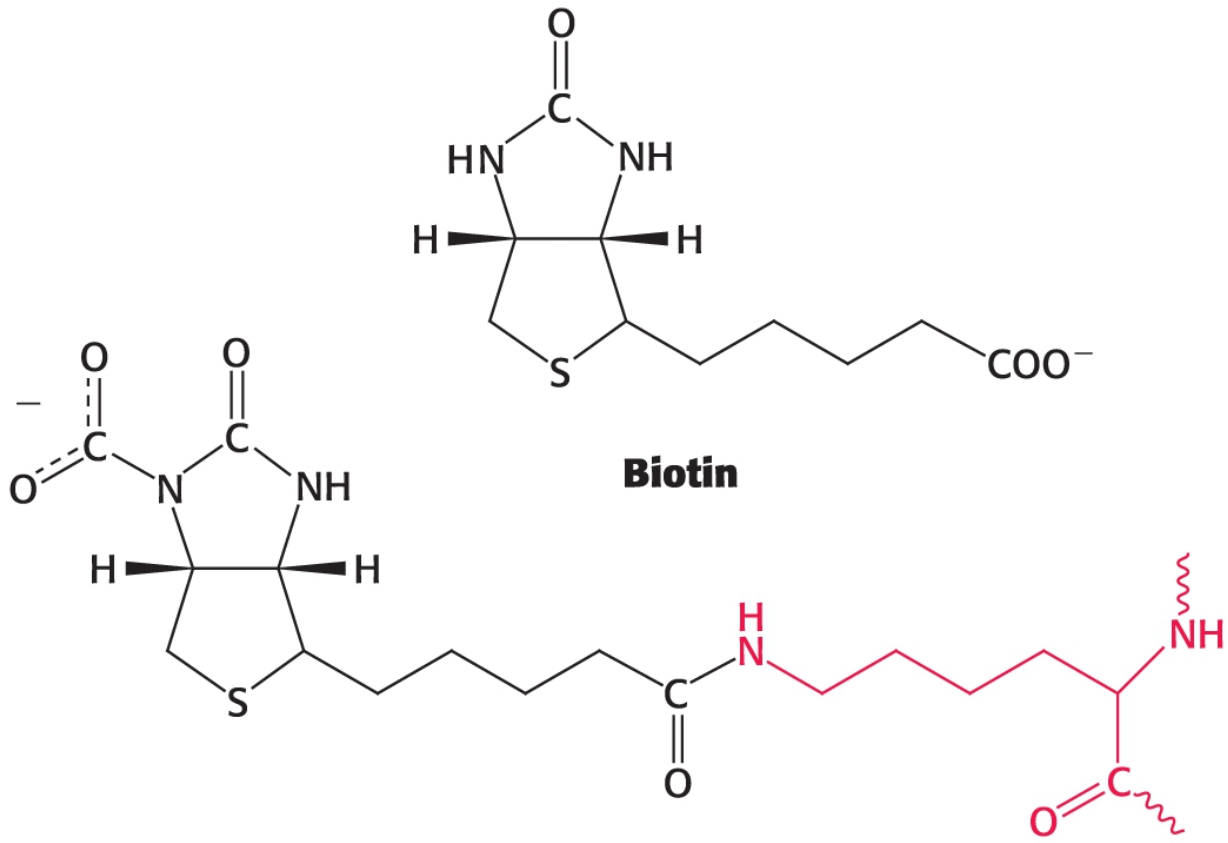
A forward reaction arrow labeled pyruvate carboxylase leads to the products.

The first product is oxaloacetate whose structure is as follows: C, single bond, C, single bond, C O O superscript minus. C 1 is double bonded to O on the upper left and single bonded to C O O superscript minus on the upper right. C 2 is single bonded to H on the left and H on the right.

The second product is A D P. The third product is P subscript i. The fourth product is 2 H superscript plus.

Return to Formation of oxaloacetate from pyruvate

Extended description for Structures of biotin and carboxybiotin covalently bound to the epsilon-amino group of a lysine



Carboxybiotin covalently bound to ε-amino group of a lysine

The structure of biotin is as follows: A 5-membered heterocyclic pentagonal ring is in a vertical orientation and consists of 2 N and 3 C atoms. First N bound to H occupies the first position, which is the top left vertex. The second N bound to H occupies the third position, which is the top right vertex. C 1 occupies the topmost vertex and is double bonded to O above. This ring is fused to another 5-membered heterocyclic pentagonal ring in a vertical orientation such that C 2

and C 3 of the first pentagonal ring are C 3 and C 2 respectively of the second ring. The second pentagonal ring consists of 1 S and 4 C atoms. S occupies the first position, which is the bottom-most vertex. C 2 is wedge bonded to H on the left. C 3 is wedge bonded to H on the right. C 4 is single bonded to a 4-carbon alkane chain depicted as a line structure using 3 zigzag lines. C 4 is single bonded to C O O superscript minus on the lower right.

The structure of carboxybiotin covalently bound to the epsilon-amino group of lysine is as follows: A 5-membered heterocyclic pentagonal ring is in a vertical orientation and consists of 2 N and 3 C atoms. The first N bound occupies the first position, which is the top left vertex. The second N bound to H occupies the third position, which is the top right vertex. C 1 occupies the topmost vertex and is double bonded to O above. N 1 is single bonded to C on the upper left. This C atom is partially double bonded to O above and O on the lower left. This C O O group has an overall negative charge. This pentagonal ring is fused to another 5-membered heterocyclic pentagonal ring in a vertical orientation such that C 2 and C 3 of the first pentagonal ring are C 3 and C 2 respectively of the second ring. The second pentagonal ring consists of 1 S and 4 C atoms. S occupies the first position, which is the bottom-most vertex. C 2 is wedge bonded to H on the left. C 3 is wedge bonded to H on the right. C 4 is single bonded to a 1 N and 10 C alkane chain depicted as a line structure using 10 zigzag lines. The N atom occupies the sixth position and is bound to H. C 5 is double bonded to O below. C 11 is single bonded to N H on the upper right with a wavy line at the top and single bonded to C below. This C atom is double bonded to O on the lower left and has a wavy line on the lower right. N 6 to C 11 and their substituent groups are shown in red.

Return to Structures of biotin and carboxybiotin covalently bound to the epsilon-amino group of a lysine

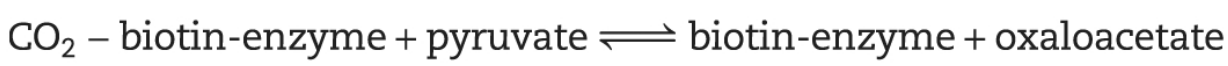
Extended description for First stage of pyruvate carboxylation



The reaction consists of two reactants and two products. The first reactant is H C O 3 superscript minus. The second reactant is A T P. The first product is H O C O 2, single bond, P O 3 superscript 2 minus. The second product is A D P.

Return to First stage of pyruvate carboxylation

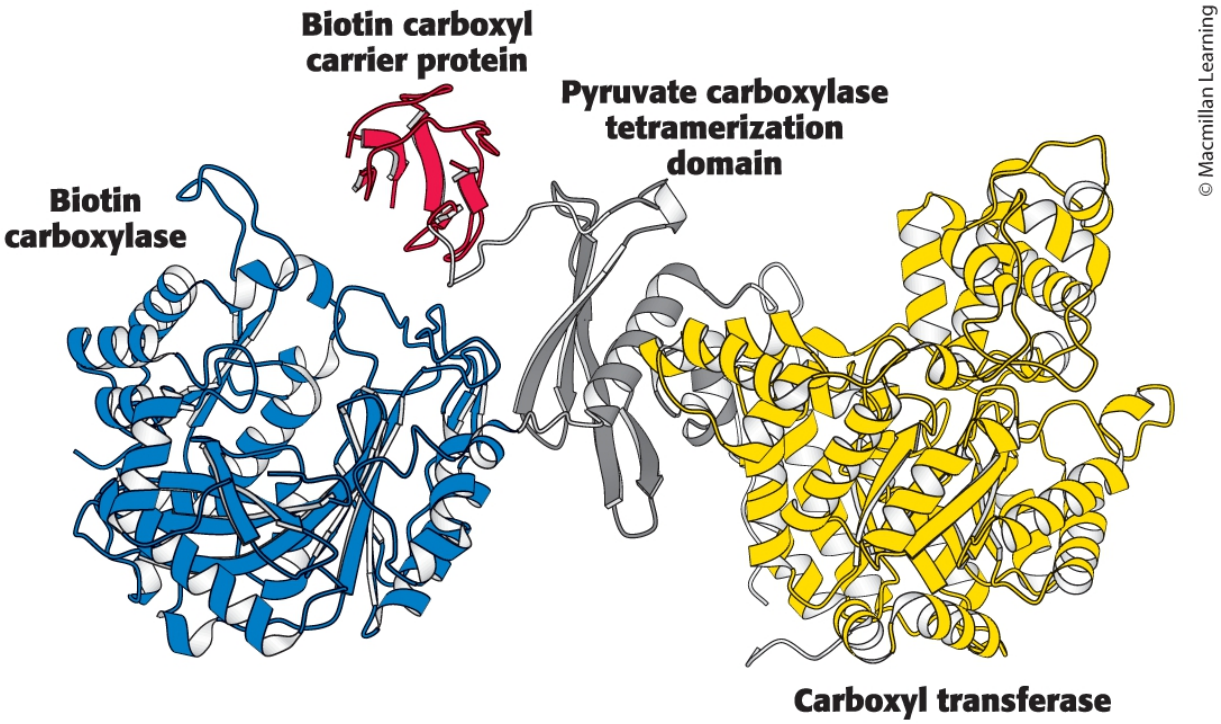
Extended description for Final stage of pyruvate carboxylation



The reaction consists of two reactants and two products. The first reactant is C O 2, single bond, Biotin-enzyme. The second reactant is pyruvate. The first product is biotin-enzyme. The second product is oxaloacetate.

Return to Final stage of pyruvate carboxylation

Extended description for Ribbon diagrams of pyruvate carboxylase subunits



The four subunits of pyruvate carboxylase are biotin carboxylase, biotin carboxyl carrier protein, pyruvate carboxylase tetramerization domain, and carboxyl transferase. The biotin carboxylase subunit consists of a compact and large cluster of several alpha-helices and beta strands. They are interconnected by long threads.

The biotin carboxyl carrier protein is a small structure composed of 5 beta-strands interconnected by long thread-like loops.

The pyruvate carboxylase tetramerization domain is located between the biotin carboxylase and carboxyl transferase subunits. It

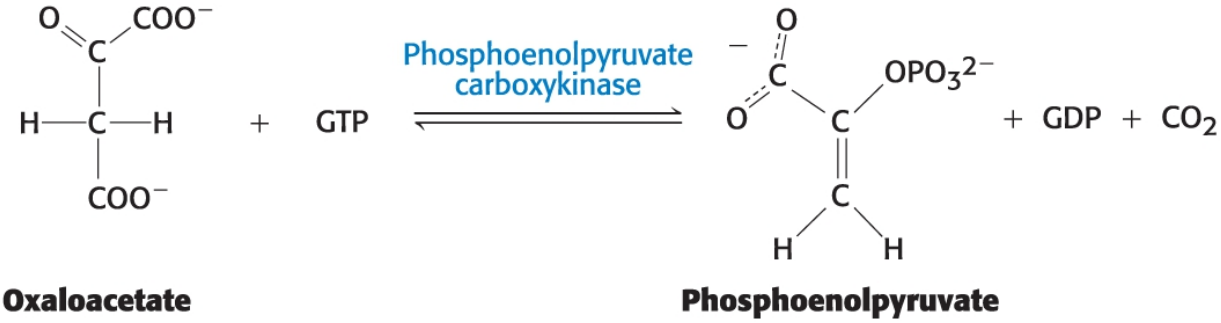
consists of four long and vertical beta-strands and two alpha-helices interconnected by thread-like loops.

The carboxyl transferase subunit consists of a large cluster of several alpha-helices and few beta-strands interconnected by thread-like loops.

The biotin carboxyl carrier protein subunit is located at the top of the junction between biotin carboxylase and pyruvate carboxylase tetramerization domain.

Return to Ribbon diagrams of pyruvate carboxylase subunits

Extended description for Formation of phosphoenolpyruvate from oxaloacetate



The chemical reaction consists of two reactants and three products. The first reactant is oxaloacetate whose structure is as follows: C, single bond, C, single bond, C O O superscript minus. C 1 is double bonded to O on the upper left and single bonded to C O O superscript minus on the upper right. C 2 is single bonded to H on the left and H on the right. The second reactant is G T P.

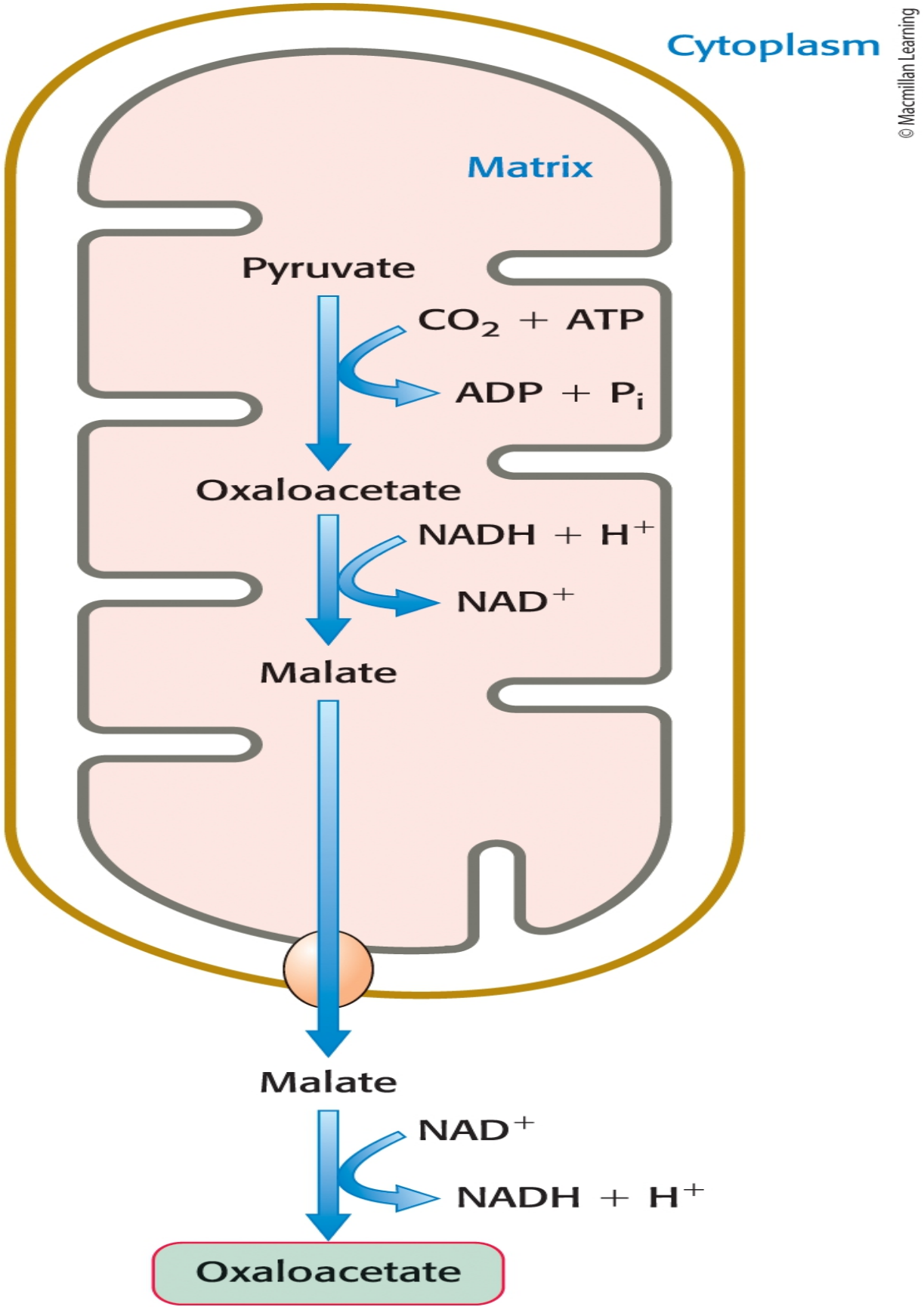
A reversible reaction arrow labeled phosphoenolpyruvate carboxykinase leads to the products.

The first product is phosphoenolpyruvate whose structure is as follows: A central C atom is double bonded to C below, single bonded to O P O 3 superscript 2 minus on the upper right, and single bonded to C on the upper left. The C atom below is single-bonded to H on the lower left and H on the lower right. The C atom on the upper left is partially double bonded to O above and O on the lower left. This C O O group has an overall negative charge. The second product is G D P. The third product is C O 2.

Return to Formation of phosphoenolpyruvate from oxaloacetate

Extended description for Transport of malate produced in the mitochondrial matrix to the cytoplasm and its

conversion to oxaloacetate

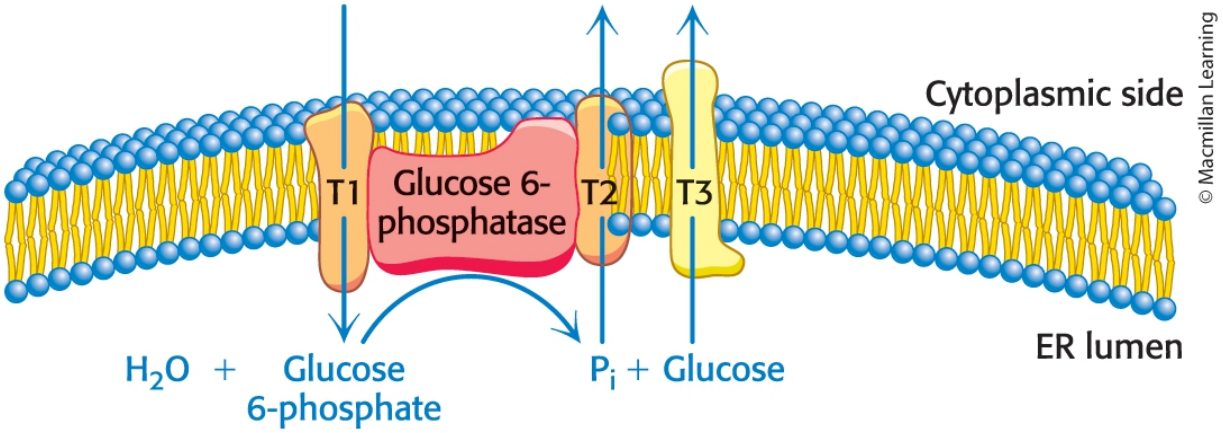


© Macmillan Learning

The mitochondrion is depicted as a big rounded rectangular structure in a vertical orientation. Its inner membrane has invaginations and encloses the matrix. The space outside the mitochondria is labeled cytoplasm. In the matrix, pyruvate is converted into oxaloacetate with the simultaneous breakdown of A T P into A D P plus P subscript i and the incorporation of C O 2. Oxaloacetate is further converted into malate with the simultaneous oxidation of N A D H plus H superscript into N A D superscript plus. The malate molecule moves into the cytoplasm through a transporter depicted as an orange circle between the inner and outer membrane of the mitochondria. In the cytoplasm, malate is converted into oxaloacetate with the simultaneous reduction of N A D superscript plus to N A D H plus H superscript plus.

Return to Transport of malate produced in the mitochondrial matrix to the cytoplasm and its conversion to oxaloacetate

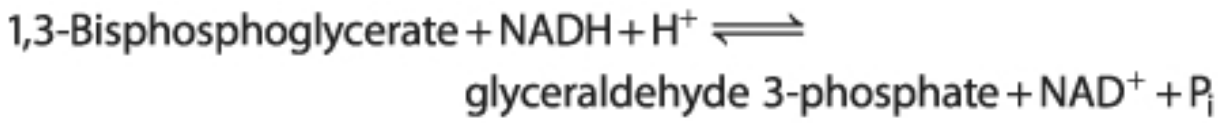
Extended description for Formation of free glucose in E R lumen



A section of the lipid bilayer is shown. The region above the bilayer is labeled the cytoplasmic side. The region below the lipid bilayer is labeled E R lumen. A square-shaped glucose 6-phosphatase enzyme with a groove at the top left is shown embedded in the bilayer. It is flanked by two tubular structures embedded in the bilayer and labeled T 1 and T 2. Another long and tubular transmembrane structure labeled T 3 is shown on the right of T 2 with a gap between them. A downward arrow across T 1 shows the entry of glucose 6-phosphate into the E R lumen. In the E R lumen, glucose plus H 2 O are converted into P subscript i plus glucose by glucose 6-phosphatase. Upward arrows across T 2 and T 3 show the exit of P subscript i and glucose respectively into the cytoplasmic side.

Return to Formation of free glucose in E R lumen

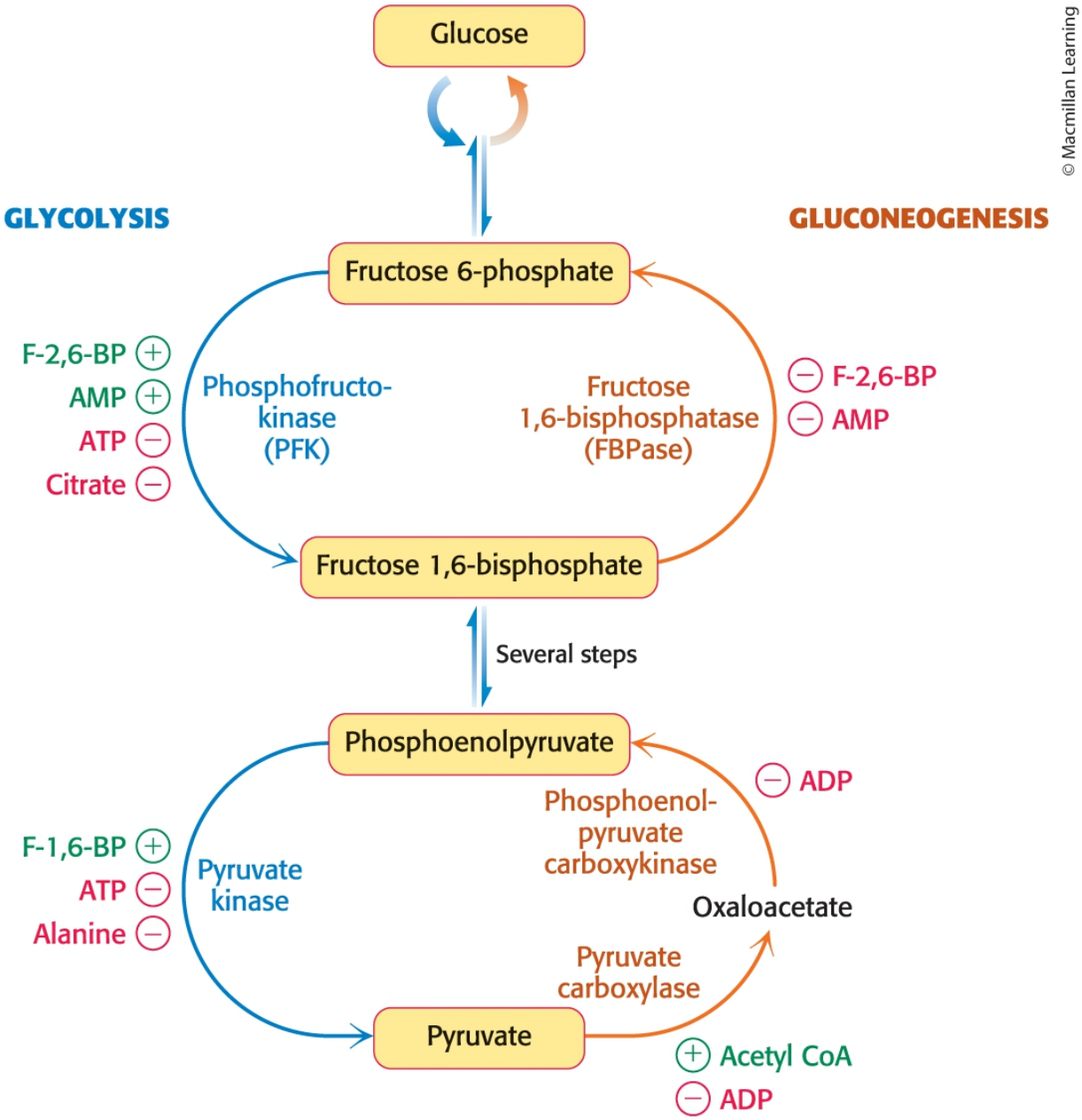
Extended description for Step 6 of gluconeogenesis



The reaction consists of 3 reactants and 3 products. The reactants are 1,3-bisphosphoglycerate, N A D H, and H superscript plus. The products are glyceraldehyde 3-phosphate, N A D superscript plus, and P subscript i.

Return to Step 6 of gluconeogenesis

Extended description for Reciprocal regulation of glycolysis and gluconeogenesis



The flowchart is depicted as follows from top to bottom:

A yellow rectangle is labeled glucose. A downward curved below and an upward curved orange arrow is shown below glucose. A blue reversible arrow is shown below the curved arrow and leads to a yellow rectangle labeled fructose 6-phosphate.

A downward curved blue arrow below fructose 6-phosphate is labeled phosphofructokinase (P F K) and leads to fructose 1, 6-bisphosphate.

An upward curved orange arrow above fructose 1, 6-bisphosphate is labeled fructose 1, 6-bisphosphatase (F B P ase) and leads to fructose 6-phosphate.

A reversible reaction arrow below fructose 1, 6-bisphosphate is labeled several steps and leads to phosphoenolpyruvate.

A downward curved blue arrow below phosphoenolpyruvate is labeled pyruvate kinase and leads to pyruvate.

An upward curved orange arrow above pyruvate is labeled pyruvate carboxylase and leads to oxaloacetate.

An upward curved orange arrow above oxaloacetate is labeled phosphoenol pyruvate carboxykinase and leads to phosphoenolpyruvate.

The left side of the flowchart shown by blue arrows depicts glycolysis and the right side shown by orange arrows depicts gluconeogenesis.

The activators of phosphofructokinase are F-2, 6-B P and A M P and its inhibitors are A T P and citrate.

The activator of pyruvate kinase is F-1, 6-B P and its inhibitors are A T P and alanine.

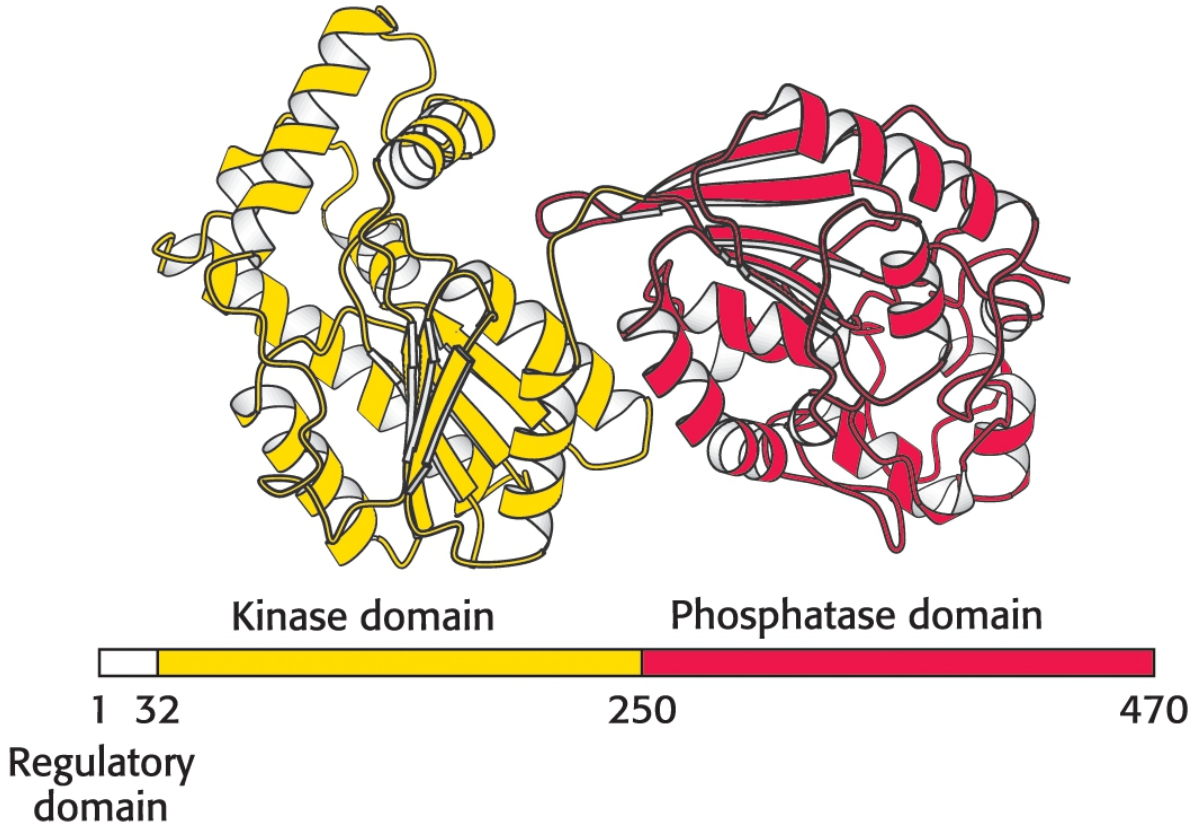
The activator of pyruvate carboxylase is acetyl C o A and its inhibitor is A D P.

The inhibitor of phosphoenolpyruvate carboxykinase is A D P.

The inhibitors of fructose 1, 6-bisphosphatase are F-2, 6-B P and A M P.

Return to Reciprocal regulation of glycolysis and gluconeogenesis

Extended description for Schematic representation and ribbon diagram of the domains of P F K 2 slash F B P ase 2



© Macmillan Learning

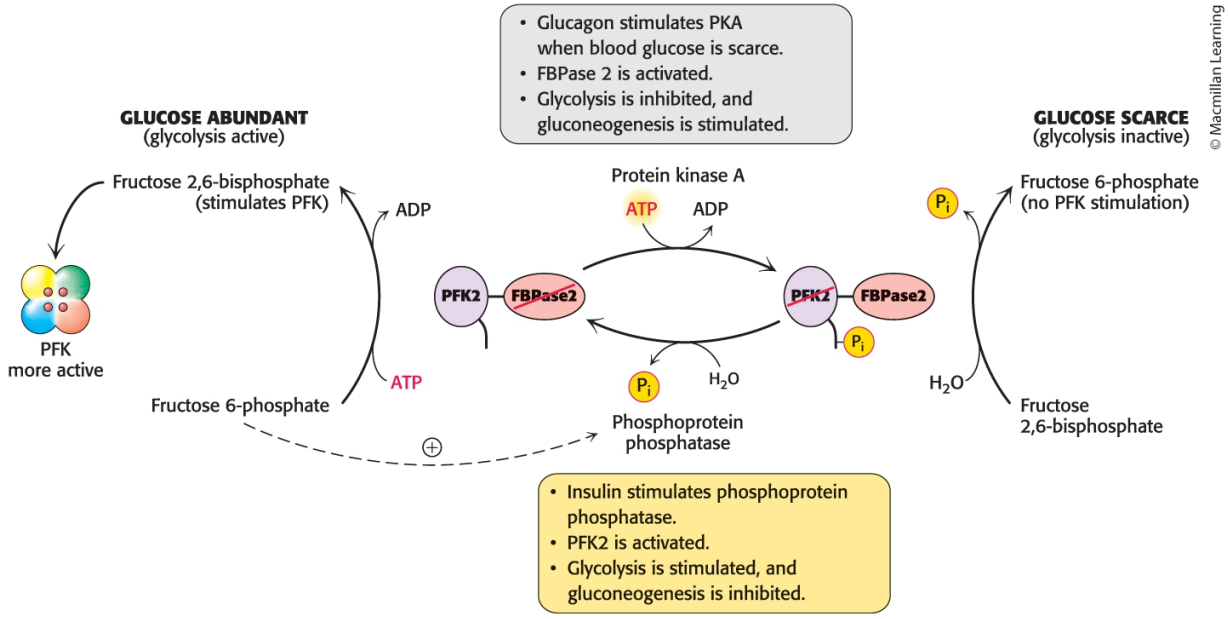
The schematic representation shows a narrow rectangular bar. Its left and right ends are labeled 1 and 470 respectively. A marking near the left end is labeled 32 and another marking in the middle is labeled 250. The region between 1 to 32 is shown in the white and labeled regulatory domain. The region between 32 and 250 is shown in the yellow and labeled kinase domain. The region between 250 and 470 is shown in red and labeled phosphatase domain.

The ribbon diagram of the kinase domain consists of several alpha-helices and a few beta-strand in the center interconnected by

thread-like loops. It is connected to a ribbon diagram of the phosphate domain composed of a few alpha-helices and beta-strands at the top interconnected by long loops.

Return to Schematic representation and ribbon diagram of the domains of P F K 2 slash F B P ase 2

Extended description for Hormonal regulation of synthesis and degradation of fructose 2, 6-bisphosphate



P F K 2 slash F B P ase 2 is depicted as a purple circle connected to a pink oval. In the initial state, F B P ase 2 has a red diagonal line. Protein kinase A carries out the phosphorylation of P F K 2 with the simultaneous breakdown of A T P to A D P. In the phosphorylated state, a red diagonal line is drawn across P F K 2 and an overhang originating from it is single bonded to P subscript i. Phosphoprotein phosphatase carries out the removal of P subscript i from P F K 2 with the simultaneous entry of H 2 O and release of P subscript i.

A text box above protein kinase A mentions the following points:

Glucagon stimulates P K A when blood glucose is scarce.

F B P ase 2 is activated.

Glycolysis is inhibited, and gluconeogenesis is stimulated.

A text box below phosphoprotein phosphatase mentions the following points:

Insulin stimulates phosphoprotein phosphatase.

P F K 2 is activated.

Glycolysis is stimulated, and gluconeogenesis is inhibited.

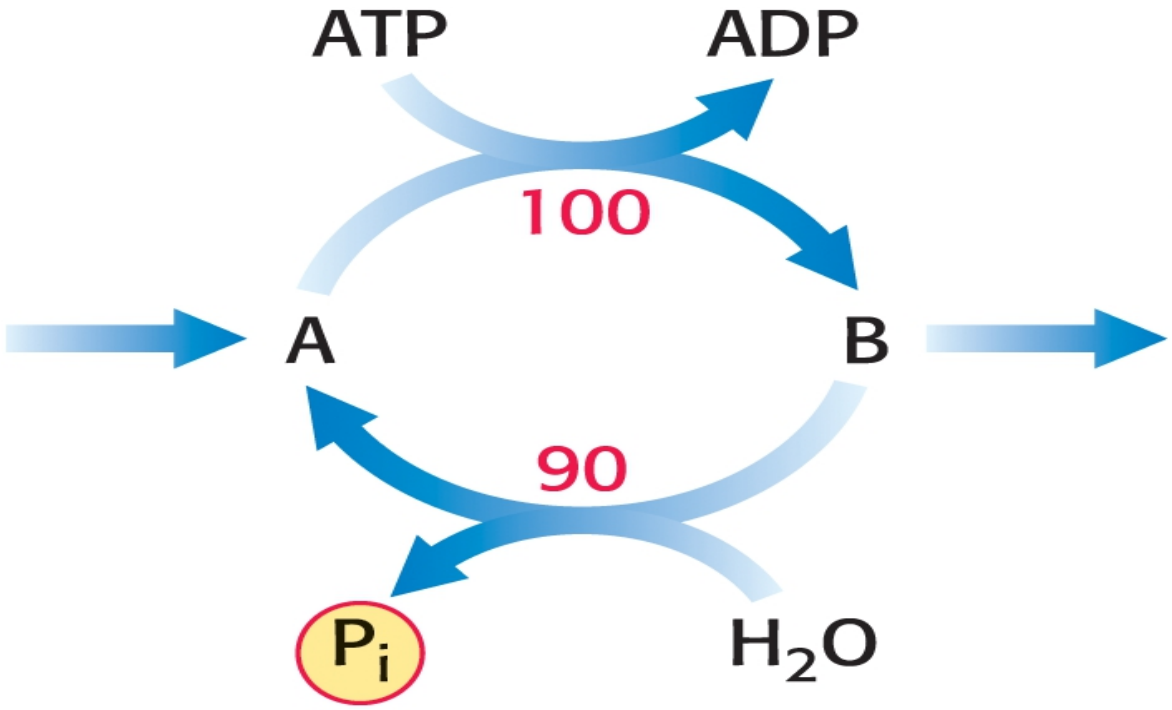
In the case of abundant glucose (glycolysis active), fructose 6-phosphate is phosphorylated to fructose 2, 6-bisphosphate with the simultaneous breakdown of A T P to A D P. Fructose 2, 6-bisphosphate stimulates P F K. It binds to P F K to make it more active. A dashed arrow from fructose 6-phosphate points toward phosphoprotein phosphatase and is labeled with a plus symbol.

In case of scarce glucose (glycolysis inactive), fructose 2, 6-bisphosphate is converted into fructose 6-phosphate with simultaneous uptake of H 2 O and release of P subscript i. Fructose 6-phosphate does not cause P F K stimulation.

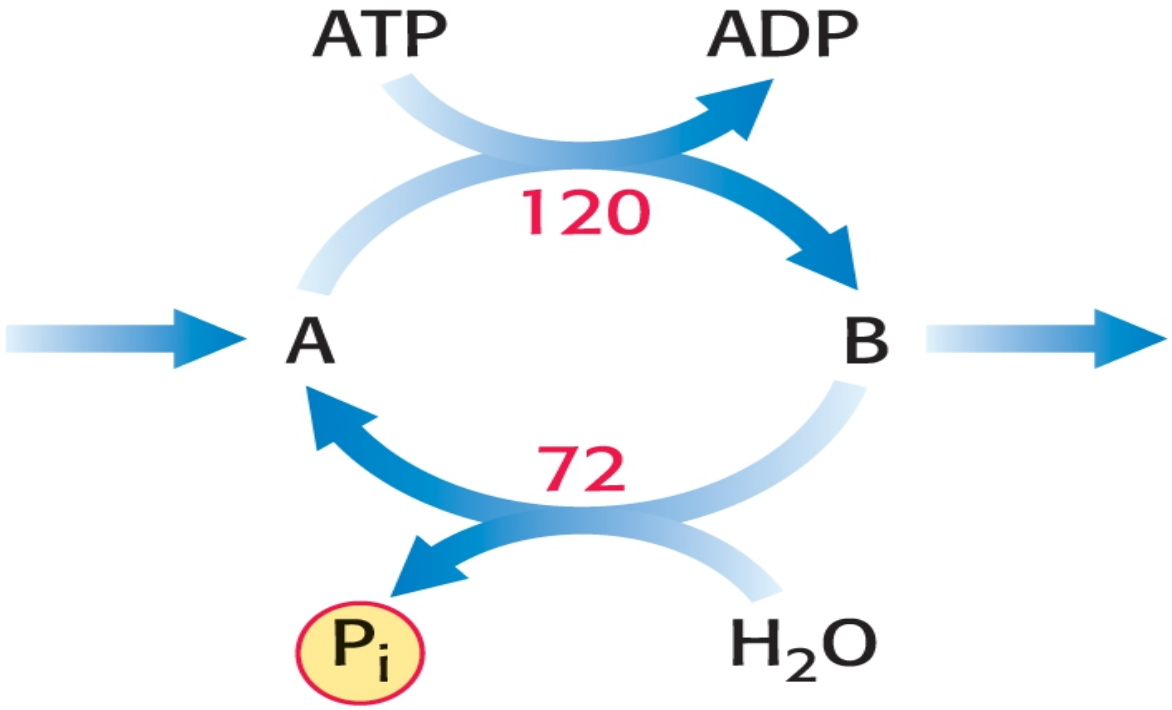
Return to Hormonal regulation of synthesis and degradation of fructose 2, 6-bisphosphate

Extended description for Different rates of operation of

a A T P-driven cycle



Net flux of B = 10



Net flux of B = 48

© Macmillan Learning

The first cycle is depicted as follows:

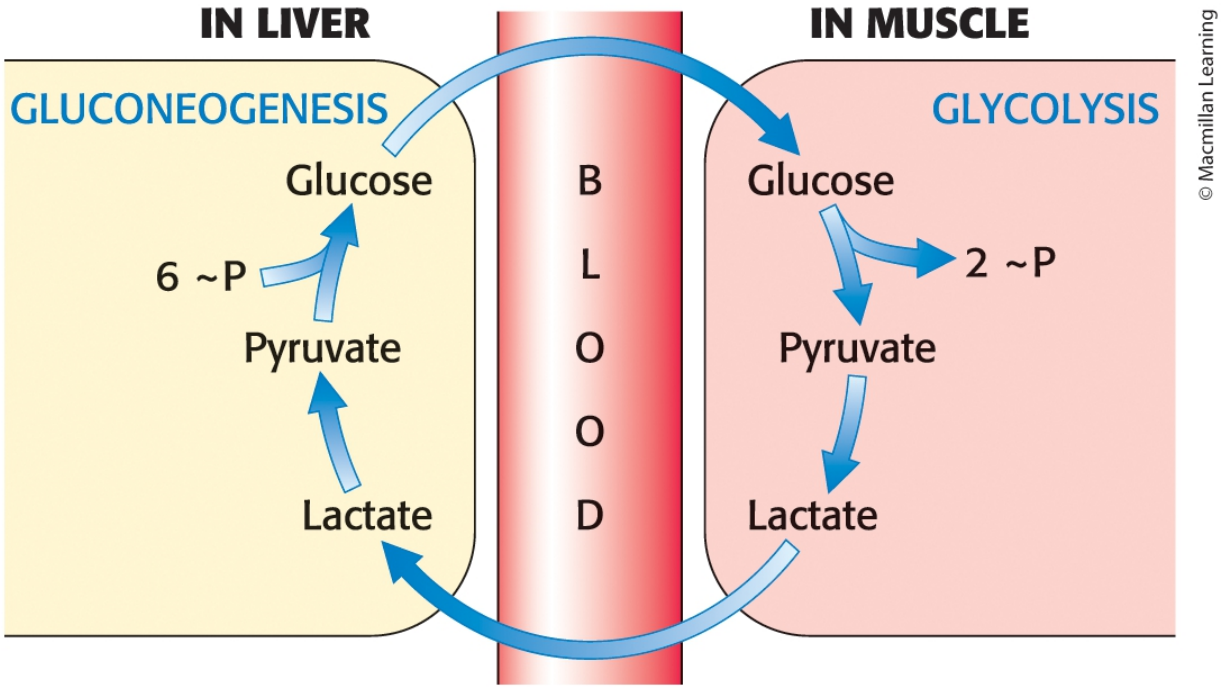
A forward arrow shows the entry of A. A curved arrow at the top of A is labeled 100 and leads to B. Another curved arrow above it shows the simultaneous breakdown of A T P into A D P. A forward arrow shows the exit of B. A curved arrow below B is labeled 90 and leads back to A. Another curved arrow below it shows the entry of H 2 O and the release of P subscript i. The net flux of B equals 10.

The second cycle is depicted as follows:

A forward arrow shows the entry of A. A curved arrow at the top of A is labeled 120 and leads to B. Another curved arrow above it shows the simultaneous breakdown of A T P into A D P. A forward arrow shows the exit of B. A curved arrow below B is labeled 72 and leads back to A. Another curved arrow below it shows the entry of H 2 O and the release of P subscript i. The net flux of B equals 48.

Return to Different rates of operation of a A T P-driven cycle

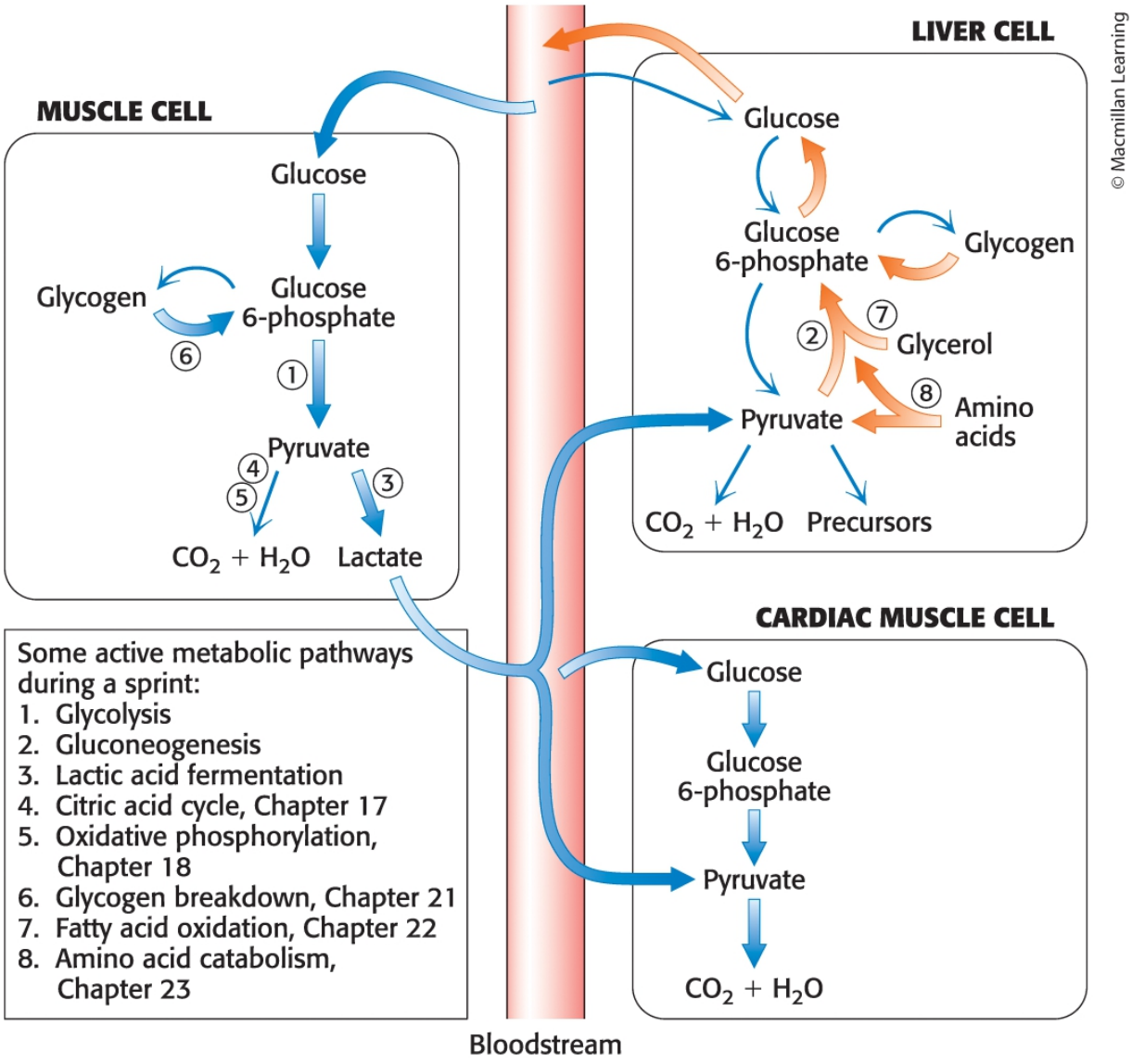
Extended description for Cori cycle



The illustration shows three different compartments. The central compartment is labeled blood and is long and cylindrical. The left compartment is a half-rectangle labeled "In liver." The right compartment is also a half-rectangle labeled "In muscle." In muscle, glycolysis is depicted as follows: Glucose is converted into pyruvate with the release of 2 wavy line P which presents 2 nucleoside triphosphates. Pyruvate is further converted into lactate. This lactate travels to the liver compartment through the blood compartment. In the liver, gluconeogenesis is depicted as follows: Lactate is converted into pyruvate. Pyruvate is further converted into glucose with the use of 6 wavy line P which represents 6 nucleoside triphosphates. The glucose molecule travels back to the muscle compartment through the blood compartment.

Return to Cori cycle

Extended description for Cooperation between glycolysis and gluconeogenesis during a sprint



© Macmillan Learning

Three rectangular compartments are shown separated by a bloodstream depicted as a long vertical cylindrical structure. These rectangular compartments are labeled muscle cell, liver cell, and cardiac muscle cell. The muscle cell is shown on the left of the

bloodstream and the liver cell and cardiac muscle cell are shown on the right of the bloodstream.

Inside the muscle cell, glucose is converted into glucose 6-phosphate. A curved arrow labeled 6 points from glycogen toward glucose 6-phosphate. Another curved arrow above it points back to glycogen. A downward arrow labeled 1 point from glucose 6-phosphate to pyruvate.

A downward arrow labeled 4 and 5 points from pyruvate to C O 2 plus H 2 O. Another downward arrow labeled 3 points from pyruvate to lactate.

Lactate moves into the liver cell and cardiac muscle cell via the bloodstream.

Glucose enters and exits the liver cell via the bloodstream. Two curved arrows pointing upward and downward are shown below glucose and they lead to glucose 6-phosphate. Two curved arrows pointing rightward and leftward are shown adjacent to glucose 6-phosphate and they lead to glycogen.

A two-way arrow labeled 8 points from amino acids in the liver cell toward pyruvate and in the upward direction. Two arrows labeled 2 and 7 from pyruvate and glycerol respectively, merge together, above the upward pointing head of arrow 8, and point toward glucose 6-phosphate. A downward curved arrow from glucose 6-phosphate point toward pyruvate below. Pyruvate is converted into C O 2 plus H 2 O or precursors.

Glucose enters the cardiac muscle cell through the bloodstream. It is converted into glucose 6-phosphate which is further converted into pyruvate. Pyruvate is ultimately converted into C O 2 plus H 2 O.

A key below the muscle cell compartment lists the following points below the heading "Some active metabolic pathways during a sprint:"

1. Glycolysis

2. Gluconeogenesis

3. Lactic acid fermentation

4. Citric acid cycle, Chapter 17

5. Oxidative phosphorylation, Chapter 18

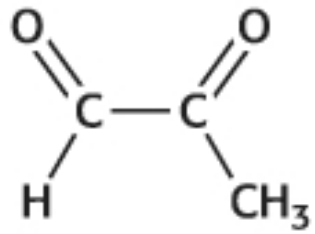
6. Glycogen breakdown, Chapter 21

7. Fatty acid oxidation, Chapter 22

8. Amino acid catabolism, Chapter 23

Return to Cooperation between glycolysis and gluconeogenesis during a sprint

Extended description for Structure of methylglyoxal

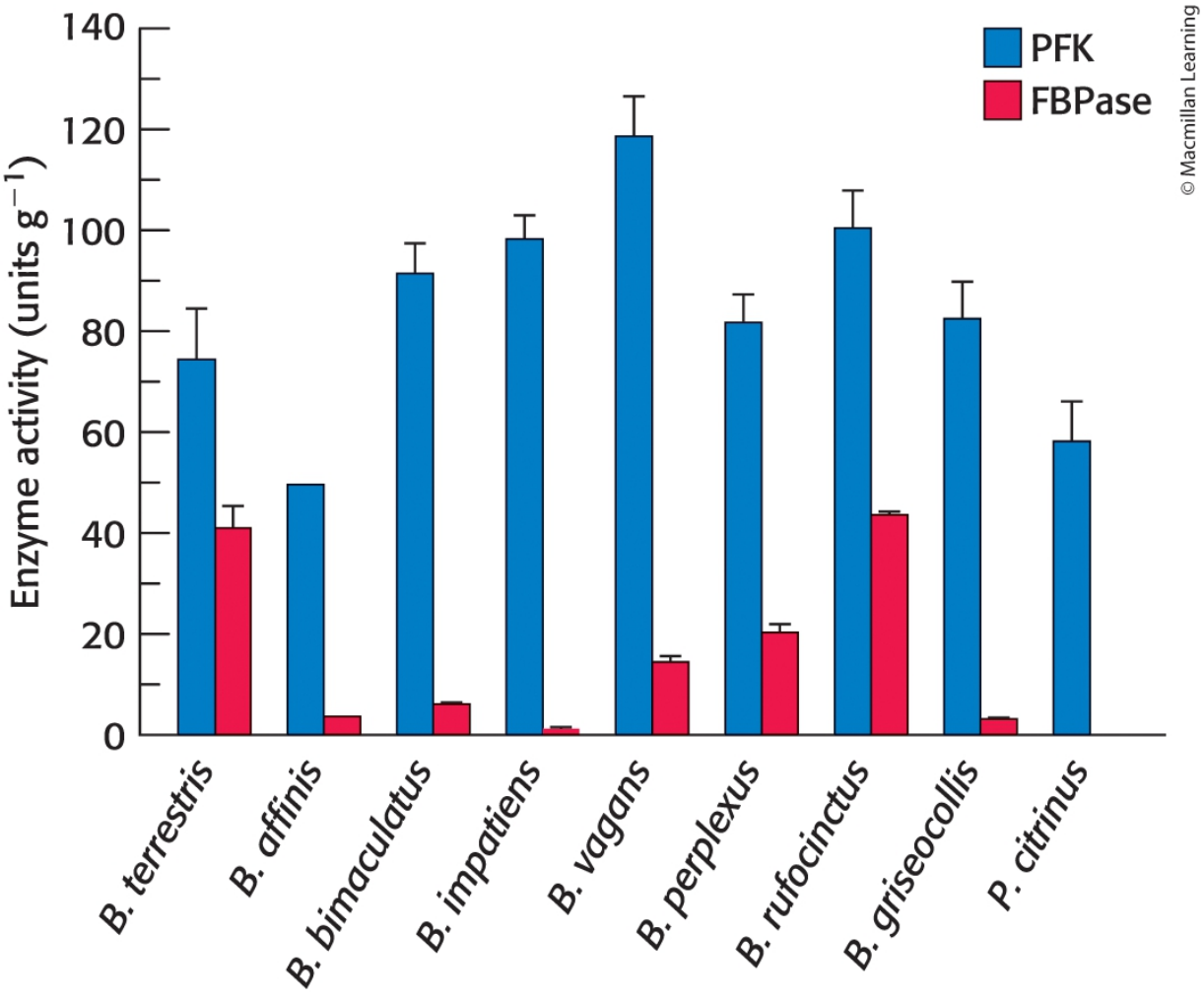


Methylglyoxal

The structure of methylglyoxal is as follows: C, single bond, C. C 1 is double bonded to O on the upper left and single bonded to H on the lower left. C 2 is double bonded to O on the upper right and single bonded to C H 3 on the lower right.

Return to Structure of methylglyoxal

Extended description for Activity of P F K and F B P ase in different bumblebee species



The horizontal axis has markings for different bumblebee species from left to right. These are *B. terrestris, B. affinis, B. bimaculatus, B. impatiens, B. vagans, B. perplexus, B. rufocinctus, B. griseocollis, P. citrinus*. The vertical axis is labeled enzyme activity in units per gram. It has markings ranging from 0 to 140 in increments of 20 units. Two vertical bars in blue and red colors are shown for each bumblebee species. The height of these vertical bars is as follows:

B. terrestris: Blue bar: 75 units per gram, Red bar: 40 units per gram.

B. affinis: Blue bar: 50 units per gram, Red bar: 5 units per gram.

B. bimaculatus: Blue bar: 92 units per gram, Red bar: 8 units per gram.

B. impatiens: Blue bar: 100 units per gram, Red bar: 0.5 units per gram.

B. vagans: Blue bar: 120 units per gram, Red bar: 20 units per gram.

B. perplexus: Blue bar: 90 units per gram, Red bar: 21 units per gram.

B. rufocinctus: Blue bar: 100 units per gram, Red bar: 50 units per gram.

B. griseocollis: Blue bar: 91 units per gram, Red bar: 5 units per gram.

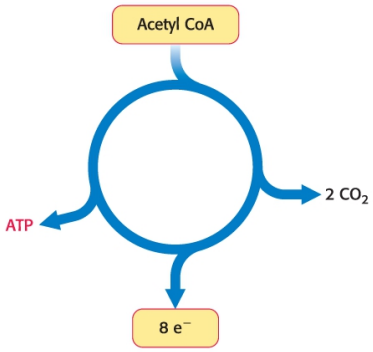
P. citrinus: Blue bar: 60 units per gram, Red bar: 0 units per gram.

All values are estimated.

Return to Activity of P F K and F B P ase in different bumblebee species

Extended description for Schematic representation of the citric acid cycle



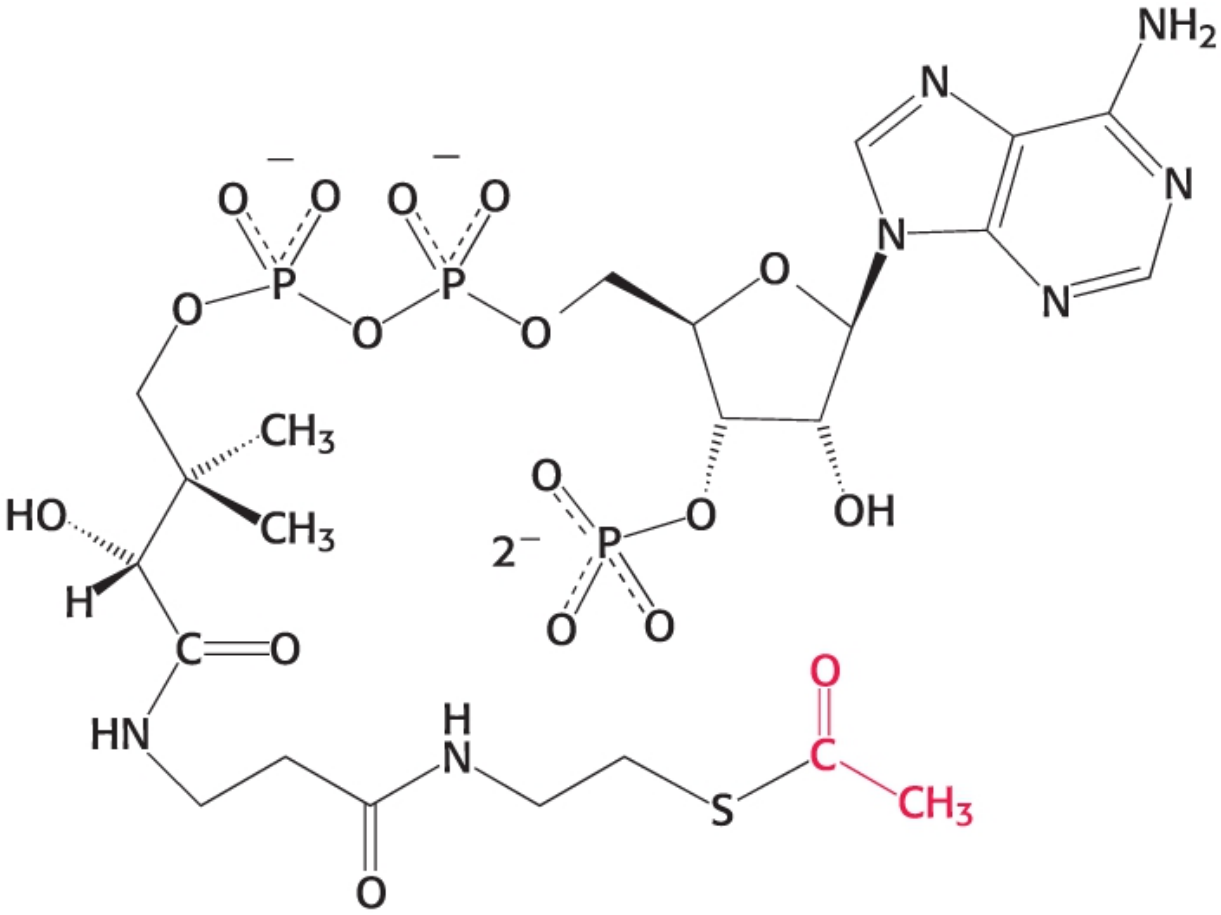


Chalermkiat Seedokmai/Getty Images
© Macmillan Learning

The citric acid cycle is depicted as a large circle with a thick blue outline. A line from a rectangle labeled acetyl C o A merges with the top of the large circle. An outward arrow from the right side of the large circle shows the exit of 2 C O 2. A downward arrow from the bottom of the large circle shows the exit of 8 electrons. An outward arrow from the bottom right of the large circle shows the exit of A T P.

Return to Schematic representation of the citric acid cycle

Extended description for Structure of acetyl coenzyme A or acetyl C o A



Acetyl coenzyme A (Acetyl CoA)

The structure of acetyl coenzyme A is as follows: A 5-membered heterocyclic pentagonal ring is in a vertical orientation and consists of 1 O and 4 C atoms. O occupies the topmost vertex. C 1 occupies the top right vertex and is wedge bonded to N 1 of another 5-membered heterocyclic pentagonal ring in a horizontal orientation. This pentagonal ring consists of 2 N and 3 C atoms. The first N occupies the first position, which is the bottom left vertex. The second N occupies the third position, which is the topmost vertex. C

1 occupies the leftmost vertex. A double bond is present between C 1 and N 2. This pentagonal ring is fused to a 6-membered heterocyclic hexagonal ring in a vertical orientation such that C 2 and C 3 of the pentagonal ring are C 3 and C 2 respectively, of the hexagonal ring. The hexagonal ring consists of 2 N and 4 C atoms. The first N occupies the first position, which is the top-right vertex. The second N occupies the third position, which is the bottommost vertex. C 1 occupies the bottom right vertex. A double bond is present between C 1 and N 2, C 2 and C 3, and C 4 and N 1. C 4 is single bonded to N H 2 above.

In the first pentagonal ring, C 2 is dash bonded to O H on the lower right, and C 3 is dashed bonded to O on the lower left. This O is single bonded to a central P atom which is further partially double bonded to O on the upper left, O on the lower left, and O on the lower right. These O atoms have an overall negative charge of 2 minus. C 4 is wedge bonded to C H 2 on the upper left in the form of a wedged line. This C H 2 is single bonded to a zigzag chain composed of O, single bond, P, single bond, O, single bond, P, single bond, O. Each P atom of this chain is partially double bonded to O on the upper left and O on the upper right. These O atoms have an overall negative charge.

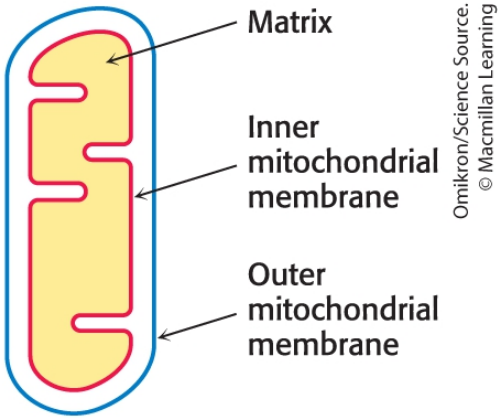
O 3 of the zigzag chain is single bonded to C 1 of a 1 S, 2 N, and 10 C alkane chain depicted as a line structure using 12 zigzag lines. The first and second N atoms occupy the fifth and ninth positions and both are bound to H. S occupies the twelfth position. C 2 is dash bonded to C H 3 on the upper right and wedge bonded to C H 3 on the lower right. C 3 is dash bonded to O H on the upper left and wedge bonded to H on the lower right. C 4 is double bonded to O on the right. C 7 is double bonded to O below. C 10 highlighted in red is double bonded to O above and single bonded to C H 3 on the lower right, both highlighted in red. The alkane chain is in a vertical

orientation from C 1 to N 1 and a horizontal orientation from C 5 to C 10.

Return to Structure of acetyl coenzyme A or acetyl C o A

Extended description for Electron micrograph and schematic illustration of a mitochondrion

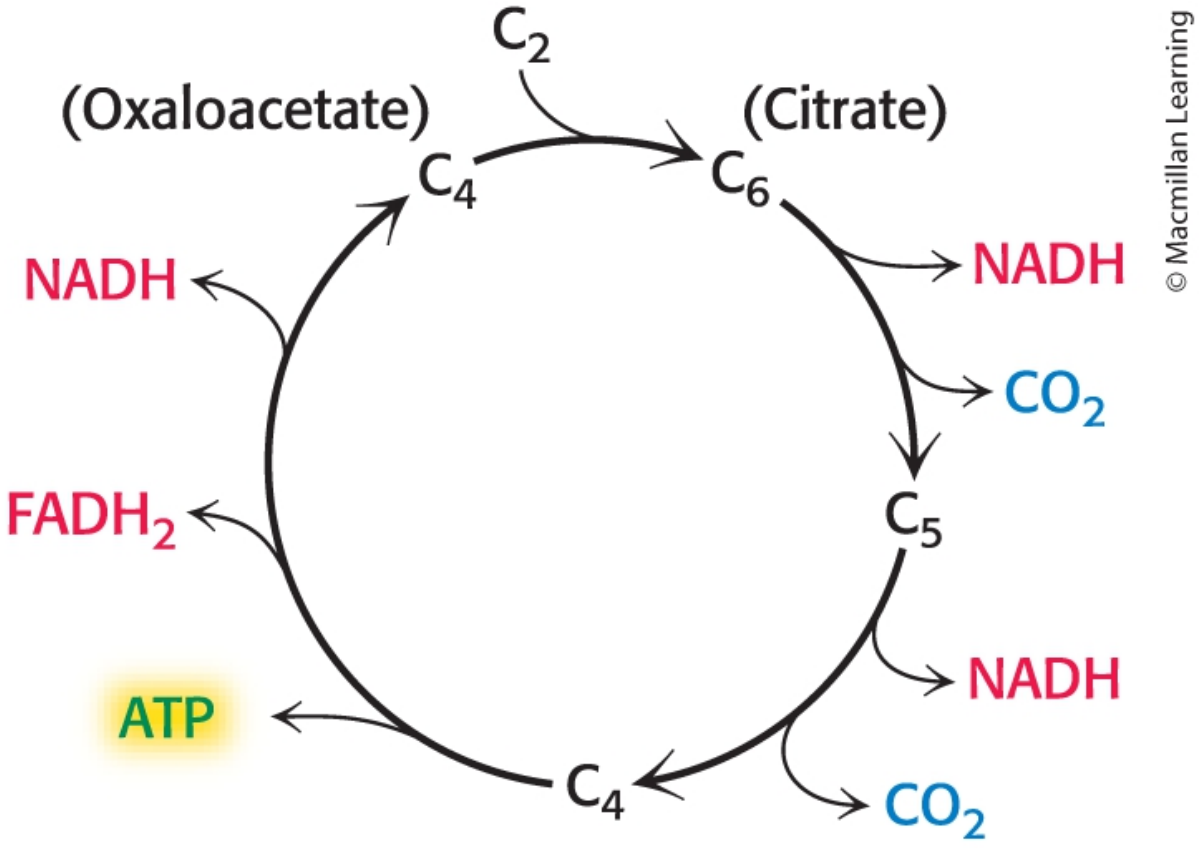




The electron micrograph shows an elongated mitochondrion with invaginations of membrane extending into the matrix. The schematic illustration shows a vertically elongated rod-shaped structure with a blue outline labeled outer mitochondrial membrane. The inner mitochondrial membrane inside the outer membrane is shown in red. It is invaginated several times to form short rectangular grooves. The space inside the inner mitochondrial membrane is labeled matrix.

Return to Electron micrograph and schematic illustration of a mitochondrion

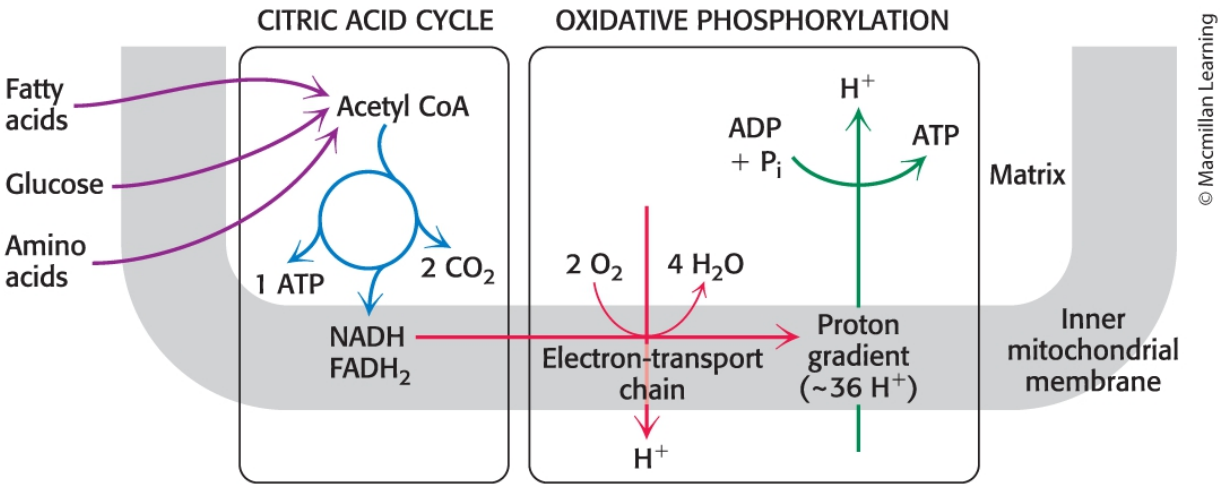
Extended description for Citric acid cycle



The citric acid cycle is depicted as follows: It begins with C 4 (oxaloacetate) and C 2 that combine to form C 6 (citrate). C 6 is converted into C 5 with the simultaneous release of N A D H and C O 2 in the same sequence. C 5 is further converted into C 4 with the simultaneous release of N A D H and C O 2 in the same sequence. C 4 is converted back to C 4 with the simultaneous release of A T P, F A D H 2, and N A D H in the same sequence.

Return to Citric acid cycle

Extended description for Citric acid cycle and oxidative phosphorylation in a mitochondrion



A long rectangular structure open at the top is shown. It has a thick grey border labeled inner mitochondrial membrane. The space enclosed by the grey border is labeled matrix. A rectangle labeled citric acid cycle is shown inside the open rectangle. Three purple arrows labeled fatty acids, glucose, and amino acids respectively, depict the movement of these molecules from external space to the matrix through the inner mitochondrial membrane. All the purple arrows point toward acetyl-C o A which enters the citric acid cycle. The cycle is depicted as a circle with a blue outline. An outward arrow is shown at the right, bottom, and bottom left of the circle to show the release of 2 C O 2; N A D H, F A D H 2; and 1 A T P respectively. N A D H and F A D H 2 are shown inside the inner mitochondrial membrane. A rectangle labeled oxidative phosphorylation is shown adjacent to the first rectangle labeled citric acid cycle. A red forward arrow from N A D H and F A D H 2 produced in the citric acid cycle is labeled electron-transport chain and its points toward proton gradient (approximately 36 H superscript). A downward arrow across it shows the movement of H

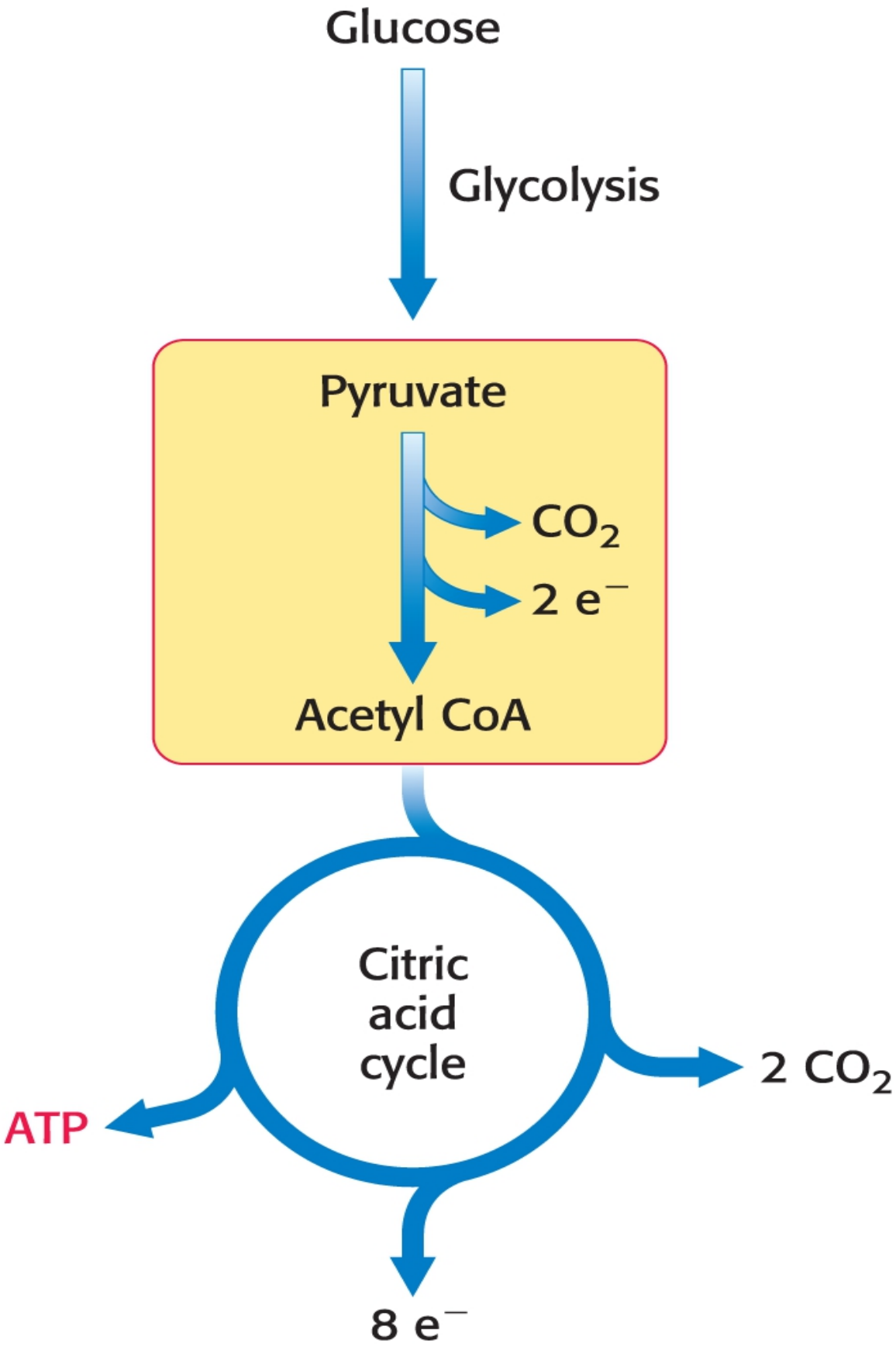
superscript plus ion from the matrix to the space outside the inner mitochondrial membrane. Another curved arrow above the forward arrow and across the downward arrow shows the simultaneous conversion of 2 O 2 to 4 H 2 O.

An upward green arrow across the proton gradient in the membrane shows the entry of H superscript plus into the matrix from a space outside the membrane. A curved arrow across it shows the simultaneous conversion of A D P plus P subscript i into A T P in the matrix.

Return to Citric acid cycle and oxidative phosphorylation in a mitochondrion

Extended description for Connection between

glycolysis and citric acid cycle

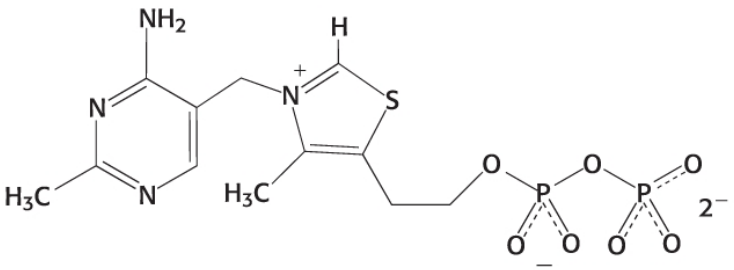


© Macmillan Learning

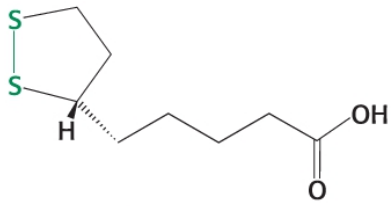
Glucose is converted into pyruvate via glycolysis. Pyruvate is further converted into acetyl C o A with the simultaneous release of C O 2 and 2 electrons. Acetyl C o A enters the citric acid cycle which is depicted as a circle with a thick blue outline. An outward arrow is shown on the right, bottom, and bottom left of the circle. These arrows represent the release of 2 C O 2, 8 electrons, and A T P respectively.

Return to Connection between glycolysis and citric acid cycle

Extended description for Structure of thiamine pyrophosphate (T P P) and lipoic acid



Thiamine pyrophosphate (TPP)



Lipoic acid

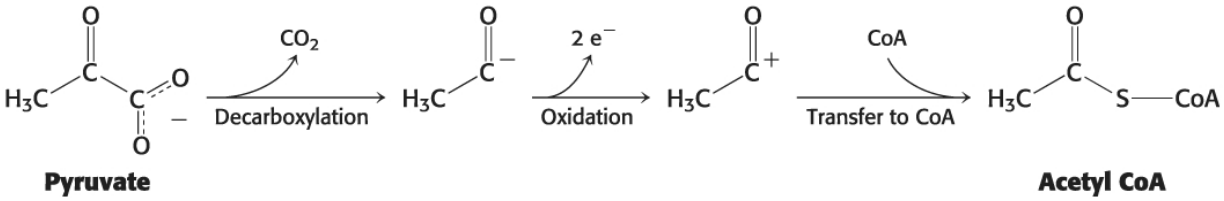
The structure of thiamine pyrophosphate (T P P) is as follows: A 6-membered heterocyclic hexagonal ring is in a vertical orientation and consists of 2 N and 4 C atoms. The first N occupies the first position, which is the bottommost vertex. The second N occupies the third position, which is the top left vertex. C 1 occupies the bottom left vertex. A double bond is present between N 1 and C 1, N 2 and C 2, and C 3 and C 4. C 1 is single bonded to C H 3 on the lower left. C 2 is single bonded to N H 2 above. C 3 is single bonded to C H 2 on the upper right in the form of a line. This C H 2 group is single-bonded to the N atom of a 5-membered heterocyclic pentagonal ring in a vertical orientation. The pentagonal ring consists of 1 N, 1 S, and 3 C atoms. N with a positive charge occupies the first position, which is the top left vertex. S occupies the third position, which is the top right vertex. C 1 occupies the topmost vertex. A double bond is present between N and C 1, and C 2 and C 3. C 1 is single bonded to H above. C 3 is single bonded to C H 3 on the lower left. C 2 is single bonded to a 2-carbon alkane chain depicted as a single line. C 2 of this alkane chain is single bonded to a zigzag chain composed of O, single bond, P, single bond, O, single bond, P. P 1 is partially double bonded to O on the lower left and O on the lower right. The O atoms have a negative charge. P 2 is partially double bonded to O on

the upper right, O on the lower left, O on the lower right. The O atoms have an overall negative charge of 2 minus.

The structure of lipoic acid is as follows: A 5-membered heterocyclic pentagonal ring is in a horizontal orientation and consists of 2 S and 3 C atoms. First S occupies the first position, which is the bottom left vertex. Second S occupies the second position, which is the top left vertex. C 1 occupies the top right vertex. C 3 is wedge bonded to H on the lower left and dash bonded to C 1 of a 5-carbon alkane chain depicted as a line structure using 4 zigzag lines. C 5 is double bonded to O below and single bonded to O H on the upper right.

Return to Structure of thiamine pyrophosphate (T P P) and lipoic acid

Extended description for Stepwise conversion pyruvate to acetyl C o A



The reaction consists of 3 steps labeled decarboxylation, oxidation, and transfer to C o A.

In the decarboxylation step, pyruvate is converted into the first intermediate with the simultaneous release of C O 2. The structure of pyruvate is as follows: A central C atom is single bonded to C H 3 on the lower left, double bonded to O above, and single bonded to C on the lower right. The lower right C atom is partially double bonded to O on the upper right and O below. These O atoms have an overall negative charge. The structure of the first intermediate is as follows: A central C atom with a negative charge is double bonded to O above and single bonded to C H 3 on the lower left.

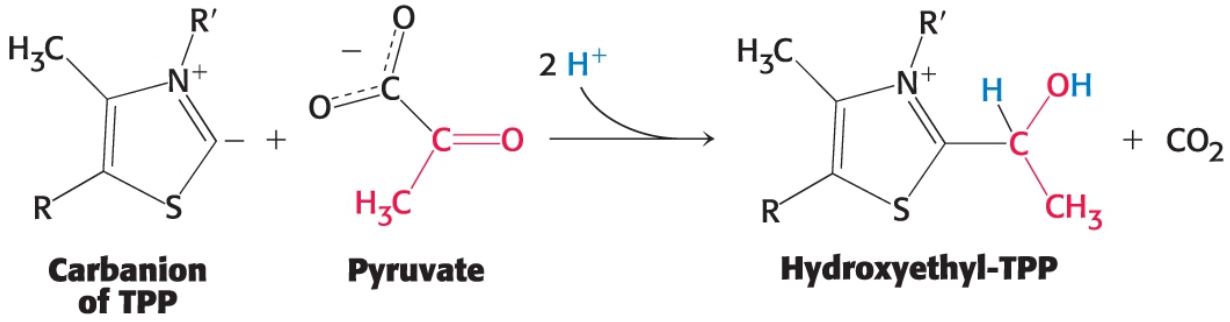
In the oxidation step, the first intermediate is converted into the second intermediate with the simultaneous release of 2 electrons.

The structure of the second intermediate is as follows: A central C atom with a positive charge is double bonded to O above and single bonded to C H 3 on the lower left. In the transfer to C o A step, the second intermediate is converted into acetyl C o A with the simultaneous entry of C o A.

The structure of acetyl C o A is as follows: A central C atom is double bonded to O above, single bonded to C H 3 on the lower left, and single bonded to S, single bond, C o A on the lower right.

Return to Stepwise conversion pyruvate to acetyl C o A

Extended description for Formation of hydroxyethyl-T P P



The chemical reaction consists of two reactants and two products. The reactants are carbanion of T P P and pyruvate. The products are hydroxyethyl-T P P and C O 2.

The structure of the carbanion of T P P is as follows: A 5-membered heterocyclic pentagonal ring is in the horizontal orientation and contains 1 N, 1 S, and 3 C atoms. N atom has a positive charge and occupies the first position, which is the top right vertex. S occupies the third position, which is the bottom right vertex. C 1 has a negative charge and occupies the rightmost vertex. A double bond is present between N and C 1 and C 2 and C 3. N is single bonded to R dash above. C 2 is single bonded to R on the lower left. C 3 is single bonded to C H 3 on the upper left.

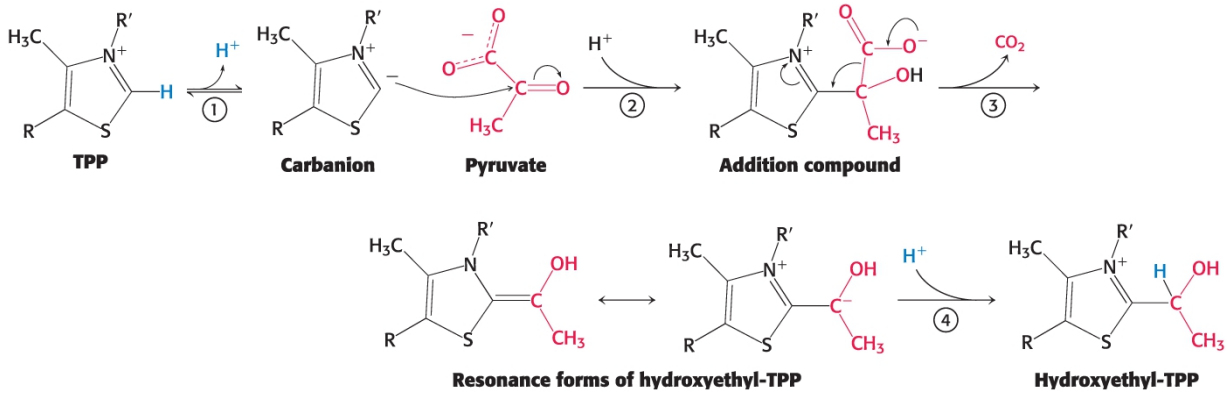
The structure of pyruvate is as follows: A central C atom is single bonded to C on the upper left, double bonded to O on the right, and single bonded to C H 3 on the lower right. The upper left C atom is partially double bonded to O on the upper right and lower left. The O atoms have an overall negative charge.

A forward arrow leads to the products. 2 H superscript plus ions enter the reaction.

The structure of hydroxyethyl-T P P is as follows: A 5-membered heterocyclic pentagonal ring is in a horizontal orientation and consists of 1 N, 1 S, and 3 C atoms. The N atom has a positive charge and occupies the first position, which is the top right vertex. S occupies the third position, which is the bottom right vertex. C 1 occupies the rightmost vertex. A double bond is present between N and C 1 and C 2 and C 3. N is single bonded to R dash above. C 1 is single bonded to C on the right. This C is single bonded to O H on the upper right, H on the upper left, and C H 3 on the lower right. C 2 is single bonded to R on the lower left. C 3 is single bonded to C H 3 on the upper left.

Return to Formation of hydroxyethyl-T P P

Extended description for Mechanism of E 1 decarboxylation reaction



The mechanism is divided into 4 main steps. The first step is reversible and the remaining steps are irreversible.

The structure of T P P is as follows: A 5-membered heterocyclic pentagonal ring is in the horizontal orientation and contains 1 N, 1 S, and 3 C atoms. N atom has a positive charge and occupies the first position, which is the top right vertex. S occupies the third position, which is the bottom right vertex. C 1 occupies the rightmost vertex. It is single bonded to H on the right. A double bond is present between N and C 1 and C 2 and C 3. N is single bonded to R dash above. C 2 is single bonded to R on the lower left. C 3 is single bonded to C H 3 on the upper left.

A reversible reaction arrow labeled 1 shows the carbanion. An upward pointing arrow above it shows the release of H superscript plus ion.

The structure of the carbanion is as follows: A 5-membered heterocyclic pentagonal ring is in the horizontal orientation and contains 1 N, 1 S, and 3 C atoms. N atom has a positive charge and

occupies the first position, which is the top right vertex. S occupies the third position, which is the bottom right vertex. C 1 has a negative charge and occupies the rightmost vertex. A double bond is present between N and C 1 and C 2 and C 3. N is single bonded to R dash above. C 2 is single bonded to R on the lower left. C 3 is single bonded to C H 3 on the upper left.

A pyruvate molecule is shown adjacent to the carbanion.

The structure of the pyruvate molecule is as follows: A central C atom is single bonded to C on the upper left, double bonded to O on the right, and single bonded to C H 3 on the lower right. The upper left C atom is partially double bonded to O on the upper right and lower left. These O atoms have an overall negative charge.

An arrow points from negatively charged C 1 of carbanion to the central C atom of pyruvate.

Another arrow points from the double bond between the central C and O of the pyruvate molecule toward the O atom.

A forward reaction arrow labeled 2 shows the addition compound. An H superscript plus ion also enters the reaction.

The structure of the addition compound is as follows: A 5-membered heterocyclic pentagonal ring is in the horizontal orientation and contains 1 N, 1 S, and 3 C atoms. N atom has a positive charge and occupies the first position, which is the top right vertex. S occupies the third position, which is the bottom right vertex. C 1 occupies the rightmost vertex. A double bond is present between N and C 1 and C 2 and C 3. N is single bonded to R dash above. C 2 is single bonded to R on the lower left. C 3 is single bonded to C H 3 on the upper left. C 1 is single bonded to C on the

right. This C atom is single bonded to C above, O H on the upper right, and C H 3 below. The C atom above is double bonded to O on the upper right and single bonded to O superscript minus on the right.

An arrow points from O superscript minus toward its single bond with the C atom located above. A second arrow points from the single bond between the C atom above and the right C atom bonded to C 1 toward the single bond between C 1 and the right C atom. A third arrow points from the double bond between the C 1 and N atom of the ring toward the N atom.

A forward arrow labeled 3 shows the resonance forms of hydroxyethyl-T P P. An upward arrow above it shows the release of C O 2.

The structures of the resonance forms are as follows:

First form: A 5-membered heterocyclic pentagonal ring is in a horizontal orientation and consists of 1 N, 1 S, and 3 C atoms. The N atom occupies the first position, which is the top right vertex. S occupies the third position, which is the bottom right vertex. C 1 occupies the rightmost vertex. A double bond is present between C 2 and C 3. N is single bonded to R dash above. C 1 is double bonded to C on the right. This C is single bonded to O H on the upper right and C H 3 on the lower right. C 2 is single bonded to R on the lower left. C 3 is single bonded to C H 3 on the upper left.

Second form: A 5-membered heterocyclic pentagonal ring is in a horizontal orientation and consists of 1 N, 1 S, and 3 C atoms. The N atom has a positive charge and occupies the first position, which is the top right vertex. S occupies the third position, which is the bottom right vertex. C 1 occupies the rightmost vertex. A double

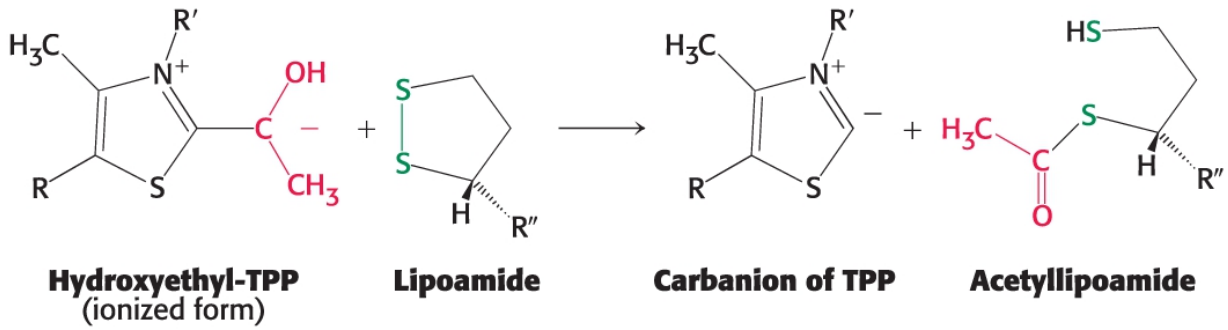
bond is present between N and C 1 and C 2 and C 3. N is single bonded to R dash above. C 1 is single bonded to C having a negative charge on the right. This C is single bonded to O H on the upper right and C H 3 on the lower right. C 2 is single bonded to R on the lower left. C 3 is single bonded to C H 3 on the upper left.

A forward reaction arrow labeled 4 shows the hydroxyethyl-T P P. An H superscript plus ion also enters the reaction.

The structure of hydroxyethyl-T P P is as follows: A 5-membered heterocyclic pentagonal ring is in a horizontal orientation and consists of 1 N, 1 S, and 3 C atoms. The N atom has a positive charge and occupies the first position, which is the top right vertex. S occupies the third position, which is the bottom right vertex. C 1 occupies the rightmost vertex. A double bond is present between N and C 1 and C 2 and C 3. N is single bonded to R dash above. C 1 is single bonded to C on the right. This C is single bonded to O H on the upper right, H on the upper left, and C H 3 on the lower right. C 2 is single bonded to R on the lower left. C 3 is single bonded to C H 3 on the upper left.

Return to Mechanism of E 1 decarboxylation reaction

Extended description for Oxidation of hydroxyethyl-T P P



The hydroxyethyl T P P (ionized form) reacts with lipoamide to give rise to the carbanion of T P P and acetyllipoamide.

The structure of hydroxyethyl T P P (ionized form) is as follows: A 5-membered heterocyclic pentagonal ring is in a horizontal orientation and consists of 1 N, 1 S, and 3 C atoms. The N atom has a positive charge and occupies the first position, which is the top right vertex. S occupies the third position, which is the bottom right vertex. C 1 occupies the rightmost vertex. A double bond is present between N and C 1 and C 2 and C 3. N is single bonded to R dash above. C 1 is single bonded to C on the right. This C is single bonded to O H on the upper right and C H 3 on the lower right. C 2 is single bonded to R on the lower left. C 3 is single bonded to C H 3 on the upper left.

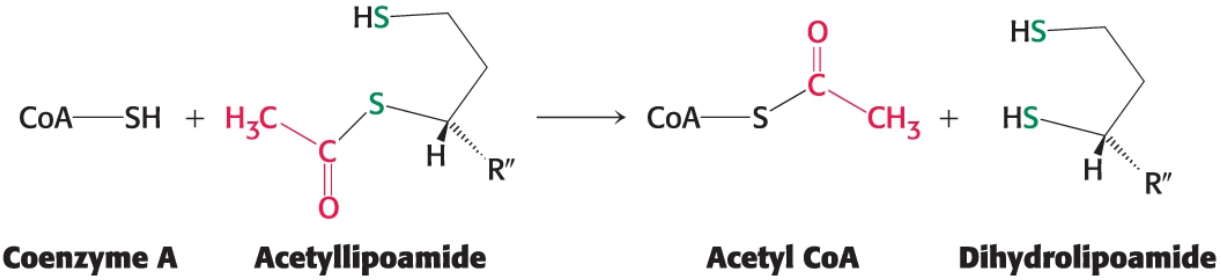
The structure of lipoamide is as follows: A 5-membered heterocyclic pentagonal ring is in a horizontal orientation and consists of 2 S and 3 C atoms. S 1 occupies the first position, which is the bottom left vertex. S 2 occupies the second position, which is the top right vertex. C 3 is wedge bonded to H on the lower left and dash bonded to R double dash on the lower right.

The structure of the carbanion of T P P is as follows: A 5-membered heterocyclic pentagonal ring is in the horizontal orientation and contains 1 N, 1 S, and 3 C atoms. N atom has a positive charge and occupies the first position, which is the top right vertex. S occupies the third position, which is the bottom right vertex. C 1 has a negative charge and occupies the rightmost vertex. A double bond is present between N and C 1 and C 2 and C 3. N is single bonded to R dash above. C 2 is single bonded to R on the lower left. C 3 is single bonded to C H 3 on the upper left.

The structure of acetyllipoamide is as follows: A 3-carbon alkane chain is depicted as a vertical line structure using 2 zigzag lines. C 1 is single bonded to S H on the left. C 3 is single bonded to S on the left. C 3 is also wedge bonded to H on the lower left and dash bonded to R double dash on the lower right. The S atom on left is single-bonded to C on the lower left. This C is single bonded to C H 3 on the upper left and double bonded to O below.

Return to Oxidation of hydroxyethyl-T P P

Extended description for Formation of acetyl C o A



The reaction consists of two reactants and two products. The reactants are coenzyme A and acetyllipoamide. The products are acetyl C o A and dihydrolipoamide.

The structure of coenzyme A is as follows: C o A, single bond, S H.

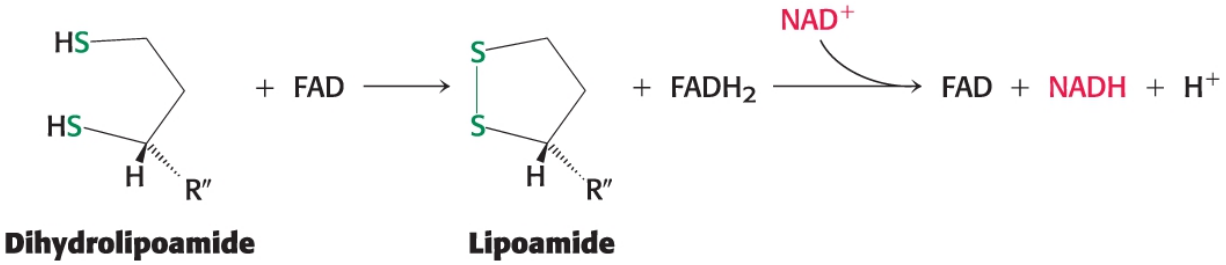
The structure of acetyllipoamide is as follows: A 3-carbon alkane chain is depicted as a vertical line structure using 2 zigzag lines. C 1 is single bonded to S H on the left. C 3 is single bonded to S on the left. C 3 is also wedge bonded to H on the lower left and dash bonded to R double dash on the lower right. The S atom is single bonded to C on the lower left. This C is single bonded to C H 3 on the upper left and double bonded to O below.

The structure of acetyl C o A is as follows: A central C atom is single bonded to C H 3 on the lower left, double bonded to O above, and single bonded to S, single bond, C o A on the lower left.

The structure of dihydrolipoamide is as follows: A 3-carbon alkane chain is depicted as a vertical line structure using 2 zigzag lines. C 1 and C 3 are each single bonded to S H on the left. C 3 is wedge bonded to H on the lower left and dash bonded to R double dash on the lower right.

Return to Formation of acetyl C o A

Extended description for Regeneration of oxidized lipoamide



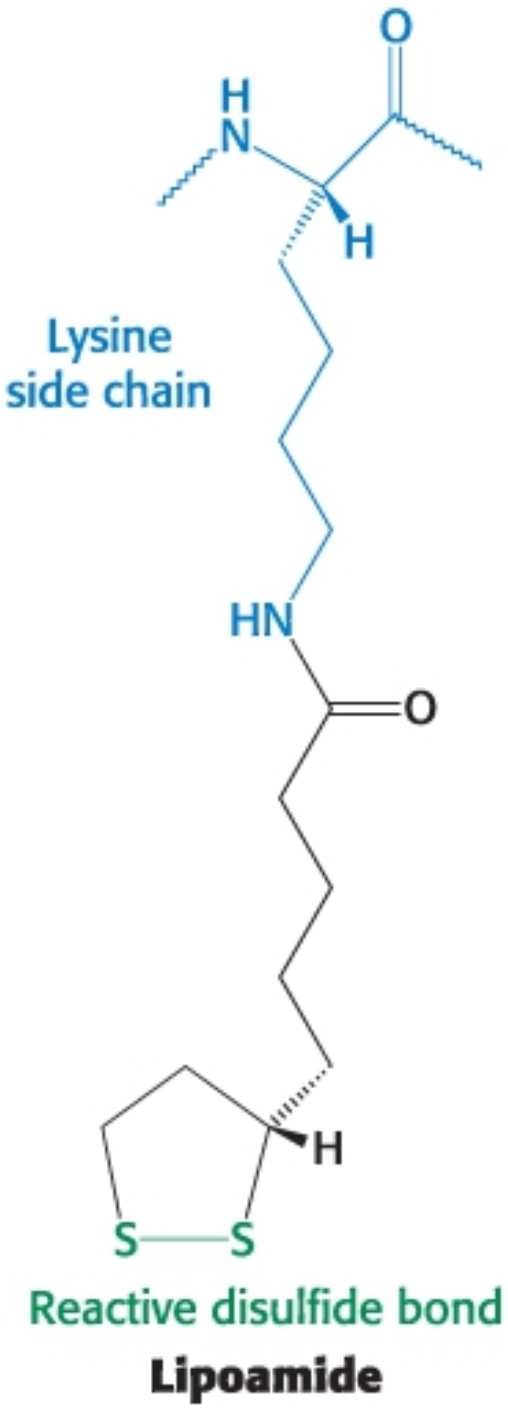
Dihydrolipoamide reacts with F A D to give rise to lipoamide. Lipoamide reacts with F A D H 2 in the presence of N A D superscript plus to give rise to F A D plus N A D H plus H superscript plus.

The structure of dihydrolipoamide is as follows: A 3-carbon alkane chain is depicted as a line structure using 2 zigzag lines vertically. C 1 and C 3 are each single bonded to S H on the left. C 3 is wedge bonded to H on the lower left and dash bonded to R double dash on the lower right.

The structure of lipoamide is as follows: A 5-membered heterocyclic pentagonal ring is in a horizontal orientation and consists of 2 S and 3 C atoms. S 1 occupies the first position, which is the bottom left vertex. S 2 occupies the second position, which is the top left vertex. C 1 occupies the top right vertex. C 3 is wedge bonded to H on the lower left and dash bonded to R double dash on the lower right.

Return to Regeneration of oxidized lipoamide

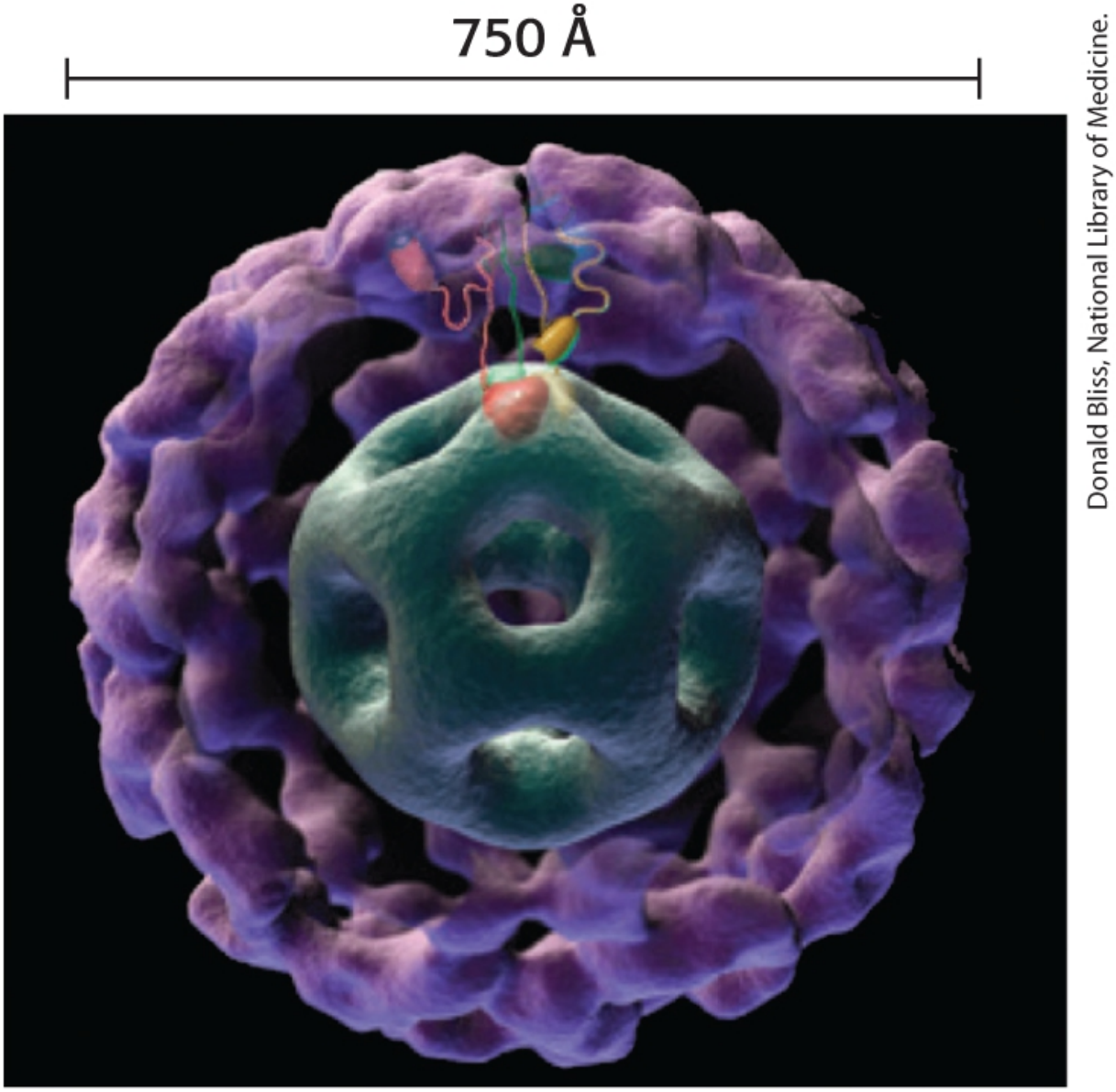
Extended description for Structure of lipoamide



The structure of lipoamide is as follows: A 5-membered heterocyclic pentagonal ring is in a vertical orientation and consists of 2 S and 3 C atoms. First S occupies the first position, which is the bottom right vertex. Second S occupies the second position, which is the bottom left vertex. C 1 occupies the top left vertex. C 3 is wedge bonded to H on the lower right and dash bonded to C 1 of a 1 N and 9 C heteronuclear alkane chain depicted as a vertical line structure using 9 zigzag lines. N bound to H occupies the sixth position. C 5 is double bonded to O on the right. C 9 is dash bonded to C 2 of a 1 N and 4 C heteronuclear alkane chain depicted as a horizontal line structure using 4 zigzag lines. N bound to H occupies the second position. C 2 is wedge bonded to H on the lower right. C 3 is double bonded to O above.

Return to Structure of lipoamide

Extended description for Photograph of bacterial pyruvate dehydrogenase complex



Donald Bliss, National Library of Medicine.

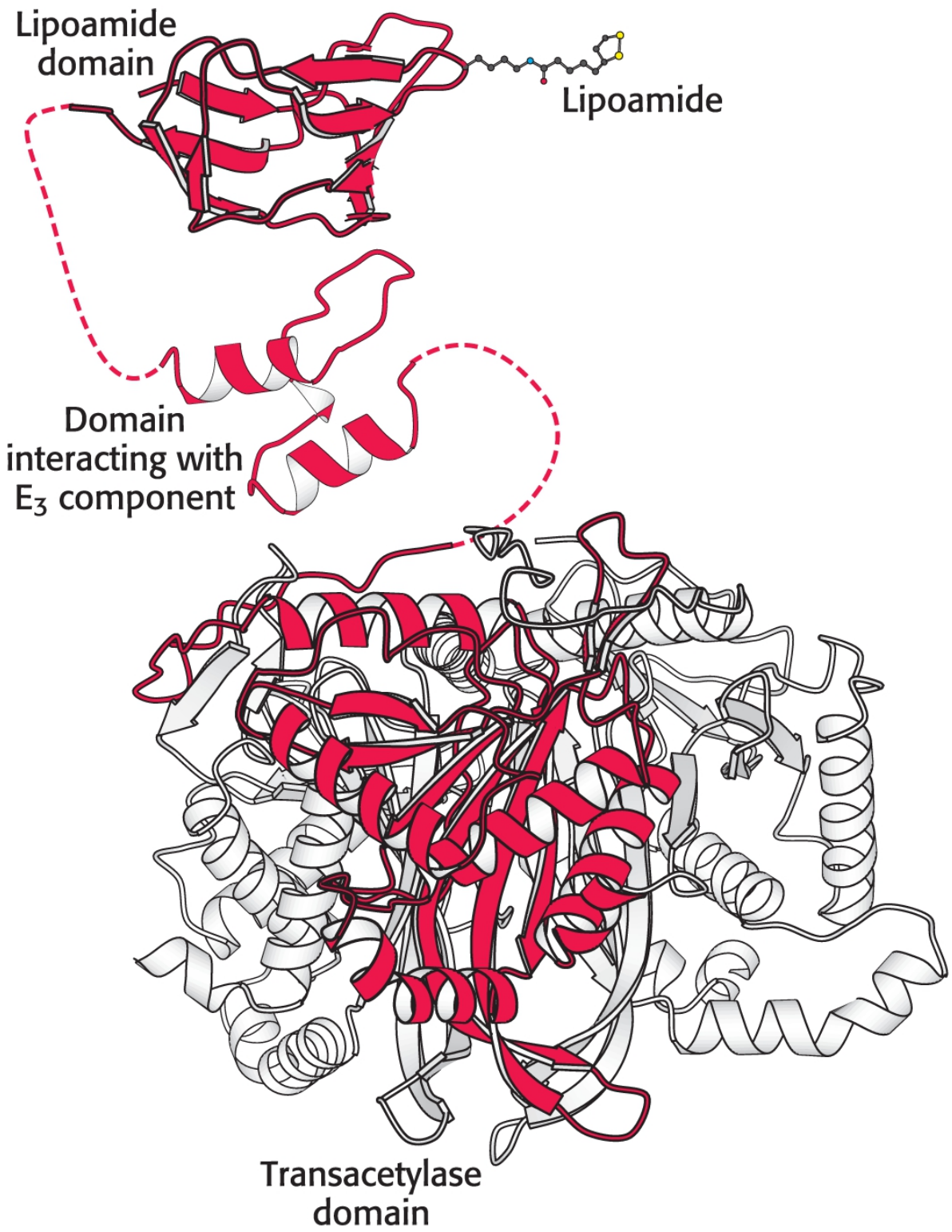
The pyruvate dehydrogenase complex consists of an inner core having several large-sized pores. The inner core is made up of the E 2 enzyme. It is surrounded by a shell composed of E 1 and E 3 enzymes. The diameter of the entire complex is 750 angstrom. Two

lipoamide arms are shown in red and yellow extending from the inner core to the shell.

Return to Photograph of bacterial pyruvate dehydrogenase complex

Extended description for Ribbon diagram of a subunit

of the transacetylase trimer

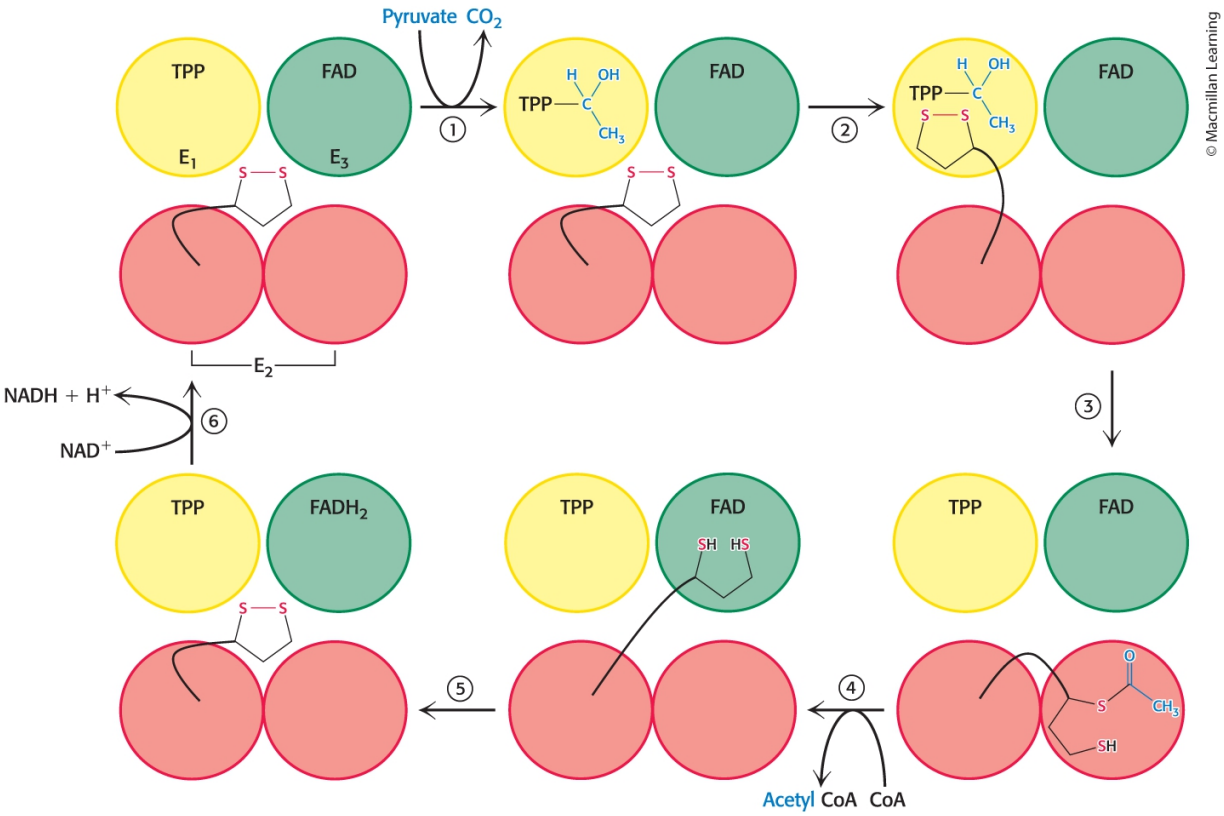


© Macmillan Learning

The ribbon diagram is composed of three domains labeled lipoamide domain, domain interacting with E 3 component, and transacetylase domain from top to bottom. The lipoamide domain is a very small cluster composed of beta-strands interconnected by long thread-like loops. A loop extending on the right is connected to a ball-and-stick model of lipoamide. A thread emerging from the left end of this domain is connected to the domain interacting with the E 3 component in the middle through a dashed-red line. This middle domain is composed of two short alpha-helices interconnected by long loops. A short thread emerging from the right end of the middle domain is connected to the transacetylase domain at the bottom through a dashed red line. The transacetylase domain is a large cluster composed of several randomly oriented alpha helices and beta-strands interconnected by thread-like loops.

Return to Ribbon diagram of a subunit of the transacetylase trimer

Extended description for Activity of pyruvate dehydrogenase complex



The activity of the pyruvate dehydrogenase complex is divided into 6 steps. The complex consists of two joined red circles labeled E 2. A yellow circle and green circle are located above the joined circles on the top left and top right respectively. The yellow circle is labeled E 1 and is bound to T P P. The green circle is labeled E 3 and is bound to F A D. A curved line from the left red sphere is connected to C 3 of a 5-membered heterocyclic pentagonal ring located in the center of the complex. The ring contains 2 S and 3 C atoms. First S occupies the first position, which is the top left vertex. Second S occupies the second position, which is the top right vertex.

A forward arrow labeled 1 lead to the complex bound to pyruvate. A curved arrow above it shows the entry of pyruvate and the release of C O 2.

T P P of E 1 subunit is single bonded to a central C atom. This C atom is single bonded to H on the upper left, O H on the upper right, C H 3 on the lower right.

A forward arrow labeled 2 leads to the next configuration of the complex. The pentagonal ring bound the E 2 subunit is located inside E 1 subunit.

A forward arrow labeled 3 shows the next configuration of the complex. The E 1 and E 3 subunits are bound to T P P and F A D respectively. The partially open pentagonal ring of E 2 is located inside the right red circle. The single bond between the S atoms is broken. S 1 is single bonded to C on the upper right. This C is double bonded to O above and single bonded to C H 3 on the lower right. S 2 is bound to H.

A forward arrow labeled 4 shows the next configuration of the complex. A curved arrow below it shows the conversion of C o A to acetyl C o A.

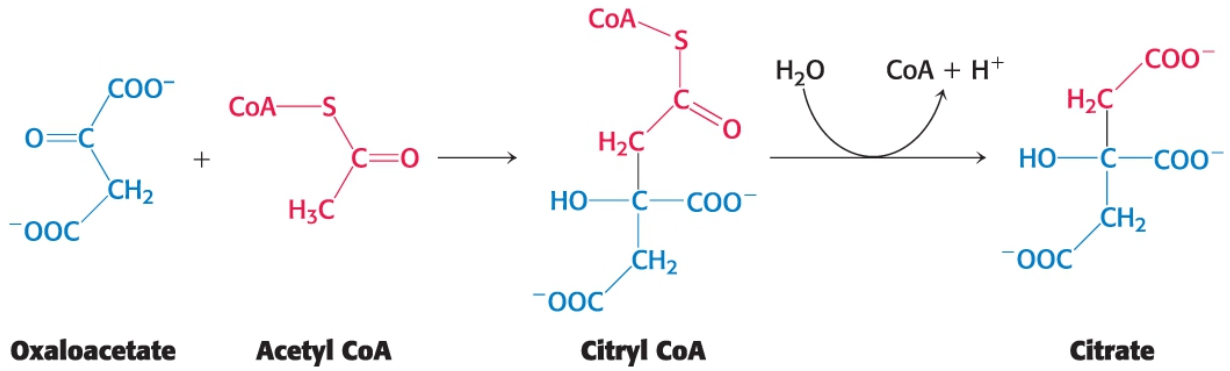
The partially open ring of the right red circle is located inside E 3 subunit. Both the S atoms are bound to H and are located at the top left and top right.

A forward arrow labeled 5 leads to the next configuration of the complex. The pentagonal ring is closed as the single bond between the S atoms is reformed. It is located in the center of the complex.

A forward arrow labeled 6 leads to the initial configuration of the complex. A curved arrow on its left shows the simultaneous reduction of N A D superscript plus to N A D H plus H superscript plus.

Return to Activity of pyruvate dehydrogenase complex

Extended description for Formation of citrate from oxaloacetate



The reaction consists of two reactants, one intermediate, and one product.

The first reactant is oxaloacetate whose structure is as follows: A central C atom is single bonded to C O O superscript minus on the upper right, double bonded to O on the left, single bonded to C H 2 on the lower right. This C H 2 is further single bonded to C O O superscript minus on the lower left.

The second reactant is acetyl C o A whose structure is as follows: A central C atom is single bonded to S, single bond, C o A on the upper left, double bonded to O on the right, and single bonded C H 3 on the lower left.

A forward reaction arrow leads to the intermediate citryl C o A.

The structure of citryl C o A is as follows: C H 2, single bond, C, single bond, C H 2. C 1 is single bonded to C, single bond, S on the upper right. The S atom is single bonded to C o A on the upper left. The C atom is double bonded to O on the lower right. C 2 of the main

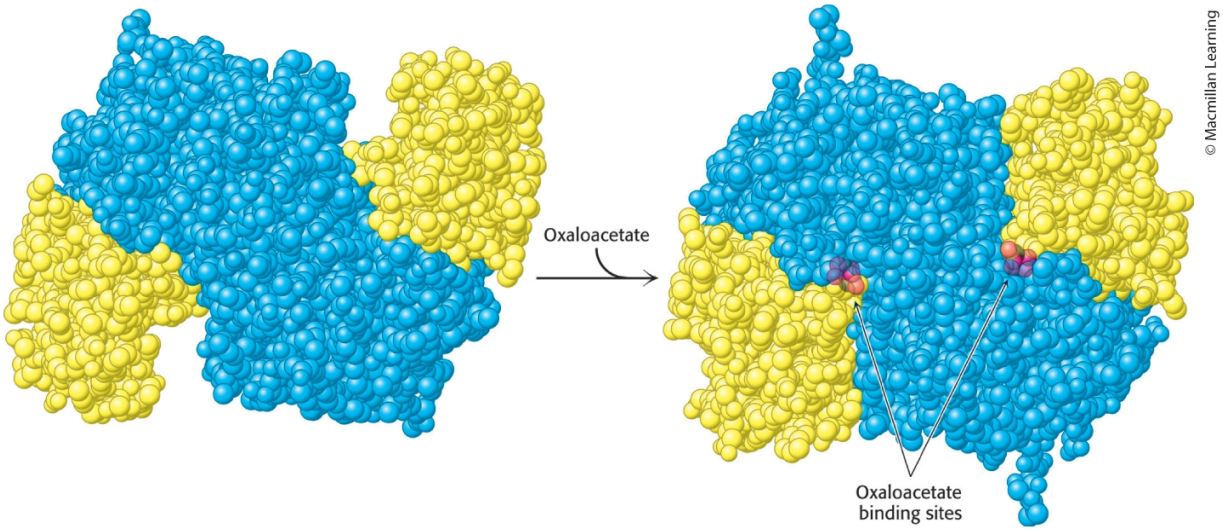
chain is single bonded to O H on the left and C O O superscript minus on the right. C 3 is single bonded to C O O superscript minus on the lower left.

A forward arrow leads to the product citrate. A curved arrow above it shows the simultaneous entry of H 2 O and exit of C o A plus H superscript plus.

The structure of citrate is as follows: C H 2, single bond, C, single bond, C H 2. C 1 is single bonded to C O O superscript minus on the upper right. C 2 is single bonded to O H on the left and single bonded to C O O superscript minus on the right. C 3 is single bonded to C O O superscript minus on the lower left.

Return to Formation of citrate from oxaloacetate

Extended description for Space filling model shows the binding of oxaloacetate to citrate synthesis

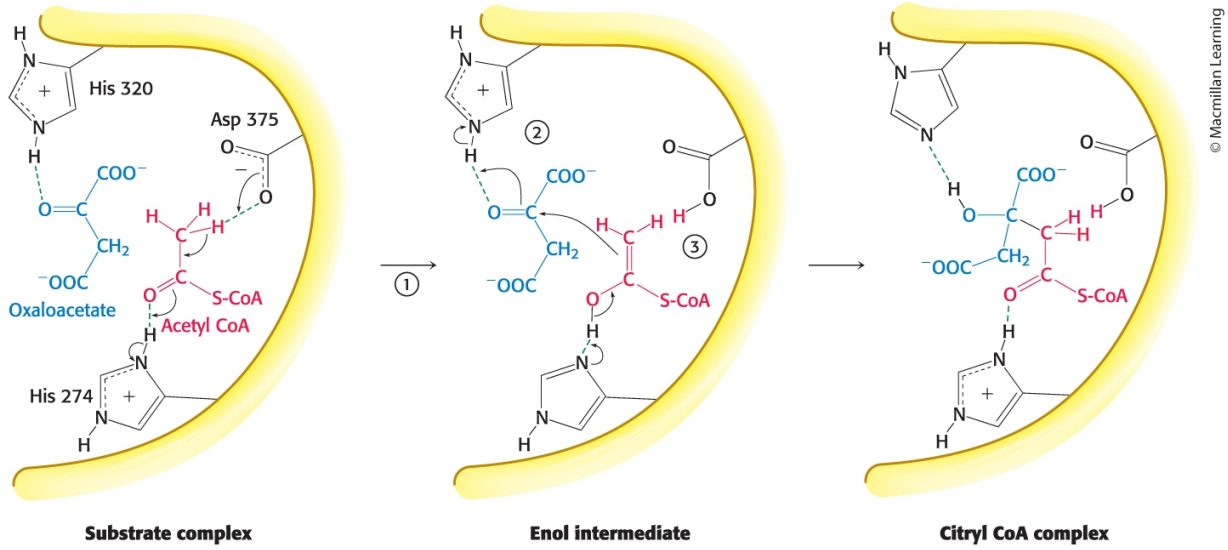


The space-filling model of citrate synthase consists of two domains. The small domain is shown as a cluster of yellow spheres. The large domain is shown as a cluster of blue spheres. The large domain is shown in the middle in a diagonal orientation. Its top left and bottom right regions are bound the small domain.

A forward arrow shows the enzyme bound to oxaloacetate. The large domain in diagonal orientation has a deep indentation on the mid left and mid right ends. These indented grooves are bound to small domains. The oxaloacetate binding sites are located in these grooves of large domain where it joins with the small domains. A few blue spheres extend upward and downward from the top and bottom ends of the large domain.

Return to Space filling model shows the binding of oxaloacetate to citrate synthesis

Extended description for Citrate synthase mechanism



The enzyme active site is depicted as a curved groove outlined with an orange line having a yellow highlight. The groove is open on the left. Its active site contains a side chain of H i s 320, A s p 375, and H i s 274 from top to bottom.

The side chain of H i s 320 and H i s 274 are as follows: A 5-membered heterocyclic pentagonal ring consists of 2 N and 3 C atoms. The first N occupies the first position, which is the bottom left vertex. The second N occupies the third position, which is the topmost vertex. Both N atoms are single-bonded to H. A partial double bond is present between C 1 and N 1 and C 1 and N 2. A double bond is present between C 2 and C 3. The ring has a plus symbol in the middle.

The side chain of A s p 375 is as follows: A central C is partially double bonded to O on the upper left and O on the lower left. The O atom has an overall negative charge.

The mechanism shows three complexes labeled substrate complex, enol intermediate, and citryl C o A complex.

The substrate complex is depicted as follows:

The oxaloacetate and acetyl-C o A molecule are shown inside the active site.

The structure of oxaloacetate is as follows: A central C atom is single bonded to C O O superscript minus on the upper right, double bonded to O on the left, and single bonded to C H 2 on the lower right. This C H 2 group is single bonded to C O O superscript minus on the lower left.

The O atom double bonded to the central C is further hydrogen bonded to the H atom bonded to N 1 of H i s 320 ring.

The structure of acetyl-C o A is as follows: C, single bond, C. C 1 is single bonded to H on the upper left, upper right, and right. C 2 is double bonded to O on the lower left and S, single bond, C o A on the lower right.

An arrow from the partial double bond between C and the lower left O atom of A s p 375 points toward the hydrogen bond between right H bonded to C 1 of acetyl C o A and the lower left O atom of the A s p 375 side chain.

A second arrow points from the single bond between this H and C 1 toward the single bond between C 1 and C 2 of acetyl C o A.

A third arrow points from the double bond between C 2 and O of acetyl C o A toward the hydrogen bond between this O and H atom bonded to N 2 of H i s 274 ring.

A forward arrow labeled 1 shows the enol intermediate which is depicted as follows:

The lower left O of A s p 375 is single bonded to H.

The structure of the intermediate product is as follows: C, double bond, C. C 1 is single bonded to H on the upper left and H on the upper right. C 2 is single bonded to O on the lower left and single bonded to S, single bond, C o A on the lower right. The lower left O is single bonded to H below.

N 2 of the H i s 274 ring is hydrogen bonded to H which is single bonded to the lower left O of the intermediate.

An arrow from N 2 points toward the hydrogen-bonded H atom.

A second arrow from the single bond between this H and lower left O of the intermediate points toward the single bond between this O and C 2 of the intermediate.

A third arrow points from the double bond between C 1 and C 2 of the intermediate toward the central C atom of oxaloacetate.

A fourth arrow points from this central C atom toward the hydrogen bond between H bonded to N 1 of H i s 320 ring and O double bonded to the central C.

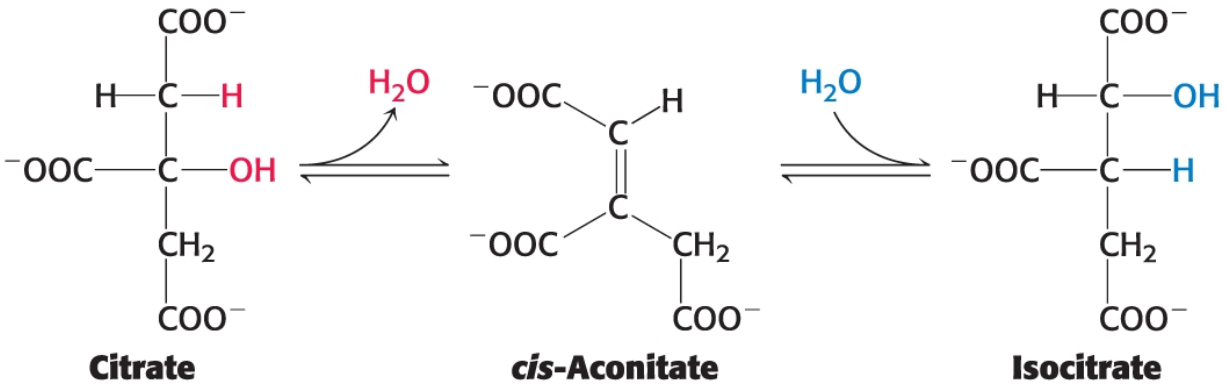
A fifth arrow points from the single bond between this H and N 1 toward N 1 of H i s 320 ring.

A forward arrow leads to the citryl C o A complex.

The central C atom of oxaloacetate and C 1 of the intermediate become single-bonded to each other. The central C is single bonded to O, single bond, H on the left. This H is hydrogen bonded to N 1 of H i s 320 ring.

Return to Citrate synthase mechanism

Extended description for Conversion of citrate to isocitrate



The conversion of citrate to isocitrate takes place in two reversible steps.

In the first step, citrate is reversibly converted into cis-aconitate. The structure of citrate is as follows: C O O superscript minus, single bond, C, single bond, C, single bond, C H 2, single bond, C O O superscript minus. C 2 is single bonded to H on the left and H on the right highlighted in red. C 3 is single bonded to C O O superscript minus on the left and O H on the right highlighted in red.

A reversible reaction arrow leads to cis-aconitate. An upward arrow above it shows the release of H 2 O highlighted in red.

The structure of cis-aconitate is as follows: A central C atom is double bonded to C above, single bonded to C O O superscript minus on the lower left, and single bonded to C H 2 on the lower right. This C H 2 group is single bonded to C O O superscript minus below. The C atom above is single bonded to C O O superscript minus on the upper right and single bonded to H on the upper right.

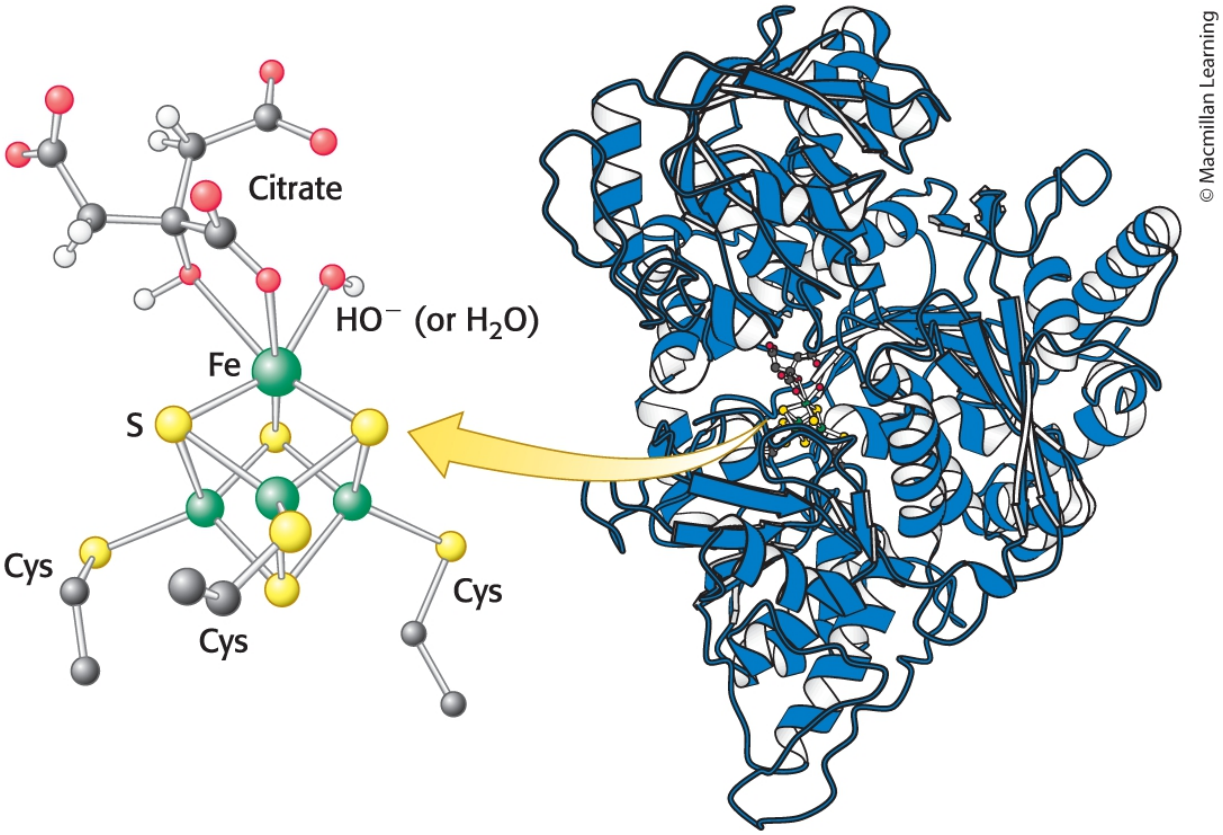
In the second step, cis-aconitate is reversibly converted into isocitrate.

A reversible reaction arrow from cis-aconitate leads to isocitrate. A line labeled H 2 O highlighted in blue is located above the arrow and shows the entry of H 2 O.

The structure of isocitrate is as follows: C O O superscript minus, single bond, C, single bond, C, single bond, C H 2, single bond, C O O superscript minus. C 2 is single bonded to H on the left and O H on the right highlighted in blue. C 3 is single bonded to C O O superscript minus on the left and single bonded to H on the right highlighted in blue.

Return to Conversion of citrate to isocitrate

Extended description for Ribbon diagram of citrate synthase and ball-and-stick model of its iron-sulfur cluster connected to citrate and side chains of amino acids



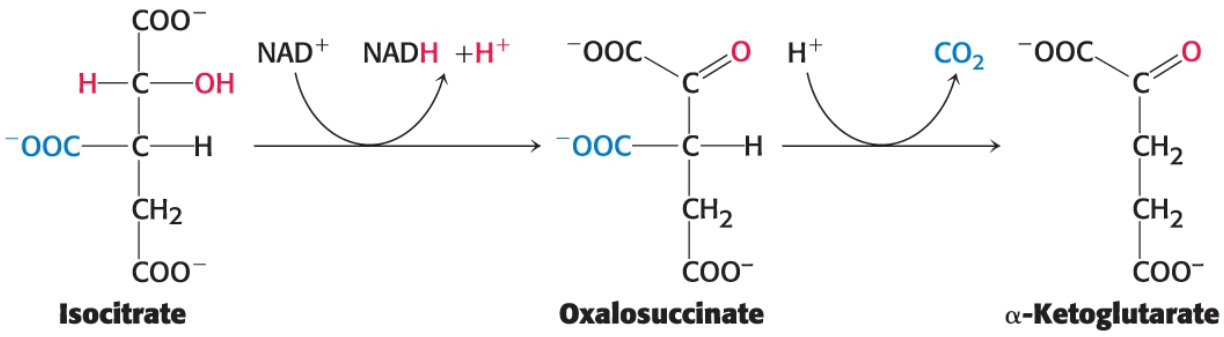
The ribbon diagram consists of several alpha-helices and a few beta-strands interconnected by thread-like loops. A narrow groove in the center is bound to a ball-and-stick model. A magnified view of the ball-and-stick model is shown on the left. It consists of a 4 F e-4 S iron-sulfur cluster connected to citrate above, O H superscript minus or H 2 O on the upper right, and the side chains of cysteine residues located on the lower left, below, and lower right. The 4 F e-4 S cluster consists of a cubical shape in which the vertices are occupied by 4 green and 4 yellow spheres. The green sphere

represents the F e atom. The yellow sphere represents the S atom. 2 green and 2 yellow spheres occupy each face of the cube.

The side chain of cysteine is depicted as a chain of two black spheres and a yellow sphere. The yellow sphere of each cysteine side chain is connected to a separate green sphere of the iron-sulfur cluster. The green sphere located at the top face of the cube, away from the observer, is connected to two red spheres of a citrate molecule and one red sphere of O H superscript minus or H 2 O molecule. The O H superscript minus molecule consists of a red sphere connected to a white sphere. The citrate molecule consists of a chain of 4 black spheres. The first black sphere is connected to two red spheres. The second black sphere is connected to two white spheres. The third black sphere is connected to a red sphere below which is further connected to a white sphere on the left and the green sphere of the iron-sulfur cluster below. The fourth black sphere is connected to a red sphere above and a red sphere below. The red sphere located below is further connected to the same green sphere of the iron-sulfur cluster. The third black sphere is connected to a chain of two black spheres above. In this chain, the first black sphere is connected to two white spheres and the second black sphere is connected to two red spheres.

Return to Ribbon diagram of citrate synthase and ball-and-stick model of its iron-sulfur cluster connected to citrate and side chains of amino acids

Extended description for Conversion of isocitrate to alpha-ketoglutarate



The conversion of isocitrate to alpha-ketoglutarate takes place in two irreversible steps.

In the first step, isocitrate is converted into oxalosuccinate.

The structure of isocitrate is as follows: C O O superscript minus, single bond, C, single bond, C, single bond, C H 2, single bond, C O O superscript minus. C 2 is single bonded to H on the left and O H on the right, both highlighted in red. C 3 is single bonded to C O O superscript minus highlighted in blue on the left and single bonded to H on the right.

A forward arrow leads to oxalosuccinate. A curved arrow above it shows the simultaneous reduction of N A D superscript plus to N A D H plus H superscript plus. H atom of N A D H and H superscript plus are highlighted in red.

The structure of oxalosuccinate is as follows: C, single bond, C, single bond, C H 2, single bond, C O O superscript minus. C 1 is single bonded to C O O superscript minus on the upper left and double bonded to O on the upper right highlighted in red. C 2 is

single bonded to C O O superscript minus on the left highlighted in blue and single bonded to H on the right.

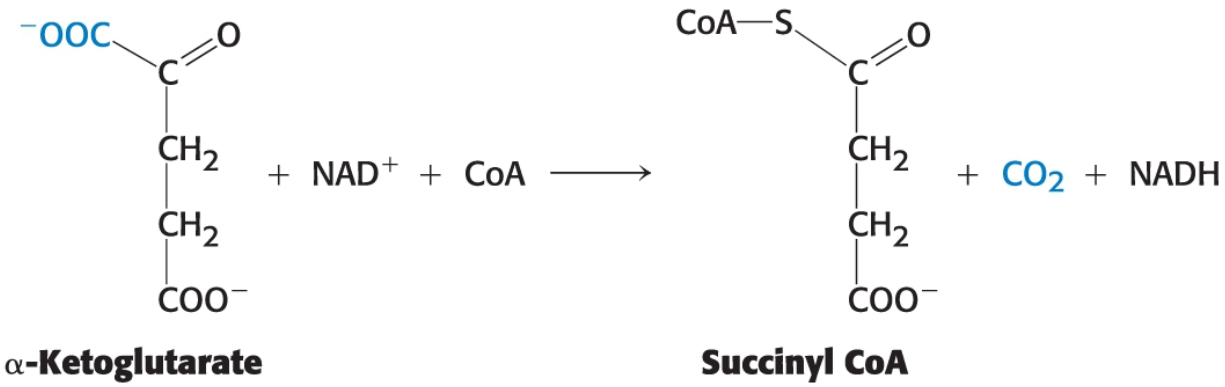
In the second step, oxalosuccinate is converted into alpha-ketoglutarate.

A forward arrow from oxalosuccinate leads to alpha-ketoglutarate. A curved arrow above it shows the entry of H superscript plus and exit of C O 2 highlighted in blue.

The structure of alpha-ketoglutarate is as follows: C, single bond, C H 2, single bond, C H 2, single bond, C O O superscript minus. C 1 is single bonded to C O O superscript minus on the upper left and double bonded to O on the upper right highlighted in red.

Return to Conversion of isocitrate to alpha-ketoglutarate

Extended description for Oxidative decarboxylation of alpha-ketoglutarate



The reaction has 3 reactants and 3 products.

The structure of the first reactant "alpha-ketoglutarate" consists of a vertical chain depicted as follows: C, single bond, C H 2, single bond, C H 2, single bond, C O O superscript minus. C 1 is double-bonded to O on the upper right and single-bonded to C O O superscript minus on the upper left highlighted in blue.

The second reactant is N A D superscript plus.

The third reactant is C o A.

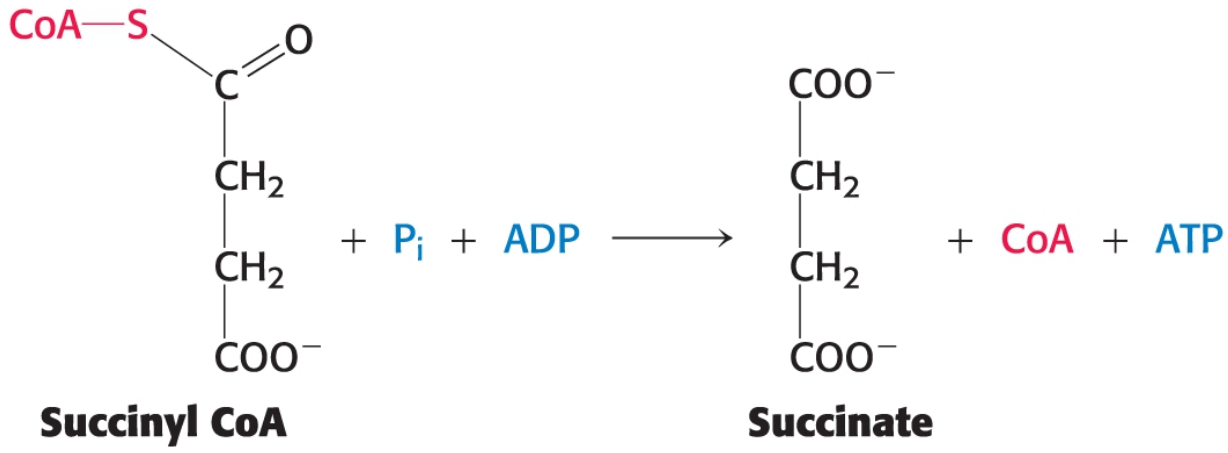
A forward arrow leads to the following three products. The first product "succinyl Co A" has the following vertical chain: C, single bond, C H 2, single bond, C H 2, single bond, C O O superscript minus. C 1 is single bonded to S, single bond, C o A on the upper left, and double bonded to O on the upper right.

The second product is C O 2 highlighted in blue.

The third product is N A D H.

Return to Oxidative decarboxylation of alpha-ketoglutarate

Extended description for Conversion of succinyl C o A into succinate



The reaction has 3 reactants and 3 products.

The first reactant "succinyl C o A" has the following vertical chain: C, single bond, C H 2, single bond, C H 2, single bond, C O O superscript minus. C 1 is single bonded to S, single bond, C o A on the upper left. C 1 is double bonded to O on the upper right.

The second reactant is P subscript i.

The third reactant is A D P.

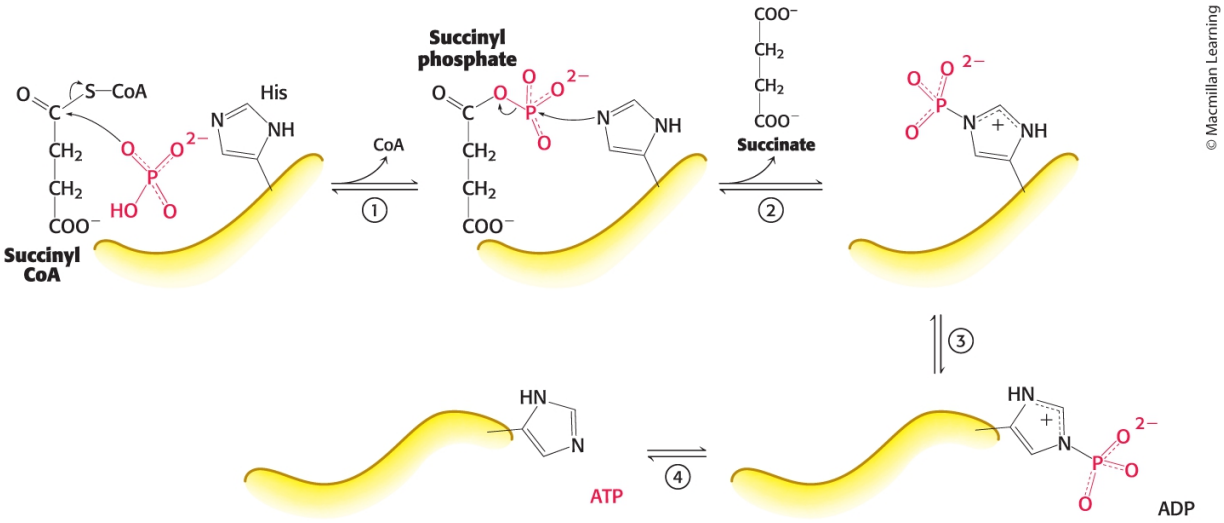
A forward arrow leads to the following three products. The first product "succinate" has the following vertical chain: C O O superscript minus, single bond, C H 2, single bond, C H 2, single bond, C O O superscript minus.

The second product is C o A.

The third product is A T P.

Return to Conversion of succinyl C o A into succinate

Extended description for Mechanism of action of succinyl C o A synthetase



The enzyme active site is depicted as a shallow groove outlined by an orange line with a yellow highlight. The active site contains an H i s side chain whose structure is as follows: A 5-membered heterocyclic pentagonal ring is in a vertical orientation and consists of 2 N and 3 C atoms. The first N occupies the first position, which is the top left vertex. The second N bound to H occupies the third position, which is the top right vertex. A double bond is present between N 1 and C 1, and C 2 and C 3.

A succinyl C o A molecule is also present in the active site. An H P O 4 superscript 2 minus molecule is present between succinyl C o A and the side chain of H i s.

The structure of succinyl C o A is as follows: C, single bond, C H 2, single bond, C H 2, single bond, C O O superscript minus. C 1 is double bonded to O on the upper left and single bonded to S, single bond, C o A on the upper right.

The structure of H P O 4 superscript 2 minus is as follows: A central P atom is partially double bonded to O on the upper left, O superscript 2 minus on the upper right, O on the lower right, and single bonded to O H on the lower left.

An arrow from the upper left O atom of H P O 4 superscript 2 minus molecule points toward C 1 of succinyl C o A. Another arrow points from the single bond between C 1 and S toward the S atom of the succinyl C o A molecule.

A reversible reaction arrow labeled 1 shows the succinyl phosphate molecule in the active site. An upward pointing arrow above it shows the release of C o A.

The structure of succinyl phosphate is as follows: C, single bond, C H 2, single bond, C H 2, single bond, C O O superscript minus. C 1 is double bonded to O on the upper left and single bonded to O on the upper right. This O is single-bonded to a central P atom. The P atom is partially double bonded to O above, O superscript 2 minus on the upper right, and O on the lower right.

An arrow from N 1 of H i s pentagonal ring points toward the central P atom. Another arrow points from the single bond between O and central P atom points toward the O atom directly bonded to C 1 of succinyl phosphate.

A reversible reaction arrow labeled 2 shows the phosphorylated H i s ring. An upward pointing arrow above it shows the release of succinate.

The structure of succinate is as follows: C O O superscript minus, single bond, C H 2, single bond, C H 2, single bond, C O O superscript minus.

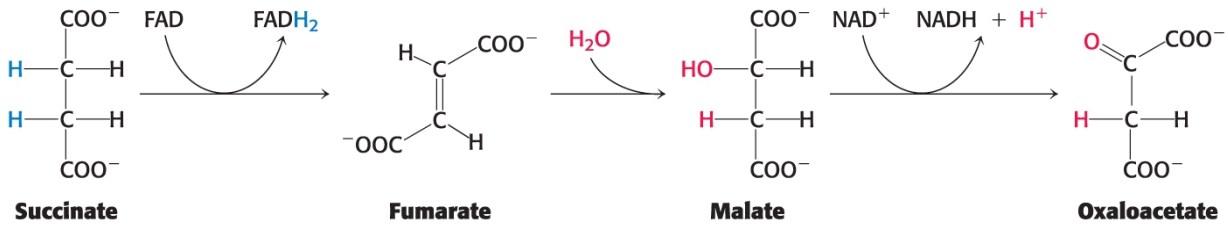
In the active site, N 1 of the H i s pentagonal ring is single bonded to a central P atom. This P is partially double bonded to O on the upper left, O superscript 2 minus above, and O on the lower left. C 1 has an overall positive charge. A partial double bond is present between C 1 and N 1, and C 1 and N 2.

A reversible reaction arrow labeled 3 shows the phosphorylated H i s pentagonal ring oriented toward A D P located in the space outside the active site.

A reversible reaction arrow labeled 4 shows the final product. The A D P molecule outside the active site is converted into A T P. The pentagonal ring of H i s loses the phosphoryl group but it is still oriented toward the outside space.

Return to Mechanism of action of succinyl C o A synthetase

Extended description for Sequential reaction showing conversion of succinate to oxaloacetate



The sequential reaction has one reactant, two intermediates, and one final product.

The structure of the reactant "Succinate" has the following vertical chain: C O O superscript minus, single bond, C, single bond, C, single bond, C O O superscript minus. C 2 and C 3 are each single bonded to H on the left and H on the right. The H atoms on the left are highlighted in blue.

A forward arrow shows the coupled conversion of F A D to F A D H 2 by the curved arrow and leads to the intermediate. H 2 of F A D H 2 is highlighted in blue.

The first intermediate "Fumarate" has the following vertical chain: C, double bond, C. C 1 is single bonded to C O O superscript minus on the upper right and H on the upper left. C 2 is single bonded to C O O superscript minus on the lower left and H on the lower right.

A forward arrow shows the entry of the H 2 O molecule highlighted in red.

The second intermediate "Malate" has the following vertical chain: C O O superscript minus, single bond, C, single bond, C, single bond,

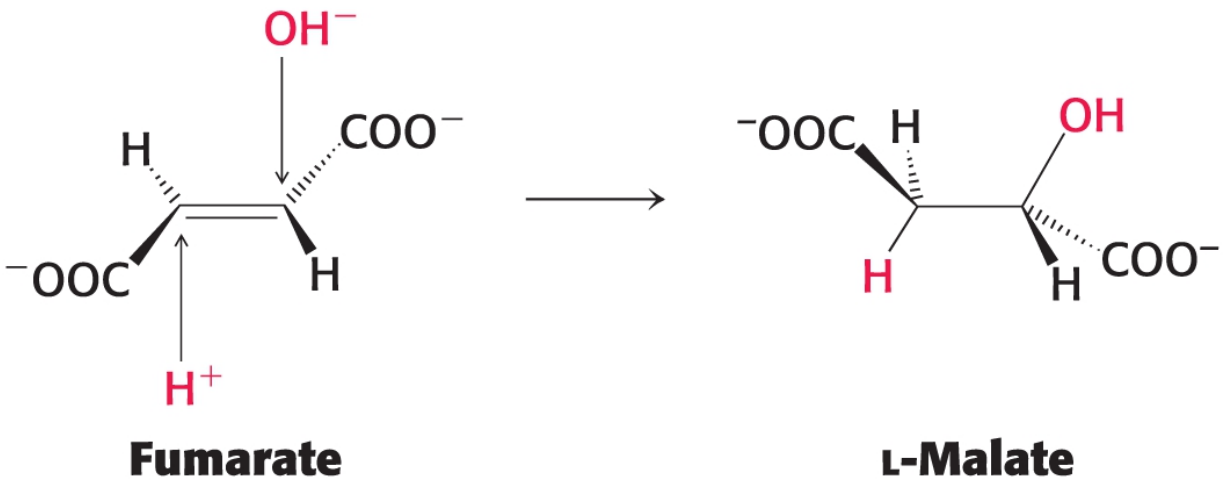
C O O superscript minus. C 2 and C 3 are each single bonded to H on the right. C 2 is single bonded to O H on the left and C 3 is single bonded to H on the left. The O H and H on the left are highlighted in red.

A forward arrow has a curved arrow above that shows coupled conversion of N A D superscript plus into N A D H and H superscript plus highlighted in red.

The final product "Oxaloacetate" has the following vertical chain: C, single bond, C, single bond, C O O superscript minus. C 1 is single bonded to C O O superscript minus on the upper right and double bonded to O on the upper left. C 2 is single bonded to H on the left and H on the right. The H atom on the left is highlighted in red.

Return to Sequential reaction showing conversion of succinate to oxaloacetate

Extended description for Conversion of fumarate into L-malate



The structure Fumarate is depicted as follows: C, double bond, C. C 1 is dash bonded to H on the upper left, and wedge bonded to C O O superscript minus on the lower left. C 2 is dash bonded to C O O superscript minus on the upper right and wedge bonded to H on the lower right.

A downward arrow points from the O H superscript minus to the dash bond between C 2 and C O O superscript minus on the upper right. An upward arrow points from the H superscript plus to the wedge bond between C 1 and C O O superscript minus on the lower left.

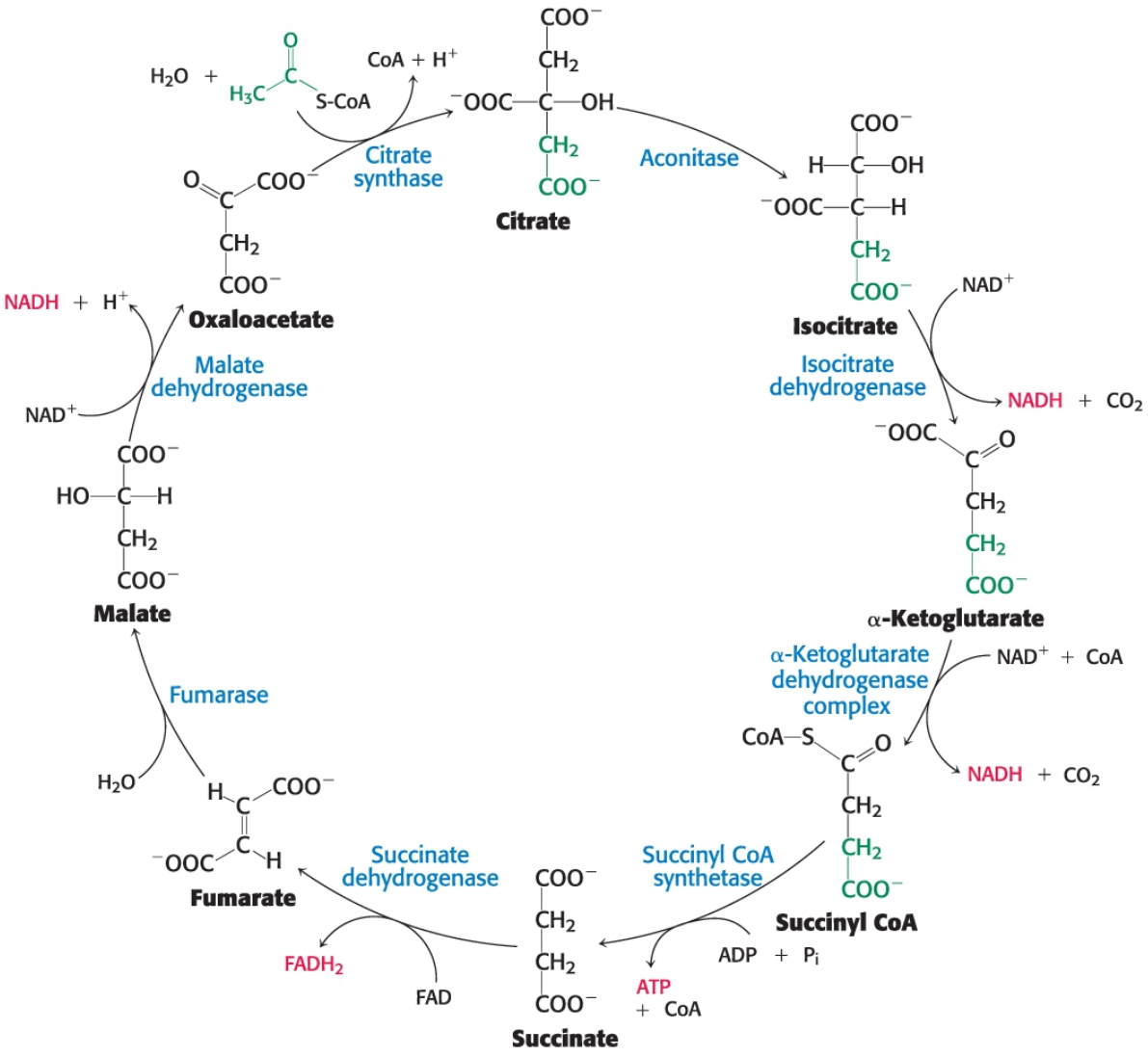
A forward arrow leads to the product.

The structure of L-Malate is depicted as follows: C, double bond, C. C 1 is dash bonded to H above, wedge bonded to C O O superscript minus on the upper left, and single bonded to H on the lower left. C 2 is dash bonded to C O O superscript minus on the lower right,

wedge bonded to H on the lower right, and single bonded to O H on the upper right.

Return to Conversion of fumarate into L-malate

Extended description for Citric acid cycle



The citric acid cycle includes 8 enzyme-catalyzed reactions depicted as follows:

1) Citrate is converted into isocitrate by the aconitase enzyme. The structure of citrate is as follows: C O O superscript minus, single bond, C H 2, single bond, C, single bond, C H 2, single bond, C O O superscript minus. C 3 is single bonded to C O O superscript minus

on the left and single bonded to O H on the right. The structure of isocitrate is as follows: C O O superscript minus, single bond, C, single bond, C, single bond, C H 2, single bond, C O O superscript minus. C 2 is single bonded to H on the left and O H on the right. C 3 is single bonded to C O O superscript minus on the left and single bonded to H.

2) Isocitrate is converted into alpha-ketoglutarate by the isocitrate dehydrogenase enzyme. It involves the reduction of N A D superscript plus to N A D H and the release of C O 2. The structure of alpha-ketoglutarate is as follows: C, single bond, C H 2, single bond, C H 2, single bond, C O O superscript minus. C 1 is single bonded to C O O superscript minus on the upper left and double bonded to O on the upper right.

3) Alpha-ketoglutarate is converted into succinyl-C o A by alpha-ketoglutarate dehydrogenase complex. It involves the reduction of N A D superscript plus to N A D H, entry of C o A, and exit of C O 2. The structure of succinyl-C o A is as follows: C, single bond, C H 2, single bond, C H 2, single bond, C O O superscript minus. C 1 is single bonded to S, single bond, C o A on the upper left, and double bonded to O on the upper right.

4) Succinyl-C o A is converted into succinate by succinyl C o A synthetase. It involves the conversion of A D P plus P subscript i to A T P and the release of C o A. The structure of succinate is as follows: C O O superscript minus, single bond, C H 2, single bond, C H 2, single bond, C O O superscript minus.

5) Succinate is converted into fumarate by succinate dehydrogenase. It involves the reduction of F A D to F A D H 2. The structure of fumarate is as follows: A central C is single bonded to H on the upper left, single bonded to C O O superscript minus on the upper right, and double bonded to C below. The C atom below is single

bonded to C O O superscript minus on the lower left and single bonded to H on the lower right.

6) Fumarate is converted into malate by fumarase. An H 2 O molecule also enters the reaction. The structure of malate is as follows: C O O superscript minus, single bond, C, single bond, C H 2, single bond, C O O superscript minus. C 2 is single bonded to O H on the left and H on the right.

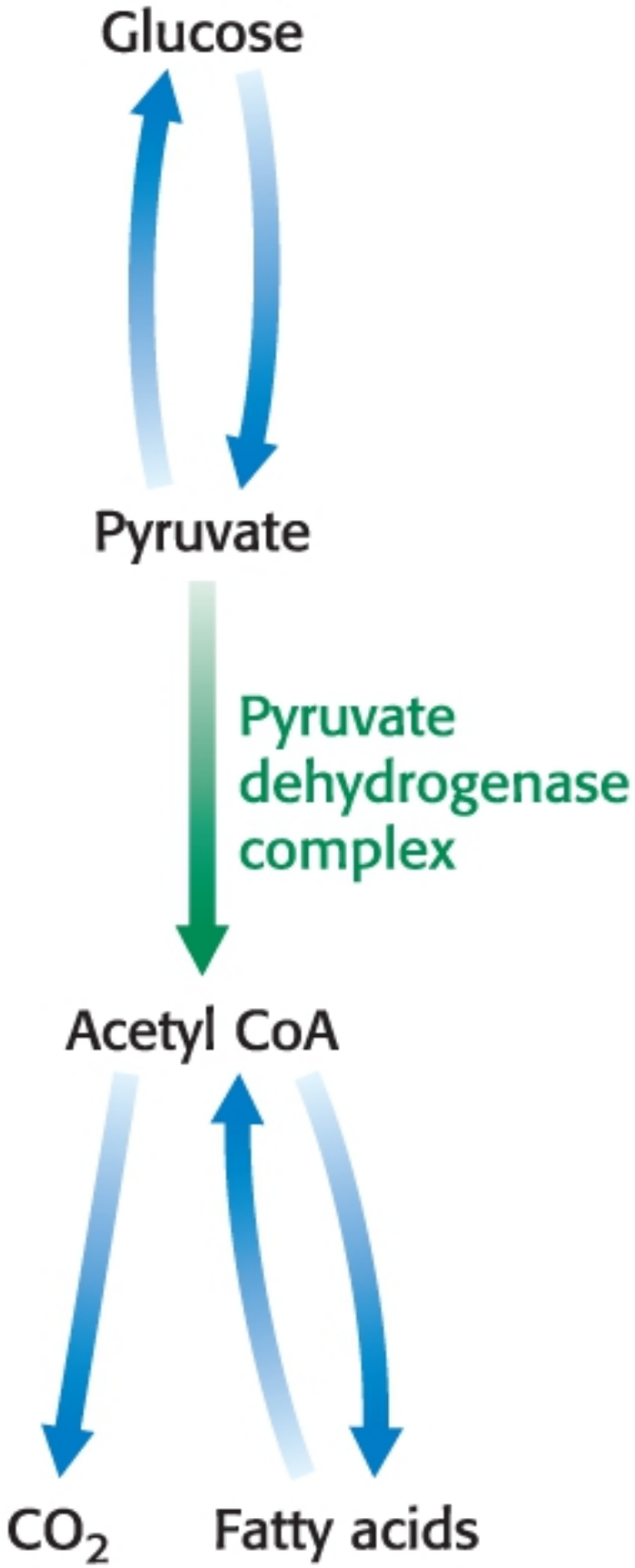
7) Malate is converted into oxaloacetate by malate dehydrogenase. It also involves the reduction of N A D superscript plus to N A D H plus H superscript plus. The structure of oxaloacetate is as follows: C, single bond, C H 2, single bond, C O O superscript minus. C 1 is double bonded to O on the upper left and single bonded to C O O superscript minus on the upper right.

8) Oxaloacetate is converted back to citrate by citrate synthase. It involves the entry of H 2 O plus a molecule whose structure is as follows: A central C atom is double bonded to O above, single bonded to C H 3 on the lower left, and single bonded to S, single bond, C o A on the lower right. C o A and H superscript plus are released during this reaction.

Return to Citric acid cycle

Extended description for Conversion of glucose to C O

2 and fatty acids

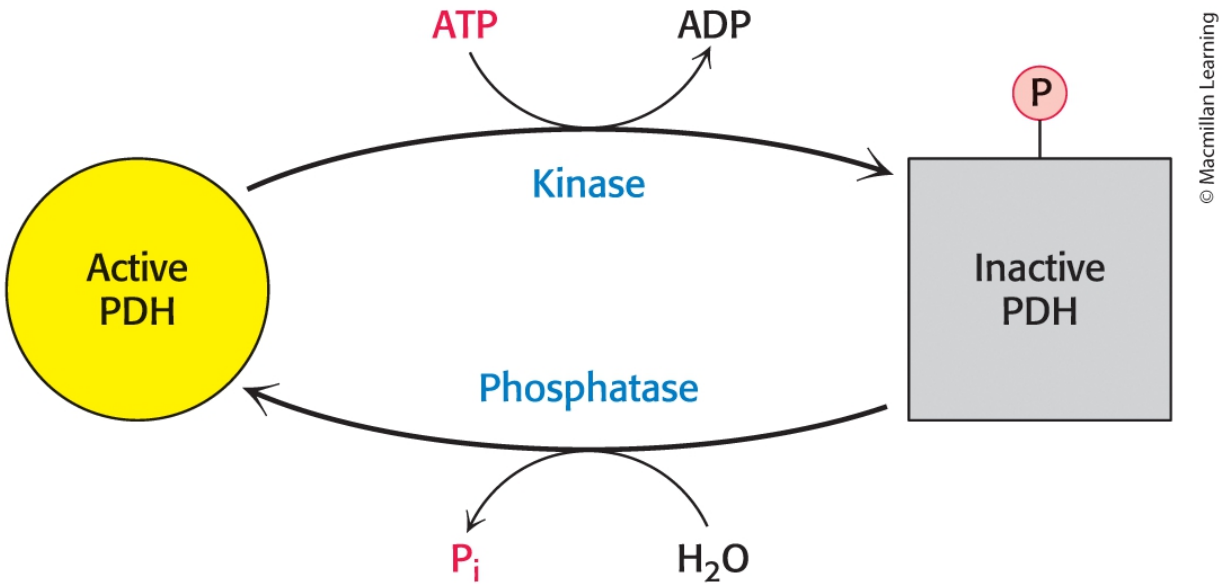


© Macmillan Learning

The flowchart is depicted as follows: Glucose, a pair of downward and upward arrows, pyruvate, a single downward arrow labeled pyruvate dehydrogenase complex, acetyl C o A, lower left arrow, and a pair of downward and upward arrows. The lower left arrow leads to C O 2 and the pair of arrows lead to fatty acids.

Return to Conversion of glucose to C O 2 and fatty acids

Extended description for Regulation of pyruvate dehydrogenase complex activity

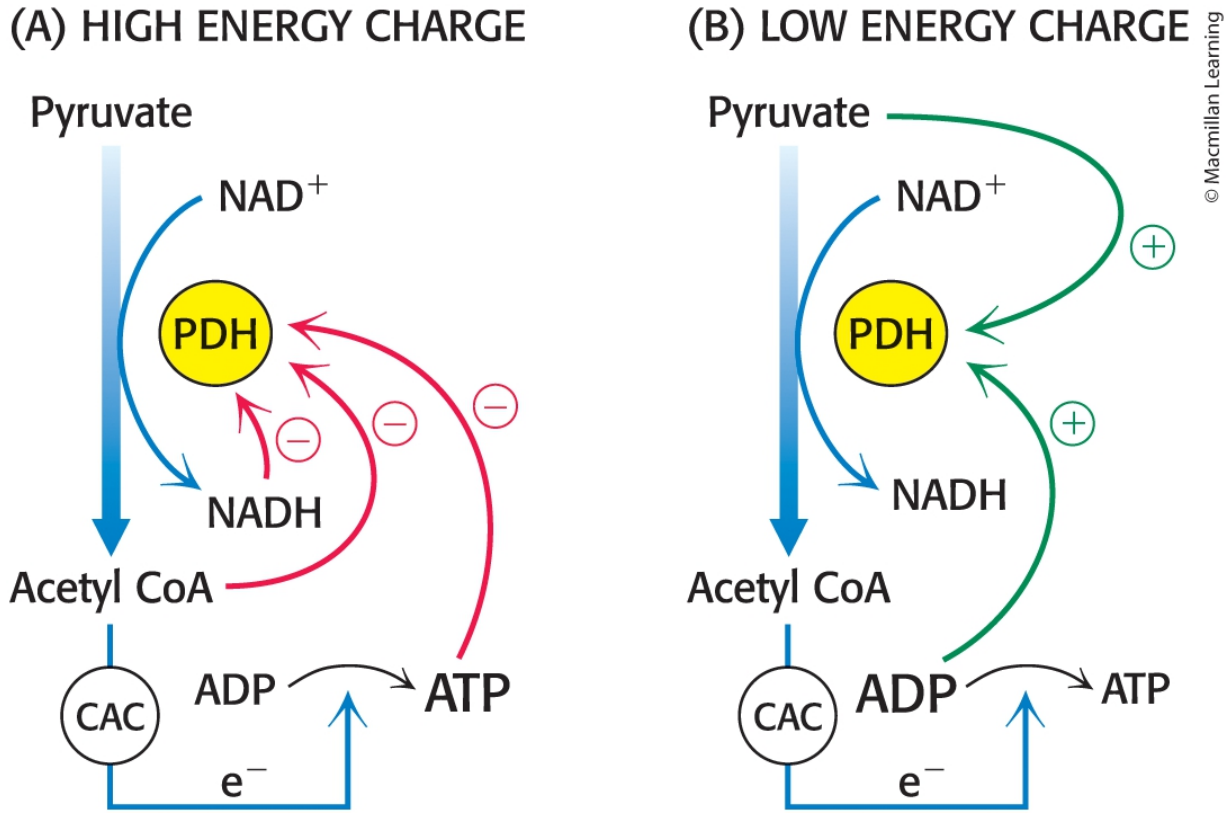


A yellow circle labeled active P D H is shown on the left. A forward arrow labeled kinase points from this circle toward a grey rectangle on the right labeled inactive P D H. A curved arrow above the forward arrow shows the simultaneous breakdown of A T P to A D P. The grey rectangle is single bonded to P above.

A backward arrow labeled phosphatase points from the grey rectangle toward the circle. A curved arrow below the backward arrow shows the simultaneous entry of H 2 O and the release of P subscript i.

Return to Regulation of pyruvate dehydrogenase complex activity

Extended description for Response of pyruvate dehydrogenase complex to changes in the energy of the cell



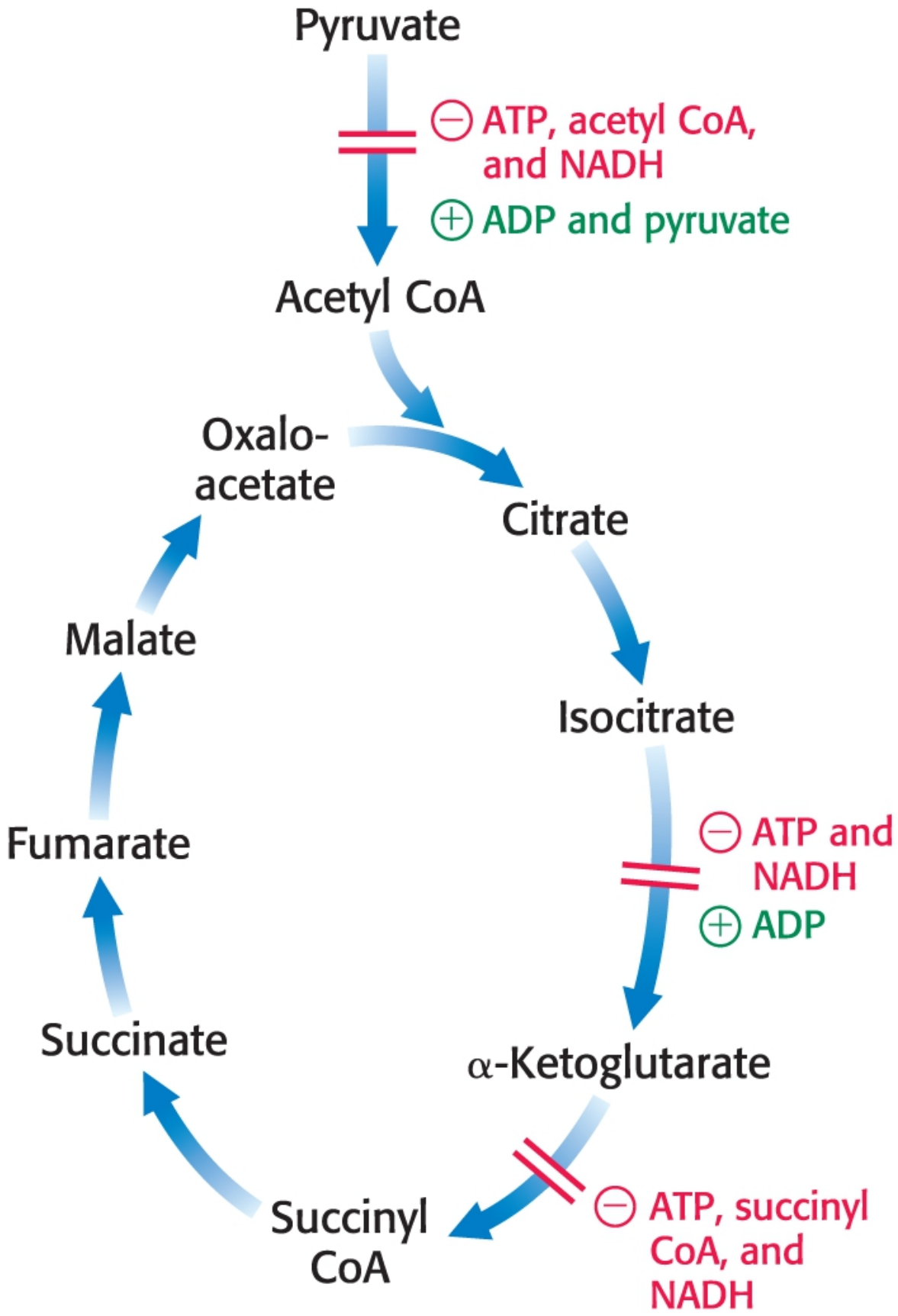
(A) High energy charge: Pyruvate, a downward arrow labeled P D H, acetyl C o A. A curved arrow on the right of the downward arrow shows the simultaneous reduction of N A D superscript plus to N A D H. An arrow from acetyl C o A passes through a circle labeled C A C. The arrow transfers electron to carry out the conversion of A D P to A T P. A red arrow with a minus symbol points from acetyl C o A to P D H, A T P to P D H, and N A D H to P D H.

(B) Low energy charge: Pyruvate, a downward arrow labeled P D H, acetyl C o A. A curved arrow on the right of the downward arrow

shows the simultaneous reduction of N A D superscript plus to N A D H. An arrow from acetyl C o A passes through a circle labeled C A C. The arrow transfers electron to carry out the conversion of A D P to A T P. A green arrow with a plus symbol points from A D P to P D H, and pyruvate to P D H.

Return to Response of pyruvate dehydrogenase complex to changes in the energy of the cell

Extended description for Regulation of citric acid cycle



© Macmillan Learning

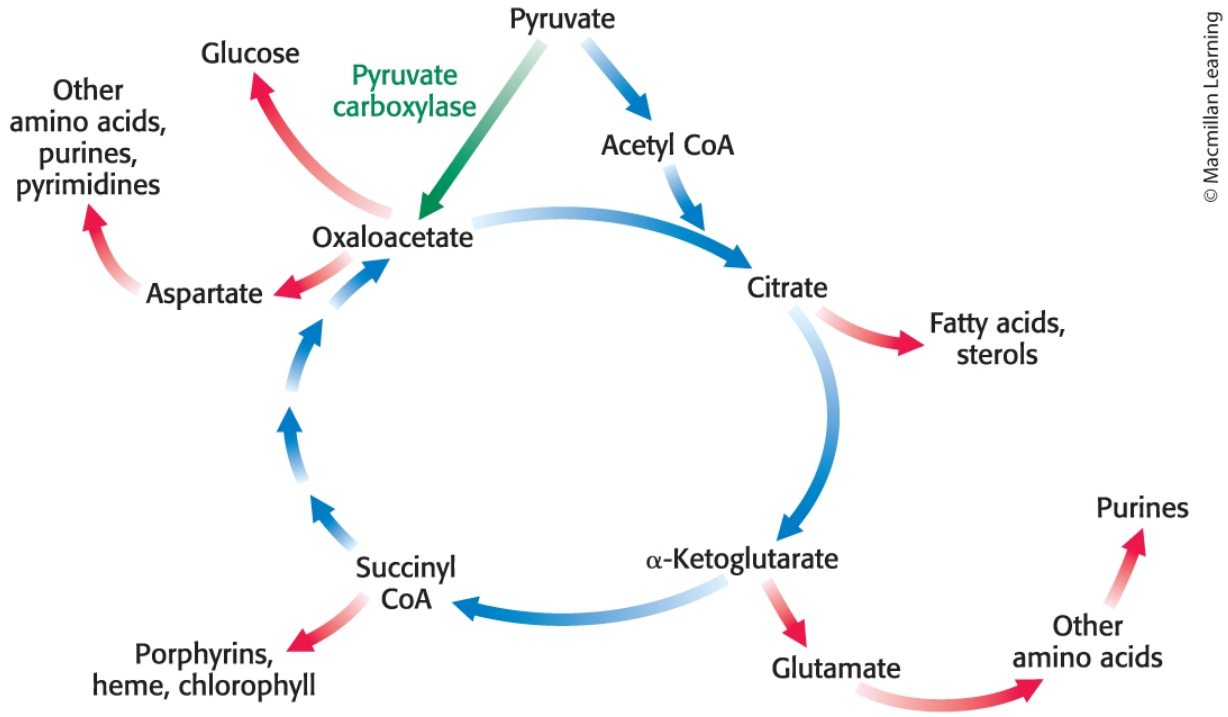
The citric acid cycle is depicted as follows: Pyruvate, downward arrow, acetyl C o A. A downward arrow from acetyl C o A leads to a forward arrow pointing from oxaloacetate to citrate. Citrate, downward arrow, isocitrate, downward arrow, alpha-ketoglutarate, lower left arrow, succinyl C o A, upper left arrow, succinate, upward arrow, fumarate, upward arrow, malate, upper right arrow, oxaloacetate. Two parallel red lines are shown over the downward arrow between pyruvate and acetyl C o A. This conversion is inhibited by A T P, acetyl C o A, and N A D H and activated by A D P and pyruvate.

Two parallel red lines are shown over the downward arrow between isocitrate and alpha-ketoglutarate. This conversion is inhibited by A T P and N A D H and activated by A D P.

Two parallel red lines are shown over the lower left arrow between alpha-ketoglutarate and succinyl C o A. This conversion is inhibited by A T P, succinyl C o A, and N A D H.

Return to Regulation of citric acid cycle

Extended description for Fates of the intermediates of citric acid cycle

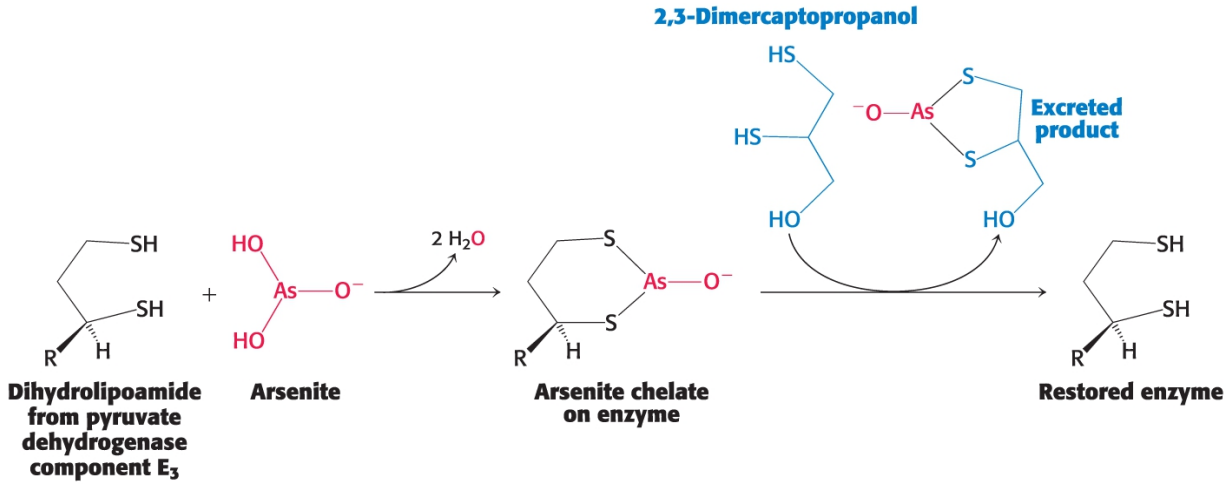


A green lower left arrow labeled pyruvate carboxylase leads from pyruvate to oxaloacetate. A lower right blue arrow leads from pyruvate to acetyl C o A. A lower right blue arrow leads from acetyl C o A toward the blue forward arrow pointing from oxaloacetate to citrate. A blue downward from citrate points toward alpha-ketoglutarate and a red arrow from citrate points toward fatty acid, sterols located outside the cycle. A blue arrow from alpha-ketoglutarate leads to succinyl C o A and a red lower right arrow from alpha-ketoglutarate points toward glutamate located outside the cycle. A red arrow from glutamate points toward other amino acids. A red arrow from other amino acids points toward purines. A red lower left arrow from succinyl C o A points toward porphyrins, heme, and chlorophyll located outside the cycle. Four blue upward arrows point from succinyl C o A points toward oxaloacetate. A red

lower left arrow from oxaloacetate points toward aspartate outside the cycle. Another arrow from aspartate points toward other amino acids, purines, and pyrimidines. A red upper left arrow from oxaloacetate points toward glucose outside the cycle.

Return to Fates of the intermediates of citric acid cycle

Extended description for Inhibition of pyruvate dehydrogenase by arsenite and its reversal by 2,3-dimercaptopropanol



The reaction is divided into two steps. In the first step, the arsenite chelate on enzyme is formed. Dihydrolipoamide from pyruvate dehydrogenase component E 3 reacts with arsenite to produce arsenite chelate on enzyme. This step is coupled with the release of 2 H 2 O. In the second step, the restored enzyme is formed. The arsenite chelate on enzyme is converted into the restored enzyme in the presence of 2, 3-Dimercaptopropanol which itself is converted into an excreted product.

The structure of dihydrolipoamide from pyruvate dehydrogenase component E 3 is as follows: A 3-carbon alkane chain is depicted as a vertical line structure using 2 zigzag lines. C 1 and C 3 are each single bonded to S H on the right. C 3 is wedge bonded to R on the lower left and dash bonded to H on the lower right.

The structure of arsenite is as follows: A central A s atom is single bonded to O superscript minus on the right, single bonded to O H on

the upper left, and single bonded to O H on the lower left.

The structure of arsenite chelate on enzyme is as follows: A 6-membered heterocyclic hexagonal ring is in a horizontal orientation and consists of 1 A s, 2 S, and 3 C atoms. S 1 occupies the first position, which is the top right vertex. A s occupies the second position, which is the rightmost vertex. A s is single bonded to O superscript minus on the right. S 2 occupies the third position, which is the bottom right vertex. C 1 occupies the bottom left vertex and is wedge bonded to R on the lower left and dash bonded to H on the lower right.

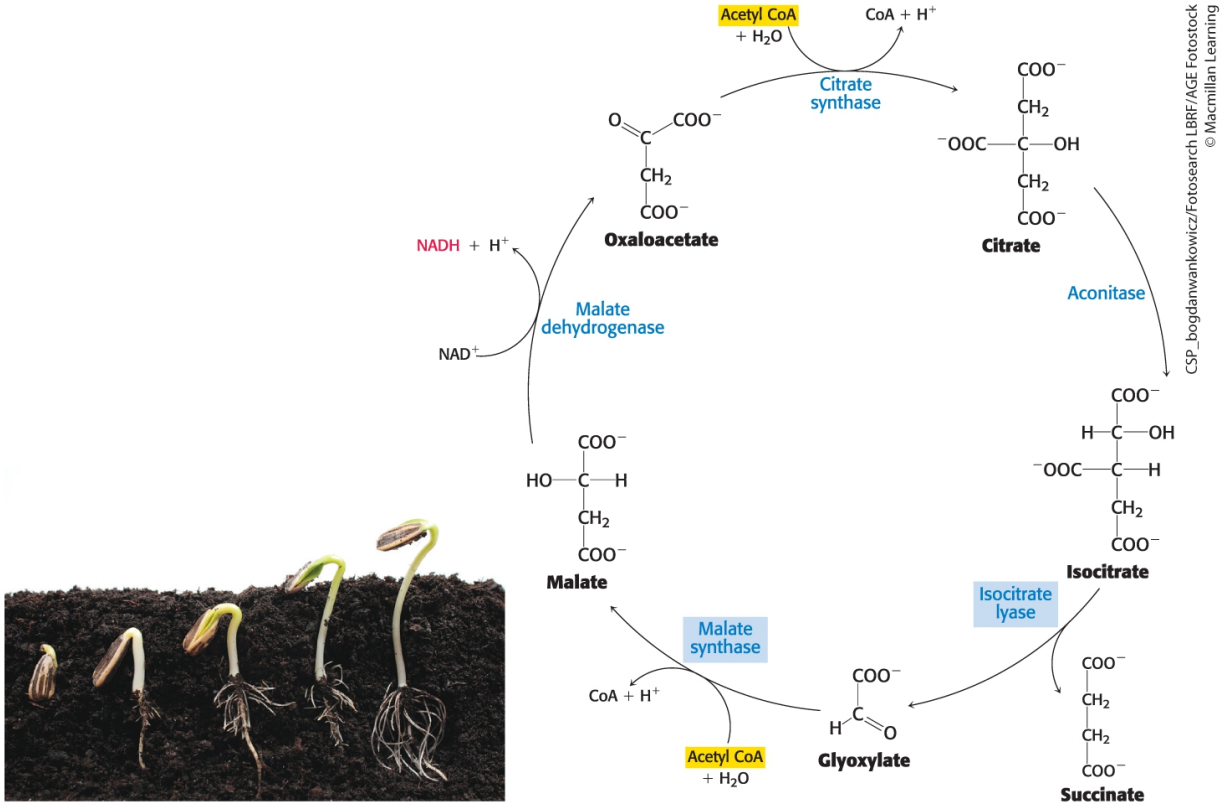
The structure of 2,3-Dimercaptopropanol is as follows: A 3-carbon alkane chain is depicted as a vertical line structure using 2 zigzag lines. C 1 is single bonded to S H on the upper left. C 2 is single bonded to S H on the left. C 3 is single bonded to O H on the lower left.

The structure of the excreted product is as follows: A 5-membered heterocyclic pentagonal ring is in a horizontal orientation with 1 A s, 2 S, and 2 C atoms. S 1 occupies the first position, which is the bottom-most vertex. A s occupies the second position, which is the leftmost vertex. A s is single bonded to O superscript minus on the right. S 2 occupies the third position, which is the top right vertex. C 2 is single bonded to C H 2 on the lower right in the form of a line. This C H 2 is single bonded to O H on the lower left.

The structure of the restored enzyme is as follows: A 3-carbon alkane chain is depicted as a vertical line structure using 2 zigzag lines vertically. C 1 and C 3 are each single bonded to S H on the right. C 3 is wedge bonded to R on the lower left and dash bonded to H on the lower right.

Return to Inhibition of pyruvate dehydrogenase by arsenite and its reversal by 2,3-dimercaptopropanol

Extended description for Glyoxylate cycle



The glyoxylate cycle consists of 5 enzyme-catalyzed reactions depicted as follows:

1) Oxaloacetate is converted into citrate by citrate synthase. It involves the simultaneous entry of acetyl C o A and H 2 O and release of C o A plus H superscript plus. The structure of oxaloacetate is as follows: C, single bond, C H 2, single bond, C O O superscript minus. C 1 is double bonded to O on the upper left and single bonded to C O O superscript minus on the upper right. The structure of citrate is as follows: C O O superscript minus, single bond, C H 2, single bond, C, single bond, C H 2, single bond, C O O superscript minus. C 3 is single bonded to C O O superscript minus on the left and O H on the right.

2) Citrate is converted into isocitrate by aconitase. The structure of isocitrate is as follows: C O O superscript minus, single bond, C, single bond, C, single bond, C H 2, single bond, C O O superscript minus. C 2 is single bonded to H on the left and O H on the right. C 3 is single bonded to C O O superscript minus on the left and H on the right.

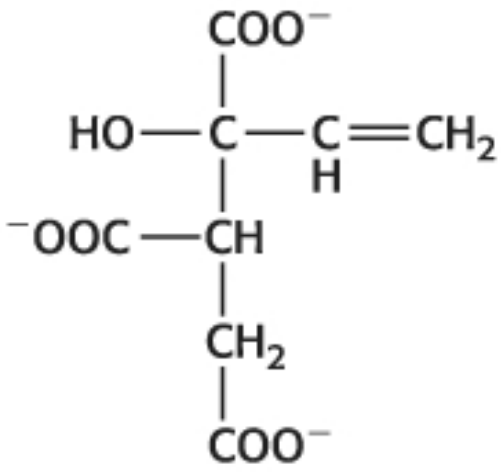
3) Isocitrate is broken down into succinate and glyoxylate by isocitrate lyase. Succinate leaves the cycle and its structure is as follows: C O O superscript minus, single bond, C H 2, single bond, C H 2, single bond, C O O superscript minus. The structure of glyoxylate is as follows: A central C atom is single bonded to H on the lower left, single bonded to C O O superscript minus above, and double bonded to O on the lower right.

4) Glyoxylate is converted into malate by malate synthase. It involves the simultaneous entry of acetyl C o A plus H 2 O and release of C o A plus H superscript plus. The structure of malate is as follows: C O O superscript minus, single bond, C, single bond, C H 2, single bond, C O O superscript minus. C 2 is single bonded to O H on the left and H on the right.

5) Malate is converted into oxaloacetate by malate dehydrogenase. It involves the simultaneous reduction of N A D superscript plus to N A D H plus H superscript plus. Oxaloacetate reenters the first reaction catalyzed by citrate synthase.

Return to Glyoxylate cycle

Extended description for Structure of 2-vinyl-isocitrate

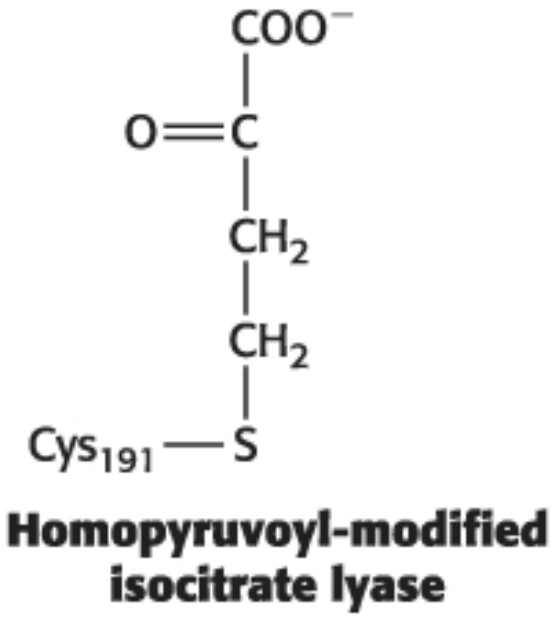


2-Vinyl-isocitrate

The structure consists of a vertical chain depicted as follows: C O O superscript minus, single bond, C, single bond, C H, single bond, C H 2, single bond, C O O superscript minus. C 2 is single bonded to O H on the left and single bonded to C H, double bond, C H 2 on the right. C 3 is single bonded to C O O superscript minus on the left.

Return to Structure of 2-vinyl-isocitrate

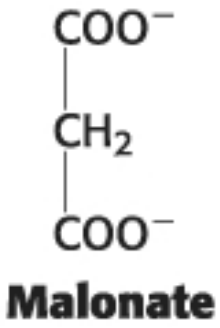
Extended description for Structure of homopyruvoyl-modified isocitrate lyase



The structure consists of a vertical chain depicted as follows: C O O superscript minus, single bond, C, single bond, C H 2, single bond, C H 2, single bond, S. C 2 is double bonded to O on the left. S is single bonded to C y s subscript 191 on the left.

Return to Structure of homopyruvoyl-modified isocitrate lyase

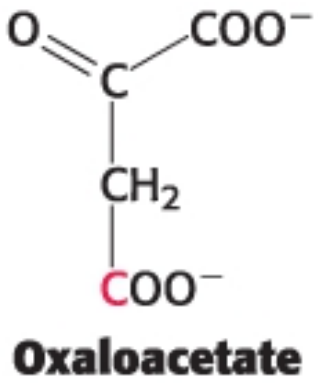
Extended description for Structure of malonate



The structure consists of a vertical chain depicted as follows: C O O superscript minus, single bond, C H 2, single bond, C O O superscript minus.

Return to Structure of malonate

Extended description for Structure of oxaloacetate



Oxaloacetate

The structure consists of a vertical chain depicted as follows: C, single bond, C H 2, single bond, C O O superscript minus. C 1 is double bonded to O on the upper left and single bonded to C O O superscript minus on the upper right. The C atom of the C O O superscript minus group at the bottom of the vertical chain is highlighted in red.

Return to Structure of oxaloacetate

Extended description for Colony-forming units in mice lungs in the weeks after an infection

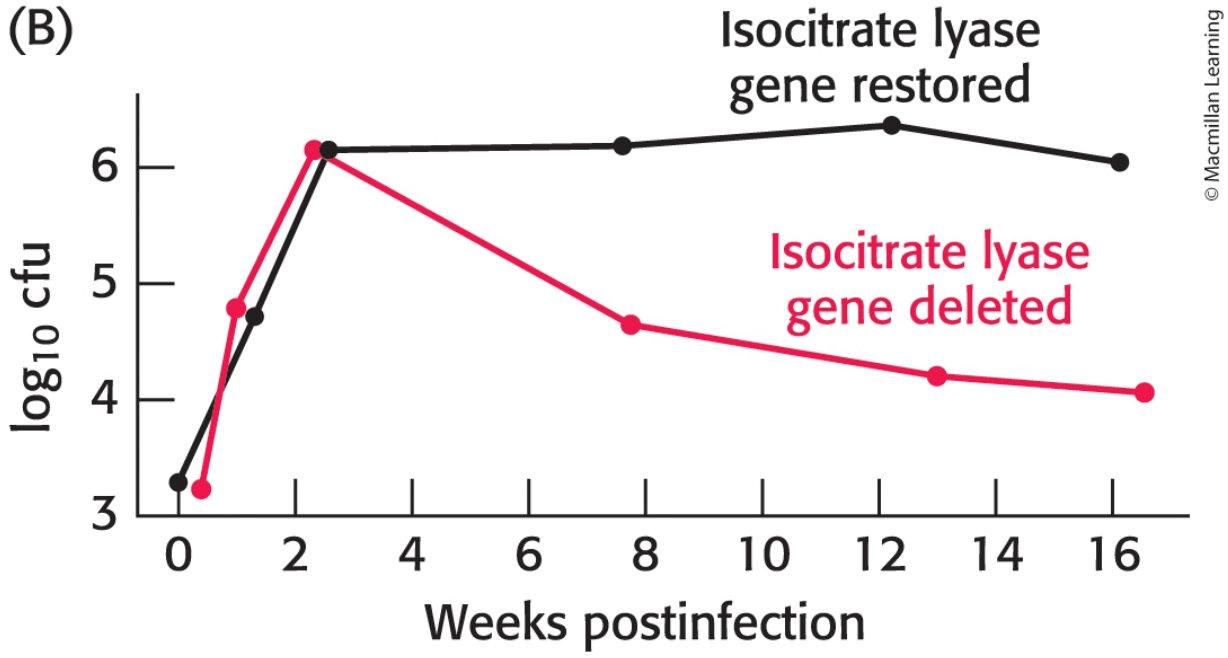


© Macmillan Learning

The horizontal axis is labeled weeks post infection. It has markings ranging from 0 to 16 in increments of 2 units. The vertical axis is labeled log base 10 c f u. It has markings ranging from 4 to 7 in increments of 1 unit. The graph contains two curves labeled wild type and isocitrate lyase gene deleted shown in black and red color respectively. The data points on the black curve are (0, 4.8), (2, 5.9), (4, 7.2), (8, 7.2), (12, 6.8), and (16, 7.2). The data points on the red curve are (negative 0.2, 4.8), (2, 5.9), (4, 7.2), (8, 5.5), (11.8, 5), and (15.9, 4.5).

Return to Colony-forming units in mice lungs in the weeks after an infection

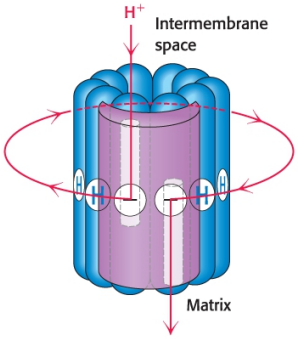
Extended description for Colony-forming units in mice lungs in the weeks after an infection



The horizontal axis is labeled weeks post infection. It has markings ranging from 0 to 16 in increments of 2 units. The vertical axis is labeled log base 10 c f u. It has markings ranging from 3 to 6 in increments of 1 unit. The graph contains two curves labeled isocitrate lyase gene restored and isocitrate lyase gene deleted shown in black and red color respectively. The data points on the black curve are (0, 3.2), (1.8, 4.7), (2.2, 6.2), (8, 6.3), (12, 6.4), and (16, 6). The data points on the red curve are (0.2, 3.2), (1, 4.8), (2, 6.2), (8, 4.8), (13, 4.3), and (16.2, 4.1).

Return to Colony-forming units in mice lungs in the weeks after an infection

Extended description for Schematic representation of proton flow across A T P synthase



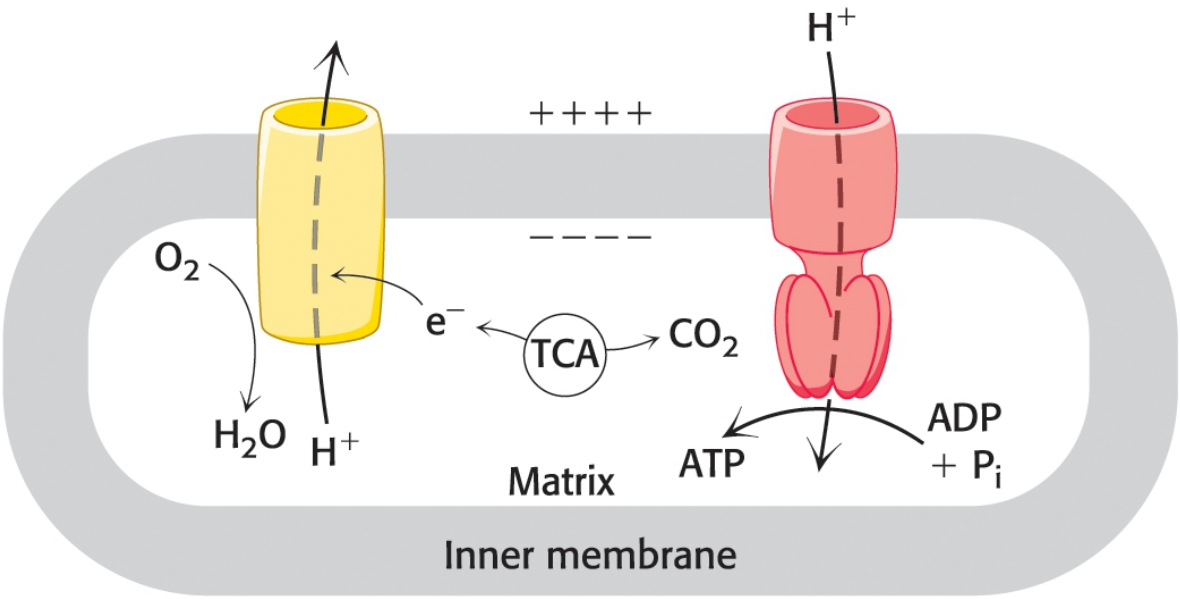


Melvyn Longhurst/Corbis Documentary/Getty Images
© Macmillan Learning

The c ring of A T P synthase is depicted as a cylindrical structure composed of 10 elongated vertical subunits. These subunits are bound to H. The region above the ring is labeled intermembrane space and the region below is labeled matrix. The front surface of the ring is enclosed by subunit a. An H superscript plus ion from the intermembrane space enters the intermembrane half-channel of subunit a. A curved circular arrow from the intermembrane half-channel moves in a clockwise direction around the c ring and returns back to the matrix half-channel of the subunit a. A downward arrow from the matrix half channel depicts the release of the H superscript plus ion into the matrix after its complete rotation around the c ring.

Return to Schematic representation of proton flow across A T P synthase

Extended description for Oxidative phosphorylation



© Macmillan Learning

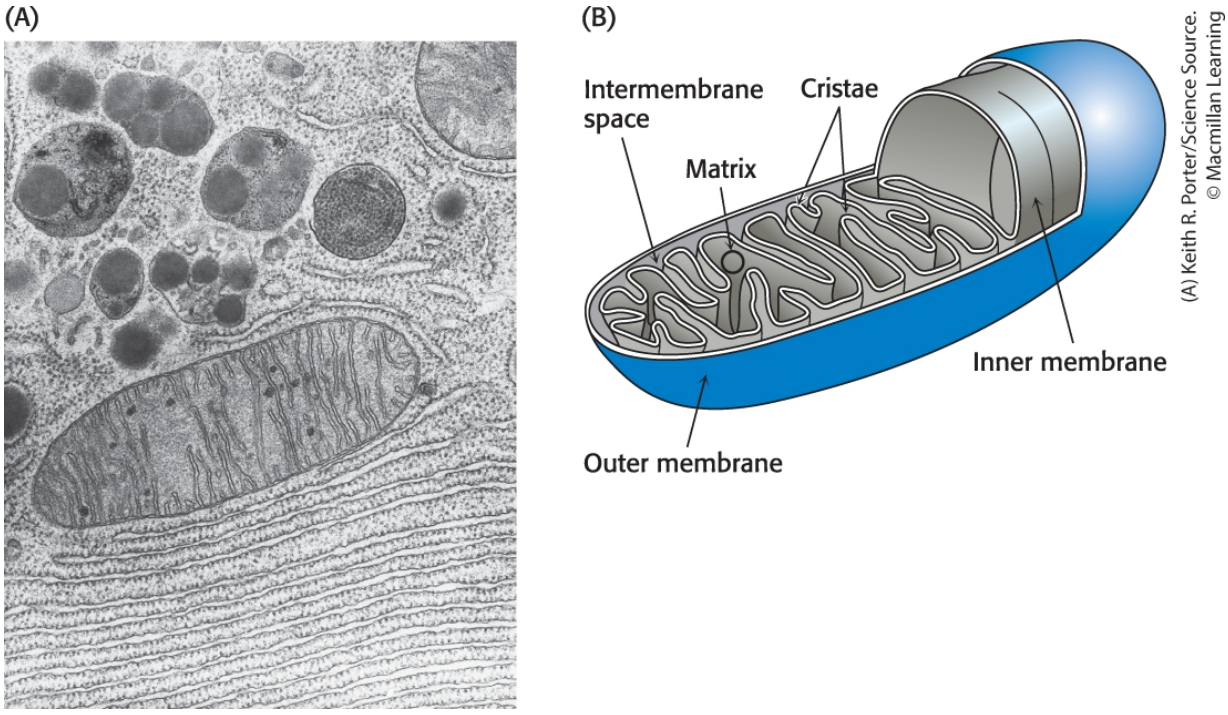
A capsule-shaped structure with a thick grey border is shown. The border is labeled inner membrane. The interior is labeled matrix. A hollow cylindrical structure spans through the inner membrane. Another hollow cylindrical structure connected to a tetramer composed of oval-shaped structures also spans through the membrane. The tetramer is located in the matrix and the hollow cylindrical portion spans through the membrane. Four plus symbols are present above the membrane and four minus symbols are present below the membrane. Inside the matrix, a circle labeled T C A is shown in the center. An arrow from this circle shows the release of C O 2 and electrons.

An upward arrow across the first hollow cylindrical structure depicts the movement of H superscript plus ion from the matrix to the outside space. The electrons from the T C A cycle are simultaneously used to convert O 2 into H 2 O by the cylindrical structure. A downward arrow across the second hollow cylindrical

structure shows the movement of the H superscript ion from outside space into the matrix. This movement is accompanied by the conversion of A D P plus P subscript i to A T P.

Return to Oxidative phosphorylation

Extended description for FIGURE 18.2 Mitochondria (A) An electron micrograph and (B) a diagram

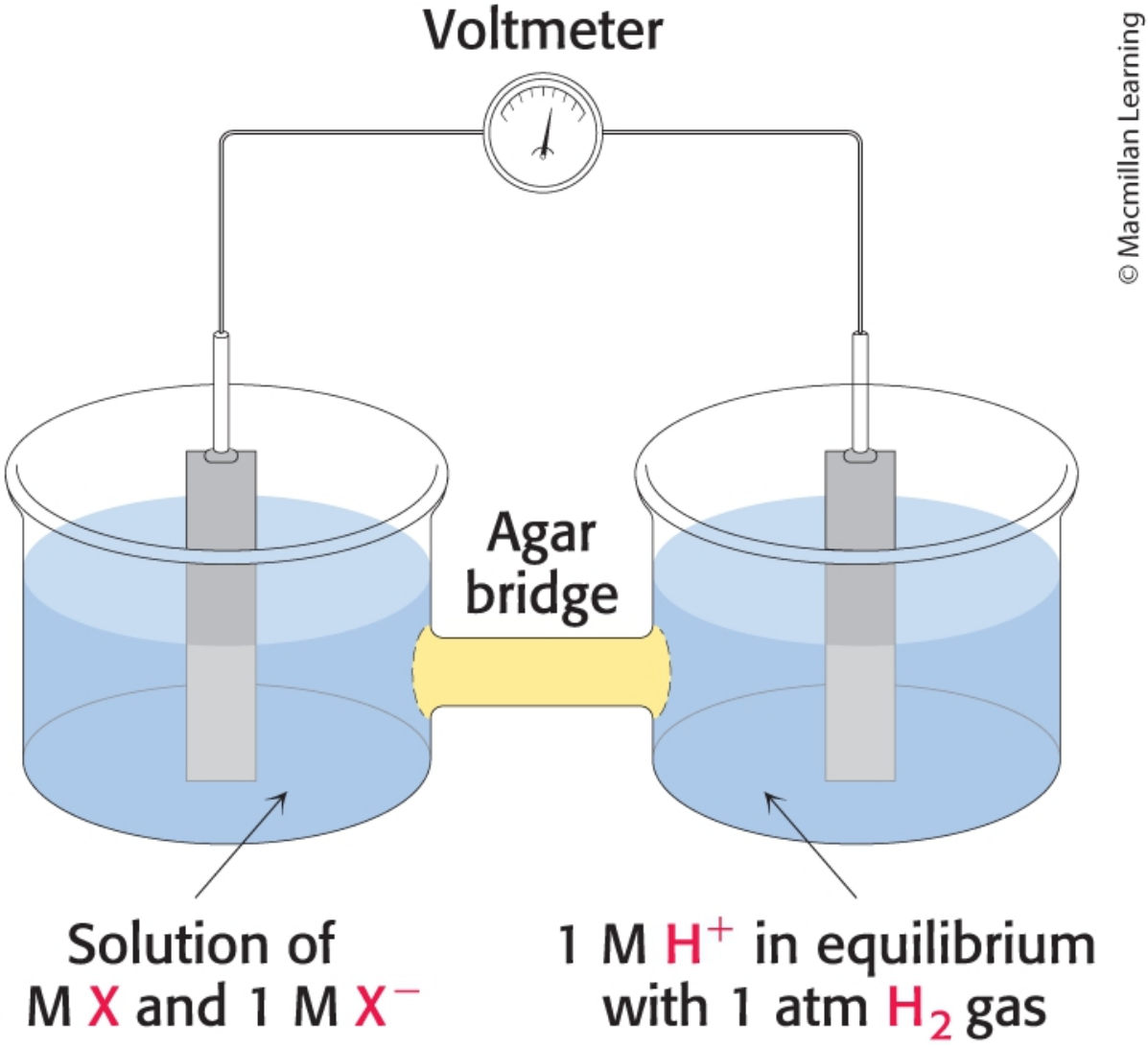


(A): The electron micrograph of mitochondria depicts a large oval structure with various thread-like projections forming stripes in the interior. Numerous granules are scattered in the interior of the organelle.

(B): The cutaway view of a 3-D mitochondrion is shown. The outer cover is labeled " Outer membrane." Inside the outer membrane, the layer is labeled "inner membrane." The space between two membranes is labeled "intermembrane space." The invaginations of the inner membrane forming numerous folds are labeled "Cristae." The space within the inner membrane is labeled "matrix."

Return to FIGURE 18.2 Mitochondria (A) An electron micrograph and (B) a diagram

Extended description for FIGURE 18.3 Redox potential can be precisely measured



© Macmillan Learning

The schematic illustration shows the apparatus composed of two glass containers joined externally and horizontally by a tubular agar bridge at the center.

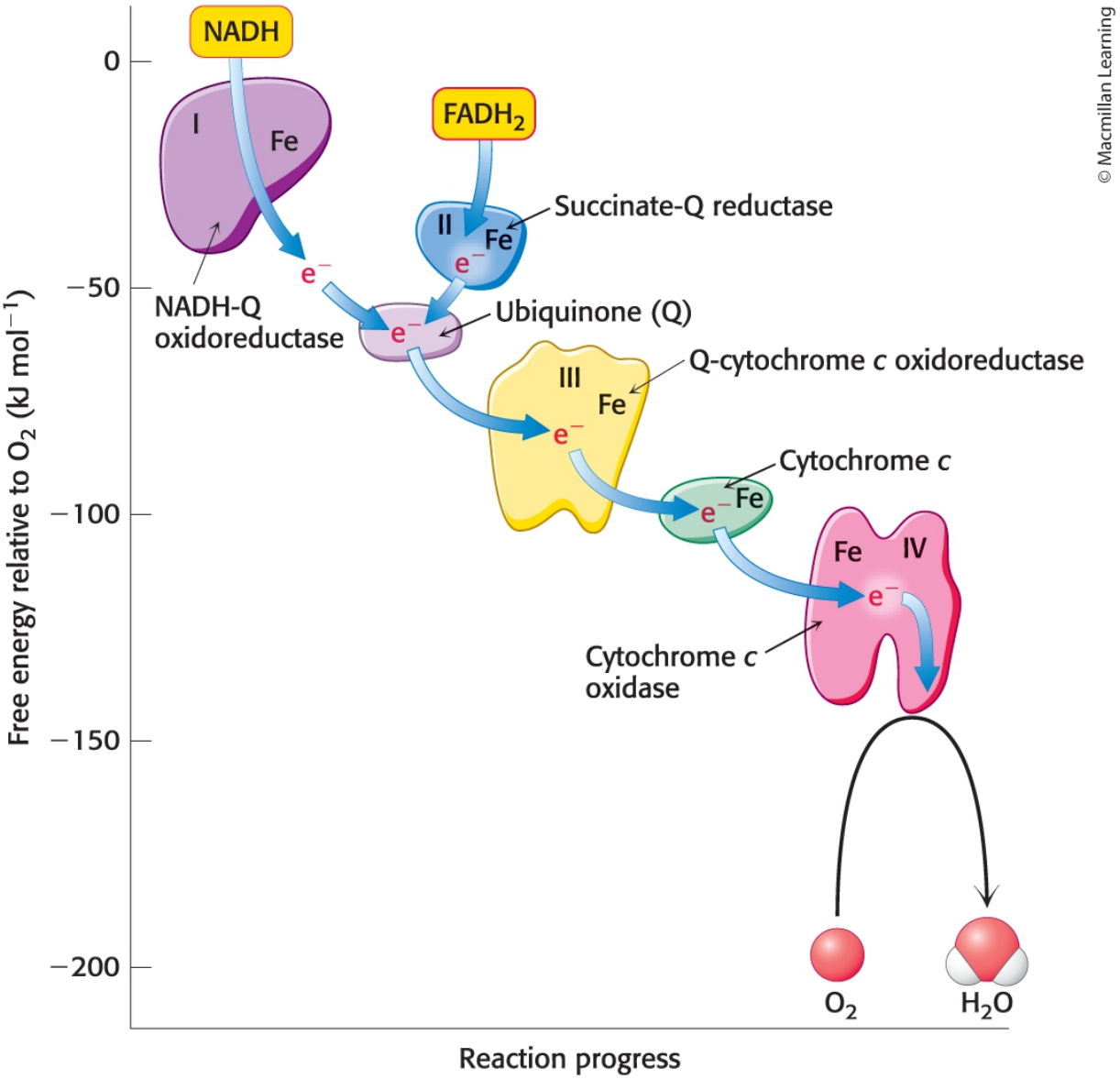
The left container has a solution of 1 Molar X and 1 molar X superscript minus. The right container has 1 molar H superscript

plus in equilibrium with 1 atmosphere H 2 gas.

Each container has a rectangular strip dipped in the solution. The strips are connected by wires to a common voltmeter at the top center.

Return to FIGURE 18.3 Redox potential can be precisely measured

Extended description for FIGURE 18.4 Components of the electron-transport chain



The schematic shows a graphical representation. The horizontal axis has label reaction progress and the vertical axis indicates free energy relative to O 2 in kilojoules per mole ranging from negative 200 to 0 in increments of 50 kilojoules per mole.

Step 1: A triangular complex I (F e) labeled N A D H- Q oxidoreductase at the top left corner of the graph is shown between negative 50 to 0 kilojoules per mole. An arrow is drawn through this complex from N A D H to an electron. Another arrow leads this electron to oval labeled ubiquinone (Q) shown in the range below negative 50 kilojoules per mole.

Step 2: An oval complex II (F e) labeled Succinate Q reductase is shown in the range of negative 50 to negative 35 kilojoules per mole. An arrow is drawn from F A D H 2 to succinate-Q reductase complex. Another arrow is drawn from an electron in the succinate Q reductase complex to an electron in ubiquinone (Q).

Step 3: A distorted polygon with a wavy border depicts complex III (F e) labeled Q- cytochrome c oxidoreductase shown in the range between negative 100 to negative 60 Kilojoules per mole. A curved arrow is drawn from an electron in ubiquinone (Q) to an electron in the Q-cytochrome c oxidoreductase complex.

Step 4: An oval labeled cytochrome c is shown at negative 100 Kilojoules per mole. An arrow is drawn from an electron in Q-cytochrome c oxidoreductase complex to the electron in cytochrome c.

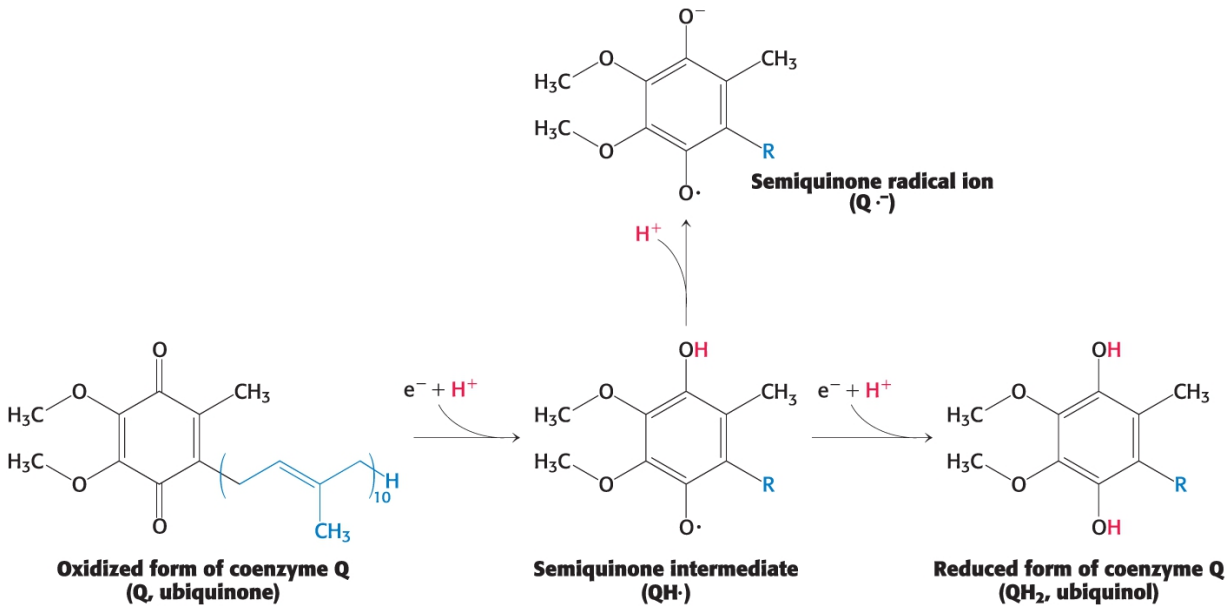
Step 5: A distorted H-shaped complex IV (F e) labeled Cytochrome c oxidase is shown in the range between negative 150 to negative 100 Kilojoules per mole. An arrow is drawn from an electron in cytochrome c to an electron in the cytochrome c oxidase complex.

Step 6: An arrow is drawn from an electron in the cytochrome c oxidase complex pointing to the coupled conversion of O 2 to H 2 O. O 2 and H 2 O is shown at negative 200 kilojoules per mole.

The coupled conversion is depicted by a curved arrow touching the lower right corner of complex IV from a sphere labeled O 2 to a triatomic space-filling model of H 2 O.

Return to FIGURE 18.4 Components of the electron-transport chain

Extended description for FIGURE 18.5 Quinones can have three different oxidation states, two of which are stable



The schematic reaction shows the following conversions.

Structure 1: An oxidized form of coenzyme Q (Q, ubiquinone) has the following structure: A 6-carbon hexagonal ring is in a vertical orientation with C 1 occupying the topmost vertex. The ring contains double bonds between C 2 and C 3, and C 5 and C 6. C 1 and C 4 are each double bonded to O and C 2 is single bonded to C H 3. C 3 is single bonded to a 4-carbon alkene chain depicted as a line structure using 3 zigzag lines. C 1 to C 4 of the alkene chain is enclosed by brackets with subscript 10. C 2 of the alkene chain is double bonded to C 3. C 3 is single bonded to C H 3 below. C 4 is single bonded to H on the lower right. C 5 and C 6 are each single bonded to O on the lower left and upper left respectively. Each O is single-bonded to C H 3. The alkene chain is blue-highlighted.

A forward arrow coupled with electron and H superscript plus ions (red highlighted) leads to the next structure.

Structure 2: Semiquinone intermediate (Q H with dot) has the following structure: A benzene ring is in a vertical orientation with C 1 occupying the topmost vertex. The ring contains double bonds between C 2 and C 3, C 4 and C 5, and C 6 and C 1. C 1 is single bonded to O H (H red highlighted) above and C 2 is single bonded to C H 3. C 3 is single bonded to R (blue highlighted). C 4 is single-bonded to O with an unpaired electron below. C 5 and C 6 are each single bonded to O on the lower left and upper left respectively. Each O is single-bonded to C H 3.

A forward arrow coupled with electron and H superscript plus ions (red highlighted) leads to the next structure.

Structure 3: The reduced form of coenzyme Q (Q H 2, ubiquinol) has the following structure: A benzene ring is in a vertical orientation with C 1 occupying the topmost vertex. The ring contains double bonds between C 2 and C 3, C 4 and C 5, and C 6 and C 1. C 1 and C 4 are each single bonded to O H (H red highlighted) and C 2 is single bonded to C H 3. C 3 is single bonded to R (blue highlighted). C 5 and C 6 are each single bonded to O on the lower left and upper left respectively. Each O is single-bonded to C H 3.

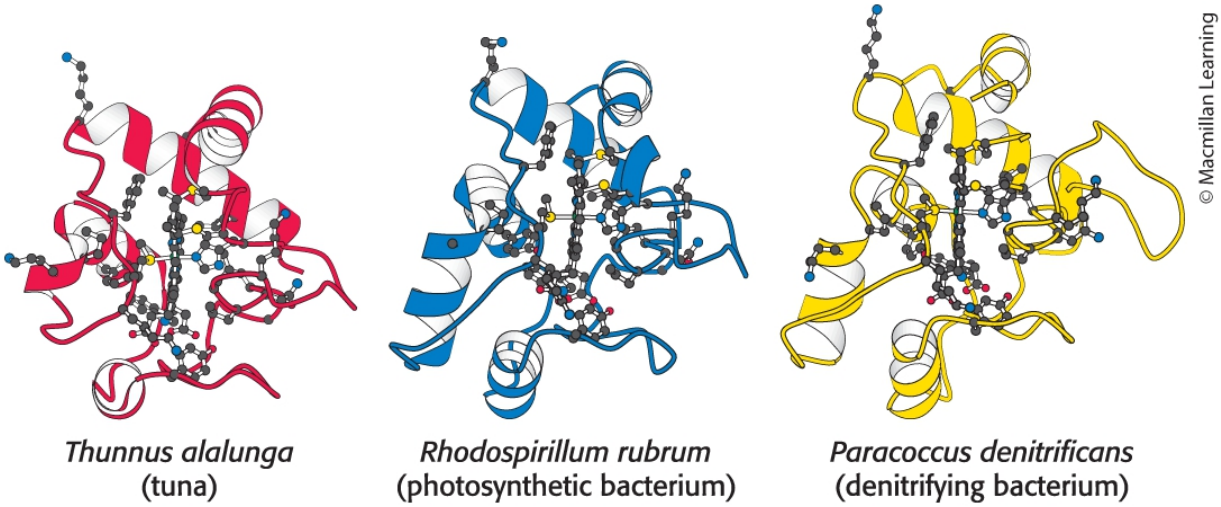
An upward arrow coupled with H superscript plus ion (red highlighted) is drawn from structure 2 leading to the next structure above.

Structure 4: Semiquinone radical ion (Q superscript minus with an unpaired electron) has the following structure: A benzene ring is in a vertical orientation with C 1 occupying the topmost vertex. The ring contains double bonds between C 2 and C 3, C 4 and C 5, and C 6

and C 1. C 1 is single bonded to O superscript minus. C 4 is single-bonded to O with an unpaired electron. C 2 is single bonded to C H 3. C 3 is single bonded to R (blue highlighted). C 5 and C 6 are each single bonded to O on the lower left and upper left respectively. Each O is single-bonded to C H 3.

Return to FIGURE 18.5 Quinones can have three different oxidation states, two of which are stable

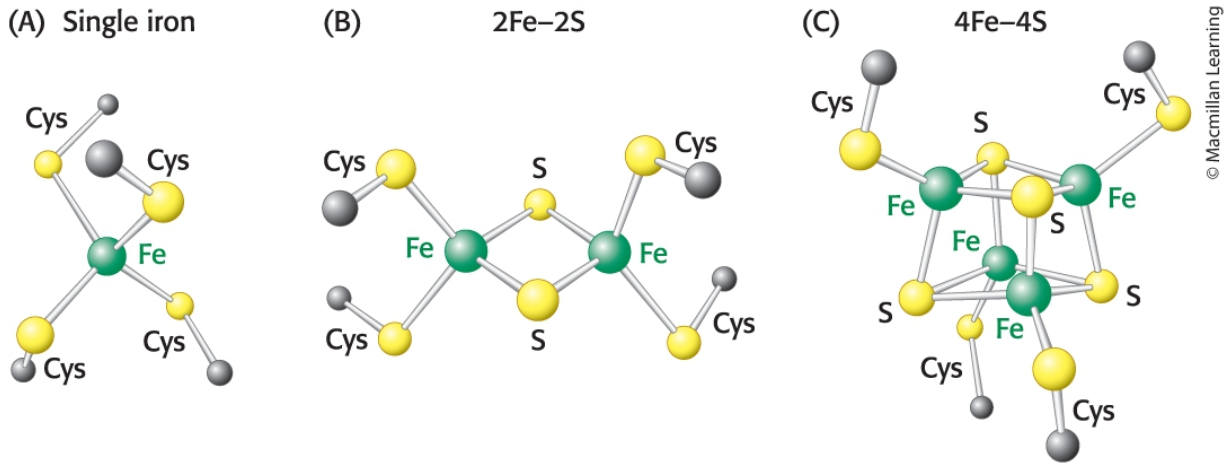
Extended description for FIGURE 18.6. The three-dimensional structure of cytochrome c is remarkably conserved among distantly related species



The ribbon diagrams of cytochrome c from Thunnus alalunga (tuna), Rhodospirillum rubrum (photosynthetic bacterium), and Paracoccus denitrificans (denitrifying bacterium) are shown. They consist of a few alpha-helices connected by long thread-like loops. Each ribbon diagram has a ball-and-stick model of the heme group in the center. The ball-and-stick models of side chain of different amino acids is shown along each ribbon diagram.

Return to FIGURE 18.6. The three-dimensional structure of cytochrome c is remarkably conserved among distantly related species

Extended description for FIGURE 18.7 Three different types of iron–sulfur clusters are commonly found in biological systems



(A): It shows a single central F e atom depicted as a green sphere connected to four cysteine resides. Each cysteine residue is composed of a yellow and a black sphere. The green sphere is connected to a yellow sphere on the upper left, upper right, lower left, and lower right. The upper right and lower left yellow spheres are located toward the observer. Each yellow sphere is connected to a black sphere.

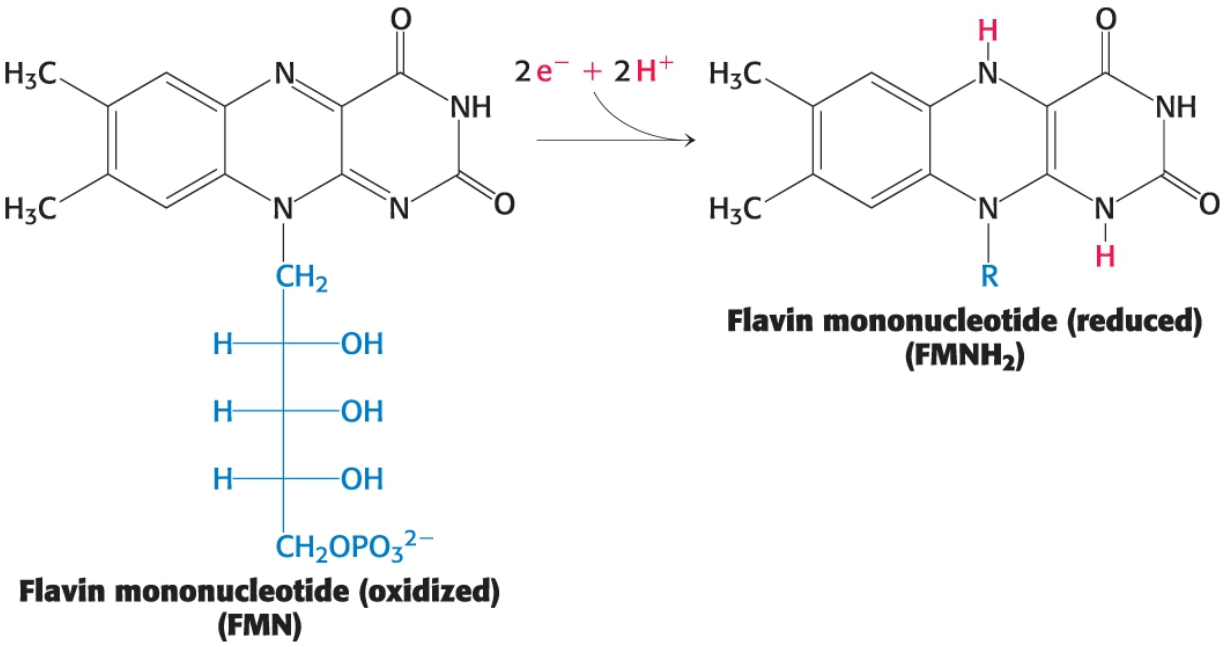
(B): It shows the 2 F e 2 S cluster. Two central green spheres depicting F e atoms are shown adjacent to each other and are separated by a short distance. They are connected to a common yellow sphere at the top center and bottom center. The yellow spheres depict S atoms. The left green sphere is further connected to a yellow sphere on the upper left and lower left. Each yellow sphere is connected to a black sphere. The right green sphere is connected to a yellow sphere on the upper right and lower right. Each yellow

sphere is connected to a black sphere. The yellow sphere connected to a black sphere depicts cysteine residue.

(C): It shows the 4 F e 4 S cluster. It is depicted as 3-D trapezium-shaped structure with four vertices at the top and bottom. Each of the vertices of the top and bottom faces are occupied by yellow and green spheres in an alternating fashion. The yellow sphere depicts the S atom and the green spheres depict the F e atom. Each green sphere is connected to a yellow sphere which is further connected to a black sphere. The yellow sphere connected to a black sphere depicts cysteine residue.

Return to FIGURE 18.7 Three different types of iron–sulfur clusters are commonly found in biological systems

Extended description for FIGURE 18.8 Flavins have two oxidation states



The reaction shows one reactant and one product.

The reactant labeled “Flavin mononucleotide (oxidized) (F M N)” has the following structure: A benzene ring is in a vertical orientation with C 1 occupying the topmost vertex and is fused to a 6-membered heterocyclic hexagonal ring consisting of 2 N and 4 C atoms in a vertical orientation with N occupying the topmost vertex. The two rings are fused such that C 2 and C 3 of the benzene ring are the C 4 and C 3 of the 6-membered hexagonal ring, respectively. The benzene ring contains alternating double bonds between C 1 and C 2, C 3 and C 4, and C 5 and C 6. C 5 and C 6 are each single bonded to C H 3. In the 6-membered heterocyclic hexagonal ring, a double bond is present between N 1 and C 1. N 2 occupies the fourth position, which is the bottom-most vertex. N 2 is single bonded to the C H 2 of the Fischer projection below.

The Fischer projection consists of a vertical line with C H 2 above and C H 2 O P O 3 superscript 2 minus below. The projection contains three C atoms placed one below the other on the vertical line. The C atoms are numbered from top to bottom. C 2, C 3, and C 4 each have a horizontal line drawn across them with H on the left and O H on the right.

The 6-membered heterocyclic hexagonal ring is fused to a second 6-membered heterocyclic hexagonal ring consisting of 2 N and 4 C atoms in a vertical orientation. In the second ring, C 1 occupies the bottom-right vertex. The two rings are fused such that C 1 and C 2 of the first hexagonal ring are the C 3 and C 2 of the second hexagonal ring, respectively.

In the second hexagonal ring, N 1 bound to H and N 2 are positioned at the top right and bottom vertices respectively. C 1 and C 4 are each double bonded to O. N 2 is double bonded to C 2.

A forward arrow is coupled with 2 electrons and 2 H superscript plus ions.

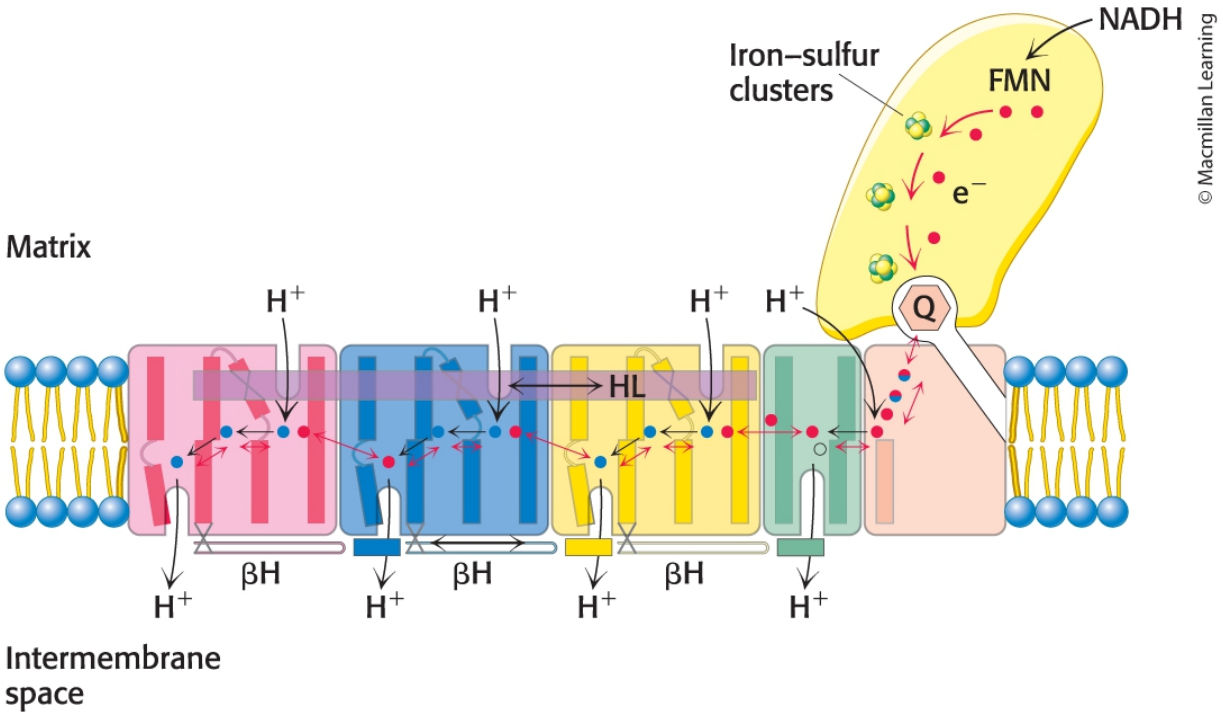
The product labeled flavin mononucleotide (reduced) (F M N H2) has the following structure: A benzene ring is in a vertical orientation with C 1 occupying the topmost vertex. It is fused to a 6-membered heterocyclic hexagonal ring consisting of 2 N and 4 C atoms in a vertical orientation with Noccupying the topmost vertex. The two rings are fused such that C 2 and C 3 of the benzene ring are the C 4 and C 3 of the 6-membered hexagonal ring, respectively. The benzene ring contains alternating double bonds between C 1 and C 2, C 3 and C 4, and C 5 and C 6. C 5 and C 6 are each single bonded to CH 3. In the 6-membered heterocyclic, N 1 occupies the topmost vertex and N 2 occupies the bottom-most vertex. N 1 is single bonded to H above and N 2 is single bonded to R below.

The 6-membered heterocyclic hexagonal ring is fused to a second 6-membered heterocyclic hexagonal ring consisting of 2 N and 4 C atoms in a vertical orientation. In the second ring, C 1 occupies the bottom-right vertex. The two rings are fused such that C 1 and C 2 of the first hexagonal ring are the C 3 and C 2 of the second hexagonal ring, respectively.

In the second hexagonal ring, N 1 bound to H and N 2 are positioned at the top right and bottom vertices respectively. C 1 and C 4 are each double bonded to O. N 2 is single bonded to H below. A double bond is present between C 2 and C 3.

Return to FIGURE 18.8 Flavins have two oxidation states

Extended description for FIGURE 18.9 Electron transfer through NADH-Q oxidoreductase is coupled to proton transfer reactions



Five different complexes are shown embedded in a lipid bilayer. The region above the bilayer is labeled matrix and the region below the bilayer is labeled intermembrane space. From the left end, three adjacent complexes are depicted as rectangles with a U-shaped groove in the top right and bottom left surface. A long horizontal and rectangular H L component spans across these three complexes. Each of the complexes contains a thin elongated and horizontal beta H complex in the intermembrane space. The next complex contains a U-shaped groove at the bottom surface. The final square-shaped complex contains a diagonal channel near the top right end. Complex 1 is depicted as a wide elongated structure in the matrix, above the square-shaped complex. N A D H enters complex 1

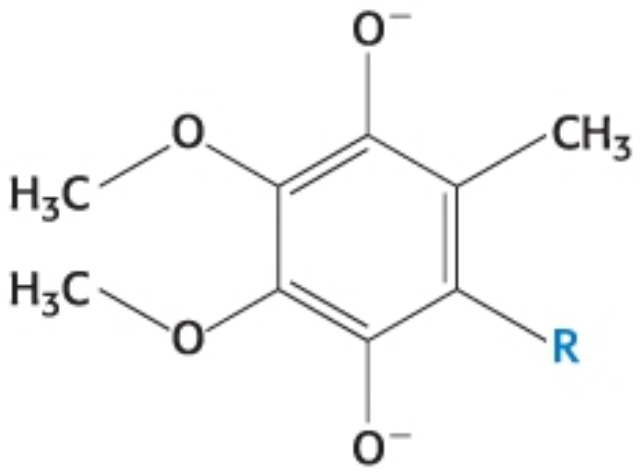
and donates electron to F M N. The electrons from F M N depicted as red dots pass through three different iron-sulfur clusters in complex 1. They travel to ubiquinone depicted as a horizontal hexagon labeled Q inside a circular groove between the junction of complex 1 and the square-shaped complex. This circular groove is continuous with the diagonal channel.

A two-way arrow depicts the movement of electrons through red and blue balls in the square-shaped complex. The electron then combines with an H superscript plus ion from the matrix. It then enters the adjacent complex and passes across it into the next adjacent complex. This movement of electrons is coupled with the release of H superscript plus ion into the intermembrane space through the bottom U-shaped groove.

The electron moves through red and blue balls leading to the alteration of the conformation of a central transmembrane helix. As a result, an H superscript plus ion enters into the top right U-shaped groove and exits through the bottom left groove into the intermembrane space. Similarly, the electrons pass through the remaining complexes with the simultaneous passage of H superscript ions from the matrix into the intermembrane space.

Return to FIGURE 18.9 Electron transfer through NADH-Q oxidoreductase is coupled to proton transfer reactions

Extended description for Structure of reduced ubiquinone



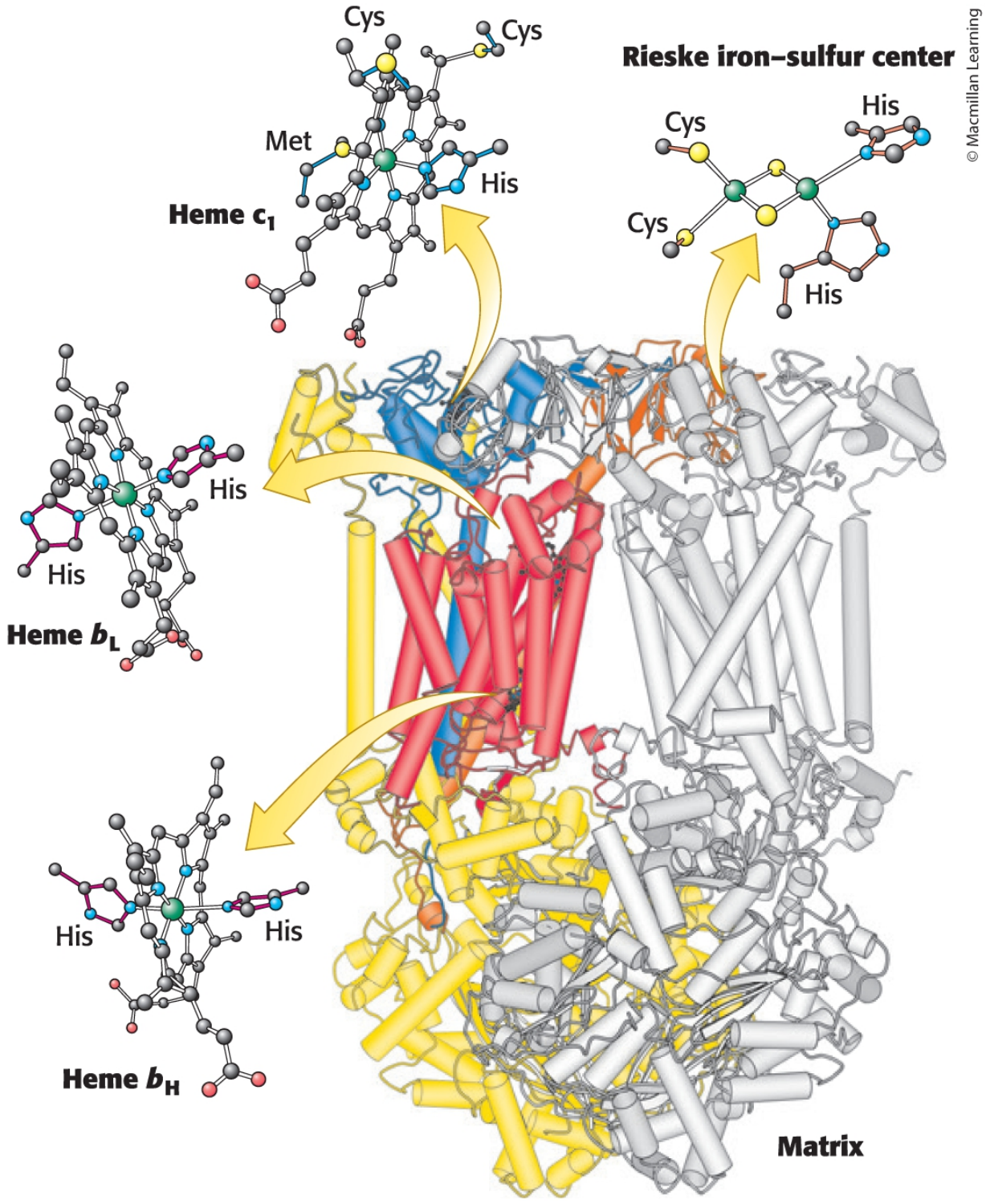
Reduced ubiquinone
(Q^{2-})

The structure of reduced ubiquinone is as follows: A benzene ring is in a vertical orientation with C 1 occupying the topmost vertex. It contains alternating double bonds between C 2 and C 3, C 4 and C 5, and C 6 and C 1. C 1 and C 4 are single bonded to O superscript minus above and below respectively. C 2 is single bonded to C H 3 on the upper right. C 3 is single bonded to R on the lower right. C 5 is single bonded to O on the lower left, which is further single bonded to C H 3 on the upper left. C 6 is single bonded to O on the upper left, which is further single bonded to C H 3 on the lower left.

Return to Structure of reduced ubiquinone

Extended description for FIGURE 18.10 Q-cytochrome c oxidoreductase is a homodimer, with each monomer

consisting of 11 distinct polypeptide chains



Q-cytochrome c oxidoreductase is a homodimer. The left half is shown in color and the right half is shown in grey. The right half shows a cluster of medium cylindrical structures at the top connected by thread-like loops. The bottom portion consists of a mixture of short and medium cylindrical structures connected by thread-like loops. A cluster of long vertical cylindrical structures is located in the middle. An arrow from the top portion points toward a Rieske iron-sulfur center. It consists of two green spheres connected to a common yellow sphere in the top center and bottom center. The left green sphere is connected to a cysteine side chain on the upper left and lower left. The right green sphere is connected to the nitrogen atom of the pentagonal ring of the histidine side chain on the upper right and lower right.

The left half shows a cluster of short and medium cylindrical structures at the top. These cylindrical structures are shown in yellow, blue, and grey colors. The bottom portion contains a cluster of short and medium yellow cylindrical structures. A cluster of long vertical cylindrical structures shown in red, blue, and yellow is located in the middle.

An arrow from the top portion of the left half points toward a ball-and-stick model of Heme c 1. It shows a central green sphere connected to blue spheres in a radial fashion. The blue spheres are further connected to black spheres that form a cage-like structure. One blue sphere is connected to the pentagonal ring of the histidine side chain and methionine side chain. The side chains of cysteine residues are connected to the black spheres on the top right and top left. An arrow from the junction between the top and middle portion of the left half points toward the ball and stick model of heme b subscript L. It consists of a central green sphere connected to blue spheres in a radial manner. The blue spheres are further connected to black spheres that form a cage-like structure. One blue sphere on

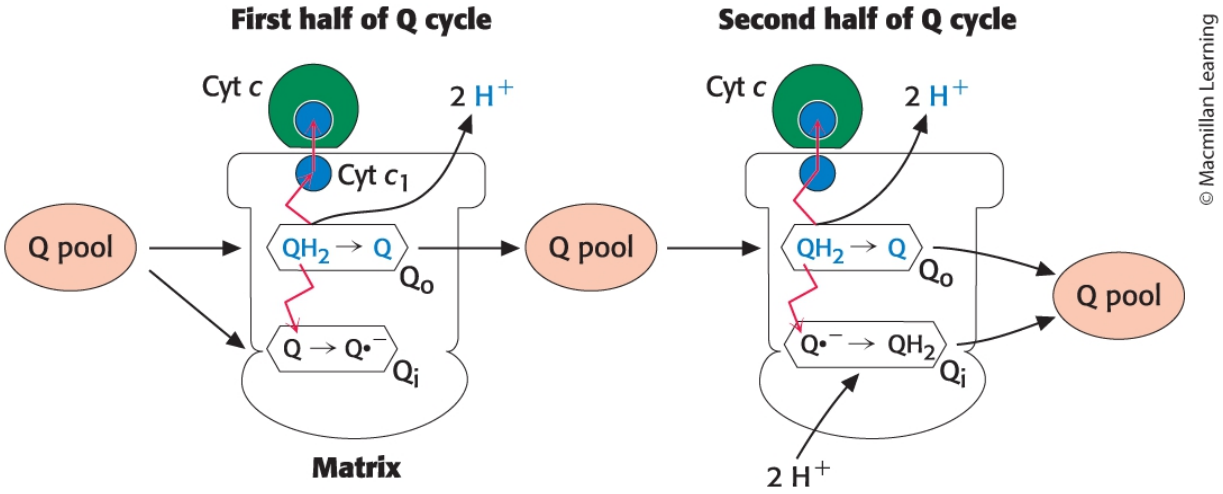
either end is connected to the pentagonal ring of the histidine side chain.

An arrow from the bottom end of the middle portion shows the ball-and-stick model of heme b subscript H. It consists of a central green sphere connected to blue spheres in a radial manner. The blue spheres are further connected to black spheres that form a cage-like structure. One blue sphere on either end is connected to the pentagonal ring of the histidine side chain.

The entire bottom portion of the oxidoreductase is in the matrix.

Return to FIGURE 18.10 Q-cytochrome c oxidoreductase is a homodimer, with each monomer consisting of 11 distinct polypeptide chains

Extended description for FIGURE 18.11 The Q cycle allows the safe transfer of electrons from Q H 2 to cytochrome c

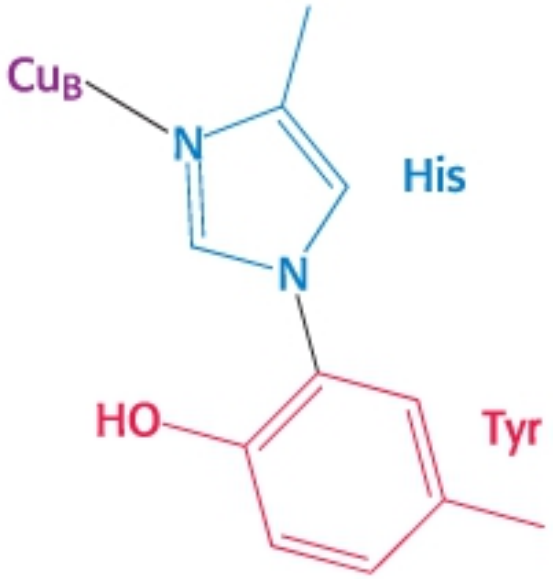


First half of Q cycle: An outline form of complex 3 is shown. Its top surface is bound to cytochrome c depicted as a medium-sized green sphere. The bottom surface is located in the matrix. Two arrows from a circle labeled Q pool point toward the inside of complex 3. The first arrow points toward the conversion of Q H 2 to Q inside a box. The box is labeled Q subscript 0. The second arrow points to the conversion of Q to semiquinone radical anion inside a box labeled Q subscript i. The semiquinone radical anion is depicted as Q superscript minus with an electron. A zigzag arrow from Q subscript 0 moves to cytochrome c 1 depicted as a small blue circle. Cytochrome c 1 then transfers the electron to cytochrome c. A black arrow from Q subscript 0 points toward 2 H superscript plus outside the complex 3. Another zigzag arrow from Q subscript 0 moves toward Q in Q subscript i. An arrow from Q subscript 0 points to a circle labeled Q pool located outside complex 3.

Second half of Q cycle: An outline form of complex 3 is shown. Its top surface is bound to cytochrome c depicted as a medium-sized green sphere. An arrow from the Q pool points toward Q subscript 0 inside complex 3. A zigzag arrow from Q subscript 0 moves to cytochrome c 1 depicted as a small blue circle. Cytochrome c 1 then transfers the electron to cytochrome c. A black arrow from Q subscript 0 points toward 2 H superscript plus outside the complex 3. Another zigzag arrow from Q subscript 0 moves toward semiquinone radical anion in Q subscript i. The box labeled Q subscript i shows the conversion of semiquinone radical anion to Q H 2. During this conversion, 2 H superscript plus ions from the matrix are used up. An arrow from Q subscript 0 and Q subscript i points toward a Q pool outside complex 3.

Return to FIGURE 18.11 The Q cycle allows the safe transfer of electrons from Q H 2 to cytochrome c

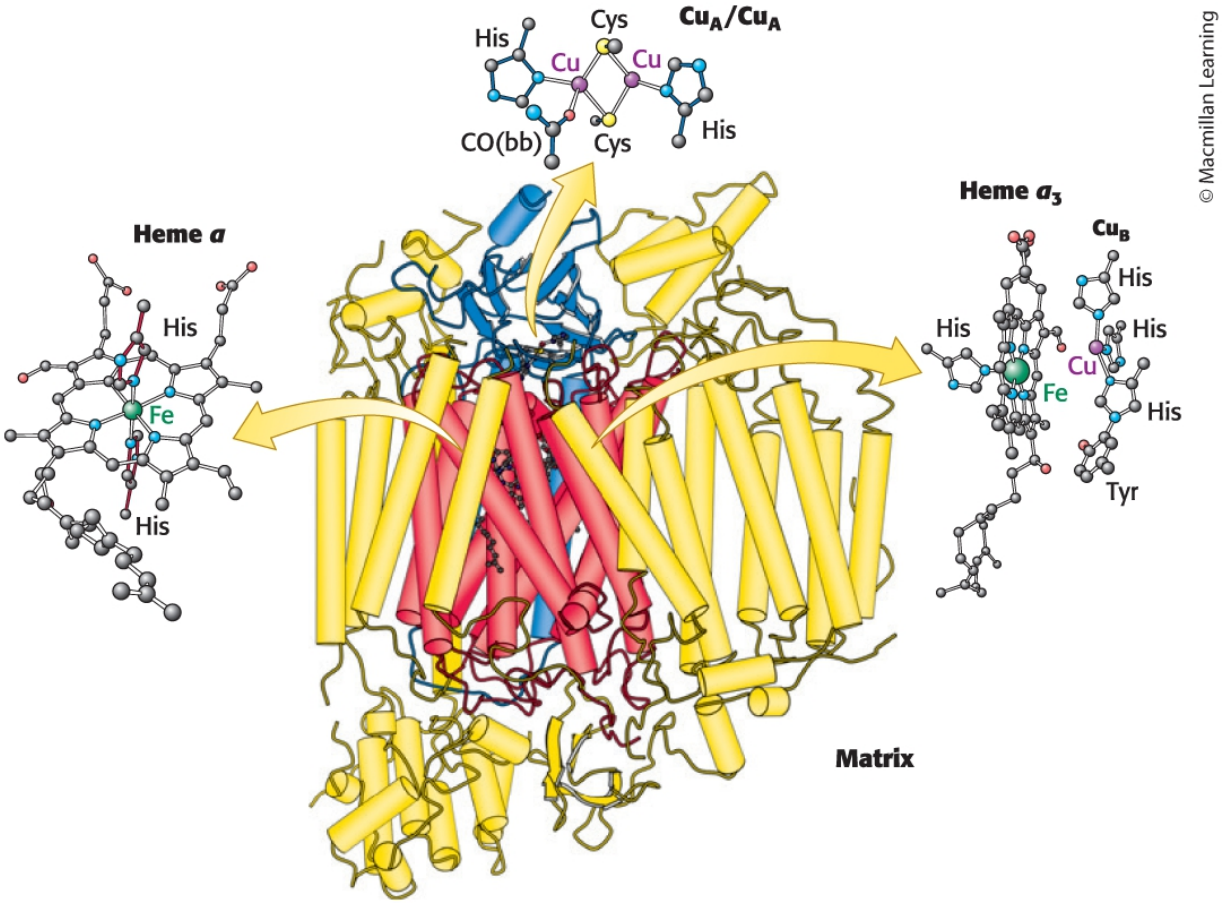
Extended description for Chemical structure of copper ion bonded to histidine residue covalently linked to a tyrosine residue



The histidine residue is depicted as a 5-membered heterocyclic pentagonal ring in a vertical orientation consisting of 2 N and 3 C atoms. First N occupies the bottom-most vertex and the second N occupies the top left vertex. A double bond is present between C 1 and N 2, and C 2 and C 3. N 2 is single bonded to C u subscript B on the upper left. C 2 has an open single bond on the upper right. N 1 is single bonded to C 5 of the tyrosine residue. The tyrosine residue is depicted as a benzene ring in a horizontal orientation with C 1 occupying the rightmost vertex. It contains alternating double bonds between C 2 and C 3, C 4 and C 5, and C 6 and C 1. C 1 has an open single bond on the right. C 4 is single-bonded to O H on the left.

Return to Chemical structure of copper ion bonded to histidine residue covalently linked to a tyrosine residue

Extended description for FIGURE 18.12 The structure of bovine cytochrome c oxidase reveals 13 polypeptide chains and numerous electron carriers



© Macmillan Learning

The bovine cytochrome c consists of a central cluster of long vertical red cylindrical structures. These are flanked by long vertical yellow cylindrical structures. A blue cylindrical structure is shown in the center of the cluster of red cylindrical structures. A few short and medium cylindrical structures are shown above them. Several short threads extend from these cylindrical structures. Just above the blue cylindrical structure, a few beta-strands are located. The bottom portion oriented toward the bottom left consists of a cluster of short and medium yellow cylindrical structures. Several short

threads are extending from the cylindrical structure. An arrow from the hollow center of the beta-strands in the top points toward C u subscript A slash C u subscript A. It shows two C u atoms depicted as purple spheres connected to a yellow sphere of a common cysteine side chain in the top center and bottom center. The left purple sphere is connected to a blue sphere of the pentagonal ring of the histidine side chain and a tiny red sphere of C O

open parenthesis b b close parenthesis. The red sphere is further connected to a black sphere. The black sphere is further connected to a blue sphere on the upper left and a black sphere below. The right purple sphere is connected to a blue sphere of the pentagonal ring of the histidine side chain.

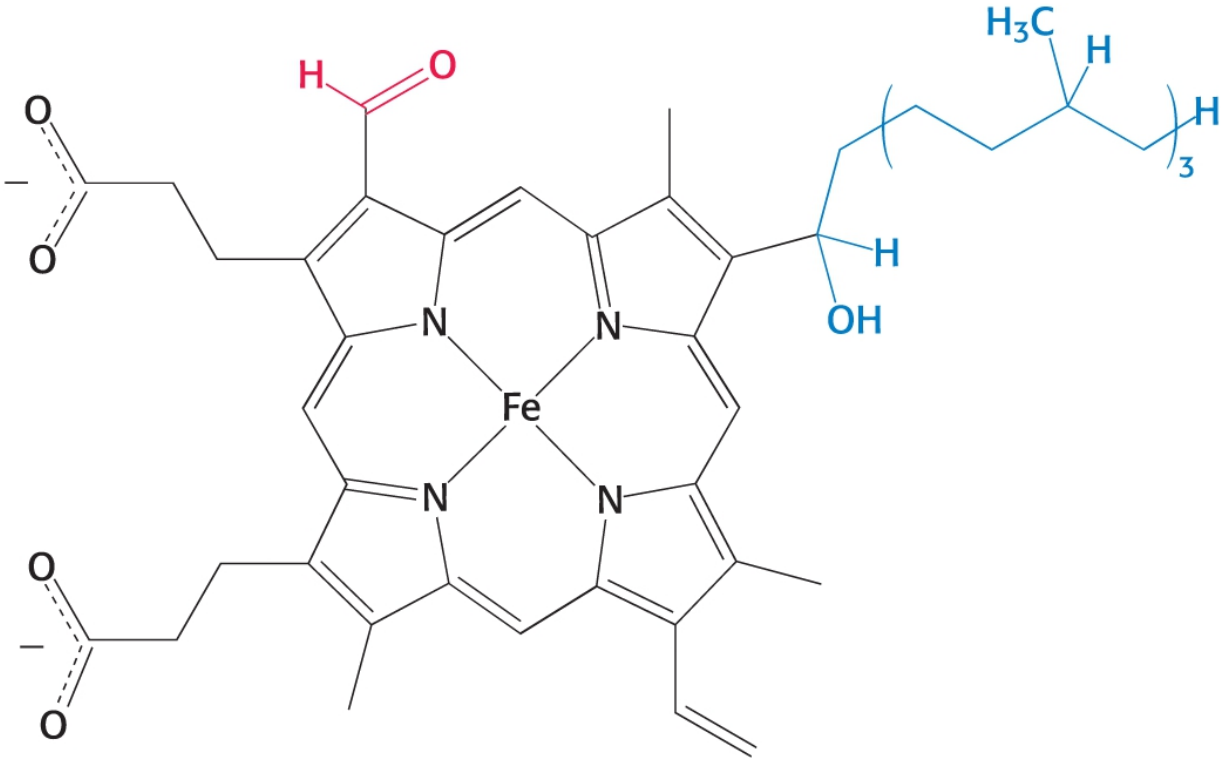
An arrow from the left end of the central cluster of red cylindrical structures point toward heme a. It consists of a central F e atom depicted as a green sphere connected to 5 blue and one black sphere in a radial manner. These blue and black spheres are further connected to black spheres to form a cage-like network. Heme a is connected to two histidine side chains.

An arrow from the right end of the central cluster of red cylindrical structures point toward heme a subscript 3 and C u subscript B. Heme a subscript 3 consists of a central green sphere connected to blue spheres that are further connected to black spheres to form a cage-like network. The heme ring is connected to the pentagonal ring of the histidine side chain. C u subscript B consists of a central purple sphere depicting C u atom connected to a blue sphere of the pentagonal ring of the histidine side chain above, on the right, and below. The second blue sphere of the pentagonal ring of the bottom histidine side chain is further connected to the tyrosine side chain.

Return to FIGURE 18.12 The structure of bovine cytochrome c oxidase reveals 13 polypeptide chains and numerous electron

carriers

Extended description for Structure of heme A



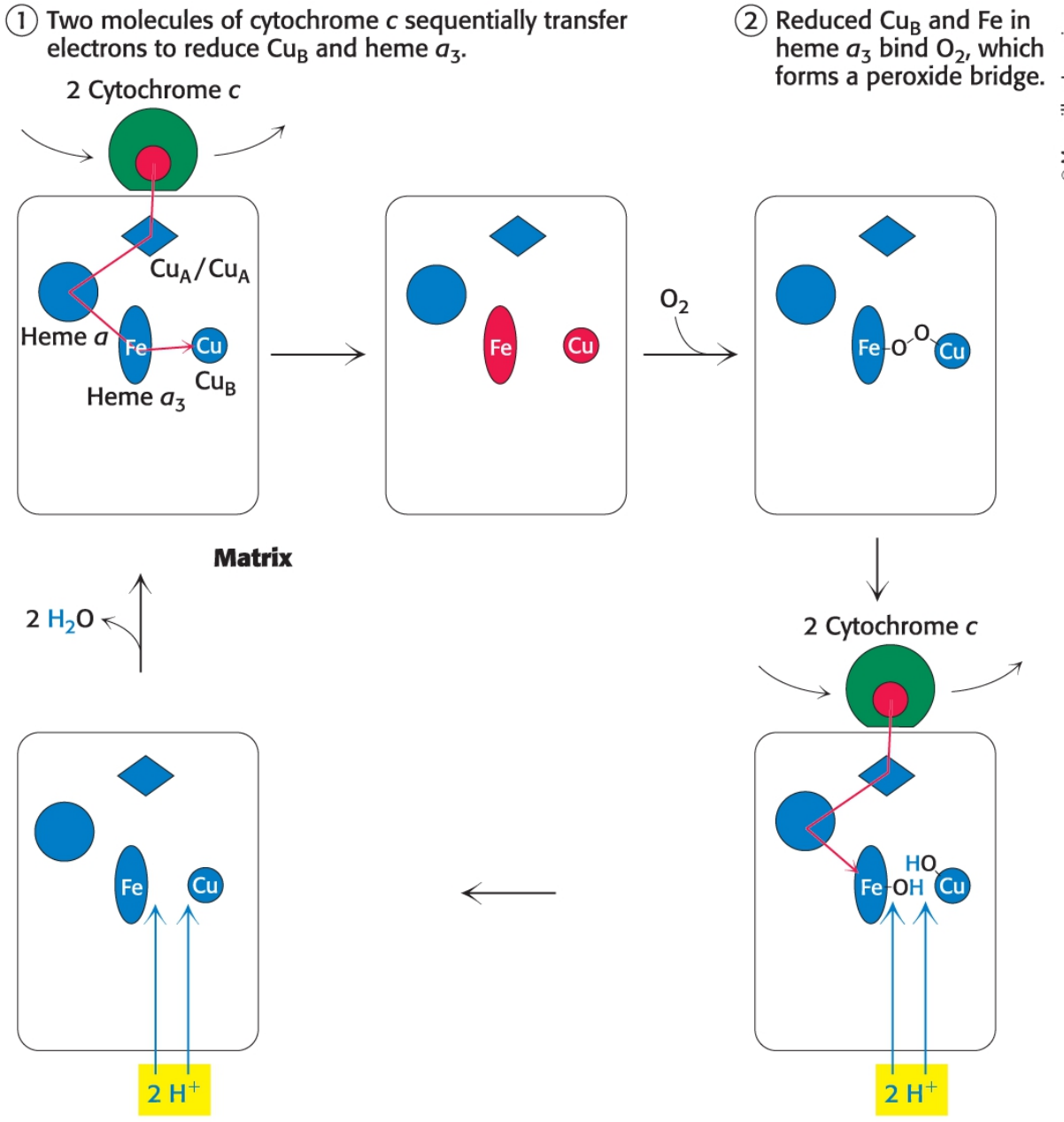
Heme A

The structure consists of a central F e atom single bonded to the N atom of a 5-membered heterocyclic pentagonal ring on the upper left, upper right, lower left, and lower right. Each ring consists of 1 N and 4 C atoms. All rings except the upper left ring contain two double bonds between any two of the following atoms: C 2 and C 3, N and C 1, C 1 and C 2, C 3 and C 4, or C 4 and N. The upper left ring contains a double bond between C 2 and C 3. C 1 and C 4 atoms of adjacent rings are connected by methylene bridges. In the upper left ring, C 2 is single bonded to a 3-carbon alkane chain depicted as a line structure using 2 lines. C 3 is partially double bonded to O on the upper left and lower left. This group has an overall negative charge. C 3 is single bonded to C above, which is further single bonded to H on the upper left and double bonded to O on the upper

right. In the upper right ring, C 2 is single-bonded to C H 3 above in the form of a line. C 3 is single-bonded to a 6-carbon alkane chain depicted as a line structure using 5 zigzag lines. C 1 is single bonded to O H on the lower right and H on the right. C 3 to C 6 are enclosed in parenthesis with subscript 3. C 6 is single bonded to H on the upper right. C 5 is single bonded to C H 3 on the upper left and H on the upper right. In the lower right ring, C 2 is single-bonded to C H 3 in the form of a line on the right. C 3 is single-bonded to a 2-carbon alkene chain depicted as two parallel lines. In the lower-left ring, C 2 is single-bonded to C H 3 below in the form of a line. C 3 is single bonded to a 3-carbon alkane chain depicted using 2 lines. C 3 is partially double-bonded to O on the upper left and O on the lower right. This group has an overall negative charge.

Return to Structure of heme A

Extended description for FIGURE 18.13 The mechanism of cytochrome c oxidase prevents early oxygen release



© Macmillan Learning

The mechanism is divided into 4 steps as follows:

Step 1: A square is shown and the region below its bottom surface is labeled matrix. The square contains the following components: A blue diamond labeled C u subscript A slash C u subscript A, a medium blue circle labeled heme a, a blue oval containing F e labeled heme a subscript 3, and a tiny blue circle containing C u labeled C u subscript B. A medium green circle with a red core is located above the top surface of the square and is labeled 2 cytochrome c. An arrow points toward cytochrome c and another arrow points away from it. A zigzag arrow starts from the red core of cytochrome c and passes through C u subscript A slash C u subscript A, heme a, and heme a subscript 3, to ultimately reach C u subscript B. The text above reads “Two molecules of cytochrome c sequentially transfer electrons to reduce C u subscript B and heme a subscript 3.

An arrow from the first square leads to the second square. The components of the second square are a blue diamond, a medium blue circle, a red oval containing F e, and a tiny red circle containing C u. It lacks cytochrome c at the top surface.

Step 2: O 2 enters and cross-links the blue oval containing Fe with the tiny blue circle containing C u through O, single bond, O. The square lacks cytochrome c at the top surface. The text above reads “Reduced C u subscript B and F e in heme a subscript 3 bind O 2, which forms a peroxide bridge.

Step 3: 2 cytochrome c binds to the surface of the square again. A zigzag arrow from the red core of cytochrome c passes through the blue diamond and medium blue circle to ultimately reach a blue oval containing Fe. The blue oval is single-bonded to O H. The tiny blue circle containing C u is also single bonded to O H. This happens as 2 H superscript plus from the matrix and electrons from

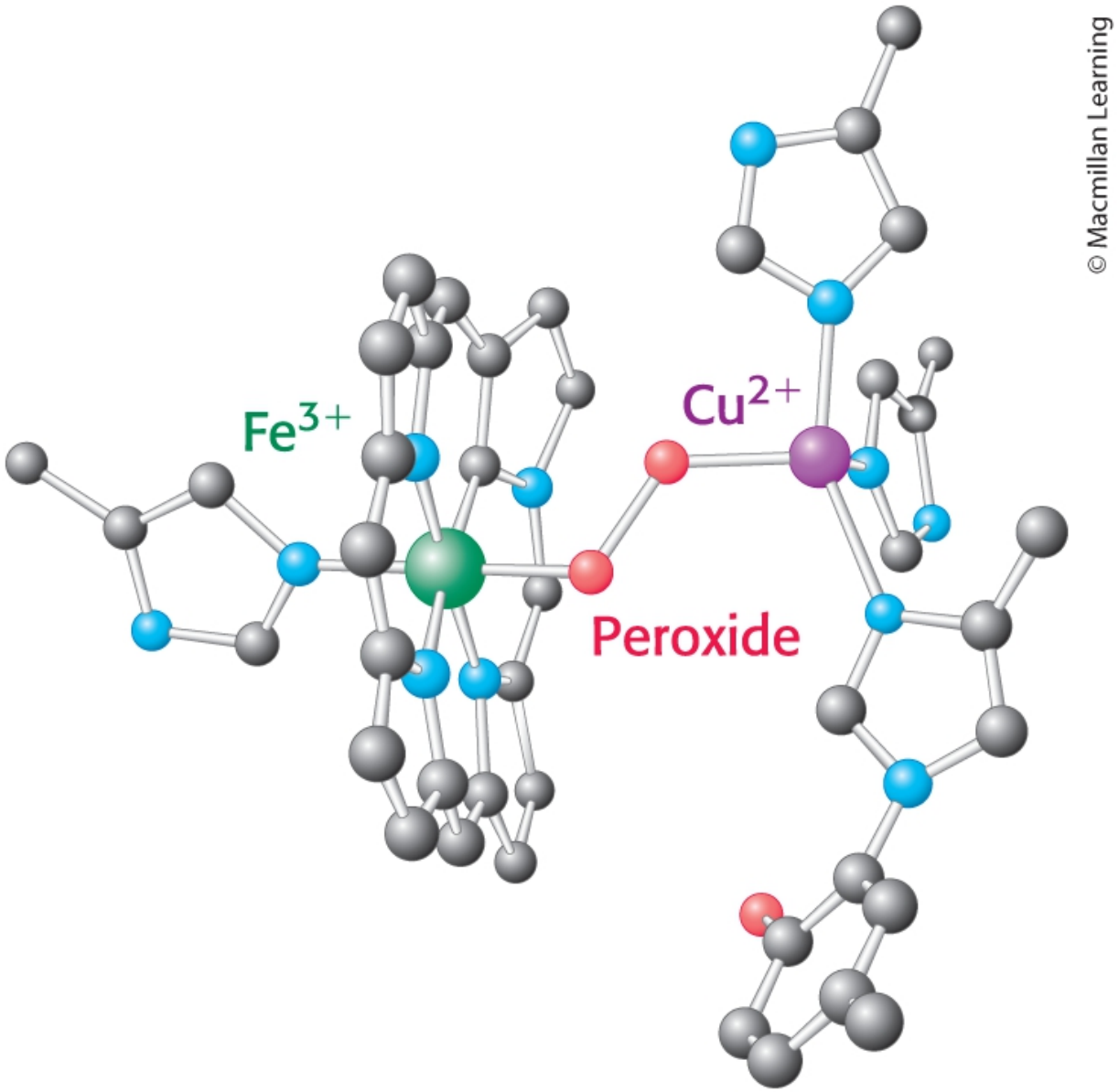
cytochrome c travel toward the peroxide bridge. The text below reads “The addition of two more electrons and two more protons cleaves the peroxide bridge.

Step 4: The square contains a blue diamond, a medium blue circle, a blue oval containing F e, and a tiny blue circle containing C u. Two arrows from 2 H superscript plus in the matrix point toward the oval and the tiny circle. The text below reads “The addition of two more protons leads to the release of water.”

2 H 2 O molecules are released and the cycle begins again.

Return to FIGURE 18.13 The mechanism of cytochrome c oxidase prevents early oxygen release

Extended description for FIGURE 18.14 Two metals form a peroxide bridge in cytochrome c oxidase



© Macmillan Learning

The ball-and-stick model of heme a subscript 3 is shown on the left and C u subscript B is shown on the right. The heme a subscript 3 molecule consists of a central green sphere depicting F e superscript 3 plus. It is connected to 4 blue spheres, one red sphere, and one

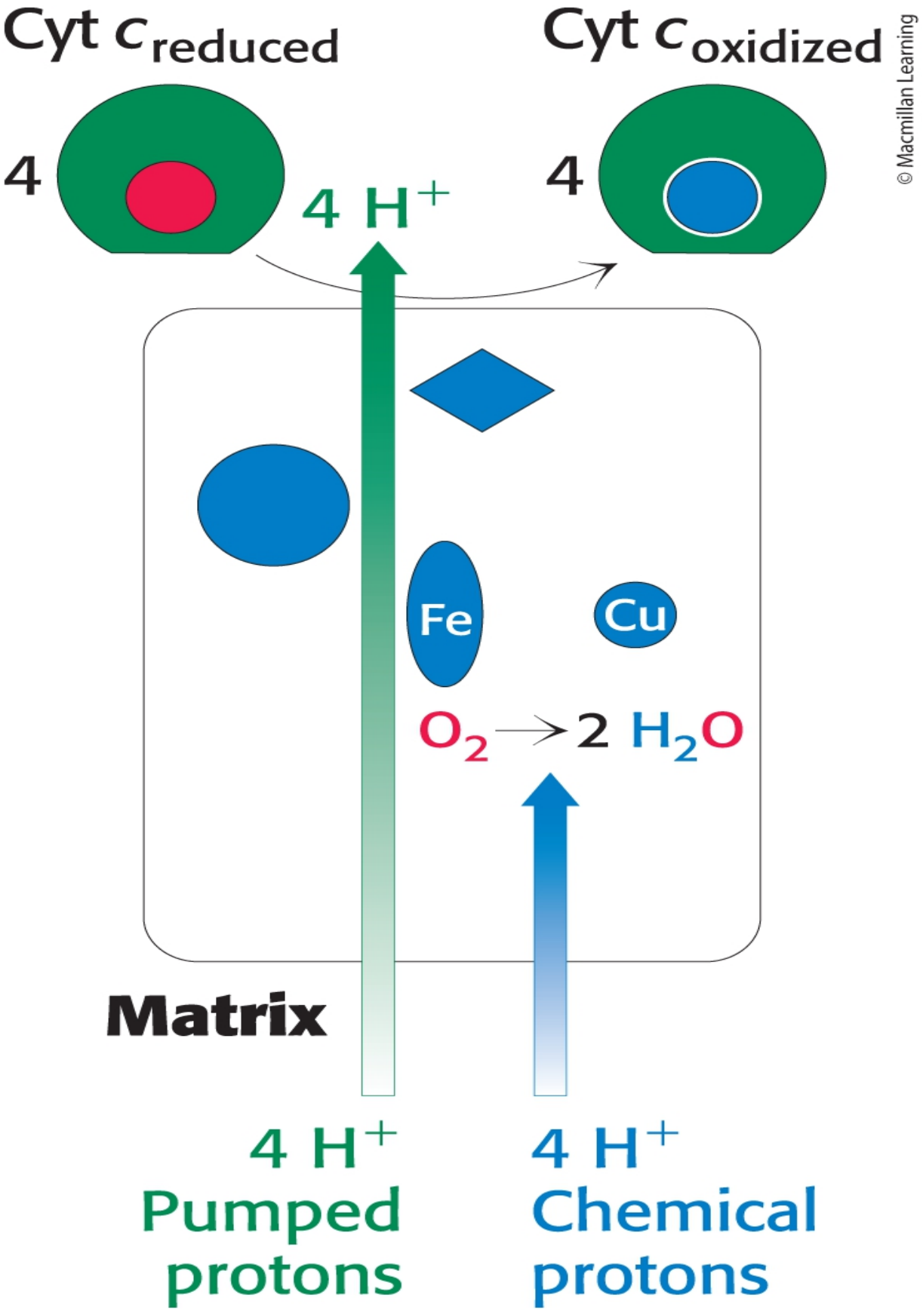
black sphere in a radial fashion. Three blue spheres and one black sphere are further connected to more black spheres to form a cage-like structure. One blue sphere is part of a pentagonal ring composed of 2 blue and 3 black spheres. The ring is located toward the left, away from the plane of the cage-like structure. The red sphere is further connected to a second red sphere. The second red sphere is in turn connected to a purple sphere depicting C u superscript 2 plus metal atom of C u subscript B. The chain of two red spheres depicts peroxide.

In C u subscript B, the central purple sphere is connected to a blue sphere of a pentagonal ring at the top, right, and bottom. The pentagonal rings consist of 2 blue and 3 black spheres. One black sphere is further connected to a black sphere. The second blue sphere of the bottom pentagonal ring is connected to a hexagonal ring composed of 6 black spheres. In the hexagonal ring, one black sphere is connected to a red sphere and another black sphere is connected to a black sphere.

Return to FIGURE 18.14 Two metals form a peroxide bridge in cytochrome c oxidase

Extended description for FIGURE 18.15 Proton transport by cytochrome c oxidase has two

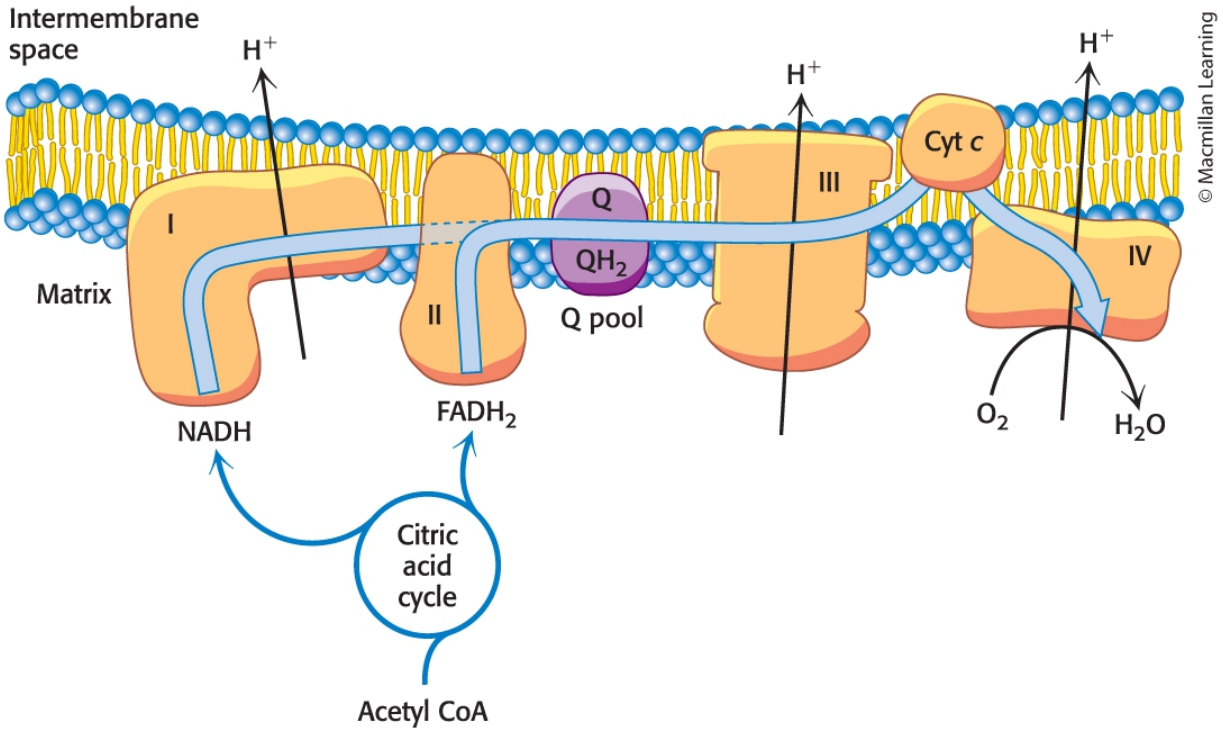
components


Cyt $c_{reduced}$
Cyt $c_{oxidized}$
4
4
4 H^+
Fe
Cu
$O_2 \rightarrow 2\ H_2O$
Matrix
4 H^+
Pumped protons
4 H^+
Chemical protons
© Macmillan Learning

A square contains a blue diamond, a medium blue circle, a blue oval containing F e, and a tiny circle containing C u. A green upward arrow passes across the square from bottom to the top surface to depict 4 H superscript plus ions or protons being pumped from the matrix into the intermembrane space. An arrow across the head of the green arrow, above the top surface of the square, depicts the conversion of 4 cytochrome c reduced to 4 cytochrome c oxidized. The reduced form is depicted as a medium-green circle with a red core. The oxidized form is depicted as a medium-green circle with a blue core. A blue upward arrow depicts the transport of 4 H superscript plus ions or chemical protons from the matrix into the square. The arrowhead points toward an irreversible reaction showing the conversion of O 2 to 2 H 2 O inside the square.

Return to FIGURE 18.15 Proton transport by cytochrome c oxidase has two components

Extended description for FIGURE 18.16 Electrons flow via two pathways through the electron-transport chain

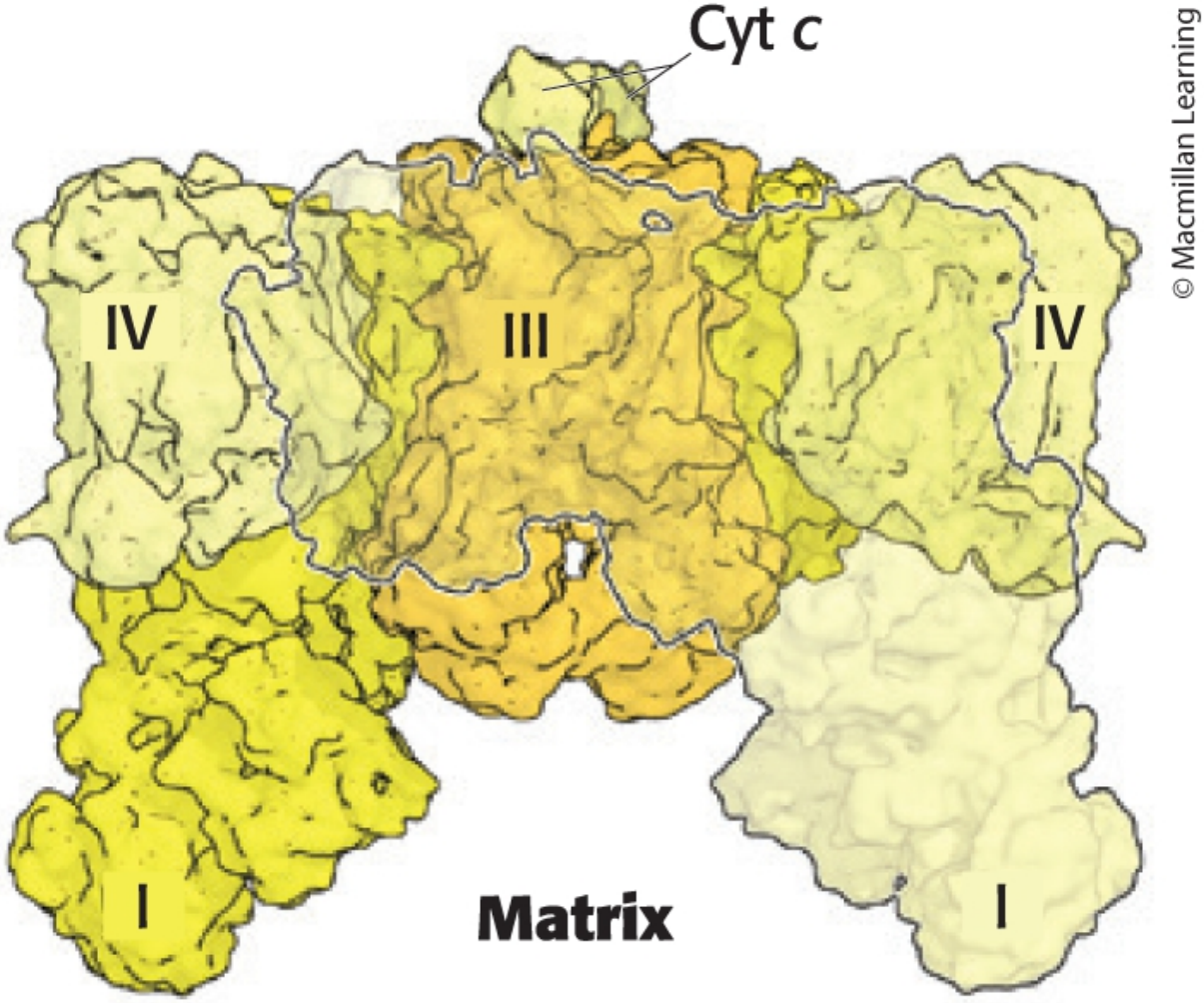


Three complexes labeled roman numbers 1, 2, and 3 are shown embedded in the lipid bilayer from left to right. The fourth complex labeled roman number 4 is attached to the inner leaflet of the bilayer. A small purple structure is embedded in the membrane between complex 2 and 3 and is labeled Q pool. Q pool alternates between Q and Q H 2 during electron transport. A small orange structure labeled cytochrome c is embedded in the membrane between complex 3 and 4. The region above the bilayer is labeled intermembrane space and the region below is labeled matrix. A very simplified citric acid cycle is shown to operate in the matrix. Its products include acetyl C o A, F A D H 2, and N A D H. Electrons from N A D H travel through complex 1, 2, Q pool, complex 3, cytochrome c, and then complex 4. Electrons from F A D H 2 travel

through complex 2, Q pool, complex 3, cytochrome c, and complex 4. An upward arrow across complex 1, 3, and 4 shows the transport of H superscript ion from the matrix to the intermembrane space. A curved arrow below complex 4 denotes the simultaneous conversion of O 2 to H 2 O.

Return to FIGURE 18.16 Electrons flow via two pathways through the electron-transport chain

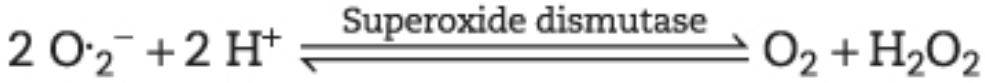
Extended description for FIGURE 18.17 Three complexes of the ETC associate to form the respirasome



The respirasome consists of a central complex 3, flanked by complex 4 on the left and right. A small cytochrome c is attached to the top surface of complex 3. The bottom surface of left complex 4 is attached to complex 1. The bottom surface of the right complex 4 is attached to complex 1.

Return to FIGURE 18.17 Three complexes of the ETC associate to form the respirasome

Extended description for Conversion of superoxide radical by enzyme superoxide dismutase



The reaction has two reactants and two products.

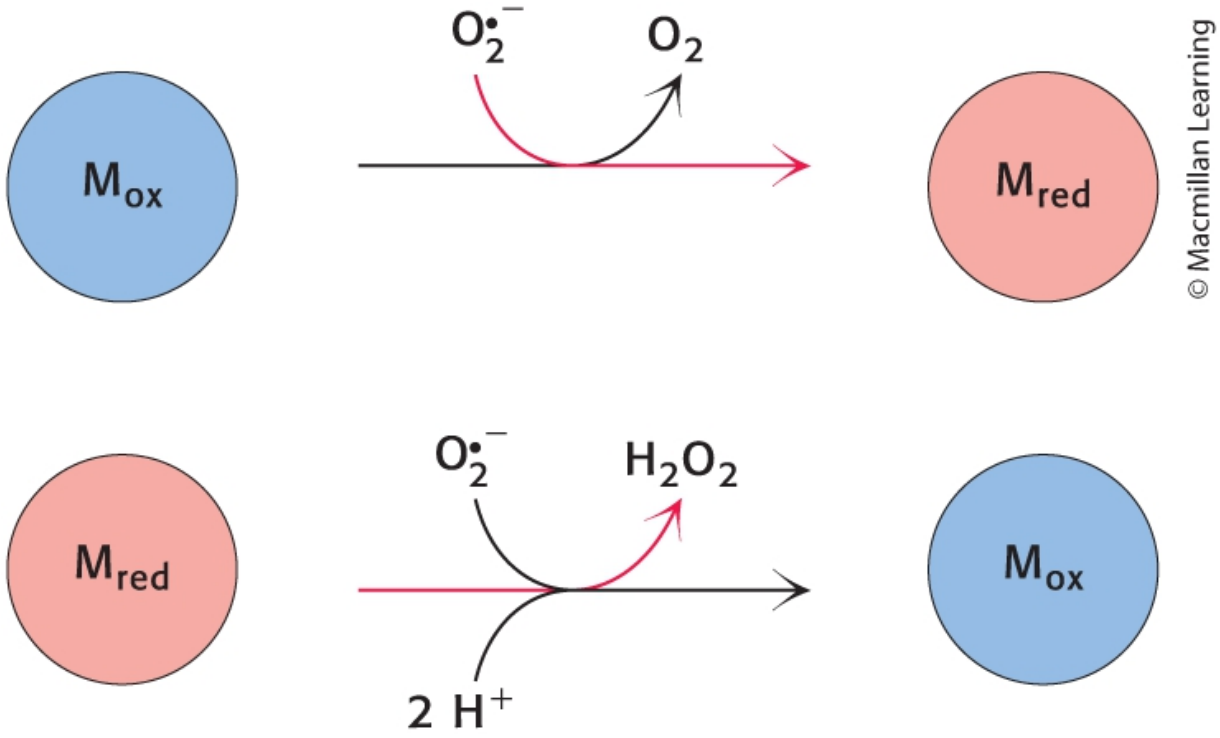
Reactants: 2 O 2 superscript minus ions with an unpaired electron; 2 H superscript plus ions.

A reversible arrow is labeled superoxide dismutase.

Products: O 2; H 2 O 2.

Return to Conversion of superoxide radical by enzyme superoxide dismutase

Extended description for FIGURE 18.18 The superoxide dismutase mechanism has two phases



© Macmillan Learning

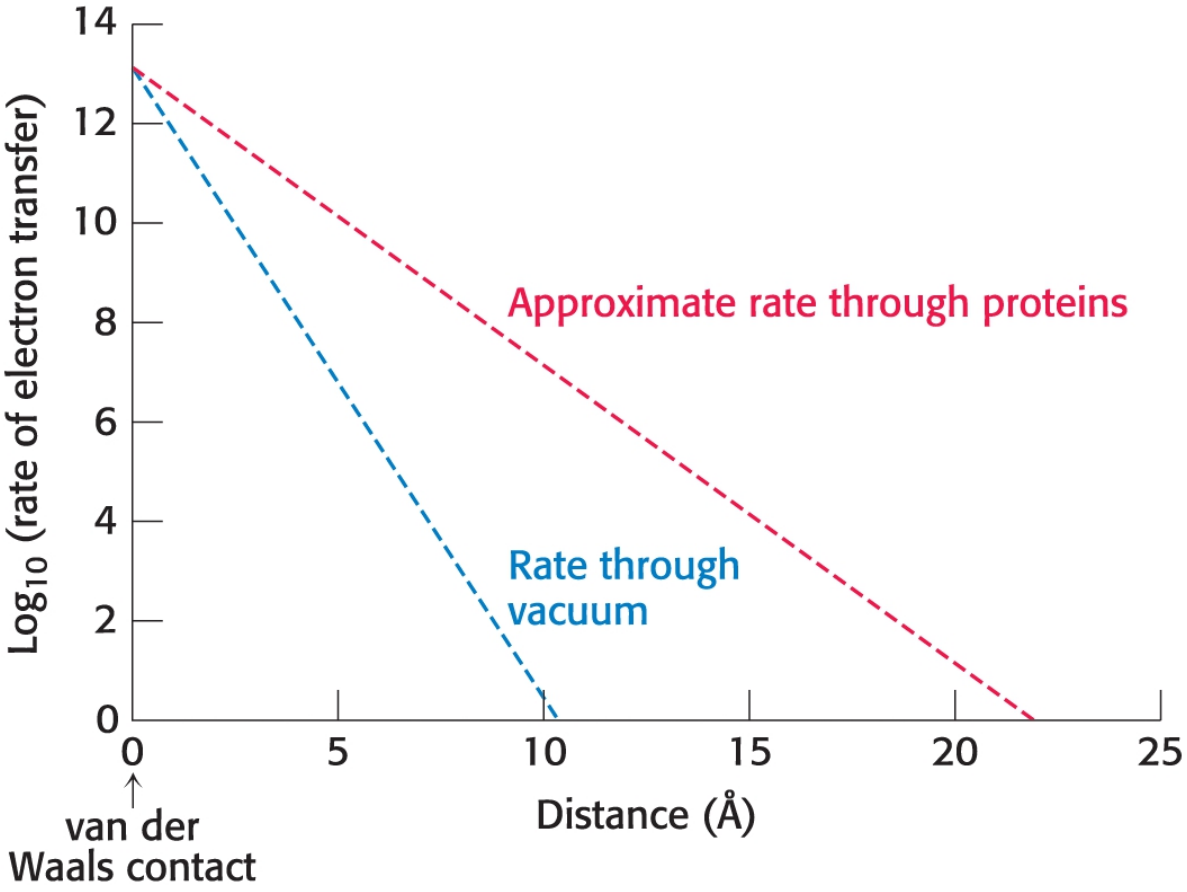
The schematic illustration shows the following conversions:

Part 1: A forward arrow coupled with the conversion of O 2 superscript minus with an unpaired electron into O 2 is drawn from a blue circle labeled “M subscript o x” to a pink circle labeled “Msubscript r e d.”

Part 2: A forward arrow coupled with the entry of 2 H superscript plus ion and conversion of O 2 superscript minus with an unpaired electron into H 2 O 2 is drawn from a pink circle labeled “M subscript r e d” to a blue circle labeled “M subscript o x.”

Return to FIGURE 18.18 The superoxide dismutase mechanism has two phases

Extended description for FIGURE 18.19 Proteins dramatically improve the rate of electron transfer



© Macmillan Learning

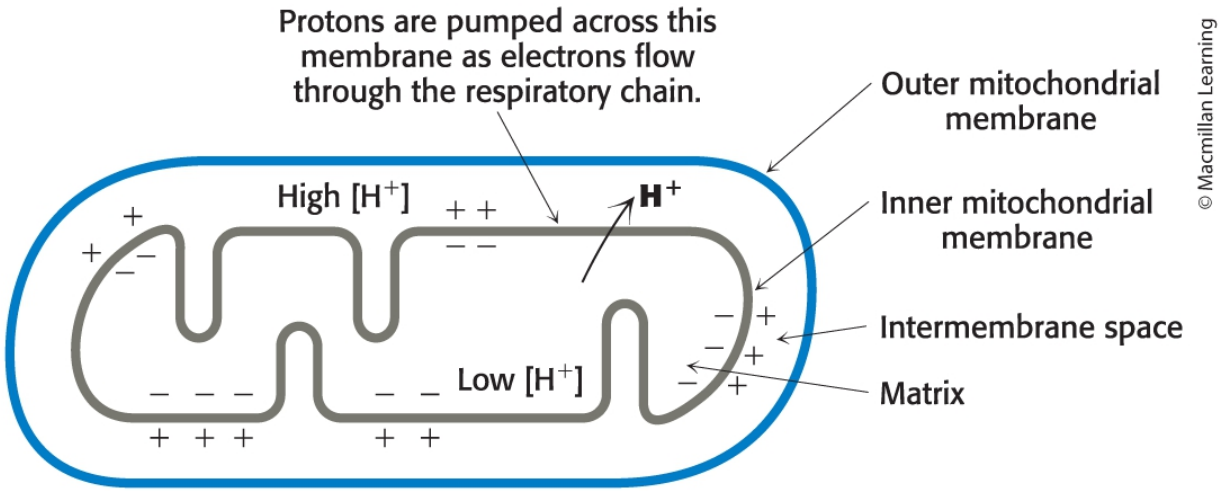
The graph has the distance in angstrom indicated on the horizontal axis ranging from 0 to 25 angstroms in increments of 5 angstroms. Van der Waals contact is indicated at 0 angstroms. The logarithm base 10 (rate of electron transfer) is indicated on the vertical axis ranging from 0 to 14 in increments of 2 units.

A linear descending steep slope depicted by a dashed blue line is labeled “Rate through vacuum.” The dashed blue line is drawn straight from (0, 13) to (10.3, 0).

The linear descending slope depicted by a dashed pink line is labeled “Approximate rate through proteins.” The dashed pink line is drawn straight from (0, 13) to (22, 0). All values are approximated.

Return to FIGURE 18.19 Proteins dramatically improve the rate of electron transfer

Extended description for FIGURE 18.20 The chemiosmotic hypothesis states that electron-driven proton transport and ATP synthesis are coupled

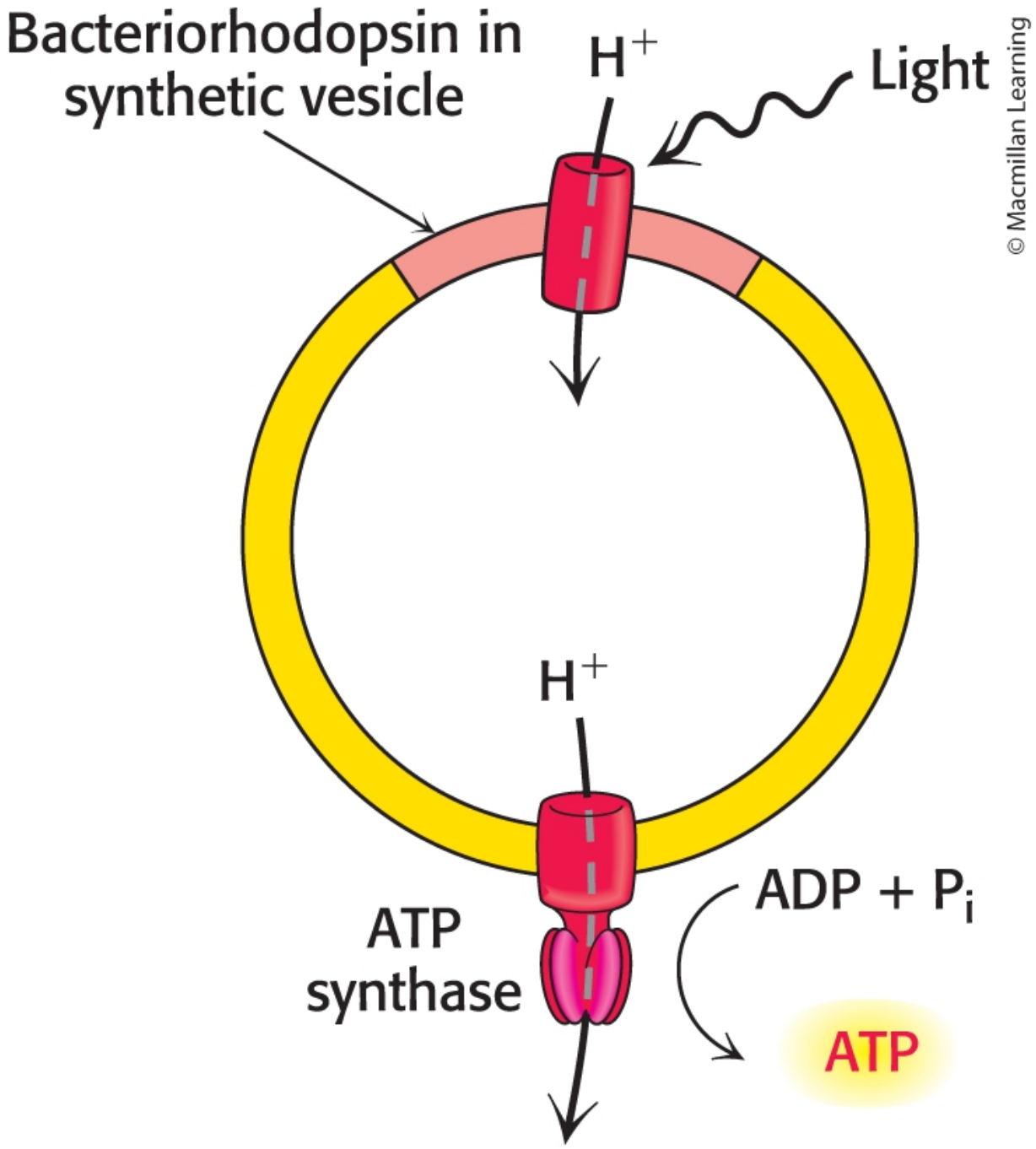


© Macmillan Learning

The mitochondrion is depicted as a large capsule-shaped structure with a solid blue outline labeled outer mitochondrial membrane. The inner mitochondrial membrane is shown as a solid grey line forming several invaginations into the matrix. The space between the inner and outer mitochondrial membrane is labeled intermembrane space. Discrete clusters of negative and positive charge are shown along the inner mitochondrial membrane. The inner surface of the inner membrane is negatively charged and the outer surface is positively charged. An arrow from the matrix points toward the intermembrane space to show the movement of the H superscript plus ion. The intermembrane space has a high H superscript plus ion concentration and the matrix has a low H superscript plus ion concentration. The text alongside an arrow pointing toward the inner mitochondrial membrane reads "Protons are pumped across this membrane as electrons flow through the respiratory chain."

Return to FIGURE 18.20 The chemiosmotic hypothesis states that electron-driven proton transport and ATP synthesis are coupled

Extended description for FIGURE 18.21 The chemiosmotic hypothesis is supported by experiments using bacterial proton pumps

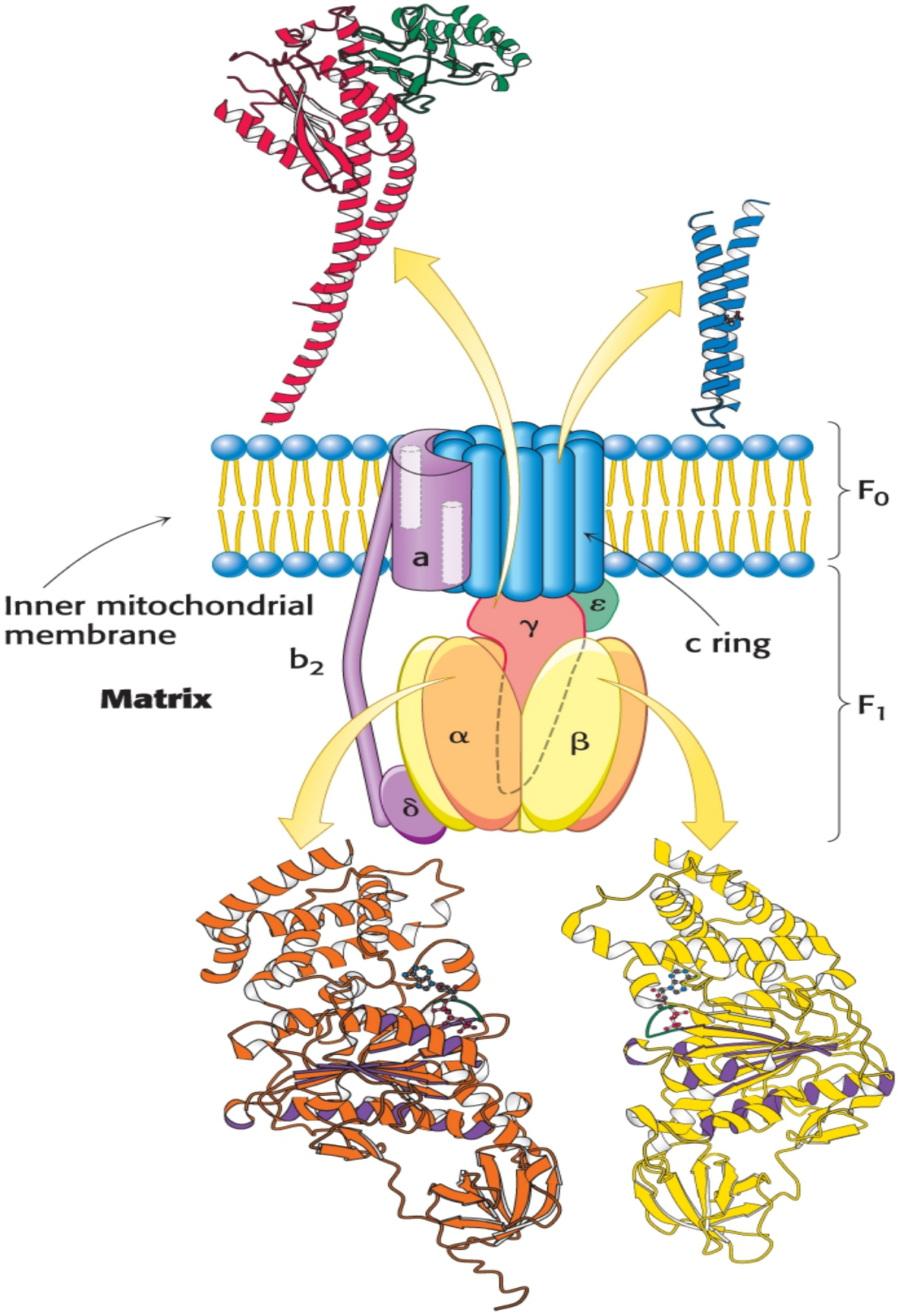


The membrane vesicle is depicted as a hollow circle with a thick yellow outline. The topmost area of the membrane vesicle has a stretch of pink area containing a hollow cylindrical structure. This region is labeled "Bacteriorhodopsin in synthetic vesicle." A wavy line labeled light points toward the hollow cylindrical structure. An inward arrow across the cylindrical structure shows the entry of H superscript plus ion. The bottom area of the membrane vesicle contains an A T P synthase. An outward arrow across it depicts the exit of the H superscript plus ion from the membrane vesicle. This movement powers the synthesis of A T P from A D P and P subscript i by the A T P synthase.

Return to FIGURE 18.21 The chemiosmotic hypothesis is supported by experiments using bacterial proton pumps

Extended description for FIGURE 18.22 The structure of ATP synthase reveals a complex molecular rotational

motor



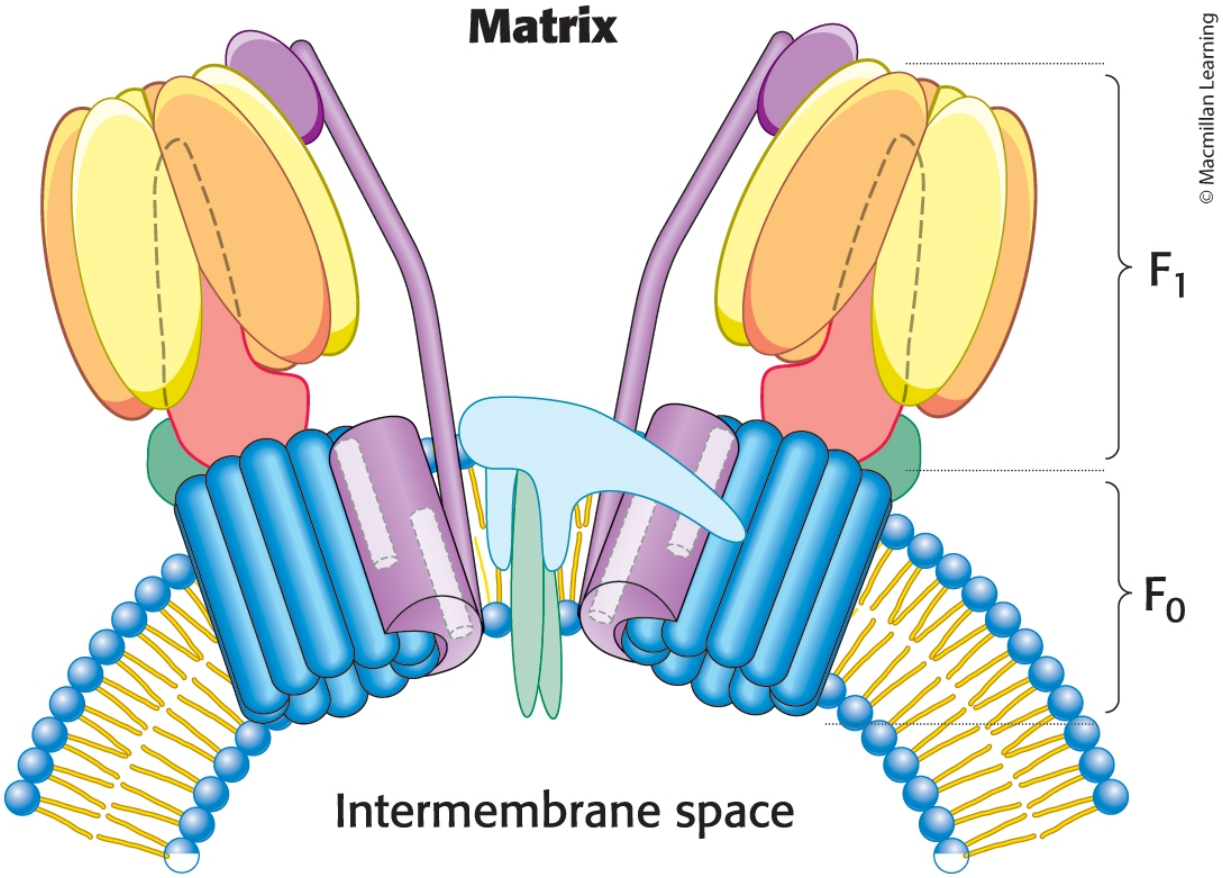
© Macmillan Learning

The A T P synthase consists of a hollow cylindrical structure embedded in the inner mitochondrial membrane. The cylindrical structure is labeled “c ring” and is lined by 10 elongated subunits. Three of these subunits are enclosed in a long cylindrical groove of a half-cut vertical cylindrical structure labeled “a.” The structure a is also embedded in the membrane. A tubular extension with a bend is labeled b 2 and its connects structure “a” with structure “delta” in the matrix. The structure delta is small oval-shaped and is part of a large complex in the matrix composed of alpha, beta, gamma, and epsilon subunits. The alpha and beta subunits are long oval-shaped structures that form a unit. The gamma subunit has a broad top and a tapered bottom. The bottom extends into the space between the alpha and beta subunits. The broad top is attached to the bottom surface of the “c ring.” The epsilon subunit is small and located on the right of the gamma subunit, just below the bottom surface of the c ring. The A T P synthase is divided into two regions, namely F 0 and F 1. F 0 includes membrane-embedded components like c-ring and structure a. F 1 includes matrix components like a portion of b 2, alpha, beta, gamma, delta, and epsilon subunits.

The elongated subunits of the c ring consist of a pair of long and vertical alpha-helices. The gamma subunit is composed of a long and slightly curved alpha-helix. Its top portion has three short and medium-sized alpha helices and a few beta-strands. One of the helices extends downward, halfway through the length of the long alpha-helix. The top right portion of the gamma subunit is attached to a small green cluster composed of two alpha-helices and a few beta-strands. The alpha subunit is composed of several alpha-helices interconnected by thread-like loops and a cluster of beta-strands at the bottom. The beta subunit is composed of several alpha-helices interconnected by thread-like loops and a cluster of beta-strands at the bottom.

Return to FIGURE 18.22 The structure of ATP synthase reveals a complex molecular rotational motor

Extended description for FIGURE 18.23 Mitochondrial ATP synthase forms homodimers

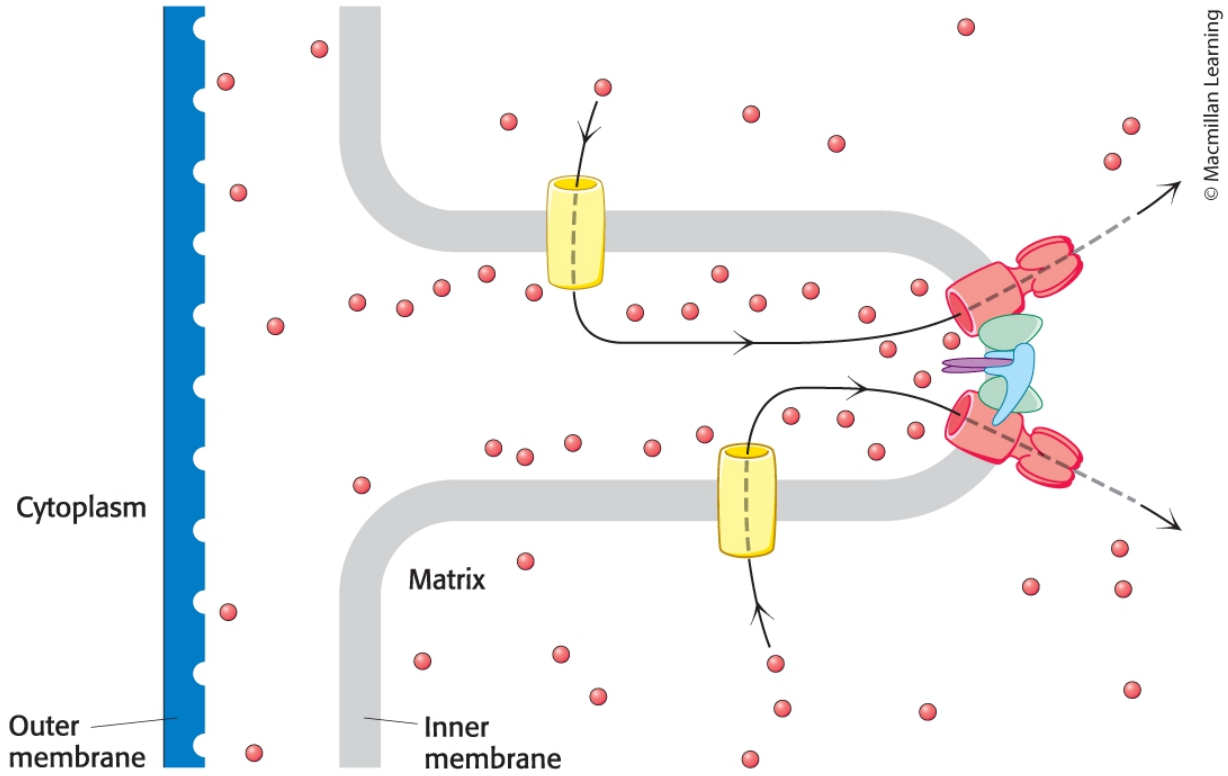


Two mitochondrial A T P synthases are shown embedded into the inner mitochondrial membrane. The membrane is curved outward and the region above it is labeled matrix and the region below is labeled intermembrane space. The F 0 component including the c ring, structure a, and portion of b 2 is embedded in the membrane. The F 1 component including alpha, beta, gamma, delta, epsilon subunits, and a portion of b 2 are located in the matrix. The dimer of A T P synthase is joined by a complex of proteins. The complex is composed of a pair of elongated oval proteins spanning the membrane. The pair has an irregularly shaped protein at the top

that extends between the b 2 subunit of one A T P synthase and the c-ring subunits of the second A T P synthase.

Return to FIGURE 18.23 Mitochondrial ATP synthase forms homodimers

Extended description for FIGURE 18.24 ATP synthase assists in the formation of cristae

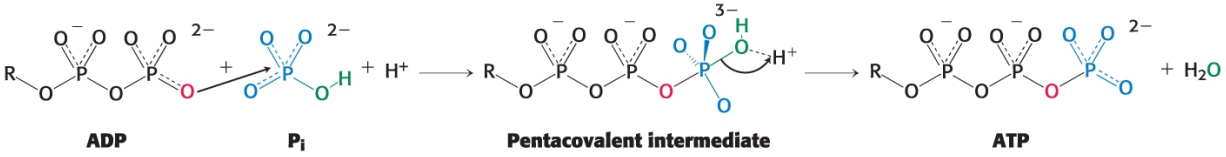


A long and vertical blue strip depicting the outer membrane contains uniformly spaced tiny semicircular grooves along its right edge. The region on its left is labeled cytoplasm. The crista is shown as a horizontal U-shaped structure formed by the inner membrane. The inner membrane is depicted as a continuous grey strip. The outer and inner membranes have a gap between them. A dimer of mitochondrial A T P synthase is shown embedded in the crista. The dimer is joined by a protein complex. Several red balls are scattered across the space between the inner and outer membrane. They are more concentrated in the U-shaped groove formed by the crista. A few red balls are also shown in the matrix, depicted as the space on the right of the inner membrane. Two yellow-colored hollow

cylindrical structures are also embedded in the inner membrane forming the side walls of the crista. A continuous arrow shows the movement of the red balls in the matrix across the cylindrical structure into the U-shaped groove and then back into the matrix through the A T P synthase.

Return to FIGURE 18.24 ATP synthase assists in the formation of cristae

Extended description for FIGURE 18.25 ATP-synthesis is catalyzed by ATP synthase



The reaction consists of three reactants, one intermediate, and two products. The first reactant is A D P whose structure is as follows: A zigzag chain is composed of 2 P and 3 O atoms. P atoms occupy the second and fourth positions and the remaining positions are occupied by O atoms. A partial double bond is present between P 2 and O 3. O 1 is single-bonded to R on the upper left. Both P atoms are partially double-bonded to O on the upper left and O on the upper right. The O atoms bonded to P 1 have an overall negative charge. The O atoms bonded to P 2 have an overall negative charge of 2 minus.

The second reactant is P subscript i whose structure is as follows: A central P atom is partially double bonded to O on the upper left, upper right, and lower left. The O atoms on the upper left and upper right have an overall negative charge of 2 minus. P atom is also single-bonded to O on the lower right which is further single-bonded to H on the upper right. The third reactant is H superscript plus ion.

A solid black arrow points from O 3 of A D P to the central P atom of P subscript i.

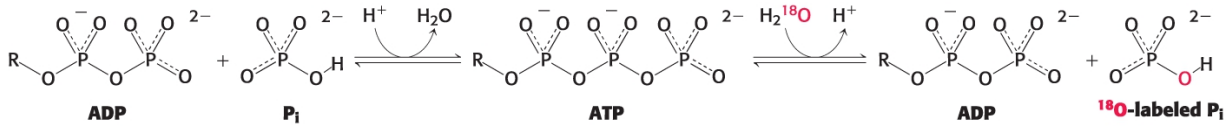
The intermediate is a pentacovalent intermediate whose structure is as follows: A zigzag chain is composed of 3 P and 3 O atoms. P atoms

occupy the second, fourth, and sixth positions, and the remaining positions are occupied by O atoms. O 1 is single-bonded to R on the upper left. P 1 and P 2 are partially double-bonded to O on the upper left and O on the upper right. The O atoms bonded to P 1 and P 2 have an overall negative charge. P 3 is dash bonded to O on the upper left, wedge bonded to O above, single bonded to O on the upper right, and single bonded to O on the lower right. The upper right O is further single bonded to H above and connected through a dashed line to H superscript minus on the lower right. The O atoms bonded to P 3 have an overall negative charge of 3 minus. A solid curved arrow from the single bond between P 3 and O on the upper right points toward the dashed line connecting the O atom and H superscript plus ion.

The first product is A T P whose structure is as follows: A zigzag chain is composed of 3 P and 4 O atoms. P atoms occupy the second, fourth, and sixth positions, and the remaining positions are occupied by O atoms. A partial double bond is present between P 3 and O 4. O 1 is single-bonded to R on the upper left. P 1, P 2, and P 3 are partially double bonded to O on the upper left and O on the upper right. The O atoms bonded to P 1 and P 2 have an overall negative charge. The O atoms bonded to P 3 have an overall charge of 2 minus. The second product is H 2 O.

Return to FIGURE 18.25 ATP-synthesis is catalyzed by ATP synthase

Extended description for FIGURE 18.26 ATP forms without a proton-motive force but is not released



The reaction consists of two reactants, one intermediate product, and two final products.

The first reactant is A D P whose structure is as follows: A zigzag chain is composed of 2 P and 3 O atoms. P atoms occupy the second and fourth positions and the remaining positions are occupied by O atoms. A partial double bond is present between P 2 and O 3. O 1 is single-bonded to R on the upper left. Both P atoms are partially double-bonded to O on the upper left and O on the upper right. The O atoms bonded to P 1 have an overall negative charge. The O atoms bonded to P 2 have an overall negative charge of 2 minus.

The second reactant is P subscript i whose structure is as follows: A central P atom is partially double bonded to O on the upper left, upper right, and lower left. The O atoms on the upper left and upper right have an overall negative charge of 2 minus. P atom is also single-bonded to O on the lower right which is further single-bonded to H on the upper right.

A reversible reaction arrow leads to the intermediate. A curved arrow above it shows the simultaneous conversion of the H superscript plus ion to H 2 O.

The intermediate product is A T P whose structure is as follows: A zigzag chain is composed of 3 P and 4 O atoms. P atoms occupy the

second, fourth, and sixth positions, and the remaining positions are occupied by O atoms. A partial double bond is present between P 3 and O 4. O 1 is single-bonded to R on the upper left. P 1, P 2, and P 3 are partially double bonded to O on the upper left and O on the upper right. The O atoms bonded to P 1 and P 2 have an overall negative charge. The O atoms bonded to P 3 have an overall charge of 2 minus.

A reversible reaction arrow leads to the final products. A curved arrow above it shows the simultaneous conversion of H 2 O superscript 18 to H superscript plus ion. O superscript 18 atom is highlighted in red.

The first final product is A D P whose structure is as follows: A zigzag chain is composed of 2 P and 3 O atoms. P atoms occupy the second and fourth positions and the remaining positions are occupied by O atoms. A partial double bond is present between P 2 and O 3. O 1 is single-bonded to R on the upper left. Both P atoms are partially double-bonded to O on the upper left and O on the upper right. The O atoms bonded to P 1 have an overall negative charge. The O atoms bonded to P 2 have an overall negative charge of 2 minus.

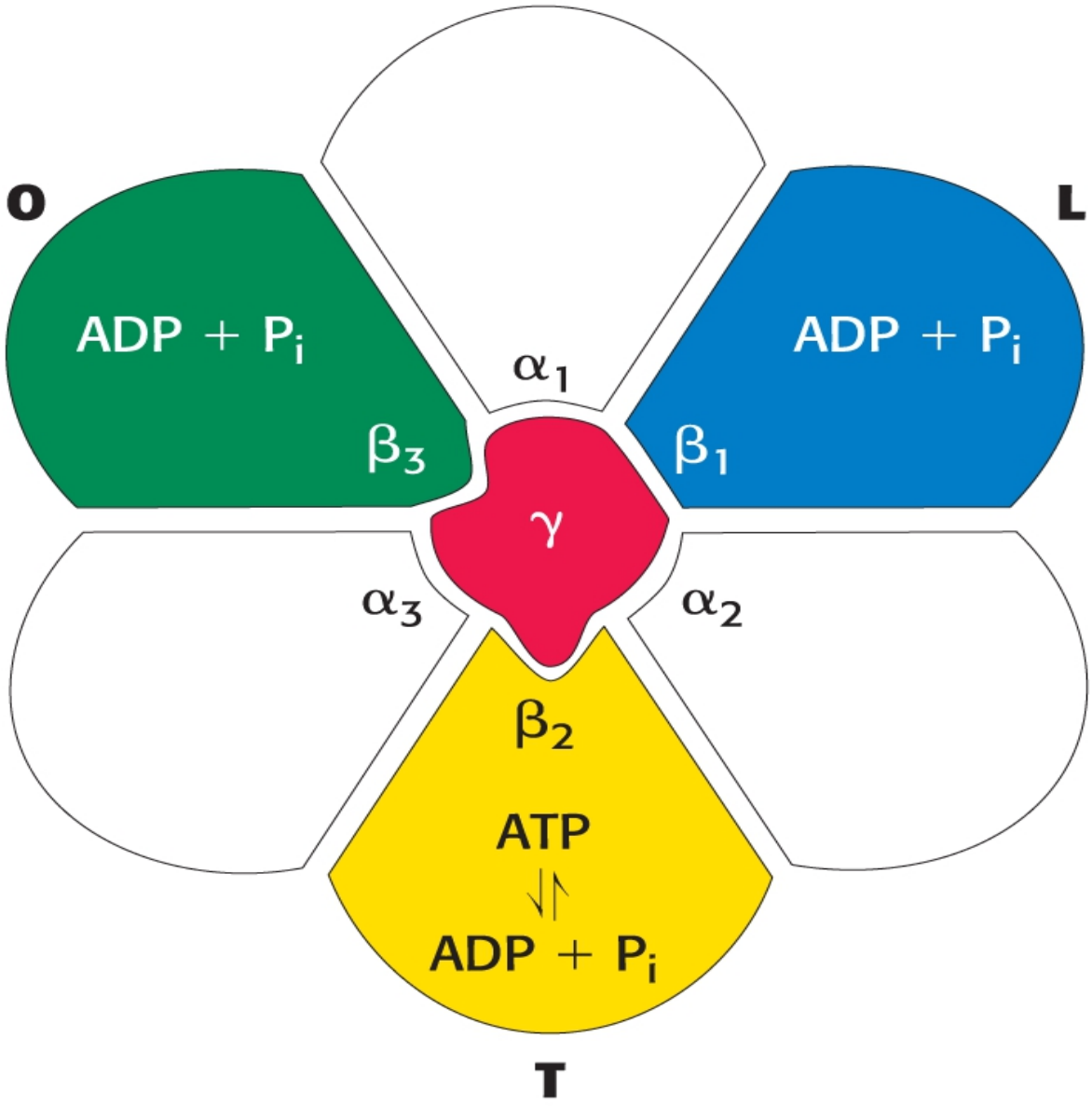
The second final product is O superscript 18-labeled P subscript i whose structure is as follows: A central P atom is partially double bonded to O on the upper left, upper right, and lower left. The O atoms on the upper left and upper right have an overall negative charge of 2 minus. P atom is also single-bonded to O on the lower right which is further single-bonded to H on the upper right. The lower right O is highlighted in red.

Return to FIGURE 18.26 ATP forms without a proton-motive force but is not released

Extended description for FIGURE 18.27 ATP synthase nucleotide-binding sites cycle through distinct

conformational states

(A)



© Macmillan Learning

(B)

β subunit 1	L → T → O → L → T → O...
β subunit 2	O → L → T → O → L → T...
β subunit 3	T → O → L → T → O → L...

Part (A): The alpha and beta subunits of the A T P synthase are arranged radially around a central gamma subunit. This arrangement resembles the petals of a flower. The alpha 1, alpha 2, and alpha 3 subunits occupy the top, bottom left, and bottom right positions respectively. Beta 1, beta 2, and beta 3 subunits occupy the top right, bottom, and top left positions respectively. The beta 1 subunit in the conformational state “L” is bound to A D P plus P subscript i. The beta 2 subunit in the conformational state “T” carries out reversible hydrolysis of A T P to A D P plus P subscript i. The beta 3 subunit in the conformational state “O” is bound to A D P plus P subscript i.

Part (B): It shows the different conformational states adopted by A T P synthase.

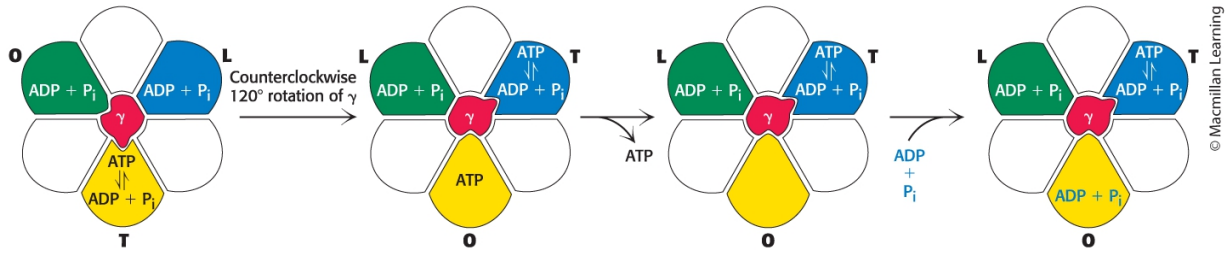
Beta subunit 1: L, forward arrow, T, forward arrow, O, forward arrow, L, forward arrow, T, forward arrow, O, dot dot dot.

Beta subunit 2: O, forward arrow, L, forward arrow, T, forward arrow, O, forward arrow, L, forward arrow, T, dot dot dot.

Beta subunit 3: T, forward arrow, O, forward arrow, L, forward arrow, T, forward arrow, O, forward arrow, L, dot dot dot.

Return to FIGURE 18.27 ATP synthase nucleotide-binding sites cycle through distinct conformational states

Extended description for FIGURE 18.28 The binding-change mechanism involves the cycling of all three β subunits through three conformations



The mechanism shows four views of the petal-like arrangement of the alpha and beta subunit around a central gamma subunit.

In the first view, the top left, top right, and bottom subunits are in O, L, and T conformational states respectively. The conformational states O and L are bound to A D P plus P subscript i. The conformational state T carries out the reversible hydrolysis of A T P to A D P plus P subscript i. The counterclockwise 120-degree rotation of gamma leads to the second view.

In the second view, the top left, top right, and bottom subunits are in the L, T, and O conformational states respectively. The conformational state L is bound to A D P plus P subscript i. The conformational state T carries out the reversible hydrolysis of A T P to A D P plus P subscript i. The conformational state O is bound to A T P.

A T P is released and leads to the third view.

In the third view, the top left, top right, and bottom subunits are in the L, T, and O conformational states respectively. The

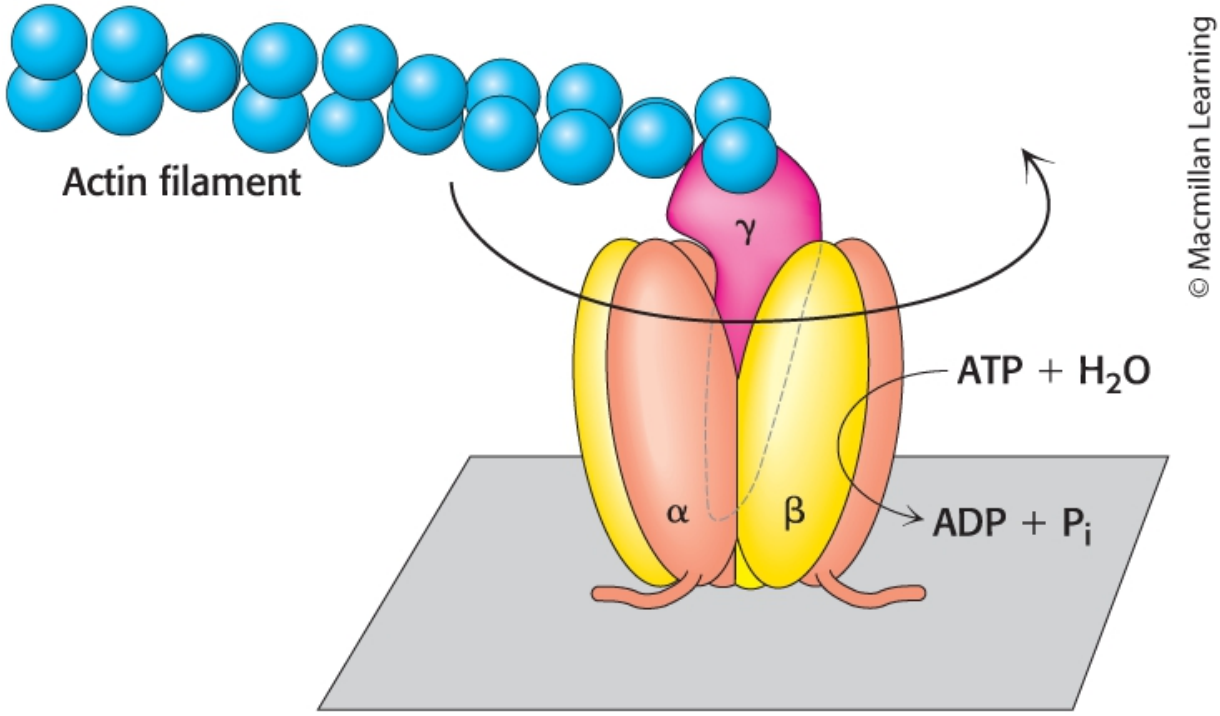
conformational state L is bound to A D P plus P subscript i. The conformational state T carries out the reversible hydrolysis of A T P to A D P plus P subscript i. The conformational state O is empty.

A D P plus P subscript i enters and leads to the fourth view.

In the fourth view, the top left, top right, and bottom subunits are in the L, T, and O conformational states respectively. The conformational state L is bound to A D P plus P subscript i. The conformational state T carries out the reversible hydrolysis of A T P to A D P plus P subscript i. The conformational state O is bound to A D P plus P subscript i.

Return to FIGURE 18.28 The binding-change mechanism involves the cycling of all three β subunits through three conformations

Extended description for FIGURE 18.29 The ATP-driven rotation in ATP synthase has been directly observed

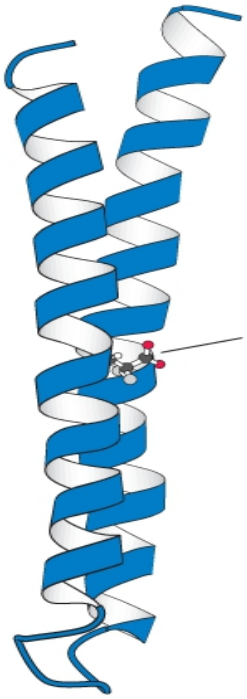


The alpha 3 beta 3 hexamers of A T P synthase are attached to a flat rectangular surface. A gamma subunit protrudes from the top center surface of the hexamer. A long actin filament depicted as a linear array of tiny circles is attached to the top surface of the gamma subunit. A curved arrow across the hexamer denotes the conversion of A T P plus H 2 O to A D P plus P subscript i. A curved counterclockwise arrow is shown around the hexamer to depict its rotation.

Return to FIGURE 18.29 The ATP-driven rotation in ATP synthase has been directly observed

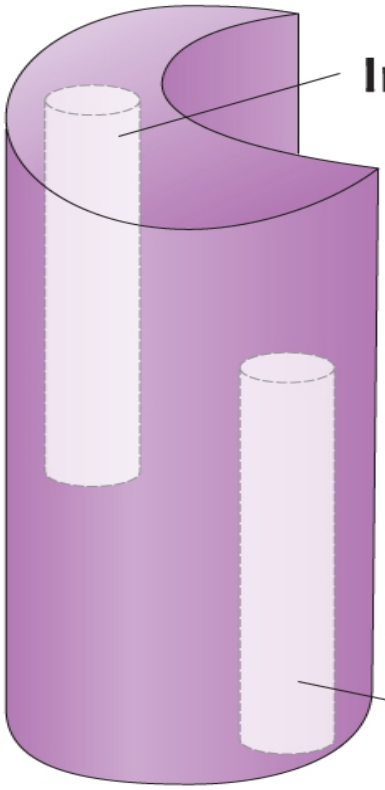
Extended description for FIGURE 18.30 Components of the proton-conducting unit of ATP synthase include

two half channels and a critical charged residue



Aspartic acid or glutamic acid

Subunit **c**



Intermembrane half-channel

Matrix half-channel

Subunit **a**

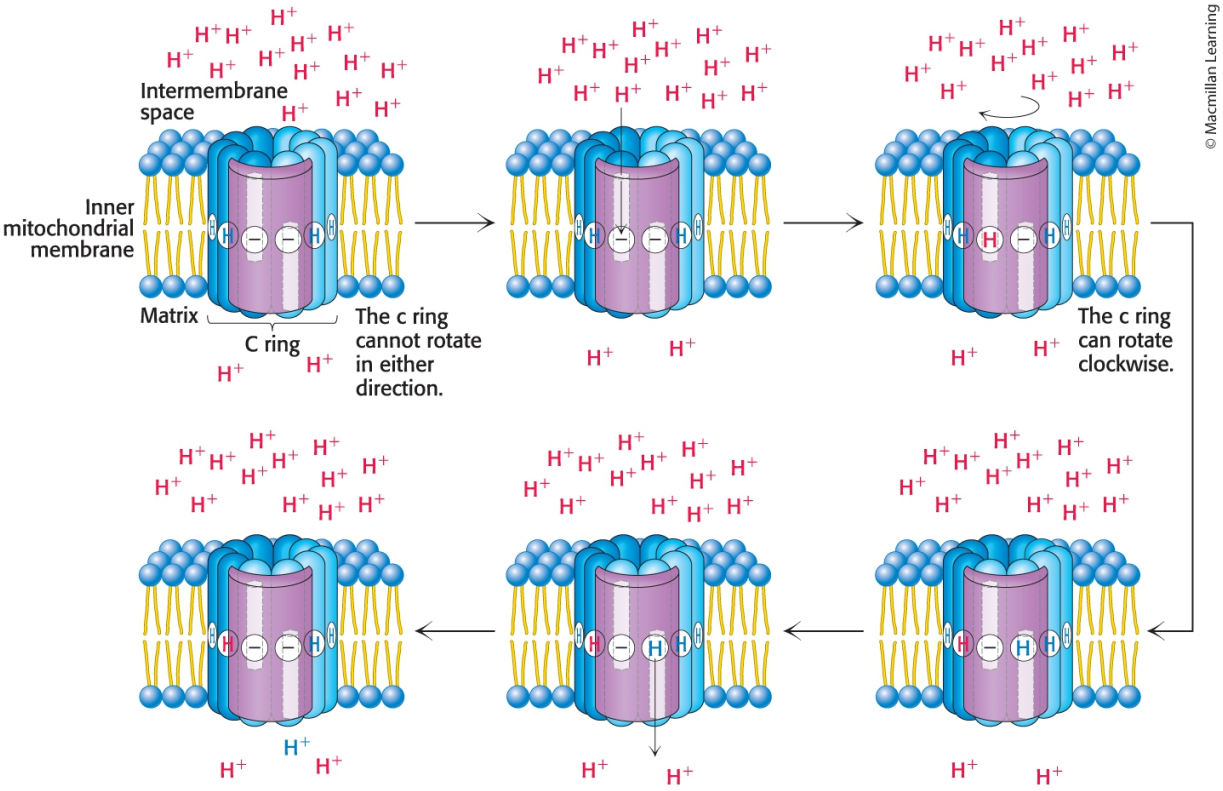
© Macmillan Learning

The ribbon diagram of subunit c consists of a pair of long and vertical alpha-helices connected by a short thread-like loop at the bottom. An aspartic acid or glutamic acid residue is shown in the center of the pair of alpha-helices.

The schematic structure of subunit a shows a thick cylindrical structure having a long and vertical cylindrical groove along its entire length. There are two half-channels inside subunit a. The intermembrane half-channel is depicted as a thin cylinder that extends from the top to a little below the center. The matrix half-channel starts a little above the center and extends to the bottom.

Return to FIGURE 18.30 Components of the proton-conducting unit of ATP synthase include two half channels and a critical charged residue

Extended description for FIGURE 18.31 Proton motion across the membrane drives rotation of the c ring



Step 1: The c ring embedded in a section of the inner mitochondrial membrane is shown. Its front surface is enclosed by subunit a. The region above the membrane is labeled intermembrane space and the region below is labeled matrix. The concentration of H superscript plus ions in the intermembrane space is much higher than in the matrix. The subunits of the c ring are bound to H. The half-channels of the subunit a have a negative charge. The text alongside reads “The c ring cannot rotate in either direction.”

Step 2: An arrow from an H superscript plus ion in the intermembrane space points toward the negative charge in the intermembrane half-channel of subunit a.

Step 3: The negative charge in the intermembrane half-channel is replaced by H transported from the intermembrane. A curved clockwise arrow is shown above the c ring. The text alongside reads “The c ring can rotate clockwise.”

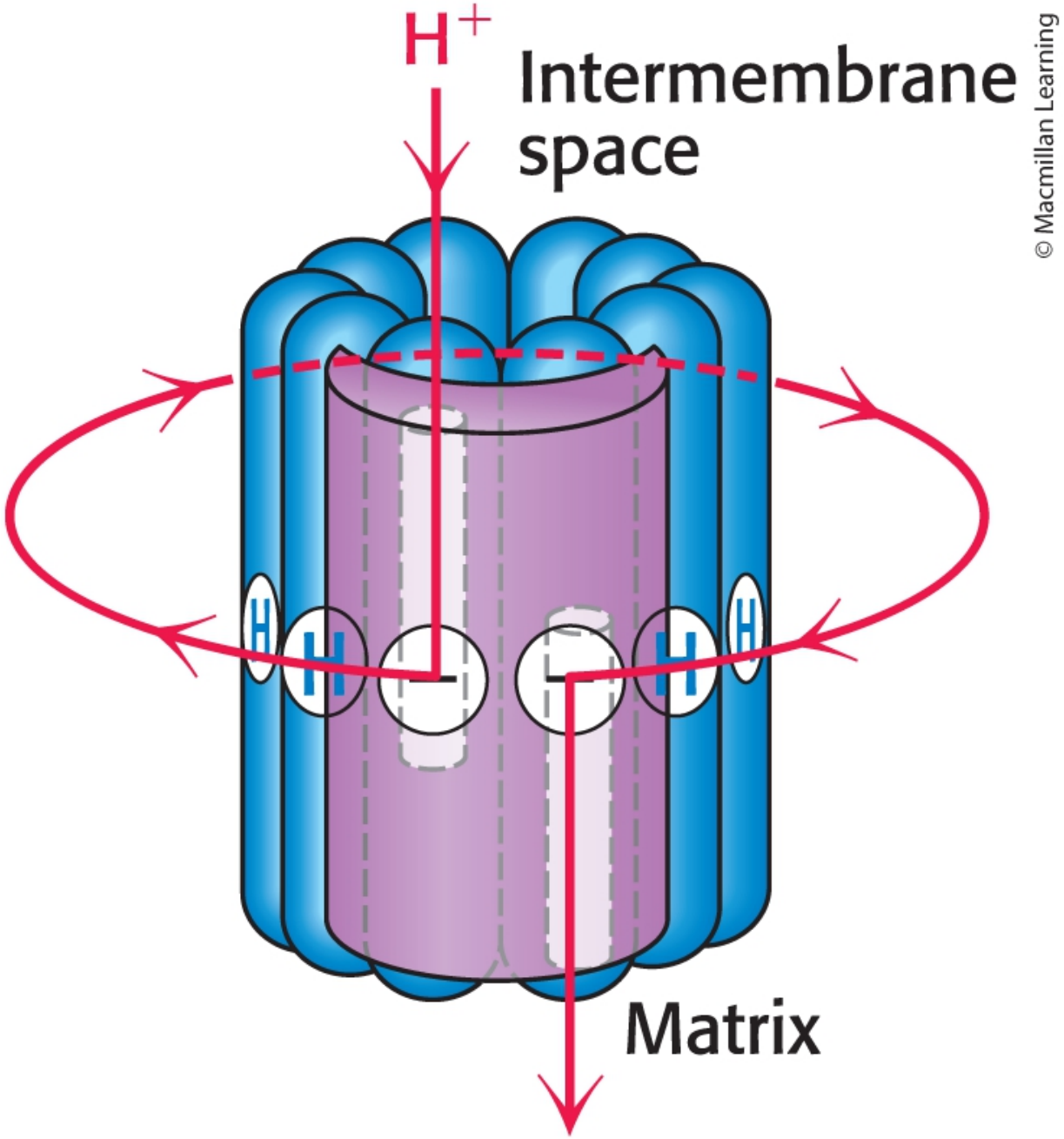
Step 4: Due to rotation of the c ring, the intermembrane half-channel again attains a negative charge and the matrix half-channel becomes bound to H. The H in the intermembrane half-channel is transferred to the rotated subunit of the c ring. The H in the matrix half-channel is transferred from the adjacent subunit of c ring.

Step 5: A downward arrow from H in the matrix half-channel points toward the matrix.

Step 6: The H atom from the matrix half-channel is released into the matrix and is depicted as H superscript plus. Both the half-channel attain the negative charge again.

Return to FIGURE 18.31 Proton motion across the membrane drives rotation of the c ring

Extended description for FIGURE 18.32 Protons must travel around the c ring to cross the membrane



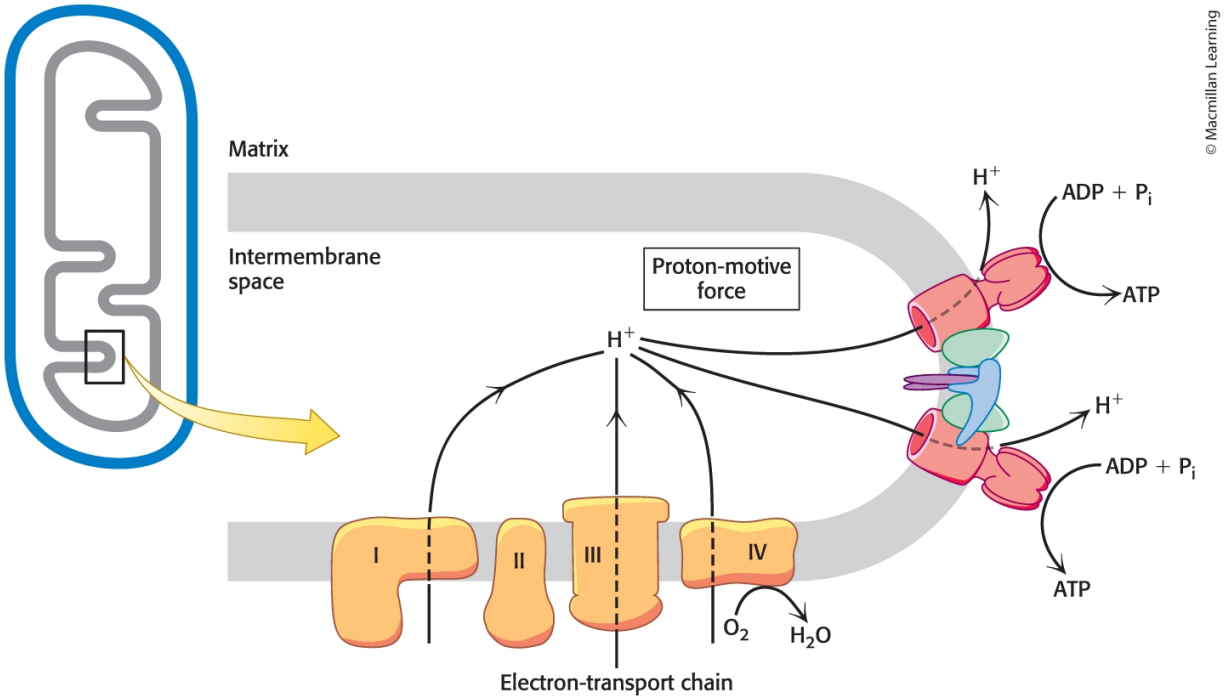
© Macmillan Learning

The c ring is depicted as a cylindrical structure composed of 10 elongated vertical subunits. These subunits are bound to H. The

region above the ring is labeled intermembrane space and the region below is labeled matrix. The front surface of the ring is enclosed by subunit a. An H superscript plus ion from the intermembrane space enters the intermembrane half-channel of subunit a. A curved circular arrow from the intermembrane half-channel moves in a clockwise direction around the c ring and returns back to the matrix half-channel of the subunit a. A downward arrow from the matrix half channel depicts the release of the H superscript plus ion into the matrix after its complete rotation around the c ring.

Return to FIGURE 18.32 Protons must travel around the c ring to cross the membrane

Extended description for FIGURE 18.33 An overview of oxidative phosphorylation shows the spatial relationship of the components



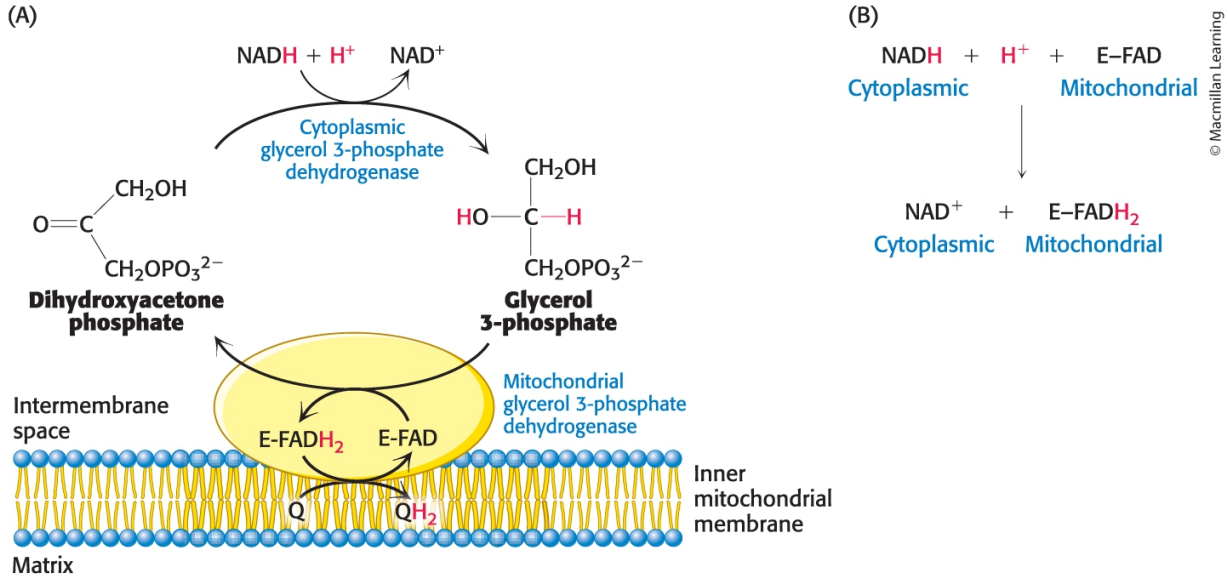
© Macmillan Learning

A schematic structure of a mitochondrion is shown. A section of the cristae formed by the inner mitochondrial membrane shows an enlarged view of a horizontal U-shaped crista. The region above the inner membrane is labeled matrix and the region inside the U-shaped structure is labeled intermembrane space. Complex 1 to 4 are shown embedded in the inner membrane. They are part of the electron transport chain. Arrows across complex 1, 3, and 4 point toward a common H superscript ion in the intermembrane space. A curved arrow below complex 4 depicts the conversion of O 2 to H 2 O in the matrix. The H superscript plus ion depicts proton motive force. Two arrows from this H superscript ion pass through a dimer of A T P synthase embedded in the inner membrane and enter the matrix. A curved arrow across the component of A T P synthase in

the matrix depicts the phosphorylation of A D P plus P subscript i to A T P.

Return to FIGURE 18.33 An overview of oxidative phosphorylation shows the spatial relationship of the components

Extended description for FIGURE 18.34 The glycerol 3-phosphate shuttle allows for rapid rates of oxidative phosphorylation at the cost of energetic efficiency



Part (A): The outer leaflet of the inner mitochondrial membrane is attached to a mitochondrial glycerol 3-phosphate dehydrogenase depicted as a large oval. The region above the membrane is labeled intermembrane space and the region below is labeled matrix. The glycerol 3-phosphate dehydrogenase catalyzes the conversion of glycerol 3-phosphate to dihydroxyacetone phosphate and the simultaneous reduction of enzyme-bound F A D to F A D H 2. F A D H 2 is again oxidized as it transfers electrons to Q in the membrane and converts them into Q H 2.

The structure of glycerol 3-phosphate is as follows: C H 2 O H, single bond, C, single bond, C H 2 O P O 3 superscript 2 minus. C 2 is single bonded to O H on the left and H on the right.

The structure of dihydroxyacetone phosphate is as follows: Acentral C atom is single bonded to C H 2 O H on the upper right, single bonded to C H 2 O P O 3 superscript 2 minus on the lower right, and double bonded to O on the left.

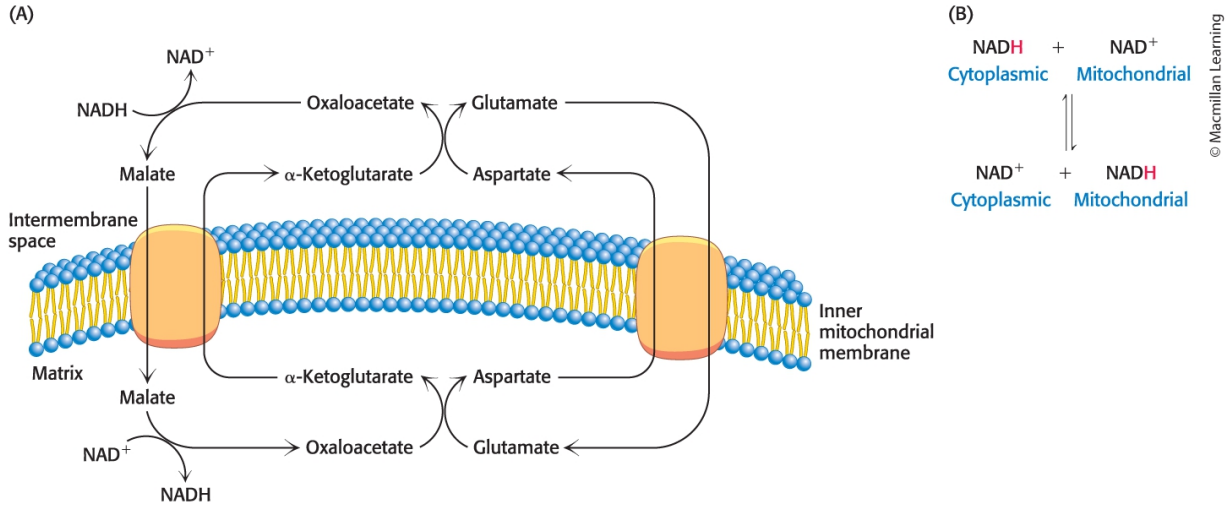
A cytoplasmic glycerol 3-phosphate dehydrogenase catalyzes the conversion of dihydroxyacetone phosphate back to glycerol 3-phosphate. It is coupled with the oxidation of N A D H plus H superscript plus to N A D superscript plus.

Part (B): It shows an equation depicted as follows:

N A D H cytoplasmic plus H superscript plus and E-F A D mitochondrial are irreversibly converted into N A D superscript plus cytoplasmic and E-F A D H 2 mitochondrial.

Return to FIGURE 18.34 The glycerol 3-phosphate shuttle allows for rapid rates of oxidative phosphorylation at the cost of energetic efficiency

Extended description for FIGURE 18.35 The malate–aspartate shuttle preserves all the chemical potential energy of cytoplasmically generated NADH



Part (A): Two cuboidal structures are embedded in the inner mitochondrial membrane on the left and right ends. The region above the membrane is labeled intermembrane space and the region below is labeled matrix. Malate from the intermembrane space enters the matrix through the left cuboidal structure. It is converted into oxaloacetate inside the matrix with the simultaneous reduction of N A D superscript plus to N A D H. The oxaloacetate is converted into alpha-ketoglutarate with the simultaneous conversion of glutamate to aspartate in the matrix. The alpha-ketoglutarate molecule moves back into the intermembrane space through the left cuboidal structure. The aspartate molecule exits the matrix and enters the intermembrane space through the right cuboidal structure. In the intermembrane space, aspartate is converted back to glutamate with the simultaneous conversion of alpha-ketoglutarate into oxaloacetate. Glutamate moves back into the matrix through the right cuboidal structure. Oxaloacetate is

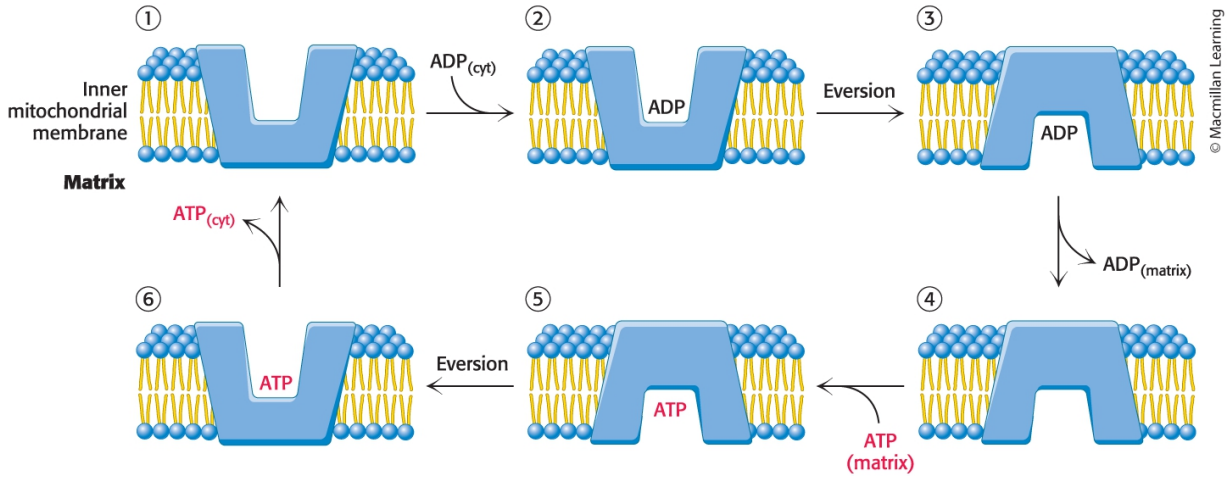
converted into malate in the intermembrane space with the simultaneous reduction of N A D superscript plus to N A D H.

Part (B): It shows an equation depicted as follows:

N A D H cytoplasmic plus N A D superscript plus mitochondrial is reversibly converted into N A D superscript plus cytoplasmic and N A D H mitochondrial.

Return to FIGURE 18.35 The malate–aspartate shuttle preserves all the chemical potential energy of cytoplasmically generated NADH

Extended description for FIGURE 18.36 The ATP-ADP translocase catalyzes the exchange of entry of ADP and ATP



The action of A T P-A D P translocase is divided into 6 steps as follows:

Step 1: An inverted V-shaped structure is shown embedded in the inner mitochondrial membrane. The region below the membrane is labeled matrix.

Step 2: A D P from the cytoplasm enters and binds to the central elongated groove in the structure.

Step 3: Eversion takes place and the groove containing A D P is now oriented toward the matrix. The A D P molecule is released into the matrix.

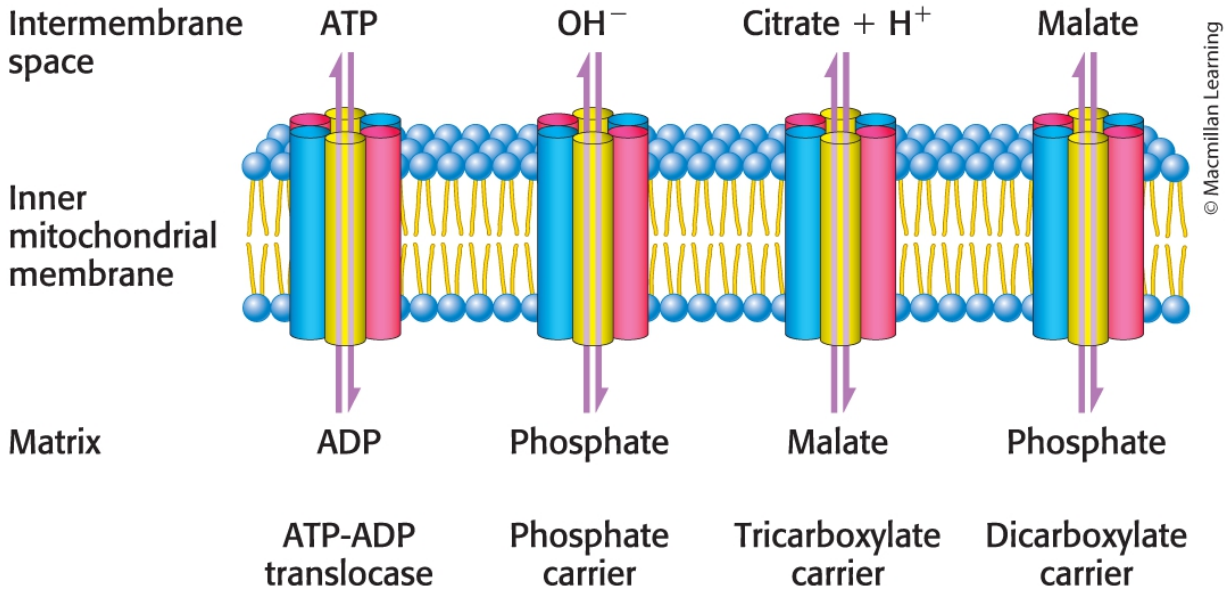
Step 4: The groove becomes empty.

Step 5: A T P from the matrix enters the groove.

Step 6: Eversion occurs again and the groove now faces upward. The A T P molecule is released into the cytoplasm.

Return to FIGURE 18.36 The ATP-ADP translocase catalyzes the exchange of entry of ADP and ATP

Extended description for FIGURE 18.37 Structurally homologous mitochondrial transporters

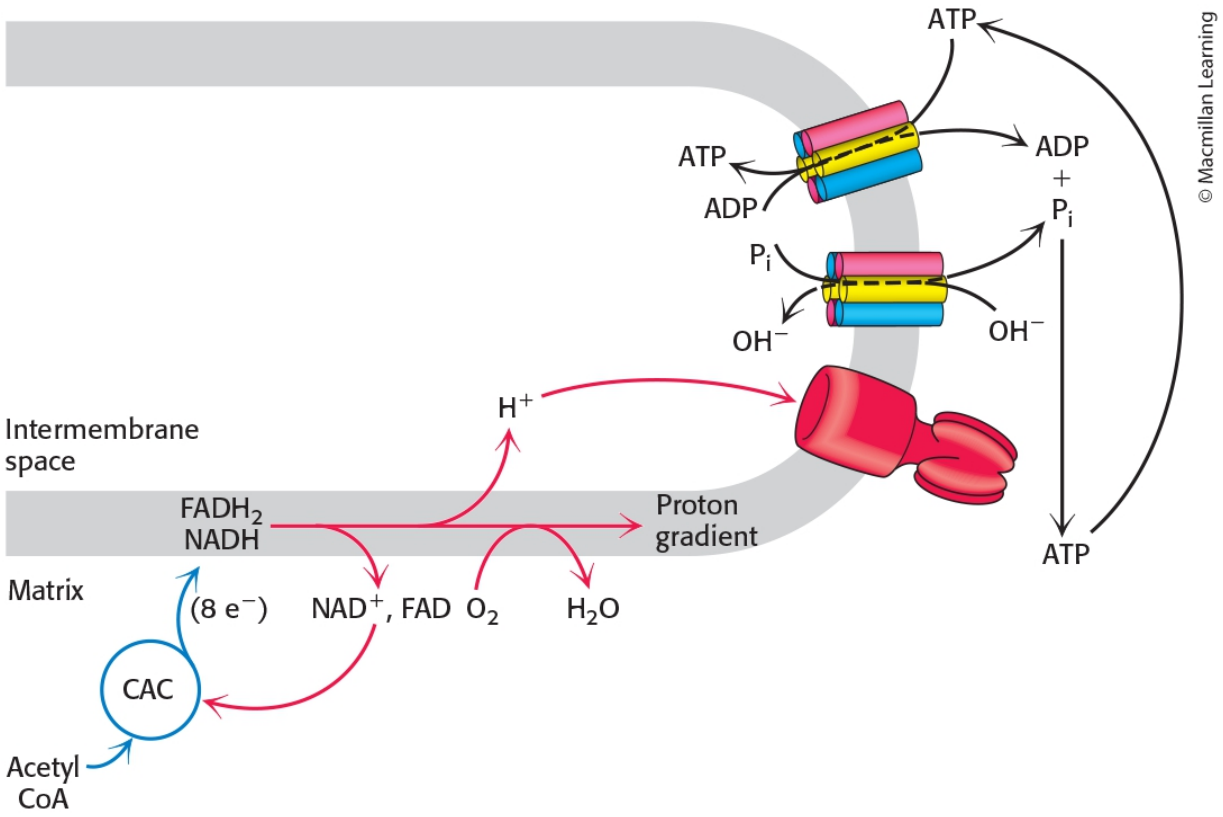


Four different transporters are shown embedded in the inner mitochondrial membrane. The region above the membrane is labeled intermembrane space and the region below is labeled matrix. From left to right, the transporters are labeled as follows: A T P-A D P translocase, phosphate carrier, tricarboxylate carrier, and dicarboxylate carrier. They are depicted as hollow structures composed of 6 thin cylindrical structures. The A T P-A D P translocase carries out the transport of A T P (intermembrane space) and A D P (matrix) across the inner mitochondrial membrane. The phosphate carrier performs the transport of O H superscript minus (intermembrane space) and phosphate (matrix) across the inner mitochondrial membrane. The tricarboxylate carrier performs the transport of citrate plus H superscript plus (intermembrane space) and malate (matrix) across the inner mitochondrial membrane. The dicarboxylate carrier performs the transport of malate

(intermembrane space) and phosphate (matrix) across the inner mitochondrial membrane.

Return to FIGURE 18.37 Structurally homologous mitochondrial transporters

Extended description for FIGURE 18.38 ATP synthase depends upon the rest of the ATP synthesome, as well as the ETC and CAC

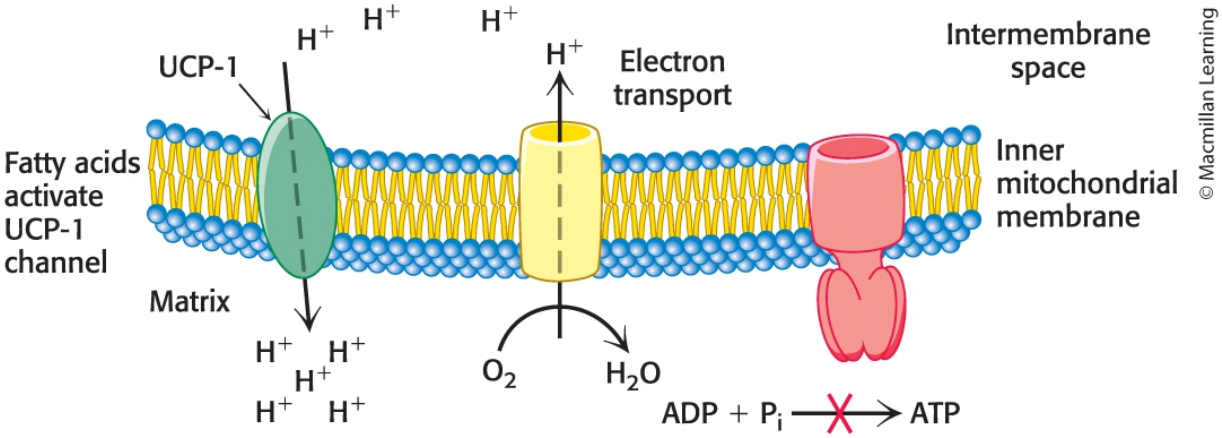


A section of crista is shown as a horizontal U-shaped structure. The region inside the crista is labeled intermembrane space and the region outside is labeled matrix. A circle labeled C A C is shown in the matrix. An arrow labeled acetyl C o A points toward the circle. An arrow labeled 8 electrons points from the circle to F A D H 2 and N A D H in the inner mitochondrial membrane lining the crista. A long arrow from F A D H 2 and N A D H points toward the proton gradient in the inner membrane. A downward arrow from the long arrow depicts the exit of N A D superscript plus and F A D into the matrix. The N A D superscript plus and F A D molecules enter into

the circle labeled C A C. A curved arrow below the long arrow depicts the conversion of O 2 to H 2 O in the matrix. An upward arrow arising from the long arrow depicts the entry of the H superscript plus ion into the intermembrane space. This H superscript plus ion enters into the A T P synthase embedded into the membrane. An A T P-A D P translocase and phosphate carrier are shown embedded into the inner membrane, adjacent to the A T P synthase. An inward arrow across the translocase depicts the entry of A T P from the matrix and the release of A D P into the intermembrane space. An outward arrow depicts the entry of P subscript i from the intermembrane space and release of A D P into the matrix. The phosphate carrier also picks the P subscript i in the intermembrane space and transfers it to the matrix. Simultaneously, it also transports the O H superscript minus from the matrix into the intermembrane space. The A D P and P subscript i in the matrix are phosphorylated by the A T P synthase to produce A T P. This A T P molecule is recycled by the A T P-A D P translocase.

Return to FIGURE 18.38 ATP synthase depends upon the rest of the ATP synthesome, as well as the ETC and CAC

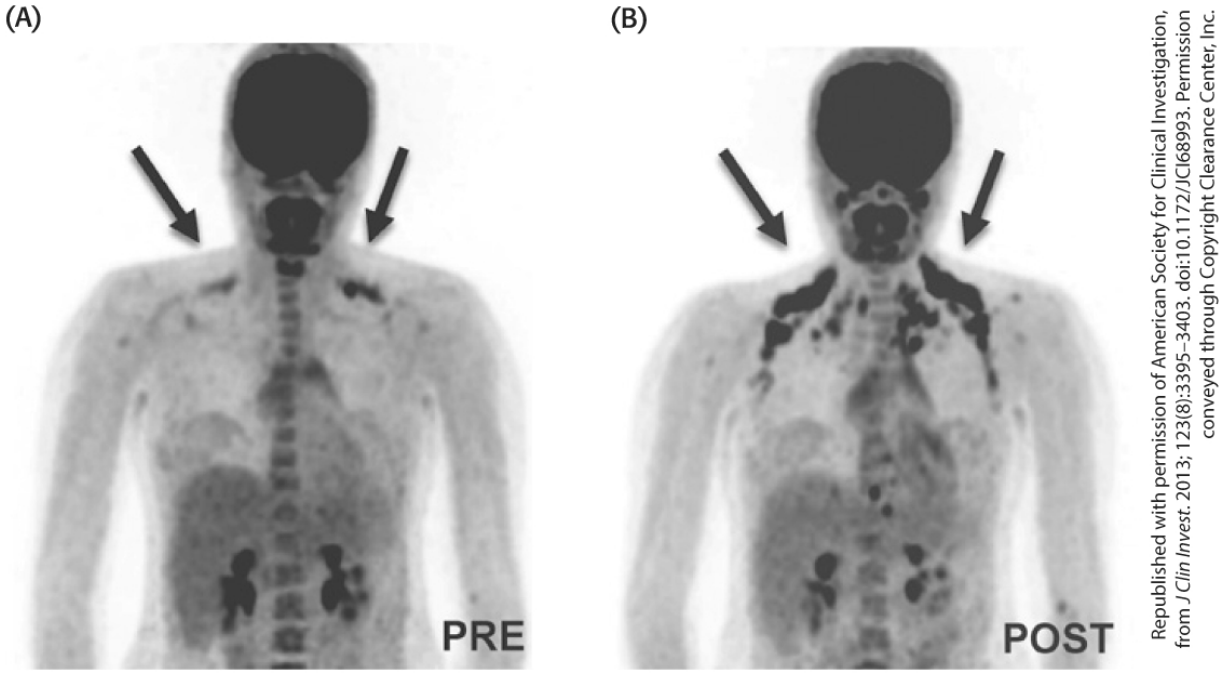
Extended description for FIGURE 18.39 Mechanism of heat generation by U C P-1



A section of the inner mitochondrial membrane is shown. The region above the membrane is labeled intermembrane space and the region below is labeled matrix. An oval-shaped protein embedded into the membrane is labeled U C P-1. A hollow cylindrical protein is shown embedded in the middle of the membrane. An A T P synthase is shown embedded in the membrane, near the right end. A few H superscript plus ions are shown in the intermembrane space, above the U C P-1 protein. A downward arrow across U C P-1 depicts the entry of H superscript plus ions from intermembrane space into the matrix. The text alongside U C P-1 reads "Fatty acids activate U C P-1 channel." The hollow cylindrical structure depicts the electron transport and shows the movement of the H superscript plus ion from the matrix into the intermembrane space. The cylindrical structure simultaneously converts O 2 into H 2 O in the matrix. The A T P synthase does not carry out the phosphorylation of A D P and P subscript i to produce A T P.

Return to FIGURE 18.39 Mechanism of heat generation by U C P-1

Extended description for FIGURE 18.40 P E T scan results of the uptake and distribution of F superscript 18-fluorodeoxyglucose in adipose tissue



Republished with permission of American Society for Clinical Investigation, from *J Clin Invest*. 2013; 123(8):3395–3403. doi:10.1172/JCI68993. Permission conveyed through Copyright Clearance Center, Inc.

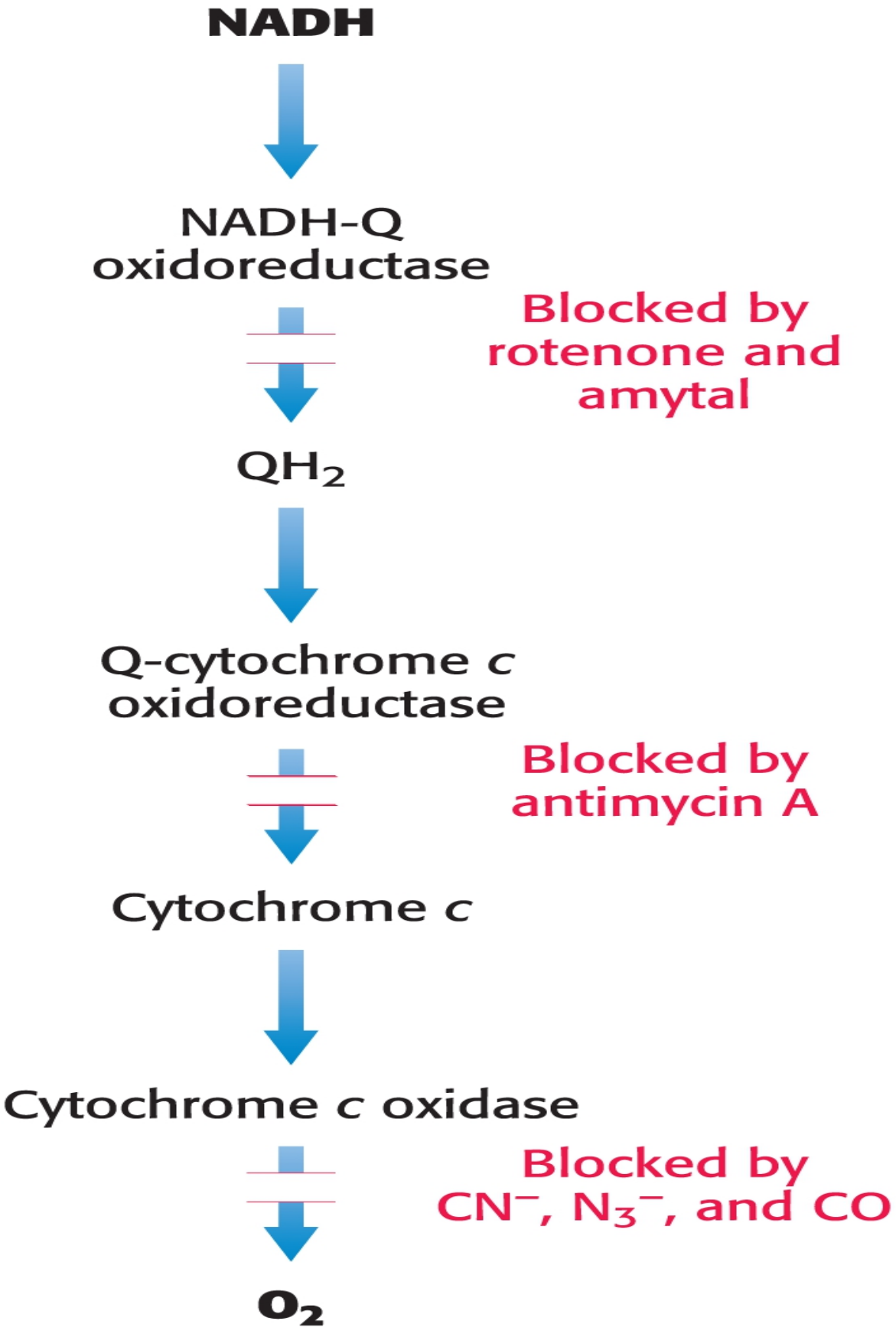
(A): The P E T scan is labeled "PRE." Two arrows point toward very small dark black patches in the shoulder region.

(B): The P E T scan is labeled "POST." Two arrows point toward relatively larger dark black patches in the shoulder region.

Return to FIGURE 18.40 P E T scan results of the uptake and distribution of F superscript 18-fluorodeoxyglucose in adipose tissue

Extended description for FIGURE 18.41 Inhibitors of the

electron transport chain

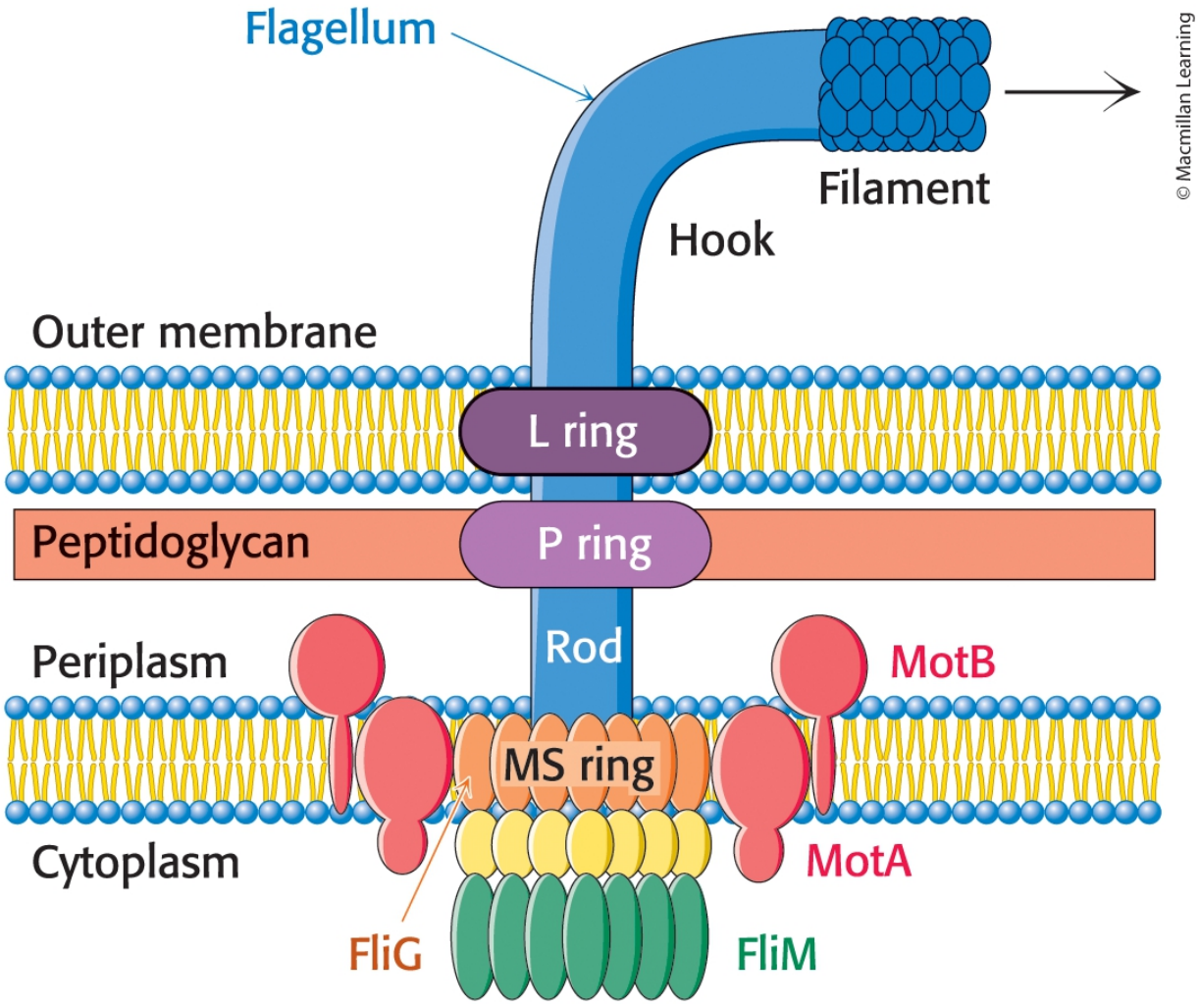


© Macmillan Learning

The flowchart is depicted as follows: N A D H, downward arrow, N A D H-Q oxidoreductase, downward arrow, Q H 2, downward arrow, Q-cytochrome c oxidoreductase, downward arrow, cytochrome c, downward arrow, cytochrome c oxidase, downward arrow O 2. The downward arrow has two parallel red lines wherever inhibition is shown. The transfer of electrons from N A D H-Q oxidoreductase to Q H 2 is blocked by rotenone and amytal. The transfer of electrons from Q-cytochrome c oxidoreductase to cytochrome c is blocked by antimycin A. The transfer of electrons from cytochrome c oxidase to O 2 is blocked by C N superscript minus, N 3 superscript minus, and C O.

Return to FIGURE 18.41 Inhibitors of the electron transport chain

Extended description for FIGURE 18.43 The flagellar motor is a complex structure containing as many as 40 distinct types of proteins

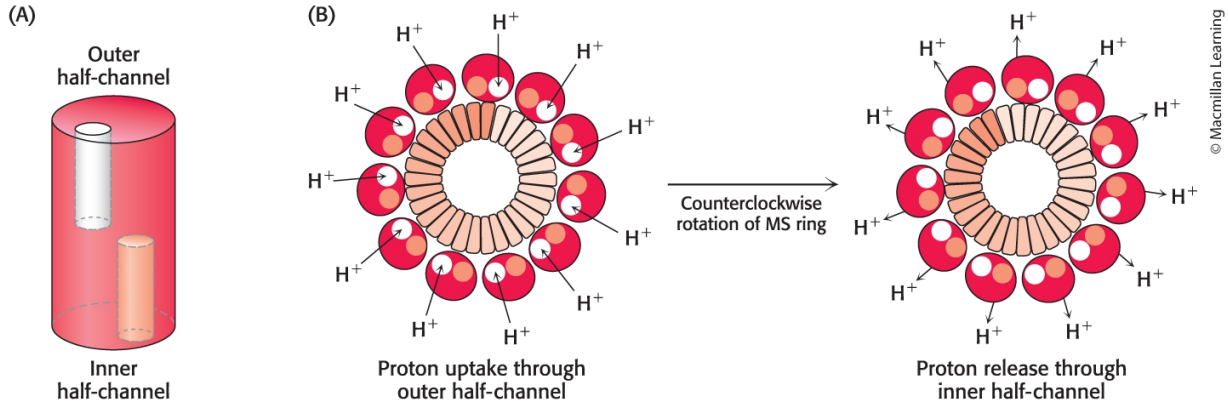


Two lipid bilayers are shown with a large gap between them. The top bilayer is labeled the outer membrane. A long rectangular strip in the gap is labeled peptidoglycan. The peptidoglycan is located closer to the outer membrane. The space between the peptidoglycan and the bottom bilayer is labeled periplasm. The region below the bottom bilayer is labeled cytoplasm. M S ring composed of several

adjacently placed orange oval-shaped structures is embedded in the bottom bilayer. The orange oval-shaped structure is labeled F l i G. A layer of yellow circles connected to a layer of green oval-shaped structures is attached to the bottom surface of the M S ring and extends into the cytoplasm. The green oval-shaped structures are labeled F l i M. A budding yeast-like structure is embedded in the bottom bilayer and flanks the M S ring. It is labeled Mot A. A circular hand-mirror-like structure labeled Mot B is embedded in the bottom bilayer and flanks the entire complex composed of the M S ring and Mot A. A cylindrical rod extends from the center of the M S ring and passes across the peptidoglycan layer and outer membrane. It protrudes above the outer membrane and is labeled flagellum. It curves toward the right, above the outer membrane and this portion is labeled hook. The right end of the flagellum is surrounded by a layer of hexagonal structures labeled filament. A rightward pointing arrow is shown next to the filament. The rod-like structure in the peptidoglycan and the outer membrane is surrounded by a P ring and L ring respectively.

Return to FIGURE 18.43 The flagellar motor is a complex structure containing as many as 40 distinct types of proteins

Extended description for FIGURE 18.44 Rotation of the flagellum involves proton half-channels like ATP synthase



Part (A): A solid cylindrical structure is shown. It contains two half-channels. The outer half-channel is depicted as a thin cylinder that extends from the top to the center. The inner half-channel starts just where the outer channel terminates and extends to the bottom.

Part (B): A hollow ring is outlined by elongated structures. The outer surface of the ring is lined by medium-sized circular structures. Each circle contains a pair of tiny circles. In each pair, one circle is white and another one is orange. Arrows labeled H superscript plus ion point toward the tiny white circle inside each medium circle. The text below the entire structure reads “Proton uptake through outer half-channel.”

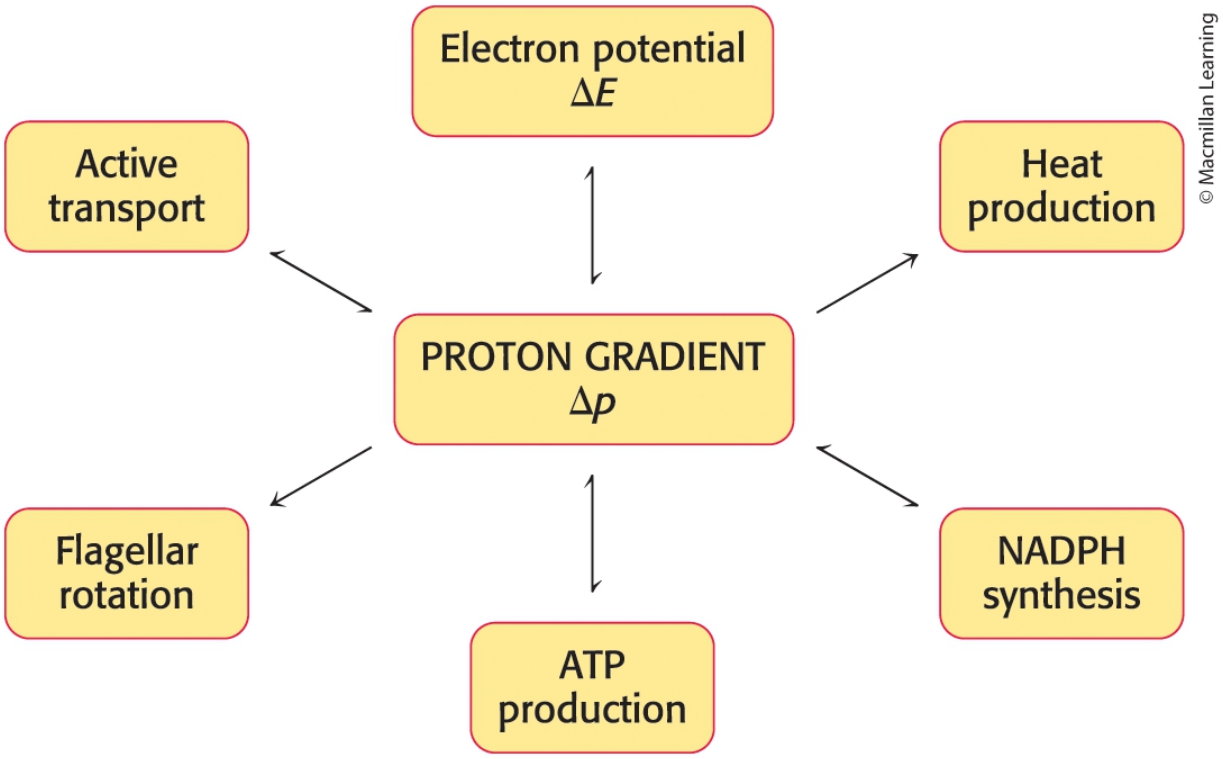
An arrow labeled “Counterclockwise rotation of M S ring” is shown.

It shows the anticlockwise rotation of the circular ring. An outward arrow from each medium circle points toward the H superscript

plus ion. The text below the entire structure reads “Proton release through inner half-channel.”

Return to FIGURE 18.44 Rotation of the flagellum involves proton half-channels like ATP synthase

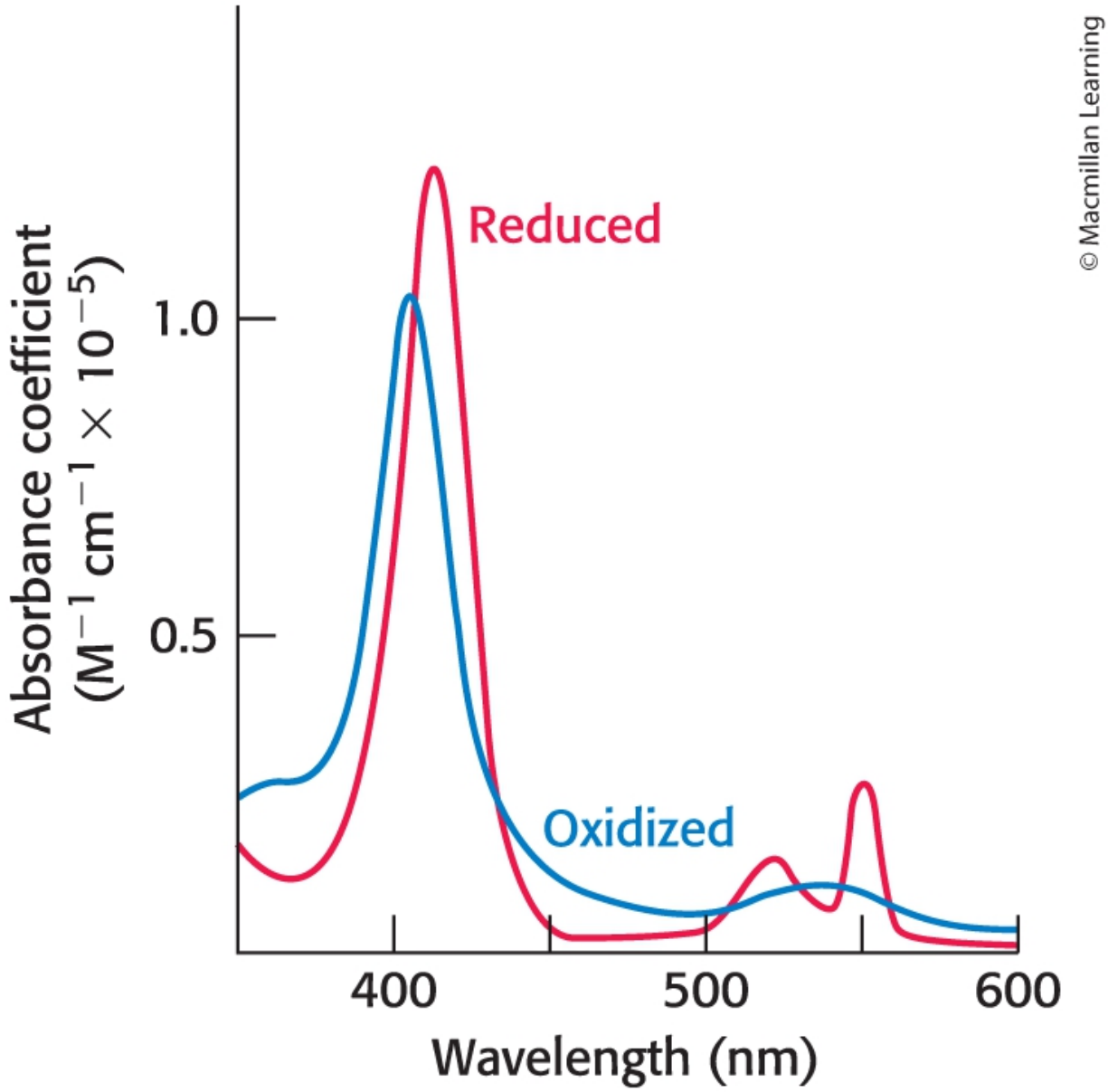
Extended description for FIGURE 18.45 Proton gradient as an interconvertible form of free energy



A rectangular box labeled proton gradient delta P is shown at the center. A two-way arrow with half arrow heads is shown above, below, on the top left, and bottom right. The arrows above, below, on the top left, and bottom right point toward different boxes labeled electron potential delta E, A T P production, active transport, and N A D P H synthesis respectively. An arrow with a complete arrowhead is shown on the top right and bottom left and points toward boxes labeled heat production and flagellar rotation.

Return to FIGURE 18.45 Proton gradient as an interconvertible form of free energy

Extended description for Absorption spectra of the reduced and oxidized forms of cytochrome c



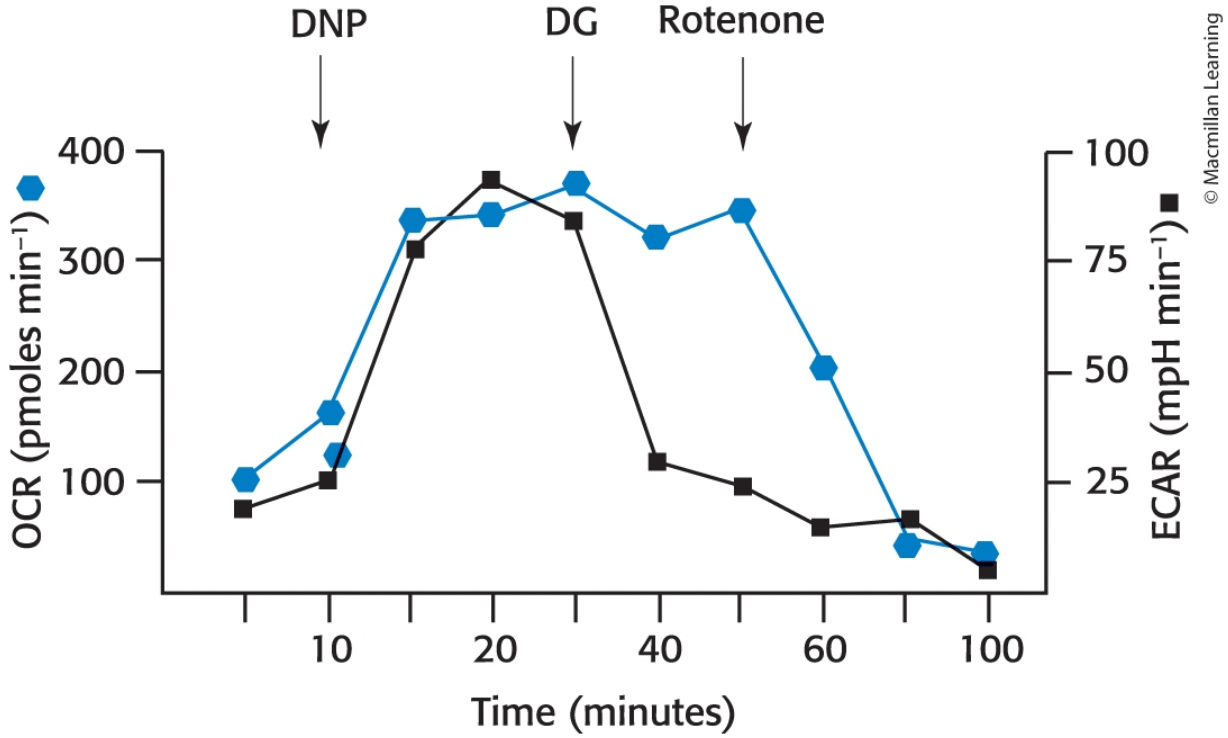
© Macmillan Learning

The horizontal axis is labeled wavelength in nanometers. It has markings ranging from 400 to 600 in increments of 100 units. The vertical axis is labeled absorbance coefficient in molar inverse centimeter inverse into 10 to the power negative 5. It has markings

ranging from 0 to 1.0 in increments of 0.5 units. The graph contains two curves. The blue curve labeled oxidized starts at 0.25 on the vertical axis and moves toward the right. It rises steeply to reach (400, 1.0), falls steeply toward the lower right to reach (430, 0.25), and then moves toward the right to reach (600, 0.2). The red curve labeled reduced starts below the red curve at 0.15 and forms a slight depression before steeply rising to (410, 1.25). It then steeply falls to (450, 0.05) and moves toward the right. During its path toward the right, it forms two tiny peaks at (520, 0.1) and (550, 0.25) and then moves along the horizontal axis. All values are estimated.

Return to Absorption spectra of the reduced and oxidized forms of cytochrome c

Extended description for Results of an experiment using the X F technology

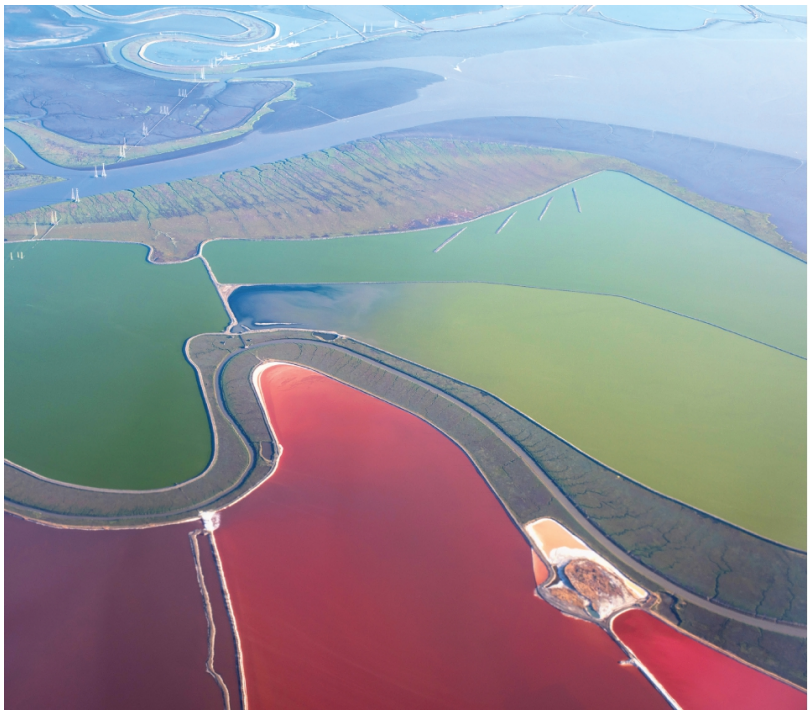


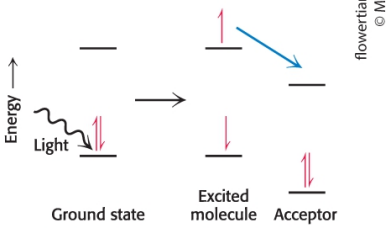
The horizontal axis is labeled time in minutes. It has markings 10, 20, 40, 60, and 100 from left to right. The left vertical axis is labeled O C R in picomoles per minute. It has markings ranging from 100 to 400 in increments of 100 units. The right vertical axis is labeled E C A R in Milli p H per minute. It has markings ranging from 25 to 100 in increments of 25 units. A blue curve with solid blue hexagonal data points represents O C R. A black curve with solid black square data points represents E C A R. The data points of the blue curve are as follows: (5, 100), (10, 180), (15, 350), (20, 351), (30, 380), (40, 320), (50, 350), (60, 210), (80, 30), and (100, 30). The data points of the blue curve are as follows: (5, 90), (10, 100), (15, 310), (20, 380), (30, 350), (40, 110), (50, 100), (60, 40), (80, 45), and (100, 10). D N P is added at

10 minutes, D G is added at 30 minutes, and rotenone is added at 50 minutes. All values are estimated.

Return to Results of an experiment using the X F technology

Extended description for Phototrophic halobacteria are visible from the air in salt ponds near the San Francisco Bay and a schematic shows electron excitation and its transfer to acceptor





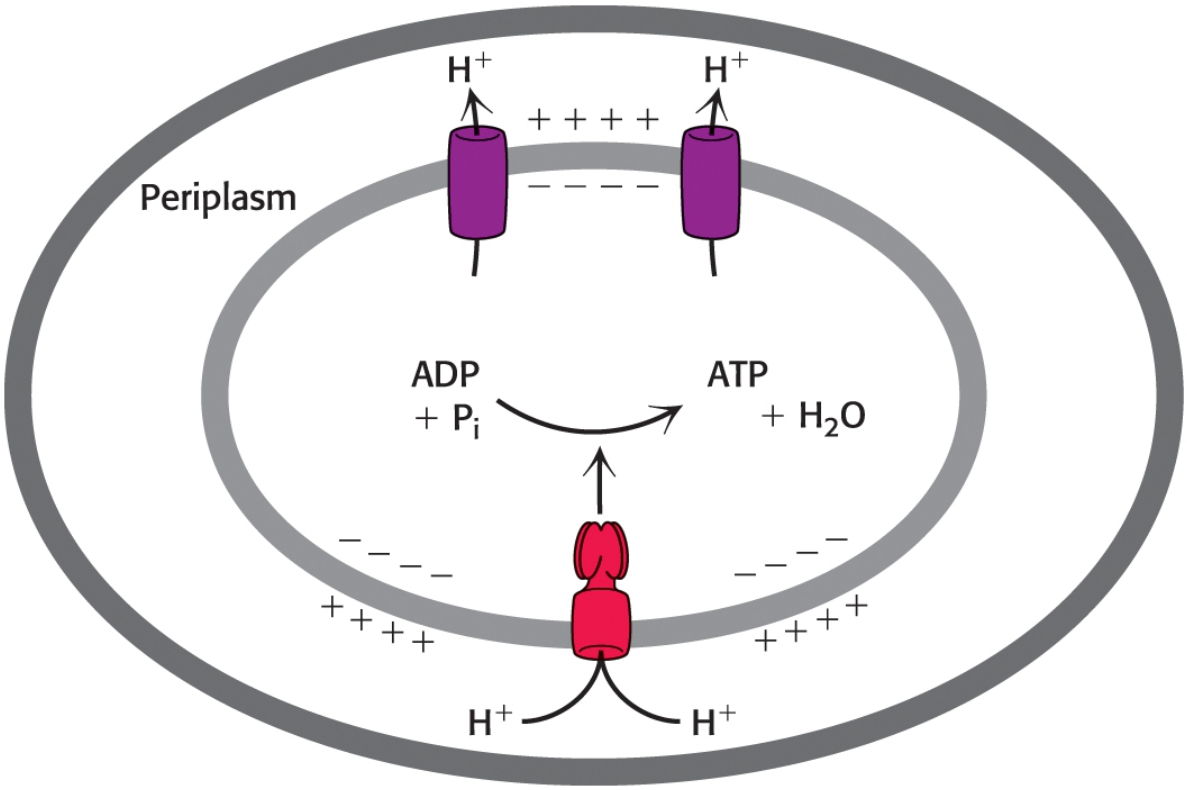
flowertiare/Deposit Photos
© Macmillan Learning

The aerial view of the salt ponds near San Francisco Bay shows the red color of the water due to the phototrophic halobacteria. The halobacteria produce distinct red and purple colors in the pond. On the right, the schematic shows the excitation of electrons. It shows a molecule in the ground state on the left and an excited molecule on the right. An upward arrow on the left side is labeled energy. On the left, an upward and downward arrow is present in the ground state. A blank is shown above the ground state at a higher energy level. An arrow from the ground state points to the excited state on the right. A downward arrow is present at the bottom excited state and an upward arrow is present in the top excited state. An arrow from the

top excited state points to the excited state of the acceptor. The excited state is blank in the acceptor. Upward and downward arrow is present in the ground state of the acceptor.

Return to Phototrophic halobacteria are visible from the air in salt ponds near the San Francisco Bay and a schematic shows electron excitation and its transfer to acceptor

Extended description for FIGURE 19.1 Phototrophy can be accomplished by the cooperation of just two proteins



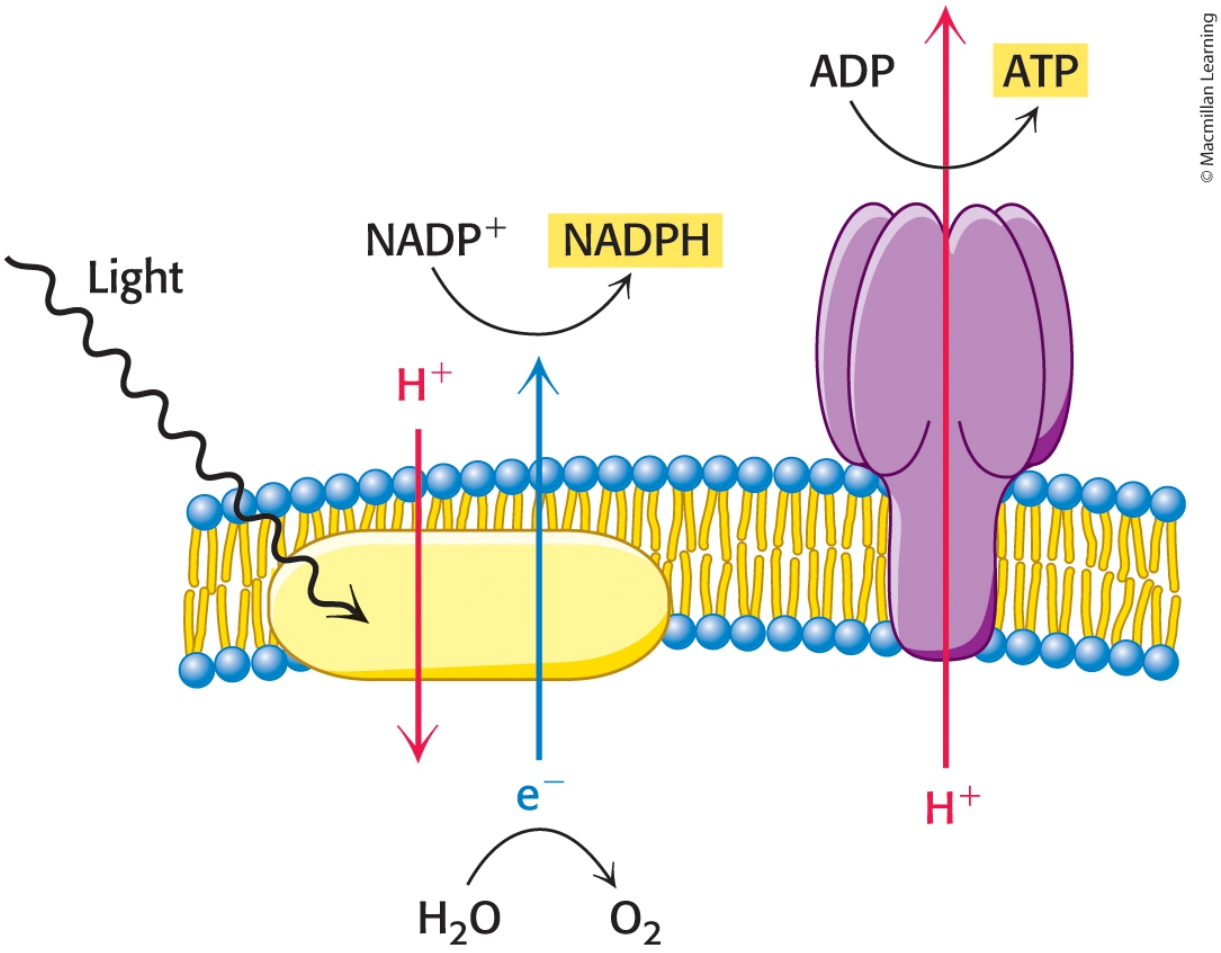
© Macmillan Learning

The cell wall is made up of two concentric circles that are separated by a space. The space between the two concentric circles is labeled periplasm. In the inner circle, a red-colored cylindrical membrane protein is present on the lower surface. 2 H plus ions enter into the inner circle through the membrane protein from the periplasm. The outer surface of the circle has a positive charge while the inner surface has a negative charge. Once the H superscript plus ions enter the circle they are used up for converting A D P and P subscript i to A T P and H 2 O. The H superscript plus ions later move into the periplasm through two purple-colored cylindered

located on the upper surface of the inner circle. Arrows indicate the outward movement of the H plus ions.

Return to FIGURE 19.1 Phototrophy can be accomplished by the cooperation of just two proteins

Extended description for FIGURE 19.2 The light reactions of oxygenic photosynthesis generate both A T P and reducing power



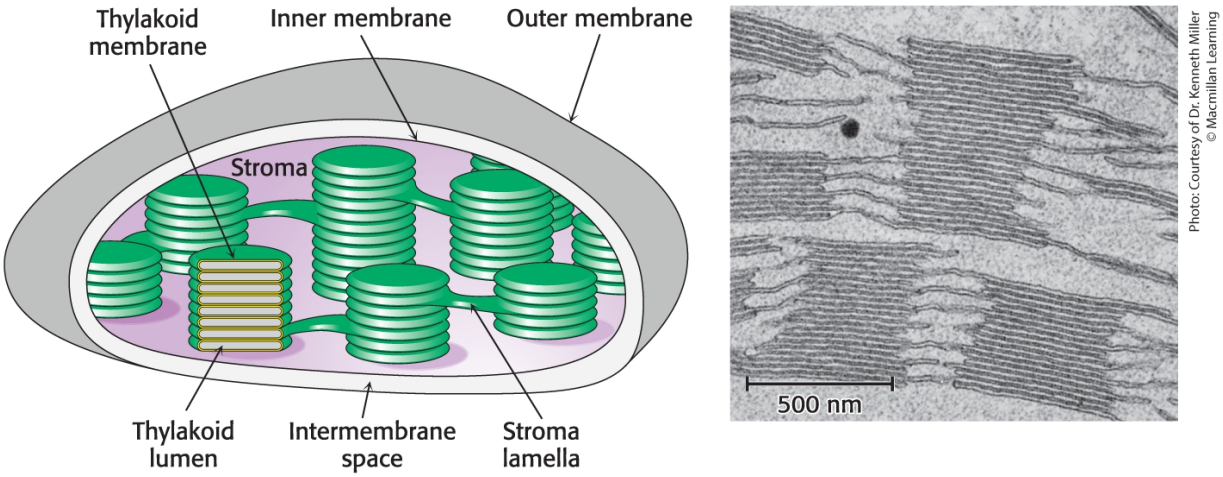
© Macmillan Learning

A capsule-shaped protein and a protein complex are embedded in a lipid bilayer. A wavy arrow labeled light strikes the capsule-shaped protein. A downward arrow across the capsule-shaped protein depicts the entry of H superscript plus into the region below the bilayer. An upward arrow across the capsule-shaped protein depicts the exit of electrons into the region above the bilayer. This movement of electrons is coupled with the conversion of H 2 O to O 2 in the region below the membrane. The electron is used to reduce

N A D P superscript plus to N A D P H above the bilayer. An upward arrow across the protein complex depicts the transfer of the H superscript plus ion from the region below the bilayer to the region above. This movement is coupled with the conversion of A D P to A T P.

Return to FIGURE 19.2 The light reactions of oxygenic photosynthesis generate both A T P and reducing power

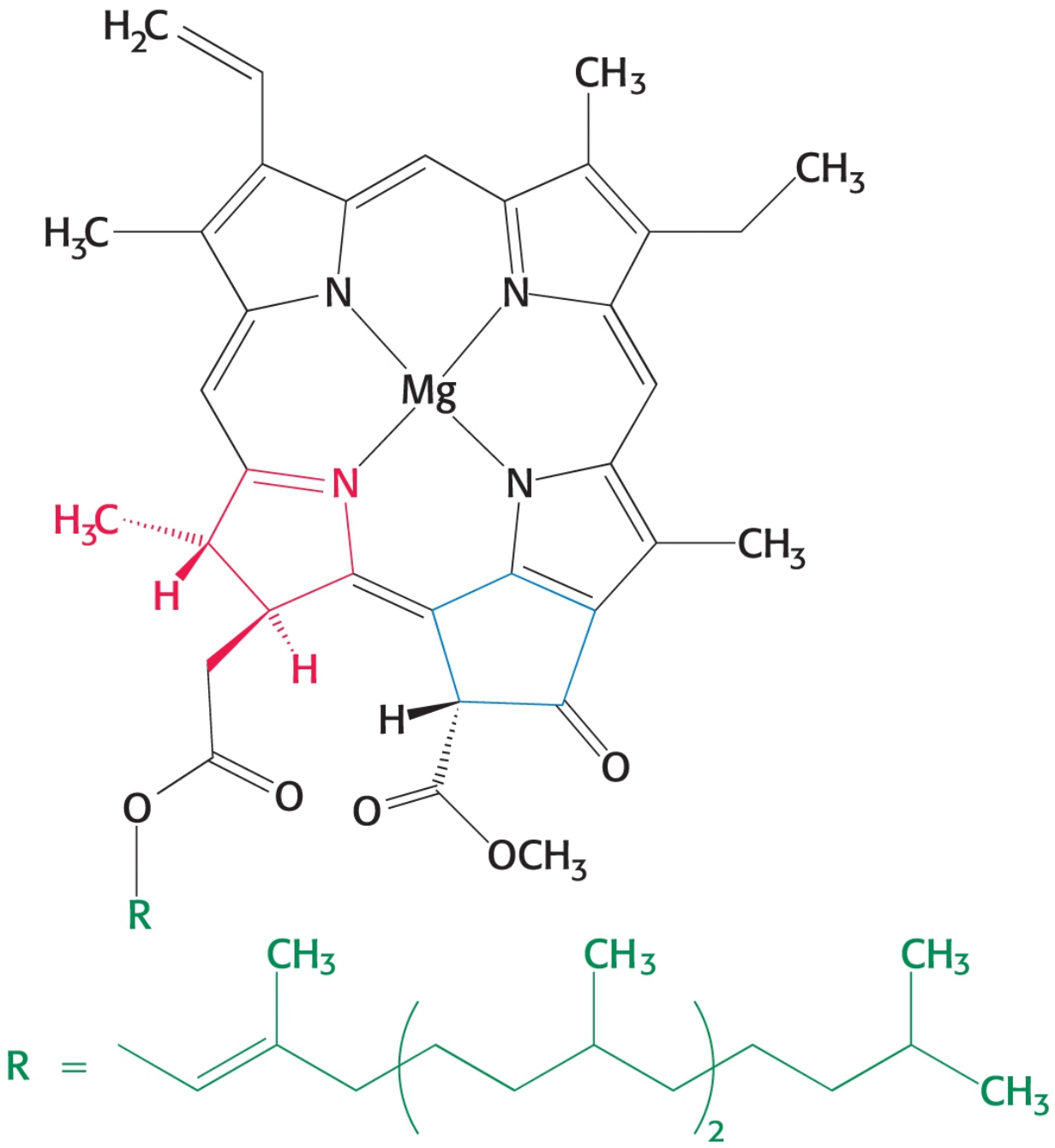
Extended description for FIGURE 19.3 The anatomy of a chloroplast reveals complex membrane-enclosed structures



The chloroplast is an oval-shaped, hollow sac-like structure that consists of two membranes labeled the outer membrane and the inner membrane. The space between the outer membrane and inner membrane is labeled intermembrane space. The hollow interior of the chloroplast is labeled stroma. The stroma of the chloroplast consists of numerous stacked discs. These discs are surrounded by thylakoid membranes. The bridges connecting the stacked discs with the neighboring stacked discs are labeled stroma lamella. One of the thylakoid membranes is cut open to expose the thylakoid lumen. An electron micrograph of a chloroplast on the right depicts the stacked grana interconnected by stroma lamella. A scale on the bottom left of the electron micrograph reads 500 nanometers.

Return to FIGURE 19.3 The anatomy of a chloroplast reveals complex membrane-enclosed structures

Extended description for FIGURE 19.5: Structure of Chlorophyll alpha



Four 5-membered heterocyclic pentagonal rings, four 6-membered heterocyclic hexagonal rings, and one 5-carbon hexagonal ring are fused together. The first 5-membered heterocyclic pentagonal ring is in a vertical orientation consisting of 1 N and 4 C atoms. In the first 5-membered heterocyclic pentagonal ring, N occupies the first position which is the bottom right vertex. In the first 5-membered heterocyclic pentagonal ring, a double bond is present between C 2 and C 3. C 2 of the first 5-membered heterocyclic pentagonal ring is single bonded to C H 3. C 3 of the first 5-membered heterocyclic pentagonal ring is single bonded to a central C H group in the form of a line. The central C H group is double bonded to C H 2 on the upper left. The first 5-membered heterocyclic pentagonal ring is fused to the first 6-membered heterocyclic hexagonal ring in a vertical orientation consisting of 1 M g, 2 N, and 3 C atoms. In the first hexagonal ring, the first N atom occupies the first position which is the bottom right vertex, M g occupies the second position which is the bottommost vertex, and the second N atom occupies the third position which is the bottom left vertex. The two rings are fused to each other such that C 4 and N of the first 5-membered heterocyclic pentagonal ring are the C 1 and the second N atom of the first hexagonal ring, respectively. In the first hexagonal ring, a double bond is present between C 1 and C 2. The first hexagonal ring is fused to the second 5-membered pentagonal ring in a vertical orientation consisting of 1 N and 4 C atoms. In the second 5-membered heterocyclic pentagonal ring, N occupies the first position which is the bottom left vertex. The two rings are fused to each other such that C 3 and the first N atom of the first hexagonal ring are the C 1 and N of the second 5-membered heterocyclic pentagonal ring, respectively. In the second 5-membered heterocyclic pentagonal ring, a double bond is present between N and C 1, and C 2 and C 3. C 2 of the second 5-membered heterocyclic pentagonal ring is single bonded to C H 3. C 3 of the second 5-membered heterocyclic pentagonal ring is single bonded to a central C H 2 group in the form of a line. The central C H 2 group is

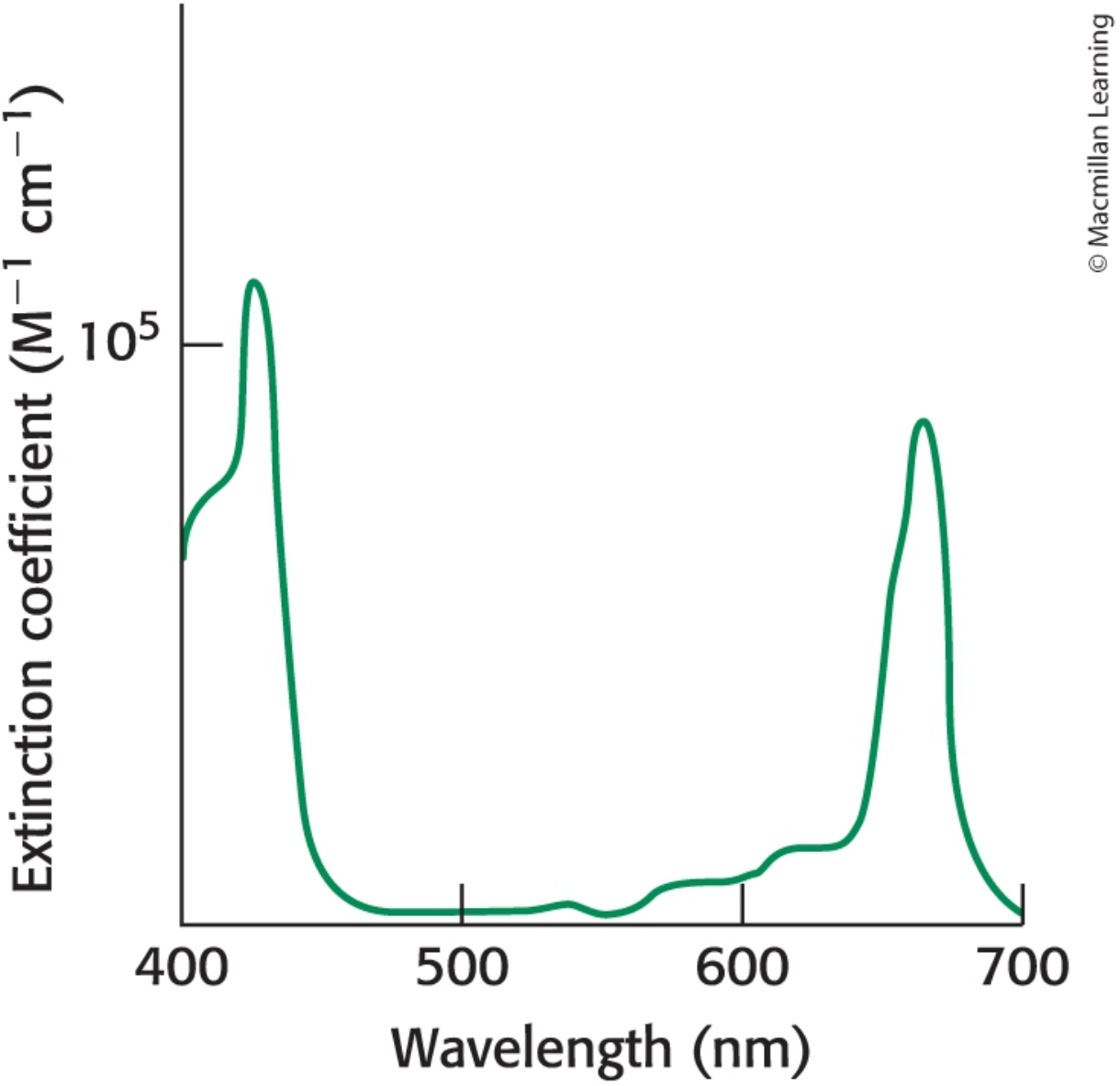
single bonded to C H 3 on the upper right. The first hexagonal ring and the second 5-membered heterocyclic pentagonal ring are fused to a second 6-membered heterocyclic hexagonal ring in a horizontal orientation consisting of 1 M g, 2 N, and 3 C atoms. In the second hexagonal ring, the first N atom occupies the first position which is the bottom left vertex, M g occupies the second position which is the leftmost vertex, and the second N atom occupies the third position which is the top left vertex. The three rings are fused to each other as follows: The first N atom and M g of the first hexagonal ring are the second N atom and M g of the second hexagonal ring, respectively. N and C 4 of the second 5-membered heterocyclic pentagonal ring are the second N atom and C 1 of the second hexagonal ring, respectively. In the second hexagonal ring, a double bond is present between C 1 and C 2. The second hexagonal ring is fused to the third 5-membered heterocyclic pentagonal ring in a horizontal orientation consisting of 1 N and 4 C atoms. In the third 5-membered heterocyclic pentagonal ring, N occupies the first position which is the top left vertex. The two rings are fused to each other such that the first N atom and C 3 of the second hexagonal ring are N and C 1 of the third 5-membered heterocyclic pentagonal ring, respectively. In the third 5-membered heterocyclic pentagonal ring, a double bond is present between C 1 and C 2, and C 3 and C 4. C 2 of the third 5-membered heterocyclic pentagonal ring is single bonded to C H 3. The second hexagonal ring and the third 5-membered heterocyclic pentagonal ring are fused to the third 6-membered heterocyclic hexagonal ring in a vertical orientation consisting of 1 M g, 2 N and 3 C atoms. In the third hexagonal ring, the first N atom occupies the first position which is the top left vertex, M g occupies the second position which is the topmost vertex, and the second N atom occupies the third position which is the top right vertex. The three rings are fused to each other as follows: M g and the first N atom of the second hexagonal ring are the M g and the second N atom of the third hexagonal ring, respectively. N and C 4 of the third 5-membered heterocyclic pentagonal ring are the second N atom

and C 1 of the third hexagonal ring, respectively. In the third hexagonal ring, a double bond is present between C 2 and C 3. The third 5-membered heterocyclic pentagonal ring and the third hexagonal ring are fused to the 5-carbon pentagonal ring in a vertical orientation highlighted in blue with C 1 occupying the topmost vertex. The three rings are fused to each other as follows: C 3 and C 4 of the third 5-membered heterocyclic pentagonal ring are the C 2 and C 1 of the 5-carbon pentagonal ring, respectively. C 1 and C 2 of the third hexagonal ring are the C 1 and C 5 of the 5-carbon pentagonal ring, respectively. C 3 of the 5-carbon pentagonal ring is double bonded to O. C 4 of the 5-carbon pentagonal ring is wedge bonded to H on the lower left and dash bonded to a central C atom on the lower left in the form of a dashed line. The central C atom is double bonded to a second O atom on the lower left and single bonded to O C H 3 on the lower right. The third hexagonal ring is fused to the fourth 5-membered heterocyclic pentagonal ring in a horizontal orientation highlighted in red consisting of 1 N and 4 C atoms. In the fourth 5-membered heterocyclic pentagonal ring, N occupies the first position which is the top right vertex. The two rings are fused to each other such that the first N atom and C 3 of the third hexagonal ring are the N and C 1 of the fourth 5-membered heterocyclic pentagonal ring, respectively. In the fourth 5-membered heterocyclic pentagonal ring, a double bond is present between C 4 and N. C 2 of the fourth 5-membered heterocyclic pentagonal ring is single bonded to H on the lower right and wedge bonded to C 1 of a 2-carbon alkane chain depicted as a line structure using 1 line. C 3 of the fourth 5-membered heterocyclic pentagonal ring is wedge bonded to H on the lower left and dash bonded to C H 3 on the upper left. The groups attached to C 1 and C 2 of the fourth 5-membered heterocyclic pentagonal ring are highlighted in red. C 2 of the 2-carbon alkane chain is double bonded to a third O atom on the lower right and single bonded to a fourth O atom on the lower left. The fourth O atom is single bonded to R below which is highlighted in green. The third hexagonal ring and the fourth 5-

membered heterocyclic pentagonal ring are fused to the fourth 6-membered heterocyclic hexagonal ring in a horizontal orientation consisting of 1 M g, 2 N, and 3 C atoms. In the fourth hexagonal ring, the first N atom occupies the first position which is the top right vertex, M g occupies the second position which is the rightmost vertex, and the second N atom occupies the third position which is the bottom right vertex. The three rings are fused to each other as follows: The first N atom and M g of the third hexagonal ring are the second N atom and M g of the fourth hexagonal ring, respectively. C 4 and N of the fourth 5-membered heterocyclic pentagonal ring are the C 1 and the second N atom of the fourth hexagonal ring, respectively. The fourth hexagonal ring, the first 5-membered heterocyclic pentagonal ring, and the first hexagonal ring are also fused to each other as follows: C 3 and the first N atom of the fourth hexagonal ring are the C 1 and N of the first 5-membered heterocyclic pentagonal ring, respectively. The first N atom and M g of the fourth hexagonal ring are the second N atom and M g of the first hexagonal ring, respectively. R has the following structure highlighted in green: A 15-carbon alkene chain is depicted as a line structure using 10 zigzag lines in which the three zigzag lines between C 4 and C 13 are enclosed within parentheses with subscript 2. A double bond is present between C 2 and C 3. C 3, C 7, and C 11 are each single bonded to C H 3 above. C 15 is single bonded to C H 3 above and C H 3 on the lower right.

Return to FIGURE 19.5: Structure of Chlorophyll alpha

Extended description for FIGURE 19.6 Chlorophyll a has a distinct absorbance spectrum in the visible range

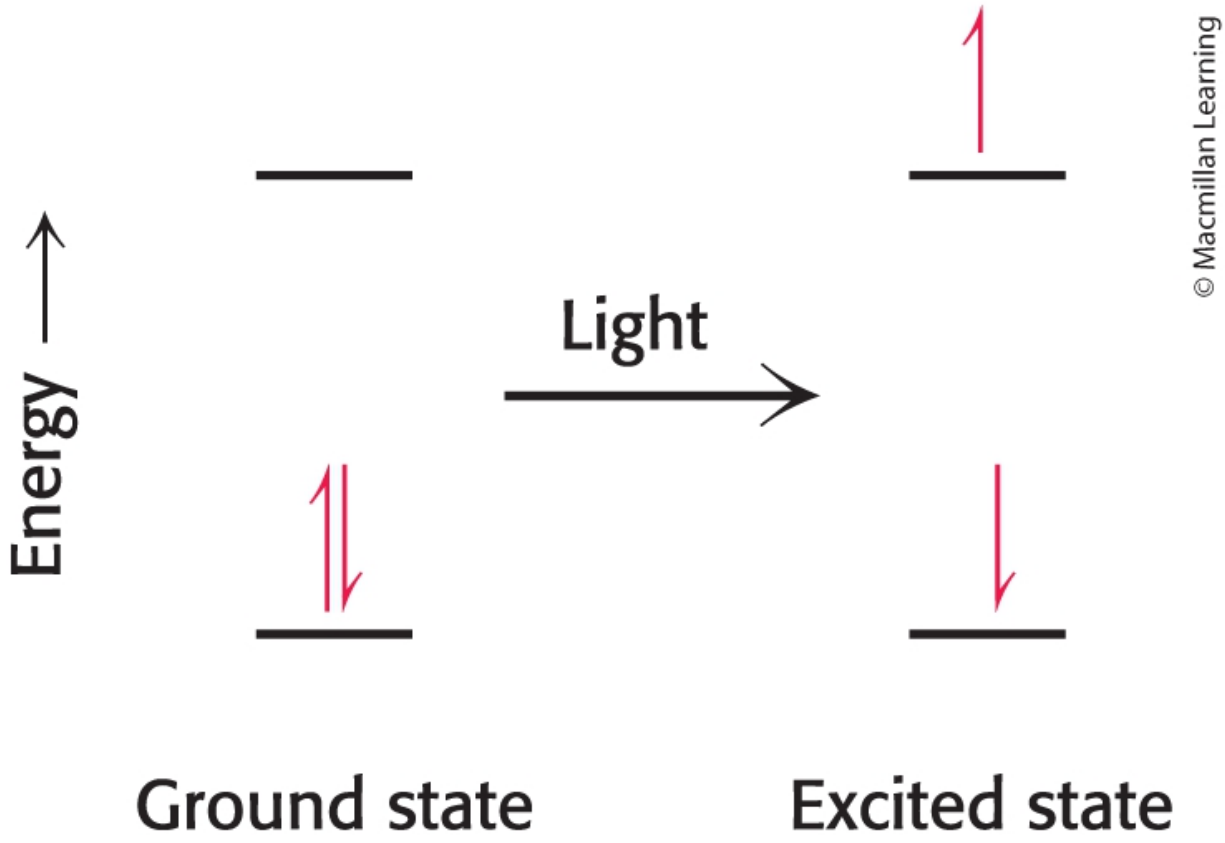


The horizontal axis, labeled wavelength in nanometers, has markings ranging from 400 to 700 in increments of 100 units. The vertical axis, labeled extinction coefficient in M inverse centimeter inverse, has the marking 10 to the power 5 much above the midpoint

of the vertical axis. The graph shows a green curve that starts from a point below 10 to power 5, peaks at 420 just above 10 to power 5, and steeply falls to 450 on the horizontal axis. It then continues moving along the horizontal axis to reach 600. The curve rises upward and peaks again at 670 nanometer and below 10 to the power 5 on the vertical axis. It then steeply falls again to terminate at 700 on the horizontal axis. All values are approximated.

Return to FIGURE 19.6 Chlorophyll a has a distinct absorbance spectrum in the visible range

Extended description for FIGURE 19.7 The absorption of light leads to the excitation of an electron from its ground state to a higher energy level

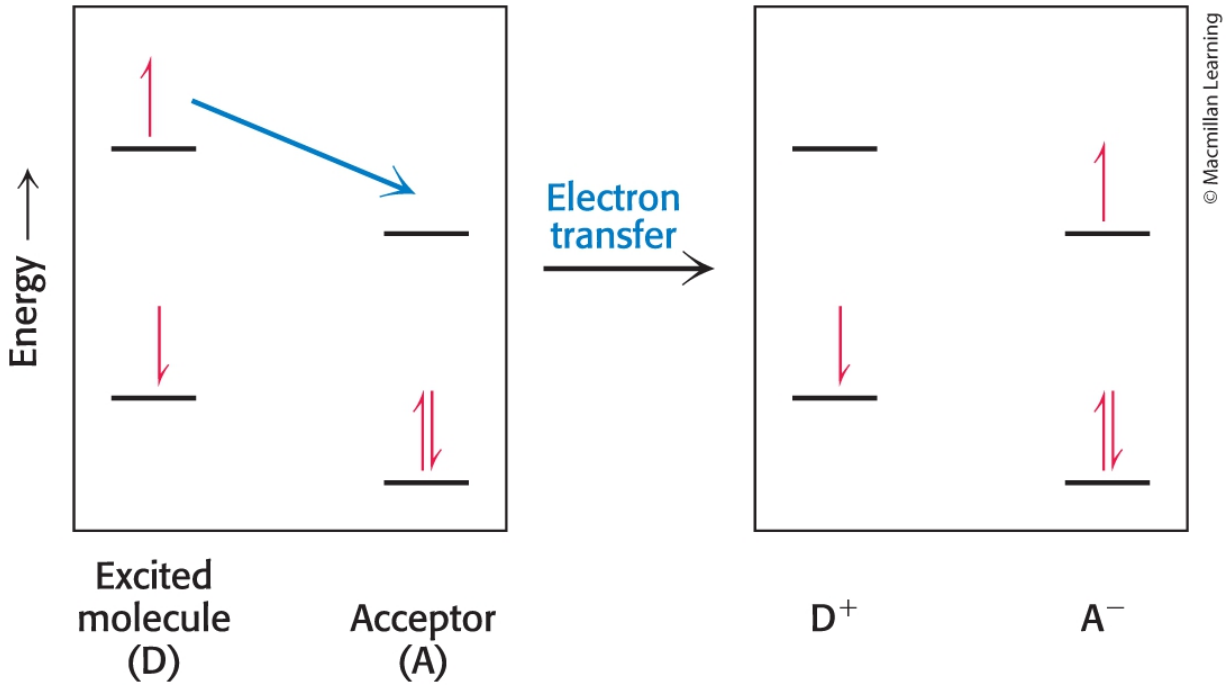


© Macmillan Learning

The figure shows the ground state of the electron on the left and the excited state of the electron on the right. An upward arrow on the left side of the figure is labeled energy. On the left, an upward and downward arrow is present in the ground state. A blank is shown above the ground state at a higher energy level. An arrow from the ground state points to the excited state on the right. The arrow is labeled light. A downward arrow is present at the bottom excited state and an upward arrow is present in the top excited state.

Return to FIGURE 19.7 The absorption of light leads to the excitation of an electron from its ground state to a higher energy level

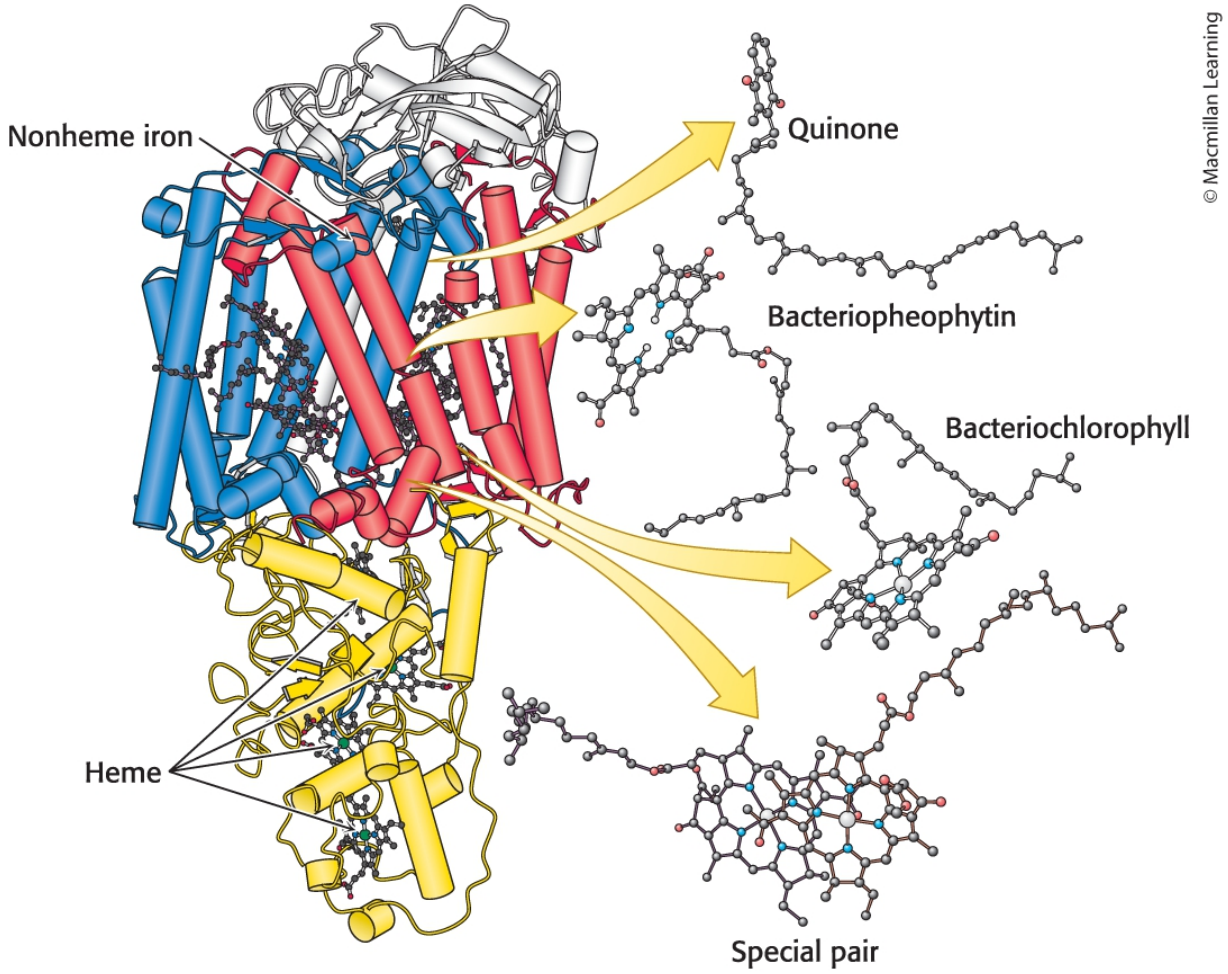
Extended description for FIGURE 19.8 The key to photosynthesis is photoinduced charge separation



The figure shows two panels. The first panel shows an excited molecule D on the left. A downward arrow is present in the bottom ground state and an upward arrow is present in the top excited state. An arrow from the excited molecule is directed toward the excited state of the acceptor A. In the ground state of acceptor A, an upward and downward arrow is present. An arrow from the first panel points to the second panel on the right and the arrow is labeled electron transfer. The second panel shows an excited molecule D superscript plus on the left. A downward arrow is present in the ground state and the top excited state is blank. In the acceptor A superscript minus, an upward arrow is present in the top excited state, and upward and downward arrow is present in the bottom ground state.

Return to FIGURE 19.8 The key to photosynthesis is photoinduced charge separation

Extended description for FIGURE 19.9 The photosynthetic reaction center in a nonsulfur purple bacterium is a large complex with many electron-carrying groups and one special pair

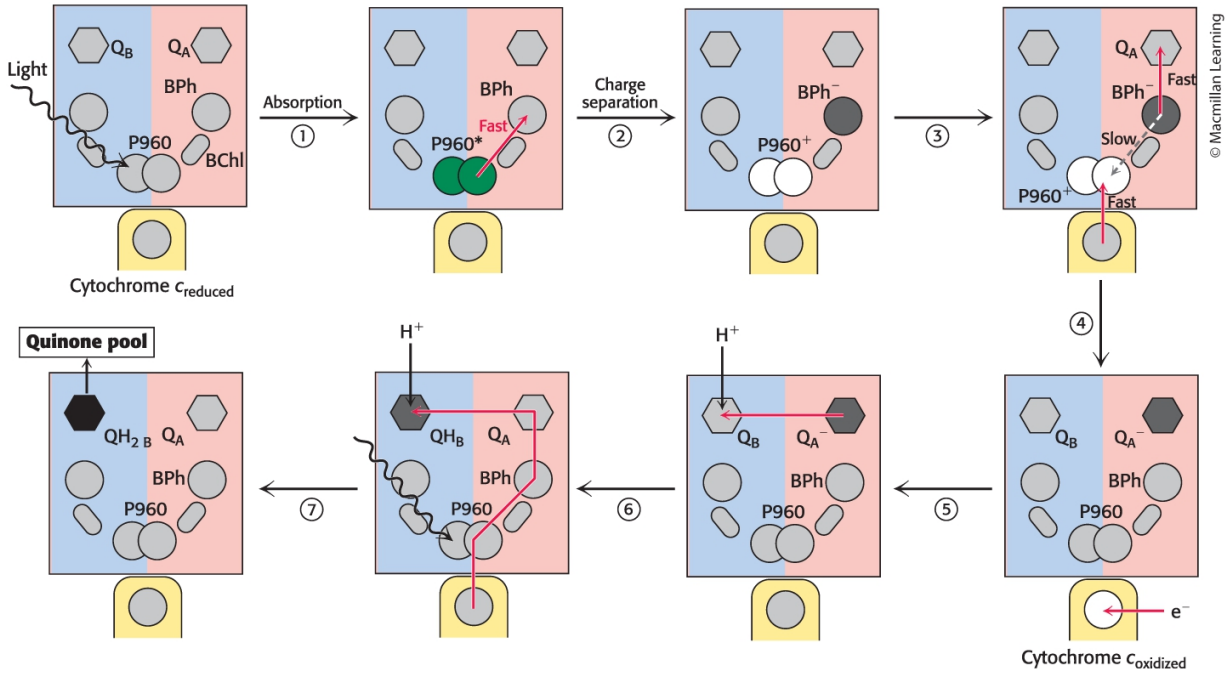


The core of the reaction center from *Rhodopseudomonas viridis* has red, blue, white, and yellow cylinders. The red cylinders represent the L chain, the blue cylinders represent the M chain, and the white chain represents the H chain. The yellow cylinders represent cytochrome subunits. The L, M, H, and cytochrome subunits are composed largely of alpha helices that span the membrane. The H

chain consists of beta sheets. A chain of electron-carrying prosthetic groups runs from the bottom to the top. It includes a special pair of bacteriochlorophylls, bacteriopheophytin, and quinone. Nonheme iron is bound to an M chain. The cytochrome subunits are bound to heme groups.

Return to FIGURE 19.9 The photosynthetic reaction center in a nonsulfur purple bacterium is a large complex with many electron-carrying groups and one special pair

Extended description for FIGURE 19.10 In the reaction center of nonsulfur purple bacteria, electrons flow from the special pair to a quinone



The figure depicts the electron flow in the reaction center in seven steps. It starts with the excitation of a pair of P 960 depicted as two overlapping circles. P 960 is present at the bottom. A wavy arrow representing light strikes P 960. Cytochrome c reduced is present below P 960. An arrow from this points to the first step and is labeled absorption and numbered 1.

In the first step, P 960 is converted to P 960 asterisk. The electron is transferred from P 960 to B P h through B C h l. The arrow is labeled fast. An arrow from the first step points toward the second step and is labeled charge separation and numbered 2.

In the second step, P 960 gives up an electron to B P h and becomes positively charged. B P h now acquires a negative charge. An arrow from the second step points to the third step and is numbered 3.

In the third step, cytochrome+ c reduced gives an electron to P 960 superscript plus. The arrow is labeled fast. A dotted arrow from B P h superscript minus points to P 960 superscript plus and is labeled slow. An arrow from B P h superscript minus points upward to Q subscript A and is labeled fast. An arrow from the third step points to the fourth step and is numbered 4.

In the fourth step, Q subscript A acquires a negative charge. An electron enters cytochrome c oxidized and converts it to cytochrome c reduced. An arrow from the fourth step points toward the fifth step and is numbered 5.

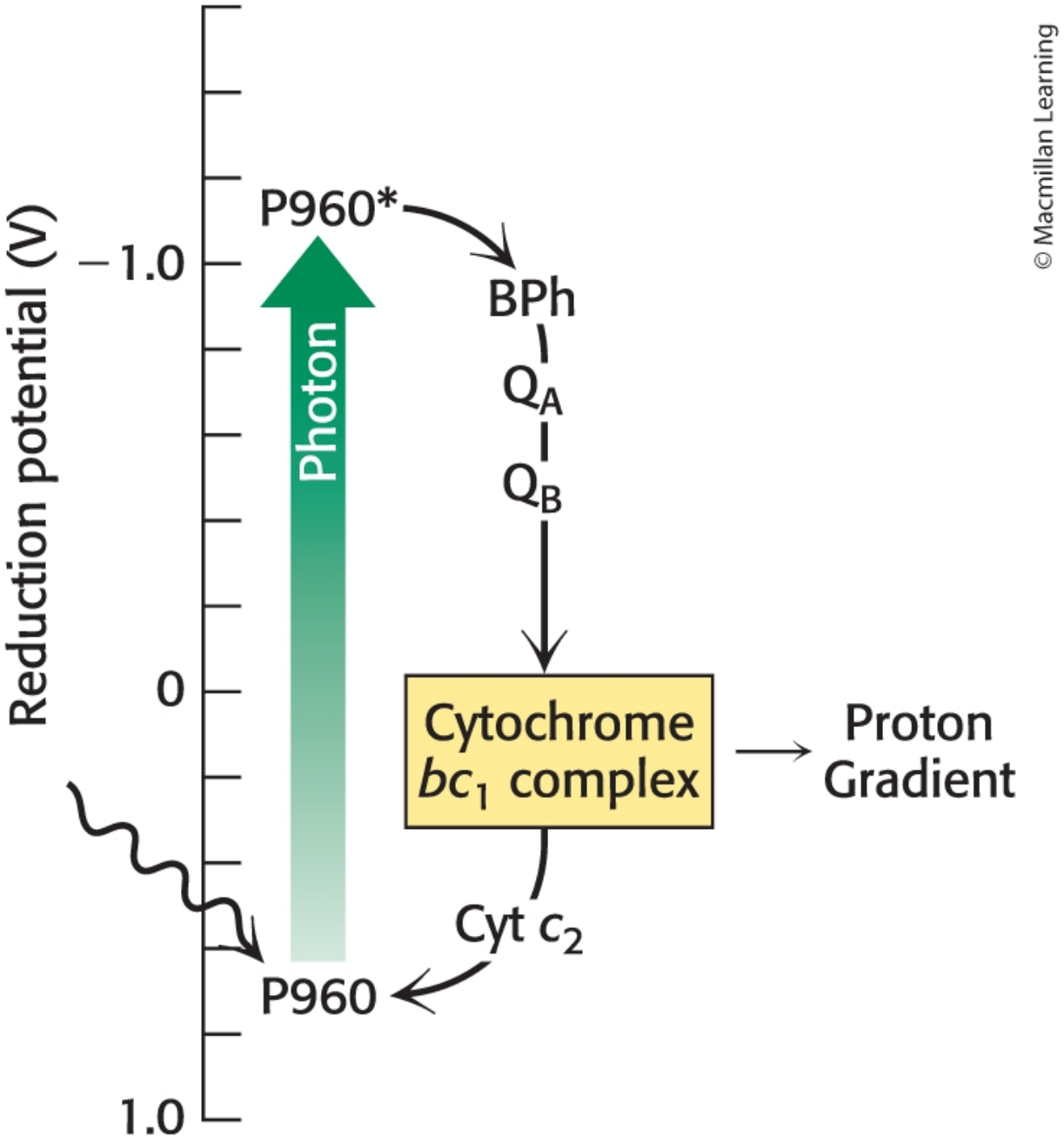
In the fifth step, Q subscript A superscript minus transfers an electron to Q subscript B. An H superscript plus ion also enters the Q subscript B. An arrow from the fifth step points to the sixth step and is numbered 6.

In the sixth step, an electron from cytochrome C reduced goes to Q H subscript B in the site Q subscript B through P 960, B P h, and Q subscript A. An H superscript plus ion also enters Q H subscript B. An arrow from the sixth step points to the seventh step and is numbered 7.

In the seventh step, Q H 2 moves into the quinone pool outside the reaction center.

Return to FIGURE 19.10 In the reaction center of nonsulfur purple bacteria, electrons flow from the special pair to a quinone

Extended description for FIGURE 19.11 Cyclic electron flow in the bacterial reaction center allows the generation of A T P but not reducing power

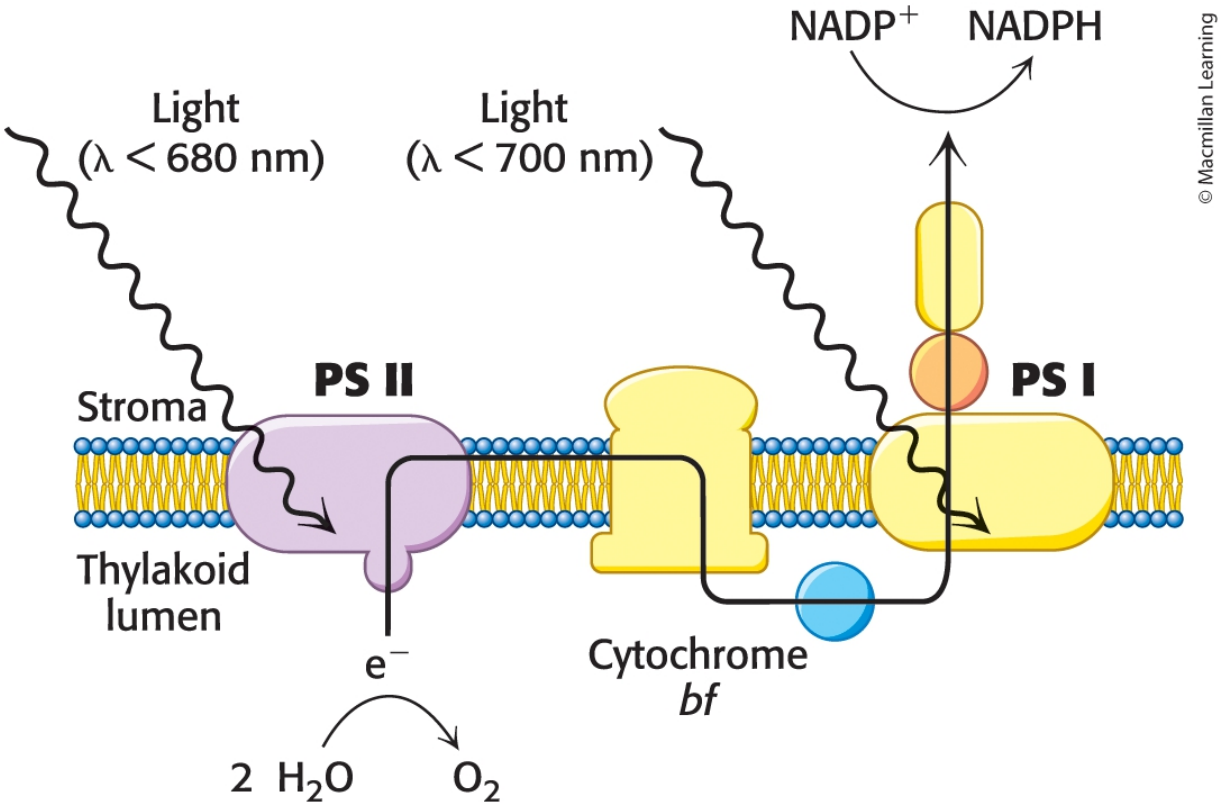


© Macmillan Learning

The vertical axis is labeled reduction potential V. It has the markings 1.0, 0, and negative 1.0 from the bottom to the top. A wavy arrow strikes P 960 corresponding to 0.8 on the vertical axis. P 960 points to the P 960 asterisk corresponding to negative 1.0. The arrow is labeled photon. P 960 asterisk leads to B P h. B P h leads to cytochrome b c subscript 1 complex through Q subscript A and Q subscript B. Cytochrome b c subscript 1 complex generates proton gradient and leads to cytochrome c subscript 2. Cytochrome c subscript 2 leads back to P 960.

Return to FIGURE 19.11 Cyclic electron flow in the bacterial reaction center allows the generation of A T P but not reducing power

Extended description for FIGURE 19.12 In green plants, electrons can flow through two photosystems



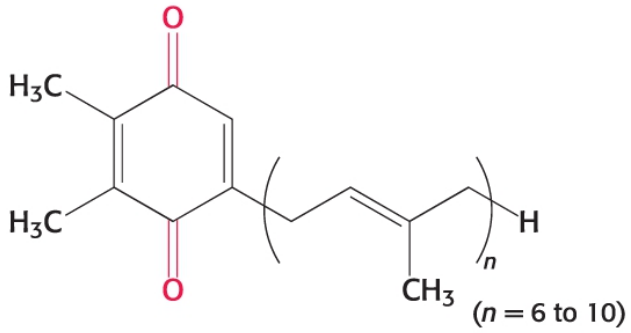
© Macmillan Learning

The figure depicts a lipid bilayer. The lipid bilayer consists of two horizontally parallel layers of lipids. The upper and lower layer consists of lipid molecules packed together compactly. Each lipid molecule is shown in a shorthand depiction. The yellow extensions of the shorthand depiction are aligned together and form the core of the bilayer. The blue spheres are located away from each other. The region above the lipid bilayer is labeled stroma and the region below the lipid bilayer is labeled thylakoid lumen. The lipid bilayer shows three membrane proteins. The first membrane protein labeled P S 2 is capsule-like and penetrates the entire lipid bilayer. The second membrane protein is rectangular with a bulb-like upper portion labeled cytochrome b f. The third membrane protein resembles a

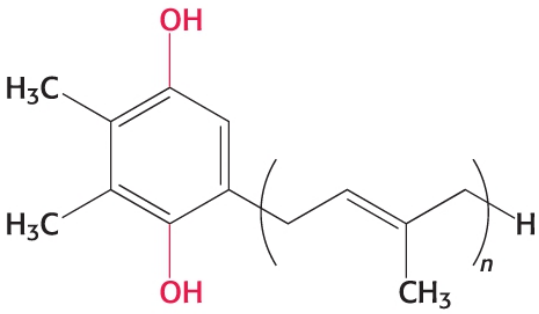
capsule and is labeled P S 1. The third membrane protein has two other structures attached to it at the upper end in the stroma. A wavy arrow labeled light lambda less than 680 nanometer strikes the P S 2. This converts 2 H 2 O to O 2. An electron in the thylakoid lumen near P S 2 moves into the P S 2 membrane protein. From P S 2 it goes to cytochrome b f. From cytochrome b f complex, it moves to a blue-colored sphere in the thylakoid lumen. It then moves into the P S 1. A wavy arrow labeled lambda less than 700 nanometers strikes P S 1. The electron exits the P S 1 and is used up for the reduction of N A D P superscript plus to N A D P H.

Return to FIGURE 19.12 In green plants, electrons can flow through two photosystems

Extended description for Structures of Plastoquinone and Plastoquinol



Plastoquinone
(oxidized form, Q)



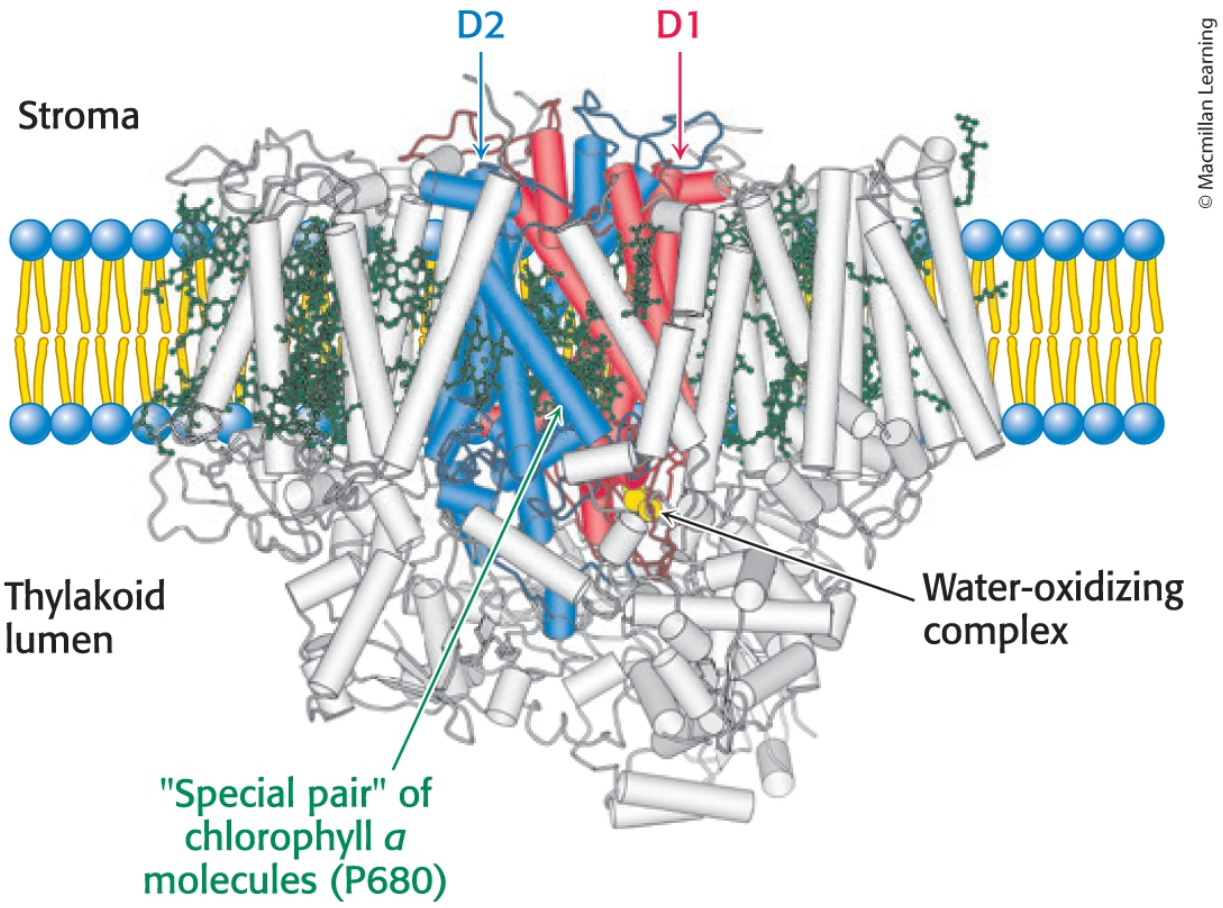
Plastoquinol
(reduced form, QH_2)

The structure of plastoquinone (oxidized form, Q) is as follows: A 6-carbon hexagonal ring is in a vertical orientation with C 1 occupying the topmost vertex. A double bond is present between C 2 and C 3 and C 5 and C 6. C 1 and C 4 are each double bonded to O highlighted in red. C 5 and C 6 are each single bonded to C H 3. C 3 is single bonded to C 1 of a 4-carbon alkene chain depicted as a line structure using 3 zigzag lines. In the alkene chain, a double bond is present between C 2 and C 3. C 3 of the alkene chain is single bonded to C H 3 below. C 4 of the alkene chain is single bonded to H on the lower right. The alkene chain is enclosed within parenthesis with subscript n. The text below reads n equals 6 to 10. The structure of plastoquinol (reduced form, Q H 2) is as follows: A benzene ring is in a vertical orientation with C 1 occupying the topmost vertex. The ring contains alternating double bonds between C 2 and C 3, C 4 and C 5, and C 6 and C 1. C 1 and C 4 are each single bonded to O H highlighted in red. C 5 and C 6 are each single bonded to C H 3. C 3 is single bonded to C 1 of a 4-carbon alkene chain depicted as a line structure using 3 zigzag lines. In the alkene chain, a double bond is present between C 2 and C 3. C 3 of the alkene chain is single bonded to C H 3 below. C 4 of the alkene chain is single bonded to H

on the lower right. The alkene chain is enclosed within parenthesis followed by subscript n.

Return to Structures of Plastoquinone and Plastoquinol

Extended description for FIGURE 19.13 Photosystem II is a large membrane protein complex with many chlorophyll molecules, one special pair, and the water-oxidizing complex

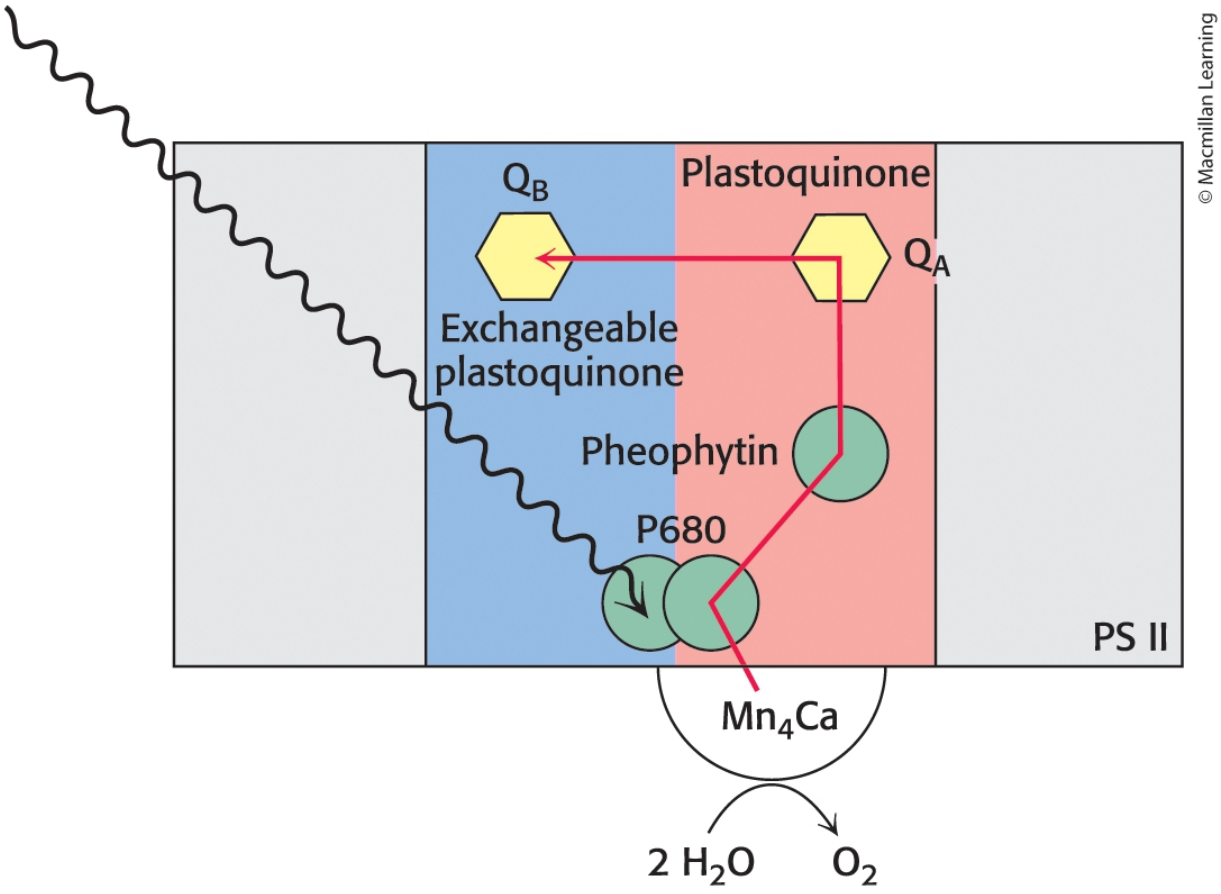


The figure depicts a lipid bilayer membrane. The lipid bilayer consists of two horizontally parallel layers of lipids. The upper and lower layer consists of lipid molecules packed together compactly. Each lipid molecule is shown in a shorthand depiction. The yellow extensions of the shorthand depiction are aligned together to form the core of the bilayer. The blue spheres are located away from each other. The region above the membrane is labeled stroma and the

region below the membrane is labeled thylakoid lumen. A cluster of red, white, and blue cylinders bound to alpha helices is embedded in the membrane. The red and blue cylinders are labeled D 1 and D 2, respectively. A yellow sphere labeled water-oxidizing complex is shown buried in the complex. The D 1 and D 2 subunits are bound to green-colored molecules labeled "special pair" of chlorophyll a molecules P 680.

Return to FIGURE 19.13 Photosystem II is a large membrane protein complex with many chlorophyll molecules, one special pair, and the water-oxidizing complex

Extended description for FIGURE 19.14 In photosystem II, electrons flow from manganese atoms to plastoquinone

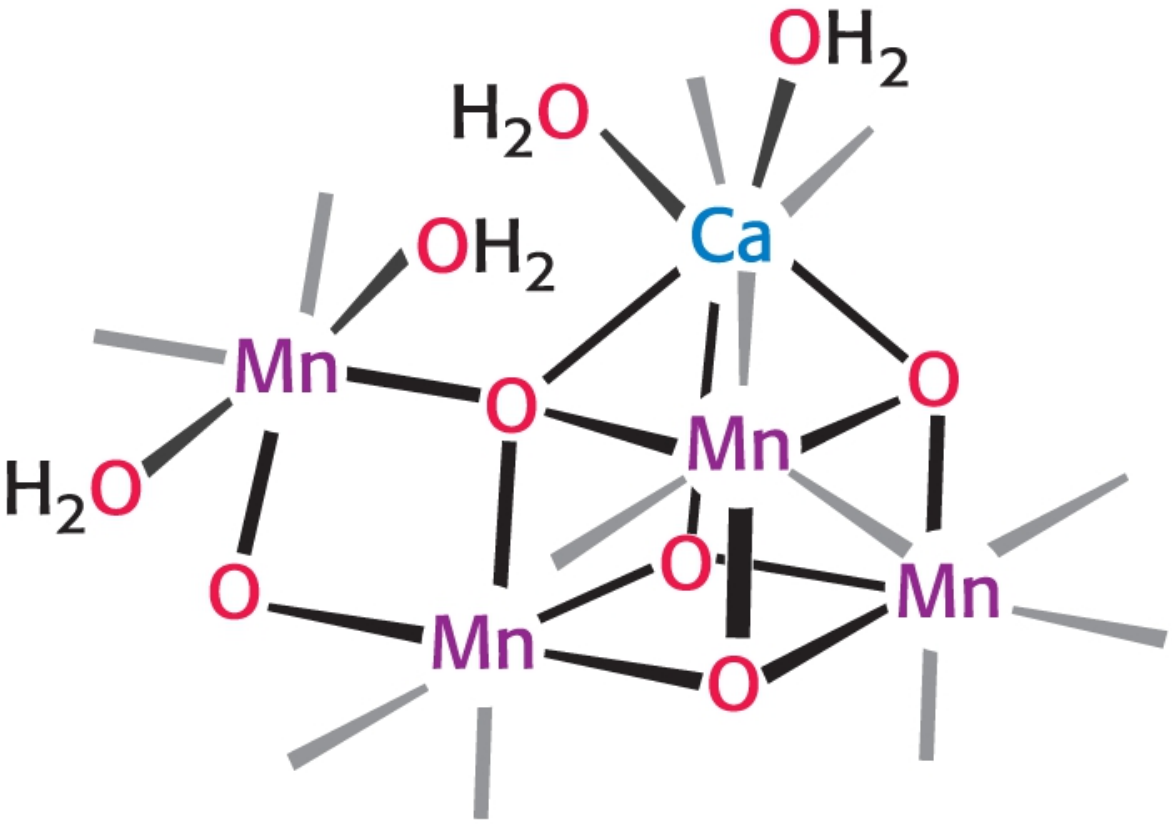


© Macmillan Learning

The electron flow in photosystem 2 starts with the excitation of a pair of chlorophyll molecules in P 680 depicted as two overlapping circles. P 680 is present at the bottom. A wavy arrow representing light strikes P 680. P 680 transfers an electron from M n 4 C a to pheophytin. From pheophytin, the electron is transferred to plastoquinone at site Q subscript A. From plastoquinone, the electron is transferred to exchangeable plastoquinone in site Q subscript B. The transfer of one electron from M n 4 C a is coupled with the conversion of 2 H 2 O to O 2.

Return to FIGURE 19.14 In photosystem II, electrons flow from manganese atoms to plastoquinone

Extended description for FIGURE 19.15 The core of the water-oxidizing complex includes four manganese ions and one calcium ion



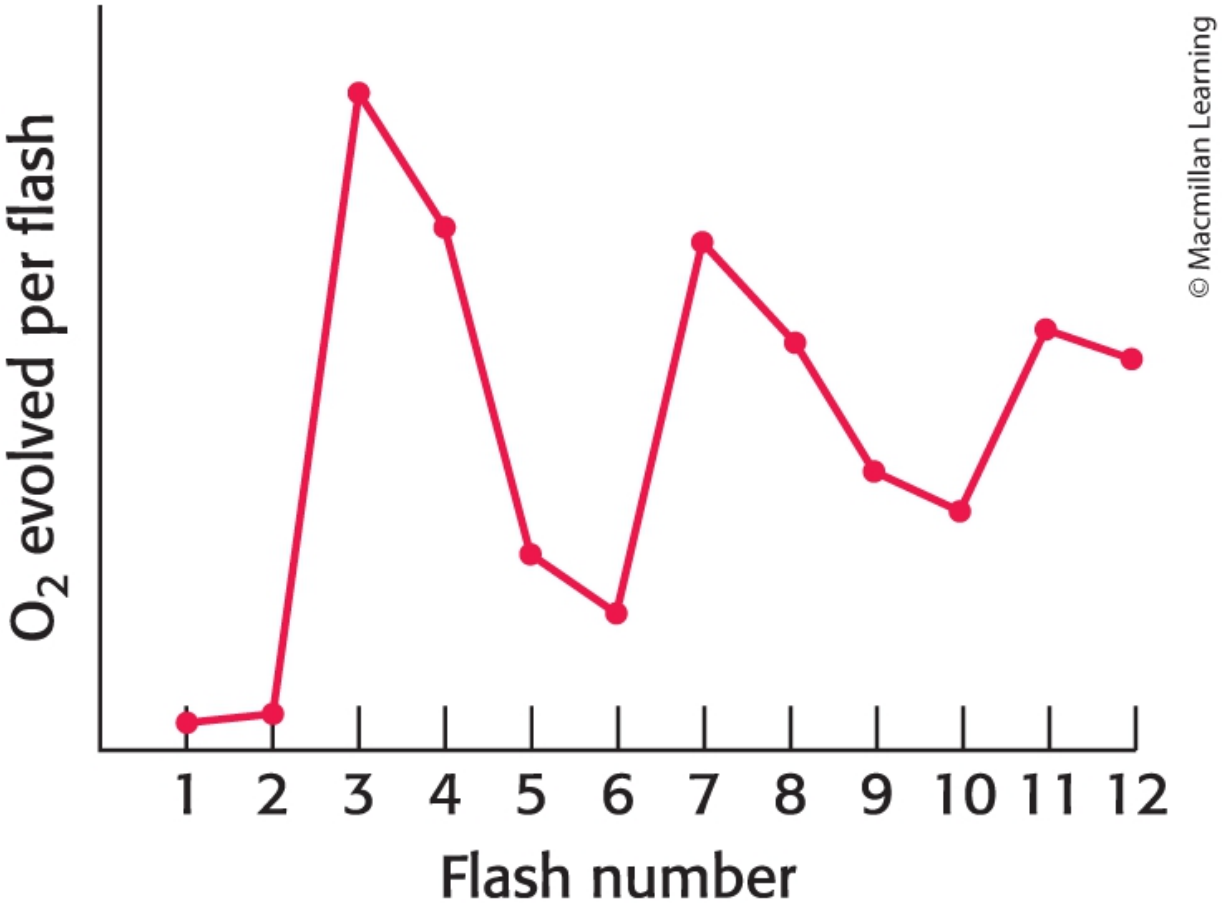
© Macmillan Learning

An 8-membered cuboid is shown consisting of 3 M n ions, 4 O atoms, and 1 C a atom. The cube is shown with its front left and front right faces toward the observer and its back left and back right faces away from the observer. Each M n ion occupies the front top vertex and the left bottom vertex, respectively. Each O atom occupies the front bottom vertex, the left top vertex, the right top vertex, and the back bottom vertex, respectively. The C a atom occupies the back top vertex. The C a atom is wedge bonded to O H 2 on the upper right and O H on the upper left, has an open single bond on the upper right and an open single bond on the upper left,

and is single bonded to M n ion at the front top vertex with the bond shaded in grey. The M n ion at the front top vertex is single bonded to the M n ion at the left bottom vertex and to the M n ion at the right bottom vertex with each bond shaded grey. The M n ion at the left bottom vertex has an open single bond on the lower left and an open single bond below. The M n ion at the right bottom vertex has an open single bond on the upper right, an open single bond on the lower right, and an open single bond below. The O atom at the left top vertex is wedge bonded to a fourth M n ion on the left which is wedge bonded to a fifth O atom below which is wedge bonded to the M n ion at the left bottom vertex of the cuboid. The fourth M ion is wedge bonded to O H 2 on the upper right and O H 2 on the lower left, and has an open single bond on the upper right and an open single bond on the upper left. All the M n ions are highlighted in purple, the C a atom is highlighted in blue, and all O atoms are highlighted in red. All the open single bonds are shaded grey.

Return to FIGURE 19.15 The core of the water-oxidizing complex includes four manganese ions and one calcium ion

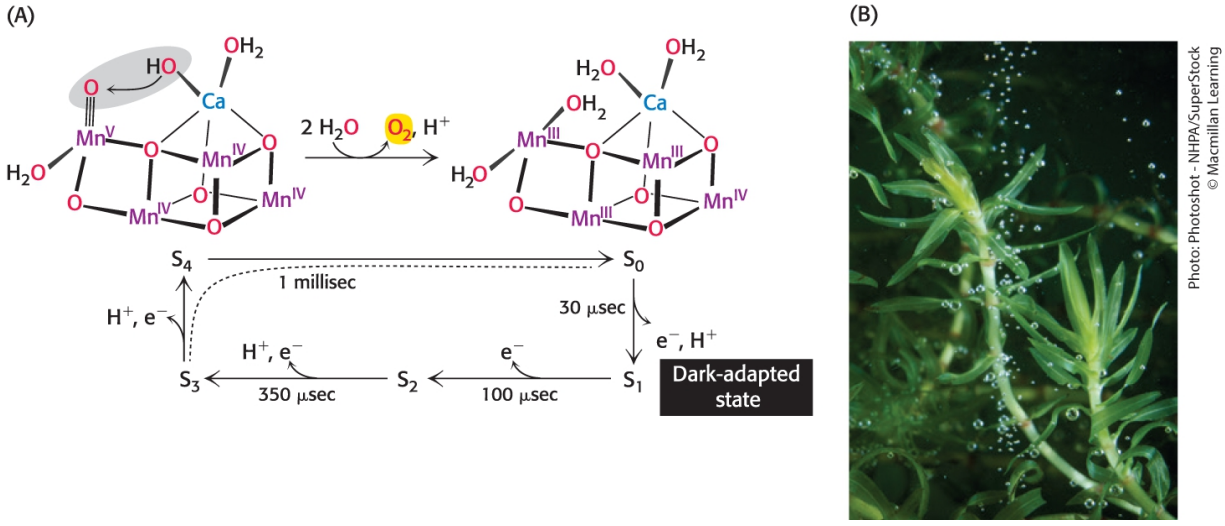
Extended description for FIGURE 19.16 Four photons are required to generate one oxygen molecule after the first cycle



The horizontal axis, labeled flash number, has markings ranging from 0 to 12 in increments of 1 unit. The vertical axis is labeled O 2 evolved per flash. The graph starts from 1 on the horizontal axis, moves toward the right to 2, shows a sharp peak at 3, slopes down to 6 slightly above the origin, peaks again at 7 much lower than the first peak, slopes down through 8, 9, and 10, and then rises upward at 11 to the midpoint of the vertical axis and terminates on the right at 12.

Return to FIGURE 19.16 Four photons are required to generate one oxygen molecule after the first cycle

Extended description for FIGURE 19.17 The model for the water-oxidizing complex explains the light-flash experiments



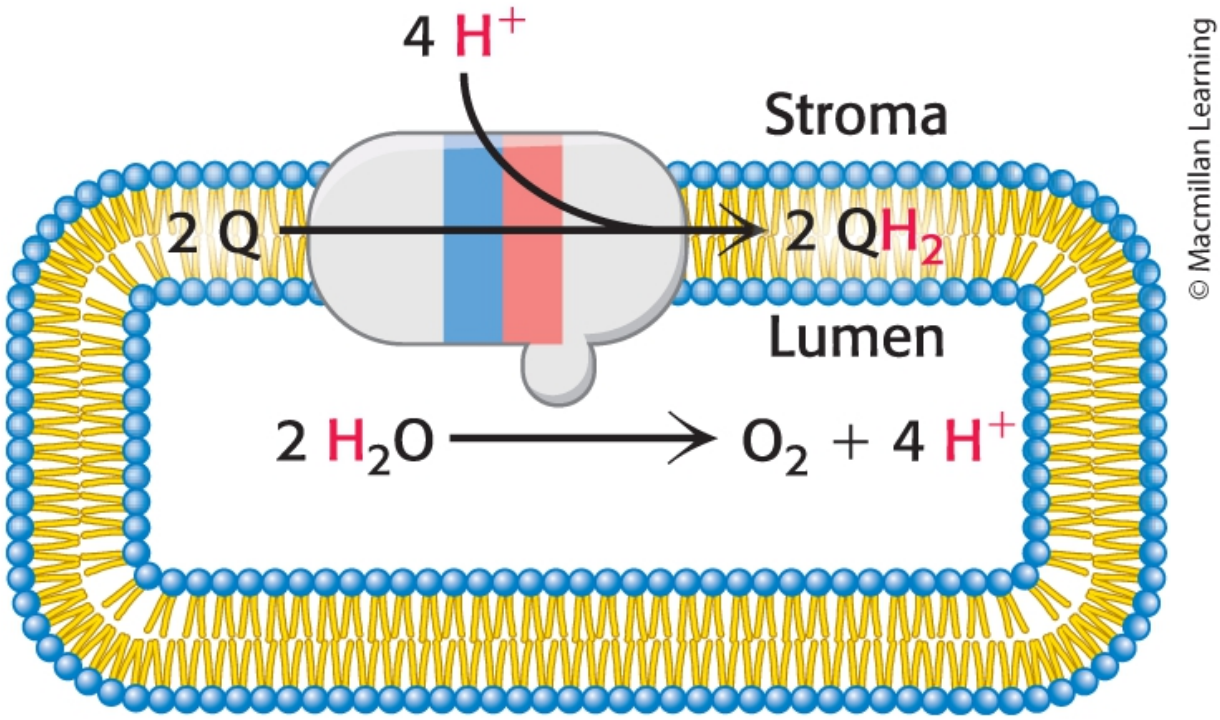
The figure has two parts labeled (A) and (B). Part (A) shows a coupled reaction of a water-oxidizing complex. The main reactant contains one reactant and one product. The reactant has the following structure: An 8-membered cuboid is shown consisting of 3 M n superscript roman numeral I V ions, 4 O atoms, and 1 C a atom. The cube is shown with its front left and front right faces toward the observer and its back left and back right faces away from the observer. Each M n superscript roman numeral I V ion occupies the front top vertex, the left bottom vertex, and the right bottom vertex, respectively. Each O atom occupies the front bottom vertex, the left top vertex, the right top vertex, and the back bottom vertex, respectively. The C a atom occupies the back top vertex. The C a atom is wedge bonded to O H 2 on the upper right and O H on the upper left. The O atom at the left top vertex is wedge bonded to M n superscript roman numeral V ion on the left which is wedge bonded to a fifth O atom below which is wedge bonded to the M n

superscript roman numeral I V ion at the left bottom vertex of the cuboid. The M n superscript roman numeral V ion is triple bonded to a sixth O atom above and is wedge bonded to O H 2 on the lower left. A curved arrow from the O H wedge bonded to C a points to the sixth O atom. The main reaction is coupled with the conversion of 2 molecules of H 2 O to O 2 shaded yellow and H superscript plus. The product has the following structure: An 8-membered cuboid is shown consisting of 2 M n superscript roman numeral I I I ions, 4 O atoms, 1 C a atom, and 1 M n superscript roman numeral I V atom. The cube is shown with its front left and front right faces toward the observer and its back left and back right faces away from the observer. Each M n superscript roman numeral I I I ion occupies the front top vertex and the left bottom vertex, respectively. Each O atom occupies the front bottom vertex, the left top vertex, the right top vertex, and the back bottom vertex, respectively. The C a atom occupies the back top vertex. The M n superscript roman numeral I V ion occupies the right bottom vertex. The C a atom is wedge bonded to O H 2 on the upper right and O H on the upper left. The O atom at the left top vertex is wedge bonded to a third M n superscript roman numeral I I I ion on the left which is wedge bonded to a fifth O atom below which is wedge bonded to the M n superscript roman numeral I I I ion at the left bottom vertex of the cuboid. The third M n superscript roman numeral I I I ion is wedge bonded to O H 2 on the upper right and is wedge bonded to O H 2 on the lower left. All the M n ions are highlighted in purple, the C a atom is highlighted in blue, and all O atoms are highlighted in red. The reactant is labeled S 4 and the product is labeled S 0. A rightward arrow from S 4 points to S 0. A downward arrow from S 0 points to S 1. The arrow is labeled 30 microseconds and depicts the release of an electron and H superscript plus ion. S 1 is labeled dark-adapted state. A leftward arrow from S 1 points to S 2 on the left. The arrow is labeled 100 microseconds and depicts the release of an electron. A leftward arrow from S 2 points to S 3 on the left. The arrow is labeled 350 microseconds and depicts the release of an

electron and H superscript plus ion. An upward arrow from S 3 points to S 4. The arrow depicts the release of an electron and H superscript plus ion. A dotted arrow from S 3 points to S 0 and is labeled 1 millisecond. The second part of the figure depicts oxygen generation by elodea plants immersed in water. The plants generate bubbles which depict the production of oxygen.

Return to FIGURE 19.17 The model for the water-oxidizing complex explains the light-flash experiments

Extended description for FIGURE 19.18 Photosystem II releases protons into the thylakoid lumen and takes them up from the stroma

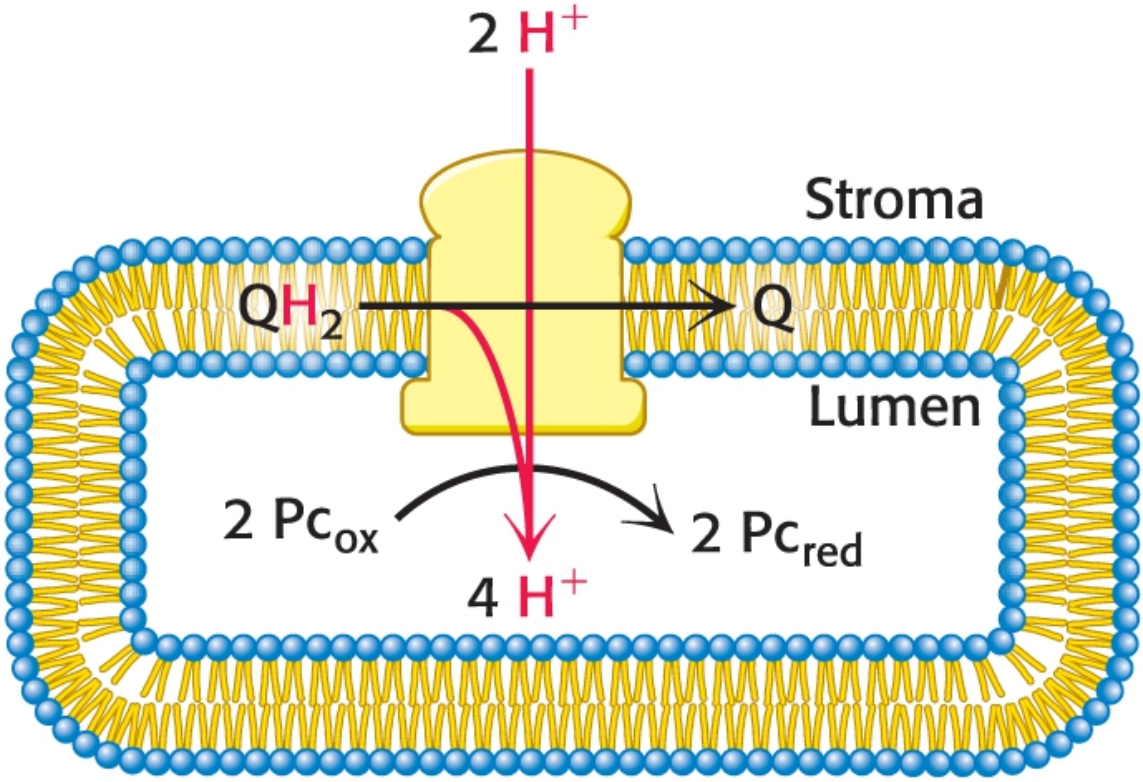


© Macmillan Learning

The figure depicts a lipid bilayer forming a rectangular loop. The lipid bilayer consists of two horizontally parallel layers of lipids. The upper and lower layer consists of lipid molecules packed together compactly. Each lipid molecule is shown in a shorthand depiction. The yellow extensions of the shorthand depiction are aligned together and form the core of the bilayer. The blue spheres are located away from each other. The region outside the lipid bilayer is labeled stroma and the region enclosed by the lipid bilayer is labeled thylakoid lumen. The lipid bilayer consists of a capsule-like membrane protein that converts 2 Q to 2 Q H 2 in the bilayer by the addition of 4 H superscript plus from the stroma. In the lumen, 2 H 2 O is converted to O 2 and 4 H superscript plus.

Return to FIGURE 19.18 Photosystem II releases protons into the thylakoid lumen and takes them up from the stroma

Extended description for FIGURE 19.19 Electron flow through cytochrome bf contributes to the proton gradient



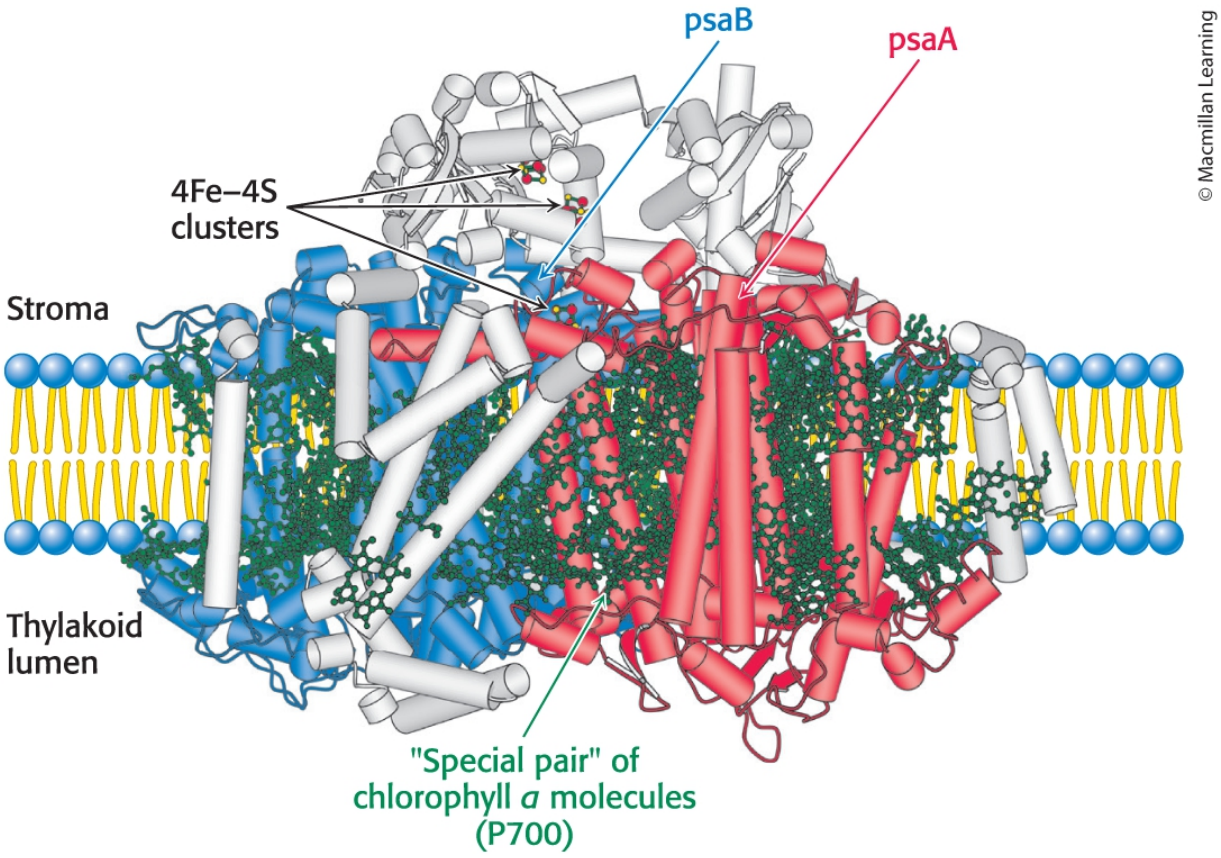
© Macmillan Learning

The figure depicts a lipid bilayer forming a rectangular loop. The lipid bilayer consists of two horizontally parallel layers of lipids. The upper and lower layer consists of lipid molecules packed together compactly. Each lipid molecule is shown in a shorthand depiction. The yellow extensions of the shorthand depiction are aligned together and form the core of the bilayer. The blue spheres are located away from each other. The region outside the lipid bilayer is labeled stroma and the region enclosed within the lipid bilayer is labeled lumen. A rectangular membrane protein is embedded in the bilayer that converts Q H 2 to Q. Q H 2 from the bilayer and 2 H superscript plus ions from the stroma enter the lumen through the

membrane protein to release 4 H superscript plus ions in the lumen. This movement is coupled with the conversion of 2 P c oxidized is converted to 2 P c reduced.

Return to FIGURE 19.19 Electron flow through cytochrome bf contributes to the proton gradient

Extended description for FIGURE 19.20 Photosystem I is a protein complex with numerous chlorophyll molecules and one special pair.



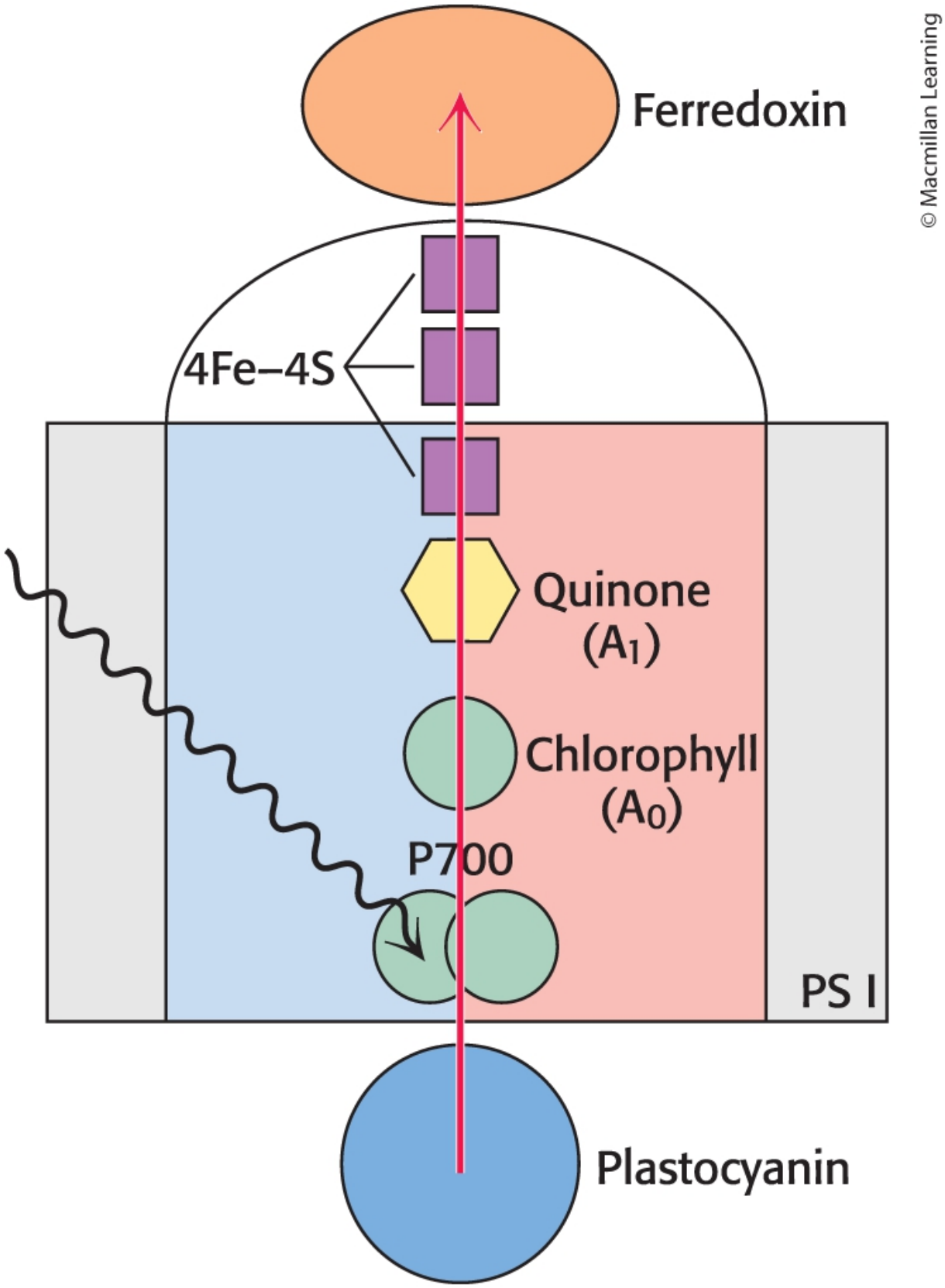
The figure depicts a lipid bilayer. The lipid bilayer consists of two horizontally parallel layers of lipids. The upper and lower layer consists of lipid molecules packed together compactly. Each lipid molecule is shown in a shorthand depiction. The yellow extensions of the shorthand depiction are aligned together and form the core of the bilayer. The blue spheres are located away from each other. The region above the lipid bilayer is labeled stroma and the region below the lipid bilayer is labeled thylakoid lumen. A cluster of red, white, and blue cylinders bound to alpha helices is embedded in the bilayer. A cluster of short white cylinders protrudes from the surface

of this complex into the stroma. The red and blue cylinders are labeled p s a A and p s a B, respectively. Interconnected red and yellow spheres labeled 4 F e 4 S clusters are buried between the cluster of white cylinders and the cluster of blue cylinders in the stroma. Green-colored molecules labeled special pair of chlorophyll a molecules P 700 are bound to the long blue and red cylinders embedded in the lipid bilayer.

Return to FIGURE 19.20 Photosystem I is a protein complex with numerous chlorophyll molecules and one special pair.

Extended description for FIGURE 19.21 In photosystem

I, electrons flow to ferredoxin



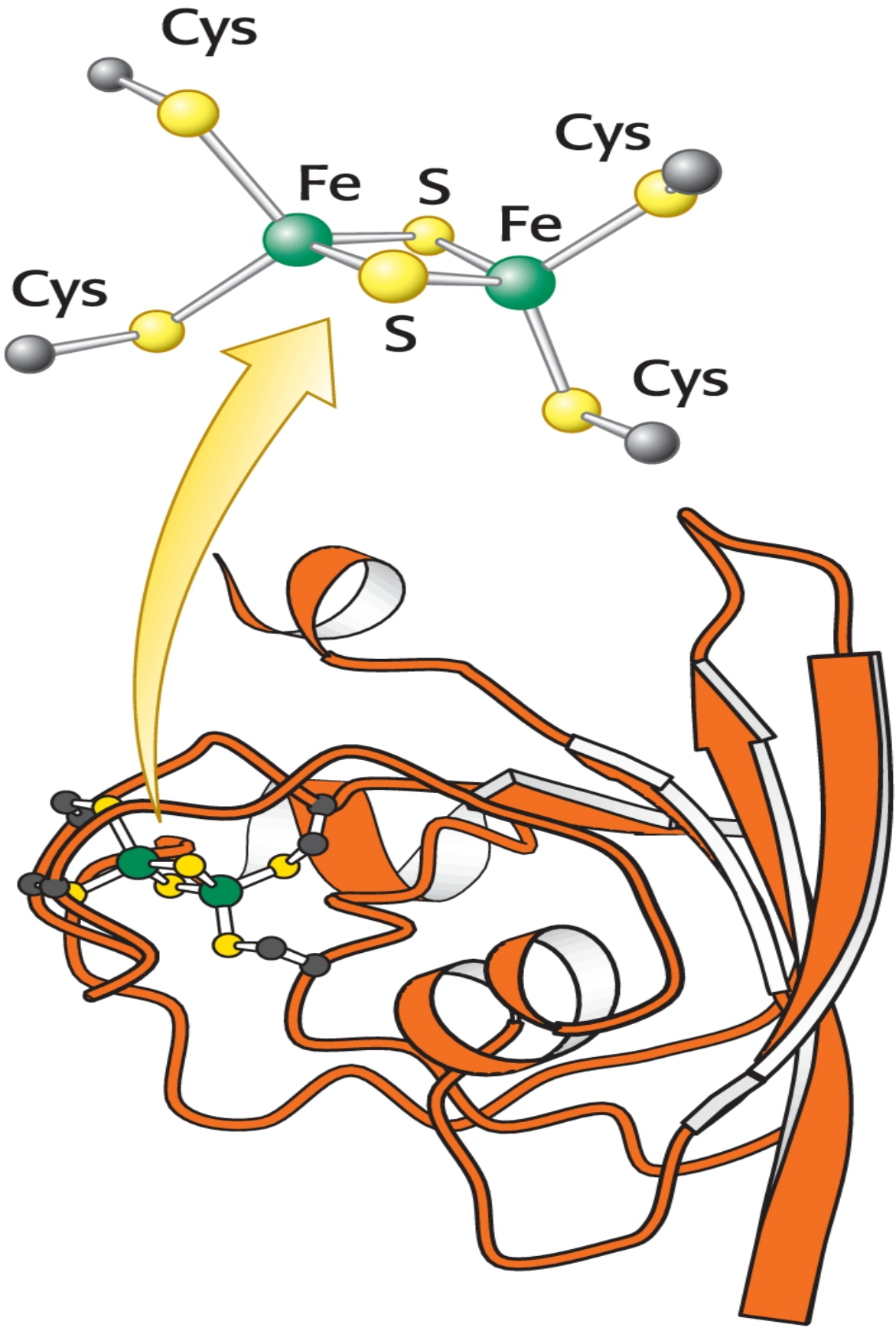
© Macmillan Learning

The electron flow in photosystem 1 starts with the excitation of a pair of chlorophyll molecules in P 700 depicted as two overlapping circles. P 700 is present at the bottom. A wavy arrow representing light strikes P 700. P 700 transfers an electron from plastocyanin to chlorophyll A subscript 0. From chlorophyll A subscript 0, the electron is transferred to Quinone A subscript 1. From quinone, it is transferred to 4 F e 4 S. From 4 F e 4 S it is finally transferred to ferredoxin.

Return to FIGURE 19.21 In photosystem I, electrons flow to ferredoxin

Extended description for FIGURE 19.22 Ferredoxin is an

electron-carrying, iron-sulfur protein

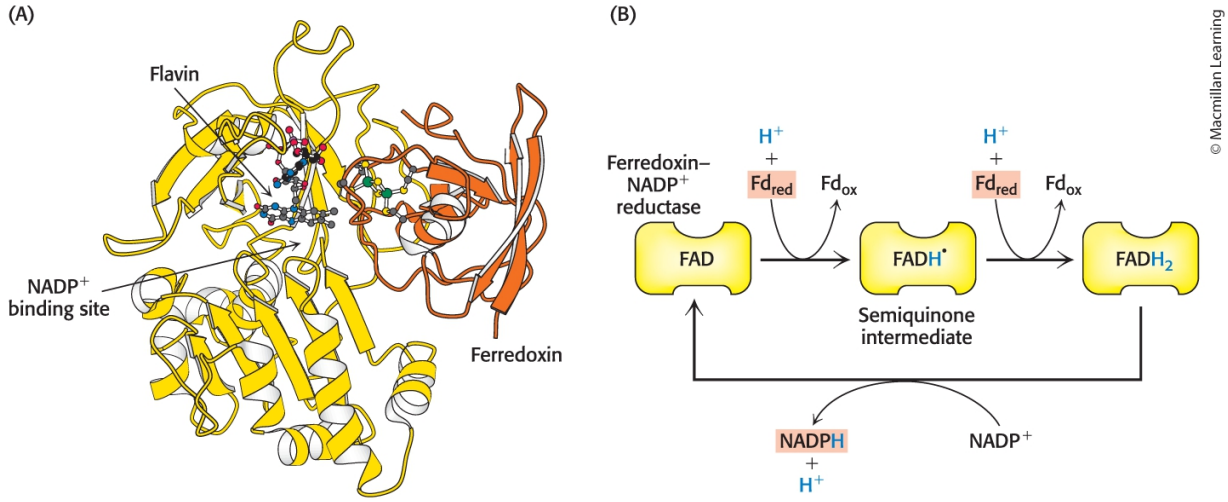


© Macmillan Learning

Ferredoxin protein is composed of four vertical beta-strands and three short alpha-helices interconnected by thread-like loops. It contains an iron and sulfur cluster attached to the thread-like loops on the left. A zoomed-in view of the ball and stick model of the iron and sulfur cluster is shown. The iron-sulfur cluster consists of green and yellow spheres. Yellows spheres represent sulfur and green sphere represents iron. Two sulfur atoms, at the top and bottom, are single-bonded to a common iron atom on the left and right. Each of the iron atoms is further single-bonded to one sulfur atom. Each sulfur atom is attached to a grey sphere labeled cysteine.

Return to FIGURE 19.22 Ferredoxin is an electron-carrying, iron-sulfur protein

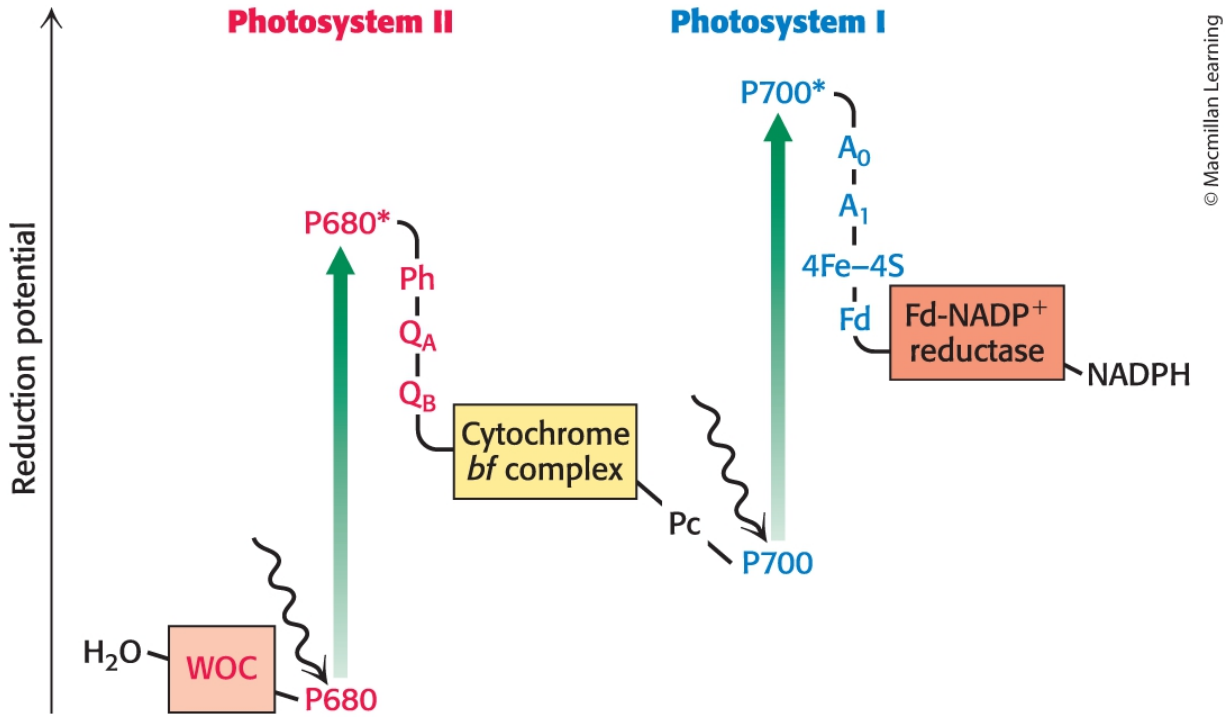
Extended description for FIGURE 19.23 Ferredoxin–N A D P + reductase transfers electrons from the protein ferredoxin to N A D P +



The figure has two parts. The first part labeled (A) shows the ribbon diagram of ferredoxin–N A D P superscript plus reductase consisting of yellow and orange alpha helices and beta strands. The orange alpha helices and beta strands are labeled ferredoxin. It is bound to an iron-sulfur cluster. The yellow alpha helices and beta strands are bound to flavin and an empty N A D P superscript plus binding site is located below it. The second part labeled (B) depicts a flowchart for the formation of N A D P H plus H superscript plus. In the first step, F A D bound to ferredoxin-N A D P superscript plus reductase is converted to F A D H coupled with the simultaneous conversion of F d reduced plus H superscript plus to F d oxidized. F A D H bound reductase is labeled semiquinone intermediate. F A D H is converted to F A D H 2 with the coupled conversion of F d reduced plus H superscript plus to F d oxidized. F A D H 2 is converted back to F A D and is used to reduce N A D P superscript plus to N A D P H and H superscript plus and cycle continues.

Return to FIGURE 19.23 Ferredoxin–N A D P + reductase transfers electrons from the protein ferredoxin to N A D P +

Extended description for FIGURE 19.24 The “Z” scheme of photosynthesis is the linear path of electrons from H 2 O to N A D P +



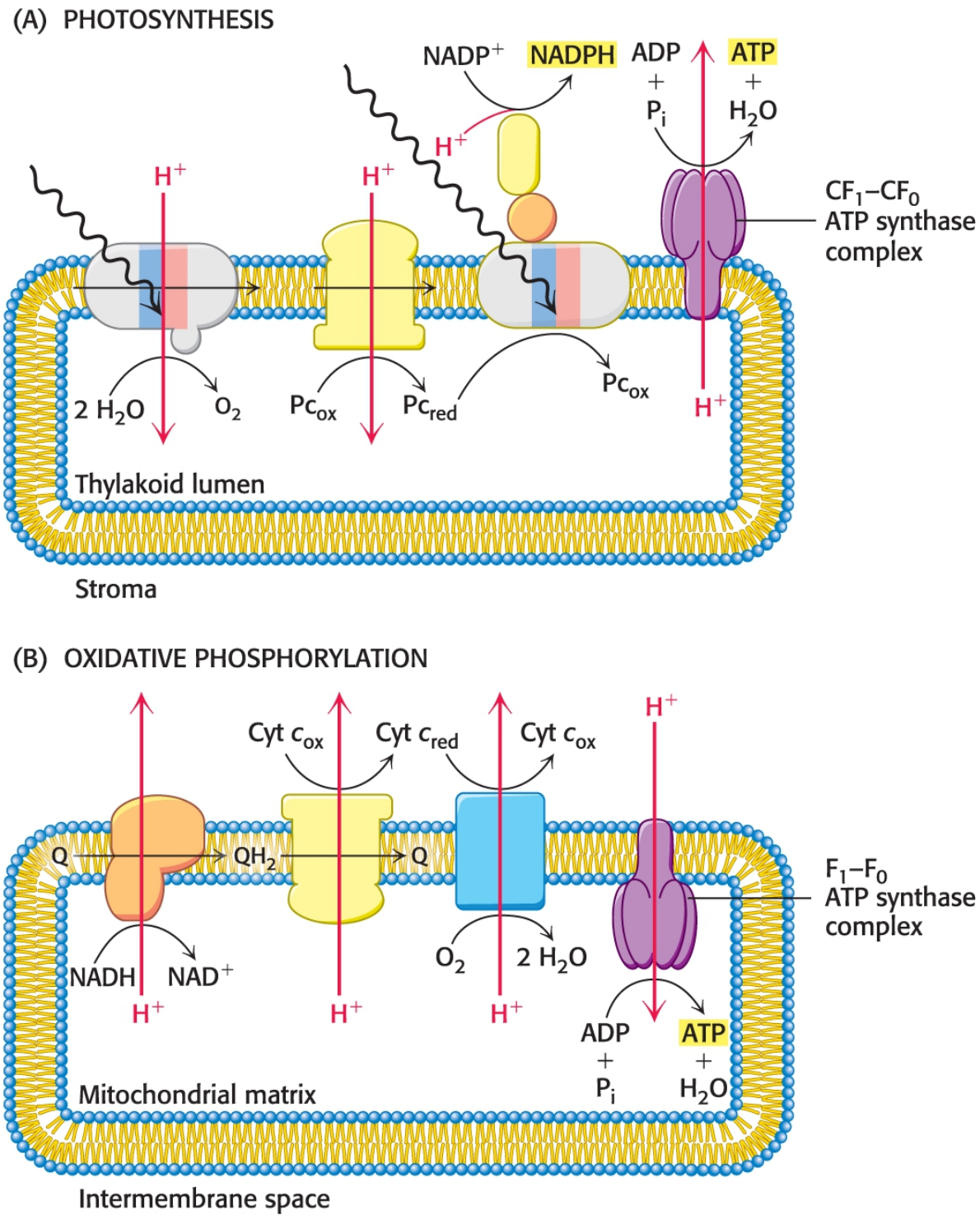
An upward arrow on the left side of the figure is labeled reduction potential. The figure is labeled photosystem 2 on the left and photosystem 1 on the right. Photosystem 2 consists of P 680 while photosystem 1 consists of P 700. In photosystem 2, P 680 is present at the bottom. A wavy arrow representing light strikes P 680 along with H 2 O through W O C. An upward arrow from P 680 points to the P 680 asterisk at the top. P 680 then leads to cytochrome b f complex on the lower right through the components namely P h, Q subscript A, and Q subscript B. Cytochrome b f complex leads to P 700 through P subscript c. A wavy arrow representing light strikes P 700. An upward arrow from P 700 points to the P 700 asterisk at the top in photosystem 1. P 700 asterisk leads to F d-N A D P superscript

plus reductase through components namely A subscript 0, A subscript 1, 4 F e 4 S, and F d. F d-N A D P superscript plus reductase leads to N A D P H.

Return to FIGURE 19.24 The “Z” scheme of photosynthesis is the linear path of electrons from H 2 O to N A D P +

Extended description for FIGURE 19.25 Photosynthesis and oxidative phosphorylation have a similar layout

but differ in a number of ways



© Macmillan Learning

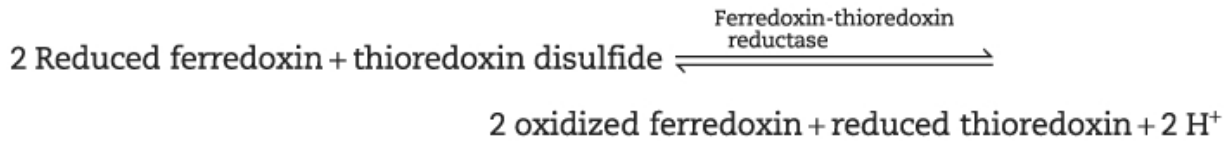
(A) Photosynthesis: The figure depicts a lipid bilayer forming a rectangular loop. The lipid bilayer consists of two horizontally parallel layers of lipids. The upper and lower layer consists of lipid molecules packed together compactly. Each lipid molecule is shown in a shorthand depiction. The yellow extensions of the shorthand depiction are aligned together and form the core of the bilayer. The blue spheres are located away from each other. The region outside the lipid bilayer is labeled stroma and the region enclosed within the lipid bilayer is labeled thylakoid lumen. Four membrane proteins are embedded in the bilayer. A wavy arrow representing light strikes the first membrane protein. H superscript plus ion from the stroma is transferred into the thylakoid lumen through the first membrane protein. This movement is coupled with the conversion of 2 H 2 O to O 2 in the thylakoid lumen. An arrow from the first membrane protein points to the second membrane protein. H plus ion from the stroma is transferred into the thylakoid lumen through the second membrane protein. This is coupled with the conversion of P c oxidized to P c reduced in the thylakoid lumen. An arrow from the second membrane protein points to the third membrane protein. A wavy arrow representing light strikes the third membrane protein. This converts P c reduced to P c oxidized in the thylakoid lumen and N A D P superscript plus and H superscript plus to N A D P H in the stroma. H superscript plus ion exits the thylakoid lumen through the fourth membrane protein. This movement is coupled with the conversion of A D P plus P subscript i to A T P and H 2 O. The fourth membrane protein is labeled C F 1-c F 0 A T P synthase complex.

(B) Oxidative phosphorylation: The figure depicts a lipid bilayer forming a rectangular loop. The lipid bilayer consists of two horizontally parallel layers of lipids. The upper and lower layer consists of lipid molecules packed together compactly. Each lipid molecule is shown in a shorthand depiction. The yellow extensions of the shorthand depiction are aligned together and form the core of the bilayer. The blue spheres are located away from each other. The

region outside the lipid bilayer is labeled intermembrane space and the region enclosed within the lipid bilayer is labeled mitochondrial matrix. Four membrane proteins are embedded in the lipid bilayer. H superscript plus ion exits the mitochondrial matrix through the first membrane protein. This is coupled with the oxidation of N A D H to N A D superscript plus in the mitochondrial matrix. Q is simultaneously converted to Q H 2 in the lipid bilayer by the first membrane protein. H superscript plus ion exits the mitochondrial matrix through the second membrane protein. It also converts cytochrome c oxidized to cytochrome c reduced. Q H 2 is simultaneously converted to Q in the lipid bilayer by the second membrane protein. H superscript plus exits the mitochondrial matrix through the third membrane protein. It converts O 2 to 2 H 2 O in the mitochondrial matrix and Cytochrome c redox to Cytochrome c oxidized in the intermembrane space. H superscript plus enters the mitochondrial matrix through the fourth membrane protein. This is coupled with the conversion of A D P and P i to A T P and H 2 O in the mitochondrial matrix. The fourth membrane protein is labeled F 1 F 0 A T P synthase complex.

Return to FIGURE 19.25 Photosynthesis and oxidative phosphorylation have a similar layout but differ in a number of ways

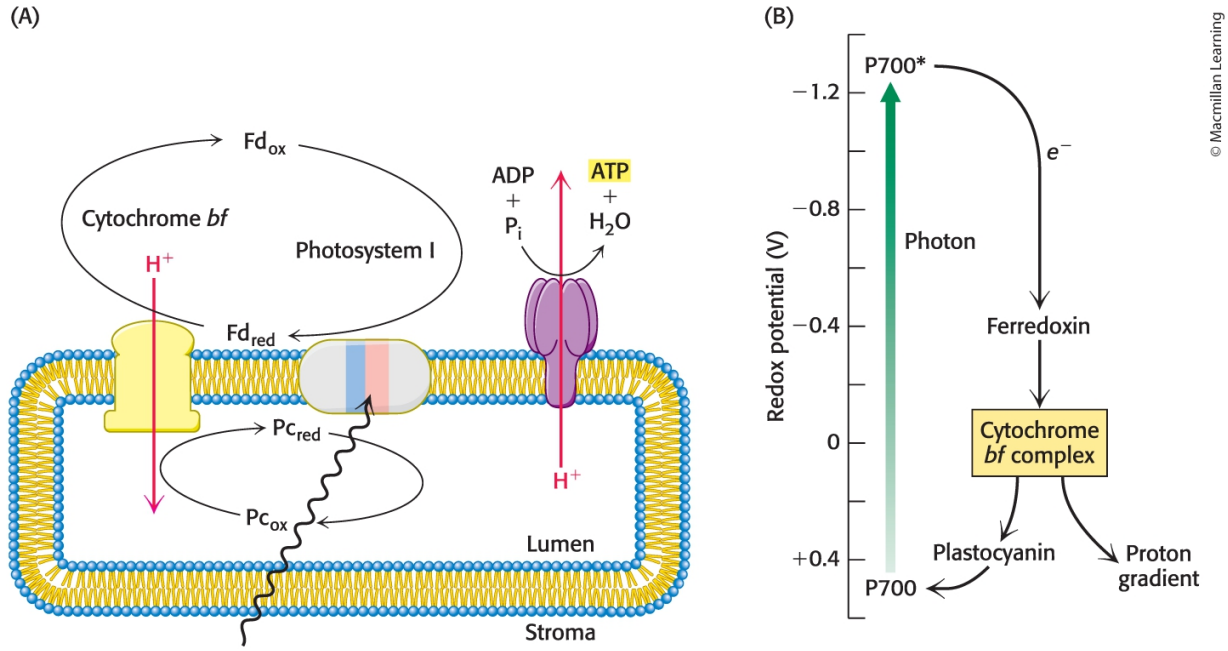
Extended description for Reversible reaction catalyzed by ferredoxin-thioredoxin reductase



2 reduced ferredoxin reacts with thioredoxin disulfide in a reversible reaction catalyzed by ferredoxin-thioredoxin reductase to form 2 oxidized ferredoxin, reduced thioredoxin, and 2 H superscript plus.

Return to Reversible reaction catalyzed by ferredoxin-thioredoxin reductase

Extended description for FIGURE 19.26 Cyclic photophosphorylation allows A T P production without a need for an electron source



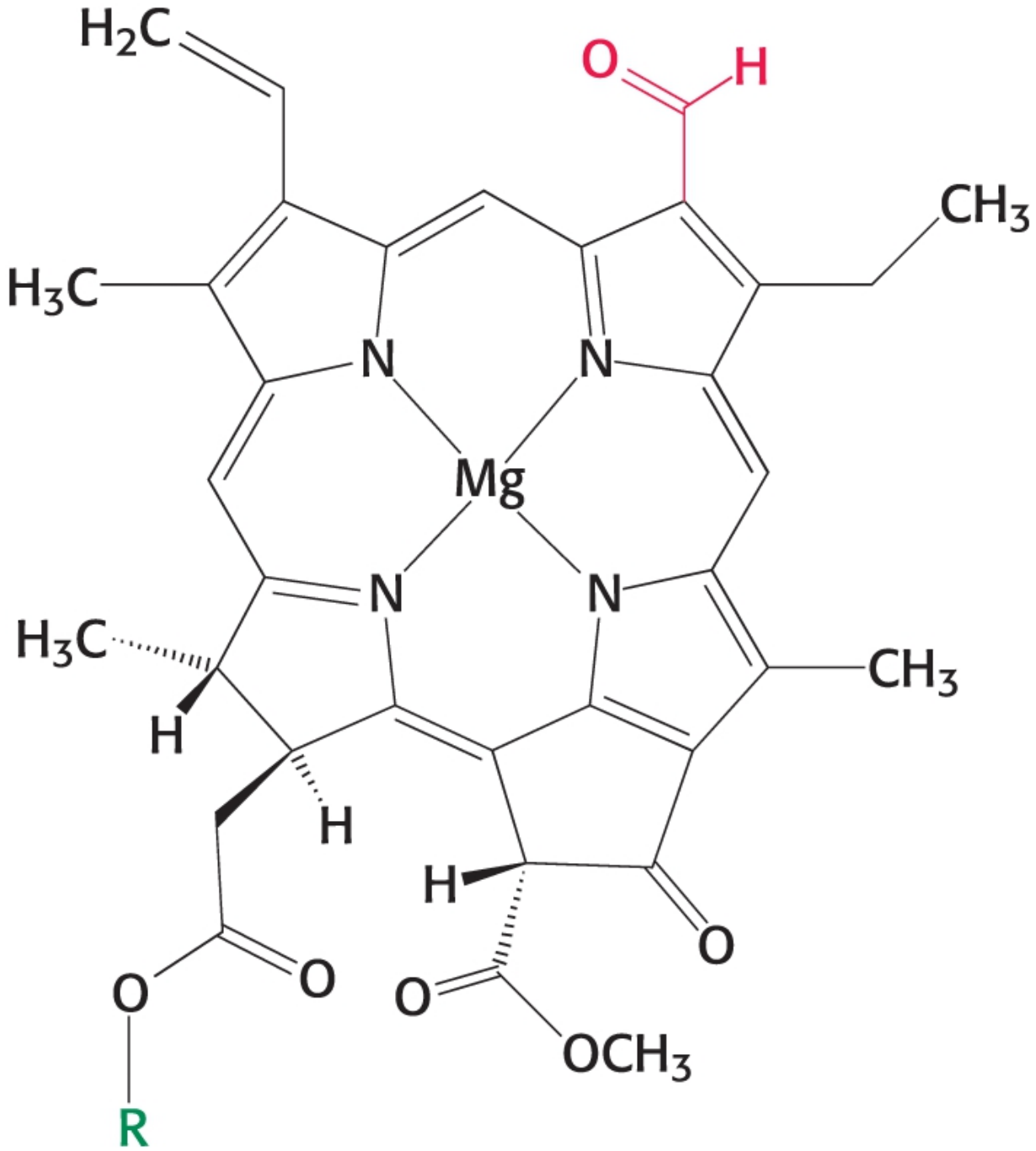
The figure has two parts. The first part depicts a lipid bilayer forming a rectangular loop. The lipid bilayer consists of two horizontally parallel layers of lipids. The upper and lower layer consists of lipid molecules packed together compactly. Each lipid molecule is shown in a shorthand depiction. The yellow extensions of the shorthand depiction are aligned together and form the core of the bilayer. The blue spheres are located away from each other. The region outside the lipid bilayer is labeled stroma and the region enclosed within the lipid bilayer is labeled lumen. The lipid bilayer has three membrane proteins. H superscript plus ion from the stroma enters the lumen through the first membrane protein. A wavy arrow representing light strikes the second membrane protein. This leads to the reversible conversion of P c reduced to P c oxidized in the lumen. In the stroma, this leads to the reversible

conversion of F d oxidized to F d reduced in photosystem 1. F d reduced is converted back to F d oxidized by cytochrome b f. H superscript plus exits the lumen through the third membrane protein. This leads to the conversion of A D P plus P subscript i to A T P and H 2 O in the stroma.

The second part shows a vertical axis labeled reduction potential V. It has markings ranging from positive 0.4 to negative 1.2 in decrements of 0.4 units. P 700 is present corresponding to positive 0.4 on the vertical axis. P 700 points to P 700 asterisk corresponding to negative 1.2. The arrow is labeled photon. P 700 asterisk transfers the electron to ferredoxin. Ferredoxin transfers the electron to cytochrome b f complex. Cytochrome b f complex then transfers the electron to plastocyanin and also produces a proton gradient. Plastocyanin leads back to P 700.

Return to FIGURE 19.26 Cyclic photophosphorylation allows A T P production without a need for an electron source

Extended description for Structure of chlorophyll b



Chlorophyll *b*

Four 5-membered heterocyclic pentagonal rings, four 6-membered heterocyclic hexagonal rings, and one 5-carbon hexagonal ring are fused together. The first 5-membered heterocyclic pentagonal ring is in a vertical orientation consisting of 1 N and 4 C atoms. In the first 5-membered heterocyclic pentagonal ring, N occupies the first position which is the bottom right vertex. In the first 5-membered heterocyclic pentagonal ring, a double bond is present between C 2 and C 3. C 2 of the first 5-membered heterocyclic pentagonal ring is single bonded to C H 3. C 3 of the first 5-membered heterocyclic pentagonal ring is single bonded to a central C H group in the form of a line. The central C H group is double bonded to C H 2 on the upper left. The first 5-membered heterocyclic pentagonal ring is fused to the first 6-membered heterocyclic hexagonal ring in a vertical orientation consisting of 1 M g, 2 N, and 3 C atoms. In the first hexagonal ring, the first N atom occupies the first position which is the bottom right vertex, M g occupies the second position which is the bottommost vertex, and the second N atom occupies the third position which is the bottom left vertex. The two rings are fused to each other such that C 4 and N of the first 5-membered heterocyclic pentagonal ring are the C 1 and the second N atom of the first hexagonal ring, respectively. In the first hexagonal ring, a double bond is present between C 1 and C 2. The first hexagonal ring is fused to the second 5-membered pentagonal ring in a vertical orientation consisting of 1 N and 4 C atoms. In the second 5-membered heterocyclic pentagonal ring, N occupies the first position which is the bottom left vertex. The two rings are fused to each other such that C 3 and the first N atom of the first hexagonal ring are the C 1 and N of the second 5-membered heterocyclic pentagonal ring, respectively. In the second 5-membered heterocyclic pentagonal ring, a double bond is present between N and C 1, and C 2 and C 3. C 2 of the second 5-membered heterocyclic pentagonal ring is single bonded to a central C atom in the form of a line. The central C atom is double bonded to O on the upper left and single bonded to H on the upper right. C 3 of the second 5-

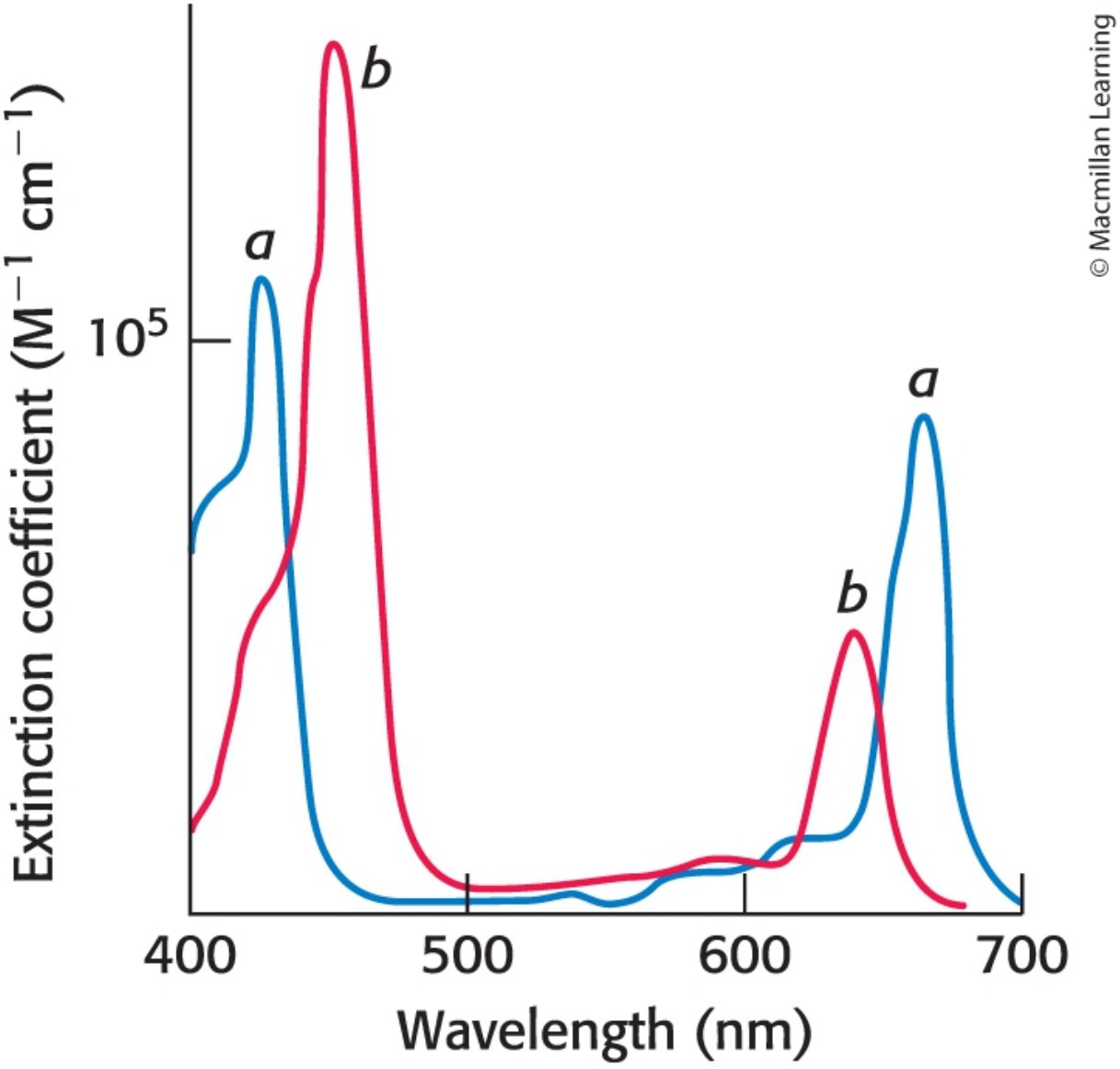
membered heterocyclic pentagonal ring is single bonded to a central C H 2 group in the form of a line. The central C H 2 group is single bonded to C H 3 on the upper right. The first hexagonal ring and the second 5-membered heterocyclic pentagonal ring are fused to a second 6-membered heterocyclic hexagonal ring in a horizontal orientation consisting of 1 M g, 2 N, and 3 C atoms. In the second hexagonal ring, the first N atom occupies the first position which is the bottom left vertex, M g occupies the second position which is the leftmost vertex, and the second N atom occupies the third position which is the top left vertex. The three rings are fused to each other as follows: The first N atom and M g of the first hexagonal ring are the second N atom and M g of the second hexagonal ring, respectively. N and C 4 of the second 5-membered heterocyclic pentagonal ring are the second N atom and C 1 of the second hexagonal ring, respectively. In the second hexagonal ring, a double bond is present between C 1 and C 2. The second hexagonal ring is fused to the third 5-membered heterocyclic pentagonal ring in a horizontal orientation consisting of 1 N and 4 C atoms. In the third 5-membered heterocyclic pentagonal ring, N occupies the first position which is the top left vertex. The two rings are fused to each other such that the first N atom and C 3 of the second hexagonal ring are N and C 1 of the third 5-membered heterocyclic pentagonal ring, respectively. In the third 5-membered heterocyclic pentagonal ring, a double bond is present between C 1 and C 2, and C 3 and C 4. C 2 of the third 5-membered heterocyclic pentagonal ring is single bonded to C H 3. The second hexagonal ring and the third 5-membered heterocyclic pentagonal ring are fused to the third 6-membered heterocyclic hexagonal ring in a vertical orientation consisting of 1 M g, 2 N and 3 C atoms. In the third hexagonal ring, the first N atom occupies the first position which is the top left vertex, M g occupies the second position which is the topmost vertex, and the second N atom occupies the third position which is the top right vertex. The three rings are fused to each other as follows: M g and the first N atom of the second hexagonal ring are the M g and the second N

atom of the third hexagonal ring, respectively. N and C 4 of the third 5-membered heterocyclic pentagonal ring are the second N atom and C 1 of the third hexagonal ring, respectively. In the third hexagonal ring, a double bond is present between C 2 and C 3. The third 5-membered heterocyclic pentagonal ring and the third hexagonal ring are fused to the 5-carbon pentagonal ring in a vertical orientation with C 1 occupying the topmost vertex. The three rings are fused to each other as follows: C 3 and C 4 of the third 5-membered heterocyclic pentagonal ring are the C 2 and C 1 of the 5-carbon pentagonal ring, respectively. C 1 and C 2 of the third hexagonal ring are the C 1 and C 5 of the 5-carbon pentagonal ring, respectively. C 3 of the 5-carbon pentagonal ring is double bonded to a second O atom. C 4 of the 5-carbon pentagonal ring is wedge bonded to H on the lower left and dash bonded to a central C atom on the lower left in the form of a dashed line. The central C atom is double bonded to a third O atom on the lower left and single bonded to O C H 3 on the lower right. The third hexagonal ring is fused to the fourth 5-membered heterocyclic pentagonal ring in a horizontal orientation consisting of 1 N and 4 C atoms. In the fourth 5-membered heterocyclic pentagonal ring, N occupies the first position which is the top right vertex. The two rings are fused to each other such that the first N atom and C 3 of the third hexagonal ring are the N and C 1 of the fourth 5-membered heterocyclic pentagonal ring, respectively. In the fourth 5-membered heterocyclic pentagonal ring, a double bond is present between C 4 and N. C 2 of the fourth 5-membered heterocyclic pentagonal ring is single bonded to H on the lower right and wedge bonded to C 1 of a 2-carbon alkane chain depicted as a line structure using 1 line. C 3 of the fourth 5-membered heterocyclic pentagonal ring is wedge bonded to H on the lower left and dash bonded to C H 3 on the upper left. C 2 of the 2-carbon alkane chain is double bonded to a fourth O atom on the lower right and single bonded to a fifth O atom on the lower left. The fifth O atom is single bonded to R below which is highlighted in green. The third hexagonal ring and the fourth 5-

membered heterocyclic pentagonal ring are fused to the fourth 6-membered heterocyclic hexagonal ring in a horizontal orientation consisting of 1 M g, 2 N, and 3 C atoms. In the fourth hexagonal ring, the first N atom occupies the first position which is the top right vertex, M g occupies the second position which is the rightmost vertex, and the second N atom occupies the third position which is the bottom right vertex. The three rings are fused to each other as follows: The first N atom and M g of the third hexagonal ring are the second N atom and M g of the fourth hexagonal ring, respectively. C 4 and N of the fourth 5-membered heterocyclic pentagonal ring are the C 1 and the second N atom of the fourth hexagonal ring, respectively. The fourth hexagonal ring, the first 5-membered heterocyclic pentagonal ring, and the first hexagonal ring are also fused to each other as follows: C 3 and the first N atom of the fourth hexagonal ring are the C 1 and N of the first 5-membered heterocyclic pentagonal ring, respectively. The first N atom and M g of the fourth hexagonal ring are the second N atom and M g of the first hexagonal ring, respectively.

Return to Structure of chlorophyll b

Extended description for FIGURE 19.27 Chlorophylls a and b absorb light maximally at different wavelengths



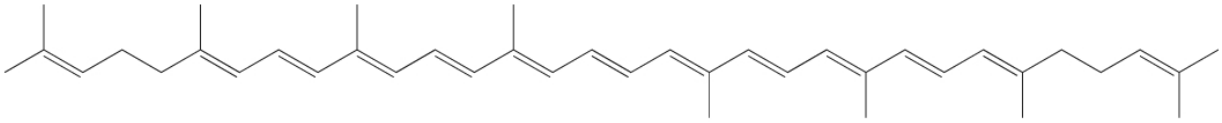
© Macmillan Learning

The horizontal axis labeled wavelength in nanometers has markings ranging from 400 to 700 in increments of 100 units. The vertical axis labeled extinction coefficient in M inverse 1-centimeter inverse has the marking 10 to the power 5 much above the midpoint. The graph shows two curves. The first blue curve labeled a starts from the

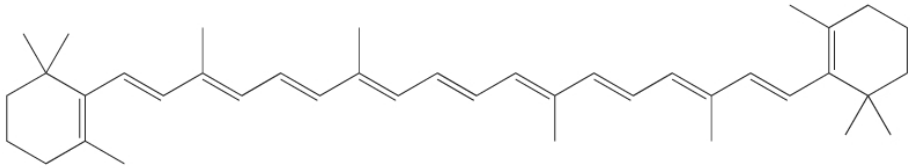
midpoint of the vertical axis and peaks at 420 on the horizontal axis slightly above 10 to the power 5 on the vertical axis, it slopes down to the lowest extinction coefficient at 470, moves toward the right to reach 600, rises upward and peaks slightly below 10 to the power 5 on the vertical axis. The second red curve labeled b starts just above the origin on the vertical axis, peaks at 470 much above the first peak of the blue curve, slopes down to 500 on the horizontal axis, moves toward the right to reach 600, peaks at 650 much below the second peak of the blue curve.

Return to FIGURE 19.27 Chlorophylls a and b absorb light maximally at different wavelengths

Extended description for Structure of Lycopene and beta carotene



Lycopene



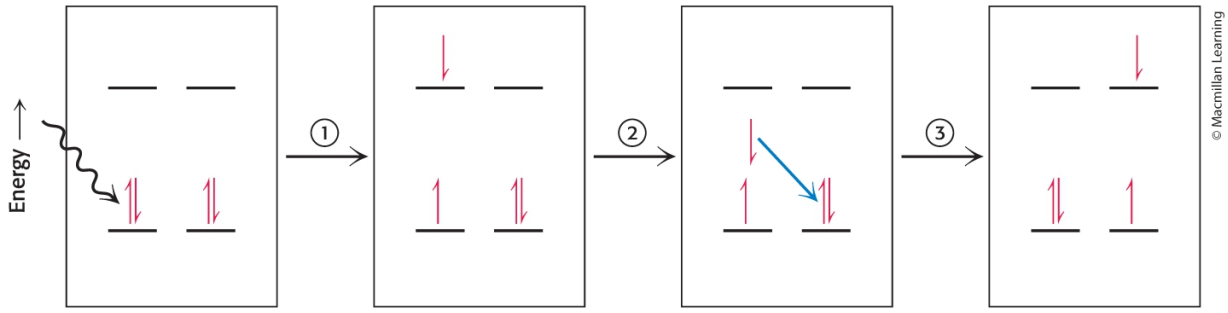
β-Carotene

The structure of lycopene is as follows: A 32-carbon alkene chain is depicted as a line structure using 31 zigzag lines. A double bond is present between C 2 and C 3, C 6 and C 7, C 8 and C 9, C 10 and C 11, C 12 and C 13, C 14 and C 15, C 16 and C 17, C 18 and C 19, C 20 and C 21, C 22 and C 23, C 24 and C 25, C 26 and C 27, and C 30 and C 31. C 2, C 6, C 10, and C 14 are each single bonded to C H 3 above in the form of a line. C 19, C 23, C 27, and C 31 are each single bonded to C H 3 below in the form of a line. The structure of beta-carotene is as follows: A 6-carbon hexagonal ring is in a vertical orientation with C 1 occupying the topmost vertex. A double bond is present between C 2 and C 3. C 1 is single bonded to C H 3 on the upper right and C H 3 on the upper left, each in the form of a line. C 3 is single bonded to C H 3 in the form of a line. C 2 is single-bonded to C 1 of an 18-carbon alkene chain depicted as a line structure using 17 zigzag lines. In the alkene chain, a double bond is present between C 1 and C 2, C 3 and C 4, C 5 and C 6, C 7 and C 8, C 9 and C 10, C 11 and C 12, C 13 and C 14, C 15 and C 16, and C 17 and C 18. In the alkene chain, C 3 and C 7 are each single bonded to C H 3 above in the form of a line. In the alkene chain, C 12 and C 16 are each single bonded to C H 3 below in the form of a line. C 18 of the alkene chain is single bonded to C 5 of

a second 6-carbon hexagonal ring in a vertical orientation with C 1 occupying the topmost vertex. In the second ring, a double bond is present between C 5 and C 6. C 4 of the second ring is single bonded to C H 3 on the lower right and C H 3 on the lower left, each in the form of a line. C 6 of the second ring is single bonded to C H 3 in the form of a line.

Return to Structure of Lycopene and beta carotene

Extended description for FIGURE 19.28 Resonance energy transfer allows electrons to transfer energy over a distance

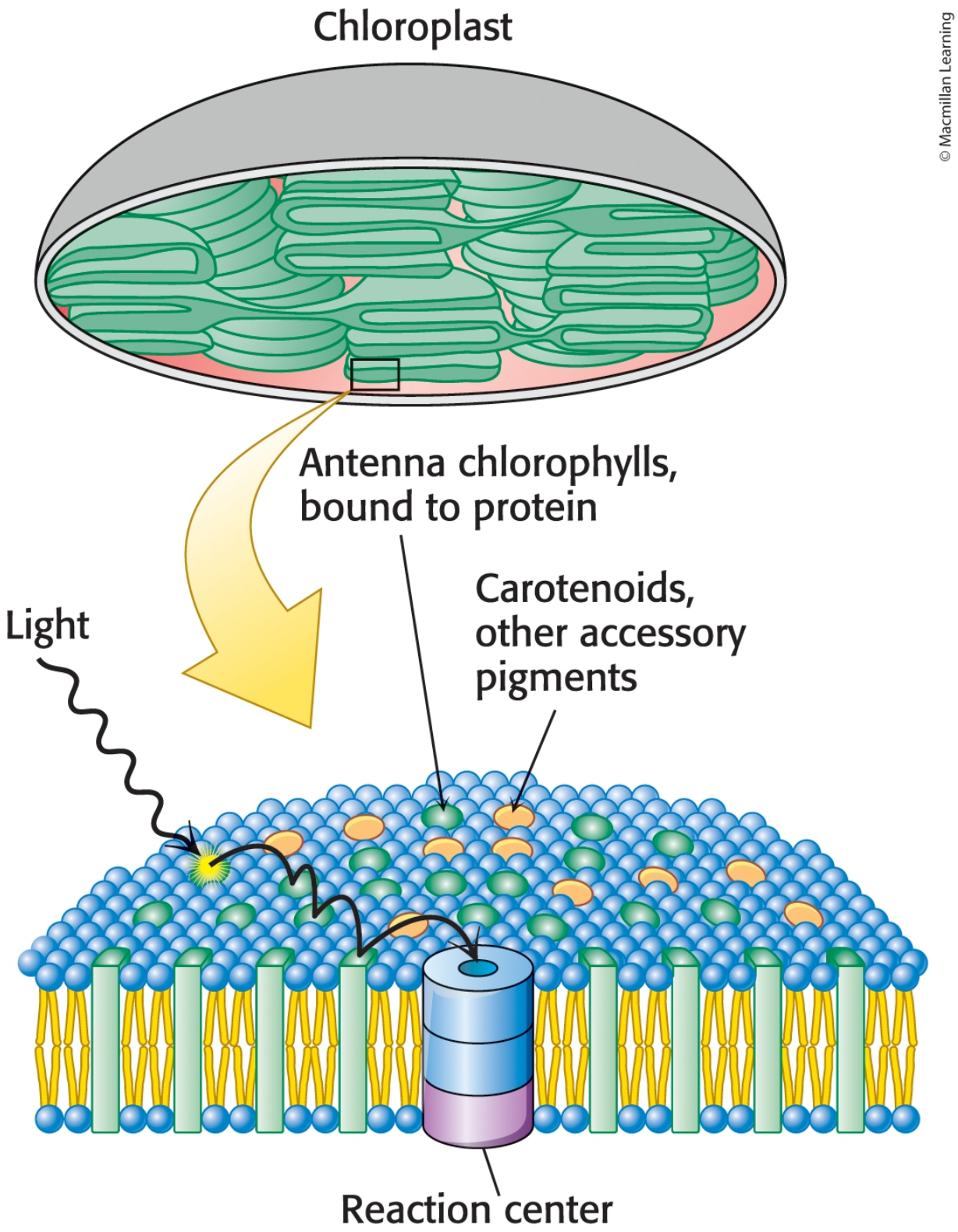


The figure has four panels. In the first panel, two pairs of upward and downward arrows are present in the ground state. The upward and downward arrows represent electrons. The excited states at the top are blank. A wavy arrow representing light strikes the first pair of upward and downward arrows. An arrow from the first panel leads to the second panel and is numbered 1. In the second panel, the first downward arrow from the first pair moves to the excited state and the upward arrow remains in the ground state. The second pair of upward and downward arrows remain in the ground state and the excited state is blank. An arrow from the second panel points to the third panel and is numbered 2. The downward arrow in the excited state is directed toward the second pair of arrows in the ground state. An arrow from the third panel points to the fourth panel and is numbered 3. In the fourth panel, the first pair of arrows are present in the ground state and the excited state is blank. The second ground state has one upward arrow and the excited state has one downward arrow.

Return to FIGURE 19.28 Resonance energy transfer allows electrons to transfer energy over a distance

Extended description for FIGURE 19.29 Energy is transferred from accessory pigments to reaction

centers

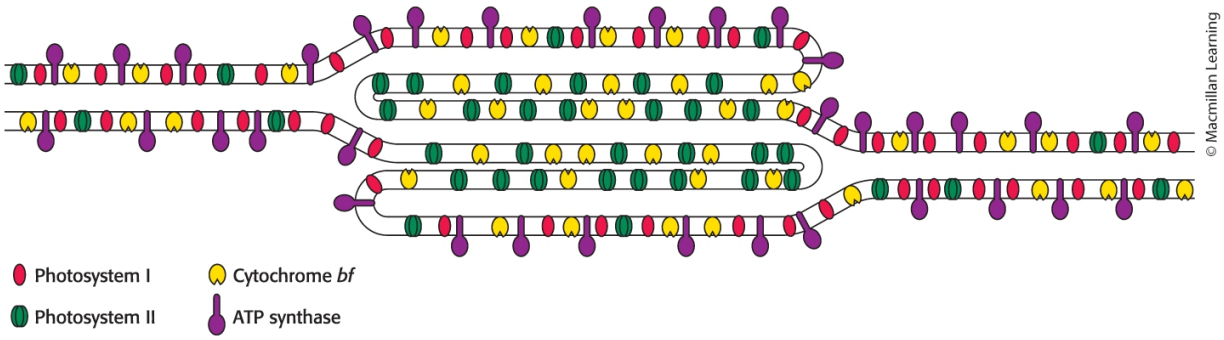


© Macmillan Learning

The figure shows a chloroplast. The chloroplast is an oval-shaped, hollow sac-like structure that consists of two membranes. The hollow interior of the chloroplast is called the stroma. The stroma of the chloroplast consists of numerous stacked discs. These discs are called thylakoids. A zoomed-in view from one of the thylakoids shows a lipid bilayer. The lipid bilayer consists of horizontally parallel layers of lipids. The upper and lower layer consists of lipid molecules packed together compactly. Each lipid molecule is shown in a shorthand depiction. The yellow extensions of the shorthand depiction are aligned together and form the core of the bilayer. The blue spheres are located away from each other. The upper layer of the lipid bilayer consists of orange and green spheres embedded in between. The orange spheres are labeled carotenoids, other accessory pigments. The green spheres are labeled antenna chlorophylls, bound to protein. Three stacked disc-like structures are embedded in the center of the lipid bilayer and labeled reaction center. A wavy arrow representing light strikes the upper layer of the lipid bilayer and is directed toward the reaction center.

Return to FIGURE 19.29 Energy is transferred from accessory pigments to reaction centers

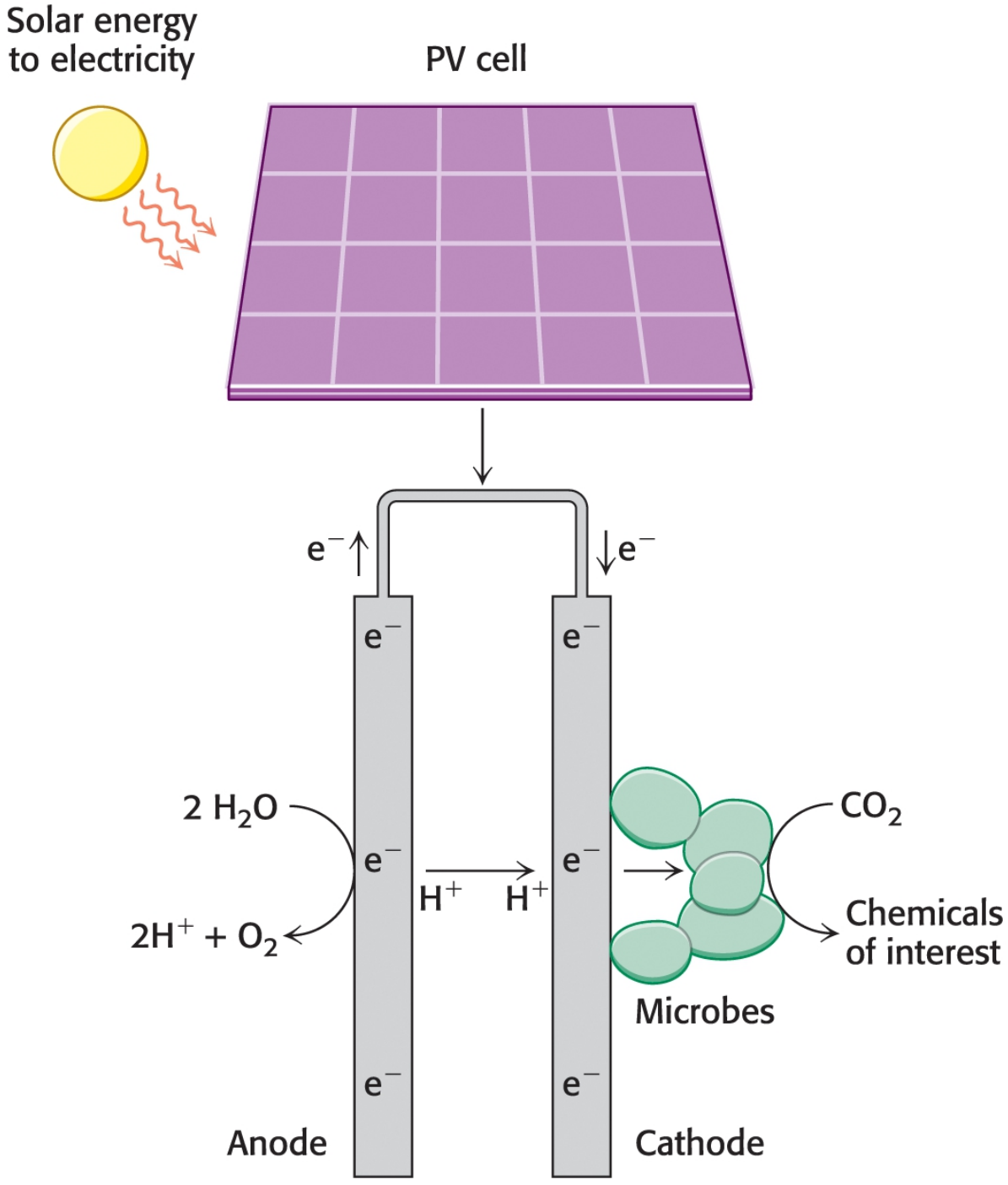
Extended description for FIGURE 19.30 Photosynthetic assemblies are differentially distributed in the stacked and unstacked regions of thylakoid membranes



The figure depicts two horizontal thick walled Y-shaped structures coinciding with one another to form a continuous bridge. The walls of these Y-shaped structures have a linear assembly of photosystem 1, photosystem 2, cytochrome b f, and A T P synthase. In the region of overlap or stacking between the two Y-shaped structures, the assembly follows an alternative pattern of photosystem 2 and cytochrome b f. In the region where there is direct contact with the stroma or there is no stacking, the assembly pattern consists of photosystem 2, photosystem 1, A T P synthase, and cytochrome b f.

Return to FIGURE 19.30 Photosynthetic assemblies are differentially distributed in the stacked and unstacked regions of thylakoid membranes

Extended description for FIGURE 19.31 Photovoltaic cells can drive artificial photosynthesis

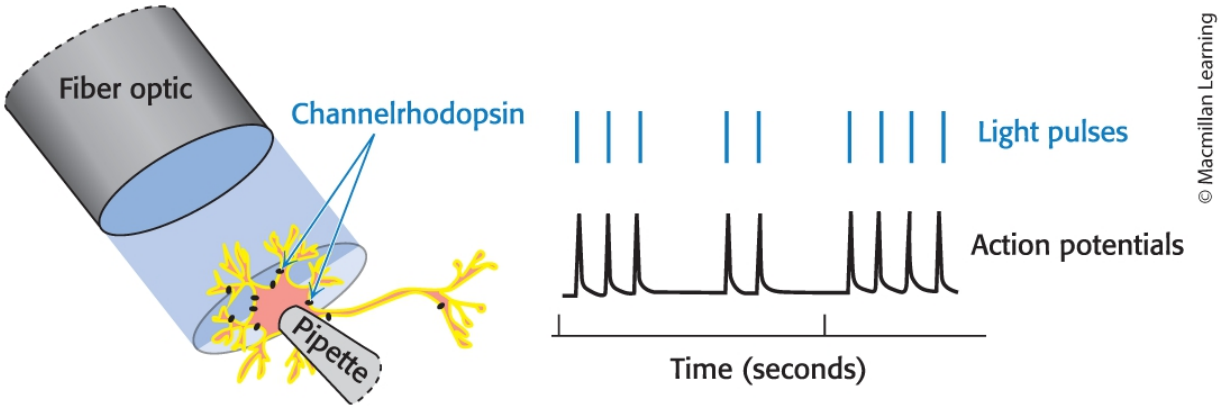


© Macmillan Learning

The photovoltaic cell shows a slab with grids. Sunlight falls on the photovoltaic cell. The sunlight is labeled solar energy to electricity. The current flows to the anode to oxidize water. The electrons that are produced move into the cathode. Spherical bacteria in contact with the cathode use up the electrons to convert C O 2 to chemicals of interest.

Return to FIGURE 19.31 Photovoltaic cells can drive artificial photosynthesis

Extended description for FIGURE 19.32 Optogenetics allows neurons to be controlled using light

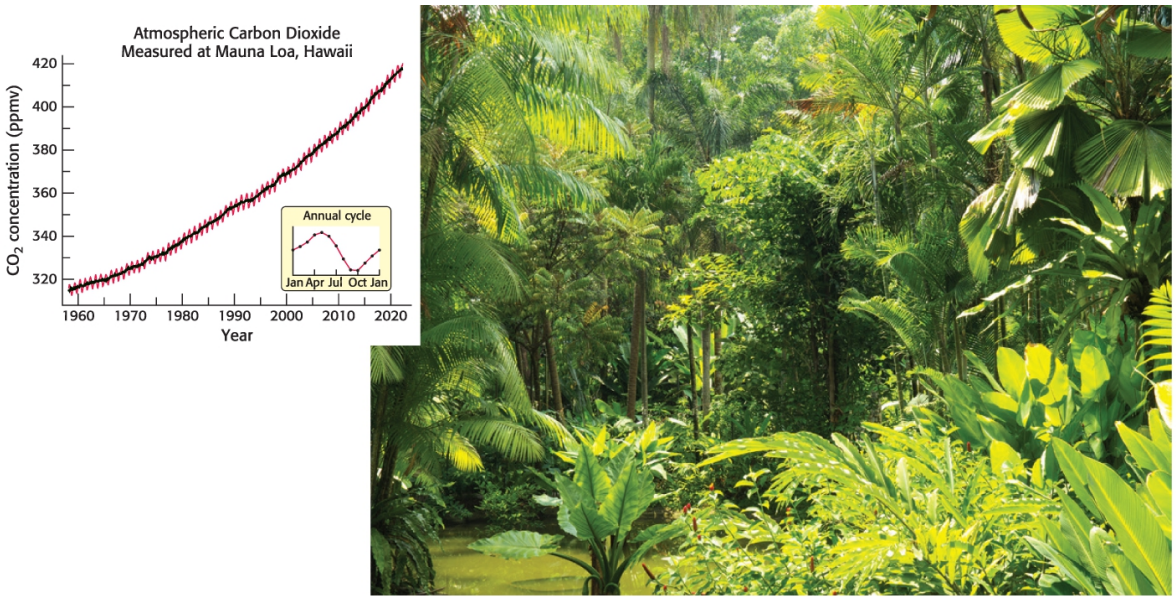


© Macmillan Learning

The figure shows a grey-colored cylinder labeled fiber optic. Light from the cylinder falls on a neuron that contains black dots on the cell membrane that represent channelrhodopsin. A micropipette is attached to the cell membrane of the neuron. On the right, a graph depicts the action potentials generated. The vertical axis is labeled time in seconds. Light pulses are depicted above the graph. Light pulses are depicted as 9 vertical lines. The first three vertical lines are grouped. The fourth and fifth vertical lines are grouped. The sixth to ninth vertical lines are grounded together. The graph below depicting the action potential shows 9 peaks corresponding to the light pulses.

Return to FIGURE 19.32 Optogenetics allows neurons to be controlled using light

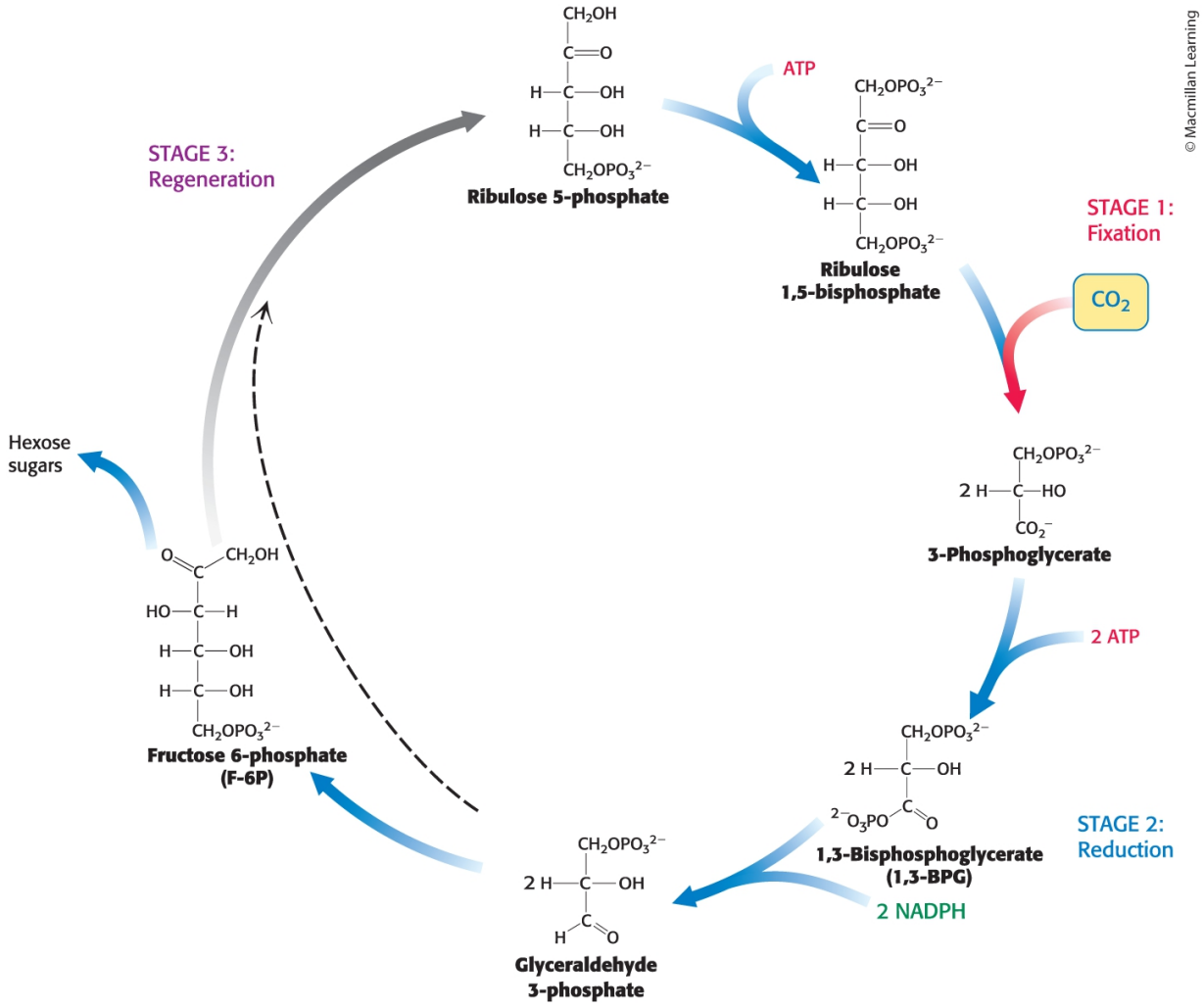
Extended description for Graph depicts atmospheric C O 2 measured at Mauna Loa, Hawaii



The horizontal axis is labeled year. It has markings ranging from 1960 to 2020 in increments of 10 units. The vertical axis is labeled C O 2 concentration (p p m v). It has markings ranging from 320 to 420 in increments of 20 units. An increasing straight line moving toward the upper right is shown. A red zigzag line overlaps with a straight line and resembles a sawtooth. An inset graph shows the markings: January, April, July, October, and January on the horizontal axis. The inset graph is titled "Annual cycle." It contains a curve that starts at the midpoint of the vertical axis and rises gradually to peak in April and then slopes down in October and then starts rising again.

Return to Graph depicts atmospheric C O 2 measured at Mauna Loa, Hawaii

Extended description for FIGURE 20.1 The Calvin–Benson cycle consists of three stages



The Calvin Benson cycle is divided into three stages as follows:

Stage 1: Fixation, Stage 2: Reduction, and Stage 3: Regeneration.

Stage 1: It involves the addition of C O 2 to ribulose 1,5-bisphosphate to produce 3-phosphoglycerate.

The structure of ribulose 1,5-bisphosphate is as follows: C H 2 O P O 3 superscript 2 minus, single bond, C, single bond, C, single bond, C, single bond, C H 2 O P O 3 superscript 2 minus. C 2 is double bonded to O on the right. C 3 and C 4 are each single bonded to H on the left and O H on the right.

The structure of 3-phosphoglycerate is as follows: C H 2 O P O 3 superscript 2 minus, single bond, C, single bond, C O 2 superscript minus. C 2 is single bonded to 2 H on the left and O H on the right.

Later 2 A T P molecules enter and convert 3-phosphoglycerate to 1,3-bisphosphoglycerate (1,3-B P G).

The structure of 1,3-bisphosphoglycerate is as follows: C H 2 O P O 3 superscript 2 minus, single bond, C, single bond, C. C 2 is single bonded to 2 H on the left and O H on the right. C 3 is single bonded to O P O 3 superscript 2 minus on the lower left and double bonded to O on the lower right.

Stage 2: It involves the reduction of 1,3-bisphosphoglycerate by 2 N A D P H to produce glyceraldehyde 3-phosphate.

The structure of glyceraldehyde 3-phosphate is as follows: C H 2 O P O 3 superscript 2 minus, single bond, C, single bond, C. C 2 is single bonded to 2 H on the left and O H on the right. C 3 is single-bonded to H on the lower left and double-bonded to O on the lower right.

Glyceraldehyde 3-phosphate can be further converted into fructose 6-phosphate (F-6 P) or enter stage 3.

The structure of fructose 6-phosphate is as follows: C, single bond, C, single bond, C, single bond, C, single bond, C H 2 O P O 3 superscript 2 minus. C 1 is double bonded to O on the upper left and

single bonded to C H 2 O H on the upper right. C 2 is single bonded to O H on the left and H on the right. C 3 and C 4 are each single bonded to H on the left and O H on the right.

Fructose 6-phosphate is further converted into hexose sugars.

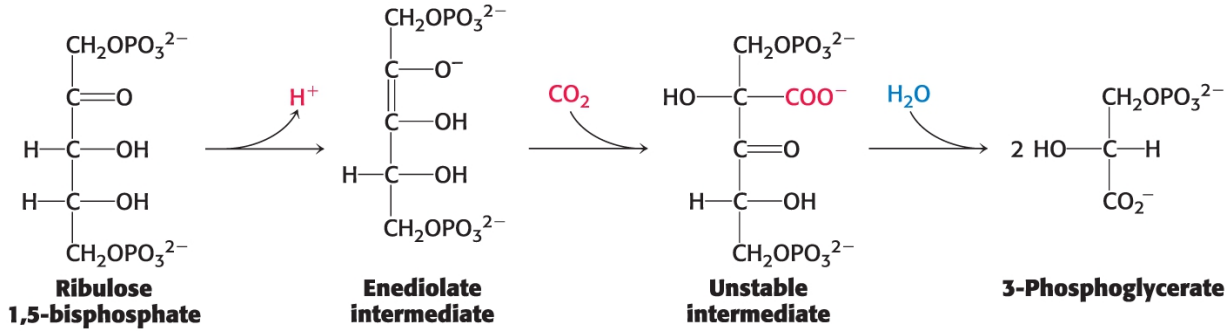
Stage 3: It involves the conversion of glyceraldehyde 3-phosphate to ribulose 5-phosphate.

The structure of ribulose 5-phosphate is as follows: C H 2 O H, single bond, C, single bond, C, single bond, C, single bond, C H 2 O P O 3 superscript 2 minus. C 3 and C 4 are each single bonded to H on the left and O H on the right.

Ribulose 5-phosphate is further converted into ribulose 1,5-bisphosphate by the addition of A T P.

Return to FIGURE 20.1 The Calvin–Benson cycle consists of three stages

Extended description for Sequential conversion of ribulose 1,5-bisphosphate to 3-phosphoglycerate



In the first step, ribulose 1,5-bisphosphate is irreversibly converted into enediolate intermediate with the simultaneous release of H superscript plus ion.

The structure of ribulose 1,5-bisphosphate is as follows: C H 2 O P O 3 superscript 2 minus, single bond, C, single bond, C, single bond, C, single bond, C H 2 O P O 3 superscript 2 minus. C 2 is double bonded to O on the right. C 3 and C 4 are each single bonded to H on the left and O H on the right.

The structure of enediolate intermediate is as follows: C H 2 O P O 3 superscript 2 minus, single bond, C, double bond, C, single bond, C, single bond, C H 2 O P O 3 superscript 2 minus. C 2 is single bonded to O superscript minus on the right. C 3 is single bonded to O H on the right. C 4 is single bonded to H on the left and O H on the right.

In the second step, the enediolate intermediate is converted into an unstable intermediate by the addition of C O 2.

The structure of the unstable intermediate is as follows: C H 2 O P O 3 superscript 2 minus, single bond, C, single bond, C, single bond, C,

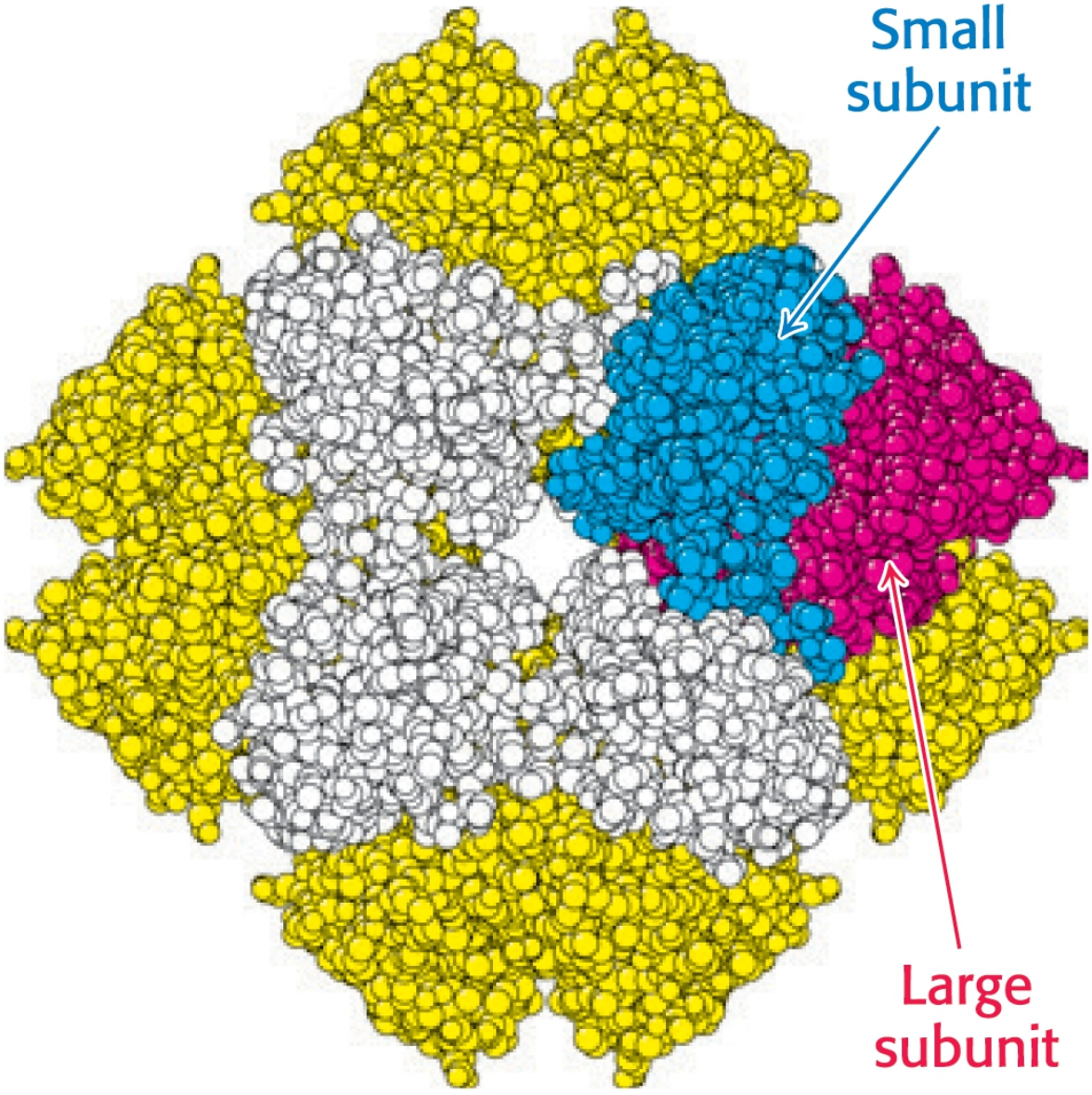
single bond, C H 2 O P O 3 superscript 2 minus. C 2 is single bonded to O H on the left C O O superscript minus on the right. C 3 is double bonded to O on the right. C 4 is single bonded to H on the left and O H on the right.

In the third step, the unstable intermediate is converted into 3-phosphoglycerate by the addition of H 2 O.

The structure of 3-phosphoglycerate is as follows: C H 2 O P O 3 superscript 2 minus, single bond, C, single bond, C O 2 superscript minus. C 2 is single bonded to 2 O H on the left and H on the right.

Return to Sequential conversion of ribulose 1,5-bisphosphate to 3-phosphoglycerate

Extended description for FIGURE 20.2 The enzyme ribulose 1,5-bisphosphate carboxylase slash oxygenase (Rubisco) comprises 16 subunits



© Macmillan Learning

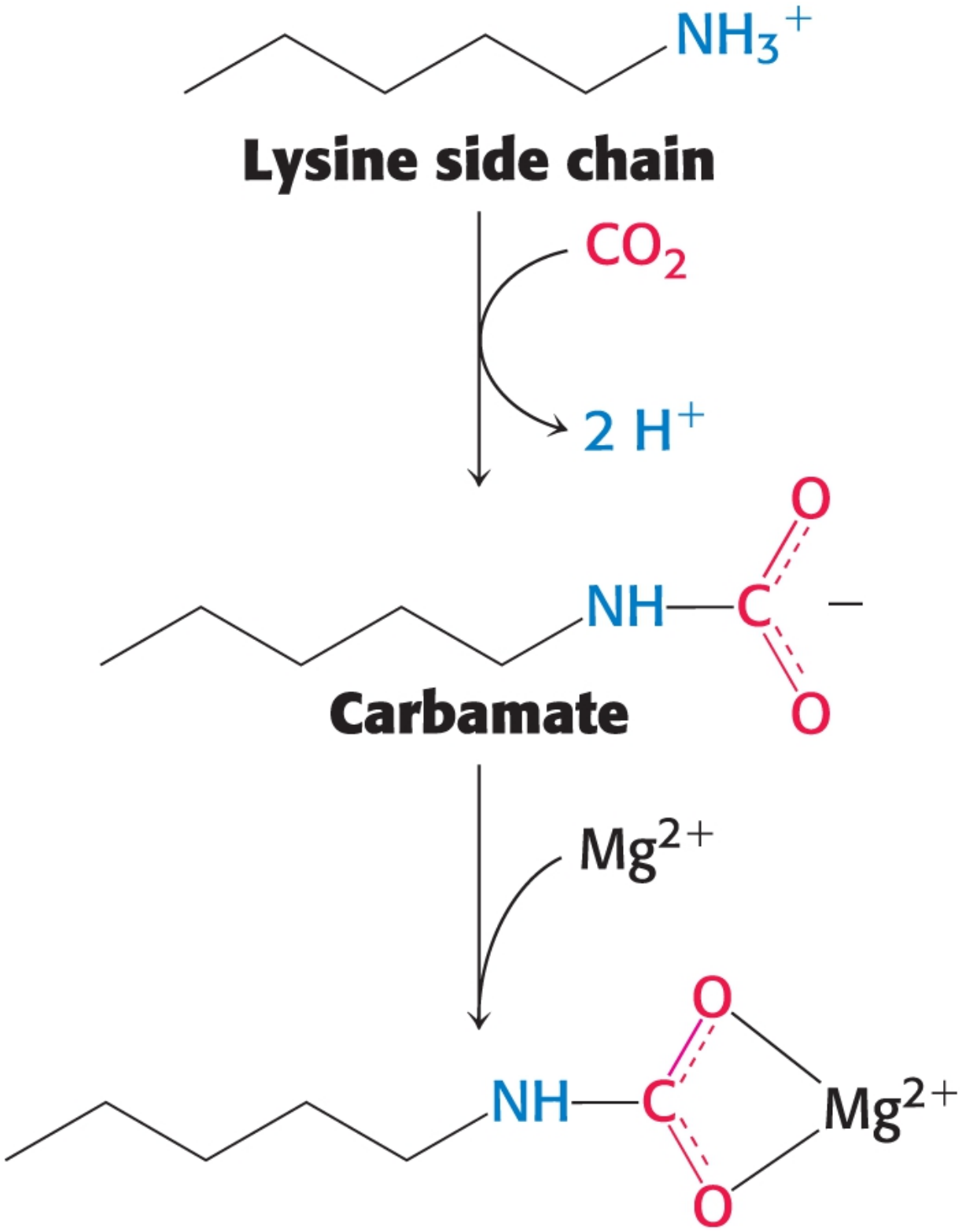
The figure shows the subunits of the enzyme ribulose 1,5-bisphosphate. Out of the sixteen subunits, 12 subunits are visible. These subunits are formed by clusters of differently colored

spheres. The figure shows four subunits in the front. The subunit on the top right is blue and is labeled small subunit. The other three subunits are white. Two subunits each are attached to the top, bottom, left, and right face of the cluster of four subunits. All these subunits are yellow except for the subunit on the top right. This subunit is pink and is labeled a large subunit.

Return to FIGURE 20.2 The enzyme ribulose 1,5-bisphosphate carboxylase slash oxygenase (Rubisco) comprises 16 subunits

Extended description for Formation of carbamate from the lysine side chain and its binding to a magnesium

ion



The lysine side chain is depicted as a 5-carbon alkane chain using 4 zigzag lines. C 5 is single bonded to N H 3 superscript plus highlighted in blue on the upper right.

A downward arrow from the lysine chain points to carbamate. It is coupled with the entry of C O 2 and the release of 2 H superscript plus.

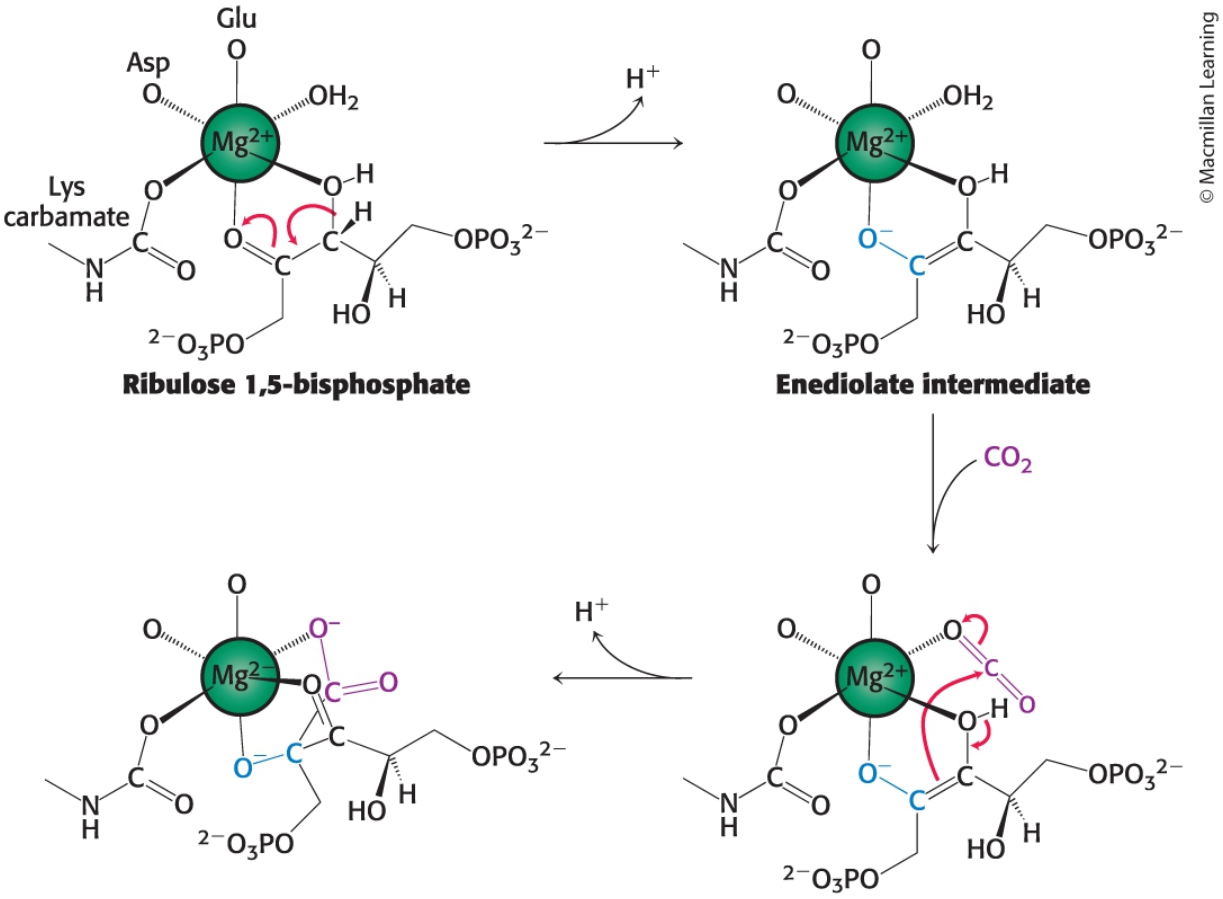
The carbamate molecule is depicted as a 5-carbon alkane chain using 4 zigzag lines. C 5 is single bonded to N H on the upper right. N H is single bonded to C on the right. This C is partially double-bonded to O on the upper right and lower right. This C O O group has a negative charge.

A downward arrow from carbamate shows the entry of M g superscript 2 plus ion.

The partially double-bonded O atoms of carbamate are single-bonded to a common M g superscript 2 plus ion.

Return to Formation of carbamate from the lysine side chain and its binding to a magnesium ion

Extended description for FIGURE 20.3 C O 2 fixation by magnesium-coordinated ribulose 1,5- bisphosphate



The process of C O 2 fixation is divided into 3 steps.

In the first step, ribulose 1,5-bisphosphate is converted to an enediolate intermediate with the simultaneous release of H superscript plus ion.

M g superscript 2 plus ion is depicted as a central green sphere. It single bonded to the O atom of glutamate above, dash bonded to O H 2 on the upper right, wedge bonded to O atom of O H group that is single bonded to C 2 of ribulose 1,5-bisphosphate, single bonded to

O atom that is double bonded to C 1 of ribulose-1,5-bisphosphate, wedge bonded to O atom of lysine carbamate, and dash bonded to O atom of aspartic acid.

Lysine carbamate consists of N, single bond, C. N bound to H has an open single bond on the upper left. C is single-bonded to O on the upper right and double-bonded to O on the lower right.

The structure of ribulose-1,5-bisphosphate is depicted as follows: C, single bond, C. C 1 is single bonded to C H 2 on the lower right in the form of a line. C H 2 is further single bonded to O P O 3 superscript 2 minus on the lower left. C 1 is also double bonded to O on the upper left. C 2 is single bonded to O, single bond, H above, and wedge bonded to H on the upper right. C 2 is also single bonded to a 2-carbon alkane chain depicted using a line. C 1 of this chain is wedge bonded to O H on the lower left and dash bonded to H on the lower right. C 2 is single bonded to O P O 3 superscript 2 minus on the right. A red curved arrow from C 1 points toward the O atom double bonded to it. A red curved arrow points from the single bond between C 2 and O points toward the single bond between C 1 and C 2.

The product of this step is the enediolate intermediate. In this intermediate, the M g superscript 2 plus ion becomes single bonded to O superscript minus below which is further single bonded to C 1 of the substrate. C 1 of the substrate becomes double bonded to C 2. The wedge bond between C 2 and H is broken down.

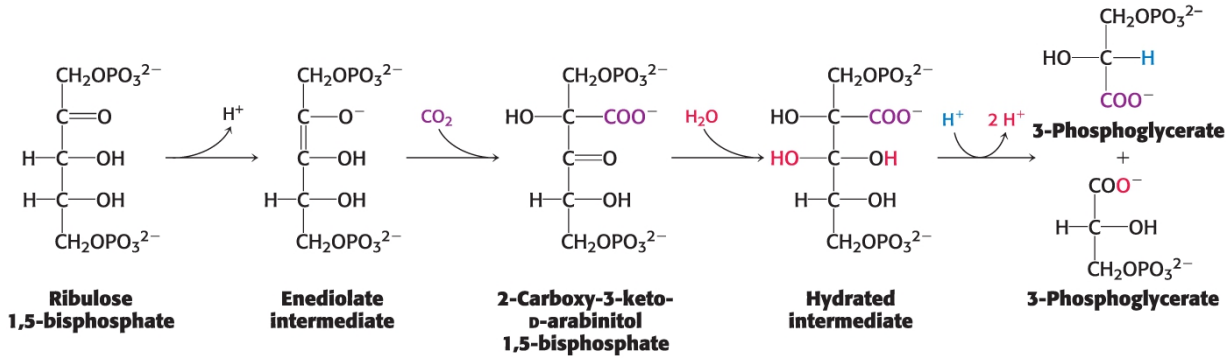
In the second step, C O 2 binds to the enediolate intermediate. In the product of this step, Mg superscript 2 plus ion becomes dash-bonded to O on the upper right. This O is double bonded to C, double bond, O on the lower right.

A red curved arrow points from the double bond between C and O bound to M g superscript 2 plus toward the O atom. A second curved arrow points from the double bond between C 1 and C 2 of the substrate toward the C atom of the C O 2 molecule bound to M g superscript 2 plus ion through the O atom. A third curved arrow points form the single bond between the O and H atom of the O H group bound to C 2 to the single bond between C 2 and O.

In the third step, the H superscript plus ion is released. The M g superscript 2 plus ion becomes dash bonded to O superscript minus on the upper right. This O superscript minus ion is further single bonded to C below. This C atom is single-bonded to C 1 of the substrate and double-bonded to O on the right. The M g superscript 2 plus ion is also wedge bonded to O on the right. This O is further double bonded to C 2 of the substrate.

Return to FIGURE 20.3 C O 2 fixation by magnesium-coordinated ribulose 1,5- bisphosphate

Extended description for FIGURE 20.4 In stage 1 of the Calvin–Benson cycle, 3-phosphoglycerate is formed



In the first step, ribulose 1,5-bisphosphate is converted into enediolate intermediate with the simultaneous release of H superscript plus ion.

The structure of ribulose 1,5-bisphosphate is as follows: C H 2 O P O 3 superscript 2 minus, single bond, C, single bond, C, single bond, C, single bond, C H 2 O P O 3 superscript 2 minus. C 2 is double bonded to O on the right. C 3 and C 4 are each single bonded to H on the left and O H on the right.

The structure of enediolate intermediate is as follows: C H 2 O P O 3 superscript 2 minus, single bond, C, double bond, C, single bond, C, single bond, C H 2 O P O 3 superscript 2 minus. C 2 is single bonded to O superscript minus on the right. C 3 is single bonded to O H on the right. C 4 is single bonded to H on the left and O H on the right.

In the second step, the enediolate intermediate is converted into 2-carboxy-3-keto-D-arabinitol 1,5-bisphosphate by the addition of C O 2.

The structure of 2-carboxy-3-keto-D-arabinitol 1,5-bisphosphate is as follows: C H 2 O P O 3 superscript 2 minus, single bond, C, single bond, C, single bond, C, single bond, C H 2 O P O 3 superscript 2 minus. C 2 is single bonded to O H on the left and C O O superscript minus on the right. C 3 is double bonded to O on the right. C 4 is single bonded to H on the left and O H on the right.

In the third step, 2-carboxy-3-keto-D-arabinitol 1,5-bisphosphate is converted into hydrate intermediate by the addition of H 2 O.

The structure of the hydrate intermediate is as follows: C H 2 O P O 3 superscript 2 minus, single bond, C, single bond, C, single bond, C, single bond, C H 2 O P O 3 superscript 2 minus. C 2 is single bonded to O H on the left and C O O superscript minus on the right. C 3 is single bonded to O H on the right and left. C 4 is single bonded to H on the left and O H on the right.

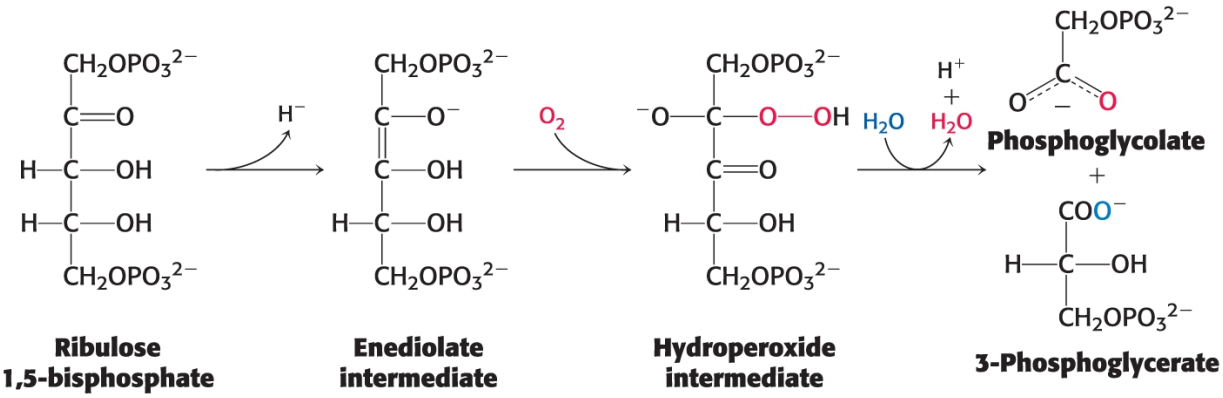
In the fourth step, the hydrated intermediate is converted into two molecules of 3-phosphoglycerate with the simultaneous entry of one H superscript plus ion and release of 2 H superscript plus ions.

The structure of the first 3-phosphoglycerate molecule is as follows: C H 2 O P O 3 superscript 2 minus, single bond, C, single bond, C O O superscript minus. C 2 is single bonded to O H on the left and H on the right.

The structure of the second 3-phosphoglycerate molecule is as follows: C O O superscript minus, single bond, C, single bond, C H 2 O P O 3 superscript 2 minus. C 2 is single bonded to H on the left and O H on the right.

Return to FIGURE 20.4 In stage 1 of the Calvin–Benson cycle, 3-phosphoglycerate is formed

Extended description for FIGURE 20.5 The enediolate on Rubisco can react with oxygen in a wasteful side reaction



In the first step, ribulose 1,5-bisphosphate is converted into enediolate intermediate with the simultaneous release of H superscript plus ion.

The structure of ribulose 1,5-bisphosphate is as follows: C H 2 O P O 3 superscript 2 minus, single bond, C, single bond, C, single bond, C, single bond, C H 2 O P O 3 superscript 2 minus. C 2 is double bonded to O on the right. C 3 and C 4 are each single bonded to H on the left and O H on the right.

The structure of enediolate intermediate is as follows: C H 2 O P O 3 superscript 2 minus, single bond, C, double bond, C, single bond, C, single bond, C H 2 O P O 3 superscript 2 minus. C 2 is single bonded to O superscript minus on the right. C 3 is single bonded to O H on the right. C 4 is single bonded to H on the left and O H on the right.

In the second step, the enediolate intermediate is converted into a hydroperoxide intermediate by the addition of O 2.

The structure of the hydroperoxide intermediate is as follows: C H 2 O P O 3 superscript 2 minus, single bond, C, single bond, C, single bond, C, single bond, C H 2 O P O 3 superscript 2 minus. C 2 is single bonded to O superscript minus on the right and single bonded to O, single bond, O H on the right. C 3 is double bonded to O on the right. C 4 is single bonded to H on the left and O H on the right.

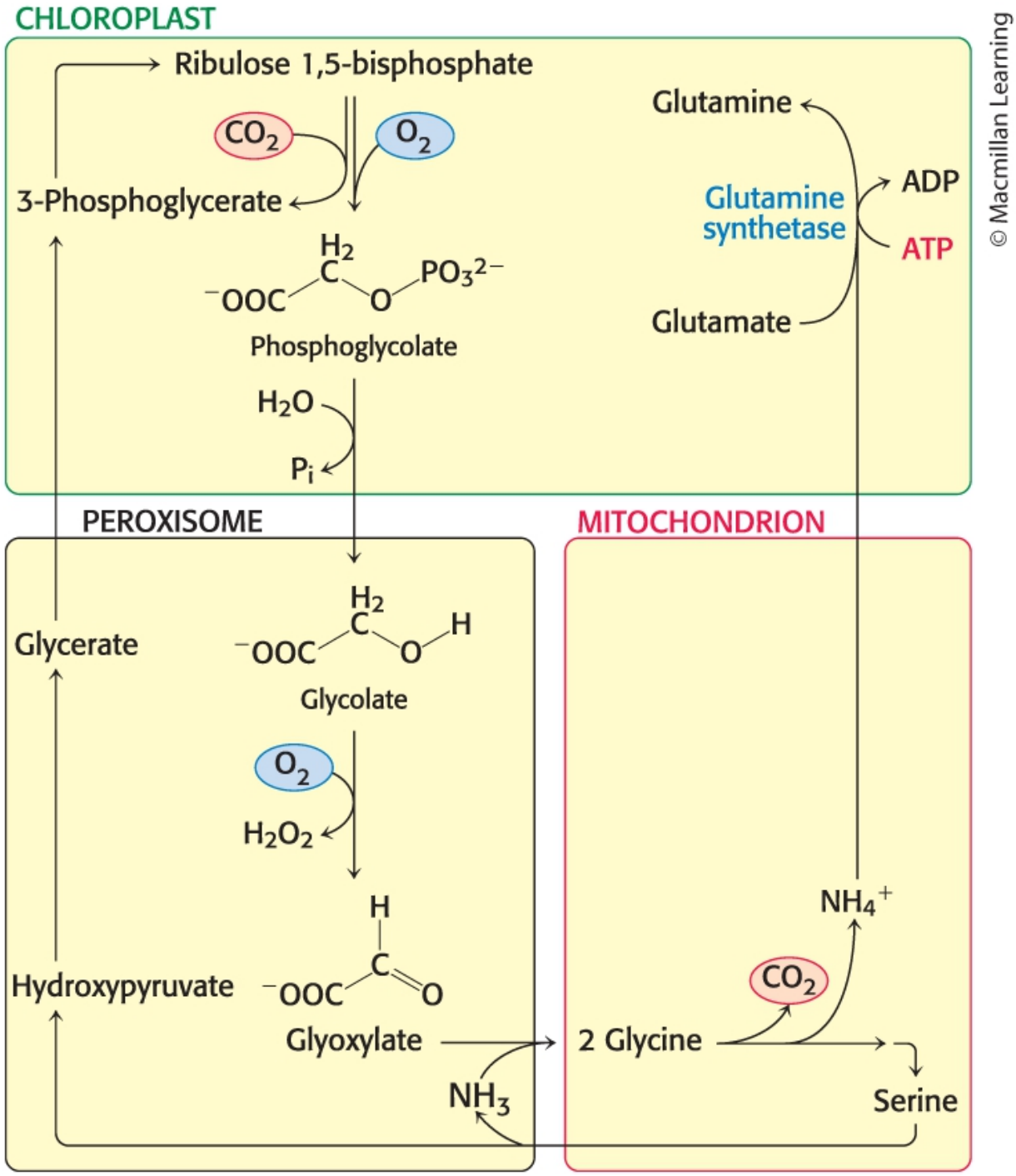
In the third step, the hydroperoxide intermediate is converted into phosphoglycolate and 3-phosphoglycerate with the simultaneous entry of H 2 O and release of H 2 O and H superscript plus ion.

The structure of phosphoglycolate is as follows: A central C atom is single bonded to C H 2 O P O 3 superscript 2 minus above and partially double bonded to O on the lower left and lower right. This C O O group has an overall negative charge.

The structure of 3-phosphoglycerate is as follows: C O O superscript minus, single bond, C, single bond, C H 2 O P O 3 superscript 2 minus. C 2 is single bonded to H on the left and O H on the right.

Return to FIGURE 20.5 The enediolate on Rubisco can react with oxygen in a wasteful side reaction

Extended description for FIGURE 20.6 Photorespiration consumes O 2 and produces C O 2



Three rectangular compartments labeled chloroplast, mitochondrion, and peroxisome are shown. In the chloroplast, ribulose 1,5-bisphosphate is irreversibly converted into phosphoglycerate by the addition of O 2. The structure of phosphoglycerate is as follows: C H 2 is single bonded to C O O superscript minus on the lower left and O on the lower right. This O is single bonded to P O 3 superscript 2 minus on the upper right. An arrow points from phosphoglycolate in the chloroplast to glycolate in the peroxisome. This arrow is coupled with another arrow showing the entry of H 2 O and the release of P subscript i in the chloroplast.

The structure of glycolate is as follows: C H 2 is single bonded to C O O superscript minus on the lower left and O on the lower right. This O is single-bonded to H on the upper right.

In the peroxisome, glycolate is irreversibly converted into glyoxylate with the simultaneous conversion of O 2 to H 2 O 2.

The structure of glyoxylate is as follows: A central C atom is single bonded to H above, single bonded to C O O superscript minus on the lower left, and double bonded to O on the lower right.

An arrow points from glyoxylate in peroxisome to 2 glycine in the mitochondrion. This arrow is coupled with the entry of N H 3.

In the mitochondrion, 2 glycine is converted into serine in two steps. The first step involves the release of C O 2 and N H 4 superscript plus. The N H 4 superscript plus molecule in the mitochondrion enters the chloroplast. In the chloroplast, it is used to convert glutamate into glutamine by glutamine synthetase with the simultaneous hydrolysis of A T P to A D P.

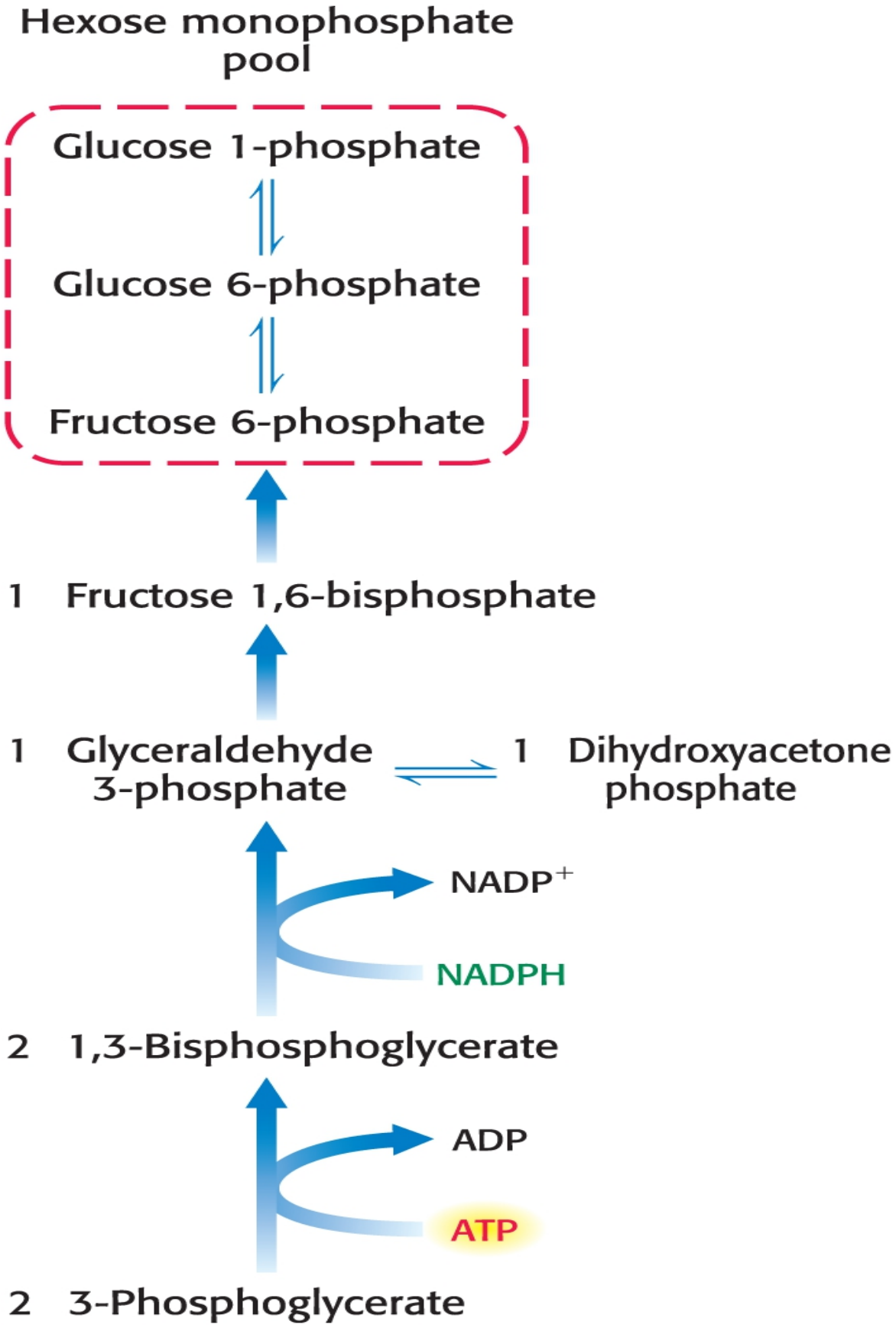
The serine molecule in the mitochondrion is transported back to the peroxisome. N H 3 molecule is released from serine to produce hydroxypyruvate. N H 3 molecule is used up to convert glyoxylate to glycine.

The hydroxypyruvate molecule is converted into glycerate in the peroxisome. The glycerate molecule enters the chloroplast where it is converted into 3-phosphoglycerate. The 3-phosphoglycerate molecule is further converted back to ribulose 1, 5-bisphosphate. The ribulose 1,5-bisphosphate molecule is converted back to 3-phosphoglycerate by the addition of C O 2.

Return to FIGURE 20.6 Photorespiration consumes O 2 and produces C O 2

Extended description for FIGURE 20.8 In stage 2 of the

Calvin–Benson cycle, hexose phosphate is formed

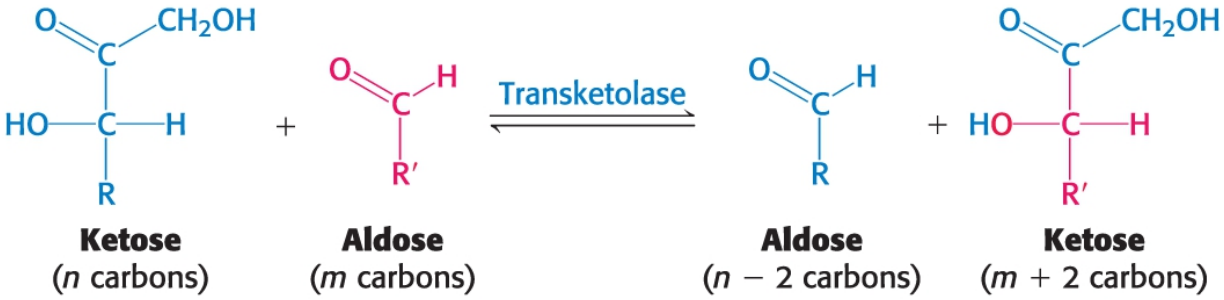


© Macmillan Learning

The cycle is depicted as a flowchart starting from the bottom to the top. In the first step, two 3-phosphoglycerate molecules are converted to two 1,3-Bisphosphoglycerate molecules with the simultaneous hydrolysis of A T P to A D P. In the second step, one glyceraldehyde 3-phosphate is formed from 1,3-Bisphosphoglycerate with the simultaneous oxidation of N A D P H to N A D P superscript plus. Alternatively, glyceraldehyde 3-phosphate produced in the second step can be reversibly converted to 1 dihydroxyacetone phosphate. In the third step, fructose 1, 6-bisphosphate is formed from glyceraldehyde 3-phosphate. Fructose 1, 6-bisphosphate is converted to fructose 6-phosphate in the fourth step. Fructose 6-phosphate is reversibly converted to glucose 6-phosphate in the fifth step. Glucose 6-phosphate is reversibly converted to glucose 1-phosphate in the sixth step. The sugar molecules fructose 6-phosphate, glucose 6-phosphate, and glucose 1-phosphate are labeled hexose monophosphate pool.

Return to FIGURE 20.8 In stage 2 of the Calvin–Benson cycle, hexose phosphate is formed

Extended description for Aldose and ketose formation



The reaction has 2 reactants and 2 products. Ketose (n carbons) reacts with aldose (m carbons) in the presence of transketolase to reversibly form aldose (n minus 2 carbons) and ketose (m plus 2 carbons).

The structure of ketose (n carbons) is as follows: The Fischer projection consists of a vertical line with C above and R below. The projection contains one C atom placed on a vertical line. The C atoms are numbered from top to bottom. C 1 is double bonded to O on the upper left and single bonded to C H 2 O H on the upper right. C 2 is single bonded to O H on the left and H on the right.

The structure of aldose (m carbons) is as follows: A central C atom is double bonded to O on the top left, single bonded to H on the top right, and single bonded to R dash below.

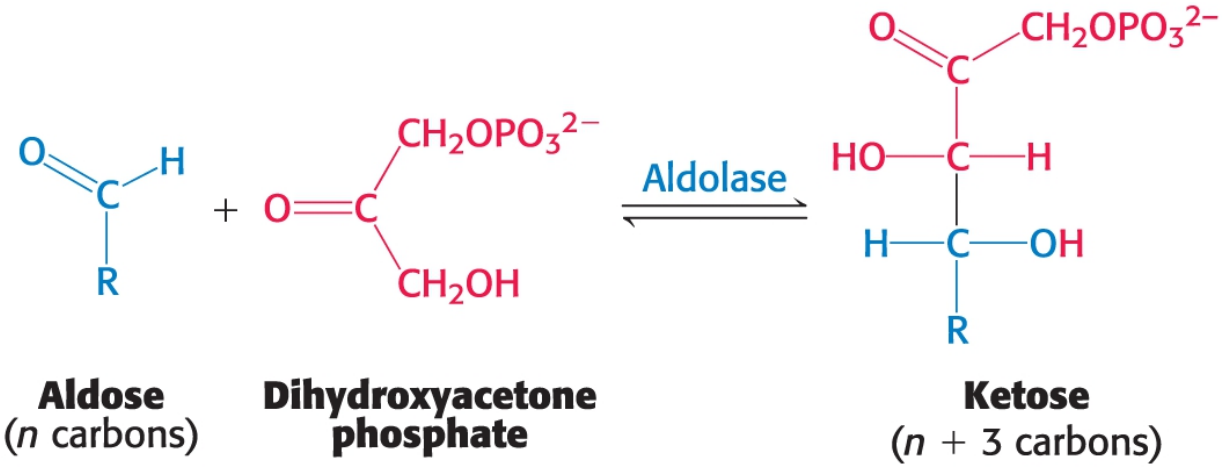
The structure of aldose (n minus 2 carbons) is as follows: A central C atom is double bonded to O on the top left, single bonded to H on the top right, and single bonded to R below.

The structure of ketose (m plus 2 carbons) is as follows: The Fischer projection consists of a vertical line with C above and R dash below. The projection contains one C atom on a vertical line. The C atoms

are numbered from top to bottom. C 1 is double bonded to O on the upper left and single bonded to C H 2 O H on the upper right. C 2 is single bonded to O H on the left and H on the right.

Return to Aldose and ketose formation

Extended description for Ketose formation



The reaction has 2 reactants and 1 product. Aldose reacts with dihydroxyacetone phosphate in the presence of aldolase to reversibly form ketose.

The structure of aldose (n carbons) is as follows: A central C atom is double bonded to O on the top left, single bonded to H on the top right, and single bonded to R below.

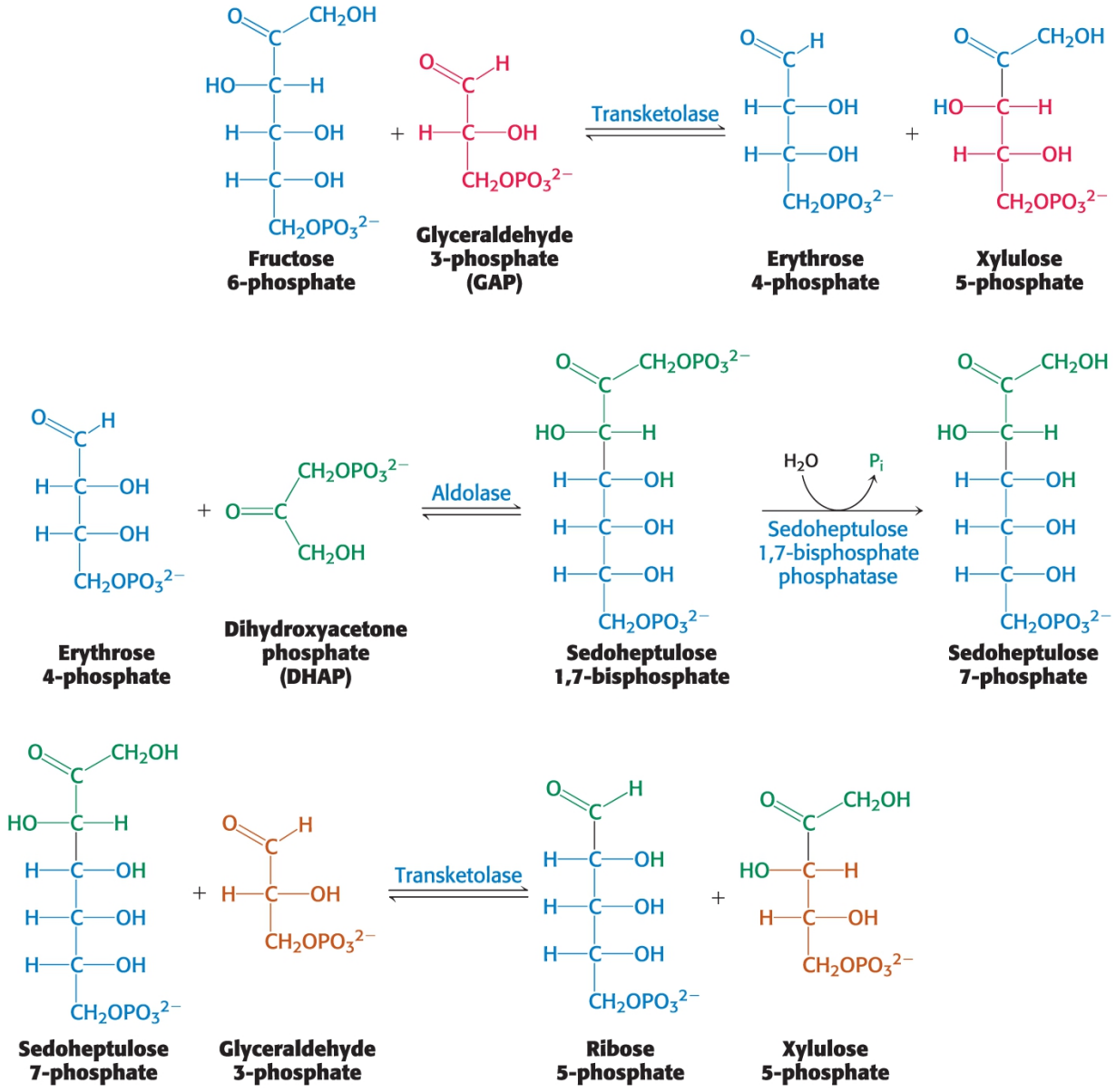
The structure of dihydroxyacetone phosphate is as follows: A central C atom is double bonded to O on the left, single bonded to C H 2 O P O 3 superscript 2 minus on the top right, and C H 2 O H on the lower right.

The structure of ketose (n plus 3 carbons) is as follows: The Fischer projection consists of a vertical line with C above and R below. The projection contains two C atoms placed one below the other on the vertical line. The C atoms are numbered from top to bottom. C 1 is double bonded to O on the upper left and single bonded to C H 2 O P O 3 superscript 2 minus on the upper right. C 2 is single bonded to O

H on the left and H on the right. C 3 is single bonded to H on the left and O H on the right.

Return to Ketose formation

Extended description for FIGURE 20.9 Five-carbon sugars are formed from six-carbon and three-carbon sugars



The first reversible chemical reaction catalyzed by transketolase depicts the formation of erythrose 4-phosphate and xylulose 5-

phosphate from fructose 6-phosphate and glyceraldehyde 3-phosphate.

The structure of fructose 6-phosphate is as follows: C, single bond, C, single bond, C, single bond, C, single bond, C H 2 O P O 3 superscript 2 minus. C 1 is double bonded to O on the upper left and single bonded to C H 2 O H on the upper right. C 2 is single bonded to O H on the left and H on the right. C 3 and C 4 are each single bonded to H on the left and O H.

The structure of glyceraldehyde 3-phosphate (G A P) is as follows: C, single bond, C, single bond, C H 2 O P O 3 superscript 2 minus. C 1 is double-bonded to O on the upper left and single-bonded to H on the upper right. C 2 is single-bonded to H on the left and O H on the right.

The structure of xylulose 5-phosphate is as follows: C, single bond, C, single bond, C, single bond, C H 2 O P O 3 superscript 2 minus. C 1 is double bonded to O on the upper left and single bonded to C H 2 O H on the upper right. C 2 is single bonded to O H on the left and H on the right. C 3 is single bonded to H on the left and O H on the right.

The second reversible chemical reaction catalyzed by aldolase depicts the formation of sedoheptulose 7-phosphate from erythrose 4-phosphate and dihydroxyacetone phosphate. Sedoheptulose 1,7-bisphosphate is formed as an intermediate.

The structure of erythrose 4-phosphate is as follows: C, single bond, C, single bond, C, single bond, C H 2 O P O 3 superscript 2 minus. C 1 is double-bonded to O on the upper left and single-bonded to H on the upper right. C 2 and C 3 are each single bonded to H on the left and O H on the right.

The structure of dihydroxyacetone phosphate (D H A P) is as follows: A central C atom is single bonded to C H 2 O P O 3 superscript 2 minus on the upper right, double bonded to O on the left, and single bonded to C H 2 O H on the lower right.

The structure of sedoheptulose 1,7-bisphosphate is as follows: C, single bond, C, single bond, C, single bond, C, single bond, C, single bond, C H 2 O P O 3 superscript 2 minus. C 1 is double bonded to O on the upper left and single bonded to C H 2 O P O 3 superscript minus on the upper right. C 2 is single bonded to O H on the left and H on the right. C 3 to C 5 are single-bonded to H on the left and O H on the right.

Sedoheptulose 1,7-bisphosphate is irreversibly converted into sedoheptulose 7-phosphate in a reaction catalyzed by sedoheptulose 1,7-bisphosphate phosphatase coupled with the entry of H 2 O and release of P subscript i.

The structure of sedoheptulose 7-phosphate is as follows: C, single bond, C, single bond, C, single bond, C, single bond, C, single bond, C H 2 O P O 3 superscript 2 minus. C 1 is double bonded to O on the upper left and single bonded to C H 2 O H on the upper right. C 2 is single bonded to O H on the left and H on the right. C 3 to C 5 are single-bonded to H on the left and O H on the right.

The third reversible chemical reaction catalyzed by transketolase depicts the formation of ribose 5-phosphate and xylulose 5-phosphate from sedoheptulose 7-phosphate and glyceraldehyde 3-phosphate.

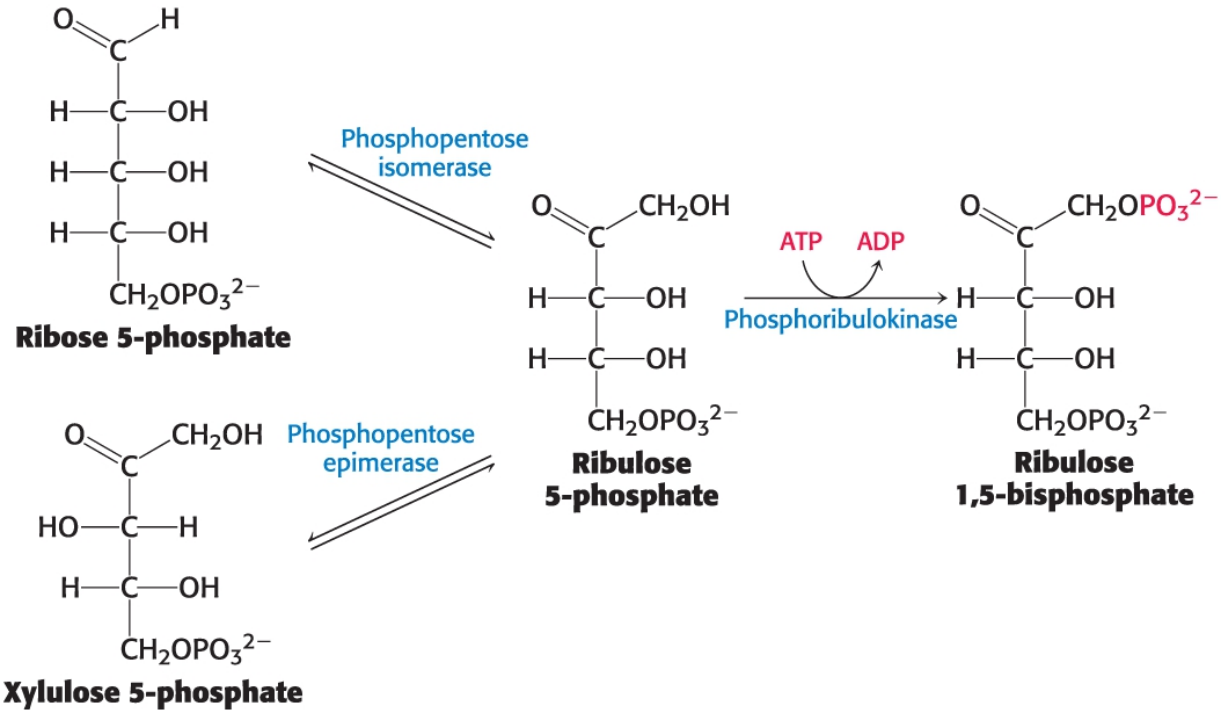
The structure of ribose 5-phosphate is as follows: C, single bond, C, single bond, C, single bond, C, single bond, C H 2 O P O 3 superscript 2 minus. C 1 is double-bonded to O on the upper left and

single-bonded to H on the upper right. C 2 to C 4 are each single bonded to H on the left and O H on the right.

The structure of xylulose 5-phosphate is as follows: C, single bond, C, single bond, C, single bond, C H 2 O P O 3 superscript 2 minus. C 1 is double bonded to O on the upper left and single bonded to C H 2 O H on the upper right. C 2 is single bonded to O H on the left and H on the right. C 3 is single bonded to H on the left and O H on the right.

Return to FIGURE 20.9 Five-carbon sugars are formed from six-carbon and three-carbon sugars

Extended description for FIGURE 20.10 In stage 3 of the Calvin–Benson cycle, ribulose 1,5-bisphosphate is regenerated



In the first step, ribose 5-phosphate and xylulose 5-phosphate produce ribulose 5-phosphate that is further converted into ribulose 1,5-bisphosphate.

Ribose 5-phosphate is reversibly converted into ribulose 5-phosphate by the enzyme phosphopentose isomerase.

Xylulose 5-phosphate is reversibly converted into ribulose 5-phosphate by the enzyme phosphopentose epimerase.

The structure of ribose 5-phosphate is as follows: C, single bond, C, single bond, C, single bond, C, single bond, C H 2 O P O 3

superscript 2 minus. C 1 is double-bonded to O on the upper left and single-bonded to H on the upper right. C 2 to C 4 are each single bonded to H on the left and O H on the right.

The structure of xylulose 5-phosphate is as follows: C, single bond, C, single bond, C, single bond, C H 2 O P O 3 superscript 2 minus. C 1 is double bonded to O on the upper left and single bonded to C H 2 O H on the upper right. C 2 is single bonded to O H on the left and H on the right. C 3 is single bonded to H on the left and O H on the right.

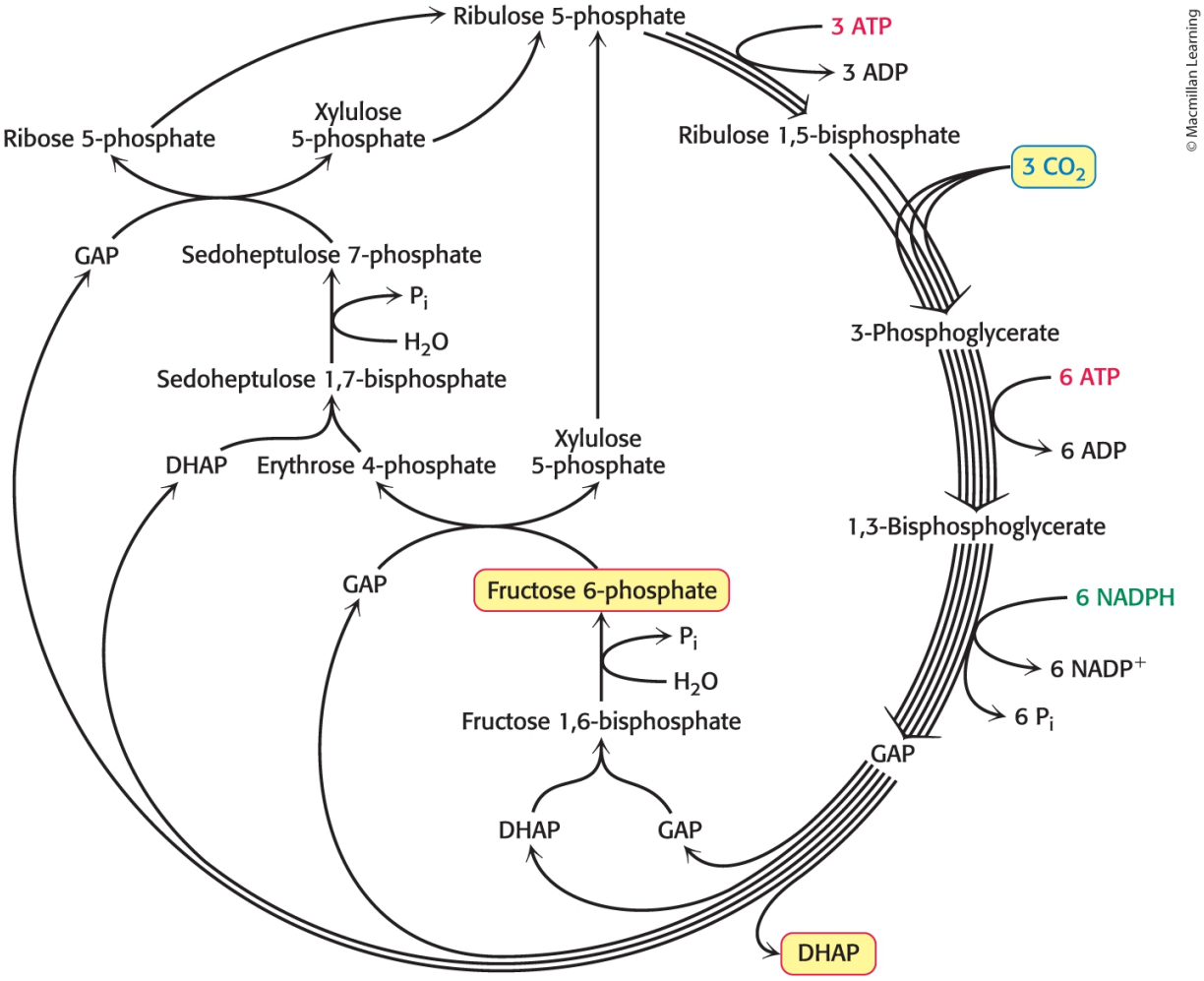
The structure of ribulose 5-phosphate is as follows: C, single bond, C, single bond, C, single bond, C H 2 O P O 3 superscript 2 minus. C 1 is double bonded to O on the upper left and single bonded to C H 2 O H on the upper right. C 2 and C 3 are each single bonded to H on the left and O H on the right.

In the second step, ribulose 5-phosphate is irreversibly converted into ribulose 1,5-bisphosphate by the enzyme phosphoribulokinase coupled with the hydrolysis of A T P to A D P.

The structure of ribulose 1,5-bisphosphate is as follows: C, single bond, C, single bond, C, single bond, C H 2 O P O 3 superscript 2 minus. C 1 is double bonded to O on the upper left and single bonded to C H 2 OP O 3 superscript 2 minus on the upper right. C 2 and C 3 are each single bonded to H on the left and O H on the right.

Return to FIGURE 20.10 In stage 3 of the Calvin–Benson cycle, ribulose 1,5-bisphosphate is regenerated

Extended description for FIGURE 20.11 The full Calvin–Benson cycle process for converting three molecules of C O 2 to dihydroxyacetone phosphate is complex



The cycle starts with ribulose 5-phosphate at the top center. An arrow with three tails leads from ribulose 5-phosphate to ribulose 1,5-bisphosphate. A coupled curved arrow depicts the hydrolysis of 3 A T P to 3 A D P. An arrow with three tails leads from ribulose 1,5-bisphosphate to 3-phosphoglycerate. 3 C O 2 also enter during this step. An arrow with 6 tails leads from 3-phosphoglycerate to 1,3-bisphosphoglycerate. A coupled curved arrow depicts the hydrolysis

of 6 A T P to 6 A D P. An arrow with 6 tails leads from 1,3-bisphosphoglycerate to G A P. A coupled curved arrow depicts the oxidation of 6 N A D P H to 6 N A D P superscript plus and release of 6 P subscript i.

Two arrows from G A P leads to G A P and D A P. One arrow leads to D H A P and the remaining three arrows lead to G A P, D H A P, and G A P. One D A P molecule exits the cycle.

The first G A P and D H A P combine to produce fructose 1, 6-bisphosphate which is further irreversibly converted to fructose 6-phosphate. This irreversible conversion is coupled with the entry of H 2 O and the release of P subscript i.

Fructose 6-phosphate and second G A P are converted into erythrose 4-phosphate and xylulose 5-phosphate which are interconvertible.

Xylulose 5-phosphate is irreversibly converted to ribulose 5-phosphate.

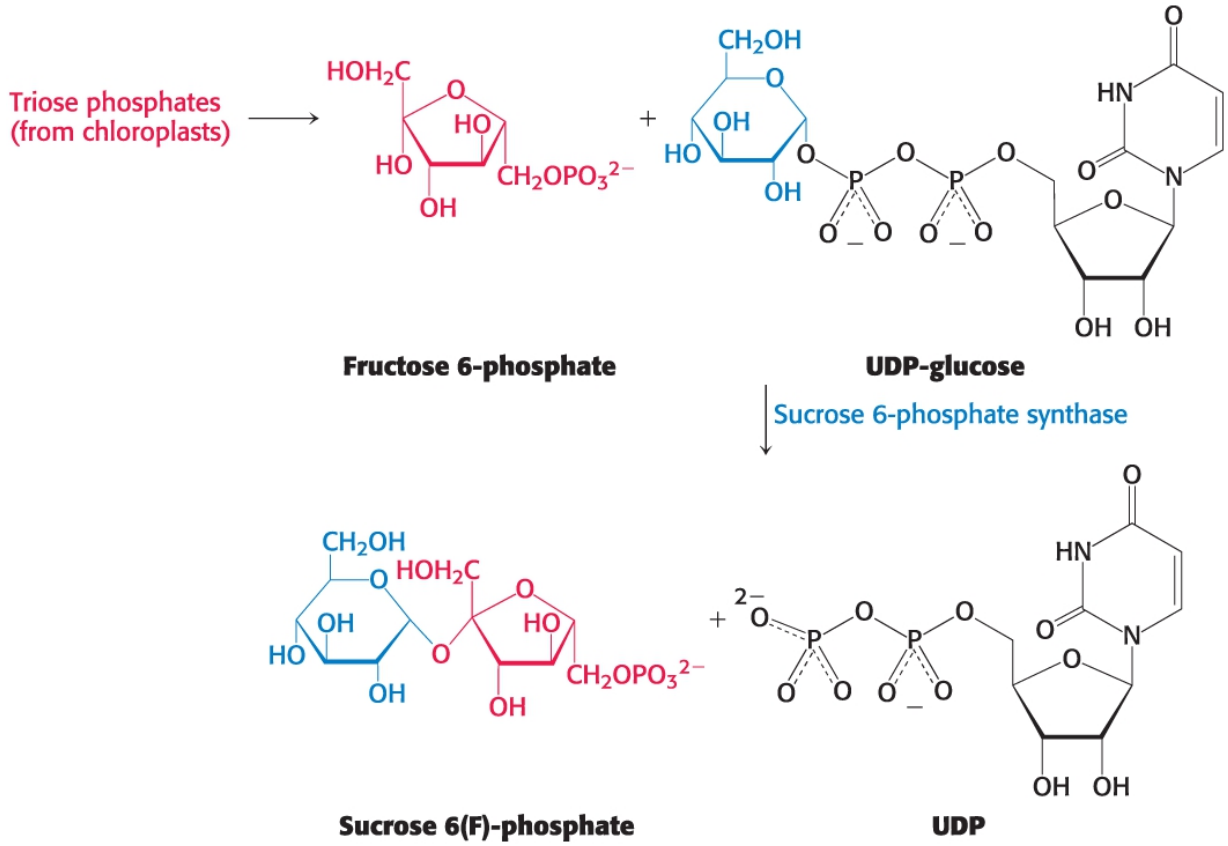
Erythrose 4-phosphate and second D H A P combine to form sedoheptulose-1,7-bisphosphate. Sedoheptulose 1,7-bisphosphate is irreversibly converted into sedoheptulose 7-phosphate coupled with the entry of H 2 O and release of P subscript i.

Sedoheptulose 7-phosphate and third G A P are converted into ribose 5-phosphate and xylulose 5-phosphate which are interconvertible.

Xylulose 5-phosphate and ribose 5-phosphate are converted to ribulose 5-phosphate.

Return to FIGURE 20.11 The full Calvin–Benson cycle process for converting three molecules of C O 2 to dihydroxyacetone phosphate is complex

Extended description for FIGURE 20.12 Carbohydrates are stored as sucrose



Triose phosphates from chloroplasts are irreversibly converted into fructose 6-phosphate.

Fructose 6-phosphate and U D P-glucose are converted into sucrose 6-phosphate and U D P by the enzyme sucrose 6-phosphate synthase.

The structure of fructose 6-phosphate is as follows: A 5-membered heterocyclic pentagonal ring is in a vertical orientation with C 1 occupying the top right vertex. It consists of 1 O and 4 C atoms. O occupies the topmost vertex. C 1 is single bonded to C H 2 O P O 3

superscript 2 minus below. C 2 is single bonded to O H above. C 3 is single bonded to O H below. C 4 is single bonded to C H 2 O H above and O H below.

The structure of U D P-glucose is as follows: A 5-membered heterocyclic pentagonal ring is in a vertical orientation with C 1 occupying the top right vertex. It consists of 1 O and 4 C atoms. O occupies the topmost vertex. C 2 and C 3 are single bonded to O H below. C 1 is single-bonded to N 1 of a 6-membered heterocyclic hexagonal ring in a vertical orientation with C 1 occupying the bottom left vertex. It consists of 2 N and 4 C atoms. First N occupies the bottom-most vertex. The second N bound to H occupies the top left vertex. C 1 and C 2 are double bonded to O. A double bond is present between C 3 and C 4.

C 4 of the pentagonal ring is single-bonded to C H 2 above in the form of a line. C H 2 is single bonded to O, single bond, P, single bond, O, single bond, P in a zigzag conformation. Both P atoms are partially double-bonded to O on the lower left and lower right. The O atoms have an overall negative charge. The terminal P atom of the zigzag chain is single-bonded to the O atom which in turn is single-bonded to C 1 of a 6-membered heterocyclic hexagonal ring in a horizontal orientation. It consists of 1 O and 5 C atoms. O occupies the top right vertex. C 2 and C 4 are each single bonded to O H below. C 3 is single bonded to O H above. C 5 is single bonded to C H 2 O H above.

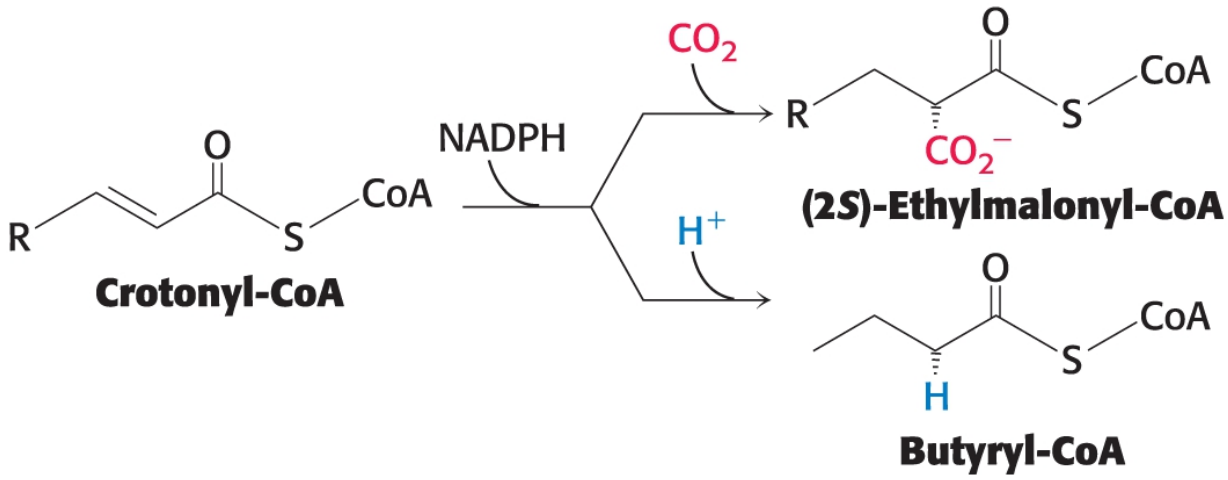
The structure of sucrose 6 (F)-phosphate is as follows: A 5-membered heterocyclic pentagonal ring is in a vertical orientation with C 1 occupying the top right vertex. It consists of 1 O and 4 C atoms. O occupies the topmost vertex. C 1 is single bonded to C H 2 O P O 3 superscript 2 minus below. C 2 is single bonded to O H above. C 3 is single bonded to O H below. C 4 is single bonded to C H 2 O H above and O on the lower left. This O atom is single-bonded to

C 1 of a 6-membered heterocyclic hexagonal ring in a horizontal orientation with C 1 occupying the rightmost vertex. It consists of 1 O and 5 C atoms. O occupies the top right vertex. C 2 and C 4 are each single bonded to O H below. C 3 is single bonded to O H above. C 5 is single bonded to C H 2 O H above.

The structure of U D P is as follows: A 5-membered heterocyclic pentagonal ring is in a vertical orientation with C 1 occupying the top right vertex. It consists of 1 O and 4 C atoms. O occupies the topmost vertex. C 2 and C 3 are single bonded to O H below. C 1 is single-bonded to N 1 of a 6-membered heterocyclic hexagonal ring in a vertical orientation with C 1 occupying the bottom left vertex. It consists of 2 N and 4 C atoms. First N occupies the bottom-most vertex. The second N bound to H occupies the top left vertex. C 1 and C 2 are double bonded to O. A double bond is present between C 3 and C 4. C 4 of the pentagonal ring is single-bonded to C H 2 above in the form of a line. C H 2 is single bonded to O, single bond, P, single bond, O, single bond, P in a zigzag conformation. The first P atom is partially double-bonded to O on the lower left and lower right. The O atoms have an overall negative charge. The terminal P atom is partially double-bonded to O on the upper left, lower left, and lower right. The O atoms have an overall negative charge of 2 minus.

Return to FIGURE 20.12 Carbohydrates are stored as sucrose

Extended description for Conversion of crotonyl-C o A to ethylmalonyl-C o A and butyryl-C o A



The structure of crotonyl-C o A is as follows: A 1 S and 3 C heteronuclear alkene chain is depicted as a line structure using 3 zigzag lines. S occupies the fourth position and is single-bonded to C o A on the upper right. C 1 is single bonded to R on the lower left. C 3 is double bonded to O above. A double bond is present between C 1 and C 2.

A bifurcated forward arrow is shown. It shows the entry of N A D P H. The top branch of the arrow shows the entry of C O 2 and leads to open parenthesis 2 S close parenthesis-Ethylmalonyl-C o A.

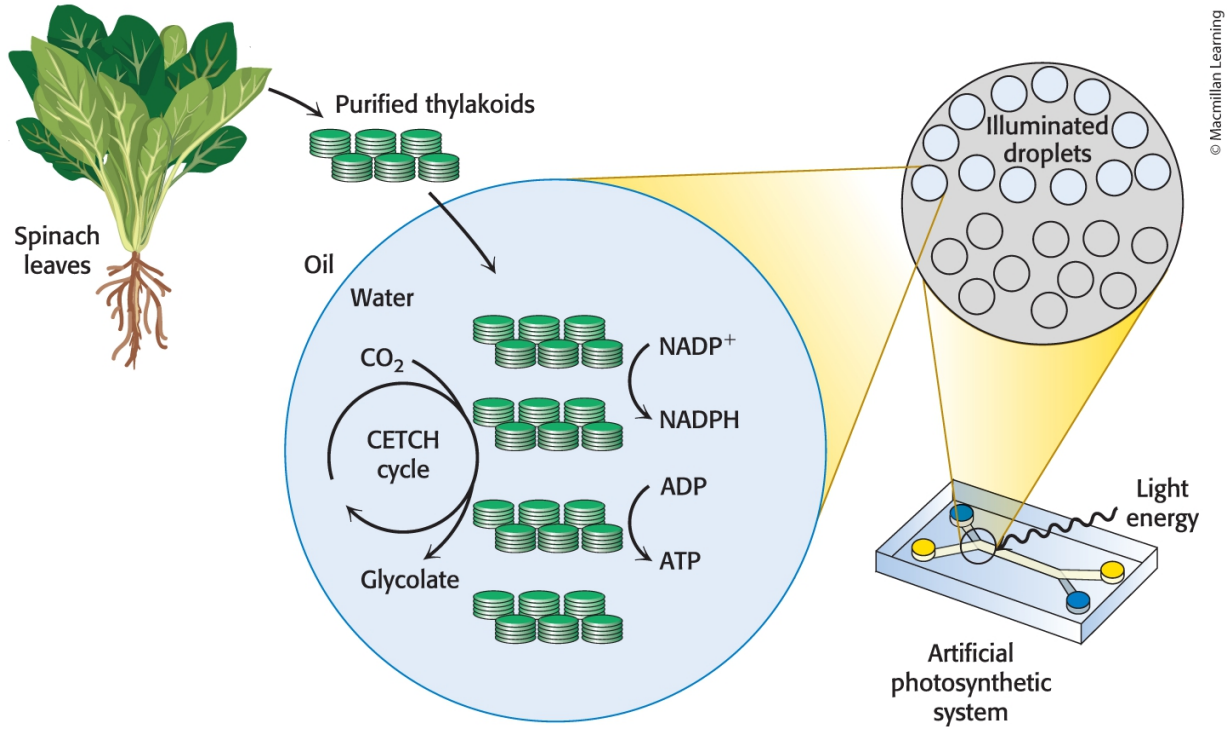
The structure of open parenthesis 2 S close parenthesis-Ethylmalonyl-C o A is as follows: A 1 S and 3 C heteronuclear alkene chain is depicted as a line structure using 3 zigzag lines. S occupies the fourth position and is single-bonded to C o A on the upper right. C 1 is single bonded to R on the lower left. C 2 is dash bonded to C O 2 superscript minus below. C 3 is double bonded to O above.

The bottom branch of the arrow shows the entry of the H superscript plus ion and leads to butyryl-C o A.

The structure of butyryl-C o A is as follows: A 1 S and 4 C heteronuclear alkene chain is depicted as a line structure using 4 zigzag lines. S occupies the fifth position and is single-bonded to C o A on the upper right. C 3 is dash bonded to H below. C 4 is double bonded to O above.

Return to Conversion of crotonyl-C o A to ethylmalonyl-C o A and butyryl-C o A

Extended description for FIGURE 20.13 Scientists have engineered artificial photosynthesis using alternative C O 2 fixation pathways

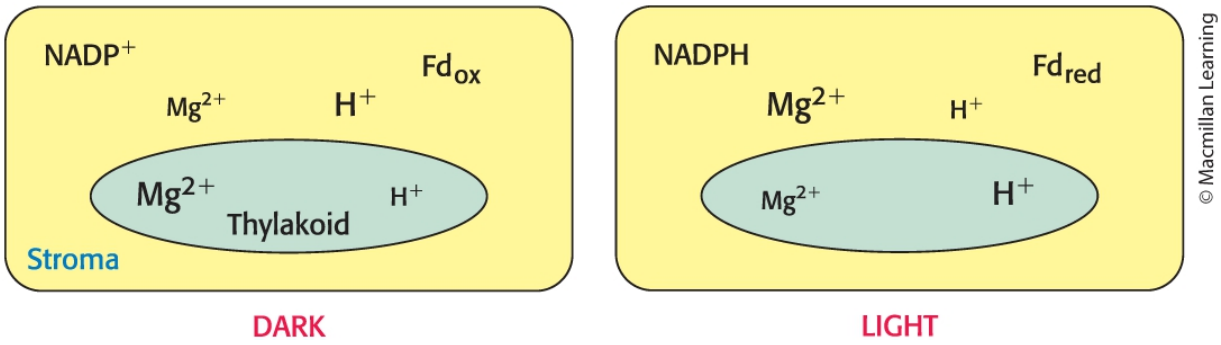


The artificial photosynthetic system is shown. A wavy arrow labeled light energy is falling on the system. An enlarged view of the part illuminated by light shows a large circle with several tiny circles. The circles at the top are shown in blue and labeled illuminated droplets. One of the blue circles is enlarged. It contains 4 sets of stacked discs of thylakoids arranged in two rows from top to the bottom. The interior of the circle is labeled water and the space outside it is labeled oil. Arrows depict the reduction of N A D P superscript plus to N A D P H and hydrolysis of A D P to A T P by the thylakoids. A curved arrow next to the thylakoid disc is labeled "CETCH cycle". C O 2 enters this cycle and glycolate is released. A bundle of spinach leaves is shown outside the circle. An arrow from

the leaves depict the purified thylakoid discs and another arrow from the purified thylakoid points toward the thylakoid discs inside the blue circle.

Return to FIGURE 20.13 Scientists have engineered artificial photosynthesis using alternative C O 2 fixation pathways

Extended description for FIGURE 20.14 Light regulates the Calvin–Benson cycle

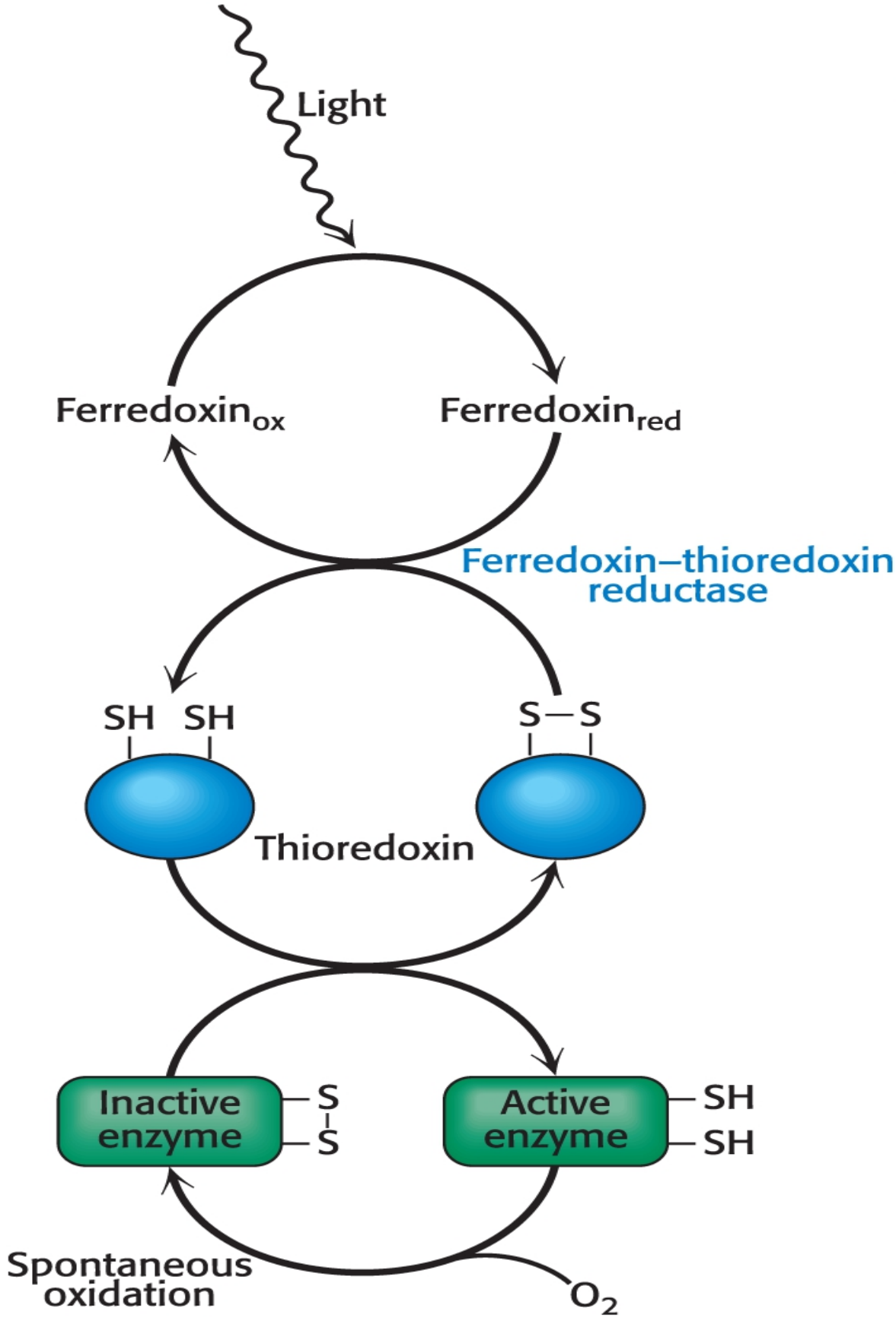


The figure has two panels. The first panel on the left is labeled dark. It consists of an oval region labeled thylakoid. The region outside the thylakoid is labeled stroma. M g superscript 2 plus and H superscript plus ions are present in the thylakoid. N A D P superscript plus, F d oxidized, M g superscript 2 plus, and H superscript plus ions are present in the stroma. The second panel on the right is labeled light. It consists of an oval region labeled thylakoid. The region outside the thylakoid is labeled stroma. M g superscript 2 plus and H superscript plus ions are present in the thylakoid. N A D P H, F d reduced, M g superscript 2 plus, and H superscript plus ions are present in the stroma.

Return to FIGURE 20.14 Light regulates the Calvin–Benson cycle

Extended description for FIGURE 20.16 Thioredoxin

can activate enzymes by reducing them

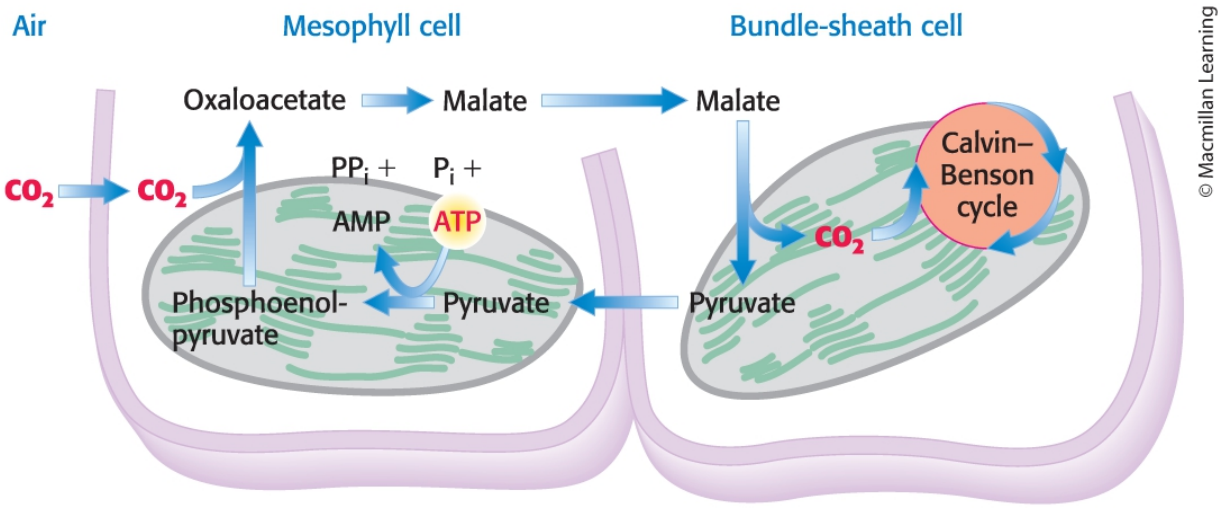


© Macmillan Learning

Light depicted as a wavy arrow stimulates the conversion of the ferredoxin oxidized form to the ferredoxin reduced form. The reduced form transfers electrons to oxidized thioredoxin in a reaction catalyzed by ferredoxin-thioredoxin reductase. The oxidized thioredoxin is depicted as a blue circle single bonded to two S atoms. These S atoms are also single-bonded. The reduced thioredoxin is depicted as a blue circle single bonded to two S H groups above. The reduced thioredoxin converts an inactive enzyme to an active enzyme. The inactive enzyme is depicted as a green rectangle single-bonded to two S atoms. These S atoms are also single-bonded to each other. The active enzyme is depicted as a green rectangle single bonded to two S H groups. Spontaneous oxidation that involves the addition of O 2 can convert the active enzyme back to its inactive form.

Return to FIGURE 20.16 Thioredoxin can activate enzymes by reducing them

Extended description for FIGURE 20.17 The C 4 pathway can concentrate C O 2

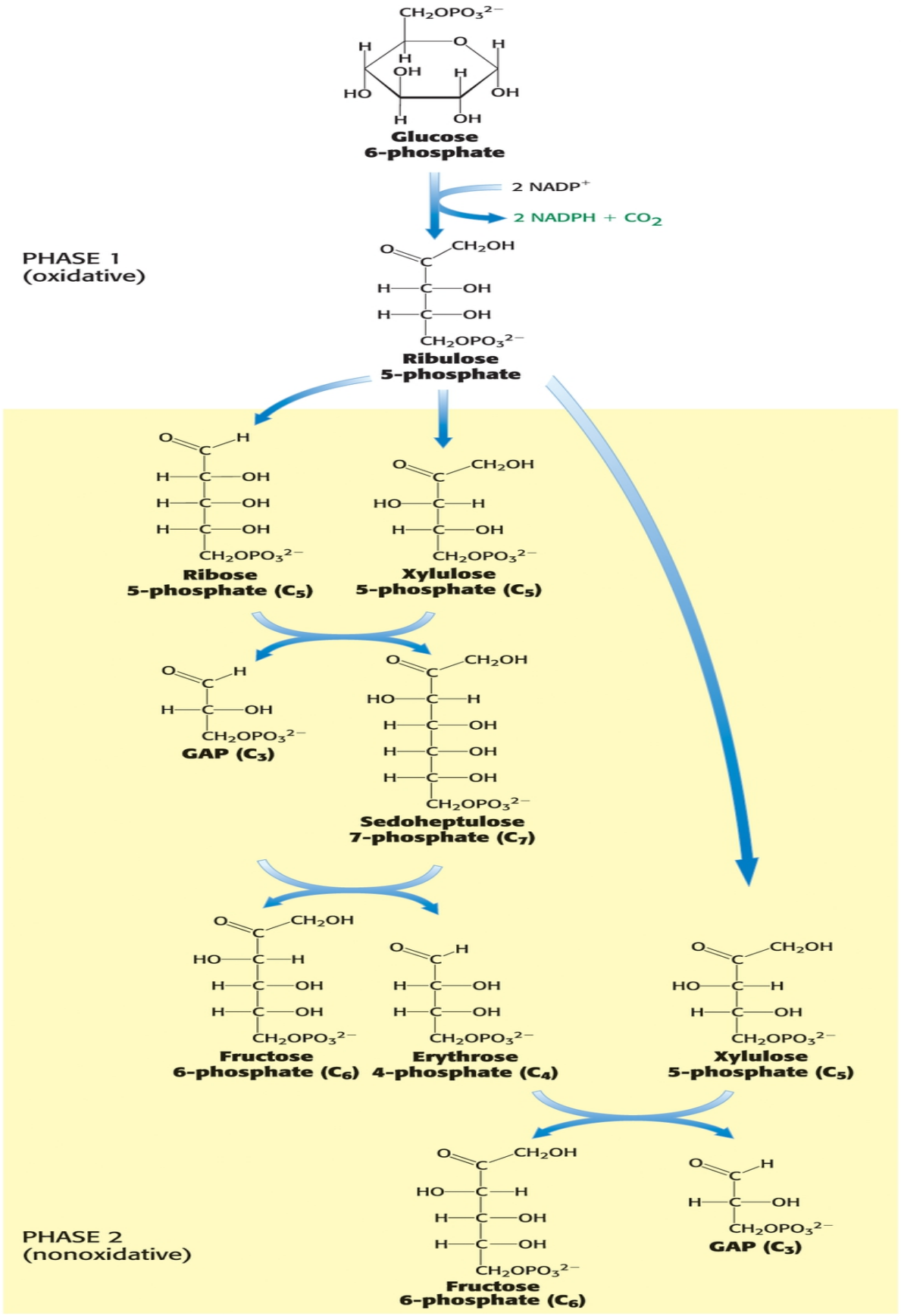


An open section of mesophyll cell attached laterally to a bundle-sheath cell is shown. The region outside the cells is labeled air. Both cells contain chloroplast with stacked thylakoids. C O 2 from the air enters the mesophyll cell. This C O 2 is combined with phosphoenolpyruvate from chloroplast to produce oxaloacetate in the cytoplasm. Oxaloacetate is converted to malate which is transported to the bundle-sheath cell. The malate molecule is converted into pyruvate and C O 2 inside the chloroplast of the bundle-sheath cell. C O 2 enters the Calvin-Benson cycle operating inside the chloroplast of the bundle-sheath cell. Pyruvate is transported back to the mesophyll cell. Inside the chloroplast of the mesophyll cell, pyruvate is converted back to phosphoenolpyruvate with the simultaneous hydrolysis of A T P to A M P.

Return to FIGURE 20.17 The C 4 pathway can concentrate C O 2

Extended description for FIGURE 20.21 The pentose phosphate pathway consists of an oxidative and a

nonoxidative phase



© Macmillan Learning

The events of phase 1 (oxidative) are as follows:

In the first step, glucose 6-phosphate is converted to ribulose 5-phosphate with the simultaneous reduction of 2 N A D P superscript plus to 2 N A D P H and release of C O 2.

The structure of glucose 6-phosphate is as follows: A 6-membered heterocyclic hexagonal ring is in a horizontal orientation and consists of 1 O and 5 C atoms. O occupies the top right vertex. C 1, C 2, and C 4 are single bonded to H above and O H below. C 3 is single bonded to O H above and H below. C 5 is single bonded to C H 2 O P O 3 superscript 2 minus above and H below.

The structure of ribulose 5-phosphate is as follows: C, single bond, C, single bond, C, single bond, C H 2 O P O 3 superscript 2 minus. C 1 is double bonded to O on the upper left and single bonded to C H 2 O H on the upper right. C 2 and C 3 are each single bonded to H on the left and O H on the right.

The events of phase 2 (non-oxidative) are as follows:

In the first step, ribulose 5-phosphate is converted into ribose 5-phosphate (C 5) and xylulose 5-phosphate (C 5). Ribulose 5-phosphate can also be directly converted into xylulose 5-phosphate. The structure of ribose 5-phosphate is as follows: C, single bond, C, single bond, C, single bond, C, single bond, C H 2 O P O 3 superscript 2 minus. C 1 is double-bonded to O on the upper left and single-bonded to H on the upper right. C 2 to C 4 are each single bonded to H on the left and O H on the right.

The structure of xylulose 5-phosphate is as follows: C, single bond, C, single bond, C, single bond, C H 2 O P O 3 superscript 2 minus. C 1 is double bonded to O on the upper left and single bonded to C H 2

O H on the upper right. C 2 is single bonded to O H on the left and H on the right. C 3 is single bonded to H on the left and O H on the right. Ribose 5-phosphate and xylulose 5-phosphate are further converted into G A P (C 3) and sedoheptulose 7-phosphate (C 7).

The structure of glyceraldehyde 3-phosphate (G A P) is as follows: C, single bond, C, single bond, C H 2 O P O 3 superscript 2 minus. C 1 is double-bonded to O on the upper left and single-bonded to H on the upper right. C 2 is single-bonded to H on the left and O H on the right. The structure of sedoheptulose 7-phosphate is as follows: C, single bond, C, single bond, C, single bond, C, single bond, C, single bond, C H 2 O P O 3 superscript 2 minus. C 1 is double bonded to O on the upper left and single bonded to C H 2 O H on the upper right. C 2 is single bonded to O H on the left and H on the right. C 3 to C 5 are single-bonded to H on the left and O H on the right.

Sedoheptulose 7-phosphate and G A P are further converted to fructose 6-phosphate (C 6) and erythrose 4-phosphate (C 4).

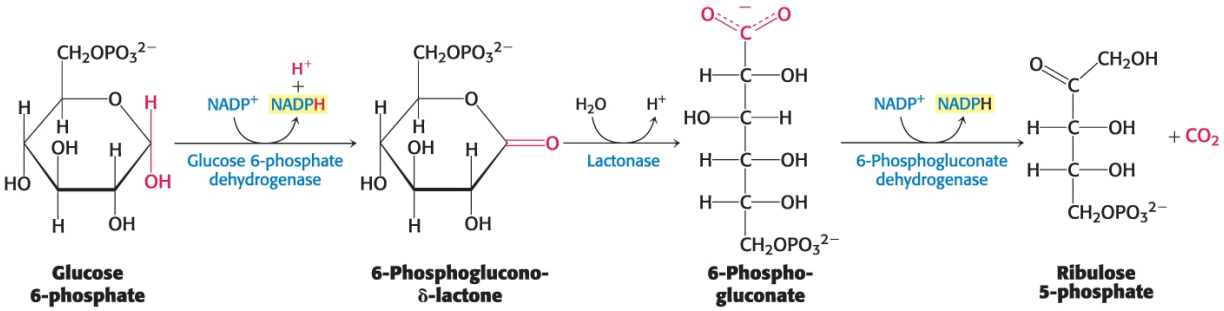
The structure of fructose 6-phosphate is as follows: C, single bond, C, single bond, C, single bond, C, single bond, C H 2 O P O 3 superscript 2 minus. C 1 is double bonded to O on the upper left and single bonded to C H 2 O H on the upper right. C 2 is single bonded to O H on the left and H on the right. C 3 and C 4 are each single bonded to H on the left and O H.

The structure of erythrose 4-phosphate is as follows: C, single bond, C, single bond, C, single bond, C H 2 O P O 3 superscript 2 minus. C 1 is double-bonded to O on the upper left and single-bonded to H on the upper right. C 2 and C 3 are each single bonded to H on the left and O H on the right.

Erythrose 4-phosphate and xylulose 5-phosphate (C 5) are converted into fructose 6-phosphate (C 6) and G A P.

Return to FIGURE 20.21 The pentose phosphate pathway consists of an oxidative and a nonoxidative phase

Extended description for FIGURE 20.22 The oxidative phase of the pentose phosphate pathway yields two molecules of NADPH



In the first step, glucose 6-phosphate is irreversibly converted into 6-phosphoglucono-delta-lactone by glucose 6-phosphate dehydrogenase. It is coupled with the reduction of N A D P superscript plus to N A D P H plus H superscript plus.

The structure of glucose 6-phosphate is as follows: A 6-membered heterocyclic hexagonal ring is in a horizontal orientation and consists of 1 O and 5 C atoms. O occupies the top right vertex. C 1, C 2, and C 4 are single bonded to H above and O H below. C 3 is single bonded to O H above and H below. C 5 is single bonded to C H 2 O P O 3 superscript 2 minus above and H below.

The structure of 6-phosphoglucono-delta-lactone is as follows: A 6-membered heterocyclic hexagonal ring is in a horizontal orientation and consists of 1 O and 5 C atoms. O occupies the top right vertex. C 1 is double bonded to O on the right. C 2 and C 4 are each single bonded to H above and O H below. C 3 is single bonded to O H above and H below. C 5 is single bonded to C H 2 O P O 3 superscript 2 minus above and H below.

In the second step, 6-phosphoglucono-delta-lactone is irreversibly converted into 6-phosphogluconate by lactonase. It is coupled with the entry of H 2 O and the release of H superscript plus ion.

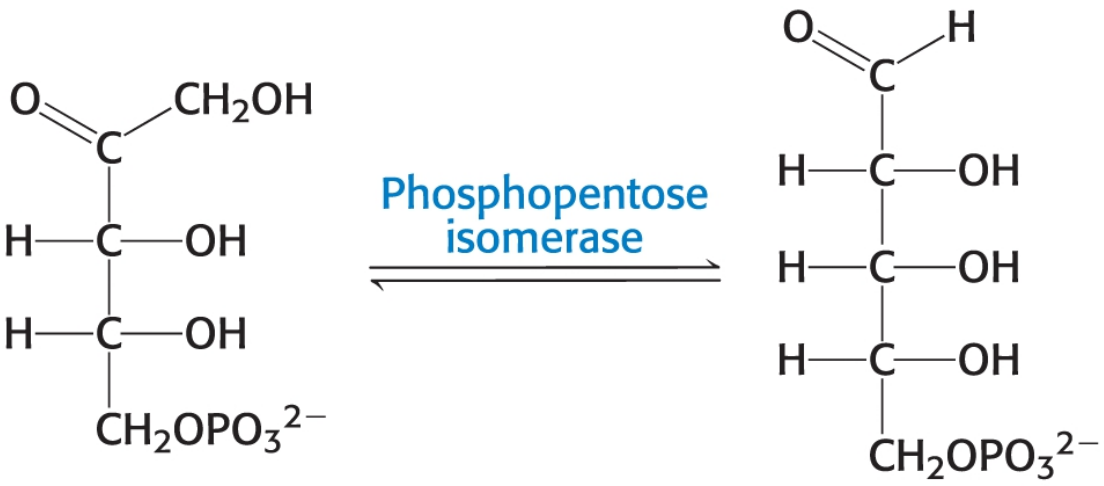
The structure of 6-phosphogluconate is as follows: C, single bond, C, single bond, C, single bond, C, single bond, C, single bond, C H 2 O P O 3 superscript 2 minus. C 1 is partially double bonded to O on the upper left and upper right. This C O O group has an overall negative charge. C 2, C 4, and C 5 are each single bonded to H on the left and O H on the right. C 3 is single bonded to O H on the left and H on the right.

In the third step, 6-phosphogluconate is irreversibly converted into ribulose 5-phosphate by 6-phosphogluconate dehydrogenase and C O 2. It is coupled with the reduction of N A D P superscript plus to N A D P H.

The structure of ribulose 5-phosphate is as follows: C, single bond, C, single bond, C, single bond, C H 2 O P O 3 superscript 2 minus. C 1 is double bonded to O on the upper left and single bonded to C H 2 O H on the upper right. C 2 and C 3 are each single bonded to H on the left and O H on the right.

Return to FIGURE 20.22 The oxidative phase of the pentose phosphate pathway yields two molecules of NADPH

Extended description for Formation of ribose 5-phosphate



Ribulose 5-phosphate **Ribose 5-phosphate**

Ribulose 5-phosphate is reversibly converted to ribose 5-phosphate in the presence of phosphopentose isomerase.

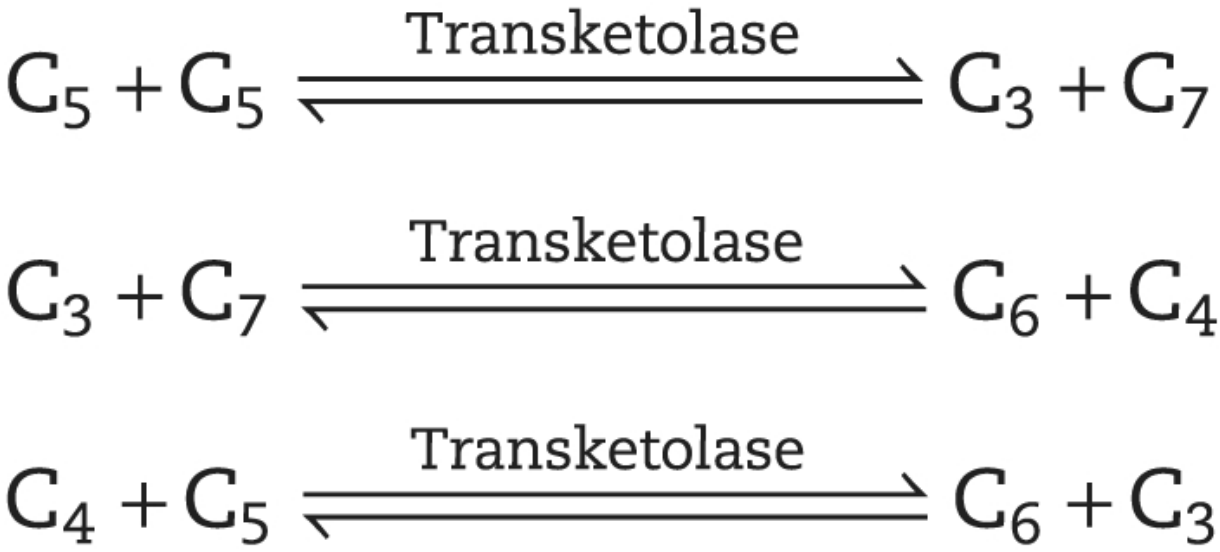
The structure of ribulose 5-phosphate is as follows: The Fischer projection consists of a vertical line with C above and C H 2 O P O 3 superscript 2 minus below. The projection contains 2 C atoms placed one below the other on a vertical line. The C atoms are numbered from top to bottom. C 1 is double bonded to O on the top left and single bonded to C H 2 O H on the top right. C 2 and C 3 are each single bonded to H on the left and O H on the right.

The structure of ribose 5-phosphate is as follows: The Fischer projection consists of a vertical line with C above and C H 2 O P O 3 superscript 2 minus below. The projection contains 3 C atoms placed one below the other on a vertical line. The C atoms are numbered from top to bottom. C 1 is double bonded to O on the top left and

single bonded to H on the top right. C 2, C 3, and C 4 are each single bonded to H on the left and O H on the right.

Return to Formation of ribose 5-phosphate

Extended description for Reactions catalyzed by transketolase



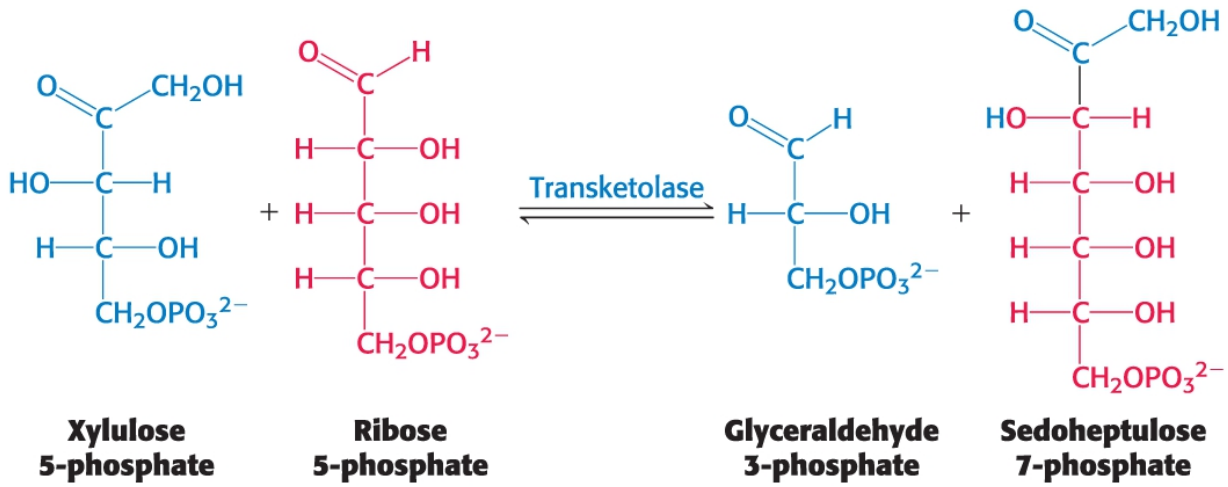
The first reaction consists of two reactants and two products. The reactants are C 5 and C 5. The products are C 3 and C 7.

The second reaction consists of two reactants and two products. The reactants are C 3 and C 7. The products are C 6 and C 4.

The third reaction consists of two reactants and two products. The reactants are C 4 and C 5. The products are C 6 and C 3.

Return to Reactions catalyzed by transketolase

Extended description for Reaction catalyzed by transketolase



Transketolase catalyzes a reversible reaction that involves the conversion of xylulose 5-phosphate and ribose 5-phosphate to glyceraldehyde 3-phosphate and sedoheptulose 7-phosphate.

The structure of xylulose 5-phosphate is as follows: C, single bond, C, single bond, C, single bond, C H 2 O P O 3 superscript 2 minus. C 1 is double bonded to O on the upper left and single bonded to C H 2 O H on the upper right. C 2 is single bonded to O H on the left and H on the right. C 3 is single bonded to H on the left and O H on the right.

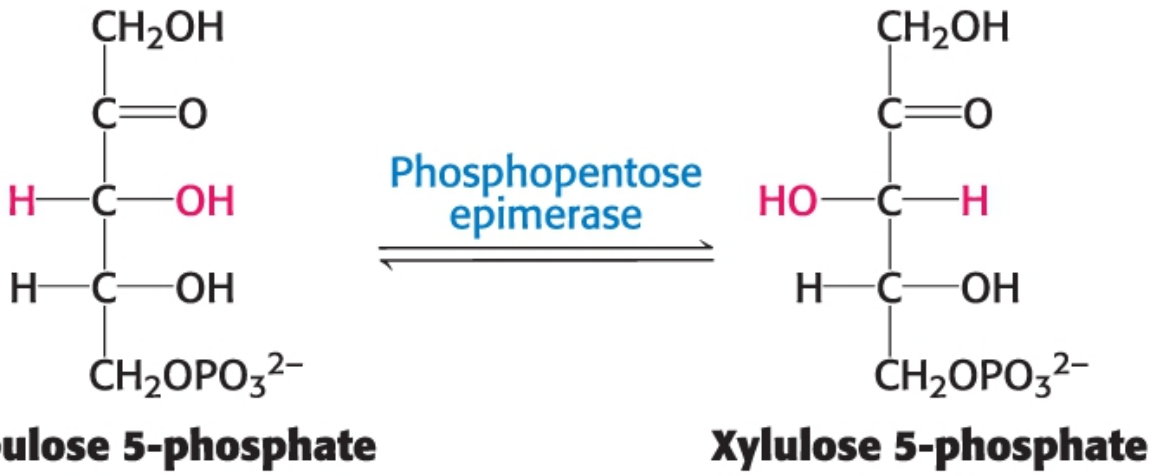
The structure of ribose 5-phosphate is as follows: C, single bond, C, single bond, C, single bond, C, single bond, C H 2 O P O 3 superscript 2 minus. C 1 is double-bonded to O on the upper left and single-bonded to H on the upper right. C 2 to C 4 are each single bonded to H on the left and O H on the right.

The structure of glyceraldehyde 3-phosphate is as follows: C, single bond, C, single bond, C H 2 O P O 3 superscript 2 minus. C 1 is double-bonded to O on the upper left and single-bonded to H on the upper right. C 2 is single-bonded to H on the left and O H on the right.

The structure of sedoheptulose 7-phosphate is as follows: C, single bond, C, single bond, C, single bond, C, single bond, C, single bond, C H 2 O P O 3 superscript 2 minus. C 1 is double bonded to O on the upper left and single bonded to C H 2 O H on the upper right. C 2 is single bonded to O H on the left and H on the right. C 3 to C 5 are single-bonded to H on the left and O H on the right.

Return to Reaction catalyzed by transketolase

Extended description for Formation of xylulose 5-phosphate



Ribulose 5-phosphate **Xylulose 5-phosphate**

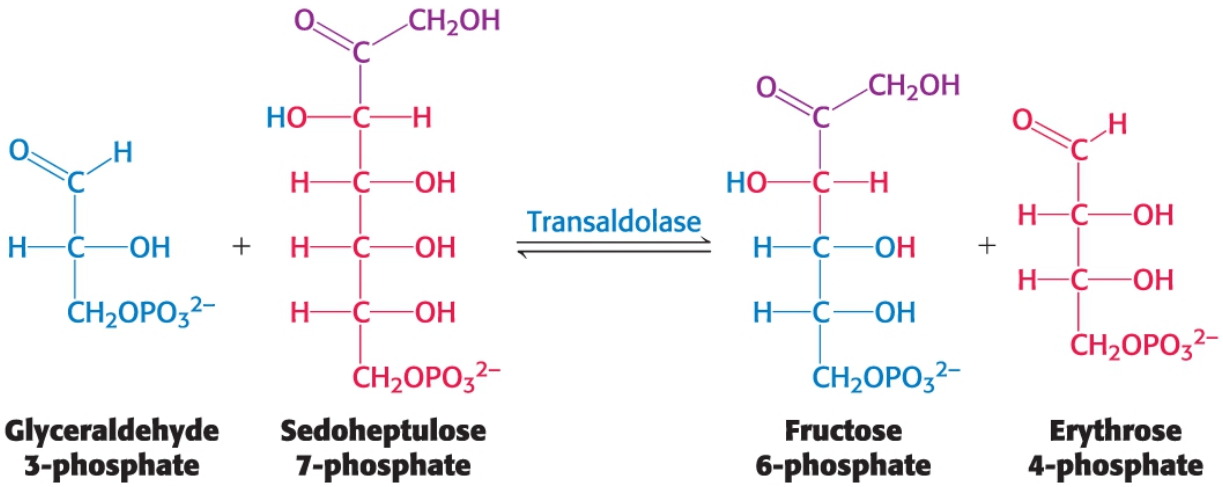
Ribulose 5-phosphate is reversibly converted to xylulose 5-phosphate in the presence of phosphopentose epimerase.

The structure of ribulose 5-phosphate is as follows: The Fischer projection consists of a vertical line with C H 2 O H above and C H 2 O P O 3 superscript 2 minus below. The projection contains 3 C atoms placed one below the other on a vertical line. The C atoms are numbered from top to bottom. C 2 is double bonded to O on the right. C 3 and C 4 are each single bonded to H on the left and O H on the right.

The structure of xylulose 5-phosphate is as follows: The Fischer projection consists of a vertical line with C H 2 O H above and C H 2 O P O 3 superscript 2 minus below. The projection contains 3 C atoms placed one below the other on a vertical line. The C atoms are numbered from top to bottom. C 2 is double bonded to O on right. C 3 is single bonded to O H on the left and H on the right. C 4 is single bonded to H on the left and O H on the right.

Return to Formation of xylulose 5-phosphate

Extended description for Reaction catalyzed by transaldolase



Transaldolase catalyzes a reversible reaction that produces fructose 6-phosphate and erythrose 4-phosphate from glyceraldehyde 3-phosphate and sedoheptulose 7-phosphate.

The structure of glyceraldehyde 3-phosphate is as follows: C, single bond, C, single bond, C H 2 O P O 3 superscript 2 minus. C 1 is double-bonded to O on the upper left and single-bonded to H on the upper right. C 2 is single-bonded to H on the left and O H on the right.

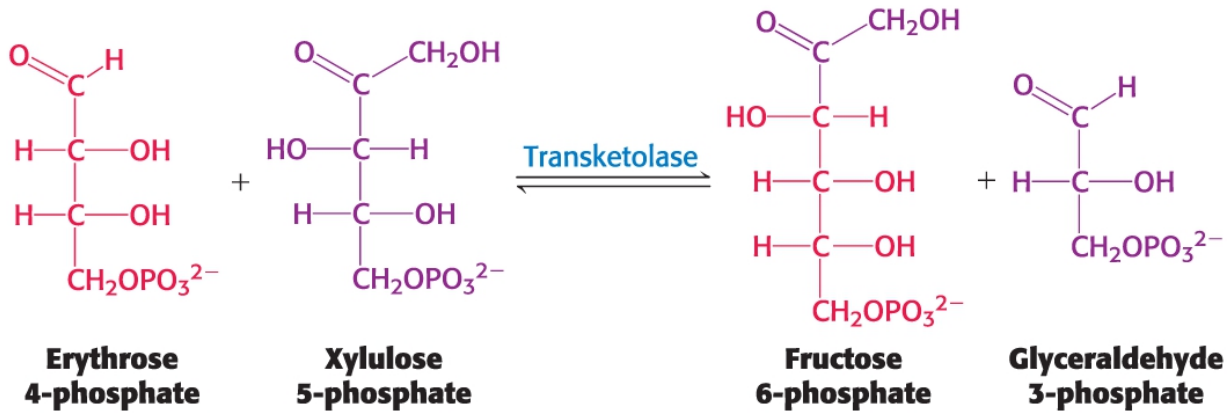
The structure of sedoheptulose 7-phosphate is as follows: C, single bond, C, single bond, C, single bond, C, single bond, C, single bond, C H 2 O P O 3 superscript 2 minus. C 1 is double bonded to O on the upper left and single bonded to C H 2 O H on the upper right. C 2 is single bonded to O H on the left and H on the right. C 3 to C 5 are single-bonded to H on the left and O H on the right.

The structure of fructose 6-phosphate is as follows: C, single bond, C, single bond, C, single bond, C, single bond, C H 2 O P O 3 superscript 2 minus. C 1 is double bonded to O on the upper left and single bonded to C H 2 O H on the upper right. C 2 is single bonded to O H on the left and H on the right. C 3 and C 4 are each single bonded to H on the left and O H.

The structure of erythrose 4-phosphate is as follows: C, single bond, C, single bond, C, single bond, C H 2 O P O 3 superscript 2 minus. C 1 is double-bonded to O on the upper left and single-bonded to H on the upper right. C 2 and C 3 are each single bonded to H on the left and O H on the right.

Return to Reaction catalyzed by transaldolase

Extended description for Reaction catalyzed by transketolase



Transketolase catalyzes a reversible reaction that involves the conversion of erythrose 4-phosphate and xylulose 5-phosphate to fructose 6-phosphate and glyceraldehyde 3-phosphate.

The structure of erythrose 4-phosphate is as follows: C, single bond, C, single bond, C, single bond, C H 2 O P O 3 superscript 2 minus. C 1 is double-bonded to O on the upper left and single-bonded to H on the upper right. C 2 and C 3 are each single bonded to H on the left and O H on the right.

The structure of xylulose 5-phosphate is as follows: C, single bond, C, single bond, C, single bond, C H 2 O P O 3 superscript 2 minus. C 1 is double bonded to O on the upper left and single bonded to C H 2 O H on the upper right. C 2 is single bonded to O H on the left and H on the right. C 3 is single bonded to H on the left and O H on the right.

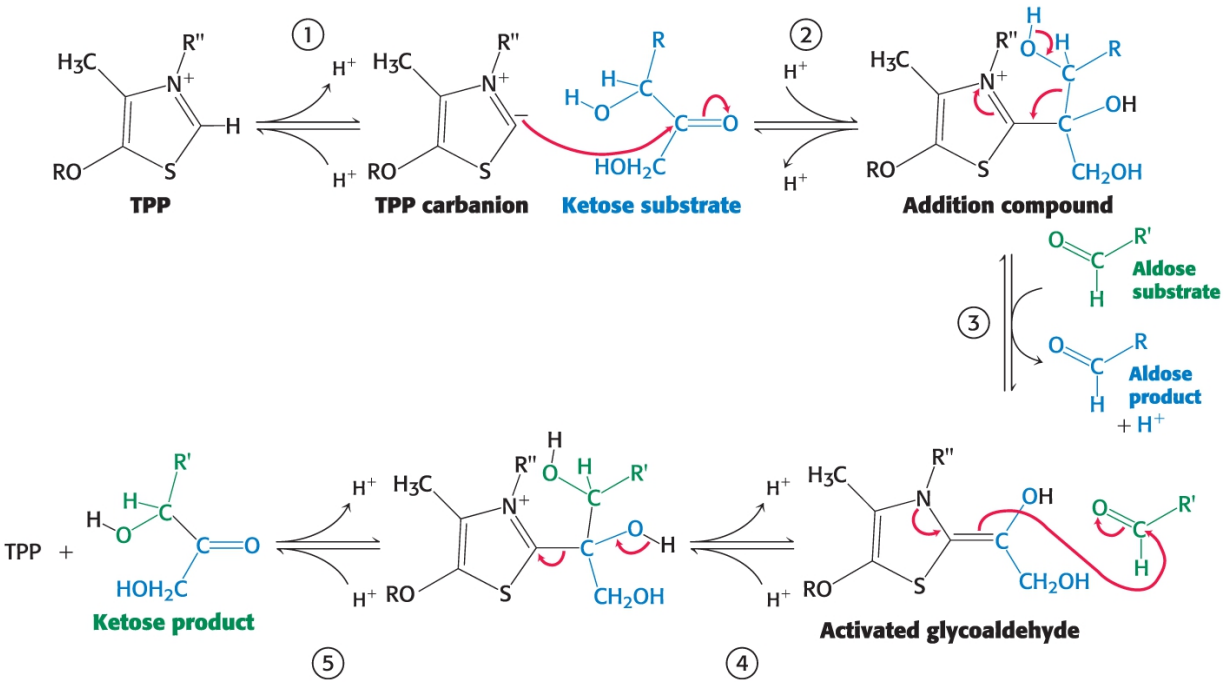
The structure of fructose 6-phosphate is as follows: C, single bond, C, single bond, C, single bond, C, single bond, C H 2 O P O 3

superscript 2 minus. C 1 is double bonded to O on the upper left and single bonded to C H 2 O H on the upper right. C 2 is single bonded to O H on the left and H on the right. C 3 and C 4 are each single bonded to H on the left and O H.

The structure of glyceraldehyde 3-phosphate is as follows: C, single bond, C, single bond, C H 2 O P O 3 superscript 2 minus. C 1 is double-bonded to O on the upper left and single-bonded to H on the upper right. C 2 is single-bonded to H on the left and O H on the right.

Return to Reaction catalyzed by transketolase

Extended description for FIGURE 20.23 The transketolase reaction takes place on thiamine pyrophosphate



The conversion of ketose substrate to ketose product takes place in five sequential steps.

In the first step, T P P is converted into a T P P carbanion.

The structure of T P P is as follows: A 5-membered heterocyclic hexagonal ring is in a horizontal orientation with C 1 occupying the rightmost vertex. It consists of 1 N, 1 S, and 3 C atoms. N with a positive charge occupies the top right vertex. S occupies the bottom right vertex. A double bond is present between N and C 1, and C 2 and C 3. N is single bonded to R double dash on the upper right. C 1 is single bonded to H on the right. C 2 is single bonded to O R on the lower left. C 3 is single bonded to C H 3 on the upper left.

A reversible reaction arrow shows the release of the H superscript plus ion as the reaction proceeds forward and the entry of the H superscript plus as the reaction proceeds backward.

The structure of the T P P carbanion is as follows: A 5-membered heterocyclic hexagonal ring is in a horizontal orientation with C 1 occupying the rightmost vertex. It consists of 1 N, 1 S, and 3 C atoms. N with a positive charge occupies the top right vertex. S occupies the bottom right vertex. A double bond is present between N and C 1, and C 2 and C 3. N is single bonded to R double dash on the upper right. C 2 is single bonded to O R on the lower left. C 3 is single bonded to C H 3 on the upper left. C 1 has a negative charge.

In the second step, the ketose substrate reacts with T P P carbanion to form an addition compound.

The structure of the ketose substrate is as follows: C, single bond, C. C 1 is single bonded to H on the left, R on the upper right, and O on the lower left. O atom is single-bonded to H on the upper left. C 2 is double bonded to O on the right and single bonded to C H 2 O H on the lower left.

A red curved arrow points from C 1 of T P P carbanion to C 2 of ketose substrate. Another red curved arrow points from the double bond between C 2 and O of the ketose substrate toward the O atom.

A reversible reaction arrow shows the entry of the H superscript plus ion as the reaction proceeds forward and the release of the H superscript plus as the reaction proceeds backward.

The structure of the addition compound is as follows: A 5-membered heterocyclic hexagonal ring is in a horizontal orientation with C 1 occupying the rightmost vertex. It consists of 1 N, 1 S, and 3

C atoms. N with a positive charge occupies the top right vertex. S occupies the bottom right vertex. A double bond is present between N and C 1, and C 2 and C 3. N is single bonded to R double dash on the upper right. C 2 is single bonded to O R on the lower left. C 3 is single bonded to C H 3 on the upper left. C 1 is single bonded to C, single bond, O H on the right. This C atom is single-bonded to C above and C H 2 O H below. The C atom above is further single bonded to O, single bond, H on the upper left, H above, and R on the upper right.

A red curved arrow points from the single bond between O and H on the upper left toward the single bond between O and the C atom located above. A second red curved arrow points from the single bond between the C atom on the right and C above toward the single bond between C 1 of the ring and the C atom on the right. A third red-curved arrow points from the double bond between N and C 1 toward the N atom of the ring.

In the third step, the addition compound is converted into activated glycoaldehyde with the simultaneous conversion of aldose substrate to aldose product.

A reversible reaction arrow leads to the activated glycoaldehyde.

The structure of the aldose substrate is as follows: A central C atom is double bonded to O on the upper left, single bonded to R dash on the upper right, and H below.

The structure of the aldose product is as follows: A central C atom is double bonded to O on the upper left, single bonded to R on the upper right, and single bonded to H below.

An H superscript plus ion is also produced during this coupled conversion.

The structure of the activated glycoaldehyde is as follows: A 5-membered heterocyclic hexagonal ring is in a horizontal orientation with C 1 occupying the rightmost vertex. It consists of 1 N, 1 S, and 3 C atoms. N occupies the top right vertex. S occupies the bottom right vertex. A double bond is present between C 2 and C 3. N is single bonded to R double dash on the upper right. C 2 is single bonded to O R on the lower left. C 3 is single bonded to C H 3 on the upper left. C 1 is double bonded to C on the right. This C atom is single-bonded to O H on the upper right and C H 2 O H on the lower right.

A red curved arrow points from the N atom to the C 1 atom of the pentagonal ring. A second red curved arrow points from the double bond between C 1 and C on the right toward the central C atom of the aldose substrate. A third red-curved arrow points from the double bond between the central C atom and O toward the O atom. In the fourth step, activated glycoaldehyde is converted into another intermediate.

A reversible reaction arrow shows the entry of the H superscript plus ion as the reaction proceeds forward and the release of the H superscript plus as the reaction proceeds backward.

The structure of the intermediate is as follows: A 5-membered heterocyclic hexagonal ring is in a horizontal orientation with C 1 occupying the rightmost vertex. It consists of 1 N, 1 S, and 3 C atoms. N with a positive charge occupies the top right vertex. S occupies the bottom right vertex. A double bond is present between N and C 1, and C 2 and C 3. N is single bonded to R double dash on the upper right. C 2 is single bonded to O R on the lower left. C 3 is single bonded to C H 3 on the upper left. C 1 is single bonded to C, single bond, O, single bond, H on the right. This C atom is single-bonded to

C above and C H 2 O H below. The C atom above is further single bonded to O, single bond, H on the upper left, H above, and R on the upper right.

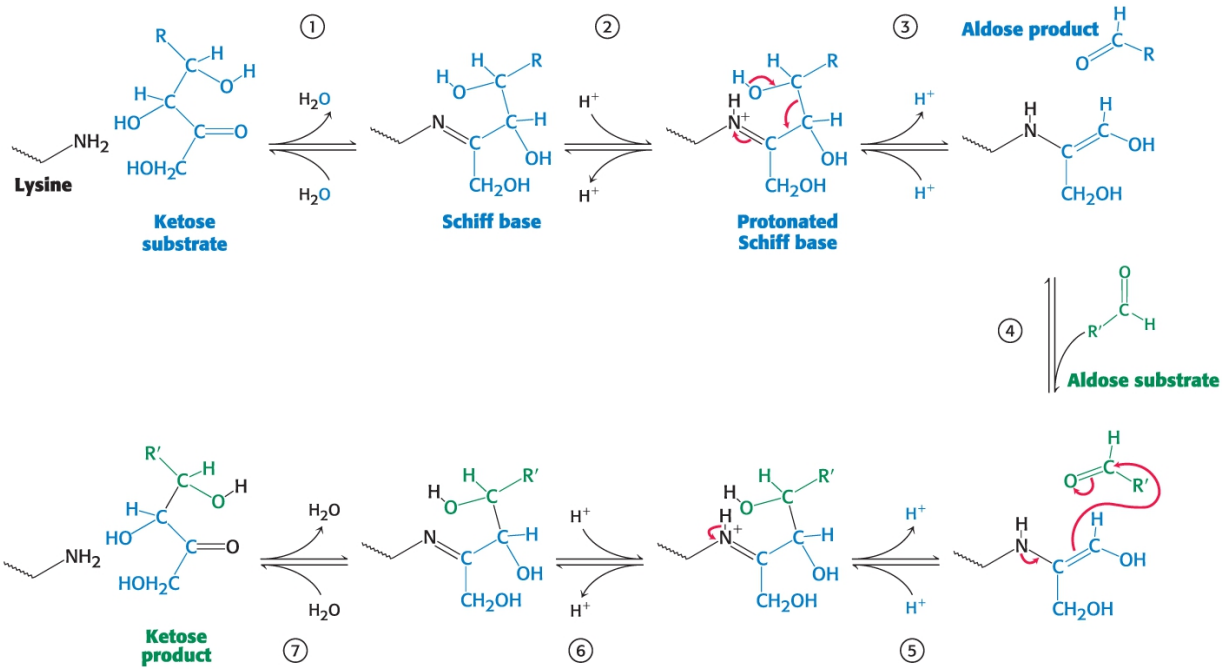
A red curved arrow points from the single bond between O and H on the right toward the single bond between the O and the C atom on the right. A second red curved arrow points from the single bond between the C atom on the right and C 1 toward the C 1 atom of the ring.

In the fifth step, the intermediate is converted into a ketose product. A reversible reaction arrow shows the entry of the H superscript plus ion as the reaction proceeds forward and the release of the H superscript plus as the reaction proceeds backward.

The structure of the ketose product is as follows: A central C atom is single-bonded to C on the upper left, C H 2 O H on the lower right, and double-bonded to O on the right. The C atom on the upper left is single bonded to O, single bond, H on the lower left, H on the upper left, and R dash on the upper right.

Return to FIGURE 20.23 The transketolase reaction takes place on thiamine pyrophosphate

Extended description for FIGURE 20.24 The transaldolase reaction involves a Schiff base intermediate



The conversion of ketose substrate into ketose product takes place in 7 steps.

In the first step, the ketose substrate and lysine side chain form a Schiff base.

The structure of the ketose substrate is as follows: A 3-carbon alkane chain is shown in a zigzag vertical orientation. From top to bottom, C 1 is single bonded to R on the upper left, H on the upper right, and O, single bond, H on the lower right. C 2 is single bonded to H on the left and O H on the lower right. C 3 is double bonded to O on the right and single bonded to C H 2 O H on the lower left.

The lysine side chain is depicted as a C atom single bonded to N H 2 on the upper right. It has a wiggly line on the upper left.

A reversible reaction arrow shows the release of H 2 O as the reaction proceeds forward and the entry of H 2 O as the reaction proceeds backward.

The structure of the Schiff base is as follows: The C 3 atom of the ketose substrate becomes double bonded to the N atom of the lysine side chain. The N atom loses 2 H and the C 3 loses the O atom.

A reversible reaction arrow shows the entry of H superscript plus ion as the reaction proceeds forward and the release of H superscript plus ion as the reaction proceeds backward.

In the second step, the Schiff base is converted into protonated Schiff base.

The structure of the protonated Schiff base is as follows: The N atom of the lysine side chain is single-bonded to H above and becomes positively charged. A curved arrow from the single bond between the O and H atoms points toward the single bond between the O atom and C 1. A second curved arrow points from the single bond between C 1 and C 2 toward the single bond between C 2 and C 3. A third curved arrow points from the double bond between C 3 and N with a positive charge toward the N atom.

A reversible reaction arrow shows the exit of the H superscript plus ion as the reaction proceeds forward and the entry of the H superscript plus ion as the reaction proceeds backward.

In the third step, the protonated Schiff base is converted into another compound and aldose product.

The structure of the compound is as follows: 1 N and 2 C alkane chains are depicted as a zigzag structure. N single-bonded to H occupies the first position. The remaining positions are occupied by C atoms. C 1 is single bonded to C H 2 O H below. A double bond is present between C 1 and C 2. C 2 is single bonded to H above and O H on the lower right. The N atom is single-bonded to C on the lower right. This C has a wiggly line on the upper left.

The structure of the aldose product is as follows: A central C atom is single bonded to H above, double bonded to O on the lower left, and single bonded to R on the lower right.

In the fourth reversible step, the aldose substrate enters.

The structure of the aldose substrate is as follows: A central C atom is double bonded to O above, single bonded to R dash on the lower left, and single bonded to H on the lower right.

The product side shows rearrangement between the compound formed in step 3 and the aldose substrate.

A curved arrow from the N atom of the substrate points toward its single bond with C 1. A second curved arrow points from the double bond between C 1 and C 2 toward the central C atom of the aldose substrate. A third curved arrow points from the double bond between the central C atom and O atom of the aldose substrate toward the O atom.

A reversible reaction arrow shows the entry of H superscript plus ion as the reaction proceeds forward and the exit of H superscript plus ion as the reaction proceeds backward.

In the fifth reversible step, the central C atom of the aldose substrate becomes single-bonded to C 2 of the compound formed in step 3. The central C atom is single bonded to O, single bond, H on the left, H above, and R dash on the upper right. The N atom of the lysine side chain becomes double bonded to C 1 and acquires a positive charge. A curved arrow from the single bond between N and H atoms points to the N atom.

A reversible reaction arrow shows the exit of the H superscript plus ion as the reaction proceeds forward and the entry of the H superscript plus ion as the reaction proceeds backward.

In the sixth step, an intermediate compound is formed.

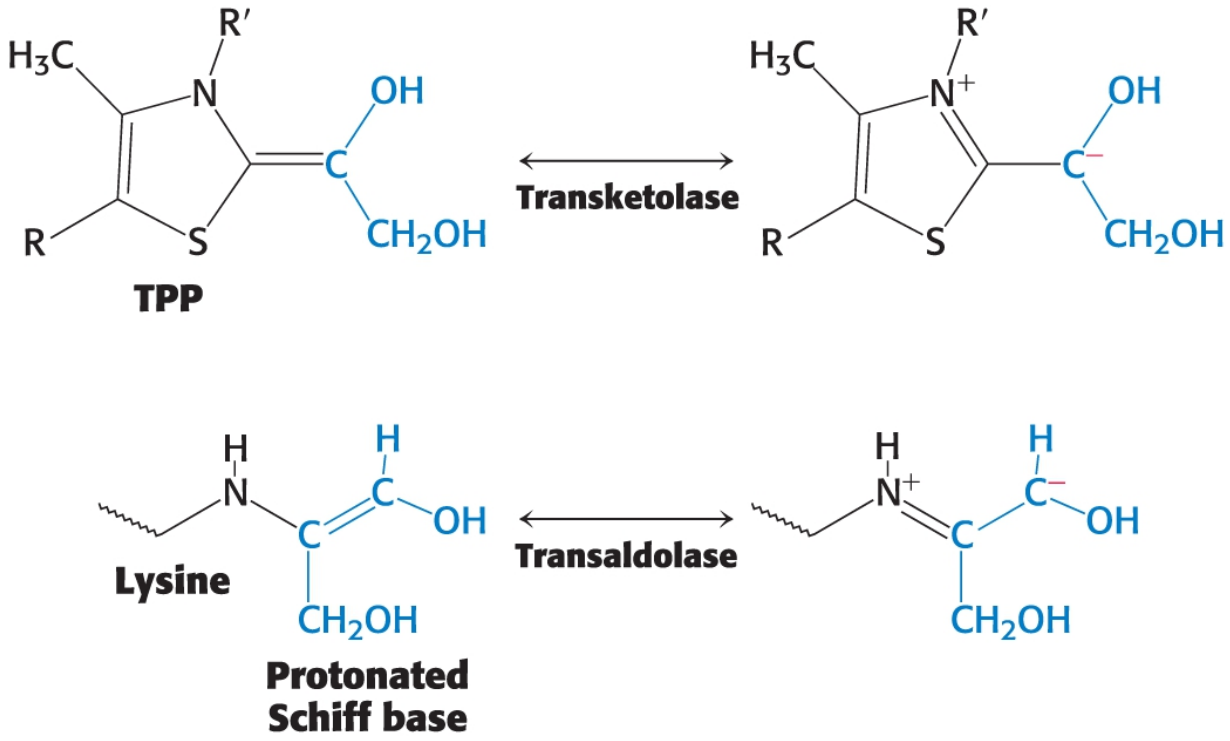
The structure of the intermediate compound is the same as the compound formed in step 5, except the N atom of the lysine side chain does not have a positive charge as the H atom is released. A reversible reaction arrow shows the entry of H 2 O as the reaction proceeds forward and the exit of H 2 O as the reaction proceeds backward.

In the seventh step, the ketose product is formed.

In the ketose product, the double bond between the N atom of the lysine side chain and C 1 is broken. The N atom binds to two H atoms to form N H 2 group. C 1 becomes double bonded to O and the remaining structure is the same as the product in step 6.

Return to FIGURE 20.24 The transaldolase reaction involves a Schiff base intermediate

Extended description for FIGURE 20.25 For transketolase and transaldolase, a carbanion intermediate is stabilized by resonance



The resonance structures of T P P bound to a compound are separated by a double-headed horizontal arrow labeled transketolase.

The left structure is as follows: A 5-membered heterocyclic hexagonal ring is in a horizontal orientation with C 1 occupying the rightmost vertex. It consists of 1 N, 1 S, and 3 C atoms. N occupies the top right vertex. S occupies the bottom right vertex. A double bond is present between C 2 and C 3. N is single-bonded to the R dash on the upper right. C 1 is double bonded to C on the right. This C is further single bonded to O H on the upper right and C H 2 O H

on the lower right. C 2 is single bonded to R on the lower left. C 3 is single bonded to C H 3 on the upper left.

The right structure is as follows: A 5-membered heterocyclic hexagonal ring is in a horizontal orientation with C 1 occupying the rightmost vertex. It consists of 1 N, 1 S, and 3 C atoms. N with a positive charge occupies the top right vertex. S occupies the bottom right vertex. A double bond is present between N and C 1, and C 2 and C 3. N is single-bonded to the R dash on the upper right. C 1 is single bonded to C superscript minus on the right. C superscript minus is further single bonded to O H on the upper right and C H 2 O H on the lower right. C 2 is single bonded to R on the lower left. C 3 is single bonded to C H 3 on the upper left.

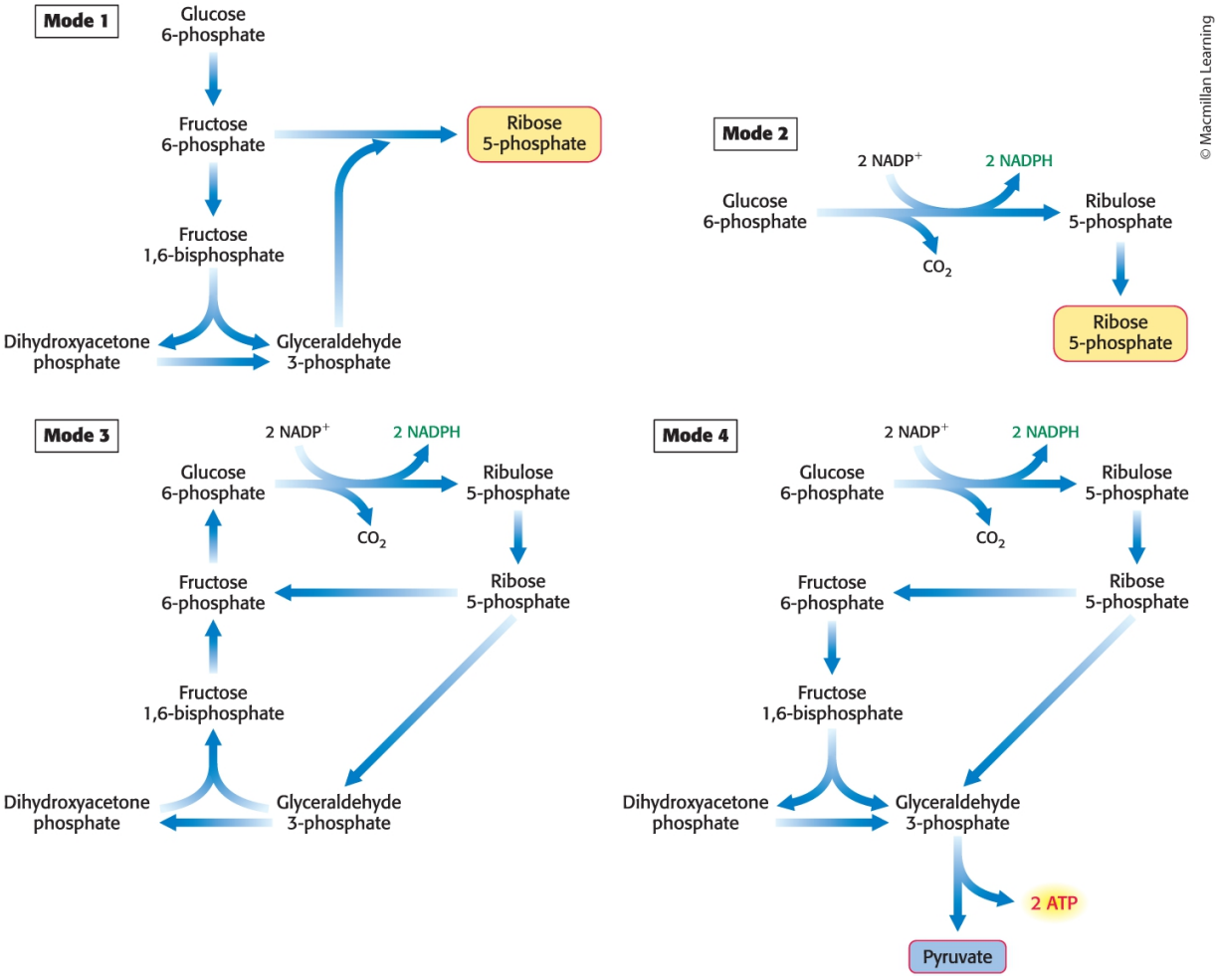
The resonance structures of protonated Schiff base bound to the lysine side chain are separated by a double-headed arrow labeled transaldolase.

The left structure is as follows: The lysine side chain consists of C single bonded to N, single bond, H on the upper right. The C atom has a wiggly line on the upper left. The N atom is single-bonded to C, double bond, C in a zigzag manner. C 1 is single bonded to C H 2 O H below. C 2 is single bonded to H above and O H on the lower right.

The right structure is as follows: The lysine side chain consists of C single bonded to N superscript plus, single bond, H on the upper right. The C atom has a wiggly line on the upper left. The N atom is single bonded to C, single bond, C superscript minus in a zigzag manner. C 1 is single bonded to C H 2 O H below. C 2 is single bonded to H above and O H on the lower right.

Return to FIGURE 20.25 For transketolase and transaldolase, a carbanion intermediate is stabilized by resonance

Extended description for FIGURE 20.26 The pentose phosphate pathway can operate in four modes



Mode 1 is depicted as follows: Glucose 6-phosphate is converted into fructose 6-phosphate. Fructose 6-phosphate is converted into fructose 1, 6-bisphosphate. Fructose 1, 6-bisphosphate is cleaved into dihydroxyacetone phosphate and glyceraldehyde 3-phosphate which are interconvertible. The glyceraldehyde 3-phosphate molecule and fructose 6-phosphate are converted into ribose 5-phosphate.

Mode 2 is depicted as follows: Glucose 6-phosphate is converted into ribulose 5-phosphate coupled with the release of C O 2 and the reduction of 2 N A D P superscript plus to 2 N A D P H. Ribulose 5-phosphate is converted into ribose 5-phosphate.

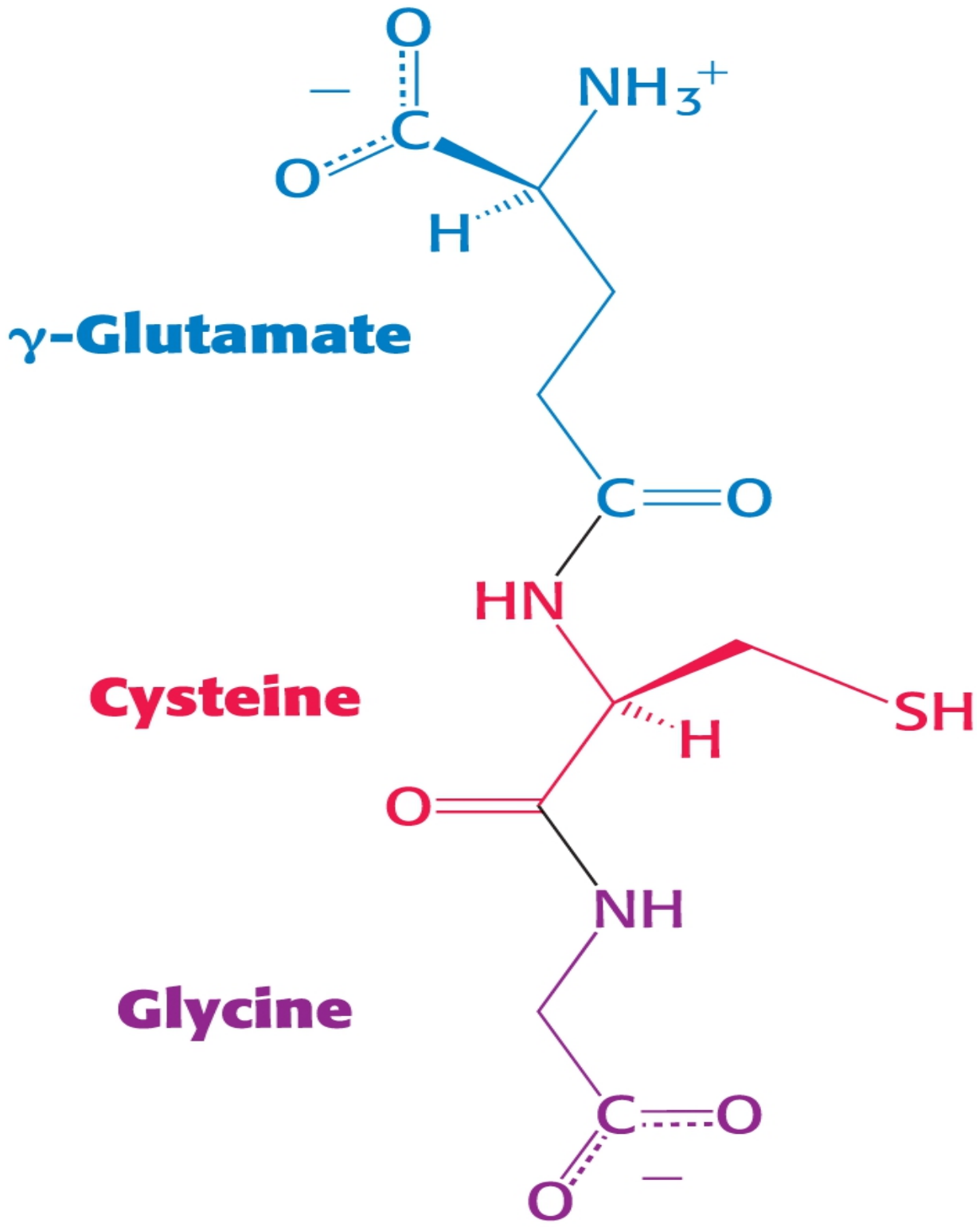
Mode 3 is depicted as follows: Glucose 6-phosphate is converted into ribulose 5-phosphate coupled with the release of C O 2 and the reduction of 2 N A D P superscript plus to 2 N A D P H. Ribulose 5-phosphate is converted into ribose 5-phosphate. Ribose 5-phosphate is further converted into fructose 6-phosphate or glyceraldehyde 3-phosphate. Glyceraldehyde 3-phosphate can be converted into dihydroxyacetone phosphate. The glyceraldehyde 3-phosphate and dihydroxyacetone phosphate molecules combine to form fructose 1, 6-bisphosphate. The fructose 1, 6-bisphosphate molecule is converted into fructose 6-phosphate which is further converted back to glucose 6-phosphate.

Mode 4 is depicted as follows: Glucose 6-phosphate is converted into ribulose 5-phosphate coupled with the release of C O 2 and the reduction of 2 N A D P superscript plus to 2 N A D P H. Ribulose 5-phosphate is converted into ribose 5-phosphate. Ribose 5-phosphate is further converted into fructose 6-phosphate or glyceraldehyde 3-phosphate. Glyceraldehyde 3-phosphate is converted into pyruvate coupled with the release of 2 A T P. The fructose 6-phosphate molecule is converted into fructose 1, 6-bisphosphate which is further broken down into dihydroxyacetone phosphate and glyceraldehyde 3-phosphate. The dihydroxyacetone phosphate molecule can be converted into glyceraldehyde 3-phosphate.

Return to FIGURE 20.26 The pentose phosphate pathway can operate in four modes

Extended description for Structure of reduced

glutathione

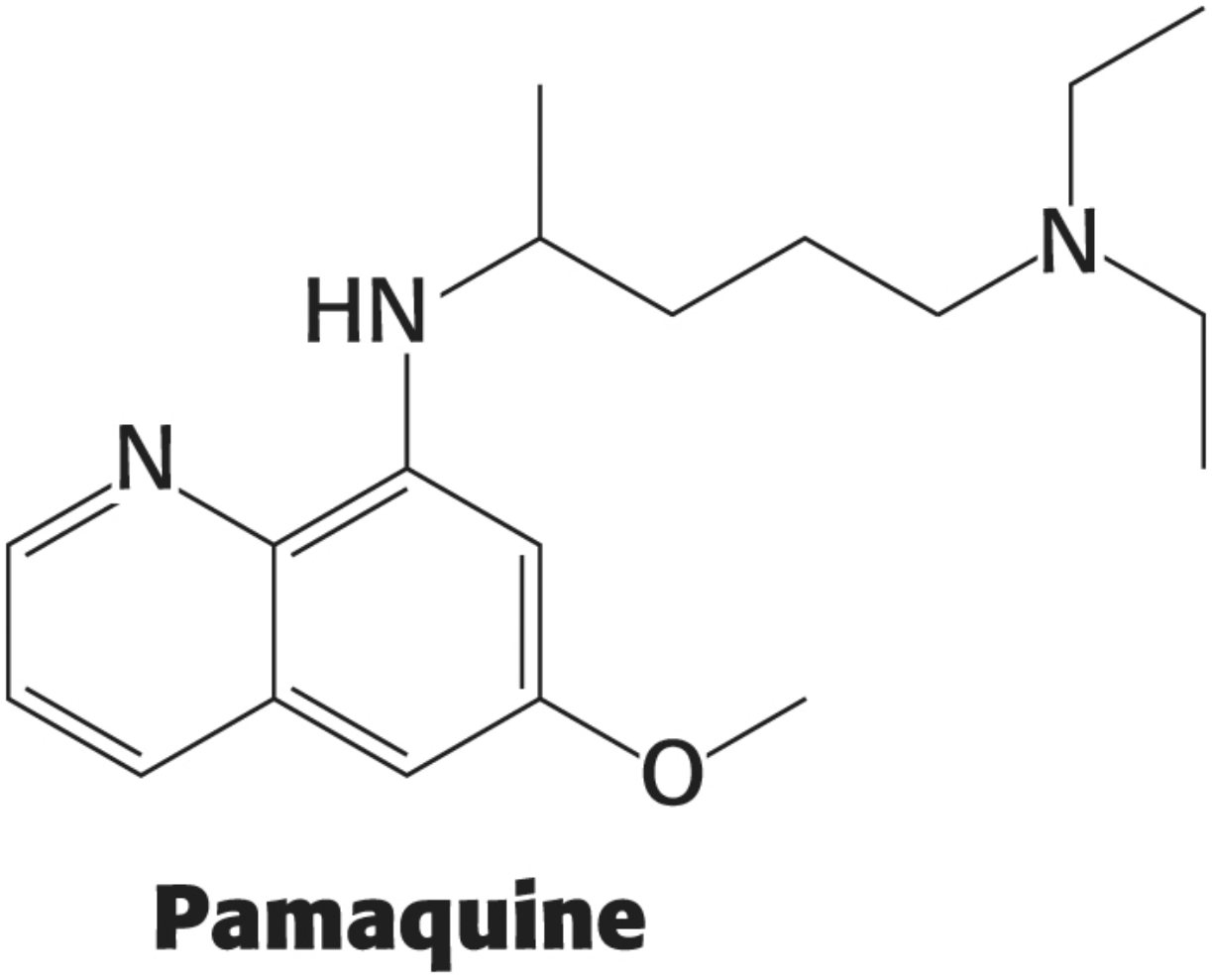


Glutathione (reduced)
(γ-Glutamylcysteinylglycine)

The structure of reduced glutathione is as follows: A 2 N and 7 C heteronuclear alkane chain is depicted as a vertical line structure using 8 zigzag lines. N atoms bound to H occupy the fifth and eighth positions. C 1 is wedge bonded to C on the upper left. This C is partially double bonded to O above and O on the lower left. This C O O group has an overall negative charge. C 1 is also single bonded to N H 3 superscript plus on the upper right and dash bonded to H on the lower left. C 4 is double bonded to O on the right. C 5 is wedge bonded to C H 2 on the upper right, which is further single bonded to S H on the lower right. C 5 is also dash bonded to H on the lower right. C 6 is double bonded to O on the left. C 7 is single bonded to C on the lower right, which is further partially double bonded to O on the right and O on the lower left. This C O O group has an overall negative charge. C 1 to C 4 and their substituents are labeled gamma-glutamate. N 1 to C 6 and their substituents are labeled cysteine. N 2 to C 7 and their substituents are labeled glycine.

Return to Structure of reduced glutathione

Extended description for Structure of pamaquine

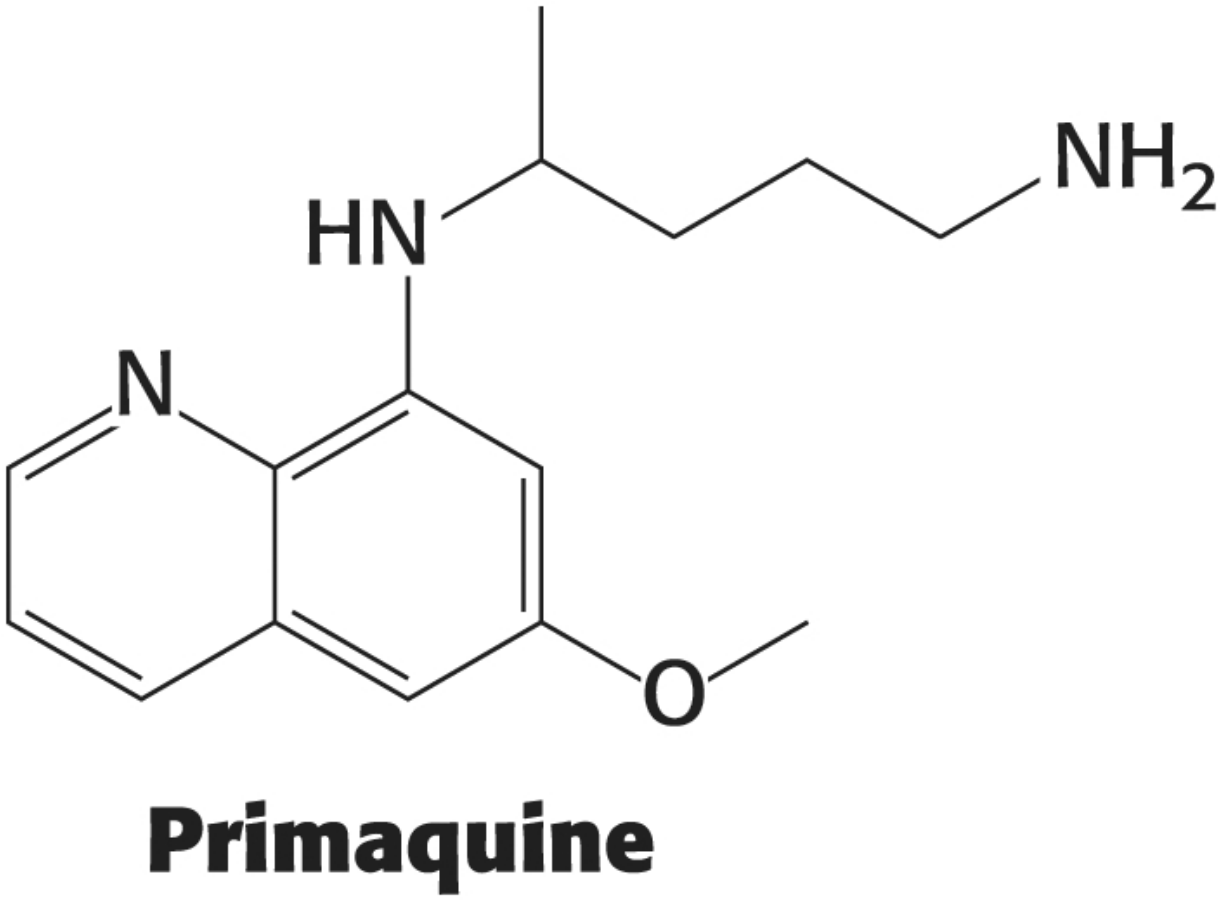


The structure of pamaquine is as follows: A 6-membered heterocyclic hexagonal ring is in a vertical orientation. It consists of 1 N and 5 C atoms. The N atom occupies the topmost vertex. C 1 occupies the top right vertex. Double bonds are present between C 3 and C 4 and C 5 and N. This ring is fused with a benzene ring in a vertical orientation such that C 1 and C 2 of the hexagonal ring are C 6 and C 5 of the benzene ring respectively. In the benzene ring, double bonds are present between C 2 and C 3, C 4 and C 5, and C 6 and C 1. C 1 is single bonded to N H on the top. N H is single bonded

to a 6-membered alkane chain depicted as a line structure using 5 zigzag lines. It consists of 1 N and 5 C atoms. N occupies the fifth position. C 1 is single bonded to C H 3 above in the form of a line. N is single bonded to C H 2 above in the form of a line. C H 2 is further single bonded to C H 3 on the upper right in the form of a line. C 5 is single bonded to C H 3 below in the form of a line. C 3 is single bonded to O on the lower right, which is further single-bonded to C H 3 on the upper right.

Return to Structure of pamaquine

Extended description for Structure of primaquine



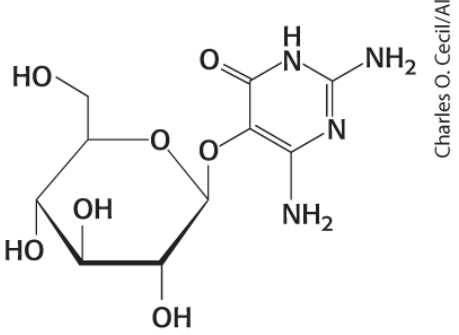
The structure of primaquine is as follows: A 6-membered heterocyclic hexagonal ring is in a vertical orientation. It consists of 1 N and 5 C atoms. The N atom occupies the topmost vertex. C 1 occupies the top right vertex. Double bonds are present between C 3 and C 4 and C 5 and N. This ring is fused with a benzene ring in a vertical orientation such that C 1 and C 2 of the hexagonal ring are C 6 and C 5 of the benzene ring respectively. In the benzene ring, double bonds are present between C 2 and C 3, C 4 and C 5, and C 6 and C 1. C 1 is single bonded to N H on the top. N H is single bonded to a 4-carbon alkane chain depicted as a line structure using 3 zigzag lines. C 4 is single bonded to N H 2 on the top right. C 1 is single

bonded to C H 3 above in the formation of a line. C 3 of the benzene ring is single bonded to O on the lower right. O is further single bonded to C H 3 on the upper right.

Return to Structure of primaquine

Extended description for FIGURE 20.27 Fava beans produce a pyrimidine glycoside





Vicine

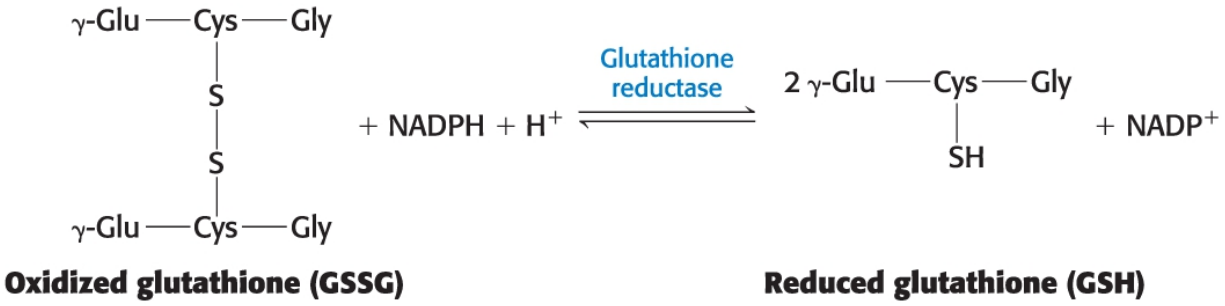
Charles O. Cecil/Alamy

The photograph shows a heap of fava beans in a marketplace.

The structure of the vicine is as follows: A 6-membered heterocyclic hexagonal ring is in a horizontal orientation with C 1 occupying the rightmost vertex. It consists of 1 O and 5 C atoms. The ring is in a plane perpendicular to the plane of the paper such that C 2 and C 3 are toward the observer and C 5 and O are away from the observer. C 2 and C 4 are each single bonded to O H below. C 3 is single bonded to O H above. C 5 is single bonded to C H 2 above in the form of a line. This C H 2 group is single-bonded to O H on the upper left. C 1 is single bonded to O above. This O atom is single-bonded to C 3 of a 6-membered heterocyclic hexagonal ring in a vertical orientation consisting of 2 N and 4 C atoms. N occupies the first and third positions. First N is bound to H. Double bonds are present between C 1 and N 2 and C 2 and C 3. C 1 is single bonded to N H 2 on the upper right. C 2 is single bonded to N H 2 below. C 4 is double bonded to O on the upper left.

Return to FIGURE 20.27 Fava beans produce a pyrimidine glycoside

Extended description for Conversion of oxidized glutathione to reduced glutathione catalyzed by glutathione reductase



The reaction consists of two reactants and two products.

The first reactant is oxidized glutathione (G S S G) whose structure is as follows: gamma glutamic acid, single bond, cysteine, single bond, glycine. Cysteine is single bonded to S, single bond, S below. The second S atom is single-bonded to cysteine below. This cysteine is further single-bonded to gamma glutamic acid on the left and glycine on the right.

The second reactant is N A D P H plus H superscript plus.

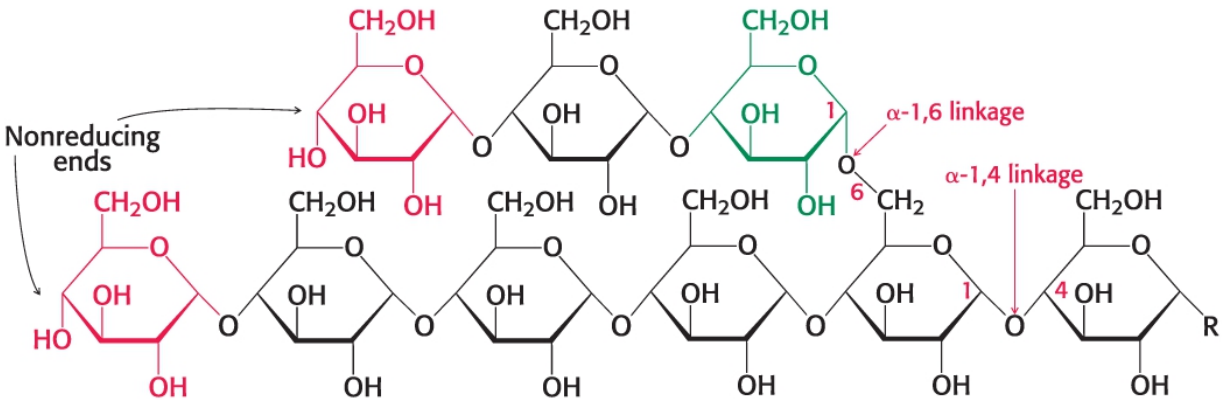
A reversible reaction arrow labeled glutathione reductase leads to the products.

The first product is reduced glutathione (G S H) whose structure is as follows: 2 gamma glutamic acid, single bond, cysteine, single bond, glycine. Cysteine is single bonded to S H below.

The second product is N A D P superscript plus.

Return to Conversion of oxidized glutathione to reduced glutathione catalyzed by glutathione reductase

Extended description for FIGURE 21.3 The fundamental structure of glycogen is a linear polymer with occasional branches



Glycogen consists of two linear chains of glucose molecules linked by alpha-1,4 linkage. The bottom chain contains 6 glucose molecules. The top chain contains 3 glucose molecules. The top chain is connected to the bottom chain through an alpha-1,6 linkage between the third and fifth glucose residues respectively.

The structure of a glucose residue is as follows: A 6-membered heterocyclic hexagonal ring is in a horizontal orientation with C 1 occupying the rightmost vertex. It consists of 1 O and 5 C atoms. O occupies the top right vertex. C 2 and C 4 are each single bonded to O H below. C 3 is single bonded to O H above. C 5 is single bonded to C H 2 O H above. The adjacent glucose residues are connected by a common O atom single bonded to C 1 and C 4 of the adjacent residues.

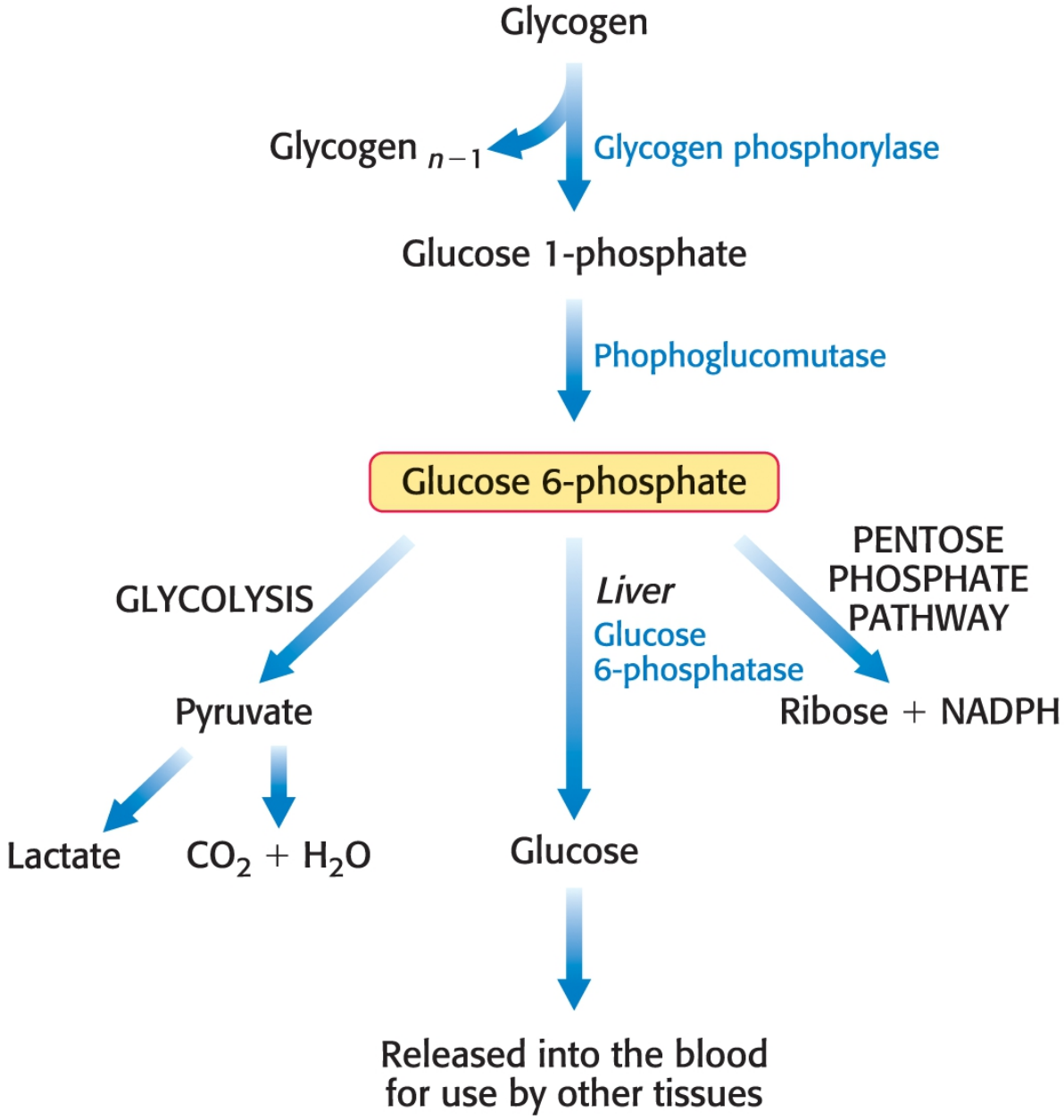
The free C 4 ends of the glucose residues of the top and bottom chains are labeled nonreducing ends. In the alpha-1,6 linkage, C 1 of the third glucose residue of the top chain is single-bonded to O

below. This O is further single-bonded to the C H 2 group bonded to the C 5 atom of the fifth glucose residue of the bottom chain.

The C 1 atom of the sixth glucose residue of the bottom chain is single-bonded to R on the lower right.

Return to FIGURE 21.3 The fundamental structure of glycogen is a linear polymer with occasional branches

Extended description for FIGURE 21.4 Glucose 6-phosphate can have many metabolic fates



© Macmillan Learning

The flowchart is described from top to bottom as follows:

Glycogen is broken down to release glucose 1-phosphate by the action of glycogen phosphorylase. This is accompanied by the release of glycogen n minus 1.

Glucose 1-phosphate is converted into glucose 6-phosphate by phosphoglucomutase.

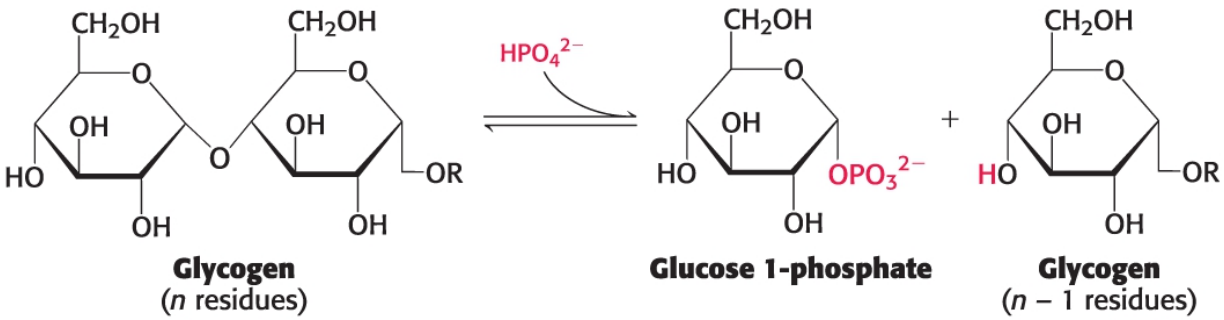
Glucose 6-phosphate has three fates: glycolysis, conversion to glucose in the liver, and pentose phosphate pathway.

In glycolysis, glucose 6-phosphate is converted to pyruvate, which is further broken down into lactate, and C O 2 plus H 2 O.

In the liver, the enzyme glucose 6-phosphatase converts glucose 6-phosphate into glucose. The glucose molecule is then released into the blood for use by other tissues. In the pentose phosphate pathway, glucose 6-phosphate is converted into ribose plus N A D P H.

Return to FIGURE 21.4 Glucose 6-phosphate can have many metabolic fates

Extended description for Cleavage of glucose 1-phosphate residue from glycogen with n residues



The reaction consists of one reactant and two products. The first reactant is glycogen with n residues.

The structure of glycogen is depicted as follows: A 6-membered heterocyclic hexagonal ring is in a horizontal orientation with C 1 occupying the rightmost vertex. It consists of 1 O and 5 C atoms. O occupies the top right vertex. C 1 is single bonded to O on the lower right. C 2 and C 4 are each single bonded to O H below. C 3 is single bonded to O H above. C 5 is single bonded to C H 2 O H above. The lower right O is single-bonded to C 4 of a second 6-membered heterocyclic hexagonal ring in a horizontal orientation. In this ring, O occupies the top right vertex. C 1 is single bonded to O R below. C 2 is single bonded to O H below. C 3 is single bonded to O H above and C 5 is single bonded to C H 2 O H above. A reversible reaction arrow shows the entry of H P O 4 superscript 2 minus.

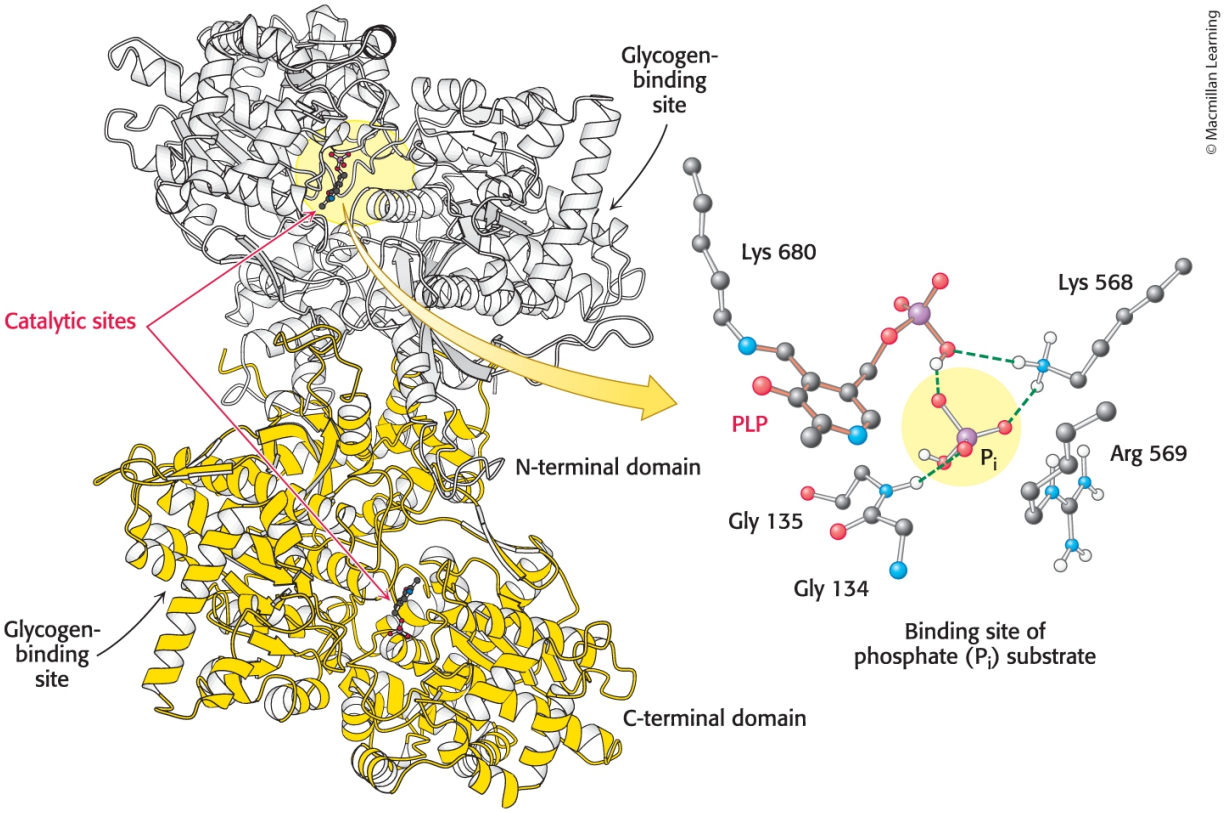
The first product is glucose 1-phosphate whose structure is as follows: A 6-membered heterocyclic hexagonal ring is in a horizontal orientation with C 1 occupying the rightmost vertex. It consists of 1 O and 5 C atoms. O occupies the top right vertex. C 1 is single bonded to O P O 3 superscript 2 minus below. C 2 and C 4 are

each single bonded to O H below. C 3 is single bonded to O H above. C 5 is single bonded to C H 2 O H above.

The second product is glycogen with n minus 1 residues whose structure is as follows: A 6-membered heterocyclic hexagonal ring is in a horizontal orientation with C 1 occupying the rightmost vertex. It consists of 1 O and 5 C atoms. O occupies the top right vertex. C 1 is single bonded to O R below. C 2 and C 4 are each single bonded to O H below. C 3 is single bonded to O H above. C 5 is single bonded to C H 2 O H above.

Return to Cleavage of glucose 1-phosphate residue from glycogen with n residues

Extended description for FIGURE 21.5 Glycogen phosphorylase forms a homodimer with a pyridoxal phosphate (P L P) group in each active site



Glycogen phosphorylase is a homodimer consisting of top and bottom subunits shown in white and yellow color respectively. The individual subunits contain several alpha-helices and some beta-strands interconnected by thread-like loops. A catalytic site is located in the center of each subunit. A glycogen binding site is shown at the top right and bottom left ends of the top and bottom subunits respectively. Each catalytic site is bound to pyridoxal phosphate. An arrow from the catalytic site of the top subunit points toward a ball-and-stick model depicted as follows:

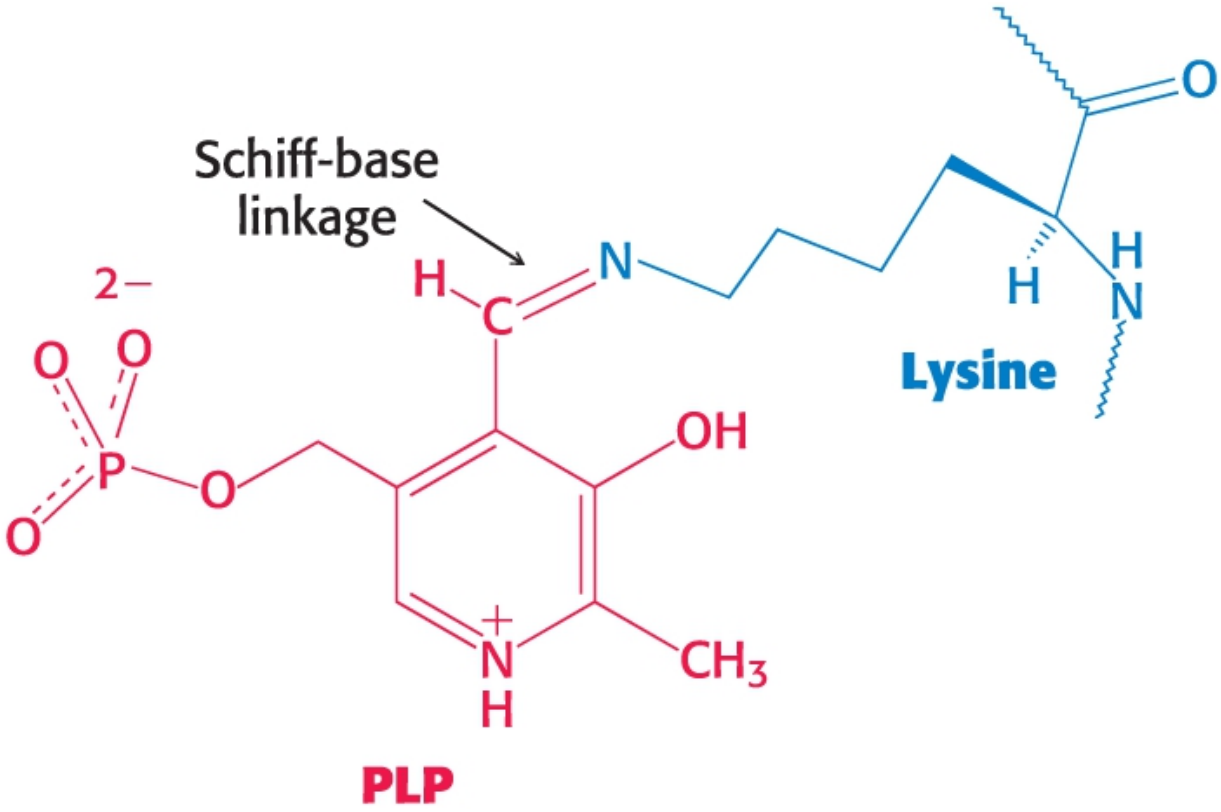
A central yellow circle depicting the catalytic site contains P subscript i or phosphate substrate. It is labeled the "Binding site of phosphate (P subscript i) substrate." It consists of a central purple sphere connected to a red sphere on the upper left, right, lower left, and front. The lower left red sphere is further connected to a white sphere.

Pyridoxal phosphate or P L P is bound to the side chain of lysine 680. P L P contains a hexagonal ring composed of 1 blue and 5 black spheres. One of the black spheres of the ring is connected to a red sphere which is further connected to a central purple sphere. The purple sphere is connected to 3 red spheres. One of the red spheres is connected to a white sphere.

The red spheres of the phosphate are connected to a white sphere of P L P, a white sphere of lysine 568, and a white sphere of glycine 135 through a dashed line. A ball and stick model of arginine 569 is shown on the bottom left of the catalytic site. A glycine 134 residue bonded to glycine 135 is also shown. A dashed line connects one white sphere of lysine 568 with the red sphere of P L P, which is connected to a white sphere.

Return to FIGURE 21.5 Glycogen phosphorylase forms a homodimer with a pyridoxal phosphate (P L P) group in each active site

Extended description for FIGURE 21.6 P L P forms a Schiff-base linkage with lysine



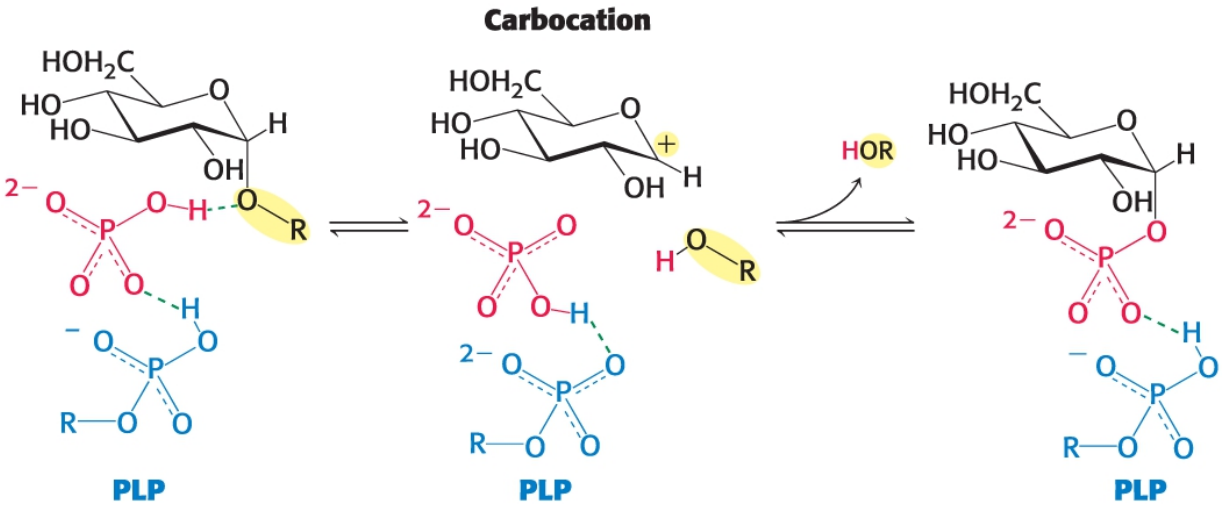
The structure of P L P is as follows: A 6-membered heterocyclic hexagonal ring is in a vertical orientation with C 1 occupying the bottom left vertex. It consists of 1 N and 5 C atoms. N with a positive charge bound to H occupies the bottom-most vertex. A double bond is present between N and C 1, C 2 and C 3, and C 4 and C 5. C 4 is single bonded to O H. C 5 is single bonded to C H 3. C 2 is single bonded to C H 2 on the upper left in the form of a line. This C H 2 is further single-bonded to O on the lower left. This O is single-bonded to a central P atom, which is further partially double-bonded to three O atoms. The O atoms have an overall negative charge of 2 minus. C 3 is single bonded to C above, which is further single bonded to H on the upper left and double bonded to N on the upper

right. The double bond between C and N is labeled "Schiff-base linkage." This N is part of the lysine residue.

The structure of lysine residue is depicted as follows: N atom of the Schiff-base linkage is single bonded to a 4-carbon alkane chain depicted as a line structure using 3 zigzag lines. C 4 is wedge bonded to C on the lower right. This C is single-bonded to another C atom on the upper right. The upper right C is double bonded to O on the right and has a wiggly line on the upper left. The lower right C is dash bonded to H on the lower left and single bonded to N H on the lower right. N has a wiggly line below.

Return to FIGURE 21.6 P L P forms a Schiff-base linkage with lysine

Extended description for FIGURE 21.7 The mechanism of phosphorylase involves P L P and the formation of a carbocation



The mechanism involves the formation of a carbocation intermediate.

The first structure shows a central phosphate molecule connected to a glycosidic bond above and P L P below. The structure of phosphate molecule is depicted as follows: A central P atom is partially double-bonded to O on the upper left, lower left, and lower right. These O atoms have an overall negative charge of 2 minus. The P atom is single bonded to O, single bond, H on the upper right.

The structure of P L P is depicted as follows: A central P atom is partially double bonded to O on the upper left, partially double bonded O on the lower right, single bonded to O, single bond, R on the lower left, and single bonded to O, single bond, H on the upper right. A dashed line connects the lower right O atom of the central

phosphate molecule with the upper right H atom of the P L P molecule.

The structure of the sugar molecule with the glycosidic bond is depicted as follows: A 6-membered heterocyclic hexagonal ring is in a chair conformation. It consists of 1 O and 5 C atoms. C 2 and C 5 are located close to each other. C 1 is single bonded to H on the upper right and single bonded to O, single bond, R on the lower right. C 2 is single bonded to O H below. C 3 is single bonded to O H on the upper left. C 4 is single bonded to O H on the lower left. C 5 is single bonded to C H 2 O H above.

A dashed line connects the O atom of the O R group to the upper right H atom of the central phosphate molecule.

A reversible reaction arrow leads to the carbocation intermediate.

The cleaved glycosidic bond produces three products as follows: The first molecule is a 6-membered heterocyclic hexagonal ring in a chair conformation. It consists of 1 O and 5 C atoms. C 2 and C 5 are located close to each other. C 1 is single bonded to H on the lower right and it has a positive charge. C 2 is single bonded to O H on the lower right. C 3 is single bonded to H on the upper left. C 4 is single bonded to O H on the lower left. C 5 is single bonded to C H 2 O H above. The second molecule consists of a central O atom single bonded to H on the lower left and R on the lower right.

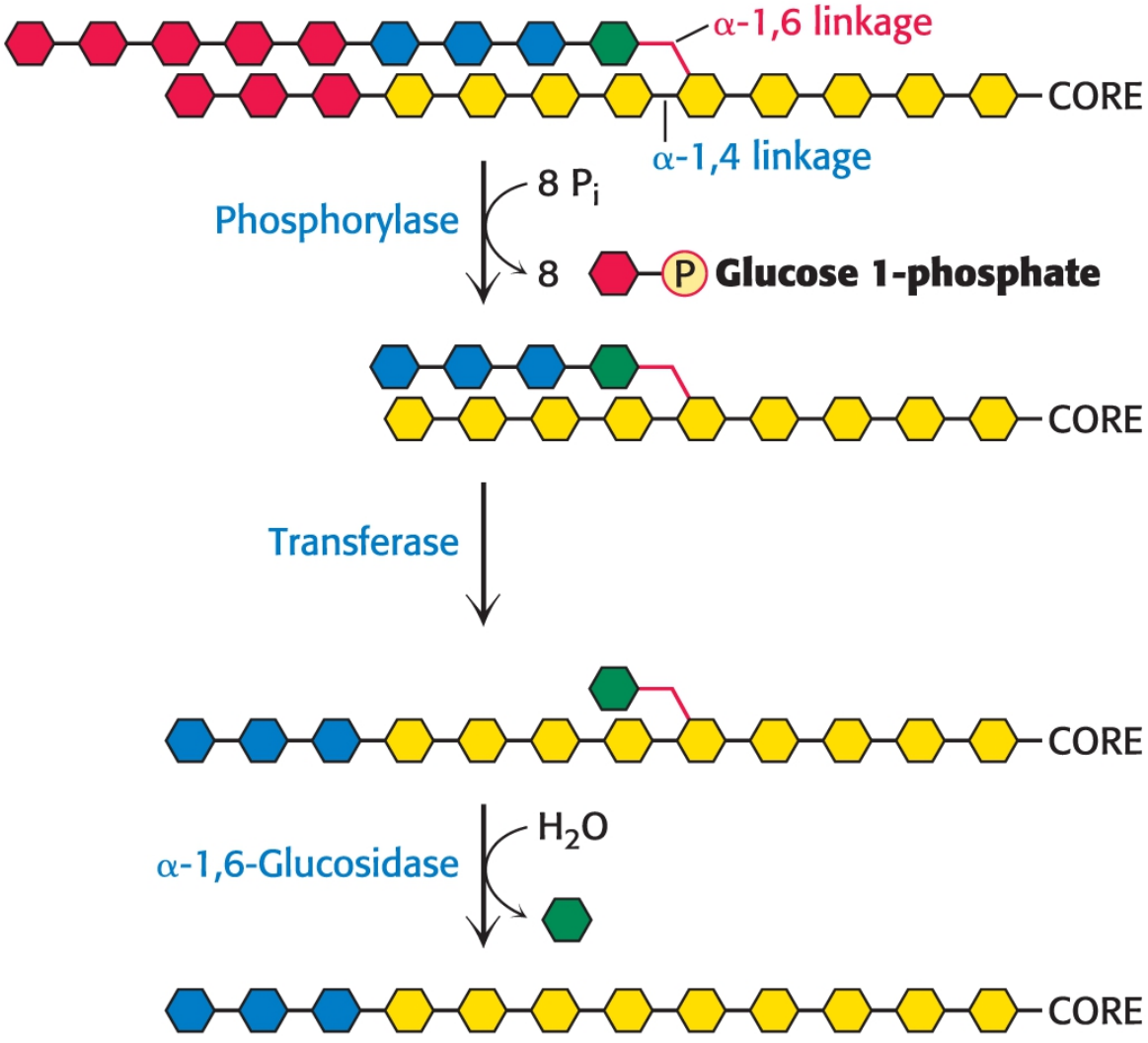
The third product consists of the central phosphate molecule single-bonded to the P L P molecule below. The central phosphate molecule has lost the upper right H atom. The lower right H atom of the central phosphate molecule is single-bonded to the upper right H atom of P L P. The H atom is further connected to the upper right O atom of P L P through a dashed line.

A reversible reaction arrow shows the release of H O R.

In the final product, the C 1 atom of the heterocyclic ring becomes single-bonded to the upper right O atom of the central phosphate. This O atom becomes single bonded to the central P atom. The lower right O atom of the phosphate molecule is connected to the upper right H atom of the P L P molecule through a dashed line. This H atom becomes single-bonded to the upper right O atom of the P L P molecule.

Return to FIGURE 21.7 The mechanism of phosphorylase involves P L P and the formation of a carbocation

Extended description for FIGURE 21.8 Glycogen remodeling requires three distinct catalytic activities



© Macmillan Learning

A linear chain is composed of three red hexagons and nine yellow hexagons connected to the core. The red hexagons are located at the left end. The fifth yellow hexagon from the left is connected to the left green hexagon of the top linear chain through an alpha-1,6 linkage. The top linear chain is composed of five red hexagons on the left, three blue hexagons in the middle, and one green hexagon on the right.

A downward arrow labeled phosphorylase is shown. A curved arrow alongside it shows the entry of 8 P subscript i and the release of 8 glucose 1-phosphate molecules. The glucose 1-phosphate molecule is depicted as a red hexagon single bonded to P on the right.

The product consists of a bottom linear chain of 9 yellow hexagons connected to the core. The fifth yellow hexagon is connected to the green hexagon of the top linear chain composed of three blue hexagons on the left and a green hexagon on the right.

A downward arrow labeled transferase leads the second product.

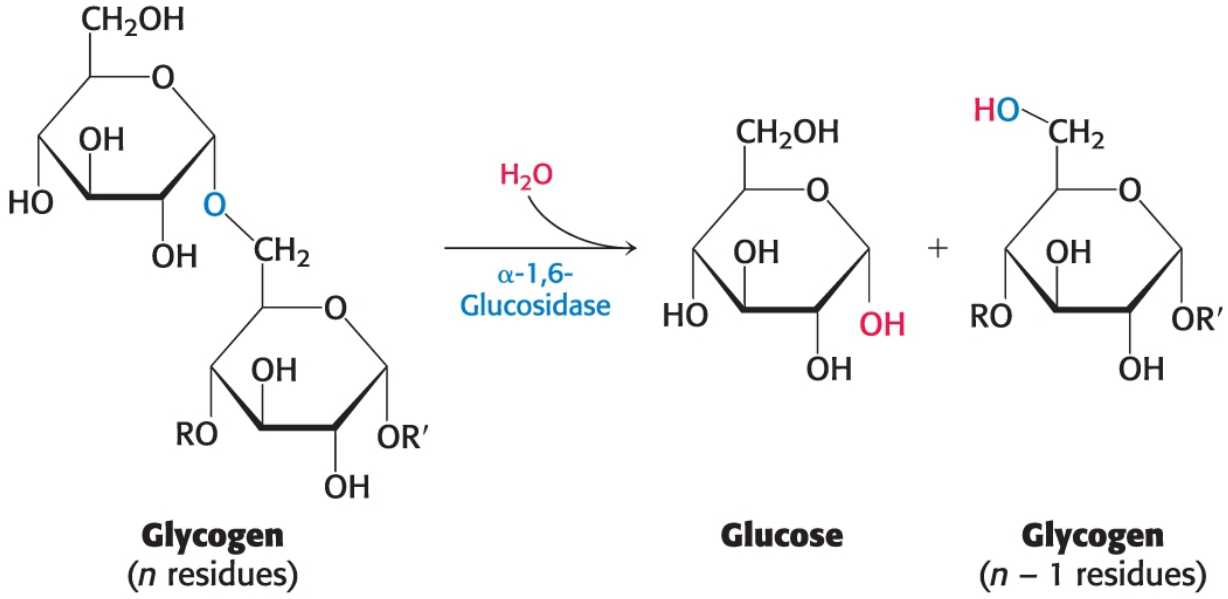
The second product consists of a linear chain composed of three blue hexagons on the left and nine yellow hexagons on the right. The rightmost yellow hexagon is connected to the core. The fifth yellow hexagon from the left is connected to a green hexagon above.

A downward arrow labeled alpha-1, 6-glucosidase leads to the product. A curved arrow alongside it shows the entry of H 2 O and the release of a green hexagon.

The third product consists of a linear chain composed of three blue hexagons on the left and nine yellow hexagons on the right. The rightmost yellow hexagon is connected to the core.

Return to FIGURE 21.8 Glycogen remodeling requires three distinct catalytic activities

Extended description for Action of alpha-1, 6-glucosidase



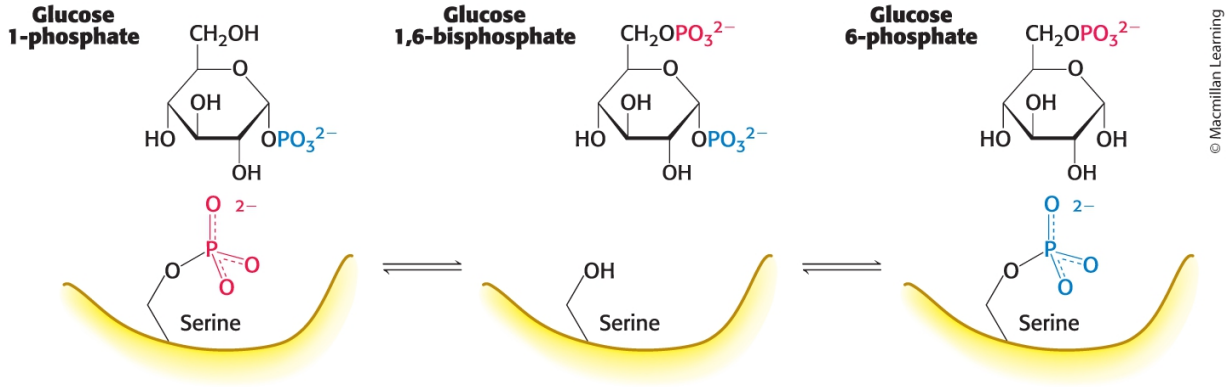
The reaction consists of one reactant and two products. The reactant is glycogen with n residues whose structure is as follows: A 6-membered heterocyclic hexagonal ring is in a horizontal orientation with C 1 occupying the rightmost vertex. It consists of 1 O and 5 C atoms. O occupies the top right vertex. C 2 and C 4 are single bonded to O H below. C 3 is single bonded to O H above. C 5 is single bonded to C H 2 O H above. C 1 is single bonded to O below, which is further single bonded to C H 2 below. This C H 2 group is single-bonded to the C 5 atom of a second 6-membered heterocyclic hexagonal ring in a horizontal orientation. It consists of 1 O and 5 C atoms. C 1 is single bonded to O R dash below. C 2 is single bonded to O H below. C 3 is single bonded to O H above. C 4 is single bonded to O R below. A forward arrow labeled alpha-1, 6-glucosidase depicts the entry of H 2 O and leads to the products.

The first product is glucose whose structure is as follows: A 6-membered heterocyclic hexagonal ring is in a horizontal orientation with C 1 occupying the rightmost vertex. It consists of 1 O and 5 C atoms. O occupies the top right vertex. C 1, C 2, and C 4 are single bonded to O H below. C 3 is single bonded to O H above. C 5 is single bonded to C H 2 O H above.

The second product is glycogen with n minus 1 residues whose structure is as follows: A 6-membered heterocyclic hexagonal ring is in a horizontal orientation with C 1 occupying the rightmost vertex. It consists of 1 O and 5 C atoms. O occupies the top right vertex. C 1 is single bonded to O R dash below. C 2 is single bonded to O H below. C 3 is single bonded to O H above. C 4 is single bonded to O R below. C 5 is single bonded to C H 2, single bond, O H below.

Return to Action of alpha-1, 6-glucosidase

Extended description for FIGURE 21.9 Phosphoglucomutase transfers a phosphoryl group to the substrate



The active site of the enzyme is depicted as a U-shaped depression with an orange outline. The side chain of the serine residue consists of C H 2 depicted as a line. This C H 2 group is single-bonded to O on the upper right. This O atom is single-bonded to a central P atom. This P atom is partially double-bonded to O above, O below, and O on the lower right. The partially double-bonded O atoms have an overall charge of 2 minus.

The glucose 1-phosphate molecule is shown above the phosphate group, outside the active site. The structure of glucose 1-phosphate is as follows: A 6-membered heterocyclic hexagonal ring is in a horizontal orientation with C 1 occupying the rightmost vertex. It consists of 1 O and 5 C atoms. O occupies the top right vertex. C 1 is single bonded to O P O 3 superscript 2 minus below. C 2 is single bonded to O H below. C 3 is single bonded to O H above. C 4 is single bonded to O H below. C 5 is single bonded to C H 2 O H above.

A reversible reaction arrow shows the side chain of the active site serine residue. It consists of C H 2 depicted as a line single bonded

to O H on the upper right.

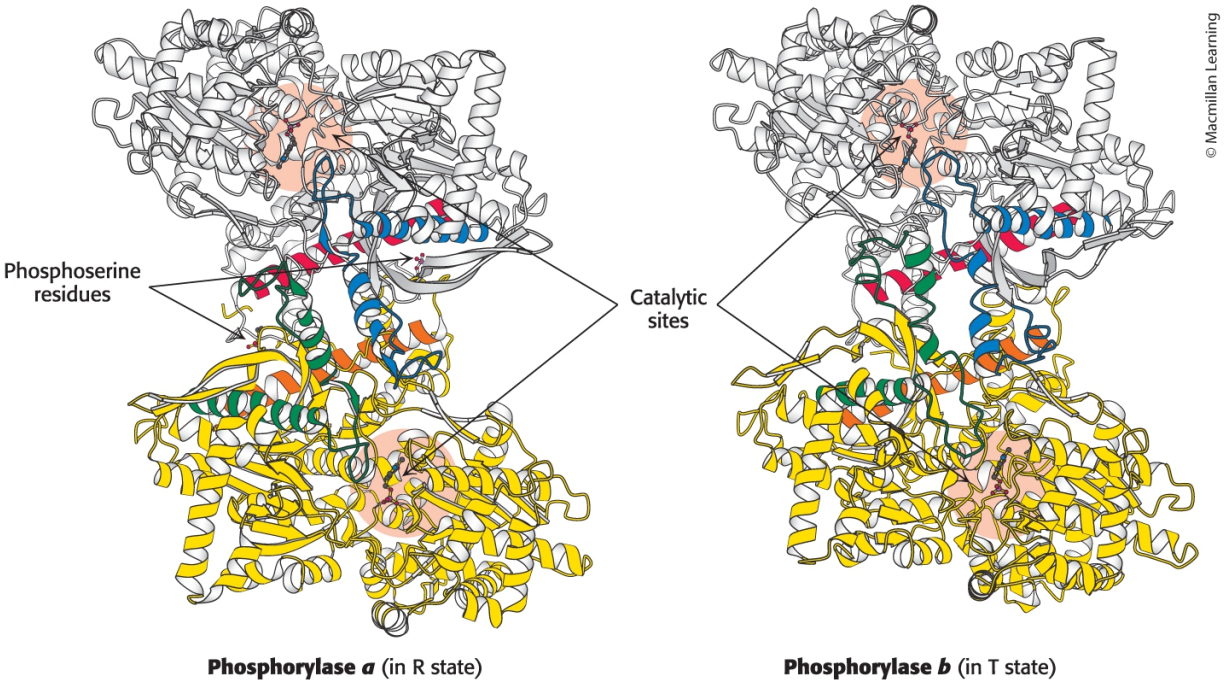
A glucose 1, 6-bisphosphate molecule is shown above the active site. Its structure is depicted as follows: A 6-membered heterocyclic hexagonal ring is in a horizontal orientation with C 1 occupying the rightmost vertex. It consists of 1 O and 5 C atoms. O occupies the top right vertex. C 1 is single bonded to O P O 3 superscript 2 minus below. C 2 is single bonded to O H below. C 3 is single bonded to O H above. C 4 is single bonded to O H below. C 5 is single bonded to C H 2 O P O 3 superscript 2 minus above.

A reversible reaction leads to the next structure. It shows the O atom of the O H group of active site serine side chain single-bonded to a central P atom. This P atom is partially double bonded to O above, O on the lower right, and O below. The O atoms have an overall negative charge of 2 minus.

A glucose 6-phosphate molecule is shown above the active site. Its structure is as follows: A 6-membered heterocyclic hexagonal ring is in a horizontal orientation with C 1 occupying the rightmost vertex. It consists of 1 O and 5 C atoms. O occupies the top right vertex. C 1 is single bonded to O H below. C 2 is single bonded to O H below. C 3 is single bonded to O H above. C 4 is single bonded to O H below. C 5 is single bonded to C H 2 O P O 3 superscript 2 minus above.

Return to FIGURE 21.9 Phosphoglucomutase transfers a phosphoryl group to the substrate

Extended description for FIGURE 21.10 Phosphorylase exists in two distinct quaternary states

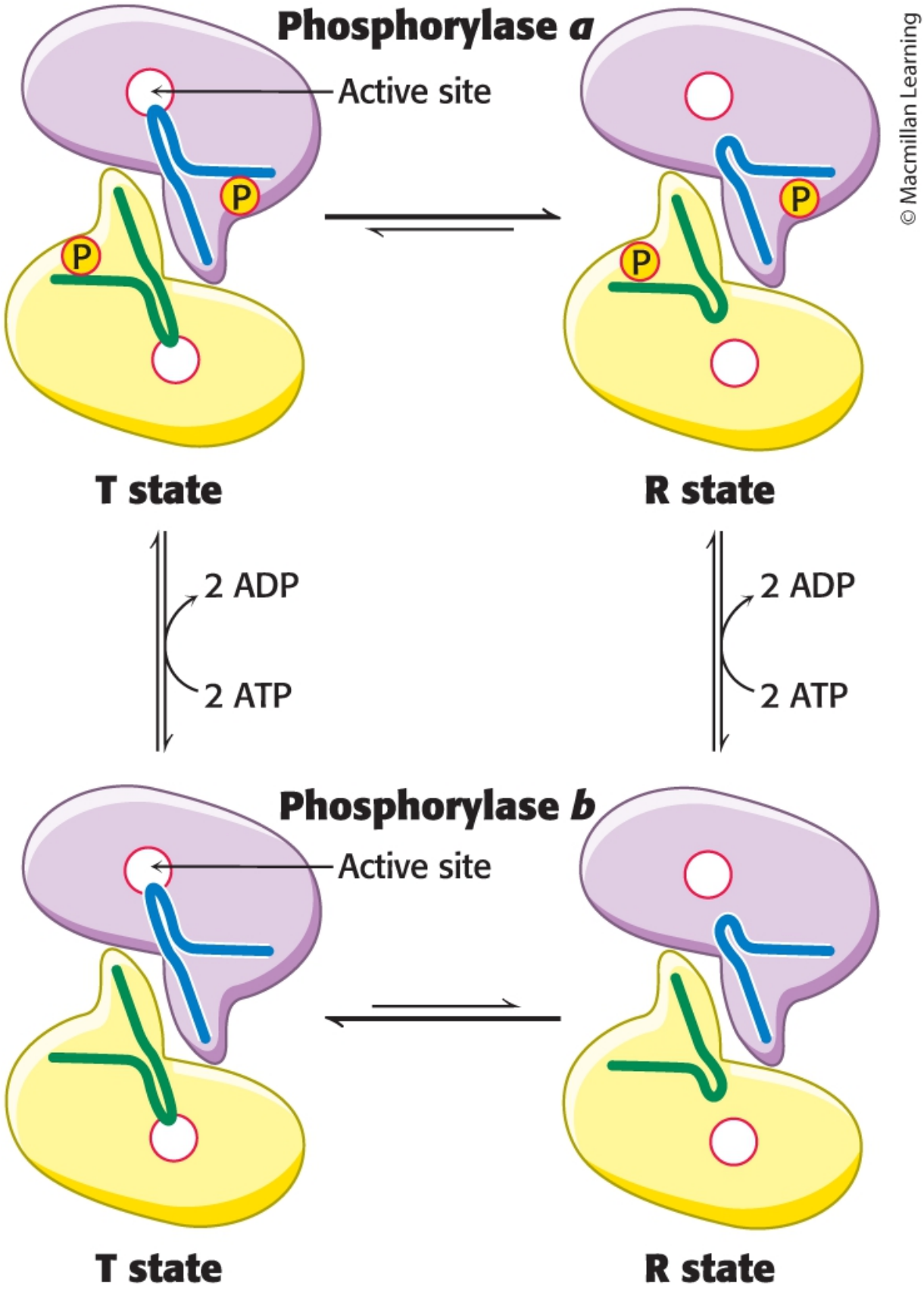


Phosphorylase a exists in the R state and phosphorylase b exists in the T state. They consist of two subunits, one at the top and the other at the bottom. The top subunit is shown in white and the bottom subunit is shown in yellow. Each subunit has a central catalytic site and is composed of several alpha-helices and beta-strands interconnected by thread-like loops. The bottom side of the top subunit contains two blue alpha-helices, one red horizontal alpha-helix, one blue beta-strand, and two blue thread-like loops. The top side of the bottom subunit contains one orange alpha-helix, two green alpha-helices, a green beta-strand, and two green thread-like loops. In phosphorylase a, a phosphoserine residue is located on the bottom right and top left sides of the top and bottom subunits respectively. The phosphorylase b lacks any phosphoserine residue.

Return to FIGURE 21.10 Phosphorylase exists in two distinct quaternary states

Extended description for FIGURE 21.11 Phosphorylase

is regulated by phosphorylation



© Macmillan Learning

The phosphorylase consists of a top purple subunit and a bottom yellow subunit. A pointed protrusion from the bottom right end of the top subunit extends toward the bottom subunit. A pointed protrusion from the top left end of the bottom subunit extends toward the top subunit. Each subunit contains an active site depicted as a small circle with a red outline.

The phosphorylase a can be reversibly converted from the T to the R state. The R state is preferred. In both states, each subunit contains a phosphate molecule depicted as a tiny circle labeled P. In the T state, a thick blue loop extends into the active site of the top subunit and a thick green loop extends into the active site of the bottom subunit. In the R state, the loops are located away from the active site.

The T state of phosphorylase a can be reversibly converted into the T state of phosphorylase b with the simultaneous hydrolysis of 2 A T P to 2 A D P.

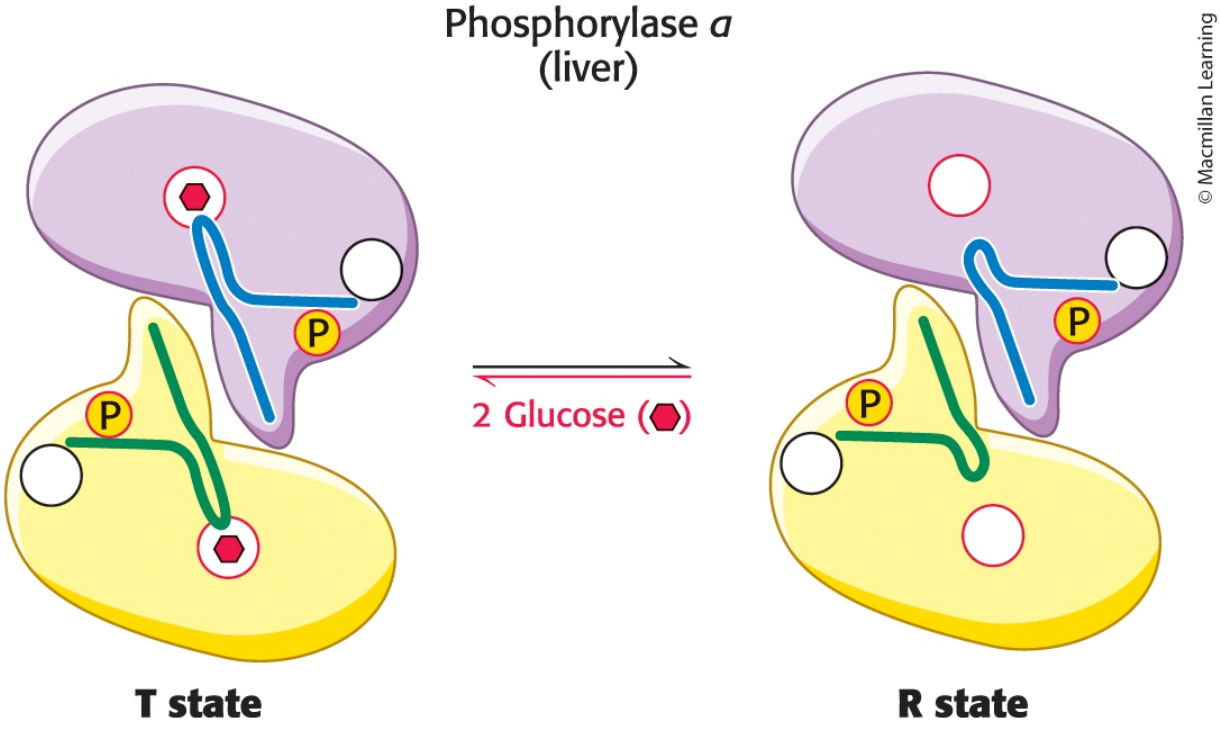
In the T state of phosphorylase b, phosphate is absent in both subunits. The respective loops, however, extend into the active site of each subunit.

The T state of phosphorylase b is preferred. It can be reversibly converted into the R state. In the R state, the loops are located away from the active site.

The R state of phosphorylase b can be reversibly converted into the R state of phosphorylase a with the simultaneous hydrolysis of 2 A T P to 2 A D P.

Return to FIGURE 21.11 Phosphorylase is regulated by phosphorylation

Extended description for FIGURE 21.12 Liver phosphorylase is allosterically inhibited by glucose



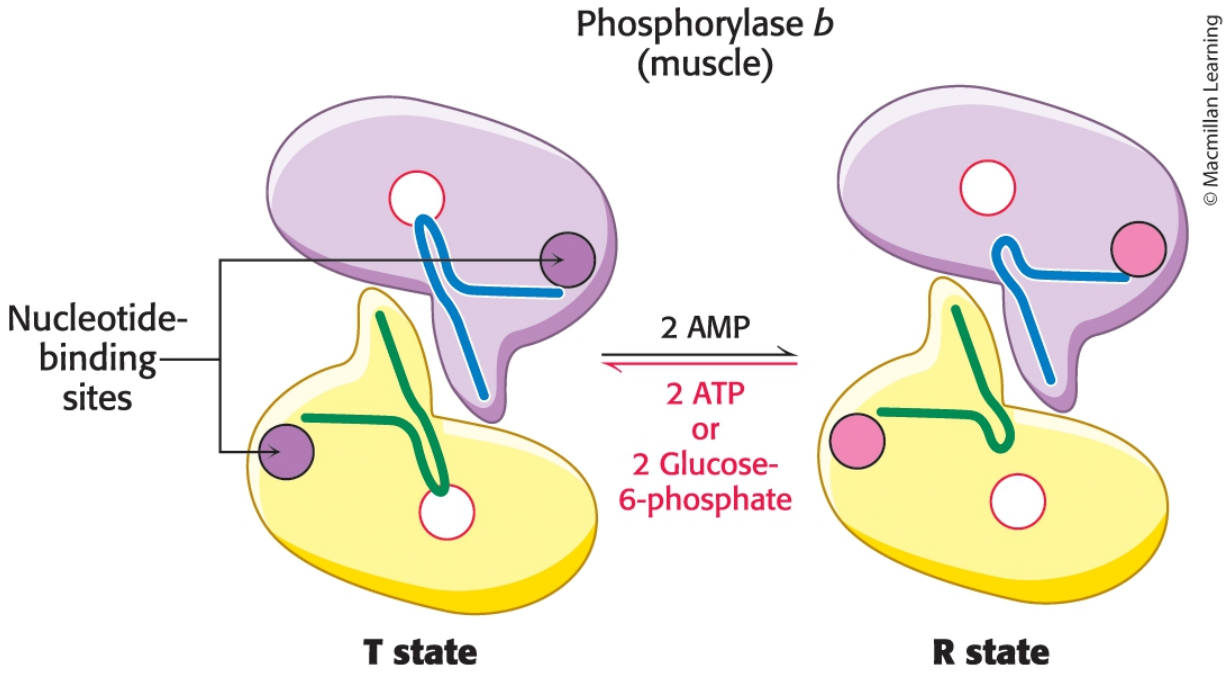
© Macmillan Learning

The T and R states of liver phosphorylase a are separated by a reversible reaction arrow. The T state is shown on the left and the R state is shown on the right. The top forward arrow is shown in black and the bottom backward arrow is shown in red and labeled 2 glucose. The glucose molecule is depicted as a red hexagon. The active site in each subunit of the phosphorylase is depicted as a central tiny circle with a red outline. A tiny circle with a black outline is also shown in each subunit. It is located away from the active site. In the T state, both active sites contain a glucose molecule. A thick blue loop extends into the active site of the top subunit. A thick green loop extends into the active site of the bottom subunit. Each subunit also contains a phosphate group. One end of each loop is attached to the empty tiny circle with a blue outline. In

the R state, the active sites are empty. The loops are also located away from the active site.

Return to FIGURE 21.12 Liver phosphorylase is allosterically inhibited by glucose

Extended description for FIGURE 21.13 Muscle phosphorylase is allosterically regulated by A T P, A M P, and glucose 6-phosphate

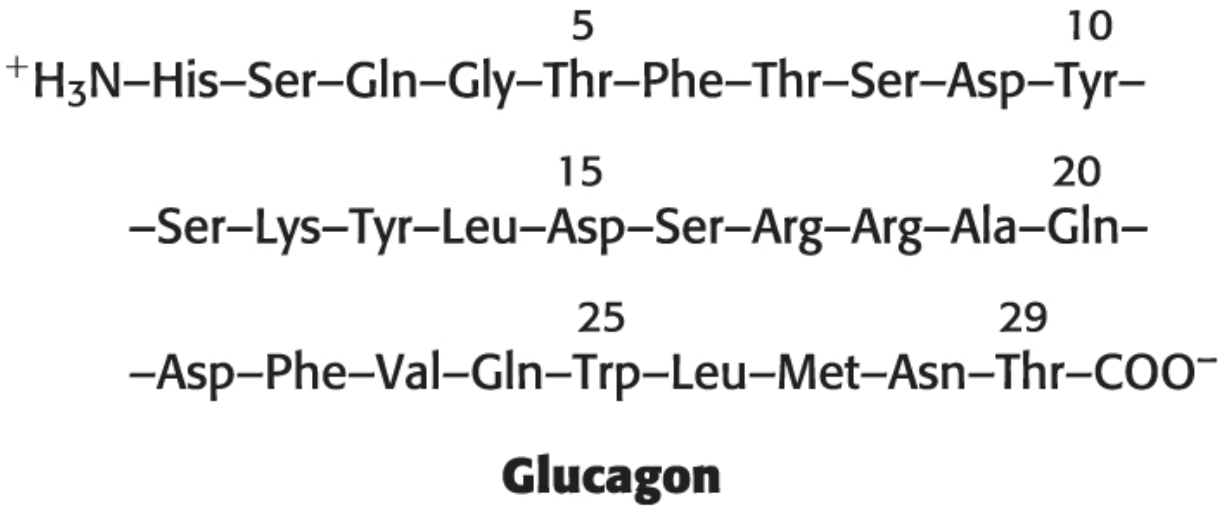


The T and R states of the muscle phosphorylase b are separated by a reversible reaction arrow. The T state is shown on the left and the R state is shown on the right. The top forward arrow is shown in black and labeled 2 A M P. The bottom backward arrow is shown in red and labeled 2 A T P or 2 glucose-6-phosphate. The active site in each subunit of the phosphorylase is depicted as a central tiny circle with a red outline. A tiny purple circle with a black outline is also shown in each subunit. It is located away from the active site and labeled nucleotide binding site. In the T state, both active sites are empty. A thick blue loop extends into the active site of the top subunit. A thick green loop extends into the active site of the bottom subunit. One end of each loop is attached to the nucleotide-binding site. In the R state, the active sites are empty. The loops are also located away

from the active site. The nucleotide-binding sites are shown in pink color.

Return to FIGURE 21.13 Muscle phosphorylase is allosterically regulated by A T P, A M P, and glucose 6-phosphate

Extended description for Amino acid sequence of glucagon



The amino acid sequence of glucagon is shown in three lines from top to the bottom.

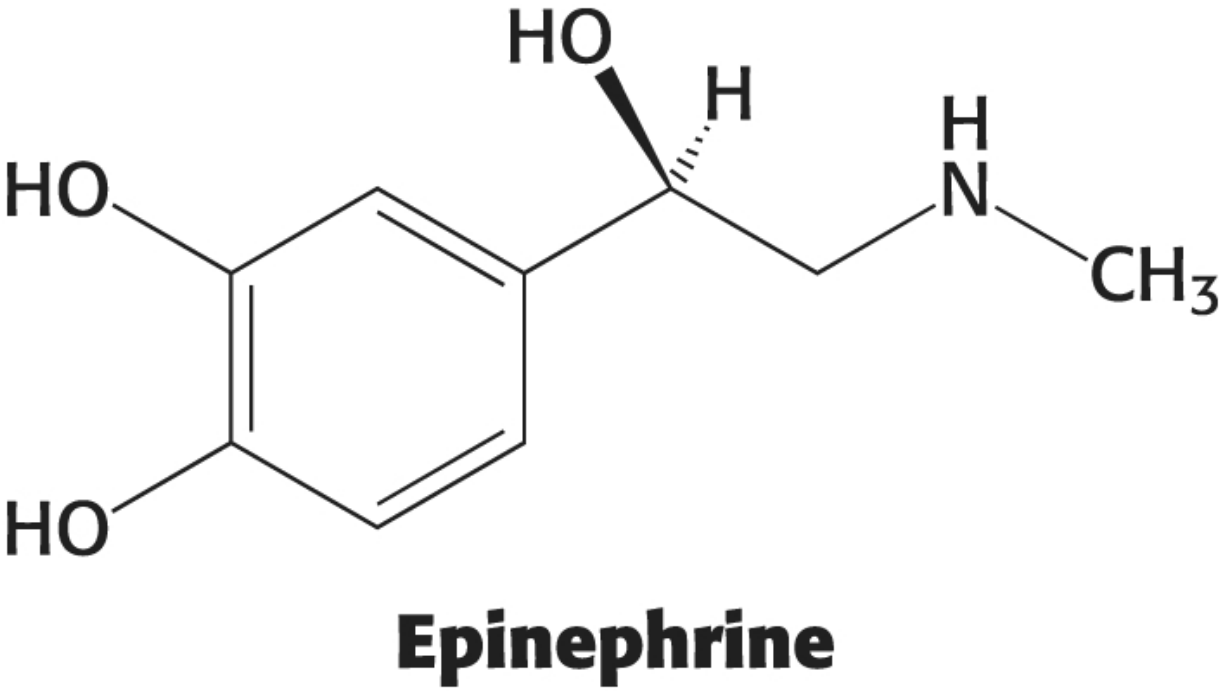
First line: N H 3 superscript plus, single bond, histidine, single bond, serine, single bond, glutamine, single bond, glycine, single bond, threonine, single bond, phenylalanine, single bond, threonine, single bond, serine, single bond, aspartic acid, single bond, tyrosine, single bond. The first threonine residue is numbered 5 at the top. The tyrosine residue is numbered 10 at the top.

Second line: single bond, serine, single bond, lysine, single bond, tyrosine, single bond, leucine, single bond, aspartic acid, single bond, serine, single bond, arginine, single bond, arginine, single bond, alanine, single bond, glutamine, single bond. The aspartic acid residue is numbered 15 at the top. The glutamine residue is numbered 20 at the top.

Third line: single bond, aspartic acid, single bond, phenylalanine, single bond, valine, single bond, glutamine, single bond, tryptophan, single bond, leucine, single bond, methionine, single bond, asparagine, single bond, threonine, single bond, C O O superscript minus. The tryptophan residue is numbered 25 at the top. The threonine residue is numbered 29 at the top.

Return to Amino acid sequence of glucagon

Extended description for Structure of epinephrine

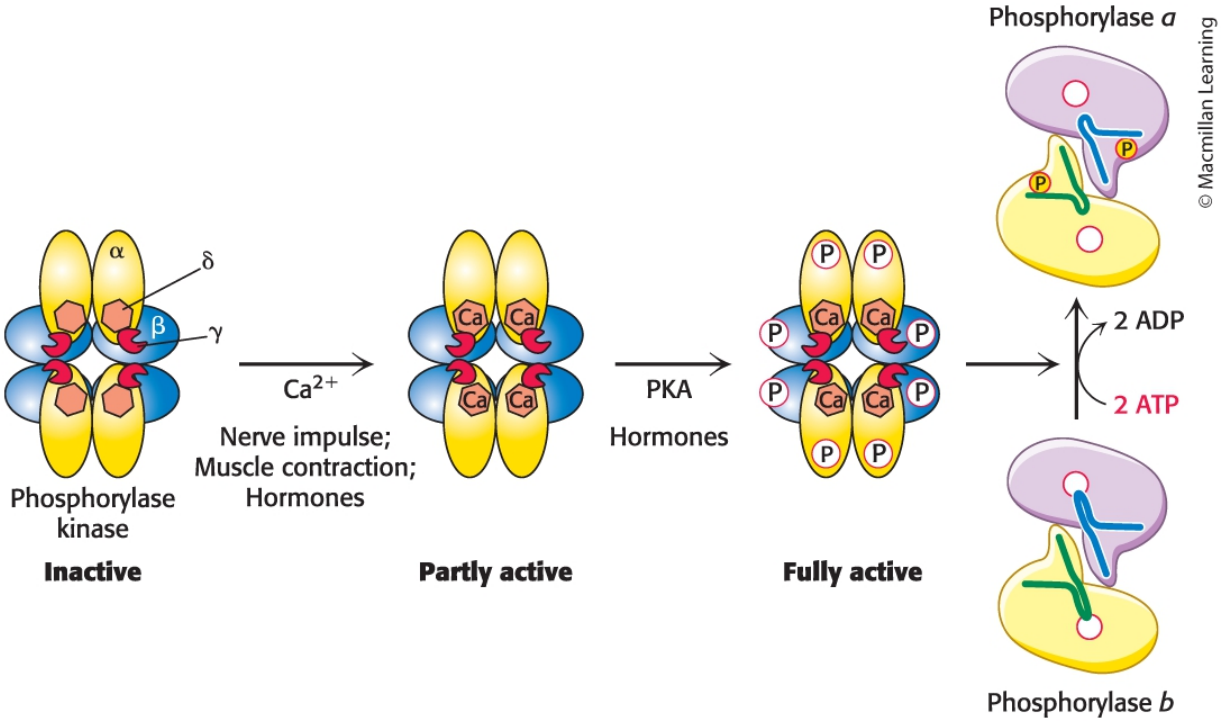


Epinephrine

The structure of epinephrine is as follows: A benzene ring is in a vertical orientation with C 1 occupying the topmost vertex. It contains alternating double bonds between C 1 and C 2, C 3 and C 4, and C 5 and C 6. C 2 is single bonded to C 1 of a 1 N and 2 C heteronuclear alkane chain depicted as a line structure using 2 zigzag lines. N bound to H occupies the third position. C 1 is wedge bonded to O H on the upper left and dash bonded to H on the upper right. N is single bonded to C H 3 on the lower right. C 5 and C 6 of the benzene ring are single bonded to O H.

Return to Structure of epinephrine

Extended description for FIGURE 21.14 Phosphorylase kinase is activated by calcium ions and hormonally controlled phosphorylation

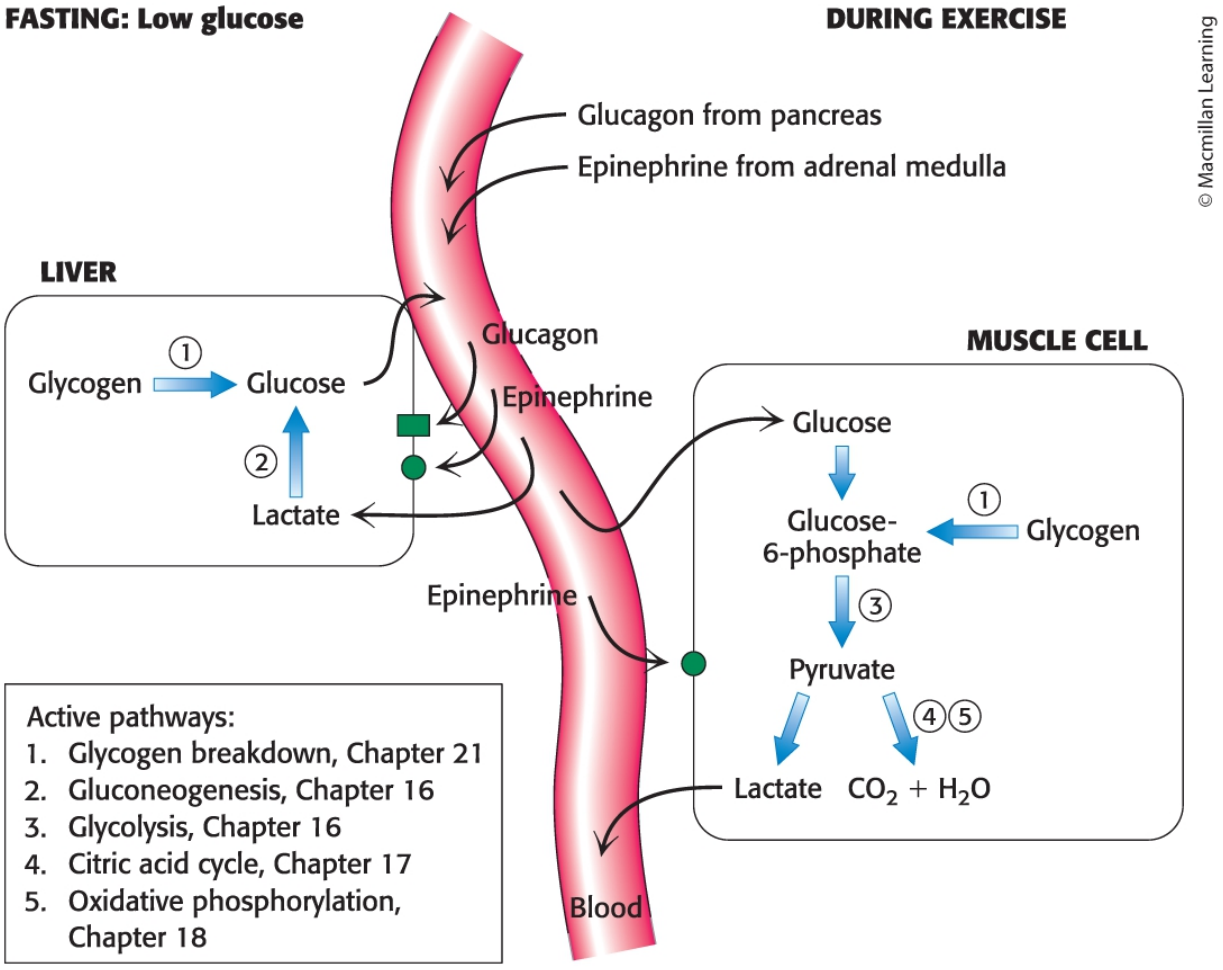


The inactive phosphorylase kinase consists of 4 alpha subunits, 4 beta subunits, 4 delta subunits, and 4 gamma subunits. The beta subunit depicted as a blue circle forms a square-like arrangement. Each beta subunit is bound to a yellow oval-shaped alpha subunit. Each alpha subunit is bound to a hexagon-shaped delta subunit in the core of the enzyme. Each delta subunit is bound to a crescent-shaped gamma subunit. A forward arrow labeled C a superscript 2 plus ion points toward the partly active kinase. The text below the arrow reads “Nerve impulse; muscle contraction; hormones.” In the partly active kinase, delta subunits of the kinase and bound to the calcium ion. A forward arrow labeled P K A hormones points toward the fully active enzyme. In the fully active enzyme, the alpha and

beta subunits are bound to phosphate groups depicted as P inside a tiny circle. The delta subunits are bound to calcium ions. A forward arrow from a fully active kinase points toward an upward arrow that depicts the conversion of phosphorylase b to phosphorylase a with the simultaneous hydrolysis of 2 A T P to 2 A D P.

Return to FIGURE 21.14 Phosphorylase kinase is activated by calcium ions and hormonally controlled phosphorylation

Extended description for FIGURE 21.15 Glycogen breakdown is controlled by the combined effects of multiple hormones in a tissue specific manner



© Macmillan Learning

A long and wavy tubular structure is shown in the center. It depicts a blood vessel containing blood. The left side is labeled “Fasting: Low glucose” and the right side is labeled “During exercise.”

During exercise, glucagon from the pancreas and epinephrine from the adrenal medulla enter the blood vessel. They travel through the bloodstream to reach the liver. Under the low glucose section, a

rectangle labeled liver is shown. Its right side contains a tiny green rectangle and a tiny green circle. The glucagon and epinephrine from the bloodstream point toward the rectangle and circle respectively. Inside the liver, a forward arrow labeled 1 point from glycogen to glucose. An arrow shows the entry of lactate from the bloodstream into the liver. An upward arrow labeled 2 points from lactate to glucose. The glucose produced in the liver is released into the bloodstream. It travels to reach the muscle cell. The muscle cell is depicted as a rectangle. Glucose from the bloodstream enters the muscle cell. It is first converted into glucose 6-phosphate. An arrow labeled 1 point from glycogen to glucose 6-phosphate. A downward arrow labeled 3 points from glucose 6-phosphate to pyruvate. Epinephrine from the bloodstream points toward a tiny green circle on the left side of the rectangle labeled muscle cell. A downward arrow from pyruvate points toward lactate. A downward arrow labeled 4 and 5 points from pyruvate to C O 2 plus H 2 O. An arrow depicts the release of lactate produced in the muscle cell into the bloodstream. A key is given inside a rectangle. It is as follows:

1. Glycogen breakdown, Chapter 21.

2. Gluconeogenesis, Chapter 16.

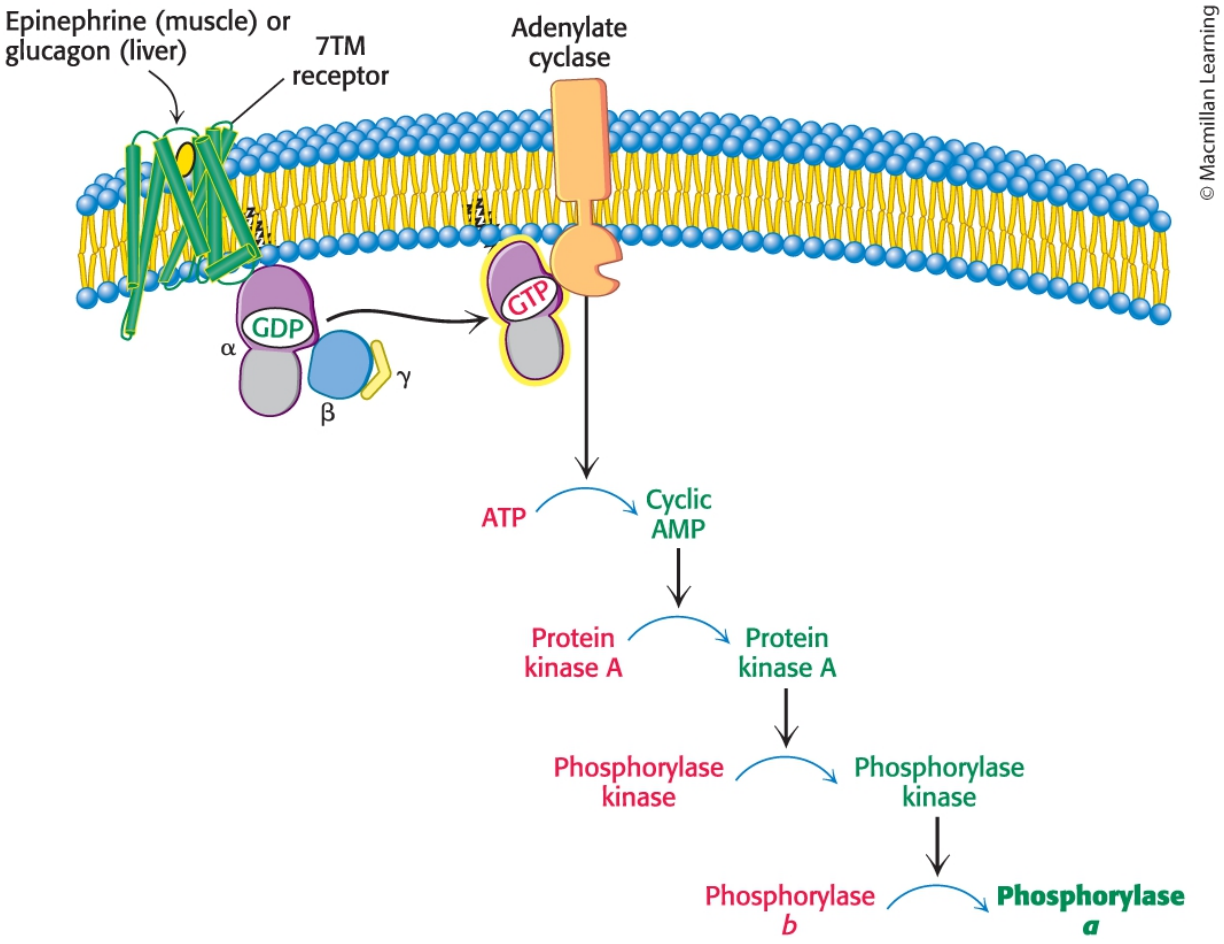
3. Glycolysis, Chapter 16.

4. Citric acid cycle, Chapter 17.

5. Oxidative phosphorylation, Chapter 18.

Return to FIGURE 21.15 Glycogen breakdown is controlled by the combined effects of multiple hormones in a tissue specific manner

Extended description for FIGURE 21.16 Glycogen degradation is stimulated by hormone binding to 7 T M receptors



A “7 T M receptor” and adenylate cyclase are embedded in a membrane. The receptor binds to epinephrine in muscle or glucagon in the liver. The epinephrine or glucagon molecule is depicted as a tiny yellow oval. The cytoplasmic region of the receptor is bound to a trimeric G-protein consisting of alpha, beta, and gamma subunits. The alpha subunit is bound to G D P. An arrow from the G protein points toward the alpha subunit bound to G T P and associated with the cytoplasmic region of the adenylate cyclase.

A downward arrow from adenylate cyclase points to the conversion of A T P highlighted in red to cyclic A M P highlighted in green.

A downward arrow from cyclic A M P points to the conversion of protein kinase A highlighted in red to protein kinase A highlighted in green.

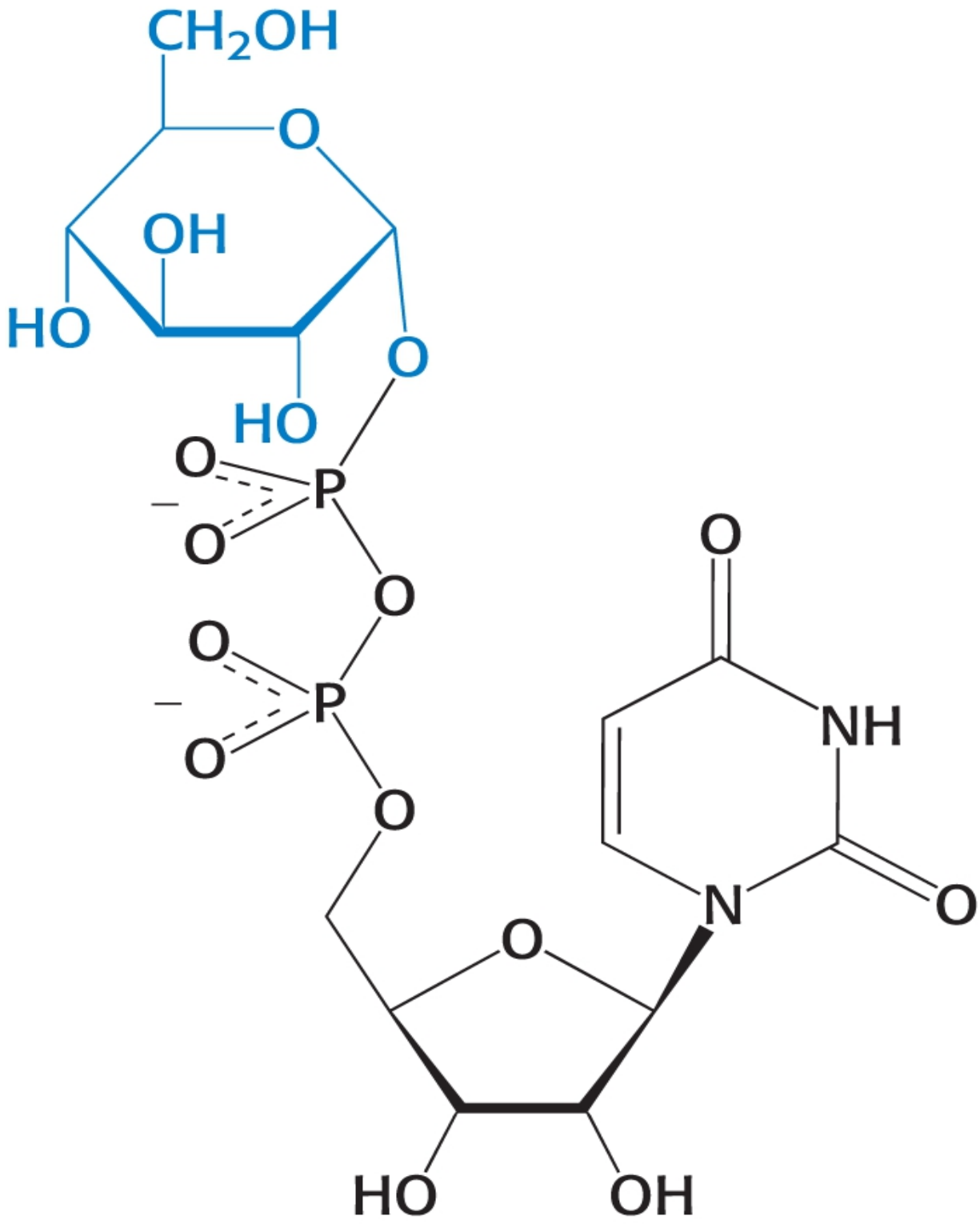
A downward arrow from green highlighted protein kinase A points to the conversion of phosphorylase kinase highlighted in red to phosphorylase kinase highlighted in green.

A downward arrow from green highlighted phosphorylase kinase points to the conversion of phosphorylase b highlighted in red to phosphorylase a highlighted in green.

Return to FIGURE 21.16 Glycogen degradation is stimulated by hormone binding to 7 T M receptors

Extended description for Structure of uridine

diphosphate glucose (U D P-glucose)

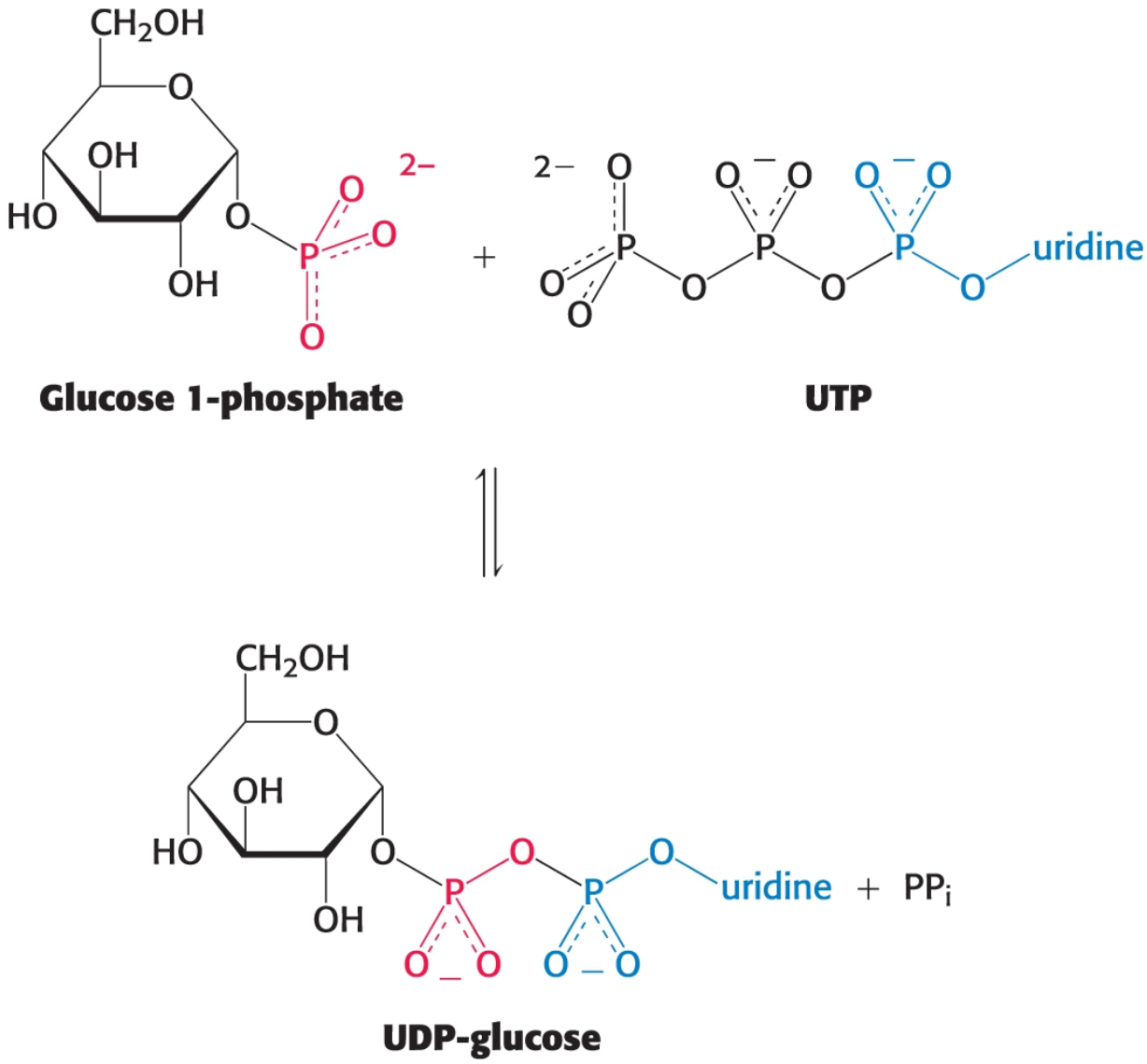


Uridine diphosphate glucose (UDP-glucose)

The structure of U D P-glucose is depicted as follows: A 5-membered heterocyclic pentagonal ring is in a vertical orientation with C 1 occupying the top right vertex. It consists of 1 O and 4 C atoms. O occupies the topmost vertex. C 1 is wedge bonded to N 2 of a 6-membered heterocyclic hexagonal ring in a vertical orientation. The hexagonal ring consists of 2 N and 4 C atoms. The first N bound to H occupies the top right vertex. The second N occupies the bottom-most vertex. C 1 occupies the bottom right vertex. C 1 and C 4 are double bonded to O. A double bond is present between C 2 and C 3. C 2 and C 3 of the pentagonal ring are single-bonded to O H below. C 4 is single-bonded to C H 2 on the upper left in the form of a line. The C H 2 group is further single bonded to a vertical zigzag chain depicted as follows: O, single bond, P, single bond, O, single bond, P. Both P atoms are partially double-bonded to two O atoms. The O atoms have an overall negative charge. The terminal P atom is single-bonded to an O atom, which is further single-bonded to C 1 of a 6-membered heterocyclic hexagonal ring in a horizontal orientation. This ring consists of 1 O and 5 C atoms. O occupies the top right vertex. C 1 occupies the rightmost vertex. C 2 and C 4 are single bonded to O H below. C 3 is single bonded to O H above. C 5 is single bonded to C H 2 O H above.

Return to Structure of uridine diphosphate glucose (U D P-glucose)

Extended description for Formation of U D P-glucose from glucose 1-phosphate and U T P



The reactant consists of two reactants and two products.

The first reactant is glucose 1-phosphate whose structure is as follows: A 6-membered heterocyclic hexagonal ring is in a horizontal orientation with C 1 occupying the rightmost vertex. It

consists of 1 O and 5 C atoms. C 1 is single bonded to O below. This O atom is single-bonded to a central P atom. This P atom is partially double bonded to O above, O on the upper right, and O below. The O atoms have an overall charge of 2 minus. C 2 and C 4 are each single bonded to O H below. C 3 is single bonded to O H above. C 5 is single bonded to C H 2 O H above.

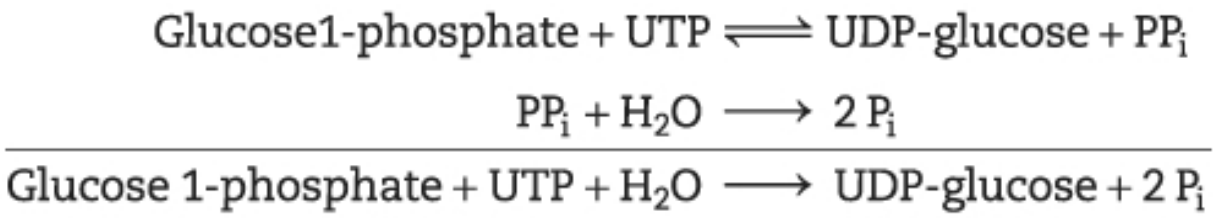
The second reactant is U T P whose structure is as follows: A horizontal zigzag chain consists of P, single bond, O, single bond, P, single bond, O, single bond, P, single bond, O. The first P atom is partially double bonded to O above, O on the lower left, and O below. These O atoms have an overall charge of 2 minus. The second and third P atoms are partially double-bonded to O on the upper left and upper right. These O atoms have an overall negative charge. O 3 atom is single-bonded to uridine on the upper right.

The first product is U D P-glucose whose structure is as follows: A 6-membered heterocyclic hexagonal ring is in a horizontal orientation with C 1 occupying the rightmost vertex. It consists of 1 O and 5 C atoms. C 2 and C 4 are each single bonded to O H below. C 3 is single bonded to O H above. C 5 is single bonded to C H 2 O H above. C 1 is single bonded to O below, which is further single bonded to a zigzag chain composed of P, single bond, O, single bond, P, single bond, O. Each P atom is partially double bonded to O on the lower left and lower right. The O atoms have an overall negative charge. O 2 of the chain is single-bonded to uridine on the lower right.

The second product is P P subscript i.

Return to Formation of U D P-glucose from glucose 1-phosphate and U T P

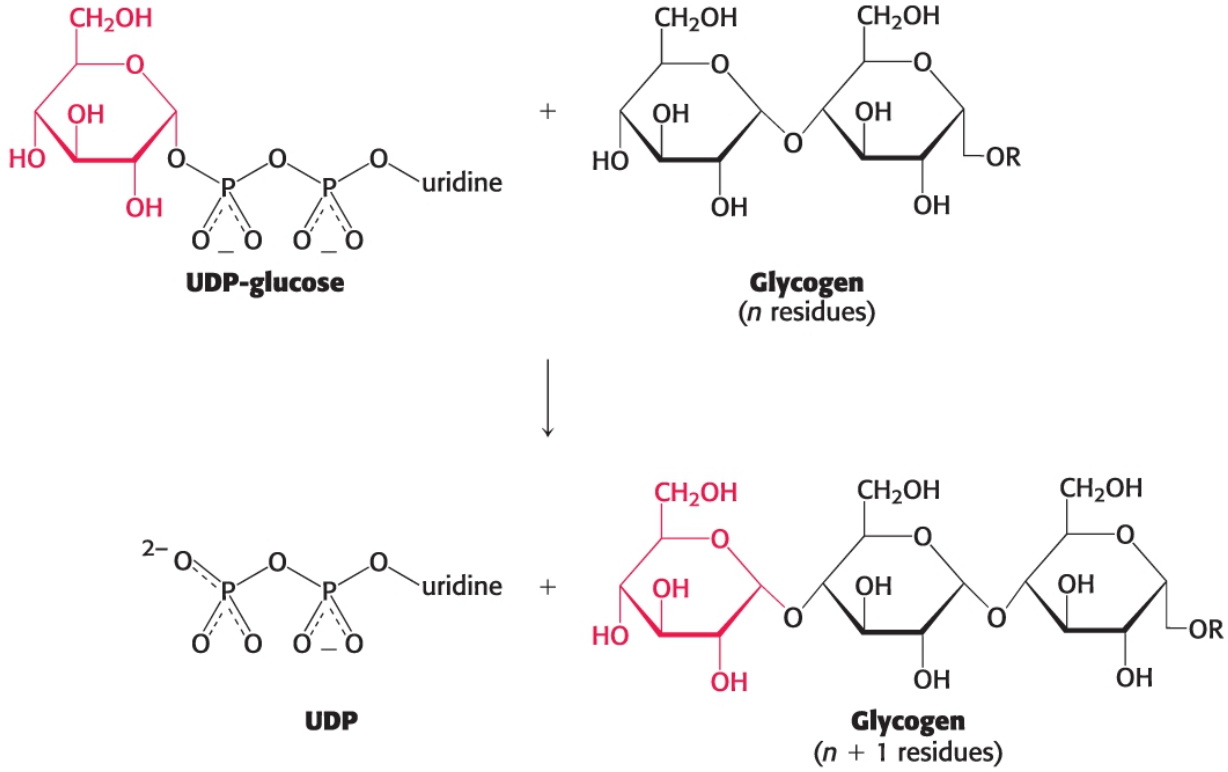
Extended description for Synthesis of U D P-glucose and the hydrolysis of pyrophosphate and the resulting reaction



Synthesis of U D P-Glucose: Glucose 1-phosphate, plus, U T P, reversible arrows, U D P-glucose, plus, P P i. Hydrolysis of Pyrophosphate: P P i, plus, H 2 O, right arrow, 2 molecules of P i. The two reactions are added to give the third reaction as follows: Glucose 1-phosphate, plus, U T P, plus, H 2 O, right arrow, U D P-glucose, plus, 2 molecules of P i.

Return to Synthesis of U D P-glucose and the hydrolysis of pyrophosphate and the resulting reaction

Extended description for Elongation of glycogen molecule by 1 glucose residue



The reactant consists of two reactants and two products.

The first reactant is glucose 1-phosphate whose structure is as follows: A 6-membered heterocyclic hexagonal ring is in a horizontal orientation with C 1 occupying the rightmost vertex. It consists of 1 O and 5 C atoms. C 1 is single bonded to O below. This O atom is single-bonded to a central P atom. This P atom is partially double bonded to O above, O on the upper right, and O below. The O atoms have an overall charge of 2 minus. C 2 and C 4 are each single bonded to O H below. C 3 is single bonded to O H above. C 5 is single bonded to C H 2 O H above.

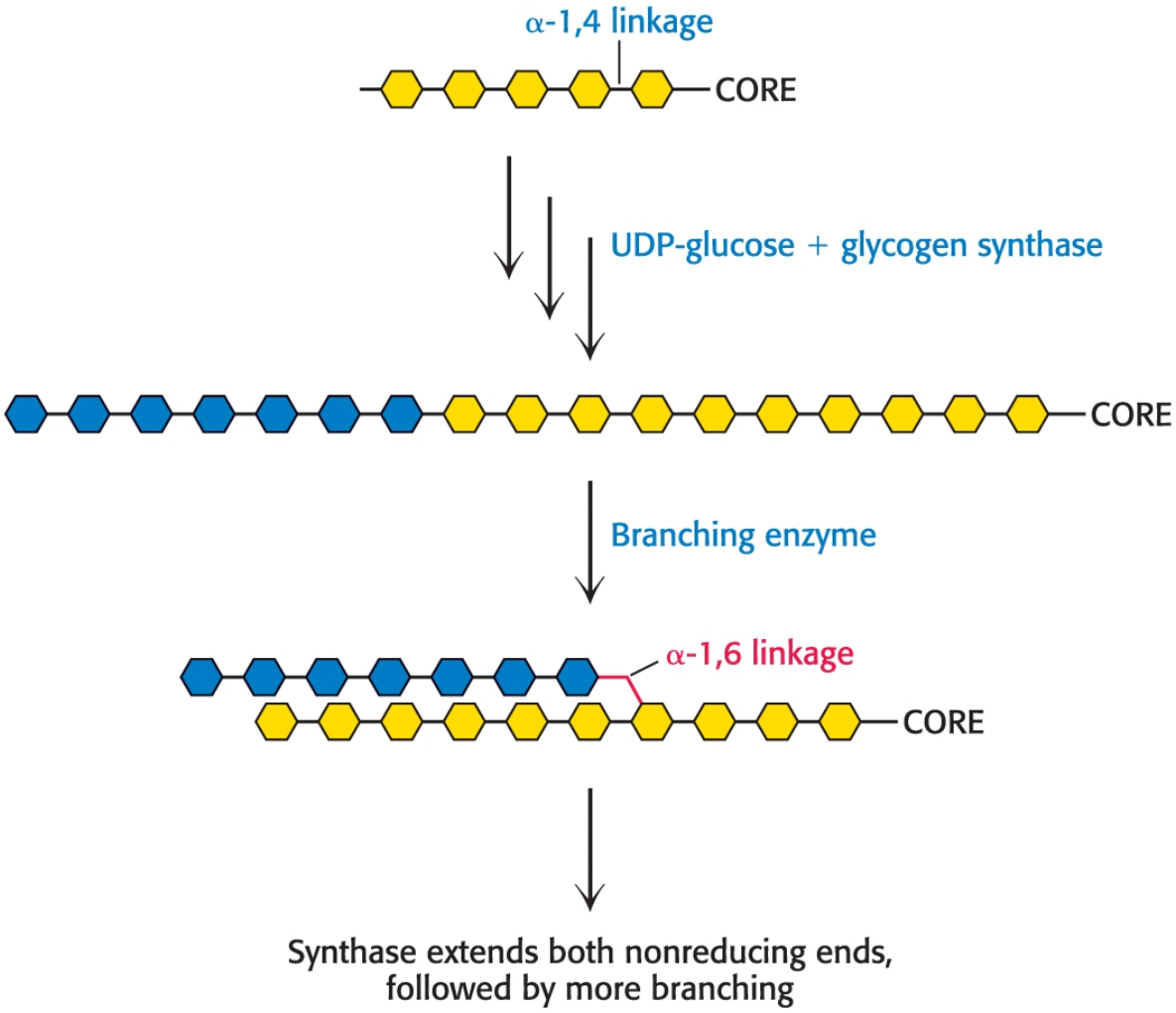
The second reactant is U T P whose structure is as follows: A horizontal zigzag chain consists of P, single bond, O, single bond, P, single bond, O, single bond, P, single bond, O. The first P atom is partially double bonded to O above, O on the lower left, and O below. These O atoms have an overall charge of 2 minus. The second and third P atoms are partially double-bonded to O on the upper left and upper right. These O atoms have an overall negative charge. O 3 atom is single-bonded to uridine on the upper right.

The first product is U D P-glucose whose structure is as follows: A 6-membered heterocyclic hexagonal ring is in a horizontal orientation with C 1 occupying the rightmost vertex. It consists of 1 O and 5 C atoms. C 2 and C 4 are each single bonded to O H below. C 3 is single bonded to O H above. C 5 is single bonded to C H 2 O H above. C 1 is single bonded to O below, which is further single bonded to a zigzag chain composed of P, single bond, O, single bond, P, single bond, O. Each P atom is partially double bonded to O on the lower left and lower right. The O atoms have an overall negative charge. O 2 of the chain is single-bonded to uridine on the lower right.

The second product is P P subscript i.

Return to Elongation of glycogen molecule by 1 glucose residue

Extended description for FIGURE 21.17 Action of a branching enzyme



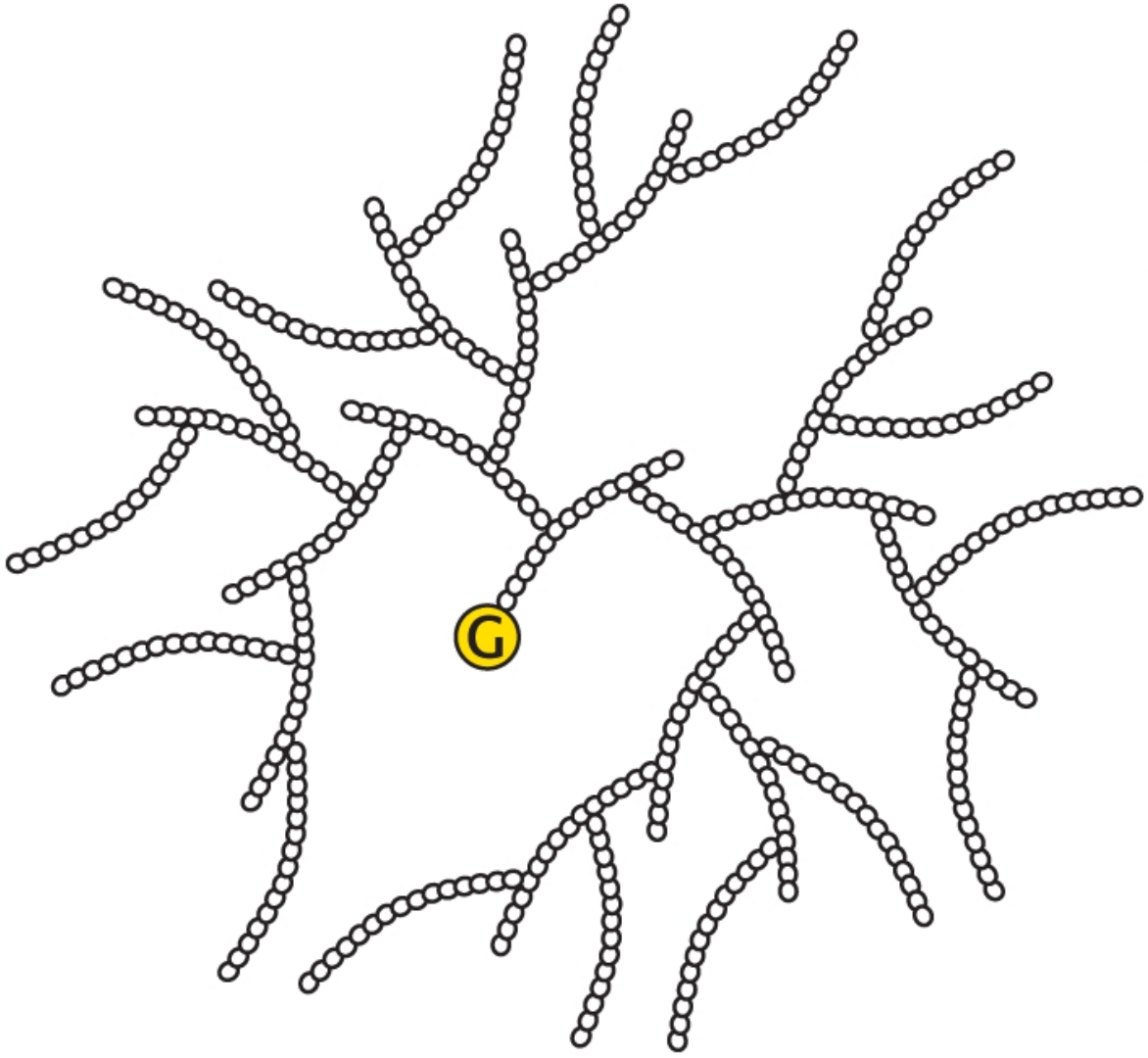
© Macmillan Learning

A linear chain composed of 5 yellow hexagons is connected to the core. The hexagons are connected by alpha-1,4 linkage. Three successive downward arrows are labeled “U D P-glucose plus glycogen synthase.” A linear chain composed of seven blue hexagons on the right and ten yellow hexagons on the right is shown below the arrows. The rightmost yellow hexagon is connected to the core. A downward arrow is labeled branching enzyme. It leads to a branched glycogen molecule below. The branched molecule consists

of a linear chain composed of ten yellow hexagons connected to another linear chain at the top composed of seven blue hexagons through an alpha-1,6 linkage. The leftmost yellow hexagon of the bottom chain is connected to the core. A downward arrow points below a text that read “Synthase extends both nonreducing ends, followed by more branching.”

Return to FIGURE 21.17 Action of a branching enzyme

Extended description for FIGURE 21.18 A cross section of a glycogen molecule reveals the basic branching structure

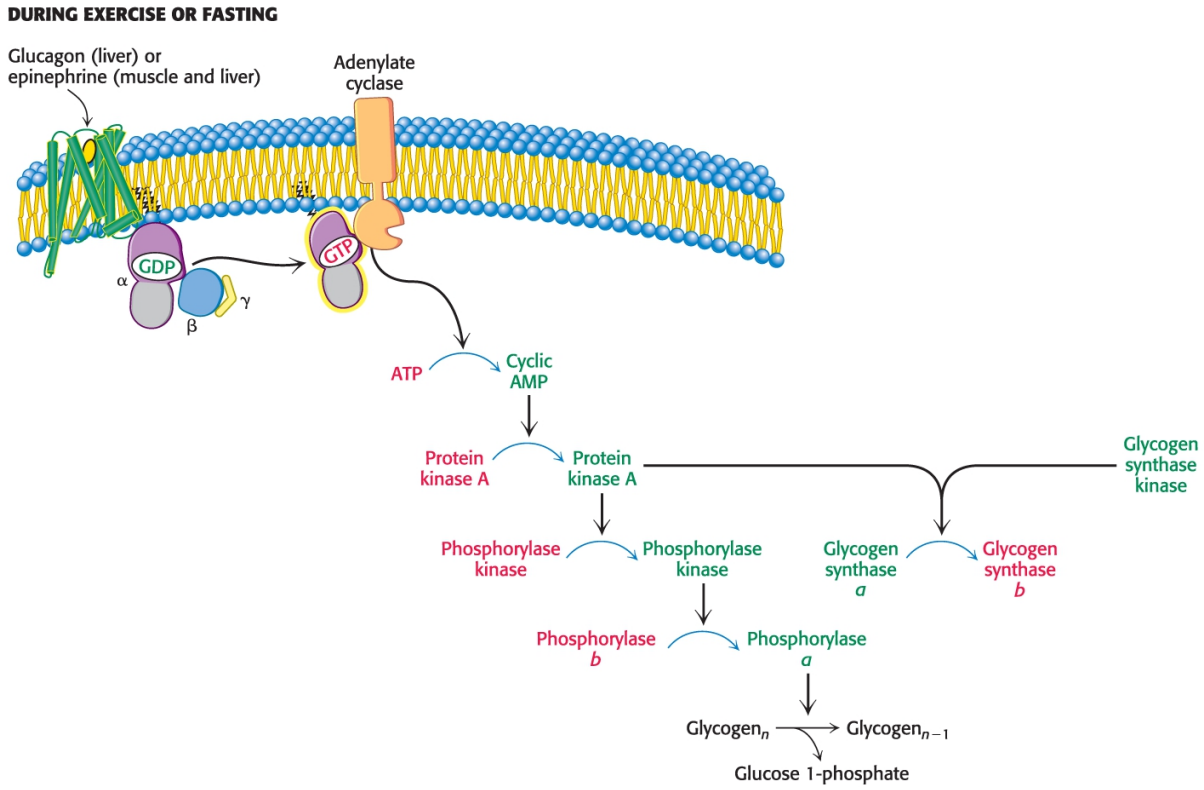


© Macmillan Learning

The cross-section contains a tiny circle labeled G at the center. It is connected to a linear chain of tiny circles oriented toward the upper right. The linear chain further undergoes extensive branching and sub-branching to form a network.

Return to FIGURE 21.18 A cross section of a glycogen molecule reveals the basic branching structure

Extended description for FIGURE 21.19 Glycogen metabolism is regulated in part by hormone-triggered cyclic A M P cascades



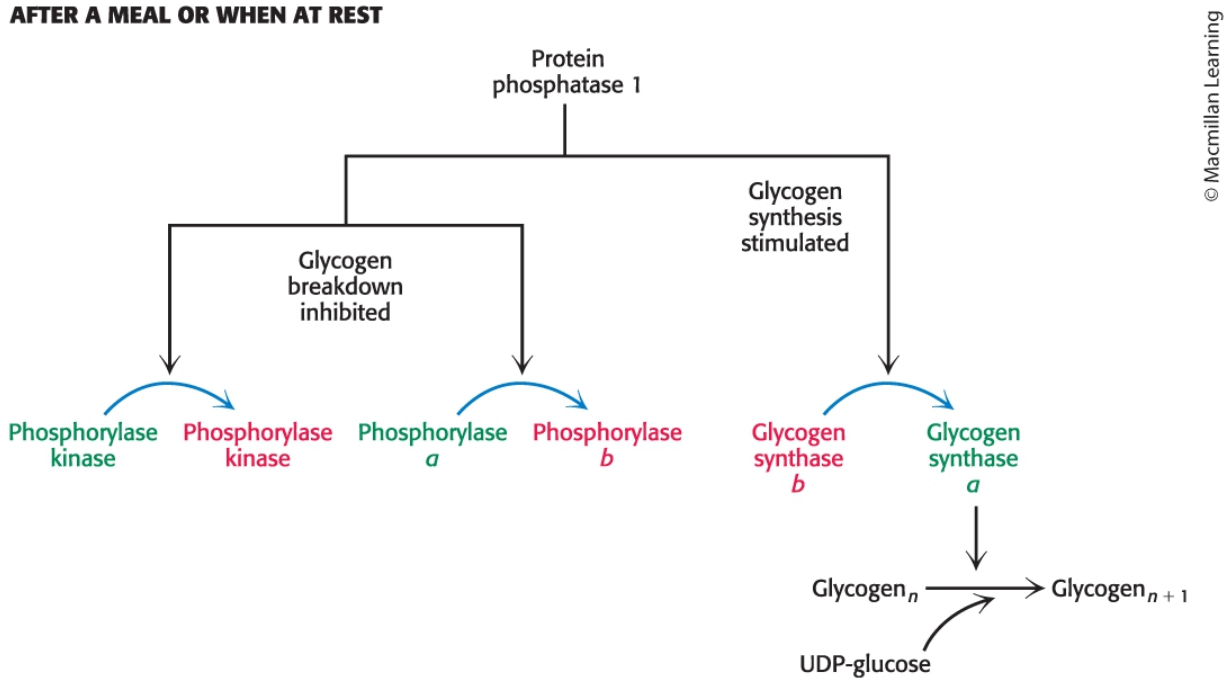
© Macmillan Learning

A “7 T M receptor” and adenylate cyclase are embedded in a membrane. The receptor binds to glucagon in the liver and epinephrine in the muscle and liver during exercise or fasting. The epinephrine or glucagon molecule is depicted as a tiny yellow oval. The cytoplasmic region of the receptor is bound to a trimeric G-protein consisting of alpha, beta, and gamma subunits. The alpha subunit is bound to G D P. An arrow from the G protein points toward the alpha subunit bound to G T P and associated with the cytoplasmic region of the adenylate cyclase. A downward arrow from adenylate cyclase points to the conversion of A T P highlighted in red to cyclic A M P highlighted in green. A downward arrow from

cyclic A M P points to the conversion of protein kinase A highlighted in red to protein kinase A highlighted in green. A downward arrow from green highlighted protein kinase A points to the conversion of phosphorylase kinase highlighted in red to phosphorylase kinase highlighted in green. A downward arrow from green highlighted phosphorylase kinase points to the conversion of phosphorylase b highlighted in red to phosphorylase a highlighted in green. The green highlighted phosphorylase a points toward a reaction depicting the conversion of glycogen subscript n into glycogen subscript n minus 1 and the release of glucose 1-phosphate. The green-highlighted protein kinase and green-highlighted glycogen synthase kinase together carry out the conversion of glycogen synthase a highlighted in green to glycogen synthase b highlighted in red.

Return to FIGURE 21.19 Glycogen metabolism is regulated in part by hormone-triggered cyclic A M P cascades

Extended description for FIGURE 21.20 Glycogen synthesis is regulated by protein phosphatase 1 (P P 1)

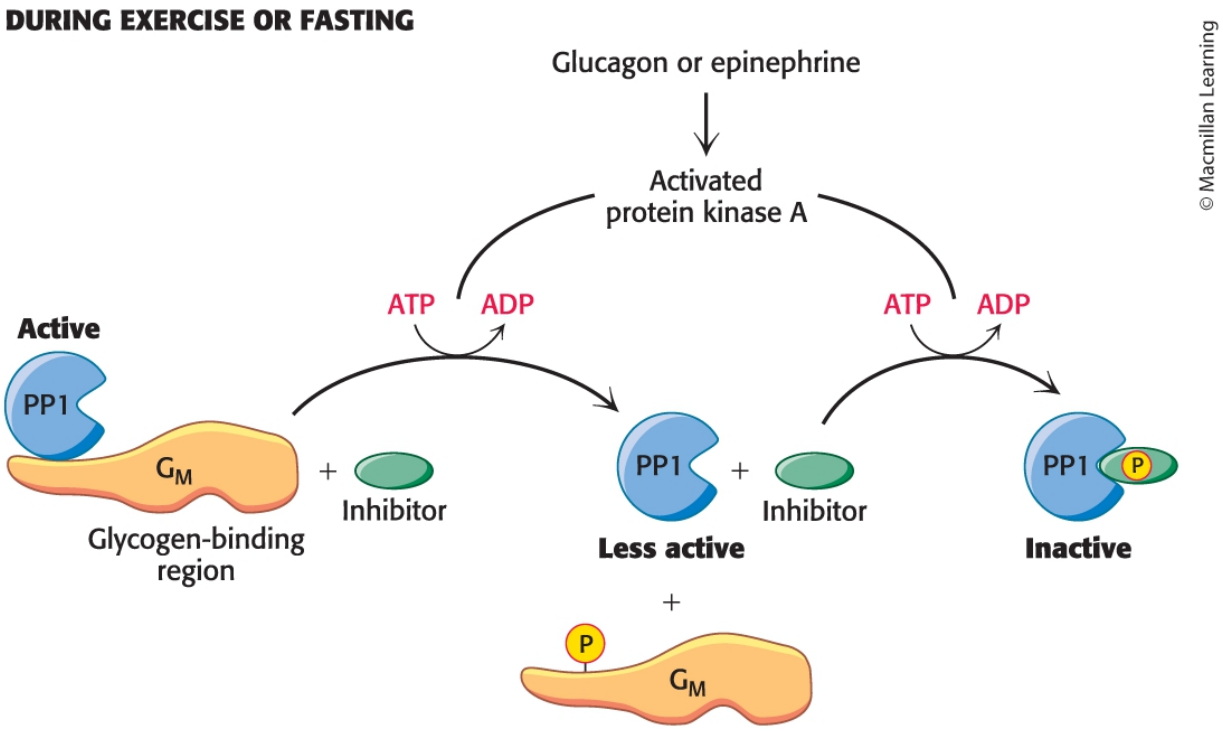


The flowchart shows the regulation of glycogen synthesis after a meal or when at rest. A line below protein phosphatase 1 splits into two branches. The right branch is labeled glycogen synthesis stimulated. It points toward the conversion of glycogen synthase b highlighted in red to glycogen synthase a highlighted in green. A downward arrow below the green-highlighted "glycogen synthase a" points toward a reaction depicting the conversion of glycogen subscript n into glycogen subscript n plus 1. A "U D P-glucose" molecule is used up during this conversion. The left branch further splits into two sub-branches and is labeled glycogen breakdown inhibited. The left sub-branch points to the conversion of phosphorylase kinase highlighted in green to phosphorylase kinase highlighted in red. The right sub-branch points to the conversion of

phosphorylase a highlighted in green to phosphorylase b highlighted in red.

Return to FIGURE 21.20 Glycogen synthesis is regulated by protein phosphatase 1 (P P 1)

Extended description for FIGURE 21.21 P P 1 is regulated by hormonally controlled cascades

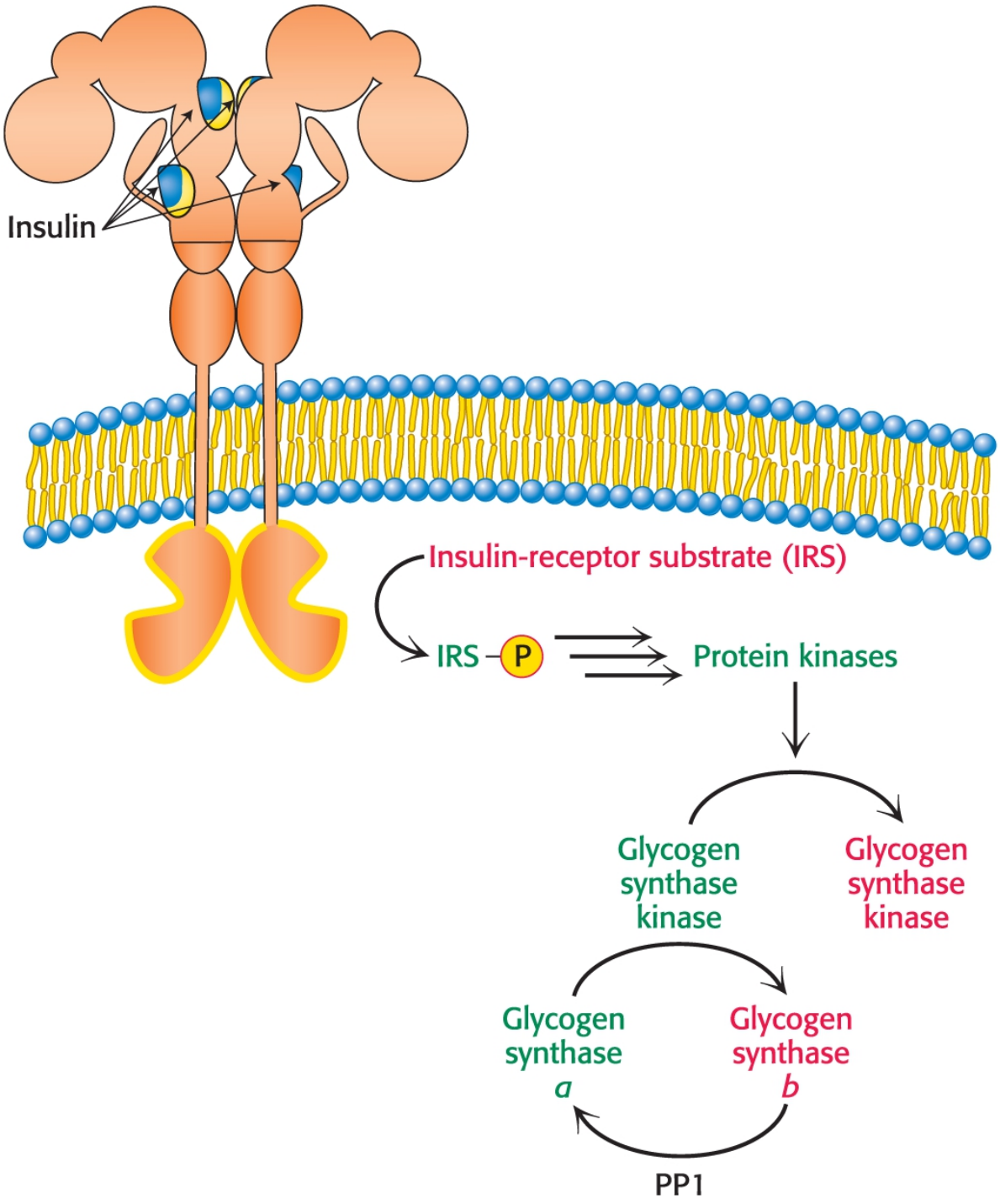


The regulation of P P 1 is depicted during exercise or fasting. A downward arrow below glucagon or epinephrine points to activated protein kinase A. The activated protein kinase A carries out the conversion of the active form of P P 1 to a less active form with the simultaneous hydrolysis of A T P to A D P. The active P P 1 is depicted as a blue circle with a triangular groove. It is bound to an elongated structure labeled G subscript M. The bottom free surface of G subscript M is labeled "Glycogen-binding region." An inhibitor depicted as a green oval is shown alongside. The less active P P 1 dissociates from the G subscript M. This occurs due to the addition of the phosphate group to G subscript M by the activated protein kinase A. The activated protein kinase A stimulates the binding of P P 1 to the inhibitor with the simultaneous hydrolysis of A T P to A D

P. The phosphorylated inhibitor binds to the triangular groove of P P 1.

Return to FIGURE 21.21 P P 1 is regulated by hormonally controlled cascades

Extended description for FIGURE 21.22 Insulin inactivates glycogen synthase kinase

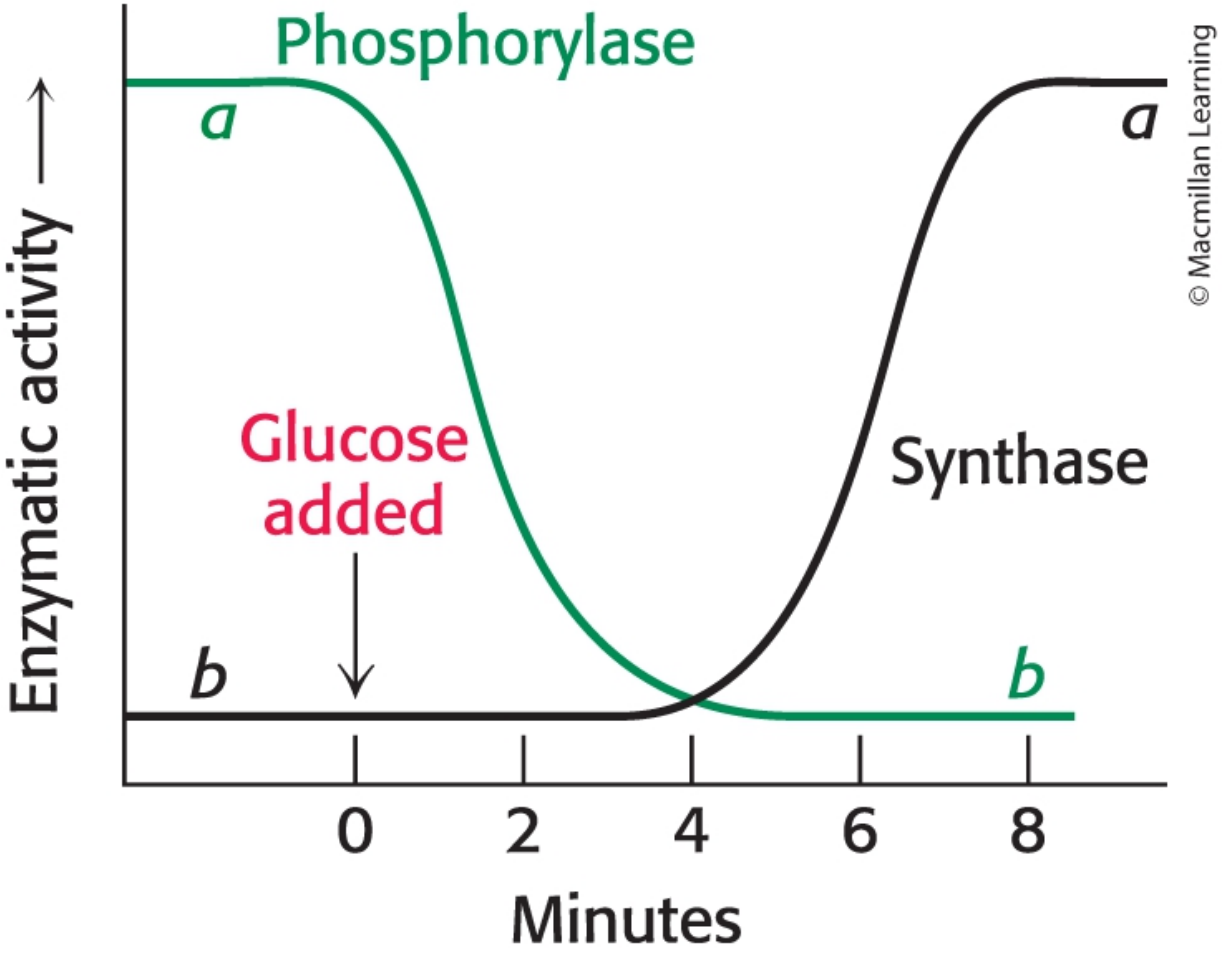


© Macmillan Learning

A transmembrane insulin receptor is embedded in the membrane. It is bound to three insulin molecules. The cytoplasmic domain of the receptor carries out the phosphorylation of insulin receptor substrate (I R S) to I R S, single, bond, P. Three successive forward arrows from phosphorylated I R S point toward protein kinases highlighted in green. A downward arrow below protein kinases shows the conversion of glycogen synthase kinase highlighted in green to glycogen synthase kinase highlighted in red. The green-highlighted glycogen synthase kinase stimulates the conversion of glycogen synthase a highlighted in green to glycogen synthase b highlighted in red. An arrow labeled P P 1 depicts the conversion of glycogen synthase b back to glycogen synthase a.

Return to FIGURE 21.22 Insulin inactivates glycogen synthase kinase

Extended description for FIGURE 21.23 Blood glucose regulates liver-glycogen metabolism

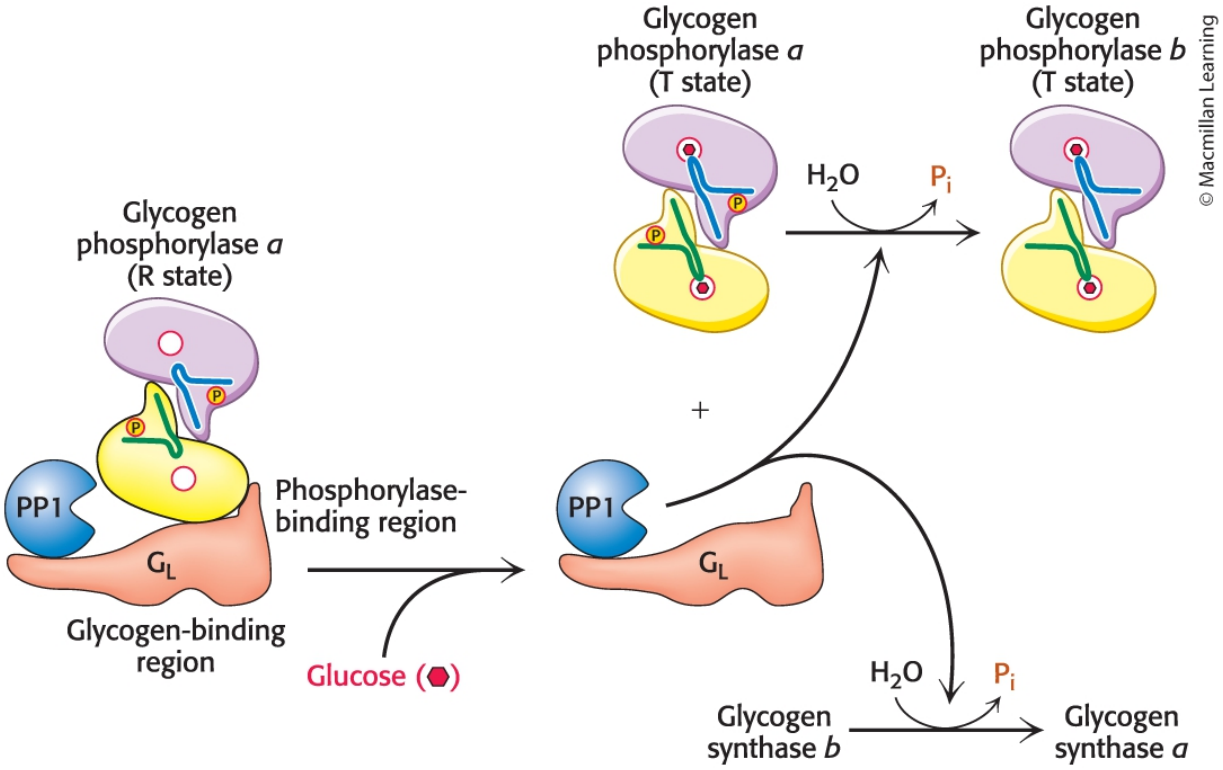


The horizontal axis is labeled minutes. It has markings ranging from 0 to 8 in increments of 2 units. The vertical axis is labeled enzymatic activity that increases from the bottom to the top. Glucose is added at 0 minutes. A green line curve labeled phosphorylase starts at the highest enzymatic activity. It moves horizontally toward the right and starts moving downward after 0 minutes. It reaches the lowest enzymatic activity at 4 minutes and then continues moving horizontally toward the right till 8 minutes. The starting point of the curve is labeled a and the endpoint is labeled b. A black line curve

starts at the lowest enzymatic activity. It moves horizontally toward the right till 4 minutes and then starts rising to reach the highest enzymatic activity at 8 minutes. The curve then moves horizontally toward the right. The starting point of the curve is labeled b and the endpoint is labeled a.

Return to FIGURE 21.23 Blood glucose regulates liver-glycogen metabolism

Extended description for FIGURE 21.24 Glucose regulates liver-glycogen metabolism

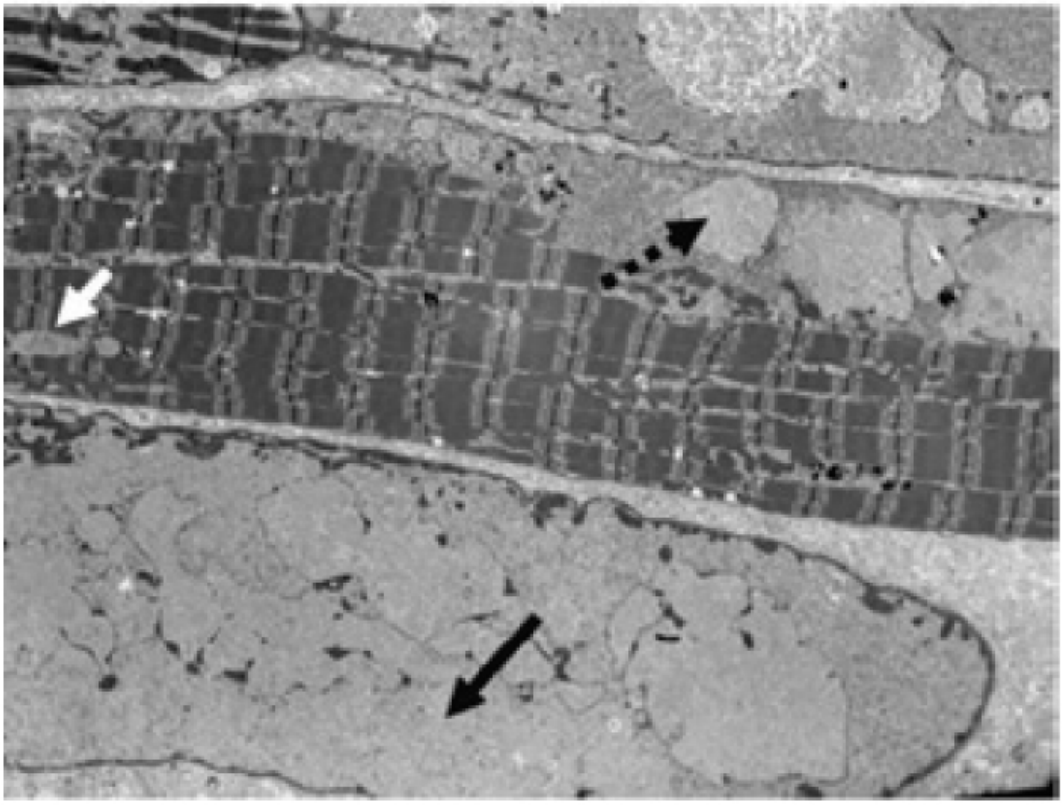


The phosphorylated R state of "glycogen phosphorylase a" is bound to an elongated protein labeled G subscript L. The top surface of G subscript L that is bound to the glycogen phosphorylase a is labeled "Phosphorylase-binding region" and the bottom free surface is labeled "Glycogen-binding region." The G subscript L protein is bound to P P 1 on the top left surface. A forward arrow shows the entry of glucose depicted as a red hexagon. The entry of glucose leads to the dissociation of glycogen phosphorylase a from G subscript L. The P P 1 protein is still attached to G subscript L. The active site of both subunits of glycogen phosphorylase a are bound to glucose and labeled T state. An arrow from P P 1 bound to G subscript L points toward a forward arrow depicting the conversion

of glycogen phosphorylase a (T state) to glycogen phosphorylase b (T state). This conversion is coupled with the entry of H 2 O and the release of P subscript i. The active site of glycogen phosphorylase b is still bound to the glucose molecule. However, both the subunits have lost the phosphate group. An arrow from P P 1 bound to G subscript L points toward a forward arrow depicting the conversion of glycogen synthase b to glycogen synthase a coupled with the entry of H 2 O and release of P subscript i.

Return to FIGURE 21.24 Glucose regulates liver-glycogen metabolism

Extended description for FIGURE 21.25 An electron micrograph of a muscle cell from a patient with Pompe disease reveals enlarged lysosomes

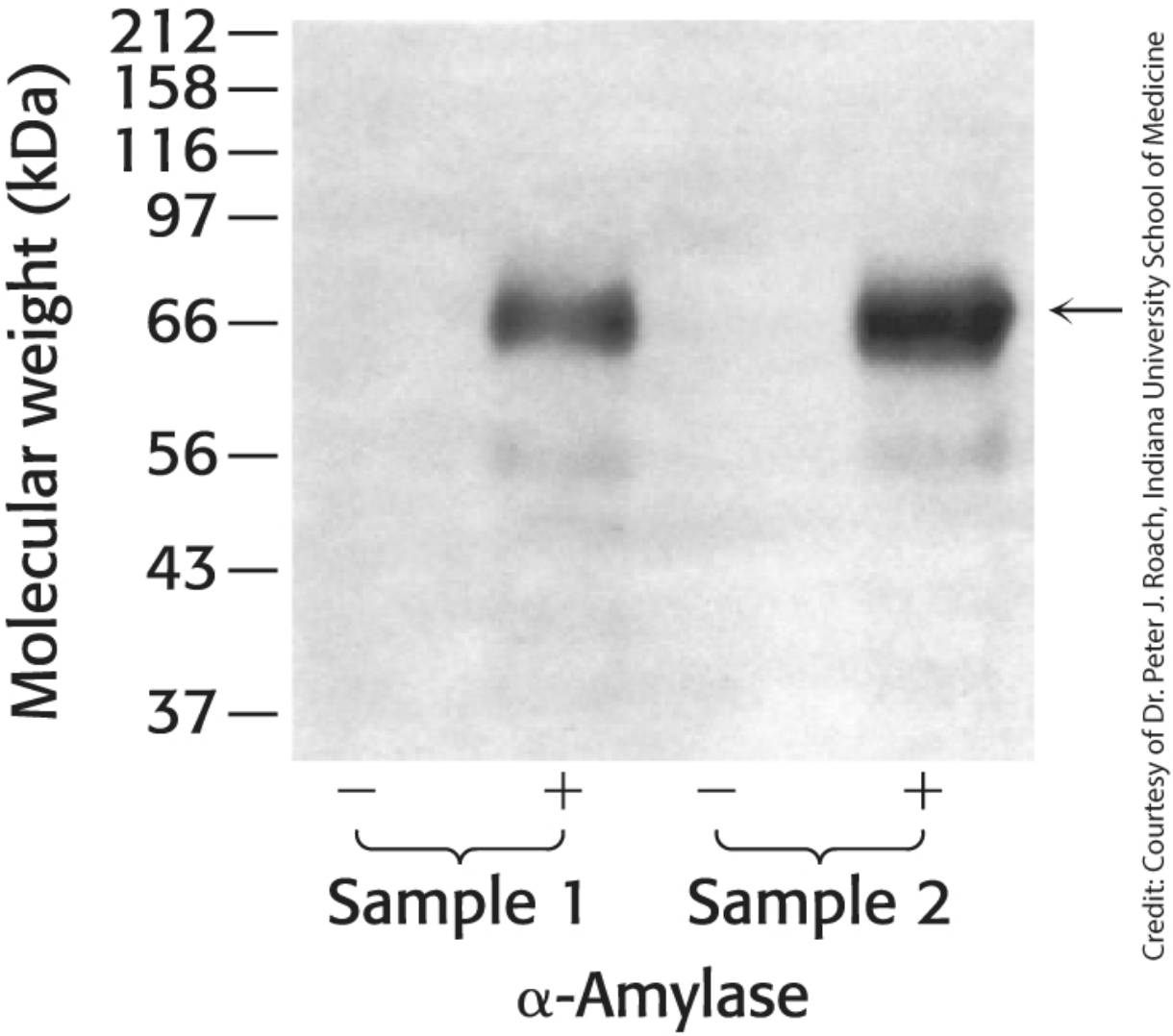


Credit: Reproduced with permission of the author, from Thurberg, B.L., et al., Characterization of pre- and post-treatment pathology after enzyme replacement for pompe disease. *Lab. Invest*, 2006 Dec: 86(12):1208–20.

The micrograph shows a striated appearance of myofibrils. A white arrow points toward a lysosome containing glycogen in the myofibril. A dashed black arrow points toward a large lysosome near the periphery of the cell. A solid black arrow points toward glycogen lakes formed by cytoplasmic accumulations of glycogen due to lysosome rupture.

Return to FIGURE 21.25 An electron micrograph of a muscle cell from a patient with Pompe disease reveals enlarged lysosomes

Extended description for Western blot photograph shows the separation of samples of glycogen



The left side of the blot has molecular weight in kilodalton markings from the bottom to the top. These are 37, 43, 56, 66, 97, 116, 158, and 212. Two lanes of sample 1 and two lanes of sample 2 are shown. For each sample, one lane is labeled minus and the other lane is labeled plus to show treatment with alpha-amylase.

The banding pattern is as follows:

Sample 1, minus lane: No band.

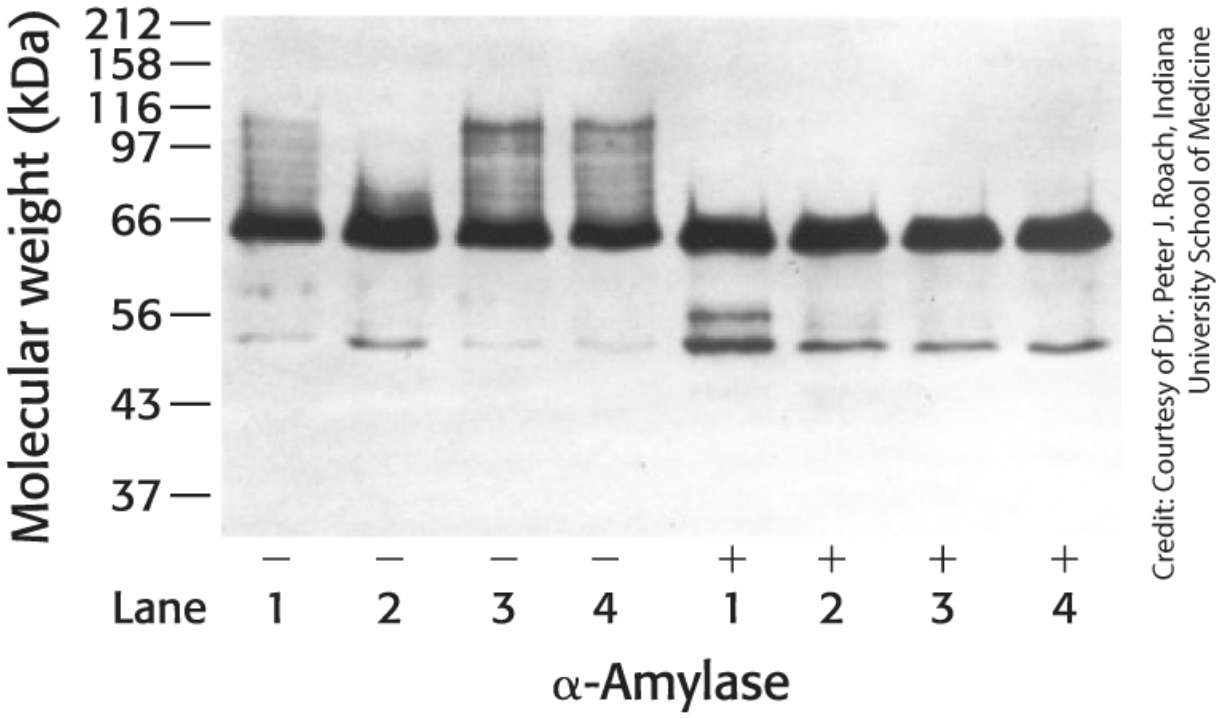
Sample 1, plus lane: A dark band at 66 kilodaltons. A faint band is visible at 56 kilodaltons and between 56 and 43 kilodaltons.

Sample 2, minus lane: No band.

Sample 2, plus lane: A dark and relatively thick band at 66 kilodaltons. A faint band is visible at 56 kilodaltons.

Return to Western blot photograph shows the separation of samples of glycogen

Extended description for Western blot photograph shows the separation of samples of glycogen isolated from a cell line



The left side of the blot has molecular weight in kilodalton markings from the bottom to the top. These are 37, 43, 56, 66, 97, 116, 158, and 212. Two sets of lanes of samples 1 to 4 are shown. The first set of lanes for each sample is labeled minus to show no treatment with alpha-amylase. The second set of lanes for each sample is labeled plus to show treatment with alpha-amylase. The banding pattern is as follows:

Sample 1, minus lane: A distinct dark band is visible at 66 kilodaltons. A faint band is present above and below 56 kilodaltons. A smear of bands is visible between 66 and 116 kilodaltons.

Sample 2, minus lane: A distinct dark band is visible at 66 kilodaltons. A faint band is present above and below 56 kilodaltons. The band below is more noticeable. A smear of bands is visible above 66 kilodaltons.

Sample 3, minus lane: A distinct dark band is visible at 66 kilodaltons. A faint band is present above and below 56 kilodaltons. A smear of bands is present between 66 and 116 kilodaltons.

Sample 4, minus lane: A distinct dark band is visible at 66 kilodaltons. A faint band is present below 56 kilodaltons. A smear of bands is present between 66 and 116 kilodaltons.

Sample 1, plus lane: A thick dark band is visible at 66 kilodaltons. A thin dark band is present above and below 56 kilodaltons.

Sample 2, plus lane: A thick dark band is visible at 66 kilodaltons. A thin dark band is present below 56 kilodaltons.

Sample 3, plus lane: A thick dark band is visible at 66 kilodaltons. A thin dark band is present below 56 kilodaltons.

Sample 4, plus lane: A thick dark band is visible at 66 kilodaltons. A thin dark band is present below 56 kilodaltons.

Return to Western blot photograph shows the separation of samples of glycogen isolated from a cell line

Extended description for Synthesis and degradation of fatty acids



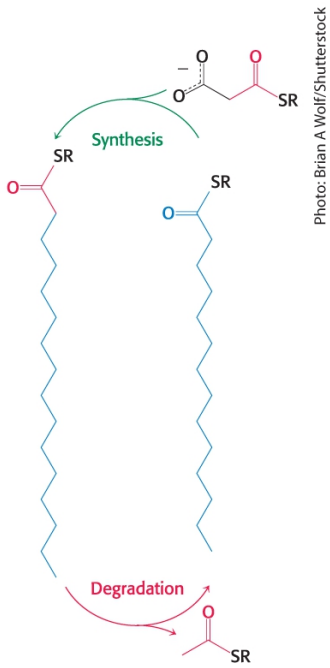


Photo: Brian A Wolf/Shutterstock

A curved arrow labeled synthesis shows the entry of a molecule and points toward a fatty acid.

The structure of the molecule is as follows: A 3-carbon alkane chain is depicted as a line structure using 2 zigzag lines. C 1 is partially double bonded to O above and O on the lower left. The O atoms have an overall negative charge. C 3 is double bonded to O above and single bonded to S R on the lower right.

The structure of the fatty acid is as follows: A 16-carbon alkane chain is depicted as a vertical line structure using 15 zigzag lines. C 1 is double bonded to O on the left and single bonded to S R on the upper right.

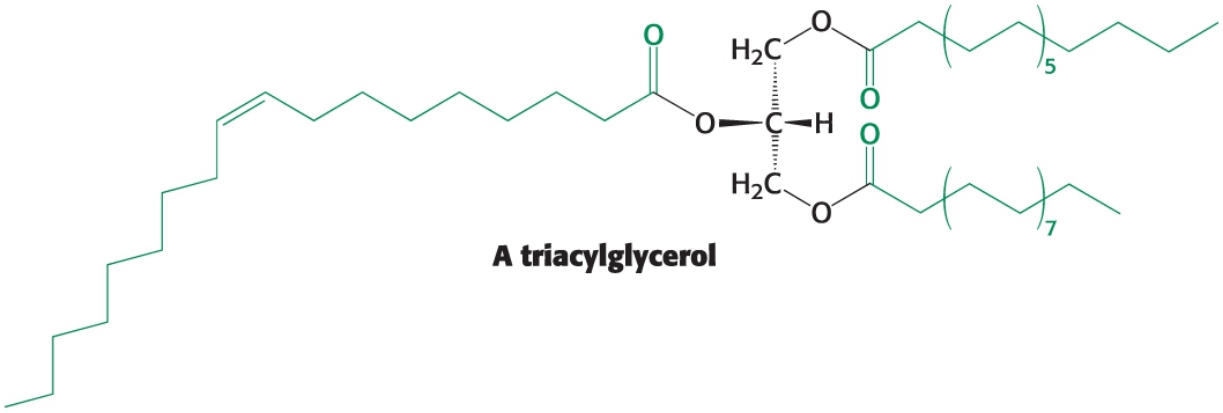
A curved arrow labeled degradation points from the fatty acid to two products.

The structure of the first product is as follows: A central C atom is double bonded to O above, single bonded to S R on the lower right, and single bonded to C H 3 on the lower left in the form of a line.

The structure of the second product is as follows: A 14-carbon alkane chain is depicted as a vertical line structure using 13 zigzag lines. C 1 is double bonded to O on the left and single bonded to S R on the upper right.

Return to Synthesis and degradation of fatty acids

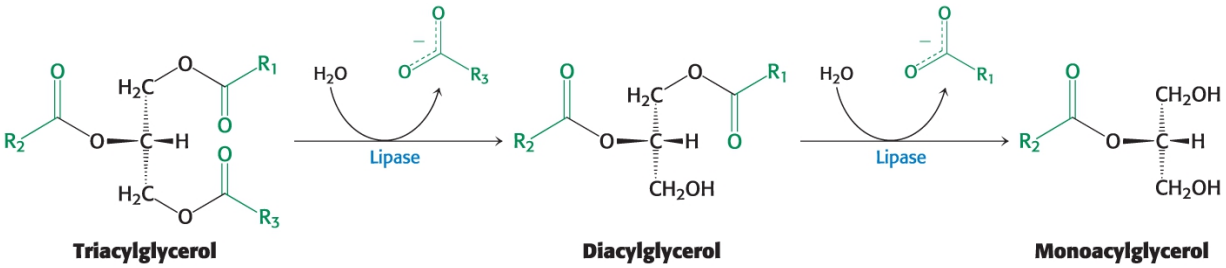
Extended description for Structure of triacylglycerol



The structure of triacylglycerol is as follows: A central C atom is dash-bonded to C H 2 above, dash-bonded to C H 2, wedge bonded to O on the left, and wedge bonded to H on the right. The C H 2 groups, located above and below, are single-bonded to an O atom. The O atom above is single-bonded to an 8-carbon alkane chain depicted as a line structure using 7 zigzag lines. C 1 is double bonded to O below. C 3 and C 4 are enclosed in parenthesis with subscript 5. The O atom below is single-bonded to a 6-carbon alkane chain depicted as a line structure using 5 zigzag lines. C 1 is double bonded to O above and C 3 and C 4 are enclosed in parenthesis with subscript 7. The left O atom, wedge bonded to the central C atom, is further single bonded to an 18-carbon alkene chain depicted as a line structure using 17 zigzag lines. A double bond is present between C 9 and C 10. C 1 is double bonded to O above. The alkene chain is bent at C 10.

Return to Structure of triacylglycerol

Extended description for FIGURE 22.2 Breakdown of triacylglycerol into monoacylglycerol and fatty acids by lipase



The first step involves the breakdown of triacylglycerol into fatty acid and diacylglycerol by lipase.

The structure of triacylglycerol is as follows: A central C atom is dash-bonded to C H 2 above, dash-bonded to C H 2 below, wedge bonded to O on the left, and wedge bonded to H on the right. The C H 2 groups, located above and below, are single-bonded to an O atom. The O atom above is single-bonded to C on the lower right. This C is double bonded to O below and single bonded to R 1 on the upper right. The O atom below is single-bonded to C on the upper right. This C is double bonded to O above and single bonded to R 3 on the lower right. The O atom, wedge bonded to the central C atom, is further single bonded to C on the upper left. This C is double bonded to O above and single bonded to R 2 on the lower left.

A forward arrow labeled lipase leads to diacylglycerol. A curved arrow above it shows the simultaneous entry of H 2 O and the release of a fatty acid.

The structure of this fatty acid is as follows: A central C atom is partially double-bonded to O above, partially double-bonded to O on

the lower left, and single-bonded to R 3 on the lower right. The O atoms have an overall negative charge.

The structure of diacylglycerol is as follows: A central C atom is dash-bonded to C H 2 above, dash bonded to C H 2 O H below, wedge bonded to O on the left, and wedge bonded to H on the right. The C H 2 group located above is single-bonded to an O atom. This O atom is single-bonded to C on the lower right. This C is double bonded to O below and single bonded to R 1 on the upper right. The O atom, wedge bonded to the central C atom, is further single bonded to C on the upper left. This C is double bonded to O above and single bonded to R 2 on the lower left.

The second step involves the breakdown of diacylglycerol into fatty acid and monoacylglycerol by lipase.

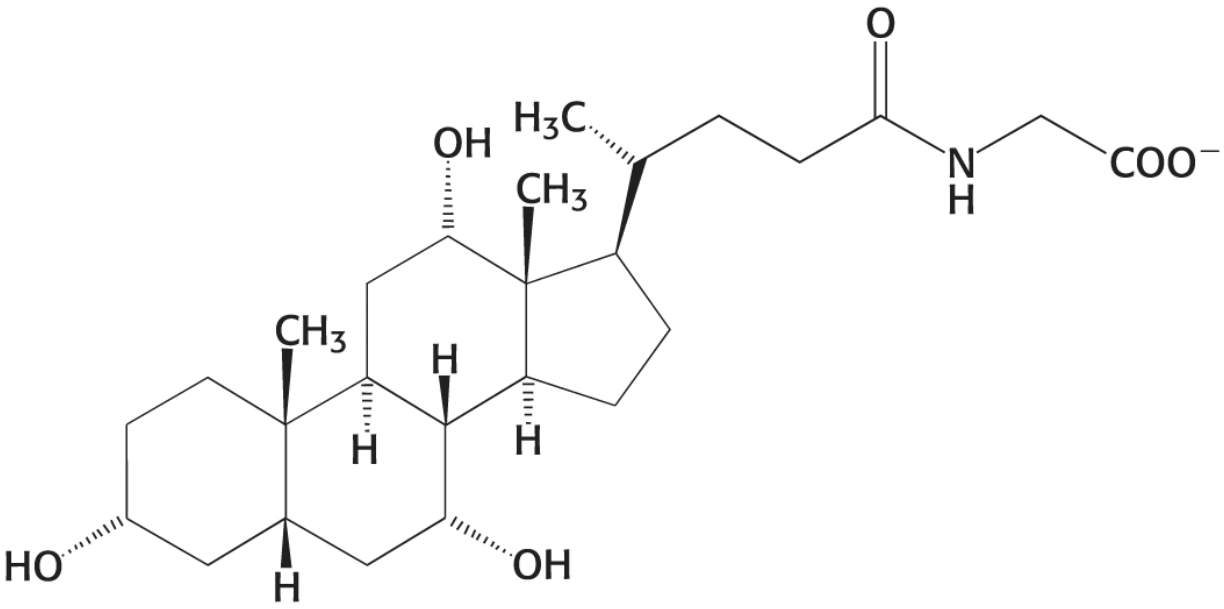
A forward arrow labeled lipase leads to monoacylglycerol. A curved arrow above it shows the simultaneous entry of H 2 O and the release of a fatty acid.

The structure of this fatty acid is as follows: A central C atom is partially double-bonded to O above, partially double-bonded to O on the lower left, and single-bonded to R 1 on the lower right. The O atoms have an overall negative charge.

The structure of monoacylglycerol is as follows: A central C atom is dash-bonded to C H 2 O H above, dash bonded to C H 2 O H below, wedge bonded to O on the left, and wedge bonded to H on the right. The O atom, wedge bonded to the central C atom, is further single bonded to C on the upper left. This C is double bonded to O above and single bonded to R 2 on the lower left.

Return to FIGURE 22.2 Breakdown of triacylglycerol into monoacylglycerol and fatty acids by lipase

Extended description for Structure of glycocholate



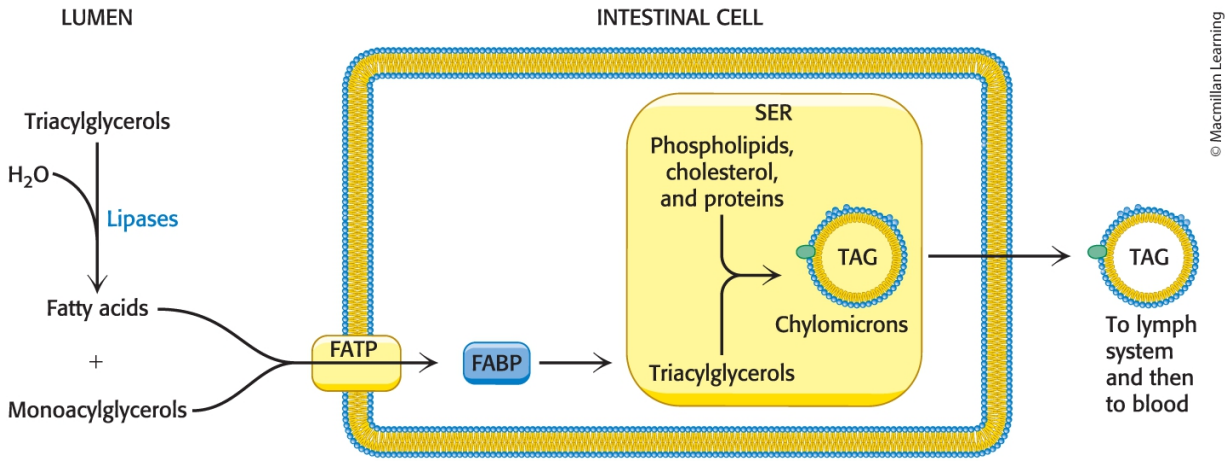
Glycocholate

The structure of glycocholate is as follows: A 6-carbon homocyclic hexagonal ring is in a vertical orientation with C 1 occupying the topmost vertex. C 5 is dash bonded to O H on the lower left. It is fused to a second 6-carbon homocyclic hexagonal ring in a vertical orientation such that C 2 and C 3 of the first ring are C 6 and C 5 respectively of the second ring. In the second ring, C 1 is dash bonded to H below. C 2 is wedge bonded to H above. C 3 is dash-bonded to O H on the lower right. C 5 is wedge bonded to H below. C 6 is wedge bonded to C H 3 above. The second ring is fused to a third 6-carbon homocyclic hexagonal ring in a vertical orientation such that C 1 and C 2 of the second ring are C 5 and C 4 respectively of the third ring. In the third ring, C 1 is dash bonded to O H above. The third ring is fused to a 5-carbon homocyclic pentagonal ring in a horizontal orientation such that C 2 and C 3 of the third ring are C 4 and C 3 respectively of the pentagonal ring. In the pentagonal ring,

C 3 is dash bonded to H below. C 4 is wedge bonded to C H 3 above. C 5 is wedge bonded to C 1 of a 1 N and 5 C alkane chain depicted as a line structure using 5 zigzag lines. N bound to H occupies the fifth position. C 1 is dash bonded to C H 3 on the upper left. C 4 is double bonded to O above. C 5 is single bonded to C O O superscript minus on the lower right.

Return to Structure of glycocholate

Extended description for FIGURE 22.4 Fat absorption and transport is a complex process involving multiple proteins

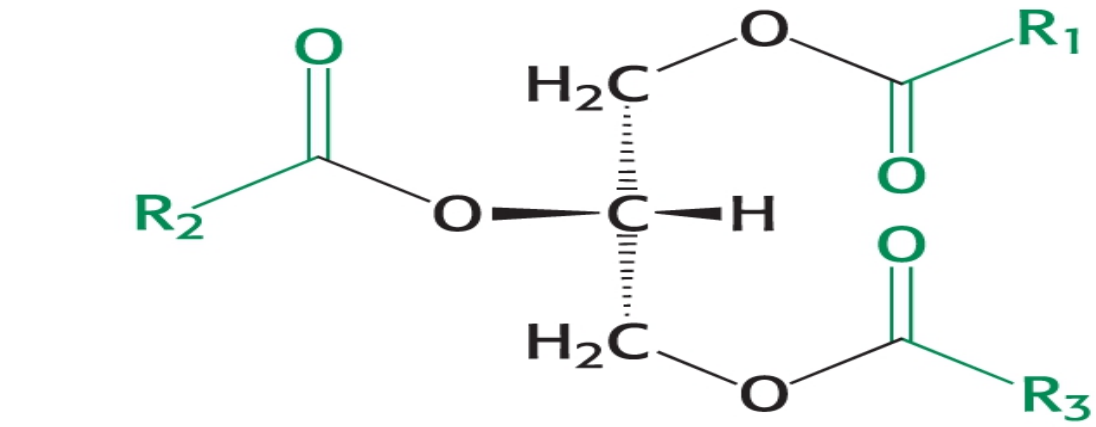


A rectangular intestine cell is shown in the center. It is surrounded by a lipid bilayer. The region on the left of the cell is labeled lumen. In the lumen, triacylglycerols are converted into fatty acids and monoacylglycerols by the action of lipases. This conversion requires the use of H 2 O. The fatty acids and monoacylglycerols in the lumen are transported to the intestinal cell through a transmembrane protein labeled F A T P. Inside the intestinal cell, the F A B P depicted as a small blue rectangle transports the fatty acids and monoacylglycerols to S E R, where they are converted back to triacylglycerols. The S E R is depicted as a large yellow rectangle inside the cell. Inside the S E R, the phospholipids, cholesterol, and proteins combine with triacylglycerol to produce chylomicrons. The chylomicron is depicted as a circular structure surrounded by a lipid monolayer. The core of the chylomicrons contains triacylglycerol abbreviated as T A G. The chylomicrons are transported out of the intestinal cell to the lymph system and then to blood.

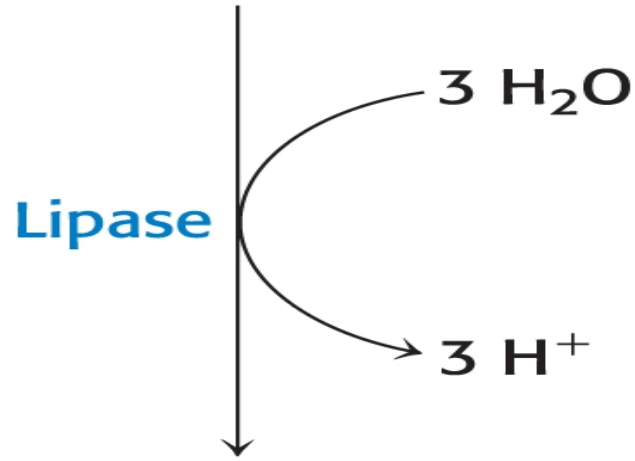
Return to FIGURE 22.4 Fat absorption and transport is a complex process involving multiple proteins

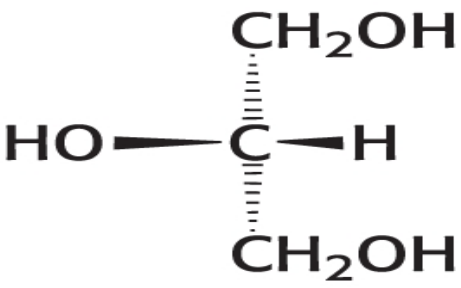
Extended description for Hydrolyzation of

triacylglycerol to yield glycerol and isolated fatty acids



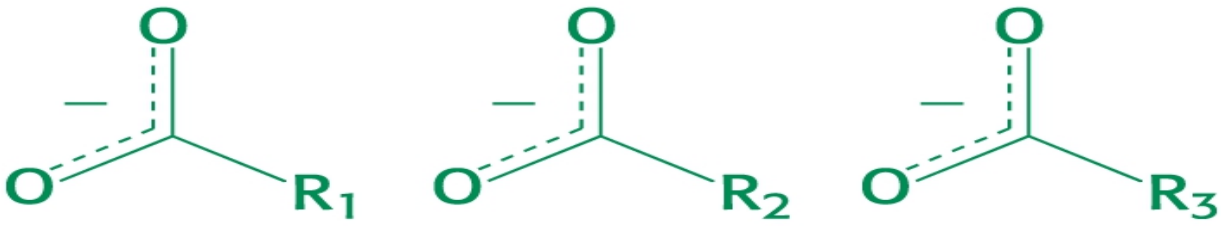
Triacylglycerol





Glycerol

+



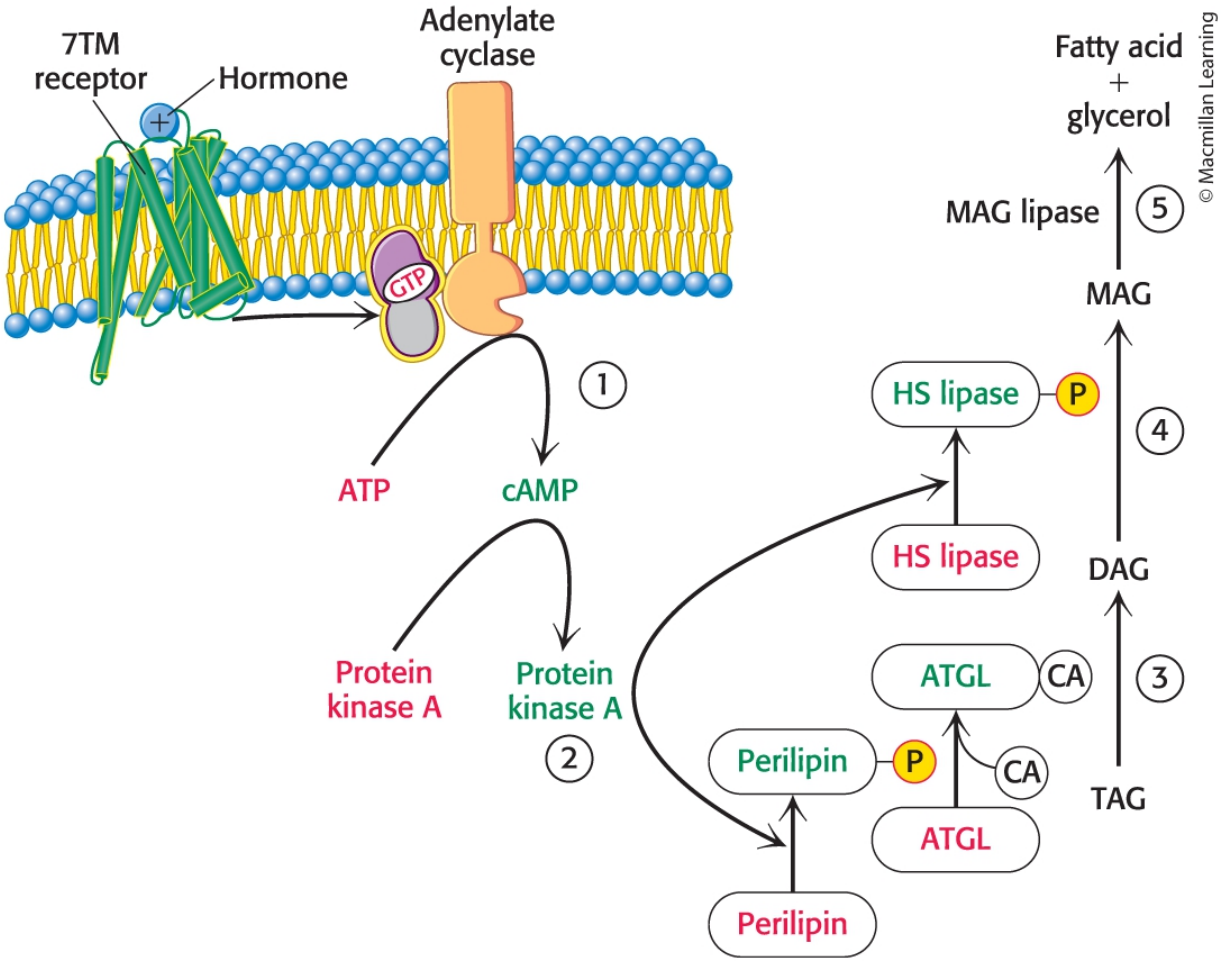
Fatty acids

The coupled reaction contains one reactant and four products. The reactant labeled Triacylglycerol has the following structure: A central C atom is dash bonded to C H 2 above, a second C H 2 group below and is wedge bonded to H on the right and O on the left. The first C H 2 group is single bonded to a second O atom on the upper right. The second O atom is single bonded to a second central C atom on the lower right in the form of a line. The second central C atom is double bonded to a third O atom below and is single bonded to R 1 on the upper right. The second central C atom and the groups attached to it are highlighted in green. The first O atom is single bonded to a third central C atom on the upper left in the form of a line. The third central C atom is double bonded to a fourth O atom above and is single bonded to R 2 on the lower left. The third central C atom and the groups attached to it are highlighted in green. The second C H 2 group is single bonded to a fifth O atom on the lower right. The fifth O atom is single bonded to a fourth central C atom on the upper right in the form of a line. The fourth central C atom is double bonded to a sixth O atom above and is single bonded to R 3 on the lower right. The fourth central C atom and the groups attached to it are highlighted in green. The reaction takes place in the presence of lipase and is coupled with the conversion of 3 H 2 O to 3 H superscript plus. The first product labeled Glycerol has the following structure: A central C atom is dash bonded to C H 2 above, a second C H 2 group below and is wedge bonded to H on the right and O H on the left. The second to the fourth products are highlighted in green and collectively labeled fatty acids. The second product has the following structure: A central C atom is partially double bonded to O above, a second O atom on the lower left and is single bonded to R 1 on the lower right. The structure carries a negative charge. The third product has the following structure: A central C atom is partially double bonded to O above, a second O atom on the lower left and is single bonded to R 2 on the lower right. The structure carries a negative charge. The fourth product has the following structure: A central C atom is partially double bonded to O

above, a second O atom on the lower left and is single bonded to R 3 on the lower right. The structure carries a negative charge.

Return to Hydrolyzation of triacylglycerol to yield glycerol and isolated fatty acids

Extended description for FIGURE 22.5 Triacylglycerols in adipose tissue are converted into free fatty acids in response to hormonal signals



A "7 T M receptor" and adenylate cyclase are embedded in a lipid bilayer. A hormone depicted as a tiny blue circle with a plus symbol is bound to the outer surface of the receptor. An arrow from the cytoplasmic surface of the receptor points toward the alpha subunit of G protein bound to G T P. The G protein is associated with the cytoplasmic region of adenylate cyclase. A curved arrow labeled 1 shows the conversion of A T P highlighted in red to c A M P

highlighted in green by adenylate cyclase. Another curved arrow depicts the conversion of protein kinase A highlighted in red to protein kinase A highlighted in green after c A M P binding. The green highlighted protein kinase A is labeled 2. It carries out the phosphorylation of perilipin to perilipin, single bond, P and H S lipase to H S lipase, single bond, P.

The phosphorylated perilipin and binding of C A cause the conversion of A T G L highlighted in red to A T G L highlighted in green.

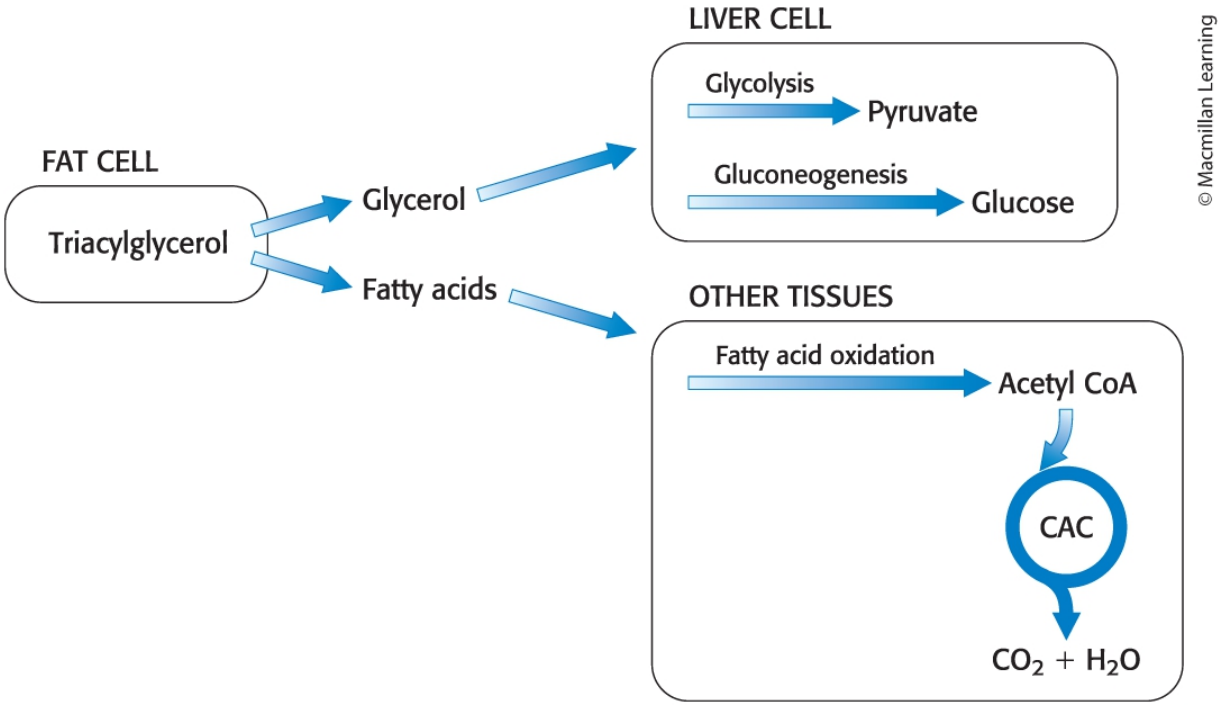
The activated A T G L bound to C A carries out the conversion of T A G to D A G depicted by an upward arrow labeled 3.

The phosphorylated H S lipase carries out the conversion of D A G to M A G depicted by an upward arrow labeled 4.

M A G is broken down by M A G lipase to produce fatty acid plus glycerol. This is depicted by an upward arrow labeled 5.

Return to FIGURE 22.5 Triacylglycerols in adipose tissue are converted into free fatty acids in response to hormonal signals

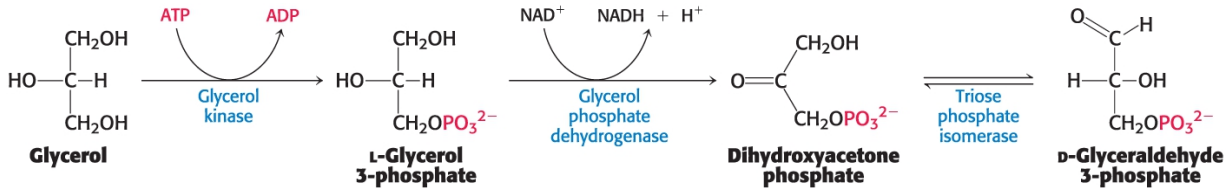
Extended description for FIGURE 22.6 Lipolysis generates fatty acids and glycerol



The fat cell is depicted as a small rectangle containing triacylglycerol. The triacylglycerol is broken down in the fat cell to release glycerol and fatty acids. The glycerol molecule travels to the liver cell depicted as a relatively larger rectangle. Inside the liver cell, glycerol is either converted into pyruvate via glycolysis or converted into glucose via gluconeogenesis. The fatty acids travel to other tissues depicted as a large square. Inside other tissues, fatty acids undergo oxidation to produce acetyl C o A. The acetyl C o A molecule enters the citric acid cycle depicted as a small circle labeled C A C. The products of the citric acid cycle are C O 2 plus H 2 O.

Return to FIGURE 22.6 Lipolysis generates fatty acids and glycerol

Extended description for Stepwise conversion of glycerol to D-Glyceraldehyde 3-phosphate



In the first step, glycerol is irreversibly converted into L-Glycerol 3-phosphate by the enzyme glycerol kinase with the simultaneous hydrolysis of A T P to A D P.

The structure of glycerol is as follows: C H 2 O H, single bond, C, single bond, C H 2 O H. C 2 is single bonded to O H on the left and H on the right.

The structure of L-Glycerol 3-phosphate is as follows: C H 2 O H, single bond, C, single bond, C H 2 O P O 3 superscript 2 minus. C 2 is single bonded to O H on the left and H on the right.

In the second step, L-Glycerol 3-phosphate is irreversibly converted into dihydroxyacetone phosphate by glycerol phosphate dehydrogenase with the simultaneous reduction of N A D superscript plus to N A D H plus H superscript plus.

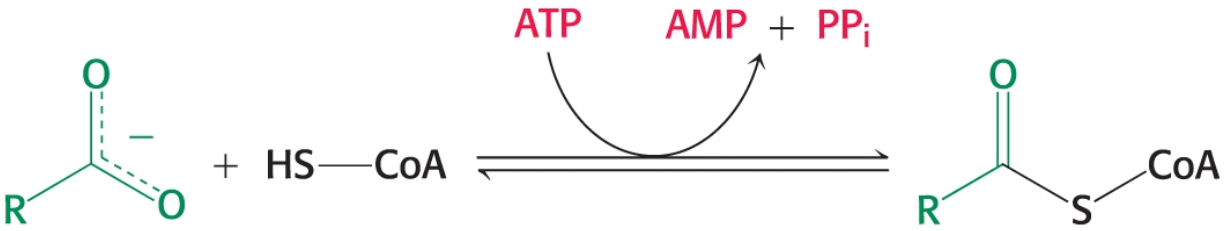
The structure of dihydroxyacetone phosphate is as follows: A central C atom is single bonded to C H 2 O H on the upper right, double bonded to O on the left, and single bonded to C H 2 O P O 3 superscript 2 minus.

the third step, dihydroxyacetone phosphate is reversibly converted into D-Glyceraldehyde 3-phosphate by triose phosphate isomerase.

The structure of D-Glyceraldehyde 3-phosphate is as follows: C, single bond, C, single bond, C H 2 O P O 3 superscript 2 minus. C 1 is double bonded to O on the upper left and single bonded to H on the upper right. C 2 is single bonded to H on the left and O H on the right.

Return to Stepwise conversion of glycerol to D-Glyceraldehyde 3-phosphate

Extended description for Thioester linkage formation between fatty acid and coenzyme A



The reaction consists of two reactants and one product. The structure of the first reactant is as follows: A central C atom is partially double-bonded to O above, partially double-bonded to O on the lower right, and single-bonded to R on the lower left. The O atoms have an overall negative charge.

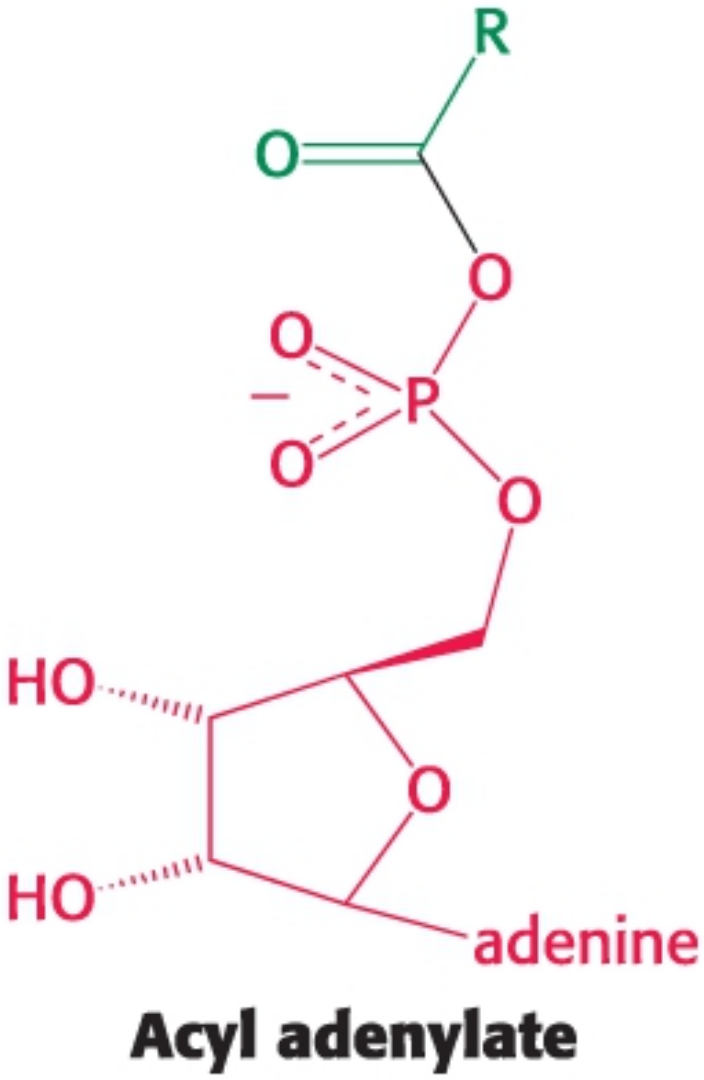
The second reactant is H S, single bond, C o A.

A reversible reaction arrow leads to the product. A curved arrow above it shows the simultaneous hydrolysis of A T P to A M P plus P P subscript i.

The structure of the product is as follows: A central C atom is double bonded to O above, single bonded to R on the lower left, and single bonded to S on the lower right. The S atom is single bonded to C o A on the upper right.

Return to Thioester linkage formation between fatty acid and coenzyme A

Extended description for Structure of acyl adenylate



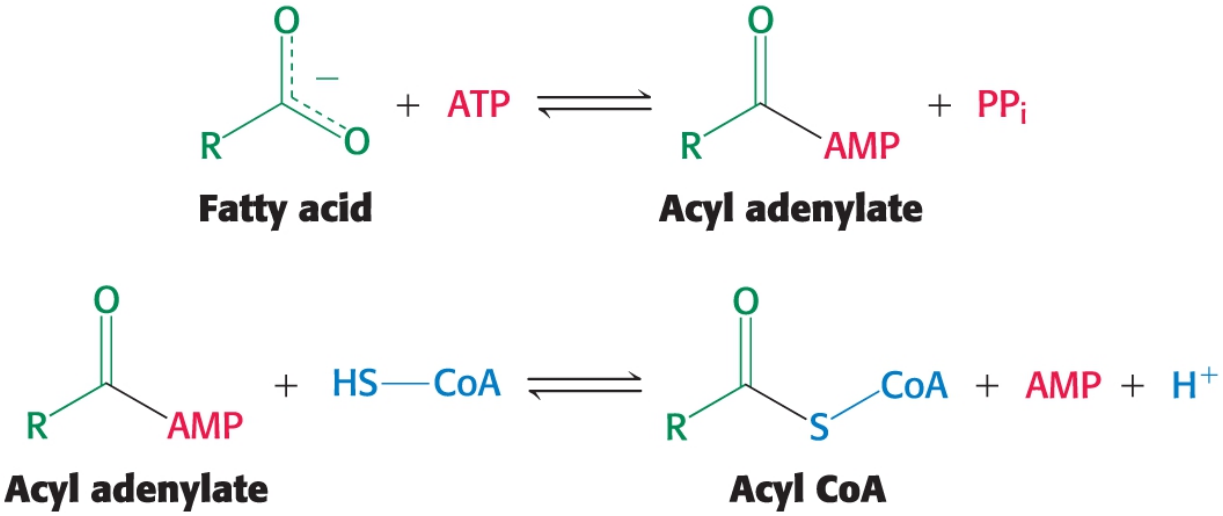
Acyl adenylate

The structure of acyl adenylate is as follows: A 5-membered heterocyclic pentagonal ring is in a horizontal orientation with C 1 occupying the bottom-right vertex. It consists of 1 O and 4 C atoms. O occupies the rightmost vertex. C 1 is single bonded to adenine on the lower right. C 2 and C 3 are dash bonded to O H on the left. C 4 is wedge bonded to C H 2 on the upper right. C H 2 is single bonded to O 1 atom of a zigzag vertical chain composed of O, single bond, P,

single bond, O. P is partially double bonded to O on the upper left and lower left. The O atoms bonded to P have an overall negative charge. O 2 of the chain is single-bonded to C on the upper left. This C atom is double-bonded to O on the left and single-bonded to R on the upper right.

Return to Structure of acyl adenylate

Extended description for Conversion of fatty acid to acyl adenylate and acyl adenylate to acyl C o A



The first reversible reaction consists of two reactants and two products. The first reactant is fatty acid whose structure is as follows: A central C atom is partially double bonded to O above, partially double bonded to O on the lower right, and single bonded to R on the lower left. The O atoms have an overall negative charge.

The second reactant is A T P.

The first product is acyl adenylate whose structure is as follows: A central C atom is double bonded to O above, single bonded to R on the lower left, and single bonded to A M P on the lower right.

The second product is P P subscript i.

The second reversible reaction consists of two reactants and three products.

The first reactant is acyl adenylate whose structure is as follows: A central C atom is double bonded to O above, single bonded to R on the lower left, and single bonded to A M P on the lower right.

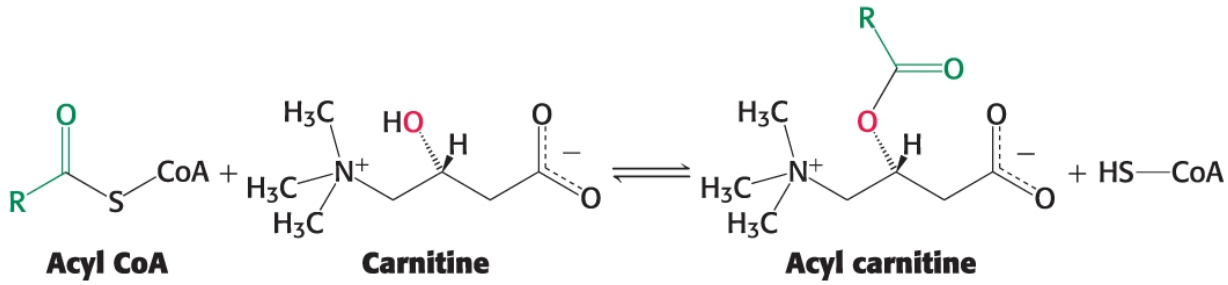
The second reactant is H S, single bond, C o A.

The first product is acyl C o A whose structure is as follows: A central C atom is single bonded to R on the lower left, double bonded to O above, and single bonded to S on the lower right. The S atom is single bonded to C o A on the upper right.

The second product is A M P. The third product is H superscript plus ion.

Return to Conversion of fatty acid to acyl adenylate and acyl adenylate to acyl C o A

Extended description for Formation of acyl carnitine from acyl C o A and carnitine



The reaction consists of two reactants and two products. The first reactant is acyl C o A whose structure is as follows: A central C atom is single bonded to R on the lower left, double bonded to O above, and single bonded to S on the lower right. The S atom is single-bonded to C o A on the upper right.

The second reactant is carnitine whose structure is as follows: A 3-carbon alkane chain is depicted as a line structure using 2 zigzag lines. C 1 is single bonded to N superscript plus on the upper left. N superscript plus is single bonded to C H 3 above, on the left, and lower left. C 2 is dash bonded to O H on the upper left and wedge bonded to H on the upper right. C 3 is single-bonded to C on the upper right. This C atom is partially double-bonded to O above and O on the lower right. The O atoms have an overall negative charge.

A reversible reaction arrow leads to the products.

The first product is acyl-carnitine whose structure is as follows: A 3-carbon alkane chain is depicted as a line structure using 2 zigzag lines. C 1 is single bonded to N superscript plus on the upper left. N superscript plus is single bonded to C H 3 above, on the left, and lower left. C 2 is dash bonded to O on the upper left and wedge

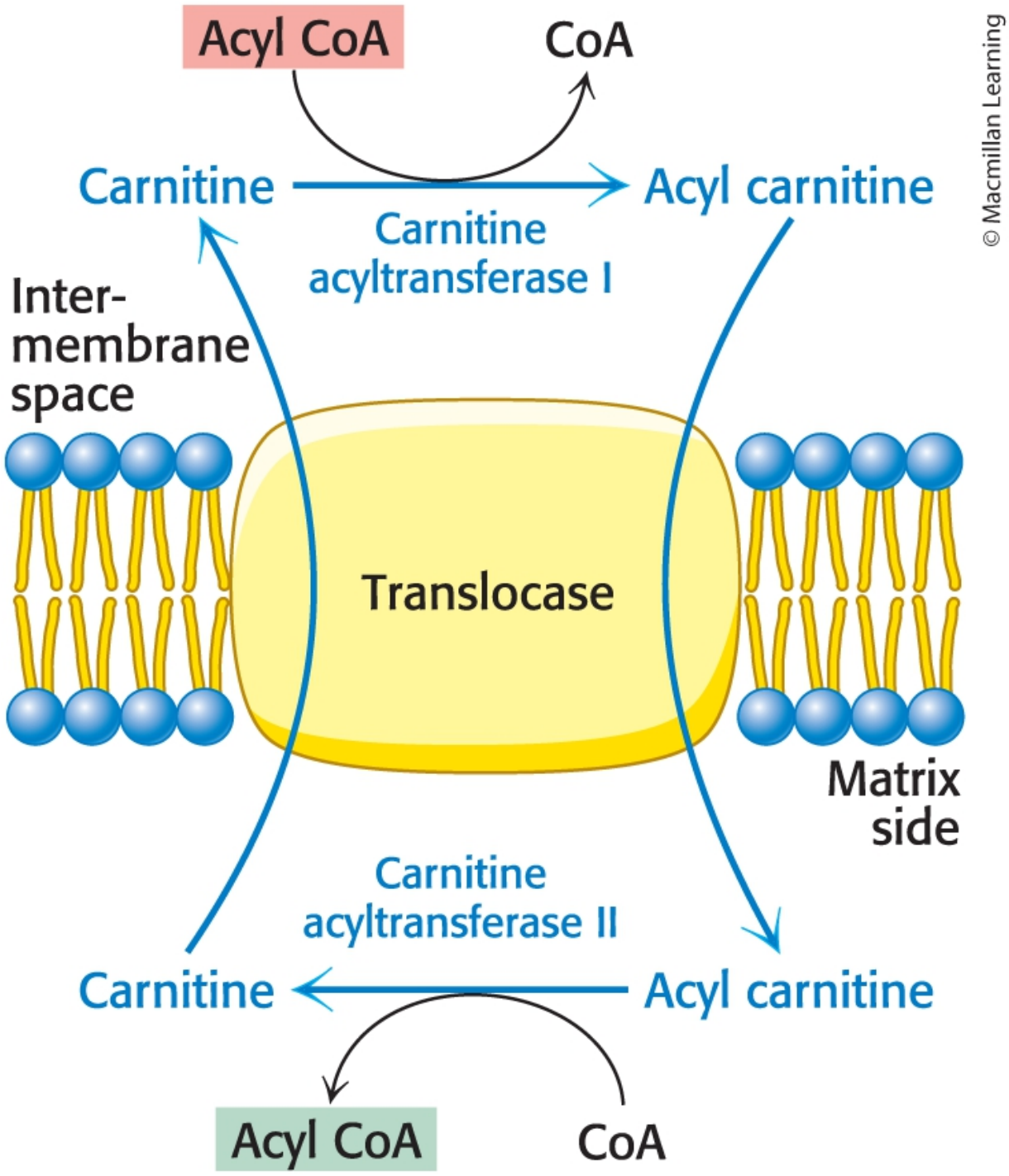
bonded to H on the upper right. The O atom is single-bonded to C on the upper right. This C is single-bonded to R on the upper left and double-bonded to O on the right. C 3 is single-bonded to C on the upper right. This C atom is partially double-bonded to O above and O on the lower right. The O atoms have an overall negative charge.

The second product is H S, single bond, C o A.

Return to Formation of acyl carnitine from acyl C o A and carnitine

Extended description for FIGURE 22.7 Acyl carnitine translocase mediates the entry of acyl carnitine into

the mitochondrial matrix



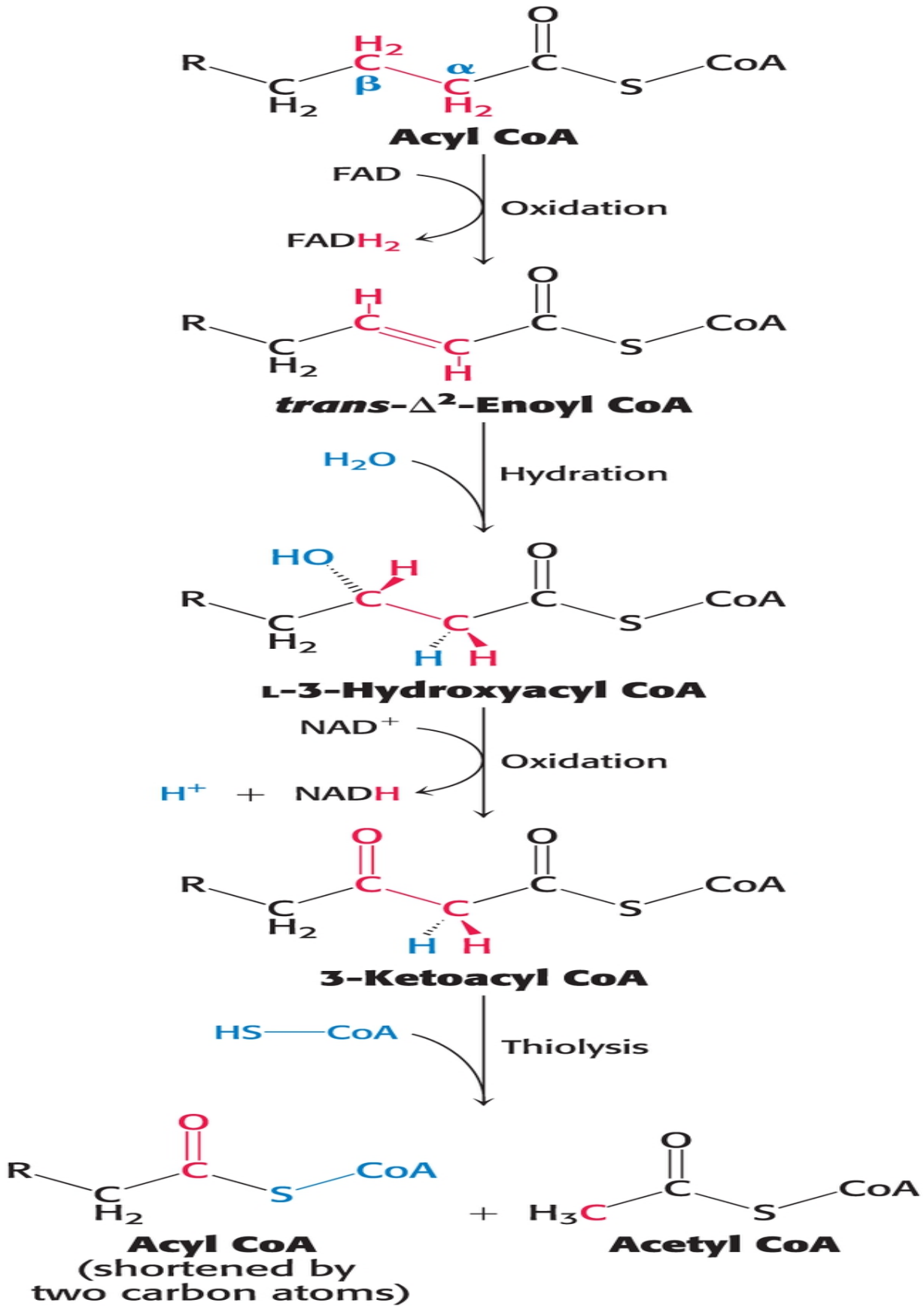
A lipid bilayer contains an oblong transport protein labeled translocase embedded in the membrane. The region above the

membrane is labeled intermembrane space and the region below is labeled matrix side. On the matrix side, acyl carnitine is irreversibly converted into carnitine by carnitine acyltransferase 2 with the simultaneous conversion of C o A to acyl C o A. The carnitine produced in the matrix side is transported into the intermembrane space by the translocase. In the intermembrane space, carnitine is irreversibly converted into acyl carnitine by carnitine acyltransferase 1 with the simultaneous conversion of acyl C o A to C o A. The acyl carnitine is then transported into the matrix site by the translocase.

Return to FIGURE 22.7 Acyl carnitine translocase mediates the entry of acyl carnitine into the mitochondrial matrix

Extended description for FIGURE 22.8 The reaction sequence for the degradation of fatty acids has four

sequential steps


Acyl CoA
FAD
FADH2
Oxidation
trans-Δ2-Enoyl CoA
H2O
Hydration
L-3-Hydroxyacyl CoA
NAD+
H+ + NADH
Oxidation
3-Ketoacyl CoA
HS—CoA
Thiolysis
Acyl CoA
(shortened by
two carbon atoms)
+
Acetyl CoA

In the first step, acyl C o A undergoes irreversible oxidation to produce trans-delta superscript 2-Enoyl C o A. It is coupled with the reduction of F A D to F A D H 2.

The structure of acyl C o A is as follows: A zigzag chain is composed of R, single bond, C H 2, single bond, C H 2, single bond, C H 2, single bond, C, single bond, S. The second C H 2 group is labeled beta and the third C H 2 group is labeled alpha. C 4 is double bonded to O above. S is single-bonded to C o A on the upper right.

The structure of trans-delta superscript 2-Enoyl C o A is as follows: A zigzag chain is composed of R, single bond, C H 2, single bond, C, double bond, C, single bond, C, single bond, S. C 2 and C 3 are each single bonded to H. C 4 is double bonded to O above. S is single-bonded to C o A on the upper right.

In the second step, trans-delta superscript 2-Enoyl C o A undergoes hydration to produce L-3-Hydroxyacyl C o A. It is coupled with the entry of H 2 O.

The structure of L-3-Hydroxyacyl C o A is as follows: A zigzag chain is composed of R, single bond, C H 2, single bond, C, single bond, C, single bond, C, single bond, S. C 2 is dash bonded to O H on the upper left and wedge bonded to H on the upper right. C 3 is dash bonded to H on the lower left and wedge bonded to H on the lower right. C 4 is double bonded to O above. S is single-bonded to C o A on the upper right.

In the third step, L-3-Hydroxyacyl C o A undergoes oxidation to produce 3-ketoacyl C o A. It is coupled with the reduction of N A D superscript plus to N A D H plus H superscript plus.

The structure of 3-ketoacyl C o A is as follows: A zigzag chain is composed of R, single bond, C H 2, single bond, C, single bond, C, single bond, C, single bond, S. C 2 is double bonded to O above. C 3 is dash bonded to H on the lower left and wedge bonded to H on the lower right. C 4 is double bonded to O above. S is single-bonded to C o A on the upper right.

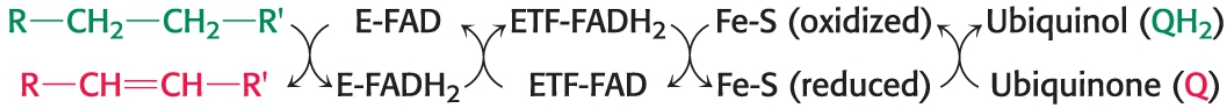
In the fourth step, 3-ketoacyl C o A undergoes thiolysis to produce acyl C o A and acetyl C o A with the simultaneous entry of H S, single bond, C o A.

The structure of acyl C o A is as follows: A zigzag chain is composed of R, single bond, C H 2, single bond, C, single bond, S. C 2 is double bonded to O above. S is single-bonded to C o A on the upper right. The acyl C o A is shortened by two carbon atoms.

The structure of acetyl C o A is as follows: A zigzag chain is composed of C H 3, single bond, C, single bond, S. C 2 is double bonded to O above. S is single-bonded to C o A on the upper right.

Return to FIGURE 22.8 The reaction sequence for the degradation of fatty acids has four sequential steps

Extended description for Sequential transfer of electrons from substrate to ubiquinone

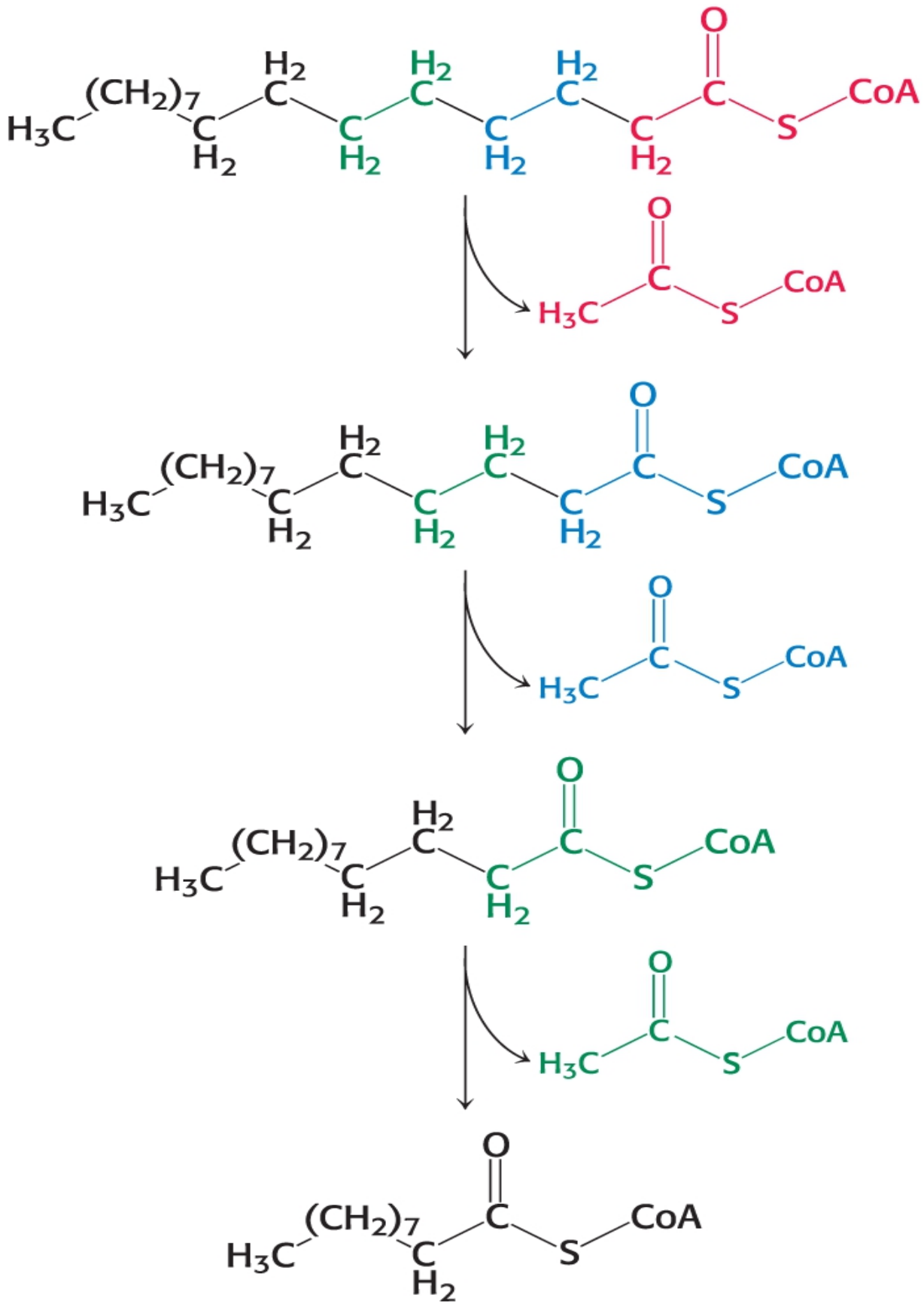


The transfer of electrons is depicted as follows: R, single bond, C H 2, single bond, C H 2, single bond, R dash is oxidized to R, single bond, C H, double bond, C H, single bond, R dash. The oxidation is coupled with the reduction of E, single bond, F A D to E, single bond, F A D H 2. E, single bond, F A D H 2 then transfers electrons to E T F, single bond, F A D to produce E T F, single bond, F A D H 2. The electrons from E T F-F A D H 2 are used to convert F e, single bond, S (oxidized) to F e, single bond, S (reduced). The reduced Fe, single bond, S donates electrons to ubiquinone (Q) to convert it into ubiquinol (Q H 2).

Return to Sequential transfer of electrons from substrate to ubiquinone

Extended description for FIGURE 22.9 Each round of

fatty acid degradation removes two carbons


O
H2
H2
H2
(CH2)7
C
C
C
C
C
C
S
CoA
H3C
H2
H2
H2
H2
O
C
CoA
H3C
S
O
H2
H2
(CH2)7
C
C
C
CoA
H3C
S
H2
H2
H2
O
C
CoA
H3C
S
O
H2
(CH2)7
C
C
CoA
H3C
S
H2
H2
O
C
CoA
H3C
S
O
C
(CH2)7
CoA
H3C
S
H2

The initial substrate has the following structure: A zigzag chain is composed of C H 3, single bond, open parenthesis C H 2 close parenthesis with subscript 7, single bond, C H 2, single bond, C H 2, single bond, C H 2, single bond, C H 2, single bond, C H 2, single bond, C H 2, single bond, C, single bond, S. C 10 is double bonded to O above. S is single-bonded to C o A on the upper right.

A downward arrow points to the product of the first round of degradation.

The leaving 2-carbon unit has the following structure: A zigzag chain is composed of C H 3, single bond, C, single bond, S. C 2 is double bonded to O above. S is single-bonded to C o A on the upper right.

The structure of the product of the first round of degradation is as follows: A zigzag chain is composed of C H 3, single bond, open parenthesis C H 2 close parenthesis with subscript 7, single bond, C H 2, single bond, C H 2, single bond, C H 2, single bond, C H 2, single bond, C H 2, single bond, C, single bond, S. C 8 is double bonded to O above. S is single-bonded to C o A on the upper right.

In the second round of degradation, another 2-carbon unit leaves from the right end of the first product. The structure of the product of the second round of degradation is as follows: A zigzag chain is composed of C H 3, single bond, open parenthesis C H 2 close parenthesis with subscript 7, single bond, C H 2, single bond, C H 2, single bond, C H 2, single bond, C H 2, single bond, C, single bond, S. C 6 is double bonded to O above. S is single-bonded to C o A on the upper right.

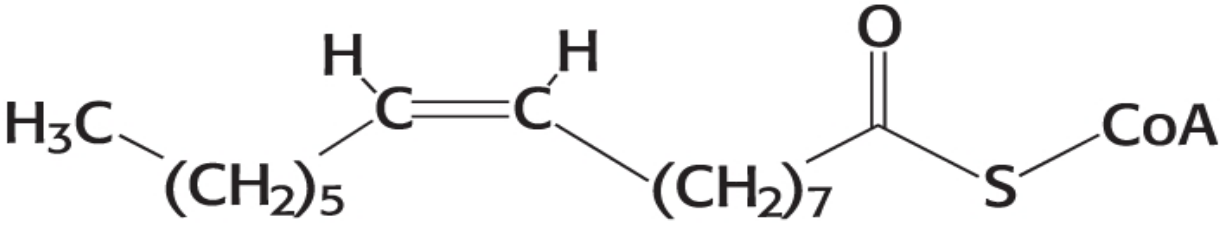
In the third round of degradation, another 2-carbon unit leaves from the right end of the second product. The structure of the product of the third round of degradation is as follows: A zigzag chain is

composed of C H 3, single bond, open parenthesis C H 2 close parenthesis with subscript 7, single bond, C H 2, single bond, C, single bond, S. C 4 is double bonded to O above. S is single-bonded to C o A on the upper right.

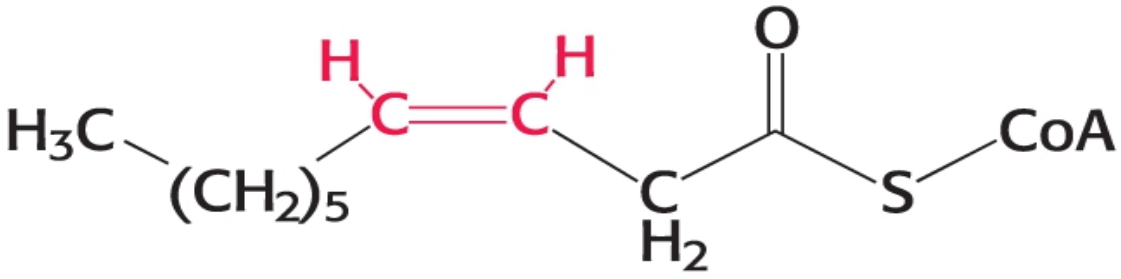
Return to FIGURE 22.9 Each round of fatty acid degradation removes two carbons

Extended description for FIGURE 22.10 The degradation of a monounsaturated fatty acid involves

an additional enzymatic step



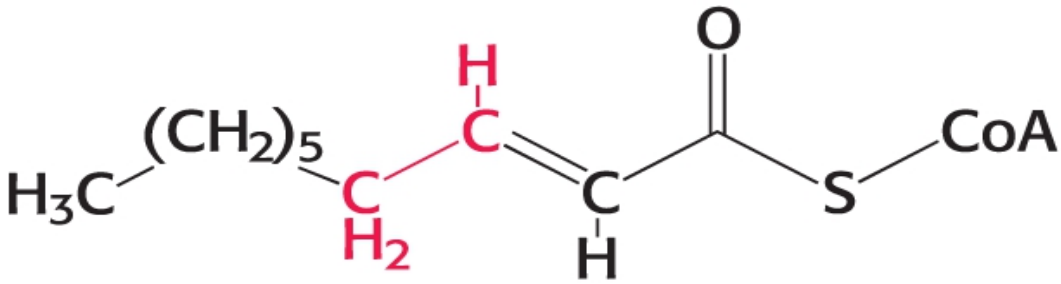
Palmitoleoyl CoA



4 3 2 1

***cis*-Δ^3-Enoyl CoA**

cis-Δ^3-Enoyl CoA isomerase



4 3 2 1

***trans*-Δ^2-Enoyl CoA**

In the first step, palmitoleoyl C o A is converted into cis-delta superscript 3-Enoyl C o A. Three successive downward arrows from palmitoleoyl C o A point to cis-delta superscript 3-Enoyl C o A.

The structure of palmitoleoyl C o A is as follows: C, double bond, C. C 1 and C 2 are single bonded to H. C 1 is single bonded to open parenthesis C H 2 close parenthesis with subscript 5, which is further single bonded to C H 3 on the upper left. C 2 is single bonded to open parenthesis C H 2 close parenthesis with subscript 7, which is further single bonded to a zigzag chain composed of C, single bond, S, single bond, C o A. C 1 of this chain is double bonded to O above.

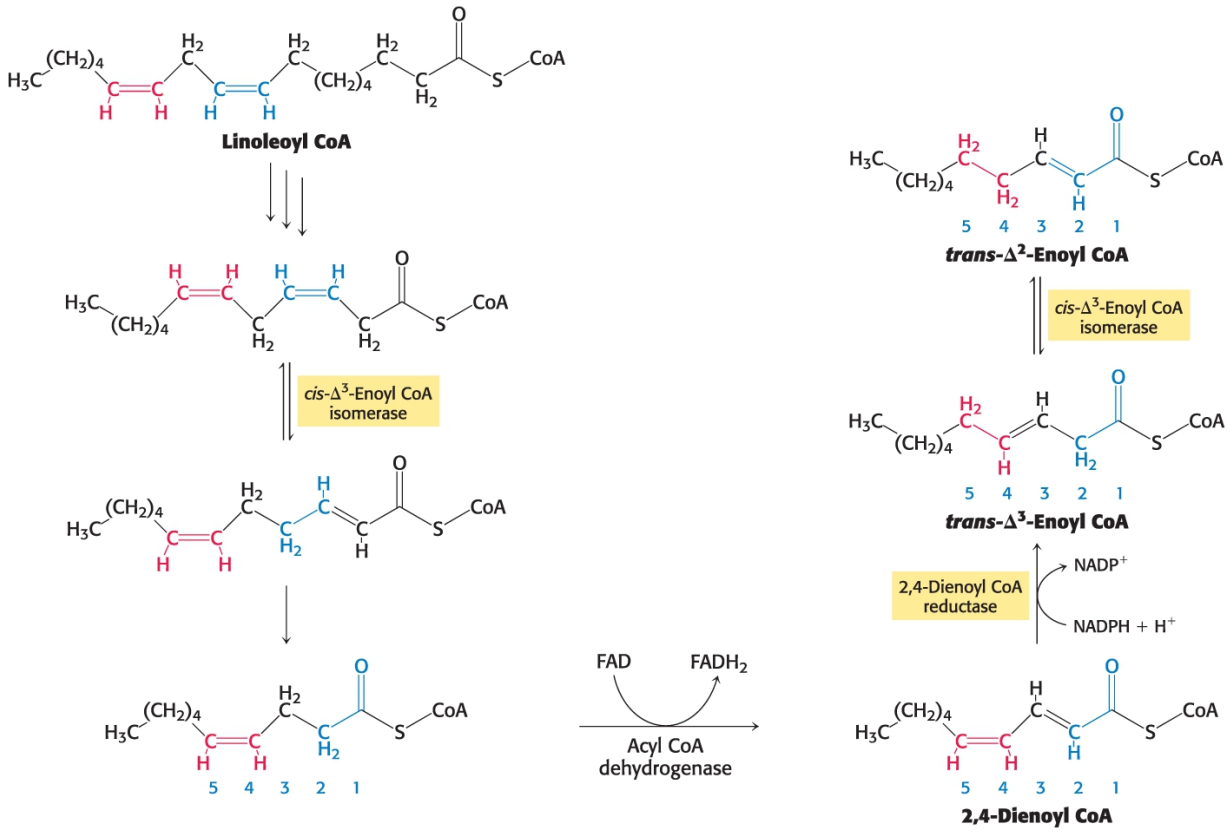
The structure of cis-delta superscript 3-Enoyl C o A is as follows: C, double bond, C. The first C is numbered 4 and the second C is numbered 3. C 3 and C 4 are single bonded to H. C 4 is single bonded to open parenthesis C H 2 close parenthesis with subscript 5, which is further single bonded to C H 3 on the upper left. C 3 is single bonded to a zigzag chain composed of C H 2, single bond, C, single bond, S, single bond, C o A. C 2 of this chain is double bonded to O above. The C atom of the C H 2 group is numbered 2 and the C atom is numbered 1.

In the second step, cis-delta superscript 3-Enoyl C o A is reversibly converted into trans-delta superscript 2-Enoyl C o A by the enzyme cis-delta superscript 3-Enoyl C o A isomerase.

The structure of trans-delta superscript 2-Enoyl C o A is as follows: A zigzag chain is composed of C H 3, single bond, open parenthesis C H 2 close parenthesis with subscript 5, single bond, C H 2, single bond, C, double bond, C, single bond, C, single bond, S, single bond, C o A. The C atoms starting with the third carbon atom from the left end are numbered 4 to 1. C 3 is single bonded to H above. C 2 is single bonded to H below. C 1 is double bonded to O above.

Return to FIGURE 22.10 The degradation of a monounsaturated fatty acid involves an additional enzymatic step

Extended description for FIGURE 22.11 Multiple additional enzymes are necessary to oxidize polyunsaturated fatty acids



The structure of linoleoyl C o A is as follows: A zigzag chain is composed of C H 3, single bond, open parenthesis C H 2 close parenthesis with subscript 4, single bond, C, double bond, C, single bond, C H 2, single bond, C, double bond, C, single bond, C H 2, single bond, open parenthesis C H 2 close parenthesis with subscript 4, single bond, C H 2, single bond, C H 2, single bond, C, single bond, S, single bond, C o A. Starting from the left end, C 3, C 4, C 6, and C 7 are single bonded to H below. C 12 is double bonded to O above.

Three successive downward arrows lead to the product.

The structure of the product is as follows: A zigzag chain is composed of C H 3, single bond, open parenthesis C H 2 close parenthesis with subscript 4, single bond, C, double bond, C, single bond, C H 2, single bond, C, double bond, C, single bond, C H 2, single bond, C, single bond, S, single bond, C o A. C 3, C 4, C 6, and C 7 are single bonded to H above. C 9 is double bonded to O above.

The enzyme cis-delta superscript 3-Enoyl C o A isomerase reversibly converts this product into a second product.

The structure of the second product is as follows: A zigzag chain is composed of C H 3, single bond, open parenthesis C H 2 close parenthesis with subscript 4, single bond, C, double bond, C, single bond, C H 2, single bond, C H 2, single bond, C, double bond, C, single bond, C, single bond, S, single bond, C o A. C 3 and C 4 are single bonded to H below. C 7 is single bonded to H above and C 8 is single bonded to H below.

The second product is irreversibly converted into a third product.

The structure of the third product is as follows: A zigzag chain is composed of C H 3, single bond, open parenthesis C H 2 close parenthesis with subscript 4, single bond, C, double bond, C, single bond, C H 2, single bond, C H 2, single bond, C, single bond, S, single bond, C o A. The carbon atoms starting with the C single bonded to S are numbered 1 to 5. C 4 and C 5 are single bonded to H below. C 1 is double bonded to O above.

A forward arrow labeled acyl C o A dehydrogenase leads to 2,4-Dienoyl C o A, which is produced by the oxidation of the third

product. This step is coupled with the reduction of F A D to F A D H 2.

The structure of 2,4-Dienoyl C o A is as follows: A zigzag chain is composed of C H 3, single bond, open parenthesis C H 2 close parenthesis with subscript 4, single bond, C, double bond, C, single bond, C, double bond, C, single bond, C, single bond, S, single bond, C o A. The carbon atoms starting with the C single bonded to S are numbered 1 to 5. C 4 and C 5 are single bonded to H below. C 2 is single bonded to H below and C 3 is single bonded to H above. C 1 is double bonded to O above.

An upward arrow labeled 2-4 dienoyl C o A reductase leads to trans-delta superscript 3-Enoyl C o A, which is produced by the reduction of 2,4-Dienoyl C o A. This step is coupled with the oxidation of N A D P H plus H superscript plus to N A D P superscript plus.

The structure of trans-delta superscript 3-Enoyl C o A is as follows: A zigzag chain is composed of C H 3, single bond, open parenthesis C H 2 close parenthesis with subscript 4, single bond, C H 2, single bond, C, double bond, C, single bond, C H 2, single bond, C, single bond, S, single bond, C o A. The carbon atoms starting with the C single bonded to S are numbered 1 to 5. C 4 is single bonded to H below. C 3 is single bonded to H above and C 1 is double bonded to O above.

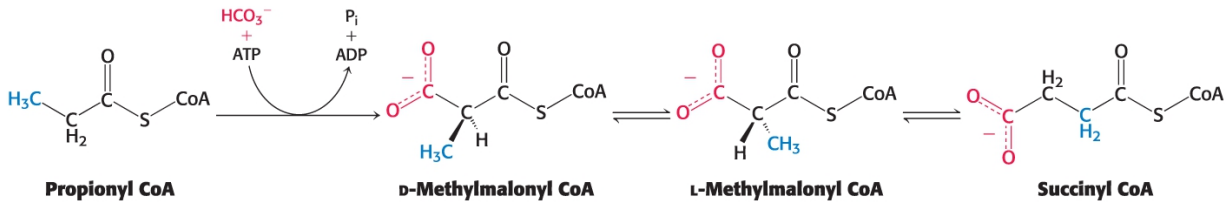
A reversible reaction arrow labeled cis-delta superscript 3-Enoyl C o A isomerase leads to trans-delta superscript 2-Enoyl C o A.

The structure of trans-delta superscript 2-Enoyl C o A is as follows: A zigzag chain is composed of C H 3, single bond, open parenthesis C H 2 close parenthesis with subscript 4, single bond, C H 2, single bond, C H 2, single bond, C, double bond, C, single bond, C, single

bond, S, single bond, C o A. The carbon atoms starting with the C single bonded to S are numbered 1 to 5. C 2 and C 3 are single bonded to H below and above respectively. C 1 is double bonded to O above.

Return to FIGURE 22.11 Multiple additional enzymes are necessary to oxidize polyunsaturated fatty acids

Extended description for FIGURE 22.12 The final product of odd-numbered fatty acid degradation is converted into a C A C intermediate



In the first irreversible step, propionyl C o A is converted into D-methylmalonyl C o A with the simultaneous entry of H C O 3 superscript minus, release of P subscript i, and the hydrolysis of A T P to A D P.

The structure of propionyl C o A is as follows: A zigzag chain is composed of C H 3, single bond, C H 2, single bond, C, single bond, S, single bond, C o A. C 3 is double bonded to O above.

The structure of D-methylmalonyl C o A is as follows: A zigzag chain is composed of C, single bond, C, single bond, C, single bond, S, single bond, C o A. C 1 is partially double bonded to O above and O on the lower left. The O atoms have an overall negative charge. C 2 is wedge bonded to C H 3 on the lower left and dash bonded to H on the lower right. C 3 is double bonded to O above.

In the second reversible step, D-methylmalonyl C o A is converted to L-Methylmalonyl C o A.

The structure of L-Methylmalonyl C o A is as follows: A zigzag chain is composed of C, single bond, C, single bond, C, single bond, S, single bond, C o A. C 1 is partially double bonded to O above and O

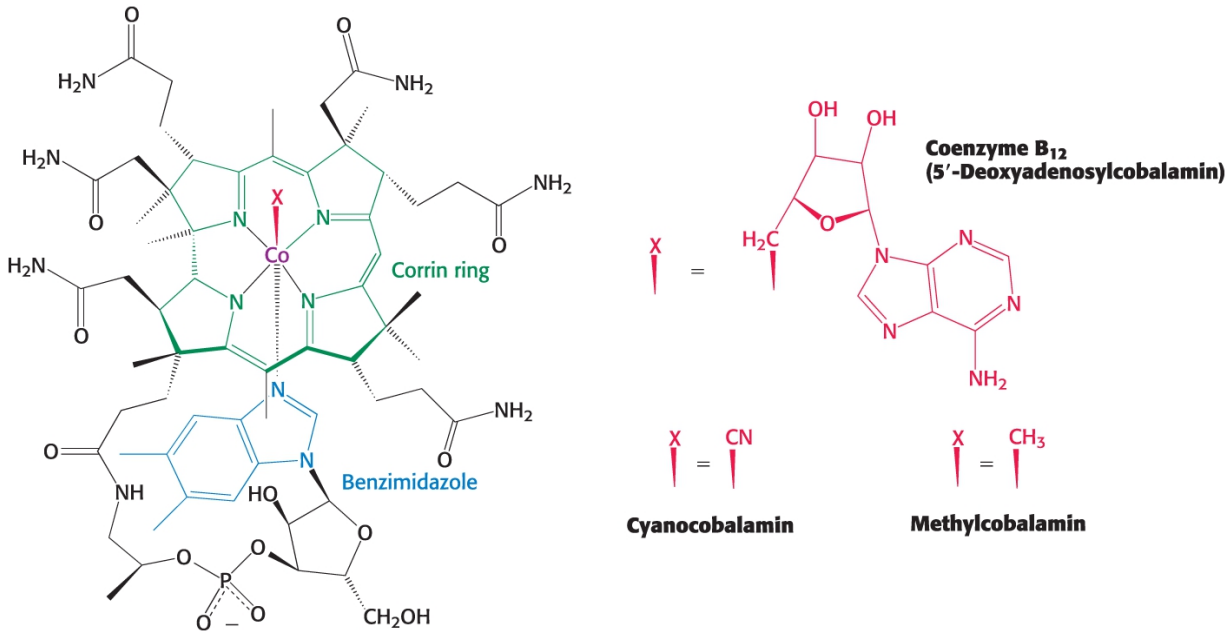
on the lower left. The O atoms have an overall negative charge. C 2 is wedge bonded to H on the lower left and dash bonded to C H 3 on the lower right. C 3 is double bonded to O above.

In the third reversible step, L-Methylmalonyl C o A is converted to succinyl C o A.

The structure of succinyl C o A is as follows: A zigzag chain is composed of C, single bond, C H 2, single bond, C H 2, single bond, C, single bond, S, single bond, C o A. C 1 is partially double bonded to O below and O on the upper left. The O atoms have an overall negative charge. C 4 is double bonded to O above.

Return to FIGURE 22.12 The final product of odd-numbered fatty acid degradation is converted into a C A C intermediate

Extended description for FIGURE 22.13 Coenzyme B 12 (cobalamin) is a class of molecules with a complex structure



The generalized structure of coenzyme B 12 is as follows: A central C o atom is single-bonded to an N atom of four different pyrrole rings located on the upper left, upper right, lower left, and lower right. The C o atom is wedge bonded to X above. The pyrrole rings are described as 5-membered heterocyclic pentagonal rings consisting of 1 N and 4 C atoms. The adjacent rings are connected by a methylene bridge between C 4 and C 1 except for two rings. The upper left and lower left rings are directly connected by a dash-bond between C 4 and C 1. The methylene bridge connecting the upper left and upper right, and the lower left and the lower right ring is single bonded to C H 3 in the form of a line.

C 2 of the upper left and upper right rings have an open dash-bond and are wedge bonded to C H 2. This C H 2 group is single-bonded to

C. The C atom is double bonded to O and single bonded to N H 2. C 3 of the upper left and upper right rings are dash bonded to C H 2 which is further single bonded to C H 2 in the form of a line. The C H 2 is single-bonded to C. This C is double bonded to O and single bonded to N H 2. C 1 of the upper left ring has an open dash bond.

C 2 of the lower right ring is dash bonded to C H 3 and wedge bonded to C H 3. C 3 is dash bonded to C H 2 which is further single bonded to C H 2 in the form of a line. The C H 2 is single-bonded to C. This C is double bonded to O and single bonded to N H 2.

C 2 of the lower left ring is wedge bonded to C H 3 and dash bonded to a 1 N and 5 C heteronuclear alkane chain depicted as a line structure using 5 zigzag lines. N occupies the fourth position and is bound to H. C 3 is double bonded to O. C 5 is wedge bonded to C H 3 and single bonded to the upper left O atom of a phosphate group. C 3 of the lower left ring is wedge bonded to C H 2, which is further single bonded to C. This C is double bonded to O and single bonded to N H 2.

The central C o atom is dash bonded below to N 1 of a 5-membered heterocyclic pentagonal ring consisting of 2 N and 3 C atoms. It contains a double bond between N 1 and C 1. This ring is fused to a benzene ring such that C 2 and C 3 of the pentagonal ring are C 3 and C 2 respectively, of the benzene ring. The benzene ring contains alternating double bonds between C 2 and C 3, C 4 and C 5, and C 6 and C 1. C 5 and C 6 are single-bonded to C H 3 in the form of a line. These fused rings are labeled benzimidazole.

N 2 of the pentagonal ring is wedge bonded to C 4 of another 5-membered heterocyclic pentagonal ring consisting of 1 O and 4 C atoms. C 1 is dash bonded to C H 2 O H. C 2 is wedge bonded to the upper right O atom of the phosphate group. C 3 is wedge bonded to O H.

In coenzyme B 12 (5 prime-deoxyadenosylcobalamin), the structure of the X group is as follows: A 5-membered heterocyclic pentagonal ring is in a horizontal orientation and consists of 2 N and 3 C atoms. A double bond is present between N 1 and C 1. The pentagonal ring is fused to a 6-membered heterocyclic hexagonal ring such that C 2 and C 3 of the pentagonal ring are C 4 and C 3 respectively of the hexagonal ring. In the hexagonal ring, N 1 occupies the topmost vertex and N 2 occupies the bottom right vertex. A double bond is present between N 1 and C 1, and N 2 and C 2. C 2 is single bonded to N H 2 below. N 2 of the pentagonal ring is single-bonded to C 4 of a 5-membered heterocyclic pentagonal ring in a vertical orientation. This pentagonal ring consists of 1 O and 4 C atoms. O occupies the bottom-most vertex. A wedge bond is present between O and C 1, and O and C 4. C 1 is single bonded to C H 2 below. This C H 2 group is wedge bonded to the central C o atom of the coenzyme B 12. C 2 and C 3 are each single bonded to O H above. In cyanocobalamin, the X group is C N. In methylcobalamin, the X group is C H 3.

Return to FIGURE 22.13 Coenzyme B 12 (cobalamin) is a class of molecules with a complex structure

Extended description for FIGURE 22.14 Cobalamin enzymes catalyze specific rearrangement reactions



The reaction consists of one reactant and one product.

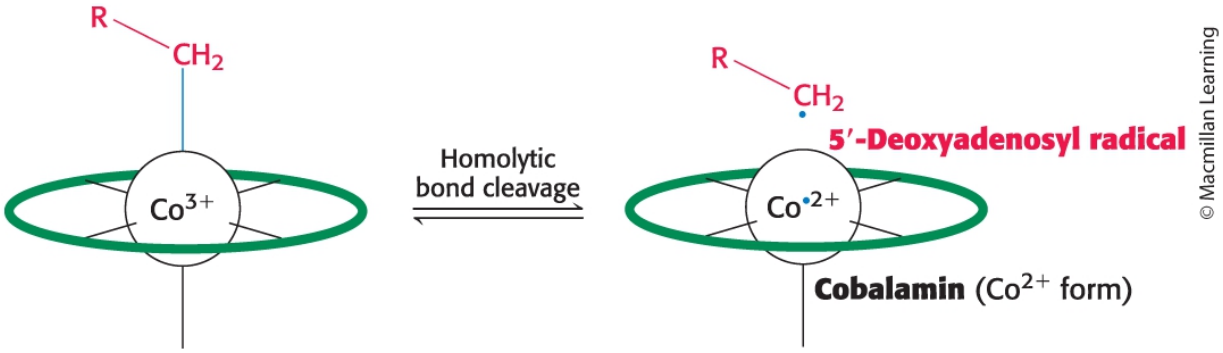
The structure of the reactant is as follows: C, single bond, C. C 1 has an open single bond above, an open single bond on the left, and is single bonded to H below. C 2 is single bonded to R above and has an open single bond on the right and below.

A reversible reaction arrow points to the product.

The structure of the product is as follows: C, single bond, C. C 1 has an open single bond above, an open single bond on the left, and is single bonded to R below. C 2 is single bonded to H above and has an open single bond on the right and below.

Return to FIGURE 22.14 Cobalamin enzymes catalyze specific rearrangement reactions

Extended description for FIGURE 22.15 Cobalamin enzymes accomplish homolytic bond cleavage to form a radical



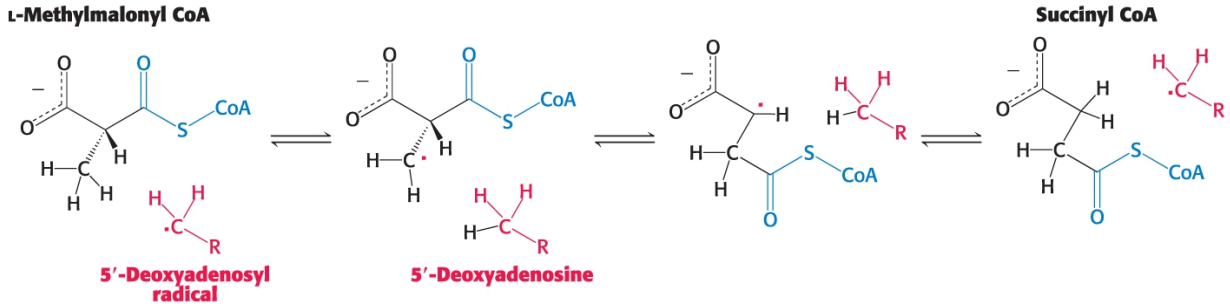
A structure on the left consists of a central white sphere depicting C o superscript 3 plus ion. It is surrounded by a green ring. The C o superscript 3 plus ion is connected to the ring through a single bond on the upper left, upper right, lower left, and lower right. It has an open single bond below and is single bonded to C H 2 above. The C H 2 group is single-bonded to R on the upper left.

A reversible reaction arrow labeled homolytic bond cleavage leads to a structure on the right.

The structure on the right is labeled cobalamin C o superscript 2 plus form. It consists of a central white sphere depicting C o superscript 2 plus with a blue dot. It is surrounded by a green ring. The C o superscript 2 plus ion is connected to the ring through a single bond on the upper left, upper right, lower left, and lower right. It has an open single bond below. An isolated C H 2 group is single-bonded to R on the upper left. The C atom of the C H 2 group has a blue dot. This structure composed of C H 2, single bond, R is labeled 5 prime-deoxyadenosyl radical.

Return to FIGURE 22.15 Cobalamin enzymes accomplish homolytic bond cleavage to form a radical

Extended description for FIGURE 22.16 Succinyl C o A is formed from methylmalonyl C o A by a rearrangement reaction



L-methylmalonyl C o A reacts with 5 prime-deoxyadenosyl radical to form two intermediate products.

The structure of L-methylmalonyl C o A is as follows: A 3-carbon alkane chain is depicted as a line structure using 2 zigzag lines. C 1 is partially double bonded to O above and O on the lower left. The O atoms have an overall negative charge. C 2 is wedge bonded to H on the lower right and dash-bonded to C on the lower left. This C atom is single-bonded to H on the left, lower left, and lower right. C 3 is double bonded to O above and single bonded to S on the lower right. The S atom is single-bonded to C o A on the upper right.

The structure of 5 prime-deoxyadenosyl radical is as follows: A central C atom with an unpaired electron is single-bonded to H on the upper left, H on the upper right, and R on the lower right.

A reversible reaction arrow leads to the intermediate products.

The first intermediate product is as follows: A 3-carbon alkane chain is depicted as a line structure using 2 zigzag lines. C 1 is partially

double bonded to O above and O on the lower left. The O atoms have an overall negative charge. C 2 is wedge bonded to H on the lower right and dash-bonded to C with an unpaired electron on the lower left. This C atom is single-bonded to H on the left and below. C 3 is double bonded to O above and single bonded to S on the lower right. The S atom is single-bonded to C o A on the upper right.

The second intermediate product is 5 prime-deoxyadenosine whose structure is as follows: A central C atom is single bonded to H on the left, H on the upper left, H on the upper right, and R on the lower right.

A reversible reaction arrow leads to the intermediate products.

The first intermediate product is as follows: A 2-carbon alkane chain is depicted as a line structure using a line. C 1 is partially double bonded to O above and O on the lower left. The O atoms have an overall negative charge. C 2 with an unpaired electron is single bonded to H on the right and C below. The C atom is single-bonded to H on the left and H on the lower left, and single-bonded to C on the lower right. The lower right C atom is double bonded to O below and single bonded to S on the upper right, which is further single bonded to C o A on the lower right.

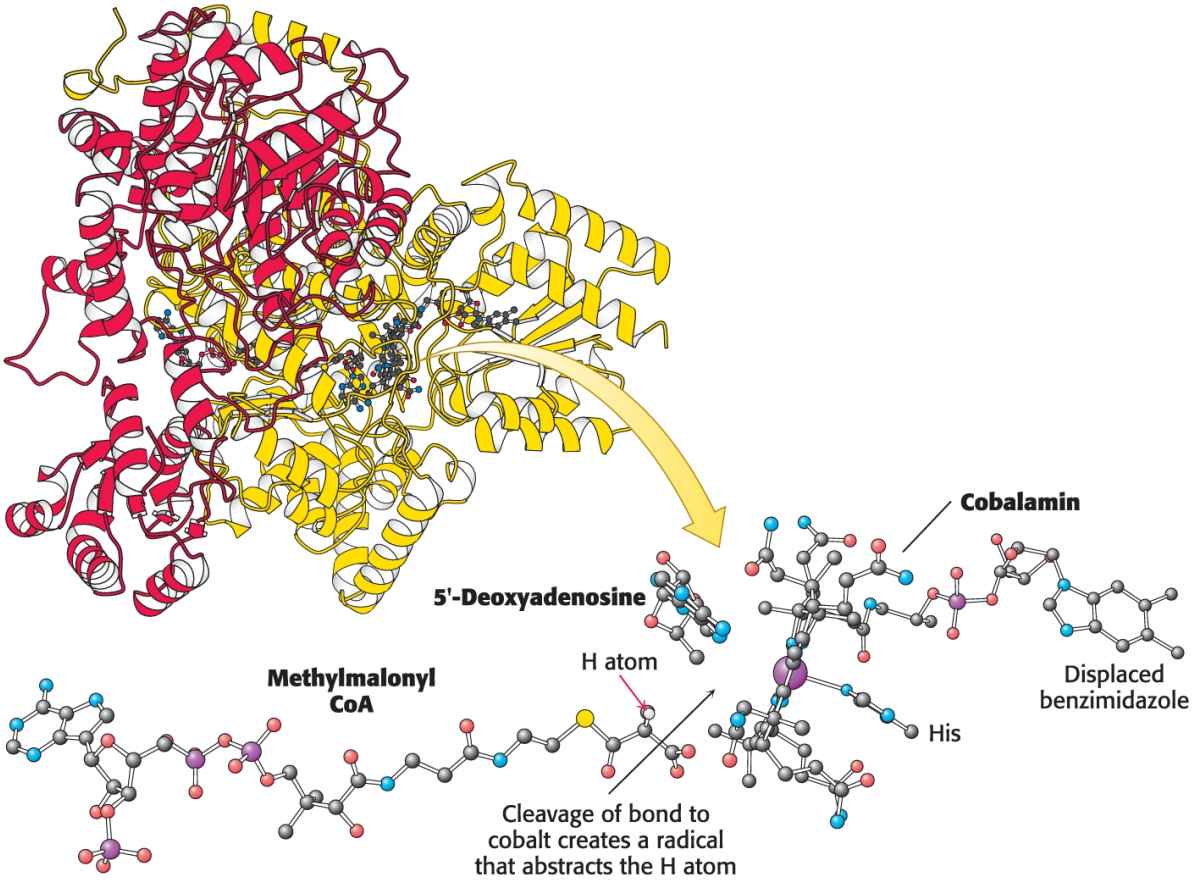
The second intermediate product is as follows: A central C atom is single-bonded to H on the left, H on the upper left, H on the upper right, and R on the lower right. A reversible reaction arrow leads to the final products. The first product is succinyl C o A whose structure is as follows: A 2-carbon alkane chain is depicted as a line structure using a line. C 1 is partially double bonded to O above and O on the lower left. The O atoms have an overall negative charge. C 2 is single bonded to H on the upper right, H on the lower right, and C below. The C atom is single-bonded to H on the left and H on the lower left, and single-bonded to C on the lower right. The C atom is

double bonded to O below and single bonded to S on the upper right, which is further single bonded to C o A on the lower right.

The second product is as follows: A central C atom with an unpaired electron is single-bonded to H on the upper left, H on the upper right, and R on the lower right.

Return to FIGURE 22.16 Succinyl C o A is formed from methylmalonyl C o A by a rearrangement reaction

Extended description for FIGURE 22.17 The active site of methylmalonyl C o A mutase reveals how radical formation is accomplished



© Macmillan Learning

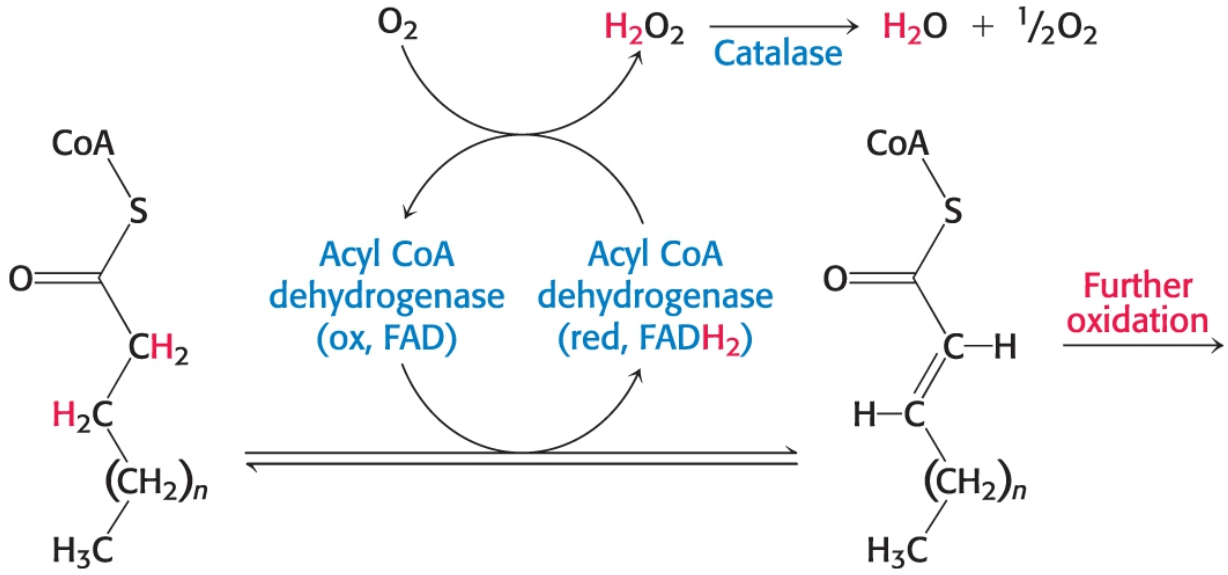
The ribbon diagram consists of two interconnected clusters. One cluster is composed of red alpha-helices and red beta-strands and the other cluster is composed of yellow alpha-helices and yellow beta-strands. The center of the enzyme contains an active site with several molecules depicted as ball-and-stick models. An arrow from the active site shows the enlarged view of the arrangement of the ball-and-stick models of the substrate, coenzymes, and amino acid residues.

A ball-and-stick model of methylmalonyl C o A is shown on the left. A white sphere connected to the second black sphere from the right end is labeled the H atom. The rightmost black sphere is connected to two red spheres. An arrow passes through the bond connecting these two black spheres. The text alongside this arrow reads "Cleavage of bond to cobalt creates a radical that abstracts the H atom."

A ball-and-stick model of cobalamin is shown on the right. Its four pyrrole rings connected to a central cobalt atom are oriented toward the right end of methylmalonyl C o A. The cobalt atom depicted as a purple sphere is connected to the histidine side chain on the lower right. The benzimidazole ring of cobalamin is displaced. A ball-and-stick model of 5 prime-deoxyadenosine is located above the right terminal of methylmalonyl C o A and the tetrapyrrole ring of cobalamin.

Return to FIGURE 22.17 The active site of methylmalonyl C o A mutase reveals how radical formation is accomplished

Extended description for FIGURE 22.18 Initiation of peroxisomal fatty acid degradation requires a flavoprotein



The reaction consists of one reactant and one product. The structure of the reactant is as follows: A vertical zigzag chain is composed of C o A, single bond, S, single bond, C, single bond, C H 2, single bond, C H 2, single bond, open parenthesis C H 2 close parenthesis with subscript n, single bond, C H 3. C 1 is double bonded to O on the left.

A reversible reaction arrow leads to the product. A curved arrow above it depicts the simultaneous conversion of acyl C o A dehydrogenase (oxidized, F A D) to acyl C o A dehydrogenase (reduced, F A D H 2).

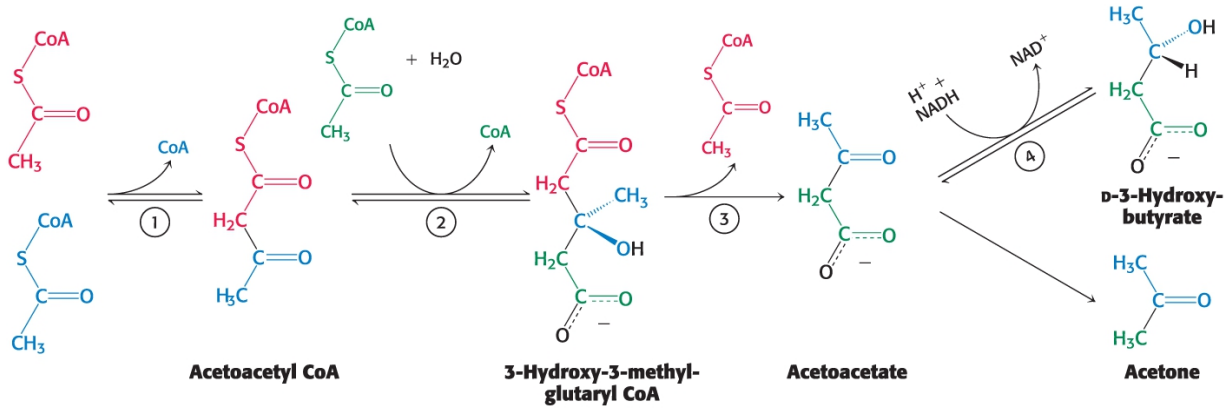
The structure of the product is as follows: A vertical zigzag chain is composed of C o A, single bond, S, single bond, C, single bond, C, double bond, C, single bond, open parenthesis C H 2 close parenthesis with subscript n, single bond, C H 3. C 1 is double

bonded to O on the left. C 2 is single bonded to H on the right. C 3 is single-bonded to H on the left. A forward arrow on the right of the product is labeled further oxidation.

The acyl C o A dehydrogenase (reduced, F A D H 2) is converted back to acyl C o A dehydrogenase (oxidized, F A D) with the simultaneous conversion of O 2 to H 2 O 2. H 2 O 2 is further converted into H 2 O and a half O 2 by the enzyme catalase.

Return to FIGURE 22.18 Initiation of peroxisomal fatty acid degradation requires a flavoprotein

Extended description for FIGURE 22.19 Ketone bodies are formed from acetyl C o A primarily in the liver



The formation of ketone bodies is divided into 4 steps.

In the first reversible step, acetoacetyl C o A is formed from two acetyl C o A molecules.

The structure of acetyl C o A is as follows: A central C atom is single bonded to C H 3 on the lower left, double bonded to O on the right, and single bonded to S, single bond, C o A on the upper left. C o A leaves the reaction.

The structure of acetoacetyl C o A is as follows: A vertical zigzag chain is composed of C o A, single bond, S, single bond, C, single bond, C H 2, single bond, C, single bond, C H 3. C 1 and C 3 are each double bonded to O on the right.

In the second reversible step, acetoacetyl C o A is converted into 3-hydroxy-3-methylglutaryl C o A. An acetyl C o A plus H 2 O molecule enters and C o A leaves the reaction.

The structure of 3-hydroxy-3-methylglutaryl C o A is as follows: A vertical zigzag chain is composed of C o A, single bond, S, single bond, C, single bond, C H 2, single bond, C, single bond, C H 2, single bond, C. C 1 is double bonded to O on the right. C 3 is dash-bonded to C H 3 on the upper right and wedge bonded to O H on the lower right. C 5 is partially double bonded to O on the right and O on the lower left. The O atoms have an overall negative charge.

In the third irreversible step, 3-hydroxy-3-methylglutaryl C o A is converted into acetoacetate. An acetyl-C o A group leaves the reaction.

The structure of acetoacetate is as follows: A vertical zigzag chain is composed of C H 3, single bond, C, single bond, C H 2, single bond, C. C 2 is double bonded to O on the right. C 4 is partially double bonded to O on the right and O on the lower left. The O atoms have an overall negative charge.

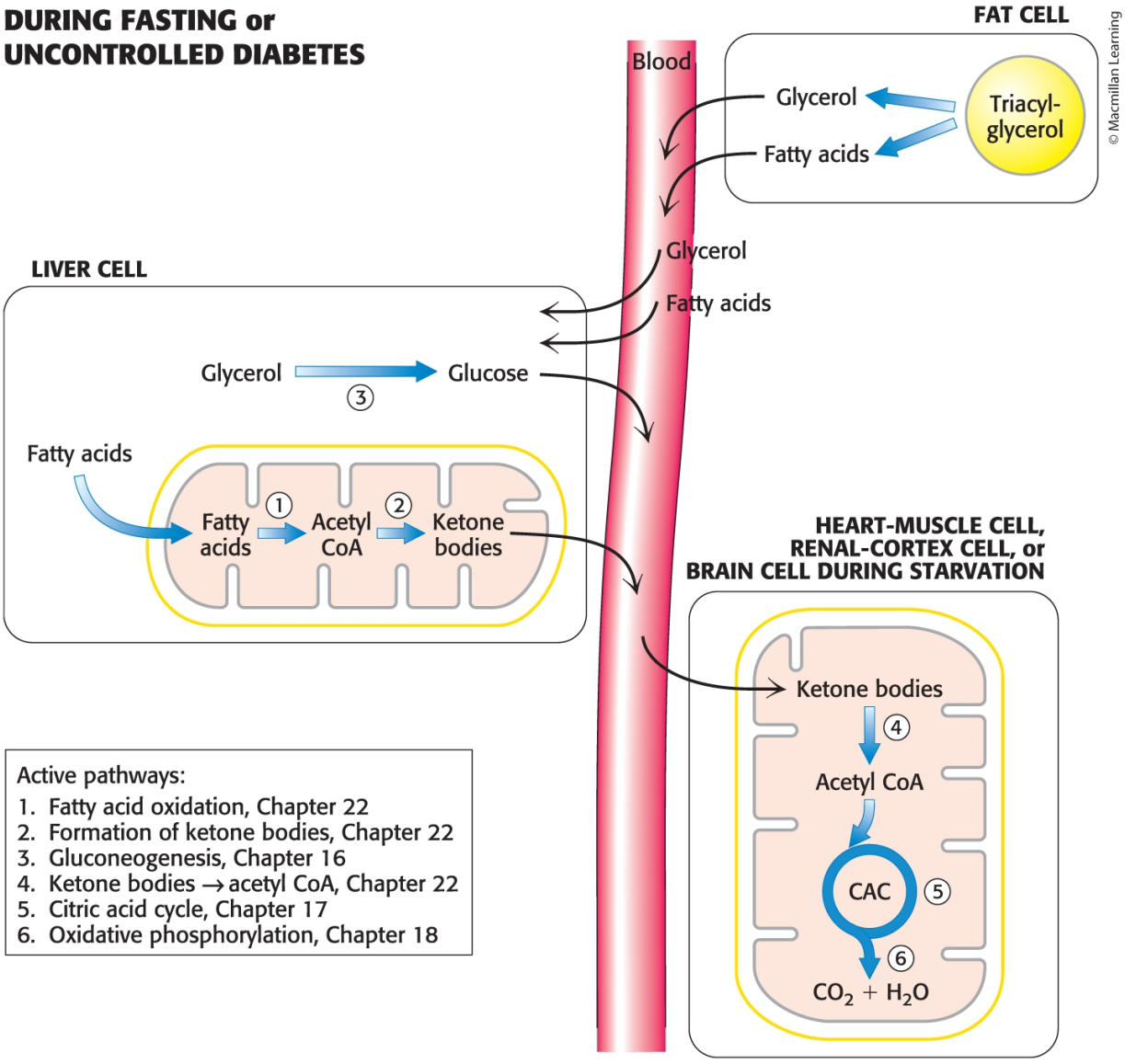
In the fourth step, D-3-hydroxy-butyrate is formed reversibly from acetoacetate with the simultaneous oxidation of N A D H plus H superscript plus to N A D superscript plus. Acetone is formed irreversibly from acetoacetate.

The structure of D-3-hydroxy-butyrate is as follows: A vertical zigzag chain is composed of C H 3, single bond, C, single bond, C H 2, single bond, C. C 2 is dash bonded to O H on the upper right and wedge bonded to H on the lower right. C 4 is partially double bonded to O on the right and O on the lower left. The O atoms have an overall negative charge.

The structure of acetone is as follows: A central C atom is single-bonded to C H 3 on the upper left, C H 3 on the lower left, and double-bonded to O on the right.

Return to FIGURE 22.19 Ketone bodies are formed from acetyl C o A primarily in the liver

Extended description for FIGURE 22.20 Pathway Integration: The liver supplies ketone bodies to the peripheral tissues



A long and tubular structure shown in the center depicts a blood vessel containing blood. A fat cell is depicted on the right as a rectangular structure. It contains a large yellow circle labeled triacylglycerol. The triacylglycerol is broken down into glycerol and

fatty acids. The glycerol and fatty acids are released into the bloodstream. They travel through the bloodstream to reach the liver cell depicted as a large rectangle. Inside the liver cell, fatty acids are transported into mitochondria. Inside the liver mitochondria, fatty acids are converted into acetyl C o A. This step is depicted as a forward arrow labeled 1. Acetyl C o A is converted into ketone bodies. This step is depicted as a forward arrow labeled 2. In the liver cell cytoplasm, glycerol is converted into glucose. This step is depicted as a forward arrow labeled 3. Glucose and ketone bodies are released into the bloodstream from the liver cell. The ketone bodies enter the heart-muscle cell, renal-cortex cell, or brain cell during starvation. Inside the mitochondria of these cells, ketone bodies are converted into acetyl C o A. This step is depicted as a forward arrow labeled 4. Acetyl C o A enters the citric acid cycle depicted as a tiny circle with a blue outline labeled C A C in the center. C A C step is numbered 5. An arrow labeled 6 from the C A C shows the release of C O 2 plus H 2 O in the mitochondria.

A key titled "active pathways" lists the following points:

1. Fatty acid oxidation, Chapter 22.

2. Formation of ketone bodies, Chapter 22.

3. Gluconeogenesis, Chapter 16.

4. Ketone bodies, forward arrow, acetyl C o A, Chapter 22.

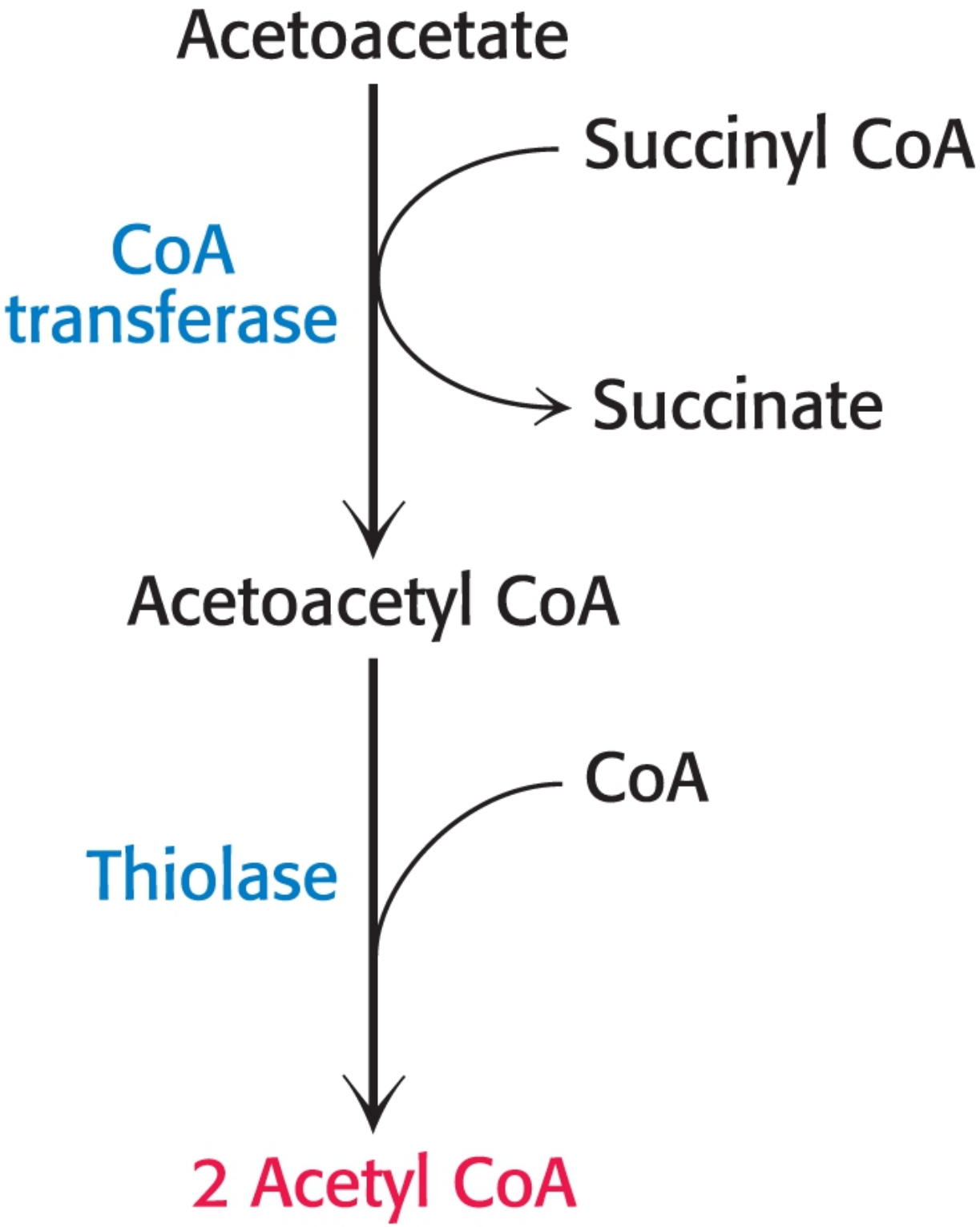
5. Citric acid cycle, Chapter 17.

6. Oxidative phosphorylation, Chapter 18.

Return to FIGURE 22.20 Pathway Integration: The liver supplies ketone bodies to the peripheral tissues

Extended description for FIGURE 22.21 Acetoacetate

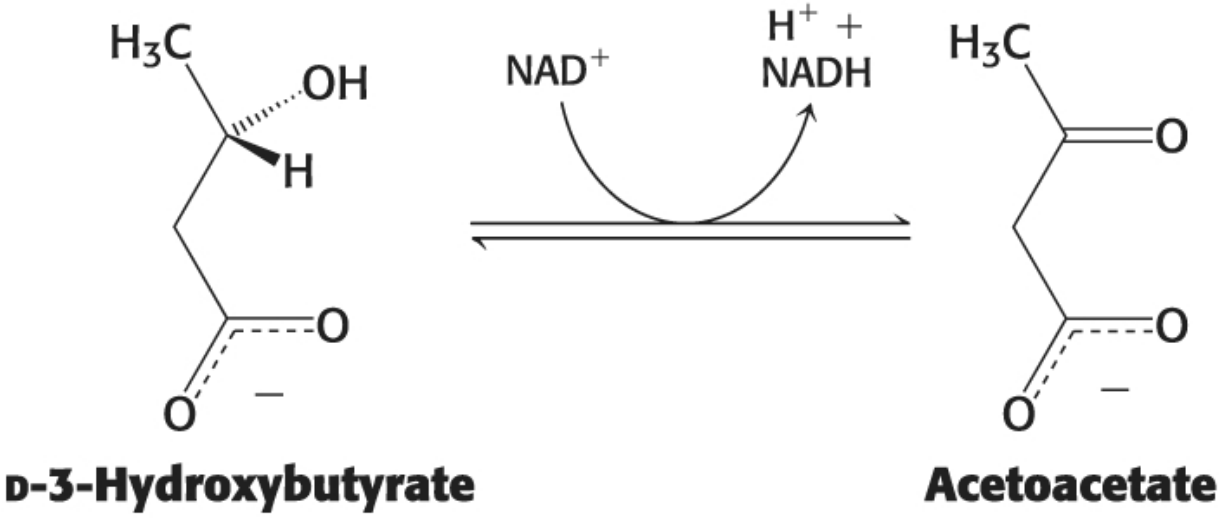
can be used as a fuel to drive A T P formation



Acetoacetate is converted into acetoacetyl C o A by C o A transferase with the simultaneous conversion of succinyl C o A to succinate. The acetoacetyl C o A is converted into 2 acetyl C o A by thiolase with the simultaneous entry of C o A.

Return to FIGURE 22.21 Acetoacetate can be used as a fuel to drive A T P formation

Extended description for Formation of acetoacetate from D-3-hydroxybutyrate



The reaction consists of one reactant and one product.

The reactant is D-3-hydroxybutyrate whose structure is as follows: A 3-carbon alkane chain is depicted as a vertical line structure using 2 zigzag lines. C 1 is single bonded to C H 3 on the upper left, dash bonded to O H on the upper right, and wedge bonded to H on the lower right. C 3 is partially double bonded to O on the lower left and right. The O atoms have an overall negative charge.

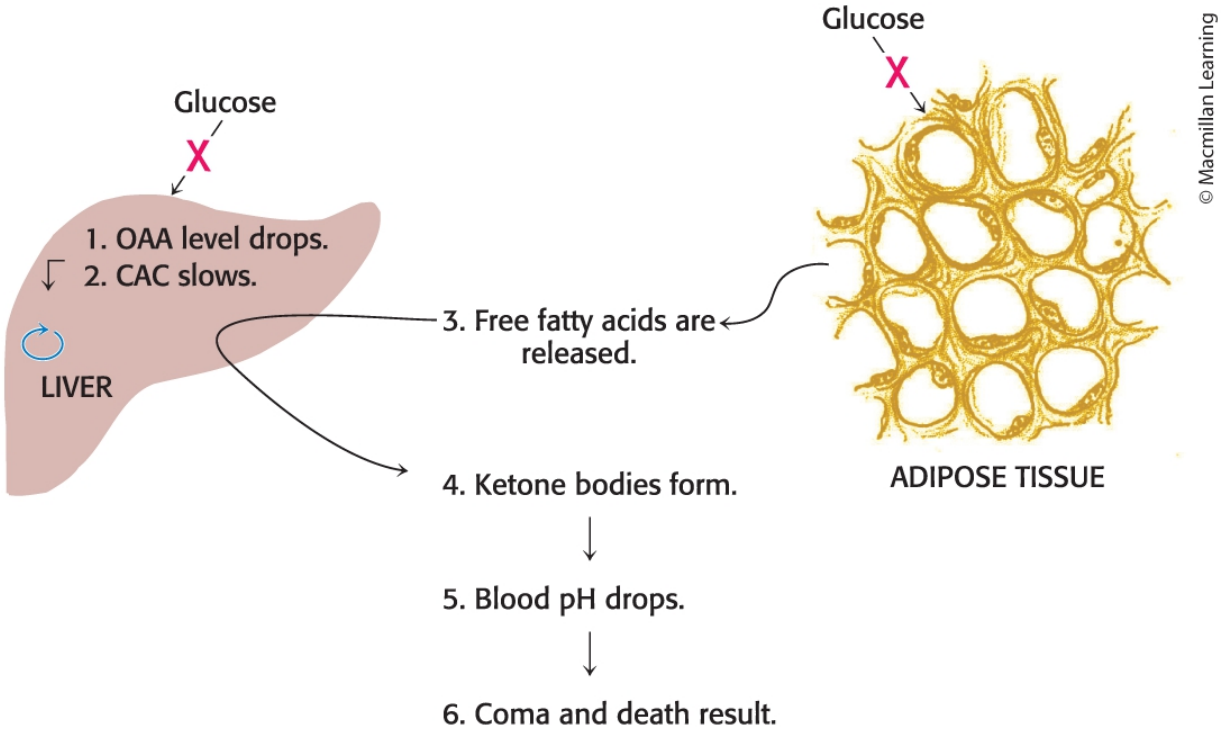
A reversible reaction arrow leads to the product. A curved arrow above it depicts the simultaneous reduction of N A D superscript plus to N A D H plus H superscript plus.

The product is acetoacetate whose structure is as follows: A 3-carbon alkane chain is depicted as a vertical line structure using 2 zigzag lines. C 1 is single bonded to C H 3 on the upper left and double bonded to O on the right. C 3 is partially double bonded to O

on the lower left and right. The O atoms have an overall negative charge.

Return to Formation of acetoacetate from D-3-hydroxybutyrate

Extended description for FIGURE 22.22 Diabetic ketosis results when insulin signaling is impaired



The liver is shown on the left and the adipose tissue is shown on the right. The adipose tissue is depicted as a cluster of cells containing large lipid droplets. A dashed arrow labeled glucose points to the liver and the adipose tissue. Both the arrows have a cross symbol. Inside the liver, the two points are listed:

1. O A A level drops.

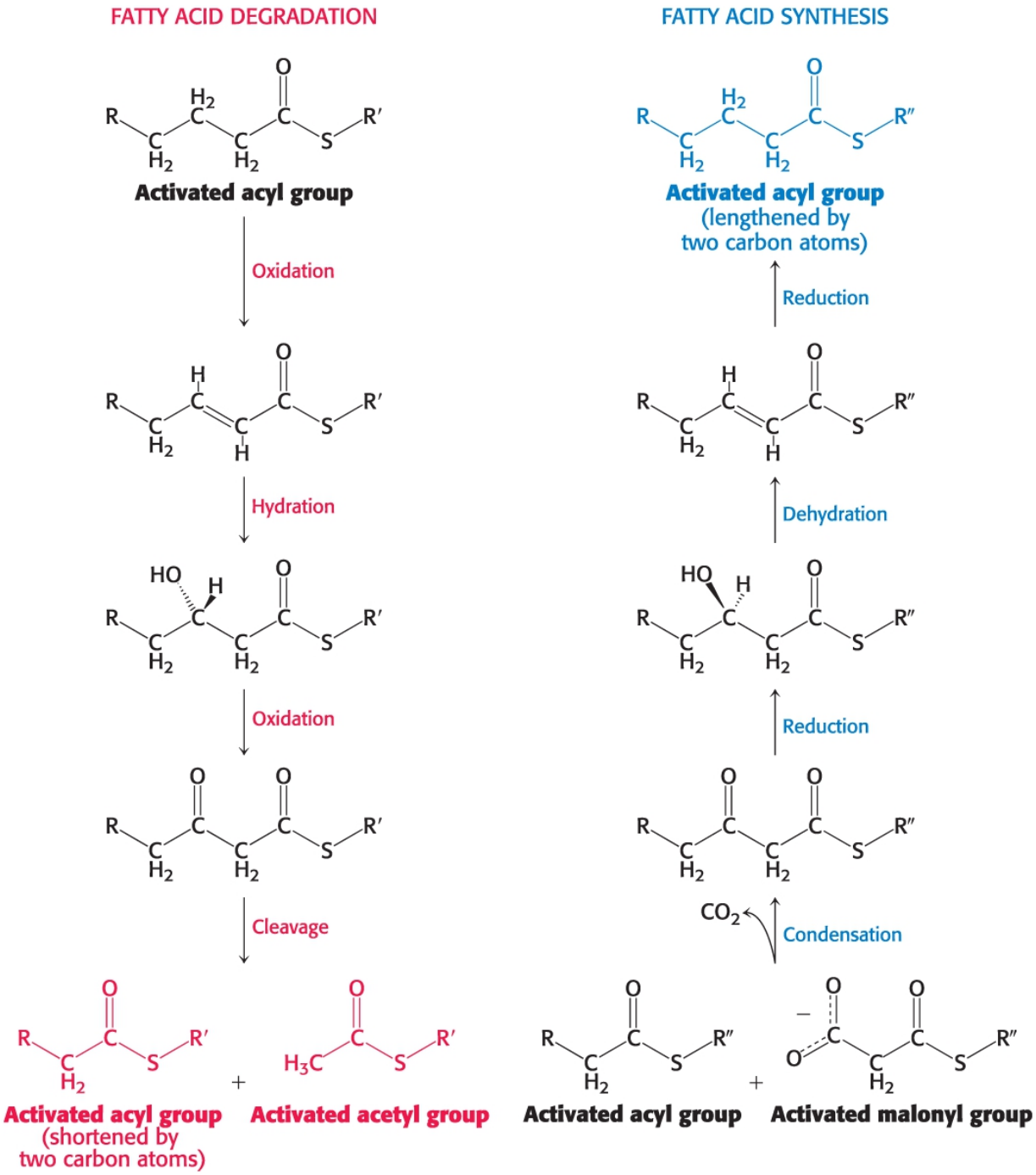
2. C A C slows.

An arrow points toward a curved clockwise arrow inside the liver.

An arrow from adipose tissue points toward point 3 with the text "Free fatty acids are released." A curved arrow from point 3 moves to the liver and then moves to point 4 with the text "Ketone bodies form." Point 4 leads to point 5 with the text "Blood p H drops." Point 5 leads to point 6 with the text "Coma and death result."

Return to FIGURE 22.22 Diabetic ketosis results when insulin signaling is impaired

Extended description for FIGURE 22.23 The steps in fatty acid degradation and synthesis are chemically similar



The reaction sequence of fatty acid degradation is depicted as follows:

In the first step, the activated acyl group undergoes irreversible oxidation.

The structure of the activated acyl group is as follows: A zigzag chain is composed of R, single bond, C H 2, single bond, C H 2, single bond, C H 2, single bond, C, single bond, S, single bond, R dash. C 4 is double bonded to O above.

The product of oxidation is as follows: A zigzag chain is composed of R, single bond, C H 2, single bond, C, double bond, C, single bond, C, single bond, S, single bond, R dash. C 2 and C 3 are single bonded to H above and H below respectively. C 4 is double bonded to O above.

In the second step, the product formed in step 1 undergoes irreversible hydration.

The product of hydration is as follows: A zigzag chain is composed of R, single bond, C H 2, single bond, C, single bond, C H 2, single bond, C, single bond, S, single bond, R dash. C 2 is dash bonded to O H on the upper left and wedge bonded to H on the upper right. C 4 is double bonded to O above.

In the third step, the product formed in step 2 undergoes irreversible oxidation.

The product of oxidation is as follows: A zigzag chain is composed of R, single bond, C H 2, single bond, C, single bond, C H 2, single bond, C, single bond, S, single bond, R dash. C 2 and C 4 are each double bonded to O above.

In the fourth step, the product formed in step 3 undergoes irreversible cleavage.

The first product of cleavage is the activated acyl group depicted as follows: A zigzag chain is composed of R, single bond, C H 2, single bond, C, single bond, S, single bond, R dash. C 2 is double bonded to O above. The activated acyl group is shortened by two carbon atoms.

The second product of cleavage is the activated acetyl group depicted as follows: A zigzag chain is composed of C H 3, single bond, C, single bond, S, single bond, R dash. C 2 is double bonded to O above.

The reaction sequence of fatty acid synthesis is depicted as follows from bottom to the top:

In the first step, the activated acyl group and activated malonyl group undergo irreversible condensation with the simultaneous release of C O 2.

The structure of the activated malonyl group is as follows: A zigzag chain is composed of C, single bond, C H 2, single bond, C, single bond, S, single bond, R double dash. C 1 is partially double bonded to O above and O on the lower left. The O atoms have an overall negative charge. C 3 is double bonded to O above.

The product of condensation is depicted as follows: A zigzag chain is composed of R, single bond, C H 2, single bond, C, single bond, C H 2, single bond, C, single bond, S, single bond, R double dash. C 2 and C 4 are each double bonded to O above.

In the second step, the product of condensation undergoes irreversible reduction.

The product of reduction is depicted as follows: A zigzag chain is composed of R, single bond, C H 2, single bond, C, single bond, C H 2, single bond, C, single bond, S, single bond, R double dash. C 2 is wedge bonded to O H on the upper left and dash bonded to H on the upper right. C 4 is double bonded to O above.

In the third step, the production of reduction undergoes irreversible dehydration.

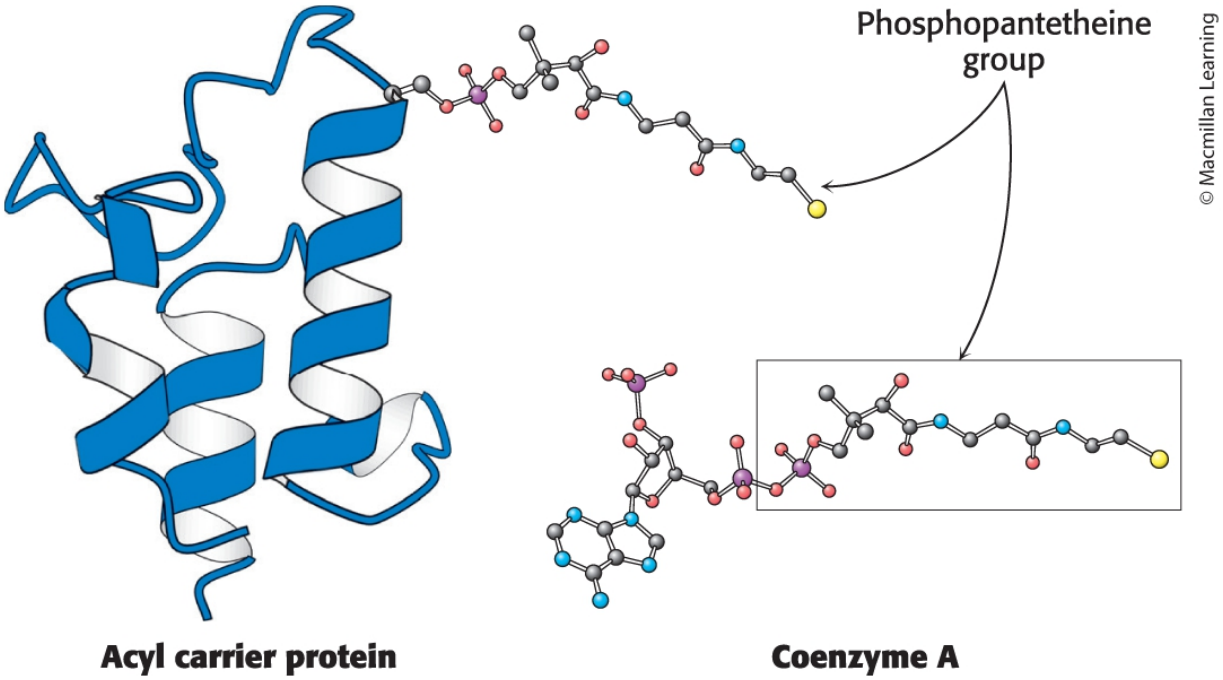
The product of dehydration is depicted as follows: A zigzag chain is composed of R, single bond, C H 2, single bond, C, double bond, C, single bond, C, single bond, S, single bond, R double dash. C 2 and C 3 are single bonded to H above and H below respectively. C 4 is double bonded to O above.

In the fourth step, the product of dehydration undergoes irreversible reduction to produce an activated acyl group.

The structure of the activated acyl group is as follows: A zigzag chain is composed of R, single bond, C H 2, single bond, C H 2, single bond, C H 2, single bond, C, single bond, S, single bond, R double dash. C 4 is double bonded to O above. The activated acyl group is lengthened by two carbon atoms.

Return to FIGURE 22.23 The steps in fatty acid degradation and synthesis are chemically similar

Extended description for FIGURE 22.24 Phosphopantetheine group in acyl carrier protein and coenzyme A



© Macmillan Learning

The acyl carrier protein consists of two medium-sized and one short alpha-helices in vertical orientation interconnected by thread-like loops. The loop at the top is connected to a ball-and-stick model composed of a zigzag chain of 1 purple sphere, 1 yellow sphere, 2 blue spheres, 2 red spheres, and 11 black spheres. The purple sphere is located at the fourth position, the red spheres are located at the third and fifth positions, the blue spheres occupy the tenth and fourteenth positions, and the yellow sphere occupies the right terminal or seventeenth position.

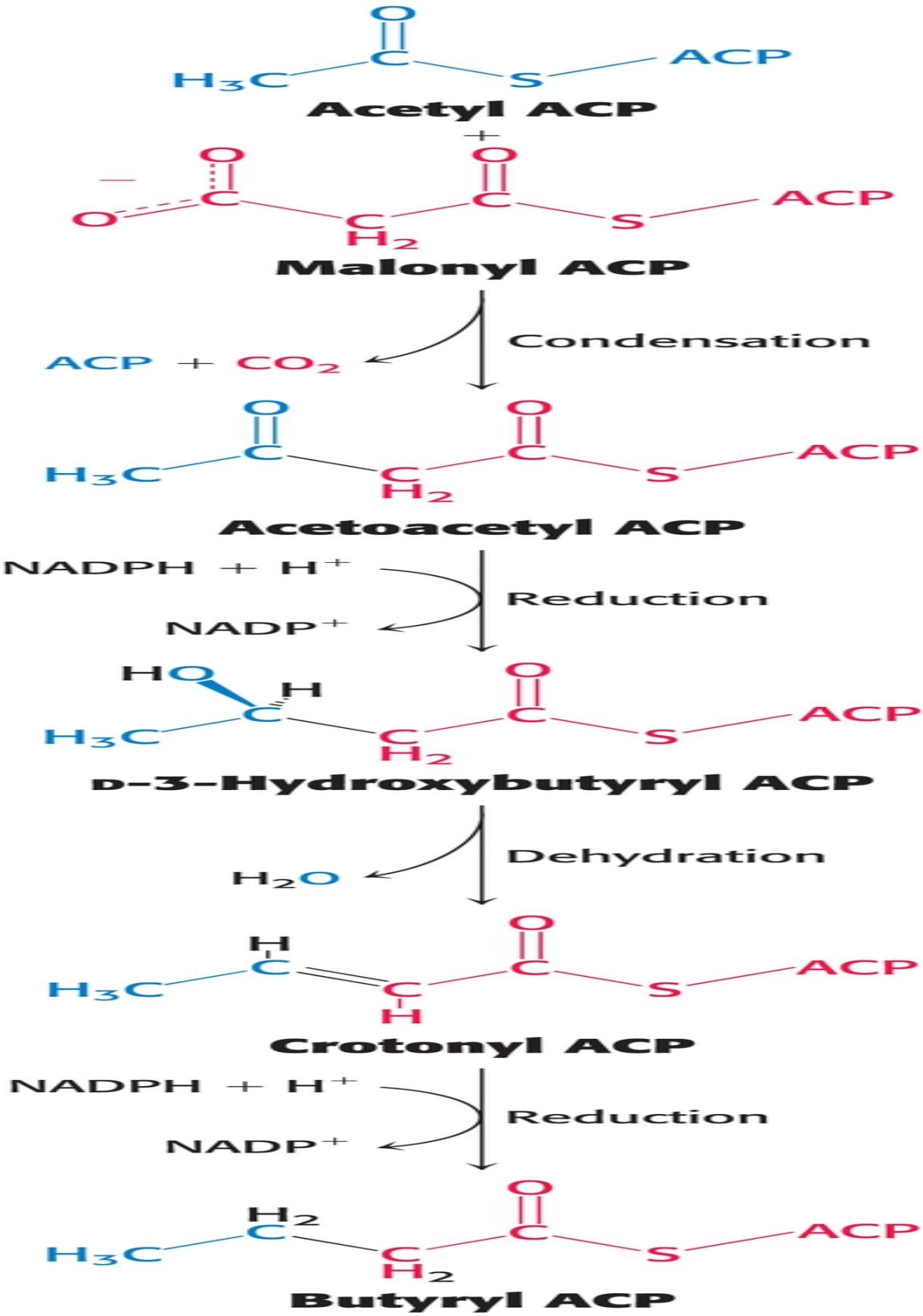
The ball-and-stick model of coenzyme A also contains an identical zigzag chain starting from the purple sphere. This region of the zigzag chain from the purple sphere to the right terminal yellow

sphere is labeled the phosphopantetheine group in both acyl carrier protein and coenzyme.

Return to FIGURE 22.24 Phosphopantetheine group in acyl carrier protein and coenzyme A

Extended description for FIGURE 22.25 Like beta-oxidation, saturated fatty acid synthesis consists of

four steps


Acetyl ACP
Malonyl ACP
Condensation
ACP + CO2
Acetoacetyl ACP
NADPH + H+
NADP+
Reduction
D–3–Hydroxybutyryl ACP
Dehydration
H2O
Crotonyl ACP
NADPH + H+
NADP+
Reduction
Butyryl ACP

In the first step, acetyl A C P and malonyl A C P undergo irreversible condensation to produce acetoacetyl A C P with the simultaneous release of A C P plus C O 2.

The structure of acetyl A C P is as follows: A zigzag chain is composed of C H 3, single bond, C, single bond, S, single bond, A C P. C 2 is double bonded to O above. The structure of malonyl A C P is as follows: A zigzag chain is composed of C, single bond, C H 2, single bond, C, single bond, S, single bond, A C P. C 1 is partially double bonded to O above and O on the lower left. The O atoms have an overall negative charge. C 3 is double bonded to O above.

The structure of acetoacetyl A C P is as follows: A zigzag chain is composed of C H 3, single bond, C, single bond, C H 2, single bond, C, single bond, S, single bond, A C P. C 2 and C 4 are each double bonded to O above.

In the second step, acetoacetyl A C P undergoes irreversible reduction to D-3-hydroxybutyryl A C P with the simultaneous oxidation of N A D P H plus H superscript plus to N A D P superscript plus.

The structure of D-3-hydroxybutyryl A C P is as follows: A zigzag chain is composed of C H 3, single bond, C, single bond, C H 2, single bond, C, single bond, S, single bond, A C P. C 2 is wedge bonded to O H on the upper left and dash bonded to H on the upper right. C 4 is double bonded to O above.

In the third step, D-3-hydroxybutyryl A C P undergoes irreversible dehydration to produce crotonyl A C P with the simultaneous release of H 2 O.

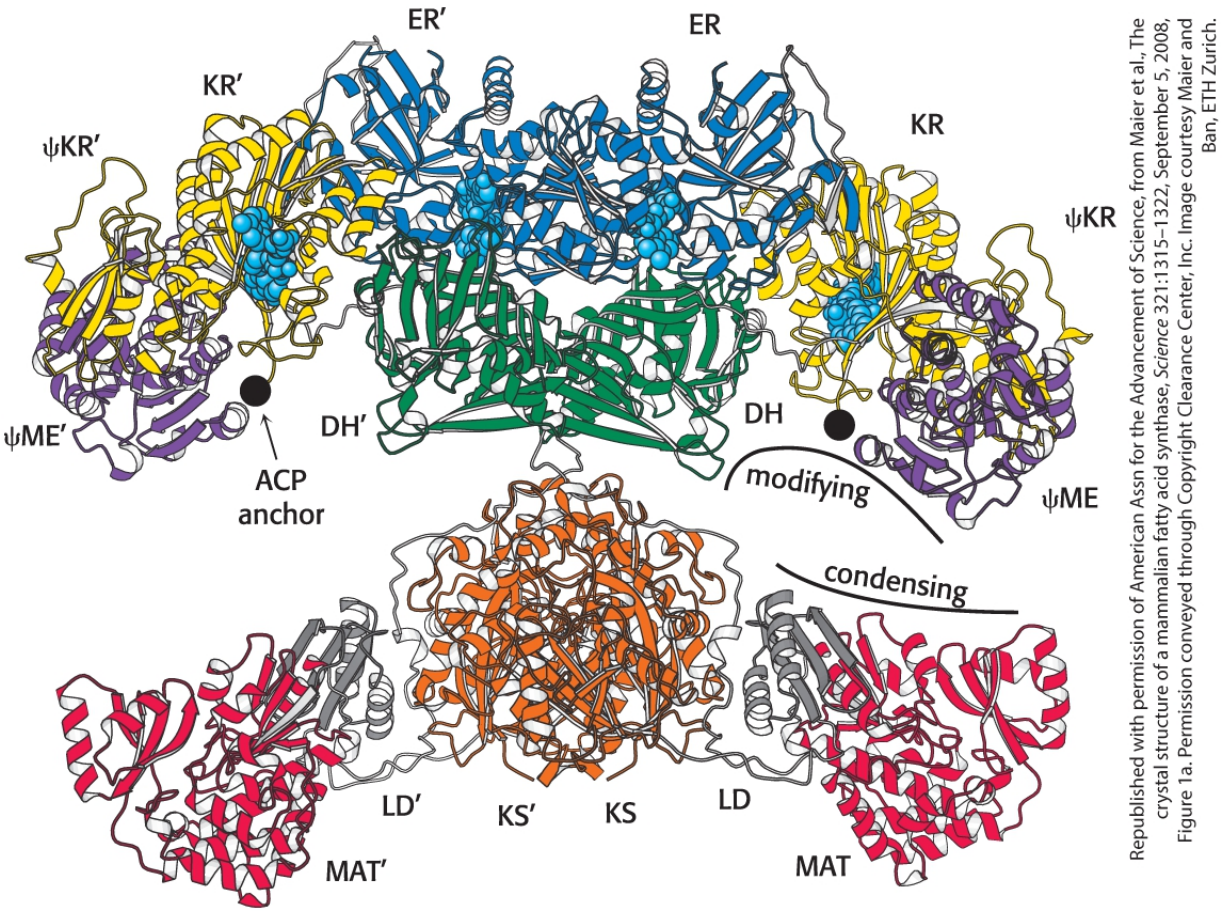
The structure of crotonyl A C P is as follows: A zigzag chain is composed of C H 3, single bond, C, double bond, C, single bond, C, single bond, S, single bond, A C P. C 2 and C 3 are single bonded to H above and below respectively. C 4 is double bonded to O above.

In the fourth step, crotonyl A C P undergoes irreversible reduction to produce butyryl A C P with the simultaneous oxidation of N A D P H plus H superscript plus to N A D P superscript plus.

The structure of butyryl A C P is as follows: A zigzag chain is composed of C H 3, single bond, C H 2, single bond, C H 2, single bond, C, single bond, S, single bond, A C P. C 4 is double bonded to O above.

Return to FIGURE 22.25 Like beta-oxidation, saturated fatty acid synthesis consists of four steps

Extended description for FIGURE 22.26 Mammalian fatty acid synthase is a large, dimeric, multidomain protein complex



Republished with permission of American Assn for the Advancement of Science, from Maier et al., The crystal structure of a mammalian fatty acid synthase, *Science* 321:1315–1322, September 5, 2008, Figure 1a. Permission conveyed through Copyright Clearance Center, Inc. Image courtesy Maier and Ban, ETH Zurich.

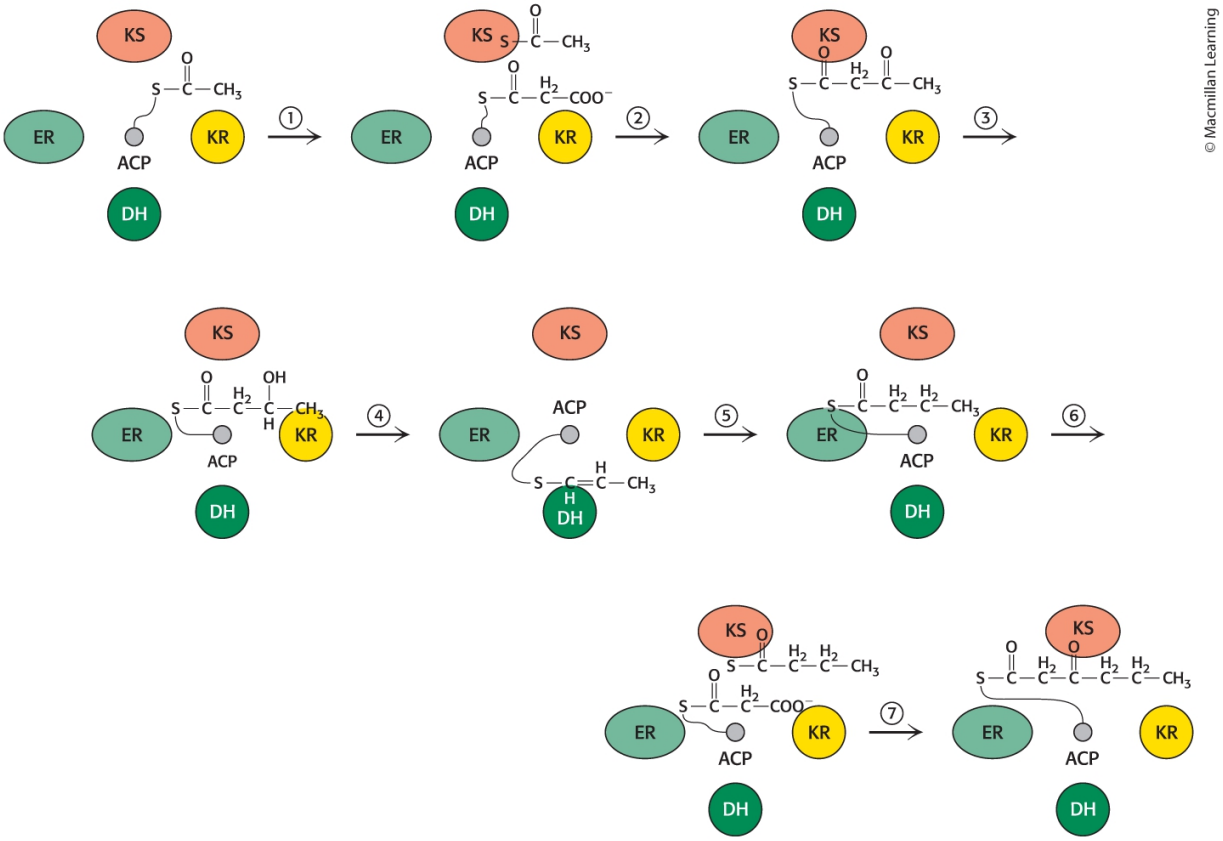
The ribbon diagram consists of two multisubunit monomers. The bottom monomer contains a central circular cluster composed of alpha-helices and beta-strands. Its left half is labeled K S prime and the right half is labeled K S. The central cluster is connected to M A T prime domain on the lower left and M A T domain on the lower right through an L D prime domain and L D domain respectively. The L D and L D prime domains are linker domains consisting of

long loops, a few alpha-helices, and beta-strands. The top surface of L D and M A T domains is together labeled condensing.

The central part of the top monomer contains a V-shaped domain composed of several beta-strands. The left half is labeled D H prime and the right half is labeled D H. A U-shaped domain is located above it. It consists of beta-strands in the center surrounded by alpha-helices which are further flanked by beta-strands on either end. The left half is labeled E R prime and the right half is labeled E R. Each half contains a cluster of blue spheres. K R prime domain and a K R domain are located on the left and right side of the central part composed of V-shaped and U-shaped domains. Both the K R prime and K R domains contain a cluster of blue spheres. The left side of the K R prime domain is attached to a psi K R prime domain and a psi M E prime domain. The right side of the K R domain is attached to a psi K R domain and psi M E domain. The black sphere depicting the A C P anchor is attached to the bottom loop of the K R prime domain and K R domain. The bottom surface of the K R and psi M E domain is labeled modifying.

Return to FIGURE 22.26 Mammalian fatty acid synthase is a large, dimeric, multidomain protein complex

Extended description for FIGURE 22.27 One catalytic cycle of mammalian fatty acid synthase consists of seven steps



© Macmillan Learning

A C P depicted as a central tiny grey circle is connected to the S atom which is further single bonded to C, single bond, C H 3. The C atom is double bonded to O above. It is surrounded by the K S domain at the top, the K R domain on the right, the D H domain below, and the E R domain on the left.

A forward arrow labeled 1 lead to the next structure. This structure consists of the tiny grey circle connected to S, single bond, C, single bond, C H 2, single bond, C O O superscript minus. C 1 is double bonded to O above. The K S domain at the top is bound to the S atom

of S, single bond, C, single bond, C H 3. The central C atom is double bonded to O above.

A forward arrow labeled 2 leads to the next structure. This structure consists of the tiny grey circle connected to S, single bond, C, single bond, C H 2, single bond, C, single bond, C H 3. C 1 and C 3 are each double bonded to O above. The O atom of C 1 is bound to the K S domain.

A forward arrow labeled 3 leads to the next structure. This structure consists of a tiny grey circle connected to S, single bond, C, single bond, C H 2, single bond, C H, single bond, C H 3. C 1 is single bonded to O above. C 3 is single bonded to O H above. C H 3 group is bound to K R domain.

A forward arrow labeled 4 leads to the next structure. This structure consists of a tiny grey circle connected to S, single bond, C H, double bond, C H, single bond, C H 3. H atom of C 1 is bound to D H.

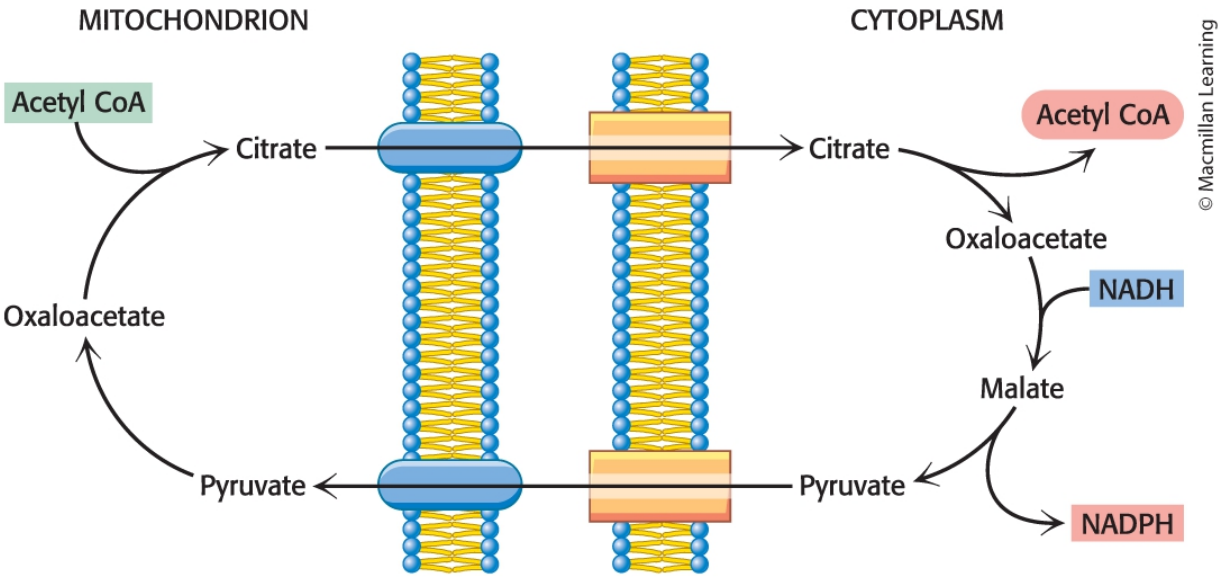
A forward arrow labeled 5 leads to the next structure. The tiny grey circle is connected to S, single bond, C, single bond, C H 2, single bond, C H 2, single bond, C H 3. C 1 is double bonded to O above. The S atom is bound to the E R domain.

A forward arrow labeled 6 leads to the next structure. A tiny grey circle is connected to S, single bond, C, single bond, C H 2, single bond, C O O superscript minus. C 1 is double bonded to O above. The S atom is located close to the E R domain and the C O O superscript minus group is located close to the K R domain. A structure composed of S, single bond, C, single bond, C H 2, single bond, C H 2, single bond, C H 3 is bound to the K S domain. C 1 is double bonded to O above which is bound to K S.

A forward arrow labeled 7 leads to the next structure. The tiny grey circle is connected to S, single bond, C, single bond, C H 2, single bond, C, single bond, C H 2, single bond, C H 2, single bond, C H 3. C 1 and C 3 are double bonded to O above. The O atom bonded to C 3 is bound to the K S domain.

Return to FIGURE 22.27 One catalytic cycle of mammalian fatty acid synthase consists of seven steps

Extended description for FIGURE 22.28 Acetyl C o A can be transferred from the mitochondrial matrix to the cytoplasm

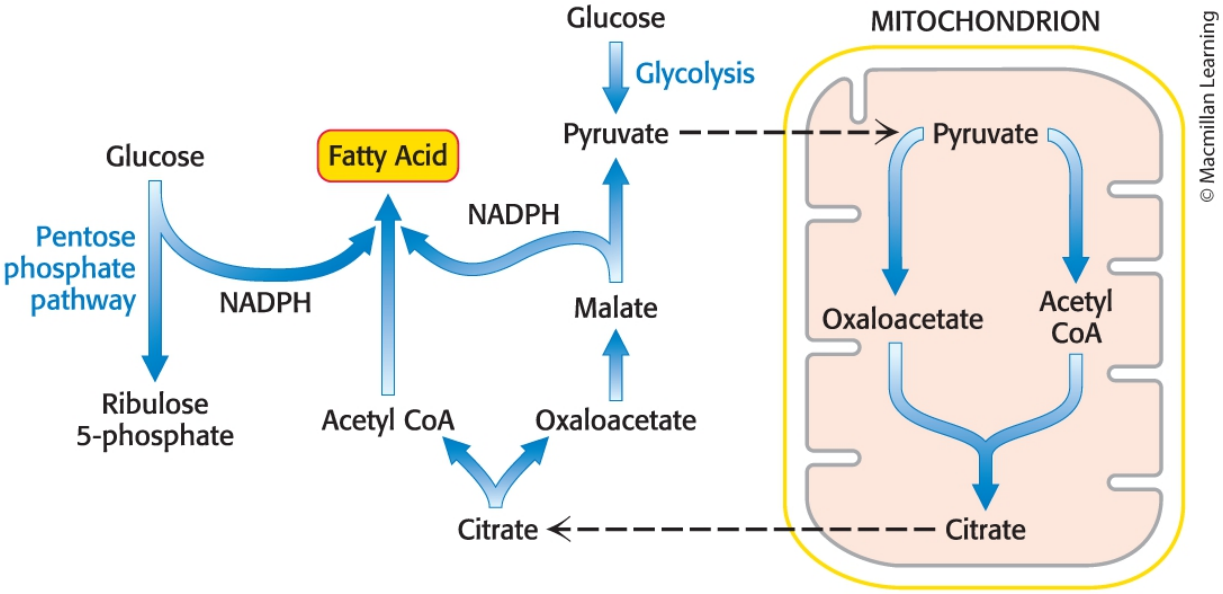


Two lipid bilayers separated by a small gap are shown in the vertical orientation. The left bilayer contains a blue oblong transport protein embedded in the membrane at the top and bottom. The right bilayer contains an orange rectangular channel at the top and bottom. The region on the left of the left bilayer is labeled mitochondrion. The region on the right of the right bilayer is labeled cytoplasm. Oxaloacetate in the mitochondrion combines with acetyl C o A to form citrate. The citrate molecule passes through the oblong transport protein in the left bilayer and then the rectangular channel in the right bilayer to enter the cytoplasm. Inside the cytoplasm, citrate breaks down into oxaloacetate and acetyl C o A. The oxaloacetate is converted into malate with the simultaneous use of N A D H. The malate molecule is converted into pyruvate with the simultaneous release of N A D P H. The pyruvate molecule passes through the bottom rectangular channel in the right bilayer and

then the bottom oblong channel in the left bilayer to reach the mitochondrion and the cycle continues.

Return to FIGURE 22.28 Acetyl C o A can be transferred from the mitochondrial matrix to the cytoplasm

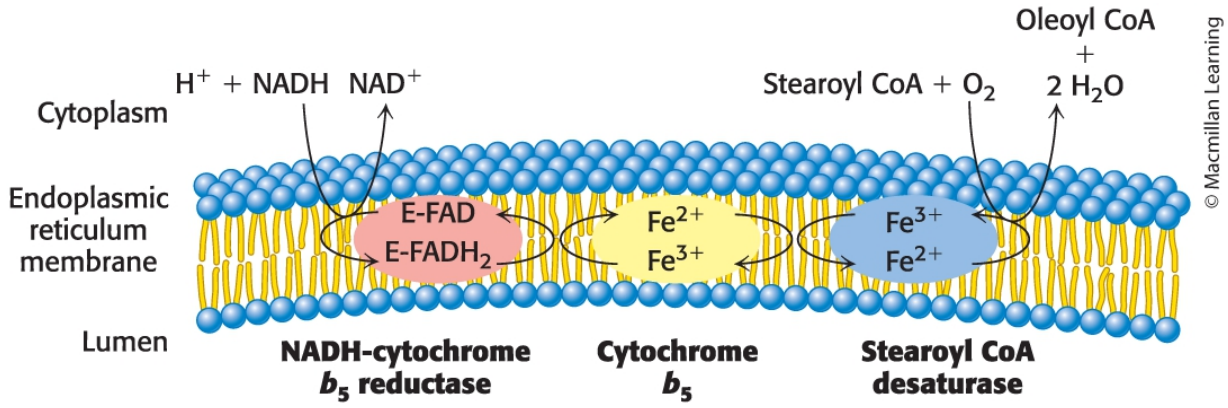
Extended description for FIGURE 22.29 Pathway Integration: Fatty acid synthesis requires the cooperation of various pathways in different cellular compartments



A mitochondrion is shown in a vertical orientation. Outside the mitochondrion, glucose is converted into pyruvate via glycolysis. Simultaneously, another glucose molecule is converted into ribulose 5-phosphate via the pentose phosphate pathway with the simultaneous release of N A D P H. Inside the mitochondrion, pyruvate is converted into oxaloacetate or acetyl C o A, both of which combine to form citrate. The citrate molecule leaves the mitochondrion and breaks down into acetyl C o A and oxaloacetate. The oxaloacetate molecule is converted into malate, which is further converted into pyruvate with the simultaneous release of N A D P H. This N A D P H and the N A D P H molecule produced by pentose phosphate pathway is used during the conversion of acetyl C o A into fatty acid.

Return to FIGURE 22.29 Pathway Integration: Fatty acid synthesis requires the cooperation of various pathways in different cellular compartments

Extended description for FIGURE 22.30 Desaturation of fatty acids by an electron transport chain in the E R membrane



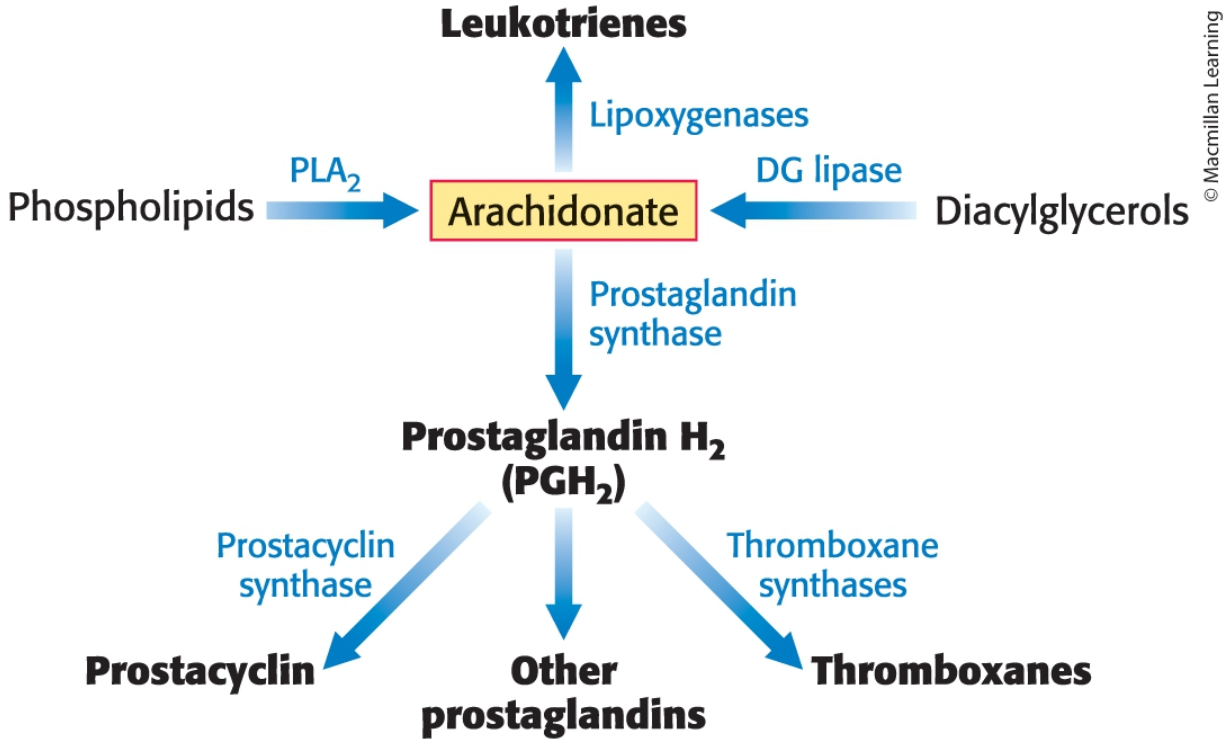
A lipid bilayer is labeled endoplasmic reticulum membrane. The region above the membrane is labeled cytoplasm and the region below is the lumen. Three proteins are embedded in the membrane from left to right. These membrane proteins are labeled N A D H-cytochrome b 5 reductase, cytochrome b 5, and stearoyl C o A desaturase. N A D H-cytochrome b 5 reductase is depicted as a pink oval. It undergoes reduction from E-F A D to E-F A D H 2 with the simultaneous oxidation of N A D H plus H superscript to N A D superscript plus in the cytoplasm. It later undergoes re-oxidation from E-F A D H 2 to E-F A D with the simultaneous reduction of F e superscript 3 plus in cytochrome b 5 to F e superscript 2 plus.

The cytochrome b 5 transfers its electrons to stearoyl C o A desaturase with the simultaneous conversion of F e superscript 2 plus to F e superscript 3 plus. The F e superscript 3 plus bound to the desaturase is reduced to F e superscript 2 plus. The desaturase transfers electrons to Stearoyl C o A plus O 2 in the cytoplasm to

produce oleoyl C o A plus 2 H 2 O. The F e superscript 2 plus in the desaturase is converted back to F e superscript 3 plus.

Return to FIGURE 22.30 Desaturation of fatty acids by an electron transport chain in the E R membrane

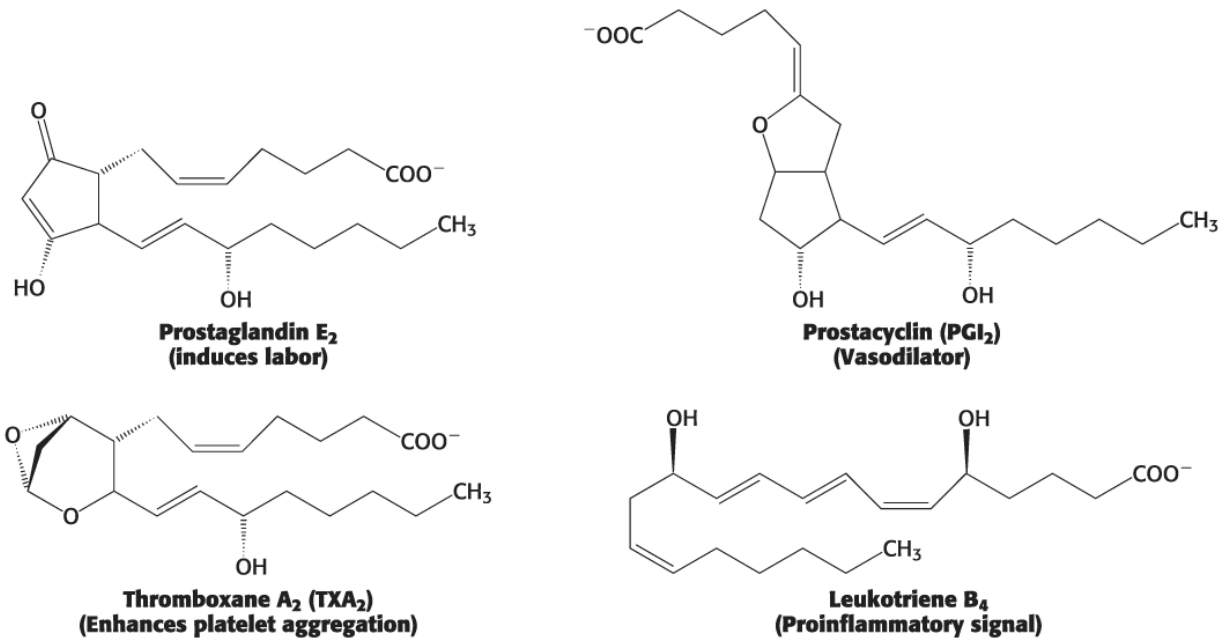
Extended description for FIGURE 22.31 Several eicosanoid hormones are produced from arachidonate by distinct enzymatic pathways



A rectangle labeled arachidonate is shown at the top center. An upward arrow labeled lipoxygenases points from arachidonate to leukotrienes. An arrow labeled P L A 2 points from phospholipids on the left to arachidonate. An arrow labeled D G lipase points from diacylglycerols on the right to arachidonate. A downward arrow labeled prostaglandin synthase points from arachidonate to prostaglandin H 2 (P G H 2). An arrow labeled prostacyclin synthase points from P G H 2 to prostacyclin. A downward arrow from P G H 2 points to other prostaglandins. An arrow labeled thromboxane synthases points from P G H 2 to thromboxanes.

Return to FIGURE 22.31 Several eicosanoid hormones are produced from arachidonate by distinct enzymatic pathways

Extended description for FIGURE 22.32 Structures of different eicosanoids



Prostaglandin E 2 which induces labor has the following structure: A 5-carbon homocyclic pentagonal ring is in a horizontal orientation with C 1 occupying the leftmost vertex. C 2 is double bonded to O on the upper left. C 5 is dash bonded to O H on the lower left. C 3 is dash bonded to C 1 of a 6-carbon alkene chain depicted as a line structure using 5 zigzag lines. A double bond is present between C 2 and C 3. C 6 is single bonded to C O O superscript minus on the lower right. C 4 of the ring is single bonded to C 1 of a 7-carbon alkene chain depicted as a line structure using 6 zigzag lines. A double bond is present between C 1 and C 2. C 3 is dash bonded to O H below. C 7 is single bonded to C H 3 on the upper right.

Thromboxane A 2 (T X A 2) which enhances platelet aggregation has the following structure: A 6-membered heterocyclic hexagonal ring is in a vertical orientation with C 1 occupying the bottom-left vertex.

It contains 1 O and 5 C atoms. O occupies the bottom-most vertex. C 1 and C 3 are dash bonded to an O atom located outside the ring. A wedge bond is present between C 1 and C 2 and C 2 and C 3. C 4 is dash bonded to C 1 of a 6-carbon alkene chain depicted as a line structure using 5 zigzag lines. A double bond is present between C 2 and C 3. C 6 is single bonded to C O O superscript minus on the lower right. C 5 of the ring is single bonded to C 1 of a 7-carbon alkene chain depicted as a line structure using 6 zigzag lines. A double bond is present between C 1 and C 2. C 3 is dash bonded to O H below. C 7 is single bonded to C H 3 on the upper right.

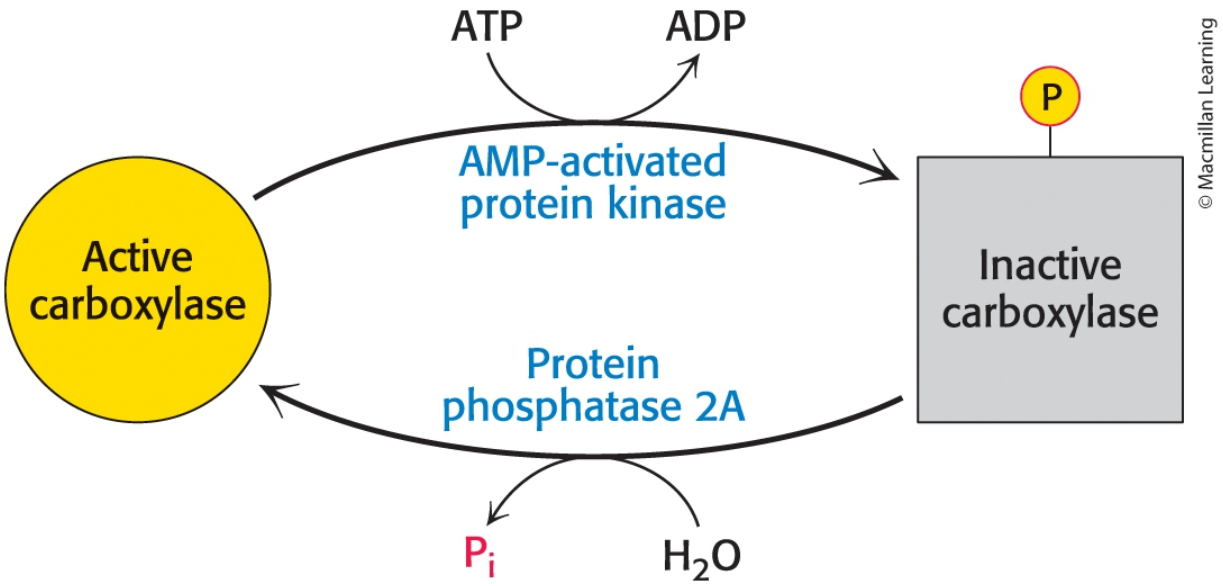
Prostacyclin (P G I 2) which is a vasodilator has the following structure: A 5-membered heterocyclic pentagonal ring is in a vertical orientation and consists of 1 O and 4 C atoms. O occupies the top left vertex. C 1 occupies the topmost vertex. C 1 is double bonded to a 4-carbon alkane chain depicted as a line structure using 3 zigzag lines. C 4 of the alkane chain is single bonded to C O O superscript minus on the lower left. The heterocyclic ring is fused to a 5-carbon homocyclic pentagonal ring in a vertical orientation such that C 3 and C 4 of the heterocyclic ring are C 4 and C 3 respectively of the homocyclic ring. In the heterocyclic pentagonal ring, C 1 occupies the bottom-most vertex and is dash-bonded to O H below. C 5 is single bonded to a 7-carbon alkene chain depicted as a line structure using 6 zigzag lines. A double bond is present between C 1 and C 2. C 3 is dash bonded to O H below. C 7 is single bonded to C H 3 on the upper right.

(d) Leukotriene B 4 which is responsible for the proinflammatory signal has the following structure: A 18-carbon alkene chain is depicted as a line structure using 17 zigzag lines. C 1 is single bonded on the upper right to C O O superscript minus. C 4 and C 11 are wedge-bonded to O H above. A double bond is present between C 5 and C 6, C 7 and C 8, C 9 and C 10, and C 13 and C 14. The alkene

chain is folded at C 12. C 18 is single bonded to C H 3 on the upper right.

Return to FIGURE 22.32 Structures of different eicosanoids

Extended description for FIGURE 22.33 Inhibition and activation of acetyl C o A carboxylase

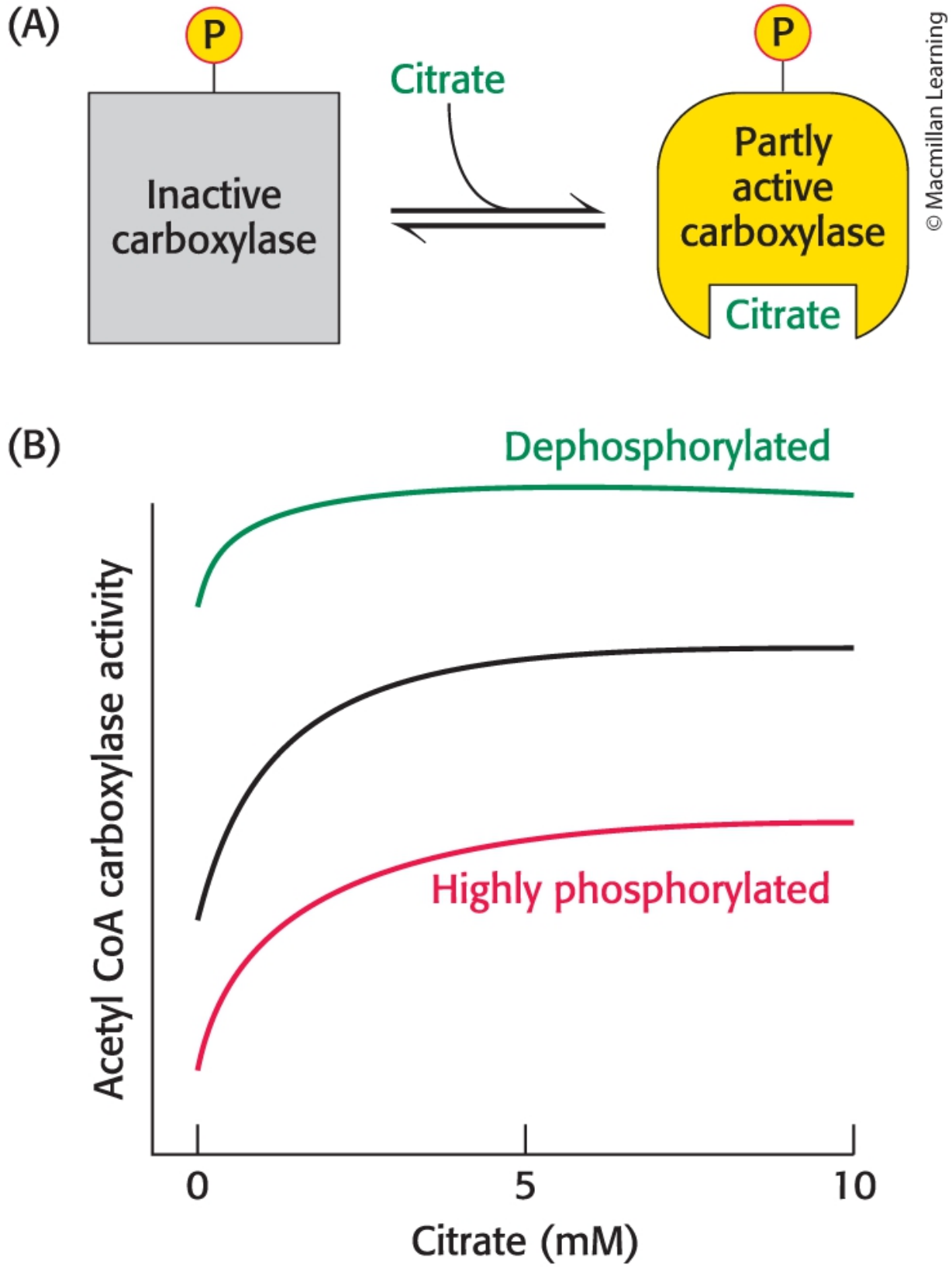


A yellow circle is labeled active carboxylase and a grey square is labeled inactive carboxylase. The inactive carboxylase is phosphorylated which is depicted as a tiny yellow circle labeled P connected to the square. A forward arrow labeled A M P-activated protein kinase points from active carboxylase to inactive carboxylase with the simultaneous hydrolysis of A T P to A D P. A backward arrow labeled protein phosphatase 2 A points from inactive carboxylase to active carboxylase with the simultaneous entry of H 2 O and release of P subscript i.

Return to FIGURE 22.33 Inhibition and activation of acetyl C o A carboxylase

Extended description for FIGURE 22.35 The catalytic activity of acetyl C o A carboxylase depends upon the

concentration of citrate



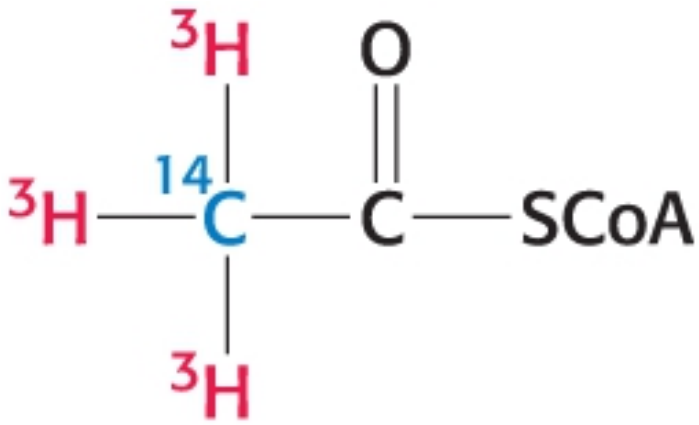
© Macmillan Learning

Part (A): It shows an inactive carboxylase as a grey square single bonded to a phosphate group. A reversible reaction arrow shows the entry of citrate and leads to a rounded yellow square labeled partly active carboxylase. The partly active carboxylase is bound to citrate and single-bonded to the phosphate group.

Part (B): It shows a graph. The horizontal axis is labeled citrate in millimolar. It has markings ranging from 0 to 10 in increments of 5 units. The vertical axis is labeled acetyl C o A carboxylase activity. It contains three curves from top to bottom. A green horizontal curve is labeled dephosphorylated. It starts at a carboxylase activity slightly less than the maximum at 0 millimolar of citrate. It rises to the highest activity and then moves horizontally toward the right. The middle black curve starts at a carboxylase activity much below the average value. It then rises gradually to a carboxylase activity much above the average value till 2.5 millimolar of citrate and then continues moving horizontally toward the right. The bottom red curve is labeled highly phosphorylated. It starts at the lowest carboxylase activity at 0 millimolar of citrate. It then rises in a concave down fashion to reach a below-average carboxylase activity at 5 millimolar and then moves horizontally toward the right. All values are estimated.

Return to FIGURE 22.35 The catalytic activity of acetyl C o A carboxylase depends upon the concentration of citrate

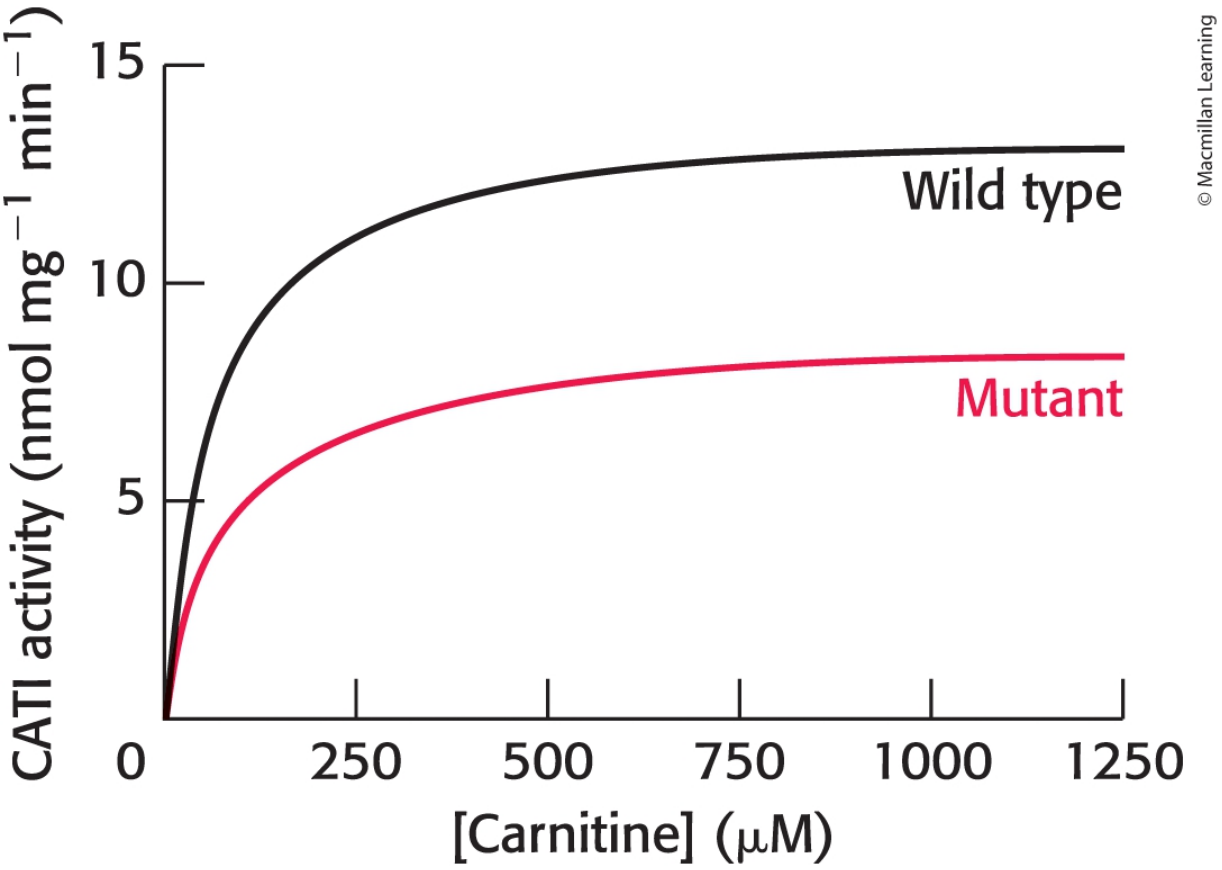
Extended description for Acetyl C o A containing radioactive carbon and hydrogen atoms



The structure of acetyl C o A is as follows: H superscript 3, single bond, C superscript 14, single bond, C, single bond, S C o A. C superscript 14 is single bonded to H superscript 3 above and below. C 2 is single bonded to O above.

Return to Acetyl C o A containing radioactive carbon and hydrogen atoms

Extended description for Relationship between carnitine acyltransferase 1 activity and concentration of carnitine



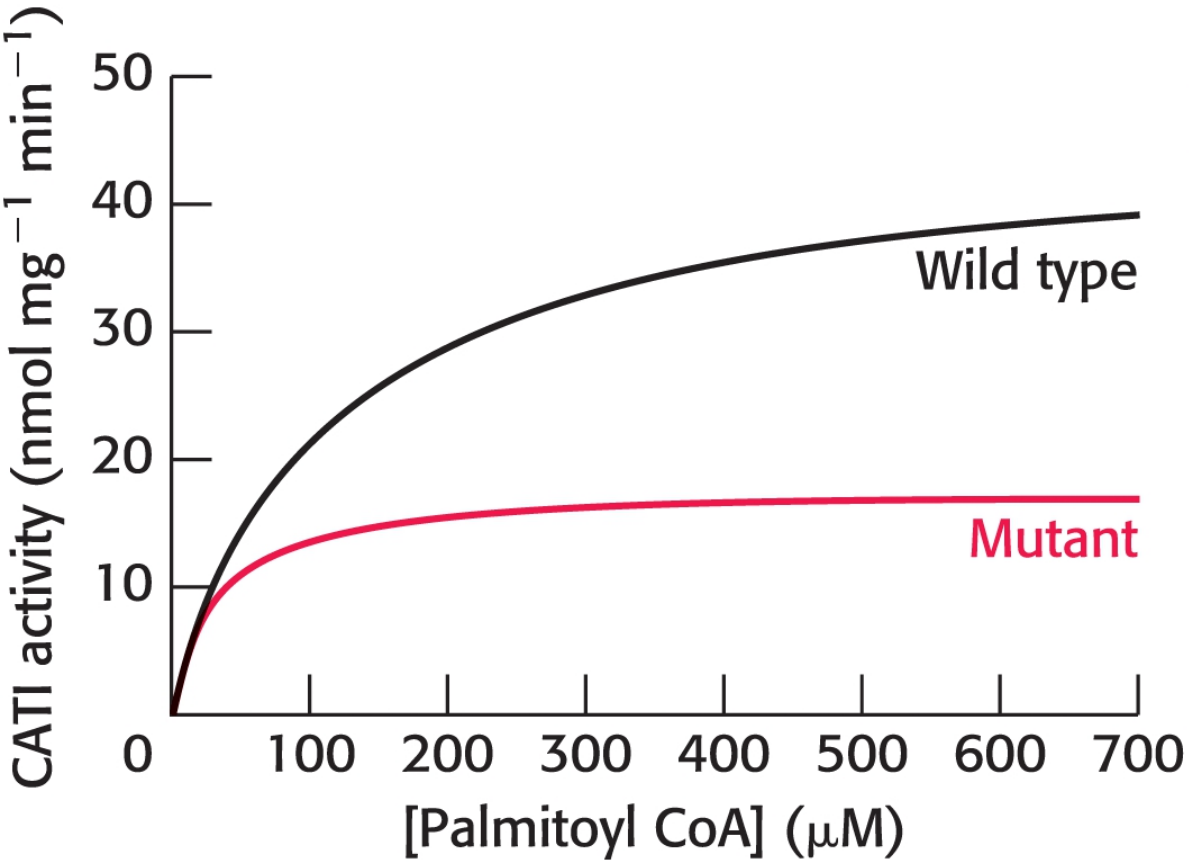
© Macmillan Learning

The horizontal axis is labeled the concentration of carnitine in micromolar. It has markings ranging from 0 to 1250 in increments of 250 units. The vertical axis is labeled CAT 1 activity in nanomoles per milligram per minute. It has markings ranging from 0 to 15 in increments of 5 units. The graph contains two concave down curves shown in black and red. The black curve is labeled wild type. It starts at (0, 0), rises steeply to (125, 10), and bends to (250, 11) in a concave-down manner. It then moves horizontally toward the right. The red curve is labeled mutant. It starts at (0, 0), rises steeply to

(125, 5), and bends to (250, 6) in a concave-down manner. It then moves horizontally toward the right. All values are estimated.

Return to Relationship between carnitine acyltransferase 1 activity and concentration of carnitine

Extended description for Relationship between carnitine acyltransferase 1 activity and concentration of palmitoyl C o A



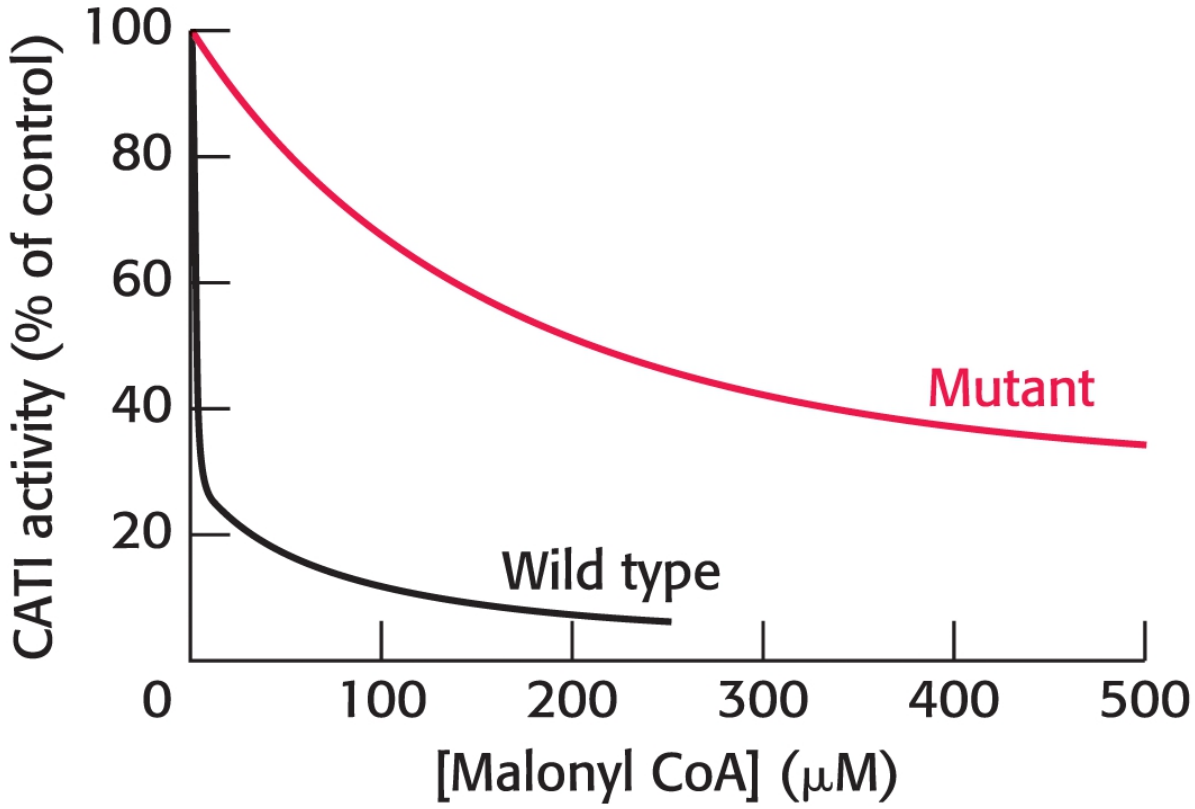
© Macmillan Learning

The horizontal axis is labeled concentration of palmitoyl C o A in micromolar. The vertical axis is labeled CAT 1 activity in nanomoles per milligram per minute. It has markings ranging from 0 to 50 in increments of 10 units. The graph contains two curves shown in black and red. The black curve is labeled wild type and the red curve is labeled mutant. The black curve starts at (0, 0), rises to the upper right in a concave-down manner to reach (500, 38), and then continues moving horizontally toward the right. The red curve starts

at (0, 0), rises to the upper right to reach (100, 12), and then moves horizontally toward the right. All values are estimated.

Return to Relationship between carnitine acyltransferase 1 activity and concentration of palmitoyl C o A

Extended description for Relationship between carnitine acyltransferase 1 activity and concentration of malonyl C o A

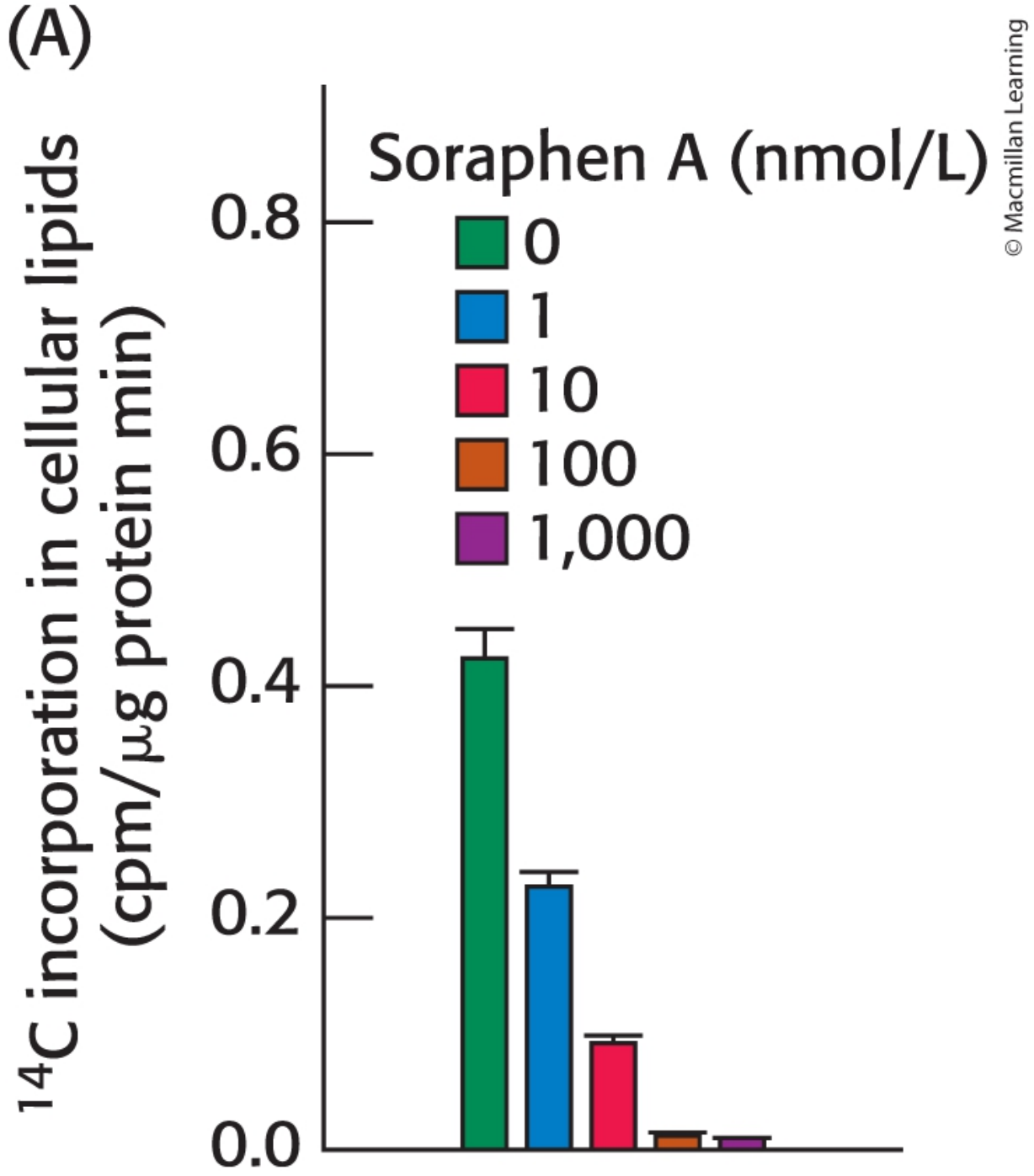


© Macmillan Learning

The horizontal axis is labeled concentration of malonyl C o A in micromolar. It has markings ranging from 0 to 500 in increments of 100 units. The vertical axis is labeled CAT 1 activity in the percentage of control. It has markings ranging from 0 to 100 in increments of 20 units. The graph contains two curves shown in black and red. The black curve is labeled wild type. It starts at (0, 100), falls vertically to (2, 29), and then moves gradually toward (250, 9) in a concave-up manner. The red curve is labeled mutant. It starts at (0, 100), moves gradually toward (500, 38) in a concave-up manner. All values are estimated.

Return to Relationship between carnitine acyltransferase 1 activity and concentration of malonyl C o A

Extended description for Effect of various amounts of soraphen A on fatty acid synthesis



The vertical axis is labeled C superscript 14 incorporation in cellular lipids in c p m per microgram protein m i n. It has markings ranging from 0.0 to 0.8 in increments of 0.2 units. Five vertical bars are shown on the horizontal axis. From left to right, these vertical bars are colored green, blue, red, brown, and purple. The different concentrations of soraphen A in nanomoles per liter are depicted by different colors as follows:

Green bar: 0 nanomoles per liter

Blue bar: 1 nanomoles per liter

Red bar: 10 nanomoles per liter

Brown bar: 100 nanomoles per liter

Purple bar: 1,000 nanomoles per liter

The incorporation of C superscript 14 in cellular lipids corresponding to these bars is as follows:

Green bar: 0.42

Blue bar: 0.22

Red bar: 0.1

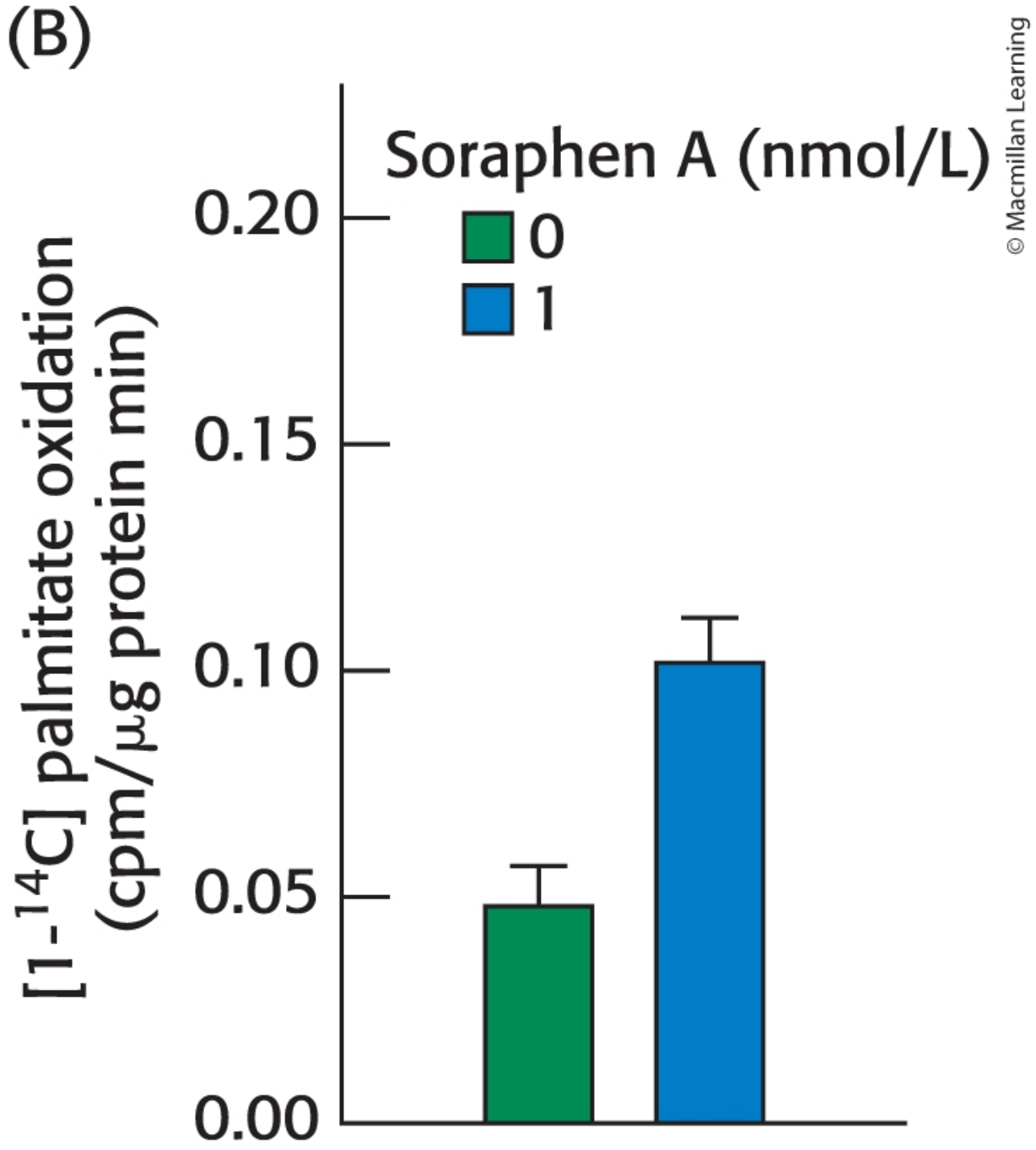
Brown bar: 0.02

Purple bar: 0.01

All values are estimated.

Return to Effect of various amounts of soraphen A on fatty acid synthesis

Extended description for Effect of various amounts of soraphen A on fatty acid oxidation



The vertical axis is labeled concentration of 1-C superscript 14 palmitate oxidation in c p m per microgram protein m i n. It has markings ranging from 0.00 to 0.20 in increments of 0.05 units. Two vertical bars are shown on the horizontal axis. The green bar depicts 0 nanomoles per liter of soraphen A and the blue bar depicts 1 nanomoles per liter of soraphen A.

The amount of palmitate oxidation depicted by different bars is as follows:

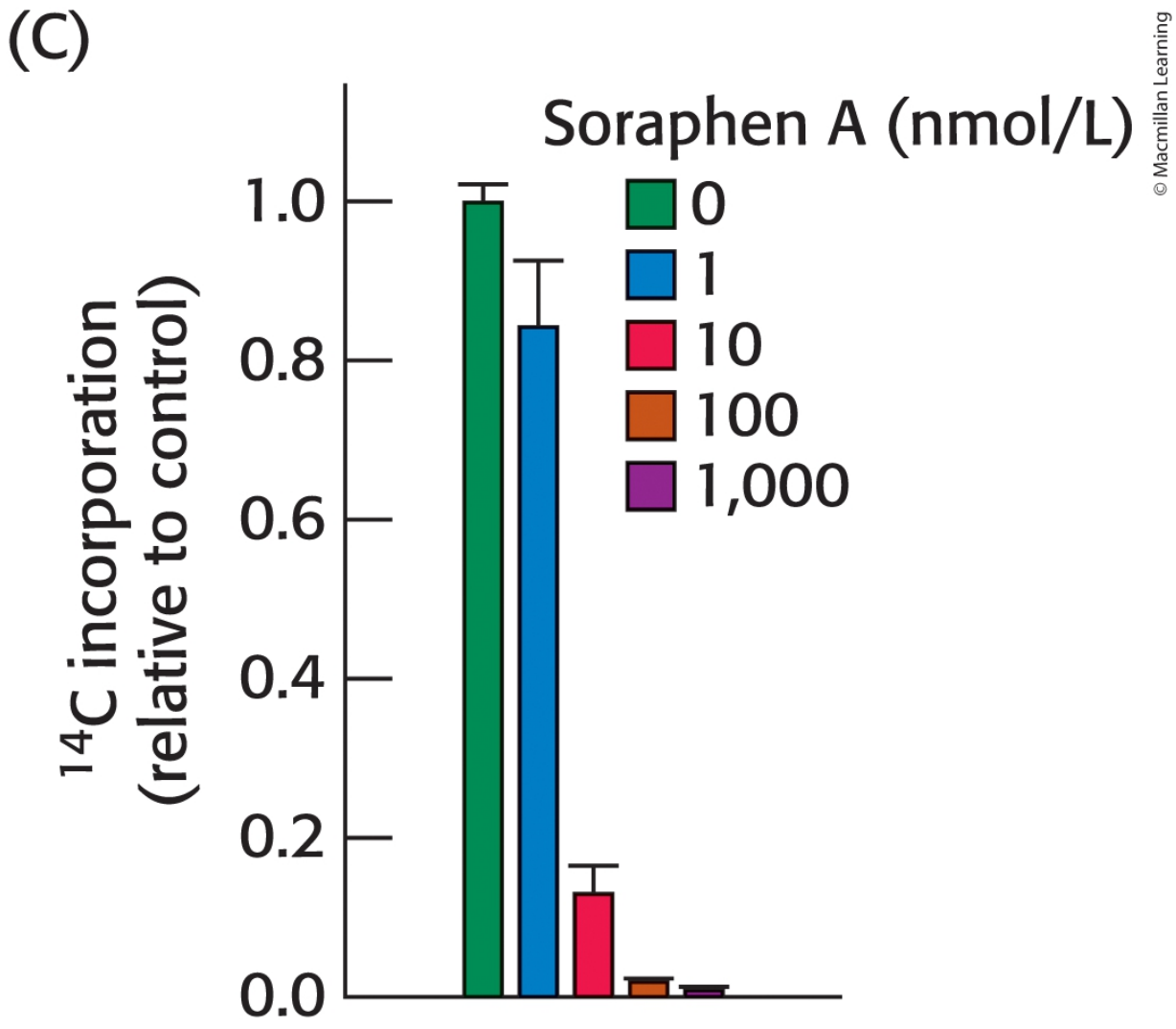
Green bar: 0.05

Blue bar: 0.10

All values are estimated.

Return to Effect of various amounts of soraphen A on fatty acid oxidation

Extended description for Effect of various amounts of soraphen A on phospholipid synthesis



© Macmillan Learning

The vertical axis is labeled C superscript 14 relative to control. It has markings ranging from 0.0 to 1.0 in increments of 0.2 units. Five vertical bars are shown on the horizontal axis. From left to right, these vertical bars are colored green, blue, red, brown, and purple. The different concentrations of soraphen A in nanomoles per liter are depicted by different colors as follows:

Green bar: 0 nanomoles per liter

Blue bar: 1 nanomoles per liter

Red bar: 10 nanomoles per liter

Brown bar: 100 nanomoles per liter

Purple bar: 1,000 nanomoles per liter

The incorporation of C superscript 14 corresponding to these bars is as follows:

Green bar: 1.0

Blue bar: 0.85

Red bar: 0.18

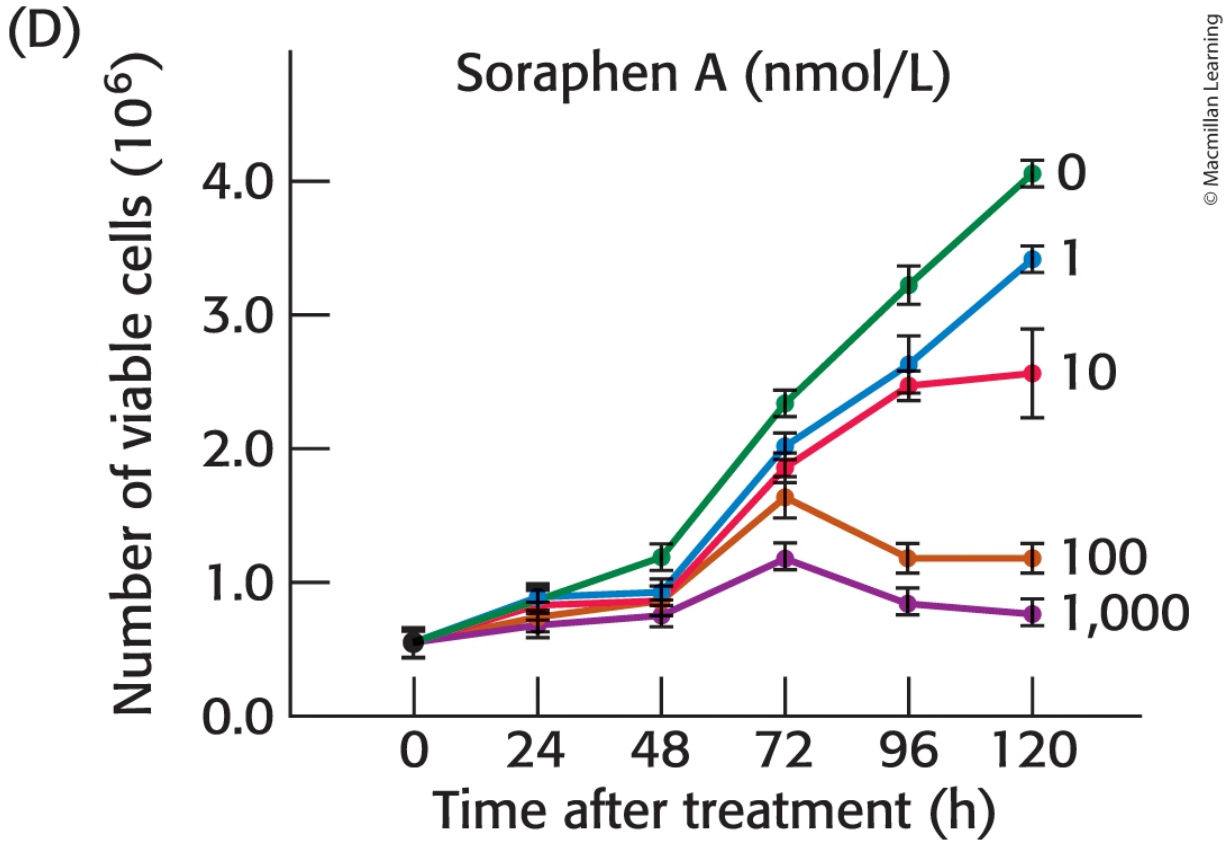
Brown bar: 0.02

Purple bar: 0.01

All values are estimated.

Return to Effect of various amounts of soraphen A on phospholipid synthesis

Extended description for Effect of different concentrations of soraphen A on the viability of cancer cells



The horizontal axis is labeled time after treatment in hours. It has markings ranging from 0 to 120 in increments of 24 hours. The vertical axis is labeled number of viable cells (10 to the power 6). It has markings ranging from 0.0 to 4.0 in increments of 1.0 units. The graph contains 5 curves depicted in green, blue, red, brown, and purple colors. The concentration of soraphen A in nanomoles per liter depicted by different colors is as follows: Green: 0, Blue: 1, Red: 10, Brown: 100, Purple: 1,000.

The green curve passes through the following data points: (0, 0.7), (24, 0.9), (48, 1.4), (72, 2.5), (96, 3.4), and (120, 4.0).

The blue curve passes through the following data points: (0, 0.7), (24, 0.9), (48, 1.0), (72, 2.1), (96, 2.7), and (120, 3.5).

The red curve passes through the following data points: (0, 0.7), (24, 0.9), (48, 1.0), (72, 2.0), (96, 2.5), and (120, 2.6).

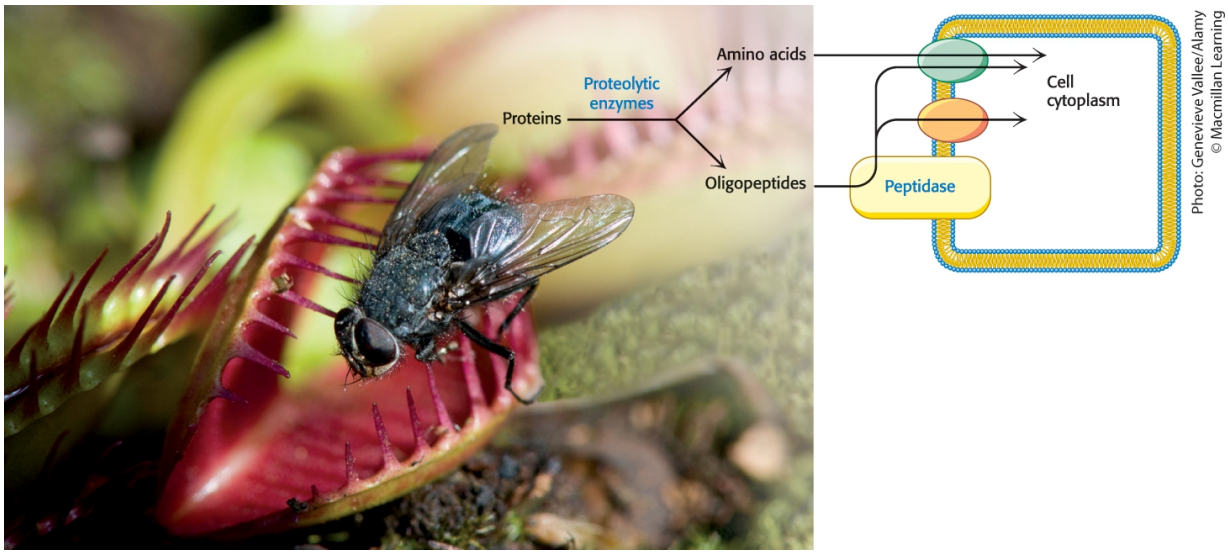
The brown curve passes through the following data points: (0, 0.7), (24, 0.8), (48, 0.9), (72, 1.8), (96, 1.2), and (120, 1.1).

The purple curve passes through the following data points: (0, 0.7), (24, 0.79), (48, 0.8), (72, 1.2), (96, 0.9), and (120, 0.8).

All values are estimated.

Return to Effect of different concentrations of soraphen A on the viability of cancer cells

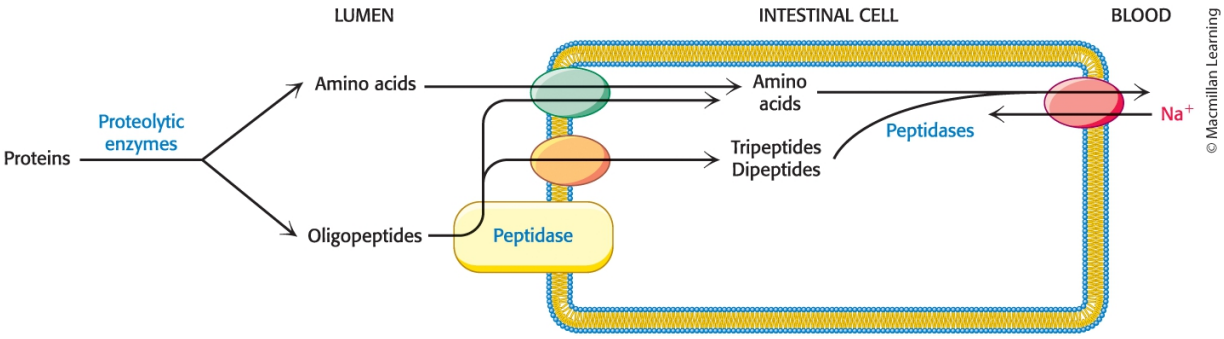
Extended description for Schematic representation of the absorption of protein digestion products by a cell



A rectangular cell is surrounded by a lipid bilayer. Two oval-shaped transport proteins shown in green and orange are embedded in the left lateral membrane of the cell. An oblong peptidase is also embedded in the left lateral membrane. In the region outside the cell, proteins are degraded into amino acids and oligopeptides by proteolytic enzymes. The oligopeptides are digested by the membrane-bound peptidase. The digestion products are transported into the cell cytoplasm through the green and orange oval transporter. The amino acids are transported into the cell cytoplasm through the green oval transporter.

Return to Schematic representation of the absorption of protein digestion products by a cell

Extended description for FIGURE 23.1 The products of protein digestion are absorbed by the small intestine

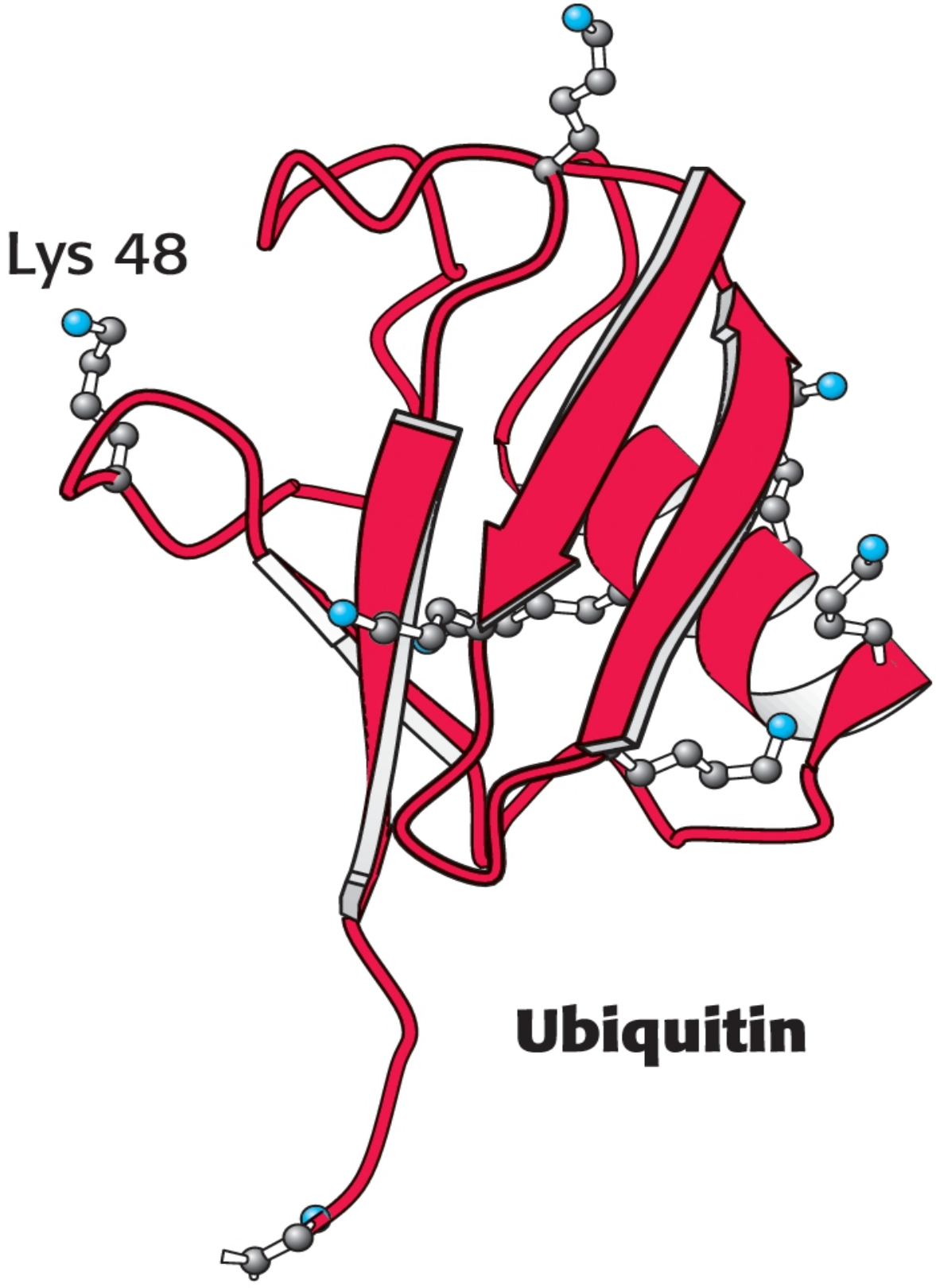


A rectangular intestine cell is surrounded by a lipid bilayer. The region on the left of the cell is labeled lumen and the region on the right is labeled blood. Two oval-shaped transport proteins shown in green and orange are embedded in the left lateral membrane of the intestine cell. An oblong peptidase is also embedded in the left lateral membrane facing the lumen. A red oval-shaped transport protein is embedded in the right lateral membrane facing the blood. Inside the lumen, proteins are degraded into amino acids and oligopeptides by proteolytic enzymes. The oligopeptides are broken down into tripeptides and dipeptides by peptidase in the membrane. The tripeptides, dipeptides, and amino acids are transported into the cell through the green oval transporter. The tripeptides and dipeptides are also transported through the orange oval transporter. The amino acids, tripeptides, and dipeptides inside the cell are transported into the blood side through the red oval transporter coupled with the entry of N a superscript plus ion into the cell.

Return to FIGURE 23.1 The products of protein digestion are absorbed by the small intestine

Extended description for FIGURE 23.2 Ubiquitin is a

small, compact protein with seven lysines

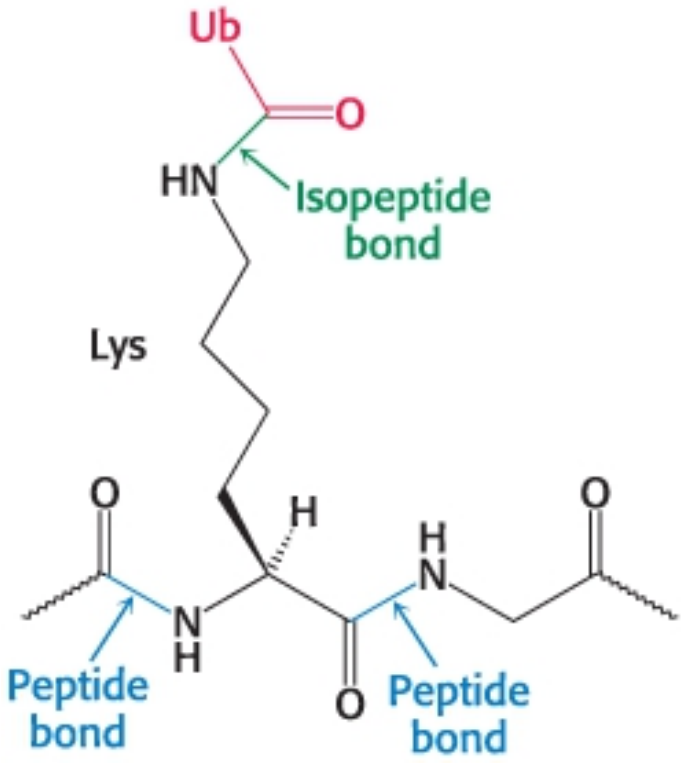


© Macmillan Learning

The ribbon diagram of ubiquitin consists of four beta-strands and one alpha-helix interconnected by long thread-like loops. The ball-and-stick models of side chains of seven different lysine residues are shown attached to the diagram at different sites. The model consists of a chain of 5 black spheres. The terminal black sphere is connected to a blue sphere. A loop at the top connected to one of the beta strands contains the side chain of lysine 48. Its adjacent beta-strand is connected to a long thread below labeled the C-terminus. The C terminus also contains a side chain of a lysine residue.

Return to FIGURE 23.2 Ubiquitin is a small, compact protein with seven lysines

Extended description for Isopeptide bond between ubiquitin and the side chain of lysine residue of the target protein

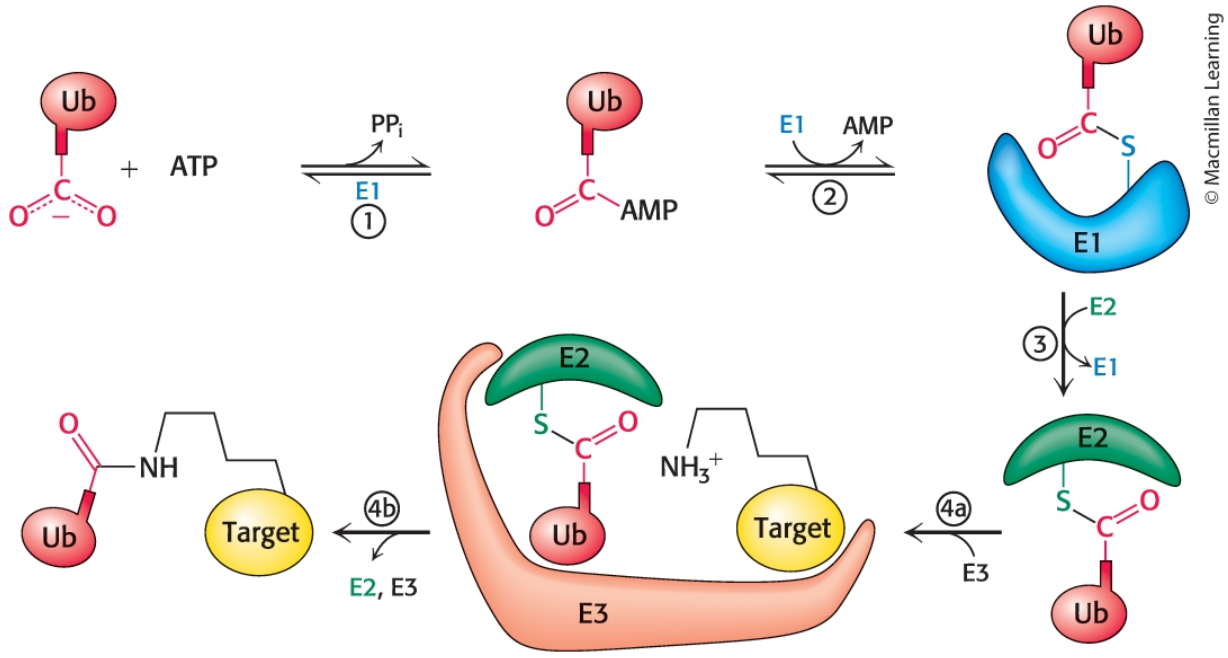


Ubiquitin depicted as U b is single bonded to C on the lower right. This C is double-bonded to O on the left and single-bonded to N H group of lysine side chain on the lower left. The single bond between C and N H is labeled an isopeptide bond. The structure of the target protein is depicted as a 2 N and 5 C heteronuclear alkane chain depicted as a line structure using 6 zigzag lines. N occupies the second and fifth positions. Both the N atoms are bound to H. C 1 is double bonded to O above and has a wiggly line on the lower left. C 2 is dash bonded to H on the upper right and wedge bonded to a 4-carbon alkane chain depicted as a line structure using 3 zigzag lines. C 4 of this alkane chain is single-bonded to N H, which is connected

to the ubiquitin through an isopeptide bond. In the heteronuclear alkane chain, C 3 and C 5 are each double bonded to O above. C 5 has a wiggly line on the lower right. The single bond between C 1 and N 1, and C 3 and N 2 is labeled peptide bond.

Return to Isopeptide bond between ubiquitin and the side chain of lysine residue of the target protein

Extended description for FIGURE 23.3 Ubiquitin conjugation requires three enzymes



In the first reversible step catalyzed by E 1, a ubiquitin-protein depicted as a small red oval connected to a short tube below is single bonded to C below. The C atom is partially double-bonded to O on the lower left and lower right. The O atoms have an overall negative charge. The ubiquitin protein reacts with A T P. The product of the first step consists of ubiquitin single bonded to C below. This C atom is double-bonded to O on the lower left and single-bonded to A M P on the lower right. P P subscript i is released during this step.

In the second reversible step, E 1 enters, and A M P is released. The ubiquitin is single-bonded to C below. This C is double-bonded to O on the lower left and single-bonded to S on the lower right. This S atom is single-bonded to E 1 which is depicted as a blue curved structure.

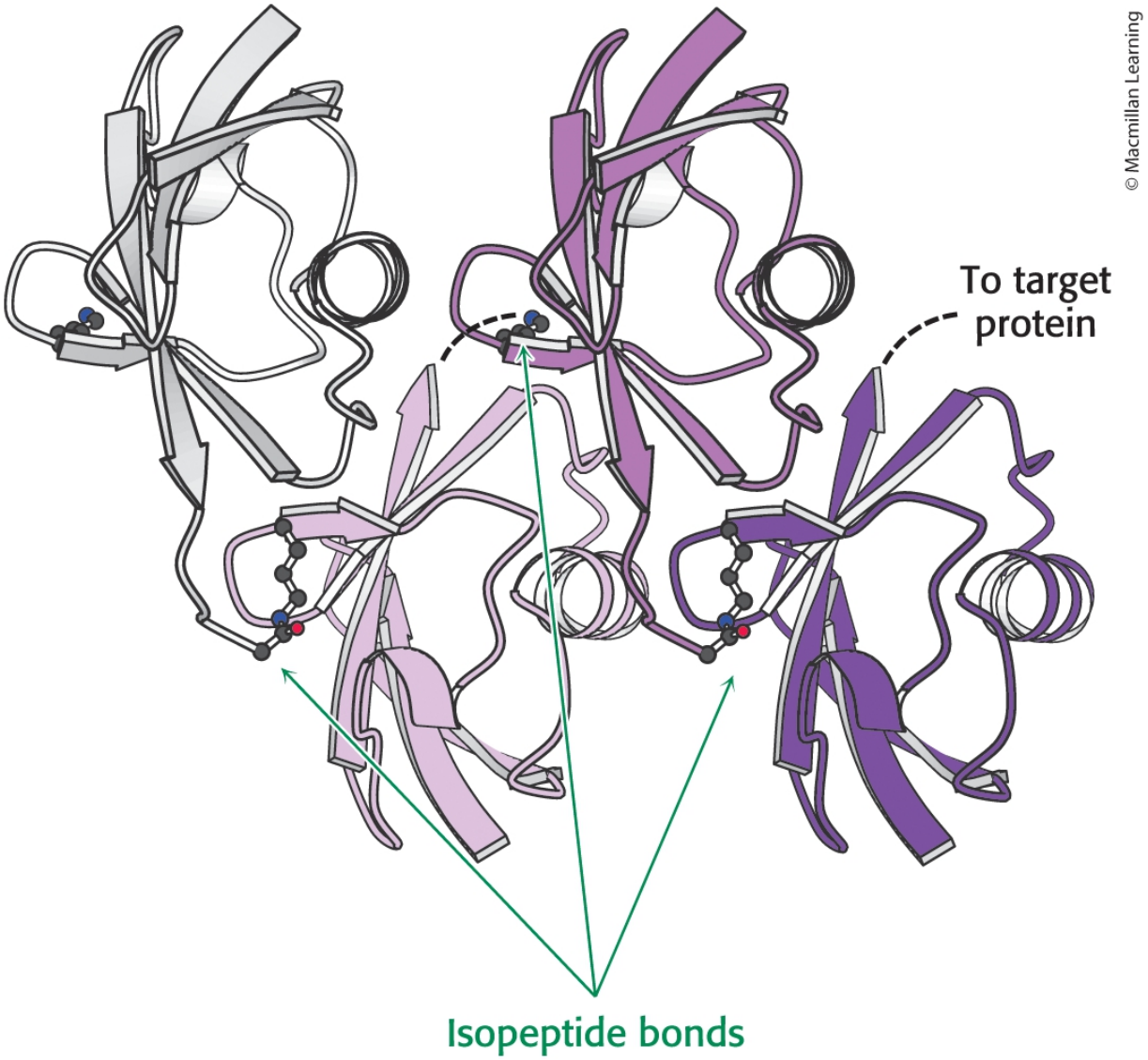
In the third irreversible step, E 2 enters and E 1 is released. The orientation of ubiquitin is reversed such that it is single-bonded to C above. This C is double-bonded to O on the upper right and single-bonded to S on the upper left. This S atom is single-bonded to E 2 which is depicted as a green crescent-shaped structure.

In the irreversible step 4 a, E 3 enters. E 3 is an elongated L-shaped protein that accommodates ubiquitin connected to E 2 and a target protein depicted as a yellow oval connected to a 4-carbon alkane chain. The alkane chain is depicted as a line structure using 3 zigzag lines. C 4 is single bonded to N H 3 superscript plus.

In irreversible step 4 b, E 2 and E 3 are released. The ubiquitin is single-bonded to C. This C is double bonded to O on the upper left and single bonded to the N H group connected to the target through a 4-carbon alkane chain.

Return to FIGURE 23.3 Ubiquitin conjugation requires three enzymes

Extended description for FIGURE 23.4 In a tetraubiquitin chain, four ubiquitin molecules are linked by isopeptide bonds



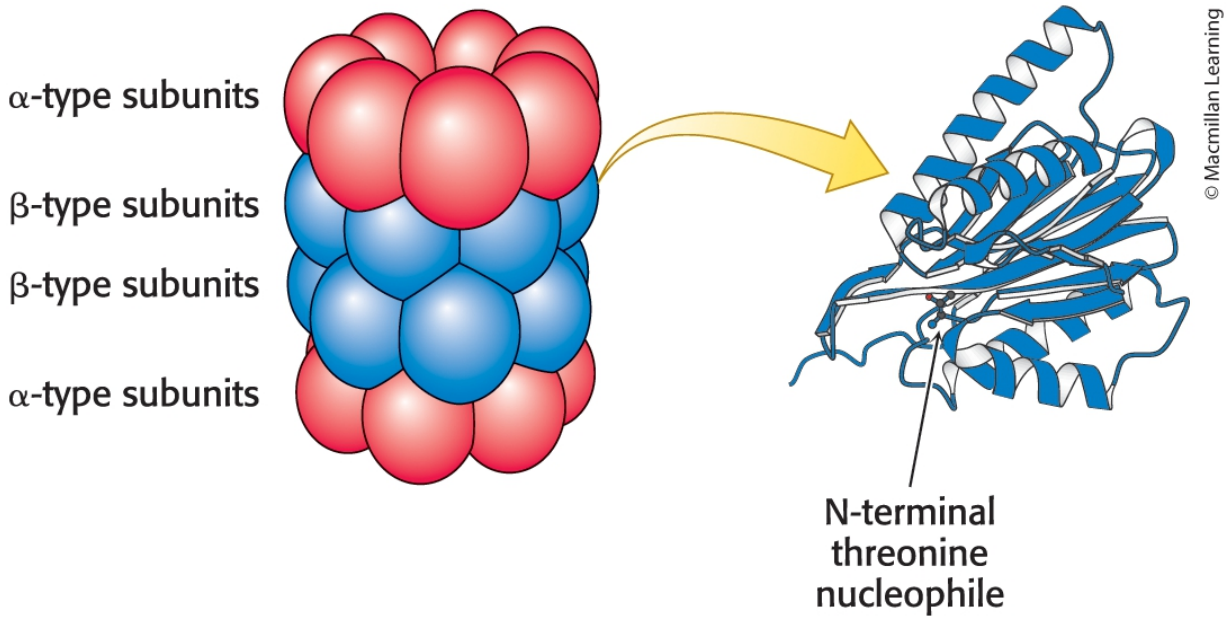
© Macmillan Learning

The ribbon diagram of four ubiquitin molecules is shown. Each molecule consists of a few beta-strands and one alpha-helix interconnected by long thread-like loops. The adjacent ubiquitin molecules are connected by isopeptide bonds. The isopeptide bond

is formed by the linkage of the carboxylate group at the end of the extended C terminus with the epsilon-amino group of a lysine residue 48. The extended C terminus of the second ubiquitin molecule is depicted as a dashed line. In the rightmost ubiquitin, a dashed line connected to one of the beta-strands is labeled "To target protein."

Return to FIGURE 23.4 In a tetraubiquitin chain, four ubiquitin molecules are linked by isopeptide bonds

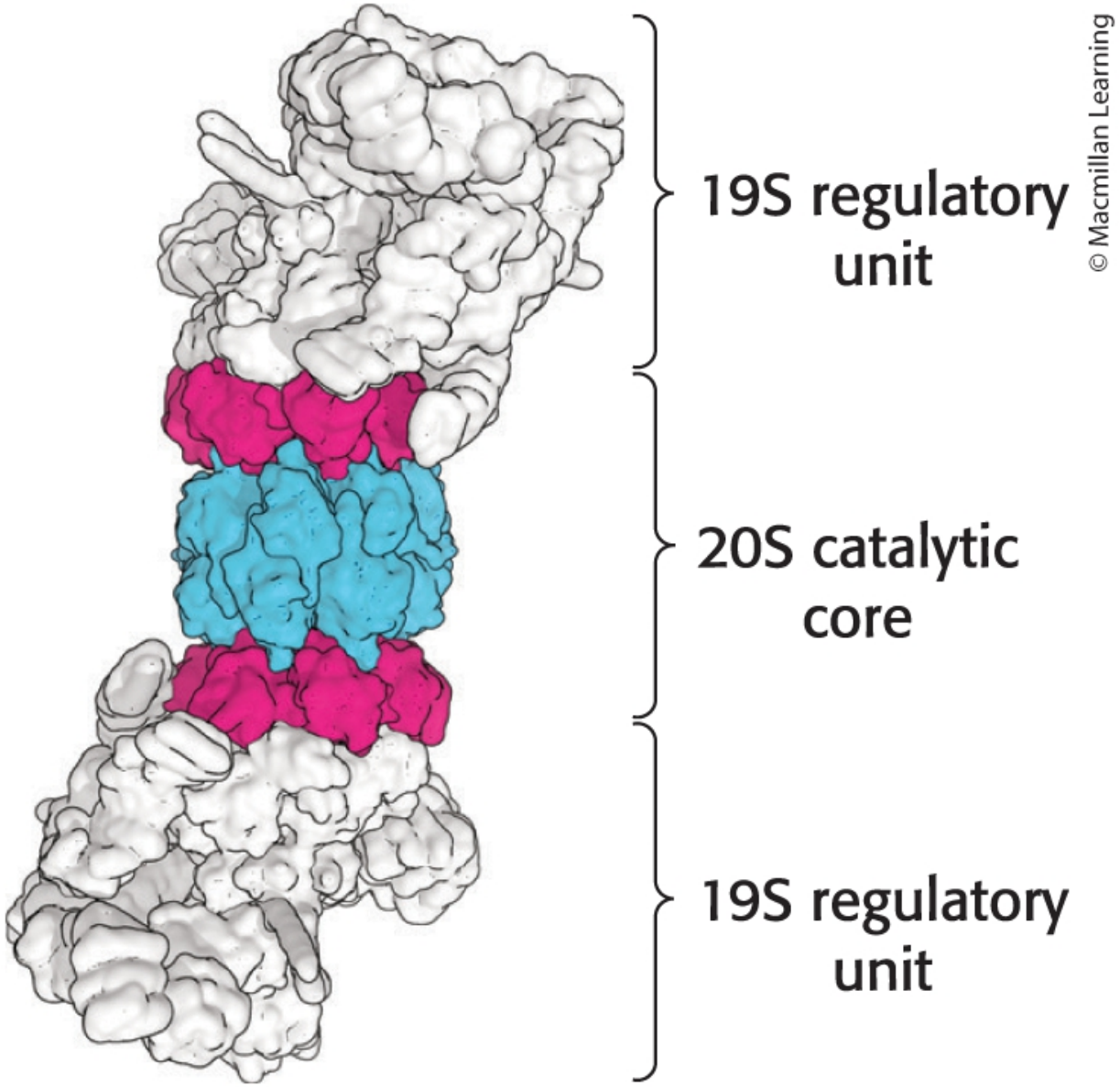
Extended description for FIGURE 23.5 The 20 S proteasome is barrel-shaped and made up of 28 homologous subunits



The 20 S proteasome is composed of 4 rings of alpha-type and beta-type subunits. Each ring is composed of 7 subunits. The alpha-type subunit is depicted as a red oval and the beta-type subunit is depicted as a blue oval. The top and bottom rings are composed of alpha-type subunits. The two rings in the middle are composed of beta-type subunits. An arrow from the beta-type subunit shows a ribbon diagram consisting of beta-strands in the middle flanked by alpha-helices at the top and bottom. An N-terminal threonine nucleophile is shown in a thread connected to one of the beta-strands.

Return to FIGURE 23.5 The 20 S proteasome is barrel-shaped and made up of 28 homologous subunits

Extended description for FIGURE 23.6 The 26 S proteasome consists of one 20 S and two 19 S subunits



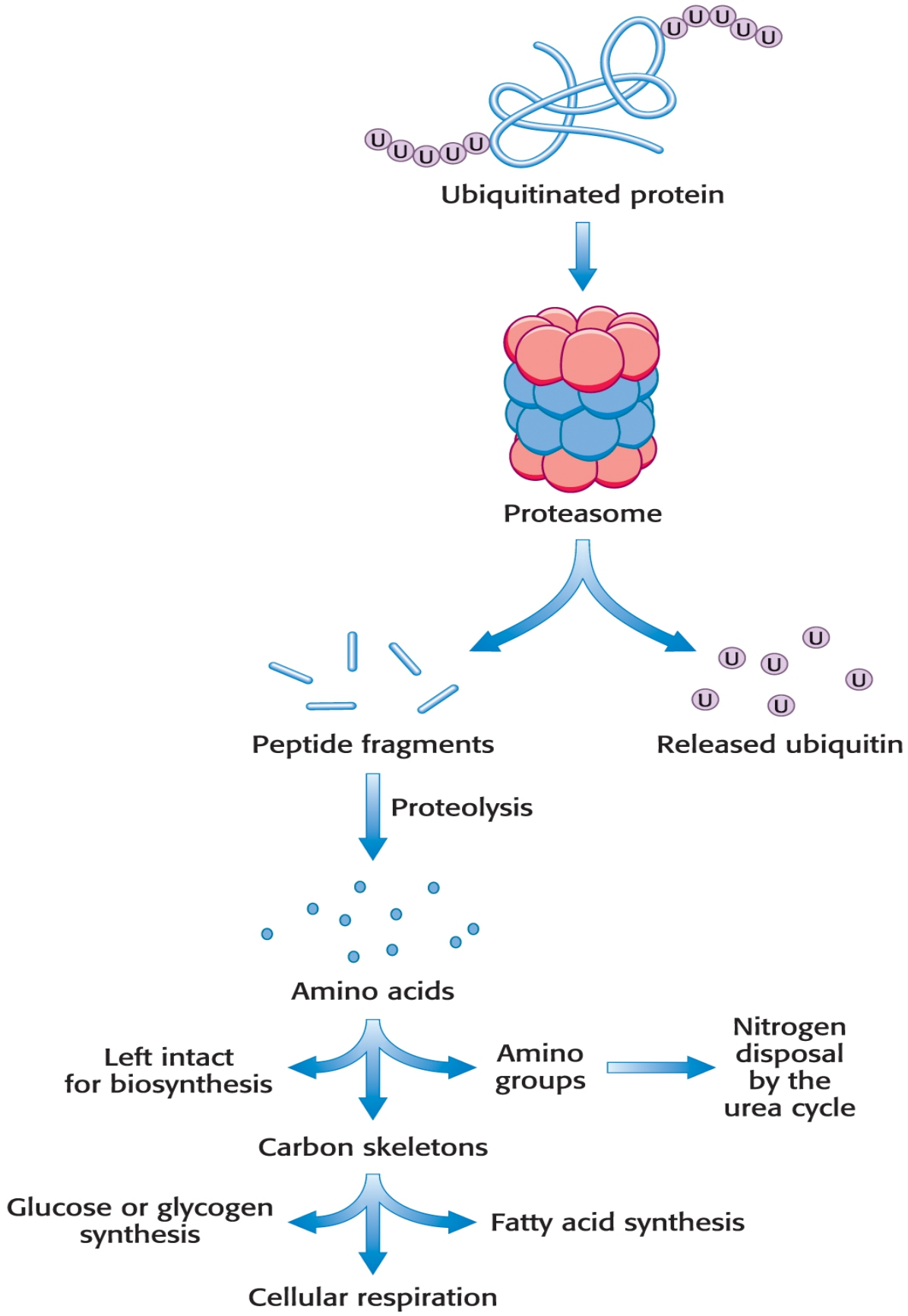
The 26 S proteasome is an elongated structure that consists of a 20 S catalytic core and a 19 S regulatory unit at the top and bottom. The 20 S catalytic core consists of thick blue subunit in the middle connected to a thin pink subunit at the top and bottom. The pink

subunits are further connected to a large white subunit having an uneven surface.

Return to FIGURE 23.6 The 26 S proteasome consists of one 20 S and two 19 S subunits

Extended description for FIGURE 23.7 The proteasome

and other proteases generate free amino acids

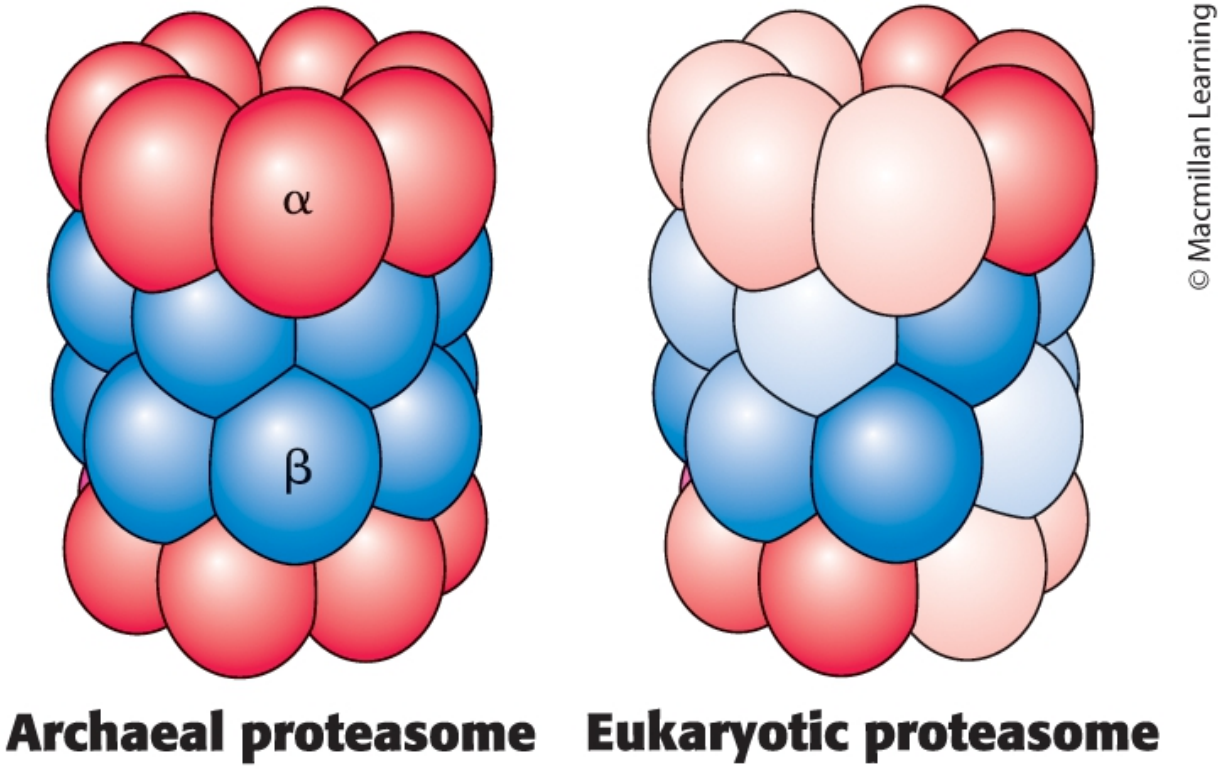


© Macmillan Learning

The ubiquitinated protein is depicted as an entangled filament. It is connected to a chain of U on the left and right. A downward arrow from ubiquitinated protein points to proteasome. Two arrows from the proteasome point toward peptide fragments and released ubiquitin. The peptide fragments are depicted as short filaments. The released ubiquitin is depicted as several isolated tiny circles labeled U. A downward arrow from peptide fragments point toward tiny blue circles depicting amino acids. Arrows from the amino acids point toward carbon skeletons, left intact for biosynthesis, and amino groups. An arrow from amino groups points toward nitrogen disposal by the urea cycle. An arrow from carbon skeletons points toward glucose or glycogen synthesis, cellular respiration, and fatty acid synthesis.

Return to FIGURE 23.7 The proteasome and other proteases generate free amino acids

Extended description for FIGURE 23.8 Proteasomes have become more complex in eukaryotes

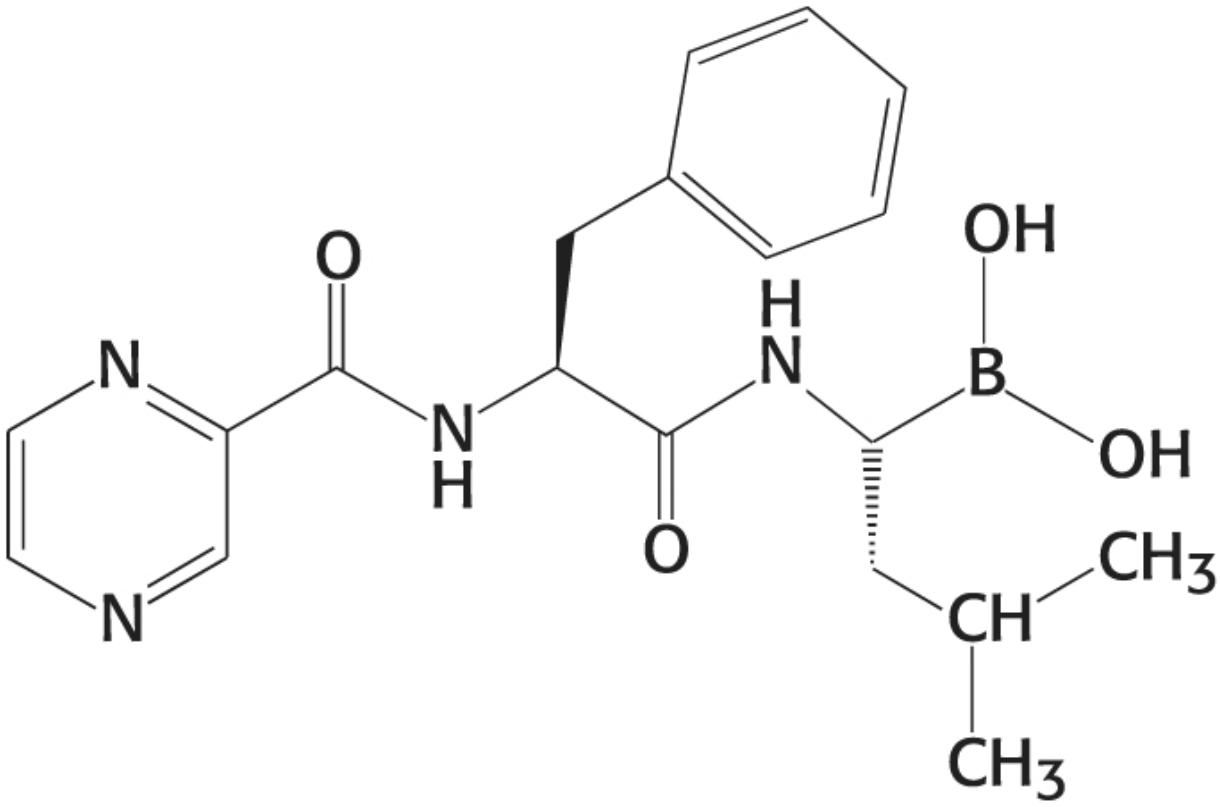


© Macmillan Learning

The archaeal proteasome is composed of 4 rings. The top and bottom rings are composed of identical alpha subunits depicted as a red oval. The two rings in the middle are composed of identical beta subunits depicted as a blue oval. The eukaryotic proteasome is composed of 4 rings. The top and bottom rings are composed of 7 distinct types of alpha subunits. The different alpha subunits are shown in red color of varying intensity. The two rings in the middle are composed of 7 distinct types of beta-subunits. The different beta subunits are shown in blue color of varying intensity.

Return to FIGURE 23.8 Proteasomes have become more complex in eukaryotes

Extended description for Structure of bortezomib



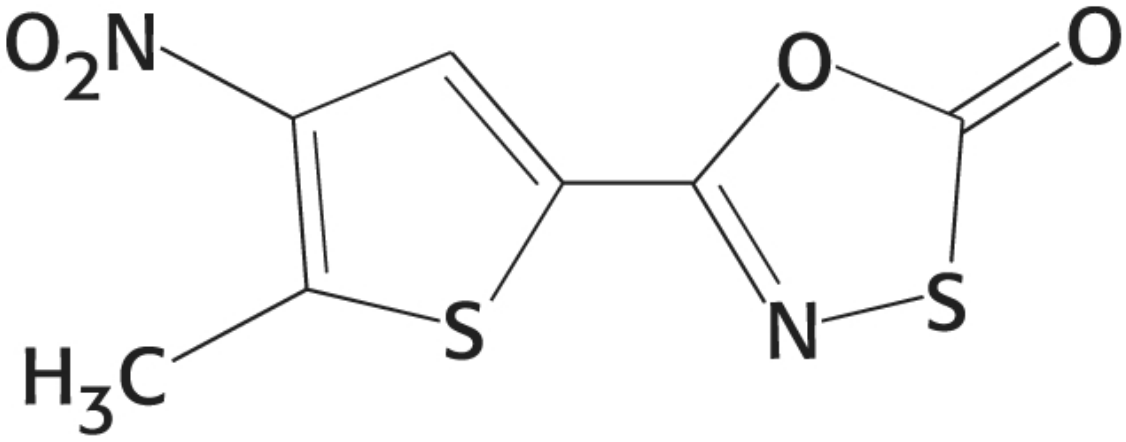
Bortezomib
(a dipeptidyl boronic acid)

The structure of bortezomib is as follows: A 6-membered heterocyclic hexagonal ring is in a vertical orientation. It consists of 2 N and 4 C atoms. C 1 occupies the top right vertex. The first N occupies the topmost vertex and the second N occupies the bottom-most vertex. A double bond is present between N 1 and C 1, C 2 and N 2, and C 3 and C 4. C 1 is single bonded to a 2 N and 3 C heteronuclear alkane chain depicted as a line structure using 4 zigzag lines. The first N bound to H occupies the second position and the second N bound to H occupies the fifth position. C 1 is double bonded to O above. C 2 is wedge bonded to C H 2 on the

upper right. This C H 2 group is single-bonded to C 1 of a benzene ring. In the benzene ring, alternating double bonds are present between C 2 and C 3, C 4 and C 5, and C 6 and C 1. C 3 of the alkane chain is double bonded to O below. N 2 of the alkane chain is single-bonded to C H 2 on the lower right. This C H 2 group is dash bonded to C H 2 below and single bonded to B on the upper right. The B atom is single-bonded to O H above and O H on the lower right. The C H 2 group below is single-bonded to C H on the lower right. The C H group is single bonded to C H 3 on the upper right and C H 3 below.

Return to Structure of bortezomib

Extended description for Structure of H T 1171



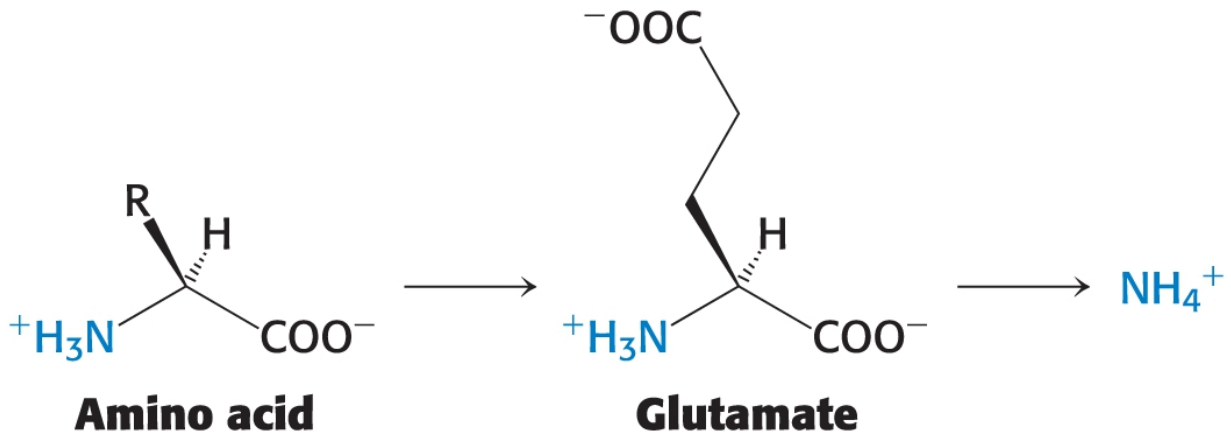
HT1171

5-(2-methyl-3-nitrothiophen-2-yl)-1,3,4-oxathiazol-2-one

The structure of H T 1171 is as follows: A 5-membered heterocyclic pentagonal ring is in a vertical orientation and consists of 1 S and 4 C atoms. S occupies the bottom-right vertex. C 1 occupies the bottom-left vertex. A double bond is present between C 1 and C 2, and C 3 and C 4. C 1 is single bonded to C H 3 on the lower left. C 2 is single bonded to N O 2 on the upper left. C 4 is single-bonded to C 2 of another 5-membered heterocyclic pentagonal ring in a vertical orientation. This ring consists of 1 O, 1 N, 1 S, and 2 C atoms. N occupies the bottom left vertex and S occupies the bottom right vertex. O occupies the topmost vertex. C 1 occupies the top right vertex. A double bond is present between N and C 2. C 1 is double bonded to O on the upper right.

Return to Structure of H T 1171

Extended description for Oxidative deamination in the liver



In oxidative deamination, the amino acid is first irreversibly converted into glutamate.

The structure of amino acid is depicted as follows: A central C atom is single bonded to N H 3 superscript plus on the lower left, single bonded to C O O superscript minus on the lower right, wedge bonded to R on the upper left, and dash bonded to H on the upper right.

The structure of glutamate is depicted as follows: A 2-carbon alkane chain is depicted using a single line. C 1 is single bonded to C O O superscript minus on the upper left. C 2 is wedge bonded to C on the lower right. This C atom is single bonded to N H 3 superscript plus on the lower left, single bonded to C O O superscript minus on the lower right, and dash bonded to H on the upper right.

In the next irreversible step, glutamate gives an ammonium ion depicted as N H 4 superscript plus.

Return to Oxidative deamination in the liver

Extended description for Transfer of the alpha-amino group from an alpha-amino acid to an alpha-ketoacid



The reversible reaction catalyzed by aminotransferase consists of two reactants and two products.

The structure of the first reactant is as follows: A central C atom is single bonded to C O O superscript minus on the lower left, single bonded to R 1 on the lower right, wedge bonded to N H 3 superscript plus on the upper left, and dash bonded to H on the upper right.

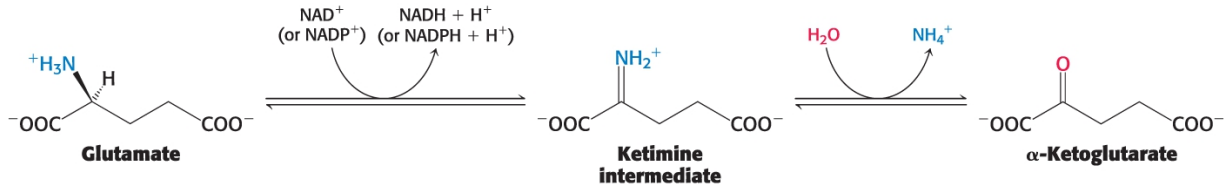
The structure of the second reactant is as follows: A central C atom is single bonded to C O O superscript minus on the lower left, single bonded to R 2 on the lower right, and double bonded to O above.

The structure of first product is as follows: A central C atom is single bonded to C O O superscript minus on the lower left, single bonded to R 1 on the lower right, and double bonded to O above.

The structure of the second product is as follows: A central C atom is single bonded to C O O superscript minus on the lower left, single bonded to R 2 on the lower right, wedge bonded to N H 3 superscript plus on the upper left, and dash bonded to H on the upper right.

Return to Transfer of the alpha-amino group from an alpha-amino acid to an alpha-ketoacid

Extended description for Formation of alpha-ketoglutarate from glutamate



The reaction consists of one reactant, one intermediate, and one product.

The reactant is glutamate whose structure is as follows: A 3-carbon alkane chain is depicted as a line structure using 2 zigzag lines. C 1 is single bonded to C O O superscript minus on the lower left, wedge bonded to N H 3 superscript plus on the upper left, and dash bonded to H on the upper right. C 3 is single bonded to C O O superscript minus on the lower right.

A reversible reaction arrow leads to the ketimine intermediate. A curved arrow above it depicts the coupled reduction of N A D superscript plus or N A D P superscript plus to N A D H plus H superscript plus or N A D P H plus H superscript plus respectively.

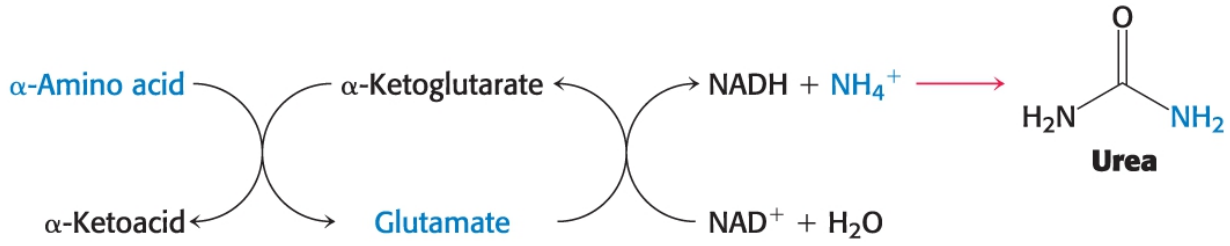
The structure of the ketimine intermediate is as follows: A 3-carbon alkane chain is depicted as a line structure using 2 zigzag lines. C 1 is single bonded to C O O superscript minus on the lower left and double bonded to N H 2 superscript plus above. C 3 is single bonded to C O O superscript minus on the lower right.

A reversible reaction arrow leads to the product. A curved arrow above it shows the entry of H 2 O and the release of N H 4 superscript plus ion.

The product is alpha-ketoglutarate whose structure is as follows: A 3-carbon alkane chain is depicted as a line structure using 2 zigzag lines. C 1 is single bonded to C O O superscript minus on the lower left and double bonded to O above. C 3 is single bonded to C O O superscript minus on the lower right.

Return to Formation of alpha-ketoglutarate from glutamate

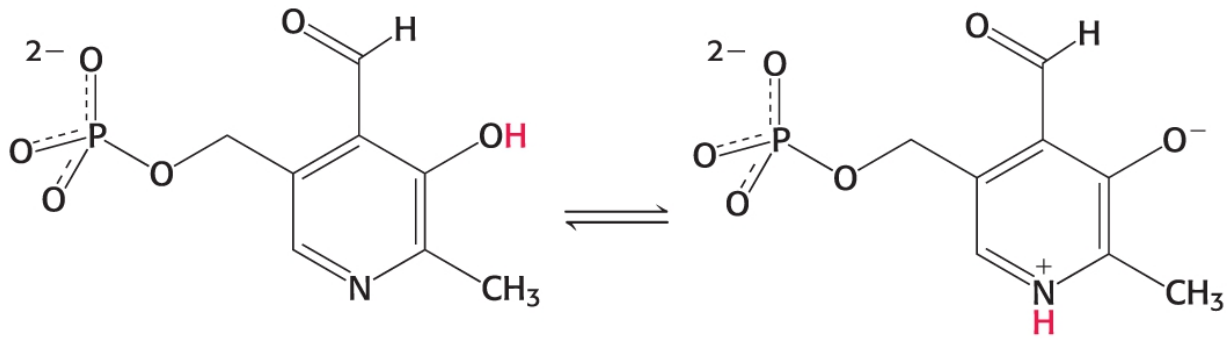
Extended description for Conversion of an ammonium ion into urea in terrestrial vertebrates



Alpha-amino acid transfers the amino group to alpha-ketoglutarate. The alpha-amino acid forms alpha-ketoacid and alpha-ketoglutarate is converted into glutamate. The glutamate molecule is converted back to alpha-ketoglutarate with the simultaneous reduction of N A D superscript plus to N A D H. H 2 O is also used up during this conversion and the N H 4 superscript plus group is also released. The N H 4 superscript plus is irreversibly converted into urea. The structure of urea consists of a central C atom single bonded to N H 2 on the lower left, N H 2 on the lower right, and double bonded to O above.

Return to Conversion of an ammonium ion into urea in terrestrial vertebrates

Extended description for Reversible conversion of P L P (phenol) to P L P (phenolate)



PLP (phenol) **PLP (phenolate)**

The structure of P L P (phenol) is as follows: A 6-membered heterocyclic hexagonal ring is in a vertical orientation and consists of 1 N and 5 C atoms. N occupies the bottom-most vertex. C 1 occupies the bottom-left vertex. A double bond is present between N and C 1, C 2 and C 3, and C 4 and C 5. C 2 is single bonded to C H 2 on the upper left in the form of a line. C H 2 is single-bonded to O on the lower left. This O is single-bonded to a P atom. The P atom is partially double-bonded to O above, O on the left, and O on the lower left. The O atoms have an overall negative charge of 2 minus. C 3 is single bonded to C above. This C is double-bonded to O on the upper left and single-bonded to H on the upper right. C 4 is single bonded to O H on the upper right. The H atom of the O H group is highlighted in red. C 5 is single bonded to C H 3 on the lower right.

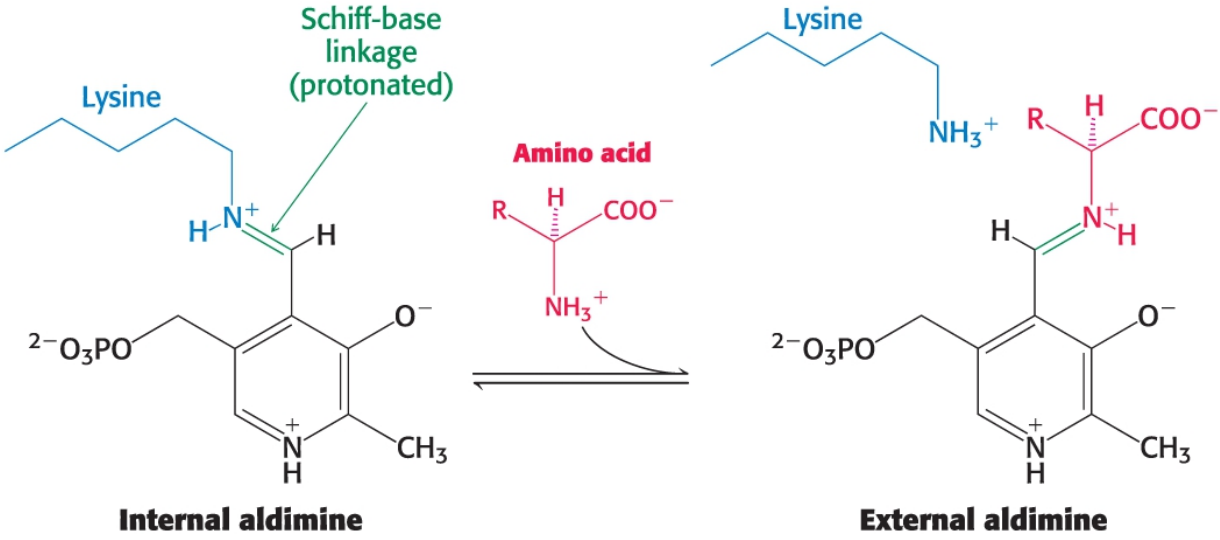
A reversible reaction arrow leads to P L P (phenolate).

The structure of P L P (phenolate) is as follows: A 6-membered heterocyclic hexagonal ring is in a vertical orientation and consists of 1 N and 5 C atoms. N with a positive charge occupies the bottom-most vertex. It is bound to H highlighted in red. C 1 occupies the

bottom-left vertex. A double bond is present between N and C 1, C 2 and C 3, and C 4 and C 5. C 2 is single bonded to C H 2 on the upper left in the form of a line. C H 2 is single-bonded to O on the lower left. This O is single-bonded to a P atom. The P atom is partially double-bonded to O above, O on the left, and O on the lower left. The O atoms have an overall negative charge of 2 minus. C 3 is single bonded to C above. This C is double-bonded to O on the upper left and single-bonded to H on the upper right. C 4 is single bonded to O superscript minus on the upper right. C 5 is single bonded to C H 3 on the lower right.

Return to Reversible conversion of P L P (phenol) to P L P (phenolate)

Extended description for Formation of external aldimine from internal aldimine



The structure of internal aldimine is as follows: A 6-membered heterocyclic hexagonal ring is in a vertical orientation and consists of 1 N and 5 C atoms. N with a positive charge occupies the bottom-most vertex. It is bound to H. C 1 occupies the bottom-left vertex. A double bond is present between N and C 1, C 2 and C 3, and C 4 and C 5. C 2 is single bonded to C H 2 on the upper left in the form of a line. C H 2 is single-bonded to O P O 3 superscript 2 minus on the lower left. C 3 is single bonded to C above. This C is double-bonded to N superscript plus on the upper left and single-bonded to H on the upper right. The double bond between the N superscript plus and the C atom is labeled "Schiff-base linkage (protonated)." The N superscript plus is single-bonded to H on the left and single-bonded to a 5-carbon alkane chain depicted as a line structure using 4 zigzag lines. The alkane chain is labeled lysine. C 4 of the ring is single bonded to O superscript minus on the upper right. C 5 is single bonded to C H 3 on the lower right.

A reversible reaction arrow leads to the external aldimine.

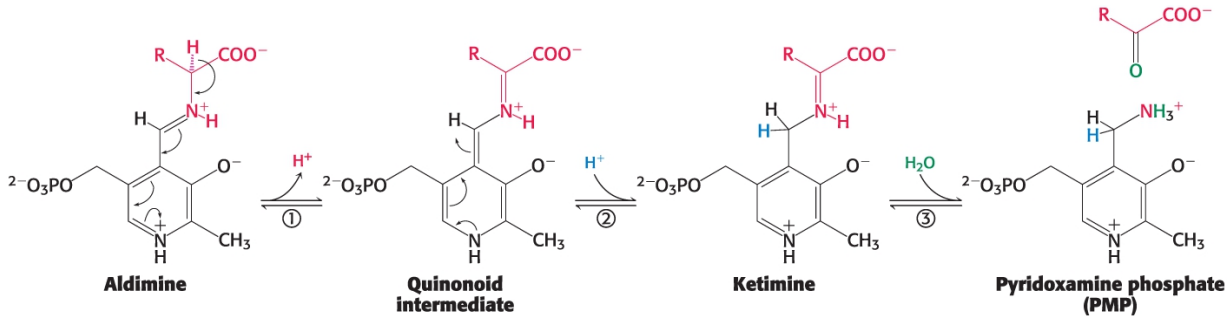
An amino acid enters the reaction. The amino acid consists of a central C atom single bonded to R on the upper left, single bonded to C O O superscript minus on the upper right, single bonded to N H 3 superscript plus, and dash bonded to H above.

The structure of external aldimine is as follows: A 6-membered heterocyclic hexagonal ring is in a vertical orientation and consists of 1 N and 5 C atoms. N with a positive charge occupies the bottom-most vertex. It is bound to H. C 1 occupies the bottom-left vertex. A double bond is present between N and C 1, C 2 and C 3, and C 4 and C 5. C 2 is single bonded to C H 2 on the upper left in the form of a line. C H 2 is single-bonded to O P O 3 superscript 2 minus on the lower left. C 3 is single bonded to C above. This C is double-bonded to N superscript plus on the upper left and single-bonded to H on the upper right. The N superscript plus atom is single-bonded to H on the lower right and single-bonded to a central C atom above. This C is single bonded to R on the upper left, single bonded to C O O superscript minus on the upper right, and dash bonded to H above.

A 5-carbon alkane chain is depicted as a line structure using 4 zigzag lines. The alkane chain is labeled lysine. C 5 is single bonded to N H 3 superscript plus below.

Return to Formation of external aldimine from internal aldimine

Extended description for FIGURE 23.9 Transaminations proceed through three steps to form P M P



In the first reversible step, aldimine is reversibly converted into a quinonoid intermediate with the concomitant release of H superscript plus.

The structure of aldimine is as follows: A 6-membered heterocyclic hexagonal ring is in a vertical orientation and consists of 1 N and 5 C atoms. N with a positive charge occupies the bottom-most vertex. It is bound to H. C 1 occupies the bottom-left vertex. A double bond is present between N and C 1, C 2 and C 3, and C 4 and C 5. C 2 is single bonded to C H 2 on the upper left in the form of a line. C H 2 is single-bonded to O P O 3 superscript 2 minus on the lower left. C 3 is single bonded to C above. This C is double-bonded to N superscript plus on the upper right and single-bonded to H on the upper left. The N superscript plus is single-bonded to H on the right and single-bonded to C above. The C atom is single bonded to R on the upper left, single bonded to C O O superscript minus on the upper right, and dash bonded to H above. An arrow from this H atom points toward the single bond between C and N superscript plus. A second arrow points from the double bond between the N superscript plus and C atom toward the single bond between this C atom and C 3 of the ring. Inside the ring, a third arrow points from the double bond

between C 2 and C 3 toward the single bond between C 1 and C 2. A fourth arrow points from the double bond between N superscript plus and C 1 of the ring toward N superscript plus.

The structure of the quinonoid intermediate is as follows: A 6-membered heterocyclic hexagonal ring is in a vertical orientation and consists of 1 N and 5 C atoms. N bound to H occupies the bottom-most vertex. C 1 occupies the bottom-left vertex. A double bond is present between C 1 and C 2, and C 4 and C 5. C 2 is single bonded to C H 2 on the upper left in the form of a line. C H 2 is single-bonded to O P O 3 superscript 2 minus on the lower left. C 3 is double bonded to C above. This C is single-bonded to N superscript plus on the upper right and single-bonded to H on the upper left. The N superscript plus is single-bonded to H on the right and double-bonded to C above. The C atom is single bonded to R on the upper left and single bonded to C O O superscript minus on the upper right. An arrow from the N atom of the ring points toward the single bond between N and C 1. A second arrow points from the double bond between C 1 and C 2 toward the single bond between C 2 and C 3. A third arrow points from the double bond between C 3 of the ring and C toward the H atom bonded to C.

In the second step, the quinonoid intermediate is reversibly converted into ketimine with the concomitant entry of H superscript plus.

The structure of ketimine is as follows: A 6-membered heterocyclic hexagonal ring is in a vertical orientation and consists of 1 N and 5 C atoms. N superscript plus bound to H occupies the bottom-most vertex. C 1 occupies the bottom-left vertex. A double bond is present between N and C 1, C 2 and C 3, and C 4 and C 5. C 2 is single bonded to C H 2 on the upper left in the form of a line. C H 2 is single-bonded to O P O 3 superscript 2 minus on the lower left. C 3 is single bonded to C above. This C is single-bonded to N superscript plus on

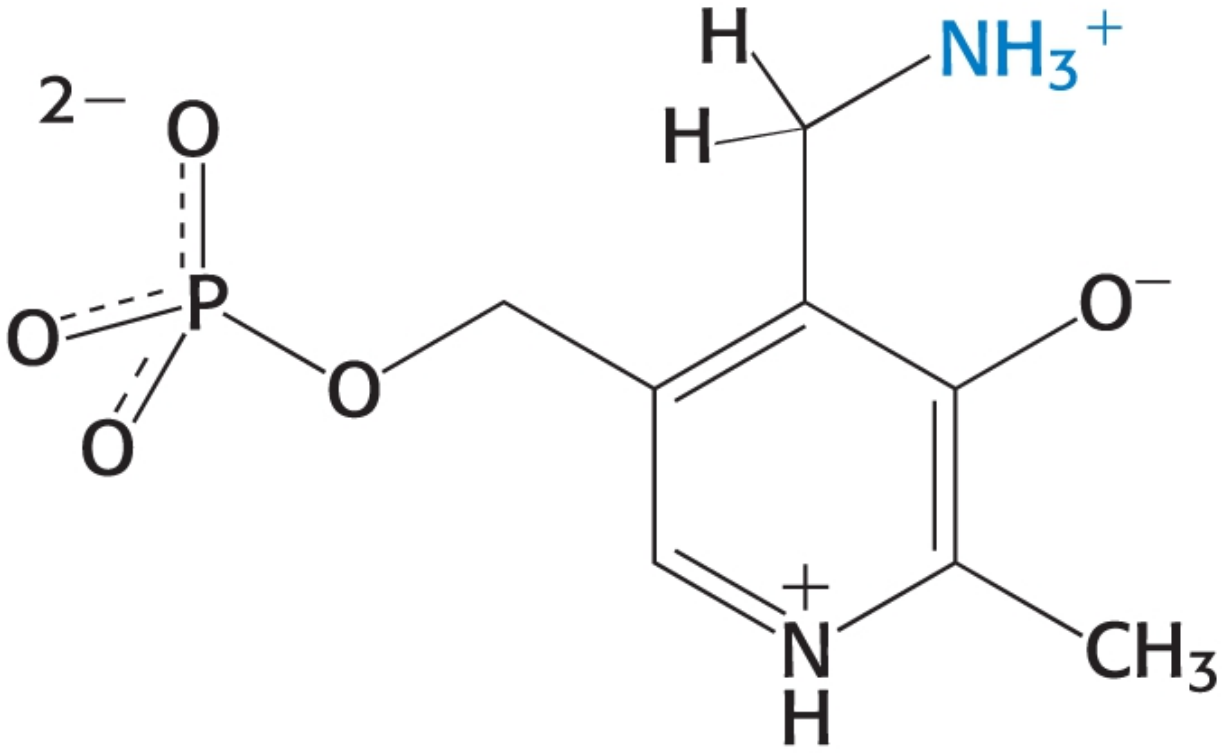
the upper right, single-bonded to H on the upper left, and single-bonded to H on the left. The N superscript plus is single-bonded to H on the right and double-bonded to C above. The C atom is single bonded to R on the upper left and single bonded to C O O superscript minus on the upper right. C 4 of the ring is single bonded to O superscript minus on the upper right. C 5 is single bonded to C H 3 on the lower right.

In the third step, ketimine is reversibly converted into pyridoxamine phosphate (P M P) and another unlabeled compound with the concomitant addition of H 2 O.

The structure of pyridoxamine phosphate (P M P) is as follows: A 6-membered heterocyclic hexagonal ring is in a vertical orientation and consists of 1 N and 5 C atoms. N superscript plus bound to H occupies the bottom-most vertex. C 1 occupies the bottom-left vertex. A double bond is present between N and C 1, C 2 and C 3, and C 4 and C 5. C 2 is single bonded to C H 2 on the upper left in the form of a line. C H 2 is single-bonded to O P O 3 superscript 2 minus on the lower left. C 3 is single bonded to C above. This C is single-bonded to N H 3 superscript plus on the upper right, single-bonded to H on the upper left, and single-bonded to H on the left. C 4 is single bonded to O superscript minus on the upper right. C 5 is single bonded to C H 3 on the lower right. The structure of the second unlabeled product is as follows: A central C atom is single bonded to R on the upper left, single bonded to C O O superscript minus on the upper right, and double bonded to O below.

Return to FIGURE 23.9 Transaminations proceed through three steps to form P M P

Extended description for Structure of pyridoxamine phosphate



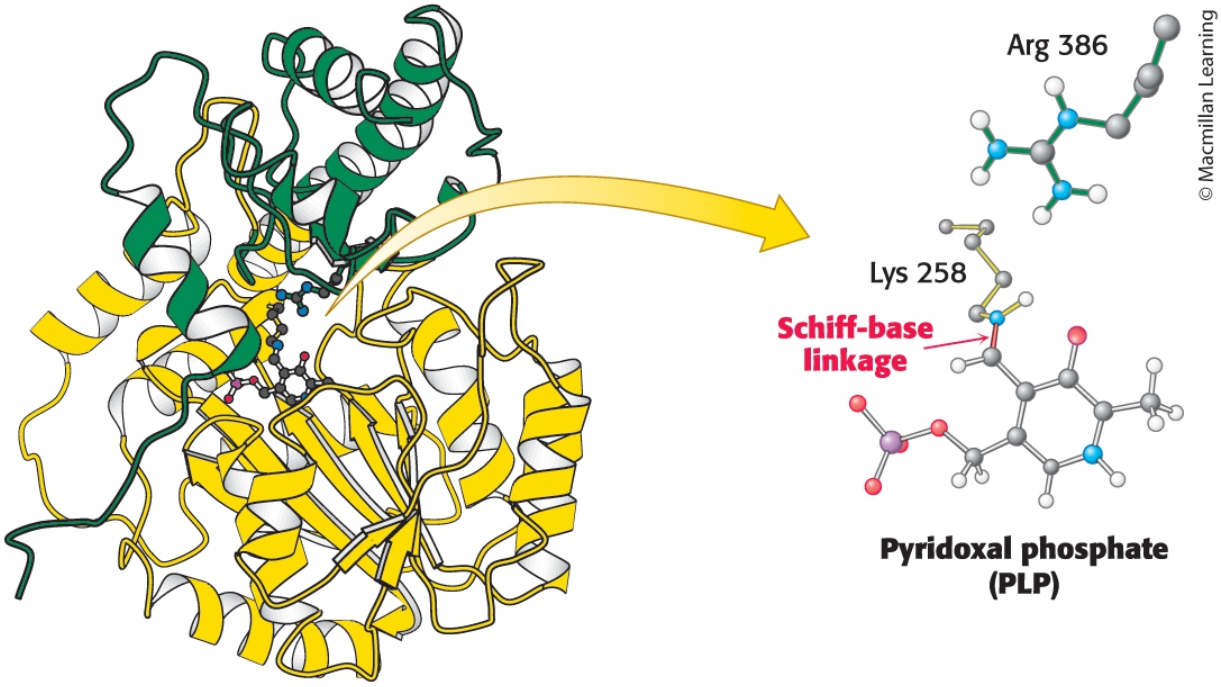
Pyridoxamine phosphate (PMP)

The structure of pyridoxamine phosphate is as follows: A 6-membered heterocyclic hexagonal ring is in a vertical orientation and consists of 1 N and 5 C atoms. N occupies the bottom-most vertex. It has a positive charge and is bound to H. C 1 occupies the bottom-left vertex. A double bond is present between N and C 1, C 2 and C 3, and C 4 and C 5. C 2 is single bonded to C H 2 on the upper left in the form of a line. C H 2 is single-bonded to O on the lower left. This O is single-bonded to a P atom. The P atom is partially

double-bonded to O above, O on the left, and O on the lower left. The O atoms have an overall negative charge of 2 minus. C 3 is single bonded to C above. This C is single bonded to H on the left, H on the upper left, and N H 3 superscript plus on the upper right. C 4 is single bonded to O superscript minus on the upper right. C 5 is single bonded to C H 3 on the lower right.

Return to Structure of pyridoxamine phosphate

Extended description for FIGURE 23.10 The active site of aspartate aminotransferase reveals P L P bound to a lysine through a Schiff-base linkage

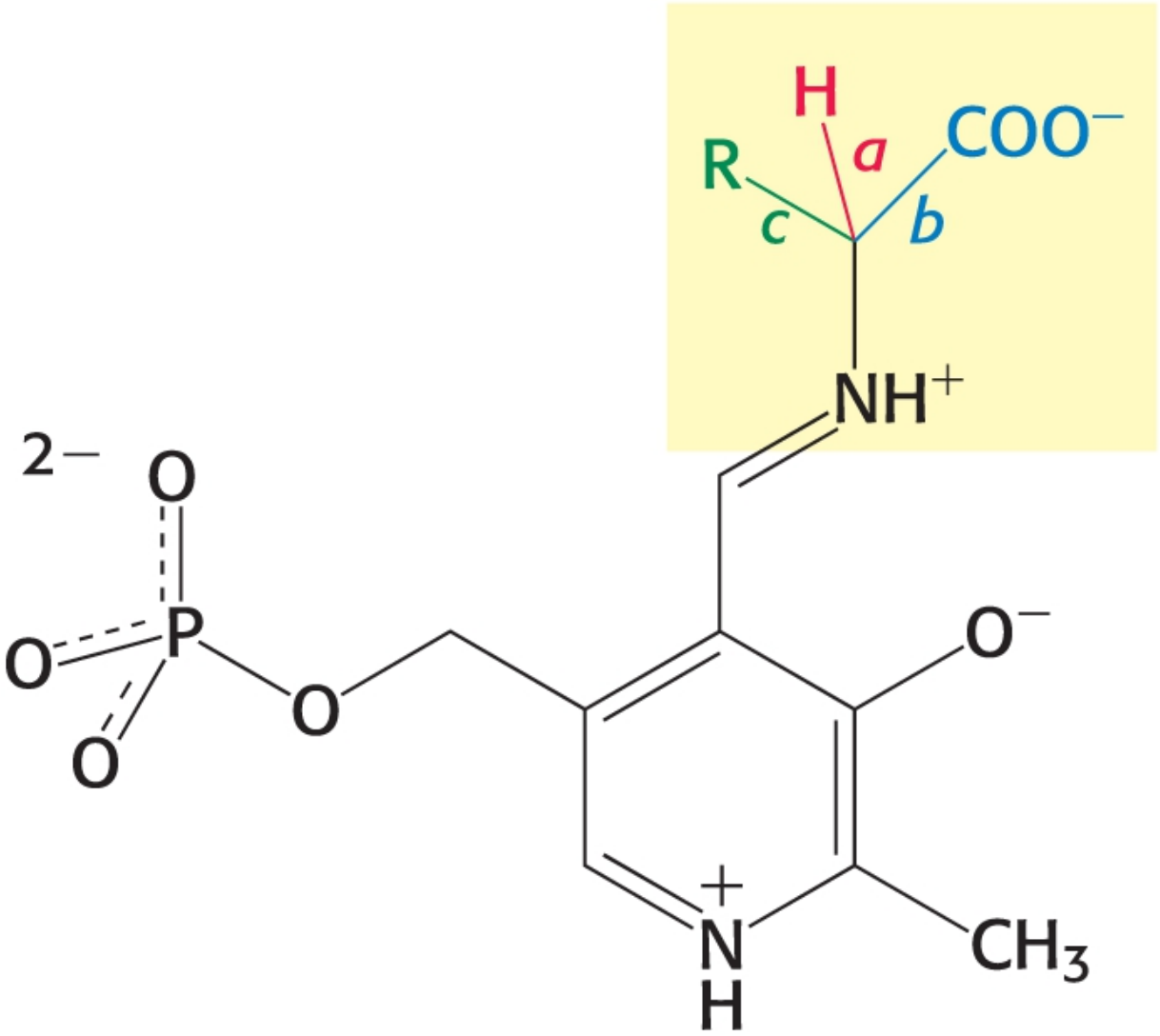


The ribbon diagram consists of a few green alpha-helices at the top interconnected by thread-like loops. A large cluster of yellow alpha-helices and beta-strands at the bottom are associated with the green helices. The center of the subunit contains a ball-and-stick model. An arrow from the center of the enzyme subunit shows an enlarged view of the Schiff-base linkage between pyridoxal phosphate (P L P) and lysine 258 residues of the active site. The ball-and-stick model of P L P consists of a hexagon composed of 1 blue and 5 black spheres. The bottom left black sphere is connected to a chain of one black, one red, and one purple sphere in the same order. The black sphere is connected to two white spheres. The terminal purple sphere is connected to three red spheres. The blue sphere is located at the bottom right vertex of the hexagon. It is connected to a white sphere

on the lower right. The bottom-most black sphere is connected to a white sphere. The top right black sphere is connected to a black sphere, which is further connected to three white spheres. The topmost black sphere is connected to a red sphere above. The top left black sphere is connected to a chain of one black and one white sphere in the same order. The black sphere of this chain is connected to the blue sphere of the lysine 258 side chain through a Schiff-base linkage. The side chain of lysine 258 is composed of a chain of 5 black spheres and 1 blue sphere. A ball-and-stick model of arginine 386 residues is composed of a chain of 2 blue and 5 black spheres. It is shown on the top right of the lysine side chain. The blue spheres occupy the first and third positions. The first blue sphere is connected to two white spheres. The first black sphere is connected to a blue sphere, which is further connected to two white spheres. The second blue sphere is connected to a white sphere above.

Return to FIGURE 23.10 The active site of aspartate aminotransferase reveals P L P bound to a lysine through a Schiff-base linkage

Extended description for FIGURE 23.11 P L P enzymes labilize one of three bonds at the alpha-carbon atom of an amino acid substrate

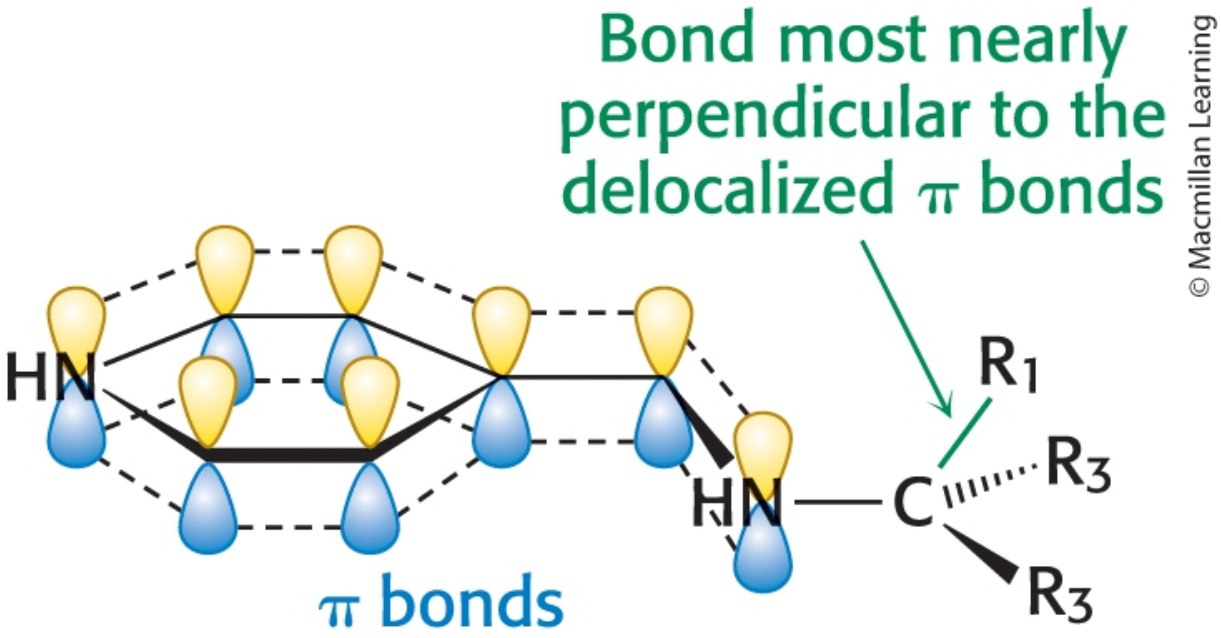


The structure is depicted as follows: A 6-membered heterocyclic hexagonal ring is in a vertical orientation and consists of 1 N and 5 C atoms. N occupies the bottom-most vertex. It has a positive charge and is bound to H. C 1 occupies the bottom-left vertex. A double bond is present between N and C 1, C 2 and C 3, and C 4 and C 5. C 2

is single bonded to C H 2 on the upper left in the form of a line. C H 2 is single-bonded to O on the lower left. This O is single-bonded to a P atom. The P atom is partially double-bonded to O above, O on the left, and O on the lower left. The O atoms have an overall negative charge of 2 minus. C 3 is single bonded to C above. This C is double-bonded to N H superscript plus on the upper left. The N H superscript plus group is single-bonded to C above. This C is single bonded to R on the upper left, H above, and C O O superscript minus. The single bond between C and R is labeled c, the single bond between C and H is labeled a, and the single bond between C and C O O superscript minus is labeled b. The N H superscript plus group and its substituents are highlighted in the yellow box.

Return to FIGURE 23.11 P L P enzymes labilize one of three bonds at the alpha-carbon atom of an amino acid substrate

Extended description for FIGURE 23.12 Stereoelectronic effects determine specific bond cleavage

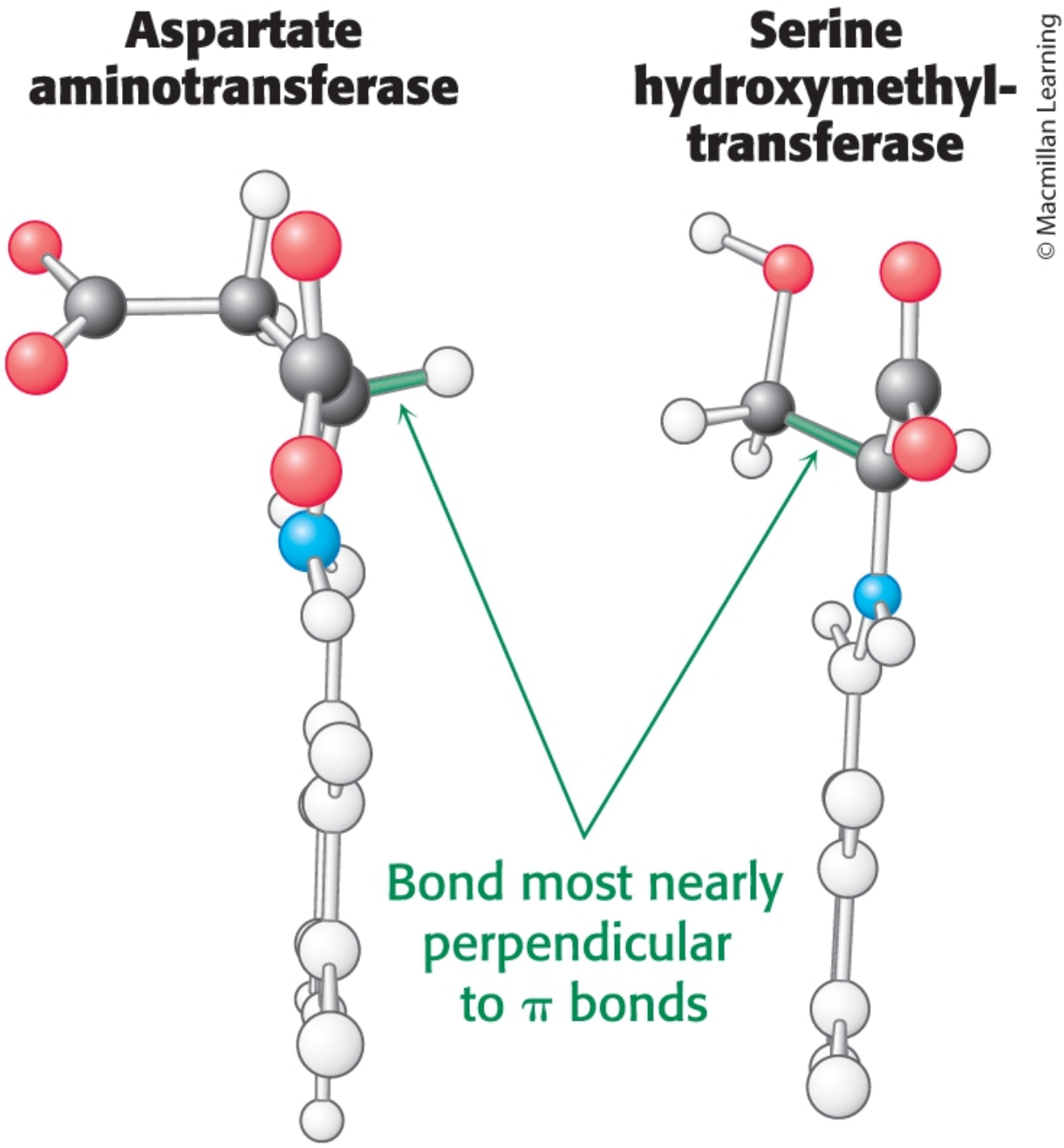


A 6-membered heterocyclic hexagonal ring is in a horizontal orientation with C 1 occupying the rightmost vertex. The ring is laying flat such that C 2 and C 3 are located toward the observer. The ring consists of 1 N and 5 C atoms. N occupies the rightmost vertex and is bound to H. C 1 is single-bonded to C H 2 on the right in the form of a line. C H 2 is further wedge bonded to N H on the lower right. N H is single bonded to C on the right. This C is single bonded to R 1 on the upper right, dash bonded to R 3 on right, and wedge bonded to R 3 on the lower right. The single bond between C 1 and R 1 is labeled with the text that reads "Bond most nearly perpendicular to the delocalized pi bonds." Each vertex of the hexagon and the positions occupied by C H 2 and N H contain dumbbell-shaped orbitals in a vertical orientation. The orbitals are composed of a tear-shaped structure located above and below the plane of the ring.

The top tear-shaped structure is shown in yellow and the bottom tear-shaped structure is shown in blue. A dashed line connects the blue tear-shaped structure below the plane of the ring. A dashed line connects the yellow tear-shaped structures, located above the plane of the ring, of all orbitals except the orbitals at C 2 and C 3.

Return to FIGURE 23.12 Stereoelectronic effects determine specific bond cleavage

Extended description for FIGURE 23.13 Bond orientation in the active site determines bond cleavage in different P L P enzymes

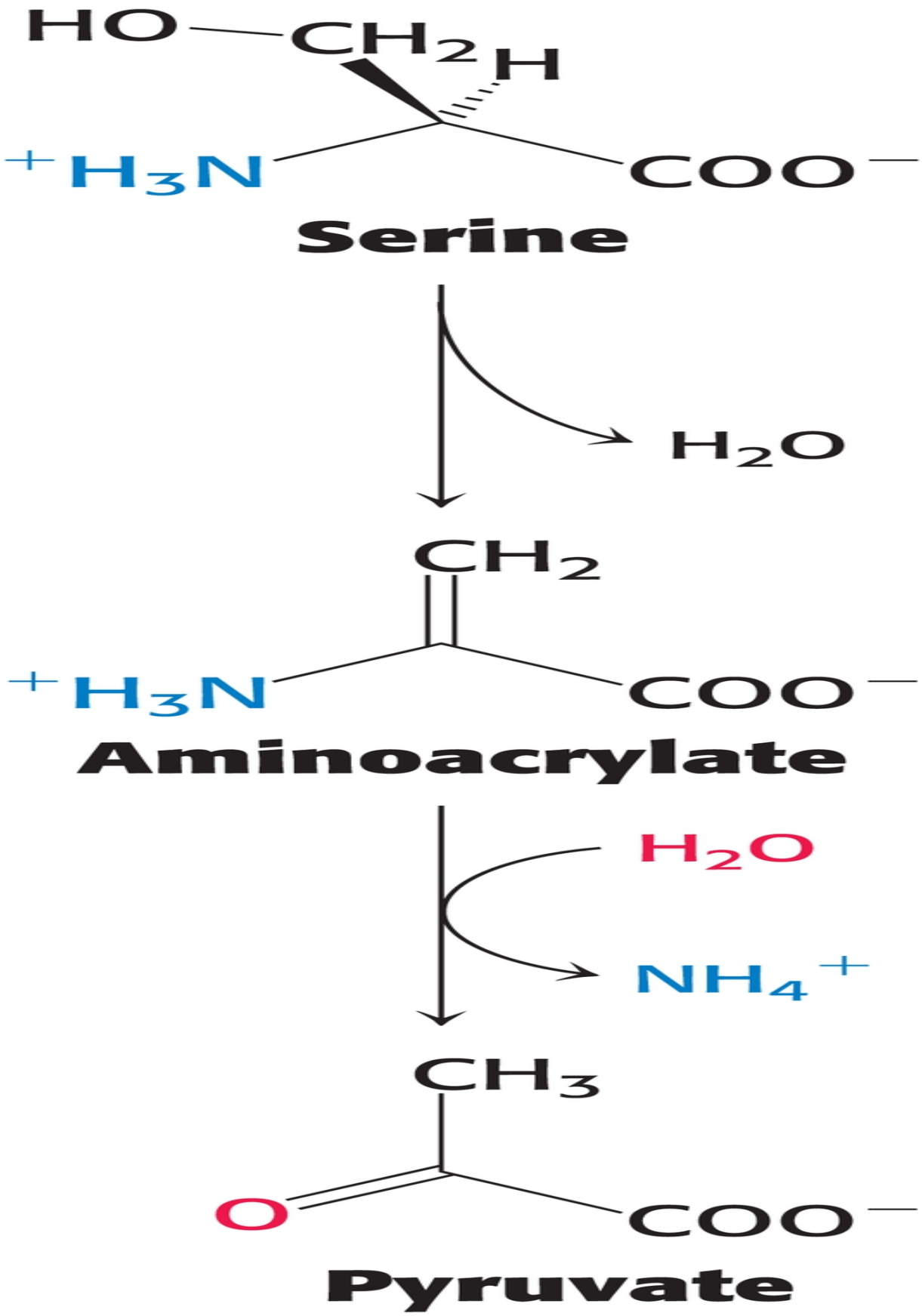


Two ball-and-stick models are shown. The left model is labeled aspartate aminotransferase and the right model is labeled serine hydroxymethyltransferase. The left model consists of several white spheres in vertical orientation connected to a blue, red, white, and two black spheres at the top. The black sphere located toward the observer is connected to a red sphere above and below. The black sphere away from the observer is connected to a white sphere on the upper right and a black sphere on the upper left. The connection between the black sphere and the upper right white sphere is labeled with a text that reads "Bond most nearly perpendicular to pi bonds." The upper left black sphere is connected to a black sphere on the left and two white spheres. The left black sphere is connected to two red spheres.

The right model consists of several white spheres in vertical orientation connected to a chain of one blue and two black spheres in the same order. The second black sphere at the top is connected to two red spheres. The first black sphere is connected to a white sphere on the upper right and a black sphere on the left. The connection between the two black spheres is labeled with a text that reads "Bond most nearly perpendicular to pi bonds." The left black sphere is connected to a red sphere above and two white spheres in the same plane. The red sphere is connected to a white sphere.

Return to FIGURE 23.13 Bond orientation in the active site determines bond cleavage in different P L P enzymes

Extended description for Deamination of serine


HO
CH2
H
+H3N
COO−
Serine
H2O
CH2
+H3N
COO−
Aminoacrylate
H2O
NH4+
CH3
O
COO−
Pyruvate

The structure of serine is as follows: A central C atom is single bonded to N H 3 superscript plus on the lower left, single bonded to C O O superscript minus on the lower right, wedge bonded to C H 2, single bond, O H on the upper left, and dash bonded to H on the upper right.

It is irreversibly converted into aminoacrylate with the simultaneous release of H 2 O.

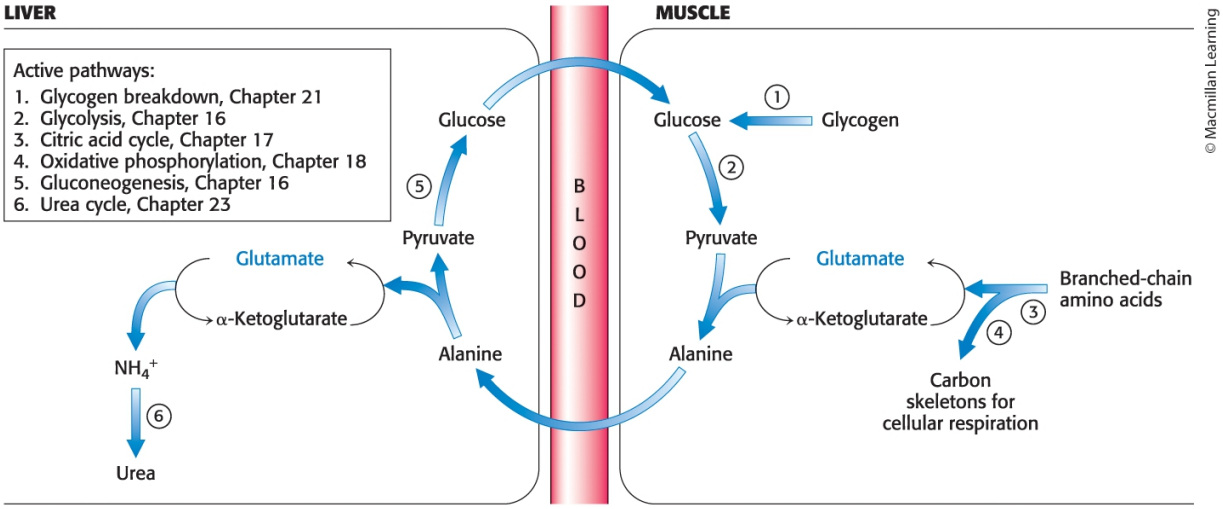
The structure of aminoacrylate is as follows: A central C atom is single bonded to N H 3 superscript plus on the lower left, single bonded to C O O superscript minus on the lower right, and double bonded to C H 2 above.

The aminoacrylate is irreversibly converted into pyruvate with the simultaneous entry of H 2 O and release of N H 4 superscript plus.

The structure of pyruvate is as follows: A central C atom is double bonded to O on the lower left, single bonded to C H 3 above, and single bonded to C O O superscript minus on the lower right.

Return to Deamination of serine

Extended description for FIGURE 23.14 PATHWAY INTEGRATION: The glucose–alanine cycle allows muscle cells to use amino acids as fuel



A central tubular structure depicts a blood vessel containing blood. A rectangular compartment on the left of the blood vessel is labeled liver and a rectangular compartment on the right is labeled muscle.

Glycogen in the muscle is converted into glucose. This step is depicted by a forward arrow labeled 1. Glucose is converted into pyruvate. This step is depicted by an arrow labeled 2.

Simultaneously, branched-chain amino acids take part in the addition of amino group to alpha-ketoglutarate to produce glutamate. Alternatively, the branched-chain amino acids also give rise to carbon skeletons for cellular respiration. This step is depicted by an arrow labeled 3 and 4. Glutamate transfers the amino group to pyruvate leading to the formation of alanine. Glutamate is itself converted back to alpha-ketoglutarate. The alanine molecule

produced in the muscle travels through the bloodstream into the liver.

Inside the liver, alanine is deaminated to produce pyruvate or convert alpha-ketoglutarate into glutamate. The pyruvate molecule is converted back into glucose. This step is depicted by an arrow labeled 5. The glucose molecule is released from the liver and travels through the bloodstream to enter the muscle and continue the cycle. The glutamate molecule further undergoes deamination to release N H 4 superscript plus and form alpha-ketoglutarate. The N H 4 superscript plus molecule is converted into urea. This step is depicted by an arrow labeled 6.

A key titled "Active pathways" lists the following points:

1. Glycogen breakdown, Chapter 21.

2. Glycolysis, Chapter 16.

3. Citric acid cycle, Chapter 17.

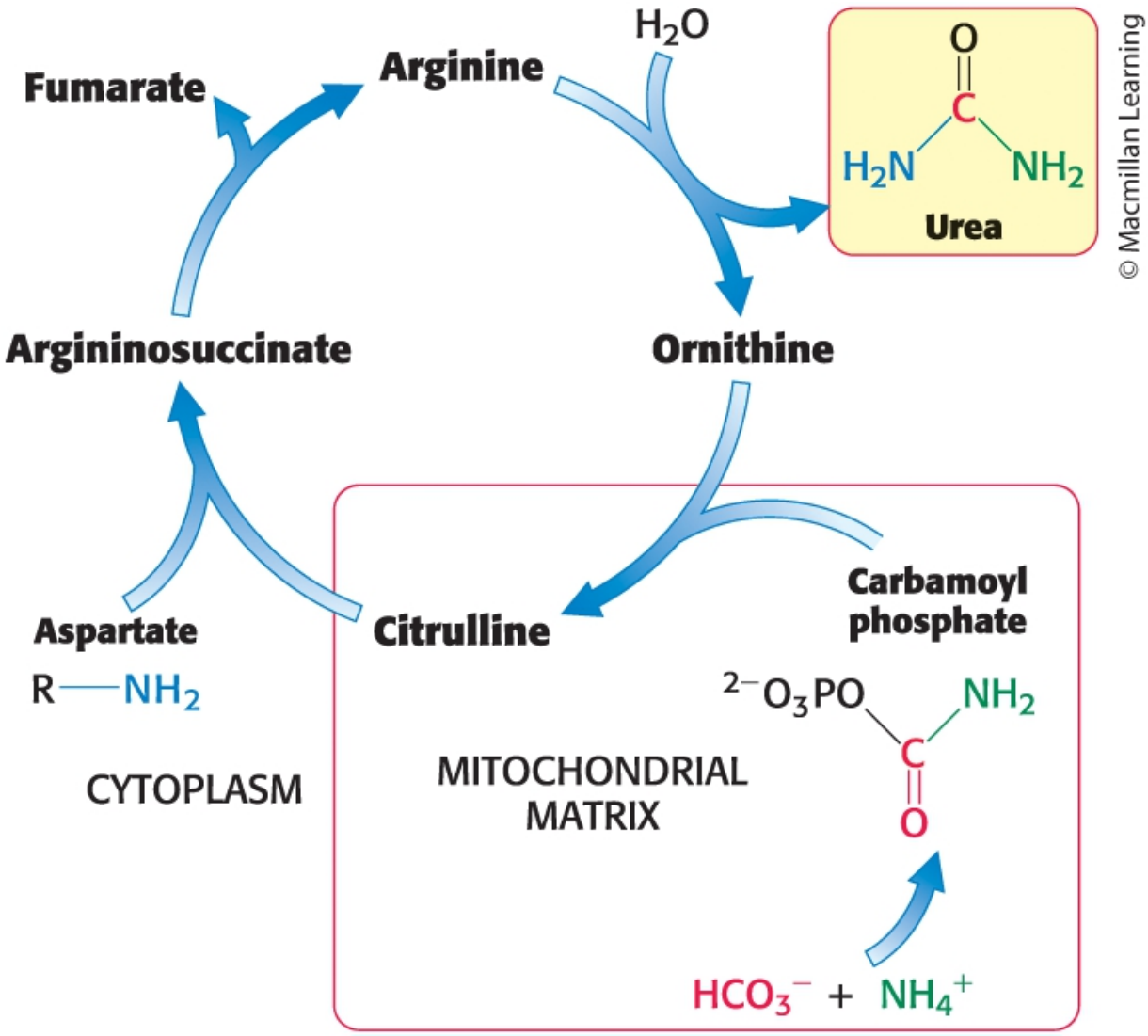
4. Oxidative phosphorylation, Chapter 18.

5. Gluconeogenesis, Chapter 16.

6. Urea cycle, Chapter 23.

Return to FIGURE 23.14 PATHWAY INTEGRATION: The glucose–alanine cycle allows muscle cells to use amino acids as fuel

Extended description for FIGURE 23.15 The urea cycle eliminates both nitrogen and carbon waste products



The urea cycle begins with arginine at the top. It is converted into ornithine with the simultaneous entry of H 2 O and release of urea. The structure of urea consists of a central C atom single-bonded to N H 2 on the lower left, single-bonded to N H 2 on the lower right, and double-bonded to O above.

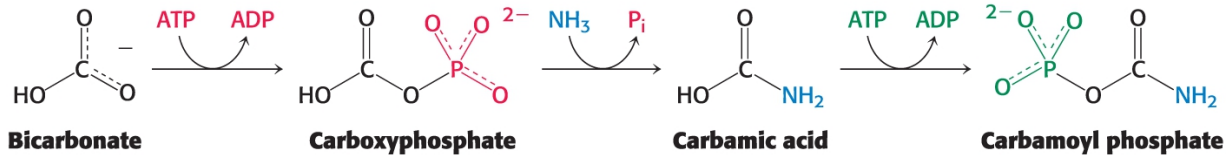
Ornithine is converted into citrulline in the mitochondrial matrix by the addition of carbamoyl phosphate. The carbamoyl phosphate is produced from H C O 3 superscript minus plus N H 4 superscript plus in the mitochondrial matrix. The structure of carbamoyl phosphate consists of a central C atom single bonded to O P O 3 superscript 2 minus on the upper left, single bonded to N H 2 on the upper right, and double bonded to O below.

Citrulline is converted into argininosuccinate in the cytoplasm by the addition of aspartate. The aspartate molecule is depicted as R, single bond, N H 2.

Argininosuccinate is converted into arginine with the release of fumarate. All reaction of the urea cycle take place in the cytoplasm except the formation of citrulline.

Return to FIGURE 23.15 The urea cycle eliminates both nitrogen and carbon waste products

Extended description for Formation of carbamoyl phosphate from bicarbonate



In the first irreversible step, bicarbonate is converted into carboxyphosphate with the simultaneous hydrolysis of A T P to A D P.

The structure of bicarbonate is as follows: A central C atom is single-bonded to O H on the lower left, partially double-bonded to O above, and partially double-bonded to O on the lower right. The O atoms have an overall negative charge.

The structure of carboxyphosphate is as follows: A central C atom is double-bonded to O above, single-bonded to O H on the lower left, and single-bonded to O on the lower right. The lower right O is single-bonded to a central P atom on the upper right. The P atom is partially double bonded to O on the upper left, O on the upper right, and O on the lower left. The O atoms have an overall negative charge of 2 minus.

In the second irreversible step, carboxyphosphate is converted into carbamic acid with the simultaneous entry of N H 3 and release of P subscript i.

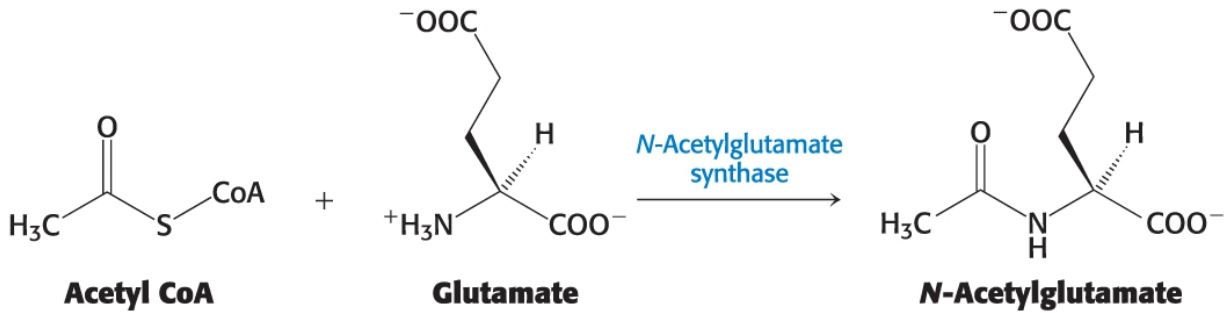
The structure of carbamic acid is as follows: A central C atom is single-bonded to O H on the lower left, single-bonded to N H 2 on the lower right, and double-bonded to O above.

In the third irreversible step, carbamic acid is converted into carbamoyl phosphate with the simultaneous hydrolysis of A T P to A D P.

The structure of carbamoyl phosphate is as follows: A central P atom is partially double-bonded to O on the upper left, O on the upper right, and O on the lower left. The O atoms have an overall negative charge of 2 minus. It is single-bonded to O on the lower right. This O atom is single-bonded to C on the upper right. This C atom is double bonded to O above and single bonded to N H 2 on the lower right.

Return to Formation of carbamoyl phosphate from bicarbonate

Extended description for Reaction catalyzed by N-acetylglutamate synthase



The reaction consists of two reactants and one product.

The first reactant is acetyl C o A whose structure is as follows: A central C atom is single bonded to C H 3 on the lower left, single bonded to S on the lower right, and double bonded to O above. S atom is single bonded to C o A on the upper right.

The second reactant is glutamate whose structure is as follows: A central C atom is single bonded to N H 3 superscript plus on the lower left, single bonded to C O O superscript minus on the lower right, wedge bonded to C H 2 on the upper left, and dash bonded to H on the upper right. The C H 2 group is single-bonded to another C H 2 group on the upper right in the form of a line. This C H 2 is single bonded to C O O superscript minus on the upper left.

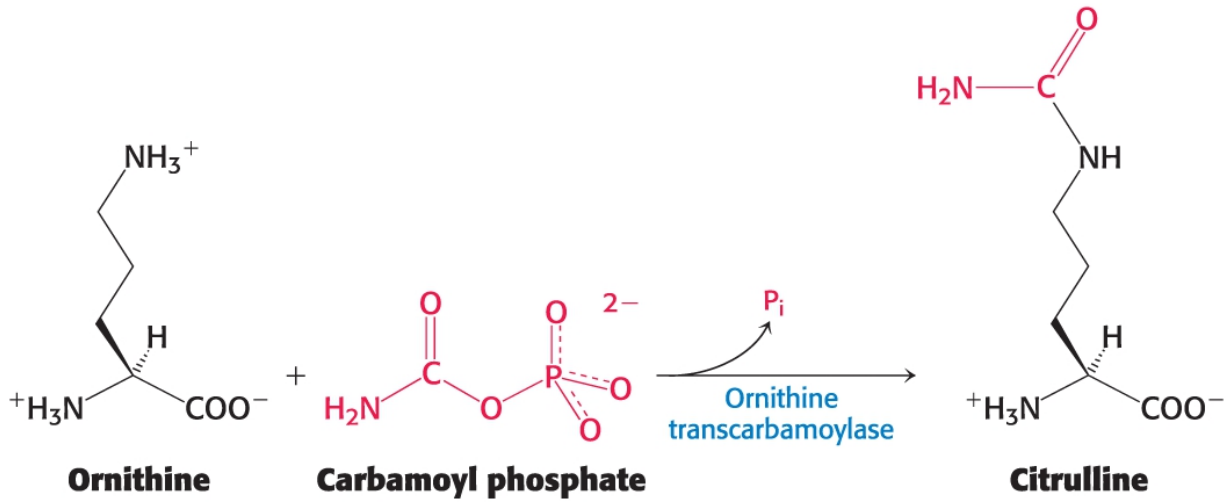
A forward arrow labeled N-acetylglutamate synthase leads to the product.

The product is N-acetylglutamate whose structure is as follows: A 1 N and 2 C heteronuclear alkane chain is depicted as a line structure using 2 zigzag lines. N bound to H occupies the second position. C 1

is double bonded to O above and single bonded to C H 3 on the lower left. C 2 is single bonded to C O O superscript minus on the lower right, wedge bonded to C H 2 on the upper left, and dash bonded to H on the upper right. The C H 2 group is single-bonded to another C H 2 group on the upper right in the form of a line. This C H 2 is single bonded to C O O superscript minus on the upper left.

Return to Reaction catalyzed by N-acetylglutamate synthase

Extended description for Reaction catalyzed by ornithine transcarbamoylase



The reaction consists of two reactants and one product.

The first reactant is ornithine whose structure is as follows: A central C atom is single bonded to N H 3 superscript plus on the lower left, single bonded to C O O superscript minus on the lower right, wedge bonded to C H 2 on the upper left, and dash bonded to H on the upper right. The C H 2 group is single-bonded to a 2-carbon alkane chain depicted using a single line. C 2 of this alkane chain is single bonded to N H 3 superscript plus on the upper right.

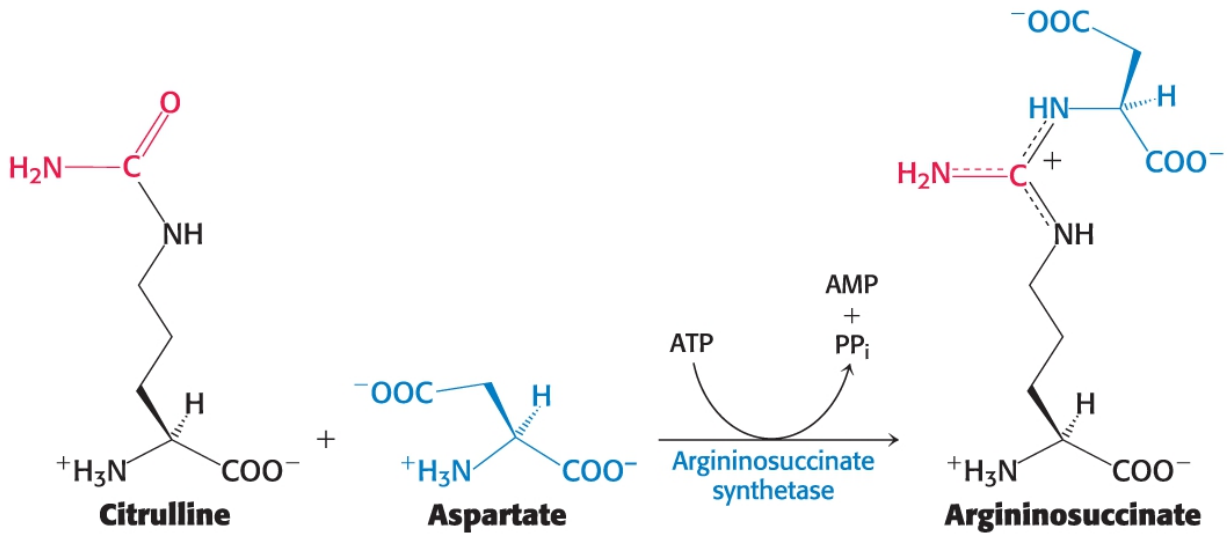
The second reactant is carbamoyl phosphate whose structure is as follows: A central C atom is double bonded to O above, single bonded to N H 2 on the lower right, and single bonded to O on the lower right. This O atom is single-bonded to a central P atom. The P atom is partially double-bonded to O above, O on the right, and O on the lower right. The O atoms have an overall negative charge of 2 minus.

A forward arrow labeled ornithine transcarbamoylase leads to the product. It also shows the release of P subscript i.

The product is citrulline whose structure is as follows: A central C atom is single bonded to N H 3 superscript plus on the lower left, single bonded to C O O superscript minus on the lower right, wedge bonded to C H 2 on the upper left, and dash bonded to H on the upper right. The C H 2 group is single-bonded to a 1 N and 2 C alkane chain depicted as a vertical line structure using 2 zigzag lines. N bound to H occupies the third position. N is single-bonded to C on the upper right. This C is single bonded to N H 2 on the left and double bonded to O on the upper right.

Return to Reaction catalyzed by ornithine transcarbamoylase

Extended description for Reaction catalyzed by argininosuccinate synthetase



The reaction consists of two reactants and one product.

The first reactant is citrulline whose structure is as follows: A central C atom is single bonded to N H 3 superscript plus on the lower left, single bonded to C O O superscript minus on the lower right, wedge bonded to C H 2 on the upper left, and dash bonded to H on the upper right. The C H 2 group is single-bonded to a 1 N and 2 C alkane chain depicted as a vertical line structure using 2 zigzag lines. N bound to H occupies the third position. N is single-bonded to C on the upper right. This C is single bonded to N H 2 on the left and double bonded to O on the upper right.

The second reactant is aspartate whose structure is as follows: A central C atom is single bonded to N H 3 superscript plus on the lower left, single bonded to C O O superscript minus on the lower right, wedge bonded to C H 2 on the upper left, and dash bonded to

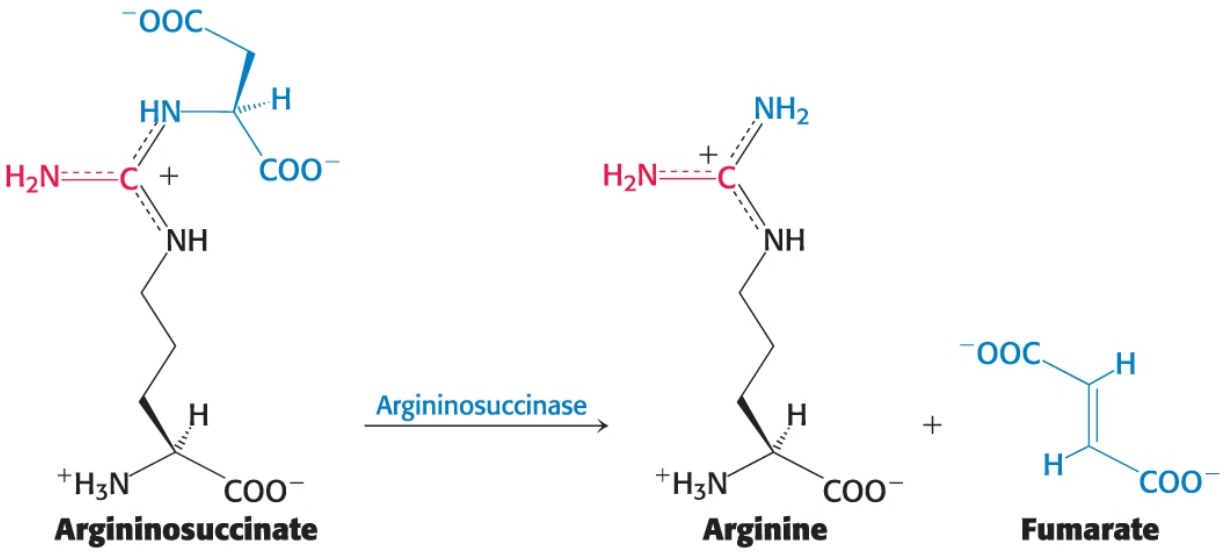
H on the upper right. The C H 2 group is single-bonded to C O O superscript minus on the left.

A forward arrow labeled argininosuccinate synthetase leads to the product. A curved arrow above it shows the coupled hydrolysis of A T P to A M P plus P P subscript i.

The product is argininosuccinate whose structure is as follows: A central C atom is single bonded to N H 3 superscript plus on the lower left, single bonded to C O O superscript minus on the lower right, wedge bonded to C H 2 on the upper left, and dash bonded to H on the upper right. The C H 2 group is single-bonded to a 1 N and 2 C alkane chain depicted as a vertical line structure using 2 zigzag lines. N bound to H occupies the third position. N is partially double-bonded to C on the upper right. This C atom has a positive charge and is partially double-bonded to N H 2 on the left and partially double-bonded to N H on the upper right. The N H group on the upper right is single-bonded to C on the right. This C is wedge bonded to C H 2 on the upper right, dash bonded to H on the right, and single bonded to C O O superscript minus on the lower right. The C H 2 group is single-bonded to C O O superscript minus on the upper left.

Return to Reaction catalyzed by argininosuccinate synthetase

Extended description for Reaction catalyzed by argininosuccinase



The reaction consists of one reactant and two products. The reactant is argininosuccinate whose structure is as follows: A central C atom is single bonded to N H 3 superscript plus on the lower left, single bonded to C O O superscript minus on the lower right, wedge bonded to C H 2 on the upper left, and dash bonded to H on the upper right. The C H 2 group is single-bonded to a 1 N and 2 C alkane chain depicted as a vertical line structure using 2 zigzag lines. N bound to H occupies the third position. N is partially double-bonded to C on the upper right. This C atom has a positive charge and is partially double-bonded to N H 2 on the left and partially double-bonded to N H on the upper right. The N H group on the upper right is single-bonded to C on the right. This C is wedge bonded to C H 2 on the upper right, dash bonded to H on the right, and single bonded to C O O superscript minus on the lower right. The C H 2 group is single-bonded to C O O superscript minus on the upper left.

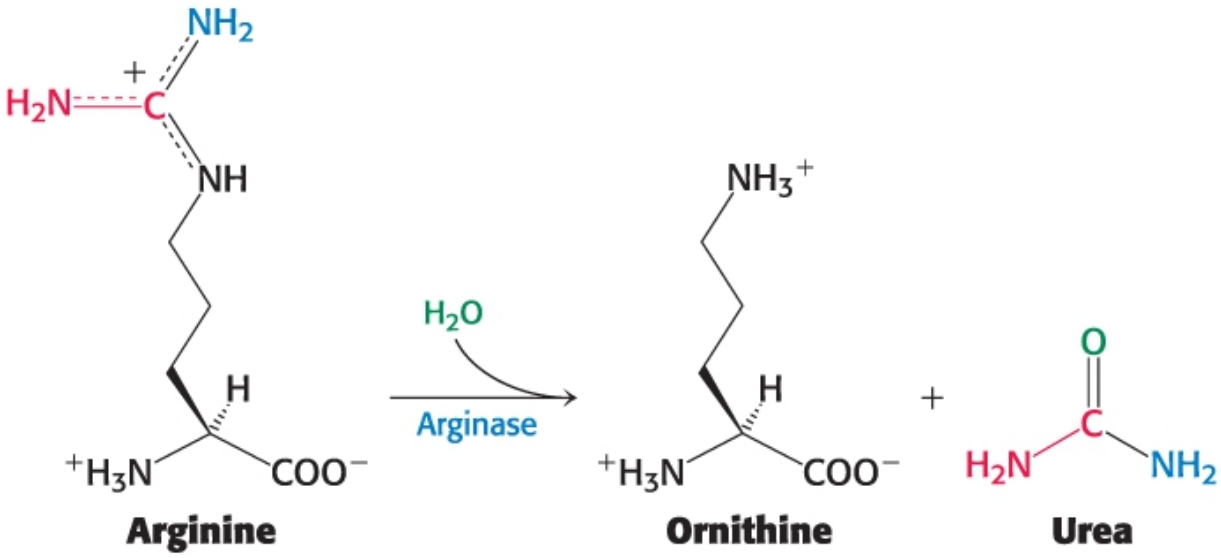
A forward arrow labeled argininosuccinase leads to the products.

The first product is arginine whose structure is as follows: A central C atom is single bonded to N H 3 superscript plus on the lower left, single bonded to C O O superscript minus on the lower right, wedge bonded to C H 2 on the upper left, and dash bonded to H on the upper right. The C H 2 group is single-bonded to a 1 N and 2 C alkane chain depicted as a vertical line structure using 2 zigzag lines. N bound to H occupies the third position. N is partially double-bonded to C on the upper right. This C atom has a positive charge and is partially double-bonded to N H 2 on the left and partially double-bonded to N H 2 on the upper right.

The second product is fumarate whose structure is as follows: A central C atom is single-bonded to H on the lower left, single-bonded to C O O superscript minus on the lower right, and double-bonded to C above. This C atom is single bonded to C O O superscript minus on the upper left and single bonded to H on the upper right.

Return to Reaction catalyzed by argininosuccinase

Extended description for Reaction catalyzed by arginase



The reaction consists of one reactant and two products. The reactant is arginine whose structure is as follows: A central C atom is single bonded to N H 3 superscript plus on the lower left, single bonded to C O O superscript minus on the lower right, wedge bonded to C H 2 on the upper left, and dash bonded to H on the upper right. The C H 2 group is single-bonded to a 1 N and 2 C alkane chain depicted as a vertical line structure using 2 zigzag lines. N bound to H occupies the third position. N is partially double-bonded to C on the upper right. This C atom has a positive charge and is partially double-bonded to N H 2 on the left and partially double-bonded to N H 2 on the upper right.

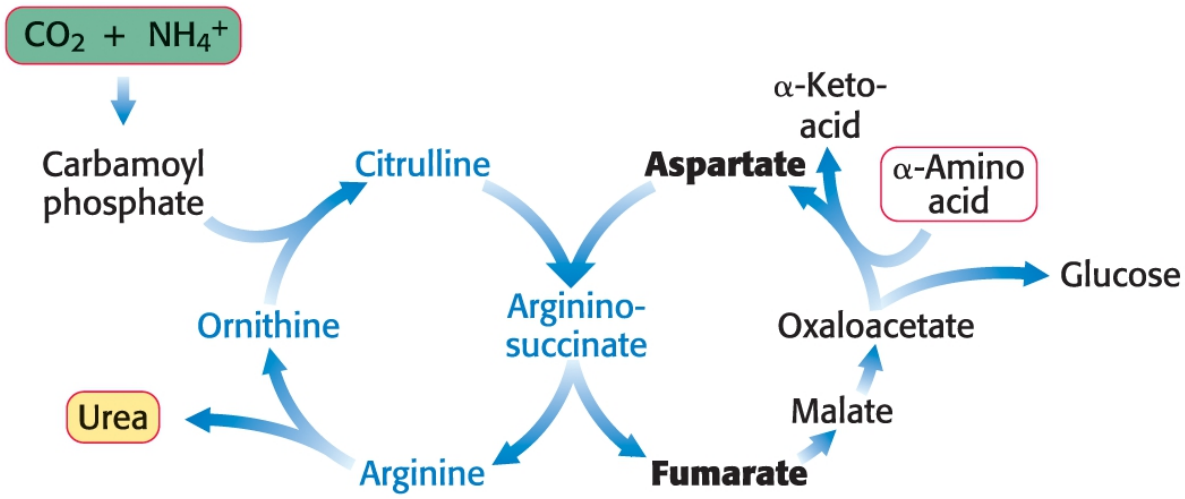
A forward arrow labeled arginase leads to the products. It also shows the entry of H 2 O.

The first product is ornithine whose structure is as follows: A central C atom is single bonded to N H 3 superscript plus on the lower left, single bonded to C O O superscript minus on the lower right, wedge bonded to C H 2 on the upper left, and dash bonded to H on the upper right. The C H 2 group is single-bonded to a 2-carbon alkane chain depicted using a single line. C 2 of this alkane chain is single bonded to N H 3 superscript plus on the upper right.

The second product is urea whose structure is as follows: A central C atom is single-bonded to N H 2 on the lower left, single-bonded to N H 2 on the lower right, and double-bonded to O above.

Return to Reaction catalyzed by arginase

Extended description for FIGURE 23.16 Nitrogen metabolism is integrated with other pathways



© Macmillan Learning

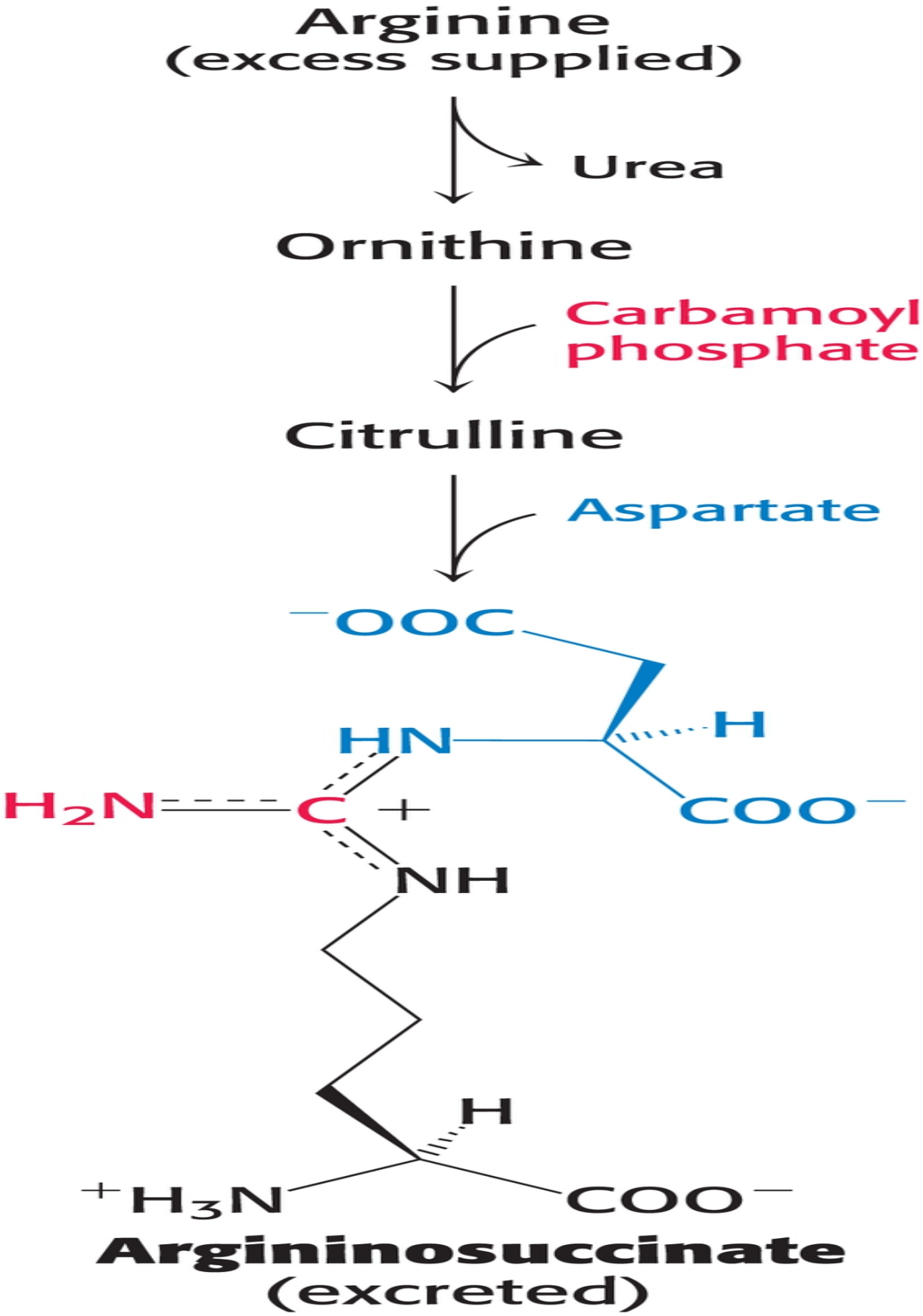
Two cyclical pathways are shown to integrate by forming a common compound named argininosuccinate. Citrulline and aspartate from the left and right cyclical pathways respectively produce argininosuccinate. The argininosuccinate molecule breaks down to produce fumarate which is channeled into the right cyclical pathway and arginine which is channeled into the left cyclical pathway.

In the right pathway, fumarate is converted into malate, which is further converted into oxaloacetate. The oxaloacetate molecule is converted back to aspartate or glucose. Glucose molecule leaves the cycle. The conversion of oxaloacetate to aspartate is coupled with the conversion of alpha-amino acid to alpha-ketoacid. In the left cyclical pathway, arginine is converted into ornithine with the simultaneous release of urea. Ornithine is converted into citrulline by the addition of carbamoyl phosphate. Carbamoyl phosphate is itself produced from C O 2 plus N H 4 superscript plus.

Return to FIGURE 23.16 Nitrogen metabolism is integrated with other pathways

Extended description for FIGURE 23.17 Argininosuccinase deficiency can be managed by

supplementing the diet with arginine

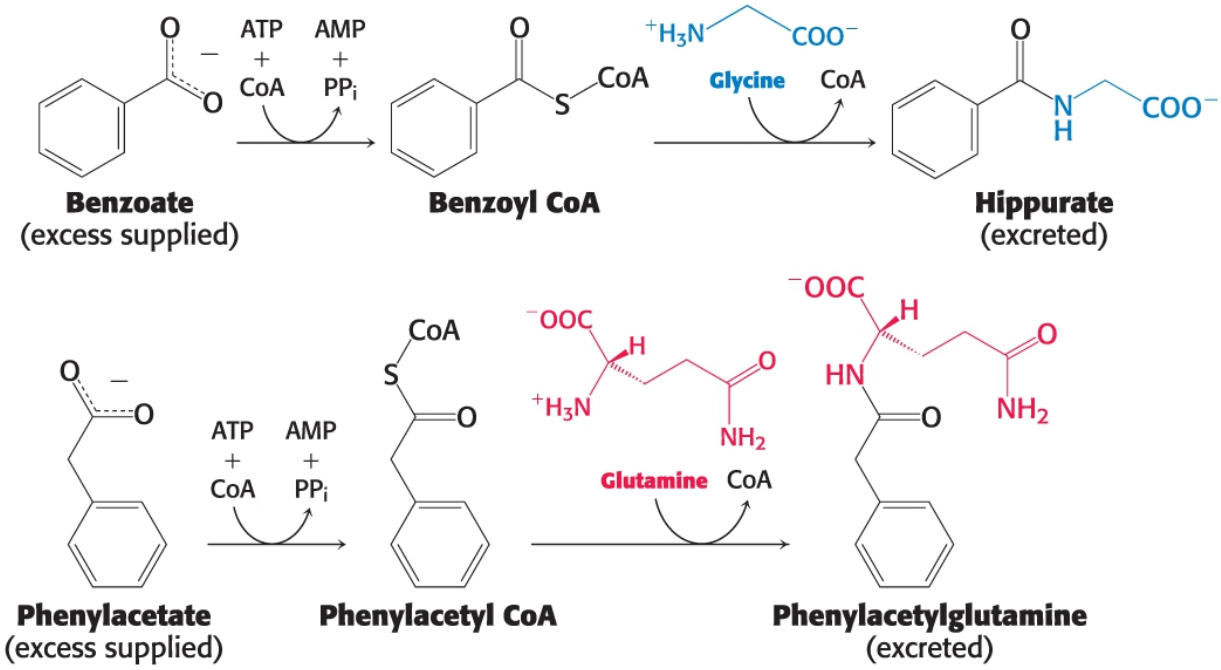

Arginine
(excess supplied)
Urea
Ornithine
Carbamoyl
phosphate
Citrulline
Aspartate
⁻OOC
HN
H
H₂N
C
+
COO⁻
NH
H
⁺H₃N
COO⁻
Argininosuccinate
(excreted)

The pathway begins with arginine (excess supplied). This arginine is converted into ornithine with the simultaneous release of urea. Ornithine is converted into citrulline by the addition of carbamoyl phosphate. The addition of aspartate leads to the conversion of citrulline to argininosuccinate, which is excreted from the body.

The structure of argininosuccinate is as follows: A central C atom is single bonded to N H 3 superscript plus on the lower left, single bonded to C O O superscript minus on the lower right, wedge bonded to C H 2 on the upper left, and dash bonded to H on the upper right. The C H 2 group is single-bonded to a 1 N and 2 C alkane chain depicted as a vertical line structure using 2 zigzag lines. N bound to H occupies the third position. N is partially double-bonded to C on the upper right. This C atom has a positive charge and is partially double-bonded to N H 2 on the left and partially double-bonded to N H on the upper right. The N H group on the upper right is single-bonded to C on the right. This C is wedge bonded to C H 2 on the upper right, dash bonded to H on the right, and single bonded to C O O superscript minus on the lower right. The C H 2 group is single-bonded to C O O superscript minus on the upper left.

Return to FIGURE 23.17 Argininosuccinase deficiency can be managed by supplementing the diet with arginine

Extended description for FIGURE 23.18 Both carbamoyl phosphate synthetase and ornithine transcarbamoylase deficiencies can be treated the same way



The benzoate (excess supplied) is converted into hippurate through a benzoyl C o A intermediate. Hippurate is excreted from the body.

The irreversible conversion of benzoate to benzoyl C o A is coupled with the hydrolysis of A T P to A M P plus P P subscript i and entry of C o A.

The structure of benzoate is as follows: A benzene ring is in a vertical orientation with C 1 occupying the topmost vertex. It contains alternating double bonds between C 2 and C 3, C 4 and C 5, and C 6 and C 1. C 2 is single-bonded to C on the upper right. This C

is partially double bonded to O above and O on the lower right. These O atoms have an overall negative charge.

The structure of benzoyl C o A is as follows: A benzene ring is in a vertical orientation with C 1 occupying the topmost vertex. It contains alternating double bonds between C 2 and C 3, C 4 and C 5, and C 6 and C 1. C 2 is single-bonded to C on the upper right. This C atom is double bonded to O above and single bonded to S on the lower right. The S atom is single-bonded to C o A on the upper right.

The benzoyl C o A is irreversibly converted into hippurate with the simultaneous entry of glycine and release of C o A. Glycine is depicted as a central C atom single bonded to N H 3 superscript plus on the lower left and single bonded to C O O superscript minus on the lower right.

The structure of hippurate is as follows: A benzene ring is in a vertical orientation with C 1 occupying the topmost vertex. It contains alternating double bonds between C 2 and C 3, C 4 and C 5, and C 6 and C 1. C 2 is single-bonded to C on the upper right. This C atom is double bonded to O above and single bonded to N H on the lower right. The N H atom is single-bonded to C H 2 on the upper right in the form of a line. The C H 2 group is further single bonded to the C O O superscript minus on the lower right.

The phenylacetate (excess supplied) is converted into phenylacetylglutamine through a phenylacetyl C o A intermediate. Phenylacetylglutamine is excreted from the body.

The irreversible conversion of phenylacetate to phenylacetyl C o A is coupled with the hydrolysis of A T P to A M P plus P P subscript i and entry of C o A.

The structure of phenylacetate is as follows: A benzene ring is in a horizontal orientation with C 1 occupying the rightmost vertex. It contains alternating double bonds between C 1 and C 2, C 3 and C 4, and C 5 and C 6. C 5 is single bonded to C H 2 on the upper left in the form of a line. The C H 2 group is further single-bonded to C. The C atom is partially double-bonded to O on the upper left and O on the right. The O atoms have an overall negative charge.

The structure of phenylacetyl C o A is as follows: A benzene ring is in a horizontal orientation with C 1 occupying the rightmost vertex. It contains alternating double bonds between C 1 and C 2, C 3 and C 4, and C 5 and C 6. C 5 is single bonded to C H 2 on the upper left in the form of a line. The C H 2 group is further single-bonded to C on the upper right. The C atom is double bonded to O on the right and single bonded to S, single bond, C o A on the upper left.

Phenylacetyl C o A is irreversibly converted into phenylacetylglutamine with the simultaneous entry of glutamine and release of C o A.

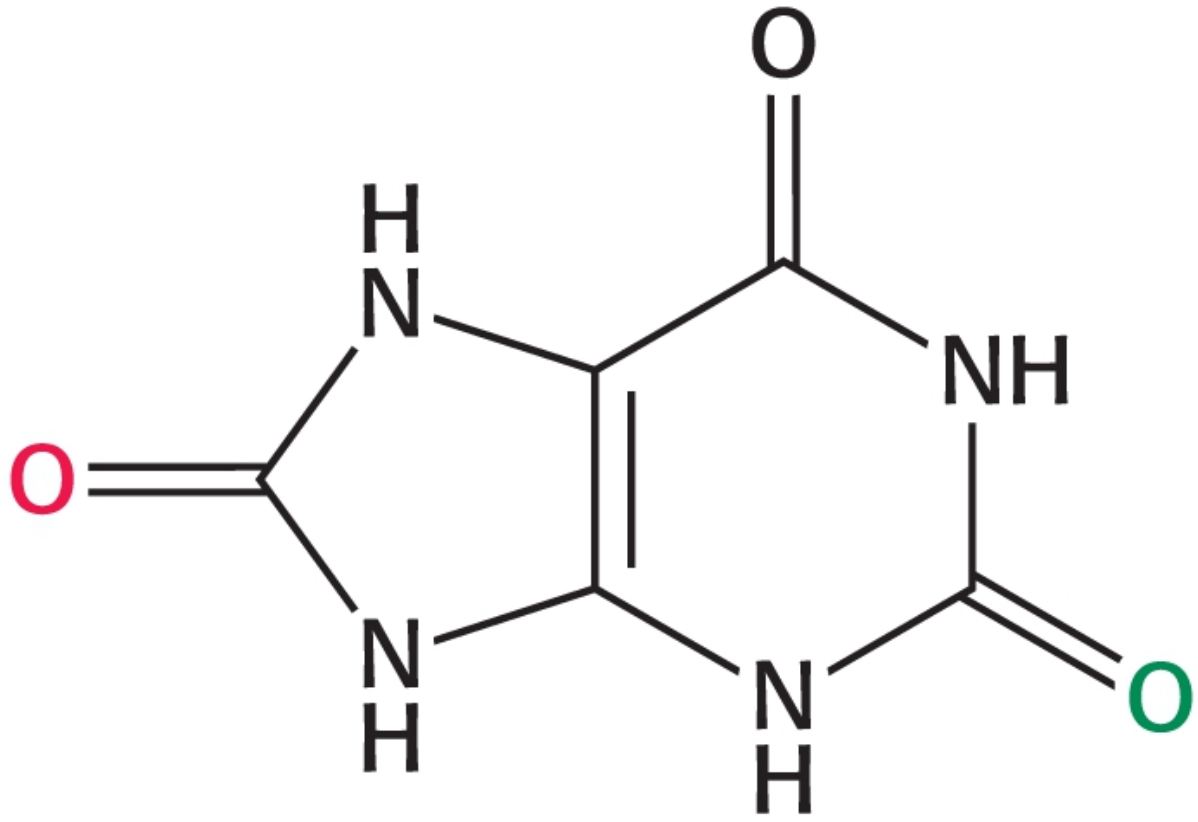
Glutamine consists of a 3-carbon alkane chain depicted as a line structure using 2 zigzag lines. C 1 is dash bonded to C on the upper left. This C atom is single bonded to C O O superscript minus on the upper left, single bonded to N H 3 superscript plus on the lower left, and wedge bonded to H on the upper right. C 3 is single bonded to N H 2 below and double bonded to O on the upper right.

The structure of phenylacetylglutamine is as follows: A benzene ring is in a horizontal orientation with C 1 occupying the rightmost vertex. It contains alternating double bonds between C 1 and C 2, C 3 and C 4, and C 5 and C 6. C 5 is single bonded to C H 2 on the upper left in the form of a line. The C H 2 group is further single-bonded to C on the upper right. The C atom is double-bonded to O on the right and single-bonded to N H on the upper left. The N H group is single-

bonded to a C atom. This C atom is single bonded to C O O superscript plus on the upper left, wedge bonded to H on the upper right, and dash bonded to a 3-carbon alkane chain depicted as a line structure using 2 zigzag lines. C 3 is double bonded to O on the upper right and single bonded to N H 2 below.

Return to FIGURE 23.18 Both carbamoyl phosphate synthetase and ornithine transcarbamoylase deficiencies can be treated the same way

Extended description for Structure of uric acid

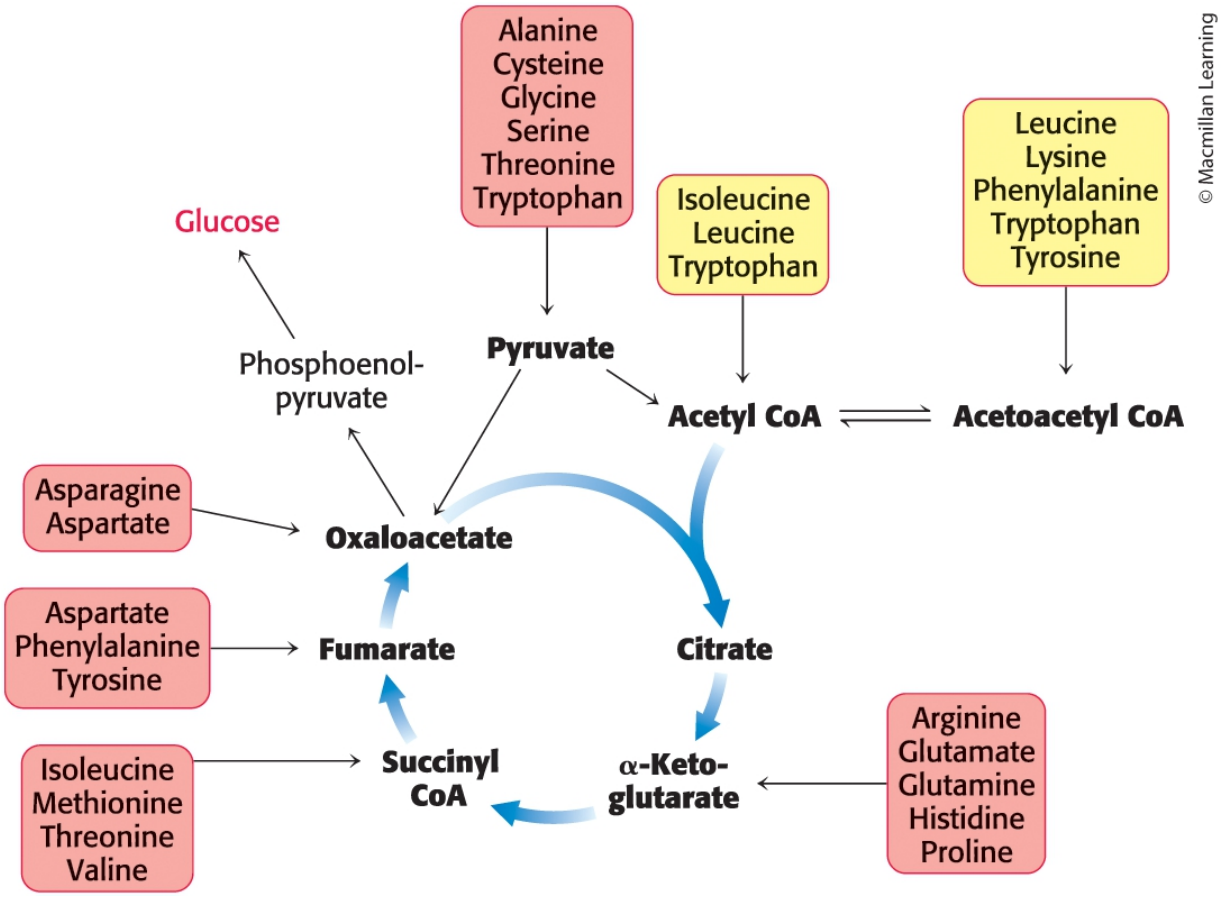


The structure of uric acid is as follows: A 5-membered heterocyclic pentagonal ring is in a horizontal orientation with C 1 occupying the leftmost vertex. It consists of 2 N and 3 C atoms. The N atoms are bound to H and occupy the bottom left and top left vertices. C 1 is double bonded to O on the left. The pentagonal ring is fused to a 6-membered heterocyclic hexagonal ring in a vertical orientation such that C 2 and C 3 of the pentagonal ring are C 3 and C 2 respectively of the hexagonal ring. The hexagonal ring consists of 2 N and 4 C atoms. The first N bound to H occupies the top right vertex and the second N bound to H occupies the bottom-most vertex. C 1 occupies

the bottom left vertex. C 1 is double bonded to O on the lower right. C 4 is double bonded to O above. A double bond is present between C 2 and C 3.

Return to Structure of uric acid

Extended description for FIGURE 23.19 The carbon skeletons of all 20 proteogenic amino acids enter central metabolism as just seven different molecules



A simplified citric acid cycle is shown in the center. Acetyl C o A and oxaloacetate combine to form citrate. Acetyl C o A and oxaloacetate are produced from pyruvate. Citrate is converted into alpha-ketoglutarate. Alpha-ketoglutarate is converted into succinyl C o A. The succinyl C o A molecule is converted into fumarate, which is further converted into oxaloacetate. The acetyl C o A entering the citric acid cycle can be alternatively converted into acetoacetyl C o A in a reversible reaction. The oxaloacetate molecule from the citric

acid cycle can form phosphoenolpyruvate, which is further converted into glucose highlighted in red.

A red box containing arginine, glutamate, glutamine, histidine, and proline points toward alpha-ketoglutarate.

A red box containing isoleucine, methionine, threonine, and valine points toward succinyl C o A.

A red box containing aspartate, phenylalanine, and tyrosine points toward fumarate.

A red box containing asparagine and aspartate points toward oxaloacetate.

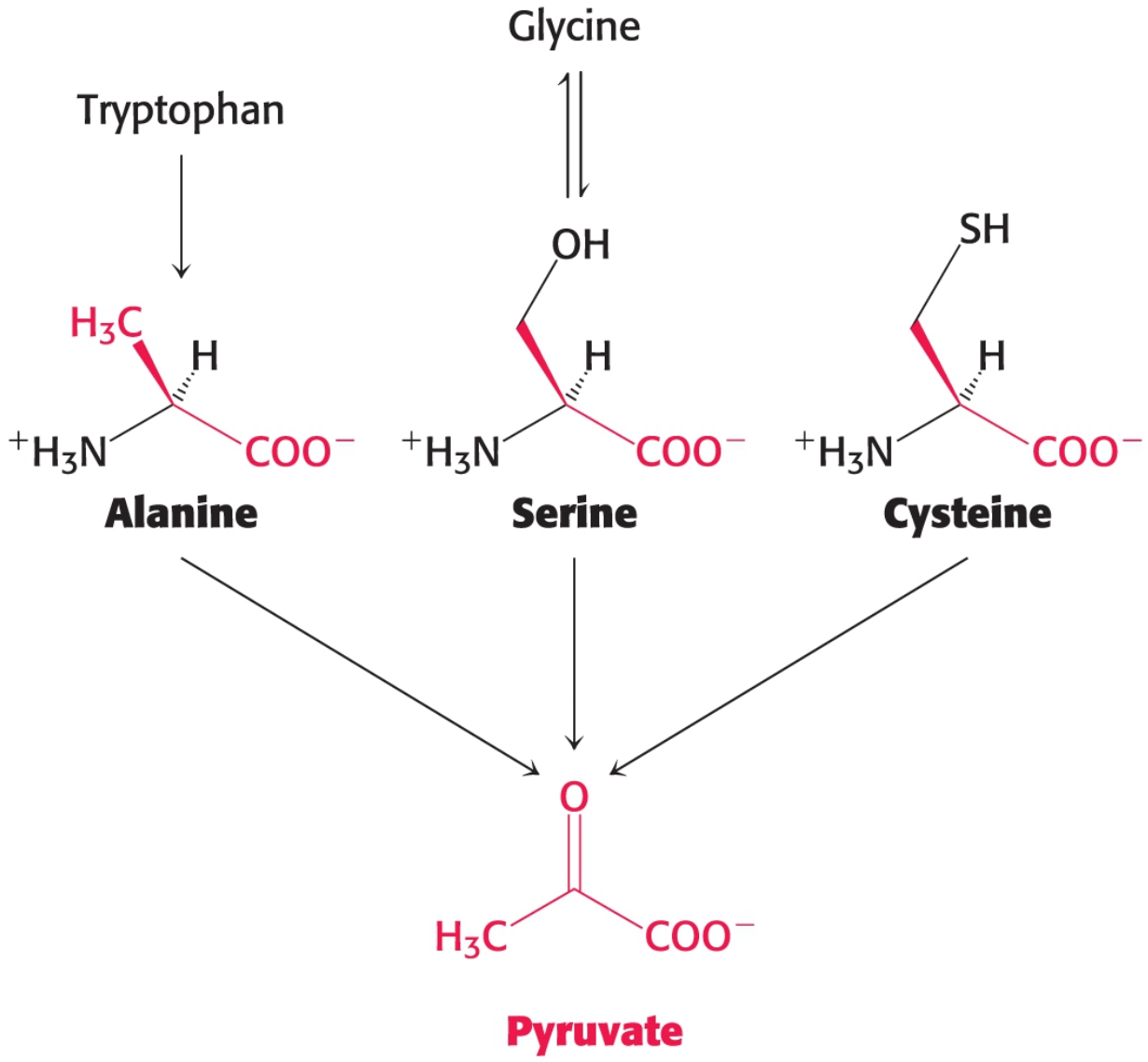
A red box containing alanine, cysteine, glycine, serine, threonine, and tryptophan points toward pyruvate.

A yellow box containing isoleucine, leucine, and tryptophan points toward acetyl C o A.

A yellow box containing leucine, lysine, phenylalanine, tryptophan, and tyrosine points toward acetoacetyl C o A.

Return to FIGURE 23.19 The carbon skeletons of all 20 proteogenic amino acids enter central metabolism as just seven different molecules

Extended description for FIGURE 23.20 Pyruvate is the metabolic entry point for the carbon skeletons from three-carbon amino acids



An arrow from alanine, serine, and cysteine points toward a common pyruvate molecule below. Alanine is produced irreversibly from tryptophan and serine is produced reversibly from glycine.

The structure of alanine is as follows: A central C atom is single bonded to N H 3 superscript plus on the lower left, wedge bonded to C H 3 on the upper left, dash bonded to H on the upper right, and single bonded to C O O superscript minus on the lower right.

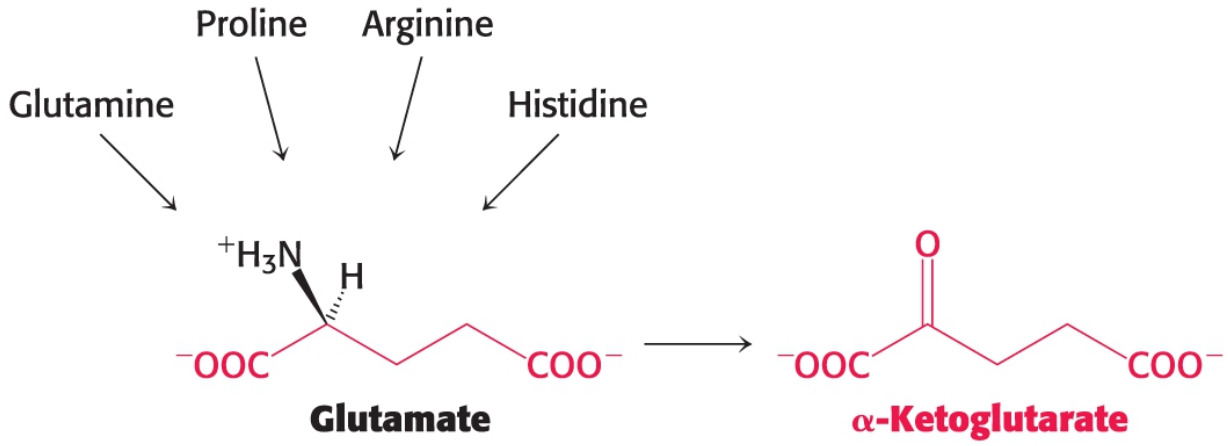
The structure of serine is as follows: A central C atom is single bonded to N H 3 superscript plus on the lower left, wedge bonded to C H 2 on the upper left, dash bonded to H on the upper right, and single bonded to C O O superscript minus on the lower right. The C H 2 group is single-bonded to O H on the upper right.

The structure of cysteine is as follows: A central C atom is single bonded to N H 3 superscript plus on the lower left, wedge bonded to C H 2 on the upper left, dash bonded to H on the upper right, and single bonded to C O O superscript minus on the lower right. The C H 2 group is single-bonded to S H on the upper right.

The structure of pyruvate is as follows: A central C atom is single bonded to C H 3 on the lower left, single bonded to C O O superscript minus on the lower right, and double bonded to O above.

Return to FIGURE 23.20 Pyruvate is the metabolic entry point for the carbon skeletons from three-carbon amino acids

Extended description for FIGURE 23.21 Four amino acids produce carbon skeletons that enter central metabolism as alpha-ketoglutarate



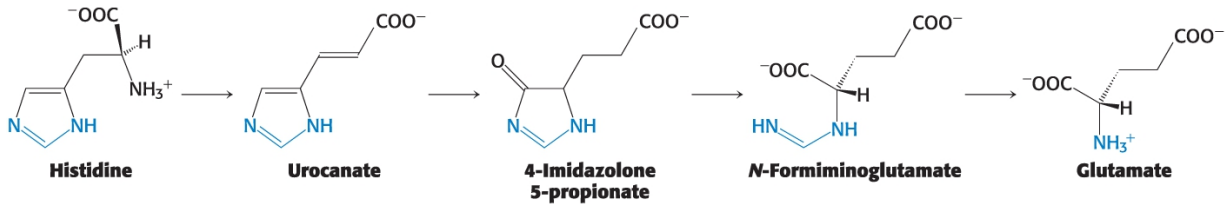
An arrow from glutamine, proline, arginine, and histidine points toward a common glutamate molecule. Glutamate is further irreversibly converted into alpha-ketoglutarate.

The structure of glutamate is as follows: A 3-carbon alkane chain is depicted as a line structure using 2 zigzag lines. C 1 is single bonded to C O O superscript minus on the lower left, wedge bonded to N H 3 superscript plus on the upper left, and dash bonded to H on the upper right. C 3 is single bonded to C O O superscript minus on the lower right.

The structure of alpha-ketoglutarate is as follows: A 3-carbon alkane chain is depicted as a line structure using 2 zigzag lines. C 1 is single bonded to C O O superscript minus on the lower left and double bonded to O above. C 3 is single bonded to C O O superscript minus on the lower right.

Return to FIGURE 23.21 Four amino acids produce carbon skeletons that enter central metabolism as alpha-ketoglutarate

Extended description for FIGURE 23.22 Stepwise conversion of histidine to glutamate



The conversion of histidine to glutamate takes place in four successive steps.

In the first step, histidine is irreversibly converted into urocanate.

The structure of histidine is as follows: A 5-membered heterocyclic pentagonal ring is in a vertical orientation with C 1 occupying the bottom-most vertex. It consists of 2 N and 3 C atoms. The first N bound to H occupies the bottom-right vertex and the second N occupies the bottom-left vertex. A double bond is present between C 1 and N 2, and C 2 and C 3. C 3 is single bonded to C H 2 on the upper right in the form of a line. The C H 2 group is further single-bonded to C on the right. The C atom is wedge bonded to C O O superscript minus above, dash bonded to H on the upper right, and single bonded to N H 3 superscript plus on the lower right.

The structure of urocanate is as follows: A 5-membered heterocyclic pentagonal ring is in a vertical orientation with C 1 occupying the bottom-most vertex. It consists of 2 N and 3 C atoms. The first N bound to H occupies the bottom-right vertex and the second N occupies the bottom-left vertex. A double bond is present between C 1 and N 2, and C 2 and C 3. C 3 is single bonded to C H on the upper right in the form of a line. The C H group is further double bonded

to C H on the right. The C H group is single-bonded to C O O superscript minus on the upper right.

In the second step, urocanate is irreversibly converted into 4-imidazolone 5-propionate.

The structure of 4-imidazolone 5-propionate is as follows: A 5-membered heterocyclic pentagonal ring is in a vertical orientation with C 1 occupying the bottom-most vertex. It consists of 2 N and 3 C atoms. The first N bound to H occupies the bottom-right vertex and the second N occupies the bottom-left vertex. A double bond is present between C 1 and N 2. C 2 is double bonded to O on the upper left. C 3 is single bonded to C H 2 on the upper right in the form of a line. The C H 2 group is further single-bonded to another C H 2 on the right in the form of a line. This C H 2 group is single bonded to C O O superscript minus on the upper right.

In the third step, 4-imidazolone 5-propionate is irreversibly converted into N-Formiminoglutamate.

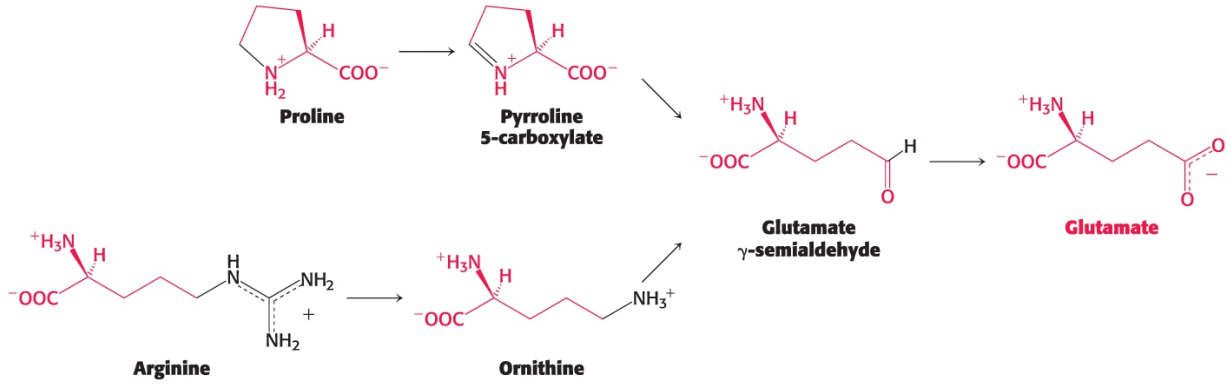
The structure of N-Formiminoglutamate is as follows: A central C atom is single bonded to C O O superscript minus on the upper left, dash bonded to C H 2 on the upper right, wedge bonded to H on the right, single bonded to N H below. The N H group is single-bonded to the C H group on the lower left. The C H group is double bonded to N H on the upper left. The upper right C H 2 group is single-bonded to C H 2 on the right in the form of a line. This C H 2 group is single bonded to C O O superscript minus on the upper right.

In the fourth step, N-Formiminoglutamate is irreversibly converted into glutamate.

The structure of glutamate is as follows: A central C atom is single bonded to C O O superscript minus on the upper left, dash bonded to C H 2 on the upper right, wedge bonded to H on the right, single bonded to N H 3 superscript plus below. The upper right C H 2 group is single-bonded to C H 2 on the right in the form of a line. The C H 2 group is single-bonded to C O O superscript minus on the upper right.

Return to FIGURE 23.22 Stepwise conversion of histidine to glutamate

Extended description for FIGURE 23.23 The degradation pathways for proline and arginine converge on a common intermediate



The degradation pathways for proline and arginine produce a common intermediate called glutamate gamma-semialdehyde. This intermediate is converted into glutamate.

Proline is first irreversibly converted into pyrroline 5-carboxylate. Simultaneously, arginine is irreversibly converted into ornithine.

The structure of proline is as follows: A central C atom is wedge bonded to C H 2 on the upper left, single bonded to N H 2 with a positive charge on the lower left, dash bonded to H on the upper right, and single bonded to C O O superscript minus on the lower right. The upper left C H 2 group is single-bonded to a 2-carbon alkane chain depicted using a line. C 2 of this chain is single-bonded to the N H 2 group on the lower left such that a cyclic pentagonal-shaped ring structure is formed.

The structure of pyrroline 5-carboxylate is as follows: A central C atom is wedge bonded to C H 2 on the upper left, single bonded to N H with a positive charge on the lower left, dash bonded to H on the

upper right, and single bonded to C O O superscript minus on the lower right. The upper left C H 2 group is single-bonded to a 2-carbon alkane chain depicted using a line. C 2 of this chain is double bonded to the N H group on the lower left such that a cyclic pentagonal-shaped ring structure is formed.

The structure of arginine is as follows: A 4-carbon alkane chain is depicted as a line structure using 3 zigzag lines. C 1 is wedge bonded to N H 3 superscript plus on the upper left, dash bonded to H on the upper right, and single bonded to C O O superscript minus on the lower left. C 4 is single bonded to N H on the upper right. This N H group is partially double-bonded to a central C atom. This C atom is partially double bonded to N H 2 on the upper right and N H 2 below. This C atom has a positive charge.

The structure of ornithine is as follows: A 4-carbon alkane chain is depicted as a line structure using 3 zigzag lines. C 1 is wedge bonded to N H 3 superscript plus on the upper left, dash bonded to H on the upper right, and single bonded to C O O superscript minus on the lower left. C 4 is single bonded to N H 3 superscript plus on the upper right.

Both pyrroline 5-carboxylate and ornithine are irreversibly converted into glutamate gamma-semialdehyde.

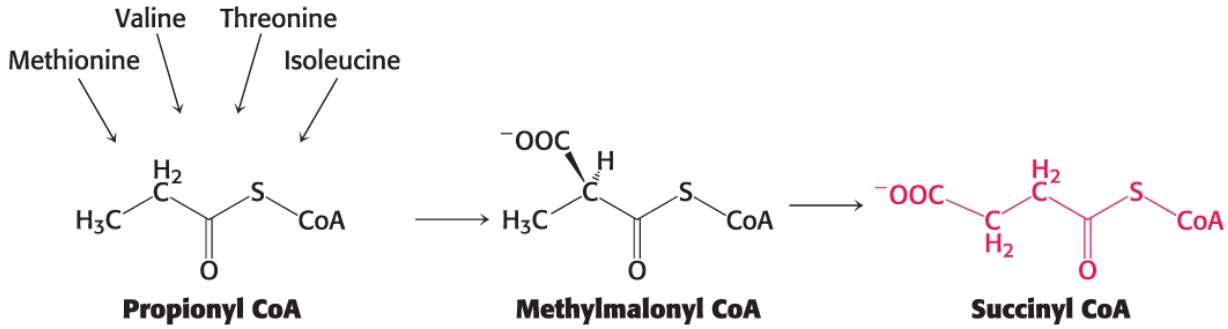
The structure of glutamate gamma-semialdehyde is as follows: A 4-carbon alkane chain is depicted as a line structure using 3 zigzag lines. C 1 is wedge bonded to N H 3 superscript plus on the upper left, dash bonded to H on the upper right, and single bonded to C O O superscript minus on the lower left. C 4 is single bonded to H on the upper right and double bonded to O below.

The common intermediate glutamate gamma-semialdehyde is irreversibly converted into glutamate.

The structure of glutamate is as follows: A 4-carbon alkane chain is depicted as a line structure using 3 zigzag lines. C 1 is wedge bonded to N H 3 superscript plus on the upper left, dash bonded to H on the upper right, and single bonded to C O O superscript minus on the lower left. C 4 is partially double bonded to O on the upper right and O below. C 4 has an overall negative charge.

Return to FIGURE 23.23 The degradation pathways for proline and arginine converge on a common intermediate

Extended description for FIGURE 23.24 Succinyl C o A is formed from methionine, isoleucine, threonine, and valine



The amino acids methionine, valine, threonine, and isoleucine give rise to propionyl C o A. The propionyl C o A molecule is irreversibly converted into methylmalonyl C o A, which is further irreversibly converted into succinyl C o A.

The structure of propionyl C o A is as follows: A central C atom is single bonded to C H 2 on the upper left, double bonded to O below, and single bonded to S on the upper right. The C H 2 group is single-bonded to C H 3 on the lower left. The S atom is single-bonded to C o A on the lower right.

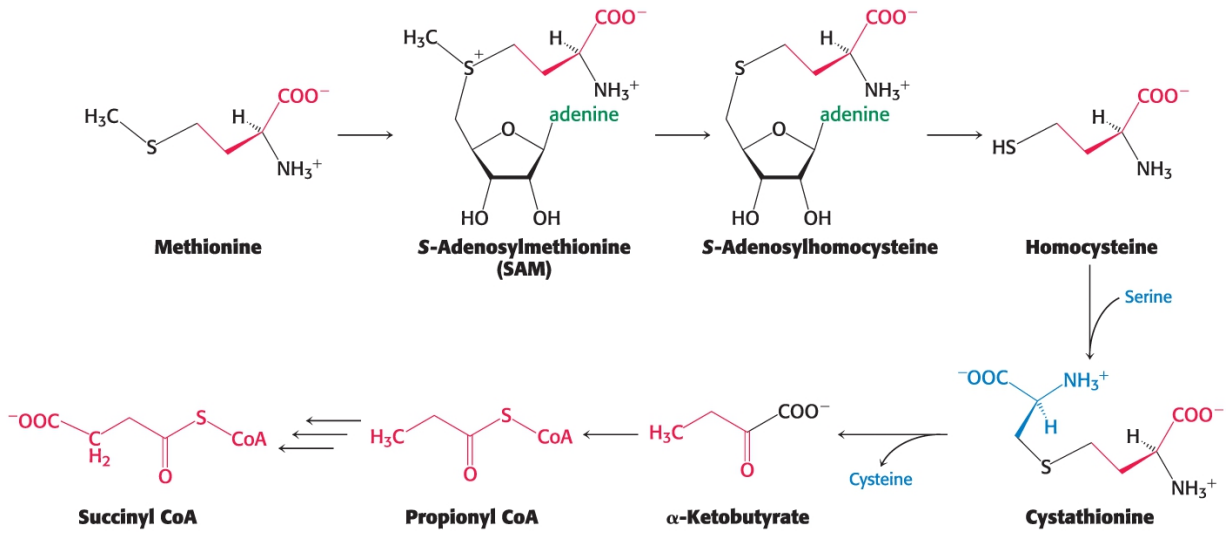
The structure of methylmalonyl C o A is as follows: A central C atom is single-bonded to C on the upper left, double-bonded to O below, and single-bonded to S on the upper right. The upper left C is single bonded to C H 3 on the lower left, wedge bonded to C O O superscript minus on the upper left, and dash bonded to H on the upper right. The S atom is single-bonded to C o A on the lower right.

The structure of succinyl C o A is as follows: A central C atom is single bonded to C H 2 on the upper left, double bonded to O below,

and single bonded to S on the upper right. The upper left C H 2 group is single bonded to C H 2 on the lower left, which is further single bonded to C O O superscript minus on the upper left. The S atom is single-bonded to C o A on the lower right.

Return to FIGURE 23.24 Succinyl C o A is formed from methionine, isoleucine, threonine, and valine

Extended description for FIGURE 23.25 Methionine catabolism proceeds through the formation of S A M



The catabolism of methionine produces succinyl C o A as the end product. It takes place in 9 irreversible steps.

In the first step, methionine is converted into S-adenosylmethionine (S A M).

The structure of methionine is as follows: A 2-carbon alkane chain is depicted using a line. C 1 is single bonded to S on the lower left. The S atom is single-bonded to C H 3 on the upper left. C 2 is wedge bonded to C on the upper right. The C atom is single bonded to C O O superscript minus on the upper right, single bonded to N H 3 superscript plus on the lower right, and dash bonded to H on the upper left.

The structure of S-adenosylmethionine is as follows: A 5-membered heterocyclic pentagonal ring is in a vertical orientation and consists of 1 O and 4 C atoms. C 1 occupies the top right vertex and is single-

bonded to adenine on the upper right. C 2 and C 3 are single bonded to O H below. C 4 is single bonded to C H 2 above, which is further single bonded to the S atom of methionine. The S atom is positively charged.

In the second step, S-adenosylmethionine is converted into S-adenosylhomocysteine.

The structure of S-adenosylhomocysteine is as follows: The C H 3 group of the methionine amino acid is removed and the S atom loses its positive charge. The remaining structure is the same as S-adenosylmethionine.

In the third step, S-adenosylhomocysteine is converted into homocysteine.

The structure of homocysteine is as follows: A 2-carbon alkane chain is depicted using a single line. C 1 is single bonded to S H on the lower left. C 2 is wedge bonded to C on the upper right. The C atom is single bonded to C O O superscript minus on the upper right, single bonded to N H 3 on the lower right, and dash bonded to H on the upper left.

In the fourth step, homocysteine is converted into cystathionine by the addition of serine.

The structure of cystathionine is as follows: A 2-carbon alkane chain is depicted using a single line. C 1 is single bonded to S on the lower left. C 2 is wedge bonded to C on the upper right. The C atom is single bonded to C O O superscript minus on the upper right, single bonded to N H 3 superscript plus on the lower right, and dash bonded to H on the upper left. The S atom is single-bonded to C H 2 on the upper left in the form of a line. This C H 2 group is wedge

bonded to a central C atom on the upper right. This C is single bonded to C O O superscript minus on the upper left, single bonded to N H 3 superscript plus on the upper right, and dash bonded to H on the lower right.

In the fifth step, cystathionine is converted into alpha-ketobutyrate with the simultaneous release of cysteine.

The structure of alpha-ketobutyrate is as follows: A 2-carbon alkane chain is depicted using a single line. C 1 is single bonded to C H 3 on the lower left. C 2 is double bonded to O below and single bonded to C O O superscript minus on the upper right.

In the sixth step, alpha-ketobutyrate is converted into propionyl C o A.

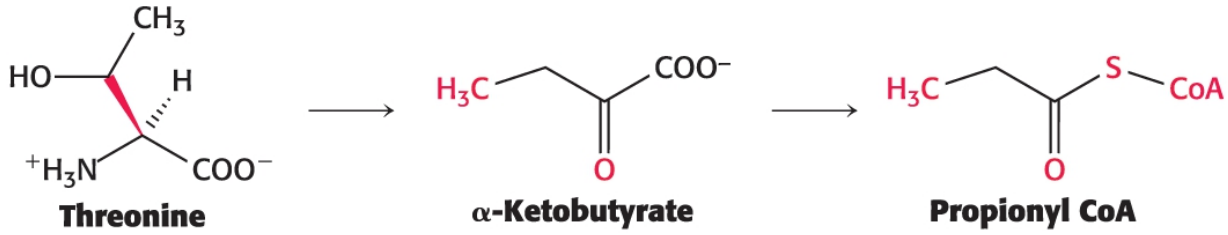
The structure of propionyl C o A is as follows: A central C atom is single bonded to C H 2 on the upper left in the form of a line, double bonded to O below, and single bonded to S on the upper right. The C H 2 group is single-bonded to C H 3 on the lower left. The S atom is single-bonded to C o A on the lower right.

The seventh, eighth, and ninth steps cause the conversion of propionyl C o A to succinyl C o A. They are depicted as three forward arrows.

The structure of succinyl C o A is as follows: A central C atom is single bonded to C H 2 on the upper left in the form of a line, double bonded to O below, and single bonded to S on the upper right. The upper left C H 2 group is single bonded to C H 2 on the lower left, which is further single bonded to C O O superscript minus on the upper left. The S atom is single-bonded to C o A on the lower right.

Return to FIGURE 23.25 Methionine catabolism proceeds through the formation of S A M

Extended description for Conversion of threonine to propionyl C o A



Threonine is irreversibly converted into propionyl C o A through an alpha-ketobutyrate intermediate.

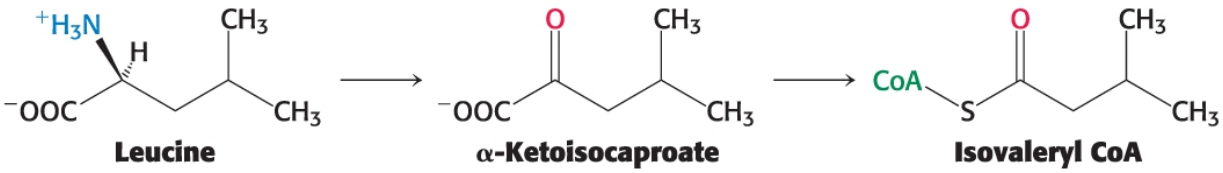
The structure of threonine is as follows: A central C atom is single bonded to N H 3 superscript plus on the lower left, single bonded to C O O superscript minus on the lower right, wedge bonded to C on the upper left, and dash bonded to H on the upper right. The upper left C atom is single-bonded to O H on the left and single-bonded to C H 3 on the upper right.

The structure of alpha-ketobutyrate is as follows: A central C atom is single bonded to C H 2 on the upper left in the form of a line, double bonded to O below, and single bonded to C O O superscript minus. The C H 2 group is single-bonded to C H 3 on the lower left.

The structure of propionyl C o A is as follows: A central C atom is single bonded to C H 2 on the upper left in the form of a line, double bonded to O below, and single bonded to S on the upper right. The C H 2 group is single-bonded to C H 3 on the lower left. The S atom is single-bonded to C o A on the lower right.

Return to Conversion of threonine to propionyl C o A

Extended description for Conversion of leucine to isovaleryl C o A



Leucine is irreversibly converted into isovaleryl C o A through an alpha-ketoisocaproate intermediate.

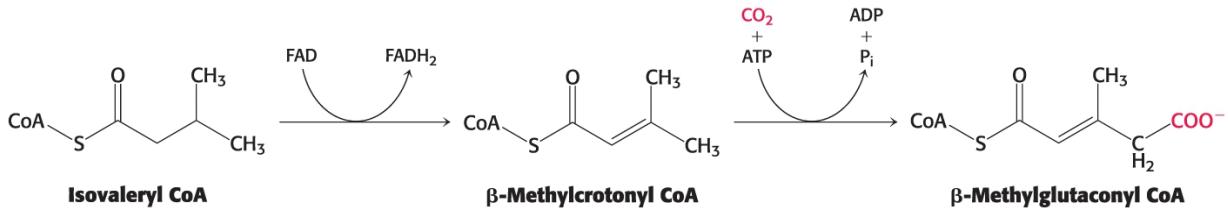
The structure of leucine is as follows: A 3-carbon alkane chain is depicted as a line structure using 2 zigzag lines. C 1 is single bonded to C O O superscript minus on the lower left, wedge bonded to N H 3 superscript plus on the upper left, and dash bonded to H on the upper right. C 3 is single bonded to C H 3 above and C H 3 on the lower right.

The structure of alpha-ketoisocaproate is as follows: A 3-carbon alkane chain is depicted as a line structure using 2 zigzag lines. C 1 is single bonded to C O O superscript minus on the lower left and double bonded to O above. C 3 is single bonded to C H 3 above and C H 3 on the lower right.

The structure of isovaleryl C o A is as follows: A 3-carbon alkane chain is depicted as a line structure using 2 zigzag lines. C 1 is single bonded to S on the lower left and double bonded to O above. S is single bonded to C o A on the upper left. C 3 is single-bonded to C H 3 above and C H 3 on the lower right.

Return to Conversion of leucine to isovaleryl C o A

Extended description for Conversion of isovaleryl C o A to beta-methylglutaconyl C o A



Isovaleryl C o A is irreversibly converted into beta-methylglutaconyl C o A through a beta-methylcrotonyl C o A intermediate.

The structure of isovaleryl C o A is as follows: A 3-carbon alkane chain is depicted as a line structure using 2 zigzag lines. C 1 is single bonded to S on the lower left and double bonded to O above. S is single bonded to C o A on the upper left. C 3 is single-bonded to C H 3 above and C H 3 on the lower right.

Isovaleryl C o A is irreversibly converted into beta-methylcrotonyl C o A with the simultaneous reduction of F A D to F A D H 2.

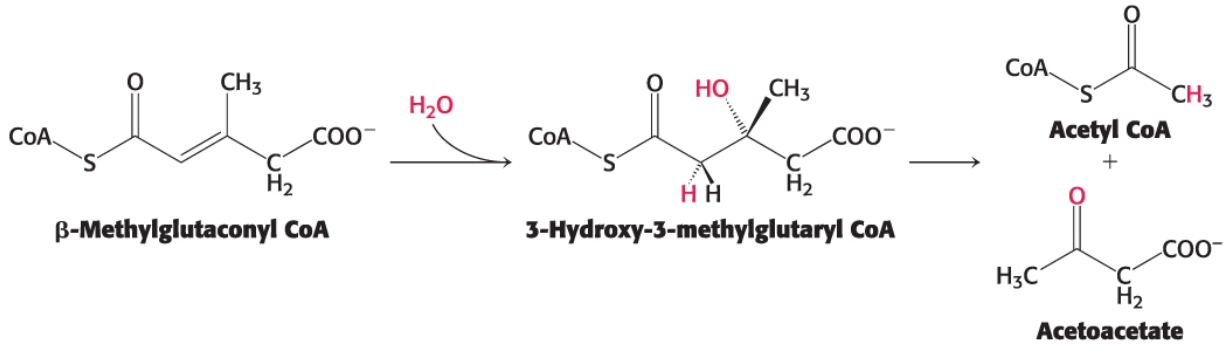
The structure of beta-methylcrotonyl C o A is as follows: A 3-carbon alkene chain is depicted as a line structure using 2 zigzag lines. C 1 is single bonded to S on the lower left and double bonded to O above. S is single bonded to C o A on the upper left. C 3 is single-bonded to C H 3 above and C H 3 on the lower right. A double bond is present between C 2 and C 3.

Beta-methylcrotonyl C o A is irreversibly converted into beta-methylglutaconyl C o A with the simultaneous hydrolysis of A T P to A D P and P subscript i and entry of C O 2.

The structure of beta-methylglutaconyl C o A is as follows: A 3-carbon alkene chain is depicted as a line structure using 2 zigzag lines. C 1 is single bonded to S on the lower left and double bonded to O above. S is single-bonded to C o A on the upper left. C 3 is single-bonded to C H 3 above and C H 2 on the lower right. C H 2 is single bonded to C O O superscript minus on the upper right. A double bond is present between C 2 and C 3.

Return to Conversion of isovaleryl C o A to beta-methylglutaconyl C o A

Extended description for Conversion of beta-methylglutaconyl C o A to acetyl C o A and acetoacetate



Beta-methylglutaconyl C o A is irreversibly converted to acetyl C o A and acetoacetate through a 3-hydroxy-3-methylglutaryl C o A intermediate.

In the first step, beta-methylglutaconyl C o A is converted into 3-hydroxy-3-methylglutaryl C o A by the addition of H 2 O.

The structure of beta-methylglutaconyl C o A is as follows: A 3-carbon alkene chain is depicted as a line structure using 2 zigzag lines. C 1 is single bonded to S on the lower left and double bonded to O above. S is single-bonded to C o A on the upper left. C 3 is single-bonded to C H 3 above and C H 2 on the lower right. C H 2 is single bonded to C O O superscript minus on the upper right. A double bond is present between C 2 and C 3.

The structure of 3-hydroxy-3-methylglutaryl C o A is as follows: A 3-carbon alkane chain is depicted as a line structure using 2 zigzag lines. C 1 is single bonded to S on the lower left and double bonded to O above. S is single-bonded to C o A on the upper left. C 2 is dash bonded to H on the lower left and wedge bonded to H on the lower right. C 3 is dash bonded to O H on the upper left, wedge bonded to

C H 3 on the upper right, and single bonded to C H 2 on the lower right. The C H 2 group is single-bonded to C O O superscript minus on the upper right.

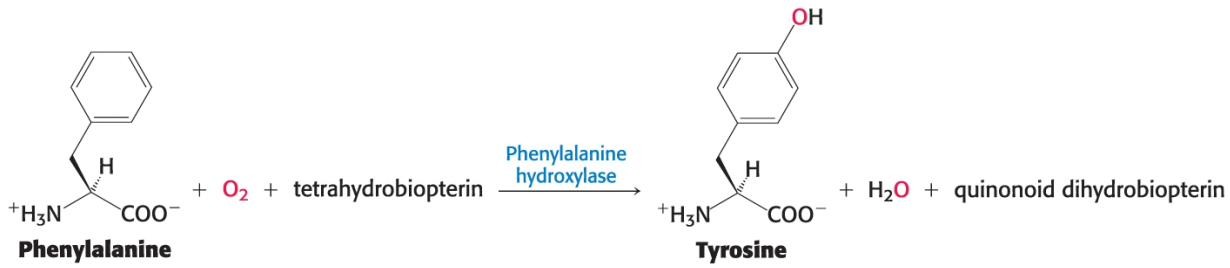
In the second step, 3-hydroxy-3-methylglutaryl C o A is converted into acetyl C o A and acetoacetate.

The structure of acetyl C o A is as follows: A central C atom is single-bonded to S on the lower left, single-bonded to C H 3 on the lower right, and double-bonded to O above. The S atom is single-bonded to C o A on the upper left.

The structure of acetoacetate is as follows: A central C atom is single-bonded to C H 3 on the lower left, single-bonded to C H 2 on the lower right, and double-bonded to O above. The lower right C H 2 group is single bonded to C O O superscript minus on the upper right.

Return to Conversion of beta-methylglutaconyl C o A to acetyl C o A and acetoacetate

Extended description for Reaction catalyzed by phenylalanine hydroxylase



The reaction consists of three reactants and three products.

The first reactant is phenylalanine whose structure is as follows: A benzene ring is in a horizontal orientation with C 1 occupying the rightmost vertex. It contains alternating double bonds between C 2 and C 3, C 4 and C 5, and C 6 and C 1. C 3 is single bonded to C H 2 on the lower left in the form of a line. The C H 2 group is wedge bonded to C on the lower right. This C atom is dash bonded to H on the upper right, single bonded to N H 3 superscript plus on the lower left, and single bonded to C O O superscript minus on the lower right.

The second reactant is O 2 and the third reactant is tetrahydrobiopterin.

A forward arrow labeled phenylalanine hydroxylase leads to the products.

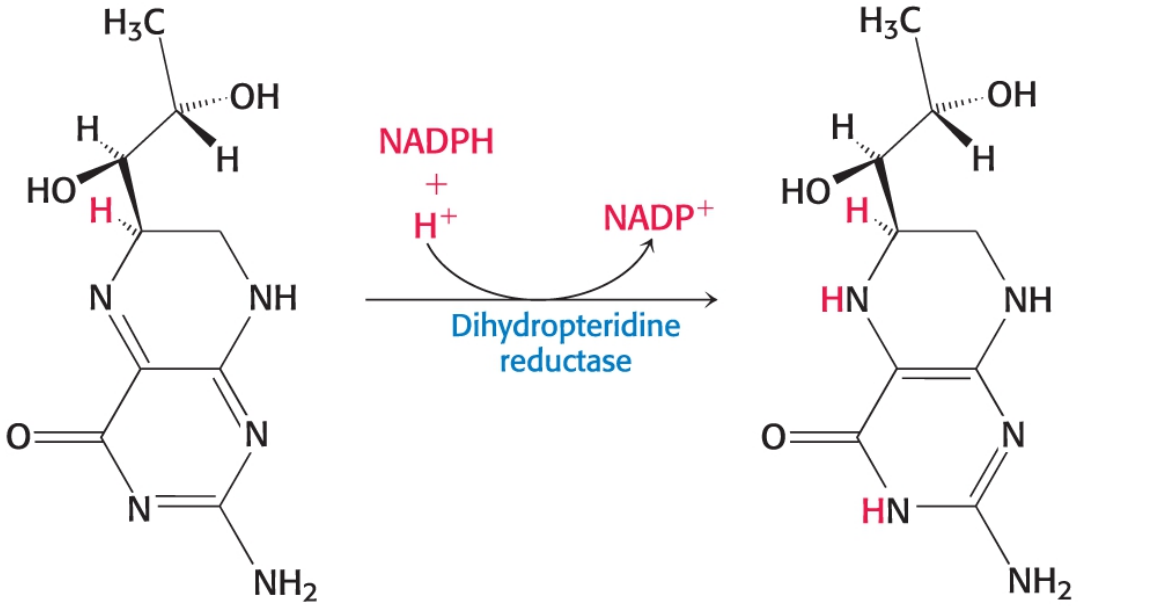
The first product is tyrosine whose structure is as follows: A benzene ring is in a horizontal orientation with C 1 occupying the rightmost vertex. It contains alternating double bonds between C 2 and C 3, C 4 and C 5, and C 6 and C 1. C 6 is single bonded to O H on the upper

right. C 3 is single bonded to C H 2 on the lower left in the form of a line. The C H 2 group is wedge bonded to C on the lower right. This C atom is dash bonded to H on the upper right, single bonded to N H 3 superscript plus on the lower left, and single bonded to C O O superscript minus on the lower right.

The second product is H 2 O and the third product is quinonoid dihydrobiopterin.

Return to Reaction catalyzed by phenylalanine hydroxylase

Extended description for Irreversible conversion of quinonoid dihydrobiopterin to tetrahydrobiopterin



Quinonoid dihydrobiopterin **Tetrahydrobiopterin**

The reaction consists of one reactant and one product. It is catalyzed by dihydropteridine reductase with the simultaneous oxidation of N A D P H plus H superscript plus to N A D P superscript plus.

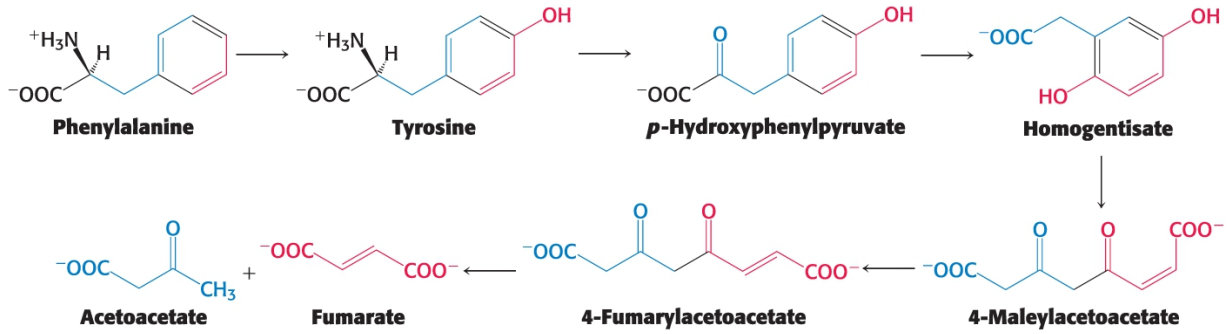
The reactant is quinonoid dihydrobiopterin whose structure is as follows: A 6-membered heterocyclic hexagonal ring is in a horizontal orientation and consists of 2 N and 4 C atoms. C 1 occupies the bottom right vertex. The first N occupies the rightmost vertex and the second N occupies the bottom left vertex. A double bond is present between C 4 and N 1 and C 1 and N 2. C 1 is single bonded to N H 2 on the lower right. C 2 is double bonded to O on the left. This hexagonal ring is fused to a second 6-membered heterocyclic hexagonal ring in a horizontal orientation such that C 3 and C 4 of the first ring are C 2 and C 1 respectively of the second ring. The second ring consists of 2 N and 4 C atoms. The first N

bound to H occupies the rightmost vertex and the second N occupies the leftmost vertex. A double bond is present between C 2 and N 2. C 3 is wedge bonded to a C atom above and dash bonded to H on the upper left. The C atom is dash bonded to H on the upper left, wedge bonded to O H on the left, and single bonded to another C atom on the upper right. The upper right C atom is single bonded to C H 3 above, dash bonded to O H on the right, and wedge bonded to H on the lower right.

The product is tetrahydrobiopterin whose structure is as follows: A 6-membered heterocyclic hexagonal ring is in a horizontal orientation and consists of 2 N and 4 C atoms. C 1 occupies the bottom right vertex. The first N occupies the rightmost vertex and the second N bound to H occupies the bottom left vertex. A double bond is present between N 1 and C 1, and C 3 and C 4. C 1 is single bonded to N H 2 on the lower right. C 2 is double bonded to O on the left. This hexagonal ring is fused to a second 6-membered heterocyclic hexagonal ring in a horizontal orientation such that C 3 and C 4 of the first ring are C 2 and C 1 respectively of the second ring. The second ring consists of 2 N and 4 C atoms. The first N bound to H occupies the rightmost vertex and the second N bound to H occupies the leftmost vertex. C 3 is wedge bonded to a C atom above and dash bonded to H on the upper left. The C atom is dash bonded to H on the upper left, wedge bonded to O H on the left, and single bonded to another C atom on the upper right. The upper right C atom is single bonded to C H 3 above, dash bonded to O H on the right, and wedge bonded to H on the lower right.

Return to Irreversible conversion of quinonoid dihydrobiopterin to tetrahydrobiopterin

Extended description for FIGURE 23.26 Phenylalanine and tyrosine degradation produce both acetoacetate and fumarate



In the first step, phenylalanine is irreversibly converted into tyrosine. The structure of phenylalanine is as follows: A benzene ring is in a vertical orientation with C 1 occupying the topmost vertex. It contains alternating double bonds between C 1 and C 2, C 3 and C 4, and C 5 and C 6. C 5 is single bonded to C H 2 on the lower left in the form of a line. This C H 2 group is single-bonded to C on the upper left. The C atom is wedge bonded to N H 3 superscript plus on the upper left, single bonded to C O O superscript minus on the lower left, and dash bonded to H on the upper right.

The structure of tyrosine is as follows: A benzene ring is in a vertical orientation with C 1 occupying the topmost vertex. It contains alternating double bonds between C 1 and C 2, C 3 and C 4, and C 5 and C 6. C 2 is single bonded to O H on the upper right. C 5 is single bonded to C H 2 on the lower left in the form of a line. This C H 2 group is single-bonded to C on the upper left. The C atom is wedge bonded to N H 3 superscript plus on the upper left, single bonded to C O O superscript minus on the lower left, and dash bonded to H on the upper right.

In the second step, tyrosine is irreversibly converted into p-hydroxyphenylpyruvate.

The structure of p-hydroxyphenylpyruvate is as follows: A benzene ring is in a vertical orientation with C 1 occupying the topmost vertex. It contains alternating double bonds between C 1 and C 2, C 3 and C 4, and C 5 and C 6. C 2 is single bonded to O H on the upper right. C 5 is single bonded to C H 2 on the lower left in the form of a line. This C H 2 group is single-bonded to C on the upper left. The C atom is double-bonded to O above and single-bonded to C O O superscript minus on the lower left.

In the third step, p-hydroxyphenylpyruvate is irreversibly converted into homogentisate.

The structure of homogentisate is as follows: A benzene ring is in a vertical orientation with C 1 occupying the topmost vertex. It contains alternating double bonds between C 1 and C 2, C 3 and C 4, and C 5 and C 6. C 2 is single bonded to O H on the upper right. C 5 is single bonded to O H on the lower left. C 6 is single bonded to C H 2 on the upper left in the form of a line. This C H 2 group is single bonded to C O O superscript minus on the lower left.

In the fourth step, homogentisate is irreversibly converted into 4-Maleylacetoacetate.

The structure of 4-Maleylacetoacetate is as follows: A 6-carbon alkene chain is depicted as a line structure using 5 zigzag lines. A double bond is present between C 5 and C 6. C 1 is single bonded to C O O superscript minus on the upper left. C 2 and C 4 are double bonded to O above. C 6 is single bonded to C O O superscript minus above.

In the fifth step, 4-Maleylacetoacetate is irreversibly converted into 4-Fumarylacetoacetate.

The structure of 4-Fumarylacetoacetate is as follows: A 6-carbon alkene chain is depicted as a line structure using 5 zigzag lines. A double bond is present between C 5 and C 6. C 1 is single bonded to C O O superscript minus on the upper left. C 2 and C 4 are double bonded to O above. C 6 is single bonded to C O O superscript minus on the lower right.

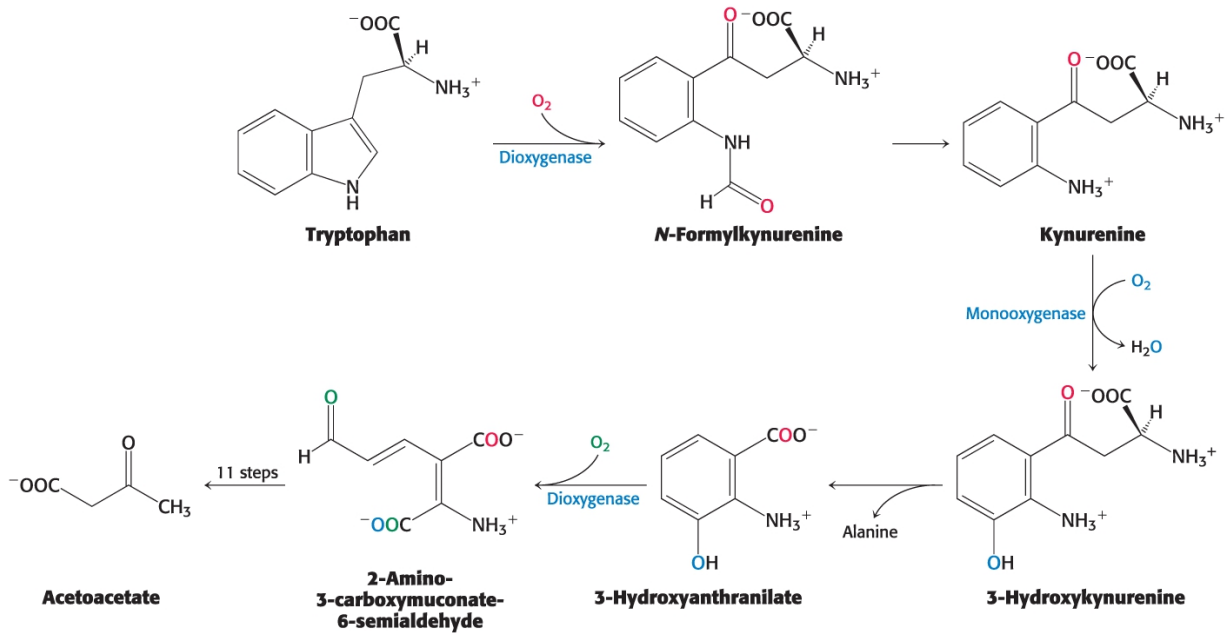
In the sixth step, 4-Fumarylacetoacetate is irreversibly converted into fumarate and acetoacetate.

The structure of fumarate is as follows: A 2-carbon alkene chain is depicted using 2 parallel lines. C 1 is single bonded to C O O superscript minus on the upper left. C 2 is single bonded to C O O superscript minus on the lower right.

The structure of acetoacetate is as follows: A central C atom is double bonded to O above, single bonded to C H 3 on the lower right, and single bonded to C H 2 on the lower left in the form of a line. The C H 2 group is single-bonded to C O O superscript minus on the upper left.

Return to FIGURE 23.26 Phenylalanine and tyrosine degradation produce both acetoacetate and fumarate

Extended description for FIGURE 23.27 Tryptophan degradation requires multiple oxygenases and numerous steps



In the first step, tryptophan is irreversibly converted into N-formylkynurenine by dioxygenase. This step requires the addition of O 2.

The structure of tryptophan is as follows: A benzene ring is a vertical orientation with C 1 occupying the topmost vertex. It contains alternating double bonds between C 2 and C 3, C 4 and C 5, and C 6 and C 1. The benzene ring is fused to a 5-membered heterocyclic pentagonal ring in a horizontal orientation such that C 2 and C 3 of the benzene ring are C 2 and C 1 respectively of the pentagonal ring. It consists of 1 N and 4 C atoms. N bound to H occupies the bottom right vertex. C 1 occupies the bottom left vertex. A double bond is present between C 3 and C 4. C 3 is single bonded to C H 2 on the upper right in the form of a line. C H 2 is

single bonded to C on the right. This C atom is wedge bonded to C O O superscript minus on the upper left, dash bonded to H on the upper right, and single bonded to N H 3 superscript plus on the right.

The structure of N-formylkynurenine is as follows: A benzene ring is a vertical orientation with C 1 occupying the topmost vertex. It contains alternating double bonds between C 2 and C 3, C 4 and C 5, and C 6 and C 1. C 2 is single bonded to a 3-carbon alkane chain depicted as a line structure using 2 zigzag lines. In the alkane chain, C 1 is double bonded to O above. C 3 is wedge bonded to C O O superscript minus on the upper left, dash bonded to H on the upper right, and single bonded to N H 3 superscript plus on the lower right. C 3 of the benzene ring is single bonded to N H on the lower right. This N H group is single bonded to C below. The C atom is single bonded to H on the lower left and double bonded to O on the lower right.

In the second step, N-formylkynurenine is irreversibly converted into kynurenine.

The structure of kynurenine is as follows: A benzene ring is a vertical orientation with C 1 occupying the topmost vertex. It contains alternating double bonds between C 2 and C 3, C 4 and C 5, and C 6 and C 1. C 2 is single bonded to a 3-carbon alkane chain depicted as a line structure using 2 zigzag lines. In the alkane chain, C 1 is double bonded to O above. C 3 is wedge bonded to C O O superscript minus on the upper left, dash bonded to H on the upper right, and single bonded to N H 3 superscript plus on the lower right. C 3 of the benzene ring is single bonded to N H 3 superscript plus on the lower right.

In the third step, kynurenine is irreversibly converted into 3-hydroxykynurenine by monooxygenase with the simultaneous

conversion of O 2 to H 2 O.

The structure of 3-hydroxykynurenine is as follows: A benzene ring is a vertical orientation with C 1 occupying the topmost vertex. It contains alternating double bonds between C 2 and C 3, C 4 and C 5, and C 6 and C 1. C 2 is single bonded to a 3-carbon alkane chain depicted as a line structure using 2 zigzag lines. In the alkane chain, C 1 is double bonded to O above. C 3 is wedge bonded to C O O superscript minus on the upper left, dash bonded to H on the upper right, and single bonded to N H 3 superscript plus on the lower right. C 3 of the benzene ring is single bonded to N H 3 superscript plus on the lower right. C 4 is single bonded to O H below.

In the fourth step, 3-hydroxykynurenine is irreversibly converted into 3-hydroxyanthranilate with the simultaneous release of alanine.

The structure of 3-hydroxyanthranilate is as follows: A benzene ring is a vertical orientation with C 1 occupying the topmost vertex. It contains alternating double bonds between C 2 and C 3, C 4 and C 5, and C 6 and C 1. C 2 is single bonded to C O O superscript minus on the upper right. C 3 is single bonded to N H 3 superscript plus on the lower right. C 4 is single bonded to O H below.

In the fifth step, 3-hydroxyanthranilate is irreversibly converted into 2-amino-3-carboxymuconate-6-semialdehyde by dioxygenase. This step requires the addition of O 2.

The structure of 2-amino-3-carboxymuconate-6-semialdehyde is as follows: A 4-carbon alkene chain is depicted as a line structure using 3 zigzag lines. A double bond is present between C 2 and C 3. C 1 is double bonded to O above and single bonded to H on the lower right. C 4 is single bonded to C O O superscript minus on the upper right and double bonded to C below. The C atom below is single

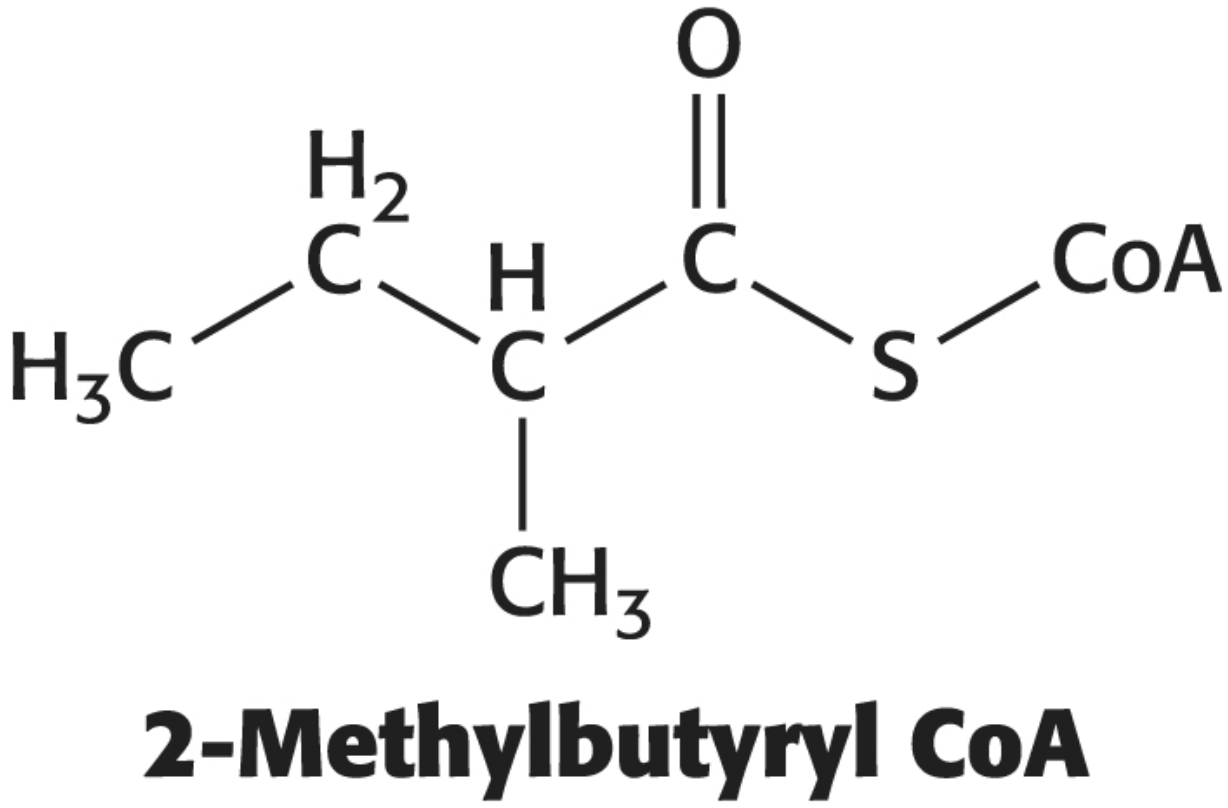
bonded to C O O superscript minus on the lower left and single bonded to N H 3 superscript plus on the lower right.

2-amino-3-carboxymuconate-6-semialdehyde is converted into acetoacetate in 11 irreversible steps.

The structure of acetoacetate is as follows: A central C atom is double bonded to O above, single bonded to C H 3 on the lower right, and single bonded to C H 2 on the lower left in the form of a line. The C H 2 group is single-bonded to C O O superscript minus on the upper left.

Return to FIGURE 23.27 Tryptophan degradation requires multiple oxygenases and numerous steps

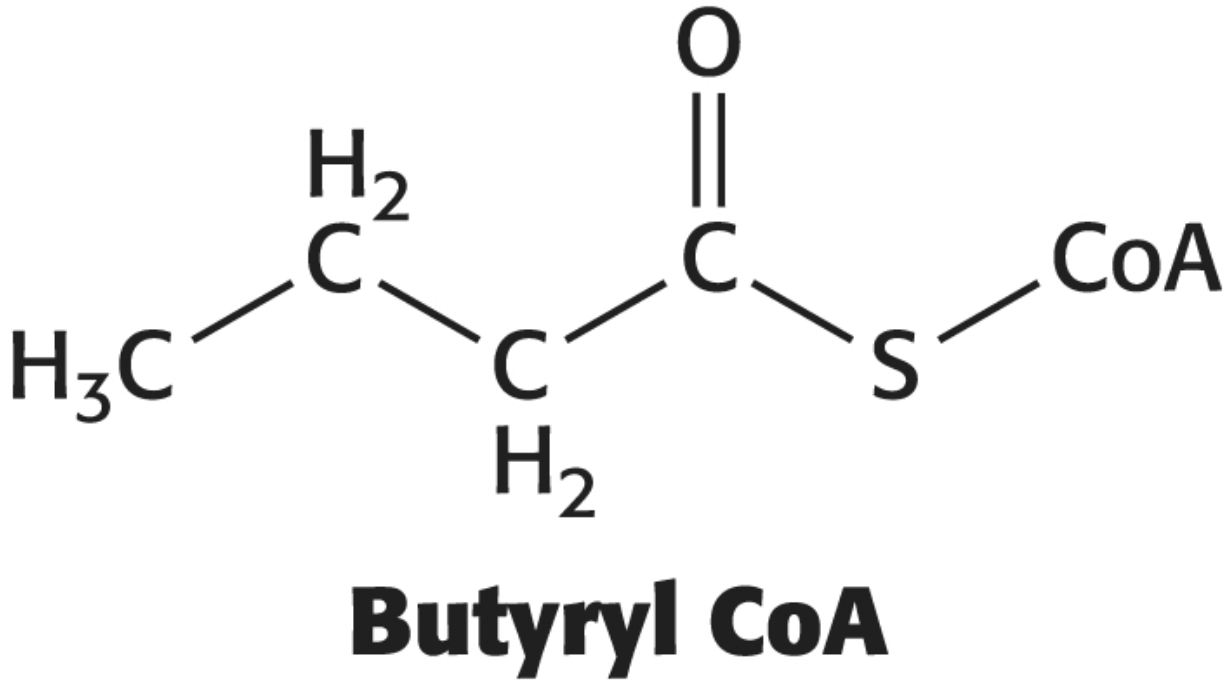
Extended description for Structure of 2-methylbutyryl C o A



The structure of 2-methylbutyryl C o A is as follows: A zigzag chain is composed of C H 3, single bond, C H 2, single bond, C H, single bond, C, single bond, S, single bond, C o A. C 3 is single bonded to C H 3 below. C 4 is double bonded to O above.

Return to Structure of 2-methylbutyryl C o A

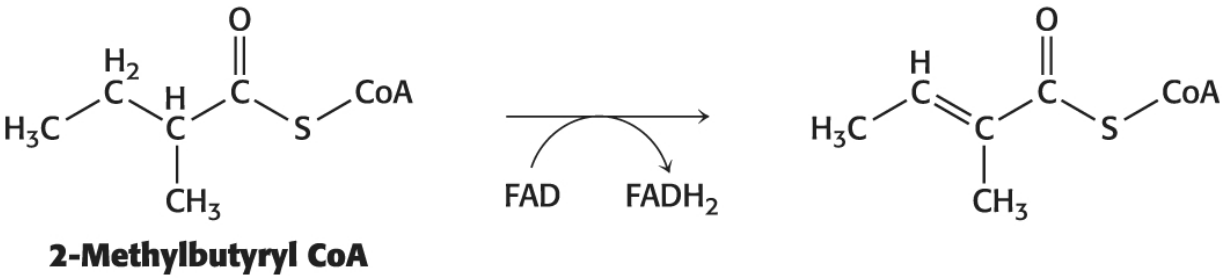
Extended description for Structure of butyryl C o A



The structure of butyryl C o A is as follows: A zigzag chain is composed of C H 3, single bond, C H 2, single bond, C H 2, single bond, C, single bond, S, single bond, C o A. C 4 is double bonded to O above.

Return to Structure of butyryl C o A

Extended description for Beta-oxidation of 2-methylbutyryl C o A



2-Methylbutyryl CoA

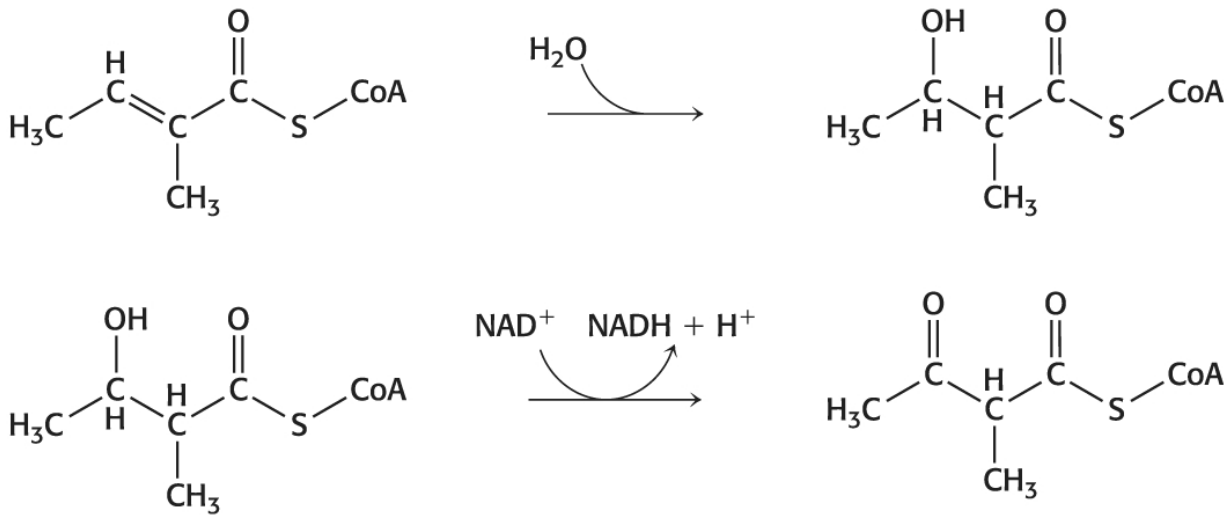
2-methylbutyryl C o A is irreversibly oxidized to another compound with the simultaneous reduction of F A D to F A D H 2.

The structure of 2-methylbutyryl C o A is as follows: A zigzag chain is composed of C H 3, single bond, C H 2, single bond, C H, single bond, C, single bond, S, single bond, C o A. C 3 is single bonded to C H 3 below. C 4 is double bonded to O above.

The structure of the compound produced after oxidation is as follows: A zigzag chain is composed of C H 3, single bond, C H, double bond, C, single bond, C, single bond, S, single bond, C o A. C 3 is single bonded to C H 3 below. C 4 is double bonded to O above.

Return to Beta-oxidation of 2-methylbutyryl C o A

Extended description for Hydration and oxidation steps of beta-oxidation



The first reaction depicts hydration as it involves the addition of H 2 O. It consists of one reactant and one product.

The structure of the reactant is as follows: A zigzag chain is composed of C H 3, single bond, C H, double bond, C, single bond, C, single bond, S, single bond, C o A. C 3 is single bonded to C H 3 below. C 4 is double bonded to O above.

The structure of the product is as follows: A zigzag chain is composed of C H 3, single bond, C H, single bond, C H, single bond, C, single bond, S, single bond, C o A. C 2 is single bonded to O H above. C 3 is single bonded to C H 3 below. C 4 is double bonded to O above.

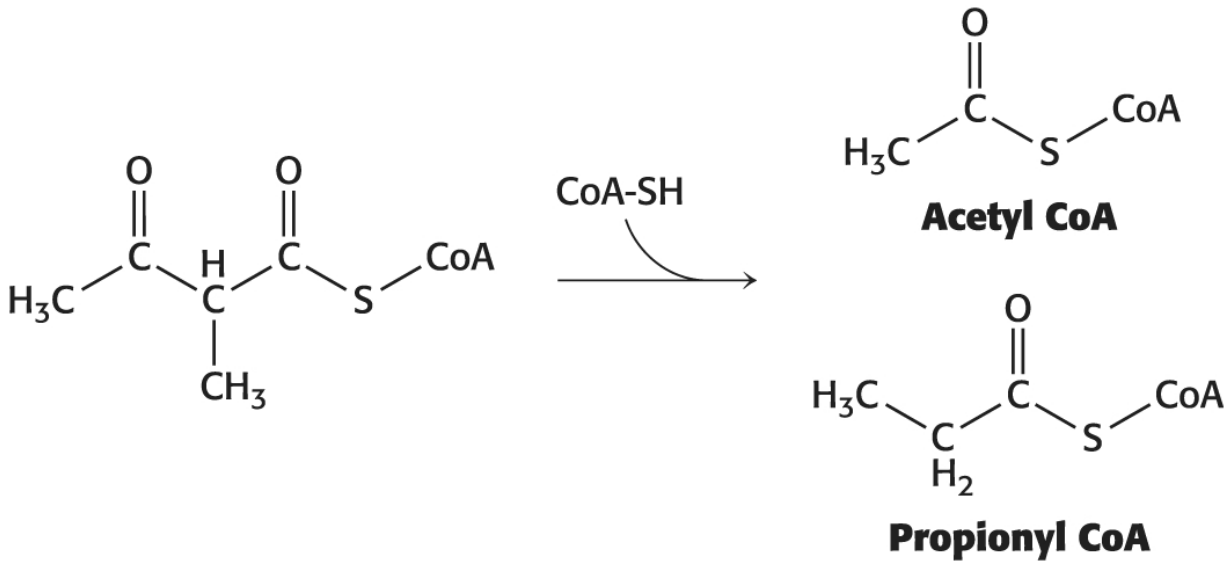
The second reaction depicts oxidation as it involves the concomitant reduction of N A D superscript plus to N A D H plus H superscript plus.

The structure of the reactant is as follows: A zigzag chain is composed of C H 3, single bond, C H, single bond, C H, single bond, C, single bond, S, single bond, C o A. C 2 is single bonded to O H above. C 3 is single bonded to C H 3 below. C 4 is double bonded to O above.

The structure of the product is as follows: A zigzag chain is composed of C H 3, single bond, C, single bond, C H, single bond, C, single bond, S, single bond, C o A. C 2 is double bonded to O above. C 3 is single bonded to C H 3 below. C 4 is double bonded to O above.

Return to Hydration and oxidation steps of beta-oxidation

Extended description for Thiolysis of the product of the oxidation step of beta-oxidation



The reaction consists of one reactant and two products. It requires the addition of C o A, single bond, S H.

The structure of the reactant is as follows: A zigzag chain is composed of C H 3, single bond, C, single bond, C H, single bond, C, single bond, S, single bond, C o A. C 2 is double bonded to O above. C 3 is single bonded to C H 3 below. C 4 is double bonded to O above.

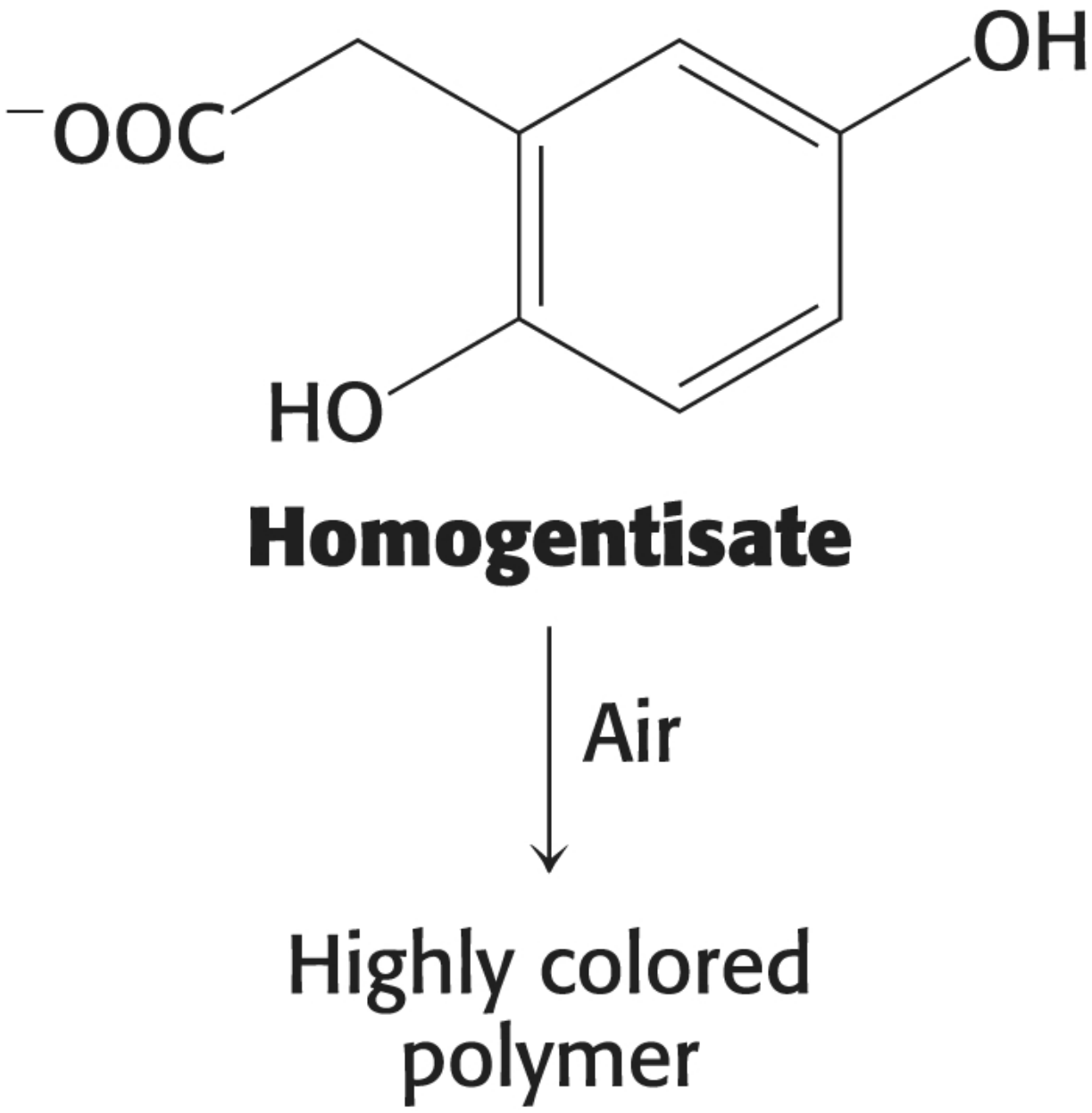
The first product is acetyl C o A whose structure is as follows: A central C atom is single bonded to C H 3 on the lower left, double bonded to O above, and single bonded to S on the lower right. The S atom is single-bonded to C o A on the upper right.

The second product is propionyl C o A whose structure is as follows: A zigzag chain is composed of C H 3, single bond, C H 2, single

bond, C, single bond, S, single bond, C o A. C 3 is double bonded to O above.

Return to Thiolysis of the product of the oxidation step of beta-oxidation

Extended description for Conversion of homogentisate to a highly colored polymer



The structure of homogentisate is as follows: A benzene ring is in a vertical orientation with C 1 occupying the topmost vertex. It contains alternating double bonds between C 1 and C 2, C 3 and C 4,

and C 5 and C 6. C 2 is single bonded to O H on the upper right. C 5 is single bonded to O H on the lower left. C 6 is single bonded to C H 2 on the upper left in the form of a line. This C H 2 group is single bonded to C O O superscript minus on the lower left.

A downward arrow labeled air points toward a highly colored polymer.

Return to Conversion of homogentisate to a highly colored polymer

Extended description for FIGURE 23.28 Urine has long been used to diagnose diseases due to the excretion of unusual biochemical products



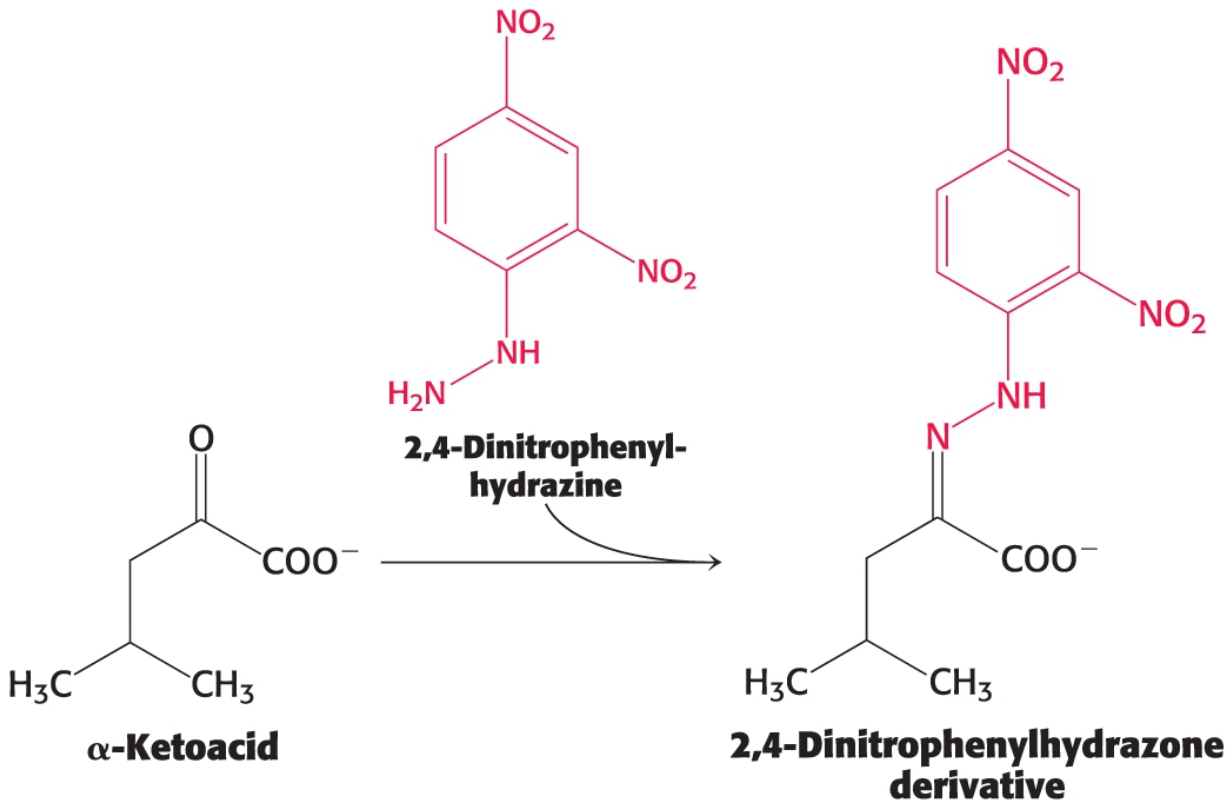
Ulrich Pinder. Epiphanie Medicorum. Speculum videndi urinas hominum. Clavis aperiendi portas pulsuum. Berillus discernendi causas & differentias febrium. Nuremberg: 1506. Rosenwald Collection. Rare Book and Special Collections Division, Library of Congress (128.2).

The center of the wheel shows a doctor sitting on a chair and inspecting a patient's urine. The patient is standing beside the doctor. The illustration of the doctor and the patient in the center is

surrounded by a radial arrangement of vials containing differently colored urine samples. A text in a foreign language is mentioned in a radial manner along the outer edge of the wheel corresponding to each vial.

Return to FIGURE 23.28 Urine has long been used to diagnose diseases due to the excretion of unusual biochemical products

Extended description for Conversion of alpha-ketoacid to 2,4-dinitrophenylhydrazone derivative



The reaction consists of one reactant and one product. It involves the addition of 2,4-Dinitrophenyl-hydrazine.

The reactant is alpha-ketoacid whose structure is as follows: A 3-carbon alkane chain is depicted as a vertical line structure using 2 zigzag lines. C 1 is single bonded to C H 3 on the lower left and C H 3 on the lower right. C 3 is double bonded to O above and single bonded to C O O superscript minus on the lower right.

The structure of 2,4-Dinitrophenyl-hydrazine is as follows: A benzene ring is in a vertical orientation with C 1 occupying the topmost vertex. It contains alternating double bonds between C 1

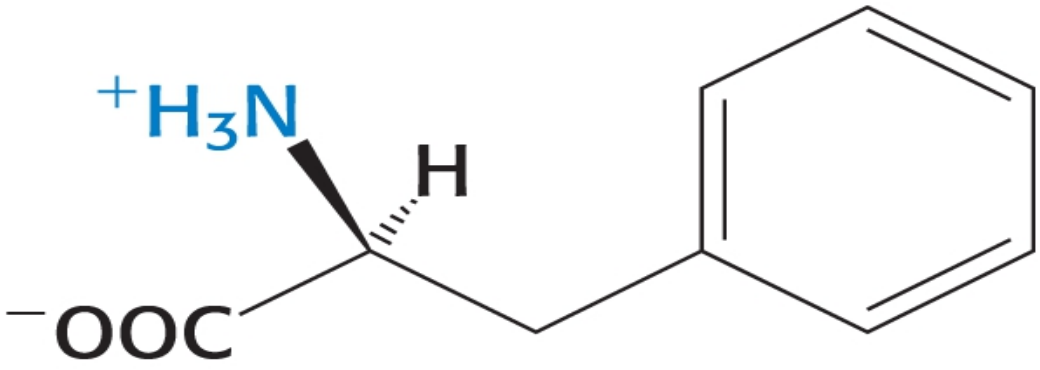
and C 2, C 3 and C 4, and C 5 and C 6. C 1 is single bonded to N O 2 above. C 3 is single bonded to N O 2 on the lower right. C 4 is single bonded to N H, single bond, N H 2 below.

The product is 2,4-dinitrophenylhydrazone derivative whose structure is as follows: A benzene ring is in a vertical orientation with C 1 occupying the topmost vertex. It contains alternating double bonds between C 1 and C 2, C 3 and C 4, and C 5 and C 6. C 1 is single bonded to N O 2 above. C 3 is single bonded to N O 2 on the lower right. C 4 is single bonded to N H, single bond, N below. The N atom is double bonded to C 3 of the alpha-ketoacid instead of the O atom.

Return to Conversion of alpha-ketoacid to 2,4-dinitrophenylhydrazone derivative

Extended description for Conversion of phenylalanine

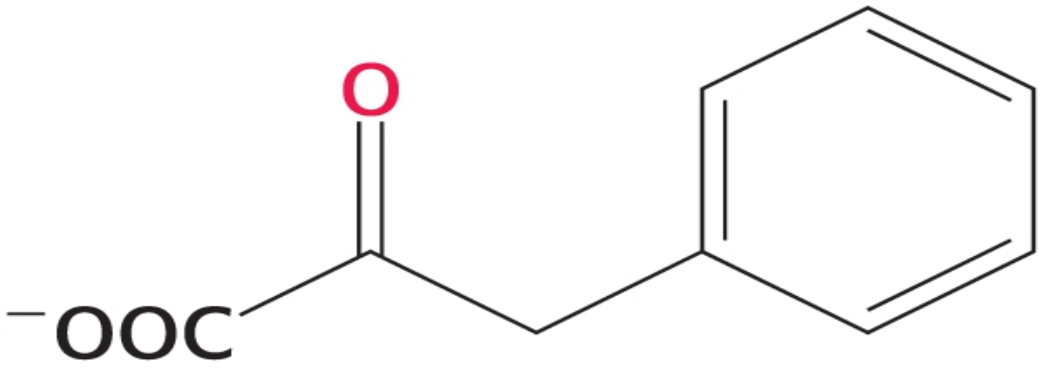
to phenylpyruvate



Phenylalanine

α-Ketoacid

α-Amino acid



Phenylpyruvate

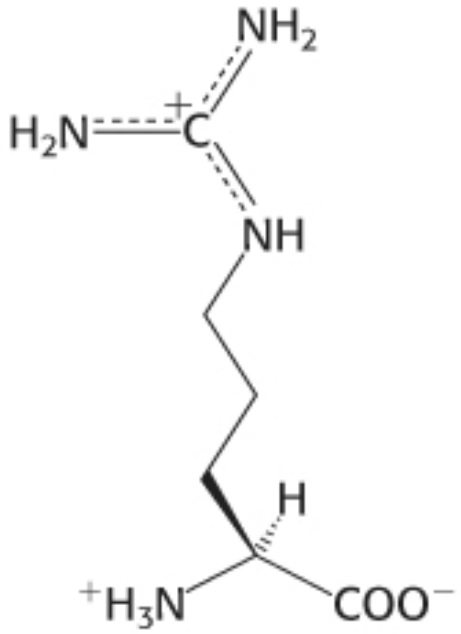
The reaction consists of one reactant and one product. It is accompanied by the simultaneous conversion of alpha-ketoacid to alpha-amino acid.

The reactant is phenylalanine whose structure is as follows: A benzene ring is in a vertical orientation with C 1 occupying the topmost vertex. It contains alternating double bonds between C 1 and C 2, C 3 and C 4, and C 5 and C 6. C 5 is single bonded to C H 2 on the lower left in the form of a line. This C H 2 group is single-bonded to C on the upper left. The C atom is wedge bonded to N H 3 superscript plus on the upper left, single bonded to C O O superscript minus on the lower left, and dash bonded to H on the upper right.

The product is phenylpyruvate whose structure is as follows: A benzene ring is in a vertical orientation with C 1 occupying the topmost vertex. It contains alternating double bonds between C 1 and C 2, C 3 and C 4, and C 5 and C 6. C 5 is single bonded to C H 2 on the lower left in the form of a line. This C H 2 group is single-bonded to C on the upper left. The C atom is double bonded to O above and single bonded to C O O superscript minus on the lower left.

Return to Conversion of phenylalanine to phenylpyruvate

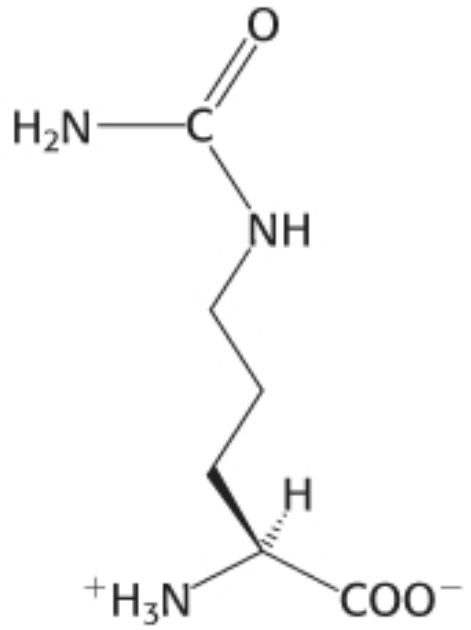
Extended description for Chemical structure



The chemical structure is depicted as follows: A central C atom is single bonded to N H 3 superscript plus on the lower left, single bonded to C O O superscript minus on the lower right, wedge bonded to C H 2 on the upper left, and dash bonded to H on the upper right. The C H 2 group is single-bonded to a 1 N and 2 C alkane chain depicted as a vertical line structure using 2 zigzag lines. N bound to H occupies the third position. N is partially double-bonded to C on the upper right. This C atom has a positive charge and is partially double-bonded to N H 2 on the left and partially double-bonded to N H 2 on the upper right.

Return to Chemical structure

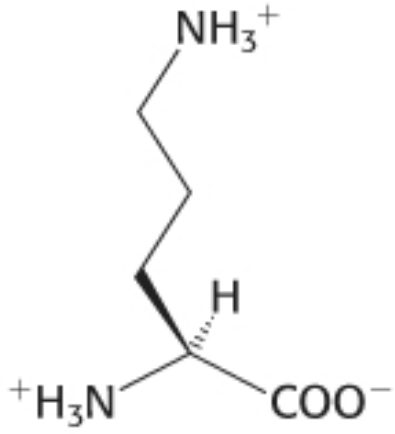
Extended description for Chemical structure



The chemical structure is depicted as follows: A central C atom is single bonded to N H 3 superscript plus on the lower left, single bonded to C O O superscript minus on the lower right, wedge bonded to C H 2 on the upper left, and dash bonded to H on the upper right. The C H 2 group is single-bonded to a 1 N and 2 C alkane chain depicted as a vertical line structure using 2 zigzag lines. N bound to H occupies the third position. N is single-bonded to C on the upper right. This C is single bonded to N H 2 on the left and double bonded to O on the upper right.

Return to Chemical structure

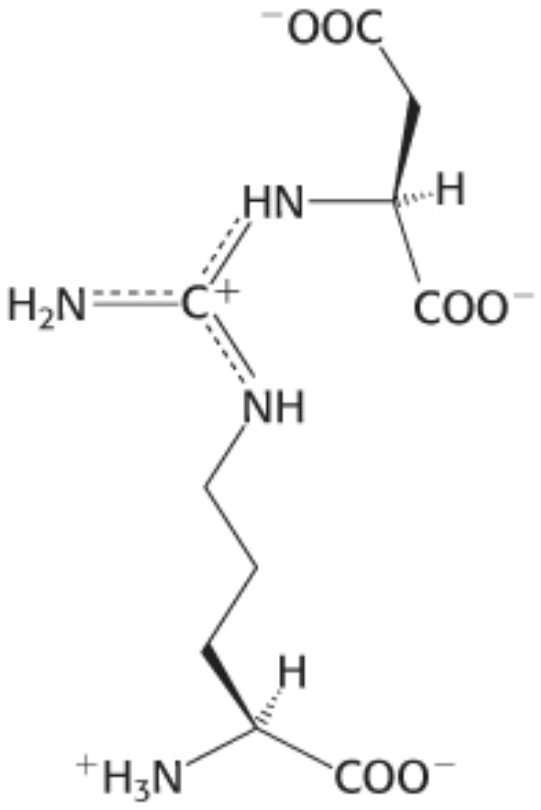
Extended description for Chemical structure



The chemical structure is depicted as follows: A central C atom is single bonded to N H 3 superscript plus on the lower left, single bonded to C O O superscript minus on the lower right, wedge bonded to C H 2 on the upper left, and dash bonded to H on the upper right. The C H 2 group is single-bonded to a 2-carbon alkane chain depicted using a single line. C 2 of this alkane chain is single bonded to N H 3 superscript plus on the upper right.

Return to Chemical structure

Extended description for Chemical structure

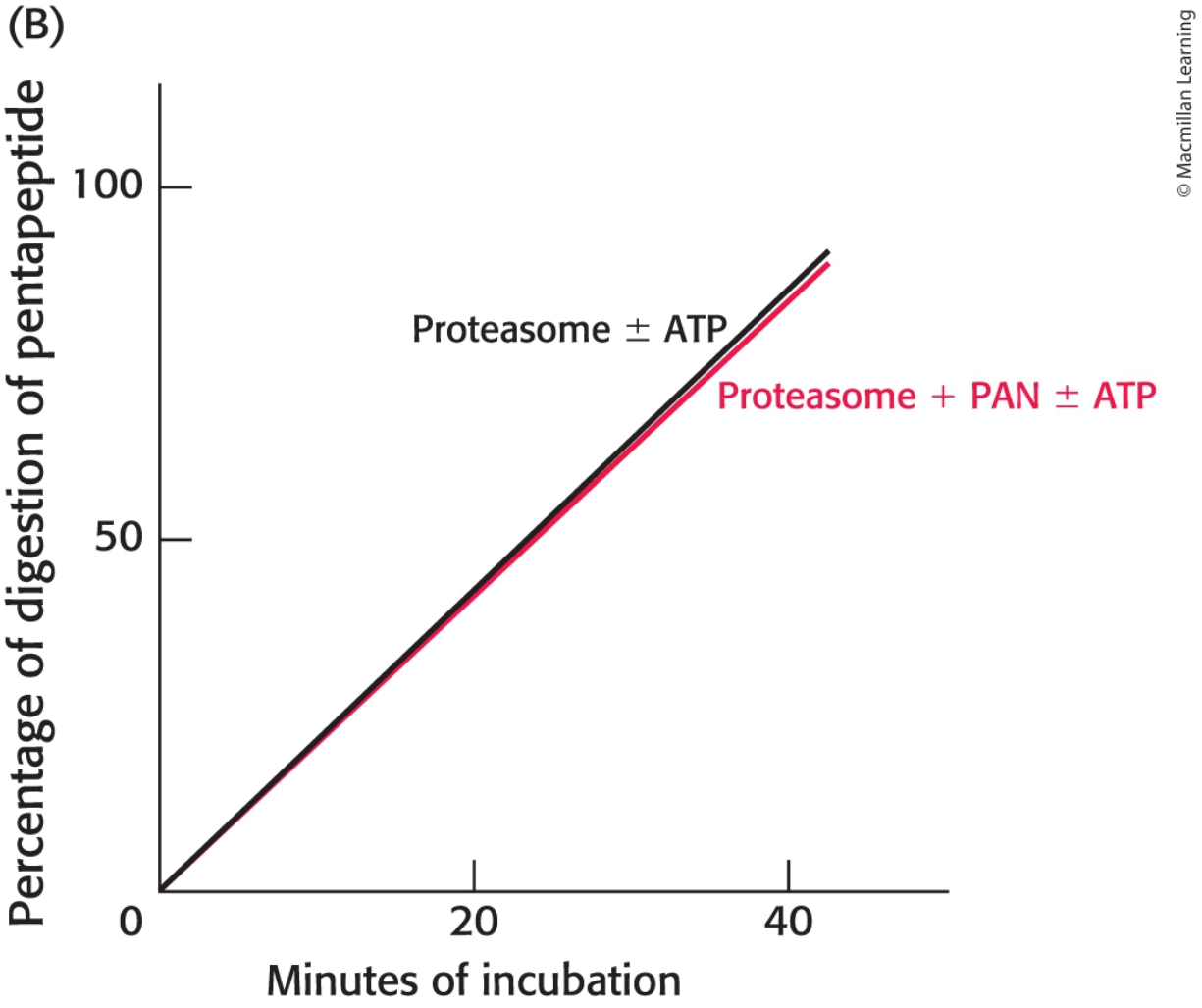


The chemical structure is depicted as follows: A central C atom is single bonded to N H 3 superscript plus on the lower left, single bonded to C O O superscript minus on the lower right, wedge bonded to C H 2 on the upper left, and dash bonded to H on the upper right. The C H 2 group is single-bonded to a 1 N and 2 C alkane chain depicted as a vertical line structure using 2 zigzag lines. N bound to H occupies the third position. N is partially double-bonded to C on the upper right. This C atom has a positive charge and is partially double-bonded to N H 2 on the left and partially double-bonded to N H on the upper right. The N H group on the upper right is single-bonded to C on the right. This C is wedge bonded to C H 2 on the upper right, dash bonded to H on the right, and single bonded to C O O superscript minus on the lower right.

The C H 2 group is single-bonded to C O O superscript minus on the upper left.

Return to Chemical structure

Extended description for Variation of percentage of digestion of pentapeptide with minutes of incubation



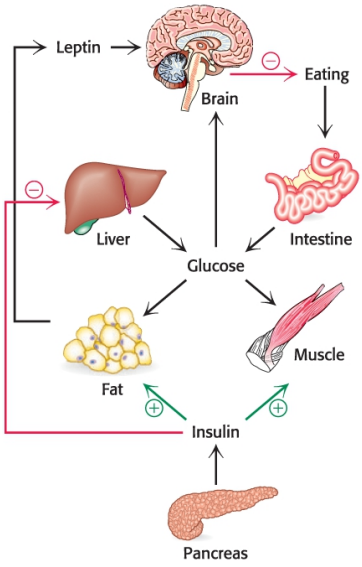
© Macmillan Learning

The horizontal axis is labeled minutes of incubation. It has markings ranging from 0 to 40 in increments of 20 units. The vertical axis is labeled the percentage of digestion of pentapeptide. It has markings ranging from 0 to 100 in increments of 50 units. The graph contains two curves shown in black and red. The black curve depicts proteasome plus minus A T P. The red curve depicts proteasome plus P A N plus minus A T P. The black curve starts at (0,

0) and moves linearly toward the upper right to reach (42, 90). The red curve starts at (0, 0) and moves linearly toward the upper right along the black curve to reach (41.5, 89). All values are estimated.

Return to Variation of percentage of digestion of pentapeptide with minutes of incubation

Extended description for Photograph of an event and schematic representation of integration of metabolic pathways for glucose homeostasis





Debbie Eckert/Alamy
© Macmillan Learning

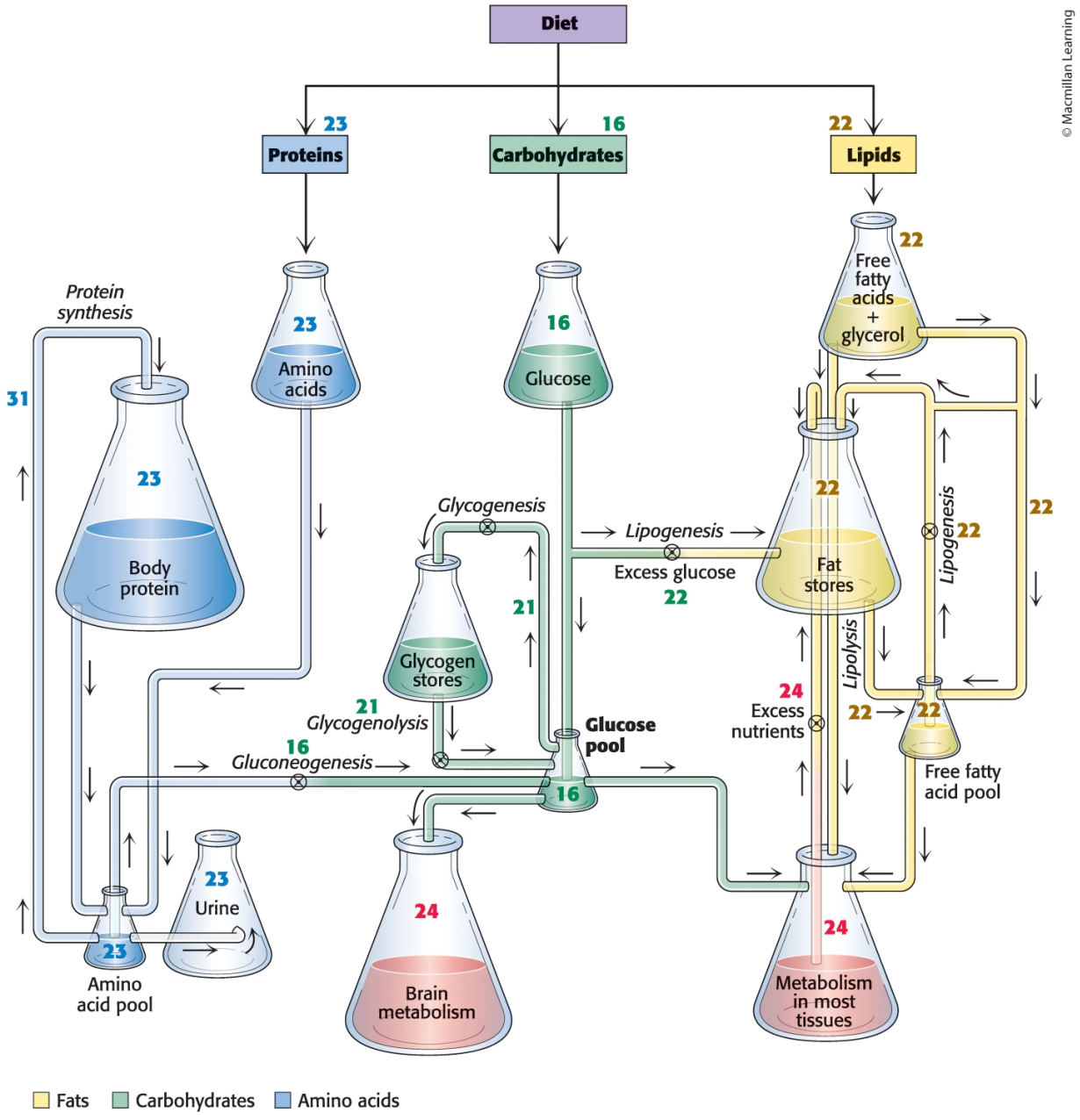
The entrance in the photograph has an arch-shaped structure. The text written on the structure is "J D R F, One Walk, For a world without type 1 diabetes."

In the schematic representation, glucose is shown in the center. An upward arrow from glucose points toward the brain at the top. A red rightward arrow with a minus symbol points from the brain to eating. A downward arrow from eating leads to the intestine. An arrow from the intestine points back to glucose. An arrow on the lower right of glucose points toward muscle and an arrow on the lower left of glucose points toward fat depicted as a cluster of cells. An arrow from fat points toward leptin at the top. Another arrow from leptin points toward the brain. Insulin is shown at the bottom. An upper left green arrow with a plus symbol leads from insulin to fat and an upper right green arrow with a plus symbol leads from

insulin to muscle. A red arrow with a minus symbol points toward the liver. A lower right arrow from liver points toward glucose. An upward arrow from the pancreas points toward insulin.

Return to Photograph of an event and schematic representation of integration of metabolic pathways for glucose homeostasis

Extended description for Coordinated use of nutrient pools to maintain homeostasis



The illustration shows different nutrient pools as conical flasks containing a solution. The flasks are interconnected by tubular

pipes. The flasks and pipes are differently numbered and each number indicates the chapters in which the topics are discussed.

A purple rectangle labeled diet is shown at the top. A line below it bifurcates into three downward arrows numbered 23, 16, and 22 from left to right. The arrow number 23 points toward a blue rectangle labeled protein. The arrow number 16 points toward a green rectangle labeled carbohydrates. The arrow number 22 points toward a yellow rectangle labeled lipids.

A downward arrow from proteins points toward flask number 23 containing amino acids. A tubular pipe containing blue solution travels toward a small flask, numbered 23, containing an amino acid pool. Three tubular pipes containing blue solution originate sideways from the small flask. A tubular pipe containing blue solution originates from the mouth of the small flask. The pipe from the right wall travels to a medium-sized flask number 23 containing urine. One of the pipes originating from the left wall is numbered 31 and labeled protein synthesis. It enters into the mouth of a large flask, numbered 23, containing body protein. A pipe from the body protein flask enters the amino acid pool flask. The pipe from the mouth of the amino acid pool flask is labeled gluconeogenesis and it travels to a small flask, numbered 16, containing a glucose pool. This pipe contains a half-blue and half-green solution. At the junction of the blue and green solution, a cross symbol is shown below the label gluconeogenesis.

A downward arrow from carbohydrates points toward a medium-sized flask, numbered 16, containing glucose. A tubular pipe from the base of this flask travels downward to the glucose pool flask. Halfway through a pipe labeled lipogenesis, excess glucose and numbered 22 branches off and travels to a large flask, numbered 22, containing fat stores. This branch of the pipe contains a half-green and half-yellow solution. At the junction of the green and yellow

solution, a cross symbol is shown below the label lipogenesis. A pipe numbered 21 and labeled glycogenesis travels from the glucose pool to a medium-sized flask containing glycogen stores. The end of the pipe closer to the mouth of the glycogen stores flask has a cross symbol below the label glycogenesis. Another pipe originates from the base of the glycogen stores flask and is labeled 21 glycogenesis. It travels back to the glucose pool flask. The end of this pipe closer to the glycogen stores flask has a cross symbol. A pipe from the glucose pool flask travels to a large flask, numbered 24 and labeled brain metabolism. Another pipe from the glucose pool flask travels to another large flask, numbered 24, and labeled metabolism in most tissues.

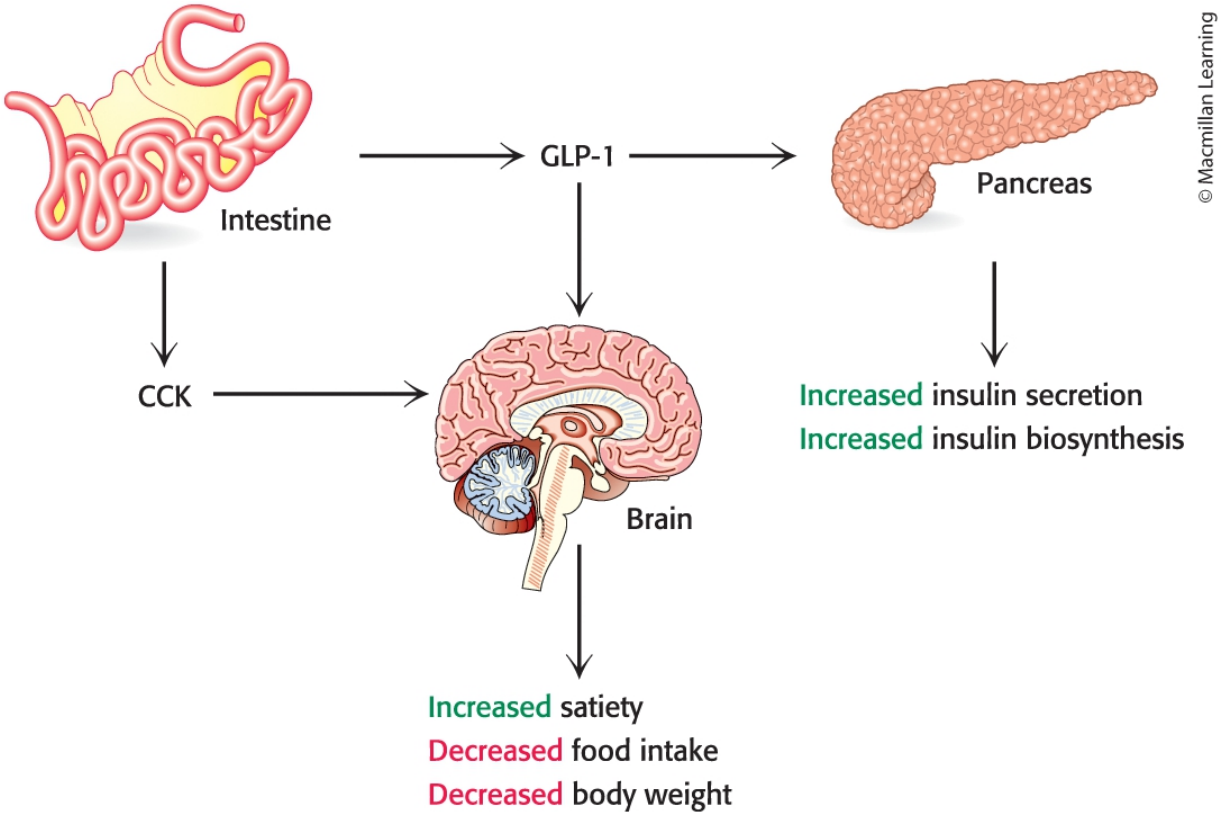
A downward arrow from lipids points toward a medium-sized flask, numbered 22, containing free fatty acids plus glycerol. A vertical pipe from the base of this flask travels through fat stores and enters into the mouth of the large flask numbered 24. Another pipe numbered 22 travels from flask number 22 to a small flask numbered 22 and labeled free fatty acid pool. A pipe originating from the mouth of the free fatty acid pool flask is numbered 22 and labeled lipogenesis. It travels to the mouth of fat stores. The pipe has a cross-symbol halfway through and it is connected above to pipe number 22 coming from the free fatty acids plus glycerol flask. Another pipe from the base of the free fatty acid pool flask travels to flask number 24 labeled metabolism in most tissues. A pipe from fat stores is numbered 22 and labeled lipolysis. It travels back to the free fatty acid pool flask.

A long pipe from flask number 24 labeled metabolism in most tissues travels to the fat stores flask and enters its mouth. This pipe is numbered 24 and labeled excess nutrients. It has a cross symbol on its end closer to the flask number 24.

Fats are depicted in yellow color, carbohydrates are depicted in green color, and amino acids are depicted in blue color.

Return to Coordinated use of nutrient pools to maintain homeostasis

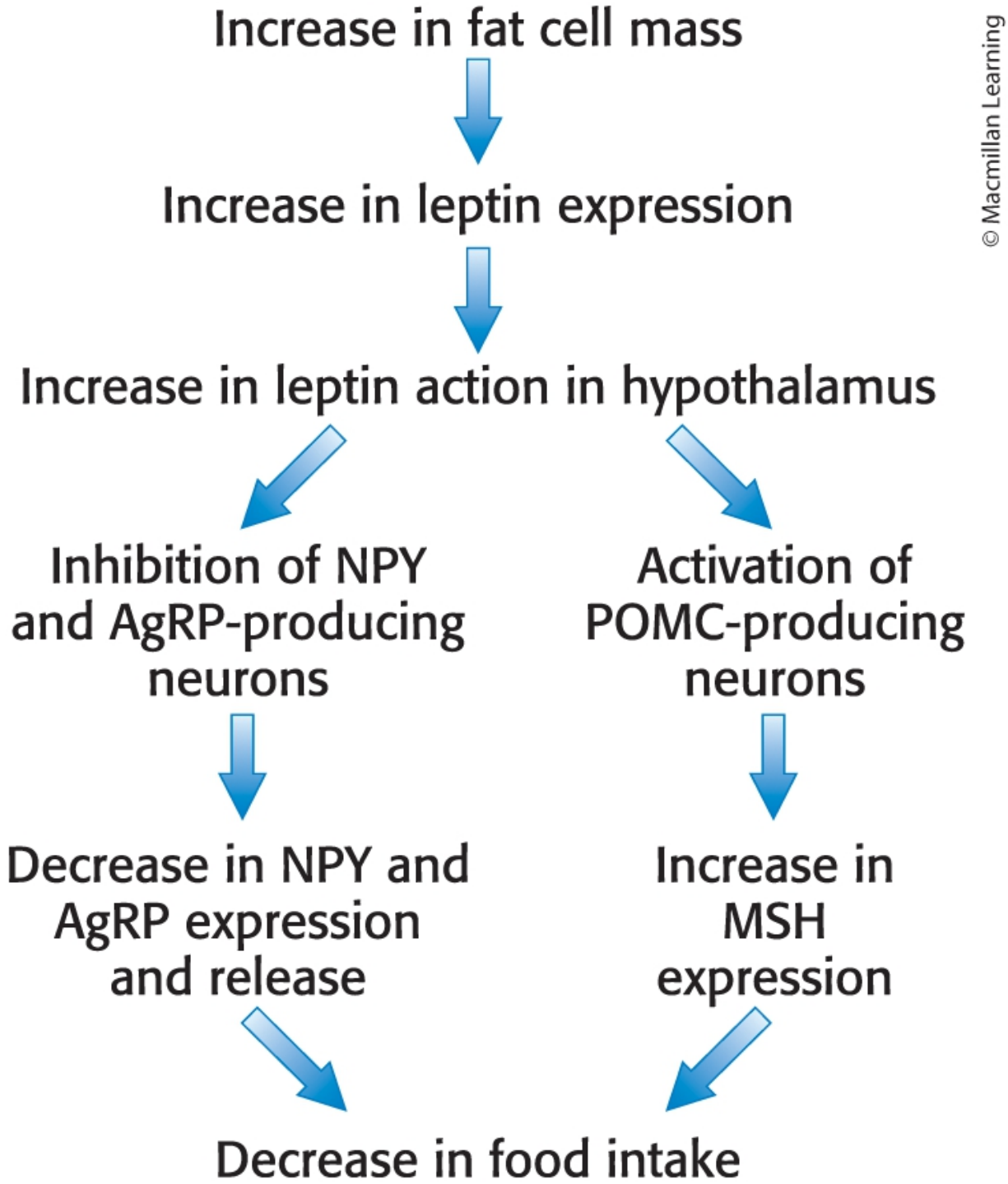
Extended description for FIGURE 24.2 Signal molecules originating from the gut induce feelings of satiety in the brain



The intestine is depicted as a looped tubular structure containing a thin membrane sheet-like structure. It produces C C K and G L P-1 that act on the brain. The sagittal section of the brain is shown. A downward arrow from the brain points to the text given as follows: Increased satiety, Decreased food intake, and Decreased body weight. An arrow from G L P-1 points toward the pancreas depicted as a tapered structure. A downward arrow from the pancreas points to the text given as follows: Increased insulin section, Increased insulin biosynthesis.

Return to FIGURE 24.2 Signal molecules originating from the gut induce feelings of satiety in the brain

Extended description for FIGURE 24.3 Leptin suppresses appetite by affecting the brain



© Macmillan Learning

The flowchart is depicted as follows:

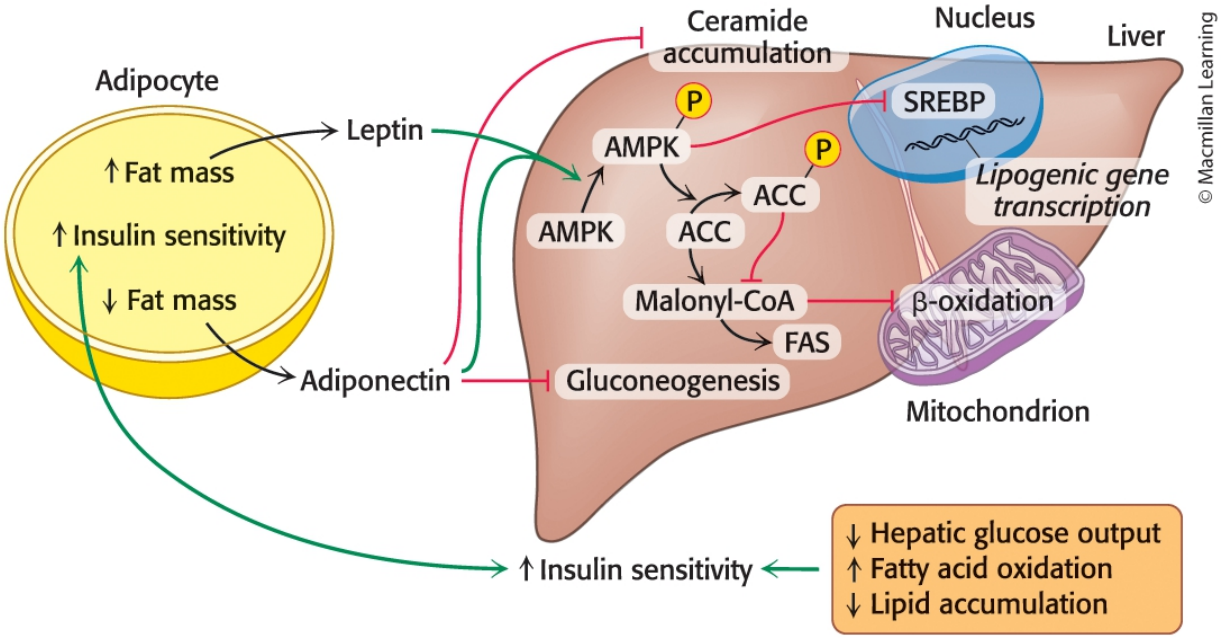
Increase in fat cell mass, downward arrow, Increased in leptin expression, downward arrow, Increase in leptin action in the hypothalamus. Two distinct paths are shown by two separate downward arrows below "Increase in leptin expression."

The left downward arrow points to the "Inhibition of N P Y and A g R P-producing neurons." A downward arrow below it points to "Decrease in N P Y and A g R P expression and release." A downward arrow below it points to "Decrease in food intake."

The right downward arrow points to the "Activation of P O M C-producing neurons." A downward arrow below it points to "Increase in M S H expression." A downward arrow below it points to "Decrease in food intake."

Return to FIGURE 24.3 Leptin suppresses appetite by affecting the brain

Extended description for FIGURE 24.4 Adipokines help to maintain systemic lipid and glucose homeostasis



The adipocyte is depicted as a half-cut sphere and the liver is depicted as a triangular organ. Increased fat mass in the adipocyte causes the release of leptin, whereas decreased fat mass cause the release of adiponectin. Leptin and adiponectin together cause the conversion of A M P K to phosphorylated A M P K in the liver. The adiponectin, independently, inhibits ceramide accumulation and gluconeogenesis in the liver. The phosphorylated A M P K in the liver inhibits S R E B P in the nucleus. S R E B P is essential for lipogenic gene transcription. The phosphorylated A M P K causes the conversion of A C C to phosphorylated A C C in the liver. A C C has an activating effect on malonyl-C o A in the liver and phosphorylated A C C has an inhibitory effect on malonyl-C o A. The malonyl-C o A inhibits beta-oxidation and activates F A S in the liver.

An orange rectangle lists the following points:

Decreased hepatic glucose output.

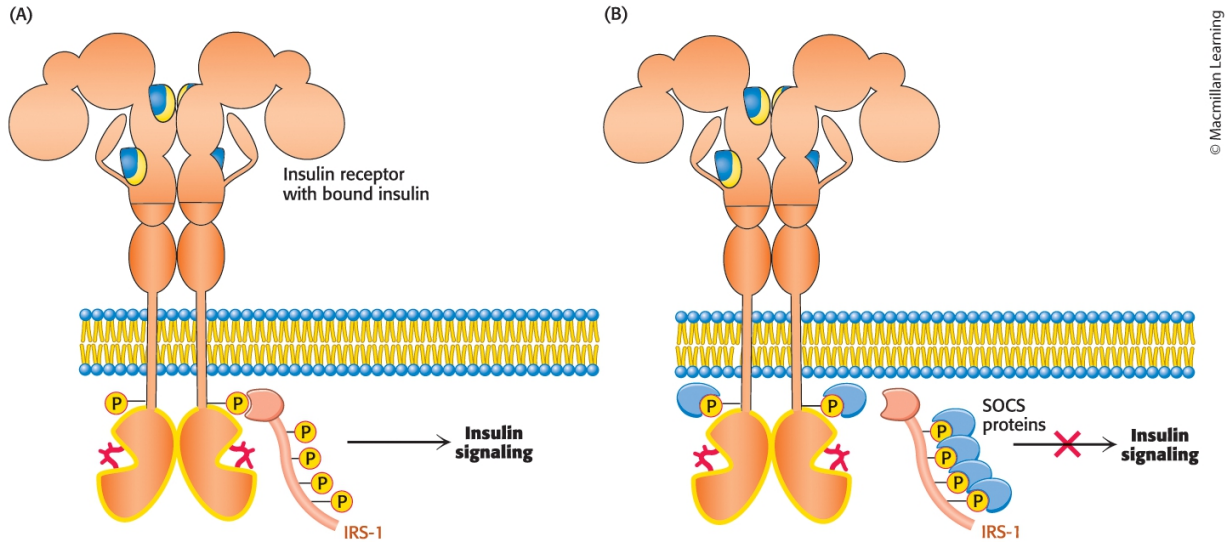
Increased fatty acid oxidation.

Decreased lipid accumulation.

An arrow from this rectangle points toward increased insulin sensitivity. A double-headed points from increased insulin sensitivity to increased insulin sensitivity inside the adipocyte.

Return to FIGURE 24.4 Adipokines help to maintain systemic lipid and glucose homeostasis

Extended description for FIGURE 24.5 Suppressors of cytokine signaling (S O C S) regulate insulin receptor function



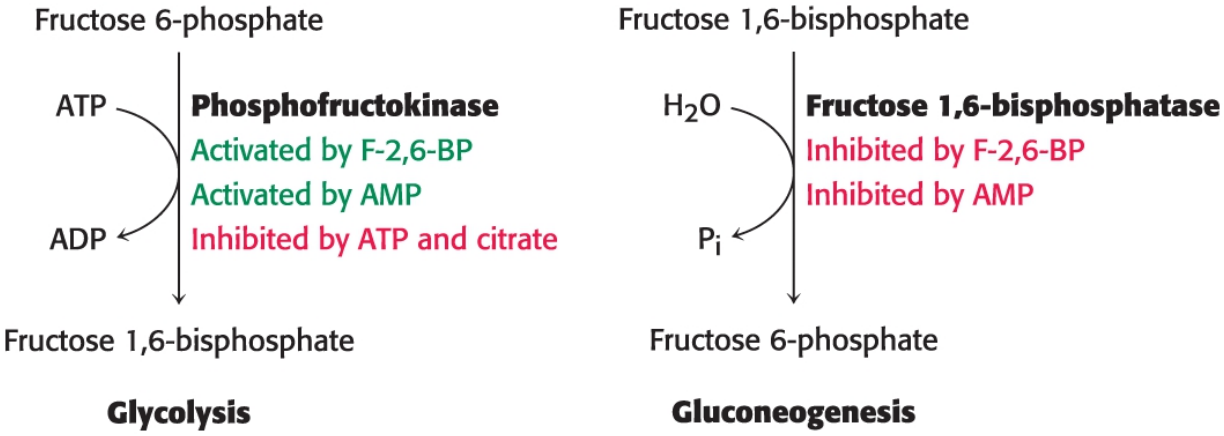
© Macmillan Learning

Part (A): An insulin receptor is embedded in the membrane. It consists of a pair of the transmembrane domain having one and a half oval above the membrane and a long tubular region passing through the membrane. Each tubular region is connected to an oval-shaped structure in the cytoplasm. The oval-shaped structure has a triangular groove. The half-oval of the transmembrane domain is connected to a region composed of one and a half oval and two spheres. The spheres are located at the terminal and oriented downward. The half-oval at the bottom is connected to a small elongated structure through a short tubular region. Insulin is bound to oval structures of the insulin receptor. The long tubular region extending into the cytoplasm is phosphorylated. The triangular groove has a thread-like structure connecting its walls. One of the phosphorylated groups is connected to a small sphere with a long tail labeled I R S-1. The tail contains 4 phosphoryl groups. A forward arrow adjacent to I R S-1 points toward insulin signaling.

Part (B): The insulin receptor is bound to insulin molecules. A blue sphere is bound to the phosphoryl group of the long tubular region in the cytoplasm. This hinders the binding of the small sphere of I R S-1. Four blue spheres are also bound to the phosphoryl groups in the tail of I R S-1. These blue spheres are labeled S C O C S proteins. The forward arrow pointing toward insulin signaling has a cross symbol over it.

Return to FIGURE 24.5 Suppressors of cytokine signaling (S O C S) regulate insulin receptor function

Extended description for FIGURE 24.6 Glycolysis and gluconeogenesis are reciprocally regulated

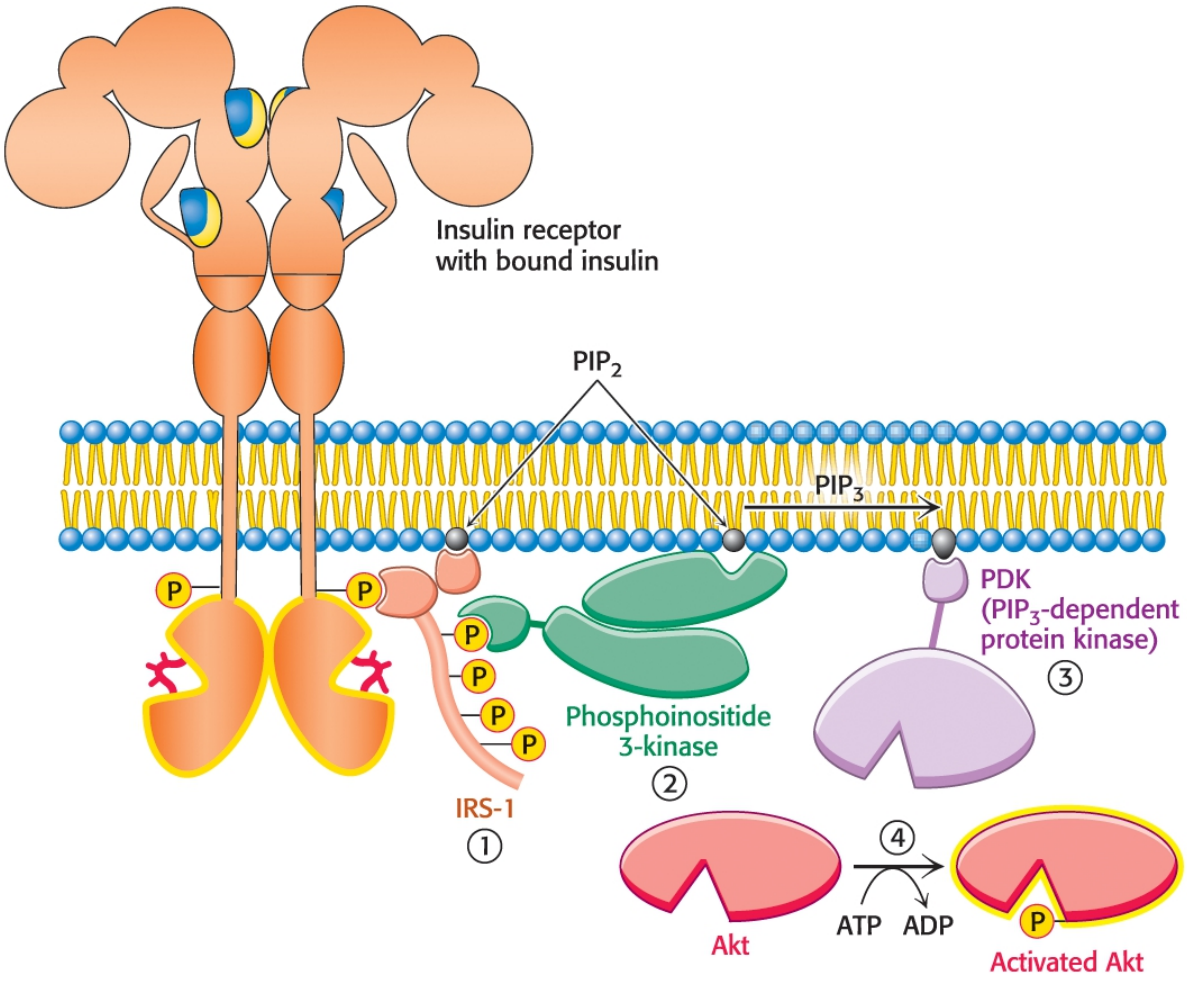


In glycolysis, fructose 6-phosphate is irreversibly converted into fructose 1, 6-bisphosphate with the concomitant hydrolysis of A T P to A D P. This step is catalyzed by phosphofructokinase. It is activated by F-2,6 B P and A M P and inhibited by A T P and citrate.

In gluconeogenesis, fructose 1, 6-bisphosphate is irreversibly converted into fructose 6-phosphate with the concomitant entry of H 2 O and release of P subscript i. This step is catalyzed by fructose 1, 6-bisphosphatase. It is inhibited by F-2, 6-B P and A M P.

Return to FIGURE 24.6 Glycolysis and gluconeogenesis are reciprocally regulated

Extended description for FIGURE 24.7 Insulin signaling activates A k t using the second messenger P I P 3



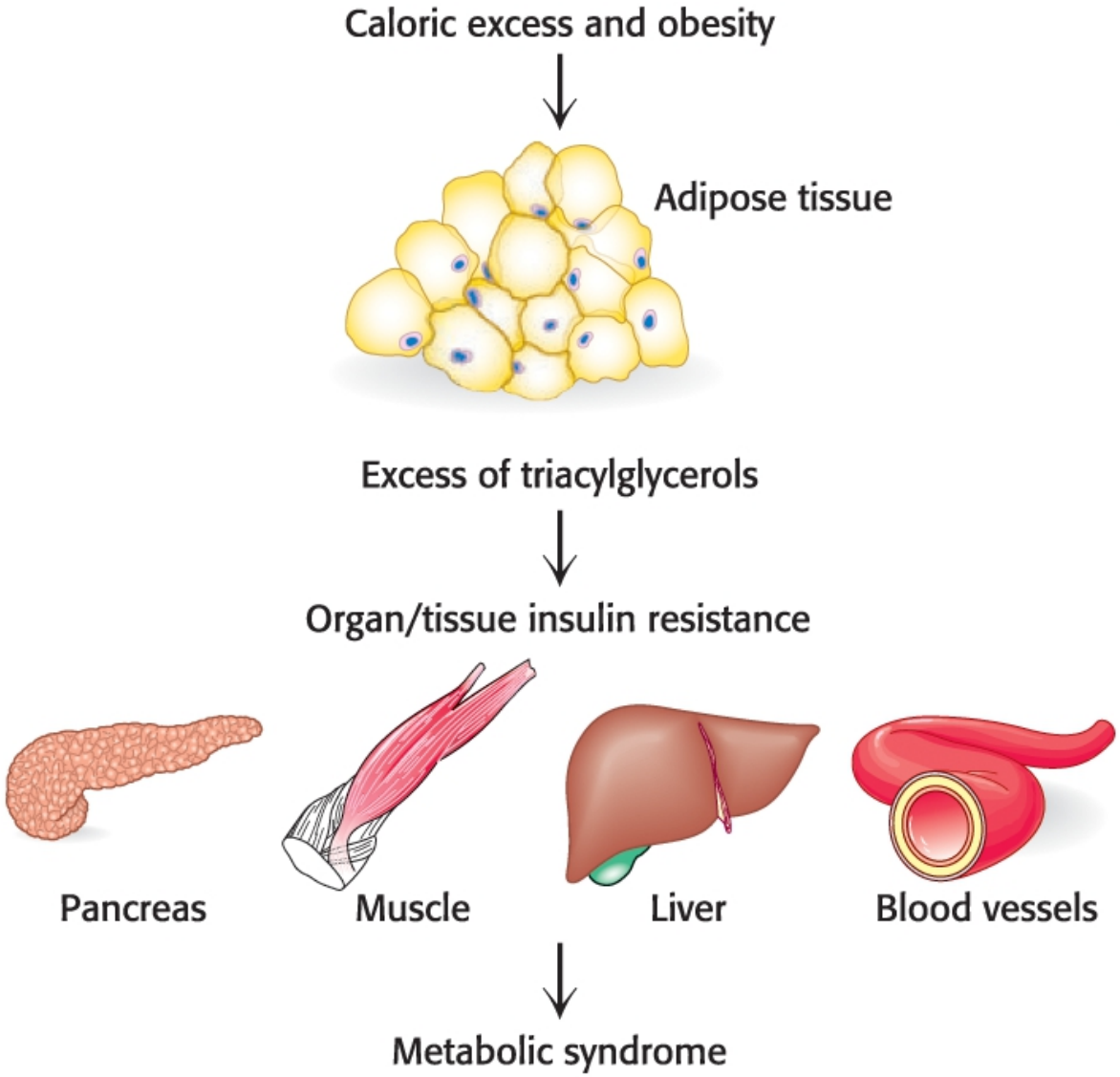
© Macmillan Learning

An insulin receptor bound to an insulin molecule is embedded in the membrane. The long tubular region of the receptor extending into the cytoplasm is phosphorylated. I R S-1 with a phosphorylated tail is bound to phosphoryl group on one of the tubular regions. The I R S-1 protein is labeled 1. The small spherical region of I R S-1 is associated with a small structure, which is further associated with P I P 2 in the inner leaflet of the membrane. One of the phosphoryl groups of the I R S-1 tail is bound by phosphoinositide 3-kinase

labeled 2. The phosphoinositide 3-kinase consists of three subunits. One small subunit is bound to the phosphoryl group on the tail of I R S-1. It is connected to a long subunit through a short and narrow bridge. The long subunit is associated with a long and horizontal oval subunit with a tiny triangular groove. The triangular groove is associated with P I P 2 in the inner leaflet of the membrane. The phosphoinositide 3-kinase converts P I P 2 into P I P 3. This P I P 3 in the inner leaflet is bound by P D K (P I P 3-dependent protein kinase) labeled 3. P D K is composed of a small subunit associated with P I P 3 and a large oval subunit connected to it through a short and narrow bridge. This oval-subunit of P D K causes the conversion of A k t to activated A k t by phosphorylation. A k t is depicted as a long oval having a triangular groove. A forward arrow labeled 4 leads to activated A k t in which the groove is bonded to a phosphoryl group. This conversion is coupled with the breakdown of A T P to A D P.

Return to FIGURE 24.7 Insulin signaling activates A k t using the second messenger P I P 3

Extended description for FIGURE 24.8 The storage capacity of fat tissue can be exceeded in obesity



© Macmillan Learning

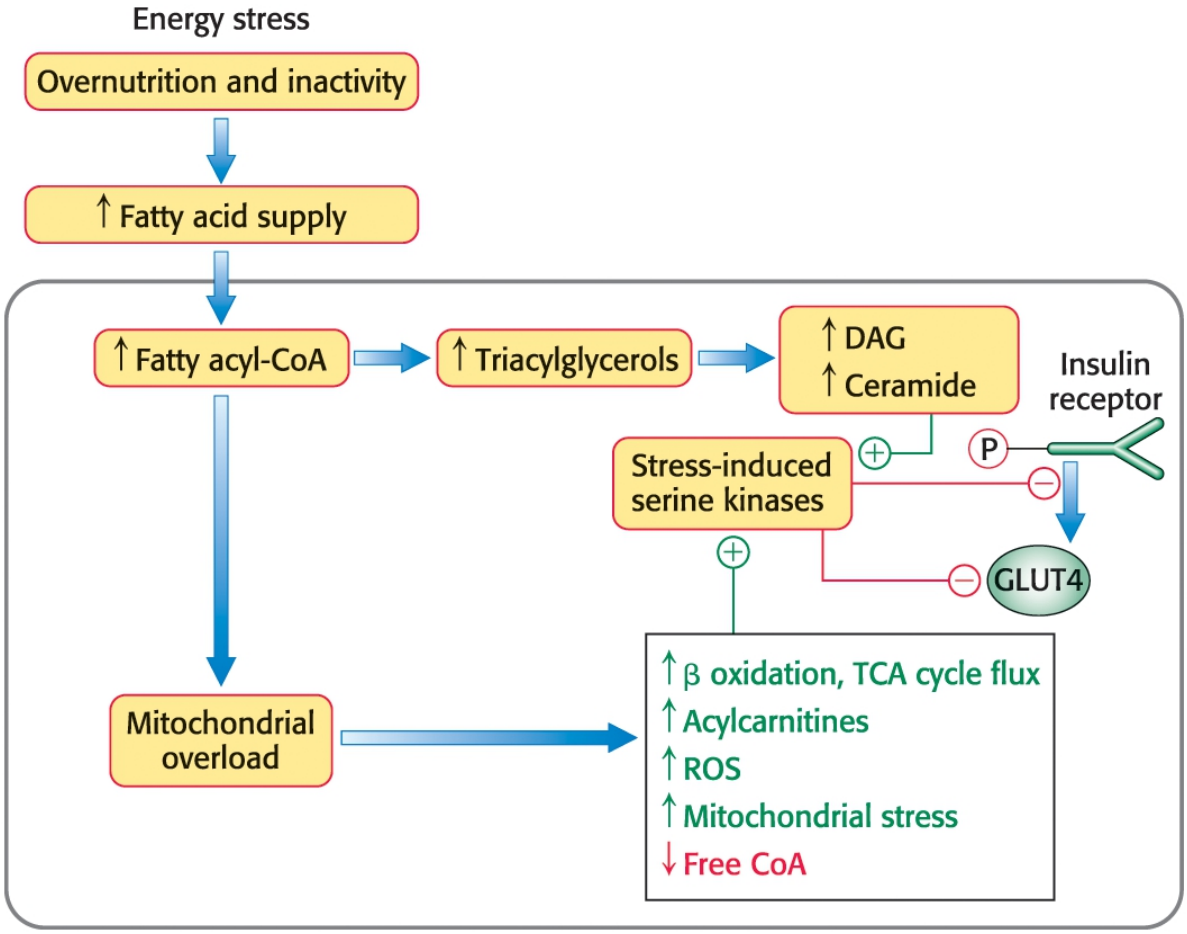
The flowchart is depicted as follows:

A downward arrow from caloric excess and obesity leads to adipose tissue depicted as a cluster of cells with irregular borders. The adipose tissue has an excess of triacylglycerols. A downward arrow

from adipose tissue leads to organ slash tissue insulin resistance. Under organ slash tissue insulin resistance, four different organs like pancreas, muscle, liver, and blood vessels are shown. A downward arrow from these organs leads to metabolic syndrome.

Return to FIGURE 24.8 The storage capacity of fat tissue can be exceeded in obesity

Extended description for FIGURE 24.9 Excess fat can disrupt signal-transduction pathways and lead to insulin insensitivity



© Macmillan Learning

A yellow rectangle with the text "Overnutrition and inactivity" is labeled energy stress on the top. Overnutrition and inactivity lead to increased fatty acid supply. A downward arrow from increased fatty acid supply points to increased fatty acyl-C o A inside a large rectangle. The remaining pathway is shown inside the large rectangle. Increased fatty acyl-C o A leads to increased triacylglycerols and mitochondrial overload. Increased triacylglycerol leads to increased D A G and ceramide. The increased

D A G and ceramide have a stimulatory effect on stress-induced serine kinases. The stimulatory effect is depicted by a plus symbol. The stress-induced serine kinases have an inhibitory effect on the action of phosphorylated insulin receptors, depicted as a Y-shaped structure bonded to P inside a circle, on G L U T 4 and G L U T 4 itself. The inhibitory effect is depicted by a minus symbol.

Mitochondrial overload leads to different effects listed below:

Increased beta-oxidation, T C A cycle flux.

Increased acylcarnitines.

Increased R O S.

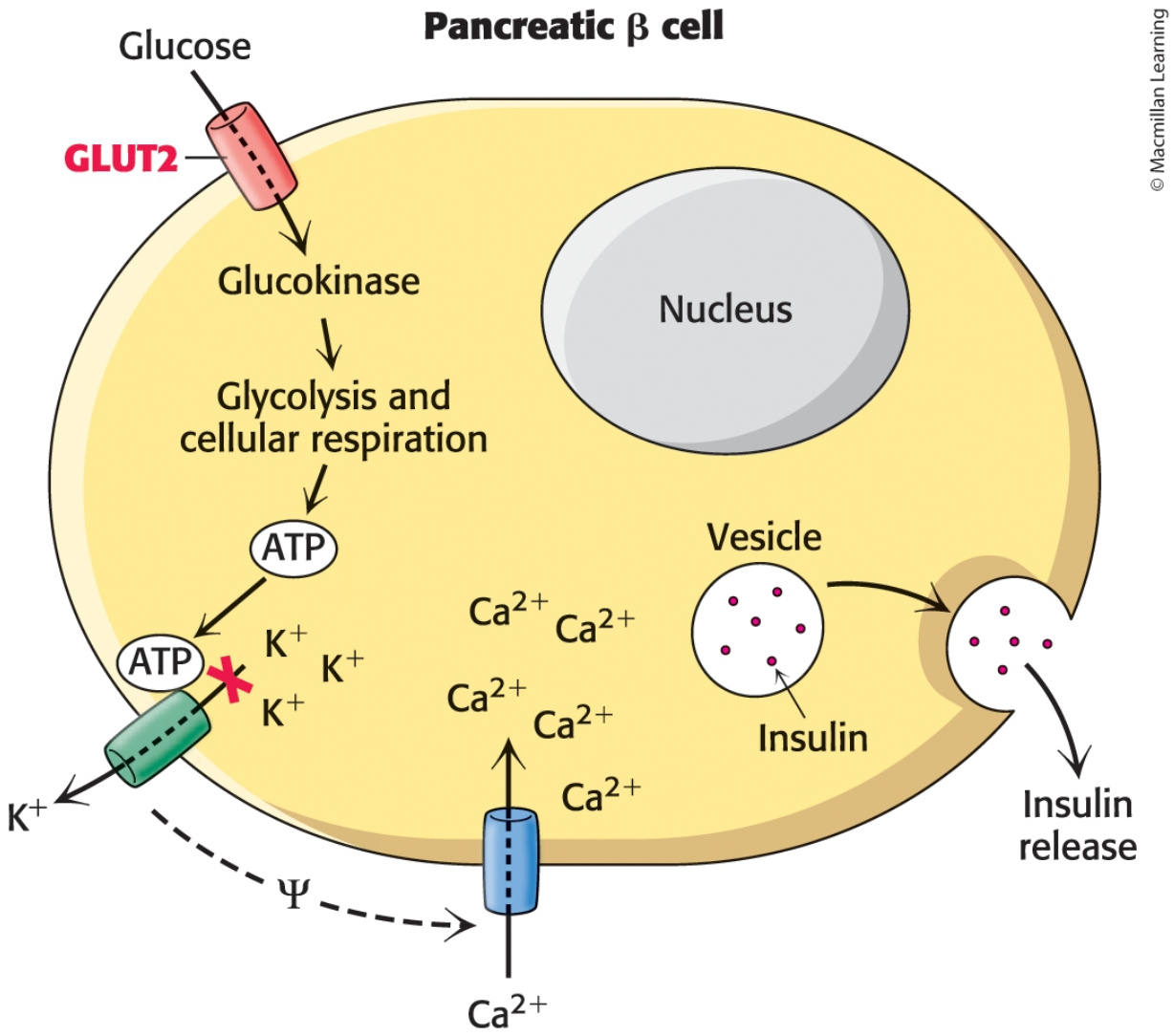
Increased mitochondrial stress.

Decrease free C o A.

All the effects listed above have a stimulatory effect on stress-induced serine kinases.

Return to FIGURE 24.9 Excess fat can disrupt signal-transduction pathways and lead to insulin insensitivity

Extended description for FIGURE 24.10 Insulin release by the pancreas is regulated by blood-glucose concentration, using A T P as a second messenger

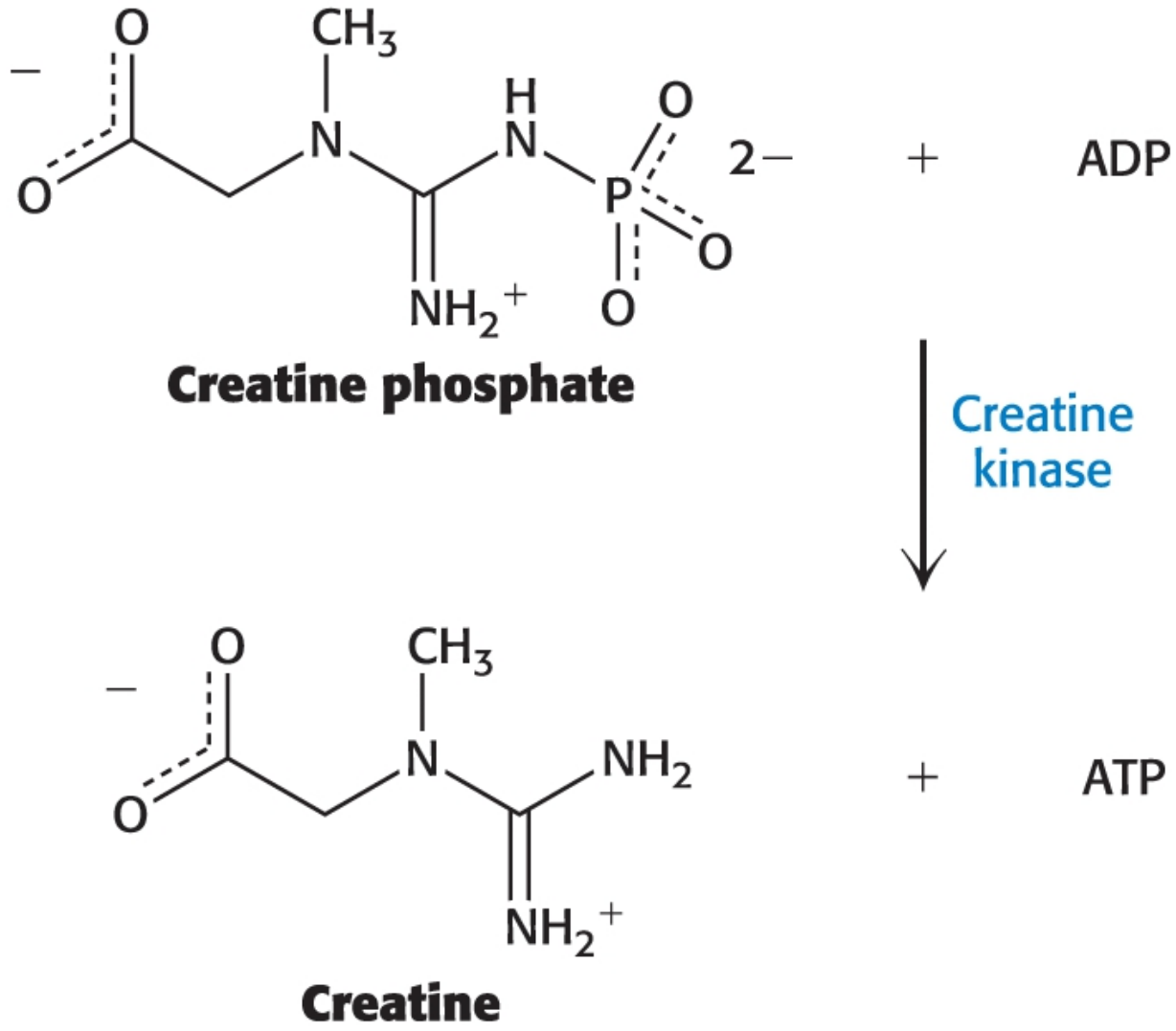


The pancreatic beta cell is depicted as a large capsule-shaped structure containing a large nucleus. A cylindrical channel on the cell surface is labeled G L U T 2. Glucose enters the pancreatic beta cell through G L U T 2. It activates glucokinase which leads to glycolysis and cellular respiration and ultimately A T P production.

A T P binds to another cylindrical channel on the cell surface. This channel is normally responsible for the transport of K superscript ions outside the cell. However, A T P binding to this channel prevents K superscript plus ion transport. A dashed arrow labeled psi points toward another channel on the cell surface which begins transporting C a superscript 2 plus ion inside the cell. The number of C a superscript 2 plus ions inside the cell increases. A vesicle containing insulin depicted as tiny dots fuses with the cell surface to release insulin.

Return to FIGURE 24.10 Insulin release by the pancreas is regulated by blood-glucose concentration, using A T P as a second messenger

Extended description for Irreversible reaction catalyzed by creatine kinase



The reaction consists of two reactants and two products. It is catalyzed by creatine kinase.

The first reactant is creatine phosphate whose structure is as follows: A 2 N and 3 C heteronuclear alkane chain is depicted as a line structure using 4 zigzag lines. First N occupies the third position

and the second N bound to H occupies the fifth position. C 1 is partially double bonded to O above and O on the lower left. The O atoms have an overall negative charge. N 1 is single bonded to C H 3 above. C 3 is double bonded to N H 2 superscript plus below. N 2 is single bonded to P on the lower right. P is partially double bonded to O on the upper right, O on the lower right, and O below. The O atoms have an overall negative charge of 2 minus.

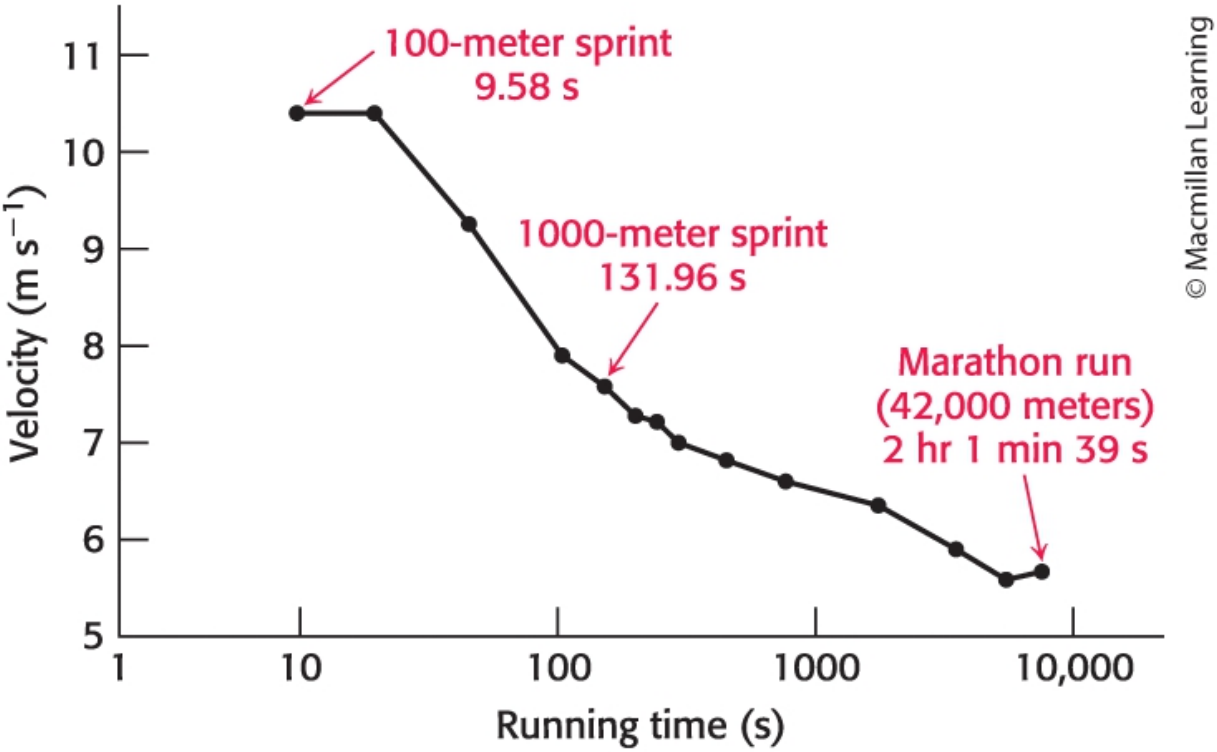
The second reactant is A D P.

The first product is creatine whose structure is as follows: A 1 N and 3 C heteronuclear alkane chain is depicted as a line structure using 3 zigzag lines. N occupies the third position. C 1 is partially double bonded to O above and O on the lower left. The O atoms have an overall negative charge. N is single bonded to C H 3 above. C 3 is double bonded to N H 2 superscript plus below and single bonded to N H 2 on the upper right.

The second product is A T P.

Return to Irreversible reaction catalyzed by creatine kinase

Extended description for FIGURE 24.11 Running velocity decreases dramatically as a function of the duration of the race

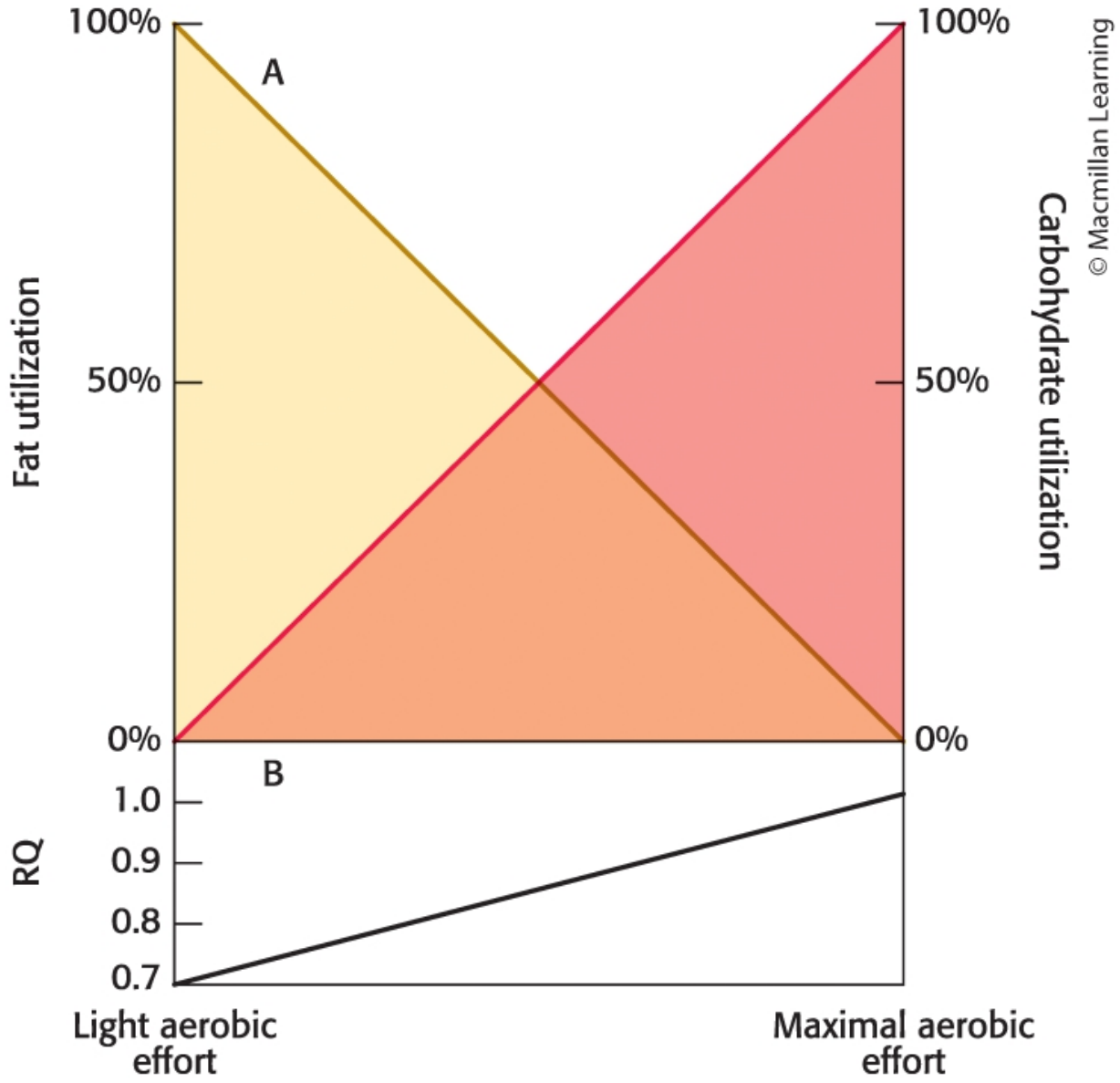


© Macmillan Learning

The horizontal axis is labeled running time in seconds. It has markings 1, 10, 100, 1000, and 10,000. The vertical axis is labeled velocity in meters per second. It has markings ranging from 5 to 11 in increments of 1 unit. The graph contains a black curve. The curve starts at (9.58, 10.5), moves horizontally toward (30, 10.5), and then falls to (7,299, 5.8). Several data points are shown on the curve and three of them are highlighted. The data point (9.58, 10.5) is labeled 100-meter sprint 9.58 seconds. The data point (131.96, 7.6) is labeled 100-meter sprint 131.96 seconds. The data point (7,299, 5.99) is labeled marathon run (42,000 meters) 2 hour 1 minute 39 seconds. All values are estimated.

Return to FIGURE 24.11 Running velocity decreases dramatically as a function of the duration of the race

Extended description for FIGURE 24.12 An idealized representation of fuel use and RQ illustrates major changes as a function of aerobic exercise intensity



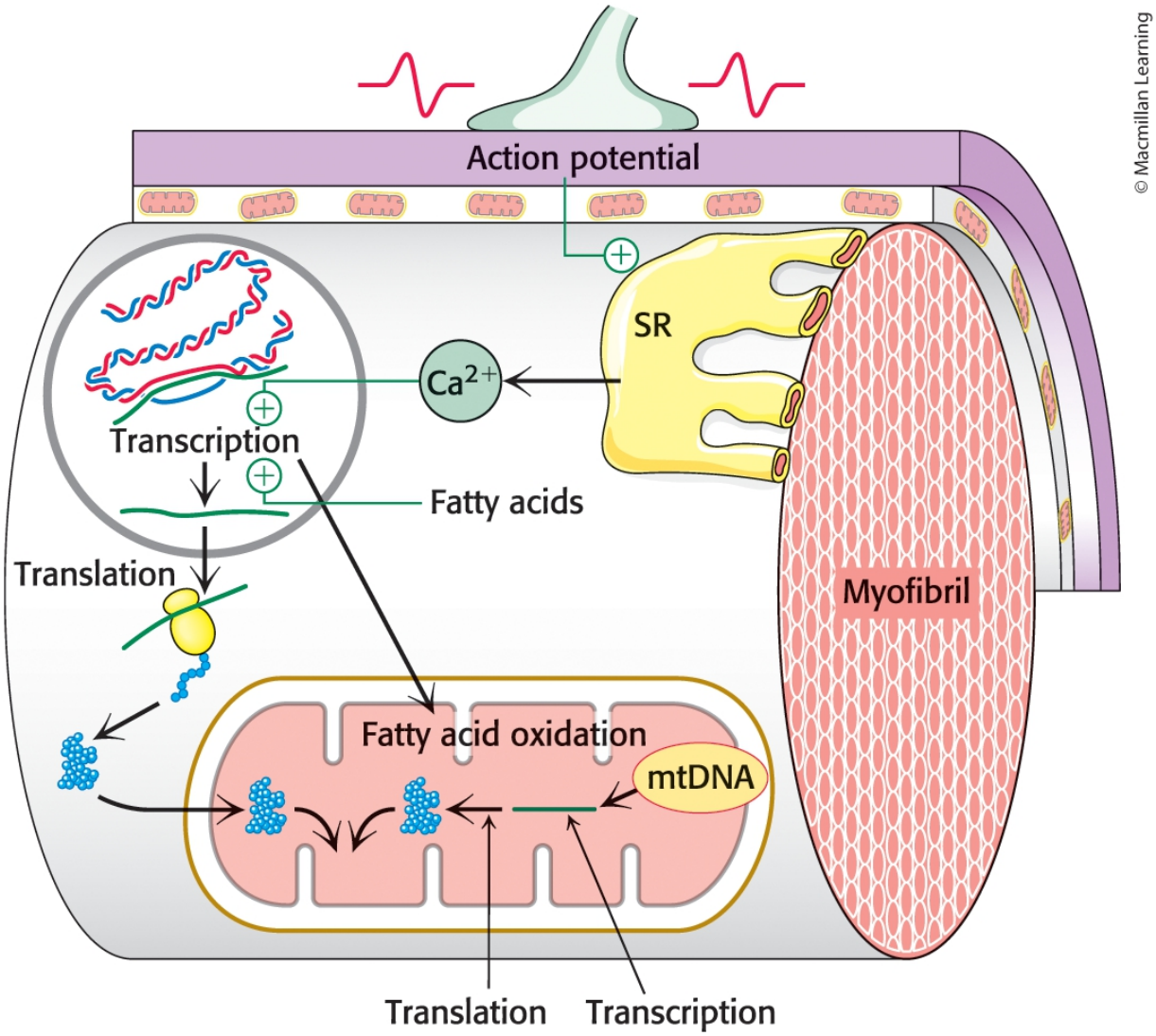
Part (A): The left vertical axis is labeled fat utilization. It has markings ranging from 0 percent to 100 percent in increments of 50 units. The right vertical axis is labeled carbohydrate utilization. It

has markings ranging from 0 to 100 percent in increments of 50 units. The horizontal axis has two markings on the extreme left and extreme right ends labeled light aerobic effort and maximal aerobic effort. A yellow decreasing line starts at 100 percent fat utilization in response to the light aerobic effort. It moves toward the lower right to reach 0 percent fat utilization in response to the maximal aerobic effort. A red decreasing line starts at 100 percent carbohydrate utilization in response to the maximal aerobic effort. It moves toward the lower left to reach 0 percent carbohydrate utilization in response to the light aerobic effort. The area under the yellow line is shown in yellow and the area under the red line is shown in red. The common triangular region below the intersection point of the two lines is shown in orange.

Part (B): The vertical axis for R Q has markings ranging from 0.7 to 1.0 in increments of 0.1 units. The horizontal axis has two markings on the extreme left and extreme right ends labeled light aerobic effort and maximal aerobic effort. An increasing straight line starts at 0. 7 R Q in response to the light aerobic effort. It moves toward the upper right to reach 1.1 R Q in response to the maximal aerobic effort.

Return to FIGURE 24.12 An idealized representation of fuel use and RQ illustrates major changes as a function of aerobic exercise intensity

Extended description for FIGURE 24.13 Exercise results in mitochondrial biogenesis and enhanced fat metabolism



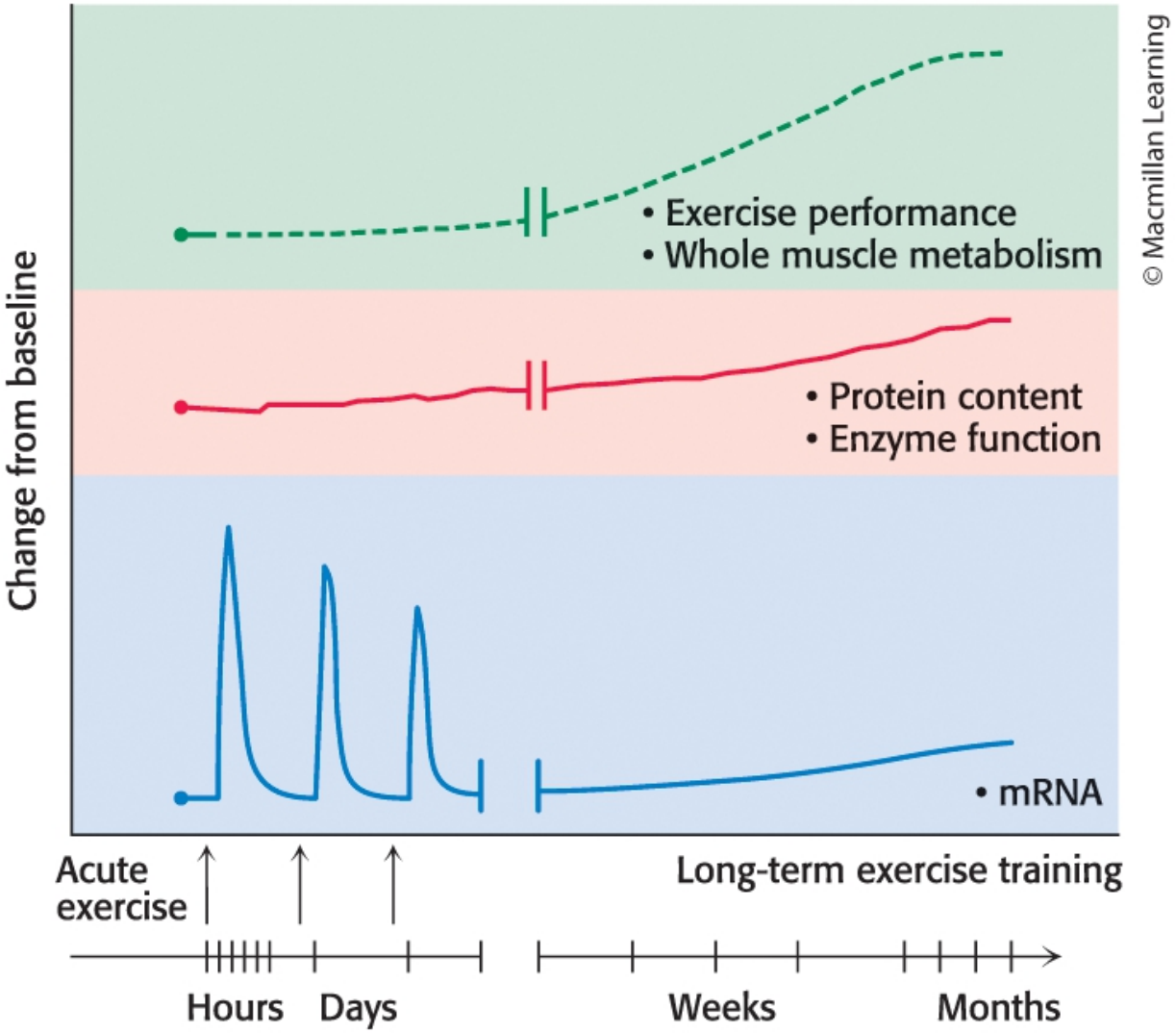
© Macmillan Learning

The myofibril is depicted as a thick horizontal cylindrical structure. Its cross-section on the right end shows vertical arrays of tiny circles. The myofibril is surrounded by a half-cut curved thick sheet containing several mitochondria. Another thick curved sheet is located above this sheet with an axon terminal attached to it for

transmission of the action potential. The action potential is also depicted as a zigzag curve. The action potential has a stimulatory effect on the sarcoplasmic reticulum (S R) depicted as a yellow irregular-shaped structure with tubular extensions. In response to stimulation, S R releases C a superscript 2 plus ions. The C a superscript 2 plus ion and fatty acids stimulate gene transcription in the nucleus containing double helical D N A. The transcribed m R N A moves to the sarcoplasm where it undergoes translation by ribosomes. The protein product of translation enters the mitochondria. Inside the mitochondria, the mitochondrial D N A also undergoes transcription followed by translation to produce proteins. The protein transported from outside and the protein produced in the mitochondria together promote mitochondrial biogenesis. Simultaneously, the genes stimulated by fatty acid in the nucleus promote fatty acid oxidation in the mitochondria.

Return to FIGURE 24.13 Exercise results in mitochondrial biogenesis and enhanced fat metabolism

Extended description for FIGURE 24.14 Biochemical adaptations to exercise vary over a range of time scales



The horizontal axis contains markings for hours, days, weeks, and months from left to right. There are 6 closely spaced markings for hours, 3 widely spaced markings for days, four widely spaced markings for weeks, and four closely spaced markings for months. The hours and days markings represent acute exercise. The weeks and months markings represent long-term exercise training. The

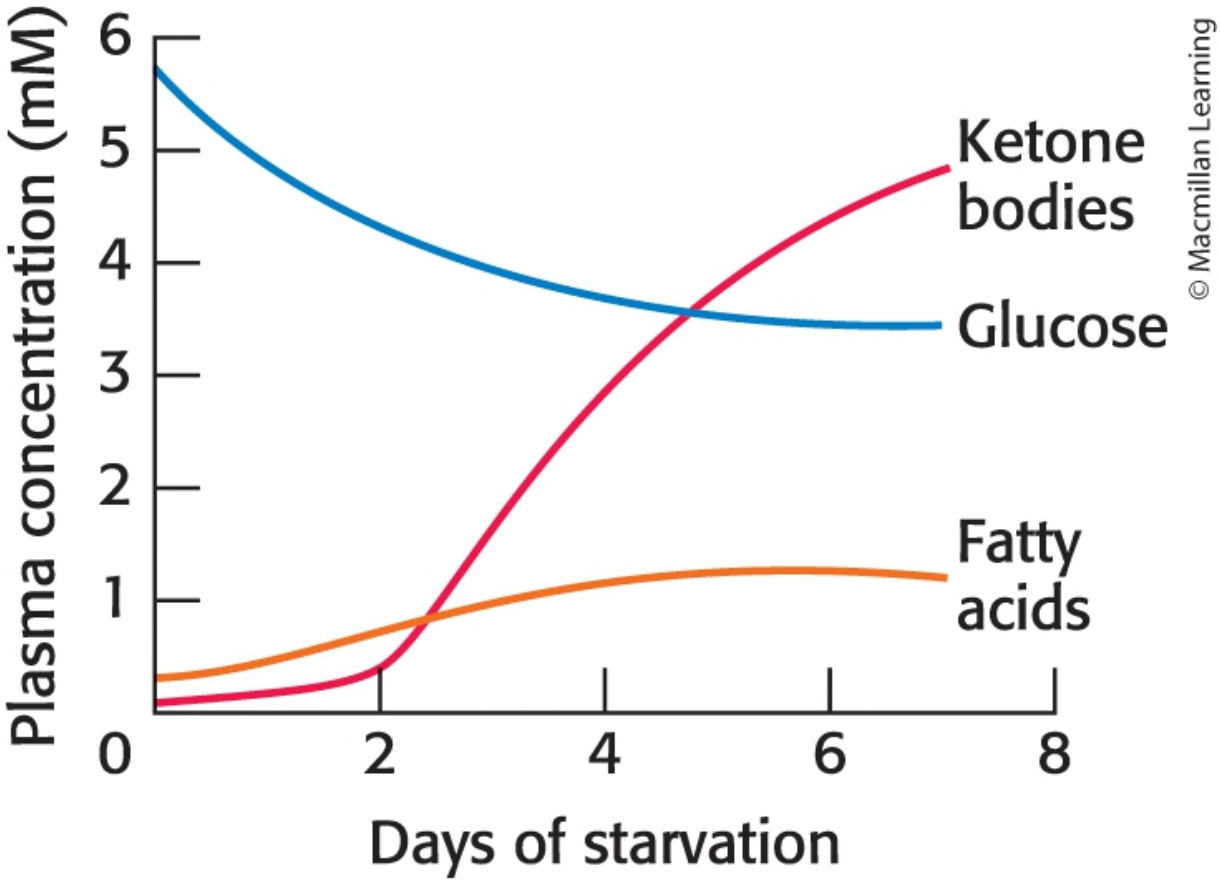
vertical axis is labeled change from baseline. The graph area is divided into three sections from top to bottom. The bottom section shown in blue depicts m R N A synthesis. During the acute exercise phase, a blue curve starts slightly above the baseline and moves horizontally till the second hour's markings. It then forms three peaks having a progressively shorter height from left to right. The peaks are separated by short baseline stretches. The first peak is formed between the second and fourth hours markings, the second peak is formed closer to the first-day marking, and the third peak is formed closer to the second-day marking. There is a break in the curve after the third-day marking. During long-term exercise training, a curve starts slightly above the baseline and slightly rises as it moves toward the right.

The middle section shown in red depicts protein content and enzyme function. It contains a red curve that starts much above the baseline during acute exercise. It moves toward the right almost horizontally. A break is shown in the curve between the third day marking and the first week marking. The curve rises gradually toward the upper right during long-term exercise training across weeks and months.

The top section shown in green depicts exercise performance and whole muscle metabolism. It contains a green dashed curve. It starts slightly above the baseline during acute exercise and moves horizontally toward the right. A break is shown in the curve between the third-day marking and the first-week marking. During the long-term exercise training, the curve rises linearly toward the upper right and then forms a plateau between second and fourth-months markings.

Return to FIGURE 24.14 Biochemical adaptations to exercise vary over a range of time scales

Extended description for FIGURE 24.15 The blood concentrations of ketone bodies glucose, and fatty acids during starvation

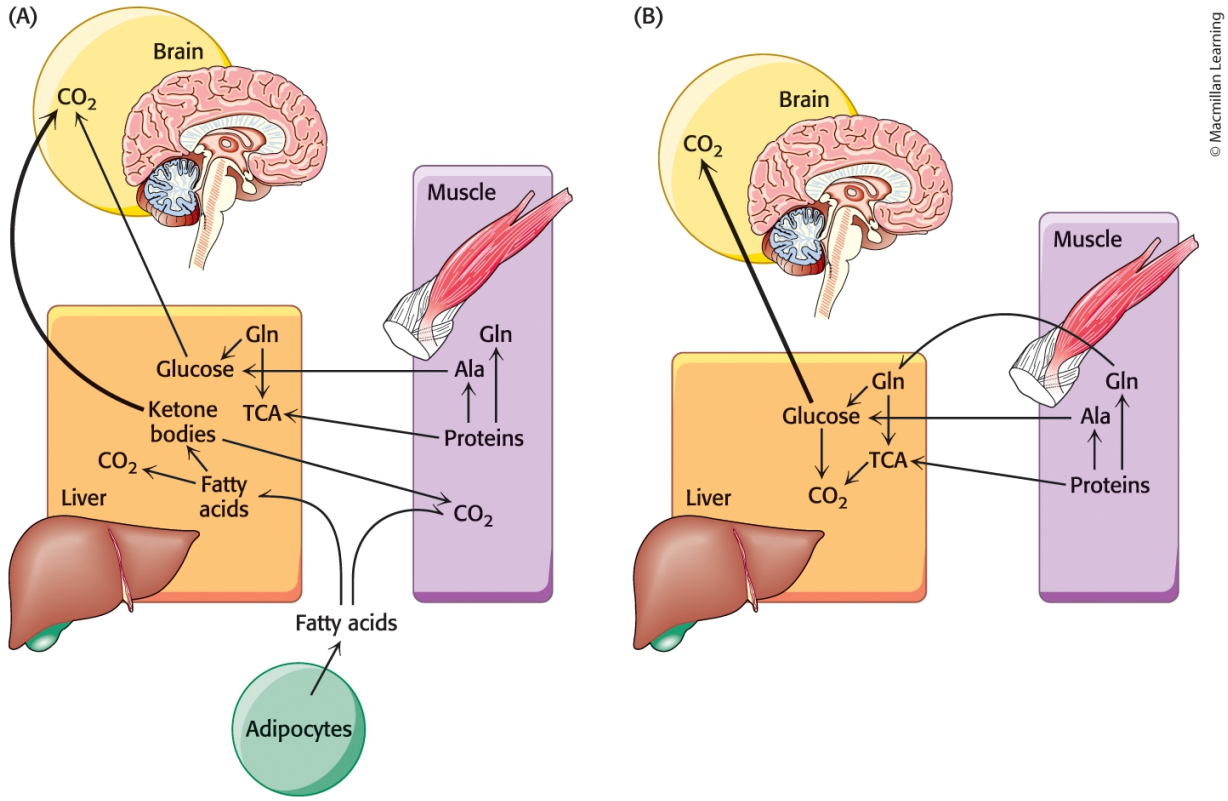


The horizontal axis is labeled days of starvation. It has markings ranging from 0 to 8 in increments of 2 units. The vertical axis is labeled plasma concentration in millimolar. It has markings ranging from 0 to 6 in increments of 1 unit. The graph contains three curves shown in orange, blue, and red. The orange curve depicts the concentration of fatty acids. It starts at (0, 0.2) and slightly rises to (7, 1.2) as it moves toward the right. The blue curve depicts glucose concentration. It starts at (0, 5.8) and falls down in a concave-up manner to reach (7, 3.6). The red curve depicts ketone bodies. It

starts at (0, 0), moves almost horizontally till (2, 0.1), and then starts rising toward the upper right in a concave-down manner to reach (7, 5). All values are estimated.

Return to FIGURE 24.15 The blood concentrations of ketone bodies glucose, and fatty acids during starvation

Extended description for FIGURE 24.16 Fuel use during prolonged starvation changes after fat mass is depleted



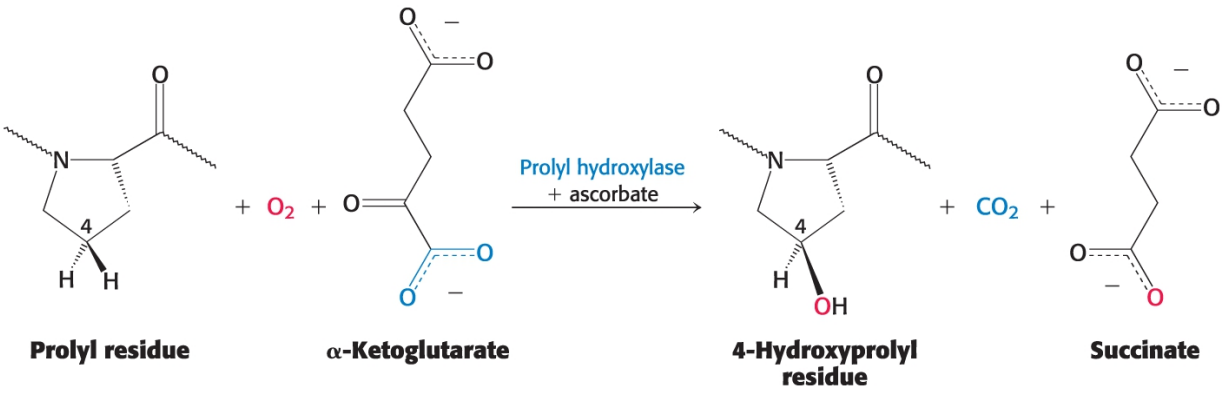
Part (A): A green circle labeled adipocytes releases fatty acids. The fatty acids are distributed to the muscle depicted as a long purple vertical rectangle and the liver depicted as an orange square. In the muscle, fatty acids are converted into C O 2. In the liver, fatty acids give rise to C O 2 and ketone bodies. The ketone bodies travel to the brain depicted as a yellow circle. Inside the brain, ketone bodies are broken down to generate C O 2. Simultaneously, in the muscle proteins are broken down to release amino acids like glutamine and alanine. These amino acids and proteins travel to the liver. In the liver, alanine gives rise to glucose and proteins enter the T C A. Glutamine can be converted into glucose or enter T C A. The glucose

produced in the liver also travels to the brain, where it is broken down to generate C O 2. A diagram of the organ is also shown alongside each depiction of the organ.

Part (B): In the muscle, proteins are broken down to release amino acids like glutamine and alanine. These amino acids and proteins travel to the liver. In the liver, alanine gives rise to glucose and proteins enter the T C A. Glutamine can be converted into glucose or enter T C A. The glucose produced in the liver also travels to the brain, where it is broken down to generate C O 2. The glucose is also broken down to generate C O 2 inside the liver. A diagram of the organ is also shown alongside each depiction of the organ.

Return to FIGURE 24.16 Fuel use during prolonged starvation changes after fat mass is depleted

Extended description for FIGURE 24.17 Formation of 4-hydroxyproline requires ascorbate



The reaction consists of three reactants and three products. It is catalyzed by prolyl hydroxylase plus ascorbate.

The first reactant is prolyl residue whose structure is as follows: A central C atom is double bonded to O above, single bonded to C H 2 on the lower left in the form of a line. It has a wiggly line on the lower right. C H 2 is single bonded to N on the left and dash bonded to C 3 of a 3-carbon alkane chain depicted as a line structure using 2 zigzag lines. N atom has a wiggly line on the upper left and is single-bonded to C 1 of the alkane chain. In the alkane chain, C 2 is numbered 4 and it is dash bonded to H on the lower left and wedge bonded to H on the lower right. The alkane chain, N atom, and C H 2 group form a pentagonal ring-like structure.

The second reactant is O 2.

The third reactant is alpha-ketoglutarate whose structure is as follows: A 5-carbon alkane chain is depicted as a vertical line structure using 4 zigzag lines. C 1 is partially double-bonded to O on the upper left and O on the right. The O atoms have an overall

negative charge. C 4 is double bonded to O on the left. C 5 is partially double bonded to O on the right and O on the lower left. The O atoms have an overall negative charge.

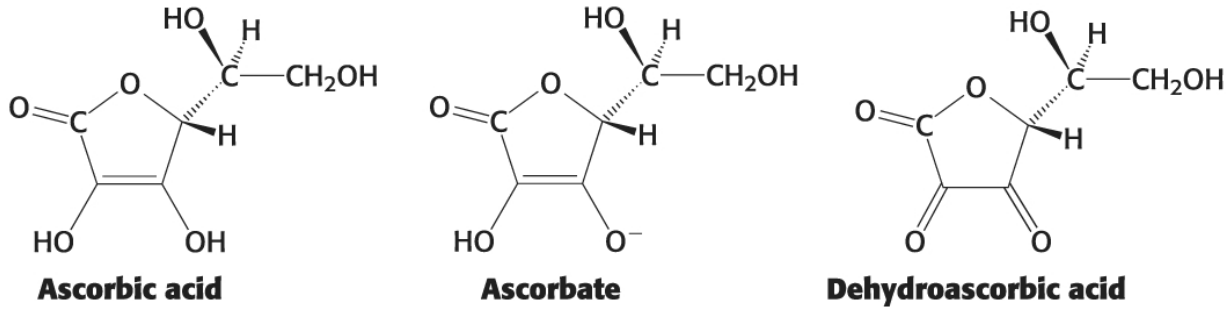
The first product is a 4-hydroxyprolyl residue whose structure is as follows: A central C atom is double bonded to O above, single bonded to C H 2 on the lower left in the form of a line. It has a wiggly line on the lower right. C H 2 is single bonded to N on the left and dash bonded to C 3 of a 3-carbon alkane chain depicted as a line structure using 2 zigzag lines. N atom has a wiggly line on the upper left and is single-bonded to C 1 of the alkane chain. In the alkane chain, C 2 is numbered 4 and it is dash bonded to H on the lower left and wedge bonded to O H on the lower right. The alkane chain, N atom, and C H 2 group form a pentagonal ring-like structure.

The second product is C O 2.

The third product is succinate whose structure is as follows: A 4-carbon alkane chain is depicted as a vertical line structure using 3 zigzag lines. C 1 is partially double-bonded to O on the upper left and O on the right. The O atoms have an overall negative charge. C 4 is partially double bonded to O on the left and O on the lower right. The O atoms have an overall negative charge.

Return to FIGURE 24.17 Formation of 4-hydroxyproline requires ascorbate

Extended description for Structure of ascorbic acid, ascorbate, and dehydroascorbic acid



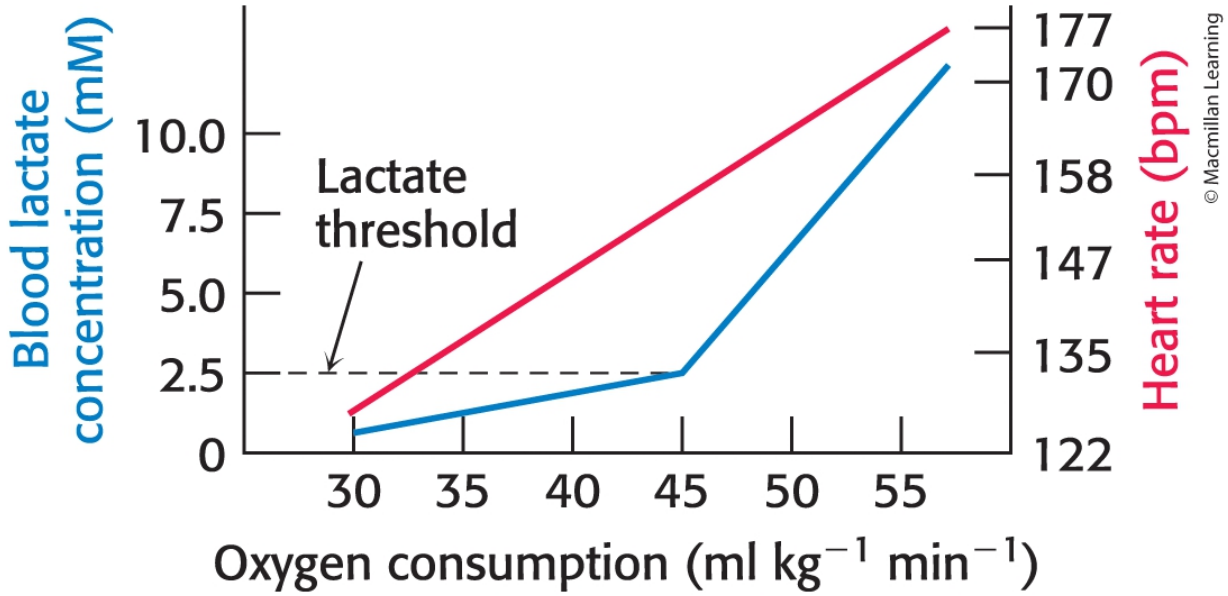
The structure of ascorbic acid is as follows: A 5-membered heterocyclic pentagonal ring is in a vertical orientation and consists of 1 O and 4 C atoms. O occupies the topmost vertex. C 1 occupies the top right vertex. A double bond is present between C 2 and C 3. C 1 is dash bonded to C on the upper right and wedge bonded to H on the lower right. The upper right C is wedge bonded to O H on the upper left, dash bonded to H on the upper right, and single bonded to C H 2 O H on the right. C 2 and C 3 are each single bonded to O H below. C 4 is double bonded to O on the upper left.

The structure of ascorbate is as follows: A 5-membered heterocyclic pentagonal ring is in a vertical orientation and consists of 1 O and 4 C atoms. O occupies the topmost vertex. C 1 occupies the top right vertex. A double bond is present between C 2 and C 3. C 1 is dash bonded to C on the upper right and wedge bonded to H on the lower right. The upper right C is wedge bonded to O H on the upper left, dash bonded to H on the upper right, and single bonded to C H 2 O H on the right. C 2 is single bonded to O superscript minus below. C 3 is single bonded to O H below. C 4 is double bonded to O on the upper left.

The structure of dehydroascorbic acid is as follows: A 5-membered heterocyclic pentagonal ring is in a vertical orientation and consists of 1 O and 4 C atoms. O occupies the topmost vertex. C 1 occupies the top right vertex. C 1 is dash bonded to C on the upper right and wedge bonded to H on the lower right. The upper right C is wedge bonded to O H on the upper left, dash bonded to H on the upper right, and single bonded to C H 2 O H on the right. C 2 and C 3 are each double bonded to O below. C 4 is double bonded to O on the upper left.

Return to Structure of ascorbic acid, ascorbate, and dehydroascorbic acid

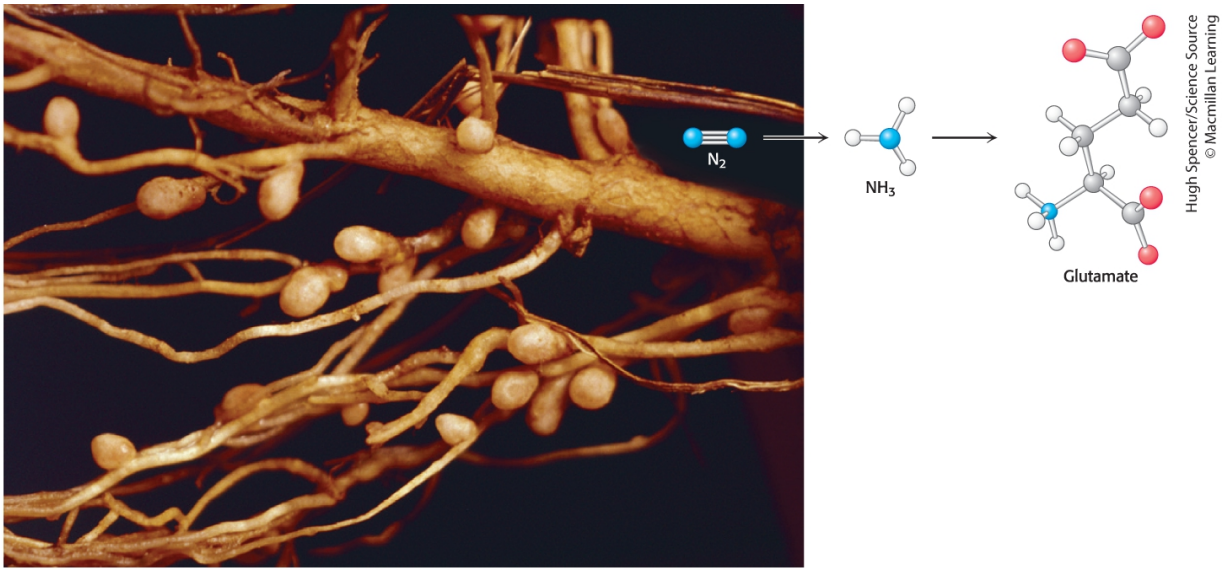
Extended description for Relation between blood-lactate levels, oxygen consumption, and heart rate during exercise of increasing intensity



The horizontal axis is labeled oxygen consumption in milliliters per kilogram per minute. It has markings ranging from 30 to 55 in increments of 5 units. The left vertical axis is labeled blood lactate concentration in millimolar. It has markings ranging from 0 to 10.0 in increments of 2.5 units. The right vertical axis is labeled heart rate in beats per minute. It has markings 122, 135, 147, 158, 170, and 177. The graph contains two curves shown in red and blue. The red curve is a straight increasing line that depicts the variation of heart rate with oxygen consumption. It starts at (30, 128) and moves toward the upper right to reach (56, 177). The blue curve depicts the variation of blood lactate concentration with oxygen consumption. It starts at (30, 0.5), moves toward (45, 2.5), and then rises upward to (56, 13). A horizontal dashed line starting from 2.5 on the left vertical axis touches the blue curve at (45, 2.5) and is labeled lactate threshold. All values are estimated.

Return to Relation between blood-lactate levels, oxygen consumption, and heart rate during exercise of increasing intensity

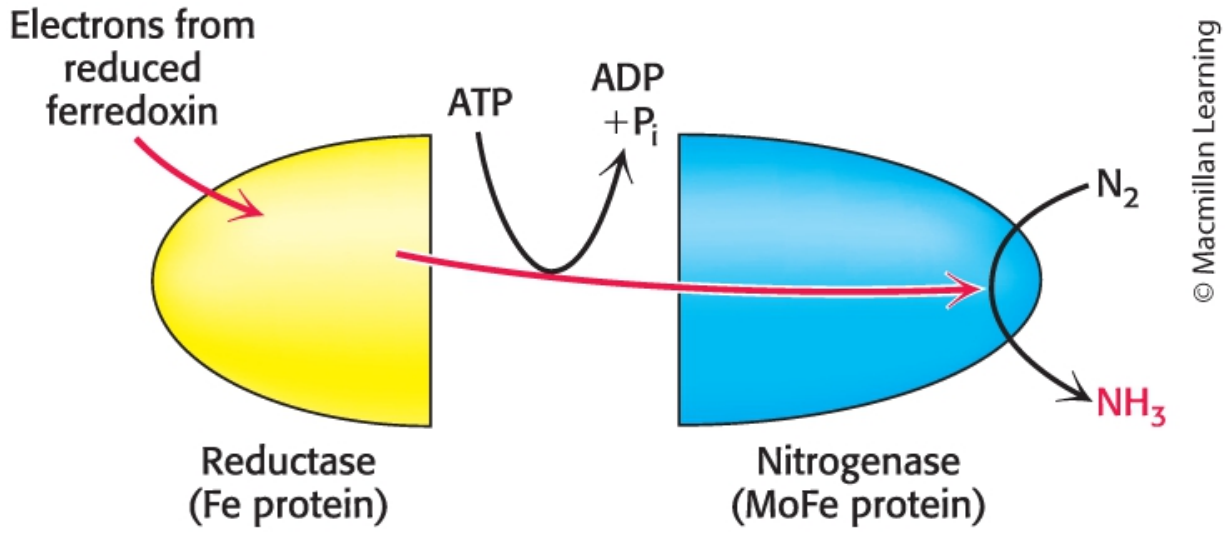
Extended description for Reaction sequence depicting the assimilation of N 2



The reaction sequence shows the conversion of N 2 to glutamate through an N H 3 intermediate. The N 2, N H 3, and glutamate molecules are depicted as ball-and-stick models. N 2 consists of two blue spheres connected by three parallel sticks. N H 3 consists of a central blue sphere connected to a white sphere on the left, upper right, and lower right. Glutamate consists of 5 grey spheres in a vertical zigzag orientation. The first grey sphere is connected to a red sphere on the left and upper right. The second and third grey sphere is connected to two white spheres. The fourth grey sphere is connected to a white sphere at the back and a blue sphere on the lower left. The blue sphere is connected to three white spheres. The fifth grey sphere is connected to two red spheres.

Return to Reaction sequence depicting the assimilation of N 2

Extended description for FIGURE 25.1 The nitrogenase complex fixes nitrogen to ammonia

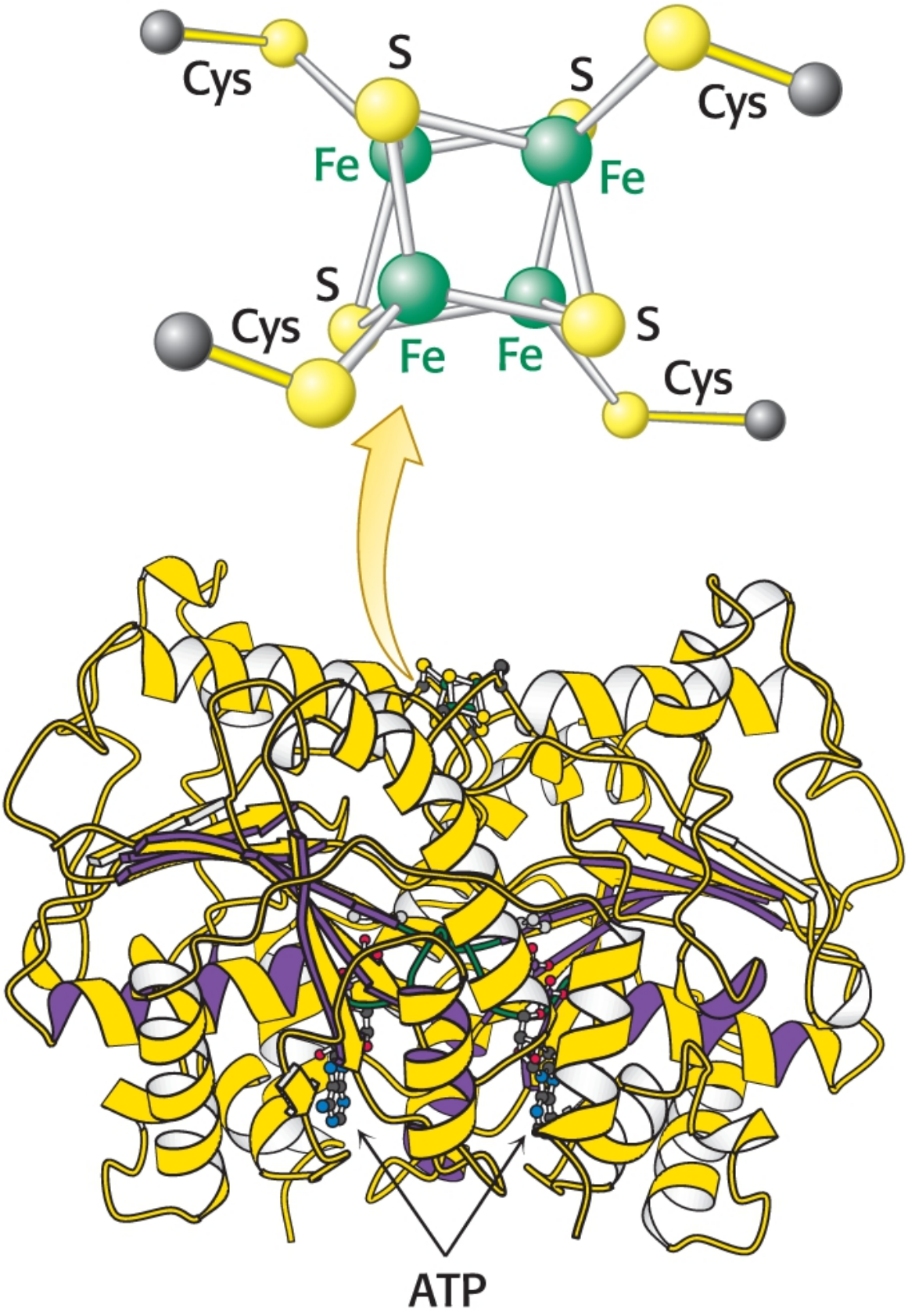


The reductase (F e protein) is depicted as a yellow-colored half-cut circle. The nitrogenase (M o F e protein) is depicted as a blue half-cut oval. Electrons from reduced ferredoxin are transferred to reductase. The reductase then transfers the electrons to nitrogenase, which uses them to convert N 2 to N H 3. The transfer of electrons from reductase to nitrogenase is coupled with the breakdown of A T P to A D P plus P subscript i.

Return to FIGURE 25.1 The nitrogenase complex fixes nitrogen to ammonia

Extended description for FIGURE 25.2 The F e protein, or reductase, transfers elections of high reducing

power

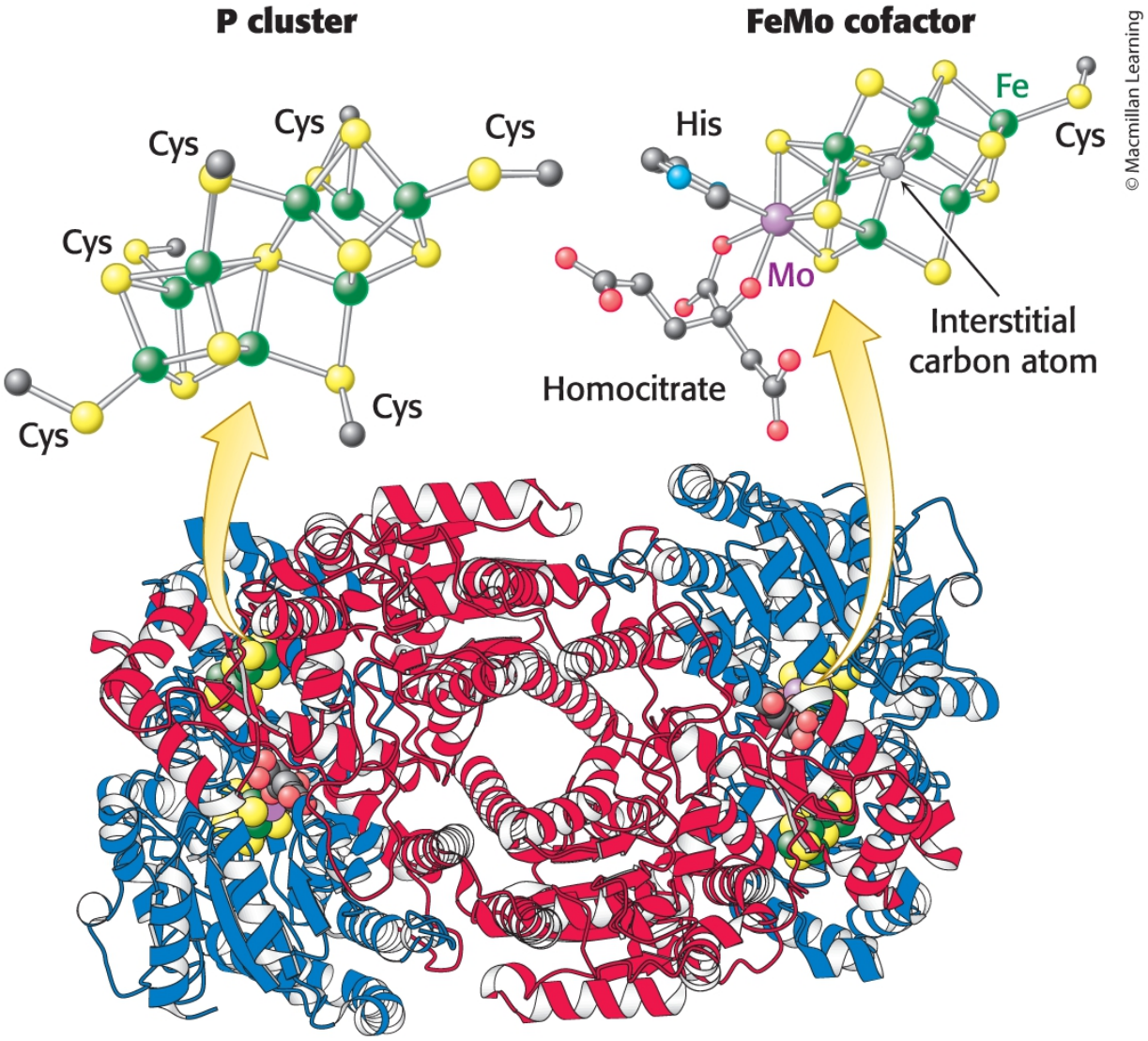


© Macmillan Learning

The ribbon diagram consists of two monomers, each composed of several alpha-helices and a few beta-strands in the center. Each monomer is bound to A T P. A ball-and-stick model of 4 F e-4 S cluster connects the two monomers at the top. An arrow shows the enlarged view of the ball-and-stick model of the 4 F e-4 S cluster. It consists of two square-shaped arrangements of F e and S atoms. The F e atoms are depicted as green spheres and the S atoms are depicted as yellow spheres. The front square arrangement consists of a yellow sphere at the top left and bottom right vertex. The green sphere occupies the top right and bottom left vertex. The rear square arrangement consists of a green sphere at the top left and bottom right vertex. The yellow sphere occupies the top right and bottom left vertex. The front and rear square arrangements are not perfectly aligned with each other. Each green sphere is connected to the side chain of cysteine residue depicted as a chain of 1 black and 1 yellow sphere.

Return to FIGURE 25.2 The F e protein, or reductase, transfers elections of high reducing power

Extended description for FIGURE 25.3 The M o F e protein, or nitrogenase, catalyzes the reduction of N 2 to N H 3



The ribbon diagram consists of the heterotetrameric nitrogenase consisting of two alpha-subunits and two beta-subunits. The alpha-subunits are depicted in red color and the beta-subunits are depicted in blue color. Each subunit is composed of several alpha-

helices and a few beta strands. The alpha subunit is located at the top left and bottom right. The beta subunit is located at the top right and bottom left. A few alpha-helices of alpha subunits form a hollow circular arrangement in the center. The alpha-subunit is bound to the P cluster and the beta-subunits are bound to the F e M o cofactor.

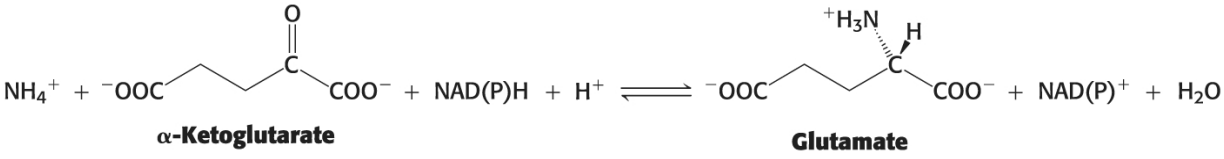
The enlarged views of the ball-and-stick model of the P cluster and F e M o are shown by arrows from the respective subunits.

Each P cluster contains eight F e atoms, depicted as green spheres, and seven S atoms, depicted as yellow spheres, interconnected to form 3 separate cage-like structures. The F e atoms are connected to 6 different cysteine residues of the protein subunit.

The F e M o cofactor contains one molybdenum atom depicted as a purple sphere, seven F e atoms depicted as a green sphere, nine S atoms depicted as yellow spheres, an interstitial carbon atom depicted as a grey sphere, and homocitrate composed of 7 black and 7 red spheres. The F e, S, and the interstitial carbon atom form a cage-like structure with the carbon atom in the center. One of the F e atoms is linked to the protein by a cysteine residue and the molybdenum atom is connected to the histidine residue. The molybdenum atom is connected to two red spheres of homocitrate.

Return to FIGURE 25.3 The M o F e protein, or nitrogenase, catalyzes the reduction of N 2 to N H 3

Extended description for Formation of glutamate



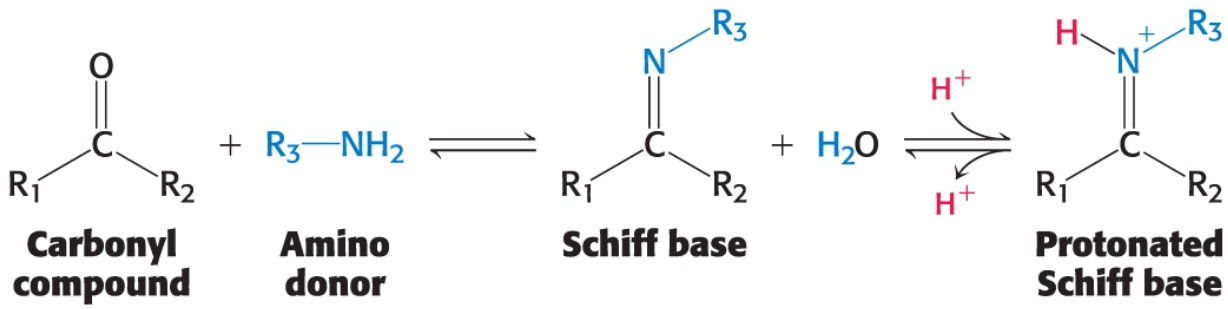
The reaction consists of four reactants and three products.

The first reactant is N H 4 superscript plus. The second reactant is alpha-ketoglutarate whose structure is as follows: A 3-carbon alkane chain is depicted as a line structure using 2 zigzag lines. C 1 is single bonded to C O O superscript minus on the lower left. C 3 is double bonded to O above and single bonded to C O O superscript minus on the lower right. The third reactant is N A D open parenthesis P close parenthesis H. The fourth reactant is H superscript plus.

The first product is glutamate whose structure is as follows: A 3-carbon alkane chain is depicted as a line structure using 2 zigzag lines. C 1 is single bonded to C O O superscript minus on the lower left. C 3 is dash bonded to N H 3 superscript plus on the upper left, wedge bonded to H on the upper right, and single bonded to C O O superscript minus on the lower right. The second product is N A D open parenthesis P close parenthesis with superscript plus. The third product is H 2 O.

Return to Formation of glutamate

Extended description for Formation of protonated Schiff base



The reaction sequence consists of two reactants, two intermediates, and one product.

The first reactant is a carbonyl compound whose structure is as follows: A central C atom is double bonded to O above, single bonded to R 1 on the lower left, and single bonded to R 2 on the lower right.

The second reactant is an amino donor which consists of R 3, single bond, N H 2.

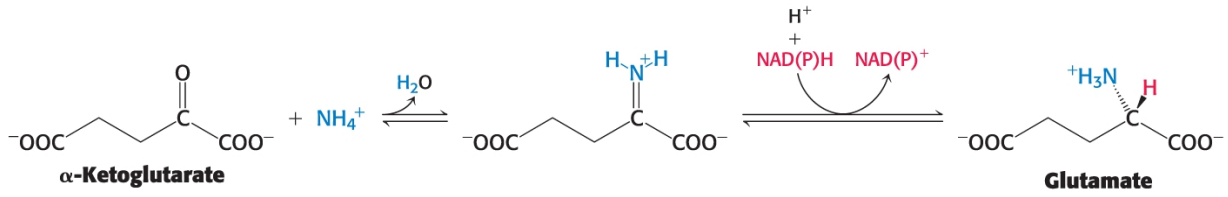
The first intermediate is Schiff base: A central C atom is single bonded to R 1 on the lower left, double bonded to N above, and single bonded to R 2 on the lower right. The N atom is single-bonded to R 3 on the upper right. The second intermediate is H 2 O.

The intermediate Schiff base is converted into protonated Schiff base after the entry of H superscript plus ion and the protonated Schiff base is converted back to the intermediate Schiff base by the removal of H superscript plus ion. The product is protonated Schiff base whose structure is as follows: A central C atom is single-bonded

to R 1 on the lower left, double-bonded to N superscript plus, and single-bonded to R 2 on the lower right. The N atom is single-bonded to R 3 on the upper right and single-bonded to H on the upper left.

Return to Formation of protonated Schiff base

Extended description for Formation of glutamate from alpha-ketoglutarate



The reaction sequence consists of two reactants, one intermediate, and one product.

The first reactant is alpha-ketoglutarate whose structure is as follows: A 3-carbon alkane chain is depicted as a line structure using 2 zigzag lines. C 1 is single bonded to C O O superscript minus on the lower left. C 3 is double bonded to O above and single bonded to C O O superscript minus on the lower right.

The second reactant is N H 4 superscript plus.

The intermediate is reversibly produced from the reactants with concomitant release of H 2 O.

The structure of the intermediate is as follows: A 3-carbon alkane chain is depicted as a line structure using 2 zigzag lines. C 1 is single bonded to C O O superscript minus on the lower left. C 3 is double bonded to N superscript plus above and single bonded to C O O superscript minus on the lower right. The N superscript plus is single-bonded to H on the upper left and H on the upper right.

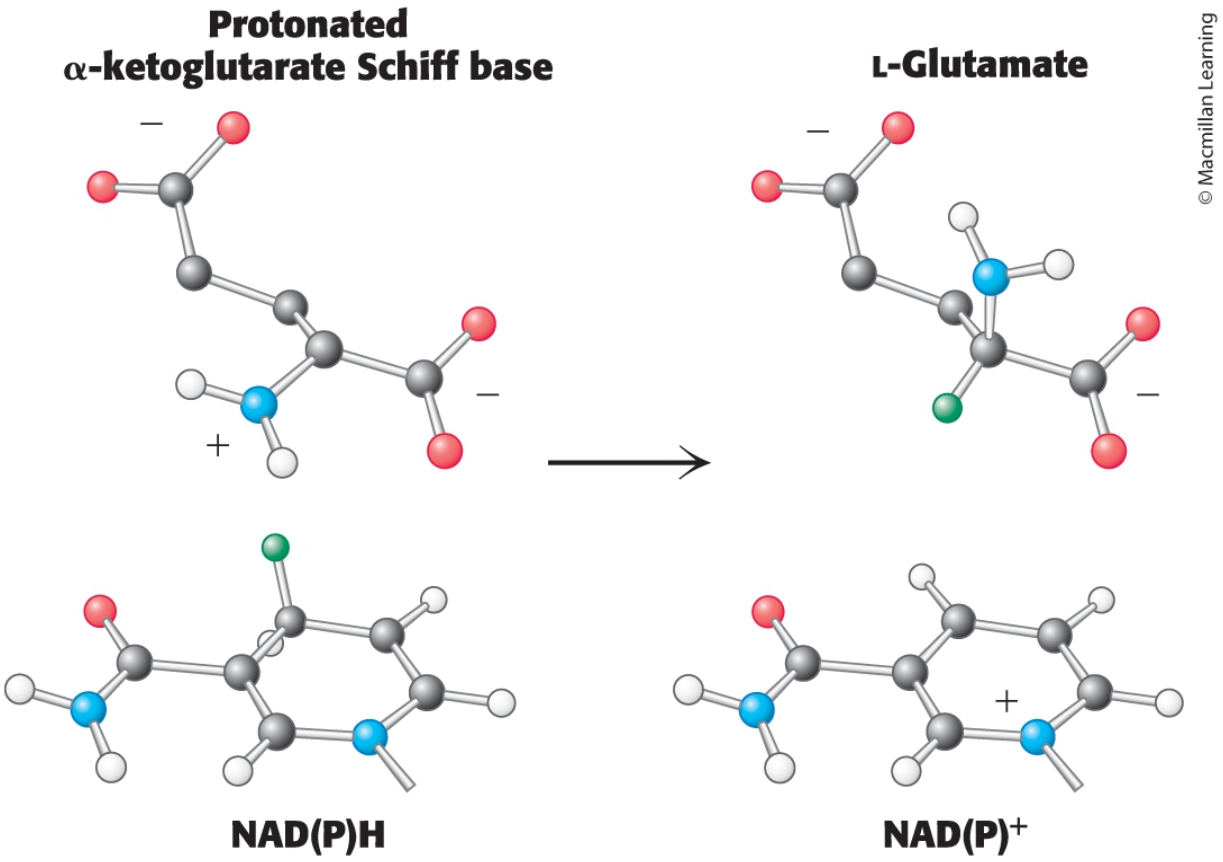
The intermediate is reversibly converted into glutamate with the concomitant oxidation of N A D open parenthesis P close

parenthesis H plus H superscript plus into N A D close parenthesis P close parenthesis with superscript plus.

The product is glutamate whose structure is as follows: A 3-carbon alkane chain is depicted as a line structure using 2 zigzag lines. C 1 is single bonded to C O O superscript minus on the lower left. C 3 is dash bonded to N H 3 superscript plus on the upper left, wedge bonded to H on the upper right, and single bonded to C O O superscript minus on the lower right.

Return to Formation of glutamate from alpha-ketoglutarate

Extended description for FIGURE 25.4 Glutamate chirality is established by hydride transfer to the Schiff base



© Macmillan Learning

The irreversible reaction consists of two reactants and two products. The reactants and products are depicted as ball-and-stick models.

The first reactant is protonated alpha-ketoglutarate Schiff base. It consists of a chain of 5 black spheres. The first and the fifth black spheres are each connected to two red spheres and have an overall negative charge. The fourth black sphere is connected to a blue sphere on the lower left. This blue sphere is further connected to two white spheres and has an overall positive charge.

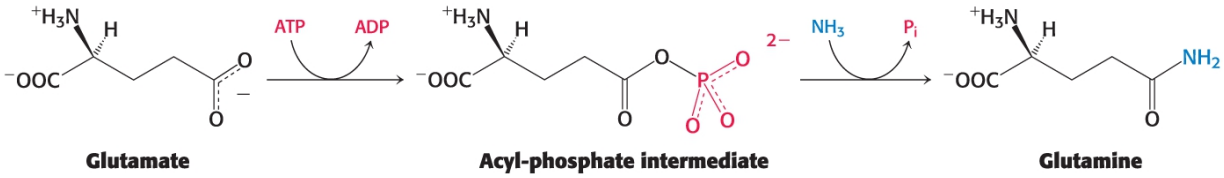
The second reactant is N A D open parenthesis P close parenthesis H. It consists of a horizontal hexagonal ring composed of 1 blue and 5 black spheres. The blue sphere occupies the bottom-right vertex. The leftmost black sphere is connected to another black sphere, which is further connected to a red sphere on the upper left and a blue sphere on the lower left. The blue sphere is connected to two white spheres. The top left black sphere is connected to a green sphere and a white sphere. The remaining black spheres are connected to a single white sphere.

The first product is L-Glutamate. It consists of a chain of 5 black spheres. The first and the fifth black spheres are each connected to two red spheres and have an overall negative charge. The fourth black sphere is connected to a blue sphere on the upper left and a green sphere on the lower left. The blue sphere is further connected to two white spheres.

The second product is N A D open parenthesis P close parenthesis with superscript plus. It consists of a horizontal hexagonal ring composed of 1 blue and 5 black spheres. The blue sphere with a positive charge occupies the bottom-right vertex. The leftmost black sphere is connected to another black sphere, which is further connected to a red sphere on the upper left and a blue sphere on the lower left. The blue sphere is connected to two white spheres. The remaining black spheres are connected to a single white sphere.

Return to FIGURE 25.4 Glutamate chirality is established by hydride transfer to the Schiff base

Extended description for Conversion of glutamate to glutamine



The reaction sequence consists of one reactant, one intermediate, and one product. The reactant is glutamate whose structure is as follows: A 4-carbon alkane chain is depicted as a line structure using 3 zigzag lines. C 1 is single bonded to C O O superscript minus on the lower left, wedge bonded to N H 3 superscript plus on the upper left, and dash bonded to H on the upper right. C 4 is partially double bonded to O on the upper right and O below. The O atoms have an overall negative charge.

Glutamate is irreversibly converted into acyl-phosphate intermediate with the simultaneous breakdown of A T P to A D P.

The structure of the acyl-phosphate intermediate is as follows: A 4-carbon alkane chain is depicted as a line structure using 3 zigzag lines. C 1 is single bonded to C O O superscript minus on the lower left, wedge bonded to N H 3 superscript plus on the upper left, and dash bonded to H on the upper right. C 4 is double bonded O below and single bonded to O on the upper right. The upper right O is further single-bonded to P on the lower right. The P atom is partially double-bonded to O on the upper right, O below, and O on the lower right. The O atoms have an overall negative charge of 2 minus.

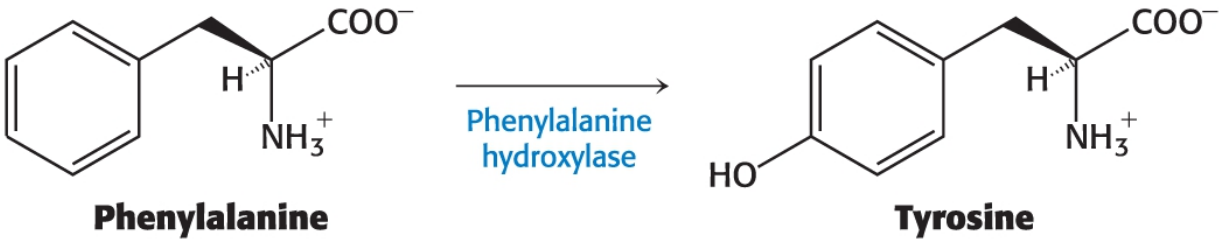
Acyl-phosphate intermediate is irreversibly converted into glutamine with the simultaneous entry of N H 3 and exit of P

subscript i.

The product is glutamine whose structure is as follows: A 4-carbon alkane chain is depicted as a line structure using 3 zigzag lines. C 1 is single bonded to C O O superscript minus on the lower left, wedge bonded to N H 3 superscript plus on the upper left, and dash bonded to H on the upper right. C 4 is double bonded O below and single bonded to N H 2 on the upper right.

Return to Conversion of glutamate to glutamine

Extended description for Irreversible reaction catalyzed by phenylalanine hydroxylase



Phenylalanine **Tyrosine**

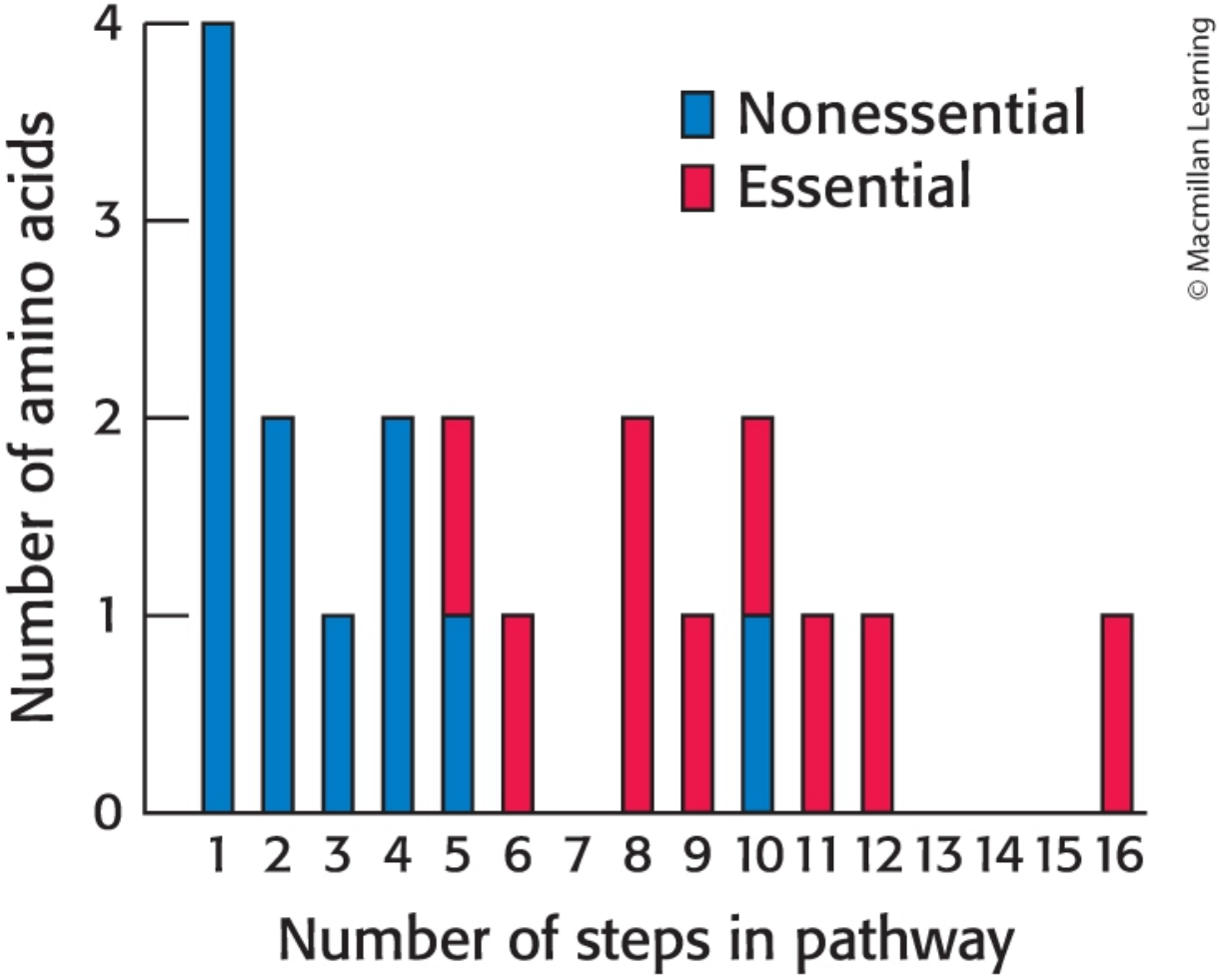
The reaction consists of one reactant and one product. It is catalyzed by phenylalanine hydroxylase.

The reactant is phenylalanine whose structure is as follows: A benzene ring is in a vertical orientation with C 1 occupying the topmost vertex. It contains alternating double bonds between C 1 and C 2, C 3 and C 4, and C 5 and C 6. C 2 is single bonded to C H 2 on the upper right in the form of a line. C H 2 is wedge bonded to C on the lower right. The C atom is single bonded to C O O superscript minus on the upper right, dash bonded to H on the lower left, and single bonded to N H 3 superscript plus below.

The product is tyrosine whose structure is as follows: A benzene ring is in a vertical orientation with C 1 occupying the topmost vertex. It contains alternating double bonds between C 1 and C 2, C 3 and C 4, and C 5 and C 6. C 2 is single bonded to C H 2 on the upper right in the form of a line. C H 2 is wedge bonded to C on the lower right. The C atom is single bonded to C O O superscript minus on the upper right, dash bonded to H on the lower left, and single bonded to N H 3 superscript plus below. C 5 of the ring is single-bonded to O H on the lower right.

Return to Irreversible reaction catalyzed by phenylalanine hydroxylase

Extended description for FIGURE 25.6 Essential and nonessential amino acids can be distinguished by the required number of biosynthetic steps



The horizontal axis is labeled "Number of steps in pathway." It has markings ranging from 1 to 16 in increments of 1 unit. The vertical axis is labeled "Number of amino acids." It has markings ranging from 0 to 4 in increments of 1 unit. Vertical bars are shown at the markings on the horizontal axis. The blue bars represent nonessential amino acids and red bars represent essential amino

acids. The values of the blue and red bars at the different markings are as follows:

1: Blue bar: 4

2: Blue bar: 2

3: Blue bar: 1

4: Blue bar: 2

5: Blue bar: 1, Red bar: spans from 1 to 2

6: Red bar: 1

7: No bar

8: Red bar: 2

9: Red bar: 1

10: Blue bar: 1, Red bar: spans from 1 to 2

11: Red bar: 1

12: Red bar: 1

13: No bar

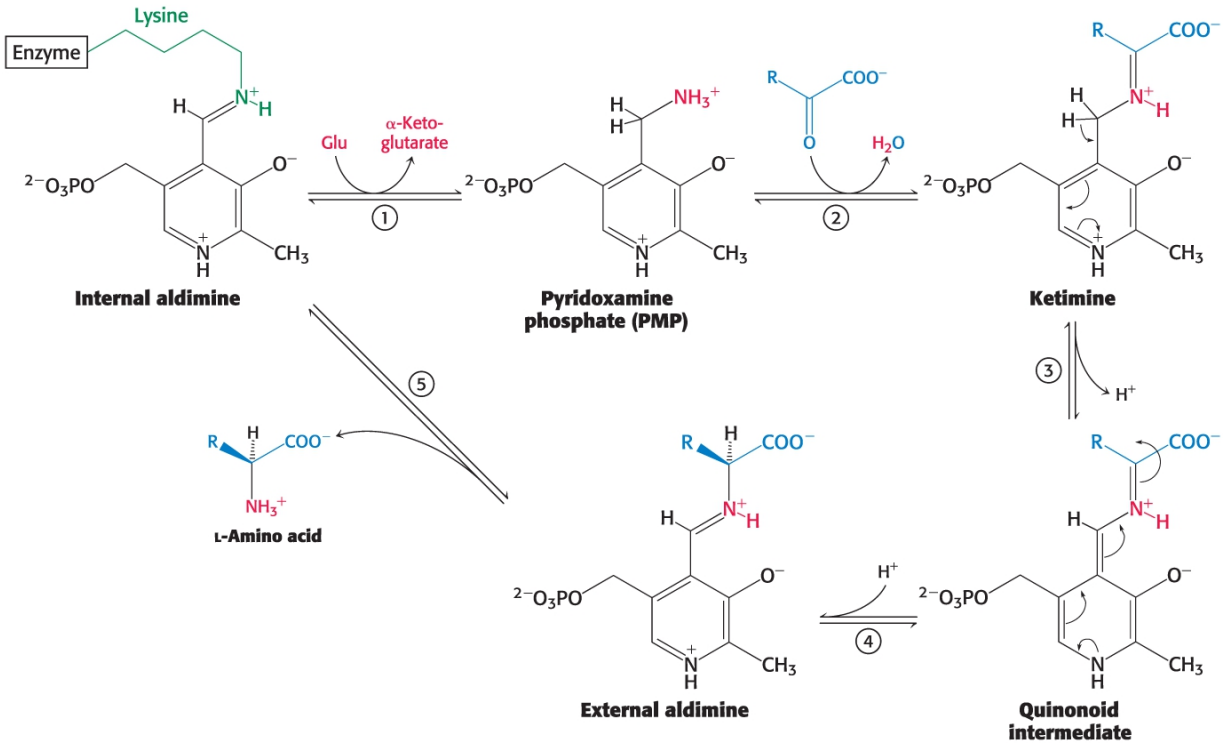
14: No bar

15: No bar

16: Red bar: 1

Return to FIGURE 25.6 Essential and nonessential amino acids can be distinguished by the required number of biosynthetic steps

Extended description for FIGURE 25.7 Transamination is a critical step in the biosynthesis of most amino acids



In the first reversible step, internal aldimine is converted into pyridoxamine phosphate (P M P) with the simultaneous conversion of glutamic acid to alpha-ketoglutarate.

The structure of internal aldimine is as follows: A 6-membered heterocyclic hexagonal ring is in a vertical orientation and consists of 1 N and 5 C atoms. N with a positive charge occupies the bottom-most vertex. It is bound to H. C 1 occupies the bottom-left vertex. A double bond is present between N and C 1, C 2 and C 3, and C 4 and C 5. C 2 is single bonded to C H 2 on the upper left in the form of a line. C H 2 is single-bonded to O P O 3 superscript 2 minus on the lower left. C 3 is single bonded to C above. This C is double-bonded

to N superscript plus on the upper left and single-bonded to H on the upper right. N superscript plus is single-bonded to H on the lower right and single-bonded to a 4-carbon alkane chain depicted as a line structure using 3 zigzag lines. The alkane chain is labeled lysine which is single-bonded to an enzyme. C 4 of the ring is single bonded to O superscript minus on the upper right. C 5 is single bonded to C H 3 on the lower right.

The structure of pyridoxamine phosphate is as follows: A 6-membered heterocyclic hexagonal ring is in a vertical orientation and consists of 1 N and 5 C atoms. N occupies the bottom-most vertex. It has a positive charge and is bound to H. C 1 occupies the bottom-left vertex. A double bond is present between N and C 1, C 2 and C 3, and C 4 and C 5. C 2 is single bonded to C H 2 on the upper left in the form of a line. C H 2 is single-bonded to O P O 3 superscript 2 minus on the lower left. C 3 is single bonded to C above. This C is single bonded to H on the left, H on the upper left, and N H 3 superscript plus on the upper right. C 4 is single bonded to O superscript minus on the upper right. C 5 is single bonded to C H 3 on the lower right.

In the second step, pyridoxamine phosphate is reversibly converted into ketimine with the simultaneous entry of a compound and release of H 2 O.

The structure of this compound is as follows: A central C atom is single bonded to R on the upper left, double bonded to O below, and single bonded to C O O superscript minus on the upper right.

The structure of ketimine is as follows: A 6-membered heterocyclic hexagonal ring is in a vertical orientation and consists of 1 N and 5 C atoms. N superscript plus bound to H occupies the bottom-most vertex. C 1 occupies the bottom-left vertex. A double bond is present between N and C 1, C 2 and C 3, and C 4 and C 5. C 2 is single bonded

to C H 2 on the upper left in the form of a line. C H 2 is single-bonded to O P O 3 superscript 2 minus on the lower left. C 3 is single bonded to C above. This C is single-bonded to N superscript plus on the upper right, single-bonded to H on the upper left, and single-bonded to H on the lower right. The N superscript plus is single-bonded to H on the right and double-bonded to C above. The C atom is single bonded to R on the upper left and single bonded to C O O superscript minus on the upper right. C 4 of the ring is single bonded to O superscript minus on the upper right. C 5 is single bonded to C H 3 on the lower right. An arrow points from H single bonded to C above toward the single bond between this C and C 3 of the ring. A second arrow points from the double bond between C 2 and C 3 toward the single bond between C 1 and C 2. A third arrow points from the double bond between C 1 and N toward the N atom.

In the third reversible step, ketimine is converted into a quinonoid intermediate with the simultaneous release of H superscript plus ion.

The structure of the quinonoid intermediate is as follows: A 6-membered heterocyclic hexagonal ring is in a vertical orientation and consists of 1 N and 5 C atoms. N bound to H occupies the bottom-most vertex. C 1 occupies the bottom-left vertex. A double bond is present between C 1 and C 2, and C 4 and C 5. C 2 is single bonded to C H 2 on the upper left in the form of a line. C H 2 is single-bonded to O P O 3 superscript 2 minus on the lower left. C 3 is double bonded to C above. This C is single-bonded to N superscript plus on the upper right and single-bonded to H on the upper left. The N superscript plus is single-bonded to H on the right and double-bonded to C above. The C atom is single bonded to R on the upper left and single bonded to C O O superscript minus on the upper right. C 4 of the ring is single bonded to O superscript minus on the upper right. C 5 is single bonded to C H 3 on the lower right. An arrow from the N atom of the ring points toward the single bond

between N and C 1. A second arrow points from the double bond between C 1 and C 2 toward the single bond between C 2 and C 3. A third arrow points from the double bond between C 3 of the ring and C toward the single bond between C and N superscript plus.

In the fourth reversible step, the quinonoid intermediate is converted into external aldimine with the simultaneous addition of H superscript plus.

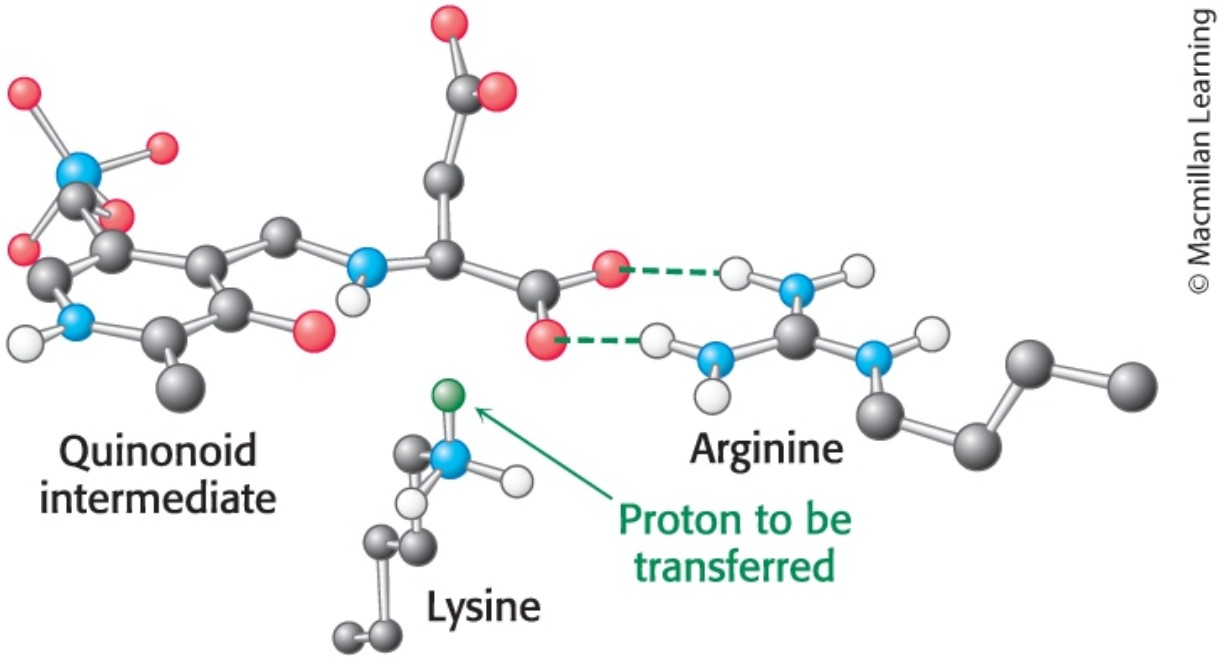
The structure of external aldimine: A 6-membered heterocyclic hexagonal ring is in a vertical orientation and consists of 1 N and 5 C atoms. N with a positive charge occupies the bottom-most vertex. It is bound to H. C 1 occupies the bottom-left vertex. A double bond is present between N and C 1, C 2 and C 3, and C 4 and C 5. C 2 is single bonded to C H 2 on the upper left in the form of a line. C H 2 is single-bonded to O P O 3 superscript 2 minus on the lower left. C 3 is single bonded to C above. This C is double-bonded to N superscript plus on the upper left and single-bonded to H on the upper right. The N superscript plus atom is single-bonded to H on the lower right and single-bonded to a central C atom above. This C is wedge bonded to R on the upper left, single bonded to C O O superscript minus on the upper right, and dash bonded to H above. C 4 of the ring is single bonded to O superscript minus on the upper right. C 5 is single bonded to C H 3 on the lower right.

In the fifth reversible step, external aldimine is converted back to internal aldimine with the simultaneous release of L-amino acid.

The structure of L-amino acid is as follows: A central C atom is single bonded to N H 3 superscript plus below, wedge bonded to R on the upper left, dash bonded to H above, and single bonded to C O O superscript minus on the upper right.

Return to FIGURE 25.7 Transamination is a critical step in the biosynthesis of most amino acids

Extended description for FIGURE 25.8 Proton addition during transamination establishes amino acid stereochemistry



© Macmillan Learning

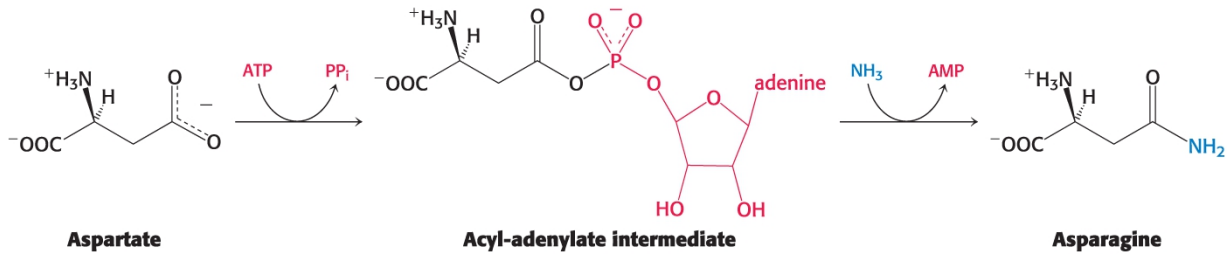
The ball-and-stick model of quinonoid intermediate, arginine, and lysine is shown. The quinonoid intermediate is laying flat. It consists of a hexagonal ring composed of 1 blue and 5 black spheres. The blue sphere is connected to a white sphere. All the black spheres except the top left sphere are connected to different substituent groups. The top right black sphere is connected to a horizontal chain composed of one blue and three black spheres. The blue sphere occupies the second position and is connected to a white sphere toward the observer. The second black sphere is connected to a vertical chain of 2 black spheres. The terminal black sphere of this chain is connected to two red spheres. The third black sphere of the horizontal chain is connected to two red spheres. A dashed line

connects these two red spheres to two different white spheres of arginine residue on the right.

The side chain of lysine residue is located below the horizontal chain connected to the top right black sphere of the ring. The side chain consists of 5 black spheres. The top black sphere is connected to a blue sphere on the right. This blue sphere is connected to a green sphere above, a white sphere on the lower left, and a white sphere on the lower right. An arrow pointing toward the green sphere is labeled "Proton to be transferred." The green sphere is aligned directly below the second black sphere of the horizontal chain.

Return to FIGURE 25.8 Proton addition during transamination establishes amino acid stereochemistry

Extended description for Conversion of aspartate to asparagine



In the first step, aspartate is irreversibly converted into acyl-adenylate intermediate with the simultaneous breakdown of A T P to P P subscript i.

The structure of aspartate is as follows: A 3-carbon alkane chain is depicted as a line structure using 2 zigzag lines. C 1 is single bonded to C O O superscript minus on the lower left, wedge bonded to N H 3 superscript plus on the upper left, and dash bonded to H on the upper right. C 3 is partially double bonded to O above and O on the lower right. The O atoms have an overall negative charge.

The structure of the acyl-adenylate intermediate is as follows: A 5-membered heterocyclic pentagonal ring is in a vertical orientation and consists of 1 O and 4 C atoms. O occupies the topmost vertex. C 1 is single bonded to adenine on the upper right. C 2 and C 3 are single bonded to O H below. C 4 is single bonded to O above. The O atom is single-bonded to P on the upper left. This P atom is partially double-bonded to O on the upper left, partially double-bonded to O on the upper right, and single-bonded to O on the lower left. The O atoms on the upper left and upper right have an overall negative charge. The lower left O is single bonded to C 3 of a 3-carbon alkane chain depicted as a line structure using 2 zigzag lines. In the alkane chain, C 1 is single bonded to C O O superscript minus on the lower

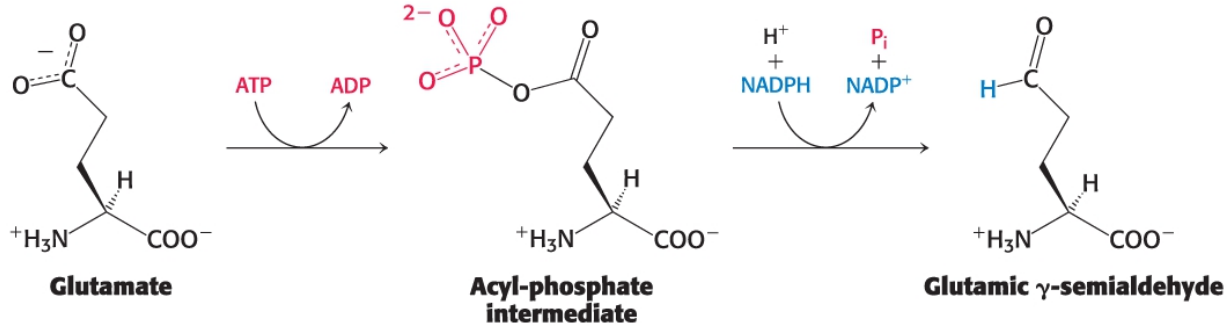
left, wedge bonded to N H 3 superscript plus on the upper left, and dash bonded to H on the upper right. C 3 is double bonded to O above.

In the second step, the acyl-adenylate intermediate is irreversibly converted into asparagine with the simultaneous entry of N H 3 and release of A M P.

The structure of asparagine is as follows: A 3-carbon alkane chain is depicted as a line structure using 2 zigzag lines. C 1 is single bonded to C O O superscript minus on the lower left, wedge bonded to N H 3 superscript plus on the upper left, and dash bonded to H on the upper right. C 3 is double bonded to O above and single bonded to N H 2 on the lower right.

Return to Conversion of aspartate to asparagine

Extended description for Conversion of glutamate to glutamic gamma-semialdehyde



In the first irreversible step, glutamate is converted into an acyl-phosphate intermediate with the simultaneous breakdown of A T P to A D P.

The structure of glutamate is as follows: A central C atom is single bonded to N H 3 superscript plus on the lower left, single bonded to C O O superscript minus on the lower right, wedge bonded to C H 2 on the upper left, and dash bonded to H on the upper right. The C H 2 group is single-bonded to another C H 2 group on the upper right in the form of a line. This C H 2 is single-bonded to C on the upper left. This C is partially double bonded to O above and O on the lower left. The O atoms have an overall negative charge.

The structure of the acyl-phosphate intermediate is as follows: A central C atom is single bonded to N H 3 superscript plus on the lower left, single bonded to C O O superscript minus on the lower right, wedge bonded to C H 2 on the upper left, and dash bonded to H on the upper right. The C H 2 group is single-bonded to another C H 2 group on the upper right in the form of a line. This C H 2 is single-bonded to C on the upper left. This C is double bonded to O above and single bonded to O on the lower left. The lower left O

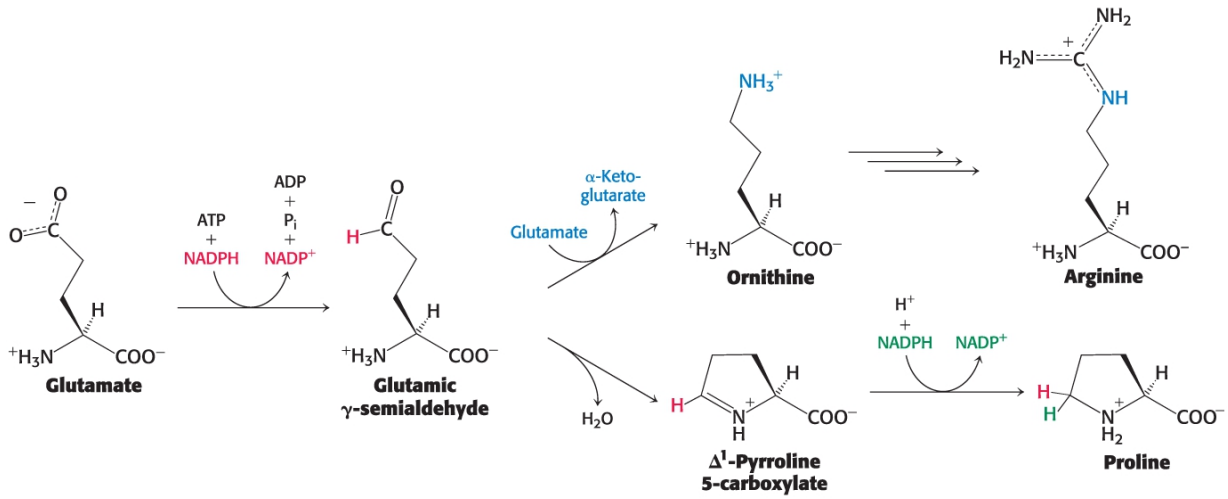
atom is single-bonded to P on the upper left. This P is partially double-bonded to O on the upper left, O on the upper right, and O on the lower left. The O atoms have an overall negative charge.

In the second irreversible step, the acyl-phosphate intermediate is converted into glutamic gamma-semialdehyde with the simultaneous oxidation of N A D P H plus H superscript plus to N A D P superscript plus and release of P subscript i.

The structure of glutamic gamma-semialdehyde is as follows: A central C atom is single bonded to N H 3 superscript plus on the lower left, single bonded to C O O superscript minus on the lower right, wedge bonded to C H 2 on the upper left, and dash bonded to H on the upper right. The C H 2 group is single-bonded to another C H 2 group on the upper right in the form of a line. This C H 2 is single-bonded to C on the upper left. This C is double bonded to O above and single bonded to H on the lower left.

Return to Conversion of glutamate to glutamic gamma-semialdehyde

Extended description for Formation of arginine and proline from glutamate



In the first irreversible step, glutamate is converted into glutamic gamma-semialdehyde with the simultaneous oxidation of N A D P H to N A D P superscript plus and breakdown of A T P to A D P plus P subscript i.

The structure of glutamate is as follows: A central C atom is single bonded to N H 3 superscript plus on the lower left, single bonded to C O O superscript minus on the lower right, wedge bonded to C H 2 on the upper left, and dash bonded to H on the upper right. The C H 2 group is single-bonded to another C H 2 group on the upper right in the form of a line. This C H 2 is single-bonded to C on the upper left. This C is partially double bonded to O above and O on the lower left. The O atoms have an overall negative charge.

The structure of glutamic gamma-semialdehyde is as follows: A central C atom is single bonded to N H 3 superscript plus on the lower left, single bonded to C O O superscript minus on the lower right, wedge bonded to C H 2 on the upper left, and dash bonded to

H on the upper right. The C H 2 group is single-bonded to another C H 2 group on the upper right in the form of a line. This C H 2 is single-bonded to C on the upper left. This C is double bonded to O above and single bonded to H on the lower left.

Glutamic gamma-semialdehyde can be channeled into two distinct paths. The first path leads to the formation of arginine. The second path leads to the formation of proline.

In the first path, glutamic gamma-semialdehyde is irreversibly converted into ornithine with the simultaneous conversion of glutamate into alpha-ketoglutarate.

The structure of ornithine is as follows: A central C atom is single bonded to N H 3 superscript plus on the lower left, single bonded to C O O superscript minus on the lower right, wedge bonded to C H 2 on the upper left, and dash bonded to H on the upper right. The C H 2 group is single-bonded to a 2-carbon alkane chain depicted using a single line. C 2 of this alkane chain is single bonded to N H 3 superscript plus on the upper right.

Three successive forward arrows from ornithine lead to arginine.

The structure of arginine is as follows: A central C atom is single bonded to N H 3 superscript plus on the lower left, single bonded to C O O superscript minus on the lower right, wedge bonded to C H 2 on the upper left, and dash bonded to H on the upper right. The C H 2 group is single-bonded to a 1 N and 2 C alkane chain depicted as a vertical line structure using 2 zigzag lines. N bound to H occupies the third position. N is partially double-bonded to C on the upper right. This C atom has a positive charge and is partially double-bonded to N H 2 on the left and partially double-bonded to N H 2 on the upper right.

In the second path, glutamic gamma-semialdehyde is irreversibly converted into delta superscript 1-pyrroline 5-carboxylate with the simultaneous release of H 2 O.

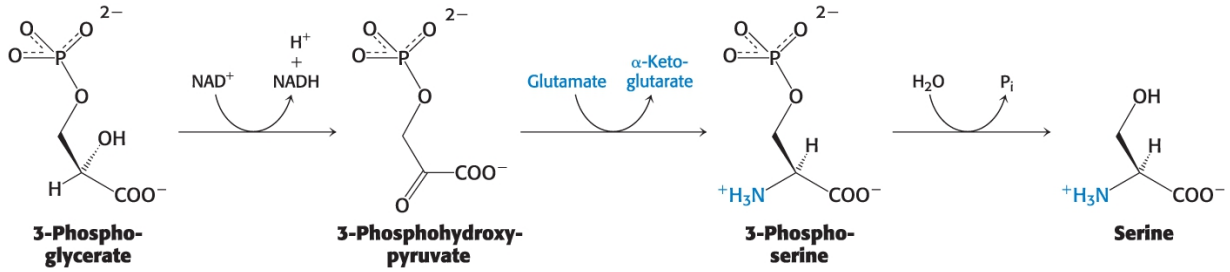
The structure of delta superscript 1-pyrroline 5-carboxylate is as follows: A central C atom is wedge bonded to C H 2 on the upper left, single bonded to N H with a positive charge on the lower left, dash bonded to H on the upper right, and single bonded to C O O superscript minus on the lower right. The upper left C H 2 group is single-bonded to a 2-carbon alkane chain depicted using a line. C 2 of this chain is double bonded to the N H group on the lower left such that a cyclic pentagonal-shaped ring structure is formed. C 2 is also single bonded to H on the lower left.

Later, delta superscript 1-pyrroline 5-carboxylate is irreversibly converted into proline with the simultaneous oxidation of N A D P H plus H superscript plus to N A D P superscript plus.

The structure of proline is as follows: A central C atom is wedge bonded to C H 2 on the upper left, single bonded to N H 2 with a positive charge on the lower left, dash bonded to H on the upper right, and single bonded to C O O superscript minus on the lower right. The upper left C H 2 group is single-bonded to a 2-carbon alkane chain depicted using a line. C 2 of this chain is single-bonded to the N H 2 group on the lower left such that a cyclic pentagonal-shaped ring structure is formed. C 2 is also single bonded to H on the upper left and lower left.

Return to Formation of arginine and proline from glutamate

Extended description for Formation of serine from 3-phosphoglycerate



In the first irreversible step, 3-phosphoglycerate is converted into 3-phosphohydroxypyruvate with the simultaneous reduction of N A D superscript plus to N A D H plus H superscript plus.

The structure of 3-phosphoglycerate is as follows: A central C atom is single bonded to H on the lower left, single bonded to C O O superscript minus on the lower right, wedge bonded to C H 2 on the upper left, and dash bonded to O H on the upper right. The C H 2 group is single-bonded to O on the upper right. This O is single-bonded to P on the upper left. This P is partially double-bonded to O on the left, O on the upper left, and O on the upper right. The O atoms have an overall negative charge of 2 minus.

The structure of 3-phosphohydroxypyruvate is as follows: A central C atom is double bonded to O on the lower left and single bonded to C O O superscript minus on the right, and single bonded to C H 2 on the upper left in the form of a line. The C H 2 group is single-bonded to O on the upper right. This O is single-bonded to P on the upper left. This P is partially double-bonded to O on the left, O on the upper left, and O on the upper right. The O atoms have an overall negative charge of 2 minus.

In the second irreversible step, 3-phosphohydroxypyruvate is converted into 3-phosphoserine with the simultaneous conversion of glutamate to alpha-ketoglutarate.

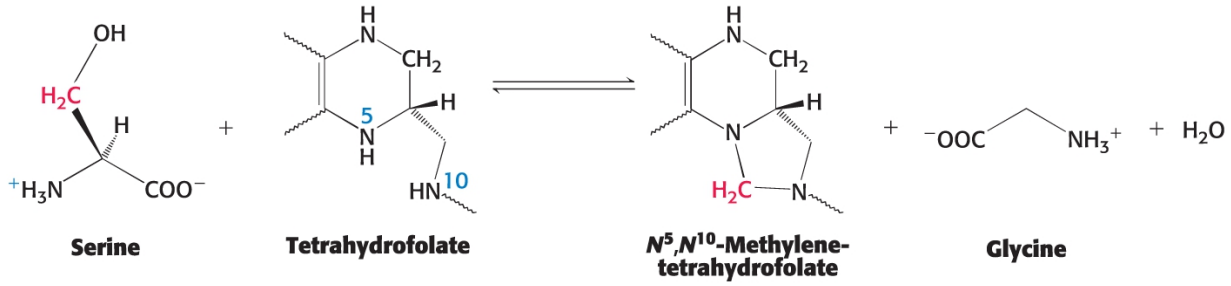
The structure of 3-phosphoserine is as follows: A central C atom is single bonded to N H 3 superscript plus on the lower left, single bonded to C O O superscript minus on the lower right, wedge bonded to C H 2 on the upper left, and dash bonded to H on the upper right. The C H 2 group is single-bonded to O on the upper right. This O is single-bonded to P on the upper left. This P is partially double-bonded to O on the left, O on the upper left, and O on the upper right. The O atoms have an overall negative charge of 2 minus.

In the third irreversible step, 3-phosphoserine is converted into serine with the simultaneous addition of H 2 O and release of P subscript i.

The structure of serine is as follows: A central C atom is single bonded to N H 3 superscript plus on the lower left, single bonded to C O O superscript minus on the lower right, wedge bonded to C H 2, single bond, O H on the upper left, and dash bonded to H on the upper right.

Return to Formation of serine from 3-phosphoglycerate

Extended description for Formation of glycine from serine



The reaction consists of two reactants and three products.

The first reactant is serine whose structure is as follows: A central C atom is single bonded to N H 3 superscript plus on the lower left, single bonded to C O O superscript minus on the lower right, wedge bonded to C H 2, single bond, O H on the upper left, and dash bonded to H on the upper right.

The second reactant is tetrahydrofolate whose structure is as follows: A 6-membered heterocyclic hexagonal ring is in a vertical orientation and consists of 2 N and 4 C atoms. First N occupies the topmost vertex and second occupies the bottom-most vertex. Both N atoms are bound to H. The second N is numbered 5. C 1 is bound to H 2. C 2 is wedge bonded to H on the upper right and dash bonded to C H 2 on the lower right. C H 2 is single bonded to N H below numbered 10. N H has a wiggly line on the lower right. C 3 and C 4 have a wiggly line and are double bonded to each other.

The first product is N superscript 5, N superscript 10-Methylene tetrahydrofolate whose structure is as follows: A 6-membered heterocyclic hexagonal ring is in a vertical orientation and consists of 2 N and 4 C atoms. First N occupies the topmost vertex and the

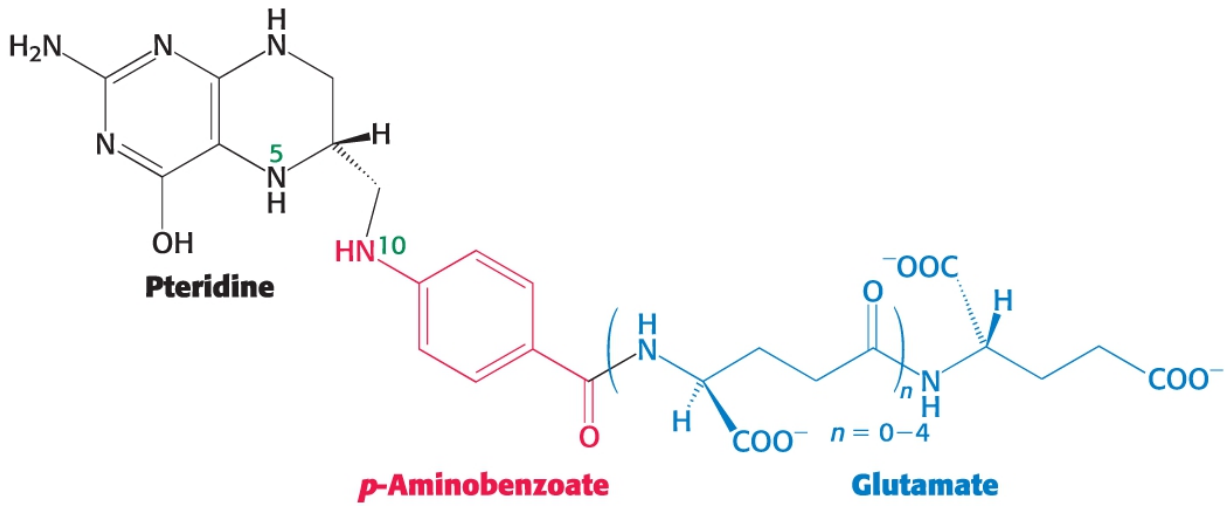
second N occupies the bottom-most vertex. First N atom is bound to H. C 1 is bound to H 2. C 2 is wedge bonded to H on the upper right and dash bonded to C H 2 on the lower right. C H 2 is single bonded to N below. N has a wiggly line on the lower right and is single-bonded to C H 2 on the left. This C H 2 is single-bonded to N 2 of the ring to form a pentagonal ring-like structure. C 3 and C 4 have a wiggly line and are double bonded to each other.

The second product is glycine whose structure is as follows: C O O superscript minus is single bonded to C H 2 on the upper right in the form of a line. C H 2 is single bonded to N H 3 superscript plus on the lower right.

The third product is H 2 O.

Return to Formation of glycine from serine

Extended description for FIGURE 25.9 Tetrahydrofolate is an important carrier of activated one-carbon units



The structure is as follows: A 6-membered heterocyclic hexagonal ring is in a vertical orientation and consists of 2 N and 4 C atoms. First N occupies the bottom left vertex and the second N occupies the topmost vertex. A double bond is present between C 1 and N 2, C 2 and C 3, and C 4 and N 1. C 1 is single bonded to N H 2 on the upper left. C 4 is single bonded to O H below. This ring is fused to a second 6-membered heterocyclic hexagonal ring in a vertical orientation such that C 2 and C 3 of the first ring are C 4 and C 3 respectively of the second ring. The second ring consists of 2 N and 4 C atoms. First N occupies the topmost vertex and the second N occupies the bottom-most vertex. Both N atoms are bound to H. The second N is numbered 5. C 2 is wedge bonded to H on the upper right and dash bonded to C H 2 on the lower right. The C H 2 group is single-bonded to the N H group of para-aminobenzoate. The fused rings are labeled pteridine.

The para-aminobenzoate consist of a benzene ring in a vertical orientation. The ring contains alternating double bonds between C 1

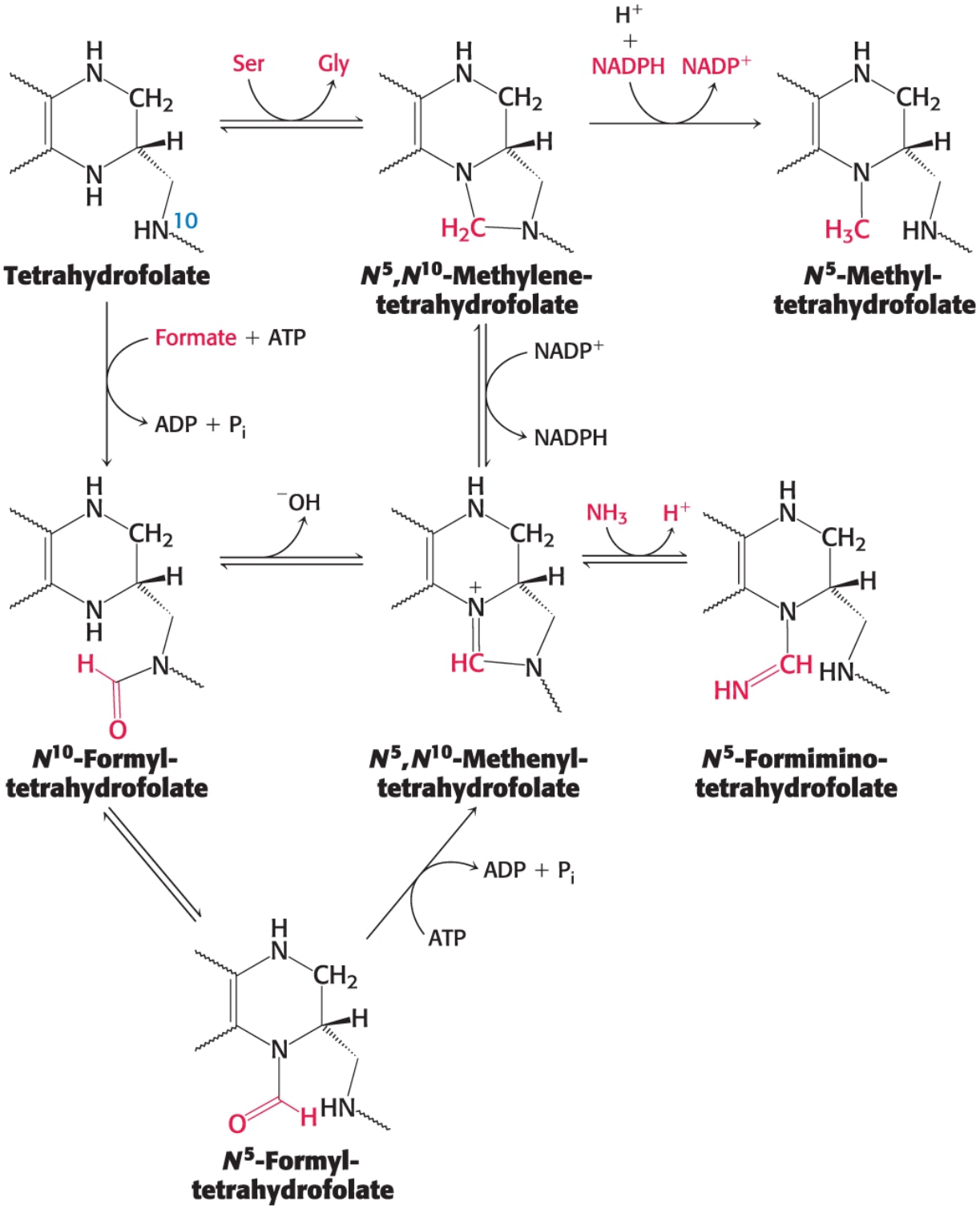
and C 2, C 3 and C 4, and C 5 and C 6. C 3 is single bonded to C on the lower right. This C is double bonded to O below and single bonded to the first N of glutamate. C 6 is single bonded to N H on the upper left numbered 10.

Glutamate consists of 2 N and 7 C heteronuclear alkane chain depicted as a line structure using 8 zigzag lines. First N bound to H occupies the first position. Second N bound to H occupies the sixth position. C 1 is dash bonded to H on the lower left and wedge bonded to C O O superscript minus on the lower right. C 4 is double bonded to O above. C 5 is dash bonded to C O O superscript minus on the upper left and wedge bonded to H on the upper right. C 7 is single bonded to C O O superscript minus on the lower right. First N to C 4 are enclosed in parenthesis with subscript n, where n equals 0 to 4.

Return to FIGURE 25.9 Tetrahydrofolate is an important carrier of activated one-carbon units

Extended description for FIGURE 25.10 Interconversion

of one carbon units attached to tetrahydrofolate



The figure shows four reaction sequences to depict the interconversion of one carbon units attached to tetrahydrofolate. The first reaction sequence shows the reversible conversion of tetrahydrofolate to N superscript 5, N superscript 10-Methylene tetrahydrofolate with the simultaneous conversion of serine to glycine. This is followed by irreversible conversion of N superscript 5, N superscript 10-Methylene tetrahydrofolate to N superscript 5-Methyl- tetrahydrofolate with the simultaneous oxidation of N A D P H plus H superscript plus to N A D P superscript plus.

The structure of tetrahydrofolate is as follows: A 6-membered heterocyclic hexagonal ring is in a vertical orientation and consists of 2 N and 4 C atoms. First N occupies the topmost vertex and second occupies the bottom-most vertex. Both N atoms are bound to H. C 1 is bound to H 2. C 2 is wedge bonded to H on the upper right and dash bonded to C H 2 on the lower right. C H 2 is single bonded to N H below numbered 10. N H has a wiggly line on the lower right. C 3 and C 4 have a wiggly line and are double bonded to each other.

The structure of N superscript 5, N superscript 10-Methylene tetrahydrofolate whose structure is as follows: A 6-membered heterocyclic hexagonal ring is in a vertical orientation and consists of 2 N and 4 C atoms. First N occupies the topmost vertex and the second N occupies the bottom-most vertex. First N atom is bound to H. C 1 is bound to H 2. C 2 is wedge bonded to H on the upper right and dash bonded to C H 2 on the lower right. C H 2 is single bonded to N below. N has a wiggly line on the lower right and is single-bonded to C H 2 on the left. This C H 2 is single-bonded to N 2 of the ring to form a pentagonal ring-like structure. C 3 and C 4 have a wiggly line and are double bonded to each other.

The structure of N superscript 5-Methyl tetrahydrofolate is as follows: A 6-membered heterocyclic hexagonal ring is in a vertical orientation and consists of 2 N and 4 C atoms. First N occupies the

topmost vertex and the second N occupies the bottom-most vertex. First N atom is bound to H. C 1 is bound to H 2. C 2 is wedge bonded to H on the upper right and dash bonded to C H 2 on the lower right. C H 2 is single bonded to N H below. N H has a wiggly line on the lower right. N 2 of the ring is single bonded to C H 3 below. C 3 and C 4 have a wiggly line and are double bonded to each other.

In the second reaction sequence, tetrahydrofolate is irreversibly converted into N superscript 10-Formyl tetrahydrofolate with the simultaneous entry of formate and the breakdown of A T P to A D P plus P subscript i. N superscript 10-Formyl tetrahydrofolate is further reversibly converted into N superscript 5-Formyl tetrahydrofolate.

The structure of N superscript 10-Formyl tetrahydrofolate is as follows: A 6-membered heterocyclic hexagonal ring is in a vertical orientation and consists of 2 N and 4 C atoms. First N occupies the topmost vertex and the second N occupies the bottom-most vertex. Both N atoms are bound to H. C 1 is bound to H 2. C 2 is wedge bonded to H on the upper right and dash bonded to C H 2 on the lower right. C H 2 is single bonded to N below. N has a wiggly line on the lower right and is single bonded to C on the lower right. This C is single bonded to H on the upper left and double bonded to O below. C 3 and C 4 have a wiggly line and are double bonded to each other.

The structure of N superscript 5-Formyl tetrahydrofolate is as follows: A 6-membered heterocyclic hexagonal ring is in a vertical orientation and consists of 2 N and 4 C atoms. First N occupies the topmost vertex and the second N occupies the bottom-most vertex. First N is bound to H. C 1 is bound to H 2. C 2 is wedge bonded to H on the upper right and dash bonded to C H 2 on the lower right. C H 2 is single bonded to N H below. N H has a wiggly line on the lower right. The second N of the ring is single bonded to C below. This C is single bonded to H on the lower right and double bonded to O on the

lower left. C 3 and C 4 have a wiggly line and are double bonded to each other.

In the third reaction sequence, N superscript 5, N superscript 10-Methylene tetrahydrofolate is reversibly converted into N superscript 5, N superscript 10-Methenyl tetrahydrofolate with the simultaneous reduction of N A D P superscript plus to N A D P H. N superscript 5, N superscript 10-Methenyl tetrahydrofolate is further irreversibly converted into N superscript 5-Formyl tetrahydrofolate with the simultaneous breakdown of A T P to A D P plus P subscript i.

The structure of N superscript 5, N superscript 10-Methenyl tetrahydrofolate is as follows: A 6-membered heterocyclic hexagonal ring is in a vertical orientation and consists of 2 N and 4 C atoms. First N occupies the topmost vertex and the second N occupies the bottom-most vertex. First N atom is bound to H. Second N has a positive charge. C 1 is bound to H 2. C 2 is wedge bonded to H on the upper right and dash bonded to C H 2 on the lower right. C H 2 is single bonded to N below. N has a wiggly line on the lower right and is single-bonded to C H on the left. This C H group is double-bonded to N 2 of the ring to form a pentagonal ring-like structure. C 3 and C 4 have a wiggly line and are double bonded to each other.

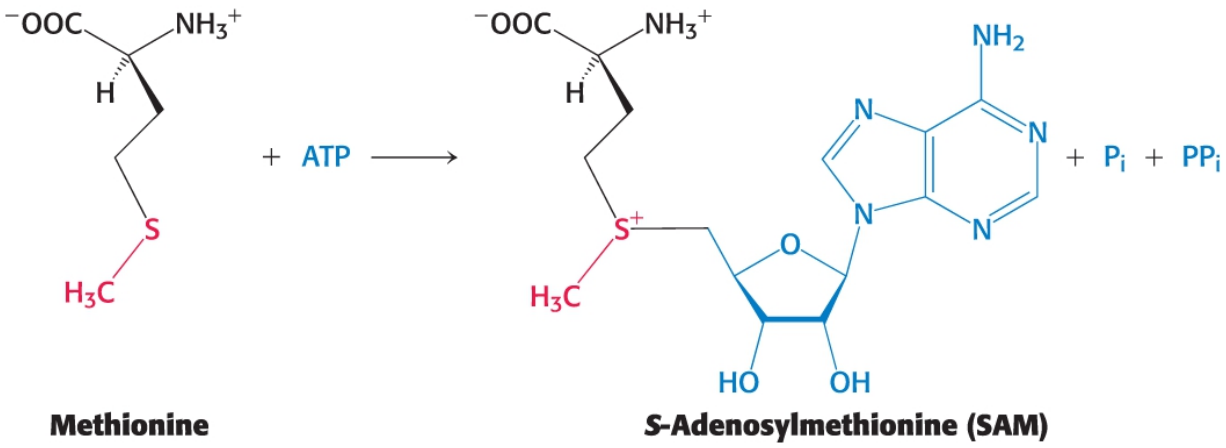
In the fourth reaction sequence, N superscript 10-Formyltetrahydrofolate is reversibly converted into N superscript 5, N superscript 10-Methenyl tetrahydrofolate with the simultaneous release of O H superscript minus. N superscript 5, N superscript 10-Methenyl tetrahydrofolate is further reversibly converted into N superscript 5-Formiminotetrahydrofolate with the simultaneous entry of N H 3 and release of H superscript plus.

The structure of N superscript 5-Formiminotetrahydrofolate is as follows: A 6-membered heterocyclic hexagonal ring is in a vertical

orientation and consists of 2 N and 4 C atoms. First N occupies the topmost vertex and the second N occupies the bottom-most vertex. The first N atom is bound to H. C 1 is bound to H 2. C 2 is wedge bonded to H on the upper right and dash bonded to C H 2 on the lower right. C H 2 is single bonded to N H below. N H has a wiggly line on the lower right. The second N is single bonded to C H below. This C H group is double-bonded to N H on the lower left. C 3 and C 4 have a wiggly line and are double bonded to each other.

Return to FIGURE 25.10 Interconversion of one carbon units attached to tetrahydrofolate

Extended description for Formation of S-adenosylmethionine from methionine



The reaction consists of two reactants and three products.

The first reactant is methionine whose structure is as follows: A central C atom is single bonded to C O O superscript minus on the upper left, single bonded to N H 3 superscript plus on the upper right, dash bonded to H on the lower left, and wedge bonded to C H 2 on the lower right. This C H 2 group is further single-bonded to C H 2 on the lower left in the form of a line. This C H 2 group is single-bonded to S on the lower right, which is further single-bonded to C H 3 on the lower left.

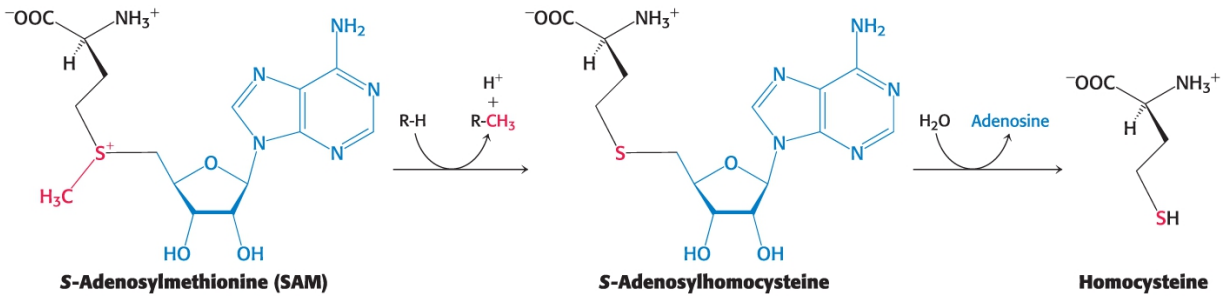
The second reactant is A T P.

The first product is S-adenosylmethionine (S A M) whose structure is as follows: A 5-membered heterocyclic pentagonal ring is in a vertical orientation and consists of 1 O and 4 C atoms. O occupies the topmost vertex. C 1 occupies the top right vertex. C 2 and C 3 are single bonded to O H below. C 4 is single-bonded to C H 2 above in the form of a line, which is further single-bonded to the S atom of

methionine. The S atom is positively charged. C 1 is single-bonded to N 1 of a 5-membered heterocyclic pentagonal ring in a horizontal orientation with C 1 occupying the leftmost vertex. This ring consists of 2 N and 3 C atoms. First N occupies the bottom left vertex and the second N occupies the topmost vertex. A double bond is present between C 1 and N 2. The pentagonal ring is fused to a 6-membered heterocyclic hexagonal ring in a vertical orientation such that C 2 and C 3 of the pentagonal ring are C 3 and C 2 of the hexagonal ring respectively. The hexagonal ring consists of 2 N and 4 C atoms. First N occupies the top right vertex and the second N occupies the bottom-most vertex. A double bond is present between C 1 and N 2, C 2 and C 3, and C 4 and N 1. C 4 is single bonded to N H 2 above. The second product is P subscript i. The third product is P P subscript i.

Return to Formation of S-adenosylmethionine from methionine

Extended description for Formation of homocysteine from S-adenosylmethionine



In the first step, S-adenosylmethionine (S A M) is irreversibly converted into S-adenosylhomocysteine with the simultaneous entry of R, single bond, H and release of R, single bond, C H 3 and H superscript plus.

The structure of S-adenosylmethionine (S A M) is as follows: A 5-membered heterocyclic pentagonal ring is in a vertical orientation and consists of 1 O and 4 C atoms. C 1 occupies the top right vertex. C 2 and C 3 are single bonded to O H below. C 4 is single-bonded to C H 2 above in the form of a line, which is further single-bonded to the S atom of methionine amino acid. The S atom is positively charged. C 1 is single-bonded to N 1 of a 5-membered heterocyclic pentagonal ring in a horizontal orientation with C 1 occupying the leftmost vertex. This ring consists of 2 N and 3 C atoms. First N occupies the bottom left vertex and the second N occupies the topmost vertex. A double bond is present between C 1 and N 2. The pentagonal ring is fused to a 6-membered heterocyclic hexagonal ring in a vertical orientation such that C 2 and C 3 of the pentagonal ring are C 3 and C 2 of the hexagonal ring respectively. The hexagonal ring consists of 2 N and 4 C atoms. First N occupies the top right vertex and the second N occupies the bottom-most vertex. A double bond is

present between C 1 and N 2, C 2 and C 3, and C 4 and N 1. C 4 is single bonded to N H 2 above.

The structure of S-adenosylhomocysteine is as follows: A 5-membered heterocyclic pentagonal ring is in a vertical orientation and consists of 1 O and 4 C atoms. O occupies the topmost vertex. C 1 occupies the top right vertex. C 2 and C 3 are single bonded to O H below. C 4 is single-bonded to C H 2 above in the form of a line, which is further single-bonded to the S atom on the left. S is single bonded to a 2-carbon alkane chain depicted using a single line. C 2 of this chain is wedge bonded to a C atom on the upper left. This C atom is single bonded to C O O superscript minus on the upper left, dash bonded to H on the lower left, and single bonded to N H 3 superscript plus on the upper right. C 1 of the pentagonal ring is single-bonded to N 1 of a 5-membered heterocyclic pentagonal ring in a horizontal orientation with C 1 occupying the leftmost vertex. This ring consists of 2 N and 3 C atoms. First N occupies the bottom left vertex and the second N occupies the topmost vertex. A double bond is present between C 1 and N 2. The pentagonal ring is fused to a 6-membered heterocyclic hexagonal ring in a vertical orientation such that C 2 and C 3 of the pentagonal ring are C 3 and C 2 of the hexagonal ring respectively. The hexagonal ring consists of 2 N and 4 C atoms. First N occupies the top right vertex and the second N occupies the bottom-most vertex. A double bond is present between C 1 and N 2, C 2 and C 3, and C 4 and N 1. C 4 is single bonded to N H 2 above.

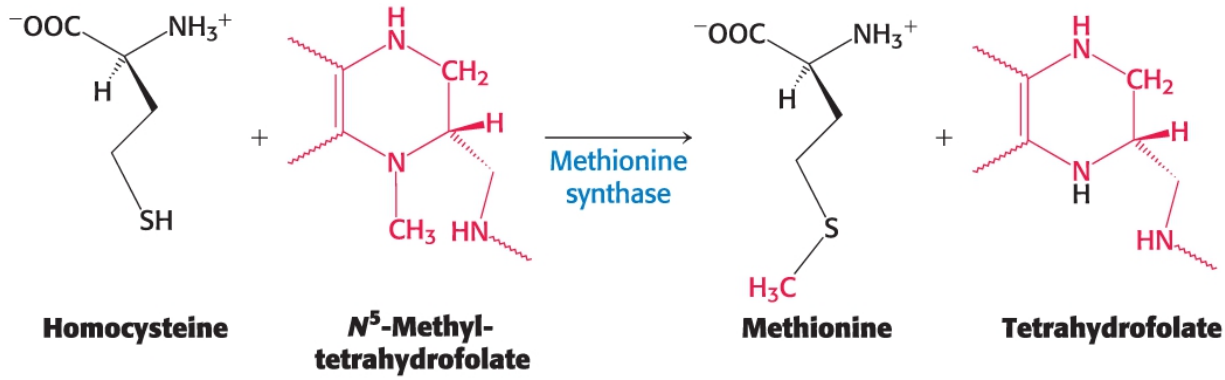
In the second step, S-adenosylhomocysteine is irreversibly converted into homocysteine with the simultaneous entry of H 2 O and release of adenosine.

The structure of homocysteine is as follows: A central C atom is single bonded to C O O superscript minus on the upper left, dash bonded to H on the lower left, single bonded to N H 3 superscript

plus on the upper right, and wedge bonded to a 2-carbon alkane chain depicted using a line. C 2 of this chain is single-bonded to S H on the lower right.

Return to Formation of homocysteine from S-adenosylmethionine

Extended description for Reaction catalyzed by methionine synthase



The reaction consists of two reactants and two products. It is catalyzed by methionine synthase.

The first reactant is homocysteine whose structure is as follows: A central C atom is single bonded to C O O superscript minus on the upper left, dash bonded to H on the lower left, single bonded to N H 3 superscript plus on the upper right, and wedge bonded to a 2-carbon alkane chain depicted using a line. C 2 of this chain is single-bonded to S H on the lower right.

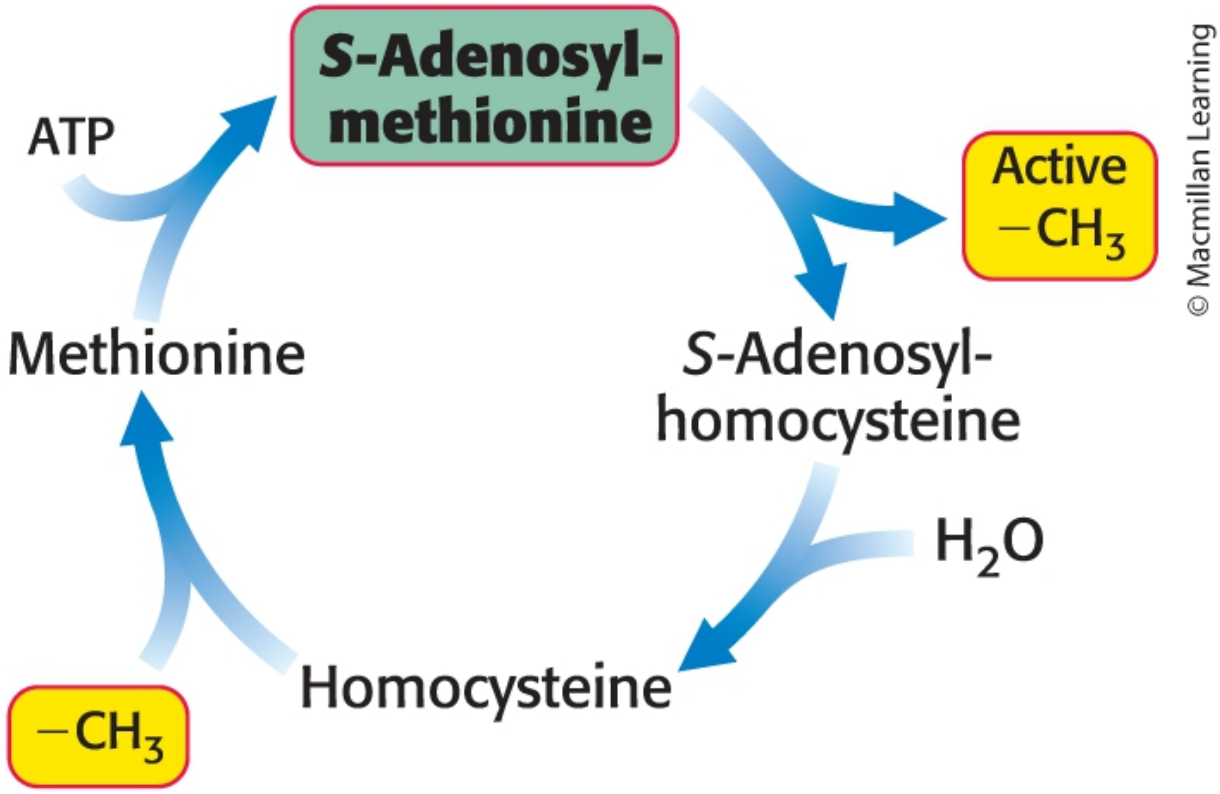
The second reactant is N superscript 5-Methyl tetrahydrofolate whose structure is as follows: A 6-membered heterocyclic hexagonal ring is in a vertical orientation and consists of 2 N and 4 C atoms. First N occupies the topmost vertex and the second N occupies the bottom-most vertex. First N atom is bound to H. C 1 is bound to H 2. C 2 is wedge bonded to H on the upper right and dash bonded to C H 2 on the lower right. C H 2 is single bonded to N H below. N H has a wiggly line on the lower right. N 2 of the ring is single bonded to C H 3 below. C 3 and C 4 have a wiggly line and are double bonded to each other.

The first product is methionine whose structure is as follows: A central C atom is single bonded to C O O superscript minus on the upper left, single bonded to N H 3 superscript plus on the upper right, dash bonded to H on the lower left, and wedge bonded to C H 2 on the lower right. This C H 2 group is further single-bonded to C H 2 on the lower left in the form of a line. This C H 2 group is single-bonded to S on the lower right, which is further single-bonded to C H 3 on the lower left.

The second product is tetrahydrofolate whose structure is as follows: A 6-membered heterocyclic hexagonal ring is in a vertical orientation and consists of 2 N and 4 C atoms. First N occupies the topmost vertex and second occupies the bottom-most vertex. Both N atoms are bound to H. C 1 is bound to H 2. C 2 is wedge bonded to H on the upper right and dash bonded to C H 2 on the lower right. C H 2 is single bonded to N H. N H has a wiggly line on the lower right. C 3 and C 4 have a wiggly line and are double bonded to each other.

Return to Reaction catalyzed by methionine synthase

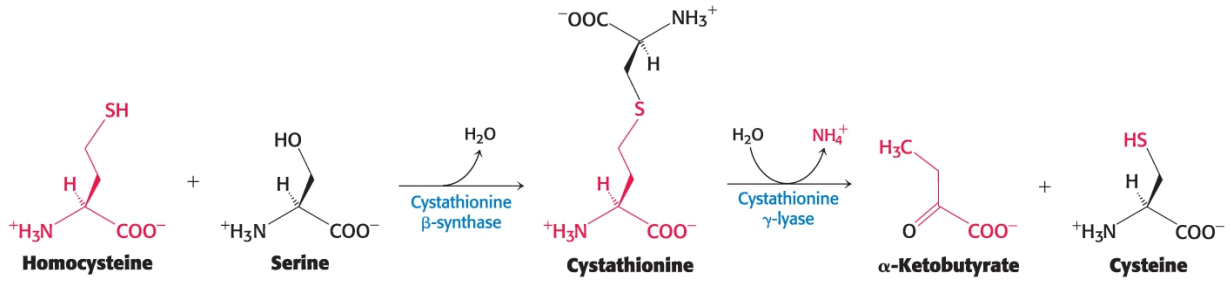
Extended description for FIGURE 25.11 The activated methyl cycle enables regeneration of methionine



The cycle is depicted as follows: S-adenosylmethionine is converted into S-adenosylhomocysteine with the simultaneous release of active C H 3. S-adenosylhomocysteine is converted into homocysteine with the concomitant entry of H 2 O. Homocysteine is further converted into methionine with the concomitant entry of C H 3. Methionine is converted back to S-adenosylmethionine with the concomitant entry of A T P.

Return to FIGURE 25.11 The activated methyl cycle enables regeneration of methionine

Extended description for Formation of alpha-ketobutyrate and cysteine



The reaction sequence consists of two reactants, one intermediate, and two products.

In the first irreversible step, homocysteine and serine are irreversibly converted into the intermediate called cystathionine by cystathionine beta-synthase. An H 2 O molecule is also released during this step.

The first reactant is homocysteine whose structure is as follows: A central C atom is single bonded to C O O superscript minus on the lower right, dash bonded to H on the upper left, single bonded to N H 3 superscript plus on the lower left, and wedge bonded on the upper right to a 2-carbon alkane chain depicted using a line. C 2 of this chain is single-bonded to S H on the upper right.

The second reactant is serine whose structure is as follows: A central C atom is single bonded to N H 3 superscript plus on the lower left, single bonded to C O O superscript minus on the lower right, wedge bonded to C H 2, single bond, O H on the upper right, and dash bonded to H on the upper left.

The intermediate is cystathione whose structure is as follows: A central C atom is single bonded to C O O superscript minus on the lower right, dash bonded to H on the upper left, single bonded to N H 3 superscript plus on the lower left, and wedge bonded on the upper right to a 2-carbon alkane chain depicted using a line. C 2 of this chain is single-bonded to S on the upper right. S is single bonded to C H 2 on the upper left. This C H 2 is wedge bonded to a C atom on the upper right. This C atom is single bonded to C O O superscript minus on the upper left, single bonded to N H 3 superscript plus on the upper right, and dash bonded to H on the lower right.

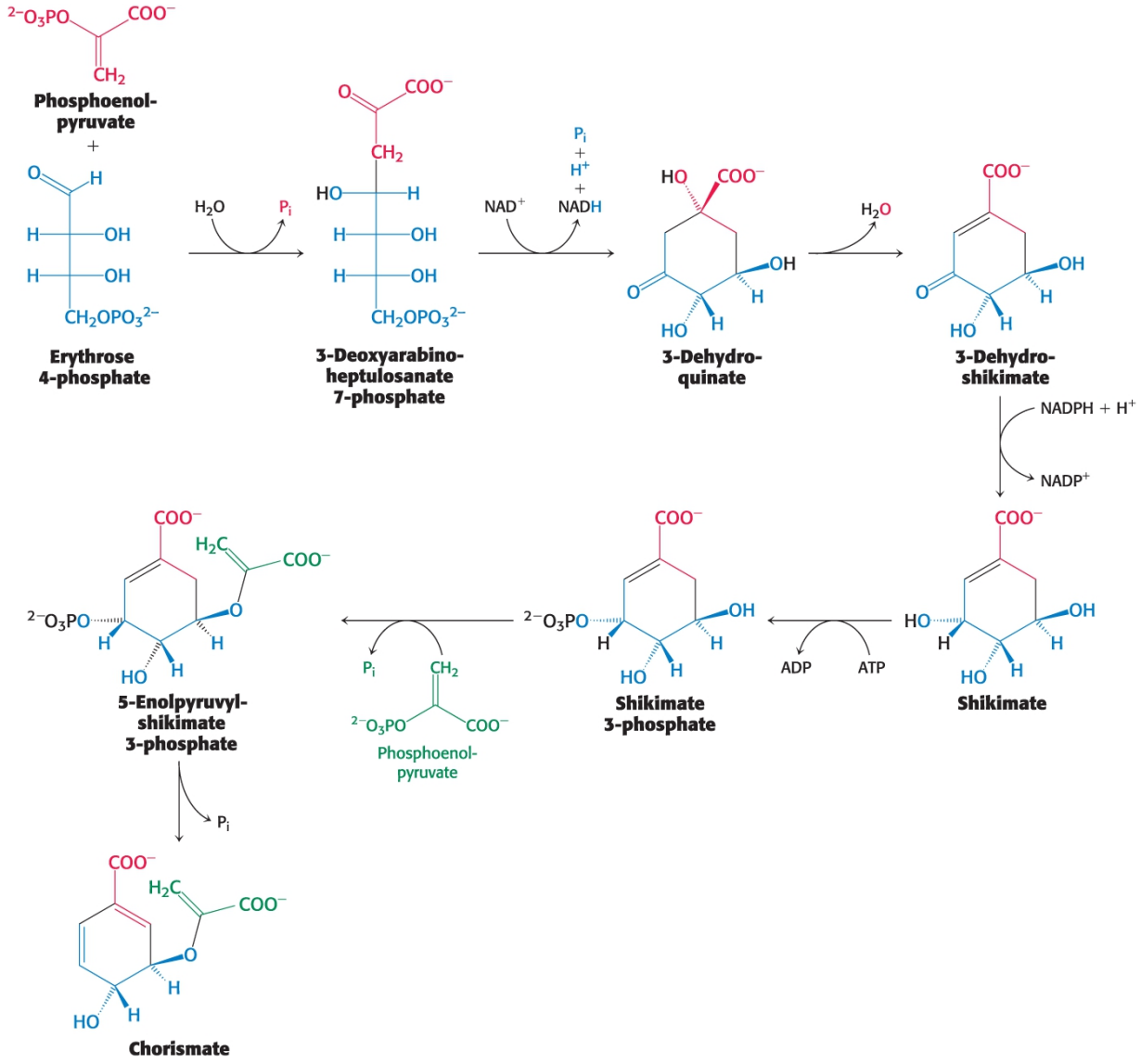
In the second irreversible step, cystathionine is converted into alpha-ketobutyrate and cysteine by cystathionine gamma-lyase. This step is coupled with the entry of H 2 O and release of N H 4 superscript plus.

The first product is alpha-ketobutyrate whose structure is as follows: A central C atom is double bonded to O on the lower left, single bonded to C O O superscript minus on the lower right, and single bonded to C H 2 above in the form of a line. This C H 2 is single bonded to C H 3 on the upper left.

The second product is cysteine whose structure is as follows: A central C atom is single bonded to N H 3 superscript plus on the lower left, wedge bonded to C H 2 on the upper right, dash bonded to H on the upper left, and single bonded to C O O superscript minus on the lower right. The C H 2 group is single-bonded to S H on the upper right.

Return to Formation of alpha-ketobutyrate and cysteine

Extended description for FIGURE 25.12 Chorismate is formed from phosphoenolpyruvate and erythrose 4-phosphate



In the first irreversible step, phosphoenolpyruvate and erythrose 4-phosphate are converted into 3-deoxyarabino-heptulosanate 7-phosphate. It is coupled with the entry of H 2 O and release of P subscript i.

The structure of phosphoenolpyruvate is as follows: A central C atom is single bonded to O P O 3 superscript 2 minus on the upper left, single bonded to C O O superscript minus on the upper right, and double bonded to C H 2 below.

The structure of erythrose 4-phosphate is as follows: C, single bond, C, single bond, C, single bond, C H 2 O P O 3 superscript 2 minus. C 1 is double-bonded to O on the upper left and single-bonded to H on the upper right. C 2 and C 3 are each single bonded to H on the left and O H on the right.

The structure of 3-deoxyarabino-heptulosanate 7-phosphate is as follows: C, single bond, C H 2, single bond, C, single bond, C, single bond, C, single bond, C H 2 O P O 3 superscript 2 minus. C 1 is double bonded to O on the upper left and single bonded to C O O superscript minus on the upper right. C 3 is single bonded to O H on the left and single bonded to H on the right. C 4 and C 5 are each single bonded to H on the left and O H on the right.

In the second irreversible step, 3-deoxyarabino-heptulosanate 7-phosphate is converted into 3-dehydroquinate. It is coupled with the reduction of N A D superscript plus to N A D H plus H superscript plus and the release of P subscript i.

The structure of 3-dehydroquinate is as follows: A 6-carbon homocyclic hexagonal ring is in a vertical orientation. C 1 occupies the topmost vertex. It is dash bonded to O H on the upper left and wedge bonded to C O O superscript minus on the upper right. C 3 is dash bonded to H on the lower right and wedge bonded to O H on the upper right. C 4 is dash bonded to O H on the lower left and wedge bonded to H on the lower right. C 5 is double bonded to O on the lower left.

In the third irreversible step, 3-dehydroquinate is converted into 3-dehydro-shikimate. It is coupled with the release of H 2 O.

The structure of 3-dehydro-shikimate is as follows: A 6-carbon homocyclic hexagonal ring is in a vertical orientation. C 1 occupies the topmost vertex. It is single bonded to C O O superscript minus above. C 3 is dash bonded to H on the lower right and wedge bonded to O H on the upper right. C 4 is dash bonded to O H on the lower left and wedge bonded to H on the lower right. C 5 is double bonded to O on the lower left. A double bond is present between C 6 and C 1.

In the fourth irreversible step, 3-dehydro-shikimate is converted into shikimate. It is coupled with the oxidation of N A D P H plus H superscript plus to N A D P superscript plus.

The structure of shikimate is as follows: A 6-carbon homocyclic hexagonal ring is in a vertical orientation. C 1 occupies the topmost vertex. It is single bonded to C O O superscript minus above. C 3 is dash bonded to H on the lower right and wedge bonded to O H on the upper right. C 4 is dash bonded to O H on the lower left and wedge bonded to H on the lower right. C 5 is dash bonded to O H on the left and wedge bonded to H on the lower left. A double bond is present between C 6 and C 1.

In the fifth irreversible step, shikimate is converted into shikimate 3-phosphate. This step is coupled with the hydrolysis of A T P to A D P.

The structure of shikimate 3-phosphate is as follows: A 6-carbon homocyclic hexagonal ring is in a vertical orientation. C 1 occupies the topmost vertex. It is single bonded to C O O superscript minus above. C 3 is dash bonded to H on the lower right and wedge bonded to O H on the upper right. C 4 is dash bonded to O H on the lower left and wedge bonded to H on the lower right. C 5 is dash bonded to

O P O 3 superscript 2 minus on the left and wedge bonded to H on the lower left. A double bond is present between C 6 and C 1.

In the sixth irreversible step, shikimate 3-phosphate is converted into 5-enolpyruvyl-shikimate 3-phosphate. This step is coupled with the entry of another molecule of phosphoenolpyruvate and the release of P subscript i.

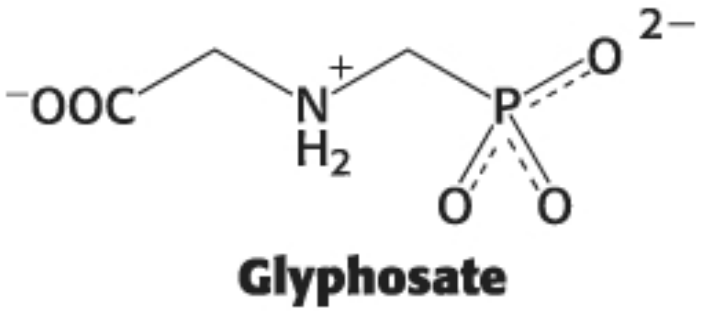
The structure of 5-enolpyruvyl-shikimate 3-phosphate is as follows: A 6-carbon homocyclic hexagonal ring is in a vertical orientation. C 1 occupies the topmost vertex. It is single bonded to C O O superscript minus above. C 3 is dash bonded to H on the lower right and wedge bonded to O on the upper right. This O is single-bonded to C on the upper right. This C is double bonded to C H 2 on the upper left and single bonded to C O O superscript minus on the upper right. C 4 is dash bonded to O H on the lower left and wedge bonded to H on the lower right. C 5 is dash bonded to O P O 3 superscript 2 minus on the left and wedge bonded to H on the lower left. A double bond is present between C 6 and C 1.

In the seventh irreversible step, 5-enolpyruvyl-shikimate 3-phosphate is converted into chorismate with the simultaneous release of P subscript i.

The structure of chorismate is as follows: A 6-carbon homocyclic hexagonal ring is in a vertical orientation. C 1 occupies the topmost vertex. It is single bonded to C O O superscript minus above. C 3 is dash bonded to H on the lower right and wedge bonded to O on the upper right. This O is single-bonded to C on the upper right. This C is double bonded to C H 2 on the upper left and single bonded to C O O superscript minus on the upper right. C 4 is dash bonded to O H on the lower left and wedge bonded to H on the lower right. A double bond is present between C 1 and C 2 and C 5 and C 6.

Return to FIGURE 25.12 Chorismate is formed from phosphoenolpyruvate and erythrose 4-phosphate

Extended description for Structure of glyphosate

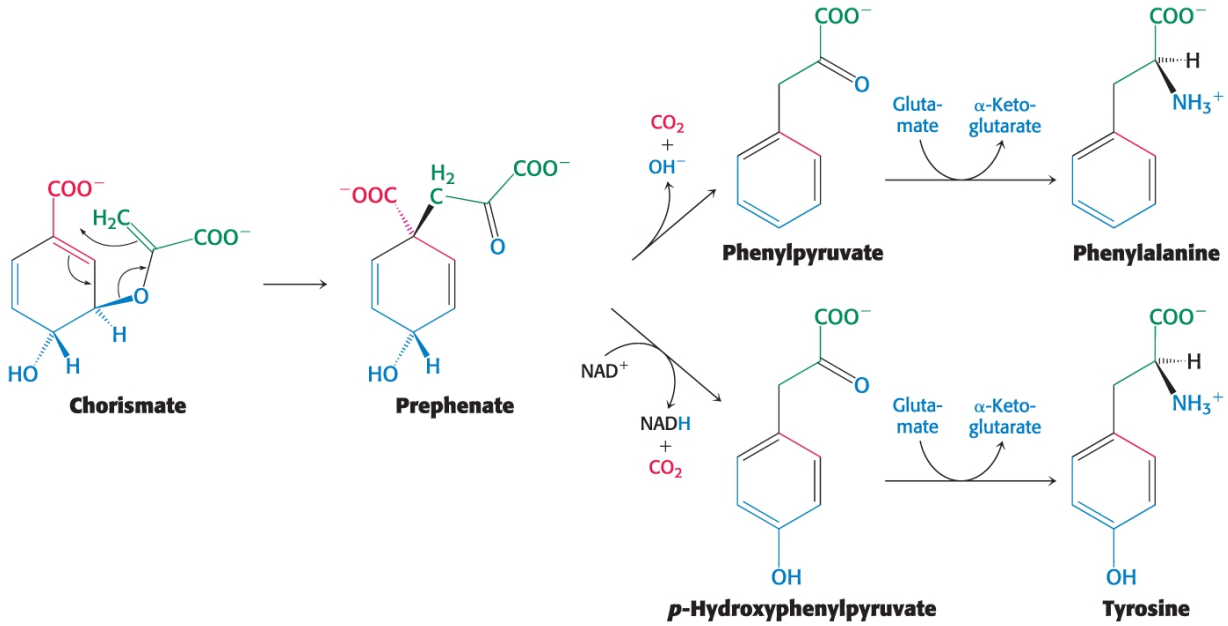


Glyphosate

The structure of glyphosate is as follows: A 1 N and 2 C heteronuclear alkane is depicted as a line structure using 2 zigzag lines. N with a positive charge occupies the second position. C 1 is single bonded to C O O superscript minus on the lower left. N with a positive charge is bound to H 2. C 2 is single bonded to P on the lower right. The P atom is partially double-bonded to O on the upper right, O on the lower left, and O on the lower right. The O atoms have an overall negative charge of 2 minus.

Return to Structure of glyphosate

Extended description for FIGURE 25.13 Phenylalanine and tyrosine are formed in the prephenate branch



In the first irreversible step, chorismate is converted into prephenate.

The structure of chorismate is as follows: A 6-carbon homocyclic hexagonal ring is in a vertical orientation. C 1 occupies the topmost vertex. It is single bonded to C O O superscript minus above. C 3 is dash bonded to H on the lower right and wedge bonded to O on the upper right. This O is single-bonded to C on the upper right. This C is double bonded to C H 2 on the upper left and single bonded to C O O superscript minus on the upper right. C 4 is dash bonded to O H on the lower left and wedge bonded to H on the lower right. A double bond is present between C 1 and C 2 and C 5 and C 6. An arrow from the double bond between C 1 and C 2 of the ring points toward the single bond between C 2 and C 3. A second arrow points from the wedge bond between C 3 and O toward the single bond

between O and upper right C. A third arrow points from the double bond between this C and C H 2 toward the single bond between C 1 and C O O superscript minus.

The structure of prephenate is as follows: A 6-carbon homocyclic hexagonal ring is in a vertical orientation. C 1 occupies the topmost vertex. It dash bonded to C O O superscript minus on the upper left, wedge bonded to C H 2 on the upper right. C H 2 is single bonded to C on the right. This C is single bonded to C O O superscript minus on the upper right and double bonded to O on the lower right. C 4 is dash bonded to O H on the lower left and wedge bonded to H on the lower right. A double bond is present between C 2 and C 3, and C 5 and C 6.

Prephenate follows two different paths. In the first path, prephenate is converted into phenylalanine. In the second path, prephenate is converted into tyrosine.

In the first path, prephenate is irreversibly converted into phenylpyruvate with the simultaneous release of C O 2 plus O H superscript minus.

The structure of phenylpyruvate is as follows: A benzene ring is in a vertical orientation with C 1 occupying the topmost vertex. It contains alternating double bonds between C 2 and C 3, C 4 and C 5, and C 6 and C 1. C 1 is single bonded to C H 2 above in the form of a line. This C H 2 is single-bonded to C on the upper right. C is single bonded to C O O superscript minus above and double bonded to O on the lower right.

Later, phenylpyruvate is irreversibly converted into phenylalanine. This step is coupled with the entry of glutamate and the release of alpha-ketoglutarate.

The structure of phenylalanine is as follows: A benzene ring is in a vertical orientation with C 1 occupying the topmost vertex. It contains alternating double bonds between C 2 and C 3, C 4 and C 5, and C 6 and C 1. C 1 is single bonded to C H 2 above in the form of a line. This C H 2 is single-bonded to C on the upper right. C is single bonded to C O O superscript minus above, dash bonded to H on the right, and wedge bonded to N H 3 superscript plus on the lower right.

In the second path, prephenate is irreversibly converted into para-hydroxyphenylpyruvate. This step is coupled with the reduction of N A D superscript plus to N A D H and the release of C O 2.

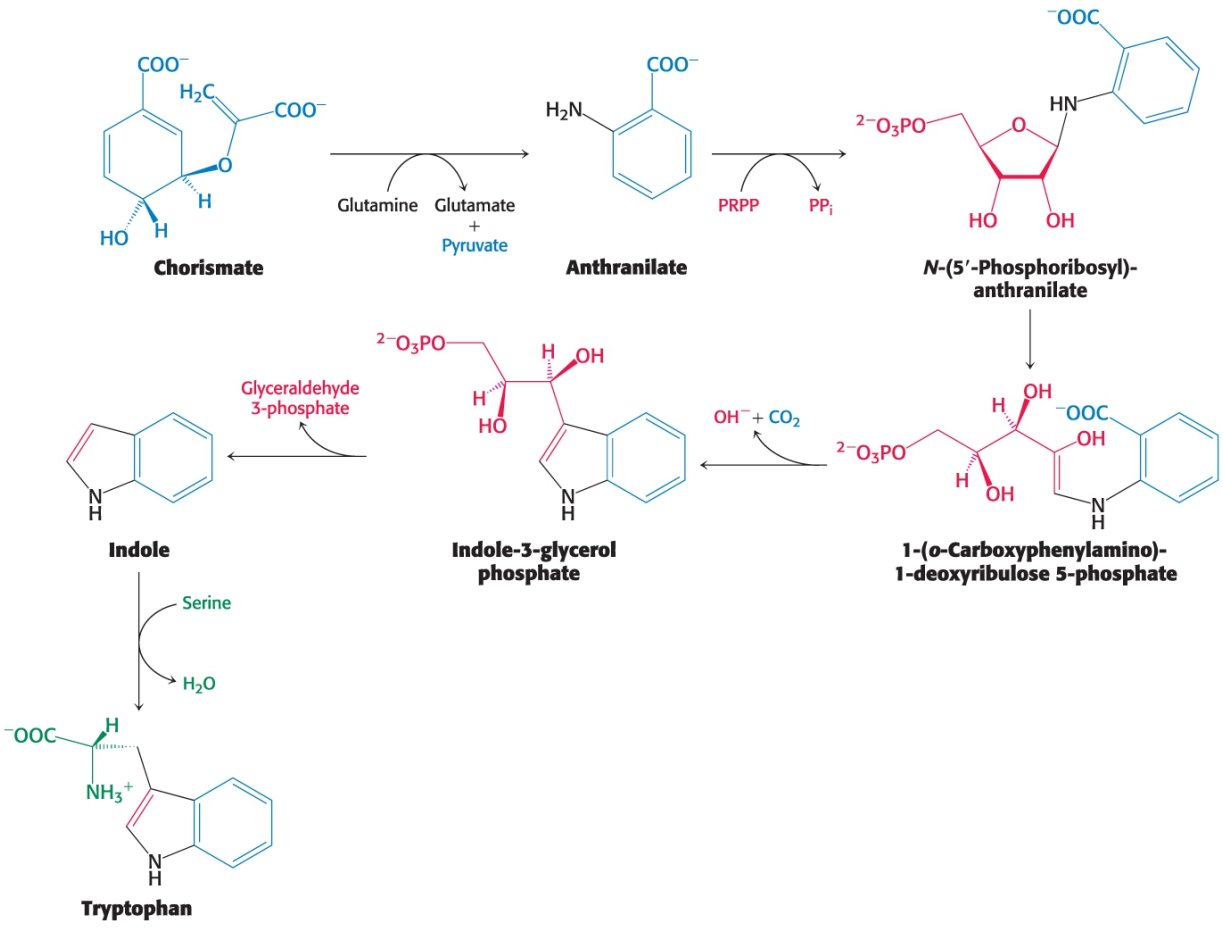
The structure of para-hydroxyphenylpyruvate is as follows: A benzene ring is in a vertical orientation with C 1 occupying the topmost vertex. It contains alternating double bonds between C 2 and C 3, C 4 and C 5, and C 6 and C 1. C 1 is single bonded to C H 2 above in the form of a line. This C H 2 is single-bonded to C on the upper right. C is single bonded to C O O superscript minus above and double bonded to O on the lower right. C 4 of the ring is single bonded to O H below.

Later, para-hydroxyphenylpyruvate is irreversibly converted into tyrosine. This step is coupled with the entry of glutamate and the release of alpha-ketoglutarate.

The structure of tyrosine is as follows: A benzene ring is in a vertical orientation with C 1 occupying the topmost vertex. It contains alternating double bonds between C 2 and C 3, C 4 and C 5, and C 6 and C 1. C 1 is single bonded to C H 2 above in the form of a line. This C H 2 is single-bonded to C on the upper right. C is single bonded to C O O superscript minus above, dash bonded to H on the right, and wedge bonded to N H 3 superscript plus on the lower right. C 4 of the ring is single bonded to O H below.

Return to FIGURE 25.13 Phenylalanine and tyrosine are formed in the prephenate branch

Extended description for FIGURE 25.14 Tryptophan is formed in the anthranilate branch



In the first irreversible step, chorismate is converted into anthranilate. It is coupled with the entry of glutamine and the release of glutamate plus pyruvate.

The structure of chorismate is as follows: A 6-carbon homocyclic hexagonal ring is in a vertical orientation. C 1 occupies the topmost vertex. It is single bonded to C O O superscript minus above. C 3 is dash bonded to H on the lower right and wedge bonded to O on the upper right. This O is single-bonded to C on the upper right. This C

is double bonded to C H 2 on the upper left and single bonded to C O O superscript minus on the upper right. C 4 is dash bonded to O H on the lower left and wedge bonded to H on the lower right. A double bond is present between C 1 and C 2 and C 5 and C 6.

The structure of anthranilate is as follows: A benzene ring is in a vertical orientation with C 1 occupying the topmost vertex. It contains alternating double bonds between C 2 and C 3, C 4 and C 5, and C 6 and C 1. C 1 is single bonded to C O O superscript minus above. C 5 is single bonded to N H 2 on the upper left.

In the second irreversible step, anthranilate is converted into N-open parenthesis 5 prime-Phosphoribosyl close parenthesis-anthranilate. This step is coupled with the entry of P R P P and release of P P subscript i.

The structure of N-open parenthesis 5 prime-Phosphoribosyl close parenthesis-anthranilate is as follows: A 5-membered heterocyclic pentagonal ring is in a vertical orientation. It consists of 1 O and 4 C atoms. O occupies the topmost vertex. C 1 is single bonded to N H. N H is further single bonded to C 5 of a benzene ring in a vertical orientation. The benzene ring contains alternating double bonds between C 1 and C 2, C 3 and C 4, and C 5 and C 6. C 6 is single bonded to C O O superscript minus on the upper left. C 2 and C 3 of the pentagonal ring are each single bonded to O H below. C 4 is single bonded to C H 2 on the upper left in the form of a line. C H 2 is single bonded to O P O 3 superscript 2 minus on the left.

In the third irreversible step, N-open parenthesis 5 prime-Phosphoribosyl close parenthesis-anthranilate is converted into 1-open parenthesis ortho-carboxyphenylamino close parenthesis-1-deoxyribulose 5-phosphate.

The structure of 1-open parenthesis ortho-carboxyphenylamino close parenthesis-1-deoxyribulose 5-phosphate is as follows: A benzene ring is in a vertical orientation with C 1 occupying the topmost vertex. It contains alternating double bonds between C 1 and C 2, C 3 and C 4, and C 5 and C 6. C 6 is single bonded to C O O superscript minus on the upper left. C 5 is single bonded to N H on the lower left. N H is single bonded to C H on the left in the form of a line. C H is double bonded to C above. This C is single bonded to O H on the upper right and single bonded to C 3 of a 3-carbon alkane chain, depicted using 2 zigzag lines, on the upper left. In the alkane chain, C 1 is single bonded to O P O 3 superscript 2 minus on the lower left. C 2 is dash bonded to H on the lower left and wedge bonded to O H on the lower right. C 3 is dash bonded to H on the upper left and wedge bonded to O H on the upper right.

In the fourth irreversible step, 1-open parenthesis ortho-carboxyphenylamino close parenthesis-1-deoxyribulose 5-phosphate is converted into indole-3-glycerol phosphate. This step is coupled with the release of C O 2 plus O H superscript minus.

The structure of indole-3-glycerol phosphate is as follows: A 5-membered heterocyclic pentagonal ring is in a horizontal orientation. It consists of 1 N and 4 C atoms. N bound to H occupies the bottom left vertex. A double bond is present between C 1 and C 2. It is fused to a benzene ring in a vertical orientation such that C 3 and C 4 of the pentagonal ring are C 6 and C 5 respectively of the benzene ring. The benzene ring contains alternating double bonds between C 1 and C 2, C 3 and C 4, and C 5 and C 6. C 2 of the pentagonal ring is single bonded to C 3 of a 3-carbon alkane chain depicted using 2 zigzag lines. In the alkane chain, C 1 is single bonded to O P O 3 superscript 2 minus on the left. C 2 is dash bonded to H on the lower left and wedge bonded to O H below. C 3 is dash bonded to H above and wedge bonded to O H on the upper right.

In the fifth irreversible step, indole-3-glycerol phosphate is converted into indole. It is coupled with the release of glyceraldehyde 3-phosphate.

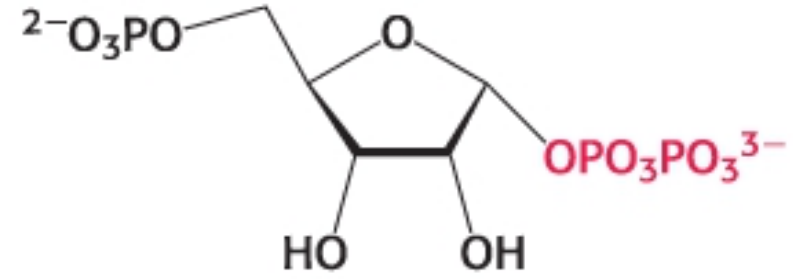
The structure of indole is as follows: A 5-membered heterocyclic pentagonal ring is in a horizontal orientation. It consists of 1 N and 4 C atoms. N bound to H occupies the bottom left vertex. A double bond is present between C 1 and C 2. It is fused to a benzene ring in a vertical orientation such that C 3 and C 4 of the pentagonal ring are C 6 and C 5 respectively of the benzene ring. The benzene ring contains alternating double bonds between C 1 and C 2, C 3 and C 4, and C 5 and C 6.

In the sixth irreversible step, indole is converted into tryptophan with the simultaneous entry of serine and release of H 2 O.

The structure of tryptophan is as follows: A 5-membered heterocyclic pentagonal ring is in a horizontal orientation. It consists of 1 N and 4 C atoms. N bound to H occupies the bottom left vertex. A double bond is present between C 1 and C 2. It is fused to a benzene ring in a vertical orientation such that C 3 and C 4 of the pentagonal ring are C 6 and C 5 respectively of the benzene ring. The benzene ring contains alternating double bonds between C 1 and C 2, C 3 and C 4, and C 5 and C 6. C 2 of the pentagonal ring is single-bonded to C H 2 on the upper left in the form of a line. C H 2 is dash bonded to C on the left. This C is single bonded to C O O superscript minus on the left, wedge bonded to H on the upper right, and single bonded to N H 3 superscript plus below.

Return to FIGURE 25.14 Tryptophan is formed in the anthranilate branch

Extended description for Structure of 5-phosphoribosyl-1-pyrophosphate



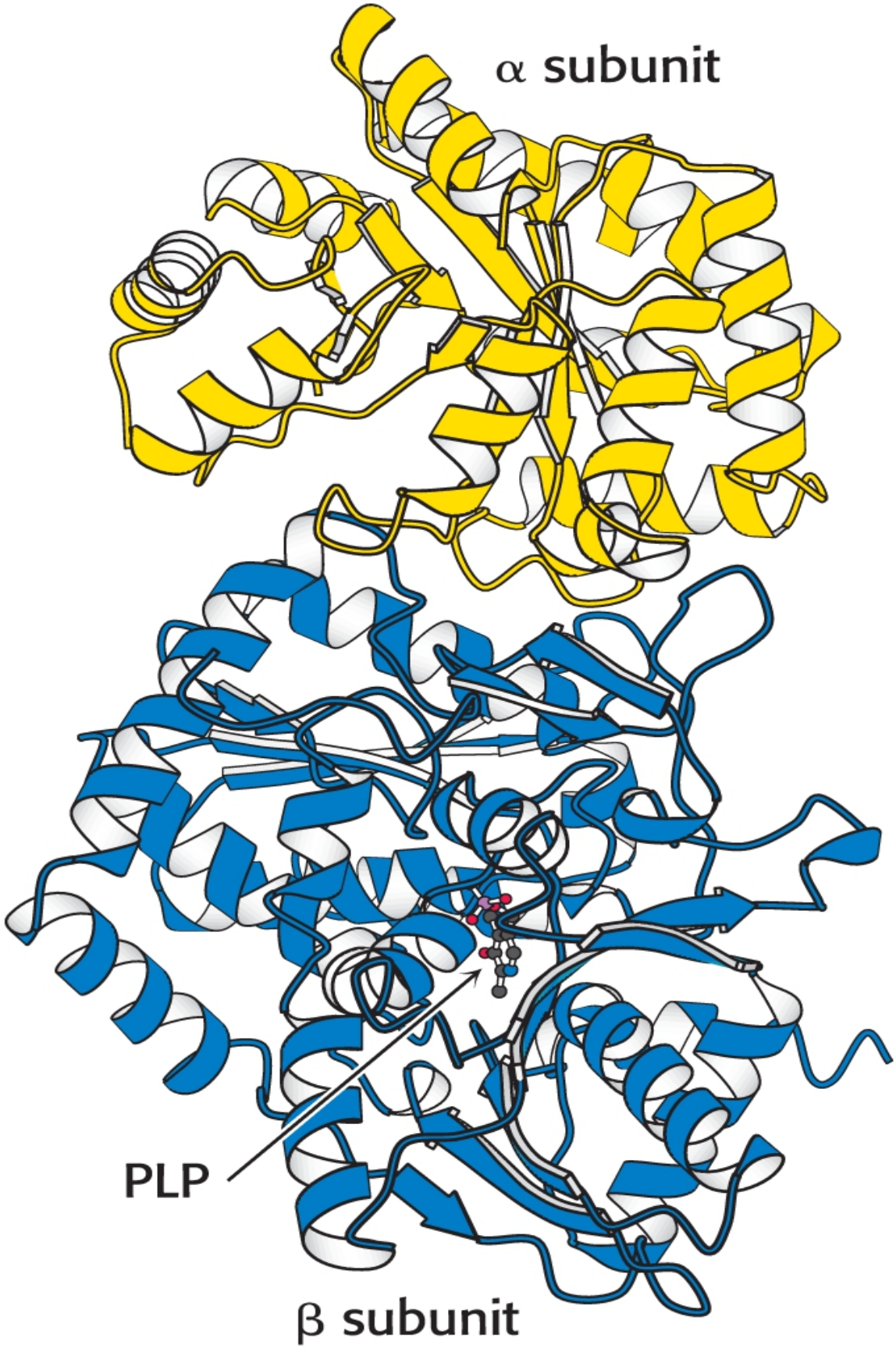
5-Phosphoribosyl-1-pyrophosphate (PRPP)

The structure of 5-phosphoribosyl-1-pyrophosphate (P R P P) is as follows: A 5-membered heterocyclic pentagonal ring is in a vertical orientation with C 1 occupying the top right vertex. It consists of 1 O and 4 C atoms. The ring is in a plane perpendicular to the plane of paper such that C 2 and C 3 are located toward the observer and O is located away from the observer. C 1 is single bonded to O P O 3 P O 3 superscript 3 minus below. C 2 and C 3 are each single bonded to O H below. C 4 is single bonded to C H 2 above in the form of a line. The C H 2 group is single bonded to O P O 3 superscript 2 minus on the left.

Return to Structure of 5-phosphoribosyl-1-pyrophosphate

Extended description for FIGURE 25.15 Tryptophan synthase contains two remotely positioned catalytic

domains



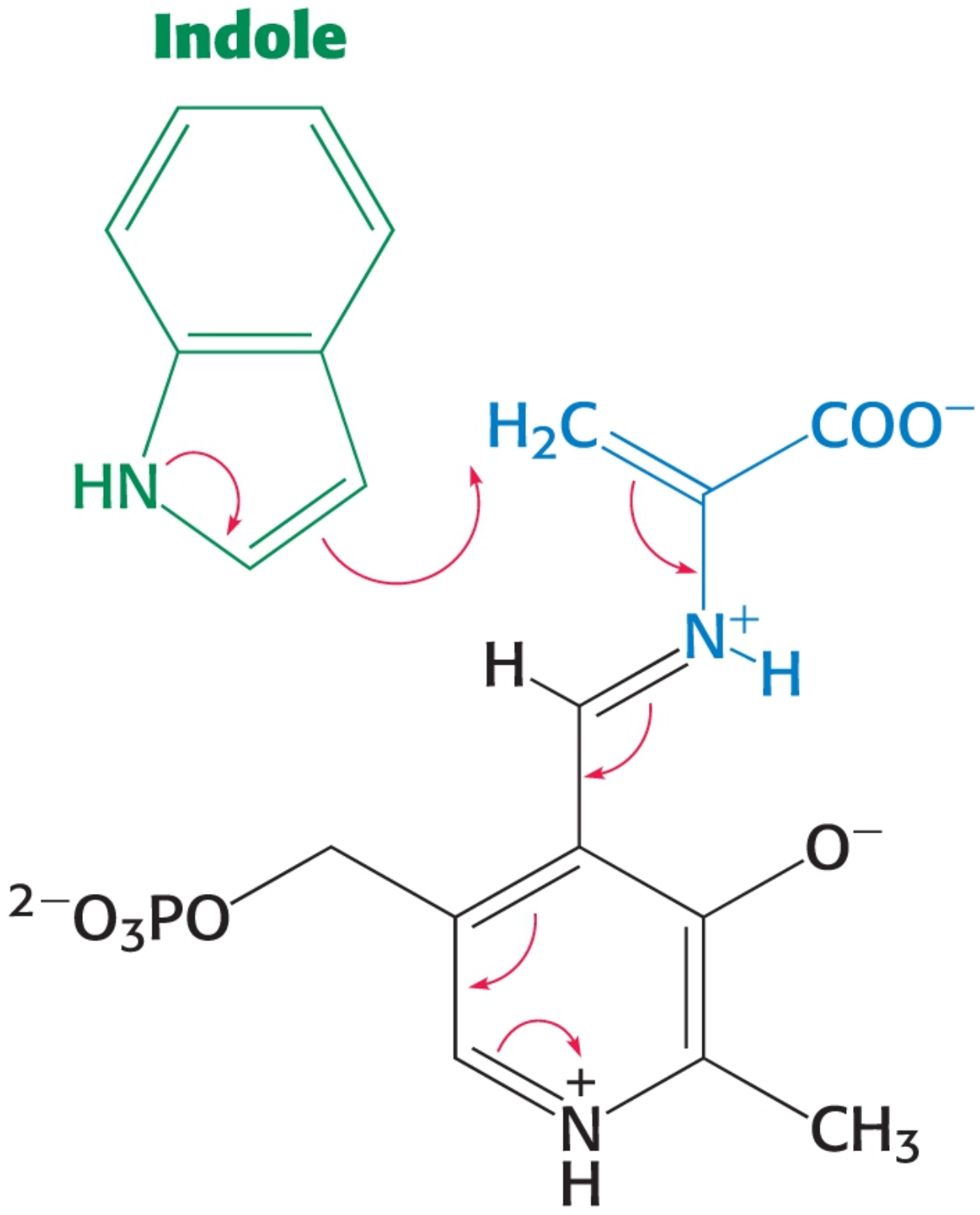
© Macmillan Learning

The ribbon diagram consists of the top alpha subunit shown in yellow and the bottom beta subunit shown in blue. The beta subunit is larger than the alpha subunit. They consist of several alpha-helices and a few beta-strands interconnected by thread-like loops. The beta subunit is bound to the ball-and-stick model of P L P in the center.

Return to FIGURE 25.15 Tryptophan synthase contains two remotely positioned catalytic domains

Extended description for Reaction between Schiff base

of aminoacrylate and indole



Schiff base of aminoacrylate
(derived from serine)

The structure of indole is as follows: A 5-membered heterocyclic pentagonal ring is in a vertical orientation. It consists of 1 N and 4 C atoms. N bound to H occupies the bottom left vertex. A double bond is present between C 3 and C 4. It is fused to a benzene ring in a horizontal orientation such that C 1 and C 2 of the pentagonal ring are C 3 and C 2 respectively of the benzene ring. The benzene ring contains alternating double bonds between C 2 and C 3, C 4 and C 5, and C 6 and C 1.

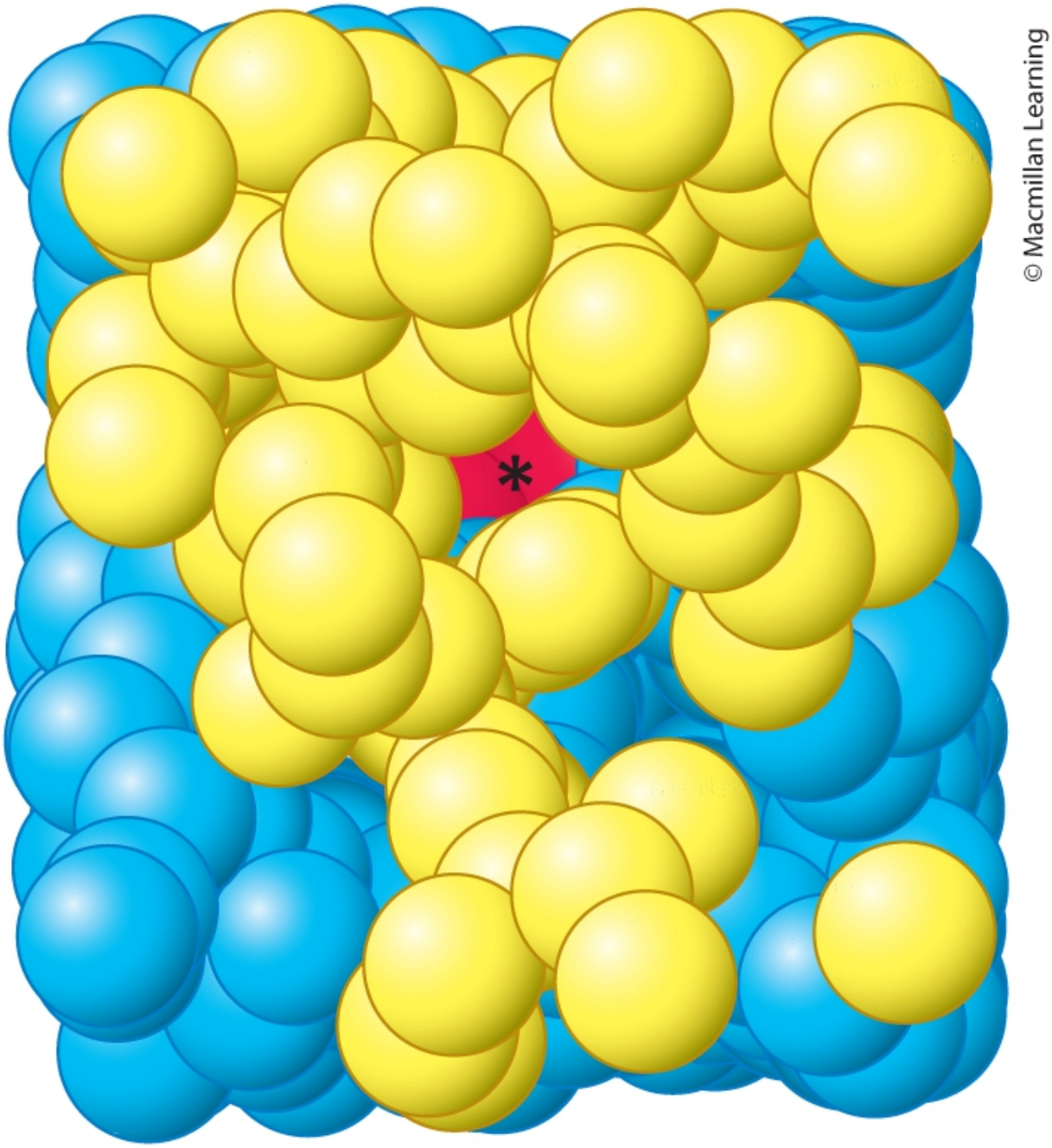
The structure of the Schiff base of aminoacrylate, derived from serine, is as follows: A 6-membered heterocyclic hexagonal ring is in a vertical orientation. It consists of 1 N and 5 C atoms. N with a positive charge bound to H occupies the bottom-most vertex. A double bond is present between N and C 1, C 2 and C 3, and C 4 and C 5. C 2 is single bonded to C H 2 on the upper left in the form of a line. C H 2 is single bonded to O P O 3 superscript 2 minus on the lower left. C 3 is single bonded to C above. This C is single bonded to H on the upper left and double bonded to N superscript plus on the upper right. This N superscript plus atom is single-bonded to H on the lower right and single-bonded to C above. This C is double bonded to C H 2 on the upper left and single bonded to C O O superscript minus on the upper right. C 4 is single bonded to O superscript minus on the upper right. C 5 is single bonded to C H 3 on the lower right.

An arrow from the N H group of indole points toward the single bond between the N H group and C 4 of the pentagonal ring. A second arrow points from the double bond between C 3 and C 4 points toward the C H 2 group of Schiff base of aminoacrylate. A third arrow from the double bond between this C H 2 group and C points toward the single bond between this C and N superscript plus atom. A fourth arrow points from the double bond between the N superscript plus atom and C toward the single bond between this C and C 3 of the ring. Inside the ring of the Schiff base, a fifth arrow

points from the double bond between C 2 and C 3 toward the single bond between C 1 and C 2. A sixth arrow points from the double bond between C 1 and N superscript plus atom toward the N superscript plus atom.

Return to Reaction between Schiff base of aminoacrylate and indole

Extended description for FIGURE 25.16 Tryptophan synthase uses substrate channeling to prevent loss of the indole intermediate

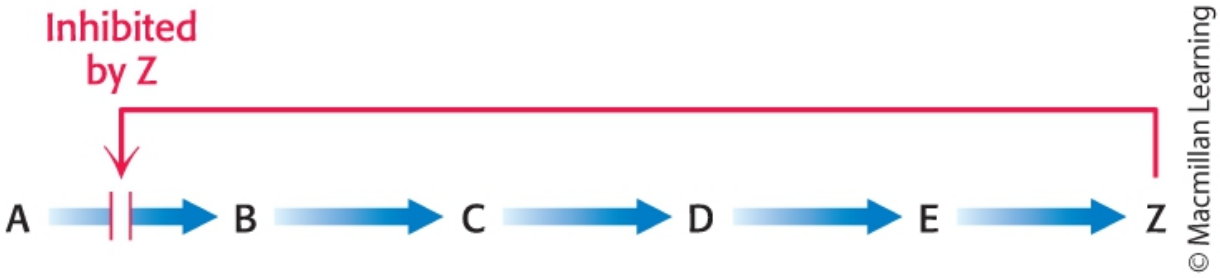


© Macmillan Learning

The top view of the tryptophan synthase is shown. The alpha subunit located in the front is depicted as an irregular cluster of yellow spheres. The beta subunit located at the back is depicted as a square-shaped structure composed of closely spaced blue spheres. A narrow central tunnel in the alpha subunit shows the P L P bound to the beta subunit. P L P is depicted in red color. An asterisk indicates the center of the tunnel.

Return to FIGURE 25.16 Tryptophan synthase uses substrate channeling to prevent loss of the indole intermediate

Extended description for Inhibition of the first irreversible step of a biosynthetic pathway

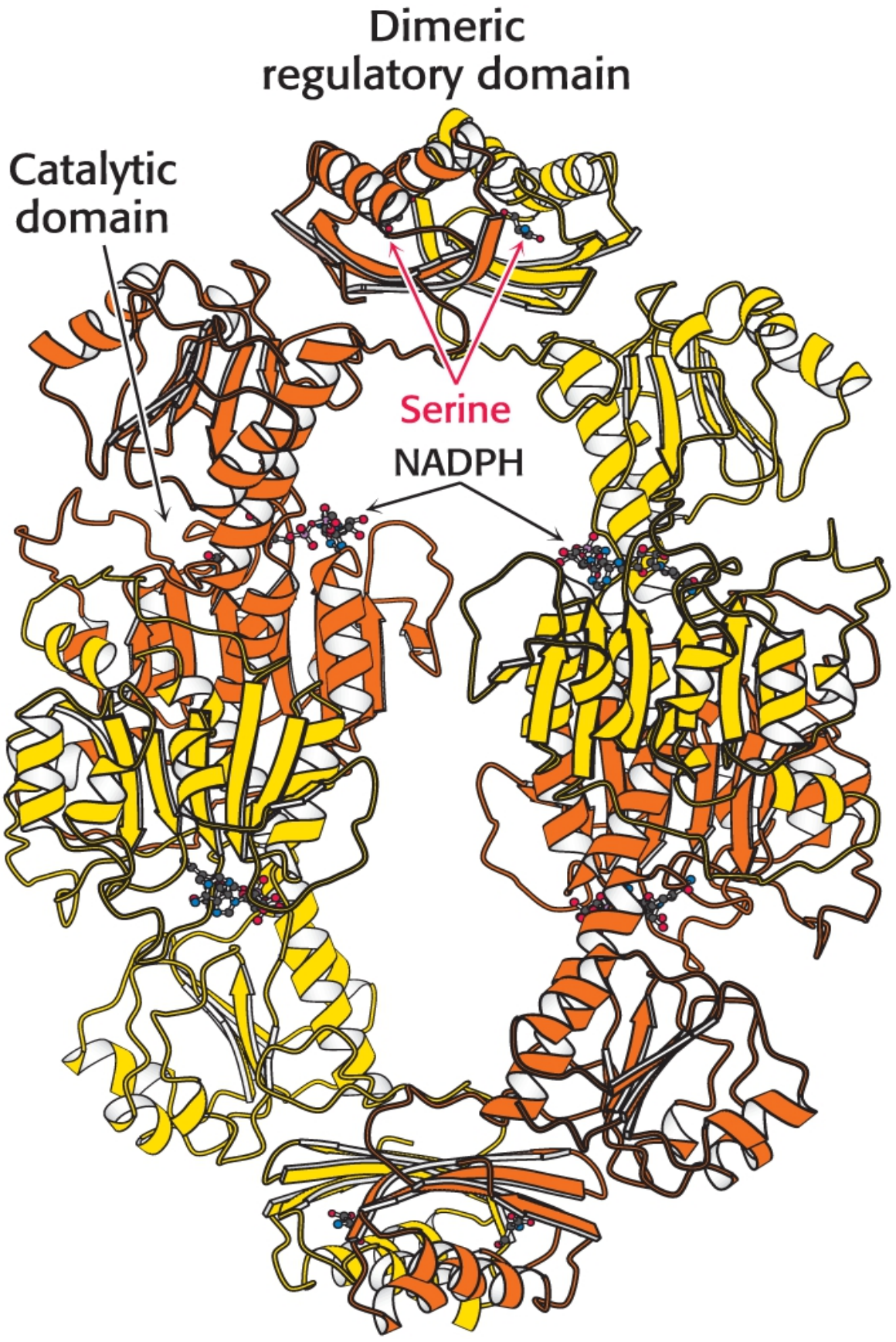


The biosynthetic pathway is depicted as follows: A, forward arrow, B, forward arrow, C, forward arrow, D, forward arrow, E, forward arrow, Z. A red arrow from Z travels toward the forward arrow leading from A to B. It is labeled inhibited by Z. Two red short parallel lines are shown above the forward arrow.

[Return to Inhibition of the first irreversible step of a biosynthetic pathway]

Extended description for FIGURE 25.17 3-

Phosphoglycerate dehydrogenase is a homotetramer

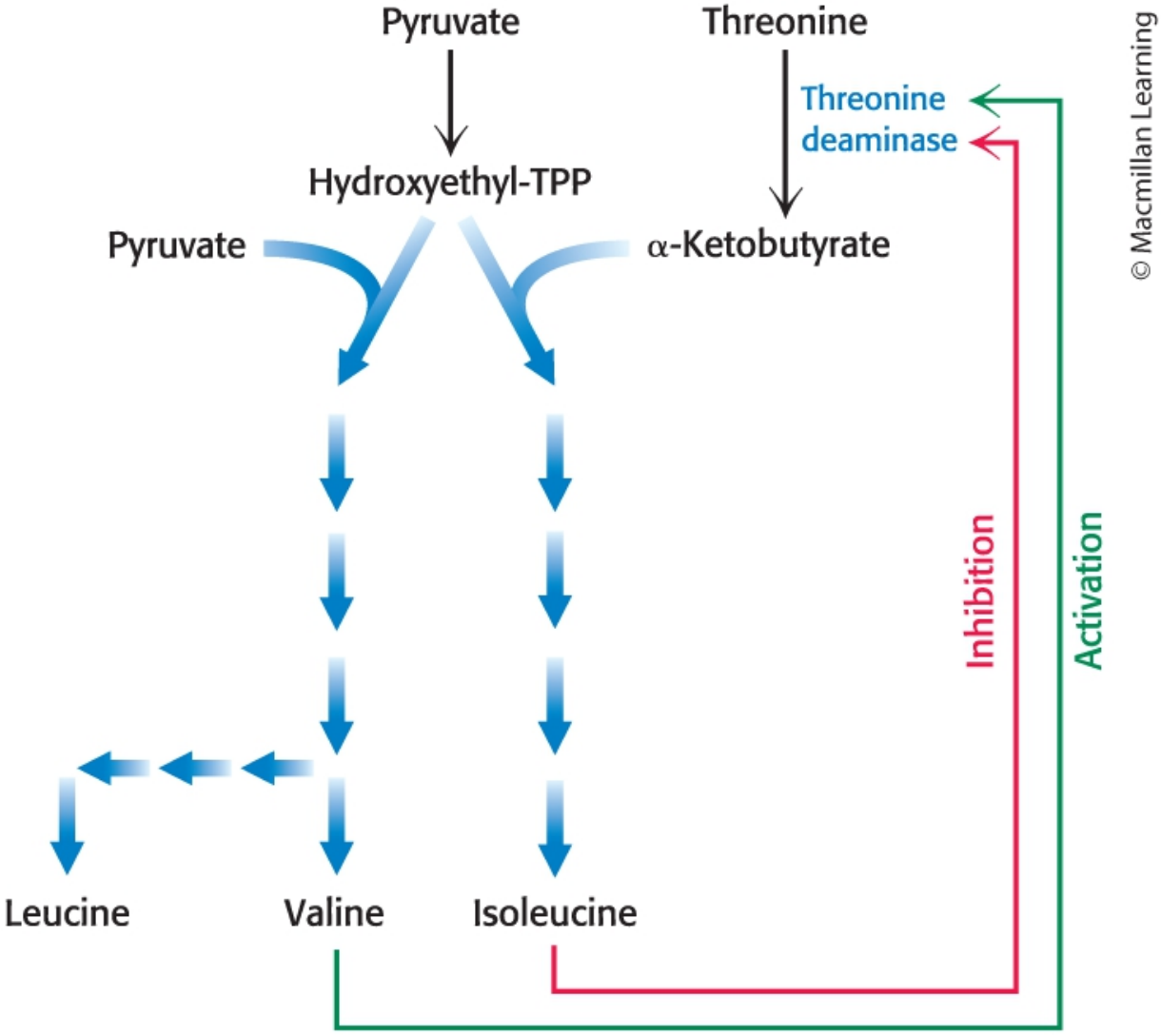


© Macmillan Learning

The ribbon diagram of phosphoglycerate dehydrogenase is depicted as a hollow oval-shaped structure. It consists of two catalytic domains, one on each side. The catalytic domain is narrow, elongated, and composed of several beta-strands and a few alpha-helices. Each of the catalytic domains is bound to N A D P H. The dimeric regulatory domain is located at the top and bottom. The regulatory domain is small and composed of beta-strands at the bottom and alpha-helices forming the top. Two adjacent hollow regions are present in each domain. These hollow regions are bound to serine amino acids. The bottom regulatory domain is inverted such that beta-strands form the top and alpha-helices constitute the bottom.

Return to FIGURE 25.17 3-Phosphoglycerate dehydrogenase is a homotetramer

Extended description for FIGURE 25.18 Threonine deaminase is regulated by feedback inhibition and activation

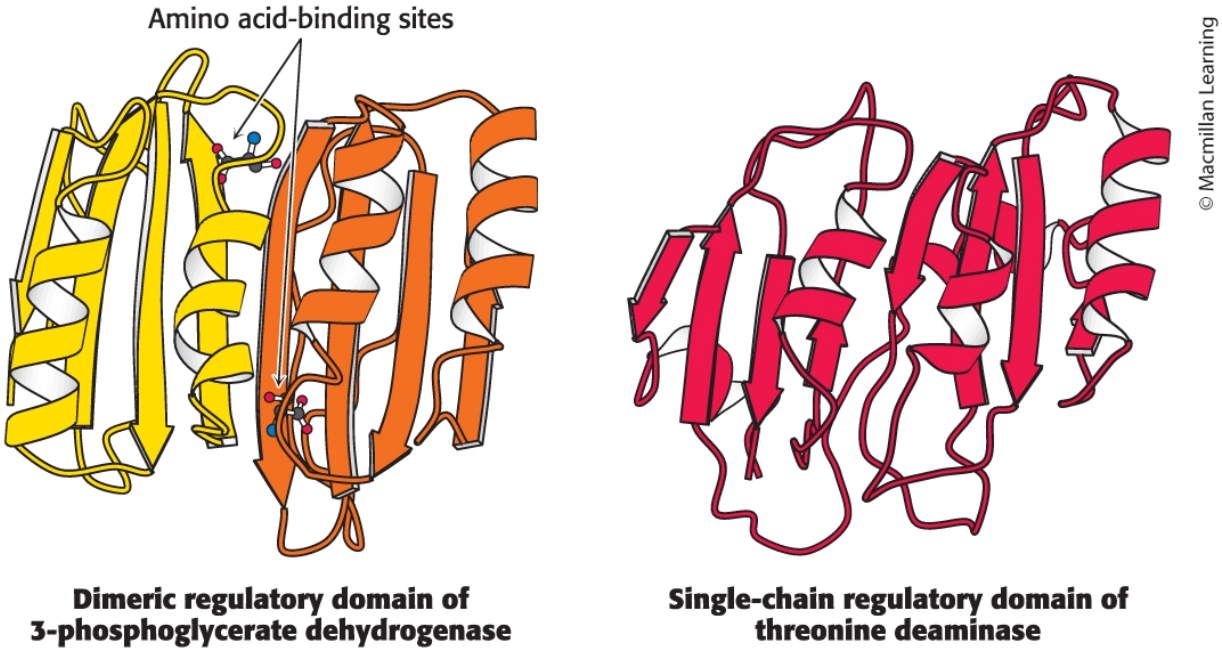


A biosynthetic pathway leading to the formation of amino acids leucine, valine, and isoleucine from pyruvate is shown. An adjacent, single-step conversion of threonine to alpha-ketobutyrate is shown. It is catalyzed by threonine deaminase. In the biosynthetic pathway, pyruvate is first irreversibly converted into hydroxyethyl-T P P,

which has two fates. It can either combine with pyruvate to form valine and leucine or combine with alpha-ketobutyrate from the single-step conversion to form isoleucine. In the first fate, four downward arrows lead to valine. Four successive arrows originating from the middle of the third and fourth downward arrows lead to leucine. In the second fate, four downward arrows lead to isoleucine. A red arrow labeled inhibition points from isoleucine to threonine deaminase. A green arrow labeled activation points from valine to threonine deaminase.

Return to FIGURE 25.18 Threonine deaminase is regulated by feedback inhibition and activation

Extended description for FIGURE 25.19 The regulatory domains of 3-phosphoglycerate dehydrogenase and threonine deaminase are related structurally



© Macmillan Learning

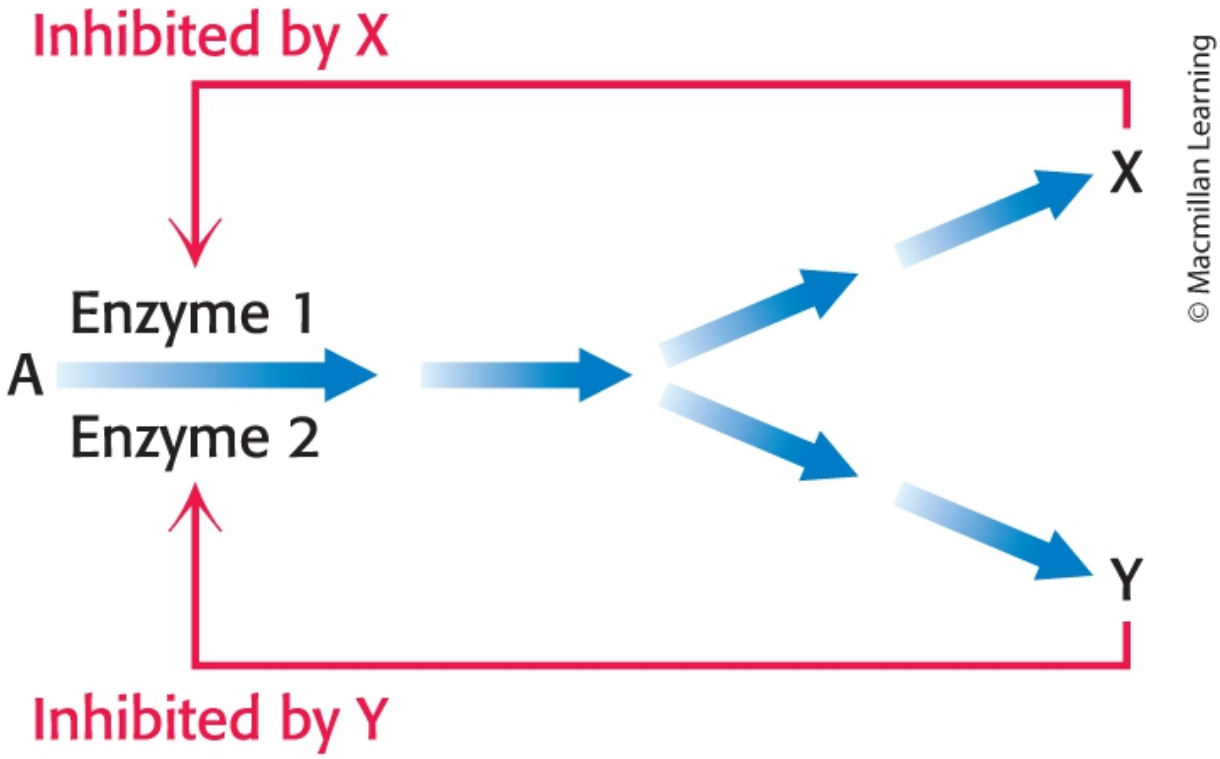
The dimeric regulatory domain of 3-phosphoglycerate dehydrogenase consists of two subunits shown in yellow and orange. The left yellow subunit consists of two vertical alpha-helices and four vertical beta-strands interconnected by thread-like loops. The right orange subunit consists of two vertical alpha-helices and four vertical beta-strands interconnected by thread-like loops. The amino acid-binding site is located on the top right and bottom left of the left and right subunits respectively. Each of these sites is bound to a ball-and-stick model of amino acid.

The single-chain regulatory domain of threonine deaminase consists of vertical and adjacently placed alpha-helices and beta-

strands interconnected by thread-like loops. It contains four alpha-helices and eight beta-strands.

Return to FIGURE 25.19 The regulatory domains of 3-phosphoglycerate dehydrogenase and threonine deaminase are related structurally

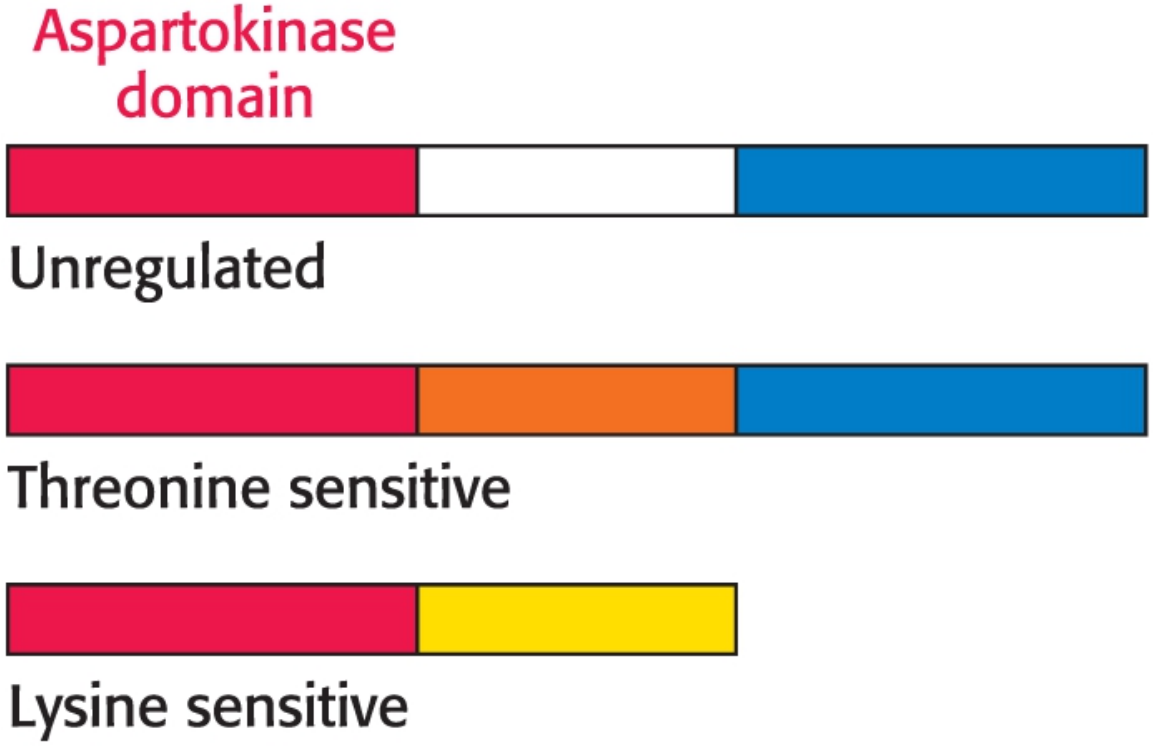
Extended description for Inhibition of enzymes by different products of a pathway



The pathway is depicted as follows: A, forward arrow labeled enzyme 1 at the top and enzyme 2 at the bottom, forward arrow. After the second forward arrow, the pathway bifurcates. Two successive forward arrows pointing toward the upper right lead to X. Two successive forward arrows pointing toward the lower right lead to Y. A red arrow from X labeled inhibited by X points toward enzyme 1. A red arrow from Y labeled inhibited by Y points toward enzyme 2.

Return to Inhibition of enzymes by different products of a pathway

Extended description for FIGURE 25.20 The three aspartokinases from *E. coli* have different regulatory domains



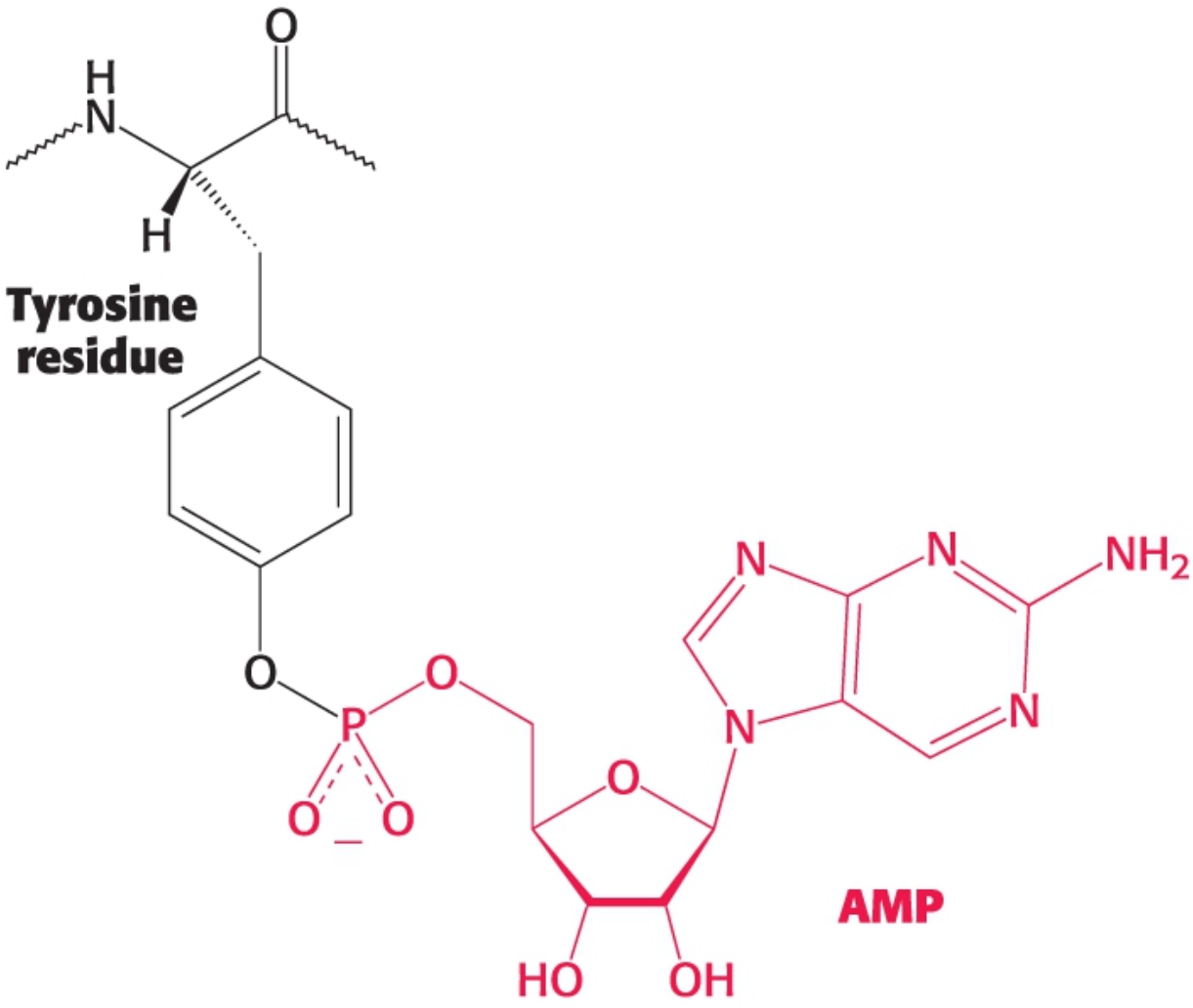
© Macmillan Learning

Three horizontal bars are shown from top to bottom. The top and middle bars have equal sizes but the bottom bar has a relatively shorter size. The top and middle bars are divided into three differently colored sections denoting different domains of aspartokinase. The bottom bar is divided into two sections. The left domain denotes the aspartokinase domain in all the bars. In the top bar, the aspartokinase domain is shown in red and labeled unregulated. The middle domain is white and the right domain is blue. In the middle bar, the aspartokinase domain is shown in red and labeled threonine sensitive. The middle domain is orange and the right domain is blue. In the bottom bar, the aspartokinase

domain is shown in red and labeled lysine sensitive and the right domain is shown in yellow.

Return to FIGURE 25.20 The three aspartokinases from *E. coli* have different regulatory domains

Extended description for Structure of tyrosine residue modified by adenylylation



Tyrosine residue modified by adenylylation

The tyrosine residue modified by adenylylation consists of tyrosine residue connected to A M P.

The structure of tyrosine is as follows: A benzene ring is in a vertical orientation with C 1 occupying the topmost vertex. It contains

alternating double bonds between C 2 and C 3, C 4 and C 5, and C 6 and C 1. C 1 is single bonded to C H 2 above in the form of a line. This C H 2 is dash-bonded to C on the upper left. C is single bonded to C on the upper right, wedge bonded to H on the lower left, and single bonded to N H on the upper left. The upper right C is double bonded to O above and has a wiggly line on the lower right. N H has a wiggly line on the lower left. C 4 of the ring is single bonded to O below. This O is single-bonded to the P atom of A M P.

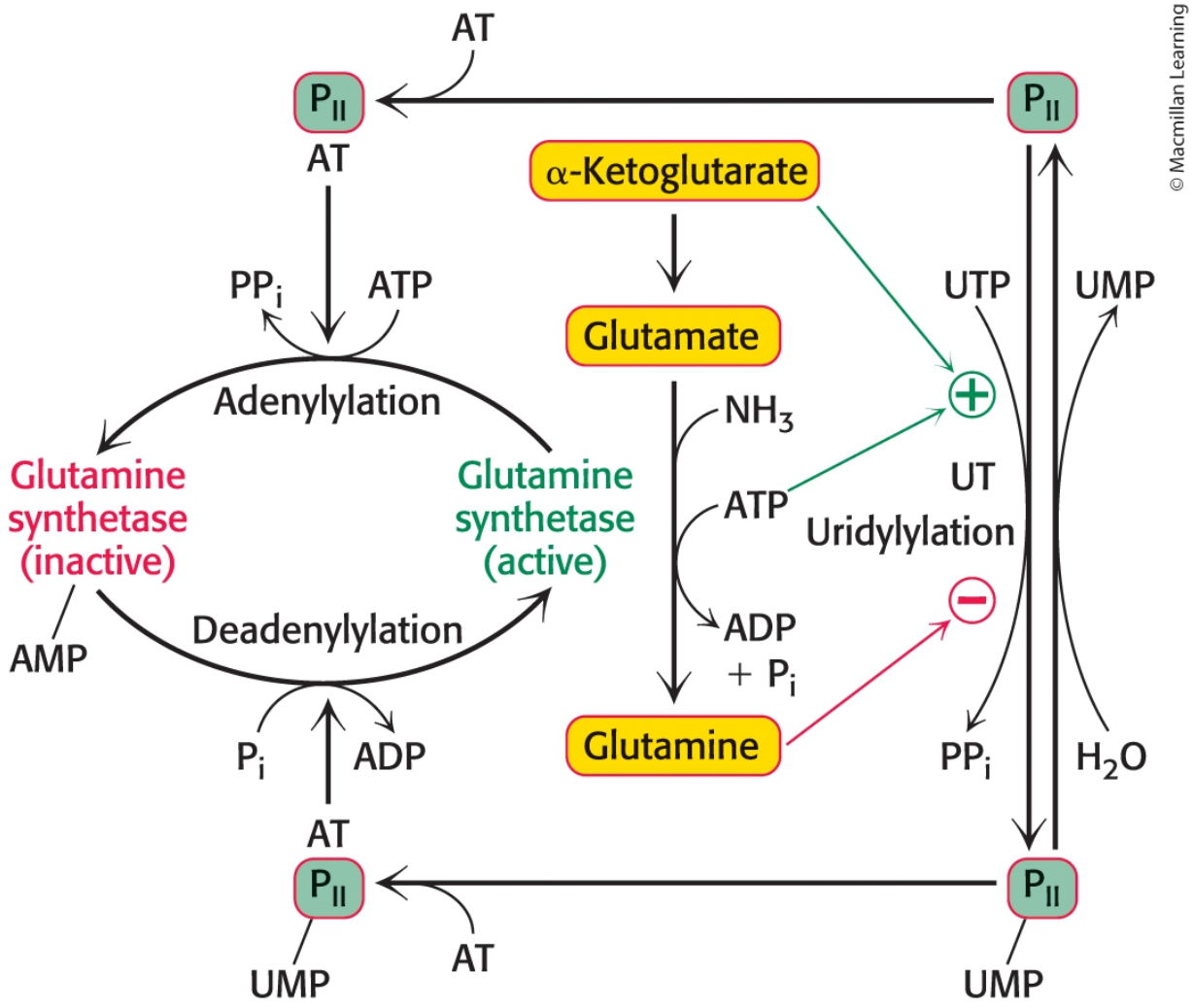
The structure of A M P is as follows: A 5-membered heterocyclic pentagonal ring is in a vertical orientation and consists of 1 O and 4 C atoms. C 1 occupies the top right vertex. C 2 and C 3 are single bonded to O H below. C 4 is single-bonded to C H 2 above in the form of a line, which is further single-bonded to the S atom of methionine amino acid. The S atom is positively charged. C 1 is single-bonded to N 1 of a 5-membered heterocyclic pentagonal ring in a horizontal orientation with C 1 occupying the leftmost vertex. This ring consists of 2 N and 3 C atoms. First N occupies the bottom left vertex and the second N occupies the topmost vertex. A double bond is present between C 1 and N 2. The pentagonal ring is fused to a 6-membered heterocyclic hexagonal ring in a vertical orientation such that C 2 and C 3 of the pentagonal ring are C 3 and C 2 of the hexagonal ring respectively. The hexagonal ring consists of 2 N and 4 C atoms. First N occupies the top right vertex and the second N occupies the bottom-most vertex. A double bond is present between C 1 and N 2, C 2 and C 3, and C 4 and N 1. C 4 is single bonded to N H 2 above.

The structure of A M P is as follows: A 5-membered heterocyclic pentagonal ring is in a vertical orientation and consists of 1 O and 4 C atoms. O occupies the topmost vertex. C 1 occupies the top right vertex. C 2 and C 3 are single bonded to O H below. C 4 is single-bonded to C H 2 above in the form of a line, which is further single-bonded to the O atom on the left. O is single-bonded to P. This P is

partially double-bonded to O on the lower left, partially double-bonded to O on the lower right, and single-bonded to the O atom of tyrosine residues. The partially double-bonded O atoms have an overall negative charge. C 1 of the pentagonal ring is single-bonded to N 1 of a 5-membered heterocyclic pentagonal ring in a horizontal orientation with C 1 occupying the leftmost vertex. This ring consists of 2 N and 3 C atoms. First N occupies the bottom left vertex and the second N occupies the topmost vertex. A double bond is present between C 1 and N 2. The pentagonal ring is fused to a 6-membered heterocyclic hexagonal ring in a vertical orientation such that C 2 and C 3 of the pentagonal ring are C 4 and C 3 of the hexagonal ring respectively. The hexagonal ring consists of 2 N and 4 C atoms. First N occupies the topmost vertex and the second N occupies the bottom-right vertex. A double bond is present between C 1 and N 1, N 2 and C 2, and C 3 and C 4. C 1 is single bonded to N H 2 on the upper right.

Return to Structure of tyrosine residue modified by adenylylation

Extended description for FIGURE 25.21 Glutamine synthetase is regulated by covalent modification



A pathway is shown in the center. It shows the irreversible conversion of alpha-ketoglutarate to glutamate. Glutamate is then irreversibly converted into glutamine by glutamine synthetase (active) with the simultaneous entry of N H 3 and breakdown of A T P to A D P plus P subscript i. A T associated with P subscript roman number 2 is shown at the top left, P subscript roman number 2 is shown at the top right, P subscript roman number 2 linked to U M P

is shown at the bottom right, A T associated with P subscript roman number 2 linked to U M P is shown at the bottom left.

P subscript roman number 2 is irreversibly converted into A T associated with P subscript roman number 2 by the addition of A T. P subscript roman number 2 undergoes reversible uridylylation to P subscript roman number 2 linked to U M P. This conversion is catalyzed by U T with the simultaneous entry of U T P and release of P P subscript i. P subscript roman number 2 linked to U M P is converted back to P subscript roman number 2 with the simultaneous entry of H 2 O and release of U M P. U T enzyme is activated by alpha-ketoglutarate, A T P and inhibited by glutamine from the pathway. Activation is depicted by a plus symbol and inhibition is depicted by a minus symbol.

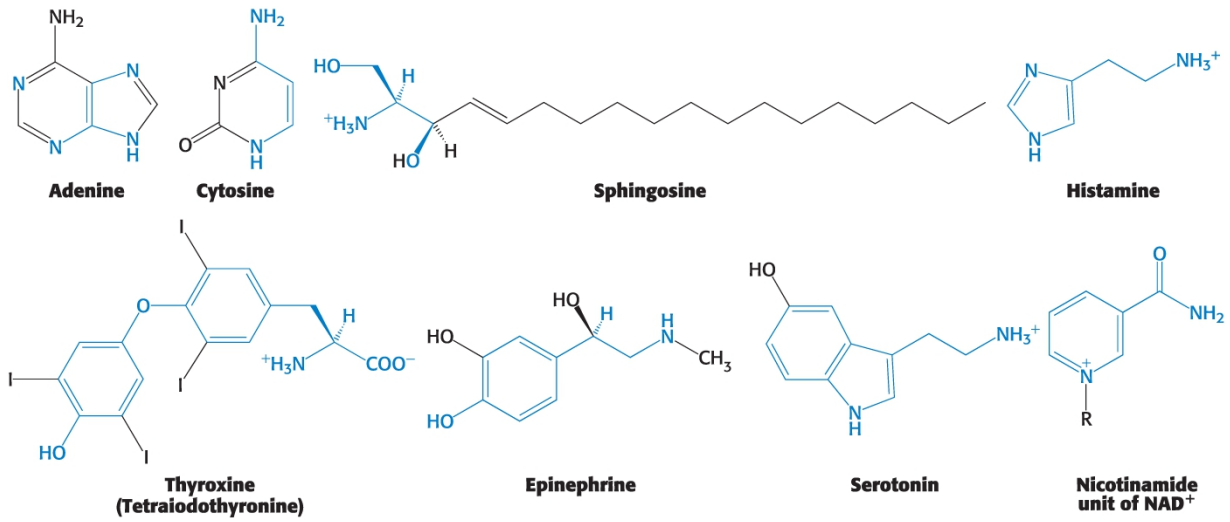
P subscript roman number 2 linked to U M P is also irreversibly converted into A T associated with P subscript roman number 2 linked to U M P by the addition of A T.

The A T associated with P subscript roman number 2 linked to U M P carries out the deadenylylation of A M P bound-glutamine synthetase (inactive) to the active form. This conversion is coupled with the entry of P subscript i and the release of A D P.

The A T associated with P subscript roman number 2 carries out the adenylylation of glutamine synthetase (active) to inactive form bound to A M P. This conversion is coupled with the entry of A T P and release of P P subscript i.

Return to FIGURE 25.21 Glutamine synthetase is regulated by covalent modification

Extended description for FIGURE 25.22 A diverse array of biomolecules are derived from amino acids



The structure of adenine is as follows: A 6-membered heterocyclic hexagonal ring is in a vertical orientation and consists of 2 N and 4 C atoms. First N occupies the bottom-most vertex and the second N occupies the top left vertex. A double bond is present between N 1 and C 1, N 2 and C 2, and C 3 and C 4. C 2 is single bonded to N H 2 above. It is fused to a 5-membered heterocyclic pentagonal ring such that C 3 and C 4 of the hexagonal ring are C 3 and C 2 respectively of the pentagonal ring. The pentagonal ring consists of 2 N and 3 C atoms. First N occupies the topmost vertex and the second N bound to H occupies the bottom right vertex. A double bond is present between N 1 and C 1. The N atoms of both rings, the H atom bound to the N atom, and the fused part of the rings are highlighted in blue.

The structure of cytosine is as follows: A 6-membered heterocyclic hexagonal ring is in a vertical orientation and consists of 2 N and 4 C atoms. The first N bound to H occupies the bottom-most vertex and

the second N occupies the top left vertex. A double bond is present between N 2 and C 2, and C 3 and C 4. C 1 is double bonded to O on the lower left. C 2 is single bonded to N H 2 above. The first N bound to H, N H 2 group, C 3, and C 4 are highlighted in blue.

The structure of sphingosine is as follows: A 2-carbon alkane chain is depicted using a single line. C 1 is wedge bonded to C H 2 on the upper left, dash bonded to H on the upper right, and single bonded to N H 3 superscript plus on the lower left. C H 2 is single-bonded to O H on the left. C 2 is wedge bonded to O H, dash bonded to H on the lower right, and single bonded to a 15-carbon alkene chain depicted using a line structure. A double bond is present between C 1 and C 2. The 2-carbon alkane chain and its substituent groups except for the 15-carbon alkene chain, lower right H, and the H atom of the lower left O H group are highlighted in blue.

The structure of histamine is as follows: A 5-membered heterocyclic pentagonal ring is in a vertical orientation and consists of 2 N and 3 C atoms. First N bound to H occupies the bottom left vertex. Second N occupies the topmost vertex. A double bond is present between C 1 and N 2, and C 2 and C 3. C 2 is single bonded to a 2-carbon alkane chain depicted using a line. C 2 of this chain is single bonded to N H 3 superscript plus on the upper right. The entire structure is highlighted in blue.

The structure of thyroxine (tetraiodothyronine) is as follows: A benzene ring is in a horizontal orientation with C 1 occupying the rightmost vertex. It contains alternating double bonds between C 1 and C 2, C 3 and C 4, and C 5 and C 6. C 1 and C 4 are single-bonded to I. C 3 is single bonded to O H on the lower left. C 6 is single bonded to O on the upper right. This O is single bonded to C 4 of another benzene ring in horizontal orientation. In the second ring, C 2 and C 3, C 4 and C 5, and C 6 and C 1. C 3 and C 5 are each single bonded to I. C 1 occupies the rightmost vertex and is single-bonded

to C H 2 on the right in the form of a line. C H 2 is wedge bonded to C on the lower right. This C is dash bonded to H on the upper right, single bonded to C O O superscript minus on the lower right, and single bonded to N H 3 superscript plus on the lower left. The entire structure except I atoms is highlighted in blue.

The structure of epinephrine is as follows: A benzene ring is in a vertical orientation with C 1 occupying the topmost vertex. It contains alternating double bonds between C 1 and C 2, C 3 and C 4, and C 5 and C 6. C 2 is single bonded to C 1 of a 1 N and 2 C heteronuclear alkane chain depicted as a line structure using 2 zigzag lines. N bound to H occupies the third position. C 1 is wedge bonded to O H on the upper left and dash bonded to H on the upper right. N is single bonded to C H 3 on the lower right. C 5 of the benzene ring is single-bonded to O H on the lower left. C 6 is single bonded to O H on the upper left. The entire benzene ring, alkane chain, H atom dashed bonded to C 1 of the alkane chain, and O H group bonded to C 5 are highlighted in blue.

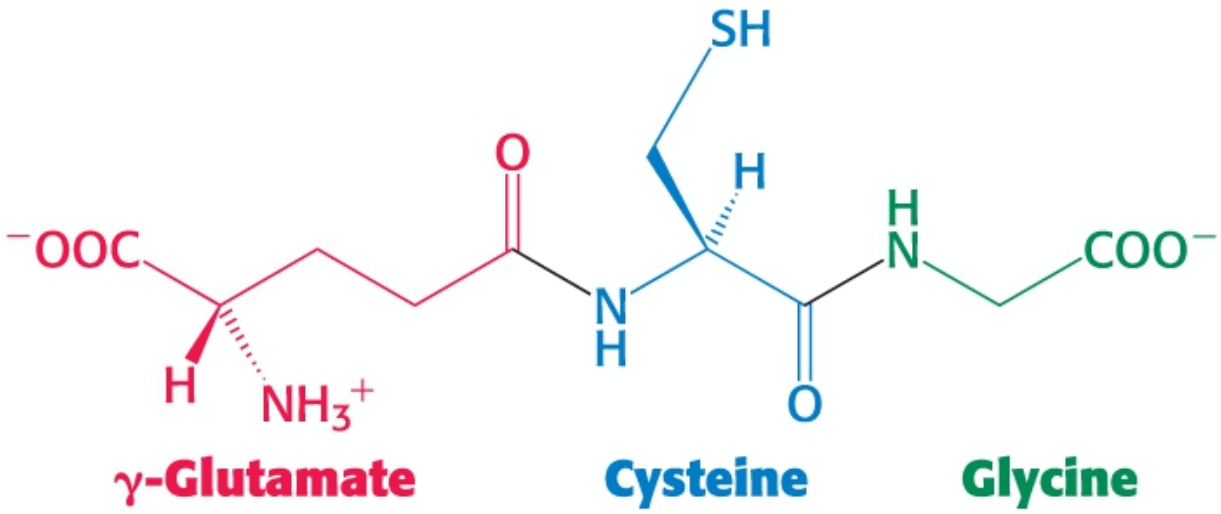
The structure of serotonin is as follows: A benzene ring is in a horizontal orientation with C 1 occupying the rightmost vertex. It contains alternating double bonds between C 1 and C 2, C 3 and C 4, and C 5 and C 6. C 5 is single bonded to O H. The benzene ring is fused to a 5-membered heterocyclic pentagonal ring in a vertical orientation such that C 1 and C 2 of the benzene ring are C 2 and C 1 respectively of the pentagonal ring. The pentagonal ring consists of 1 N and 4 C atoms. N bound to H occupies the bottom-most vertex. A double bond is present between C 3 and C 4. C 3 is single bonded to a 2-carbon alkane chain depicted using a line. C 2 of this chain is single bonded to N H 3 superscript plus on the upper right. The entire structure except the O H group is highlighted in blue.

The structure of the nicotinamide unit of N A D superscript plus is as follows: A 6-membered heterocyclic hexagonal ring is in a vertical

orientation. It consists of 1 N and 5 C atoms. N with a positive charge occupies the bottom-most vertex. N is single bonded to R below. A double bond is present between N and C 1, C 2 and C 3, and C 4 and C 5. C 4 is single bonded to C on the upper right. This C is double bonded to O above and single bonded to N H 2 on the lower right. The entire structure except the R group is highlighted in blue.

Return to FIGURE 25.22 A diverse array of biomolecules are derived from amino acids

Extended description for FIGURE 25.23 Glutathione structure



Glutathione is composed of 3 amino acids namely gamma-glutamate, cysteine, and glycine from left to right.

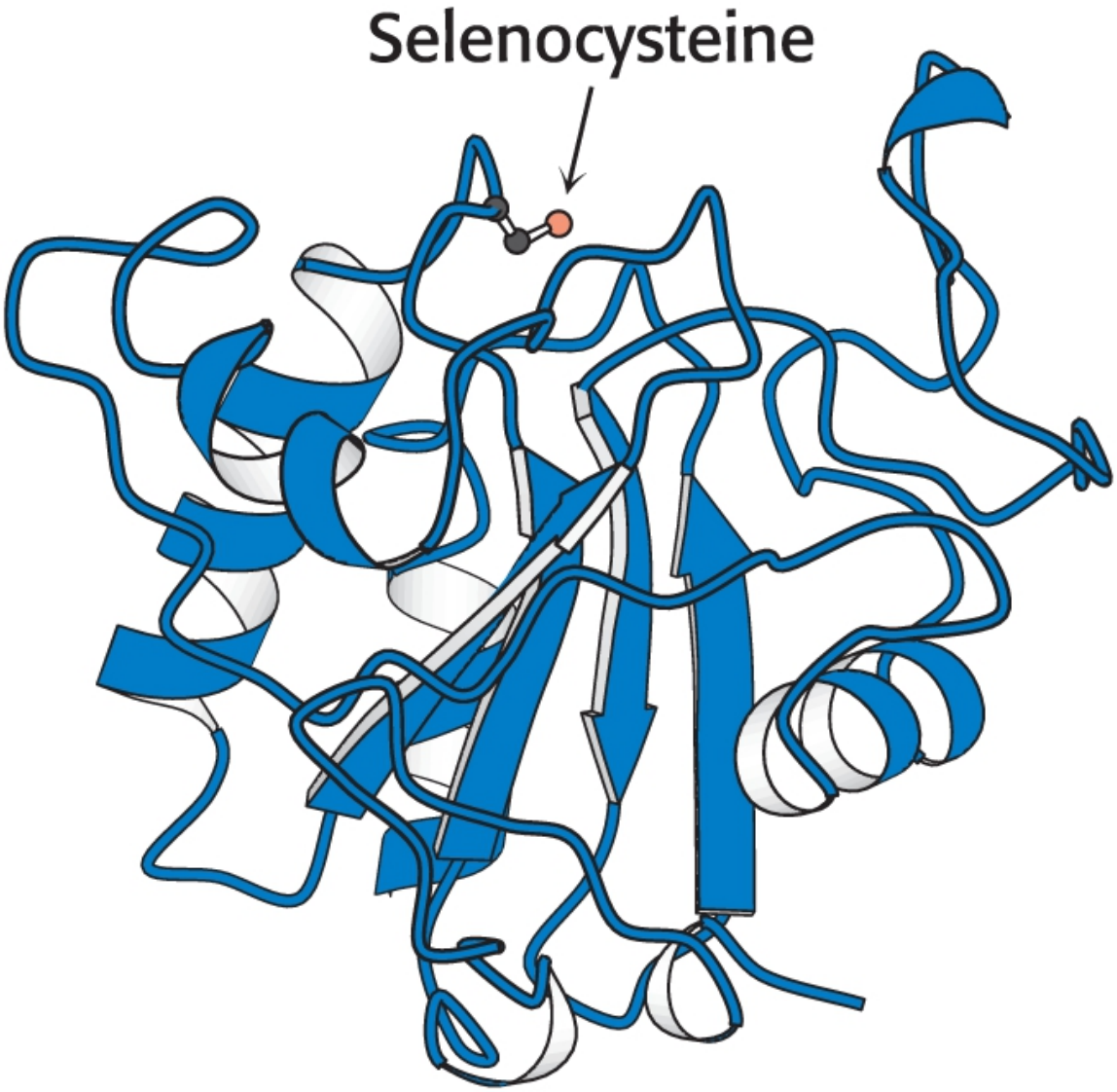
Gamma-glutamate consists of 4 carbon alkane chain depicted as a line structure using 3 zigzag lines. C 1 is single bonded to C O O superscript minus on the upper left, wedge bonded to H on the lower left, and dash bonded to N H 3 superscript plus on the lower right. C 4 is double bonded to O above and single bonded to N H of a cysteine residue.

Cysteine consists of a central C atom single bonded to N H on the lower left, wedge bonded to C H 2 on the upper left, dash bonded to H on the upper right, and single bonded to C on the lower right. This C atom is double bonded to O below and single bonded to N H of glycine on the upper right. The upper left C H 2 is single-bonded to S H on the upper right.

Glycine consists of N H single bonded to C H 2 on the lower right in the form of a line. C H 2 is single bonded to C O O superscript minus on the upper right.

Return to FIGURE 25.23 Glutathione structure

Extended description for FIGURE 25.24 Ribbon diagram of glutathione peroxidase

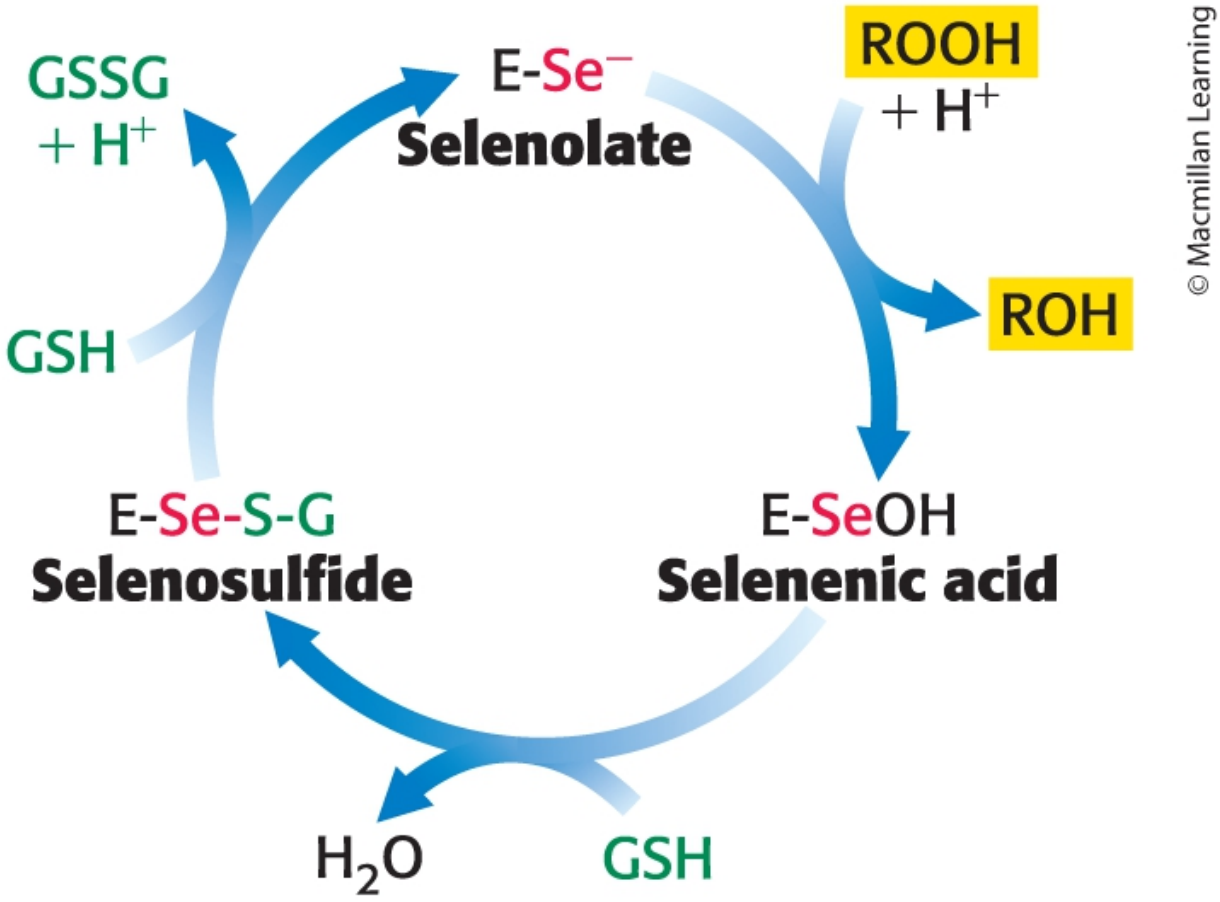


© Macmillan Learning

The ribbon diagram consists of 4 beta-strands in the middle and a few alpha-helices on either side interconnected by long thread-like loops. A ball-and-stick model of selenocysteine residue is connected to a loop extending above the ribbon diagram.

Return to FIGURE 25.24 Ribbon diagram of glutathione peroxidase

Extended description for FIGURE 25.25 Regeneration of selenolate active site after peroxide cleavage

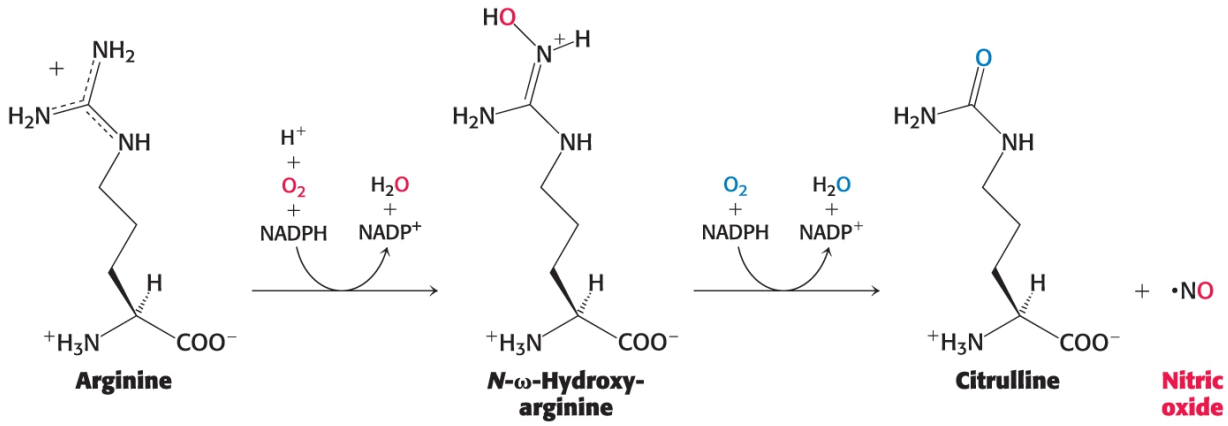


© Macmillan Learning

The cycle is depicted as follows: E, single bond, S e superscript minus labeled selenolate is converted into selenenic acid depicted as E, single bond, S e O H. This conversion is coupled with the entry of R O O H plus H superscript plus and release of R O H. Selenenic acid is further converted into selenosulfide depicted as E, single bond, S e, single bond, S, single bond, G. This conversion is coupled with the entry of G S H and release of H 2 O. The selenosulfide is converted back to selenolate with the simultaneous entry of G S H and release of G S S G plus H superscript plus.

Return to FIGURE 25.25 Regeneration of selenolate active site after peroxide cleavage

Extended description for FIGURE 25.26 Generation of nitric oxide from arginine



In the first irreversible step, arginine is converted into N-omega-hydroxy-arginine. This step is coupled with the entry of H superscript plus and O 2, the release of H 2 O, and the oxidation of N A D P H to N A D P superscript plus.

The structure of arginine is as follows: A central C is wedge bonded to C H 2 on the upper left, dash bonded to H on the upper right, single bonded to C O O superscript minus on the lower right, and single bonded to N H 3 superscript plus on the lower left. C H 2 is single bonded to 1 N and 2 C heteronuclear alkane chain depicted as vertical line structure using 2 zigzag lines. N bound to H occupies the third position. This N H group is partially double-bonded to a central C atom on the upper left. This C atom is partially double-bonded to N H 2 on the upper right and N H 2 on the lower left. The N H 2 groups have an overall positive charge.

The structure of N-omega-hydroxy-arginine is as follows: A central C is wedge bonded to C H 2 on the upper left, dash bonded to H on the upper right, single bonded to C O O superscript minus on the lower

right, and single bonded to N H 3 superscript plus on the lower left. C H 2 is single bonded to 1 N and 2 C heteronuclear alkane chain depicted as vertical line structure using 2 zigzag lines. N bound to H occupies the third position. This N H group is single-bonded to a central C atom on the upper left. This C atom is double bonded to N superscript plus on the upper right and single bonded to N H 2 on the lower left. The N atom is single-bonded to H on the upper right and single-bonded to the O H group on the upper left.

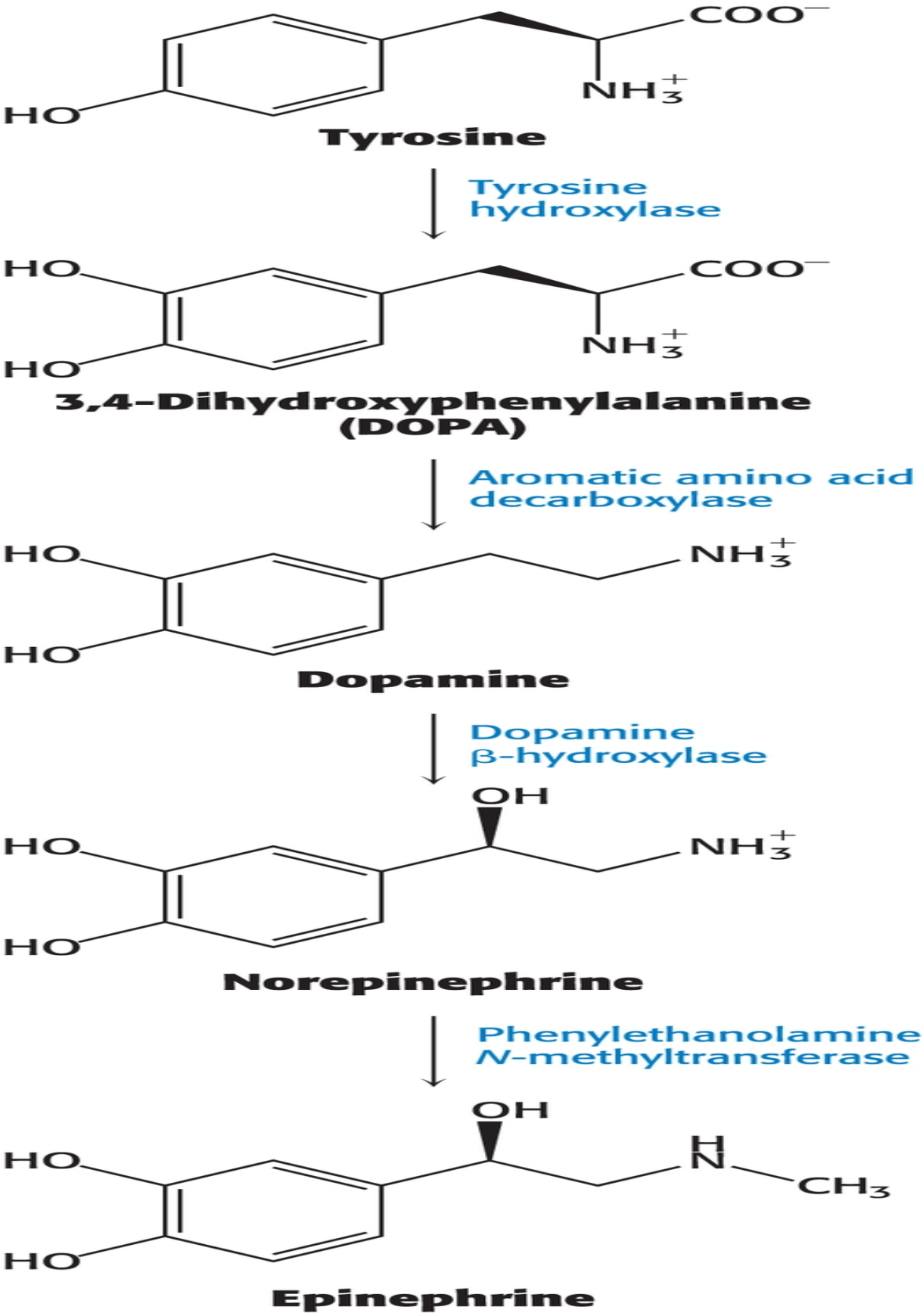
In the second irreversible step, N-omega-hydroxy-arginine is converted into citrulline and nitric oxide. This step is coupled with the entry of O 2, the release of H 2 O, and the oxidation of N A D P H to N A D P superscript plus.

The structure of citrulline is as follows: A central C atom is single bonded to N H 3 superscript plus on the lower left, single bonded to C O O superscript minus on the lower right, wedge bonded to C H 2 on the upper left, and dash bonded to H on the upper right. The C H 2 group is single-bonded to a 1 N and 2 C alkane chain depicted as a vertical line structure using 2 zigzag lines. N bound to H occupies the third position. N is single-bonded to C on the upper right. This C is single bonded to N H 2 on the left and double bonded to O on the upper right. The formula of nitric oxide is N O. N atom has an unpaired electron.

Return to FIGURE 25.26 Generation of nitric oxide from arginine

Extended description for FIGURE 25.27 Tyrosine is a

precursor for the catecholamines


COO⁻
NH3+
HO
Tyrosine
Tyrosine hydroxylase
HO
HO
COO⁻
NH3+
3,4-Dihydroxyphenylalanine (DOPA)
Aromatic amino acid decarboxylase
HO
HO
NH3+
Dopamine
Dopamine β-hydroxylase
OH
HO
HO
NH3+
Norepinephrine
Phenylethanolamine N-methyltransferase
OH
HO
HO
H N
CH3
Epinephrine

In the first irreversible step catalyzed by tyrosine hydroxylase, tyrosine is converted into 3,4-Dihydroxyphenylalanine (D O P A).

The structure of tyrosine is as follows: A benzene ring is in a vertical orientation with C 1 occupying the topmost vertex. It contains alternating double bonds between C 1 and C 2, C 3 and C 4, and C 5 and C 6. C 2 is single bonded to C H 2 on the upper right in the form of a line. C H 2 is wedge bonded to C on the lower right. The C atom is single bonded to C O O superscript minus on the upper right and single bonded to N H 3 superscript plus below. C 5 of the ring is single-bonded to O H on the lower right.

The structure of 3,4-Dihydroxyphenylalanine is as follows: A benzene ring is in a vertical orientation with C 1 occupying the topmost vertex. It contains alternating double bonds between C 1 and C 2, C 3 and C 4, and C 5 and C 6. C 2 is single bonded to C H 2 on the upper right in the form of a line. C H 2 is wedge bonded to C on the lower right. The C atom is single bonded to C O O superscript minus on the upper right and single bonded to N H 3 superscript plus below. C 5 and C 6 of the ring are each single-bonded to O H.

In the second irreversible step catalyzed by aromatic amino acid decarboxylase, 3,4-Dihydroxyphenylalanine is converted into dopamine.

The structure of dopamine is as follows: A benzene ring is in a vertical orientation with C 1 occupying the topmost vertex. It contains alternating double bonds between C 1 and C 2, C 3 and C 4, and C 5 and C 6. C 2 is single bonded to a 2-carbon alkane chain depicted using a line. C 2 of this chain is single bonded to N H 3 superscript plus on the upper right. C 5 and C 6 of the ring are each single-bonded to O H.

In the third irreversible step catalyzed by dopamine beta-hydroxylase, dopamine is converted into norepinephrine.

The structure of norepinephrine is as follows: A benzene ring is in a vertical orientation with C 1 occupying the topmost vertex. It contains alternating double bonds between C 1 and C 2, C 3 and C 4, and C 5 and C 6. C 2 is single bonded to a 2-carbon alkane chain depicted using a line. C 1 of this chain is wedge bonded to O H above. C 2 of this chain is single bonded to N H 3 superscript plus on the upper right. C 5 and C 6 of the ring are each single-bonded to O H.

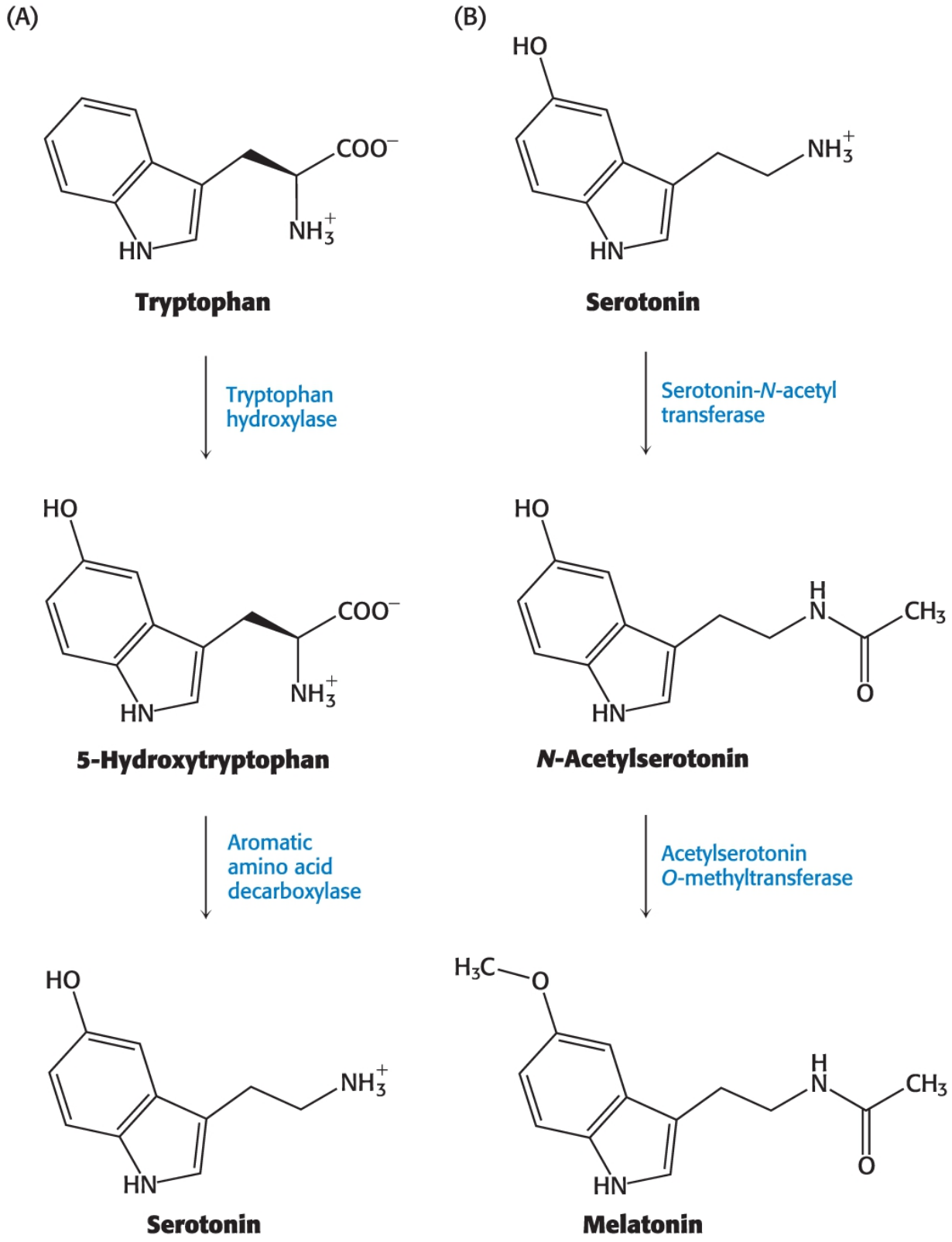
In the fourth irreversible step catalyzed by phenylethanolamine N-methyltransferase, norepinephrine is converted into epinephrine.

The structure of epinephrine is as follows: A benzene ring is in a vertical orientation with C 1 occupying the topmost vertex. It contains alternating double bonds between C 1 and C 2, C 3 and C 4, and C 5 and C 6. C 2 is single bonded to C 1 of a 1 N and 2 C alkane chain depicted using 2 zigzag lines. N bound to H occupies the third position. C 1 of this chain is wedge bonded to O H above. N H is single bonded to C H 3 on the lower right. C 5 and C 6 of the ring are each single-bonded to O H.

Return to FIGURE 25.27 Tyrosine is a precursor for the catecholamines

Extended description for FIGURE 25.28 The neurotransmitters serotonin and melatonin are

synthesized from tryptophan



Reaction sequence (A): In the first irreversible step catalyzed by tryptophan hydroxylase, tryptophan is converted into 5-hydroxytryptophan.

The structure of tryptophan is as follows: A 5-membered heterocyclic pentagonal ring is in a vertical orientation. It consists of 1 N and 4 C atoms. N bound to H occupies the bottom-most vertex. A double bond is present between C 3 and C 4. It is fused to a benzene ring in a vertical orientation such that C 1 and C 2 of the pentagonal ring are C 3 and C 2 respectively of the benzene ring. The benzene ring contains alternating double bonds between C 2 and C 3, C 4 and C 5, and C 6 and C 1. C 3 of the pentagonal ring is single-bonded to C H 2 on the upper right in the form of a line. C H 2 is wedge bonded to C on the right. This C is single bonded to C O O superscript minus on the upper right and single bonded to N H 3 superscript plus below.

The structure of 5-hydroxytryptophan is as follows: A 5-membered heterocyclic pentagonal ring is in a vertical orientation. It consists of 1 N and 4 C atoms. N bound to H occupies the bottom-most vertex. A double bond is present between C 3 and C 4. It is fused to a benzene ring in a vertical orientation such that C 1 and C 2 of the pentagonal ring are C 3 and C 2 respectively of the benzene ring. The benzene ring contains alternating double bonds between C 2 and C 3, C 4 and C 5, and C 6 and C 1. C 6 of the benzene ring is single-bonded to O H. C 3 of the pentagonal ring is single-bonded to C H 2 on the upper right in the form of a line. C H 2 is wedge bonded to C on the right. This C is single bonded to C O O superscript minus on the upper right and single bonded to N H 3 superscript plus below.

In the second irreversible step catalyzed by aromatic amino acid decarboxylase, 5-hydroxytryptophan is converted into serotonin.

The structure of serotonin is as follows: A 5-membered heterocyclic pentagonal ring is in a vertical orientation. It consists of 1 N and 4 C atoms. N bound to H occupies the bottom-most vertex. A double bond is present between C 3 and C 4. It is fused to a benzene ring in a vertical orientation such that C 1 and C 2 of the pentagonal ring are C 3 and C 2 respectively of the benzene ring. The benzene ring contains alternating double bonds between C 2 and C 3, C 4 and C 5, and C 6 and C 1. C 6 of the benzene ring is single-bonded to O H. C 3 of the pentagonal ring is single-bonded to a 2-carbon alkane chain on the upper right depicted using a line. C 2 is single bonded to N H 3 superscript plus on the upper right.

Reaction sequence (B): In the first irreversible step catalyzed by serotonin-N-acetyl transferase, serotonin is converted into N-acetylserotonin.

The structure of N-acetylserotonin is as follows: A 5-membered heterocyclic pentagonal ring is in a vertical orientation. It consists of 1 N and 4 C atoms. N bound to H occupies the bottom-most vertex. A double bond is present between C 3 and C 4. It is fused to a benzene ring in a vertical orientation such that C 1 and C 2 of the pentagonal ring are C 3 and C 2 respectively of the benzene ring. The benzene ring contains alternating double bonds between C 2 and C 3, C 4 and C 5, and C 6 and C 1. C 6 of the benzene ring is single-bonded to O H. C 3 of the pentagonal ring is single-bonded to C 1 of a 1 N and 2 C alkane chain on the upper right depicted as line structure using 2 zigzag lines. N bound to H occupies the third position. N is further single-bonded to C on the lower right. This C is single bonded to C H 3 on the upper right and double bonded to O below.

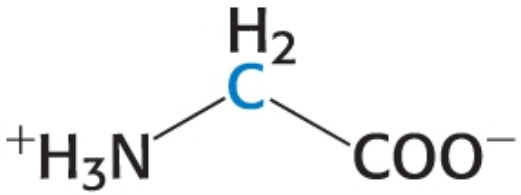
In the second irreversible step catalyzed by acetylserotonin O-methyltransferase, N-acetylserotonin is converted into melatonin.

The structure of melatonin is as follows: A 5-membered heterocyclic pentagonal ring is in a vertical orientation. It consists of 1 N and 4 C atoms. N bound to H occupies the bottom-most vertex. A double bond is present between C 3 and C 4. It is fused to a benzene ring in a vertical orientation such that C 1 and C 2 of the pentagonal ring are C 3 and C 2 respectively of the benzene ring. The benzene ring contains alternating double bonds between C 2 and C 3, C 4 and C 5, and C 6 and C 1. C 6 of the benzene ring is single bonded to O, single bond, C H 3. C 3 of the pentagonal ring is single-bonded to C 1 of a 1 N and 2 C alkane chain on the upper right depicted as a line structure using 2 zigzag lines. N bound to H occupies the third position. N is further single-bonded to C on the lower right. This C is single bonded to C H 3 on the upper right and double bonded to O below.

Return to FIGURE 25.28 The neurotransmitters serotonin and melatonin are synthesized from tryptophan

Extended description for FIGURE 25.29 The origins of atoms in heme were revealed by isotope-labeling

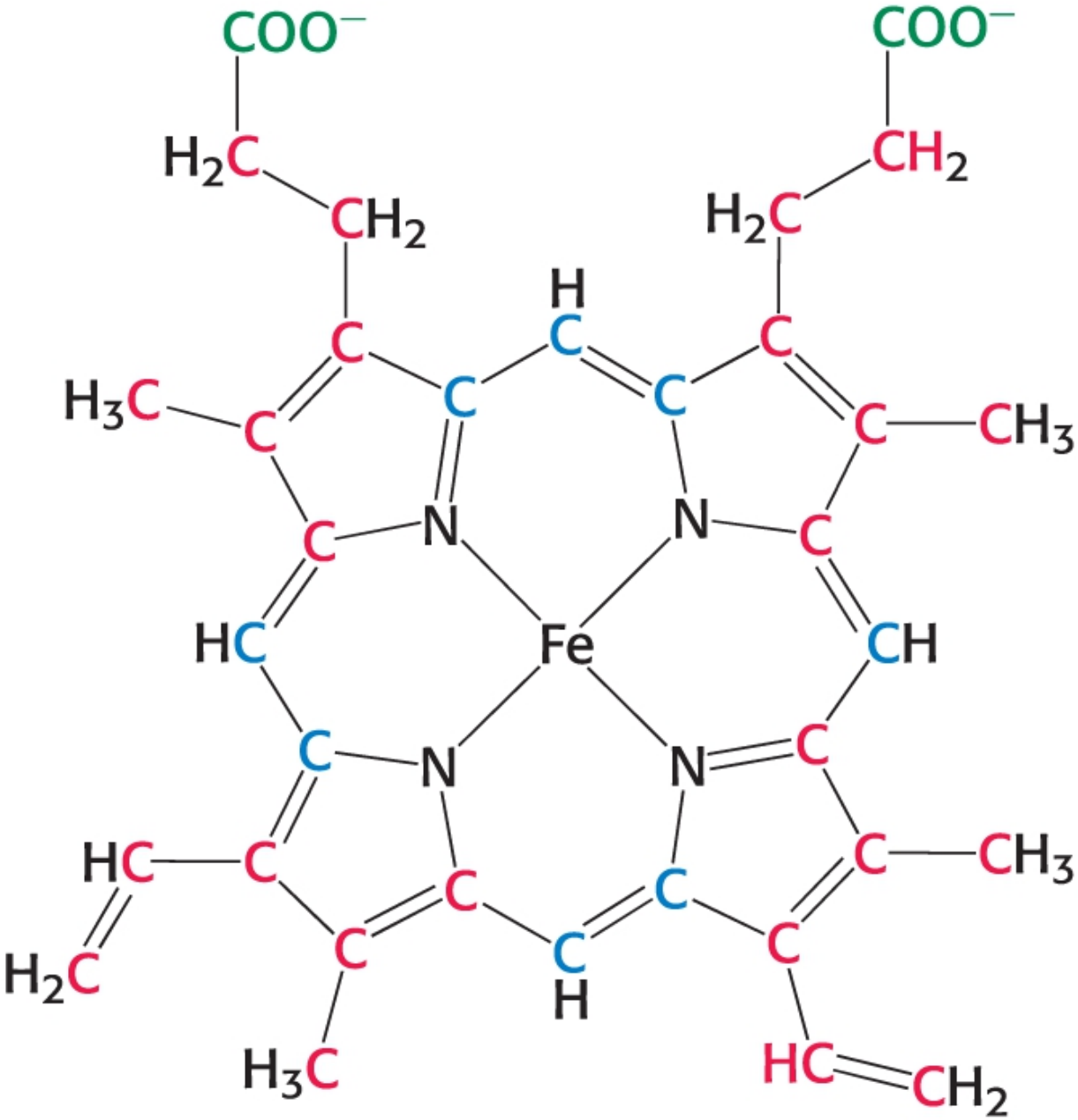
studies



Glycine



Acetate



Heme

A structure of glycine and acetate is shown above the heme ring. Glycine consists of C H 2 single bonded to N H 3 superscript plus on the lower left and single bonded to C O O superscript minus on the lower right. The C atom of the C H 2 group is highlighted in blue.

Acetate is composed of C H 3, single bond, C O O superscript minus. C O O is highlighted in green and the C atom of C H 3 is highlighted in red.

Heme consists of a central C atom single bonded to the N atom of a pentagonal ring on the upper left, upper right, lower left, and lower right. Each pentagonal ring consists of 1 N and 4 C atoms. C 1 and C 4 of adjacent rings are connected by a methylene bridge composed of C 1, single bond, C H, double bond, C 4 or C 4, single bond, C H, double bond, C 1. The C atom of the C H group in the bridge is highlighted in blue. In the upper left ring, C 1, C 2, and C 3 are highlighted in red. C 4 is highlighted in blue. A double bond is present between C 2 and C 3. C 2 is single bonded to C H 3. The C atom of C H 3 is highlighted in red. C 3 is single bonded to C H 2, single bond, C H 2, single bond, C O O superscript minus. The C atom of C H 2 groups are highlighted in red. C O O group is highlighted in green.

In the upper right ring, C 2, C 3, and C 4 are highlighted in red. C 1 is highlighted in blue. A double bond is present between C 2 and C 3. C 2 is single bonded to C H 2, single bond, C H 2, single bond, C O O superscript minus. The C atom of C H 2 groups are highlighted in red. C O O group is highlighted in green. C 3 is single bonded to C H 3. The C atom of C H 3 is highlighted in red.

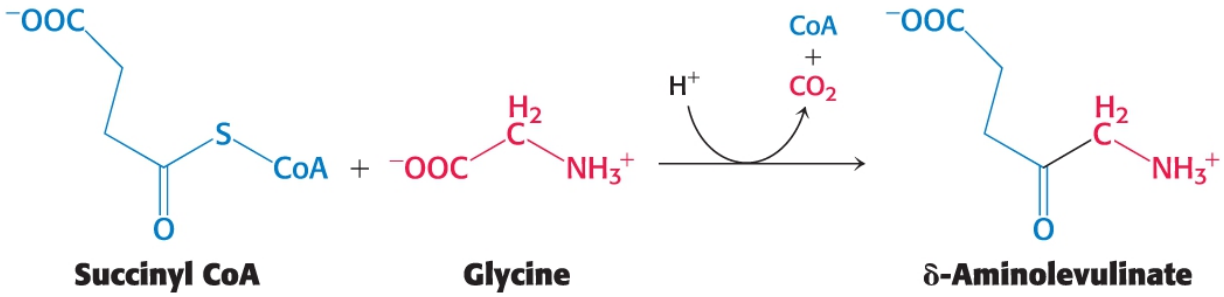
In the lower right ring, C 1, C 2, and C 3 are highlighted in red. C 4 is highlighted in blue. A double bond is present between N and C 1, and C 2 and C 3. C 2 is single bonded to C H 3. The C atom of C H 3 is

highlighted in red. C 3 is single bonded to C H, double bond, C H 2. The C atom of C H 2 and C H groups are highlighted in red.

In the lower-left ring, C 1, C 2, and C 3 are highlighted in red. C 4 is highlighted in blue. A double bond is present between C 1 and C 2, and C 3 and C 4. C 2 is single bonded to C H 3. The C atom of C H 3 is highlighted in red. C 3 is single bonded to C H, double bond, C H 2. The C atom of C H 2 and C H groups are highlighted in red.

Return to FIGURE 25.29 The origins of atoms in heme were revealed by isotope-labeling studies

Extended description for Formation of delta-aminolevulinate



The reaction consists of two reactants and one product. It is coupled with the entry of H superscript plus and release of C o A plus C O 2.

The first reactant is succinyl C o A whose structure is as follows: A central C atom is single bonded to C H 2 on the upper left in the form of a line, double bonded to O below, and single bonded to S on the upper right. S is single bonded to C o A on the lower right. C H 2 is single bonded to C H 2 above in the form of a line. This C H 2 group is further single bonded to C O O superscript minus on the upper left.

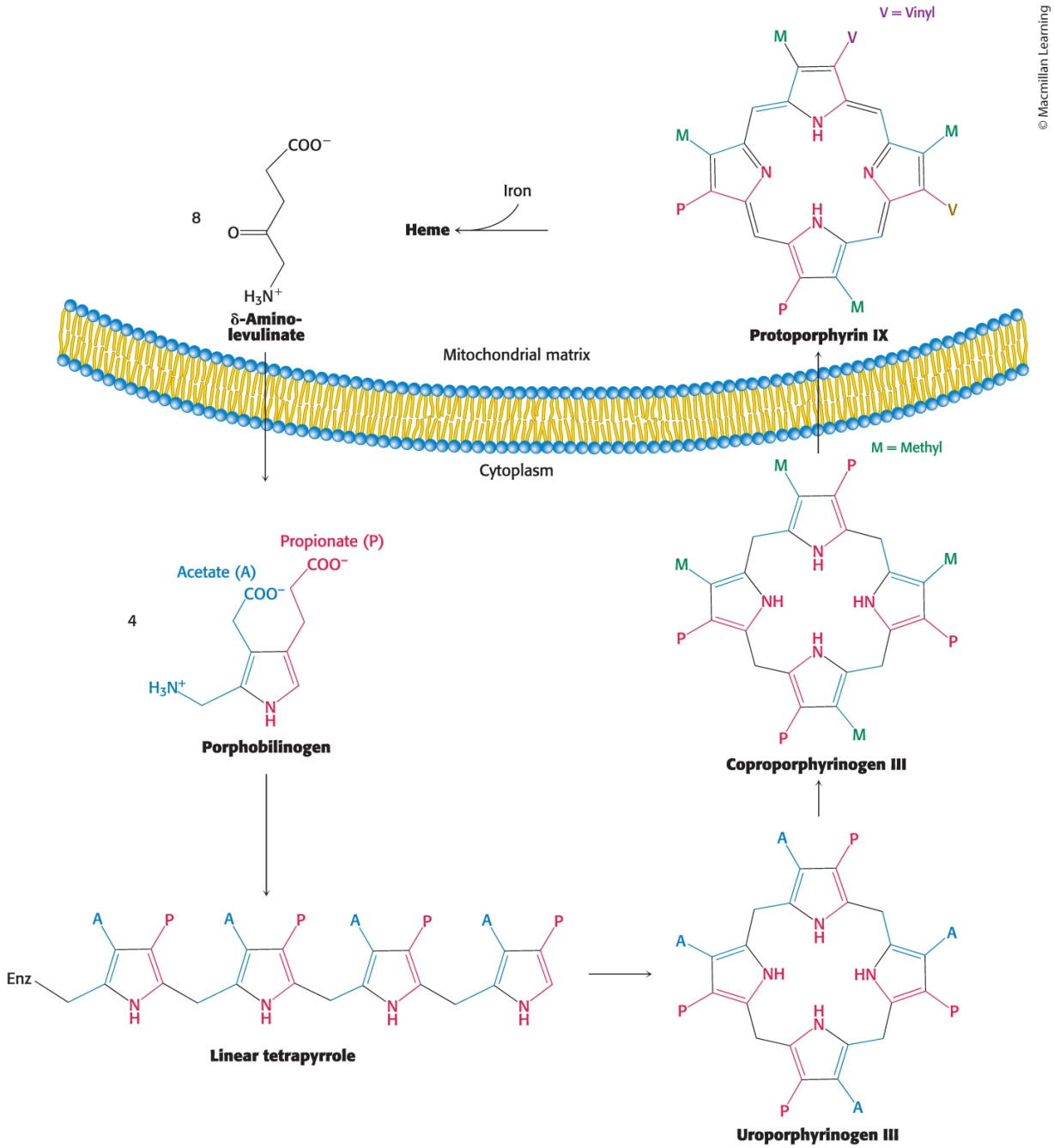
The second reactant is glycine whose structure is as follows: A central C atom bound to H 2 is single bonded to C O O superscript minus on the lower left and single bonded to N H 3 superscript plus on the lower right.

The product is delta-aminolevulinate whose structure is as follows: A central C atom is single bonded to C H 2 on the upper left in the form of a line, double bonded to O below, and single bonded to C H 2 on the upper right. The upper right C H 2 is single bonded to N H 3 superscript plus on the lower right. The upper left C H 2 is further single bonded to C H 2 above in the form of a line. This C H 2 group

is further single bonded to C O O superscript minus on the upper left.

Return to Formation of delta-aminolevulinate

Extended description for FIGURE 25.30 Heme is synthesized from eight molecules of delta-aminolevulinate



© Macmillan Learning

A lipid bilayer is shown. The region above the bilayer is labeled mitochondrial matrix and the region below is labeled cytoplasm. Eight delta-aminolevulinate molecules from the matrix enter the cytoplasm.

The structure of delta-aminolevulinate is as follows: A 4-carbon alkane chain is depicted as a vertical line structure using 3 zigzag lines. C 1 is single bonded to C O O superscript minus on the upper right. C 3 is double bonded to O on the left. C 4 is single bonded to N H 3 superscript plus on the lower left.

Inside the cytoplasm, delta-aminolevulinate molecules are converted into 4 porphobilinogen molecules.

The structure of 4 porphobilinogen is as follows: A 5-membered heterocyclic pentagonal ring is in a vertical orientation. It consists of 1 N and 4 C atoms. N bound to H occupies the bottom-most vertex. C 1 is single bonded to C H 2, single bond, N H 3 superscript plus on the left. C 2 is single bonded to C H 2, single bond, C O O superscript minus. C 3 is single bonded to C H 2, single bond, C H 2, single bond, C O O superscript minus above. A double bond is present between C 1 and C 2, and C 3 and C 4. C 1, C 2, and their substituent groups are highlighted in blue and labeled acetate (A). N H, C 3, C 4, and their substituent groups are highlighted in red and labeled propionate (P).

Porphobilinogen is converted into linear tetrapyrrole inside the cytoplasm.

The linear tetrapyrrole consists of four 5-membered heterocyclic pentagonal rings composed of 1 N and 4 C atoms. N bound to H occupies the bottom-most vertex. A double bond is present between C 1 and C 2, and C 3 and C 4. C 2 is single-bonded to A and C 3 is

single-bonded to P. The adjacent rings are connected by C 4, single bond, C H 2, single bond, C 1. C 1 of the leftmost ring is single-bonded to C H 2, which is further single-bonded to an enzyme.

Linear tetrapyrrole is converted into uroporphyrinogen 3 inside the cytoplasm.

Uroporphyrinogen 3 consists of a ring-like arrangement of tetrapyrrole. The N H groups of the individual rings face the interior and A and P substituents are located toward the exterior.

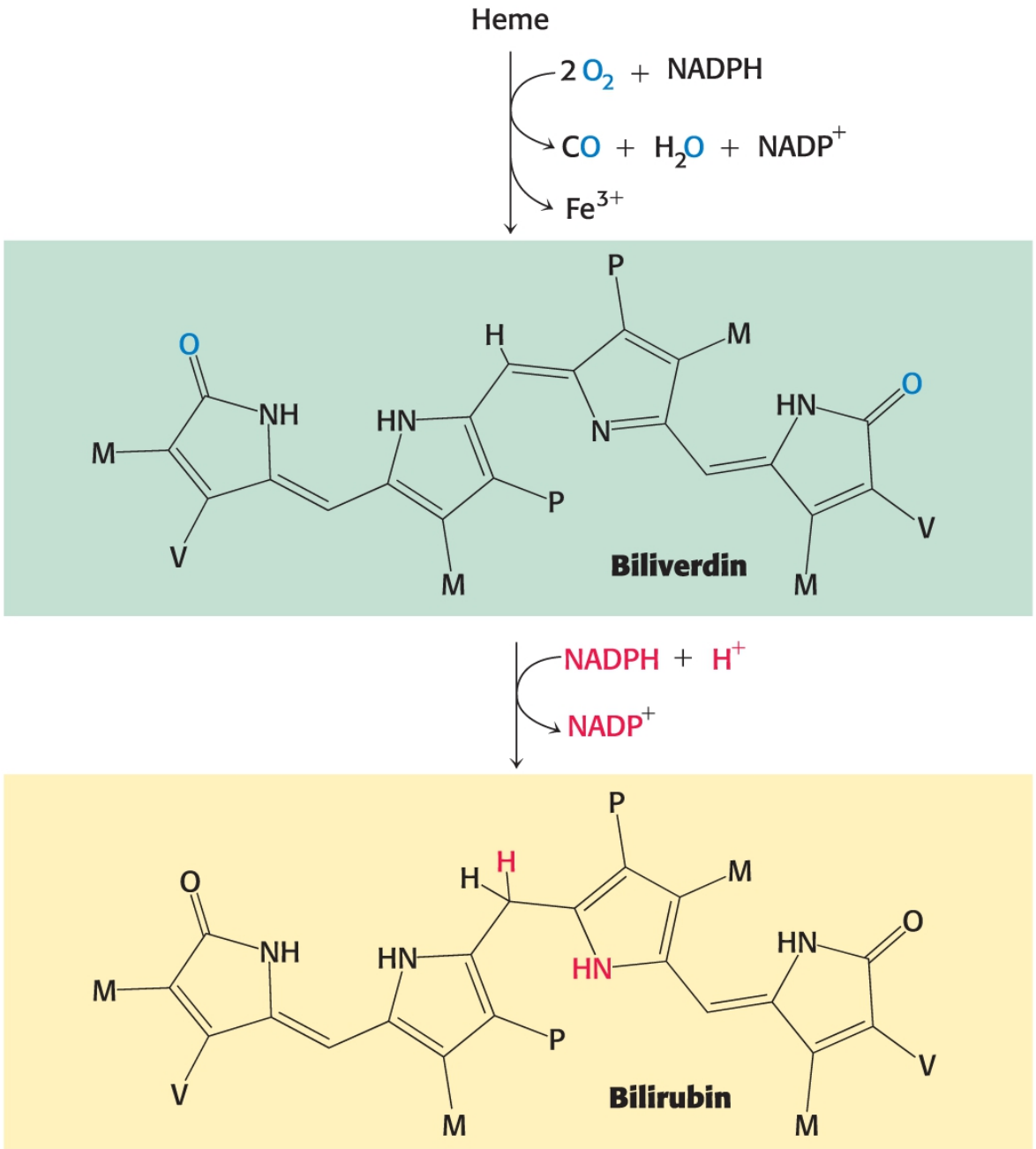
Uroporphyrinogen 3 is converted into coproporphyrinogen 3 inside the cytoplasm. In coproporphyrinogen 3, A is replaced with M. M depicts the methyl group.

Coproporphyrinogen 3 crosses the bilayer to enter the mitochondrial matrix. In the matrix, protoporphyrin 9 is formed. In protoporphyrin 9, P bonded to C 3 of the topmost and right pyrrole rings is replaced with V. V depicts the vinyl group. In addition, the adjacent rings are connected by C 4, double bond, C H, single bond, C 1 or C 4, single bond, C H, double bond, C 1. The topmost ring contains only one double bond between C 2 and C 3. The position of double bonds is altered in the left and right rings.

In the matrix, iron is added to protoporphyrin 9 to produce heme.

Return to FIGURE 25.30 Heme is synthesized from eight molecules of delta-aminolevulinate

Extended description for FIGURE 25.31 Heme is degraded into biliverdin and bilirubin



© Macmillan Learning

In the first irreversible step, heme is converted into biliverdin. This step is coupled with the entry of 2 O 2, the release of C O 2 plus H 2 O

and F e superscript 3 plus, and the oxidation of N A D P H to N A D P superscript plus.

The structure of the biliverdin is shown inside a green rectangle. It is composed of four 5-membered heterocyclic pentagonal rings. The adjacent rings are connected by a methylene bridge. In the methylene bridge, the adjacent rings are connected by a double bond, C H, single bond or single bond, C H, double bond.

Each ring consists of 1 N and 4 C atoms. In the first ring from left, C 2 is single bonded to V, C 3 is single bonded to M, and C 4 is double bonded to O above. A double bond is present between C 2 and C 3.

In the second ring, a double bond is present between C 1 and C 2, and C 3 and C 4. C 2 is single-bonded to P and C 3 is single-bonded to M.

In the third ring, a double bond is present between C 2 and C 3, and C 4 and N. C 2 is single bonded to P, and C 3 is single bonded to M.

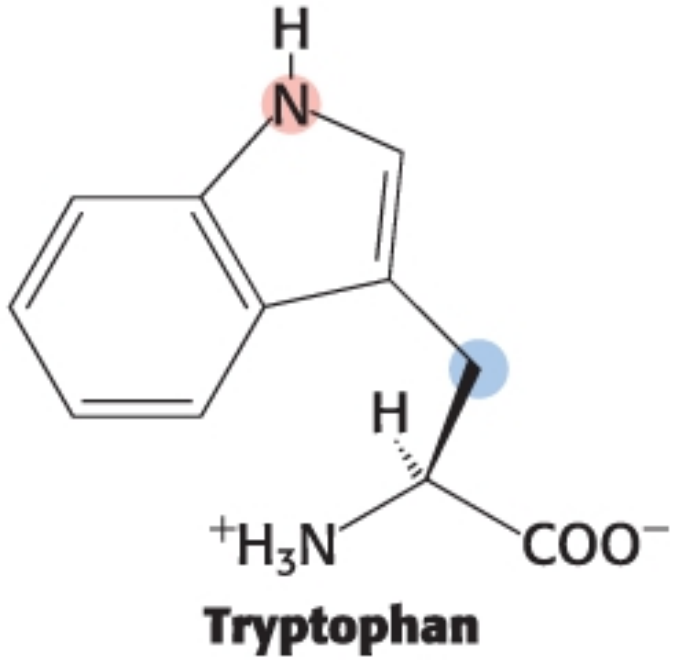
In the fourth ring, C 2 is single bonded to V, C 3 is single bonded to M, and C 1 is double bonded to O above. A double bond is present between C 2 and C 3.

In the second irreversible step, biliverdin is converted into bilirubin with the simultaneous oxidation of N A D P H plus H superscript plus into N A D P superscript plus. The structure of bilirubin is shown inside a yellow rectangle.

Bilirubin is similar to biliverdin except the methylene bridge connecting the second and third ring is altered to single bond, C H 2, single bond. In addition, N of the third ring is bound to H and the position of double bonds is altered in the third ring.

Return to FIGURE 25.31 Heme is degraded into biliverdin and bilirubin

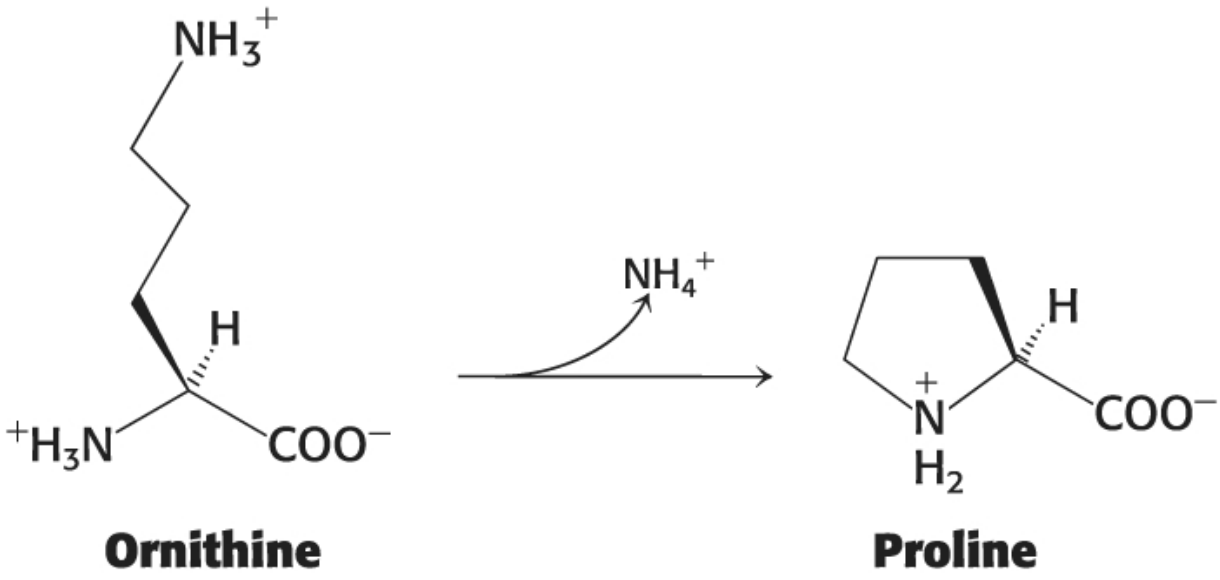
Extended description for Structure of tryptophan



The structure of tryptophan is as follows: A 5-membered heterocyclic pentagonal ring is in a vertical orientation. It consists of 1 N and 4 C atoms. N single bonded to H occupies the topmost vertex and is highlighted inside a pink circle. A double bond is present between C 1 and C 2. It is fused to a benzene ring in a horizontal orientation such that C 3 and C 4 of the pentagonal ring are C 1 and C 6 respectively of the benzene ring. The benzene ring contains alternating double bonds between C 2 and C 3, C 4 and C 5, and C 6 and C 1. C 2 of the pentagonal ring is single-bonded to C H 2 on the lower right in the form of a line. C H 2 is highlighted inside a blue circle. It is wedge bonded to C on the lower left. This C is single bonded to C O O superscript minus on the lower right, dash bonded to H on the upper left, and single bonded to N H 3 superscript plus on the lower left.

Return to Structure of tryptophan

Extended description for Formation of proline from ornithine



The reaction consists of one reactant and one product. It is coupled with the release of N H 4 superscript plus molecule. The reactant is ornithine and the product is proline.

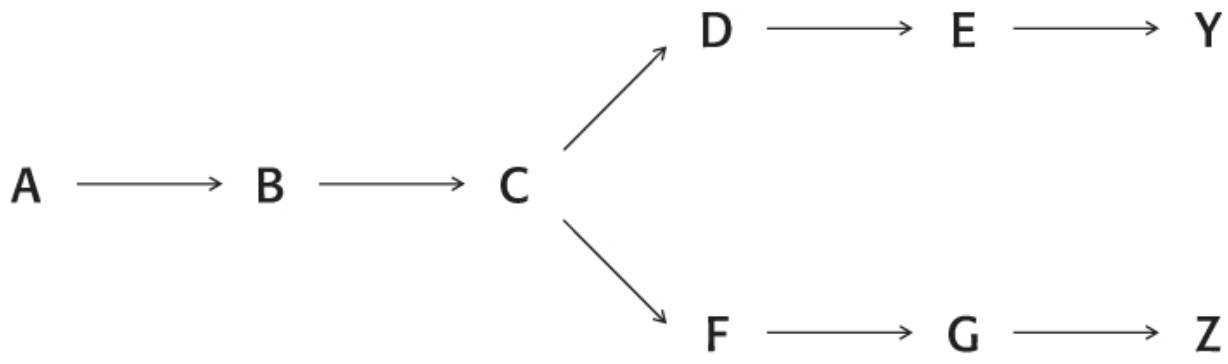
The structure of ornithine is as follows: A central C atom is single bonded to N H 3 superscript plus on the lower left, single bonded to C O O superscript minus on the lower right, wedge bonded to C H 2 on the upper left, and dash bonded to H on the upper right. The C H 2 group is single-bonded to a 2-carbon alkane chain depicted using a single line. C 2 of this alkane chain is single bonded to N H 3 superscript plus on the upper right.

The structure of proline is as follows: A central C atom is wedge bonded to C H 2 on the upper left, single bonded to N H 2 with a positive charge on the lower left, dash bonded to H on the upper right, and single bonded to C O O superscript minus on the lower

right. The upper left C H 2 group is single-bonded to a 2-carbon alkane chain depicted using a line. C 2 of this chain is single-bonded to the N H 2 group on the lower left such that a cyclic pentagonal-shaped ring structure is formed.

Return to Formation of proline from ornithine

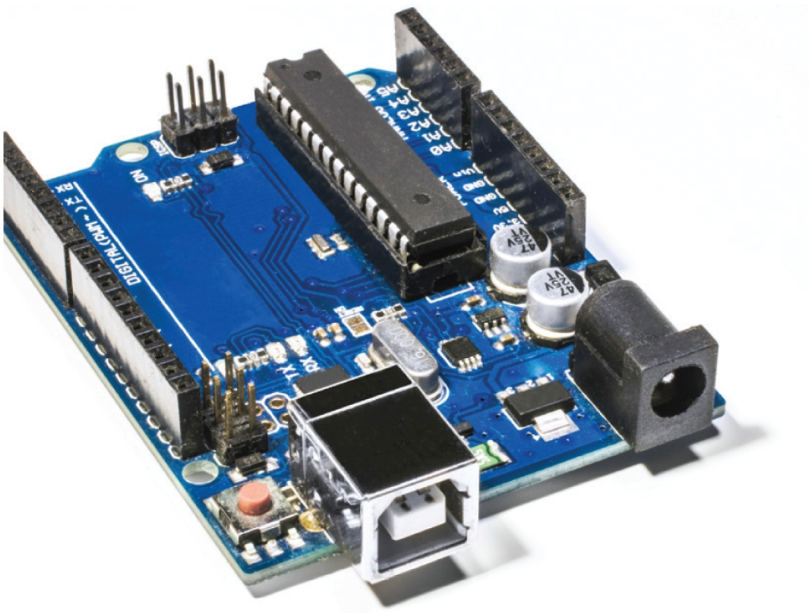
Extended description for Schematic representation of a branched pathway



The pathway is depicted as follows: A, forward arrow, B, forward arrow, C. After the formation of C, the pathway bifurcates or branches to form Y and Z. The top branch is depicted as follows: C, upper right arrow, D, forward arrow, E, forward arrow, Y. The bottom branch is depicted as follows: C, lower right arrow, F, forward arrow, G, forward arrow, Z.

Return to Schematic representation of a branched pathway

Extended description for Ribbon diagram of A T P grasp domain



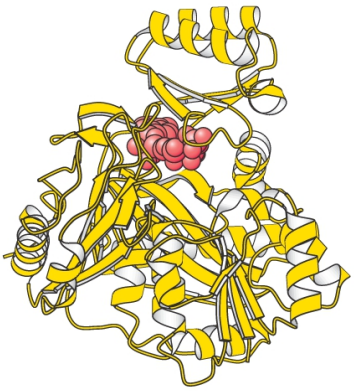
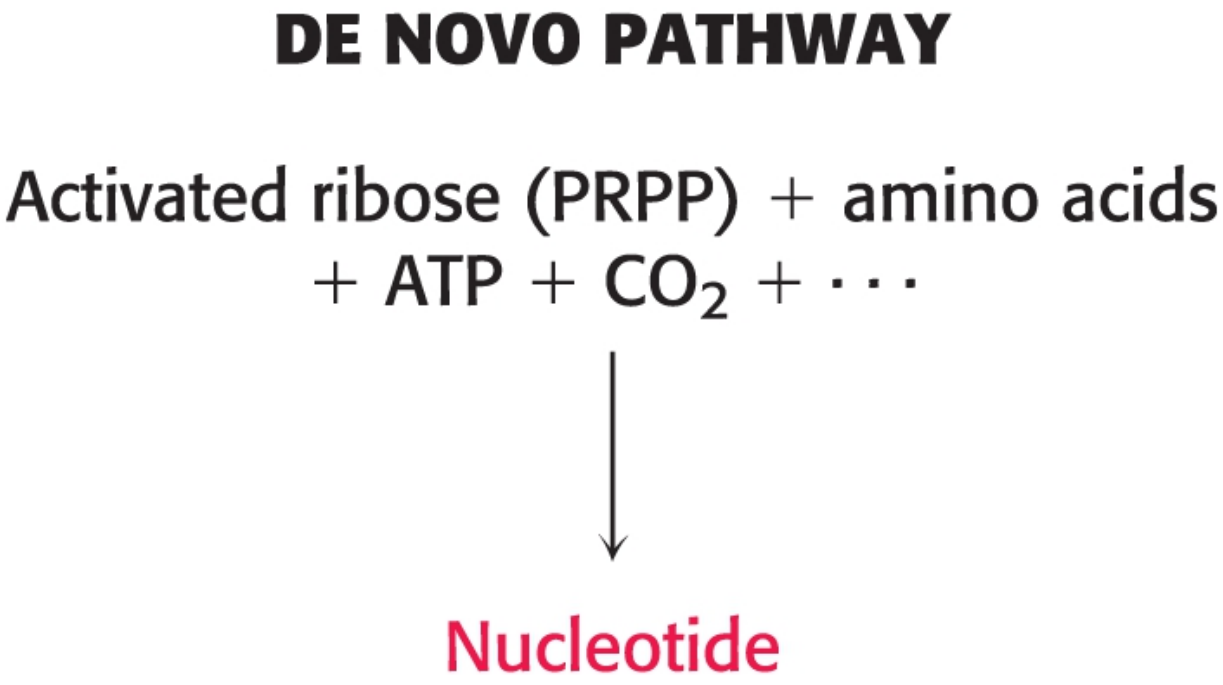


Photo: Sergey Privalov/Shutterstock
© Macmillan Learning

The A T P grasp domain consists of several beta-strands in the center and alpha-helices in the periphery. The alpha-helices and beta-strands are interconnected by thread-like loops. A cluster of red spheres is located inside a hollow space near the top of the ribbon diagram.

Return to Ribbon diagram of A T P grasp domain

Extended description for FIGURE 26.1 Nucleotides can be synthesized by de novo and salvage pathways



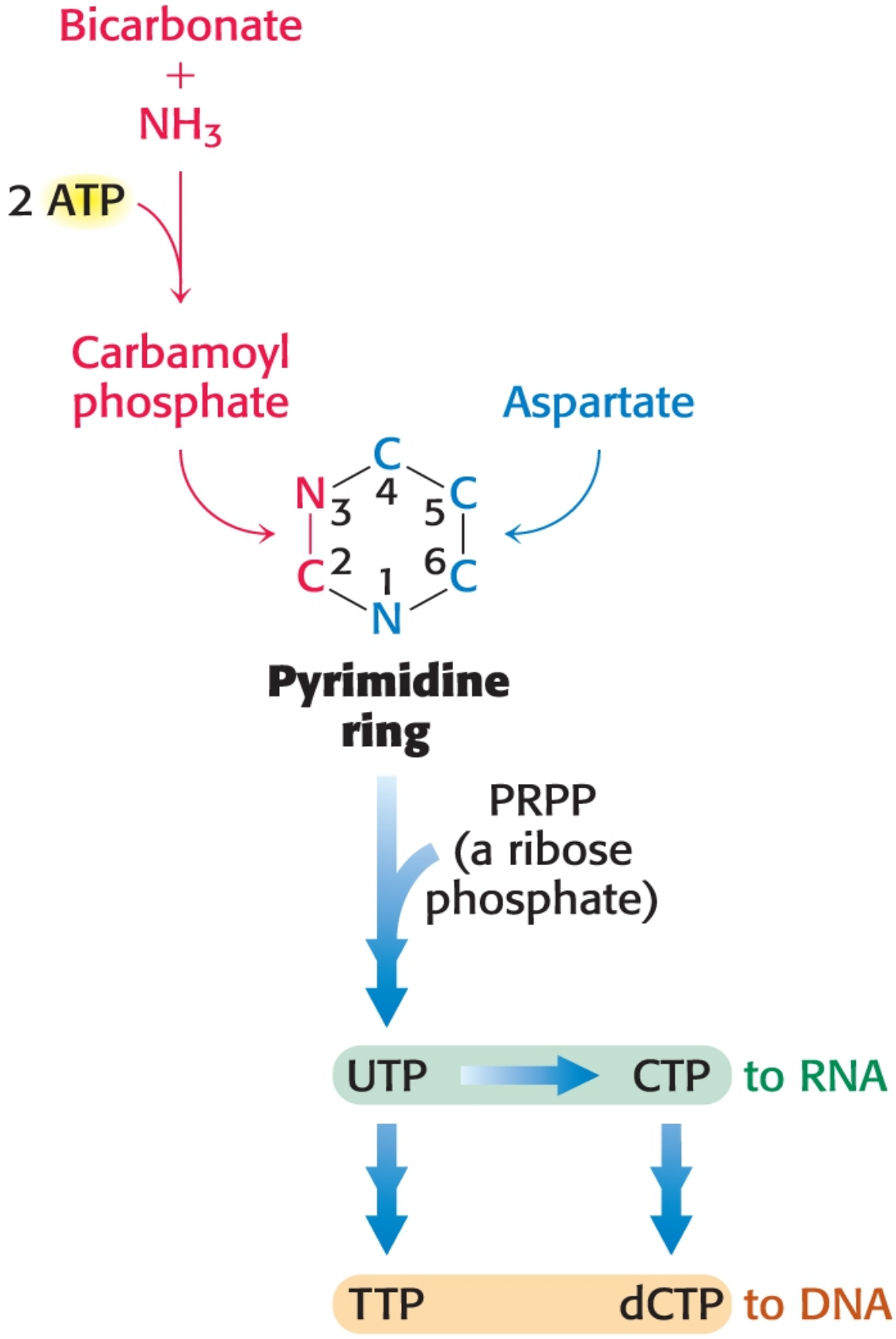
The first pathway for nucleotide biosynthesis is the de novo pathway. The precursor materials for this pathway are depicted as follows: Activated ribose (P R P P) plus amino acids plus A T P plus C O 2 plus dot dot. A downward arrow from these precursors leads to the nucleotide.

The second pathway for nucleotide biosynthesis is the salvage pathway. The precursor materials for this pathway are depicted as follows: Activated ribose (P R P P) plus base. A downward arrow from these precursors leads to the nucleotide.

Return to FIGURE 26.1 Nucleotides can be synthesized by de novo and salvage pathways

Extended description for FIGURE 26.2 Pyrimidine

nucleotides can be synthesized de novo



© Macmillan Learning

The de novo synthesis of pyrimidine nucleotides is depicted as follows:

Bicarbonate plus N H 3 are irreversibly converted into carbamoyl phosphate with the addition of 2 A T P.

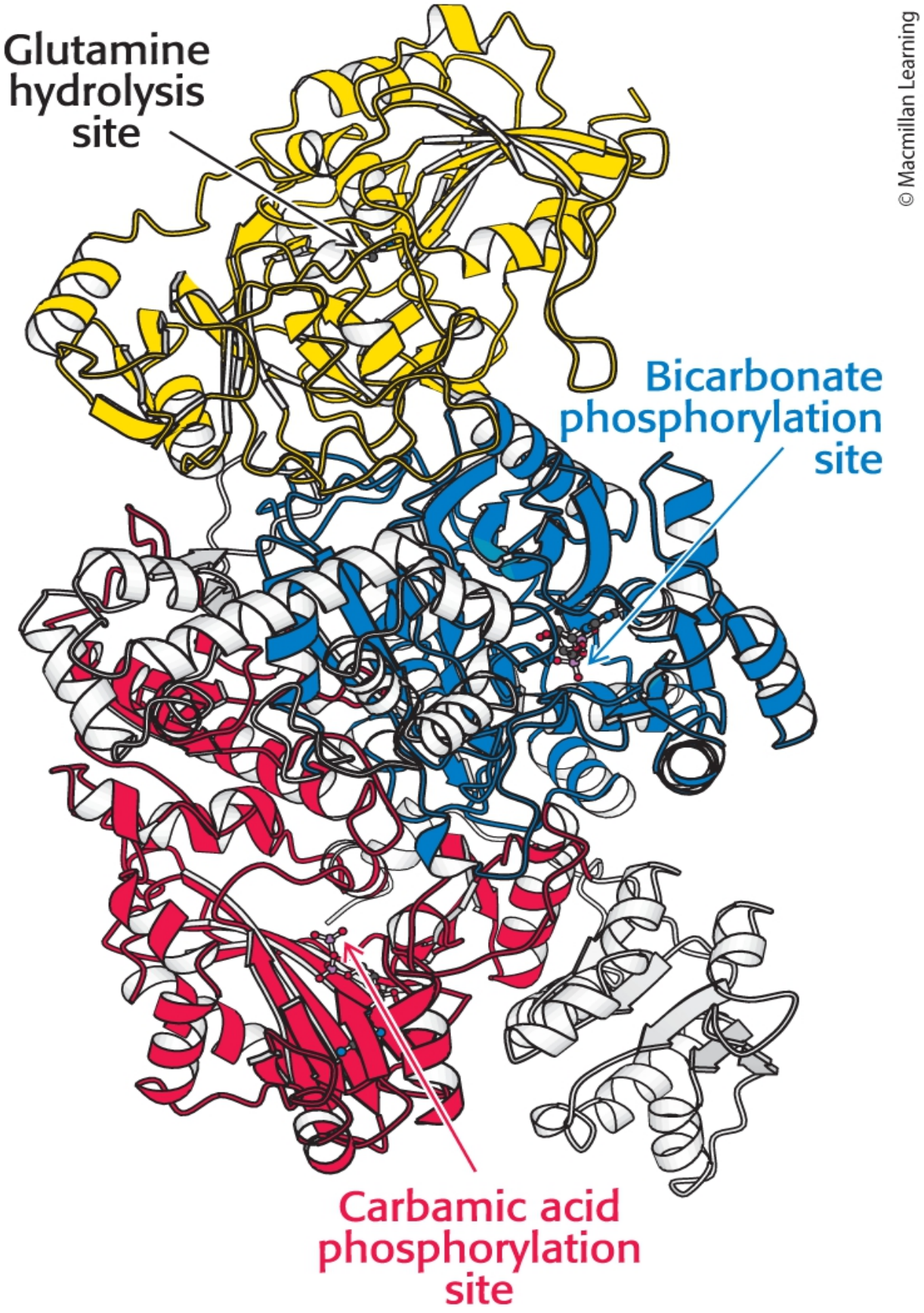
A 6-membered heterocyclic hexagonal ring in vertical orientation is shown below. The ring is labeled pyrimidine ring. It consists of 2 N and 4 C atoms. First N occupies the bottom-most vertex and the second N occupies the top left vertex. The remaining positions are occupied by C atoms. The atoms of the ring are numbered 1 to 6 in a clockwise manner starting from the bottom-most N atom. C 2 occupying the bottom left vertex and N 3 occupying the top left vertex are highlighted in red. The remaining atoms are highlighted in blue. The red highlighted atoms are derived from carbamoyl phosphate and the blue highlighted atoms are derived from aspartate.

A downward arrow from the pyrimidine ring leads to U T P with the simultaneous addition of P R P P (a ribose phosphate). A single forward arrow from U T P leads to C T P. U T P and C T P are labeled "to R N A." Two successive downward arrows below U T P and C T P lead to T P P and d C T P respectively. T T P and d C T P are labeled "to D N A."

Return to FIGURE 26.2 Pyrimidine nucleotides can be synthesized de novo

Extended description for FIGURE 26.3 Carbamoyl phosphate synthetase 2 includes sites for three

reactions

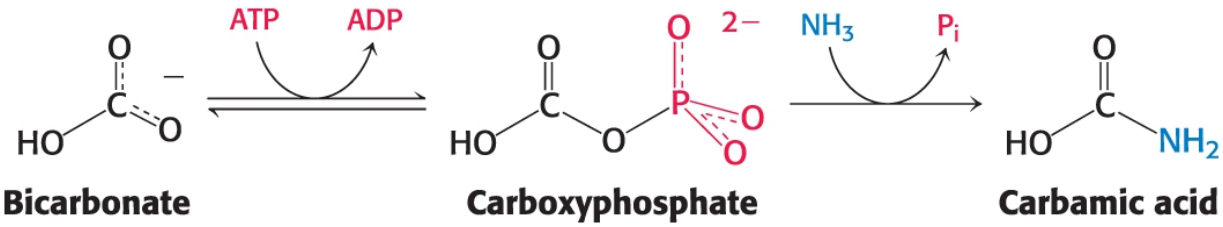


© Macmillan Learning

The carbamoyl phosphate synthetase 2 consists of a small domain at the top, a large domain in the middle, and a tiny domain at the bottom right. The top domain is shown in yellow. A glutamine hydrolysis site is located in the center of this domain. The middle large domain is composed of two A T P-grasp domains shown in blue and red. The blue domain is located above the red domain and contains a bicarbonate phosphorylation site. The red domain contains a carbamic acid phosphorylation site. The tiny bottom right domain is shown in white. It consists of a few alpha-helices and short beta-strands.

Return to FIGURE 26.3 Carbamoyl phosphate synthetase 2 includes sites for three reactions

Extended description for Formation of carbamic acid from bicarbonate



In the first reversible step, bicarbonate is converted into carboxyphosphate. It is coupled with the breakdown of A T P to A D P.

The structure of bicarbonate is as follows: A central C atom is partially double-bonded to O above, partially double-bonded to O on the lower right, and single-bonded to O H on the lower left. The partially double-bonded O atoms have an overall negative charge.

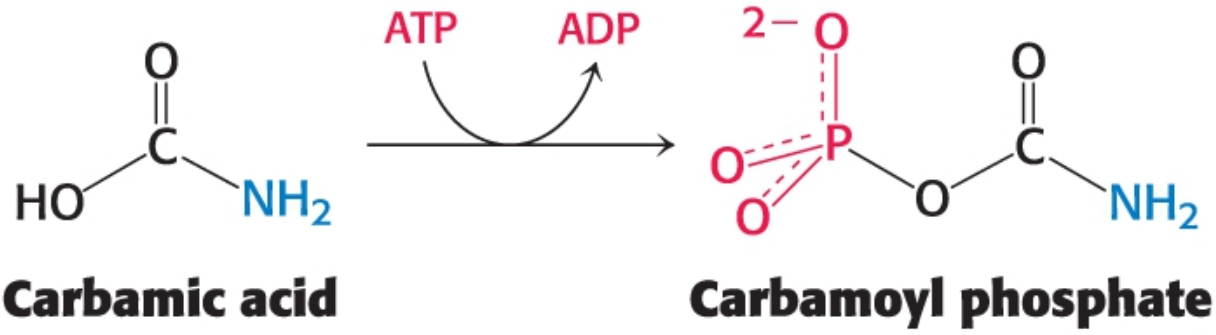
The structure of carboxyphosphate is as follows: A central C atom is double bonded to O above, single bonded to O H on the lower left, and single bonded to O on the lower right. The lower right O is single-bonded to P on the upper right. P is partially double bonded to O above, O on the right, and O on the lower right. The partially double bonded O atoms have an overall negative charge of 2 minus.

In the second irreversible step, carboxyphosphate is converted into carbamic acid. It is coupled with the entry of N H 3 and the release of P subscript i.

The structure of carbamic acid is as follows: A central C atom is double bonded to O above, single bonded to O H on the lower left, and single bonded to N H 2 on the lower right.

Return to Formation of carbamic acid from bicarbonate

Extended description for Formation of carbamoyl phosphate from carbamic acid



The reaction consists of one reactant and one product. It is coupled with the breakdown of A T P to A D P. The reactant is carbamic acid and the product is carbamoyl phosphate.

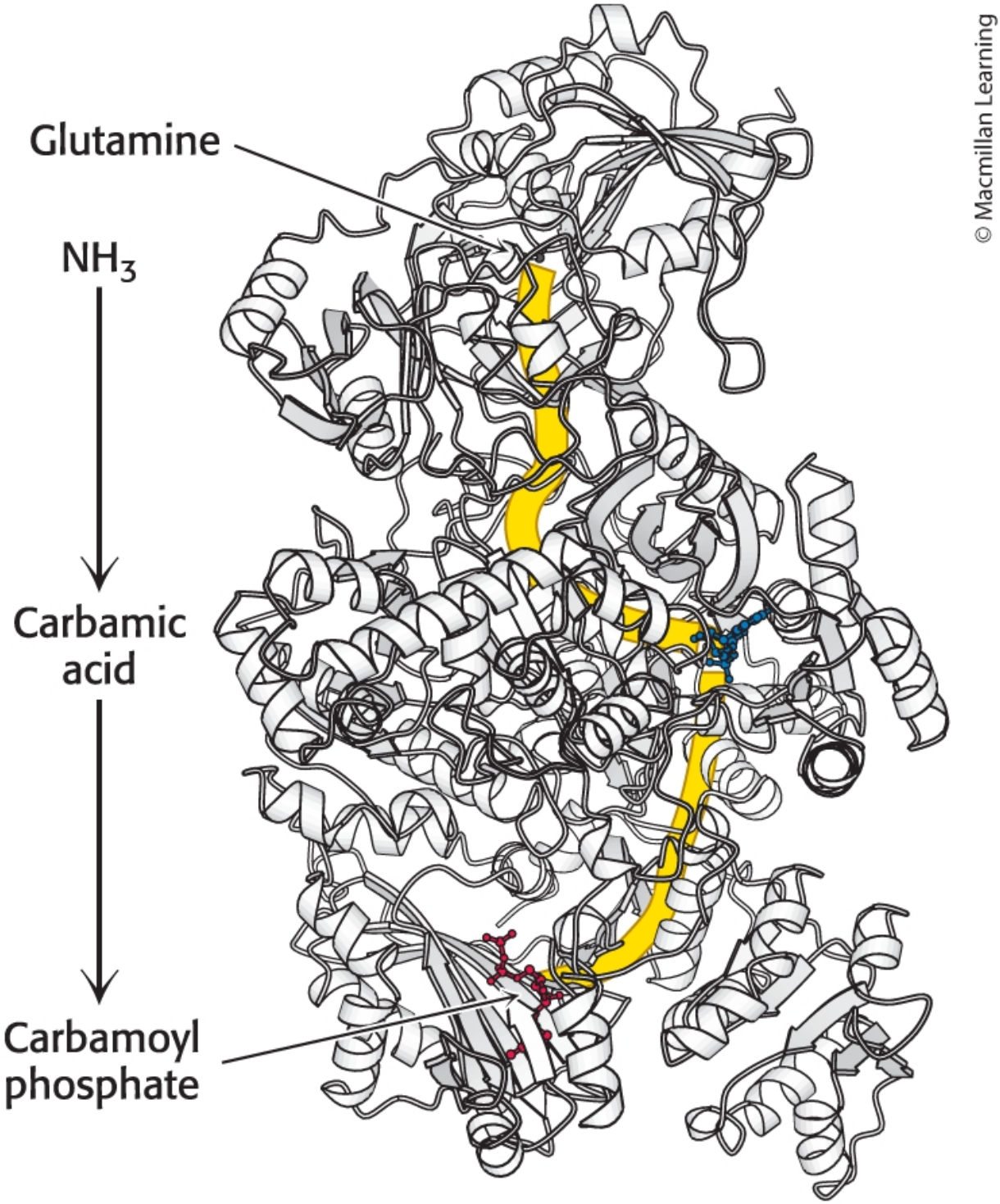
The structure of carbamic acid is as follows: A central C atom is double bonded to O above, single bonded to O H on the lower left, and single bonded to N H 2 on the lower right.

The structure of carbamoyl phosphate is as follows: A central C atom is double bonded to O above, single bonded to O on the lower left, and single bonded to N H 2 on the lower right. The lower left O is single-bonded to P on the upper left. P is partially double bonded to O above, O on the left, and O on the lower left. The partially double bonded O atoms have an overall negative charge of 2 minus.

Return to Formation of carbamoyl phosphate from carbamic acid

Extended description for FIGURE 26.4 The three active sites of carbamoyl phosphate synthetase 2 are linked

by a channel through which intermediates pass

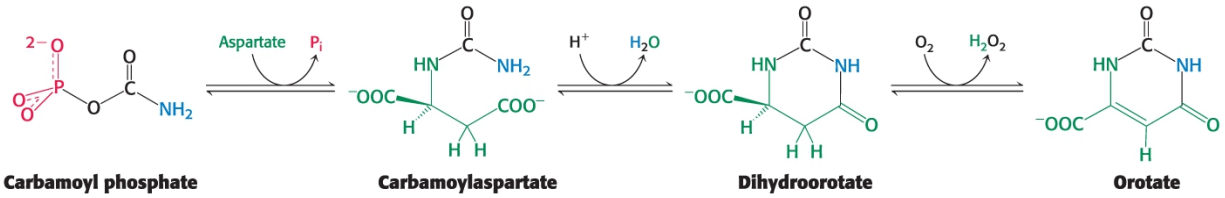


© Macmillan Learning

The ribbon diagram shows an elongated structure composed of several alpha helices and a few-beta strands interconnected by thread-like loops. A yellow tubular channel moves vertically down from top to the bottom in a slightly wavy manner. It passes through the three active sites. An arrow pointing toward the top mouth of the channel is labeled glutamine. An arrow pointing toward the bottom end of the channel is labeled carbamoyl phosphate. An irreversible conversion of N H 3 to carbamoyl phosphate is shown outside the ribbon diagram, along the channel. N H 3 near the top mouth of the channel is irreversibly converted into carbamic acid, corresponding to the middle of the channel. Carbamic acid is later irreversibly converted into carbamoyl phosphate.

Return to FIGURE 26.4 The three active sites of carbamoyl phosphate synthetase 2 are linked by a channel through which intermediates pass

Extended description for Formation of orotate from carbamoyl phosphate



In the first irreversible step, carbamoyl phosphate is converted into carbamoylaspartate. It is coupled with the entry of aspartate and release of P subscript i.

The structure of carbamoyl phosphate is as follows: A central C atom is double bonded to O above, single bonded to O on the lower left, and single bonded to N H 2 on the lower right. The lower left O is single-bonded to P on the upper left. P is partially double bonded to O above, O on the left, and O on the lower left. The partially double-bonded O atoms have an overall negative charge of 2 minus.

The structure of carbamoylaspartate is as follows: A central C atom is double bonded to O above, single bonded to N H on the lower left, and single bonded to N H 2 on the lower right. The lower left N H is single-bonded to C 1 of a 2-carbon alkane chain depicted using a line. C 1 is wedge bonded to C O O superscript minus on the upper left, dash bonded to H on the lower left. C 2 is single bonded to C O O superscript minus on the upper right, single bonded to H on the lower left and lower right.

In the second reversible step, carbamoylaspartate is converted into dihydroorotate. It is coupled with the entry of H superscript plus ion and release of H 2 O.

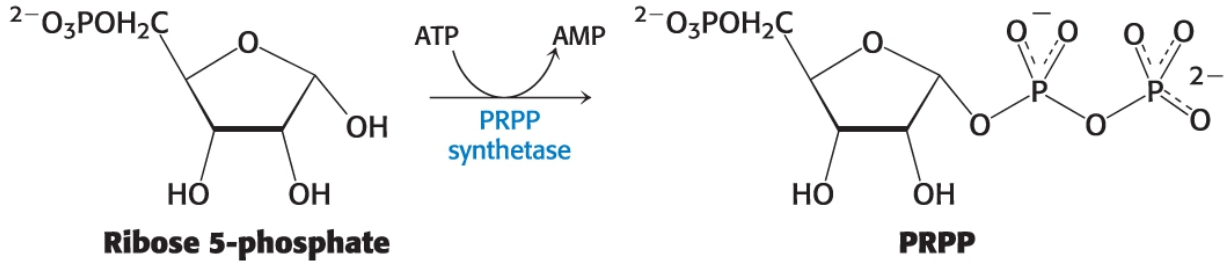
The structure of dihydroorotate is as follows: A 6-membered heterocyclic hexagonal ring is in a vertical orientation. It consists of 2 N and 4 C atoms. The first N bound to H occupies the top left vertex and the second N bound to H occupies the top right vertex. C 1 occupies the topmost vertex and is double bonded to O above. C 2 is double bonded to O on the lower right. C 3 is single bonded to H on the lower left and H on the lower right. C 4 is wedge bonded to C O O superscript minus on the left and dash bonded to H on the lower left.

In the third reversible step, dihydroorotate is converted into orotate. It is coupled with the entry of O 2 and the release of H 2 O 2.

The structure of orotate is as follows: A 6-membered heterocyclic hexagonal ring is in a vertical orientation. It consists of 2 N and 4 C atoms. The first N bound to H occupies the top left vertex and the second N bound to H occupies the top right vertex. C 1 occupies the topmost vertex and is double bonded to O above. A double bond is present between C 3 and C 4. C 2 is double bonded to O on the lower right. C 3 is single bonded to H below. C 4 is single bonded to C O O superscript minus on the lower left.

Return to Formation of orotate from carbamoyl phosphate

Extended description for Reaction catalyzed by P R P P synthetase



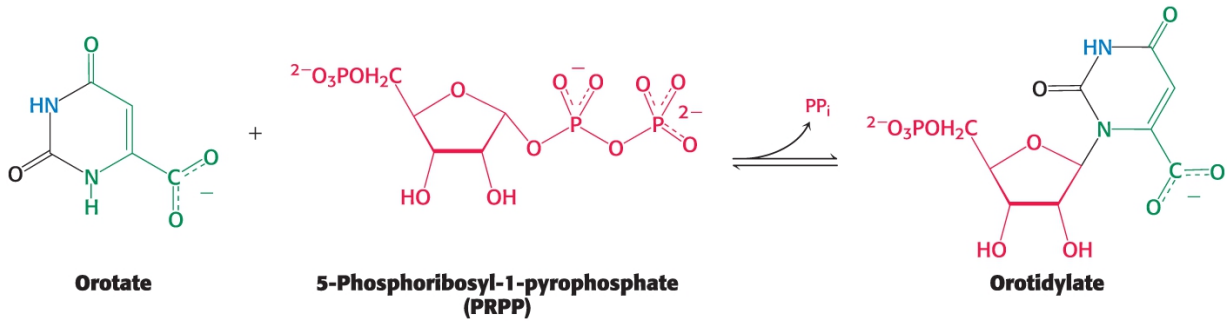
The reaction consists of one reactant and one product. It is catalyzed by P R P P synthetase and is coupled with the breakdown of A T P to A M P.

The reactant is ribose 5-phosphate whose structure is as follows: A 5-membered heterocyclic pentagonal ring is in a vertical orientation with C 1 occupying the top right vertex. It consists of 1 O and 4 C atoms. O occupies the topmost vertex. C 1, C 2, and C 3 are single bonded to O H below. C 4 is single bonded to C H 2 O P O 3 superscript 2 minus on the upper left.

The product is P R P P whose structure is as follows: A 5-membered heterocyclic pentagonal ring is in a vertical orientation with C 1 occupying the top right vertex. It consists of 1 O and 4 C atoms. O occupies the topmost vertex. C 1 is single bonded to a zigzag chain composed of O, single bond, P, single bond, O, single bond, P. P 1 is partially double bonded to O on the upper left and O on the upper right. The O atoms have an overall negative charge. P 2 is partially double bonded to O on the upper left, upper right, and lower right. The O atoms have an overall negative charge of 2 minus. C 2 and C 3 are single bonded to O H below. C 4 is single bonded to C H 2 O P O 3 superscript 2 minus on the upper left.

Return to Reaction catalyzed by P R P P synthetase

Extended description for Formation of orotidylate



The reaction consists of two reactants and one product. It is coupled with the release of P P subscript i.

The first reactant is orotate whose structure is as follows: A 6-membered heterocyclic hexagonal ring is in a vertical orientation. It consists of 2 N and 4 C atoms. The first N single bonded to H occupies the bottom-most vertex and the second N bound to H occupies the top left vertex. A double bond is present between C 3 and C 4. C 1 occupies the bottom left vertex and is double bonded to O on the lower left. C 2 is double bonded to O above. C 4 is single bonded to C on the lower left. This C is partially double bonded on the upper right and O below. The O atoms have an overall negative charge.

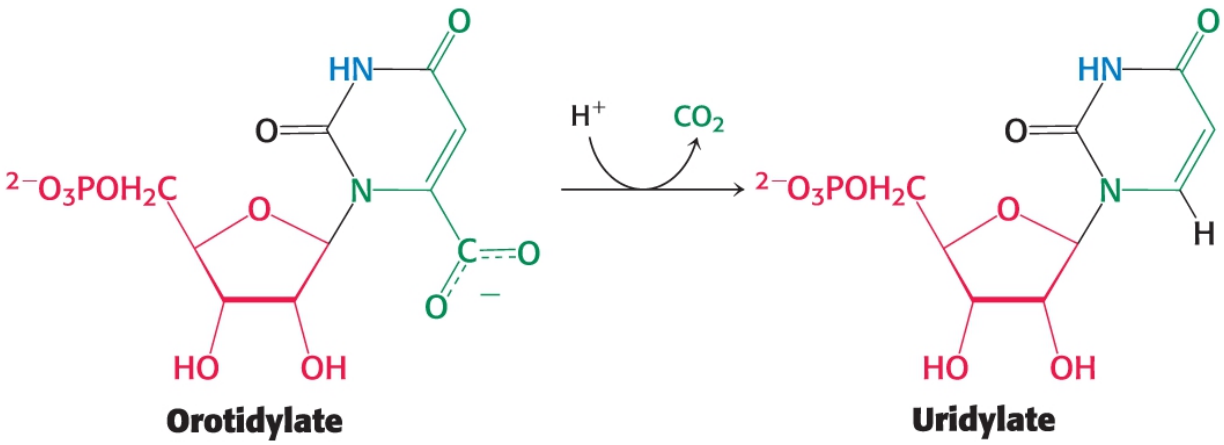
The second reactant is 5-phosphoribosyl1-pyrophosphate (P R P P) whose structure is as follows: A 5-membered heterocyclic pentagonal ring is in a vertical orientation with C 1 occupying the top right vertex. It consists of 1 O and 4 C atoms. O occupies the topmost vertex. C 1 is single bonded to a zigzag chain composed of O, single bond, P, single bond, O, single bond, P. P 1 is partially double bonded to O on the upper left and O on the upper right. The O atoms have an overall negative charge. P 2 is partially double

bonded to O on the upper left, upper right, and lower right. The O atoms have an overall negative charge of 2 minus. C 2 and C 3 are single bonded to O H below. C 4 is single bonded to C H 2 O P O 3 superscript 2 minus on the upper left.

The product is orotidylate whose structure is as follows: A 5-membered heterocyclic pentagonal ring is in a vertical orientation with C 1 occupying the top right vertex. It consists of 1 O and 4 C atoms. O occupies the topmost vertex. C 1 is single bonded to N 1 of orotate in horizontal orientation. C 2 and C 3 are single bonded to O H below. C 4 is single bonded to C H 2 O P O 3 superscript 2 minus on the upper left.

Return to Formation of orotidylate

Extended description for Formation of uridylate from orotidylate



The reaction consists of one reactant and one product. It is coupled with the entry of H superscript plus ion and release of C O 2.

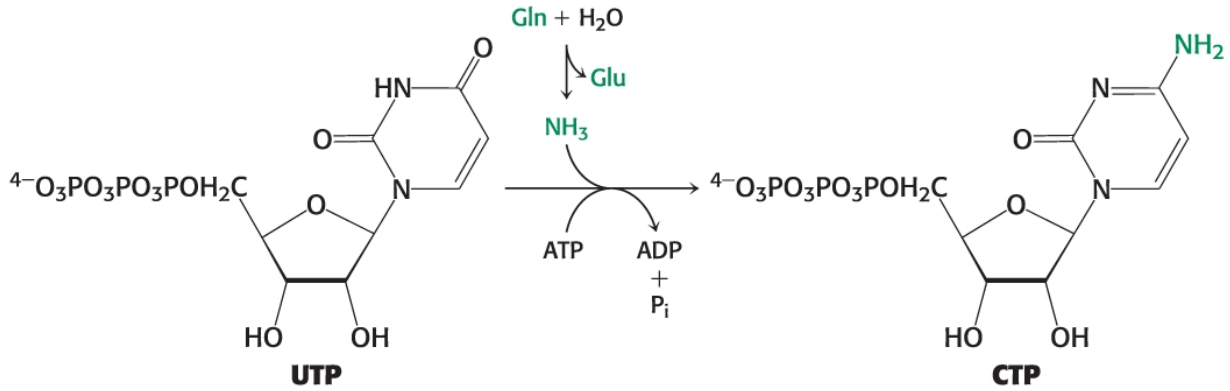
The reactant is orotidylate whose structure is as follows: A 5-membered heterocyclic pentagonal ring is in a vertical orientation with C 1 occupying the top right vertex. It consists of 1 O and 4 C atoms. O occupies the topmost vertex. C 1 is single-bonded to N 1 of a 6-membered heterocyclic hexagonal ring in a horizontal orientation. C 2 and C 3 are single bonded to O H below. C 4 is single bonded to C H 2 O P O 3 superscript 2 minus on the upper left. The hexagonal ring consists of 2 N and 4 C atoms. First N occupies the bottom left vertex and second N bound to H occupies the top left vertex. A double bond is present between C 3 and C 4. C 1 is double bonded to O on the left. C 2 is double bonded to O on the upper right. C 4 is single bonded to C on the lower right. This C is partially double-bonded to O on the right and O on the lower left.

The product is uridylate whose structure is as follows: A 5-membered heterocyclic pentagonal ring is in a vertical orientation

with C 1 occupying the top right vertex. It consists of 1 O and 4 C atoms. O occupies the topmost vertex. C 1 is single-bonded to N 1 of a 6-membered heterocyclic hexagonal ring in a horizontal orientation. C 2 and C 3 are single bonded to O H below. C 4 is single bonded to C H 2 O P O 3 superscript 2 minus on the upper left. The hexagonal ring consists of 2 N and 4 C atoms. First N occupies the bottom left vertex and second N bound to H occupies the top left vertex. A double bond is present between C 3 and C 4. C 1 is double bonded to O on the left. C 2 is double bonded to O on the upper right. C 4 is single bonded to H on the lower right.

Return to Formation of uridylate from orotidylate

Extended description for Formation of C T P from U T P



The reaction consists of one reactant and one product. The reactant is U T P and the product is C T P. This reaction is coupled with the entry of N H 3 and breakdown of A T P to A D P plus P subscript i. N H 3 is derived from glutamine. Glutamine reacts with H 2 O to form N H 3 and releases glutamic acid.

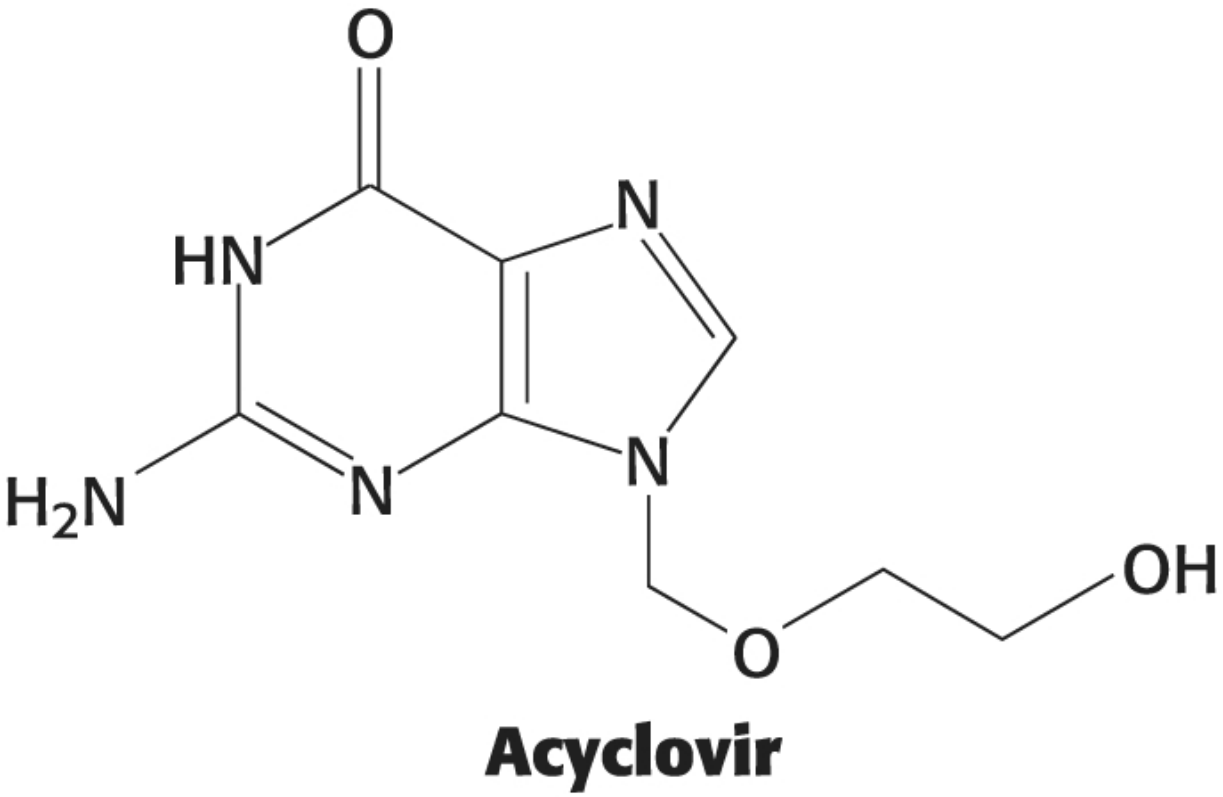
The structure of U T P is as follows: A 5-membered heterocyclic pentagonal ring is in a vertical orientation with C 1 occupying the top right vertex. It consists of 1 O and 4 C atoms. O occupies the topmost vertex. C 1 is single-bonded to N 1 of a 6-membered heterocyclic hexagonal ring in a horizontal orientation. C 2 and C 3 are single bonded to O H below. C 4 is single bonded to C H 2 O P O 3 P O 3 P O 3 superscript 4 minus on the upper left. The hexagonal ring consists of 2 N and 4 C atoms. First N occupies the bottom left vertex and second N bound to H occupies the top left vertex. A double bond is present between C 3 and C 4. C 1 is double bonded to O on the left. C 2 is double bonded to O on the upper right.

The structure of C T P is as follows: A 5-membered heterocyclic pentagonal ring is in a vertical orientation with C 1 occupying the top right vertex. It consists of 1 O and 4 C atoms. O occupies the

topmost vertex. C 1 is single-bonded to N 1 of a 6-membered heterocyclic hexagonal ring in a horizontal orientation. C 2 and C 3 are single bonded to O H below. C 4 is single bonded to C H 2 O P O 3 P O 3 P O 3 superscript 4 minus on the upper left. The hexagonal ring consists of 2 N and 4 C atoms. First N occupies the bottom left vertex and the second N occupies the top left vertex. A double bond is present between N 2 and C 2, and C 3 and C 4. C 1 is double bonded to O on the left. C 2 is single bonded to N H 2 on the upper right.

Return to Formation of C T P from U T P

Extended description for Structure of acyclovir



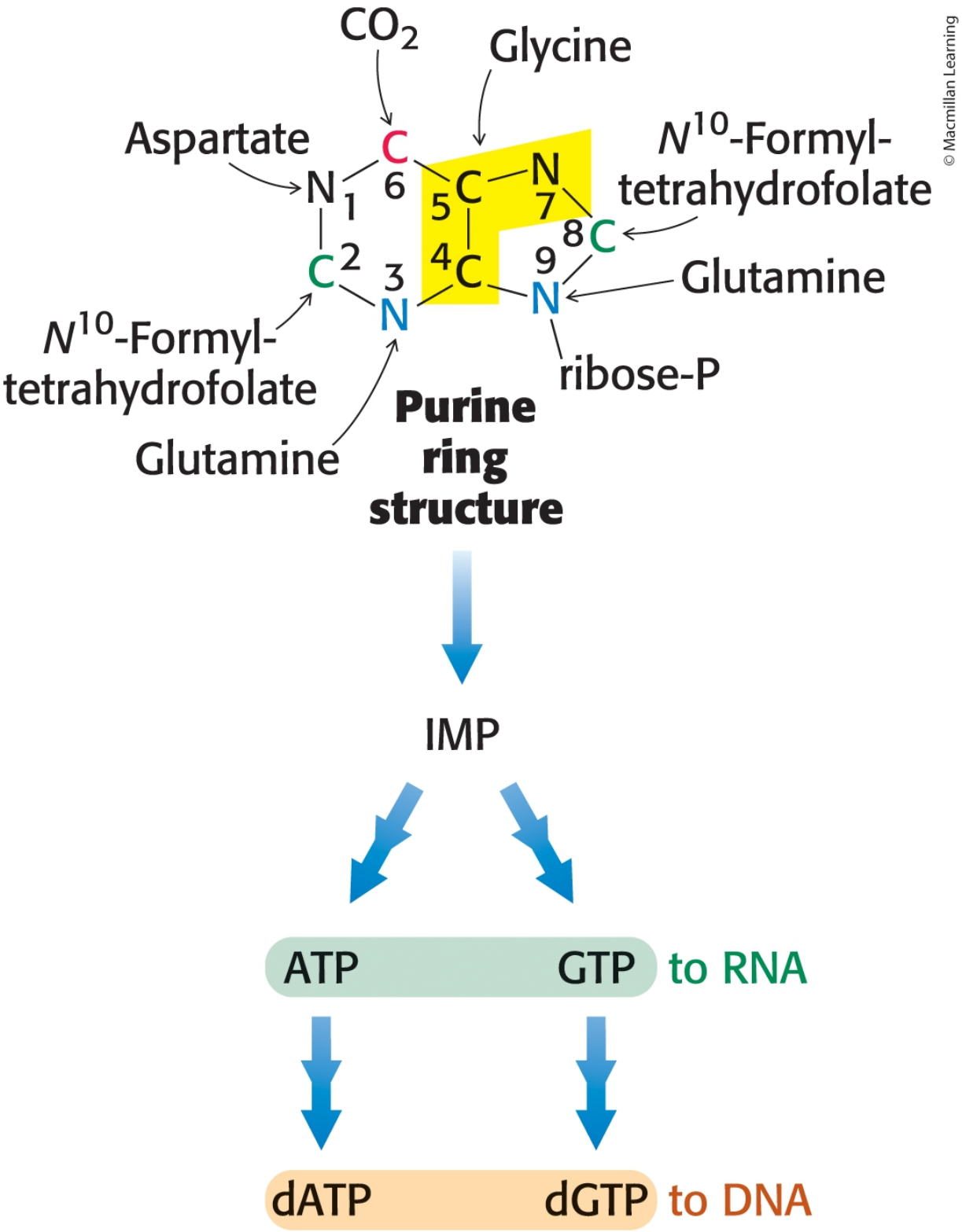
The structure of acyclovir is as follows: A 6-membered heterocyclic hexagonal ring is in a vertical orientation with C 1 occupying the bottom left vertex. It consists of 2 N and 4 C atoms. First N occupies the bottom-most vertex. The second N bound to H occupies the top left vertex. A double bond is present between N 1 and C 1. C 1 is single bonded to N H 2 on the lower left. C 2 is double bonded to O above. The hexagonal ring is fused to a 5-membered heterocyclic pentagonal ring in a horizontal orientation such that C 3 and C 4 of the hexagonal ring are C 3 and C 2 respectively of the pentagonal ring. The pentagonal ring consists of 2 N and 3 C atoms. First N occupies the topmost vertex and the second N occupies the bottom right vertex. A double bond is present between N 1 and C 1, and C 2 and C 3. N 2 is single bonded to a 1 O and 3 C heteronuclear alkane

chain depicted as a line structure using 3 zigzag lines. O occupies the second position. C 3 is single bonded to O H on the upper right.

Return to Structure of acyclovir

Extended description for FIGURE 26.5 Purine

nucleotides can be synthesized de novo



© Macmillan Learning

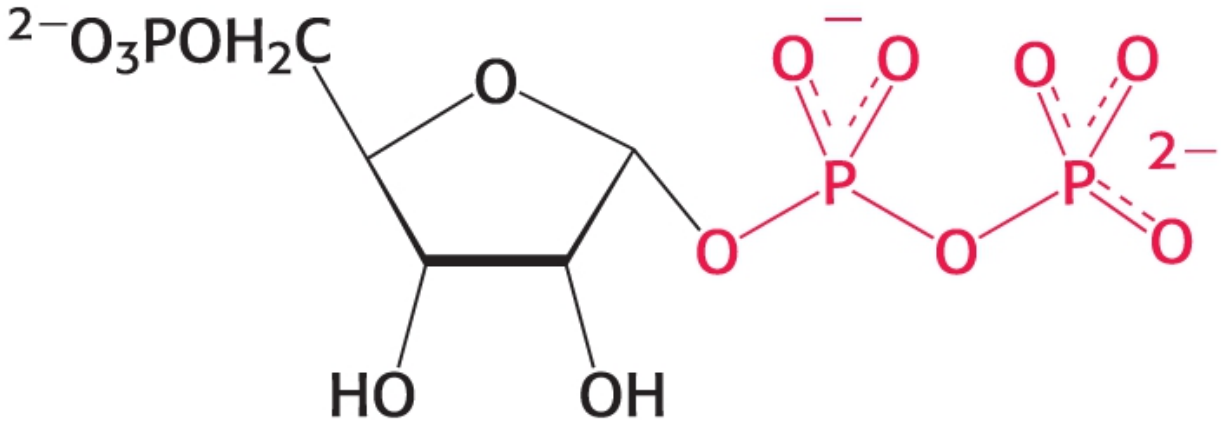
The purine ring structure is shown at the top. It consists of a 6-membered heterocyclic hexagonal ring in a vertical orientation. The ring consists of 2 N and 4 C atoms. First N occupies the bottom-most vertex and the second N occupies the top left vertex. The remaining positions are occupied by C atoms. The atoms of the ring are numbered 1 to 6 in an anticlockwise manner starting from the top-left N atom. N 1 occupying the top left vertex is derived from aspartate. C 2 occupying the bottom left vertex, highlighted in green, is derived from N superscript 10-Formyl-tetrahydrofolate. N 3 occupying the bottom-most vertex, highlighted in blue, is derived from glutamine. C 6 occupying the topmost vertex, highlighted in red, is derived from C O 2. The hexagonal ring is fused to a 5-membered heterocyclic pentagonal ring in a horizontal orientation such the C 4 and C 5 atoms are shared between them. The pentagonal ring consists of 2 N and 3 C atoms. First N occupies the topmost vertex. Second N occupies the bottom right vertex. First N, C 1, and second N are numbered 7, 8, and 9 respectively. N 7, C 4, and C 5, highlighted in yellow, are derived from glycine. C 8, highlighted in green, is derived from N superscript 10-Formyl-tetrahydrofolate. N 9, highlighted in blue, is derived from glutamine. N 9 is single bonded to ribose, single bond, P.

A downward arrow from the purine ring structure leads to I M P. I M P has two fates. It can either produce A T P or G T P. A T P and G T P are highlighted in a green bar labeled "to R N A." Two successive downward arrows from A T P lead to d A T P. Two successive downward arrows from G T P lead to d G T P. d A T P and d G T P are highlighted in an orange bar labeled "to D N A."

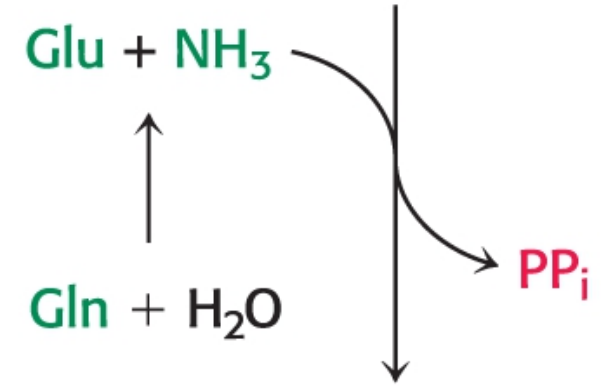
Return to FIGURE 26.5 Purine nucleotides can be synthesized de novo

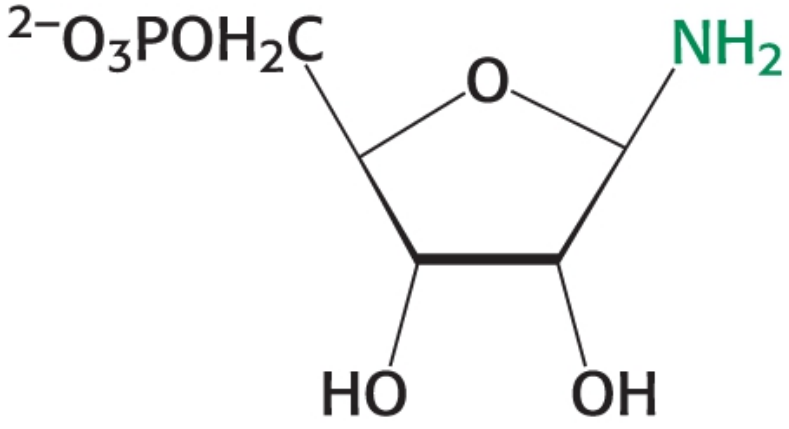
Extended description for Formation of 5-

phosphoribosyl-1-amine from P R P P



PRPP





5-Phosphoribosyl-1-amine

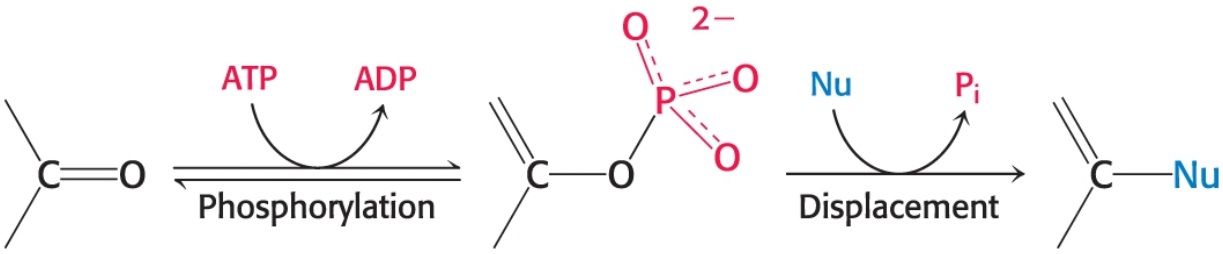
The reaction consists of one reactant and one product. The reactant is P R P P and the product is 5-phosphoribosyl-1-amine. It is coupled with the entry of glutamic acid plus N H 3 and the release of P P subscript i. Glutamic acid plus N H 3 is produced from glutamine plus H 2 O.

The structure of P R P P is as follows: A 5-membered heterocyclic pentagonal ring is in a vertical orientation with C 1 occupying the top right vertex. It consists of 1 O and 4 C atoms. O occupies the topmost vertex. C 1 is single bonded to a zigzag chain composed of O, single bond, P, single bond, O, single bond, P. P 1 is partially double bonded to O on the upper left and O on the upper right. The O atoms have an overall negative charge. P 2 is partially double bonded to O on the upper left, upper right, and lower right. The O atoms have an overall negative charge of 2 minus. C 2 and C 3 are single bonded to O H below. C 4 is single bonded to C H 2 O P O 3 superscript 2 minus on the upper left.

The structure of 5-phosphoribosyl-1-amine is as follows: A 5-membered heterocyclic pentagonal ring is in a vertical orientation with C 1 occupying the top right vertex. It consists of 1 O and 4 C atoms. O occupies the topmost vertex. C 1 is single bonded to N H 2 on the upper right. C 2 and C 3 are single bonded to O H below. C 4 is single bonded to C H 2 O P O 3 superscript 2 minus on the upper left.

Return to Formation of 5-phosphoribosyl-1-amine from P R P P

Extended description for Activation of the carbonyl oxygen atom followed by the displacement of the phosphoryl group by a nucleophile



In the first reversible step, a carbonyl oxygen atom is phosphorylated. It is coupled with the breakdown of A T P to A D P.

The structure of the reactant is as follows: A central C atom is double-bonded to O on the right and has an open single bond on the upper left and lower left.

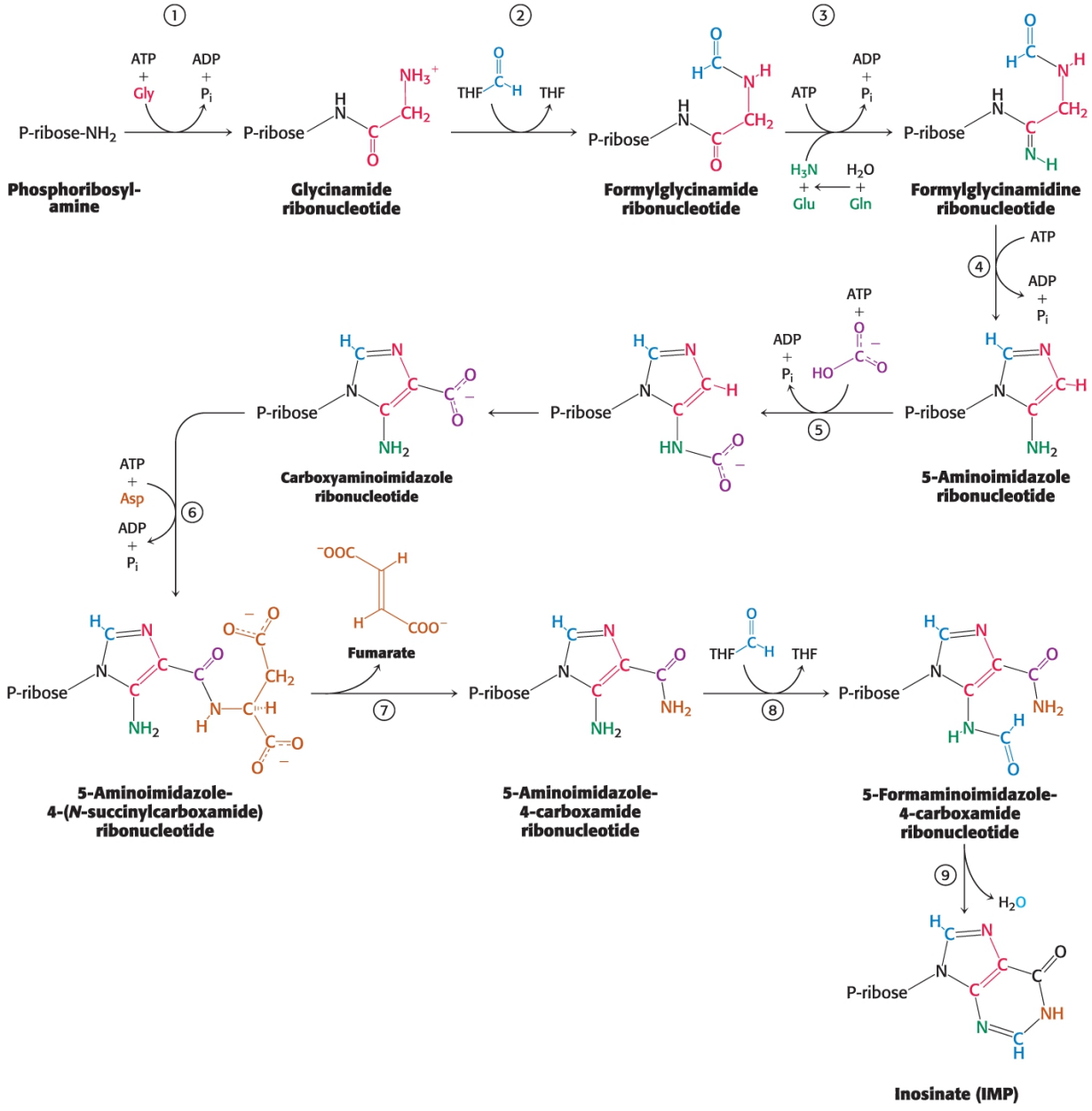
The structure of the product is as follows: A central C atom is single-bonded to O on the right and has an open double bond on the upper left and an open single bond on the lower left. The right O atom is single-bonded to P on the upper right. P is partially double bonded to O above, O on the upper right, and O on the lower right. The O atoms have an overall negative charge of 2 minus.

In the second irreversible step, the phosphoryl group or P subscript i in the product of the first step is displaced by a nucleophile depicted as N u.

The structure of the product of displacement is as follows: A central C is single bonded to N u on the right and has an open double bond on the upper left and an open single bond on the lower left.

Return to Activation of the carbonyl oxygen atom followed by the displacement of the phosphoryl group by a nucleophile

Extended description for FIGURE 26.6 The de novo purine biosynthesis pathway involves nine steps



In the first irreversible step, phosphoribosyl-amine is converted into glycinamide ribonucleotide. It is coupled with the entry of A T P plus glycine and the release of A D P plus P subscript i.

Phosphoribosyl-amine consists of P, single bond, ribose, single bond, N H 2.

Glycinamide ribonucleotide consists of P, single bond, ribose, single bond, N H, single bond, C, single bond, C H 2. C 1 is double bonded to O below. C H 2 is single bonded to N H 3 superscript plus above.

In the second irreversible step, glycinamide ribonucleotide is converted into formylglycinamide ribonucleotide. It is coupled with the entry of the formyl group bonded to T H F and release of T H F. The structure of formylglycinamide ribonucleotide is as follows: P, single bond, ribose, single bond, N H, single bond, C, single bond, C H 2. C 1 is double bonded to O below. C H 2 is single bonded to N above. N is single-bonded to H on the upper right and C on the upper left. C is double bonded to O above and single bonded to H on the lower left.

In the third irreversible step, formylglycinamide ribonucleotide is converted into formylglycinamidine ribonucleotide. It is coupled with the entry of N H 3 and the breakdown of A T P to A D P plus P subscript i. N H 3 and glutamic acid are derived from a reaction between glutamine and H 2 O.

The structure of formylglycinamidine ribonucleotide is as follows: P, single bond, ribose, single bond, N H, single bond, C, single bond, C H 2. C 1 is double bonded to N, single bond, H below. C H 2 is single bonded to N above. N is single-bonded to H on the upper right and C on the upper left. C is double bonded to O above and single bonded to H on the lower left.

In the fourth irreversible step, formylglycinamidine ribonucleotide is converted into 5-aminoimidazole ribonucleotide. It is coupled with the breakdown of A T P to A D P plus P subscript i.

The structure of 5-aminoimidazole ribonucleotide is as follows: A 5-membered heterocyclic pentagonal ring is in a vertical orientation. It consists of 2 N and 3 C atoms. First N occupies the bottom left vertex and the second N occupies the top right vertex. The remaining positions are occupied by C atoms. C 1 occupies the top left vertex. A double bond is present between C 1 and N 2, and C 2 and C 3. N 1 is single bonded to ribose, single bond, P on the lower left. C 1 and C 2 are each single bonded to H. C 3 is single bonded to N H 2 below.

In the fifth irreversible step, 5-aminoimidazole ribonucleotide is converted into another unlabeled compound with the simultaneous entry of bicarbonate and breakdown of A T P to A D P plus P subscript i. The bicarbonate ion is composed of a central C partially double-bonded to O above, partially double-bonded to O on the lower right, and single-bonded to O H on the lower left. The partially double-bonded O atoms have an overall negative charge.

The structure of the unlabeled compound is as follows: A 5-membered heterocyclic pentagonal ring is in a vertical orientation. It consists of 2 N and 3 C atoms. First N occupies the bottom left vertex and the second N occupies the top right vertex. The remaining positions are occupied by C atoms. C 1 occupies the top left vertex. A double bond is present between C 1 and N 2, and C 2 and C 3. N 1 is single bonded to ribose, single bond, P on the lower left. C 1 and C 2 are each single bonded to H. C 3 is single bonded to N H. N H is single bonded to C on the right. This C is partially double-bonded to O on the upper right and lower right. The O atoms have an overall negative charge.

This unlabeled compound is irreversibly converted into carboxyaminoimidazole ribonucleotide.

The structure of carboxyaminoimidazole ribonucleotide is as follows: A 5-membered heterocyclic pentagonal ring is in a vertical orientation. It consists of 2 N and 3 C atoms. First N occupies the bottom left vertex and the second N occupies the top right vertex. The remaining positions are occupied by C atoms. C 1 occupies the top left vertex. A double bond is present between C 1 and N 2, and C 2 and C 3. N 1 is single bonded to ribose, single bond, P on the lower left. C 1 is single bonded to H. C 2 is single bonded to C on the lower right, which is further partially double bonded to O on the upper right and O on the lower right. The O atoms have an overall negative charge. C 3 is single bonded to N H 2 below.

In the sixth irreversible step, carboxyaminoimidazole ribonucleotide is irreversibly converted into 5-aminoimidazole-4-open parenthesis N-succinylcarboxamide close parenthesis ribonucleotide. It is coupled with the simultaneous entry of aspartic acid and breakdown of A T P to A D P plus P subscript i.

The structure of 5-aminoimidazole-4-open parenthesis N-succinylcarboxamide close parenthesis ribonucleotide is as follows: A 5-membered heterocyclic pentagonal ring is in a vertical orientation. It consists of 2 N and 3 C atoms. First N occupies the bottom left vertex and the second N occupies the top right vertex. The remaining positions are occupied by C atoms. C 1 occupies the top left vertex. A double bond is present between C 1 and N 2, and C 2 and C 3. N 1 is single bonded to ribose, single bond, P on the lower left. C 1 is single bonded to H. C 2 is single bonded to C on the right. This C is single-bonded to N on the lower right and double-bonded to O on the upper right. N is single-bonded to H on the lower left and single-bonded to C 2 of a 2-carbon alkane chain in a vertical orientation. C 1 of this chain is single bonded to C above, which is further partially double bonded to O on the upper left and O on the upper right. The O atoms have an overall negative charge. C 2 is single-bonded to H on the right and single-bonded to C on the lower

right. This C is partially double-bonded to O on the right and lower left. The O atoms have an overall negative charge. C 3 of the ring is single bonded to N H 2 below.

In the seventh irreversible step, 5-aminoimidazole-4-open parenthesis N-succinylcarboxamide close parenthesis ribonucleotide is converted into 5-aminoimidazole-4-carboxamide ribonucleotide. It is coupled with the release of fumarate.

The structure of fumarate is as follows: A central C atom is single-bonded to H on the lower left, single-bonded to C O O superscript minus on the lower right, and double-bonded to C above. The C atom above is single bonded to C O O superscript minus on the upper left and single bonded to H on the upper right.

The structure of 5-aminoimidazole-4-carboxamide ribonucleotide is as follows: A 5-membered heterocyclic pentagonal ring is in a vertical orientation. It consists of 2 N and 3 C atoms. First N occupies the bottom left vertex and the second N occupies the top right vertex. The remaining positions are occupied by C atoms. C 1 occupies the top left vertex. A double bond is present between C 1 and N 2, and C 2 and C 3. N 1 is single bonded to ribose, single bond, P on the lower left. C 1 is single bonded to H. C 2 is single bonded to C on the right. This C is single-bonded to N H 2 on the lower right and double-bonded to O on the upper right. C 3 is single bonded to N H 2 below.

In the eighth irreversible step, 5-aminoimidazole-4-carboxamide ribonucleotide is converted into 5-formaminoimidazole-4-carboxamide ribonucleotide. It is coupled with the entry of T H F bonded to the formyl group and the release of T H F.

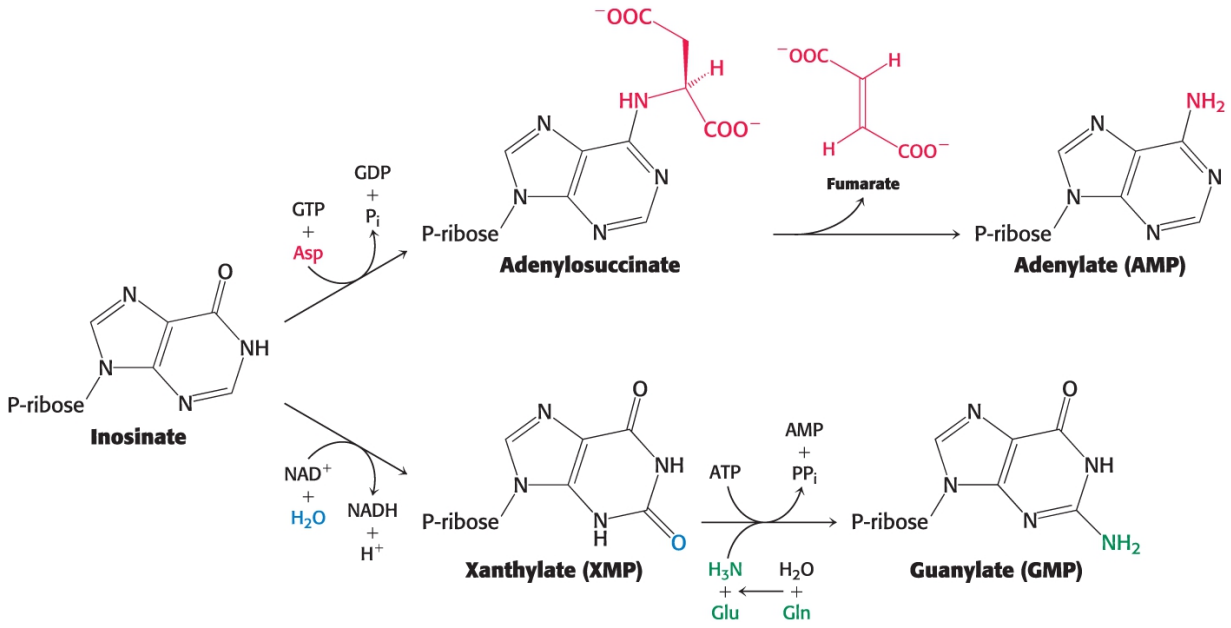
The structure of 5-formaminoimidazole-4-carboxamide ribonucleotide is as follows: A 5-membered heterocyclic pentagonal ring is in a vertical orientation. It consists of 2 N and 3 C atoms. First N occupies the bottom left vertex and the second N occupies the top right vertex. The remaining positions are occupied by C atoms. C 1 occupies the top left vertex. A double bond is present between C 1 and N 2, and C 2 and C 3. N 1 is single bonded to ribose, single bond, P on the lower left. C 1 is single bonded to H. C 2 is single bonded to C on the right. This C is single-bonded to N H 2 on the lower right and double-bonded to O on the upper right. C 3 is single bonded to N H below. N H is single bonded to C on the lower right. This C is single bonded to H on the upper right and double bonded to O below.

In the ninth step, 5-formaminoimidazole-4-carboxamide ribonucleotide is converted into inosinate (I M P). It is coupled with the release of H 2 O.

The structure of inosinate is as follows: A 5-membered heterocyclic pentagonal ring is in a vertical orientation. It consists of 2 N and 3 C atoms. First N occupies the bottom left vertex and the second N occupies the top right vertex. The remaining positions are occupied by C atoms. C 1 occupies the top left vertex. A double bond is present between C 1 and N 2, and C 2 and C 3. N 1 is single bonded to ribose, single bond, P on the lower left. C 1 is single bonded to H. It is fused to a 6-membered heterocyclic hexagonal ring in a vertical orientation such that C 2 and C 3 of the pentagonal ring are C 3 and C 2 respectively of the hexagonal ring. The hexagonal ring is composed of 2 N and 4 C atoms. The first N bound to H occupies the bottom right vertex and the second N occupies the bottom left vertex. A double bond is present between C 1 and N 2, and C 2 and C 3. C 1 is bound to H. C 4 is double bonded to O on the upper right.

Return to FIGURE 26.6 The de novo purine biosynthesis pathway involves nine steps

Extended description for FIGURE 26.7 Inosinate can be converted to A M P and G M P



The formation of adenylate (A M P) from inosinate is depicted as follows:

In the first irreversible step, inosinate is converted into adenylosuccinate. It is coupled with the entry of G T P plus aspartic acid and the release of G D P plus P subscript i.

The structure of inosinate is as follows: A 6-membered heterocyclic hexagonal ring is in a vertical orientation with C 1 occupying the bottom right vertex. It consists of 2 N and 4 C atoms. First N bound to H occupies the top right vertex. The second N occupies the bottom-most vertex. A double bond is present between C 1 and N 2, and C 2 and C 3. C 4 is double bonded to O above. The hexagonal ring is fused to a 5-membered heterocyclic pentagonal ring in a horizontal orientation such that C 2 and C 3 of the hexagonal ring

are C 3 and C 2 respectively of the pentagonal ring. The pentagonal ring consists of 2 N and 3 C atoms. First N occupies the bottom left vertex and the second N occupies the topmost vertex. A double bond is present between C 1 and N 2, and C 2 and C 3. N 1 is single bonded to ribose, single bond, P on the lower left.

The structure of adenylosuccinate is as follows: A 6-membered heterocyclic hexagonal ring is in a vertical orientation with C 1 occupying the bottom right vertex. It consists of 2 N and 4 C atoms. The first N bound occupies the top right vertex. The second N occupies the bottom-most vertex. A double bond is present between C 1 and N 2, and C 2 and C 3. C 4 is double bonded to N H above. This N H is single-bonded to a central C atom on the upper right. This C is wedge bonded to C H 2, single bond, C O O superscript minus above, dash bonded to H on the upper right, and single bonded to C O O superscript minus on the lower right. The hexagonal ring is fused to a 5-membered heterocyclic pentagonal ring in a horizontal orientation such that C 2 and C 3 of the hexagonal ring are C 3 and C 2 respectively of the pentagonal ring. The pentagonal ring consists of 2 N and 3 C atoms. First N occupies the bottom left vertex and the second N occupies the topmost vertex. A double bond is present between C 1 and N 2, and C 2 and C 3. N 1 is single bonded to ribose, single bond, P on the lower left.

In the second irreversible step, adenylosuccinate is converted into adenylate (A M P). It is coupled with the release of fumarate.

The structure of fumarate is as follows: A central C atom is single-bonded to H on the lower left, single-bonded to C O O superscript minus on the lower right, and double-bonded to C above. The C atom above is single bonded to C O O superscript minus on the upper left and single bonded to H on the upper right.

The structure of adenylate (A M P) is as follows: A 6-membered heterocyclic hexagonal ring is in a vertical orientation with C 1 occupying the bottom right vertex. It consists of 2 N and 4 C atoms. First N occupies the top right vertex. The second N occupies the bottom-most vertex. A double bond is present between C 1 and N 2, and C 2 and C 3. C 4 is single bonded to N H 2 above. The hexagonal ring is fused to a 5-membered heterocyclic pentagonal ring in a horizontal orientation such that C 2 and C 3 of the hexagonal ring are C 3 and C 2 respectively of the pentagonal ring. The pentagonal ring consists of 2 N and 3 C atoms. First N occupies the bottom left vertex and the second N occupies the topmost vertex. A double bond is present between C 1 and N 2, and C 2 and C 3. N 1 is single bonded to ribose, single bond, P on the lower left.

The formation of guanylate (G M P) from inosinate is depicted as follows:

In the first irreversible step, inosinate is converted into xanthylate (X M P). It is coupled with the reduction of N A D superscript plus to N A D H plus H superscript plus and the entry of H 2 O.

The structure of xanthylate (X M P) is as follows: A 6-membered heterocyclic hexagonal ring is in a vertical orientation with C 1 occupying the bottom right vertex. It consists of 2 N and 4 C atoms. First N bound to H occupies the top right vertex. The second N bound to H occupies the bottom-most vertex. A double bond is present between C 2 and C 3. C 1 and C 4 are double bonded to O. The hexagonal ring is fused to a 5-membered heterocyclic pentagonal ring in a horizontal orientation such that C 2 and C 3 of the hexagonal ring are C 3 and C 2 respectively of the pentagonal ring. The pentagonal ring consists of 2 N and 3 C atoms. First N occupies the bottom left vertex and the second N occupies the topmost vertex. A double bond is present between C 1 and N 2, and

C 2 and C 3. N 1 is single bonded to ribose, single bond, P on the lower left.

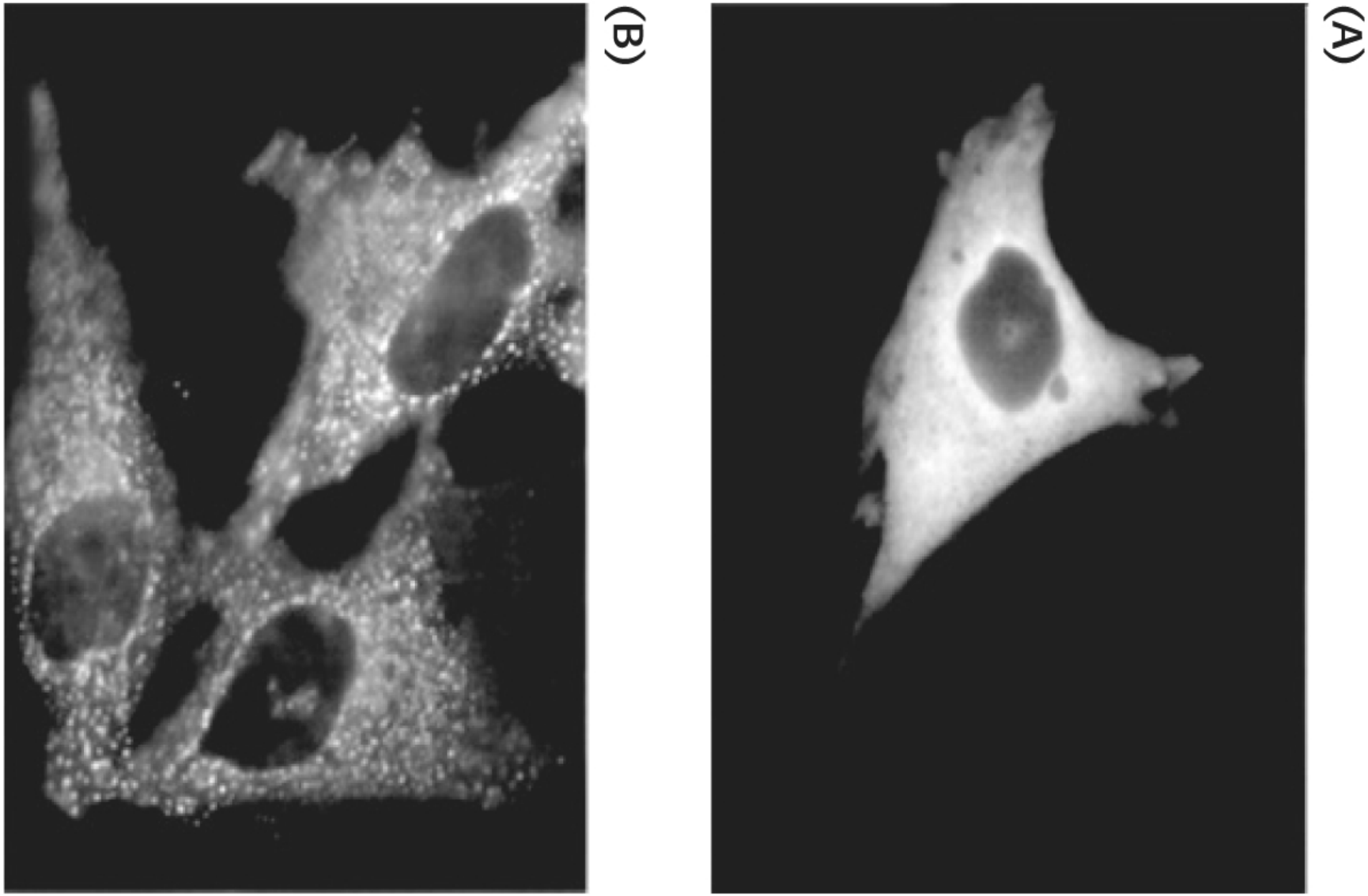
In the second irreversible step, xanthylate (X M P) is converted into guanylate (G M P). It is coupled with the breakdown of A T P to A M P plus P P subscript i and entry of N H 3. N H 3 and glutamic acid are derived from the reaction of glutamine with H 2 O.

The structure of guanylate (G M P) is as follows: A 6-membered heterocyclic hexagonal ring is in a vertical orientation with C 1 occupying the bottom right vertex. It consists of 2 N and 4 C atoms. First N bound to H occupies the top right vertex. The second N occupies the bottom-most vertex. A double bond is present between C 1 and N 2, and C 2 and C 3. C 1 is single bonded to N H 2. C 4 is double bonded to O above. The hexagonal ring is fused to a 5-membered heterocyclic pentagonal ring in a horizontal orientation such that C 2 and C 3 of the hexagonal ring are C 3 and C 2 respectively of the pentagonal ring. The pentagonal ring consists of 2 N and 3 C atoms. First N occupies the bottom left vertex and the second N occupies the topmost vertex. A double bond is present between C 1 and N 2, and C 2 and C 3. N 1 is single bonded to ribose, single bond, P on the lower left.

Return to FIGURE 26.7 Inosinate can be converted to A M P and G M P

Extended description for FIGURE 26.8 Hela cells in the presence and absence respectively of purine in the

medium



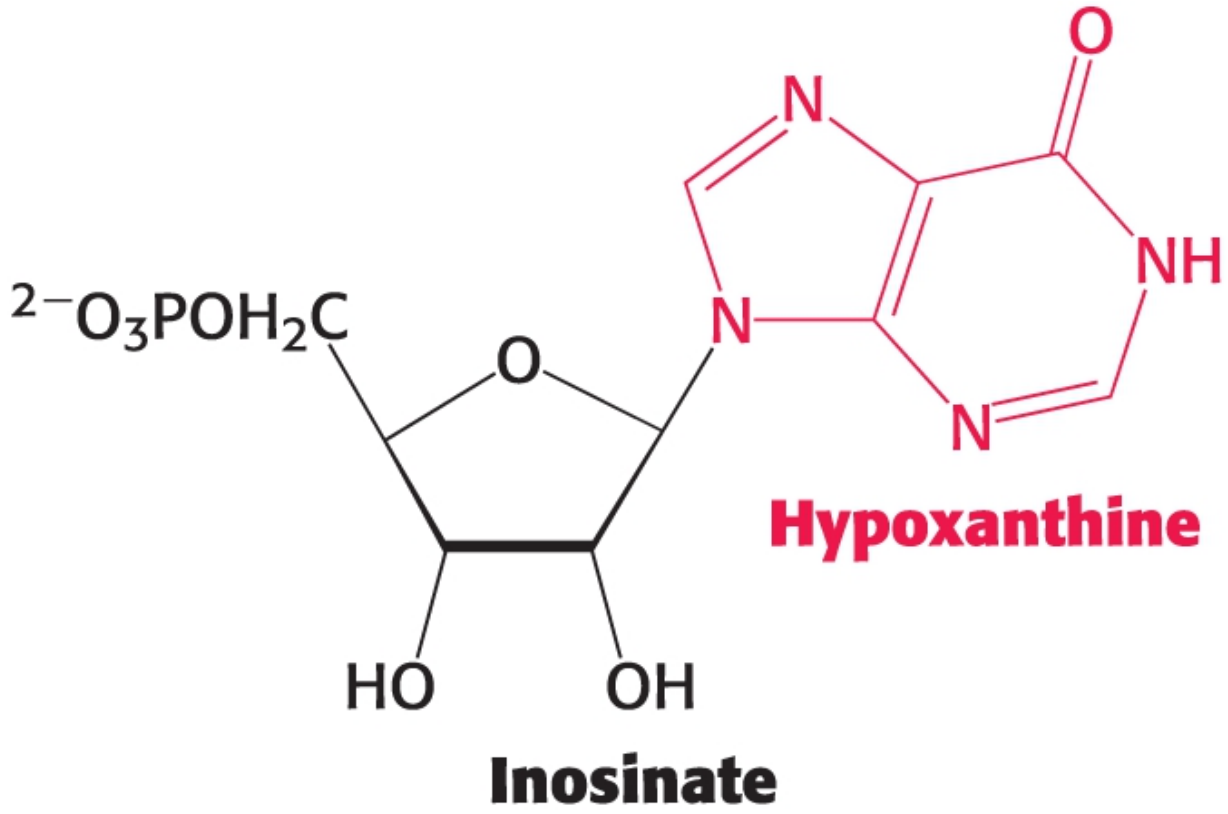
Republished with permission of AAAS, from An, S., Kumar, R., Sheets, E. D., and Benkovic, S. J. 2. Reversible compartmentalization of de novo purine biosynthetic complexes in living cells. *Science* 320: 103–106, 2008; permission conveyed through Copyright Clearance Center, Ltd.

Photomicrograph (A): It shows a single cell against a dark background. The cell has a central nucleus and short projections at the top, left, and right. The entire cytoplasm is uniformly bright.

Photomicrograph (B): It shows three irregular-shaped cells against a dark background. The cytoplasm of these cells contains tiny bright granules.

Return to FIGURE 26.8 Hela cells in the presence and absence respectively of purine in the medium

Extended description for Structure of inosinate



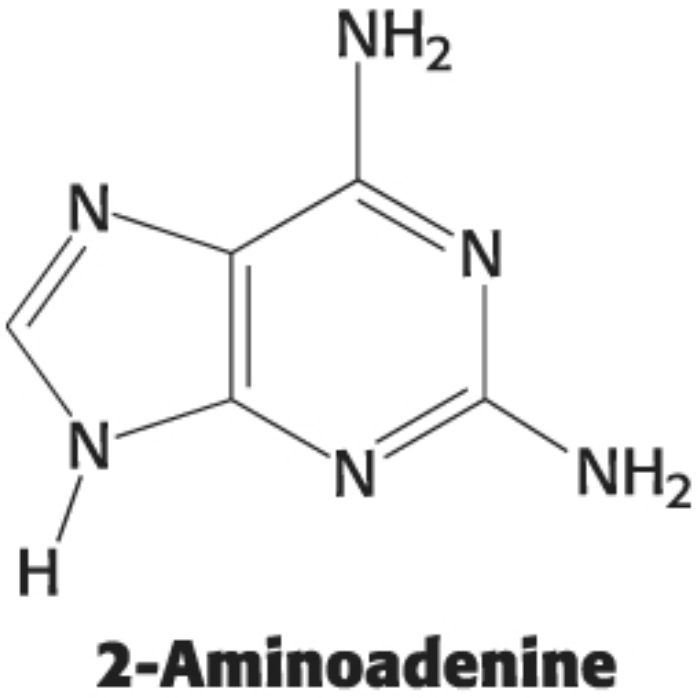
The structure of inosinate is as follows: A 5-membered heterocyclic pentagonal ring is in a vertical orientation with C 1 occupying the top right vertex. It consists of 1 O and 4 C atoms. O occupies the topmost vertex. C 2 and C 3 are single bonded to O H below. C 4 is single bonded to C H 2 O P O 3 superscript 2 minus on the upper left. C 1 is single bonded to N 1 of the pentagonal ring of hypoxanthine.

The structure of hypoxanthine is as follows: A 5-membered heterocyclic pentagonal ring is in a horizontal orientation. It consists of 2 N and 3 C atoms. First N occupies the bottom left vertex and the second N occupies the topmost vertex. C 1 occupies the leftmost vertex. A double bond is present between C 1 and N 2, and C 2 and C 3. It is fused to a 6-membered heterocyclic hexagonal ring

in a vertical orientation such that C 2 and C 3 of the pentagonal ring are C 3 and C 2 respectively of the hexagonal ring. The hexagonal ring is composed of 2 N and 4 C atoms. The first N bound to H occupies the top right vertex and the second N occupies the bottom-most vertex. A double bond is present between C 1 and N 2, and C 2 and C 3. C 4 is double bonded to O above.

Return to Structure of inosinate

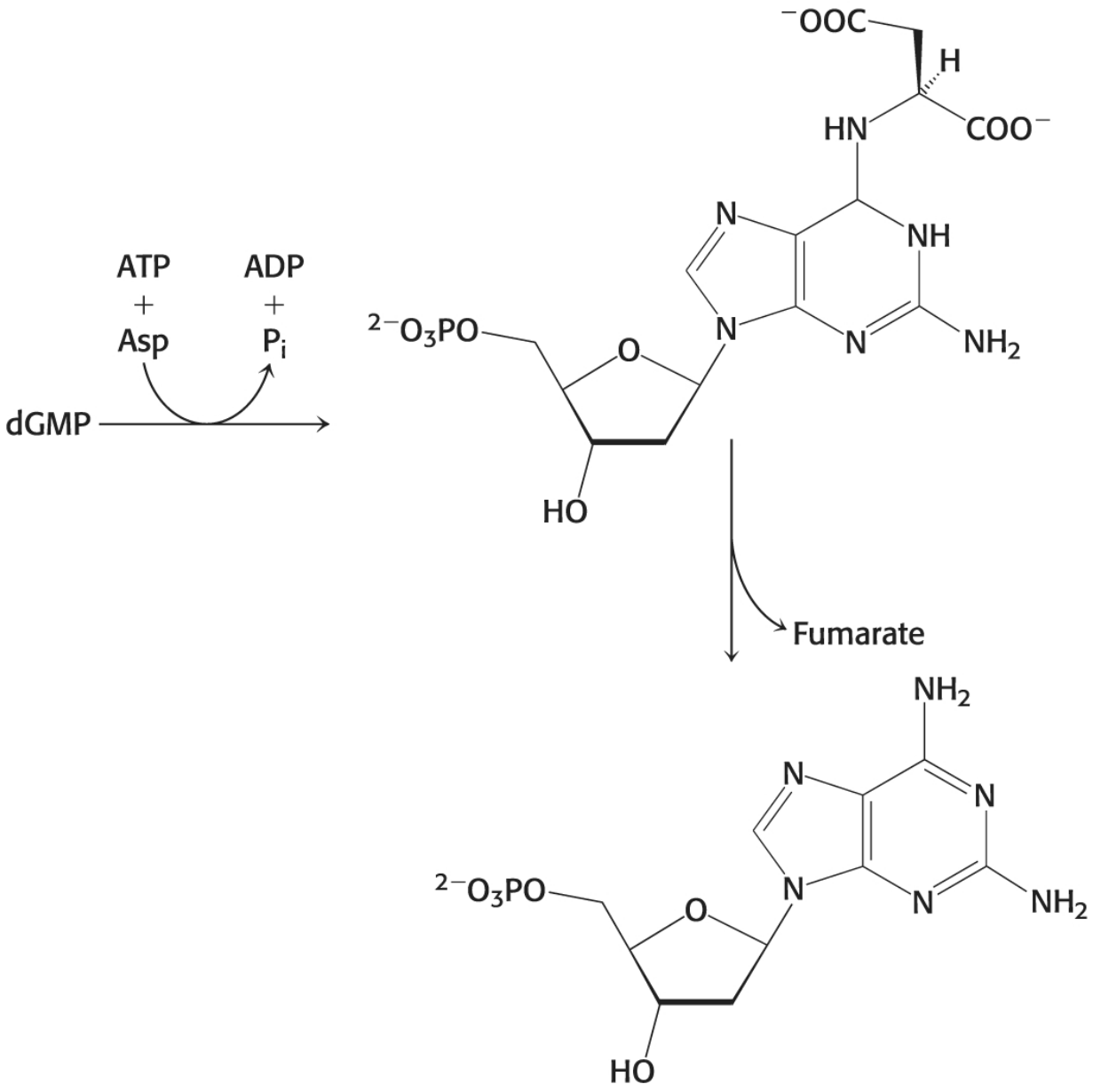
Extended description for Structure of 2-aminoadenine



The structure of 2-aminoadenine is as follows: A 5-membered heterocyclic pentagonal ring is in a horizontal orientation. It consists of 2 N and 3 C atoms. First N occupies the bottom left vertex and the second N occupies the top left vertex. C 1 occupies the leftmost vertex. A double bond is present between C 1 and N 2, and C 2 and C 3. N 1 is single bonded to H. It is fused to a 6-membered heterocyclic hexagonal ring in a vertical orientation such that C 2 and C 3 of the pentagonal ring are C 3 and C 2 respectively of the hexagonal ring. The hexagonal ring is composed of 2 N and 4 C atoms. The first N occupies the top right vertex and the second N occupies the bottom-most vertex. A double bond is present between C 1 and N 2, C 2 and C 3, and C 4 and N 1. C 1 and C 4 are each single bonded to N H 2.

Return to Structure of 2-aminoadenine

Extended description for FIGURE 26.9 The nucleotide containing 2-aminoadenine is synthesized from deoxyguanylate



In the first irreversible step, d G M P is converted into an unlabeled compound. It is coupled with the entry of aspartic acid and the

breakdown of A T P to A D P plus P subscript i.

The structure of the unlabeled compound is as follows: A 5-membered heterocyclic pentagonal ring is in a vertical orientation. It consists of 1 O and 4 C atoms. O occupies the topmost vertex. C 3 is single bonded to O H below. C 4 is single bonded to C H 2 on the upper left in the form of a line. C H 2 in single bonded to O P O 3 superscript 2 minus on the left. C 1 is single-bonded to N 1 of a 5-membered heterocyclic pentagonal ring in a horizontal orientation. The pentagonal ring consists of 2 N and 3 C atoms. First N occupies the bottom left vertex and the second N occupies the top left vertex. A double bond is present between C 1 and N 2, and C 2 and C 3. It is fused to a 6-membered heterocyclic hexagonal ring in a vertical orientation such that C 2 and C 3 of the pentagonal ring are C 3 and C 2 respectively of the hexagonal ring. The hexagonal ring consists of 2 N and 4 C atoms. First N bound to H occupies the top right vertex. The second N occupies the bottom-most vertex. A double bond is present between C 1 and N 2, and C 2 and C 3. C 4 is single bonded to N H above. N H is single bonded to C on the upper right. This C is wedge bonded to C H 2, single bond, C O O superscript minus above, dash bonded to H on the upper right, and single bonded to C O O superscript minus on the lower right.

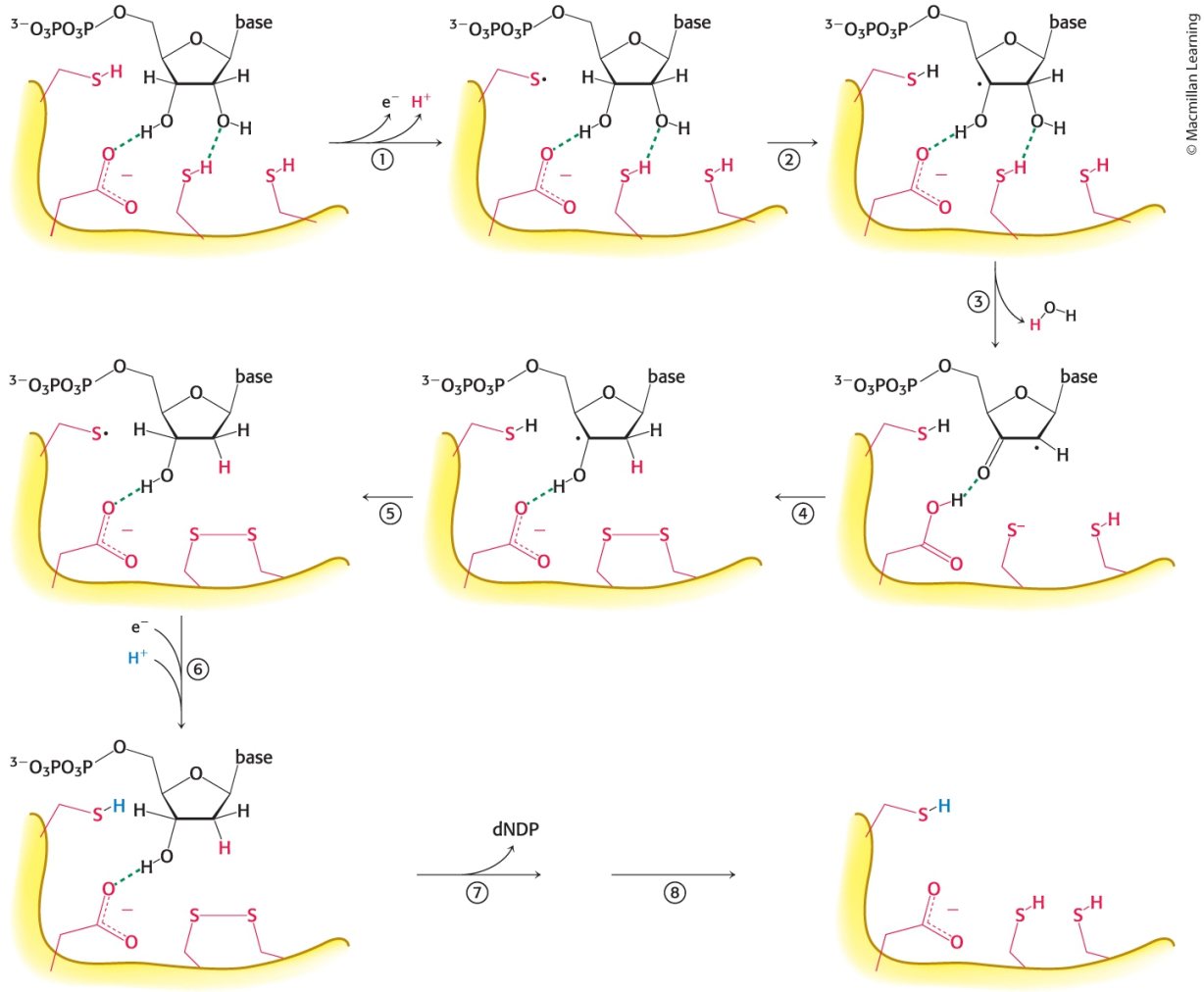
In the second irreversible step, fumarate is released leading to the formation of the final product.

The structure of the final product is as follows: A 5-membered heterocyclic pentagonal ring is in a vertical orientation. It consists of 1 O and 4 C atoms. O occupies the topmost vertex. C 3 is single bonded to O H below. C 4 is single bonded to C H 2 on the upper left in the form of a line. C H 2 in single bonded to O P O 3 superscript 2 minus on the left. C 1 is single-bonded to N 1 of a 5-membered heterocyclic pentagonal ring in a horizontal orientation. The pentagonal ring consists of 2 N and 3 C atoms. First N occupies the

bottom left vertex and the second N occupies the top left vertex. A double bond is present between C 1 and N 2, and C 2 and C 3. It is fused to a 6-membered heterocyclic hexagonal ring in a vertical orientation such that C 2 and C 3 of the pentagonal ring are C 3 and C 2 respectively of the hexagonal ring. The hexagonal ring consists of 2 N and 4 C atoms. First N occupies the top right vertex. The second N occupies the bottom-most vertex. A double bond is present between C 1 and N 2, C 2 and C 3, and C 4 and N 1. C 1 and C 4 are each single bonded to N H 2.

Return to FIGURE 26.9 The nucleotide containing 2-aminoadenine is synthesized from deoxyguanylate

Extended description for FIGURE 26.10 Ribonucleotide reductase uses a radical mechanism to produce deoxyribonucleotides



© Macmillan Learning

The active site of the ribonucleotide reductase is depicted as a cleft with an orange outline. The outline has a yellow highlight. It contains side chains of three cysteine residues and one tyrosine residue.

The side chain of cysteine is depicted as C H 2, single bond, S, single bond, H. The side chain of tyrosine is depicted as C H 2, single bond, C. C is partially double bonded to O above and O on the lower right. The O atoms have an overall negative charge.

A pentagonal ring is shown in the active site of the enzyme. The structure of the ring is as follows: A 5-membered heterocyclic pentagonal ring is in a vertical orientation. It consists of 1 O and 4 C atoms. O occupies the topmost vertex. C 1 is single-bonded to base. C 2 is single bonded to H and O, single bond, H. C 3 is single bonded to H and O, single bond, H. C 4 is single bonded to C H 2, single bond, O, single bond, P O 3 P O 3 superscript 3 minus. A dashed line connects the H atom of O H groups bonded to C 2 and C 3 with the H atom of one cysteine side chain and the O atom of the tyrosine side chain.

In step 1, an electron and H superscript plus ion are released. This electron and H atom are released from the side chain of one of the cysteine side chains. As a result, the S atom of the cysteine side chain contains an unpaired electron.

In step 2, the H atom bonded to C 3 of the ring is transferred to the S atom with an unpaired electron of the cysteine side chain. As a result, C 3 contains an unpaired electron.

In step 3, H, single bond, O, single bond, H is released from the active site. C 3 of the ring becomes double bonded to O, which is further connected to H through a dashed line. This H becomes single-bonded to the O atom of the tyrosine side chain. This O becomes single-bonded to C of the tyrosine side chain and the other O becomes double-bonded to the C atom. C 2 of the ring loses its O H group. As a result, C 2 contains an unpaired electron and the S atom of the cysteine side chain with which it was previously bonded becomes negatively charged.

In step 4, a single bond forms between the negatively charged S atom of one cysteine side chain and the S atom of the adjacent side chain. This happens as the H atom of one cysteine side chain is transferred to C 2. As a result, C 2 is single-bonded to two H atoms. C 3 contains an unpaired electron and it is single bonded to O, single bond, H below. H is connected to the O atom of the tyrosine side chain through a dashed line. The double bonds between C and O atoms of the tyrosine side chain again start resonating.

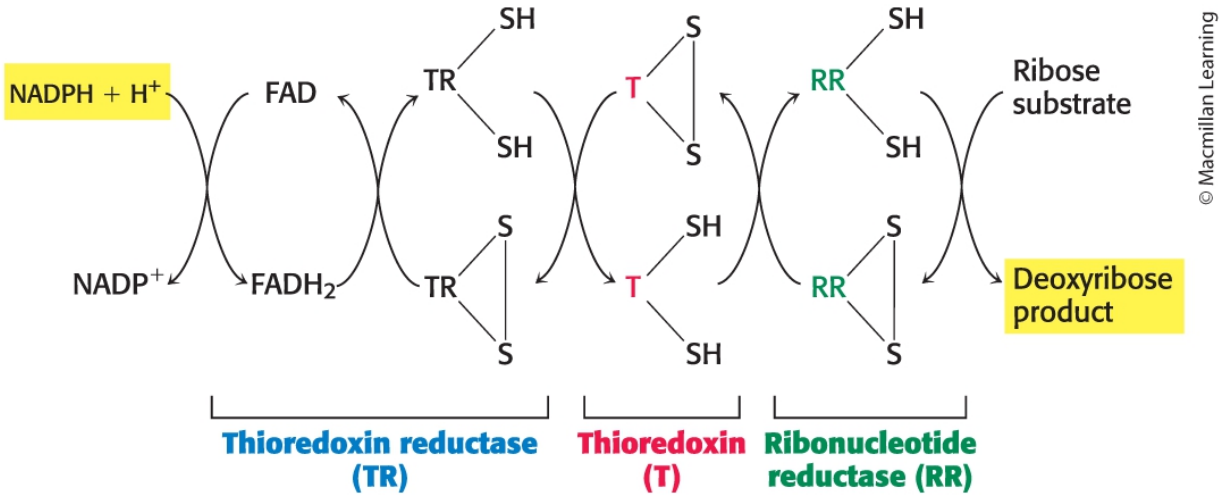
In step 5, the H atom from the S H group of the same cysteine side chain is transferred to C 3. This S atom contains an unpaired electron similar to step 1.

In step 6, H superscript plus ion and electron enter the active site. The S atom with an unpaired electron becomes single-bonded to this H.

In step 7, d N D P is released. It is followed by step 8, which leads to an empty active site. The empty active site contains the side chains of three cysteine residues and one tyrosine residue in their native configuration.

Return to FIGURE 26.10 Ribonucleotide reductase uses a radical mechanism to produce deoxyribonucleotides

Extended description for Oxidation of N A D P H coupled with the reduction of ribose substrate



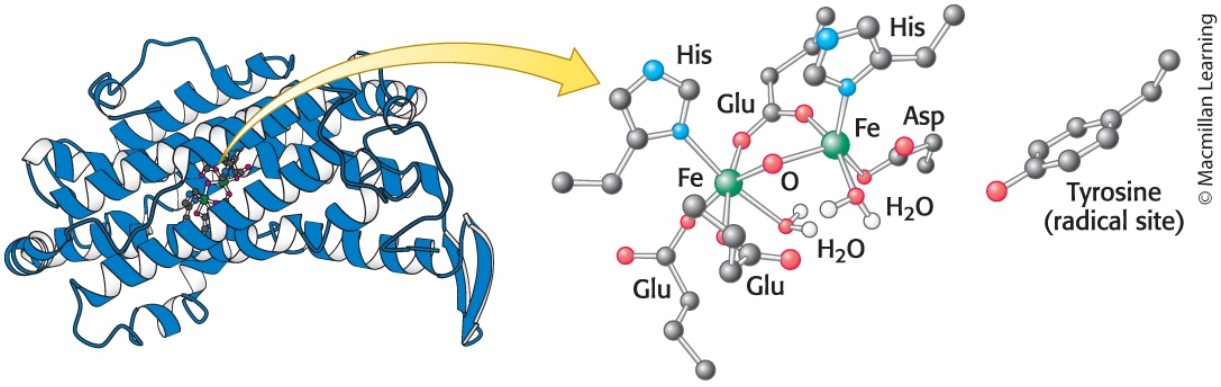
© Macmillan Learning

N A D P H plus H superscript plus highlighted in yellow transfers electron to F A D bound to thioredoxin reductase (T R). As a result, it is converted into N A D P superscript plus, and F A D is converted to F A D H 2. F A D H 2 of T R transfer electrons to the disulfide linkage of T R. The disulfide linkage is depicted as T R single bonded to S on the upper right and S on the lower right. Both S atoms are single-bonded to each other. After electron transfer, the disulfide linkage is broken and T R is single-bonded to S H on the upper right and S H on the lower right. Electrons from the S H groups are transferred to the disulfide linkage of thioredoxin (T). The disulfide linkage is depicted as T single bonded to S on the upper right and S on the lower right. Both S atoms are single-bonded to each other. After electron transfer, the disulfide linkage is broken and T is single-bonded to S H on the upper right and S H on the lower right. Electrons from the S H group are transferred to the disulfide linkage of ribonucleotide reductase (R R). The disulfide linkage is depicted as R R single bonded to S on the upper right and S on the lower right. Both S atoms are single-bonded to each other. After electron

transfer, the disulfide linkage is broken and R R is single-bonded to S H on the upper right and S H on the lower right. Electrons from the S H group are transferred to the ribose substrate to produce the deoxyribose product highlighted in yellow.

Return to Oxidation of N A D P H coupled with the reduction of ribose substrate

Extended description for FIGURE 26.11 The ribonucleotide reductase R 2 subunit contains a stable free radical on a tyrosine residue



The ribonucleotide reductase R 2 subunit is composed of several horizontally oriented alpha-helices and 2 vertical beta-strands on the bottom right interconnected by thread-like loops. An arrow from the center of the R 2 subunit points toward a ball-and-stick on the right. The model shows a central O atom connected to F e on the lower left and O on the upper right. O is depicted as a red sphere and F e is depicted as a green sphere. The lower left F e is connected to a histidine residue on the top, glutamic acid on the lower left and below, H 2 O on the lower right, and glutamic acid on the upper right. The upper right F e is connected to the upper left glutamic acid, which is also connected to the lower left F e. It is also connected to a histidine residue on the upper right, aspartic acid on the lower right, and H 2 O below.

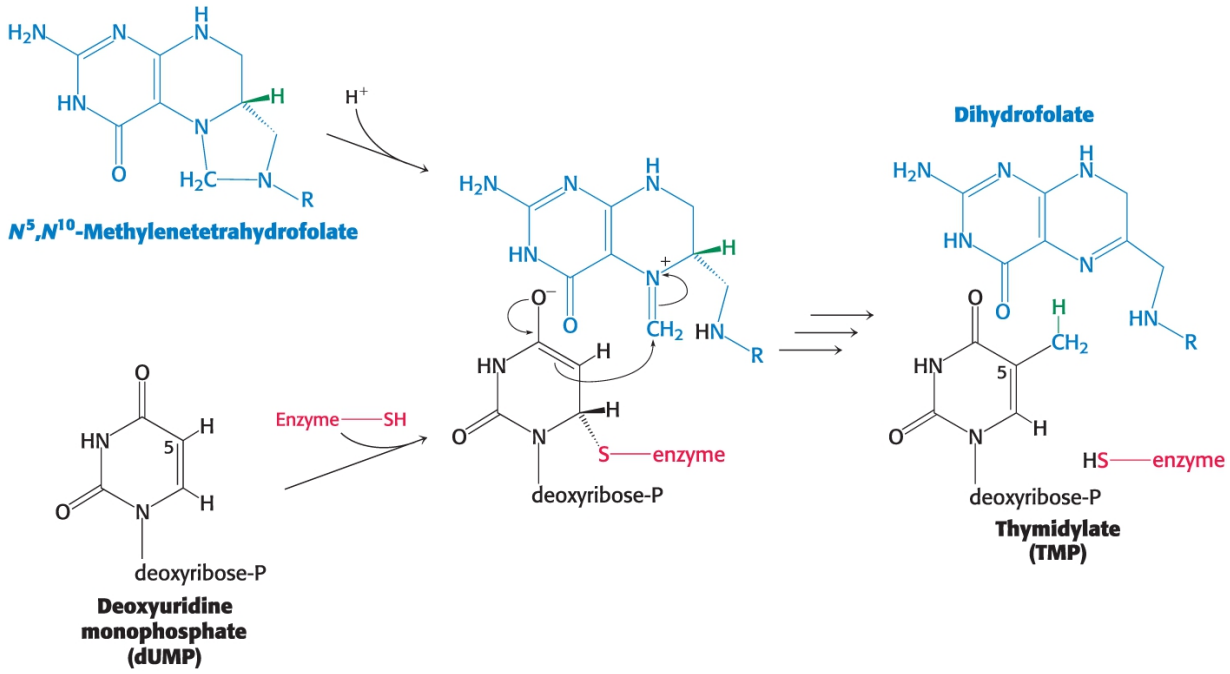
The histidine residue contains a pentagonal ring composed of 2 blue and 3 black spheres. The F e atom is connected to one of the blue spheres. One of the black spheres is further connected to a chain of two black spheres. The glutamic acid residue is composed of a chain of 4 black spheres. One of the black spheres is connected to two red

spheres. The F e atom is connected to the red sphere. The H 2 O molecule is composed of a red sphere connected to a white sphere on either side. The F e atom is connected to the red sphere of H 2 O. The aspartic acid residue is composed of 3 black spheres. One of the black spheres is connected to a red sphere.

A tyrosine (radical site) is located on the right side of the ball-and-stick model. The side view of the radical site is shown. Tyrosine consists of a hexagonal ring composed of 6 black spheres. One of the black spheres is connected to a chain of two black spheres on the upper right and another black sphere, opposite to it, is connected to a red sphere on the lower left.

Return to FIGURE 26.11 The ribonucleotide reductase R 2 subunit contains a stable free radical on a tyrosine residue

Extended description for FIGURE 26.12 Thymidylate synthase catalyzes the addition of a methyl group to d U M P to form T M P



In the first irreversible step, deoxyuridine monophosphate (d U M P) binds to an enzyme with an S H group. Simultaneously, N superscript 5, N superscript 10-Methylenetetrahydrofolate gains an H superscript plus ion.

The structure of deoxyuridine monophosphate (d U M P) is as follows: A 6-membered heterocyclic hexagonal ring is in a vertical orientation with C 1 occupying the bottom left vertex. It consists of 2 N and 4 C atoms. First N occupies the bottom-most vertex. The second N bound to H occupies the top left vertex. C 1 and C 2 are double bonded to O. C 3 is numbered 5. C 3 and C 4 are single-bonded to H and double-bonded to each other. N 1 is single bonded to deoxyribose, single bond, P.

The structure of N superscript 5, N superscript 10-Methylenetetrahydrofolate is as follows: A 6-membered heterocyclic hexagonal ring is in a vertical orientation and consists of 2 N and 4 C atoms. First N occupies the topmost vertex and the second N occupies the bottom-most vertex. First N atom is bound to H. C 2 is wedge bonded to H on the upper right and dash bonded to C H 2 on the lower right. C H 2 is single bonded to N below. N is single-bonded to R on the lower right and single-bonded to C H 2 on the left. This C H 2 is single-bonded to N 2 of the ring to form a pentagonal ring-like structure. The ring is fused to a second 6-membered heterocyclic hexagonal ring in a vertical orientation such that C 3 and C 4 of the first hexagonal ring are C 3 and C 2 respectively of the second hexagonal ring. The second ring consists of 2 N and 4 C atoms. First N bound to H occupies the bottom left vertex. Second N occupies the topmost vertex. A double bond is present between C 1 and N 2, and C 2 and C 3. C 1 is single bonded to N H 2. C 4 is double bonded to O below.

After enzyme addition, the S atom of the enzyme forms a dash bond with C 4 of d U M P. C 4 also forms a wedge bond with H. The double bond between C 3 and C 4 is broken. A double bond is formed between C 2 and C 3. C 2 is single bonded to O superscript minus above. The remaining structure is the same.

In N superscript 5, N superscript 10-Methylenetetrahydrofolate, H superscript plus ion binds to N below, which is single bonded to C H 2. As a result, the single bond between this N and C H 2 on the left is broken and the C H 2 group forms a double bond with N 2 of the first ring. N2 acquires a positive charge.

An arrow points from O superscript minus toward its single bond with C 2 of d U M P. An arrow from the double bond between C 2 and C 3 points toward the C H 2 of protonated N superscript 5, N superscript 10-Methylenetetrahydrofolate. An arrow from the

double bond between this C H 2 group and the second N with positive charge points toward the second N atom.

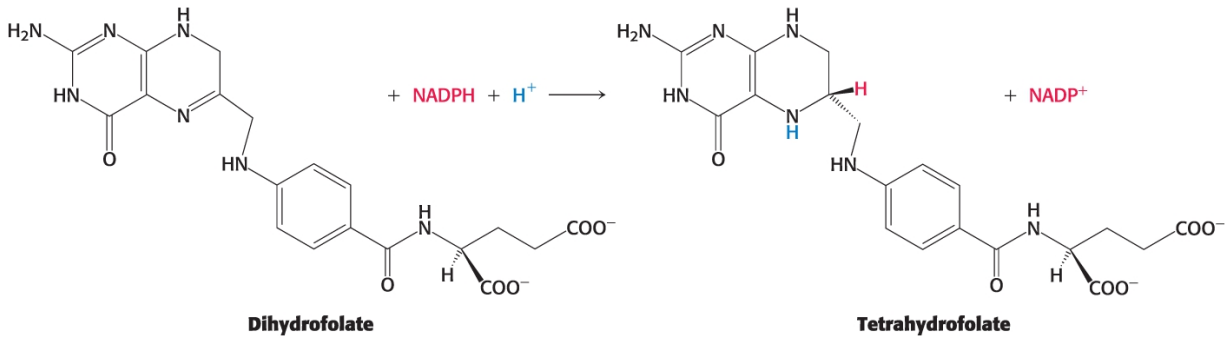
Three forward arrows lead to the products that are thymidylate (T M P) and dihydrofolate. The enzyme bound to S H is released.

The structure of thymidylate (T M P) is as follows: A 6-membered heterocyclic hexagonal ring is in a vertical orientation with C 1 occupying the bottom left vertex. It consists of 2 N and 4 C atoms. First N occupies the bottom-most vertex. The second N bound to H occupies the top left vertex. C 1 and C 2 are double bonded to O. C 3 is numbered 5. C 3 is single bonded to CH 2, single bond, H on the upper right. C 4 is single bonded to H on the lower right. A double bond is present between C 3 and C 4. N 1 is single bonded to deoxyribose, single bond, P.

The structure of dihydrofolate is as follows: A 6-membered heterocyclic hexagonal ring is in a vertical orientation and consists of 2 N and 4 C atoms. First N occupies the topmost vertex and the second N occupies the bottom-most vertex. First N atom is bound to H. C 2 is single-bonded to C H 2 on the lower right in the form of a line. C H 2 is single bonded to N H below. N H is single bonded to R on the lower right. The ring is fused to a second 6-membered heterocyclic hexagonal ring in a vertical orientation such that C 3 and C 4 of the first hexagonal ring are C 3 and C 2 respectively of the second hexagonal ring. The second ring consists of 2 N and 4 C atoms. First N bound to H occupies the bottom left vertex. Second N occupies the topmost vertex. A double bond is present between C 1 and N 2, and C 2 and C 3. C 1 is single bonded to N H 2. C 4 is double bonded to O below.

Return to FIGURE 26.12 Thymidylate synthase catalyzes the addition of a methyl group to d U M P to form T M P

Extended description for Reduction of dihydrofolate to tetrahydrofolate



The reaction consists of two reactants and two products.

The first reactant is dihydrofolate whose structure is as follows: A 6-membered heterocyclic hexagonal ring is in a vertical orientation and consists of 2 N and 4 C atoms. First N occupies the topmost vertex and the second N occupies the bottom-most vertex. The first N atom is bound to H. A double bond is present between C 2 and N 2. C 2 is single-bonded to C H 2 on the lower right in the form of a line. C H 2 is single bonded to N H below. The ring is fused to a second 6-membered heterocyclic hexagonal ring in a vertical orientation such that C 3 and C 4 of the first hexagonal ring are C 3 and C 2 respectively of the second hexagonal ring. The second ring consists of 2 N and 4 C atoms. First N bound to H occupies the bottom left vertex. Second N occupies the topmost vertex. A double bond is present between C 1 and N 2, and C 2 and C 3. C 1 is single bonded to N H 2. C 4 is double bonded to O below. N H group connected to the first ring is single bonded to C 6 of a benzene ring in a vertical orientation on the lower right. The benzene ring contains alternating double bonds between C 1 and C 2, C 3 and C 4, and C 5 and C 6. C 3 is single bonded to C 1 of a 1 N and 4 C heteronuclear alkane chain depicted as a line structure using 4

zigzag lines. N bound to H occupies the second position. C 1 is double bonded to O below. C 2 is dash bonded to H on the lower left and single bonded to C O O superscript minus on the lower right. C 4 is single bonded to C O O superscript minus on the upper right.

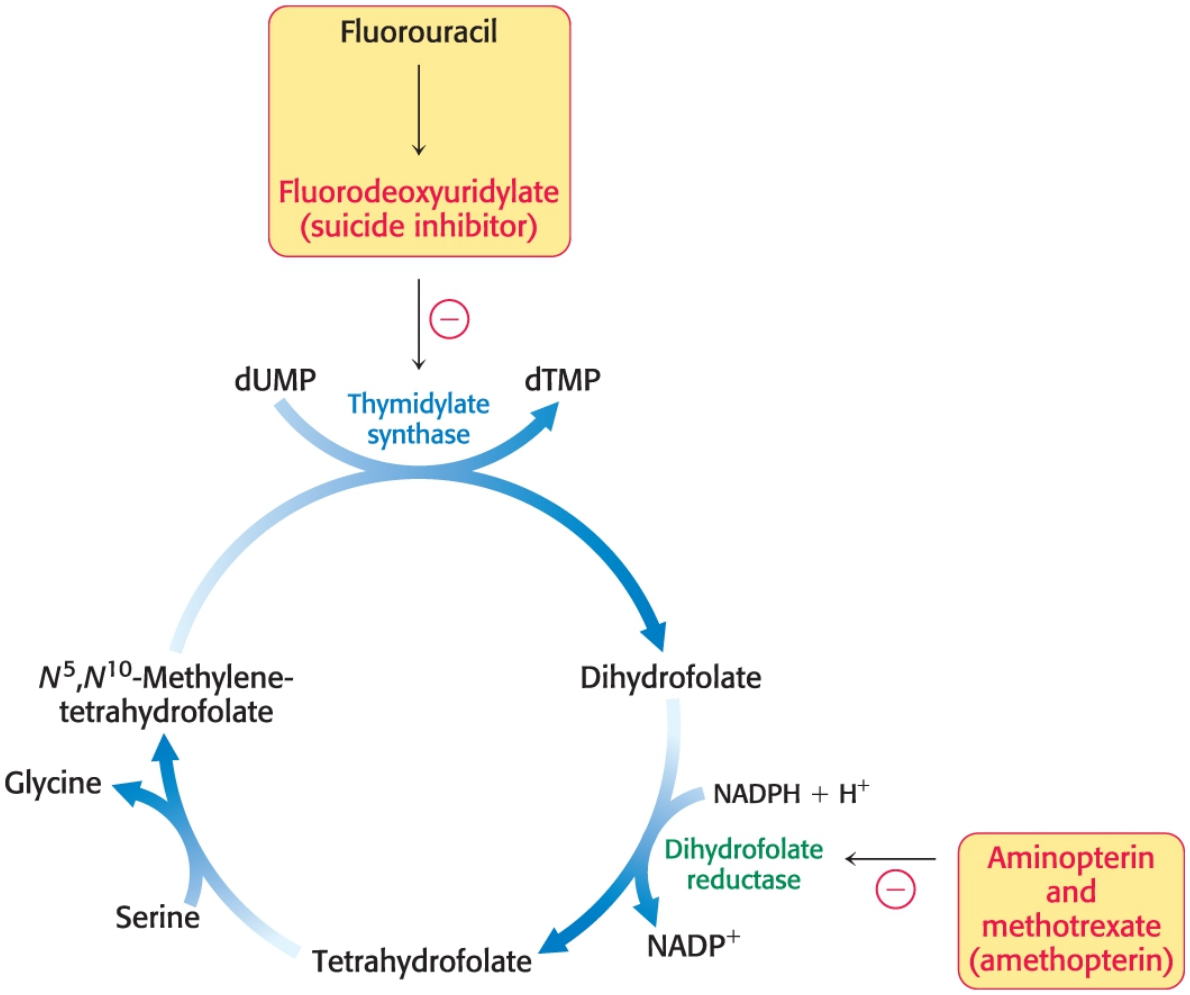
The second reactant is N A D P H plus H superscript plus.

The first product is tetrahydrofolate whose structure is as follows: A 6-membered heterocyclic hexagonal ring is in a vertical orientation and consists of 2 N and 4 C atoms. The first N occupies the topmost vertex and the second N occupies the bottom-most vertex. Both N atoms are bound to H. C 2 is dash bonded to C H 2 on the lower right and wedge bonded to H on the right. C H 2 is single bonded to N H below. The ring is fused to a second 6-membered heterocyclic hexagonal ring in a vertical orientation such that C 3 and C 4 of the first hexagonal ring are C 3 and C 2 respectively of the second hexagonal ring. The second ring consists of 2 N and 4 C atoms. First N bound to H occupies the bottom left vertex. Second N occupies the topmost vertex. A double bond is present between C 1 and N 2, and C 2 and C 3. C 1 is single bonded to N H 2. C 4 is double bonded to O below. N H group connected to the first ring is single bonded to C 6 of a benzene ring in a vertical orientation on the lower right. The benzene ring contains alternating double bonds between C 1 and C 2, C 3 and C 4, and C 5 and C 6. C 3 is single bonded to C 1 of a 1 N and 4 C heteronuclear alkane chain depicted as a line structure using 4 zigzag lines. N bound to H occupies the second position. C 1 is double bonded to O below. C 2 is dash bonded to H on the lower left and wedge bonded to C O O superscript minus on the lower right. C 4 is single bonded to C O O superscript minus on the upper right.

The second product is N A D P superscript plus.

Return to Reduction of dihydrofolate to tetrahydrofolate

Extended description for FIGURE 26.13 Enzymes crucial for nucleotide synthesis are anticancer drug targets



© Macmillan Learning

A cycle shows the site of action of thymidylate synthase and dihydrofolate reductase.

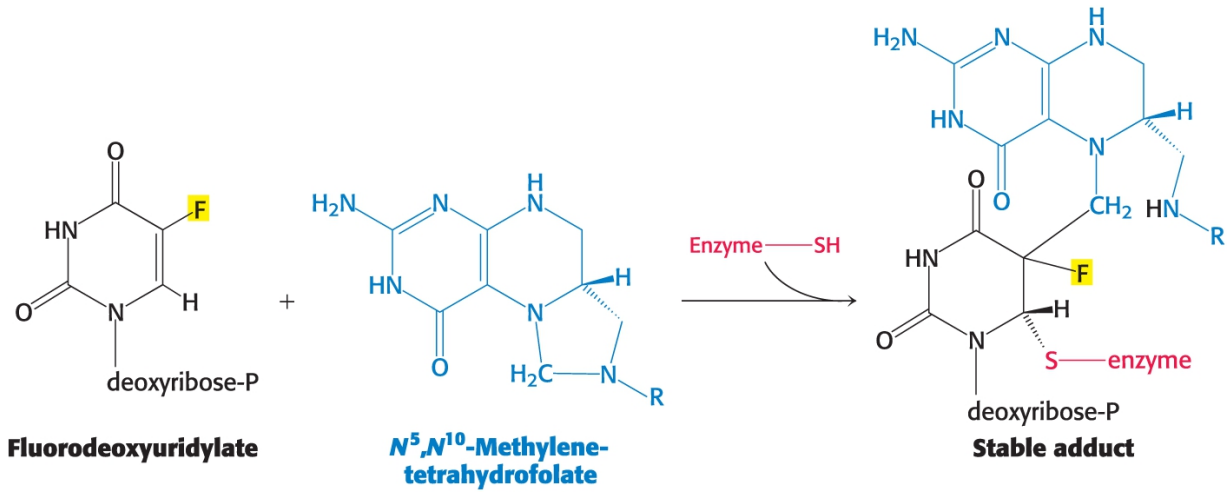
N superscript 5, N superscript 10-Methylene tetrahydrofolate is converted into dihydrofolate by thymidylate synthase. It is coupled with the conversion of d U M P to d T M P. Dihydrofolate is converted into tetrahydrofolate by dihydrofolate reductase. It is

coupled with the oxidation of N A D P H plus H superscript plus to N A D P superscript plus.

Tetrahydrofolate is converted back to N superscript 5, N superscript 10-Methylene tetrahydrofolate. It is coupled with the entry of serine and the release of glycine. The cycle continues in this manner. A yellow square shows the conversion of fluorouracil to fluorodeoxyuridylate (suicide inhibitor) highlighted in red. A downward arrow with a minus symbol points from this yellow square toward thymidylate synthase. Another yellow square contains aminopterin and methotrexate (amethopterin). An arrow with a minus symbol points from this square to dihydrofolate reductase.

Return to FIGURE 26.13 Enzymes crucial for nucleotide synthesis are anticancer drug targets

Extended description for FIGURE 26.14 Fluoruracil acts by suicide inhibition



The reaction consists of two reactants and one product.

The first reactant is fluorodeoxyuridylate whose structure is as follows: A 6-membered heterocyclic hexagonal ring is in a vertical orientation with C 1 occupying the bottom left vertex. It consists of 2 N and 4 C atoms. First N occupies the bottom-most vertex. The second N bound to H occupies the top left vertex. C 1 and C 2 are double bonded to O. C 3 is single bonded to F on the upper right. C 4 is single-bonded to H on the lower right. A double bond is present between C 3 and C 4. N 1 is single bonded to deoxyribose, single bond, P.

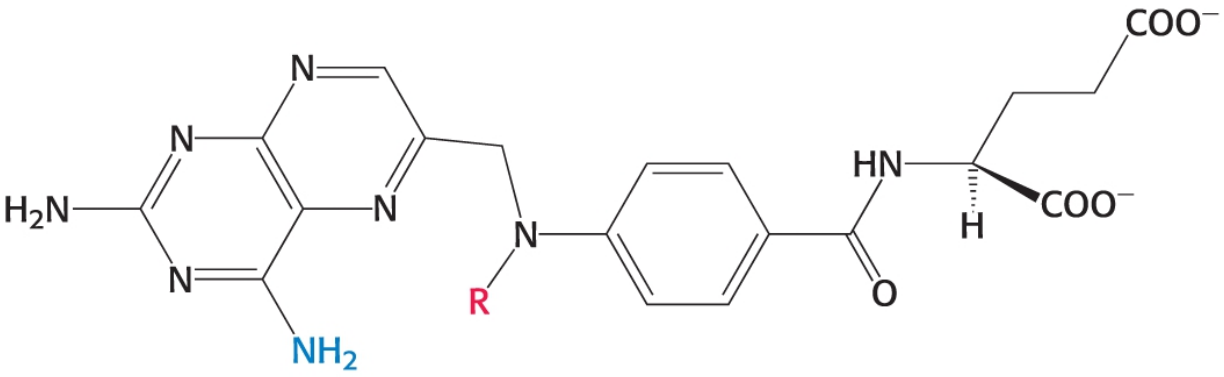
The structure of N superscript 5, N superscript 10-Methylene tetrahydrofolate is as follows: A 6-membered heterocyclic hexagonal ring is in a vertical orientation and consists of 2 N and 4 C atoms. First N occupies the topmost vertex and the second N occupies the bottom-most vertex. First N atom is bound to H. C 2 is wedge bonded to H on the upper right and dash bonded to C H 2 on the

lower right. C H 2 is single bonded to N below. N is single-bonded to R on the lower right and single-bonded to C H 2 on the left. This C H 2 is single-bonded to N 2 of the ring to form a pentagonal ring-like structure. The ring is fused to a second 6-membered heterocyclic hexagonal ring in a vertical orientation such that C 3 and C 4 of the first hexagonal ring are C 3 and C 2 respectively of the second hexagonal ring. The second ring consists of 2 N and 4 C atoms. First N bound to H occupies the bottom left vertex. Second N occupies the topmost vertex. A double bond is present between C 1 and N 2, and C 2 and C 3. C 1 is single bonded to N H 2. C 4 is double bonded to O below.

An enzyme bound to the S H group enters the reaction. The product is a stable adduct between fluorodeoxyuridylate, N superscript 5, N superscript 10-Methylene tetrahydrofolate, and the enzyme. The C 4 of fluorodeoxyuridylate is dash bonded to S, single bond, enzyme. It becomes wedge bonded to H. C 3 of fluorodeoxyuridylate is single bonded to C H 2 group of the pentagonal ring-like structure of N superscript 5, N superscript 10-Methylene tetrahydrofolate. The single bond between N and this C H 2 group breaks. As a result, N becomes bound to H.

Return to FIGURE 26.14 Fluoruracil acts by suicide inhibition

Extended description for Generalized structure of aminopterin and methotrexate



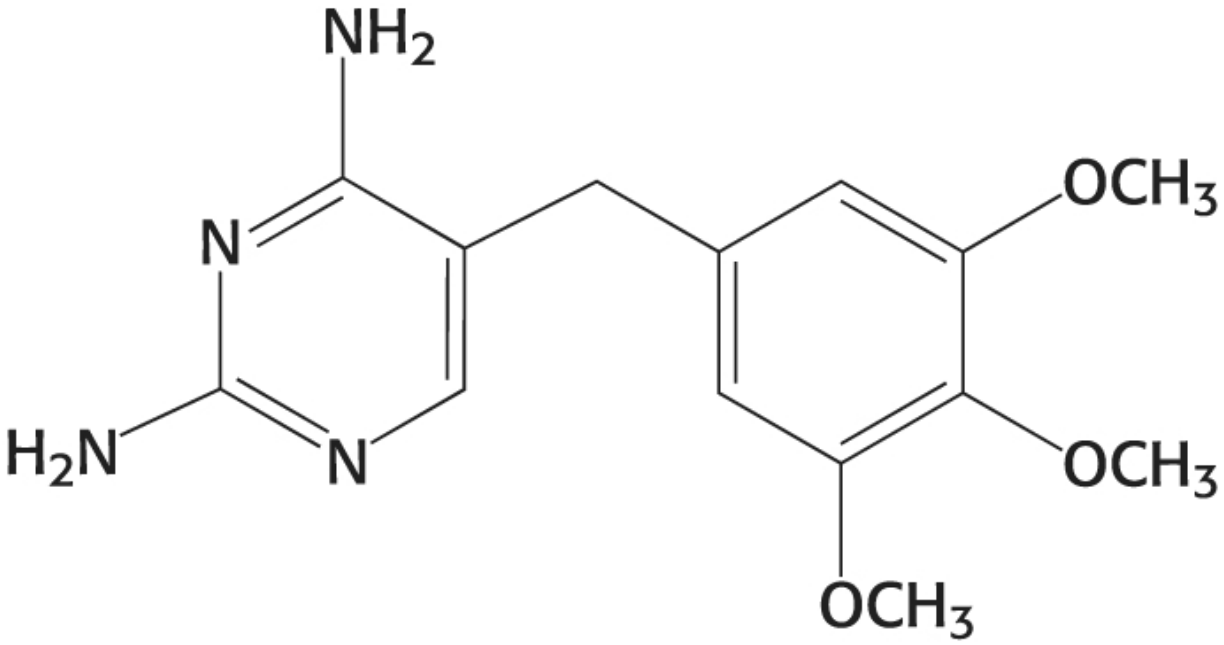
Aminopterin (R = H) or methotrexate (R = CH_3)

The generalized structure is as follows: A 6-membered heterocyclic hexagonal ring is in a horizontal orientation with C 1 occupying the rightmost vertex. It consists of 2 N and 4 C atoms. First N occupies the bottom-left vertex and the second N occupies the top-left vertex. A double bond is present between C 1 and N 2, C 2 and C 3, and C 4 and N 1. C 1 is single bonded to N H 2 on the left. C 4 is single bonded to N H 2 on the lower right. It is fused to another 6-membered heterocyclic hexagonal ring in a horizontal orientation such that C 2 and C 3 of the first ring are C 4 and C 3 respectively of the second ring. The second hexagonal ring consists of 2 N and 4 C atoms. First N occupies the top left vertex and the second N occupies the bottom right vertex. A double bond is present between N 1 and C 1, and C 2 and N 2. C 2 is single bonded to C H 2 on the lower right in the form of a line. This C H 2 is single bonded to N below. N is single bonded to R on the lower right and single bonded to C 4 of a benzene ring in horizontal orientation. The benzene ring contains alternating double bonds between C 1 and C 2, C 3 and C 4, and C 5 and C 6. C 1 is single-bonded to C on the right. This C is single-bonded to N H on the upper right and double-bonded to O on

the lower right. N H is single bonded to C on the right. This C is dash bonded to H below, wedge bonded to C O O superscript minus on the lower right, and single bonded to a 2-carbon alkane chain depicted using a line on the upper right. C 2 of this chain is single bonded to C O O superscript minus on the upper right. In aminopterin, R equals H, and in methotrexate, R equals C H 3.

Return to Generalized structure of aminopterin and methotrexate

Extended description for Structure of trimethoprim

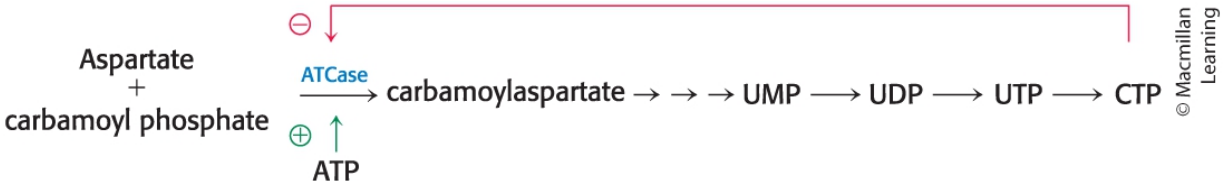


Trimethoprim

The structure of trimethoprim is as follows: A 6-membered heterocyclic hexagonal ring is in a vertical orientation with C 1 occupying the bottom left vertex. First N occupies the bottom-most vertex and the second N occupies the top left vertex. A double bond is present between N 1 and C 1, N 2 and C 2, and C 2 and C 3. C 1 and C 2 are each single bonded to N H 2. C 3 is single bonded to C H 2 on the upper right in the form of a line. This C H 2 is single bonded to C 6 of a benzene ring in a vertical orientation. The benzene ring contains alternating double bonds between C 1 and C 2, C 3 and C 4, and C 5 and C 6. C 2, C 3, and C 4 are each single bonded to O C H 3.

Return to Structure of trimethoprim

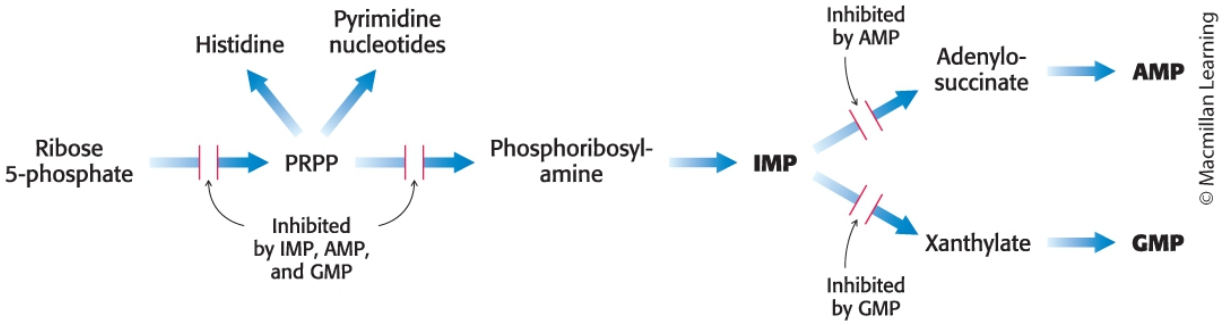
Extended description for Regulation of aspartate transcarbamoylase



A horizontal sequence shows the formation of C T P from aspartate and carbamoyl phosphate. Aspartate plus carbamoyl phosphate combine to form carbamoylaspartate. This step is catalyzed by A T C ase (aspartate transcarbamoylase). Carbamoylaspartate is converted into U M P in three irreversible steps depicted as three successive forward arrows. The remaining steps consist of U M P, forward arrow, U D P, forward arrow, U T P, forward arrow, C T P. A red arrow with a minus symbol points from C T P to A T C ase. A green arrow labeled A T P has a plus symbol and it points toward A C T ase.

Return to Regulation of aspartate transcarbamoylase

Extended description for FIGURE 26.15 Purine biosynthesis is regulated at many steps

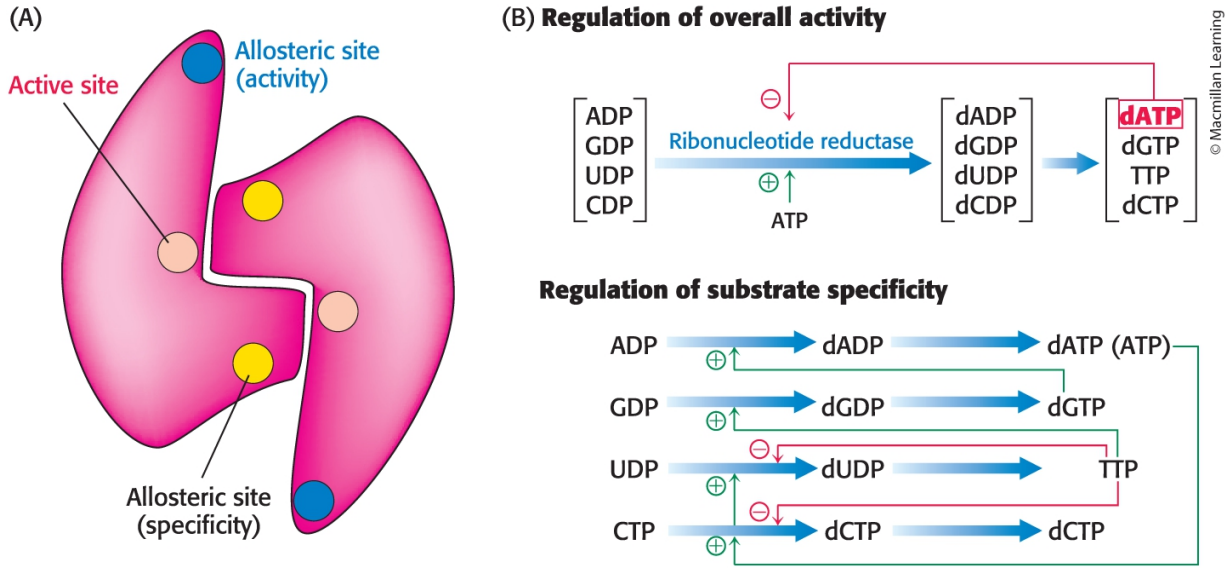


A horizontal sequence shows the conversion of ribose 5-phosphate to I M P. It is depicted as follows: Ribose 5-phosphate, forward arrow, P R P P, forward arrow, phosphoribosyl amine, forward arrow, I M P. The first and second forward arrows have two red parallel lines. These parallel lines depict inhibition by I M P, A M P, and G M P. An upper left arrow points from P R P P toward histidine. An upper right arrow points from P R P P toward pyrimidine nucleotides.

I M P has two fates. An upper left arrow from I M P points toward adenylosuccinate. A forward arrow from adenylosuccinate leads to A M P. A lower left arrow from I M P points toward xanthylate. A forward arrow from xanthylate leads to G M P. Two parallel red lines are shown over the upper left and lower left arrows. The parallel lines over the upper left arrow depict inhibition by A M P. The parallel lines over the lower left arrow depict inhibition by G M P.

Return to FIGURE 26.15 Purine biosynthesis is regulated at many steps

Extended description for FIGURE 26.16 Ribonucleotide reductase is highly regulated to balance the pool of deoxyribonucleotides



Part (A): The ribonucleotide reductase R 1 dimer consists of two subunits. The subunits are elongated and hooked to each other at the center. Each subunit contains an active site, an allosteric site (specificity), and an allosteric site (activity). The left subunit protrudes upward and the right subunit protrudes downward.

Part (B): A horizontal sequence labeled "Regulation of overall activity" is depicted as follows: left square bracket, A D P, G D P, U D P, C D P, right square bracket; forward arrow labeled ribonucleotide reductase; left square bracket, d A D P, d G D P, d U D P, and d C T P, right square bracket; forward arrow, left square bracket, d A T P, d G T P, T T P, d C T P. d A T P is highlighted in red. A red arrow with a minus symbol points from d A T P to ribonucleotide reductase. A green upward arrow labeled A T P with a plus symbol points toward ribonucleotide reductase.

Four horizontal sequences labeled "Regulation of substrate specificity" are depicted as follows:

First sequence: A D P, forward arrow, d A D P, forward arrow, d A T P open parenthesis A T P close parenthesis.

Second sequence: G D P, forward arrow, d G D P, forward arrow, d G T P.

Third sequence: U D P, forward arrow, d U D P, forward arrow, T T P.

Fourth sequence: C T P, forward arrow, d C T P, forward arrow, d C T P.

A green arrow with a plus symbol points from d G T P to the first forward arrow of the first sequence.

A green arrow with a plus symbol points from T T P to the first forward arrow of the second sequence.

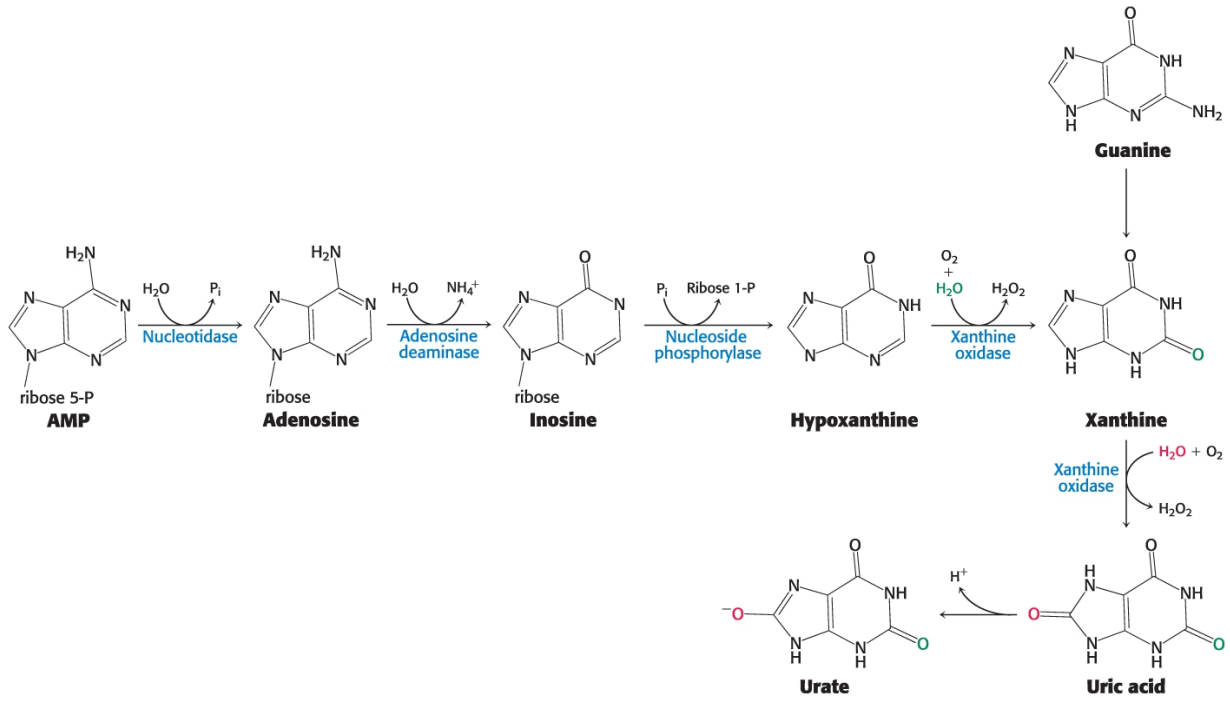
A green upward arrow with a plus symbol points from the first forward arrow of the fourth sequence to the first forward arrow of the third sequence.

A green arrow with a plus symbol points from d A T P open parenthesis A T P close parenthesis points toward the first forward arrow of the fourth sequence.

A red arrow with a minus symbol points from T T P to the first forward arrow of the third sequence. Another red arrow with a minus symbol points from T T P toward the first forward arrow of the fourth sequence.

Return to FIGURE 26.16 Ribonucleotide reductase is highly regulated to balance the pool of deoxyribonucleotides

Extended description for FIGURE 26.17 Purines are catabolized for excretion



In the first irreversible step catalyzed by nucleotidase, A M P is converted into adenosine. It is coupled with the addition of H 2 O and the release of P subscript i.

The structure of A M P is as follows: A 5-membered heterocyclic pentagonal ring is in a horizontal orientation. It consists of 2 N and 3 C atoms. First N occupies the bottom left vertex and the second N occupies the top left vertex. C 1 occupies the leftmost vertex. A double bond is present between C 1 and N 2, and C 2 and C 3. N 1 is single-bonded to ribose 5-phosphate. It is fused to a 6-membered heterocyclic hexagonal ring in a vertical orientation such that C 2 and C 3 of the pentagonal ring are C 3 and C 2 respectively of the hexagonal ring. The hexagonal ring is composed of 2 N and 4 C atoms. The first N occupies the top right vertex and the second N

occupies the bottom-most vertex. A double bond is present between C 1 and N 2, C 2 and C 3, and C 4 and N 1. C 4 is single bonded to N H 2.

The structure of adenosine is as follows: A 5-membered heterocyclic pentagonal ring is in a horizontal orientation. It consists of 2 N and 3 C atoms. First N occupies the bottom left vertex and the second N occupies the top left vertex. C 1 occupies the leftmost vertex. A double bond is present between C 1 and N 2, and C 2 and C 3. N 1 is single-bonded to ribose below. It is fused to a 6-membered heterocyclic hexagonal ring in a vertical orientation such that C 2 and C 3 of the pentagonal ring are C 3 and C 2 respectively of the hexagonal ring. The hexagonal ring is composed of 2 N and 4 C atoms. The first N occupies the top right vertex and the second N occupies the bottom-most vertex. A double bond is present between C 1 and N 2, C 2 and C 3, and C 4 and N 1. C 4 is single bonded to N H 2.

In the second irreversible step, adenosine is converted into inosine by adenosine deaminase. It is coupled with the entry of H 2 O and release of N H 4 superscript plus.

The structure of inosine is as follows: A 5-membered heterocyclic pentagonal ring is in a horizontal orientation. It consists of 2 N and 3 C atoms. First N occupies the bottom left vertex and the second N occupies the top left vertex. C 1 occupies the leftmost vertex. A double bond is present between C 1 and N 2, and C 2 and C 3. N 1 is single-bonded to ribose below. It is fused to a 6-membered heterocyclic hexagonal ring in a vertical orientation such that C 2 and C 3 of the pentagonal ring are C 3 and C 2 respectively of the hexagonal ring. The hexagonal ring is composed of 2 N and 4 C atoms. The first N occupies the top right vertex and the second N occupies the bottom-most vertex. A double bond is present between C 1 and N 2, and C 2 and C 3. C 4 is double bonded to O above.

In the third irreversible step, inosine is converted into hypoxanthine by nucleoside phosphorylase. It is coupled with the entry of P subscript i and the release of ribose 1-phosphate.

The structure of hypoxanthine is as follows: A 5-membered heterocyclic pentagonal ring is in a horizontal orientation. It consists of 2 N and 3 C atoms. First N occupies the bottom left vertex and the second N occupies the top left vertex. C 1 occupies the leftmost vertex. A double bond is present between C 1 and N 2, and C 2 and C 3. It is fused to a 6-membered heterocyclic hexagonal ring in a vertical orientation such that C 2 and C 3 of the pentagonal ring are C 3 and C 2 respectively of the hexagonal ring. The hexagonal ring is composed of 2 N and 4 C atoms. The first N bound to H occupies the top right vertex and the second N occupies the bottom-most vertex. A double bond is present between C 1 and N 2, and C 2 and C 3. C 4 is double bonded to O above.

In the fourth irreversible step, hypoxanthine is converted into xanthine by xanthine oxidase. It is coupled with the entry of H 2 O plus O 2 and the release of H 2 O 2.

The structure of xanthine is as follows: A 5-membered heterocyclic pentagonal ring is in a horizontal orientation. It consists of 2 N and 3 C atoms. First N occupies the bottom left vertex and the second N occupies the top left vertex. C 1 occupies the leftmost vertex. A double bond is present between C 1 and N 2, and C 2 and C 3. It is fused to a 6-membered heterocyclic hexagonal ring in a vertical orientation such that C 2 and C 3 of the pentagonal ring are C 3 and C 2 respectively of the hexagonal ring. The hexagonal ring is composed of 2 N and 4 C atoms. The first N bound to H occupies the top right vertex and the second N bound to H occupies the bottom-most vertex. A double bond is present between C 2 and C 3. C 1 and C 4 are each double bonded to O.

A downward arrow from guanine leads to xanthine below.

The structure of guanine is as follows: A 5-membered heterocyclic pentagonal ring is in a horizontal orientation. It consists of 2 N and 3 C atoms. The first N bound to H occupies the bottom left vertex and the second N occupies the top left vertex. C 1 occupies the leftmost vertex. A double bond is present between C 1 and N 2, and C 2 and C 3. It is fused to a 6-membered heterocyclic hexagonal ring in a vertical orientation such that C 2 and C 3 of the pentagonal ring are C 3 and C 2 respectively of the hexagonal ring. The hexagonal ring is composed of 2 N and 4 C atoms. The first N bound to H occupies the top right vertex and the second N occupies the bottom-most vertex. A double bond is present between C 1 and N 2, and C 2 and C 3. C 1 is single bonded to N H 2. C 4 is double bonded to O above.

In the fifth irreversible step, xanthine is converted into uric acid by xanthine oxidase. It is coupled with the entry of H 2 O plus O 2 and the release of H 2 O 2.

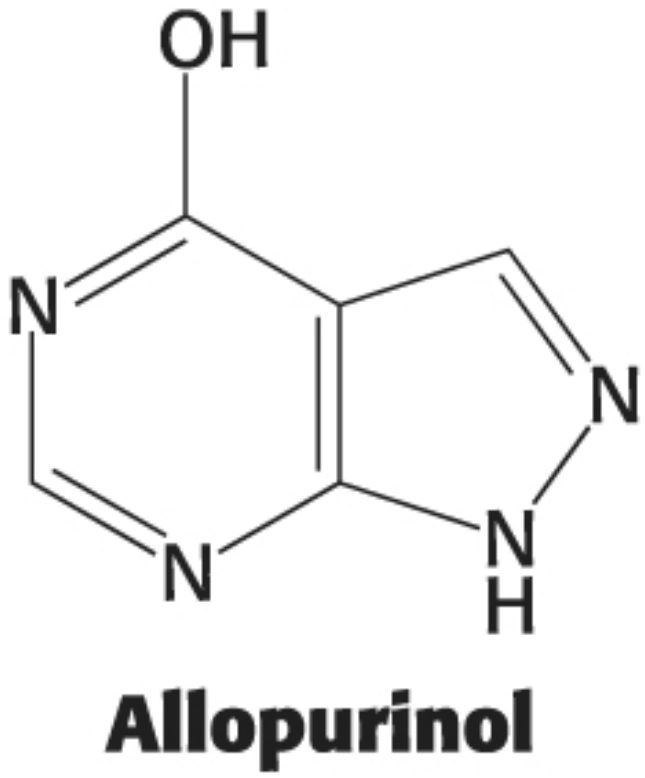
The structure of uric acid is as follows: A 5-membered heterocyclic pentagonal ring is in a horizontal orientation. It consists of 2 N and 3 C atoms. The first N bound to H occupies the bottom left vertex and the second N bound to H occupies the top left vertex. C 1 occupies the leftmost vertex. A double bond is present between C 2 and C 3. C 1 is double bonded to O on the left. It is fused to a 6-membered heterocyclic hexagonal ring in a vertical orientation such that C 2 and C 3 of the pentagonal ring are C 3 and C 2 respectively of the hexagonal ring. The hexagonal ring is composed of 2 N and 4 C atoms. The first N bound to H occupies the top right vertex and the second N bound to H occupies the bottom-most vertex. A double bond is present between C 2 and C 3. C 1 and C 4 are each double bonded to O.

In the sixth irreversible step, uric acid is converted into urate. It is coupled with the release of urate.

The structure of the urate is as follows: A 5-membered heterocyclic pentagonal ring is in a horizontal orientation. It consists of 2 N and 3 C atoms. The first N bound to H occupies the bottom left vertex and the second N occupies the top left vertex. C 1 occupies the leftmost vertex. A double bond is present between C 1 and N 2. C 1 is single bonded to O superscript minus on the left. It is fused to a 6-membered heterocyclic hexagonal ring in a vertical orientation such that C 2 and C 3 of the pentagonal ring are C 3 and C 2 respectively of the hexagonal ring. The hexagonal ring is composed of 2 N and 4 C atoms. The first N bound to H occupies the top right vertex and the second N bound to H occupies the bottom-most vertex. A double bond is present between C 2 and C 3. C 1 and C 4 are each double bonded to O.

Return to FIGURE 26.17 Purines are catabolized for excretion

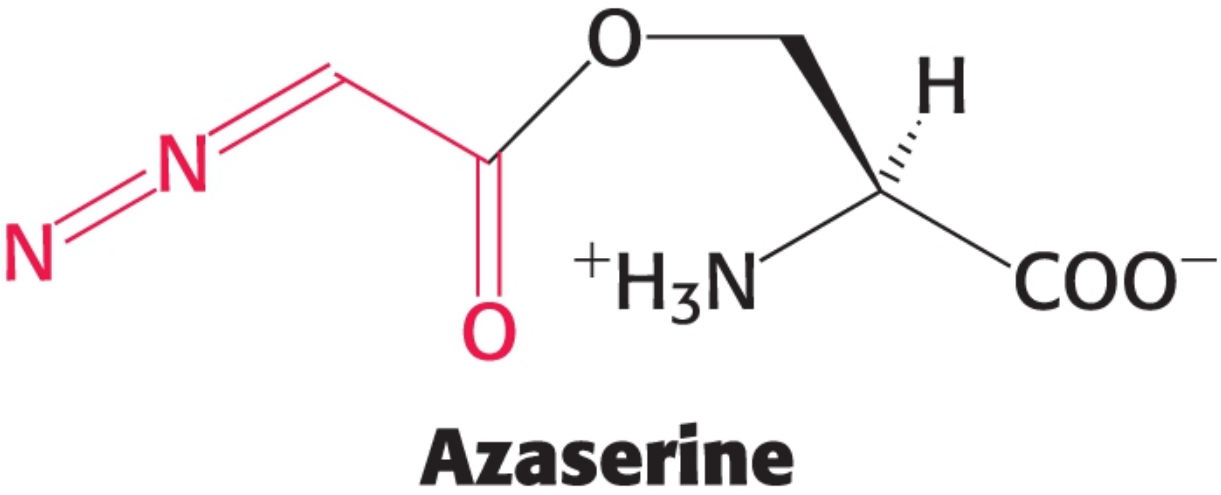
Extended description for Structure of allopurinol



The structure of allopurinol is as follows: A 6-membered heterocyclic hexagonal ring is in a vertical orientation with C 1 occupying the bottom left vertex. First N occupies the bottom-most vertex and the second N occupies the top left vertex. A double bond is present between N 1 and C 1, N 2 and C 2, and C 3 and C 4. C 2 is single bonded to O H above. The ring is fused to a 5-membered heterocyclic pentagonal ring in a horizontal orientation such that C 3 and C 4 of the hexagonal ring are C 2 and C 1 respectively of the pentagonal ring. The pentagonal ring consists of 2 N and 3 C atoms. First N occupies the rightmost vertex. The second N bound to H occupies the bottom right vertex. A double bond is present between C 3 and N 1.

Return to Structure of allopurinol

Extended description for Structure of azaserine



The structure of azaserine is as follows: A central C atom is single-bonded to C H on the upper left in the form of a line, double-bonded to O below, and single-bonded to O on the upper right. C H is double bonded to N, double bond, N on the lower left. The upper right O is single-bonded to C H 2 on the right in the form of a line. C H 2 is wedge bonded to a central C atom on the lower right. This C is dash bonded to H on the upper right, single bonded to N H 3 superscript plus on the lower left, and single bonded to C O O superscript minus on the lower right.

Return to Structure of azaserine

Extended description for Action of statins on cholesterol level and photograph of medicines targeting lipid biosynthesis

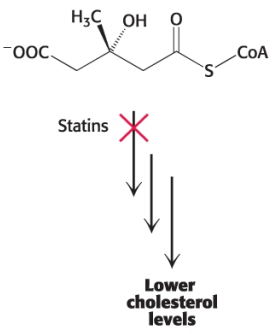




Photo: Kumar Sriskandan/Alamy

The structure of a compound is as follows: A 4-carbon alkane chain is depicted as a line structure using 3 zigzag lines. C 1 is single bonded to C O O superscript minus on the upper left. C 2 is wedge bonded to C H 3 on the upper left and dash bonded to O H on the upper right. C 4 is double bonded to O above and single bonded to S on the lower right. This S is single bonded to C o A on the upper right.

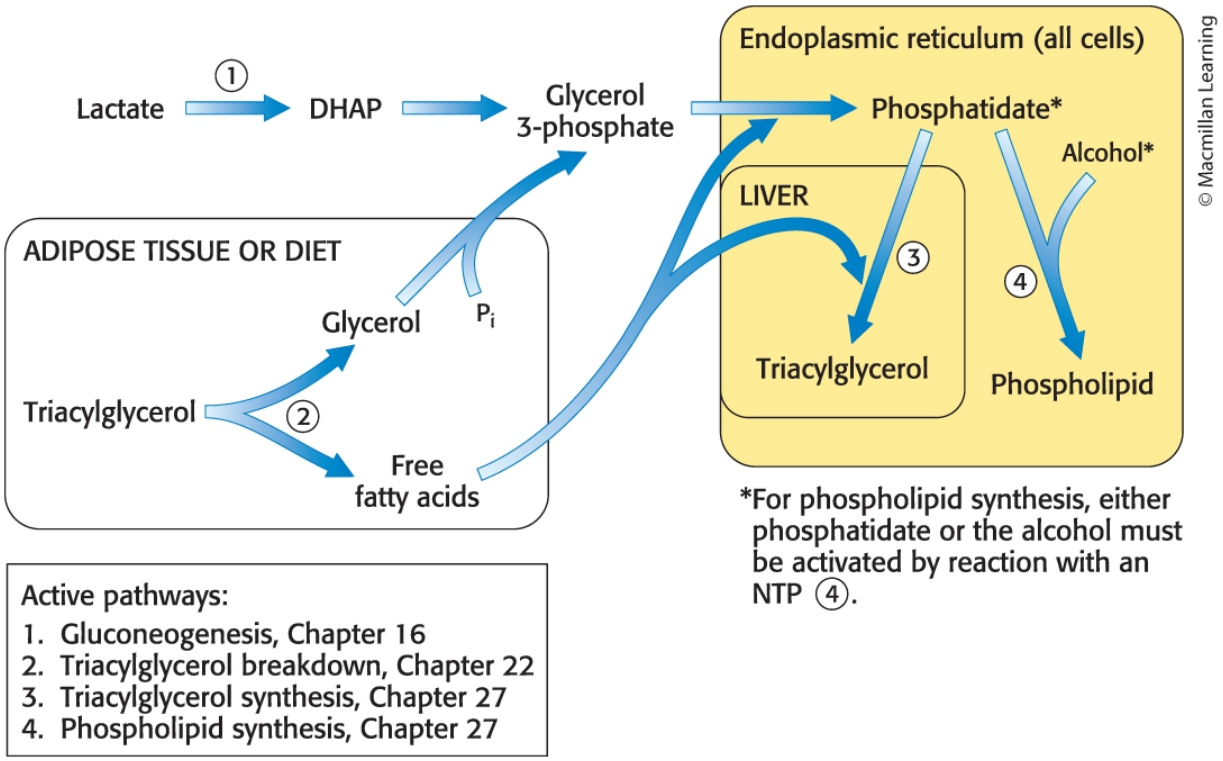
Three successive downward arrows are shown below the structure. The third arrow points to "Lower cholesterol levels." The first arrow has a cross symbol to depict the inhibitory action of statins.

The photograph shows several medicine packets and tablets. These packets contain the medicines atorvastatin, pravastatin sodium, and

simvastatin and others. Some of the medium packets have the brand name "Lipitor."

Return to Action of statins on cholesterol level and photograph of medicines targeting lipid biosynthesis

Extended description for FIGURE 27.1 Phosphatidate is a key intermediate in lipid biosynthesis



The illustration shows adipose tissue or diet as a rectangle on the lower left. The endoplasmic reticulum of all cells is depicted as a yellow square on the upper right. Inside the endoplasmic reticulum, a smaller square is present and is labeled liver. The process starts with lactate which is present outside the adipose tissue. Lactate is transformed into D H A P which is depicted by a forward arrow numbered 1. D H A P is then converted to glycerol 3-phosphate. Simultaneously, in the adipose tissue triacylglycerol is broken down into glycerol and free fatty acids depicted by a bifurcated arrow numbered 2. Glycerol combines with P subscript i and leaves the adipose tissue to combine with glycerol 3-phosphate outside the adipose tissue. Glycerol 3-phosphate enters into the endoplasmic reticulum of all cells and gets transformed to phosphatidate with an

asterisk. Free fatty acids from the adipose tissue also enter the endoplasmic reticulum of all cells. In the endoplasmic reticulum of all cells, it combines with glycerol 3-phosphate to get transformed to phosphatidate with an asterisk. Phosphatidate with an asterisk has two fates. In the liver, it forms triacylglycerol by combining with free fatty acids from the adipose tissue. This process is depicted by a downward arrow numbered 3. In the endoplasmic reticulum of all cells, it combines with alcohol with an asterisk to form a phospholipid depicted by a downward arrow numbered 4.

A text marked with an asterisk is given below the yellow square. The text reads "For phospholipid synthesis, either phosphatidate or the alcohol must be activated by reaction with an N T P numbered 4."

A key titled active pathways is given below the schematic illustration which lists the following points:

1. Gluconeogenesis, Chapter 16.

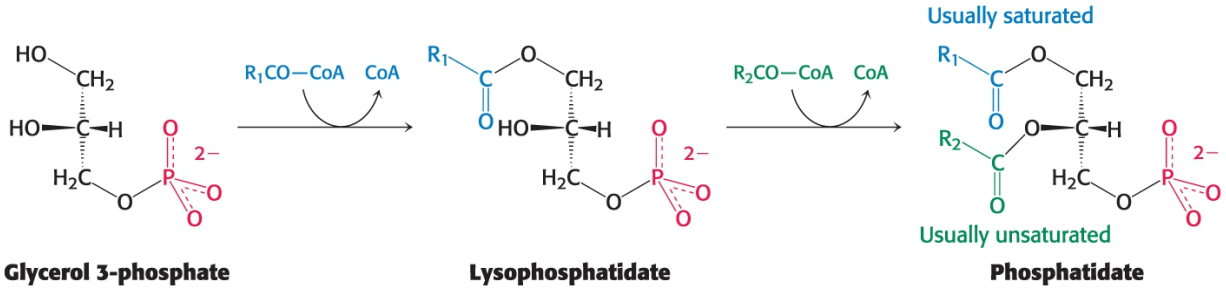
2. Triacylglycerol breakdown, Chapter 22.

3. Triacylglycerol synthesis, Chapter 27.

4. Phospholipid synthesis, Chapter 27.

Return to FIGURE 27.1 Phosphatidate is a key intermediate in lipid biosynthesis

Extended description for A reaction depicting the conversion of glycerol 3-phosphate to phosphatidate



In the first irreversible step, glycerol 3-phosphate is converted to lysophosphatidate coupled with the entry of R subscript 1 C O, single bond, C o A, and release of C o A.

The structure of glycerol 3-phosphate is as follows: A central C atom is dash bonded to C H 2 above and C H 2 below. The central C atom is also wedge bonded to O H on the left and H on the right. C H 2 above is single-bonded to O H on the upper left. C H 2 below is single-bonded to O on the lower right. This O atom is single-bonded to P on the upper right. P is partially double-bonded to O above, O on the lower right, and O below. The P O O group has an overall charge of 2 minus.

The structure lysophosphatidate is as follows: A central C atom is dash bonded to C H 2 above and C H 2 below. The central C atom is also wedge bonded to O H on the left and H on the right. C H 2 above is single-bonded to O on the upper left. O is single-bonded to C on the lower left. This C atom is single-bonded to R subscript 1 on the upper left and double-bonded to O below. C H 2 below is single-bonded to O on the lower right. This O atom is single-bonded to P on the upper right. P is partially double-bonded to O above, O on the

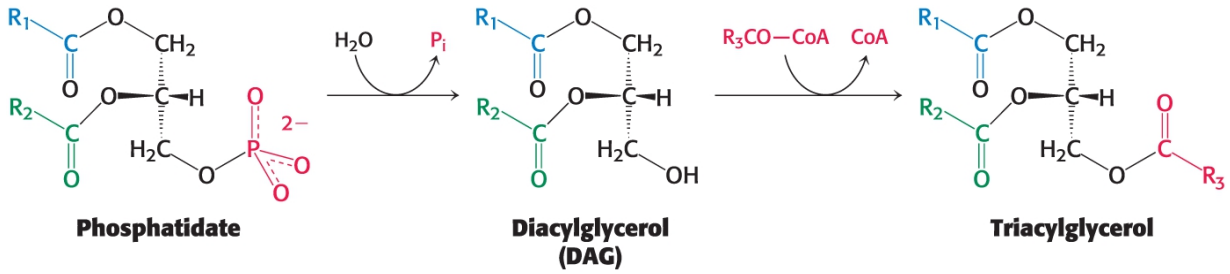
lower right, and O below. The P O O group has an overall charge of 2 minus.

In the second irreversible step, lysophosphatidate is converted to phosphatidate coupled with the entry of R subscript 2 C O, single bond, C o A, and release of C o A.

The structure of phosphatidate is as follows: A central C atom is dash bonded to C H 2 above and C H 2 below. The central C atom is also wedge bonded to O on the left and H on the right. C H 2 above is single-bonded to O on the upper left. O is single-bonded to C on the lower left. This C atom is single-bonded to R subscript 1 on the upper left and double-bonded to O below. The left O wedge bonded to the central C atom is single-bonded to C on the lower left. C is single-bonded to R 2 on the upper left and double-bonded to O below. C H 2 dash bonded to the central C atom below is single-bonded to O on the lower right. This O atom is single-bonded to P on the upper right. P is partially double-bonded to O above, O on the lower right, and O below. The P O O group has an overall charge of 2 minus. The R subscript 1 C O group bonded to the upper left O and left O are labeled "Usually saturated."

Return to A reaction depicting the conversion of glycerol 3-phosphate to phosphatidate

Extended description for A reaction depicting the conversion of phosphatidate to triacylglycerol



In the first irreversible step, phosphatidate is converted to diacylglycerol (D A G) coupled with the entry of H 2 O and release of P subscript i.

The structure of phosphatidate is as follows: A central C atom is dash bonded to C H 2 above and C H 2 below. The central C atom is also wedge bonded to O on the left and H on the right. C H 2 above is single-bonded to O on the upper left. O is single-bonded to C on the lower left. This C atom is single-bonded to R subscript 1 on the upper left and double-bonded to O below. The left O wedge bonded to the central C atom is single-bonded to C on the lower left. C is single-bonded to R subscript 2 on the upper left and double-bonded to O below. C H 2 dash bonded to the central C atom below is single-bonded to O on the lower right. This O atom is single-bonded to P on the upper right. P is partially double-bonded to O above, O on the lower right, and O below. The P O O group has an overall charge of 2 minus.

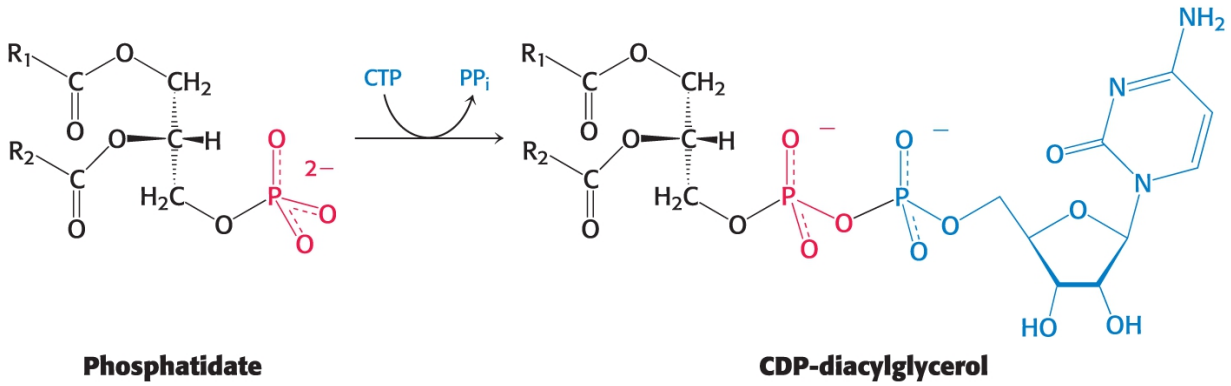
The structure of diacylglycerol (D A G) is as follows: The structure of D A G is the same as phosphatidate except for the absence of the P O O group. The C H 2 that is dash bonded to the central C atom below is single-bonded to O H on the lower right.

In the second irreversible step, diacylglycerol is converted to triacylglycerol. It is coupled with the entry of R 3 C O, single bond, C o A, and release of C o A.

The structure of triacylglycerol is as follows: The structure of triacylglycerol is the same as D A G except that the C H 2 that is dash bonded to the central C atom below is single-bonded to O on the lower right. This O atom is single-bonded to C on the upper right. C is double-bonded to O above and single-bonded to R subscript 3 on the lower right.

Return to A reaction depicting the conversion of phosphatidate to triacylglycerol

Extended description for Conversion of phosphatidate to C D P diacylglycerol



The conversion of phosphatidate to C D P diacylglycerol is coupled with the entry of C T P and P P subscript i.

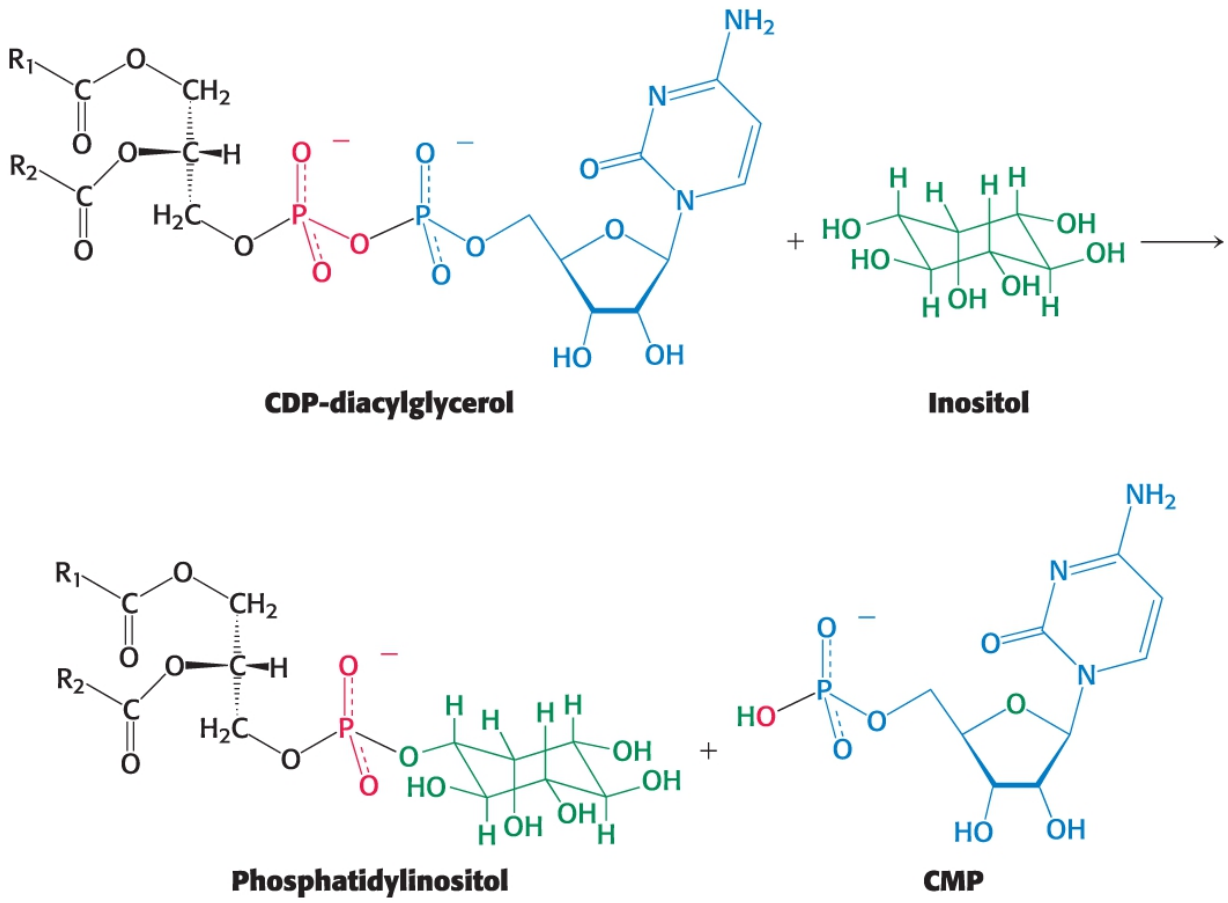
The structure of phosphatidate is as follows: A central C atom is dash bonded to C H 2 above and C H 2 below. The central C atom is also wedge bonded to O on the left and H on the right. C H 2 above is single-bonded to O on the upper left. O is single-bonded to C on the lower left. This C atom is single-bonded to R subscript 1 on the upper left and double-bonded to O below. The left O wedge bonded to the central C atom is single-bonded to C on the lower left. C is single-bonded to R subscript 2 on the upper left and double-bonded to O below. C H 2 dash bonded to the central C atom below is single-bonded to O on the lower right. This O atom is single-bonded to P on the upper right. P is partially double-bonded to O above, O on the lower right, and O below. The P O O group has an overall charge of 2 minus.

The structure of C D P diacylglycerol is as follows: The lower right O atom of the P O O group of phosphatidate is single-bonded to another P atom on the upper right. The P atom is partially double-

bonded to O above and O below. P is also single-bonded to O on the lower right. This P O O group has an overall negative charge. The O atom on the lower right is single-bonded to C H 2 on the upper right in the form of a line. This C H 2 is single-bonded to C 4 of a 5-membered heterocyclic pentagonal ring in a vertical orientation with 1 O and 4 C atoms. C 2 and C 3 of the pentagonal ring are each single-bonded to O H. C 1 of the pentagonal ring is single-bonded to N 1 of a 6-membered heterocyclic hexagonal ring in a vertical orientation with 2 N and 4 C atoms. N 1 occupies the first position which is the bottommost vertex and N 2 occupies the third position which is the top left vertex. Double bonds are present between N 2 and C 2 and C 3 and C 4. C 1 is double-bonded to O on the lower left. C 2 is single-bonded to N H 2 above.

Return to Conversion of phosphatidate to C D P diacylglycerol

Extended description for Conversion of C D P diacylglycerol to phosphatidylinositol and C M P



C D P diacylglycerol reacts with inositol to produce phosphatidylinositol and C M P.

The structure of C D P diacylglycerol is as follows: A central C atom is dash bonded to C H 2 above and C H 2 below. The central C atom is also wedge bonded to O on the left and H on the right. C H 2 above is single-bonded to O on the upper left. O is single-bonded to C on the lower left. This C atom is single-bonded to R subscript 1 on the upper left and double-bonded to O below. The left O wedge bonded to the central C atom is single-bonded to C on the lower left. C is

single-bonded to R subscript 2 on the upper left and double-bonded to O below. C H 2 dash bonded to the central C atom below is single-bonded to O on the lower right. This O atom is single-bonded to P on the upper right. P is partially double-bonded to O above, O below, and single-bonded to O on the lower right. The P O O group has an overall negative charge. The O atom on the lower right is single-bonded to a P atom on the upper right. The P atom is partially double-bonded to O above and O below. P is also single-bonded to O on the lower right. The P O O group has an overall negative charge. The O atom on the lower right is single-bonded to C H 2 on the upper right in the form of a line. C H 2 is single-bonded to C 4 of a 5-membered heterocyclic pentagonal ring in a vertical orientation with 1 O and 4 C atoms. C 2 and C 3 of the pentagonal ring are each single-bonded to O H. C 1 of the pentagonal ring is single-bonded to N 1 of a 6-membered heterocyclic hexagonal ring in a vertical orientation with 2 N and 4 C atoms. N 1 occupies the first position which is the bottommost vertex and N 2 occupies the third position which is the top left vertex. Double bonds are present between N 2 and C 2 and C 3 and C 4. C 1 is double-bonded to O on the lower left. C 2 is single-bonded to N H 2 above.

The structure of inositol is as follows: A 6-carbon hexagonal ring is in a chair conformation. C 1 occupies the bottom right vertex and C 4 occupies the top left vertex. C 2 and C 5 are close to each other. C 1 is single-bonded to O H on the top right and H below. C 2 is single-bonded to H above and O H on the lower right. C 3 is single-bonded to O H on the top left and H below. C 4 is single-bonded to H above and O H on the lower left. C 5 is single-bonded to H on the top left and O H below. C 6 is single-bonded to H above and O H on the right.

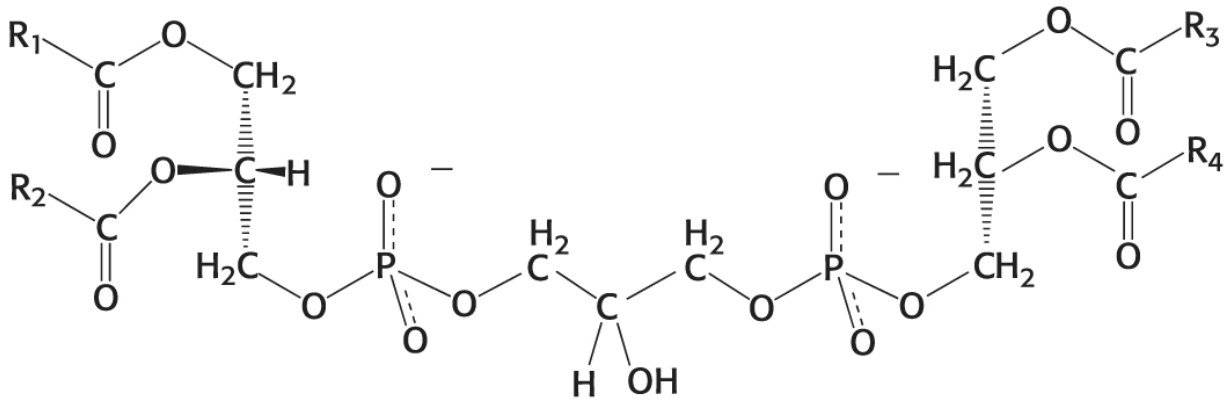
The structure of phosphatidylinositol is as follows: The structure of phosphatidylinositol is the same as C D P diacylglycerol except for the absence of the second P O O group and the addition of inositol.

The lower right O atom of the first P O O group is single-bonded to an O atom bonded to C 4 of inositol.

The structure of C M P is as follows: O H atom on the lower left is single-bonded to a P atom on the upper right. The P atom is partially double-bonded to O above and O below. P is also single-bonded to O on the lower right. The P O O group has an overall negative charge. The O atom on the lower right is single-bonded to C H 2 on the upper right in the form of a line. The C H 2 group is single-bonded to C 4 of a 5-membered heterocyclic pentagonal ring in a vertical orientation with 1 O and 4 C atoms. C 2 and C 3 of the pentagonal ring are each single-bonded to O H. C 1 of the pentagonal ring is single-bonded to N 1 of a 6-membered heterocyclic hexagonal ring in a vertical orientation with 2 N and 4 C atoms. N 1 occupies the first position which is the bottommost vertex and N 2 occupies the third position which is the upper left vertex. Double bonds are present between N 2 and C 2 and C 3 and C 4. C 1 is double-bonded to O on the lower left. C 2 is single-bonded to N H 2 above.

Return to Conversion of C D P diacylglycerol to phosphatidylinositol and C M P

Extended description for Structure of diphosphatidylglycerol (cardiolipin)



Diphosphatidylglycerol (Cardiolipin)

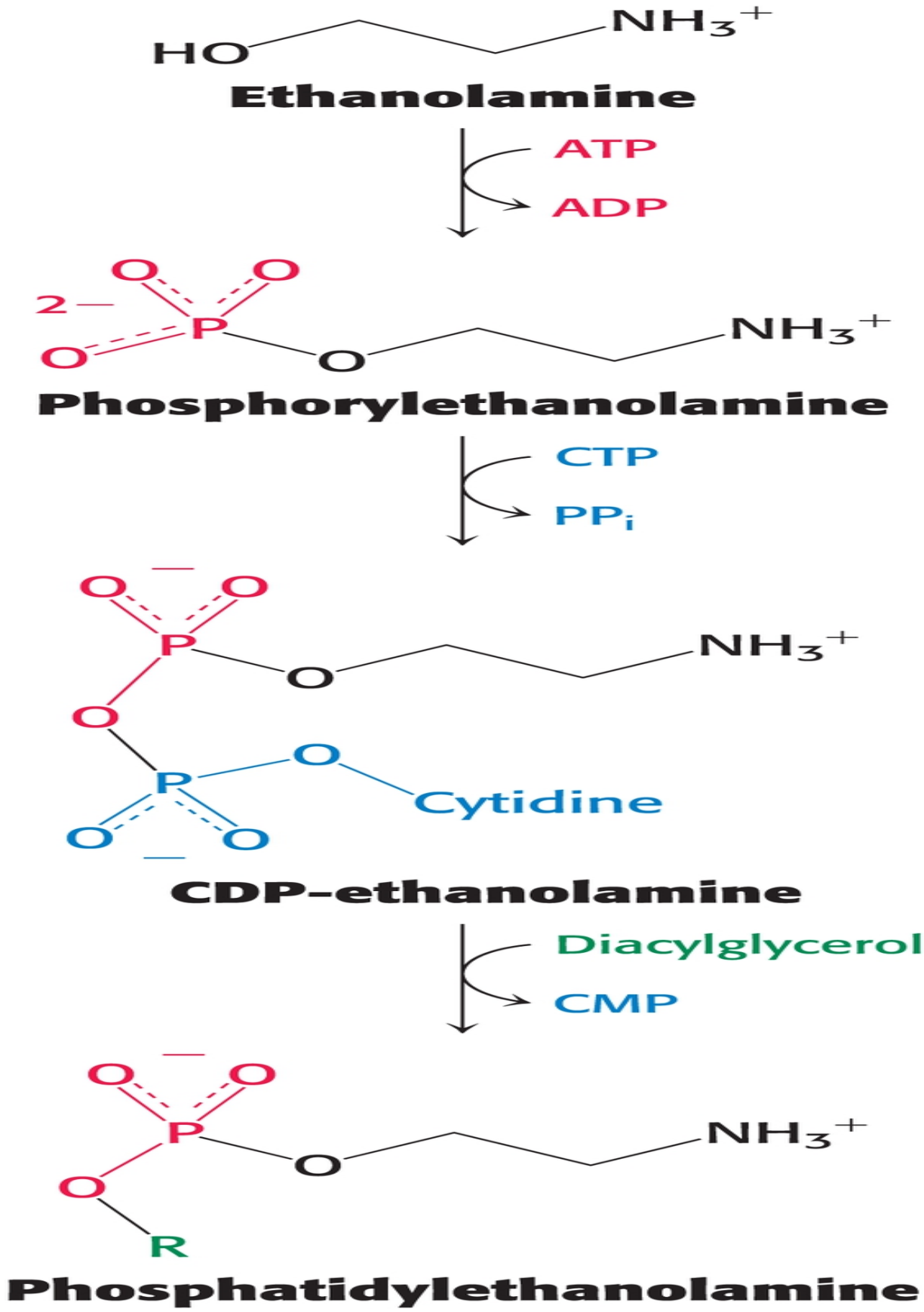
The structure of diphosphatidylglycerol (cardiolipin) is as follows: A central C atom is dash bonded to C H 2 above and C H 2 below. The central C atom is also wedge bonded to O on the left and H on the right. C H 2 above is single-bonded to O on the upper left. O is single-bonded to C on the lower left. This C atom is single-bonded to R subscript 1 on the upper left and double-bonded to O below. The left O wedge bonded to the central C atom is single-bonded to C on the lower left. C is single-bonded to R subscript 2 on the upper left and double-bonded to O below. C H 2 dash bonded to the central C atom below is single-bonded to O, single bond, P, single bond, O, single bond, C H 2, single bond, C, single bond, C H 2, single bond, O, single bond, P, single bond, O, single bond, C H 2 in a zigzag pattern. P 1 and P 2 at the second and eighth positions are each partially double-bonded to O above and O on the lower right. Both the P O O groups have a negative charge. C at the fifth position is single-bonded to H on the lower left and O H on the lower right. C H 2 at the tenth position is dash bonded to C H 2 above. This C H 2 is single-bonded on the top right to O, single bond, C, single bond, R subscript 4. C is double-bonded to O below. The C H 2 group that is

dash bonded to C H 2 at the tenth position is further dash bonded to C H 2 above. This C H 2 is single-bonded on the top right to O, single bond, C, single bond, R subscript 3. C is double-bonded to O below.

Return to Structure of diphosphatidylglycerol (cardiolipin)

Extended description for Conversion of ethanolamine

to phosphatidylethanolamine


HO
NH3+
Ethanolamine
ATP
ADP
2−
O
P
NH3+
Phosphorylethanolamine
CTP
PPi
Cytidine
CDP–ethanolamine
Diacylglycerol
CMP
R
Phosphatidylethanolamine

In the first irreversible step, ethanolamine is converted to phosphorylethanolamine coupled with the breakdown of A T P to A D P.

The structure of ethanolamine is as follows: A 2-carbon alkane chain is depicted using a line. C 1 is single bonded to O H on the lower left. C 4 is single bonded to N H 3 superscript plus on the upper right.

The structure of phosphorylethanolamine is as follows: A 1 O and 2 C heteronuclear alkane is depicted as a line structure using 2 zigzag lines. O occupies the first position and is single-bonded to P on the upper left. P is partially double-bonded to O on the upper right, O on the upper left, and O on the lower left. The P O O group has an overall charge of 2 minus. C 2 is single bonded to N H 3 superscript plus on the upper right.

In the second irreversible step, phosphorylethanolamine is converted to C D P ethanolamine coupled with the entry of C T P and release of P P subscript i.

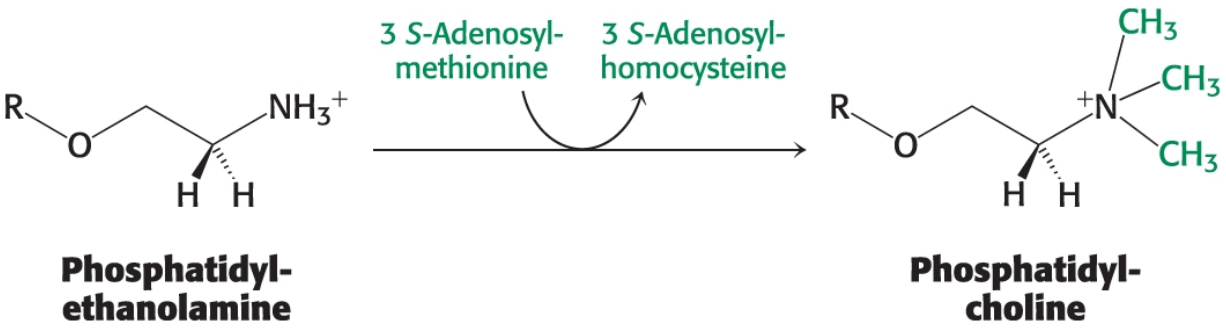
The structure of C D P ethanolamine is as follows: A 1 O and 2 C heteronuclear alkane is depicted as a line structure using 2 zigzag lines. O occupies the first position and is single-bonded to P on the upper left. P is partially double-bonded to O on the upper right, O on the upper left, and single-bonded to O on the lower left. The P O O group has an overall charge of 2 minus. C 2 is single bonded to N H 3 superscript plus on the upper right. The lower left O is single-bonded to another P on the lower right. This P is partially double-bonded to O on the lower left and lower right with an overall negative charge. P is also single-bonded to O on the upper right. The O on the upper right is single-bonded to cytidine on the lower right.

In the third irreversible step, C D P ethanolamine is converted to phosphatidylethanolamine coupled with the entry of diacylglycerol and release of C M P.

The structure of phosphatidylethanolamine is as follows: A 1 O and 2 C heteronuclear alkane is depicted as a line structure using 2 zigzag lines. O occupies the first position and is single-bonded to P on the upper left. P is partially double-bonded to O on the upper right, O on the upper left, and single-bonded to O on the lower left. The P O O group has an overall charge of 2 minus. The lower left O is single-bonded to R on the lower right. C 2 of the alkane chain is single bonded to N H 3 superscript plus on the upper right.

Return to Conversion of ethanolamine to phosphatidylethanolamine

Extended description for Formation of phosphatidylcholine



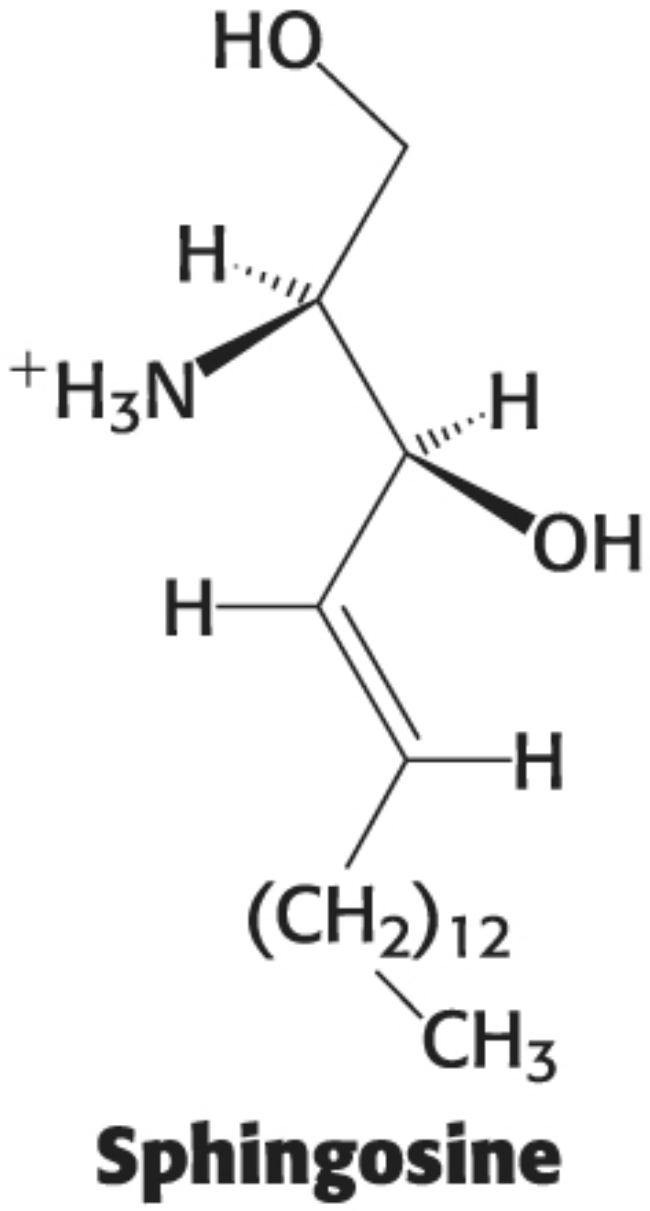
An irreversible reaction depicts the transformation of phosphatidylethanolamine to phosphatidylcholine coupled with the entry of 3 S-adenosyl-methionine and the release of 3 S-adenosyl-homocysteine.

The structure of phosphatidylethanolamine is as follows: A 2-carbon alkane chain is depicted as a line structure using a line. C 1 is single-bonded to O on the lower left. The O atom is single-bonded to R on the upper left. C 2 is single bonded to N H 3 superscript plus on the upper right. C 2 is wedge bonded to H on the lower left and dash bonded to H on the lower right.

The structure of phosphatidylcholine is as follows: A 1 N and 2 C heteronuclear alkane chain is depicted as a line structure using 2 zigzag lines. N superscript plus occupies the third position. C 1 is single-bonded to O on the lower left. The O atom is single-bonded to R on the upper left. C 2 is wedge bonded to H on the lower left and dash bonded to H on the lower right. N superscript plus is single bonded to C H 3 above, C H 3 on the upper right, and C H 3 on the lower right.

Return to Formation of phosphatidylcholine

Extended description for Structure of sphingosine

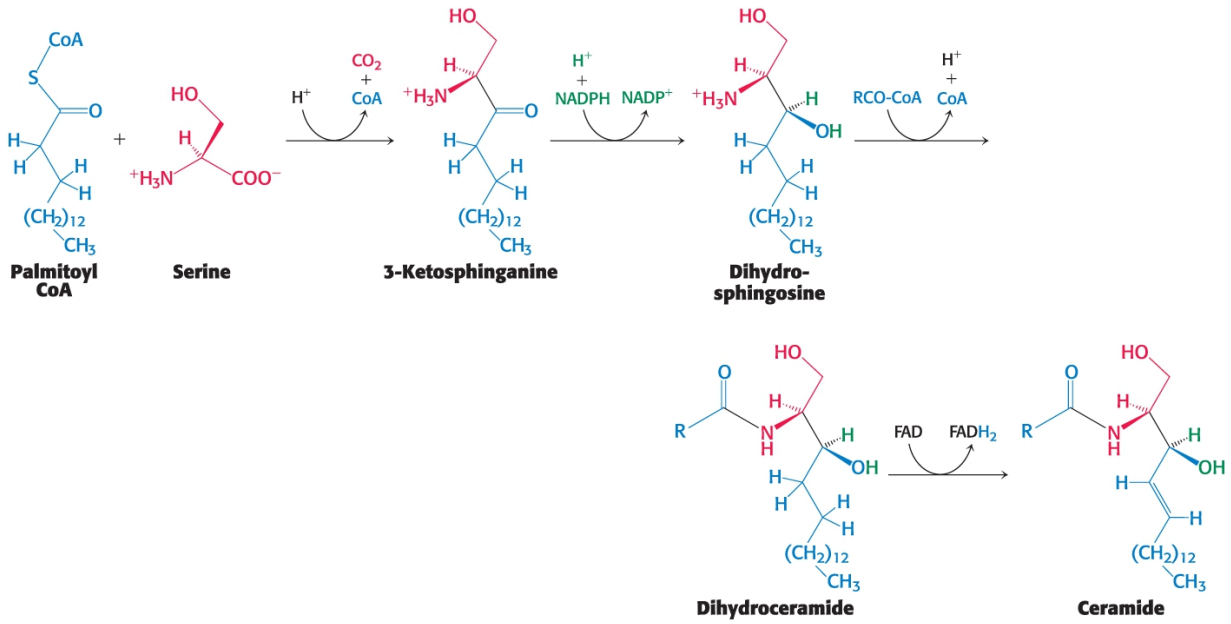


The structure of sphingosine is as follows: A 5-carbon alkene chain is depicted vertically as a line structure using 4 zigzag lines. A double bond is present between C 4 and C 5. C 1 is single bonded to O H on the upper left. C 2 is dash bonded to H on the upper left and wedge bonded to N H 3 superscript plus on the lower left. C 3 is dash

bonded to H on the upper right and wedge bonded to O H on the lower right. C 4 is single-bonded to H on the left. C 5 is single bonded to H on the right. C 5 is single bonded to open parenthesis C H 2 close parenthesis with subscript 12 on the lower left. Open parenthesis C H 2 close parenthesis with subscript 12 is single bonded to C H 3 on the lower right.

Return to Structure of sphingosine

Extended description for FIGURE 27.2 Biosynthesis of ceramide involves four steps



In the first irreversible step, palmitoyl C o A combines with serine to give rise to 3-ketosphinganine coupled with the entry of H superscript plus ion and release of C O 2 and C o A.

The structure of palmitoyl C o A is as follows: A 3-carbon alkane chain is depicted as a vertical line structure using two zig-zag lines. C 1 is single bonded to S on the upper left and double bonded to O on the right. S is further single bonded to C o A on the upper right. C 2 is single bonded to H on the upper left and H on the lower left. C 3 is single bonded to H on the upper right and H on the lower right. C 3 is also single bonded to open parenthesis C H 2 close parenthesis with subscript 12 on the lower left. Open parenthesis C H 2 close parenthesis 12 is single bonded to C H 3 on the lower right.

The structure of serine is as follows: A central C atom is single bonded to N H 3 superscript plus on the lower left and C O O superscript minus on the lower right. The central C atom is dash bonded to H on the upper left and wedge bonded to another C atom on the upper right. The upper right C atom is single-bonded to O H on the upper left.

The structure of 3-ketosphinganine is as follows: A 5-carbon alkane chain is depicted as a vertical line structure using 4 zig-zag lines. C 1 is single bonded to O H on the upper left. C 2 is dash bonded to H on the upper left and wedge bonded to N H 3 superscript plus on the lower left. C 3 is double bonded to O on the right. C 4 is single bonded to H on the upper left and H on the lower left. C 5 is single bonded to H on the upper right, H on the lower right, and open parenthesis C H 2 close parenthesis with subscript 12 on the lower left. Open parenthesis C H 2 close parenthesis 12 is single bonded to C H 3 on the lower right.

In the second irreversible step, 3-ketosphinganine is converted to dihydro-sphingosine coupled with oxidation of N A D P H plus H superscript plus to N A D P superscript plus.

The structure of dihydro-sphingosine is as follows: A 5-carbon alkane chain is depicted as a vertical line structure using 4 zigzag lines. C 1 is single bonded to O H on the upper left. C 2 is dash bonded to H on the upper left and wedge bonded to N H 3 superscript plus on the lower left. C 3 is dash bonded to H on the upper right and wedge bonded to O H on the lower right. C 4 is single bonded to H on the upper left and H on the lower left. C 5 is single bonded to H on the upper right, H on the lower right, and single bonded to open parenthesis C H 2 close parenthesis with subscript 12 on the lower left. Open parenthesis C H 2 close parenthesis with subscript 12 is single bonded to C H 3 on the lower right.

In the third irreversible step, dihydro-sphingosine is converted to dihydroceramide coupled with the entry of R C O, single bond, C o A, and release of C o A and H superscript plus.

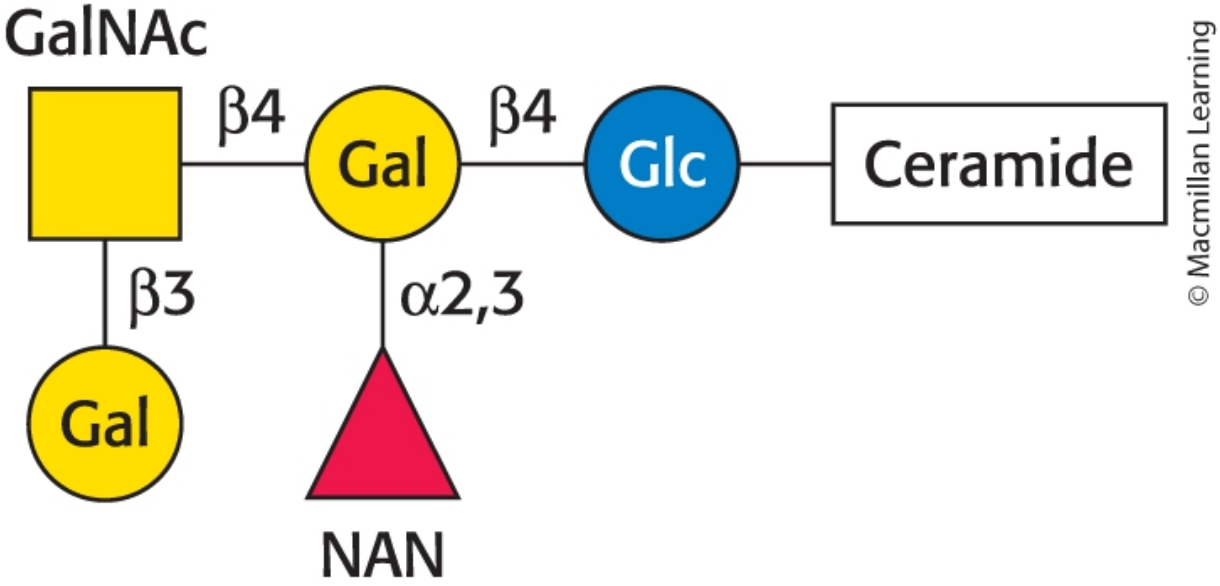
The structure of dihydroceramide is as follows: A 5-carbon alkane chain is depicted as a vertical line structure using 4 zigzag lines. C 1 is single bonded to O H on the upper left. C 2 is dash bonded to H on the upper left and wedge bonded to N H on the lower left. N H is further single-bonded to a central C atom on the upper left. The central C atom is single-bonded to R on the lower left and double-bonded to O above. C 3 of the alkane chain is dash bonded to H on the upper right and wedge bonded to O H on the lower right. C 4 is single bonded to H on the upper left and H on the lower left. C 5 is single bonded to H on the upper right, H on the lower right, and open parenthesis C H 2 close parenthesis with subscript 12 on the lower left. Open parenthesis C H 2 close parenthesis 12 is single bonded to C H 3 on the lower right.

In the fourth irreversible step, dihydroceramide is converted to ceramide coupled with the reduction of F A D to F A D H 2.

The structure of ceramide is as follows: A 5-carbon alkene chain is depicted as a vertical line structure using 4 zigzag lines. A double bond is present between C 4 and C 5. C 1 is single bonded to O H on the upper left. C 2 is dash bonded to H on the upper left and wedge bonded to N H on the lower left. N H is further single-bonded to a central C atom on the upper left. The central C atom is single-bonded to R on the lower left and double-bonded to O above. C 3 of the alkene chain is dash bonded to H on the upper right and wedge bonded to O H on the lower right. C 4 is single-bonded to H on the left. C 5 is single bonded to H on the right and single bonded to open parenthesis C H 2 close parenthesis with subscript 12 on the lower left. Open parenthesis C H 2 close parenthesis with subscript 12 is single bonded to C H 3 on the lower right.

Return to FIGURE 27.2 Biosynthesis of ceramide involves four steps

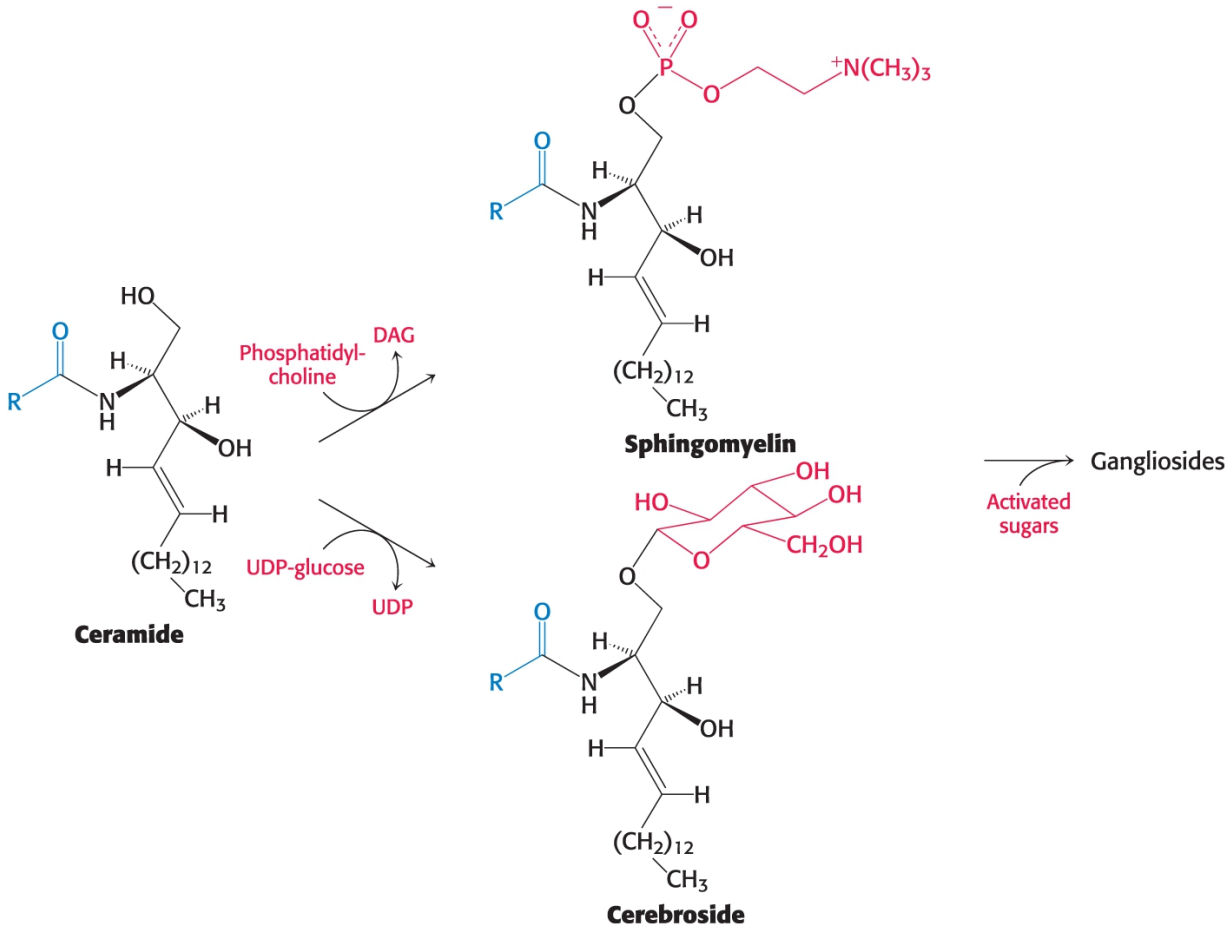
Extended description for FIGURE 27.3 The ganglioside G subscript M 1 consists of five monosaccharides linked to ceramide



The structure of ganglioside is as follows: A rectangle labeled ceramide is connected to a blue circle on the left. The blue circle is labeled G l c. G l c is connected to a yellow circle on the left by a beta 4 linkage. The yellow circle is labeled G a l. G a l is connected to a yellow square on the left by a beta 4 linkage and a red triangle below by an alpha 2, 3 linkage. The yellow square is labeled G a l N A c and the triangle is labeled N A N. G a l N A c is connected to another yellow circle below by a beta 3 linkage. The yellow circle is labeled G a l.

Return to FIGURE 27.3 The ganglioside G subscript M 1 consists of five monosaccharides linked to ceramide

Extended description for FIGURE 27.4 Ceramide can be converted into sphingomyelin, cerebroside, and gangliosides



Ceramide has two fates. It can either get converted to sphingomyelin or cerebroside. The conversion of ceramide to sphingomyelin is coupled with the entry of phosphatidylcholine and release of D A G. The conversion of ceramide to cerebroside is coupled with the entry of U D P-glucose and release of U D P. Later, sphingomyelin and cerebroside are converted to gangliosides with the addition of activated sugars.

The structure of ceramide is as follows: A 5-carbon alkene chain is depicted as a vertical line structure using 4 zigzag lines. A double bond is present between C 4 and C 5. C 1 is single bonded to O H on the upper left. C 2 is dash bonded to H on the upper left and wedge bonded to N H on the lower left. N H is further single-bonded to a central C atom on the upper left. The central C atom is single-bonded to R on the lower left and double-bonded to O above. C 3 of the alkene chain is dash bonded to H on the upper right and wedge bonded to O H on the lower right. C 4 is single-bonded to H on the left. C 5 is single bonded to H on the right and single bonded to open parenthesis C H 2 close parenthesis with subscript 12 on the lower left. Open parenthesis C H 2 close parenthesis with subscript 12 is single bonded to C H 3 on the lower right.

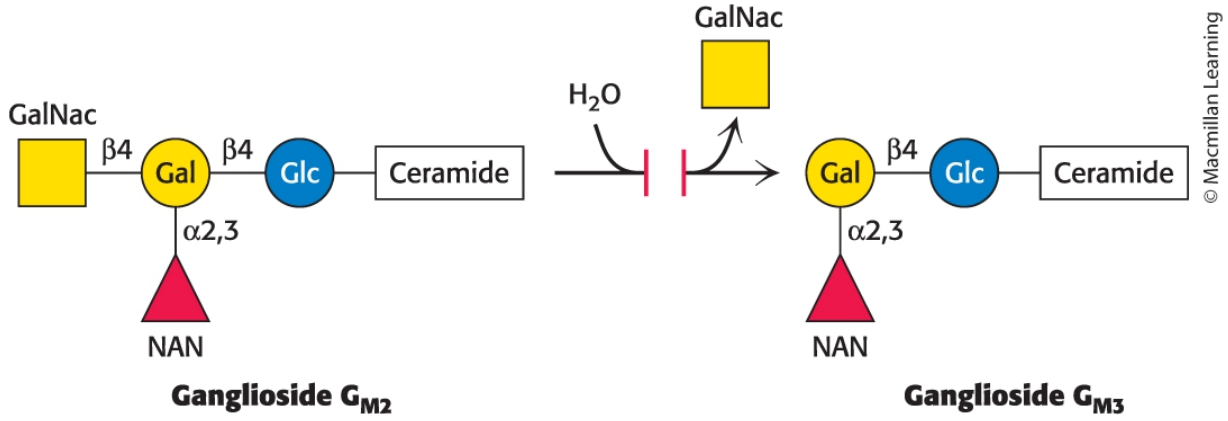
The structure of sphingomyelin is as follows: A 5-carbon alkene chain is depicted as a vertical line structure using 4 zigzag lines. A double bond is present between C 4 and C 5. C 1 is single-bonded to O on the upper left. This O is single-bonded to P on the upper right. The P atom is partially double-bonded to O on the upper left and O on the upper right. The P O O group has an overall negative charge. The P atom is single-bonded to O on the lower right. The O atom is single-bonded to a 2-carbon alkane chain depicted as a line structure using a line. C 2 of the alkane chain is single bonded to N superscript plus open parenthesis C H 3 close parenthesis with subscript 3. C 2 of the alkene chain is dash bonded to H on the upper left and wedge bonded to N H on the lower left. N H is further single-bonded to a central C atom on the upper left. The central C atom is single-bonded to R on the lower left and double-bonded to O above. C 3 of the alkene chain is dash bonded to H on the upper right and wedge bonded to O H on the lower right. C 4 is single-bonded to H on the left. C 5 is single bonded to H on the right and single bonded to open parenthesis C H 2 close parenthesis with subscript 12 on the lower left. Open parenthesis C H 2 close

parenthesis with subscript 12 is single bonded to C H 3 on the lower right.

The structure of the cerebroside is as follows: A 5-carbon alkene chain is depicted as a vertical line structure using 4 zigzag lines. A double bond is present between C 4 and C 5. C 2 is dash bonded to H on the upper left and wedge bonded to N H on the lower left. N H is further single-bonded to a central C atom on the upper left. The central C atom is single-bonded to R on the lower left and double-bonded to O above. C 3 of the alkene chain is dash bonded to H on the upper right and wedge bonded to O H on the lower right. C 4 is single-bonded to H on the left. C 5 is single bonded to H on the right and single bonded to open parenthesis C H 2 close parenthesis with subscript 12 on the lower left. Open parenthesis C H 2 close parenthesis with subscript 12 is single bonded to C H 3 on the lower right. C 1 is single-bonded to O on the upper left. The O atom is single-bonded to C 1 of a 6-membered heterocyclic ring in a chair conformation consisting of 1 O and 5 C atoms. The O atom occupies the first position, which is the bottom left vertex. C 2 and C 5 are close to each other. C 2, C 3, and C 4 are each single bonded to O H and C 5 is single bonded to C H 2 O H.

Return to FIGURE 27.4 Ceramide can be converted into sphingomyelin, cerebroside, and gangliosides

Extended description for Conversion of ganglioside G subscript M 2 to ganglioside G subscript M 3



An irreversible reaction depicts the formation of ganglioside G subscript M 3 from ganglioside G subscript M 2 coupled with the entry of H 2 O and release of G a l N a c depicted as a yellow square. Two red parallel lines are shown over the forward arrow pointing from ganglioside G subscript M 2 to ganglioside G subscript M 3.

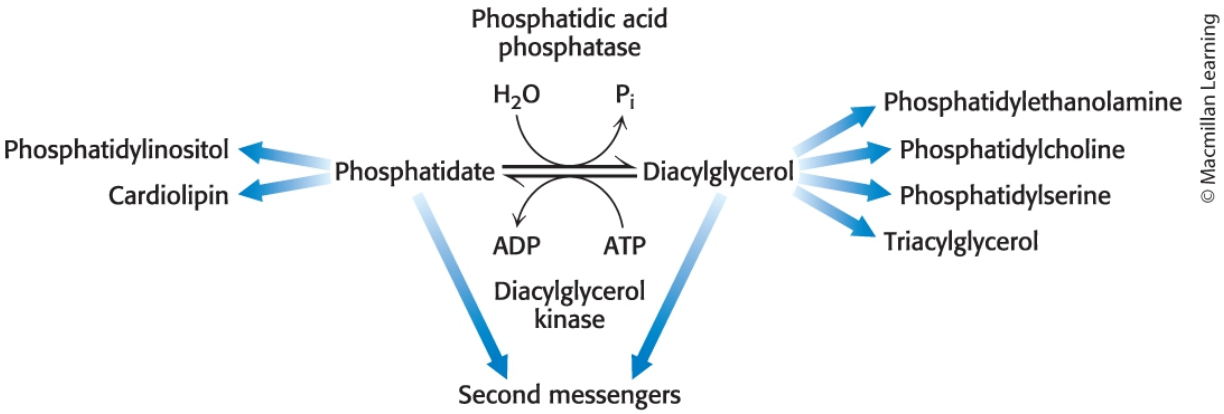
The structure of ganglioside G subscript M 2 is depicted as follows: A rectangle labeled ceramide is connected to a blue circle on the left. The blue circle is labeled G l c. G l c is connected to a yellow circle on the left by a beta 4 linkage. The yellow circle is labeled G a l. G a l is connected to a yellow square on the left by a beta 4 linkage and a red triangle below by an alpha 2, 3 linkage. The yellow square is labeled G a l N A c and the triangle is labeled N A N.

The structure of ganglioside G subscript M 3 is as follows: A rectangle labeled ceramide is connected to a blue circle on the left. The blue circle is labeled G l c. G l c is connected to a yellow circle on the left by a beta 4 linkage. The yellow circle is labeled G a l. G a l

is connected to a red triangle below by an alpha 2, 3 linkage. The triangle is labeled N A N.

Return to Conversion of ganglioside G subscript M 2 to ganglioside G subscript M 3

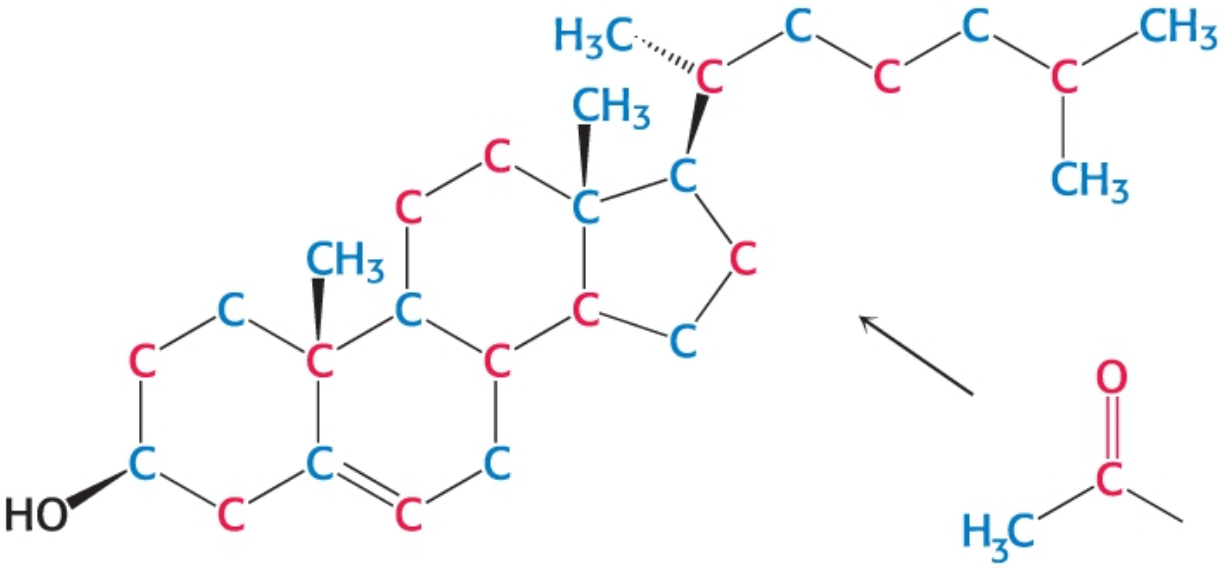
Extended description for FIGURE 27.6 Phosphatidic acid phosphatase is a key regulatory enzyme in lipid synthesis



The figure shows a reversible reaction in which phosphatidate is converted to diacylglycerol by the action of phosphatidic acid phosphatase. It is coupled with the entry of H 2 O and the release of P subscript i. Diacylglycerol can be converted back to phosphatidate by the action of diacylglycerol kinase. It is coupled with the breakdown of A T P to A D P. Phosphatidate gives rise to phosphatidylinositol and cardiolipin. Diacylglycerol gives rise to phosphatidylethanolamine, phosphatidylcholine, phosphatidylserine, and triacylglycerol. Phosphatidate and diacylglycerol are labeled second messengers.

Return to FIGURE 27.6 Phosphatidic acid phosphatase is a key regulatory enzyme in lipid synthesis

Extended description for FIGURE 27.7 Isotope-labeling experiments have revealed the source of carbon atoms in cholesterol synthesized from acetate



Cholesterol has the following structure: Two 6-carbon hexagonal rings in vertical orientation have C 1 at the topmost vertex. The second ring has a double bond between C 4 and C 5. Both the rings are fused such that C 2 and C 3 of the first ring are C 6 and C 5 respectively of the second ring. C 2 of the first ring is wedge bonded to C H 3 above. C 5 of the first ring is wedge bonded to O H on the lower left. Another 6-carbon hexagonal ring in vertical orientation is fused with the second ring such that C 1 and C 2 of the second ring are C 5 and C 4 respectively of the third ring. A 5-membered pentagonal ring in horizontal orientation with C 1 occupying the top right vertex is fused with the third ring such that C 2 and C 3 of the third ring are C 5 and C 4 respectively of the fourth ring. C 5 of the pentagonal ring is wedge bonded to C H 3 above. C 1 of the fourth ring is wedge bonded to C 1 of a 5-carbon alkane chain depicted using 4 zigzag lines. C 1 of the alkane chain is dash bonded to C H 3

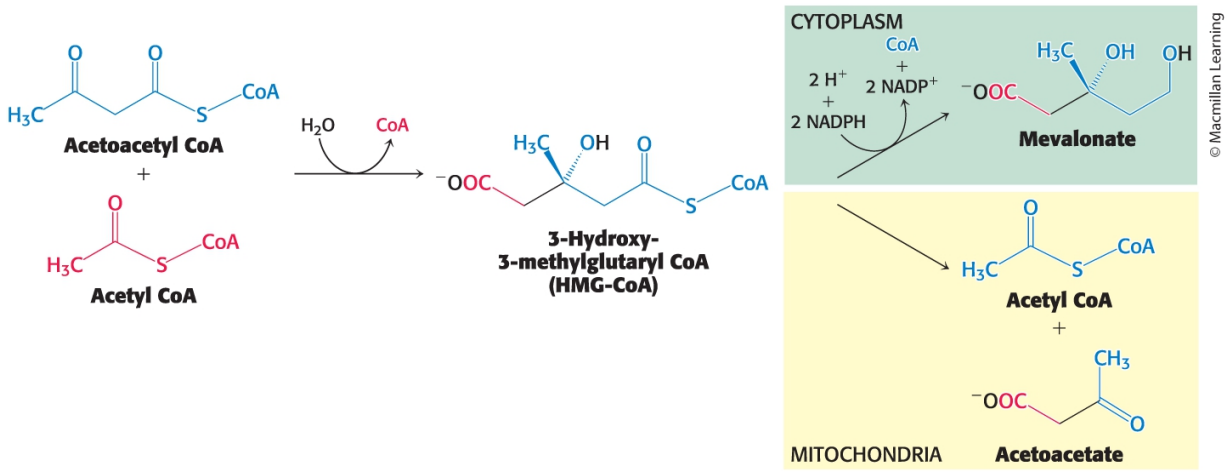
on the top left. C 5 of the alkane chain is single bonded to C H 3 on the top right and C H 3 below.

The structure of the acetate molecule is shown on the bottom right. An arrow from the acetate molecule points toward the structure of cholesterol. The structure of the acetate molecule is as follows: A central C atom is single bonded to C H 3 on the lower left and double bonded to O above and has an open single bond on the lower right.

In cholesterol, C 1, C 3, and C 5 of the first two rings are highlighted in blue. C H 3 wedge bonded to C 2 of the first ring and C 2 of the third ring are also highlighted in blue. C 2 and C 5 of the third ring are highlighted in blue. C 1, C 3, and C 5 of the fourth ring are highlighted in blue. C 2 and C 4 of the alkane chain are highlighted in blue. C H 3 groups bound to the alkane chain are highlighted in blue. The rest of the C atoms are highlighted in red.

Return to FIGURE 27.7 Isotope-labeling experiments have revealed the source of carbon atoms in cholesterol synthesized from acetate

Extended description for FIGURE 27.8 3-Hydroxy-3-methylglutaryl C o A has different fates



In the first irreversible step, acetoacetyl C o A reacts with acetyl C o A to give rise to 3-hydroxy-3-methylglutaryl C o A coupled with the entry of H 2 O and release of C o A.

The structure of acetoacetyl C o A is as follows: A zigzag chain is composed of C H 3, single bond, C, single bond, C, single bond, C, single bond, S, single bond, C o A. C 1 and C 3 are each double bonded to O above.

The structure of acetyl C o A is as follows: A zigzag chain is composed of C H 3, single bond, C, single bond, S, single bond, C o A. C is double bonded to O above.

The structure of 3-hydroxy-3-methylglutaryl C o A (H M G C o A) is as follows: A zigzag chain is composed of C O O superscript minus, single bond, C, single bond, C, single bond, C, single bond, C, single bond, S, single bond, C o A. C 2 is wedge bonded to C H 3 on the

upper left and dash bonded to O H on the upper right. C 4 is double bonded to O above.

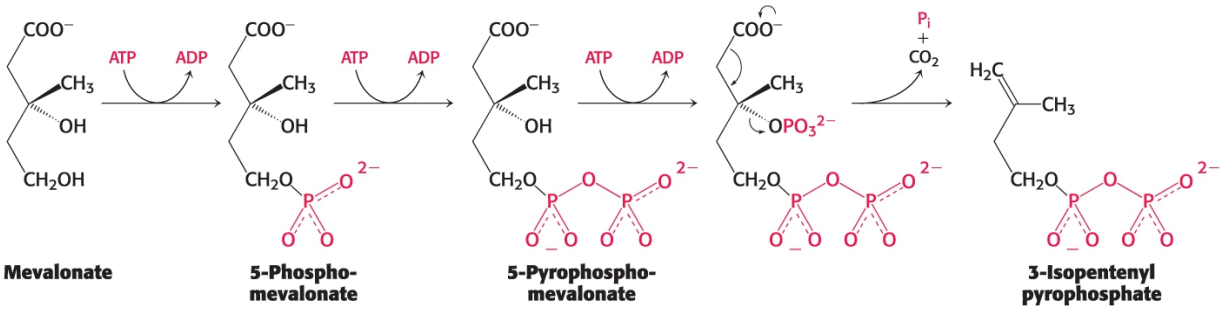
3-hydroxy-3-methylglutaryl C o A (H M G C o A) has two fates. H M G C o A enters the cytoplasm and gets transformed to mevalonate coupled with the entry of 2 H superscript plus and 2 N A D P H and release of 2 N A D P superscript plus and C o A. H M G C o A enters the mitochondria and is transformed to acetyl C o A and acetoacetate.

The structure of mevalonate is as follows: A zigzag chain is composed of C O O superscript minus, single bond, C, single bond, C, single bond, C, single bond, C. C 2 is wedge bonded to C H 3 on the top left and dash bonded to O H on the top right. C 4 is single bonded to O H above.

The structure of acetoacetate is as follows: A zigzag chain is composed of C O O superscript minus, single bond, C, single bond C. C 2 is single bonded to C H 3 on the top and double bonded to O on the lower right.

Return to FIGURE 27.8 3-Hydroxy-3-methylglutaryl C o A has different fates

Extended description for FIGURE 27.9 Mevalonate is converted into isopentenyl pyrophosphate



In the first irreversible step, mevalonate is converted to 5-phospho-mevalonate coupled with the breakdown of A T P to A D P.

The structure of mevalonate is as follows: A 3-carbon alkane chain is depicted vertically as a line structure using 2 zigzag lines. C 1 is single bonded to C O O superscript minus on the upper right. C 2 is wedge bonded to C H 3 on the upper right and dash bonded to O H on the lower right. C 3 is single bonded to C H 2 O H on the lower right.

The structure of 5-phospho-mevalonate is as follows: A 3-carbon alkane chain is depicted vertically as a line structure using 2 zigzag lines. C 1 is single bonded to C O O superscript minus on the upper right. C 2 is wedge bonded to C H 3 on the upper right and dash bonded to O H on the lower right. C 3 is single bonded to C H 2 O on the lower right. C H 2 O is single-bonded to P on the lower right. P is partially double-bonded to O on the upper right, O on the lower left, and O on the lower right. The P O O group has an overall charge of 2 minus.

In the second irreversible step, 5-phospho-mevalonate is transformed to 5-pyrophospho-mevalonate coupled with the breakdown of A T P to A D P.

The structure of 5-pyrophospho-mevalonate is as follows: A 3-carbon alkane chain is depicted vertically as a line structure using 2 zigzag lines. C 1 is single bonded to C O O superscript minus on the upper right. C 2 is wedge bonded to C H 3 on the upper right and dash bonded to O H on the lower right. C 3 is single bonded to C H 2 O on the lower right. C H 2 O is single-bonded to P on the lower right. P is single-bonded to O on the upper right. O is single-bonded to P on the lower right. The first P atom is partially double-bonded to O on the lower left, and O on the lower right. The second P atom is partially double-bonded to O on the upper right, O on the lower left, and O on the lower right. The first P O O group has an overall negative charge. The second P O O group has an overall negative charge of 2 minus.

In the third irreversible step, 5-pyrophospho-mevalonate is transformed into an unlabeled intermediate by the breakdown of A T P to A D P.

The structure of the intermediate is as follows: A 3-carbon alkane chain is depicted vertically as a line structure using 2 zigzag lines. C 1 is single bonded to C O O superscript minus on the upper right. C 2 is wedge bonded to C H 3 on the upper right and dash bonded to O P O 3 superscript 2 minus on the lower right. C 3 is single bonded to C H 2 O on the lower right. C H 2 O is single-bonded to P on the lower right. P is single-bonded to O on the upper right. O is single-bonded to P on the lower right. The first P atom is partially double-bonded to O on the lower left, and O on the lower right. The second P atom is partially double-bonded to O on the upper right, O on the lower left, and O on the lower right. The first P O O group has an overall negative charge. The second P O O group has an overall negative

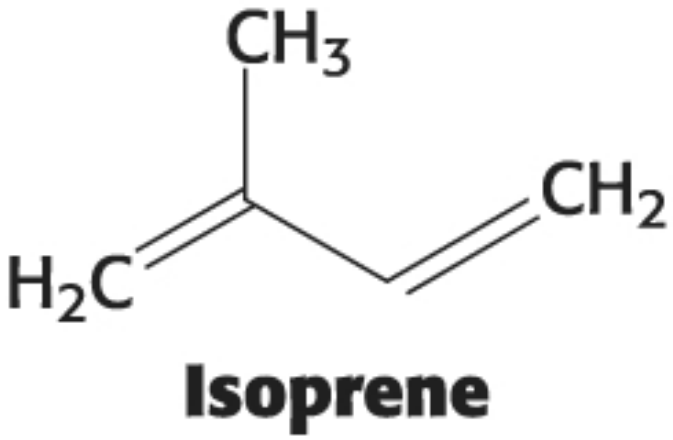
charge of 2 minus. An arrow from superscript minus in C O O superscript minus points toward C O O. An arrow from the single bond between C 1 and C O O superscript minus points to the single bond between C 1 and C 2. An arrow from C 2 points toward O P O 3 superscript 2 minus.

In the fourth irreversible step, the intermediate is transformed to 3-isopentenyl pyrophosphate coupled with the release of P subscript i and C O 2.

The structure of 3-isopentenyl pyrophosphate is as follows: A 2-carbon alkane chain is depicted vertically as a line structure using a line. C 1 is double bonded to C H 2 on the upper left and single bonded to C H 3 on the right. C 2 is single bonded to C H 2 O on the lower right. C H 2 O is single-bonded to P on the lower right. P is single-bonded to O on the upper right. O is single-bonded to P on the lower right. The first P atom is partially double-bonded to O on the lower left, and O on the lower right. The second P atom is partially double-bonded to O on the upper right, O on the lower left, and O on the lower right. The first P O O group has an overall negative charge. The second P O O group has an overall charge of 2 minus.

Return to FIGURE 27.9 Mevalonate is converted into isopentenyl pyrophosphate

Extended description for Structure of isoprene

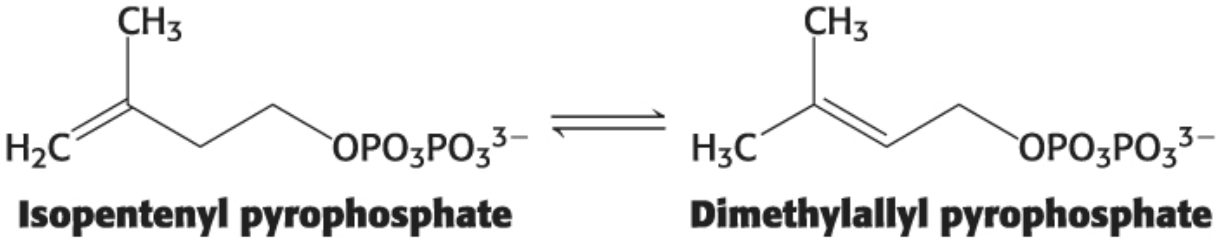


Isoprene

The structure of isoprene is as follows: A 2-carbon alkane chain is depicted as a line structure using a line. C 1 is double bonded to C H 2 on the lower left and single bonded to C H 3 above. C 2 is double bonded to C H 2 on the upper right.

Return to Structure of isoprene

Extended description for Formation of dimethylallyl pyrophosphate from isopentenyl pyrophosphate

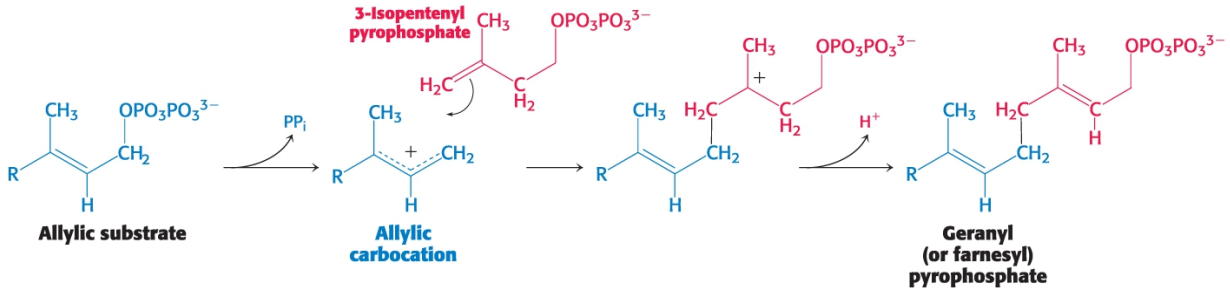


The structure of isopentenyl pyrophosphate is as follows: A 3-carbon alkane chain is depicted as a line structure using 2 zigzag lines. C 1 is double bonded to C H 2 on the lower left and single bonded to C H 3 above. C 3 is single bonded to O P O 3 P O 3 superscript 3 minus on the lower right.

The structure of dimethylallyl pyrophosphate is as follows: A 3-carbon alkene chain is depicted as a line structure using 2 zigzag lines. A double bond is present between C 1 and C 2. C 1 is single bonded to C H 3 above and C H 3 on the lower left. C 3 is single bonded to O P O 3 P O 3 superscript 3 minus on the lower right.

Return to Formation of dimethylallyl pyrophosphate from isopentenyl pyrophosphate

Extended description for FIGURE 27.10 Condensation reactions build carbon–carbon bonds that eventually form the cholesterol skeleton



In the first irreversible step, the allylic substrate is transformed to allylic carbocation coupled with the release of P P subscript i.

The structure of the allylic substrate is as follows: A 3-carbon alkene chain is depicted as a line structure using 2 zigzag lines. C bound to H 2 occupies the third position. A double bond is present between C 1 and C 2. C 1 is single-bonded to R on the lower left and C H 3 above. C 2 is single bonded to H below. C H 2 is single-bonded to O P O 3 P O 3 superscript 3 minus above.

The structure of allylic carbocation is as follows: A 3-carbon alkene chain is depicted as a line structure using 2 zigzag lines. C bound to H 2 occupies the third position. A partial double bond is present between C 1 and C 2 and C 2 and C 3 along with a positive charge at C 2. C 1 is single-bonded to R on the lower left and C H 3 above. C 2 is single bonded to H below.

In the second irreversible step, 3-isopentenyl pyrophosphate attacks allylic carbocation to give rise to an unlabeled intermediate.

The structure of 3-isopentenyl pyrophosphate is as follows: A 3-carbon alkane chain is depicted as a line structure using 2 zigzag lines. C H 2 occupies the second position. C 1 is single-bonded to C H 3 above and double-bonded to C H 2 on the lower left. C 3 is single bonded to O P O 3 P O 3 superscript 3 minus above. An arrow from the double bond between C 1 and C H 2 attacks C H 3 of the allylic carbocation.

The structure of the intermediate is as follows: A 3-carbon alkene chain is depicted as a line structure using 2 zigzag lines. C bound to H 2 occupies the third position. A double bond is present between C 1 and C 2. C 1 is single-bonded to R on the lower left and C H 3 above. C 2 is single-bonded to H below. C H 2 is single bonded to C 1 of a 4-carbon alkane chain depicted as a line structure using 3 zigzag lines. C H 2 occupies the first and third positions. C 2 atom has a positive charge. C 2 is single bonded to C H 3 above. C 4 is single bonded to O P O 3 P O 3 superscript 3 minus above.

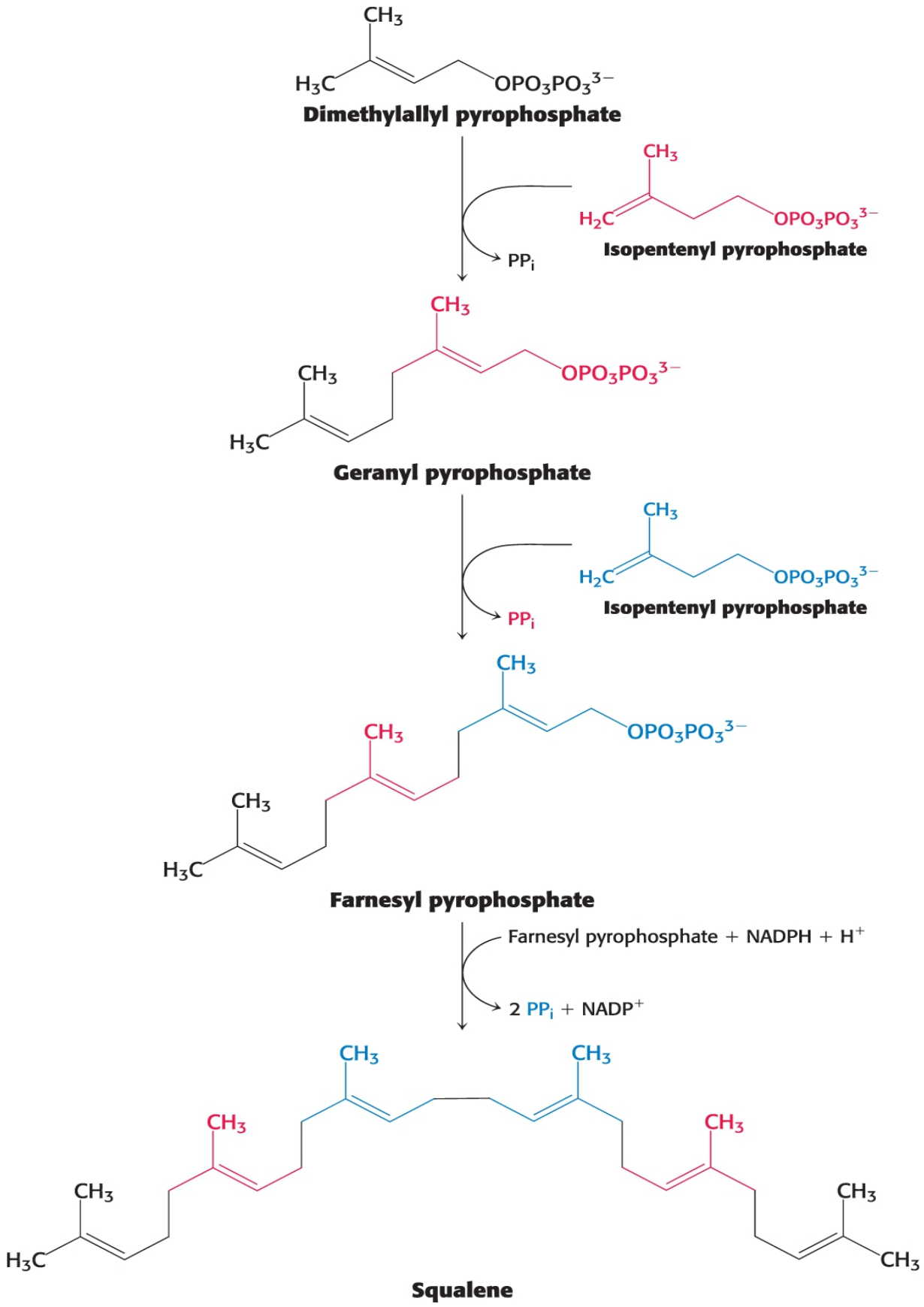
In the third irreversible step, the intermediate is transformed into geranyl or farnesyl pyrophosphate coupled with the release of H superscript plus ion.

The structure of geranyl or farnesyl pyrophosphate is as follows: A 3-carbon alkene chain is depicted as a line structure using 2 zigzag lines. C H 2 occupies the third position. A double bond is present between C 1 and C 2. C 1 is single bonded to R on the lower left and C H 3 above. C 2 is single bonded to H below. C H 2 is single bonded to C 1 of a 4-carbon alkene chain depicted as a line structure using 3 zigzag lines. C H 2 occupies the first position. A double bond is present between C 2 and C 3. C 2 is single-bonded to C H 3 above. C 3 is single bonded to H below. C 4 is single-bonded to O P O 3 P O 3 superscript 3 minus above.

Return to FIGURE 27.10 Condensation reactions build carbon–carbon bonds that eventually form the cholesterol skeleton

Extended description for FIGURE 27.11 Two molecules

of farnesyl pyrophosphate are linked to form squalene


CH3
H3C
OPO3PO3 3−
Dimethylallyl pyrophosphate
CH3
H2C
OPO3PO3 3−
Isopentenyl pyrophosphate
PPi
CH3
CH3
H3C
OPO3PO3 3−
Geranyl pyrophosphate
CH3
H2C
OPO3PO3 3−
Isopentenyl pyrophosphate
PPi
CH3
CH3
CH3
H3C
OPO3PO3 3−
Farnesyl pyrophosphate
Farnesyl pyrophosphate + NADPH + H+
2 PPi + NADP+
CH3
CH3
CH3
CH3
CH3
CH3
H3C
CH3
Squalene

In the first irreversible step, dimethylallyl pyrophosphate is transformed to geranyl pyrophosphate coupled with the entry of isopentenyl pyrophosphate and the release of P P subscript i.

The structure of dimethylallyl pyrophosphate is as follows: A 4-carbon alkene chain is depicted as a line structure using 3 zigzag lines. C H 3 occupies the first position. A double bond is present between C 2 and C 3. C 2 is single bonded to C H 3 above. C 4 is single bonded to O P O 3 P O 3 superscript 3 minus on the lower right.

The structure of isopentenyl pyrophosphate is as follows: A 4-carbon alkene chain is depicted as a line structure using 3 zigzag lines. C H 2 occupies the first position. A double bond is present between C 1 and C 2. C 2 is single bonded to C H 3 above. C 4 is single bonded to O P O 3 P O 3 superscript 2 minus on the lower right.

The structure of geranyl pyrophosphate is as follows: A 4-carbon alkene chain is depicted as a line structure using 3 zigzag lines. C H 3 occupies the first position. A double bond is present between C 2 and C 3. C 2 is single bonded to C H 3 above. C 4 is single bonded to C 1 of a 4-carbon alkene chain depicted as a line structure using 3 zigzag lines. A double bond is present between C 2 and C 3. C 2 is single bonded to C H 3 above. C 4 is single bonded to O P O 3 P O 3 superscript 3 minus.

In the second irreversible step, geranyl pyrophosphate is transformed to farnesyl pyrophosphate coupled with the entry of isopentenyl pyrophosphate and the release of P P subscript i.

The structure of farnesyl pyrophosphate is as follows: A 4-carbon alkene chain is depicted as a line structure using 3 zigzag lines. C H 3 occupies the first position. A double bond is present between C 2

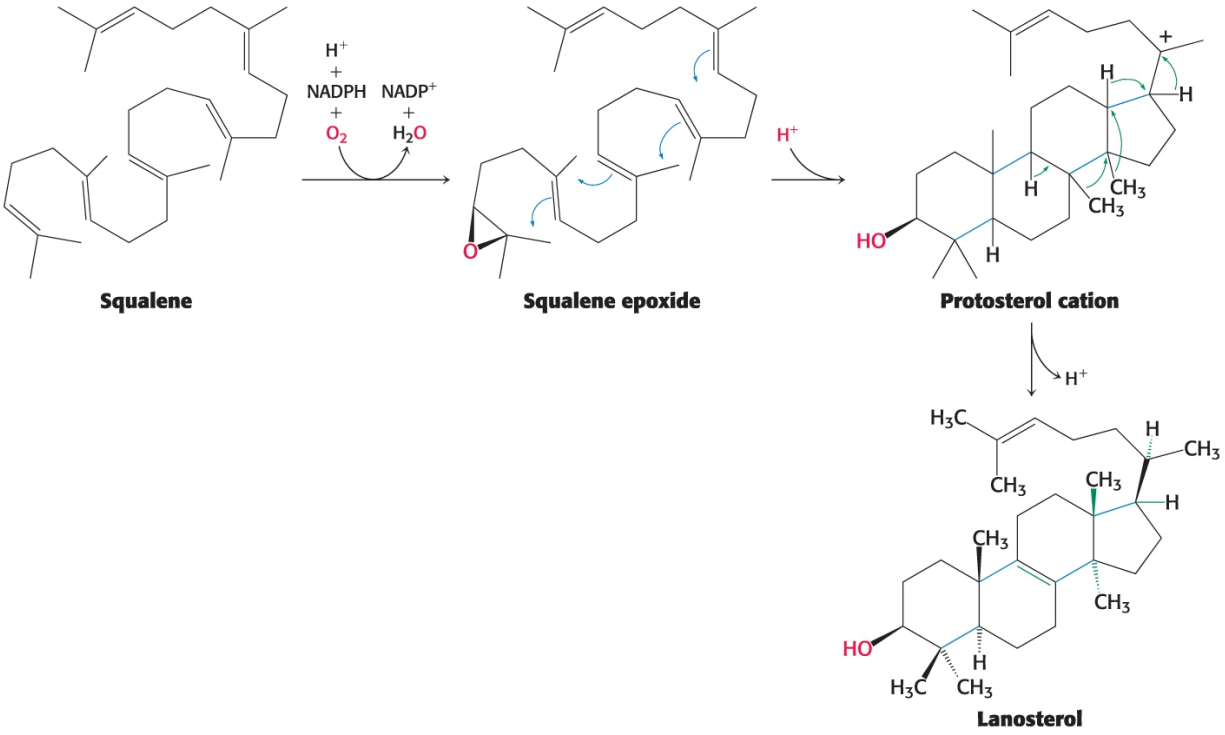
and C 3. C 2 is single bonded to C H 3 above. C 4 is single bonded to C 1 of a 4-carbon alkene chain depicted as a line structure using 3 zigzag lines. A double bond is present between C 2 and C 3. C 2 is single bonded to C H 3 above. C 4 is single bonded to C 1 of another 4-carbon alkene chain depicted as a line structure using 3 zigzag lines. A double bond is present between C 2 and C 3. C 2 is single bonded to C H 3 above. C 4 is single bonded to O P O 3 P O 3 superscript 3 minus.

In the third irreversible step, farnesyl pyrophosphate is transformed to squalene coupled with the entry of farnesyl pyrophosphate, N A D P H plus H superscript plus, and release of 2 P P subscript i and N A D P superscript plus.

The structure of squalene is as follows: A 4-carbon alkene chain is depicted as a line structure using 3 zigzag lines. C H 3 occupies the first position. A double bond is present between C 2 and C 3. C 2 is single bonded to C H 3 above. C 4 is single bonded to C 1 of an alkene chain depicted as a line structure using 3 zigzag lines. A double bond is present between C 2 and C 3. C 2 is single bonded to C H 3 above. C 4 of the alkene chain is single bonded to an 8-carbon alkene chain depicted as a line structure using 7 zigzag lines. A double bond is present between C 2 and C 3 and C 6 and C 7. C 2 and C 7 are each single bonded to C H 3 above. C 8 is single bonded to a 4-carbon alkene chain depicted as a line structure using 3 zigzag lines. A double bond is present between C 2 and C 3. C 3 is single bonded to C H 3 above. C 4 is single bonded to another 4-carbon alkene chain depicted as a line structure using 3 zigzag lines. C H 3 occupies the fourth position. A double bond is present between C 2 and C 3. C 3 is single bonded to C H 3 above.

Return to FIGURE 27.11 Two molecules of farnesyl pyrophosphate are linked to form squalene

Extended description for FIGURE 27.12 Squalene cyclization leads to the steroid skeleton in the form of lanosterol



In the first irreversible step, squalene is transformed to squalene epoxide coupled with the entry of N A D P H plus H superscript plus and O 2 and release of N A D P superscript plus and H 2 O.

The structure of squalene is as follows: A 5-carbon alkene chain is depicted as a line structure using 4 zigzag lines. A double bond is present between C 1 and C 2. C 1 is single bonded to C H 3 on the upper left and C H 3 below in the form of a line. C 5 is single bonded to C H 3 in the form of a line on the upper right and double bonded to C H below. This C H group is single-bonded to a C H 2 group on the lower right in the form of a line. This C H 2 group is single-bonded to C H 2 on the lower left in the form of a line. This C H 2 is

single-bonded to C 1 of a 14-carbon alkene chain on the left depicted as a line structure using 13 zigzag lines. A double bond is present between C 1 and C 2, C 5 and C 6, C 9 and C 10, and C 13 and C 14. C 1 is single-bonded to C H 3 in the form of a line on the lower left. C 6 is single bonded to C H 3 on the lower right in the form of a line. C 10 is single bonded to C H 3 on the upper right in the form of a line. C 14 is single bonded to C H 3 in the form of a line on the lower left and lower right.

The structure of squalene epoxide is as follows: The structure of squalene epoxide is the same as squalene except C 13 and C 14 are each wedge bonded to a common O atom. An arrow points from the double bond between C 5 of the alkene chain and the C H 2 group points toward C 2 of the 14-carbon alkene chain. An arrow from the double bond between C 1 and C 2 of the 14-carbon alkene chain points toward the C H 3 group single-bonded to C 6 of the 14-carbon alkene chain. An arrow from the double bond between C 5 and C 6 points to C H 3 single bonded to C 10. An arrow from the double bond between C 9 and C 10 points toward C H 3 group single-bonded to C 14.

In the second irreversible step, squalene epoxide is transformed into protosterol cation coupled with the entry of H superscript plus.

The structure of the protosterol cation is as follows: Two 6-carbon hexagonal rings in vertical orientation have C 1 at the topmost vertex. Both the rings are fused such that C 2 and C 3 of the first ring are C 6 and C 5 respectively of the second ring. In the first ring, C 2 is single bonded to C H 3 above in the form of a line, C 3 is single bonded to H below, C 4 is single bonded to C H 3 on the lower left, and C H 3 on the lower right in the form of a line. C 5 is wedge bonded to O H on the lower left. In the second ring, C 1 is single-bonded to H below. Another 6-carbon hexagonal ring in vertical orientation is fused with the second ring such that C 1 and C 2 of the

second ring are C 5 and C 4 respectively of the third ring. C 2 is single bonded to H above. C 3 and C 4 are each single bonded to C H 3. A 5-membered pentagonal ring in horizontal orientation with C 1 occupying the top right vertex is fused with the third ring such that C 2 and C 3 of the third ring are C 5 and C 4 respectively of the fourth ring. C 1 is single bonded to H on the right and single bonded to C 6 of a 7-carbon alkene chain depicted using 6 zigzag lines. A double bond is present between C 2 and C 3. C 6 of the alkene chain has a positive charge. C 2 of the alkane chain is single-bonded to C H 3 below in the form of a line. An arrow from the H atom bonded to C 1 of the second ring points toward the single bond between C 4 and C 5 of the third ring. An arrow from C H 3 bonded to C 4 of the third ring points toward C 3. An arrow from C H 3 bonded to C 3 of the third ring points toward C 2 of the third ring. An arrow from H bonded to C 2 of the third ring points toward C 1 of the fourth ring. An arrow from the H bonded to C 1 of the fourth ring points toward C 6 of the alkene chain.

In the third irreversible step, protosterol cation is converted to lanosterol coupled with the release of H superscript plus ion.

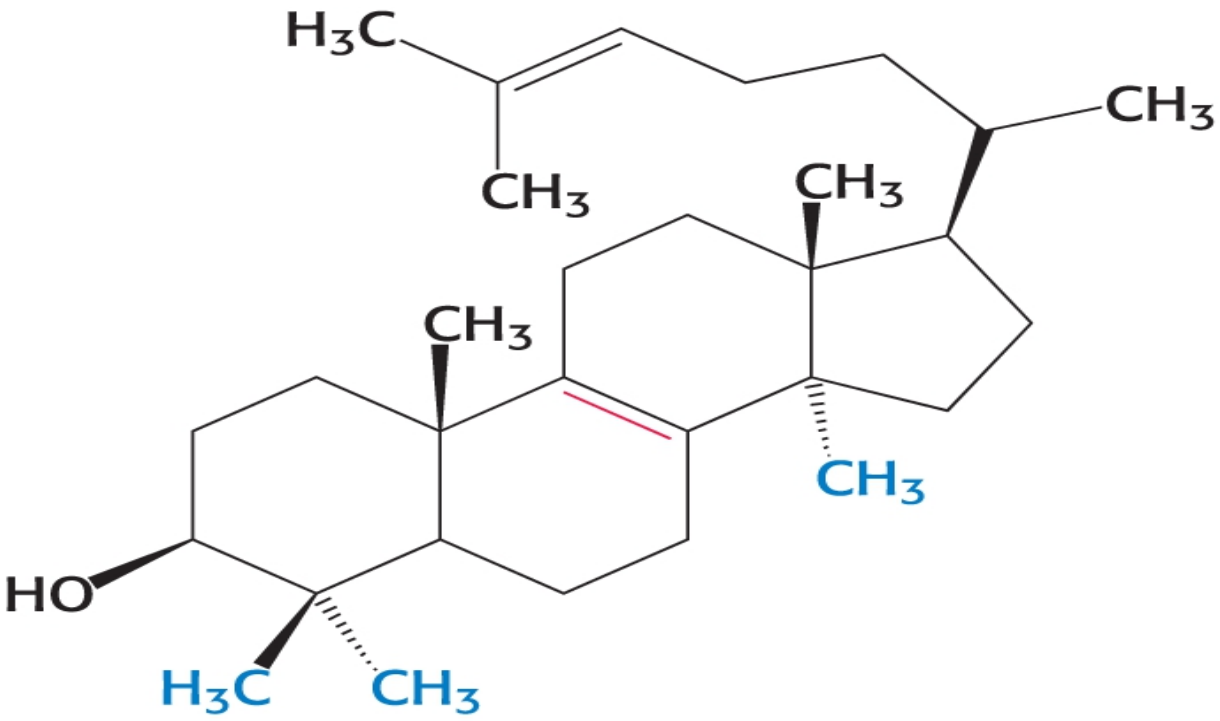
The structure of lanosterol is as follows: Two 6-carbon hexagonal rings in vertical orientation have C 1 at the topmost vertex. The second ring has a double bond between C 1 and C 2. Both the rings are fused such that C 2 and C 3 of the first ring are C 6 and C 5 respectively of the second ring. C 2 of the first ring is wedge bonded to C H 3 above. C 3 is dash bonded to H below. C 4 of the first ring is wedge bonded to C H 3 on the lower left and dash bonded to C H 3 on the lower right. C 5 is wedge bonded to O H. A double bond is present between C 1 and C 2 of the second ring. Another 6-carbon hexagonal ring in vertical orientation is fused with the second ring such that C 1 and C 2 of the second ring are C 5 and C 4 respectively of the third ring. A 5-membered pentagonal ring in horizontal orientation with C 1 occupying the top right vertex is fused with the

third ring such that C 2 and C 3 of the third ring are C 5 and C 4 respectively of the fourth ring. C 5 of the pentagonal ring is wedge bonded to C H 3 above and C 4 is dash bonded to C H 3 below. C 1 of the fourth ring is single bonded to H on the right and wedge bonded to C 5 of a 5-carbon alkene chain depicted as a line structure using 4 zigzag lines. A double bond is present between C 1 and C 2. C 1 of the alkene chain is single-bonded to C H 3 on the upper left and C H 3 below. C 5 is single bonded to C H 3 on the top right and dash bonded to H above.

Return to FIGURE 27.12 Squalene cyclization leads to the steroid skeleton in the form of lanosterol

Extended description for FIGURE 27.13 Cholesterol is

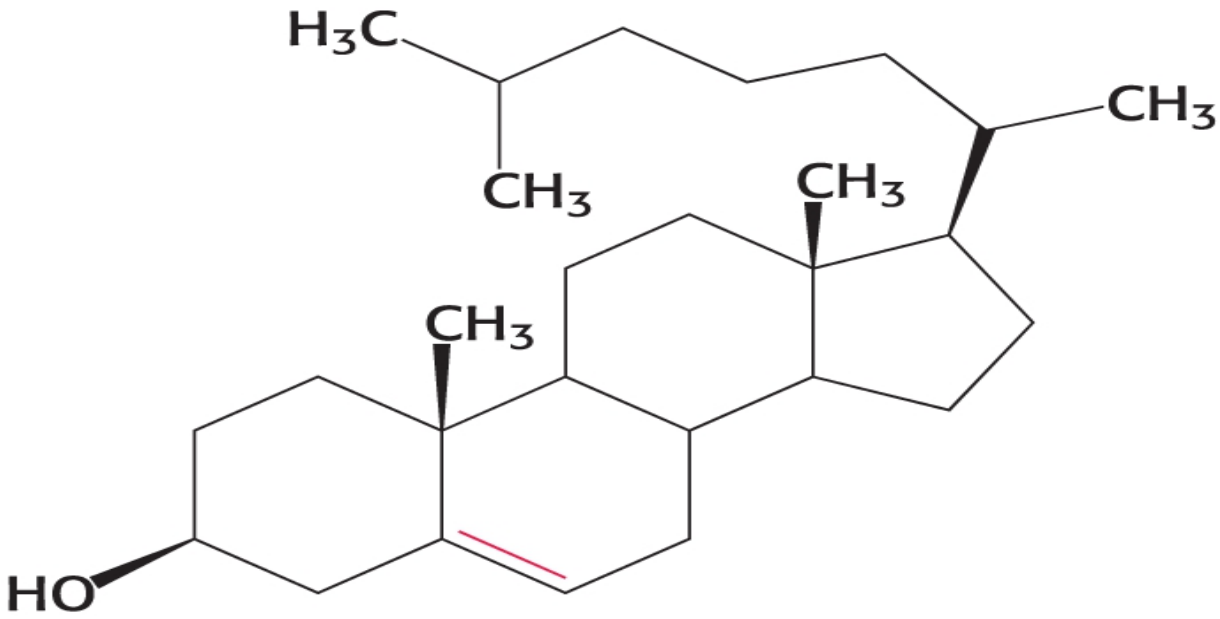
formed from lanosterol



Lanosterol

19 steps

HCOOH + 2 CO_2



Cholesterol

Lanosterol is transformed into cholesterol and this transformation is depicted by a downward arrow labeled 19 steps. It is coupled with the release of H C O O H and 2 C O 2.

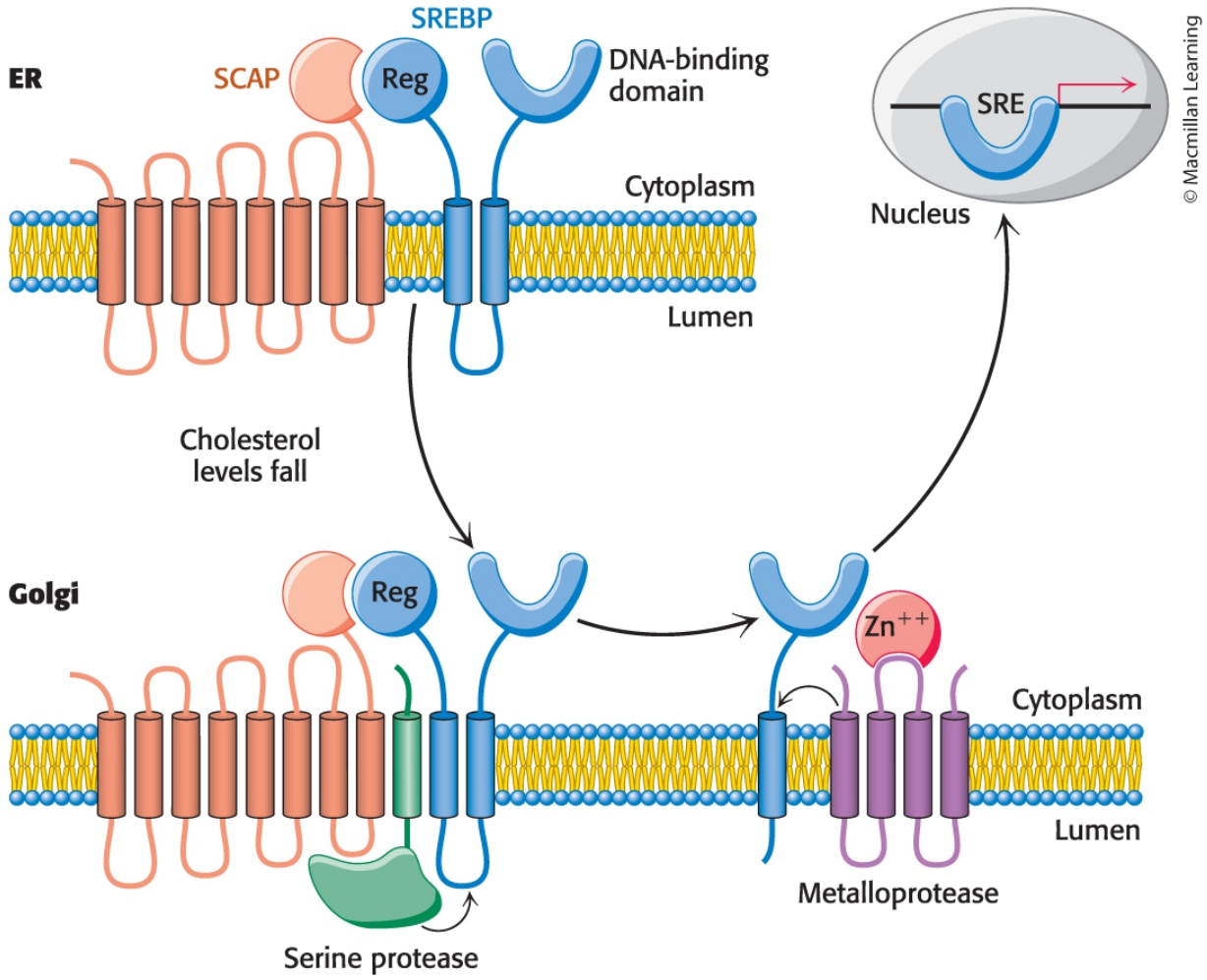
The structure of lanosterol is as follows: Two 6-carbon hexagonal rings in vertical orientation have C 1 at the topmost vertex. The second ring has a double bond between C 1 and C 2 and is highlighted in red. Both the rings are fused such that C 2 and C 3 of the first ring are C 6 and C 5 respectively of the second ring. C 2 of the first ring is wedge bonded to C H 3 above. C 4 of the first ring is wedge bonded to C H 3 on the lower left and dash bonded to C H 3 on the lower right. C 5 is wedge bonded to O H. Another 6-carbon hexagonal ring in vertical orientation is fused with the second ring such that C 1 and C 2 of the second ring are C 5 and C 4 respectively of the third ring. A 5-membered pentagonal ring in horizontal orientation with C 1 occupying the top right vertex is fused with the third ring such that C 2 and C 3 of the third ring are C 5 and C 4 respectively of the fourth ring. C 5 of the pentagonal ring is wedge bonded to C H 3 above and C 4 is dash bonded to C H 3 below. C 1 of the fourth ring is wedge bonded to C 5 of a 5-carbon alkene chain depicted as a line structure using 4 zigzag lines. A double bond is present between C 1 and C 2. C 1 of the alkene chain is single-bonded to C H 3 on the upper left and C H 3 below. C 5 is single bonded to C H 3 on the top right.

The structure of cholesterol is as follows: Two 6-carbon hexagonal rings in vertical orientation have C 1 at the topmost vertex. The second ring has a double bond between C 4 and C 5 and is highlighted in red. Both the rings are fused such that C 2 and C 3 of the first ring are C 6 and C 5 respectively of the second ring. C 2 of the first ring is wedge bonded to C H 3 above. C 5 of the first ring is wedge bonded to O H on the lower left. Another 6-carbon hexagonal ring in vertical orientation is fused with the second ring such that C 1 and C 2 of the second ring are C 5 and C 4 respectively of the third

ring. A 5-membered pentagonal ring in horizontal orientation with C 1 occupying the top right vertex is fused with the third ring such that C 2 and C 3 of the third ring are C 5 and C 4 respectively of the fourth ring. C 5 of the pentagonal ring is wedge bonded to C H 3 above. C 1 of the fourth ring is wedge bonded to a C 5 of a 5-carbon alkane chain depicted as a line structure using 4 zigzag lines. C 1 of the alkane chain is single-bonded to C H 3 on the upper left and C H 3 below. C 5 is single bonded to C H 3 on the top right.

Return to FIGURE 27.13 Cholesterol is formed from lanosterol

Extended description for FIGURE 27.14 S R E B P regulates gene expression in response to cholesterol levels

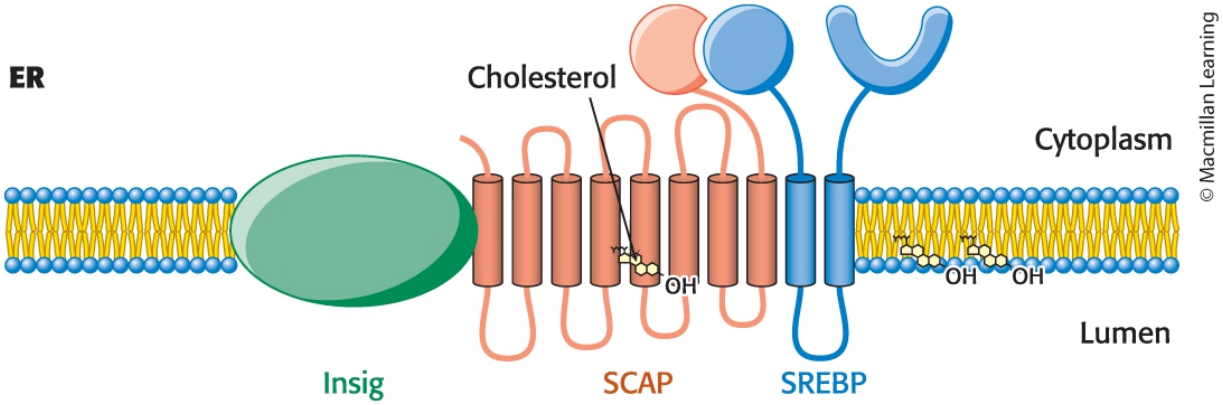


The figure depicts a lipid bilayer of the endoplasmic reticulum. The region above the lipid bilayer is labeled cytoplasm and the region below the lipid bilayer is labeled lumen. The membrane proteins are embedded in the lipid bilayer. The first membrane protein labeled S C A P consists of 8 vertically oriented cylindrical transmembrane domains placed adjacent to each other. The cylindrical domains are connected by thread-like loops at the bottom and top in an

alternating manner. A loop emerging into the cytoplasm from the eighth cylindrical domain is connected to a circular domain with an oval-shaped groove. The second membrane protein labeled S R E B P consists of 2 vertically oriented cylindrical transmembrane domains placed adjacent to each other. A thread-like loop connects the cylindrical domains in the lumen. A loop extending into the cytoplasm from the first cylindrical domain is connected to a circular domain labeled "R e g". A loop extending into the cytoplasm from the second cylindrical domain is connected to a curved elongated structure with a concave groove labeled D N A binding domain. An arrow from the lipid bilayer of the endoplasmic reticulum points to the D N A binding domain of the S R E B P protein embedded in the membrane of the Golgi complex. The membrane lipid bilayer of the Golgi complex consists of an additional membrane protein between S C A P and S R E B P which is labeled serine protease. This membrane protein has an irregular-shaped structure in the lumen. This irregular structure is connected to a single vertically oriented cylindrical transmembrane domain with a loop extending into the cytoplasm. An arrow from serine protease points to S R E B P. An arrow from the D N A binding domain of S R E B P in the Golgi membrane points toward another D N A binding domain on the right connected to a single vertical cylindrical transmembrane domain. Four vertically oriented cylindrical transmembrane domains labeled metalloprotease are connected by thread-like loops at the bottom and top in an alternating manner. The metalloprotease is connected to an oval structure in the cytoplasm. The oval structure is bound to Z n superscript plus plus ion. An arrow from metalloprotease points to the S R E B P. An arrow from the D N A binding domain points to an oval-shaped structure at the top labeled nucleus. The nucleus contains the D N A binding domain of S R E B P bound to S R E. An arrow from S R E points to the right.

Return to FIGURE 27.14 S R E B P regulates gene expression in response to cholesterol levels

Extended description for FIGURE 27.15 Insig regulates S C A P-S R E B P movement

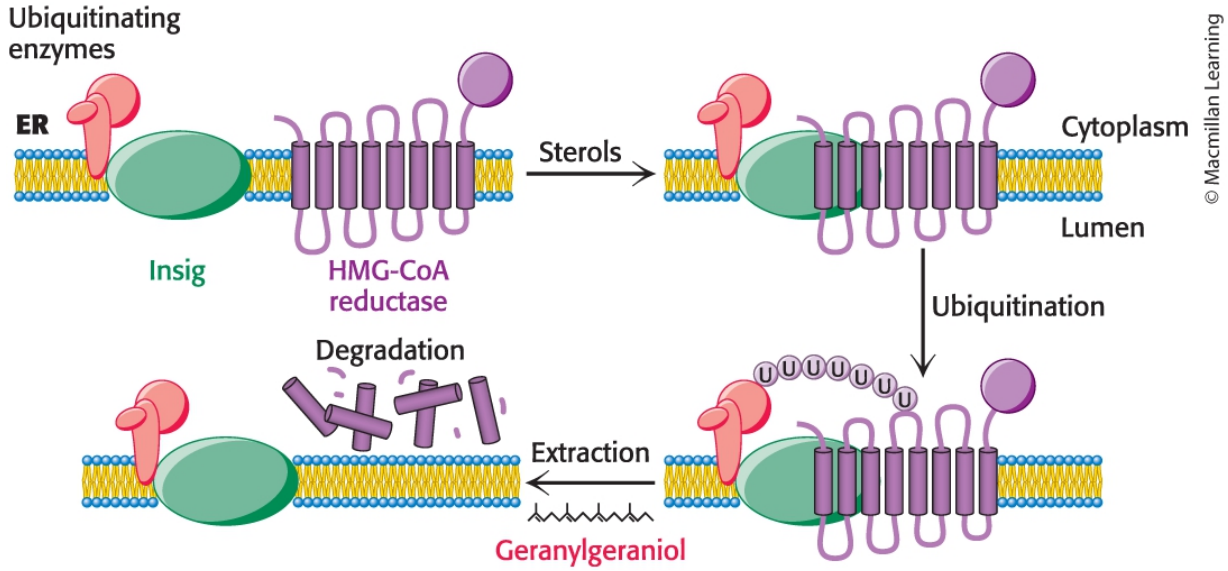


The figure depicts a lipid bilayer of the endoplasmic reticulum. The region above the lipid bilayer is labeled cytoplasm and the region below the lipid bilayer is labeled lumen. The membrane proteins are embedded in the lipid bilayer. The first membrane protein is oval in shape and is labeled Insig. The second membrane protein labeled S C A P consists of 8 vertically oriented cylindrical transmembrane domains placed adjacent to each other. The cylindrical domains are connected by thread-like loops at the bottom and top in an alternating manner. A loop emerging into the cytoplasm from the eighth cylindrical domain is connected to a circular domain with an oval-shaped groove. The third membrane protein labeled S R E B P consists of 2 vertically oriented cylindrical transmembrane domains placed adjacent to each other. A thread-like loop connects the cylindrical domains in the lumen. A loop extending into the cytoplasm from the first cylindrical domain is connected to an oval-shaped domain. A loop extending into the cytoplasm from the second cylindrical domain is connected to a curved elongated structure with a concave center. Two cholesterol molecules are embedded in the lipid bilayer. One cholesterol molecule is bound to

S C A P. The cholesterol molecules are depicted as four-fused rings connected to an O H group.

Return to FIGURE 27.15 Insig regulates S C A P-S R E B P movement

Extended description for FIGURE 27.16 Insig facilitates the degradation of H M G-C o A reductase



The lipid bilayer of the endoplasmic reticulum is shown. The region above the lipid bilayer is labeled cytoplasm and the region below the lipid bilayer is labeled lumen. The membrane proteins are embedded in the lipid bilayer. The first membrane protein has three subunits of which one subunit is embedded into the membrane. This protein is labeled ubiquitinating enzymes. The second membrane protein is oval-shaped and labeled Insig. The third membrane protein labeled H M G C o A reductase consists of 8 vertically oriented cylindrical transmembrane domains placed adjacent to each other. The cylindrical domains are connected by thread-like loops at the bottom and top in an alternating manner. A loop emerging into the cytoplasm from the eighth cylindrical domain is connected to a circular domain.

In the first step, Insig associated with ubiquitinating enzymes binds H M G-C o A reductase in the presence of sterols. Insig directly

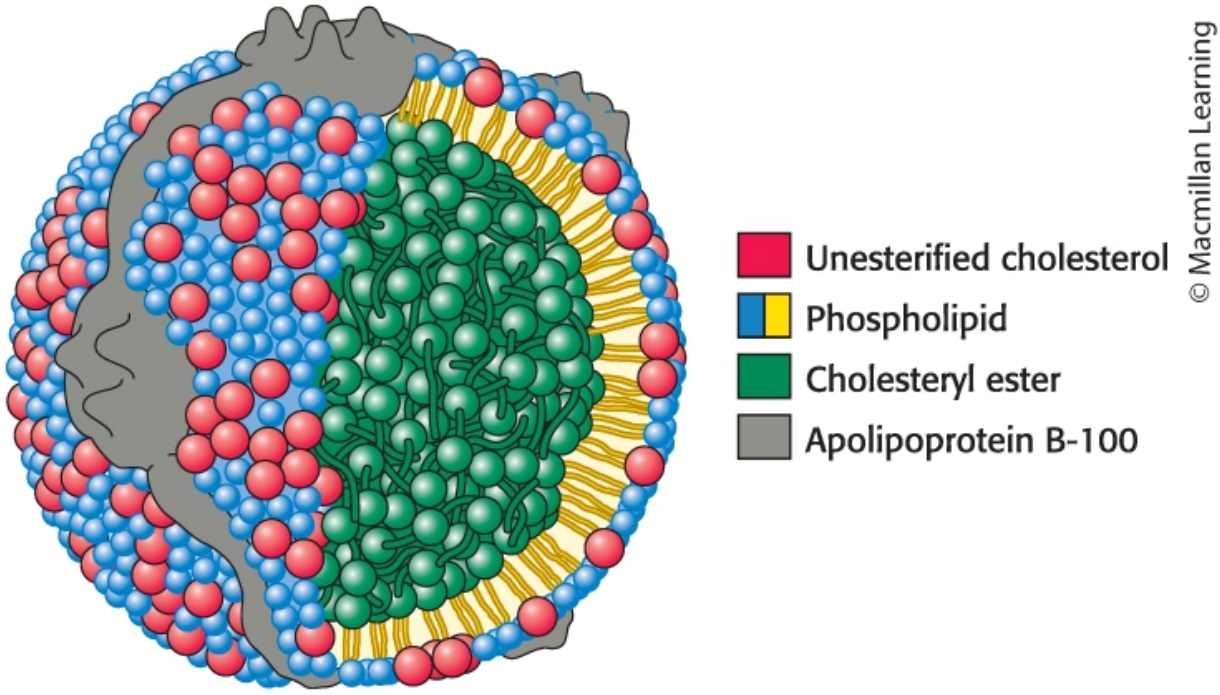
interacts with H M G-C o A reductase.

In the second step, H M G-C o A reductase undergoes ubiquitination. 7 spheres labeled U are connected to each other in the form of a string. This string of U is connected to H M G C o A reductase.

In the third step, ubiquitination and the presence of geranylgeraniol lead to the extraction of the H M G-C o A reductase from the bilayer. Later, the reductase undergoes degradation by the proteasome to release the cylindrical domains into the cytoplasm.

Return to FIGURE 27.16 Insig facilitates the degradation of H M G-C o A reductase

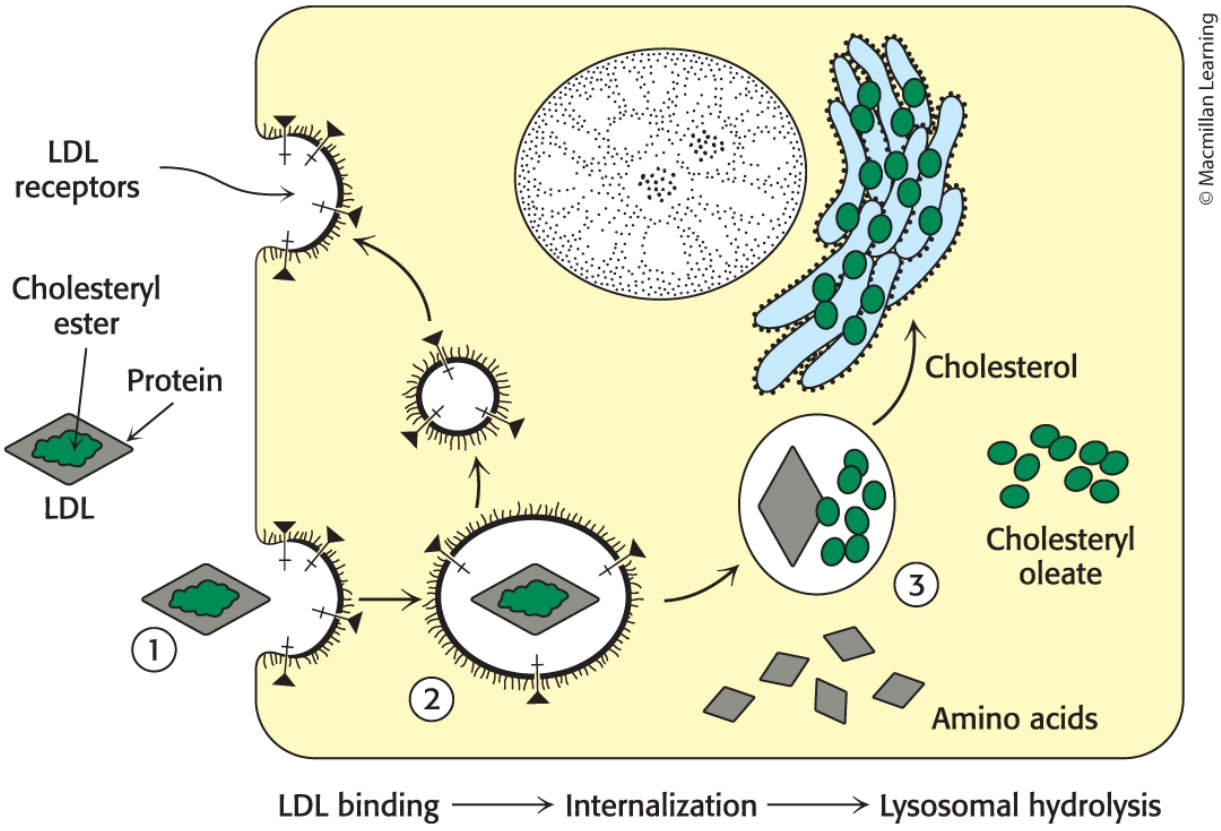
Extended description for FIGURE 27.18 L D L consists of a core of cholesterol esters surrounded by a single molecule of apolipoprotein B-100



The L D L particle is spherical in shape. A part of the L D L particle Is cut open to expose the internal molecules. The core of the L D L particle is composed of green-colored spheres with tail-like structures attached to them. These represent the cholesteryl esters. The cholesteryl esters are surrounded by a layer of phospholipids depicted as blue spheres with two yellow tails. Red spheres embedded in between the blue spheres of the phospholipid represent the unesterified cholesterol. A single grey-colored irregular structure with conical protrusions is embedded in the phospholipid layer of the L D L particle. It represents the apolipoprotein B-100.

Return to FIGURE 27.18 L D L consists of a core of cholesterol esters surrounded by a single molecule of apolipoprotein B-100

Extended description for FIGURE 27.19 L D L enters cells through receptor-mediated endocytosis



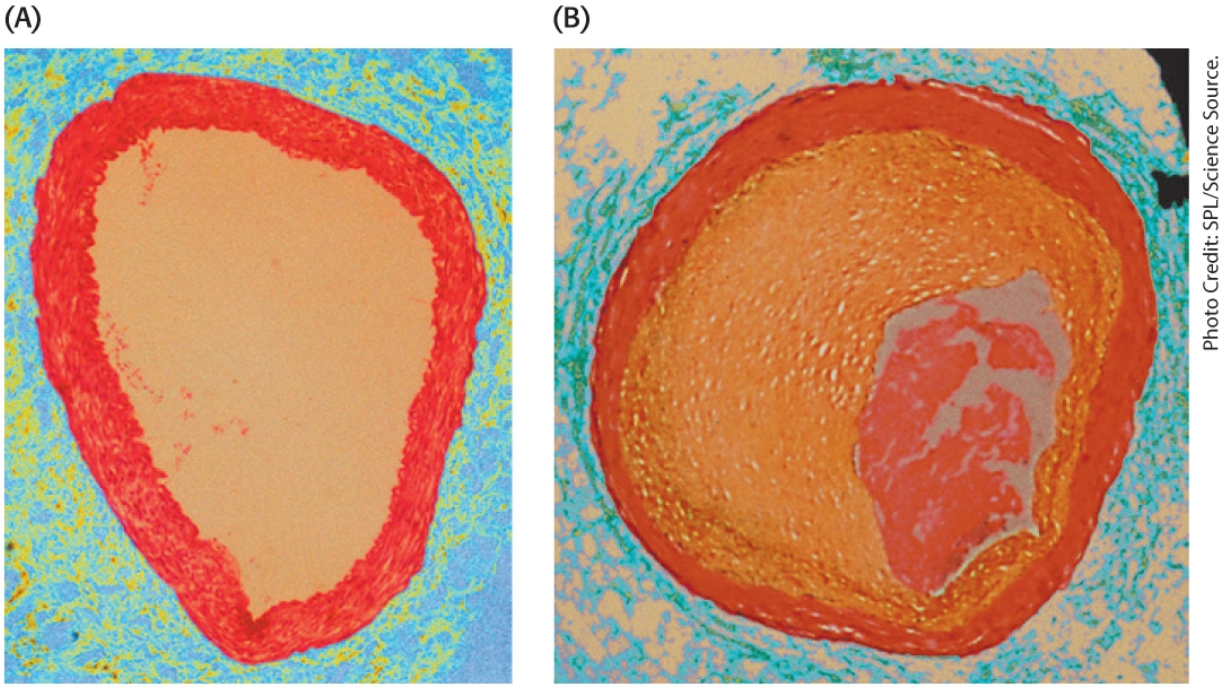
The figure depicts a square-shaped cell with two grooves on the left. The grooves are lined by L D L receptors. Outside the cell, a rhomboid-shaped L D L is present. L D L contains a cloud-like structure inside it labeled cholesteryl ester. In the first step, the L D L binds to the L D L receptors in the second groove. In the second step, the groove containing L D L bound to the L D L receptor undergoes invagination to form an endosome vesicle inside the cell. In the third step, the L D L is separated from the vesicle containing the L D L receptors. The vesicle containing the receptor moves back to the first groove to replenish the pool of L D L receptors in the membrane. Simultaneously, L D L undergoes degradation in

lysosomes to release amino acids, cholesteryl oleate, and cholesterol. The cholesterol and cholesteryl oleate are depicted as tiny green circles and amino acids are depicted as grey diamond-shaped structures. The cholesterol molecules enter into a clump of long sacs-like structures. The remaining molecules are released into the cytoplasm.

A horizontal sequence below the figure shows the process corresponding to each step of L D L processing. This sequence is as follows: L D L binding, forward arrow, internalization, forward arrow, lysosomal hydrolysis.

Return to FIGURE 27.19 L D L enters cells through receptor-mediated endocytosis

Extended description for FIGURE 27.20 Arterial plaques are one of the effects of excess cholesterol

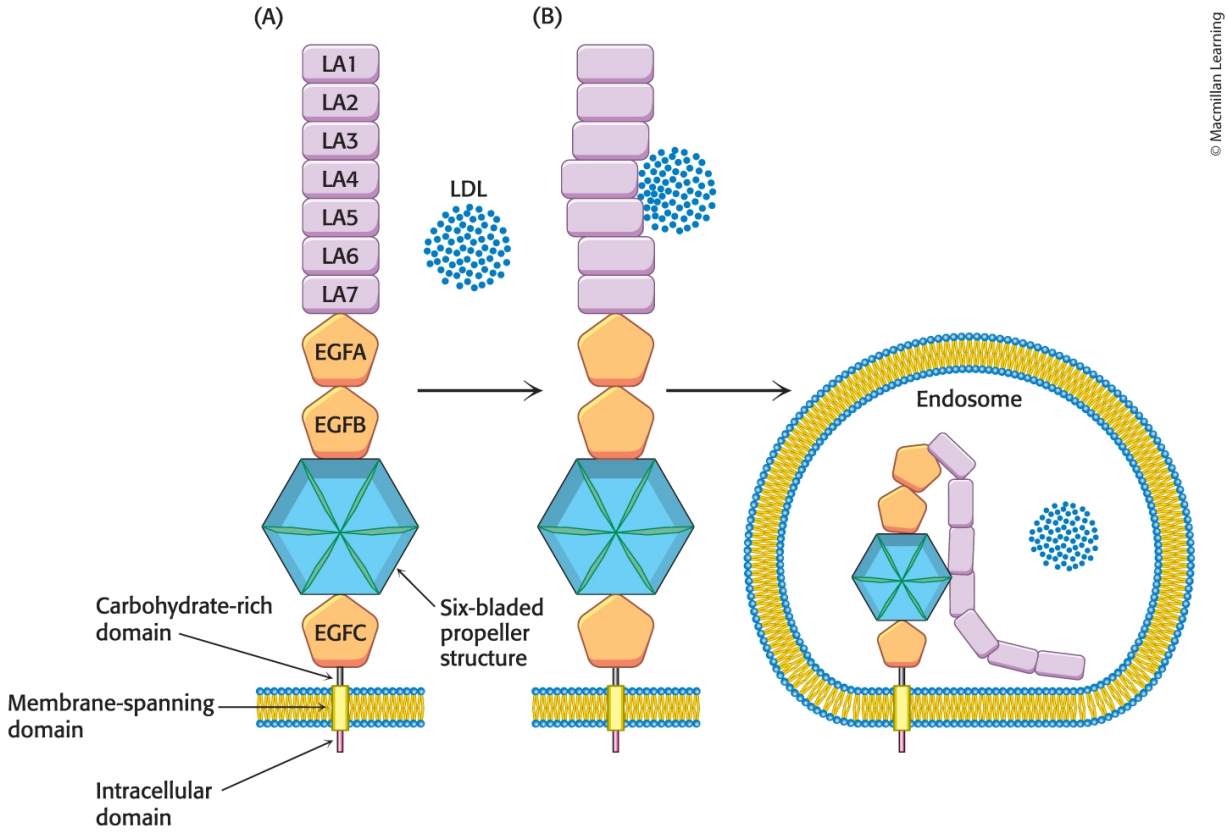


(A): The normal artery is oval-shaped with thick walls. It has a hollow interior.

(B): The blocked artery is circular with thick walls. A plaque is formed due to the deposition of cholesterol in the walls of the artery. The plaque extends into the interior thereby narrowing the hollow region of the artery.

Return to FIGURE 27.20 Arterial plaques are one of the effects of excess cholesterol

Extended description for FIGURE 27.21 The L D L receptor releases L D L in the endosome



© Macmillan Learning

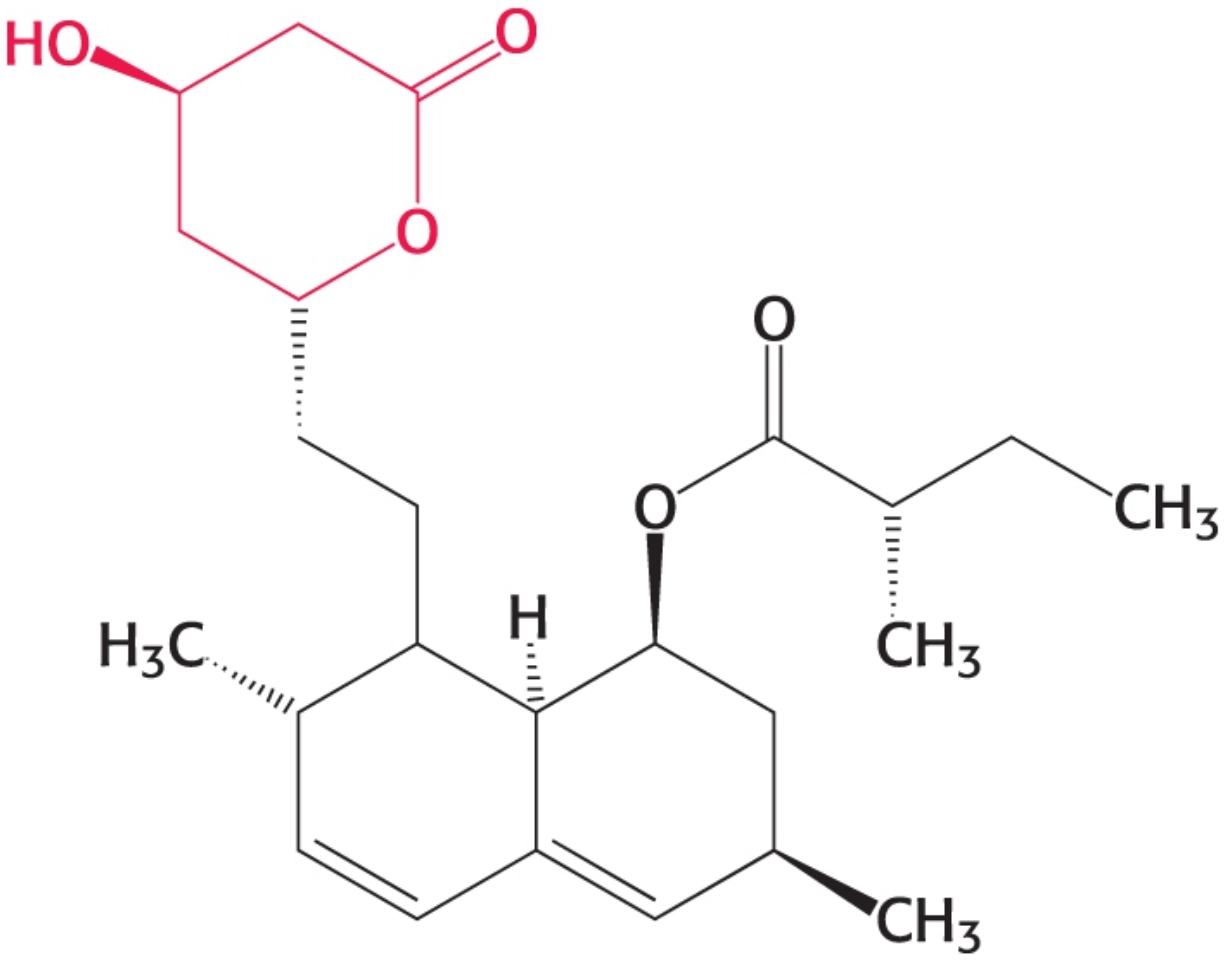
(A): The domain structure of the L D L receptor is shown. The structure consists of a membrane-spanning domain in the lipid bilayer. The membrane-spanning domain is attached to a thin structure in the lumen labeled intracellular domain. In the cytoplasm, the membrane-spanning domain is attached to a short tubular labeled carbohydrate-rich domain. The carbohydrate-rich domain is attached to a pentagonal structure labeled E G F C at the top. E G F C is attached to a six-bladed propeller structure at the top. This is further attached to two pentagonal structures one above the other labeled E G F B and E G F A. E G F A is further attached to 7 blocks labeled from L A 1 to L A 7 from top to bottom. An L D L

molecule depicted as a sphere with small dots is shown on the right side of the L A blocks.

Part (B): The L D L particle attaches to the blocks numbered L A 4 and L A 5 shifting them slightly toward the left. An arrow points toward the L D L receptor inside an endosome. A lipid bilayer lines the circular endosome. The open structure of L D L converts into the closed structure inside the endosome by bending of L A blocks. This leads to the release of L D L in the endosome.

Return to FIGURE 27.21 The L D L receptor releases L D L in the endosome

Extended description for FIGURE 27.22 Structure of lovastatin



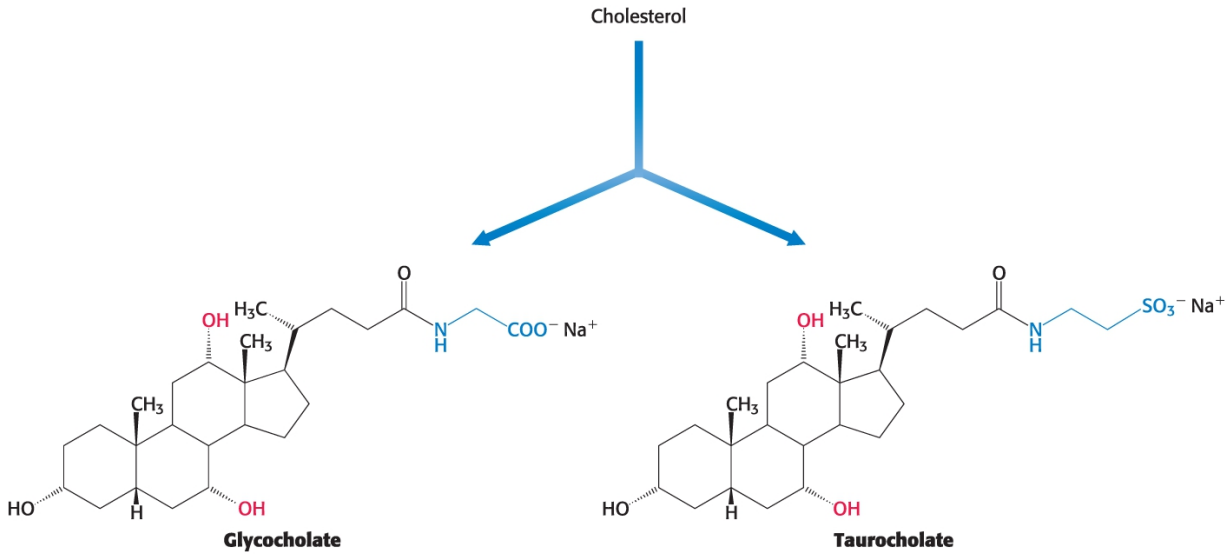
Lovastatin

The structure of lovastatin is as follows: Two 6-carbon hexagonal rings in vertical orientation have C 1 at the topmost vertex. Both the rings have double bonds between C 4 and C 5. Both the rings are fused such that C 2 and C 3 of the first ring are C 6 and C 5 respectively of the second ring. C 2 of the first ring is dash bonded to H above. C 6 of the first ring is dash bonded to C H 3. C 1 of the second ring is wedge bonded to O above and C 3 is wedge bonded to

C H 3. The O atom is single-bonded to a 3-carbon alkane chain depicted as a line structure using 2 zigzag lines. C 1 of the alkane chain is double bonded to O above. C 2 is dash bonded to C H 3 below. C 3 is single bonded to C H 3 on the lower right. C 1 of the first ring is single-bonded to a 2-carbon alkane chain depicted by a line. C 2 of the alkane chain is dash bonded to C 1 of a 6-membered heterocyclic hexagonal ring in a vertical orientation with 1 O and 5 C atoms. O occupies the first position, which is the bottom right vertex. C 3 is wedge bonded to O H. C 5 is double bonded to O.

Return to FIGURE 27.22 Structure of lovastatin

Extended description for FIGURE 27.23 Bile salts are synthesized from cholesterol



The figure shows a bifurcated arrow from cholesterol that points to glycocholate and taurocholate.

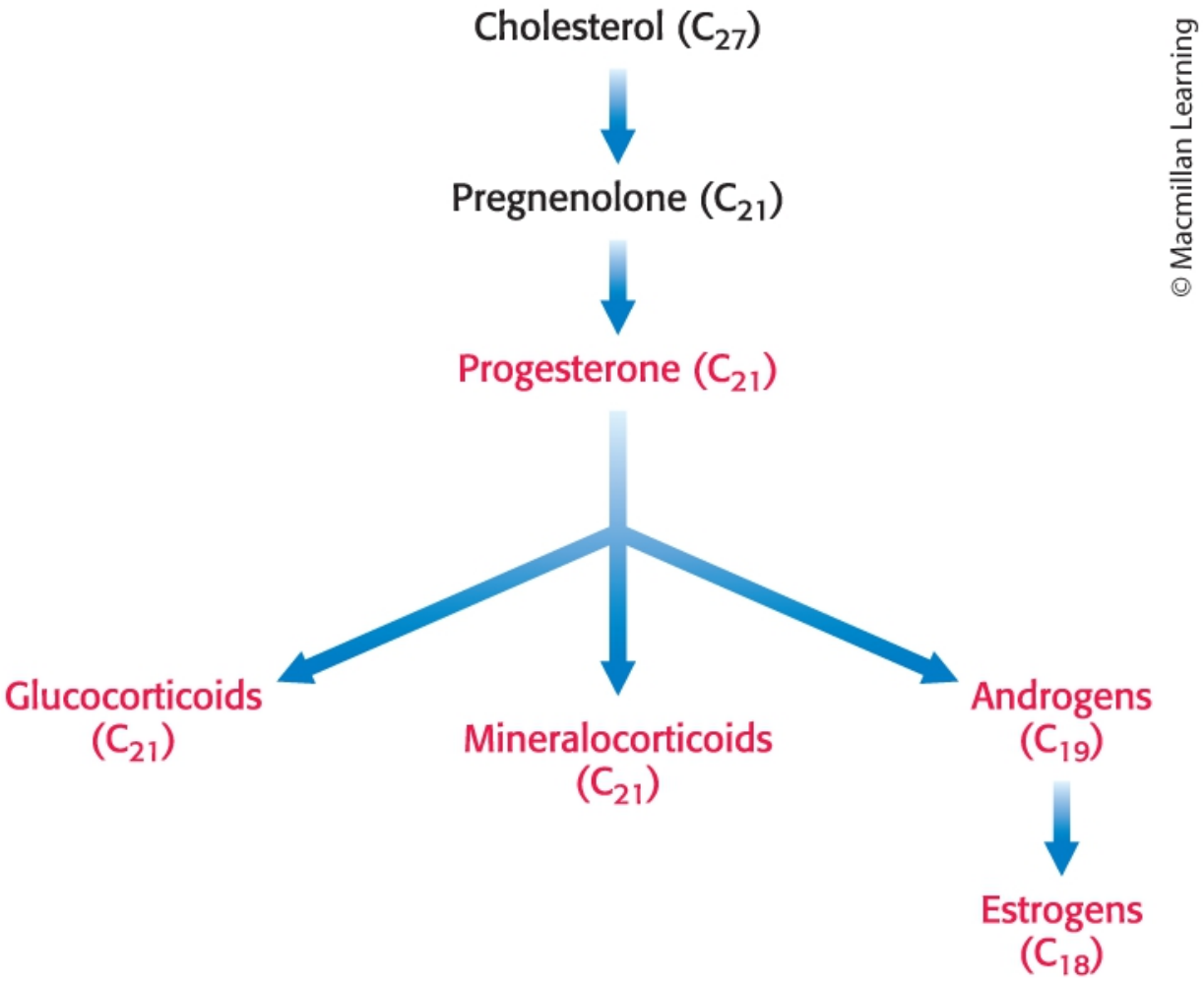
The structure of glycocholate is as follows: Two 6-carbon hexagonal rings in vertical orientation have C 1 at the topmost vertex. Both the rings are fused such that C 2 and C 3 of the first ring are C 6 and C 5 respectively of the second ring. C 2 of the first ring is wedge bonded to C H 3 above. C 3 is wedge bonded to H below. C 5 is dash bonded to O H on the lower left. C 3 of the second ring is dash bonded to O H. Another 6-carbon hexagonal ring in vertical orientation is fused with the second ring such that C 1 and C 2 of the second ring are C 5 and C 4 respectively of the third ring. C 1 of this ring is dash bonded to O H above. A 5-membered pentagonal ring in horizontal orientation with C 1 occupying the top right vertex is fused with the third ring such that C 2 and C 3 of the third ring are C 5 and C 4 respectively of the fourth ring. C 5 of the pentagonal ring is wedge bonded to C H 3 above. C 1 of the fourth ring is wedge bonded to a C

1 of a 1 N and 5 C heteronuclear alkane chain depicted as a line structure using 5 zigzag lines. N bound to H occupies the fifth position. C 1 is dash bonded to C H 3 on the upper left. C 4 is double bonded to O above. C 5 is single bonded to C O O superscript minus N a superscript plus.

The structure of taurocholate is as follows: Two 6-carbon hexagonal rings in vertical orientation have C 1 at the topmost vertex. Both the rings are fused such that C 2 and C 3 of the first ring are C 6 and C 5 respectively of the second ring. C 2 of the first ring is wedge bonded to C H 3 above. C 3 is wedge bonded to H below. C 5 is dash bonded to O H on the lower left. C 3 of the second ring is dash bonded to O H. Another 6-carbon hexagonal ring in vertical orientation is fused with the second ring such that C 1 and C 2 of the second ring are C 5 and C 4 respectively of the third ring. C 1 of this ring is dash bonded to O H above. A 5-membered pentagonal ring in horizontal orientation with C 1 occupying the top right vertex is fused with the third ring such that C 2 and C 3 of the third ring are C 5 and C 4 respectively of the fourth ring. C 5 of the pentagonal ring is wedge bonded to C H 3 above. C 1 of the fourth ring is wedge bonded to C 1 of a 1 N and 6 C heteronuclear alkane chain depicted as a line structure using 6 zigzag lines. N bound to H occupies the fifth position. C 1 is dash bonded to C H 3 on the upper left. C 4 is double bonded to O above. C 6 is single bonded to S O 3 superscript minus N a superscript plus on the upper right.

Return to FIGURE 27.23 Bile salts are synthesized from cholesterol

Extended description for FIGURE 27.24 Different classes of steroid hormones are derived from cholesterol

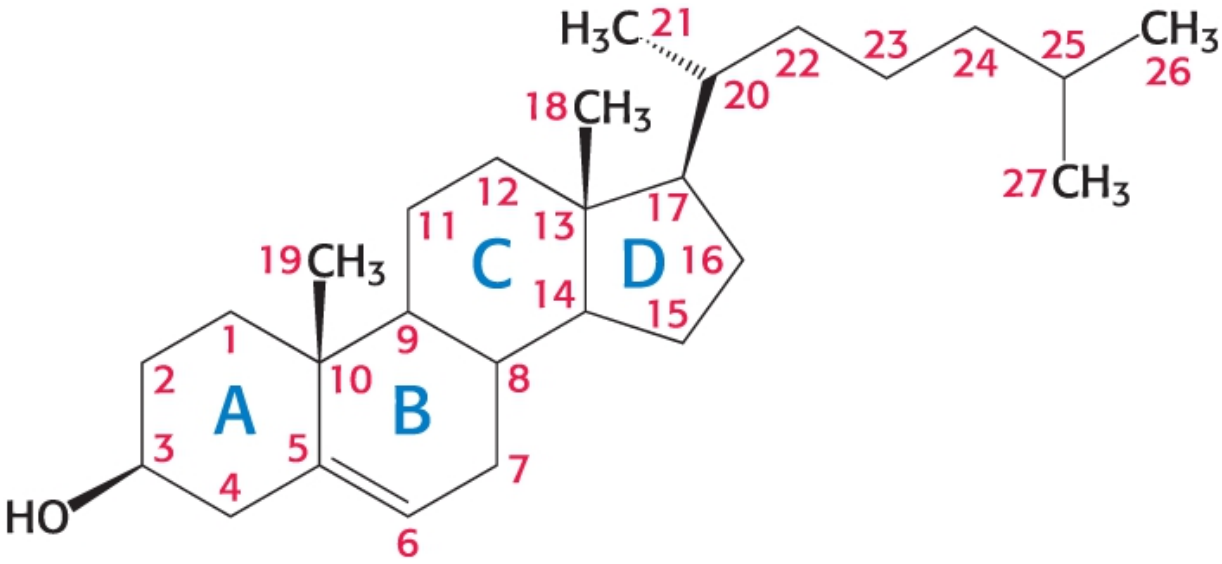


© Macmillan Learning

The schematic illustration starts with cholesterol C 27. A downward arrow from cholesterol C 27 points to pregnenolone C 21. A downward arrow from pregnenolone C 21 leads to progesterone C 21. Three downward arrows from progesterone C 21 lead to glucocorticoids C 21, mineralocorticoids C 21, and androgens C 19. A downward arrow from androgens C 19 leads to estrogens C 18.

Return to FIGURE 27.24 Different classes of steroid hormones are derived from cholesterol

Extended description for FIGURE 27.25 A common numbering system is used for cholesterol and other steroids

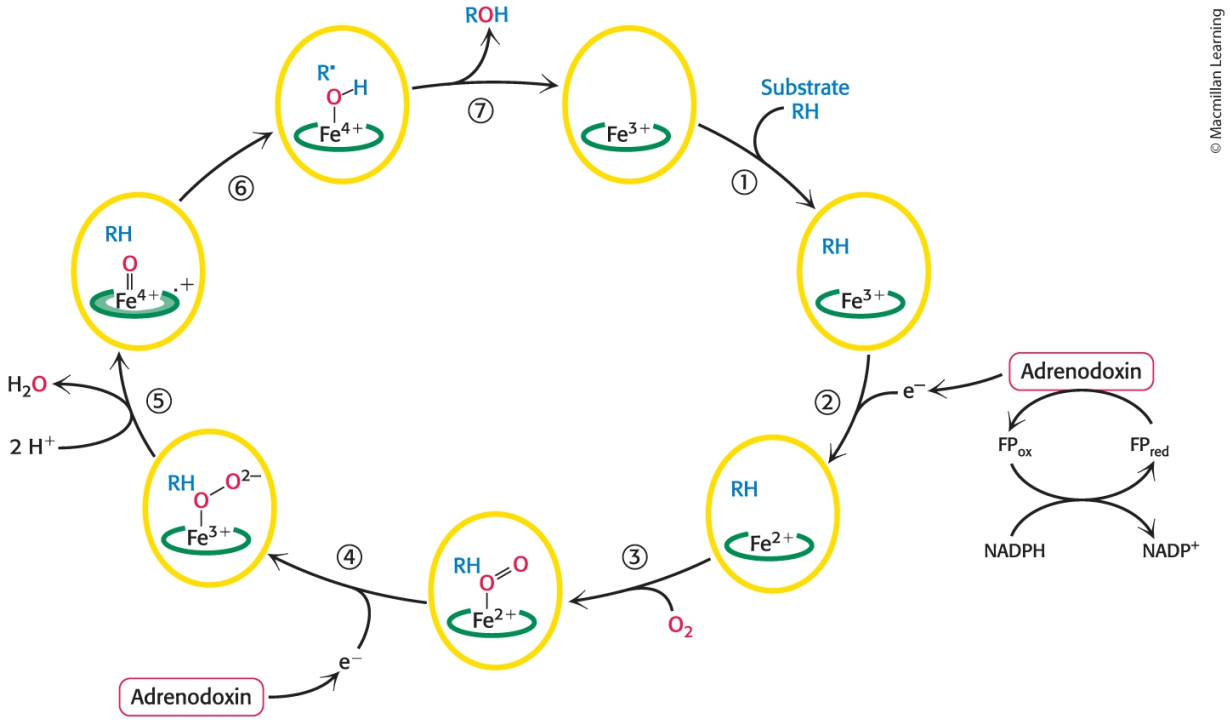


The structure of cholesterol is as follows: Two 6-carbon hexagonal rings in vertical orientation have C 1 at the topmost vertex. The first hexagonal ring is labeled A and the second hexagonal ring is labeled B. The ring labeled B has a double bond between C 4 and C 5. Both the rings are fused such that C 2 and C 3 of ring A are C 6 and C 5 respectively of ring B. C 2 of the first ring is wedge bonded to C H 3 above. C 5 of ring A is wedge bonded to O H on the lower left. Another 6-carbon hexagonal ring in vertical orientation labeled C is fused with ring B such that C 1 and C 2 of ring B are C 5 and C 4 respectively of ring C. A 5-membered pentagonal ring in horizontal orientation with C 1 occupying the top right vertex is labeled D and fused with ring C such that C 2 and C 3 of ring C are C 4 and C 3 respectively of ring D. C 5 of ring D is wedge bonded to C H 3 above. C 1 of ring D is single bonded to C 1 of a 6-carbon alkane chain depicted as a line structure using 5 zigzag lines. C bond to H 3

occupies the sixth position. C 1 is dash bonded to C H 3 on the upper left. C 5 is single bonded to C H 3 below. In the first ring, C 1, C 6, C 5, C 4, and C 3 are numbered from 1 to 5 respectively. In the second ring, C 4, C 3, C 2, C 1, and C 6 are numbered from 6 to 10, respectively. In the third ring, C 6, C 1, C 2, and C 3 are numbered from 11 to 14, respectively. In the fourth ring, C 1, C 2, and C 3 are numbered 17, 16, and 15, respectively. C H 3 bound to C 5 of ring D is numbered 18. C H 3 bound to C 2 of ring A is numbered 19. C 1 of the alkane chain is numbered 20. C H 3 group dash bonded to C 1 of the alkane chain is numbered 21. C 2, C 3, C 4, C 5, and C 6 of the alkane chain are numbered from 22 to 26. C H 3 single bonded to C 5 of the alkane chain is numbered 27.

Return to FIGURE 27.25 A common numbering system is used for cholesterol and other steroids

Extended description for FIGURE 27.26 The reaction mechanism for cytochrome P 450 enzymes reveals how oxygen is inserted into R-H bonds



© Macmillan Learning

The figure shows an oval-shaped enzyme with F e superscript 3 plus. In the first step, substrate R H binds to the enzyme.

In the second step, adrenodoxin donates an electron. Simultaneously, adrenodoxin also converts F P reduced to F P oxidized. F P oxidized is converted back to F P reduced, coupled with the oxidation of N A D P H to N A D P superscript plus. The electron is accepted by F e superscript 3 plus to become F e superscript 2 plus. In the third step, O 2 enters the enzyme. This leads to the formation of a single bond between F e superscript 2 plus and O. This O is double-bonded to another O on the top right.

In the fourth step, another adrenodoxin donates an electron. This removes the double bond between the O atoms. The top right O is converted to O superscript 2 minus along with the oxidation of F e superscript 2 plus to F e superscript 3 plus.

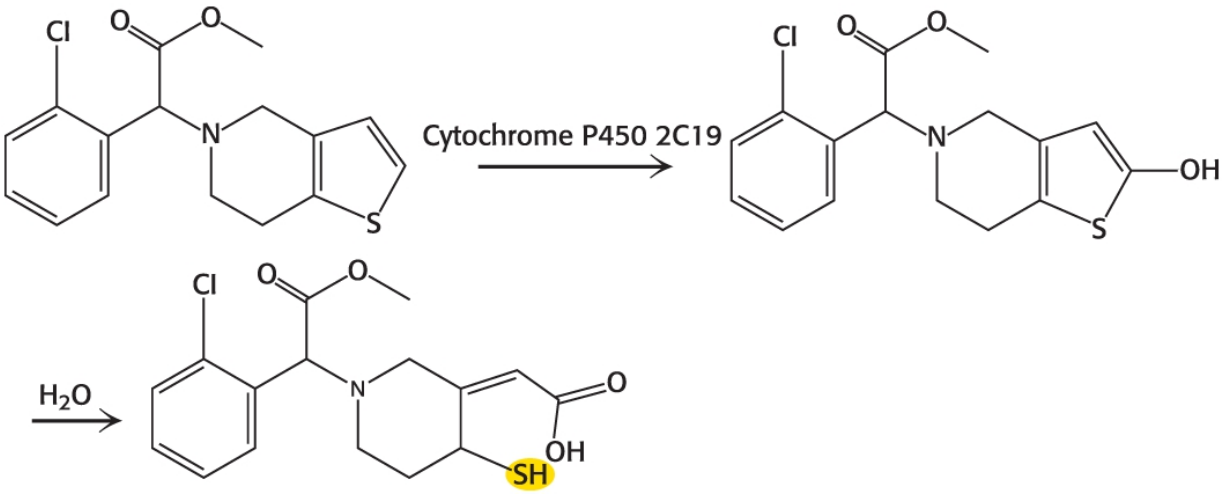
In the fifth step, F e superscript 3 plus is further oxidized to F e superscript 4 plus. F e superscript 4 plus is double-bonded to O above. This is coupled with the entry of 2 H superscript plus and release of H 2 O.

In the sixth step, F e superscript 4 plus is single-bonded to O on the top. The H from the R H becomes single-bonded to O on the top right. R with an unpaired electron is shown above it.

In the seventh step, R O H is released from the enzyme to give rise to back the enzyme with F e superscript 3 plus.

Return to FIGURE 27.26 The reaction mechanism for cytochrome P 450 enzymes reveals how oxygen is inserted into R-H bonds

Extended description for FIGURE 27.27 Cytochrome P 450 2 C 19 converts the prodrug clopidogrel to an active form



In the first irreversible step, prodrug clopidogrel is hydroxylated by cytochrome P 450 2 C 19 to form an intermediate.

The structure of prodrug clopidogrel is as follows: A benzene ring is in a vertical orientation with C 1 occupying the topmost vertex. The ring contains alternating double bonds between C 2 and C 3, C 4 and C 5, and C 6 and C 1. C 1 is single bonded to C l above. C 2 is single-bonded to a central C atom on the top right. The central C atom is single-bonded to another C atom above. This C atom is double-bonded to O on the upper left and single-bonded to O on the upper right. The O on the upper right is single-bonded to C H 3 on the lower right in the form of a line. The central C atom is single-bonded to N of a 6-membered heterocyclic hexagonal ring in a vertical orientation with 1 N and 5 C atoms. N occupies the first position which is the top left vertex. This ring is fused with another 5-membered pentagonal ring in a horizontal orientation with 1 S and 4 C atoms. S occupies the first position which is the bottom right

vertex. C 1 occupies the second position, which is the bottom left vertex. Double bonds are present between C 1 and C 2 and C 3 and C 4. The rings are fused such that C 2 and C 3 of the heterocyclic ring are C 2 and C 1 respectively of the pentagonal ring.

The structure of the intermediate is as follows: A benzene ring is in a vertical orientation with C 1 occupying the topmost vertex. The ring contains alternating double bonds between C 2 and C 3, C 4 and C 5, and C 6 and C 1. C 1 is single bonded to C l above. C 2 is single-bonded to a central C atom on the top right. The central C atom is single-bonded to another C atom above. This C atom is double-bonded to O on the upper left and single-bonded to O on the upper right. The O on the upper right is single-bonded to C H 3 on the lower right in the form of a line. The central C atom is single-bonded to N of a 6-membered heterocyclic hexagonal ring in a vertical orientation with 1 N and 5 C atoms. N occupies the first position, which is the top left vertex. This ring is fused with another 5-membered heterocyclic pentagonal ring in a horizontal orientation with 1 S and 4 C atoms. S occupies the first position, which is the bottom right vertex. C 1 occupies the second position, which is the bottom left vertex. Double bonds are present between C 1 and C 2 and C 3 and C 4. C 4 is single bonded to O H on the right. The rings are fused such that C 2 and C 3 of the heterocyclic ring are C 2 and C 1 respectively of the pentagonal ring.

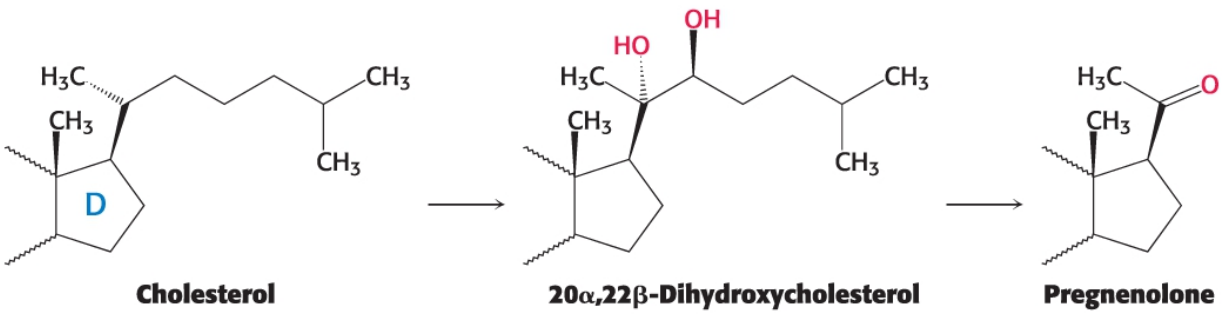
In the second irreversible step, the intermediate product undergoes spontaneous hydrolysis to produce a compound with a reactive thiol group.

The structure of the product is as follows: A benzene ring is in a vertical orientation with C 1 occupying the topmost vertex. The ring contains alternating double bonds between C 2 and C 3, C 4 and C 5, and C 6 and C 1. C 1 is single bonded to C l above. C 2 is single-bonded to a central C atom on the top right. The central C atom is

single-bonded to another C atom above. This C atom is double-bonded to O on the upper left and single-bonded to O on the upper right. The O on the upper right is single-bonded to C H 3 on the lower right in the form of a line. The central C atom is single-bonded to N of a 6-membered heterocyclic hexagonal ring in a vertical orientation with 1 N and 5 C atoms. N occupies the first position, which is the top left vertex. C 2 is double bonded to C H on the upper right. C H is single-bonded to C on the lower right. This C is double bonded to O on the upper right and single bonded to O H below. C 3 is single bonded to S H on the lower right highlighted in yellow.

Return to FIGURE 27.27 Cytochrome P 450 2 C 19 converts the prodrug clopidogrel to an active form

Extended description for Conversion of cholesterol to pregnenolone



An irreversible reaction depicts the transformation of cholesterol to 20 alpha, 22 beta-dihydroxycholesterol.

The structure of cholesterol is as follows: A 5-carbon pentagonal ring in horizontal orientation with C 1 occupying the top right vertex is labeled D. C 1 is wedge bonded to a C 1 of a 5-carbon alkane chain depicted as a line structure using 4 zigzag lines. C 1 of the alkane chain is dash bonded to C H 3 on the upper left. C 5 is single bonded to C H 3 on the upper right and C H 3 below. C 4 of the pentagonal ring has an open wiggly line on the lower left. C 5 has a wiggly line on the top left and is wedge bonded to C H 3 on the top.

The structure of 20 alpha, 22 beta-dihydroxycholesterol is as follows: A 5-carbon pentagonal ring is in horizontal orientation with C 1 occupying the top right vertex. C 1 is wedge bonded to a C 1 of a 5-carbon alkane chain depicted as a line structure using 4 zigzag lines. C 1 of the alkane chain is single bonded to C H 3 on the upper left and dash bonded to O H above. C 2 is wedge bonded to O H above. C 5 is single bonded to C H 3 on the upper right and C H 3 below. C 4 of the pentagonal ring has a wiggly line on the lower left. C 5 has a

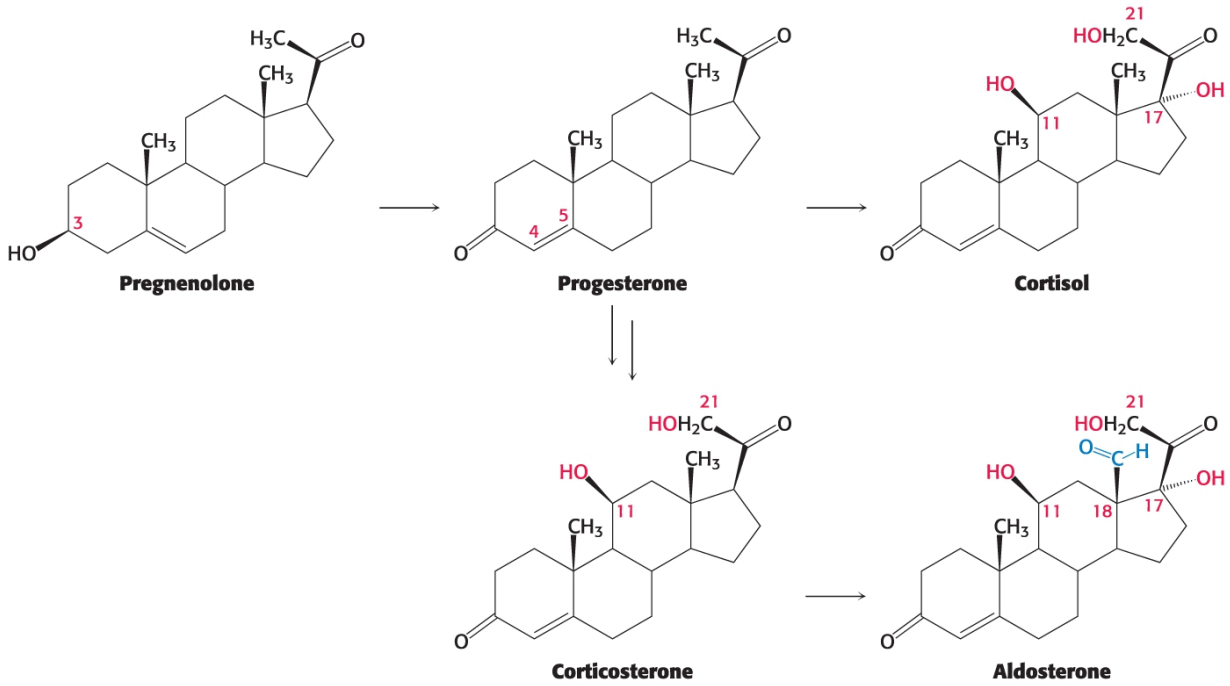
wiggly line on the upper left and is wedge bonded to C H 3 on the top.

20 alpha, 22 beta-dihydroxycholesterol is irreversibly converted into pregnenolone.

The structure of pregnenolone is as follows: A 5-carbon pentagonal ring is in horizontal orientation with C 1 occupying the top right vertex. C 1 is wedge bonded to a central C atom above. The central C atom is single-bonded to C H 3 on the upper left and double-bonded to O on the upper right. C 4 of the pentagonal ring has a wiggly line on the lower left. C 5 has a wiggly line on the upper left and is wedge bonded to C H 3 on the top.

Return to Conversion of cholesterol to pregnenolone

Extended description for FIGURE 27.28 Pregnenolone is converted into progesterone, cortisol, and aldosterone



In the first irreversible step, pregnenolone is converted to progesterone.

The structure of pregnenolone is as follows: Two 6-carbon hexagonal rings in vertical orientation have C 1 at the topmost vertex. The second ring has a double bond between C 4 and C 5. Both the rings are fused such that C 2 and C 3 of the first ring are C 6 and C 5 respectively of the second ring. C 2 of the first ring is wedge bonded to C H 3 above. C 5 numbered 3 is wedge bonded to O H. Another 6-carbon hexagonal ring in vertical orientation is fused with the second ring such that C 1 and C 2 of the second ring are C 5 and C 4 respectively of the third ring. A 5-membered pentagonal ring in horizontal orientation with C 1 occupying the top-right

vertex is fused with the third ring such that C 2 and C 3 of the third ring are C 5 and C 4 respectively of the fourth ring. C 5 of the pentagonal ring is wedge bonded to C H 3 above. C 1 of the fourth ring is wedge bonded to a central C atom. The central C atom is wedge bonded to C H 3 on the upper left and double-bonded to O on the upper right.

The structure of progesterone is as follows: Two 6-carbon hexagonal rings in vertical orientation have C 1 at the topmost vertex. The first ring has a double bond between C 3 and C 4. C 3 and C 4 are numbered 5 and 4 respectively. Both the rings are fused such that C 2 and C 3 of the first ring are C 6 and C 5 respectively of the second ring. C 2 of the first ring is wedge bonded to C H 3 above. C 5 is double bonded to O. Another 6-carbon hexagonal ring in vertical orientation is fused with the second ring such that C 1 and C 2 of the second ring are C 5 and C 4 respectively of the third ring. A 5-membered heterocyclic pentagonal ring in horizontal orientation with C 1 occupying the top right vertex is fused with the third ring such that C 2 and C 3 of the third ring are C 5 and C 4 respectively of the fourth ring. C 5 of the pentagonal ring is wedge bonded to C H 3 above. C 1 of the fourth ring is wedge bonded to a central C atom. The central C atom is wedge bonded to C H 3 on the upper left and double-bonded to O on the upper right.

In the second irreversible step, progesterone has two fates, the first being transformation to cortisol and the second being transformation to corticosterone. The conversion of progesterone to corticosterone is depicted using 2 forward arrows.

The structure of cortisol is as follows: Two 6-carbon hexagonal rings in vertical orientation have C 1 at the topmost vertex. The first ring has a double bond between C 3 and C 4. Both the rings are fused such that C 2 and C 3 of the first ring are C 6 and C 5 respectively of the second ring. C 2 of the first ring is wedge bonded to C H 3 above.

C 5 is double bonded to O. Another 6-carbon hexagonal ring in vertical orientation is fused with the second ring such that C 1 and C 2 of the second ring are C 5 and C 4 respectively of the third ring. C 6 of the third ring is numbered 11 and wedge bonded to O H. A 5-membered pentagonal ring in horizontal orientation with C 1 occupying the top right vertex is fused with the third ring such that C 2 and C 3 of the third ring are C 5 and C 4 respectively of the fourth ring. C 5 of the pentagonal ring is wedge bonded to C H 3 above. C 1 of the fourth ring, numbered 17, is dash bonded to O H on the upper right and wedge bonded to a central C atom above. The central C atom is wedge bonded to C H 2 O H on the upper left and double-bonded to O on the upper right. C H 2 O H is numbered 21.

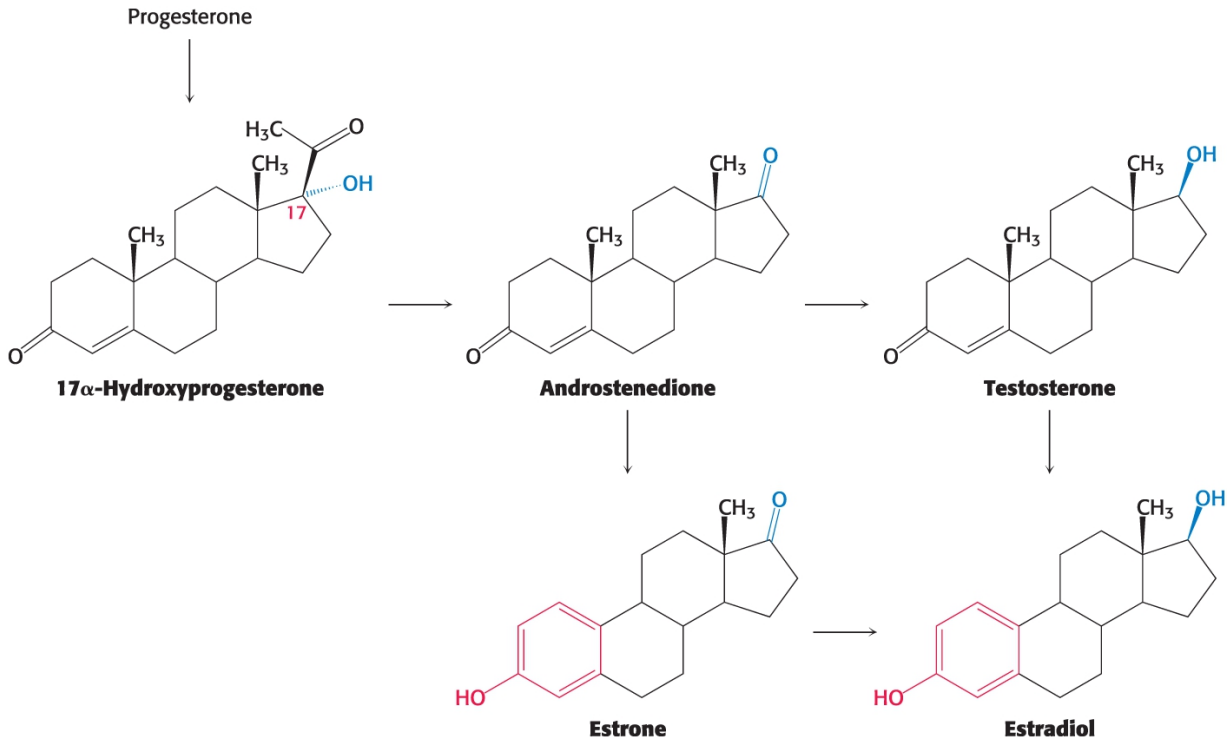
The structure of corticosterone is as follows: Two 6-carbon hexagonal rings in vertical orientation have C 1 at the topmost vertex. The first ring has a double bond between C 3 and C 4. Both the rings are fused such that C 2 and C 3 of the first ring are C 6 and C 5 respectively of the second ring. C 2 of the first ring is wedge bonded to C H 3 above. C 5 is double bonded to O. Another 6-carbon hexagonal ring in vertical orientation is fused with the second ring such that C 1 and C 2 of the second ring are C 5 and C 4 respectively of the third ring. C 6 of the third ring is numbered 11 and wedge bonded to O H. A 5-membered pentagonal ring in horizontal orientation with C 1 occupying the top right vertex is fused with the third ring such that C 2 and C 3 of the third ring are C 5 and C 4 respectively of the fourth ring. C 5 of the pentagonal ring is wedge bonded to C H 3 above. C 1 of the fourth ring is wedge bonded to a central C atom above. The central C atom is wedge bonded to C H 2 O H on the upper left and double-bonded to O on the upper right. C H 2 O H is numbered 21.

In the third irreversible step, corticosterone is converted to aldosterone.

The structure of aldosterone is as follows: Two 6-carbon hexagonal rings in vertical orientation have C 1 at the topmost vertex. The first ring has a double bond between C 3 and C 4. Both the rings are fused such that C 2 and C 3 of the first ring are C 6 and C 5 respectively of the second ring. C 2 of the first ring is wedge bonded to C H 3 above. C 5 is double bonded to O. Another 6-carbon hexagonal ring in vertical orientation is fused with the second ring such that C 1 and C 2 of the second ring are C 5 and C 4 respectively of the third ring. C 6 of the third ring is numbered 11 and is wedge bonded to O H. C 2 of the third ring is numbered 18. A 5-membered pentagonal ring in horizontal orientation with C 1 occupying the top right vertex is fused with the third ring such that C 2 and C 3 of the third ring are C 5 and C 4 respectively of the fourth ring. C 5 of the pentagonal ring is wedge bonded to C above. This C atom is double-bonded to O on the upper left and single-bonded to H on the upper right. C 1 of the fourth ring, numbered 17, is dash bonded to O H on the upper right and wedge bonded to a central C atom above. The central C atom is wedge bonded to C H 2 O H on the upper left and double-bonded to O on the upper right. C H 2 O H is numbered 21.

Return to FIGURE 27.28 Pregnenolone is converted into progesterone, cortisol, and aldosterone

Extended description for FIGURE 27.29 Progesterone is converted into testosterone and estradiol



In the first irreversible step, progesterone is converted to 17 alpha-hydroxyprogesterone.

The structure of 17 alpha-hydroxyprogesterone is as follows: Two 6-carbon hexagonal rings in vertical orientation have C 1 at the topmost vertex. The first ring has a double bond between C 3 and C 4. Both the rings are fused such that C 2 and C 3 of the first ring are C 6 and C 5 respectively of the second ring. C 2 of the first ring is wedge bonded to C H 3 above. C 5 is double-bonded to O. Another 6-carbon hexagonal ring in vertical orientation is fused with the second ring such that C 1 and C 2 of the second ring are C 5 and C 4 respectively of the third ring. A 5-membered pentagonal ring in horizontal orientation with C 1 occupying the top right vertex is

fused with the third ring such that C 2 and C 3 of the third ring are C 5 and C 4 respectively of the fourth ring. C 5 of the pentagonal ring is wedge bonded to C H 3 above. C 1 of the fourth ring numbered 17 is dash bonded to O H on the upper right and wedge bonded to a central C atom above. The central C atom is single-bonded to C H 3 on the upper left and double-bonded to O on the upper right.

In the second irreversible step, 17 alpha-hydroxyprogesterone is converted to androstenedione. The structure of androstenedione is as follows: Two 6-carbon hexagonal rings in vertical orientation have C 1 at the topmost vertex. The first ring has a double bond between C 3 and C 4. Both the rings are fused such that C 2 and C 3 of the first ring are C 6 and C 5 respectively of the second ring. C 2 of the first ring is wedge bonded to C H 3 above. C 5 is double-bonded to O. Another 6-carbon hexagonal ring in vertical orientation is fused with the second ring such that C 1 and C 2 of the second ring are C 5 and C 4 respectively of the third ring. A 5-membered pentagonal ring in horizontal orientation with C 1 occupying the top right vertex is fused with the third ring such that C 2 and C 3 of the third ring are C 5 and C 4 respectively of the fourth ring. C 5 of the pentagonal ring is wedge bonded to C H 3 above. C 1 of the fourth ring is double-bonded to O above.

In the third irreversible step, androstenedione has two fates, first is conversion to testosterone and the second is conversion to estrone.

The structure of testosterone is as follows: Two 6-carbon hexagonal rings in vertical orientation have C 1 at the topmost vertex. Both the rings are fused such that C 2 and C 3 of the first ring are C 6 and C 5 respectively of the second ring. A double bond is present between C 3 and C 4 of the first ring. C 2 of the first ring is wedge bonded to C H 3. C 5 of the first ring is double-bonded to O on the lower left. Another 6-carbon hexagonal ring in vertical orientation is fused with the second ring such that C 1 and C 2 of the second ring are C 5

and C 4 respectively of the third ring. A 5-membered pentagonal ring in horizontal orientation with C 1 occupying the top right vertex is fused with the third ring such that C 2 and C 3 of the third ring are C 5 and C 4 respectively of the fourth ring. C 5 of the pentagonal ring is wedge bonded to C H 3 above. C 1 of the fourth ring is wedge bonded to O H.

The structure of estrone is as follows: A benzene ring in a vertical orientation consists of double bonds between C 1 and C 2, C 3 and C 4, and C 6 and C 1. C 5 is single bonded to O H. The benzene ring is fused with another 6-membered hexagonal ring in a vertical orientation such that C 2 and C 3 of the benzene ring are C 6 and C 5 of the hexagonal ring. The second hexagonal ring is fused to a third ring hexagonal ring in a vertical orientation such that C 1 and C 2 of the second ring are C 5 and C 4 of the third ring. The third ring is fused with another 5-membered pentagonal ring in a horizontal orientation such that C 2 and C 3 of the third ring are C 5 and C 4 respectively of the pentagonal ring. In the pentagonal ring, C 1 occupies the top right vertex. C 1 is double-bonded to O above. C 5 of the pentagonal ring is wedge bonded to C H 3 above.

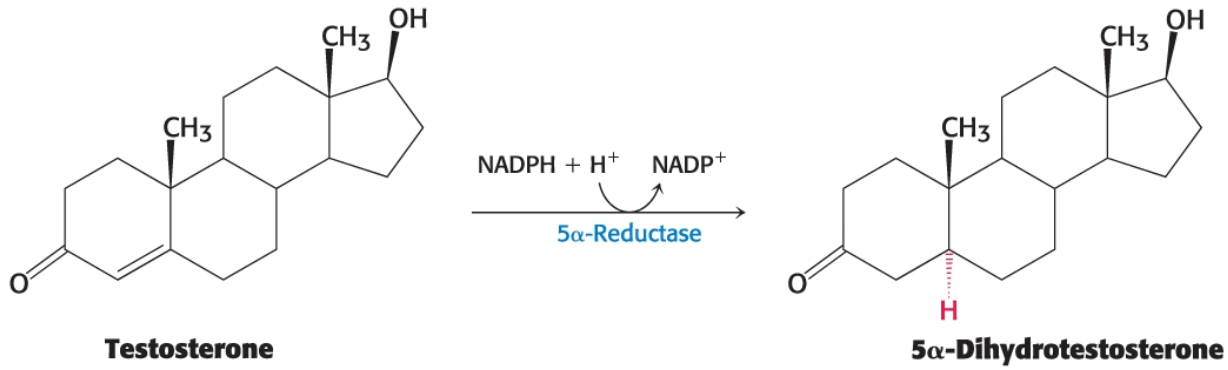
In the fourth irreversible step, testosterone and estrone are both transformed into estradiol.

The structure of estradiol is as follows: A benzene ring in a vertical orientation consists of double bonds between C 1 and C 2, C 3 and C 4, and C 6 and C 1. C 5 is single bonded to O H. The benzene ring is fused with another 6-carbon hexagonal ring in a vertical orientation such that C 2 and C 3 of the benzene ring are C 6 and C 5 respectively of the hexagonal ring. The hexagonal ring is fused to a third ring hexagonal ring in a vertical orientation such that C 1 and C 2 of the second ring are C 5 and C 4 respectively of the third ring. The third ring is fused with another 5-membered pentagonal ring in a horizontal orientation such that C 2 and C 3 of the third ring are C 5

and C 4 respectively of the pentagonal ring. C 1 of the pentagonal ring is dash bonded to O H above. C 5 of the pentagonal ring is wedge bonded to C H 3 above.

Return to FIGURE 27.29 Progesterone is converted into testosterone and estradiol

Extended description for Formation of 5 alpha-dihydrotestosterone



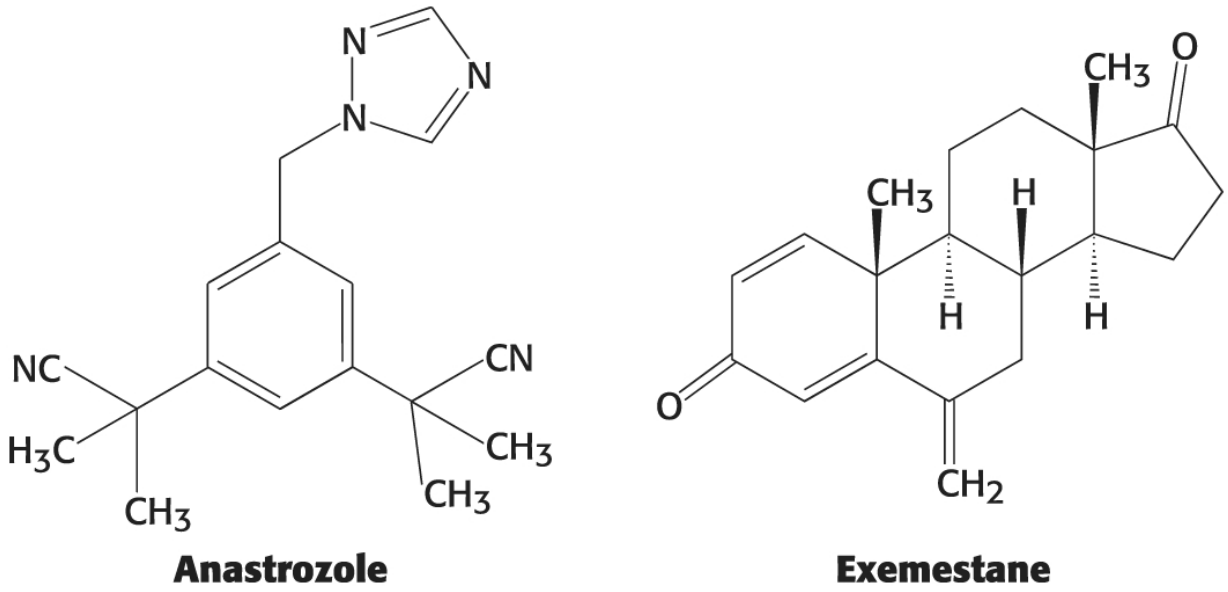
The irreversible reaction depicts the transformation of testosterone to 5 alpha-dihydrotestosterone coupled with the oxidation of N A D P H plus H superscript plus to form N A D P superscript plus. The reaction is catalyzed by 5 alpha-Reductase.

The structure of testosterone is as follows: Two 6-carbon hexagonal rings in vertical orientation have C 1 at the topmost vertex. The first ring has a double bond between C 3 and C 4. Both the rings are fused such that C 2 and C 3 of the first ring are C 6 and C 5 respectively of the second ring. C 2 of the first ring is wedge bonded to C H 3. C 5 of the first ring is double bonded to O on the lower left. Another 6-carbon hexagonal ring in vertical orientation is fused with the second ring such that C 1 and C 2 of the second ring are C 5 and C 4 respectively of the third ring. A 5-membered pentagonal ring in horizontal orientation with C 1 occupying the top right vertex is fused with the third ring such that C 2 and C 3 of the third ring are C 5 and C 4 respectively of the fourth ring. C 5 of the pentagonal ring is wedge bonded to C H 3 above. C 1 of the fourth ring is wedge bonded to O H.

The structure of 5 alpha-dihydrotestosterone is as follows: Two 6-carbon hexagonal rings in vertical orientation have C 1 at the topmost vertex. Both the rings are fused such that C 2 and C 3 of the first ring are C 6 and C 5 respectively of the second ring. C 2 of the first ring is wedge bonded to C H 3. C 3 is dash bonded to H below. C 5 of the first ring is double bonded to O on the lower left. Another 6-carbon hexagonal ring in vertical orientation is fused with the second ring such that C 1 and C 2 of the second ring are C 5 and C 4 respectively of the third ring. A 5-membered pentagonal ring in horizontal orientation with C 1 occupying the top right vertex is fused with the third ring such that C 2 and C 3 of the third ring are C 5 and C 4 respectively of the fourth ring. C 5 of the pentagonal ring is wedge bonded to C H 3 above. C 1 of the fourth ring is wedge bonded to O H.

Return to Formation of 5 alpha-dihydrotestosterone

Extended description for FIGURE 27.30 Structure of anastrozole and exemestane



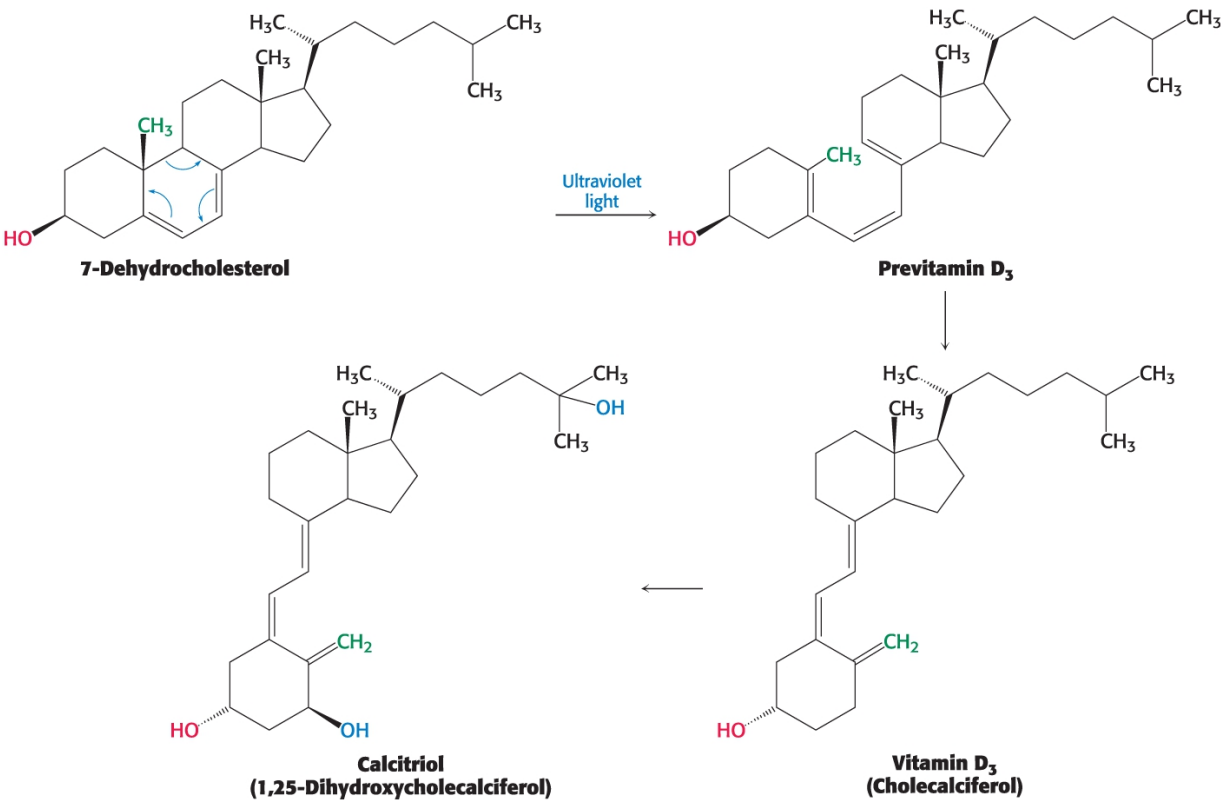
Anastrozole **Exemestane**

The structure of anastrozole is as follows: A benzene ring is in a vertical orientation with C 1 occupying the topmost vertex. The ring contains alternating double bonds between C 2 and C 3, C 4 and C 5, and C 6 and C 1. C 1 is single-bonded to a central C atom above. The central C atom is single-bonded to N 1 of a 5-membered heterocyclic pentagonal ring in a horizontal orientation with 2 C and 3 N atoms. N occupies the first, second, and fourth positions respectively. The first N atom occupies the bottom left vertex. Double bonds are present between N 2 and C 1 and N 3 and C 2. C 3 of the benzene ring is single-bonded to a central C atom on the lower right. This C atom is single-bonded to C N on the upper right, C H 3 on the lower right, and C H 3 below. C 5 of the benzene ring is single-bonded to a central C atom on the lower left. This C atom is single-bonded to C N on the upper left, C H 3 on the lower left, and C H 3 below.

The structure of exemestane is as follows: A 6-carbon hexagonal ring is in a vertical orientation with C 1 at the topmost vertex. Double bonds are present between C 3 and C 4 and C 6 and C 1. C 2 is wedge bonded to C H 3 above and C 5 is double bonded to O. The ring is fused with another 6-membered hexagonal ring in a vertical orientation with C 1 at the topmost vertex. C 1 is dash bonded to H below. C 4 is double bonded to C H 2 below. The first ring is fused with the second ring such that C 2 and C 3 of the first ring are C 6 and C 5 respectively of the second ring. The second ring is fused with the third hexagonal ring in a vertical orientation with C 1 at the topmost vertex. C 2 is wedge bonded to C H 3 above. C 3 is dash bonded to H below. C 4 is wedge bonded to H above. The second and third rings are fused such that C 1 and C 2 of the second ring are C 5 and C 4 of the third ring. The third hexagonal ring is fused with a 5-membered pentagonal ring in a horizontal orientation such that C 2 and C 3 of the hexagonal ring are C 5 and C 4 respectively of the pentagonal ring. C 1 is double bonded to O above.

Return to FIGURE 27.30 Structure of anastrozole and exemestane

Extended description for FIGURE 27.31 Vitamin D is synthesized from 7-dehydrocholesterol in a process initiated by absorption of ultraviolet light



In the first irreversible step, 7-dehydrocholesterol is converted to previtamin D 3 by the action of ultraviolet light.

The structure of 7-dehydrocholesterol is as follows: Two 6-carbon hexagonal rings in vertical orientation have C 1 at the topmost vertex. The second ring has double bonds between C 2 and C 3, and C 4 and C 5. An arrow from the double bond between C 2 and C 3 points toward the single bond between C 3 and C 4. An arrow from the double bond between C 4 and C 5 points to the single bond between C 5 and C 6. An arrow from the single bond between C 6 and C 1 points to the single bond between C 1 and C 2. Both the rings

are fused such that C 2 and C 3 of the first ring are C 6 and C 5 respectively of the second ring. C 2 of the first ring is wedge bonded to C H 3 above. C 5 of the first ring is wedge bonded to O H on the lower left. Another 6-carbon hexagonal ring in vertical orientation is fused with the second ring such that C 1 and C 2 of the second ring are C 5 and C 4 respectively of the third ring. A 5-carbon pentagonal ring in horizontal orientation with C 1 occupying the top right vertex is fused with the third ring such that C 2 and C 3 of the third ring are C 5 and C 4 respectively of the fourth ring. C 5 of the pentagonal ring is wedge bonded to C H 3 above. C 1 of the fourth ring is wedge bonded to a C 1 of a 5-carbon alkane chain depicted as a line structure using 4 zigzag lines. C 1 of the alkane chain is dash bonded to C H 3 on the upper left. C 5 is single-bonded to C H 3 on the upper right and C H 3 below.

The structure of previtamin D 3 is as follows: A 6-carbon hexagonal ring is in a vertical orientation with C 1 occupying the topmost vertex. C 2 is single bonded to C H 3 on the upper right. C 5 is wedge bonded to O H. A double is present between C 2 and C 3. C 3 is single bonded to C H on the lower right in the form of a line. C H is double bonded to another C H on the upper right. This C H is single bonded to C 4 of a second 6-carbon hexagonal ring in a vertical orientation. In the second ring, a double bond is present between C 4 and C 5. The second ring is fused to a 5-carbon pentagonal ring in a horizontal orientation such that C 2 and C 3 of the second ring are C 5 and C 4 respectively of the pentagonal ring. C 1 of the pentagonal ring is wedge bonded to C 1 of a 5-carbon alkane chain depicted as a line structure using 4 zigzag lines. In the alkane chain, C 1 is dash bonded to C H 3 on the upper left. C 5 is single bonded to C H 3 on the upper right and C H 3 below. C 5 of the pentagonal ring is wedge bonded to C H 3 above.

In the second irreversible step, previtamin D 3 is transformed into vitamin D 3 (cholecalciferol).

The structure of vitamin D 3 (cholecalciferol) is as follows: A 6-carbon hexagonal ring in vertical orientation has C 1 occupying the topmost vertex. The hexagonal ring is fused to a 5-membered pentagonal ring in a horizontal orientation with C 1 occupying the top right vertex. The rings are fused such that C 2 and C 3 of the hexagonal ring are C 5 and C 4 respectively of the pentagonal ring. C 5 of the pentagonal ring is wedge bonded to C H 3 above. C 1 of the pentagonal ring is wedge bonded to C 1 of a 5-carbon alkane chain depicted as a line structure using 4 zigzag lines. In the alkane chain, C 1 is dash bonded to C H 3 on the upper left. C 5 is single-bonded to C H 3 on the upper right and C H 3 below. C 4 of the hexagonal ring is double-bonded to a 2-carbon alkane chain depicted as a line structure using a line. C 2 of the alkane chain is double-bonded to C 1 of a 6-carbon hexagonal ring in a vertical orientation. C 2 of the hexagonal ring is double-bonded to C H 2 and C 5 is dash bonded to O H.

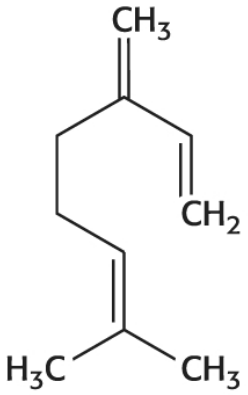
In the third irreversible step, vitamin D 3 (cholecalciferol) is converted to calcitriol (1, 25-dihydroxycholecalciferol).

The structure of calcitriol (1, 25-dihydroxycholecalciferol) is as follows: A 6-carbon hexagonal ring in vertical orientation has C 1 occupying the topmost vertex. The hexagonal ring is fused to a 5-membered pentagonal ring in a horizontal orientation with C 1 occupying the top right vertex. The rings are fused such that C 2 and C 3 of the hexagonal ring are C 5 and C 4 respectively of the pentagonal ring. C 5 of the pentagonal ring is wedge bonded to C H 3 above. C 1 of the pentagonal ring is wedge bonded to C 1 of a 5-carbon alkane chain depicted as a line structure using 4 zigzag lines. C 1 is dash bonded to C H 3 on the upper left. C 5 is single-bonded to C H 3 on the upper right, O H on the right, and C H 3 below. C 4 of the hexagonal ring is double-bonded to a 2-carbon alkane chain depicted as a line structure using a line. C 2 of the alkane chain is double-bonded to C 1 of a 6-carbon hexagonal ring in a vertical

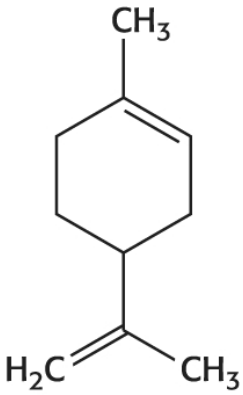
orientation. C 2 of the hexagonal ring is double-bonded to C H 2. C 3 is wedge bonded to O H, and C 5 is dash bonded to O H.

Return to FIGURE 27.31 Vitamin D is synthesized from 7-dehydrocholesterol in a process initiated by absorption of ultraviolet light

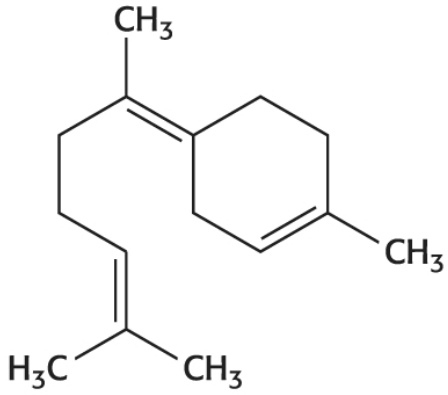
Extended description for FIGURE 27.32 Some terpenes are familiar from everyday life



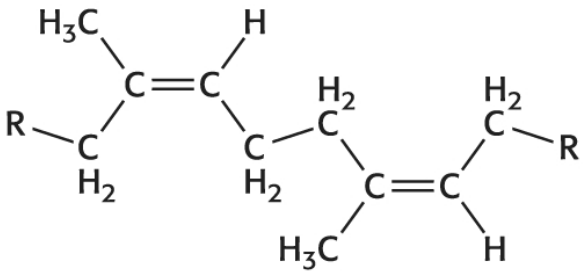
Myrcene
(found in bay leaves, hops, and cannabis)



Limonene
(natural lemon scent)



Zingiberene
(gives ginger its distinct flavor)



***cis*-Polyisoprene**
(natural rubber)

The structure of myrcene (found in bay leaves, hops, and cannabis) is as follows: A 6-carbon alkene chain is depicted as a line structure using 5 zigzag lines. A double bond is present between C 5 and C 6. C 1 is double bonded to C H 2 below. C 2 is double bonded to C H 3 above. C 6 is single bonded to C H 3 on the lower left and C H 3 on the lower right.

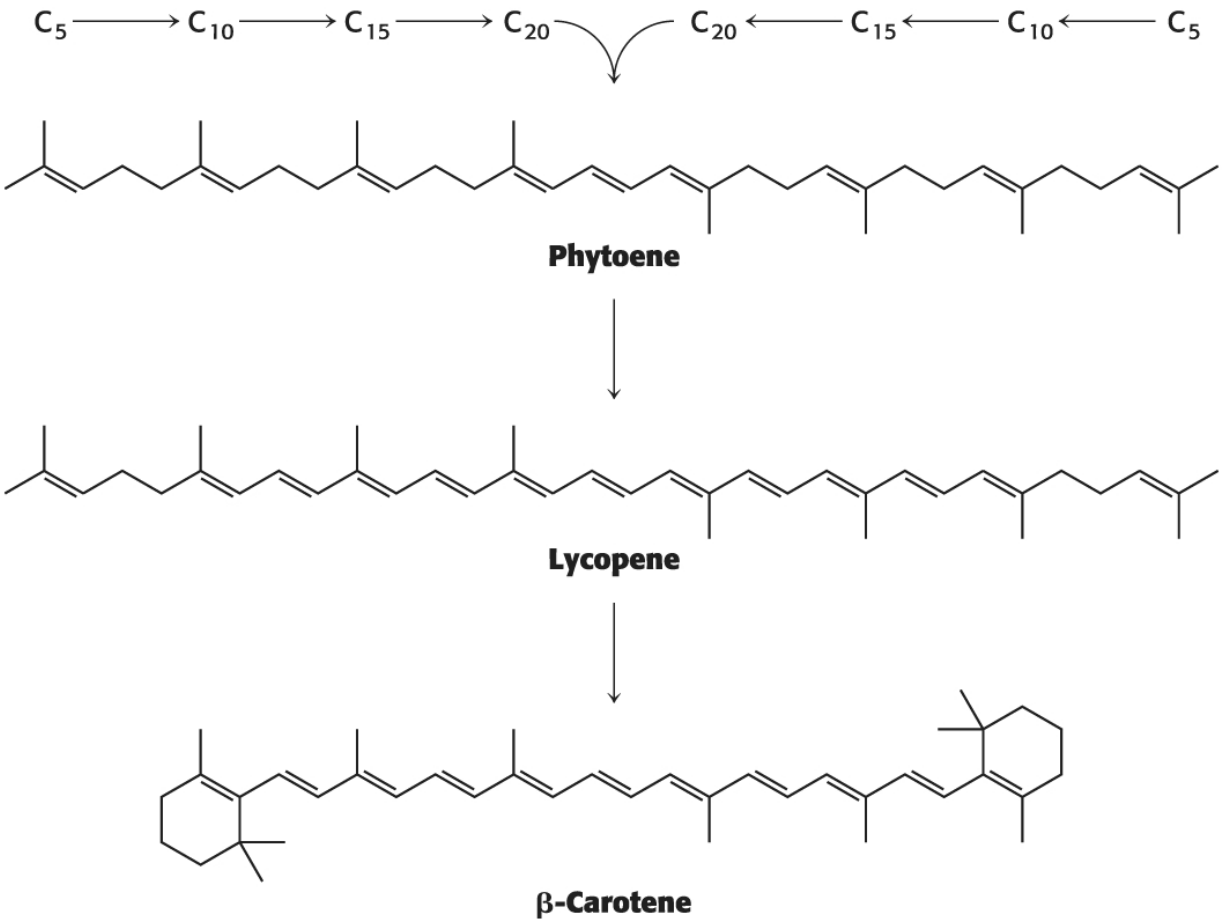
The structure of limonene (natural lemon scent) is as follows: A 6-carbon hexagonal ring is in a vertical orientation with C 1 at the topmost vertex. A double bond is present between C 1 and C 2. C 1 is single bonded to C H 3 above. C 4 is single-bonded to a central C atom below. The central C atom is double-bonded to C H 2 on the lower left and single-bonded to C H 3 on the lower right.

The structure of zingiberene that gives ginger its distinct flavor is as follows: A 6-carbon hexagonal ring is in a vertical orientation with C 1 at the topmost vertex. A double bond is present between C 3 and C 4. C 3 is single bonded to C H 3 on the lower right. C 6 is double bonded to a 5-carbon alkene chain depicted as a line structure using 4 zigzag lines. A double bond is present between C 4 and C 5. C 1 is single bonded to C H 3 above. C 5 is single bonded to C H 3 on the lower left and C H 3 on the lower right.

The structure of cis-polyisoprene (natural rubber) is as follows: C, double bond, C. C 1 is single bonded to C H 3 on the upper left and single bonded to C H 2 on the lower left. C H 2 is single bonded to R on the upper left. C 2 is single bonded to H on the upper right and single bonded to C H 2 on the lower right. C H 2 is single-bonded to C H 2 on the upper right. This C H 2 is single bonded to C on the lower right. C is single-bonded to C H 3 on the lower left and double-bonded to another C on the right. The right C is single bonded to C H 2 on the upper right and single bonded to H on the lower right. C H 2 on the upper right is single-bonded to R on the right.

Return to FIGURE 27.32 Some terpenes are familiar from everyday life

Extended description for FIGURE 27.33 Two carotenoids responsible for the color of tomatoes and carrots are large isotrenes



In the first irreversible step, phytoene is transformed into lycopene.

The structure of phytoene is as follows: A 32-carbon alkene chain is depicted as a line structure using 31 zigzag lines. Double bonds are present between C 2 and C 3, C 6 and C 7, C 10 and C 11, C 14 and C 15, C 16 and C 17, C 18 and C 19, C 22 and C 23, C 26 and C 27, and C 30 and C 31. C 2, C 6, C 10, and C 14 are each single bonded to C H 3

above in the form of a line. C 19, C 23, C 27, and C 31 are each single bonded to C H 3 below in the form of a line.

The structure of lycopene is as follows: A 32-carbon alkene chain is depicted as a line structure using 31 zigzag lines. Double bonds are present between C 2 and C 3, C 6 and C 7, C 8 and C 9, C 10 and C 11, C 12 and C 13, C 14 and C 15, C 16 and C 17, C 18 and C 19, C 20 and C 21, C 22 and C 23, C 24 and C 25, C 26 and C 27, and C 30 and C 31. C 2, C 6, C 10, and C 14 are each single bonded to C H 3 above in the form of a line. C 19, C 23, C 27, and C 31 are each single bonded to C H 3 below in the form of a line.

In the second irreversible step, lycopene undergoes cyclization to form beta-carotene.

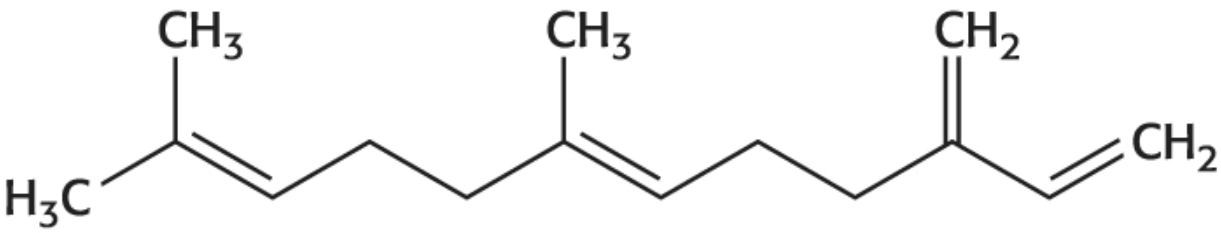
The structure of beta-carotene is as follows: A 6-carbon hexagonal ring is in a vertical orientation with C 1 at the topmost vertex. A double bond is present between C 1 and C 2. C 1 is single bonded to C H 3 above in the form of a line. C 3 is single bonded to C H 3 on the right and C H 3 on the lower right in the form of a line. C 2 of the hexagonal ring is single-bonded to C 1 of an 18-carbon alkene chain depicted as a line structure using 17 zigzag lines. Double bonds are present between C 1 and C 2, C 3 and C 4, C 5 and C 6, C 7 and C 8, C 9 and C 10, C 11 and C 12, C 13 and C 14, C 15 and C 16, and C 17 and C 18. C 3 and C 7 are each single bonded to C H 3 above in the form of a line. C 12 and C 16 are each single bonded to C H 3 below in the form of a line. C 18 of the alkene chain is single-bonded to C 5 of a hexagonal ring in a vertical orientation with C 1 at the topmost vertex. A double bond is present between C 4 and C 5. C 4 is single bonded to C H 3 below in the form of a line. C 6 is single bonded to C H 3 on the right and C H 3 on the top right in the form of a line.

On the top of phytoene, a flow chart is present horizontally. The flowchart from both sides converges at C 16 of the alkene chain of

phytoene. From left to right the flow chart is as follows: C 5, forward arrow, C 10, forward arrow, C 15, forward arrow, C 20. The flow chart from right to left is C 5, left arrow, C 10, left arrow, C 15, left arrow, C 20. C 20 from the left and right flow chart converges above C 16 of the alkene chain and points downward.

Return to FIGURE 27.33 Two carotenoids responsible for the color of tomatoes and carrots are large isotrenes

Extended description for Structure of farnesene

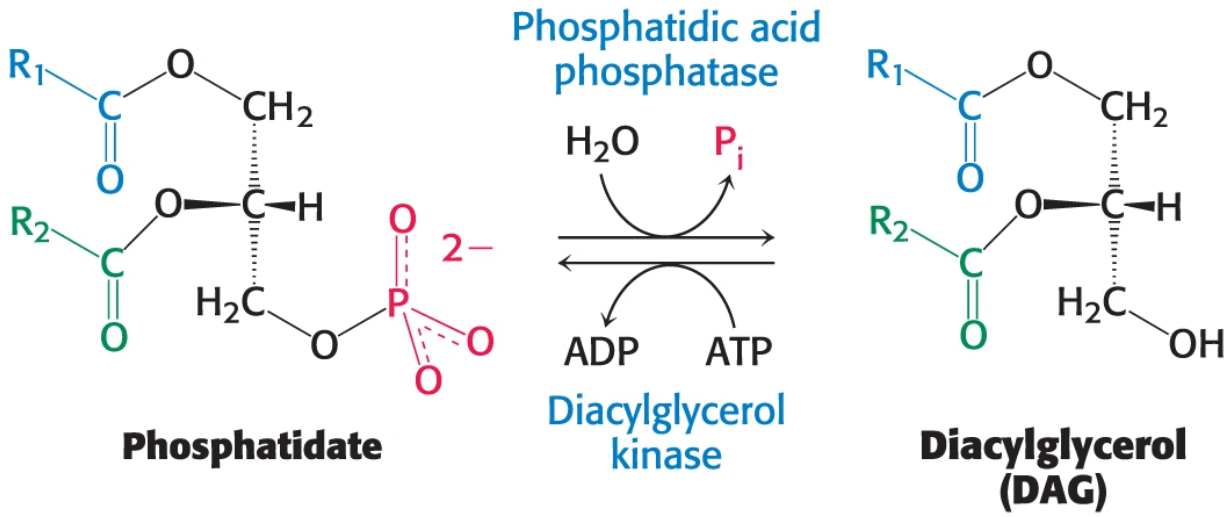


Farnesene

The structure of farnesene is as follows: A 10-carbon alkene chain is depicted as a line structure using 9 zigzag lines. Double bonds are present between C 1 and C 2, and C 5 and C 6. C 1 is single bonded to C H 3 on the lower left and C H 3 above. C 5 is single bonded to C H 3 above. C 9 is double bonded to C H 2 above. C 10 is double bonded to C H 2 on the upper right.

Return to Structure of farnesene

Extended description for Formation of diacylglycerol from phosphatidate



The figure shows a reversible reaction in which phosphatidate is converted to diacylglycerol by the action of phosphatidic acid phosphatase. It is coupled with the entry of H 2 O and the release of P subscript i. Diacylglycerol can be converted back to phosphatidate by the action of diacylglycerol kinase. It is coupled with the breakdown of A T P to A D P.

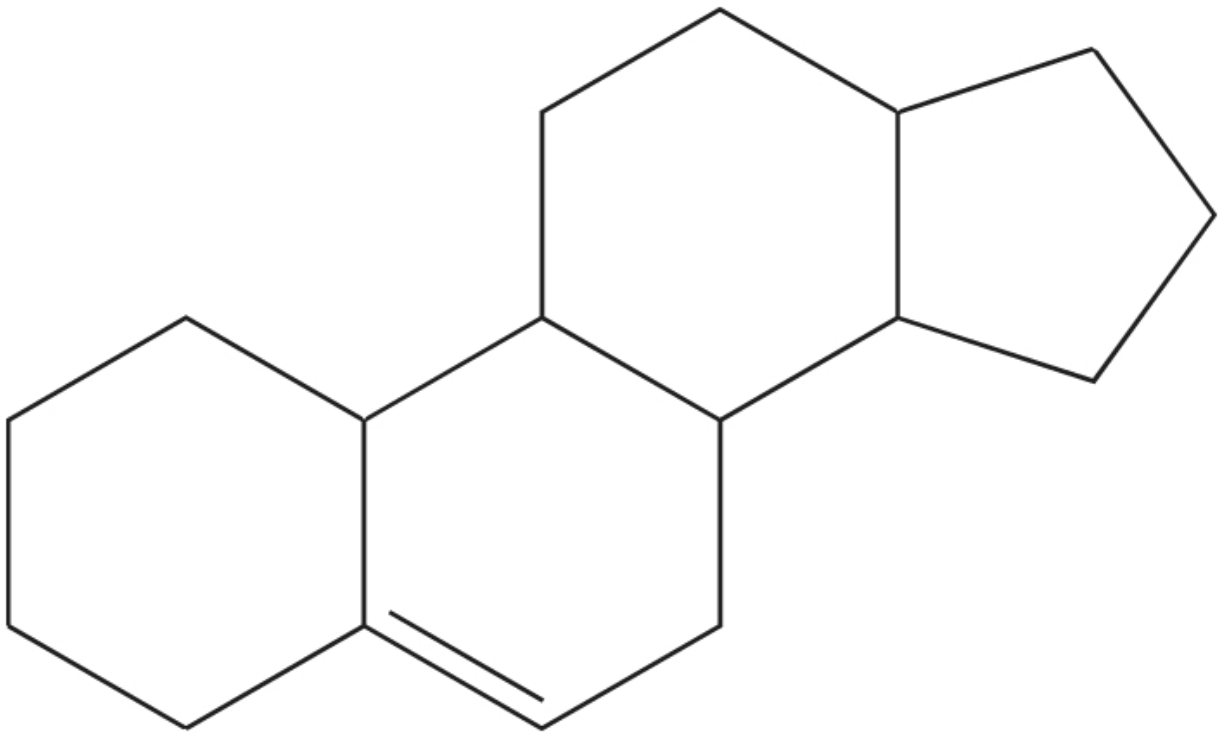
The structure of phosphatidate is as follows: A central C atom is dash bonded to C H 2 above and C H 2 below. The central C atom is also wedge bonded to O on the left and H on the right. C H 2 above is single-bonded to O on the upper left. O is single-bonded to C on the lower left. This C atom is single-bonded to R subscript 1 on the upper left and double-bonded to O below. The left O wedge bonded to the central C atom is single-bonded to C on the lower left. C is single-bonded to R subscript 2 on the upper left and double-bonded to O below. C H 2 dash bonded to the central C atom below is single-bonded to O on the lower right. This O atom is single-bonded to P on

the upper right. P is partially double-bonded to O above, O on the lower right, and O below. The P O O group has an overall charge of 2 minus.

The structure of diacylglycerol (D A G) is as follows: The structure of D A G is the same as phosphatidate except for the absence of the P O O group. The C H 2 that is dash bonded to the central C atom below is single-bonded to O H on the lower right.

Return to Formation of diacylglycerol from phosphatidate

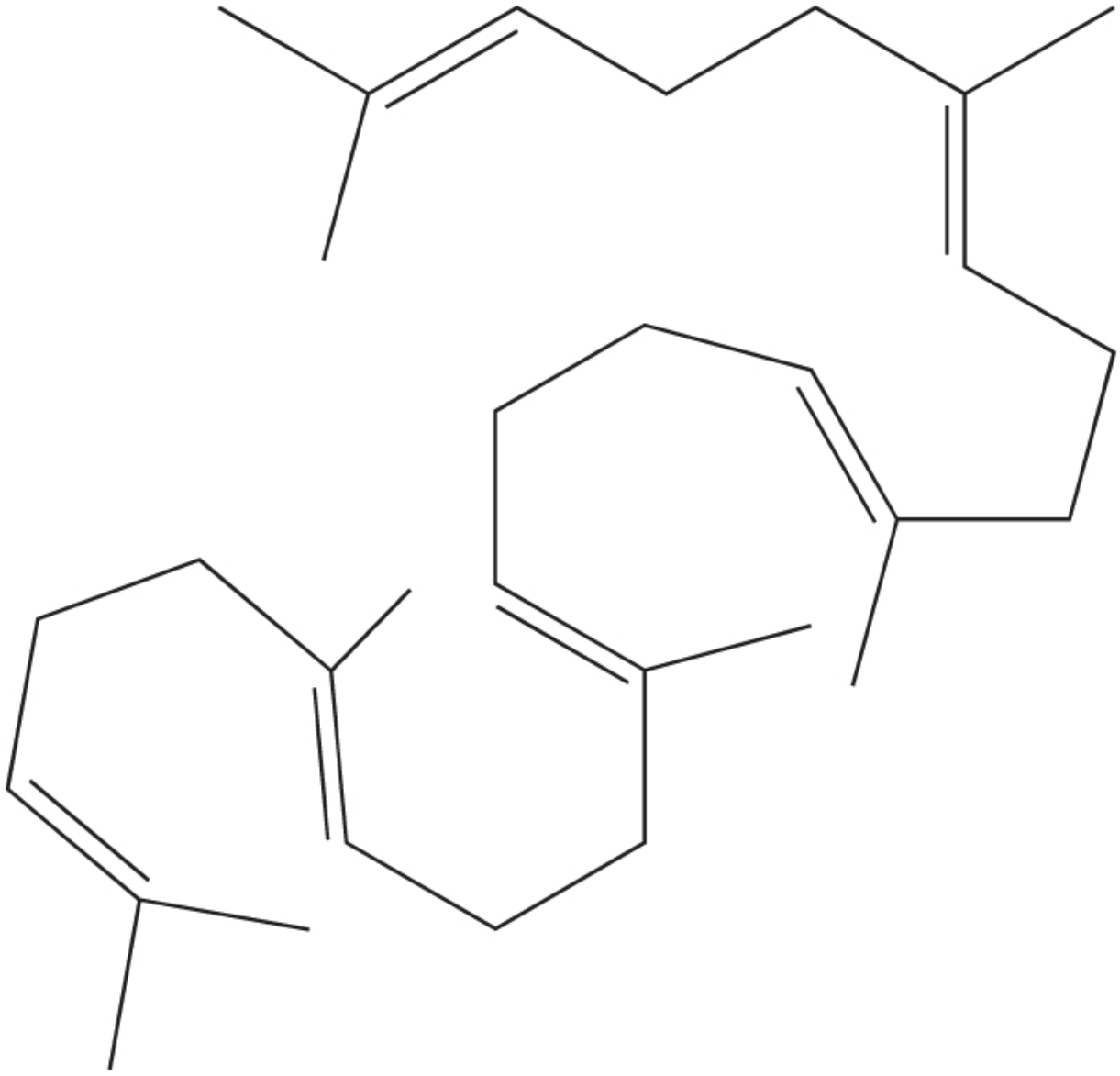
Extended description for Fused-ring core structure of a steroid



The structure is as follows: Two 6-carbon hexagonal rings in vertical orientation have C 1 at the topmost vertex. The second ring has a double bond between C 4 and C 5. Both the rings are fused such that C 2 and C 3 of the first ring are C 6 and C 5 respectively of the second ring. Another 6-carbon hexagonal ring in vertical orientation is fused with the second ring such that C 1 and C 2 of the second ring are C 5 and C 4 respectively of the third ring. A 5-carbon pentagonal ring in horizontal orientation with C 1 occupying the top right vertex is fused with the third ring such that C 2 and C 3 of the third ring are C 5 and C 4 respectively of the fourth ring.

Return to Fused-ring core structure of a steroid

Extended description for Structure of a compound

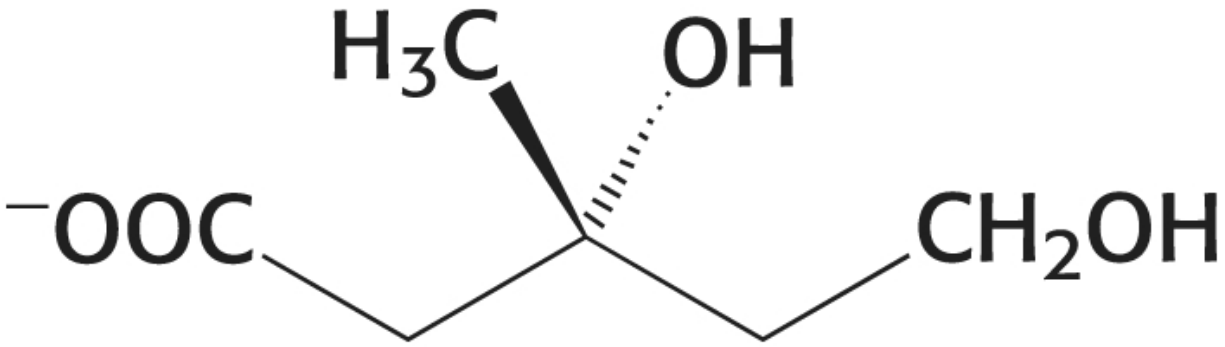


The structure of the compound is as follows: A 5-carbon alkene chain is depicted as a line structure using 4 zigzag lines. A double bond is present between C 1 and C 2. C 1 is single bonded to C H 3 on the upper left and C H 3 below in the form of a line. C 5 is single bonded to C H 3 in the form of a line on the upper right and double bonded to C H below. This C H group is single-bonded to a C H 2

group on the lower right in the form of a line. This C H 2 group is single-bonded to C H 2 on the lower left in the form of a line. This C H 2 is single-bonded to C 1 of a 14-carbon alkene chain on the left depicted as a line structure using 13 zigzag lines. A double bond is present between C 1 and C 2, C 5 and C 6, C 9 and C 10, and C 13 and C 14. C 1 is single-bonded to C H 3 in the form of a line on the lower left. C 6 is single bonded to C H 3 on the lower right in the form of a line. C 10 is single bonded to C H 3 on the upper right in the form of a line. C 14 is single bonded to C H 3 in the form of a line on the lower left and lower right.

Return to Structure of a compound

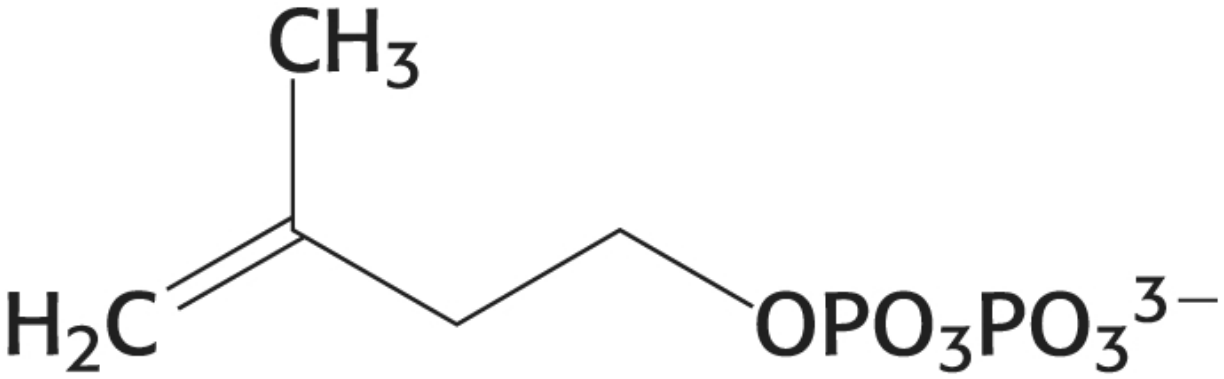
Extended description for Structure of a compound



A 3-carbon alkane chain is depicted as a line structure using 2 zigzag lines. C 1 is single bonded to C O O superscript minus on the upper left. C 2 is wedge bonded to C H 3 on the upper left and dash bonded to O H on the upper right. C 3 is single bonded to C H 2 O H on the upper right.

Return to Structure of a compound

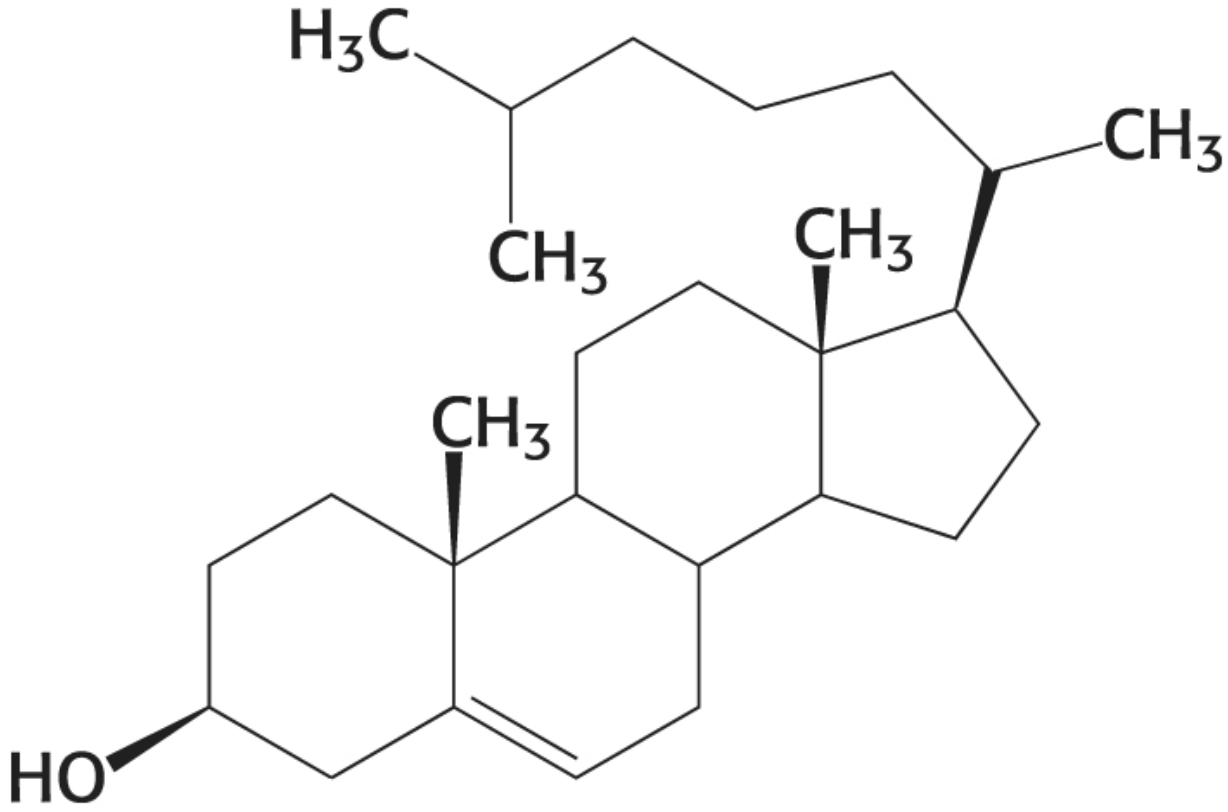
Extended description for Structure of a compound



A 3-carbon alkane chain is depicted as a line structure using 2 zigzag lines. C 1 is double bonded to C H 2 on the lower left and single bonded to C H 3 above. C 3 is single bonded to O P O 3 P O 3 superscript 3 minus on the lower right.

Return to Structure of a compound

Extended description for Structure of a compound

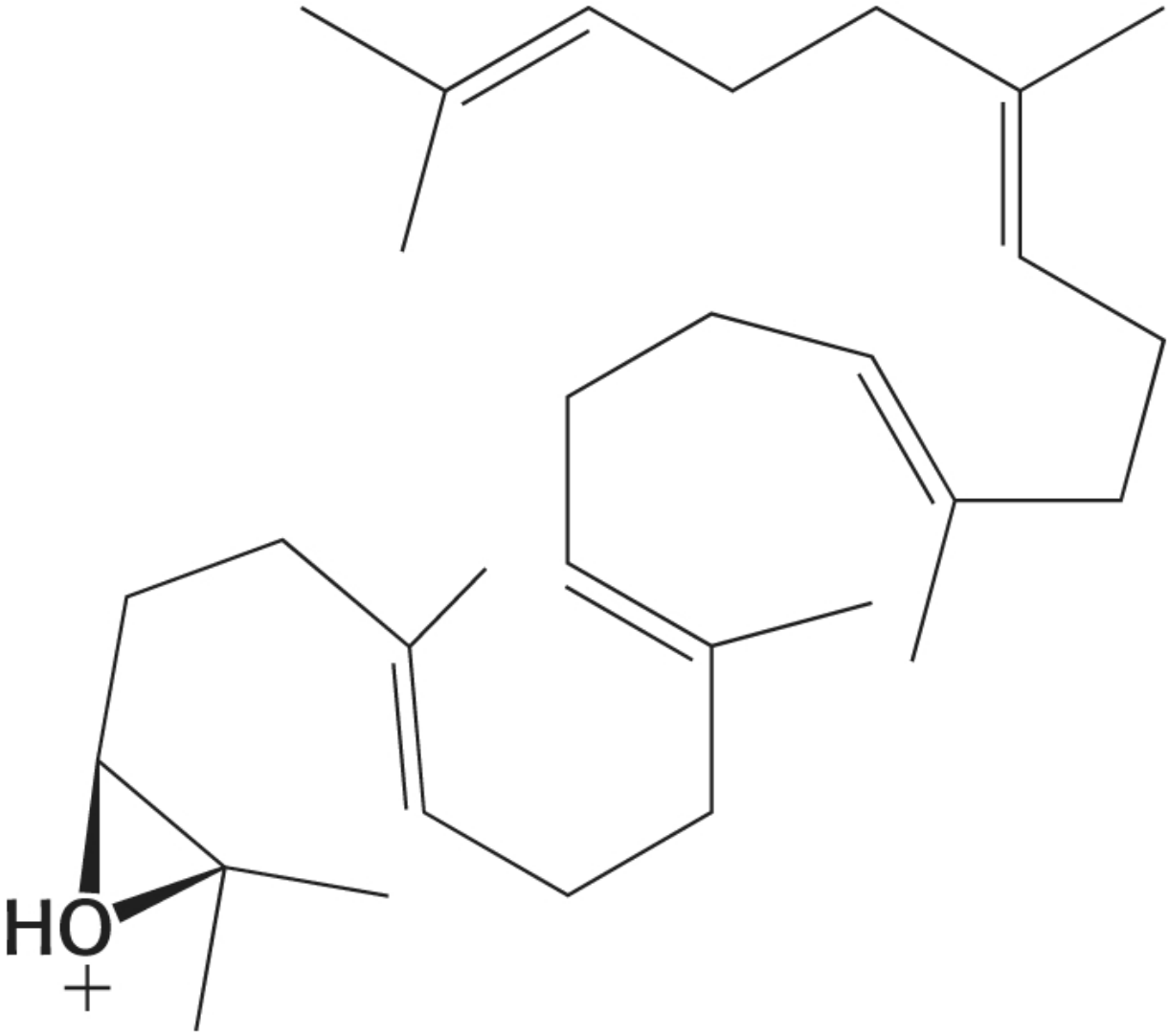


Two 6-carbon hexagonal rings in vertical orientation have C 1 at the topmost vertex. The second ring has a double bond between C 4 and C 5. Both the rings are fused such that C 2 and C 3 of the first ring are C 6 and C 5 respectively of the second ring. C 2 of the first ring is wedge bonded to C H 3 above. C 5 of the first ring is wedge bonded to O H on the lower left. Another 6-carbon hexagonal ring in vertical orientation is fused with the second ring such that C 1 and C 2 of the second ring are C 5 and C 4 respectively of the third ring. A 5-carbon pentagonal ring in horizontal orientation with C 1 occupying the top right vertex is fused with the third ring such that C 2 and C 3 of the second ring are C 5 and C 4 respectively of the fourth ring. C 5 of the pentagonal ring is wedge bonded to C H 3 above. C 1 of the fourth ring is wedge bonded to a C 5 of a 5-carbon alkane chain depicted as

a line structure using 4 zigzag lines. C 1 of the alkane chain is single-bonded to C H 3 on the upper left and C H 3 below. C 5 is single bonded to C H 3 on the top right.

Return to Structure of a compound

Extended description for Structure of a compound



The structure of the compound is as follows: A 5-carbon alkene chain is depicted as a line structure using 4 zigzag lines. A double bond is present between C 1 and C 2. C 1 is single bonded to C H 3 on the upper left and C H 3 below in the form of a line. C 5 is single bonded to C H 3 in the form of a line on the upper right and double bonded to C H below. This C H group is single bonded to a C H 2 group on the lower right in the form of a line. This C H 2 group is

single bonded to C H 2 on the lower left in the form of a line. This C H 2 is single bonded to C 1 of a 14-carbon alkene chain on the left depicted as a line structure using 13 zigzag lines. A double bond is present between C 1 and C 2, C 5 and C 6, and C 9 and C 10. C 1 is single bonded to C H 3 in the form of a line on the lower left. C 6 is single bonded to C H 3 on the lower right in the form of a line. C 10 is single bonded to C H 3 on the upper right in the form of a line. C 14 is single bonded to C H 3 in the form of a line on the lower left and lower right. C 13 and C 14 are each wedge bonded to a common O H group with an overall positive charge.

Return to Structure of a compound

Extended description for Ribbon diagram of D N A polymerase copying D N A

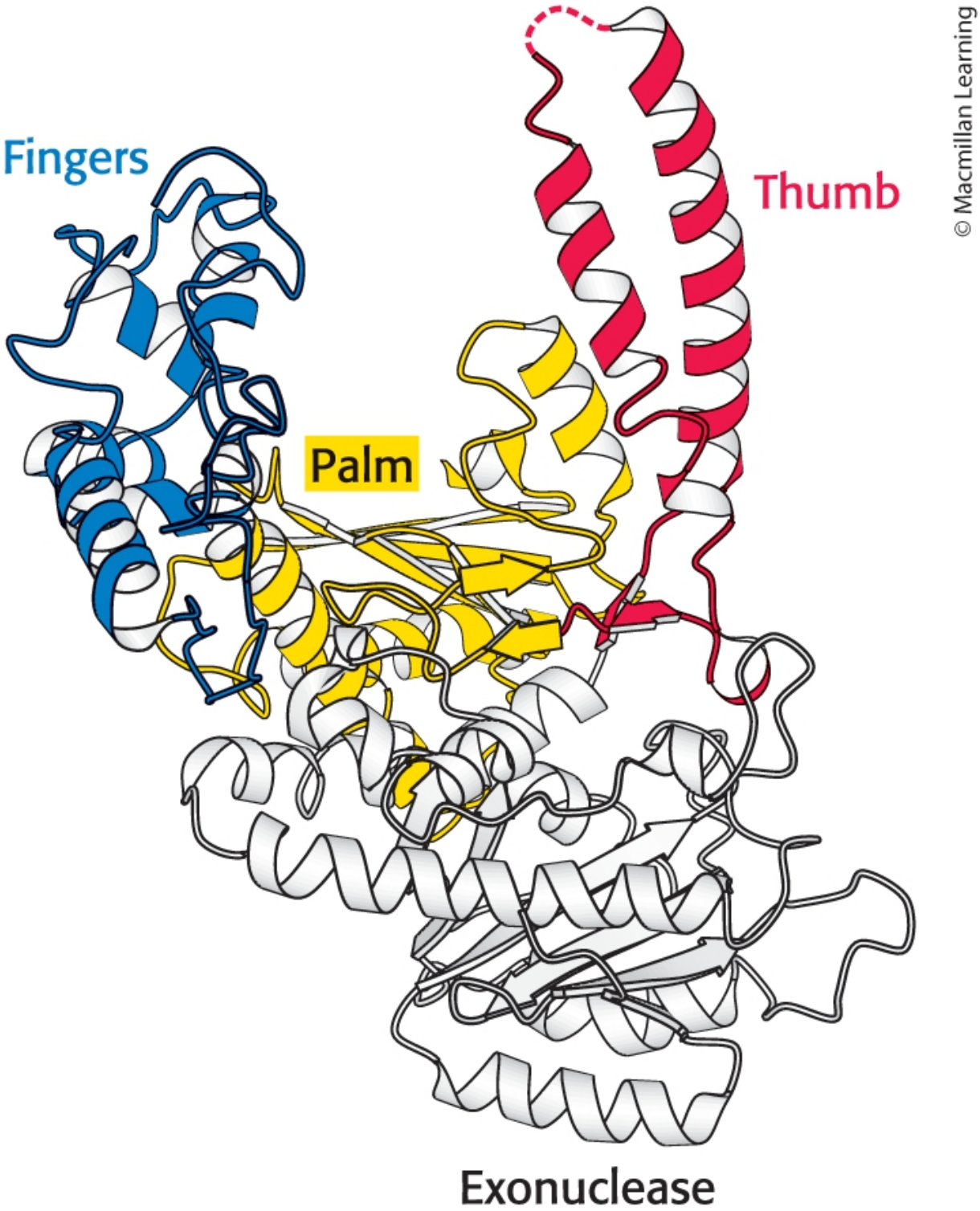


The ribbon diagram of D N A polymerase consists of several alpha-helices and a few beta-strands. A large hollow space is located in the center of the polymerase. A section of a double helix with a single complete turn is shown entering the hollow space of the polymerase. The D N A is composed of red and blue strands. The red strand is labeled template D N A. It extends outside the hollow center. A short blue fragment depicting newly synthesized D N A is shown outside the hollow center.

Return to Ribbon diagram of D N A polymerase copying D N A

Extended description for FIGURE 28.1 The structure of the *E.coli* D N A polymerase I Klenow fragment

resembles a hand

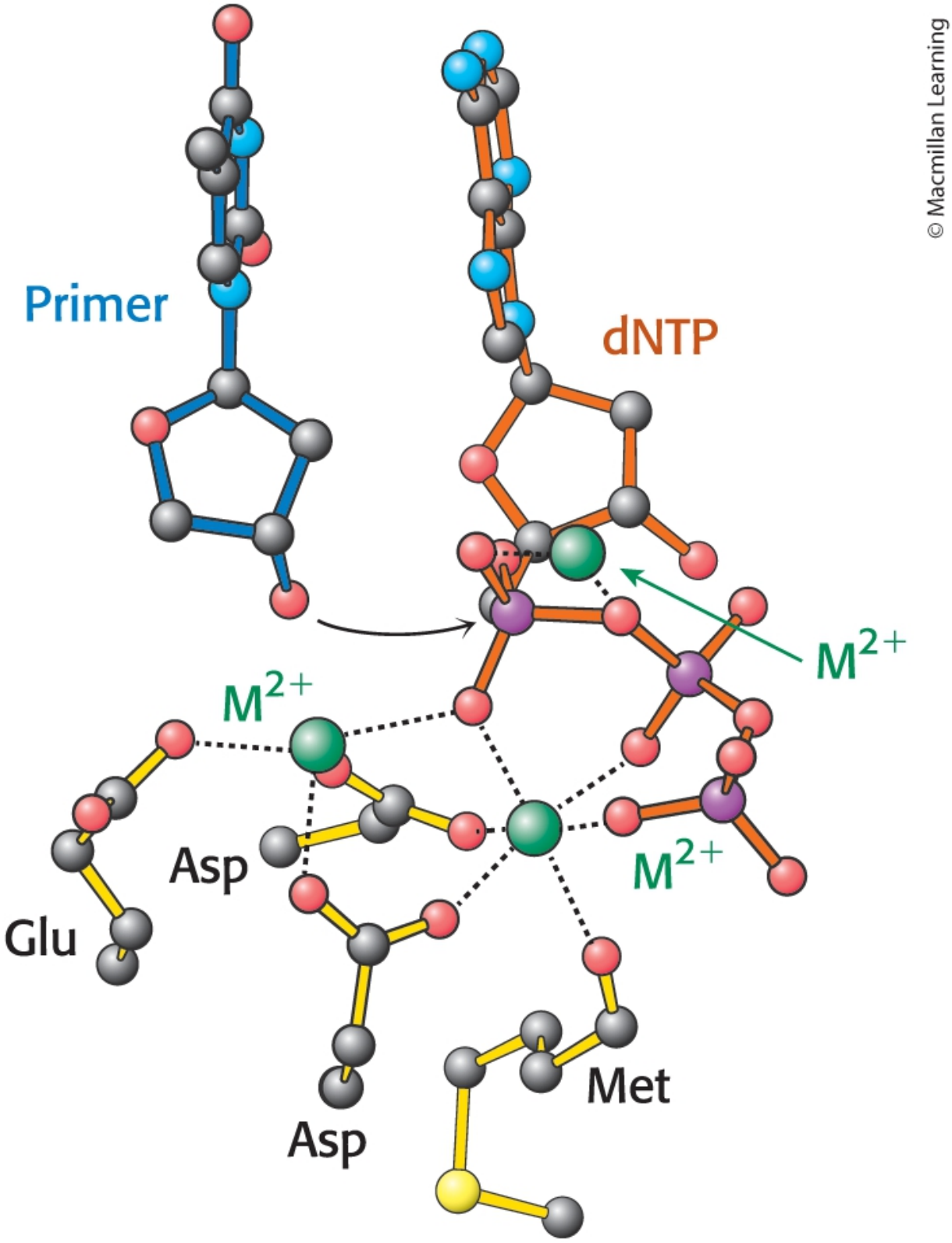


The D N A polymerase 1 Klenow fragment has a structure resembling the right hand. A few blue-colored alpha-helices extending upward on the left side are labeled fingers. A pair of red color alpha-helices and one beta-strand on the right side are labeled thumb. The palm is formed by a few yellow-colored alpha-helices and beta-strands. Several white-colored alpha-helices in horizontal orientation are located below the palm.

Return to FIGURE 28.1 The structure of the *E.coli* D N A polymerase I Klenow fragment resembles a hand

Extended description for FIGURE 28.2 Three metal ions (typically, M g superscript 2 plus) participate in the D N

A polymerase reaction



© Macmillan Learning

The metal ions, primer, d N T P, and amino acid residues are depicted as ball-and-stick models. The primer is shown on the top left. It consists of a pentagonal ring in vertical orientation composed of 1 red and 4 black spheres. The red sphere occupies the top left vertex. The topmost black sphere is connected to a 6-membered heterocyclic hexagonal ring. The side view of the hexagonal ring is shown. The ring consists of 2 blue and 4 black spheres. Two of the black spheres are connected to a red sphere. The bottom right black sphere of the pentagonal ring is connected to a red sphere. In the primer, the spheres are connected by blue-colored sticks.

A similar d N T P molecule is shown on the top right. Its structure is the same as a primer, except the bottom left sphere is connected to a chain of 2 red and 3 purple spheres through a black sphere. The red spheres occupy the second and fourth positions. The purple spheres occupy the remaining positions. The first and third purple spheres are connected to 3 red spheres. The second purple sphere is connected to two red spheres. In d N T P, the spheres are connected by red-colored sticks.

The first green sphere depicting M superscript 2 plus ion is located below the pentagonal ring of d N T P. It is connected to the second red sphere of the chain through a dashed line. An arrow from the red sphere connected to the bottom right black sphere of the pentagonal ring of the primer points toward the black sphere connected to the chain of red and purple spheres.

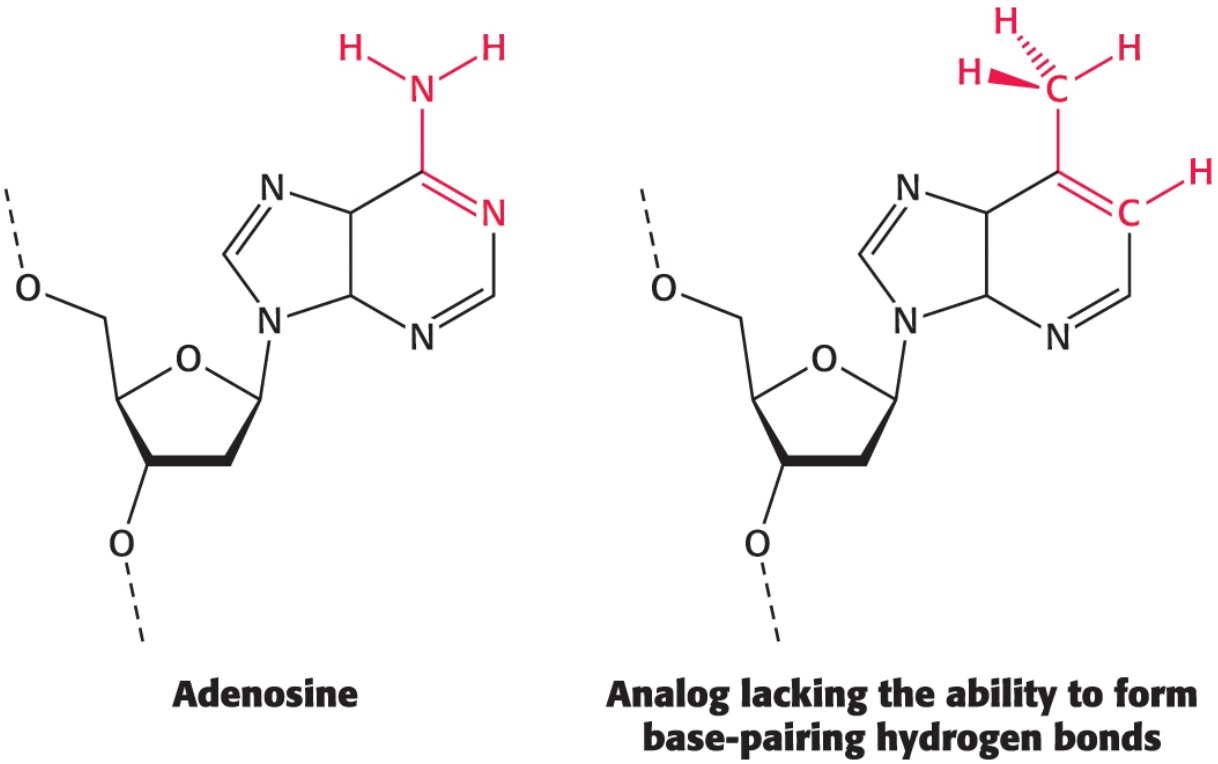
The side chain of glutamic acid, two aspartic acids, and one methionine residue is located below. The glutamic acid side chain consists of a chain of 2 red and 4 black spheres. The aspartic acid side chain consists of 3 black spheres. One of the black spheres is connected to two red spheres. The methionine side chain is composed of a chain of 1 yellow, 1 red, and 5 black spheres.

One red sphere of the two aspartic acid side chains and the methionine side chain is connected to a second central green sphere through a dashed line. One red sphere connected to the first, second, and third purple spheres of the chain is also connected to the second green sphere through a dashed line. The green sphere depicts M superscript 2 plus.

The third green sphere is connected to the red sphere of the glutamic acid side chain, red sphere of the second aspartic acid side chain, and the red sphere connected to the first purple sphere, through a dashed line.

Return to FIGURE 28.2 Three metal ions (typically, M g superscript 2 plus) participate in the D N A polymerase reaction

Extended description for FIGURE 28.3 Base analogs that have the same shape as normal bases can participate in D N A replication



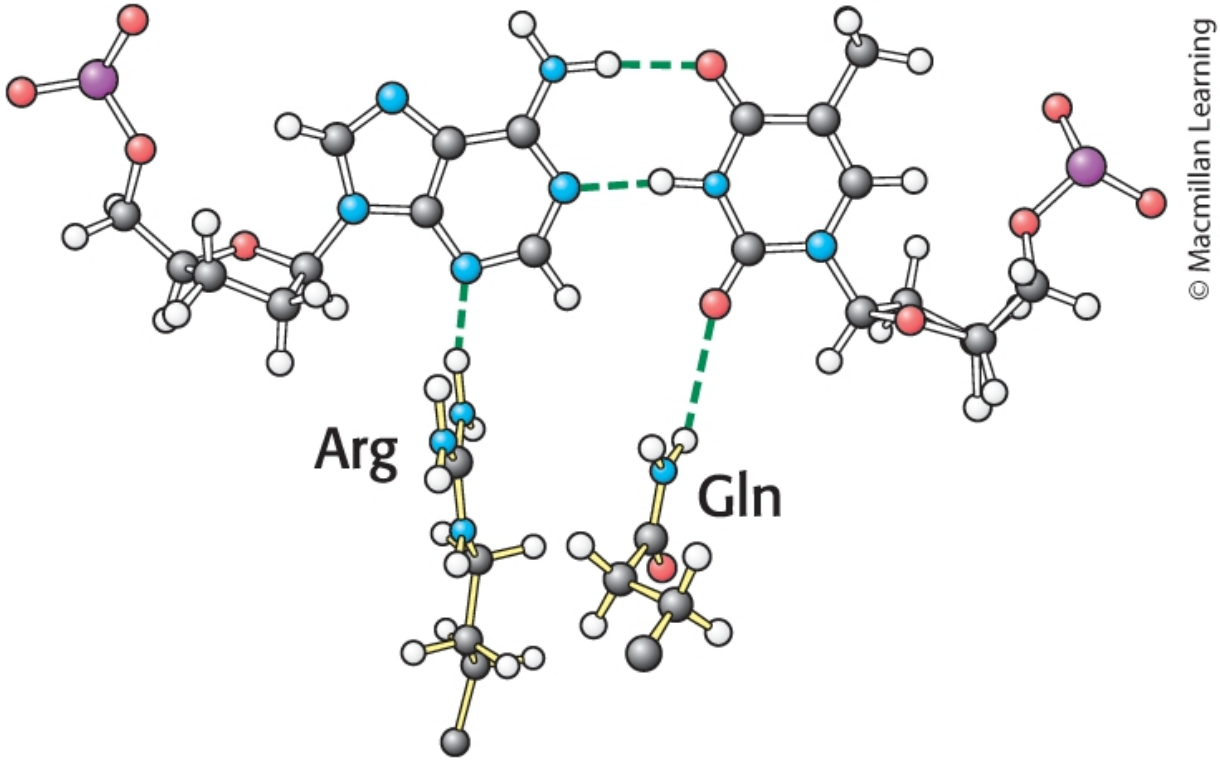
The structure of adenosine is as follows: A 5-membered heterocyclic pentagonal ring is in a vertical orientation and consists of 1 O and 4 C atoms. O occupies the topmost vertex. C 1 occupies the top right vertex. C 3 is single bonded to O below, which has a dashed line below. C 4 is single bonded to C H 2 above in the form of a line. C H 2 is single-bonded to O on the upper left. O has a dashed line above. C 1 is single-bonded to N 1 of a 5-membered heterocyclic pentagonal ring in a horizontal orientation. It consists of 2 N and 3 C atoms. First N occupies the bottom left vertex and the second N occupies the top left vertex. C 1 occupies the leftmost vertex. A double bond is present between C 1 and N 2. It is fused to a 6-membered

heterocyclic hexagonal ring in a vertical orientation such that C 2 and C 3 of the pentagonal ring are C 3 and C 2 respectively of the hexagonal ring. The hexagonal ring is composed of 2 N and 4 C atoms. The first N occupies the top right vertex and the second N occupies the bottom-most vertex. A double bond is present between C 1 and N 2, and C 4 and N 1. C 4 is single bonded to N above. N is single-bonded to H on the upper left and H on the upper right.

The structure of the analog of adenosine is as follows: A 5-membered heterocyclic pentagonal ring is in a vertical orientation and consists of 1 O and 4 C atoms. O occupies the topmost vertex. C 1 occupies the top right vertex. C 3 is single bonded to O below, which has a dashed line below. C 4 is single bonded to C H 2 above in the form of a line. C H 2 is single-bonded to O on the upper left. O has a dashed line above. C 1 is single-bonded to N 1 of a 5-membered heterocyclic pentagonal ring in a horizontal orientation. It consists of 2 N and 3 C atoms. First N occupies the bottom left vertex and the second N occupies the top left vertex. C 1 occupies the leftmost vertex. A double bond is present between C 1 and N 2. It is fused to a 6-membered heterocyclic hexagonal ring in a vertical orientation such that C 2 and C 3 of the pentagonal ring are C 3 and C 2 respectively of the hexagonal ring. The hexagonal ring is composed of 1 N and 5 C atoms. N occupies the bottom-most vertex. A double bond is present between C 3 and C 4, and C 5 and N. C 3 is single bonded to C above. This C is wedge bonded to H on the left, dash bonded to H on the upper left, and single bonded to H on the upper right. C 4 is single bonded to H on the upper right. The text below the analog of adenosine reads "Analog lacking the ability to form base-pairing hydrogen bonds."

Return to FIGURE 28.3 Base analogs that have the same shape as normal bases can participate in D N A replication

Extended description for FIGURE 28.4 Minor-groove interactions promote the specificity of D N A replication



The ball-and-stick model of the A T base pair is shown. Base A consists of a fused pentagonal and hexagonal ring. The pentagonal ring is composed of 2 blue and 3 black spheres. The top left black sphere is connected to a white sphere. The hexagonal ring is composed of 2 blue and 4 black spheres. The blue sphere of the pentagonal ring is connected to the black sphere of a flat pentagonal ring composed of 1 red and 4 black spheres. The top left black sphere of this ring is connected to a black sphere on the upper left, which is further connected to a red sphere. The black sphere is also connected to two white spheres. The red sphere is connected to a purple sphere on the upper left. The purple sphere is connected to

two different red spheres. The two black spheres of the flat pentagonal ring, facing toward the observer, are connected to two white spheres. The remaining black spheres of this ring are connected to a single white sphere. The topmost black sphere of the hexagonal ring is connected to a blue sphere, which is further connected to two white spheres. The bottom right black sphere is connected to a white sphere. In the hexagonal ring, one white sphere is connected to the topmost black sphere through the blue sphere and the top right blue sphere is connected to a red sphere and the leftmost blue sphere respectively of the base T. This connection is depicted by a dashed green line.

The base T consists of a horizontal hexagonal ring composed of 2 blue and 4 black spheres. The blue sphere occupies the bottom right and leftmost vertex respectively. The remaining positions are occupied by black spheres. The top left black sphere is connected to a red sphere on the upper left. The top right black sphere is connected to a black sphere on the upper right, which is further connected to two white spheres. The rightmost black sphere is connected to a white sphere on the right. The bottom left black sphere is connected to a red sphere. The bottom right blue sphere is connected to a black sphere of a flat pentagonal ring composed of 1 red and 4 black spheres. The red sphere of this ring faces the observer. Two black spheres of the ring are connected to two white spheres. The remaining black spheres are connected to a single white sphere. One of the black spheres of this ring is connected to a black sphere on the upper right. The upper right black sphere is connected to a red sphere above, which is further connected to a purple sphere on the upper right. The purple sphere is connected to two red spheres.

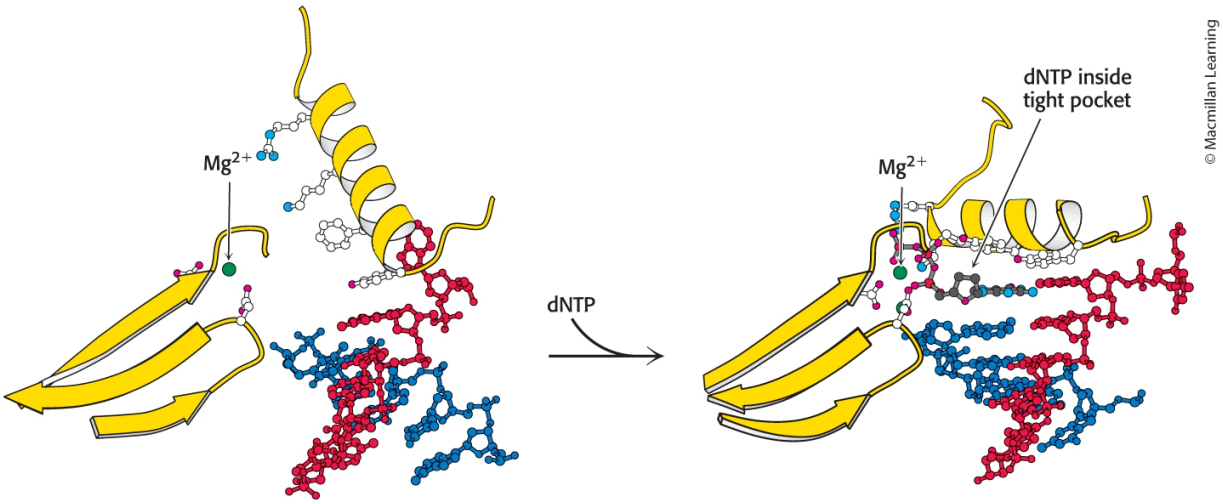
The ball-and-stick models of arginine and glutamine are shown below the A T base pair.

Arginine is located below A and glutamine is located below T. Arginine is composed of a vertical chain of 5 black spheres. The topmost black sphere is connected to two blue spheres. Each of these blue spheres is connected to two white spheres. One of these white spheres is connected to the bottom left blue sphere of the hexagonal ring of base A. The second black sphere from the top is connected to a chain of 1 blue and 1 white sphere, and two different white spheres. The third and fourth black sphere is connected to two white spheres.

Glutamine is composed of a zigzag chain of 4 black spheres. The topmost black sphere is connected to a blue sphere above. This blue sphere is connected to two white spheres. One of these white spheres is connected to a red sphere which in turn is connected to the bottom left black sphere of the hexagonal ring of base T. This connection between the white and red spheres is depicted through a green dashed line. The topmost black sphere of glutamine is also connected to a red sphere. The second and third red spheres of the chain are connected to two white spheres.

Return to FIGURE 28.4 Minor-groove interactions promote the specificity of D N A replication

Extended description for FIGURE 28.5 Shape selectivity promotes the specificity of DNA replication



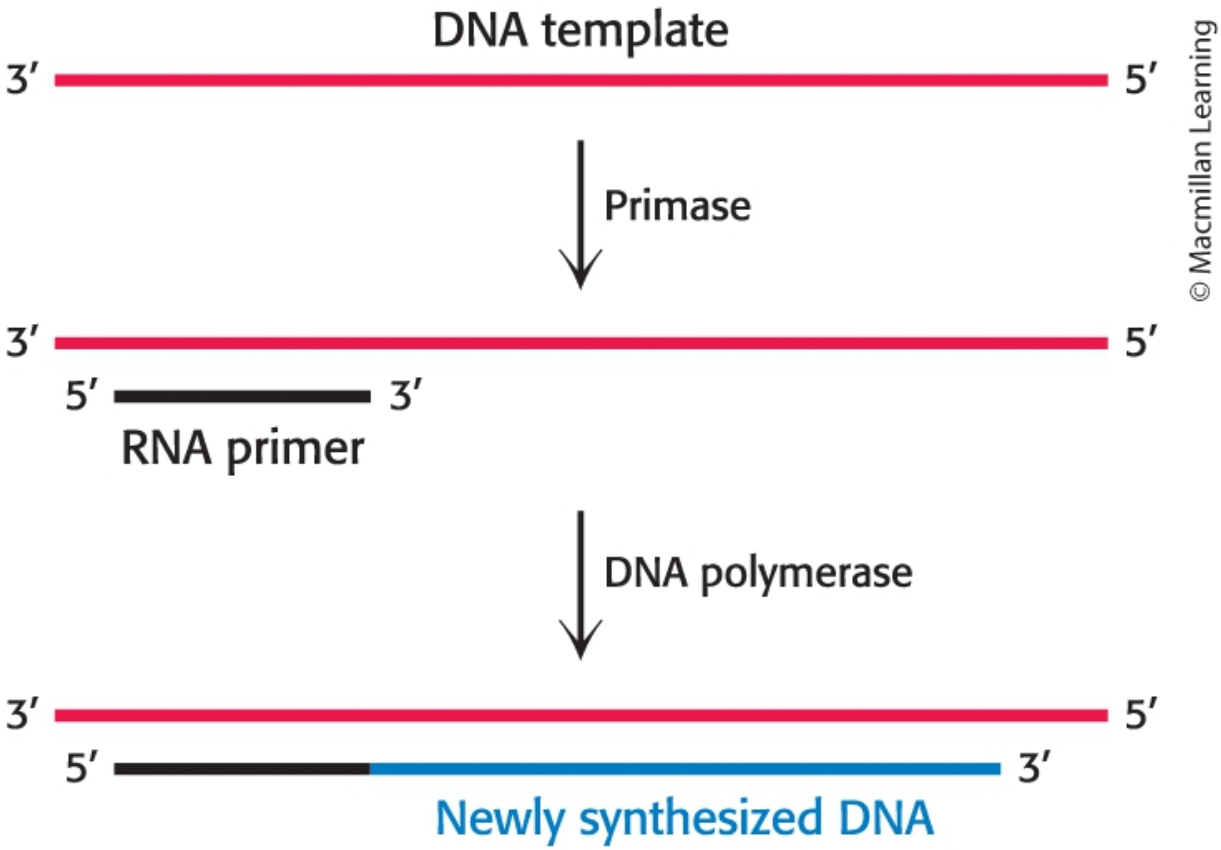
An alpha-helix in diagonal orientation is shown on the top right. Three anti-parallel beta-strands in diagonal orientation are connected by thread-like loops and shown on the bottom right. These secondary structures are separated by a gap. A ball-and-stick model of the D N A double helix is shown below. The different strands of D N A are composed of blue and red spheres. The alpha-helix contains side chains of different amino acids. One of the beta-strand and the loop connecting them also contains a side chain of amino acids. A green sphere labeled M g superscript 2 plus is located above the top-most beta-strand. The D N A strand composed of red spheres extends toward the alpha-helix and is unpaired in this extended region.

A forward arrow shows the conformational change after the addition of d N T P. After the conformational change, the alpha-helix becomes horizontally oriented. The orientation of the beta-strands remains the same. A "d N T P" is shown inside the tight pocket formed after shifting of the position of the helix. This d N T P is

aligned with the unpaired base of the D N A strand composed of red spheres. The location of the M g superscript 2 plus ion is the same.

Return to FIGURE 28.5 Shape selectivity promotes the specificity of DNA replication

Extended description for FIGURE 28.6 D N A polymerases require a primer



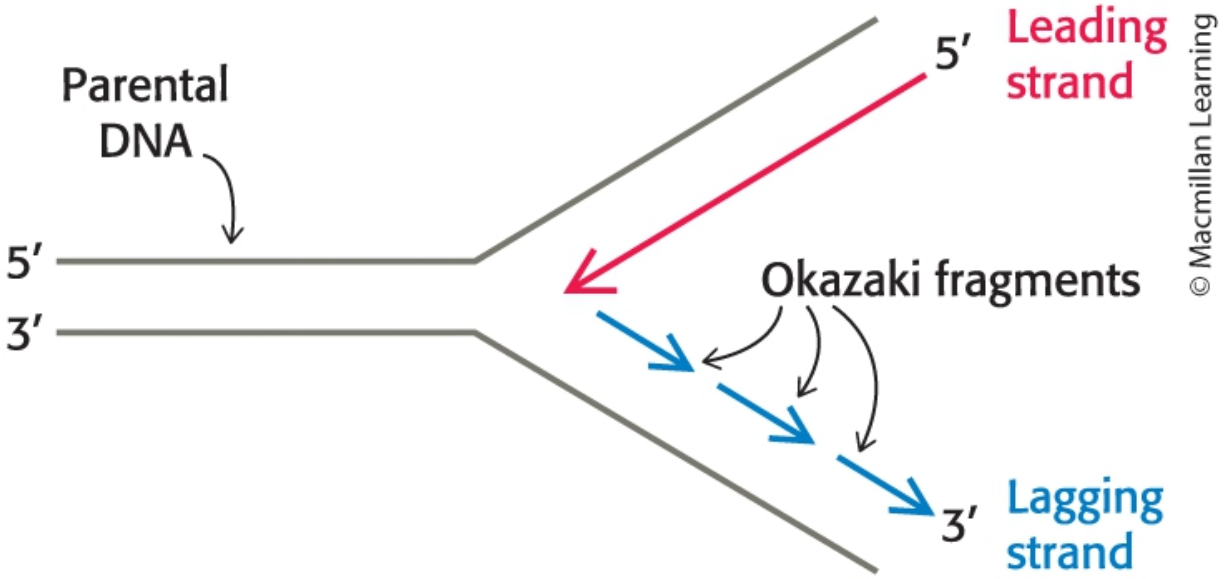
The D N A template is depicted as a horizontal red line. The left end of the D N A template is labeled 3 prime and the right end is labeled 5 prime.

A downward arrow labeled primase is shown below. It shows the attachment of the R N A primer near the 3 prime ends of the D N A template. The R N A primer is depicted as a short horizontal black line. Its left end is labeled 5 prime and the right end is labeled 3 prime. The 5 prime ends of R N A primer is located close to the 3 prime ends.

A downward arrow labeled D N A polymerase is shown below. It shows the synthesis of D N A. A newly synthesized D N A strand is located below the D N A template. It is composed of a short R N A primer at the 5 prime end and the remaining 3 prime region is newly synthesized and shown as a continuous blue line.

Return to FIGURE 28.6 D N A polymerases require a primer

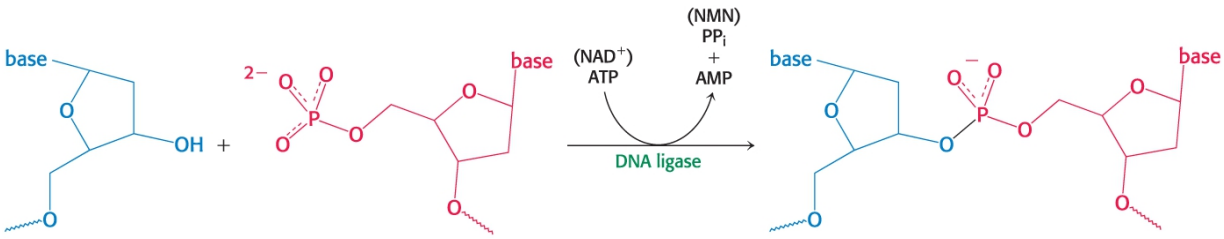
Extended description for FIGURE 28.7 The lagging strand is made in short pieces called Okazaki fragments



A horizontal Y-shaped replication fork is shown. The double-stranded D N A is labeled parental D N A. The 5 prime end of the top D N A strand and 3 prime end of the bottom D N A strand are aligned together. The 3 prime and 5 prime ends of the top and bottom strands are separated to form a Y-shaped structure. The 3 prime end of the top strand is oriented toward the upper right. The 5 prime end of the bottom strand is oriented toward the lower right. A red line parallel to the upper right 3 prime end is labeled leading strand. Its top end is labeled 5 prime and bottom end has an arrowhead pointing toward the replication fork. Three short blue lines separated by short gaps are aligned parallel with the lower right 5 prime end. The bottom end of each blue line has an arrowhead. These short blue lines depict Okazaki fragments. The arrowhead of the terminal Okazaki fragment is labeled 3 prime. These Okazaki fragments are collectively labeled lagging strand.

Return to FIGURE 28.7 The lagging strand is made in short pieces called Okazaki fragments

Extended description for FIGURE 28.8 D N A ligase catalyzes the joining of two D N A strands



The reaction consists of two reactants and one product. It is catalyzed by D N A ligase and coupled with the entry of A T P (N A D superscript plus) and release of A M P plus (N M N) P P subscript i.

The structure of the first reactant is as follows: A 5-membered heterocyclic pentagonal ring is in a horizontal orientation with C 1 occupying the top right vertex. It consists of 1 O and 4 C atoms. O occupies the leftmost vertex. C 1 is single-bonded to base on the upper right. C 3 is single bonded to O H on the right. C 4 is single bonded to C H 2 on the lower left in the form of a line. C H 2 is single bonded to O below. This O has a wiggly line on the lower left.

The structure of the second reactant is as follows: A 5-membered heterocyclic pentagonal ring is in a vertical orientation with C 1 occupying the top right vertex. It consists of 1 O and 4 C atoms. O occupies the topmost vertex. C 1 is single-bonded to the base above. C 3 is single bonded to O on the lower left. This O has a wiggly line on the lower right. C 4 is single bonded to C H 2 on the upper left in the form of a line. C H 2 is single-bonded to O on the lower left. This O is single-bonded to P on the upper left. P is partially double-bonded to O on the upper left, O on the upper right, and O on the lower left. The P O O group has an overall negative charge of 2 minus.

The structure of the product is as follows: A 5-membered heterocyclic pentagonal ring is in a horizontal orientation with C 1 occupying the top right vertex. It consists of 1 O and 4 C atoms. O occupies the leftmost vertex. C 1 is single-bonded to base on the upper right. C 3 is single bonded to O on the right. C 4 is single bonded to C H 2 on the lower left in the form of a line. C H 2 is single bonded to O below. This O has a wiggly line on the lower left. The O bonded to C 3 of the ring is further single bonded to P on the upper right. This P is partially double-bonded to O on the upper left and upper right, and single-bonded to O on the lower right. The lower right O is single bonded to C H 2 on the upper right in the form of a line. This C H 2 is single-bonded to C 4 of a 5-membered heterocyclic pentagonal ring in a vertical orientation with C 1 occupying the top right vertex. It consists of 1 O and 4 C atoms. O occupies the topmost vertex. C 1 is single-bonded to the base above. C 3 is single bonded to O on the lower left. This O has a wiggly line on the lower right.

Return to FIGURE 28.8 D N A ligase catalyzes the joining of two D N A strands

Extended description for FIGURE 28.9 Helicases are hexamers



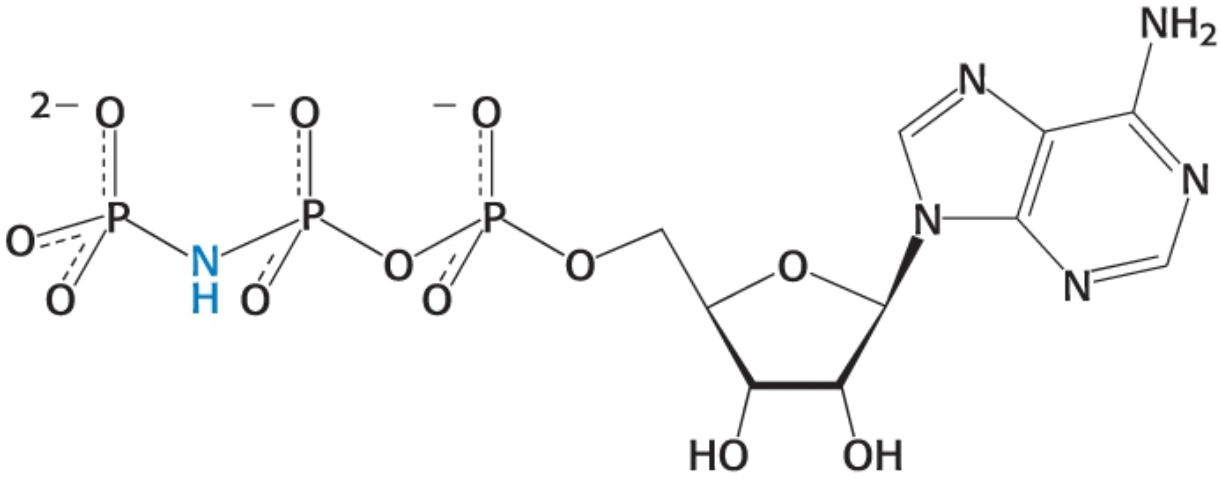
© Macmillan Learning

The helicase is a hexamer composed of 6 subunits. The subunits are arranged in a circular fashion with a hollow center. The subunits are located at the top, bottom, top left, bottom left, top right, and bottom right. Each subunit is composed of several alpha-helices and

a few beta-strands interconnected by loops. Loops from each subunit line the hollow center. The loop of the top subunit is highlighted inside a yellow oval.

Return to FIGURE 28.9 Helicases are hexamers

Extended description for Structure of A M P-P N P



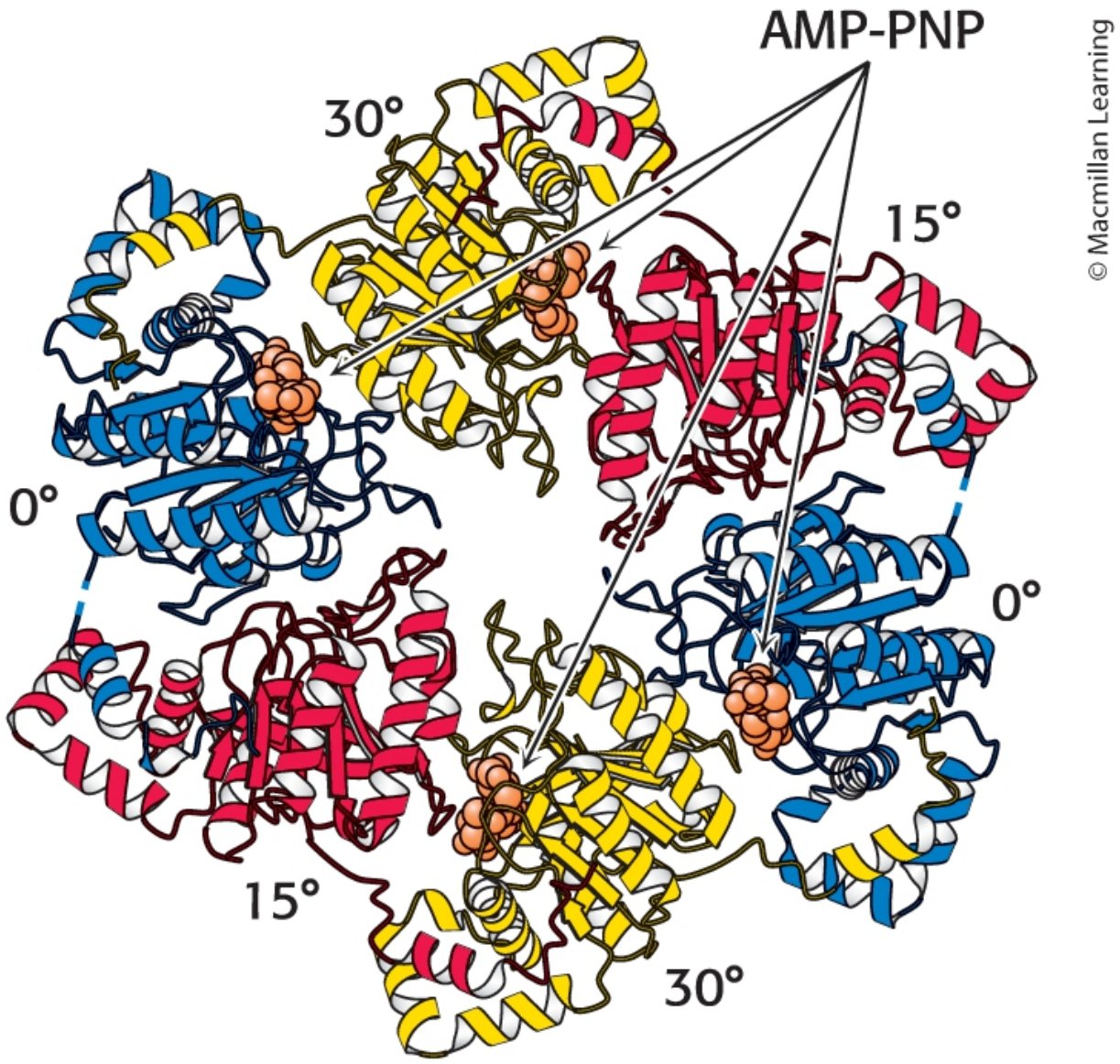
AMP-PNP

The structure of A M P-P N P is as follows: A 5-membered heterocyclic pentagonal ring is in a vertical orientation with C 1 occupying the top right vertex. It consists of 1 O and 4 C atoms. O occupies the topmost vertex. C 2 and C 3 are single bonded to O H below. C 4 is single bonded to C H 2 on the upper left in the form of a line. This C H 2 group is single bonded to a zigzag chain composed of O, single bond, P, single bond, O, single bond, P, single bond, N, single bond, P. N atom of this chain is bound to H and both are highlighted in blue. P 1 and P 2 are each partially double bonded to O above and O on the lower left. The top O has an overall negative charge. P 3 is partially double bonded to O above, O on the left, and O on the lower left. These O atoms have an overall charge of 2 minus. C 1 of the ring is wedge bonded to N 1 of a 5-membered heterocyclic pentagonal ring in a horizontal orientation with C 1 occupying the leftmost vertex. The pentagonal ring consists of 2 N and 3 C atoms. First N occupies the bottom left vertex and the second N occupies the topmost vertex. A double bond is present between C 1 and N 2. This pentagonal ring is fused with a 6-

membered heterocyclic hexagonal ring in a vertical orientation such that C 2 and C 3 of the pentagonal ring are C 3 and C 2 respectively of the hexagonal ring. In the hexagonal ring, C 1 occupies the bottom right vertex. First N occupies the top right vertex and the second N occupies the bottom-most vertex. A double bond is present between C 1 and N 2, C 2 and C 3, and C 4 and N 1. C 1 is single bonded to N H 2 above.

Return to Structure of A M P-P N P

Extended description for FIGURE 28.10 Helicases have intrinsic asymmetry



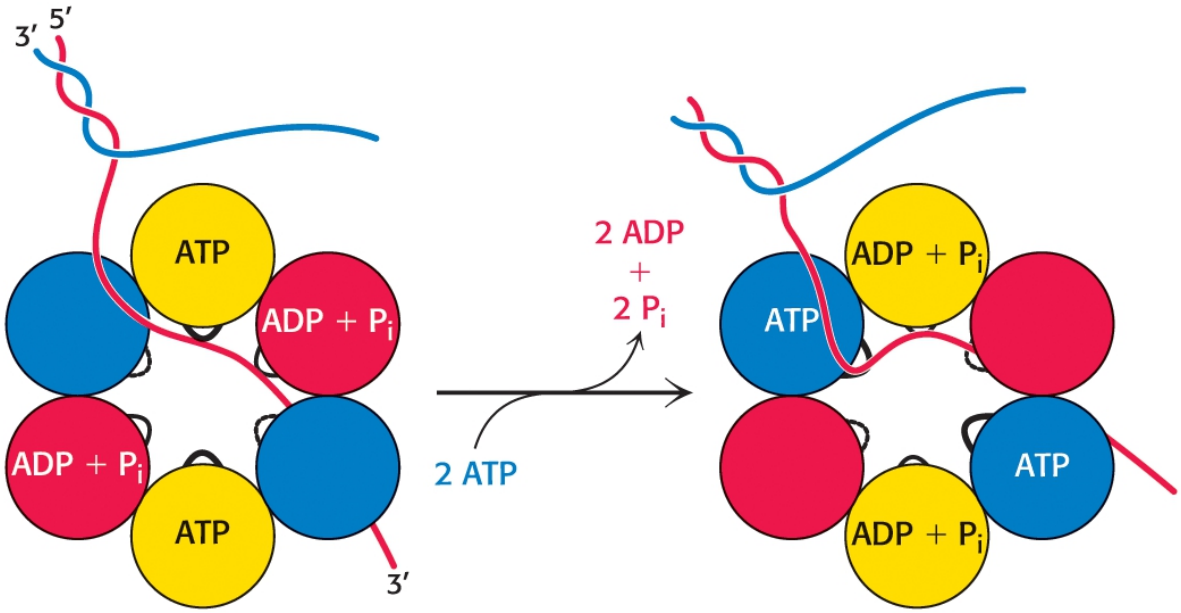
© Macmillan Learning

The helicase is composed of six subunits arranged in a circular fashion. The subunits are located at the top, bottom, top left, bottom left, top right, and bottom right. The top and bottom subunits are shown in yellow. The top left and bottom right subunits are shown in blue. The top right and bottom left subunits are shown in red. The

top and bottom subunits are rotated 30 degrees relative to the plane of the hexamer. The top right and bottom left subunits are rotated 15 degrees relative to the plane of the hexamer. The top left and bottom right subunits are rotated 0 degrees relative to the plane of the hexamer. A cluster of orange spheres depicting A M P-P N P is bound to all the subunits except the top right and bottom left subunits.

Return to FIGURE 28.10 Helicases have intrinsic asymmetry

Extended description for FIGURE 28.11 Helicases unwind D N A



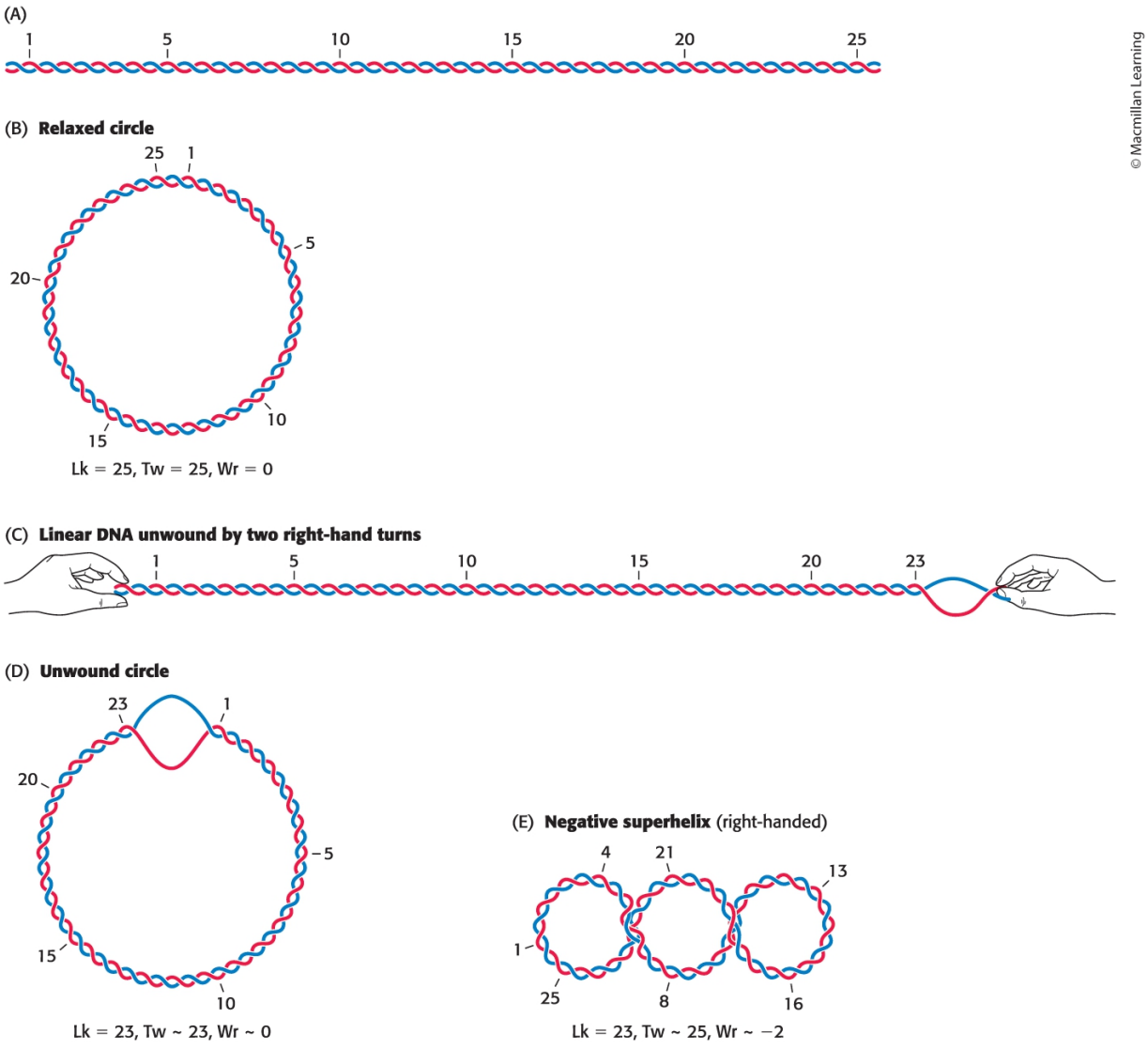
© Macmillan Learning

The helicase is depicted as a ring-like structure composed of 6 subunits depicted as medium-sized circles. It has a hollow interior. The top and bottom circles are yellow colored. The top right and bottom left circles are red colored. The top left and bottom right circles are blue-colored. The top and bottom subunits are bound to A T P. The top right and bottom left subunits are bound to A D P plus P subscript i. A small loop from each circle lines the hollow interior. A "D N A helix" is shown on the top right. It is composed of two strands shown in red and blue. The 3 prime and 5 prime ends of the strands are aligned with each other. The D N A helix is unwound such that the red D N A strands pass through the hollow interior of the helicase. It is attached with the loops of the top yellow and top right red circles. The other end of the red strand that extends outside through the helicase is labeled 3 prime.

A forward arrow shows the conformational change in helicase hexamer after A T P binding to the top left and bottom right blue circles and release of A D P plus P subscript i from the top right and bottom left subunits. In the hexamer, the top and bottom yellow circles are bound to A D P plus P subscript i. The red strand of the helix is pulled through the helicase. It is attached to the loops of the top and top left circles.

Return to FIGURE 28.11 Helicases unwind D N A

Extended description for FIGURE 28.12 The linking number (L k), twist (T w), and writhe (W r) of circular DNA are related



© Macmillan Learning

Part (A): A linear D N A double helix is shown in horizontal orientation. The first complete turn of the strands around each other is numbered 1. From left to right, the number of complete turns is numbered 1, 5, 10, 15, 20, and 25.

Part (B): A relaxed circular double helical D N A is shown. It is marked 1, 5, 10, 15, 20, and 25 starting from the top in a clockwise direction. The markings depict the number of complete turns. Note: Linking number equals 25, twist equals 25, and writhe equals 0.

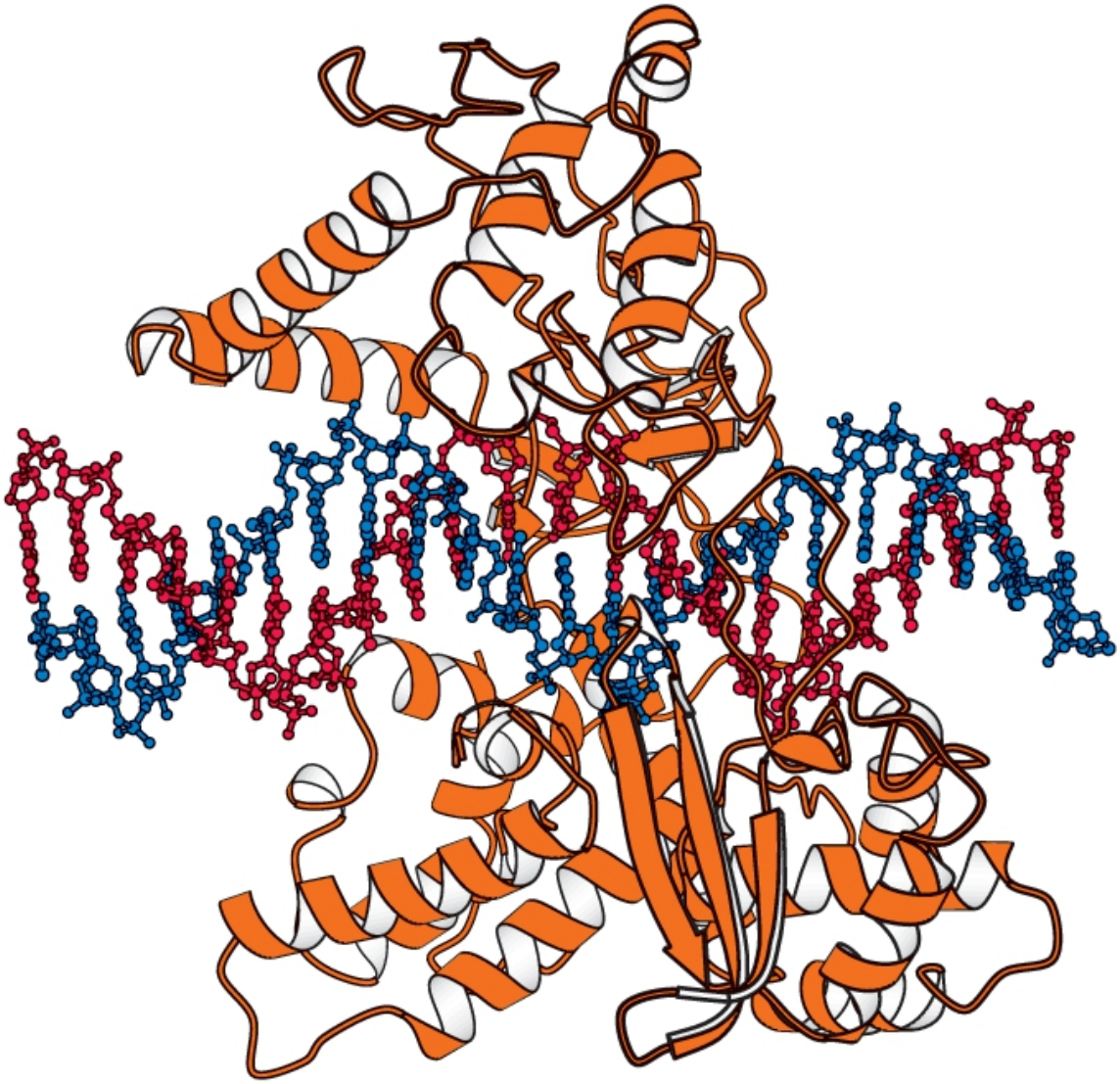
Part (C): A linear D N A double helix unwound by two right-hand turns is shown in horizontal orientation. The first complete turn of the strands around each other is numbered 1. From left to right, the number of complete turns is numbered 1, 5, 10, 15, 20, and 23. A hand is holding the left end of the linear D N A. The right end is unwound and another hand is holding the unwound end.

Part (D): An unwound circular double helical D N A is shown. It is marked 1, 5, 10, 15, 20, and 23 starting from the top right in a clockwise direction. The markings depict the number of complete turns. The topmost region of the circular helix is unwound to form a bubble. Note: Linking number equals 23, the twist is approximately 23, and the writhe is approximately 0.

Part (E): It shows a right-handed negative superhelix. The circular D N A double helix is twisted upon itself to form three adjacent and continuous ring-like structures. The left ring is marked 1, 4, and 25 in a clockwise direction starting at the left end. The middle ring is marked 21 and 8 at the top and bottom. The right ring is marked 13 and 16 at the top right and bottom. Note: Linking number equals 23, the twist is approximately 23, and writhe is negative 2.

Return to FIGURE 28.12 The linking number (L k), twist (T w), and writhe (W r) of circular DNA are related

Extended description for FIGURE 28.14 Topoisomerase 1 binds to D N A



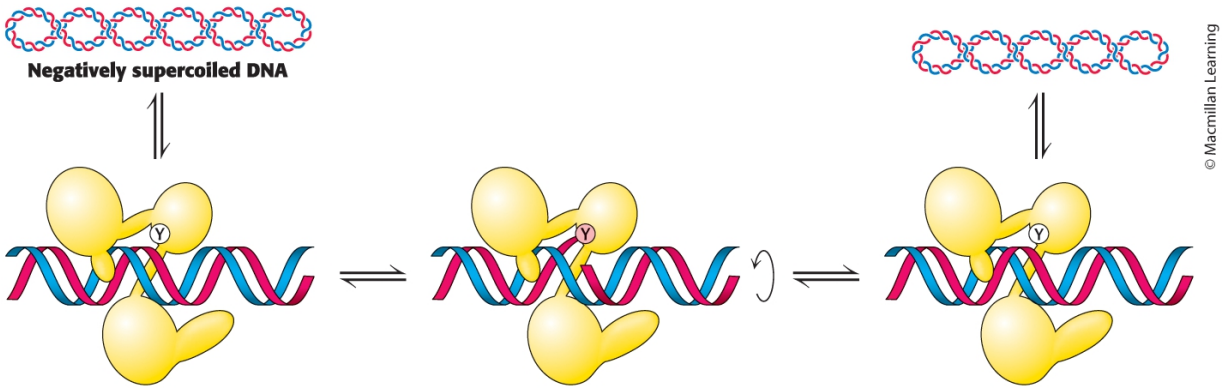
© Macmillan Learning

The fragment of human topoisomerase 1 is bound to D N A double helix in horizontal orientation. The strands of the double helix are composed of blue and red spheres. The helix passes through a central cavity in the topoisomerase. Topoisomerase 1 is composed of a cluster of alpha-helices and beta-strands at the top and bottom. These clusters are separated by a small gap or central cavity through

which the D N A helix passes. The clusters are connected by long threads.

Return to FIGURE 28.14 Topoisomerase 1 binds to D N A

Extended description for FIGURE 28.15 Topoisomerase 1 relaxes supercoiled D N A



© Macmillan Learning

A negatively supercoiled double helical D N A contains six adjacent and continuous ring-like structures. It reversibly binds to topoisomerase 1. A short stretch of D N A double helix in horizontal orientation is bound to topoisomerase 1.

Topoisomerase 1 is composed of 3 spherical structures interconnected by short tubes. Two spherical structures are located above and the third spherical structure is located below the helix. The second spherical structure contains a tyrosine residue depicted as a tiny circle labeled Y.

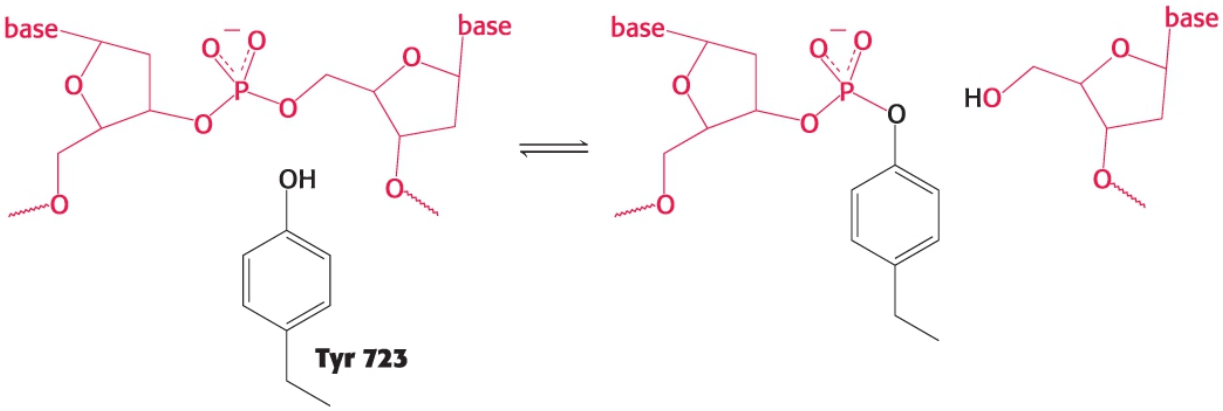
An irreversible arrow shows the topoisomerase 1 bound to the D N A helix. One of the strands is nicked such that one end of the nicked strand is bound to the tyrosine residue. An anticlockwise arrow depicts the rotation of the cleaved strand.

An irreversible arrow shows the topoisomerase bound to the re-ligated D N A.

An irreversible arrow shows a coiled double helical D N A composed of five adjacent and continuous ring-like structures.

Return to FIGURE 28.15 Topoisomerase 1 relaxes supercoiled D N A

Extended description for Cleavage of phosphodiester bond by the tyrosine residue of topoisomerase



The reaction includes two reactants and two products.

The structure of the first reactant is as follows: A 5-membered heterocyclic pentagonal ring is in a horizontal orientation with C 1 occupying the top right vertex. It consists of 1 O and 4 C atoms. O occupies the leftmost vertex. C 1 is single-bonded to base on the upper right. C 3 is single bonded to O on the right. C 4 is single bonded to C H 2 on the lower left in the form of a line. C H 2 is single bonded to O below. This O has a wiggly line on the lower left. The O bonded to C 3 of the ring is further single bonded to P on the upper right. This P is partially double-bonded to O on the upper left and upper right, and single-bonded to O on the lower right. The lower right O is single bonded to C H 2 on the upper right in the form of a line. This C H 2 is single-bonded to C 4 of a 5-membered heterocyclic pentagonal ring in a vertical orientation with C 1 occupying the top right vertex. It consists of 1 O and 4 C atoms. O occupies the topmost vertex. C 1 is single-bonded to the base above. C 3 is single bonded to O on the lower left. This O has a wiggly line on the lower right.

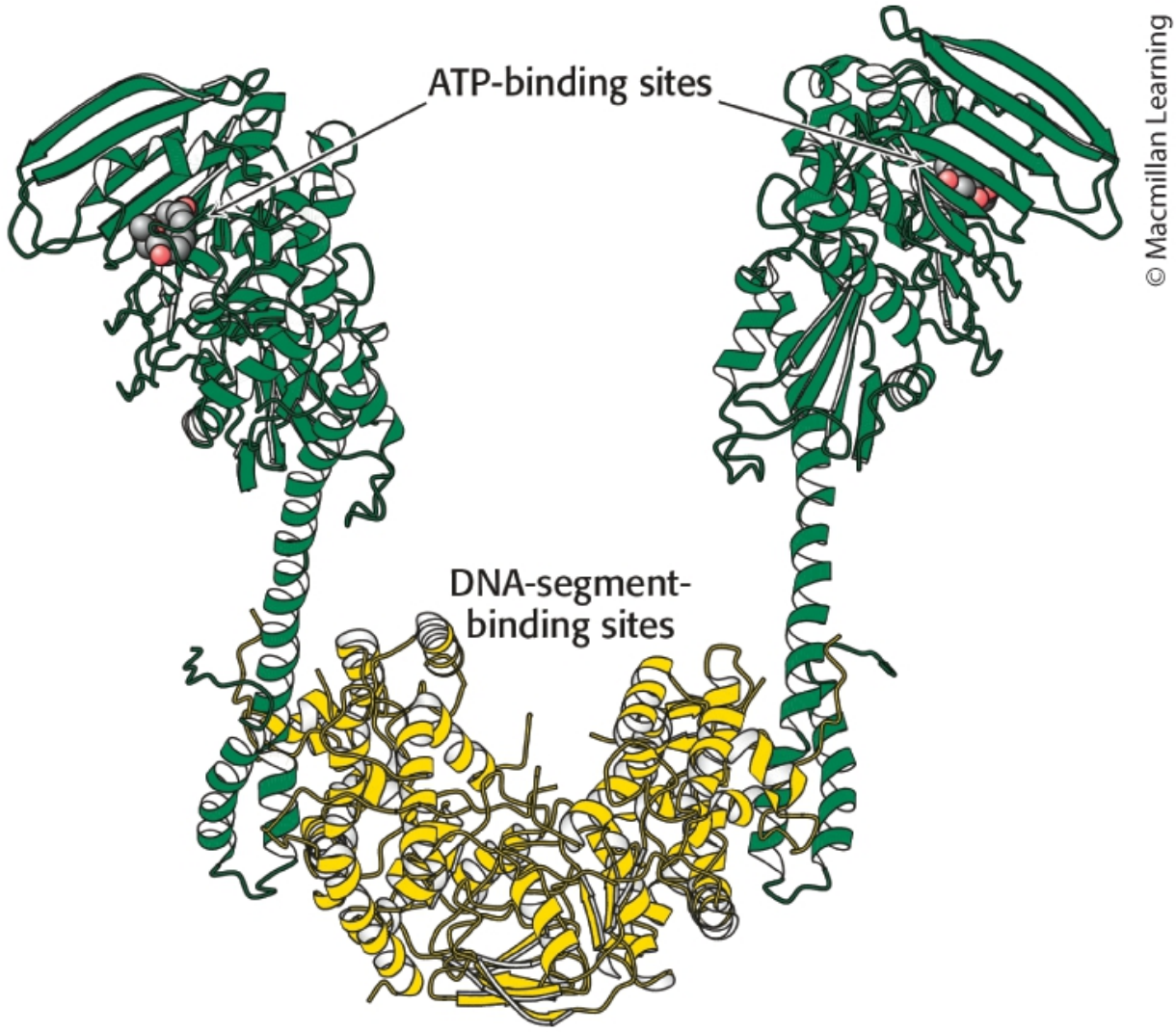
The second reactant is tyrosine 723 whose structure is as follows: A benzene ring is in a vertical orientation with C 1 occupying the topmost vertex. It contains alternating double bonds between C 1 and C 2, C 3 and C 4, and C 5 and C 6. C 4 is single bonded to C H 2 below in the form of a line. C H 2 has an open single bond on the lower right.

The structure of the first product is as follows: A 5-membered heterocyclic pentagonal ring is in a horizontal orientation with C 1 occupying the top right vertex. It consists of 1 O and 4 C atoms. O occupies the leftmost vertex. C 1 is single-bonded to base on the upper right. C 3 is single bonded to O on the right. C 4 is single bonded to C H 2 on the lower left in the form of a line. C H 2 is single bonded to O below. This O has a wiggly line on the lower left. The O bonded to C 3 of the ring is further single bonded to P on the upper right. This P is partially double-bonded to O on the upper left and upper right, and single-bonded to O on the lower right. The lower right O is single-bonded to C 1 of a benzene ring in a vertical orientation. The benzene ring contains alternating double bonds between C 1 and C 2, C 3 and C 4, and C 5 and C 6. C 4 is single bonded to C H 2 below in the form of a line. C H 2 has an open single bond on the lower right.

The structure of the second product is as follows: A 5-membered heterocyclic pentagonal ring is in a vertical orientation with C 1 occupying the top right vertex. It contains 1 O and 4 C atoms. O occupies the topmost vertex. C 1 is single-bonded to the base above. C 3 is single bonded to O on the lower left. This O has a wiggly line on the lower right. C 4 is single bonded to C H 2 on the upper left in the form of a line. This C H 2 is single-bonded to O H on the lower left.

Return to Cleavage of phosphodiester bond by the tyrosine residue of topoisomerase

Extended description for FIGURE 28.16 Topoisomerase 2 is a dimer

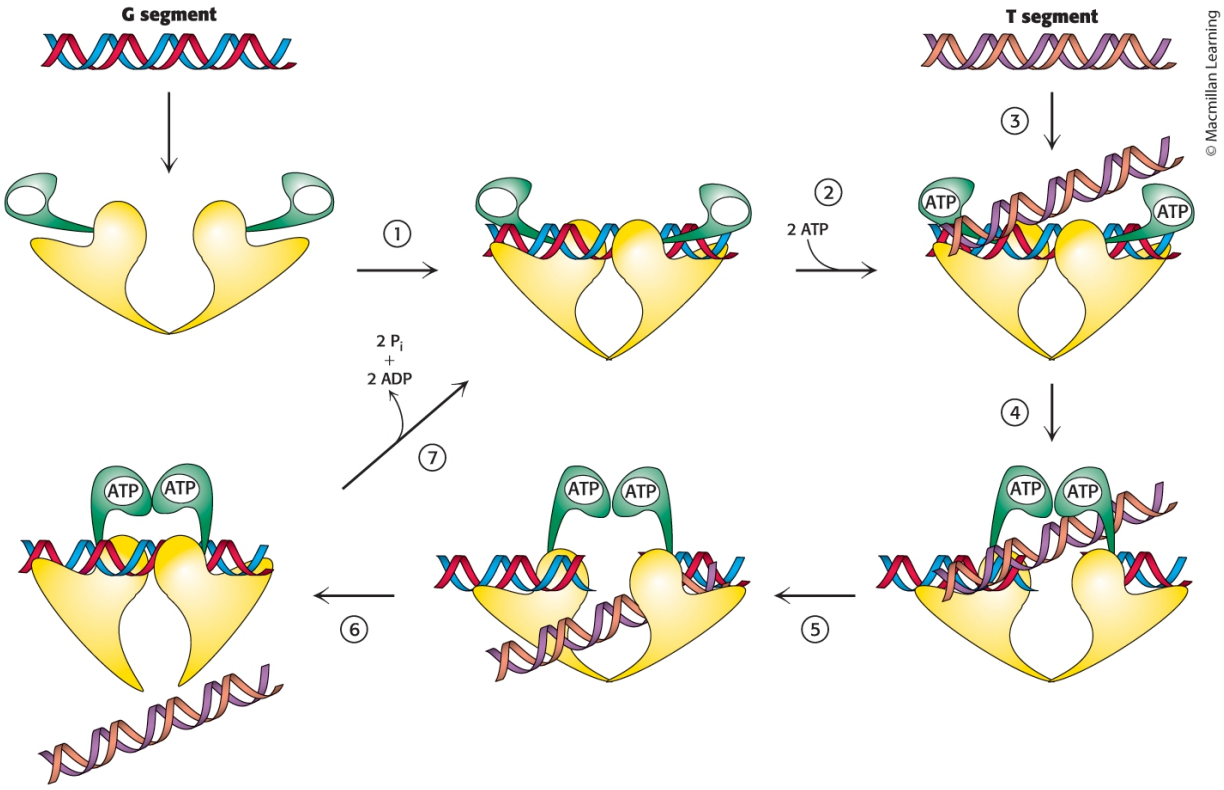


Topoisomerase 2 is a dimer composed of the left and right subunits. Each subunit has two domains. The bottom domain shown in yellow is small and composed of several alpha-helices. The top domain is shown in green and is composed of a cluster of alpha-helices and beta-strands at the top. A long and vertical alpha-helix extends below the top domain and is connected with another short alpha-

helix. These alpha-helices are associated with the bottom domain. The top cluster of the top domain contains an A T P-binding site bound to a cluster of spheres. The bottom domain contains D N A-segment binding sites.

Return to FIGURE 28.16 Topoisomerase 2 is a dimer

Extended description for FIGURE 28.17 Topoisomerase 2 uses A T P hydrolysis to introduce negative supercoils into D N A



In the first step, a double helical D N A fragment labeled G segment binds to topoisomerase 2. The topoisomerase is depicted as a pair of yellow-colored structures connected at the bottom. The top portion of the yellow structure is broad and the bottom portion is tapered and pointed. In the unbound state, the top portion of the yellow structures is separated. A small green structure is connected to the top of each yellow structure through its pointed tail. The broad portion of each green structure contains an empty site. The G segment is binds to the top portion of the yellow structure. In the D N A bound state, the top portion of the yellow structures is joined.

In the second step, 2 A T P molecules enter the complex. These A T P molecules bind to the empty site of each small green structure.

In the third step, the T segment of D N A binds to the complex of the topoisomerase and G segment. The T segment is in diagonal orientation and bound to the top of the left yellow structure.

In the fourth step, the G segment is cleaved and the top portions of the yellow structures are separated. The small green structures bound to A T P join together to form an arch-shaped structure above the yellow structure. The T segment passes diagonally below the arch-shaped structure.

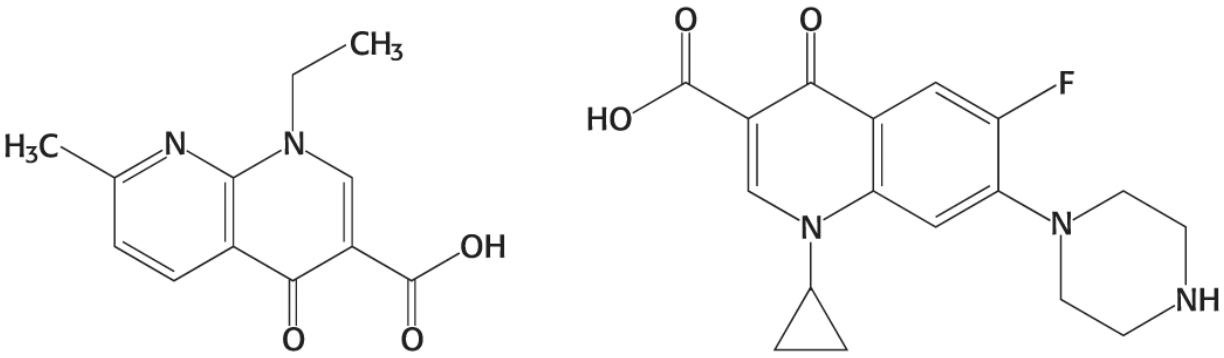
In the fifth step, the T segment is shifted below and it passes diagonally through the hollow cavity between the left and right yellow structures.

In the sixth step, the pointed bottom ends of the yellow structures separate to release the T segment. The G segment is re-ligated.

In the seventh step, 2 A D P plus 2 P subscript i are released from the small green structures due to A T P hydrolysis. The green structures separate from each again and the topoisomerase bound to re-ligated D N A attains the original conformation as observed in step 1.

Return to FIGURE 28.17 Topoisomerase 2 uses A T P hydrolysis to introduce negative supercoils into D N A

Extended description for Structure of nalidixic acid and ciprofloxacin



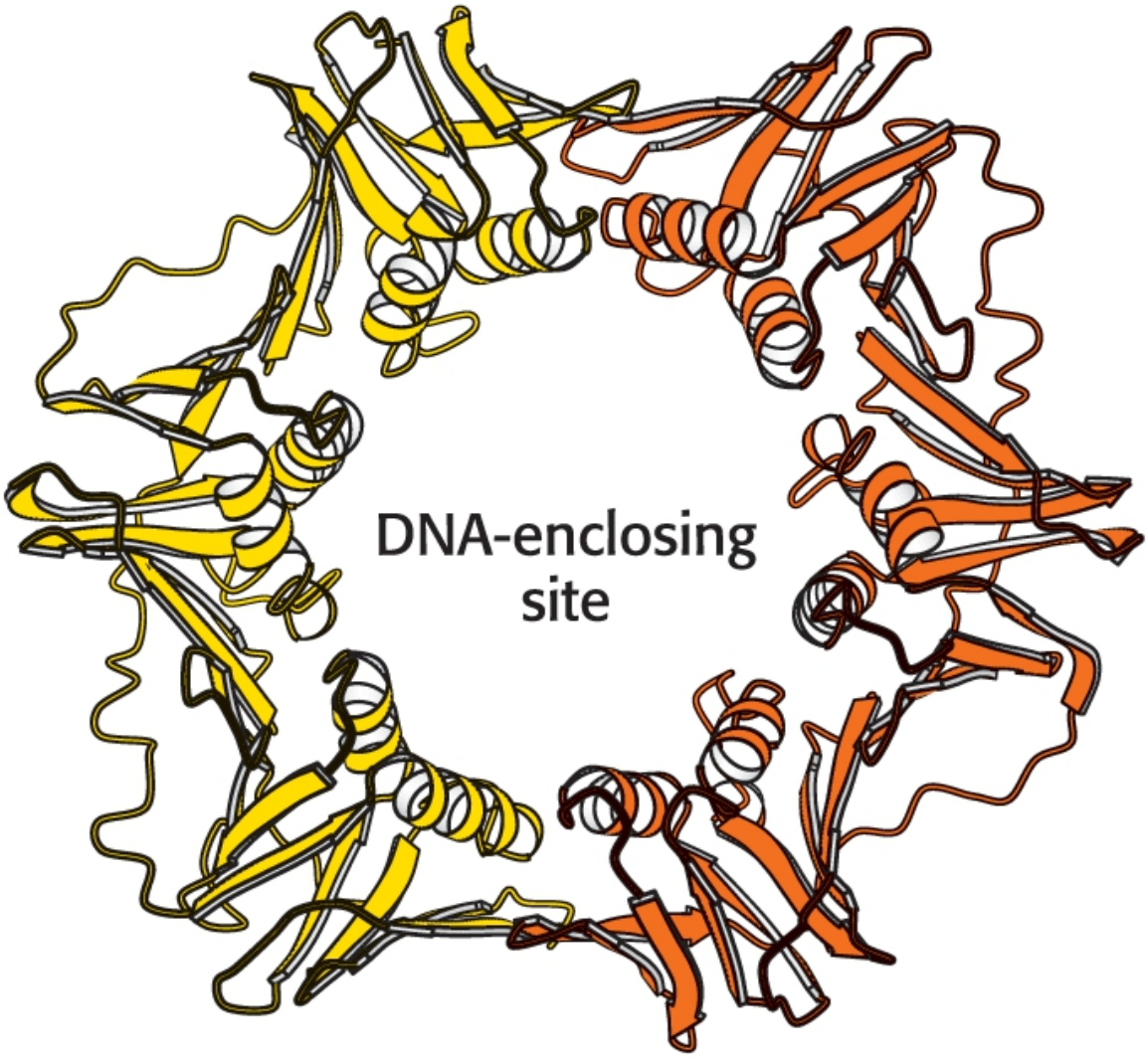
The structure of nalidixic acid is as follows: A 6-membered heterocyclic hexagonal ring is in a vertical orientation with C 1 occupying the top right vertex. It consists of 1 N and 5 C atoms. N occupies the topmost vertex. A double bond is present between C 1 and C 2, C 3 and C 4, and C 5 and N. C 5 is single bonded to C H 3 on the upper left. This hexagonal ring is fused to a second 6-membered heterocyclic hexagonal ring in a vertical orientation such that C 1 and C 2 of the first ring are C 5 and C 4 respectively of the second ring. The second hexagonal ring consists of 1 N and 5 C atoms. N occupies the topmost vertex. A double bond is present between C 1 and C 2. N is single bonded to C H 2 above in the form of a line, which is further single bonded to C H 3 on the upper right. C 2 is single bonded to C on the lower right. This C is double bonded to O below and single bonded to O H on the upper right. C 3 is double bonded to O below.

The structure of ciprofloxacin is as follows: A 6-membered heterocyclic hexagonal ring is in a vertical orientation with C 1 occupying the bottom left vertex. It contains 1 N and 5 C atoms. N occupies the bottom-most vertex. A double bond is present between

C 1 and C 2. C 2 is single-bonded to C on the upper left. This C is double bonded to O above and single bonded to O H on the lower left. C 3 is double bonded to O above. N is single-bonded to C 1 of a triangular ring. The hexagonal ring is fused to a benzene ring in a vertical orientation such that C 4 and C 5 of the hexagonal ring are C 6 and C 5 respectively of the benzene ring. The benzene ring contains alternating double bonds between C 1 and C 2, C 3 and C 4, and C 5 and C 6. C 2 is single bonded to F on the upper right. C 3 is single-bonded to N 1 of a 6-membered heterocyclic hexagonal ring in a vertical orientation. This hexagonal ring consists of 2 N and 4 C atoms. First N occupies the top left vertex. The second N bound to H occupies the bottom right vertex.

Return to Structure of nalidixic acid and ciprofloxacin

Extended description for FIGURE 28.18 The sliding clamp subunit of D N A polymerase 3 is a dimer

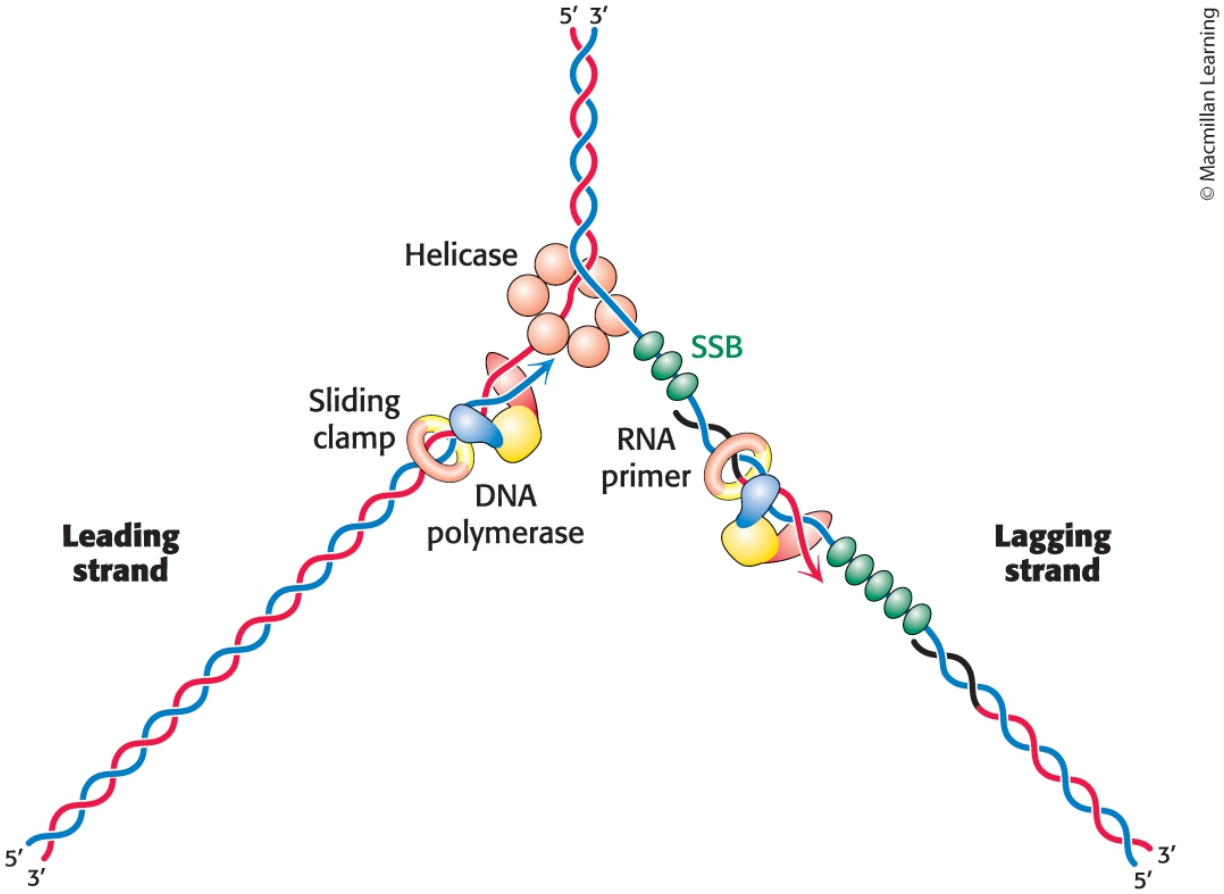


© Macmillan Learning

The sliding clamp subunit is depicted as a hollow ring-like structure. It is a dimer composed of left and right subunits. The left subunit is shown in yellow and the right subunit is shown in orange. Each subunit is composed of three clusters of beta-strands. Each cluster is connected to a few alpha-helices. These alpha-helices line the hollow interior of the ring. The hollow interior is labeled the "D N A-enclosing site."

Return to FIGURE 28.18 The sliding clamp subunit of D N A polymerase 3 is a dimer

Extended description for FIGURE 28.19 D N A synthesis at the replication fork is highly coordinated



© Macmillan Learning

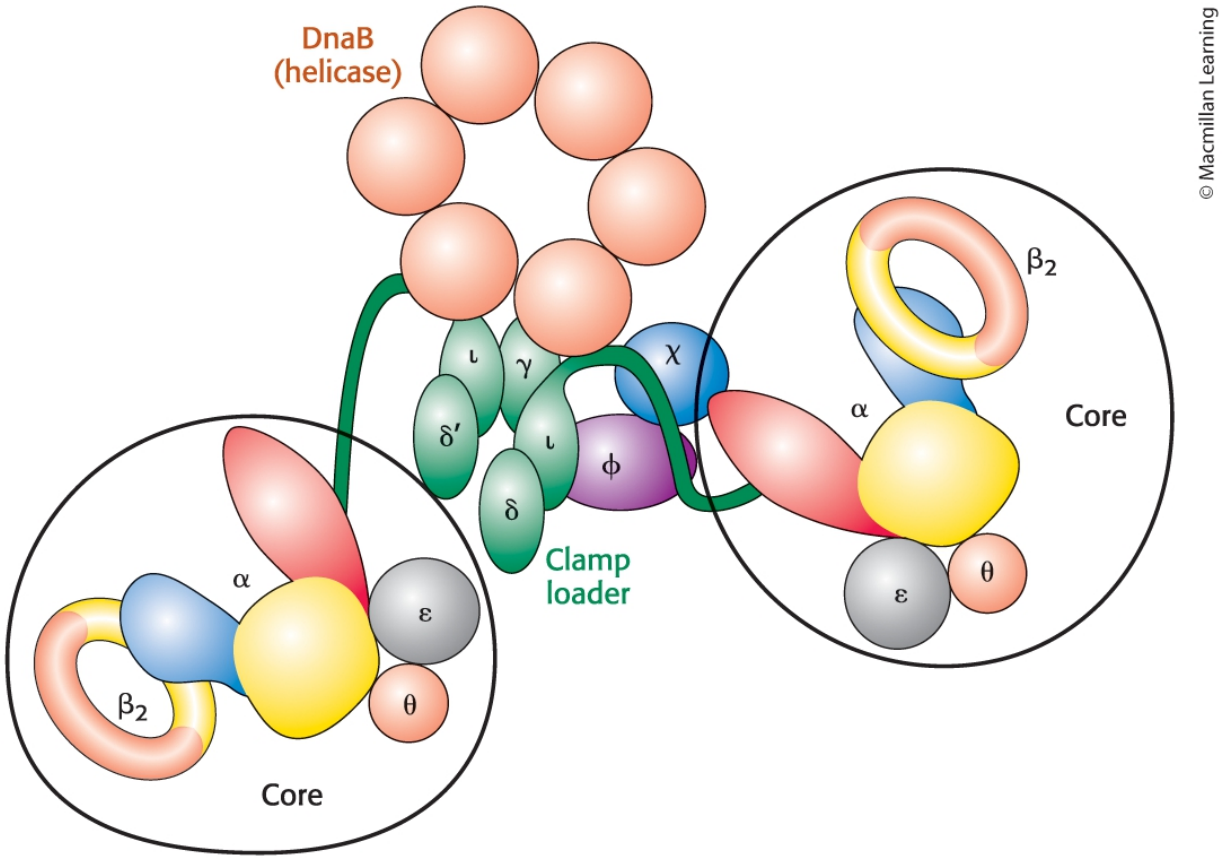
The replication fork is depicted as an inverted Y-shaped structure. The 5 prime and 3 prime ends of the parental D N A are aligned together. The lower left segment is labeled leading strand and the lower right segment is labeled lagging strand. The leading strand is synthesized using the red strand of the parental D N A as the template. It is synthesized in 5 prime to 3 prime direction from the 3 prime end of the parental strand, away from the replication fork. The red parental strand is surrounded by a helicase at the replication fork. The helicase is a hollow ring-like structure composed of 6 spherical subunits. The D N A polymerase is bound at

the 3 prime end of the leading strand, near the replication fork. The hollow ring-like sliding clamp of D N A polymerase allows the passage of a newly formed double helix through it.

The lagging strand is synthesized using the blue strand of the parental D N A ad the template. It is synthesized discontinuously in 5 prime to 3 prime direction from the 3 prime end of the parental strand near the replication fork. Two short Okazaki fragments of the lagging strand are synthesized. Each fragment contains the primer at the 5 prime end. Several S S B depicted as green ovals are bound to the blue parental strand near the replication and between the Okazaki fragments. The D N A polymerase is bound to the 3 prime end of one Okazaki fragment. The newly synthesized double helix passes through the sliding clamp of D N A polymerase.

Return to FIGURE 28.19 D N A synthesis at the replication fork is highly coordinated

Extended description for FIGURE 28.20 The D N A polymerase holoenzyme consists of multiple subunits



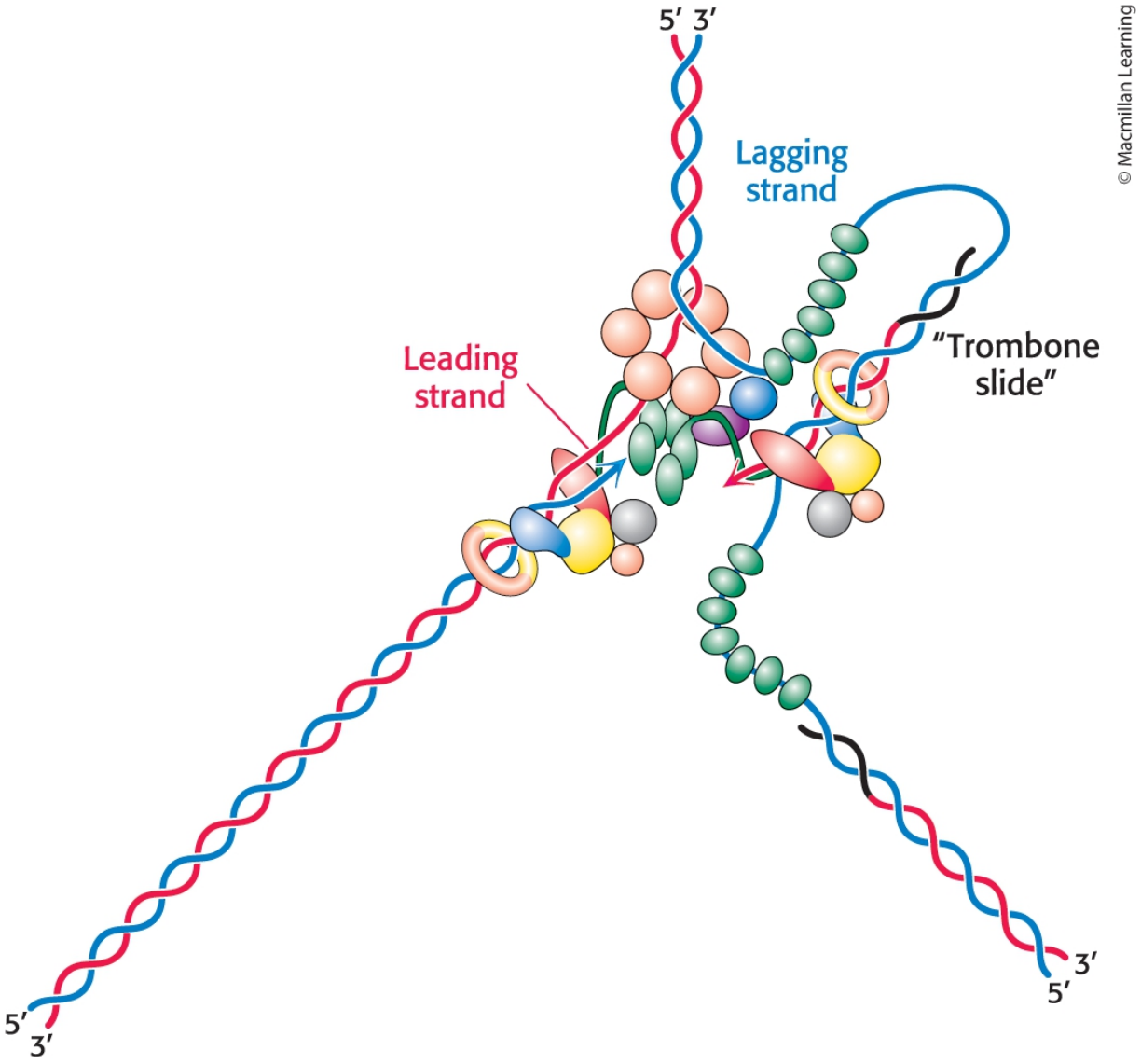
© Macmillan Learning

The D N A polymerase holoenzyme is composed of a central structure connected to two copies of the polymerase core enzyme. Each core enzyme is shown inside a circle with a black outline. It contains an alpha subunit, an epsilon subunit, a theta subunit, and a beta 2 subunit. The alpha subunit is depicted as a round structure connected to two vertical elongated structures on the top left and top right. One of these elongated structures is connected to the hollow ring-like beta 2 subunit. The epsilon and theta subunits are depicted as small round structures.

The central structure is composed of a clamp loader and D n a B (helicase). The helicase is a hollow ring-like structure composed of six circular subunits. It is connected to the elongated structure of the alpha subunit of one of the polymerase core enzymes. The clamp loader is composed of one gamma subunit, two tau subunits, one delta subunit, and one delta prime subunit. These subunits are depicted as green ovals. The other two subunits of the central structure are phi and chi. One of the tau subunits of the clamp loader is connected to the elongated structure of the alpha subunit of the second polymerase core enzyme.

Return to FIGURE 28.20 The D N A polymerase holoenzyme consists of multiple subunits

Extended description for FIGURE 28.21 The trombone model describes the coordination of D N A synthesis at the replication fork



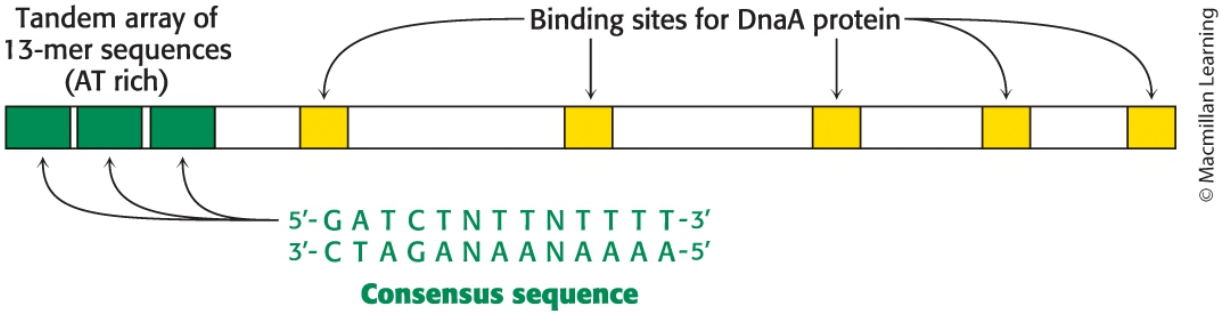
© Macmillan Learning

D N A replication is shown at the replication fork. The model shows the coordination of lagging strand and leading strand replication. The blue parental strand serving as the template of the lagging strand is looped out. It leads to the formation of a trombone slide-

like structure by the looped-out blue strand. D N A polymerase holoenzyme is associated with the replication fork. A polymerase core enzyme is involved in the synthesis of the leading and lagging strands.

Return to FIGURE 28.21 The trombone model describes the coordination of D N A synthesis at the replication fork

Extended description for FIGURE 28.22 The *E. coli* chromosome has a single origin of replication



The *ori* C is depicted as a horizontal bar. The left end of the bar contains three green square boxes separated by a narrow gap. These boxes depict the tandem array of 13-mer sequences (A T rich). The consensus sequence of 13-mer sequence is as follows:

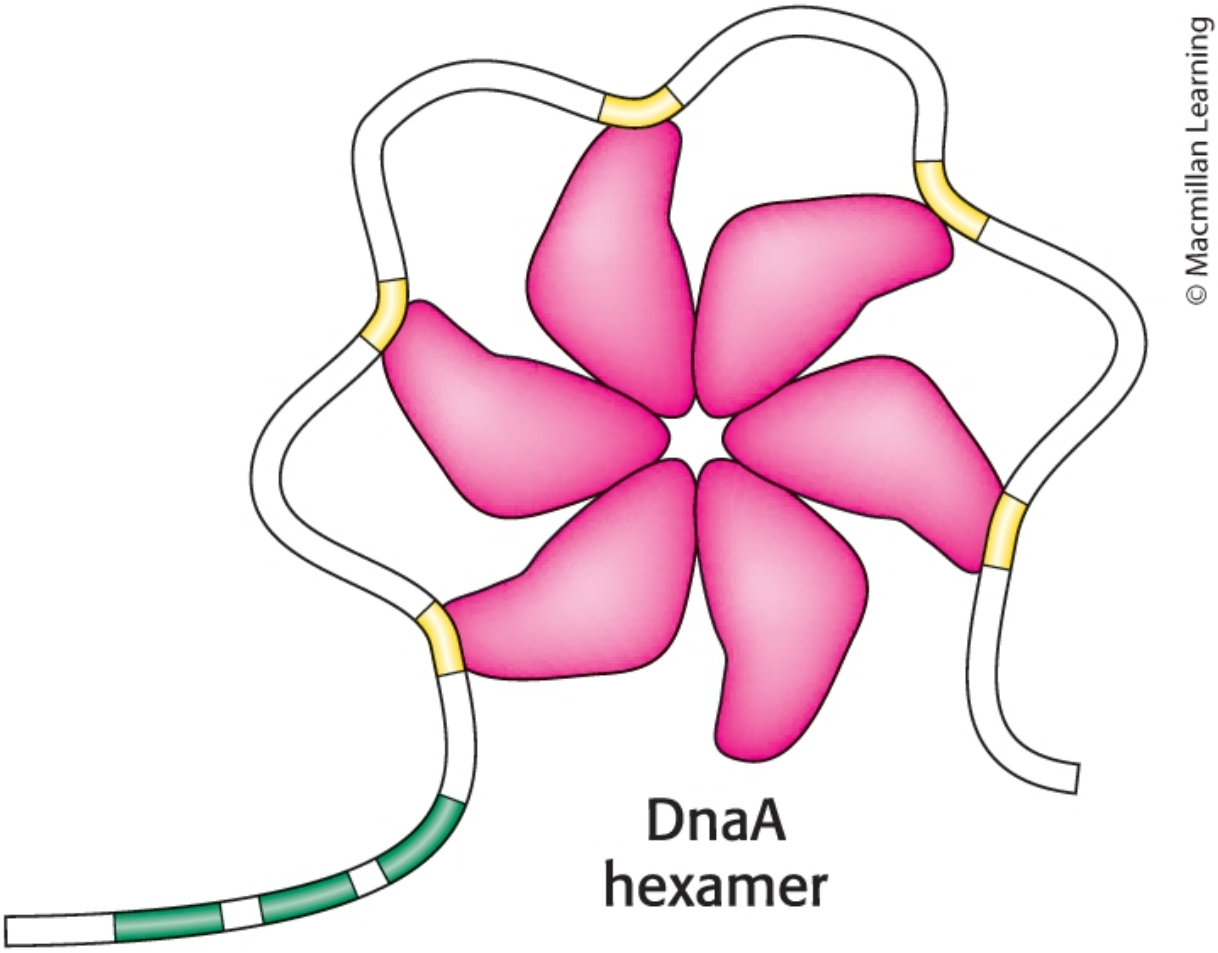
Top strand: 5 prime, G A T C T N T T N T T T T, 3 prime.

Bottom strand: 3 prime, C T A G A N A A N A A A A, 5 prime.

The 13-mer sequences are followed by binding sites for D n a A protein depicted as five yellow square boxes separated by a large gap. The fifth box is located at the right end.

Return to FIGURE 28.22 The *E. coli* chromosome has a single origin of replication

Extended description for FIGURE 28.23 The assembly of D n a A proteins initiates D N A replication

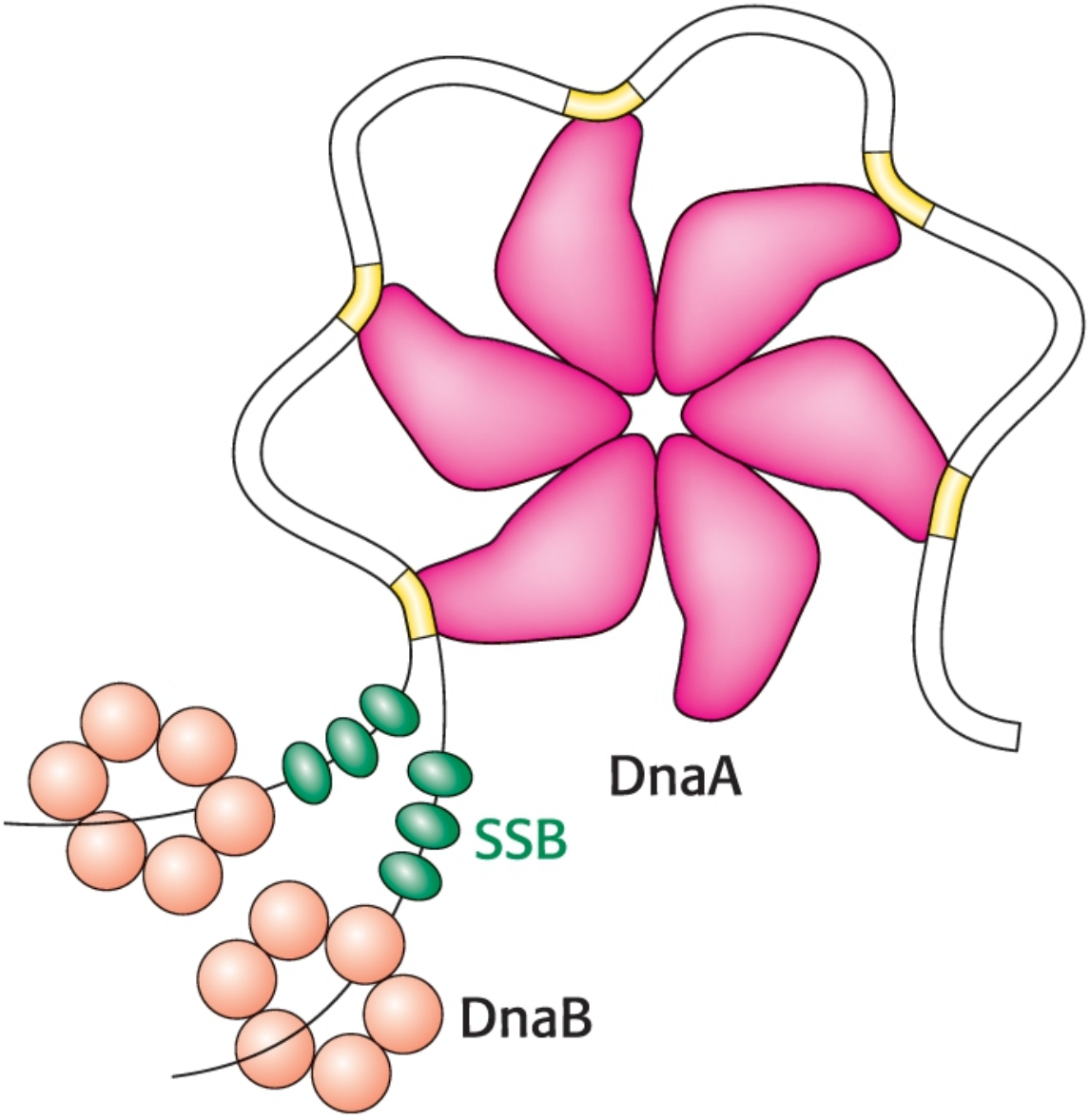


© Macmillan Learning

The large and slightly curved D n a A protein monomers are bound to the yellow sites on the *ori* C. The monomers bound to different yellow sites on *ori* C join together at a common central point to form a D n a A hexamer having a flower-like structure. The protein monomers resemble the petals of a flower. The hexamer is surrounded by the *ori* C segment containing the yellow sites. The segment of ori C containing a tandem array of 13-mer sequence extends toward the lower left.

Return to FIGURE 28.23 The assembly of D n a A proteins initiates D N A replication

Extended description for FIGURE 28.24 The prepriming complex prepares the template strands for D N A synthesis



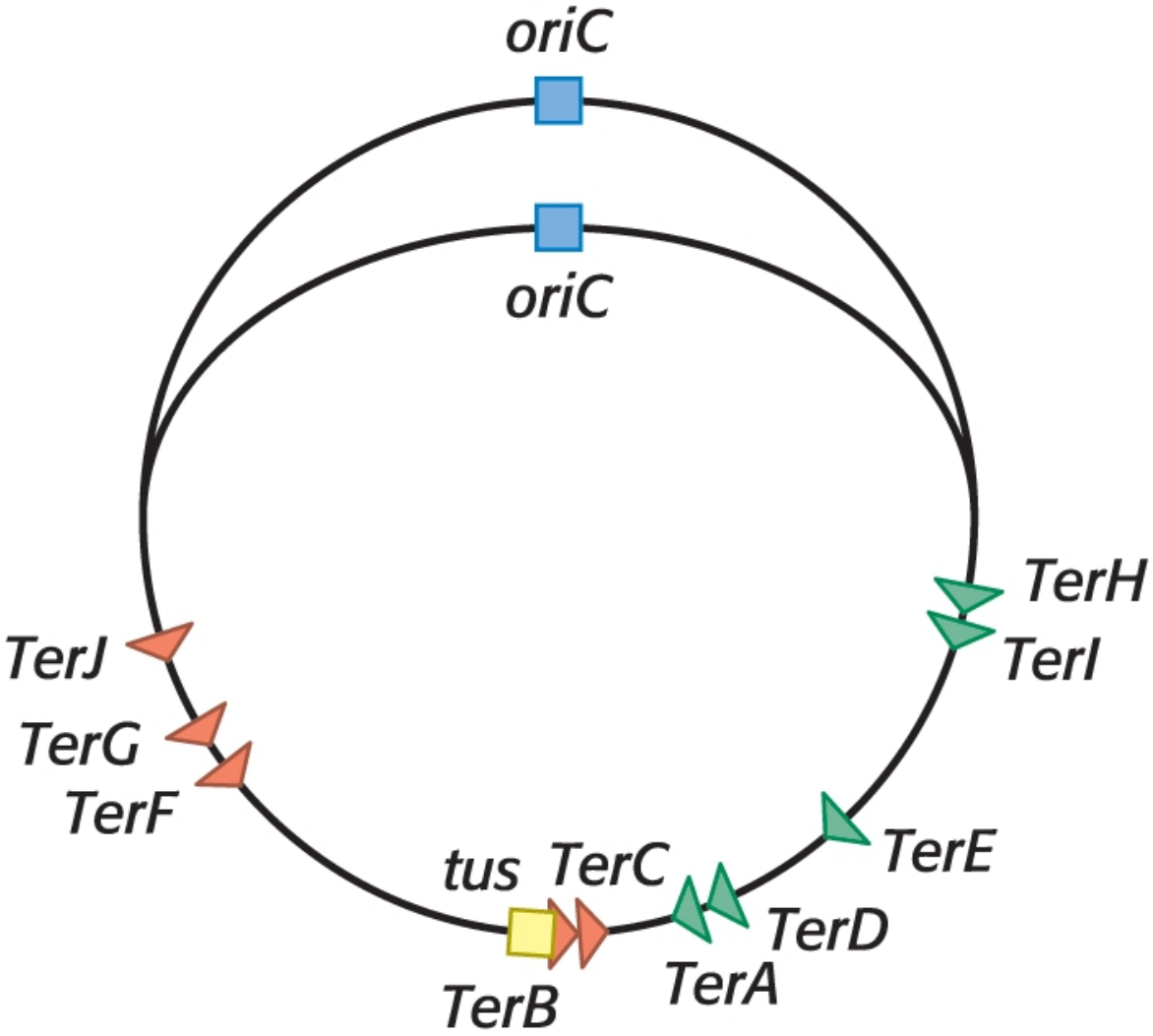
© Macmillan Learning

The D n a A hexamer is attached to the yellow sites on *ori* C. The segment of *ori* C containing a tandem array of 13-mer sequence extends toward the lower left. The 13-mer sequences are unwound

and bound by S S B depicted as green ovals. D n a B hexamer depicted as a hollow ring-like structure composed of 6 spheres is loaded on each strand behind the S S B proteins.

Return to FIGURE 28.24 The prepriming complex prepares the template strands for D N A synthesis

Extended description for FIGURE 28.25 Replication termination in *E. coli* occurs at T e r sites



© Macmillan Learning

The circular E. coli genome with replicated ori C at the top is shown. The replication starts at the ori C and proceeds bidirectionally. The remaining bottom portion of the genome is not yet replicated. Three T e r sites are shown on the bottom left portion of genome. These sites are labeled T e r J, T e r G, and T e r F from top to bottom and are depicted as orange downward-pointing triangles. Five T e r sites are spread from right to bottom right. These are depicted as green

triangles with their apex oriented below. These sites are labeled T e r H, T e r I, T e r E, T e r D, and T e r A from top to bottom. T e r H and T e r I, and T e r D, and T e r A are tandemly located. T e r B and T e r C are tandemly located at the bottom and depicted as orange triangles with their apex oriented toward the right. A tiny yellow square depicting tus is bound to T e r B.

Return to FIGURE 28.25 Replication termination in *E. coli* occurs at T e r sites

Extended description for FIGURE 28.26 Eukaryotic chromosomes have multiple origins of replication



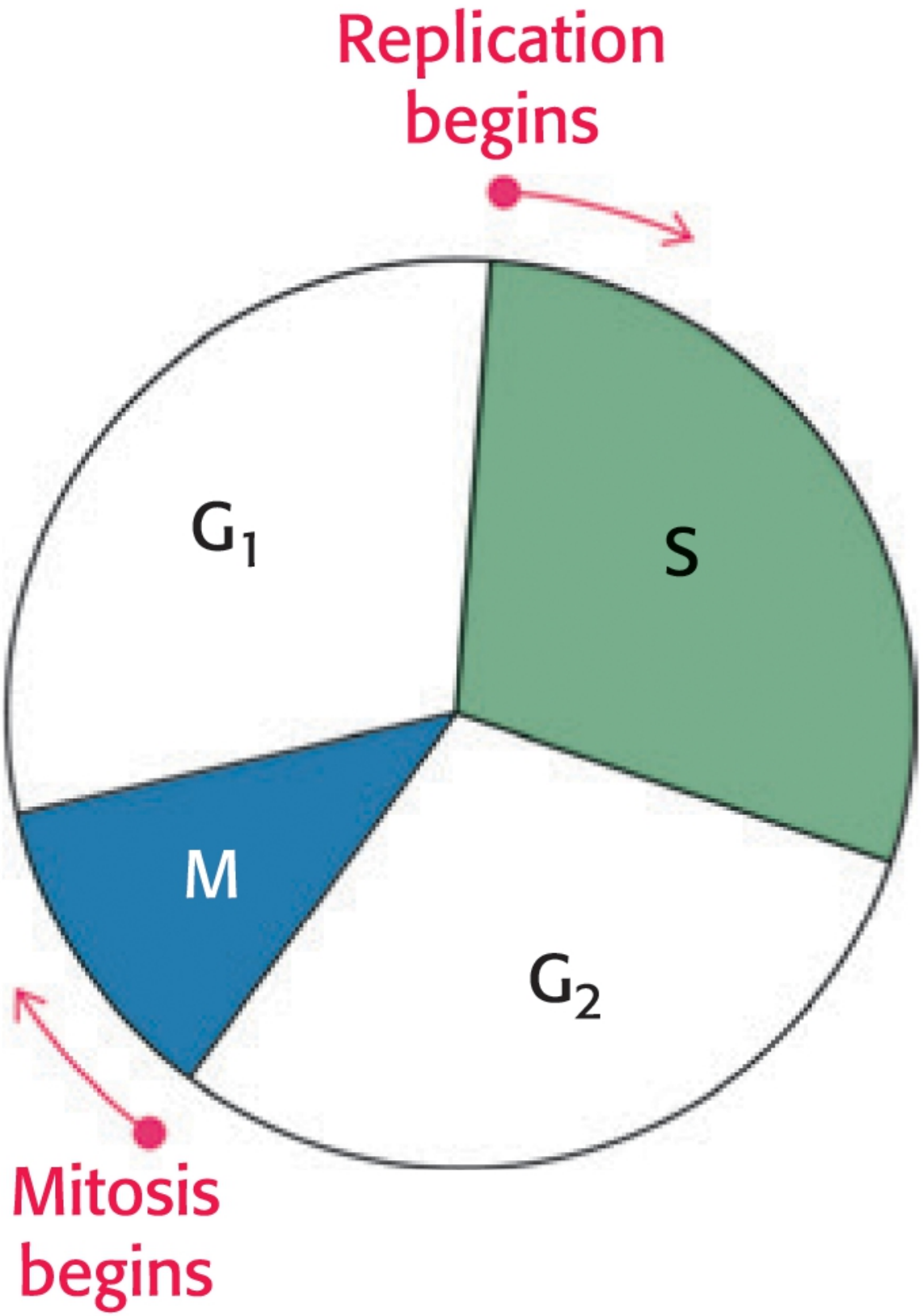
Courtesy Aaron Bensimon.

Four horizontal short and narrow bands are shown against a dark background. These bands are separated by gaps. Each band has a red left region and a green right region. Green depicts I d U and red depicts C I d U. The gaps between the two bands on the left and right are labeled the origin of replication. The label "origin of replication" is flanked by arrows pointing toward the left and right respectively. The leftward pointing arrow corresponds to the first and third bands. The rightward pointing arrow corresponds to the second and fourth bands.

Return to FIGURE 28.26 Eukaryotic chromosomes have multiple origins of replication

Extended description for FIGURE 28.27 Eukaryotic D N

A replication and cell division are highly coordinated



© Macmillan Learning

A circle is divided into four sectors. The top left sector depicts G 1 phase, the top right sector depicts the S phase, the bottom sector depicts G 2 phase, and the bottom left sector depicts the M phase. The sector depicting the S phase is filled with green color, and the sector depicting the M phase is filled with blue color. The smallest sector is M and the remaining sectors have almost equivalent sizes. An arrow from the start of the S phase is labeled replication begins. An arrow from the start of the M phase is labeled mitosis begins.

Return to FIGURE 28.27 Eukaryotic D N A replication and cell division are highly coordinated

Extended description for FIGURE 28.28 Telomeres may form duplex loops

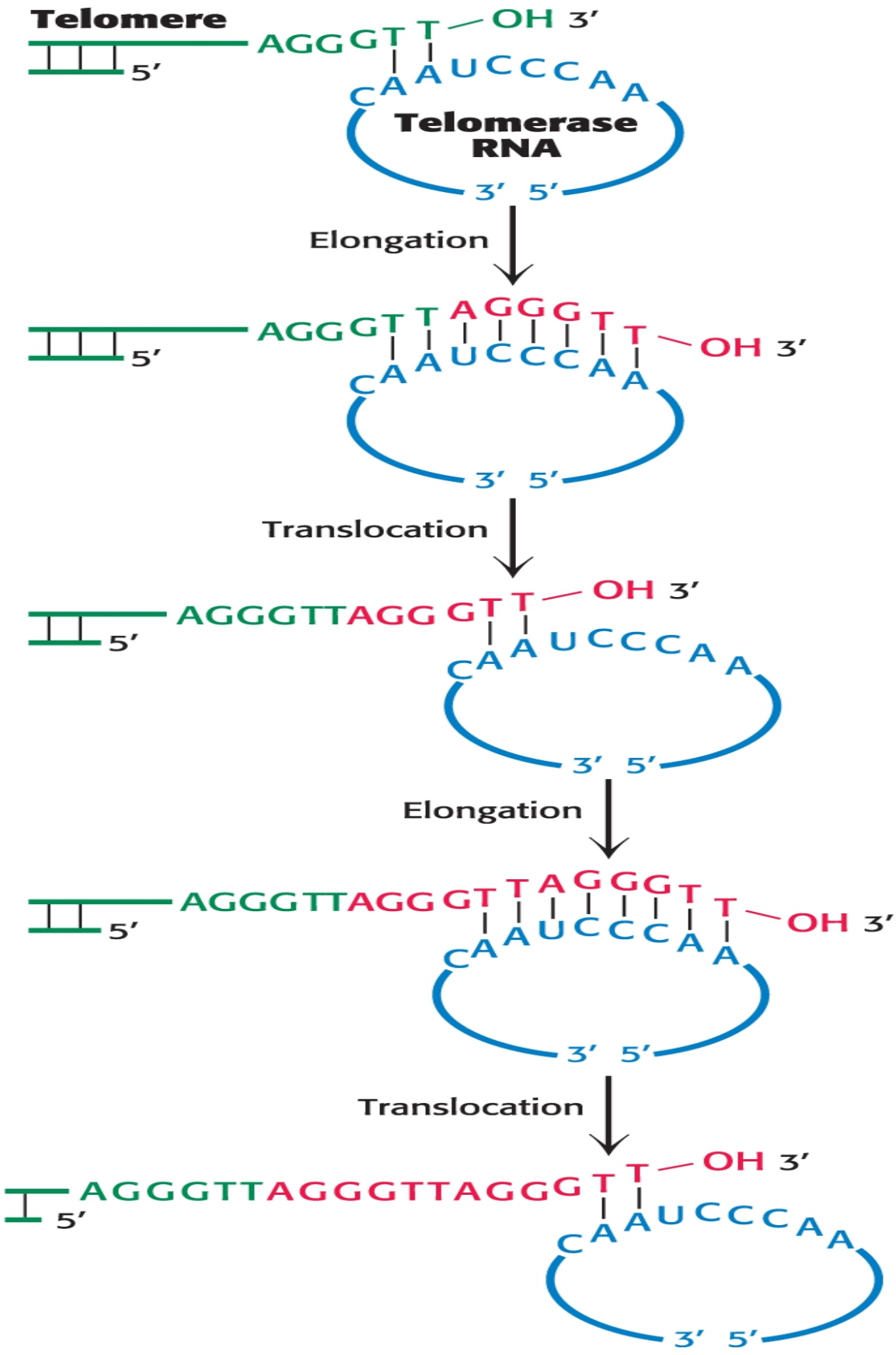


A G-rich strand is depicted as two parallel lines. The top line is solid red and its right end extends beyond the right end of the bottom blue line. A forward arrow shows the duplex loop formed by the G-rich strand. It shows the folding back of the G-rich strand to form a loop. The extended red line enters into a bubble formed by the red line near its left end.

Return to FIGURE 28.28 Telomeres may form duplex loops

Extended description for FIGURE 28.29 Telomerase uses its R N A template to synthesize the G-rich strand

of telomeres



© Macmillan Learning

The telomere is depicted as a double-stranded D N A segment. The right end of the bottom strand is labeled 5 prime. The right end of the top strand is extended and contains the sequence A G G G T T, single bond, O H, 3 prime. The T residues of this sequence are hydrogen bonded to the first and second A residues of the telomerase R N A. The telomerase R N A is depicted as an open circle with the sequence 3 prime C A A U C C C A A 5 prime. The free 3 prime and 5 prime ends are shown at the bottom.

The first step is elongation. The telomerase R N A is used as a template to extend the 3 prime end of the top strand of telomerase. The sequence of the 3 prime end of the top strand of telomere is A G G G T T A G G G T T, single bond, O H, 3 prime. The sequence from the first T to the fourth T is hydrogen bonded with the telomerase R N A.

The second step is translocation. The sequence of the 3 prime end of the top strand of the telomere is translocated toward the left such that only the two terminal T residues are hydrogen bonded to the first and second A residues of telomerase R N A. The remaining bases of the R N A are unpaired.

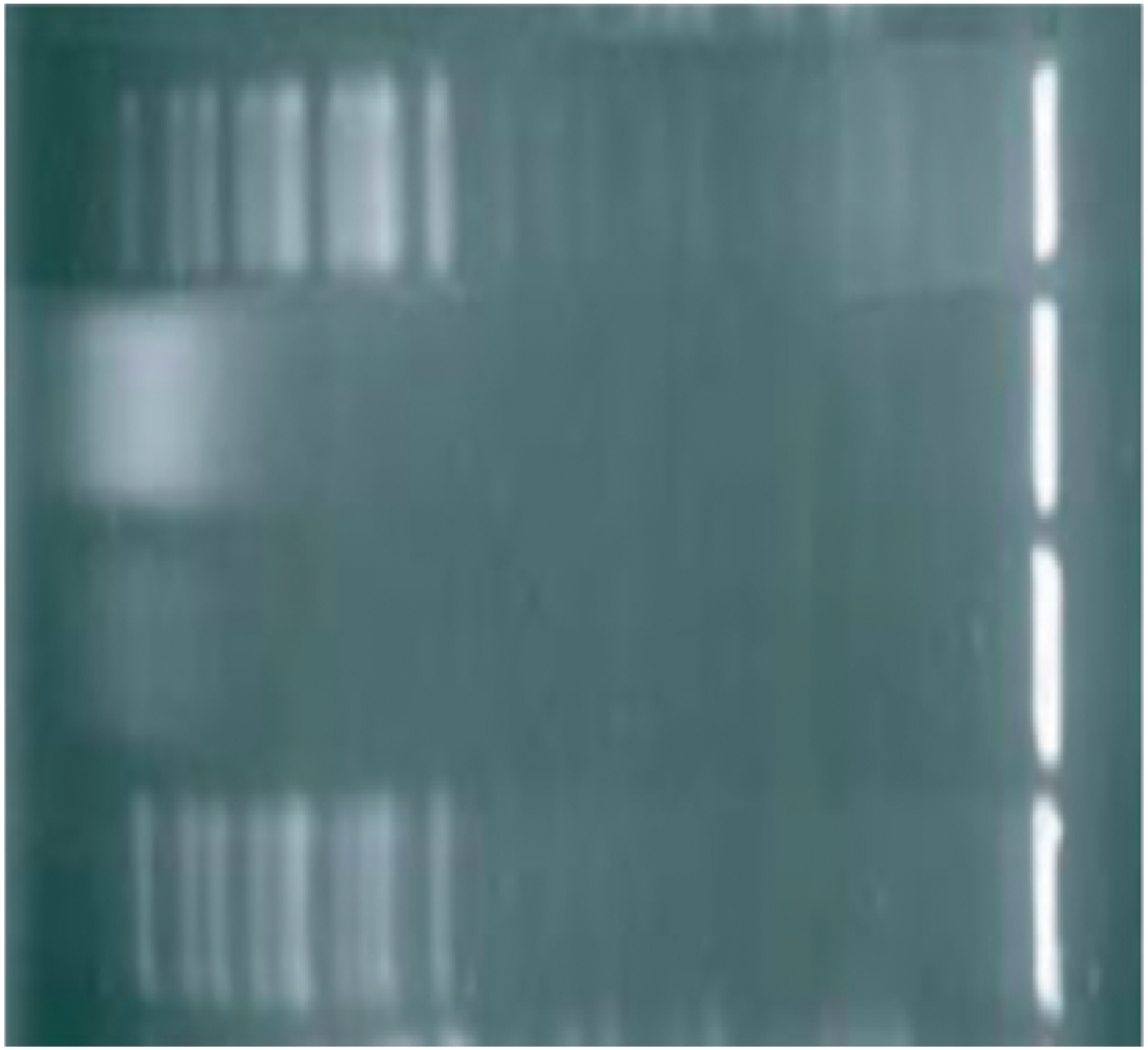
The third step is elongation. The telomerase R N A is again used as a template to extend the 3 prime end of the top strand of telomerase. The sequence of the 3 prime end of the top strand of the telomere is A G G G T T A G G G T T A G G G T T, single bond, O H, 3 prime. The terminal A G G G T T sequence is hydrogen bonded with the telomerase R N A.

The fourth step is translocation. The sequence of the 3 prime end of the top strand of the telomere is again translocated toward the left such that only the two terminal T residues are hydrogen bonded to the first and second A residues of telomerase R N A. The remaining bases of the R N A are unpaired.

Return to FIGURE 28.29 Telomerase uses its R N A template to synthesize the G-rich strand of telomeres

Extended description for FIGURE 28.30 The bacterium

Deinococcus radiodurans repairs DNA damage quickly

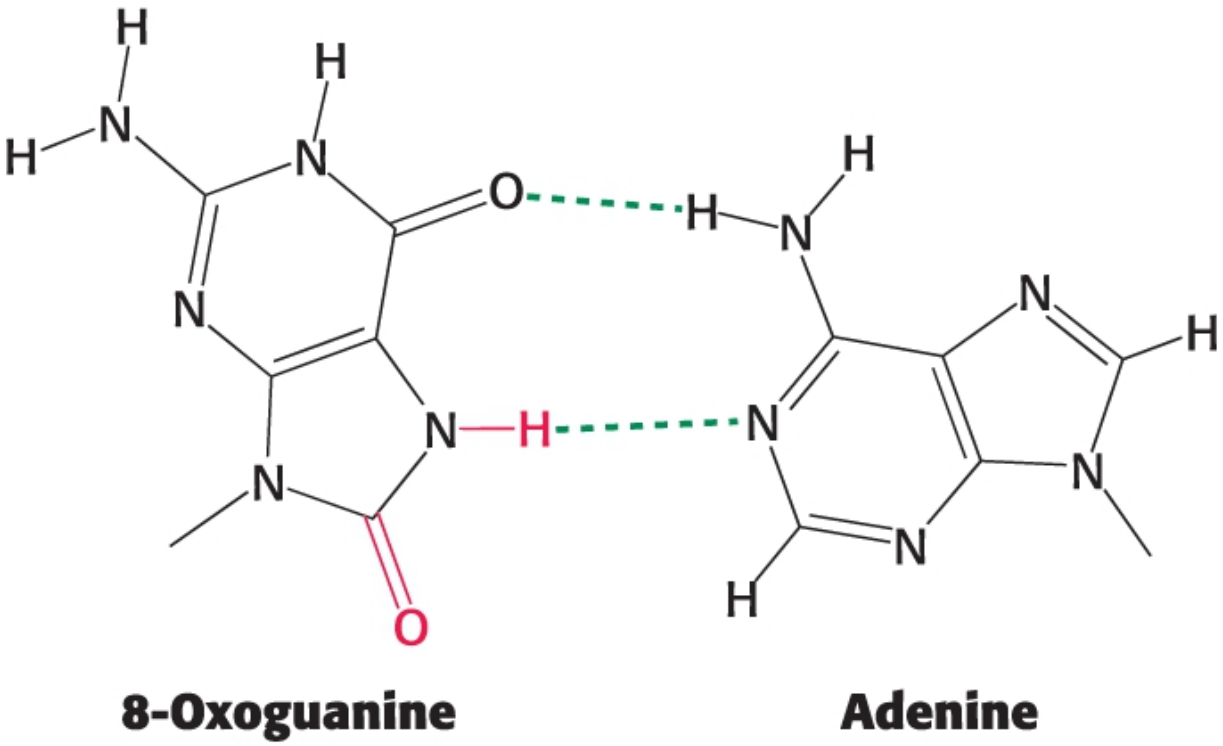


Reprinted with permission of Macmillan Publishers Ltd, from Zahradka, K., Slade, D., Bailone, A. et al. Reassembly of shattered chromosomes in Deinococcus radiodurans. Nature 443, 569–573 (2006); permission conveyed through Copyright Clearance Cener, Inc.

The gel contains four lanes. From left to right, the lanes are labeled C, 0 hours, 1.5 hours, and 3 hours. C depicts starting genome, 0 hour depicts the irradiated fragmented genome, and 3 hours depict the spontaneously reassembled genome. In lane C, a thick and bright band is seen at the top which is followed by a series of relatively faint bands near the bottom. In lane 0 hours, a thick and bright band is seen at the top. A thick smear is seen at the bottom of the lane. In lane 1.5, a thick and bright band is seen at the top. A very light and small smear is seen near the bottom of the lane. In lane 3 hours, the banding pattern is almost identical to lane C.

Return to FIGURE 28.30 The bacterium *Deinococcus radiodurans* repairs DNA damage quickly

Extended description for FIGURE 28.31 Damaged D N A bases can form base pairs



The structure of 8-oxoguanine is as follows: A 6-membered heterocyclic hexagonal ring is in a vertical orientation with C 1 occupying the top left vertex. It consists of 2 N and 4 C atoms. First N occupies the bottom left vertex and the second N occupies the topmost vertex. A double bond is present between N 1 and C 1, and C 3 and C 4. C 1 is single bonded to N on the upper left. This N is single bonded to H above and H on the lower left. C 2 is single-bonded to O on the upper right. Second N is single bonded to H above. It is fused with a 5-membered heterocyclic pentagonal ring in a horizontal orientation such that C 3 and C 4 of the hexagonal ring are C 3 and C 2 respectively of the pentagonal ring. The pentagonal ring consists of 2 N and 3 C atoms. First N occupies the bottom right vertex and the second N occupies the bottom left vertex. C 1

occupies the bottom-most vertex and is double bonded to O below. N 2 has an open single bond on the lower left. N 1 is single bonded to H on the right.

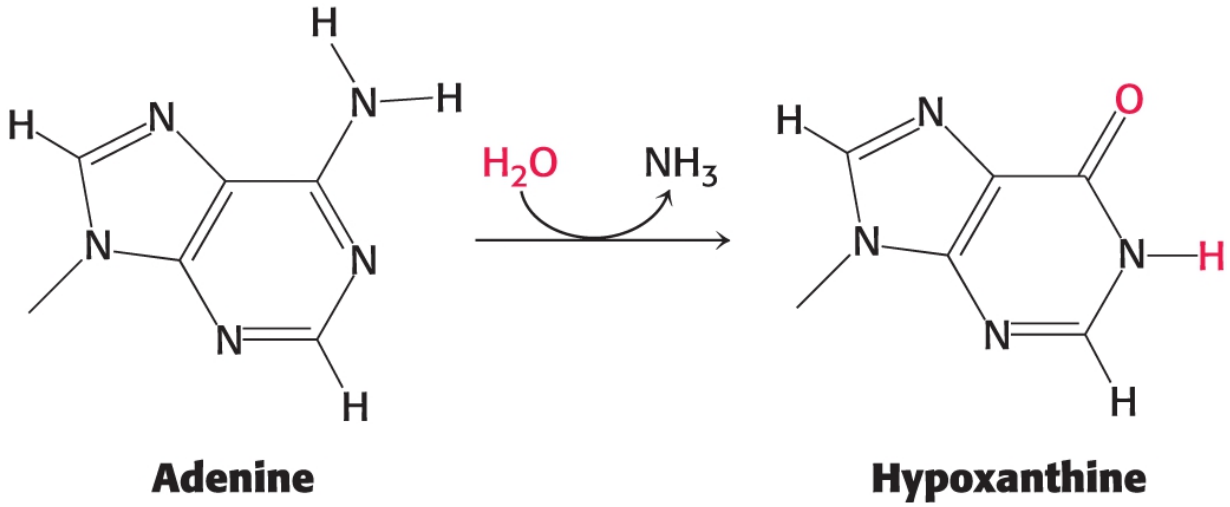
The structure of adenine is as follows: A 6-membered heterocyclic hexagonal ring is in a vertical orientation with C 1 occupying the bottom left vertex. It consists of 2 N and 4 C atoms. First N occupies the bottom-most vertex and the second N occupies the top left vertex. A double bond is present between N 1 and C 1, N 2 and C 2, and C 3 and C 4. C 1 is single-bonded to H on the lower left. C 2 is single bonded to N above, which is further single bonded to two different H. The hexagonal ring is fused with a 5-membered heterocyclic pentagonal ring such that C 3 and C 4 of the hexagonal ring are C 2 and C 3 respectively of pentagonal ring. The pentagonal ring consists of 2 N and 3 C atoms. First N occupies the top right vertex and the second N occupies the bottom right vertex. C 1 occupies the rightmost vertex. A double bond is present between N 1 and C 1. C 1 is single bonded to H on the right. N 2 has an open single bond below.

The O atom double bonded to C 2 of the hexagonal ring of 8-oxoguanine is connected to the H atom of the N H 2 group bonded to the hexagonal ring of adenine. This connection is depicted through a green dashed line.

The H atom single bonded to N 1 of the pentagonal ring of 8-oxoguanine is connected to N 2 of the hexagonal ring of adenine. This connection is depicted through a green dashed line.

Return to FIGURE 28.31 Damaged D N A bases can form base pairs

Extended description for FIGURE 28.32 Adenine can be deaminated to form hypoxanthine



The conversion of adenine to hypoxanthine is coupled with the entry of H 2 O and the release of N H 3.

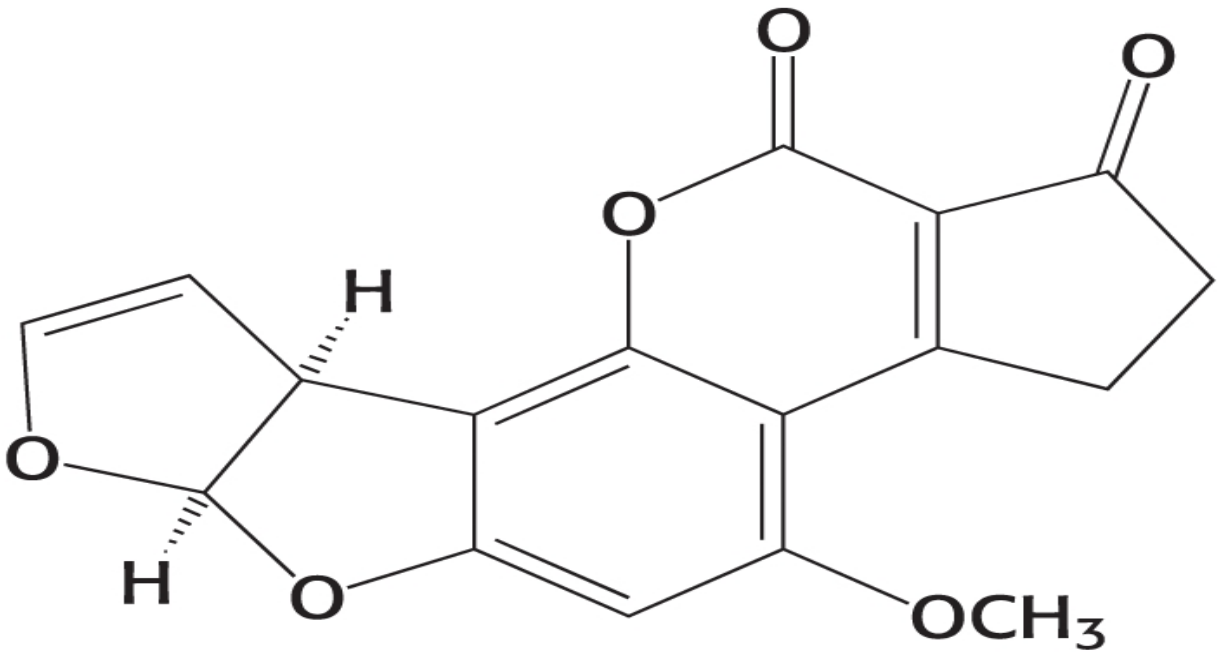
The structure of adenine is as follows: A 6-membered heterocyclic hexagonal ring is in a horizontal orientation with C 1 occupying the bottom right vertex. First N occupies the rightmost vertex and the second N occupies the bottom left vertex. A double bond is present between C 1 and N 2, C 2 and C 3, and C 4 and N 1. C 1 is single bonded to H. C 4 is single bonded to N on the upper right, which is further single bonded to H on the upper left and H on the right. The hexagonal ring is fused to a 5-membered heterocyclic pentagonal ring in a vertical orientation such that C 2 and C 3 of the hexagonal ring are C 3 and C 2 respectively of the pentagonal ring. The pentagonal ring consists of 2 N and 3 C atoms. First N occupies the bottom left vertex and the second N occupies the topmost vertex. A double bond is present between C 1 and N 2. C 1 is single-bonded to H on the upper left. N 1 has an open single bond on the lower left.

The structure of hypoxanthine is as follows: A 6-membered heterocyclic hexagonal ring is in a horizontal orientation with C 1 occupying the bottom right vertex. First N occupies the rightmost vertex and the second N occupies the bottom left vertex. A double bond is present between C 1 and N 2, and C 2 and C 3. C 1 is single bonded to H. C 4 is double bonded to O on the upper right. N 1 is single bonded to H on the right. The hexagonal ring is fused to a 5-membered heterocyclic pentagonal ring in a vertical orientation such that C 2 and C 3 of the hexagonal ring are C 3 and C 2 respectively of the pentagonal ring. The pentagonal ring consists of 2 N and 3 C atoms. First N occupies the bottom left vertex and the second N occupies the topmost vertex. A double bond is present between C 1 and N 2. C 1 is single-bonded to H on the upper left. N 1 has an open single bond on the lower left.

Return to FIGURE 28.32 Adenine can be deaminated to form hypoxanthine

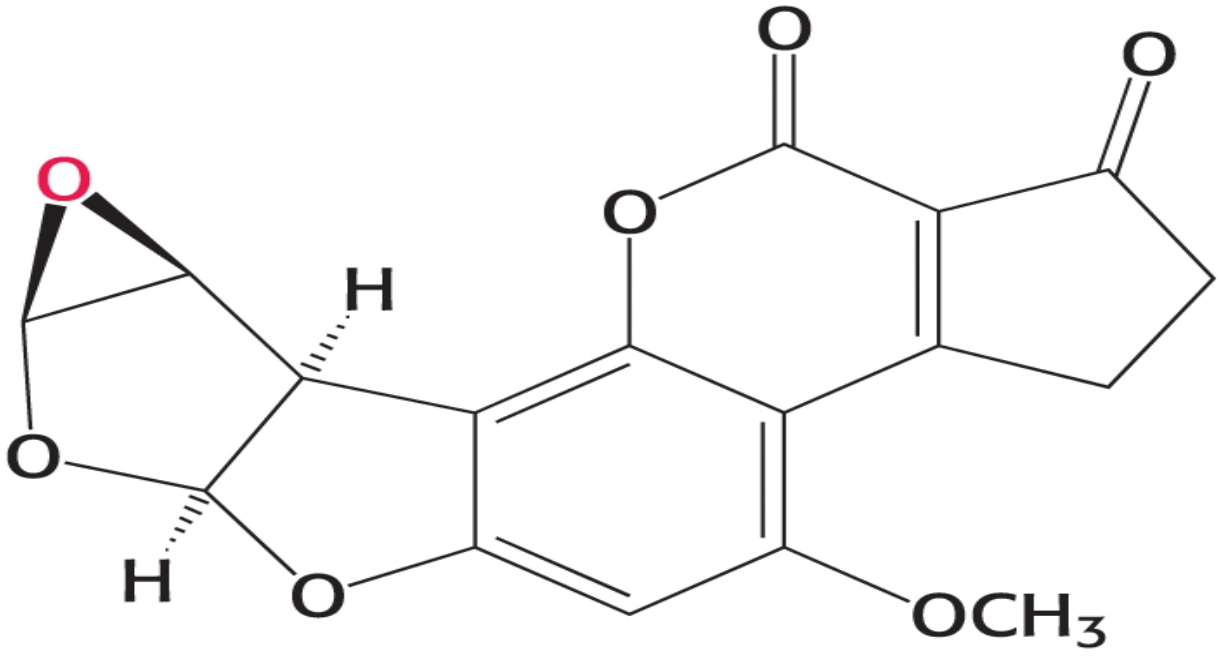
Extended description for FIGURE 28.33 Aflatoxin can be

activated into a mutagen



Aflatoxin B_1

Cytochrome P450



Active DNA-modifying agent

The structure of aflatoxin B 1 is as follows: A 5-membered heterocyclic pentagonal ring is in vertical orientation with C 1 occupying the top left vertex. It consists of 1 O and 4 C atoms. O occupies the bottom left vertex. A double bond is present between C 1 and C 2. It is fused with another 5-membered heterocyclic pentagonal ring in a vertical orientation such that C 3 and C 4 of the first ring are C 2 and C 1 respectively of the pentagonal ring. The pentagonal ring consists of 1 O and 4 C atoms. O occupies the bottom-most vertex. C 1 and C 2 are each dash bonded to H. The second pentagonal ring fused to a benzene ring in vertical orientation such that C 3 and C 4 of the second ring are C 6 and C 5 respectively of the benzene ring. In the benzene ring, alternating double bonds are present between C 2 and C 3, C 4 and C 5, and C 6 and C 1. C 3 is single bonded to O C H 3 on the lower right. The benzene ring is fused with a 6-membered heterocyclic hexagonal ring in a vertical orientation such that C 1 and C 2 of the benzene ring are C 5 and C 4 respectively of the hexagonal ring. The hexagonal ring consists of 1 O and 5 C atoms. O occupies the top left vertex. C 1 occupies the topmost vertex and is double bonded to O above. A double bond is present between C 2 and C 3. The hexagonal ring is fused with a 5-carbon pentagonal ring in vertical orientation such that C 2 and C 3 of the hexagonal ring are C 5 and C 4 of the pentagonal ring. In the pentagonal ring, C 1 occupies the topmost vertex and is double bonded to O above.

A downward arrow labeled cytochrome P 450 leads to active D N A-modifying agent.

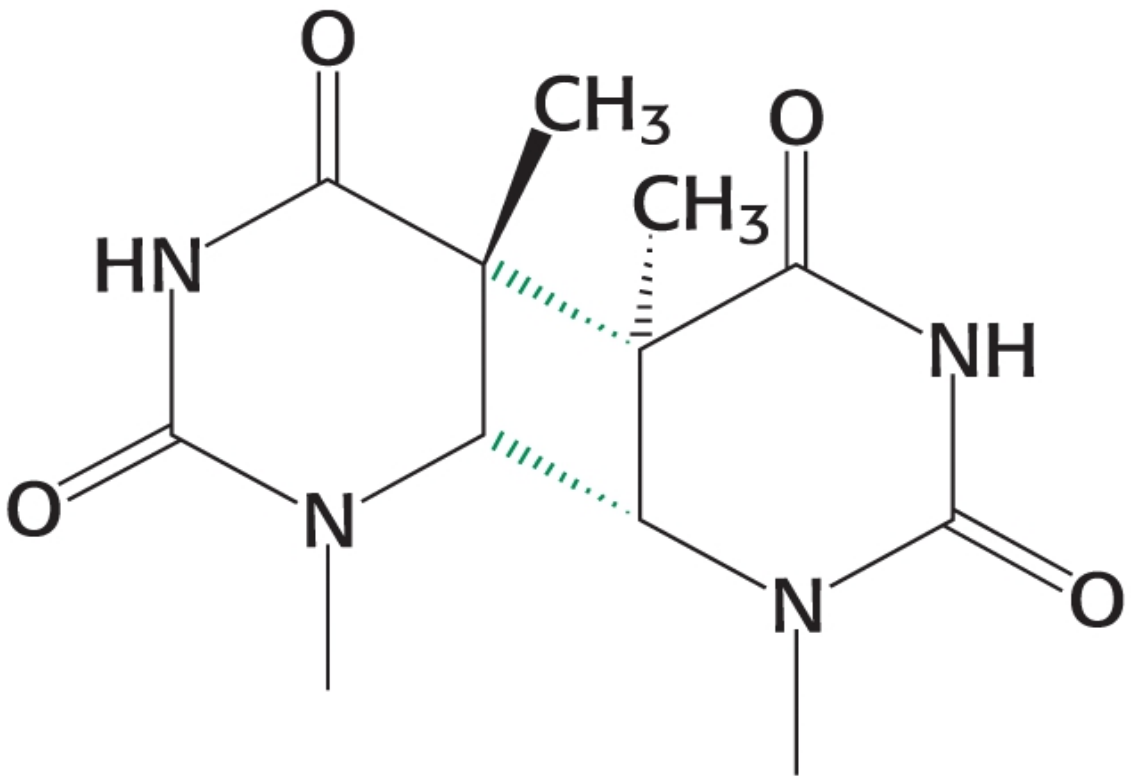
The structure of the active D N A-modifying agent is as follows: A 5-membered heterocyclic pentagonal ring is in vertical orientation with C 1 occupying the top left vertex. It consists of 1 O and 4 C atoms. O occupies the bottom left vertex. C 1 and C 2 are wedge-bonded to a common O atom on the upper left. It is fused with another 5-membered heterocyclic pentagonal ring in a vertical

orientation such that C 3 and C 4 of the first ring are C 2 and C 1 respectively of the pentagonal ring. The pentagonal ring consists of 1 O and 4 C atoms. O occupies the bottom-most vertex. C 1 and C 2 are each dash bonded to H. The second pentagonal ring fused to a benzene ring in vertical orientation such that C 3 and C 4 of the second ring are C 6 and C 5 respectively of the benzene ring. In the benzene ring, alternating double bonds are present between C 2 and C 3, C 4 and C 5, and C 6 and C 1. C 3 is single bonded to O C H 3 on the lower right. The benzene ring is fused with a 6-membered heterocyclic hexagonal ring in a vertical orientation such that C 1 and C 2 of the benzene ring are C 5 and C 4 respectively of the hexagonal ring. The hexagonal ring consists of 1 O and 5 C atoms. O occupies the top left vertex. C 1 occupies the topmost vertex and is double bonded to O above. A double bond is present between C 2 and C 3. The hexagonal ring is fused with a 5-carbon pentagonal ring in vertical orientation such that C 2 and C 3 of the hexagonal ring are C 5 and C 4 of the pentagonal ring. In the pentagonal ring, C 1 occupies the topmost vertex and is double bonded to O above.

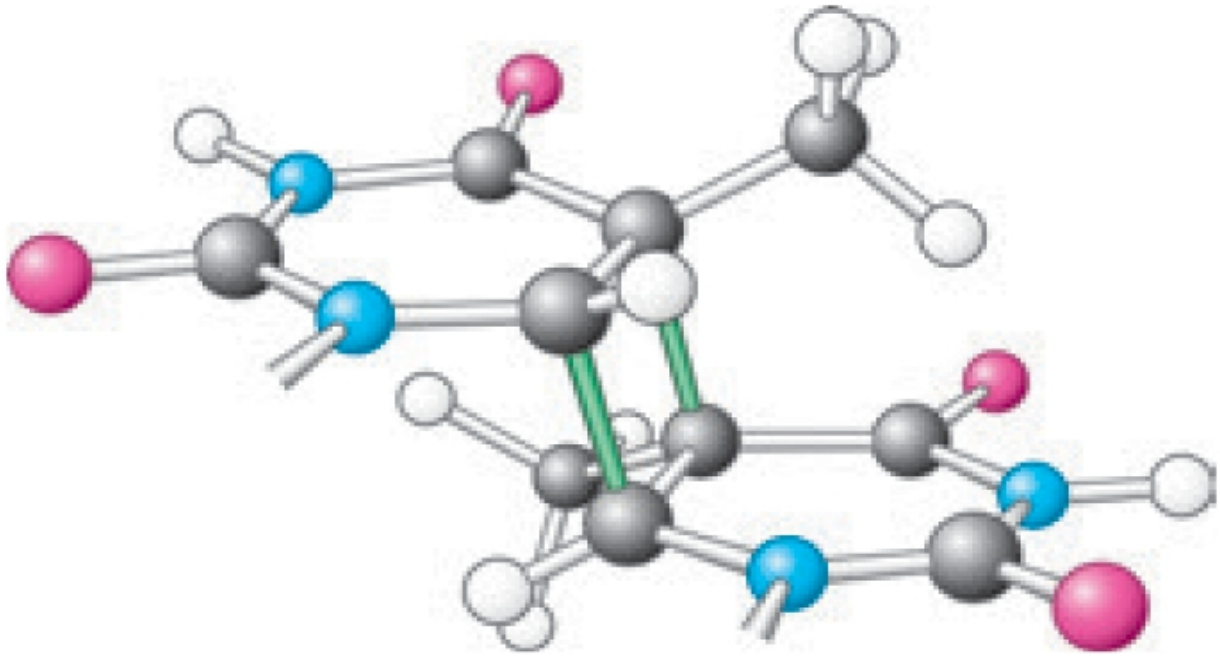
Return to FIGURE 28.33 Aflatoxin can be activated into a mutagen

Extended description for FIGURE 28.34 Chemical

structure and ball-and-stick model of thymine dimer



Thymine dimer



The thymine dimer is composed of two thymine molecules dash bonded to each other.

The structure of the left thymine molecule is as follows: A 6-membered heterocyclic hexagonal ring is in a vertical orientation with C 1 occupying the bottom left vertex. It consists of 2 N and 4 C atoms. First N occupies the bottom-most vertex and the second N bound to H occupies the top-left vertex. N 1 has an open single bond below. C 1 and C 2 are double bonded to O. C 3 is wedge bonded to C H 3 on the upper right.

The structure of the right thymine molecule is as follows: A 6-membered heterocyclic hexagonal ring is in a vertical orientation with C 1 occupying the bottom right vertex. It consists of 2 N and 4 C atoms. The first N bound to H occupies the top right vertex and the second N occupies the bottom-most vertex. N 2 has an open single bond below. C 1 and C 4 are double bonded to O. C 3 is dash bonded to C H 3 above. C 3 of the left thymine molecule is dash bonded to C 3 of the right thymine molecule. C 4 of the left thymine molecule is dash bonded to C 2 of the right thymine molecule.

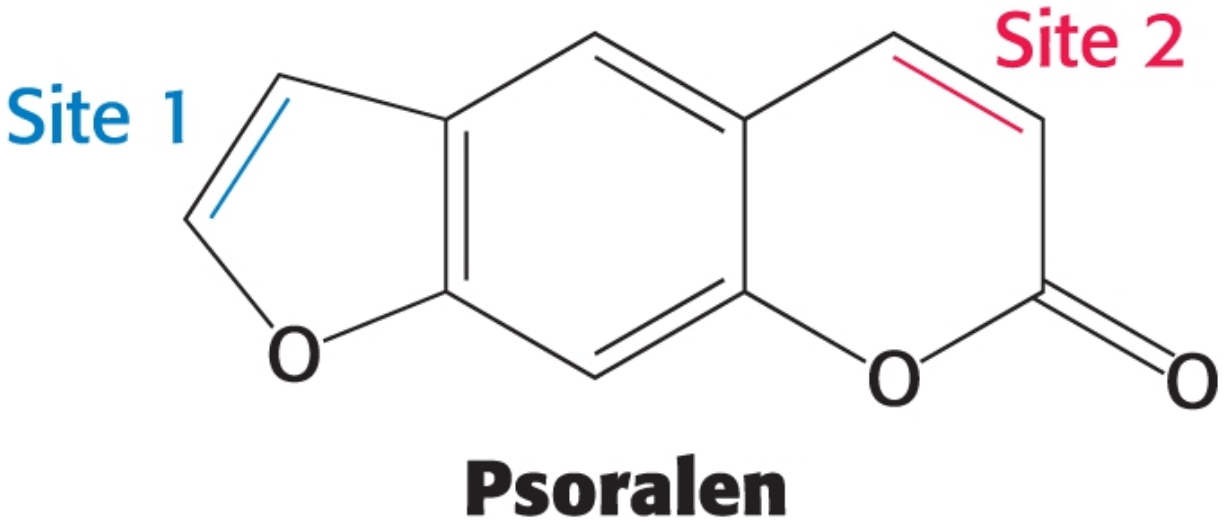
In the ball-and-stick model, two flat hexagonal rings are shown. Each ring is composed of 2 blue and 4 black spheres. In the top ring, the blue sphere occupies the bottommost and top left vertex. The remaining positions are occupied by black spheres. The top left blue sphere is connected to a white sphere. The bottom left and topmost black spheres are each connected to a pink sphere. The top right black sphere is connected to another black sphere on the upper right, which is further connected to three white spheres. The bottom right black sphere is connected to a white sphere on the upper right.

The bottom ring is the non-superimposable mirror image of the top ring. The top right and bottom right black spheres of the top ring are

connected to the top left and bottom left black spheres respectively of the bottom ring through a green stick.

Return to FIGURE 28.34 Chemical structure and ball-and-stick model of thymine dimer

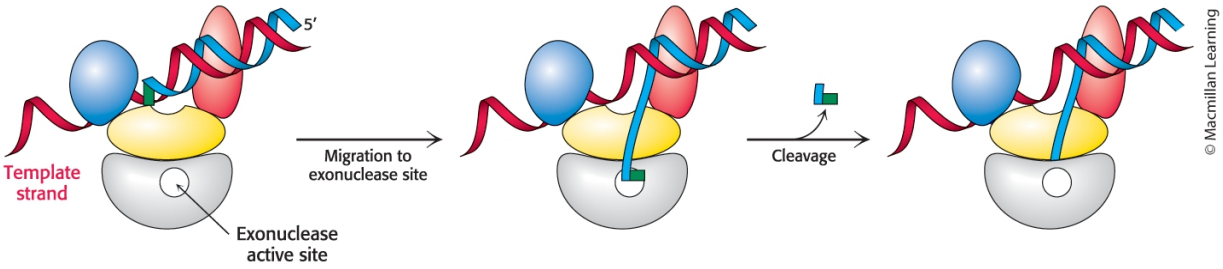
Extended description for FIGURE 28.35 Psoralen is a cross-linking agent



The structure of psoralen is as follows: A 5-membered heterocyclic pentagonal ring is in horizontal orientation with C 1 occupying the leftmost vertex. It consists of 1 O and 4 C atoms. O occupies the bottom-most vertex. A double bond between C 1 and C 2 is highlighted in blue and labeled site 1. It is fused with a benzene ring in a vertical orientation such that C 3 and C 4 of the pentagonal ring are C 6 and C 5 of the benzene ring. In the benzene ring, alternating double bonds are present between C 1 and C 2, C 3 and C 4, and C 5 and C 6. The benzene ring is fused with a 6-membered heterocyclic hexagonal ring in a vertical orientation such that C 2 and C 3 of the benzene ring are C 2 and C 1 respectively of the hexagonal ring. The hexagonal ring consists of 1 O and 5 C atoms. O occupies the bottom-most vertex. C 5 is double bonded to O on the lower right. A double bond between C 3 and C 4 is highlighted in red and labeled site 2.

Return to FIGURE 28.35 Psoralen is a cross-linking agent

Extended description for FIGURE 28.36 D N A polymerases have proofreading activities



The D N A polymerase is bound to a replicating double helical D N A. In the helix, the red strand is the template and the blue strand is the replicating strand. The 3 prime end of the blue strand contains a short green block to depict a wrong nucleotide. The D N A polymerase consists of a semi-circular structure at the bottom with an empty exonuclease active site. A horizontally oriented oval-shaped structure is located above it. It has a narrow concave groove at the top center. A blue round subunit is attached to the top left of the oval and an elongated red subunit in vertical orientation is attached to the top right of the oval. The replicating double helix passes through the space between the round and elongated structures.

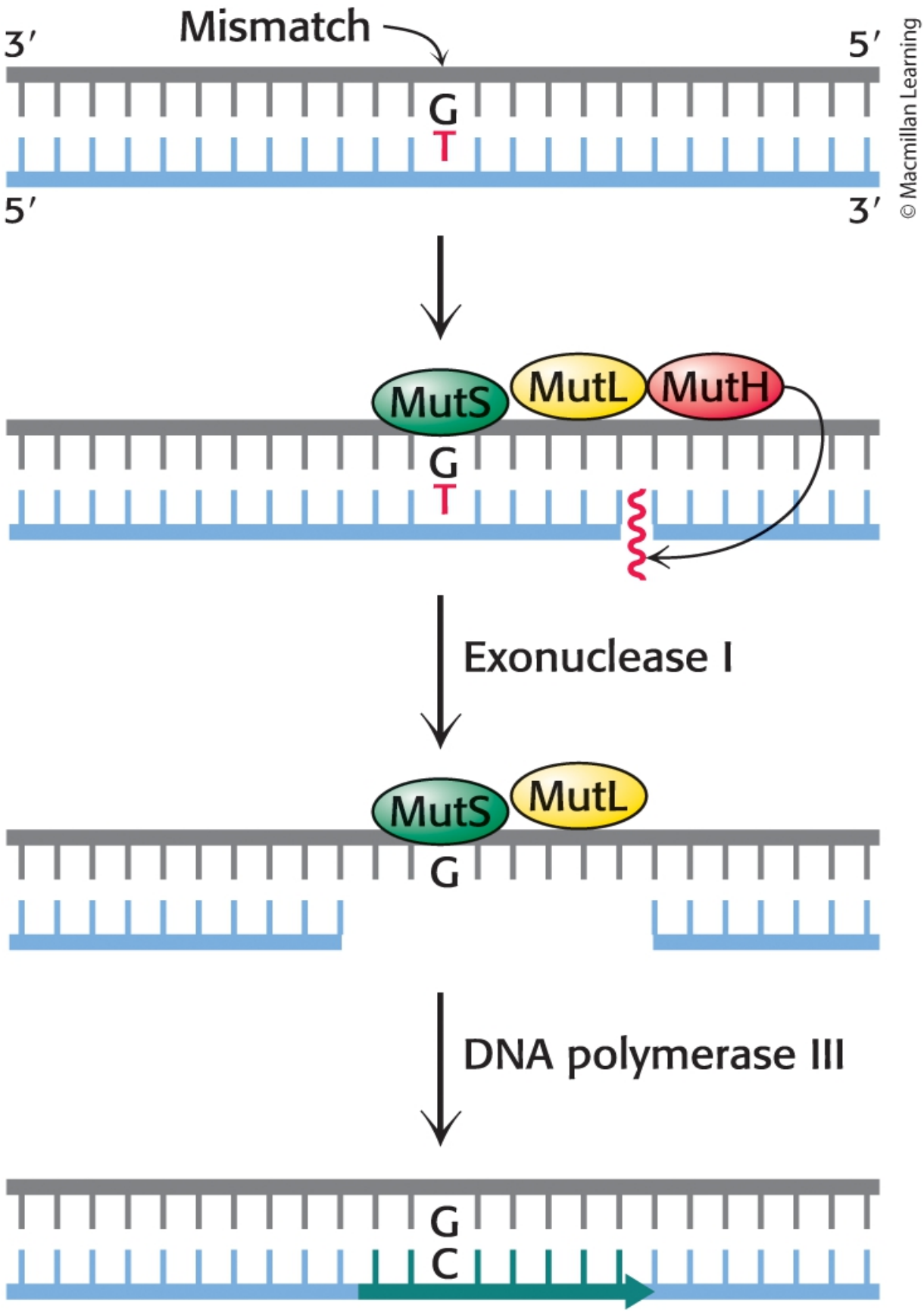
the first step, the free 3 prime end of replicating blue strand migrates to the exonuclease site. The position of the template strand remains the same.

In the second step, cleavage occurs and the green block along with a short blue stretch is removed from the 3 prime end of the replicating strand. The exonuclease active site becomes empty again.

Return to FIGURE 28.36 D N A polymerases have proofreading activities

Extended description for FIGURE 28.37 D N A mismatch

repair in *E. coli* involves multiple proteins



© Macmillan Learning

A double-stranded D N A is shown. The top strand is grey and its left and right ends are labeled 3 prime and 5 prime respectively. The bottom strand is blue and its left and right ends are labeled 5 prime and 3 prime respectively. Short regularly spaced line emerging from the top and bottom strands depicts base pairing. The G base is located in the middle of the top strand corresponding to the T base in the bottom strand. The G T pair depicts a mismatch. T is highlighted in red.

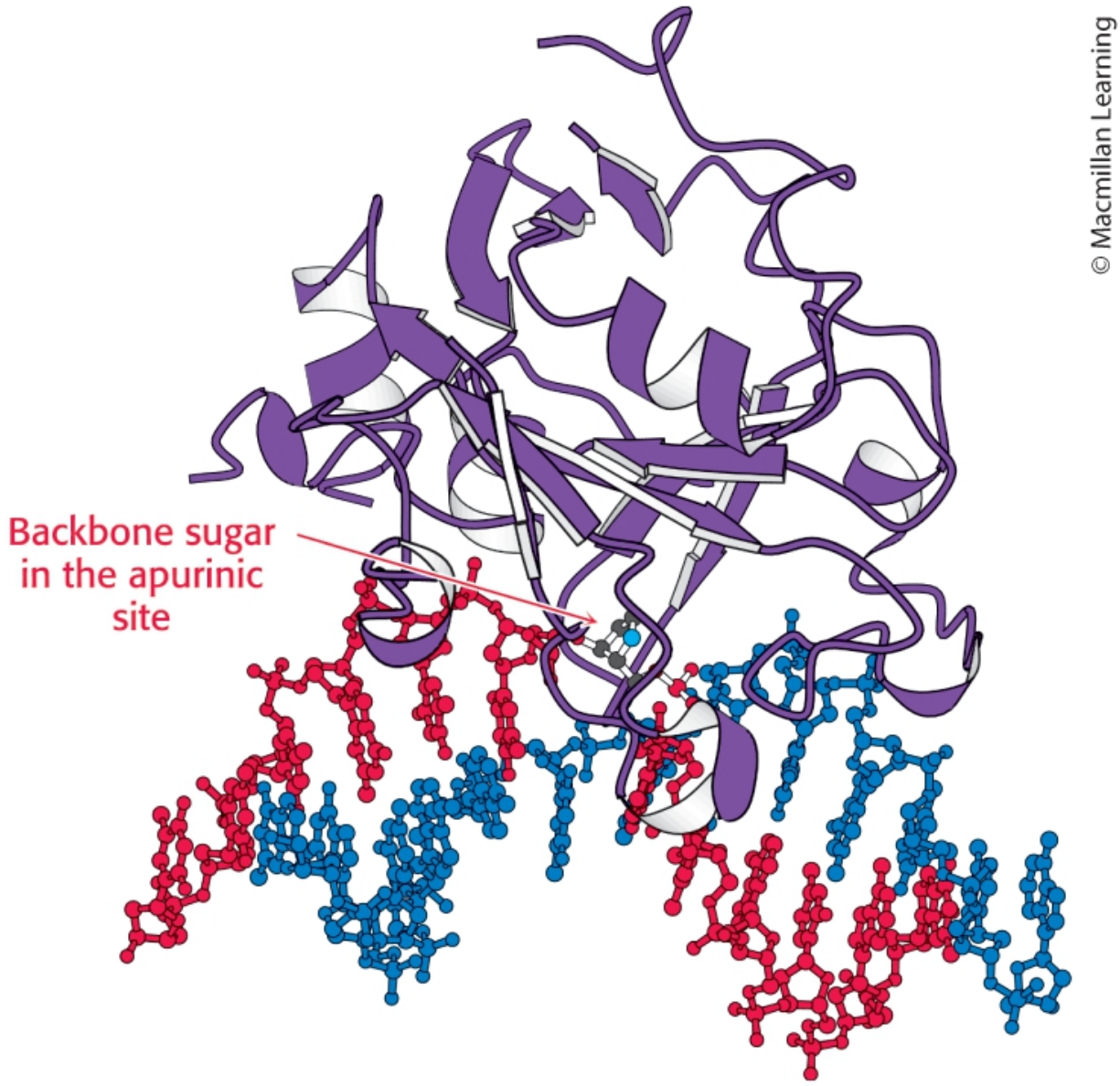
In the second step, Mut S, Mut L, and Mut H are bound to the top strand. Mut S is directly bound to the G T base pair. Mut H creates a nick in the bottom strand five base pairs away from the mismatch. This nick is created toward the right of the mismatch.

In the third step, exonuclease 1 enters. It cleaves the bottom strand starting from the nick up to 2 base pairs on the left of the mismatch in the 3 prime to 5 prime direction.

In the fourth step, D N A polymerase 3 enters. It re-synthesizes the cleaved bottom strand in the 5 prime to 3 prime direction. The correct base C is added opposite G.

Return to FIGURE 28.37 D N A mismatch repair in *E. coli* involves multiple proteins

Extended description for FIGURE 28.38 Base-excision repair enzymes remove damaged bases



© Macmillan Learning

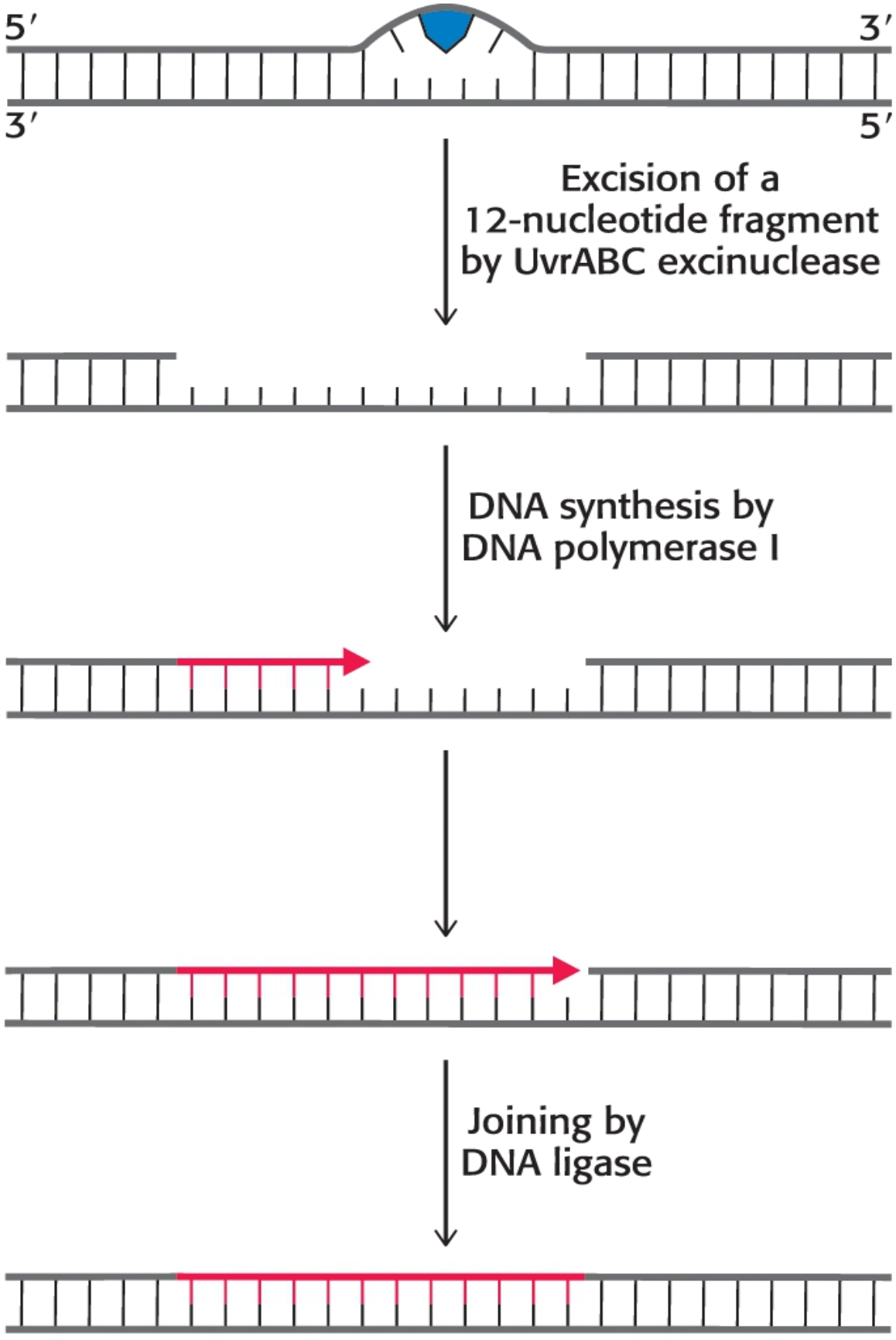
The D N A double helix is slightly curved. It consists of two strands composed of red and blue spheres. The repair enzyme consists of several beta-strands and a few alpha-helices interconnected by thread-like loops. It is associated with the top groove of the double

helix. The backbone sugar in the apurinic site is flipped out of the helix into the repair enzyme's enzyme active site. The active site is depicted as a small hollow space surrounded by thread-like loops.

Return to FIGURE 28.38 Base-excision repair enzymes remove damaged bases

Extended description for FIGURE 28.39 Nucleotide-excision repair involves the removal of a section of

damaged D N A



© Macmillan Learning

A double-stranded D N A is shown. The left and right ends of the top strand are labeled 5 prime and 3 prime respectively. The left and right ends of the bottom strand are labeled 3 prime and 5 prime respectively. A thymine dimer in the middle of the top strand is depicted as a blue block. It causes the bulging out of the top strand.

In the first step, the excision of a 12-nucleotide fragment by U v r A B C excinuclease takes place. In the top strand, a fragment containing the thymine dimer and its flanking region is removed.

In the second step, D N A synthesis by D N A polymerase 1 is initiated. The cleaved region of the top strand is re-filled by the D N A synthesizing activity of D N A polymerase 1. The synthesis takes place in 5 prime to 3 prime direction.

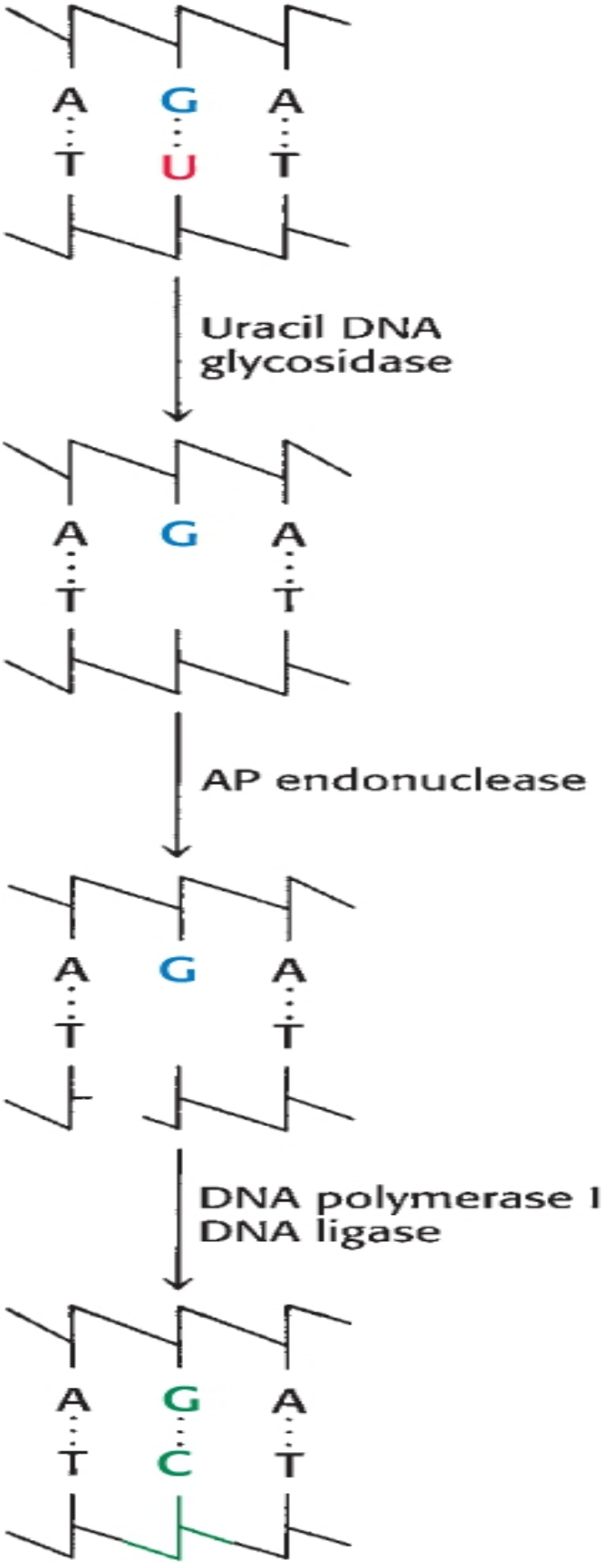
In the third step, D N A synthesis on the top strand is completed. The free 3 prime end of the newly synthesized D N A strand is depicted as an arrowhead pointing toward the right.

In the fourth step, the free 3 prime end of the newly synthesized D N A on the top strand is joined with the free 5 prime end of the adjacent nucleotide by D N A ligase.

Return to FIGURE 28.39 Nucleotide-excision repair involves the removal of a section of damaged D N A

Extended description for FIGURE 28.40 Excision and

replacement of uridine bases in D N A by cytidine



© Macmillan Learning

A section of a double-stranded D N A is shown. The top and bottom strands are depicted as zigzag lines. Short lines from the top and bottom strands are attached to different bases. From left to right, the sequence in these strands is as follows:

Top strand: A G A

Bottom strand: T U T

The complementary bases are connected by hydrogen bonds depicted as a dotted line.

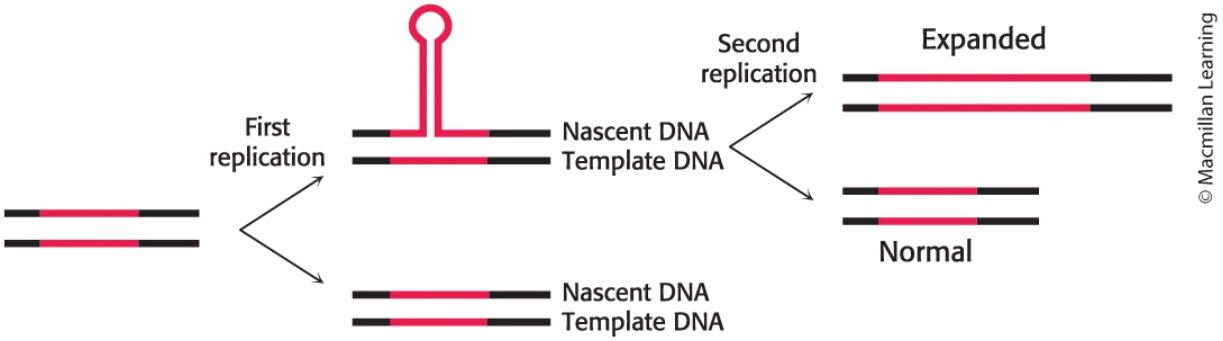
In the first step, uracil D N A glycosidase removes "U" from the bottom strand.

In the second step, A P endonuclease breaks the bond between the apyrimidinic site and the left nucleotide having the base T in the bottom strand.

In the third step, the nucleotide in the apyrimidinic site is removed and replaced with a new nucleotide having the base C by D N A polymerase 1. The D N A ligase seals the gap between the newly added nucleotide and its adjacent nucleotides.

Return to FIGURE 28.40 Excision and replacement of uridine bases in D N A by cytidine

Extended description for FIGURE 28.41 Trinucleotide repeats can form structures that lead to their expansion during D N A replication

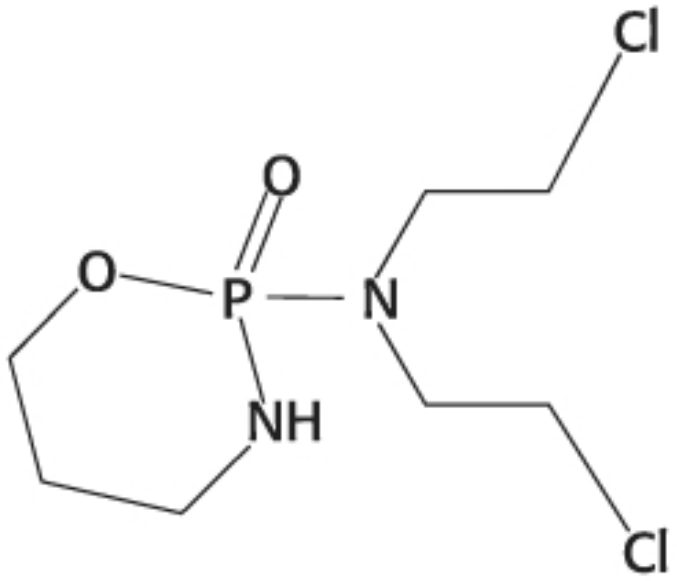


A double-stranded D N A is depicted as two parallel solid lines. The central large portion of each strand is shown in red and it is flanked by short black stretches. After the first replication round, two daughter D N A molecules are formed. One daughter D N A is linear double-stranded. In this D N A, the top strand is labeled nascent D N A and the bottom strand is labeled template D N A. Another daughter D N A is double-stranded with a hairpin loop. In this D N A, the red region of the nascent D N A strand forms a hairpin loop structure.

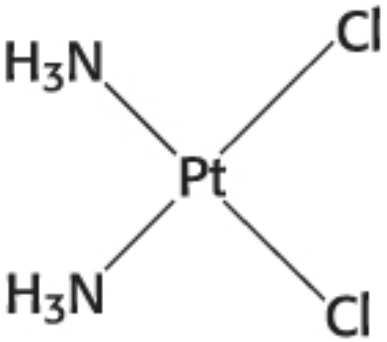
After the second replication round in the double-stranded D N A containing the hairpin loop, the red region is expanded in one daughter D N A. However, in the other daughter D N A, the size of the red region is similar to the parental D N A and is labeled normal.

Return to FIGURE 28.41 Trinucleotide repeats can form structures that lead to their expansion during D N A replication

Extended description for Structure of cyclophosphamide and cisplatin



Cyclophosphamide



Cisplatin

The structure of cyclophosphamide is as follows: A 6-membered heterocyclic hexagonal ring is in a horizontal orientation with C 1 occupying the bottom right vertex. It contains 1 O, 1 P, 1 N, and 3 C

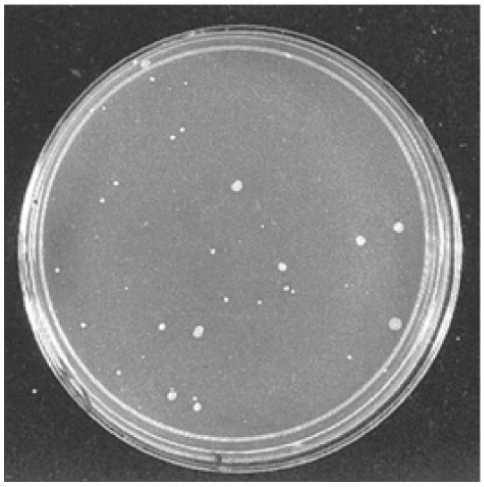
atoms. O occupies the top left vertex. P occupies the top right vertex. N bound to H occupies the rightmost vertex. P is double bonded to O on the upper right. P is single-bonded to N on the right. This N is single-bonded to a 2-carbon alkane chain depicted as a line on the upper right and lower right. C 2 of the upper right alkane chain is single-bonded to C l on the upper right. C 2 of the lower right alkane chain is single bonded to C l on the lower right.

The structure of cisplatin is as follows: A central P t atom is single-bonded to N H 3 on the upper left and N H 3 on the lower left. It is single-bonded to C l on the upper right and C l on the lower right.

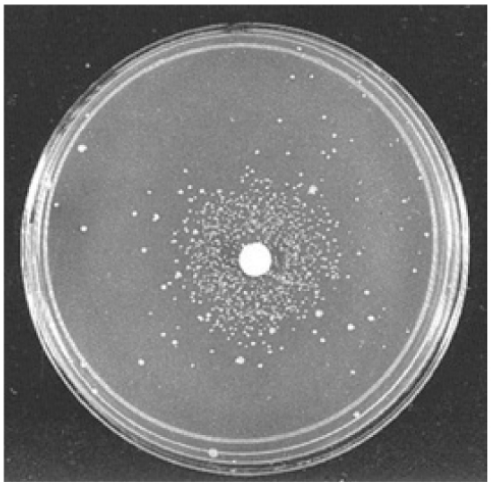
Return to Structure of cyclophosphamide and cisplatin

Extended description for FIGURE 28.42 The Ames test determines the mutagenicity of various compounds

(A)



(B)



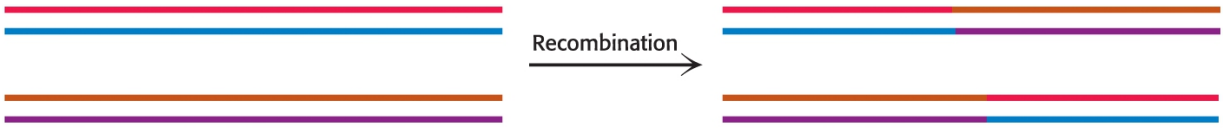
Republished with permission of Elsevier, from Mutation Research/Environmental Mutagenesis and Related Subjects, 31:6, Ames, B.N., et al. Methods for detecting carcinogens and mutagens with the salmonella/mammalian-microsome mutagenicity test, pp. 347–363, Copyright 1975; permission conveyed through Copyright Clearance Center, Ltd.

Photograph (A): It shows a circular agar plate containing a few widely scattered white bacterial colonies.

Photograph (B): It shows a circular agar plate containing a tiny circular filter paper disc in the center. Several tiny white bacterial colonies are clustered around the disc in a ring-like arrangement.

Return to FIGURE 28.42 The Ames test determines the mutagenicity of various compounds

Extended description for FIGURE 28.43 D N A recombination



© Macmillan Learning

Two double-stranded D N A molecules are depicted as two solid parallel lines. The top D N A molecule contains a red top strand and a blue bottom strand. The bottom D N A molecule contains an orange top strand and a purple bottom strand.

A forward arrow labeled recombination leads to the product of D N A recombination.

In the top D N A molecule, the top strand is half red and half orange, and the bottom strand is half blue and half purple. In the bottom D N A molecule, the top strand is half orange and half red and the bottom strand is half purple and half blue.

Return to FIGURE 28.43 D N A recombination

Extended description for FIGURE 28.44 Strand invasion can initiate recombination



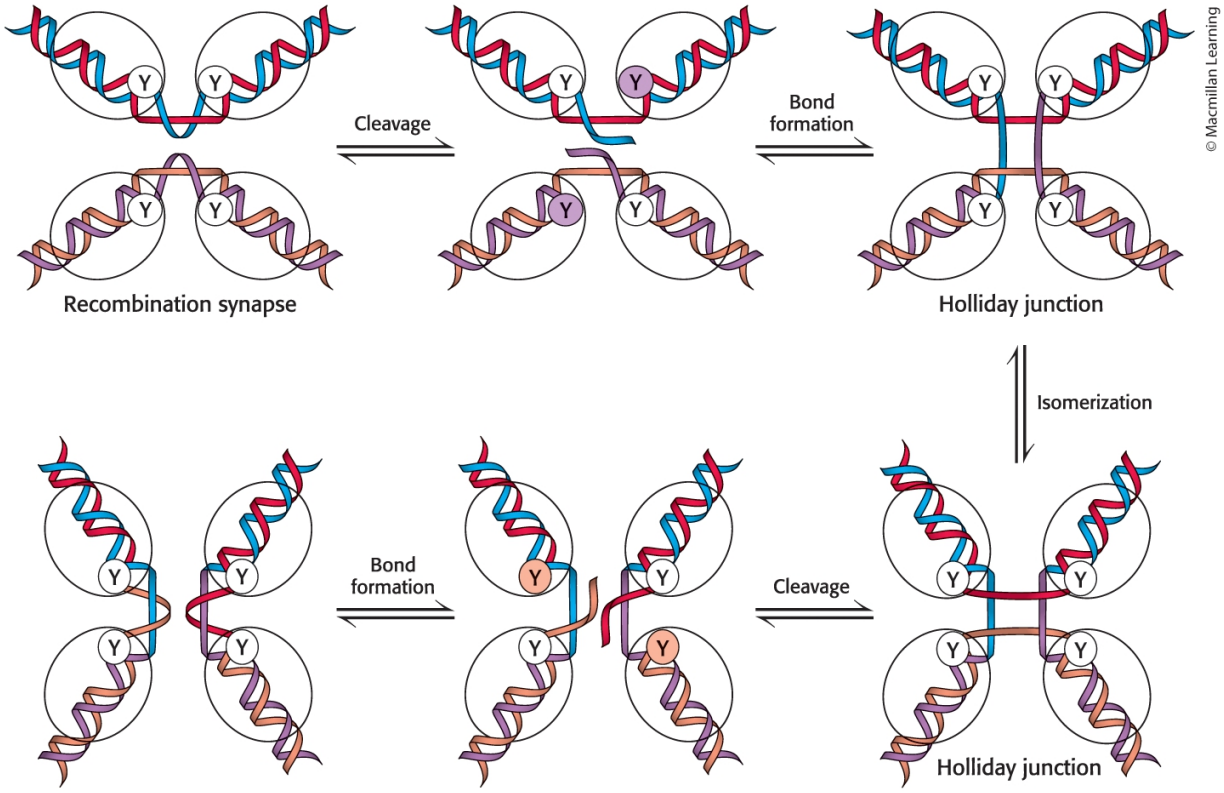
Two double-stranded D N A molecules are depicted as two solid parallel lines. The top D N A molecule is relatively shorter than the bottom D N A molecule. In the top D N A molecule, the bottom strand is relatively longer than the top strand such that its left end extends out. The strands of both D N A molecules are differently colored.

A forward arrow labeled strand invasion shows the formation of a displacement loop in the bottom D N A molecule due to strand invasion.

The left end of the bottom strand of the top D N A molecule enters into the space between the strands of the bottom D N A molecule. As a result, a displacement loop is formed due to the bulging out of the top strand of the bottom D N A molecule.

Return to FIGURE 28.44 Strand invasion can initiate recombination

Extended description for FIGURE 28.45 Holliday junctions are formed and resolved by recombinases



Two double-helical D N A molecules are each bound to two recombinases. The recombinase is depicted as a large white oval. Two recombinases in diagonal orientation are bound to the top helix such that it forms a V-shaped structure. Two recombinases in diagonal orientation are bound to the bottom helix such that it forms an inverted V-shaped structure. Each recombinase contains a tyrosine residue depicted as a tiny circle labeled Y. These residues are located close to the bound helix.

In the first reversible step, cleavage takes place. One strand of the top helix and the bottom helix is cleaved. One end of each cleaved strand is linked to the tyrosine residue of the associated

recombinase. In the top helix, one end of the cleaved strand is linked to the tyrosine of the right recombinase. In the bottom helix, one end of the cleaved strand is linked to the tyrosine of the left recombinase.

In the second reversible step, bond formation takes place leading to the formation of the Holliday junction. The free end of the cleaved strand of the top helix links with the tyrosine residue of the left recombinase of the bottom helix. The free end of the cleaved strand of the bottom helix links with the tyrosine residue of the right recombinase of the top helix. This creates an interlinked D N A having a junction resembling the letter H of the alphabet.

In the third reversible step, isomerization takes place such that the intact strands of both helices are located toward the observer.

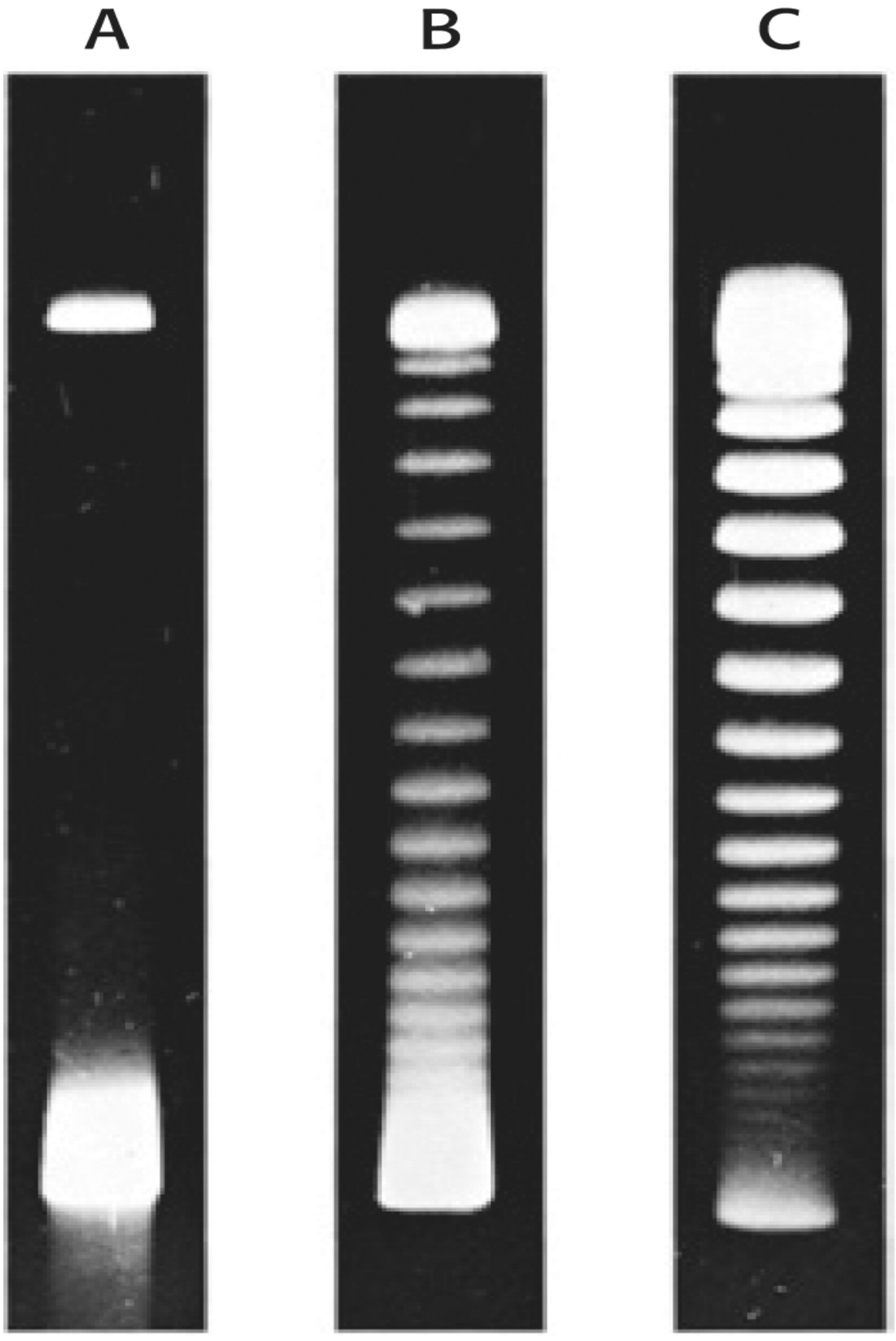
In the fourth reversible step, the previously intact strands of both helices are cleaved. One end of the newly cleaved strand of the top helix links with the tyrosine residue of the left recombinase. One end of the newly cleaved strand of the bottom helix links with the tyrosine residue of the right recombinase.

In the fifth reversible step, bond formation takes place. The free end of the cleaved strand of the bottom helix joins with the linked end of the cleaved strand of the top helix. Similarly, the free end of the cleaved strand of the top helix joins with the linked end of the cleaved strand of the bottom helix.

Return to FIGURE 28.45 Holliday junctions are formed and resolved by recombinases

Extended description for D N A banding pattern in

lanes A, B, and C



From W. Keller. PNAS 72(1975):2553.

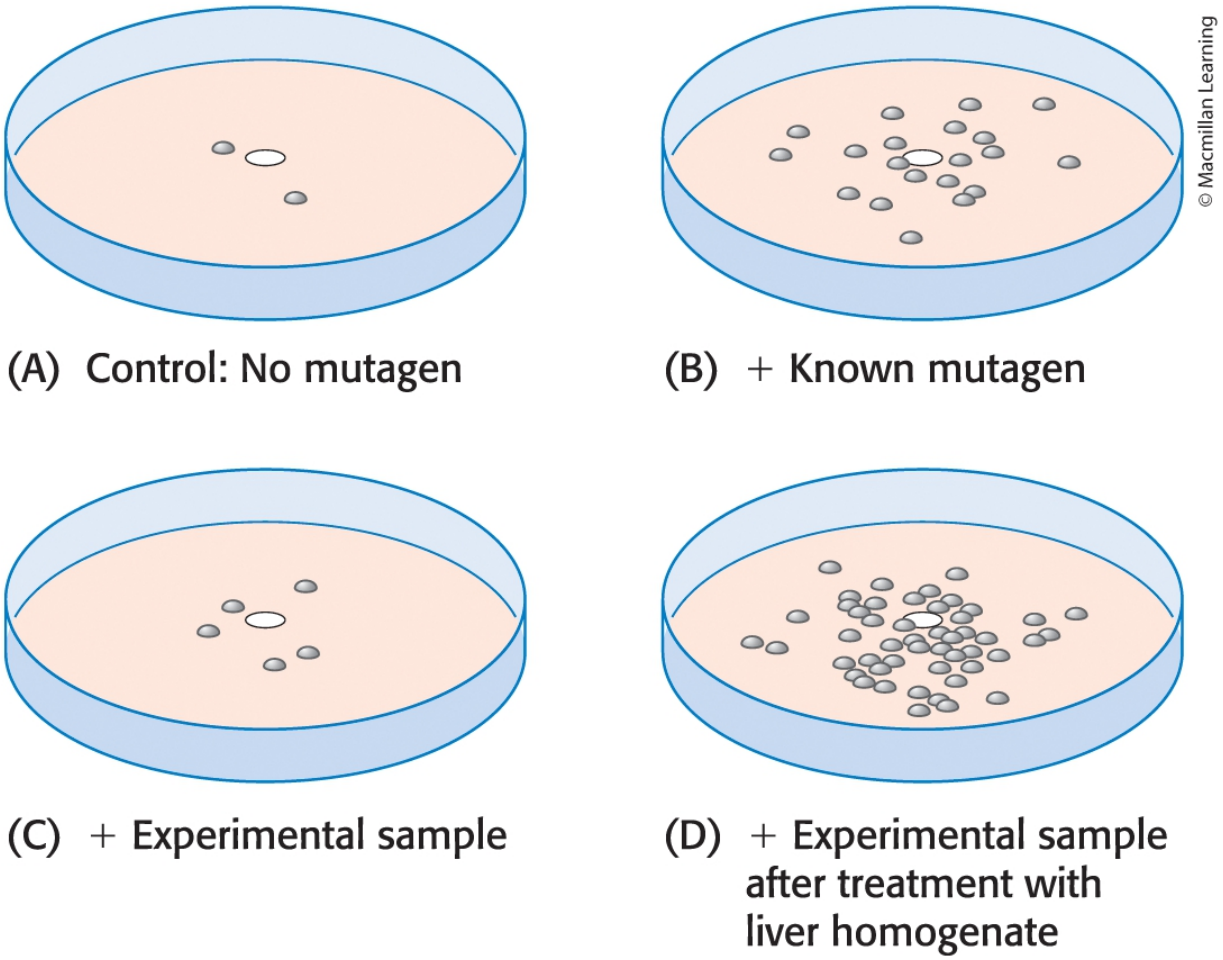
In lane A, a bright band is present at the top and a thick and bright smear is located at the bottom.

In lane B, a bright band is seen at the top at the same level as the bright band of lane A. It is followed by a series of evenly spaced thin bands from top to bottom. The bottom contains a thick and bright smear.

In lane C, a thick bright band is seen at the top. It is followed by a series of bands whose thickness and intensity decrease from top to bottom. A thin smear is located at the bottom.

Return to D N A banding pattern in lanes A, B, and C

Extended description for Illustration of four agar plates used for Ames test



The agar plates are labeled (A) to (D).

Plate (A) is labeled "Control: No mutagen." It contains a tiny circular filter paper disk in the center. Two bacterial colonies are present around the disk.

Plate (B) is labeled "Plus known mutagen." It contains a tiny circular filter paper disk in the center. Several scattered bacterial colonies

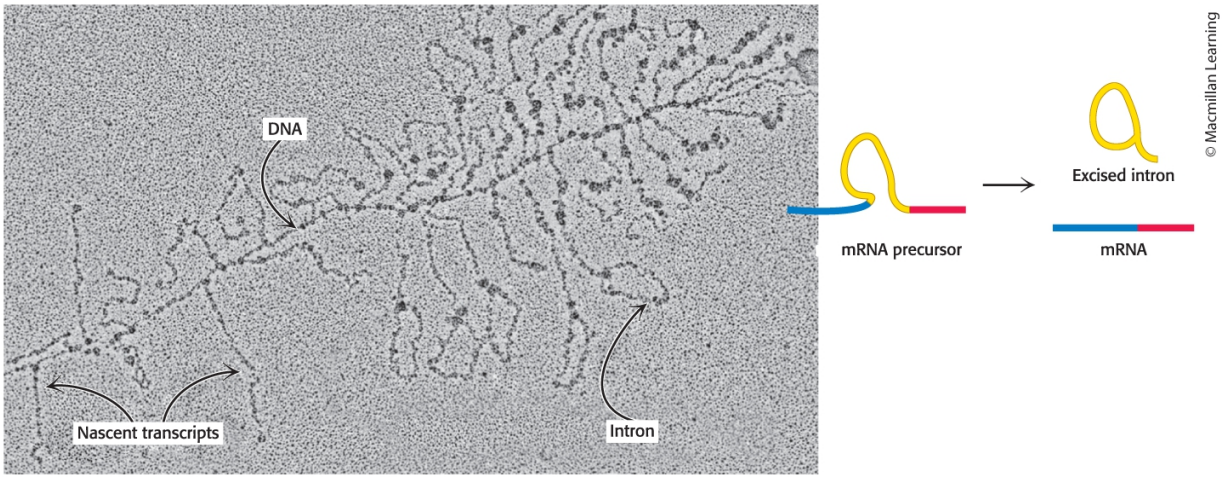
are present around the disk.

Plate (C) is labeled "Plus experimental sample." It contains a tiny circular filter paper disk in the center. 5 bacterial colonies are present around the disk.

Plate (D) is labeled "Plus experimental sample after treatment with liver homogenate." A dense cluster of a large number of bacterial colonies is present around the disk.

Return to Illustration of four agar plates used for Ames test

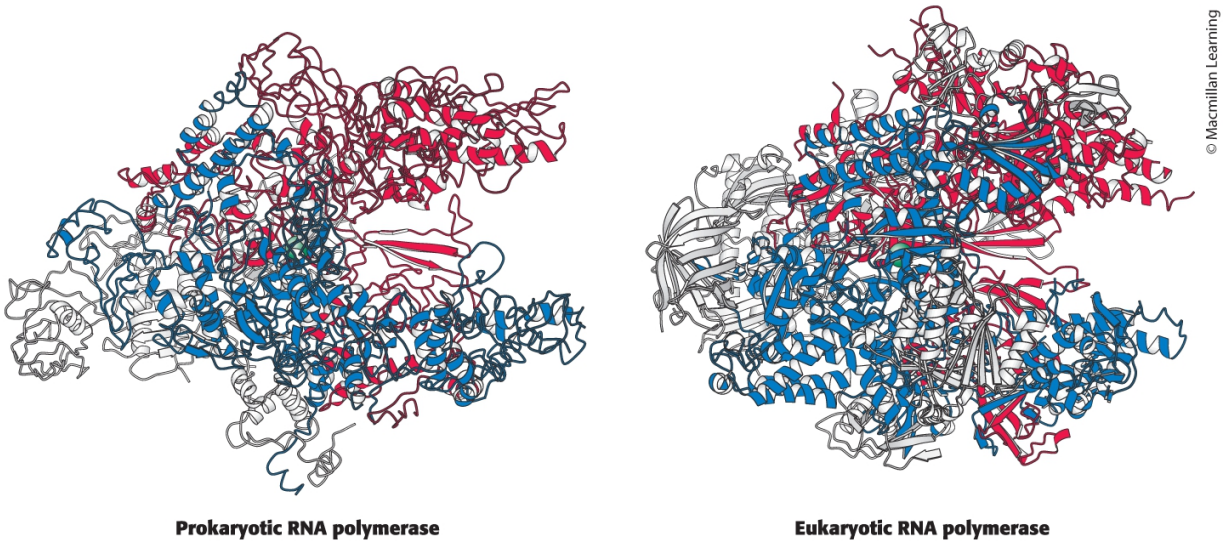
Extended description for Electron micrograph and schematic representation of R N A synthesis and splicing respectively



The figure illustrates two images. The first image is an electron micrograph that shows a D N A template from a fruity fly that is being transcribed into R N A. Nascent transcripts, Introns, and D N A are shown with curved arrows on the electron micrograph. The central narrow thread-like D N A has several short threads arising from it labeled nascent transcripts. A loop-like structure at the end of one transcript is labeled introns. The schematic representation depicts the conversion of m R N A precursor into excised intron and m R N A. The m R N A precursor is depicted as a tube-like structure containing three differently colored components shown in red, yellow, and blue. The yellow region forms a loop. The yellow region is cleaved out and labeled excised intron. The blue-colored and red colored components of the m R N A precursor are joined together to form an m R N A.

Return to Electron micrograph and schematic representation of R N A synthesis and splicing respectively

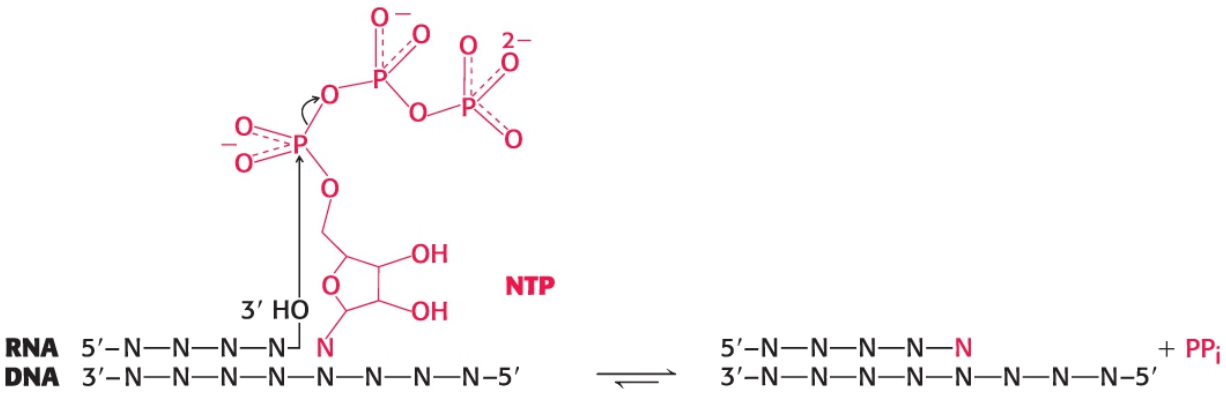
Extended description for FIGURE 29.1 R N A polymerase structures in prokaryotes and eukaryotes resemble each other



The prokaryotic and eukaryotic R N A polymerase consists of a large dense cluster of several alpha-helices and beta-strands. Each polymerase consists of two subunits shown in dark red and dark blue colors. Both the polymerases have a cleft on the right side. The cleft of the prokaryotic R N A polymerase is relatively deeper and wider than the cleft of the eukaryotic R N A polymerase.

Return to FIGURE 29.1 R N A polymerase structures in prokaryotes and eukaryotes resemble each other

Extended description for R N A synthesis using D N A as a template



The reactant shows a hybrid of R N A and D N A.

The sequence of D N A is 3 prime, single bond, N, single bond, N, single bond, N, single bond, N, single bond, N, single bond, N, single bond, N, single bond, N, single bond, 5 prime.

The sequence of R N A strand undergoing synthesis is 5 prime, single bond, N, single bond, N, single bond, N, single bond, N, single bond, 3 prime O H.

An incoming nucleoside triphosphate (N T P) is located near the 3 prime end of R N A. The N base of this N T P is aligned opposite to the fifth N base from the 3 prime end of the D N A.

The structure of N T P is as follows: A 5-membered heterocyclic pentagonal ring is in a horizontal orientation with C 1 occupying the top left vertex. It consists of 1 O and 4 C atoms. O occupies the leftmost vertex. C 2 and C 3 are each single bonded to H. C 4 is single bonded to N on the lower left. C 1 is single bonded to C H 2 on the upper left in the form of a line. C H 2 is single bonded to O on the

upper right. O is single bonded to a zigzag chain composed of P, single bond, O, single bond, P, single bond, O, single bond, P. P 1 and P 2 are each partially double bonded to two different O. The P O O groups have an overall negative charge. P 3 is partially double bonded to three O. This P O 3 group has an overall negative charge of 2 minus.

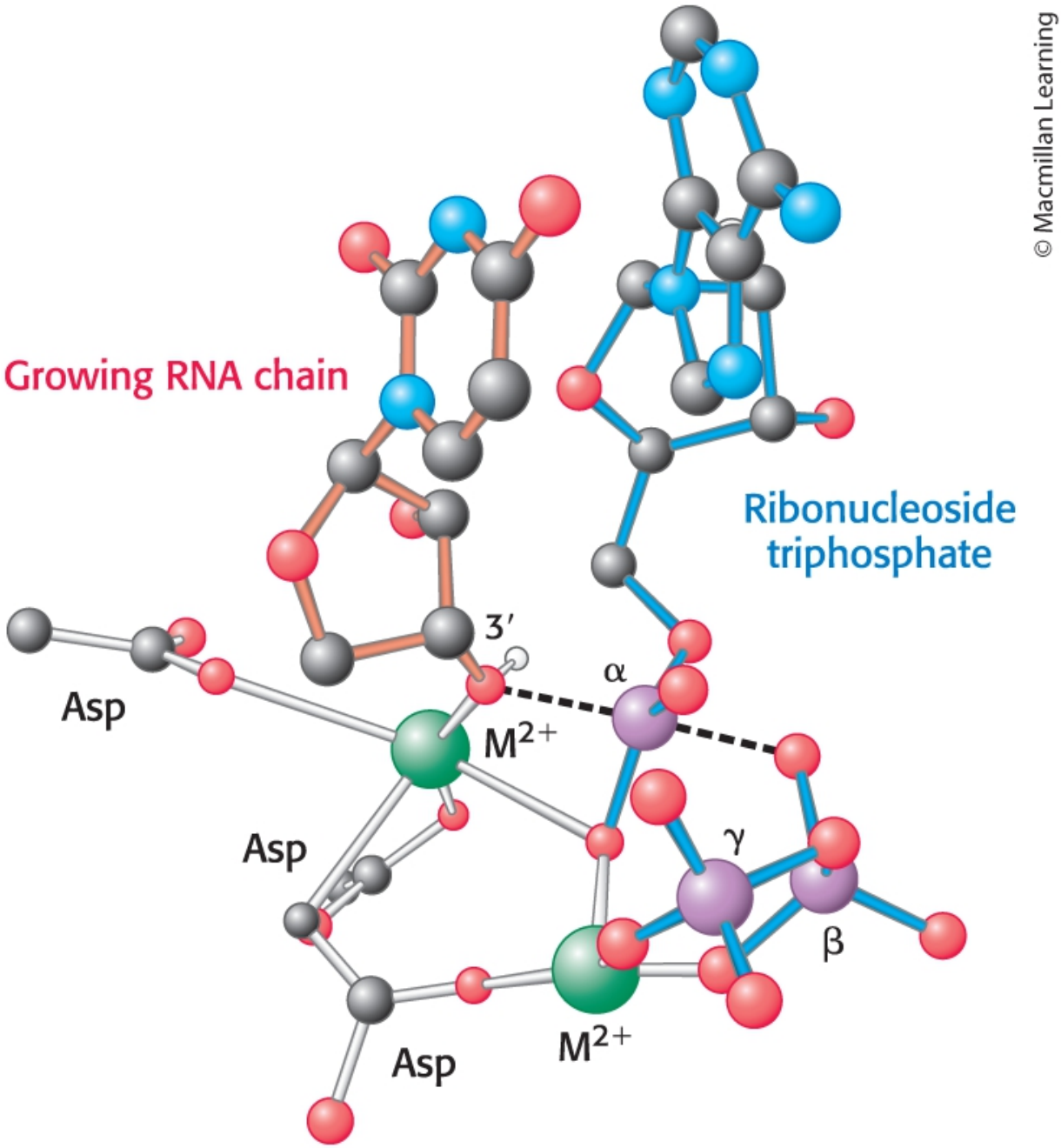
An arrow from the 3 prime O H of R N A points toward P 1 of the zigzag chain. Another arrow from the single bond between this P and O 1 points toward O 1.

The first product of the N T P addition includes an R N A and D N A hybrid with a newly added N to the 3 prime end of R N A.

The sequence of D N A is 3 prime, single bond, N, single bond, N, single bond, N, single bond, N, single bond, N, single bond, N, single bond, N, single bond, N, single bond, N, single bond, 5 prime. The sequence of the extended R N A strand is 5 prime, single bond, N, single bond, N, single bond, N, single bond, N, single bond, N. The second product is P P subscript i.

Return to R N A synthesis using D N A as a template

Extended description for FIGURE 29.2 The R N A polymerase active site contains metal ions



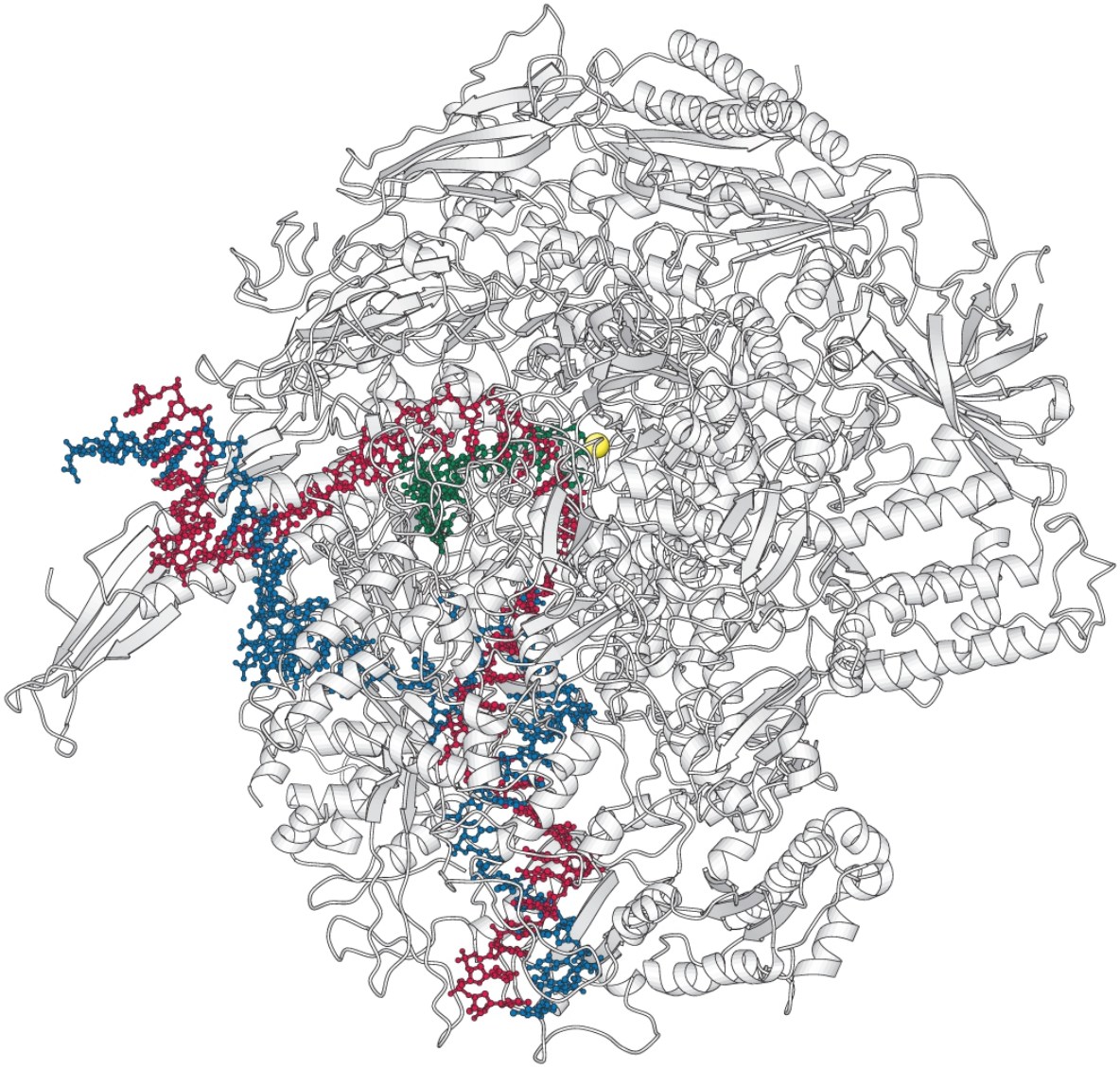
© Macmillan Learning

The growing R N A chain is shown on the top left and the ribonucleoside triphosphate is shown on the top right. The growing R N A chain consists of a pentagonal ring connected to a hexagonal ring. The pentagonal ring consists of 1 red and 4 black spheres. The hexagonal ring consists of 2 blue and 4 black spheres. The ribonucleoside triphosphate consists of a pentagonal ring connected to a hexagonal ring. The pentagonal ring consists of 1 red and 4 black spheres. The hexagonal ring consists of 2 blue and 4 black spheres. A green sphere depicting M superscript 2 plus is shown below the pentagonal ring of the growing R N A chain. It is connected to the red or black sphere in the side chain of aspartic acid residue on the left, lower left, and bottom. It is also connected to a red sphere on the upper right, which is further connected to a black sphere at the 3 prime position of the pentagonal ring. This red sphere is also connected to a white sphere. A second green sphere depicting M superscript 2 plus is connected to the red sphere of aspartic acid residue on the left, the red sphere of the beta phosphoryl group, the red sphere of gamma phosphoryl group, the red sphere of the alpha-phosphoryl group connected to the pentagonal ring of ribonucleoside triphosphate. This red sphere of the alpha phosphoryl group is also connected to the first green sphere.

The pyrophosphate consists of two purple spheres. Each purple sphere is connected to three red spheres. The purple sphere connected to red spheres depicts beta and gamma phosphoryl groups. The gamma phosphoryl group is located toward the observer. The red sphere of the beta phosphoryl group is connected to the red sphere which is, in turn, connected to the 3 prime position of the pentagonal ring of the growing R N A chain. This connection is represented by a dashed line.

Return to FIGURE 29.2 The R N A polymerase active site contains metal ions

Extended description for FIGURE 29.3 R N A polymerase separates a region of the double helix to form the transcription bubble



© Macmillan Learning

The R N A polymerase is depicted as a large dense cluster composed of several alpha-helices and beta-strands. A ball-and-stick model of D N A double helix passes from the left end of the polymerase to the bottom. The double helix is separated inside the polymerase to form

a large transcription bubble. The strands of D N A are composed of red and blue spheres. The strand composed of red spheres depicts the template. A yellow sphere depicting magnesium is located in the center of the polymerase adjacent to the template strand in the bubble. A short R N A strand composed of a green sphere is bonded to the template strand in the bubble.

Return to FIGURE 29.3 R N A polymerase separates a region of the double helix to form the transcription bubble

Extended description for FIGURE 29.4 R N A transcript complementary to the template strand



The sequence of the template or antisense (minus) strand is as follows from left to right: ellipsis, G C A T A C A A C A C A C C T T G C A T C C A G T G T A G, ellipsis.

The sequence of the coding or sense (plus) strand is as follows from left to right: ellipsis, C G T A T G T T G T G T G G A A C G T A G G G T C A C A T C, ellipsis.

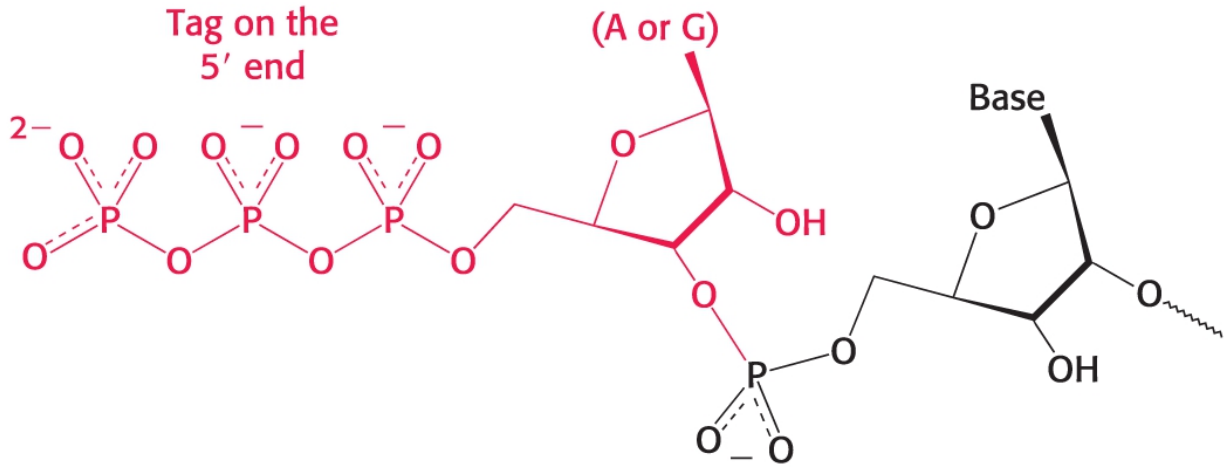
The sequence of R N A transcript complementary to the template strand is as follows from left to right: A A C G U A G G G U C A C A U C, ellipsis.

The first A of R N A corresponds to C at the 14th position of the template. The fourth C of the R N A corresponds to G at the 30th position of the template.

A vertical line passes from the left side of first A in R N A, through the space between C T and G A of the coding strand. The base G on the left of this vertical line in the coding strand is numbered minus 1. The first base A on the right of the vertical line in the coding strand is numbered plus 1. The second A, located on the right of the first A numbered plus 1, is numbered plus 2.

Return to FIGURE 29.4 R N A transcript complementary to the template strand

Extended description for Structure of a molecule

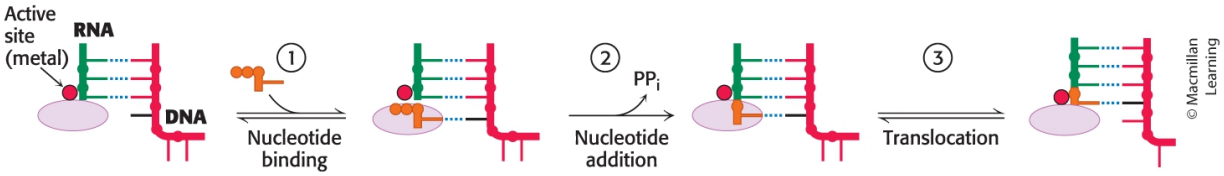


The structure is as follows: A 5-membered heterocyclic pentagonal ring is in a vertical orientation and consists of 1 O and 4 C atoms. The O atom occupies the first position, which is the topmost vertex. The ring is in a plane perpendicular to the plane of the paper such that O is away from the observer and C 2 and C 3 are toward the observer. C 1 is wedge bonded to (A or G). C 2 is single bonded to O H. C 3 is single-bonded to O. O is single-bonded to a central P atom of the first phosphate group on the lower right. A central P is single-bonded to the first O on the upper right, partially double-bonded to O superscript minus on the lower right, and partially double-bonded to the second O on the lower left. The first O atom of the phosphate group is single-bonded to C H 2 on the upper right in the form of a line. C H 2 is single-bonded to C 4 of the second 5-membered heterocyclic pentagonal ring in a vertical orientation. The 5-membered heterocyclic pentagonal ring is in a vertical orientation and consists of 1 O and 4 C atoms. The O atom occupies the first position, which is the topmost vertex. The ring is in a plane perpendicular to the plane of the paper such that O is away from the observer and C 2 and C 3 are toward the observer. C 1 is wedge bonded to the base. C 2 is single-bonded to O. O has a wiggly line on

the lower right. C 3 is single-bonded to O H. C 4 of the first pentagonal ring is single-bonded to C H 2 in the form of a line. C H 2 is single-bonded to O on the lower left. O is further single-bonded to a central P atom of the first phosphate group. The central P atom is single-bonded to the first O on the lower left, partially double-bonded to the second O on the upper right, and partially double-bonded to the O superscript minus on the upper left. The first O of the first phosphate group is single-bonded to a central P atom of the second phosphate group. The central P atom is single-bonded to the first O on the lower left, partially double-bonded to the second O on the upper right, and partially double-bonded to the O superscript minus on the upper left. The first O of the second phosphate group is single-bonded to a central P atom of the third phosphate group. The central P atom is partially double-bonded to the first O on the lower left, partially double-bonded to the second O on the upper right, and partially double-bonded to O superscript 2 minus on the upper left. The three phosphate groups are aligned in a zigzag manner. The three phosphate groups in the chain and first pentagonal ring are highlighted in red color and labeled "Tag on the 5 prime end."

Return to Structure of a molecule

Extended description for FIGURE 29.5 The elongation mechanism involves a series of steps



An R N A-D N A hybrid is shown. The R N A is depicted as a solid green vertical line. The D N A is depicted as a solid red vertical line. R N A and D N A molecules are connected by three base pairs. The bottom end of the D N A is curved toward the lower right. It has an unpaired base. A purple oval with a tiny red circle at the top is located at the bottom end of R N A. The red circle is labeled active site (metal).

In the first reversible step, nucleotide binding takes place. The nucleotide is depicted as a short vertical stick with three orange circles at the top left and a short stick on the middle right. It aligns below the bottom end of the R N A inside the purple oval. It forms hydrogen bonds with the free unpaired base of the D N A molecule.

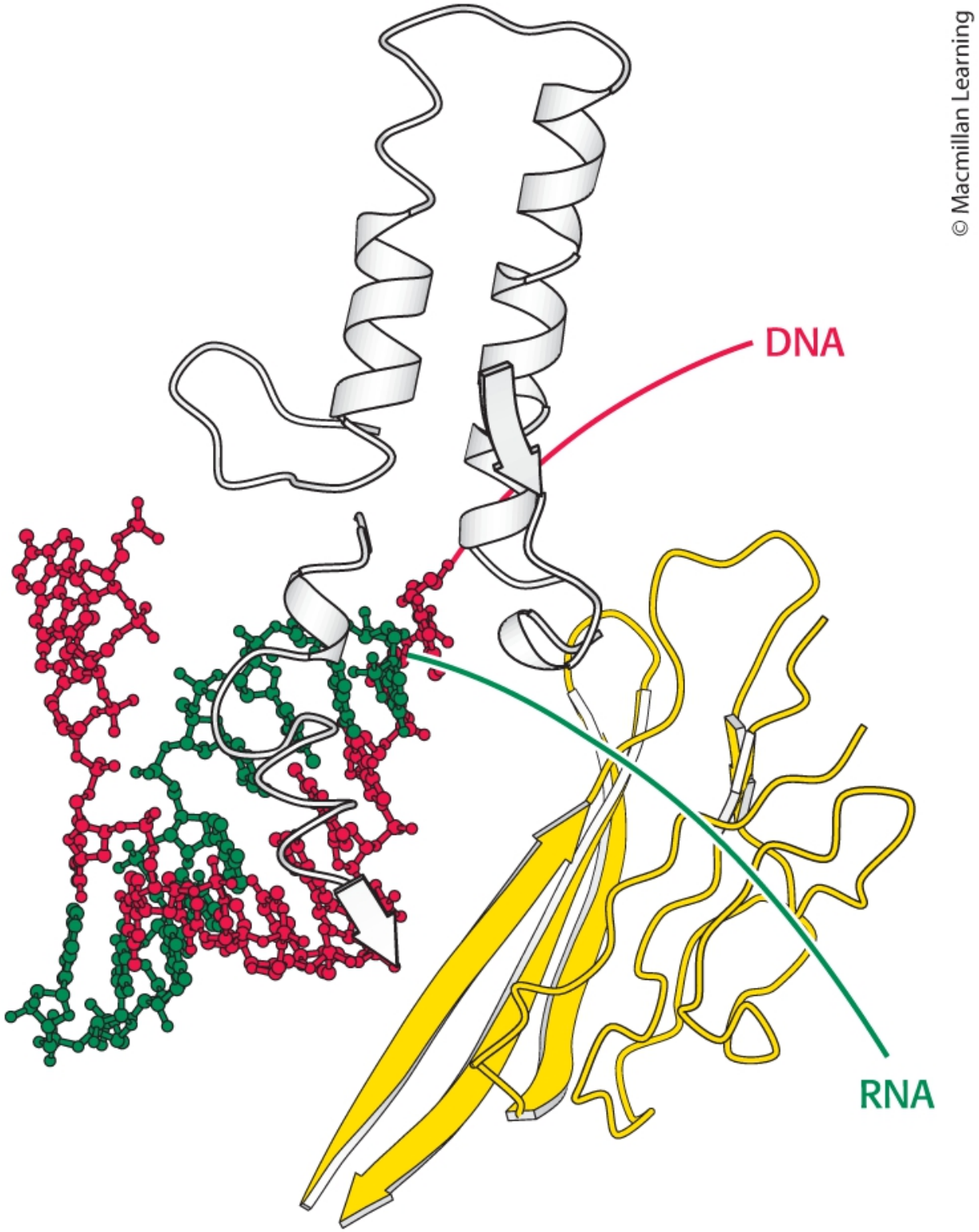
In the second irreversible step, P P subscript i is released and nucleotide addition takes place. The two terminal circles of the nucleotide are removed. The gap between the bottom end of R N A and incoming nucleotide is sealed.

In the third reversible step, translocation takes. The purple oval translocates downward such that it is located opposite the next free unpaired base of D N A.

Return to FIGURE 29.5 The elongation mechanism involves a series of steps

Extended description for FIGURE 29.6 A structure within R N A polymerase forces the separation of the R

N A–D N A hybrid

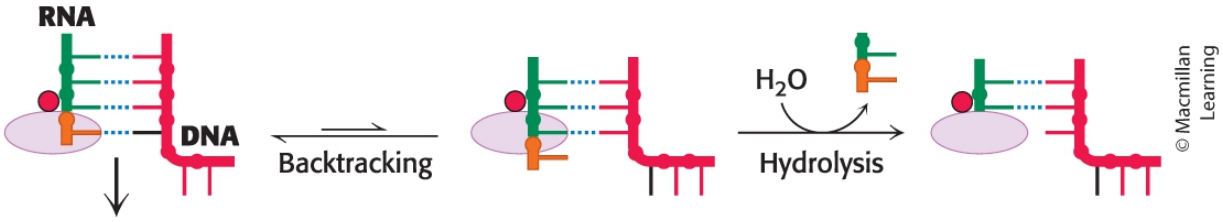


© Macmillan Learning

A helix-loop-helix is shown at the top. A beta-strand is shown in front of the right helix. Three anti-parallel beta strands in diagonal orientation are shown on the lower right of the helix-loop-helix. The beta strands are connected to several loops on the right. The ball-and-stick model of an R N A-D N A hybrid is located below the helix-loop-helix and on the left of the beta-strands. A short helix connected to a short beta-strand through a long loop passes over the R N A-D N A hybrid. The D N A composed of red spheres forms a U-shaped orientation such that the free end of D N A is located toward the upper left. The R N A composed of green spheres is in a diagonal orientation such that its free end is located toward the lower left, below the D N A.

Return to FIGURE 29.6 A structure within R N A polymerase forces the separation of the R N A–D N A hybrid

Extended description for FIGURE 29.7 The R N A–D N A hybrid can occasionally backtrack within the R N A polymerase



An R N A-D N A hybrid is shown. The R N A is depicted as a solid green vertical line. The D N A is depicted as a solid red vertical line. R N A and D N A molecules are connected by four base pairs. The bottom end of the D N A is curved toward the lower right. It has two unpaired nucleotides. A purple oval with a tiny red circle at the top is located at the bottom end of R N A. The oval structure encloses the newly added nucleotide depicted in orange color.

In the first reversible step, backtracking takes place. The oval moves upward and encloses the nucleotide located above the orange nucleotide. The base in the D N A previously hydrogen bonded with the orange nucleotide becomes unpaired and moves toward the lower right.

In the second irreversible step, hydrolysis takes place with the entry of H 2 O and removal of dinucleotide from the bottom end of R N A. The released dinucleotide includes the orange nucleotide and the nucleotide located above it. The purple oval is bound to the bottom end of the R N A. In the hybrid, R N A and D N A molecules are connected by two base pairs. The D N A contains three unpaired nucleotides at the lower right.

Return to FIGURE 29.7 The R N A–D N A hybrid can occasionally backtrack within the R N A polymerase

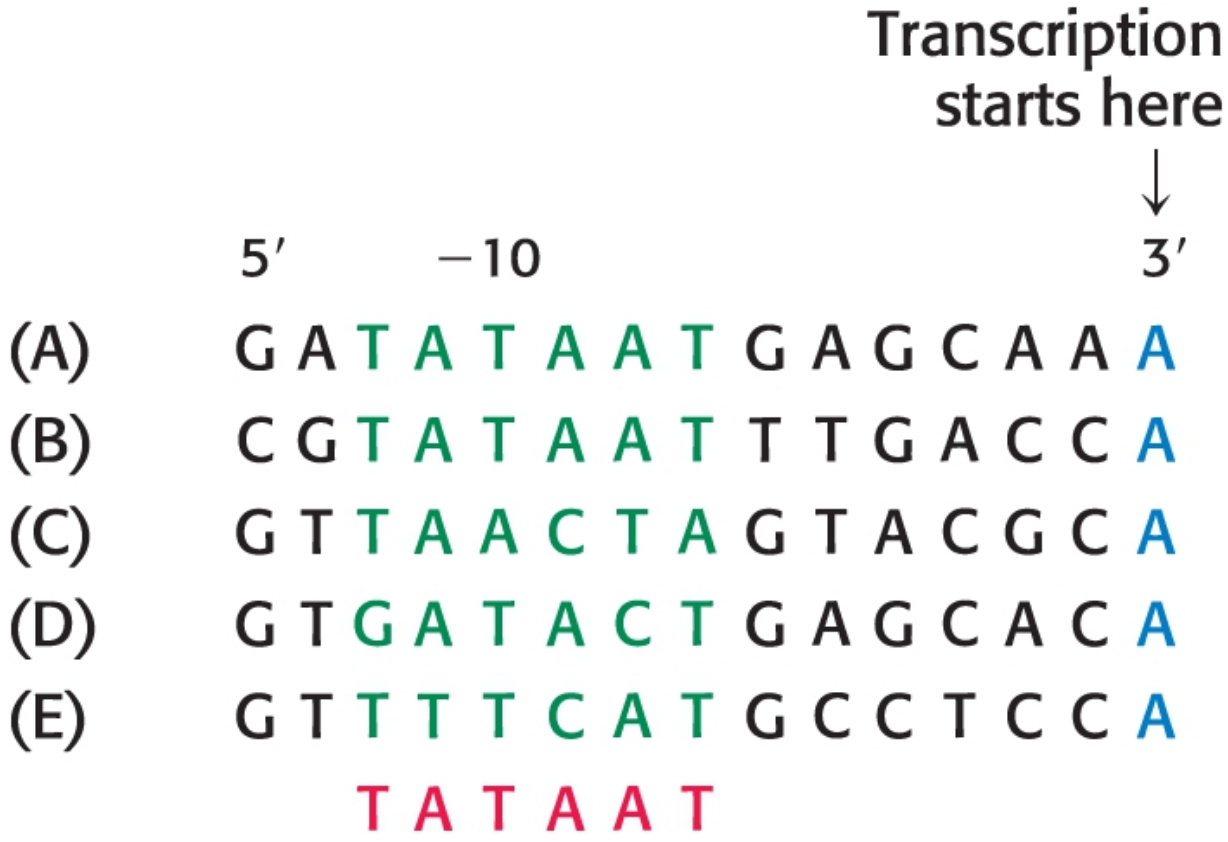
Extended description for Consensus sequence for the core promoter



The consensus sequence deduced from the analyses of the many promoters is as follows: 5 prime, small wiggly line, T T G A C A, large wiggly line, T A T A A T, medium wiggly line, start site. The first and the second sequence are highlighted in red and labeled minus 35 and minus 10 respectively. The start site mentioned at the end of the sequence is labeled plus 1.

Return to Consensus sequence for the core promoter

Extended description for FIGURE 29.8 Bacterial promoters contain conserved sequences



The sequences are labeled (A) to (E).

Sequence (A) reads 5 prime, G A T A T A A T G A G C A A A, 3 prime.

Sequence (B) reads 5 prime, C G T A T A A T T T G A C C A, 3 prime.

Sequence (C) reads 5 prime, G T T A A C T A G T A C G C A, 3 prime.

Sequence (D) reads 5 prime, G T G A T A C T G A G C A C A, 3 prime.

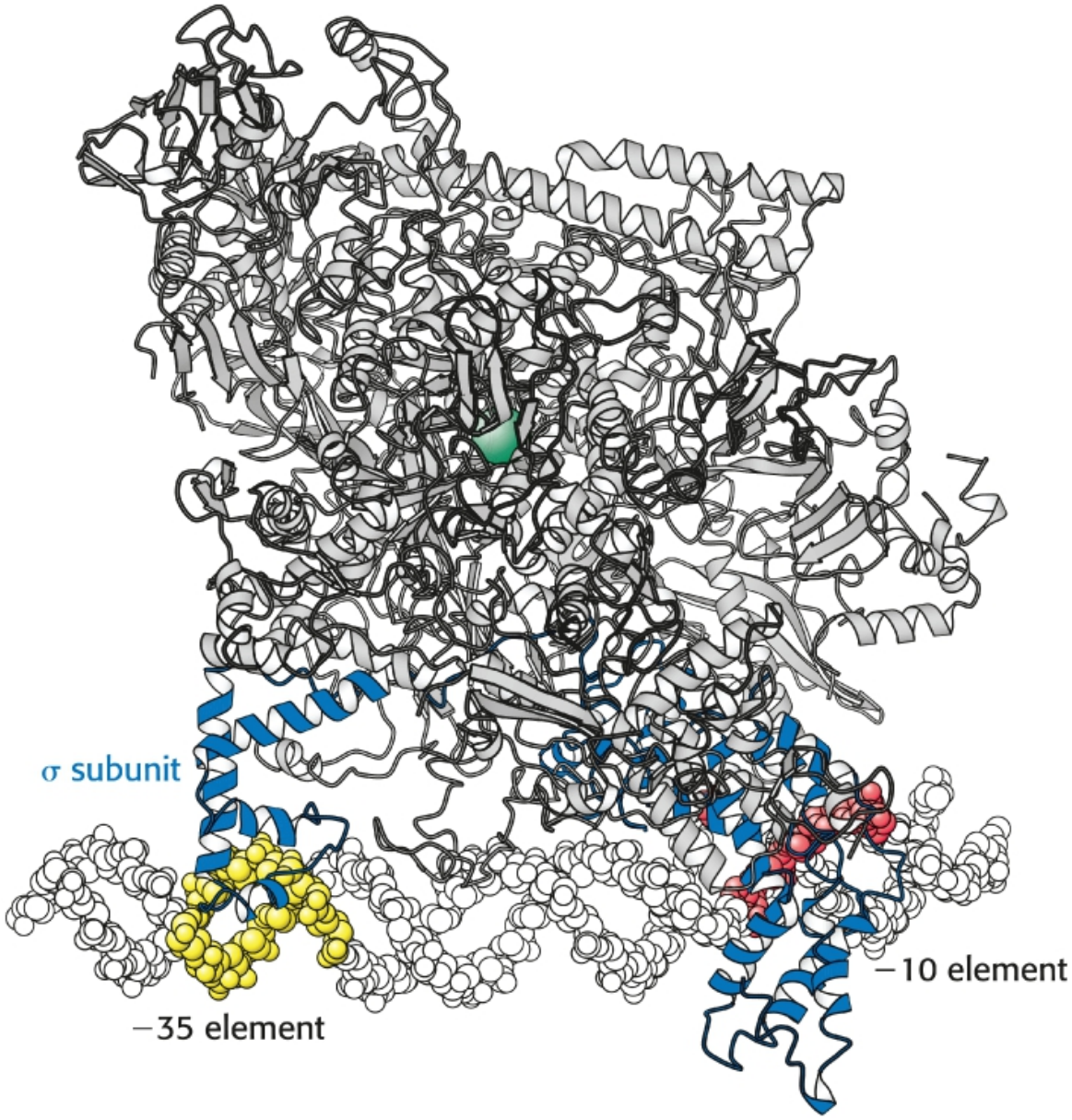
Sequence (E) reads 5 prime, G T T T T C A T G C C T C C A, 3 prime.

The base A at the 3 prime ends is highlighted in blue and labeled "Transcription starts here."

The bases at the fifth position from the 5 prime end in each sequence, occupy the minus 10 position. The sequence T A T A A T highlighted in red corresponds to the consensus sequence at the minus 10 position.

Return to FIGURE 29.8 Bacterial promoters contain conserved sequences

Extended description for FIGURE 29.9 E. coli R N A polymerase holoenzyme complex binds to conserved promoter sequences



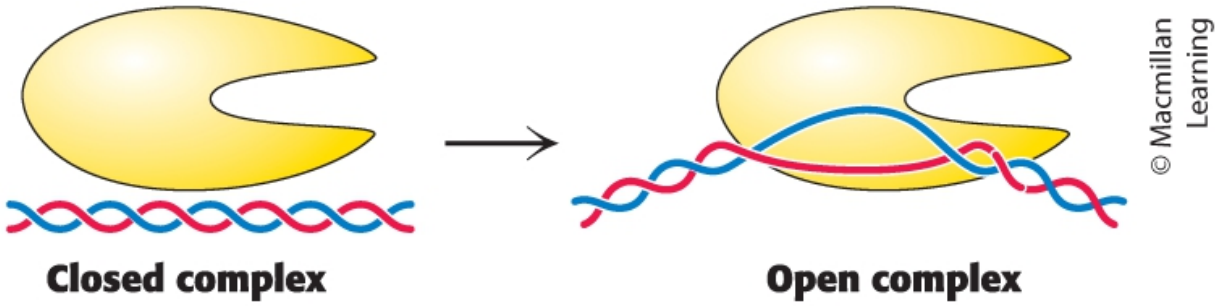
© Macmillan Learning

The R N A polymerase holoenzyme consists of a dense and large cluster of alpha-helices and beta-strands. A few alpha-helices of the

sigma subunit extend from the bottom right and bottom left of the holoenzyme. The alpha-helices on the bottom left are bound to the minus 35 element of D N A. The alpha-helices on the bottom right are bound to the minus 10 element of D N A. D N A double helix in horizontal orientation is depicted as two strands composed of white spheres. The minus 35 element is highlighted in yellow and the minus 10 element is highlighted in red.

Return to FIGURE 29.9 E. coli R N A polymerase holoenzyme complex binds to conserved promoter sequences

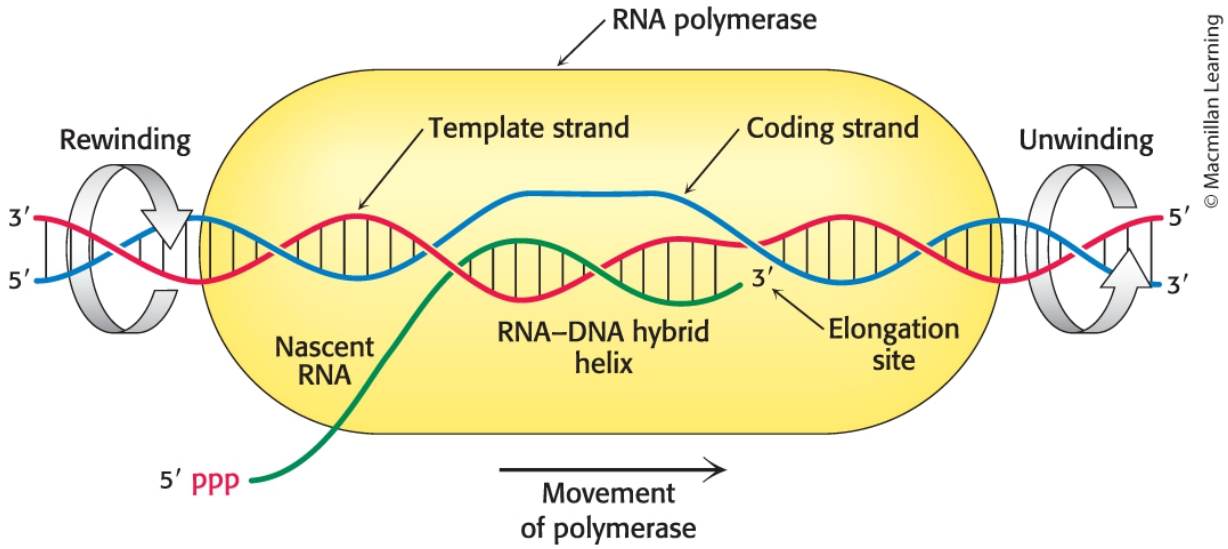
Extended description for FIGURE 29.10 E. coli R N A polymerase binds to a promoter sequence



In the closed complex, R N A polymerase depicted as a yellow oval with a deep cleft on the right is shown above a double helical D N A. A forward arrow leads to the open complex. In the open complex, the D N A is bent downward and its strands are unwound in the middle to form a bubble. The bubble is bound by the polymerase.

Return to FIGURE 29.10 E. coli R N A polymerase binds to a promoter sequence

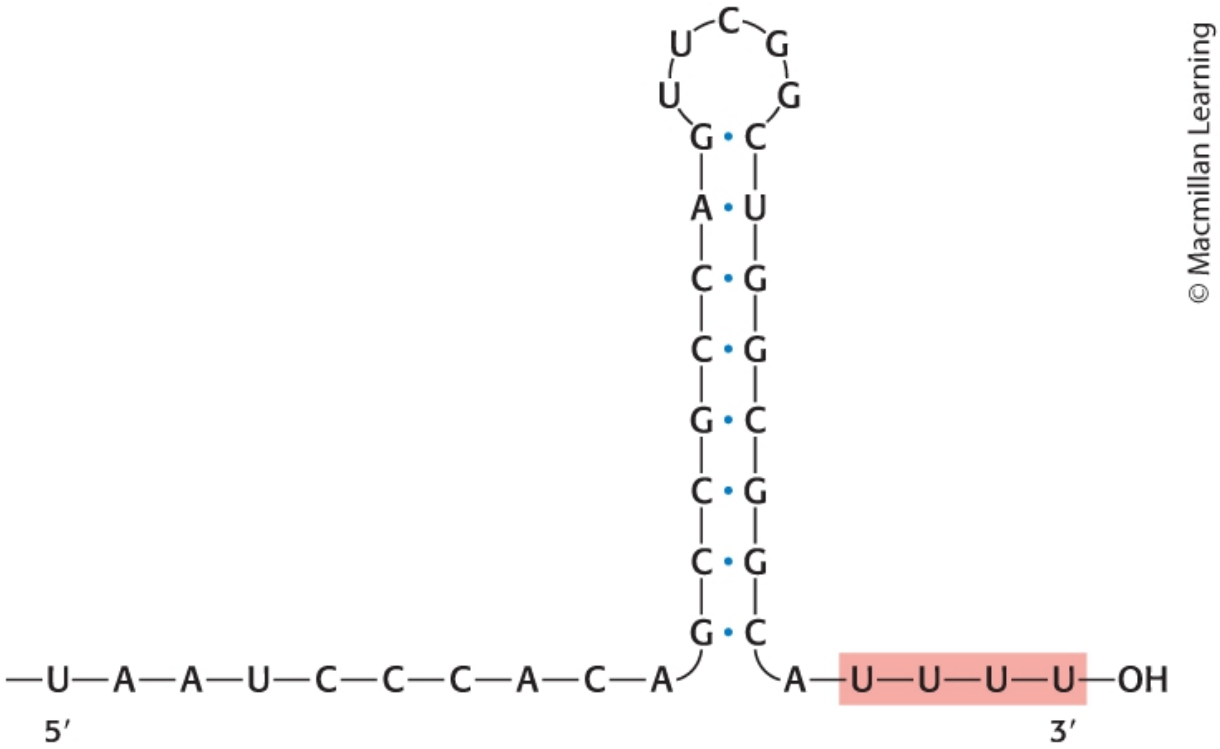
Extended description for FIGURE 29.11 The transcription bubble moves with the R N A polymerase during elongation



A double-helical D N A is shown in a horizontal orientation. It is composed of a red and a blue strand. The red strand is labeled the template strand. The blue strand is labeled the coding strand. The ends of the D N A double helix are located outside the R N A polymerase. The R N A polymerase is depicted as a large yellow capsule-shaped structure. Rewinding occurs at the left end and is depicted as a clockwise arrow. Unwinding occurs at the right end and is depicted as an anticlockwise arrow. A transcription bubble is formed in the double helix inside the R N A polymerase. A nascent R N A strand is depicted in green. It is bound to the template strand in the bubble to form an R N A-D N A hybrid helix. The nascent R N A exits out of the R N A polymerase and its 5 prime end contains three P. The free 3 prime of the R N A is labeled elongation sites as the polymerase moves in 5 prime to 3 prime direction.

Return to FIGURE 29.11 The transcription bubble moves with the R N A polymerase during elongation

Extended description for FIGURE 29.12 Some genes contain intrinsic termination signals

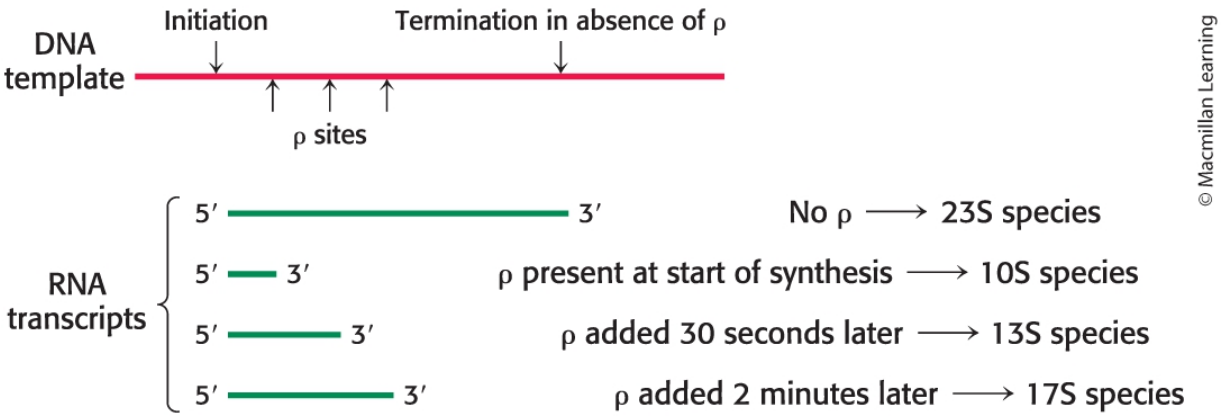


© Macmillan Learning

The intrinsic terminal signal consists of a stem-loop structure. The linear 5 prime sequence is U A A U C C C A C A. The stem-loop consists of G C, A U, C G, C G, G C, C G, C G, and G C base pairs from top to bottom of the stem region. The loop region consists of U U C G G in an anti-clockwise orientation starting from the bottom left. The linear 3 prime sequence is A U U U U, single bond, O H. The continuous string of U residues is highlighted inside a pink rectangle.

Return to FIGURE 29.12 Some genes contain intrinsic termination signals

Extended description for FIGURE 29.13 Rho protein promotes the termination of transcription



© Macmillan Learning

The D N A template is depicted as a solid red horizontal line. The initiation site is present near the left end and a site near the right end is labeled "Termination in absence of rho." Three rho sites are present between the initiation and rho-independent sites.

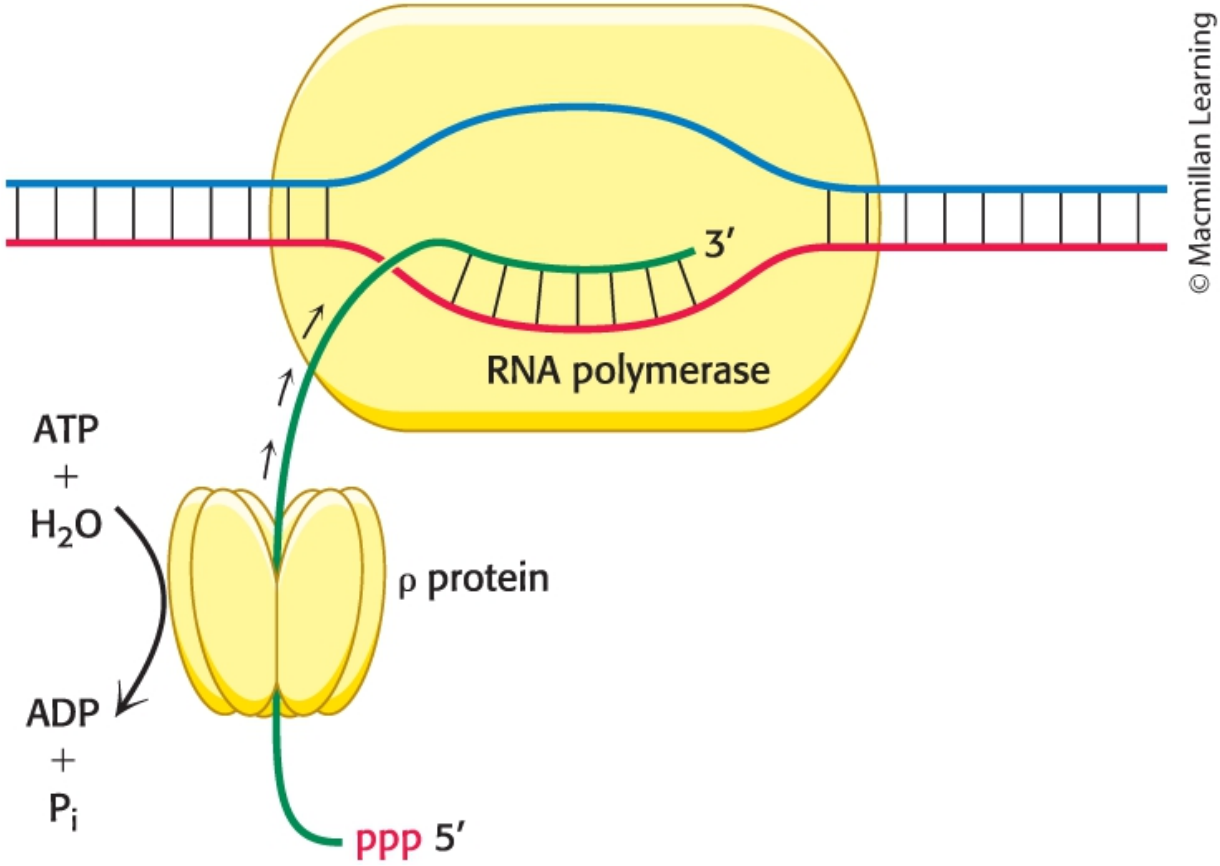
Four R N A transcripts of different lengths are shown below the D N A template. They are depicted as solid green lines. The left end is labeled 5 prime and the right end is labeled 3 prime. The first R N A transcript corresponds to termination in the absence of rho. It has the largest size. A label alongside this transcript reads "No rho, forward arrow, 23 S species."

The second R N A transcript corresponds to termination at the first rho site. It has the smallest size. A label alongside this transcript reads "Rho present at the start of synthesis, forward arrow, 10 S species." The third R N A transcript corresponds to termination at the second rho site. Its size is relatively larger than the second transcript but smaller than the first transcript. A label alongside this transcript reads "Rho added 30 seconds later, forward arrow, 13 S

species." The fourth R N A transcript corresponds to termination at the third rho site. Its size is relatively larger than the third transcript but smaller than the first transcript. A label alongside this transcript reads "Rho added 2 minutes later, forward arrow, 17 S species."

Return to FIGURE 29.13 Rho protein promotes the termination of transcription

Extended description for FIGURE 29.14 Rho protein is an A T P-dependent helicase

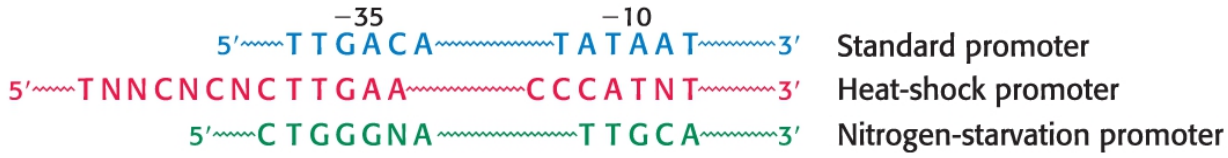


R N A polymerase depicted as a large capsule-shaped structure is bound to the transcription bubble of a double-stranded D N A. An R N A strand is hydrogen bonded to the red strand of the helix in the transcription bubble. The free 3 prime end of the R N A is located inside the polymerase. The 5 prime region of the R N A strand is located outside the polymerase. The 5 prime end contains three P. The rho protein composed of 6 elongated subunits is bound near the 5 prime end of the R N A. The R N A strand passes through the hollow core of the rho protein. Three upward arrows point from the rho protein toward the transcription bubble to depict its movement.

The movement of rho protein is coupled with the hydrolysis of A T P plus H 2 O to A D P plus P subscript i.

Return to FIGURE 29.14 Rho protein is an A T P-dependent helicase

Extended description for FIGURE 29.15 Alternative promoters vary in their consensus sequences at conserved sites



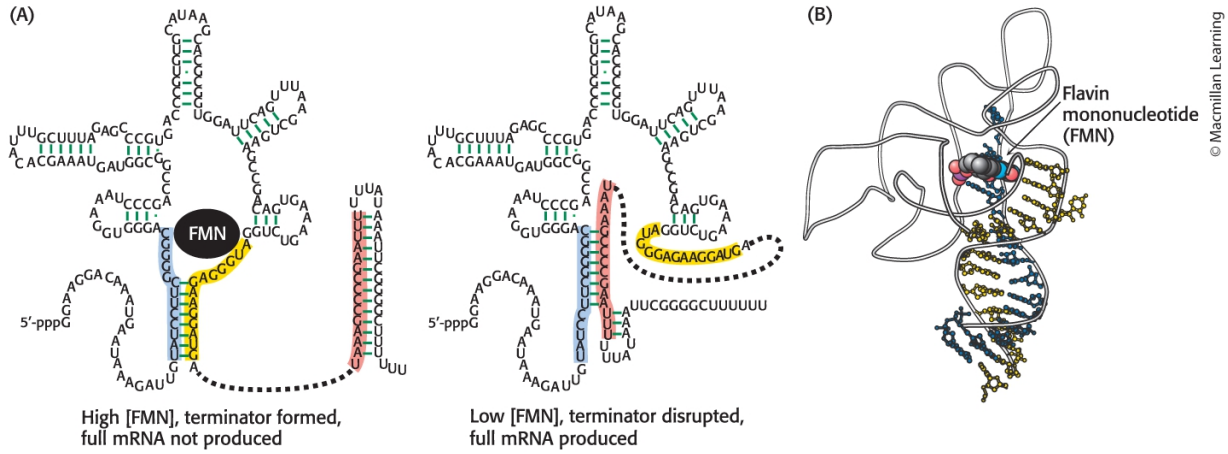
The sequence of a standard promoter is as follows: 5 prime, wiggly line, T T G A C A, wiggly line, T A T A A T, wiggly line, 3 prime. T T G A C A is located at minus 35 position and T A T A A T is located at minus 10 position.

The sequence of heat-shock promoter is as follows: 5 prime, wiggly line, T N N C N C N C T T G A A, wiggly line, C C C A T N T, wiggly line, 3 prime. T N N C N C N C T T G A A is located at minus 35 position and C C C A T N T is located at minus 10 position.

The sequence of nitrogen-starvation promoter is as follows: 5 prime, wiggly line, C T G G G N A, wiggly line, T T G C A, wiggly line, 3 prime. C T G G G N A is located at minus 35 position and T T G C A is located at minus 10 position.

Return to FIGURE 29.15 Alternative promoters vary in their consensus sequences at conserved sites

Extended description for FIGURE 29.16 Riboswitches use metabolite concentrations to regulate transcription



Part (A): The first riboswitch is bound to F M N. It has a short 5 prime region followed by stem-loop structures. The loop portion is larger and further contains five stem-loop structures on the bottom left, top left, top, top right, and bottom right. The loop of the main stem-loop is bound to F M N. The main stem-loop is followed by a short linear stretch and a terminator composed of a long stem region and a small loop region. The left side of the stem region of the main stem-loop is highlighted in blue. The right side of the stem region of the main stem-loop is highlighted in yellow. The left side of the stem region of the terminator is highlighted in pink. The text below the riboswitch reads "High concentration of F M N, terminator formed, full m R N A not produced."

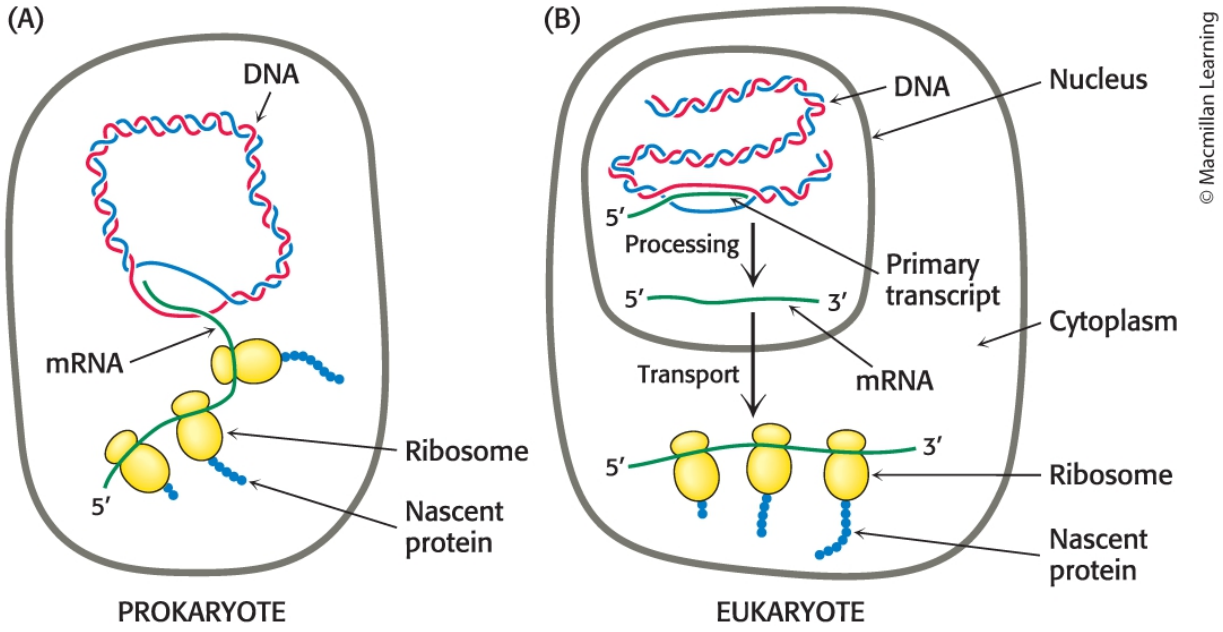
Under low F M N concentration, the terminator is disrupted, and full m R N A is produced. The main stem-loop is also disrupted and the terminator disappears. The blue highlighted sequence partially

base pairs with the pink highlighted sequence to form a stem loop. The yellow sequence is free.

Part (B): A double-helical structure with a complete single turn is shown below. It continues into an irregular wavy structure at the top. A cluster of black, pink, and blue spheres is bound to the top region and labeled "Flavin mononucleotide (F M N)." The helical region contain ball-and-stick models of nucleotide residues. In the bottom half turn, the right side of the helix contains blue highlighted nucleotides and the left side contains yellow highlighted nucleotides. In the top half turn, the right side contains yellow highlighted nucleotides and the left side contains blue highlighted nucleotides.

Return to FIGURE 29.16 Riboswitches use metabolite concentrations to regulate transcription

Extended description for FIGURE 29.17 Transcription and translation are closely coupled in prokaryotes, whereas they are spatially and temporally separate in eukaryotes



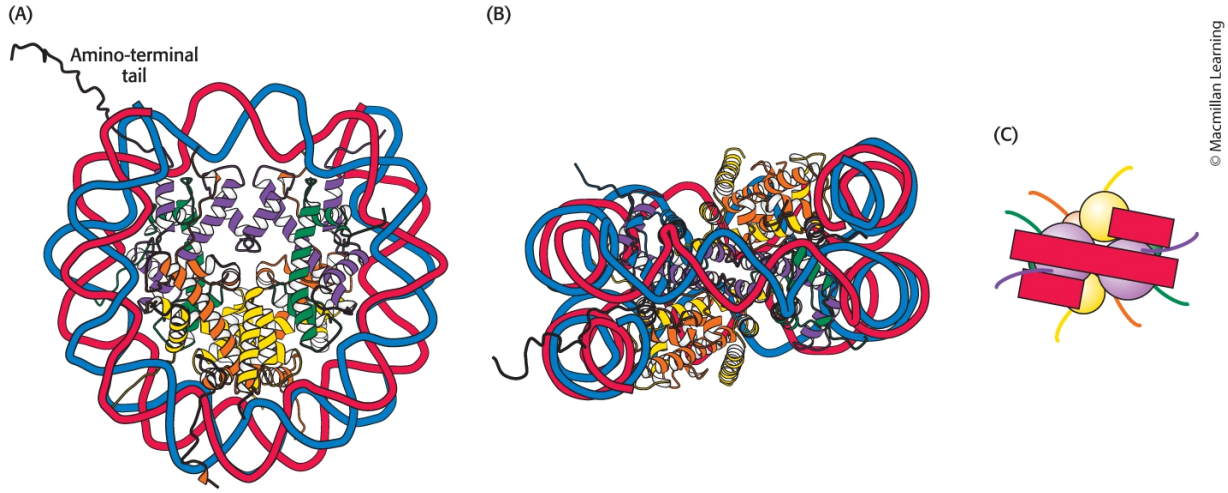
Part (A): In a capsule-shaped prokaryote, D N A depicted as a circular double helix is undergoing transcription to produce m R N A. The newly synthesized m R N A strand binds to ribosomes as it emerges from the transcription bubble. Multiple ribosomes are bound to the free end of the m R N A strand. Each ribosome is producing nascent proteins depicted as chains of tiny blue circles. All the activities are taking place in the cytoplasm.

Part (B): In the nucleus of a eukaryote, a linear D N A molecule is undergoing transcription to produce a primary transcript. The transcript undergoes processing within the nucleus to produce m R N A. The m R N A molecule is transported into the cytoplasm. In the

cytoplasm, m R N A is bound by multiple ribosomes. Each ribosome is producing nascent proteins depicted as chains of tiny blue circles.

Return to FIGURE 29.17 Transcription and translation are closely coupled in prokaryotes, whereas they are spatially and temporally separate in eukaryotes

Extended description for FIGURE 29.19 The structure of the nucleosome consists of eight histone proteins surrounded by D N A



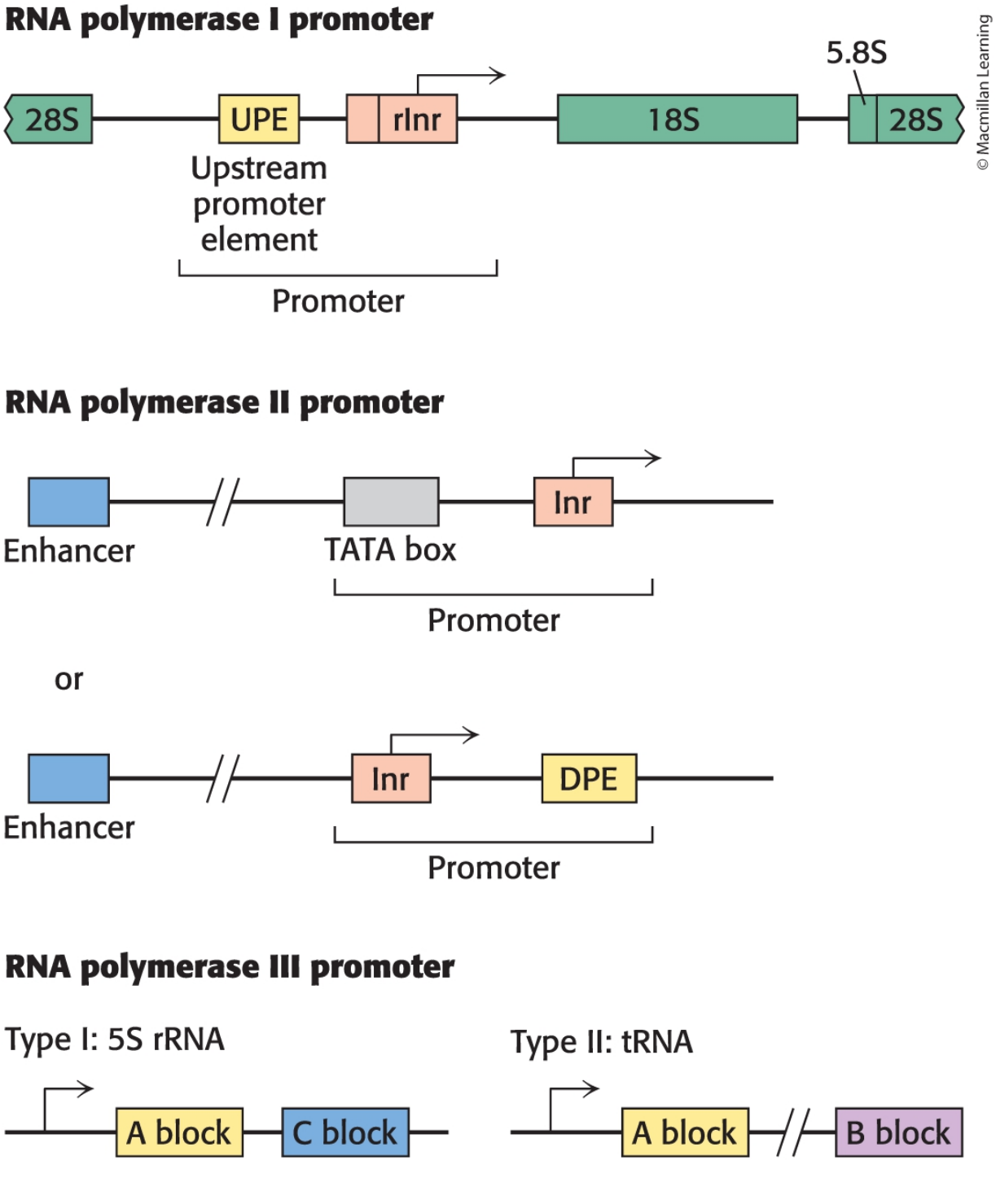
(A): In this view, D N A double helix is circularly wrapped around the histone core. The core consists of the ribbon structures of different histone proteins depicted in different colors. The tails of these histone core proteins are extending outward. One such tail extends out of the double helix and is labeled "Amino-terminal tail."

(B): It shows the 90-degree rotation of the view shown in (A). It shows the side view of a compressed helix with a histone core.

(C): It shows a schematic view consisting of a cluster of purple and yellow spheres. Short tails extend outward from each sphere. Three parallel red bars in diagonal orientation are shown in front of the cluster. The top right and bottom left bars are short. The middle bar is long.

Return to FIGURE 29.19 The structure of the nucleosome consists of eight histone proteins surrounded by D N A

Extended description for FIGURE 29.21 Eukaryotic promoters share common elements



© Macmillan Learning

The R N A polymerase 1 promoter is depicted as follows: A linear stretch contains U P E and r I n r. U P E is the upstream promoter element depicted as a yellow box. The r I n r is a ribosomal initiator depicted as a pink box. U P E and r I n r are located close together and collectively labeled promoter. An arrow pointing toward the right is shown above r I n r. A long rectangular box labeled 18 S is located downstream of the ribosomal initiator. It is followed by 5.8 S and 28 S that are joined together. 28 S is also located upstream of the promoter.

The R N A polymerase 2 promoter is depicted as follows: A linear stretch contains a blue box labeled enhancer at the left end. It is followed by a break depicted as two parallel diagonal lines. On the right side of the break is the T A T A box depicted as a grey rectangle. The T A T A box is followed by the initiator depicted as a pink box labeled "I n r." An arrow pointing toward the right is shown originating from the initiator. T A T A box and initiator are together labeled promoter.

Alternatively, the T A T A box is absent, and the initiator is followed by the downstream promoter element depicted as a yellow box labeled "D P E." The initiator and D P E are together labeled promoter.

The R N A polymerase 3 promoters are depicted as follows: Type 1 promoter is for 5 S r R N A. It consists of a linear stretch composed of two elements downstream of the start site. The start site is depicted as an arrow pointing toward the right. This arrow originates near the left end. The first element is an A block depicted as a yellow rectangle and the second element is a C block depicted as a blue rectangle.

Type 2 promoter is for t R N A. It consists of a linear stretch composed of two elements downstream of the start site. The

elements are separated by a break depicted as two parallel diagonal lines. The start site is depicted as an arrow pointing toward the right. This arrow originates near the left end. The first element is A block depicted as a yellow rectangle and the second element is B block depicted as a purple rectangle.

Return to FIGURE 29.21 Eukaryotic promoters share common elements

Extended description for FIGURE 29.22 The sequence of the T A T A box is highly conserved



The consensus sequence in 5 prime to 3 prime direction is as follows: T subscript 82, A subscript 97, T subscript 93, A subscript 85, A subscript 63, A subscript 88, A subscript 50. The first and third T and second and fourth A are highlighted in red.

Return to FIGURE 29.22 The sequence of the T A T A box is highly conserved

Extended description for FIGURE 29.23 The sequences of the C A A T box and G C box are also highly conserved

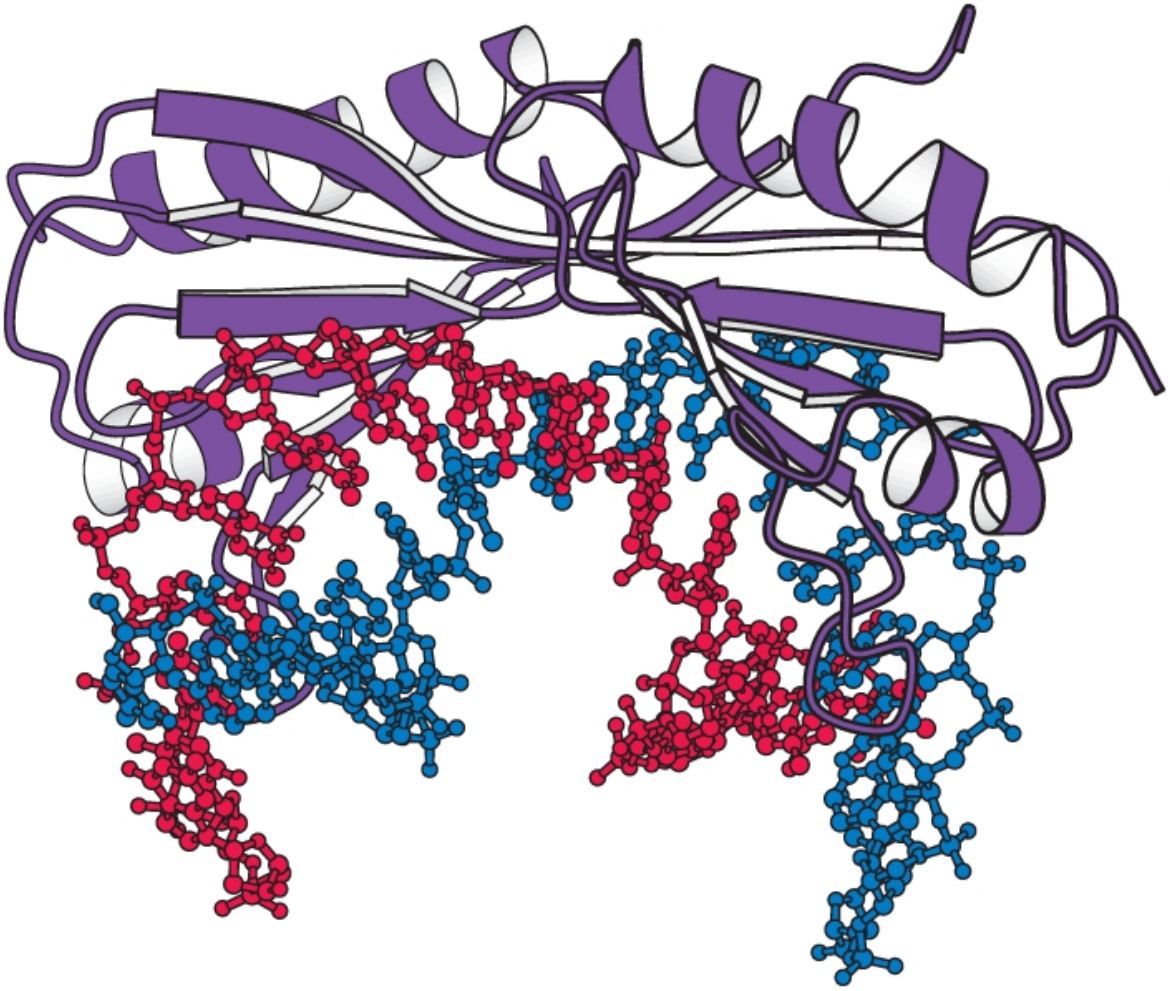


The consensus sequence of the C A A T box in 5 prime to 3 prime direction is as follows: G G N C A A T C T. The C A A T sequence is highlighted in red.

The consensus sequence of the G C box in 5 prime to 3 prime direction is as follows: G G G C G G. The G C sequence in the middle is highlighted in red.

Return to FIGURE 29.23 The sequences of the C A A T box and G C box are also highly conserved

Extended description for FIGURE 29.24 The T A T A-box-binding protein binds to D N A



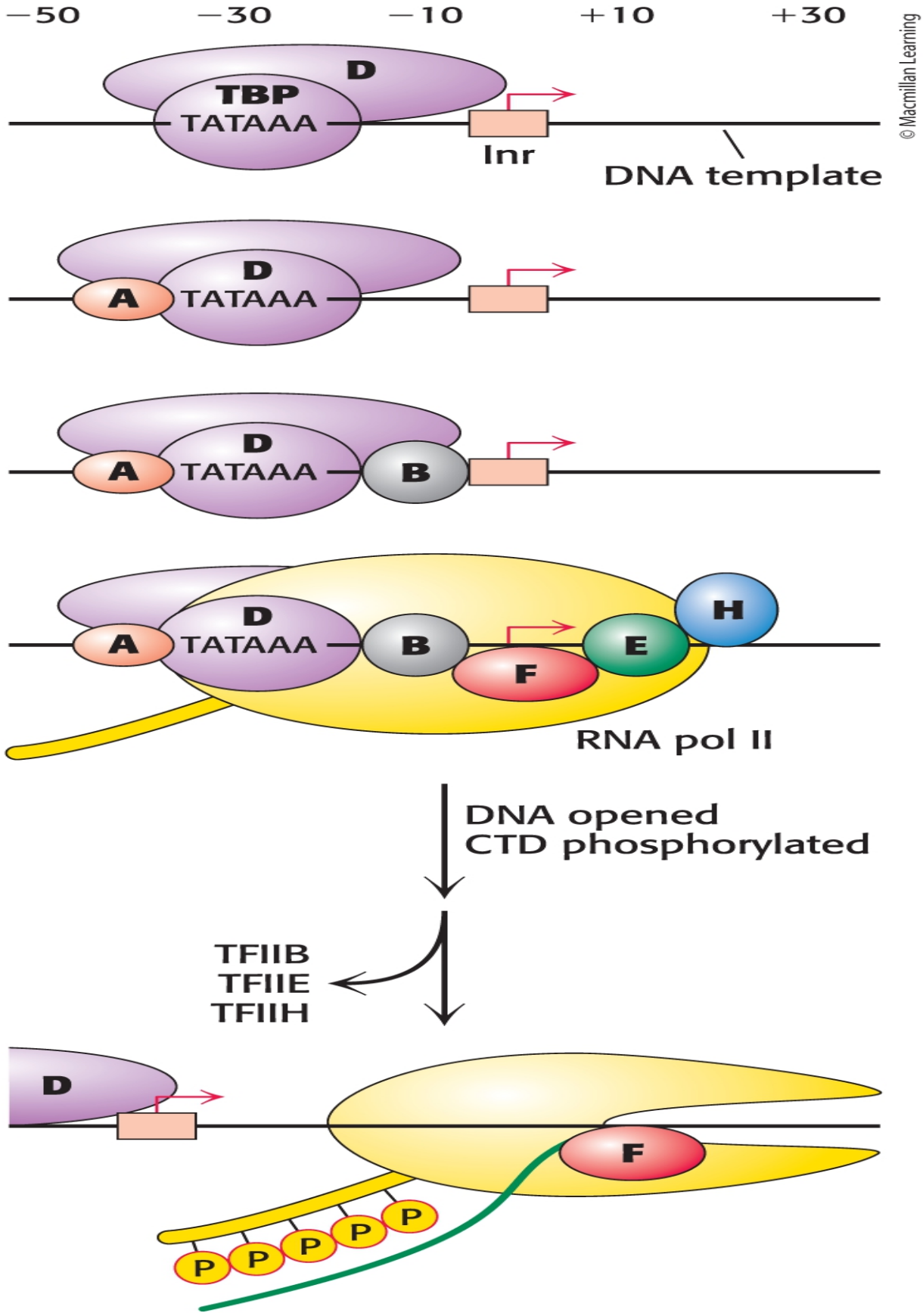
The T A T A box binding protein is a saddle-shaped protein that sits on the top of the D N A double helix. It consists of two similar domains located on either side of the helix. The protein consists of two long and antiparallel beta-strands crisscrossing each other at the center. On either side of this intersection point, a few short beta-strands and an alpha-helix are located at the bottom and directly attached to the D N A. A slightly curved alpha-helix is located on top of the protein on either side of the intersection point. These

secondary structures are interconnected by thread-like loops. The double helix is curved downward. It is composed of two strands, one composed of red spheres and another one composed of blue spheres.

Return to FIGURE 29.24 The T A T A-box-binding protein binds to D N A

Extended description for FIGURE 29.25 General transcription factors are essential in initiating

transcription by RNA polymerase 2



© Macmillan Learning

The D N A template is depicted as a solid horizontal line. A pink box labeled "I n r" is shown in the D N A template. An arrow pointing toward the right is shown above the "I n r" box. The region of the D N A template downstream of the I n r box is numbered plus 10 and plus 30. The region of the D N A template upstream of the I n r box is numbered minus 10, minus 30, minus 50. A purple oval in horizontal orientation labeled D, associated with T B P depicted as a sphere, is bound to the T A T A A A sequence located around minus 30 position. T B P is directly bound to the sequence.

In the second step, a small circular orange structure labeled A associates with T B P between minus 30 and minus 50 positions.

In the third step, a small circular grey structure labeled B associates with T B P at minus 10 position.

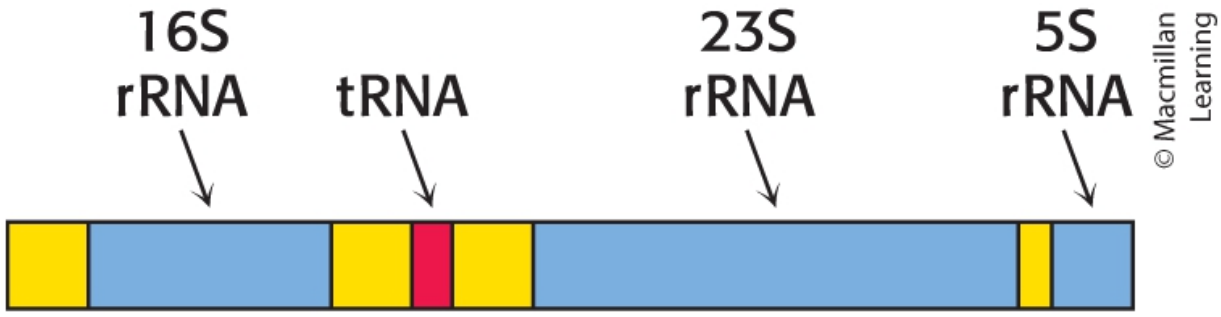
In the fourth step, R N A polymerase 2 binds to the D N A template between minus 30 and plus 10 positions. The "I n r" box is bound to F. F is further bound to E, which is bound to H. The R N A polymerase has a short tail extending toward the lower left.

Two successive downward arrows are shown below the assembly depicted in the fourth step. The first arrow is labeled "D N A opened C T D phosphorylated." The second arrow shows the release of T F 2 B, T F 2 E, and T F 2 H.

In the last step, initiation occurs which is depicted as the downstream movement of the R N A polymerase. The tail of the polymerase is bonded to 5 different phosphoryl groups depicted as tiny circles labeled P. An R N A strand depicted as a solid green line emerges from the cleft of the polymerase on the right side. F is bound near the cleft of the polymerase.

Return to FIGURE 29.25 General transcription factors are essential in initiating transcription by RNA polymerase 2

Extended description for FIGURE 29.26 Cleavage of a primary R N A transcript in *E. coli* produces 5 S, 16 S, and 23 S r R N A molecules and a t R N A molecule

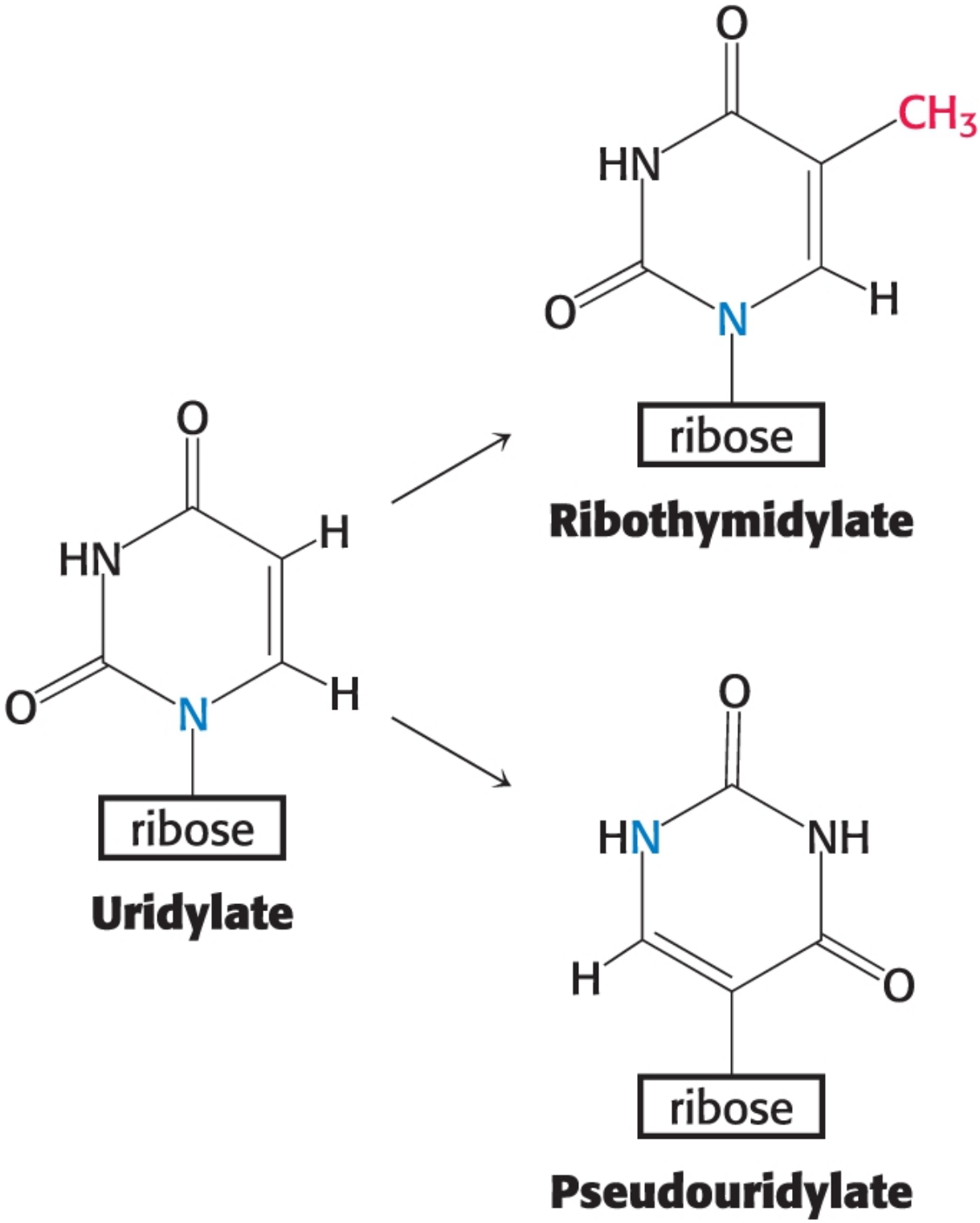


A horizontal bar containing differently colored sections is shown. The left end contains a small yellow section. It is followed by 16 S r R N A depicted as a short blue section. 16 S r R N A is followed by a very narrow red region labeled t R N A, flanked by small yellow sections. t R N A is followed by a long blue section labeled 23 S r R N A. Its size is relatively larger than 16 S r R N A. 23 S r R N A is followed by a narrow yellow region and a small blue section at the right end labeled 5 S r R N A.

Return to FIGURE 29.26 Cleavage of a primary R N A transcript in *E. coli* produces 5 S, 16 S, and 23 S r R N A molecules and a t R N A molecule

Extended description for Modification of uridylate into

ribothymidylate and pseudouridylate



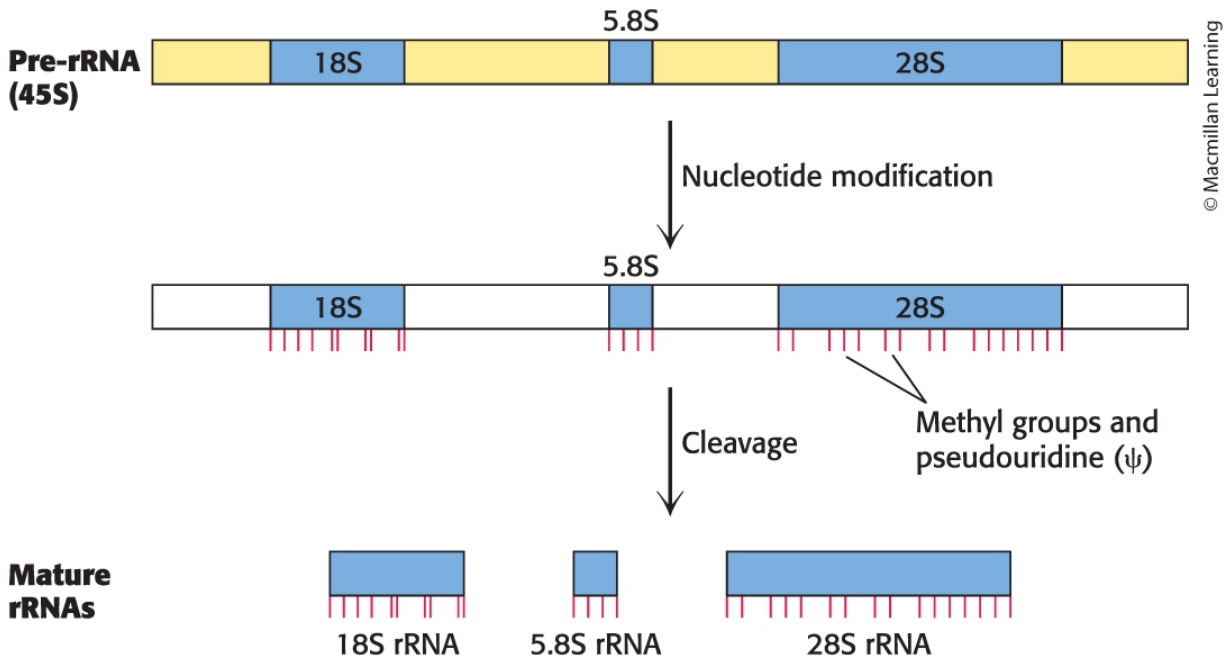
Uridylate has the following structure: A 6-membered heterocyclic hexagonal ring is in a vertical orientation and consists of 1 N, 1 N bound to H, and 4 C atoms. The first N atom occupies the first position which is the bottommost vertex and the second N atom bound to H occupies the third position, which is the top left vertex. A double bond is present between C 3 and C 4. C 1 and C 2 are each double bonded to O. C 3 and C 4 are each single bonded to H. First N is single-bonded to ribose.

Ribothymidylate has the following structure: A 6-membered heterocyclic hexagonal ring is in a vertical orientation and consists of 1 N, 1 N bound to H, and 4 C atoms. The first N atom occupies the first position which is the bottommost vertex and the second N atom bound to H occupies the third position, which is the top left vertex. A double bond is present between C 3 and C 4. C 1 and C 2 are each double bonded to O. C 3 is single bonded to C H 3 and C 4 is single bonded to H. First N is single-bonded to ribose.

Pseudouridylate has the following structure: A 6-membered heterocyclic hexagonal ring in a vertical orientation consists of 2 N bound to H and 4 C atoms. The first N atom bound to H occupies the first position which is the top left vertex and the second N atom bound to H occupies the third position which is the top right vertex. A double bond is present between C 3 and C 4. C 1 and C 2 are each double bonded to O. C 3 is single bonded to ribose and C 4 is single bonded to H.

Return to Modification of uridylate into ribothymidylate and pseudouridylate

Extended description for FIGURE 29.27 The processing of eukaryotic pre-r R N A produces mature r R N As



The pre-r R N A (45 S) is depicted as a horizontal bar. It contains 18 S, 5.8 S, and 28 S segments depicted in blue color from left to right. These segments are separated by yellow sections. The increasing order of the size of these segments is 5.8 S, 18 S, and 28 S.

A downward arrow labeled nucleotide modification is shown below. It leads to the horizontal bar containing modified nucleotides.

The 18 S segment contains 10 modifications depicted as short red lines below the segment. The 5.8 S segment contains three short red lines. The 28 S segment contains 16 short red lines. Two red lines below the 28 S segment are labeled “Methyl groups and pseudouridine (psi).” The intervening sections between these segments are shown in white instead of yellow.

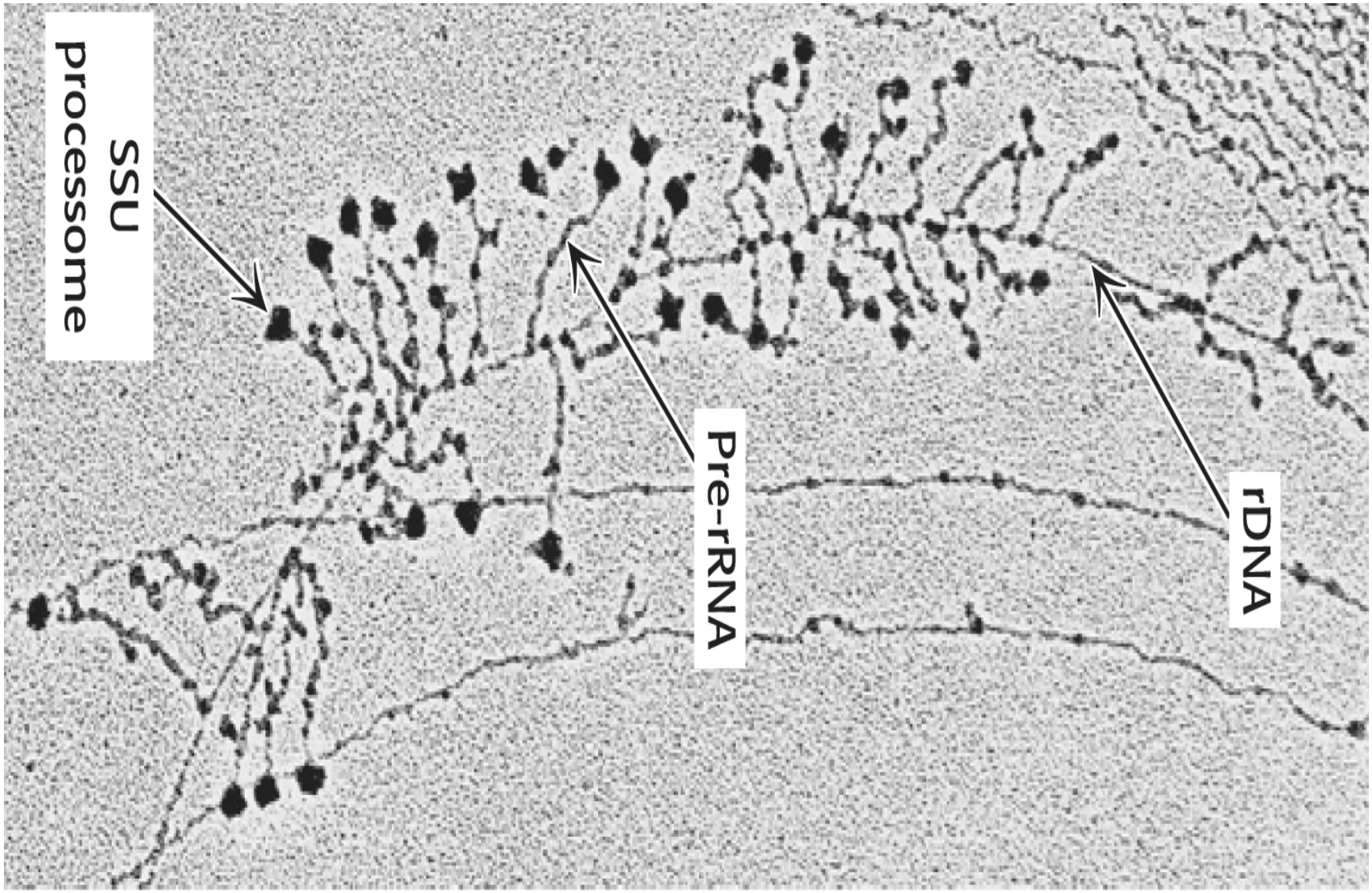
A downward arrow labeled cleavage leads to the mature r R N As.

The 18 S, 5.8 S, and 28 S segments are cleaved out to release free r R N A segments containing modified nucleotides.

Return to FIGURE 29.27 The processing of eukaryotic pre-r R N A produces mature r R N As

Extended description for FIGURE 29.28 Electron microscopy gives a window into r R N A transcription

and processing in eukaryotes

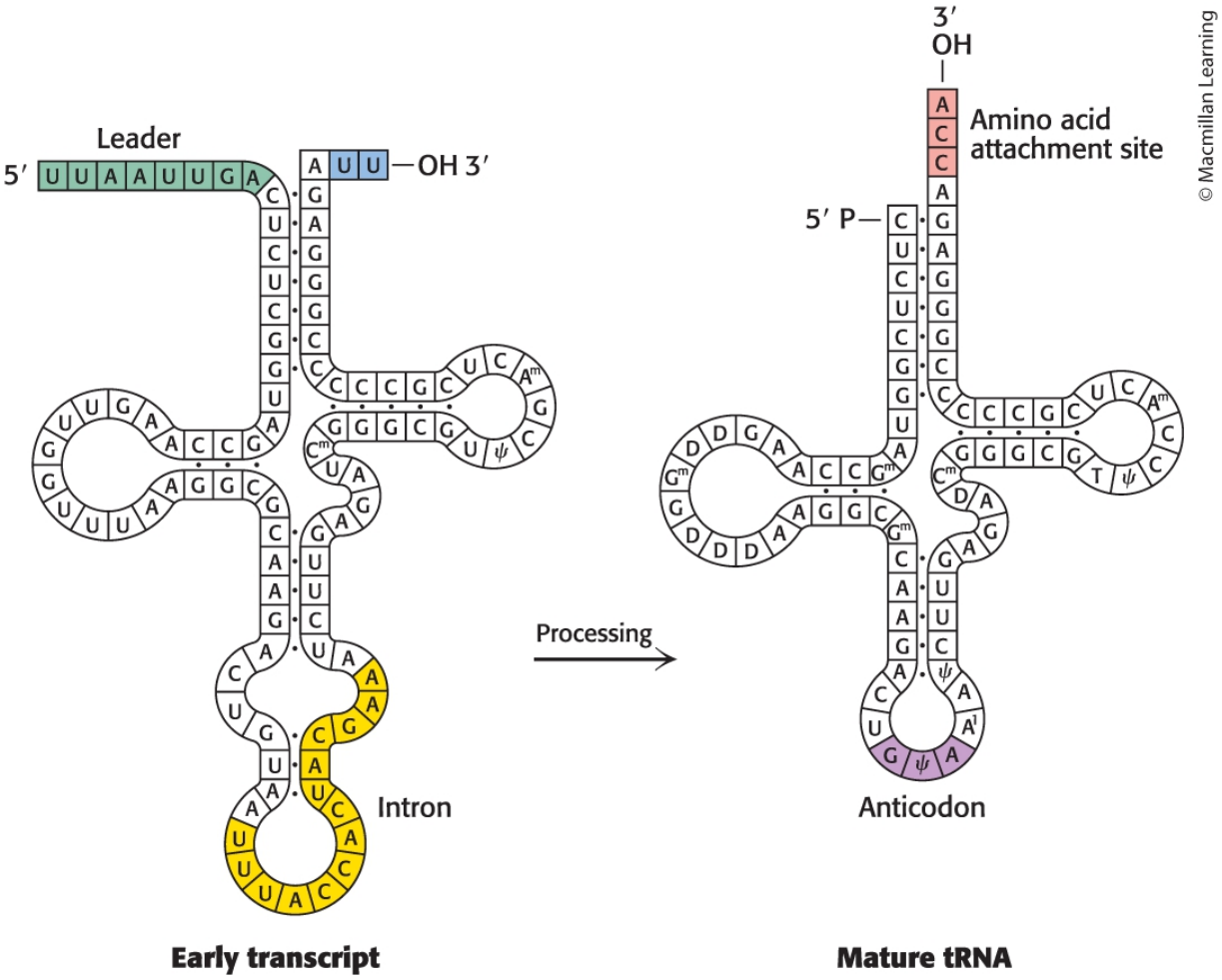


Reprinted by permission from Macmillan Publishers Ltd, from Dragon, F., Gallagher, J., Compagnone-Post, P. et al. A large nucleolar U3 ribonucleoprotein required for 18S ribosomal RNA biogenesis. Nature 417, 967–970 (2002); permission conveyed through Copyright Clearance Center, ltd.

It shows several threads in a vertical orientation. These threads are labeled r D N A. Short horizontal threads originate from either side of the main thread resembling a fir tree. These short threads are labeled pre-r R N A. The length of these threads increases from top to bottom. Most of these threads contain thick knobs at the free end labeled "S S U processome."

Return to FIGURE 29.28 Electron microscopy gives a window into r R N A transcription and processing in eukaryotes

Extended description for FIGURE 29.29 Transfer R N A precursors are processed



The early transcript consists of a linear leader sequence at the 5 prime end followed by several stem loops at the bottom. The stem-loops cause the folding back of the transcript such that 5 prime and 3 prime ends are aligned together at the top. The leader sequence U U A A U U G A is highlighted in green. The 3 prime sequence is A U U, single bond, O H. The last two U residues are highlighted in blue. An intron sequence highlighted in yellow spans through the bottom two loops.

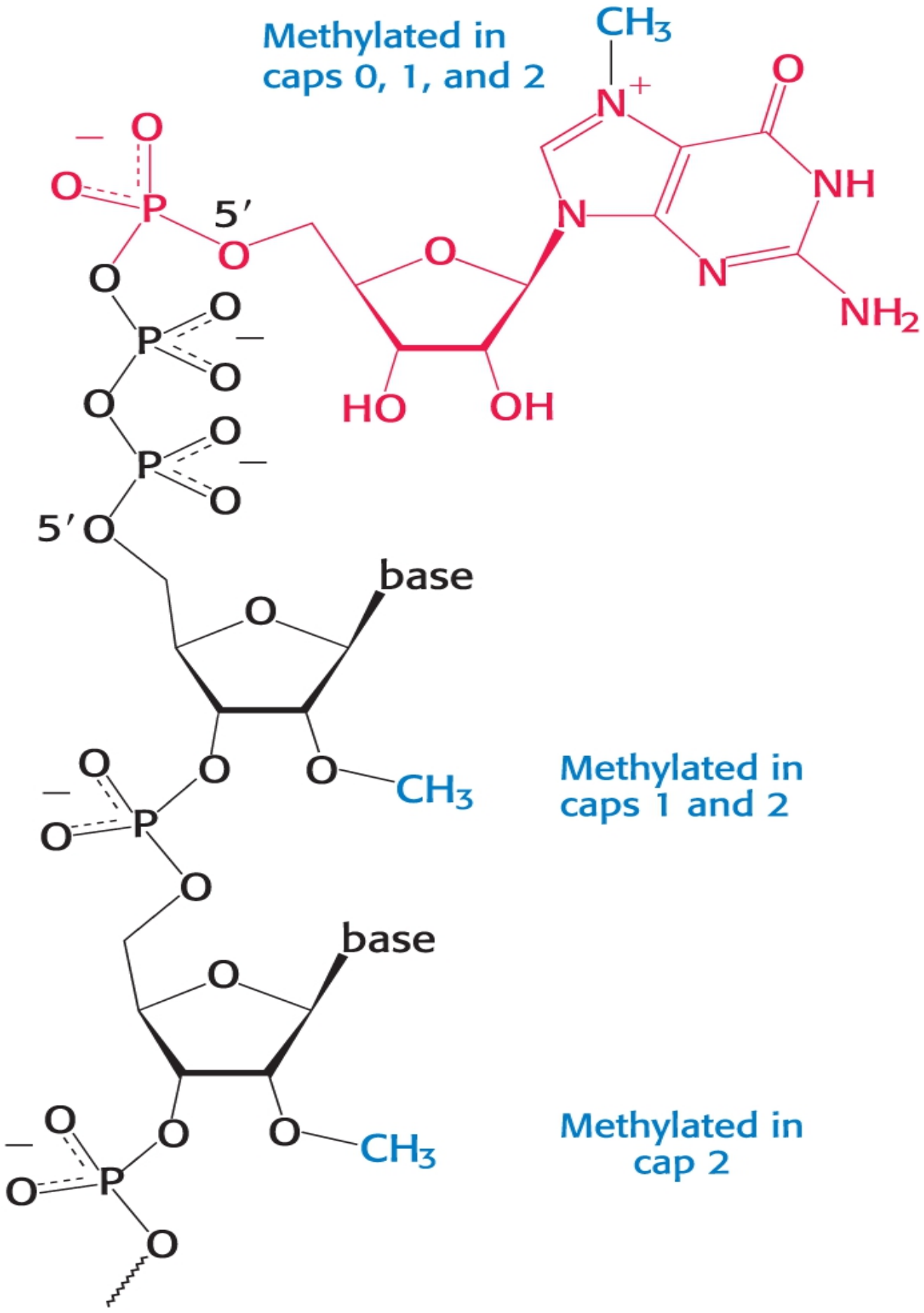
The early transcript undergoes processing to produce the mature t R N A.

The mature t R N A contains a stem-loop on the left, bottom, and right. The 5 prime and 3 prime regions are aligned vertically together at the top of the t R N A. A small bulge is located between the right and bottom stem-loops. The 3 prime end extends above the 5 prime end. The sequence C C A at the 3 prime of the t R N A is highlighted in red and labeled "amino acid attachment site." The 3 prime end contains an O H group. The bottom-most region of the bottom loop contains the sequence G psi A highlighted in purple.

Return to FIGURE 29.29 Transfer R N A precursors are processed

Extended description for FIGURE 29.30 The 5 prime

ends of eukaryotic m R N As are capped


Methylated in caps 0, 1, and 2
CH3
N+
O
NH
N
N
NH2
O
5′
O
HO
OH
base
CH3
Methylated in caps 1 and 2
base
CH3
Methylated in cap 2

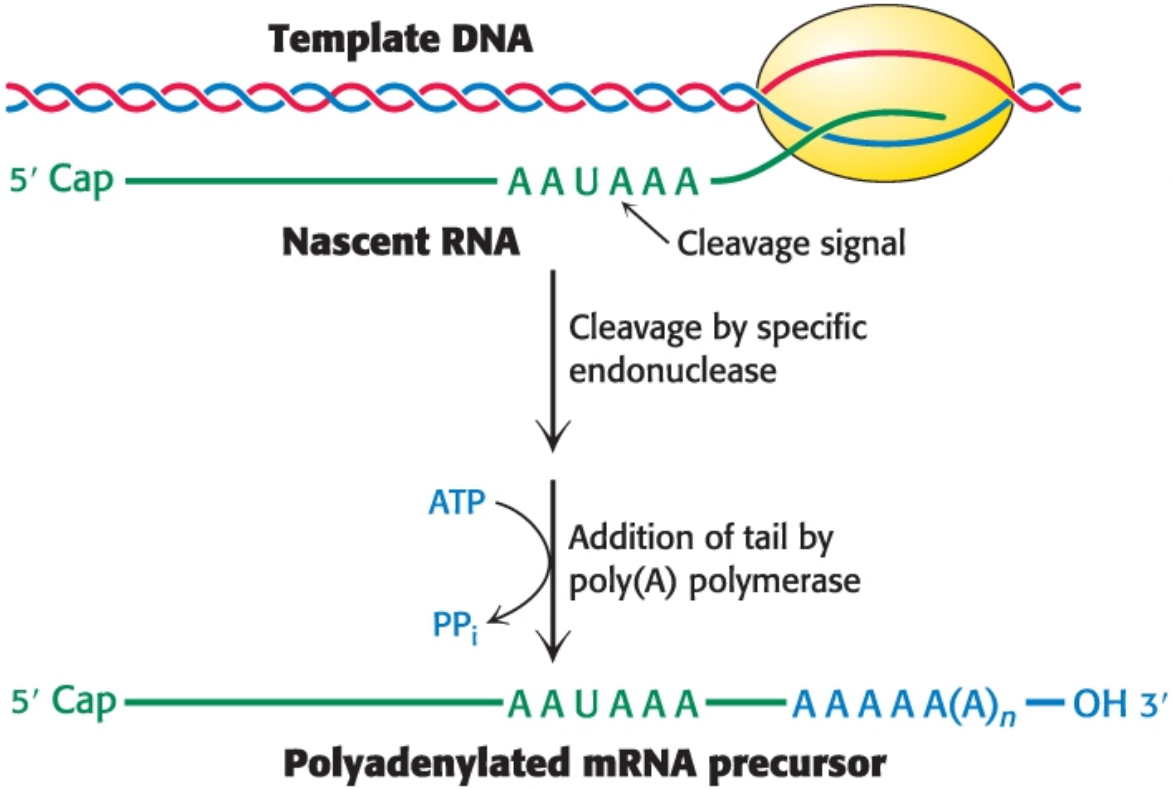
The structure is as follows: A 5-membered heterocyclic pentagonal ring is in a vertical orientation and consists of 1 O and 4 C atoms. The O atom occupies the first position, which is the topmost vertex. The ring is in a plane perpendicular to the plane of the paper such that O is away from the observer and C 2 and C 3 are toward the observer. C 1 is wedge bonded to the base. C 2 is single bonded to O. O is single bonded to C H 3 on the lower right. C H 3 is highlighted in blue color and labeled "Methylated in Caps 1 and 2." C 3 is single-bonded to O. O is single-bonded to a central P atom of the phosphate group on the lower left. The central P atom is single-bonded to the first O on the lower right, partially double-bonded to the second O on the lower left, and partially double-bonded to the O superscript minus on the upper left. The first O is single bonded to C H 3 on the lower left in the form of the line. C H 3 is single-bonded to C 4 of a second heterocyclic pentagonal ring in a vertical orientation. The second 5-membered heterocyclic pentagonal ring is in a vertical orientation and consists of 1 O and 4 C atoms. The O atom occupies the first position, which is the topmost vertex. The ring is in a plane perpendicular to the plane of the paper such that O is away from the observer and C 2 and C 3 are toward the observer. C 1 is wedge bonded to the base. C 2 is single bonded to O. O is single bonded to C H 3 on the lower right. C H 3 is highlighted in blue color and labeled "Methylated in cap 2." C 3 of the second pentagonal ring is single-bonded to O. O is single-bonded to a central P atom of the second phosphate group. The central P atom is single-bonded to O on the lower right, partially double-bonded to the second O atom on the lower left, and partially double-bonded to O superscript minus on the upper left. A wiggly line is shown on the lower left of the O atom. C 4 of the first pentagonal ring is single-bonded to C H 2 in the form of a line. C H 2 is single-bonded to O on the upper left. O is labeled 5 prime. O is single-bonded to the first central P atom of the zigzag chain containing three phosphate groups aligned in a zigzag manner. The first central P atom of the first phosphate group is partially double-bonded to O superscript minus on the lower right,

partially double-bonded to O on the upper right, and single-bonded to the second O on the upper left. The second O atom of the first phosphate group is single-bonded to the central P atom of the second phosphate group. The central P atom is partially double-bonded to O superscript minus on the lower right, partially double-bonded to O on the upper right, and single-bonded to the second O on the upper left. The second O atom of the second phosphate group is single-bonded to the central P atom of the third phosphate group. The central P atom is partially double-bonded to the first O atom on the upper left, partially double-bonded to the O superscript minus above, and single-bonded to the second O atom on the lower right. The second O atom of the third phosphate group is labeled 5 prime and single bonded to C H 2 on the upper right in the form of a line. C H 2 is single-bonded to C 4 of a third heterocyclic pentagonal ring in a vertical orientation. The 5-membered heterocyclic pentagonal ring is in a vertical orientation and consists of 1 O and 4 C atoms. The O atom occupies the first position, which is the topmost vertex. The ring is in a plane perpendicular to the plane of the paper such that O is away from the observer and C 2 and C 3 are toward the observer. C 1 of the third heterocyclic pentagonal ring is single-bonded to the first N of the fourth heterocyclic pentagonal ring in a vertical orientation. The 5-membered heterocyclic pentagonal ring is in a vertical orientation and consists of 2 N and 3 C atoms. The first N occupies the first position, which is the bottom leftmost vertex and the second N occupies the third position which is the topmost vertex. A double bond is present between C 1 and second N. The second N atom carries a positive charge and is single-bonded to C H 3 above. C H 3 is highlighted in blue and labeled "Methylated in caps 0, 1, and 2." The fourth heterocyclic pentagonal ring is fused to a 6-membered heterocyclic hexagonal ring in a vertical orientation such that C 2 and C 3 of the pentagonal ring are C 3 and C 2 respectively of the hexagonal ring. The hexagonal ring consists of 1 N, 1 N bound to H, and 4 C atoms. In the 6-membered heterocyclic hexagonal ring, the first N bound to occupies the first position which is the top right

vertex and the second N occupies the third position which is the top bottom-most vertex. A double bond is present between C 1 and N 2, and C 2 and C 3. C 4 is double bonded to O and C 1 is single bonded to N H 2. C 3 and C 4 of the third pentagonal ring are each single bonded to O H. Third phosphate group, third pentagonal ring, and two fused ring structures are highlighted in red color.

Return to FIGURE 29.30 The 5 prime ends of eukaryotic m R N As are capped

Extended description for FIGURE 29.31 Primary transcripts in eukaryotes are polyadenylated



© Macmillan Learning

A double helical template D N A is bound to a large yellow oval near the right end. The strands of the D N A are unwound to form a transcription bubble inside the oval. A newly synthesized R N A strand emerges out of the transcription bubble. The 5 prime end of the R N A has a cap. It is followed by a cleavage signal sequence A A U A A A near the 3 prime end.

Two downward arrows are shown below.

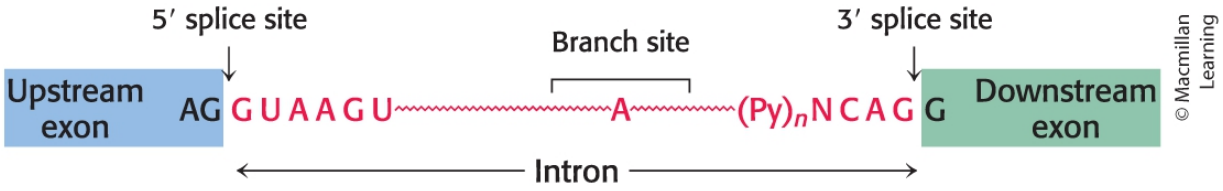
The first downward arrow is labeled "Cleavage by specific endonuclease." The second downward arrow is labeled "Addition of

tail by poly (A) polymerase. It is coupled with the breakdown of A T P to P P subscript i.

The second arrow leads to a polyadenylated m R N A precursor. The polyadenylated m R N A precursor consists of a 5 prime cap and 3 prime O H group. The sequence A A U A A A is located close to the 3 prime end. It is followed by the sequence A A A A A open parenthesis A close parenthesis with subscript n at the 3 prime end.

Return to FIGURE 29.31 Primary transcripts in eukaryotes are polyadenylated

Extended description for FIGURE 29.32 Splice sites are identified by conserved sequences



The consensus sequence is: A G G U A A G U, a long wiggly line, A, a medium-sized wiggly line, open parenthesis P y close parenthesis with subscript n end subscript N C A G G. The first A and first G from left are enclosed in a blue colored rectangular box labeled upstream exon. A downward-facing arrow labeled 5 prime splice site points toward the sequence A G G U A A G U. The sequence from the second G on the left till the second last G on the right is marked using a horizontal double-headed arrow labeled "Intron." The middle A with wiggly lines on both sides is marked with the square bracket on the top and labeled branch site. The rightmost G at the end of the right sequence is enclosed in a rectangular green-colored box labeled "Downstream exon. The space between the last G and second last G of the right sequence is marked with a downward-facing arrow labeled 3 prime splice site.

Return to FIGURE 29.32 Splice sites are identified by conserved sequences

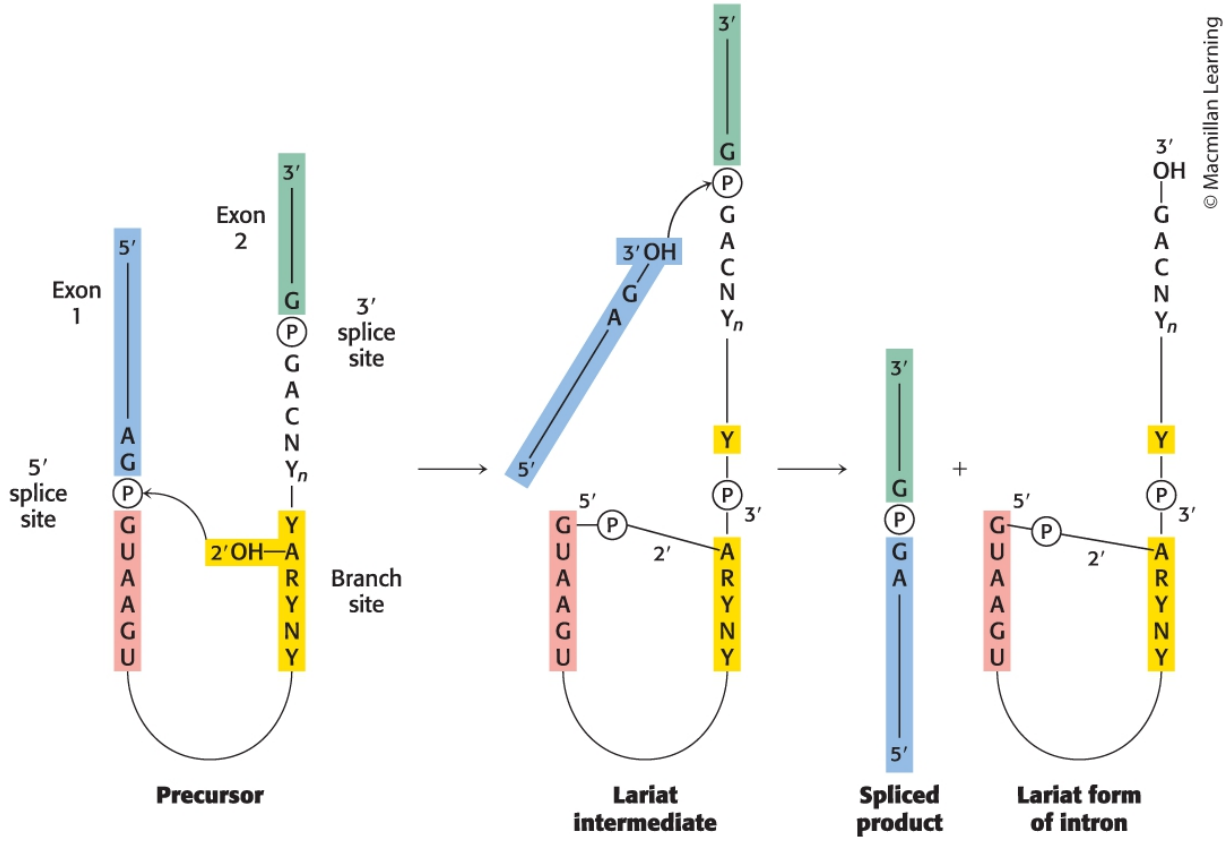
Extended description for Reversible transesterification reaction



The reaction contains two reactants and two products. The reactant has the following structure: A zigzag chain is composed of R 1, single bond, O, single bond, P, single bond, O, single bond, R 2. P is partially double bonded to O on the upper left and O superscript minus on the upper right. The second reactant has the following structure: A zigzag chain is composed of H, single bond, O, single bond, R 3. The first product has the following structure: A zigzag chain is composed of R 1, single bond, O, single bond, P, single bond, O, single bond, R 3. P is partially double bonded to O on the upper left and O superscript minus on the upper right. The second product has the following structure: A zigzag chain is composed of H, single bond, O, single bond, R 2.

Return to Reversible transesterification reaction

Extended description for FIGURE 29.33 The splicing mechanism for m R N A precursors involves a lariat intermediate



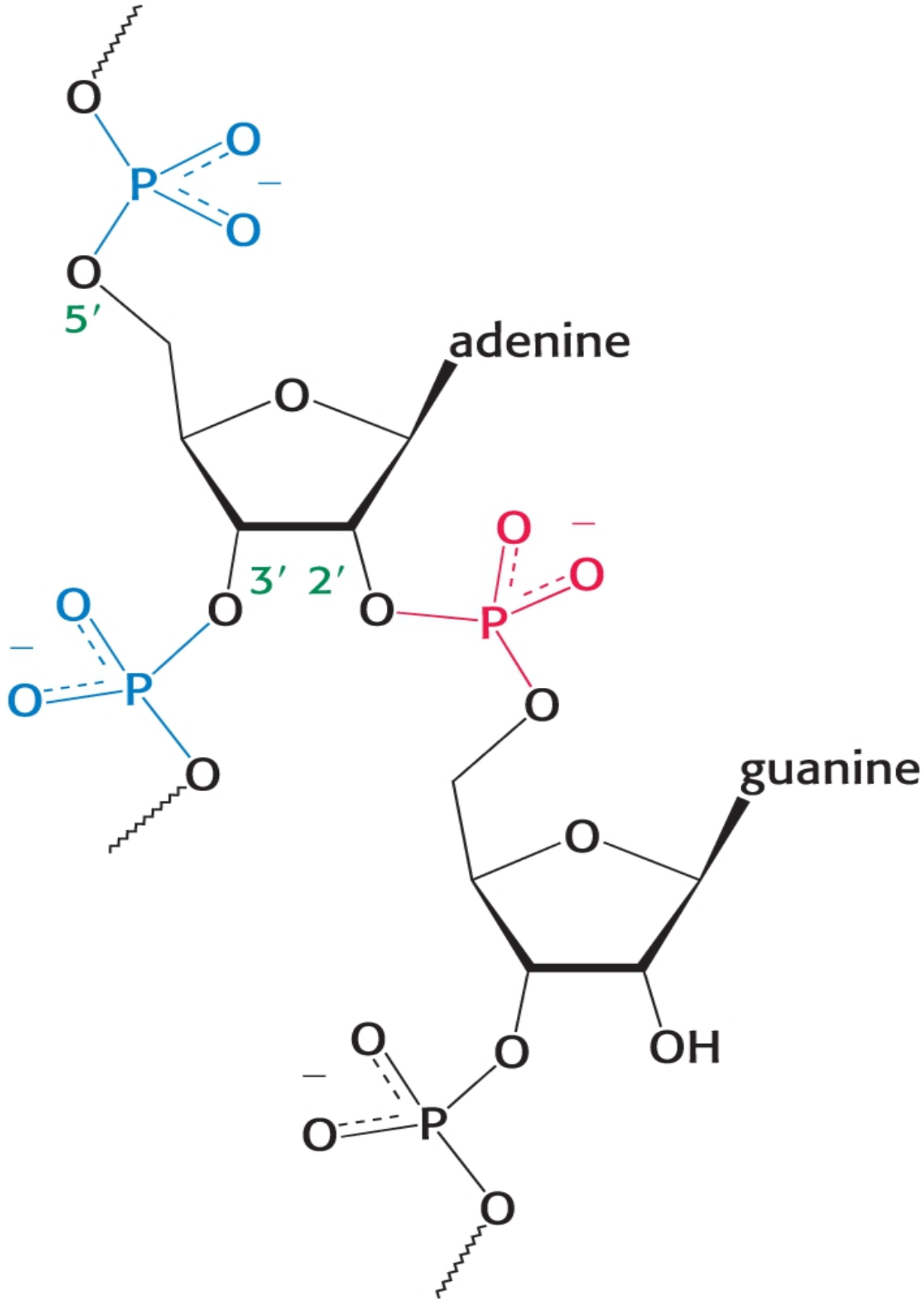
The precursor is depicted as a U-shaped structure. Its 5 prime end at the top left contains exon 1 followed by a 5 prime splice site. Its 3 prime end at the top right contains exon 2 followed by 3 prime splice site. The branch site is located below the 3 prime splice sites. The 5 prime splice site is A G G U A A G U. The phosphodiester bond between first G and second G is depicted as a tiny circle labeled P. The initial A G sequence is part of the 3 prime end of exon 1. The 3 prime splice site is G G A C N Y subscript n. The phosphodiester bond between the first and second G is depicted as a tiny circle labeled P. The first G is part of the 5 prime end of exon 2. The

sequence of the branch site is Y N Y R A Y in 5 prime to 3 prime direction. The 2 prime O H of the nucleotide containing base A in the branch site extends into the U-shaped interior of the precursor. An arrow points from 2 prime O H to the phosphodiester linkage between first G and second G in the 5 prime splice site. This attack leads to the formation of a lariat intermediate. The bond between the first G and second G of the 5 prime splice site is broken. This generates a short fragment containing exon 1 and A G at the 3 prime end with a free O H group. The second G of the splice site forms a phosphodiester bond with the 2 prime end of nucleotide containing A in the branch site. The 3 prime O H of the short fragment attacks the 3 prime splice site. It attacks the phosphodiester bond between the first and second G.This leads to the formation of the spliced product containing joined exon 1 and exon 2. The 3 prime end of exon 1 contains A G. The 5 prime end of exon 2 contains G. This G and G of exon 1 are connected by a phosphodiester bond. The second product is a lariat form of intron having a U-shaped formation with 3 prime end extending much above the 5 prime end. The 5 prime end has the sequence G U A A G U in 5 prime to 3 prime direction. The 3 prime end contains the sequence G A C N Y subscript n in 3 prime to 5 prime direction. The 5 prime end is connected to the 2 prime end of A in the branch site.

Return to FIGURE 29.33 The splicing mechanism for m R N A precursors involves a lariat intermediate

Extended description for FIGURE 29.34 The splicing

branch point has a unique structure


adenine
guanine
5′
3′
2′
OH

The structure of R N A with splicing branch point is as follows: A 5-membered heterocyclic pentagonal ring is in a vertical orientation and consists of 1 O and 4 C atoms. The O atom occupies the first position, which is the topmost vertex. The ring is in a plane perpendicular to the plane of the paper such that O is away from the observer and C 2 and C 3 are toward the observer. C 1 is wedge bonded to adenine. C 2 labeled 2 prime is single-bonded to O. O is single-bonded to a central P atom of the first phosphate group on the lower right. A central P is partially double-bonded to the first O on the upper right, partially double-bonded to O superscript minus on the upper right, and single-bonded to the second O on the lower right. The phosphate group is highlighted in red color. The second O atom of the phosphate group is single-bonded to C H 2 on the lower left in the form of a line. C H 2 is single-bonded to C 4 of the second 5-membered heterocyclic pentagonal ring in a vertical orientation. The 5-membered heterocyclic pentagonal ring is in a vertical orientation and consists of 1 O and 4 C atoms. The O atom occupies the first position, which is the topmost vertex. The ring is in a plane perpendicular to the plane of the paper such that O is away from the observer and C 2 and C 3 are toward the observer. C 1 is wedge bonded to guanine. C 2 is single-bonded to O H. C 3 is single-bonded to O. O is single-bonded to a central P atom of the second phosphate group on the lower left. The central P atom is single-bonded to O on the lower right, partially double-bonded to the second O on the lower left, and partially double-bonded to O superscript minus on the upper left. A wiggly line is shown on the lower left of the lower right O atom. C 3 of the first pentagonal ring is labeled 3 prime and single bonded to O below. O is single-bonded to a central P atom of the third phosphate group. The central P atom is single-bonded to O on the lower right, partially double-bonded to the second O on the lower left, and partially double-bonded to O superscript minus on the upper left. A wiggly line is shown on the lower left of the lower right O atom. C 4 of the first pentagonal ring is single-bonded to C H 2 in the form of a line. C H 2 is single-bonded to O on the upper left.

The O is labeled 5 prime. O is single-bonded to a central P atom of the fourth phosphate group. The central P is single-bonded to the first O on the upper left, partially double-bonded to O superscript minus on the lower right, and partially double-bonded to the second O on the upper right. A wiggly line is shown on the upper right of the upper left O atom. The first phosphate group is highlighted in red color, third and fourth phosphate groups are highlighted in blue color.

Return to FIGURE 29.34 The splicing branch point has a unique structure

Extended description for FIGURE 29.35 The spliceosome consists of proteins and R N As



© Macmillan Learning

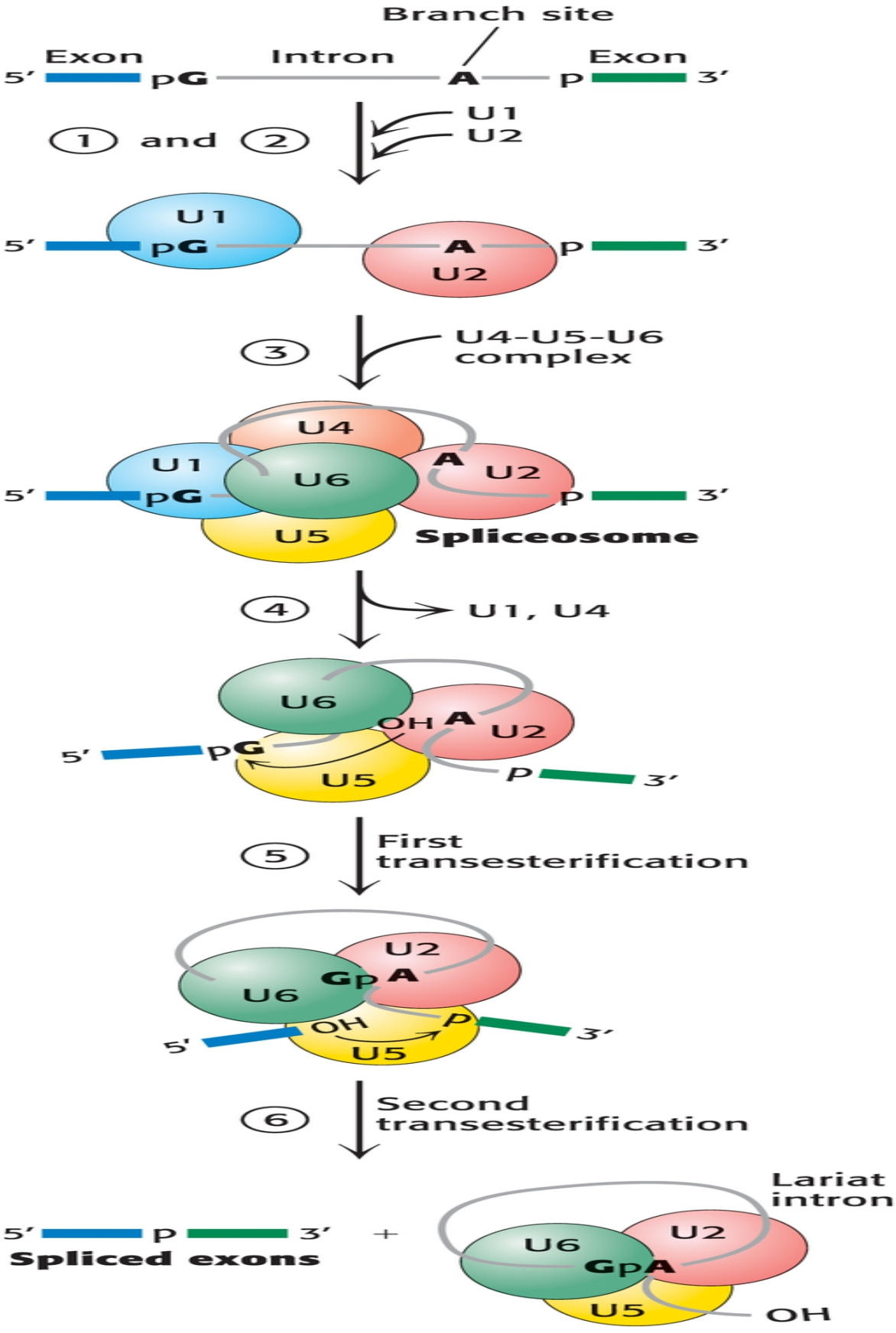
The structure is a helically coiled ribbon-like structure with folds and loops. The structure consists of three different colored tube-like

structures corresponding to different R N A components. U 2, U 5, and U 6 are shown as red, yellow, and blue tube-like structures.

Return to FIGURE 29.35 The spliceosome consists of proteins and R N As

Extended description for FIGURE 29.36 The

spliceosome promotes the splicing of some genes



© Macmillan Learning

The pre-m R N A exons are located at the 5 prime and 3 prime ends. The exons are separated by an intron. The junction of the upstream exon and the intron contains p G. G is part of the intron. The branch site A is located near the 3 prime end of the intron.

In steps 1 and 2, U 1 and U 2 enter. U 2 binds to p G and U 2 binds to branch site A.

In step 3, U 4-U 5-U 6 complex enters. This complex interacts with U 1 and U 2 to constitute a spliceosome. The spliceosome brings U 1 and U 2 closer to form an intron loop.

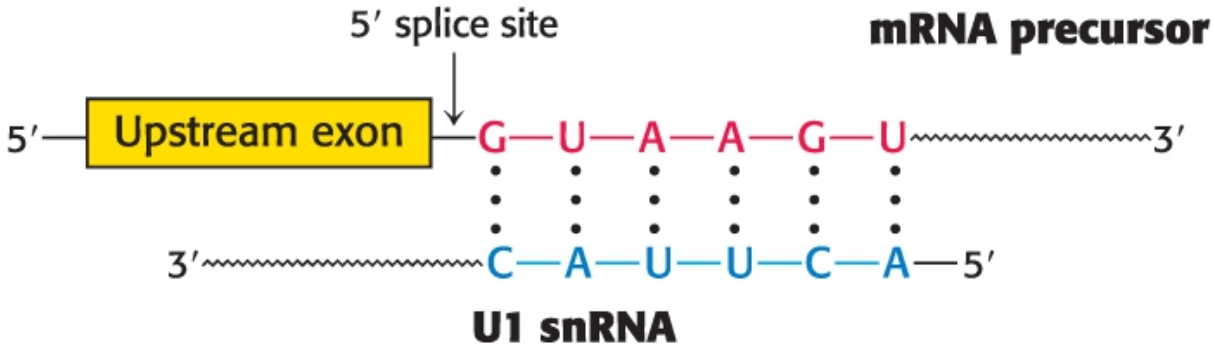
In step 4, U 1 and U 4 are released. The O H group of the branch site A attacks the phosphodiester bond between G and the 3 prime of the first exon.

In step 5, the first transesterification takes place. The first attack by the branch site A cleaves the phosphodiester bond between the first exon and the 5 prime end of the intron. The free 3 prime O H of the first exon attacks the phosphodiester bond between the 3 prime end of the intron and the second intron.

In step 6, the second transesterification takes place leading to the formation of spliced exons and lariat intron. The lariat intron is bound to the U 2, U 5, and U 6 components of the spliceosomes. The 5 prime G of the intron forms a phosphodiester bond with branch site A. The 3 prime region of the intron extends out of the lariat structure.

Return to FIGURE 29.36 The spliceosome promotes the splicing of some genes

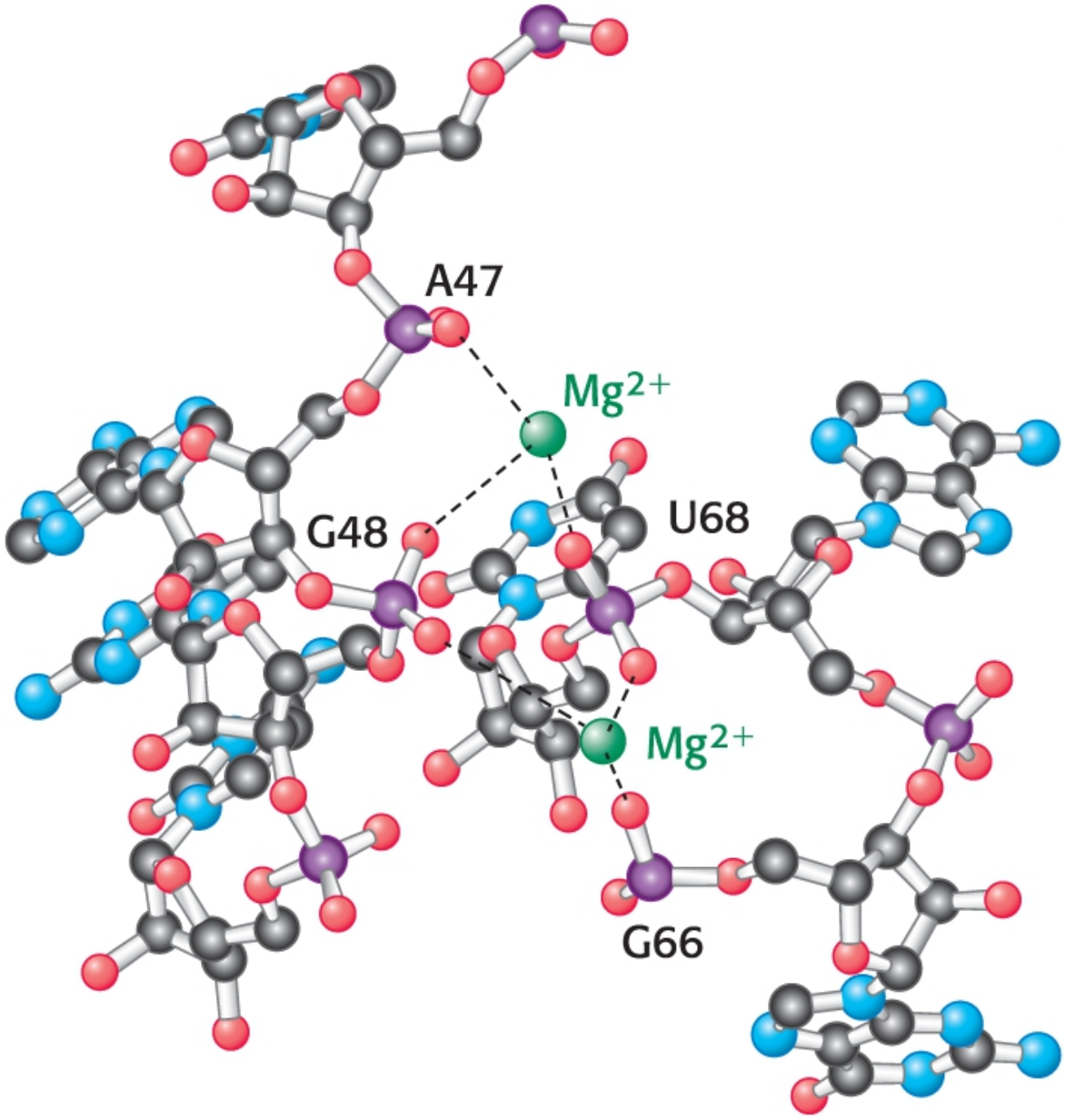
Extended description for Base-pairing of the 5 prime splice site of the pre-m R N A with the conserved sequence of U 1 s n R N A



The figure illustrates a strand of the m R N A precursor and U 1 s n R N A. The first strand at the top depicts m R N A precursor. It is labeled 5 prime on the left and 3 prime on the right. A yellow-colored rectangular box labeled "Upstream exon" is placed next to 5 prime end. It is followed by the sequence G, single bond, U, single bond, A, single bond, A, single bond, G, single bond, U, a long wiggly line, 3 prime. The sequence from G to U is highlighted in red color. The second strand for U 1 s n R N A has the following sequence: 3 prime, a long wiggly line, C, single bond, A, single bond, U, single bond, U, single bond, C, single bond, A, a small line 5 prime. Three dots indicating hydrogen bonds are present between the first G of the first sequence and the first C of the second sequence, the first U of the first sequence and the first A of the second sequence, the first A of the first sequence and the first U of the second sequence, second A of the first sequence and second U of the second sequence, second G of the first sequence and second C of the second sequence, and second U of the first sequence and second A of the second sequence.

Return to Base-pairing of the 5 prime splice site of the pre-m R N A with the conserved sequence of U 1 s n R N A

Extended description for FIGURE 29.37 The spliceosome's catalytic center includes two key magnesium ions



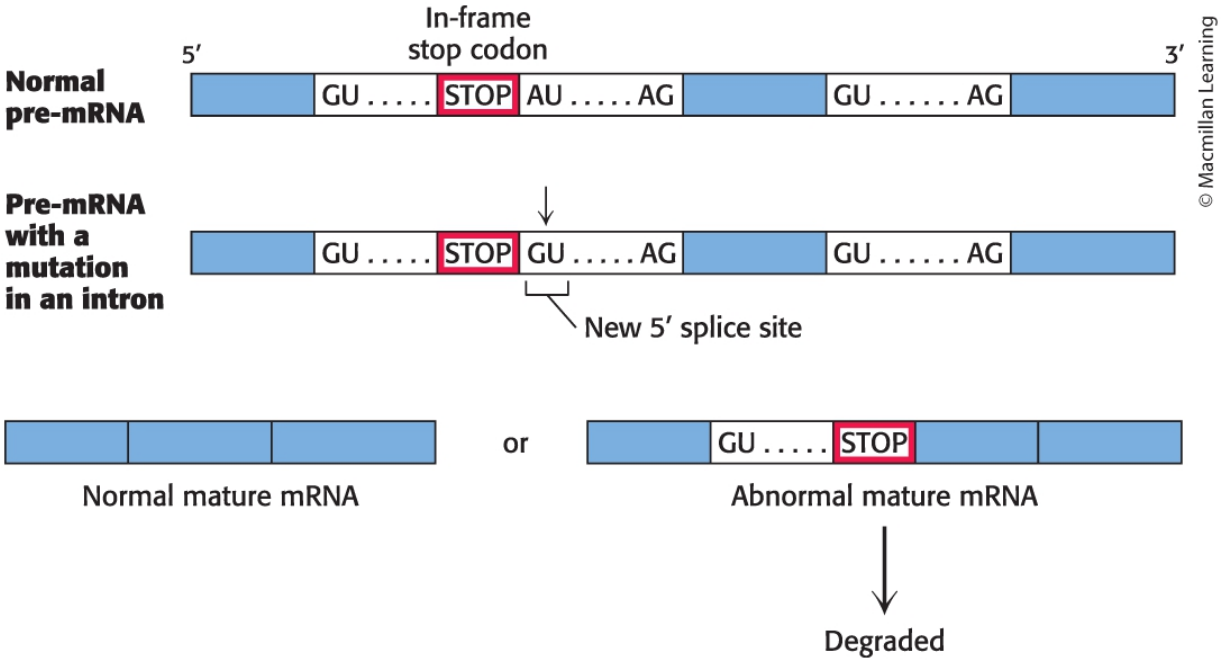
© Macmillan Learning

The figure illustrates the ball and stick model of the catalytic center of the spliceosome. It contains black, red, blue, purple, and green

colored small spheres. The size of the black, blue, green, and red colored spheres are similar while the purple colored spheres are slightly bigger than the others. The two green-colored spheres are present at the center of the structure and are labeled M g superscript 2 plus. The first M g superscript 2 plus atom at the top is partially bonded to the three red-colored spheres on the upper left, lower left, and lower right. These red spheres are part of the phosphate groups of A 47, G 48, and U 68 residues. The second green-colored M g superscript 2 plus ion is partially bonded to red-colored spheres on the upper right, lower right, and upper left. These red spheres are part of the phosphate groups of U 68, G 48, and G 66 residues. These phosphate groups are further connected to pentagonal rings composed of 1 red and 4 black spheres. These pentagonal rings are further connected to the fused pentagonal and hexagonal rings or only hexagonal rings in different orientations.

Return to FIGURE 29.37 The spliceosome's catalytic center includes two key magnesium ions

Extended description for FIGURE 29.38 Mutations in splice sites can cause diseases such as thalassemia



The normal pre-m R N A is depicted as a horizontal bar whose left end is labeled 5 prime and right end is labeled 3 prime. The exons are depicted as short blue sections separated by white gaps. There are 3 exons and 2 introns. The first intron contains an in-frame stop codon. The 5 prime end of the first intron contains G U and the 3 prime end contains A G. A stop codon is located in the middle followed by A U. The 5 prime end of the second intron contains G U and the 3 prime end contains A G.

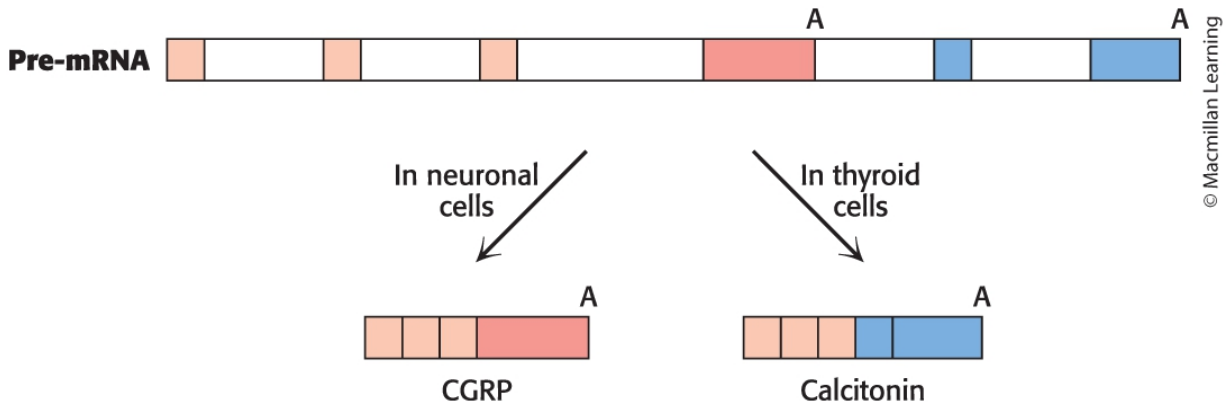
The pre-m R N A with a mutation in an intron is also depicted as a horizontal bar. The exons are depicted as short blue sections separated by white gaps. There are 3 exons and 2 introns. The sequence of the introns are same, except the first intron contains G U instead of A U after the stop codon. This G U is labeled the "New 5 prime splice site."

A normal mature m R N A is shown below. It consists of three short blue sections depicting exons joined together.

Alternatively, an abnormal mature m R N A can be formed due to the mutation. In this m R N A, the 5 prime region of the first intron from G U to the stop codon is retained between the first and second exons. This abnormal mature m R N A is degraded.

Return to FIGURE 29.38 Mutations in splice sites can cause diseases such as thalassemia

Extended description for FIGURE 29.39 Alternative splicing produces different m R N As

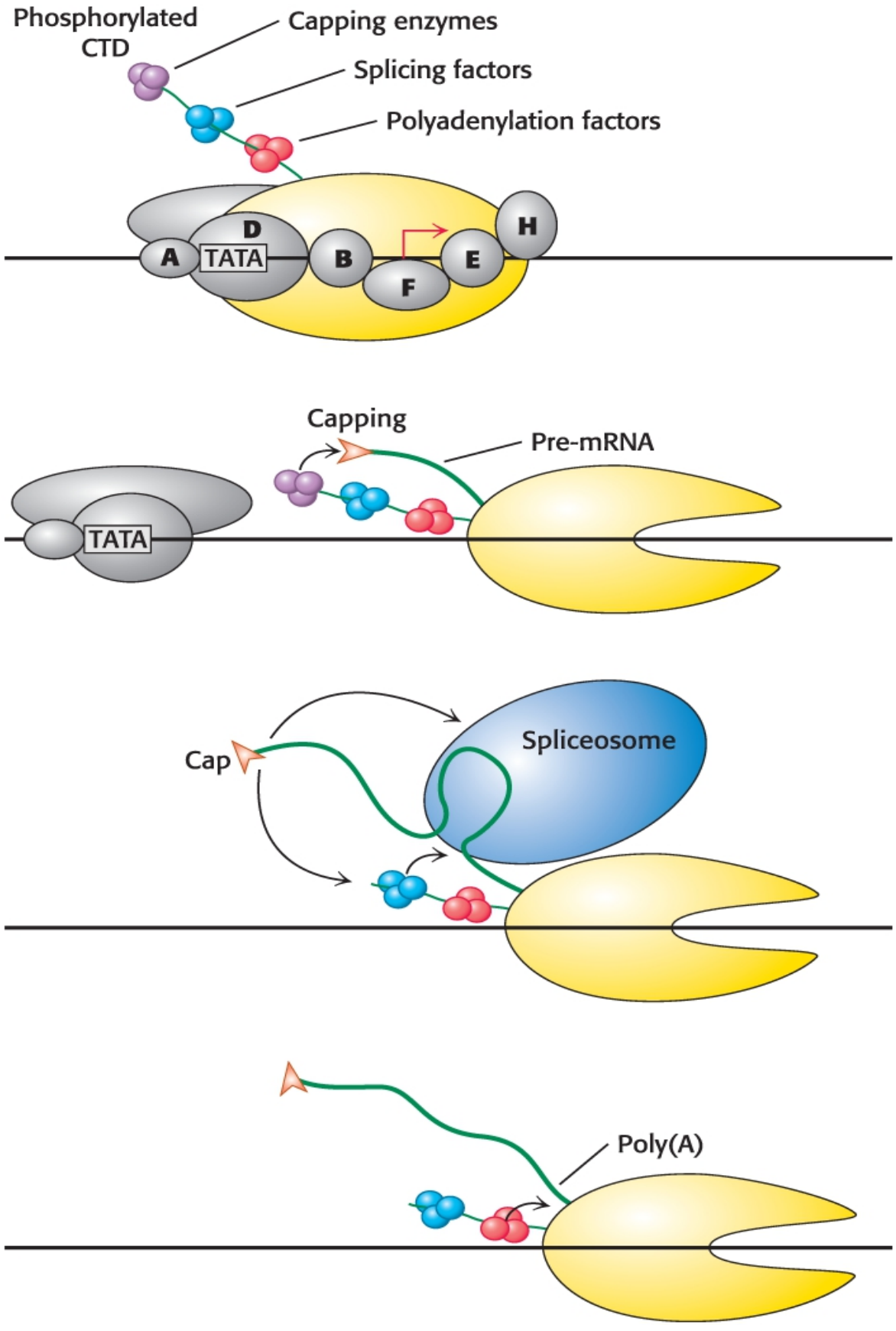


The pre-m R N A is depicted as a horizontal bar. It contains three equally spaced small face-colored sections from starting from the left end. It is followed by a relatively larger pink section labeled A, a small blue section, and a blue section labeled A at the right end. The space or gaps between these colored sections is shown in white. In the neuronal cells, the three face-colored sections and the pink section labeled A are joined together from left to right. This segment is labeled C G R P. In the thyroid cells, the three-face-colored sections, the small blue section, and the blue section labeled A are joined together from left to right. This segment is labeled calcitonin.

Return to FIGURE 29.39 Alternative splicing produces different m R N As

Extended description for FIGURE 29.40 The C T D

couples transcription to pre-m R N A processing



© Macmillan Learning

A linear D N A is depicted as a solid line. The promoter region of the D N A contains a T A T A box bound to a structure labeled D. The polymerase is associated with the promoter along with other transcription factors labeled A, B, F, E, and H. The tail of the polymerase is labeled phosphorylated C T D. It is bound to capping enzymes, splicing factors, and polyadenylation factors depicted as separate clusters of tiny spheres.

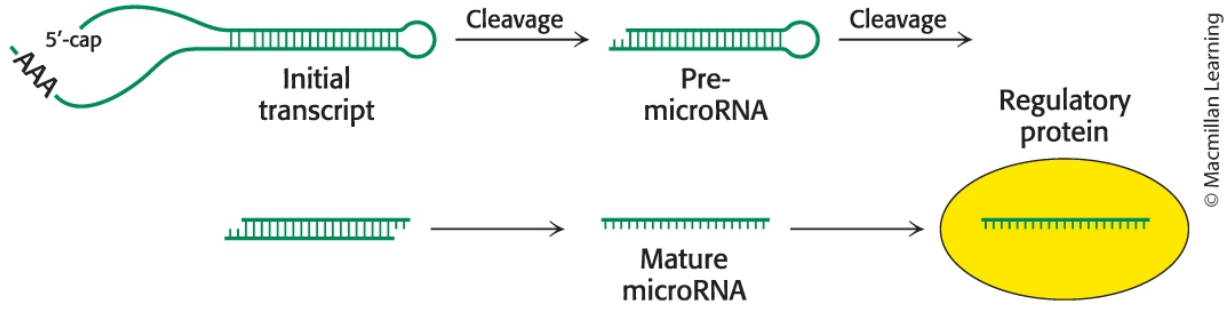
In the first step, the R N A polymerase escapes the promoter and starts the transcription of D N A. The pre-m R N A is depicted as a green strand emerging out of the polymerase as it moves forward. The free end of the pre-m R N A undergoes capping by the capping enzymes bound to the tail.

In the second step, an arrow from the cap at the free end of the pre-m R N A points toward a large oval-shaped structure labeled spliceosome. The spliceosome is bound to the pre-m R N A exiting the polymerase. Another arrow from the cap points toward splicing factors bound to the C T D. An arrow from the splicing factors points toward the spliceosome. The capping enzymes are already released from the C T D.

In the third step, the polyadenylation factors add poly (A) to the m R N A emerging out of the polymerase.

Return to FIGURE 29.40 The C T D couples transcription to pre-m R N A processing

Extended description for FIGURE 29.41 Small regulatory R N As are involved in gene regulation



The initial transcript is depicted as a horizontal stem-loop structure. The 5 prime end contains a cap and the 3 prime end contains three A residues. These ends are free and have a wavy orientation.

In the first step, the initial transcript undergoes cleavage to produce pre-micro R N A. The free 3 prime and 5 prime ends are cleaved such that only the stem-loop structure is left. The top strand of the stem region is cleaved by two extra nucleotides such that the bottom strand of the stem region has an overhang at the 3 prime end.

In the second step, the pre-micro R N A again undergoes cleavage. The loop region is cleaved such that a double-stranded R N A with overhangs of 2 nucleotides is produced.

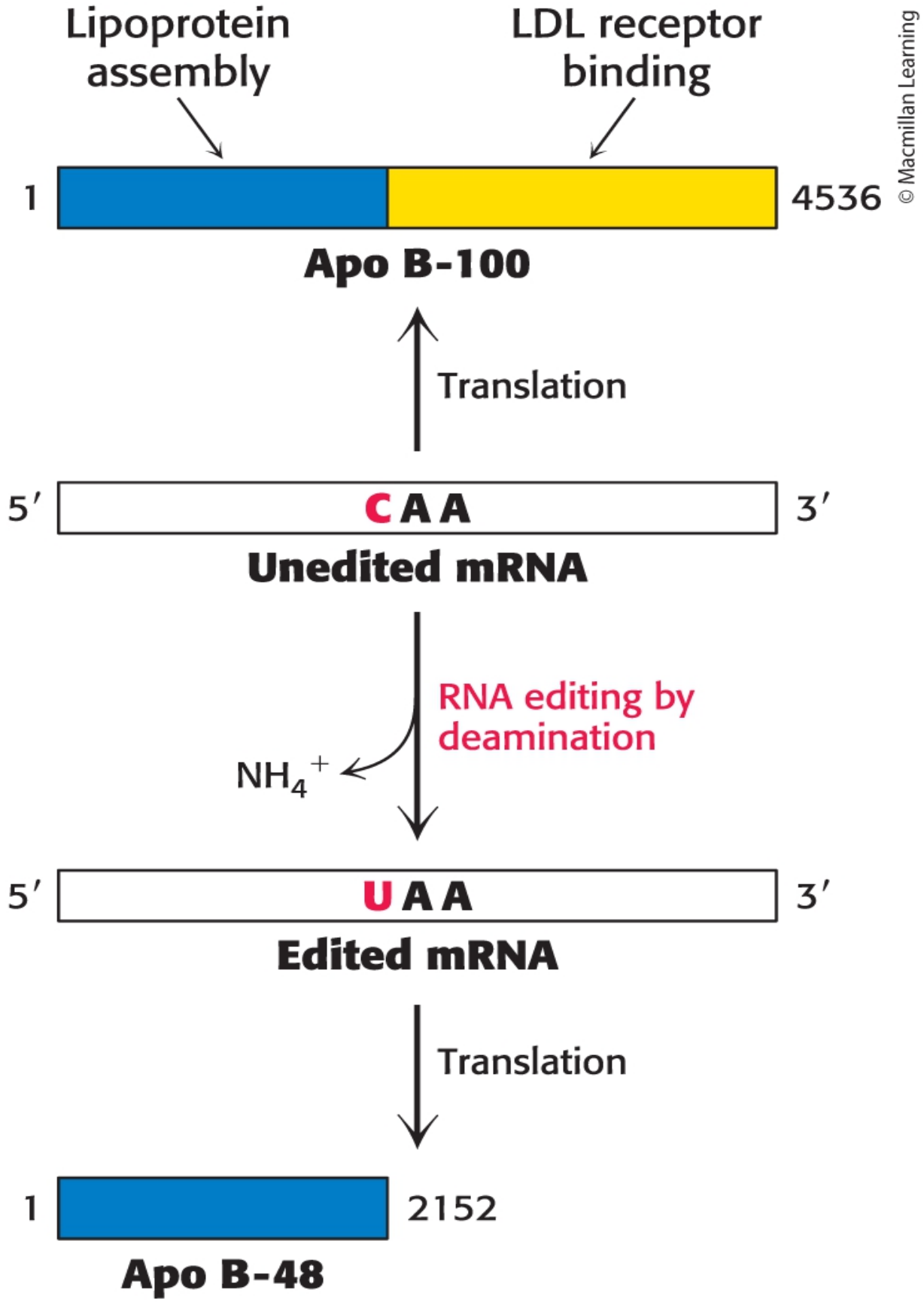
In the third step, mature micro R N A is produced which is a linear single-stranded R N A.

In the fourth step, it associates with a yellow large circular regulatory protein.

Return to FIGURE 29.41 Small regulatory R N As are involved in gene regulation

Extended description for FIGURE 29.42 R N A editing

alters the coding sequence of m R N As



© Macmillan Learning

A white horizontal bar contains the sequence C A A in the middle. Its left end is 5 prime and the right end is 3 prime end. It depicts the unedited m R N A.

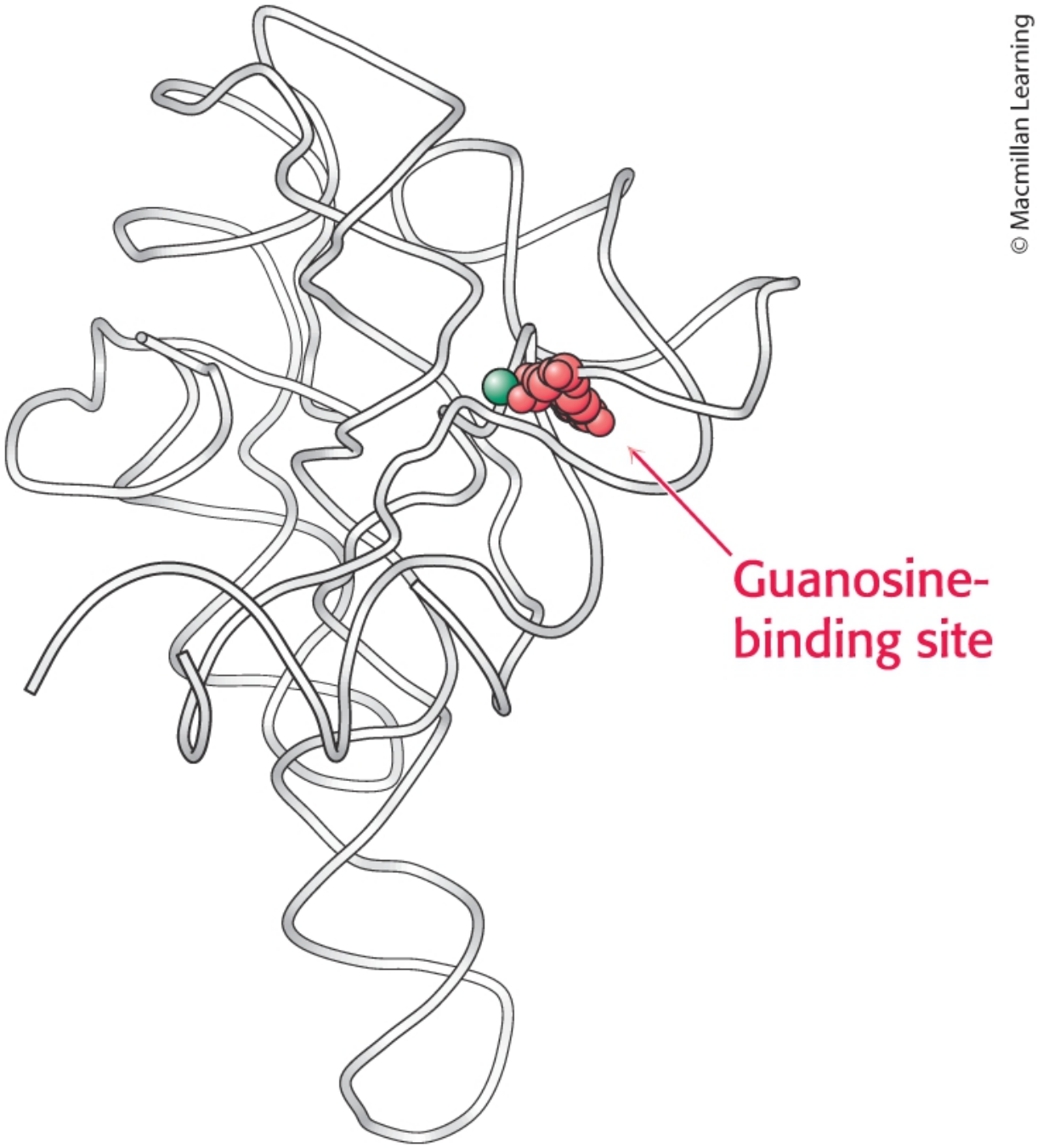
An upward arrow from the unedited m R N A leads to another horizontal bar labeled A p o B-100. Its left part is colored blue and the right part is colored yellow. The blue part is labeled lipoprotein assembly. The yellow part is labeled L D L receptor binding. The left end is numbered 1 and the right end is numbered 4536.

A downward arrow below the unedited m R N A is labeled "R N A editing by deamination." It shows the release of N H 4 superscript plus.

It leads to edited m R N A depicted as a horizontal bar containing the sequence U A A in the middle. The edited m R N A undergoes translation to produce A p o B-48 depicted as a short blue horizontal bar. Its left end is numbered 1 and the right end is numbered 2152.

Return to FIGURE 29.42 R N A editing alters the coding sequence of m R N As

Extended description for FIGURE 29.44 Self-splicing introns have a complex structure



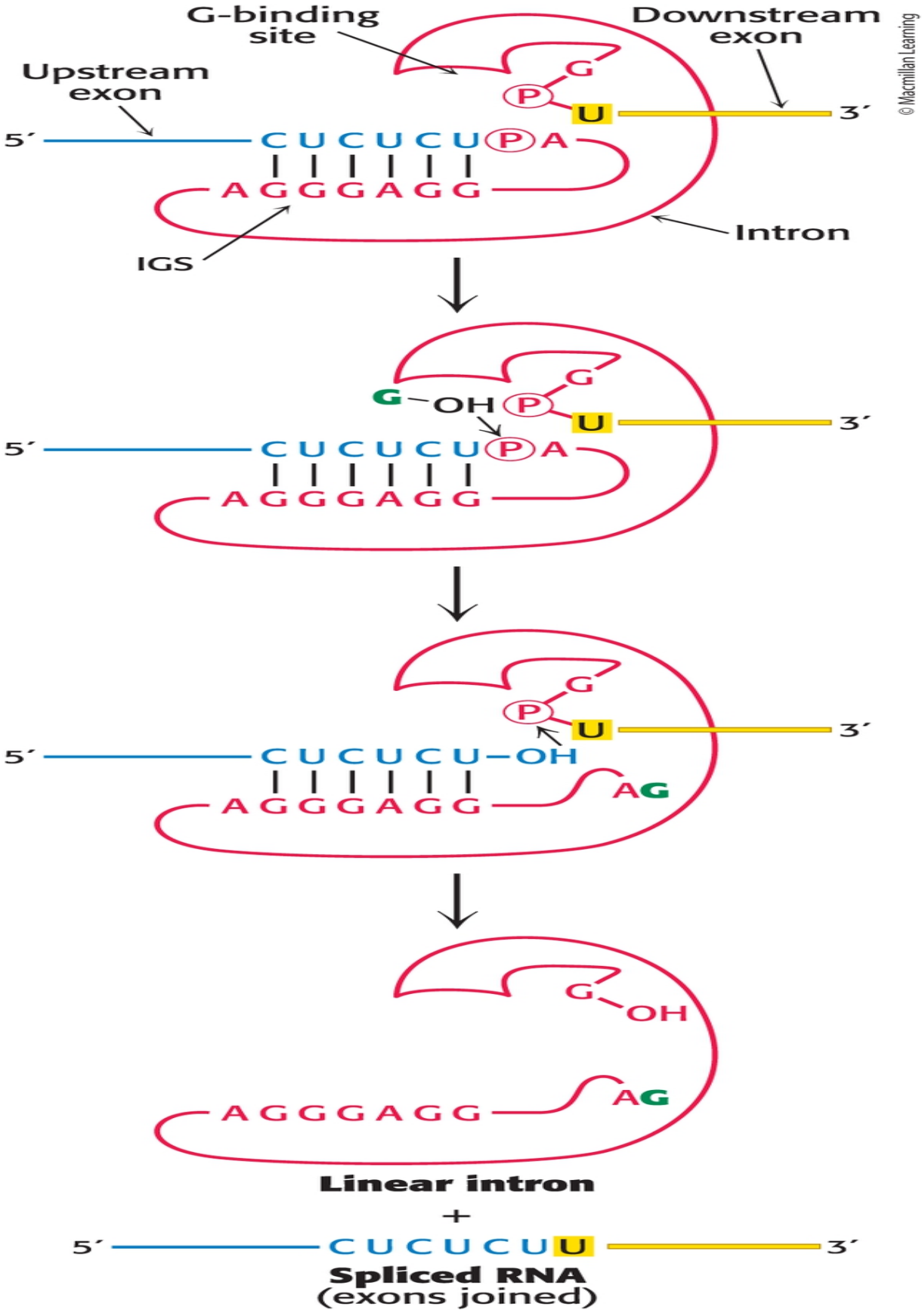
© Macmillan Learning

The figure illustrates a folded tube-like structure of a large fragment of the self-splicing intron. It has a complex folding pattern composed of helices and loops. The guanosine binding site is depicted as a small cluster of few red-colored spheres and one blue-colored sphere at the top right.

Return to FIGURE 29.44 Self-splicing introns have a complex structure

Extended description for FIGURE 29.45 The catalytic mechanism of the group 1 self-splicing intron includes

a series of transesterification reactions


G-binding site
Downstream exon
Upstream exon
G
P
U
3′
5′
C U C U C U P A
A G G G A G G
IGS
Intron
G OH
5′–C U C U C U–OH
A G
Linear intron
+
5′–C U C U C U U–3′
Spliced RNA
(exons joined)
© Macmillan Learning

The upstream exon is located at the 5 prime end and the downstream exon is located at the 3 prime end. The long intron between the exons is folded into a structure to bring the exons close to each other. The sequence at the 3 prime end of the upstream exon is C U C U C U. A is present at the 5 prime end of the intron at its junction with the upstream exon. A phosphodiester bond depicted as a tiny circle labeled P is shown between the last U of the upstream exon and A of the intron. The sequence C U C U C U is based paired with the sequence 3 prime G G G A G G 5 prime of the intron. A is located at the 3 prime end of the first G of this sequence labeled "I G S." The 3 prime end of the intron contains G which is connected to 5 prime U of the downstream exon by a phosphodiester bond. The 3 prime end of the intron creates a cleft labeled G-binding site.

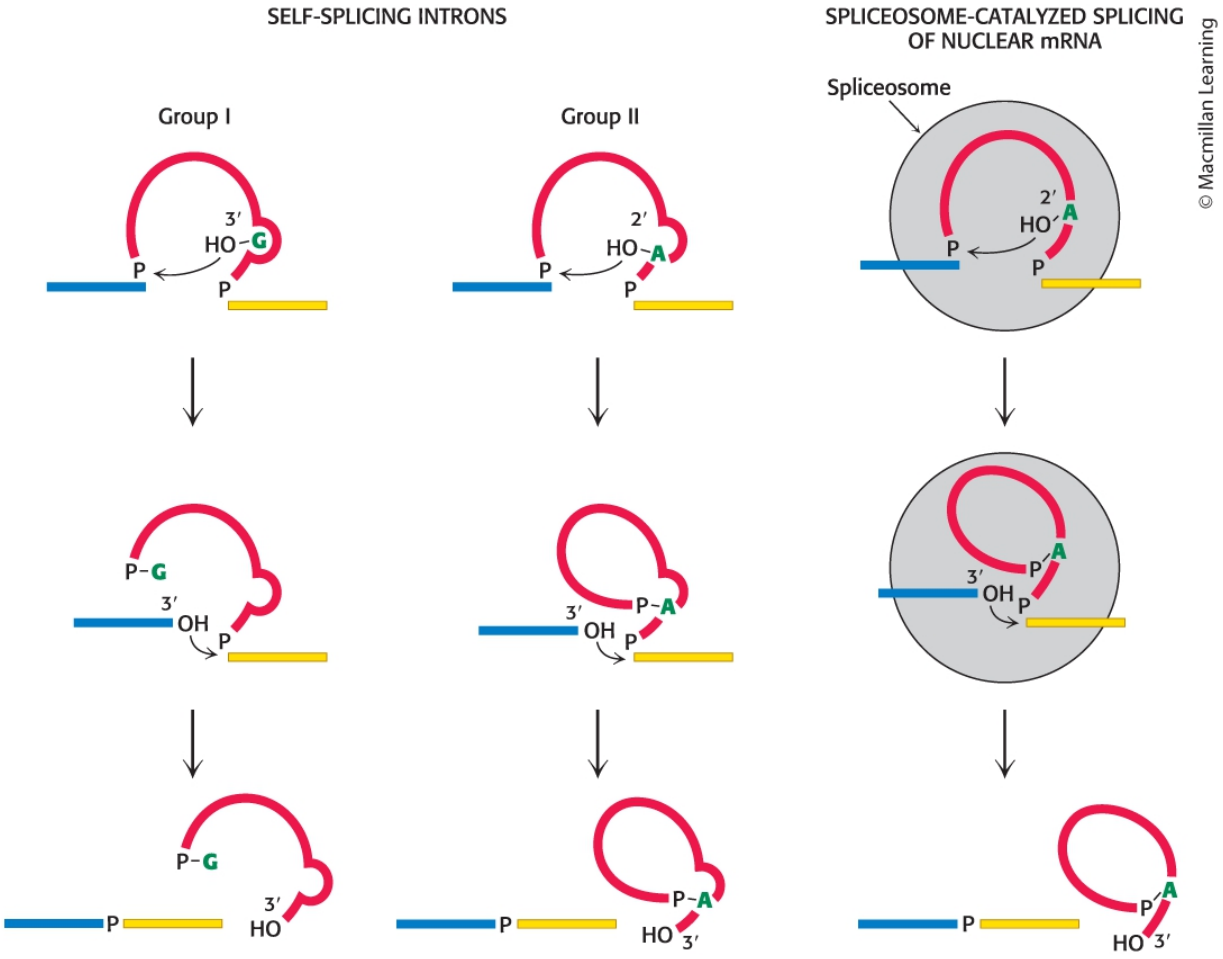
In the next step, a G nucleotide with a free O H group binds to its site. This O H group attacks the phosphodiester bond between U and A at the junction of the upstream exon and intron.

In the next step, the phosphodiester bond between U and A is cleaved. G binds to the 5 prime end of the intron. G is followed by A residue. The 3 prime O H of the upstream exon becomes free and attacks the phosphodiester bond between G and U at the 3 prime intron and downstream exon junction.

This attack leads to the formation of a spliced R N A containing the joined exons. The upstream exon is at the 5 prime end and the downstream exon is at the 3 prime end. The sequence at their junction is C U C U C U U. The linear intron is released such that its 3 prime G nucleotide contains a free O H.

Return to FIGURE 29.45 The catalytic mechanism of the group 1 self-splicing intron includes a series of transesterification reactions

Extended description for FIGURE 29.46 In self-splicing mechanisms, the catalytic site is formed by the intron itself



The self-splicing introns are of two types: group 1 and group 2.

In group 1, two exons on either ends are separated by a circular loop-like intron. The intron has a tiny semi-circular groove near its 3 prime end. A "G-nucleotide" with a free 3 prime O H is bound to the groove. O H attacks the phosphodiester bond between the 3 prime end of the upstream exon and the 5 prime end of the intron. In the

next step, the G nucleotide is bound to the free 5 prime end of the intron. The 3 prime O H of the upstream exon also becomes free and attacks the phosphodiester bond between the 3 prime end of the intron and downstream exon.

This attacks results in the joining of the two exons and the release of a semi-circular loop like intron. The 5 prime end of the intron contains G nucleotide and its 3 prime end contains a free O H group.

In group 2, An "A nucleotide" is located near the 3 prime end of the intron. It has a free 2 prime O H group. This O H attacks the phosphodiester bond between the upstream exon and the 5 prime end of the intron.

In the next step, the intron circularizes as its 5 prime end becomes bonded with 2 prime O H of A nucleotide near its 3 prime end. The free 3 prime O H of the upstream exon attacks the phosphodiester bond between the 3 prime end of the intron and the downstream exon. This attack results in the joining of the two exons and the release of the intron. The intron is loop-like with the short 3 prime end extending out of the loop.

In the spliceosome-catalyzed splicing of nuclear m R N A, the process is identical to group 2 self-splicing intron. The difference is that the transesterification reaction takes place inside a large spliceosome depicted as a large grey circle.

Return to FIGURE 29.46 In self-splicing mechanisms, the catalytic site is formed by the intron itself

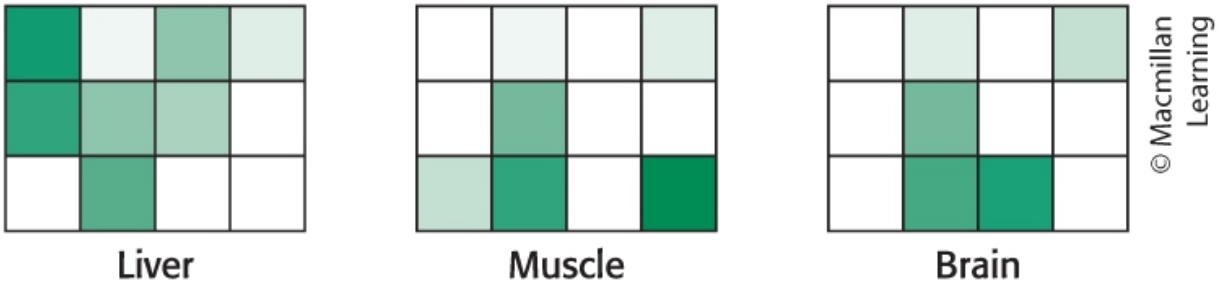
Extended description for Three genes on a double-stranded D N A



Three genes, labeled gene A, gene B, and gene C, are present from left to right between two template strands. The first template strand at the top is blue-colored with 5 prime label at the left end and 3 prime label at the right end. The bottom strand is green colored and labeled 3 prime at the left end and 5 prime at the right end. Gene A is at the left, Gene C is at the right, and Gene B is in the middle of the two genes.

Return to Three genes on a double-stranded D N A

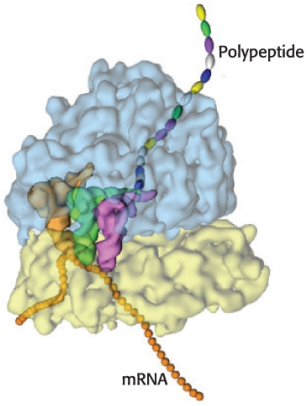
Extended description for Graphs for the liver, muscle, and brain indicating how much m R N A has attached to each D N A sequence

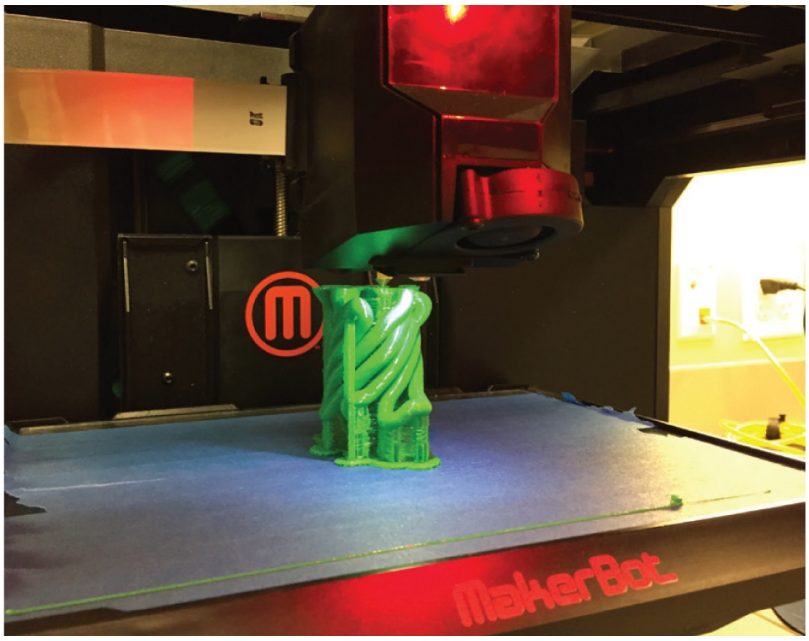


The figure depicts three graphs for the liver, muscle, and brain. In each graph, the intensity of the shading indicates approximately how much m R N A has attached to each D N A sequence. Each graph contains 12 equally sized boxes arranged in three rows and 4 columns. In the first graph for the liver three extra dark boxes, 3 medium intensity boxes, and one light-colored box are present. In the second graph for muscle, two extra dark, one medium intensity, and two light-colored boxes are present. In the third graph for the brain one extra dark, two medium-intensity, and two light-colored boxes are present.

Return to Graphs for the liver, muscle, and brain indicating how much m R N A has attached to each D N A sequence

Extended description for The ribosome, shown above, is a cellular machine that is not unlike a 3 D printer



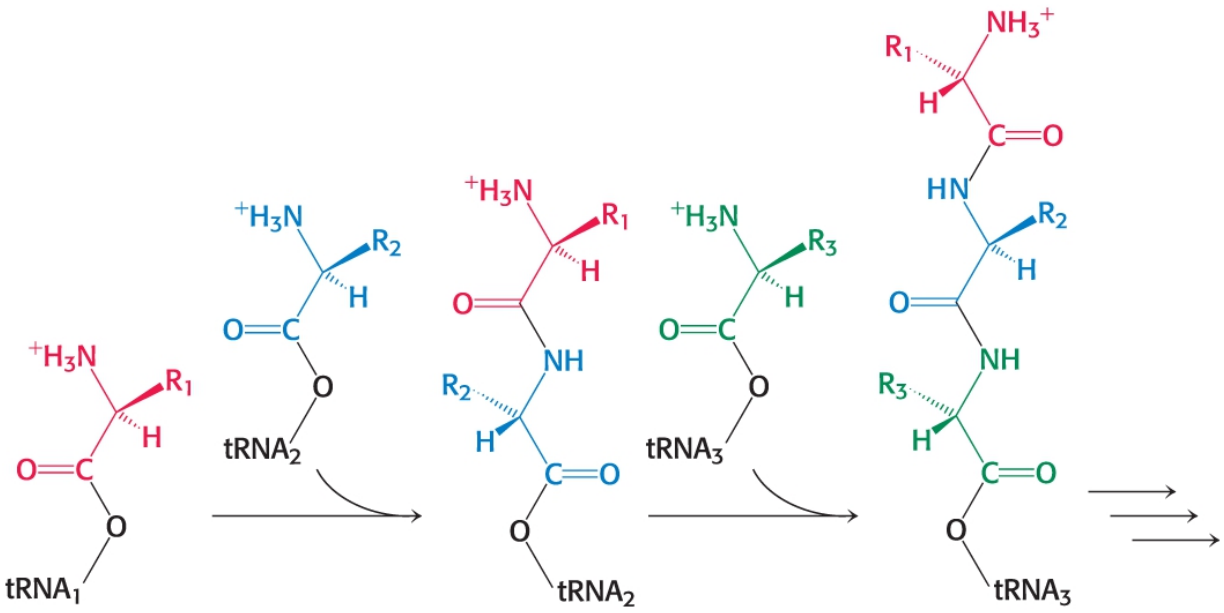


© Jess Petree
© Macmillan Learning

The figure has two parts. The first part depicts the 2 subunits of a ribosome depicted as two cloud-like structures with the smaller subunit at the bottom and the larger subunit at the top. The smaller subunit consists of an m R N A. Three t R N A binding sites of the 70 S ribosome are depicted as yellow, green, and purple double-helix structures arranged in series. The t R N A molecules are connected to the smaller and larger subunit of the ribosome. A beaded chain emerging upward from the larger subunit is labeled polypeptide. The second part depicts a photograph of a 3-D printer with a label that reads MakerBot.

Return to The ribosome, shown above, is a cellular machine that is not unlike a 3 D printer

Extended description for FIGURE 30.1 Polypeptides are synthesized by the successive addition of amino acids to the carboxyl terminus



In the first step, an amino acid is converted into a polypeptide. It is coupled with the entry of the second amino acid.

The structure of the amino acid is as follows: A central C atom is double bonded to O on the left and single bonded to a second central C atom in the form of a line. The second central C atom is dash bonded to H on the lower right, wedge bonded to R 1 on the upper right, and single bonded to N H 3 superscript plus on the upper left. This part of the structure is highlighted in red. The first central C atom is single bonded to a second O atom on the lower right. The second O atom is single bonded to t R N A subscript 1 on the lower left.

The structure of the amino acid that is added to the first amino acid is as follows: A central C atom is double bonded to O on the left and single bonded to a second central C atom in the form of a line. The second central C atom is dash bonded to H on the lower right, wedge bonded to R 2 on the upper right, and single bonded to N H 3 superscript plus on the upper left. This part of the structure is highlighted in blue. The first central C atom is single bonded to a second O atom on the lower right. The second O atom is single bonded to t R N A subscript 2 on the lower left.

The structure of the polypeptide formed by the addition of the second amino acid is as follows: A 1 N and 3 C heteronuclear alkane chain is depicted as a line structure using 3 zigzag lines. N bound to H occupies the third position. C 1 is wedge bonded to R 1 on the upper right, dash bonded to H on the lower right, and is single bonded to N H 3 superscript plus on the upper left. C 2 is double bonded to O on the left. C 3 is dash bonded to R 2 on the upper left, wedge bonded to H on the lower left, and is single bonded to a central C atom on the lower right. The central C atom is double bonded to a second O atom on the right and is single bonded to a third O atom on the lower left. The third O atom is single bonded to t R N A subscript 2 on the lower right. In the alkane chain, C 1 to C 2 part of the structure is highlighted in red, and N H to the C atom part of the structure is highlighted in blue.

In the second step, the polypeptide is further transformed to form a longer polypeptide. It is coupled with the entry of the third amino acid.

The structure of the third amino acid is as follows: A central C atom is double bonded to O on the left and single bonded to a second central C atom in the form of a line. The second central C atom is dash bonded to H on the lower right, wedge bonded to R 3 on the upper right, and single bonded to N H 3 superscript plus on the

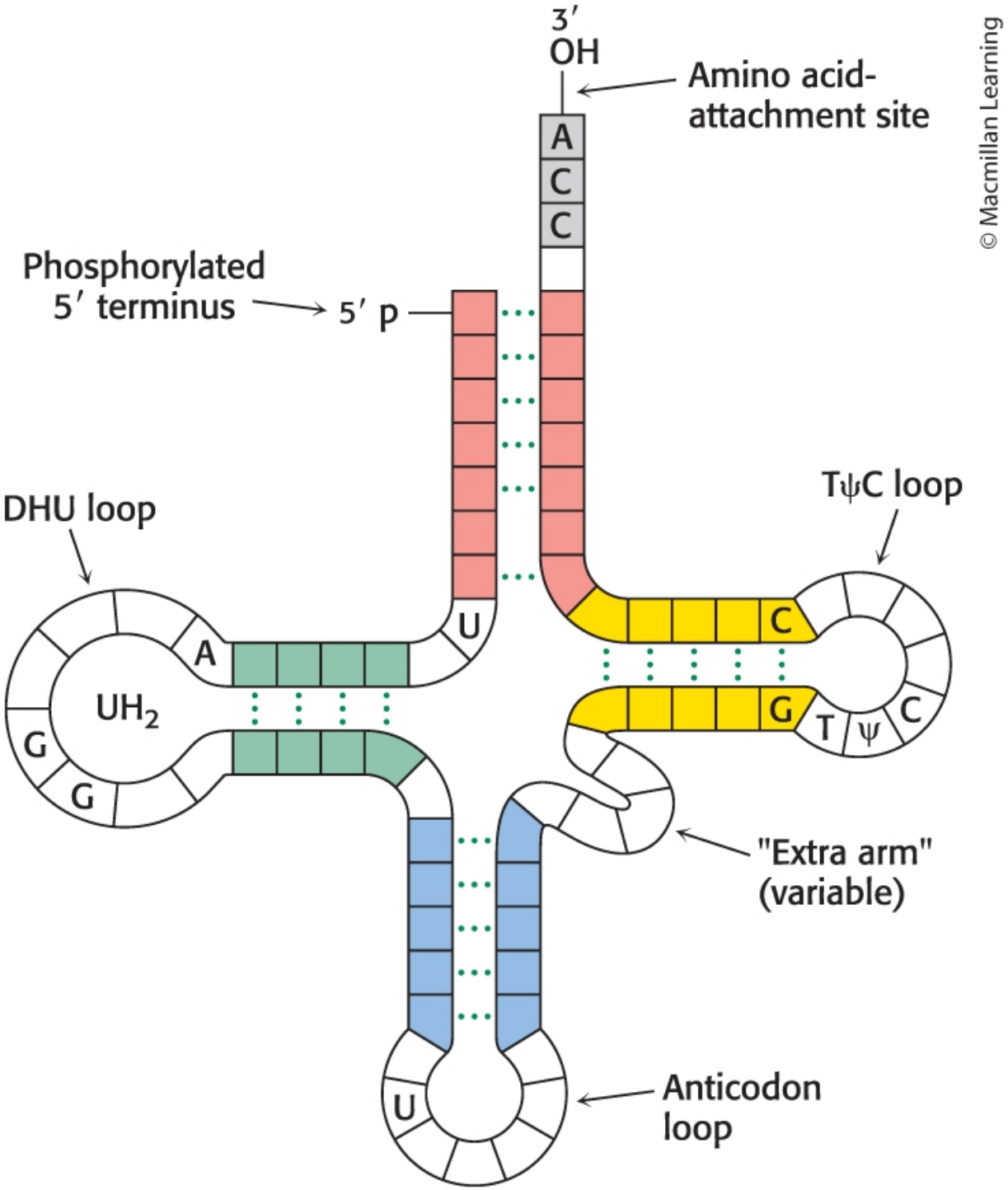
upper left. This part of the structure is highlighted in green. The first central C atom is single bonded to a second O atom on the lower right. The second O atom is single bonded to t R N A subscript 3 on the lower left.

The structure of the polypeptide formed by the addition of the third amino acid is as follows: A 2 N and 3 C heteronuclear alkane chain is depicted as a line structure using 4 zigzag lines. N bound to H occupies the first and the fourth positions. The first N atom is single bonded to a central C atom on the upper right. The central C atom is double bonded to O on the right and is single bonded to a second central C atom on the upper left in the form of a line. The second central C atom is single bonded to N H 3 superscript plus on the upper right, dash bonded to R 1 on the upper left, and is wedge bonded to H on the lower left. C 1 of the alkane chain is wedge bonded to R 2 on the upper right and dash bonded to H on the lower right. C 2 of the alkane chain is double bonded to a second O atom on the left. C 3 of the alkane chain is dash bonded to R 3 on the upper left, wedge bonded to H on the lower left, and is single bonded to a third central C atom on the lower right. The third central C atom is double bonded to a third O atom on the right and is single bonded to a fourth O atom on the lower left. The fourth O atom is single bonded to t R N A subscript 3 on the lower right. In the alkane chain, the first and second central C atoms and the groups attached to them are highlighted in red. In the alkane chain, the first N atom to C 2 part of the chain and groups attached to them is highlighted in blue. In the alkane chain the second N atom to third central C atom part of the chain and groups attached to them is highlighted in green.

Three forward arrows drawn from the product of the second step indicate that the reaction continues.

Return to FIGURE 30.1 Polypeptides are synthesized by the successive addition of amino acids to the carboxyl terminus

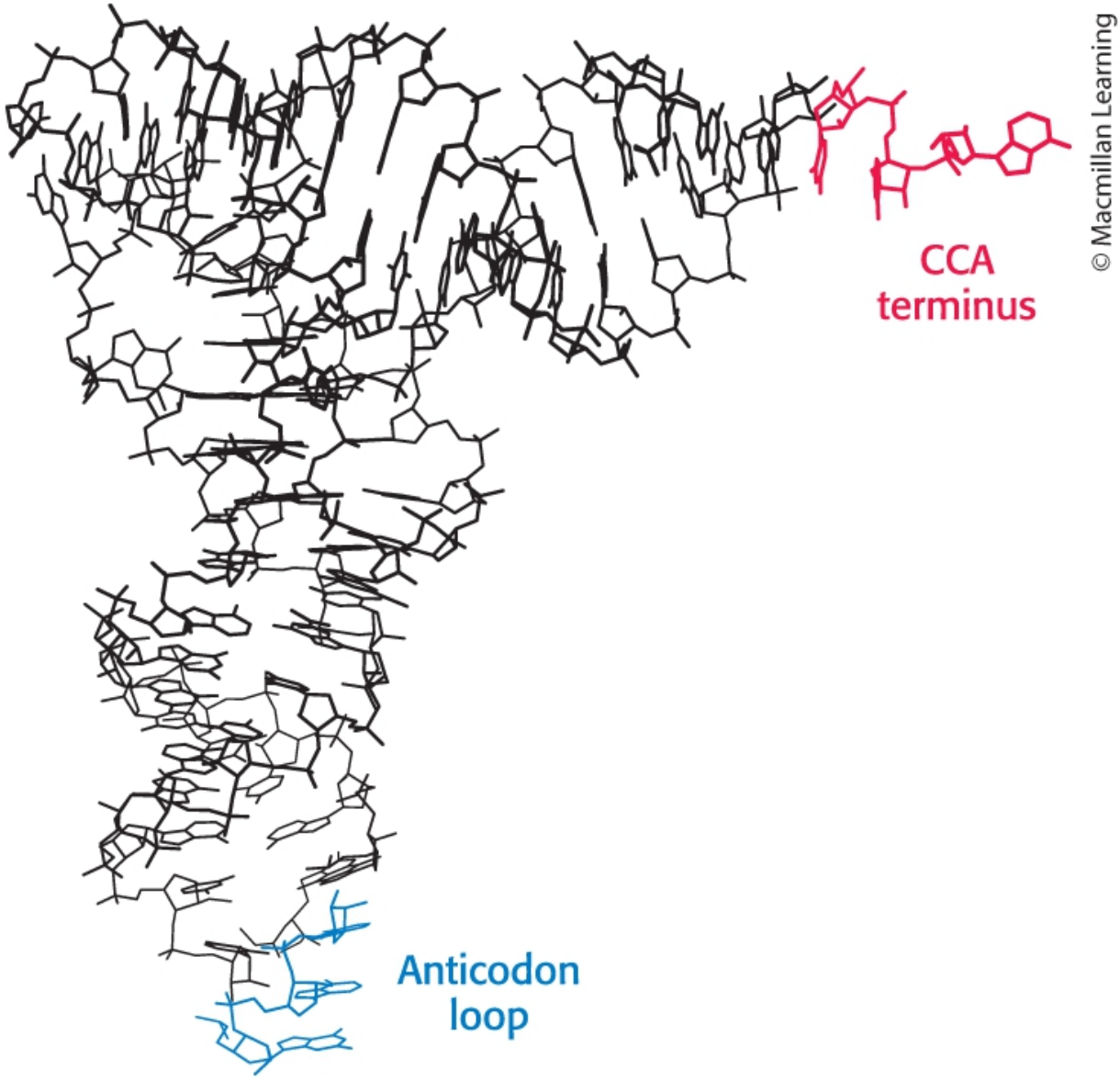
Extended description for FIGURE 30.2 The secondary structure of all transfer R N A s resembles a cloverleaf



The secondary structure of R N A resembles a cloverleaf. A single chain of t R N A is folded to form five arms which results in 3 prime and 5 prime ends that lie adjacent to each other at the top. Each arm consists of a loop and a basal stalk. The 3 prime and 5 prime ends of the t R N A are at the top. They do not form a loop and hence are in the form of two parallel lines. The stalk representing 5 prime terminus is shorter than the 3 prime stalk. The second arm on the right is the T loop and it is labeled T psi C loop. It consists of a bases C, T, and C-G base pair. The third arm at the bottom is labeled the anticodon loop. The loop consists of a base U. The fourth arm on the left is the D loop and it is labeled D H U loop. The center of the loop reads U H 2. The loop consists of bases A, G, and G. G and G are present side by side while A lies away from it. The fifth arm is a short extra arm that lies between the second and third arms. It is labeled extra arm (variable). The 3 prime strand at the top consists of a codon. From top to bottom, the codon reads A C C. The 3 prime end is attached to an O H group at the top. The 5 prime end is single bonded to a phosphate group and is labeled phosphorylated 5 prime terminus. The base pairs in each arm are highlighted in different colors. The base pairs in the free 5 prime and 3 prime ends are highlighted in pink. The base pairs in the stalk of the T loop are highlighted in yellow. The base pairs in the stalk of the anticodon loop are highlighted in blue. The base pairs in the stalk of the D loop are highlighted in green.

Return to FIGURE 30.2 The secondary structure of all transfer R N A s resembles a cloverleaf

Extended description for FIGURE 30.3 Transfer R N A s have an L-shaped tertiary structure

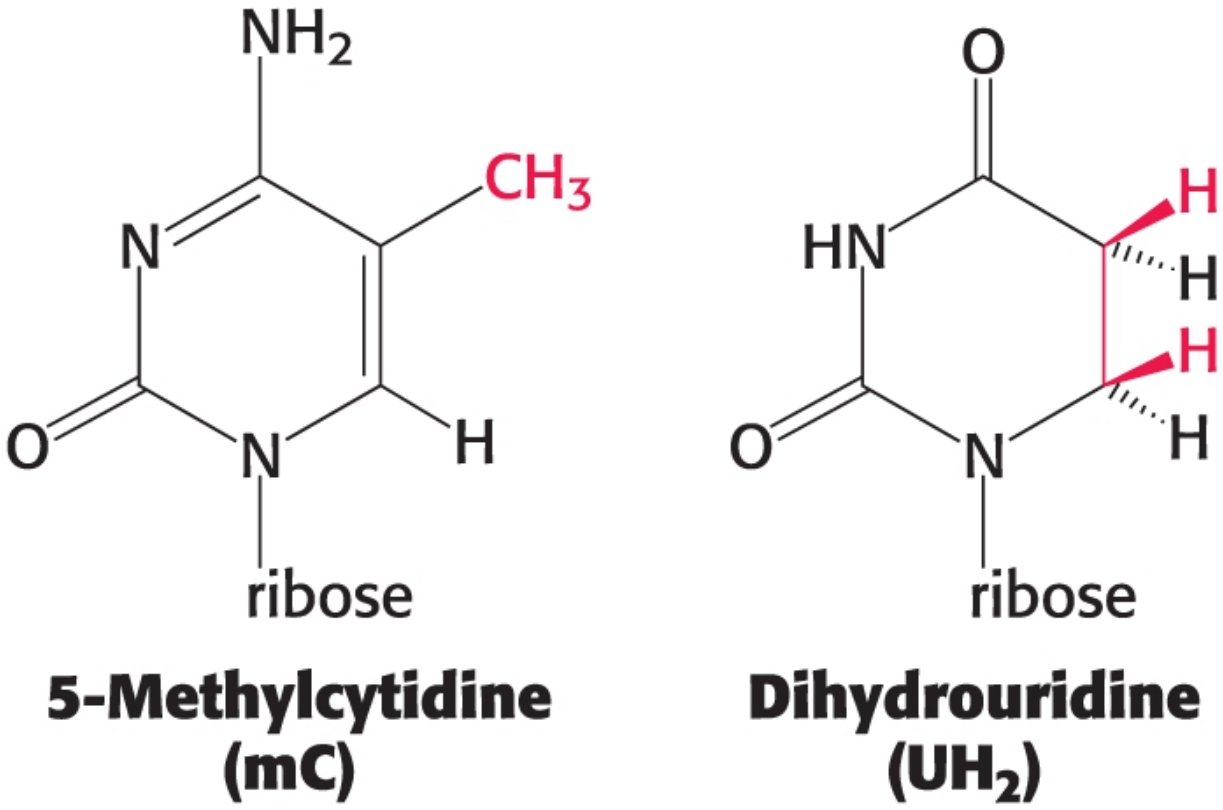


The tertiary structure of t R N A is depicted in the form of an inverted L. The t R N A is composed of ball-and-stick models composed of pentagonal rings attached by sticks to the neighboring pentagonal rings in a haphazard manner. A red-colored ball-and-

stick model attached to the upper right of the t R N A is labeled C C A terminus. A blue-colored ball-and-stick model attached to the lower end of the t R N A is labeled an anticodon loop.

Return to FIGURE 30.3 Transfer R N A s have an L-shaped tertiary structure

Extended description for Structures of 5-methycytidine and dihydrouridine

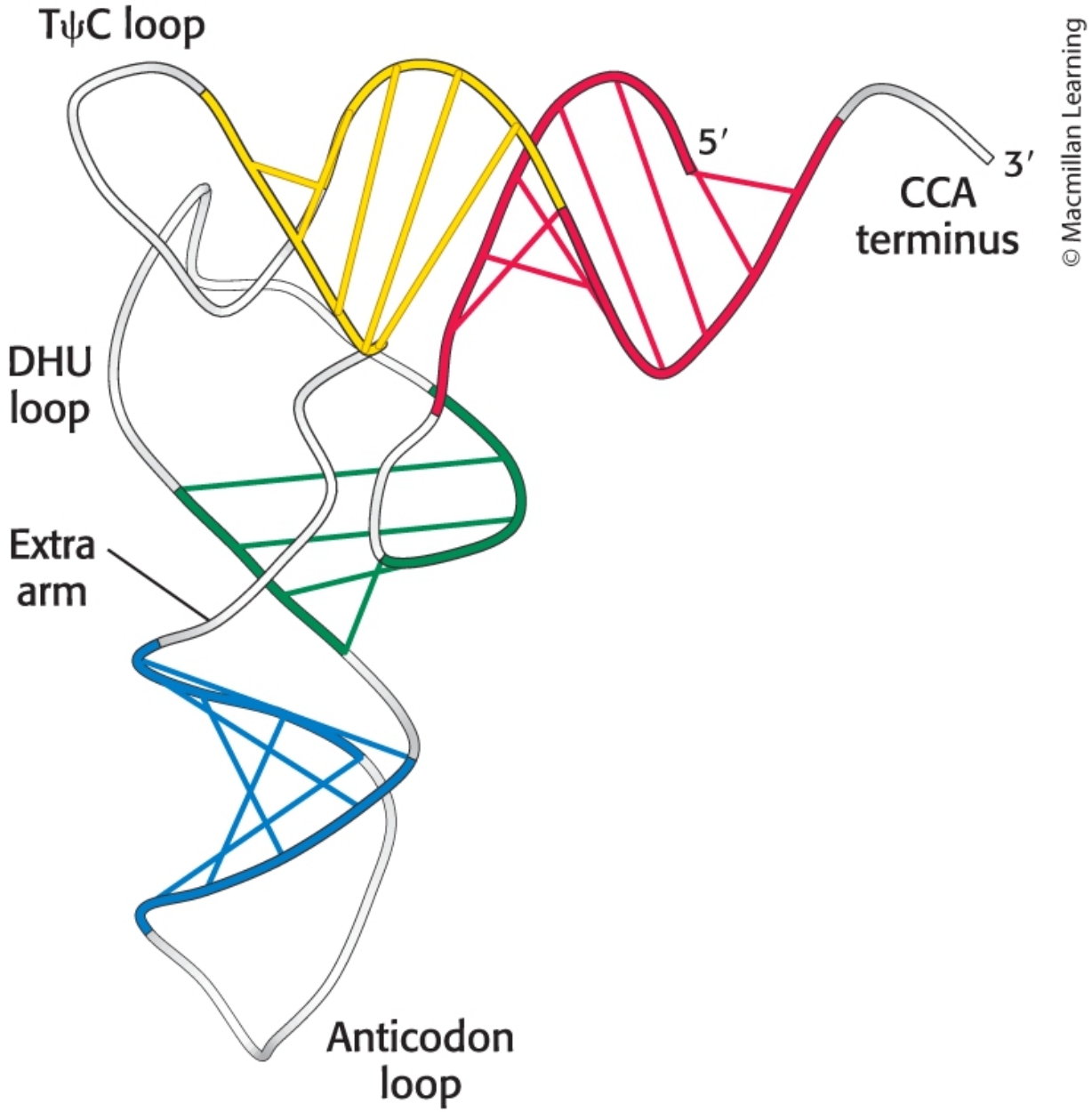


The structure of 5-methycytidine (m C) is as follows: A 6-membered heterocyclic hexagonal ring is in a vertical orientation and consists of 2 N and 4 C atoms. The first N atom occupies the first position, which is the bottommost vertex. The second N atom occupies the third position which is the top left vertex. A double bond is present between the second N atom and C 2 and C 3 and C 4. The first N atom is single bonded to ribose. C 1 is double bonded to O. C 2 is single bonded to N H 2. C 3 is single bonded to C H 3. C H 3 is highlighted in red. C 4 is single bonded to H. The structure of dihydrouridine (U H 2) is as follows: A 6-membered heterocyclic hexagonal ring is in a vertical orientation and consists of 2 N and 4 C atoms. The first N atom occupies the first position, which is the

bottommost vertex. The second N atom bound to H occupies the third position which is the top left vertex. The first N atom is single bonded to ribose. C 1 is double bonded to O. C 2 is double bonded to O. C 3 and C 4 are each wedge bonded to H on the upper right and dash bonded to H on the lower right. The wedge bonded H atoms in both C 3 are C 4 are highlighted in red.

Return to Structures of 5-methycytidine and dihydrouridine

Extended description for FIGURE 30.4 The four double-stranded regions of a t R N A stack to form an L-shaped structure



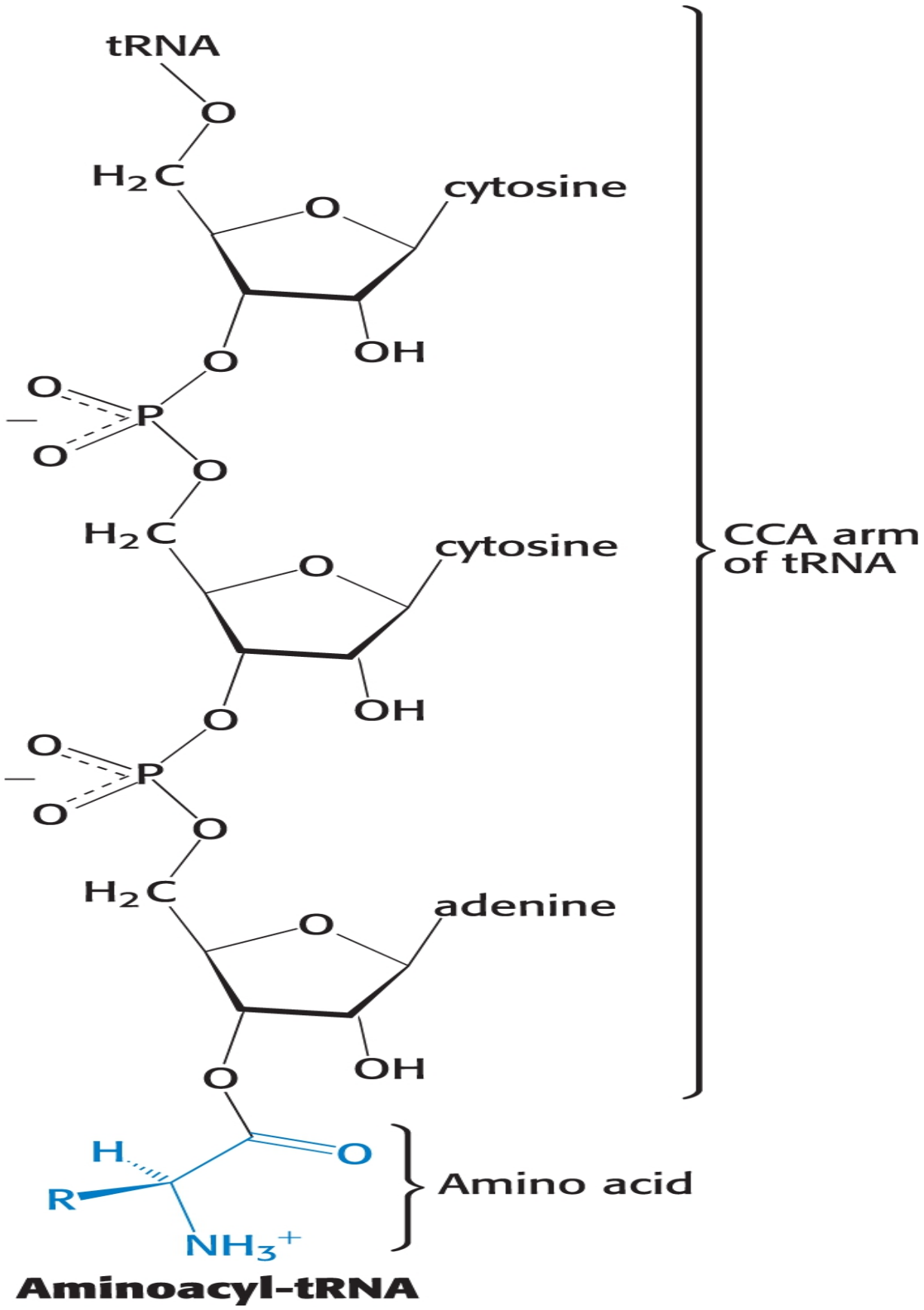
The tertiary structure of t R N A is depicted in the form of an inverted L-shaped structure composed of four double-stranded

regions. These include red, yellow, green, and blue helices. These helices are attached by white helices in between. The helices have 5 prime and 3 prime ends. The region of the helix on the upper right is labeled C C A terminus. The region of the helix on the top left is labeled T psi C loop. The region of the helix at the lower end of the t R N A is labeled the anticodon loop. The region between the T psi loop and anticodon loop consists of the D H U loop and the extra arm.

Return to FIGURE 30.4 The four double-stranded regions of a t R N A stack to form an L-shaped structure

Extended description for FIGURE 30.5 Ester linkages

couple amino acids to t R N A s



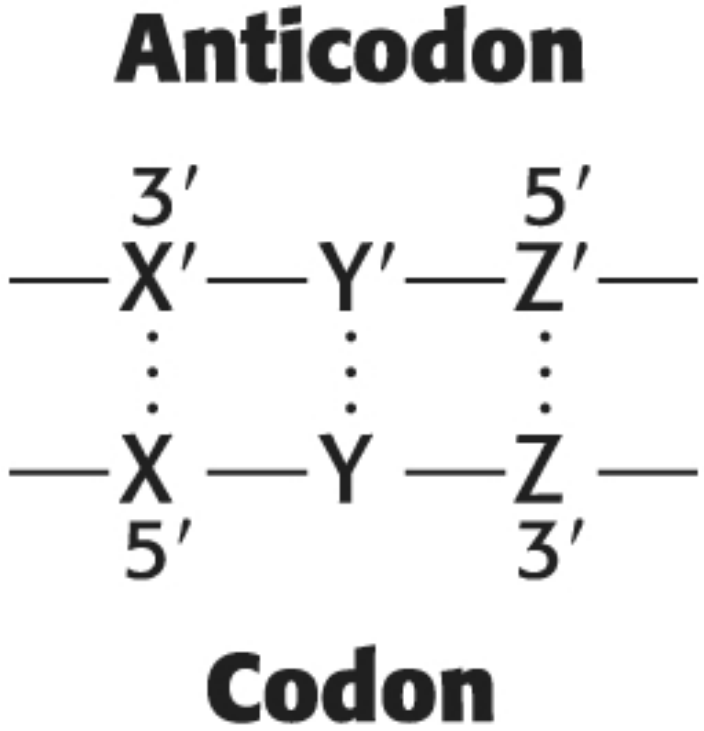
Aminoacyl-tRNA

The structure of aminoacyl- t R N A shows an amino acid attached to the C C A arm of t R N A. The structure is as follows: A 5-membered heterocyclic pentagonal ring in a vertical orientation and consists of 1 O and 4 C atoms. O occupies the first position which is the topmost vertex. The ring is in a plane perpendicular to the plane of the paper such that C 2 and C 3 are toward the observer, and O is away from the observer. C 1 is single bonded to cytosine. C 2 is single bonded to O H. C 4 is single bonded to C H 2. C H 2 is further single bonded to O on the upper right. O on the upper right is single bonded to t R N A on the upper left. C 3 is single bonded to a second O atom. The second O atom is single bonded to a central P atom on the lower left. The central P atom is partially double bonded to a third O atom on the upper left and a fourth O atom on the lower left. The P O O group has an overall negative charge. The central P atom is single bonded to a fifth O atom on the lower right. The fifth O atom is single bonded to a second C H 2 group on the lower left. The second C H 2 group is single bonded to C 4 of a second 5-membered pentagonal ring in a vertical orientation consisting of 1 O and 4 C atoms. In the second ring, O occupies the first position which is the topmost vertex. The second ring is in a plane perpendicular to the plane of the paper such that C 2 and C 3 are toward the observer, and O is away from the observer. C 1 of the second ring is single bonded to cytosine. C 2 of the second ring is single bonded to O H. C 3 of the second is single bonded to a sixth O atom. The sixth O atom is single bonded to a second central P atom on the lower left. The second central P atom is partially double bonded to a seventh O atom on the upper left and an eighth O atom on the lower left. The P O O group has an overall negative charge. The second central P atom is also single bonded to a ninth O atom on the lower right. The ninth O atom is further single bonded to a third C H 2 group on the lower left. The third C H 2 group is single bonded to C 4 of a third 5-membered pentagonal ring in a vertical orientation consisting of 1 O and 4 C atoms. In the third ring, O occupies the first position which is the topmost vertex. The third ring is in a plane perpendicular to

the plane of the paper such that C 2 and C 3 are toward the observer, and O is away from the observer. C 1 of the third ring is single bonded to adenine. C 2 of the third ring is single bonded to O H. C 3 of the third ring is single bonded to a tenth O atom. The tenth O atom is single bonded to C 2 of a 2-carbon alkane chain depicted as a line structure using 1 line. C 1 of the alkane chain is single bonded to H on the upper left, and N H 3 superscript plus on the lower right and is wedge bonded to R on the left. C 2 of the alkane chain is double bonded to a eleventh O atom on the lower right. The 2-carbon alkane chain and the groups attached to it are highlighted in blue.

Return to FIGURE 30.5 Ester linkages couple amino acids to t R N A s

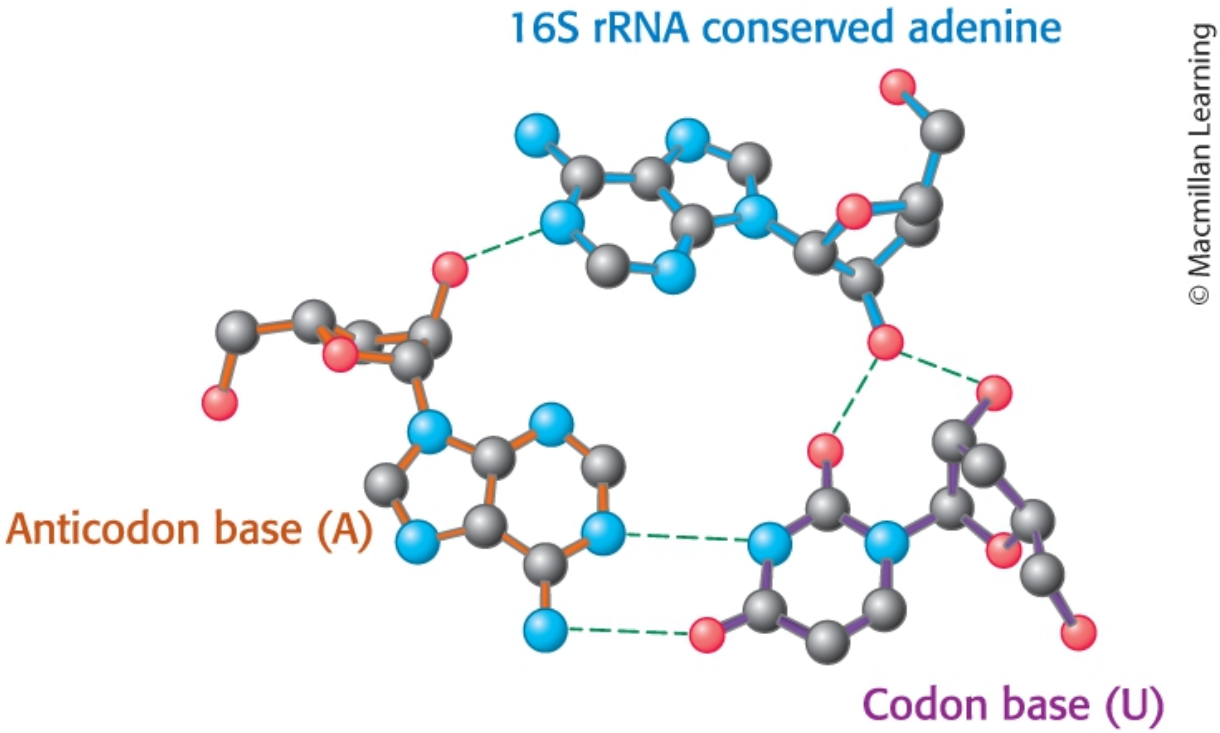
Extended description for Anticodon and codon sequence



The anticodon sequence at the top is in the 3 prime to 5 prime direction while the codon sequence below is in the 5 prime to 3 prime direction. The anticodon sequence reads X prime, Y prime, and Z prime from left to right and is connected by bonds. The X and Z on the left and right also have bonds on the left and right, respectively. The codon sequence reads X, Y, and Z from left to right and is connected by bonds. The X and Z on the left and right also have bonds on the left and right, respectively. The anticodons at the top are vertically base paired with the corresponding codons below such that X prime is paired with X, Y prime is paired with Y, and Z prime is paired with Z.

Return to Anticodon and codon sequence

Extended description for FIGURE 30.6 16 S r R N A monitors base-pairing between the codon and the anticodon



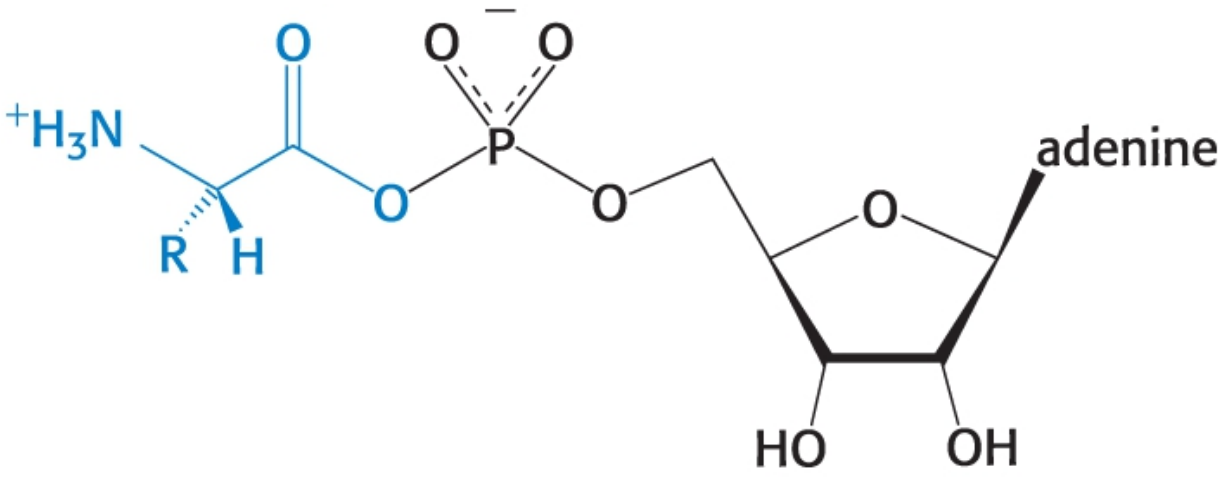
© Macmillan Learning

The figure depicts the ball-and-stick model of 16 S r R N A conserved adenine at the top. The ball-and-stick model consists of grey, blue, and red spheres. C atoms are depicted as a grey spheres, N atoms are depicted as a blue spheres, and O atoms are depicted as a red spheres. The ball-and-stick model consists of a 6-membered heterocyclic, hexagonal ring. The hexagonal ring consists of four grey and two blue spheres. A grey sphere on the top left is attached to a blue sphere. The hexagonal ring is fused with a pentagonal ring consisting of 2 blue spheres and three grey spheres. One of the blue spheres in the pentagonal ring is attached to a grey sphere of another pentagonal ring consisting of one red and four grey spheres. One of the grey spheres of the pentagonal ring is attached

to a grey sphere that is further attached to a red sphere. Another grey sphere in the pentagonal ring is attached to a red sphere at the bottom. A blue sphere from the hexagonal ring in the 16 S r R N A is hydrogen bonded to a red sphere in the anticodon base adenine. A red sphere attached to the pentagonal ring in the 16 S r R N A is hydrogen bonded to codon base uracil. The anticodon base adenine consists of five grey spheres attached side by side. The first, fourth, and fifth spheres are each attached to red spheres. The red sphere attached to the fourth grey sphere is the place where the hydrogen bond is formed. The fifth sphere is also attached to a pentagonal ring consisting of two blue and three grey spheres. The pentagonal ring is fused with a hexagonal ring consisting of two blue and three grey spheres. One of the grey spheres is attached to a blue sphere. The codon base uracil consists of a hexagonal ring consisting of four grey and two blue spheres. Two grey spheres are attached to one red sphere each. One of the red spheres directly forms a hydrogen bond with the 16 S r R N A. One of the blue spheres of the hexagonal ring is attached to a pentagonal ring consisting of one red and four grey spheres. One of the grey spheres is attached to a grey sphere at the bottom. This grey sphere is attached to a red sphere. One of the grey spheres at the top is attached to a red sphere. The red sphere forms a hydrogen bond with the 16 S r R N A. Two hydrogen bonds are formed between anticodon base adenine and codon base uracil.

Return to FIGURE 30.6 16 S r R N A monitors base-pairing between the codon and the anticodon

Extended description for Structure of aminoacyl A M P

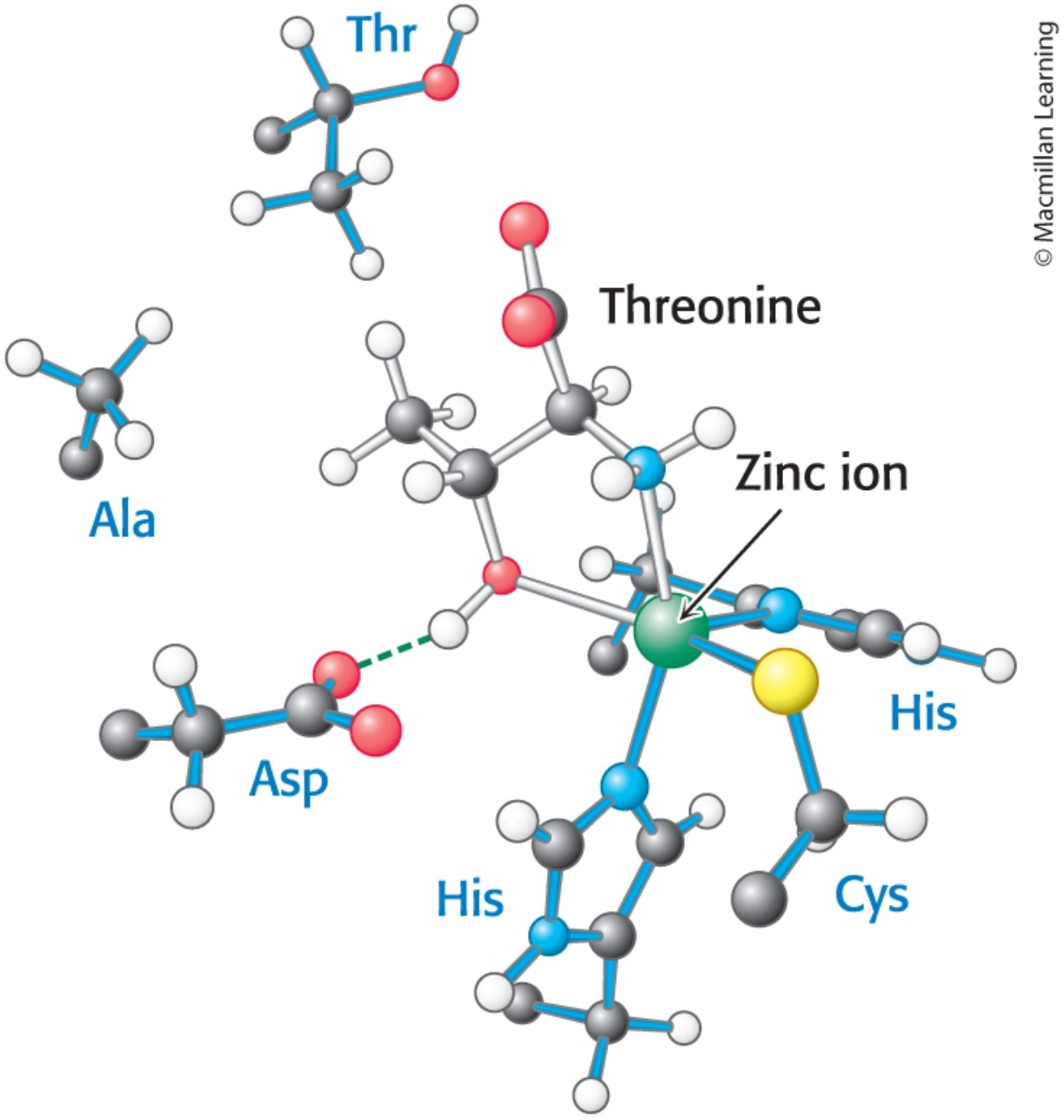


Aminoacyl-AMP

The structure of aminoacyl A M P is as follows: A 5-membered heterocyclic pentagonal ring in a horizontal orientation consists of 1 O and 4 C atoms. O occupies the first position which is the topmost vertex. C 1 is wedge bonded to adenine. C 2 is single bonded to O H. C 3 is single bonded to O H. C 4 is single bonded to C 3 of a 1 N H 3 superscript plus, 1 P, 2 O, and 3 C heteronuclear alkane chain consisting of depicted as a line structure using 6 zigzag lines. N H 3 superscript plus occupies the first position. The first O atom occupies the fourth position, P occupies the fifth position, and the second O occupies the sixth position. C 1 is dash bonded to R on the lower left and wedge bonded to H on the lower right. C 2 is double bonded to O above. P is partially double bonded to O on the upper left and O on the upper right. The P O O group has an overall negative charge. The structures in the alkane chain upto the fourth position are highlighted in blue.

Return to Structure of aminoacyl A M P

Extended description for FIGURE 30.7 The amino acid-binding site of threonyl- t R N A synthetase contains a zinc ion



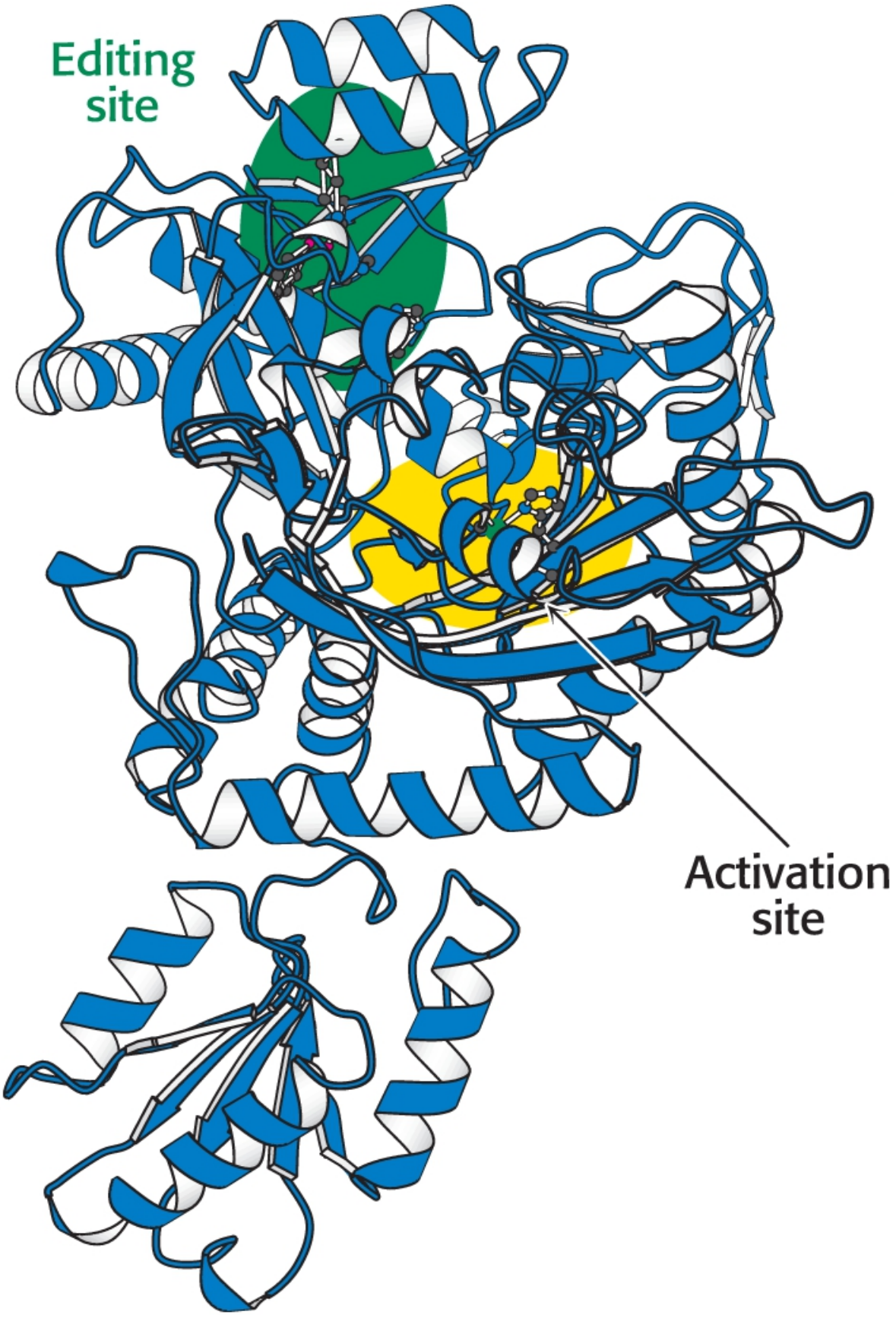
© Macmillan Learning

The figure shows the ball-and-stick mode of threonyl- t R N A synthase. The ball-and-stick model consists of grey, blue, red, and green spheres. C atoms are depicted as a grey spheres, N atoms are depicted as a blue spheres, O atoms are depicted as a red spheres, and zinc ion is depicted as a large green sphere. The zinc ion at the center is bound to the amino and hydroxyl groups of threonine at the top. These bonds are depicted in white. The zinc ion is also attached to a few amino acids at the bottom. The attachment with the amino acids are depicted by blue bonds. The amino acids bound to the zinc ion are histidine on the lower left, cysteine on the lower right, and histidine on the right. Aspartic acid is hydrogen bonded to threonine on the left. Two amino acids labeled alanine and threonine are free.

Return to FIGURE 30.7 The amino acid-binding site of threonyl- t R N A synthetase contains a zinc ion

Extended description for FIGURE 30.8 Threonyl- t R N A

synthetase also contains an editing site

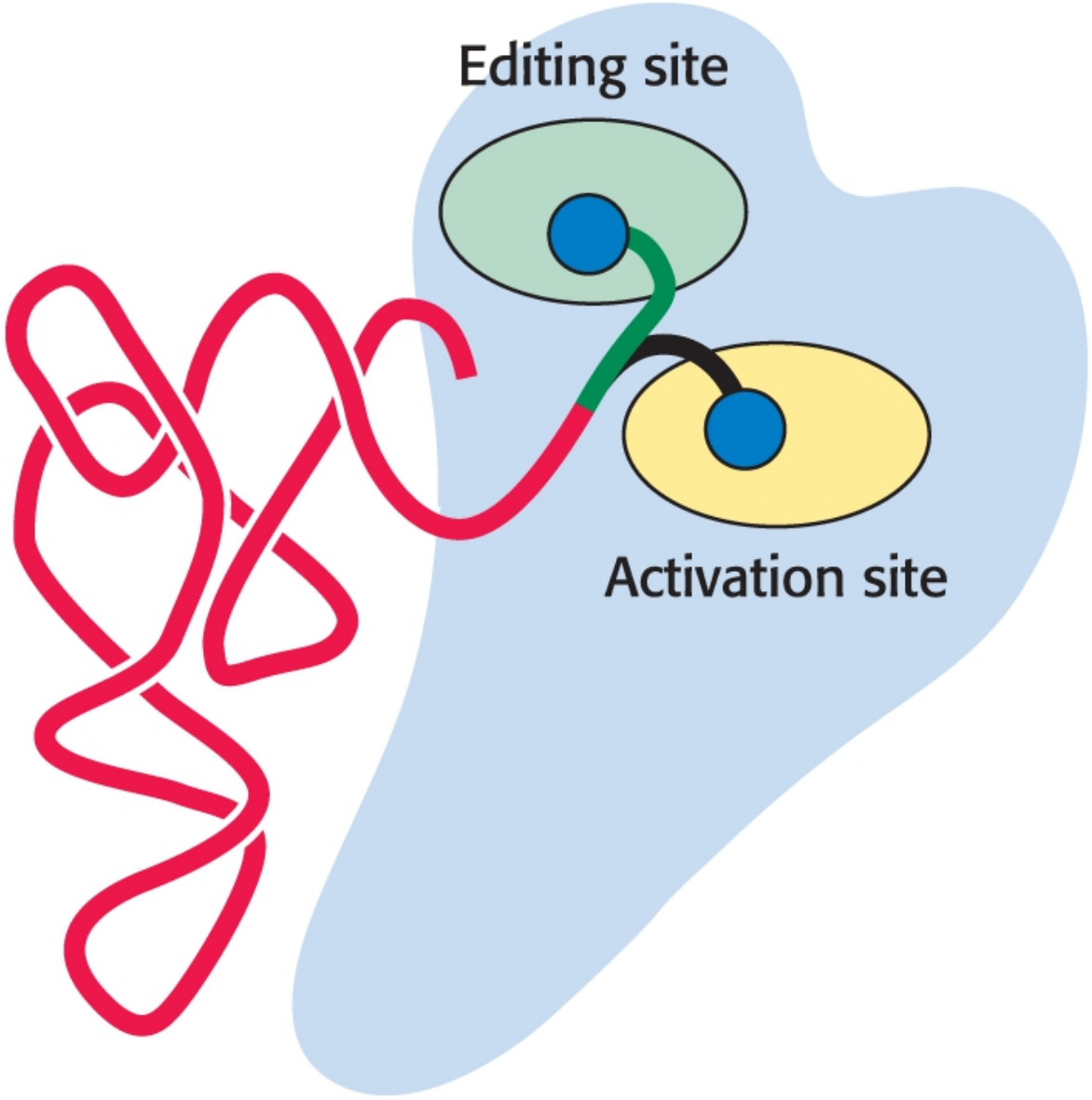


© Macmillan Learning

The ribbon diagram of threonyl- t R N A synthetase is a dimer. Only one subunit of the dimer is depicted in the figure. The subunit roughly has a heart-shaped appearance. It consists of blue-colored alpha helices and beta strands interconnected by thread-like loops. A green-colored oval structure in the upper region of the subunit is labeled the editing site. A yellow-colored oval structure, slightly above the center of the subunit and below the editing site is labeled activation site. Both the editing site and activation site consist of ball-and-stick models of amino acids attached to the ribbon diagram.

Return to FIGURE 30.8 Threonyl- t R N A synthetase also contains an editing site

Extended description for FIGURE 30.9 Amino acids move between the activation site and the editing site of an aminoacyl- t R N A synthetase



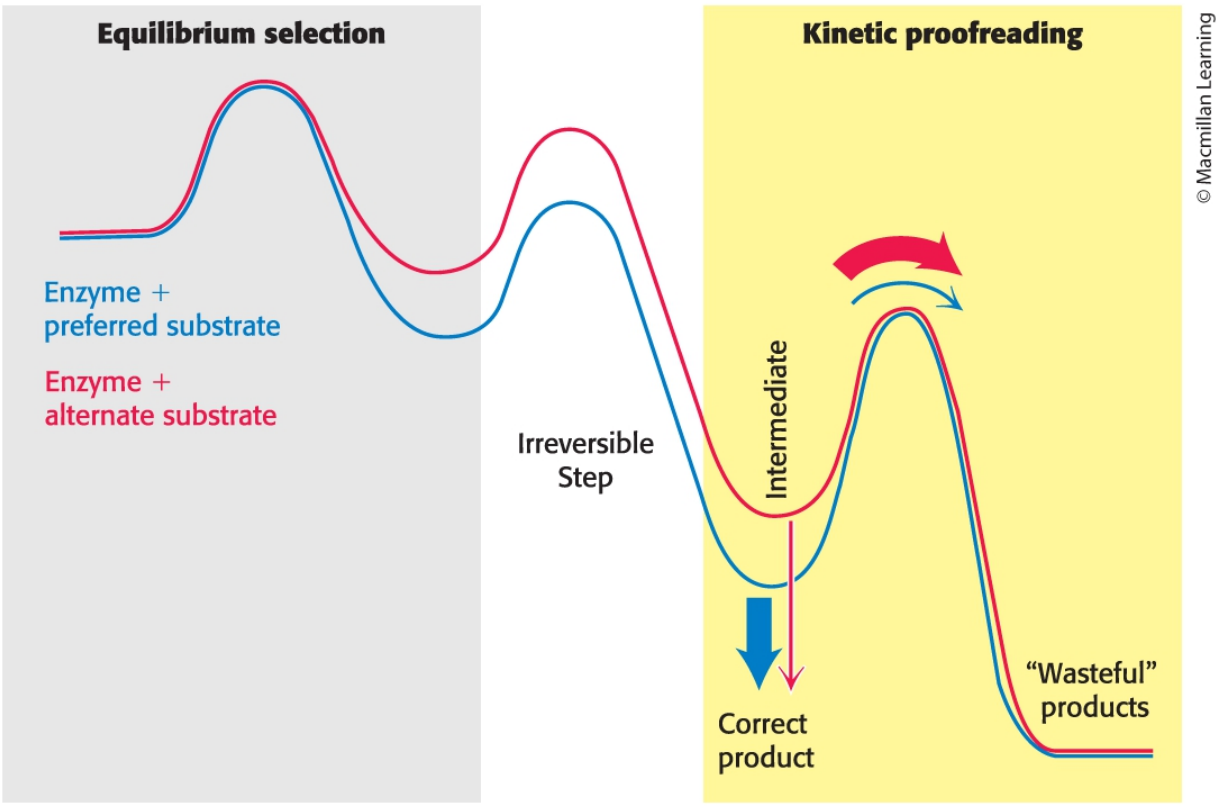
© Macmillan Learning

The figure depicts a subunit of threonyl- t R N A which roughly has a heart-shaped appearance. It consists of a green-colored oval structure in the upper region of the subunit is labeled the editing

site. A yellow-colored oval structure, slightly above the center of the subunit and below the editing site is labeled activation site. A red-colored double-stranded inverted L-shaped t R N A has an acceptor stem on the upper right. The acceptor stem consists of an amino acid in the terminal end of one of its strands. The amino acid is depicted as a blue sphere that can swing between the editing site and the activation site. Only one amino acid can attach with the t R N A at a time.

Return to FIGURE 30.9 Amino acids move between the activation site and the editing site of an aminoacyl- t R N A synthetase

Extended description for FIGURE 30.10 Kinetic proofreading can increase reaction specificity

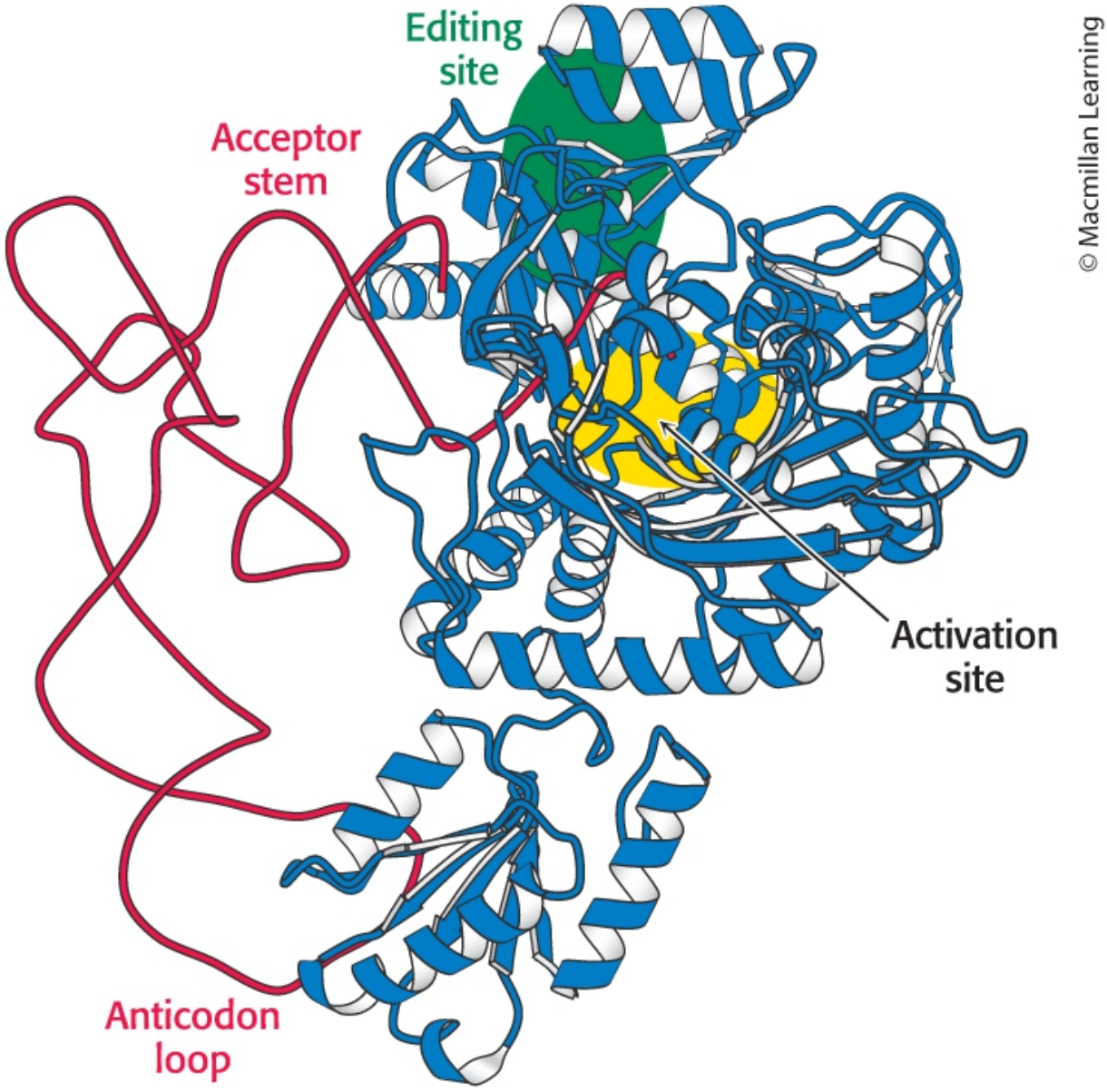


The figure shows two panels, one on the left labeled equilibrium and the other on the right labeled kinetic proofreading. The figure shows a substrate that binds to an enzyme more tightly (curve shown in blue) than an alternate substrate (curve shown in red). The red and blue curves show the simultaneous rise and fall throughout the panels. On the upper region of the equilibrium selection panels, the two curves start from the left, move upward, and slope down, showing a peak between the two panels labeled irreversible step. The curves, then show a dip in the kinetic proofreading panel labeled intermediate. The space between the blue and red curves is slightly larger in the intermediate. A downward arrow from the intermediate shows that it can form a final correct product or the

intermediate shows another peak that gradually slopes down and terminates on the right depicting the formation of wasteful products. The wasteful products are formed faster for the alternate substrate.

Return to FIGURE 30.10 Kinetic proofreading can increase reaction specificity

Extended description for FIGURE 30.11 Aminoacyl- t R N A synthetases bind to both the acceptor stem and the anticodon loop of a t R N A

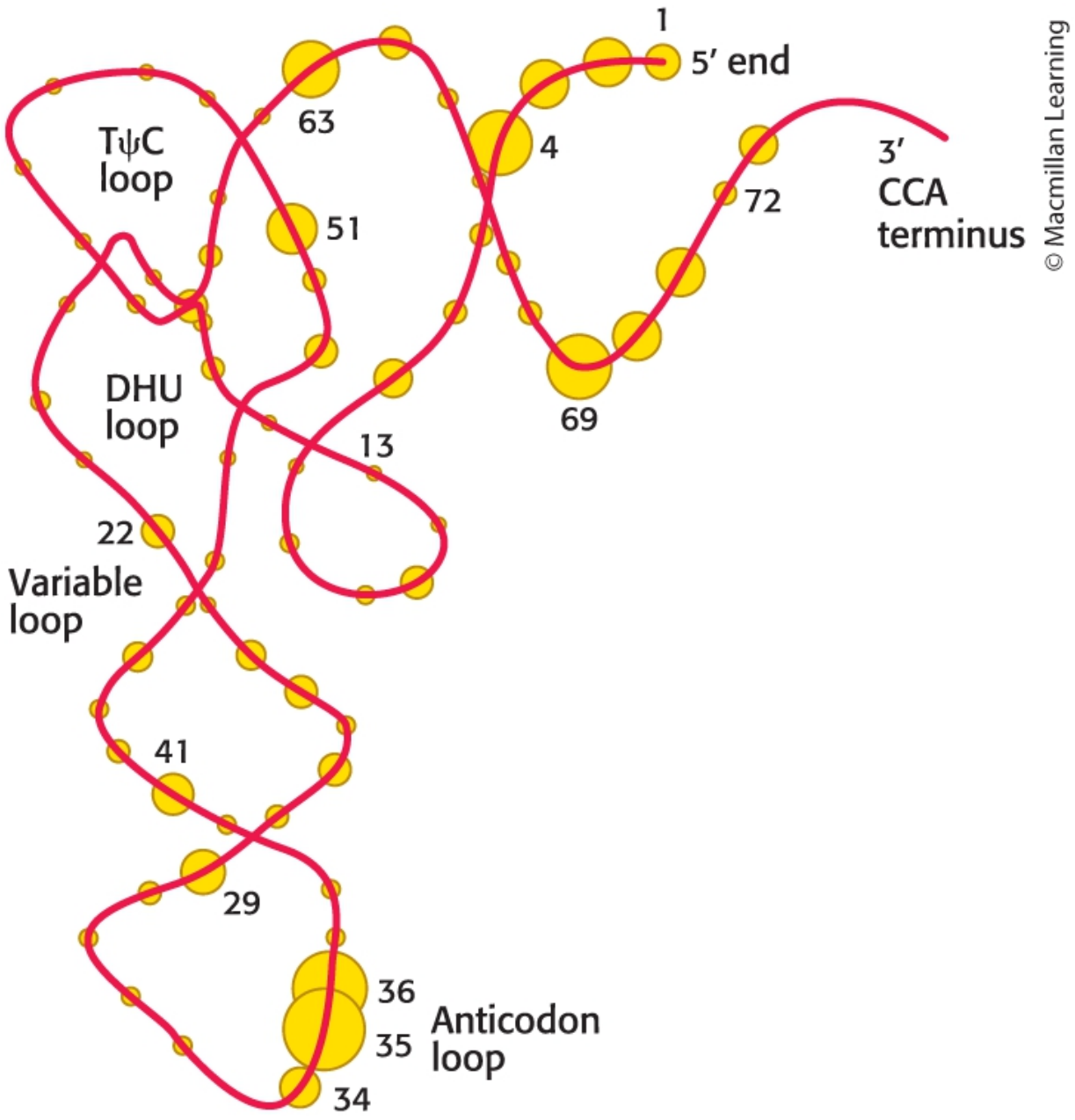


The ribbon diagram of threonyl- t R N A synthetase is a dimer. Only one subunit of the dimer is depicted in the figure. The subunit roughly has a heart-shaped appearance. It consists of blue-colored

alpha helices and beta strands interconnected by thread-like loops. A green-colored oval structure in the upper region of the subunit is labeled the editing site. A yellow-colored oval structure, slightly above the center of the subunit and below the editing site is labeled activation site. A red-colored double-stranded inverted L-shaped t R N A is present on the left. It consists of an acceptor on the upper right and an anticodon loop on the lower end. Both the acceptor stem and the anticodon loop are bound to the aminoacyl- t R N A synthetase.

Return to FIGURE 30.11 Aminoacyl- t R N A synthetases bind to both the acceptor stem and the anticodon loop of a t R N A

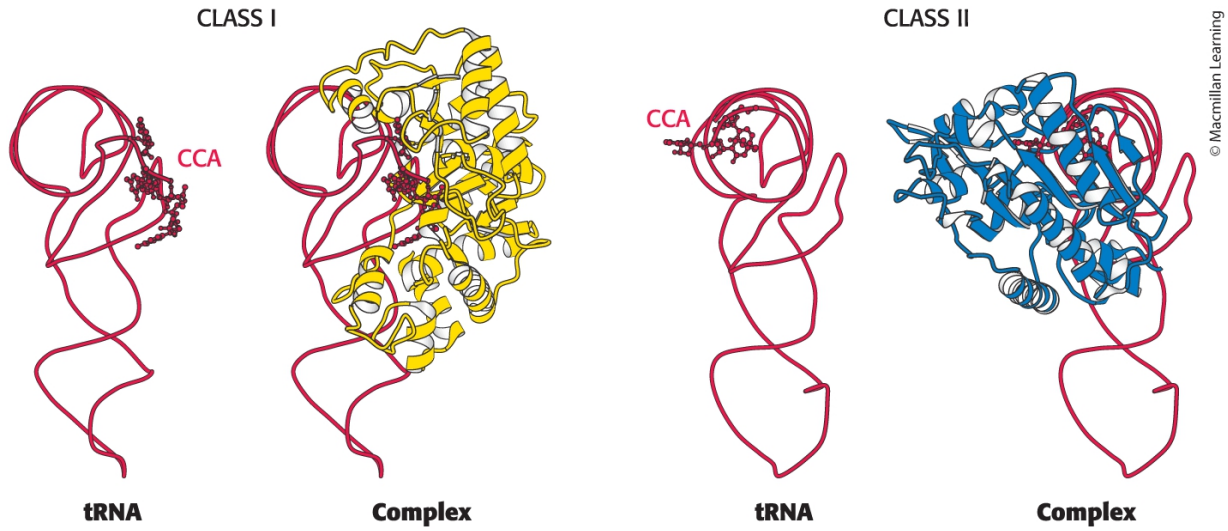
Extended description for FIGURE 30.12 t R N A s have multiple recognition sites for aminoacyl- t R N A synthetases



The tertiary structure of t R N A is depicted in the form of an inverted L. The t R N A is composed of a continuous double helix that has free 5 prime and 3 prime ends on the upper right, where the latter is labeled C C A terminus. The region of the helix on the top left is labeled T psi C loop. The region of the helix at the lower end of the t R N A is labeled the anticodon loop. The region between the T psi loop and anticodon loop consists of the D H U loop and the variable arm. The helix consists of yellow-colored circles of different sizes that represent the nucleotides in the base sequence starting from the 5 prime ends of the t R N A molecule. The numbers on the nucleotides represent the positions of the nucleotides in the base sequence. The numbering starts from 1 to 72 between 5 prime and to 3 prime C C A terminus.

Return to FIGURE 30.12 t R N A s have multiple recognition sites for aminoacyl- t R N A synthetases

Extended description for FIGURE 30.13 Class I and class II aminoacyl-t R N A synthetases recognize different faces of the t R N A molecule



In class roman numeral I, the tertiary structure of t R N A is depicted in the form of an inverted L that is turned toward the viewer. The t R N A is depicted as a double helix with the C C A terminus on the upper right. A ball-and-stick model of an amino acid is attached to the C C A terminus of the t R N A on the right.

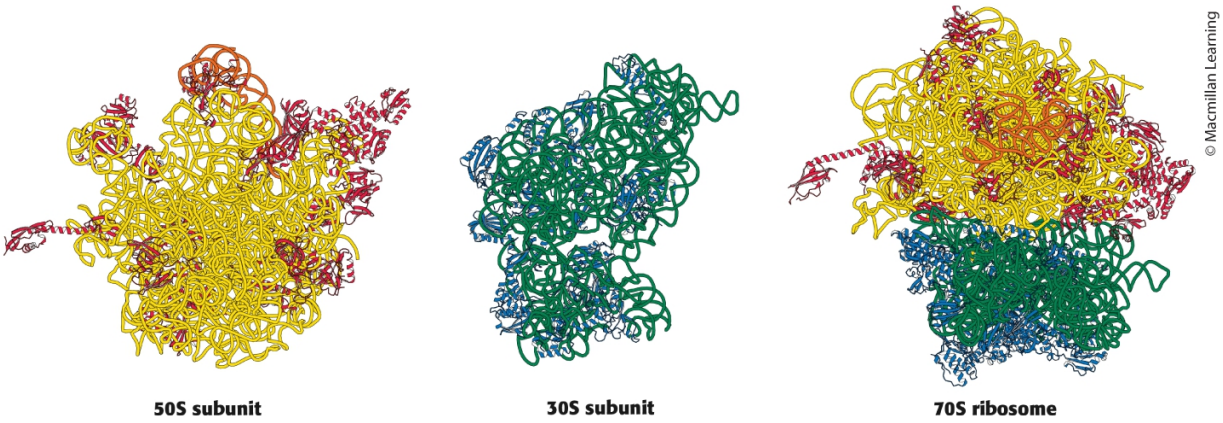
In class roman numeral I, the tertiary structure of t R N A is complex with the ball-and-stick model and a yellow-colored ribbon diagram that is attached to the right side of the t R N A. The ribbon diagram consists of alpha helices and beta strands.

In class roman numeral I I, the tertiary structure of t R N A is depicted in the form of an inverted L that is turned toward the viewer. The t R N A is depicted as a double helix with the C C A terminus on the upper left. A ball-and-stick model of an amino acid is attached to the C C A terminus of the t R N A on the left.

In class roman numeral I I, the tertiary structure of t R N A is complex with the ball-and-stick model and a blue-colored ribbon diagram that is attached to the left side of the t R N A. The ribbon diagram consists of alpha helices and beta strands connected by turns and loops.

Return to FIGURE 30.13 Class I and class II aminoacyl-t R N A synthetases recognize different faces of the t R N A molecule

Extended description for FIGURE 30.14 The ribosome consists of a large subunit and a small subunit



The figure has three parts.

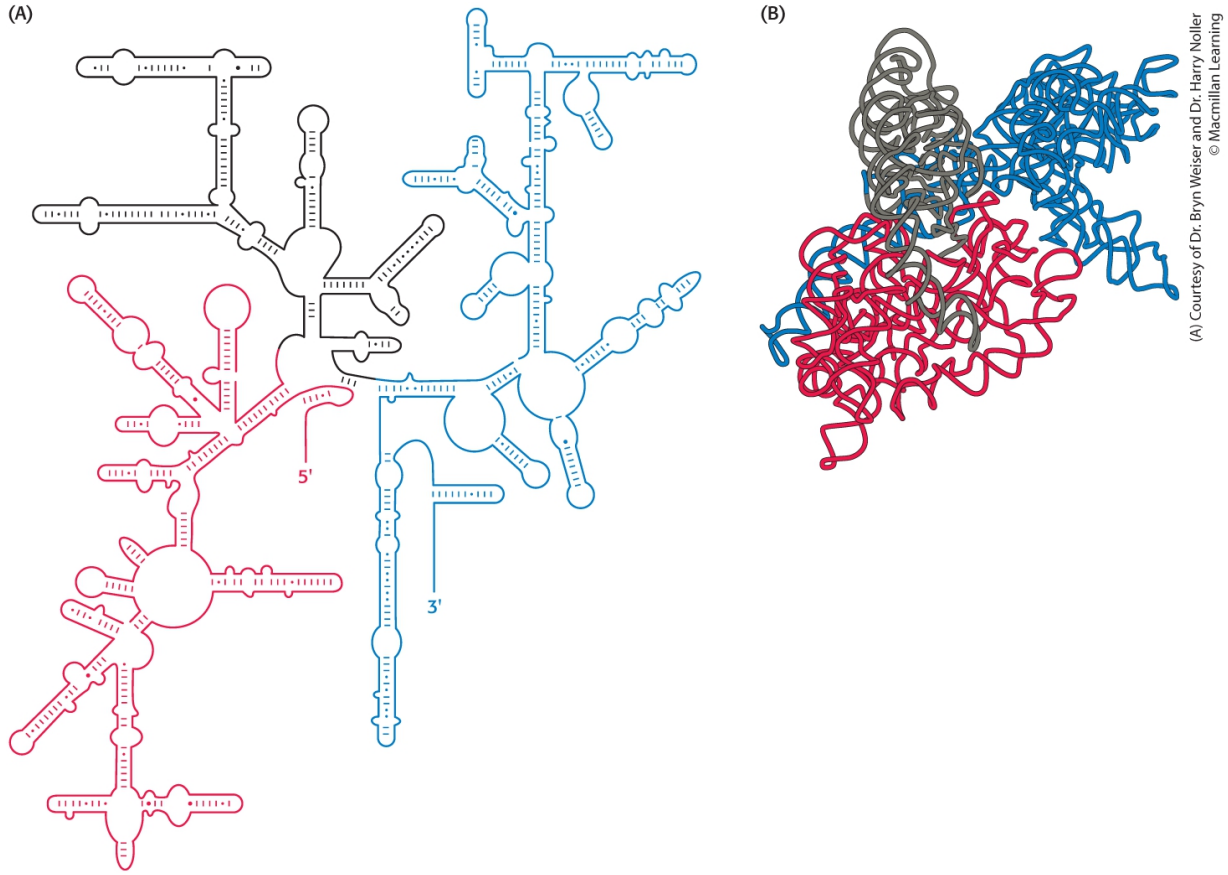
The first part labeled the 50 S subunit shows the view of the part of the 50 S subunit that interacts with the 30 S subunit. It consists of yellow-colored thread-like structures. Red-colored alpha helices and beta strands project from the upper end and lateral sides of the yellow-colored structures. Additionally, orange-colored thread-like structures also project from the upper end. The yellow-colored structures represent the 50 S subunit while the red alpha helices and beta strands represent the 30 S subunit.

The second part labeled 30 S subunit shows the view of the part of the 30 S subunit that interacts with the 50 S subunit. It consists of green-colored thread-like structures. Blue-colored alpha helices and beta strands project from the upper, lower, and lateral sides of the green-colored structures. The green-colored structures represent the 30 S subunit while the blue alpha helices and beta strands represent the 50 S subunit.

The third part labeled 70 S ribosome shows the view of the 70 S ribosome that is rotated with respect to the other two views. It shows two subunits. The subunit at the top consists of yellow-colored thread-like structures. Red-colored alpha helices and beta strands project from the upper end and lateral sides of the yellow-colored structures. Orange-colored thread-like structures emerge from the front. The subunit at the bottom consists of green-colored thread-like structures. Blue-colored alpha helices and beta strands project from the upper, lower, and lateral sides of the green-colored structures. 23 S r R N A are shown in yellow, 5 S r R N A are shown in orange, 16 S r R N A are shown in green, proteins of the 50 S subunit are in red, and proteins of the 30 S subunit are in blue. The interface between the 50 S and the 30 S subunits consists primarily of R N A.

Return to FIGURE 30.14 The ribosome consists of a large subunit and a small subunit

Extended description for FIGURE 30.15 Ribosomal R N A s form intramolecular base pairs



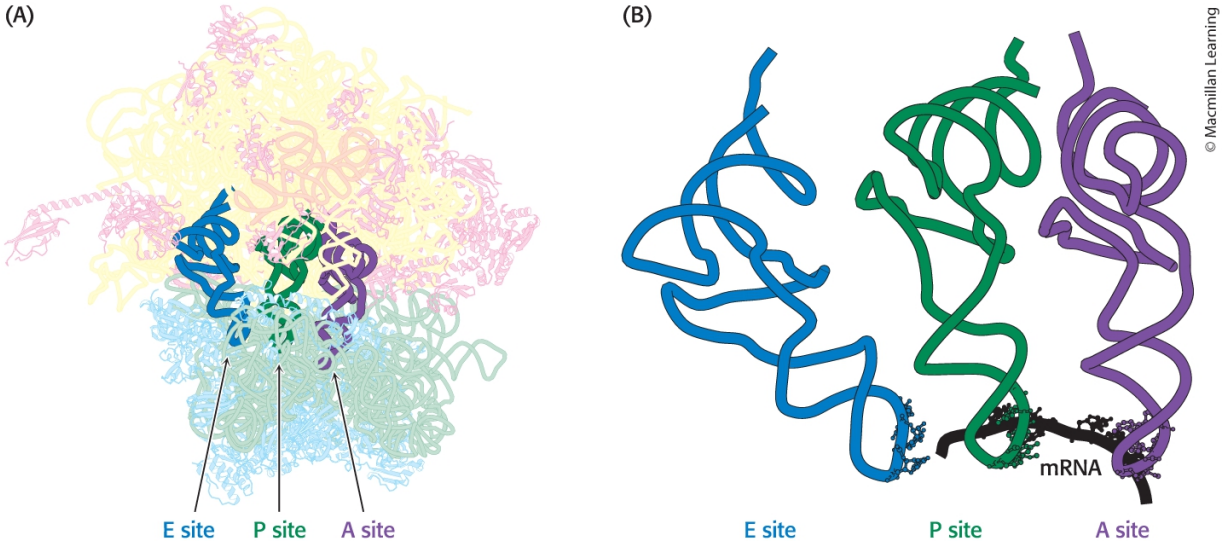
The figure has two parts.

Part A depicts the secondary structure of 16 S r R N A consisting of codon loops that emerge in different directions. The codon loops have 5 prime and 3 prime ends. The codon loops on the top left are black, the codon loops on the top and bottom right are blue, and the codon loops below the black loops at the bottom left position are red. The stem of the codon loops has dashes and dots. Dashes represent standard Watson–Crick base pairs and dots represent non-Watson–Crick base pairs.

Part B depicts the tertiary structure of 16 S r R N A which consists of three types of thread-like structures. Black thread-like structures are present on the top left, blue thread-like structures are present on the top right, and red thread-like structures are present below the black thread-like structures.

Return to FIGURE 30.15 Ribosomal R N A s form intramolecular base pairs

Extended description for FIGURE 30.16 The ribosome has three binding sites for transfer R N A s



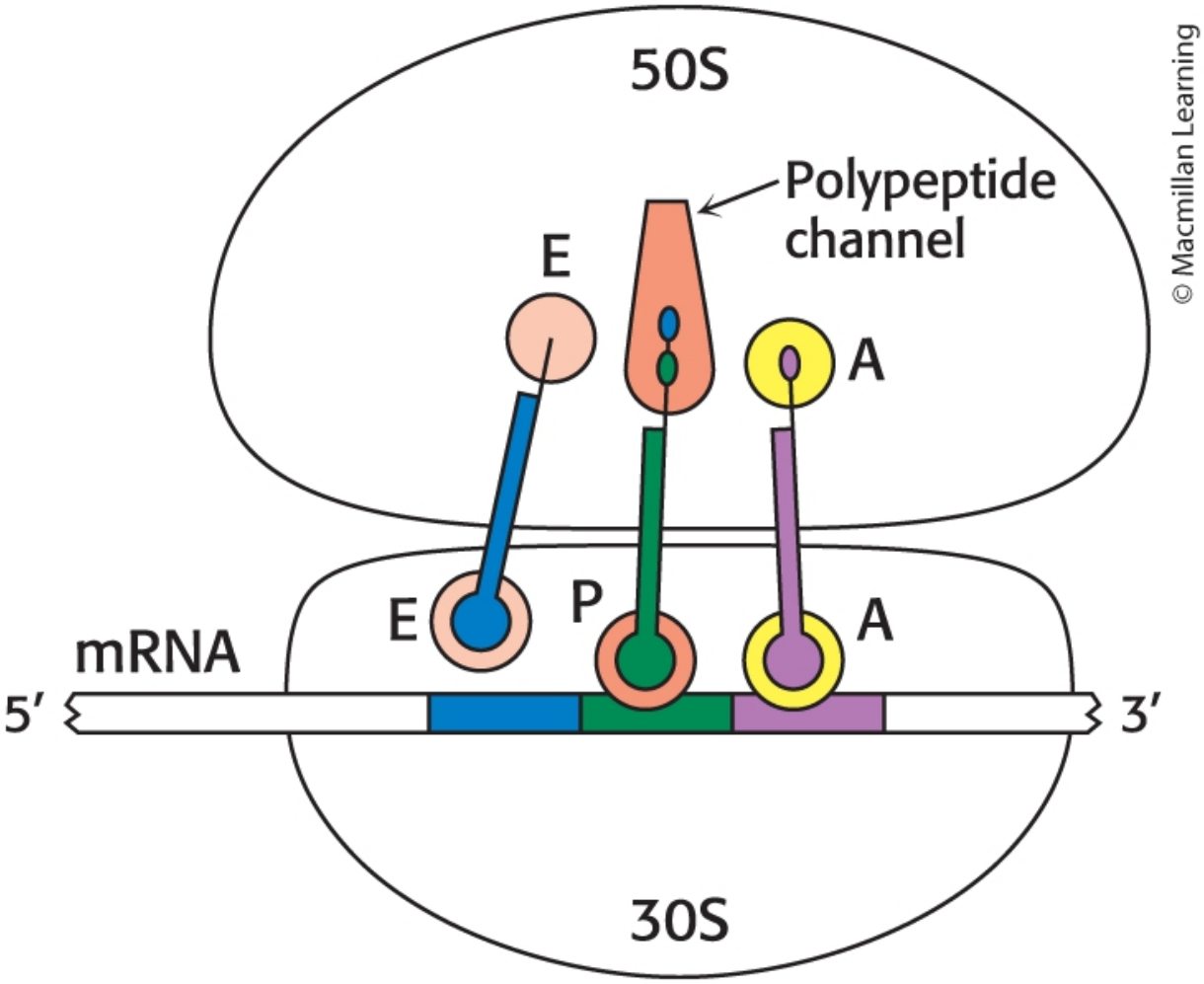
The figure has two parts.

Part A depicts a 70 S ribosome consisting of 30 S and 50 Ssubunits. The 30 S subunit at the top consists of yellow-colored thread-like structures. Pink-colored alpha helices and beta strands project from the upper end and lateral sides of the yellow-colored structures. Additionally, orange-colored thread-like structures also project from the upper end. The 50 Ssubunit at the bottom consists of green-colored thread-like structures. Blue-colored alpha helices and beta strands project from the upper, lower, and lateral sides of the green-colored structures. The three t R N A binding sites of the 70 S ribosome are called the E site, P site, and A site. The t R N A in these sites are depicted as blue, green, and purple double-helix structures that are in the form of an inverted L. The t R N A molecules are connected to the 30 S and 50 S subunits of the 70 S ribosome.

Part B depicts the t R N A molecules isolated from the E, P, and A sites. Each t R N A molecule consists of a ball-and-stick model in the anticodon loop. Each t R N A molecule in sites P and A is base-paired with m R N A. m R N A is depicted as a black continuous strand connected horizontally.

Return to FIGURE 30.16 The ribosome has three binding sites for transfer R N A s

Extended description for FIGURE 30.17 The key components of the translation machinery interact on an active ribosome

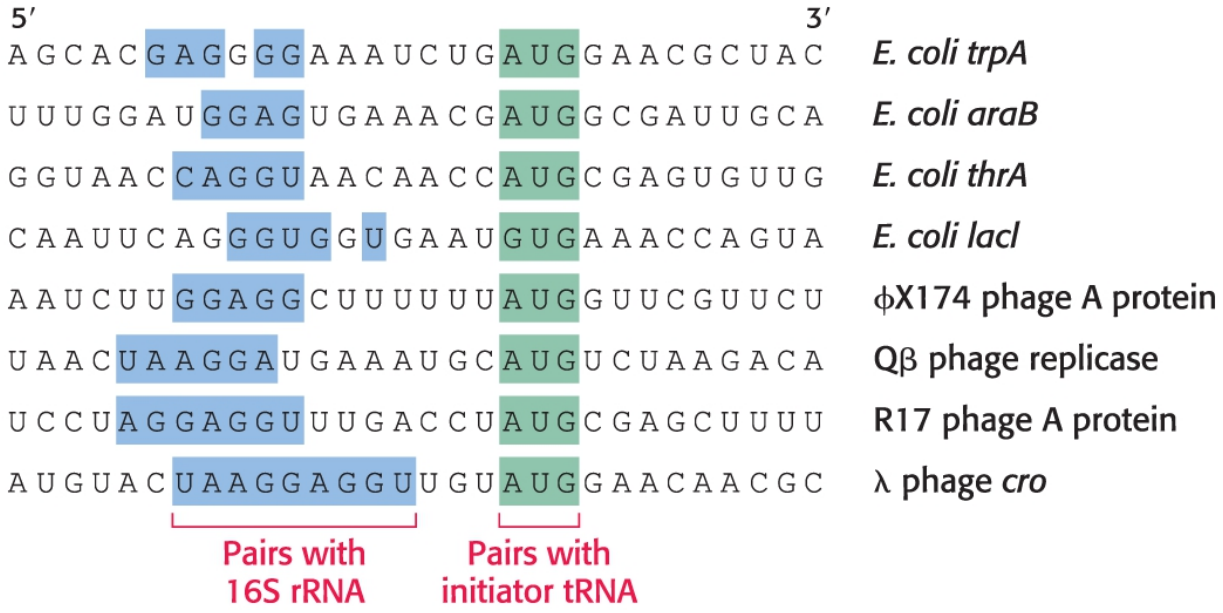


The figure has a horizontal m R N A consisting of 5 prime ends on the left and 3 prime ends on the right. A ribosome consisting of two oval-shaped subunits is shown. The smaller 30 S subunit is bound to the m R N A while the larger 50 S m R N A is at the top. The m R N A consists of three segments. The segments from left to right are blue, green, and purple, respectively. These represent the binding sites for t R N A molecules. The blue segment is labeled E site, the green

is labeled P site, and the purple is labeled A site. The 50 S subunit at the top consists of a polypeptide channel that connects the A and P sites from the back end of the ribosome. The t R N A molecules are depicted as stem-loops whose stems are in the 50 S subunit of the ribosome and the loops are in the 30 S subunit. Each t R N A molecule in sites P and A in the 30 S subunit is base-paired with m R N A. The t R N A molecule in site E remains free.

Return to FIGURE 30.17 The key components of the translation machinery interact on an active ribosome

Extended description for FIGURE 30.18 Initiator regions in m R N A determine where protein biosynthesis starts



The figure shows 8 sequences in 5 prime to 3 prime directions.

The first sequence labeled *E. coli t r p A* reads A G C A C G A G G G G A A A U C U G A U G G A A C G C U A C. G A G in the sixth, seventh, and eighth positions and G G in the tenth and eleventh positions are highlighted in blue. A U G in the nineteenth, twentieth, and twenty-first positions is highlighted in green.

The second sequence labeled *E. coli a r a B* reads U U U G G A U G G A G U G A A A C G A U G G C G A U U G C A. G G A G in the eighth, ninth, tenth, and eleventh positions are highlighted in blue. A U G in the nineteenth, twentieth, and twenty-first positions is highlighted in green.

The third sequence labeled *E. coli t h r A* reads G G U A A C C A G G U A A C A A C C A U G C G A G U G U U G. C A G G U in the seventh, eighth, ninth, tenth, and eleventh positions in highlighted in blue. A U G in the nineteenth, twentieth, and twenty-first positions is highlighted in green.

The fourth sequence labeled *E. coli l a d* l reads C A A U U C A G G G U G G U G A A U G U G A A A C C A G U A. G G U G in the ninth, tenth, eleventh, and twelfth positions and U in the fourteenth positions is highlighted in blue. G U G in the nineteenth, twentieth, and twenty-first positions are highlighted in green.

The fifth sequence labeled phi X 174 phage A protein reads A A U C U U G G A G G C U U U U U U A U G G U U C G U U C U. G G A G G in the seventh, eighth, ninth, tenth, and eleventh positions in highlighted in blue. A U G in the nineteenth, twentieth, and twenty-first positions is highlighted in green.

The sixth sequence labeled Q beta phage replicase reads U A A C U A A G G A U G A A A U G C A U G U C U A A G A C A. U A A G G A in the fifth, sixth, seventh, eighth, ninth, and tenth positions is highlighted in blue. A U G in the nineteenth, twentieth, and twenty-first positions is highlighted in green.

The seventh sequence labeled R 17 phage A protein reads U C C U A G G A G G U U U G A C C U A U G C G A G C U U U U. A G G A G G U in the fifth, sixth, seventh, eighth, ninth, tenth, and eleventh positions is highlighted in blue. A U G in the nineteenth, twentieth, and twenty-first positions is highlighted in green.

The eighth sequence labeled lambda phage *cro* reads A U G U A C U A A G G A G G U U G U A U G G A A C A A C G C. U A A G G A G G U in the seventh, eighth, ninth, tenth, eleventh, twelfth, thirteenth,

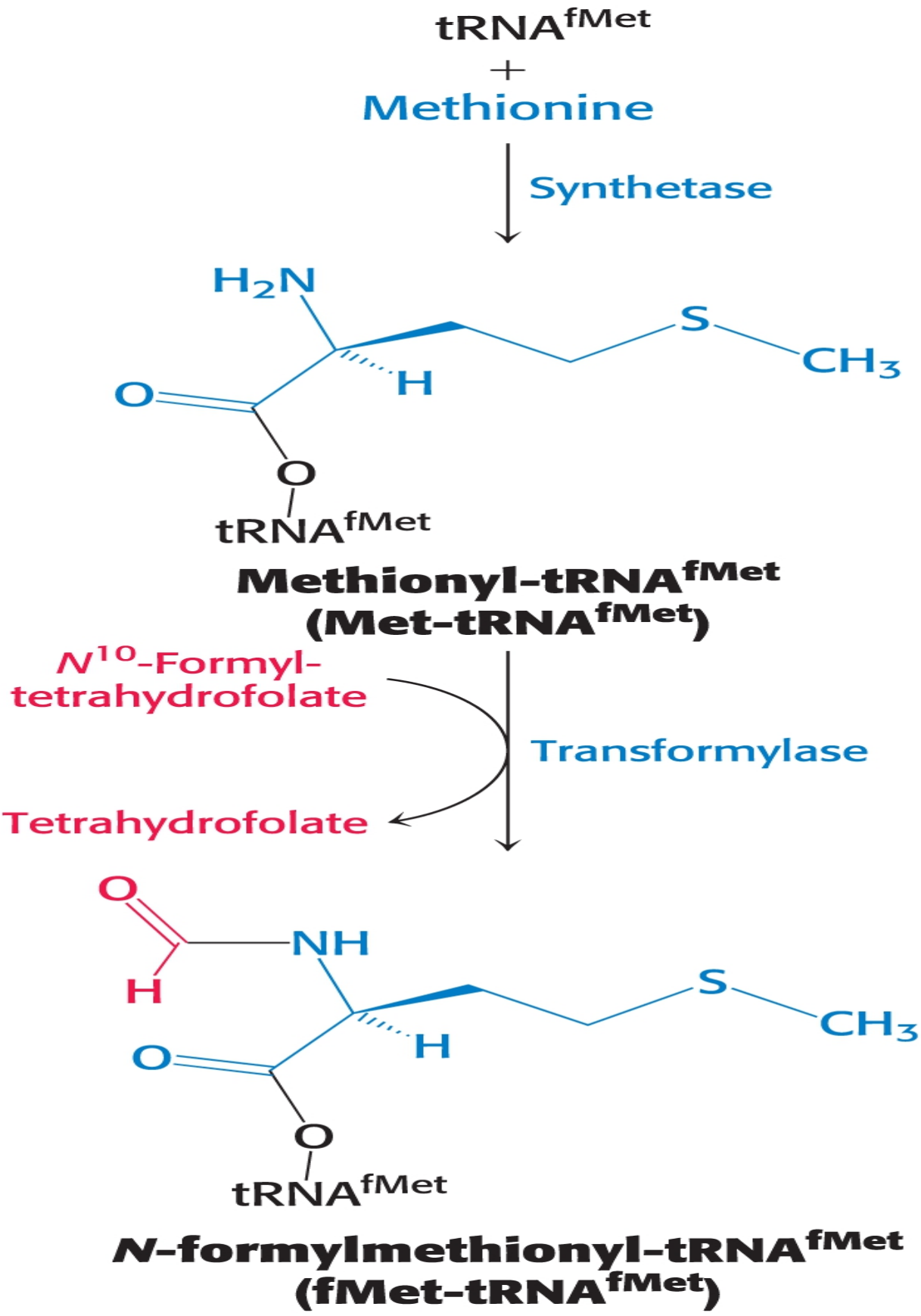
fourteenth, and fifteenth positions is highlighted in blue. A U G in the nineteenth, twentieth, and twenty-first positions is highlighted in green.

The sequences highlighted in blue are labeled pairs with 16 S r R N A. The sequences highlighted in green are labeled pairs with initiator t R N A.

Return to FIGURE 30.18 Initiator regions in m R N A determine where protein biosynthesis starts

Extended description for FIGURE 30.19 Methionyl-t R N

A is formylated to create a modified amino acid


tRNA^fMet
+
Methionine
Synthetase
H2N
S
CH3
H
O
O
tRNA^fMet
Methionyl-tRNA^fMet
(Met-tRNA^fMet)
N10-Formyl-
tetrahydrofolate
Transformylase
Tetrahydrofolate
O
NH
H
S
CH3
H
O
O
tRNA^fMet
N-formylmethionyl-tRNA^fMet
(fMet-tRNA^fMet)

In the first irreversible step, t R N A superscript f Met reacts with methionine in the presence of synthetase to give rise to methionyl t R N A superscript f Met (Met t R N A superscript f Met).

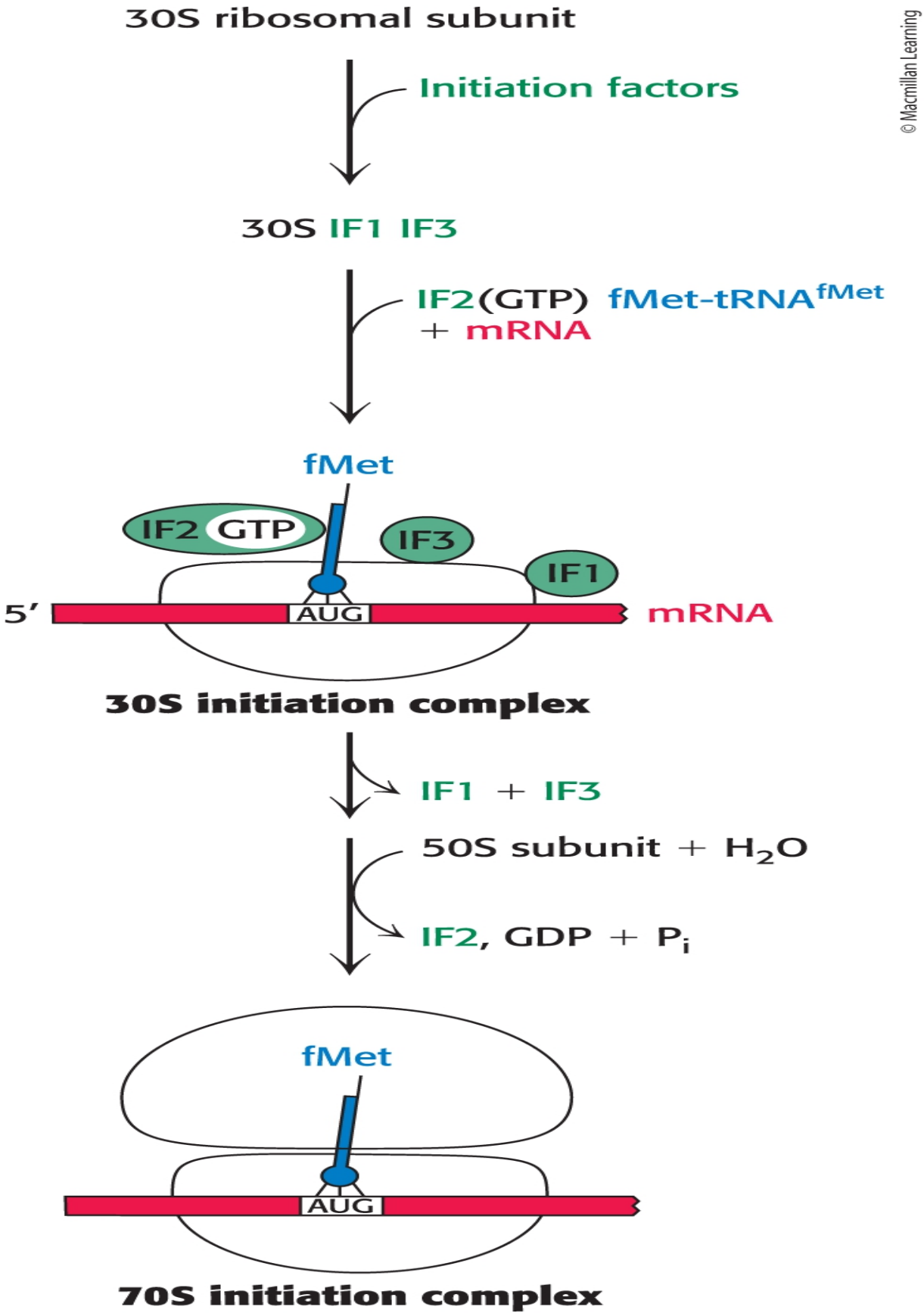
The structure of methionyl t R N A superscript f Met (Met t R N A superscript f Met) is as follows: A 1 S, 1 C H 3, and 2 C heteronuclear alkane chain is depicted as a line structure using 3 zigzag lines. S and C H 3 occupy the third and fourth positions, respectively. C 1 is wedge bonded to C 1 of another 1 N H 2, 1 O, and 2 C heteronuclear alkane chain depicted vertically as a line structure using 3 zigzag lines. N H 2 occupies the first position. O occupies the fourth position. C 1 is dash bonded to H on the lower right. C 2 is double bonded to O on the left. O is single bonded to t R N A superscript f Met below. The O atom and the t R N A is black and the rest of the structure is highlighted in blue. In the second irreversible step, Met (Met t R N A superscript f Met) is transformed to N-formylmethionyl t R N A superscript f Met (f Met t R N A superscript f Met). It is coupled with the entry of N superscript 10 Formyl-tetrahydrofolate and the release of tetrahydrofolate in the presence of transformylase.

The structure of N-formylmethionyl t R N A superscript f Met (f Met t R N A superscript f Met) is as follows: 1 S, 1 C H 3, and 2 C heteronuclear alkane chain is depicted as a line structure using 3 zigzag lines. S and C H 3 occupy the third and fourth positions respectively. C 1 is wedge bonded to C 1 of another 1 N H, 1 O, and 2 C heteronuclear alkane chain depicted vertically as a line structure using 3 zigzag lines. N H occupies the first position. N H is single bonded to a central C on the left. The central C atom is double bonded to O on the upper left and H on the lower left. O occupies the fourth position in the alkane chain. C 1 is dash bonded to H on the lower right. C 2 is double bonded to O on the left. O is single bonded to t R N A superscript f Met below. The central C atom and the structures attached to it on the left are highlighted in red.

Return to FIGURE 30.19 Methionyl-t R N A is formylated to create a modified amino acid

Extended description for FIGURE 30.20 Prokaryotic initiation factors aid the assembly of initiation

complexes



© Macmillan Learning

In the first irreversible step, the 30 S ribosomal subunit is transformed to 30 S I F 1 I F 3 coupled with the entry of initiation factors. Initiation factors are highlighted in green. In the second irreversible step, 30 S I F 1 I F 3 is transformed into a 30 S initiation complex coupled with the entry of I F 2 (G T P) f met t R N A superscript f Met and m R N A. I F 1 I F 3 are highighted in green m R N A is highlighted in red. f met t R N A superscript f Met is highlighted in blue.

The 30 S initiation complex shows the 30 S ribosomal subunit bound to m R N A. The m R N A is in 5 prime to 3 prime direction. The m R N A has a codon at the center that reads A U G. The f Met t R N A is depicted as a stem-loop with the loop embedded in the 30 S ribosome and the stem lies outside. The loop of the t R N A is base paired with the A U G codon in the m R N A. The ribosome is attached to three spheres at the top labeled I F 2 (G T P), I F 3, and I F 1. I F 1 bind near the A site and prevents any t R N A from binding with the m R N A.

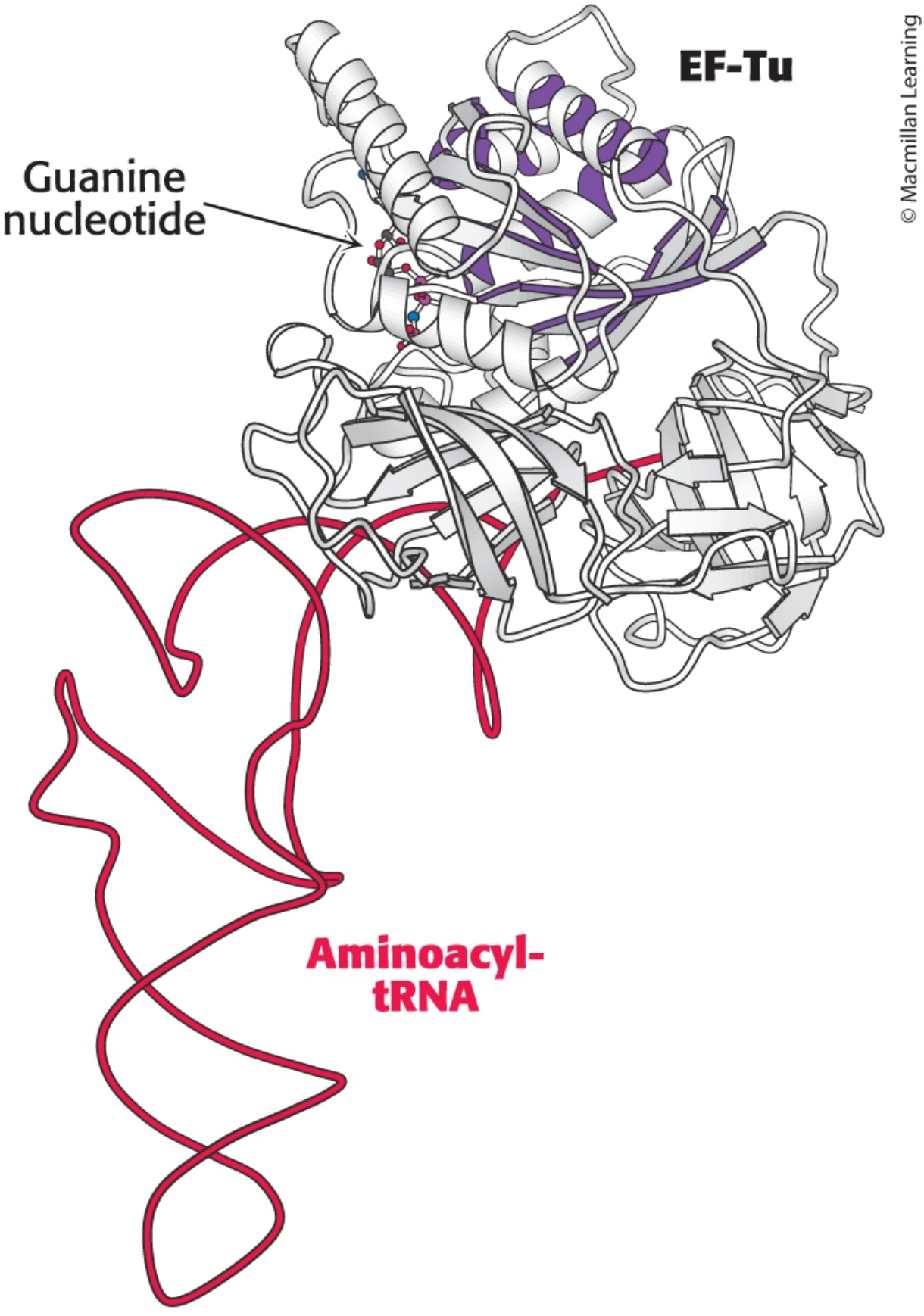
In the third irreversible step, the 50 S t R N A interacts with the 30 S t R N A to form the 70 S initiation complex. It is coupled with the release of I F 1 and I F 3. It is also coupled with the entry of 50 S subunit and H 2 O and release of I F 2, G D P, and P subscript i.

The 50 S ribosomal subunit binds with the 30 S subunit from the top. The 50 S subunit is larger than the 30 S subunit. The stem of the f Met t R N A lies in the 50 S subunit while its loop is base paired with the A U G codon in the m R N A.

Return to FIGURE 30.20 Prokaryotic initiation factors aid the assembly of initiation complexes

Extended description for FIGURE 30.21 The structure of elongation factor T u (E F-T u) and an aminoacyl-t R N A

resembles those of other G proteins

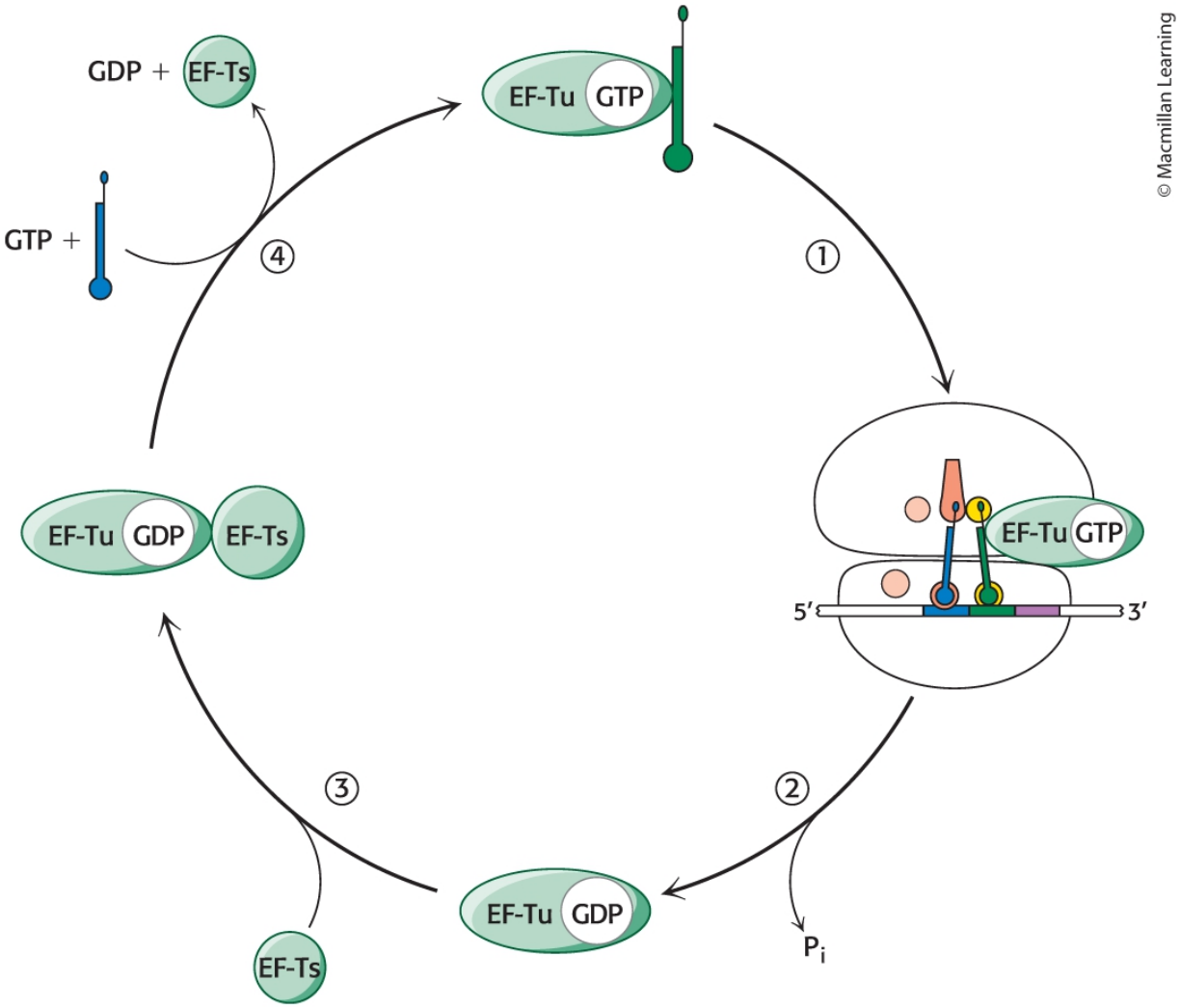


© Macmillan Learning

A red-colored double-stranded inverted L-shaped t R N A is present on the bottom left. It consists of an acceptor on the upper right and an anticodon loop on the lower end. The acceptor on the upper right is bound to E F T u consisting of white-colored alpha helices and beta strands interconnected by thread-like structures. The amino-terminal end of E F T u on the upper end highlighted in purple represents the P loop N T Pase domain. The E F T u consists of a ball-and-stick model on the top left labeled guanine nucleotide.

Return to FIGURE 30.21 The structure of elongation factor T u (E F-T u) and an aminoacyl-t R N A resembles those of other G proteins

Extended description for FIGURE 30.22 The G T P ase E F T u binds aminoacyl t R N A only in its G T P form



The cycle has four steps. In the first step, an oval-shaped E F T u along with the G T P binds with a green t R N A that is depicted by a stem loop with the stem at the top and a loop at the bottom. The E F T u G T P binds aminoacyl t R N A and delivers it to the A site of the ribosome.

The ribosome consists of two oval-shaped subunits. The smaller 30 S subunit is bound to the m R N A while the larger 50 S m R N A is at the top. The m R N A consists of three segments. The segments from left to right are blue, green, and purple, respectively. These represent the binding sites for t R N A molecules. The blue segment is labeled E site, green is labeled P site, and purple is labeled A site. The 50 S subunit at the top consists of a polypeptide channel that connects the A and P sites from the back end of the ribosome. The t R N A molecules are depicted as stem loops whose stems are in the 50 S subunit of the ribosome and the loops are in the 30 S subunit. Each t R N A molecule in sites E and P in the 30 S subunit are base-paired with m R N A. The t R N A molecule in site A remains free. The sphere E F T u G T P binds to the 50 S ribosome.

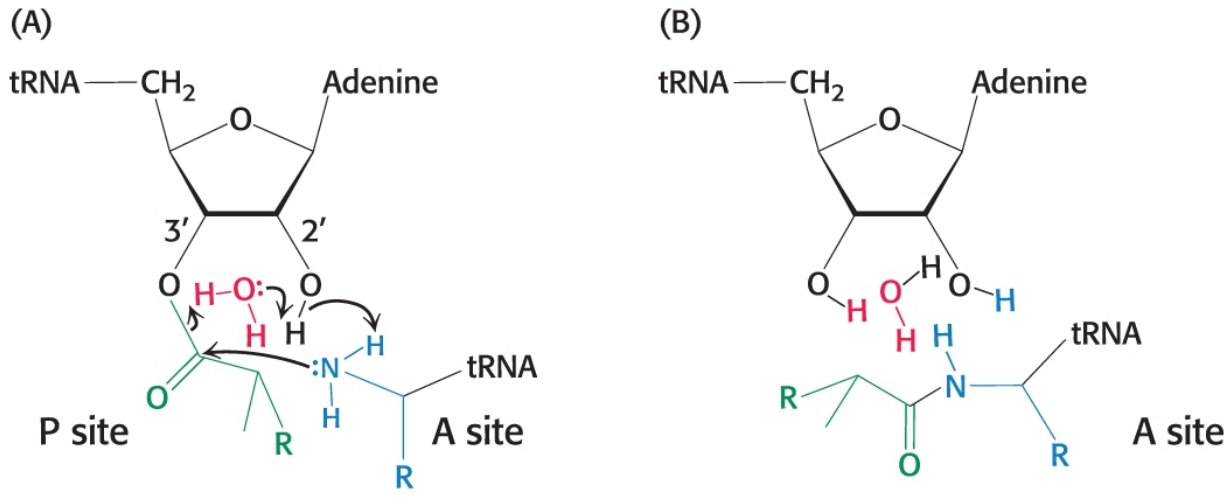
In the second step, the G T P from the E F T u G T P is converted to G D P coupled with the release of P subscript i.

In the third step, the oval E F T u G D P is attached to a sphere E F T s. It is coupled with the entry of E F T s.

In the fourth step, the oval and sphere are transformed to E F T u G T P with a t R N A attached to it. It is coupled with the entry of G T P and a blue t R N A and the release of G D P and E F T s.

Return to FIGURE 30.22 The G T P ase E F T u binds aminoacyl t R N A only in its G T P form

Extended description for FIGURE 30.23 Peptide-bond formation links amino acids



Part A shows a 5-membered heterocyclic pentagonal ring in a vertical orientation consisting of 1 O and 4 C atoms. O occupies the first position which is the topmost vertex. C 1 is single bonded to adenine. C 2 and C 3 are each single bonded to O and they are labeled 2 prime and 3 prime, respectively. C 4 is single bonded to C H 2. C H 2 is further single bonded to t R N A on the left. O bound to C 2 is single bonded to H. O bound to C 3 is single bonded to C 1 of a 2 C alkane chain depicted as a line structure using a line. C 1 is double bonded to O on the lower left. C 2 is single bonded to C H 3 on the lower left and R on the lower right. The alkane chain is labeled P site. An aminoacyl t R N A with an A site is depicted on the right. The A site consists of a central C atom that is single bonded to t R N A on the upper right, single bonded to R below, and single bonded to N on the upper left. N carries a pair of electrons. It is single bonded to H on the upper right and H below. The amino group of the A site attacks the carbonyl group of the P site. A water molecule is added in the next step. The water molecule consists of an O atom with a pair of electrons. The O atom is attached to two H

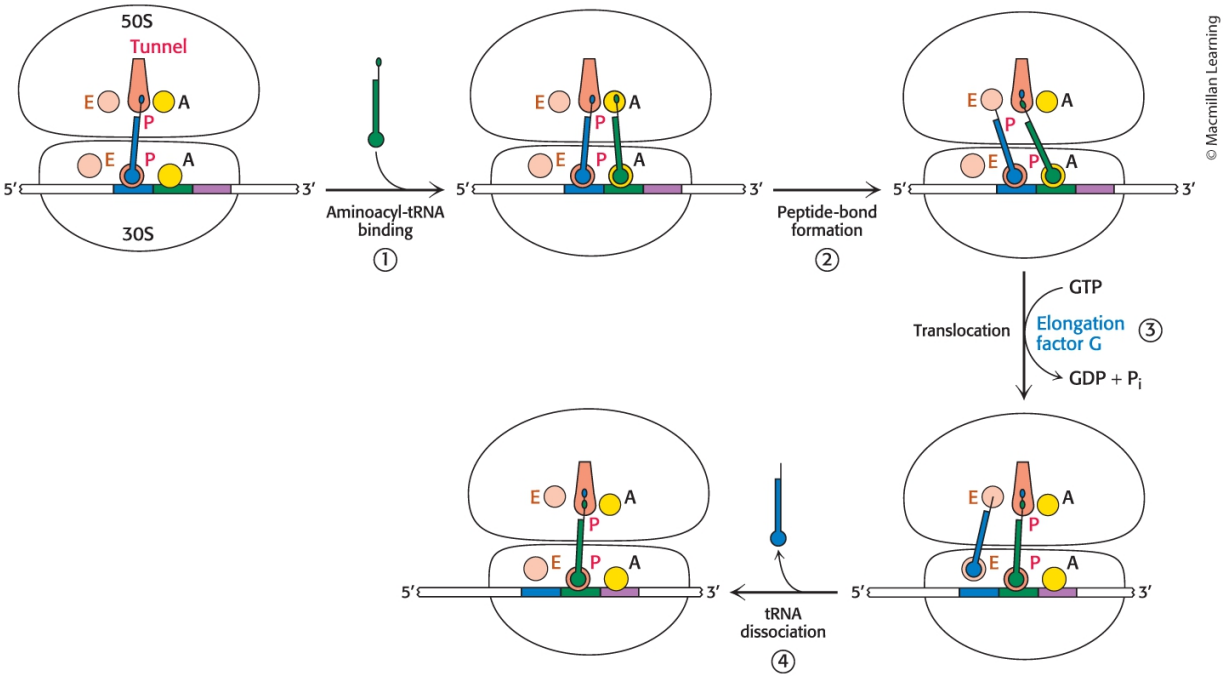
atoms. The water molecule attacks the O atom attached to C 3 and C 4 of the pentagonal ring simultaneously. The O atom attached to C 2 attacks the A site.

Part B shows a 5-membered heterocyclic pentagonal ring in a vertical orientation consisting of 1 O and 4 C atoms. O occupies the first position which is the topmost vertex. C 1 is single bonded to adenine. C 2 and C 3 are each single bonded to O. C 4 is single bonded to C H 2. C H 2 is single bonded to t R N A on the left. O bound to C 2 and C 3 are each single bonded to H. The transition results in the formation of the peptide bond and the release of deacylated t R N A. The water molecule is free and consists of an O atom bound to 2 H atoms.

The deacylated t R N A that is released consists of a 1 N and 3 C heteronuclear alkane chain depicted as a line structure using 3 zigzag lines. N occupies the third position. C 1 is single bonded to R on the left and C H 3 on the lower left. C 2 is double bonded to O below. N is single bonded to H. C 3 is single bonded to t R N A on the upper right and R on the lower right.

Return to FIGURE 30.23 Peptide-bond formation links amino acids

Extended description for FIGURE 30.24 Protein biosynthesis is a cyclical process



The cycle has four steps. The cycle begins with peptidyl t R N A in the P site. The figure has a horizontal m R N A consisting of 5 prime end on the left and 3 prime end on the right. A ribosome consisting of two oval-shaped subunits is shown. The smaller 30 S subunit is bound to the m R N A while the larger 50 S m R N A is at the top. The m R N A consists of three segments. The segments from left to right are blue, green, and purple, respectively. These represent the binding sites for t R N A molecules. The blue segment is labeled E site, the green is labeled P site, and the purple is labeled A site. The 50 S subunit at the top consists of a polypeptide tunnel. The t R N A molecule is depicted as a stem-loop whose stem is in the 50 S subunit of the ribosome and the loop is in the 30 S subunit. The t R N A molecule in site P in the 30 S subunit is base-paired with m R N A. There are no t R N A molecules in sites E and A.

In the first step, an aminoacyl t R N A molecule in site A in the 30 S subunit is base-paired with m R N A.

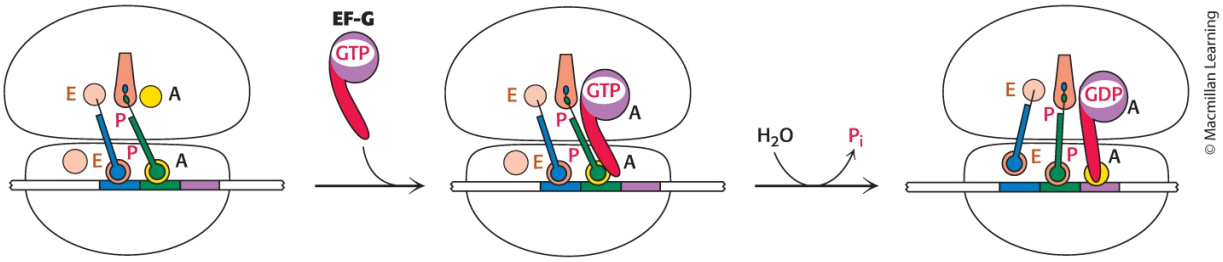
In the second step, peptide-bond formation takes place. When both the sites are occupied a peptide bond is formed in the tunnel in the 50 S subunit where the stem of the t R N A is attached.

In the third step, the translocation of the t R N A s and the m R N A occurs through the action of elongation factor G. This is coupled with the entry of G T P and release of G D P and P subscript i. In this step, the deacylated t R N A moves to the E site.

In the fourth step t R N A dissociation occurs due to the release of the t R N A from the E site.

Return to FIGURE 30.24 Protein biosynthesis is a cyclical process

Extended description for FIGURE 30.25 Translocation repositions t R N A s and m R N A with respect to the ribosome



The figure has three steps.

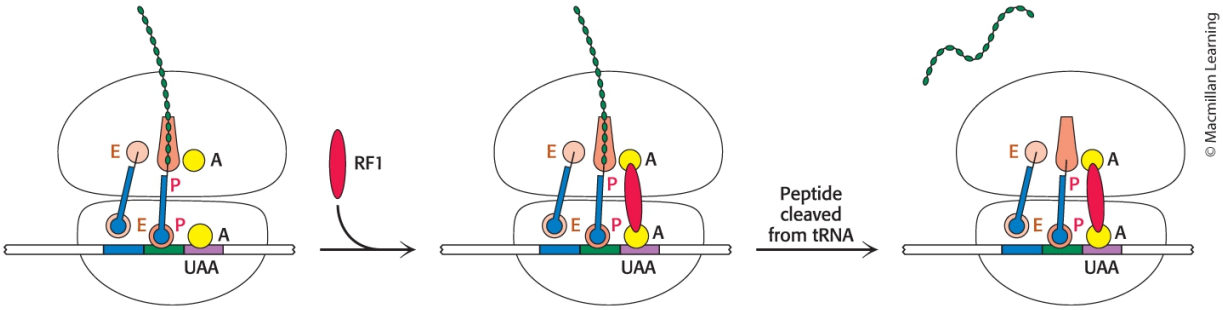
In the first step, a horizontal m R N A consists of 5 prime end on the left and 3 prime end on the right. A ribosome consisting of two oval-shaped subunits is shown. The smaller 30 S subunit is bound to the m R N A while the larger 50 S m R N A is at the top. The m R N A consists of three segments. The segments from left to right are blue, green, and purple, respectively. These represent the binding sites for t R N A molecules. The blue segment is labeled E site, the green is labeled P site, and the purple is labeled A site. The 50 S subunit at the top consists of a polypeptide channel that connects the A and P sites from the back end of the ribosome. The t R N A molecules are depicted as stem-loops whose stems are in the 50 S subunit of the ribosome and the loops are in the 30 S subunit. Each t R N A molecule in sites E and P in the 30 S subunit are base-paired with m R N A. There is no t R N A in site A.

In the second step, the E F G in the G T P form binds to the A site of the 50 S subunit.

In the third step, the G T P bound to the 50 S subunit is converted to G D P, and the E F G is attached to the A site of the m R N A in the 30 S subunit. This is coupled with the entry of H 2 O and the release of P subscript i.

Return to FIGURE 30.25 Translocation repositions t R N A s and m R N A with respect to the ribosome

Extended description for FIGURE 30.27 Release factors facilitate the termination of protein biosynthesis



The figure has three steps.

In the first step, a horizontal m R N A consists of 5 prime end on the left and 3 prime end on the right. A ribosome consisting of two oval-shaped subunits is shown. The smaller 30 S subunit is bound to the m R N A while the larger 50 S m R N A is at the top. The m R N A consists of three segments. The segments from left to right are blue, green, and purple, respectively. These represent the binding sites for t R N A molecules. The blue segment is labeled E site, the green is labeled P site, and the purple is labeled A site. The A site has a codon U A A. The 50 S subunit at the top consists of a polypeptide channel that connects the A and P sites from the back end of the ribosome. A polypeptide chain emerges from the polypeptide channel that resembles a beaded string. The t R N A molecules are depicted as stem-loops whose stems are in the 50 S subunit of the ribosome and the loops are in the 30 S subunit. The t R N A in the E site in the 30 S subunit is free while the t R N A in the P site is base-paired with m R N A. There is no t R N A in site A.

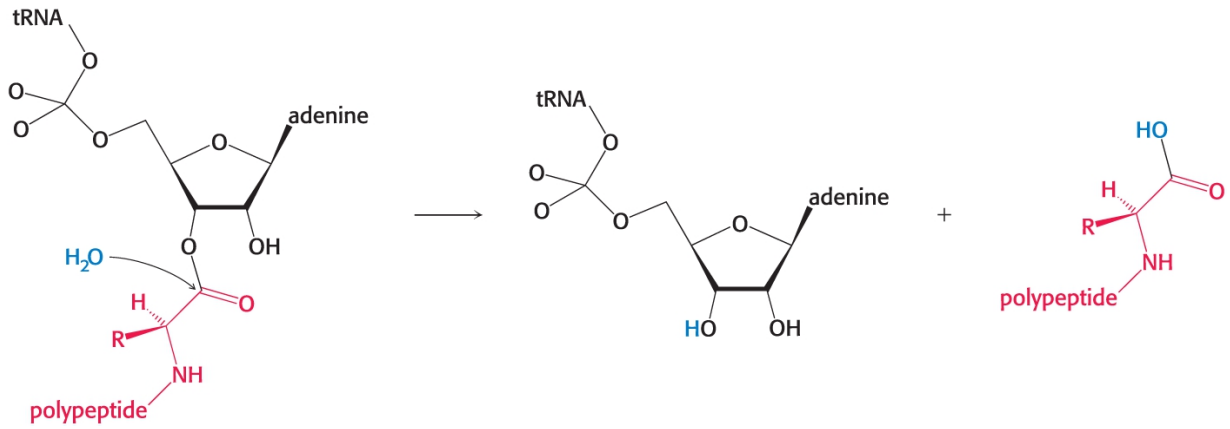
In the second step, the entry of R F 1 causes the R F 1 to bind to the A site of the 50 S and 30 S subunits of the ribosome. The R F 1

recognizes the stop codon in the A site.

In the third step, the R F 1 stimulates the release of the peptide from the peptide channel. The peptide channel is depicted as a free-beaded structure at the top.

Return to FIGURE 30.27 Release factors facilitate the termination of protein biosynthesis

Extended description for Release of complete protein from t R N A



The reactant undergoes cleavage to form two products.

The structure of the reactant is as follows: A 5-membered heterocyclic pentagonal ring in a vertical orientation consists of 1 O and 4 C atoms. O occupies the first position which is the topmost vertex. C 1 is wedge bonded to adenine. C 2 is single bonded to O H. C 3 is single bonded to O of a 1 O, 1 N, and 2 C heteronuclear alkane chain depicted as a line structure vertically using 3 zigzag lines. O occupies the first position. N bound to H occupies the fourth position. C 1 is double bonded to O on the lower right. C 2 is dash bonded to H on the upper left and wedge bonded to R on the lower left. N H is single bonded to a polypeptide on the lower left. A H 2 O molecule attacks C 1 of the alkane chain. The structures from C 1 upto the polypeptide are highlighted in red. C 4 of the pentagonal ring is single bonded to a central C atom on the upper left. The central C atom is single bonded to O on the lower left. This O is further single bonded to a second C atom on the upper left. The second C atom is single bonded to a second O on the lower left, third

O on the upper left, and fourth O on the upper right. The fourth O atom is single bonded to t R N A on the upper left.

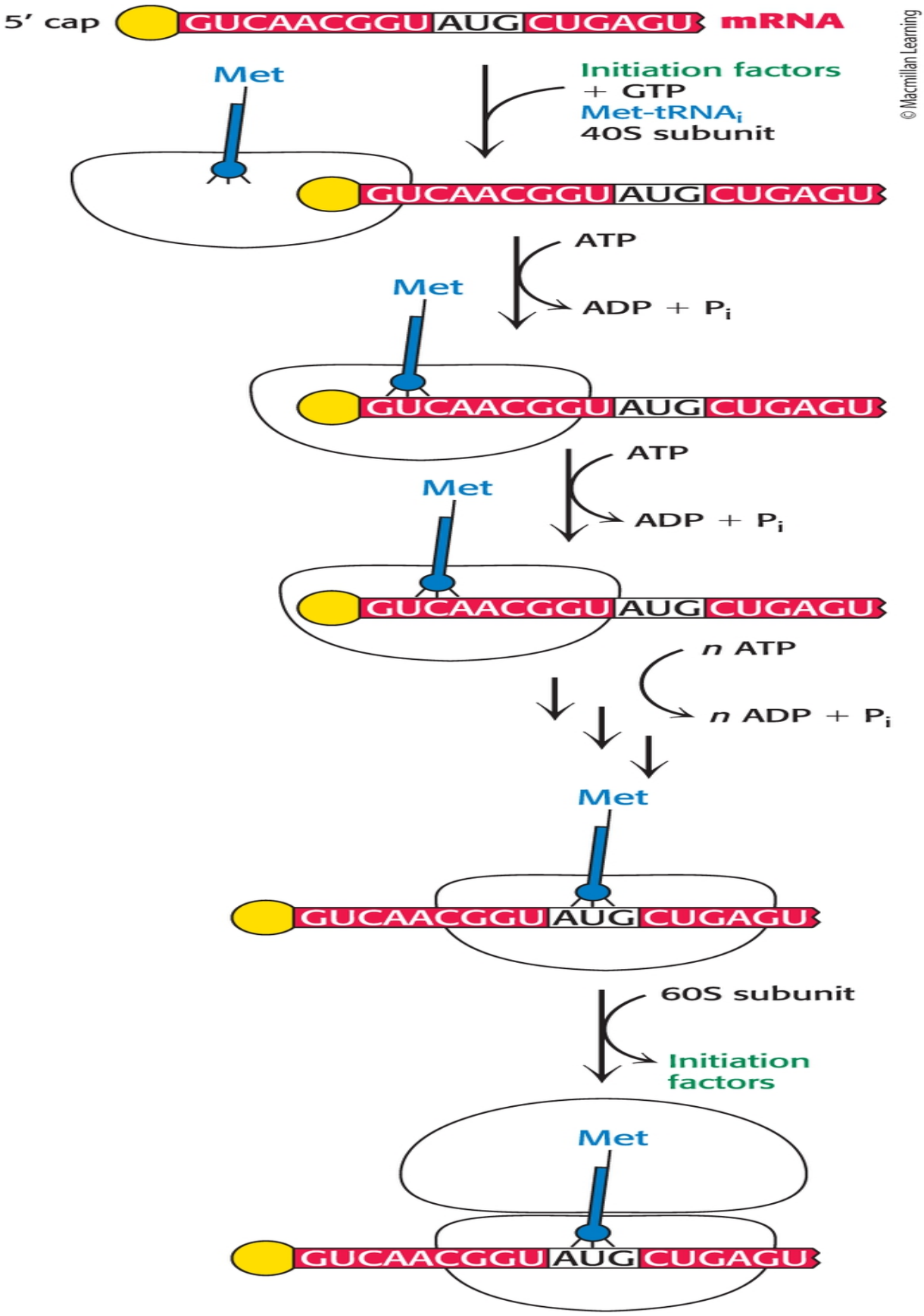
The structure of the first product is as follows: A 5-membered heterocyclic pentagonal ring in a horizontal orientation consists of 1 O and 4 C atoms. O occupies the first position which is the topmost vertex. C 1 is wedge bonded to adenine. C 2 is single bonded to O H. C 3 is single bonded to O H. H from the O H is highlighted in blue. C 4 is single bonded to a central C atom on the upper left. The central C atom is single bonded to O on the lower left. This O is further single bonded to a second C atom on the upper left. The second C atom is single bonded to a second O on the lower left, third O on the upper left, and fourth O on the upper right. The fourth O atom is single bonded to t R N A on the upper left.

The structure of the second product is as follows: A 1 O H, 1 N, and 2 C heteronuclear alkane chain is depicted as a line structure vertically using 3 zigzag lines. O H occupies the first position. N H occupies the fourth position. C 1 is double bonded to O on the lower right. C 2 is dash bonded to H on the upper left and wedge bonded to R on the lower left. N H is single bonded to a polypeptide on the lower left. O H in the first position is highlighted in blue and the rest of the structures are highlighted in red.

Return to Release of complete protein from t R N A

Extended description for FIGURE 30.28 Translation initiation differs in eukaryotes as compared with

prokaryotes



© Macmillan Learning

The figure has five steps. In all steps, the codon A U G is highlighted.

In the first step, the m R N A strand is depicted as a horizontal bar with a yellow sphere on the left which has the following sequence G U C A A C G G U A U G C U G A G U. A 40 S ribosomal subunit binds with the m R N A. A downward arrow depicts the entry of initiation factors plus G T P, Met t R N A, and 40 S subunit.

In the first step, a 40 S ribosomal subunit with a met t R N A binds to the left side of the m R N A such that the ribosome does not fully overlap with the m R N A. The Met t R N A is depicted as a stem-loop with the stem facing up and the loop embedded in the subunit.

In the second step, the ribosome completely overlaps with the m R N A. This is coupled with the entry of A T P and release of A D P and P subscript i. The Met t R N A is base paired with G U C of the m R N A.

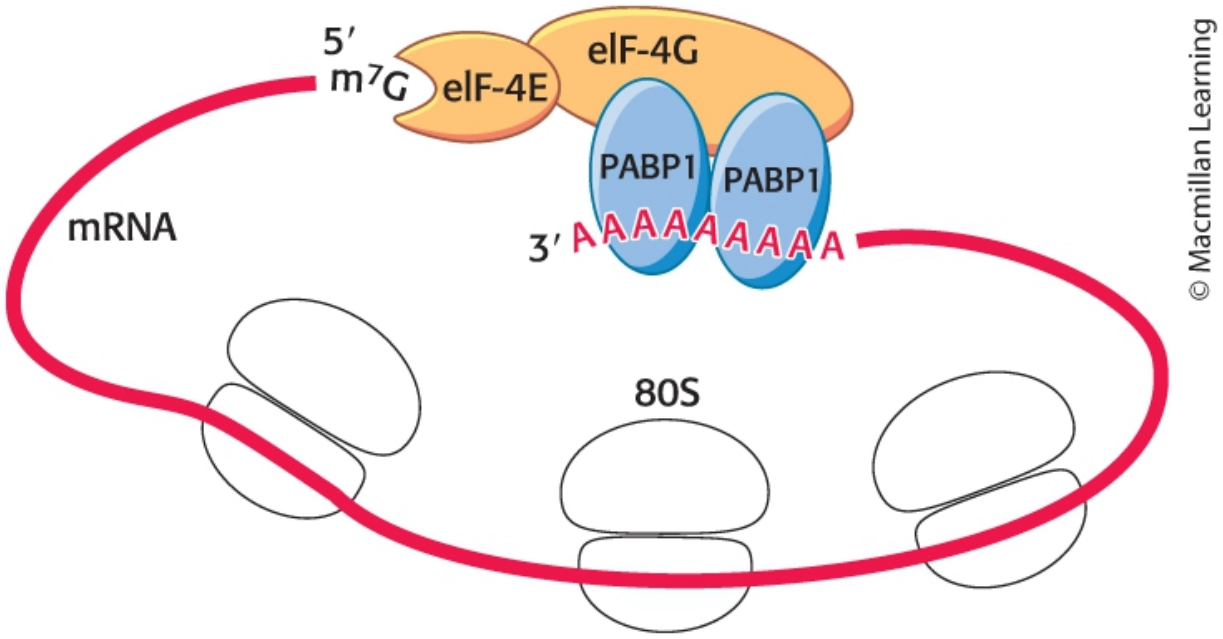
In the third step, the ribosome moves slightly to the right. This is coupled with the entry of A T P and release of A D P and P subscript i. The Met t R N A base pairing slightly shifts to the right. Now it is base paired with U C A.

In the fourth step, the ribosome moves to the right. This is coupled with the entry of n A T P and release of n A D P and P subscript i. This indicates that the shift is continuous. The Met t R N A is now base paired with the codon A U G in the m R N A.

In the fifth step, the 60 S ribosome binds with the 40 S subunit at the top. This is coupled with the entry of 60 S ribosome and the release of initiation factors. The Met t R N A remains attached to the A U G codon in the m R N A.

Return to FIGURE 30.28 Translation initiation differs in eukaryotes as compared with prokaryotes

Extended description for FIGURE 30.29 Protein interactions circularize eukaryotic m R N A

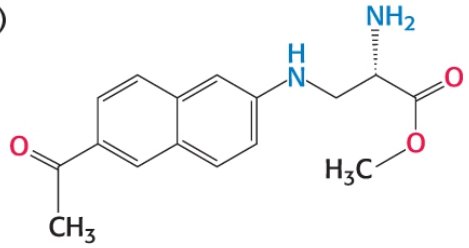


The figure shows a single-stranded m R N A that forms a circular loop such that the 5 prime and 3 prime ends of the loop are at the top. An oval structure with a groove on the left is labeled e l F 4 E. The groove on the left side of e l F 4 E is labeled m 7 G. This e l F 4 E binds with the 5 prime end of the m R N A. Another oval labeled e l F 4 G is attached to the right side of e l F 4 E. Two oval-shaped structures attached to one another are labeled P A B P 1. P A B P 1 overlap with e l F 4 G. The 3 prime end of the m R N A with sequence A A A A A A A A A overlap the P A B P 1. The lower end of the loop of m R N A consists of three ribosomal subunits. The smaller subunits are bound to the m R N A while the larger subunits are at the top. One of the larger subunits is labeled 80 S.

Return to FIGURE 30.29 Protein interactions circularize eukaryotic m R N A

Extended description for FIGURE 30.30 Unnatural amino acids can be incorporated into proteins

(A)



(2S)-3-[(6-Acetylnaphthalen-2-yl)amino]-2-aminopropanoic acid (L-ANAP)

(B)

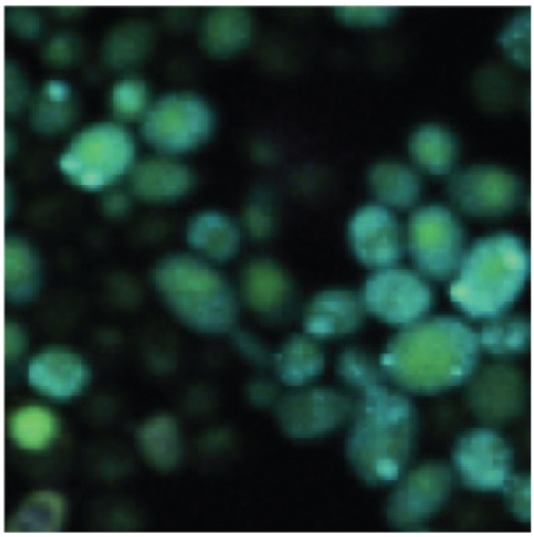


Image from Hsieh et al. 2014. Monitoring Protein Misfolding by Site-Specific Labeling of Proteins In Vivo. PLoS ONE 9:e99395, 10.1371/journal.pone.0099395.

The figure has two parts.

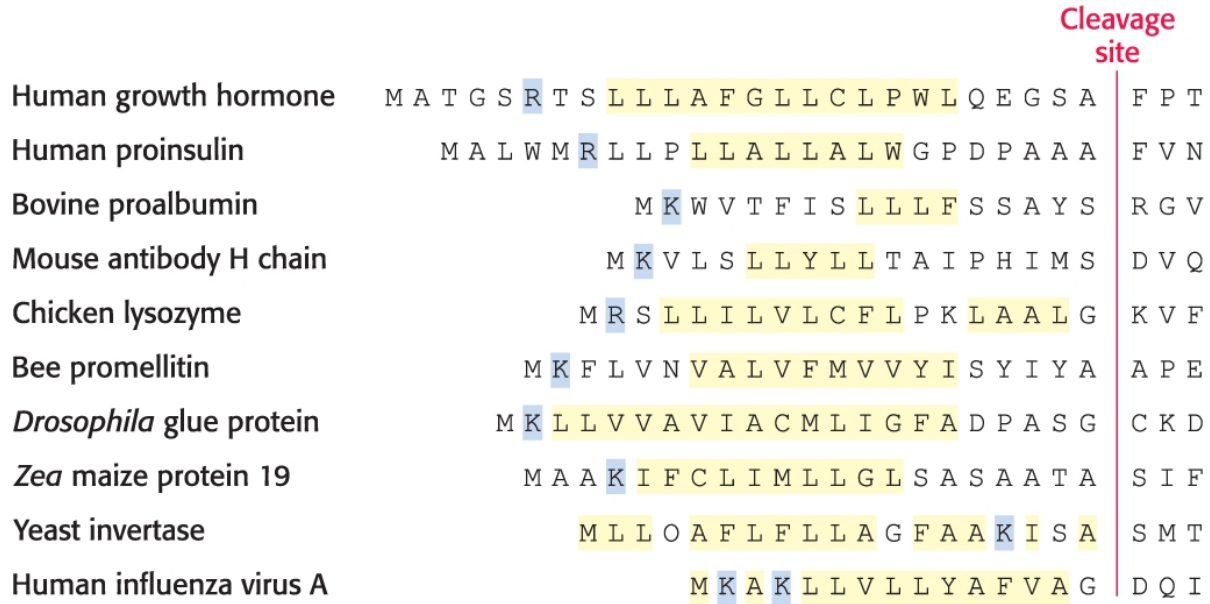
The first part depicts the structure of L A N A P ((2 S)-3-[(6-Acetylnaphthalen-2-y l)amino]-2-aminopropanoic acid), a fluorescent unnatural amino acid. The structure is as follows: A 6-carbon hexagonal ring in a vertical orientation with C 1 occupying the topmost vertex. A double bond is present between C 4 and C 5 and C 6 and C 1. C 5 is single bonded to a central C atom. The central C atom is double bonded to O on the upper left and single bonded to C H 3 below. This ring is fused to a benzene ring in a vertical orientation with C 1 occupying the topmost vertex. The ring contains alternating double bonds between C 2 and C 3, C 4 and C5, and C 6 and C 1. The two rings are fused to each other such that C 2 and C 3 of the 6-carbon hexagonal ring are the C 6 and C 5 of the benzene ring, respectively. C 2 of the benzene ring is single bonded to N of a 1 N and 3 C heteronuclear alkane chain depicted as a line

structure using 3 zigzag lines. N bound to H occupies the first position. C 2 is dash bonded to N H 2 above. C 3 is double bonded to O on the upper right and single bonded to O below. O is further single bonded to C H 3 on the lower left.

The second part depicts a photomicrograph of yeast cells with green fluorescence due to the presence of protein L A N A P.

Return to FIGURE 30.30 Unnatural amino acids can be incorporated into proteins

Extended description for FIGURE 30.32 The signal sequences of eukaryotic secretory and plasma membrane proteins contain hydrophobic residues



The sequences are aligned to the right side. A vertical line labeled cleavage site is drawn. The line is drawn before the set of three amino acid residues of each sequence at the terminal end. The sequence of human growth hormones reads M A T G S R T S L L L A F G L L C L P W L Q E G S A F P T. R in the sixth position is highlighted in blue. The sequence L L L A F G L L C L P W L is highlighted in yellow. F P T, in the end, comes after the cleavage site.

The sequence of human proinsulin reads M A L W M R L L P L L A L L A L W G P D P A A A F V N. R in the sixth position is highlighted in blue. F V N in the end comes after the cleavage site.

The sequence of bovine proalbumin reads M K W V T F I S L L L F S S A Y S R G V. K in the second position is highlighted in blue. The

sequence L L A L L A L W is highlighted in yellow. R G V in the end comes after the cleavage site.

The sequence of the mouse antibody H chain reads M K V L S L L Y L L T A I P H I M S D V Q. K in the second position is highlighted in blue. The sequence L L L F is highlighted in yellow. D V Qin the end comes after the cleavage site.

The sequence of chicken lysozyme reads M R S L L I L Y L C F L P K L A A L G K V F. R in the second position is highlighted in blue. The sequences L L I L Y L C F L and L A A L are highlighted in yellow. K V F, in the end, comes after the cleavage site.

The sequence of bee promellitin reads M K F L V N V A L V F M V V Y I S Y I Y A A P E. K in the second position is highlighted in blue. The sequence V A L V F M V V Y I is highlighted in yellow. A P E, in the end, comes after the cleavage site.

The sequence of drosophila glue protein reads M K L L V V A V I A C M L I G F A D P A S G C K D. K in the second position is highlighted in blue. The sequence L L V V A V I A C M L I G F A is highlighted in yellow. C K D in the end comes after the cleavage site.

The sequence of zea maize 19 reads M A A K I F C L I M L L G L S A S A A T A S I F. K in the fourth position is highlighted in blue. The sequence I F C L I M L L G L is highlighted in yellow. S I F in the end comes after the cleavage site.

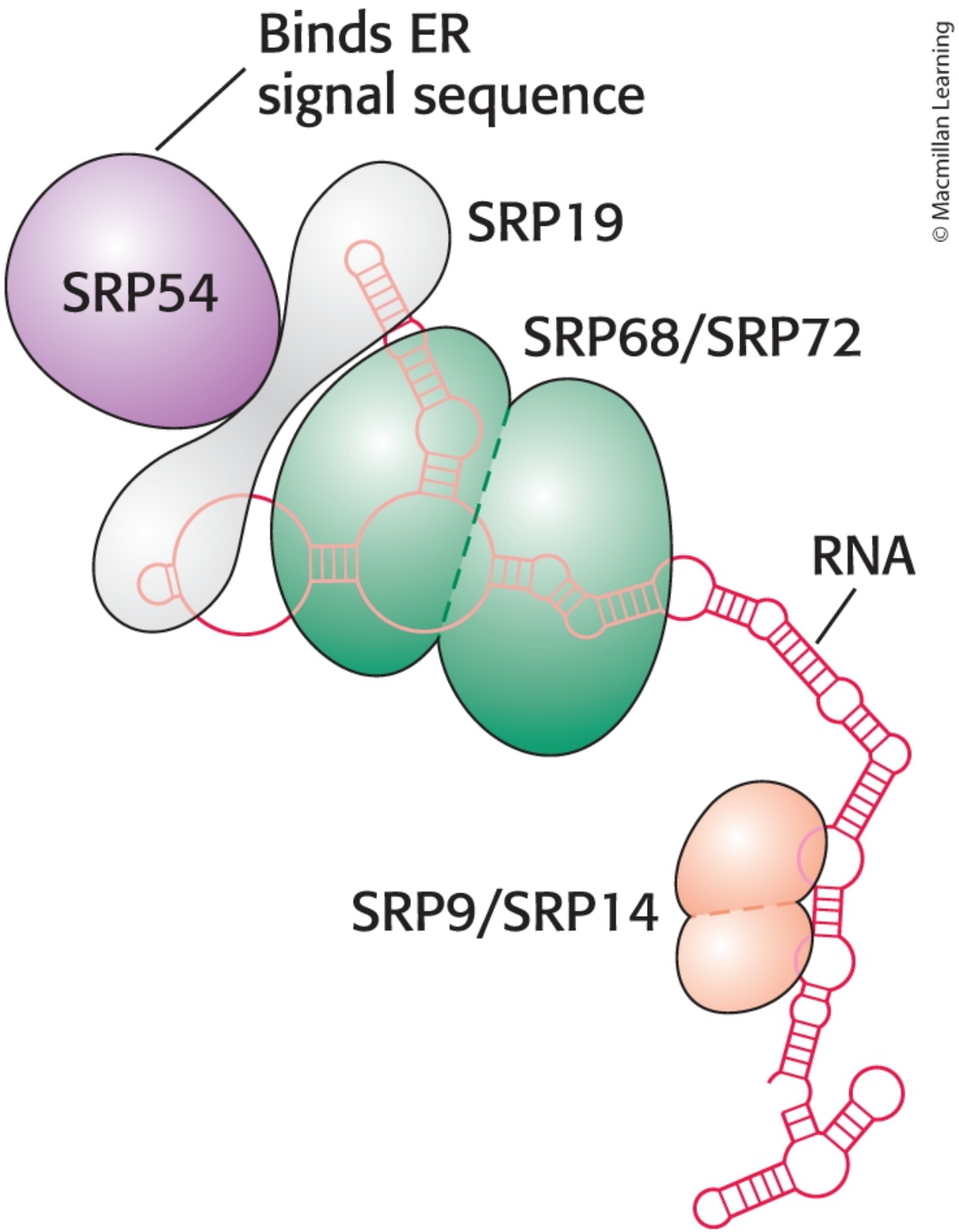
The sequence of yeast invertase reads M L L O A F L F L L A G F A A K I S A S M T. K in the sixteenth position is highlighted in blue. The sequences M L L, A F L F L L A, F A A, I, and A are highlighted in yellow. S M T in the end comes after the cleavage site.

The sequence of human influenza virus A reads M K A K L L V L L Y A F V A G D Q I. K in the second and fourth positions is highlighted in blue. The sequences M, A, L L V L L Y A F V A are highlighted in yellow. D Q I in the end comes after the cleavage site.

Return to FIGURE 30.32 The signal sequences of eukaryotic secretory and plasma membrane proteins contain hydrophobic residues

Extended description for FIGURE 30.33 The signal-recognition particle (S R P) consists of six proteins and

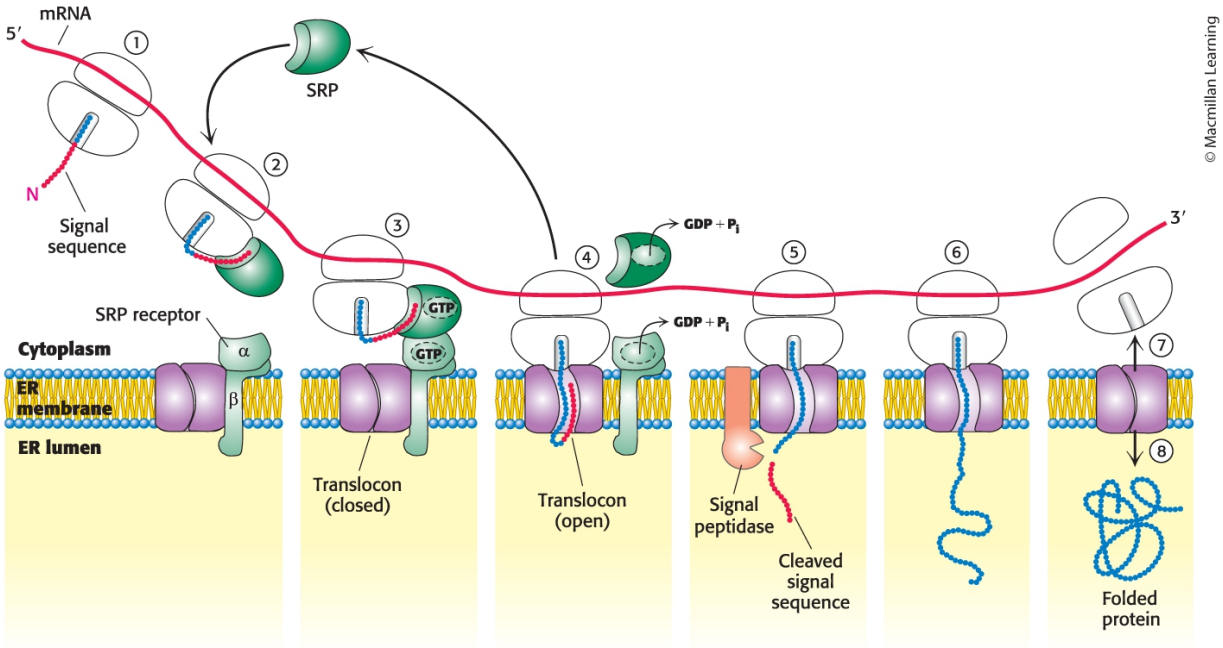
one 300-nucleotide R N A



A figure depicts the structure of R N A consisting of codon loops and stem-like extensions. The stems have horizontal lines on them. The loops on the R N A vary in size. The S R P is composed of six proteins and a 300 nucleotide R N A. The first protein on the upper left is labeled S R P 54. A callout from this protein reads "binds E R signal sequence." The next protein that is present on the right side of the S R P 54 has a dumbbell-shaped appearance and is labeled S R P 19. The next set of proteins is found in pairs which are oval-shaped structures attached side by side. They are labeled S R P 68 or S R P 72. The next set of proteins is also found in pairs with two oval-shaped structures attached one below the other. These proteins are not attached to the previous pair of proteins but are found at a distance and are labeled S R P 9 or S R P 14. The codon loop of R N A start from the bottom and moves upward attaches with the S R P or S R P 14 proteins on the left, takes a left turn overlaps the S R P 68 or S R P 72 proteins. It finally branches into two separate codon loops and terminates in the S R P 19.

Return to FIGURE 30.33 The signal-recognition particle (S R P) consists of six proteins and one 300-nucleotide R N A

Extended description for FIGURE 30.34 The S R P targeting cycle delivers nascent proteins containing a signal sequence to the E R



© Macmillan Learning

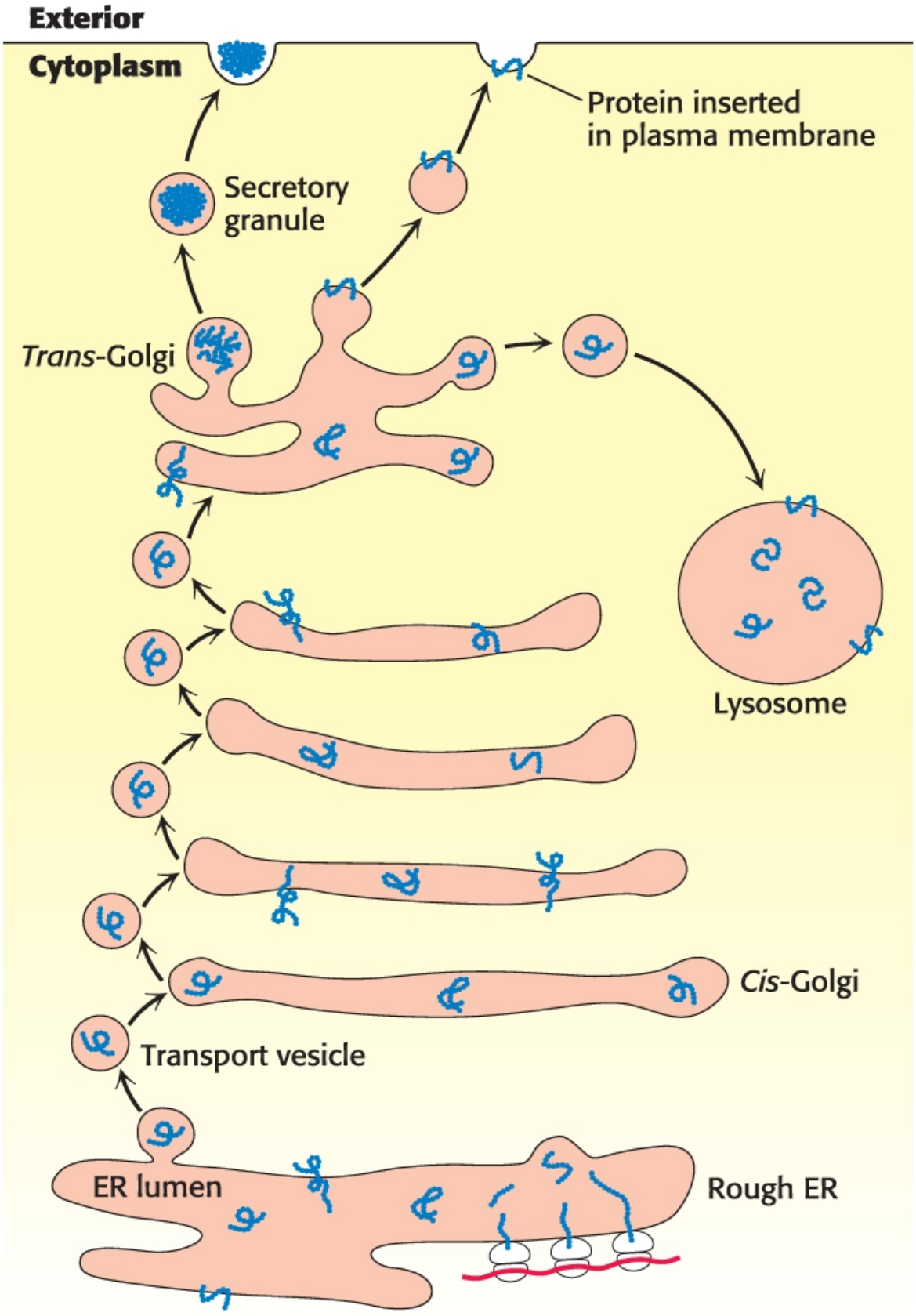
The figure depicts a lipid bilayer of the E R membrane with the cytoplasm at the top and the lumen at the bottom. The E R membrane consists of a translocon that has two subunits. The translocon opens and closes as per requirement. The translocon is attached to a green-colored S R P receptor consisting of alpha and beta subunits. The beta subunit is embedded in the E R membrane while the alpha subunit is in the cytoplasm. The series of events consists of eight steps. These steps are shown subsequently in eight parts. An m R N A in 5 prime to 3 prime direction bound to a ribosome is shown at the top in the first step. The larger subunit of the m R N A is at the bottom and the smaller subunit is at the top. The larger subunit consists of a polypeptide channel through which a beaded string-like structure emerges. The beaded structure

represents a protein. The beaded structure within the ribosome is blue and that emerging out chain is red and is labeled signal sequence. In the second step, a green-colored S R P binds with the larger subunit of the ribosome. This leads to the bending of the signal sequence into the S R P. In the third step, the S R P bound with the ribosome binds with the S R P receptor. Both S R P and S R P receptors consist of G T P. In the fourth step, the S R P is released along with the hydrolysis of G T P in the S R P and S R P receptors. Simultaneously, the ribosome now binds with the translocon. The translocon now opens to allow the entry of the signal sequence. In the fifth step, a membrane protein labeled signal peptidase removes the signal sequence from the peptide channel. The peptide sequence enters the lumen of the E R and is labeled cleaved signal sequence. In the sixth step, the protein biosynthesis continues directly into the E R. In the seventh step, the ribosomes are released. In the eighth step, the translocon closes and the peptide sequence is shown in a uniquely folded condition.

Return to FIGURE 30.34 The S R P targeting cycle delivers nascent proteins containing a signal sequence to the E R

Extended description for FIGURE 30.35 Protein-sorting

pathways deliver proteins to their final destinations

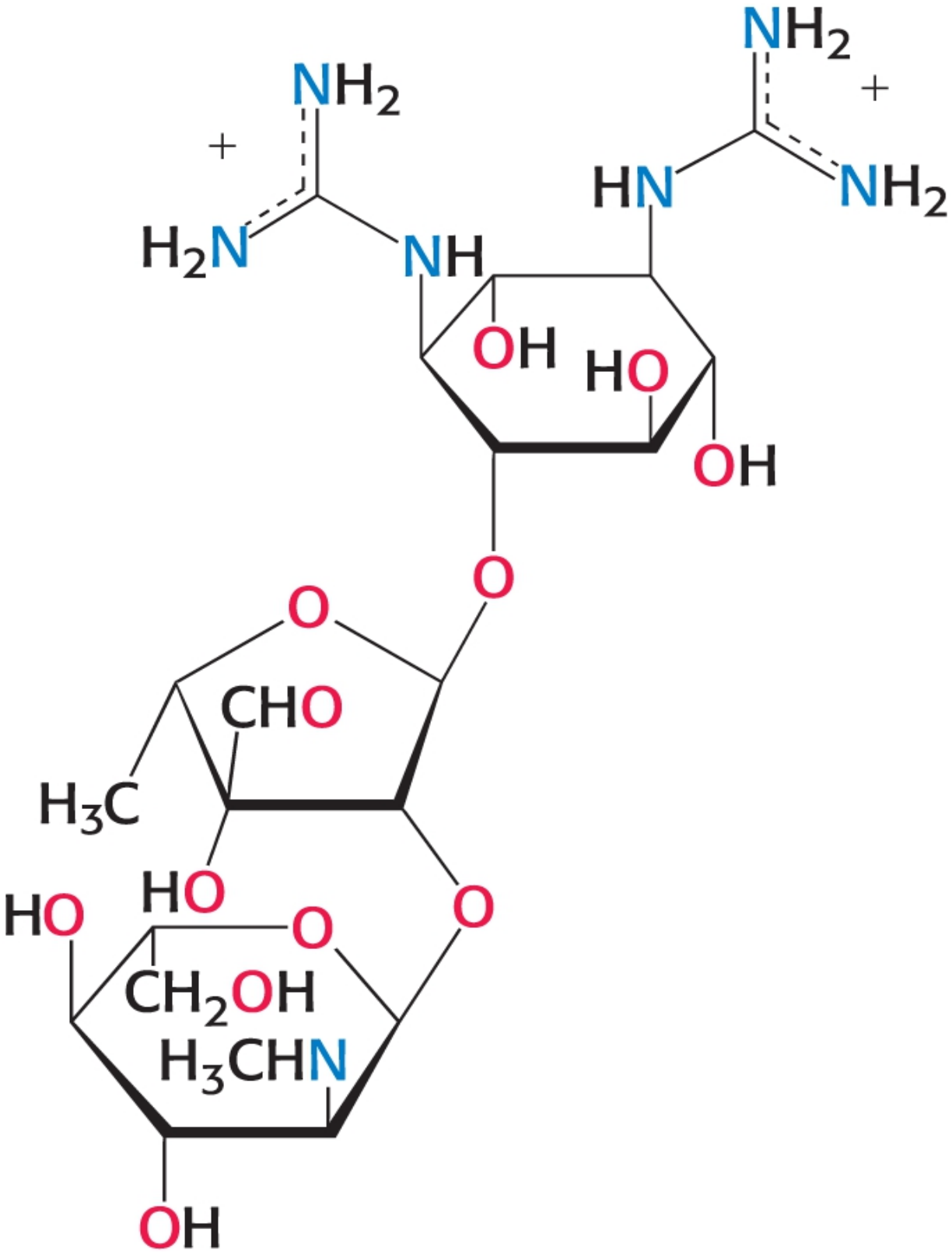


© Macmillan Learning

The figure depicts the organelles Golgi body and rough E R within a cell. The interior of the cell is labeled cytoplasm and the outer region of the cell is labeled exterior. The cell interior consists of a two-dimensional array of flattened sacs that extend across the cytoplasm labeled rough E R. The inner region of the E R is labeled E R lumen. Above the E R, the Golgi apparatus is depicted as a series of stacked flat cisternae with two distinct faces called the trans-Golgi and cis-Golgi. The trans-Golgi is at the top and the cis-Golgi is at the bottom near the rough E R. An m R N A with three ribosomes is attached to the lower side of the rough E R. The proteins synthesized by the ribosomes are released into the E R lumen. The protein from the E R lumen pinches off as a vesicle labeled transport vesicle. The transport vesicle enters the cis side of the Golgi. The proteins go through a series of modifications as they move from the cis side of the Golgi to the trans side. On the trans side, these proteins are packaged properly. The proteins are released into the cytoplasm in the form of a secretory granule. The secretory granule is then sent to the exterior. On the other hand, one of the proteins is shown inserted into the plasma membrane. The rest of the proteins are sent to the lysosome in the cytoplasm.

Return to FIGURE 30.35 Protein-sorting pathways deliver proteins to their final destinations

Extended description for Structure of streptomycin

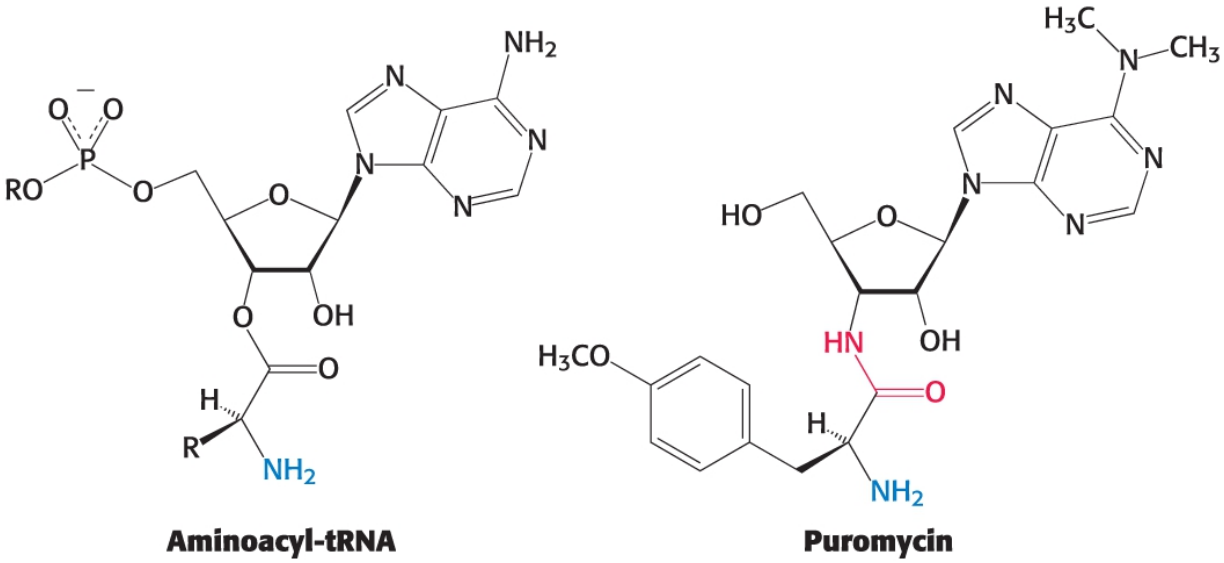


Streptomycin

A 6-membered heterocyclic hexagonal ring is in a horizontal orientation and consists of 1 O and 5 C atoms. The O atom occupies the first position, which is the top right vertex. The ring is in a plane perpendicular to the plane of the paper such that C 5 and O are away from the observer and C 2 and C 3 are towards the observer. C 2 is single bonded to C H 3 N H. N in C H 3 N H is highlighted in blue. C 3 is single bonded to O H below. O in the O H is higlighted in red. C 4 is single bonded to O H above. O in the O H is higlighted in red. C 5 is single bonded to C H 2 O H below. O in the C H 2 O H is higlighted in red. C 1 is single bonded to O on the upper right. The O is highlighted in red. The O atom single bonded to C 2 of the 5-membered heterocyclic pentagonal ring in a vertical orientation and consists of 1 O and 4 C atoms. The O atom is at the topmost vertex. The ring is in a plane perpendicular to the plane of the paper such that C 2 and C 3 are towards the observer and O is away from the observer. C 3 is single bonded to C H O above and O H below. The O in both C H O and O H are highlighted in red. C 4 is single bonded to C H 3 below. C 1 is single bonded to O above and is highlighted in red. The O atom is single bonded to C 3 of a 6-carbon hexagonal ring in a horizontal orientation with C 1 occupying the rightmost vertex. The ring is in a plane perpendicular to the plane of the paper such that C 2 and C 3 are towards the observer and C 5 and C 6 are away from the observer. C 1 and C 5 are each single bonded to O H below. C 2 is single bonded to O H above. O in the O H are highlighted in red. C 4 of the hexagonal ring is single bonded to N H above. N H is single bonded to a central C atom on the upper left. The central C atom is partially double bonded to N H 2 above and N H 2 on the lower left. The N H 2 atoms have an overall positive charge. C 6 of the hexagonal ring is single bonded to N H above. N H is single bonded to a central C atom on the upper right. The central C atom is partially double bonded to N H 2 above and N H 2 on the lower right. The N H 2 atoms have an overall positive charge. The N in the N H and N H 2 atoms are highlighted in blue.

Return to Structure of streptomycin

Extended description for FIGURE 30.36 The antibiotic puromycin resembles the aminoacyl terminus of an aminoacyl-t R N A



The structure of aminoacyl- t R N A is as follows: A 5-membered heterocyclic pentagonal ring in a vertical orientation consists of 1 O and 4 C atoms. O occupies the first position which is the topmost vertex. C 2 is single bonded to O H. C 3 is single bonded to O of a 1 O and 2 C heteronuclear alkane chain depicted as a line structure vertically using 2 zigzag lines. O ccupies the first position C 1 is double bonded to O on the right. C 2 is dash bonded to H on the upper left, wedge bonded to R on the lower left, and single bonded to N H 2 on the lower right. N H 2 is highlighted in blue. C 4 of the pentagonal ring is single bonded to a central C atom. The central C atom is further single bonded to O on the lower left. This O is further single bonded to a central P on the upper left. The central P atom is single bonded to O R on the lower left and partially double bonded to O on the upper left and O on the upper right. The P O O group has an overall negative charge. C 1 of the pentagonal ring is

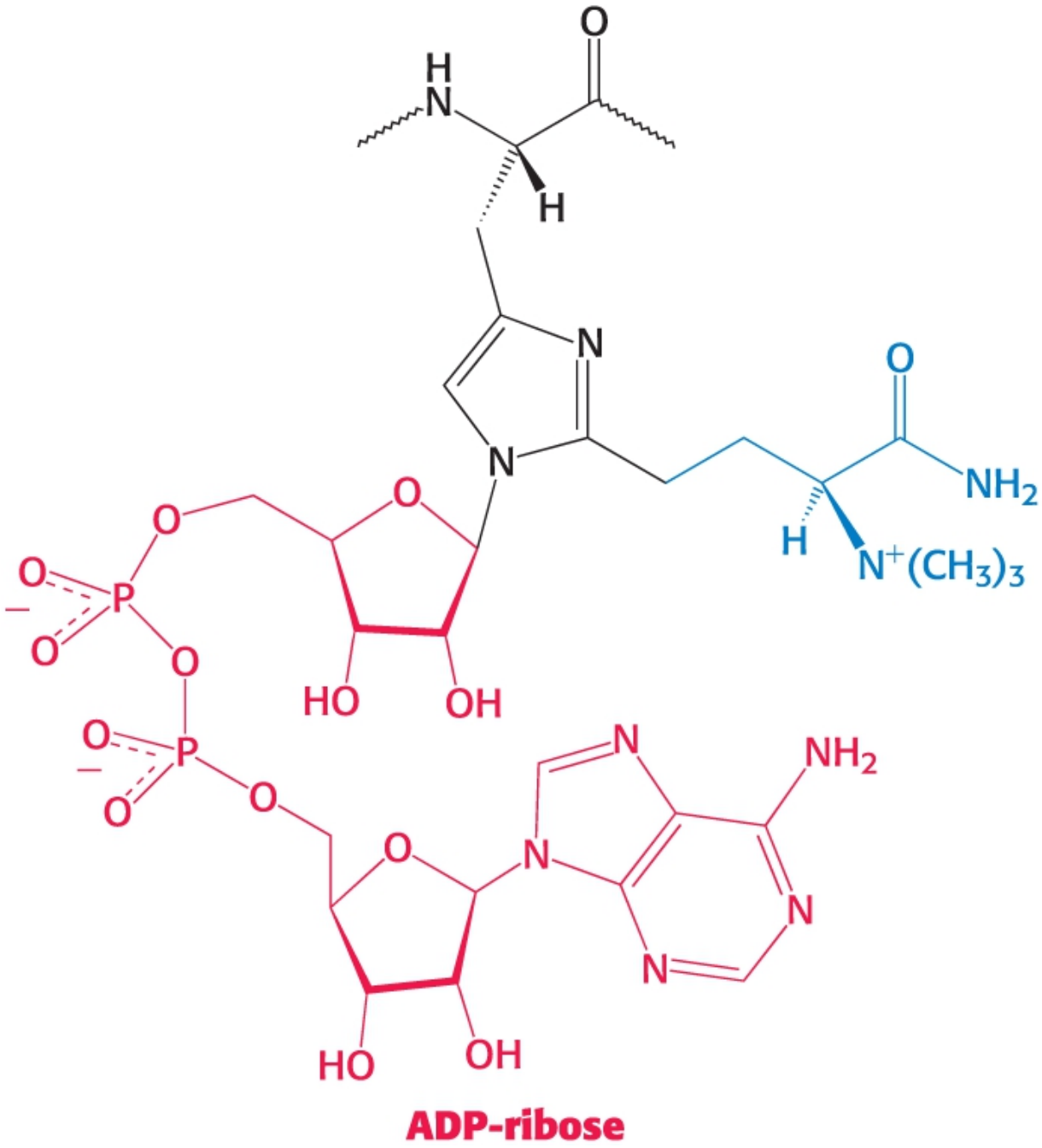
single bonded to the first N atom of a 5-membered heterocyclic pentagonal ring is in a vertical orientation consisting of 2 N and 3 C atoms. The first N atom occupies the first position, which is the bottom left vertex. The second N atom occupies the third position which is the topmost vertex. A double bond is present between C 1 and the second N atom. The 5-membered ring is fused to a 6-membered heterocyclic hexagonal ring in a vertical orientation consisting of 2 N and 4 C atoms. In the 6-membered ring, the first N atom occupies the first position, which is the top right vertex. The second N atom occupies the third position which is the bottommost vertex. The 6-membered ring contains double bonded between C 1 and the second N atom, C 2 and C 3, and C 4 and the second N atom. C 4 is single bonded to N H 2 above. The two rings are fused to each other such that C 2 and C 3 of the 5-membered ring are the C 3 and C 2 of the 6-membered ring, respectively.

The structure of puromycin is as follows: A 5-membered heterocyclic pentagonal ring in a vertical orientation consists of 1 O and 4 C atoms. O occupies the first position which is the topmost vertex. C 2 is single bonded to O H. C 3 is single bonded to N H of a 1 N H and 2 C heteronuclear alkane chain depicted as a line structure vertically using 2 zigzag lines. N H occupies the first position. C 1 is double bonded to O on the right. These structures of the alkane chain are highlighted in red. C 2 is dash bonded to H on the upper left, wedge bonded to a central C atom on the lower left, and single bonded to N H 2 on the lower right. N H 2 is highlighted in blue. The central C atom is further single bonded to C 3 of a benzene ring in vertical orientation with C 1 occupying the topmost vertex. Double bonds are present between C 2 and C 3, C 4 and C 5, and C 6 and C 1. C 6 is single bonded to O C H 3. C 4 of the pentagonal ring is single bonded to a central C atom. The central C atom is further single bonded to O H on the lower left. C 1 of the pentagonal ring is single bonded to the first N atom of a 5-membered heterocyclic pentagonal ring and in a vertical orientation consisting of 2 N and 3 C atoms.

The first N atom occupies the first position, which is the bottom left vertex. The second N atom occupies the third position which is the topmost vertex. A double bond is present between C 1 and the second N atom. The 5-membered ring is fused to a 6-membered heterocyclic hexagonal ring in a vertical orientation consisting of 2 N and 4 C atoms. In the 6-membered ring, the first N atom occupies the first position, which is the top right vertex. The second N atom occupies the third position which is the bottommost vertex. The 6-membered ring contains double bonded between C 1 and the second N atom, C 2 and C 3, and C 4 and the first N atom. C 4 is single bonded to N above. This N is further single bonded to C H 3 on the upper left and C H 3 on the upper right. The two rings are fused to each other such that C 2 and C 3 of the 5-membered ring are the C 3 and C 2 of the 6-membered ring, respectively.

Return to FIGURE 30.36 The antibiotic puromycin resembles the aminoacyl terminus of an aminoacyl-t R N A

Extended description for FIGURE 30.37 Diphtheria toxin inhibits protein biosynthesis in eukaryotes

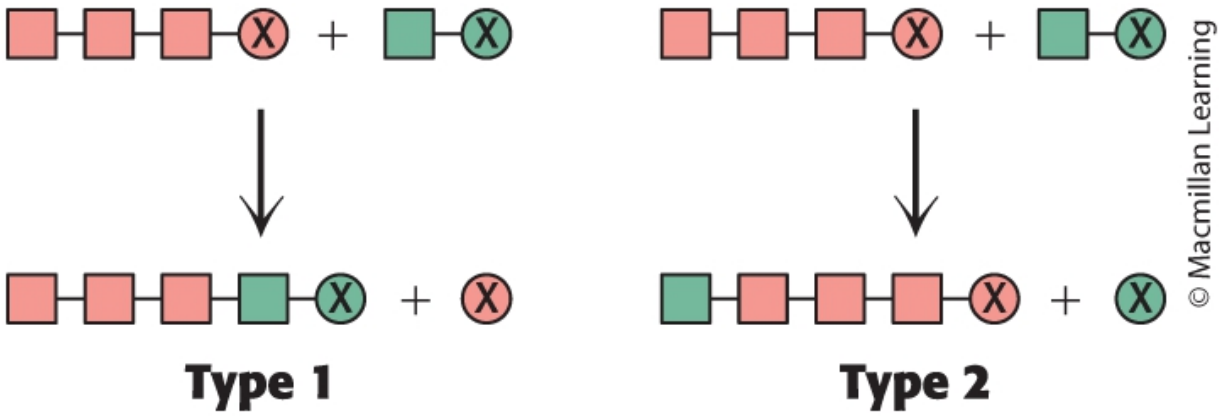


The structure of diphtheria toxin is as follows: A 5-membered heterocyclic pentagonal ring in a vertical orientation consists of 1 O and 4 C atoms. O occupies the first position which is the topmost vertex. C 2 and C 3 are each single bonded to O H. C 1 of the pentagonal ring is single bonded to the first N atom of a 5-membered heterocyclic pentagonal ring in a horizontal orientation consisting of 2 N and 3 C atoms. The first N atom occupies the first position, which is the bottom left vertex. The second N atom occupies the third position which is the top right vertex. A double bond is present between C 1 and the second N atom. The 5-membered ring is fused to a 6-membered heterocyclic hexagonal ring in a horizontal orientation consisting of 2 N and 4 C atoms. In the 6-membered ring, the first N atom occupies the first position, which is the rightmost vertex. The second N atom occupies the third position which is the bottom left vertex. The 6-membered ring contains double bonded between C 1 and the second N atom, C 2 and C 3, and C 4 and the first N atom. C 4 is single bonded to N H 2 above. The two rings are fused to each other such that C 2 and C 3 of the 5-membered ring are the C 3 and C 2 of the 6-membered ring, respectively. C 4 of the first heterocyclic pentagonal ring is single bonded to a central C atom above. The central C atom is further single bonded to O on the upper left. This O is further single bonded to a central P on the upper left. The central P atom is single bonded to O above and partially double bonded to O on the upper left and O on the lower left. The P O O group has an overall negative charge. O that is single bonded to P above is further single bonded to a second P atom on the upper left. The second P atom is partially double bonded to O on the upper left and O on the lower left. The P O O group has an overall negative charge. P is also single bonded to O on the upper right. O is single bonded to a central C atom. The central C atom is single bonded to C 4 of a 5-membered heterocyclic pentagonal ring in a vertical orientation consisting of 1 O and 4 C atoms. O occupies the first position which is the topmost vertex. C 2 and C 3 are each single bonded to O H. The structures upto this

pentagonal ring are highlighted in red. C 1 of the pentagonal ring is single bonded to the first N atom of a 5-membered heterocyclic pentagonal ring in a horizontal orientation consisting of 2 N and 3 C atoms. The first N atom occupies the first position, which is the bottom left vertex. The second N atom occupies the fourth position which is the top right vertex. A double bond is present between C 1 and C 2 and the second N atom and C 3. C 2 is single bonded to a central C atom above. The central C atom is dash bonded to C 1 of a 1 N and 2 C heteronuclear alkane chain depicted as a line structure using 2 zigzag lines. N bound to H occupies the first position. C 1 is wedge bonded to H on the lower right. C 2 is double bonded to O above. N bound to H has a wiggly bond on the lower left. C 2 has a wiggly bond on the lower right The pentagonal ring and the alkane chain are highlighted in black. C 3 of the 5-membered ring is single bonded to a 1 N H 2 and 4 C heteronuclear alkane chain depicted as a line structure using 4 zigzag lines. N H 2 occupies the fifth position. C 3 is dash bonded to H on the lower left and wedge bonded to N superscript plus open parenthesis C H 3 close parenthesis subscript 3. C 4 is double bonded to O above. This alkane chain is highlighted in blue.

Return to FIGURE 30.37 Diphtheria toxin inhibits protein biosynthesis in eukaryotes

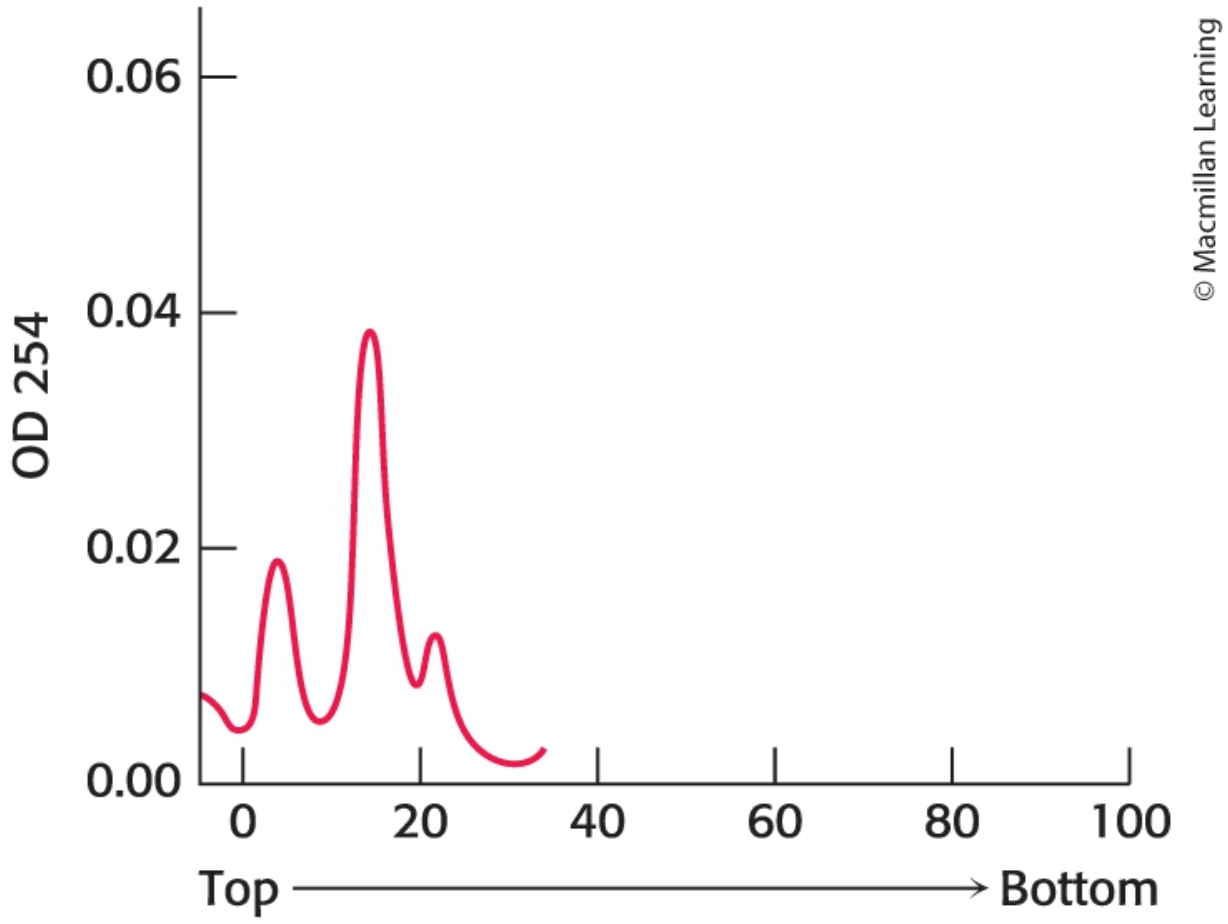
Extended description for The two basic mechanisms for the elongation of biomolecules are represented in the adjoining illustration



In the first mechanism labeled type 1, two biomolecules, each with an activating group is depicted. These biomolecules are separated by a plus sign. The first biomolecule is pink and consists of three squares connected by single bonds from left to right. The third square on the right is single-bonded to a circle marked with an X. The X mark represents the activating group of the biomolecule. The second biomolecule in green consists of one square connected to a circle marked with an X on the right. When the reaction proceeds, the activating group from the first biomolecule is released and the second biomolecule with its activating group is added to the right side of the first biomolecule.

Return to The two basic mechanisms for the elongation of biomolecules are represented in the adjoining illustration

Extended description for Graphical representation of optical density gradient for each fraction

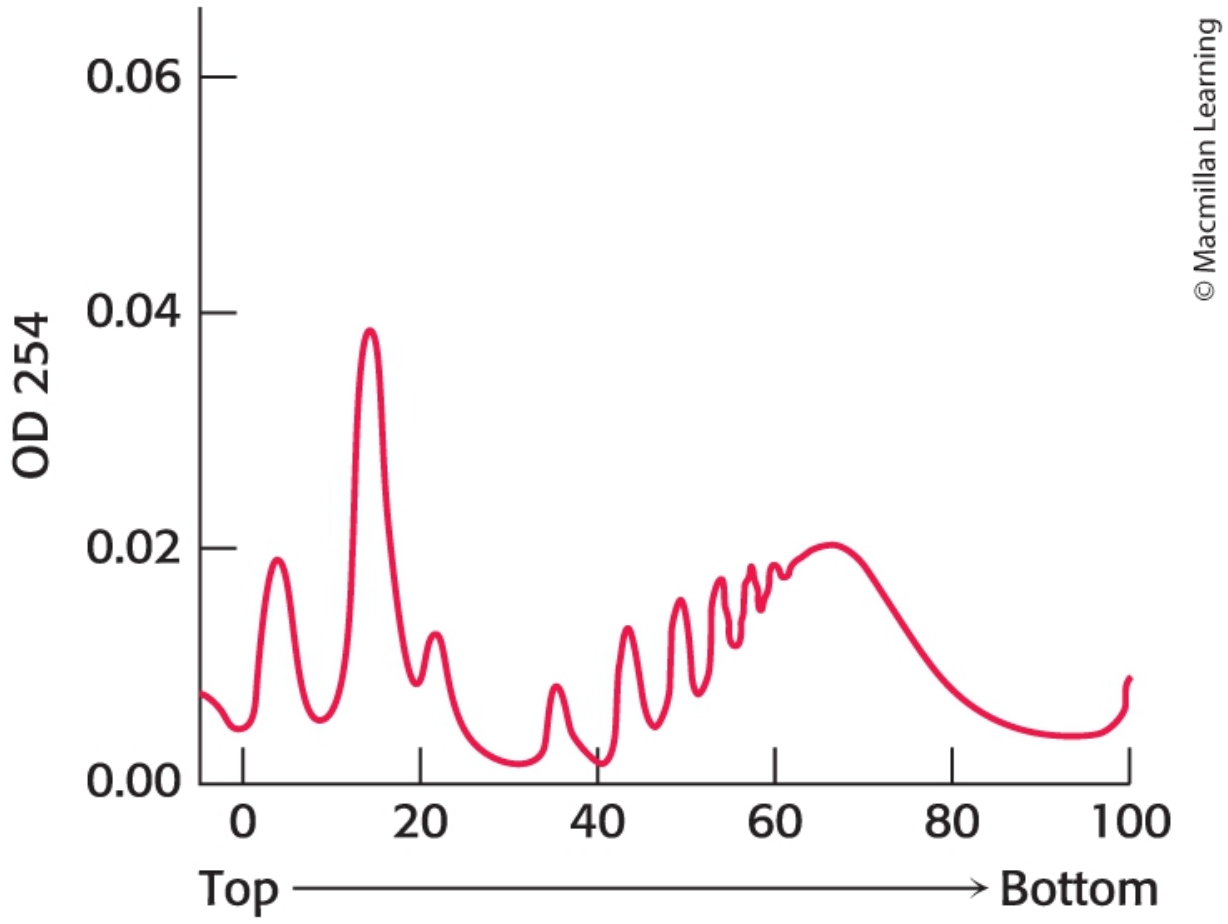


© Macmillan Learning

The horizontal axis is indicated by a rightward arrow labeled top on the left and bottom on the right. It has markings ranging from 0 to 100 in increments of 20 units. The vertical axis, labeled optical density at 254 nanometers, has markings ranging from 0.00 to 0.06 in increments of 0.02 units. The graph starts from 0.008 on the vertical axis, slopes down to (0, 0.005), rises to (2, 0.018), slopes down to (10, 0.005), reaches a peak at (18, 0.038), slopes down to (20, 0.008), shows a small peak at (21, 0.01), slopes down to (30, 0.001), and terminates at (36, 0.003). All values are approximated.

Return to Graphical representation of optical density gradient for each fraction

Extended description for Graphical representation of optical density gradient for each fraction



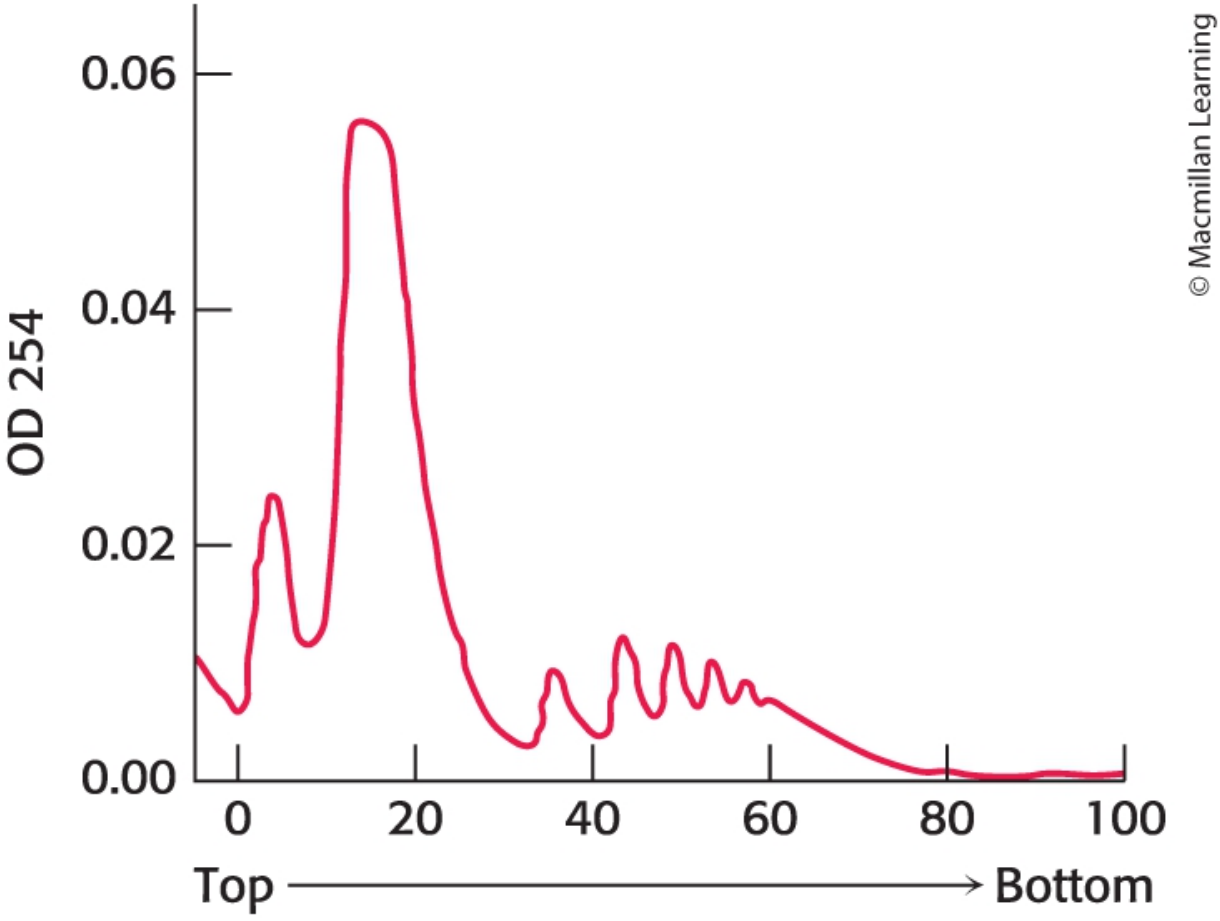
© Macmillan Learning

The horizontal axis is indicated by a rightward arrow labeled top on the left and bottom on the right. It has markings ranging from 0 to 100 in increments of 20 units. The vertical axis, labeled optical density at 254 nanometers, has markings ranging from 0.00 to 0.06 in increments of 0.02 units. The graph starts from 0.008 on the vertical axis, slopes down to (0, 0.005), rises to (2, 0.018), slopes down to (10, 0.005), reaches a peak at (18, 0.038), slopes down to (20, 0.008), shows a small peak at (21, 0.01), slopes down to (30, 0.001), it again shows a series of small peaks at coordinates (42, 0.01), (50,

0.014), (55, 0.016), (60, 0.018), (65, 0.02), slopes down to (80, 0.008), moves to the right at terminates at (100, 0.008). All values are approximated.

Return to Graphical representation of optical density gradient for each fraction

Extended description for Graphical representation of optical density gradient for each fraction



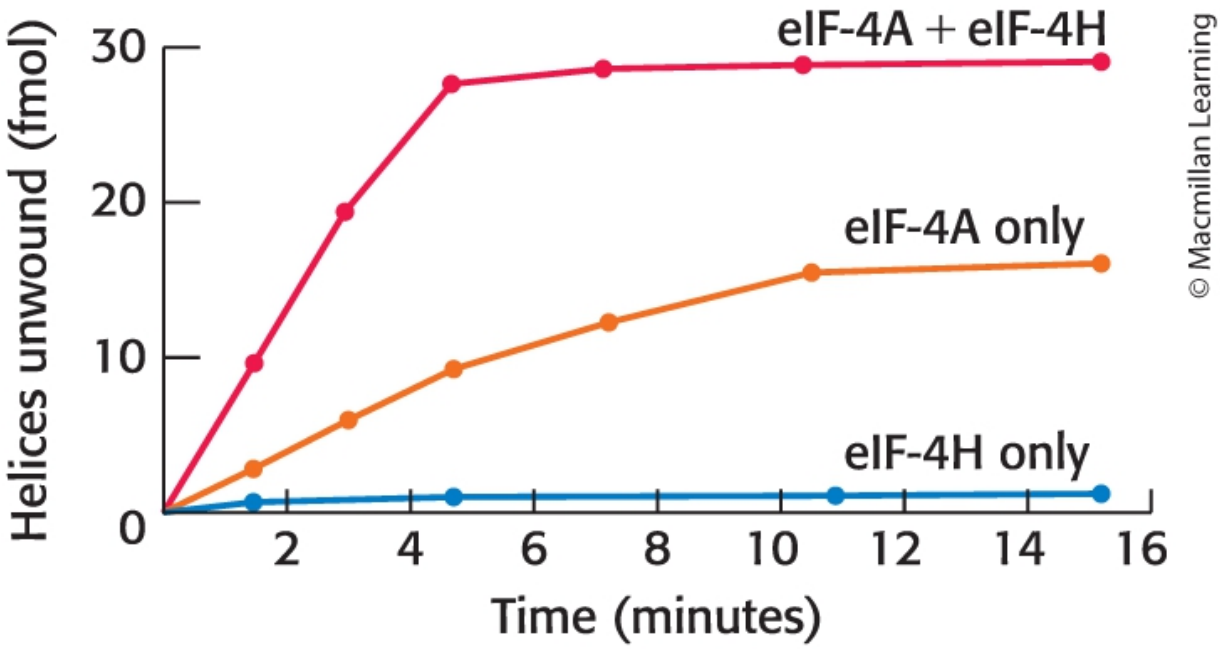
© Macmillan Learning

The horizontal axis is indicated by a rightward arrow labeled top on the left and bottom on the right. It has markings ranging from 0 to 100 in increments of 20 units. The vertical axis, labeled optical density at 254 nanometers, has markings ranging from 0.00 to 0.06 in increments of 0.02 units. The graph starts from 0.008 on the vertical axis, slopes down to (0, 0.005), rises to (4, 0.024), slopes down to (10, 0.012), reaches a peak at (18, 0.056), slopes down to (35, 0.004), shows a series of small peaks at coordinates (36, 0.006), (42, 0.01), (50, 0.008), (55, 0.007), (58, 0.005), (60, 0.004), slopes down to

(80, 0.00), moves to the right at terminates at (100, 0.00). All values are approximated.

Return to Graphical representation of optical density gradient for each fraction

Extended description for Graphical representation of helices unwound versus time in minutes



The horizontal axis, labeled time in minutes, has markings ranging from 0 to 16 in increments of 2 units. The vertical axis labeled helices unwound in femtomoles has markings ranging from 0 to 30 in increments of 10 units.

The first curve in blue labeled e l F 4 H only starts from (0, 0), moves to the right through coordinates (1.8, 0.5), (4.8, 1), (11, 1), and terminates at (15.2, 1).

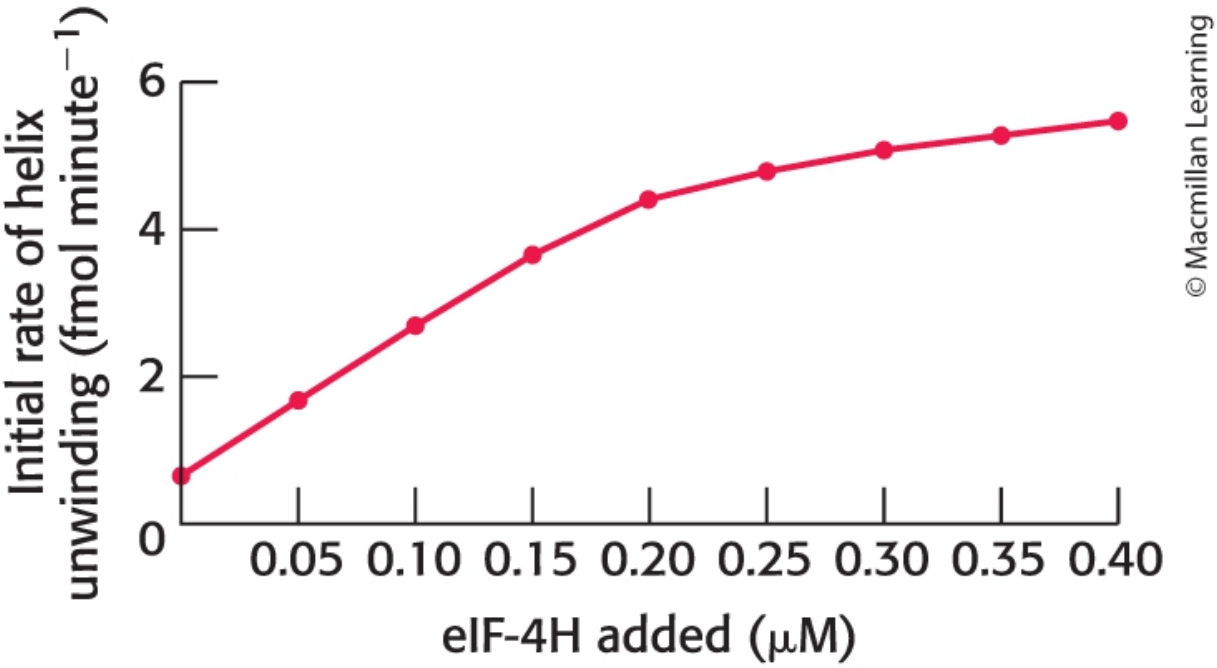
The second curve in orange labeled e l F 4 A only starts from (0, 0), and rises upward through coordinates (1.8, 2), (3, 5), (4.8, 9), (7.8, 11), (11, 14), and terminates at (15.2, 15).

The third curve in red labeled e l F 4 A plus e L F 4 H starts from (0, 0), rises upward through coordinates (1.8, 10), (3, 20), (4.8, 27), move

to the right through coordinates (7.8, 28), (11, 28), and terminates at (15.2, 29). All values are approximated.

Return to Graphical representation of helices unwound versus time in minutes

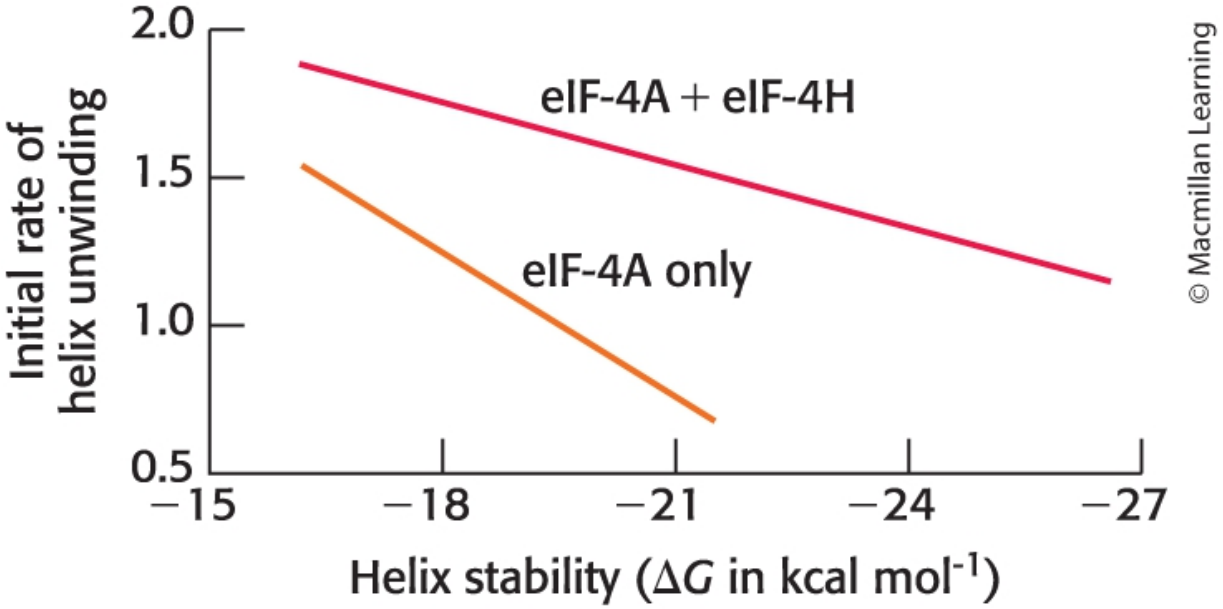
Extended description for Graphical representation of helicase activity



The horizontal axis, labeled e l F 4 H added in microMolars, has markings ranging from 0 to 0.40 in increments of 0.05 units. The vertical axis labeled initial rate of helix unwinding in femtomoles per minute has markings ranging from 0 to 6 in increments of 2 units. The graph starts from (0, 0.8), and rises upward through coordinates (0.05, 1.8), (0.10, 2.6), (0.15, 3.8), (0.20, 4.2), (0.25, 4.5), (0.35, 5), and terminates at (0.40, 5.6). All values are approximated.

Return to Graphical representation of helicase activity

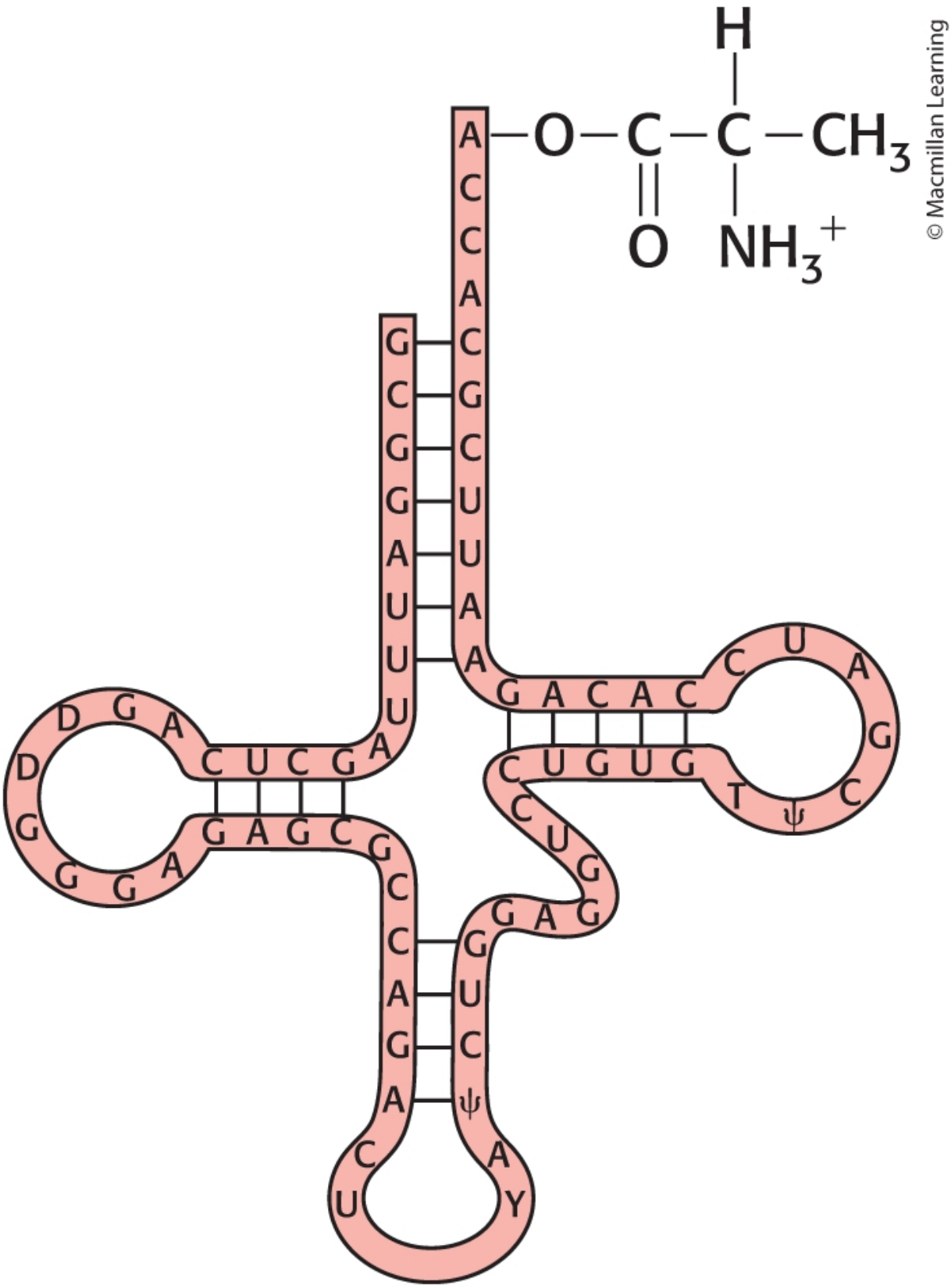
Extended description for Graphical representation of effects of R N A R N A on helix stability



The horizontal axis, labeled helix stability in delta G in kilocalories per mole, has markings ranging from negative 15 to negative 27 in decrements of 3 units. The vertical axis labeled initial rate of helix unwinding has markings ranging from 0.5 to 2.0 in increments of 0.5 units. The graph has two decreasing lines. The first line in orange labeled e l F 4 A only starts from (negative 16.5, 1.51), slopes down to (negative 18, 1.25), and terminates at (negative 21.5, 0.7). The second line in red labeled e l F 4 A plus e l F 4 H starts from (negative 16.5, 1.8), slopes down to (negative 21, 1.7), and terminates at (negative 27, 1.25) All values are approximated.

Return to Graphical representation of effects of R N A R N A on helix stability

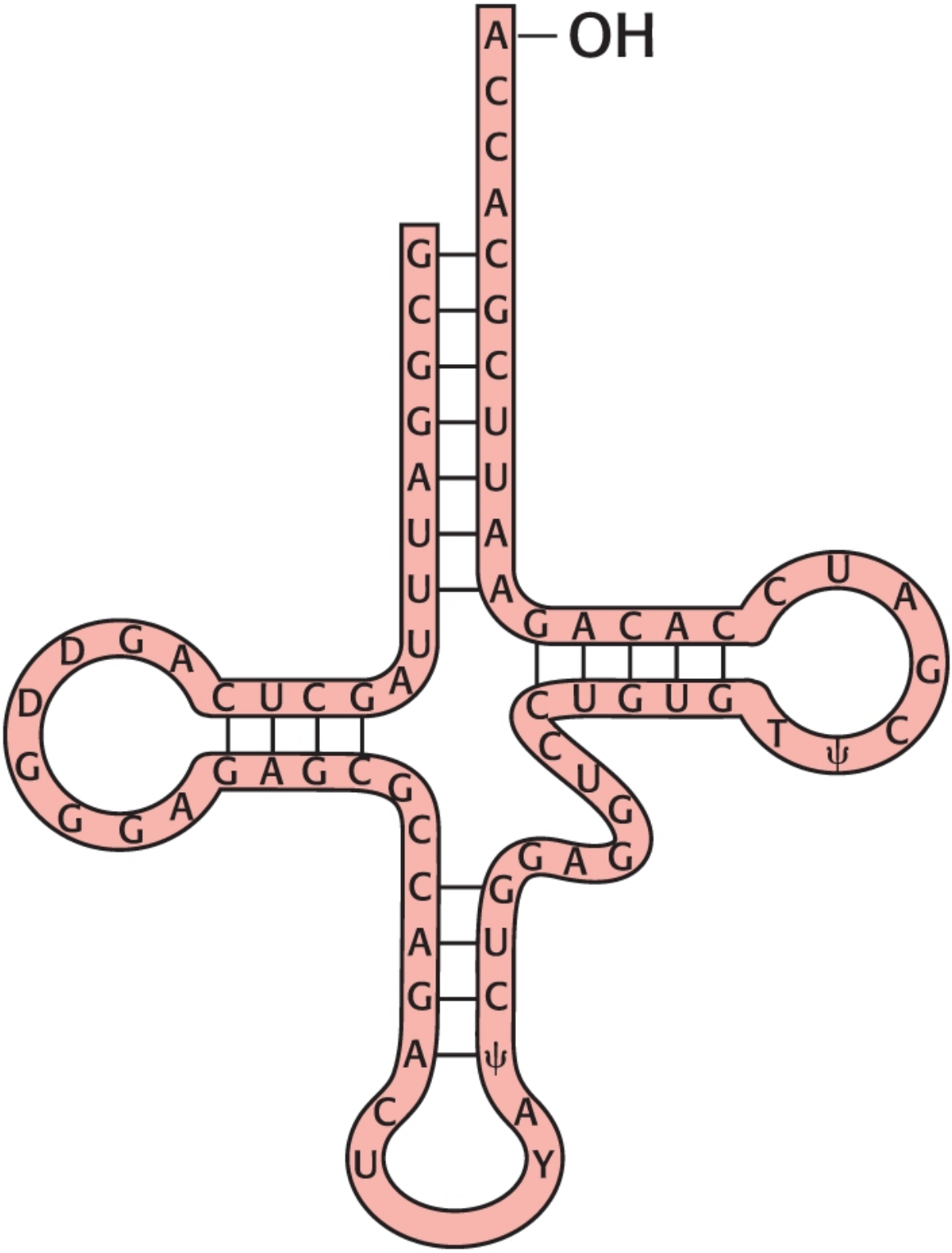
Extended description for Structure of a t R N A


H
O
C
C
CH3
O
NH3+
A
C
C
A
C
G
C
G
G
A
U
U
A
U
U
A
G
A
C
A
C
C
U
A
G
T
ψ
C
C
U
G
U
G
U
G
D
G
A
C
U
C
G
A
D
G
G
A
G
G
A
G
C
G
C
C
A
G
A
C
U
G
A
G
G
U
C
ψ
A
Y
© Macmillan Learning

The secondary structure of R N A resembles a cloverleaf. A single chain of t R N A is folded to form five arms which results in 3 prime and 5 prime ends that lie adjacent to each other at the top. Each arm consists of a loop and a basal stalk. The 3 prime and 5 prime ends of the t R N A are at the top. They do not form a loop and hence are in the form of two parallel lines. The stalk representing 5 prime terminus is shorter than the 3 prime stalk. The 3 prime stalk is attached to O, single bond, C, single bond, C, single bond, C H 3. C 1 is double bonded to O below. C 2 is single bonded to H above and N H 3 superscript plus below. The R N A consists of bases that are based paired with complementary bases.

Return to Structure of a t R N A

Extended description for Structure of a t R N A



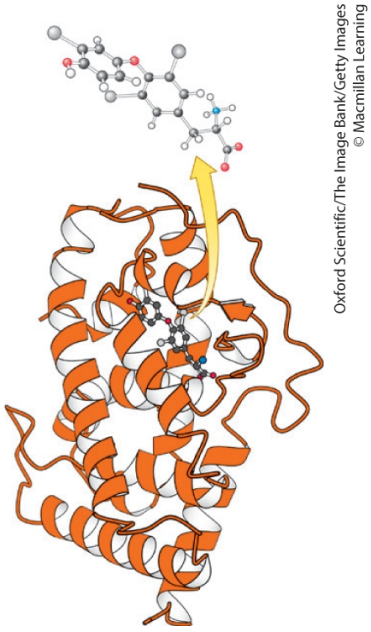
© Macmillan Learning

The secondary structure of R N A resembles a cloverleaf. A single chain of t R N A is folded to form five arms which results in 3 prime and 5 prime ends that lie adjacent to each other at the top. Each arm consists of a loop and a basal stalk. The 3 prime and 5 prime ends of the t R N A are at the top. They do not form a loop and hence are in the form of two parallel lines. The stalk representing 5 prime terminus is shorter than the 3 prime stalk. The 3 prime stalk is single bonded to OH. The R N A consists of bases that are based paired with complementary bases.

Return to Structure of a t R N A

Extended description for Complex biological processes often require coordinated control of the expression of many genes





Oxford Scientific/The Image Bank/Getty Images
© Macmillan Learning

The tadpole on the left has a short oval-shaped body with a broad translucent tail. The ribbon structure of thyroid hormone consists of 6 orange-colored alpha helices and 1 beta sheet attached by loops and turns. The core of the ribbon structure consists of a ball-and-stick model of the thyroid hormone receptor. A zoomed-in view of the ball-and-stick model shows 15 black spheres, 12 white spheres, 3 grey spheres, 4 red spheres, and 1 blue sphere.

Return to Complex biological processes often require coordinated control of the expression of many genes

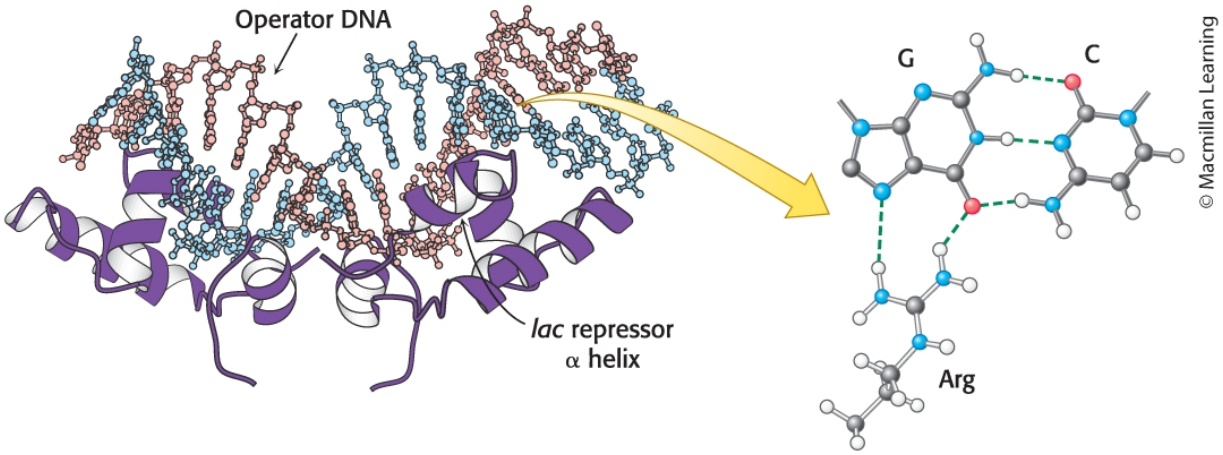
Extended description for FIGURE 31.1 The sequence of the lac regulatory site is a nearly perfect inverted repeat



The sequence of the top strand of the regulatory site in 5 prime to 3 prime direction reads T G T G T G G A A T T G T G A G C G G A T A A C A A T T T C A C A C A. The sequence of the bottom strand in 3 prime to 5 prime direction reads A C A C A C C T T A A C A C T C G C C T A T T G T T A A A G T G T G T. The base G at the eighteenth position of the top strand is paired with C at the eighteenth position of the bottom strand. The bases from positions 1 to 6 and 30 to 35 in the top and bottom strands are highlighted in blue. The bases at the seventh, fourteenth, sixteenth, eighteenth, twentieth, twenty-second, and twenty-ninth positions in the top and bottom strands are highlighted in black. The bases from positions 8 to 13 and 23 to 28 in the top and bottom strands are highlighted in red. The bases at the fifteenth and twenty-first positions in the top and bottom strands are highlighted in purple.

Return to FIGURE 31.1 The sequence of the lac regulatory site is a nearly perfect inverted repeat

Extended description for FIGURE 31.2 The lac repressor binds to operator D N A

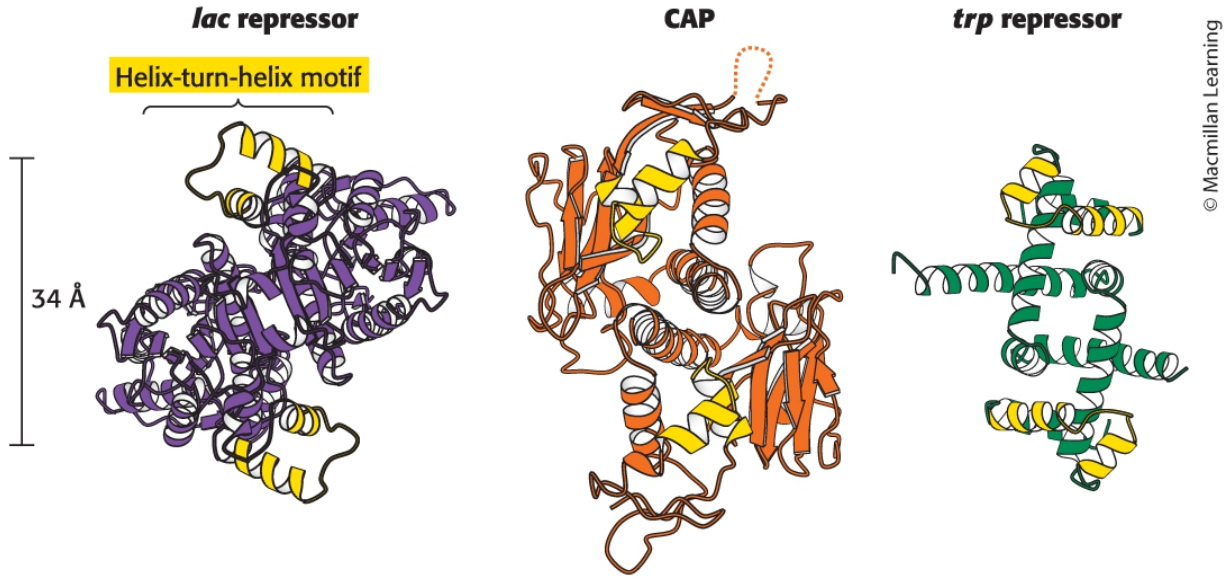


The figure shows a ribbon diagram of the D N A-binding subunit of the lac repressor. It is a dimer composed of two subunits. Each subunit is composed of 3 alpha helices. The subunits are bound to a ball-and-stick model of an operator D N A that consists of blue and orange spheres. One alpha-helix of each repressor extends into the major groove of the operator D N A. A zoomed-in view shows the interaction between the G-C pair of operator D N A and the arginine residue of the repressor. The base G on the left has the following structure: A 6-membered heterocyclic hexagonal ring in a horizontal orientation consists of three grey and two blue spheres. The blue spheres occupy the top left and the rightmost vertices which are the first and third positions, respectively. The first grey sphere is single bonded to a central blue sphere which is further single bonded to a white sphere on the right and a white sphere on the upper left. The second grey sphere of the ring is single bonded to a red sphere. The ring is fused to a 5-membered heterocyclic pentagonal ring in a vertical orientation consisting of 2 blue and three grey spheres. In the pentagonal ring, the blue spheres occupy the bottommost and the top left vertices which are the first and third positions,

respectively. The two rings are fused to each other such that the third and the fourth grey spheres of the hexagonal ring are the third and the second grey spheres of the pentagonal ring, respectively. An open single bond is shown on the upper left of the second blue sphere of the pentagonal ring. The base C on the right has the following structure: A 6-membered heterocyclic hexagonal ring in a horizontal orientation consists of three grey and two blue spheres. The blue spheres occupy the leftmost and the top right vertices which are the first and third positions, respectively. The first grey sphere is single bonded to a red sphere. The fourth grey sphere is single bonded to a central blue sphere which is further single bonded to a white sphere on the left and a white sphere on the lower right. The second blue sphere has an open single bond on the upper right. The second and third grey spheres are each single bonded to a white sphere. The arginine residue has the following structure: A zigzag chain consists of four grey spheres and one blue sphere with the blue sphere occupying the fourth position. The first, second, and third grey spheres are each single bonded to two white spheres. The blue sphere is single bonded to a white sphere. The fourth grey sphere is single bonded to a second blue sphere on the upper right and a third blue sphere on the upper left. Each of the second and third blue spheres are single bonded to two white spheres. The interaction between the spheres of one molecule with that of the other molecule is depicted by dotted lines. In the guanine structure, the white sphere attached to the central blue sphere, the second blue sphere of the hexagonal ring, and the red sphere interact with the red sphere, the first blue sphere, and the white sphere attached to the central blue sphere in the cytosine structure, respectively. In the guanine structure, the first blue sphere of the pentagonal ring and the red sphere interacts with the white spheres attached to the third and second blue spheres of the arginine residue, respectively.

Return to FIGURE 31.2 The lac repressor binds to operator D N A

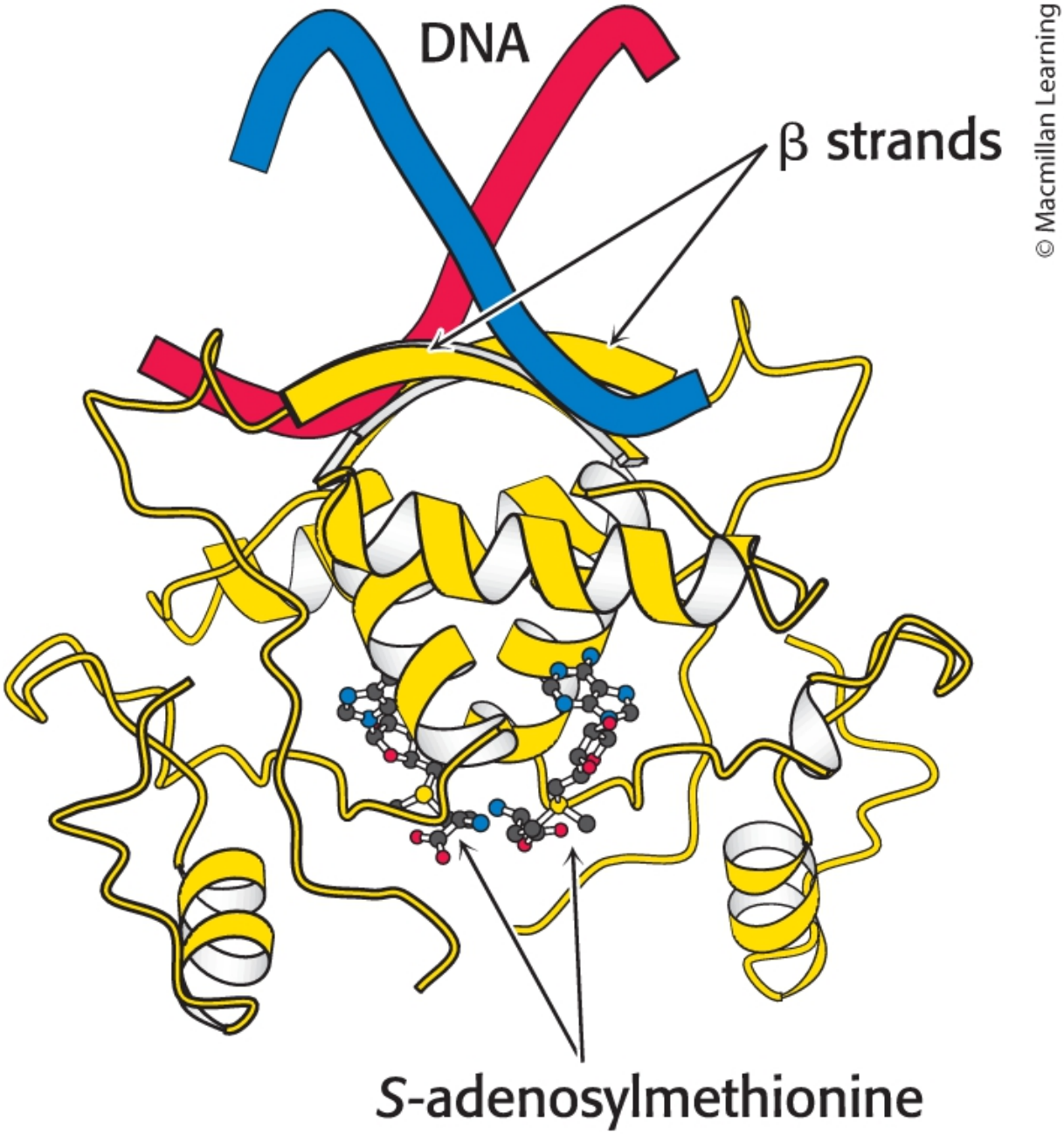
Extended description for FIGURE 31.3 Sequence-specific D N A-binding proteins interact with D N A through a helix-turn-helix motif



The figure shows the ribbon diagrams of the lac repressor, C A P, and t r p repressor. The ribbon diagram of the lac repressor consists of purple-colored alpha helices and beta strands that are coiled together to form two clusters. Each cluster consists of two yellow-colored alpha-helices interconnected by a short loop. These are present at the top and bottom edges of the lac repressor and labeled helix-turn-helix motif. These motifs range about 34 Angstrom. The ribbon diagram of C A P consists of orange-colored alpha helices and beta strands that are coiled together to form two clusters. Each cluster consists of two yellow-colored alpha-helices interconnected by a short loop. The ribbon diagram of the t r p repressor consists of green-colored alpha helices. The alpha helices are attached to yellow-colored alpha helices.

Return to FIGURE 31.3 Sequence-specific D N A-binding proteins interact with D N A through a helix-turn-helix motif

Extended description for FIGURE 31.4 Some D N A-binding proteins recognize specific D N A sequences through beta strands

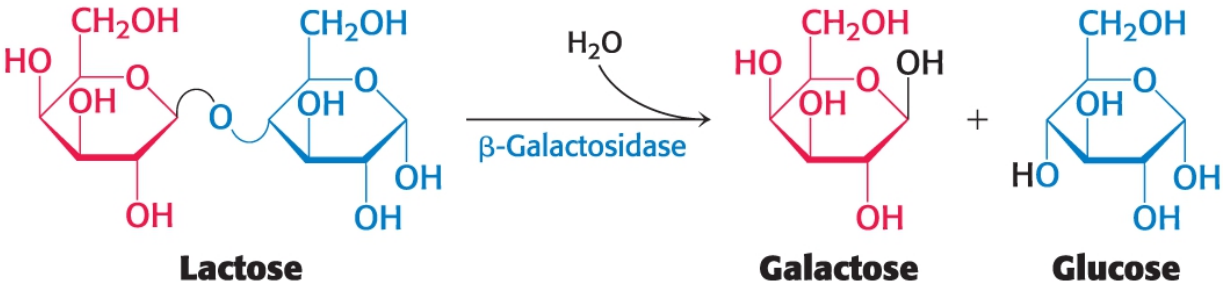


© Macmillan Learning

The methionine repressor consists of yellow-colored alpha helices and beta strands. A ball-and-stick model of S-adenosylmethionine is attached to the core of the beta strands of the methionine repressor. The ball and stick model consists of grey, blue, and red spheres. One of the beta-strands of the methionine repressor at the top is bound to an X-shaped blue and red flat ribbon structure labeled D N A.

Return to FIGURE 31.4 Some D N A-binding proteins recognize specific D N A sequences through beta strands

Extended description for Formation of galactose and glucose

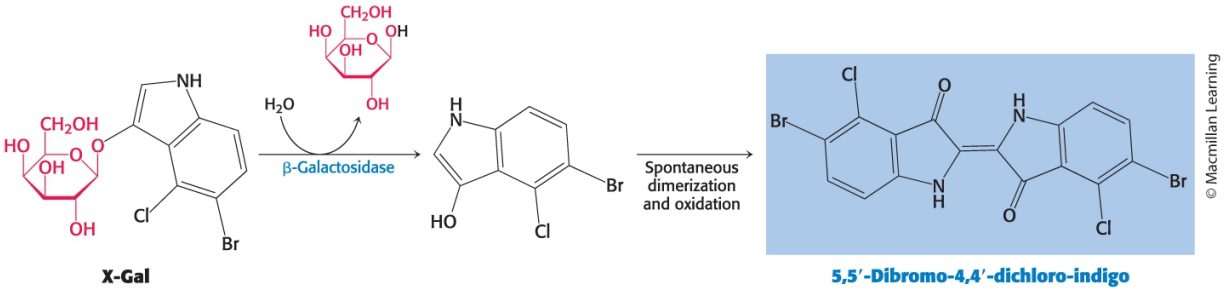


Lactose undergoes hydrolysis in the presence of beta-galactosidase to give rise to galactose and glucose. The structure of lactose is as follows: A 6-membered heterocyclic hexagonal ring is in a horizontal orientation and consists of 1 O and 5 C atoms. The O atom occupies the first position, which is the top right vertex. The ring is in a plane perpendicular to the plane of the observer such that C 5 and O are away from the observer and C 2 and C 3 are toward the observer. C 2 is single-bonded to O H below. C 3 and C 4 are each single-bonded to O H above. C 5 is single-bonded to C H 2 O H above. C 1 is single-bonded to O on the right. The ring and its attached groups are highlighted in red. The O attached to C 1 is single-bonded to C 4 of a second 6-membered heterocyclic hexagonal ring in a horizontal orientation consisting of 1 O and 5 C atoms. In the second ring, the O atom occupies the first position, which is the top right vertex. The second ring is in a plane perpendicular to the plane of the observer such that C 5 and O are away from the observer and C 2 and C 3 are toward the observer. In the second ring, C 1 and C 2 are each single bonded to O H below, C 3 is single bonded to O H above, and C 5 is single-bonded to C H 2 O H above. The second ring and its attached groups are highlighted in blue. The structure of galactose is as follows: A 6-membered heterocyclic hexagonal ring is in a horizontal orientation and consists of 1 O and 5 C atoms. O occupies

the top right vertex. The ring is in a plane perpendicular to the plane of the observer such that C 5 and O are away from the observer and C 2 and C 3 are toward the observer. C 1, C 3, and C 4 are each single bonded to O H above. C 2 is single-bonded to O H below. C 5 is single-bonded to C H 2 O H above. The ring and all its attached groups except for O H attached to C 1 are highlighted in red. The structure of glucose is as follows: A 6-membered heterocyclic hexagonal ring is in a horizontal orientation and consists of 1 O and 5 C atoms. O occupies the top right vertex. The ring is in a plane perpendicular to the plane of the observer such that C 5 and O are away from the observer and C 2 and C 3 are toward the observer. C 1, C 2, and C 4 are each single-bonded to O H below. C 3 is single-bonded to O H above. C 5 is single-bonded to C H 2 O H above.

Return to Formation of galactose and glucose

Extended description for FIGURE 31.5 The Beta-galactosidase reaction can be monitored using a colored indicator.



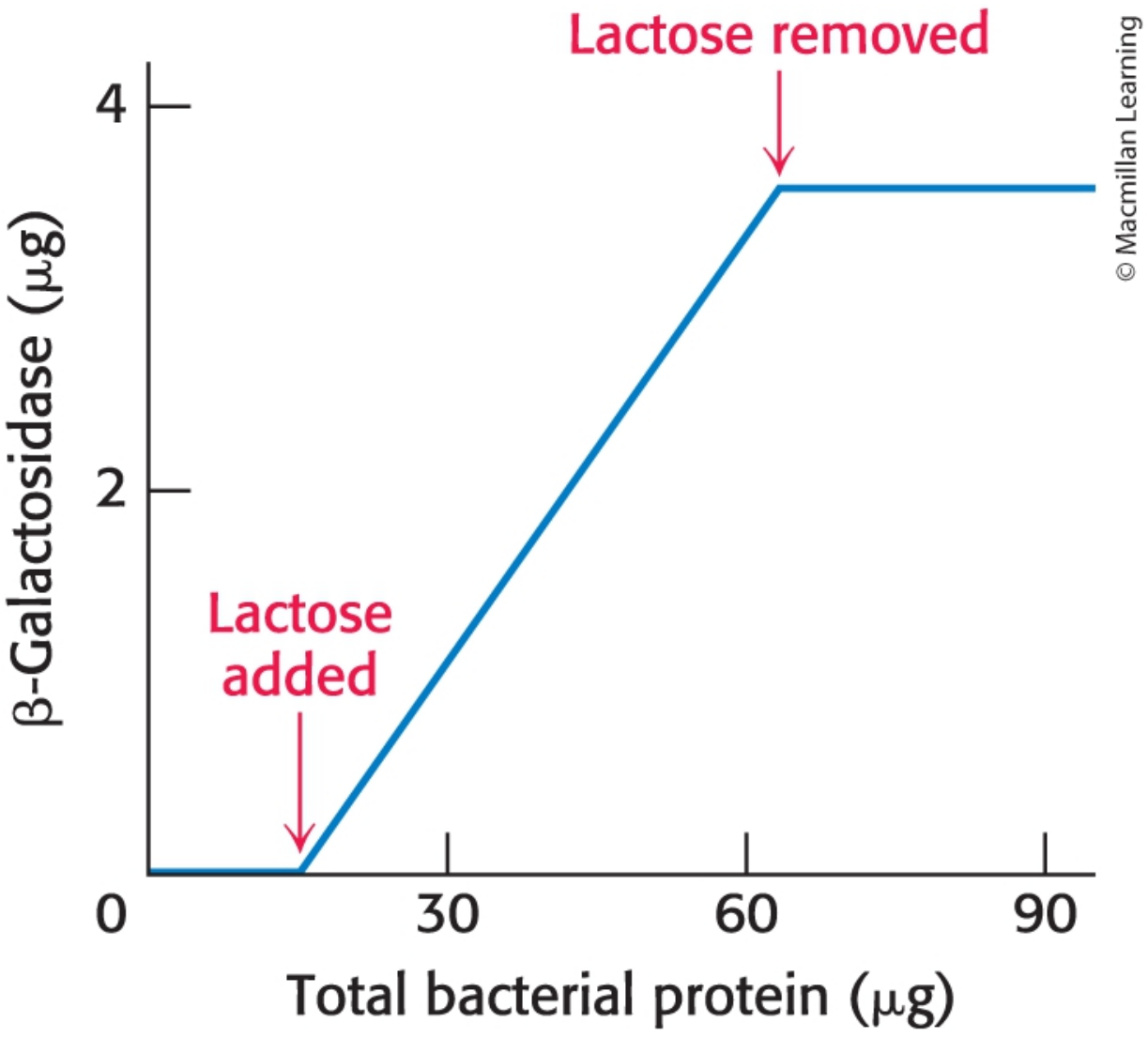
The coupled reaction consists of two steps and contains one reactant, one intermediate, and one product. In the first step, X-Gal is transformed to an intermediate by the action of betagalactosidase. This is coupled with the entry of H 2 O and release of galactose. The structure of X-Gal is as follows: A 5-membered heterocyclic pentagonal ring is in a horizontal orientation and consists of 1 N and 4 C atoms. N bound to H occupies the first position, which is the top right vertex. A double bond is present between C 3 and C 4. This ring is fused to a benzene ring in a vertical orientation with C 1 occupying the topmost vertex. The benzene ring contains alternating double bonds between C 2 and C 3, C 4 and C 5, and C 6 and C 1. The two rings are fused to each other such that C 1 and C 2 of the 5-membered ring are the C 1 and C 6 of the benzene ring, respectively. In the benzene ring, C 4 is single bonded to B r and C 5 is single bonded to C l. C 3 of the 5-membered ring is single-bonded to O on the lower left. O is single bonded to C 1 of a 6-membered heterocyclic hexagonal ring in a horizontal orientation consisting of 1 O and 5 C atoms. In the hexagonal ring, the O atom occupies the first position, which is the top right vertex. The hexagonal ring is in a plane perpendicular to the plane of the paper such that C 5 and O are away from the observer and C 2 and C 3 are toward the observer.

In the hexagonal ring, C 2 is single bonded to O H below, C 3 and C 4 are each single bonded to O H above, and C 5 is single bonded to C H 2 O H above. The hexagonal ring and its attached groups are highlighted in red. The structure of Galactose is as follows: A 6-membered heterocyclic hexagonal ring is in a horizontal orientation consisting of 1 O and 5 C atoms. The O atom occupies the first position, which is the top right vertex. The ring is in a plane perpendicular to the plane of the paper such that C 5 and O are away from the observer and C 2 and C 3 are towards the observer. C 1 is single bonded to O H above. C 2 is single bonded to O H below. C 3 and C 4 are each single bonded to O H above. C 5 is single bonded to C H 2 O H above. The ring is highlighted in red with the exception of H of O H single bonded to C 1. The structure of the intermediate is as follows: A 5-membered heterocyclic pentagonal ring is in a horizontal orientation and consists of 1 N and 4 C atoms. N bound to H occupies the first position, which is the top left vertex. A double bond is present between C 3 and C 4. C 3 is single bonded to O H. This ring is fused to a benzene ring in a vertical orientation with C 1 occupying the topmost vertex. The two rings are fused to each other such that C 1 and C 2 of the pentagonal ring are the C 6 and C 5 of the benzene ring, respectively. In the benzene ring, double bonds are present between C 1 and C 2, C 3 and C 4, and C 5 and C 6. In the benzene ring, C 3 is single bonded to B r and C 4 is single bonded to C l. In the second step, the intermediate is transformed to 5, 5 prime Dibromo-4, 4 prime dichloro indigo through spontaneous dimerization and oxidation. The structure of 5, 5 prime Dibromo-4, 4 prime dichloro indigo is as follows: A benzene ring is in a vertical orientation with C 1 occupying the topmost vertex. The ring contains alternating double bonds between C 2 and C 3, C 4 and C 5, and C 6 and C 1. C 1 is single bonded to C l and C 6 is single bonded to B r. The benzene ring is fused to a 5-membered heterocyclic pentagonal ring in a horizontal orientation with 1 N and 4 C atoms. In the pentagonal ring, N bound to H occupies the first position which is the bottom right vertex. The two rings are fused such that C

2 and C 3 of the benzene ring are C 2 and C 1 of the 5-membered ring, respectively. In the pentagonal ring, C 3 is double bonded to O. C 4 of the 5-membered ring is double bonded to C 4 of a second 5-membered heterocyclic pentagonal ring in horizontal orientation with 1 N and 4 C atoms. In the second pentagonal ring, N bound to H occupies the top left vertex. In the second pentagonal ring, C 3 is double bonded to O. The second 5-membered ring is fused to a second benzene ring in a vertical orientation with C 1 occupying the topmost vertex. In the second benzene ring, double bonds are present between C 1 and C 2, C 3 and C 4, and C 5 and C 6. The two rings are fused such that C 1 and C 2 of the second 5-membered ring are the C 6 and C 5 of the second benzene ring, respectively. In the second benzene ring, C 3 is single bonded to B r and C 4 is single bonded to C l.

Return to FIGURE 31.5 The Beta-galactosidase reaction can be monitored using a colored indicator.

Extended description for FIGURE 31.6 The production of β-galactosidase can be increased by the addition of lactose

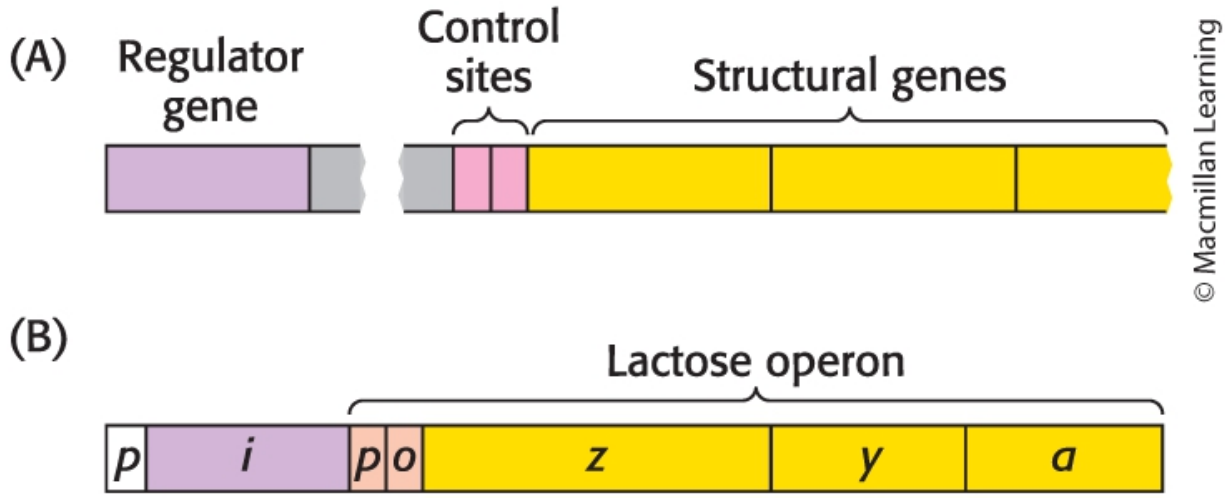


The horizontal axis, labeled total bacterial protein in micrograms, has markings ranging from 0 to 90 in increments of 30 units. The vertical axis, labeled beta-galactosidase in micrograms, has markings ranging from 0 to 4 in increments of 2 units. The graph starts from (18, 0), moves linearly to the upper right to (60, 3.5),

moves to the right, and terminates at (90, 3.5). The coordinate (18, 0) is labeled lactose added and the coordinate (60, 3.5) is labeled lactose removed. All values are approximated.

Return to FIGURE 31.6 The production of β-galactosidase can be increased by the addition of lactose

Extended description for FIGURE 31.7 Operons are clusters of genes under a common control



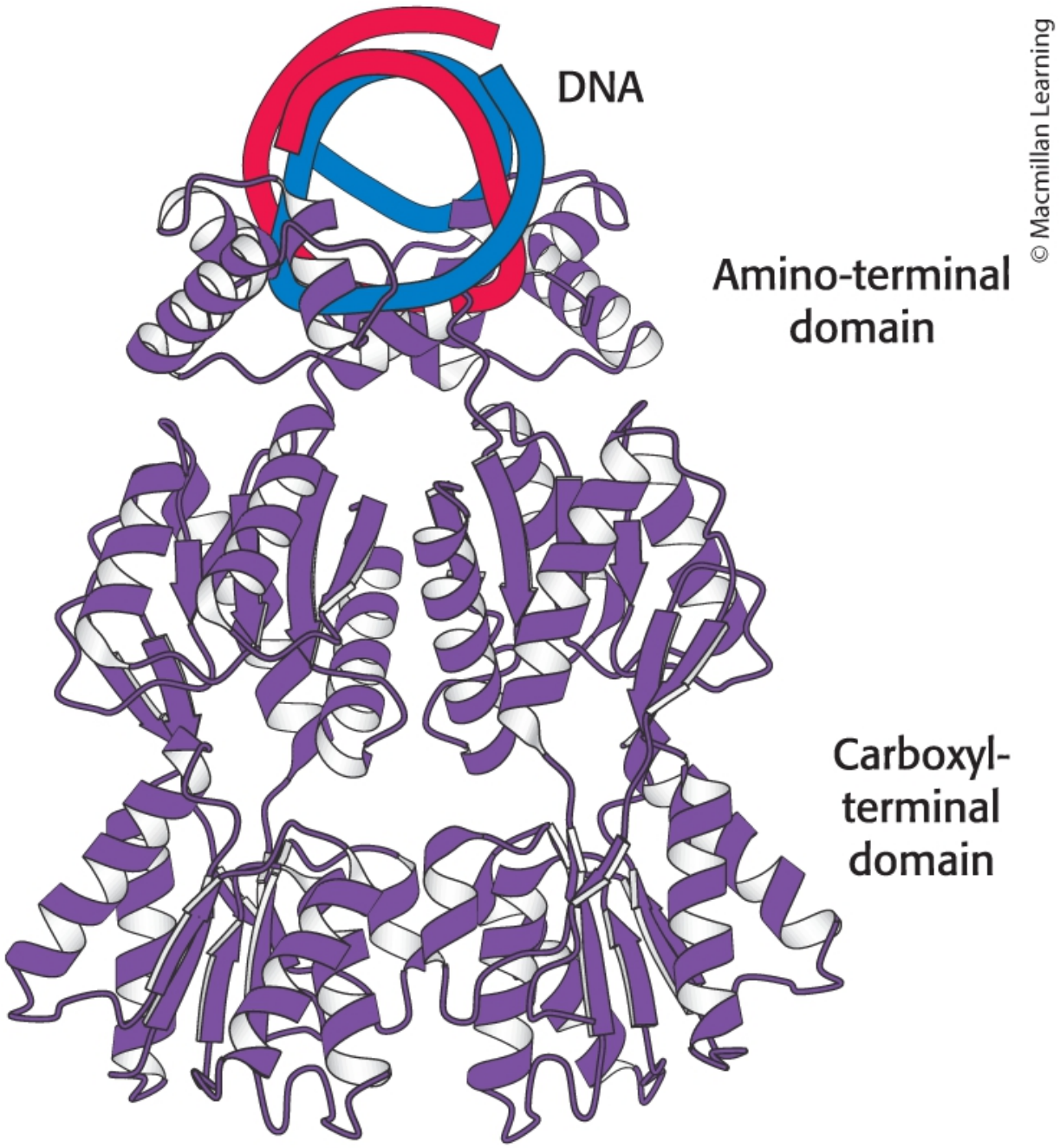
© Macmillan Learning

(A) General structure of operon: The figure shows a horizontal bar with regulator genes, control sites, and structural genes. The regulator gene is separated from the control sites and structural genes by a break. There are two control sites depicted in pink and three yellow structural genes depicted in yellow.

(B) Structure of Lactose operon: The figure shows a horizontal bar with a regulator gene attached to the lactose operon. The regulator gene is divided into two parts and is labeled p and i. The lactose operon has two control sites depicted in pink labeled p and o and three structural genes depicted in yellow labeled z, y, and a.

Return to FIGURE 31.7 Operons are clusters of genes under a common control

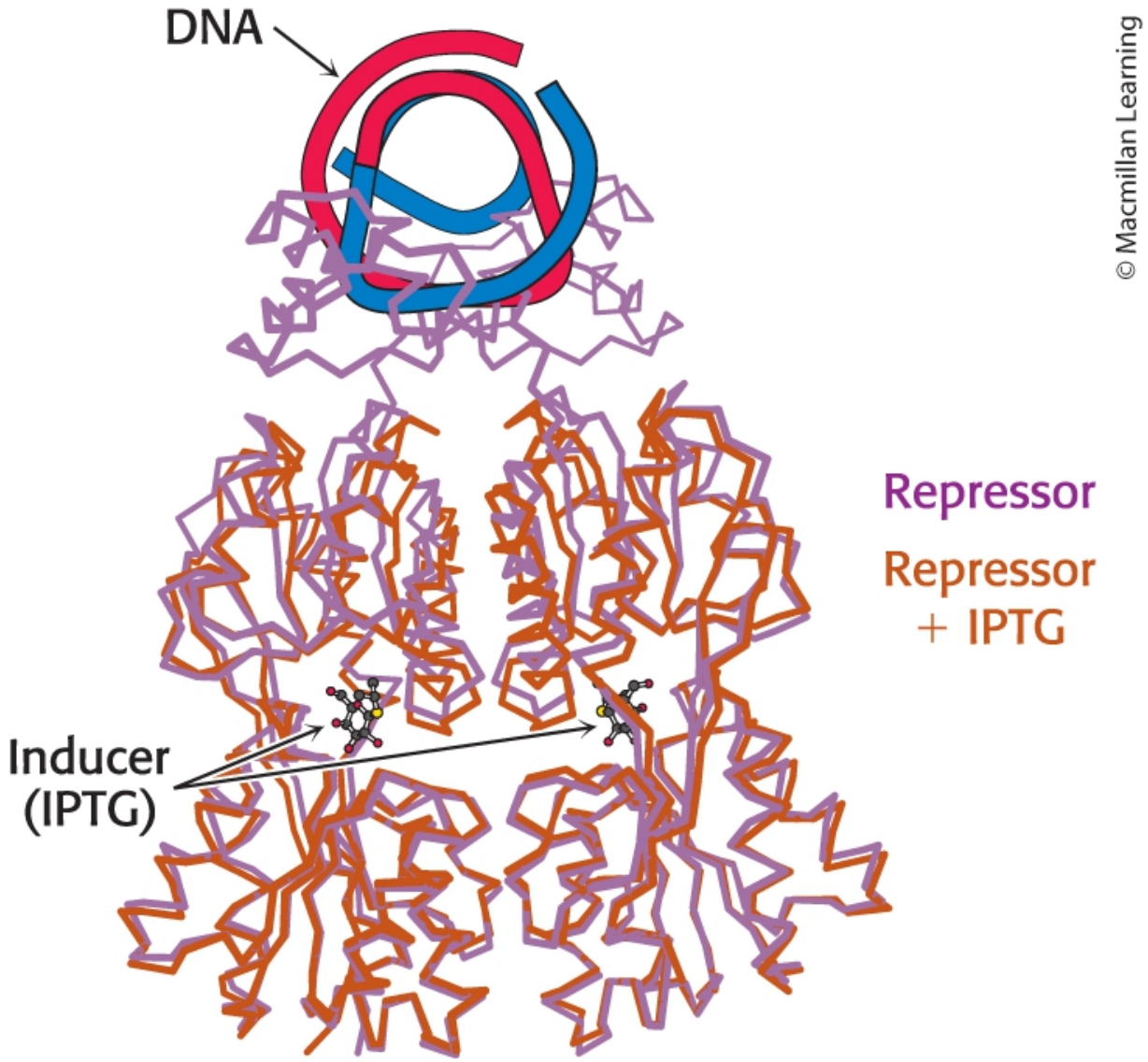
Extended description for FIGURE 31.8 The lac repressor binds to D N A as a dimer



The figure shows a lac repressor consisting of three functional regions. The upper region is labeled amino-terminal domain and the lower region is labeled carboxyl-terminal domain. Two red and two blue colored flat ribbon-like structures labeled D N A are attached to the amino-terminal domain of the lac repressor. The amino-terminal region consists of four parallel purple-colored beta strands. The middle functional region consists of six parallel purple-colored beta strands. The carboxyl-terminal domain consists of four parallel purple-colored beta strands. These functional regions are connected through alpha helices.

Return to FIGURE 31.8 The lac repressor binds to D N A as a dimer

Extended description for FIGURE 31.9 Binding of I P T G alters the lac repressor structure and affects its ability to bind D N A

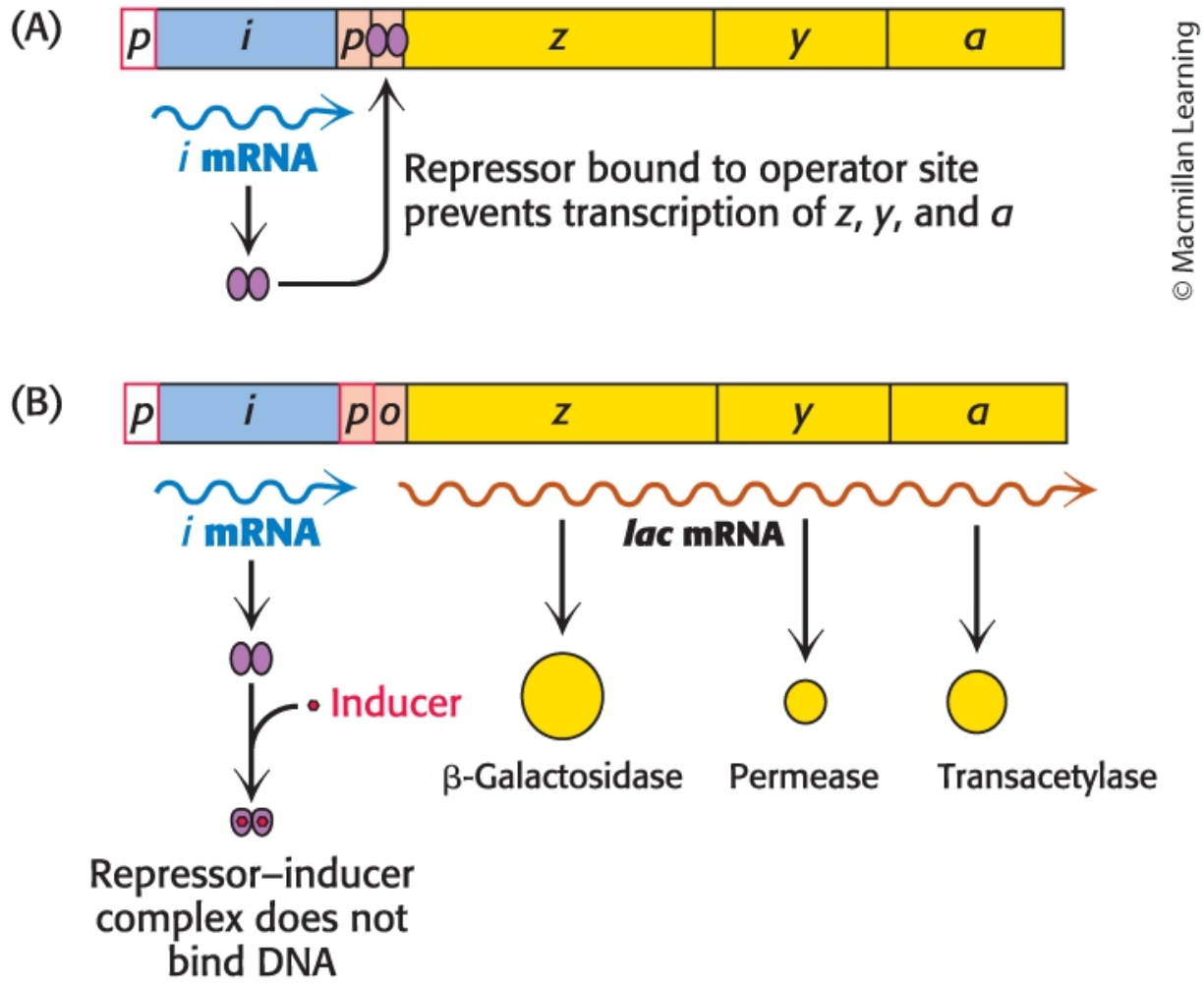


The figure shows two red and two blue colored flat ribbon-like structures labeled D N A attached to the lac repressor. The lac repressor consists of three functional regions from top to bottom. It is depicted as purple-colored zigzag strands. Orange-colored zigzag

strands superimposed on the lac repressor are labeled repressor I P T G. The repressor plus I P T G consists of two ball and stick models attached at the core of the functional region.

Return to FIGURE 31.9 Binding of I P T G alters the lac repressor structure and affects its ability to bind D N A

Extended description for FIGURE 31.10 The lac operon can be induced



© Macmillan Learning

The figure has two parts.

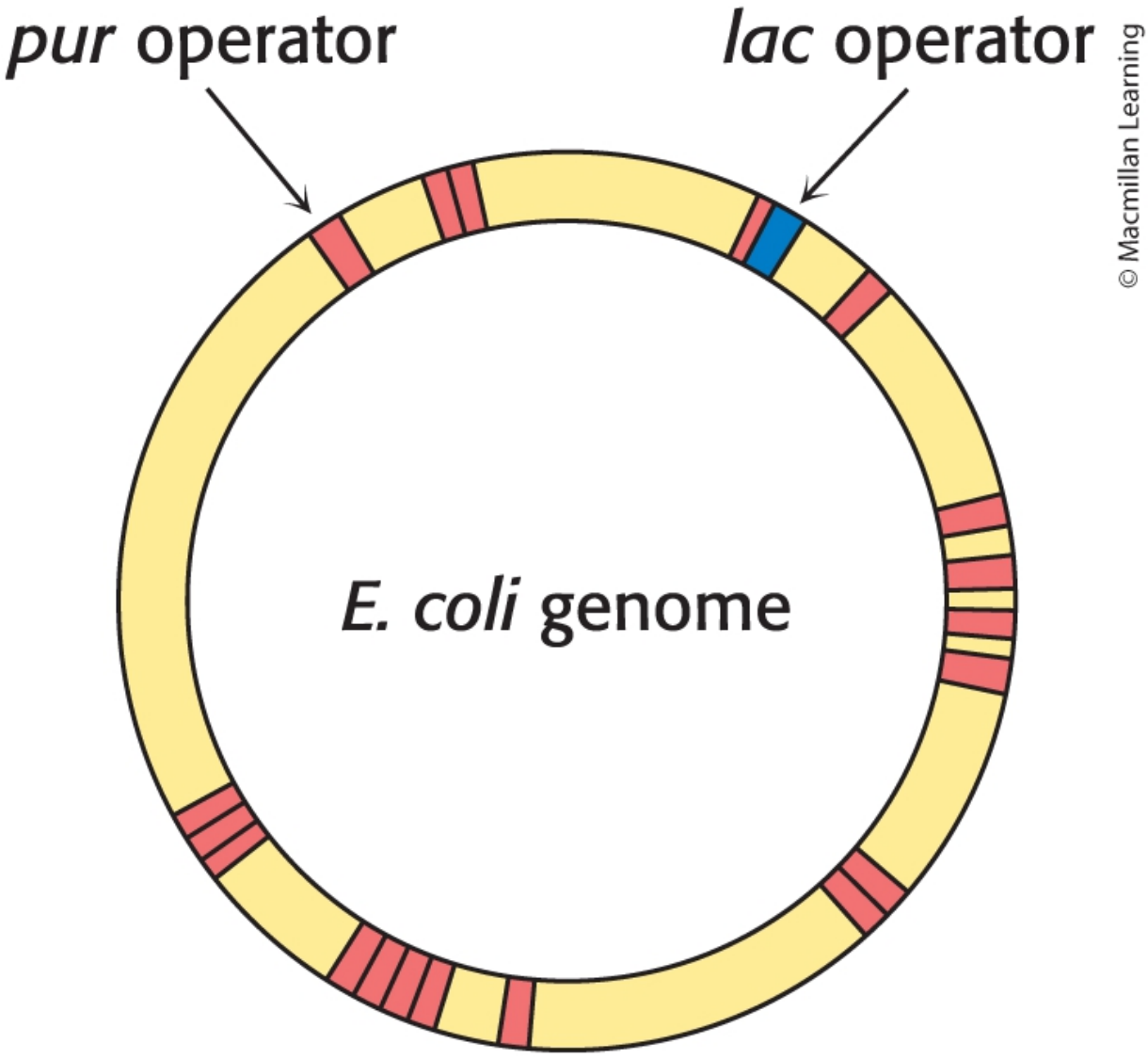
Part A: The figure shows a horizontal bar with a regulator gene attached to the lactose operon. The regulator gene is divided into two parts and is labeled p and i. The lactose operon has two control sites depicted in pink labeled p and o and three structural genes depicted in yellow labeled z, y, and a. Below the regulator gene a right wavy arrow labeled i m R N A is present. A downward arrow

from i m R N A points to two spheres attached side by side. The spheres represent the repressor. An arrow from the repressor points to the operator site on the horizontal bar. The arrow reads the repressor bound to the operator site and prevents transcription of z, y, and a.

Part B: The figure shows a horizontal bar with a regulator gene attached to the lactose operon. The regulator gene is divided into two parts and is labeled p and i. The lactose operon has two control sites depicted in pink labeled p and o and three structural genes depicted in yellow labeled z, y, and a. Below the regulator gene a right wavy arrow labeled i m R N A is present. A downward arrow from i m R N A points to two spheres attached side by side. The spheres represent the repressor. Small pink-colored structures labeled inducer bind to the repressor. The text below the repressor bound to the inducer reads repressor-inducer complex does not bind to D N A. A right wavy arrow below the lactose operon region of the horizontal bar is labeled lac m R N A. Three downward arrows from the z, y, and a point down to three yellow spheres at the bottom. The yellow spheres are labeled beta-galactosidase, permease, and transacetylase, respectively.

Return to FIGURE 31.10 The lac operon can be induced

Extended description for FIGURE 31.11 Operator sites are not distributed evenly across the E. coli genome

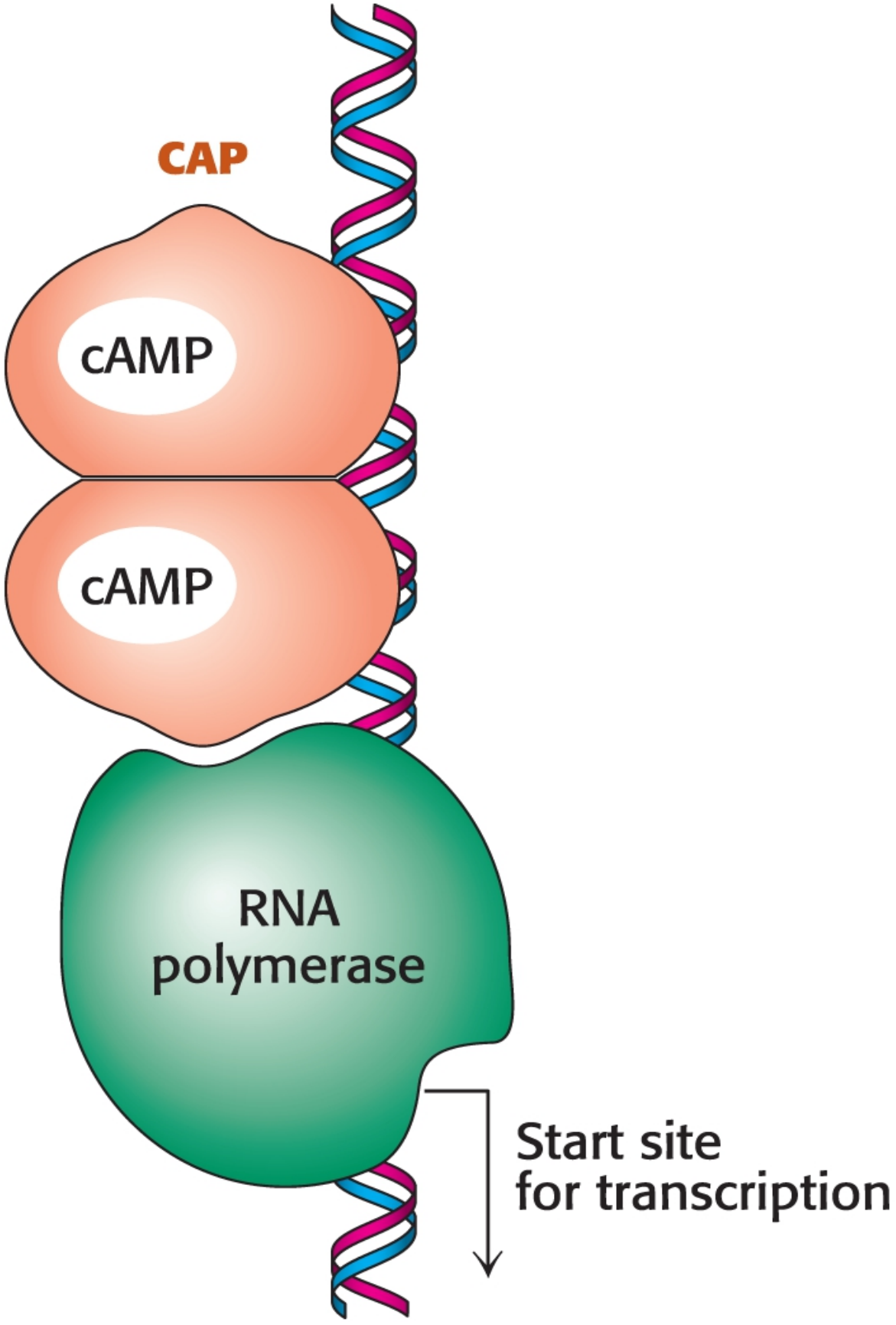


The circular genome of E.coli consists of 19 bands of pur operator shown as red bands in clusters or individually throughout the genome. It also consists of a single band of lac operator shown as a blue band in the genome.

Return to FIGURE 31.11 Operator sites are not distributed evenly across the E. coli genome

Extended description for FIGURE 31.12 The catabolite

activator protein (CAP) binds to DNA as a dimer

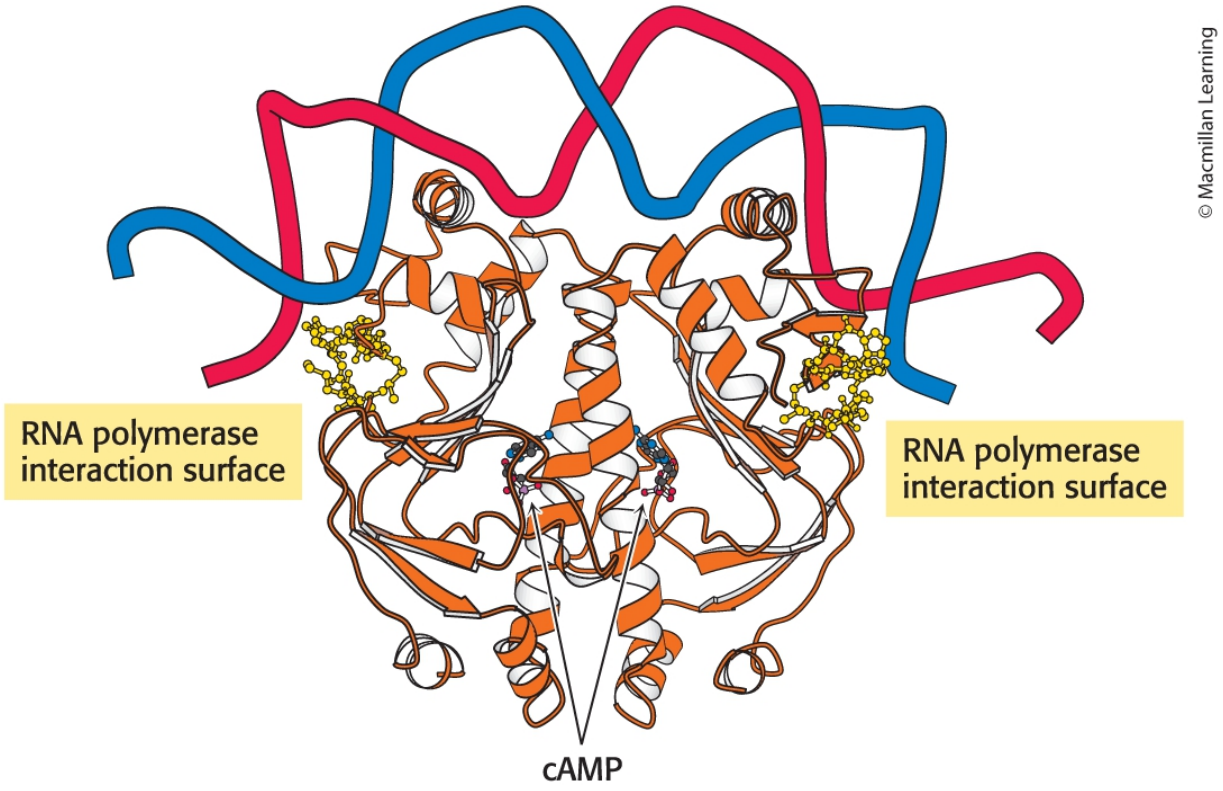


© Macmillan Learning

The figure shows a vertical double helix consisting of red and blue strands wrapped around each other. The upper end of the double helix is attached to two c A M P receptor proteins. c A M P is bound to CAP. R N A polymerase binds to the double helix below the c A M P and it is the site where the transcription starts.

Return to FIGURE 31.12 The catabolite activator protein (CAP) binds to DNA as a dimer

Extended description for The CAP dimer binds to D N A and to R N A polymerase

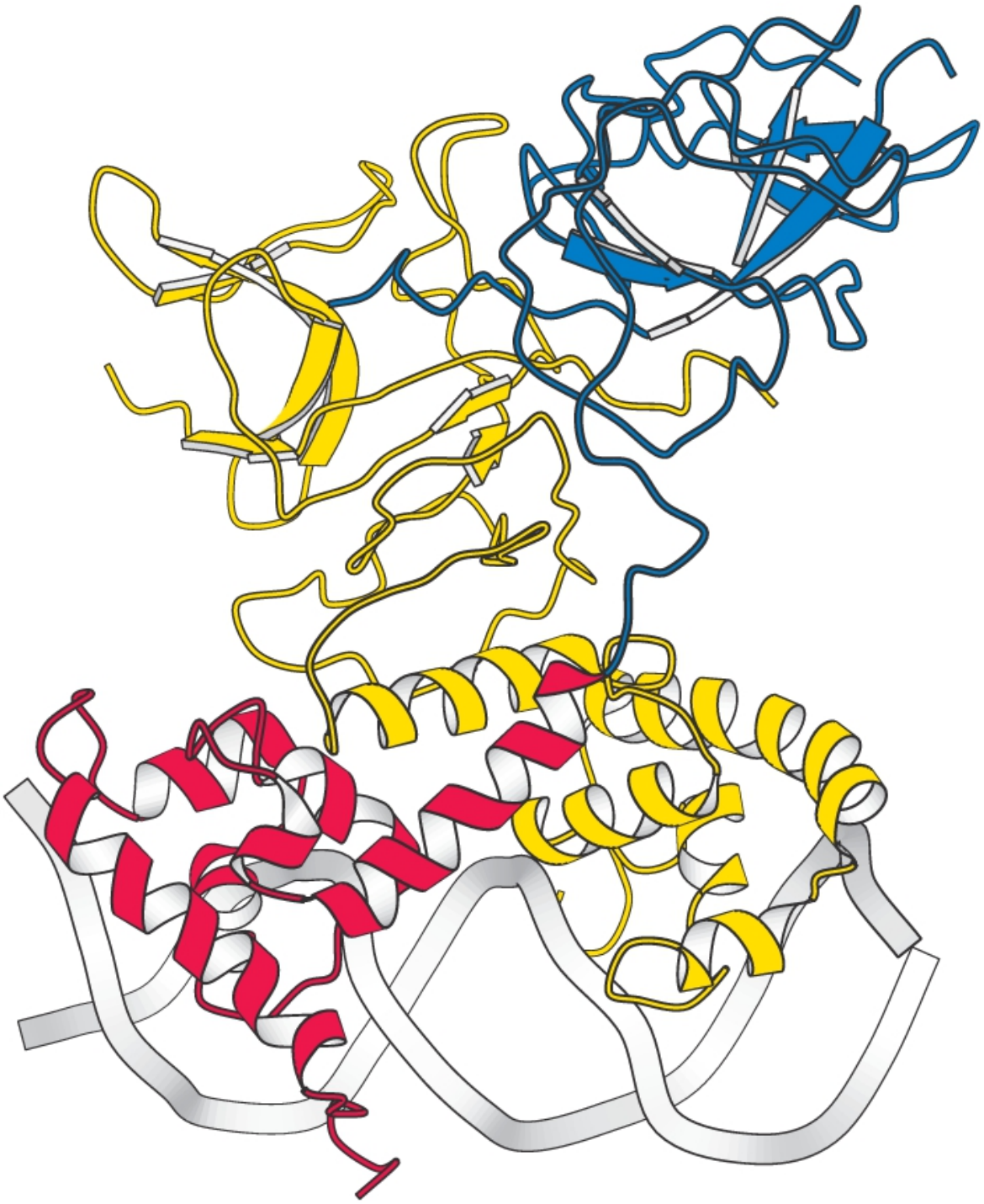


© Macmillan Learning

The figure shows a D N A double helix consisting of red and blue flat-ribbon-like structures at the top. The D N A binds to a CAP dimer at the bottom. The CAP dimer is formed by two CAP monomers. The CAP dimer consists of alpha helices and beta strands. The alpha helices of each monomer consisting of a ball-and-stick model. The region of attachment of the space-filling ball-and stick-model to the alpha helices is labeled R N A polymerase interaction surface. The core of each CAP monomer consists of a space-filling ball-and-stick model with blue and red spheres. These space-filling models are labeled c A M P.

Return to The CAP dimer binds to D N A and to R N A polymerase

Extended description for FIGURE 31.14 The lambda repressor binds to D N A as a dimer

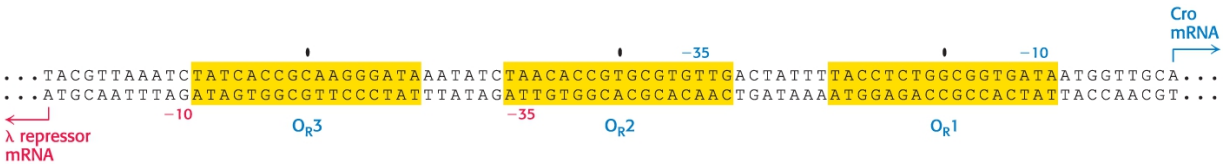


© Macmillan Learning

The figure shows a double-stranded grey-colored D N A in a horizontal orientation. Red and yellow ribbon structures with alpha helices and beta strands are attached to the major groove of the D N A from the top. The red and yellow ribbon structures represent the two subunits of the amino-terminal domain. The alpha helices of the two subunits extend upward and attach to the ribbon diagram with beta strands shown in blue and yellow at the top via loops and turns. The blue and yellow beta strands and the loops represent the carboxyl-terminal domain.

Return to FIGURE 31.14 The lambda repressor binds to D N A as a dimer

Extended description for FIGURE 31.15 The sequence of the lambda right operator is a binding target for regulatory proteins



The figure shows two sequences.

The sequence of the top strand reads ellipses A T A C G T T A A A T C T A T C A C C G C A A G G G A T A A A T A T C T A A C A C C G T G C G T G T T G A C T A T T T T A C C T C T G G C G G T G A T A A T G G T T G C A ellipses. An arrow from the top strand points toward the right. The arrow is labeled Cro m R N A.

The sequence of the bottom strand reads ellipses A T G C A A T T T A G A T A G T G G C G T T C C C T A T T T A T A G A T T G T G G C A C G C A C A A C T G A T A A A A T G G A G A C C G C C A C T A T T A C C A A C G T ellipses. An arrow from the bottom strand points toward the left. The arrow is labeled lambda repressor m R N A.

The bases from the twelfth position to the twenty-eighth position of both strands are highlighted in yellow and labeled O R 3. The bases from the thirty-fourth position to the fiftieth position of both strands are highlighted in yellow and labeled O R 2. The bases from the fifty-eighth position to the seventy-fourth position of both strands are highlighted in yellow and labeled O R 1.

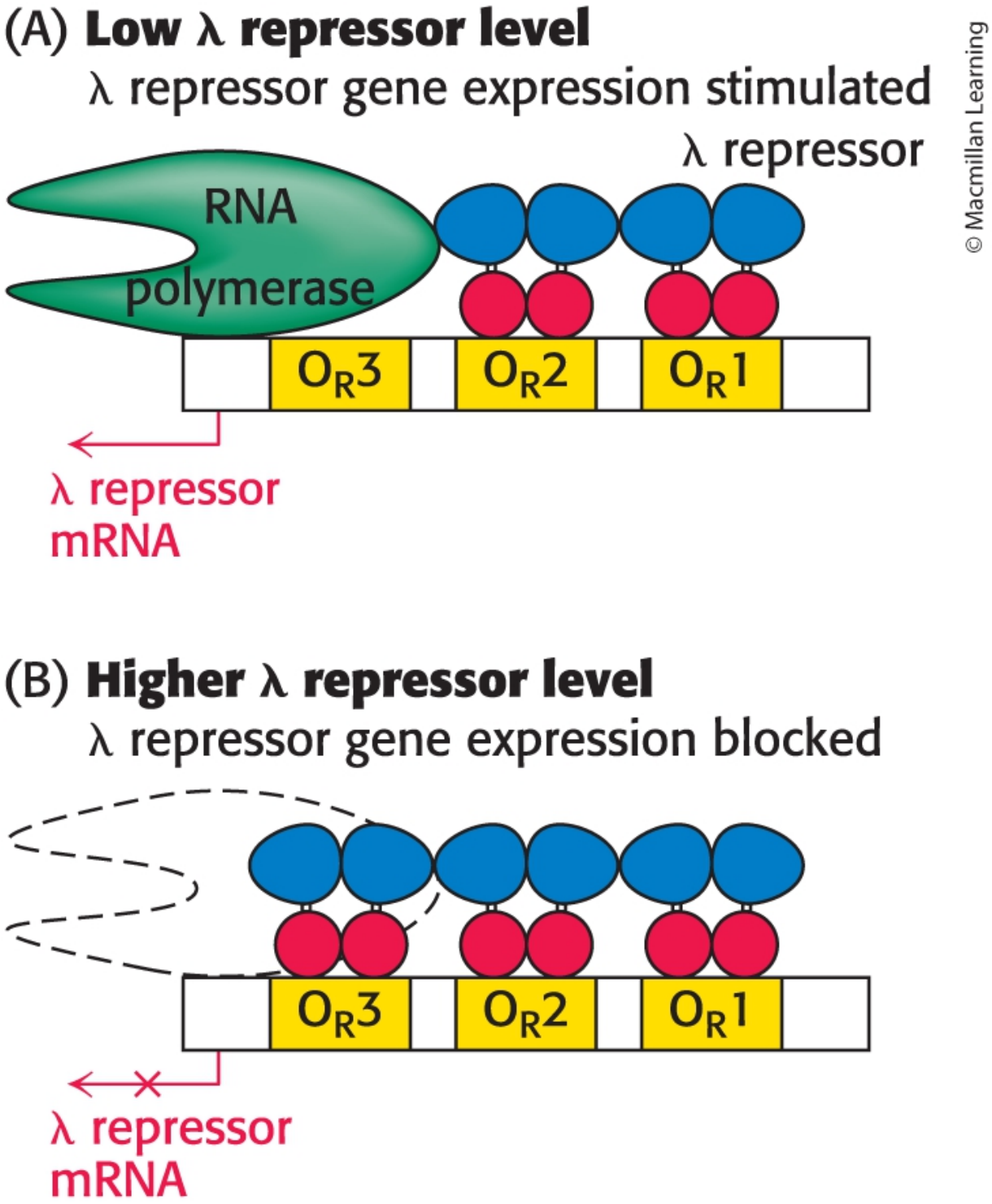
O R 1, O R 2, and O R 3 represent the operator sites. The centers of each of the operator sites are indicated by a small stroke at the top.

The right side of the O R 2 and O R 1 regions of the top strand is labeled negative 35 and negative 10, respectively. The left side of O R 3 and O R 2 regions of the bottom strand are labeled negative 10 and negative 35, respectively.

Return to FIGURE 31.15 The sequence of the lambda right operator is a binding target for regulatory proteins

Extended description for FIGURE 31.16 The lambda

repressor controls its own synthesis



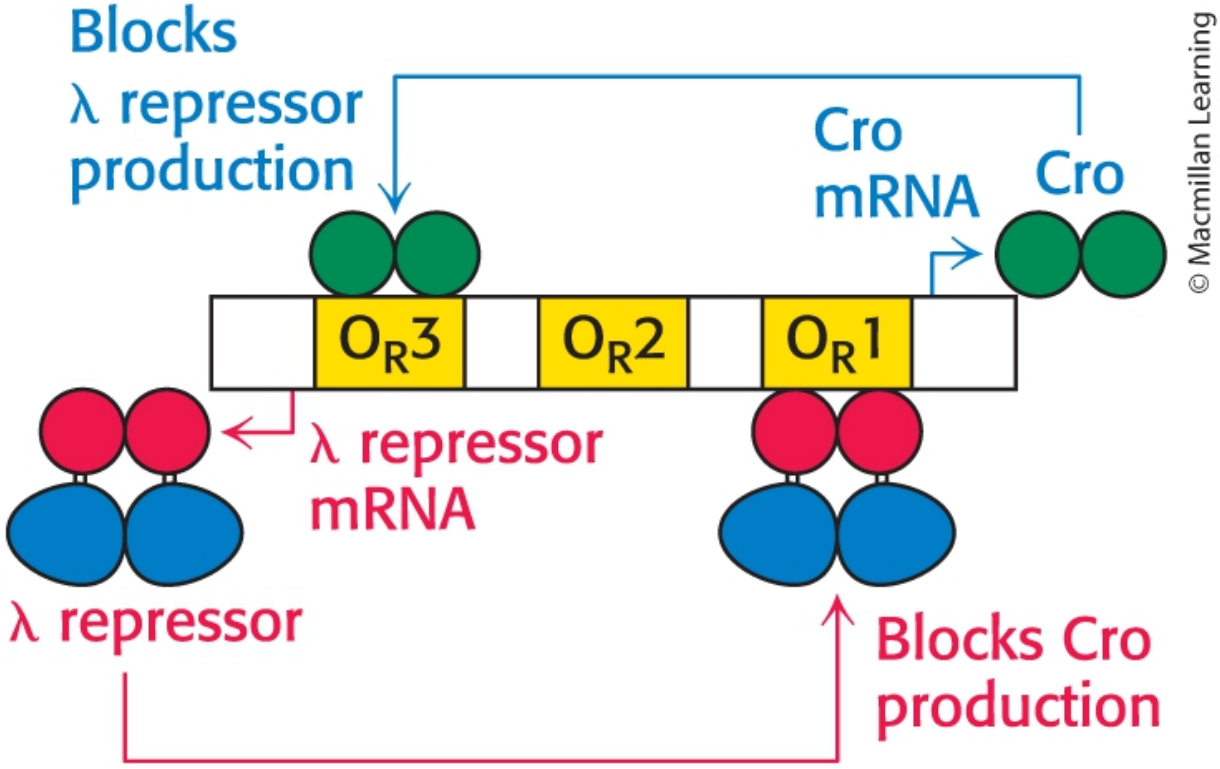
© Macmillan Learning

Part A: Low lambda repressor level: A figure depicts a repressor strand with sequence O R 3-O R 2-O R 1 each depicted as a yellow box in a horizontal set of boxes. A green-colored oval structure with a groove on the left labeled R N A polymerase binds to the site O R 3 at the top. A lambda repressor binds to O R 2 and O R 1. Lambda repressor consists of two red spheres attached to two blue oval-shaped structures at the top. An arrow from the repressor strand pointing toward the left is labeled lambda repressor m R N A. A text at the top reads lambda repressor gene expression stimulated.

Part B: Higher lambda repressor level: The figure shows a repressor strand with sequence O R 3-O R 2-O R 1 each depicted as a yellow box in a horizontal set of boxes. A dotted oval structure with a groove on the left labeled R N A polymerase binds to the site O R 3 at the top. A lambda repressor binds to each O R 3, O R 2, and O R 1 at the top. An arrow from the repressor strand pointing toward the left is cross marked and is labeled lambda repressor m R N A. A text at the top reads lambda repressor gene expression blocked.

Return to FIGURE 31.16 The lambda repressor controls its own synthesis

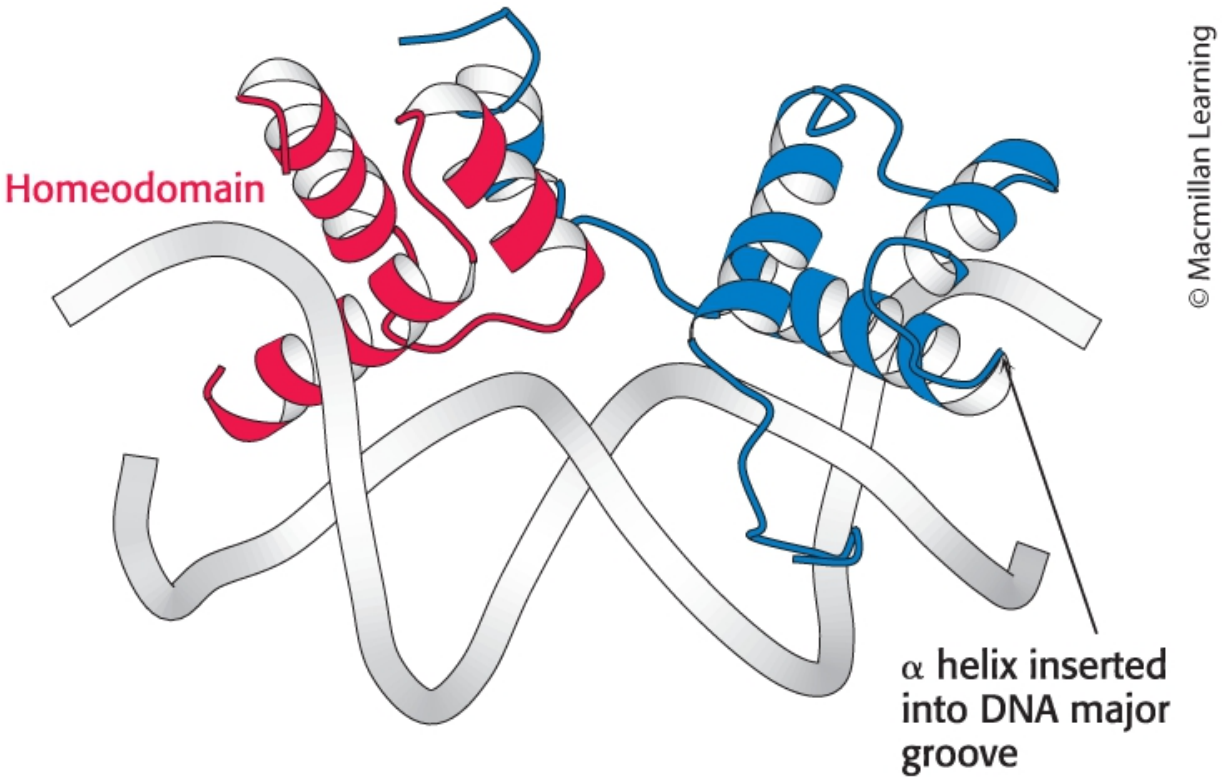
Extended description for FIGURE 31.17 The lambda repressor and Cro form a genetic circuit



The figure depicts a repressor strand with sequence O R 3-O R 2-O R 1 each depicted as a yellow box in a horizontal set of boxes. Two green spheres attached side by side representing Cro are present on the top right. Two red spheres attached to two blue oval-shaped structures representing lambda repressor is present on the bottom left. Cro binds to O R 3 and blocks the lambda repressor production. Lambda repressor binds to O R 1 and blocks the production of Cro. An arrow from the repressor strand on the top right pointing toward cro is labeled Cro m R N A. An arrow from the repressor strand on the bottom left pointing toward lambda repressor is labeled lambda repressor m R N A.

Return to FIGURE 31.17 The lambda repressor and Cro form a genetic circuit

Extended description for FIGURE 31.18 Two different D N A-binding homeodomains can form a heterodimer

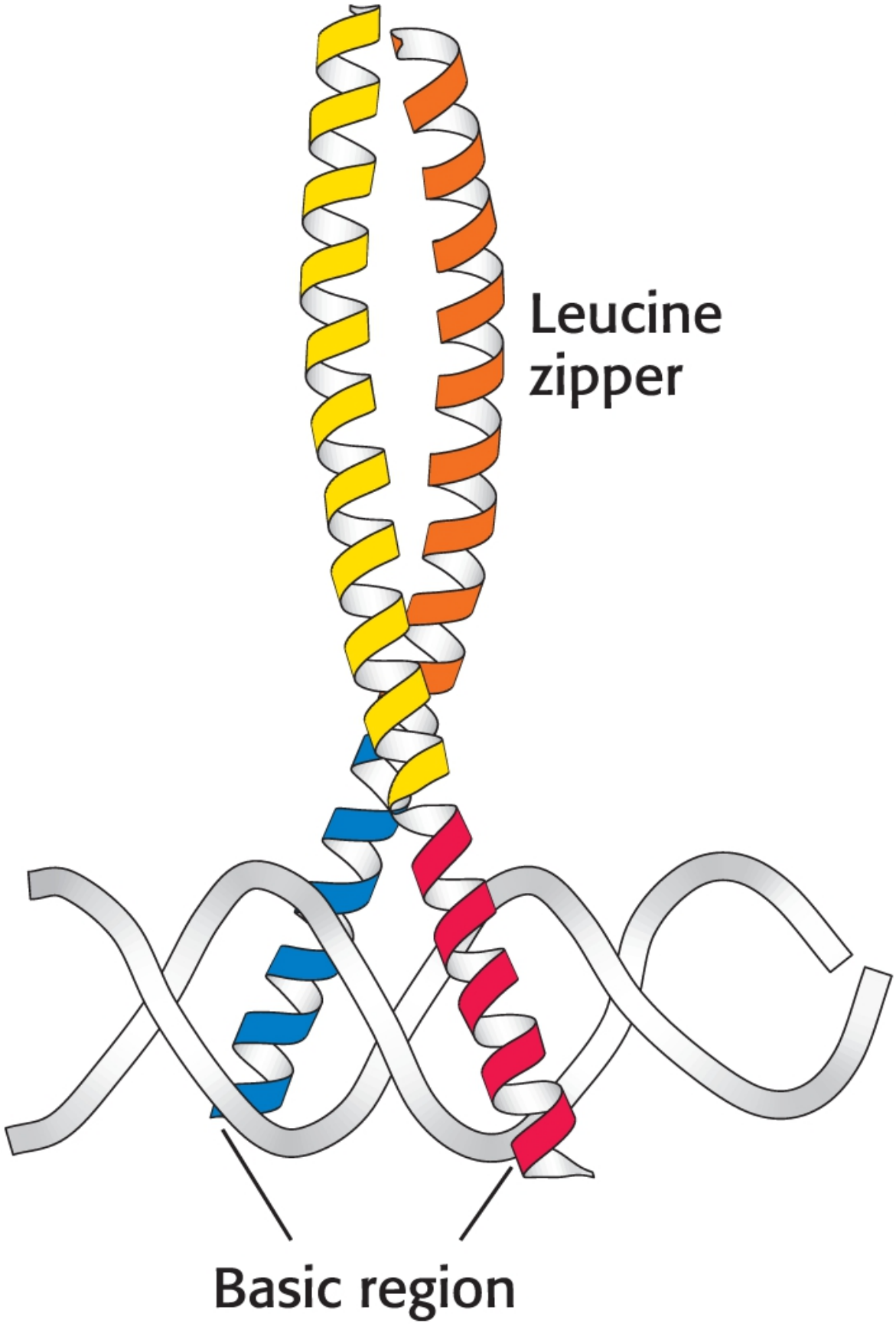


The figure shows a double-stranded grey colored D N A in a horizontal orientation. The D N A is attached to two ribbon structures at the top. The first ribbon structure is red and consists of 3 alpha helices and beta strands are attached to it and is labeled homeodomain. The second ribbon structure is blue and consists of 3 beta strands and alpha helices attached to it. The alpha helix of the blue ribbon structure is inserted into the major D N A groove.

Return to FIGURE 31.18 Two different D N A-binding homeodomains can form a heterodimer

Extended description for FIGURE 31.19 Two basic-

leucine zipper proteins can form a heterodimer

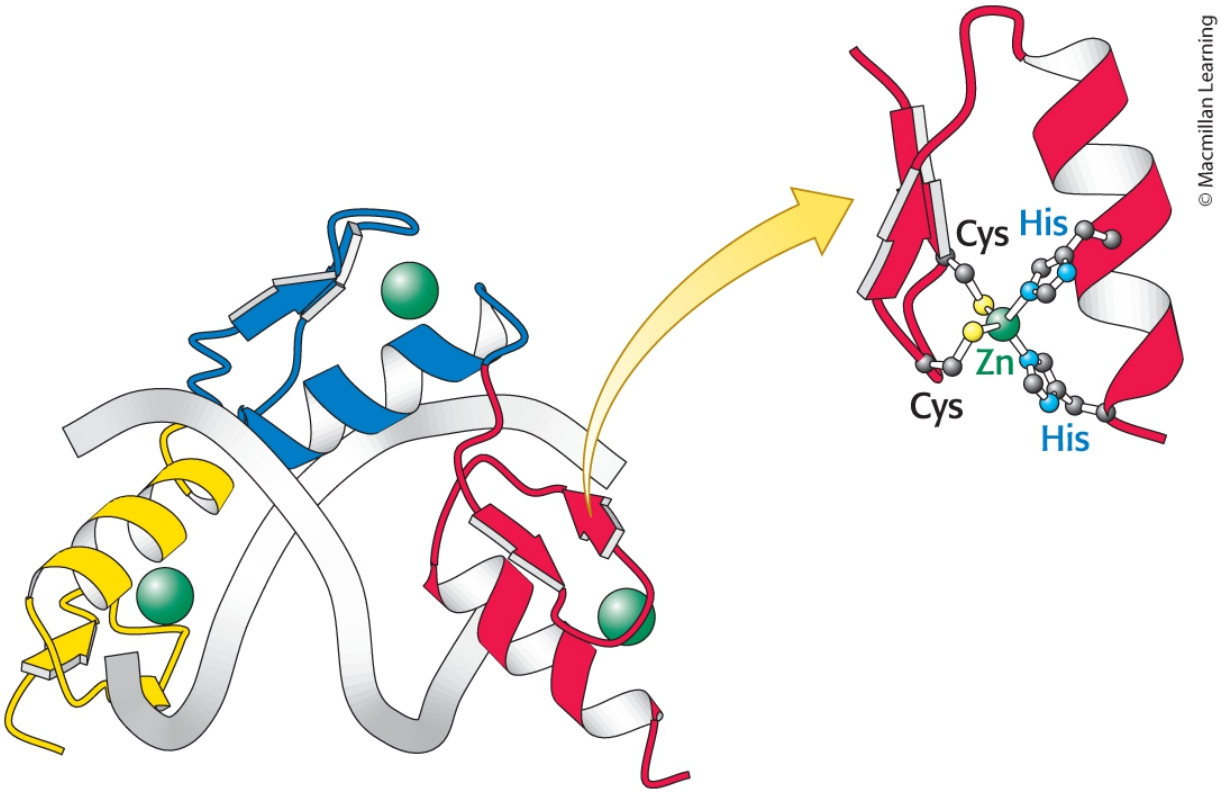


© Macmillan Learning

The figure shows a leucine zipper composed of a pair of long alpha helices that form an X shape. A double-stranded grey-colored D N A is in a horizontal orientation. The first part of each alpha helix at the top is spaced appropriately. The second part of each alpha helix present below represents the basic region that lies in the major groove of D N A at the bottom.

Return to FIGURE 31.19 Two basic-leucine zipper proteins can form a heterodimer

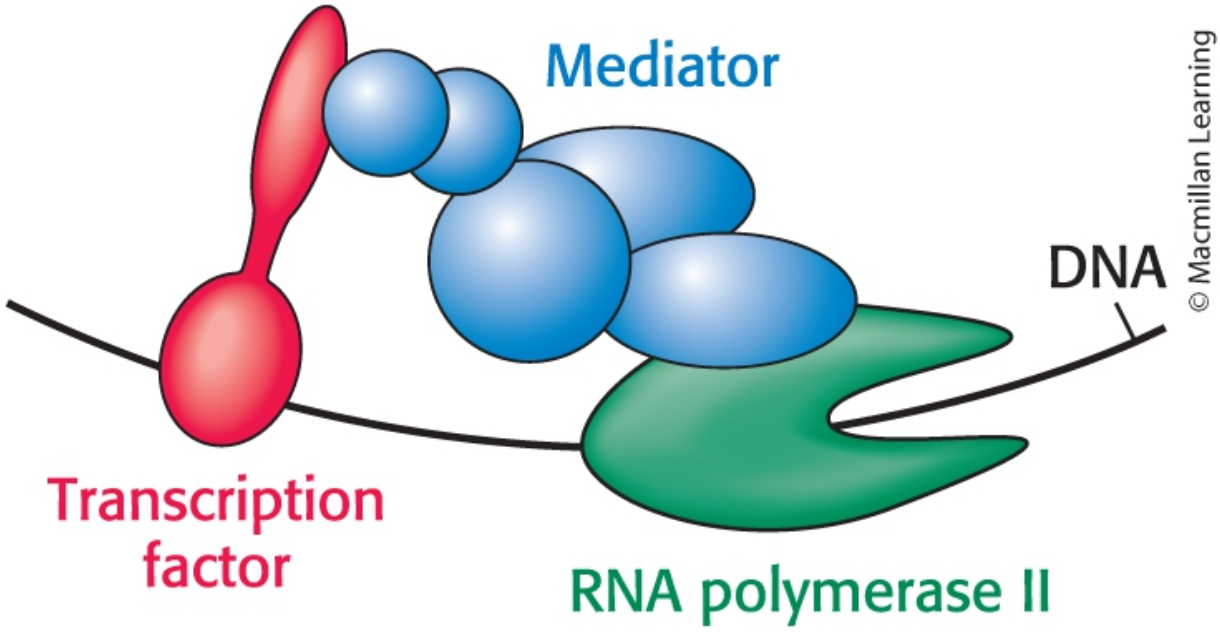
Extended description for FIGURE 31.20 Zinc-finger domains bind to D N A



The figure shows a double-stranded grey-colored D N A in a horizontal orientation. The D N A is attached to yellow, blue, and red ribbon alpha helix and beta strand structures at the top. Each ribbon structure represents a zinc finger. A green sphere is bound to each zinc finger. A zoomed-in view of the red zinc finger is depicted on the right. The red zinc finger consists of an alpha-helix and beta-strand. The core of the zinc finger is bound to a space-filling ball-and-stick model consisting of cysteine and histidine residues with a green sphere at the center. The central green sphere is labeled zinc.

Return to FIGURE 31.20 Zinc-finger domains bind to D N A

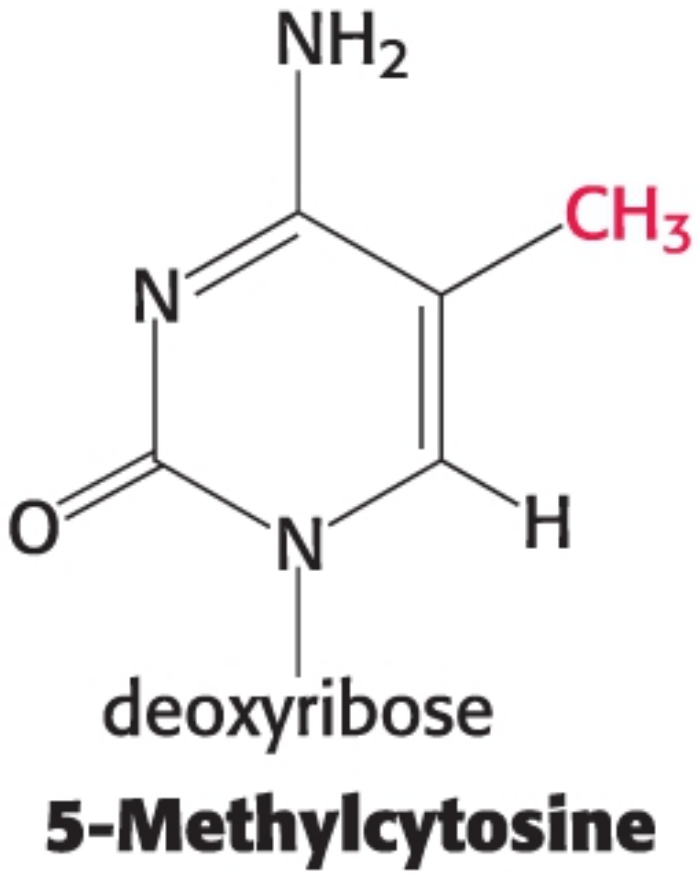
Extended description for FIGURE 31.21 The mediator complex binds to transcription factors and to R N A polymerase II



The figure shows an upward concave curve lying horizontally and is labeled D N A. A circular structure with a constriction projects upward to form a thin elongated tube. This structure is labeled transcription factor. The transcription factor is bound to the D N A on the left. A green-colored oval structure with a groove on the right is labeled R N A polymerase roman numeral I, which is bound to the D N A on the right. A mediator comprised of five subunits acts as a bridge between the transcription factor and R N A polymerase roman numeral I I.

Return to FIGURE 31.21 The mediator complex binds to transcription factors and to R N A polymerase II

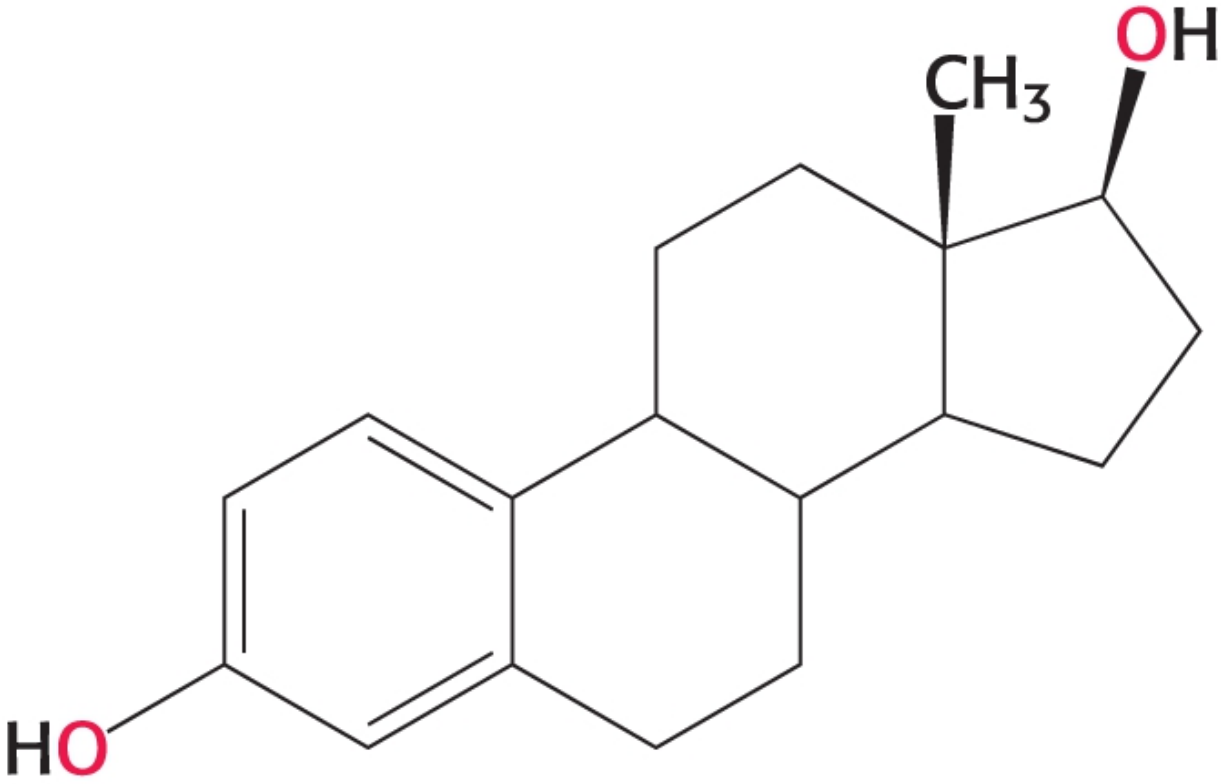
Extended description for Structure of 5-methylcytosine



The structure of 5-methylcytosine is as follows: A 6-membered heterocyclic hexagonal ring is in a vertical orientation and consists of 2 N and 4 C atoms. The first N atom occupies the first position, which is the bottommost vertex. The second N atom occupies the second position, which is the top left vertex. A double bond is present between the second N atom and C 2, and C 3 and C 4. C 1 is double bonded to O. C 2 is single bonded to N H 2. C 3 is single bonded to C H 3 which is highlighted in red. C 4 is single bonded to H. The first N atom is single bonded to deoxyribose.

Return to Structure of 5-methylcytosine

Extended description for Structure of estradiol



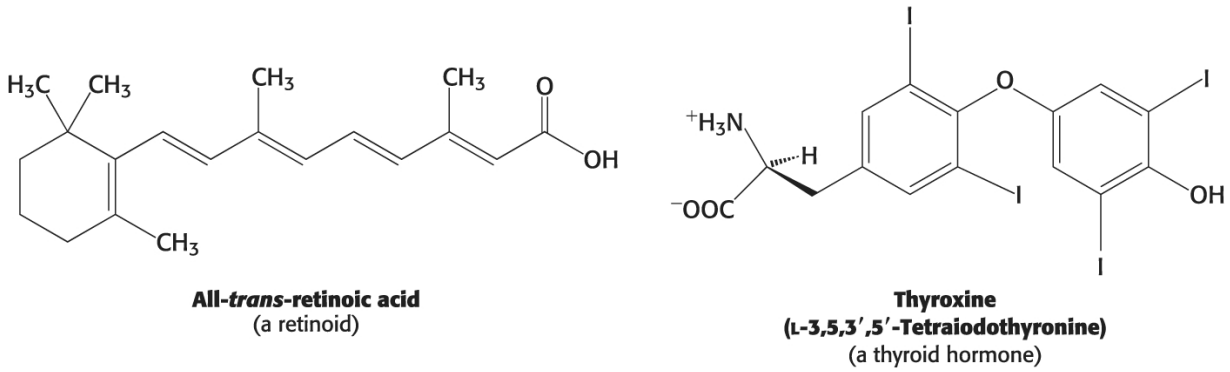
Estradiol
(an estrogen)

A benzene ring is in a vertical orientation with C 1 occupying the topmost vertex. The ring contains alternating double bonds between C 1 and C 2, C 3 and C 4, and C 5 and C 6. C 5 is single bonded to O H in which O is highlighted in red. The benzene ring is fused to a 6-carbon hexagonal ring in a vertical orientation with C 1 occupying the topmost vertex. The two rings are fused such that C 2 and C 3 of the benzene ring are C 6 and C 5 of the 6-carbon hexagonal ring, respectively. In the second 6-carbon ring, C 2 is wedge bonded to O H above. The 6-carbon hexagonal ring is fused to a second 6-carbon

hexagonal ring in a vertical orientation with C 1 occupying the topmost vertex. In the second hexagonal ring, C 2 is wedge bonded to C H 3 above The two rings are fused such that C 1 and C 2 of the first 6-carbon ring are C 5 and C 4 of the second 6-carbon ring, respectively. The second 6-carbon ring is fused to a five-membered pentagonal ring in a horizontal orientation with C 1 occupying the rightmost vertex. The two rings are fused such that C 2 and C 3 of the second hexagonal ring are the C 4 and C 3 of the pentagonal ring, respectively. In the pentagonal ring, C 5 is wedge bonded to O H of which O is highlighted in red.

Return to Structure of estradiol

Extended description for Structure of all-trans-retinoic acid (a retinoid) and thyroxine (L-3,5,39,59-tetraiodothyronine) (a thyroid hormone)



All-*trans*-retinoic acid
(a retinoid)

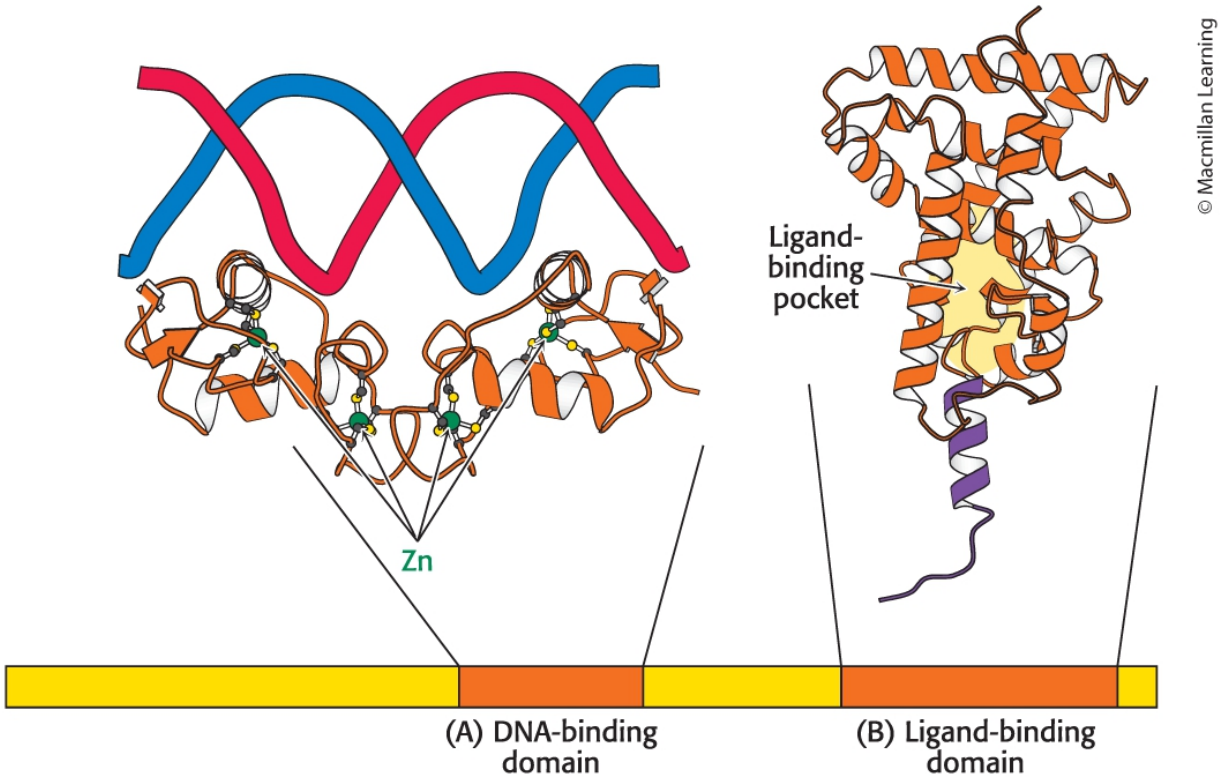
Thyroxine
(L-3,5,3′,5′-Tetraiodothyronine)
(a thyroid hormone)

The structure of the retinoid is as follows: A 6-carbon hexagonal ring is in a vertical orientation with C 1 occupying the topmost vertex. A double bond is present between C 2 and C 3. C 1 is single bonded to C H 3 on the upper left and C H 3 on the upper right. C 3 is single bonded to C H 3. C 2 is single bonded to C 1 of a 9-carbon alkene chain depicted as a line structure using 8 zigzag lines. In the alkene chain, double bonds are present between C 1 and C 2, C 3 and C 4, C 5 and C 6, and C 7 and C 8. In the alkene chain, C 3 and C 7 are each single bonded to C H 3 above. In the alkene chain, C 9 is double bonded to O above and single bonded to O H on the lower right. The structure of thyroid hormone is as follows: A benzene ring is in a vertical orientation with C 1 occupying the topmost vertex. The ring contains alternating double bonds between C 1 and C 2, C 3 and C 4, and C 5 and C 6. C 1 and C 3 are each single bonded to I. C 5 is single bonded to C 1 of a 2-carbon alkane chain depicted as a line structure using 1 wedged line. C 2 of the 2-carbon alkene chain is single bonded to N H 3 superscript plus on the upper left, C O O superscript minus on the lower left, and dash bonded to H on the upper right. C 2 of the benzene ring is single bonded to O. The O

atom is single bonded to C 6 of a second benzene ring in a vertical orientation with C 1 occupying the topmost vertex. The second benzene ring contains alternating double bonds between C 1 and C 2, C 3 and C 4, and C 5 and C 6. In the second benzene ring, C 2 and C 4 are each single bonded to I and C 3 is single bonded to O H.

Return to Structure of all-trans-retinoic acid (a retinoid) and thyroxine (L-3,5,39,59-tetraiodothyronine) (a thyroid hormone)

Extended description for FIGURE 31.24 Nuclear hormone receptors contain two important conserved domains



© Macmillan Learning

The figure depicts a nuclear hormone receptor depicted in the form of a horizontal bar. The bar consists of two conserved domains highlighted in orange. The first domain lies toward the center of the horizontal bar while the second domain lies on the right. The first domain is labeled D N A binding domain and the second domain is labeled ligand-binding domain.

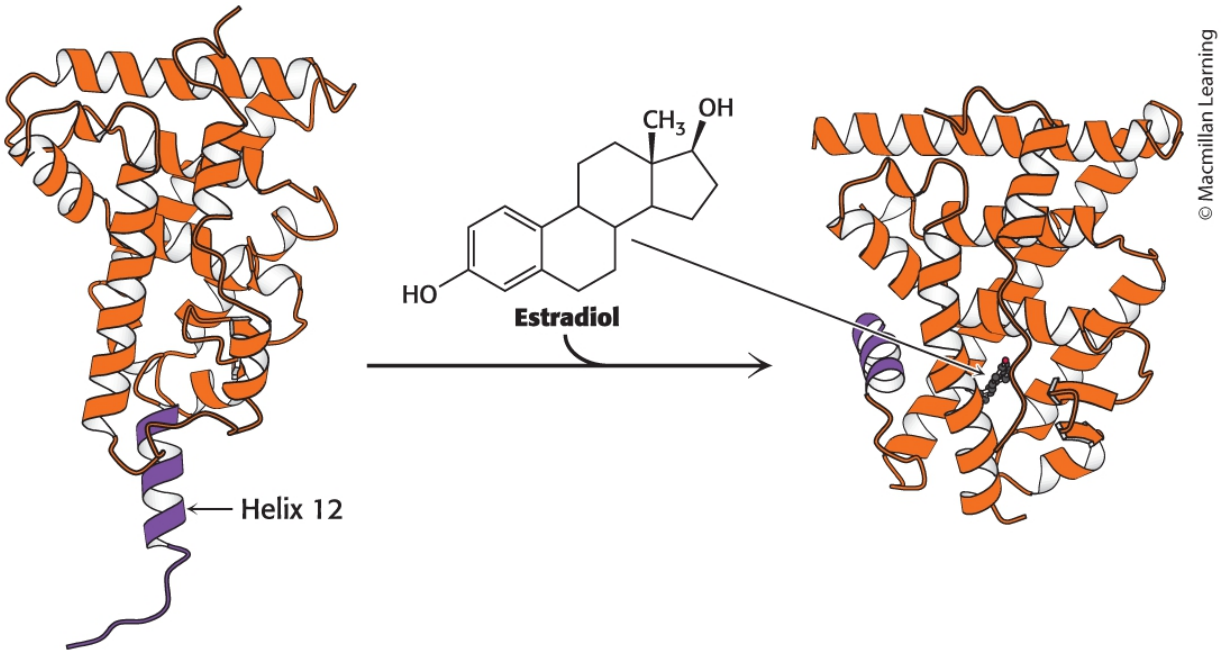
A zoomed-in view from the D N A binding domain on the top shows an orange-colored ribbon structure consisting of alpha helices and beta strands. The ribbon structure is accompanied by a D N A double-helix in a horizontal orientation. The D N A double helix

consists of red and blue flat ribbon-like structures. The ribbon structure is bound to four space-filling ball-and-stick models. Each ball-and-stick model consists of a green sphere along with a few grey and yellow spheres. The green sphere is labeled zinc.

A zoomed-in view from the ligand-binding domain on the top shows two alpha helices. A circular hydrophobic pocket is present at the center of the helices.

Return to FIGURE 31.24 Nuclear hormone receptors contain two important conserved domains

Extended description for FIGURE 31.25 Nuclear hormone receptors interact with ligands

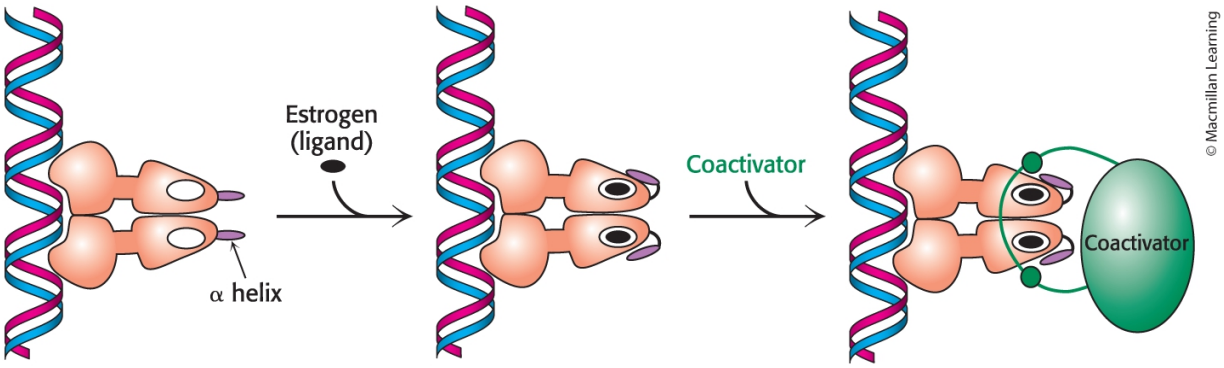


The figure shows an unbound ligand-binding domain of the left. An arrow from the ligand binding domain points to the right to a ligand binding domain bound to an estradiol molecule. The structure of estradiol molecule is shown entering the reaction. In the unbound state, the figure shows two ribbon structures. One ribbon structure consists of orange-colored alpha helices and beta strands while the second ribbon structure consists of a purple colored alpha helix and beta strand. The purple colored alpha helix labeled helix 12 is attached at the bottom. The structure of estradiol is as follows: A benzene ring is in a vertical orientation with C 1 occupying the topmost vertex. The ring contains alternating double bonds between C 1 and C 2, C 3 and C 4, and C 5 and C 6. C 5 is single bonded to O H. The benzene ring is fused to a 6-carbon hexagonal ring in a vertical orientation with C 1 occupying the topmost vertex. The two rings are fused such that C 2 and C 3 of the benzene ring are C 6 and C 5 of the

6-carbon hexagonal ring, respectively. In the second 6-carbon ring, C 2 is wedge bonded to O H above. The 6-carbon hexagonal ring is fused to a second 6-carbon hexagonal ring in a vertical orientation with C 1 occupying the topmost vertex. In the second hexagonal ring, C 2 is wedge bonded to C H 3 above The two rings are fused such that C 1 and C 2 of the first 6-carbon ring are C 5 and C 4 of the second 6-carbon ring, respectively. The second 6-carbon ring is fused to a five-membered pentagonal ring in a horizontal orientation with C 1 occupying the rightmost vertex. The two rings are fused such that C 2 and C 3 of the second hexagonal ring are the C 4 and C 3 of the pentagonal ring, respectively. In the pentagonal ring, C 5 is wedge bonded to O H. On the right, an estradiol molecule is bound to the ligand binding domain. In the bound state, the figure shows an estradiol molecule bound to two ribbon structures. One ribbon structure consists of orange-colored alpha helices and beta strands while the second ribbon structure consists of a purple colored alpha helix and beta strand. The purple colored alpha helix labeled helix 12 is attached to the left of the orange-colored alpha helices. A space-filling model of estradiol is attached to the core of the ribbon structure.

Return to FIGURE 31.25 Nuclear hormone receptors interact with ligands

Extended description for FIGURE 31.26 Nuclear hormone receptors recruit coactivators upon ligand binding



© Macmillan Learning

The process is given in a series of three sequential steps. In the first step, a vertical double helix consists of red and blue flat ribbon-like structures wrapped around each other. The vertical double helix consists of two receptors on the right. Each receptor consists of an irregularly oval structure on the left that continues on the right as a triangular head with a constriction. The triangular head consists of an oval-shaped ligand binding site. Each receptor is attached to a short oval-shaped structure on the right labeled alpha helix.

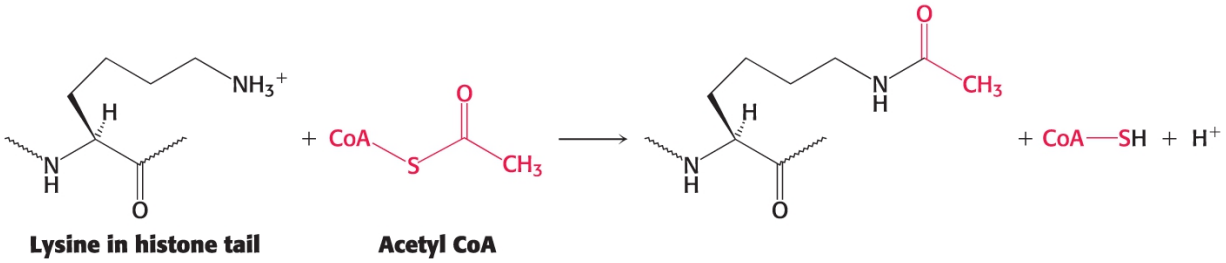
An arrow from the first step points to the second step. The arrow depicts the entry of an oval-shaped structure labeled estrogen or ligand.

In the second step, the estrogen binds to the ligand-binding site of the receptor. This induces a conformational change in the alpha helix. The alpha helix bends and attaches to the sides of the triangular heads.

An arrow from the second step points to the third step. The arrow depicts the binding of the coactivator to the receptors. In the third step, an oval-shaped structure labeled coactivator is present on the right side of the receptor. A loop-like structure from the coactivator attaches to the receptor. The loop consists of two bead-like structures.

Return to FIGURE 31.26 Nuclear hormone receptors recruit coactivators upon ligand binding

Extended description for A chemical reaction



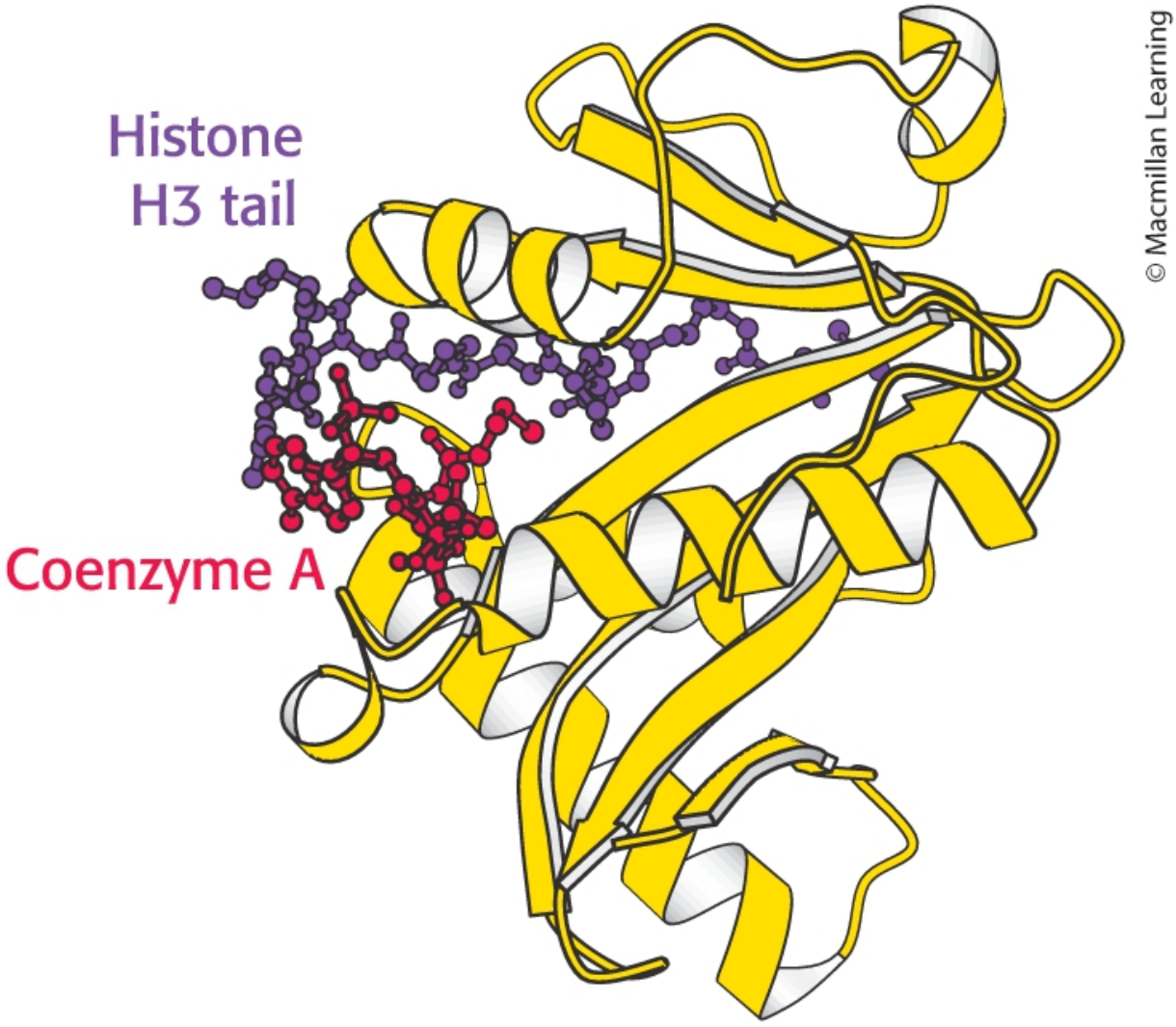
Lysine in histone tail Acetyl CoA

Lysine in histone tail reacts with acetyl C o A to give rise to three products. The structure of lysine in histone tail is as follows: A 4-carbon alkane chain is depicted as line structure using 3 zigzag lines. C 4 is single bonded to N H 3 superscript minus on the lower right. C 1 is wedge bonded to C 1 of a 2-carbon alkane chain depicted as a line structure using a line. C 1 of the second alkane chain is dash bonded to H on the upper right and single bonded to N H on the lower left. This N H has an open wavy bond on the upper left. C 2 is double bonded to O below and has an open wavy bond on the upper right. The structure of acetyl C o A highlighted in red is as follows: A central C atom is double bonded to O above. C is single bonded to C H 3 on the lower right and S on the lower left. S is further single bonded to C o A on the upper left. The structure of the first product is as follows: A 1 N and 5 C heteronuclear alkane chain is depicted as a line structure using 5 zigzag lines. N bound to H occupies the fifth position. C 5 is double bonded to O above and single bonded to C H 3 on the lower right, both of which are highlighted in red. C 1 is wedge bonded to C 1 of a 2-carbon alkane chain depicted as a line structure using a line. C 1 of the second alkane chain is dash bonded to H on the upper right and single bonded to N H on the lower left. This N H has an open wavy bond on the upper left. In the second alkane chain, C 2 is double bonded to O below and has an open wavy bond on the upper right. The second

product is C o A, single bond, S H, in which except for H the rest are highlighted in red. The third product is H superscript plus.

Return to A chemical reaction

Extended description for FIGURE 31.27 Histone acetyltransferase modifies histone tails

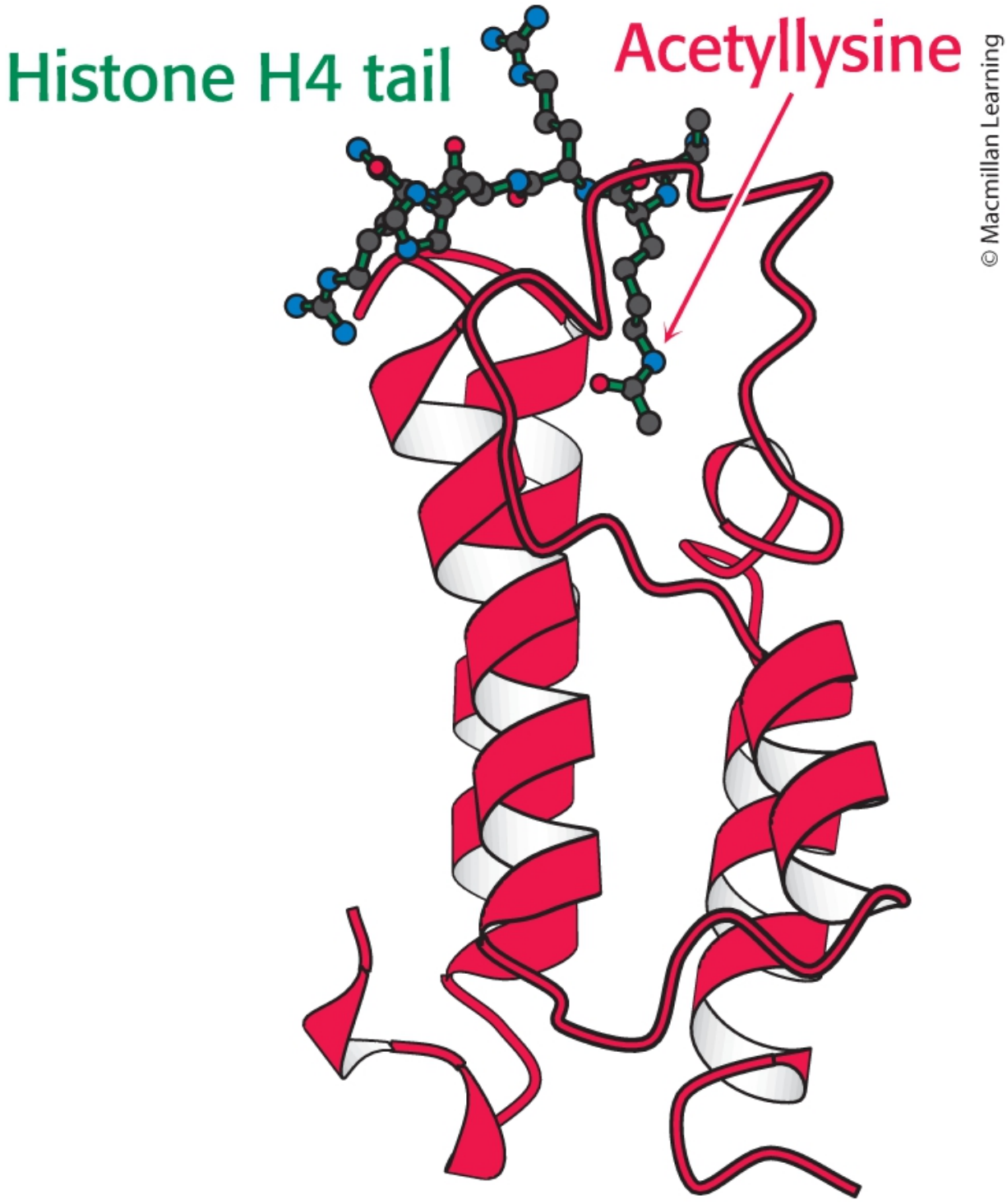


© Macmillan Learning

The ribbon structure consists of three alpha helices and beta strands interconnected by thread-like structures. A ball-and-stick model of purple-colored histone H 3 tail is attached to the amino-terminal domain of the histone acetyltransferase. The ball-and-stick model of the histone H 3 tail is attached to another space-filling ball-and-stick model of red-colored coenzyme A.

Return to FIGURE 31.27 Histone acetyltransferase modifies histone tails

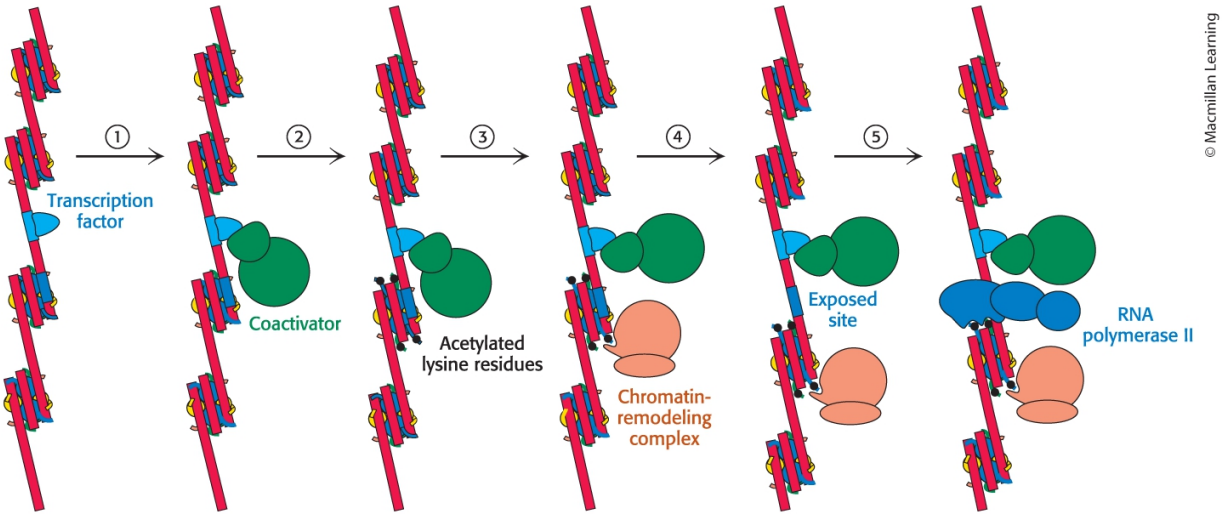
Extended description for FIGURE 31.28 Bromodomains interact with acetyllysine



The ribbon structure consists of four vertical alpha helix bundles interconnected by thread-like structures of loops and turns. The upper end of the helix bundles is attached to ball-and-stick models of histone H 4 tail and acetyllysine.

Return to FIGURE 31.28 Bromodomains interact with acetyllysine

Extended description for FIGURE 31.29 Gene regulation can involve chromatin remodeling



In the first step, chromatin strands are packaged in such a way that it appears vertically with four monomeric nucleotides arranged in vertical series. Each unit is composed of 2 small blue spheres combined with two yellow spheres without any protrusions. From top to bottom between the second and third monomeric unit, an irregular triangular structure is attached and is labeled transcription factor. An arrow numbered 1, from the first step, points to the second step.

In the second step, two green-colored spheres are attached to the transcription factor. One sphere is smaller than the other. These spheres represent the coactivator.

An arrow numbered 2, from the second step, points to the third step.

In the third step, black spherical protrusions are seen in the third monomeric unit. These black spheres represent the acetylated lysine residues.

An arrow numbered 3, from the third step, points to the fourth step.

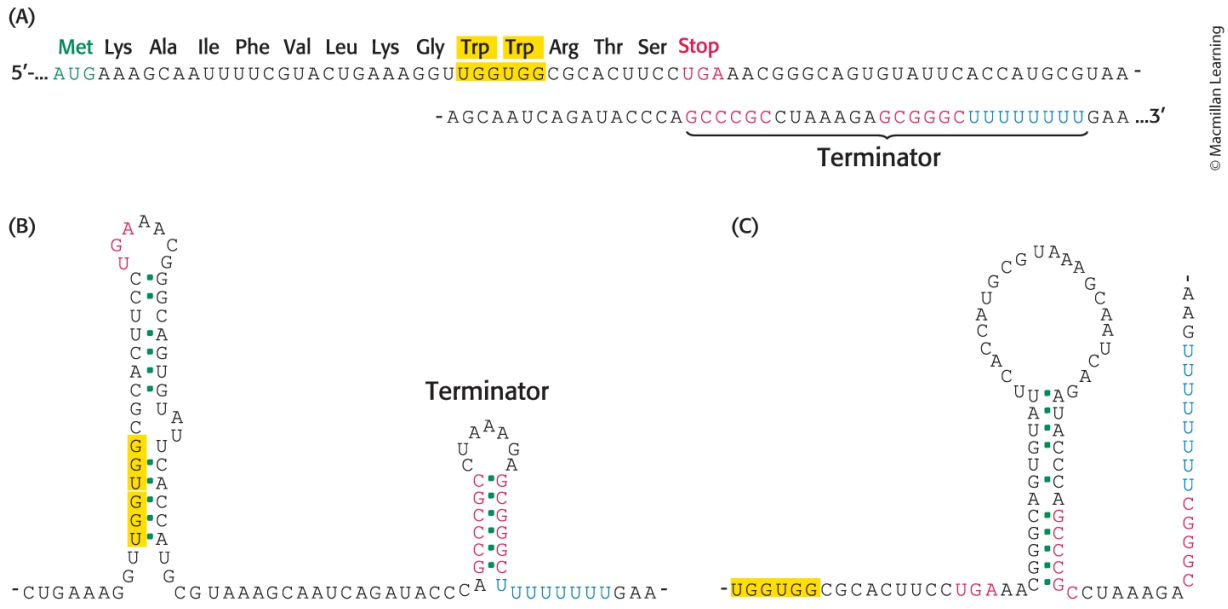
In the fourth step, two subunits consisting of two spheres are attached to the third monomeric unit. The first subunit is larger than the second one. The subunits are labeled chromatin-remodeling complex.

An arrow numbered 4, from the fourth step, points to the fifth step.

In the fifth step, a short fragment from the chromatin between the second and third monomeric units is exposed. This fragment is labeled exposed site. An arrow numbered 5, from the fifth step, points to the sixth step. In the sixth step, R N A polymerase roman numeral I I is attached to the exposed site. R N A polymerase roman numeral I I consists of three irregular spherical subunits.

Return to FIGURE 31.29 Gene regulation can involve chromatin remodeling

Extended description for FIGURE 31.30 The leader region of t r p m R N A includes tryptophan codons



Part A shows a nucleotide sequence in 5 prime to 3 prime direction. The nucleotide sequence reads A U G A A A G C A A U U U U C G U A C U G A A A G G U U G G U G G C G C A C U U C C U G A A A C G G G C A G U G U A U U C A C C A U G C G U A A A G C A A U C A G A U A C C C A G C C C G C C U A A A G A G C G G G C U U U U U U U U U G A A. The nucleotide sequence of the 5 prime ends of t r p m R N A encodes a peptide comprising 14 amino acids which include methionine, lysine, alanine, isoleucine, phenylalanine, valine, leucine, lysine, glycine, tryptophan, tryptophan, arginine, threonine, and serine followed by a stop codon which is U G A. The part of the sequence A G C A A U C A G A U A C C C A G C C C G C C U A A A G A G C G G G C U U U U U U U U U is labeled terminator.

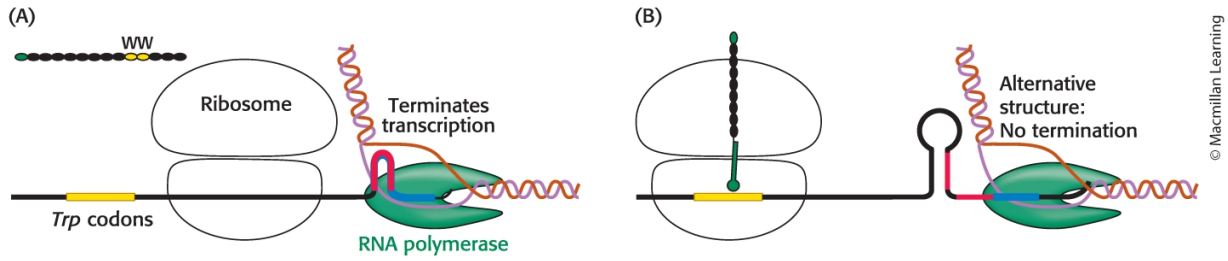
Part B shows the formation of two stem loops in the attenuator region. The first stem-loop is formed from the peptide comprising the 14 amino acid sequences such that the stop codon forms the

peak of the stem loop. The loop then moves down becomes horizontal and again shows a smaller stem loop that is formed from the terminator sequence. The loop again moves down and becomes horizontal in the U U U U U U U U sequence.

Part C shows the formation of a single stem loop. The nucleotide sequence remains horizontal up to the stop codon, rises upward to form the stem-loop, moves down at the terminator nucleotide becomes horizontal for about 8 bases and again rises upward and terminates on the top right.

Return to FIGURE 31.30 The leader region of t r p m R N A includes tryptophan codons

Extended description for FIGURE 31.31 Attenuation regulates transcription



Part A shows a horizontal nucleotide consisting of t r p codons on the left and a stem loop on the right. A ribosome consisting of two oval-shaped subunits is present between the t r p codons and the stem loop. The lower subunit lies on the nucleotide sequence. On the right side of the stem loop, R N A polymerase is present. The R N A polymerase is an oval-shaped structure with a groove on the right. A double helix starts from the region above the stem loop, moves down, makes a larger loop, and terminates on the right side of the R N A polymerase. A text above the nucleotide reads terminates transcription. A horizontal beaded strand with 14 beads is present above the t r p codons. The first bead is green, the eleventh and twelfth beads are yellow, and the rest of the beads are green. The yellow beads are labeled W W.

Part B shows a vertical beaded structure above the t r p codons. A ribosome is found occupying the t r p codons site. A green bead with a long tubular extension above is in contact with the lower subunit of the ribosome and about 10 beaded structures are arranged along the length of the large subunit of the ribosome. Out of 10, 9 are black beads, and the tenth bead is green which is located outside the larger subunit of the ribosome. At the right end, a stem-loop is seen where the right half of the loop is seen with alternating pink strands, post which R N A polymerase is seen bound to. The R N A

polymerase is an oval-shaped structure with a groove on the right. A double helix starts from the region above the stem loop, moves down, makes a larger loop, and terminates on the right side of the R N A polymerase. A text above the nucleotide reads alternative structure: no termination.

Return to FIGURE 31.31 Attenuation regulates transcription

Extended description for FIGURE 31.32 The leader sequences of several operons contain codons for the specific amino acid that they regulate



Part A shows the leader sequence of the threonine operon. The nucleotide sequence of threonine operon in 5 prime to 3 prime direction reads A U G A A A C G C A U U A G C A C C A C C A U U A C C A C C A C C A U C A C C A U U A C C A C A. The nucleotide sequence codes for the following amino acids: methionine, lysine, arginine, isoleucine, serine, threonine, threonine, isoleucine, threonine, threonine, threonine, isoleucine, threonine, isoleucine, threonine, and threonine.

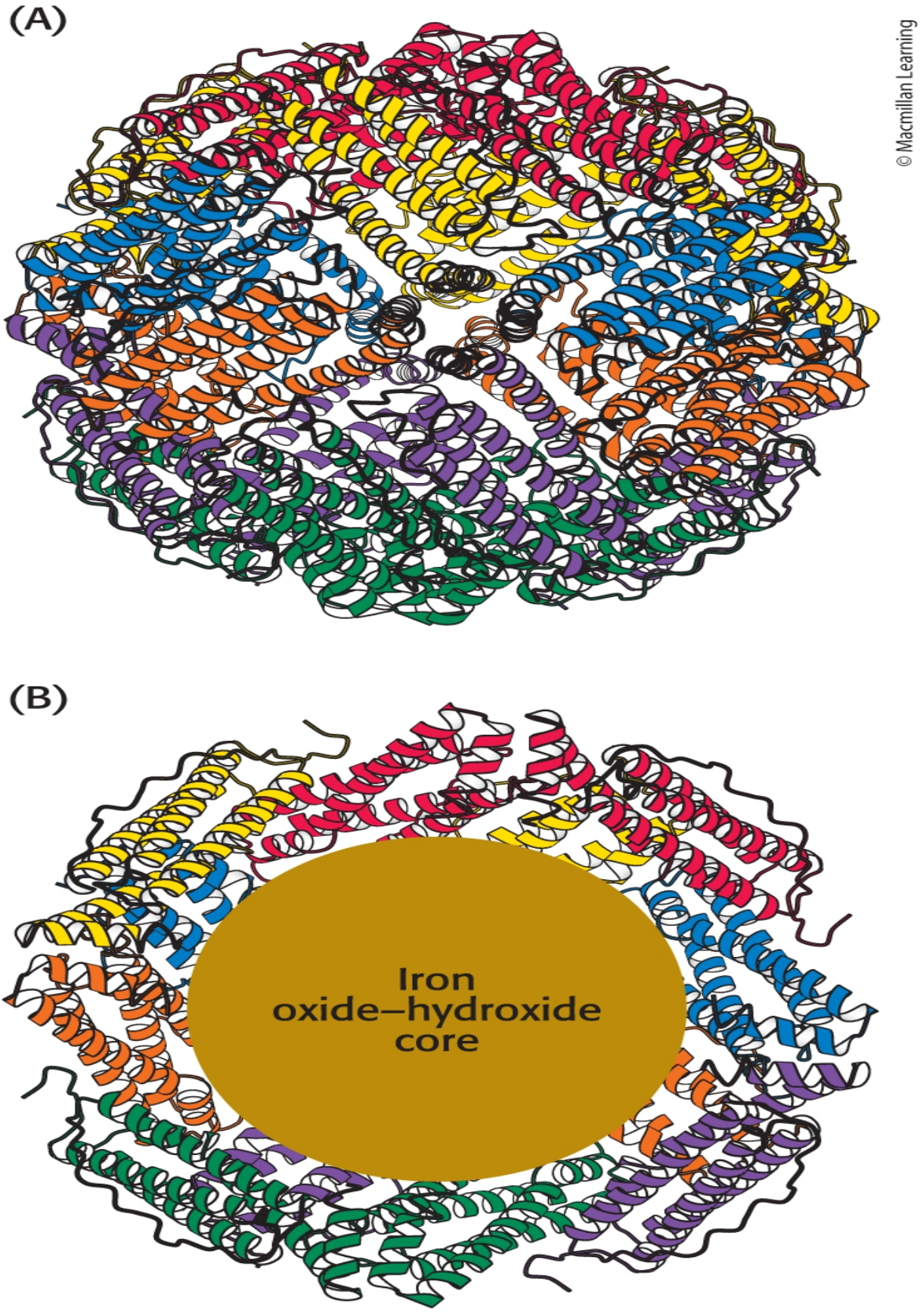
Part B shows the leader sequence of the phenylalanine operon. The nucleotide sequence of phenylalanine operon in 5 prime to 3 prime direction reads A U G A A A C A C A U A C C G U U U U U U C G C A U U C U U U U U U U A C C U U C C C C U G A. The nucleotide sequence codes for the following amino acids: methionine, lysine, histidine, isoleucine, proline, phenylalanine, phenylalanine, phenylalanine, alanine, phenylalanine, phenylalanine, phenylalanine, threonine, phenylalanine, proline, followed by a stop codon.

Part C shows the nucleotide sequence of the histidine operon. The nucleotide sequence of histidine operon in 5 prime to 3 prime direction reads A U G A C A C G C G U U C A A U U U A A A C A C C A C C A U C A U C A C C A U C A U C C U G A C. The nucleotide sequence codes for the following amino acids: methionine, threonine, arginine, valine, glutamine, phenylalanine, lysine, histidine, histidine, histidine, histidine, histidine, histidine, histidine, proline, and aspartic acid.

Return to FIGURE 31.32 The leader sequences of several operons contain codons for the specific amino acid that they regulate

Extended description for FIGURE 31.33 The structure of

ferritin forms a sphere



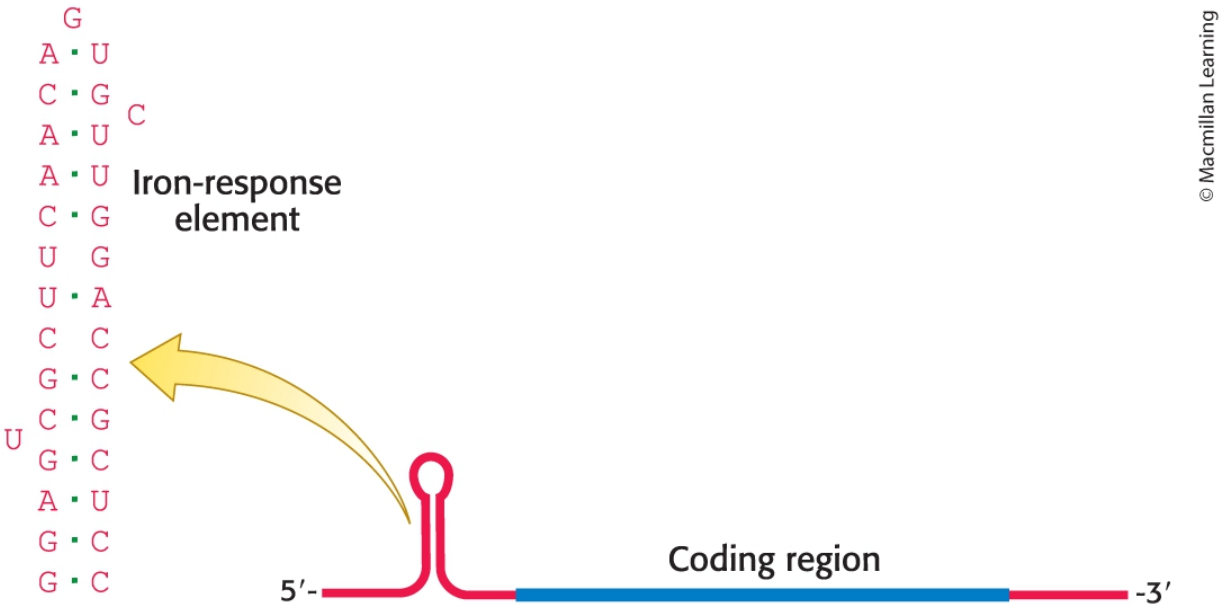
© Macmillan Learning

Part A shows the ribbon diagram of ferritin. The ribbon diagram consists of 24 polypeptides composed of alpha helices and beta strands. The 24 polypeptides are clustered to form a spherical shell.

Part B shows the cutaway view of the core of ferritin. The cutaway view reveals the core of the spherical shell that consists of iron oxide-hydroxide.

Return to FIGURE 31.33 The structure of ferritin forms a sphere

Extended description for FIGURE 31.34 Ferritin m R N A includes an iron-response element in its 5 prime untranslated region

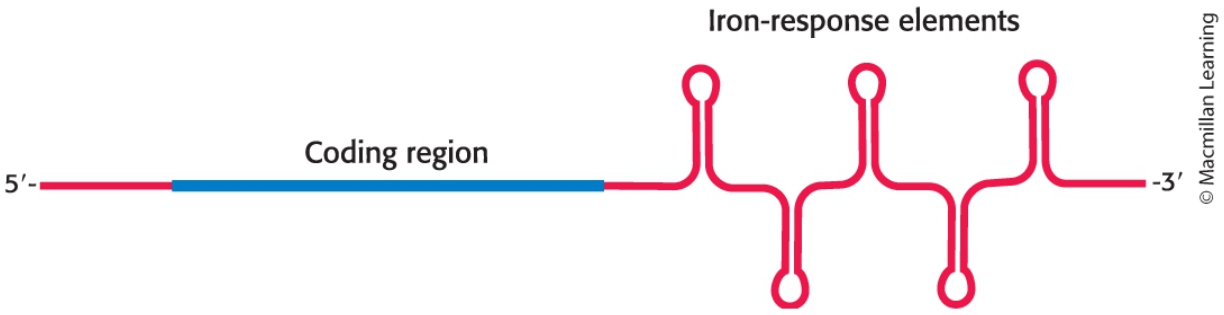


© Macmillan Learning

The figure depicts the ferritin m R N A in a 5 prime to 3 prime direction. A stem-loop is present near the 5 prime end of the m R N A. The stem loop represents the iron-response element. The coding region of the m R N A on the right side of the stem loop is depicted in blue. A zoomed-in view from the stem loop shows the bases given in linear parallel rows from bottom to top and back to bottom as follows. G G A G U C G C U U C A A C A G U G C U U G G A C C G C U C C.

Return to FIGURE 31.34 Ferritin m R N A includes an iron-response element in its 5 prime untranslated region

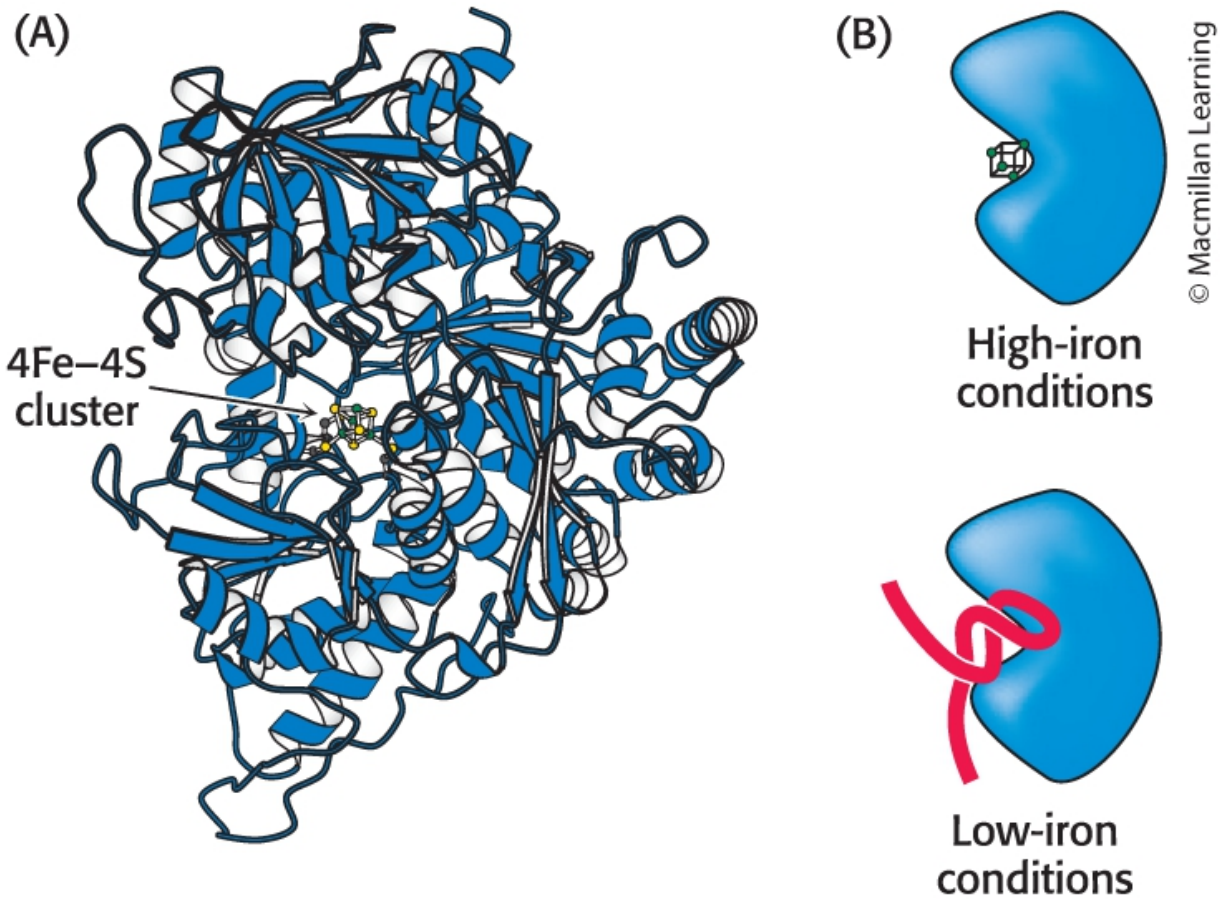
Extended description for FIGURE 31.35 Transferring receptor m R N A has a set of iron-response elements (I R E s) in its 3 prime untranslated region



The figure depicts the transferring receptor m R N A in a 5 prime to 3 prime direction. The coding region of the m R N A is present near the 5 prime end of the m R N A. In the 3 prime untranslated regions, the m R N A has a series of five stem-loops. The stem loops represent the iron-response elements. The five stem loops project upward and downward in an alternating manner until the 3 prime end of the m R N A.

Return to FIGURE 31.35 Transferring receptor m R N A has a set of iron-response elements (I R E s) in its 3 prime untranslated region

Extended description for FIGURE 31.36 The I R P is an aconitase

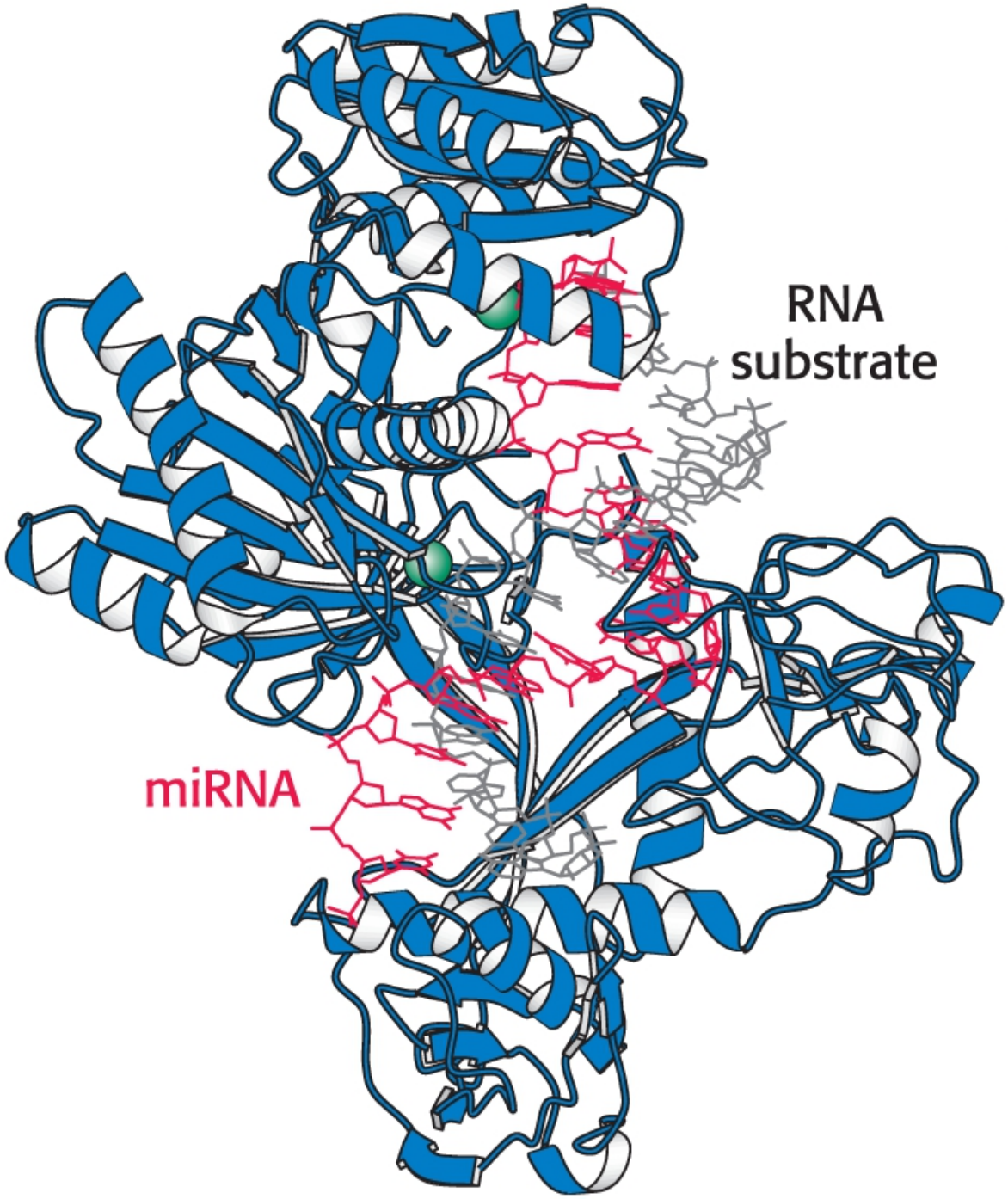


Part A shows a ribbon structure forming a cluster of alpha helices and beta strands. The core of the ribbon structure consists of a ball-and-stick model of 4 F e to 4 S cluster.

Part B shows the binding and dissociation of 4 F e 4 S clusters to aconitase under high and low iron conditions. Aconitase is depicted as a bean-shaped structure with a concavity on the left. Under high-iron conditions, a 4 F e 4 S cluster attaches to the concave side of the aconitase. Under low-iron conditions, a ribbon-like structure attaches to the concave side of the aconitase.

Return to FIGURE 31.36 The I R P is an aconitase

Extended description for FIGURE 31.37 Micro R N A s bind to the Argonaute complex

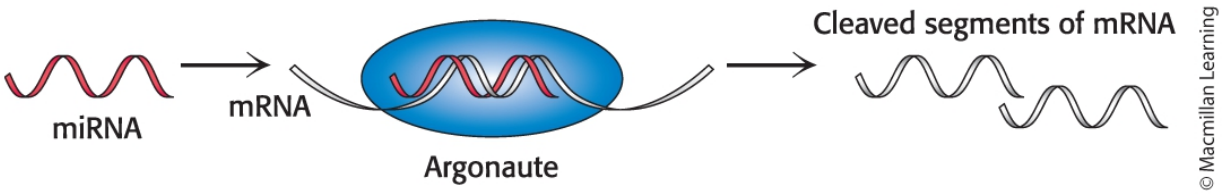


© Macmillan Learning

The figure shows a ribbon structure of an argonaute complex forming two clusters. The clusters are composed of alpha helices and beta strands joined by loops and turns. Thin ribbon strands representing m i R N A are shown in red and R N A substrate is shown in grey along with two magnesium ions. The magnesium ions are represented as green spheres found bound to the argonaute complex.

Return to FIGURE 31.37 Micro R N A s bind to the Argonaute complex

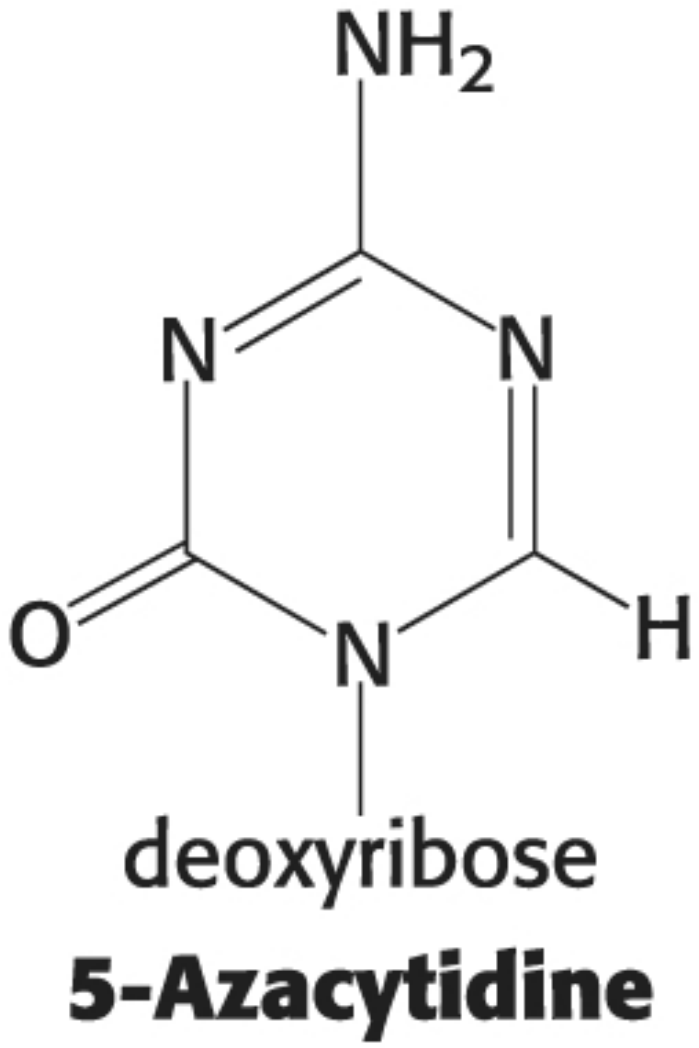
Extended description for FIGURE 31.38 Micro R N A–Argonaute complexes target specific m R N A molecules for cleavage



In the first step, a red-colored single-stranded, coiled, ribbon-like structure labeled m i R N A is shown. An arrow from the first step points to the second step. In the second step, an oval-shaped structure with the m i R N A from the first step is labeled argonaute. Argonaute consists of a white-colored single-stranded ribbon-like structure protruding outside from either side. The white-colored ribbon-like structure is labeled m R N A. The m i R N A binds to the m R N A inside the Argonaute. An arrow from the second step points to the third step. In the third step, two cleaved segments of m R N A are shown as small fragments of two white-coiled, single strands.

Return to FIGURE 31.38 Micro R N A–Argonaute complexes target specific m R N A molecules for cleavage

Extended description for Structure of 5-azacytidine

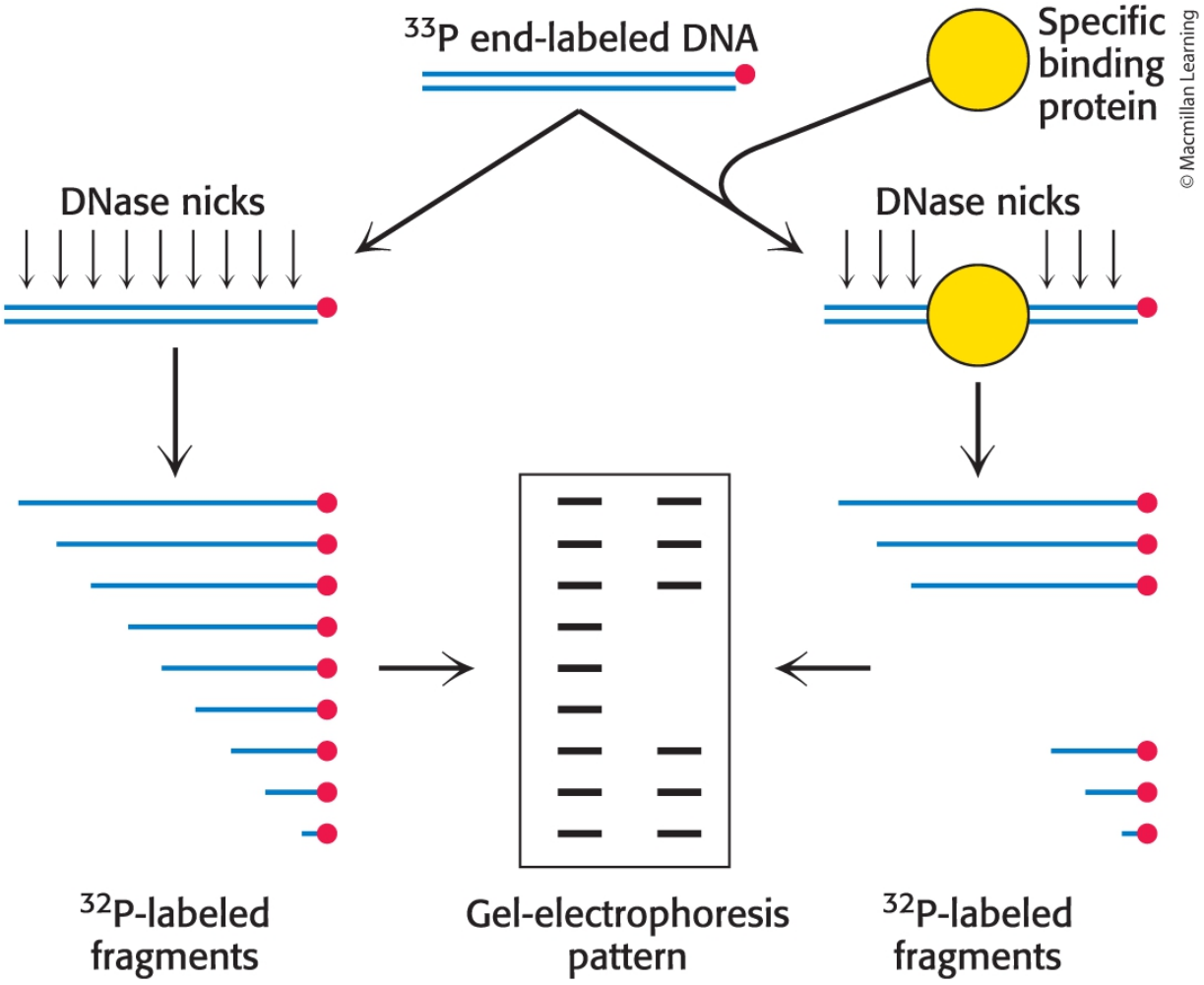


The structure of 5-azacytidine is as follows: A 6-membered heterocyclic hexagonal ring is in a vertical orientation and consists of 3 N and 3 C atoms. The first N atom occupies the first position which is the bottommost vertex, the second N atom occupies the third position which is the top left vertex, and the third N atom occupies the fifth position which is the top right vertex. Double bonds are present between the second N atom and C 2, and the third N atom and C 3. C 2 is single bonded to N H 2, C 3 is single bonded to

H, and C 1 is double bonded to O. The first N atom is single bonded to deoxyribose below.

Return to Structure of 5-azacytidine

Extended description for Patterns of D N A fragments in Gel electrophoresis

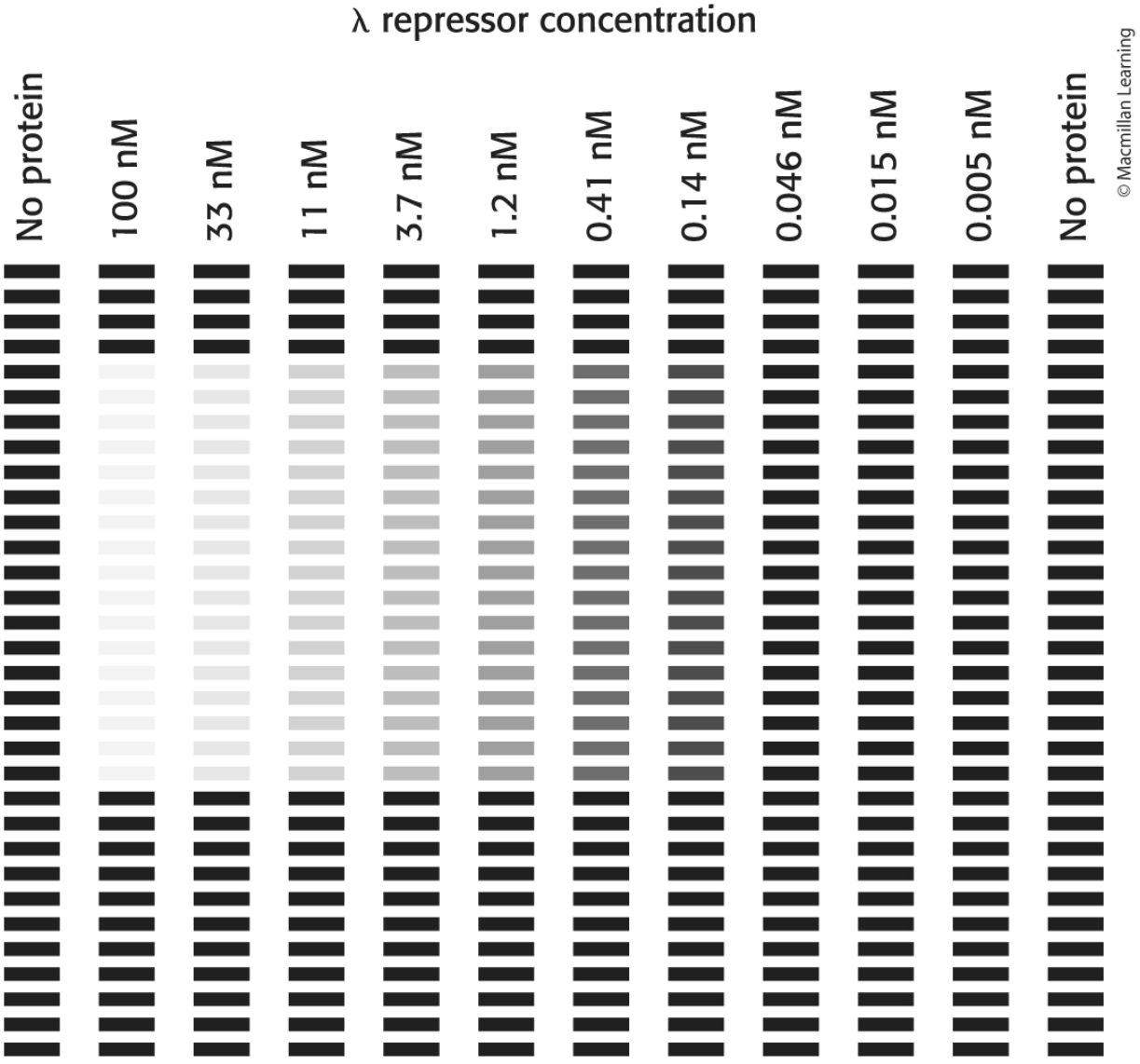


The figure depicts a double-stranded D N A labeled superscript 33 baseline uppercase P end-labeled D N A. The strand at the top is attached to a red sphere on the right. The bottom strand does not have any sphere. A bifurcated arrow from the double-stranded D N A points down. On the left, the top strand of D N A is subjected to nicks by the enzyme D N ase in the absence of proteins. On the right, the bottom strand of D N A is subjected to nicks by the enzyme D N ase in the presence of a specific binding protein. In the absence

of proteins, the top strand of D N A is broken down into 9 fragments labeled superscript 32 baseline uppercase P- labeled fragments. The fragments are depicted as horizontal lines from top to bottom. The fragment size decreases from top to bottom such that the first strand is the longest and the ninth strand is the shortest. Each fragment is attached to a red sphere on the right. In the presence of a specific binding protein, the top strand of D N A is broken down into 6 fragments labeled superscript 32 baseline uppercase P- labeled fragments. The fragments are depicted as horizontal lines from top to bottom. The fragment size decreases from top to bottom such that the first strand is the longest and the sixth strand is the shortest. Each strand is attached to a red sphere on the right. The cleaved D N A fragments are subjected to gel electrophoresis. The gel electrophoresis plate has two lanes. The first lane consists of 9 fragments placed one below the other continuously. The second lane consists of 6 fragments. The first three fragments are present at the top and the other three fragments are present at the bottom.

Return to Patterns of D N A fragments in Gel electrophoresis

Extended description for Autoradiograph of lambda repressor concentration

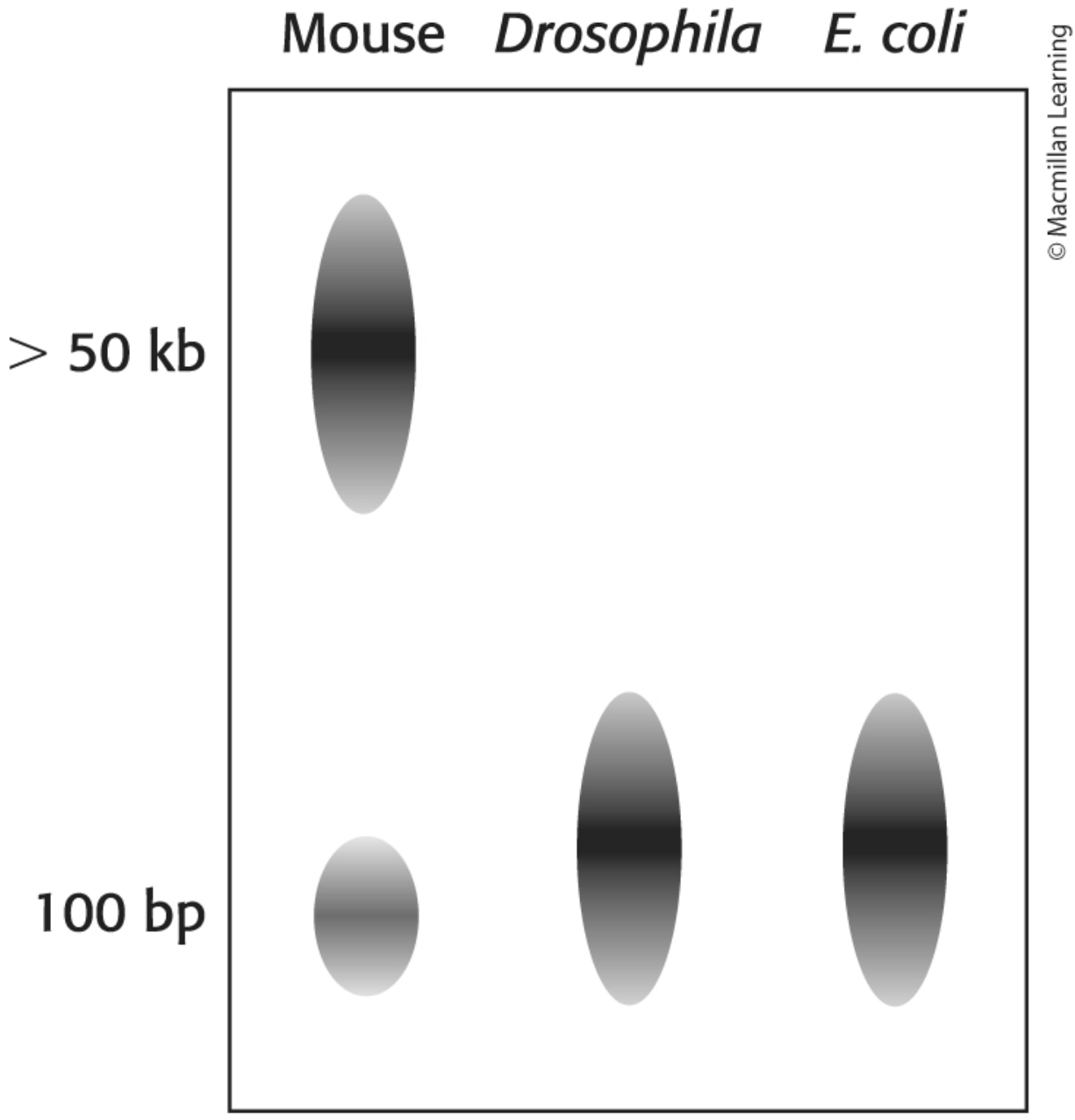


The autoradiograph shows twelve columns and thirty-two rows. The column headings from left to right are no protein, 100 n M, 33 n M, 11 n M, 3.7 n M, 1.2 n M, 0.41 n M, 0.14 n M, 0.046 n M, 0.015 n M, 0.005 n M, and no protein. The column headings have a common title as lambda repressor concentration. Each column consists of 32

fragments. The second, third, fourth, fifth, sixth, and seventh columns have light-colored bands between rows five to twenty-one. The rest of the bands in all other rows have dark fragments.

Return to Autoradiograph of lambda repressor concentration

Extended description for Gel electrophoresis showing results of D N A from different organisms treated with H p a 2



The gel electrophoresis consists of three lanes. The first lane is labeled mouse, the second lane is labeled *Drosophila*, and the third lane is labeled *E. coli*. The gel electrophoresis plate shows two rows. The first row is labeled greater than 50 k b and the second row is labeled 100 b p.

The row entries are as follows.

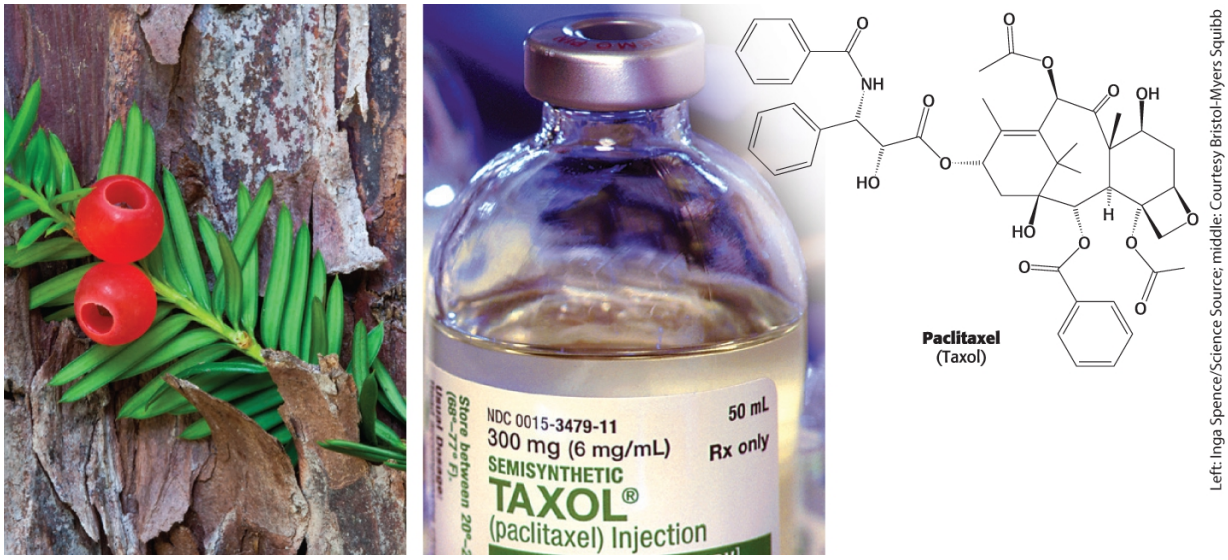
Row Lesser than 50 k b: Mouse lane: A thick horizontal fragment inside a sphere. *Drosophila* and *E. coli* lanes are blank.

Row 100 b p: Mouse lane: A small sphere has a thin horizontal fragment inside.

Drosophila lane: A large sphere has a thick horizontal fragment inside. *E. coli* lane: A large sphere has a thick horizontal fragment inside.

Return to Gel electrophoresis showing results of D N A from different organisms treated with H p a 2

Extended description for Structure of Paclitaxel



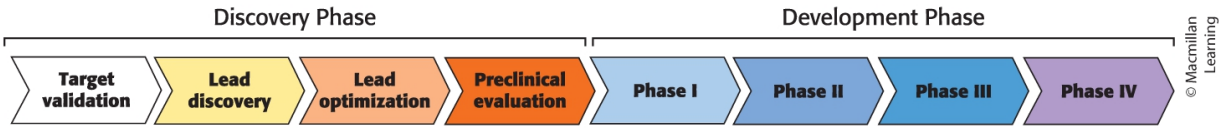
The structure is as follows: A benzene ring is in a vertical orientation with C 1 occupying the rightmost vertex. The ring contains alternating double bonds between C 2 and C 3, C 4 and C 5, and C 6 and C 1. C 1 is single bonded to C 1 of a 1 N and 4 C heteronuclear alkane chain is depicted as a line structure using 4 zigzag lines. In the alkane chain, N bound to H occupies the second position. In the alkane chain, a dash bond is present between N H and C 2. C 1 of the alkane chain is double bonded to O on the upper right. C 2 of the alkane chain is single bonded on the lower left to C 2 of a second ring in a vertical orientation with C 1 occupying the topmost vertex. The second benzene ring contains alternating double bonds between C 1 and C 2, C 3 and C 4, and C 5 and C 6. C 3 of the alkane chain is dash bonded to O H on the lower left. C 4 of the alkane chain is double bonded to a second O atom on the upper right and is single bonded to a third O atom on the lower right. The third O atom is dash bonded on the right to C 4 of a 6-carbon hexagonal ring in a horizontal orientation with C 1 occupying the rightmost vertex. In the 6-carbon ring, a double bond is present

between C 5 and C 6. C 5 of the 6-carbon ring is single bonded to C H 3 in the form of a line. C 1 of the 6-carbon ring is single bonded to C H 3 on the upper right and C H 3 on the lower right, each in the form of a line. C 2 of the 6-carbon ring is wedge bonded to O H on the lower left and is single bonded to a central C atom on the lower right in the form of a line. The central C atom is dash bonded to a fourth O atom on the lower right. The fourth O atom is single bonded to a second central C atom on the lower left in the form of a line. The second central C atom is double bonded to a fifth O atom on the upper left and is single bonded on the lower right to C 5 of a third benzene ring in a horizontal orientation with C 1 occupying the rightmost vertex. The third benzene ring contains alternating double bonds between C 2 and C 3, C 4 and C 5, and C 6 and C 1. The first central C atom is single bonded on the upper right to C 5 of a second 6-carbon hexagonal ring in a vertical orientation with C 1 occupying the topmost vertex. C 1 of the second 6-carbon ring is wedge bonded to O H. C 5 of the second 6-carbon ring is dash bonded to H below. C 6 of the second 6-carbon ring is wedge bonded to C H 3 on the upper right in the form of a wedged line. C 4 of the second 6-carbon ring is dash bonded on the lower left to a sixth O atom. The sixth O atom is single bonded on the lower right to a third central C atom in the form of a line. The third central C atom is double bonded to a seventh O atom on the lower left and is single bonded to C H 3 on the upper right in the form of a line. The second 6-carbon ring is fused to a 4-membered heterocyclic square ring in a vertical orientation consisting of 1 O and 3 C atoms. In the square ring, O occupies the first position which is the rightmost vertex. The two rings are fused to each other such that C 3 and C 4 of the second 6-carbon ring are the C 3 and C 2 of the square ring, respectively. In the square ring, a wedge bond is present between C 1 and C 2, and C 3 and O. C 6 of the second 6-carbon ring is single bonded on the upper left to C 2 of a 2-carbon alkane chain depicted as a line structure using 1 line. C 2 of the 2-carbon alkane chain is double bonded to an eighth O atom on the upper right. C 1 of the 2-carbon

alkane chain is single bonded o the lower left to C 6 of the first 6-carbon ring and is wedge bonded on the upper left to a ninth O atom. The ninth O atom is single bonded on the upper left to a fourth central C atom in the form of a line. The fourth central C atom is double bonded to a tenth O atom above and is single bonded on the lower left to C H 3 in the form of a line.

Return to Structure of Paclitaxel

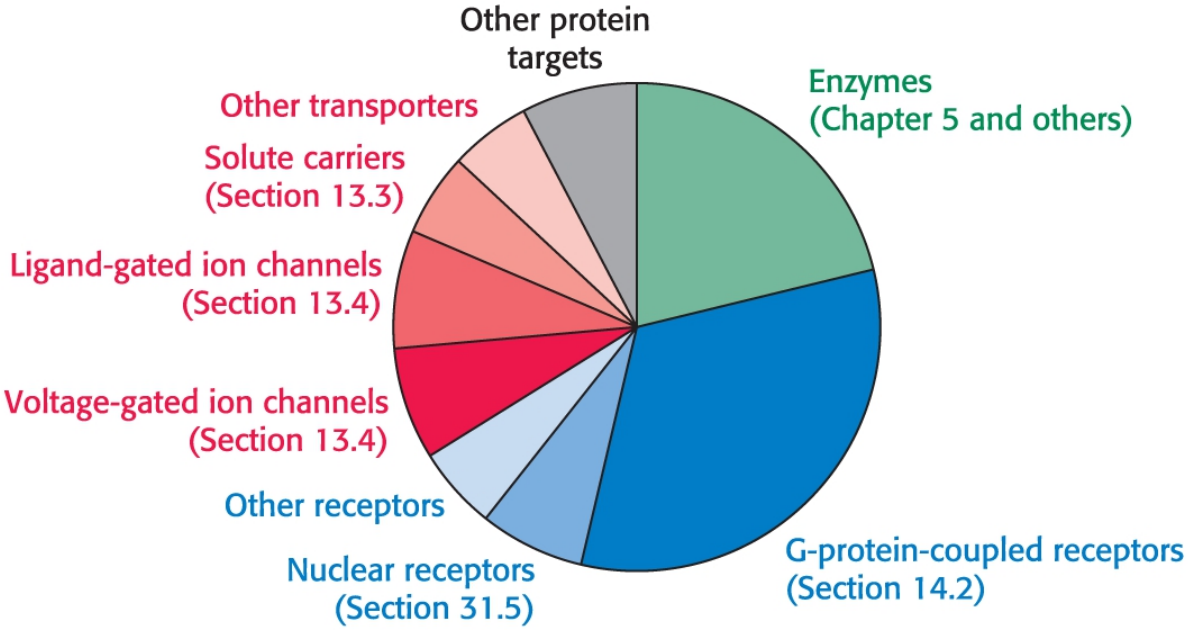
Extended description for FIGURE 32.1 The journey to an approved drug is divided into a discovery phase and a development phase



From the left to the right the discovery phase is followed by the development phase. In the discovery phase, the following stages are shown from the left to the right: Target validation, Lead discovery, Lead optimization, and Preclinical evaluation. The Preclinical evaluation stage points to the first stage of the development phase. In the development phase the following stages are shown from the left to the right: Phase roman numeral i, Phase roman numeral i i, Phase roman numeral i i i, and Phase roman numeral i v.

Return to FIGURE 32.1 The journey to an approved drug is divided into a discovery phase and a development phase

Extended description for FIGURE 32.2 Drug targets span a variety of protein classes

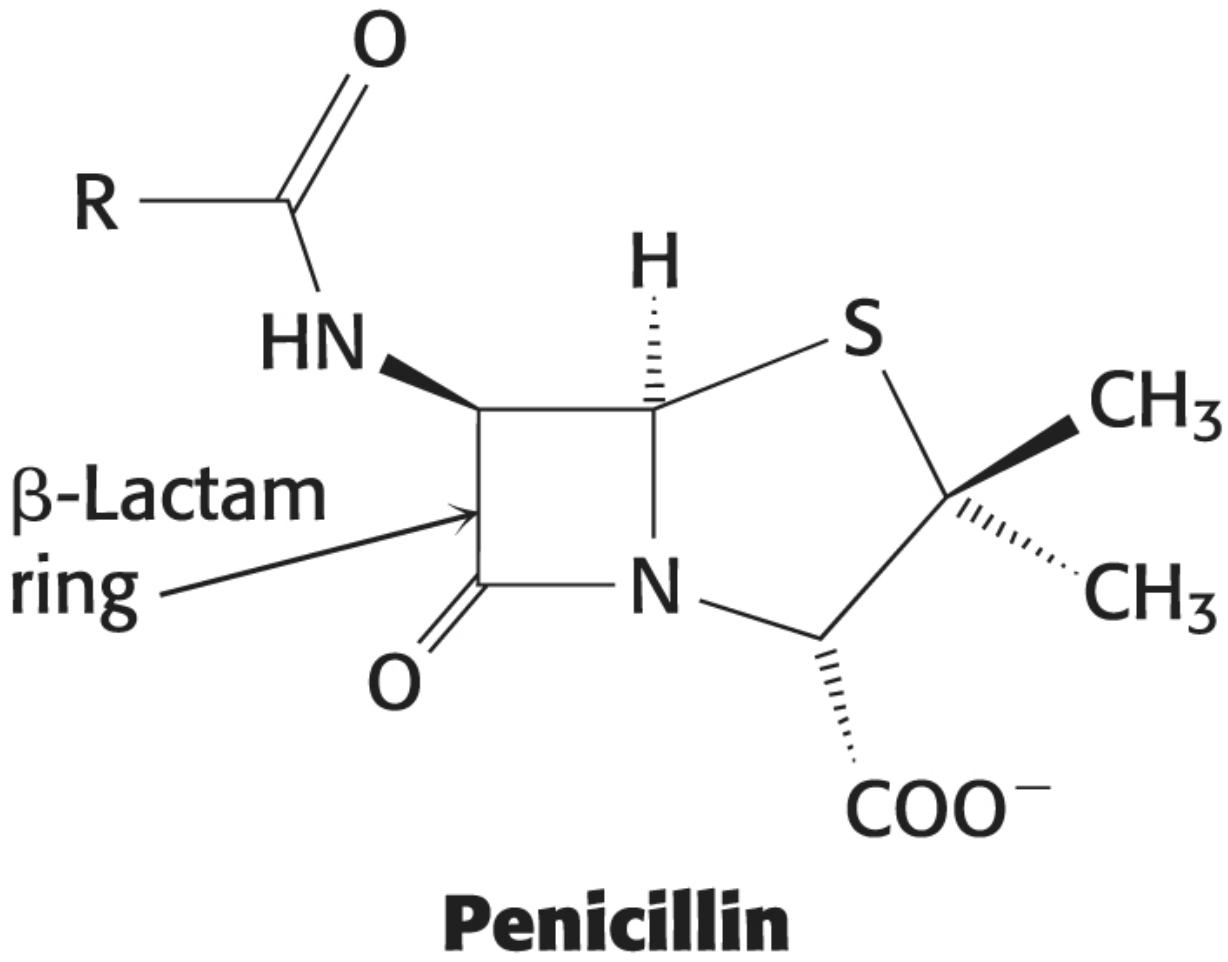


© Macmillan Learning

In the pie-chart, approximately 20 percent is shaded green and labeled Enzymes (Chapter 5 and others). Approximately 35 percent is shaded dark blue and labeled G-protein-coupled receptors (Section 4.2). Approximately 6 percent is shaded medium blue and labeled Nuclear receptors (Section 31.5). Approximately 5 percent is shaded light blue and labeled Other receptors. Approximately 8 percent is shaded dark red and labeled Voltage-gated ion channels (Section 13.4). Approximately 8 percent is shaded medium red and labeled Ligand-gated ion channels (Section 13.4). Approximately 6 percent is shaded medium red and labeled Solute carriers (Section 13.3). Approximately 5 percent is shaded light red and labeled Other transporters. Approximately 7 percent is shaded gray and labeled Other protein targets.

Return to FIGURE 32.2 Drug targets span a variety of protein classes

Extended description for Structure of Penicillin

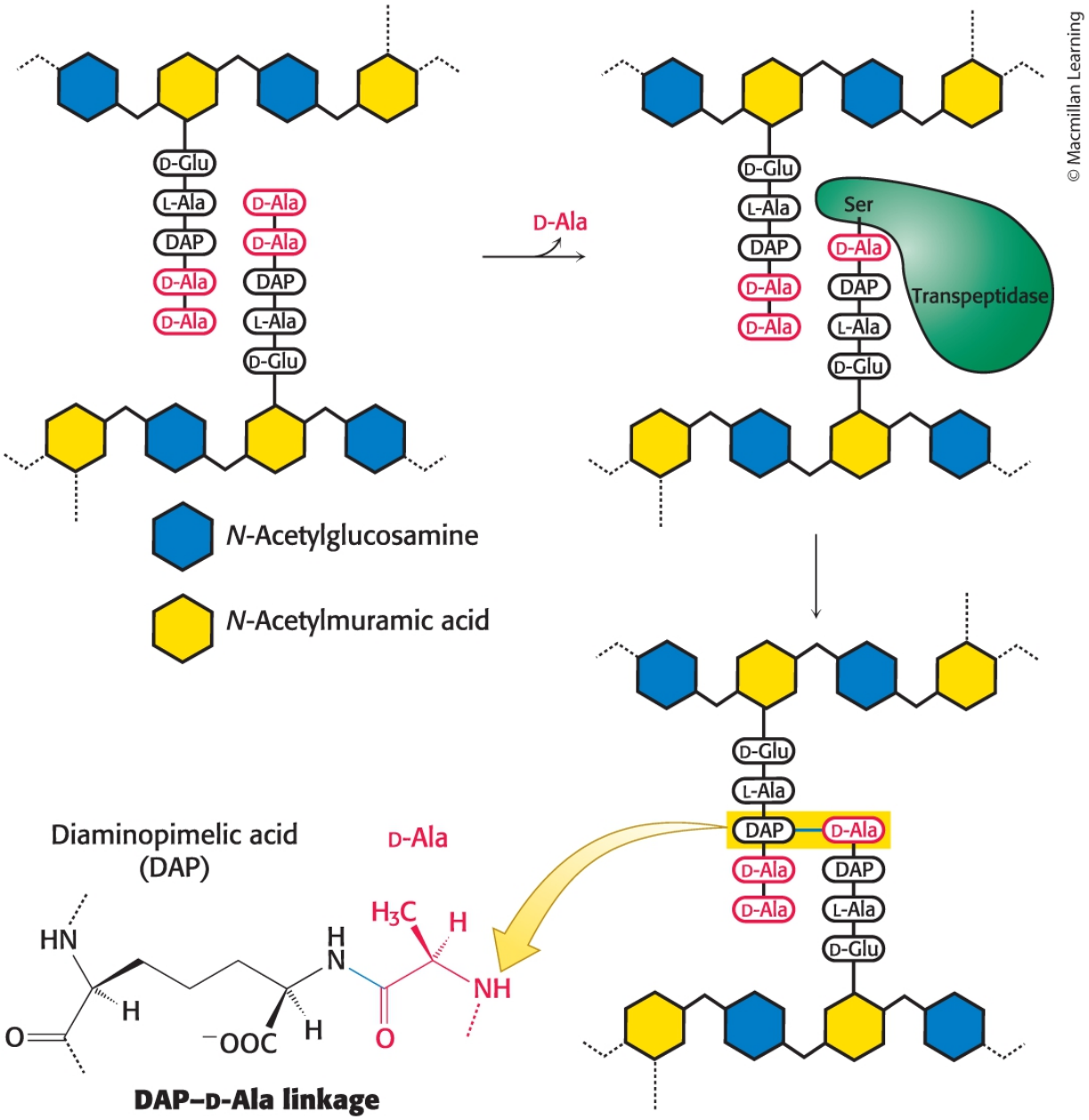


A 4-membered heterocyclic square ring labeled Beta-Lactam ring is in a horizontal orientation consisting of 1 N and 3 C atoms. N occupies the first position which is the bottom right vertex. C 1 is double bonded to O. C 3 is dash bonded to H above. C 2 is wedge bonded to N H. N H is single bonded to a central C atom on the upper left in the form of a line. The central C atom is double bonded to a second O atom on the upper right and single bonded to R on the left. The ring is fused to a 5-membered heterocyclic pentagonal ring in a horizontal orientation consisting of 1 N, 1 S, and 3 C atoms. In the pentagonal ring, N occupies the first position which is the

bottom left vertex, and S occupies the third position which is the top right vertex. The two rings are fused to each other such that C 3 and N of the square ring are the C 1 and N of the pentagonal ring, respectively. C 2 of the pentagonal ring is wedge bonded to C H 3 on the upper right and dash bonded to C H 3 on the lower right. C 3 of the pentagonal ring is dash bonded to C O O superscript minus.

Return to Structure of Penicillin

Extended description for FIGURE 32.3 Penicillin disrupts the biosynthesis of the bacterial cell wall



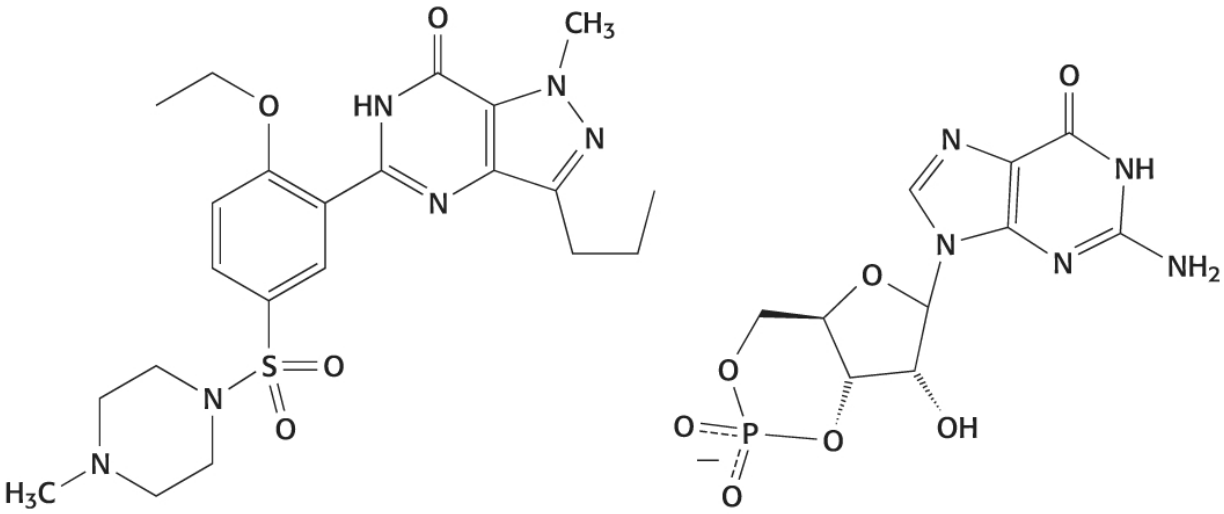
The reaction consists of two steps. In the first step two peptidoglycan groups are shown. The peptidoglycan group has the following structure: Four hexagonal rings each in a vertical

orientation are bonded together in a chain. From the left to the right, the first and the third hexagonal rings are shaded blue and represent N-Acetylglucosamine, and the second and fourth hexagonal rings are shaded yellow and represent N-Acetylmuramic acid. C 3 of each of the first and third hexagonal rings are single bonded to a C H group in the form of a line, which is single bonded on the upper right to C 5 of each of the second and fourth hexagonal rings. C 2 of the second hexagonal ring is single bonded to a C H 2 group which is single bonded on the lower right to C 6 of the third hexagonal ring. Open bonds are present at C 6 of the first hexagonal ring, C 1 and C 2 of the fourth hexagonal ring. C 4 of the second hexagonal ring is single bonded to D-G l u of the following vertical chain: D-G l u, single bond, L-A l a, single bond, D A P, single bond, D-A l a, single bond, D-A l a. In each of the peptidoglycan groups, the D-A l a molecules are highlighted in red. The second D-A l a molecule of the second peptidoglycan group is released and the first D-A l a molecule of the second peptidoglycan group is single bonded to S e r contained in Transpeptidase depicted as an irregular shaped green structure. In the second step, D A P of the first peptidoglycan group forms a linkage with D-A l a of the second peptidoglycan group. The structure of the linkage is as follows: A 2 N and 8 C heteronuclear alkane chain is depicted as a line structure using 9 zigzag lines. N bound to H occupies the seventh and tenth positions. A wedge bond is present between C 2 and C 3. C 1 is double bonded to O on the left and has an open single bond on the lower right. C 2 is dash bonded to H on the lower right and is single bonded to N H on the upper left which has an open single bond on the upper right. C 6 is dash bonded to H on the lower right and is wedge bonded to C O O superscript minus on the lower left. C 7 is double bonded to a second O atom below. C 8 is wedge bonded to C H 3 on the upper left, and dash bonded to H on the upper right. The second N atom has an open single bond on the lower left. C 1 to the first N atom part of the chain is in black and labeled Diaminopimelic acid (D A P)

and the first N atom to the second N atom part of the chain is in red and labeled D-A l a.

Return to FIGURE 32.3 Penicillin disrupts the biosynthesis of the bacterial cell wall

Extended description for FIGURE 32.4 Structures of Sildenafil and c G M P



Sildenafil has the following structure: A 6-membered heterocyclic hexagonal ring is in a vertical orientation consisting of 2 N and 4 C atoms. The first N atom is in the first position which is the top right vertex. The second N atom is in the fourth position which is the bottom left vertex. The second N atom is single bonded to C H 3. The first N atom is single bonded to a central S atom. The central S atom is double bonded to O on the right and a second O atom on the lower right, and single bonded above to C 4 of a benzene ring in a vertical orientation with C 1 occupying the topmost vertex. The benzene ring contains alternating double bonds between C 1 and C 2, C 3 and C 4, and C 5 and C 6. C 1 of the benzene ring is single bonded to a third O atom. The third O atom is single bonded on the upper left to C 2 of a 2-carbon alkane chain depicted as a line structure using 1 line. C 2 of the benzene ring is single bonded to C 1 of a second 6-membered heterocyclic hexagonal ring in a vertical orientation consisting of 2 N and 4 C atoms. In the second 6-membered ring, the first N atom occupies the first position which is the bottommost

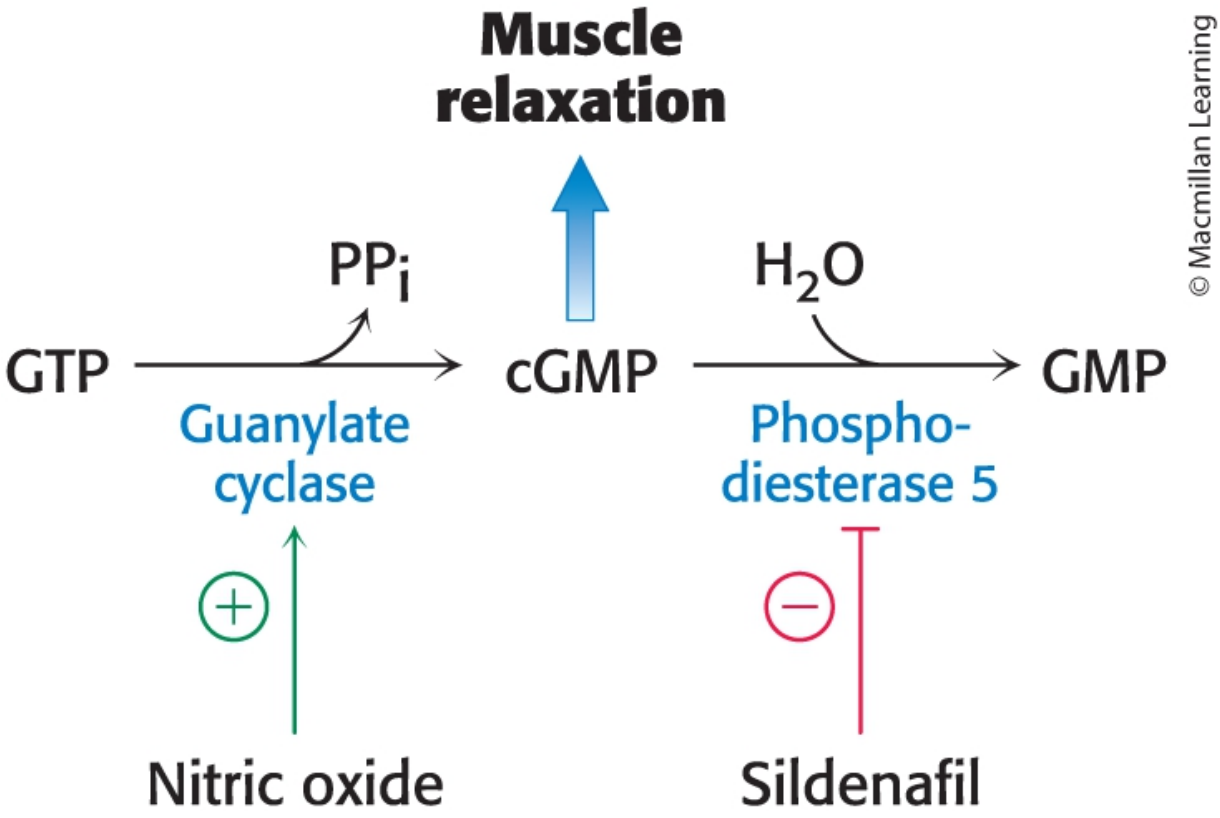
vertex, and the second N atom bound to H occupies the third position which is the top left vertex. In the second 6-membered ring, a double bond is present between the first N atom and C 1, and C 3 and C 4. C 2 of the second 6-membered ring is double bonded to a fourth O atom. The second 6-membered ring is fused to a 5-membered heterocyclic pentagonal ring in a horizontal orientation consisting of 2 N and 3 C atoms. In the pentagonal ring, the first N atom occupies the first position which is the top right vertex, and the second N atom occupies the second position which is the rightmost vertex. In the pentagonal ring, a double bond is present between the second N atom and C 1. The first N atom of the pentagonal ring is single bonded to C H 3. C 1 of the pentagonal ring is single bonded to C 1 of a 3-carbon alkane chain depicted as a line structure using 2 zigzag lines.

c G M P has the following structure: A 6-membered heterocyclic hexagonal ring is in a horizontal orientation consisting of 2 O, 1 P, and 3 C atoms. The first O atom occupies the first position which is the bottom right vertex, P occupies the second position which is the bottom left vertex, and the third O atom occupies the third position which is the leftmost vertex. A wedge bond is present between C 1 and C 2, and a dash bond is present between C 3 and O. P carries a negative charge and is partially double bonded to O on the lower left and a second O atom on the upper left. The ring is fused to a 5-membered heterocyclic pentagonal ring in a vertical orientation consisting of 1 O and 4 C atoms. In the pentagonal ring, O occupies the first position which is the topmost vertex. The two rings are fused to each other such that C 2 and C 3 of the hexagonal ring are the C 4 and C 3 of the 5-membered ring, respectively. C 2 of the pentagonal ring is dash bonded to O H. C 1 of the pentagonal ring is single bonded to the first N atom of a second 5-membered heterocyclic pentagonal ring in a horizontal orientation consisting of 2 N and 3 C atoms. In the second pentagonal ring, the first N atom occupies the first position which is the bottom left vertex and the

second N atom occupies the third position which is the top left vertex. In the second pentagonal ring, a double bond is present between C 1 and the second N atom. The second pentagonal ring is fused to a second 6-membered heterocyclic hexagonal ring in a vertical orientation consisting of 2 N and 4 C atoms. In the second hexagonal ring, the first N atom bound to H occupies the first position which is the top right vertex, and the second N atom occupies the third position which is the bottommost vertex. The two rings are fused to each other such that C 2 and C 3 of the second pentagonal ring are the C 3 and C 2 of the second hexagonal ring, respectively. In the second hexagonal ring, a double bond is present between C 1 and the second N atom, and C 2 and C 3. C 1 of the second hexagonal ring is single bonded to N H 2. C 4 of the second hexagonal ring is double bonded to a third O atom.

Return to FIGURE 32.4 Structures of Sildenafil and c G M P

Extended description for FIGURE 32.5 c G M P stimulates muscle relaxation

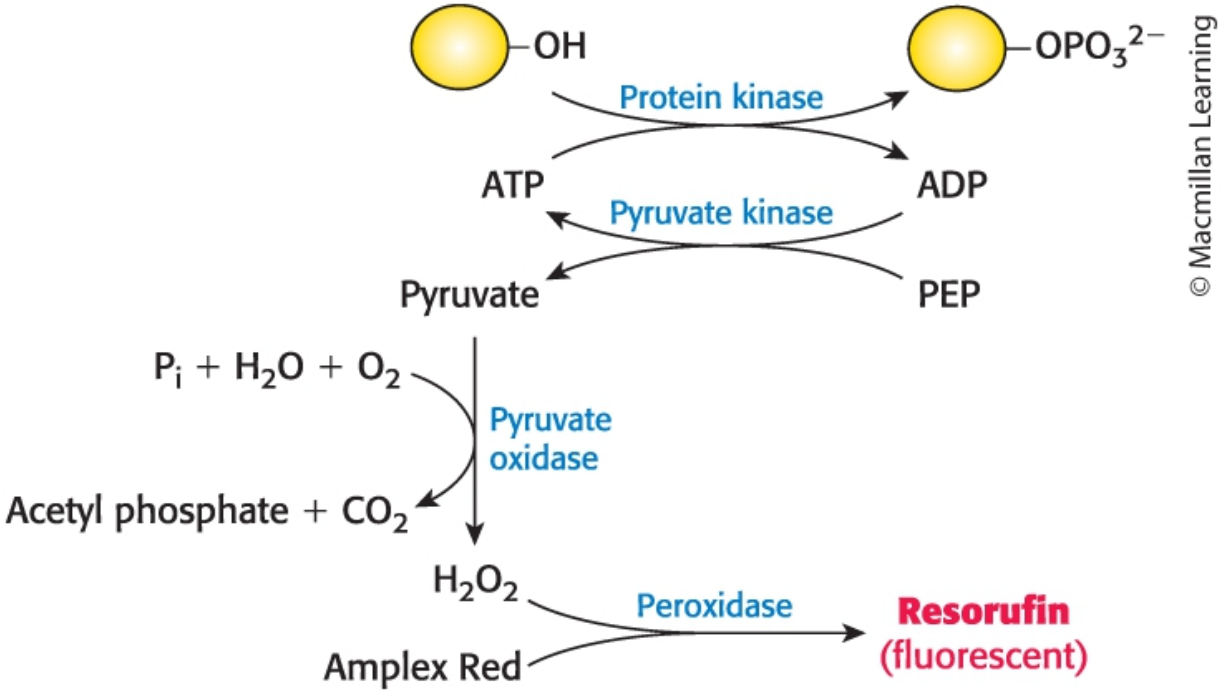


© Macmillan Learning

In the first step, G T P is converted to c G M P by releasing P P i. The first step of the reaction takes place in the presence of Guanylate cyclase which is stimulated by increase in nitric oxide levels. In the second step, c G M P stimulates muscle relaxation and is converted to G M P with the inclusion of H 2 O. The second step of the reaction take place in the presence of Phospho-diesterase 5 which lowers c G M P concentration. Phospho-diesterase 5 is inhibited by Sildenafil.

Return to FIGURE 32.5 c G M P stimulates muscle relaxation

Extended description for FIGURE 32.7 Coupled assays link the activity of an enzyme to the production of a fluorescent product

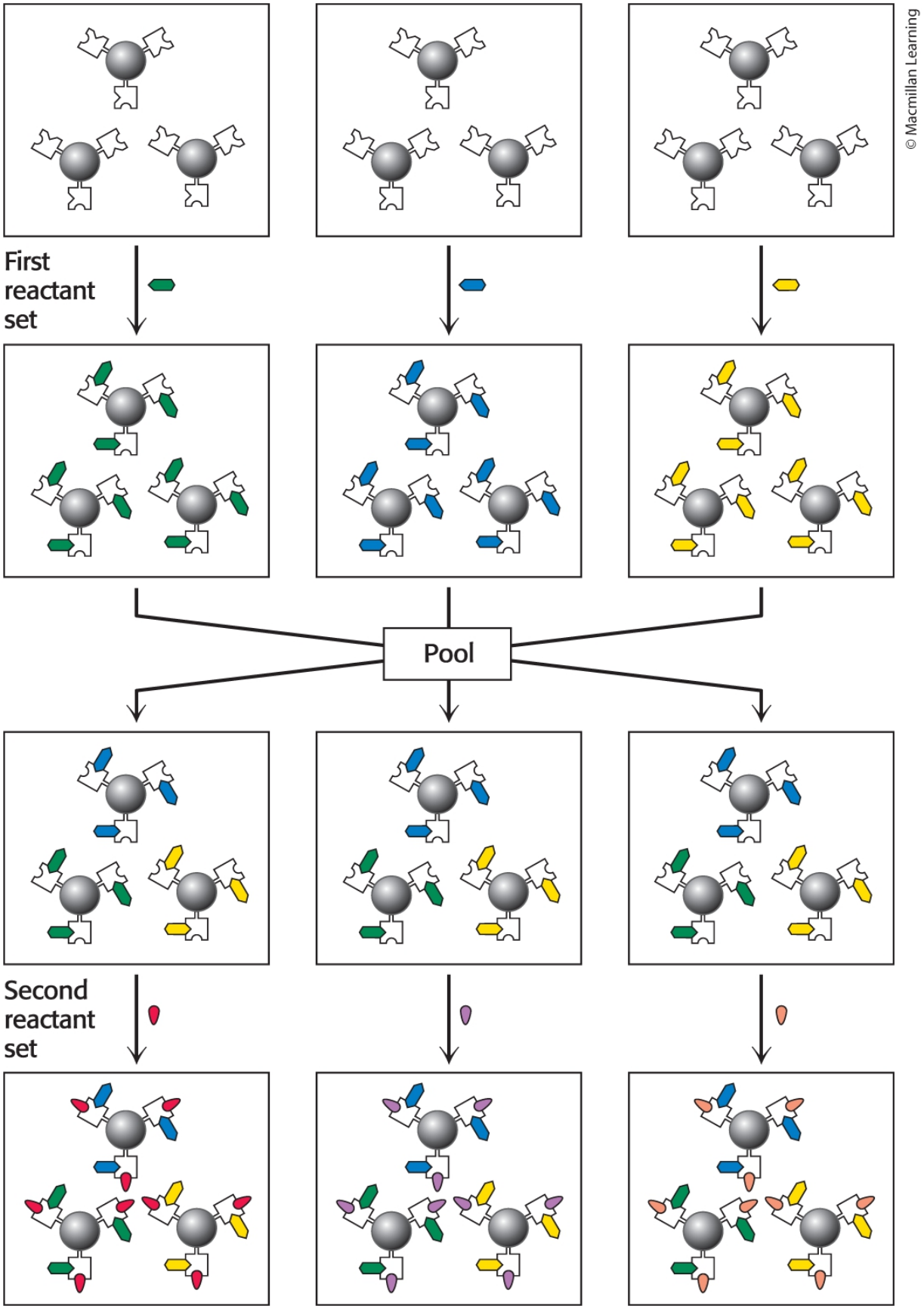


In the first step, A T P depicted as a sphere single bonded to O H converts to A D P depicted as a sphere single bonded to O P O 3 superscript 2 minus, in the presence of Protein kinase. In the second step a coupled reaction shows the conversion of A D P back to A T P and P E P to Pyruvate in the presence of Pyruvate kinase. In the third step, a coupled reaction shows the conversion of Pyruvate to H 2 O 2 and P i plus H 2 O plus O 2 to Acetyl phosphate plus C O 2, in the presence of Pyruvate oxidase. In the fourth step, H 2 O 2 and Amplex Red convert to Resorufin (fluorescent) in the presence of Peroxidase.

Return to FIGURE 32.7 Coupled assays link the activity of an enzyme to the production of a fluorescent product

Extended description for FIGURE 32.8 Compound

libraries can be generated by split-pool synthesis



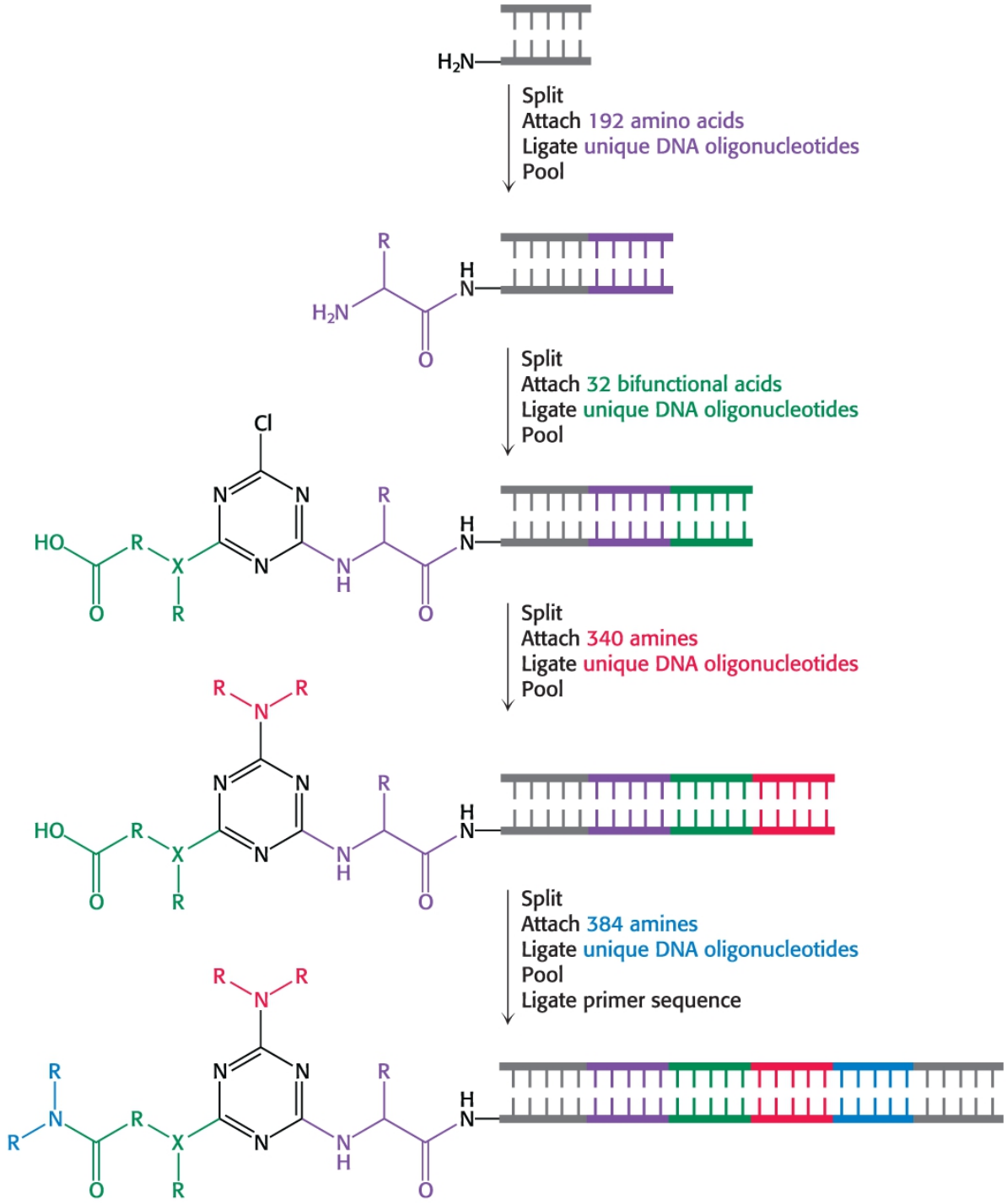
© Macmillan Learning

Each set of compounds consists of three beads shown in gray. Each bead contains an initial structural scaffold depicted as three white arrows attached to the circumference of the bead and tangent to it. In the first step, three set of compounds are shown. Each of the compound set reacts with the first reactant set. The first compound set reacts with a green oval-shaped reactant, the second compound set reacts with a blue oval-shaped reactant, and the third compound reacts with a yellow oval-shaped reactant. Each of these reactions produce a compound set with three beads with the corresponding reactant attached to each arrow of the scaffold structure of the bead. In the second step, the three compound sets are mixed in a box labeled Pool. Three arrows from the pool show the new three compound sets. In each of the new compound sets, the three arrows on each bead are attached with the blue, green and yellow reactants, respectively. In the third step, each of the three new compound sets react with the second reactant set. The first new compound set reacts with a red oval-shaped reactant, the second new compound set reacts with a purple oval-shaped reactant, and the third new compound set reacts with a yellow oval-shaped reactant. Each of these reactions produce a compound set with three beads with the corresponding reactant attached to each arrow of the scaffold structure of the bead.

Return to FIGURE 32.8 Compound libraries can be generated by split-pool synthesis

Extended description for FIGURE 32.10 Diverse D N A-

encoded libraries are generated by split pool synthesis



© Macmillan Learning

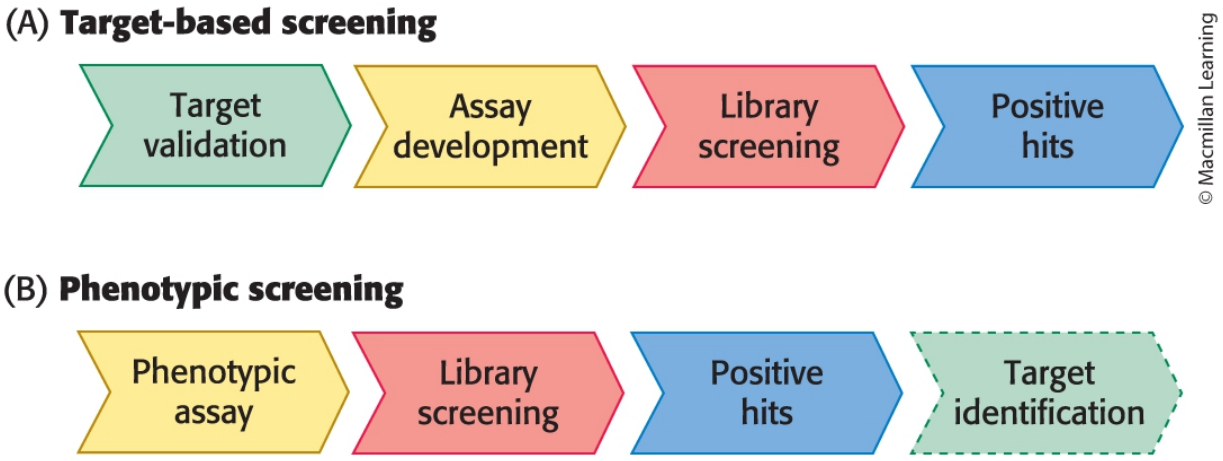
DNA-encoded library containing 802,160,640 unique molecules

The process shows the initial four steps in the synthesis. In the first step, a short D N A strand is shown with the main bottom strand and the complementary top strand each consisting of 5 bases colored gray. The bottom strand is single bonded to N H 2 on the left. The D N A strand undergoes the following process: Split, Attach, 192 amino acids, Ligate unique D N A oligonucleotides, and pool. The resulting D N A strand shows a new strand consisting of 5 bases colored purple attached on the right of the original D N A strand. N H is single bonded on the lower left to C 2 of a 2-carbon alkane chain depicted as a line structure using 1 line. C 1 of the alkane chain is single bonded to R above and N H 2 on the lower left. C 2 is double bonded to O below. The structure is colored purple. In the second step, the resulting D N A strand of the first step undergoes the following process: Split, Attach, 32 bifunctional acids, Ligate unique D N A oligonucleotides, and pool. The resulting D N A strand shows a new strand consisting of 5 bases colored green attached on the right of the resulting D N A strand of the first step. C 1 of the alkane chain is single bonded to R above and N H on the lower left instead of N H 2. This part is colored purple. N H is single bonded on the upper left to C 1 of a 6-membered heterocyclic hexagonal ring in a vertical orientation consisting of 3 N and 3 C atoms. In the hexagonal ring, the first N atom occupies the first position which is the top right vertex, the second N atom occupies the third position which is the bottommost vertex, and the third N atom occupies the fifth position which is the top left vertex. In the hexagonal ring, a double bond is present between the first N atom and C 1, the second N atom and C 2, and the third N atom and C 3. C 3 of the hexagonal ring is single bonded to C l. C 2 of the hexagonal ring is single bonded to X on the lower left. X is single bonded to R below and a second R group on the upper left. The second R group is single bonded to a central C atom on the lower left in the form of a line. The central C atom is double bonded to a second O atom below and single bonded to O H on the upper left. The X to central C atom part of the structure with its attached groups is highlighted in green. In

the third step, the resulting D N A strand of the second step undergoes the following process: Split, Attach, 34 amines, Ligate unique D N A oligonucleotides, and pool. The resulting D N A strand shows a new strand consisting of 5 bases colored red attached on the right of the resulting D N A strand of the second step. C 3 of the hexagonal ring is single bonded to a central N atom instead of C l. The central N atom is single bonded to a third R group on the upper right and a fourth R group on the upper left. The central N atom and its attached groups is highlighted in red. In the fourth step, the resulting D N A strand of the third step undergoes the following process: Split, Attach, 384 amines, Ligate unique D N A oligonucleotides, pool, and ligate primer sequence. The resulting D N A strand shows a new strand consisting of 10 bases, with the first 5 colored blue and the next 5 colored gray attached on the right of the resulting D N A strand of the third step. The central C atom is single bonded to a second central N atom instead of O H on the upper left. The second central N atom is single bonded to a fourth R group above and a fifth R group on the lower left. The second central N atom and its attached groups is highlighted in blue.

Return to FIGURE 32.10 Diverse D N A-encoded libraries are generated by split pool synthesis

Extended description for FIGURE 32.11 Target-based screening and phenotypic screening are two paths to early drug discovery



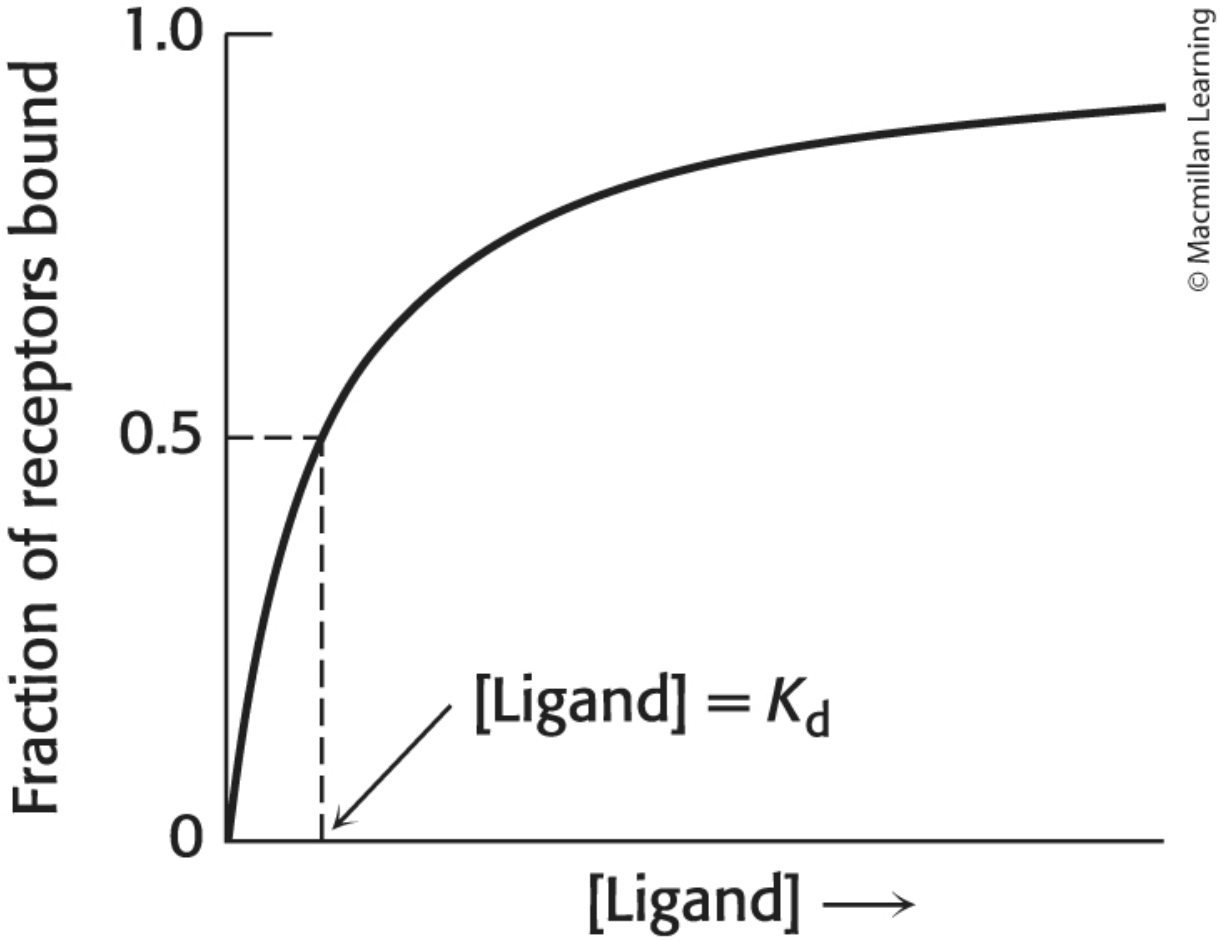
© Macmillan Learning

Target-based screening labeled (A) shows the following stages from the left to the right: Target validation, Assay development, Library screening, and Positive hits.

Phenotypic screening labeled (B) shows the following stages from the left to the right: Phenotypic assay, Library screening, Positive hits, and Target identification.

Return to FIGURE 32.11 Target-based screening and phenotypic screening are two paths to early drug discovery

Extended description for FIGURE 32.12 Simple ligand binding results in a hyperbolic curve

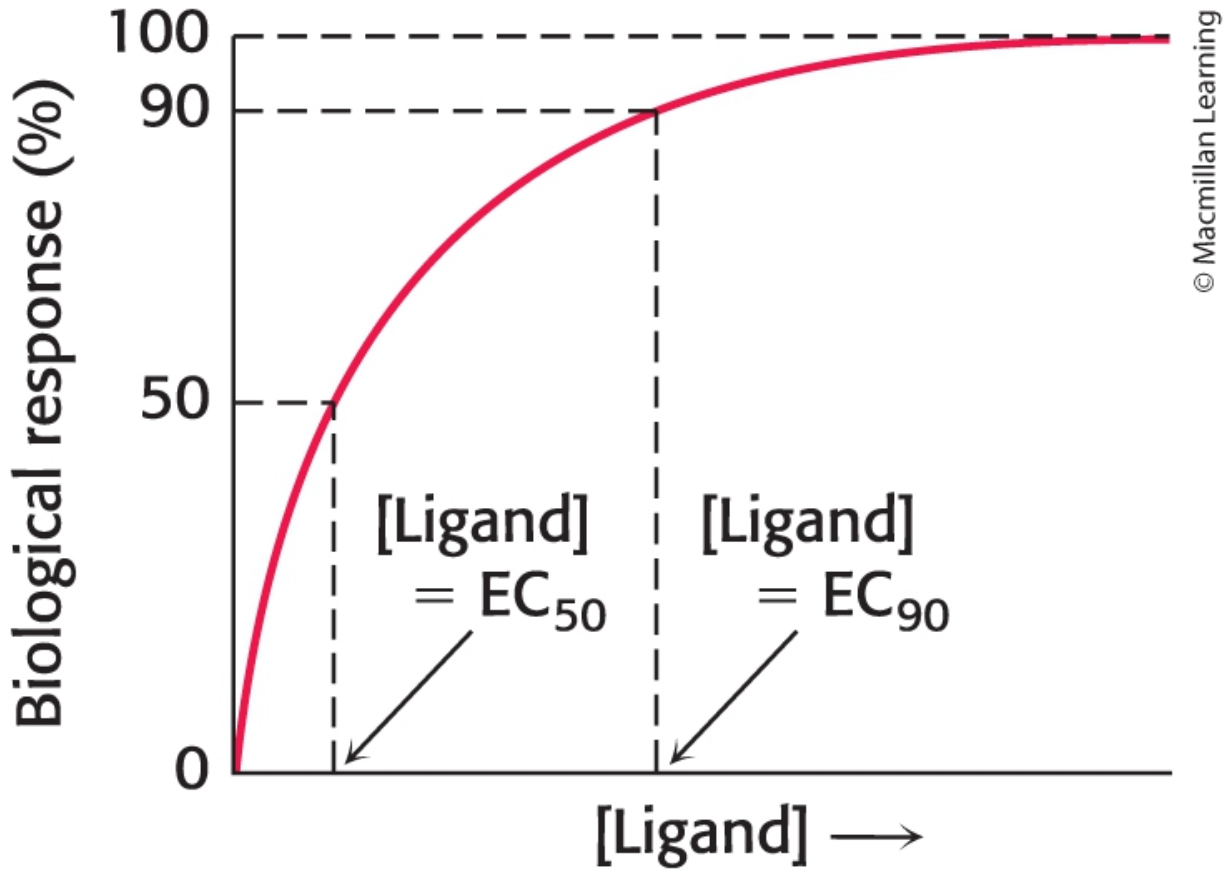


The horizontal axis is labeled open square bracket Ligand close square bracket indicated by a rightward arrow. The vertical axis is labeled Fraction of receptors bound and ranges from 0 to 1.0 in increments of 0.5 units. The two axes intersect at the bottom left. A black hyperbolic curve starts at the intersection of the axes, rises to the upper right with a decreasing slope up to 0.75 value on the vertical axis, and moves almost horizontally to the right to 0.9 value on the vertical axis. A point on the black curve is shown with coordinates (open square bracket Ligand close square bracket

equals K subscript d Baseline, 0.5). A vertical dotted line and a horizontal dotted line are drawn from the point to the horizontal and vertical axes, respectively.

Return to FIGURE 32.12 Simple ligand binding results in a hyperbolic curve

Extended description for FIGURE 32.13 Effective concentration (E C) describes the amount of compound required to elicit a particular biological response

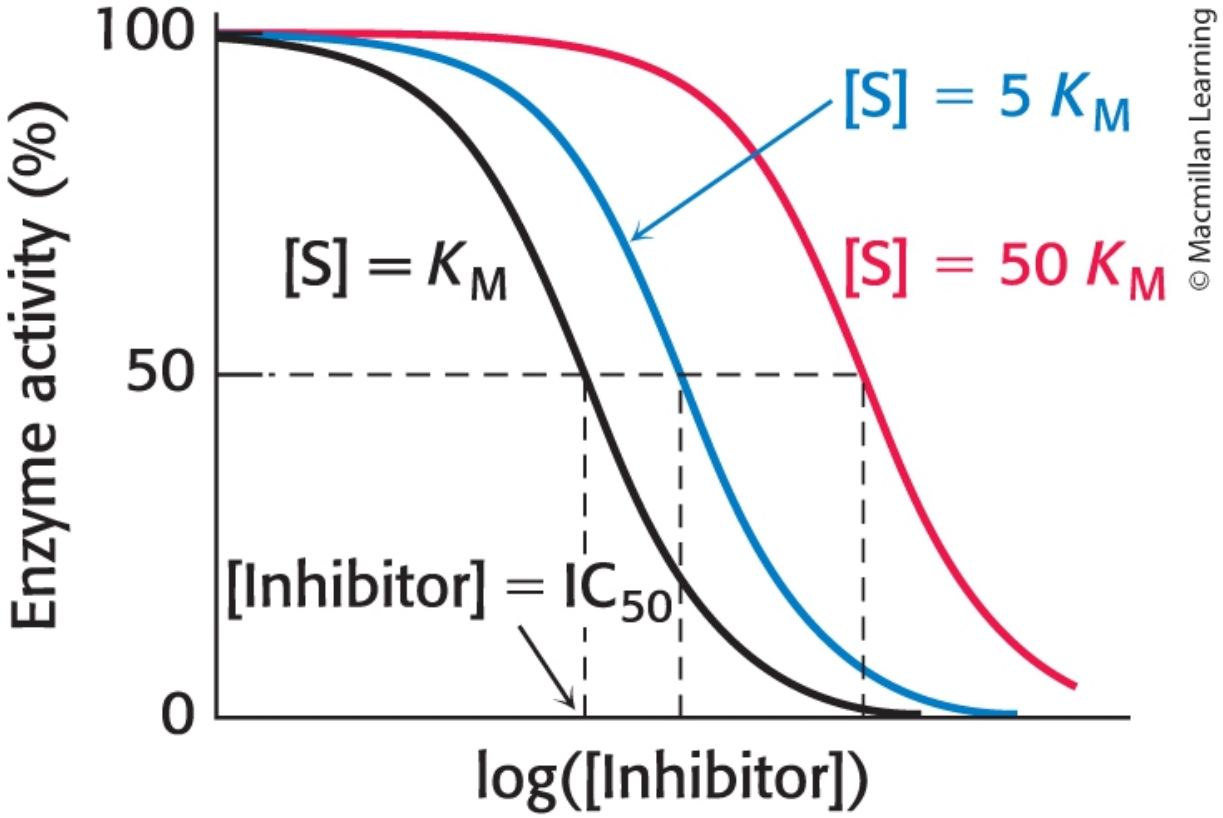


The horizontal axis is labeled open square bracket Ligand close square bracket indicated by a rightward arrow. The vertical axis is labeled Biological response (percent) and has the markings 0, 50, 90, and 100 from the bottom to the top. The two axes intersect at the bottom left. A red curve starts at the intersection of the axes and rises to the upper right with a decreasing slope passing through points (open square bracket Ligand close square bracket equals E C subscript 50 Baseline, 50) and (open square bracket Ligand close square bracket equals E C subscript 90 Baseline, 90), and moves

almost horizontally to the right to 100 value on the vertical axis. Vertical dotted lines and horizontal dotted lines are drawn from the points to the horizontal and vertical axes, respectively.

Return to FIGURE 32.13 Effective concentration (E C) describes the amount of compound required to elicit a particular biological response

Extended description for FIGURE 32.14 Inhibitors compete with substrates for enzyme active sites

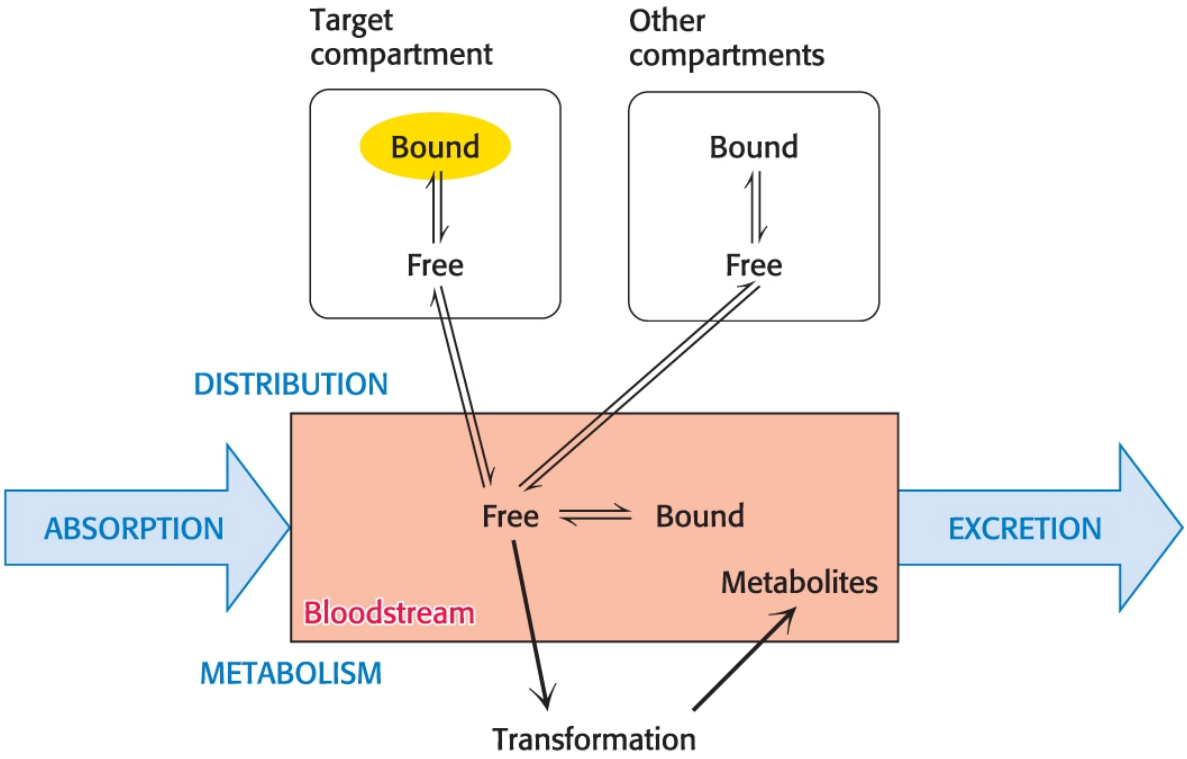


The horizontal axis is labeled log (open square bracket inhibitor close square bracket). The vertical axis is labeled Enzyme activity (percent) and ranges from 0 to 100 in increments of 50 units. A black curve for concentration of S equals K subscript M Baseline starts from 100 on the vertical axis, and falls with an increasing slope concave down up to 50 units value on the vertical axis, falls further with a decreasing slope concave up to intersect the horizontal axis. A blue curve for concentration of S equals 5 K subscript M Baseline starts from 100 on the vertical axis, falls with an increasing slope concave down up to 50 units value on the vertical axis to the right of the black curve, and falls further with a decreasing slope concave up to intersect the horizontal axis to the right of the end point of the

black curve. A red curve for concentration of S equals 50 K subscript M Baseline starts from 100 on the vertical axis, falls with an increasing slope concave down up to 50 units value on the vertical axis to the right of the blue curve, and falls further with a decreasing slope concave up to intersect the horizontal axis to the right of the end point of the blue curve. A horizontal dotted line is drawn from 50 units value on the vertical axis. Three vertical dotted lines are drawn from each point of the three curves at 50 units value on the vertical axis. The vertical dotted line from the point on the black curve at 50 units value on the vertical axis intersects the horizontal axis at (open square bracket Inhibitor close square bracket) equals I C subscript 50 Baseline.

Return to FIGURE 32.14 Inhibitors compete with substrates for enzyme active sites

Extended description for FIGURE 32.15 The pharmacokinetics of a compound in a living organism is described by its absorption, distribution, metabolism, and excretion (A D M E) properties



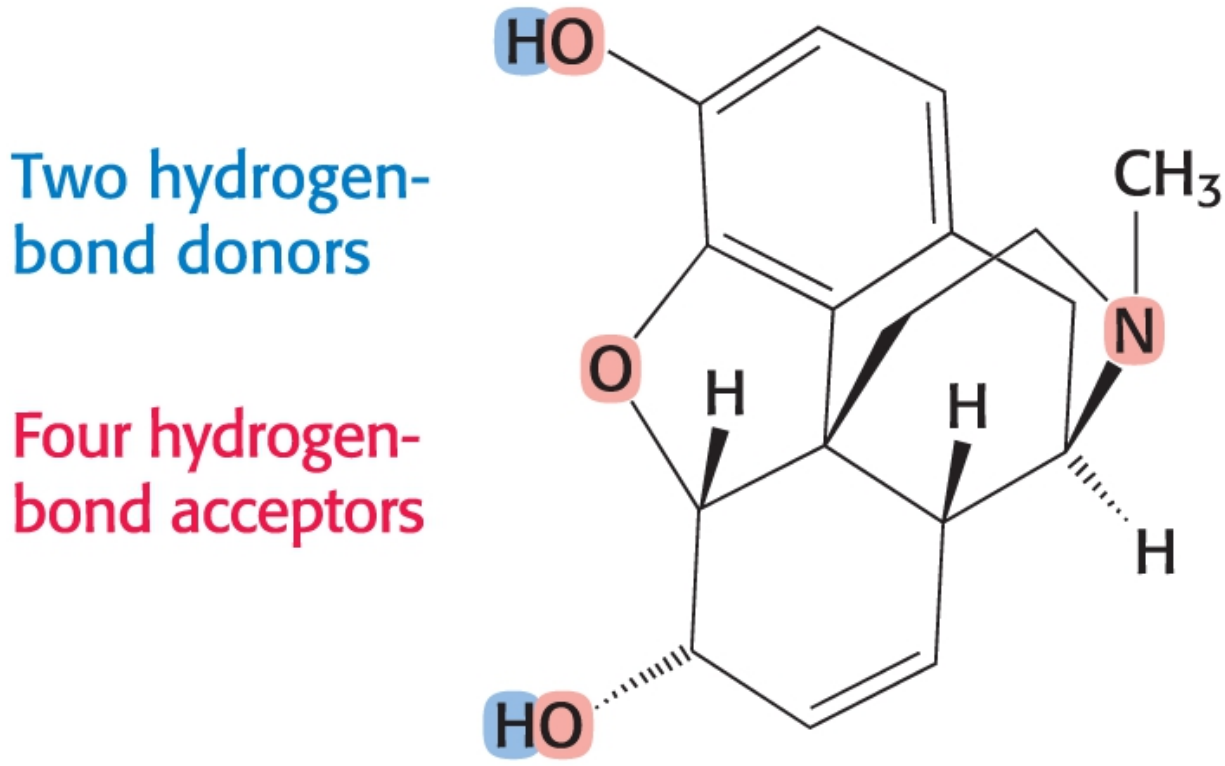
© Macmillan Learning

The bloodstream is depicted as a horizontal red rectangle. A large blue arrow labeled Absorption from the left points to the bloodstream. The free compound converts reversibly to a bound compound in the bloodstream. The area above the bloodstream is labeled Distribution and the area below the bloodstream is labeled Metabolism. The free compound in the bloodstream also converts reversibly to a free compound in a target compartment shown in the distribution area. In the target compartment the free compound converts reversibly to a bound compound shaded yellow. The free compound in the bloodstream also converts reversibly to a free

compound in other compartments shown in the distribution area. In other compartments the free compound converts reversibly to a bound compound. The free compound in the bloodstream also undergoes transformation in the metabolism area and is converted to metabolites back in the bloodstream. A large blue arrow labeled excretion from the bloodstream points to the right.

Return to FIGURE 32.15 The pharmacokinetics of a compound in a living organism is described by its absorption, distribution, metabolism, and excretion (A D M E) properties

Extended description for FIGURE 32.16 Lipinski's rules serve as a guide to predict oral bioavailability



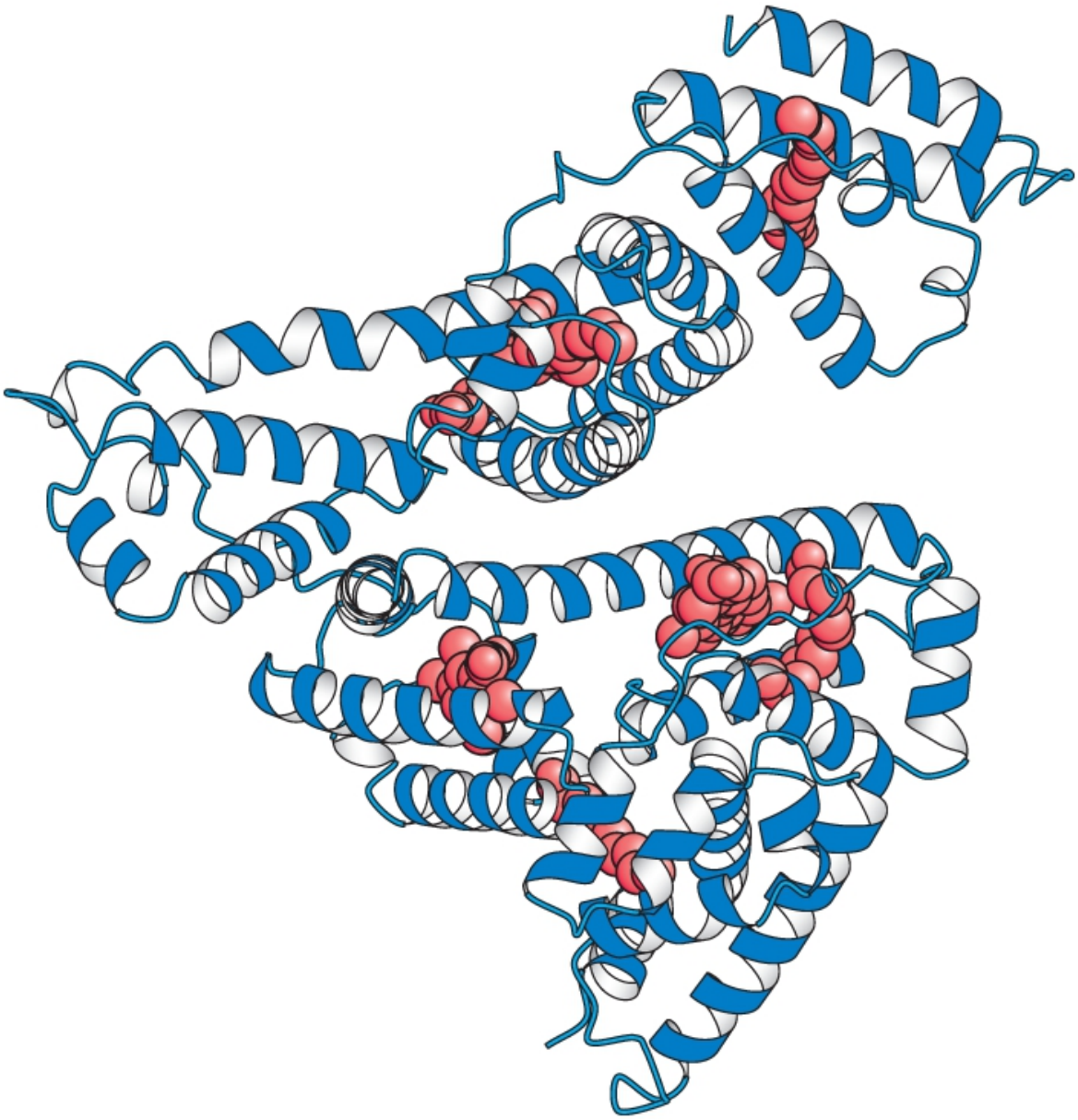
A benzene ring is in a vertical orientation with C 1 occupying the topmost vertex. The benzene ring contains alternating double bonds between C 2 and C 3, C 4 and C 5, and C 6 and C 1. C 6 of the benzene ring is single bonded to O H. The benzene ring is fused to a bridged bicyclic ring which is as follows: A non-planar cyclic heterocyclic ring consisting of 1 N and 7 C atoms is shown. N occupies the first

position. N is single bonded to C 1 on the upper left. C 1 is single bonded to C 2 on the lower left. C 2 is wedge bonded to C 3 on the lower left. C 3 is single bonded to C 4 above. C 4 is single bonded to C 5 on the upper right. C 5 is single bonded to C 6 on the lower right. C 6 is single bonded to C 7 below. C 7 is wedge bonded to N on the upper right, completing the ring. C 3 and C 7 are each single bonded to a common C 8 below the ring. The benzene ring and the bridged bicyclic ring are fused to each other such that C 3 and C 4 of the benzene ring are the C 5 and C 4 of the bridged bicyclic ring, respectively. N of the bridged bicyclic ring is single bonded to C H 3 above. C 7 of the bridged bicyclic ring is dash bonded to H on the lower right. C 8 of the bridged bicyclic ring is wedge bonded to H above. The bridged bicyclic ring is fused to a 6-carbon hexagonal ring in a vertical orientation with C 1 occupying the topmost vertex. The two rings are fused to each other such that C 3 and C 8 of the bridged bicyclic ring are the C 1 and C 2 of the 6-carbon hexagonal ring, respectively. In the 6-carbon hexagonal ring, a double bond is present between C 3 and C 4. C 5 of the 6-carbon hexagonal ring is dash bonded to O H. The 6-carbon hexagonal ring, the bridged bicyclic ring, and the benzene ring are fused to a 5-membered heterocyclic pentagonal ring in a horizontal orientation consisting of 1 O and 4 C atoms. In the pentagonal ring, O occupies the first position which is the leftmost vertex. The 6-carbon hexagonal ring and the pentagonal ring are fused to each other such that C 6 and C 1 of the 6-carbon hexagonal ring are the C 4 and C 3 of the pentagonal ring, respectively. The bridged bicyclic ring and the pentagonal ring are fused to each other such that C 3 and C 4 of the bridged bicyclic ring are the C 3 and C 2 of the pentagonal ring, respectively. The benzene ring and the pentagonal ring are fused to each other such that C 4 and C 5 of the benzene ring are the C 2 and C 1 of the pentagonal ring, respectively. O of the O H groups, O of the pentagonal ring, and N of the bridged bicyclic ring are highlighted in red and are the four hydrogen-bond receptors. H of the O H

groups are the two hydrogen-bond donors. Note: Molecular weight equals 285. Log of (P) equals 1.27.

Return to FIGURE 32.16 Lipinski's rules serve as a guide to predict oral bioavailability

Extended description for FIGURE 32.17 Albumin is abundant in the bloodstream and binds hydrophobic compounds

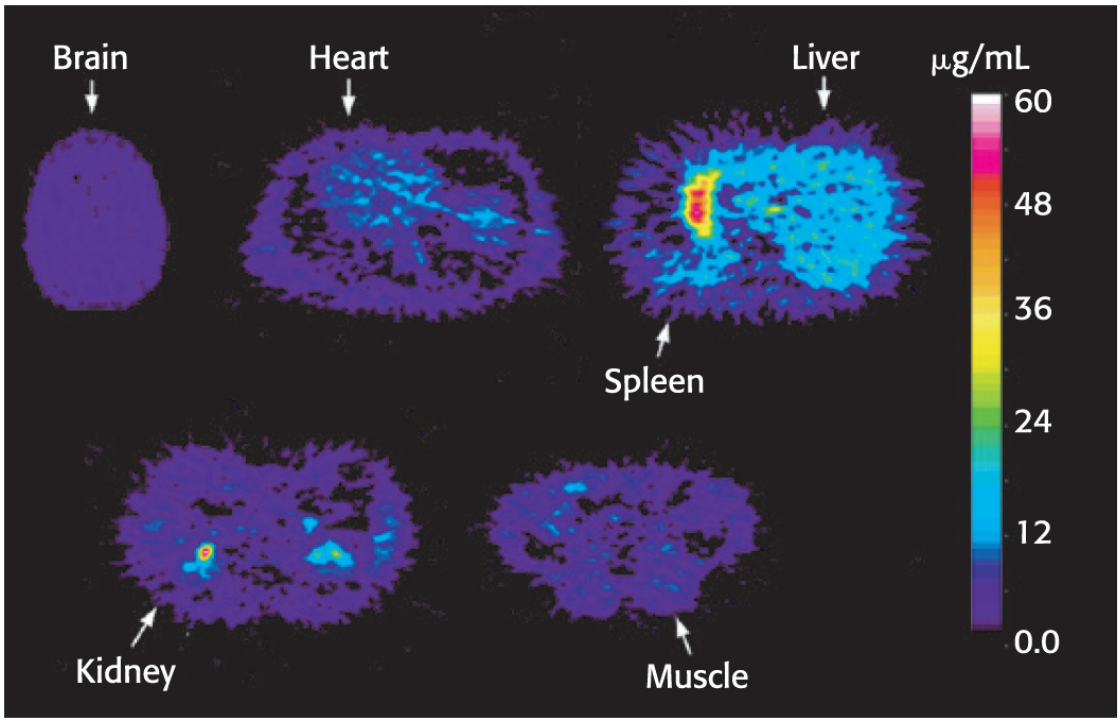


The three-dimensional ribbon diagram shows the heart-shaped tertiary structure of the serum albumin composed of numerous

coiled blue alpha helices homologous domains interconnected by thin thread-like loops. The space-filling model of seven hydrophobic compounds each composed of fused red spheres. The seven hydrophobic compounds are shown bound to the serum albumin in the following locations: on the upper right, 2 on the lower right, 2 on the upper left, and a few on the lower left region.

Return to FIGURE 32.17 Albumin is abundant in the bloodstream and binds hydrophobic compounds

Extended description for FIGURE 32.18 Once absorbed, compounds distribute to various organs within the body



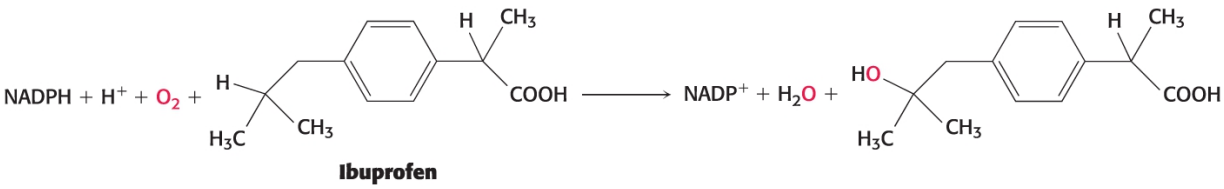
Reprinted by permission from Macmillan Publishers Ltd: Nature Reviews Drug Discovery, Rudin, M., and Weissleder, R., "Molecular imaging in drug discovery and development," 2: 2, pp. 123–131, (2003); permission conveyed through Copyright Clearance Center, Inc.

The composite P E T scanned image shows the distribution of fluconazole labeled with the positron-emitting isotope superscript 18 F into the following target compartments: Brain, Heart, Liver, spleen, Kidney, and Muscle. A color gradient scale is shown on the right ranging from a concentration of 0.0 to 60 micrograms per milliliter in increments of 12 micrograms per milliliter. 0 to 12 micrograms per milliliter represent purple. 12 to 20 micrograms per milliliter represent blue. 20 to 28 micrograms per milliliter represent green. 24 to 36 micrograms per milliliter represent yellow. 36 to 48 orange. 48 to 54 micrograms per milliliter represent pink. 54 to 60 micrograms per milliliter represent white. First target compartment Brain: The distribution of fluconazole all over the

brain ranges from approximately 0 to 10 micrograms per milliliter. Second target compartment Heart: The distribution of fluconazole in the heart ranges from approximately 12 to 18 micrograms per milliliter in the center and the lower right regions lightly and the remaining area has 0 to 10 micrograms per milliliter predominantly. Third target compartment Liver on the upper right and spleen on the lower left: The distribution of fluconazole in the liver ranges from approximately 12 to 18 micrograms per milliliter dispersing from the center to the upper right and the lower right regions predominantly and the remaining outlining area has a concentration of 0 to 10 micrograms per milliliter. The distribution of fluconazole in the spleen ranges from approximately 48 to 52 micrograms per milliliter concentrated at the core, surrounded by 30 to 36 micrograms per milliliter at the center-left, 12 to 18 micrograms per milliliter dispersing toward lower left regions and the remaining are has a concentration of 0 to 10 micrograms per milliliter. Fourth target compartment kidney. The distribution of fluconazole in the kidney ranges from approximately 12 to 18 micrograms per milliliter predominantly and feeble concentration of 12 to 18 micrograms per milliliter in the lower left and the lower right regions, and minute concentration of 36 to 52 micrograms per milliliter in the lower left region. Fifth target compartment muscle. The distribution of fluconazole in the muscle ranges from approximately 0 to 10 micrograms per milliliter predominantly and a minute concentration of 12 to 18 micrograms per milliliter on the upper left and lower right regions.

Return to FIGURE 32.18 Once absorbed, compounds distribute to various organs within the body

Extended description for FIGURE 32.19 Cytochrome P450 isozymes catalyze xenobiotic metabolic reactions such as hydroxylation

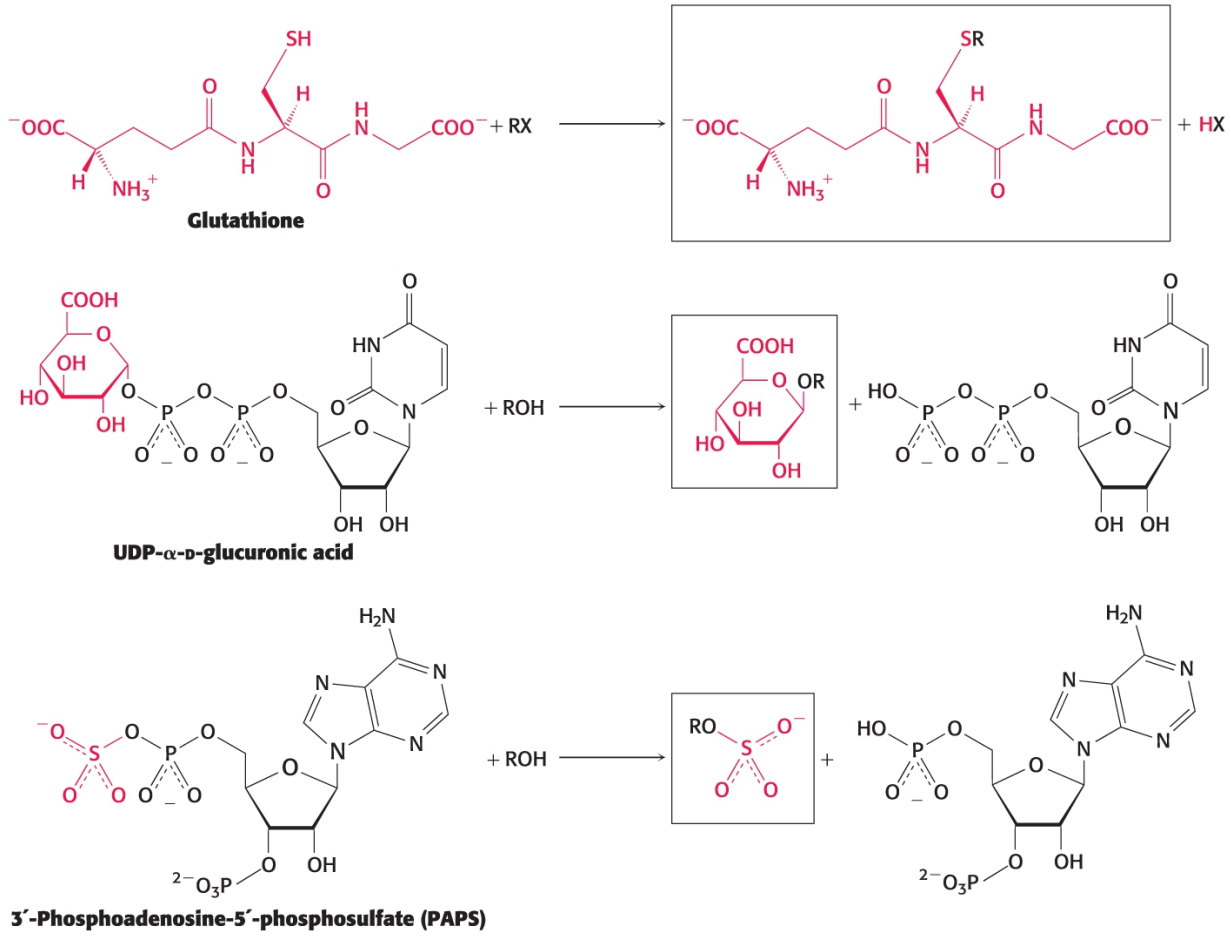


The reaction contains four reactants and three products. The first reactant is N A D P H. The second reactant is H superscript plus. The third reactant is O 2 highlighted in red. The fourth reactant is labeled Ibuprofen and has the following structure: A benzene ring is in a horizontal orientation with C 1 occupying the rightmost vertex. The ring contains alternating double bonds between C 1 and C 2, C 3 and C 4, and C 5 and C 6. C 1 is single bonded to a central C atom in the form of a line. The central C atom is single bonded to H on the upper left, C H 3 on the upper right, and C O O H on the lower right. C 4 of the benzene ring is single bonded to C 2 of a 2-carbon alkane chain depicted as a line structure using 1 line. C 1 of the alkane chain is single bonded to H on the upper left, C H 3 on the lower left, and C H 3 on the lower right. The first product is N A D P superscript plus. The second product is H 2 O of which O is highlighted in red. The third product has the following structure: A benzene ring is in a horizontal orientation with C 1 occupying the rightmost vertex. The ring contains alternating double bonds between C 1 and C 2, C 3 and C 4, and C 5 and C 6. C 1 is single bonded to a central C atom in the form of a line. The central C atom is single bonded to H on the upper left, C H 3 on the upper right, and C O O H on the lower right. C 4 of the benzene ring is single bonded to C 2 of a 2-carbon alkane chain depicted as a line structure using 1 line. C 1 of the alkane

chain is single bonded to C H 3 on the lower left, C H 3 on the lower right, and O H on the upper left of which O is highlighted in red.

Return to FIGURE 32.19 Cytochrome P450 isozymes catalyze xenobiotic metabolic reactions such as hydroxylation

Extended description for FIGURE 32.20 Compounds that have certain functional groups are often modified by conjugation reactions



The first reaction contains two reactants and two products. The first reactant labeled Glutathione and highlighted in red has the following structure: A 2 N and 7 C heteronuclear alkane chain is depicted as a line structure using 8 zigzag lines. N bound to H occupies the fifth and the eighth positions. C 1 is single bonded to C O O superscript minus on the upper left, wedge bonded to H on the lower left, and dash bonded to N H 3 superscript plus on the lower right. C 4 is double bonded to O above. C 5 is dash bonded to H on

the upper right and wedge bonded to a central C H 2 group on the upper left. The central C H 2 group is single bonded to S H on the upper right. C 6 is double bonded to a second O atom below. C 7 is single bonded to C O O superscript minus on the upper right. The second reactant is R X. The first product enclosed in a box has the following structure: A 2 N and 7 C heteronuclear alkane chain is depicted as a line structure using 8 zigzag lines. N bound to H occupies the fifth and the eighth positions. C 1 is single bonded to C O O superscript minus on the upper left, wedge bonded to H on the lower left, and dash bonded to N H 3 superscript plus on the lower right. C 4 is double bonded to O above. C 5 is dash bonded to H on the upper right and wedge bonded to a central C H 2 group on the upper left. The central C H 2 group is single bonded to S R on the upper right. C 6 is double bonded to a second O atom below. C 7 is single bonded to C O O superscript minus on the upper right. The entire structure except for R of S R is highlighted in red. The second reactant is H X of which H is highlighted in red.

The second reaction contains two reactants and two products. The first reactant labeled U D P-alpha-D-glucuronic acid has the following structure: A 6-membered heterocyclic hexagonal ring is in a horizontal orientation consisting of 1 O and 5 C atoms. O occupies the first position which is the top right vertex. The ring is in a plane perpendicular to the plane of the paper such that C 2 and C 3 are toward the observer, and C 5 and O are away from the observer. C 2 and C 4 are each single bonded to O H below. C 3 is single bonded to O H above. C 5 is single bonded to C O O H above. The ring is highlighted in red. C 1 is single bonded below to the first O atom of the following horizontal zigzag chain: O, single bond, P, single bond, O, single bond, P, single bond, O. Each P atom of the horizontal zigzag chain carries a negative charge and is partially double bonded to an O atom on the lower right and an O atom on the lower left. The third O atom of the main horizontal zigzag chain is single bonded to a central C H 2 group on the lower right in the form of a line. The

central C H 2 group is single bonded below to C 4 of a 5-membered heterocyclic pentagonal ring in a vertical orientation consisting of 1 O and 4 C atoms. In the pentagonal ring, O occupies the first position which is the topmost vertex. The pentagonal ring is in a plane perpendicular to the plane of the paper such that C 2 and C 3 are toward the observer, and O is away from the observer. In the pentagonal ring, C 2 and C 3 are each single bonded to O H below. C 1 of the pentagonal ring is single bonded to the first N atom of a second 6-membered heterocyclic hexagonal ring in a vertical orientation consisting of 2 N and 4 C atoms. In the second 6-membered ring, the first N atom occupies the first position which is the bottommost vertex and the second N atom bound to H occupies the third position which is the top left vertex. In the second 6-membered ring, a double bond is present between C 3 and C 4. In the second 6-membered ring, C 1 and C 2 are each double bonded to O. The second reactant is R O H. The first product is enclosed in a box and has the following structure: A 6-membered heterocyclic hexagonal ring is in a horizontal orientation consisting of 1 O and 5 C atoms. O occupies the first position which is the top right vertex. The ring is in a plane perpendicular to the plane of the paper such that C 2 and C 3 are toward the observer, and C 5 and O are away from the observer. C 2 and C 4 are each single bonded to O H below. C 3 is single bonded to O H above. C 5 is single bonded to C O O H above. The ring is highlighted in red. C 1 is single bonded to O R above. The second product has the following structure: A horizontal zigzag chain is illustrated by: H O, single bond, P, single bond, O, single bond, P, single bond, O. Each P atom of the horizontal zigzag chain carries a negative charge and is partially double bonded to an O atom on the lower right and an O atom on the lower left. The second O atom of the main horizontal zigzag chain is single bonded to a central C H 2 group on the lower right in the form of a line. The central C H 2 group is single bonded below to C 4 of a 5-membered heterocyclic pentagonal ring in a vertical orientation consisting of 1 O and 4 C atoms. In the pentagonal ring, O occupies the first

position which is the topmost vertex. The pentagonal ring is in a plane perpendicular to the plane of the paper such that C 2 and C 3 are toward the observer, and O is away from the observer. In the pentagonal ring, C 2 and C 3 are each single bonded to O H below. C 1 of the pentagonal ring is single bonded to the first N atom of a second 6-membered heterocyclic hexagonal ring in a vertical orientation consisting of 2 N and 4 C atoms. In the second 6-membered ring, the first N atom occupies the first position which is the bottommost vertex and the second N atom bound to H occupies the third position which is the top left vertex. In the second 6-membered ring, a double bond is present between C 3 and C 4. In the second 6-membered ring, C 1 and C 2 are each double bonded to O.

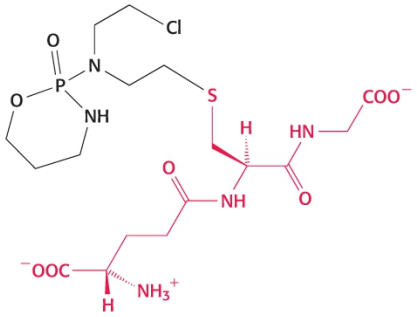
The third reaction contains two reactants and two products. The first reactant labeled 3 prime-Phosphoadenosine-5 prime-phosphosulfate (P A P S) has the following structure: A horizontal zigzag chain is illustrated by: O superscript minus, single bond, S, single bond, O, single bond, P, single bond, O. The P atom carries a negative charge. The S and the P atoms are each partially double bonded to an O atom on the lower right and an O atom on the lower left. O superscript minus, the S atom and the groups attached to it are highlighted in red. The second O atom of the main horizontal zigzag chain is single bonded to a central C H 2 group on the lower right in the form of a line. The central C H 2 group is single bonded below to C 4 of a 5-membered heterocyclic pentagonal ring in a vertical orientation consisting of 1 O and 4 C atoms. In the pentagonal ring, O occupies the first position which is the topmost vertex. The pentagonal ring is in a plane perpendicular to the plane of the paper such that C 2 and C 3 are toward the observer, and O is away from the observer. In the pentagonal ring, C 2 is single bonded to O H below. C 3 of the pentagonal ring is single bonded to O below which is further single bonded to P O 3 superscript 2 minus. C 1 of the pentagonal ring is single bonded to the first N atom of a second

5-membered heterocyclic pentagonal ring in a horizontal orientation consisting of 2 N and 3 C atoms. In the second pentagonal ring, the first N atom occupies the first position which is the bottom left vertex and the second N atom occupies the third position which is the top left vertex. In the second pentagonal ring, a double bond is present between C 1 and the second N atom. The second pentagonal ring is fused to a 6-membered heterocyclic hexagonal ring in a vertical orientation consisting of 2 N and 4 C atoms. In the 6-membered ring, the first N atom occupies the first position which is the top right vertex and the second N atom occupies the third position which is the bottommost vertex. The two rings are fused to each other such that C 2 and C 3 of the second pentagonal ring are the C 3 and C 2 of the 6-membered ring, respectively. In the 6-membered ring, a double bond is present between C 1 and the second N atom, C 2 and C 3, and C 4 and the first N atom. In the second 6-membered ring, C 4 is single bonded to N H 2. The second reactant is R O H. The first product enclosed in a box has the following structure: A central S atom is partially double bonded to O superscript minus on the upper right, O on the lower right, and a second O atom on the lower left. This part is highlighted in red. The central S atom is single bonded to O R on the upper left. The second product has the following structure: A horizontal zigzag chain is illustrated by: O H, single bond, P, single bond, O. The P atom carries a negative charge and is partially double bonded to an O atom on the lower right and an O atom on the lower left. O of the main horizontal zigzag chain is single bonded to a central C H 2 group on the lower right in the form of a line. The central C H 2 group is single bonded below to C 4 of a 5-membered heterocyclic pentagonal ring in a vertical orientation consisting of 1 O and 4 C atoms. In the pentagonal ring, O occupies the first position which is the topmost vertex. The pentagonal ring is in a plane perpendicular to the plane of the paper such that C 2 and C 3 are toward the observer, and O is away from the observer. In the pentagonal ring, C 2 is single bonded to O H below. C 3 of the pentagonal ring is single

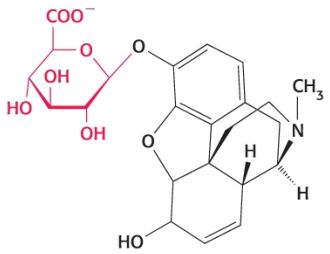
bonded to O below which is further single bonded to P O 3 superscript 2 minus. C 1 of the pentagonal ring is single bonded to the first N atom of a second 5-membered heterocyclic pentagonal ring in a horizontal orientation consisting of 2 N and 3 C atoms. In the second pentagonal ring, the first N atom occupies the first position which is the bottom left vertex and the second N atom occupies the third position which is the top left vertex. In the second pentagonal ring, a double bond is present between C 1 and the second N atom. The second pentagonal ring is fused to a 6-membered heterocyclic hexagonal ring in a vertical orientation consisting of 2 N and 4 C atoms. In the 6-membered ring, the first N atom occupies the first position which is the top right vertex and the second N atom occupies the third position which is the bottommost vertex. The two rings are fused to each other such that C 2 and C 3 of the second pentagonal ring are the C 3 and C 2 of the 6-membered ring, respectively. In the 6-membered ring, a double bond is present between C 1 and the second N atom, C 2 and C 3, and C 4 and the first N atom. In the second 6-membered ring, C 4 is single bonded to N H 2.

Return to FIGURE 32.20 Compounds that have certain functional groups are often modified by conjugation reactions

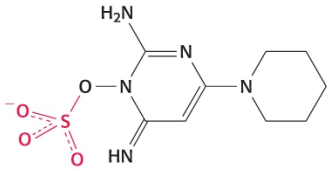
Extended description for Structures of Cyclophosphamide-glutathione conjugate, Morphine glucuronidate, and Minoxidil sulfate



Cyclophosphamide-glutathione conjugate



Morphine glucuronidate



Minoxidil sulfate

Cyclophosphamide-glutathione conjugate has the following structure: A 6-membered heterocyclic hexagonal ring is in a vertical orientation consisting of 1 O 1 P, 1 N, and 3 C atoms. O occupies the first position which is the top left vertex. P occupies the second position which is the topmost vertex. N bound to H occupies the third position which is the top right vertex. P is double bonded to a second O atom on the upper left and is single bonded on the upper right to N of 1 N and 4 C heteronuclear alkane chain depicted as a line structure using 4 zigzag lines. In the alkane chain, N occupies the third position. C 1 of the alkane chain is single bonded to C l on the lower right. C 4 of the alkane chain is single bonded to S on the lower right. S is single bonded to a central C H 2 group below in the form of a line. The central C H 2 group is wedge bonded on the lower right to C 5 of a 2 N and 6 C heteronuclear alkane chain depicted as a line structure using 6 zigzag lines. In the 2 N and 6 C heteronuclear alkane chain, N bound to H occupies the fifth and the eighth positions. C 1 of the 2 N and 6 C heteronuclear alkane chain, is dash bonded to N H 3 superscript plus on the lower right, wedge bonded to H below, and single bonded to C O O superscript minus

on the left. C 4 is double bonded to a third O atom on the upper left. C 5 is dash bonded to H above. C 6 is double bonded to a fourth O atom on the lower right. C 6 is single bonded to C O O superscript minus on the upper right. The S atom and the 2 N and 6 C heteronuclear alkane chain along with its attached groups is highlighted in red.

Morphine glucuronidate has the following structure: A 6-membered heterocyclic hexagonal ring is in a horizontal orientation and consists of 1 O and 5 C atoms. O occupies the first position which is the top right vertex. The ring is in a plane perpendicular to the plane of the paper such that C 2 and C 3 are toward the observer, and C 5 and O are away from the observer. C 2 is single bonded to O H below. C 3 is single bonded to O H above. C 4 is single bonded to O H on the lower left. C 5 is single bonded to C O O superscript minus. The ring and the groups attached to the vertices are highlighted in red. C 1 is single bonded to a second O atom on the upper right. The second O atom is single bonded on the lower right to C 5 of a benzene ring in a vertical orientation with C 1 occupying the topmost vertex. The benzene ring contains alternating double bonds between C 2 and C 3, C 4 and C 5, and C 6 and C 1. The benzene ring is fused to a bridged bicyclic ring which is as follows: A non-planar cyclic heterocyclic ring consisting of 1 N and 7 C atoms is shown. N occupies the first position. N is single bonded to C 1 on the upper left. C 1 is single bonded to C 2 on the lower left. C 2 is wedge bonded to C 3 on the lower left. C 3 is single bonded to C 4 above. C 4 is single bonded to C 5 on the upper right. C 5 is single bonded to C 6 on the lower right. C 6 is single bonded to C 7 below. C 7 is wedge bonded to N on the upper right, completing the ring. C 3 and C 7 are each single bonded to a common C 8 below the ring. The benzene ring and the bridged bicyclic ring are fused to each other such that C 3 and C 4 of the benzene ring are the C 5 and C 4 of the bridged bicyclic ring, respectively. N of the bridged bicyclic ring is single bonded to C H 3 above. C 7 of the bridged bicyclic ring is dash

bonded to H on the lower right. C 8 of the bridged bicyclic ring is wedge bonded to H above. The bridged bicyclic ring is fused to a 6-carbon hexagonal ring in a vertical orientation with C 1 occupying the topmost vertex. The two rings are fused to each other such that C 3 and C 8 of the bridged bicyclic ring are the C 1 and C 2 of the 6-carbon hexagonal ring, respectively. In the 6-carbon hexagonal ring, a double bond is present between C 3 and C 4. C 5 of the 6-carbon hexagonal ring is dash bonded to O H. The 6-carbon hexagonal ring, the bridged bicyclic ring, and the benzene ring are fused to a 5-membered heterocyclic pentagonal ring in a horizontal orientation consisting of 1 O and 4 C atoms. In the pentagonal ring, O occupies the first position which is the leftmost vertex. The 6-carbon hexagonal ring and the pentagonal ring are fused to each other such that C 6 and C 1 of the 6-carbon hexagonal ring are the C 4 and C 3 of the pentagonal ring, respectively. The bridged bicyclic ring and the pentagonal ring are fused to each other such that C 3 and C 4 of the bridged bicyclic ring are the C 3 and C 2 of the pentagonal ring, respectively. The benzene ring and the pentagonal ring are fused to each other such that C 4 and C 5 of the benzene ring are the C 2 and C 1 of the pentagonal ring, respectively.

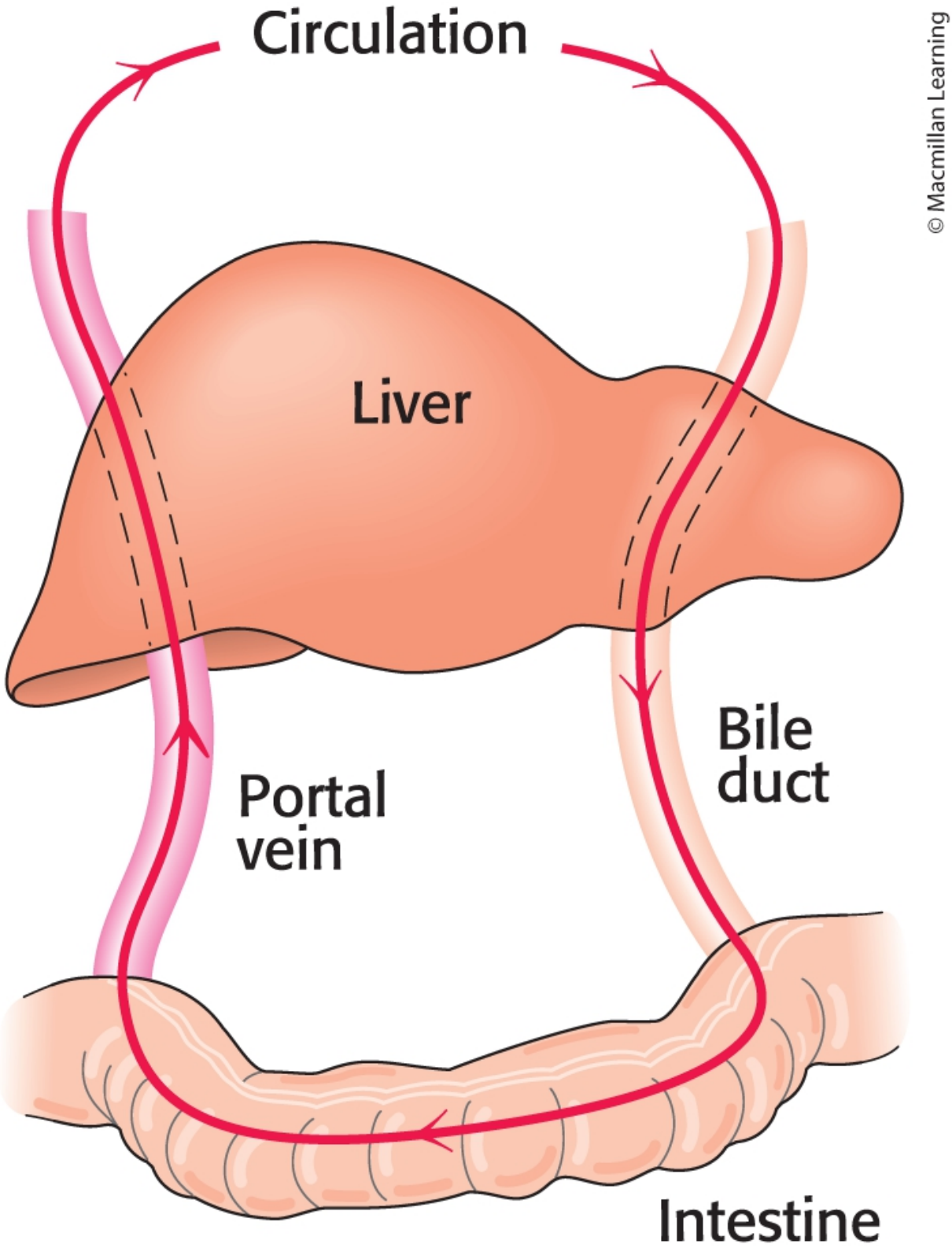
Minoxidil sulfate has the following structure: A 6-membered heterocyclic hexagonal ring is in a horizontal orientation consisting of 2 N and 4 C atoms. The first N atom occupies the first position which is the leftmost vertex. The second N atom occupies the third position which is the top right vertex. A double bond is present between C 1 and the second N atom, and C 2 and C 3. C 1 is single bonded to N H 2. C 4 is double bonded to N H. C 2 is single bonded to N of a second 6-membered heterocyclic hexagonal ring in a horizontal orientation consisting of 1 N and 5 C atoms. In the second ring, N occupies the first position which is the leftmost vertex. The first N atom of the first ring is single bonded to O. O is single bonded to a central S atom on the lower left. The central S atom is partially double bonded to O on the lower right, a second O atom on the

lower left, and O superscript minus on the upper left. The central S atom and the groups attached to it are highlighted in red.

Return to Structures of Cyclophosphamide-glutathione conjugate, Morphine glucuronidate, and Minoxidil sulfate

Extended description for FIGURE 32.21 Drugs can move between the intestine and the circulation via

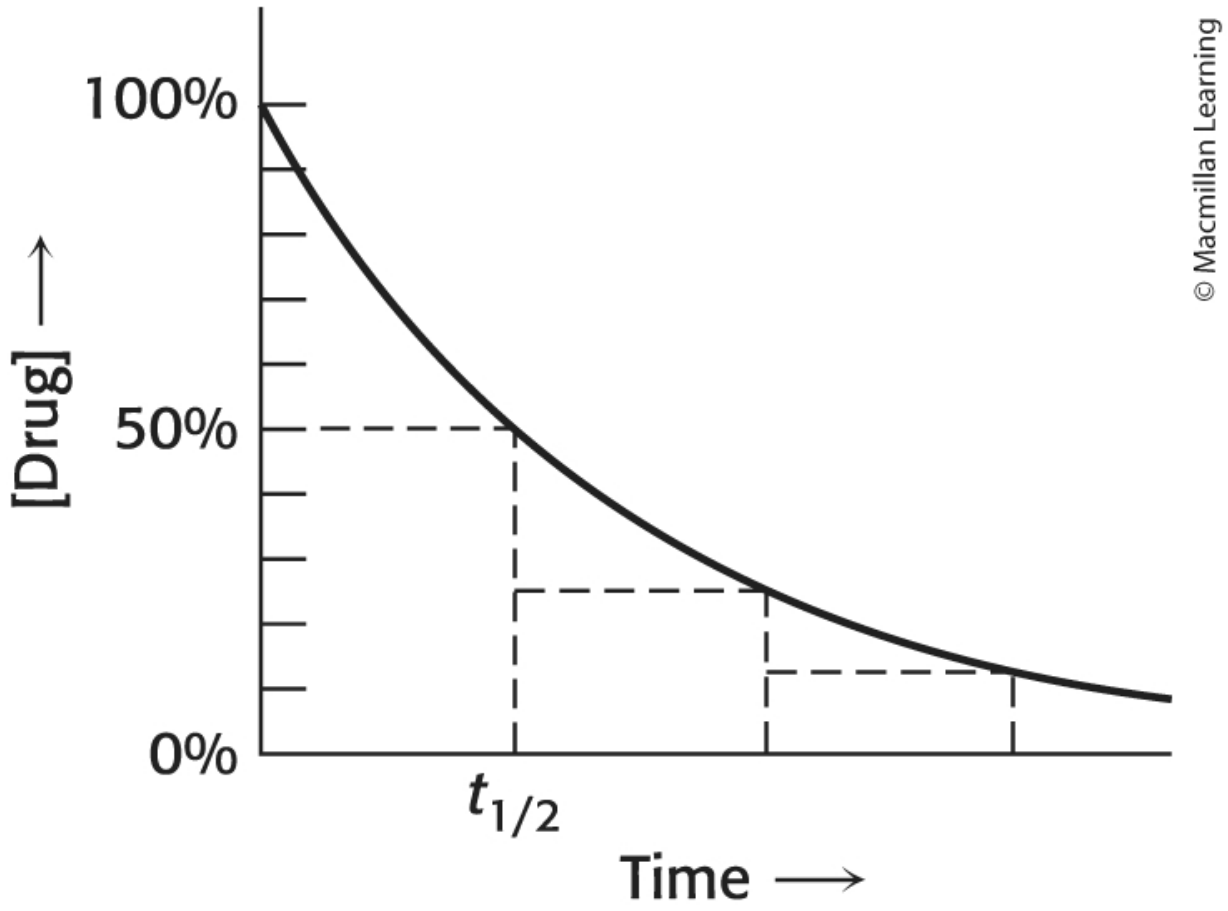
enterohepatic cycling



The illustration shows the cone-shaped muscular organ liver and the long horizontal muscular tube of the intestine with numerous folds running at the bottom. The liver is connected to the intestine by two thin tubular structures: the bile duct on the right and the portal vein on the left. The enterohepatic drug circulation indicated by arrows is shown from the liver to the intestine via the bile duct and back to the liver via the portal vein.

Return to FIGURE 32.21 Drugs can move between the intestine and the circulation via enterohepatic cycling

Extended description for FIGURE 32.22 Drug excretion may be measured by its half-life

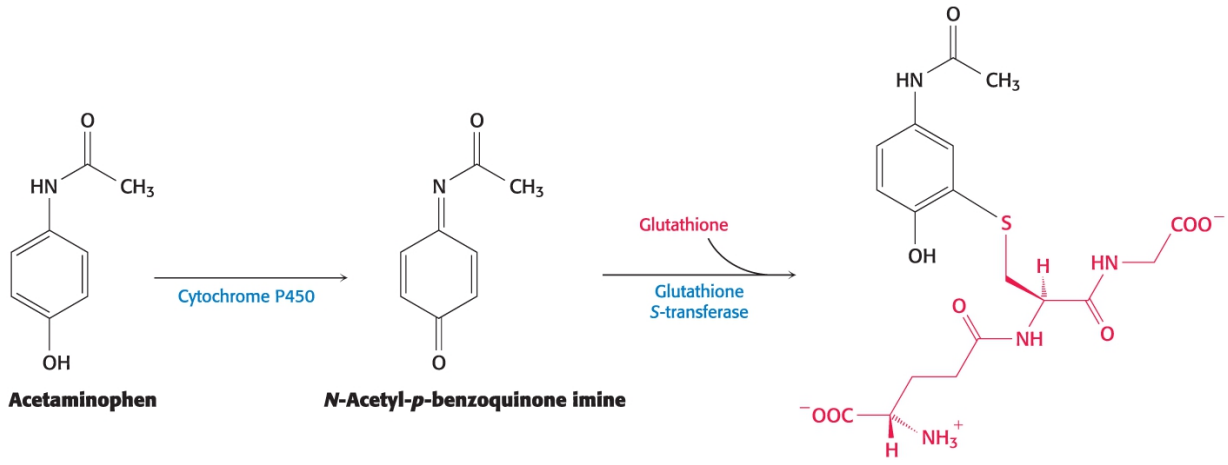


© Macmillan Learning

The horizontal axis is labeled time indicated by a rightward arrow. The vertical axis is labeled concentration of drug indicated by an upward arrow and ranges from 0 to 100 percent in increments of 50 percent. A black elliptical curve starts at 100 percent on the vertical axis, and falls to the lower right concave up till it almost becomes parallel to the horizontal axis. A point is shown on the curve at 50 percent ordinate with an abscissa of t subscript one-half Baseline. Vertical dashed lines and horizontal dashed lines are drawn from this point and two other points on the lower half of the curve to the horizontal and the vertical axes, respectively.

Return to FIGURE 32.22 Drug excretion may be measured by its half-life

Extended description for FIGURE 32.23 Acetaminophen metabolism results in its toxicity

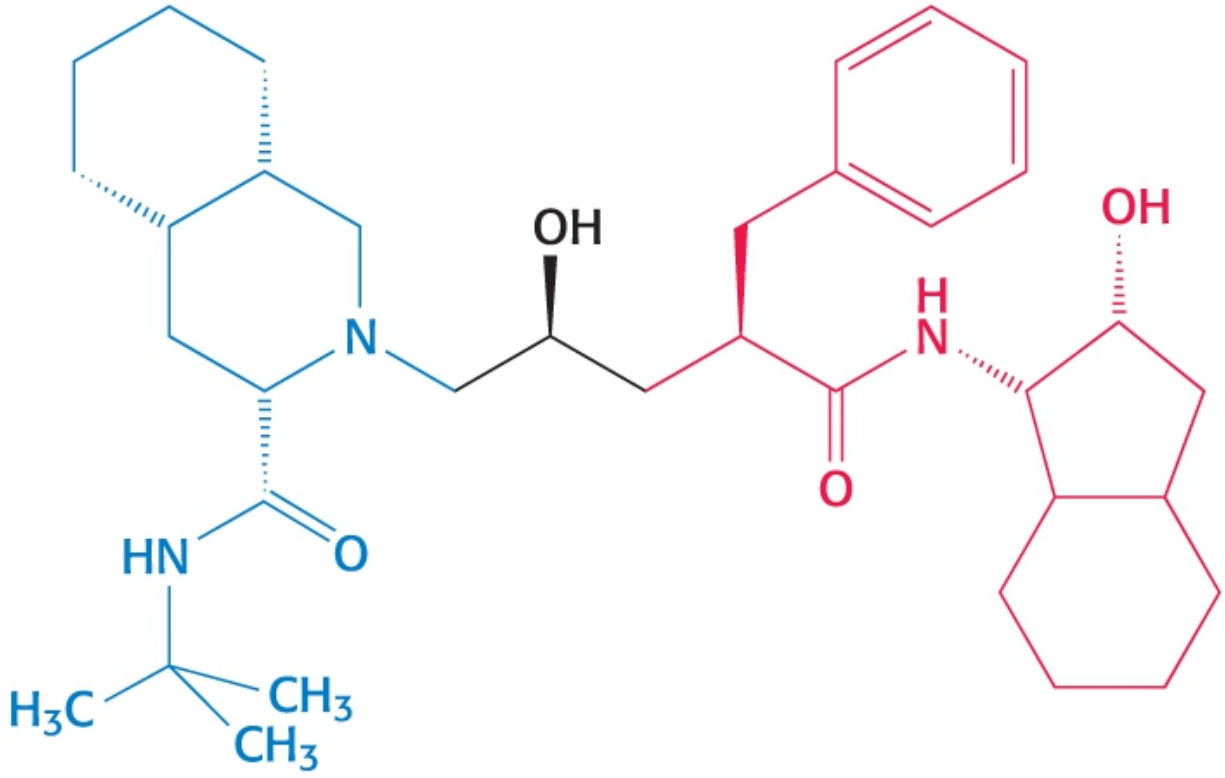


A two-step reaction contains two reactants, one intermediate, and one product. In the first step, the first reactant converts to the intermediate in the presence of Cytochrome P 450 which is highlighted in blue. The first reactant labeled Acetaminophen has the following structure: A benzene ring is in a vertical orientation with C 1 occupying the topmost vertex. The ring contains alternating double bonds between C 2 and C 3, C 4 and C 5, and C 6 and C 1. C 4 is single bonded to O H. C 1 is single bonded to N H. N H is single bonded to a central C atom on the upper right in the form of a line. The central C atom is double bonded to O above and is single bonded to C H 3 on the lower right. The intermediate labeled N-Acetyl-p-benzoquinone imine has the following structure: A 6-carbon hexagonal ring is in a vertical orientation with C 1 occupying the topmost vertex. A double bond is present between C 2 and C 3, and C 5 and C 6. C 4 is double bonded to O. C 1 is double bonded to N. N is single bonded to a central C atom on the upper right in the form of a line. The central C atom is double bonded to O above and is single bonded to C H 3 on the lower right. In the second step, the second reactant Glutathione highlighted in red, reacts with the

intermediate in the presence of Glutathione 5-transferase highlighted in blue. The product has the following structure: A benzene ring is in a vertical orientation with C 1 occupying the topmost vertex. The ring contains alternating double bonds between C 1 and C 2, C 3 and C 4, and C 5 and C 6. C 4 is single bonded to O H. C 1 is single bonded to N H. N H is single bonded to a central C atom on the upper right in the form of a line. The central C atom is double bonded to O above and is single bonded to C H 3 on the lower right. C 3 is single bonded to S. S is single bonded to a central C H 2 group below in the form of a line. The central C H 2 group is wedge bonded on the lower right to C 5 of a 2 N and 6 C heteronuclear alkane chain depicted as a line structure using 6 zigzag lines. In the 2 N and 6 C heteronuclear alkane chain, N bound to H occupies the fifth and the eighth positions. C 1 of the 2 N and 6 C heteronuclear alkane chain, is dash bonded to N H 3 superscript plus on the lower right, wedge bonded to H below, and single bonded to C O O superscript minus on the left. C 4 is double bonded to a second O atom on the upper left. C 5 is dash bonded to H above. C 6 is double bonded to a third O atom on the lower right. C 6 is single bonded to C O O superscript minus on the upper right. The S atom and the 2 N and 6 C heteronuclear alkane chain along with its attached groups is highlighted in red.

Return to FIGURE 32.23 Acetaminophen metabolism results in its toxicity

Extended description for FIGURE 32.24 Structural information led to the initial design of an H I V protease inhibitor

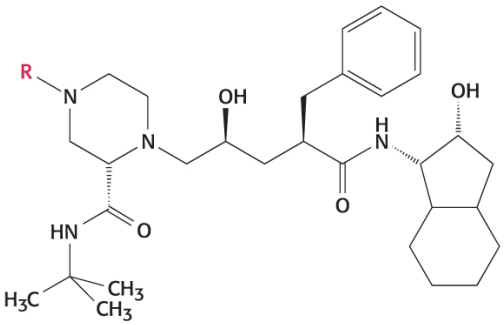


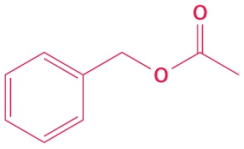
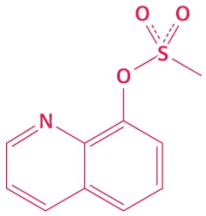
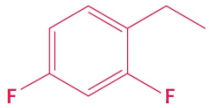
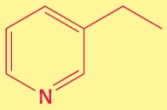
The molecule has the following structure: A 6-carbon hexagonal ring is in a vertical orientation with C 1 occupying the topmost vertex. A dash bond is present between C 2 and C 3, and C 4 and C 5. The ring is fused to a 6-membered heterocyclic hexagonal ring in a vertical orientation consisting of 1 N and 5 C atoms. In the 6-membered ring, N occupies the first position which is the bottom right vertex. The two rings are fused to each other such that C 3 and C 4 of the 6-carbon ring are the C 4 and C 3 of the 6-membered ring, respectively. C 3 of the 6-membered ring is dash bonded to a central C atom in the form of a dashed line. The central C atom is double bonded to O on the lower right and single bonded to N H on the

lower left. N H is single bonded to a second central C atom below in the form of a line. The second central C atom is single bonded to C H 3 on the right, C H 3 on the lower right, and C H 3 on the lower left. The structures until this point is highlighted in blue. The second N atom of the 6-membered ring is single bonded on the lower right to C 1 of a 5-carbon alkane chain depicted as a line structure using 4 zigzag lines. C 2 of the alkane chain is wedge bonded to O H above. C 4 of the alkane chain is wedge bonded to a C H 2 group in the form of a wedged line. The C H 2 group is single bonded on the upper right to C 4 of a benzene ring in a vertical orientation with C 1 occupying the topmost vertex. The benzene ring contains alternating double bonds between C 2 and C 3, C 4 and C 5, and C 6 and C 1. C 5 of the alkane chain is double bonded to O below and single bonded to N H on the upper right. N H is dash bonded on the lower right to C 5 of a 5-carbon pentagonal ring in a vertical orientation with C 1 occupying the topmost vertex. C 1 of the pentagonal ring is dash bonded to O H. The pentagonal ring is fused to a second 6-carbon hexagonal ring in a horizontal orientation with C 1 occupying the rightmost vertex. The two rings are fused to each other such that C 3 and C 4 of the pentagonal ring are the C 6 and C 5 of the second 6-carbon ring, respectively. The part of the structure from C 3 of the 5-carbon alkane chain onwards is highlighted in red.

Return to FIGURE 32.24 Structural information led to the initial design of an H I V protease inhibitor

Extended description for FIGURE 32.25. Optimizing lead molecules requires the balancing of multiple compound properties



R group	IC_{50} (nM)	log(*P*)	c_{max} (μM)
	0.4	4.67	< 0.1
	0.01	3.70	< 0.1
	0.3	3.69	0.7
	0.6	2.92	11

The base structure of a drug compound is as follows: A 6-membered heterocyclic hexagonal ring is in a vertical orientation consisting of 2 N and 4 C atoms. The first N atom occupies the first position which is the top left vertex and the second N atom occupies the third position which is the bottom right vertex. The first N atom is single bonded to R which is highlighted in red. C 3 is dash bonded to a central C atom in the form of a dashed line. The central C atom is double bonded to O on the lower right and single bonded to N H on the lower left. N H is single bonded to a second central C atom below in the form of a line. The second central C atom is single bonded to C H 3 on the right, C H 3 on the lower right, and C H 3 on the lower left. The second N atom of the ring is single bonded on the

lower right to C 1 of a 5-carbon alkane chain depicted as a line structure using 4 zigzag lines. C 2 of the alkane chain is wedge bonded to O H above. C 4 of the alkane chain is wedge bonded to a C H 2 group in the form of a wedged line. The C H 2 group is single bonded on the upper right to C 4 of a benzene ring in a vertical orientation with C 1 occupying the topmost vertex. The benzene ring contains alternating double bonds between C 2 and C 3, C 4 and C 5, and C 6 and C 1. C 5 of the alkane chain is double bonded to O below and single bonded to N H on the upper right. N H is wedge bonded on the lower right to C 5 of a 5-carbon pentagonal ring in a vertical orientation with C 1 occupying the topmost vertex. C 1 of the pentagonal ring is wedge bonded to O H. The pentagonal ring is fused to a 6-carbon hexagonal ring in a horizontal orientation with C 1 occupying the rightmost vertex. The two rings are fused to each other such that C 3 and C 4 of the pentagonal ring are the C 6 and C 5 of the 6-carbon ring, respectively.

The table consists of 4 columns and 4 rows. The column headers are as follows: R group, I C subscript 50 Baseline (nanoMolars), log of (P), and c subscript maximum Baseline (microMolars). The row entries are as follows:

Row 1: R group, A benzene ring is in a vertical orientation with C 1 occupying the topmost vertex. The ring contains alternating double bonds between C 1 and C 2, C 3 and C 4, and C 5 and C 6. C 2 is single bonded to C 1 of a 1 O and 2 C heteronuclear alkane chain depicted as a line structure using 2 zigzag lines. In the alkane chain, O occupies the second position. C 2 is double bonded to a second O atom above and has an open single bond on the lower right. I C subscript 50 Baseline (nanoMolars), 0.4. log of (P), 4.67. c subscript maximum Baseline (microMolars), less than 0.1.

Row 2: R group, A 6-membered heterocyclic hexagonal ring is in a vertical orientation consisting of 1 N and 5 C atoms. N occupies the

first position which is the topmost vertex. A double bond is present between C 3 and C 4, and C 5 and N. The ring is fused to a benzene ring in a vertical orientation with C 1 occupying the topmost vertex. The two rings are fused to each other such that C 1 and C 2 of the 6-membered ring are the C 6 and C 5 of the benzene ring, respectively. The benzene ring contains alternating double bonds between C 2 and C 3, C 4 and C 5, and C 6 and C 1. C 1 of the benzene ring is single bonded to O. O is single bonded to a central S atom on the upper right. The central S atom is partially double bonded to a second O atom on the upper right, a third O atom on the upper left and has an open single bond on the lower right. I C subscript 50 Baseline (nanoMolars), 0.01. log of (P), 3.70. c subscript maximum Baseline (microMolars), less than 0.1.

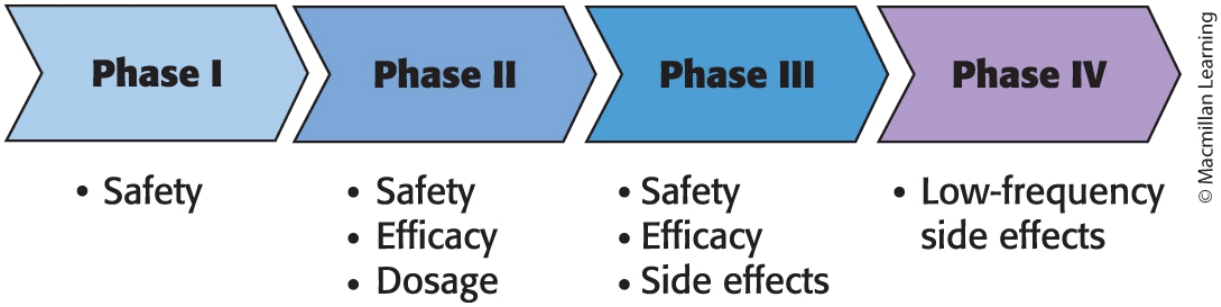
Row 3: R group, A benzene ring is in a vertical orientation with C 1 occupying the topmost vertex. The ring contains alternating double bonds between C 1 and C 2, C 3 and C 4, and C 5 and C 6. C 3 and C 5 are each single bonded to F. C 2 is single bonded to a central C H 2 group in the form of a line. The central C H 2 group has an open bond on the lower right. I C subscript 50 Baseline (nanoMolars), 0.3. log of (P), 3.69. c subscript maximum Baseline (microMolars), 0.7.

Row 4: R group, A 6-membered heterocyclic hexagonal ring is in a vertical orientation consisting of 1 N and 5 C atoms. N occupies the first position which is the bottommost vertex. A double bond is present between C 1 and C 2, C 3 and C 4, and C 5 and N. C 4 is single bonded to a central C H 2 group in the form of a line. The central C H 2 group has an open single bond on the lower right. I C subscript 50 Baseline (nanoMolars), 0.6. log of (P), 2.92. c subscript maximum Baseline (microMolars), 11.

The R group column structures are highlighted in red and Row 4 is highlighted in yellow.

Return to FIGURE 32.25. Optimizing lead molecules requires the balancing of multiple compound properties

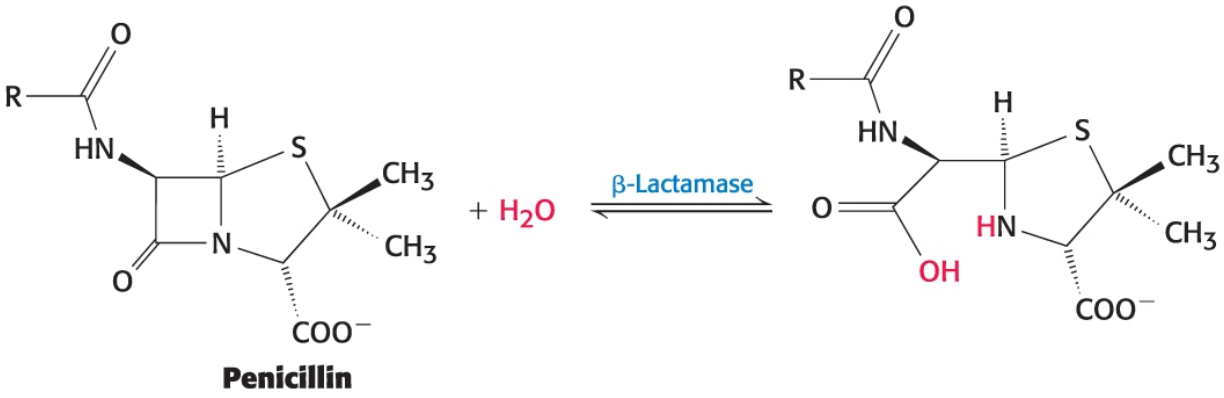
Extended description for FIGURE 32.26 Clinical trials proceed in phases examining safety and efficacy in increasingly large groups



The flowchart from the left to the right shows the following phases: Phase roman numeral I, phase roman numeral I I, phase roman numeral I I I, and phase roman numeral I V. Phase roman numeral I examines Safety. Phase roman numeral I I examines Safety, Efficacy, and Dosage. Phase roman numeral I I I examines Safety, Efficacy, and Side Effects. Phase roman numeral I V examines Low-frequency side effects.

Return to FIGURE 32.26 Clinical trials proceed in phases examining safety and efficacy in increasingly large groups

Extended description for Hydrolyzation of penicillin by Beta-Lactamase



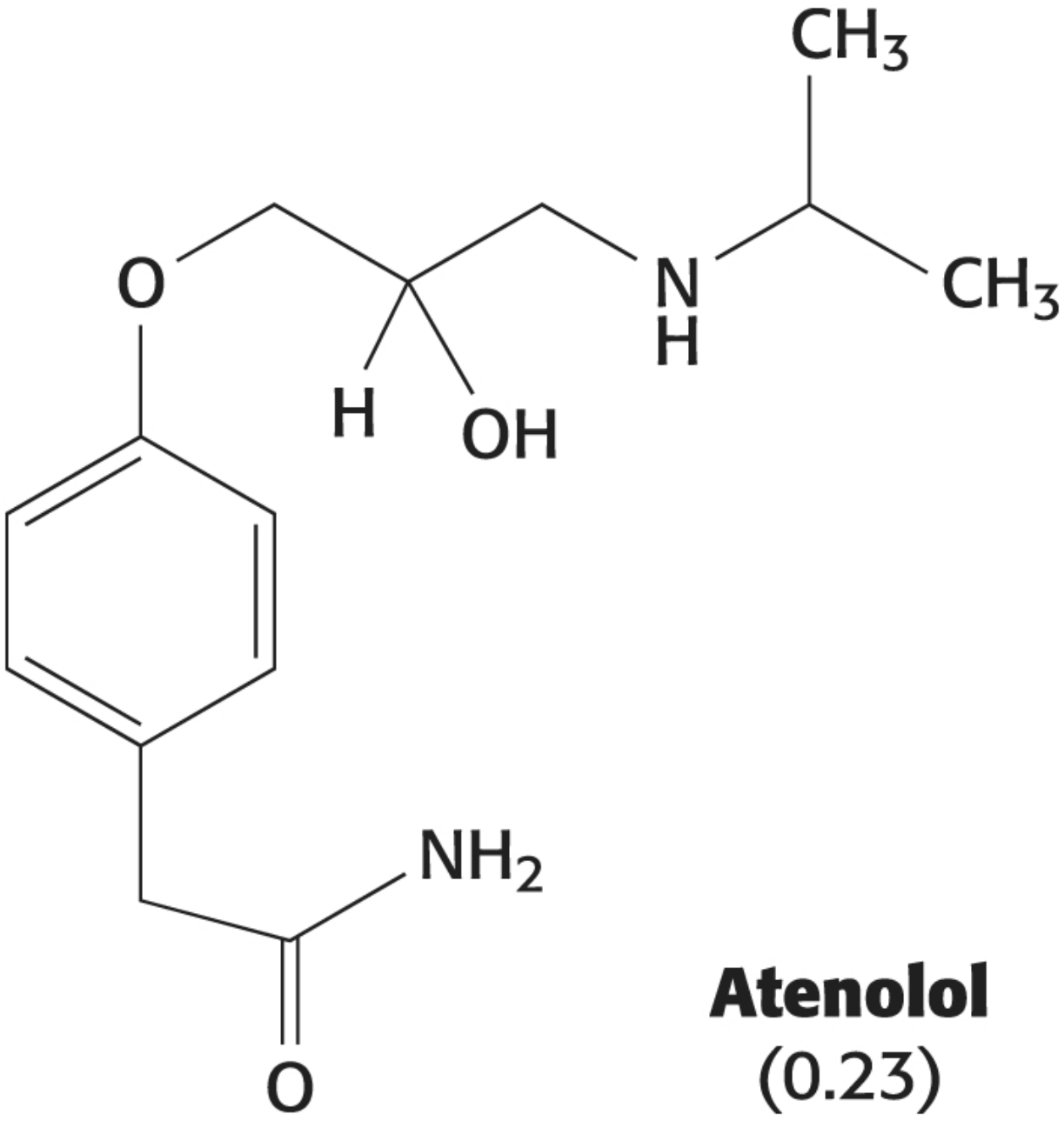
Penicillin

The reversible reaction contains two reactants and one product. The first reactant labeled Penicillin has the following structure: A 4-membered heterocyclic square ring is in a horizontal orientation consisting of 1 N and 3 C atoms. N occupies the first position which is the bottom right vertex. C 1 is double bonded to O. C 3 is dash bonded to H above. C 2 is wedge bonded to N H. N H is single bonded to a central C atom on the upper left in the form of a line. The central C atom is double bonded to a second O atom on the upper right and single bonded to R on the left. The ring is fused to a 5-membered heterocyclic pentagonal ring in a horizontal orientation consisting of 1 N, 1 S, and 3 C atoms. In the pentagonal ring, N occupies the first position which is the bottom left vertex, and S occupies the third position which is the top right vertex. The two rings are fused to each other such that C 3 and N of the square ring are the C 1 and N of the pentagonal ring, respectively. C 2 of the pentagonal ring is wedge bonded to C H 3 on the upper right and dash bonded to C H 3 on the lower right. C 3 of the pentagonal ring is dash bonded to C O O superscript minus. The second reactant is H 2 O highlighted in red. The reaction takes place in the presence of Beta-Lactamase highlighted in blue and written over the reversible

reaction arrow. The product has the following structure: A 1 N and 3 C heteronuclear alkane chain is depicted as a line structure using 3 zigzag lines. N bound to H occupies the second position. A wedge bond is present between N H and C 2. C 1 is double bonded to O on the upper right and is single bonded to R on the left. C 3 is double bonded to a second O atom on the left and is single bonded to O H on the lower right. O H is highlighted in red. C 2 is single bonded on the right to C 1 of a 5-membered heterocyclic pentagonal ring in a horizontal orientation consisting of 1 N, 1 S, and 3 C atoms. In the pentagonal ring, N occupies the first position which is the bottom left vertex, and S occupies the third position which is the top right vertex. H of N H of the pentagonal ring is highlighted in red. C 1 of the pentagonal ring is dash bonded to H above. C 2 of the pentagonal ring is wedge bonded to C H 3 on the upper right and dash bonded to C H 3 on the lower right. C 3 of the pentagonal ring is dash bonded to C O O superscript minus.

Return to Hydrolyzation of penicillin by Beta-Lactamase

Extended description for Structure of Atenolol

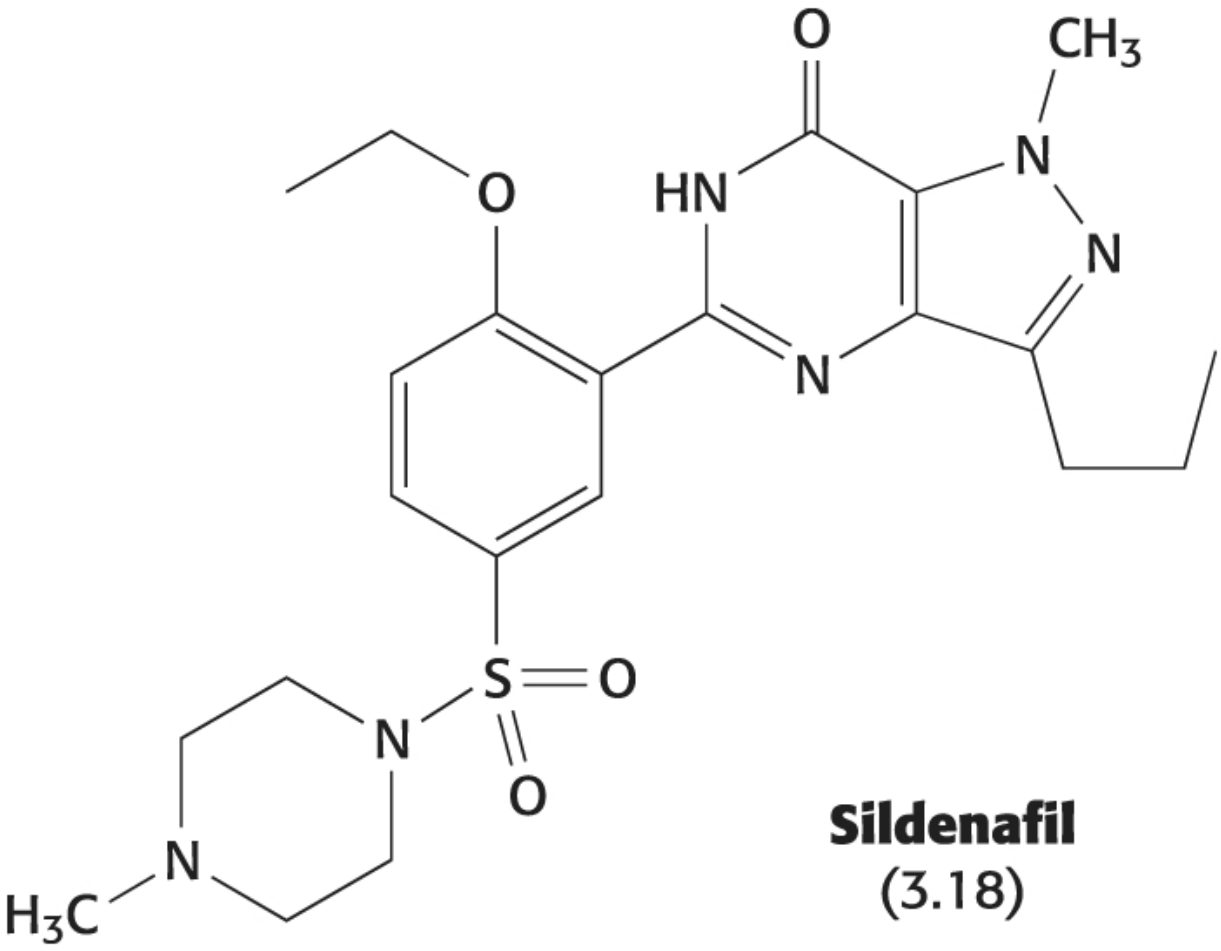


A benzene ring is in a vertical orientation with C 1 occupying the topmost vertex. The ring contains alternating double bonds between C 2 and C 3, C 4 and C 5, and C 6 and C 1. C 4 is single bonded to C 1

of a 2-carbon alkane chain depicted as a line structure using 1 line. C 2 of the alkane chain is double bonded to O below and single bonded to N H 2 on the upper right. C 1 of the benzene ring is single bonded to a second O atom. The second O atom is single bonded on the upper right to C 1 of a 1 N and 4 C heteronuclear alkane chain depicted as a line structure using 4 zigzag lines. In the heteronuclear alkane chain, N bound to H occupies the fourth position. C 2 of the heteronuclear alkane chain is single bonded to H on the lower left and O H on the lower right. C 4 of the heteronuclear alkane chain is single bonded to C H 3 above and C H 3 on the lower right.

Return to Structure of Atenolol

Extended description for Structure of Sildenafil



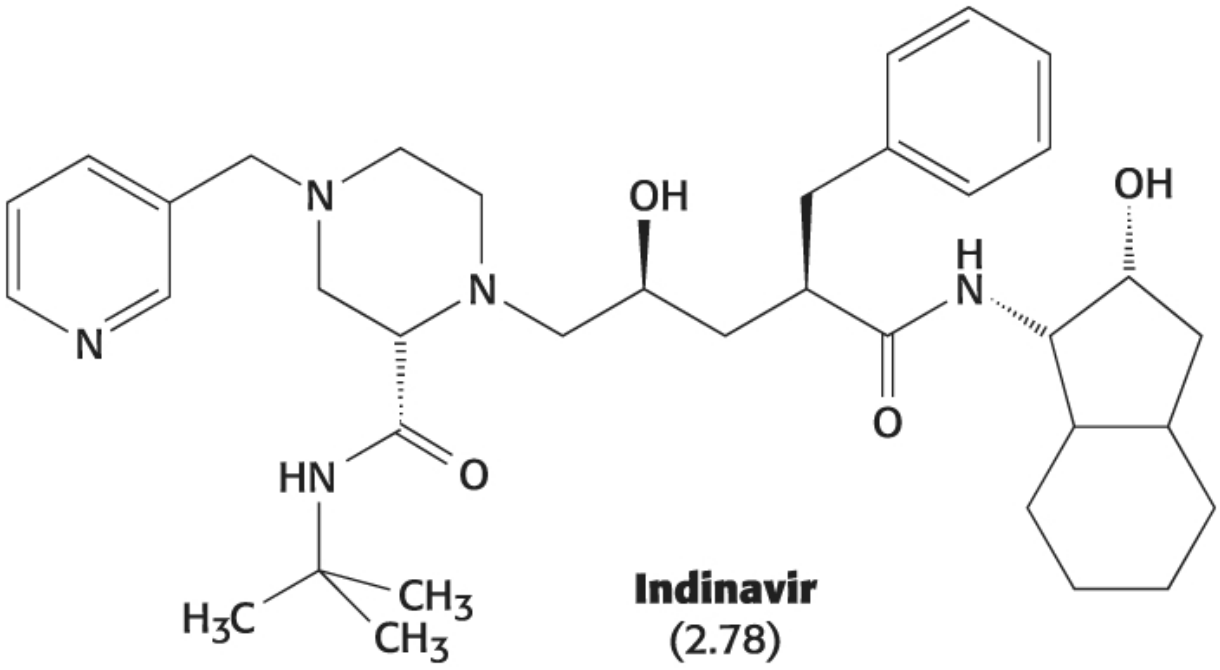
Sildenafil
(3.18)

A 6-membered heterocyclic hexagonal ring is in a vertical orientation consisting of 2 N and 4 C atoms. The first N atom is in the first position which is the top right vertex. The second N atom is in the fourth position which is the bottom left vertex. The second N atom is single bonded to C H 3. The first N atom is single bonded to a central S atom. The central S atom is double bonded to O on the right and a second O atom on the lower right, and single bonded above to C 4 of a benzene ring in a vertical orientation with C 1 occupying the topmost vertex. The benzene ring contains alternating double bonds between C 1 and C 2, C 3 and C 4, and C 5

and C 6. C 1 of the benzene ring is single bonded to a third O atom. The third O atom is single bonded on the upper left to C 2 of a 2-carbon alkane chain depicted as a line structure using 1 line. C 2 of the benzene ring is single bonded to C 1 of a second 6-membered heterocyclic hexagonal ring in a vertical orientation consisting of 2 N and 4 C atoms. In the second 6-membered ring, the first N atom occupies the first position which is the bottommost vertex, and the second N atom bound to H occupies the third position which is the top left vertex. In the second 6-membered ring, a double bond is present between the first N atom and C 1, and C 3 and C 4. C 2 of the second 6-membered ring is double bonded to a fourth O atom. The second 6-membered ring is fused to a 5-membered heterocyclic pentagonal ring in a horizontal orientation consisting of 2 N and 3 C atoms. In the pentagonal ring, the first N atom occupies the first position which is the top right vertex, and the second N atom occupies the second position which is the rightmost vertex. In the pentagonal ring, a double bond is present between the second N atom and C 1. The first N atom of the pentagonal ring is single bonded to C H 3. C 1 of the pentagonal ring is single bonded to C 1 of a 3-carbon alkane chain depicted as a line structure using 2 zigzag lines.

Return to Structure of Sildenafil

Extended description for Structure of Indinavir



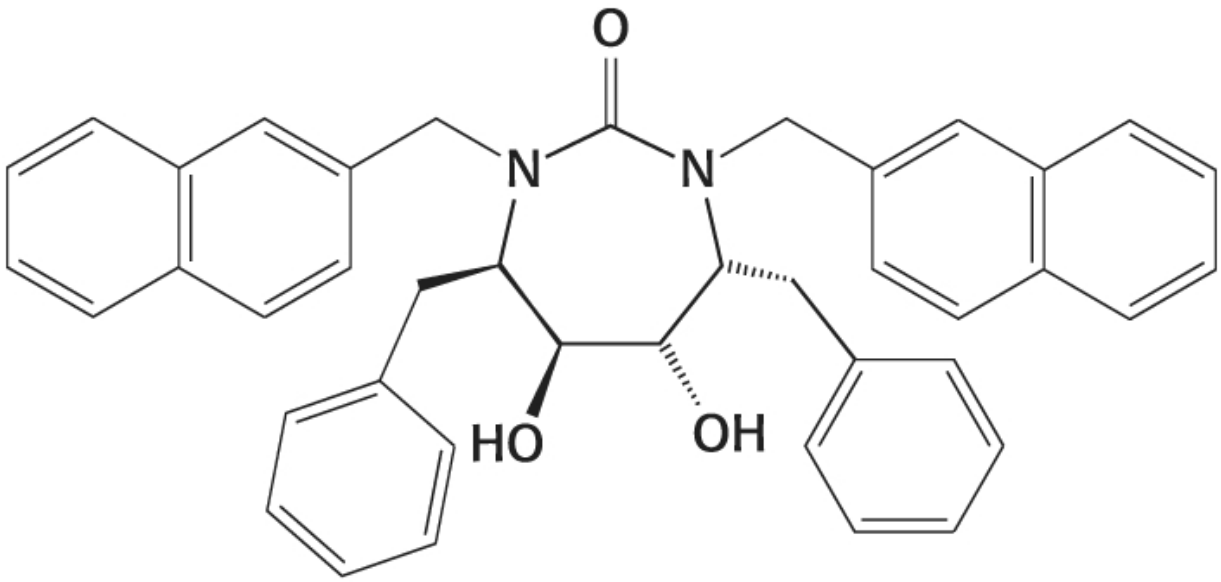
Indinavir
(2.78)

A 6-membered heterocyclic hexagonal ring is in a vertical orientation consisting of 1 N and 5 C atoms. N occupies the first position which is the bottommost vertex. A double bond is present between C 1 and C 2, C 3 and C 4, and C 5 and N. C 4 is single bonded to a central C H 2 group in the form of a line. The central C H 2 group is single bonded on the lower right to the first N atom of a second 6-membered heterocyclic hexagonal ring in a vertical orientation consisting of 2 N and 4 C atoms. In the second ring, the first N atom occupies the first position which is the top left vertex and the second N atom occupies the third position which is the bottom right vertex. C 3 of the second ring is dash bonded to a central C atom in the form of a dashed line. The central C atom is double bonded to O on the lower right and single bonded to N H on the lower left. N H is single bonded to a second central C atom below in the form of a line. The second central C atom is single bonded to C H 3 on the right, C H 3 on the lower right, and C H 3 on

the lower left. The second N atom of the second ring is single bonded on the lower right to C 1 of a 5-carbon alkane chain depicted as a line structure using 4 zigzag lines. C 2 of the alkane chain is wedge bonded to O H above. C 4 of the alkane chain is wedge bonded to a second C H 2 group in the form of a wedged line. The second C H 2 group is single bonded on the upper right to C 4 of a benzene ring in a vertical orientation with C 1 occupying the topmost vertex. The benzene ring contains alternating double bonds between C 2 and C 3, C 4 and C 5, and C 6 and C 1. C 5 of the alkane chain is double bonded to O below and single bonded to N H on the upper right. N H is single bonded on the lower right to C 5 of a 5-carbon pentagonal ring in a vertical orientation with C 1 occupying the topmost vertex. C 1 of the pentagonal ring is single bonded to O H. The pentagonal ring is fused to a 6-carbon hexagonal ring in a horizontal orientation with C 1 occupying the rightmost vertex. The two rings are fused to each other such that C 3 and C 4 of the pentagonal ring are the C 6 and C 5 of the 6-carbon ring, respectively.

Return to Structure of Indinavir

Extended description for Structure of Compound A



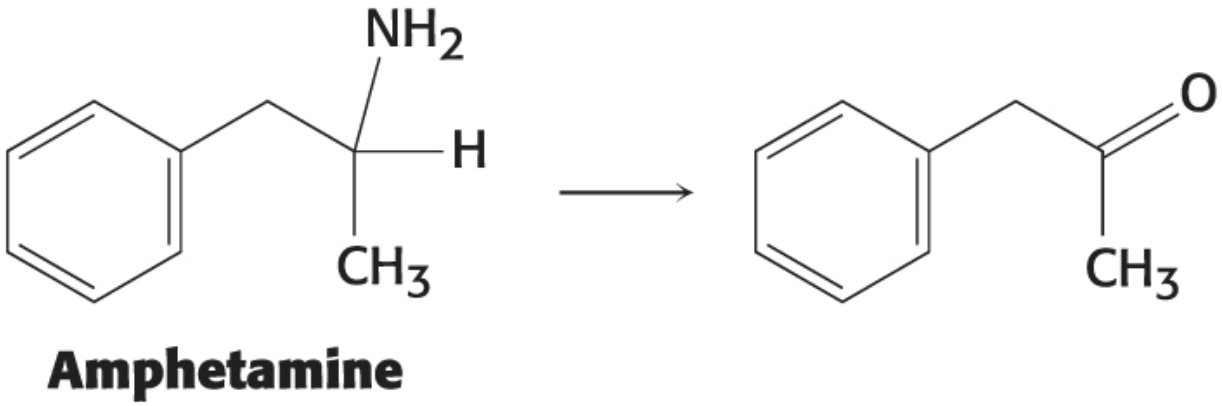
Compound A

A 7-membered heterocyclic heptagonal ring is in a vertical orientation and consists of 2 N and 5 C atoms. The first N atom is in the first position which occupies the top left vertex. The second N atom is in the third position which occupies the top right vertex. C 1 is double bonded to O. C 3 is dash bonded to O H. C 4 is wedge bonded to O H. The first N atom is single bonded to a central C H 2 group in the form of a line. The central C H 2 group is single bonded on the lower left to C 2 of a benzene ring in a vertical orientation with C 1 occupying the topmost vertex. The ring contains alternating double bonds between C 1 and C 2, C 3 and C 4, and C 5 and C 6. The ring is fused to a 6-carbon hexagonal ring in a vertical orientation with C 1 occupying the topmost vertex. The two rings are fused to each other such that C 5 and C 6 of the benzene ring are the C 3 and C 2 of the 6-carbon hexagonal ring in a orientation with C 1 occupying the vertex ring, respectively. In the 6-carbon ring, a double bond is present between C 4 and C 5, and C 6 and C 1. The

second N atom of the heptagonal ring is single bonded to a second central C H 2 group in the form of a line. The second central C H 2 group is single bonded on the lower right to C 6 of a second benzene ring in a vertical orientation with C 1 occupying the topmost vertex. The second benzene ring contains alternating double bonds between C 2 and C 3, C 4 and C 5, and C 6 and C 1. The second benzene ring is fused to a second 6-carbon hexagonal ring in a vertical orientation with C 1 occupying the topmost vertex. The two rings are fused to each other such that C 2 and C 3 of the second benzene ring are the C 6 and C 5 of the second 6-carbon ring, respectively. C 2 of the heptagonal ring is dash bonded to a third central C H 2 group in the form of a dashed line. The third central C H 2 group is single bonded to C 5 of a third benzene ring in a horizontal orientation with C 1 occupying the rightmost vertex. The third benzene ring contains alternating double bonds between C 2 and C 3, C 4 and C 5, and C 6 and C 1. C 5 of the heptagonal ring is wedge bonded to a fourth central C H 2 group in the form of a wedged line. The fourth central C H 2 group is single bonded to C 1 of a fourth benzene ring in a vertical orientation with C 1 occupying the topmost vertex. The fourth benzene ring contains alternating double bonds between C 2 and C 3, C 4 and C 5, and C 6 and C 1.

Return to Structure of Compound A

Extended description for Metabolism of Amphetamine

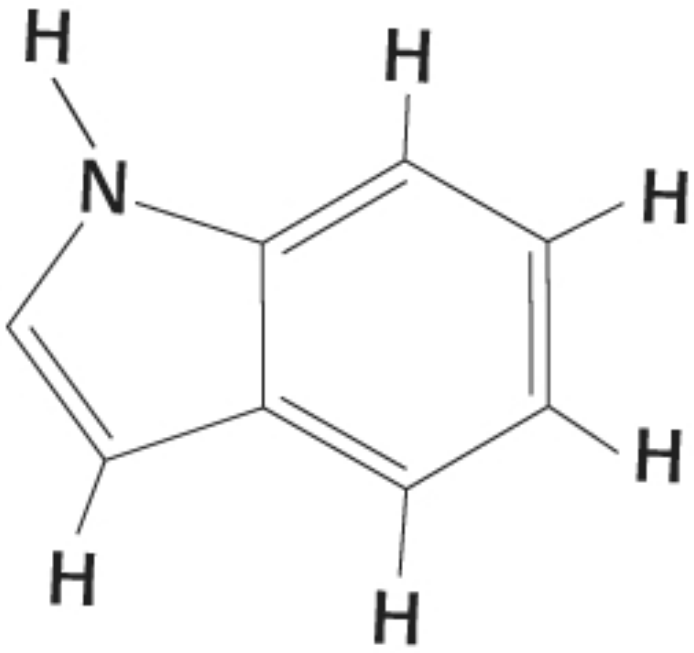


Amphetamine

The reaction contains one reactant and one product. The reactant labeled Amphetamine has the following structure: A benzene ring is in a vertical orientation with C 1 occupying the topmost vertex. The ring contains alternating double bonds between C 2 and C 3, C 4 and C 5, and C 6 and C 1. C 1 is single bonded to C 1 of a 2-carbon alkane chain depicted as a line structure using 1 line. C 2 of the alkane chain is single bonded to N H 2 on the upper right, H on the right, and C H 3 below. The product has the following structure: A benzene ring is in a vertical orientation with C 1 occupying the topmost vertex. The ring contains alternating double bonds between C 2 and C 3, C 4 and C 5, and C 6 and C 1. C 1 is single bonded to C 1 of a 2-carbon alkane chain depicted as a line structure using 1 line. C 2 of the alkane chain is double bonded to O on the upper right and single bonded to C H 3 below.

Return to Metabolism of Amphetamine

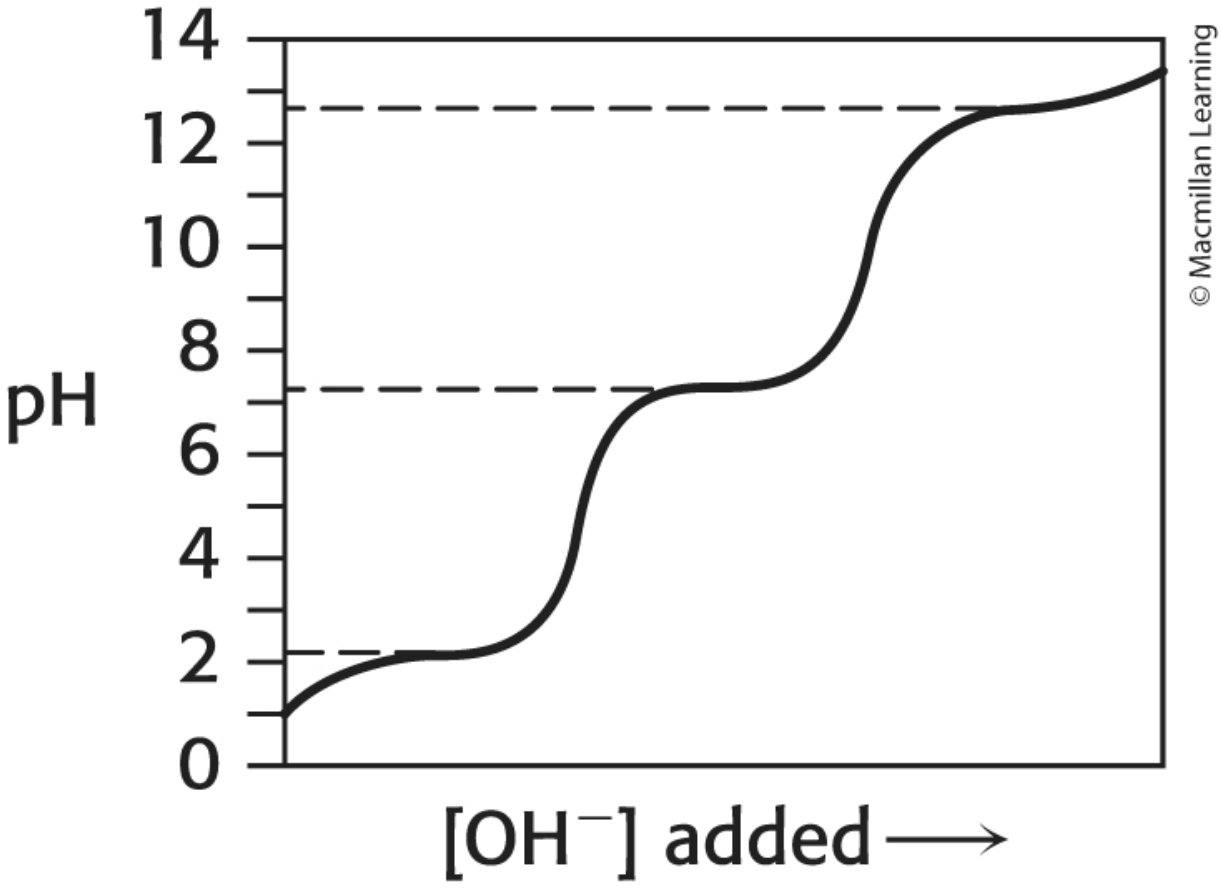
Extended description for Structure of two fused rings



The structure of the fused rings is as follows: A 5-membered heterocyclic pentagonal ring is in a horizontal orientation with C 1 occupying the top right vertex. It consists of 1 N and 4 C atoms. First N occupies the top left vertex. A double bond is present between C 3 and C 4. C 3 is single bonded to H on the lower left. N is single-bonded to H on the upper left. The pentagonal ring is fused to a benzene ring such that C 1 and C 2 of the pentagonal ring are C 6 and C 5 of the benzene ring respectively. The benzene ring contains alternating double bonds between C 2 and C 3, C 4 and C 5, and C 6 and C 1. C 1, C 2, C 3, and C 4 are each single bonded to H.

Return to Structure of two fused rings

Extended description for Variation of p H with the addition of O H superscript minus

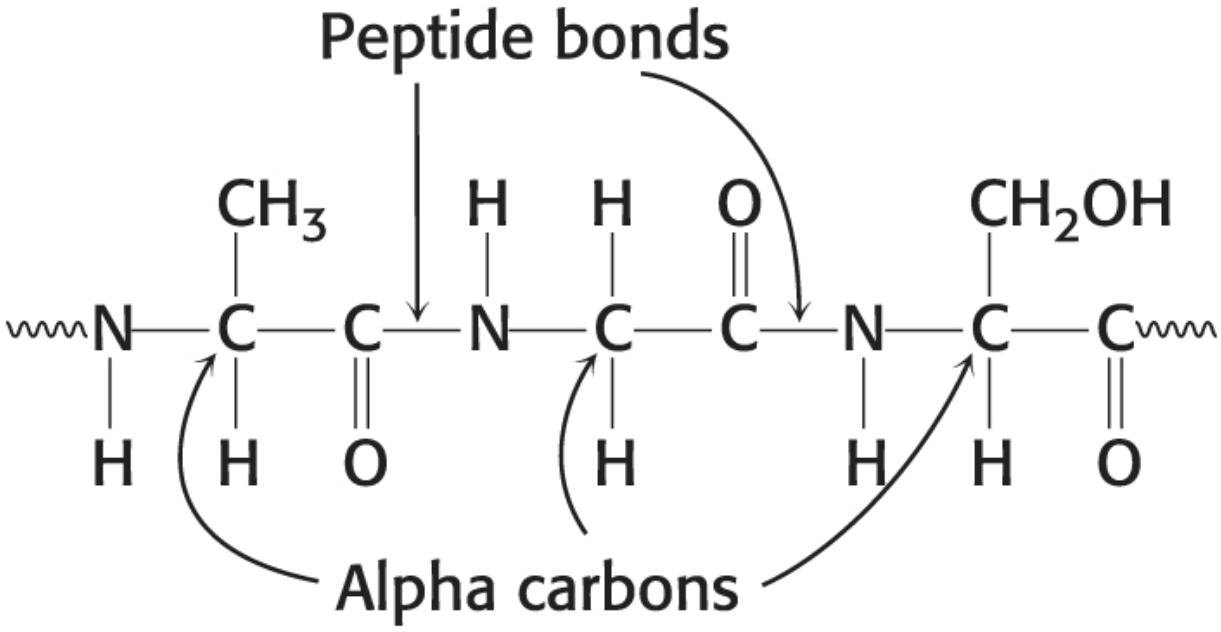


The horizontal axis is labeled concentration of O H superscript minus added. The concentration of O H superscript minus increases from left to right. The vertical axis is labeled p H. It has markings ranging from 0 to 14 in increments of 2 units. The graph contains a wavy ladder-like curve that moves from the bottom left to the top right. The curve starts at (0, 1) and ends at the highest concentration of O H superscript minus at p H 13. A dashed line starts from p H 2 and moves toward the first ladder of the curve. A second dashed line starts from p H 7.1 and moves toward the second ladder. A third

dashed line starts from p H 12.8 and moves toward the third ladder. All values are estimated.

Return to Variation of p H with the addition of O H superscript minus

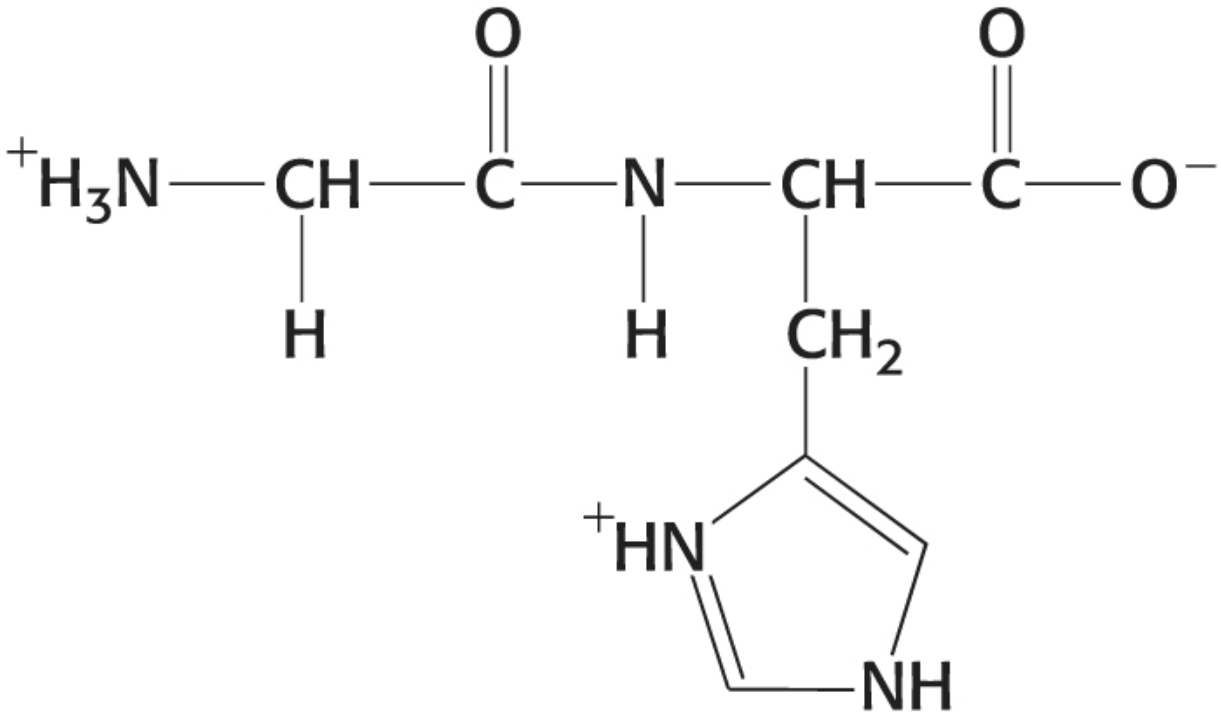
Extended description for Structure of a peptide



The structure of the peptide is as follows: N, single bond, C, single bond, C, single bond, N, single bond, C, single bond, C, single bond, N, single bond, C, single bond, C. N 1 has a wiggly line on the left. C 9 has a wiggly line on the right. N 1 is single bonded to H below. C 2 is single bonded to C H 3 above and H below. C 3 is double bonded to O below. N 4 is single bonded to H above. C 5 is single bonded to H above and H below. C 6 is double bonded to O above. N 7 is single bonded to H below. C 8 is single bonded to C H 2 O H above and H below. C 9 is double bonded to O below. C 2, C 5, and C 8 are labeled alpha carbons. The single bond between C 3 and N 4 and C 6 and N 7 are labeled peptide bonds.

Return to Structure of a peptide

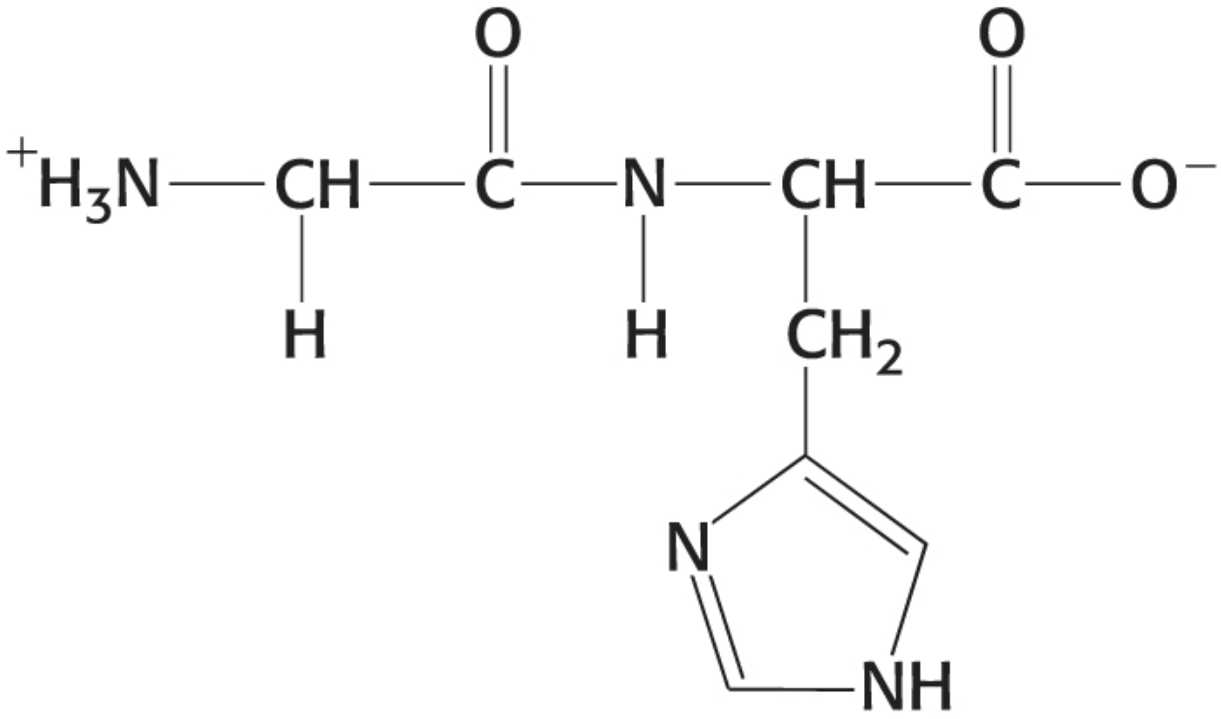
Extended description for Structure of a peptide at p H 5.5



The structure of the peptide is as follows: C H, single bond, C, single bond, N, single bond, C H, single bond, C, single bond, O superscript minus. C 1 is single bonded to H below and single bonded to N H 3 superscript plus on the left. C 2 is double bonded to O above. N 3 is single bonded to H below. C 4 is single bonded to C H 2 below. C H 2 is further single-bonded to C 2 of a 5-membered heterocyclic pentagonal ring in a vertical orientation. The pentagonal ring consists of 2 N and 3 C atoms. First N bound to H occupies the bottom right vertex. Second N bound to H occupies the top left vertex and it has an overall positive charge. A double bond is present between C 1 and N 2, and C 2 and C 3. C 5 of the main chain is double bonded to O above.

Return to Structure of a peptide at p H 5.5

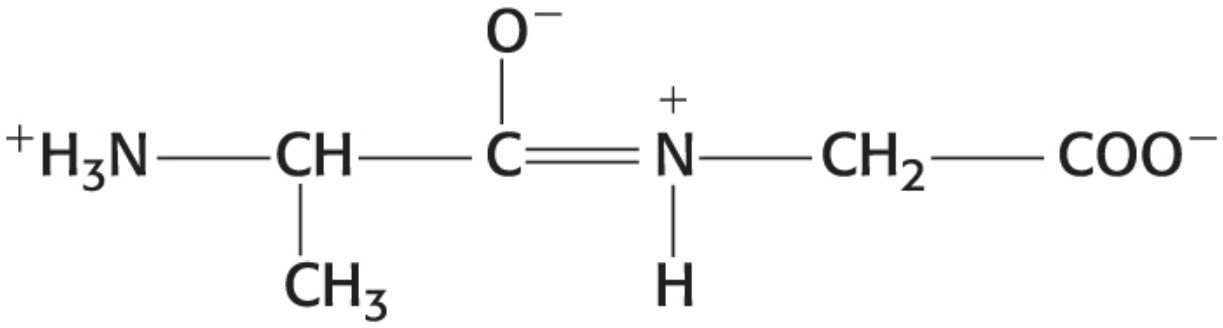
Extended description for Structure of a peptide at p H 7.5



The structure of the peptide is as follows: C H, single bond, C, single bond, N, single bond, C H, single bond, C, single bond, O superscript minus. C 1 is single bonded to H below and single bonded to N H 3 superscript plus on the left. C 2 is double bonded to O above. N 3 is single bonded to H below. C 4 is single bonded to C H 2 below. C H 2 is further single-bonded to C 2 of a 5-membered heterocyclic pentagonal ring in a vertical orientation. The pentagonal ring consists of 2 N and 3 C atoms. First N bound to H occupies the bottom right vertex. Second N occupies the top left vertex. A double bond is present between C 1 and N 2, and C 2 and C 3. C 5 of the main chain is double bonded to O above.

Return to Structure of a peptide at p H 7.5

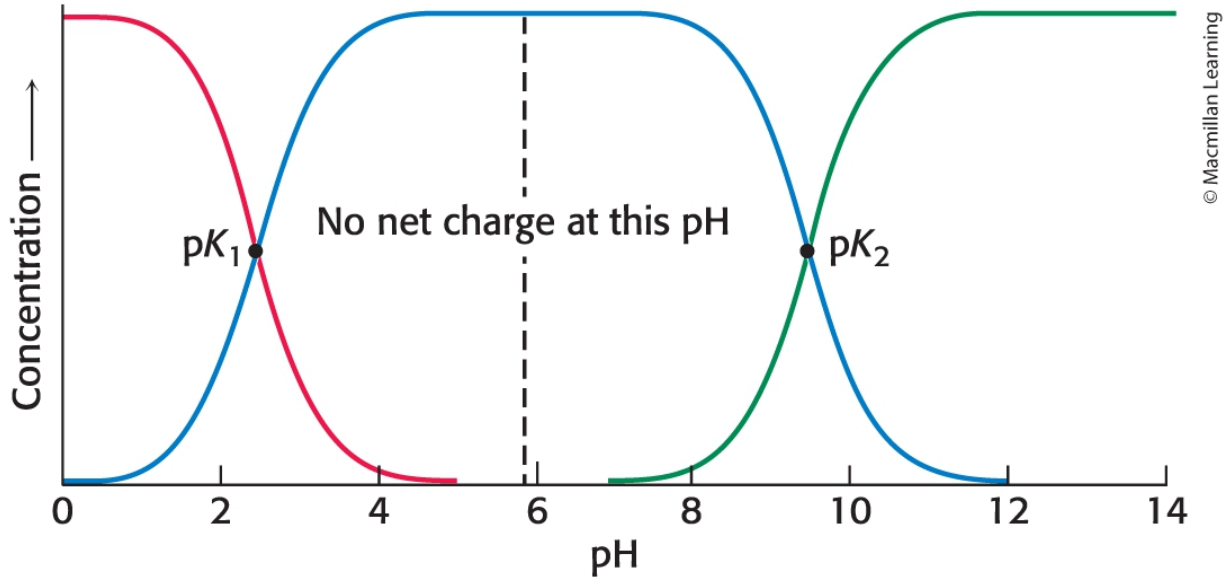
Extended description for Chemical structure



The chemical structure is as follows: N H 3 superscript plus, single bond, C H, single bond, C, double bond, N superscript plus, single bond, C H 2, single bond, C O O superscript minus. C 1 is single bonded to C H 3 below. C 2 is single bonded to O superscript minus above. N superscript plus is single bonded to H below.

Return to Chemical structure

Extended description for Relationship between concentration and p H

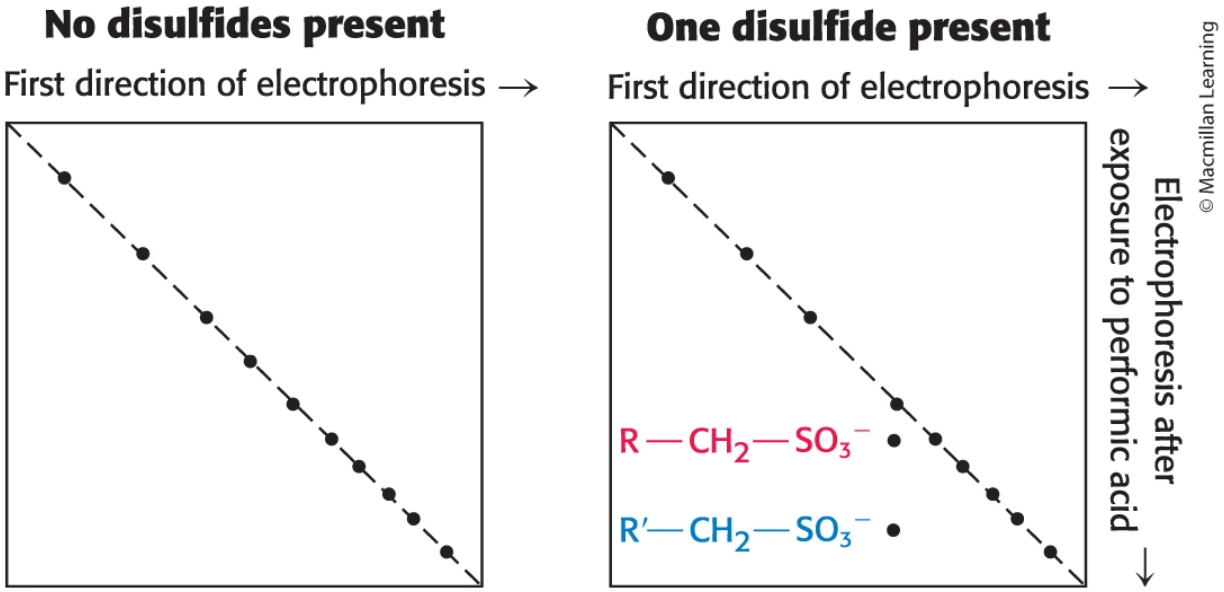


The horizontal axis is labeled p H. It has markings ranging from 0 to 14 in increments of 2 units. The vertical axis is labeled concentration. The graph contains three curves depicted in red, blue, and green colors. The first red curve starts at the highest concentration, moves horizontally till p H 1.2, and then gradually declines to reach p H 5 on the horizontal axis. The second blue curve is a bell-shaped curve with a broad and flat peak. It starts at the lowest concentration at p H 0, moves horizontally till p H 0. 8, and then rises toward the upper right to reach the highest concentration at p H 4. The curves then move horizontally toward the right till p H 8 and then fall gradually to reach p H 12 on the horizontal axis. The point of the intersection of the downward slope of the red curve and the upward slope of the blue curve at an average concentration and p H of 2.2 is labeled p K subscript 1. A dashed vertical line originates from p H 5.8 on the horizontal axis and touches the horizontal part of the blue curve. The third green starts at p H 6.9 on the horizontal

axis, moves horizontally till p H 7.5, and then rises gradually toward the upper right to reach the highest concentration at p H 11.5. The curve continues moving horizontally toward the right. The point of intersection between the downward slope of the blue curve and the upward slope of the green curve at an average concentration and p H of 9.7 is labeled p K subscript 2. All values are estimated.

Return to Relationship between concentration and p H

Extended description for Electrophoretic mobility of a protein with no disulfide bond or one disulfide bond

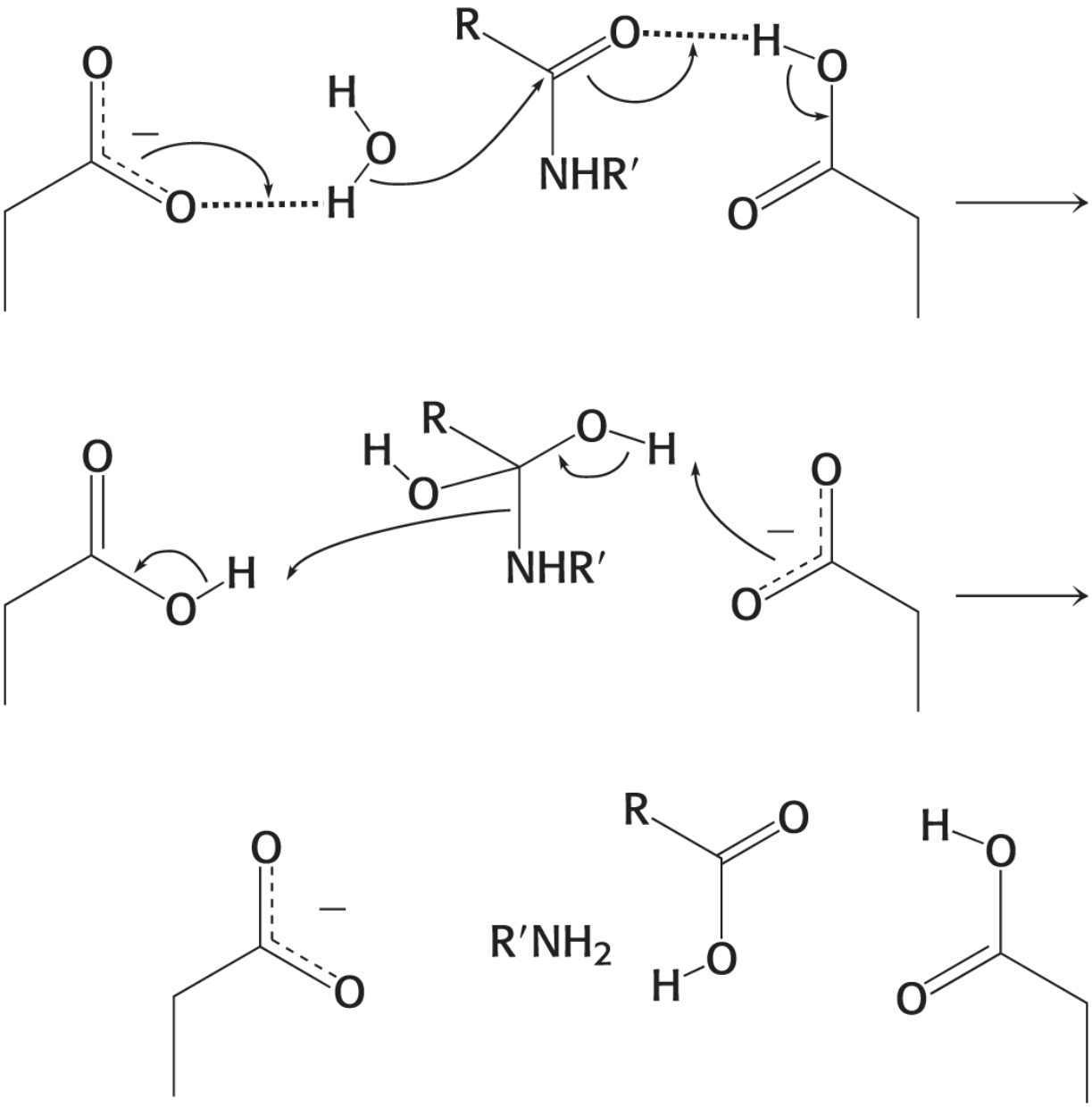


The first square-shaped chromatography paper depicts the mobility of protein with no disulfides present. The top of the paper is labeled "First direction of electrophoresis" which is from left to right. The right side is labeled "Electrophoresis after exposure to performic acid." Its direction is from top to bottom. The paper contains a diagonal dashed line from the top left to the bottom right vertex. A series of dots are placed across the diagonal line.

The second chromatography paper depicts the mobility of protein with one disulfide present. It contains a diagonal dashed line from the top left to the bottom right vertex. A series of dots are placed across the diagonal line. Two dots are located on the bottom left side of the diagonal line. The top dot is for R, single bond, C H 2, single bond, S O 3 superscript minus. The bottom dot is for R dash, single bond, C H 2, single bond, S O 3 superscript minus.

Return to Electrophoretic mobility of a protein with no disulfide bond or one disulfide bond

Extended description for Reaction mechanism of aspartyl protease



A 2-carbon alkane chain is depicted as a vertical line. C 2 is single-bonded to C on the upper right. This C is partially double bonded to O above and O on the lower right. The C O O group has an overall

negative charge. An arrow from the partial double bond between C and lower right O points toward a dashed line connecting the lower right O with H of H 2 O. H 2 O consists of a central O single bonded to H on the upper left and lower left. An arrow from the single bond between O and lower left H of H 2 O points toward a central C atom of a compound. This C is single bonded to R on the upper left, single bonded to N H R dash, and double bonded to O on the upper right. The upper right O of this compound is connected to the H of another compound through a dashed line. H is single-bonded to O on the lower right. This O is single-bonded to a central C below. This C is double bonded to O on the lower left and C 1 of a 2-carbon alkane chain is depicted as a vertical line. An arrow from the single bond between H and O of this compound points toward the single bond between O and C.

In the next step, a 2-carbon alkane chain is depicted as a vertical line. C 2 is single-bonded to C on the upper right. This C is double bonded to O above and single bonded to O, single bond, H on the lower right. An arrow from the single bond between O and H points toward the single bond between C and O.

A compound located on the right has the following structure: A central C atom is single bonded to R on the upper left, single bonded to O on the lower left, single bonded to N H R dash below, and single bonded to O on the upper right. Both the O atoms are single-bonded to H.

An arrow from the single bond between upper right O and H points toward the single bond between O and C. An arrow from the single bond between N H R dash and C points toward the H atom of the first alkane chain.

A second 2-carbon alkane chain is depicted as a vertical line on the right. C 1 of this chain is single-bonded to C on the upper left. This C

is partially double-bonded to O above and partially double-bonded to O on the lower left. The C O O group has a negative charge. An arrow from the partial double bond between C and the lower left O of the C O O group points toward H of the compound in the middle.

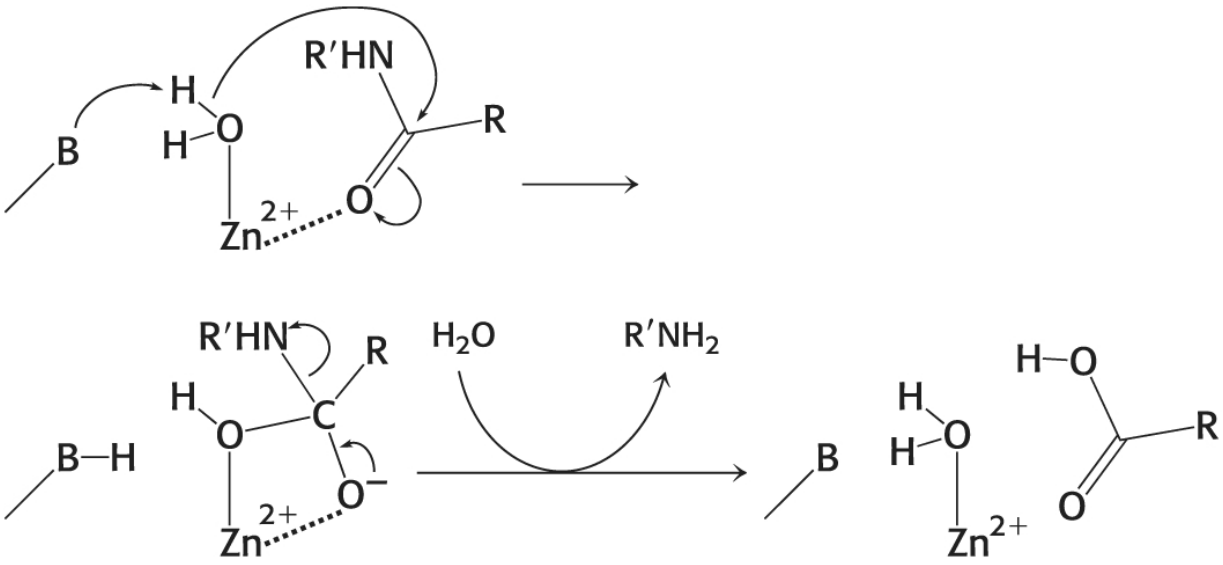
In the final step, two products are formed. The first product is R dash N H 2. The structure of the second product is as follows: A central C is single bonded to R on the upper left, double bonded to O on the upper right, single bonded to O below. The O atom below is single-bonded to H on the lower left.

A 2-carbon alkane chain is depicted as a vertical line on the right. C 1 of this chain is single-bonded to C on the upper left. This C is partially double-bonded to O above and partially double-bonded to O on the lower left. The C O O group has a negative charge.

A 2-carbon alkane chain is depicted as a vertical line on the left. C 1 of this chain is single-bonded to C on the upper left. This C is single bonded O, single bond, H above, and double bonded to O on the lower left.

Return to Reaction mechanism of aspartyl protease

Extended description for Reaction mechanism of metalloprotease



In the first step, a central Z n superscript 2 plus atom is shown below. It is single-bonded to O above. This O is single-bonded to H on the upper left and lower left. A dashed line connects the Z n superscript plus atom with the O atom of another compound. This compound consists of a central C atom double bonded to O on the lower left, single bonded to R dash H N on the upper left, and single bonded to R on the upper right. B with an open single bond on the lower left attacks the upper left H of H 2 O. An arrow from the single bond between this H and O of H 2 O points toward the central C atom. An arrow from the double bond between the central C atom and the lower left O points toward O.

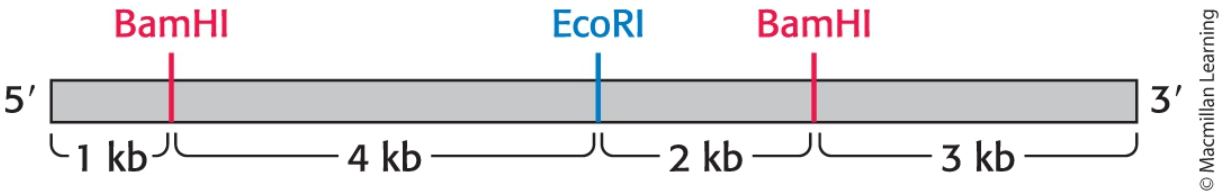
In the second step, B with an open single bond is single-bonded to H on the right. Z n superscript 2 plus is single bonded to O above, which is further single bonded to H on the upper left. This O is also single-bonded to C on the right. C is single bonded to N H R dash on the upper left, single bonded to R on the upper right, and single

bonded to O superscript minus on the lower left. A dashed line connects O superscript minus with Z n superscript 2 plus. An arrow from O superscript minus points toward its single bond with the C atom. An arrow from the single bond between this C and N H R dash points toward the N H R dash.

In the third step, H 2 O enters, and R dash N H 2 leaves. B with an open single bond is located on the left. A central O single bonded to Z n superscript 2 plus below, single bonded to H on the upper left and lower left is shown in the middle. The third compound consists of a central C atom double bonded to O on the lower left, single bonded to R on the right, and single bonded to O above. This O is single-bonded to H on the left.

Return to Reaction mechanism of metalloprotease

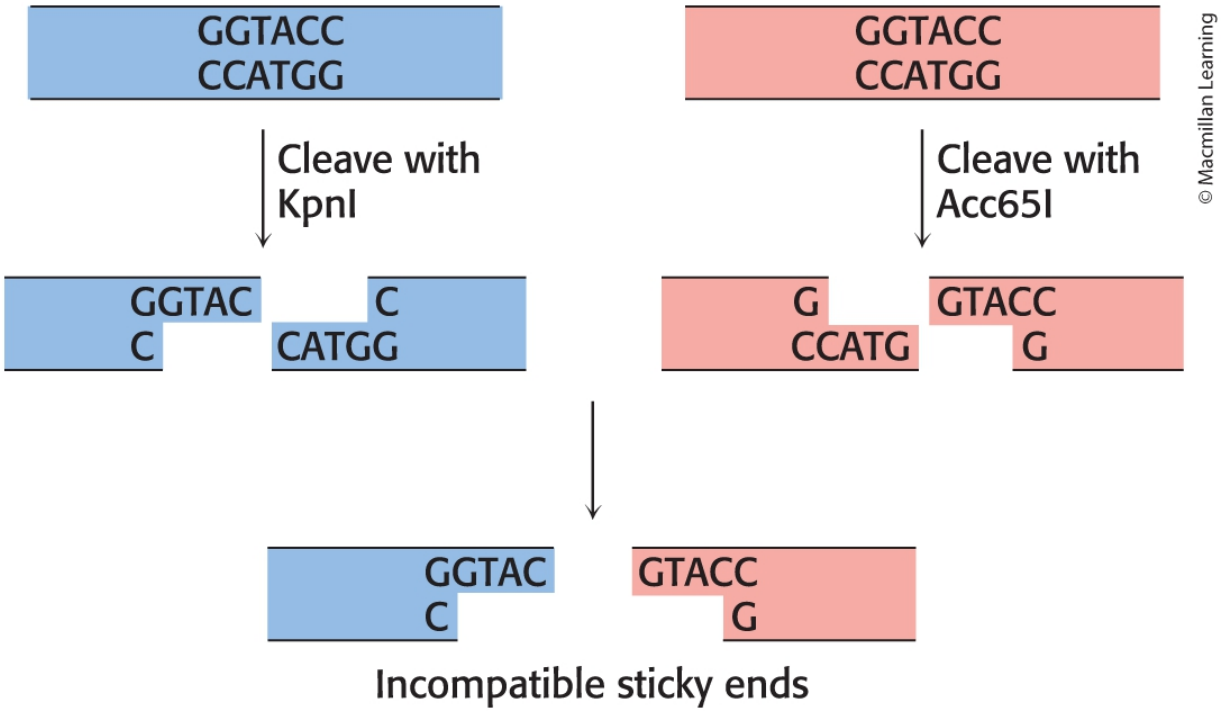
Extended description for Restriction map of a linear D N A



The D N A is depicted as a horizontal bar with its left end labeled 5 prime and right end labeled 3 prime. It contains two B a m H 1 sites and one Eco R 1 site. The first B a m H 1 site is located near the 5 prime end and the second site is located close to the 3 prime end. The Eco R 1 site is located in the middle of the D N A. The distance between the 5 prime end and the first B a m H 1 site is 1 k b. The distance between the second B a m H 1 site and the 3 prime end is 3 k b. The distance between the first B a m H 1 and Eco R 1 site is 4 k b. The distance between the Eco R 1 site and the second B a m H 1 site is 2 k b.

Return to Restriction map of a linear D N A

Extended description for Formation of incompatible sticky ends



A short blue horizontal bar depicts a D N A segment containing the sequence G G T A C C. G G T A C C is base paired with C C A T G G. This D N A is cleaved with K p n roman number 1. The bond between the first C and second C of the top sequence and the first C and second C of the bottom sequence is cleaved. This creates an overhang sequence containing G G T A C at the top and C at the bottom. The first G of the top sequence is base paired with C.

A short pink horizontal bar depicts a D N A segment containing the sequence G G T A C C. G G T A C C is base paired with C C A T G G. The D N A segment is cleaved with A c c 65 roman number 1. The bond between the first and second G of the top sequence and the first G and second G of the bottom sequence is cleaved. This creates

an overhang sequence containing G T A C C at the top and G at the bottom. The second C of the top sequence is base paired with G.

These overhang sequences produced from the two different D N A segments are labeled "incompatible sticky ends."

Return to Formation of incompatible sticky ends

Extended description for Three pairs of aligned protein sequences



In the first pair, the aligned sequences are as follows:

The first sequence is as follows: W Y L G K I T R M D A E V L L K K P T V R D G H F L V T Q C E S S P G E F.

The second sequence is as follows: W Y F G K I T R R E S E R L L L N P E N P R G T F L V R E S E T T K G A Y.

In the second pair, the aligned sequences are as follows:

The first sequence is as follows: S I S V R F G D S V Q, five dashes, H F K V L R D Q N G K Y Y L W A V K, single dash, F N. The second sequence is as follows: C L S V S D F D N A K G L N V K H Y K I R K L D S G G F Y I T S R T Q F S.

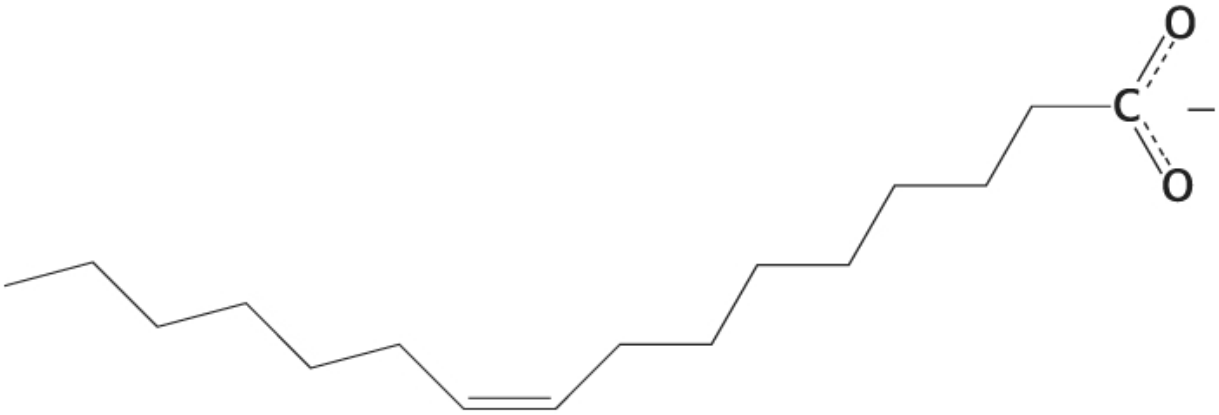
In the third pair, the aligned sequences are as follows: The first sequence is as follows: S L N E L V A Y H R T A S V S R T H T I L L S D M N V.

The second sequence is as follows: S S L Q Q L V A Y Y S K H A D G L C H R L T N V.

The identical amino acid residues in the aligned pairs are highlighted in yellow.

Return to Three pairs of aligned protein sequences

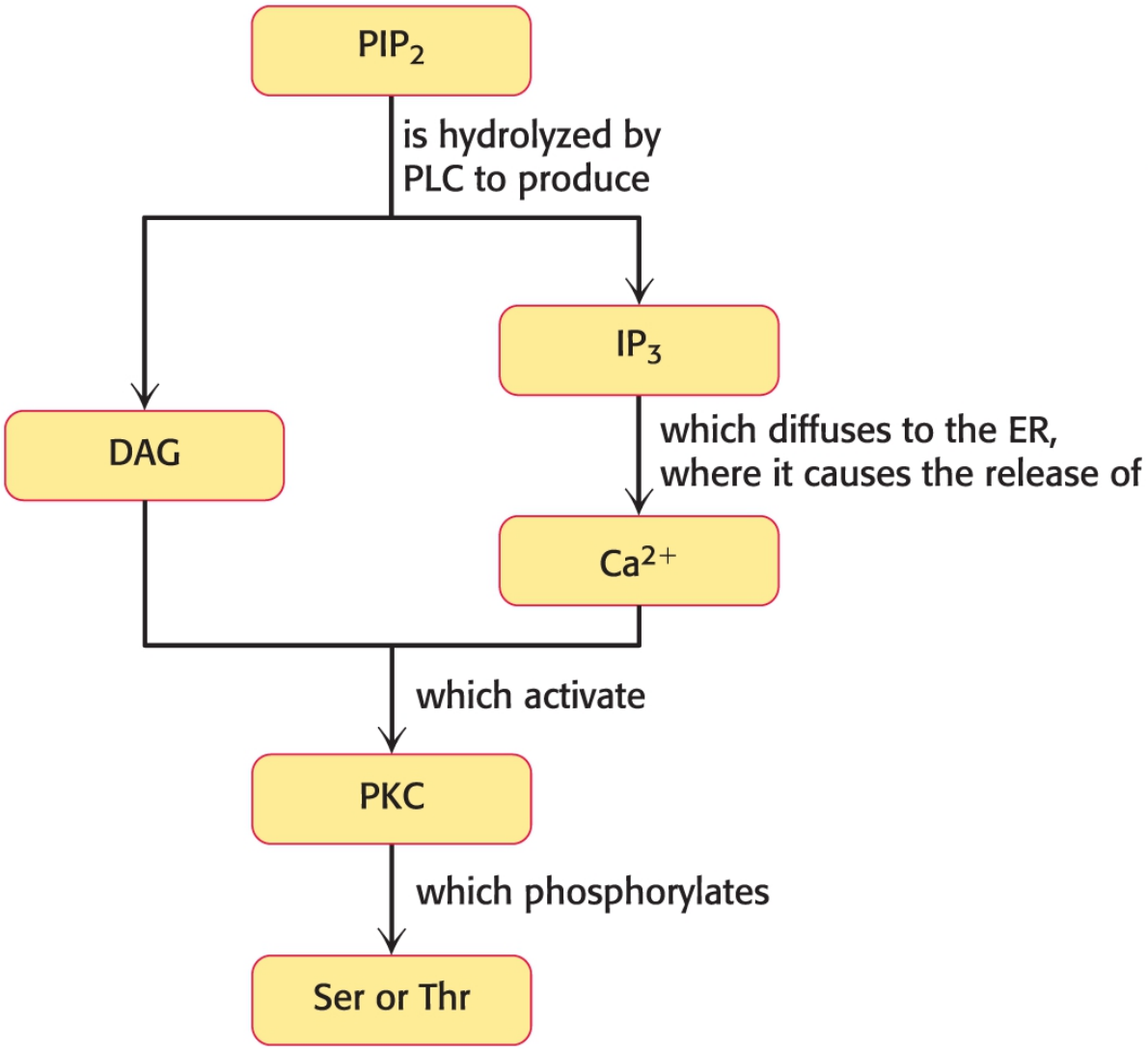
Extended description for Chemical structure



The chemical structure is depicted as follows: A 15-carbon alkene chain is depicted as a line structure using 14 zigzag lines. A double bond is present between C 7 and C 8. C 15 is single bonded to C on the right. This C is partially double-bonded to O on the upper right and O on the lower right. The C O O group has an overall negative charge.

Return to Chemical structure

Extended description for Flowchart depicts a signaling pathway



© Macmillan Learning

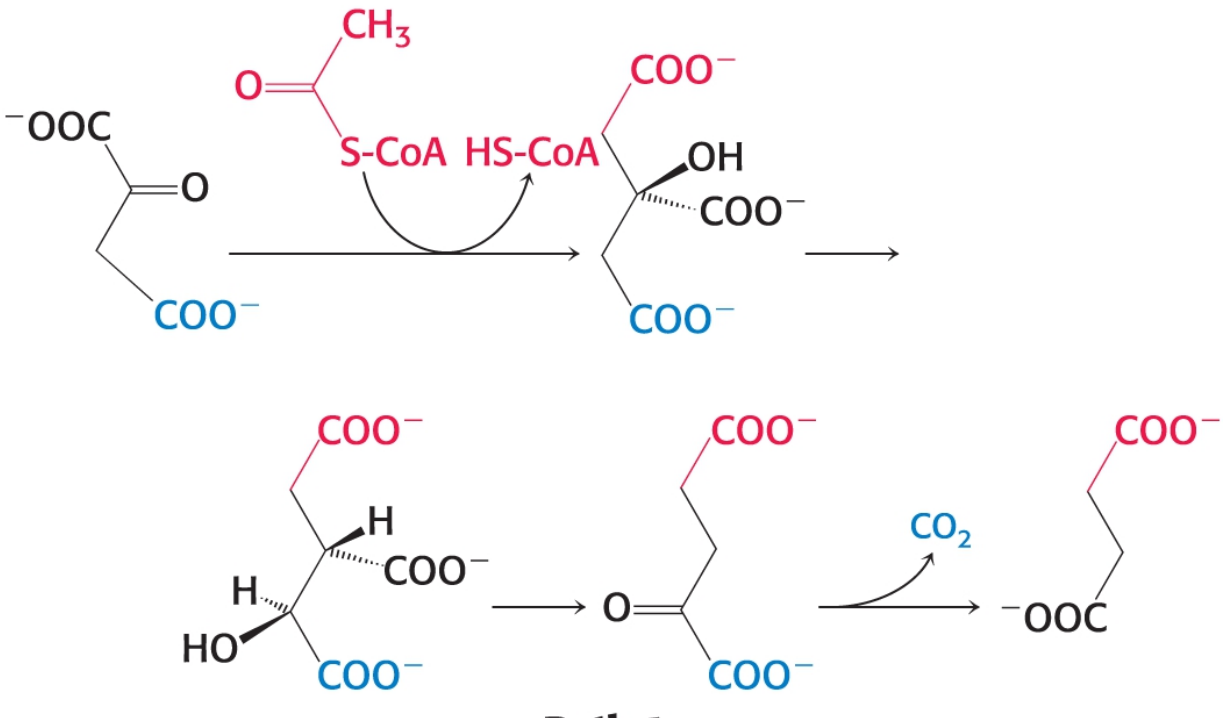
A rectangular yellow box labeled P I P 2 is shown at the top. A line below this box is labeled "is hydrolyzed by P L C to produce." The line bifurcates into two downward arrows. The left arrow leads to a yellow box labeled D A G. The right arrow leads to a box labeled I P 3. A downward arrow labeled "which diffuses to the E R, where it causes the release of." leads to a yellow box labeled C a superscript 2

plus. Lines from D A G and C a superscript 2 plus combine into a single downward arrow labeled "which activate." This arrow leads to a yellow box labeled P K C. A downward arrow below P K C is labeled "which phosphorylates" and it leads to a box labeled serine or threonine.

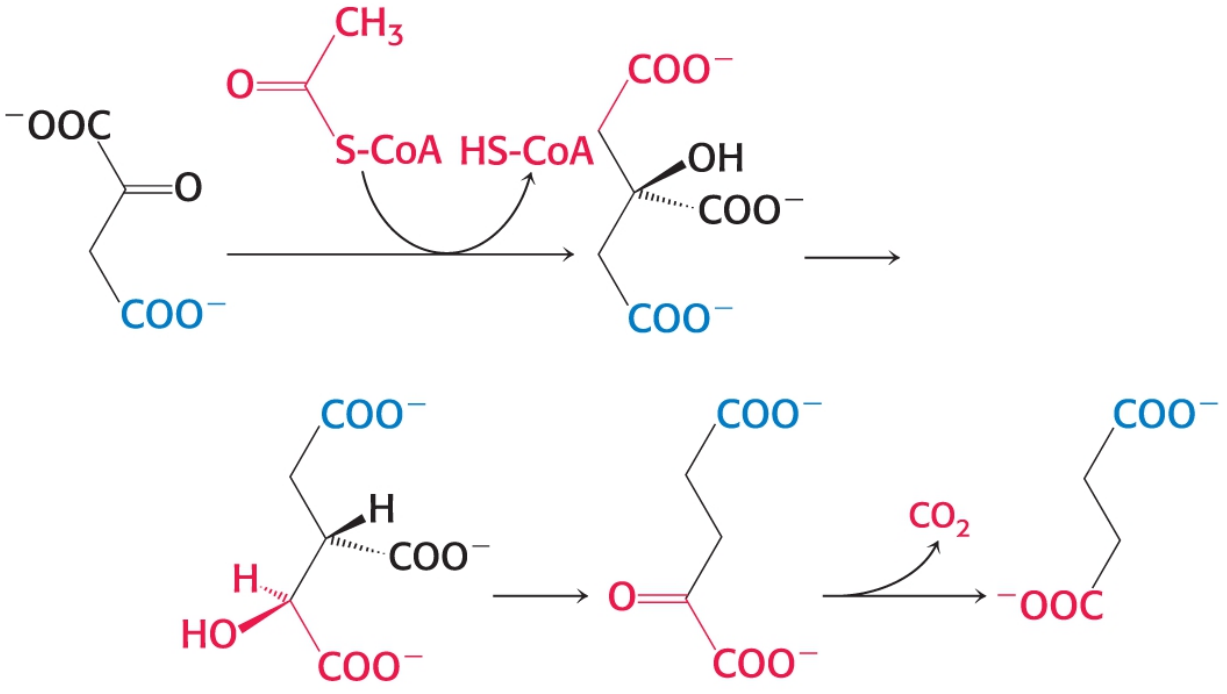
Return to Flowchart depicts a signaling pathway

Extended description for Citrate molecule undergoing

a series of reactions



Path 1



Path 2 (does not occur)

Path 1 is depicted as follows:

In the first irreversible, there is one reactant and one product. It is coupled with the entry of acetyl-C o A and release of H S, single bond, C o A.

The structure of the reactant is as follows: A central C atom is single bonded to C H 2 on the lower left in the form of a line, double bonded to O on the right, and single bonded to C O O superscript minus on the upper left. C H 2 is single bonded to C O O superscript minus on the lower right.

The structure of acetyl C o A is as follows: A central C atom is double bonded to O on the left, single bonded to C H 3 on the upper right, and single bonded to S, single bond, C o A on the lower right.

The structure of the product is as follows: A 3-carbon alkane chain is depicted as a vertical line structure using 2 zigzag lines. C 1 is single bonded to C O O superscript minus on the upper right. C 2 is wedge bonded to O H on the upper right and dash bonded to C O O superscript minus on the lower right. C 3 is single bonded to C O O superscript minus on the lower right.

In the second irreversible step, the product of the first step serves as the reactant and is converted into another product.

The structure of the product is as follows: A 3-carbon alkane chain is depicted as a line structure using 2 zigzag lines. C 1 is single bonded to C O O superscript minus on the upper right. The C O O group is highlighted in red. C 2 is wedge bonded to H on the upper right and dash bonded to C O O superscript minus on the right. C 3 is dash bonded to H on the left, wedge bonded to O H on the lower left, and

single bonded to C O O superscript minus on the lower right. The C O O group is highlighted in blue.

In the third irreversible step, the product of the second step is converted into another product.

The structure of the product is as follows: A 3-carbon alkane chain is depicted as a line structure using 2 zigzag lines. C 1 is single bonded to C O O superscript minus on the upper right. C 3 is double bonded to O on the left and single bonded to C O O superscript on the lower right.

In the fourth irreversible step, C O 2 is released and the product of the third step is converted into the final product. C O 2 is highlighted in blue.

The structure of the final product is as follows: A 2-carbon alkane chain is depicted as a diagonal line. C 1 is single bonded to C O O superscript minus on the upper right and single bonded to C O O superscript minus on the lower left. The upper right C O O group is highlighted in red.

Path 2 is depicted as follows:

In the first irreversible, there is one reactant and one product. It is coupled with the entry of acetyl-C o A and release of H S, single bond, C o A.

The structure of the reactant is as follows: A central C atom is single bonded to C H 2 on the lower left in the form of a line, double bonded to O on the right, and single bonded to C O O superscript minus on the upper left. C H 2 is single bonded to C O O superscript minus on the lower right.

The structure of acetyl C o A is as follows: A central C atom is double bonded to O on the left, single bonded to C H 3 on the upper right, and single bonded to S, single bond, C o A on the lower right.

The structure of the product is as follows: A 3-carbon alkane chain is depicted as a vertical line structure using 2 zigzag lines. C 1 is single bonded to C O O superscript minus on the upper right. C 2 is wedge bonded to O H on the upper right and dash bonded to C O O superscript minus on the lower right. C 3 is single bonded to C O O superscript minus on the lower right. In the second irreversible step, the product of the first step serves as the reactant and is converted into another product.

The structure of the product is as follows: A 3-carbon alkane chain is depicted as a line structure using 2 zigzag lines. C 1 is single bonded to C O O superscript minus on the upper right. The C O O group is highlighted in blue. C 2 is wedge bonded to H on the upper right and dash bonded to C O O superscript minus on the right. C 3 is dash bonded to H on the left, wedge bonded to O H on the lower left, and single bonded to C O O superscript minus on the lower right. The substituents of C 3 are highlighted in red.

In the third irreversible step, the product of the second step is converted into another product.

The structure of the product is as follows: A 3-carbon alkane chain is depicted as a line structure using 2 zigzag lines. C 1 is single bonded to C O O superscript minus on the upper right highlighted in blue. C 3 is double bonded to O on the left and single bonded to C O O superscript on the lower right. Both O and C O O superscript minus are highlighted in red.

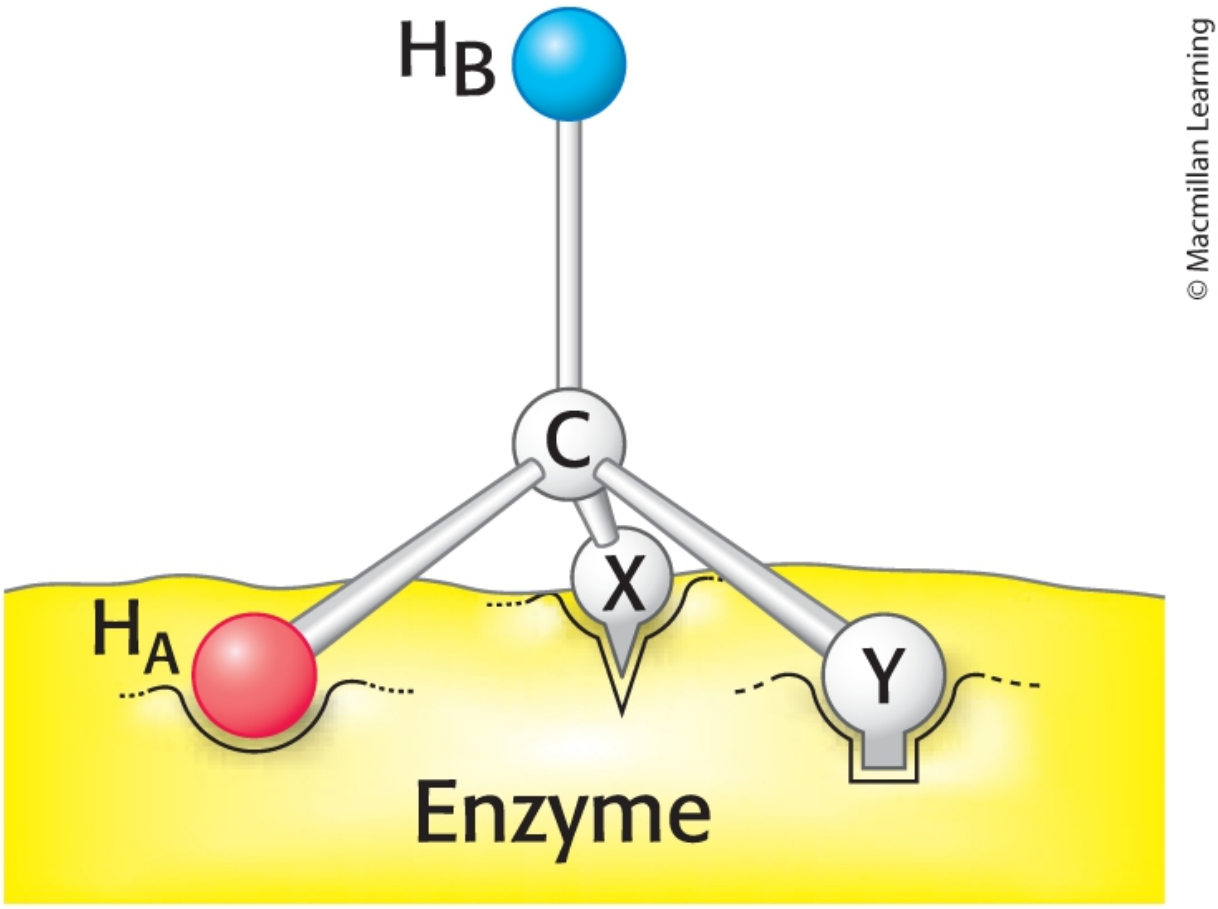
In the fourth irreversible step, C O 2 is released and the product of the third step is converted into the final product. C O 2 is highlighted in red.

The structure of the final product is as follows: A 2-carbon alkane chain is depicted as a diagonal line. C 1 is single bonded to C O O superscript minus on the upper right and single bonded to C O O superscript minus on the lower left. The upper right C O O group is highlighted in blue and the lower left C O O group is highlighted in red.

Note: Path 2 does not occur.

Return to Citrate molecule undergoing a series of reactions

Extended description for Illustration of an enzyme bound to a substrate



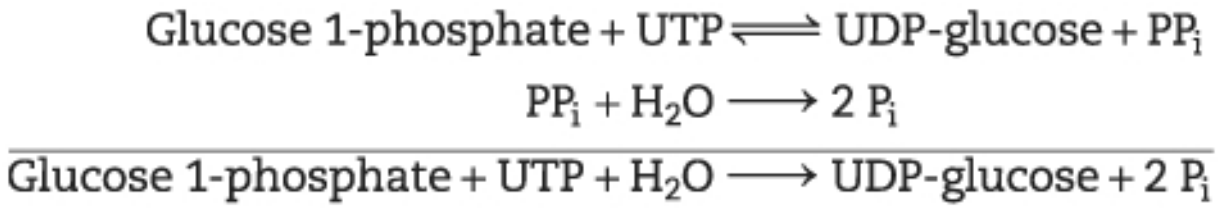
© Macmillan Learning

The top surface of the enzyme is shown. The substrate is depicted in a ball-and-stick model. It consists of a central white sphere depicting C connected to a blue sphere above, a red sphere on the lower left, a white sphere labeled Y on the lower right, and a small white sphere labeled X below. The blue sphere is labeled H subscript B and the red sphere is labeled H subscript A. The red sphere and the white sphere labeled Y are located toward the observer. Both these spheres are bound to a cleft on the top surface of the enzyme. The sphere labeled Y has a small rectangular portion that fits inside a rectangular groove. The white sphere labeled X has a conical

protrusion at the bottom that fits inside a complementary groove on the top surface of the enzyme.

Return to Illustration of an enzyme bound to a substrate

Extended description for Two reactions and their overall summation



The first reversible reaction consists of two reactants and two products. The first reactant is glucose 1-phosphate. The second reactant is U T P. The first product is U D P-glucose. The second reactant is P P subscript i.

The second irreversible reaction consists of two reactants and one product. The first reactant is P P subscript i. The second reactant is H 2 O. The product is 2 P subscript i.

The overall summation reaction is irreversible and consists of three reactants and two products. The first reactant is glucose 1-phosphate. The second reactant is U T P. The third reactant is H 2 O. The first product is U D P-glucose. The second product is 2 P subscript i.

Return to Two reactions and their overall summation

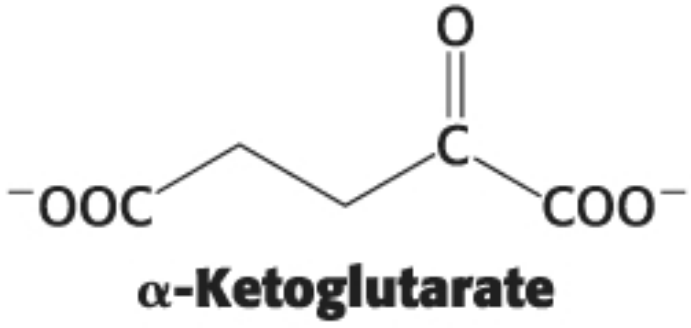
Extended description for Reversible chemical reaction



The reaction consists of two reactants and two products. The first reactant is oxaloacetate and second reactant is N A D H plus H superscript plus. The first product is malate and the second product is N A D superscript plus.

Return to Reversible chemical reaction

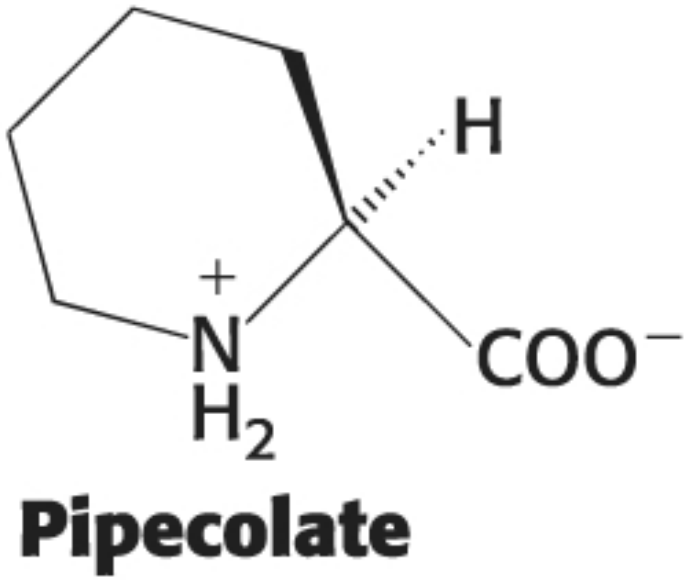
Extended description for Structure of alpha-ketoglutarate



The structure of alpha-ketoglutarate is as follows: A 3-carbon alkane chain is depicted as a line structure using 2 zigzag lines. C 1 is single bonded to C O O superscript minus on the lower left. C 3 is double bonded to O above and single bonded to C O O superscript minus on the lower right.

Return to Structure of alpha-ketoglutarate

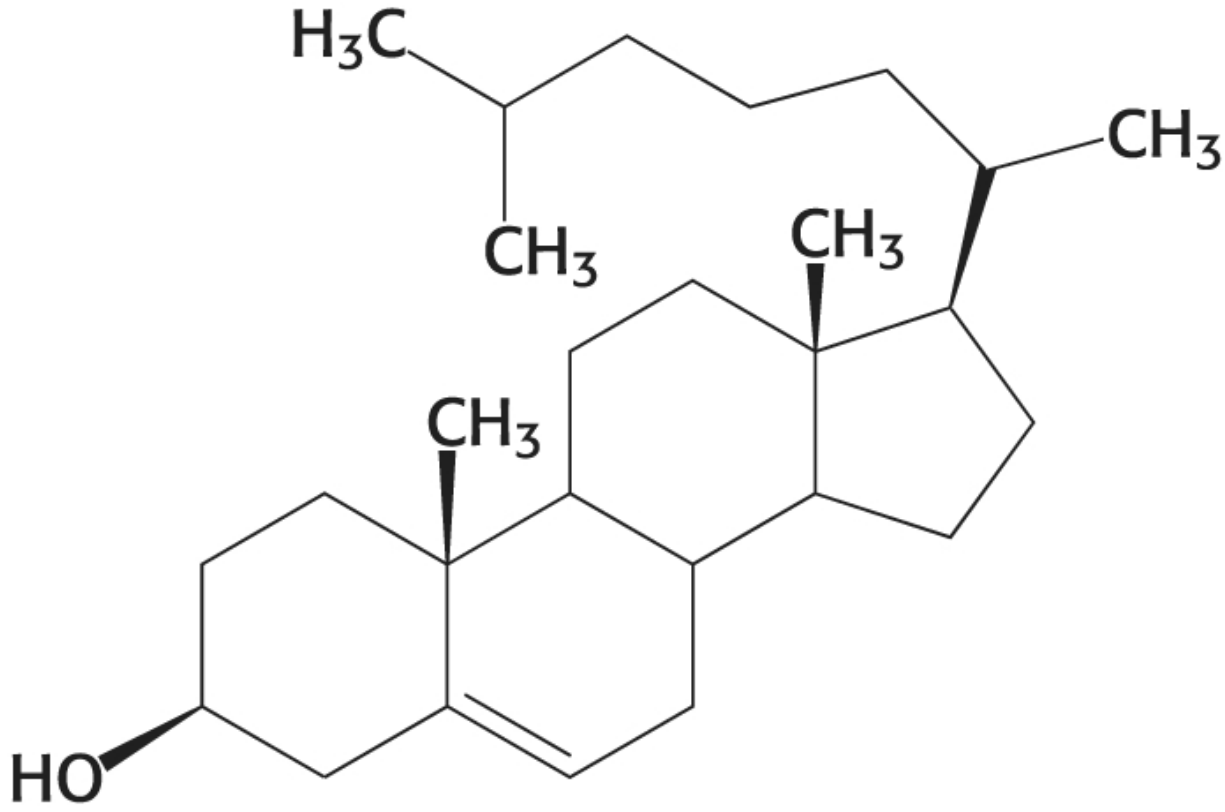
Extended description for Structure of pipecolate



A 6-membered heterocyclic hexagonal ring is in a horizontal orientation with C 1 occupying the bottom left vertex. It consists of 1 N and 5 C atoms. N with a positive charge occupies the bottom right vertex and is bound to H 2. C 5 is wedge bonded to C 4. C 5 is dash bonded to H on the upper right and single bonded to C O O superscript minus on the lower right.

Return to Structure of pipecolate

Extended description for Chemical structure of four fused rings

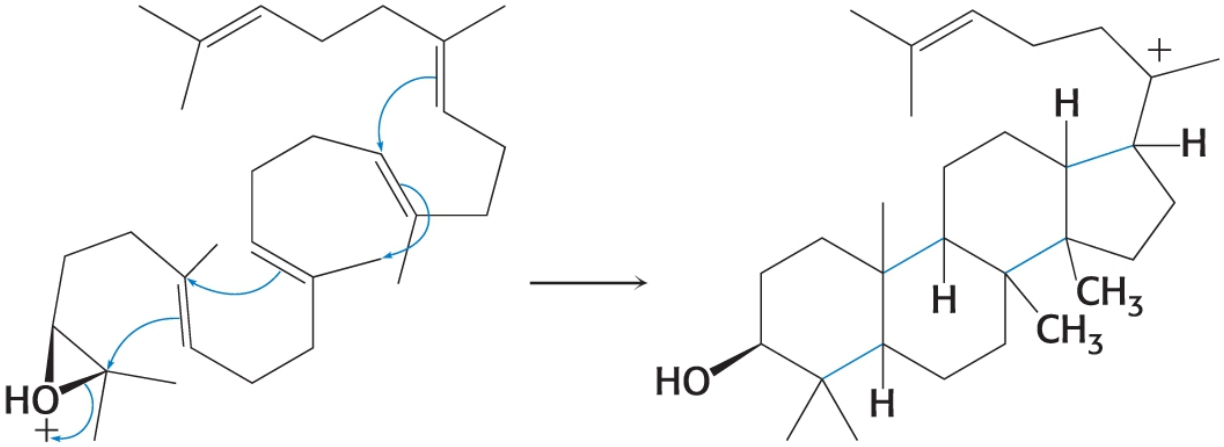


The structure is as follows: A 6-carbon homocyclic hexagonal ring is in a vertical orientation with C 1 occupying the topmost vertex. C 5 is wedge bonded to O H on the lower left. It is fused to a second 6-carbon homocyclic hexagonal ring in a vertical orientation such that C 2 and C 3 of the first ring are C 6 and C 5 respectively of the second ring. In the second ring, C 6 is wedge bonded to C H 3 above. A double bond is present between C 4 and C 5. The second ring is fused to a third 6-carbon homocyclic hexagonal ring in a vertical orientation such that C 1 and C 2 of the second ring are C 5 and C 4 respectively of the third ring. The third ring is fused to a 5-carbon homocyclic pentagonal ring in a horizontal orientation such that C 2 and C 3 of the third ring are C 4 and C 3 respectively of the

pentagonal ring. C 4 is wedge bonded to C H 3 above. C 5 is wedge bonded to C 5 of a 5 carbon alkane chain depicted as a line structure using 4 zigzag lines. C 1 of the alkane chain is single bonded to C H 3 on the upper right and C H 3 below. C 5 is single bonded to C H 3 on the upper left.

Return to Chemical structure of four fused rings

Extended description for Formation of protosterol cation



Protosterol cation

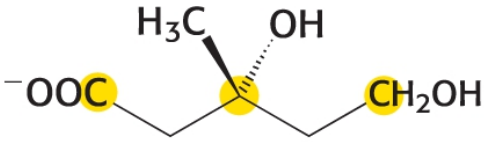
The structure of the reactant is as follows: A 5-carbon alkene chain is depicted as a line structure using 4 zigzag lines. A double bond is present between C 1 and C 2. C 1 is single bonded to C H 3 on the upper left and C H 3 below in the form of a line. C 5 is single bonded to C H 3 in the form of a line on the upper right and double bonded to C H below. This C H group is single-bonded to a C H 2 group on the lower right in the form of a line. This C H 2 group is single-bonded to C H 2 on the lower left in the form of a line. This C H 2 is single-bonded to C 1 of a 14-carbon alkene chain on the left depicted as a line structure using 13 zigzag lines. A double bond is present between C 1 and C 2, C 5 and C 6, and C 9 and C 10. C 1 is single-bonded to C H 3 in the form of a line on the lower left. C 6 is single bonded to C H 3 on the lower right in the form of a line. C 10 is single bonded to C H 3 on the upper right in the form of a line. C 13 and C 14 are each wedge bonded to a common O H superscript plus group atom. C 14 is single bonded to C H 3 on the lower right and lower left in the formation of a line. An arrow from the double bond between C 5 of the alkene chain and the C H group points toward C 2

of the 14-carbon alkene chain. An arrow from the double bond between C 1 and C 2 of the 14-carbon alkene chain points toward the C H 3 group single-bonded to C 6 of the 14-carbon alkene chain. An arrow from the double bond between C 5 and C 6 points to C H 3 single bonded to C 10. An arrow from the double bond between C 9 and C 10 points toward C H 3 group single-bonded to C 14.

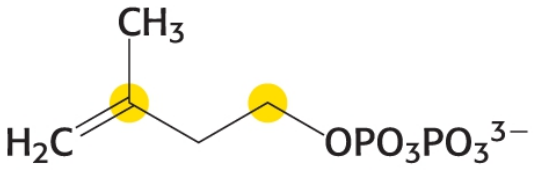
The product is a protosterol cation whose structure is as follows: Two 6-carbon hexagonal rings in vertical orientation have C 1 at the topmost vertex. Both the rings are fused such that C 2 and C 3 of the first ring are C 6 and C 5 respectively of the second ring. In the first ring, C 2 is single bonded to C H 3 above in the form of a line, C 3 is single bonded to H below, C 4 is single bonded to C H 3 on the lower left, and C H 3 on the lower right in the form of a line. C 5 is wedge bonded to O H on the lower left. In the second ring, C 1 is single-bonded to H below. Another 6-carbon hexagonal ring in vertical orientation is fused with the second ring such that C 1 and C 2 of the second ring are C 5 and C 4 respectively of the third ring. C 2 is single bonded to H above. C 3 and C 4 are each single bonded to C H 3. A 5-membered pentagonal ring in horizontal orientation with C 1 occupying the top right vertex is fused with the third ring such that C 2 and C 3 of the third ring are C 5 and C 4 respectively of the fourth ring. C 1 is single bonded to H on the right and single bonded to C 6 of a 7-carbon alkene chain depicted using 6 zigzag lines. In the alkane chain, a double bond is present between C 2 and C 3. C 6 of the alkene chain has a positive charge. C 2 of the alkane chain is single-bonded to C H 3 below in the form of a line.

Return to Formation of protosterol cation

Extended description for Structure of labeled mevalonate and labeled isopentenyl pyrophosphate



Labeled mevalonate



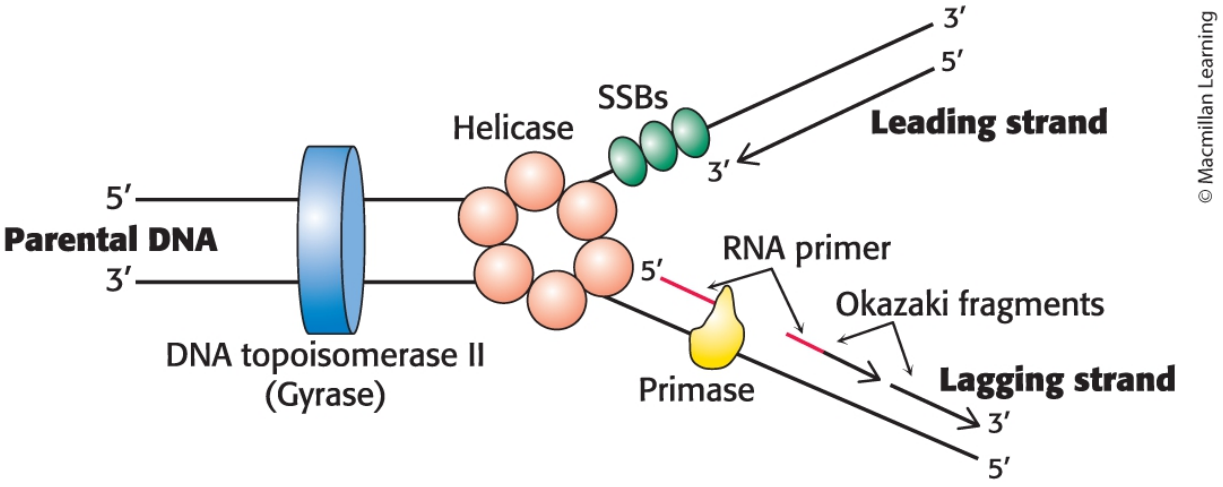
Labeled isopentenyl pyrophosphate

The structure of labeled mevalonate is as follows: A 3-carbon alkane chain is depicted as a line structure using 2 zigzag lines. C 1 is single bonded to C O O superscript minus. The C atom of the C O O group is highlighted in yellow. C 2 highlighted in yellow is wedge bonded to C H 3 on the upper left and dash bonded to O H on the upper right. C 3 is single bonded to C H 2 O H on the upper right. The C atom of the C H 2 O H group is highlighted in yellow.

The structure of labeled isopentenyl pyrophosphate is as follows: A 3-carbon alkane chain is depicted as a line structure using 2 zigzag lines. C 1 and C 3 are highlighted in yellow. C 1 is double bonded to C H 2 on the lower left and single bonded to C H 3 above. C 3 is single bonded to O P O 3 P O 3 superscript 3 minus on the lower right.

Return to Structure of labeled mevalonate and labeled isopentenyl pyrophosphate

Extended description for Illustration of the replication fork



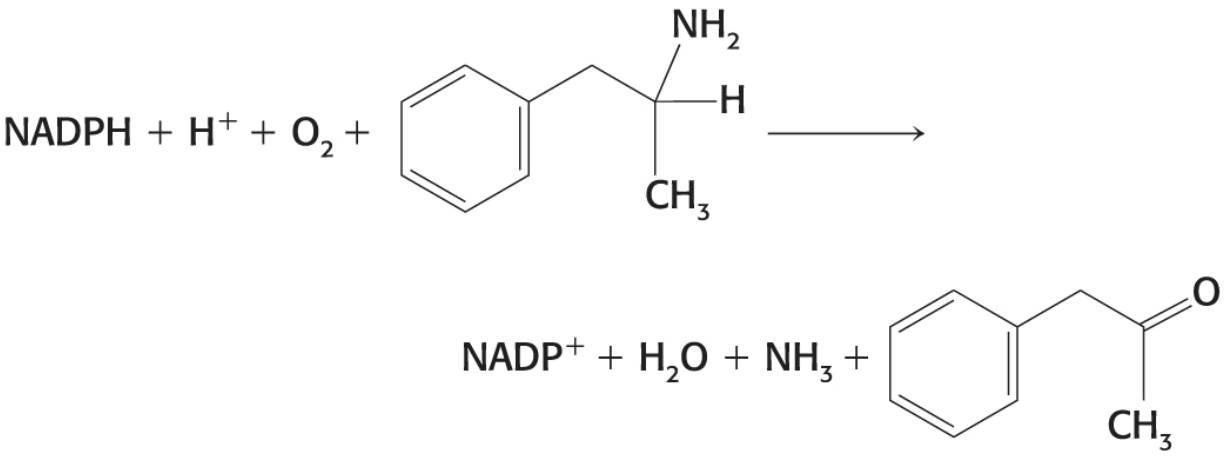
© Macmillan Learning

A horizontal Y-shaped replication fork is shown. The double-stranded D N A is labeled parental D N A. It is bound by a D N A topoisomerase 2 (gyrase) depicted as a thick circular disc. The side view of the disc is visible to the observer. The 5 prime end of the top D N A strand and 3 prime end of the bottom D N A strand are aligned together. The 3 prime and 5 prime ends of the top and bottom strands are separated to form a Y-shaped structure. The 3 prime end of the top strand is oriented toward the upper right. The 5 prime end of the bottom strand is oriented toward the lower right. A line parallel to the upper right 3 prime end is labeled leading strand. Its top end is labeled 5 prime and the bottom end has an arrowhead pointing toward the replication fork. The arrowhead end is labeled 3 prime. Two short lines separated by short gaps are aligned parallel with the lower right 5 prime end. The bottom end of each line has an arrowhead. These short lines depict Okazaki fragments. The arrowhead of the terminal Okazaki fragment is labeled 3 prime. These Okazaki fragments are collectively labeled lagging strand. The Okazaki fragment closer to the fork contains an R N A primer

depicted as a short red stretch. A primase is bound to the lagging strand template near the replication fork. It is engaged in the synthesis of a R N A primer. A helicase depicted as a hollow ring-like structure composed of 6 small spherical structures is bound to the replication fork. The single-stranded region of the leading strand template is bound by S S Bs depicted as small green ovals.

Return to Illustration of the replication fork

Extended description for Oxidative deamination reaction

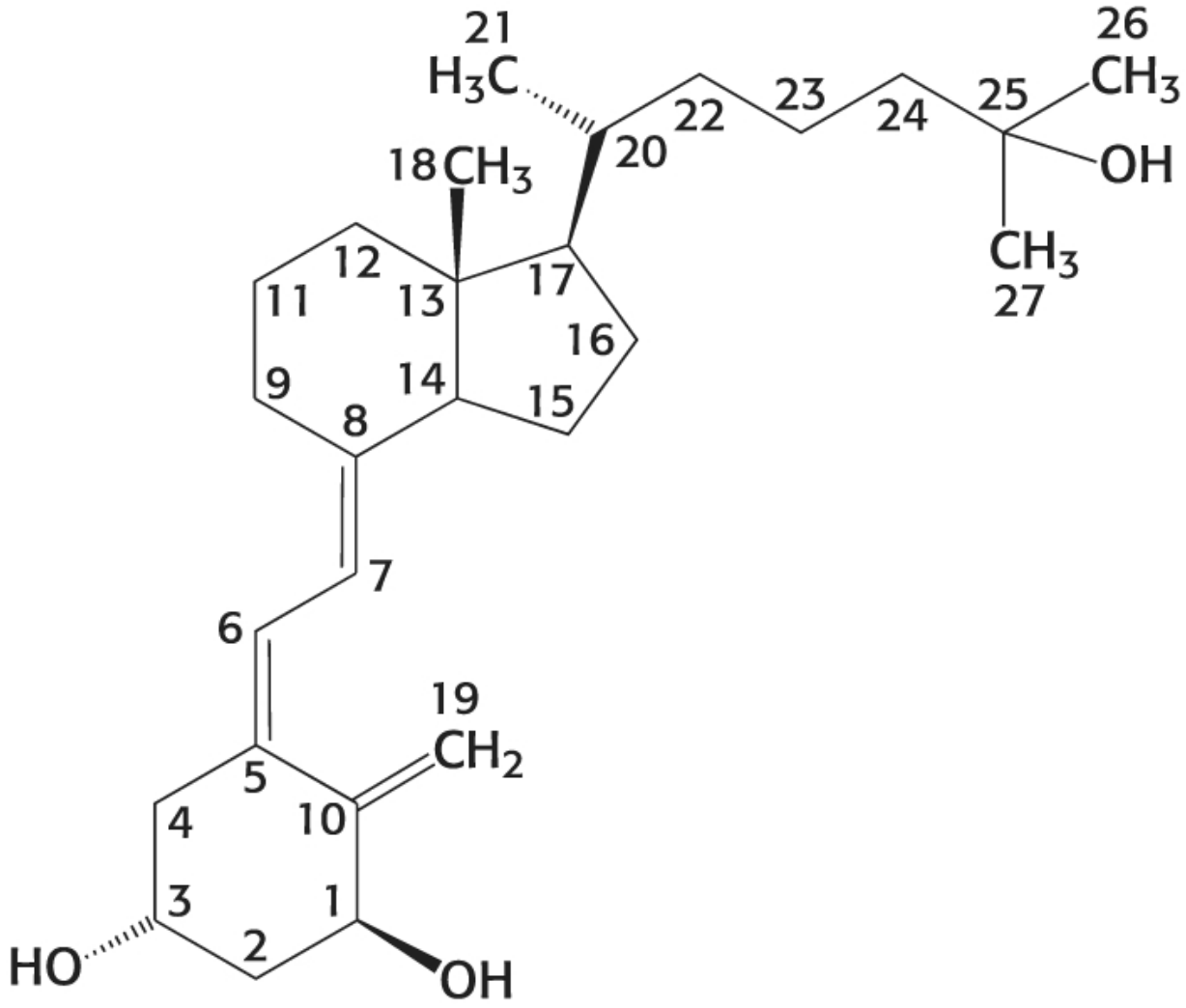


The reaction consists of three reactants and four products. The first reactant is N A D P H plus H superscript plus. The second reactant is O 2. The structure of the third reactant is as follows: A benzene ring is in a vertical orientation with C 1 occupying the topmost vertex. It contains alternating double bonds between C 2 and C 3, C 4 and C 5, and C 6 and C 1. C 2 is single bonded to C H 2 on the upper right in the form of a line. This C H 2 is single bonded to C on the lower right. The C atom is single-bonded to N H 2 on the upper right, H on the right, and C H 3 below.

The first product is N A D P superscript plus. The second product is H 2 O. The third product is N H 3. The structure of the fourth product is as follows: A benzene ring is in a vertical orientation with C 1 occupying the topmost vertex. It contains alternating double bonds between C 2 and C 3, C 4 and C 5, and C 6 and C 1. C 2 is single bonded to C H 2 on the upper right in the form of a line. This C H 2 is single bonded to C on the lower right. The C atom is double-bonded to O on the upper right and single-bonded to C H 3.

Return to Oxidative deamination reaction

Extended description for Chemical structure

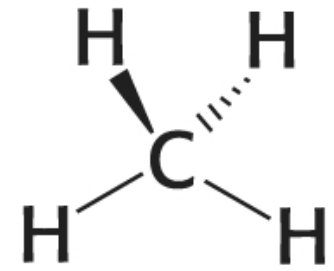


The structure is as follows: A 6-carbon hexagonal ring is in a vertical orientation with C 1 occupying the topmost vertex. C 2 is double bonded to C H 2 on the upper right, numbered 19. C 3 is wedge bonded to O H on the lower right. C 5 is dash bonded to O H on the lower left. C 3, C 4, C 5, C 6, C 1, and C 2 of this ring are numbered 1, 2, 3, 4, 5, and 10 respectively. C 1 is double bonded to C H above, numbered 6. C H is single bonded to C H on the upper right, numbered 7. This C H is double bonded to C 4 of a 6-carbon

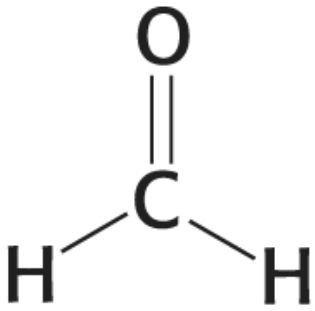
hexagonal ring in a vertical orientation with C 1 occupying the topmost vertex. C 4, C 5, C 6, C 1, C 2, and C 3 of this ring are numbered 8, 9, 11, 12, 13, and 14 respectively. The hexagonal ring is fused with a 5-carbon pentagonal ring in a horizontal orientation such that C 2 and C 3 of the hexagonal ring are C 4 and C 3 respectively of the pentagonal ring. C 4 of the pentagonal ring is wedge bonded to C H 3 above, numbered 18. C 2, C 1, and C 5 of this ring are numbered 15, 16, and 17 respectively. C 5 is wedge bonded to C 1 of a 5-carbon alkane chain depicted as a line structure using 4 zigzag lines. C 1 is dash bonded to C H 3 on the upper left, numbered 21. C 5 is single bonded to C H 3 on the upper right, numbered 26, O H on the lower right, and C H 3 below numbered 27. C 1, C 2, C 3, C 4, and C 5 are numbered 20, 22, 23, 24, and 25 respectively.

Return to Chemical structure

Extended description for Structure of methane and formaldehyde



Methane



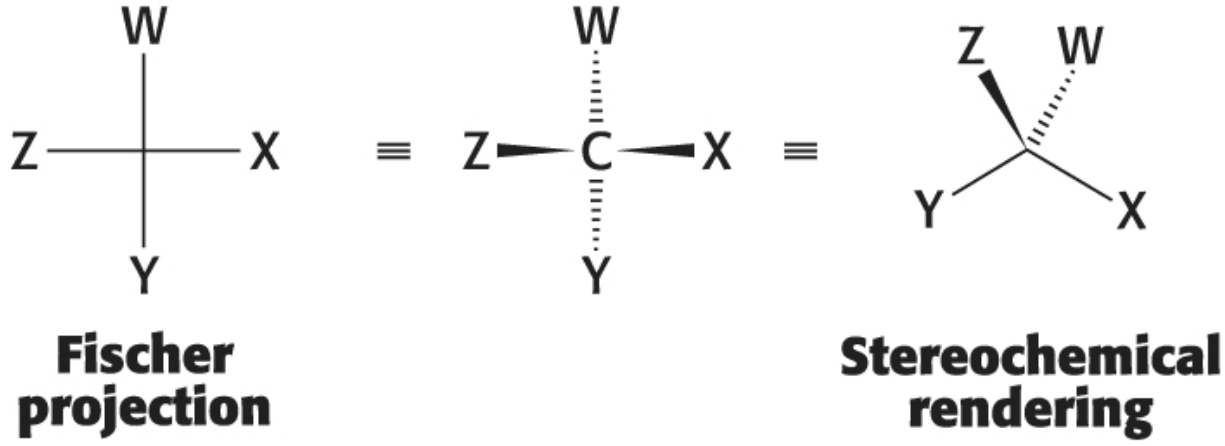
Formaldehyde

Methane has the following structure: A central C atom is dash bonded to H on the upper right, single bonded to H on the lower right and H on the lower left, and is wedge bonded to H on the upper left.

Formaldehyde has the following structure: A central C atom is double bonded to O above and is single bonded to H on the lower right and H on the lower left.

Return to Structure of methane and formaldehyde

Extended description for Structure of a molecule with its Fischer projection and stereochemical rendering



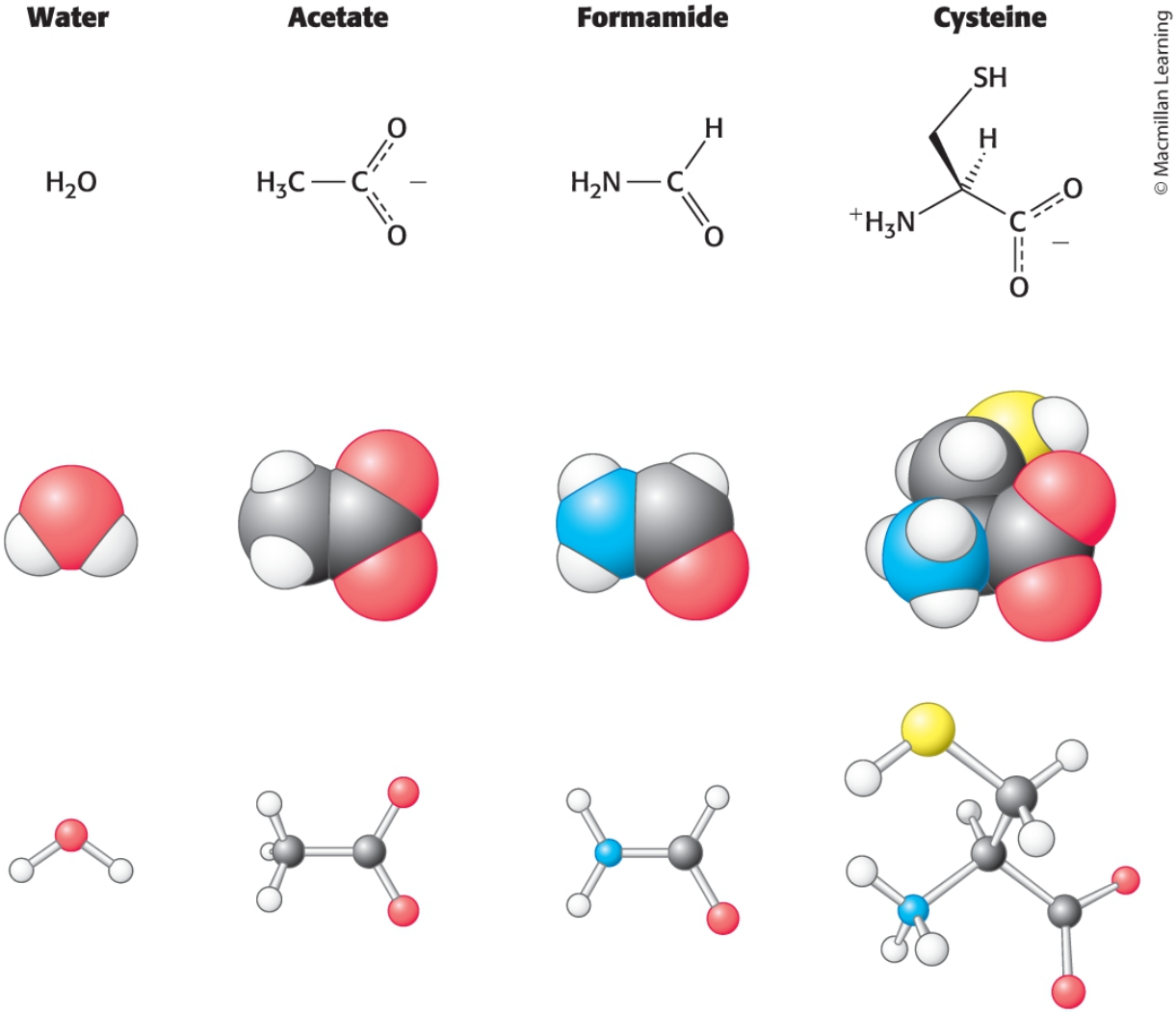
The molecule has the following structure: A central C atom is dash bonded to W above, wedge bonded to X on the right, dash bonded to Y below, and wedge bonded to Z on the left.

The Fischer projection consists of a central C atom depicted as a dot with a vertical line passing through it with W at the top and Y at the bottom, and a horizontal line passing through it with X on the right and Z on the left.

The stereochemical rendering shows a central C atom dash bonded to W on the upper right, single bonded to X on the lower right and Y on the lower left, and wedge bonded to Z on the upper left.

Return to Structure of a molecule with its Fischer projection and stereochemical rendering

Extended description for FIGURE 1 Molecules are depicted in various ways



© Macmillan Learning

In each space-filling and ball-and-stick model, an H atom is depicted as a small white sphere, an O atom is depicted as a red sphere, a C atom is depicted as a black sphere, an N atom is depicted as a blue sphere, and an S atom is depicted as a large yellow sphere.

Water: Structural formula: H 2 O.

Space-filling model: A large central red sphere is fused to a white sphere on the lower right and a white sphere on the lower left.

Ball-and-stick model: A central red sphere is single bonded to a white sphere on the lower right and a white sphere on the lower left.

Acetate: Structural formula: A central C atom carrying a negative charge is partially double bonded to O on the upper right, partially double bonded to a second O atom on the lower right, and is single bonded to C H 3 on the left.

Space-filling model: Two black spheres are fused horizontally. The first black sphere on the left is fused to a white sphere on the upper left toward the observer, a white sphere on the lower left toward the observer, and a white sphere on the left away from the observer. The second black sphere on the right is fused to a red sphere on the upper right toward the observer and a second red sphere on the lower right toward the observer.

Ball-and-stick model: Two black spheres are single bonded to each other. The first black sphere on the left is single bonded to a white sphere on the upper left toward the observer, a white sphere on the lower left toward the observer, and a white sphere on the left away from the observer. The second black sphere on the right is single bonded to a red sphere on the upper right toward the observer and a second red sphere on the lower right toward the observer.

Formamide: Structural Formula: A central C atom is single bonded to H on the upper right, double bonded to O on the lower right, and single bonded to N H 2 on the left.

Space-filling model: A blue sphere is fused to a black sphere on the right. The blue sphere is fused to a white sphere on the upper left

toward the observer, and a white sphere on the lower left toward the observer. The black sphere is fused to a white sphere on the upper right toward the observer and a red sphere on the lower right toward the observer.

Ball-and-stick model: A blue sphere is single bonded to a black sphere on the right. The blue sphere is single bonded to a white sphere on the upper left toward the observer, and a white sphere on the lower left toward the observer. The black sphere is single bonded to a white sphere on the upper right toward the observer and is double bonded to a red sphere on the lower right toward the observer.

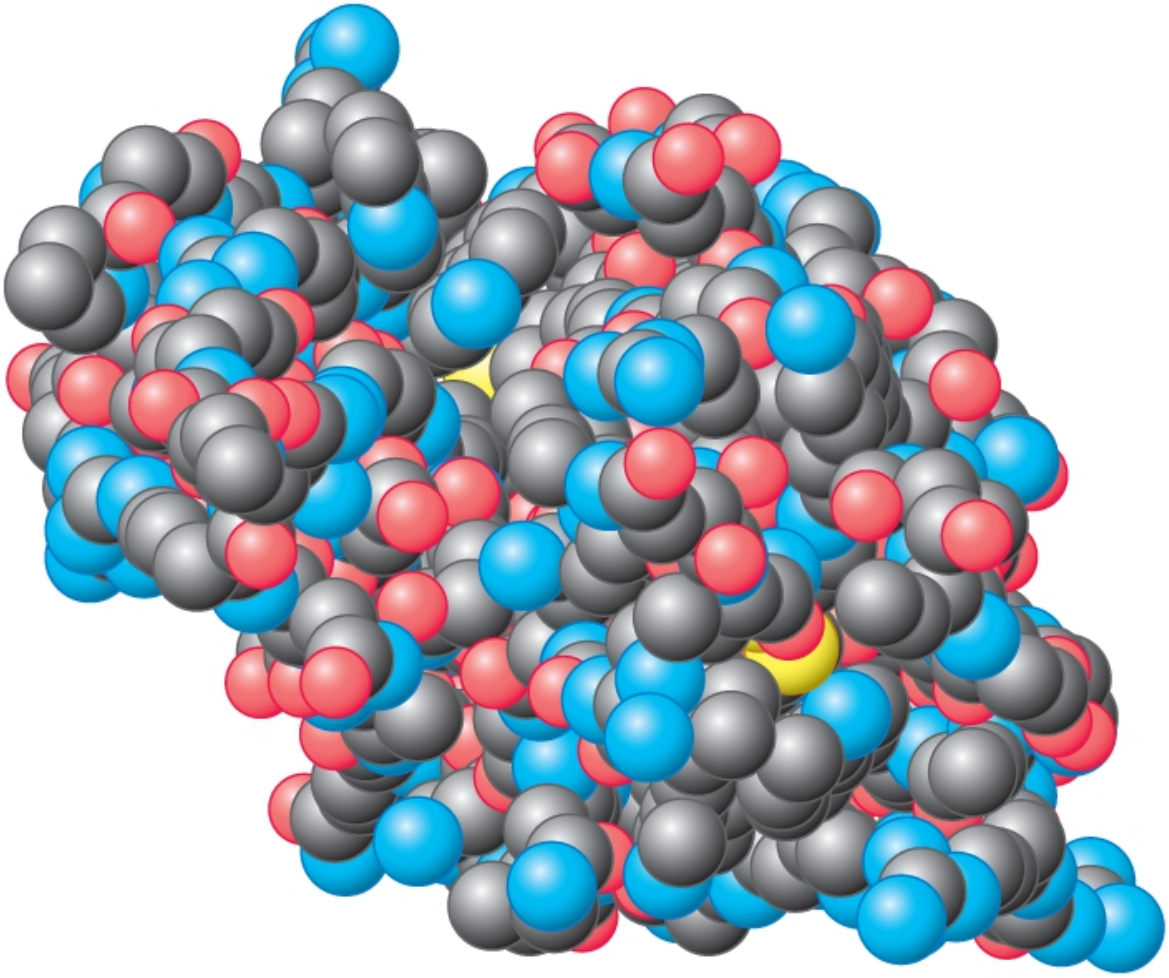
Cysteine: Structural Formula: A 2-carbon alkane chain is depicted as a line structure using 1 wedged line. C 1 is single bonded to S H on the upper right. C 2 is dash bonded to H on the upper right, single bonded to N H 3 superscript plus on the lower left, and is single bonded to a central C atom carrying a negative charge on the lower right. The central C atom is partially double bonded to O on the upper right and a second O atom below.

Space-filling model: A central black sphere is fused to a second black sphere on the upper left away from the observer, a third black sphere on the upper right toward the observer, a blue sphere on the lower left toward the observer, and a white sphere not visible to the observer. The second black sphere is fused to a white sphere on the upper right toward the observer, a white sphere on the upper left away from the observer, and a yellow sphere on the upper right away from the observer. The yellow sphere is fused to a white sphere on the upper right away from the observer. The second black sphere is fused to a red sphere on the upper right and a second red sphere on the lower right. The blue sphere is fused to a white sphere on the upper right toward the observer, a white sphere below, and a white sphere on the upper left away from the observer.

Ball-and-stick model: A central black sphere is single bonded to a white sphere on the upper left away from the observer, a second black sphere on the upper right toward the observer, a third black sphere on the lower right, and a blue sphere on the lower left. The second black sphere is single bonded to a white sphere on the upper right away from the observer, a white sphere on the lower right toward the observer, and a yellow sphere on the upper left. The yellow sphere is single bonded to a white sphere on the lower left toward the observer. The third black sphere is single bonded to a red sphere on the upper right away from the observer, and a second red sphere below. The blue sphere is single bonded to a white sphere on the lower right toward the observer, a white sphere on the lower left away from the observer, and a white sphere on the upper left toward the observer.

Return to FIGURE 1 Molecules are depicted in various ways

Extended description for FIGURE 2 A space-filling model shows the atoms tightly packed

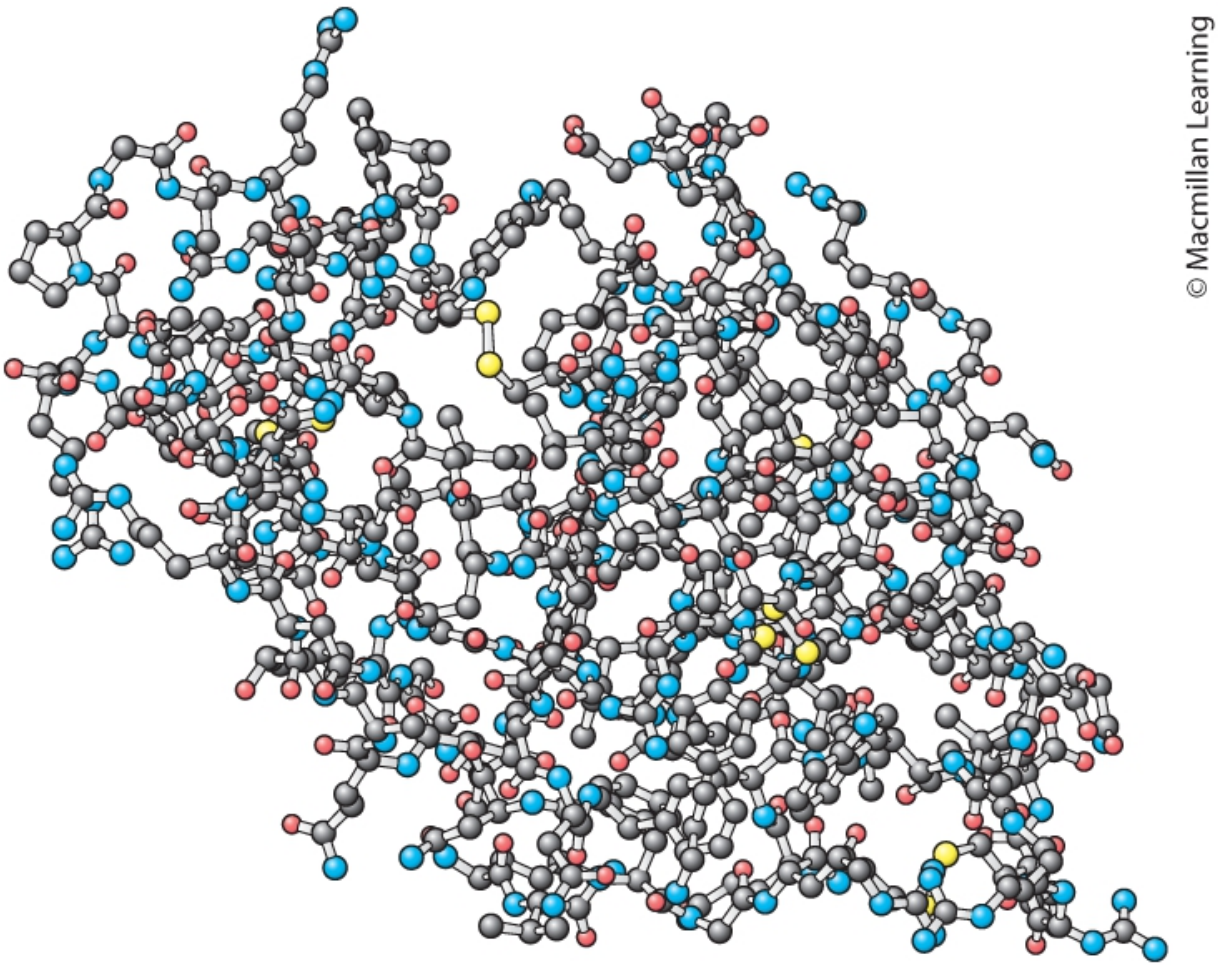


© Macmillan Learning

In the space-filling model, an O atom is depicted as a red sphere, a C atom is depicted as a black sphere, an N atom is depicted as a blue sphere, and an S atom is depicted as a large yellow sphere. The model shows a large number of red, blue, and black spheres and one yellow sphere fused together forming an aggregated cluster.

Return to FIGURE 2 A space-filling model shows the atoms tightly packed

Extended description for FIGURE 3 In a ball-and-stick model, bonds are represented by sticks

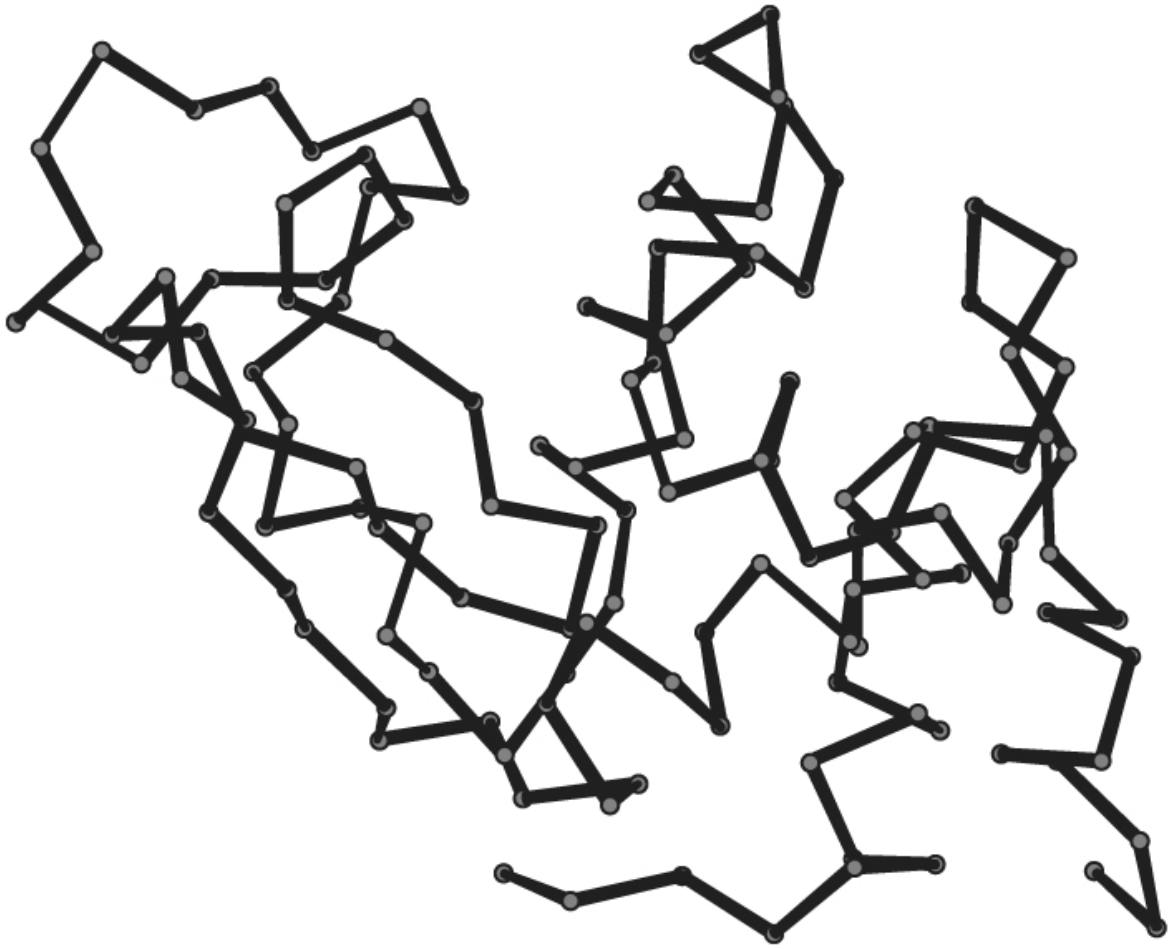


© Macmillan Learning

In the ball-and-stick model, an O atom is depicted as a red sphere, a C atom is depicted as a black sphere, an N atom is depicted as a blue sphere, and an S atom is depicted as a large yellow sphere. The model shows a large number of red, blue, and black spheres and one yellow sphere bonded to each other with the bonds represented as sticks.

Return to FIGURE 3 In a ball-and-stick model, bonds are represented by sticks

Extended description for FIGURE 4 In a backbone model, only the backbone polypeptide chain is represented

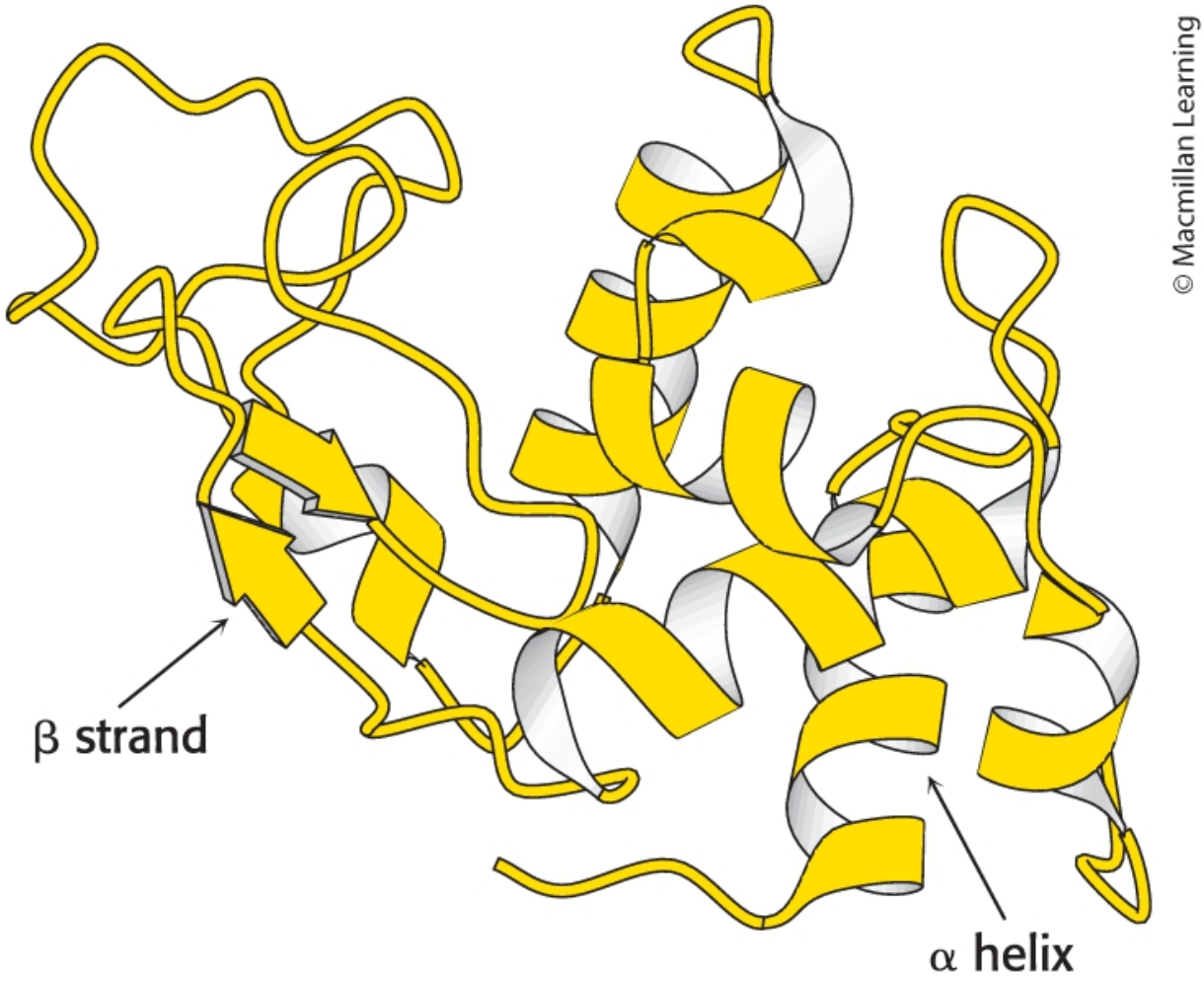


© Macmillan Learning

In the backbone model, alpha carbons of the adjacent amino acids are depicted as gray spheres. The model consists of several gray spheres bonded to each other with the bonds depicted as black zigzag lines.

Return to FIGURE 4 In a backbone model, only the backbone polypeptide chain is represented

Extended description for FIGURE 5 In a simple ribbon diagram, the *α* helices are shown as coiled ribbons and a strands are depicted as arrows

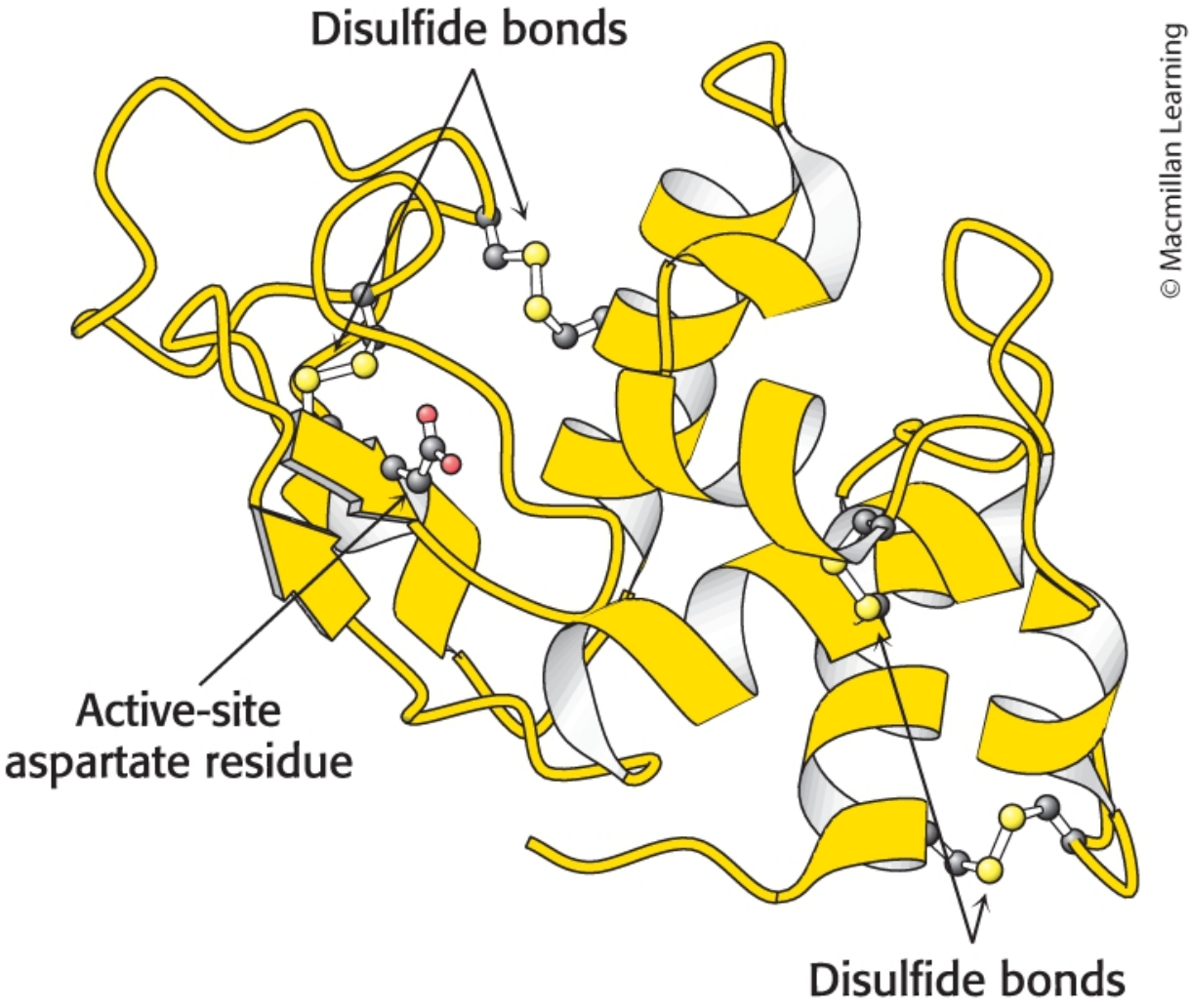


© Macmillan Learning

In the simple ribbon diagram, three alpha helices depicted as coiled yellow ribbons are shown on the right connected by thin thread-like loops. Two antiparallel beta strands are shown on the lower left depicted as arrows pointing toward the upper left and lower right, respectively.

Return to FIGURE 5 In a simple ribbon diagram, the *α* helices are shown as coiled ribbons and a strands are depicted as arrows

Extended description for FIGURE 6 An enhanced ribbon diagram may show functionally important areas using ball-and-stick

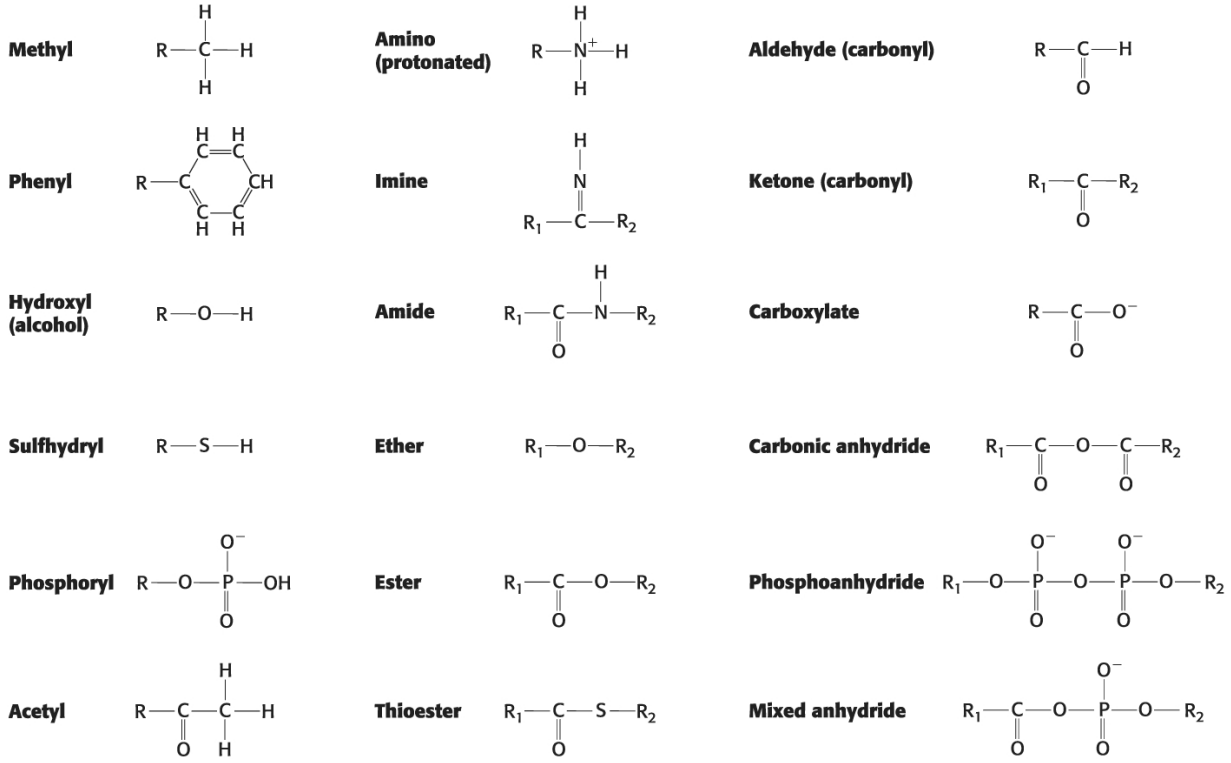


In the enhanced ribbon diagram, three alpha helices depicted as coiled yellow ribbons are shown on the right connected by thin thread-like loops. Two antiparallel beta strands are shown on the lower left depicted as arrows pointing toward the upper left and lower right, respectively. Five ball-and-stick models are shown in which an O atom is depicted as a red sphere, a C atom is depicted as

a black sphere, and an S atom is depicted as a large yellow sphere. A disulfide bond consists of a zigzag chain of four black spheres and two yellow spheres, in which the yellow spheres occupy the third and fourth positions. Two disulfide bonds are present on the upper left, one on the center right, and one on the lower right. An active-site aspartate residue shown on the lower left, consists of a zigzag chain of three black spheres. The third black sphere is double bonded to a red sphere above and is single bonded to a second red sphere on the lower right.

Return to FIGURE 6 An enhanced ribbon diagram may show functionally important areas using ball-and-stick

Extended description for FIGURE 7 Structures of various functional groups



Methyl: A central C atom is single bonded to H above, H on the right, H below, and R on the left.

Amino (protonated): A central N atom carrying a positive charge is single bonded to H above, H on the right, H below, and R on the left.

Aldehyde (carbonyl): A central C atom is single bonded to H on the right, double bonded to O below, and single bonded to R on the left.

Phenyl: A benzene ring is in a horizontal orientation with a C atom occupying each vertex and C 1 occupying the rightmost vertex. The ring contains alternating double bonds between C 1 and C 2, C 3 and

C 4, and C 5 and C 6. C 1 to C 3, C 5, and C 6 are each bound to H. C 4 is single bonded to R.

Imine: A vertical chain is illustrated by H, single bond, N, double bond, C. C is single bonded to R 1 on the left and R 2 on the right.

Ketone (carbonyl): A central C atom is double bonded to O below, and single bonded to R 1 on the left and R 2 on the right.

Hydroxyl (alcohol): A central O atom is single bonded to H on the right, and R on the left.

Amide: R 1, single bond, C, single bond, N, single bond, R 2. C is double bonded to O below. N is single bonded to H above.

Carboxylate: A central C atom is single bonded to O superscript minus on the right, double bonded to O below, and is single bonded to R on the left.

Sulfhydryl: A central S atom is single bonded to H on the right and R on the left.

Ether: A central O atom is single bonded to R 1 on the left and R 2 on the right.

Carbonic anhydride: R 1, single bond, C, single bond, O, single bond, C, single bond, R 2. C 1 and C 2 are each double bonded to O below.

Phosphoryl: R, single bond, O, single bond, P, single bond, O H. P is single bonded to O superscript minus above and is double bonded to a second O atom below.

Ester: R 1, single bond, C, single bond, O, single bond, R 2. C is double bonded to a second O atom below. Phosphoanhydride: R 1, single bond, O, single bond, P, single bond, O, single bond, P, single bond, O, single bond, R 2. Each P atom is single bonded to O superscript minus above and is double bonded to an O atom below.

Acetyl: R, single bond, C, single bond, C, single bond, H. C 1 is double bonded to O below. C 2 is single bonded to H above and H below.

Thioester: R 1, single bond, C, single bond, S, single bond, R 2. C is double bonded to a second O atom below.

Mixed anhydride: R 1, single bond, C, single bond, O, single bond, P, single bond, O, single bond, R 2. C is double bonded to a third O atom below. P is single bonded to O superscript minus above and is double bonded to a fourth O atom below.

Return to FIGURE 7 Structures of various functional groups

Extended description for Reaction between ammonia, N H 3, and methyl iodide, H 3 C, single bond, I and its mechanism



The reaction contains two reactants and two products. The first reactant is H 3 N in which N has a lone pair of electrons. The second reactant is H 3 C, single bond, I. A curved arrow from the lone pair of electrons in the first reactant points to C of H 3 C in the second reactant. A second curved arrow from the single bond in the second reactant between H 3 C and I points to I. The first product is H 3 N superscript plus, single bond, C H 3. The second product is I superscript minus.

Return to Reaction between ammonia, N H 3, and methyl iodide, H 3 C, single bond, I and its mechanism

Reference Tables

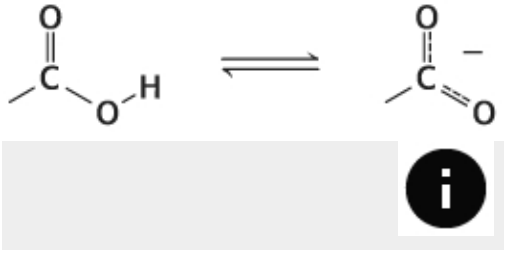
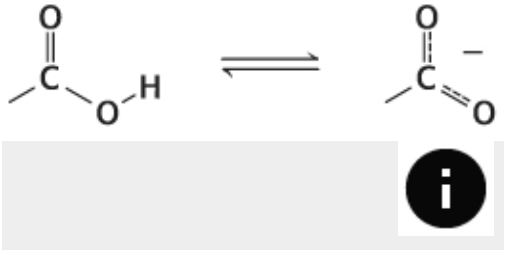
Typical pK_a values of some acids

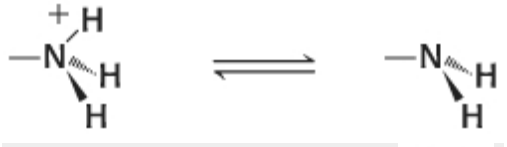
Acid	pK_a (at 25°C)
Acetic acid	4.76
Acetoacetic acid	3.58
Ammonium ion	9.25
Ascorbic acid	pK_1 4.10 pK_2 11.79
Benzoic acid	4.20
n-Butyric acid	4.81
Cacodylic acid	6.19
Citric acid	pK_1 3.14 pK_2 4.77 pK_3 6.39
Ethylammonium ion	10.81

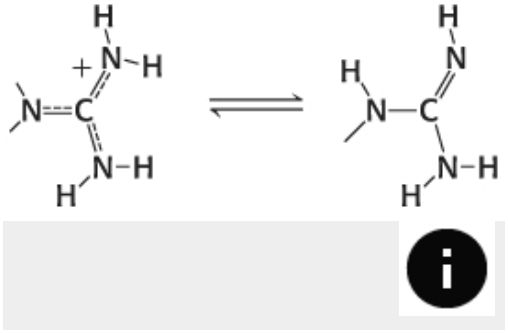
Formic acid	3.75
Glycine	pK_1 2.35 pK_2 9.78
Imidazolium ion	6.95
Lactic acid	3.86
Fumaric acid	pK_1 3.03 p pK_2 4.44
Malic acid	pK_1 3.40 pK_2 5.11
Phenol	9.89
Phosphoric acid	pK_1 2.12 pK_2 7.21 pK_3 12.67
Pyridinium ion	5.25
Pyrophosphoric acid	pK_1 0.85 pK_2 1.49 pK_3 5.77 pK_4 8.22
Succinic acid	pK_1 4.21 pK_2 5.64

Trimethylammonium ion	9.79
Tris (hydroxymethyl) aminomethane	8.08
Water, assuming $[H^+][OH^-] = 10^{-14}$; $[H_2O] = 55.5$ M	15.74

Typical pK_a values of ionizable groups in proteins

Group	Acid ⇌ Base	Typical pK_a
Terminal α-carboxyl group		3.1
Aspartic acid Glutamic acid		3.9 (Asp) 4.3 (Glu)

Histidine		6.0
Terminal α-amino group		8.0
Cysteine		8.3
Tyrosine		10.0

Lysine	10.4
	
Arginine	12.5
	

Note: pK_a values depend on temperature, ionic strength, and the microenvironment of the ionizable group

Standard bond lengths

Bond	Structure	Length (Å)
C—H	R_2CH_2 Aromatic RCH_3	1.07 1.08 1.10
C—C	Hydrocarbon Aromatic	1.54 1.40
C═C	Ethylene	1.33

C≡C	Acetylene	1.20
C—N	RNH_2 O═C—N	1.47 1.34
C—O	Alcohol Ester	1.43 1.36
C═O	Aldehyde Amide	1.22 1.24
C—S	R_2S	1.82
N—H	Amide	0.99
O—H	Alcohol	0.97
O—O	O_2	1.21
P—O	Ester	1.56
S—H	Thiol	1.33
S—S	Disulfide	2.05